

REVIEW OF PARTICLE PHYSICS*

Particle Data Group

Abstract

The *Review* summarizes much of particle physics and cosmology. Using data from previous editions, plus 2,143 new measurements from 709 papers, we list, evaluate, and average measured properties of gauge bosons and the recently discovered Higgs boson, leptons, quarks, mesons, and baryons. We summarize searches for hypothetical particles such as supersymmetric particles, heavy bosons, axions, dark photons, etc. Particle properties and search limits are listed in Summary Tables. We give numerous tables, figures, formulae, and reviews of topics such as Higgs Boson Physics, Supersymmetry, Grand Unified Theories, Neutrino Mixing, Dark Energy, Dark Matter, Cosmology, Particle Detectors, Colliders, Probability and Statistics. Among the 120 reviews are many that are new or heavily revised, including a new review on Machine Learning, and one on Spectroscopy of Light Meson Resonances.

The *Review* is divided into two volumes. Volume 1 includes the Summary Tables and 97 review articles. Volume 2 consists of the Particle Listings and contains also 23 reviews that address specific aspects of the data presented in the Listings.

The complete *Review* (both volumes) is published online on the website of the Particle Data Group (pdg.lbl.gov) and in a journal. Volume 1 is available in print as the *PDG Book*. A *Particle Physics Booklet* with the Summary Tables and essential tables, figures, and equations from selected review articles is available in print, as a web version optimized for use on phones, and as an Android app.

The 2022 edition of the *Review of Particle Physics* should be cited as:
R.L. Workman *et al.* (Particle Data Group), *Prog. Theor. Exp. Phys.* **2022**, 083C01 (2022)

DOI: 10.1093/ptep/ptac097

For the online version see pdg.lbl.gov:



© 2022

Except where otherwise noted, content of this work (the *Review of Particle Physics*) is licensed under a Creative Commons Attribution-NonCommercial 4.0 International (CC BY-NC 4.0) license.

*The publication of the *Review of Particle Physics* is supported by the Director, Office of Science, Office of High Energy Physics of the U.S. Department of Energy under Contract No. DE-AC02-05CH11231; by an implementing arrangement between the governments of Japan (MEXT: Ministry of Education, Culture, Sports, Science and Technology) and the United States (DOE) on cooperative research and development; by the Italian National Institute of Nuclear Physics (INFN); by the Physical Society of Japan (JPS); and by the European Laboratory for Particle Physics (CERN). Individual collaborators receive support for their PDG activities from their respective institutes or funding agencies.

Particle Data Group

R.L. Workman,¹ V.D. Burkert,² V. Crede,³ E. Klempt,⁴ U. Thoma,⁴ L. Tiator,⁵ K. Agashe,⁶ G. Aielli,⁷ B.C. Allanach,⁸ C. Amsler,⁹ M. Antonelli,¹⁰ E.C. Aschenauer,¹¹ D.M. Asner,¹¹ H. Baer,¹² Sw. Banerjee,¹³ R.M. Barnett,¹⁴ L. Baudis,¹⁵ C.W. Bauer,¹⁴ J.J. Beatty,¹⁶ V.I. Belousov,¹⁷ J. Beringer,¹⁴ A. Bettini*,¹⁸ O. Biebel,¹⁹ K.M. Black,²⁰ E. Blucher,²¹ R. Bonventre,¹⁴ V.V. Bryzgalov,¹⁷ O. Buchmuller,²² M.A. Bychkov,²³ R.N. Cahn,¹⁴ M. Carena,^{24,21,25} A. Ceccucci,²⁶ A. Cerri,²⁷ R. Sekhar Chivukula,²⁸ G. Cowan,²⁹ K. Cranmer,³⁰ O. Cremonesi,³¹ G. D'Ambrosio,³² T. Damour,³³ D. de Florian,³⁴ A. de Gouvêa,³⁵ T. DeGrand,³⁶ P. de Jong,³⁷ S. Demers,³⁸ B.A. Dobrescu,²⁴ M. D'Onofrio,³⁹ M. Doser,²⁶ H.K. Dreiner,⁴⁰ P. Eerola,⁴¹ U. Egede,⁴² S. Eidelman†,^{43,44} A.X. El-Khadra,⁴⁵ J. Ellis,^{46,26} S. C. Eno,⁶ J. Erler,⁵ V.V. Ezhela,¹⁷ W. Fetscher,⁴⁷ B.D. Fields,^{48,45} A. Freitas,⁴⁹ H. Gallagher,⁵⁰ Y. Gershtein,⁵¹ T. Gherghetta,⁵² M.C. Gonzalez-Garcia,^{53,54,55} M. Goodman,⁵⁶ C. Grab,⁴⁷ A.V. Gritsan,⁵⁷ C. Grojean,^{58,59} D.E. Groom,¹⁴ M. Grünewald,⁶⁰ A. Gurtu,^{26,61} T. Gutsche,⁶² H.E. Haber,⁶³ Matthieu Hamel,⁶⁴ C. Hanhart,⁶⁵ S. Hashimoto,⁶⁶ Y. Hayato,^{67,68} A. Hebecker,⁶⁹ S. Heinemeyer,⁷⁰ J. J. Hernández-Rey†,⁷¹ K. Hikasa,^{72,73,74} J. Hisano,⁷⁵ A. Höcker,²⁶ J. Holder,^{76,77} L. Hsu,²⁴ J. Huston,⁷⁸ T. Hyodo,⁷⁹ Al. Ianni,⁸⁰ M. Kado,^{81,82,83} M. Karliner,⁸⁴ U.F. Katz,⁸⁵ M. Kenzie,⁸⁶ V.A. Khoze,⁸⁷ S.R. Klein,^{88,89} F. Krauss,⁸⁷ M. Kreps,⁸⁶ P. Krizan,^{90,91} B. Krusche†,⁹² Y. Kwon,⁹³ O. Lahav,⁹⁴ J. Laiho,⁹⁵ L.P. Lellouch,⁹⁶ J. Lesgourgues,⁹⁷ A.R. Liddle,⁹⁸ Z. Ligeti,¹⁴ C.-J. Lin,¹⁴ C. Lippmann,⁹⁹ T.M. Liss,¹⁰⁰ L. Littenberg,¹¹ C. Lourenço,²⁶ K.S. Lugovsky,^{14,17} S.B. Lugovsky,¹⁷ A. Lusiani,^{101,102} Y. Makida,⁶⁶ F. Maltoni,^{103,104} T. Mannel,¹⁰⁵ A.V. Manohar,²⁸ W.J. Marciano,¹¹ A. Masoni,¹⁰⁶ J. Matthews,¹⁰⁷ U.-G. Meißner,^{4,65} I.-A. Melzer-Pellmann,⁵⁸ M. Mikhasenko,¹⁹ D.J. Miller,¹⁰⁸ D. Milstead,¹⁰⁹ R.E. Mitchell,¹¹⁰ K. Mönig,¹¹¹ P. Molaro,^{112,113} F. Moortgat,^{26,114} M. Moskvic,²⁶ K. Nakamura,^{66,68} M. Narain,¹¹⁵ P. Nason,^{31,116} S. Navas†,¹¹⁷ A. Nelles,^{111,85} M. Neubert,¹¹⁸ P. Nevski§,¹¹ Y. Nir,¹¹⁹ K.A. Olive,⁵² C. Patrignani,¹²⁰ J.A. Peacock,¹²¹ V.A. Petrov,¹⁷ E. Pianori,¹⁴ A. Pich,⁷¹ A. Piepke,¹²² F. Pietropaolo,^{26,123} A. Pomarol,^{124,125} S. Pordes,²⁴ S. Profumo,⁶³ A. Quadt,¹²⁶ K. Rabbertz,¹²⁷ J. Rademacker,¹²⁸ G. Raffelt,¹²⁹ M. Ramsey-Musolf,^{130,131,132} B.N. Ratcliff,¹³³ P. Richardson,⁸⁷ A. Ringwald,⁵⁸ D.J. Robinson,¹⁴ S. Roesler,²⁶ S. Rolli,¹³⁴ A. Romaniouk,^{135,136} L. J. Rosenberg,¹³⁷ J.L. Rosner,²¹ G. Rybka,¹³⁷ M.G. Ryskin,¹³⁸ R.A. Ryutin,¹⁷ Y. Sakai,⁶⁶ S. Sarkar,¹³⁹ F. Sauli§,²⁶ O. Schneider,¹⁴⁰ S. Schönert,¹⁴¹ K. Scholberg,¹⁴² A.J. Schwartz,¹⁴³ J. Schwiening,⁹⁹ D. Scott,¹⁴⁴ F. Sefkow,⁵⁸ U. Seljak,^{89,14} V. Sharma,²⁸ S.R. Sharpe,¹³⁷ V. Shiltsev¶,²⁴ G. Signorelli,¹⁰² M. Silari,²⁶ F. Simon,¹²⁹ T. Sjöstrand,¹⁴⁵ P. Skands,⁴² T. Skwarnicki,⁹⁵ G.F. Smoot,^{146,89,14,147,148} A. Soffer,⁸⁴ M.S. Sozzi,¹⁴⁹ S. Spanier,¹⁵⁰ C. Spiering,¹¹¹ A. Stahl,¹⁵¹ S.L. Stone†,⁹⁵ Y. Sumino,⁷⁴ M.J. Syphers,^{152,24} F. Takahashi,⁷⁴ M. Tanabashi,^{153,75} J. Tanaka,¹⁵⁴ M. Taševský,¹⁵⁵ K. Terao,^{133,156} K. Terashi,¹⁵⁴ J. Terning,¹⁵⁷ R.S. Thorne,⁹⁴ M. Titov,¹⁵⁸ N.P. Tkachenko,¹⁷ D.R. Tovey,¹⁵⁹ K. Trabelsi,⁸³ P. Urquijo,¹⁶⁰ G. Valencia,⁴² R. Van de Water,²⁴ N. Varelas,¹⁶¹ G. Venanzoni,¹⁰² L. Verde,^{55,54} I. Vivarelli,²⁷ P. Vogel,¹⁶² W. Vogelsang,⁶² V. Vorobyev,^{43,44} S.P. Wakely,^{21,25} W. Walkowiak,¹⁰⁵ C.W. Walter,¹⁴² D. Wands,¹⁶³ D.H. Weinberg,¹⁶⁴ E.J. Weinberg,¹⁶⁵ N. Vermes,⁴⁰ M. White,^{89,14} L.R. Wiencke,¹⁶⁶ S. Willocq,¹³² C.G. Wohl,¹⁴ C.L. Woody,¹¹ W.-M. Yao,¹⁴ M. Yokoyama,^{167,68} R. Yoshida,⁵⁶ G. Zanderighi,¹⁶⁸ G.P. Zeller,²⁴ O.V. Zenin,^{17,169} R.-Y. Zhu,¹⁷⁰ Shi-Lin Zhu,¹⁷¹ F. Zimmermann,²⁶ P.A. Zyla¹⁴

Technical Associates: J. Anderson,¹⁴ T. Basaglia,²⁶ P. Schaffner,¹⁴ W. Zheng,¹⁷²

1. *George Washington University, Department of Physics, Washington, D.C., USA*
2. *Jefferson Lab, Newport News, VA, USA*
3. *Florida State University, Department of Physics, Tallahassee, FL, USA*
4. *Universität Bonn, Helmholtz-Institut für Strahlen- und Kernphysik, Bonn, Germany*
5. *Institut für Kernphysik, Johannes Gutenberg University, Mainz, Germany*
6. *University of Maryland, Department of Physics, College Park, MD, USA*
7. *Università degli Studi di Roma "Tor Vergata", Rome, Italy*
8. *Department of Applied Mathematics and Theoretical Physics, University of Cambridge, Cambridge, UK*
9. *Stefan Meyer Institute for Subatomic Physics, Austrian Academy of Sciences, Vienna, Austria*
10. *Lab. Nazionali di Frascati dell'INFN, Frascati, Italy*
11. *Brookhaven National Laboratory, Nuclear and Particle Physics Directorate, Upton, NY, USA*
12. *University of Oklahoma, Department of Physics and Astronomy, Norman, OK, USA*
13. *University of Louisville, Louisville, KY, USA*
14. *Physics Division, Lawrence Berkeley National Laboratory, Berkeley, CA, USA*
15. *Universität Zürich, Physik-Institut, Zürich, Switzerland*
16. *Ohio State University, Department of Physics, Columbus, OH, USA*

*Coordination activities supported directly by INFN.

†Deceased.

‡Support from Programa Estatal de Generación de Conocimiento MCIU, Spain and ERDF of the European Union (PGC2018-096663-B-C41 and C44).

§Retired.

¶Supported by Fermi Research Alliance, LLC under Contract No. DE-AC02-07CH11359 with DOE.

17. *Institute for High Energy Physics of the National Research Centre Kurchatov Institute, COMPAS Group, Protvino, Russia*
18. *INFN and Dipartimento di Fisica e Astronomia, Università di Padova, Padova, Italy*
19. *Ludwig-Maximilians-Universität, Fakultät für Physik, München, Germany*
20. *University of Wisconsin, Department of Physics, Madison, WI, USA*
21. *University of Chicago, Enrico Fermi Institute and Department of Physics, Chicago, IL, USA*
22. *Imperial College, High Energy Physics Group, Blackett Laboratory, London, UK*
23. *University of Virginia, Department of Physics, Charlottesville, VA, USA*
24. *Fermi National Accelerator Laboratory, Batavia, IL, USA*
25. *University of Chicago, Kavli Institute for Cosmological Physics, Chicago, IL, USA*
26. *CERN, European Organization for Nuclear Research, Genève, Switzerland*
27. *Department of Physics and Astronomy, University of Sussex, Brighton, UK*
28. *Department of Physics, University of California at San Diego, La Jolla, CA, USA*
29. *Department of Physics, Royal Holloway, University of London, London, UK*
30. *State University of New York, Institute for Theoretical Physics, Stony Brook, NY, USA*
31. *INFN Sezione di Milano-Bicocca, Piazza della Scienza, Milano, Italy*
32. *INFN Sezione di Napoli, Napoli, Italy*
33. *Institut des Hautes Etudes Scientifiques, Bures-sur-Yvette, France*
34. *UNSAM - Universidad Nacional de San Martín, International Center for Advanced Studies (ICAS) and Instituto de Ciencias Físicas (ICIFI), Buenos Aires, Argentina*
35. *Northwestern University, Department of Physics and Astronomy, Evanston, IL, USA*
36. *University of Colorado at Boulder, Department of Physics, Boulder, CO, USA*
37. *Nikhef and University of Amsterdam, Amsterdam, The Netherlands*
38. *Yale University, New Haven, CT, USA*
39. *University of Liverpool, Department of Physics, Liverpool, UK*
40. *Universität Bonn, Physikalisches Institut, Bonn, Germany*
41. *University of Helsinki, Department of Physics, Helsinki, Finland*
42. *Monash University, School of Physics and Astronomy, Melbourne, Australia*
43. *Budker Institute of Nuclear Physics SB RAS, Novosibirsk, Russia*
44. *Novosibirsk State University, Novosibirsk, Russia*
45. *University of Illinois, Department of Physics, Urbana, IL, USA*
46. *King's College London, Department of Physics, London, UK*
47. *ETH Zurich, Institute for Particle Physics and Astrophysics, Zurich, Switzerland*
48. *University of Illinois, Department of Astronomy, Urbana, IL, USA*
49. *University of Pittsburgh, Department of Physics and Astronomy, Pittsburgh, PA, USA*
50. *Tufts University, Department of Physics and Astronomy, Medford, MA, USA*
51. *Department of Physics and Astronomy, Rutgers University, NJ, USA*
52. *University of Minnesota, School of Physics and Astronomy, Minneapolis, MN, USA*
53. *CN Yang Institute for Theoretical Physics, Stony Brook University, Stony Brook, NY, USA*
54. *Institució Catalana de Recerca i Estudis Avancats, Barcelona, Spain*
55. *Instituto de ciencias del Cosmos (ICC), University of Barcelona, Barcelona, Spain*
56. *Argonne National Laboratory, Argonne, IL, USA*
57. *Johns Hopkins University, Baltimore, MD, USA*
58. *Deutsches Elektronen-Synchrotron DESY, Hamburg, Germany*
59. *Institut für Physik, Humboldt-Universität zu Berlin, Berlin, Germany*
60. *University College Dublin, School of Physics, Dublin, Ireland*
61. *TIFR, Mumbai, India*
62. *Universität Tübingen, Institut für Theoretische Physik, Tübingen, Germany*
63. *Santa Cruz Institute for Particle Physics, University of California, Santa Cruz, CA, USA*
64. *Université Paris-Saclay, CEA, LIST, F-91120 Palaiseau, France*
65. *Institut für Kernphysik and Institute for Advanced Simulation, Forschungszentrum Jülich, Jülich, Germany*
66. *KEK, High Energy Accelerator Research Organization, Tsukuba, Japan*
67. *Kamioka Observatory, ICRR, The University of Tokyo, Tokyo, Japan*
68. *The University of Tokyo, Kavli IPMU (WPI), The University of Tokyo Institutes for Advanced Study, Kashiwa, Japan*
69. *Heidelberg University, Institute for Theoretical Physics, Heidelberg, Germany*

70. *Instituto de Física Teórica (UAM/CSIC), Universidad Autónoma de Madrid, Madrid, Spain*
71. *IFIC — Instituto de Física Corpuscular, Universitat de València — C.S.I.C., Valencia, Spain*
72. *Division for Interdisciplinary Advanced Research and Education, Tohoku University, Sendai, Japan*
73. *Institute of Liberal Arts and Sciences, Tohoku University, Sendai, Japan*
74. *Tohoku University, Department of Physics, Sendai, Japan*
75. *Nagoya University, Kobayashi-Maskawa Institute, Nagoya, Japan*
76. *University of Delaware, Department of Physics and Astronomy, Newark, DE, USA*
77. *University of Delaware, Bartol Research Institute, Newark, DE, USA*
78. *Michigan State University, Dept. of Physics and Astronomy, East Lansing, MI, USA*
79. *Department of Physics, Tokyo Metropolitan University, Tokyo, Japan*
80. *INFN - Laboratori Nazionali del Gran Sasso, Assergi, Italy*
81. *Dipartimento di Fisica, Sapienza Università di Roma, Rome, Italy*
82. *INFN Sezione di Roma, Rome, Italy*
83. *IJCLab, CNRS/IN2P3, Université Paris-Saclay, Orsay, France*
84. *Department of Particle Physics, Tel-Aviv University, Tel Aviv, Israel*
85. *Friedrich-Alexander-Universität Erlangen-Nürnberg, Erlangen Centre for Astroparticle Physics, Erlangen, Germany*
86. *University of Warwick, Department of Physics, Coventry, UK*
87. *University of Durham, Institute for Particle Physics Phenomenology, Department of Physics, Durham, UK*
88. *Nuclear Science Division, Lawrence Berkeley National Laboratory, Berkeley, CA, USA*
89. *University of California, Department of Physics, Berkeley, CA, USA*
90. *Faculty of Mathematics and Physics, University of Ljubljana, Jadranska, Slovenia*
91. *Jozef Stefan Institute, Ljubljana, Slovenia*
92. *University of Basel, Institute of Physics, Basel, Switzerland*
93. *Yonsei University, Department of Physics, Seoul, Republic of Korea*
94. *University College London, Department of Physics and Astronomy, London, UK*
95. *Syracuse University, Department of Physics, Syracuse, NY, USA*
96. *Aix-Marseille Univ, Université de Toulon, CNRS, CPT, Marseille, France*
97. *Institute of Theoretical Particle Physics and Cosmology (TTK), RWTH, Aachen, Germany*
98. *Instituto de Astrofísica e Ciências do Espaço, Universidade de Lisboa, Lisbon, Portugal*
99. *GSI, Helmholtzzentrum für Schwerionenforschung, Darmstadt, Germany*
100. *The City College of New York, New York, NY, USA*
101. *Scuola Normale Superiore, Pisa, Italy*
102. *INFN Sezione di Pisa, Pisa, Italy*
103. *Université catholique de Louvain, Centre for Cosmology, Particle Physics and Phenomenology (CP3), Louvain-la-Neuve, Belgium*
104. *Università di Bologna and INFN, Dipartimento di Fisica e Astronomia, Bologna, Italy*
105. *Universität Siegen, Department für Physik, Siegen, Germany*
106. *INFN Sezione di Cagliari, Monserrato, Italy*
107. *Louisiana State University, Department of Physics and Astronomy, Baton Rouge, LA, USA*
108. *University of Glasgow, School of Physics and Astronomy, Glasgow, UK*
109. *Stockholms Universitet, AlbaNova University Centre, Fysikum, Stockholm, Sweden*
110. *Indiana University, Department of Physics, Bloomington, IN, USA*
111. *Deutsches Elektronen-Synchrotron DESY, Zeuthen, Germany*
112. *INAF-OATS, Trieste, Italy*
113. *Institute for Fundamental Physics of the Universe, Trieste, Italy*
114. *University of Ghent, Dept. of Physics and Astronomy, Ghent, Belgium*
115. *Brown University, Department of Physics, Providence, RI, USA*
116. *Dip. di Fisica "G. Occhialini", Università di Milano-Bicocca, Milano, Italy*
117. *Universidad de Granada, Dpto. de Física Teórica y del Cosmos & C.A.F.P.E., Granada, Spain*
118. *Johannes Gutenberg University, PRISMA Cluster of Excellence and Mainz Institute for Theoretical Physics, Mainz, Germany*
119. *Department of Particle Physics and Astrophysics, Weizmann Institute of Science, Rehovot, Israel*
120. *Università di Bologna and INFN, Dip. Scienze per la Qualità della Vita, Rimini, Italy*
121. *University of Edinburgh, Royal Observatory, Institute for Astronomy, Edinburgh, UK*
122. *University of Alabama, Department of Physics and Astronomy, Tuscaloosa, AL, USA*

123. *INFN Sezione di Padova, Padova, Italy*
124. *Universitat Autònoma de Barcelona, Departament de Física, Barcelona, Spain*
125. *IFAE, Universitat Autònoma de Barcelona, Barcelona, Spain*
126. *Georg-August-Universität Göttingen, II. Physikalisches Institut, Göttingen, Germany*
127. *Karlsruhe Institute of Technology, Karlsruhe, Germany*
128. *University of Bristol, HH Wills Physics Laboratory, Bristol, UK*
129. *Max-Planck-Institut für Physik (Werner-Heisenberg-Institut), München, Germany*
130. *Tsung-Dao Lee Institute, Shanghai Jiao Tong University, Shanghai, China*
131. *Shanghai Jiao Tong University, Shanghai, China*
132. *University of Massachusetts, Department of Physics, Amherst, MA, USA*
133. *SLAC National Accelerator Laboratory, Menlo Park, CA, USA*
134. *DOE, Washington, DC, USA*
135. *Institut für Astro- und Teilchenphysik, Leopold-Franzens-Universität, Innsbruck, Austria*
136. *National Research Nuclear University "MEPhI", Moscow, Russia*
137. *University of Washington, Department of Physics, Seattle, WA, USA*
138. *Petersburg Nuclear Physics Institute, Petersburg, Russia*
139. *University of Oxford, Rudolf Peierls Centre for Theoretical Physics, Oxford, UK*
140. *Institute of Physics, Ecole Polytechnique Fédérale de Lausanne (EPFL), Lausanne, Switzerland*
141. *Department of Physics, Technical University Munich, Munich, Germany*
142. *Duke University, Physics Department, Durham, NC, USA*
143. *University of Cincinnati, Department of Physics, Cincinnati, OH, USA*
144. *University of British Columbia, Department of Physics and Astronomy, Vancouver, BC, Canada*
145. *Lund University, Department of Astronomy and Theoretical Physics, Lund, Sweden*
146. *The Hong Kong University of Science and Technology, Kowloon, Hong Kong*
147. *Donostia International Physics Center (DIPC), Donostia-San Sebastián, Spain*
148. *Paris Centre for Cosmological Physics, APC (CNRS), Université de Paris, Paris, France*
149. *Pisa University, Pisa, Italy*
150. *University of Tennessee, Department of Physics and Astronomy, Knoxville, TN, USA*
151. *III. Physikalisches Institut, Physikzentrum, RWTH Aachen University, Aachen, Germany*
152. *Department of Physics, Northern Illinois University, DeKalb, IL, USA*
153. *Department of Physics, Nagoya University, Nagoya, Japan*
154. *International Center for Elementary Particle Physics (ICEPP), The University of Tokyo, Tokyo, Japan*
155. *Institute of Physics, Czech Academy of Sciences, Prague, Czech Republic*
156. *Stanford University, Stanford, CA, USA*
157. *Department of Physics, University of California, Davis, CA, USA*
158. *IRFU, CEA, Université Paris-Saclay, F-91191 Gif-sur-Yvette, France*
159. *University of Sheffield, Department of Physics and Astronomy, Sheffield, UK*
160. *University of Melbourne, School of Physics, Victoria, Australia*
161. *University of Illinois at Chicago, Chicago, IL, USA*
162. *California Institute of Technology, Kellogg Radiation Laboratory, Pasadena, CA, USA*
163. *University of Portsmouth, Institute of Cosmology and Gravitation, Portsmouth, UK*
164. *Ohio State University, Department of Astronomy and CCAPP, Columbus, OH, USA*
165. *Columbia University, Department of Physics, New York, NY, USA*
166. *Dept. of Physics, Colorado School of Mines, Golden, CO, USA*
167. *The University of Tokyo, Department of Physics, Tokyo, Japan*
168. *Max-Planck-Institute of Physics, Munich, Germany*
169. *Moscow Institute of Physics and Technology, Dolgoprudny, Russia*
170. *California Institute of Technology, High Energy Physics, Pasadena, CA, USA*
171. *School of Physics, Peking University, Beijing, China*
172. *Institute of High Energy Physics, Beijing, China*

HIGHLIGHTS OF THE 2022 EDITION OF THE REVIEW OF PARTICLE PHYSICS

All PDG data and review articles are available online at pdg.lbl.gov.

709 new papers with 2,143 new measurements

120 reviews (most are revised)

- 267 new papers from *LHC* experiments (ATLAS, CMS and LHCb).
- Extensive up-to-date *Higgs boson* coverage from 58 new papers with 88 measurements, including latest results on mass, couplings, decay width and branching ratios, plus searches for other neutral and charged Higgs bosons.
- *Supersymmetry*: 62 new papers with major exclusions.
- *Top quark*: 24 new papers provide latest results on mass, coupling, and the first direct evidence of four top quark production at LHC.
- Latest from *b-hadron physics*: 83 papers and 326 measurements provide the world-best data on CKM angles, mixing, CP violation, and constraints on new physics from b-flavored hadrons.
- Substantial reorganization of several *meson resonances* sections. Also, recently observed states such as tetraquark candidates are included, several mesons now considered established are added to Summary Tables, and complex pole positions are listed when available.
- Revised naming and status of the Lambda and Sigma resonances.
- New most precise measurement of neutron lifetime.
- Naming scheme for hadrons extended to accommodate states with quantum numbers not allowed for $q\bar{q}$ and qqq states.
- New reviews on:
 - *Machine Learning*.
 - *Spectroscopy of Light Meson Resonances*.
- Significant update/revision to reviews on:
 - Major revision of review on *Accelerator Physics of Colliders*.
 - New section *LAr Time Projection Chamber* added to *Particle Detectors at Accelerators* review; extensive revision of sections on *Organic scintillators*, *Gaseous detectors*, *Semiconductor detectors*, *Low-noise detector readout*, and *Hadronic calorimeters*.
 - Major updates of sections on *Sub-Kelvin detectors*, *Low-radioactivity background techniques*, and *Radio emission from (ultra-)high energy particle showers* in *Particle Detectors for Non-Accelerator Physics* review.
 - Updated EWK fit in *Electroweak Model and Constraints on New Physics* review.
 - *Quark Model* review includes new discussion on magnetic moments and charmed and bottom baryons.
 - *Top Quark* review summarizes latest LHC results and constraints on new physics from top quark.
 - Review on *Semileptonic B Hadron Decays, Determination of V_{cb} and V_{ub}* summarizes latest results and discusses long-standing issues with inclusive and exclusive measurements.
 - Curated *Online Particle Physics Information* review now paired with more extensive online version on github open to community contributions.

VOLUME 1: SUMMARY TABLES AND REVIEWS

Highlights	6	Experimental Methods and Colliders	
Introduction	11	31. Accelerator physics of colliders (rev.)	533
History plots	19	32. High-energy collider parameters (rev.)	543
Online particle physics information (rev.)	20	33. Neutrino beam lines at high-energy proton synchrotrons (rev.)	548
SUMMARY TABLES		34. Passage of particles through matter (rev.)	549
Gauge and Higgs bosons	25	35. Particle detectors at accelerators (rev.)	565
Leptons	28	36. Particle detectors for non-accelerator phys. (rev.)	618
Quarks	32	37. Radioactivity and radiation protection (rev.)	646
Mesons	33	38. Commonly used radioactive sources (rev.)	652
Meson quick reference table	88	Mathematical Tools	
Baryon quick reference table	89	39. Probability (rev.)	655
Baryons	90	40. Statistics (rev.)	660
Searches not in Other Sections	108	41. Machine Learning (new)	676
Tests of conservation laws	110	42. Monte Carlo techniques (rev.)	713
REVIEWS, TABLES, AND PLOTS		43. Monte Carlo event generators (rev.)	717
Constants, Units, Atomic and Nuclear Properties		44. Monte Carlo neutrino event generators (rev.)	729
1. Physical constants (rev.)	133	45. Monte Carlo particle numbering scheme (rev.)	733
2. Astrophysical constants and parameters (rev.)	134	46. Clebsch-Gordan coefficients, spherical harmonics, and d functions	737
3. International system of units (SI) (rev.)	136	47. SU(3) isoscalar factors and representation matrices	738
4. Periodic table of the elements (rev.)	137	48. SU(n) multiplets and Young diagrams	739
5. Electronic structure of the elements	138	Kinematics, Cross-Section Formulae, and Plots	
6. Atomic and nuclear properties of materials (rev.)	140	49. Kinematics (rev.)	743
7. Electromagnetic relations	142	50. Resonances (rev.)	747
8. Naming scheme for hadrons (rev.)	144	51. Cross-section formulae for specific processes (rev.)	756
Standard Model and Related Topics		52. Neutrino cross section measurements (rev.)	765
9. Quantum chromodynamics (rev.)	149	53. Plots of cross sections and related quantities (rev.)	770
10. Electroweak model and constraints on new physics (rev.)	177	Particle Properties	
11. Higgs boson physics, status of (rev.)	201	<u>Gauge Bosons</u>	
12. CKM quark-mixing matrix (rev.)	261	54. Mass and width of the W boson (rev.)	789
13. CP violation in the quark sector (rev.)	271	55. Z boson	791
14. Neutrino masses, mixing, and oscillations (rev.)	285	<u>Charged Leptons</u>	
15. Quark model (rev.)	312	56. Muon anomalous magnetic moment (rev.)	796
16. Heavy-quark & soft-collinear effective theory	329	57. Muon decay parameters (rev.)	800
17. Lattice quantum chromodynamics (rev.)	337	58. τ branching fractions (rev.)	803
18. Structure functions (rev.)	353	59. τ -lepton decay parameters (rev.)	806
19. Fragmentation functions in e^+e^- , ep and pp collisions (rev.)	375	<u>Quarks</u>	
20. High Energy Soft QCD and Diffraction	392	60. Quark masses (rev.)	808
Astrophysics and Cosmology		61. Top quark (rev.)	817
21. Experimental tests of gravitational theory (rev.)	417		
22. Big-Bang cosmology (rev.)	430		
23. Inflation (rev.)	443		
24. Big-Bang nucleosynthesis (rev.)	459		
25. Cosmological parameters (rev.)	467		
26. Neutrinos in cosmology (rev.)	476		
27. Dark matter (rev.)	483		
28. Dark energy (rev.)	499		
29. Cosmic microwave background (rev.)	509		
30. Cosmic rays (rev.)	520		

(Continued on next page.)

<u>Mesons</u>	
62. Form factors for semileptonic kaon ($K_{\ell 3}$), radiative pion ($\pi_{\ell 2\gamma}$) & kaon ($K_{\ell 2\gamma}$) decays (rev.)	842
63. Spectroscopy of light meson resonances (new)	845
64. Scalar mesons below 1 GeV (rev.)	858
65. Rare kaon decays (rev.)	865
66. CPT invariance tests in neutral kaon decay (rev.)	871
67. V_{ud}, V_{us} , Cabibbo angle, and CKM unitarity (rev.)	873
68. CP -violation in K_L decays (rev.)	877
69. Review of multibody charm analyses (rev.)	880
70. $D^0-\bar{D}^0$ mixing (rev.)	885
71. D_s^+ branching fractions (rev.)	895
72. Leptonic decays of charged pseudoscalar mesons (rev.)	897
73. Production and decay of b -flavored hadrons (rev.)	908
74. Polarization in B decays (rev.)	919
75. $B^0-\bar{B}^0$ mixing (rev.)	923
76. Semileptonic B -hadron decays, V_{cb} and V_{ub} (rev.)	930
77. CKM angles from B hadrons, determination of (rev.)	946
78. Spectroscopy of mesons containing two heavy quarks (rev.)	951
79. Heavy non- $q\bar{q}$ mesons (rev.)	959
<u>Baryons</u>	
80. Baryon decay parameters	964
81. N and Δ resonances	965
82. Λ and Σ resonances (rev.)	970
83. Pole structure of the $\Lambda(1405)$ region (rev.)	973
84. Pentaquarks (rev.)	975
Hypothetical Particles and Concepts	
85. Extra dimensions (rev.)	983
86. W' -boson searches (rev.)	991
87. Z' -boson searches (rev.)	995
88. Supersymmetry: theory (rev.)	1000
89. Supersymmetry: experiment (rev.)	1019
90. Axions and other similar particles (rev.)	1038
91. Quark and lepton compositeness, searches for (rev.)	1055
92. Dynamical electroweak symmetry breaking: implications of the H^0 (rev.)	1061
93. Grand unified theories	1076
94. Leptoquarks (rev.)	1090
95. Magnetic monopoles (rev.)	1093
INDEX (Volumes 1 and 2 combined)	1101

VOLUME 2: PARTICLE LISTINGS (available online only)

Illustrative key and abbreviations

Illustrative key	1127
Abbreviations	1128

Gauge and Higgs bosons

(γ , gluon, graviton, W , Z , Higgs, Axions)	1141
--	------

Leptons

(e , μ , τ , Heavy-charged lepton searches, Neutrino properties, Number of neutrino types, Double- β decay, Neutrino mixing, Heavy-neutral lepton searches)	1239
---	------

Quarks

(u , d , s , c , b , t , b' , t' (4^{th} gen.), Free quarks)	1311
--	------

Mesons

Light unflavored (π , ρ , a , b) (η , ω , f , ϕ , h)	1349
Strange (K , K^*)	1473
Charmed (D , D^*)	1527
Charmed, strange (D_s , D_s^* , D_{sJ})	1588
Bottom (B , V_{cb}/V_{ub} , B^* , B_J^*)	1609
Bottom, strange (B_s , B_s^* , B_{sJ}^*)	1786
Bottom, charmed (B_c)	1813
$c\bar{c}$ (η_c , $J/\psi(1S)$, χ_c , h_c , ψ)	1818
$b\bar{b}$ (η_b , Υ , χ_b , h_b)	1940
Other mesons	1980

Baryons

N	1987
Δ	2042
Λ	2065
Σ	2090
Ξ	2121
Ω	2133
Charmed (Λ_c , Σ_c , Ξ_c , Ω_c)	2136
Doubly charmed (Ξ_{cc})	2160
Bottom (Λ_b , Σ_b , Ξ_b , Ω_b , b -baryon admixture)	2161
Exotic baryons (P_c pentaquarks)	2181

Searches not in Other Sections

Magnetic monopole searches	2185
Supersymmetric particle searches	2187
Technicolor	2238
Searches for quark and lepton compositeness	2239
Extra dimensions	2243
WIMP and dark matter searches	2249
Other particle searches	2263

INTRODUCTION

1. Overview	11
2. Particle Listings responsibilities	11
3. Consultants	12
4. Naming scheme for hadrons	15
5. Procedures	15
5.1 Selection and treatment of data	15
5.2 Averages and fits	15
5.2.1 Treatment of errors	15
5.2.2 Unconstrained averaging	16
5.2.3 Constrained fits	16
5.3 Rounding	17
5.4 Discussion	17
History plots	19

ONLINE PARTICLE PHYSICS INFORMATION

1. Introduction	20
2. Particle Data Group (PDG) resources	20
3. Particle physics information platform	20
4. Literature databases	20
5. Journals	21
6. Conference and seminars databases	21
7. Research institutions	21
8. People	21
9. Experiments	21
10. Jobs	21
11. Software packages and repositories	21
12. Data repositories and preservation	21
13. Particle physics education and outreach	21

Introduction

1 Overview

The *Review of Particle Physics* is a comprehensive review of the field of Particle Physics and of related areas in Cosmology. It is divided into two volumes. Volume 1 includes the “Summary Tables” and “Reviews, Tables, and Plots”. Volume 2 consists of the “Particle Listings”.

The *Review* is updated each year and made available on the PDG website (pdg.lbl.gov). In even-numbered years, the *Review* is also published in a journal and printed as the *PDG Book* together with an abridged *Particle Physics Booklet* containing Summary Tables and essential tables, figures, and equations from selected review articles. This edition is an updating through January 2022.

The Summary Tables give our best values and limits for particle properties such as masses, widths or lifetimes, and branching fractions, as well as an extensive summary of searches for hypothetical particles and a summary of experimental tests of conservation laws.

The 95 review articles in Reviews, Tables and Plots cover a wide variety of theoretical and experimental topics. Together with the Summary Tables they provide a quick reference for the practicing particle physicist. Two more review articles, Online Particle Physics Information and Tests of Conservation Laws, can be found in the introduction and Summary Tables, respectively.

The Particle Listings are a compilation/evaluation of data on particle properties. They contain all the data used to get the values given in the Summary Tables. They also give information on unconfirmed particles and particle searches. In this edition, the Particle Listings include 2,143 new measurements from 709 papers, in addition to the 44,695 measurements from 12,200 papers that first appeared in previous editions [1]. 23 review articles are part of the Particle Listings and address specific aspects of the data presented in the Listings. Because of the large quantity of data, the Particle Listings are not an archive of all published data on particle properties. We refer interested readers to earlier editions for data now considered to be obsolete.

We organize the particles into six categories:

- Gauge and Higgs bosons
- Leptons
- Quarks
- Mesons
- Baryons
- Searches not in other sections

The last category only includes searches for particles that do not belong to the previous groups. For example, it includes searches for supersymmetric particles, compositeness and extra dimensions, while searches for heavy charged leptons are with the leptons.

In Sec. 2 of this Introduction, we list the main areas of responsibility of the authors of the Particle Listings. Our many consultants, without whom we would not have been able to produce this *Review*, are acknowledged in Sec. 3. In Sec. 4, we mention briefly the naming scheme for hadrons, and in Sec. 5, we discuss our procedures for choosing among measurements of particle properties and for obtaining best values of the properties from the measurements.

The accuracy and usefulness of this *Review* depend in large part on interaction between its users and the authors. We appreciate comments, criticisms, and suggestions for improvements of any kind. Please send them to the appropriate author, according to the list of responsibilities in Sec. 2 below, or to pdg@lbl.gov.

In addition to the online publication at pdg.lbl.gov, the *Review* is available in different formats:

- The printed *PDG Book* includes volume 1 only, *i.e.* it contains the Summary Tables and most review articles. Since the 2016 edition [2] the detailed tables from the Particle Listings are no longer printed.
- The *Particle Physics Booklet* includes the Summary Tables plus essential tables, figures, and equations from selected review articles. Starting with the Booklets of the 2018 edi-

tion, we have excluded most text and explanations in order to revert back to a more pocket-sized format. The Booklet is available in print, as a web version optimized for use on phones, and as an Android app (see pdg.lbl.gov/booklet).

- *pdgLive* (pdgLive.lbl.gov) is a web application giving more interactive access to PDG data than the static web pages and PDF files that are also available.
- Files that can be downloaded from the PDG website include a table of masses, widths, and PDG Monte Carlo particle ID numbers; PDF files of volume 1 (PDG Book), volume 2 (Particle Listings) and Booklet; individual review articles; all figures; and an archive file containing the complete PDG website (except for pdgLive).

Copies of the *PDG Book* or the *Particle Physics Booklet* can be ordered from our website or directly at pdg.lbl.gov/order. For special requests only, please email pdg@lbl.gov in North and South America, Australia, and the Far East, and pdg-products@cern.ch in all other areas.

This *Review* is considered to be a single comprehensive review of particle physics and related areas. Therefore we prefer that it be cited as a whole, rather than citing *e.g.* an individual review article that is part of this *Review*. For the 2022 edition, the proper citation is:

R.L. Workman *et al.* (Particle Data Group), Prog. Theor. Exp. Phys. **2022**, 083C01 (2022).

If you wish to refer to a specific part of the *Review*, for example to the Higgs boson review article, the following form should be used:

Status of Higgs Boson Physics in R.L. Workman *et al.* (Particle Data Group), Prog. Theor. Exp. Phys. **2022**, 083C01 (2022).

2 Particle Listings responsibilities

* Asterisk indicates the people to contact with questions or comments about Particle Listings sections.

• Gauge and Higgs bosons

γ	A. Bettini, D.E. Groom*
Gluons	R.M. Barnett,* A.V. Manohar
Graviton	A. Bettini,* D.E. Groom
W, Z	M. Grünewald,* A. Gurtu*
Higgs bosons	S. Heinemeyer,* K. Hikasa, J. Tanaka
Heavy bosons	R. Bonventre,* K.A. Olive, M. Tanabashi
Axions	K.A. Olive, G. Raffelt,* F. Takahashi

• Leptons

Neutrinos	M. Goodman, C.-J. Lin,* K. Nakamura, K.A. Olive, A. Piepke
Double- β decay	A. Piepke, A. Bettini*
e, μ	A. Bettini,* C. Grab
τ	A. Lusiani, K. Mönig*

• Quarks

Quarks	R.M. Barnett,* A.V. Manohar
Top quark	W.-M. Yao,* Y. Sumino
b', t'	W.-M. Yao,* Y. Sumino
Free quark	A. Bettini,* C.-J. Lin

• Mesons

π, η	A. Bettini,* C. Grab
Unstable mesons	C. Amsler,* T. Gutsche, C. Hanhart, J.J. Hernández-Rey, C. Lourenco, A. Masoni, M. Mikhasenko, R.E. Mitchell, S. Navas, C. Patrignani, S. Spanier, G. Venanzoni, V. Vorobyev
K (stable)	G. D'Ambrosio, C.-J. Lin*
D (stable, no mix.)	D.M. Asner, R. Bonventre, J. Rademacker, D. Robinson*
D^0 mixing	D.M. Asner, R. Bonventre, J. Rademacker, D. Robinson*
B (stable)	A. Cerri,* P. Eerola, M. Kreps, Y. Kwon, W.-M. Yao*

- Baryons
 - Stable baryons C. Grab, D. Robinson*
 - Unstable baryons V. Burkert, V. Crede, U. Thoma, L. Tiator, R.L. Workman*
 - Charmed baryons R. Bonventre, J. Rademacker, D. Robinson*
 - Bottom baryons A. Cerri,* P. Eerola, M. Kreps, Y. Kwon, W.-M. Yao*
- Miscellaneous searches
 - Monopole A. Bettini,* D. Milstead
 - Supersymmetry H.K. Dreiner,* I.-A. Melzer-Pellmann, A. de Gouvêa, K.A. Olive, I. Vivarelli
 - Technicolor K. Agashe,* K.A. Olive, M. Tanabashi
 - Compositeness M. Tanabashi, J. Terning*
 - Extra Dimensions T. Gherghetta, K.A. Olive, D. Robinson*
 - WIMP, DM, Other H. Baer, A. Bettini,* W.-M. Yao*

3 Consultants

The Particle Data Group benefits greatly from the assistance of hundreds of physicists who are asked to referee review articles and verify every piece of data entered into this *Review*. Of special value is the advice of the PDG Advisory Committee, which meets biennially and thoroughly reviews all aspects of our operation. The members of the 2022 committee are:

S. Demers (Yale)
 D. d'Enterria (CERN)
 J. Frieman (FNAL)
 T. Nakada (EPFL)
 M. Yokoyama (Tokyo)
 Q. Zhao (IHEP Beijing)

We have especially relied on the expertise of the following people for advice on particular topics:

- K.N. Abazajian (UC Irvine)
- I. Abt (MPI Munich)
- R. Acciarri (FNAL)
- M. Achasov (Budker Inst., Novosibirsk)
- E.G. Adelberger (FNAL)
- J. Aebischer (Munich Tech. U.)
- F. Afzal (Bonn U.)
- M. Aleksa (CERN)
- P. Alvarez (CERN)
- L. Alvarez-Ruso (IFIC, Valencia)
- L. An (CERN)
- A. Antognini (ETH Zurich)
- F. Anulli (INFN, Rome)
- E. Aprile (Columbia U.)
- F. Archilli (CERN)
- G. Arduini (CERN)
- C. Armand (LAPTH)
- E. Armengaud (CEA Saclay, DSM/IRFU/SPP)
- M. Artuso (Syracuse U.)
- P. Athron (Nanjing U.)
- Avnish (Physics U. Bhubaneswar)
- G. Azuelos (U. de Montreal)
- P. Azzurri (INFN, Pisa)
- C. Balazs (Monash U.)
- A. Baldini (INFN, Pisa)
- A. Ball (CERN)
- D. Barney (CERN)
- R. Beck (Bonn U.)
- O. Behnke (DESY, Hamburg)
- V. Belyaev (ITEP)
- G. Bertone (Amsterdam U.)
- M. Bettler (CERN)
- T. Biekötter (DESY, Hamburg)
- T. Blum (UConn)
- S. Bolognesi (CERN)
- A. Bolz (Heidelberg U.)
- M. Bona (QMUL)
- A. Bondar (Budker Inst., Novosibirsk)
- M. Borsato (CERN)
- M. Boulay (Carleton U.)
- A. Boyarsky (Leiden U.)
- P. Brady (Wisconsin U.)
- E. Bratkovskaya (GSI Darmstadt; Frankfurt U.)
- J.E. Brau (Oregon U.)
- R.A. Briere (Carnegie Mellon U.)
- J. Brod (U. of Cincinnati)
- J. Brodzicka (IFJ PAN)
- G. Brooijmans (Columbia U.)
- R. Bruce (CERN)
- O. Bruning (CERN)
- D.A. Bryman (TRIUMF)
- A. Buckley (Glasgow U.)
- A. Buras (Munich Tech. U.)
- A. Cabrera (APC, Paris)
- L. Calibbi (NKU)
- J. Camalich (IAC)
- I. Campos Plasencia (CSIC)
- P. Carenza (Stockholm U.)
- T. Carli (CERN)
- N. Cartiglia (INFN, Torino)
- G. Casarosa (Pisa U.; INFN, Pisa)
- V. Cavaliere (BNL)
- G. Cavallero (CERN)
- G. Cavoto (Rome U.; INFN, Rome)
- S. Cebrian Guajardo (U. de Zaragoza)
- M. Cepeda (CIEMAT)
- F. Cerutti (LBNL)
- M. Charles (CNRS)
- A.E. Chavarria (U. Washington)
- K. Chen (Taiwan National U. Physics Dep.)
- Y. Chen (MIT)
- D. Chiesa (Milano-Bicocca U.; INFN, Milano-Bicocca)
- V. Chobanova (CERN)
- J. Chou (Rutgers U.)
- M. Cirelli (LPTHE, Paris)
- C. Clement (Stockholm U.)
- G. Colangelo (Bern U.)
- J.I. Collar (Chicago U.)
- P. Coloma (UAM/CSIC, U. Autónoma de Madrid)
- N. Crisosto (U. Washington)
- P. Crivelli (ETH Zurich)
- A. Cukierman (Stanford U.; SLAC)
- J.P. Cumalat (Colorado U.)
- A. Dainese (INFN, Padua)
- S. Dalla Torre (SISSA/INFN, Trieste)
- J. Dalseno (Santiago de Compostela U.)
- J. Darling (Colorado U.)
- C. Da Via (Manchester U.)
- C. Davies (Glasgow U.)
- A. De Angelis (INFN, Padova)
- C. De La Taille (OMEGA-CNRS-Ecole Polytechnique)

- M. Delmastro (CERN; LAPP)
- Z. Demiragli (Boston U.)
- P.B. Denton (BNL)
- F. Deppisch (UCL)
- A. Derbin (NRC Kurchatov Inst. PNPI)
- A. Di Domenico (INFN, Rome)
- L. Dong (IHEP)
- A. Dragone (SLAC)
- J.J. Dudek (IReS)
- K. Dundas (Columbia U.)
- M. Dunford (CERN)
- B. Dutta (TAMU)
- V. Dutta (UC Santa Barbara)
- D.A. Dwyer (LBNL)
- S.R. Elliott (LANL)
- K. Ellis (Durham U.)
- C. Englert (Glasgow U.)
- D. Epifanov (Budker Inst., Novosibirsk)
- J. Erdmann (TU)
- S. Esen (CERN)
- R. Essig (YITP, Stony Brook)
- I. Esteban (Ohio State U.)
- J. Estrada (FNAL)
- P. Everaerts (MIT)
- S. Fang (IHEP Beijing)
- M. Fedderke (Stanford U.)
- T. Ferber (KIT)
- A. Ferrari (CERN)
- A. Ferrari (Uppsala U.)
- C. Finley (Stockholm U.)
- W. Fischer (BNL)
- P. Fonte (LIP)
- J. Formaggio (MIT)
- S. Forte (INFN, Milano-Bicocca)
- M. Frank (Concordia U.)
- S. Friedrich (LLNL)
- T. Fujii (Kyoto U.)
- K. Fujikura (UTokyo)
- E. Gabriel (CERN)
- P. Gambino (INFN, Torino)
- J. Gao (IHEP Beijing)
- Y. Gao (IHEP Beijing)
- O. Gaponenko (INR, Moscow)
- R. Garisto (APS)
- M. Garny (Munich Tech. U.)
- A. Gasparian (Jefferson Lab)
- C. Gatti (INFN, LNF)
- P. Gauzzi (INFN, Rome; Rome U. Sapienza)
- M. Gazdzicki (CERN)
- S. Ghosh (Yale U.)
- M. Giovannozzi (CERN)
- T.A. Girard (Lisbon U.)
- C. Giunti (INFN, Torino)
- L. Gladilin (SINP)
- S. Gleyzer (Alabama U.)
- V. Gligorov (CNRS)
- S.N. Gninenko (Russian Academy of Sciences)
- J. Gomez Cadenas (DIPC)
- G. Gomez-Ceballos (CERN)
- J. Goodman (U. Maryland)
- M. Goodsell (LPTHE, Paris)
- S.A. Gottlieb (Indiana U.)
- P. Govoni (INFN, Milano-Bicocca)
- P. Grabmayr (Tübingen U.)
- G. Gratta (Stanford U.)
- E. Graziani (INFN, Rome)
- P. Guzowski (Manchester U.)
- C. Gwenlan (Phys. Dep. Oxford U.)
- F. Halzen (Wisconsin U.)
- S. Hannestad (Aarhus U.)
- F.A. Harris (Hawaii U.)
- F. Hartmann (KIT)
- J. He (CERN)
- B. Heacock (NIST)
- A. Heijboen (NIKHEF)
- W. Heil (JGU, Mainz)
- B. Heinemann (DESY, Hamburg; Freiburg U.)
- F. Hesse (MPIK)
- J. Heitger (WWU)
- K.H. Hicks (Ohio State U.)
- A. Hinzmann (Hamburg U.)
- F. Hiskens (School of Phys. U. of Melbourne)
- A. Hoang (HEPHY, Vienna)
- M. Hoferichter (Bern U.)
- N. Houston (BJUT)
- T. Huege (KIT)
- T. Ikeda (Kyoto U.)
- N. Ilic (Toronto U.)
- S. Ito (Osaka U.)
- L. Jacob (LPSC, IN2P3)
- N. Jafari (DESY, Zeuthen)
- C. James (CIRA)
- B. Jayatilaka (FNAL)
- L. Jeanty (CERN)
- I. John (Stockholm U.)
- D. Johnson (CERN)
- B. Jose (Adelaide U.)
- A. Jung (Purdue U.)
- N. Jurik (CERN)
- A. Juste (IFAE; ICREA, Barcelona)
- M. Kagan (SLAC)
- A. Kahn (MPIK)
- D. Karlen (Victoria U.)
- S. Karshenboim (Pulkovo Obs., St.Petersburg)
- K. Kawagoe (Kyushu U.)
- O. Kepka (CERN)
- S. Kim (Seoul National U.)
- Y. Kim (IBS, Daejeon)
- K. Kirch (ETH Zurich)
- R. Klanner (DESY, Hamburg)
- M. Knecht (CPT, Marseille)
- B. Ko (IBS, Daejeon)
- Y. Kolomensky (LBNL)
- B. Kopf (Ruhr U. Bochum)
- A. Kopylov (INR, Moscow)
- U. Kose (ETH Zurich)
- T. Koseki (KEK)
- S. Kraml (LPSC, Grenoble)
- N. Krasnikov (INR, Moscow; JINR, Dubna)
- G. Kribs (Oregon U.)
- A. Krieger (LBNL)
- P. Krokovny (Budker Inst., Novosibirsk)

- A. Kronfeld (FNAL)
- C. Lange (CERN)
- F. Lanusse (CEA Saclay)
- C. Lazzeroni (Birmingham U.)
- K. Leney (Southern Methodist U.)
- A. Lenz (Siegen U.)
- O. Leroy (CPPM Marseille)
- H. Li (IHEP Beijing)
- P. Li (Heidelberg U.)
- J. Libby (Indian Inst. Tech., Madras)
- E. Lisi (INFN, Bari)
- L. Lista (INFN, Napoli U.)
- J. Liu (School of Physics, Peking U.)
- J. Liu (SJTU)
- S. Lloyd (Phys. Dep. Durham U.)
- L. Longke (DESY, Hamburg)
- S. Lowette (ULB, Brussels)
- G. Lucente (INFN, Bari)
- M. Lucio (Santiago de Compostela U.)
- X. Luo (UC Santa Barbara)
- H. Ma (IHEP Beijing)
- F. Mahmoudi (IP2I, Lyon)
- P. Maksimovic (Johns Hopkins U.)
- B. Malaescu (LPNHE Paris)
- R. Manzoni (ETH Zurich)
- A. Marchionni (FNAL)
- M. Margoni (INFN, Padova)
- F. Marianna (LPNHE Paris)
- D. Marsh (King's Coll. London)
- C. Marshall (Rochester U.)
- M. Martinez-Perez (IFAE)
- T. Masubuchi (UTokyo)
- A. Mathad (ETH Zurich)
- M. Mazziotta (INFN, Bari)
- M. Mihovilovic (Jozef Stefan Inst.)
- C. Milardi (INFN, LNF)
- E. Minucci (CERN)
- R. Mizuk (MIPT Moscow)
- S. Moch (Hamburg U.)
- R.N. Mohapatra (U. Maryland)
- P. Mohr (NIST)
- D. Moore (Yale U.)
- M. Morello (SNS, Pisa)
- S. Moriyama (ICRR)
- V.M. Mostepanenko (Pulkovo Obs., St.Petersburg)
- M. Mulder (CERN)
- E. Myers (Florida State U.)
- B. Nachman (LBNL)
- P. Nadav (Stanford U.)
- P. Naik (Bristol U.)
- S. Narison (Montpellier U.)
- K. Ng (MIT)
- J. Nico (NIST)
- V. Obraztsov (IHEP, Protvino)
- A. Ochi (Kobe U.)
- H.B. O'Connell (FNAL)
- S. OGURI (JAXA)
- C. O'Hare (Sydney U.)
- K. Oide (KEK)
- F. Olness (Southern Methodist U.)
- P.E. Onyisi (Texas U. Austin)
- W. Ootani (ICEPP, UTokyo)
- G. Orebi Gann (LBNL)
- J.L. Ouellet (MIT)
- L. Pagnanini (GSSI)
- A. Palano (INFN, Bari)
- N. Palanque-Delabrouille (Paris U.)
- L. PDG-BMesons-verifiers (CERN)
- P. Pedroni (INFN, Pavia)
- H. Peiris (UCL; Stockholm U.)
- J.R. Pelaez (UCM, Madrid)
- M. Peruzzi (CERN)
- F. Petricca (MPI Munich)
- M. Pierini (CERN)
- L. Piilonen (Virginia Tech)
- P. Piminov (Budker Inst., Novosibirsk)
- T. Plehn (Heidelberg U.)
- S. Polikarpov (MEPhI Moscow)
- I. Polyakov (Syracuse U.)
- A. Pompili (INFN, Bari)
- A. Popov (IHEP, Protvino)
- W. Porod (Würzburg U.)
- J. Pradler (HEPHY, Vienna)
- G. Pugliese (INFN, Bari)
- A. Read (Oslo U.)
- A. Rebhan (TU Vienna)
- M. REGIS (INFN, Torino; Torino U.)
- F. Resnati (ETH Zurich)
- J. Richard (IP2I, Lyon)
- C.D. Roberts (Nanjing U.)
- A. Rodas (UCM, Madrid)
- M. Rotondo (INFN, Frascati)
- T. Roussy (Colorado U.)
- G. Ruggiero (Lancaster U.)
- T. Saab (Florida State U.)
- B. Safdi (UC Berkeley)
- R. Salerno (CNRS)
- D. Salvat (Indiana U.)
- N. Saoulidou (Athens U.)
- A.V. Sarantsev (Bonn U.)
- M. Sarsa (U. de Zaragoza)
- K. Schmidt-Hoberg (DESY, Hamburg)
- M. Schott (JGU, Mainz)
- S. Schramm (Geneva U.)
- K. Schutz (MIT; McGill U.)
- C. Schwanda (HEPHY, Vienna)
- B. Schwingenheur (MPIK)
- S. Scorza (Adelaide U.)
- Y.K. Semertzidis (IBS, Daejeon; KAIST)
- S. Seo (IBS, Daejeon)
- A.P. Serebrov (Petersburg Nuclear Phys. Inst.)
- L. Sestini (INFN, Padua)
- L. Shao (Beijing U. Kavli Inst. for Astronomy and Astrophysics)
- D. Shwartz (Budker Inst., Novosibirsk)
- C.V. Sierra (CERN)
- R. Simoniello (CERN)
- S. Simula (INFN, Rome)
- J. Smiga (JGU, Mainz; GSI Darmstadt)
- E. Smith (CERN)
- J. Sobczyk (Wrocław U.)
- F. Spano (RHUL)

- J. Steggemann (ETH Zurich)
- L. Sun (ANU)
- A. Sushkov (Boston U.)
- A. Suzuki (LBNL)
- E.S. Swanson (Pittsburgh U.)
- R. Tesarek (FNAL)
- J. Thaler (MIT)
- D. Tonelli (Trieste U.)
- D. Tovey (Sheffield U.)
- N. Tran (FNAL)
- R. Trotta (Imperial Coll. Physics Dep.)
- Y. Tsai (UC Irvine)
- J. Tyson (UC Davis)
- S. Ulmer (RIKEN)
- Y. Unno (KEK)
- P.L. Vahle (William and Mary Coll.)
- R.G. Van De Water (LANL)
- D. Vanegas (UdeMedellín)
- C. van Eldik (Erlangen U.)
- R. Van Kooten (Indiana U.)
- D. Veberic (KIT)
- J. Vlimant (CALTECH)
- B. von Krosigk (Hamburg U.; KIT)
- M. Vos (IFIC, Valencia)
- D. Wang (School of Physics, Peking U.)
- N. Wardle (Imperial Coll. Physics Dep.)
- A. Watson (Leeds U.)
- G. Watt (Durham U.)
- M. Weber (Bern U.)
- R. Wendell (Kyoto U.)
- A.P. White (Texas U.)
- M. Wilkinson (U. of Cincinnati)
- C. Will (Florida State U.)
- M. Williams (Manchester U.)
- J. Wilson (Johns Hopkins U.)
- M. Wilson (Toronto U.)
- Z. Xu (CERN)
- A. Yamamoto (KEK)
- T. Yamanaka (Osaka U.)
- N. Yamasaki (JAXA)
- S. Yang (Sun Yat-sen U.)
- P. Yin (IHEP Beijing)
- K. Yokoya (KEK)
- C. Yuan (IHEP Beijing)
- Q. Yue (Tsinghua U.)
- D. Zerwas (LAL Orsay)
- C. Zhang (IHEP Beijing)
- J. Zhang (IHEP)
- B. Zheng (South China U.)
- K. Zhu (IHEP Beijing)
- K. Zioutas (U. Patras)
- B. Zou (Academia Sinica, Inst. of Physics)

4 Naming scheme for hadrons

We introduced in the 1986 edition [3] a new naming scheme for the hadrons. Changes from older terminology affected mainly the heavier mesons made of u , d , and s quarks. Otherwise, the only important change to known hadrons was that the F^\pm became the D_s^\pm . None of the lightest pseudoscalar or vector mesons changed names, nor did the $c\bar{c}$ or $b\bar{b}$ mesons (we do, however, now use χ_c for the $c\bar{c}$ χ states), nor did any of the established baryons. The Summary Tables give both the new and old names whenever a change has occurred.

In the 2018 edition [4], the naming scheme was extended to address the naming of charmonium and bottomonium states that are commonly referred to as X, Y or Z states in the literature. The current scheme is described in “Naming Scheme for Hadrons” (p. 1) of this *Review*. A table details the correspondence between the names newly adopted by the PDG and those that have appeared in the literature. For this edition the naming scheme was further extended to accommodate states with quantum numbers not allowed for $q\bar{q}$ and qqq states.

We give here our conventions on type-setting style. Particle symbols are italic (or slanted) characters: e^- , p , Λ , π^0 , K_L , D_s^+ , b . Charge is indicated by a superscript: B^- , Δ^{++} . Charge is not normally indicated for p , n , or the quarks, and is optional for neutral isosinglets: η or η^0 . Antiparticles and particles are distinguished by charge for charged leptons and mesons: τ^+ , K^- . Otherwise, distinct antiparticles are indicated by a bar (overline): $\bar{\nu}_\mu$, \bar{l} , \bar{p} , \bar{K}^0 , and $\bar{\Sigma}^+$ (the antiparticle of the Σ^-).

5 Procedures

5.1 Selection and treatment of data

The Particle Listings contain all relevant data known to us that are published in journals. With very few exceptions, we do not include results from preprints or conference reports. Nor do we include data that are of historical importance only (the Listings are not an archival record). We search every volume of 30 journals through our cutoff date for relevant data. We also include later published papers that are sent to us by the authors (or others).

In the Particle Listings, we clearly separate measurements that are used to calculate or estimate values given in the Summary Tables from measurements that are not used. We give explanatory comments in many such cases. Among the reasons a measurement might be excluded are the following:

- It is superseded by or included in later results.
- No error is given.
- It involves assumptions we question.
- It has a poor signal-to-noise ratio, low statistical significance, or is otherwise of poorer quality than other data available.
- It is clearly inconsistent with other results that appear to be more reliable. Usually we then state the criterion, which sometimes is quite subjective, for selecting “more reliable” data for averaging. See Sec. 5.4.
- It is not independent of other results.
- It is not the best limit (see below).
- It is quoted from a preprint or a conference report.

In some cases, *none* of the measurements is entirely reliable and no average is calculated. For example, the masses of many of the baryon resonances, obtained from partial-wave analyses, are quoted as estimated ranges thought to probably include the true values, rather than as averages with errors. This is discussed in the Baryon Particle Listings.

For upper limits, we normally quote in the Summary Tables the strongest limit. We do not average or combine upper limits except in a very few cases where they may be re-expressed as measured numbers with Gaussian errors.

As is customary, we assume that particle and antiparticle share the same spin, mass, and mean life. The Tests of Conservation Laws table, following the Summary Tables, lists tests of CPT as well as other conservation laws.

We use the following indicators in the Particle Listings to tell how we get values from the tabulated measurements:

- OUR AVERAGE —From a weighted average of selected data.
- OUR FIT —From a constrained or overdetermined multiparameter fit of selected data.
- OUR EVALUATION —Not from a direct measurement, but evaluated from measurements of related quantities.
- OUR ESTIMATE —Based on the observed range of the data. Not from a formal statistical procedure.

- **OUR LIMIT** —For special cases where the limit is evaluated by us from measured ratios or other data. Not from a direct measurement.

An experimentalist who sees indications of new a particle will of course want to know what has been seen in that region in the past. Hence, we include in the Particle Listings all reported states that, in our opinion, have sufficient statistical merit and that have not been disproved by more reliable data. However, we promote to the Summary Tables only those states that we feel are well-established. This judgment is, of course, somewhat subjective and no precise criteria can be given. For more detailed discussions, see the reviews section on Particle Properties.

5.2 Averages and fits

We divide this discussion on obtaining averages and errors into three sections: (1) treatment of errors; (2) unconstrained averaging; (3) constrained fits.

5.2.1 Treatment of errors

In what follows, the “error” δx means that the range $x \pm \delta x$ is intended to be a 68.3% confidence interval about the central value x . We treat this error as if it were Gaussian. Thus, when the error is Gaussian, δx is the usual one standard deviation (1σ). Many experimenters now give statistical and systematic errors separately, in which case we usually quote both errors, with the statistical error first. For averages and fits, we then add the two errors in quadrature and use this combined error for δx .

When experimenters quote asymmetric errors $(\delta x)^+$ and $(\delta x)^-$ for a measurement x , the error that we use for that measurement in making an average or a fit with other measurements is a continuous function of these three quantities. When the resultant average or fit \bar{x} is less than $x - (\delta x)^-$, we use $(\delta x)^-$; when it is greater than $x + (\delta x)^+$, we use $(\delta x)^+$. In between, the error we use is a linear function of x . Since the errors we use are functions of the result, we iterate to get the final result. Asymmetric output errors are determined from the input errors assuming a linear relation between the input and output quantities.

In fitting or averaging, we usually do not include correlations between different measurements, but we try to select data in such a way as to reduce correlations. Correlated errors are, however, treated explicitly when there are a number of results of the form $A_i \pm \sigma_i \pm \Delta$ that have identical systematic errors Δ . In this case, one can first average the $A_i \pm \sigma_i$ and then combine the resulting statistical error with Δ . One obtains, however, the same result by averaging $A_i \pm (\sigma_i^2 + \Delta_i^2)^{1/2}$, where $\Delta_i = \sigma_i \Delta [\sum (1/\sigma_j^2)]^{1/2}$. This procedure has the advantage that, with the modified systematic errors Δ_i , each measurement may be treated as independent and averaged in the usual way with other data. Therefore, when appropriate, we adopt this procedure. We tabulate Δ and invoke an automated procedure that computes Δ_i before averaging, and we include a note saying that there are common systematic errors.

Another common case of correlated errors occurs when experimenters measure two quantities and then quote the two and their difference, e.g., m_1 , m_2 , and $\Delta = m_2 - m_1$. We cannot enter all of m_1 , m_2 and Δ into a constrained fit because they are not independent. In some cases, it is a good approximation to ignore the quantity with the largest error and put the other two into the fit. However, in some cases correlations are such that the errors on m_1 , m_2 and Δ are comparable and none of the three values can be ignored. In this case, we put all three values into the fit and invoke an automated procedure to increase the errors prior to fitting such that the three quantities can be treated as independent measurements in the constrained fit. We include a note saying that this has been done.

5.2.2 Unconstrained averaging

To average data, we use a standard weighted least-squares procedure and in some cases, discussed below, increase the errors with a “scale factor.” We begin by assuming that measurements of a given quantity are uncorrelated, and calculate a weighted average and error as

$$\bar{x} \pm \delta \bar{x} = \frac{\sum_i w_i x_i}{\sum_i w_i} \pm \left(\sum_i w_i \right)^{-1/2}, \quad (1)$$

where

$$w_i = 1/(\delta x_i)^2.$$

Here x_i and δx_i are the value and error reported by the i th experiment, and the sums run over the N experiments. We then calculate $\chi^2 = \sum w_i (\bar{x} - x_i)^2$ and compare it with $N - 1$, which is the expectation value of χ^2 if the measurements are from a Gaussian distribution.

If $\chi^2/(N - 1)$ is less than or equal to 1, and there are no known problems with the data, we accept the results.

If $\chi^2/(N - 1)$ is very large, we may choose not to use the average at all. Alternatively, we may quote the calculated average, but then make an educated guess of the error, a conservative estimate designed to take into account known problems with the data.

Finally, if $\chi^2/(N - 1)$ is greater than 1, but not greatly so, we still average the data, but then also do the following:

- (a) We increase our quoted error, $\delta \bar{x}$ in Eq. (1), by a scale factor S defined as

$$S = \left[\chi^2/(N - 1) \right]^{1/2}. \quad (2)$$

Our reasoning is as follows. The large value of the χ^2 is likely to be due to underestimation of errors in at least one of the experiments. Not knowing which of the errors are underestimated, we assume they are all underestimated by the same factor S . If we scale up all the input errors by this factor, the χ^2 becomes $N - 1$, and of course the output error $\delta \bar{x}$ scales up by the same factor. See Ref. [5].

When combining data with widely varying errors, we modify this procedure slightly. We evaluate S using only the experiments with smaller errors. Our cutoff or ceiling on δx_i is arbitrarily chosen to be

$$\delta_0 = 3N^{1/2} \delta \bar{x},$$

where $\delta \bar{x}$ is the unscaled error of the mean of all the experiments. Our reasoning is that although the low-precision experiments have little influence on the values \bar{x} and $\delta \bar{x}$, they can make significant contributions to the χ^2 , and the contribution of the high-precision experiments thus tends to be obscured. Note that if each experiment has the same error δx_i , then $\delta \bar{x}$ is $\delta x_i/N^{1/2}$, so each δx_i is well below the cutoff. (More often, however, we simply exclude measurements with relatively large errors from averages and fits: new, precise data chase out old, imprecise data.)

Our scaling procedure has the property that if there are two values with comparable errors separated by much more than their stated errors (with or without a number of other values of lower accuracy), the scaled-up error $\delta \bar{x}$ is approximately half the interval between the two discrepant values.

We emphasize that our scaling procedure for *errors* in no way affects central values. And if you wish to recover the unscaled error $\delta \bar{x}$, simply divide the quoted error by S .

- (b) If the number M of experiments with an error smaller than δ_0 is at least three, and if $\chi^2/(M - 1)$ is greater than 1.25, we show in the Particle Listings an ideogram of the data. Figure 1 is an example. Sometimes one or two data points lie apart from the main body; other times the data split into two or more groups. We extract no numbers from these ideograms; they are simply visual aids, which the reader may use as he or she sees fit.

Each measurement in an ideogram is represented by a Gaussian with a central value x_i , error δx_i , and area proportional to $1/\delta x_i$. The choice of $1/\delta x_i$ for the area is somewhat arbitrary. With this choice, the center of gravity of the ideogram corresponds to an average that uses weights $1/\delta x_i$ rather than the $(1/\delta x_i)^2$ actually used in the averages. This may be appropriate when some of the experiments have seriously underestimated systematic errors. However, since for this choice of area the height of the Gaussian for each measurement is proportional to $(1/\delta x_i)^2$, the peak position of the ideogram will often favor the high-precision measurements at least as much as does the least-squares average. See our 1986 edition [3] for a detailed discussion of the use of ideograms.

5.2.3 Constrained fits

In some cases, such as branching ratios or masses and mass differences, a constrained fit may be needed to obtain the best values of a set of parameters. For example, most branching ratios

and rate measurements are analyzed by making a simultaneous least-squares fit to all the data and extracting the partial decay fractions P_i , the partial widths Γ_i , the full width Γ (or mean life), and the associated error matrix.

Assume, for example, that a state has m partial decay fractions P_i , where $\sum P_i = 1$. These have been measured in N_r different ratios R_r , where, e.g., $R_1 = P_1/P_2$, $R_2 = P_1/P_3$, etc. [We can handle any ratio R of the form $\sum \alpha_i P_i / \sum \beta_i P_i$, where α_i and β_i are constants, usually 1 or 0. The forms $R = P_i P_j$ and $R = (P_i P_j)^{1/2}$ are also allowed.] Further, assume that each ratio R has been measured by N_k experiments (we designate each experiment with a subscript k , e.g., R_{1k}). We then find the best values of the fractions P_i by minimizing the χ^2 as a function of the $m - 1$ independent parameters:

$$\chi^2 = \sum_{r=1}^{N_r} \sum_{k=1}^{N_k} \left(\frac{R_{rk} - R_r}{\delta R_{rk}} \right)^2, \quad (3)$$

where the R_{rk} are the measured values and R_r are the fitted values of the branching ratios.

In addition to the fitted values \bar{P}_i , we calculate an error matrix $(\delta \bar{P}_i \delta \bar{P}_j)$. We tabulate the diagonal elements of $\delta \bar{P}_i = \langle \delta \bar{P}_i \delta \bar{P}_i \rangle^{1/2}$ (except that some errors are scaled as discussed below). In the Particle Listings, we give the complete correlation matrix; we also calculate the fitted value of each ratio, for comparison with the input data, and list it above the relevant input, along with a simple unconstrained average of the same input.

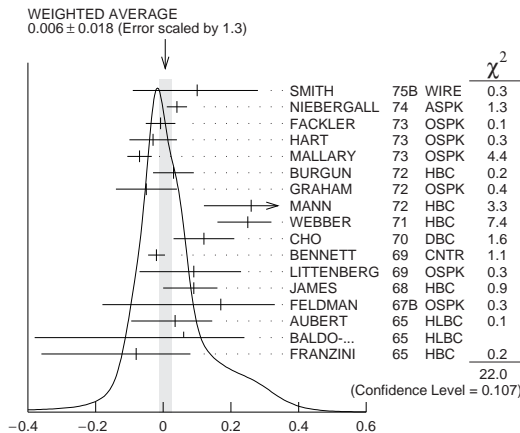


Figure 1: A typical ideogram. The arrow at the top shows the position of the weighted average, while the width of the shaded pattern shows the error in the average after scaling by the factor S . The column on the right gives the χ^2 contribution of each of the experiments. Note that the next-to-last experiment, denoted by the incomplete error flag (\perp), is not used in the calculation of S (see the text).

Three comments on the example above:

(1) There was no connection assumed between measurements of the full width and the branching ratios. But often we also have information on partial widths Γ_i as well as the total width Γ . In this case we must introduce Γ as a parameter in the fit, along with the P_i , and we give correlation matrices for the widths in the Particle Listings.

(2) We try to pick those ratios and widths that are as independent and as close to the original data as possible. When one experiment measures all the branching fractions and constrains their sum to be one, we leave one of them (usually the least well-determined one) out of the fit to make the set of input data more nearly independent. We now do allow for correlations between input data.

(3) We calculate scale factors for both the R_r and P_i when the measurements for any R give a larger-than-expected contribution to the χ^2 . According to Eq. (3), the double sum for χ^2 is first summed over experiments $k = 1$ to N_k , leaving a single sum over

ratios $\chi^2 = \sum \chi_r^2$. One is tempted to define a scale factor for the ratio r as $S_r^2 = \chi_r^2 / \langle \chi_r^2 \rangle$. However, since $\langle \chi_r^2 \rangle$ is not a fixed quantity (it is somewhere between N_k and N_{k-1}), we do not know how to evaluate this expression. Instead, we define

$$S_r^2 = \frac{1}{N_k} \sum_{k=1}^{N_k} \frac{(R_{rk} - \bar{R}_r)^2}{\langle (R_{rk} - \bar{R}_r)^2 \rangle}. \quad (4)$$

With this definition the expected value of S_r^2 is one. We can show that

$$\langle (R_{rk} - \bar{R}_r)^2 \rangle = \langle (\delta R_{rk})^2 \rangle - (\delta \bar{R}_r)^2, \quad (5)$$

where $\delta \bar{R}_r$ is the fitted error for ratio r .

The fit is redone using errors for the branching ratios that are scaled by the larger of S_r and unity, from which new and often larger errors $\delta \bar{P}_i'$ are obtained. The scale factors we finally list in such cases are defined by $S_i = \delta \bar{P}_i' / \delta \bar{P}_i$. However, in line with our policy of not letting S affect the central values, we give the values of \bar{P}_i obtained from the original (unscaled) fit.

There is one special case in which the errors that are obtained by the preceding procedure may be changed. When a fitted branching ratio (or rate) \bar{P}_i turns out to be less than three standard deviations $(\delta \bar{P}_i')$ from zero, a new smaller error $(\delta \bar{P}_i'')^-$ is calculated on the low side by requiring the area under the Gaussian between $\bar{P}_i - (\delta \bar{P}_i'')^-$ and \bar{P}_i to be 68.3% of the area between zero and \bar{P}_i . A similar correction is made for branching fractions that are within three standard deviations of one. This keeps the quoted errors from overlapping the boundary of the physical region.

5.3 Rounding

While the results shown in the Particle Listings are usually exactly those published by the experiments, the numbers that appear in the Summary Tables (means, averages and limits) are subject to a set of rounding rules.

The basic rule states that if the three highest order digits of the error lie between 100 and 354, we round to two significant digits. If they lie between 355 and 949, we round to one significant digit. Finally, if they lie between 950 and 999, we round up to 1000 and keep two significant digits. In all cases, the central value is given with a precision that matches that of the error. So, for example, the result (coming from an average) 0.827 ± 0.119 would appear as 0.83 ± 0.12 , while 0.827 ± 0.367 would turn into 0.8 ± 0.4 .

In cases where there are asymmetric errors, if these errors differ by less than 10 percent of the average of the two errors, the average is instead used as a symmetric error in the displayed result and the rounding is determined by this average. Otherwise, the narrower of the two asymmetric errors is used to determine the rounding on both.

Rounding of this form is also performed on the value of limits that come from calculations (but not on limits that are directly taken from a single source).

Finally, we should point out that in several instances, when a group of results come from a single fit to a set of data, we have chosen to keep two significant digits for all the results. This happens, for instance, for several properties of the W and Z bosons and the τ lepton.

5.4 Discussion

The problem of averaging data containing discrepant values is nicely discussed by Taylor in Ref. [6]. He considers a number of algorithms that attempt to incorporate inconsistent data into a meaningful average. However, it is difficult to develop a procedure that handles simultaneously in a reasonable way two basic types of situations: (a) data that lie apart from the main body of the data are incorrect (contain unreported errors); and (b) the opposite—it is the main body of data that is incorrect. Unfortunately, as Taylor shows, case (b) is not infrequent. He concludes that the choice of procedure is less significant than the initial choice of data to include or exclude.

We place much emphasis on this choice of data. Often we solicit the help of outside experts (consultants). Sometimes, however, it

is simply impossible to determine which of a set of discrepant measurements are correct. Our scale-factor technique is an attempt to address this ignorance by increasing the error. In effect, we are saying that present experiments do not allow a precise determination of this quantity because of unresolvable discrepancies, and one must await further measurements. The reader is warned of this situation by the size of the scale factor, and if he or she desires can go back to the literature (via the Particle Listings) and redo the average with a different choice of data.

Our situation is less severe than most of the cases Taylor considers, such as estimates of the fundamental constants like h , *etc.* Most of the errors in his case are dominated by systematic effects. For our data, statistical errors are often at least as large as systematic errors, and statistical errors are usually easier to estimate. A notable exception occurs in partial-wave analyses, where different techniques applied to the same data yield different results. In this case, as stated earlier, we often do not make an average but just quote a range of values.

A brief history of early Particle Data Group averages is given in Ref. [5]. Our History Plots show the time evolution of some of our values of a few particle properties. Sometimes large changes occur. These usually reflect the introduction of significant new data or the discarding of older data. Older data are discarded in favor of newer data when it is felt that the newer data have smaller systematic errors, or have more checks on systematic errors, or have made corrections unknown at the time of the older experiments, or simply have much smaller errors. Sometimes, the scale factor becomes large near the time at which a large jump takes place, reflecting the uncertainty introduced by the new and inconsistent data. By and large, however, a full scan of our history plots shows a dull progression toward greater precision at central values quite consistent with the first data points shown.

We conclude that the reliability of the combination of experimental data and our averaging procedures is usually good, but it is important to be aware that fluctuations outside of the quoted errors can and do occur.

ACKNOWLEDGMENTS

The publication of the *Review of Particle Physics* is supported by the Director, Office of Science, Office of High Energy Physics

of the U.S. Department of Energy under Contract No. DE-AC02-05CH11231; by an implementing arrangement between the governments of Japan (MEXT: Ministry of Education, Culture, Sports, Science and Technology) and the United States (DOE) on cooperative research and development; by the Italian National Institute of Nuclear Physics (INFN); by the Physical Society of Japan (JPS); and by the European Laboratory for Particle Physics (CERN). Individual collaborators receive support for their PDG activities from their respective institutes or funding agencies.

We thank all those who have assisted in the many phases of preparing this *Review*. We particularly thank the many who have responded to our requests for verification of data entered in the Listings, and those who have made suggestions or pointed out errors.

We are grateful to the staff at CERN, IHEP Beijing, KEK, and LBNL who take care of the mailing and distribution of our products.

This work used resources of the National Energy Research Scientific Computing Center, a DOE Office of Science User Facility supported by the Office of Science of the U.S. Department of Energy under Contract No. DE-AC02-05CH11231.

References

- [1] The previous edition was: P.A. Zyla *et al.* (Particle Data Group), *Prog. Theor. Exp. Phys.* **2020**, 083C01 (2020).
- [2] C. Patrignani *et al.* (Particle Data Group), *Chin. Phys.* **C40**, 10, 100001 (2016).
- [3] M. Aguilar-Benitez *et al.* (Particle Data Group), *Phys. Lett.* **170B**, 1 (1986).
- [4] M. Tanabashi *et al.* (Particle Data Group), *Phys. Rev. D* **98**, 3, 030001 (2018).
- [5] A. H. Rosenfeld, *Ann. Rev. Nucl. Part. Sci.* **25**, 555 (1975).
- [6] B.N. Taylor, "Numerical Comparisons of Several Algorithms for Treating Inconsistent Data in a Least-Squares Adjustment of the Fundamental Constants," U.S. National Bureau of Standards NBSIR 81-2426 (1982).

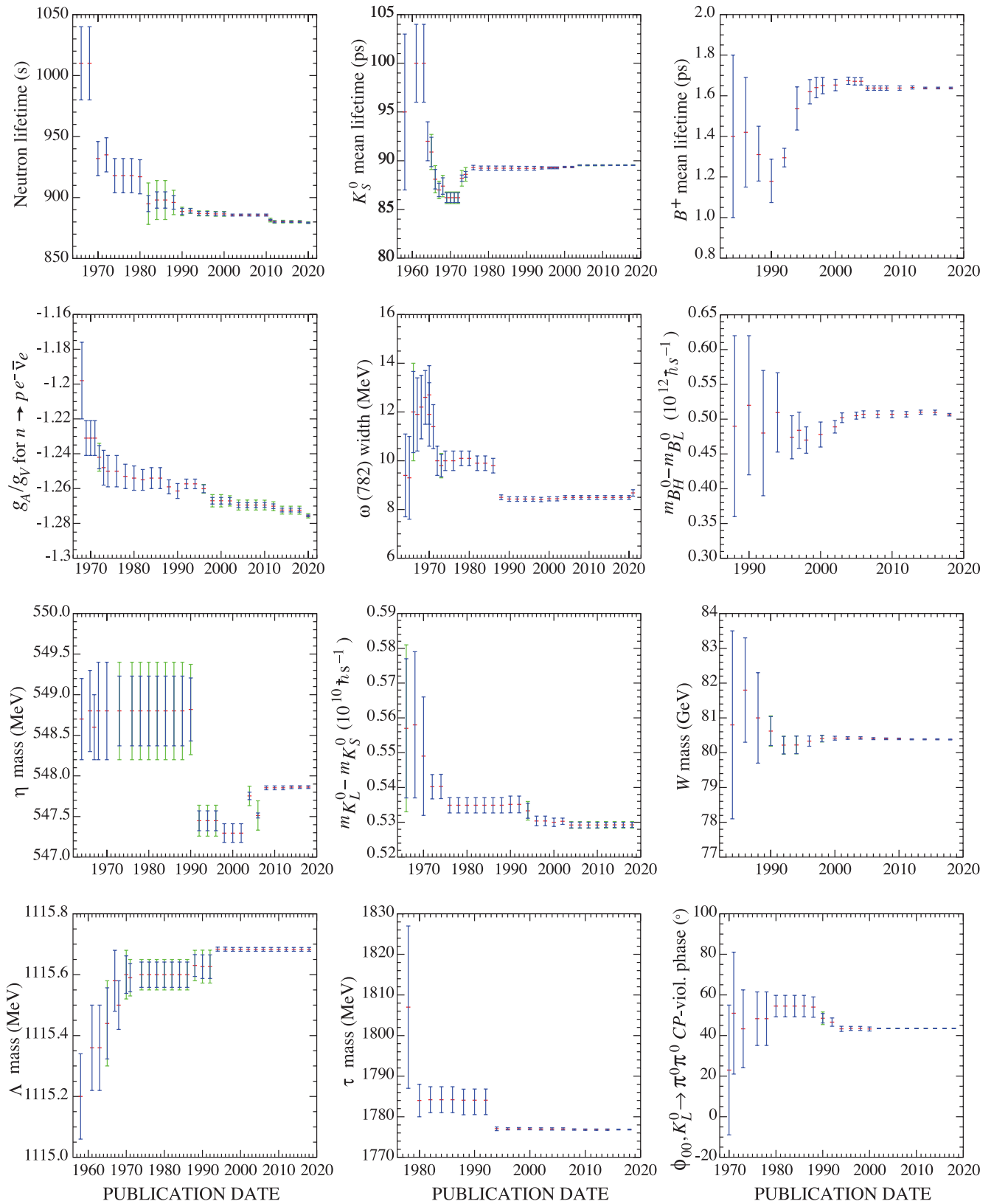


Figure 1: A historical perspective of values of a few particle properties tabulated in this *Review* as a function of date of publication of the *Review*. A full error bar indicates the quoted error; a thick-lined portion indicates the same but without the “scale factor.”

Online Particle Physics Information

Revised August 2021 by S. Demers (Yale U.) and M. Moskvic (CERN).

1	Introduction	20
2	Particle Data Group (PDG) resources	20
3	Particle physics information platform	20
4	Literature databases	20
5	Journals	21
6	Conference and seminars databases	21
7	Research institutions	21
8	People	21
9	Experiments	21
10	Jobs	21
11	Software packages and repositories	21
12	Data repositories and preservation	21
13	Particle physics education and outreach	21

1 Introduction

Online resources are used in a diverse and expanding set of ways in particle physics. Many of these resources have become central to our collective work. We provide a brief curated selection of the major resources here. An expanded and regularly updated online repository is referred to below and can be found at

<https://github.com/particledatagroup/hep-resources>

By contrast, it is meant to be inclusive and catalog all useful resources related to particle physics. The community is warmly invited to contribute in order to ensure a broad and up to date coverage of relevant resources. Practical details are available online.

2 Particle Data Group (PDG) resources

- **Review of Particle Physics (RPP):** A comprehensive report on the fields of particle physics and related areas of cosmology and astrophysics, including both review articles and a compilation/evaluation of data on particle properties. The review section includes articles, tables and plots on a wide variety of theoretical and experimental topics of interest to particle physicists and astrophysicists. The particle properties section provides tables of published measurements as well as the Particle Data Group's best values and limits for particle properties such as masses, widths, lifetimes, and branching fractions, as well as an extensive summary of searches for hypothetical particles. RPP is published as a large book every two years, with partial updates made available once each year on the web.

All the contents of the book version of RPP are available online:

<https://pdg.lbl.gov>

The printed book can be ordered:

https://pdg.lbl.gov/current/receive_our_products.html

[//pdg.lbl.gov/current/receive_our_products.html](https://pdg.lbl.gov/current/receive_our_products.html)

Of historical interest is the complete RPP collection which can be found online:

<https://pdg.lbl.gov/rpp-archive/>

<https://scientific-info.cern/search-and-read/online-resources/review-particle-physics>

- **Particle Physics booklet:** An abridged version of the Review of Particle Physics, available as a pocket-sized 250-page booklet. It is one of the most useful summaries of physics data. The booklet contains an abbreviated set of reviews and the summary tables from the most recent edition of the Review of Particle Physics.

The PDF file of the booklet can be downloaded:

<https://pdg.lbl.gov/current/booklet.pdf>

The printed booklet can be ordered:

https://pdg.lbl.gov/current/receive_our_products.html

[//pdg.lbl.gov/current/receive_our_products.html](https://pdg.lbl.gov/current/receive_our_products.html)

- **PDGLive:** A web application for browsing the contents of the PDG database that contains the information published in the Review of Particle Physics. It allows one to navigate to a

particle of interest, see a summary of the information available, and then proceed to the detailed information published in the Review of Particle Physics. Data entries are directly linked to the corresponding bibliographic information in INSPIRE.

<https://pdglive.lbl.gov>

- **Computer-readable files:** Data files that can be downloaded from the PDG include tables of particle masses and widths, PDG Monte Carlo particle numbers, and cross-section data. The files are updated with each new edition of the Review of Particle Physics.

https://pdg.lbl.gov/current/html/computer_read.html

3 Particle physics information platform

INSPIRE: INSPIRE serves as a one-stop information platform for the particle physics community, comprising interlinked databases on literature, authors, jobs, seminars, conferences, institutions and experiments (each described in more detail below). Run in collaboration by CERN, DESY, Fermilab, IHEP, IN2P3, and SLAC, it has been serving the scientific community for almost 50 years. Previously known as SPIRES, it was the first website outside Europe and the first database on the web. Close interaction with the user community and with arXiv, ADS, HEPData, ORCID, PDG and publishers is the backbone of INSPIRE's evolution. Since 2020, it is running on a modernized platform that is continuously being improved.

<https://inspirehep.net/>

4 Literature databases

Most research articles in the field of high-energy physics are first made available on the arXiv eprint server, where researchers can learn about the latest developments by browsing through the new announcements five days a week. They are indexed, together with all other publications in high-energy physics and related fields, in the INSPIRE literature collection. For neighboring fields such as astrophysics or mathematics, other databases are more exhaustive.

- **arXiv.org:** A repository of full-text articles in physics, astronomy, mathematics, computer science, statistics, nonlinear sciences, quantitative finance, quantitative biology, electrical engineering and systems science, and economics. Papers are submitted by registered authors to arXiv, often as preprints in advance of submission to a journal for publication; includes postprints, working papers, and other relevant material. Established in 1991, the repository is interlinked with ADS and INSPIRE, among others. Readers can browse subject categories or search by author, title, abstract, date, and other fields. Receive daily update alerts for subfields by email or RSS.

<https://arXiv.org>

- **INSPIRE Literature:** The literature collection, the flagship of the INSPIRE suite, serves more than 1.4 million bibliographic records with a growing number of full-text articles attached and metadata including author affiliations, abstracts, references, experiments, keywords as well as links to arXiv, ADS, PDG, HEPData, publisher platforms and other servers. It provides fast metadata searches that can be easily refined using facets, plots extracted from full text, author disambiguation, author profile pages and citation analysis.

<https://inspirehep.net/literature>

- **ADS:** The SAO/NASA Astrophysics Data System is a Digital Library portal offering access to 15 million bibliographic records in Astronomy and Physics. The ADS search engine also indexes the full-text for many publications in this collection and tracks citations. The system also provides access and links to a wealth of external resources, including electronic articles hosted by publishers and arXiv, data catalogs and a variety of data products hosted by the astronomy archives worldwide. The ADS can be accessed at:

<http://ads.harvard.edu/>

- **MathSciNet:** This database of almost 4 million items provides reviews, abstracts and bibliographic information for

much of the mathematical sciences literature. Over 100,000 new items, most of them classified according to the Mathematics Subject Classification, and more than 80,000 reviews of the current published literature are added each year. Author identification allows users to search for publications by author and citation data allows users to track the history and influence of research publications.

<https://www.ams.org/mathscinet>

5 Journals

SCOAP³ Journals: A list of journals currently financed by the SCOAP³ consortium. All HEP publications in those journals are made freely available under Open Access conditions at no cost for the authors.

<https://www.scoap3.org/phase3-journals/>

6 Conference and seminars databases

- **INSPIRE Conferences:** The database of more than 24,000 past, present, and future conferences, schools, and meetings relevant to high-energy physics and related fields is searchable by title, acronym, series, date and location. Included are information about published proceedings, links to conference contributions in the INSPIRE HEP database, and links to the conference website when available. New conferences can be submitted from the entry page.

<https://inspirehep.net/conferences>

- **INSPIRE Seminars:** Created to support the surge of online seminars during the COVID19 pandemic, this database already contains more than 1,500 seminars in high-energy physics and related fields. Seminars can be filtered by date, series and subject and exported to a calendar. Direct links to join the online seminar and external resources are included. All seminars are community-maintained and can be submitted from the entry page.

<https://inspirehep.net/seminars>

7 Research institutions

INSPIRE Institutions: INSPIRE Institutions contains over 11,500 institutes, laboratories, and universities, where research on particle physics and astrophysics is led. Every record includes, whenever possible, as detailed information, such as address, web links, experiments, and links to INSPIRE papers authored by people affiliated to that institution. One can search for a particular institution by name, acronym, and location.

<https://inspirehep.net/institutions>

8 People

- **INSPIRE Authors:** Searchable worldwide database of more than a hundred thousand active, departed, retired, and deceased people associated with particle physics and related fields. The affiliation history of these researchers, their e-mail addresses, ORCIDs, web pages, experiments they participated in, PhD advisor, information on their graduate students and links to their papers and seminars are provided, as well as a user interface to update this information.

<https://inspirehep.net/authors>

- **ORCID:** Registry providing persistent digital identifiers allowing to unambiguously identify researchers. Through integration in key research workflows such as manuscript and grant submission, it supports automated linkages between scientists and their professional activities ensuring that their work is recognized.

<https://orcid.org>

9 Experiments

INSPIRE Experiments: Contains more than 3,700 past, present, and future experiments in particle physics. It lists and classifies both accelerator and non-accelerator experiments as well as theory collaborations. Includes official experiment name and number, location, and collaboration lists. Simple searches by participant, title, experiment number, institution, date approved, accelerator, or detector, return a description of the experiment, including a complete list of authors, title, overview of the experiment's goals and methods, and a link to the experiment's web page if available. Recently, it has expanded its scope to include particle accelerators besides experiments and to link them together.

<https://inspirehep.net/experiments>

10 Jobs

INSPIRE Jobs: Lists academic and research jobs in high energy physics, nuclear physics, accelerator physics and astrophysics with the option to post a job or to receive email notices of new job listings. Several hundreds of jobs are listed all year round, with more activity during the application season.

<https://inspirehep.net/jobs>

11 Software packages and repositories

A vast number of software tools are used for various aspects of high-energy physics research. Due to their number, their often specialized purpose and the quickly-changing nature of software, no attempt has been made to present them in this chapter. The accompanying online version contains an extensive categorized list of software.

12 Data repositories and preservation

Initiatives to preserve and disseminate data produced during different stages of research, from Monte Carlo events to machine-readable versions of tables in papers, have grown in recent years. Unfortunately, there currently exists no central resource aggregating all these data as is the case for the more established means of scholarly communication. Instead, there are a number of repositories targeting different types of data and research subjects. They are listed in the online version.

13 Particle physics education and outreach

Particle physics public engagement efforts are widespread, with laboratories, experiments, universities and individual researchers engaged in a range of efforts. The online version of this chapter provides links to resources for particle physicists wanting to become engaged in public education as well as resources that physicists can provide directly to students or lay people. There are classroom activities, interactive websites, films, and direct links to education offices at institutions and experiments. Additionally, news sites relevant for experts and for the general public are provided.

SUMMARY TABLES OF PARTICLE PHYSICS

Gauge and Higgs bosons	25
Leptons	28
Quarks	32
Mesons	33
Baryons	90
Searches not in Other Sections*	108
Tests of conservation laws	110
Meson Quick Reference Table	88
Baryon Quick Reference Table	89

* There are also search limits in the Summary Tables for the Gauge and Higgs Bosons, the Leptons, the Quarks, and the Mesons.



SUMMARY TABLES OF PARTICLE PROPERTIES

Extracted from the Particle Listings of the
Review of Particle Physics
 R.L. Workman *et al.* (Particle Data Group),
 Prog. Theor. Exp. Phys. **2022**, 083C01 (2022)
 Available at <https://pdg.lbl.gov>

Particle Data Group

R.L. Workman, V.D. Burkert, V. Crede, E. Klempt, U. Thoma, L. Tiator, K. Agashe, G. Aielli, B.C. Allanach, C. Amsler, M. Antonelli, E.C. Aschenauer, D.M. Asner, H. Baer, Sw. Banerjee, R.M. Barnett, L. Baudis, C.W. Bauer, J.J. Beatty, V.I. Belousov, J. Beringer, A. Bettini, O. Biebel, K.M. Black, E. Blucher, R. Bonventre, V.V. Bryzgalov, O. Buchmuller, M.A. Bychkov, R.N. Cahn, M. Carena, A. Ceccucci, A. Cerri, R. Sekhar Chivukula, G. Cowan, K. Cranmer, O. Cremonesi, G. D'Ambrosio, T. Damour, D. de Florian, A. de Gouvêa, T. DeGrand, P. de Jong, S. Demers, B.A. Dobrescu, M. D'Onofrio, M. Doser, H.K. Dreiner, P. Eerola, U. Egede, S. Eidelman, A.X. El-Khadra, J. Ellis, S. C. Eno, J. Erler, V.V. Ezhela, W. Fetscher, B.D. Fields, A. Freitas, H. Gallagher, Y. Gershtein, T. Gherghetta, M.C. Gonzalez-Garcia, M. Goodman, C. Grab, A.V. Gritsan, C. Grojean, D.E. Groom, M. Grünewald, A. Gurtu, T. Gutsche, H.E. Haber, Matthieu Hamel, C. Hanhart, S. Hashimoto, Y. Hayato, A. Hebecker, S. Heinemeyer, J. J. Hernández-Rey, K. Hikasa, J. Hisano, A. Höcker, J. Holder, L. Hsu, J. Huston, T. Hyodo, Al. Ianni, M. Kado, M. Karliner, U.F. Katz, M. Kenzie, V.A. Khoze, S.R. Klein, F. Krauss, M. Kreps, P. Križan, B. Krusche, Y. Kwon, O. Lahav, J. Laiho, L.P. Lellouch, J. Lesgourgues, A.R. Liddle, Z. Ligeti, C.-J. Lin, C. Lippmann, T.M. Liss, L. Littenberg, C. Lourenço, K.S. Lugovsky, S.B. Lugovsky, A. Lusiani, Y. Makida, F. Maltoni, T. Mannel, A.V. Manohar, W.J. Marciano, A. Masoni, J. Matthews, U.-G. Meißner, I.-A. Melzer-Pellmann, M. Mikhasenko, D.J. Miller, D. Milstead, R.E. Mitchell, K. Mönig, P. Molaro, F. Moortgat, M. Moskvic, K. Nakamura, M. Narain, P. Nason, S. Navas, A. Nelles, M. Neubert, P. Nevski, Y. Nir, K.A. Olive, C. Patrignani, J.A. Peacock, V.A. Petrov, E. Pianori, A. Pich, A. Piepke, F. Pietropaolo, A. Pomarol, S. Pordes, S. Profumo, A. Quadt, K. Rabbertz, J. Rademacker, G. Raffelt, M. Ramsey-Musolf, B.N. Ratcliff, P. Richardson, A. Ringwald, D.J. Robinson, S. Roesler, S. Rolli, A. Romaniouk, L. J. Rosenberg, J.L. Rosner, G. Rybka, M.G. Ryskin, R.A. Ryutin, Y. Sakai, S. Sarkar, F. Sauli, O. Schneider, S. Schnert, K. Schölberg, A.J. Schwartz, J. Schwiening, D. Scott, F. Sefkow, U. Seljak, V. Sharma, S.R. Sharpe, V. Shiltsev, G. Signorelli, M. Silari, F. Simon, T. Sjöstrand, P. Skands, T. Skwarnicki, G.F. Smoot, A. Soffer, M.S. Sozzi, S. Spanier, C. Spiering, A. Stahl, S.L. Stone, Y. Sumino, M.J. Syphers, F. Takahashi, M. Tanabashi, J. Tanaka, M. Taševský, K. Terao, K. Terashi, J. Terning, R.S. Thorne, M. Titov, N.P. Tkachenko, D.R. Tovey, K. Trabelsi, P. Urquijo, G. Valencia, R. Van de Water, N. Varelas, G. Venanzoni, L. Verde, I. Vivarelli, P. Vogel, W. Vogelsang, V. Vorobyev, S.P. Wakely, W. Walkowiak, C.W. Walter, D. Wands, D.H. Weinberg, E.J. Weinberg, N. Vermes, M. White, L.R. Wiencke, S. Willocq, C.G. Wohl, C.L. Woody, W.-M. Yao, M. Yokoyama, R. Yoshida, G. Zanderighi, G.P. Zeller, O.V. Zenin, R.-Y. Zhu, Shi-Lin Zhu, F. Zimmermann, P.A. Zyla

Technical Associates:

J. Anderson, T. Basaglia, P. Schaffner, W. Zheng

©2022

(Approximate closing date for data: January 15, 2022)

GAUGE AND HIGGS BOSONS

 γ (photon)

$$I(J^{PC}) = 0.1(1^{--})$$

$$\text{Mass } m < 1 \times 10^{-18} \text{ eV}$$

$$\text{Charge } q < 1 \times 10^{-46} e \quad (\text{mixed charge})$$

$$\text{Charge } q < 1 \times 10^{-35} e \quad (\text{single charge})$$

$$\text{Mean life } \tau = \text{Stable}$$

 g
or gluon

$$I(J^P) = 0(1^-)$$

$$\text{Mass } m = 0 [^a]$$

$$\text{SU}(3) \text{ color octet}$$

graviton

$$J = 2$$

W

$$J = 1$$

$$\text{Charge} = \pm 1 e$$

$$\text{Mass } m = 80.377 \pm 0.012 \text{ GeV}$$

$$W/Z \text{ mass ratio} = 0.88145 \pm 0.00013$$

$$m_Z - m_W = 10.811 \pm 0.012 \text{ GeV}$$

$$m_{W^+} - m_{W^-} = -0.029 \pm 0.028 \text{ GeV}$$

$$\text{Full width } \Gamma = 2.085 \pm 0.042 \text{ GeV}$$

$$\langle N_{\pi^\pm} \rangle = 15.70 \pm 0.35$$

$$\langle N_{K^\pm} \rangle = 2.20 \pm 0.19$$

$$\langle N_p \rangle = 0.92 \pm 0.14$$

$$\langle N_{\text{charged}} \rangle = 19.39 \pm 0.08$$

W^- modes are charge conjugates of the modes below.

W^+ DECAY MODES	Fraction (Γ_i/Γ)	Confidence level	P (MeV/c)
$\ell^+ \nu$	[b] (10.86 ± 0.09) %		–
$e^+ \nu$	(10.71 ± 0.16) %		40189
$\mu^+ \nu$	(10.63 ± 0.15) %		40189
$\tau^+ \nu$	(11.38 ± 0.21) %		40170
hadrons	(67.41 ± 0.27) %		–
$\pi^+ \gamma$	< 7 × 10 ⁻⁶	95%	40189
$D_s^+ \gamma$	< 1.3 × 10 ⁻³	95%	40165
cX	(33.3 ± 2.6) %		–
$c\bar{3}$	(31 + ¹³ / ₋₁₁) %		–
invisible	[c] (1.4 ± 2.9) %		–
$\pi^+ \pi^+ \pi^-$	< 1.01 × 10 ⁻⁶	95%	40189

Z

$$J = 1$$

$$\text{Charge} = 0$$

$$\text{Mass } m = 91.1876 \pm 0.0021 \text{ GeV } [^d]$$

$$\text{Full width } \Gamma = 2.4952 \pm 0.0023 \text{ GeV}$$

$$\Gamma(\ell^+ \ell^-) = 83.984 \pm 0.086 \text{ MeV } [^d]$$

$$\Gamma(\text{invisible}) = 499.0 \pm 1.5 \text{ MeV } [^e]$$

$$\Gamma(\text{hadrons}) = 1744.4 \pm 2.0 \text{ MeV}$$

$$\Gamma(\mu^+ \mu^-) / \Gamma(e^+ e^-) = 1.0001 \pm 0.0024$$

$$\Gamma(\tau^+ \tau^-) / \Gamma(e^+ e^-) = 1.0020 \pm 0.0032 [^f]$$

Average charged multiplicity

$$\langle N_{\text{charged}} \rangle = 20.76 \pm 0.16 \quad (S = 2.1)$$

Couplings to quarks and leptons

$$g_V^\ell = -0.03783 \pm 0.00041$$

$$g_V^u = 0.266 \pm 0.034$$

$$g_V^d = -0.38^{+0.04}_{-0.05}$$

$$g_A^\ell = -0.50123 \pm 0.00026$$

$$g_A^u = 0.519^{+0.028}_{-0.033}$$

$$g_A^d = -0.527^{+0.040}_{-0.028}$$

$$g_V^\ell = 0.5008 \pm 0.0008$$

$$g_V^e = 0.53 \pm 0.09$$

$$g_V^\mu = 0.502 \pm 0.017$$

Gauge & Higgs Boson Summary Table

Asymmetry parameters [8]

$$\begin{aligned}
A_e &= 0.1515 \pm 0.0019 \\
A_\mu &= 0.142 \pm 0.015 \\
A_\tau &= 0.143 \pm 0.004 \\
A_s &= 0.90 \pm 0.09 \\
A_c &= 0.670 \pm 0.027 \\
A_b &= 0.923 \pm 0.020
\end{aligned}$$

Charge asymmetry (%) at Z pole

$$\begin{aligned}
A_{FB}^{(0\ell)} &= 1.71 \pm 0.10 \\
A_{FB}^{(0u)} &= 4 \pm 7 \\
A_{FB}^{(0s)} &= 9.8 \pm 1.1 \\
A_{FB}^{(0c)} &= 7.07 \pm 0.35 \\
A_{FB}^{(0b)} &= 9.92 \pm 0.16
\end{aligned}$$

Z DECAY MODES	Fraction (Γ_i/Γ)	Scale factor/ Confidence level	p (MeV/c)
e^+e^-	[h] (3.3632±0.0042) %		45594
$\mu^+\mu^-$	[h] (3.3662±0.0066) %		45594
$\tau^+\tau^-$	[h] (3.3696±0.0083) %		45559
$\ell^+\ell^-$	[b,h] (3.3658±0.0023) %		—
$\ell^+\ell^-\ell^+\ell^-$	[j] (4.55 ±0.17) × 10 ⁻⁶		45594
invisible	[h] (20.000 ±0.055) %		—
hadrons	[h] (69.911 ±0.056) %		—
($u\bar{u} + c\bar{c}$)/2	(11.6 ±0.6) %		—
($d\bar{d} + s\bar{s} + b\bar{b}$)/3	(15.6 ±0.4) %		—
$c\bar{c}$	(12.03 ±0.21) %		—
$b\bar{b}$	(15.12 ±0.05) %		—
$b\bar{b}b\bar{b}$	(3.6 ±1.3) × 10 ⁻⁴		—
$g g g$	< 1.1 %	CL=95%	—
$\pi^0\gamma$	< 2.01 × 10 ⁻⁵	CL=95%	45594
$\eta\gamma$	< 5.1 × 10 ⁻⁵	CL=95%	45592
$\rho^0\gamma$	< 2.5 × 10 ⁻⁵	CL=95%	45591
$\omega\gamma$	< 6.5 × 10 ⁻⁴	CL=95%	45590
$\eta'(958)\gamma$	< 4.2 × 10 ⁻⁵	CL=95%	45589
$\phi\gamma$	< 9 × 10 ⁻⁷	CL=95%	45588
$\gamma\gamma$	< 1.46 × 10 ⁻⁵	CL=95%	45594
$\pi^0\pi^0$	< 1.52 × 10 ⁻⁵	CL=95%	45594
$\gamma\gamma\gamma$	< 2.2 × 10 ⁻⁶	CL=95%	45594
$\pi^\pm W^\mp$	[j] < 7 × 10 ⁻⁵	CL=95%	10167
$\rho^\pm W^\mp$	[j] < 8.3 × 10 ⁻⁵	CL=95%	10142
$J/\psi(1S)X$	(3.51 \pm $\frac{0.23}{-0.25}$) × 10 ⁻³	S=1.1	—
$J/\psi(1S)\gamma$	< 1.4 × 10 ⁻⁶	CL=95%	45541
$\psi(2S)X$	(1.60 ±0.29) × 10 ⁻³		—
$\psi(2S)\gamma$	< 4.5 × 10 ⁻⁶	CL=95%	45519
$J/\psi(1S)J/\psi(1S)$	< 2.2 × 10 ⁻⁶	CL=95%	45489
$\chi_{c1}(1P)X$	(2.9 ±0.7) × 10 ⁻³		—
$\chi_{c2}(1P)X$	< 3.2 × 10 ⁻³	CL=90%	—
$\Upsilon(1S)X + \Upsilon(2S)X$	(1.0 ±0.5) × 10 ⁻⁴		—
$\Upsilon(1S)X$	< 4.4 × 10 ⁻⁵	CL=95%	—
$\Upsilon(1S)\gamma$	< 2.8 × 10 ⁻⁶	CL=95%	45103
$\Upsilon(2S)X$	< 1.39 × 10 ⁻⁴	CL=95%	—
$\Upsilon(2S)\gamma$	< 1.7 × 10 ⁻⁶	CL=95%	45043
$\Upsilon(3S)X$	< 9.4 × 10 ⁻⁵	CL=95%	—
$\Upsilon(3S)\gamma$	< 4.8 × 10 ⁻⁶	CL=95%	45006
$\Upsilon(1, 2, 3S) \Upsilon(1, 2, 3S)$	< 1.5 × 10 ⁻⁶	CL=95%	—
$(D^0/\bar{D}^0)X$	(20.7 ±2.0) %		—
$D^\pm X$	(12.2 ±1.7) %		—
$D^*(2010)^\pm X$	[j] (11.4 ±1.3) %		—
$D_{s1}(2536)^\pm X$	(3.6 ±0.8) × 10 ⁻³		—
$D_{sJ}(2573)^\pm X$	(5.8 ±2.2) × 10 ⁻³		—
$D^{*'}(2629)^\pm X$	searched for		—
B^+X	[k] (6.08 ±0.13) %		—
$B_s^0 X$	[k] (1.59 ±0.13) %		—
$B_c^+ X$	searched for		—
$A_c^+ X$	(1.54 ±0.33) %		—
$\Xi_c^0 X$	seen		—
$\Xi_b X$	seen		—
b -baryon X	[k] (1.38 ±0.22) %		—
anomalous γ + hadrons	[l] < 3.2 × 10 ⁻³	CL=95%	—
$e^+e^-\gamma$	[l] < 5.2 × 10 ⁻⁴	CL=95%	45594
$\mu^+\mu^-\gamma$	[l] < 5.6 × 10 ⁻⁴	CL=95%	45594
$\tau^+\tau^-\gamma$	[l] < 7.3 × 10 ⁻⁴	CL=95%	45559

$\ell^+\ell^-\gamma\gamma$	[n] < 6.8 × 10 ⁻⁶	CL=95%	—
$q\bar{q}\gamma\gamma$	[n] < 5.5 × 10 ⁻⁶	CL=95%	—
$\nu\bar{\nu}\gamma\gamma$	[n] < 3.1 × 10 ⁻⁶	CL=95%	45594
$e^\pm\mu^\mp$	LF [j] < 7.5 × 10 ⁻⁷	CL=95%	45594
$e^\pm\tau^\mp$	LF [j] < 5.0 × 10 ⁻⁶	CL=95%	45576
$\mu^\pm\tau^\mp$	LF [j] < 6.5 × 10 ⁻⁶	CL=95%	45576
pe	L,B < 1.8 × 10 ⁻⁶	CL=95%	45589
$p\mu$	L,B < 1.8 × 10 ⁻⁶	CL=95%	45589

H⁰

J = 0

Mass $m = 125.25 \pm 0.17$ GeV (S = 1.5)
 Full width $\Gamma = 3.2^{+2.8}_{-2.2}$ MeV (assumes equal
 on-shell and off-shell effective couplings)

H⁰ Signal Strengths in Different Channels

Combined Final States = 1.13 ± 0.06

 $WW^* = 1.19 \pm 0.12$ $ZZ^* = 1.01 \pm 0.07$ $\gamma\gamma = 1.10 \pm 0.07$ $c\bar{c}$ Final State = 37 ± 20 $b\bar{b} = 0.98 \pm 0.12$ $\mu^+\mu^- = 1.19 \pm 0.34$ $\tau^+\tau^- = 1.15^{+0.16}_{-0.15}$ $Z\gamma < 3.6$, CL = 95% $\gamma^*\gamma$ Final State = 1.5 ± 0.5 $t\bar{t}H^0$ Production = 1.10 ± 0.18 tH^0 production = 6 ± 4 H^0 Production Cross Section in pp Collisions at $\sqrt{s} = 13$ TeV =
56 ± 4 pb

H ⁰ DECAY MODES	Fraction (Γ_i/Γ)	Confidence level	p (MeV/c)
e^+e^-	< 3.6 × 10 ⁻⁴	95%	62625
$Z\rho(770)$	< 1.21 %	95%	29423
$Z\phi(1020)$	< 3.6 × 10 ⁻³	95%	29417
$J/\psi\gamma$	< 3.5 × 10 ⁻⁴	95%	62587
$J/\psi J/\psi$	< 1.8 × 10 ⁻³	95%	62548
$\psi(2S)\gamma$	< 2.0 × 10 ⁻³	95%	62571
$\Upsilon(1S)\gamma$	< 4.9 × 10 ⁻⁴	95%	62268
$\Upsilon(2S)\gamma$	< 5.9 × 10 ⁻⁴	95%	62224
$\Upsilon(3S)\gamma$	< 5.7 × 10 ⁻⁴	95%	62197
$\Upsilon(nS) \Upsilon(mS)$	< 1.4 × 10 ⁻³	95%	—
$\rho(770)\gamma$	< 8.8 × 10 ⁻⁴	95%	62623
$\phi(1020)\gamma$	< 4.8 × 10 ⁻⁴	95%	62621
$e\mu$	LF < 6.1 × 10 ⁻⁵	95%	62625
$e\tau$	LF < 2.2 × 10 ⁻³	95%	62612
$\mu\tau$	LF < 1.5 × 10 ⁻³	95%	62612
invisible	< 19 %	95%	—

Neutral Higgs Bosons, Searches for**Mass limits for heavy neutral Higgs bosons (H_2^0, A^0) in the MSSM** $m > 389$ GeV, CL = 95% ($\tan\beta = 10$) $m > 863$ GeV, CL = 95% ($\tan\beta = 20$) $m > 1157$ GeV, CL = 95% ($\tan\beta = 30$) $m > 1341$ GeV, CL = 95% ($\tan\beta = 40$) $m > 1496$ GeV, CL = 95% ($\tan\beta = 50$) $m > 1613$ GeV, CL = 95% ($\tan\beta = 60$)**Charged Higgs Bosons (H^\pm and $H^{\pm\pm}$),
Searches for****Mass limits for $m_{H^\pm} < m(\text{top})$** $m > 155$ GeV, CL = 95%**Mass limits for $m_{H^\pm} > m(\text{top})$** $m > 181$ GeV, CL = 95% ($\tan\beta = 10$) $m > 249$ GeV, CL = 95% ($\tan\beta = 20$) $m > 390$ GeV, CL = 95% ($\tan\beta = 30$) $m > 894$ GeV, CL = 95% ($\tan\beta = 40$) $m > 1017$ GeV, CL = 95% ($\tan\beta = 50$) $m > 1103$ GeV, CL = 95% ($\tan\beta = 60$)

**New Heavy Bosons
(W' , Z' , leptoquarks, etc.),
Searches for**

Additional W Bosons

- W' with standard couplings
Mass $m > 6000$ GeV, CL = 95% ($p\bar{p}$ direct search)
 W_R (Right-handed W Boson)
Mass $m > 715$ GeV, CL = 90% (electroweak fit)

Additional Z Bosons

- Z'_{SM} with standard couplings
Mass $m > 5150$ GeV, CL = 95% ($p\bar{p}$ direct search)
 Z_{LR} of $SU(2)_L \times SU(2)_R \times U(1)$ (with $g_L = g_R$)
Mass $m > 630$ GeV, CL = 95% ($p\bar{p}$ direct search)
Mass $m > 1162$ GeV, CL = 95% (electroweak fit)
 Z_χ of $SO(10) \rightarrow SU(5) \times U(1)_\chi$ (with $g_\chi = e/\cos\theta_W$)
Mass $m > 4800$ GeV, CL = 95% ($p\bar{p}$ direct search)
 Z_ψ of $E_6 \rightarrow SO(10) \times U(1)_\psi$ (with $g_\psi = e/\cos\theta_W$)
Mass $m > 4560$ GeV, CL = 95% ($p\bar{p}$ direct search)
 Z_η of $E_6 \rightarrow SU(3) \times SU(2) \times U(1) \times U(1)_\eta$ (with $g_\eta = e/\cos\theta_W$)
Mass $m > 3.900 \times 10^3$ GeV, CL = 95% ($p\bar{p}$ direct search)

Scalar Leptoquarks

- $m > 1800$ GeV, CL = 95% (1st gen., pair prod., $B(eq)=1$)
 $m > 1755$ GeV, CL = 95% (1st gen., single prod., $B(eq)=1$)
 $m > 1700$ GeV, CL = 95% (2nd gen., pair prod., $B(\mu q)=1$)
 $m > 660$ GeV, CL = 95% (2nd gen., single prod., $B(\mu q)=1$)
 $m > 1430$ GeV, CL = 95% (3rd gen., pair prod., $B(\tau t)=1$)
 $m > 740$ GeV, CL = 95% (3rd gen., single prod., $B(\tau b)=1$)
(See the Particle Listings for assumptions on leptoquark quantum numbers and branching fractions.)

Diquarks

- Mass $m > 7200$ GeV, CL = 95% (E_6 diquark)

Axiglun

- Mass $m > 6600$ GeV, CL = 95%

**Axions (A^0) and Other
Very Light Bosons, Searches for**

See the review on "Axions and other similar particles."

The best limit for the half-life of neutrinoless double beta decay with Majoron emission is $> 7.2 \times 10^{24}$ years (CL = 90%).

NOTES

In this Summary Table:

When a quantity has "($S = \dots$)" to its right, the error on the quantity has been enlarged by the "scale factor" S , defined as $S = \sqrt{\chi^2/(N-1)}$, where N is the number of measurements used in calculating the quantity. We do this when $S > 1$, which often indicates that the measurements are inconsistent. When $S > 1.25$, we also show in the Particle Listings an ideogram of the measurements. For more about S , see the Introduction.

A decay momentum p is given for each decay mode. For a 2-body decay, p is the momentum of each decay product in the rest frame of the decaying particle. For a 3-or-more-body decay, p is the largest momentum any of the products can have in this frame.

- [a] Theoretical value. A mass as large as a few MeV may not be precluded.
[b] ℓ indicates each type of lepton (e , μ , and τ), not sum over them.
[c] This represents the width for the decay of the W boson into a charged particle with momentum below detectability, $p < 200$ MeV.
[d] The Z -boson mass listed here corresponds to a Breit-Wigner resonance parameter. It lies approximately 34 MeV above the real part of the position of the pole (in the energy-squared plane) in the Z -boson propagator.
[e] This partial width takes into account Z decays into $\nu\bar{\nu}$ and any other possible undetected modes.
[f] This ratio has not been corrected for the τ mass.
[g] Here $A \equiv 2g_V g_A / (g_V^2 + g_A^2)$.
[h] This parameter is not directly used in the overall fit but is derived using the fit results; see the note "The Z boson" and ref. LEP-SLC 06 (Physics Reports (Physics Letters C) **427** 257 (2006)).
[i] Here ℓ indicates e or μ .
[j] The value is for the sum of the charge states or particle/antiparticle states indicated.
[k] This value is updated using the product of (i) the $Z \rightarrow b\bar{b}$ fraction from this listing and (ii) the b -hadron fraction in an unbiased sample of weakly decaying b -hadrons produced in Z -decays provided by the Heavy Flavor Averaging Group (HFLAV, <http://www.slac.stanford.edu/xorg/hflav/osc/PGD.2009/#FRACZ>).
[l] See the Z Particle Listings for the γ energy range used in this measurement.
[n] For $m_{\gamma\gamma} = (60 \pm 5)$ GeV.

Lepton Summary Table

LEPTONS

e

$$J = \frac{1}{2}$$

Mass $m = (548.579909065 \pm 0.000000016) \times 10^{-6} \text{ u}$
 Mass $m = 0.51099895000 \pm 0.0000000015 \text{ MeV}$
 $|m_{e^+} - m_{e^-}|/m < 8 \times 10^{-9}$, CL = 90%
 $|q_{e^+} + q_{e^-}|/e < 4 \times 10^{-8}$
 Magnetic moment anomaly
 $(g-2)/2 = (1159.65218076 \pm 0.00000028) \times 10^{-6}$
 $(g_{e^+} - g_{e^-}) / g_{\text{average}} = (-0.5 \pm 2.1) \times 10^{-12}$
 Electric dipole moment $d < 0.11 \times 10^{-28} \text{ ecm}$, CL = 90%
 Mean life $\tau > 6.6 \times 10^{28} \text{ yr}$, CL = 90% [a]

 μ

$$J = \frac{1}{2}$$

Mass $m = 0.1134289259 \pm 0.0000000025 \text{ u}$
 Mass $m = 105.6583755 \pm 0.0000023 \text{ MeV}$
 Mean life $\tau = (2.1969811 \pm 0.0000022) \times 10^{-6} \text{ s}$
 $\tau_{\mu^+}/\tau_{\mu^-} = 1.00002 \pm 0.00008$
 $c\tau = 658.6384 \text{ m}$
 Magnetic moment anomaly $(g-2)/2 = (11659206 \pm 4) \times 10^{-10}$
 $(g_{\mu^+} - g_{\mu^-}) / g_{\text{average}} = (-0.11 \pm 0.12) \times 10^{-8}$
 Electric dipole moment $|d| < 1.8 \times 10^{-19} \text{ ecm}$, CL = 95%

Decay parameters [b]

$\rho = 0.74979 \pm 0.00026$
 $\eta = 0.057 \pm 0.034$
 $\delta = 0.75047 \pm 0.00034$
 $\xi P_{\mu} = 1.0009^{+0.0016}_{-0.0007} [c]$
 $\xi P_{\mu} \delta / \rho = 1.0018^{+0.0016}_{-0.0007} [c]$
 $\xi' = 1.00 \pm 0.04$
 $\xi'' = 0.98 \pm 0.04$
 $\alpha/A = (0 \pm 4) \times 10^{-3}$
 $\alpha'/A = (-10 \pm 20) \times 10^{-3}$
 $\beta/A = (4 \pm 6) \times 10^{-3}$
 $\beta'/A = (2 \pm 7) \times 10^{-3}$
 $\overline{\eta} = 0.02 \pm 0.08$

μ^{\pm} modes are charge conjugates of the modes below.

μ^- DECAY MODES	Fraction (Γ_i/Γ)	Confidence level	ρ (MeV/c)
$e^- \overline{\nu}_e \nu_{\mu}$	$\approx 100\%$		53
$e^- \overline{\nu}_e \nu_{\mu} \gamma$	[d] $(6.0 \pm 0.5) \times 10^{-8}$		53
$e^- \overline{\nu}_e \nu_{\mu} e^+ e^-$	[e] $(3.4 \pm 0.4) \times 10^{-5}$		53
Lepton Family number (LF) violating modes			
$e^- \nu_e \overline{\nu}_{\mu}$	LF [f] < 1.2	%	90% 53
$e^- \gamma$	LF < 4.2	$\times 10^{-13}$	90% 53
$e^- e^+ e^-$	LF < 1.0	$\times 10^{-12}$	90% 53
$e^- 2\gamma$	LF < 7.2	$\times 10^{-11}$	90% 53

 τ

$$J = \frac{1}{2}$$

Mass $m = 1776.86 \pm 0.12 \text{ MeV}$
 $(m_{\tau^+} - m_{\tau^-})/m_{\text{average}} < 2.8 \times 10^{-4}$, CL = 90%
 Mean life $\tau = (290.3 \pm 0.5) \times 10^{-15} \text{ s}$
 $c\tau = 87.03 \mu\text{m}$
 Magnetic moment anomaly > -0.052 and < 0.013 , CL = 95%
 $\text{Re}(d_{\tau}) = -0.220$ to $0.45 \times 10^{-16} \text{ ecm}$, CL = 95%
 $\text{Im}(d_{\tau}) = -0.250$ to $0.0080 \times 10^{-16} \text{ ecm}$, CL = 95%

Weak dipole moment

$\text{Re}(d_{\tau}^W) < 0.50 \times 10^{-17} \text{ ecm}$, CL = 95%
 $\text{Im}(d_{\tau}^W) < 1.1 \times 10^{-17} \text{ ecm}$, CL = 95%

Weak anomalous magnetic dipole moment

$\text{Re}(\alpha_{\tau}^W) < 1.1 \times 10^{-3}$, CL = 95%
 $\text{Im}(\alpha_{\tau}^W) < 2.7 \times 10^{-3}$, CL = 95%
 $\tau^{\pm} \rightarrow \pi^{\pm} K_S^0 \nu_{\tau}$ (RATE DIFFERENCE) / (RATE SUM) = $(-0.36 \pm 0.25)\%$

Decay parameters

See the τ Particle Listings for a note concerning τ -decay parameters.

$\rho(e \text{ or } \mu) = 0.745 \pm 0.008$
 $\rho(e) = 0.747 \pm 0.010$
 $\rho(\mu) = 0.763 \pm 0.020$
 $\xi(e \text{ or } \mu) = 0.985 \pm 0.030$
 $\xi(e) = 0.994 \pm 0.040$
 $\xi(\mu) = 1.030 \pm 0.059$
 $\eta(e \text{ or } \mu) = 0.013 \pm 0.020$
 $\eta(\mu) = 0.094 \pm 0.073$
 $(\delta\xi)(e \text{ or } \mu) = 0.746 \pm 0.021$
 $(\delta\xi)(e) = 0.734 \pm 0.028$
 $(\delta\xi)(\mu) = 0.778 \pm 0.037$
 $\xi(\pi) = 0.993 \pm 0.022$
 $\xi(\rho) = 0.994 \pm 0.008$
 $\xi(a_1) = 1.001 \pm 0.027$
 $\xi(\text{all hadronic modes}) = 0.995 \pm 0.007$
 $\overline{\eta}(\mu) = -1.3 \pm 1.7$
 $(\xi\kappa)(e \text{ or } \mu) \text{ PARAMETER} = 0.5 \pm 0.4$
 $(\xi\kappa)(e) = -0.4 \pm 1.2$
 $(\xi\kappa)(\mu) = 0.8 \pm 0.6$

τ^{\pm} modes are charge conjugates of the modes below. " h^{\pm} " stands for π^{\pm} or K^{\pm} . " e " stands for e or μ . "Neutrals" stands for γ 's and/or π^0 's.

τ^- DECAY MODES	Fraction (Γ_i/Γ)	Scale factor / Confidence level	ρ (MeV/c)
Modes with one charged particle			
particle $^- \geq 0$ neutrals $\geq 0K^0 \nu_{\tau}$ ("1-prong")	$(85.24 \pm 0.06) \%$		-
particle $^- \geq 0$ neutrals $\geq 0K_L^0 \nu_{\tau}$	$(84.58 \pm 0.06) \%$		-
$\mu^- \overline{\nu}_{\mu} \nu_{\tau}$	[g] $(17.39 \pm 0.04) \%$		885
$\mu^- \overline{\nu}_{\mu} \nu_{\tau} \gamma$	[e] $(3.67 \pm 0.08) \times 10^{-3}$		885
$e^- \overline{\nu}_e \nu_{\tau}$	[g] $(17.82 \pm 0.04) \%$		888
$e^- \overline{\nu}_e \nu_{\tau} \gamma$	[e] $(1.83 \pm 0.05) \%$		888
$h^- \geq 0K_L^0 \nu_{\tau}$	$(12.03 \pm 0.05) \%$		883
$h^- \nu_{\tau}$	$(11.51 \pm 0.05) \%$		883
$\pi^- \nu_{\tau}$	[g] $(10.82 \pm 0.05) \%$		883
$K^- \nu_{\tau}$	[g] $(6.96 \pm 0.10) \times 10^{-3}$		820
$h^- \geq 1$ neutrals ν_{τ}	$(37.01 \pm 0.09) \%$		-
$h^- \geq 1\pi^0 \nu_{\tau}$ (ex. K^0)	$(36.51 \pm 0.09) \%$		-
$h^- \pi^0 \nu_{\tau}$	$(25.93 \pm 0.09) \%$		878
$\pi^- \pi^0 \nu_{\tau}$	[g] $(25.49 \pm 0.09) \%$		878
$\pi^- \pi^0$ non- $\rho(770) \nu_{\tau}$	$(3.0 \pm 3.2) \times 10^{-3}$		878
$K^- \pi^0 \nu_{\tau}$	[g] $(4.33 \pm 0.15) \times 10^{-3}$		814
$h^- \geq 2\pi^0 \nu_{\tau}$	$(10.81 \pm 0.09) \%$		-
$h^- 2\pi^0 \nu_{\tau}$	$(9.48 \pm 0.10) \%$		862
$h^- 2\pi^0 \nu_{\tau}$ (ex. K^0)	$(9.32 \pm 0.10) \%$		862
$\pi^- 2\pi^0 \nu_{\tau}$ (ex. K^0)	[g] $(9.26 \pm 0.10) \%$		862
$\pi^- 2\pi^0 \nu_{\tau}$ (ex. K^0), scalar	< 9	$\times 10^{-3}$ CL=95%	862
$\pi^- 2\pi^0 \nu_{\tau}$ (ex. K^0), vector	< 7	$\times 10^{-3}$ CL=95%	862
$K^- 2\pi^0 \nu_{\tau}$ (ex. K^0)	[g] $(6.5 \pm 2.2) \times 10^{-4}$		796
$h^- \geq 3\pi^0 \nu_{\tau}$	$(1.34 \pm 0.07) \%$		-
$h^- \geq 3\pi^0 \nu_{\tau}$ (ex. K^0)	$(1.25 \pm 0.07) \%$		-
$h^- 3\pi^0 \nu_{\tau}$	$(1.18 \pm 0.07) \%$		836
$\pi^- 3\pi^0 \nu_{\tau}$ (ex. K^0)	[g] $(1.04 \pm 0.07) \%$		836
$K^- 3\pi^0 \nu_{\tau}$ (ex. K^0)	[g] $(4.8 \pm 2.1) \times 10^{-4}$		765
$h^- 4\pi^0 \nu_{\tau}$ (ex. K^0)	$(1.6 \pm 0.4) \times 10^{-3}$		800
$h^- 4\pi^0 \nu_{\tau}$ (ex. K^0, η)	[g] $(1.1 \pm 0.4) \times 10^{-3}$		800
$a_1(1260) \nu_{\tau} \rightarrow \pi^- \gamma \nu_{\tau}$	$(3.8 \pm 1.5) \times 10^{-4}$		-
$K^- \geq 0\pi^0 \geq 0K^0 \geq 0\gamma \nu_{\tau}$	$(1.552 \pm 0.029) \%$		820
$K^- \geq 1(\pi^0 \text{ or } K^0 \text{ or } \gamma) \nu_{\tau}$	$(8.59 \pm 0.28) \times 10^{-3}$		-
Modes with K^0 's			
$K_S^0(\text{particles})^- \nu_{\tau}$	$(9.43 \pm 0.28) \times 10^{-3}$		-
$h^- \overline{K}^0 \nu_{\tau}$	$(9.87 \pm 0.14) \times 10^{-3}$		812
$\pi^- \overline{K}^0 \nu_{\tau}$	[g] $(8.38 \pm 0.14) \times 10^{-3}$		812
$\pi^- \overline{K}^0$	$(5.4 \pm 2.1) \times 10^{-4}$		812
$(\text{non-}K^*(892)^- \nu_{\tau})$			
$K^- K^0 \nu_{\tau}$	[g] $(1.486 \pm 0.034) \times 10^{-3}$		737
$K^- K^0 \geq 0\pi^0 \nu_{\tau}$	$(2.99 \pm 0.07) \times 10^{-3}$		737
$h^- \overline{K}^0 \pi^0 \nu_{\tau}$	$(5.32 \pm 0.13) \times 10^{-3}$		794
$\pi^- \overline{K}^0 \pi^0 \nu_{\tau}$	[g] $(3.82 \pm 0.13) \times 10^{-3}$		794

Lepton Summary Table

$\bar{K}^0 \rho^- \nu_\tau$	(2.2 ± 0.5) × 10 ⁻³	612	$K^- K^+ K^- \nu_\tau$ (ex. ϕ)	< 2.5	× 10 ⁻⁶ CL=90%	-
$K^- K^0 \pi^0 \nu_\tau$	[g] (1.50 ± 0.07) × 10 ⁻³	685	$K^- K^+ K^- \pi^0 \nu_\tau$	< 4.8	× 10 ⁻⁶ CL=90%	345
$\pi^- \bar{K}^0 \geq 1\pi^0 \nu_\tau$	(4.08 ± 0.25) × 10 ⁻³	-	$\pi^- K^+ \pi^- \geq 0$ neut. ν_τ	< 2.5	× 10 ⁻³ CL=95%	794
$\pi^- \bar{K}^0 \pi^0 \pi^0 \nu_\tau$ (ex. K^0)	[g] (2.6 ± 2.3) × 10 ⁻⁴	763	$e^- e^- e^+ \bar{\nu}_e \nu_\tau$	(2.8 ± 1.5) × 10 ⁻⁵		888
$K^- K^0 \pi^0 \pi^0 \nu_\tau$	< 1.6 × 10 ⁻⁴ CL=95%	619	$\mu^- e^- e^+ \bar{\nu}_e \mu \nu_\tau$	< 3.2	× 10 ⁻⁵ CL=90%	885
$\pi^- K^0 \bar{K}^0 \nu_\tau$	(1.55 ± 0.24) × 10 ⁻³	682	$\pi^- e^- e^+ \nu_\tau$	seen		883
$\pi^- K_S^0 K_S^0 \nu_\tau$	[g] (2.35 ± 0.06) × 10 ⁻⁴	682	$\pi^- \mu^- \mu^+ \nu_\tau$	< 1.14	× 10 ⁻⁵ CL=90%	870
$\pi^- K_S^0 K_L^0 \nu_\tau$	[g] (1.08 ± 0.24) × 10 ⁻³	682	Modes with five charged particles			
$\pi^- K_L^0 K_S^0 \nu_\tau$	(2.35 ± 0.06) × 10 ⁻⁴	682	$3h^- 2h^+ \geq 0$ neutrals ν_τ	(9.9 ± 0.4) × 10 ⁻⁴		794
$\pi^- K^0 \bar{K}^0 \pi^0 \nu_\tau$	(3.6 ± 1.2) × 10 ⁻⁴	614	(ex. $K_S^0 \rightarrow \pi^- \pi^+$)			
$\pi^- K_S^0 K_S^0 \pi^0 \nu_\tau$	[g] (1.82 ± 0.21) × 10 ⁻⁵	614	("5-prong")			
$K^{*-} K^0 \pi^0 \nu_\tau \rightarrow$	(1.08 ± 0.21) × 10 ⁻⁵	-	$3h^- 2h^+ \nu_\tau$ (ex. K^0)	(8.29 ± 0.31) × 10 ⁻⁴		794
$\pi^- K_S^0 K_S^0 \pi^0 \nu_\tau$			$3\pi^- 2\pi^+ \nu_\tau$ (ex. K^0, ω)	(8.27 ± 0.31) × 10 ⁻⁴		794
$f_1(1285) \pi^- \nu_\tau \rightarrow$	(6.8 ± 1.5) × 10 ⁻⁶	-	$3\pi^- 2\pi^+ \nu_\tau$ (ex. K^0, ω ,	[g] (7.75 ± 0.30) × 10 ⁻⁴		-
$\pi^- K_S^0 K_S^0 \pi^0 \nu_\tau$			$f_1(1285)$)			
$f_1(1420) \pi^- \nu_\tau \rightarrow$	(2.4 ± 0.8) × 10 ⁻⁶	-	$K^- 2\pi^- 2\pi^+ \nu_\tau$ (ex. K^0)	[g] (6 ± 1.2) × 10 ⁻⁷		716
$\pi^- K_S^0 K_S^0 \pi^0 \nu_\tau$			$K^+ 3\pi^- \pi^+ \nu_\tau$	< 5.0	× 10 ⁻⁶ CL=90%	716
$\pi^- K_S^0 K_L^0 \pi^0 \nu_\tau$	[g] (3.2 ± 1.2) × 10 ⁻⁴	614	$K^+ K^- 2\pi^- \pi^+ \nu_\tau$	< 4.5	× 10 ⁻⁷ CL=90%	528
$\pi^- K_L^0 K_L^0 \pi^0 \nu_\tau$	(1.82 ± 0.21) × 10 ⁻⁵	614	$3h^- 2h^+ \pi^0 \nu_\tau$ (ex. K^0)	(1.65 ± 0.11) × 10 ⁻⁴		746
$K^- K_S^0 K_S^0 \nu_\tau$	< 6.3 × 10 ⁻⁷ CL=90%	466	$3\pi^- 2\pi^+ \pi^0 \nu_\tau$ (ex. K^0)	(1.63 ± 0.11) × 10 ⁻⁴		746
$K^- K_S^0 K_S^0 \pi^0 \nu_\tau$	< 4.0 × 10 ⁻⁷ CL=90%	337	$3\pi^- 2\pi^+ \pi^0 \nu_\tau$ (ex. K^0, η ,	(1.11 ± 0.10) × 10 ⁻⁴		-
$K^0 h^+ h^- h^- \geq 0$ neutrals ν_τ	< 1.7 × 10 ⁻³ CL=95%	760	$f_1(1285)$)			
$K^0 h^+ h^- h^- \nu_\tau$	[g] (2.5 ± 2.0) × 10 ⁻⁴	760	$3\pi^- 2\pi^+ \pi^0 \nu_\tau$ (ex. K^0, η ,	[g] (3.8 ± 0.9) × 10 ⁻⁵		-
Modes with three charged particles			$\omega, f_1(1285)$)			
$h^- h^- h^+ \geq 0$ neutrals $\geq 0 K_L^0 \nu_\tau$	(15.20 ± 0.06) %	861	$K^- 2\pi^- 2\pi^+ \pi^0 \nu_\tau$ (ex. K^0)	[g] (1.1 ± 0.6) × 10 ⁻⁶		657
$h^- h^- h^+ \geq 0$ neutrals ν_τ	(14.55 ± 0.06) %	861	$K^+ 3\pi^- \pi^+ \pi^0 \nu_\tau$	< 8	× 10 ⁻⁷ CL=90%	657
(ex. $K_S^0 \rightarrow \pi^+ \pi^-$)			$3h^- 2h^+ 2\pi^0 \nu_\tau$	< 3.4	× 10 ⁻⁶ CL=90%	687
("3-prong")			Miscellaneous other allowed modes			
$h^- h^- h^+ \nu_\tau$	(9.80 ± 0.05) %	861	$(5\pi)^- \nu_\tau$	(7.8 ± 0.5) × 10 ⁻³		800
$h^- h^- h^+ \nu_\tau$ (ex. K^0)	(9.46 ± 0.05) %	861	$4h^- 3h^+ \geq 0$ neutrals ν_τ	< 3.0	× 10 ⁻⁷ CL=90%	682
$h^- h^- h^+ \nu_\tau$ (ex. K^0, ω)	(9.43 ± 0.05) %	861	("7-prong")			
$\pi^- \pi^+ \pi^- \nu_\tau$	(9.31 ± 0.05) %	861	$4h^- 3h^+ \nu_\tau$	< 4.3	× 10 ⁻⁷ CL=90%	682
$\pi^- \pi^+ \pi^- \nu_\tau$ (ex. K^0)	(9.02 ± 0.05) %	861	$4h^- 3h^+ \pi^0 \nu_\tau$	< 2.5	× 10 ⁻⁷ CL=90%	612
$\pi^- \pi^+ \pi^- \nu_\tau$ (ex. K^0),	< 2.4 %	861	$X^- (S=-1) \nu_\tau$	(2.92 ± 0.04) %		-
non-axial vector			$K^*(892)^0 \geq 0$ neutrals \geq	(1.42 ± 0.18) %	S=1.4	665
$\pi^- \pi^+ \pi^- \nu_\tau$ (ex. K^0, ω)	[g] (8.99 ± 0.05) %	861	$0 K_L^0 \nu_\tau$			
$h^- h^- h^+ \geq 1$ neutrals ν_τ	(5.29 ± 0.05) %	-	$K^*(892)^- \nu_\tau$	(1.20 ± 0.07) %	S=1.8	665
$h^- h^- h^+ \geq 1\pi^0 \nu_\tau$ (ex. K^0)	(5.09 ± 0.05) %	-	$K^*(892)^- \nu_\tau \rightarrow \pi^- \bar{K}^0 \nu_\tau$	(7.82 ± 0.26) × 10 ⁻³		-
$h^- h^- h^+ \pi^0 \nu_\tau$	(4.76 ± 0.05) %	834	$K^*(892)^0 K^- \geq 0$ neutrals ν_τ	(3.2 ± 1.4) × 10 ⁻³		542
$h^- h^- h^+ \pi^0 \nu_\tau$ (ex. K^0)	(4.57 ± 0.05) %	834	$K^*(892)^0 K^- \nu_\tau$	(2.1 ± 0.4) × 10 ⁻³		542
$h^- h^- h^+ \pi^0 \nu_\tau$ (ex. K^0, ω)	(2.79 ± 0.07) %	834	$\bar{K}^*(892)^0 \pi^- \geq 0$ neutrals ν_τ	(3.8 ± 1.7) × 10 ⁻³		655
$\pi^- \pi^+ \pi^- \pi^0 \nu_\tau$	(4.62 ± 0.05) %	834	$\bar{K}^*(892)^0 \pi^- \nu_\tau$	(2.2 ± 0.5) × 10 ⁻³		655
$\pi^- \pi^+ \pi^- \pi^0 \nu_\tau$ (ex. K^0)	(4.49 ± 0.05) %	834	$(\bar{K}^*(892) \pi)^- \nu_\tau \rightarrow$	(1.0 ± 0.4) × 10 ⁻³		-
$\pi^- \pi^+ \pi^- \pi^0 \nu_\tau$ (ex. K^0, ω)	[g] (2.74 ± 0.07) %	834	$\pi^- \bar{K}^0 \pi^0 \nu_\tau$			
$h^- h^- h^+ \geq 2\pi^0 \nu_\tau$ (ex. K^0)	(5.17 ± 0.31) × 10 ⁻³	-	$K_1(1270)^- \nu_\tau$	(4.7 ± 1.1) × 10 ⁻³		447
$h^- h^- h^+ 2\pi^0 \nu_\tau$	(5.05 ± 0.31) × 10 ⁻³	797	$K_1(1400)^- \nu_\tau$	(1.7 ± 2.6) × 10 ⁻³	S=1.7	335
$h^- h^- h^+ 2\pi^0 \nu_\tau$ (ex. K^0)	(4.95 ± 0.31) × 10 ⁻³	797	$K^*(1410)^- \nu_\tau$	(1.5 ± 1.4) × 10 ⁻³		326
$h^- h^- h^+ 2\pi^0 \nu_\tau$ (ex. K^0, ω, η)	[g] (10 ± 4) × 10 ⁻⁴	797	$K_0^0(1430)^- \nu_\tau$	< 5	× 10 ⁻⁴ CL=95%	317
$h^- h^- h^+ 3\pi^0 \nu_\tau$	(2.13 ± 0.30) × 10 ⁻⁴	749	$K_2^0(1430)^- \nu_\tau$	< 3	× 10 ⁻³ CL=95%	315
$2\pi^- \pi^+ 3\pi^0 \nu_\tau$ (ex. K^0)	(1.95 ± 0.30) × 10 ⁻⁴	749	$\eta \pi^- \nu_\tau$	< 9.9	× 10 ⁻⁵ CL=95%	797
$2\pi^- \pi^+ 3\pi^0 \nu_\tau$ (ex. K^0, η ,	(1.7 ± 0.4) × 10 ⁻⁴	-	$\eta \pi^- \pi^0 \nu_\tau$	[g] (1.39 ± 0.07) × 10 ⁻³		778
$f_1(1285)$)			$\eta \pi^- \pi^0 \pi^0 \nu_\tau$	[g] (2.0 ± 0.4) × 10 ⁻⁴		746
$2\pi^- \pi^+ 3\pi^0 \nu_\tau$ (ex. K^0, η ,	[g] (1.4 ± 2.7) × 10 ⁻⁵	-	$\eta K^- \nu_\tau$	[g] (1.55 ± 0.08) × 10 ⁻⁴		719
$\omega, f_1(1285)$)			$\eta K^*(892)^- \nu_\tau$	(1.38 ± 0.15) × 10 ⁻⁴		511
$K^- h^+ h^- \geq 0$ neutrals ν_τ	(6.29 ± 0.14) × 10 ⁻³	794	$\eta K^- \pi^0 \nu_\tau$	[g] (4.8 ± 1.2) × 10 ⁻⁵		665
$K^- h^+ \pi^- \nu_\tau$ (ex. K^0)	(4.37 ± 0.07) × 10 ⁻³	794	$\eta K^- \pi^0$ (non- $K^*(892)$) ν_τ	< 3.5	× 10 ⁻⁵ CL=90%	-
$K^- h^+ \pi^- \pi^0 \nu_\tau$ (ex. K^0)	(8.6 ± 1.2) × 10 ⁻⁴	763	$\eta \bar{K}^0 \pi^- \nu_\tau$	[g] (9.4 ± 1.5) × 10 ⁻⁵		661
$K^- \pi^+ \pi^- \geq 0$ neutrals ν_τ	(4.77 ± 0.14) × 10 ⁻³	794	$\eta \bar{K}^0 \pi^- \pi^0 \nu_\tau$	< 5.0	× 10 ⁻⁵ CL=90%	590
$K^- \pi^+ \pi^- \geq$	(3.73 ± 0.13) × 10 ⁻³	794	$\eta K^- K^0 \nu_\tau$	< 9.0	× 10 ⁻⁶ CL=90%	430
$0\pi^0 \nu_\tau$ (ex. K^0)			$\eta \pi^+ \pi^- \pi^- \geq 0$ neutrals ν_τ	< 3	× 10 ⁻³ CL=90%	744
$K^- \pi^+ \pi^- \nu_\tau$	(3.45 ± 0.07) × 10 ⁻³	794	$\eta \pi^- \pi^+ \pi^- \nu_\tau$ (ex. K^0)	[g] (2.20 ± 0.13) × 10 ⁻⁴		744
$K^- \pi^+ \pi^- \nu_\tau$ (ex. K^0)	(2.93 ± 0.07) × 10 ⁻³	794	$\eta \pi^- \pi^+ \pi^- \nu_\tau$ (ex. $K^0, f_1(1285)$)	(9.9 ± 1.6) × 10 ⁻⁵		-
$K^- \pi^+ \pi^- \nu_\tau$ (ex. K^0, ω)	[g] (2.93 ± 0.07) × 10 ⁻³	794	$\eta a_1(1260)^- \nu_\tau \rightarrow \eta \pi^- \rho^0 \nu_\tau$	< 3.9	× 10 ⁻⁴ CL=90%	-
$K^- \rho^0 \nu_\tau \rightarrow$	(1.4 ± 0.5) × 10 ⁻³	-	$\eta \eta \pi^- \nu_\tau$	< 7.4	× 10 ⁻⁶ CL=90%	637
$K^- \pi^+ \pi^- \nu_\tau$			$\eta \eta \pi^- \pi^0 \nu_\tau$	< 2.0	× 10 ⁻⁴ CL=95%	559
$K^- \pi^+ \pi^- \pi^0 \nu_\tau$	(1.31 ± 0.12) × 10 ⁻³	763	$\eta \eta K^- \nu_\tau$	< 3.0	× 10 ⁻⁶ CL=90%	382
$K^- \pi^+ \pi^- \pi^0 \nu_\tau$ (ex. K^0)	(7.9 ± 1.2) × 10 ⁻⁴	763	$\eta'(958) \pi^- \nu_\tau$	< 4.0	× 10 ⁻⁶ CL=90%	620
$K^- \pi^+ \pi^- \pi^0 \nu_\tau$ (ex. K^0, η)	(7.6 ± 1.2) × 10 ⁻⁴	763	$\eta'(958) \pi^- \pi^0 \nu_\tau$	< 1.2	× 10 ⁻⁵ CL=90%	591
$K^- \pi^+ \pi^- \pi^0 \nu_\tau$ (ex. K^0, ω)	(3.7 ± 0.9) × 10 ⁻⁴	763	$\eta'(958) K^- \nu_\tau$	< 2.4	× 10 ⁻⁶ CL=90%	495
$K^- \pi^+ \pi^- \pi^0 \nu_\tau$ (ex. K^0, ω, η)	[g] (3.9 ± 1.4) × 10 ⁻⁴	763	$\phi \pi^- \nu_\tau$	(3.4 ± 0.6) × 10 ⁻⁵		585
$K^- \pi^+ K^- \geq 0$ neut. ν_τ	< 9 × 10 ⁻⁴ CL=95%	685	$\phi K^- \nu_\tau$	[g] (4.4 ± 1.6) × 10 ⁻⁵		445
$K^- K^+ \pi^- \geq 0$ neut. ν_τ	(1.496 ± 0.033) × 10 ⁻³	685	$f_1(1285) \pi^- \nu_\tau$	(3.9 ± 0.5) × 10 ⁻⁴	S=1.9	408
$K^- K^+ \pi^- \nu_\tau$	[g] (1.435 ± 0.027) × 10 ⁻³	685	$f_1(1285) \pi^- \nu_\tau \rightarrow$	(1.18 ± 0.07) × 10 ⁻⁴	S=1.3	-
$K^- K^+ \pi^- \pi^0 \nu_\tau$	[g] (6.1 ± 1.8) × 10 ⁻⁵	618	$\eta \pi^- \pi^+ \pi^- \nu_\tau$			
$K^- K^+ K^- \nu_\tau$	(2.2 ± 0.8) × 10 ⁻⁵	472	$f_1(1285) \pi^- \nu_\tau \rightarrow$	[g] (5.2 ± 0.4) × 10 ⁻⁵		-
			$3\pi^- 2\pi^+ \nu_\tau$			

Lepton Summary Table

$\pi(1300)^- \nu_\tau \rightarrow (\rho\pi)^- \nu_\tau \rightarrow (3\pi)^- \nu_\tau$	< 1.0	$\times 10^{-4}$ CL=90%	-
$\pi(1300)^- \nu_\tau \rightarrow ((\pi\pi)_{S\text{-wave}} \pi)^- \nu_\tau \rightarrow (3\pi)^- \nu_\tau$	< 1.9	$\times 10^{-4}$ CL=90%	-
$h^- \omega \geq 0$ neutrals ν_τ	(2.40 ± 0.08) %		708
$h^- \omega \nu_\tau$	(1.99 ± 0.06) %		708
$\pi^- \omega \nu_\tau$	[g] (1.95 ± 0.06) %		708
$K^- \omega \nu_\tau$	[g] (4.1 ± 0.9) $\times 10^{-4}$		610
$h^- \omega \pi^0 \nu_\tau$	[g] (4.1 ± 0.4) $\times 10^{-3}$		684
$h^- \omega 2\pi^0 \nu_\tau$	(1.4 ± 0.5) $\times 10^{-4}$		644
$\pi^- \omega 2\pi^0 \nu_\tau$	[g] (7.2 ± 1.6) $\times 10^{-5}$		644
$h^- 2\omega \nu_\tau$	< 5.4	$\times 10^{-7}$ CL=90%	250
$2h^- h^+ \omega \nu_\tau$	(1.20 ± 0.22) $\times 10^{-4}$		641
$2\pi^- \pi^+ \omega \nu_\tau$ (ex. K^0)	[g] (8.4 ± 0.6) $\times 10^{-5}$		641

Lepton Family number (LF), Lepton number (L), or Baryon number (B) violating modes

L means lepton number violation (e.g. $\tau^- \rightarrow e^+ \pi^- \pi^-$). Following common usage, LF means lepton family violation and not lepton number violation (e.g. $\tau^- \rightarrow e^- \pi^+ \pi^-$). B means baryon number violation.

$e^- \gamma$	LF	< 3.3	$\times 10^{-8}$ CL=90%	888
$e^- \gamma \gamma$		< 2.5	$\times 10^{-4}$ CL=90%	888
$\mu^- \gamma$	LF	< 4.2	$\times 10^{-8}$ CL=90%	885
$\mu^- \gamma \gamma$		< 5.8	$\times 10^{-4}$ CL=90%	885
$e^- \pi^0$	LF	< 8.0	$\times 10^{-8}$ CL=90%	883
$\mu^- \pi^0$	LF	< 1.1	$\times 10^{-7}$ CL=90%	880
$e^- K_S^0$	LF	< 2.6	$\times 10^{-8}$ CL=90%	819
$\mu^- K_S^0$	LF	< 2.3	$\times 10^{-8}$ CL=90%	815
$e^- \eta$	LF	< 9.2	$\times 10^{-8}$ CL=90%	804
$\mu^- \eta$	LF	< 6.5	$\times 10^{-8}$ CL=90%	800
$e^- \rho^0$	LF	< 1.8	$\times 10^{-8}$ CL=90%	719
$\mu^- \rho^0$	LF	< 1.2	$\times 10^{-8}$ CL=90%	715
$e^- \omega$	LF	< 4.8	$\times 10^{-8}$ CL=90%	716
$\mu^- \omega$	LF	< 4.7	$\times 10^{-8}$ CL=90%	711
$e^- K^*(892)^0$	LF	< 3.2	$\times 10^{-8}$ CL=90%	665
$\mu^- K^*(892)^0$	LF	< 5.9	$\times 10^{-8}$ CL=90%	659
$e^- \bar{K}^*(892)^0$	LF	< 3.4	$\times 10^{-8}$ CL=90%	665
$\mu^- \bar{K}^*(892)^0$	LF	< 7.0	$\times 10^{-8}$ CL=90%	659
$e^- \eta'(958)$	LF	< 1.6	$\times 10^{-7}$ CL=90%	630
$\mu^- \eta'(958)$	LF	< 1.3	$\times 10^{-7}$ CL=90%	625
$e^- f_0(980) \rightarrow e^- \pi^+ \pi^-$	LF	< 3.2	$\times 10^{-8}$ CL=90%	-
$\mu^- f_0(980) \rightarrow \mu^- \pi^+ \pi^-$	LF	< 3.4	$\times 10^{-8}$ CL=90%	-
$e^- \phi$	LF	< 3.1	$\times 10^{-8}$ CL=90%	596
$\mu^- \phi$	LF	< 8.4	$\times 10^{-8}$ CL=90%	590
$e^- e^+ e^-$	LF	< 2.7	$\times 10^{-8}$ CL=90%	888
$e^- \mu^+ \mu^-$	LF	< 2.7	$\times 10^{-8}$ CL=90%	882
$e^+ \mu^- \mu^-$	LF	< 1.7	$\times 10^{-8}$ CL=90%	882
$\mu^- e^+ e^-$	LF	< 1.8	$\times 10^{-8}$ CL=90%	885
$\mu^+ e^- e^-$	LF	< 1.5	$\times 10^{-8}$ CL=90%	885
$\mu^- \mu^+ \mu^-$	LF	< 2.1	$\times 10^{-8}$ CL=90%	873
$e^- \pi^+ \pi^-$	LF	< 2.3	$\times 10^{-8}$ CL=90%	877
$e^+ \pi^- \pi^-$	L	< 2.0	$\times 10^{-8}$ CL=90%	877
$\mu^+ \pi^- \pi^-$	LF	< 2.1	$\times 10^{-8}$ CL=90%	866
$\mu^- \pi^+ \pi^-$	L	< 3.9	$\times 10^{-8}$ CL=90%	866
$e^- \pi^+ K^-$	LF	< 3.7	$\times 10^{-8}$ CL=90%	813
$e^- \pi^- K^+$	LF	< 3.1	$\times 10^{-8}$ CL=90%	813
$e^+ \pi^- K^-$	L	< 3.2	$\times 10^{-8}$ CL=90%	813
$e^- K_S^0 K_S^0$	LF	< 7.1	$\times 10^{-8}$ CL=90%	736
$e^- K^+ K^-$	LF	< 3.4	$\times 10^{-8}$ CL=90%	738
$e^+ K^- K^-$	L	< 3.3	$\times 10^{-8}$ CL=90%	738
$\mu^- \pi^+ K^-$	LF	< 8.6	$\times 10^{-8}$ CL=90%	800
$\mu^- \pi^- K^+$	LF	< 4.5	$\times 10^{-8}$ CL=90%	800
$\mu^+ \pi^- K^-$	L	< 4.8	$\times 10^{-8}$ CL=90%	800
$\mu^- K_S^0 K_S^0$	LF	< 8.0	$\times 10^{-8}$ CL=90%	696
$\mu^- K^+ K^-$	LF	< 4.4	$\times 10^{-8}$ CL=90%	699
$\mu^+ K^- K^-$	L	< 4.7	$\times 10^{-8}$ CL=90%	699
$e^- \pi^0 \pi^0$	LF	< 6.5	$\times 10^{-6}$ CL=90%	878
$\mu^- \pi^0 \pi^0$	LF	< 1.4	$\times 10^{-5}$ CL=90%	867
$e^- \eta \eta$	LF	< 3.5	$\times 10^{-5}$ CL=90%	699
$\mu^- \eta \eta$	LF	< 6.0	$\times 10^{-5}$ CL=90%	653
$e^- \pi^0 \eta$	LF	< 2.4	$\times 10^{-5}$ CL=90%	798
$\mu^- \pi^0 \eta$	LF	< 2.2	$\times 10^{-5}$ CL=90%	784
$p e^- e^-$	L,B	< 3.0	$\times 10^{-8}$ CL=90%	641
$\bar{p} e^+ e^-$	L,B	< 3.0	$\times 10^{-8}$ CL=90%	641
$\bar{p} e^+ \mu^-$	L,B	< 2.0	$\times 10^{-8}$ CL=90%	635
$\bar{p} e^- \mu^+$	L,B	< 1.8	$\times 10^{-8}$ CL=90%	635

$p \mu^- \mu^-$	L,B	< 4.0	$\times 10^{-8}$ CL=90%	618
$\bar{p} \mu^+ \mu^-$	L,B	< 1.8	$\times 10^{-8}$ CL=90%	618
$\bar{p} \gamma$	L,B	< 3.5	$\times 10^{-6}$ CL=90%	641
$\bar{p} \pi^0$	L,B	< 1.5	$\times 10^{-5}$ CL=90%	632
$\bar{p} 2\pi^0$	L,B	< 3.3	$\times 10^{-5}$ CL=90%	604
$\bar{p} \eta$	L,B	< 8.9	$\times 10^{-6}$ CL=90%	475
$\bar{p} \pi^0 \eta$	L,B	< 2.7	$\times 10^{-5}$ CL=90%	360
$\Lambda \pi^-$	L,B	< 7.2	$\times 10^{-8}$ CL=90%	525
$\bar{\Lambda} \pi^-$	L,B	< 1.4	$\times 10^{-7}$ CL=90%	525
e^- light boson	LF	< 2.7	$\times 10^{-3}$ CL=95%	-
μ^- light boson	LF	< 5	$\times 10^{-3}$ CL=95%	-

Heavy Charged Lepton Searches

L^\pm - charged lepton

Mass $m > 100.8$ GeV, CL = 95% ^[h] Decay to νW .

L^\pm - stable charged heavy lepton

Mass $m > 102.6$ GeV, CL = 95%

Neutrino Properties

See the note on "Neutrino properties listings" in the Particle Listings.

Mass $m < 1.1$ eV, CL = 90% (tritium decay)

Mean life/mass, $\tau/m > 300$ s/eV, CL = 90% (reactor)

Mean life/mass, $\tau/m > 7 \times 10^9$ s/eV (solar)

Mean life/mass, $\tau/m > 15.4$ s/eV, CL = 90% (accelerator)

Magnetic moment $\mu < 0.28 \times 10^{-10} \mu_B$, CL = 90% (solar + radiochemical)

Number of Neutrino Types

Number $N = 2.996 \pm 0.007$ (Standard Model fits to LEP-SLC data)

Number $N = 2.92 \pm 0.05$ ($S = 1.2$) (Direct measurement of invisible Z width)

Neutrino Mixing

The following values are obtained through data analyses based on the 3-neutrino mixing scheme described in the review "Neutrino Masses, Mixing, and Oscillations."

$$\sin^2(\theta_{12}) = 0.307 \pm 0.013$$

$$\Delta m_{21}^2 = (7.53 \pm 0.18) \times 10^{-5} \text{ eV}^2$$

$$\sin^2(\theta_{23}) = 0.539 \pm 0.022 \text{ (S = 1.1) (Inverted order)}$$

$$\sin^2(\theta_{23}) = 0.546 \pm 0.021 \text{ (Normal order)}$$

$$\Delta m_{32}^2 = (-2.536 \pm 0.034) \times 10^{-3} \text{ eV}^2 \text{ (Inverted order)}$$

$$\Delta m_{32}^2 = (2.453 \pm 0.033) \times 10^{-3} \text{ eV}^2 \text{ (Normal order)}$$

$$\sin^2(\theta_{13}) = (2.20 \pm 0.07) \times 10^{-2}$$

$$\delta, \text{ CP violating phase} = 1.36^{+0.20}_{-0.16} \pi \text{ rad}$$

$$\langle \Delta m_{21}^2 - \Delta \bar{m}_{21}^2 \rangle < 1.1 \times 10^{-4} \text{ eV}^2, \text{ CL} = 99.7\%$$

$$\langle \Delta m_{32}^2 - \Delta \bar{m}_{32}^2 \rangle = (-0.12 \pm 0.25) \times 10^{-3} \text{ eV}^2$$

NOTES

In this Summary Table:

When a quantity has "(S = ...)" to its right, the error on the quantity has been enlarged by the "scale factor" S, defined as $S = \sqrt{\chi^2/(N-1)}$, where N is the number of measurements used in calculating the quantity. We do this when $S > 1$, which often indicates that the measurements are inconsistent. When $S > 1.25$, we also show in the Particle Listings an ideogram of the measurements. For more about S, see the Introduction.

A decay momentum p is given for each decay mode. For a 2-body decay, p is the momentum of each decay product in the rest frame of the decaying particle. For a 3-or-more-body decay, p is the largest momentum any of the products can have in this frame.

[a] This is the best limit for the mode $e^- \rightarrow \nu \gamma$. The best limit for Nuclear de-excitation experiments is 6.4×10^{24} yr.

[b] See the review on "Muon Decay Parameters" for definitions and details.

[c] P_μ is the longitudinal polarization of the muon from pion decay. For V-A coupling, $P_\mu = 1$ and $\rho = \delta = 3/4$.

Lepton Summary Table

[d] This only includes events with energy of $e > 45$ MeV and energy of $\gamma > 40$ MeV. Since the $e^- \bar{\nu}_e \nu_\mu$ and $e^- \bar{\nu}_e \nu_\mu \gamma$ modes cannot be clearly separated, we regard the latter mode as a subset of the former.

[e] See the relevant Particle Listings for the energy limits used in this measurement.

[f] A test of additive vs. multiplicative lepton family number conservation.

[g] Basis mode for the τ .

[h] L^\pm mass limit depends on decay assumptions; see the Full Listings.

Quark Summary Table

QUARKS

The u -, d -, and s -quark masses are the $\overline{\text{MS}}$ masses at the scale $\mu = 2$ GeV. The c - and b -quark masses are the $\overline{\text{MS}}$ masses renormalized at the $\overline{\text{MS}}$ mass, i.e. $\overline{m} = \overline{m}(\mu = \overline{m})$. The t -quark mass is extracted from event kinematics (see the review "The Top Quark").

u	$I(J^P) = \frac{1}{2}(\frac{1}{2}^+)$
$m_u = 2.16^{+0.49}_{-0.26}$ MeV	Charge = $\frac{2}{3} e$ $I_z = +\frac{1}{2}$
$m_u/m_d = 0.474^{+0.056}_{-0.074}$	
d	$I(J^P) = \frac{1}{2}(\frac{1}{2}^+)$
$m_d = 4.67^{+0.48}_{-0.17}$ MeV	Charge = $-\frac{1}{3} e$ $I_z = -\frac{1}{2}$
$m_s/m_d = 17-22$	
$\overline{m} = (m_u + m_d)/2 = 3.45^{+0.35}_{-0.15}$ MeV	
s	$I(J^P) = 0(\frac{1}{2}^+)$
$m_s = 93.4^{+8.6}_{-3.4}$ MeV	Charge = $-\frac{1}{3} e$ Strangeness = -1
$m_s / ((m_u + m_d)/2) = 27.33^{+0.67}_{-0.77}$	
c	$I(J^P) = 0(\frac{1}{2}^+)$
$m_c = 1.27 \pm 0.02$ GeV	Charge = $\frac{2}{3} e$ Charm = $+1$
$m_c/m_s = 11.76^{+0.05}_{-0.10}$	
$m_b/m_c = 4.58 \pm 0.01$	
$m_b - m_c = 3.45 \pm 0.05$ GeV	
b	$I(J^P) = 0(\frac{1}{2}^+)$
$m_b = 4.18^{+0.03}_{-0.02}$ GeV	Charge = $-\frac{1}{3} e$ Bottom = -1
t	$I(J^P) = 0(\frac{1}{2}^+)$
	Charge = $\frac{2}{3} e$ Top = $+1$
	Mass (direct measurements) $m = 172.69 \pm 0.30$ GeV [a,b] (S = 1.3)
	Mass (from cross-section measurements) $m = 162.5^{+2.1}_{-1.5}$ GeV [a]
	Mass (Pole from cross-section measurements) $m = 172.5 \pm 0.7$ GeV
	$m_t - m_{\overline{t}} = -0.15 \pm 0.20$ GeV (S = 1.1)
	Full width $\Gamma = 1.42^{+0.19}_{-0.15}$ GeV (S = 1.4)
	$\Gamma(Wb)/\Gamma(Wq(q = b, s, d)) = 0.957 \pm 0.034$ (S = 1.5)
	t-quark EW Couplings
	$F_0 = 0.693 \pm 0.013$
	$F_- = 0.315 \pm 0.010$
	$F_+ = -0.005 \pm 0.007$
	$F_{V+A} < 0.29$, CL = 95%

t DECAY MODES	Fraction (Γ_i/Γ)	Confidence level	ρ (MeV/c)
$Wq(q = b, s, d)$			—
Wb			—
$e\nu_e b$	(11.10 ± 0.30) %		—
$\mu\nu_\mu b$	(11.40 ± 0.20) %		—
$\tau\nu_\tau b$	(10.7 ± 0.5) %		—
$q\overline{q}b$	(66.5 ± 1.4) %		—
$\gamma q(q = u, c)$	[c] < 1.8	$\times 10^{-4}$	95%

$\Delta T = 1$ weak neutral current (T1) modes

$Zq(q = u, c)$	T1	[d] < 5	$\times 10^{-4}$	95%	—
Hu	T1	< 1.2	$\times 10^{-3}$	95%	—
Hc	T1	< 1.1	$\times 10^{-3}$	95%	—
$\ell^+ \overline{q} q' (q = d, s, b; q' = u, c)$	T1	< 1.6	$\times 10^{-3}$	95%	—

b' (4th Generation) Quark, Searches for

Mass $m > 190$ GeV, CL = 95%	($p\overline{p}$, quasi-stable b')
Mass $m > 1390$ GeV, CL = 95%	($B(b' \rightarrow Zb) = 1$)
Mass $m > 1350$ GeV, CL = 95%	($B(b' \rightarrow Wt) = 1$)
Mass $m > 1570$ GeV, CL = 95%	($B(b' \rightarrow Hb) = 1$)
Mass $m > 46.0$ GeV, CL = 95%	($e^+ e^-$, all decays)

t' (4th Generation) Quark, Searches for

$m(t'(2/3)) > 1280$ GeV, CL = 95%	($B(t' \rightarrow Zt) = 1$)
$m(t'(2/3)) > 1295$ GeV, CL = 95%	($B(t' \rightarrow Wb) = 1$)
$m(t'(2/3)) > 1310$ GeV, CL = 95%	(singlet t')
$m(t'(2/3)) > 1350$ GeV, CL = 95%	(t' in a weak isospin doublet (t', b'))
$m(t'(5/3)) > 1.350 \times 10^3$ GeV, CL = 95%	($t'(5/3) \rightarrow tW^+$)

Free Quark Searches

All searches since 1977 have had negative results.

NOTES

- [a] A discussion of the definition of the top quark mass in these measurements can be found in the review "The Top Quark."
- [b] Based on published top mass measurements using data from Tevatron Run-I and Run-II and LHC at $\sqrt{s} = 7$ TeV. Including the most recent unpublished results from Tevatron Run-II, the Tevatron Electroweak Working Group reports a top mass of 173.2 ± 0.9 GeV. See the note "The Top Quark" in the Quark Particle Listings of this Review.
- [c] This limit is for $\Gamma(t \rightarrow \gamma q)/\Gamma(t \rightarrow Wb)$.
- [d] This limit is for $\Gamma(t \rightarrow Zq)/\Gamma(t \rightarrow Wb)$.

LIGHT UNFLAVORED MESONS ($S = C = B = 0$)

For $I = 1$ (π, b, ρ, a): $u\bar{d}, (u\bar{u}-d\bar{d})/\sqrt{2}, d\bar{u}$;
for $I = 0$ ($\eta, \eta', h, h', \omega, \phi, f, f'$): $c_1(u\bar{u} + d\bar{d}) + c_2(s\bar{s})$

 π^\pm

$$J^G(J^P) = 1^-(0^-)$$

Mass $m = 139.57039 \pm 0.00018$ MeV ($S = 1.8$)
Mean life $\tau = (2.6033 \pm 0.0005) \times 10^{-8}$ s ($S = 1.2$)
 $c\tau = 7.8045$ m

$\pi^\pm \rightarrow \ell^\pm \nu \gamma$ form factors [a]

$F_V = 0.0254 \pm 0.0017$
 $F_A = 0.0119 \pm 0.0001$
 F_V slope parameter $a = 0.10 \pm 0.06$
 $R = 0.059^{+0.009}_{-0.008}$

π^- modes are charge conjugates of the modes below.

For decay limits to particles which are not established, see the section on Searches for Axions and Other Very Light Bosons.

π^\pm DECAY MODES	Fraction (Γ_i/Γ)	Confidence level	p (MeV/c)
$\mu^+ \nu_\mu$	[b] (99.98770 \pm 0.00004) %		30
$\mu^+ \nu_\mu \gamma$	[c] (2.00 \pm 0.25) $\times 10^{-4}$		30
$e^+ \nu_e$	[b] (1.230 \pm 0.004) $\times 10^{-4}$		70
$e^+ \nu_e \gamma$	[c] (7.39 \pm 0.05) $\times 10^{-7}$		70
$e^+ \nu_e \pi^0$	(1.036 \pm 0.006) $\times 10^{-8}$		4
$e^+ \nu_e e^+ e^-$	(3.2 \pm 0.5) $\times 10^{-9}$		70
$\mu^+ \nu_\mu \nu \bar{\nu}$	< 9 $\times 10^{-6}$	90%	30
$e^+ \nu_e \nu \bar{\nu}$	< 1.6 $\times 10^{-7}$	90%	70

Lepton Family number (LF) or Lepton number (L) violating modes			
$\mu^+ \bar{\nu}_e$	L [d] < 1.5 $\times 10^{-3}$	90%	30
$\mu^+ \nu_e$	LF [d] < 8.0 $\times 10^{-3}$	90%	30
$\mu^- e^+ e^+ \nu$	LF < 1.6 $\times 10^{-6}$	90%	30

 π^0

$$J^G(J^{PC}) = 1^-(0^{-+})$$

Mass $m = 134.9768 \pm 0.0005$ MeV ($S = 1.1$)
 $m_{\pi^\pm} - m_{\pi^0} = 4.5936 \pm 0.0005$ MeV
Mean life $\tau = (8.43 \pm 0.13) \times 10^{-17}$ s ($S = 1.2$)
 $c\tau = 25.3$ nm

For decay limits to particles which are not established, see the appropriate Search sections (A^0 (axion) and Other Light Boson (X^0) Searches, etc.).

π^0 DECAY MODES	Fraction (Γ_i/Γ)	Scale factor/ Confidence level	p (MeV/c)
2γ	(98.823 \pm 0.034) %	S=1.5	67
$e^+ e^- \gamma$	(1.174 \pm 0.035) %	S=1.5	67
γ positronium	(1.82 \pm 0.29) $\times 10^{-9}$		67
$e^+ e^+ e^- e^-$	(3.34 \pm 0.16) $\times 10^{-5}$		67
$e^+ e^-$	(6.46 \pm 0.33) $\times 10^{-8}$		67
4γ	< 2 $\times 10^{-8}$	CL=90%	67
$\nu \bar{\nu}$	[e] < 4.4 $\times 10^{-9}$	CL=90%	67
$\nu_e \bar{\nu}_e$	< 1.7 $\times 10^{-6}$	CL=90%	67
$\nu_\mu \bar{\nu}_\mu$	< 1.6 $\times 10^{-6}$	CL=90%	67
$\nu_\tau \bar{\nu}_\tau$	< 2.1 $\times 10^{-6}$	CL=90%	67
$\gamma \nu \bar{\nu}$	< 1.9 $\times 10^{-7}$	CL=90%	67

Charge conjugation (C) or Lepton Family number (LF) violating modes			
3γ	C < 3.1 $\times 10^{-8}$	CL=90%	67
$\mu^+ e^-$	LF < 3.8 $\times 10^{-10}$	CL=90%	26
$\mu^- e^+$	LF < 3.2 $\times 10^{-10}$	CL=90%	26
$\mu^+ e^- + \mu^- e^+$	LF < 3.6 $\times 10^{-10}$	CL=90%	26

 η

$$J^G(J^{PC}) = 0^+(0^{-+})$$

Mass $m = 547.862 \pm 0.017$ MeV
Full width $\Gamma = 1.31 \pm 0.05$ keV

C-nonconserving decay parameters

$\pi^+ \pi^- \pi^0$ left-right asymmetry = $(0.09^{+0.11}_{-0.12}) \times 10^{-2}$
 $\pi^+ \pi^- \pi^0$ sextant asymmetry = $(0.12^{+0.10}_{-0.11}) \times 10^{-2}$
 $\pi^+ \pi^- \pi^0$ quadrant asymmetry = $(-0.09 \pm 0.09) \times 10^{-2}$
 $\pi^+ \pi^- \gamma$ left-right asymmetry = $(0.9 \pm 0.4) \times 10^{-2}$
 $\pi^+ \pi^- \gamma$ β (D-wave) = -0.02 ± 0.07 ($S = 1.3$)

CP-nonconserving decay parameters

$\pi^+ \pi^- e^+ e^-$ decay-plane asymmetry $A_\phi = (-0.6 \pm 3.1) \times 10^{-2}$

Other decay parameters

$\pi^0 \pi^0 \pi^0$ Dalitz plot $\alpha = -0.0288 \pm 0.0012$ ($S = 1.1$)
Parameter Λ in $\eta \rightarrow \ell^+ \ell^- \gamma$ decay = 0.716 ± 0.011 GeV/ c^2

η DECAY MODES	Fraction (Γ_i/Γ)	Scale factor/ Confidence level	p (MeV/c)
Neutral modes			
neutral modes	(71.96 \pm 0.30) %	S=1.3	-
2γ	(39.36 \pm 0.18) %	S=1.1	274
$3\pi^0$	(32.57 \pm 0.21) %	S=1.2	179
$\pi^0 2\gamma$	(2.55 \pm 0.22) $\times 10^{-4}$		257
$2\pi^0 2\gamma$	< 1.2 $\times 10^{-3}$	CL=90%	238
4γ	< 2.8 $\times 10^{-4}$	CL=90%	274
invisible	< 1.0 $\times 10^{-4}$	CL=90%	-
Charged modes			
charged modes	(28.04 \pm 0.30) %	S=1.3	-
$\pi^+ \pi^- \pi^0$	(23.02 \pm 0.25) %	S=1.2	174
$\pi^+ \pi^- \gamma$	(4.28 \pm 0.07) %	S=1.1	236
$e^+ e^- \gamma$	(6.9 \pm 0.4) $\times 10^{-3}$	S=1.2	274
$\mu^+ \mu^- \gamma$	(3.1 \pm 0.4) $\times 10^{-4}$		253
$e^+ e^-$	< 7 $\times 10^{-7}$	CL=90%	274
$\mu^+ \mu^-$	(5.8 \pm 0.8) $\times 10^{-6}$		253
$2e^+ 2e^-$	(2.40 \pm 0.22) $\times 10^{-5}$		274
$\pi^+ \pi^- e^+ e^- (\gamma)$	(2.68 \pm 0.11) $\times 10^{-4}$		235
$e^+ e^- \mu^+ \mu^-$	< 1.6 $\times 10^{-4}$	CL=90%	253
$2\mu^+ 2\mu^-$	< 3.6 $\times 10^{-4}$	CL=90%	161
$\mu^+ \mu^- \pi^+ \pi^-$	< 3.6 $\times 10^{-4}$	CL=90%	113
$\pi^+ e^- \bar{\nu}_e + c.c.$	< 1.7 $\times 10^{-4}$	CL=90%	256
$\pi^+ \pi^- 2\gamma$	< 2.1 $\times 10^{-3}$		236
$\pi^+ \pi^- \pi^0 \gamma$	< 6 $\times 10^{-4}$	CL=90%	174
$\pi^0 \mu^+ \mu^- \gamma$	< 3 $\times 10^{-6}$	CL=90%	210

Charge conjugation (C), Parity (P), Charge conjugation \times Parity (CP), or Lepton Family number (LF) violating modes

$\pi^0 \gamma$	C [f] < 9 $\times 10^{-5}$	CL=90%	257
$\pi^+ \pi^-$	P, CP < 4.4 $\times 10^{-6}$	CL=90%	236
$2\pi^0$	P, CP < 3.5 $\times 10^{-4}$	CL=90%	238
$2\pi^0 \gamma$	C < 5 $\times 10^{-4}$	CL=90%	238
$3\pi^0 \gamma$	C < 6 $\times 10^{-5}$	CL=90%	179
3γ	C < 1.6 $\times 10^{-5}$	CL=90%	274
$4\pi^0$	P, CP < 6.9 $\times 10^{-7}$	CL=90%	40
$\pi^0 e^+ e^-$	C [g] < 8 $\times 10^{-6}$	CL=90%	257
$\pi^0 \mu^+ \mu^-$	C [g] < 5 $\times 10^{-6}$	CL=90%	210
$\mu^+ e^- + \mu^- e^+$	LF < 6 $\times 10^{-6}$	CL=90%	264

 $f_0(500)$

$$J^G(J^{PC}) = 0^+(0^{++})$$

also known as σ ; was $f_0(600)$

See the review on "Scalar Mesons below 1 GeV."

Mass (T-Matrix Pole \sqrt{s}) = $(400-550) - i(200-350)$ MeV

Mass (Breit-Wigner) = 400 to 800 MeV

Full width (Breit-Wigner) = 100 to 800 MeV

$f_0(500)$ DECAY MODES	Fraction (Γ_i/Γ)	p (MeV/c)
$\pi \pi$	seen	-
$\gamma \gamma$	seen	-

 $\rho(770)$

$$J^G(J^{PC}) = 1^+(1^{--})$$

See the review on "Spectroscopy of Light Meson Resonances."

Mass $m = 775.26 \pm 0.23$ MeV

Full width $\Gamma = 149.1 \pm 0.8$ MeV

Meson Summary Table

$\rho(770)$ DECAY MODES	Fraction (Γ_i/Γ)	Scale factor/ Confidence level	ρ (MeV/c)
$\pi\pi$	~ 100	%	363
$\rho(770)^\pm$ decays			
$\pi^\pm\gamma$	(4.5 \pm 0.5) $\times 10^{-4}$	S=2.2	375
$\pi^\pm\eta$	< 6 $\times 10^{-3}$	CL=84%	152
$\pi^\pm\pi^+\pi^-\pi^0$	< 2.0 $\times 10^{-3}$	CL=84%	254
$\rho(770)^0$ decays			
$\pi^+\pi^-\gamma$	(9.9 \pm 1.6) $\times 10^{-3}$		362
$\pi^0\gamma$	(4.7 \pm 0.8) $\times 10^{-4}$	S=1.7	376
$\eta\gamma$	(3.00 \pm 0.21) $\times 10^{-4}$		194
$\pi^0\pi^0\gamma$	(4.5 \pm 0.8) $\times 10^{-5}$		363
$\mu^+\mu^-$	[h] (4.55 \pm 0.28) $\times 10^{-5}$		373
e^+e^-	[h] (4.72 \pm 0.05) $\times 10^{-5}$		388
$\pi^+\pi^-\pi^0$	(1.01 \pm 0.54 \pm 0.34) $\times 10^{-4}$		323
$\pi^+\pi^-\pi^+\pi^-$	(1.8 \pm 0.9) $\times 10^{-5}$		251
$\pi^+\pi^-\pi^0\pi^0$	(1.6 \pm 0.8) $\times 10^{-5}$		257
$\pi^0e^+e^-$	< 1.2 $\times 10^{-5}$	CL=90%	376

 $\omega(782)$

$$J^G(J^{PC}) = 0^-(1^{--})$$

Mass $m = 782.66 \pm 0.13$ MeV (S = 2.0)
Full width $\Gamma = 8.68 \pm 0.13$ MeV

$\omega(782)$ DECAY MODES	Fraction (Γ_i/Γ)	Scale factor/ Confidence level	ρ (MeV/c)
$\pi^+\pi^-\pi^0$	(89.2 \pm 0.7) %		327
$\pi^0\gamma$	(8.35 \pm 0.27) %	S=2.2	380
$\pi^+\pi^-$	(1.53 \pm 0.11 \pm 0.13) %	S=1.2	366
neutrals (excluding $\pi^0\gamma$)	(7 \pm 8) $\times 10^{-3}$	S=1.1	-
$\eta\gamma$	(4.5 \pm 0.4) $\times 10^{-4}$	S=1.1	200
$\pi^0e^+e^-$	(7.7 \pm 0.6) $\times 10^{-4}$		380
$\pi^0\mu^+\mu^-$	(1.34 \pm 0.18) $\times 10^{-4}$	S=1.5	349
e^+e^-	(7.38 \pm 0.22) $\times 10^{-5}$	S=1.9	391
$\pi^+\pi^-\pi^0\pi^0$	< 2 $\times 10^{-4}$	CL=90%	262
$\pi^+\pi^-\gamma$	< 3.6 $\times 10^{-3}$	CL=95%	366
$\pi^+\pi^-\pi^+\pi^-$	< 1 $\times 10^{-3}$	CL=90%	256
$\pi^0\pi^0\gamma$	(6.7 \pm 1.1) $\times 10^{-5}$		367
$\eta\pi^0\gamma$	< 3.3 $\times 10^{-5}$	CL=90%	162
$\mu^+\mu^-$	(7.4 \pm 1.8) $\times 10^{-5}$		377
3γ	< 1.9 $\times 10^{-4}$	CL=95%	391

Charge conjugation (C) violating modes

$\eta\pi^0$	C	< 2.1 $\times 10^{-4}$	CL=90%	162
$2\pi^0$	C	< 2.2 $\times 10^{-4}$	CL=90%	367
$3\pi^0$	C	< 2.3 $\times 10^{-4}$	CL=90%	330
invisible		< 7 $\times 10^{-5}$	CL=90%	-

 $\eta'(958)$

$$J^G(J^{PC}) = 0^+(0^{-+})$$

Mass $m = 957.78 \pm 0.06$ MeV
Full width $\Gamma = 0.188 \pm 0.006$ MeV

$\eta'(958)$ DECAY MODES	Fraction (Γ_i/Γ)	Confidence level	ρ (MeV/c)
$\pi^+\pi^-\eta$	(42.5 \pm 0.5) %		232
$\rho^0\gamma$ (including non-resonant)	(29.5 \pm 0.4) %		165
$\pi^+\pi^-\pi^-\gamma$			
$\pi^0\pi^0\eta$	(22.4 \pm 0.5) %		239
$\omega\gamma$	(2.52 \pm 0.07) %		159
ωe^+e^-	(2.0 \pm 0.4) $\times 10^{-4}$		159
$\gamma\gamma$	(2.307 \pm 0.033) %		479
$3\pi^0$	(2.50 \pm 0.17) $\times 10^{-3}$		430
$\mu^+\mu^-\gamma$	(1.13 \pm 0.28) $\times 10^{-4}$		467
$\pi^+\pi^-\mu^+\mu^-$	(2.0 \pm 0.4) $\times 10^{-5}$		401
$\pi^+\pi^-\pi^0$	(3.61 \pm 0.17) $\times 10^{-3}$		428
($\pi^+\pi^-\pi^0$) S-wave	(3.8 \pm 0.5) $\times 10^{-3}$		428
$\pi^\mp\rho^\pm$	(7.4 \pm 2.3) $\times 10^{-4}$		106
$\pi^0\rho^0$	< 4 %	90%	111
$2(\pi^+\pi^-)$	(8.4 \pm 0.9) $\times 10^{-5}$		372
$\pi^+\pi^-2\pi^0$	(1.8 \pm 0.4) $\times 10^{-4}$		376
$2(\pi^+\pi^-)$ neutrals	< 1 %	95%	-

$2(\pi^+\pi^-)\pi^0$	< 1.8 $\times 10^{-3}$	90%	298
$2(\pi^+\pi^-)2\pi^0$	< 1 %	95%	197
$3(\pi^+\pi^-)$	< 3.1 $\times 10^{-5}$	90%	189
$K^\pm\pi^\mp$	< 4 $\times 10^{-5}$	90%	334
$\pi^+\pi^-e^+e^-$	(2.42 \pm 0.10) $\times 10^{-3}$		458
$\pi^+e^-\nu_e + c.c.$	< 2.1 $\times 10^{-4}$	90%	469
γe^+e^-	(4.91 \pm 0.27) $\times 10^{-4}$		479
$\pi^0\gamma\gamma$	(3.20 \pm 0.24) $\times 10^{-3}$		469
$\pi^0\gamma\gamma$ (non resonant)	(6.2 \pm 0.9) $\times 10^{-4}$		-
$\eta\gamma\gamma$	< 1.33 $\times 10^{-4}$	90%	322
$4\pi^0$	< 4.94 $\times 10^{-5}$	90%	380
e^+e^-	< 5.6 $\times 10^{-9}$	90%	479
invisible	< 6 $\times 10^{-4}$	90%	-

**Charge conjugation (C), Parity (P),
Lepton family number (LF) violating modes**

$\pi^+\pi^-$	P,CP	< 1.8 $\times 10^{-5}$	90%	458
$\pi^0\pi^0$	P,CP	< 4 $\times 10^{-4}$	90%	459
$\pi^0e^+e^-$	C	[g] < 1.4 $\times 10^{-3}$	90%	469
ηe^+e^-	C	[g] < 2.4 $\times 10^{-3}$	90%	322
3γ	C	< 1.0 $\times 10^{-4}$	90%	479
$\mu^+\mu^-\pi^0$	C	[g] < 6.0 $\times 10^{-5}$	90%	445
$\mu^+\mu^-\eta$	C	[g] < 1.5 $\times 10^{-5}$	90%	273
$e\mu$	LF	< 4.7 $\times 10^{-4}$	90%	473

 $f_0(980)$

$$J^G(J^{PC}) = 0^+(0^{++})$$

See the review on "Scalar Mesons below 1 GeV."

T-matrix pole $\sqrt{s} = (980-1010) - i(20-35)$ MeV [1]
Mass $m = 990 \pm 20$ MeV [1]
Full width $\Gamma = 10$ to 100 MeV [1]

$f_0(980)$ DECAY MODES	Fraction (Γ_i/Γ)	ρ (MeV/c)
$\pi\pi$	seen	476
$K\bar{K}$	seen	36
$\gamma\gamma$	seen	495

 $a_0(980)$

$$J^G(J^{PC}) = 1^-(0^{++})$$

See the review on "Scalar Mesons below 1 GeV."

T-matrix pole $\sqrt{s} = (960-1030) - i(20-70)$ MeV [1]
Mass $m = 980 \pm 20$ MeV [1]
Full width $\Gamma = 50$ to 100 MeV [1]

$a_0(980)$ DECAY MODES	Fraction (Γ_i/Γ)	ρ (MeV/c)
$\eta\pi$	seen	319
$K\bar{K}$	seen	†
$\eta'\pi$	seen	†
$\rho\pi$	not seen	137
$\gamma\gamma$	seen	490

 $\phi(1020)$

$$J^G(J^{PC}) = 0^-(1^{--})$$

Mass $m = 1019.461 \pm 0.016$ MeV
Full width $\Gamma = 4.249 \pm 0.013$ MeV (S = 1.1)

$\phi(1020)$ DECAY MODES	Fraction (Γ_i/Γ)	Scale factor/ Confidence level	ρ (MeV/c)
K^+K^-	(49.1 \pm 0.5) %	S=1.3	127
$K_L^0K_S^0$	(33.9 \pm 0.4) %	S=1.2	110
$\rho\pi + \pi^+\pi^-\pi^0$	(15.4 \pm 0.4) %	S=1.2	-
$\eta\gamma$	(1.301 \pm 0.025) %	S=1.2	363
$\pi^0\gamma$	(1.32 \pm 0.05) $\times 10^{-3}$		501
$\ell^+\ell^-$	-		510
e^+e^-	(2.979 \pm 0.033) $\times 10^{-4}$	S=1.3	510
$\mu^+\mu^-$	(2.85 \pm 0.19) $\times 10^{-4}$		499
ηe^+e^-	(1.08 \pm 0.04) $\times 10^{-4}$		363
$\pi^+\pi^-$	(7.3 \pm 1.3) $\times 10^{-5}$		490
$\omega\pi^0$	(4.7 \pm 0.5) $\times 10^{-5}$		171
$\omega\gamma$	< 5 %	CL=84%	209
$\rho\gamma$	< 1.2 $\times 10^{-5}$	CL=90%	215
$\pi^+\pi^-\gamma$	(4.1 \pm 1.3) $\times 10^{-5}$		490
$f_0(980)\gamma$	(3.22 \pm 0.19) $\times 10^{-4}$	S=1.1	29

Meson Summary Table

$\pi^0 \pi^0 \gamma$	$(1.12 \pm 0.06) \times 10^{-4}$	492
$\pi^+ \pi^- \pi^+ \pi^-$	$(3.9 \pm 2.8) \times 10^{-6}$	410
$\pi^+ \pi^+ \pi^- \pi^- \pi^0$	$< 4.6 \times 10^{-6}$ CL=90%	342
$\pi^0 e^+ e^-$	$(1.33 \pm 0.10) \times 10^{-5}$	501
$\pi^0 \eta \gamma$	$(7.27 \pm 0.30) \times 10^{-5}$ S=1.5	346
$a_0(980) \gamma$	$(7.6 \pm 0.6) \times 10^{-5}$	39
$K^0 \bar{K}^0 \gamma$	$< 1.9 \times 10^{-8}$ CL=90%	110
$\eta'(958) \gamma$	$(6.21 \pm 0.21) \times 10^{-5}$	60
$\eta \pi^0 \pi^0 \gamma$	$< 2 \times 10^{-5}$ CL=90%	293
$\mu^+ \mu^- \gamma$	$(1.4 \pm 0.5) \times 10^{-5}$	499
$\rho \gamma \gamma$	$< 1.2 \times 10^{-4}$ CL=90%	215
$\eta \pi^+ \pi^-$	$< 1.8 \times 10^{-5}$ CL=90%	288
$\eta \mu^+ \mu^-$	$< 9.4 \times 10^{-6}$ CL=90%	321
$\eta U \rightarrow \eta e^+ e^-$	$< 1 \times 10^{-6}$ CL=90%	-
invisible	$< 1.7 \times 10^{-4}$ CL=90%	-

Lepton Family number (LF) violating modes

$e^\pm \mu^\mp$	LF	$< 2 \times 10^{-6}$ CL=90%	504
-----------------	----	-----------------------------	-----

 $h_1(1170)$

$$I^G(J^{PC}) = 0^-(1^+ -)$$

Mass $m = 1166 \pm 6$ MeV
Full width $\Gamma = 375 \pm 35$ MeV

$h_1(1170)$ DECAY MODES	Fraction (Γ_i/Γ)	ρ (MeV/c)
$\rho \pi$	seen	305

 $b_1(1235)$

$$I^G(J^{PC}) = 1^+(1^+ -)$$

Mass $m = 1229.5 \pm 3.2$ MeV (S = 1.6)
Full width $\Gamma = 142 \pm 9$ MeV (S = 1.2)

$b_1(1235)$ DECAY MODES	Fraction (Γ_i/Γ)	Confidence level	ρ (MeV/c)
$\omega \pi$	seen		348
	[D/S amplitude ratio = 0.277 ± 0.027]		
$\pi^\pm \gamma$	$(1.6 \pm 0.4) \times 10^{-3}$		607
$\eta \rho$	seen		†
$\pi^+ \pi^+ \pi^- \pi^0$	< 50 %	84%	535
$K^*(892)^\pm K^\mp$	seen		†
$(K\bar{K})^\pm \pi^0$	< 8 %	90%	248
$K_S^0 K_L^0 \pi^\pm$	< 6 %	90%	235
$K_S^0 K_S^0 \pi^\pm$	< 2 %	90%	235
$\phi \pi$	< 1.5 %	84%	147

 $a_1(1260)$ [1]

$$I^G(J^{PC}) = 1^-(1^+ +)$$

Mass $m = 1230 \pm 40$ MeV [1]
Full width $\Gamma = 250$ to 600 MeV [1]

$a_1(1260)$ DECAY MODES	Fraction (Γ_i/Γ)	ρ (MeV/c)
3π	seen	577
$(\rho\pi)_{S\text{-wave}}, \rho \rightarrow \pi\pi$	seen	353
$(\rho\pi)_{D\text{-wave}}, \rho \rightarrow \pi\pi$	seen	353
$(\rho(1450)\pi)_{S\text{-wave}}, \rho \rightarrow \pi\pi$	seen	†
$(\rho(1450)\pi)_{D\text{-wave}}, \rho \rightarrow \pi\pi$	seen	†
$f_0(500)\pi, f_0 \rightarrow \pi\pi$	seen	-
$f_0(980)\pi, f_0 \rightarrow \pi\pi$	not seen	179
$f_0(1370)\pi, f_0 \rightarrow \pi\pi$	seen	†
$f_2(1270)\pi, f_2 \rightarrow \pi\pi$	seen	†
$\pi^+ \pi^- \pi^0$	seen	576
$\pi^0 \pi^0 \pi^0$	not seen	577
$KK\pi$	seen	250
$K^*(892)K$	seen	†
$\pi\gamma$	seen	608

 $f_2(1270)$

$$I^G(J^{PC}) = 0^+(2^+ +)$$

Mass $m = 1275.5 \pm 0.8$ MeV
Full width $\Gamma = 186.7 \pm 2.2$ MeV (S = 1.4)

 $f_2(1270)$ DECAY MODES

DECAY MODES	Fraction (Γ_i/Γ)	Scale factor/ Confidence level	ρ (MeV/c)
$\pi\pi$	$(84.2 \pm 2.9) \%$	S=1.1	623
$\pi^+ \pi^- 2\pi^0$	$(7.7 \pm 1.1) \%$	S=1.2	563
$K\bar{K}$	$(4.6 \pm 0.5) \%$	S=2.7	404
$2\pi^+ 2\pi^-$	$(2.8 \pm 0.4) \%$	S=1.2	560
$\eta\eta$	$(4.0 \pm 0.8) \times 10^{-3}$	S=2.1	326
$4\pi^0$	$(3.0 \pm 1.0) \times 10^{-3}$		565
$\gamma\gamma$	$(1.42 \pm 0.24) \times 10^{-5}$	S=1.4	638
$\eta\pi\pi$	$< 8 \times 10^{-3}$	CL=95%	478
$K^0 K^- \pi^+ + \text{c.c.}$	$< 3.4 \times 10^{-3}$	CL=95%	293
$e^+ e^-$	$< 6 \times 10^{-10}$	CL=90%	638

 $f_1(1285)$

$$I^G(J^{PC}) = 0^+(1^+ +)$$

Mass $m = 1281.9 \pm 0.5$ MeV (S = 1.8)
Full width $\Gamma = 22.7 \pm 1.1$ MeV (S = 1.5)

 $f_1(1285)$ DECAY MODES

DECAY MODES	Fraction (Γ_i/Γ)	Scale factor/ Confidence level	ρ (MeV/c)
4π	$(32.7 \pm 1.9) \%$	S=1.2	568
$\pi^0 \pi^0 \pi^+ \pi^-$	$(21.8 \pm 1.3) \%$	S=1.2	566
$2\pi^+ 2\pi^-$	$(10.9 \pm 0.6) \%$	S=1.2	563
$\rho^0 \pi^+ \pi^-$	$(10.9 \pm 0.6) \%$	S=1.2	336
$\rho^0 \rho^0$	seen		†
$4\pi^0$	$< 7 \times 10^{-4}$	CL=90%	568
$\eta\pi^+ \pi^-$	$(35 \pm 15) \%$		479
$\eta\pi\pi$	$(52.2 \pm 2.0) \%$	S=1.2	482
$a_0(980)\pi$ [ignoring $a_0(980) \rightarrow K\bar{K}$]	$(38 \pm 4) \%$		238
$\eta\pi\pi$ [excluding $a_0(980)\pi$]	$(14 \pm 4) \%$		482
$K\bar{K}\pi$	$(9.0 \pm 0.4) \%$	S=1.1	308
$K\bar{K}^*(892)$	not seen		†
$\pi^+ \pi^- \pi^0$	$(3.0 \pm 0.9) \times 10^{-3}$		603
$\rho^\pm \pi^\mp$	$< 3.1 \times 10^{-3}$	CL=95%	390
$\gamma\rho^0$	$(6.1 \pm 1.0) \%$	S=1.7	406
$\phi\gamma$	$(7.4 \pm 2.6) \times 10^{-4}$		236
$e^+ e^-$	$< 9.4 \times 10^{-9}$	CL=90%	641

 $\eta(1295)$

$$I^G(J^{PC}) = 0^+(0^- +)$$

See the review on "Spectroscopy of Light Meson Resonances."

Mass $m = 1294 \pm 4$ MeV (S = 1.6)
Full width $\Gamma = 55 \pm 5$ MeV

 $\eta(1295)$ DECAY MODES

DECAY MODES	Fraction (Γ_i/Γ)	ρ (MeV/c)
$\eta\pi^+ \pi^-$	seen	487
$a_0(980)\pi$	seen	248
$\eta\pi^0 \pi^0$	seen	490
$\eta(\pi\pi)_{S\text{-wave}}$	seen	-

 $\pi(1300)$

$$I^G(J^{PC}) = 1^-(0^- +)$$

Mass $m = 1300 \pm 100$ MeV [1]
Full width $\Gamma = 200$ to 600 MeV [1]

 $\pi(1300)$ DECAY MODES

DECAY MODES	Fraction (Γ_i/Γ)	ρ (MeV/c)
$\rho\pi$	seen	404
$\pi(\pi\pi)_{S\text{-wave}}$	seen	-

 $a_2(1320)$

$$I^G(J^{PC}) = 1^-(2^+ +)$$

Mass $m = 1318.2 \pm 0.6$ MeV (S = 1.2)
Full width $\Gamma = 107 \pm 5$ MeV [1]

 $a_2(1320)$ DECAY MODES

DECAY MODES	Fraction (Γ_i/Γ)	Scale factor/ Confidence level	ρ (MeV/c)
3π	$(70.1 \pm 2.7) \%$	S=1.2	624
$\eta\pi$	$(14.5 \pm 1.2) \%$		535
$\omega\pi\pi$	$(10.6 \pm 3.2) \%$	S=1.3	366
$K\bar{K}$	$(4.9 \pm 0.8) \%$		437
$\eta'(958)\pi$	$(5.5 \pm 0.9) \times 10^{-3}$		288

Meson Summary Table

$\pi^\pm \gamma$	$(2.91 \pm 0.27) \times 10^{-3}$	652
$\gamma \gamma$	$(9.4 \pm 0.7) \times 10^{-6}$	659
$e^+ e^-$	$< 5 \times 10^{-9}$ CL=90%	659

$$f_0(1370) \quad I^G(J^{PC}) = 0^+(0^{++})$$

See the review on "Spectroscopy of Light Meson Resonances."
Mass $m = 1200$ to 1500 MeV
Full width $\Gamma = 200$ to 500 MeV

$f_0(1370)$ DECAY MODES	Fraction (Γ_i/Γ)	ρ (MeV/c)
$\pi \pi$	seen	672
4π	seen	617
$4\pi^0$	seen	617
$2\pi^+ 2\pi^-$	seen	612
$\pi^+ \pi^- 2\pi^0$	seen	615
$\rho \rho$	seen	†
$2(\pi\pi)$ s-wave	seen	–
$\pi(1300)\pi$	seen	†
$a_1(1260)\pi$	seen	35
$\eta \eta$	seen	411
$K \bar{K}$	seen	475
$K \bar{K} \eta \pi$	not seen	†
6π	not seen	508
$\omega \omega$	not seen	†
$\gamma \gamma$	seen	685
$e^+ e^-$	not seen	685

$$\pi_1(1400) \quad I^G(J^{PC}) = 1^-(1^{-+})$$

Coupled channel analyses favor the existence of only one broad 1^- isovector state consistent with $\pi_1(1600)$ in the 1400 – 1600 MeV region. See the review on "Spectroscopy of Light Meson Resonances." See also $\pi_1(1600)$.
Mass $m = 1354 \pm 25$ MeV ($S = 1.8$)
Full width $\Gamma = 330 \pm 35$ MeV

$\pi_1(1400)$ DECAY MODES	Fraction (Γ_i/Γ)	ρ (MeV/c)
$\eta \pi^0$	seen	557
$\eta \pi^-$	seen	556
$\rho(770)\pi$	not seen	442

$$\eta(1405) \quad I^G(J^{PC}) = 0^+(0^{-+})$$

See the review on "Spectroscopy of Light Meson Resonances." See also $\eta(1475)$.
Mass $m = 1408.8 \pm 2.0$ MeV ($S = 2.2$)
Full width $\Gamma = 50.1 \pm 2.6$ MeV ($S = 1.7$)

$\eta(1405)$ DECAY MODES	Fraction (Γ_i/Γ)	Confidence level	ρ (MeV/c)
$K \bar{K} \pi$	seen		424
$\eta \pi \pi$	seen		562
$a_0(980)\pi$	seen		345
$\eta(\pi\pi)$ s-wave	seen		–
$f_0(980)\pi^0 \rightarrow \pi^+ \pi^- \pi^0$	not seen		–
$f_0(980)\eta$	seen		†
4π	seen		639
$\rho \rho$	$< 58\%$	99.85%	†
$\rho^0 \gamma$	seen		491
$K^*(892)K$	seen		123

$$h_1(1415) \quad I^G(J^{PC}) = 0^-(1^{+-})$$

was $h_1(1380)$
Mass $m = 1416 \pm 8$ MeV ($S = 1.5$)
Full width $\Gamma = 90 \pm 15$ MeV

$$f_1(1420) \quad I^G(J^{PC}) = 0^+(1^{++})$$

See the review on "Spectroscopy of Light Meson Resonances."
Mass $m = 1426.3 \pm 0.9$ MeV ($S = 1.1$)
Full width $\Gamma = 54.5 \pm 2.6$ MeV

$f_1(1420)$ DECAY MODES	Fraction (Γ_i/Γ)	ρ (MeV/c)
$K \bar{K} \pi$	seen	438
$K \bar{K}^*(892) + \text{c.c.}$	seen	163
$\eta \pi \pi$	possibly seen	573
$\phi \gamma$	seen	349

$$\omega(1420) [K] \quad I^G(J^{PC}) = 0^-(1^{--})$$

Mass $m = 1410 \pm 60$ MeV [I]
Full width $\Gamma = 290 \pm 190$ MeV [I]

$\omega(1420)$ DECAY MODES	Fraction (Γ_i/Γ)	ρ (MeV/c)
$\rho \pi$	seen	480
$\omega \pi \pi$	seen	437
$b_1(1235)\pi$	seen	112
$e^+ e^-$	seen	705

$$a_0(1450) \quad I^G(J^{PC}) = 1^-(0^{++})$$

See the review on "Spectroscopy of Light Meson Resonances."
Mass $m = 1474 \pm 19$ MeV
Full width $\Gamma = 265 \pm 13$ MeV
Branching fractions are given relative to the one **DEFINED AS 1**.

$a_0(1450)$ DECAY MODES	Fraction (Γ_i/Γ)	ρ (MeV/c)
$\pi \eta$	0.093 ± 0.020	627
$\pi \eta'(958)$	0.033 ± 0.017	410
$K \bar{K}$	0.082 ± 0.028	547
$\omega \pi \pi$	DEFINED AS 1	484
$a_0(980)\pi \pi$	seen	342
$\gamma \gamma$	seen	737

$$\rho(1450) \quad I^G(J^{PC}) = 1^+(1^{--})$$

See the review on "Spectroscopy of Light Meson Resonances."
Mass $m = 1465 \pm 25$ MeV [I]
Full width $\Gamma = 400 \pm 60$ MeV [I]

$\rho(1450)$ DECAY MODES	Fraction (Γ_i/Γ)	ρ (MeV/c)
$\pi \pi$	seen	720
$\pi^+ \pi^-$	seen	719
4π	seen	669
$e^+ e^-$	seen	732
$\eta \rho$	seen	311
$a_2(1320)\pi$	not seen	55
$K \bar{K}$	seen	541
$K^+ K^-$	seen	541
$K \bar{K}^*(892) + \text{c.c.}$	possibly seen	229
$\eta \gamma$	seen	630
$f_0(500)\gamma$	not seen	–
$f_0(980)\gamma$	not seen	398
$f_0(1370)\gamma$	not seen	92
$f_2(1270)\gamma$	not seen	177

$$\eta(1475) \quad I^G(J^{PC}) = 0^+(0^{-+})$$

See the review on "Spectroscopy of Light Meson Resonances." See also $\eta(1405)$.
Mass $m = 1475 \pm 4$ MeV ($S = 1.4$)
Full width $\Gamma = 90 \pm 9$ MeV ($S = 1.6$)

$\eta(1475)$ DECAY MODES	Fraction (Γ_i/Γ)	ρ (MeV/c)
$K \bar{K} \pi$	seen	477
$K \bar{K}^*(892) + \text{c.c.}$	seen	244
$a_0(980)\pi$	seen	396
$\gamma \gamma$	seen	738
$K_S^0 K_S^0 \eta$	possibly seen	†
$\gamma \phi(1020)$	possibly seen	385

Meson Summary Table

 $f_0(1500)$

$$I^G(J^{PC}) = 0^+(0^{++})$$

See the review on "Spectroscopy of Light Meson Resonances."

Mass $m = 1506 \pm 6$ MeV ($S = 1.4$)

Full width $\Gamma = 112 \pm 9$ MeV

$f_0(1500)$ DECAY MODES	Fraction (Γ_i/Γ)	Scale factor	ρ (MeV/c)
$\pi\pi$	(34.5±2.2) %	1.2	741
$\pi^+\pi^-$	seen		740
$2\pi^0$	seen		741
4π	(48.9±3.3) %	1.2	692
$4\pi^0$	seen		692
$2\pi^+2\pi^-$	seen		687
$2(\pi\pi)S$ -wave	seen		—
$\rho\rho$	seen		†
$\pi(1300)\pi$	seen		145
$a_1(1260)\pi$	seen		219
$\eta\eta$	(6.0±0.9) %	1.1	517
$\eta\eta'(958)$	(2.2±0.8) %	1.4	20
$K\bar{K}$	(8.5±1.0) %	1.1	569
$\gamma\gamma$	not seen		753

 $f'_2(1525)$

$$I^G(J^{PC}) = 0^+(2^{++})$$

Mass $m = 1517.4 \pm 2.5$ MeV ($S = 2.8$)

Full width $\Gamma = 86 \pm 5$ MeV ($S = 2.2$)

$f'_2(1525)$ DECAY MODES	Fraction (Γ_i/Γ)	Scale factor	ρ (MeV/c)
$K\bar{K}$	(87.6±2.2) %	1.1	576
$\eta\eta$	(11.6±2.2) %	1.1	525
$\pi\pi$	(8.3±1.6) $\times 10^{-3}$		747
$\gamma\gamma$	(9.5±1.1) $\times 10^{-7}$	1.1	759

 $\pi_1(1600)$

$$I^G(J^{PC}) = 1^-(1^{-+})$$

See the review on "Spectroscopy of Light Meson Resonances" and a note in PDG 06, Journal of Physics **G33** 1 (2006). See also

$\pi_1(1400)$.

Mass $m = 1661^{+15}_{-11}$ MeV ($S = 1.2$)

Full width $\Gamma = 240 \pm 50$ MeV ($S = 1.7$)

$\pi_1(1600)$ DECAY MODES	Fraction (Γ_i/Γ)	ρ (MeV/c)
$\pi\pi\pi$	seen	803
$\rho^0\pi^-$	seen	641
$f_2(1270)\pi^-$	not seen	318
$b_1(1235)\pi$	seen	357
$\eta'(958)\pi^-$	seen	543
$f_1(1285)\pi$	seen	314

 $a_1(1640)$

$$I^G(J^{PC}) = 1^-(1^{++})$$

Mass $m = 1655 \pm 16$ MeV ($S = 1.2$)

Full width $\Gamma = 254 \pm 40$ MeV ($S = 1.8$)

$a_1(1640)$ DECAY MODES	Fraction (Γ_i/Γ)	ρ (MeV/c)
$\pi\pi\pi$	seen	800
$f_2(1270)\pi$	seen	314
$\sigma\pi$	seen	—
$\rho\pi$ S-wave	seen	638
$\rho\pi$ D-wave	seen	638
$\omega\pi\pi$	seen	607
$f_1(1285)\pi$	seen	309
$a_1(1260)\eta$	not seen	†

 $\eta_2(1645)$

$$I^G(J^{PC}) = 0^+(2^{-+})$$

Mass $m = 1617 \pm 5$ MeV

Full width $\Gamma = 181 \pm 11$ MeV

 $\eta_2(1645)$ DECAY MODES

	Fraction (Γ_i/Γ)	ρ (MeV/c)
$a_2(1320)\pi$	seen	242
$K\bar{K}\pi$	seen	580
$K^*\bar{K}$	seen	404
$\eta\pi^+\pi^-$	seen	685
$a_0(980)\pi$	seen	499
$f_2(1270)\eta$	not seen	†

 $\omega(1650)$ [1]

$$I^G(J^{PC}) = 0^-(1^{--})$$

Mass $m = 1670 \pm 30$ MeV [1]

Full width $\Gamma = 315 \pm 35$ MeV [1]

 $\omega(1650)$ DECAY MODES

	Fraction (Γ_i/Γ)	ρ (MeV/c)
$\rho\pi$	seen	647
$\rho(1450)\pi$	seen	145
$\omega\pi\pi$	seen	617
$\omega\eta$	seen	500
e^+e^-	seen	835
$\pi^0\gamma$	not seen	830

 $\omega_3(1670)$

$$I^G(J^{PC}) = 0^-(3^{--})$$

Mass $m = 1667 \pm 4$ MeV

Full width $\Gamma = 168 \pm 10$ MeV

 $\omega_3(1670)$ DECAY MODES

	Fraction (Γ_i/Γ)	ρ (MeV/c)
$\rho\pi$	seen	645
$\omega\pi\pi$	seen	615
$b_1(1235)\pi$	possibly seen	361

 $\pi_2(1670)$

$$I^G(J^{PC}) = 1^-(2^{-+})$$

Mass $m = 1670.6^{+2.9}_{-1.2}$ MeV ($S = 1.3$)

Full width $\Gamma = 258^{+8}_{-9}$ MeV ($S = 1.2$)

 $\pi_2(1670)$ DECAY MODES

	Fraction (Γ_i/Γ)	Confidence level	ρ (MeV/c)
3π	(95.8±1.4) %		808
$f_2(1270)\pi$	(56.3±3.2) %		327
$\rho\pi$	(31 ± 4) %		647
$\sigma\pi$	(10 ± 4) %		—
$\pi(\pi\pi)S$ -wave	(8.7±3.4) %		—
$\pi^\pm\pi^+\pi^-$	(53 ± 4) %		806
$K\bar{K}^*(892) + c.c.$	(4.2±1.4) %		453
$\omega\rho$	(2.7±1.1) %		302
$\pi^\pm\gamma$	(7.0±1.2) $\times 10^{-4}$		829
$\gamma\gamma$	< 2.8 $\times 10^{-7}$	90%	835
$\eta\pi$	< 5 %		739
$\pi^\pm 2\pi^+ 2\pi^-$	< 5 %		735
$\rho(1450)\pi$	< 3.6 $\times 10^{-3}$	97.7%	145
$b_1(1235)\pi$	< 1.9 $\times 10^{-3}$	97.7%	364
$f_1(1285)\pi$	possibly seen		322
$a_2(1320)\pi$	not seen		291

 $\phi(1680)$

$$I^G(J^{PC}) = 0^-(1^{--})$$

Mass $m = 1680 \pm 20$ MeV [1]

Full width $\Gamma = 150 \pm 50$ MeV [1]

 $\phi(1680)$ DECAY MODES

	Fraction (Γ_i/Γ)	ρ (MeV/c)
$K\bar{K}^*(892) + c.c.$	seen	462
$K_S^0 K\pi$	seen	621
$K\bar{K}$	seen	680
e^+e^-	seen	840
$\omega\pi\pi$	not seen	623
$K^+K^-\pi^+\pi^-$	seen	544
$\eta\phi$	seen	290
$\eta\gamma$	seen	751

Meson Summary Table

 $\rho_3(1690)$

$$I^G(J^{PC}) = 1^+(3^{--})$$

Mass $m = 1688.8 \pm 2.1$ MeVFull width $\Gamma = 161 \pm 10$ MeV ($S = 1.5$)

$\rho_3(1690)$ DECAY MODES	Fraction (Γ_i/Γ)	Scale factor	ρ (MeV/c)
4π	(71.1 \pm 1.9) %		790
$\pi^\pm \pi^+ \pi^- \pi^0$	(67 \pm 22) %		787
$\omega \pi$	(16 \pm 6) %		655
$\pi \pi \pi$	(23.6 \pm 1.3) %		834
$K \bar{K} \pi$	(3.8 \pm 1.2) %		629
$K \bar{K}$	(1.58 \pm 0.26) %	1.2	685
$\eta \pi^+ \pi^-$	seen		727
$\rho(770) \eta$	seen		520
$\pi \pi \rho$	seen		633
$a_2(1320) \pi$	seen		307
$\rho \rho$	seen		335

 $\rho(1700)$

$$I^G(J^{PC}) = 1^+(1^{--})$$

See the review on "Spectroscopy of Light Meson Resonances."

Mass $m = 1720 \pm 20$ MeV [1] ($\eta \rho^0$ and $\pi^+ \pi^-$ modes)Full width $\Gamma = 250 \pm 100$ MeV [1] ($\eta \rho^0$ and $\pi^+ \pi^-$ modes)

$\rho(1700)$ DECAY MODES	Fraction (Γ_i/Γ)	ρ (MeV/c)
$2(\pi^+ \pi^-)$	seen	803
$\rho \pi \pi$	seen	653
$\rho^0 \pi^+ \pi^-$	seen	651
$\rho^\pm \pi^\mp \pi^0$	seen	652
$a_1(1260) \pi$	seen	404
$h_1(1170) \pi$	seen	450
$\pi(1300) \pi$	seen	349
$\rho \rho$	seen	372
$\pi^+ \pi^-$	seen	849
$\pi \pi$	seen	849
$K \bar{K}^*(892) + c.c.$	seen	496
$\eta \rho$	seen	545
$a_2(1320) \pi$	not seen	334
$K \bar{K}$	seen	704
$e^+ e^-$	seen	860
$\pi^0 \omega$	seen	674
$\pi^0 \gamma$	not seen	855

 $a_2(1700)$

$$I^G(J^{PC}) = 1^-(2^{++})$$

Mass $m = 1698 \pm 40$ MeVFull width $\Gamma = 265 \pm 60$ MeV

$a_2(1700)$ DECAY MODES	Fraction (Γ_i/Γ)	ρ (MeV/c)
$\eta \pi$	(3.6 \pm 1.1) %	754
$\gamma \gamma$	(1.13 \pm 0.30) $\times 10^{-6}$	849
$\rho \pi$	seen	664
$f_2(1270) \pi$	seen	350
$K \bar{K}$	(1.9 \pm 1.2) %	691
$\omega \pi^- \pi^0$	seen	634
$\omega \rho$	seen	338

 $f_0(1710)$

$$I^G(J^{PC}) = 0^+(0^{++})$$

See the review on "Spectroscopy of Light Meson Resonances."

Mass $m = 1704 \pm 12$ MeVFull width $\Gamma = 123 \pm 18$ MeV

$f_0(1710)$ DECAY MODES	Fraction (Γ_i/Γ)	ρ (MeV/c)
$K \bar{K}$	seen	694
$\eta \eta$	seen	652
$\pi \pi$	seen	841
$\gamma \gamma$	seen	852
$\omega \omega$	seen	337

 $\pi(1800)$

$$I^G(J^{PC}) = 1^-(0^{-+})$$

Mass $m = 1810^{+9}_{-11}$ MeV ($S = 2.2$)Full width $\Gamma = 215^{+7}_{-8}$ MeV

$\pi(1800)$ DECAY MODES	Fraction (Γ_i/Γ)	ρ (MeV/c)
$\pi^+ \pi^- \pi^-$	seen	878
$f_0(500) \pi^-$	seen	-
$f_0(980) \pi^-$	seen	624
$f_0(1370) \pi^-$	seen	366
$f_0(1500) \pi^-$	not seen	247
$\rho \pi^-$	not seen	731
$\eta \eta \pi^-$	seen	660
$a_0(980) \eta$	seen	471
$a_2(1320) \eta$	not seen	†
$f_2(1270) \pi$	not seen	441
$f_0(1370) \pi^-$	not seen	366
$f_0(1500) \pi^-$	seen	247
$\eta \eta'(958) \pi^-$	seen	373
$K_0^*(1430) K^-$	seen	†
$K^*(892) K^-$	not seen	568

 $\phi_3(1850)$

$$I^G(J^{PC}) = 0^-(3^{--})$$

Mass $m = 1854 \pm 7$ MeVFull width $\Gamma = 87^{+28}_{-23}$ MeV ($S = 1.2$)

$\phi_3(1850)$ DECAY MODES	Fraction (Γ_i/Γ)	ρ (MeV/c)
$K \bar{K}$	seen	785
$K \bar{K}^*(892) + c.c.$	seen	602

 $\eta_2(1870)$

$$I^G(J^{PC}) = 0^+(2^{-+})$$

Mass $m = 1842 \pm 8$ MeVFull width $\Gamma = 225 \pm 14$ MeV

$\eta_2(1870)$ DECAY MODES	Fraction (Γ_i/Γ)	ρ (MeV/c)
$\eta \pi \pi$	seen	816
$a_2(1320) \pi$	seen	434
$f_2(1270) \eta$	seen	119
$a_0(980) \pi$	seen	651
$\gamma \gamma$	seen	921

 $\pi_2(1880)$

$$I^G(J^{PC}) = 1^-(2^{-+})$$

Mass $m = 1874^{+26}_{-5}$ MeV ($S = 1.6$)Full width $\Gamma = 237^{+33}_{-30}$ MeV ($S = 1.2$)

$\pi_2(1880)$ DECAY MODES	Fraction (Γ_i/Γ)	ρ (MeV/c)
$\eta \eta \pi^-$	seen	702
$a_0(980) \eta$	seen	528
$a_2(1320) \eta$	seen	76
$f_0(1500) \pi$	seen	308
$f_1(1285) \pi$	seen	485
$\omega \pi^- \pi^0$	seen	744

 $f_2(1950)$

$$I^G(J^{PC}) = 0^+(2^{++})$$

Mass $m = 1936 \pm 12$ MeV ($S = 1.3$)Full width $\Gamma = 464 \pm 24$ MeV

$f_2(1950)$ DECAY MODES	Fraction (Γ_i/Γ)	ρ (MeV/c)
$K^*(892) \bar{K}^*(892)$	seen	377
$\pi^+ \pi^-$	seen	958
$\pi^0 \pi^0$	seen	959
4π	seen	921
$\eta \eta$	seen	798
$K \bar{K}$	seen	833
$\gamma \gamma$	seen	968
$\rho \bar{\rho}$	seen	238

$a_4(1970)$

$$J^G(J^{PC}) = 1^-(4^{++})$$

was $a_4(2040)$

Mass $m = 1967 \pm 16$ MeV ($S = 2.1$)
 Full width $\Gamma = 324^{+15}_{-18}$ MeV

$a_4(1970)$ DECAY MODES	Fraction (Γ_i/Γ)	ρ (MeV/c)
$K\bar{K}$	seen	851
$\pi^+\pi^-\pi^0$	seen	959
$\rho\pi$	seen	825
$f_2(1270)\pi$	seen	559
$\omega\pi^-\pi^0$	seen	801
$\omega\rho$	seen	601
$\eta\pi$	seen	902
$\eta'(958)\pi$	seen	743

 $f_2(2010)$

$$J^G(J^{PC}) = 0^+(2^{++})$$

Mass $m = 2011^{+60}_{-80}$ MeV
 Full width $\Gamma = 202 \pm 60$ MeV

$f_2(2010)$ DECAY MODES	Fraction (Γ_i/Γ)	ρ (MeV/c)
$\phi\phi$	seen	†
$K\bar{K}$	seen	876

 $f_4(2050)$

$$J^G(J^{PC}) = 0^+(4^{++})$$

Mass $m = 2018 \pm 11$ MeV ($S = 2.1$)
 Full width $\Gamma = 237 \pm 18$ MeV ($S = 1.9$)

$f_4(2050)$ DECAY MODES	Fraction (Γ_i/Γ)	ρ (MeV/c)
$\omega\omega$	seen	637
$\pi\pi$	(17.0±1.5) %	1000
$K\bar{K}$	(6.8 ^{+3.4} _{-1.8}) × 10 ⁻³	880
$\eta\eta$	(2.1±0.8) × 10 ⁻³	848
$4\pi^0$	< 1.2 %	964
$\gamma\gamma$	seen	1009
$a_2(1320)\pi$	seen	567

 $\phi(2170)$

$$J^G(J^{PC}) = 0^-(1^{--})$$

Mass $m = 2162 \pm 7$ MeV [I] ($S = 1.1$)
 Full width $\Gamma = 100^{+31}_{-23}$ MeV [I] ($S = 2.5$)

$\phi(2170)$ DECAY MODES	Fraction (Γ_i/Γ)	ρ (MeV/c)
e^+e^-	seen	1081
$\phi f_0(980)$	seen	399
$K^+K^-f_0(980) \rightarrow$ $K^+K^-\pi^+\pi^-$	seen	-
$K^+K^-f_0(980) \rightarrow K^+K^-\pi^0\pi^0$	seen	-
$K^{*0}K^\pm\pi^\mp$	not seen	761
$K^*(892)^0\bar{K}^*(892)^0$	not seen	612

 $f_2(2300)$

$$J^G(J^{PC}) = 0^+(2^{++})$$

Mass $m = 2297 \pm 28$ MeV
 Full width $\Gamma = 149 \pm 40$ MeV

$f_2(2300)$ DECAY MODES	Fraction (Γ_i/Γ)	ρ (MeV/c)
$\phi\phi$	seen	529
$K\bar{K}$	seen	1037
$\gamma\gamma$	seen	1149
$\Lambda\bar{\Lambda}$	seen	273

 $f_2(2340)$

$$J^G(J^{PC}) = 0^+(2^{++})$$

Mass $m = 2345^{+50}_{-40}$ MeV
 Full width $\Gamma = 322^{+70}_{-60}$ MeV

$f_2(2340)$ DECAY MODES	Fraction (Γ_i/Γ)	ρ (MeV/c)
$\phi\phi$	seen	580
$\eta\eta$	seen	1037

STRANGE MESONS
($S = \pm 1, C = B = 0$)

$K^+ = u\bar{s}, K^0 = d\bar{s}, \bar{K}^0 = \bar{d}s, K^- = \bar{u}s$, similarly for K^* 's

 K^\pm

$$J^G(J^{PC}) = \frac{1}{2}(0^-)$$

Mass $m = 493.677 \pm 0.016$ MeV [n] ($S = 2.8$)
 Mean life $\tau = (1.2380 \pm 0.0020) \times 10^{-8}$ s ($S = 1.8$)
 $c\tau = 3.711$ m

CPT violation parameters ($\Delta = \text{rate difference/sum}$)

$$\Delta(K^\pm \rightarrow \mu^\pm \nu_\mu) = (-0.27 \pm 0.21)\%$$

$$\Delta(K^\pm \rightarrow \pi^\pm \pi^0) = (0.4 \pm 0.6)\% [o]$$

CP violation parameters ($\Delta = \text{rate difference/sum}$)

$$\Delta(K^\pm \rightarrow \pi^\pm e^+ e^-) = (-2.2 \pm 1.6) \times 10^{-2}$$

$$\Delta(K^\pm \rightarrow \pi^\pm \mu^+ \mu^-) = 0.010 \pm 0.023$$

$$\Delta(K^\pm \rightarrow \pi^\pm \pi^0 \gamma) = (0.0 \pm 1.2) \times 10^{-3}$$

$$\Delta(K^\pm \rightarrow \pi^\pm \pi^+ \pi^-) = (0.04 \pm 0.06)\%$$

$$\Delta(K^\pm \rightarrow \pi^\pm \pi^0 \pi^0) = (-0.02 \pm 0.28)\%$$

T violation parameters

$$K^+ \rightarrow \pi^0 \mu^+ \nu_\mu \quad P_T = (-1.7 \pm 2.5) \times 10^{-3}$$

$$K^+ \rightarrow \mu^+ \nu_\mu \gamma \quad P_T = (-0.6 \pm 1.9) \times 10^{-2}$$

$$K^+ \rightarrow \pi^0 \mu^+ \nu_\mu \quad \text{Im}(\xi) = -0.006 \pm 0.008$$

Slope parameter $g^{[p]}$

(See Particle Listings for quadratic coefficients and alternative parametrization related to $\pi\pi$ scattering)

$$K^\pm \rightarrow \pi^\pm \pi^+ \pi^- \quad g = -0.21134 \pm 0.00017$$

$$K^\pm \rightarrow \pi^\pm \pi^0 \pi^0 \quad g = 0.626 \pm 0.007$$

$$(g_+ - g_-) / (g_+ + g_-) = (-1.5 \pm 2.2) \times 10^{-4}$$

$$(g_+ - g_-) / (g_+ + g_-) = (1.8 \pm 1.8) \times 10^{-4}$$

 K^\pm decay form factors [a,q]

Assuming μ - e universality

$$\lambda_+(K_{\mu 3}^+) = \lambda_+(K_{e 3}^+) = (2.959 \pm 0.025) \times 10^{-2}$$

$$\lambda_0(K_{\mu 3}^+) = (1.76 \pm 0.25) \times 10^{-2} \quad (S = 2.7)$$

Not assuming μ - e universality

$$\lambda_+(K_{e 3}^+) = (2.956 \pm 0.025) \times 10^{-2}$$

$$\lambda_+(K_{\mu 3}^+) = (3.09 \pm 0.25) \times 10^{-2} \quad (S = 1.5)$$

$$\lambda_0(K_{\mu 3}^+) = (1.73 \pm 0.27) \times 10^{-2} \quad (S = 2.6)$$

K_{e3} form factor quadratic fit

$$\lambda'_+(K_{e 3}^\pm) \text{ linear coeff.} = (2.59 \pm 0.04) \times 10^{-2}$$

$$\lambda''_+(K_{e 3}^\pm) \text{ quadratic coeff.} = (0.186 \pm 0.021) \times 10^{-2}$$

$$\lambda'_+(K_{\mu 3}^\pm) \text{ (LINEAR } K_{\mu 3}^\pm \text{ FORM FACTOR FROM QUADRATIC FIT)}$$

$$= (24 \pm 4) \times 10^{-3}$$

$$\lambda''_+(K_{\mu 3}^\pm) \text{ (QUADRATIC } K_{\mu 3}^\pm \text{ FORM FACTOR)} = (1.8 \pm 1.5) \times 10^{-3}$$

M_V (VECTOR POLE MASS FOR $K_{e 3}^\pm$ DECAY) = 890.3 ± 2.8 MeV

M_V (VECTOR POLE MASS FOR $K_{\mu 3}^\pm$ DECAY) = 878 ± 12 MeV

M_S (SCALAR POLE MASS FOR $K_{\mu 3}^\pm$ DECAY) = 1215 ± 50 MeV

Λ_+ (DISPERSIVE VECTOR FORM FACTOR IN $K_{e 3}^\pm$ DECAY) = (2.460 ± 0.017) × 10⁻²

Λ_+ (DISPERSIVE VECTOR FORM FACTOR IN $K_{\mu 3}^\pm$ DECAY) = (25.4 ± 0.9) × 10⁻³

$\ln(C)$ (DISPERSIVE SCALAR FORM FACTOR in $K_{\mu 3}^\pm$ decays) = (182 ± 16) × 10⁻³

$$K_{e 3}^+ \quad |f_S/f_+| = (-0.08^{+0.34}_{-0.40}) \times 10^{-2}$$

$$K_{e 3}^+ \quad |f_T/f_+| = (-1.2^{+1.3}_{-1.1}) \times 10^{-2}$$

$$K_{\mu 3}^+ \quad |f_S/f_+| = (0.2 \pm 0.6) \times 10^{-2}$$

$$K_{\mu 3}^+ \quad |f_T/f_+| = (-0.1 \pm 0.7) \times 10^{-2}$$

$$K^+ \rightarrow e^+ \nu_e \gamma \quad |F_A + F_V| = 0.133 \pm 0.008 \quad (S = 1.3)$$

$$K^+ \rightarrow \mu^+ \nu_\mu \gamma \quad |F_A + F_V| = 0.165 \pm 0.013$$

$$K^+ \rightarrow e^+ \nu_e \gamma \quad |F_A - F_V| < 0.49, \text{ CL} = 90\%$$

$$K^+ \rightarrow \mu^+ \nu_\mu \gamma \quad |F_A - F_V| = -0.153 \pm 0.033 \quad (S = 1.1)$$

Meson Summary Table

Charge radius

$$\langle r \rangle = 0.560 \pm 0.031 \text{ fm}$$

Forward-backward asymmetry

$$A_{FB}(K_{\pi\mu\mu}^{\pm}) = \frac{\Gamma(\cos(\theta_{K\mu}) > 0) - \Gamma(\cos(\theta_{K\mu}) < 0)}{\Gamma(\cos(\theta_{K\mu}) > 0) + \Gamma(\cos(\theta_{K\mu}) < 0)} < 2.3 \times 10^{-2}, \text{ CL} = 90\%$$

K^- modes are charge conjugates of the modes below.

K⁺ DECAY MODES	Fraction (Γ_i/Γ)	Scale factor/ Confidence level (MeV/c)	ρ
Leptonic and semileptonic modes			
$e^+ \nu_e$	$(1.582 \pm 0.007) \times 10^{-5}$		247
$\mu^+ \nu_\mu$	$(63.56 \pm 0.11) \%$	S=1.2	236
$\pi^0 e^+ \nu_e$	$(5.07 \pm 0.04) \%$	S=2.1	228
Called K_{e3}^+ .			
$\pi^0 \mu^+ \nu_\mu$	$(3.352 \pm 0.033) \%$	S=1.9	215
Called $K_{\mu 3}^+$.			
$\pi^0 \pi^0 e^+ \nu_e$	$(2.55 \pm 0.04) \times 10^{-5}$	S=1.1	206
$\pi^+ \pi^- e^+ \nu_e$	$(4.247 \pm 0.024) \times 10^{-5}$		203
$\pi^+ \pi^- \mu^+ \nu_\mu$	$(1.4 \pm 0.9) \times 10^{-5}$		151
$\pi^0 \pi^0 \pi^0 e^+ \nu_e$	$< 3.5 \times 10^{-6}$	CL=90%	135
Hadronic modes			
$\pi^+ \pi^0$	$(20.67 \pm 0.08) \%$	S=1.2	205
$\pi^+ \pi^0 \pi^0$	$(1.760 \pm 0.023) \%$	S=1.1	133
$\pi^+ \pi^+ \pi^-$	$(5.583 \pm 0.024) \%$		125
Leptonic and semileptonic modes with photons			
$\mu^+ \nu_\mu \gamma$	$[r,s] (6.2 \pm 0.8) \times 10^{-3}$		236
$\mu^+ \nu_\mu \gamma (\text{SD}^+)$	$[a,t] (1.33 \pm 0.22) \times 10^{-5}$		-
$\mu^+ \nu_\mu \gamma (\text{SD}^+ \text{INT})$	$[a,t] < 2.7 \times 10^{-5}$	CL=90%	-
$\mu^+ \nu_\mu \gamma (\text{SD}^- + \text{SD}^- \text{INT})$	$[a,t] < 2.6 \times 10^{-4}$	CL=90%	-
$e^+ \nu_e \gamma$	$(9.4 \pm 0.4) \times 10^{-6}$		247
$\pi^0 e^+ \nu_e \gamma$	$[r,s] (2.66 \pm 0.09) \times 10^{-4}$		228
$\pi^0 e^+ \nu_e \gamma (\text{SD})$	$[a,t] < 5.3 \times 10^{-5}$	CL=90%	228
$\pi^0 \mu^+ \nu_\mu \gamma$	$[r,s] (1.25 \pm 0.25) \times 10^{-5}$		215
$\pi^0 \pi^0 e^+ \nu_e \gamma$	$< 5 \times 10^{-6}$	CL=90%	206
Hadronic modes with photons or $\ell\bar{\ell}$ pairs			
$\pi^+ \pi^0 \gamma (\text{INT})$	$(-4.2 \pm 0.9) \times 10^{-6}$		-
$\pi^+ \pi^0 \gamma (\text{DE})$	$[r,u] (6.0 \pm 0.4) \times 10^{-6}$		205
$\pi^+ \pi^0 e^+ e^-$	$(4.24 \pm 0.14) \times 10^{-6}$		205
$\pi^+ \pi^0 \pi^0 \gamma$	$[r,s] (7.6 \pm 6.0_{-3.0}) \times 10^{-6}$		133
$\pi^+ \pi^+ \pi^- \gamma$	$[r,s] (7.1 \pm 0.5) \times 10^{-6}$		125
$\pi^+ \gamma \gamma$	$[r] (1.01 \pm 0.06) \times 10^{-6}$		227
$\pi^+ 3\gamma$	$[r] < 1.0 \times 10^{-4}$	CL=90%	227
$\pi^+ e^+ e^- \gamma$	$(1.19 \pm 0.13) \times 10^{-8}$		227
Leptonic modes with $\ell\bar{\ell}$ pairs			
$e^+ \nu_e \nu\bar{\nu}$	$< 6 \times 10^{-5}$	CL=90%	247
$\mu^+ \nu_\mu \nu\bar{\nu}$	$< 1.0 \times 10^{-6}$	CL=90%	236
$e^+ \nu_e e^+ e^-$	$(2.48 \pm 0.20) \times 10^{-8}$		247
$\mu^+ \nu_\mu e^+ e^-$	$(7.06 \pm 0.31) \times 10^{-8}$		236
$e^+ \nu_e \mu^+ \mu^-$	$(1.7 \pm 0.5) \times 10^{-8}$		223
$\mu^+ \nu_\mu \mu^+ \mu^-$	$< 4.1 \times 10^{-7}$	CL=90%	185
Lepton family number (LF), Lepton number (L), $\Delta S = \Delta Q$ (SQ) violating modes, or $\Delta S = 1$ weak neutral current (S1) modes			
$\pi^+ \pi^+ e^- \bar{\nu}_e$	SQ $< 1.3 \times 10^{-8}$	CL=90%	203
$\pi^+ \pi^+ \mu^- \bar{\nu}_\mu$	SQ $< 3.0 \times 10^{-6}$	CL=95%	151
$\pi^+ e^+ e^-$	S1 $(3.00 \pm 0.09) \times 10^{-7}$		227
$\pi^+ \mu^+ \mu^-$	S1 $(9.4 \pm 0.6) \times 10^{-8}$	S=2.6	172
$\pi^+ \nu\bar{\nu}$	S1 $(1.14 \pm 0.40_{-0.33}) \times 10^{-10}$		227
$\pi^+ \pi^0 \nu\bar{\nu}$	S1 $< 4.3 \times 10^{-5}$	CL=90%	205
$\mu^- \nu e^+ e^+$	LF $< 2.1 \times 10^{-8}$	CL=90%	236
$\mu^+ \nu_e$	LF $[d] < 4 \times 10^{-3}$	CL=90%	236
$\pi^+ \mu^+ e^-$	LF $< 1.3 \times 10^{-11}$	CL=90%	214
$\pi^+ \mu^- e^+$	LF $< 6.6 \times 10^{-11}$	CL=90%	214
$\pi^- \mu^+ e^+$	L $< 4.2 \times 10^{-11}$	CL=90%	214
$\pi^- e^+ e^+$	L $< 2.2 \times 10^{-10}$	CL=90%	227
$\pi^- \mu^+ \mu^+$	L $< 4.2 \times 10^{-11}$	CL=90%	172
$\mu^+ \bar{\nu}_e$	L $[d] < 3.3 \times 10^{-3}$	CL=90%	236
$\pi^0 e^+ \bar{\nu}_e$	L $< 3 \times 10^{-3}$	CL=90%	228
$\pi^+ \gamma$	$[v] < 2.3 \times 10^{-9}$	CL=90%	227

K⁰

$$I(J^P) = \frac{1}{2}(0^-)$$

50% K_S , 50% K_L

$$\text{Mass } m = 497.611 \pm 0.013 \text{ MeV} \quad (S = 1.2)$$

$$m_{K^0} - m_{K^\pm} = 3.934 \pm 0.020 \text{ MeV} \quad (S = 1.6)$$

Mean square charge radius

$$\langle r^2 \rangle = -0.077 \pm 0.010 \text{ fm}^2$$

T-violation parameters in K^0 - \bar{K}^0 mixing [q]

$$\text{Asymmetry } A_T \text{ in } K^0\text{-}\bar{K}^0 \text{ mixing} = (6.6 \pm 1.6) \times 10^{-3}$$

CP-violation parameters

$$\text{Re}(\epsilon) = (1.596 \pm 0.013) \times 10^{-3}$$

CPT-violation parameters [q]

$$\text{Re } \delta = (2.5 \pm 2.3) \times 10^{-4}$$

$$\text{Im } \delta = (-1.5 \pm 1.6) \times 10^{-5}$$

$$\text{Re}(y), K_{e3} \text{ parameter} = (0.4 \pm 2.5) \times 10^{-3}$$

$$\text{Re}(x_-), K_{e3} \text{ parameter} = (-2.9 \pm 2.0) \times 10^{-3}$$

$$|m_{K^0} - m_{\bar{K}^0}| / m_{\text{average}} < 6 \times 10^{-19}, \text{ CL} = 90\% [x]$$

$$(\Gamma_{K^0} - \Gamma_{\bar{K}^0}) / m_{\text{average}} = (8 \pm 8) \times 10^{-18}$$

Tests of $\Delta S = \Delta Q$

$$\text{Re}(x_+), K_{e3} \text{ parameter} = (-0.9 \pm 3.0) \times 10^{-3}$$

K_S⁰

$$I(J^P) = \frac{1}{2}(0^-)$$

Mean life $\tau = (0.8954 \pm 0.0004) \times 10^{-10} \text{ s}$ (S = 1.1) Assuming CPT

Mean life $\tau = (0.89564 \pm 0.00033) \times 10^{-10} \text{ s}$ Not assuming CPT

$$c\tau = 2.6844 \text{ cm} \quad \text{Assuming CPT}$$

CP-violation parameters [y]

$$\text{Im}(\eta_{+-0}) = -0.002 \pm 0.009$$

$$\text{Im}(\eta_{000}) = -0.001 \pm 0.016$$

$$|\eta_{000}| = |A(K_S^0 \rightarrow 3\pi^0)/A(K_L^0 \rightarrow 3\pi^0)| < 0.0088, \text{ CL} = 90\%$$

$$\text{CP asymmetry } A \text{ in } \pi^+ \pi^- e^+ e^- = (-0.4 \pm 0.8)\%$$

K_S⁰ DECAY MODES

	Fraction (Γ_i/Γ)	Scale factor/ Confidence level (MeV/c)	ρ
Hadronic modes			
$\pi^0 \pi^0$	$(30.69 \pm 0.05) \%$		209
$\pi^+ \pi^-$	$(69.20 \pm 0.05) \%$		206
$\pi^+ \pi^- \pi^0$	$(3.5 \pm 1.1_{-0.9}) \times 10^{-7}$		133
Modes with photons or $\ell\bar{\ell}$ pairs			
$\pi^+ \pi^- \gamma$	$[s,z] (1.79 \pm 0.05) \times 10^{-3}$		206
$\pi^+ \pi^- e^+ e^-$	$(4.79 \pm 0.15) \times 10^{-5}$		206
$\pi^0 \gamma \gamma$	$[z] (4.9 \pm 1.8) \times 10^{-8}$		230
$\gamma \gamma$	$(2.63 \pm 0.17) \times 10^{-6}$	S=3.1	249
Semileptonic modes			
$\pi^\pm e^\mp \nu_e$	$[aa] (7.04 \pm 0.08) \times 10^{-4}$		229
CP violating (CP) and $\Delta S = 1$ weak neutral current (S1) modes			
$3\pi^0$	CP $< 2.6 \times 10^{-8}$	CL=90%	139
$\mu^+ \mu^-$	S1 $< 2.1 \times 10^{-10}$	CL=90%	225
$e^+ e^-$	S1 $< 9 \times 10^{-9}$	CL=90%	249
$\pi^0 e^+ e^-$	S1 $[z] (3.0 \pm 1.5_{-1.2}) \times 10^{-9}$		230
$\pi^0 \mu^+ \mu^-$	S1 $(2.9 \pm 1.5_{-1.2}) \times 10^{-9}$		177

K_L⁰

$$I(J^P) = \frac{1}{2}(0^-)$$

$$m_{K_L} - m_{K_S}$$

$$= (0.5293 \pm 0.0009) \times 10^{10} \hbar \text{ s}^{-1} \quad (S = 1.3) \quad \text{Assuming CPT}$$

$$= (3.484 \pm 0.006) \times 10^{-12} \text{ MeV} \quad \text{Assuming CPT}$$

$$= (0.5289 \pm 0.0010) \times 10^{10} \hbar \text{ s}^{-1} \quad \text{Not assuming CPT}$$

$$\text{Mean life } \tau = (5.116 \pm 0.021) \times 10^{-8} \text{ s} \quad (S = 1.1)$$

$$c\tau = 15.34 \text{ m}$$

Slope parameters [p]

(See Particle Listings for other linear and quadratic coefficients)

$$K_V^0 \rightarrow \pi^+ \pi^- \pi^0: g = 0.678 \pm 0.008 \quad (S = 1.5)$$

$$K_L^0 \rightarrow \pi^+ \pi^- \pi^0: h = 0.076 \pm 0.006$$

$$K_L^0 \rightarrow \pi^+ \pi^- \pi^0: k = 0.0099 \pm 0.0015$$

$$K_L^0 \rightarrow \pi^0 \pi^0 \pi^0: h = (0.6 \pm 1.2) \times 10^{-3}$$

 K_L decay form factors [q]Linear parametrization assuming μ -e universality

$$\lambda_+(K_{\mu 3}^0) = \lambda_+(K_{e 3}^0) = (2.82 \pm 0.04) \times 10^{-2} \quad (S = 1.1)$$

$$\lambda_0(K_{\mu 3}^0) = (1.38 \pm 0.18) \times 10^{-2} \quad (S = 2.2)$$

Quadratic parametrization assuming μ -e universality

$$\lambda'_+(K_{\mu 3}^0) = \lambda'_+(K_{e 3}^0) = (2.40 \pm 0.12) \times 10^{-2} \quad (S = 1.2)$$

$$\lambda''_+(K_{\mu 3}^0) = \lambda''_+(K_{e 3}^0) = (0.20 \pm 0.05) \times 10^{-2} \quad (S = 1.2)$$

$$\lambda_0(K_{\mu 3}^0) = (1.16 \pm 0.09) \times 10^{-2} \quad (S = 1.2)$$

Pole parametrization assuming μ -e universality

$$M_V^{\mu}(K_{\mu 3}^0) = M_V^e(K_{e 3}^0) = 878 \pm 6 \text{ MeV} \quad (S = 1.1)$$

$$M_S^{\mu}(K_{\mu 3}^0) = 1252 \pm 90 \text{ MeV} \quad (S = 2.6)$$

Dispersive parametrization assuming μ -e universality

$$\Lambda_+ = (2.51 \pm 0.06) \times 10^{-2} \quad (S = 1.5)$$

$$\ln(C) = (1.75 \pm 0.18) \times 10^{-1} \quad (S = 2.0)$$

$$K_{e 3}^0 \quad |f_S/f_+| = (1.5^{+1.4}_{-1.6}) \times 10^{-2}$$

$$K_{e 3}^0 \quad |f_T/f_+| = (5^{+4}_{-5}) \times 10^{-2}$$

$$K_{\mu 3}^0 \quad |f_T/f_+| = (12 \pm 12) \times 10^{-2}$$

$$K_L \rightarrow \ell^+ \ell^- \gamma, K_L \rightarrow \ell^+ \ell^- \ell'^+ \ell'^-: \alpha_{K^*} = -0.205 \pm 0.022 \quad (S = 1.8)$$

$$K_L \rightarrow \ell^+ \ell^- \gamma, K_L^0 \rightarrow \ell^+ \ell^- \ell'^+ \ell'^-: \alpha_{DIP} = -1.69 \pm 0.08 \quad (S = 1.7)$$

$$K_L \rightarrow \pi^+ \pi^- e^+ e^-: a_1/a_2 = -0.737 \pm 0.014 \text{ GeV}^2$$

$$K_L \rightarrow \pi^0 2\gamma: a_V = -0.43 \pm 0.06 \quad (S = 1.5)$$

CP-violation parameters [v]

$$A_L = (0.332 \pm 0.006)\%$$

$$|\eta_{00}| = (2.220 \pm 0.011) \times 10^{-3} \quad (S = 1.8)$$

$$|\eta_{+-}| = (2.232 \pm 0.011) \times 10^{-3} \quad (S = 1.8)$$

$$|\epsilon| = (2.228 \pm 0.011) \times 10^{-3} \quad (S = 1.8)$$

$$|\eta_{00}/\eta_{+-}| = 0.9950 \pm 0.0007^{[bb]} \quad (S = 1.6)$$

$$\text{Re}(\epsilon'/\epsilon) = (1.66 \pm 0.23) \times 10^{-3}^{[bb]} \quad (S = 1.6)$$

Assuming CPT

$$\phi_{+-} = (43.51 \pm 0.05)^\circ \quad (S = 1.2)$$

$$\phi_{00} = (43.52 \pm 0.05)^\circ \quad (S = 1.3)$$

$$\phi_\epsilon = \phi_{SW} = (43.52 \pm 0.05)^\circ \quad (S = 1.2)$$

$$\text{Im}(\epsilon'/\epsilon) = -(\phi_{00} - \phi_{+-})/3 = (-0.002 \pm 0.005)^\circ \quad (S = 1.7)$$

Not assuming CPT

$$\phi_{+-} = (43.4 \pm 0.5)^\circ \quad (S = 1.2)$$

$$\phi_{00} = (43.7 \pm 0.6)^\circ \quad (S = 1.2)$$

$$\phi_\epsilon = (43.5 \pm 0.5)^\circ \quad (S = 1.3)$$

$$\text{CP asymmetry } A \text{ in } K_L^0 \rightarrow \pi^+ \pi^- e^+ e^- = (13.7 \pm 1.5)\%$$

$$\beta_{CP} \text{ from } K_L^0 \rightarrow e^+ e^- e^+ e^- = -0.19 \pm 0.07$$

$$\gamma_{CP} \text{ from } K_L^0 \rightarrow e^+ e^- e^+ e^- = 0.01 \pm 0.11 \quad (S = 1.6)$$

$$j \text{ for } K_L^0 \rightarrow \pi^+ \pi^- \pi^0 = 0.0012 \pm 0.0008$$

$$f \text{ for } K_L^0 \rightarrow \pi^+ \pi^- \pi^0 = 0.004 \pm 0.006$$

$$|\eta_{+-\gamma}| = (2.35 \pm 0.07) \times 10^{-3}$$

$$\phi_{+-\gamma} = (44 \pm 4)^\circ$$

$$|\epsilon'_{+-\gamma}|/\epsilon < 0.3, \text{ CL} = 90\%$$

$$|\bar{g}_{E1}| \text{ for } K_L^0 \rightarrow \pi^+ \pi^- \gamma < 0.21, \text{ CL} = 90\%$$

T-violation parameters

$$\text{Im}(\xi) \text{ in } K_{\mu 3}^0 = -0.007 \pm 0.026$$

CPT invariance tests

$$\phi_{00} - \phi_{+-} = (0.34 \pm 0.32)^\circ$$

$$\text{Re}(\frac{2}{3}\eta_{+-} + \frac{1}{3}\eta_{00}) - \frac{A}{2} = (-3 \pm 35) \times 10^{-6}$$

 $\Delta S = -\Delta Q$ in $K_{\mu 3}^0$ decay

$$\text{Re } x = -0.002 \pm 0.006$$

$$\text{Im } x = 0.0012 \pm 0.0021$$

 K_L^0 DECAY MODES

K_L^0 DECAY MODES	Fraction (Γ_i/Γ)	Scale factor/ Confidence level (MeV/c)	p
Semileptonic modes			
$\pi^\pm e^\mp \nu_e$ Called $K_{e 3}^0$.	[aa] (40.55 \pm 0.11) %	S=1.7	229
$\pi^\pm \mu^\mp \nu_\mu$ Called $K_{\mu 3}^0$.	[aa] (27.04 \pm 0.07) %	S=1.1	216
$(\pi \mu \text{atom}) \nu$	(1.05 \pm 0.11) $\times 10^{-7}$		188
$\pi^0 \pi^\pm e^\mp \nu$	[aa] (5.20 \pm 0.11) $\times 10^{-5}$		207
$\pi^\pm e^\mp \nu e^+ e^-$	[aa] (1.26 \pm 0.04) $\times 10^{-5}$		229
Hadronic modes, including Charge conjugation \times Parity Violating (CPV) modes			
$3\pi^0$	(19.52 \pm 0.12) %	S=1.6	139
$\pi^+ \pi^- \pi^0$	(12.54 \pm 0.05) %		133
$\pi^+ \pi^-$	CPV [cc] (1.967 \pm 0.010) $\times 10^{-3}$	S=1.5	206
$\pi^0 \pi^0$	CPV (8.64 \pm 0.06) $\times 10^{-4}$	S=1.8	209
Semileptonic modes with photons			
$\pi^\pm e^\mp \nu_e \gamma$	[s,aa,dd] (3.79 \pm 0.06) $\times 10^{-3}$		229
$\pi^\pm \mu^\mp \nu_\mu \gamma$	(5.65 \pm 0.23) $\times 10^{-4}$		216
Hadronic modes with photons or $\ell\bar{\ell}$ pairs			
$\pi^0 \pi^0 \gamma$	< 2.43 $\times 10^{-7}$	CL=90%	209
$\pi^+ \pi^- \gamma$	[s,dd] (4.15 \pm 0.15) $\times 10^{-5}$	S=2.8	206
$\pi^+ \pi^- \gamma$ (DE)	(2.84 \pm 0.11) $\times 10^{-5}$	S=2.0	206
$\pi^0 2\gamma$	[dd] (1.273 \pm 0.033) $\times 10^{-6}$		230
$\pi^0 \gamma e^+ e^-$	(1.62 \pm 0.17) $\times 10^{-8}$		230
Other modes with photons or $\ell\bar{\ell}$ pairs			
2γ	(5.47 \pm 0.04) $\times 10^{-4}$	S=1.1	249
3γ	< 7.4 $\times 10^{-8}$	CL=90%	249
$e^+ e^- \gamma$	(9.4 \pm 0.4) $\times 10^{-6}$	S=2.0	249
$\mu^+ \mu^- \gamma$	(3.59 \pm 0.11) $\times 10^{-7}$	S=1.3	225
$e^+ e^- \gamma \gamma$	[dd] (5.95 \pm 0.33) $\times 10^{-7}$		249
$\mu^+ \mu^- \gamma \gamma$	[dd] (1.0 \pm 0.8 \pm 0.6) $\times 10^{-8}$		225
Charge conjugation \times Parity (CP) or Lepton Family number (LF) violating modes, or $\Delta S = 1$ weak neutral current (S1) modes			
$\mu^+ \mu^-$	S1 (6.84 \pm 0.11) $\times 10^{-9}$		225
$e^+ e^-$	S1 (9 \pm 4) $\times 10^{-12}$		249
$\pi^+ \pi^- e^+ e^-$	S1 [dd] (3.11 \pm 0.19) $\times 10^{-7}$		206
$\pi^0 \pi^0 e^+ e^-$	S1 < 6.6 $\times 10^{-9}$	CL=90%	209
$\pi^0 \pi^0 \mu^+ \mu^-$	S1 < 9.2 $\times 10^{-11}$	CL=90%	57
$\mu^+ \mu^- e^+ e^-$	S1 (2.69 \pm 0.27) $\times 10^{-9}$		225
$e^+ e^- e^+ e^-$	S1 (3.56 \pm 0.21) $\times 10^{-8}$		249
$\pi^0 \mu^+ \mu^-$	CP,S1 [ee] < 3.8 $\times 10^{-10}$	CL=90%	177
$\pi^0 e^+ e^-$	CP,S1 [ee] < 2.8 $\times 10^{-10}$	CL=90%	230
$\pi^0 \nu \bar{\nu}$	CP,S1 [ff] < 3.0 $\times 10^{-9}$	CL=90%	230
$\pi^0 \pi^0 \nu \bar{\nu}$	S1 < 8.1 $\times 10^{-7}$	CL=90%	209
$e^\pm \mu^\mp$	LF [aa] < 4.7 $\times 10^{-12}$	CL=90%	238
$e^\pm e^\pm \mu^\mp \mu^\mp$	LF [aa] < 4.12 $\times 10^{-11}$	CL=90%	225
$\pi^0 \mu^\pm e^\mp$	LF [aa] < 7.6 $\times 10^{-11}$	CL=90%	217
$\pi^0 \pi^0 \mu^\pm e^\mp$	LF < 1.7 $\times 10^{-10}$	CL=90%	159
Lorentz invariance violating modes			
$\pi^0 \gamma$	< 1.7 $\times 10^{-7}$	CL=90%	230

 $K_0^*(700)$

$$I(J^P) = \frac{1}{2}(0^+)$$

also known as κ ; was $K_0^*(800)$

See the review on "Scalar Mesons below 1 GeV."

$$\text{Mass (T-Matrix Pole } \sqrt{s}) = (630-730) - i(260-340) \text{ MeV}$$

$$\text{Mass (Breit-Wigner)} = 845 \pm 17 \text{ MeV}$$

$$\text{Full width (Breit-Wigner)} = 468 \pm 30 \text{ MeV}$$

 $K_0^*(700)$ DECAY MODES

$K_0^*(700)$ DECAY MODES	Fraction (Γ_i/Γ)	p (MeV/c)
$K \pi$	100 %	256

Meson Summary Table

$K^*(892)$	$I(J^P) = \frac{1}{2}(1^-)$
Mass (T-Matrix Pole \sqrt{s}) = $(890 \pm 14) - i(26 \pm 6)$ MeV	
$K^*(892)^\pm$ hadroproduced mass $m = 891.67 \pm 0.26$ MeV	
$K^*(892)^\pm$ in τ decays mass $m = 895.5 \pm 0.8$ MeV	
$K^*(892)^0$ mass $m = 895.55 \pm 0.20$ MeV ($S = 1.7$)	
$K^*(892)^\pm$ hadroproduced full width $\Gamma = 51.4 \pm 0.8$ MeV	
$K^*(892)^\pm$ in τ decays full width $\Gamma = 46.2 \pm 1.3$ MeV	
$K^*(892)^0$ full width $\Gamma = 47.3 \pm 0.5$ MeV ($S = 1.9$)	

$K^*(892)$ DECAY MODES	Fraction (Γ_i/Γ)	Confidence level	ρ (MeV/c)
$K\pi$	~ 100	%	289
$K^0\gamma$	$(2.46 \pm 0.21) \times 10^{-3}$		307
$K^\pm\gamma$	$(9.8 \pm 0.9) \times 10^{-4}$		309
$K\pi\pi$	< 7	$\times 10^{-4}$	95% 223

$K_1(1270)$	$I(J^P) = \frac{1}{2}(1^+)$		
Mass $m = 1253 \pm 7$ MeV ($S = 2.2$)			
Full width $\Gamma = 90 \pm 20$ MeV [1]			
$K_1(1270)$ DECAY MODES	Fraction (Γ_i/Γ)	Scale factor	ρ (MeV/c)
$K\rho$	(38 ± 13) %	2.2	†
$K_0^*(1430)\pi$	(28 ± 4) %		†
$K^*(892)\pi$	(21 ± 10) %	2.2	286
$K\omega$	(11.0 ± 2.0) %		†
$Kf_0(1370)$	(3.0 ± 2.0) %		†
γK^0	seen		528

$K_1(1400)$	$I(J^P) = \frac{1}{2}(1^+)$	
Mass $m = 1403 \pm 7$ MeV		
Full width $\Gamma = 174 \pm 13$ MeV ($S = 1.6$)		
$K_1(1400)$ DECAY MODES	Fraction (Γ_i/Γ)	ρ (MeV/c)
$K^*(892)\pi$	(94 ± 6) %	402
$K\rho$	(3.0 ± 3.0) %	293
$Kf_0(1370)$	(2.0 ± 2.0) %	†
$K\omega$	(1.0 ± 1.0) %	284
$K_0^*(1430)\pi$	not seen	†
γK^0	seen	613
$K\phi$	seen	†

$K^*(1410)$	$I(J^P) = \frac{1}{2}(1^-)$		
Mass $m = 1414 \pm 15$ MeV ($S = 1.3$)			
Full width $\Gamma = 232 \pm 21$ MeV ($S = 1.1$)			
$K^*(1410)$ DECAY MODES	Fraction (Γ_i/Γ)	Confidence level	ρ (MeV/c)
$K^*(892)\pi$	> 40 %	95%	410
$K\pi$	(6.6 ± 1.3) %		612
$K\rho$	< 7 %	95%	305
γK^0	< 2.3 $\times 10^{-4}$	90%	619
$K\phi$	seen		†

$K_0^*(1430)$	$I(J^P) = \frac{1}{2}(0^+)$	
Mass $m = 1425 \pm 50$ MeV [1]		
Full width $\Gamma = 270 \pm 80$ MeV [1]		
$K_0^*(1430)$ DECAY MODES	Fraction (Γ_i/Γ)	ρ (MeV/c)
$K\pi$	(93 ± 10) %	619
$K\eta$	(8.6 ± 2.7) %	486
$K\eta'(958)$	seen	†

$K_2^*(1430)$	$I(J^P) = \frac{1}{2}(2^+)$
$K_2^*(1430)^\pm$ mass $m = 1427.3 \pm 1.5$ MeV ($S = 1.3$)	
$K_2^*(1430)^0$ mass $m = 1432.4 \pm 1.3$ MeV	
$K_2^*(1430)^\pm$ full width $\Gamma = 100.0 \pm 2.1$ MeV	
$K_2^*(1430)^0$ full width $\Gamma = 109 \pm 5$ MeV ($S = 1.9$)	

$K_2^*(1430)$ DECAY MODES	Fraction (Γ_i/Γ)	Scale factor/ Confidence level	ρ (MeV/c)
$K\pi$	(49.9 ± 1.2) %		620
$K^*(892)\pi$	(24.7 ± 1.5) %		420
$K^*(892)\pi\pi$	(13.4 ± 2.2) %		373
$K\rho$	(8.7 ± 0.8) %	$S=1.2$	320
$K\omega$	(2.9 ± 0.8) %		313
$K^+\gamma$	$(2.4 \pm 0.5) \times 10^{-3}$	$S=1.1$	628
$K\eta$	$(1.5 \pm 3.4) \times 10^{-3}$	$S=1.3$	488
$K\omega\pi$	< 7.2 $\times 10^{-4}$	CL=95%	106
$K^0\gamma$	< 9 $\times 10^{-4}$	CL=90%	627

$K(1460)$	$I(J^P) = \frac{1}{2}(0^-)$	
$K(1460)$ DECAY MODES	Fraction (Γ_i/Γ)	ρ (MeV/c)
$K^*(892)\pi$	seen	–
$K\rho$	seen	–
$K_0^*(1430)\pi$	seen	–
$K\phi$	seen	–

$K_1(1650)$	$I(J^P) = \frac{1}{2}(1^+)$
Mass $m = 1650 \pm 50$ MeV	
Full width $\Gamma = 150 \pm 50$ MeV	

$K^*(1680)$	$I(J^P) = \frac{1}{2}(1^-)$
Mass $m = 1718 \pm 18$ MeV	
Full width $\Gamma = 322 \pm 110$ MeV ($S = 4.2$)	

$K^*(1680)$ DECAY MODES	Fraction (Γ_i/Γ)	ρ (MeV/c)
$K\pi$	(38.7 ± 2.5) %	782
$K\rho$	(31.4 ± 5.0) %	571
$K^*(892)\pi$	(29.9 ± 2.2) %	618
$K\phi$	seen	387
$K\eta$	(1.4 ± 1.0) %	683

$K_2(1770)$ [sg]	$I(J^P) = \frac{1}{2}(2^-)$
Mass $m = 1773 \pm 8$ MeV	
Full width $\Gamma = 186 \pm 14$ MeV	

$K_2(1770)$ DECAY MODES	Fraction (Γ_i/Γ)	ρ (MeV/c)
$K\pi\pi$		794
$K_2^*(1430)\pi$	seen	287
$K^*(892)\pi$	seen	654
$Kf_2(1270)$	seen	53
$K\phi$	seen	441
$K\omega$	seen	607

$K_3^*(1780)$	$I(J^P) = \frac{1}{2}(3^-)$
Mass $m = 1779 \pm 8$ MeV ($S = 1.2$)	
Full width $\Gamma = 161 \pm 17$ MeV ($S = 1.1$)	

$K_3^*(1780)$ DECAY MODES	Fraction (Γ_i/Γ)	Confidence level	ρ (MeV/c)
$K\rho$	(31 ± 9) %		616
$K^*(892)\pi$	(20 ± 5) %		657
$K\pi$	(18.8 ± 1.0) %		815
$K\eta$	(30 ± 13) %		721
$K_2^*(1430)\pi$	< 16 %	95%	292

Meson Summary Table

 $K_2(1820)$ [sg]

$$I(J^P) = \frac{1}{2}(2^-)$$

Mass $m = 1819 \pm 12$ MeV
Full width $\Gamma = 264 \pm 34$ MeV

$K_2(1820)$ DECAY MODES	Fraction (Γ_i/Γ)	ρ (MeV/c)
$K\pi\pi$	seen	819
$K_2^*(1430)\pi$	seen	328
$K^*(892)\pi$	seen	683
$Kf_2(1270)$	seen	191
$K\omega$	seen	640
$K\phi$	seen	483

 $K_2^*(1980)$

$$I(J^P) = \frac{1}{2}(2^+)$$

Mass $m = 1994^{+60}_{-50}$ MeV ($S = 2.8$)
Full width $\Gamma = 348^{+50}_{-30}$ MeV ($S = 1.3$)

$K_2^*(1980)$ DECAY MODES	Fraction (Γ_i/Γ)	ρ (MeV/c)
$K^*(892)\pi$	possibly seen	791
$K\rho$	possibly seen	762
$Kf_2(1270)$	possibly seen	424
$K\phi$	seen	627
$K\eta$	seen	850

 $K_4^*(2045)$

$$I(J^P) = \frac{1}{2}(4^+)$$

Mass $m = 2048^{+8}_{-9}$ MeV ($S = 1.1$)
Full width $\Gamma = 199^{+27}_{-19}$ MeV

$K_4^*(2045)$ DECAY MODES	Fraction (Γ_i/Γ)	ρ (MeV/c)
$K\pi$	(9.9 ± 1.2) %	960
$K^*(892)\pi\pi$	(9 ± 5) %	804
$K^*(892)\pi\pi\pi$	(7 ± 5) %	770
$\rho K\pi$	(5.7 ± 3.2) %	744
$\omega K\pi$	(5.0 ± 3.0) %	740
$\phi K\pi$	(2.8 ± 1.4) %	597
$\phi K^*(892)$	(1.4 ± 0.7) %	368

CHARMED MESONS ($C = \pm 1$)

$D^+ = c\bar{d}, D^0 = c\bar{u}, \bar{D}^0 = \bar{c}u, D^- = \bar{c}d$, similarly for D^{*s}

 D^\pm

$$I(J^P) = \frac{1}{2}(0^-)$$

Mass $m = 1869.66 \pm 0.05$ MeV
Mean life $\tau = (1033 \pm 5) \times 10^{-15}$ s
 $c\tau = 309.8$ μm

c-quark decays

$\Gamma(c \rightarrow \ell^+ \text{anything})/\Gamma(c \rightarrow \text{anything}) = 0.096 \pm 0.004$ [hh]
 $\Gamma(c \rightarrow D^*(2010)^+ \text{anything})/\Gamma(c \rightarrow \text{anything}) = 0.255 \pm 0.017$

CP-violation decay-rate asymmetries

$A_{CP}(\mu^\pm \nu) = (8 \pm 8)\%$
 $A_{CP}(K_S^0 e^\pm \nu) = (-0.6 \pm 1.6)\%$
 $A_{CP}(K_S^0 \pi^\pm) = (-0.41 \pm 0.09)\%$
 $A_{CP}(K_L^0 K^\pm) \text{ in } D^\pm \rightarrow K_L^0 K^\pm = (-4.2 \pm 3.4) \times 10^{-2}$
 $A_{CP}(K^\pm 2\pi^\pm) = (-0.18 \pm 0.16)\%$
 $A_{CP}(K^\pm \pi^\pm \pi^\pm \pi^0) = (-0.3 \pm 0.7)\%$
 $A_{CP}(K_S^0 \pi^\pm \pi^0) = (-0.1 \pm 0.7)\%$
 $A_{CP}(K_S^0 \pi^\pm \eta) \text{ in } D^\pm \rightarrow K_S^0 \pi^\pm \eta = (-0.9 \pm 3.1) \times 10^{-2}$
 $A_{CP}(K_S^0 \pi^\pm \pi^+ \pi^-) = (0.0 \pm 1.2)\%$
 $A_{CP}(K^\pm \pi^+ \pi^- \pi^0) \text{ in } D^\pm \rightarrow K^\pm \pi^+ \pi^- \pi^0 = -0.04 \pm 0.06$
 $A_{CP}(\pi^\pm \pi^0) = (0.4 \pm 1.3)\%$ ($S = 1.7$)
 $A_{CP}(\pi^\pm \eta) = (0.3 \pm 0.8)\%$ ($S = 1.2$)
 $A_{CP}(\pi^\pm \pi^0 \eta) \text{ in } D^\pm \rightarrow \pi^\pm \pi^0 \eta = (-6 \pm 7) \times 10^{-2}$
 $A_{CP}(\pi^\pm \eta \eta) \text{ in } D^\pm \rightarrow \pi^\pm \eta \eta = (8 \pm 9) \times 10^{-2}$
 $A_{CP}(\pi^\pm \eta'(958)) = (-0.6 \pm 0.7)\%$

$A_{CP}(\bar{K}^0/K^0 K^\pm) = (0.11 \pm 0.17)\%$
 $A_{CP}(K_S^0 K^\pm) = (-0.01 \pm 0.07)\%$
 $A_{CP}(K_S^0 K^\pm \pi^0) \text{ in } D^\pm \rightarrow K_S^0 K^\pm \pi^0 = (1 \pm 4) \times 10^{-2}$
 $A_{CP}(K_L^0 K^\pm \pi^0) \text{ in } D^\pm \rightarrow K_L^0 K^\pm \pi^0 = (-1 \pm 4) \times 10^{-2}$
 $A_{CP}(K^\pm K^- \pi^\pm) = (0.37 \pm 0.29)\%$
 $A_{CP}(K^\pm K^*0) = (-0.3 \pm 0.4)\%$
 $A_{CP}(\phi \pi^\pm) = (0.01 \pm 0.09)\%$ ($S = 1.8$)
 $A_{CP}(K^\pm K_0^*(1430)^0) = (8^{+7}_{-6})\%$
 $A_{CP}(K^\pm K_2^*(1430)^0) = (43^{+20}_{-26})\%$
 $A_{CP}(K^\pm K_0^*(700)) = (-12^{+18}_{-13})\%$
 $A_{CP}(a_0(1450)^0 \pi^\pm) = (-19^{+14}_{-16})\%$
 $A_{CP}(\phi(1680) \pi^\pm) = (-9 \pm 26)\%$
 $A_{CP}(\pi^+ \pi^- \pi^\pm) = (-2 \pm 4)\%$
 $A_{CP}(\pi^+ \pi^- \pi^\pm \eta) \text{ in } D^\pm \rightarrow \pi^+ \pi^- \pi^\pm \eta = (3 \pm 5) \times 10^{-2}$
 $A_{CP}(K_S^0 K^\pm \pi^+ \pi^-) = (-4 \pm 7)\%$
 $A_{CP}(K^\pm \pi^0) = (-3 \pm 5)\%$
 $A_{CP}(K^\pm \eta) \text{ in } D^\pm \rightarrow K^\pm \eta = (-6 \pm 11) \times 10^{-2}$

 χ^2 tests of CP-violation (CPV)

Local CPV in $D^\pm \rightarrow \pi^+ \pi^- \pi^\pm = 78.1\%$
Local CPV in $D^\pm \rightarrow K^+ K^- \pi^\pm = 31\%$

CP violating asymmetries of P-odd (T-odd) moments

$A_T(K_S^0 K^\pm \pi^+ \pi^-) = (-12 \pm 11) \times 10^{-3}$ [ii]

 D^+ form factors

$f_+(0)|V_{cs}| \text{ in } \bar{K}^0 \ell^+ \nu_\ell = 0.719 \pm 0.011$ ($S = 1.6$)
 $r_1 \equiv a_1/a_0 \text{ in } \bar{K}^0 \ell^+ \nu_\ell = -2.13 \pm 0.14$
 $r_2 \equiv a_2/a_0 \text{ in } \bar{K}^0 \ell^+ \nu_\ell = -3 \pm 12$ ($S = 1.5$)
 $f_+(0)|V_{cd}| \text{ in } \pi^0 \ell^+ \nu_\ell = 0.1407 \pm 0.0025$
 $r_1 \equiv a_1/a_0 \text{ in } \pi^0 \ell^+ \nu_\ell = -2.00 \pm 0.13$
 $r_2 \equiv a_2/a_0 \text{ in } \pi^0 \ell^+ \nu_\ell = -4 \pm 5$
 $f_+(0)|V_{cd}| \text{ in } D^+ \rightarrow \eta \ell^+ \nu_\ell (\ell = e \text{ or } \nu) = (8.4 \pm 0.4) \times 10^{-2}$
 $r_1 \equiv a_1/a_0 \text{ in } D^+ \rightarrow \eta e^+ \nu_e = -5.3 \pm 2.7$ ($S = 1.9$)
 $r_\nu \equiv V(0)/A_1(0) \text{ in } D^+ \rightarrow \omega e^+ \nu_e = 1.24 \pm 0.11$
 $r_2 \equiv A_2(0)/A_1(0) \text{ in } D^+ \rightarrow \omega e^+ \nu_e = 1.06 \pm 0.16$
 $r_\nu \equiv V(0)/A_1(0) \text{ in } D^+, D^0 \rightarrow \rho e^+ \nu_e = 1.64 \pm 0.10$ ($S = 1.2$)
 $r_2 \equiv A_2(0)/A_1(0) \text{ in } D^+, D^0 \rightarrow \rho e^+ \nu_e = 0.84 \pm 0.06$
 $r_\nu \equiv V(0)/A_1(0) \text{ in } \bar{K}^*(892)^0 \ell^+ \nu_\ell = 1.49 \pm 0.05$ ($S = 2.1$)
 $r_2 \equiv A_2(0)/A_1(0) \text{ in } \bar{K}^*(892)^0 \ell^+ \nu_\ell = 0.802 \pm 0.021$
 $r_3 \equiv A_3(0)/A_1(0) \text{ in } \bar{K}^*(892)^0 \ell^+ \nu_\ell = 0.0 \pm 0.4$
 $\Gamma_L/\Gamma_T \text{ in } \bar{K}^*(892)^0 \ell^+ \nu_\ell = 1.13 \pm 0.08$
 $\Gamma_+/ \Gamma_- \text{ in } \bar{K}^*(892)^0 \ell^+ \nu_\ell = 0.22 \pm 0.06$ ($S = 1.6$)

Most decay modes (other than the semileptonic modes) that involve a neutral K meson are now given as K_S^0 modes, not as \bar{K}^0 modes. Nearly always it is a K_S^0 that is measured, and interference between Cabibbo-allowed and doubly Cabibbo-suppressed modes can invalidate the assumption that $2\Gamma(K_S^0) = \Gamma(\bar{K}^0)$.

 D^+ DECAY MODES

	Fraction (Γ_i/Γ)	Scale factor/ Confidence level	ρ (MeV/c)
Inclusive modes			
e^+ semileptonic	(16.07 ± 0.30) %		—
μ^+ anything	(17.6 ± 3.2) %		—
K^- anything	(25.7 ± 1.4) %		—
\bar{K}^0 anything + K^0 anything	(61 ± 5) %		—
K^+ anything	(5.9 ± 0.8) %		—
$K^*(892)^-$ anything	(6 ± 5) %		—
$\bar{K}^*(892)^0$ anything	(23 ± 5) %		—
$K^*(892)^0$ anything	< 6.6 %	CL=90%	—
η anything	(6.3 ± 0.7) %		—
η' anything	(1.04 ± 0.18) %		—
ϕ anything	(1.12 ± 0.04) %		—
Leptonic and semileptonic modes			
$e^+ \nu_e$	< 8.8	$\times 10^{-6}$ CL=90%	935
$\gamma e^+ \nu_e$	< 3.0	$\times 10^{-5}$ CL=90%	935
$\mu^+ \nu_\mu$	(3.74 ± 0.17) %	$\times 10^{-4}$	932
$\tau^+ \nu_\tau$	(1.20 ± 0.27) %	$\times 10^{-3}$	90
$\bar{K}^0 e^+ \nu_e$	(8.72 ± 0.09) %		869
$\bar{K}^0 \mu^+ \nu_\mu$	(8.76 ± 0.19) %		865
$K^- \pi^+ e^+ \nu_e$	(4.02 ± 0.18) %	S=3.2	864
$\bar{K}^*(892)^0 e^+ \nu_e, \bar{K}^*(892)^0 \rightarrow K^- \pi^+$	(3.77 ± 0.17) %		722
$(K^- \pi^+) [0.8-1.0] \text{ GeV } e^+ \nu_e$	(3.39 ± 0.09) %		864
$(K^- \pi^+)_{S\text{-wave}} e^+ \nu_e$	(2.28 ± 0.11) %	$\times 10^{-3}$	—

Meson Summary Table

$\bar{K}^*(1410)^0 e^+ \nu_e$, $\bar{K}^*(1410)^0 \rightarrow K^- \pi^+$	< 6	$\times 10^{-3}$ CL=90%	-	$\bar{K}^*(892)^0 2\pi^+ \pi^-$, $\bar{K}^*(892)^0 \rightarrow K^- \pi^+$	$(1.2 \pm 0.4) \times 10^{-3}$	645
$\bar{K}_2^*(1430)^0 e^+ \nu_e$, $\bar{K}_2^*(1430)^0 \rightarrow K^- \pi^+$	< 5	$\times 10^{-4}$ CL=90%	-	$\bar{K}^*(892)^0 \rho^0 \pi^+$, $\bar{K}^*(892)^0 \rightarrow K^- \pi^+$	$(2.3 \pm 0.4) \times 10^{-3}$	239
$K^- \pi^+ e^+ \nu_e$ nonresonant $\bar{K}^*(892)^0 e^+ \nu_e$	< 7	$\times 10^{-3}$ CL=90%	864	$\bar{K}^*(892)^0 a_1(1260)^+$ [nn]	$(9.3 \pm 1.9) \times 10^{-3}$	†
$K^- \pi^+ \mu^+ \nu_\mu$	$(5.40 \pm 0.10) \%$	S=1.1	722	$K^- \rho^0 2\pi^+$	$(1.72 \pm 0.28) \times 10^{-3}$	524
$\bar{K}^*(892)^0 \mu^+ \nu_\mu$	$(3.65 \pm 0.34) \%$		851	$K^- 3\pi^+ \pi^-$ nonresonant	$(4.0 \pm 2.9) \times 10^{-4}$	772
$\bar{K}^*(892)^0 \rightarrow K^- \pi^+$	$(3.52 \pm 0.10) \%$		717	$K^+ 2K_S^0$	$(2.54 \pm 0.13) \times 10^{-3}$	545
$K^- \pi^+ \mu^+ \nu_\mu$ nonresonant	$(1.9 \pm 0.5) \times 10^{-3}$		851	$K^+ K^- K_S^0 \pi^+$	$(2.4 \pm 0.5) \times 10^{-4}$	436
$\bar{K}^*(892)^0 \mu^+ \nu_\mu$	$(5.27 \pm 0.15) \%$		717	Pionic modes		
$K^- \pi^+ \pi^0 \mu^+ \nu_\mu$	< 1.5	$\times 10^{-3}$ CL=90%	825	$\pi^+ \pi^0$	$(1.247 \pm 0.033) \times 10^{-3}$	925
$\bar{K}_1(1270)^0 e^+ \nu_e$, $\bar{K}_1^0 \rightarrow$ $K^- \pi^+ \pi^0$	$(1.06 \pm 0.15) \times 10^{-3}$		-	$2\pi^+ \pi^-$	$(3.27 \pm 0.18) \times 10^{-3}$	909
$\bar{K}_0^*(1430)^0 \mu^+ \nu_\mu$	< 2.3	$\times 10^{-4}$ CL=90%	380	$\rho^0 \pi^+$	$(8.3 \pm 1.5) \times 10^{-4}$	767
$\bar{K}^*(1680)^0 \mu^+ \nu_\mu$	< 1.5	$\times 10^{-3}$ CL=90%	105	$\pi^+ (\pi^+ \pi^-)_{S\text{-wave}}$	$(1.83 \pm 0.16) \times 10^{-3}$	909
$\pi^0 e^+ \nu_e$	$(3.72 \pm 0.17) \times 10^{-3}$	S=2.0	930	$\sigma \pi^+, \sigma \rightarrow \pi^+ \pi^-$	$(1.38 \pm 0.12) \times 10^{-3}$	-
$\pi^0 \mu^+ \nu_\mu$	$(3.50 \pm 0.15) \times 10^{-3}$		927	$f_0(980) \pi^+$	$(1.56 \pm 0.33) \times 10^{-4}$	669
$\eta e^+ \nu_e$	$(1.11 \pm 0.07) \times 10^{-3}$		855	$f_0(980) \rightarrow \pi^+ \pi^-$		-
$\eta \mu^+ \nu_\mu$	$(1.04 \pm 0.11) \times 10^{-3}$		851	$f_0(1370) \pi^+$	$(8 \pm 4) \times 10^{-5}$	-
$\pi^- \pi^+ e^+ \nu_e$	$(2.45 \pm 0.10) \times 10^{-3}$		924	$f_0(1370) \rightarrow \pi^+ \pi^-$		-
$f_0(500)^0 e^+ \nu_e$, $f_0(500)^0 \rightarrow$ $\pi^+ \pi^-$	$(6.3 \pm 0.5) \times 10^{-4}$		-	$f_2(1270) \pi^+$	$(5.0 \pm 0.9) \times 10^{-4}$	485
$\rho^0 e^+ \nu_e$	$(2.18 \pm 0.17) \times 10^{-3}$		774	$f_2(1270) \rightarrow \pi^+ \pi^-$		-
$\rho^0 \mu^+ \nu_\mu$	$(2.4 \pm 0.4) \times 10^{-3}$		770	$\rho(1450)^0 \pi^+$	< 8	$\times 10^{-5}$ CL=95%
$\omega e^+ \nu_e$	$(1.69 \pm 0.11) \times 10^{-3}$		771	$\rho(1450)^0 \rightarrow \pi^+ \pi^-$		-
$\omega \mu^+ \nu_\mu$	$(1.77 \pm 0.21) \times 10^{-3}$		767	$f_0(1500) \pi^+$	$(1.1 \pm 0.4) \times 10^{-4}$	-
$\eta'(958) e^+ \nu_e$	$(2.0 \pm 0.4) \times 10^{-4}$		690	$f_0(1500) \rightarrow \pi^+ \pi^-$		-
$a(980)^0 e^+ \nu_e$, $a(980)^0 \rightarrow \eta \pi^0$	$(1.7 \pm 0.8) \times 10^{-4}$		-	$f_0(1710) \pi^+$	< 5	$\times 10^{-5}$ CL=95%
$b_1(1235)^0 e^+ \nu_e$, $b_1^0 \rightarrow \omega \pi^0$	< 1.75	$\times 10^{-4}$ CL=90%	-	$f_0(1710) \rightarrow \pi^+ \pi^-$		-
$\phi e^+ \nu_e$	< 1.3	$\times 10^{-5}$ CL=90%	657	$f_0(1790) \pi^+$	< 7	$\times 10^{-5}$ CL=95%
$D^0 e^+ \nu_e$	< 1.0	$\times 10^{-4}$ CL=90%	5	$f_0(1790) \rightarrow \pi^+ \pi^-$		-
Hadronic modes with a \bar{K} or $\bar{K}K\bar{K}$				$(\pi^+ \pi^+)_{S\text{-wave}} \pi^-$	< 1.2	$\times 10^{-4}$ CL=95%
$K_S^0 \pi^+$	$(1.562 \pm 0.031) \%$	S=1.7	863	$2\pi^+ \pi^-$ nonresonant	< 1.1	$\times 10^{-4}$ CL=95%
$K_L^0 \pi^+$	$(1.46 \pm 0.05) \%$		863	$\pi^+ 2\pi^0$	$(4.7 \pm 0.4) \times 10^{-3}$	910
$K^- 2\pi^+$	[ij] $(9.38 \pm 0.16) \%$	S=1.6	846	$2\pi^+ \pi^- \pi^0$	$(1.16 \pm 0.08) \%$	883
$(K^- \pi^+)_{S\text{-wave}} \pi^+$	$(7.52 \pm 0.17) \%$		846	$3\pi^+ 2\pi^-$	$(1.66 \pm 0.16) \times 10^{-3}$	S=1.1 845
$\bar{K}_0^*(1430)^0 \pi^+$, [kk]	$(1.25 \pm 0.06) \%$		382	$\eta \pi^+$	$(3.77 \pm 0.09) \times 10^{-3}$	848
$\bar{K}_0^*(1430)^0 \rightarrow K^- \pi^+$			714	$\eta \pi^+ \pi^0$	$(2.05 \pm 0.35) \times 10^{-3}$	S=2.2 831
$\bar{K}^*(892)^0 \pi^+$, $\bar{K}^*(892)^0 \rightarrow K^- \pi^+$	$(1.04 \pm 0.12) \%$		714	$\eta 2\pi^+ \pi^-$	$(3.41 \pm 0.20) \times 10^{-3}$	798
$\bar{K}^*(1410)^0 \pi^+$, $\bar{K}^{*0} \rightarrow$ $K^- \pi^+$	not seen		381	$\eta \pi^+ 2\pi^0$	$(3.20 \pm 0.33) \times 10^{-3}$	801
$\bar{K}_2^*(1430)^0 \pi^+$, [kk]	$(2.3 \pm 0.7) \times 10^{-4}$		371	$\eta \eta \pi^+$	$(2.96 \pm 0.26) \times 10^{-3}$	700
$\bar{K}_2^*(1430)^0 \rightarrow K^- \pi^+$			58	$\omega \pi^+$	$(2.8 \pm 0.6) \times 10^{-4}$	764
$\bar{K}^*(1680)^0 \pi^+$, [kk]	$(2.2 \pm 1.1) \times 10^{-4}$		58	$\omega \pi^+ \pi^0$	$(3.9 \pm 0.9) \times 10^{-3}$	742
$\bar{K}^*(1680)^0 \rightarrow K^- \pi^+$			-	$\eta'(958) \pi^+$	$(4.97 \pm 0.19) \times 10^{-3}$	681
$K^- (2\pi^+)_{I=2}$	$(1.45 \pm 0.26) \%$		-	$\eta'(958) \pi^+ \pi^0$	$(1.6 \pm 0.5) \times 10^{-3}$	654
$K_S^0 \pi^+ \pi^0$ [ij]	$(7.36 \pm 0.21) \%$		845	Hadronic modes with a $K\bar{K}$ pair		
$K_S^0 \rho^+$	$(6.14 \pm 0.35) \%$		677	$K_S^0 K^+$	$(3.04 \pm 0.09) \times 10^{-3}$	S=2.2 793
$K_S^0 \rho(1450)^+$, $\rho^+ \rightarrow \pi^+ \pi^0$	$(1.5 \pm 1.2) \times 10^{-3}$		-	$K_S^0 K^+$	$(3.21 \pm 0.16) \times 10^{-3}$	793
$\bar{K}^*(892)^0 \pi^+$, $\bar{K}^*(892)^0 \rightarrow K_S^0 \pi^0$	$(2.64 \pm 0.32) \times 10^{-3}$		714	$K_S^0 K^+ \pi^0$	$(5.07 \pm 0.30) \times 10^{-3}$	744
$\bar{K}_0^*(1430)^0 \pi^+$, $\bar{K}_0^{*0} \rightarrow$ $K_S^0 \pi^0$	$(2.7 \pm 0.9) \times 10^{-3}$		-	$K^*(892)^+ + K_S^0$	$(2.89 \pm 0.30) \times 10^{-3}$	612
$\bar{K}_0^*(1680)^0 \pi^+$, $\bar{K}_0^{*0} \rightarrow$ $K_S^0 \pi^0$	$(10 \pm 7) \times 10^{-4}$		-	$\bar{K}^*(892)^0 K^+$	$(5.2 \pm 1.4) \times 10^{-4}$	613
$\bar{\pi}^0 \pi^+$, $\bar{\pi}^0 \rightarrow K_S^0 \pi^0$	$(6 \pm 5) \times 10^{-3}$		-	$K_L^0 K^+ \pi^0$	$(5.24 \pm 0.31) \times 10^{-3}$	744
$K_S^0 \pi^+ \pi^0$ nonresonant	$(3 \pm 4) \times 10^{-3}$		845	$K^+ K^- \pi^+$ [ij]	$(9.68 \pm 0.18) \times 10^{-3}$	744
$K_S^0 \pi^+ \pi^0$ nonresonant and $\bar{\pi}^0 \pi^+$	$(1.37 \pm 0.21) \%$		-	$K^+ \bar{K}^*(892)^0$, $\bar{K}^*(892)^0 \rightarrow K^- \pi^+$	$(2.49 \pm 0.08) \times 10^{-3}$	613
$(K_S^0 \pi^0)_{S\text{-wave}} \pi^+$	$(1.27 \pm 0.27) \%$		845	$K^+ \bar{K}_0^*(1430)^0$, $\bar{K}_0^*(1430)^0 \rightarrow K^- \pi^+$	$(1.82 \pm 0.35) \times 10^{-3}$	-
$K_S^0 \pi^+ \eta$	$(1.31 \pm 0.05) \%$		722	$K^+ \bar{K}_2^*(1430)^0$, $\bar{K}_2^{*0} \rightarrow$ $K^- \pi^+$	$(1.6 \pm 1.2) \times 10^{-4}$	-
$K_S^0 \pi^+ \eta'(958)$	$(1.90 \pm 0.21) \times 10^{-3}$		481	$K^+ \bar{K}_0^*(700)$, $\bar{K}_0^{*0} \rightarrow K^- \pi^+$	$(6.8 \pm 3.5) \times 10^{-4}$	-
$K^- 2\pi^+ \pi^0$ [ll]	$(6.25 \pm 0.18) \%$		817	$a_0(1450)^0 \pi^+$, $a_0^0 \rightarrow$ $K^+ K^-$	$(4.5 \pm 7.0) \times 10^{-4}$	-
$K_S^0 2\pi^+ \pi^-$ [ll]	$(3.10 \pm 0.09) \%$		814	$\phi(1680) \pi^+$, $\phi \rightarrow K^+ K^-$	$(4.9 \pm 4.0) \times 10^{-5}$	-
$K^- 2\pi^+ \eta$	$(1.35 \pm 0.12) \times 10^{-3}$		657	$\phi \pi^+$, $\phi \rightarrow K^+ K^-$	$(2.69 \pm 0.07) \times 10^{-3}$	647
$K_S^0 \pi^+ \pi^0 \eta$	$(1.22 \pm 0.25) \times 10^{-3}$		657	$\phi \pi^+$	$(5.70 \pm 0.14) \times 10^{-3}$	647
$K^- 3\pi^+ \pi^-$ [jj]	$(5.7 \pm 0.5) \times 10^{-3}$	S=1.1	772	$K^+ K^- \pi^+ \pi^0$	$(6.62 \pm 0.32) \times 10^{-3}$	682
				$K_S^0 K_S^0 \pi^+$	$(2.70 \pm 0.13) \times 10^{-3}$	741
				$K_S^0 K_S^0 \pi^+ \pi^0$	$(1.34 \pm 0.21) \times 10^{-3}$	679
				$K_S^0 K^+ \eta$	$(1.8 \pm 0.5) \times 10^{-4}$	516
				$K^+ K_S^0 \pi^+ \pi^-$	$(1.89 \pm 0.13) \times 10^{-3}$	678
				$K_S^0 K^+ \pi^0 \pi^0$	$(5.8 \pm 1.3) \times 10^{-4}$	683
				$K_S^0 K^- 2\pi^+$	$(2.27 \pm 0.13) \times 10^{-3}$	678
				$K^+ K^- 2\pi^+ \pi^-$	$(2.3 \pm 1.2) \times 10^{-4}$	601

Meson Summary Table

A few poorly measured branching fractions:

$\phi\pi^+\pi^0$	$(2.3 \pm 1.0) \%$	619
$\phi\rho^+$	$< 1.5 \%$	260
$K^+K^-\pi^+\pi^0$ non- ϕ	$(1.5 \pm_{-0.6}^{+0.7}) \%$	682

Doubly Cabibbo-suppressed modes

$K^+\pi^0$	$(2.08 \pm 0.21) \times 10^{-4}$	$S=1.4$	864
$K^+\eta$	$(1.25 \pm 0.16) \times 10^{-4}$	$S=1.1$	776
$K^+\eta'(958)$	$(1.85 \pm 0.20) \times 10^{-4}$		571
$K^+\pi^+\pi^-$	$(4.91 \pm 0.09) \times 10^{-4}$		846
$K^+\rho^0$	$(1.9 \pm 0.5) \times 10^{-4}$		679
$K^*(892)^0\pi^+, K^*(892)^0 \rightarrow$	$(2.3 \pm 0.4) \times 10^{-4}$		714
$K^+\pi^-$			
$K^+f_0(980), f_0(980) \rightarrow$	$(4.4 \pm 2.6) \times 10^{-5}$		-
$K_2^+(1430)^0\pi^+, K_2^*(1430)^0 \rightarrow$	$(3.9 \pm 2.7) \times 10^{-5}$		-
$K^+\pi^-$			
$K^+\pi^+\pi^-$ nonresonant	not seen		846
$K^+\pi^+\pi^-\pi^0$	$(1.21 \pm 0.09) \times 10^{-3}$		817
$K^+\pi^+\pi^-\pi^0$ nonresonant	$(1.10 \pm 0.07) \times 10^{-3}$		817
$K^+\omega$	$(5.7 \pm_{-2.1}^{+2.5}) \times 10^{-5}$		675
$2K^+K^-$	$(6.14 \pm 0.11) \times 10^{-5}$		550
$\phi(1020)^0 K^+$	$< 2.1 \times 10^{-5}$	$CL=90\%$	-
$K^+\phi(1020), \phi \rightarrow K^+K^-$	$(4.4 \pm 0.6) \times 10^{-6}$		-
$K^+(K^+K^-)_{S-wave}$	$(5.77 \pm 0.12) \times 10^{-5}$		550

$\Delta C = 1$ weak neutral current (CI) modes, or Lepton Family number (LF), or Lepton number (L), or Baryon number (B) violating modes

$\pi^+e^+e^-$	CI	$< 1.1 \times 10^{-6}$	$CL=90\%$	930
$\pi^+\pi^0e^+e^-$		$< 1.4 \times 10^{-5}$	$CL=90\%$	925
$\pi^+\phi, \phi \rightarrow e^+e^-$	[oo]	$(1.7 \pm_{-0.9}^{+1.4}) \times 10^{-6}$		-
$\pi^+\mu^+\mu^-$	CI	$< 6.7 \times 10^{-8}$	$CL=90\%$	918
$\pi^+\phi, \phi \rightarrow \mu^+\mu^-$	[oo]	$(1.8 \pm 0.8) \times 10^{-6}$		-
$\rho^+\mu^+\mu^-$	CI	$< 5.6 \times 10^{-4}$	$CL=90\%$	757
$K^+e^+e^-$	[pp]	$< 8.5 \times 10^{-7}$	$CL=90\%$	870
$K^+\pi^0e^+e^-$		$< 1.5 \times 10^{-5}$	$CL=90\%$	864
$K_S^0\pi^+e^+e^-$		$< 2.6 \times 10^{-5}$	$CL=90\%$	-
$K_S^0K^+e^+e^-$		$< 1.1 \times 10^{-5}$	$CL=90\%$	792
$K^+\mu^+\mu^-$	[pp]	$< 5.4 \times 10^{-8}$	$CL=90\%$	856
$\pi^+e^+\mu^-$	LF	$< 2.1 \times 10^{-7}$	$CL=90\%$	927
$\pi^+e^-\mu^+$	LF	$< 2.2 \times 10^{-7}$	$CL=90\%$	927
$K^+e^+\mu^-$	LF	$< 7.5 \times 10^{-8}$	$CL=90\%$	866
$K^+e^-\mu^+$	LF	$< 1.0 \times 10^{-7}$	$CL=90\%$	866
π^-2e^+	L	$< 5.3 \times 10^{-7}$	$CL=90\%$	930
$\pi^-2\mu^+$	L	$< 1.4 \times 10^{-8}$	$CL=90\%$	918
$\pi^-e^+\mu^+$	L	$< 1.3 \times 10^{-7}$	$CL=90\%$	927
$\rho^-2\mu^+$	L	$< 5.6 \times 10^{-4}$	$CL=90\%$	757
K^-2e^+	L	$< 9 \times 10^{-7}$	$CL=90\%$	870
$K_S^0\pi^-2e^+$		$< 3.3 \times 10^{-6}$	$CL=90\%$	863
$K^- \pi^0 2e^+$		$< 8.5 \times 10^{-6}$	$CL=90\%$	864
$K^-2\mu^+$	L	$< 1.0 \times 10^{-5}$	$CL=90\%$	856
$K^-e^+\mu^+$	L	$< 1.9 \times 10^{-6}$	$CL=90\%$	866
$K^*(892)^-2\mu^+$	L	$< 8.5 \times 10^{-4}$	$CL=90\%$	703
Λe^+	L,B	$< 1.1 \times 10^{-6}$	$CL=90\%$	602
$\bar{\Lambda} e^+$	L,B	$< 6.5 \times 10^{-7}$	$CL=90\%$	602
$\Sigma^0 e^+$	L,B	$< 1.7 \times 10^{-6}$	$CL=90\%$	554
$\bar{\Sigma}^0 e^+$	L,B	$< 1.3 \times 10^{-6}$	$CL=90\%$	554

D⁰

$$I(J^P) = \frac{1}{2}(0^-)$$

Mass $m = 1864.84 \pm 0.05$ MeV
 $m_{D^\pm} - m_{D^0} = 4.822 \pm 0.015$ MeV
 Mean life $\tau = (410.3 \pm 1.0) \times 10^{-15}$ s
 $c\tau = 123.01 \mu\text{m}$

Mixing and related parameters

$|m_{D_1^0} - m_{D_2^0}| = (0.997 \pm 0.116) \times 10^{10} \hbar \text{ s}^{-1}$
 $(\Gamma_{D_1^0} - \Gamma_{D_2^0})/\Gamma = 2\gamma = (1.23 \pm 0.11) \times 10^{-2}$
 $|q/p| = 0.995 \pm 0.016$
 $A_\Gamma = (0.089 \pm 0.113) \times 10^{-3}$
 $\phi^{K_S^0\pi\pi} = 0.02 \pm_{-0.05}^{+0.04}$
 $K^+\pi^-$ relative strong phase: $\cos \delta = 0.97 \pm 0.11$
 $K^-\pi^+\pi^0$ coherence factor $R_{K\pi\pi^0} = 0.792 \pm 0.033$
 $K^-\pi^+\pi^0$ average relative strong phase $\delta^{K\pi\pi^0} = (198 \pm 10)^\circ$
 $K^-\pi^-2\pi^+$ coherence factor $R_{K3\pi} = 0.52 \pm_{-0.09}^{+0.10}$

$K^-\pi^-2\pi^+$ average relative strong phase $\delta^{K3\pi} = (149 \pm_{-16}^{+26})^\circ$ ($S = 1.4$)

$D^0 \rightarrow K^-\pi^-2\pi^+, R_{K3\pi}$ ($y \cos \delta^{K3\pi} - x \sin \delta^{K3\pi}$) = $(-3.0 \pm 0.7) \times 10^{-3} \text{ TeV}^{-1}$

$K_S^0 K^+\pi^-$ coherence factor $R_{K_S^0 K\pi} = 0.70 \pm 0.08$

$K_S^0 K^+\pi^-$ average relative strong phase $\delta^{K_S^0 K\pi} = (0 \pm 16)^\circ$

K^*K coherence factor $R_{K^*K} = 0.94 \pm 0.12$

K^*K average relative strong phase $\delta^{K^*K} = (-17 \pm 18)^\circ$

CP-violation decay-rate asymmetries (labeled by the D⁰ decay)

$A_{CP}(K^+K^-) = (-0.07 \pm 0.11)\%$
 $A_{CP}(2K_S^0) = (-1.9 \pm 1.1)\%$ ($S = 1.1$)
 $A_{CP}(\pi^+\pi^-) = (0.13 \pm 0.14)\%$
 $A_{CP}(\pi^0\pi^0) = (0.0 \pm 0.6)\%$
 $A_{CP}(\rho\gamma) = (6 \pm 15) \times 10^{-2}$
 $A_{CP}(\phi\gamma) = (-9 \pm 7) \times 10^{-2}$
 $A_{CP}(K^*(892)^0\gamma) = (-0.3 \pm 2.0) \times 10^{-2}$
 $A_{CP}(\pi^+\pi^-\pi^0) = (0.3 \pm 0.4)\%$
 $A_{CP}(\eta\pi^+\pi^-)$ in $D^0, \bar{D}^0 \rightarrow \eta\pi^+\pi^- = (0.9 \pm 1.3) \times 10^{-2}$
 $A_{CP}(\rho(770)^+\pi^- \rightarrow \pi^+\pi^-\pi^0) = (1.2 \pm 0.9)\%$ [qq]
 $A_{CP}(\rho(770)^0\pi^0 \rightarrow \pi^+\pi^-\pi^0) = (-3.1 \pm 3.0)\%$ [qq]
 $A_{CP}(\rho(770)^-\pi^+ \rightarrow \pi^+\pi^-\pi^0) = (-1.0 \pm 1.7)\%$ [qq]
 $A_{CP}(\rho(1450)^+\pi^- \rightarrow \pi^+\pi^-\pi^0) = (0 \pm 70)\%$ [qq]
 $A_{CP}(\rho(1450)^0\pi^0 \rightarrow \pi^+\pi^-\pi^0) = (-20 \pm 40)\%$ [qq]
 $A_{CP}(\rho(1450)^-\pi^+ \rightarrow \pi^+\pi^-\pi^0) = (6 \pm 9)\%$ [qq]
 $A_{CP}(\rho(1700)^+\pi^- \rightarrow \pi^+\pi^-\pi^0) = (-5 \pm 14)\%$ [qq]
 $A_{CP}(\rho(1700)^0\pi^0 \rightarrow \pi^+\pi^-\pi^0) = (13 \pm 9)\%$ [qq]
 $A_{CP}(\rho(1700)^-\pi^+ \rightarrow \pi^+\pi^-\pi^0) = (8 \pm 11)\%$ [qq]
 $A_{CP}(f_0(980)\pi^0 \rightarrow \pi^+\pi^-\pi^0) = (0 \pm 35)\%$ [qq]
 $A_{CP}(f_0(1370)\pi^0 \rightarrow \pi^+\pi^-\pi^0) = (25 \pm 18)\%$ [qq]
 $A_{CP}(f_0(1500)\pi^0 \rightarrow \pi^+\pi^-\pi^0) = (0 \pm 18)\%$ [qq]
 $A_{CP}(f_0(1710)\pi^0 \rightarrow \pi^+\pi^-\pi^0) = (0 \pm 24)\%$ [qq]
 $A_{CP}(f_2(1270)\pi^0 \rightarrow \pi^+\pi^-\pi^0) = (-4 \pm 6)\%$ [qq]
 $A_{CP}(\sigma(400)\pi^0 \rightarrow \pi^+\pi^-\pi^0) = (6 \pm 8)\%$ [qq]
 $A_{CP}(\text{nonresonant } \pi^+\pi^-\pi^0) = (-13 \pm 23)\%$ [qq]
 $A_{CP}(a_1(1260)^+\pi^- \rightarrow 2\pi^+2\pi^-) = (5 \pm 6)\%$
 $A_{CP}(a_1(1260)^-\pi^+ \rightarrow 2\pi^+2\pi^-) = (14 \pm 18)\%$
 $A_{CP}(\pi(1300)^+\pi^- \rightarrow 2\pi^+2\pi^-) = (-2 \pm 15)\%$
 $A_{CP}(\pi(1300)^-\pi^+ \rightarrow 2\pi^+2\pi^-) = (-6 \pm 30)\%$
 $A_{CP}(a_1(1640)^+\pi^- \rightarrow 2\pi^+2\pi^-) = (9 \pm 26)\%$
 $A_{CP}(\pi_2(1670)^+\pi^- \rightarrow 2\pi^+2\pi^-) = (7 \pm 18)\%$
 $A_{CP}(\sigma f_0(1370) \rightarrow 2\pi^+2\pi^-) = (-15 \pm 19)\%$
 $A_{CP}(\sigma\rho(770)^0 \rightarrow 2\pi^+2\pi^-) = (3 \pm 27)\%$
 $A_{CP}(2\rho(770)^0 \rightarrow 2\pi^+2\pi^-) = (-6 \pm 6)\%$
 $A_{CP}(2f_2(1270) \rightarrow 2\pi^+2\pi^-) = (-28 \pm 24)\%$
 $A_{CP}(\pi^+\pi^-\pi^0\eta)$ in $D^0, \bar{D}^0 \rightarrow \pi^+\pi^-\pi^0\eta = (-6 \pm 6) \times 10^{-2}$
 $A_{CP}(K^+K^-\pi^0) = (-1.0 \pm 1.7)\%$
 $A_{CP}(K^*(892)^+K^- \rightarrow K^+K^-\pi^0) = (-0.9 \pm 1.3)\%$ [qq]
 $A_{CP}(K^*(1410)^+K^- \rightarrow K^+K^-\pi^0) = (-21 \pm 24)\%$ [qq]
 $A_{CP}((K^+\pi^0)_{S-wave}K^- \rightarrow K^+K^-\pi^0) = (7 \pm 15)\%$ [qq]
 $A_{CP}(\phi(1020)\pi^0 \rightarrow K^+K^-\pi^0) = (1.1 \pm 2.2)\%$ [qq]
 $A_{CP}(f_0(980)\pi^0 \rightarrow K^+K^-\pi^0) = (-3 \pm 19)\%$ [qq]
 $A_{CP}(a_0(980)^0\pi^0 \rightarrow K^+K^-\pi^0) = (-5 \pm 16)\%$ [qq]
 $A_{CP}(f_2'(1525)\pi^0 \rightarrow K^+K^-\pi^0) = (0 \pm 160)\%$ [qq]
 $A_{CP}(K^*(892)^-K^+ \rightarrow K^+K^-\pi^0) = (-5 \pm 4)\%$ [qq]
 $A_{CP}(K^*(1410)^-K^+ \rightarrow K^+K^-\pi^0) = (-17 \pm 29)\%$ [qq]
 $A_{CP}((K^-\pi^0)_{S-wave}K^+ \rightarrow K^+K^-\pi^0) = (-10 \pm 40)\%$ [qq]
 $A_{CP}(K^+K^-\eta)$ in $D^0, \bar{D}^0 \rightarrow K^+K^-\eta = (-1.4 \pm 3.5) \times 10^{-2}$
 $A_{CP}(\phi(1020)\eta \rightarrow K^+K^-\eta)$ in $D^0, \bar{D}^0 \rightarrow \phi(1020)\eta = (-2 \pm 4) \times 10^{-2}$
 $A_{CP}(K_S^0\pi^0) = (-0.20 \pm 0.17)\%$
 $A_{CP}(K_S^0\eta) = (0.5 \pm 0.5)\%$
 $A_{CP}(K_S^0\eta') = (1.0 \pm 0.7)\%$
 $A_{CP}(K_S^0\phi) = (-3 \pm 9)\%$
 $A_{CP}(K^-\pi^+) = (0.2 \pm 0.5)\%$
 $A_{CP}(K^+\pi^-) = (-0.9 \pm 1.4)\%$
 $A_{CP}(D_{CP(\pm 1)} \rightarrow K^\mp\pi^\pm) = (12.7 \pm 1.5)\%$
 $A_{CP}(K^-\pi^+\pi^0) = (0.1 \pm 0.5)\%$
 $A_{CP}(K^+\pi^-\pi^0) = (0 \pm 5)\%$
 $A_{CP}(K_S^0\pi^+\pi^-) = (-0.1 \pm 0.8)\%$
 $A_{CP}(K^\mp\pi^\pm\eta)$ in $D^0, \bar{D}^0 \rightarrow K^\mp\pi^\pm\eta = (-1.9 \pm 1.6) \times 10^{-2}$
 $A_{CP}(K_S^0\pi^0\eta)$ in $D^0, \bar{D}^0 \rightarrow K_S^0\pi^0\eta = (-3.9 \pm 3.3) \times 10^{-2}$

Meson Summary Table

$A_{CP}(K^\mp \pi^\pm \pi^0 \eta)$ in $D^0, \bar{D}^0 \rightarrow K^\mp \pi^\pm \pi^0 \eta = (-8 \pm 5) \times 10^{-2}$
 $A_{CP}(K^*(892)^- \pi^+ \rightarrow K_S^0 \pi^+ \pi^-) = (0.4 \pm 0.5)\%$
 $A_{CP}(K^*(892)^+ \pi^- \rightarrow K_S^0 \pi^+ \pi^-) = (1 \pm 6)\%$
 $A_{CP}(\bar{K}^0 \rho^0 \rightarrow K_S^0 \pi^+ \pi^-) = (-0.1 \pm 0.5)\%$
 $A_{CP}(\bar{K}^0 \omega \rightarrow K_S^0 \pi^+ \pi^-) = (-13 \pm 7)\%$
 $A_{CP}(\bar{K}^0 f_0(980) \rightarrow K_S^0 \pi^+ \pi^-) = (-0.4 \pm 2.7)\%$
 $A_{CP}(\bar{K}^0 f_2(1270) \rightarrow K_S^0 \pi^+ \pi^-) = (-4 \pm 5)\%$
 $A_{CP}(\bar{K}^0 f_0(1370) \rightarrow K_S^0 \pi^+ \pi^-) = (-1 \pm 9)\%$
 $A_{CP}(\bar{K}^0 \rho^0(1450) \rightarrow K_S^0 \pi^+ \pi^-) = (-4 \pm 10)\%$
 $A_{CP}(\bar{K}^0 f_0(600) \rightarrow K_S^0 \pi^+ \pi^-) = (-3 \pm 5)\%$
 $A_{CP}(K^*(1410)^- \pi^+ \rightarrow K_S^0 \pi^+ \pi^-) = (-2 \pm 9)\%$
 $A_{CP}(K_S^0(1430)^- \pi^+ \rightarrow K_S^0 \pi^+ \pi^-) = (4 \pm 4)\%$
 $A_{CP}(K_S^0(1430)^+ \pi^- \rightarrow K_S^0 \pi^+ \pi^-) = (12 \pm 15)\%$
 $A_{CP}(K_2^*(1430)^- \pi^+ \rightarrow K_S^0 \pi^+ \pi^-) = (3 \pm 6)\%$
 $A_{CP}(K_2^*(1430)^+ \pi^- \rightarrow K_S^0 \pi^+ \pi^-) = (-10 \pm 32)\%$
 $A_{CP}(K^- \pi^+ \pi^+ \pi^-) = (0.2 \pm 0.5)\%$
 $A_{CP}(K^+ \pi^- \pi^+ \pi^-) = (-2 \pm 4)\%$
 $A_{CP}(K^+ K^- \pi^+ \pi^-) = (1.3 \pm 1.7)\%$
 $A_{CP}(K_1^*(1270)^+ K^- \rightarrow K^+ K^- \pi^+ \pi^-) = (-2.3 \pm 1.7)\%$
 $A_{CP}(K_1^*(1270)^+ K^- \rightarrow K^{*0} \pi^+ K^-) = (-1 \pm 10)\%$
 $A_{CP}(K_1^*(1270)^- K^+ \rightarrow \bar{K}^{*0} \pi^- K^+) = (-10 \pm 32)\%$
 $A_{CP}(K_1^*(1270)^- K^+ \rightarrow K^+ K^- \pi^+ \pi^-) = (1.7 \pm 3.5)\%$
 $A_{CP}(K_1^*(1270)^+ K^- \rightarrow \rho^0 K^+ K^-) = (-7 \pm 17)\%$
 $A_{CP}(K_1^*(1270)^- K^+ \rightarrow \rho^0 K^- K^+) = (10 \pm 13)\%$
 $A_{CP}(K_1(1400)^+ K^- \rightarrow K^+ K^- \pi^+ \pi^-) = (-4.4 \pm 2.1)\%$
 $A_{CP}(K^*(1410)^+ K^- \rightarrow K^{*0} \pi^+ K^-) = (-20 \pm 17)\%$
 $A_{CP}(K^*(1410)^- K^+ \rightarrow \bar{K}^{*0} \pi^- K^+) = (-1 \pm 14)\%$
 $A_{CP}(K^*(1680)^+ K^- \rightarrow K^+ K^- \pi^+ \pi^-) = (-17 \pm 29)\%$
 $A_{CP}(K^{*0} \bar{K}^{*0})$ in $D^0, \bar{D}^0 \rightarrow K^{*0} \bar{K}^{*0} = (-5 \pm 14)\%$
 $A_{CP}(K^{*0} \bar{K}^{*0} S\text{-wave}) = (-3.9 \pm 2.2)\%$
 $A_{CP}(\phi \rho^0)$ in $D^0, \bar{D}^0 \rightarrow \phi \rho^0 = (1 \pm 9)\%$
 $A_{CP}(\phi \rho^0 S\text{-wave}) = (-3 \pm 5)\%$
 $A_{CP}(\phi \rho^0 D\text{-wave}) = (-37 \pm 19)\%$
 $A_{CP}(\phi(\pi^+ \pi^-)_{S\text{-wave}}) = (6 \pm 6)\%$
 $A_{CP}(K^*(892)^0 (K^- \pi^+)_{S\text{-wave}}) = (-10 \pm 40)\%$
 $A_{CP}(K^+ K^- \pi^+ \pi^- \text{ non-resonant}) = (8 \pm 20)\%$
 $A_{CP}((K^- \pi^+)_{P\text{-wave}} (K^+ \pi^-)_{S\text{-wave}}) = (3 \pm 11)\%$
 $A_{CP}(K^+ K^- \mu^+ \mu^-)$ in $D^0, \bar{D}^0 \rightarrow K^+ K^- \mu^+ \mu^- = (0 \pm 11)\%$
 $A_{CP}(\pi^+ \pi^- \mu^+ \mu^-)$ in $D^0, \bar{D}^0 \rightarrow \pi^+ \pi^- \mu^+ \mu^- = (5 \pm 4)\%$

CP-even fractions (labeled by the D^0 decay)

$CP\text{-even fraction in } D^0 \rightarrow \pi^+ \pi^- \pi^0 \text{ decays} = (97.3 \pm 1.7)\%$
 $CP\text{-even fraction in } D^0 \rightarrow K^+ K^- \pi^0 \text{ decays} = (73 \pm 6)\%$
 $CP\text{-even fraction in } D^0 \rightarrow \pi^+ \pi^- \pi^+ \pi^- \text{ decays} = (76.9 \pm 2.3)\%$
 $CP\text{-even fraction in } D^0 \rightarrow K_S^0 \pi^+ \pi^- \pi^0 \text{ decays} = (23.8 \pm 1.7)\%$
 $CP\text{-even fraction in } D^0 \rightarrow K^+ K^- \pi^+ \pi^- \text{ decays} = (75 \pm 4)\%$

CP-violation asymmetry difference

$\Delta A_{CP} = A_{CP}(K^+ K^-) - A_{CP}(\pi^+ \pi^-) = (-0.154 \pm 0.029)\%$

χ^2 tests of CP-violation (CPV) p-values

Local CPV in $D^0, \bar{D}^0 \rightarrow \pi^+ \pi^- \pi^0 = 4.9\%$
 Local CPV in $D^0, \bar{D}^0 \rightarrow \pi^+ \pi^- \pi^+ \pi^- = (0.6 \pm 0.2)\%$
 Local CPV in $D^0, \bar{D}^0 \rightarrow K_S^0 \pi^+ \pi^- = 96\%$
 Local CPV in $D^0, \bar{D}^0 \rightarrow K^+ K^- \pi^0 = 16.6\%$
 Local CPV in $D^0, \bar{D}^0 \rightarrow K^+ K^- \pi^+ \pi^- = 9.1\%$

T-violation decay-rate asymmetry

$A_T(K^+ K^- \pi^+ \pi^-) = (2.9 \pm 2.2) \times 10^{-3}$ [ii]
 $A_{T\text{viol}}(K_S \pi^+ \pi^- \pi^0)$ in $D^0, \bar{D}^0 \rightarrow K_S \pi^+ \pi^- \pi^0 = (-0.3 \pm 1.4) \times 10^{-3}$

CPT-violation decay-rate asymmetry

$A_{CPT}(K^\mp \pi^\pm) = 0.008 \pm 0.008$

Form factors

$r_V \equiv V(0)/A_1(0)$ in $D^0 \rightarrow K^*(892)^- \ell^+ \nu_\ell = 1.46 \pm 0.07$
 $r_2 \equiv A_2(0)/A_1(0)$ in $D^0 \rightarrow K^*(892)^- \ell^+ \nu_\ell = 0.68 \pm 0.06$
 $f_+(0)$ in $D^0 \rightarrow K^- \ell^+ \nu_\ell = 0.736 \pm 0.004$
 $f_+(0)|V_{cs}|$ in $D^0 \rightarrow K^- \ell^+ \nu_\ell = 0.7166 \pm 0.0030$
 $r_1 \equiv a_1/a_0$ in $D^0 \rightarrow K^- \ell^+ \nu_\ell = -2.40 \pm 0.16$
 $r_2 \equiv a_2/a_0$ in $D^0 \rightarrow K^- \ell^+ \nu_\ell = 5 \pm 4$
 $f_+(0)$ in $D^0 \rightarrow \pi^- \ell^+ \nu_\ell = 0.637 \pm 0.009$
 $f_+(0)|V_{cd}|$ in $D^0 \rightarrow \pi^- \ell^+ \nu_\ell = 0.1436 \pm 0.0026$ ($S = 1.5$)
 $r_1 \equiv a_1/a_0$ in $D^0 \rightarrow \pi^- \ell^+ \nu_\ell = -1.97 \pm 0.28$ ($S = 1.4$)
 $r_2 \equiv a_1/a_0$ in $D^0 \rightarrow \pi^- \ell^+ \nu_\ell = -0.2 \pm 2.2$ ($S = 1.7$)

Most decay modes (other than the semileptonic modes) that involve a neutral K meson are now given as K_S^0 modes, not as \bar{K}^0 modes. Nearly always it is a K_S^0 that is measured, and interference between Cabibbo-allowed and doubly Cabibbo-suppressed modes can invalidate the assumption that $2\Gamma(K_S^0) = \Gamma(\bar{K}^0)$.

D^0 DECAY MODES	Fraction (Γ_i/Γ)	Scale factor/ Confidence level (MeV/c)	p
Topological modes			
0-prongs	[rr] (15 ± 6) %		-
2-prongs	(71 ± 6) %		-
4-prongs	[ss] (14.6 ± 0.5) %		-
6-prongs	[tt] (6.5 ± 1.3) × 10 ⁻⁴		-
Inclusive modes			
e^+ anything	[uu] (6.49 ± 0.11) %		-
μ^+ anything	(6.8 ± 0.6) %		-
K^- anything	(54.7 ± 2.8) %	S=1.3	-
\bar{K}^0 anything + K^0 anything	(47 ± 4) %		-
K^+ anything	(3.4 ± 0.4) %		-
$K^*(892)^-$ anything	(15 ± 9) %		-
$\bar{K}^*(892)^0$ anything	(9 ± 4) %		-
$K^*(892)^+$ anything	< 3.6 %	CL=90%	-
$K^*(892)^0$ anything	(2.8 ± 1.3) %		-
η anything	(9.5 ± 0.9) %		-
η' anything	(2.48 ± 0.27) %		-
ϕ anything	(1.08 ± 0.04) %		-
invisibles	< 9.4 × 10 ⁻⁵	CL=90%	-
Semileptonic modes			
$K^- e^+ \nu_e$	(3.549 ± 0.026) %	S=1.2	867
$K^- \mu^+ \nu_\mu$	(3.41 ± 0.04) %		864
$K^*(892)^- e^+ \nu_e$	(2.15 ± 0.16) %		719
$K^*(892)^- \mu^+ \nu_\mu$	(1.89 ± 0.24) %		714
$K^- \pi^0 e^+ \nu_e$	(1.6 ± 1.3) %		861
$\bar{K}^0 \pi^- e^+ \nu_e$	(1.44 ± 0.04) %		860
$(\bar{K}^0 \pi^-) S\text{-wave } e^+ \nu_e$	(7.9 ± 1.7) × 10 ⁻⁴		860
$K^- \pi^+ \pi^- e^+ \nu_e$	(2.8 ± 1.4) × 10 ⁻⁴		843
$K_1(1270)^- e^+ \nu_e$	(1.01 ± 0.18) × 10 ⁻³		511
$K^- \pi^+ \pi^- \mu^+ \nu_\mu$	< 1.3 × 10 ⁻³	CL=90%	821
$(\bar{K}^*(892) \pi^-) \mu^+ \nu_\mu$	< 1.5 × 10 ⁻³	CL=90%	692
$\pi^- e^+ \nu_e$	(2.91 ± 0.04) × 10 ⁻³		927
$\pi^- \mu^+ \nu_\mu$	(2.67 ± 0.12) × 10 ⁻³	S=1.3	924
$\pi^- \pi^0 e^+ \nu_e$	(1.45 ± 0.07) × 10 ⁻³		922
$\rho^- e^+ \nu_e$	(1.50 ± 0.12) × 10 ⁻³	S=1.9	771
$\rho^- \mu^+ \nu_\mu$	(1.35 ± 0.13) × 10 ⁻³		767
$a(980)^- e^+ \nu_e, a^- \rightarrow \eta \pi^-$	(1.33 ± 0.34) × 10 ⁻⁴		-
$b_1(1235)^- e^+ \nu_e, b_1^- \rightarrow \omega \pi^-$	< 1.12 × 10 ⁻⁴	CL=90%	-
Hadronic modes with one \bar{K}			
$K^- \pi^+$	(3.947 ± 0.030) %	S=1.2	861
$K_S^0 \pi^0$	(1.240 ± 0.022) %		860
$K_L^0 \pi^0$	(10.0 ± 0.7) × 10 ⁻³		860
$K_S^0 \pi^+ \pi^-$	[ij] (2.80 ± 0.18) %	S=1.1	842
$K_S^0 \rho^0$	(6.3 ± 0.8) × 10 ⁻³		674
$K_S^0 \omega, \omega \rightarrow \pi^+ \pi^-$	(2.0 ± 0.6) × 10 ⁻⁴		670
$K_S^0 (\pi^+ \pi^-)_{S\text{-wave}}$	(3.3 ± 0.8) × 10 ⁻³		842
$K_S^0 f_0(980), f_0 \rightarrow \pi^+ \pi^-$	(1.20 ± 0.40) × 10 ⁻³		549
$K_S^0 f_0(1370), f_0 \rightarrow \pi^+ \pi^-$	(2.8 ± 0.9) × 10 ⁻³		†
$K_S^0 f_2(1270), f_2 \rightarrow \pi^+ \pi^-$	(9 ± 10) × 10 ⁻⁵		262
$K^*(892)^- \pi^+, K^{*-} \rightarrow$	(1.64 ± 0.14) %		711
$K_S^0 \pi^-$			
$K_S^0(1430)^- \pi^+, K_S^{*0} \rightarrow$	(2.67 ± 0.40) × 10 ⁻³		378
$K_S^0 \pi^-$			
$K_2^*(1430)^- \pi^+, K_2^{*-} \rightarrow$	(3.4 ± 1.9) × 10 ⁻⁴		367
$K_S^0 \pi^-$			
$K^*(1680)^- \pi^+, K^{*-} \rightarrow$	(4.4 ± 3.5) × 10 ⁻⁴		46
$K_S^0 \pi^-$			
$K^*(892)^+ \pi^-, K^{*+} \rightarrow$	[w] (1.13 ± 0.60) × 10 ⁻⁴		711
$K_S^0 \pi^+$			
$K_S^0(1430)^+ \pi^-, K_S^{*0} \rightarrow$	[w] < 1.4 × 10 ⁻⁵	CL=95%	-
$K_S^0 \pi^+$			

Meson Summary Table

				Fractions of some of the following modes with resonances have already appeared above as submodes of particular charged-particle modes. These nine modes below are all corrected for unseen decays of the resonances.			
$K_2^*(1430)^+ \pi^-, K_2^{*+} \rightarrow$	$[w] < 3.4$	$\times 10^{-5}$	CL=95%	-			
$K_S^0 \pi^+ \pi^-$							
$K_S^0 \pi^+ \pi^-$ nonresonant	$(2.5 \pm 6.0 / 1.6) \times 10^{-4}$			842	$K_S^0 \eta$	$(5.09 \pm 0.13) \times 10^{-3}$	772
$K^- \pi^+ \pi^0$	$[jj] (14.4 \pm 0.5) \%$		S=2.0	844	$K_S^0 \omega$	$(1.11 \pm 0.06) \%$	670
$K^- \rho^+$	$(11.2 \pm 0.7) \%$			675	$K_S^0 \eta'(958)$	$(9.49 \pm 0.32) \times 10^{-3}$	565
$K^- \rho(1700)^+, \rho^+ \rightarrow \pi^+ \pi^0$	$(8.2 \pm 1.8) \times 10^{-3}$			†	$\overline{K}^*(892)^0 \pi^+ \pi^- \pi^0$	$(1.9 \pm 0.9) \%$	643
$K^*(892)^- \pi^+, K^*(892)^- \rightarrow$	$(2.31 \pm 0.40 / 0.20) \%$			711	$\overline{K}^*(892)^0 \eta$	$(1.41 \pm 0.12) \%$	583
$K^- \pi^+ \pi^0$					$K^- \pi^+ \omega$	$(3.1 \pm 0.6) \%$	605
$\overline{K}^*(892)^0 \pi^0, \overline{K}^*(892)^0 \rightarrow$	$(1.95 \pm 0.24) \%$			711	$\overline{K}^*(892)^0 \omega$	$(1.1 \pm 0.5) \%$	410
$K^- \pi^+ \pi^0$					$K^- \pi^+ \eta'(958)$	$(6.43 \pm 0.34) \times 10^{-3}$	479
$K_0^*(1430)^- \pi^+, K_0^{*-} \rightarrow$	$(4.8 \pm 2.2) \times 10^{-3}$			378	$K_S^0 \eta'(958) \pi^0$	$(2.52 \pm 0.27) \times 10^{-3}$	479
$K^- \pi^0$					$\overline{K}^*(892)^0 \eta'(958)$	$< 1.0 \times 10^{-3}$	CL=90% 119
$\overline{K}_0^*(1430)^0 \pi^0, \overline{K}_0^{*0} \rightarrow$	$(5.9 \pm 5.0 / 1.6) \times 10^{-3}$			379			
$K^- \pi^+$							
$K^*(1680)^- \pi^+, K^{*-} \rightarrow$	$(1.9 \pm 0.7) \times 10^{-3}$			46	Hadronic modes with three K's		
$K^- \pi^0$					$K_S^0 K^+ K^-$	$(4.42 \pm 0.32) \times 10^{-3}$	544
$K^- \pi^+ \pi^0$ nonresonant	$(1.15 \pm 0.60 / 0.20) \%$			844	$K_S^0 a_0(980)^0, a_0^0 \rightarrow K^+ K^-$	$(2.9 \pm 0.4) \times 10^{-3}$	-
$K_S^0 2\pi^0$	$(9.1 \pm 1.1) \times 10^{-3}$		S=2.2	843	$K^- a_0(980)^+, a_0^+ \rightarrow$	$(5.9 \pm 1.8) \times 10^{-4}$	-
$K_S^0(2\pi^0)_{S\text{-wave}}$	$(2.6 \pm 0.7) \times 10^{-3}$			-	$K^+ K_S^0$		
$\overline{K}^*(892)^0 \pi^0, \overline{K}^{*0} \rightarrow K_S^0 \pi^0$	$(8.1 \pm 0.7) \times 10^{-3}$			711	$K^+ a_0(980)^-, a_0^- \rightarrow$	$< 1.1 \times 10^{-4}$	CL=95% -
$\overline{K}^*(1430)^0 \pi^0, \overline{K}^{*0} \rightarrow$	$(4 \pm 23) \times 10^{-5}$			-	$K^- K_S^0$		
$K_S^0 \pi^0$					$K^0 f_0(980), f_0 \rightarrow K^+ K^-$	$< 9 \times 10^{-5}$	CL=95% -
$\overline{K}^*(1680)^0 \pi^0, \overline{K}^{*0} \rightarrow$	$(1.0 \pm 0.4) \times 10^{-3}$			-	$K_S^0 \phi, \phi \rightarrow K^+ K^-$	$(2.03 \pm 0.15) \times 10^{-3}$	520
$K_S^0 \pi^0$					$K_S^0 f_0(1370), f_0 \rightarrow K^+ K^-$	$(1.7 \pm 1.1) \times 10^{-4}$	-
$K_S^0 f_2(1270), f_2 \rightarrow 2\pi^0$	$(2.3 \pm 1.1) \times 10^{-4}$			-	$3K_S^0$	$(7.5 \pm 0.7) \times 10^{-4}$	S=1.4 539
$2K_S^0, \text{one } K_S^0 \rightarrow 2\pi^0$	$(3.2 \pm 1.1) \times 10^{-4}$			-	$K^+ 2K^- \pi^+$	$(2.25 \pm 0.32) \times 10^{-4}$	434
$K^- 2\pi^+ \pi^-$	$[jj] (8.22 \pm 0.14) \%$		S=1.1	813	$K^+ K^- \overline{K}^*(892)^0, \overline{K}^{*0} \rightarrow$	$(4.5 \pm 1.8) \times 10^{-5}$	†
$K^- \pi^+ \rho^0$ total	$(6.87 \pm 0.31) \%$			609	$K^- \pi^+$		
$K^- \pi^+ \rho^0$ 3-body	$(6.1 \pm 1.6) \times 10^{-3}$			609	$K^- \pi^+ \phi, \phi \rightarrow K^+ K^-$	$(4.0 \pm 1.7) \times 10^{-5}$	422
$\overline{K}^*(892)^0 \rho^0, \overline{K}^{*0} \rightarrow$	$(1.01 \pm 0.05) \%$			416	$\phi \overline{K}^*(892)^0, \phi \rightarrow K^+ K^-,$	$(1.08 \pm 0.21) \times 10^{-4}$	†
$K^- \pi^+$					$\overline{K}^{*0} \rightarrow K^- \pi^+$		
$\overline{K}^*(892)^0 \rho^0$ transverse,	$(1.2 \pm 0.4) \%$			417	$K^+ 2K^- \pi^+$ nonresonant	$(3.4 \pm 1.5) \times 10^{-5}$	434
$\overline{K}^{*0} \rightarrow K^- \pi^+$					$2K_S^0 K^\pm \pi^\mp$	$(5.9 \pm 1.3) \times 10^{-4}$	427
$K^- a_1(1260)^+, a_1^+ \rightarrow$	$(4.32 \pm 0.32) \%$			327			
$\rho^0 \pi^+$							
$K_1(1270)^- \pi^+, K_1^- \rightarrow$	$(3.9 \pm 0.4) \times 10^{-3}$			-	Pionic modes		
$K^- \pi^+ \pi^-$ total					$\pi^+ \pi^-$	$(1.454 \pm 0.024) \times 10^{-3}$	S=1.4 922
$K_1(1270)^- \pi^+, K_1^- \rightarrow$	$(6.6 \pm 2.3) \times 10^{-4}$			484	$2\pi^0$	$(8.26 \pm 0.25) \times 10^{-4}$	923
$\overline{K}^*(892)^0 \pi^-, \overline{K}^{*0} \rightarrow$					$\pi^+ \pi^- \pi^0$	$(1.49 \pm 0.06) \%$	S=2.1 907
$K^- \pi^+$					$\rho^+ \pi^-$	$(1.01 \pm 0.04) \%$	764
$K^- 2\pi^+ \pi^-$ nonresonant	$(1.81 \pm 0.07) \%$			813	$\rho^0 \pi^0$	$(3.86 \pm 0.23) \times 10^{-3}$	764
$K_S^0 \pi^+ \pi^- \pi^0$	$[xx] (5.2 \pm 0.6) \%$			813	$\rho^- \pi^+$	$(5.15 \pm 0.25) \times 10^{-3}$	764
$K_S^0 \eta, \eta \rightarrow \pi^+ \pi^- \pi^0$	$(1.17 \pm 0.03) \times 10^{-3}$			772	$\rho(1450)^+ \pi^-, \rho^+ \rightarrow \pi^+ \pi^0$	$(1.6 \pm 2.1) \times 10^{-5}$	-
$K_S^0 \omega, \omega \rightarrow \pi^+ \pi^- \pi^0$	$(9.9 \pm 0.6) \times 10^{-3}$			670	$\rho(1450)^0 \pi^0, \rho^0 \rightarrow \pi^+ \pi^-$	$(4.5 \pm 2.0) \times 10^{-5}$	-
$K^- \pi^+ 2\pi^0$	$(8.86 \pm 0.23) \%$			815	$\rho(1450)^- \pi^+, \rho^- \rightarrow \pi^- \pi^0$	$(2.7 \pm 0.4) \times 10^{-4}$	-
$K^- 2\pi^+ \pi^- \pi^0$	$(4.3 \pm 0.4) \%$			771	$\rho(1700)^+ \pi^-, \rho^+ \rightarrow \pi^+ \pi^0$	$(6.1 \pm 1.5) \times 10^{-4}$	-
$\overline{K}^*(892)^0 \pi^+ \pi^- \pi^0, \overline{K}^{*0} \rightarrow$	$(1.3 \pm 0.6) \%$			643	$\rho(1700)^0 \pi^0, \rho^0 \rightarrow \pi^+ \pi^-$	$(7.4 \pm 1.8) \times 10^{-4}$	-
$K^- \pi^+$					$\rho(1700)^- \pi^+, \rho^- \rightarrow \pi^- \pi^0$	$(4.8 \pm 1.1) \times 10^{-4}$	-
$K^- \pi^+ \omega, \omega \rightarrow \pi^+ \pi^- \pi^0$	$(2.8 \pm 0.5) \%$			605	$f_0(980) \pi^0, f_0 \rightarrow \pi^+ \pi^-$	$(3.7 \pm 0.9) \times 10^{-5}$	-
$\overline{K}^*(892)^0 \omega, \overline{K}^{*0} \rightarrow$	$(6.5 \pm 3.0) \times 10^{-3}$			410	$f_0(500) \pi^0, f_0 \rightarrow \pi^+ \pi^-$	$(1.22 \pm 0.22) \times 10^{-4}$	-
$K^- \pi^+, \omega \rightarrow$					$f_0(1370) \pi^0, f_0 \rightarrow \pi^+ \pi^-$	$(5.5 \pm 2.1) \times 10^{-5}$	-
$\pi^+ \pi^- \pi^0$					$f_0(1500) \pi^0, f_0 \rightarrow \pi^+ \pi^-$	$(5.8 \pm 1.6) \times 10^{-5}$	-
$K_S^0 \eta \pi^0$	$(1.01 \pm 0.05) \%$			721	$f_0(1710) \pi^0, f_0 \rightarrow \pi^+ \pi^-$	$(4.6 \pm 1.6) \times 10^{-5}$	-
$K_S^0 a_0(980), a_0 \rightarrow \eta \pi^0$	$(1.20 \pm 0.28) \%$			-	$f_2(1270) \pi^0, f_2 \rightarrow \pi^+ \pi^-$	$(1.97 \pm 0.21) \times 10^{-4}$	-
$\overline{K}^*(892)^0 \eta, \overline{K}^{*0} \rightarrow K_S^0 \pi^0$	$(2.9 \pm 0.7) \times 10^{-3}$			-	$\pi^+ \pi^- \pi^0$ nonresonant	$(1.3 \pm 0.4) \times 10^{-4}$	907
$K^- \pi^+ \eta$	$(1.88 \pm 0.05) \%$		S=1.4	721	$3\pi^0$	$(2.0 \pm 0.5) \times 10^{-4}$	908
$K^*(892)^0 \eta, K^{*0} \rightarrow K^- \pi^+$	$(8.9 \pm 0.8 / 0.6) \times 10^{-3}$			-	$2\pi^+ 2\pi^-$	$(7.56 \pm 0.20) \times 10^{-3}$	880
$a_0(980)^+ K^-, a_0^+ \rightarrow \eta \pi^+$	$(7.4 \pm 0.9 / 0.7) \times 10^{-3}$			-	$a_1(1260)^+ \pi^-, a_1^+ \rightarrow$	$(4.53 \pm 0.31) \times 10^{-3}$	-
$K_2^*(1980)^- \pi^+, K_2^{*-} \rightarrow$	$(2.2 \pm 1.7 / 1.9) \times 10^{-4}$			-	$2\pi^+ \pi^-$ total		
$K^- \eta$					$a_1(1260)^+ \pi^-, a_1^+ \rightarrow$	$(3.13 \pm 0.21) \times 10^{-3}$	-
$K^- \pi^+ \pi^0 \eta$	$(4.49 \pm 0.27) \times 10^{-3}$			656	$\rho^0 \pi^+ S\text{-wave}$		
$K_S^0 \pi^+ \pi^- \eta$	$(2.80 \pm 0.21) \times 10^{-3}$			651	$a_1(1260)^+ \pi^-, a_1^+ \rightarrow$	$(1.9 \pm 0.5) \times 10^{-4}$	-
$K_S^0 2\pi^0 \eta$	$(1.76 \pm 0.26) \times 10^{-3}$			656	$\rho^0 \pi^+ D\text{-wave}$		
$K_S^0 2\pi^+ 2\pi^-$	$(2.66 \pm 0.30) \times 10^{-3}$			768	$a_1(1260)^+ \pi^-, a_1^+ \rightarrow$	$(6.4 \pm 0.7) \times 10^{-4}$	-
$K_S^0 \rho^0 \pi^+ \pi^-, \text{no } K^*(892)^-$	$(1.1 \pm 0.7) \times 10^{-3}$			-	$\sigma \pi^+$		
$K^*(892)^- 2\pi^+ \pi^-,$	$(5 \pm 7) \times 10^{-4}$			642	$a_1(1260)^- \pi^+, a_1^- \rightarrow$	$(2.3 \pm 0.9) \times 10^{-4}$	-
$K^*(892)^- \rightarrow K_S^0 \pi^-,$					$\rho^0 \pi^- S\text{-wave}$		
$\text{no } \rho^0$					$a_1(1260)^- \pi^+, a_1^- \rightarrow \sigma \pi^-$	$(6.0 \pm 3.4) \times 10^{-5}$	-
$K^*(892)^- \rho^0 \pi^+,$	$(1.6 \pm 0.6) \times 10^{-3}$			230	$\pi(1300)^+ \pi^-, \pi(1300)^+ \rightarrow$	$(5.1 \pm 2.7) \times 10^{-4}$	-
$K^*(892)^- \rightarrow K_S^0 \pi^-$					$\sigma \pi^+$		
$K_S^0 2\pi^+ 2\pi^-$ nonresonant	$< 1.2 \times 10^{-3}$		CL=90%	768	$\pi(1300)^- \pi^+, \pi(1300)^- \rightarrow$	$(2.3 \pm 2.2) \times 10^{-4}$	-
$K^- 3\pi^+ 2\pi^-$	$(2.2 \pm 0.6) \times 10^{-4}$			713	$\sigma \pi^-$		
					$a_1(1640)^+ \pi^-, a_1^+ \rightarrow$	$(3.2 \pm 1.6) \times 10^{-4}$	-
					$\rho^0 \pi^+ D\text{-wave}$		
					$a_1(1640)^+ \pi^-, a_1^+ \rightarrow \sigma \pi^+$	$(1.8 \pm 1.4) \times 10^{-4}$	-
					$\pi_2(1670)^+ \pi^-, \pi_2^+ \rightarrow$	$(2.0 \pm 0.9) \times 10^{-4}$	-
					$f_2(1270)^0 \pi^+, f_2^0 \rightarrow$		
					$\pi^+ \pi^-$		

Meson Summary Table

$\pi_2(1670)^+ \pi^-, \pi_2^+ \rightarrow \sigma \pi^+$	$(2.6 \pm 1.0) \times 10^{-4}$	-	$K^*(892)^- K^+, K^*(892)^- \rightarrow$	$(5.4 \pm 0.4) \times 10^{-4}$	-
$2\rho^0$ total	$(1.85 \pm 0.13) \times 10^{-3}$	518	$K^- \pi^0$		
$2\rho^0$, parallel helicities	$(8.3 \pm 3.2) \times 10^{-5}$	-	$(K^+ \pi^0)_{S\text{-wave}} K^-$	$(2.43 \pm 0.18) \times 10^{-3}$	743
$2\rho^0$, perpendicular helicities	$(4.8 \pm 0.6) \times 10^{-4}$	-	$(K^- \pi^0)_{S\text{-wave}} K^+$	$(1.3 \pm 0.5) \times 10^{-4}$	743
$2\rho^0$, longitudinal helicities	$(1.27 \pm 0.10) \times 10^{-3}$	-	$f_0(980) \pi^0, f_0 \rightarrow K^+ K^-$	$(3.6 \pm 0.6) \times 10^{-4}$	-
$2\rho(770)^0$, S-wave	$(1.8 \pm 1.3) \times 10^{-4}$	-	$\phi \pi^0, \phi \rightarrow K^+ K^-$	$(6.6 \pm 0.4) \times 10^{-4}$	-
$2\rho(770)^0$, P-wave	$(5.3 \pm 1.3) \times 10^{-4}$	-	$2K_S^0 \pi^0$	$< 5.9 \times 10^{-4}$	740
$2\rho(770)^0$, D-wave	$(6.2 \pm 3.0) \times 10^{-4}$	-	$K^+ K^- \eta$	$(5.9 \pm 1.9) \times 10^{-5}$	514
Resonant $(\pi^+ \pi^-) \pi^+ \pi^-$	$(1.51 \pm 0.12) \times 10^{-3}$	-	$\phi(1020) \eta$	$(1.84 \pm 0.12) \times 10^{-4}$	489
3-body total		-	$K^+ K^- \eta$ nonresonant	$(9.9 \pm 0.9) \times 10^{-5}$	514
$\sigma \pi^+ \pi^-$	$(6.2 \pm 0.9) \times 10^{-4}$	-	$2K_S^0 \eta$	$(1.3 \pm 0.6) \times 10^{-4}$	508
$\sigma \rho(770)^0$	$(5.0 \pm 2.5) \times 10^{-4}$	-	$K^+ K^- \pi^0 \pi^0$	$(6.9 \pm 0.8) \times 10^{-4}$	681
$f_0(980) \pi^+ \pi^-, f_0 \rightarrow$	$(1.8 \pm 0.5) \times 10^{-4}$	-	$K^+ K^- \pi^+ \pi^-$	$(2.47 \pm 0.11) \times 10^{-3}$	677
$\pi^+ \pi^-$		-	$\phi(\pi^+ \pi^-)_{S\text{-wave}}, \phi \rightarrow$	$(10 \pm 5) \times 10^{-5}$	614
$f_2(1270) \pi^+ \pi^-, f_2 \rightarrow$	$(3.7 \pm 0.6) \times 10^{-4}$	-	$K^+ K^-$		
$\pi^+ \pi^-$		-	$(\phi \rho^0)_{S\text{-wave}}, \phi \rightarrow K^+ K^-$	$(6.9 \pm 0.6) \times 10^{-4}$	250
$2f_2(1270), f_2 \rightarrow \pi^+ \pi^-$	$(1.6 \pm 1.8) \times 10^{-4}$	-	$(\phi \rho^0)_{P\text{-wave}}, \phi \rightarrow K^+ K^-$	$(4.0 \pm 1.9) \times 10^{-5}$	-
$f_0(1370) \sigma, f_0 \rightarrow$	$(1.6 \pm 0.5) \times 10^{-3}$	-	$(\phi \rho^0)_{D\text{-wave}}, \phi \rightarrow K^+ K^-$	$(4.2 \pm 1.4) \times 10^{-5}$	-
$\pi^+ \pi^-$		-	$(K^*(892)^0 \bar{K}^*(892)^0)_{S\text{-wave}},$	$(2.24 \pm 0.13) \times 10^{-4}$	-
$\pi^+ \pi^- 2\pi^0$	$(1.02 \pm 0.09) \%$	882	$K^* \rightarrow K^\pm \pi^\mp$		
$\eta \pi^0$ [yy]	$(6.3 \pm 0.6) \times 10^{-4}$	S=1.1 846	$(K^*(892)^0 \bar{K}^*(892)^0)_{P\text{-wave}},$	$(1.20 \pm 0.08) \times 10^{-4}$	-
$\omega \pi^0$ [yy]	$(1.17 \pm 0.35) \times 10^{-4}$	761	$K^* \rightarrow K^\pm \pi^\mp$		
$\omega \eta$	$(1.98 \pm 0.18) \times 10^{-3}$	S=1.1 648	$(K^*(892)^0 \bar{K}^*(892)^0)_{D\text{-wave}},$	$(4.7 \pm 0.4) \times 10^{-5}$	-
$2\pi^+ 2\pi^- \pi^0$	$(4.2 \pm 0.5) \times 10^{-3}$	844	$K^* \rightarrow K^\pm \pi^\mp$		
$\eta \pi^+ \pi^-$ [yy]	$(1.16 \pm 0.07) \times 10^{-3}$	827	$K^*(892)^0 (K^- \pi^+)_{S\text{-wave}}$	$(1.4 \pm 0.6) \times 10^{-4}$	-
$\omega \pi^+ \pi^-$ [yy]	$(1.33 \pm 0.20) \times 10^{-3}$	738	3-body, $K^* \rightarrow K^+ \pi^-$		
$\omega \pi^0 \pi^0$	$< 1.10 \times 10^{-3}$	CL=90% 740	$K_1(1270)^+ K^-, K_1^+ \rightarrow$	$(1.4 \pm 0.9) \times 10^{-4}$	-
$\eta 2\pi^0$	$(3.8 \pm 1.3) \times 10^{-4}$	829	$K^* \pi^+$		
$\pi^+ \pi^- \pi^0 \eta$	$(3.23 \pm 0.22) \times 10^{-3}$	797	$K_1(1270)^+ K^-, K_1^+ \rightarrow$	$(1.5 \pm 0.5) \times 10^{-4}$	-
$3\pi^+ 3\pi^-$	$(4.3 \pm 1.2) \times 10^{-4}$	795	$K^*(1430)^0 \pi^+, K^* \rightarrow$		
$\eta'(958) \pi^0$	$(9.2 \pm 1.0) \times 10^{-4}$	678	$K^+ \pi^-$		
$\eta'(958) \pi^+ \pi^-$	$(4.5 \pm 1.7) \times 10^{-4}$	650	$K_1(1270)^+ K^-, K_1^+ \rightarrow$	$(2.2 \pm 0.6) \times 10^{-4}$	-
2η	$(2.11 \pm 0.19) \times 10^{-3}$	S=2.2 754	$\rho^0 K^+$		
$2\eta \pi^0$	$(7.3 \pm 2.2) \times 10^{-4}$	699	$K_1(1270)^+ K^-, K_1^+ \rightarrow$	$(1.5 \pm 1.2) \times 10^{-5}$	-
3η	$< 1.3 \times 10^{-4}$	CL=90% 421	$\omega(782) K^+, \omega \rightarrow \pi^+ \pi^-$		
$\eta \eta'(958)$	$(1.01 \pm 0.19) \times 10^{-3}$	537	$K_1(1270)^- K^+, K_1^- \rightarrow$	$(1.3 \pm 0.4) \times 10^{-4}$	-
Hadronic modes with a $K\bar{K}$ pair					
$K^+ K^-$	$(4.08 \pm 0.06) \times 10^{-3}$	S=1.6 791	$\rho^0 K^-$		
$2K_S^0$	$(1.41 \pm 0.05) \times 10^{-4}$	S=1.1 789	$K_1(1400)^+ K^-, K_1^+ \rightarrow$	$(4.6 \pm 0.4) \times 10^{-4}$	-
$K_S^0 K^- \pi^+$	$(3.3 \pm 0.5) \times 10^{-3}$	S=1.1 739	$K^*(892)^0 \pi^+, K^* \rightarrow$		
$\bar{K}^*(892)^0 K_S^0, \bar{K}^{*0} \rightarrow$	$(8.2 \pm 1.6) \times 10^{-5}$	608	$K^+ \pi^-$		
$K^*(892)^+ K^-, K^* \rightarrow$	$(1.89 \pm 0.30) \times 10^{-3}$	-	$K^*(1410)^- K^+, K^* \rightarrow$	$(7.0 \pm 1.1) \times 10^{-5}$	-
$K_S^0 \pi^+$		-	$K^* \pi^-$		
$\bar{K}^*(1410)^0 K_S^0, \bar{K}^{*0} \rightarrow$	$(1.3 \pm 1.9) \times 10^{-4}$	-	$K_1(1680)^+ K^-, K_1^+ \rightarrow$	$(8.9 \pm 3.2) \times 10^{-5}$	-
$K^*(1410)^+ K^-, K^* \rightarrow$	$(3.2 \pm 1.9) \times 10^{-4}$	-	$K^* \pi^+, K^* \rightarrow K^+ \pi^-$		
$K_S^0 \pi^+$		-	$K^+ K^- \pi^+ \pi^-$ non-resonant	$(2.7 \pm 0.6) \times 10^{-4}$	-
$(K^- \pi^+)_{S\text{-wave}} K_S^0$	$(6.0 \pm 2.9) \times 10^{-4}$	739	$2K_S^0 \pi^+ \pi^-$	$(5.3 \pm 0.9) \times 10^{-4}$	673
$(K_S^0 \pi^+)_{S\text{-wave}} K^-$	$(3.9 \pm 1.0) \times 10^{-4}$	739	$K_S^0 K^- \pi^+ \pi^0$	$(1.32 \pm 0.16) \times 10^{-3}$	677
$a_0(980)^- \pi^+, a_0^- \rightarrow K_S^0 K^-$	$(1.3 \pm 1.4) \times 10^{-4}$	-	$K_S^0 K^+ \pi^- \pi^0$	$(6.5 \pm 0.7) \times 10^{-4}$	677
$a_0(1450)^- \pi^+, a_0^- \rightarrow$	$(2.5 \pm 2.0) \times 10^{-5}$	-	$K_S^0 K^- 2\pi^+ \pi^-$	$< 1.4 \times 10^{-4}$	CL=90% 595
$K_S^0 K^-$		-	$K^+ K^- \pi^+ \pi^- \pi^0$	$(3.1 \pm 2.0) \times 10^{-3}$	600
$a_2(1320)^- \pi^+, a_2^- \rightarrow$	$(5 \pm 5) \times 10^{-6}$	-	Other $K\bar{K}X$ modes. They include all decay modes of the $\phi, \eta,$ and ω .		
$K_S^0 K^-$		-	$\phi \pi^0$	$(1.17 \pm 0.04) \times 10^{-3}$	645
$\rho(1450)^- \pi^+, \rho^- \rightarrow K_S^0 K^-$	$(4.6 \pm 2.5) \times 10^{-5}$	-	$\phi \eta$	$(1.8 \pm 0.5) \times 10^{-4}$	489
$K_S^0 K^+ \pi^-$		-	$\phi \omega$	$(6.5 \pm 1.0) \times 10^{-4}$	238
$K_S^*(892)^0 K_S^0, K^* \rightarrow$	$(1.12 \pm 0.21) \times 10^{-4}$	608	Radiative modes		
$K^+ \pi^-$		-	$\rho^0 \gamma$	$(1.82 \pm 0.32) \times 10^{-5}$	771
$K^*(892)^- K^+, K^* \rightarrow$	$(6.2 \pm 1.0) \times 10^{-4}$	-	$\omega \gamma$	$< 2.4 \times 10^{-4}$	CL=90% 768
$K_S^0 \pi^-$		-	$\phi \gamma$	$(2.81 \pm 0.19) \times 10^{-5}$	654
$K^*(1410)^0 K_S^0, K^* \rightarrow$	$(5 \pm 8) \times 10^{-5}$	-	$\bar{K}^*(892)^0 \gamma$	$(4.1 \pm 0.7) \times 10^{-4}$	719
$K^+ \pi^+$		-	Doubly Cabibbo suppressed (DC) modes or $\Delta C = 2$ forbidden via mixing ($C2M$) modes		
$K^*(1410)^- K^+, K^* \rightarrow$	$(2.6 \pm 2.0) \times 10^{-4}$	-	$K^+ \ell^- \bar{\nu}_\ell$ via \bar{D}^0	$< 2.2 \times 10^{-5}$	CL=90% -
$K_S^0 \pi^-$		-	K^+ or $K^*(892)^+ e^- \bar{\nu}_e$ via \bar{D}^0	$< 6 \times 10^{-5}$	CL=90% -
$(K^+ \pi^-)_{S\text{-wave}} K_S^0$	$(3.7 \pm 1.9) \times 10^{-4}$	739	$K^+ \pi^-$ DC	$(1.50 \pm 0.07) \times 10^{-4}$	S=3.0 861
$(K_S^0 \pi^-)_{S\text{-wave}} K^+$	$(1.4 \pm 0.6) \times 10^{-4}$	739	$K^+ \pi^-$ via DCS	$(1.363 \pm 0.025) \times 10^{-4}$	-
$a_0(980)^+ \pi^-, a_0^+ \rightarrow K_S^0 K^+$	$(6 \pm 4) \times 10^{-4}$	-	$K^+ \pi^-$ via \bar{D}^0	$< 1.6 \times 10^{-5}$	CL=95% 861
$a_0(1450)^+ \pi^-, a_0^+ \rightarrow$	$(3.2 \pm 2.5) \times 10^{-5}$	-	$K_S^0 \pi^+ \pi^-$ in $D^0 \rightarrow \bar{D}^0$	$< 1.8 \times 10^{-4}$	CL=95% -
$K_S^0 K^+$		-	$K^*(892)^+ \pi^-, K^* \rightarrow$ DC	$(1.13 \pm 0.60) \times 10^{-4}$	711
$\rho(1700)^+ \pi^-, \rho^+ \rightarrow K_S^0 K^+$	$(1.1 \pm 0.6) \times 10^{-5}$	-	$K_S^0 \pi^+$		
$K^+ K^- \pi^0$	$(3.42 \pm 0.14) \times 10^{-3}$	743	$K_0^*(1430)^+ \pi^-, K_0^* \rightarrow$ DC	$< 1.4 \times 10^{-5}$	-
$K^*(892)^+ K^-, K^*(892)^+ \rightarrow$	$(1.52 \pm 0.07) \times 10^{-3}$	-	$K_S^0 \pi^+$		
$K^+ \pi^0$		-	$K_2^*(1430)^+ \pi^-, K_2^* \rightarrow$ DC	$< 3.4 \times 10^{-5}$	-
		-	$K_S^0 \pi^+$		

Meson Summary Table

$K^+ \pi^- \pi^0$	DC	$(3.05 \pm 0.15) \times 10^{-4}$	844
$K^+ \pi^- \pi^0$ via \overline{D}^0		$(7.6 \pm_{-0.6}^{+0.5}) \times 10^{-4}$	-
$K^+ \pi^+ 2\pi^-$ via DC		$(2.49 \pm 0.07) \times 10^{-4}$	-
$K^+ \pi^+ 2\pi^-$	DC	$(2.65 \pm 0.06) \times 10^{-4}$	813
$K^+ \pi^+ 2\pi^-$ via \overline{D}^0		$(7.9 \pm 3.0) \times 10^{-6}$	812
μ^- anything via \overline{D}^0		$< 4 \times 10^{-4}$	CL=90%

**$\Delta C = 1$ weak neutral current (CI) modes,
Lepton Family number (LF) violating modes,
Lepton (L) or Baryon (B) number violating modes**

$\gamma\gamma$	CI	$< 8.5 \times 10^{-7}$	CL=90%	932
e^+e^-	CI	$< 7.9 \times 10^{-8}$	CL=90%	932
$\mu^+\mu^-$	CI	$< 6.2 \times 10^{-9}$	CL=90%	926
$\pi^0 e^+e^-$	CI	$< 4 \times 10^{-6}$	CL=90%	928
$\pi^0 \mu^+\mu^-$	CI	$< 1.8 \times 10^{-4}$	CL=90%	915
ηe^+e^-	CI	$< 3 \times 10^{-6}$	CL=90%	852
$\eta \mu^+\mu^-$	CI	$< 5.3 \times 10^{-4}$	CL=90%	838
$\pi^+ \pi^- e^+e^-$	CI	$< 7 \times 10^{-6}$	CL=90%	922
$\rho^0 e^+e^-$	CI	$< 1.0 \times 10^{-4}$	CL=90%	771
$\pi^+ \pi^- \mu^+\mu^-$	CI	$(9.6 \pm 1.2) \times 10^{-7}$		894
$\pi^+ \pi^- \mu^+\mu^-$ (non-res)		$< 5.5 \times 10^{-7}$	CL=90%	-
$\rho^0 \mu^+\mu^-$	CI	$< 2.2 \times 10^{-5}$	CL=90%	754
ωe^+e^-	CI	$< 6 \times 10^{-6}$	CL=90%	768
$\omega \mu^+\mu^-$	CI	$< 8.3 \times 10^{-4}$	CL=90%	751
$K^- K^+ e^+e^-$	CI	$< 1.1 \times 10^{-5}$	CL=90%	791
ϕe^+e^-	CI	$< 5.2 \times 10^{-5}$	CL=90%	654
$K^- K^+ \mu^+\mu^-$	CI	$(1.54 \pm 0.32) \times 10^{-7}$		710
$K^- K^+ \mu^+\mu^-$ (non-res)		$< 3.3 \times 10^{-5}$	CL=90%	-
$\phi \mu^+\mu^-$	CI	$< 3.1 \times 10^{-5}$	CL=90%	631
$\overline{K}^0 e^+e^-$	[pp]	$< 2.4 \times 10^{-5}$	CL=90%	866
$\overline{K}^0 \mu^+\mu^-$	[pp]	$< 2.6 \times 10^{-4}$	CL=90%	852
$K^- \pi^+ e^+e^-$, 675 < $m_{ee} < 875$ MeV		$(4.0 \pm 0.5) \times 10^{-6}$		-
$K^- \pi^+ e^+e^-$, 1.005 < $m_{ee} < 1.035$ GeV		$< 5 \times 10^{-7}$	CL=90%	-
$\overline{K}^*(892)^0 e^+e^-$	[pp]	$< 4.7 \times 10^{-5}$	CL=90%	719
$K^- \pi^+ \mu^+\mu^-$	CI	$< 3.59 \times 10^{-4}$	CL=90%	829
$K^- \pi^+ \mu^+\mu^-$, 675 < $m_{\mu\mu} < 875$ MeV		$(4.2 \pm 0.4) \times 10^{-6}$		-
$\overline{K}^*(892)^0 \mu^+\mu^-$	[pp]	$< 2.4 \times 10^{-5}$	CL=90%	700
$\pi^+ \pi^- \pi^0 \mu^+\mu^-$	CI	$< 8.1 \times 10^{-4}$	CL=90%	863
$\mu^\pm e^\mp$	LF [aa]	$< 1.3 \times 10^{-8}$	CL=90%	929
$\pi^0 e^\pm \mu^\mp$	LF [aa]	$< 8.0 \times 10^{-7}$	CL=90%	924
$\eta e^\pm \mu^\mp$	LF [aa]	$< 2.25 \times 10^{-6}$	CL=90%	848
$\pi^+ \pi^- e^\pm \mu^\mp$	LF [aa]	$< 1.71 \times 10^{-6}$	CL=90%	911
$\rho^0 e^\pm \mu^\mp$	LF [aa]	$< 5.0 \times 10^{-7}$	CL=90%	767
$\omega e^\pm \mu^\mp$	LF [aa]	$< 1.71 \times 10^{-6}$	CL=90%	764
$K^- K^+ e^\pm \mu^\mp$	LF [aa]	$< 1.00 \times 10^{-6}$	CL=90%	754
$\phi e^\pm \mu^\mp$	LF [aa]	$< 5.1 \times 10^{-7}$	CL=90%	648
$\overline{K}^0 e^\pm \mu^\mp$	LF [aa]	$< 1.74 \times 10^{-6}$	CL=90%	863
$K^- \pi^+ e^\pm \mu^\mp$	LF [aa]	$< 1.90 \times 10^{-6}$	CL=90%	848
$\overline{K}^*(892)^0 e^\pm \mu^\mp$	LF [aa]	$< 1.25 \times 10^{-6}$	CL=90%	714
$2\pi^- 2e^+$	L	$< 9.1 \times 10^{-7}$	CL=90%	922
$2\pi^- 2\mu^+$	L	$< 1.52 \times 10^{-6}$	CL=90%	894
$K^- \pi^- 2e^+$	L	$< 5.0 \times 10^{-7}$	CL=90%	861
$K^- \pi^- 2\mu^+$	L	$< 5.3 \times 10^{-7}$	CL=90%	829
$2K^- 2e^+$	L	$< 3.4 \times 10^{-7}$	CL=90%	791
$2K^- 2\mu^+$	L	$< 1.0 \times 10^{-7}$	CL=90%	710
$\pi^- \pi^- e^+ \mu^+$	L	$< 3.06 \times 10^{-6}$	CL=90%	911
$K^- \pi^- e^+ \mu^+$	L	$< 2.10 \times 10^{-6}$	CL=90%	848
$2K^- e^+ \mu^+$	L	$< 5.8 \times 10^{-7}$	CL=90%	754
$p e^-$	L,B [zz]	$< 1.0 \times 10^{-5}$	CL=90%	696
$\overline{p} e^+$	L,B [aa]	$< 1.1 \times 10^{-5}$	CL=90%	696

 $D^*(2007)^0$

$$I(J^P) = \frac{1}{2}(1^-)$$

I, J, P need confirmation.

Mass $m = 2006.85 \pm 0.05$ MeV ($S = 1.1$)
 $m_{D^{*0}} - m_{D^0} = 142.014 \pm 0.030$ MeV ($S = 1.5$)
 Full width $\Gamma < 2.1$ MeV, CL = 90%

$\overline{D}^*(2007)^0$ modes are charge conjugates of modes below.

$D^*(2007)^0$ DECAY MODES	Fraction (Γ_i/Γ)	ρ (MeV/c)
$D^0 \pi^0$	$(64.7 \pm 0.9) \%$	43
$D^0 \gamma$	$(35.3 \pm 0.9) \%$	137
$D^0 e^+ e^-$	$(3.91 \pm 0.33) \times 10^{-3}$	137

 $D^*(2010)^\pm$

$$I(J^P) = \frac{1}{2}(1^-)$$

I, J, P need confirmation.

Mass $m = 2010.26 \pm 0.05$ MeV
 $m_{D^*(2010)^+} - m_{D^+} = 140.603 \pm 0.015$ MeV
 $m_{D^*(2010)^-} - m_{D^0} = 145.4258 \pm 0.0017$ MeV
 Full width $\Gamma = 83.4 \pm 1.8$ keV

$D^*(2010)^-$ modes are charge conjugates of the modes below.

$D^*(2010)^\pm$ DECAY MODES	Fraction (Γ_i/Γ)	ρ (MeV/c)
$D^0 \pi^+$	$(67.7 \pm 0.5) \%$	39
$D^+ \pi^0$	$(30.7 \pm 0.5) \%$	38
$D^+ \gamma$	$(1.6 \pm 0.4) \%$	136

 $D_0^*(2300)$

$$I(J^P) = \frac{1}{2}(0^+)$$

was $D_0^*(2400)$

Mass $m = 2343 \pm 10$ MeV ($S = 1.5$)
 Full width $\Gamma = 229 \pm 16$ MeV

$D_0^*(2300)$ DECAY MODES	Fraction (Γ_i/Γ)	ρ (MeV/c)
$D \pi^\pm$	seen	411

 $D_1(2420)$

$$I(J^P) = \frac{1}{2}(1^+)$$

Mass $m = 2422.1 \pm 0.6$ MeV ($S = 1.7$)
 $m_{D_1(2420)^0} - m_{D^{*+}} = 411.8 \pm 0.6$ MeV ($S = 1.7$)
 $m_{D_1(2420)^\pm} - m_{D_1(2420)^0} = 4 \pm 4$ MeV
 Full width $\Gamma = 31.3 \pm 1.9$ MeV ($S = 2.8$)

$\overline{D}_1(2420)$ modes are charge conjugates of modes below.

$D_1(2420)$ DECAY MODES	Fraction (Γ_i/Γ)	ρ (MeV/c)
$D^*(2007)^0 \pi$	seen	359

 $D_1(2430)^0$

$$I(J^P) = \frac{1}{2}(1^+)$$

Mass $m = 2412 \pm 9$ MeV
 Full width $\Gamma = 314 \pm 29$ MeV

$D_1(2430)^0$ DECAY MODES	Fraction (Γ_i/Γ)	ρ (MeV/c)
$D^*(2010)^+ \pi^-$	seen	345

 $D_2^*(2460)$

$$I(J^P) = \frac{1}{2}(2^+)$$

Mass $m = 2461.1 \pm_{-0.8}^{+0.7}$ MeV ($S = 6.2$)
 $m_{D_2^*(2460)^0} - m_{D^+} = 591.5 \pm_{-0.8}^{+0.7}$ MeV ($S = 5.9$)
 $m_{D_2^*(2460)^0} - m_{D^{*+}} = 450.9 \pm_{-0.8}^{+0.7}$ MeV ($S = 5.9$)
 $m_{D_2^*(2460)^\pm} - m_{D_2^*(2460)^0} = 2.4 \pm 1.7$ MeV
 Full width $\Gamma = 47.3 \pm 0.8$ MeV ($S = 1.5$)

$\overline{D}_2^*(2460)$ modes are charge conjugates of modes below.

$D_2^*(2460)$ DECAY MODES	Fraction (Γ_i/Γ)	ρ (MeV/c)
$D \pi^-$	seen	509
$D^*(2010) \pi^-$	seen	389

 $D_3^*(2750)$

$$I(J^P) = \frac{1}{2}(3^-)$$

Mass $m = 2763.1 \pm 3.2$ MeV ($S = 2.1$)
 Full width $\Gamma = 66 \pm 5$ MeV

$D_3^*(2750)$ DECAY MODES	Fraction (Γ_i/Γ)	ρ (MeV/c)
$D \pi$	seen	743
$D^+ \pi^-$	seen	739
$D^0 \pi^\pm$	seen	743
$D^* \pi$	seen	639
$D^{*+} \pi^-$	seen	639

Meson Summary Table

CHARMED, STRANGE MESONS
($C = \pm 1, S = \pm 1$)
(including possibly non- $q\bar{q}$ states)

$$D_s^+ = c\bar{s}, D_s^- = \bar{c}s, \text{ similarly for } D_s^{* \pm}$$

D_s^\pm

$$J(J^P) = 0(0^-)$$

$$\text{Mass } m = 1968.35 \pm 0.07 \text{ MeV}$$

$$m_{D_s^\pm} - m_{D^\pm} = 98.69 \pm 0.05 \text{ MeV}$$

$$\text{Mean life } \tau = (504 \pm 4) \times 10^{-15} \text{ s } (S = 1.2)$$

$$c\tau = 151.2 \mu\text{m}$$

CP-violating decay-rate asymmetries

$$A_{CP}(\mu^\pm \nu) = (-0.2 \pm 2.5)\%$$

$$A_{CP}(\tau^\pm \nu) \text{ in } D_s^\pm \rightarrow \tau^\pm \nu_\tau, D_s^\mp \rightarrow \tau^\mp \bar{\nu}_\tau = (3 \pm 5)\%$$

$$A_{CP}(K^\pm K_S^0) = (0.09 \pm 0.26)\%$$

$$A_{CP}(K^\pm K_L^0) \text{ in } D_s^\pm \rightarrow K^\pm K_L^0 = (-1.1 \pm 2.7) \times 10^{-2}$$

$$A_{CP}(K^+ K^- \pi^\pm) = (-0.5 \pm 0.9)\%$$

$$A_{CP}(\phi \pi^\pm) = (-0.38 \pm 0.27)\%$$

$$A_{CP}(K^\pm K_S^0 \pi^0) = (-2 \pm 6)\%$$

$$A_{CP}(2K_S^0 \pi^\pm) = (3 \pm 5)\%$$

$$A_{CP}(K^+ K^- \pi^\pm \pi^0) = (0.0 \pm 3.0)\%$$

$$A_{CP}(K^\pm K_S^0 \pi^+ \pi^-) = (-6 \pm 5)\%$$

$$A_{CP}(K_S^0 K^\mp 2\pi^\pm) = (4.1 \pm 2.8)\%$$

$$A_{CP}(\pi^+ \pi^- \pi^\pm) = (-0.7 \pm 3.1)\%$$

$$A_{CP}(\pi^\pm \eta) = (0.3 \pm 0.4)\%$$

$$A_{CP}(\pi^\pm \eta') = (-0.9 \pm 0.5)\%$$

$$A_{CP}(\eta \pi^\pm \pi^0) = (-1 \pm 4)\%$$

$$A_{CP}(\eta' \pi^\pm \pi^0) = (0 \pm 8)\%$$

$$A_{CP}(K^\pm \pi^0) = (2 \pm 4)\% (S = 1.2)$$

$$A_{CP}(\bar{K}^0 / K^0 \pi^\pm) = (0.4 \pm 0.5)\%$$

$$A_{CP}(K_S^0 \pi^\pm) = (0.20 \pm 0.18)\%$$

$$A_{CP}(K^\pm \pi^+ \pi^-) = (4 \pm 5)\%$$

$$A_{CP}(K_S^0 \pi^+ \pi^0) \text{ in } D_s^\pm \rightarrow K_S^0 \pi^+ \pi^0 = (3 \pm 6)\%$$

$$A_{CP}(K^\pm \eta) = (1.8 \pm 1.9)\%$$

$$A_{CP}(K^\pm \eta'(958)) = (6 \pm 19)\%$$

CP violating asymmetries of P-odd (T-odd) moments

$$A_T(K_S^0 K^\pm \pi^+ \pi^-) = (-14 \pm 8) \times 10^{-3} [ii]$$

$D_s^\pm \rightarrow \phi \ell^+ \nu_\ell$ form factors

$$r_2 = 0.84 \pm 0.11 (S = 2.4)$$

$$r_V = 1.80 \pm 0.08$$

$$\Gamma_L / \Gamma_T = 0.72 \pm 0.18$$

$$f_+(0) |V_{cs}| \text{ in } D_s^\pm \rightarrow \eta e^+ \nu_e = 0.446 \pm 0.007$$

$$f_+(0) |V_{cs}| \text{ in } D_s^\pm \rightarrow \eta' e^+ \nu_e = 0.48 \pm 0.05$$

$$f_+(0) |V_{cd}| \text{ in } D_s^\pm \rightarrow K^0 e^+ \nu_e = 0.162 \pm 0.019$$

$$r_V \equiv V(0)/A_1(0) \text{ in } D_s^\pm \rightarrow K^*(892)^0 e^+ \nu_e = 1.7 \pm 0.4$$

$$r_2 \equiv A_2(0)/A_1(0) \text{ in } D_s^\pm \rightarrow K^*(892)^0 e^+ \nu_e = 0.77 \pm 0.29$$

$$f_{D_s^\pm} |V_{cs}| \text{ in } D_s^\pm \rightarrow \mu^+ \nu_\mu = 243 \pm 5 \text{ MeV}$$

$$f_{D_s^\pm} |V_{cs}| \text{ in } D_s^\pm \rightarrow \tau^+ \nu_\tau = 245.3 \pm 3.0 \text{ MeV}$$

Unless otherwise noted, the branching fractions for modes with a resonance in the final state include all the decay modes of the resonance. D_s^- modes are charge conjugates of the modes below.

D_s^\pm DECAY MODES	Fraction (Γ_i/Γ)	Scale factor/ p	
		Confidence level	(MeV/c)
Inclusive modes			
e^+ semileptonic	[bbb] (6.33 \pm 0.15) %	—	—
π^+ anything	(119.3 \pm 1.4) %	—	—
π^- anything	(43.2 \pm 0.9) %	—	—
π^0 anything	(123 \pm 7) %	—	—
K^- anything	(18.7 \pm 0.5) %	—	—
K^+ anything	(28.9 \pm 0.7) %	—	—
K_S^0 anything	(19.0 \pm 1.1) %	—	—
η anything	[ccc] (29.9 \pm 2.8) %	—	—
ω anything	(6.1 \pm 1.4) %	—	—

η' anything	[ddd] (10.3 \pm 1.4) %	S=1.1	—
$f_0(980)$ anything, $f_0 \rightarrow \pi^+ \pi^-$	< 1.3	CL=90%	—
ϕ anything	(15.7 \pm 1.0) %	—	—
$K^+ K^-$ anything	(15.8 \pm 0.7) %	—	—
$K_S^0 K^+$ anything	(5.8 \pm 0.5) %	—	—
$K_S^0 K^-$ anything	(1.9 \pm 0.4) %	—	—
$2K_S^0$ anything	(1.70 \pm 0.32) %	—	—
$2K^+$ anything	< 2.6	$\times 10^{-3}$ CL=90%	—
$2K^-$ anything	< 6	$\times 10^{-4}$ CL=90%	—

Leptonic and semileptonic modes

$e^+ \nu_e$	< 8.3	$\times 10^{-5}$ CL=90%	984
$\mu^+ \nu_\mu$	(5.43 \pm 0.15) $\times 10^{-3}$		981
$\tau^+ \nu_\tau$	(5.32 \pm 0.11) %		182
$\gamma e^+ \nu_e$	< 1.3	$\times 10^{-4}$ CL=90%	984
$K^+ K^- e^+ \nu_e$	—		851
$\phi e^+ \nu_e$	[eee] (2.39 \pm 0.16) %	S=1.3	720
$\phi \mu^+ \nu_\mu$	(1.9 \pm 0.5) %		715
$\eta e^+ \nu_e + \eta'(958) e^+ \nu_e$	[eee] (3.03 \pm 0.24) %		—
$\eta e^+ \nu_e$	[eee] (2.32 \pm 0.08) %		908
$\eta'(958) e^+ \nu_e$	[eee] (8.0 \pm 0.7) $\times 10^{-3}$		751
$\eta \mu^+ \nu_\mu$	(2.4 \pm 0.5) %		905
$\eta'(958) \mu^+ \nu_\mu$	(1.1 \pm 0.5) %		747
$\omega e^+ \nu_e$	[fff] < 2.0	$\times 10^{-3}$ CL=90%	829
$K^0 e^+ \nu_e$	(3.4 \pm 0.4) $\times 10^{-3}$		921
$K^*(892)^0 e^+ \nu_e$	[eee] (2.15 \pm 0.28) $\times 10^{-3}$	S=1.1	782
$a_0(980)^0 e^+ \nu_e, a_0(980)^0 \rightarrow \pi^0 \eta$	< 1.2	$\times 10^{-4}$ CL=90%	—

Hadronic modes with a $K\bar{K}$ pair

$K^+ K_S^0$	(1.453 \pm 0.035) %		850
$K^+ K_L^0$	(1.49 \pm 0.06) %		850
$K^+ \bar{K}^0$	(2.95 \pm 0.14) %		850
$K^+ K^- \pi^+$	[jj] (5.38 \pm 0.10) %	S=1.1	805
$\phi \pi^+$	[eee,ggg] (4.5 \pm 0.4) %		712
$\phi \pi^+, \phi \rightarrow K^+ K^-$	[ggg] (2.22 \pm 0.06) %		712
$K^+ \bar{K}^*(892)^0, \bar{K}^{*0} \rightarrow K^- \pi^+$	(2.58 \pm 0.06) %		416
$f_0(980) \pi^+, f_0 \rightarrow K^+ K^-$	(1.11 \pm 0.19) %		732
$f_0(1370) \pi^+, f_0 \rightarrow K^+ K^-$	(7.1 \pm 2.9) $\times 10^{-4}$		—
$f_0(1710) \pi^+, f_0 \rightarrow K^+ K^-$	(6.7 \pm 2.8) $\times 10^{-4}$		198
$K^+ \bar{K}_0^*(1430)^0, \bar{K}_0^* \rightarrow K^+ K^- \pi^+$	(1.76 \pm 0.25) $\times 10^{-3}$		218
$K^+ K_S^0 \pi^+$	(1.52 \pm 0.22) %		805
$2K_S^0 \pi^+$	(7.7 \pm 0.6) $\times 10^{-3}$		802
$K^0 \bar{K}^0 \pi^+$	—		802
$K^*(892)^+ \bar{K}^0$	[eee] (5.4 \pm 1.2) %		683
$K^+ K^- \pi^+ \pi^0$	(5.50 \pm 0.24) %	S=1.3	748
$\phi \rho^+$	[eee] (5.59 \pm 0.34) %		401
$\bar{K}_1(1270)^0 K^+, \bar{K}_1(1270)^0 \rightarrow K^- \rho^+$	(5.7 \pm 0.6) $\times 10^{-3}$		—
$\bar{K}_1(1270)^0 K^+, \bar{K}_1(1270)^0 \rightarrow K^*(892) \pi$	(1.31 \pm 0.25) %		—
$\bar{K}_1(1400)^0 K^+, \bar{K}_1(1400)^0 \rightarrow K^*(892) \pi$	(2.0 \pm 0.4) %		—
$a_0(980)^0 \rho^+, a_0(980)^0 \rightarrow K^+ K^-$	(1.9 \pm 0.4) $\times 10^{-3}$		—
$f_1(1420)^0 \pi^+, f_1(1420)^0 \rightarrow K^*(892)^\mp K^\pm$	(3.9 \pm 0.7) $\times 10^{-3}$		—
$f_1(1420)^0 \pi^+, f_1(1420)^0 \rightarrow a_0(980)^0 \pi^0, a_0(980)^0 \rightarrow K^+ K^-$	(4.0 \pm 1.4) $\times 10^{-4}$		—
$\eta(1475) \pi^+, \eta(1475) \rightarrow a_0(980)^0 \pi^0, a_0(980)^0 \rightarrow K^+ K^-$	(7.0 \pm 2.8) $\times 10^{-4}$		—
$K_S^0 K^- 2\pi^+$	(1.53 \pm 0.08) %	S=1.5	744
$K^*(892)^+ \bar{K}^*(892)^0$	[eee] (5.64 \pm 0.35) %		417
$\eta(1475) K_S^0, \eta \rightarrow K^*(892)^0 \pi^+, K^{*0} \rightarrow K^- \pi^+$	(3.4 \pm 1.0) $\times 10^{-4}$		—
$\eta(1475) \pi^+, \eta \rightarrow \bar{K}^*(892)^+ K^-, \bar{K}^{*+} \rightarrow K_S^0 \pi^+$	(3.4 \pm 1.0) $\times 10^{-4}$		—
$\eta(1475) \pi^+, \eta \rightarrow a_0(980)^- \pi^+, a_0^- \rightarrow K_S^0 K^-$	(1.7 \pm 0.9) $\times 10^{-3}$		—

Meson Summary Table

$D_s^\pm \pi^+ \pi^-$	$< 4 \times 10^{-3}$	90%	194
$D_s^\pm \pi^0 \pi^0$	not seen		205

 $D_{s1}(2460)^\pm$

$$I(J^P) = 0(1^+)$$

See the review on "Heavy Non- $q\bar{q}$ Mesons."

$$\text{Mass } m = 2459.5 \pm 0.6 \text{ MeV } (S = 1.1)$$

$$m_{D_{s1}(2460)^\pm} - m_{D_s^{*\pm}} = 347.3 \pm 0.7 \text{ MeV } (S = 1.2)$$

$$m_{D_{s1}(2460)^\pm} - m_{D_s^\pm} = 491.1 \pm 0.6 \text{ MeV } (S = 1.1)$$

$$\text{Full width } \Gamma < 3.5 \text{ MeV, CL} = 95\%$$

$D_{s1}(2460)^\pm$ modes are charge conjugates of the modes below.

$D_{s1}(2460)^\pm$ DECAY MODES	Fraction (Γ_i/Γ)	Scale factor/ Confidence level	ρ (MeV/c)
$D_s^{*+} \pi^0$	(48 ± 11) %		297
$D_s^+ \gamma$	(18 ± 4) %		442
$D_s^\pm \pi^+ \pi^-$	(4.3 ± 1.3) %	S=1.1	363
$D_s^{*+} \gamma$	< 8 %	CL=90%	323
$D_{s0}^*(2317)^+ \gamma$	(3.7 ± 5.0 / 2.4) %		138

 $D_{s1}(2536)^\pm$

$$I(J^P) = 0(1^+)$$

J, P need confirmation.

$$\text{Mass } m = 2535.11 \pm 0.06 \text{ MeV}$$

$$m_{D_{s1}(2536)^\pm} - m_{D_s^*(2111)} = 422.9 \pm 0.4 \text{ MeV}$$

$$m_{D_{s1}(2536)^\pm} - m_{D^*(2010)^\pm} = 524.85 \pm 0.04 \text{ MeV}$$

$$m_{D_{s1}(2536)^\pm} - m_{D^*(2007)^0} = 528.26 \pm 0.05 \text{ MeV } (S = 1.2)$$

$$\text{Full width } \Gamma = 0.92 \pm 0.05 \text{ MeV}$$

Branching fractions are given relative to the one **DEFINED AS 1**.

$D_{s1}(2536)^\pm$ modes are charge conjugates of the modes below.

$D_{s1}(2536)^\pm$ DECAY MODES	Fraction (Γ_i/Γ)	Confidence level	ρ (MeV/c)
$D^*(2010)^+ K^0$	0.85 ± 0.12		149
$(D^*(2010)^+ K^0)_{S\text{-wave}}$	0.61 ± 0.09		149
$D^+ \pi^- K^+$	0.028 ± 0.005		176
$D^*(2007)^0 K^+$	DEFINED AS 1		167
$D^+ K^0$	< 0.34	90%	381
$D^0 K^+$	< 0.12	90%	391
$D_s^{*+} \gamma$	possibly seen		388
$D_s^\pm \pi^+ \pi^-$	seen		437

 $D_{s2}^*(2573)$

$$I(J^P) = 0(2^+)$$

$$\text{Mass } m = 2569.1 \pm 0.8 \text{ MeV } (S = 2.4)$$

$$m_{D_{s2}^*(2573)} - m_{D^0} = 704 \pm 3.2 \text{ MeV}$$

$$\text{Full width } \Gamma = 16.9 \pm 0.7 \text{ MeV}$$

$D_{s2}^*(2573)^\pm$ modes are charge conjugates of the modes below.

$D_{s2}^*(2573)^\pm$ DECAY MODES	Fraction (Γ_i/Γ)	ρ (MeV/c)
$D^0 K^+$	seen	431
$D^*(2007)^0 K^+$	not seen	238
$D^+ K_S^0$	seen	422
$D^{*+} K_S^0$	seen	225

 $D_{s1}^*(2700)^\pm$

$$I(J^P) = 0(1^-)$$

$$\text{Mass } m = 2714 \pm 5 \text{ MeV } (S = 1.5)$$

$$\text{Full width } \Gamma = 122 \pm 10 \text{ MeV}$$

$D_{s1}^*(2700)^\pm$ DECAY MODES	Fraction (Γ_i/Γ)	ρ (MeV/c)
$D^0 K^+$	seen	579
$D^+ K_S^0$	seen	573
$D^{*0} K^+$	seen	438
$D^{*+} K_S^0$	seen	431

 $D_{s3}^*(2860)^\pm$

$$I(J^P) = 0(3^-)$$

$$\text{Mass } m = 2860 \pm 7 \text{ MeV}$$

$$\text{Full width } \Gamma = 53 \pm 10 \text{ MeV}$$

 $D_{s3}^*(2860)^\pm$ DECAY MODES

DECAY MODES	Fraction (Γ_i/Γ)	ρ (MeV/c)
$D^0 K^+$	seen	710
$D^+ K_S^0$	seen	704
$D^{*0} K^+$	seen	589
$D^{*+} K_S^0$	seen	584

**BOTTOM MESONS
($B = \pm 1$)**

$$B^+ = u\bar{b}, B^0 = d\bar{b}, \bar{B}^0 = \bar{d}b, B^- = \bar{u}b, \text{ similarly for } B^{*s}$$

B-particle organization

Many measurements of B decays involve admixtures of B hadrons. Previously we arbitrarily included such admixtures in the B^\pm section, but because of their importance we have created two new sections: " B^\pm/B^0 Admixture" for $\Upsilon(4S)$ results and " $B^\pm/B^0/B_s^0/b$ -baryon Admixture" for results at higher energies. Most inclusive decay branching fractions and χ_b at high energy are found in the Admixture sections. B^0 - \bar{B}^0 mixing data are found in the B^0 section, while B_s^0 - \bar{B}_s^0 mixing data and B - \bar{B} mixing data for a B^0/B_s^0 admixture are found in the B_s^0 section. CP -violation data are found in the B^\pm, B^0 , and B^\pm/B^0 Admixture sections. b -baryons are found near the end of the Baryon section.

The organization of the B sections is now as follows, where bullets indicate particle sections and brackets indicate reviews.

- B^\pm
mass, mean life, CP violation, branching fractions
- B^0
mass, mean life, B^0 - \bar{B}^0 mixing, CP violation, branching fractions
- B^\pm/B^0 Admixtures
 CP violation, branching fractions
- $B^\pm/B^0/B_s^0/b$ -baryon Admixtures
mean life, production fractions, branching fractions
- B^*
mass
- $B_1(5721)^+$
mass
- $B_1(5721)^0$
mass
- $B_2^+(5747)^+$
mass
- $B_2^+(5747)^0$
mass
- $B_2^+(5970)^+$
mass
- $B_2^+(5970)^0$
mass
- B_s^0
mass, mean life, B_s^0 - \bar{B}_s^0 mixing, CP violation, branching fractions
- B_s^*
mass
- $B_{s1}(5830)^0$
mass
- $B_{s2}^*(5840)^0$
mass
- B_c^\pm

mass, mean life, branching fractions
At the end of Baryon Listings:

- Λ_b
mass, mean life, branching fractions
- $\Lambda_b(5912)^0$
mass, mean life
- $\Lambda_b(5920)^0$
mass, mean life
- Σ_b
mass
- Σ_b^*
mass
- Ξ_b^0, Ξ_b^-
mass, mean life, branching fractions
- $\Xi_b(5935)^-$
mass
- $\Xi_b(5945)^0$
mass
- $\Xi_b(5955)^-$
mass
- Ω_b^-
mass, branching fractions
- b -baryon Admixture
mean life, branching fractions

B[±]

$$I(J^P) = \frac{1}{2}(0^-)$$

I, J, P need confirmation. Quantum numbers shown are quark-model predictions.

Mass $m_{B^\pm} = 5279.34 \pm 0.12$ MeV
Mean life $\tau_{B^\pm} = (1.638 \pm 0.004) \times 10^{-12}$ s
 $c\tau = 491.1$ μ m

CP violation

- $A_{CP}(B^+ \rightarrow J/\psi(1S)K^+) = (1.8 \pm 3.0) \times 10^{-3}$ (S = 1.5)
 $A_{CP}(B^+ \rightarrow J/\psi(1S)\pi^+) = (1.8 \pm 1.2) \times 10^{-2}$ (S = 1.3)
 $A_{CP}(B^+ \rightarrow J/\psi\rho^+) = -0.05 \pm 0.05$
 $A_{CP}(B^+ \rightarrow J/\psi K^*(892)^+) = -0.048 \pm 0.033$
 $A_{CP}(B^+ \rightarrow \eta_c K^+) = 0.01 \pm 0.07$ (S = 2.2)
 $A_{CP}(B^+ \rightarrow \psi(2S)\pi^+) = 0.03 \pm 0.06$
 $A_{CP}(B^+ \rightarrow \psi(2S)K^+) = 0.012 \pm 0.020$ (S = 1.5)
 $A_{CP}(B^+ \rightarrow \psi(2S)K^*(892)^+) = 0.08 \pm 0.21$
 $A_{CP}(B^+ \rightarrow \chi_{c1}(1P)\pi^+) = 0.07 \pm 0.18$
 $A_{CP}(B^+ \rightarrow \chi_{c0}K^+) = -0.20 \pm 0.18$ (S = 1.5)
 $A_{CP}(B^+ \rightarrow \chi_{c1}K^+) = -0.009 \pm 0.033$
 $A_{CP}(B^+ \rightarrow \chi_{c1}K^*(892)^+) = 0.5 \pm 0.5$
 $A_{CP}(B^+ \rightarrow D^0 \ell^+ \nu_\ell) = (-0.14 \pm 0.20) \times 10^{-2}$
 $A_{CP}(B^+ \rightarrow \bar{D}^0 \pi^+) = -0.007 \pm 0.007$
 $A_{CP}(B^+ \rightarrow D_{CP(+1)}\pi^+) = -0.0080 \pm 0.0024$
 $A_{CP}(B^+ \rightarrow D_{CP(-1)}\pi^+) = 0.017 \pm 0.026$
 $A_{CP}([K^\mp \pi^\pm \pi^\pm \pi^\mp]_D \pi^+) = 0.02 \pm 0.05$
 $A_{CP}(B^+ \rightarrow [\pi^+ \pi^+ \pi^- \pi^-]_D K^+) = 0.10 \pm 0.04$
 $A_{CP}(B^+ \rightarrow [\pi^+ \pi^- \pi^+ \pi^-]_D K^*(892)^+) = 0.02 \pm 0.11$
 $A_{CP}(B^+ \rightarrow \bar{D}^0 K^+) = -0.017 \pm 0.005$
 $A_{CP}([K^\mp \pi^\pm \pi^\pm \pi^\mp]_D K^+) = -0.31 \pm 0.11$
 $A_{CP}(B^+ \rightarrow [\pi^+ \pi^+ \pi^- \pi^-]_D \pi^+) = (-4 \pm 8) \times 10^{-3}$
 $A_{CP}(B^+ \rightarrow [K^- \pi^+]_D K^+) = -0.58 \pm 0.21$
 $A_{CP}(B^+ \rightarrow [K^- \pi^+ \pi^0]_D K^+) = 0.07 \pm 0.30$ (S = 1.5)
 $A_{CP}(B^+ \rightarrow [K^+ K^- \pi^0]_D K^+) = 0.30 \pm 0.20$
 $A_{CP}(B^+ \rightarrow [\pi^+ \pi^- \pi^0]_D K^+) = 0.05 \pm 0.09$
 $A_{CP}(B^+ \rightarrow \bar{D}^0 K^*(892)^+) = -0.007 \pm 0.019$
 $A_{CP}(B^+ \rightarrow [K^- \pi^+]_D K^*(892)^+) = -0.75 \pm 0.16$
 $A_{CP}(B^+ \rightarrow [K^- \pi^+ \pi^- \pi^+]_D K^*(892)^+) = -0.45 \pm 0.25$
 $A_{CP}(B^+ \rightarrow [K^- \pi^+]_D \pi^+) = 0.00 \pm 0.09$
 $A_{CP}(B^+ \rightarrow [K^- \pi^+ \pi^0]_D \pi^+) = 0.35 \pm 0.16$
 $A_{CP}(B^+ \rightarrow [K^+ K^- \pi^0]_D \pi^+) = -0.03 \pm 0.04$
 $A_{CP}(B^+ \rightarrow [\pi^+ \pi^- \pi^0]_D \pi^+) = -0.016 \pm 0.020$

- $A_{CP}(B^+ \rightarrow [K^- \pi^+]_{(D\pi)} \pi^+) = -0.09 \pm 0.27$
 $A_{CP}(B^+ \rightarrow [K^- \pi^+]_{(D\gamma)} \pi^+) = -0.7 \pm 0.6$
 $A_{CP}(B^+ \rightarrow [K^- \pi^+]_{(D\pi)} K^+) = 0.8 \pm 0.4$
 $A_{CP}(B^+ \rightarrow [K^- \pi^+]_{(D\gamma)} K^+) = 0.4 \pm 1.0$
 $A_{CP}(B^+ \rightarrow [\pi^+ \pi^- \pi^0]_D K^+) = -0.02 \pm 0.15$
 $A_{CP}(B^+ \rightarrow [K_S^0 K^+ \pi^-]_D K^+) = 0.10 \pm 0.09$
 $A_{CP}(B^+ \rightarrow [K_S^0 K^- \pi^+]_D K^+) = -0.04 \pm 0.08$
 $A_{CP}(B^+ \rightarrow [K_S^0 K^- \pi^+]_D \pi^+) = 0.003 \pm 0.015$
 $A_{CP}(B^+ \rightarrow [K_S^0 K^+ \pi^-]_D \pi^+) = -0.034 \pm 0.020$
 $A_{CP}(B^+ \rightarrow [K^*(892)^- K^+]_D K^+) = 0.08 \pm 0.05$
 $A_{CP}(B^+ \rightarrow [K^*(892)^+ K^-]_D K^+) = 0.02 \pm 0.10$
 $A_{CP}(B^+ \rightarrow [K^*(892)^+ K^-]_D \pi^+) = 0.007 \pm 0.017$
 $A_{CP}(B^+ \rightarrow [K^*(892)^- K^+]_D \pi^+) = -0.020 \pm 0.011$
 $A_{CP}(B^+ \rightarrow D_{CP(+1)}K^+) = 0.132 \pm 0.015$ (S = 1.8)
 $A_{ADS}(B^+ \rightarrow D K^+) = -0.451 \pm 0.026$
 $A_{ADS}(B^+ \rightarrow D \pi^+) = 0.129 \pm 0.014$
 $A_{ADS}(B^+ \rightarrow D^*(D\gamma)K^+) = -0.6 \pm 1.3$
 $A_{ADS}(B^+ \rightarrow D^*(D\pi^0)K^+) = 0.72 \pm 0.29$
 $A_{ADS}(B^+ \rightarrow D^*(D\gamma)\pi^+) = 0.08 \pm 0.13$
 $A_{ADS}(B^+ \rightarrow D^*(D\pi^0)\pi^+) = -0.14 \pm 0.06$
 $A_{ADS}(B^+ \rightarrow [K^- \pi^+]_D K^+ \pi^- \pi^+) = -0.33 \pm 0.35$
 $A_{ADS}(B^+ \rightarrow [K^- \pi^+]_D \pi^+ \pi^- \pi^+) = -0.01 \pm 0.09$
 $A_{CP}(B^+ \rightarrow D_{CP(-1)}K^+) = -0.10 \pm 0.07$
 $A_{CP}(B^+ \rightarrow [K^+ K^-]_D K^+ \pi^- \pi^+) = -0.04 \pm 0.06$
 $A_{CP}(B^+ \rightarrow [\pi^+ \pi^-]_D K^+ \pi^- \pi^+) = -0.05 \pm 0.10$
 $A_{CP}(B^+ \rightarrow [K^- \pi^+]_D K^+ \pi^- \pi^+) = 0.013 \pm 0.023$
 $A_{CP}(B^+ \rightarrow [K^+ K^-]_D \pi^+ \pi^- \pi^+) = -0.019 \pm 0.015$
 $A_{CP}(B^+ \rightarrow [\pi^+ \pi^-]_D \pi^+ \pi^- \pi^+) = -0.013 \pm 0.019$
 $A_{CP}(B^+ \rightarrow [K^- \pi^+]_D \pi^+ \pi^- \pi^+) = -0.002 \pm 0.011$
 $A_{CP}(B^+ \rightarrow \bar{D}^{*0} \pi^+) = -0.0004 \pm 0.0021$ (S = 1.1)
 $A_{CP}(B^+ \rightarrow (D_{CP(+1)}^*)^0 \pi^+) = 0.010 \pm 0.007$
 $A_{CP}(B^+ \rightarrow (D_{CP(-1)}^*)^0 \pi^+) = -0.09 \pm 0.05$
 $A_{CP}(B^+ \rightarrow D^{*0} K^+) = 0.012 \pm 0.010$ (S = 1.5)
 $A_{CP}(B^+ \rightarrow D_{CP(+1)}^{*0} K^+) = -0.09 \pm 0.05$ (S = 2.6)
 $A_{CP}(B^+ \rightarrow D_{CP(-1)}^{*0} K^+) = 0.07 \pm 0.10$
 $A_{CP}(B^+ \rightarrow D_{CP(+1)} K^*(892)^+) = 0.08 \pm 0.06$
 $A_{CP}(B^+ \rightarrow D_{CP(-1)} K^*(892)^+) = -0.23 \pm 0.22$
 $A_{CP}(B^+ \rightarrow D_S^+ \phi) = 0.0 \pm 0.4$
 $A_{CP}(B^+ \rightarrow D_S^+ \bar{D}^0) = (-0.4 \pm 0.7)\%$
 $A_{CP}(B^+ \rightarrow D^{*+} \bar{D}^{*0}) = -0.15 \pm 0.11$
 $A_{CP}(B^+ \rightarrow D^{*+} \bar{D}^0) = -0.06 \pm 0.13$
 $A_{CP}(B^+ \rightarrow D^+ \bar{D}^{*0}) = 0.13 \pm 0.18$
 $A_{CP}(B^+ \rightarrow D^+ \bar{D}^0) = 0.016 \pm 0.025$
 $A_{CP}(B^+ \rightarrow K_S^0 \pi^+) = -0.017 \pm 0.016$
 $A_{CP}(B^+ \rightarrow K^+ \pi^0) = 0.030 \pm 0.013$
 $A_{CP}(B^+ \rightarrow \eta' K^+) = 0.004 \pm 0.011$
 $A_{CP}(B^+ \rightarrow \eta' K^*(892)^+) = -0.26 \pm 0.27$
 $A_{CP}(B^+ \rightarrow \eta' K_S^0(1430)^+) = 0.06 \pm 0.20$
 $A_{CP}(B^+ \rightarrow \eta' K_S^0(1430)^+) = 0.15 \pm 0.13$
 $A_{CP}(B^+ \rightarrow \eta K^+) = -0.37 \pm 0.08$
 $A_{CP}(B^+ \rightarrow \eta K^*(892)^+) = 0.02 \pm 0.06$
 $A_{CP}(B^+ \rightarrow \eta K_S^0(1430)^+) = 0.05 \pm 0.13$
 $A_{CP}(B^+ \rightarrow \eta K_S^0(1430)^+) = -0.45 \pm 0.30$
 $A_{CP}(B^+ \rightarrow \omega K^+) = -0.02 \pm 0.04$
 $A_{CP}(B^+ \rightarrow \omega K^{*+}) = 0.29 \pm 0.35$
 $A_{CP}(B^+ \rightarrow \omega(K\pi)_0^{*+}) = -0.10 \pm 0.09$
 $A_{CP}(B^+ \rightarrow \omega K_S^0(1430)^+) = 0.14 \pm 0.15$
 $A_{CP}(B^+ \rightarrow K^{*0} \pi^+) = -0.04 \pm 0.09$ (S = 2.1)
 $A_{CP}(B^+ \rightarrow K^*(892)^+ \pi^0) = -0.39 \pm 0.21$ (S = 1.6)
 $A_{CP}(B^+ \rightarrow K^+ \pi^- \pi^+) = 0.027 \pm 0.008$
 $A_{CP}(B^+ \rightarrow K^+ K^- K^+ \text{nonresonant}) = 0.06 \pm 0.05$
 $A_{CP}(B^+ \rightarrow f(980)^0 K^+) = -0.08 \pm 0.09$
 $A_{CP}(B^+ \rightarrow f_2(1270)K^+) = -0.68^{+0.19}_{-0.17}$
 $A_{CP}(B^+ \rightarrow f_0(1500)K^+) = 0.28 \pm 0.30$
 $A_{CP}(B^+ \rightarrow f_2'(1525)^0 K^+) = -0.08^{+0.05}_{-0.04}$
 $A_{CP}(B^+ \rightarrow \rho^0 K^+) = 0.37 \pm 0.10$
 $A_{CP}(B^+ \rightarrow K^0 \pi^+ \pi^0) = 0.07 \pm 0.06$
 $A_{CP}(B^+ \rightarrow K_S^0(1430)^0 \pi^+) = 0.061 \pm 0.032$
 $A_{CP}(B^+ \rightarrow K_S^0(1430)^+ \pi^0) = 0.26^{+0.18}_{-0.14}$
 $A_{CP}(B^+ \rightarrow K_S^0(1430)^0 \pi^+) = 0.05^{+0.29}_{-0.24}$

Meson Summary Table

$A_{CP}(B^+ \rightarrow K^+ \pi^0 \pi^0) = -0.06 \pm 0.07$
 $A_{CP}(B^+ \rightarrow K^0 \rho^+) = -0.03 \pm 0.15$
 $A_{CP}(B^+ \rightarrow K^{*+} \pi^+ \pi^-) = 0.07 \pm 0.08$
 $A_{CP}(B^+ \rightarrow \rho^0 K^*(892)^+) = 0.31 \pm 0.13$
 $A_{CP}(B^+ \rightarrow K^*(892)^+ f_0(980)) = -0.15 \pm 0.12$
 $A_{CP}(B^+ \rightarrow a_1^+ K^0) = 0.12 \pm 0.11$
 $A_{CP}(B^+ \rightarrow b_1^+ K^0) = -0.03 \pm 0.15$
 $A_{CP}(B^+ \rightarrow K^*(892)^0 \rho^+) = -0.01 \pm 0.16$
 $A_{CP}(B^+ \rightarrow b_1^0 K^+) = -0.46 \pm 0.20$
 $A_{CP}(B^+ \rightarrow K^0 K^+) = 0.04 \pm 0.14$
 $A_{CP}(B^+ \rightarrow K_S^0 K^+) = -0.21 \pm 0.14$
 $A_{CP}(B^+ \rightarrow K^+ K_S^0 K_S^0) = 0.025 \pm 0.031$
 $A_{CP}(B^+ \rightarrow K^+ K^- \pi^+) = -0.122 \pm 0.021$
 $A_{CP}(B^+ \rightarrow K^+ K^- \pi^+ \text{ nonresonant}) = -0.11 \pm 0.06$
 $A_{CP}(B^+ \rightarrow K^+ \bar{K}^*(892)^0) = 0.12 \pm 0.10$
 $A_{CP}(B^+ \rightarrow K^+ \bar{K}_0^*(1430)^0) = 0.10 \pm 0.17$
 $A_{CP}(B^+ \rightarrow \phi \pi^+) = 0.1 \pm 0.5$
 $A_{CP}(B^+ \rightarrow \pi^+ (K^+ K^-)_{S\text{-wave}}) = -0.66 \pm 0.04$
 $A_{CP}(B^+ \rightarrow K^+ K^- K^+) = -0.033 \pm 0.008$
 $A_{CP}(B^+ \rightarrow \phi K^+) = 0.024 \pm 0.028 \quad (S = 2.3)$
 $A_{CP}(B^+ \rightarrow X_0(1550) K^+) = -0.04 \pm 0.07$
 $A_{CP}(B^+ \rightarrow K^{*+} K^+ K^-) = 0.11 \pm 0.09$
 $A_{CP}(B^+ \rightarrow \phi K^*(892)^+) = -0.01 \pm 0.08$
 $A_{CP}(B^+ \rightarrow \phi (K \pi)_0^{*+}) = 0.04 \pm 0.16$
 $A_{CP}(B^+ \rightarrow \phi K_1(1270)^+) = 0.15 \pm 0.20$
 $A_{CP}(B^+ \rightarrow \phi K_2^*(1430)^+) = -0.23 \pm 0.20$
 $A_{CP}(B^+ \rightarrow K^+ \phi \phi) = -0.08 \pm 0.07$
 $A_{CP}(B^+ \rightarrow K^+ [\phi \phi]_{\eta_c}) = 0.10 \pm 0.08$
 $A_{CP}(B^+ \rightarrow K^*(892)^+ \gamma) = 0.014 \pm 0.018$
 $A_{CP}(B^+ \rightarrow X_S \gamma) = 0.028 \pm 0.019$
 $A_{CP}(B^+ \rightarrow \eta K^+ \gamma) = -0.12 \pm 0.07$
 $A_{CP}(B^+ \rightarrow \phi K^+ \gamma) = -0.13 \pm 0.11 \quad (S = 1.1)$
 $A_{CP}(B^+ \rightarrow \rho^+ \gamma) = -0.11 \pm 0.33$
 $A_{CP}(B^+ \rightarrow \pi^+ \pi^0) = 0.03 \pm 0.04$
 $A_{CP}(B^+ \rightarrow \pi^+ \pi^- \pi^+) = 0.057 \pm 0.013$
 $A_{CP}(B^+ \rightarrow \rho^0 \pi^+) = 0.009 \pm 0.019$
 $A_{CP}(B^+ \rightarrow f_2(1270) \pi^+) = 0.40 \pm 0.06$
 $A_{CP}(B^+ \rightarrow \rho^0(1450) \pi^+) = -0.11 \pm 0.05$
 $A_{CP}(B^+ \rightarrow \rho_3(1690) \pi^+) = -0.80 \pm 0.28$
 $A_{CP}(B^+ \rightarrow f_0(1370) \pi^+) = 0.72 \pm 0.22$
 $A_{CP}(B^+ \rightarrow \pi^+ \pi^- \pi^+ \text{ nonresonant}) = -0.14^{+0.23}_{-0.16}$
 $A_{CP}(B^+ \rightarrow \rho^+ \pi^0) = 0.02 \pm 0.11$
 $A_{CP}(B^+ \rightarrow \rho^+ \rho^0) = -0.05 \pm 0.05$
 $A_{CP}(B^+ \rightarrow \omega \pi^+) = -0.04 \pm 0.05$
 $A_{CP}(B^+ \rightarrow \omega \rho^+) = -0.20 \pm 0.09$
 $A_{CP}(B^+ \rightarrow \eta \pi^+) = -0.14 \pm 0.07 \quad (S = 1.4)$
 $A_{CP}(B^+ \rightarrow \eta \rho^+) = 0.11 \pm 0.11$
 $A_{CP}(B^+ \rightarrow \eta' \pi^+) = 0.06 \pm 0.16$
 $A_{CP}(B^+ \rightarrow \eta' \rho^+) = 0.26 \pm 0.17$
 $A_{CP}(B^+ \rightarrow b_1^0 \pi^+) = 0.05 \pm 0.16$
 $A_{CP}(B^+ \rightarrow \rho \bar{\rho} \pi^+) = 0.00 \pm 0.04$
 $A_{CP}(B^+ \rightarrow \rho \bar{\rho} K^+) = 0.00 \pm 0.04 \quad (S = 2.2)$
 $A_{CP}(B^+ \rightarrow \rho \bar{\rho} K^*(892)^+) = 0.21 \pm 0.16 \quad (S = 1.4)$
 $A_{CP}(B^+ \rightarrow \rho \bar{\rho} \gamma) = 0.17 \pm 0.17$
 $A_{CP}(B^+ \rightarrow \rho \bar{\rho} \pi^0) = 0.01 \pm 0.17$
 $A_{CP}(B^+ \rightarrow K^+ \ell^+ \ell^-) = -0.02 \pm 0.08$
 $A_{CP}(B^+ \rightarrow K^+ e^+ e^-) = 0.14 \pm 0.14$
 $A_{CP}(B^+ \rightarrow K^+ \mu^+ \mu^-) = 0.011 \pm 0.017$
 $A_{CP}(B^+ \rightarrow \pi^+ \mu^+ \mu^-) = -0.11 \pm 0.12$
 $A_{CP}(B^+ \rightarrow K^* \ell^+ \ell^-) = -0.09 \pm 0.14$
 $A_{CP}(B^+ \rightarrow K^* e^+ e^-) = -0.14 \pm 0.23$
 $A_{CP}(B^+ \rightarrow K^* \mu^+ \mu^-) = -0.12 \pm 0.24$
 $\gamma = (65.9^{+3.5}_{-3.5})^\circ$
 $\Gamma_B(B^+ \rightarrow D^0 K^+) = 0.0994 \pm 0.0026$
 $\delta_B(B^+ \rightarrow D^0 K^+) = (127.7^{+3.6}_{-3.9})^\circ$
 $\Gamma_B(B^+ \rightarrow D^0 K^{*+}) = 0.101^{+0.016}_{-0.034}$
 $\delta_B(B^+ \rightarrow D^0 K^{*+}) = (48^{+59}_{-16})^\circ$
 $\Gamma_B(B^+ \rightarrow D^{*0} K^+) = 0.104^{+0.013}_{-0.014}$
 $\delta_B(B^+ \rightarrow D^{*0} K^+) = (314.8^{+7.9}_{-9.9})^\circ$

B^- modes are charge conjugates of the modes below. Modes which do not identify the charge state of the B are listed in the B^\pm/B^0 ADMIXTURE section.

The branching fractions listed below assume 50% $B^0 \bar{B}^0$ and 50% $B^+ B^-$ production at the $\Upsilon(4S)$. We have attempted to bring older measurements up to date by rescaling their assumed $\Upsilon(4S)$ production ratio to 50:50 and their assumed D, D_S, D^* , and ψ branching ratios to current values whenever this would affect our averages and best limits significantly.

Indentation is used to indicate a subchannel of a previous reaction. All resonant subchannels have been corrected for resonance branching fractions to the final state so the sum of the subchannel branching fractions can exceed that of the final state.

For inclusive branching fractions, e.g., $B \rightarrow D^\pm X$, the values usually are multiplicities, not branching fractions. They can be greater than one.

B^- DECAY MODES	Fraction (Γ_i/Γ)	Scale factor/ Confidence level (MeV/c)	p
Semileptonic and leptonic modes			
$\ell^+ \nu_\ell X$	[iii] (10.99 ± 0.28) %		–
$e^+ \nu_e X_c$	(10.8 ± 0.4) %		–
$\ell^+ \nu_\ell X_u$	(1.65 ± 0.21) × 10 ⁻³		–
$D \ell^+ \nu_\ell X$	(9.6 ± 0.7) %		–
$\bar{D}^0 \ell^+ \nu_\ell$	[iii] (2.30 ± 0.09) %		2310
$\bar{D}^0 \tau^+ \nu_\tau$	(7.7 ± 2.5) × 10 ⁻³		1911
$\bar{D}^{*0}(2007)^0 \ell^+ \nu_\ell$	[iii] (5.58 ± 0.22) %		2258
$\bar{D}^{*0}(2007)^0 \tau^+ \nu_\tau$	(1.88 ± 0.20) %		1839
$D^- \pi^+ \ell^+ \nu_\ell$	(4.4 ± 0.4) × 10 ⁻³		2306
$\bar{D}_0^*(2420)^0 \ell^+ \nu_\ell, \bar{D}_0^{*0} \rightarrow$	(2.5 ± 0.5) × 10 ⁻³		–
$\bar{D}_2^*(2460)^0 \ell^+ \nu_\ell, \bar{D}_2^{*0} \rightarrow$	(1.53 ± 0.16) × 10 ⁻³		2065
$D^{*-} \pi^+$			
$D^{(*)-} n \pi \ell^+ \nu_\ell (n \geq 1)$	(1.85 ± 0.25) %		–
$D^{*-} \pi^+ \ell^+ \nu_\ell$	(6.0 ± 0.4) × 10 ⁻³		2254
$\bar{D}_1^-(2420)^0 \ell^+ \nu_\ell, \bar{D}_1^0 \rightarrow$	(3.03 ± 0.20) × 10 ⁻³		2084
$\bar{D}_1^{*-} \pi^+$			
$\bar{D}_1^-(2430)^0 \ell^+ \nu_\ell, \bar{D}_1^0 \rightarrow$	(2.7 ± 0.6) × 10 ⁻³		–
$\bar{D}_2^{*-} \pi^+$			
$\bar{D}_2^-(2460)^0 \ell^+ \nu_\ell,$	(1.01 ± 0.24) × 10 ⁻³	S=2.0	2065
$\bar{D}_2^0 \rightarrow D^{*-} \pi^+$			
$\bar{D}^0 \pi^+ \pi^- \ell^+ \nu_\ell$	(1.6 ± 0.4) × 10 ⁻³		2301
$\bar{D}^{*0} \pi^+ \pi^- \ell^+ \nu_\ell$	(8 ± 5) × 10 ⁻⁴		2248
$D_S^{(*)-} K^+ \ell^+ \nu_\ell$	(6.1 ± 1.0) × 10 ⁻⁴		–
$D_S^- K^+ \ell^+ \nu_\ell$	(3.0 ± 1.4) × 10 ⁻⁴		2242
$D_S^{*-} K^+ \ell^+ \nu_\ell$	(2.9 ± 1.9) × 10 ⁻⁴		2185
$\pi^0 \ell^+ \nu_\ell$	(7.80 ± 0.27) × 10 ⁻⁵		2638
$\eta \ell^+ \nu_\ell$	(3.9 ± 0.5) × 10 ⁻⁵		2611
$\eta' \ell^+ \nu_\ell$	(2.3 ± 0.8) × 10 ⁻⁵		2553
$\omega \ell^+ \nu_\ell$	[iii] (1.19 ± 0.09) × 10 ⁻⁴		2582
$\rho^0 \ell^+ \nu_\ell$	[iii] (1.58 ± 0.11) × 10 ⁻⁴		2583
$\pi^+ \pi^- \ell^+ \nu_\ell$	(2.3 ± 0.4) × 10 ⁻⁴		2636
$\rho \bar{\rho} \ell^+ \nu_\ell$	(5.8 ± 2.6) × 10 ⁻⁶		2467
$\rho \bar{\rho} \mu^+ \nu_\mu$	(5.32 ± 0.34) × 10 ⁻⁶		2446
$\rho \bar{\rho} e^+ \nu_e$	(8.2 ± 4.0) × 10 ⁻⁶		2467
$e^+ \nu_e$	< 9.8 × 10 ⁻⁷	CL=90%	2640
$\mu^+ \nu_\mu$	< 8.6 × 10 ⁻⁷	CL=90%	2639
$\tau^+ \nu_\tau$	(1.09 ± 0.24) × 10 ⁻⁴	S=1.2	2341
$\ell^+ \nu_\ell \gamma$	< 3.0 × 10 ⁻⁶	CL=90%	2640
$e^+ \nu_e \gamma$	< 4.3 × 10 ⁻⁶	CL=90%	2640
$\mu^+ \nu_\mu \gamma$	< 3.4 × 10 ⁻⁶	CL=90%	2639
$\mu^+ \mu^- \mu^+ \nu_\mu$	< 1.6 × 10 ⁻⁸	CL=95%	2634
Inclusive modes			
$D^0 X$	(8.6 ± 0.7) %		–
$\bar{D}^0 X$	(79 ± 4) %		–
$D^+ X$	(2.5 ± 0.5) %		–
$D^- X$	(9.9 ± 1.2) %		–
$D_S^+ X$	(7.9 ± 1.4) %		–
$D_S^- X$	(1.10 ± 0.40) %		–
$\Lambda_c^+ X$	(2.1 ± 0.9) %		–
$\bar{\Lambda}_c^- X$	(2.8 ± 1.1) %		–
$\bar{\Sigma} X$	(97 ± 4) %		–
$c X$	(23.4 ± 2.2) %		–
$c/\bar{c} X$	(120 ± 6) %		–

Meson Summary Table

D, D*, or D_s modes							
$\bar{D}^0 \pi^+$		(4.68 ± 0.13) × 10 ⁻³	2308	$\bar{D}^{*0} 3\pi^+ 2\pi^-$	(5.7 ± 1.2) × 10 ⁻³	2196	
$D_{CP(+1)} \pi^+$	[<i>ijj</i>]	(2.05 ± 0.20) × 10 ⁻³	-	$D^*(2010) + K^0$	< 3.6	× 10 ⁻⁶	2255
$D_{CP(-1)} \pi^+$	[<i>ijj</i>]	(2.1 ± 0.4) × 10 ⁻³	-	$D^*(2010) + K^0$	< 9.0	× 10 ⁻⁶	CL=90% 2225
$\bar{D}^0 \rho^+$		(1.34 ± 0.18) %	2237	$D^*(2010) - \pi^+ \pi^+ \pi^0$	(1.5 ± 0.7) %		2235
$\bar{D}^0 K^+$		(3.69 ± 0.16) × 10 ⁻⁴	2281	$D^*(2010) - \pi^+ \pi^+ \pi^+ \pi^-$	(2.6 ± 0.4) × 10 ⁻³		2217
$D_{CP(+1)} K^+$	[<i>ijj</i>]	(1.83 ± 0.08) × 10 ⁻⁴	-	$\bar{D}^{*0} \pi^+$	[<i>mn</i>]	(5.7 ± 1.2) × 10 ⁻³	-
$D_{CP(-1)} K^+$	[<i>ijj</i>]	(1.99 ± 0.19) × 10 ⁻⁴	-	$\bar{D}_1^*(2420) \pi^+$	(1.5 ± 0.6) × 10 ⁻³	S=1.3	2081
$D^0 K^+$		(3.64 ± 0.25) × 10 ⁻⁶	2281	$\bar{D}_1(2420) \pi^+ + B(\bar{D}_1^0 \rightarrow$	(2.5 ± 1.6 / 1.4) × 10 ⁻⁴	S=3.9	2081
$[K^- \pi^+]_D K^+$	[<i>kkk</i>]	< 2.8	× 10 ⁻⁷	$\bar{D}_1(2420) \pi^+ + B(\bar{D}_1^0 \rightarrow$	(2.2 ± 1.0) × 10 ⁻⁴		2081
$[K^+ \pi^-]_D K^+$	[<i>kkk</i>]	< 2.0	× 10 ⁻⁵	$\bar{D}_1(2420) \pi^+ + B(\bar{D}_1^0 \rightarrow$	(3.5 ± 0.6) × 10 ⁻⁴		2079
$[K^- \pi^+ \pi^0]_D K^+$	seen	-	-	$\bar{D}_1(2420) \pi^+ + B(\bar{D}_1^0 \rightarrow$	(7.2 ± 1.4) × 10 ⁻⁵		-
$[K^+ \pi^- \pi^0]_D K^+$	seen	-	-	$\bar{D}_1(2420) \pi^+ + B(\bar{D}_1^0 \rightarrow$	(6.8 ± 1.3) × 10 ⁻⁵		-
$[K^- \pi^+ \pi^+ \pi^-]_D K^+$	seen	-	-	$\bar{D}_1(2420) \pi^+ + B(\bar{D}_1^0 \rightarrow$	(3.56 ± 0.24) × 10 ⁻⁴		-
$[K^+ \pi^- \pi^+ \pi^-]_D K^+$	seen	-	-	$\bar{D}_1(2420) \pi^+ + B(\bar{D}_1^0 \rightarrow$	(2.2 ± 1.0) × 10 ⁻⁴		-
$[K^- \pi^+]_D \pi^+$	[<i>kkk</i>]	(6.3 ± 1.1) × 10 ⁻⁷	-	$\bar{D}_1(2420) \pi^+ + B(\bar{D}_1^0 \rightarrow$	(2.2 ± 1.1) × 10 ⁻⁴		-
$[K^+ \pi^-]_D \pi^+$	[<i>kkk</i>]	(1.7 ± 0.4) × 10 ⁻⁴	-	$\bar{D}_1(2420) \pi^+ + B(\bar{D}_1^0 \rightarrow$	(6.4 ± 1.4) × 10 ⁻⁴		2136
$[K^- \pi^+ \pi^0]_D \pi^+$	seen	-	-	$\bar{D}_1(2420) \pi^+ + B(\bar{D}_1^0 \rightarrow$	(7.4 ± 1.0) × 10 ⁻⁴		-
$[K^+ \pi^- \pi^0]_D \pi^+$	seen	-	-	$\bar{D}_1(2420) \pi^+ + B(\bar{D}_1^0 \rightarrow$	(1.98 ± 0.30) × 10 ⁻⁴		-
$[K^- \pi^+ \pi^+ \pi^-]_D \pi^+$	seen	-	-	$\bar{D}_1(2420) \pi^+ + B(\bar{D}_1^0 \rightarrow$	(3.5 ± 0.9) × 10 ⁻⁴	S=1.5	-
$[K^+ \pi^- \pi^+ \pi^-]_D \pi^+$	seen	-	-	$\bar{D}_1(2420) \pi^+ + B(\bar{D}_1^0 \rightarrow$	< 6	× 10 ⁻⁶	CL=90% 2081
$[\pi^+ \pi^- \pi^0]_D K^-$		(4.6 ± 0.9) × 10 ⁻⁶	-	$\bar{D}_1(2420) \pi^+ + B(\bar{D}_1^0 \rightarrow$	< 1.4	× 10 ⁻³	CL=90% 1996
$[K_S^0 K^+ \pi^-]_D K^+$	seen	-	-	$\bar{D}_1(2420) \pi^+ + B(\bar{D}_1^0 \rightarrow$	< 1.3	× 10 ⁻³	CL=90% 2063
$[K_S^0 K^- \pi^+]_D K^+$	seen	-	-	$\bar{D}_1(2420) \pi^+ + B(\bar{D}_1^0 \rightarrow$	< 2.2	× 10 ⁻⁵	CL=90% 2063
$[K^*(892)^+ K^-]_D K^+$	seen	-	-	$\bar{D}_1(2420) \pi^+ + B(\bar{D}_1^0 \rightarrow$	(8.4 ± 2.1) × 10 ⁻⁵		-
$[K_S^0 K^- \pi^+]_D \pi^+$	seen	-	-	$\bar{D}_1(2420) \pi^+ + B(\bar{D}_1^0 \rightarrow$	(3.3 ± 1.5) × 10 ⁻⁵		-
$[K^*(892)^+ K^-]_D \pi^+$	seen	-	-	$\bar{D}_1(2420) \pi^+ + B(\bar{D}_1^0 \rightarrow$	(1.10 ± 0.32) × 10 ⁻⁵		1913
$[K_S^0 K^+ \pi^-]_D \pi^+$	seen	-	-	$\bar{D}_1(2420) \pi^+ + B(\bar{D}_1^0 \rightarrow$	(1.00 ± 0.22) × 10 ⁻⁵		-
$[K^*(892)^+ K^-]_D \pi^+$	seen	-	-	$\bar{D}_1(2420) \pi^+ + B(\bar{D}_1^0 \rightarrow$	(2.0 ± 1.4) × 10 ⁻⁶		-
$\bar{D}^0 K^*(892)^+$		(5.3 ± 0.4) × 10 ⁻⁴	2213	$\bar{D}_1(2420) \pi^+ + B(\bar{D}_1^0 \rightarrow$	< 4.7	× 10 ⁻³	CL=90% 1977
$D_{CP(-1)} K^*(892)^+$	[<i>ijj</i>]	(2.7 ± 0.8) × 10 ⁻⁴	-	$\bar{D}_1(2420) \pi^+ + B(\bar{D}_1^0 \rightarrow$	(9.0 ± 0.9) × 10 ⁻³		1815
$D_{CP(+1)} K^*(892)^+$	[<i>ijj</i>]	(6.2 ± 0.7) × 10 ⁻⁴	-	$\bar{D}_1(2420) \pi^+ + B(\bar{D}_1^0 \rightarrow$	(8.0 ± 1.6 / 1.3) × 10 ⁻⁴		1605
$D^0 K^*(892)^+$		(5.4 ± 1.8 / 4.0) × 10 ⁻⁶	2213	$\bar{D}_1(2420) \pi^+ + B(\bar{D}_1^0 \rightarrow$	< 7.6	× 10 ⁻⁴	CL=90% 1605
$\bar{D}^0 K^+ \pi^+ \pi^-$		(5.2 ± 2.1) × 10 ⁻⁴	2237	$\bar{D}_1(2420) \pi^+ + B(\bar{D}_1^0 \rightarrow$	(3.1 ± 1.0 / 0.9) × 10 ⁻³		-
$\bar{D}^0 K^+ \bar{K}^0$		(5.5 ± 1.6) × 10 ⁻⁴	2189	$\bar{D}_1(2420) \pi^+ + B(\bar{D}_1^0 \rightarrow$	(4.6 ± 1.3 / 1.1) × 10 ⁻⁴		-
$\bar{D}^0 K^+ \bar{K}^*(892)^0$		(7.5 ± 1.7) × 10 ⁻⁴	2072	$\bar{D}_1(2420) \pi^+ + B(\bar{D}_1^0 \rightarrow$	< 2.2	× 10 ⁻⁴	CL=90% -
$\bar{D}^0 \pi^+ \pi^+ \pi^-$		(5.6 ± 2.1) × 10 ⁻³	S=3.6 2289	$\bar{D}_1(2420) \pi^+ + B(\bar{D}_1^0 \rightarrow$	< 2.7	× 10 ⁻⁴	CL=90% -
$\bar{D}^0 \pi^+ \pi^+ \pi^-$ nonresonant		(5 ± 4) × 10 ⁻³	2289	$\bar{D}_1(2420) \pi^+ + B(\bar{D}_1^0 \rightarrow$	< 2.7	× 10 ⁻⁴	CL=90% -
$\bar{D}^0 \pi^+ \rho^0$		(4.2 ± 3.0) × 10 ⁻³	2208	$\bar{D}_1(2420) \pi^+ + B(\bar{D}_1^0 \rightarrow$	< 9.8	× 10 ⁻⁴	CL=90% -
$\bar{D}^0 a_1(1260)^+$		(4 ± 4) × 10 ⁻³	2123	$\bar{D}_1(2420) \pi^+ + B(\bar{D}_1^0 \rightarrow$	(1.20 ± 0.30) %		-
$\bar{D}^0 \omega \pi^+$		(4.1 ± 0.9) × 10 ⁻³	2206	$\bar{D}_1(2420) \pi^+ + B(\bar{D}_1^0 \rightarrow$	(1.4 ± 0.7 / 0.6) × 10 ⁻³		-
$D^*(2010) - \pi^+ \pi^+$		(1.35 ± 0.22) × 10 ⁻³	2247	$\bar{D}_1(2420) \pi^+ + B(\bar{D}_1^0 \rightarrow$	(4.0 ± 1.0) × 10 ⁻⁴		1447
$D^*(2010) - K^+ \pi^+$		(8.2 ± 1.4) × 10 ⁻⁵	2206	$\bar{D}_1(2420) \pi^+ + B(\bar{D}_1^0 \rightarrow$			
$\bar{D}_1(2420) \pi^+, \bar{D}_1^0 \rightarrow$		(8.4 ± 1.5) × 10 ⁻⁴	2081	$\bar{D}_1(2420) \pi^+ + B(\bar{D}_1^0 \rightarrow$			
$D^- \pi^+ \pi^+$		(1.07 ± 0.05) × 10 ⁻³	2299	$\bar{D}_1(2420) \pi^+ + B(\bar{D}_1^0 \rightarrow$			
$D^- K^+ \pi^+$		(7.7 ± 0.5) × 10 ⁻⁵	2260	$\bar{D}_1(2420) \pi^+ + B(\bar{D}_1^0 \rightarrow$			
$D_2^*(2300)^0 K^+, D_2^{*0} \rightarrow$		(6.1 ± 2.4) × 10 ⁻⁶	-	$\bar{D}_1(2420) \pi^+ + B(\bar{D}_1^0 \rightarrow$			
$D_2^*(2460)^0 K^+, D_2^{*0} \rightarrow$		(2.32 ± 0.23) × 10 ⁻⁵	-	$\bar{D}_1(2420) \pi^+ + B(\bar{D}_1^0 \rightarrow$			
$D_1^*(2760)^0 K^+, D_1^{*0} \rightarrow$		(3.6 ± 1.2) × 10 ⁻⁶	-	$\bar{D}_1(2420) \pi^+ + B(\bar{D}_1^0 \rightarrow$			
$D^+ K^0$		< 2.9	× 10 ⁻⁶	CL=90% 2278			
$D^+ K^+ \pi^-$		(5.6 ± 1.1) × 10 ⁻⁶	2260				
$D_2^*(2460)^0 K^+, D_2^{*0} \rightarrow$		< 6.3	× 10 ⁻⁷	CL=90% -			
$D^+ K^* \pi^-$		< 4.9	× 10 ⁻⁷	CL=90% 2211			
$D^+ \bar{K}^* \pi^-$		< 1.4	× 10 ⁻⁶	CL=90% 2211			
$\bar{D}^*(2007)^0 \pi^+$		(5.18 ± 0.15) × 10 ⁻³	2256				
$\bar{D}_{CP(+1)}^* \pi^+$	[<i>ijj</i>]	(2.9 ± 0.6) × 10 ⁻³	-				
$\bar{D}_{CP(-1)}^* \pi^+$	[<i>ijj</i>]	(2.6 ± 1.0) × 10 ⁻³	-				
$\bar{D}^*(2007)^0 \omega \pi^+$		(4.5 ± 1.2) × 10 ⁻³	2149				
$\bar{D}^*(2007)^0 \rho^+$		(9.8 ± 1.7) × 10 ⁻³	2181				
$\bar{D}^*(2007)^0 K^+$		(4.20 ± 0.31 / 0.28) × 10 ⁻⁴	2227				
$\bar{D}_{CP(+1)}^* K^+$	[<i>ijj</i>]	(2.75 ± 0.35) × 10 ⁻⁴	-				
$\bar{D}_{CP(-1)}^* K^+$	[<i>ijj</i>]	(2.31 ± 0.31) × 10 ⁻⁴	-				
$D^*(2007)^0 K^+$		(4.5 ± 1.2) × 10 ⁻⁶	2227				
$\bar{D}^*(2007)^0 K^* (892)^+$		(8.1 ± 1.4) × 10 ⁻⁴	2156				
$\bar{D}^*(2007)^0 K^+ \bar{K}^0$		< 1.06	× 10 ⁻³	CL=90% 2132			
$\bar{D}^*(2007)^0 K^+ \bar{K}^*(892)^0$		(1.5 ± 0.4) × 10 ⁻³	2009				
$\bar{D}^*(2007)^0 \pi^+ \pi^+ \pi^-$		(1.03 ± 0.12) %	2236				
$\bar{D}^*(2007)^0 a_1(1260)^+$		(1.9 ± 0.5) %	2063				
$\bar{D}^*(2007)^0 \pi^- \pi^+ \pi^+ \pi^0$		(1.8 ± 0.4) %	2219				

Meson Summary Table

$\bar{D}^0 D_{s1}(2536)^+ \times$ $B(D_{s1}(2536)^+ \rightarrow$ $D^*(2007)^0 K^+)$	$(2.2 \pm 0.7) \times 10^{-4}$	1447	$\eta_c K^+ \pi^+ \pi^-$	< 3.9	$\times 10^{-4}$	CL=90%	1684
$\bar{D}^*(2007)^0 D_{s1}(2536)^+ \times$ $B(D_{s1}(2536)^+ \rightarrow$ $D^*(2007)^0 K^+)$	$(5.5 \pm 1.6) \times 10^{-4}$	1339	$\eta_c K^+ \omega(782)$	< 5.3	$\times 10^{-4}$	CL=90%	1475
$\bar{D}^0 D_{s1}(2536)^+ \times$ $B(D_{s1}(2536)^+ \rightarrow$ $D^*(2007)^0 K^+)$	$(2.3 \pm 1.1) \times 10^{-4}$	1447	$\eta_c K^+ \eta$	< 2.2	$\times 10^{-4}$	CL=90%	1588
$\bar{D}^0 D_{s1}(2536)^+ \times$ $B(D_{s1}(2536)^+ \rightarrow D^{*+} K^0)$	$(5.6 \pm 1.8) \times 10^{-4}$	S=1.7	$\eta_c K^+ \pi^0$	< 6.2	$\times 10^{-5}$	CL=90%	1723
$\bar{D}^0 D_{sJ}(2700)^+ \times$ $B(D_{sJ}(2700)^+ \rightarrow D^0 K^+)$	$(3.9 \pm 2.6) \times 10^{-4}$	1339	$\eta_c(2S) K^+$	$(4.4 \pm 1.0) \times 10^{-4}$			1320
$\bar{D}^{*0} D_{s1}(2536)^+, D_{s1}^+ \rightarrow$ $D^{*+} K^0$	$(8 \pm 15) \times 10^{-6}$	-	$\eta_c(2S) K^+, \eta_c \rightarrow p\bar{p}$	$(3.5 \pm 0.8) \times 10^{-8}$			-
$\bar{D}^0 D_{sJ}(2573)^+, D_{sJ}^+ \rightarrow$ $D^0 K^+$	< 2	$\times 10^{-4}$	$\eta_c(2S) K^+, \eta_c \rightarrow p\bar{p} \pi^+ \pi^-$	$(3.4 \pm 2.3) \times 10^{-6}$			-
$\bar{D}^{*0} D_{sJ}(2573), D_{sJ}^+ \rightarrow$ $D^0 K^+$	< 5	$\times 10^{-4}$	$K_S^0 K^+ \pi^\pm$	$(1.12 \pm 0.18) \times 10^{-6}$			-
$\bar{D}^0 D_s^{*+}$	$(7.6 \pm 1.6) \times 10^{-3}$	1734	$\eta_c(2S) K^+, \eta_c \rightarrow p\bar{p} \pi^+ \pi^-$	< 3.4	$\times 10^{-6}$	CL=90%	1401
$\bar{D}^*(2007)^0 D_s^+$	$(8.2 \pm 1.7) \times 10^{-3}$	1737	$h_c(1P) K^+, h_c \rightarrow J/\psi \pi^+ \pi^-$	< 4.6	$\times 10^{-5}$	CL=90%	-
$\bar{D}^*(2007)^0 D_s^+$	$(1.71 \pm 0.24) \%$	1651	$X(3730)^0 K^+, X^0 \rightarrow \eta_c \eta$	< 5.7	$\times 10^{-6}$	CL=90%	-
$D_s^{*+} \bar{D}^{*0}$	$(2.7 \pm 1.2) \%$	-	$X(3730)^0 K^+, X^0 \rightarrow \eta_c \pi^0$	< 3.7	$\times 10^{-5}$	CL=90%	-
$\bar{D}^*(2007)^0 D^*(2010)^+$	$(8.1 \pm 1.7) \times 10^{-4}$	1713	$\eta_{c2}(1D) K^+, \eta_{c2} \rightarrow h_c \gamma$	< 1.1	$\times 10^{-4}$	CL=90%	-
$\bar{D}^0 D^*(2010)^+ +$ $\bar{D}^*(2007)^0 D^+$	< 1.30	$\%$	$\eta_{c2}(1D) \pi^+ K_S^0, \eta_{c2} \rightarrow h_c \gamma$	$< 2.8 \pm 0.6) \times 10^{-7}$			-
$\bar{D}^0 D^*(2010)^+$	$(3.9 \pm 0.5) \times 10^{-4}$	1792	$\psi_2(3823) K^+, \psi_2 \rightarrow$ $J/\psi \pi^+ \pi^-$	$(2.1 \pm 0.7) \times 10^{-4}$			1141
$\bar{D}^0 D^+$	$(3.8 \pm 0.4) \times 10^{-4}$	1866	$X_{c1}(3872) K^+$	< 2.8	$\times 10^{-4}$	CL=90%	1101
$\bar{D}^0 D^+ K^0$	$(1.55 \pm 0.21) \times 10^{-3}$	1571	$X_{c0}(3915) K^+$	$< 8.1 \pm 3.3) \times 10^{-6}$			-
$D^+ \bar{D}^*(2007)^0$	$(6.3 \pm 1.7) \times 10^{-4}$	1791	$X_{c0}(3915) K^+, X_{c0} \rightarrow D^+ D^-$	< 4.7	$\times 10^{-5}$	CL=90%	-
$\bar{D}^*(2007)^0 D^+ K^0$	$(2.1 \pm 0.5) \times 10^{-3}$	1475	$X_{c0}(3915) K^+, X_{c0} \rightarrow \eta_c \eta$	< 1.7	$\times 10^{-5}$	CL=90%	-
$\bar{D}^0 D^*(2010)^+ K^0$	$(3.8 \pm 0.4) \times 10^{-3}$	1476	$(X_{chi})_{c0}(3915) K^+, X_{c0} \rightarrow$ $\eta_c \pi^0$	< 3.9	$\times 10^{-5}$	CL=90%	-
$\bar{D}^*(2007)^0 D^*(2010)^+ K^0$	$(9.2 \pm 1.2) \times 10^{-3}$	1362	$X(4014)^0 K^+, X^0 \rightarrow \eta_c \eta$	< 1.2	$\times 10^{-5}$	CL=90%	-
$\bar{D}^0 D^0 K^+$	$(1.45 \pm 0.33) \times 10^{-3}$	S=2.6	$X(4014)^0 K^+, X^0 \rightarrow \eta_c \pi^0$	< 4.7	$\times 10^{-5}$	CL=90%	-
$\bar{D}^*(2007)^0 D^0 K^+$	$(2.26 \pm 0.23) \times 10^{-3}$	1481	$Z_c(3900)^0 K^+, Z_c^0 \rightarrow$ $\eta_c \pi^+ \pi^-$	< 1.6	$\times 10^{-5}$	CL=90%	-
$\bar{D}^0 D^*(2007)^0 K^+$	$(6.3 \pm 0.5) \times 10^{-3}$	1481	$X(4020)^0 K^+, X^0 \rightarrow$ $\eta_c \pi^+ \pi^-$	< 6	$\times 10^{-4}$	CL=90%	940
$\bar{D}^*(2007)^0 D^*(2007)^0 K^+$	$(1.12 \pm 0.13) \%$	1368	$X_{c1}(3872) K^*, X_{c1} \rightarrow$ $J/\psi \pi^+ \pi^0$	< 6.1	$\times 10^{-6}$	CL=90%	-
$D^- D^+ K^+$	$(2.2 \pm 0.7) \times 10^{-4}$	1571	$X_{c1}(3872) K^*, X_{c1} \rightarrow$ $J/\psi \pi^+ \pi^0$	$(2.8 \pm 1.2) \times 10^{-4}$			1085
$X_0(2900) D^+, X_0 \rightarrow$ $D^- K^+$	$(1.2 \pm 0.5) \times 10^{-5}$	-	$Z_c(4430)^+ K^0, Z_c^+ \rightarrow J/\psi \pi^+$	< 1.5	$\times 10^{-5}$	CL=95%	-
$X_1(2900) D^+, X_1 \rightarrow$ $D^- K^+$	$(6.7 \pm 2.3) \times 10^{-5}$	-	$Z_c(4430)^+ K^0, Z_c^+ \rightarrow$ $J/\psi \pi^+$	< 4.7	$\times 10^{-5}$	CL=95%	-
$D^- D^+ K^+$ nonresonant	$(5.3 \pm 1.8) \times 10^{-5}$	1571	$\psi(2S) \pi^+$	< 1.56	$\times 10^{-5}$	CL=95%	-
$D^- D^*(2010)^+ K^+$	$(6.3 \pm 1.1) \times 10^{-4}$	1475	$\psi(4230)^0 K^+, \psi^0 \rightarrow$ $J/\psi \pi^+ \pi^-$	< 1.4	$\times 10^{-5}$	CL=90%	-
$D^*(2010)^- D^+ K^+$	$(6.0 \pm 1.3) \times 10^{-4}$	1475	$X_{c0}(3915) K^+, X_{c0} \rightarrow J/\psi \gamma$	< 3.8	$\times 10^{-5}$	CL=90%	-
$D^*(2010)^- D^*(2010)^+ K^+$	$(1.32 \pm 0.18) \times 10^{-3}$	1363	$X_{c0}(3915) K^+, X_{c0} \rightarrow$ $J/\psi \gamma$	< 2.5	$\times 10^{-6}$	CL=90%	-
$(\bar{D} + \bar{D}^*)(D + D^*) K$	$(4.05 \pm 0.30) \%$	-	$X_{c1}(1P) \pi^0$	$< 1.020 \pm 0.019) \times 10^{-3}$			1684
$D_s^+ \pi^0$	$(1.6 \pm 0.5) \times 10^{-5}$	2270	$X(3930)^0 K^+, X^0 \rightarrow J/\psi \gamma$	$(1.14 \pm 0.11) \times 10^{-3}$			1651
$D_s^+ \pi^0$	< 2.6	$\times 10^{-4}$	$J/\psi(1S) K^+$	$(8.1 \pm 1.3) \times 10^{-4}$		S=2.5	1612
$D_s^+ \eta$	< 4	$\times 10^{-4}$	$J/\psi(1S) K^0 \pi^+$	$(3.37 \pm 0.29) \times 10^{-5}$			1252
$D_s^+ \eta$	< 6	$\times 10^{-4}$	$J/\psi(1S) K^+ \pi^+ \pi^-$	< 7.1	$\times 10^{-8}$	CL=95%	-
$D_s^+ \rho^0$	< 3.0	$\times 10^{-4}$	$J/\psi(1S) K^+ \pi^+ \pi^-$	$< 1.43 \pm 0.08) \times 10^{-3}$			1571
$D_s^+ \rho^0$	< 4	$\times 10^{-4}$	$J/\psi(1S) K^+ K^- K^+$	$(1.8 \pm 0.5) \times 10^{-3}$			1402
$D_s^+ \omega$	< 4	$\times 10^{-4}$	$X_{c0}(3915) K^+, X_{c0} \rightarrow p\bar{p}$	< 5	$\times 10^{-4}$	CL=90%	1308
$D_s^+ \omega$	< 6	$\times 10^{-4}$	$J/\psi(1S) \eta K^+$	$(1.24 \pm 0.14) \times 10^{-4}$			1510
$D_s^+ a_1(1260)^0$	< 1.8	$\times 10^{-3}$	$X_{c1-odd}(3872) K^+,$ $X_{c1-odd} \rightarrow J/\psi \eta$	< 3.8	$\times 10^{-6}$	CL=90%	-
$D_s^+ a_1(1260)^0$	< 1.3	$\times 10^{-3}$	$\psi(4160) K^+, \psi \rightarrow J/\psi \eta$	< 7.4	$\times 10^{-6}$	CL=90%	-
$D_s^+ K^+ K^-$	$(7.2 \pm 1.1) \times 10^{-6}$	2149	$J/\psi(1S) \eta' K^+$	< 8.8	$\times 10^{-5}$	CL=90%	1273
$D_s^+ \phi$	< 4.2	$\times 10^{-7}$	$J/\psi(1S) \phi K^+$	$(5.0 \pm 0.4) \times 10^{-5}$			1227
$D_s^+ \phi$	< 1.2	$\times 10^{-5}$	$J/\psi(1S) K_1(1650), K_1 \rightarrow$ ϕK^+	$(6 \pm 10/6) \times 10^{-6}$			-
$D_s^+ \bar{K}^0$	< 8	$\times 10^{-4}$	$J/\psi(1S) K^*(1680)^+, K^* \rightarrow$ ϕK^+	$(3.4 \pm 1.9/2.2) \times 10^{-6}$			-
$D_s^+ \bar{K}^0$	< 9	$\times 10^{-4}$	$J/\psi(1S) K_2^*(1980), K_2^* \rightarrow$ ϕK^+	$(1.5 \pm 0.9/0.5) \times 10^{-6}$			-
$D_s^+ \bar{K}^*(892)^0$	< 4.4	$\times 10^{-6}$	$J/\psi(1S) K(1830)^+,$ $K(1830)^+ \rightarrow \phi K^+$	$(1.3 \pm 1.3/1.1) \times 10^{-6}$			-
$D_s^+ K^*0$	< 3.5	$\times 10^{-6}$	$X_{c1}(4140) K^+, X_{c1} \rightarrow$ $J/\psi(1S) \phi$	$(10 \pm 4) \times 10^{-6}$			-
$D_s^+ \bar{K}^*(892)^0$	< 3.5	$\times 10^{-4}$	$X_{c1}(4274) K^+, X_{c1} \rightarrow$ $J/\psi(1S) \phi$	$(3.6 \pm 2.2/1.8) \times 10^{-6}$			-
$D_s^- \pi^+ K^+$	$(1.80 \pm 0.22) \times 10^{-4}$	2222	$X_{c0}(4500) K^+, X_{c0} \rightarrow$ $J/\psi(1S) \phi$	$(3.3 \pm 2.1/1.7) \times 10^{-6}$			-
$D_s^- \pi^+ K^+$	$(1.45 \pm 0.24) \times 10^{-4}$	2164	$X_{c0}(4700) K^+, X_{c0} \rightarrow$ $J/\psi(1S) \phi$	$(6 \pm 5/4) \times 10^{-6}$			-
$D_s^- \pi^+ K^*(892)^+$	< 5	$\times 10^{-3}$	$J/\psi(1S) \omega K^+$	$(3.20 \pm 0.60/0.32) \times 10^{-4}$			1388
$D_s^- \pi^+ K^*(892)^+$	< 7	$\times 10^{-3}$	$X_{c0}(3915) K^+, X_{c0} \rightarrow$ $J/\psi \omega$	$(3.0 \pm 0.9/0.7) \times 10^{-5}$			1103
$D_s^- K^+ K^+$	$(9.7 \pm 2.1) \times 10^{-6}$	2149					
$D_s^- K^+ K^+$	< 1.5	$\times 10^{-5}$					
Charmonium modes							
$\eta_c K^+$	$(1.09 \pm 0.08) \times 10^{-3}$	1751					
$\eta_c K^+, \eta_c \rightarrow K_S^0 K^\mp \pi^\pm$	$(2.7 \pm 0.6) \times 10^{-5}$	-					
$\eta_c K^*(892)^+$	$(1.1 \pm 0.5/0.4) \times 10^{-3}$	1646					

Meson Summary Table

$J/\psi(1S)\pi^+$	$(3.92 \pm 0.08) \times 10^{-5}$	1728	$\omega K^*(892)^+$	$< 7.4 \times 10^{-6}$	CL=90%	2503
$J/\psi(1S)\pi^+\pi^+\pi^-\pi^-$	$(1.17 \pm 0.13) \times 10^{-5}$	1635	$\omega(K\pi)_0^{*+}$	$(2.8 \pm 0.4) \times 10^{-5}$		-
$\psi(2S)\pi^+\pi^-\pi^-$	$(1.9 \pm 0.4) \times 10^{-5}$	1304	$\omega K_0^*(1430)^+$	$(2.4 \pm 0.5) \times 10^{-5}$		-
$J/\psi(1S)\rho^+$	$(4.1 \pm 0.5) \times 10^{-5}$	S=1.4 1611	$\omega K_2^*(1430)^+$	$(2.1 \pm 0.4) \times 10^{-5}$		2379
$J/\psi(1S)\pi^+\pi^0$ nonresonant	$< 7.3 \times 10^{-6}$	CL=90% 1717	$a_0(980) + K^0 \times B(a_0(980)^+ \rightarrow \eta\pi^+)$	$< 3.9 \times 10^{-6}$	CL=90%	-
$J/\psi(1S)a_1(1260)^+$	$< 1.2 \times 10^{-3}$	CL=90% 1415	$a_0(980)^0 K^+ \times B(a_0(980)^0 \rightarrow \eta\pi^0)$	$< 2.5 \times 10^{-6}$	CL=90%	-
$J/\psi(1S)p\bar{p}\pi^+$	$< 5.0 \times 10^{-7}$	CL=90% 643	$K^*(892)^0 \pi^+$	$(1.01 \pm 0.08) \times 10^{-5}$		2562
$J/\psi(1S)p\bar{p}\pi^-$	$(1.46 \pm 0.12) \times 10^{-5}$	567	$K^*(892)^+ \pi^0$	$(6.8 \pm 0.9) \times 10^{-6}$		2563
$J/\psi(1S)\Sigma^0 p$	$< 1.1 \times 10^{-5}$	CL=90% -	$K^+ \pi^- \pi^+$	$(5.10 \pm 0.29) \times 10^{-5}$		2609
$J/\psi(1S)D^+$	$< 1.2 \times 10^{-4}$	CL=90% 871	$K^+ \pi^- \pi^+$ nonresonant	$(1.63 \pm 0.21) \times 10^{-5}$		2609
$J/\psi(1S)\bar{D}^0 \pi^+$	$< 2.5 \times 10^{-5}$	CL=90% 665	$\omega(782) K^+$	$(6 \pm 9) \times 10^{-6}$		2558
$\psi(2S)\pi^+$	$(2.44 \pm 0.30) \times 10^{-5}$	1347	$K^+ f_0(980) \times B(f_0(980) \rightarrow \pi^+ \pi^-)$	$(9.4 \pm 1.0) \times 10^{-6}$		2522
$\psi(2S)K^+$	$(6.24 \pm 0.20) \times 10^{-4}$	1284	$f_2(1270)^0 K^+$	$(1.07 \pm 0.27) \times 10^{-6}$		-
$\psi(2S)K^*(892)^+$	$(6.7 \pm 1.4) \times 10^{-4}$	S=1.3 1116	$f_0(1370)^0 K^+ \times B(f_0(1370)^0 \rightarrow \pi^+ \pi^-)$	$< 1.07 \times 10^{-5}$	CL=90%	-
$\psi(2S)K^+\pi^+\pi^-$	$(4.3 \pm 0.5) \times 10^{-4}$	1179	$\rho^0(1450) K^+ \times B(\rho^0(1450) \rightarrow \pi^+ \pi^-)$	$< 1.17 \times 10^{-5}$	CL=90%	-
$\psi(2S)\phi(1020)K^+$	$(4.0 \pm 0.7) \times 10^{-6}$	418	$f_2'(1525) K^+ \times B(f_2'(1525) \rightarrow \pi^+ \pi^-)$	$< 3.4 \times 10^{-6}$	CL=90%	2394
$\psi(3770)K^+$	$(4.3 \pm 1.1) \times 10^{-4}$	1218	$K^+ \rho^0$	$(3.7 \pm 0.5) \times 10^{-6}$		2559
$\psi(3770)K^+, \psi \rightarrow D^0 \bar{D}^0$	$(1.5 \pm 0.5) \times 10^{-4}$	S=1.4 1218	$K_0^*(1430)^0 \pi^+$	$(3.9 \pm 0.6) \times 10^{-5}$	S=1.4	2445
$\psi(3770)K^+, \psi \rightarrow D^+ D^-$	$(9.4 \pm 3.5) \times 10^{-5}$	1218	$K_2^*(1430)^0 \pi^+$	$(5.6 \pm 2.2) \times 10^{-6}$		2445
$\psi(3770)K^+, \psi \rightarrow p\bar{p}$	$< 2 \times 10^{-7}$	CL=95% -	$K^*(1410)^0 \pi^+$	$< 4.5 \times 10^{-5}$	CL=90%	2448
$\psi(4040)K^+$	$< 1.3 \times 10^{-4}$	CL=90% 1003	$K^*(1680)^0 \pi^+$	$< 1.2 \times 10^{-5}$	CL=90%	2358
$\psi(4040)K^+, \psi \rightarrow D^+ D^-$	$(1.1 \pm 0.5) \times 10^{-5}$	-	$K^+ \pi^0 \pi^0$	$(1.62 \pm 0.19) \times 10^{-5}$		2610
$\psi(4160)K^+$	$(5.1 \pm 2.7) \times 10^{-4}$	868	$f_0(980)K^+ \times B(f_0 \rightarrow \pi^0 \pi^0)$	$(2.8 \pm 0.8) \times 10^{-6}$		2522
$\psi(4160)K^+, \psi \rightarrow \bar{D}^0 D^0$	$(8 \pm 5) \times 10^{-5}$	-	$K^- \pi^+ \pi^+$	$< 4.6 \times 10^{-8}$	CL=90%	2609
$\psi(4160)K^+, \psi \rightarrow D^+ D^-$	$(1.5 \pm 0.6) \times 10^{-5}$	-	$K^- \pi^+ \pi^+$ nonresonant	$< 5.6 \times 10^{-5}$	CL=90%	2609
$\psi(4415)K^+, \psi \rightarrow D^+ D^-$	$(2.0 \pm 0.8) \times 10^{-5}$	-	$K_1(1270)^0 \pi^+$	$< 4.0 \times 10^{-5}$	CL=90%	2489
$\chi_{c0}\pi^+, \chi_{c0} \rightarrow \pi^+ \pi^-$	$< 1 \times 10^{-7}$	CL=90% 1531	$K_1(1400)^0 \pi^+$	$< 3.9 \times 10^{-5}$	CL=90%	2451
$\chi_{c0}K^+$	$(1.51 \pm 0.15) \times 10^{-4}$	1478	$K^0 \pi^+ \pi^0$	$< 6.6 \times 10^{-5}$	CL=90%	2609
$\chi_{c0}K^*(892)^+$	$< 2.1 \times 10^{-4}$	CL=90% 1341	$K_0^*(1430)^+ \pi^0$	$(1.19 \pm 0.20) \times 10^{-5}$		-
$\chi_{c1}(1P)\pi^+$	$(2.2 \pm 0.5) \times 10^{-5}$	1468	$K^0 \rho^+$	$(7.3 \pm 1.0) \times 10^{-6}$		2558
$\chi_{c1}(1P)K^+$	$(4.74 \pm 0.22) \times 10^{-4}$	1412	$K^*(892)^+ \pi^+ \pi^-$	$(7.5 \pm 1.0) \times 10^{-5}$		2557
$\chi_{c1}(1P)K^*(892)^+$	$(3.0 \pm 0.6) \times 10^{-4}$	S=1.1 1265	$K^*(892)^+ \rho^0$	$(4.6 \pm 1.1) \times 10^{-6}$		2504
$\chi_{c1}(1P)K^0 \pi^+$	$(5.8 \pm 0.4) \times 10^{-4}$	1370	$K^*(892)^+ f_0(980)$	$(4.2 \pm 0.7) \times 10^{-6}$		2466
$\chi_{c1}(1P)K^+ \pi^0$	$(3.29 \pm 0.35) \times 10^{-4}$	1373	$a_1^+ K^0$	$(3.5 \pm 0.7) \times 10^{-5}$		-
$\chi_{c1}(1P)K^+ \pi^+ \pi^-$	$(3.74 \pm 0.30) \times 10^{-4}$	1319	$b_1^+ K^0 \times B(b_1^+ \rightarrow \omega \pi^+)$	$(9.6 \pm 1.9) \times 10^{-6}$		-
$\chi_{c1}(2P)K^+, \chi_{c1}(2P) \rightarrow \pi^+ \pi^- \chi_{c1}(1P)$	$< 1.1 \times 10^{-5}$	CL=90% -	$K^*(892)^0 \rho^+$	$(9.2 \pm 1.5) \times 10^{-6}$		2504
$\chi_{c2}K^+$	$(1.1 \pm 0.4) \times 10^{-5}$	1379	$K_1(1400)^+ \rho^0$	$< 7.8 \times 10^{-4}$	CL=90%	2388
$\chi_{c2}K^+, \chi_{c2} \rightarrow p\bar{p}\pi^+ \pi^-$	$< 1.9 \times 10^{-7}$	-	$K_2^*(1430)^+ \rho^0$	$< 1.5 \times 10^{-3}$	CL=90%	2381
$\chi_{c2}K^*(892)^+$	$< 1.2 \times 10^{-4}$	CL=90% 1228	$b_1^0 K^+ \times B(b_1^0 \rightarrow \omega \pi^0)$	$(9.1 \pm 2.0) \times 10^{-6}$		-
$\chi_{c2}K^0 \pi^+$	$(1.16 \pm 0.25) \times 10^{-4}$	1336	$b_1^+ K^* \times B(b_1^+ \rightarrow \omega \pi^+)$	$< 5.9 \times 10^{-6}$	CL=90%	-
$\chi_{c2}K^+ \pi^0$	$< 6.2 \times 10^{-5}$	CL=90% 1339	$b_1^0 K^* \times B(b_1^0 \rightarrow \omega \pi^0)$	$< 6.7 \times 10^{-6}$	CL=90%	-
$\chi_{c2}K^+ \pi^+ \pi^-$	$(1.34 \pm 0.19) \times 10^{-4}$	1284	$K^+ \bar{K}^0$	$(1.31 \pm 0.17) \times 10^{-6}$	S=1.2	2593
$\chi_{c2}(3930)K^+, \chi_{c2} \rightarrow D^+ D^-$	$(1.6 \pm 0.6) \times 10^{-5}$	-	$\bar{K}^0 K^+ \pi^0$	$< 2.4 \times 10^{-5}$	CL=90%	2578
$\chi_{c2}(3930)\pi^+, \chi_{c2} \rightarrow \pi^+ \pi^-$	$< 1 \times 10^{-7}$	CL=90% 1437	$K^+ K_S^0 K_S^0$	$(1.05 \pm 0.04) \times 10^{-5}$		2521
$h_c(1P)K^+$	$(3.7 \pm 1.2) \times 10^{-5}$	1401	$f_0(980)K^+, f_0 \rightarrow K_S^0 K_S^0$	$(1.47 \pm 0.33) \times 10^{-5}$		-
$h_c(1P)K^+, h_c \rightarrow p\bar{p}$	$< 6.4 \times 10^{-8}$	CL=95% -	$f_0(1710)K^+, f_0 \rightarrow K_S^0 K_S^0$	$(4.8 \pm 4.0) \times 10^{-7}$		-
K or K* modes			$K^+ K_S^0 K_S^0$ nonresonant	$(2.0 \pm 0.4) \times 10^{-5}$		2521
$K^0 \pi^+$	$(2.37 \pm 0.08) \times 10^{-5}$	2614	$K_S^0 K_S^0 \pi^+$	$< 5.1 \times 10^{-7}$	CL=90%	2577
$K^+ \pi^0$	$(1.29 \pm 0.05) \times 10^{-5}$	2615	$K^+ K^- \pi^+$	$(5.2 \pm 0.4) \times 10^{-6}$		2578
$\eta' K^+$	$(7.04 \pm 0.25) \times 10^{-5}$	2528	$K^+ K^- \pi^+$ nonresonant	$(1.68 \pm 0.26) \times 10^{-6}$		2578
$\eta' K^*(892)^+$	$(4.8 \pm 1.8) \times 10^{-6}$	2472	$K^+ \bar{K}^*(892)^0$	$(5.9 \pm 0.8) \times 10^{-7}$		2540
$\eta' K_0^*(1430)^+$	$(5.2 \pm 2.1) \times 10^{-6}$	-	$K^+ \bar{K}_0^*(1430)^0$	$(3.8 \pm 1.3) \times 10^{-7}$		2421
$\eta' K_2^*(1430)^+$	$(2.8 \pm 0.5) \times 10^{-5}$	2346	$\pi^+ (K^+ K^-) s\text{-wave}$	$(8.5 \pm 0.9) \times 10^{-7}$		2578
ηK^+	$(2.4 \pm 0.4) \times 10^{-6}$	S=1.7 2588	$K^+ K^+ \pi^-$	$< 1.1 \times 10^{-8}$	CL=90%	2578
$\eta K^*(892)^+$	$(1.93 \pm 0.16) \times 10^{-5}$	2534	$K^+ K^+ \pi^-$ nonresonant	$< 8.79 \times 10^{-5}$	CL=90%	2578
$\eta K_0^*(1430)^+$	$(1.8 \pm 0.4) \times 10^{-5}$	-	$f_2'(1525) K^+$	$(1.8 \pm 0.5) \times 10^{-6}$	S=1.1	2394
$\eta K_2^*(1430)^+$	$(9.1 \pm 3.0) \times 10^{-6}$	2414	$K^* \pi^+ K^-$	$< 1.18 \times 10^{-5}$	CL=90%	2524
$\eta(1295)K^+ \times B(\eta(1295) \rightarrow \eta\pi\pi)$	$(2.9 \pm 0.8) \times 10^{-6}$	2455	$K^*(892)^+ K^*(892)^0$	$(9.1 \pm 2.9) \times 10^{-7}$		2485
$\eta(1405)K^+ \times B(\eta(1405) \rightarrow \eta\pi\pi)$	$< 1.3 \times 10^{-6}$	CL=90% 2425	$K^* \pi^+ K^-$	$< 6.1 \times 10^{-6}$	CL=90%	2524
$\eta(1405)K^+ \times B(\eta(1405) \rightarrow K^* K)$	$< 1.2 \times 10^{-6}$	CL=90% 2425	$K^+ K^- K^+$	$(3.40 \pm 0.14) \times 10^{-5}$	S=1.4	2523
$\eta(1475)K^+ \times B(\eta(1475) \rightarrow K^* K)$	$(1.38 \pm 0.21) \times 10^{-5}$	2407	$K^+ \phi$	$(8.8 \pm 0.7) \times 10^{-6}$	S=1.1	2516
$f_1(1285)K^+$	$< 2.0 \times 10^{-6}$	CL=90% 2458	$f_0(980)K^+ \times B(f_0(980) \rightarrow K^+ K^-)$	$(9.4 \pm 3.2) \times 10^{-6}$		2522
$f_1(1420)K^+ \times B(f_1(1420) \rightarrow \eta\pi\pi)$	$< 2.9 \times 10^{-6}$	CL=90% 2420	$a_2(1320)K^+ \times B(a_2(1320) \rightarrow K^+ K^-)$	$< 1.1 \times 10^{-6}$	CL=90%	2449
$f_1(1420)K^+ \times B(f_1(1420) \rightarrow K^* K)$	$< 4.1 \times 10^{-6}$	CL=90% 2420				
$\phi(1680)K^+ \times B(\phi(1680) \rightarrow K^* K)$	$< 3.4 \times 10^{-6}$	CL=90% 2344				
$f_0(1500)K^+$	$(3.7 \pm 2.2) \times 10^{-6}$	2398				
ωK^+	$(6.5 \pm 0.4) \times 10^{-6}$	2558				

Meson Summary Table

$X_0(1550) K^+ \times$ $B(X_0(1550) \rightarrow K^+ K^-)$	$(4.3 \pm 0.7) \times 10^{-6}$	-	$\rho^0 a_1(1260)^+$	< 6.2	$\times 10^{-4}$	CL=90%	2433		
$\phi(1680) K^+ \times B(\phi(1680) \rightarrow$ $K^+ K^-)$	< 8	$\times 10^{-7}$	CL=90%	2344	$\rho^0 a_2(1320)^+$	< 7.2	$\times 10^{-4}$	CL=90%	2410
$f_0(1710) K^+ \times B(f_0(1710) \rightarrow$ $K^+ K^-)$	$(1.1 \pm 0.6) \times 10^{-6}$			2336	$b_1^0 \pi^+, b_1^0 \rightarrow \omega \pi^0$	$(6.7 \pm 2.0) \times 10^{-6}$			-
$K^+ K^- K^+$ nonresonant	$(2.38 \pm 0.28) \times 10^{-5}$			2523	$b_1^+ \pi^0, b_1^+ \rightarrow \omega \pi^+$	< 3.3	$\times 10^{-6}$	CL=90%	-
$K^*(892)^+ K^+ K^-$	$(3.6 \pm 0.5) \times 10^{-5}$			2466	$\pi^+ \pi^+ \pi^+ \pi^- \pi^- \pi^0$	< 6.3	$\times 10^{-3}$	CL=90%	2592
$K^*(892)^+ \phi$	$(10.0 \pm 2.0) \times 10^{-6}$	S=1.7		2460	$b_1^+ \rho^0, b_1^+ \rightarrow \omega \pi^+$	< 5.2	$\times 10^{-6}$	CL=90%	-
$\phi(K\pi)_0^{*+}$	$(8.3 \pm 1.6) \times 10^{-6}$			-	$a_1(1260)^+ a_1(1260)^0$	< 1.3	%	CL=90%	2336
$\phi K_1(1270)^+$	$(6.1 \pm 1.9) \times 10^{-6}$			2380	$b_1^0 \rho^+, b_1^0 \rightarrow \omega \pi^0$	< 3.3	$\times 10^{-6}$	CL=90%	-
$\phi K_1(1400)^+$	< 3.2	$\times 10^{-6}$	CL=90%	2339	Charged particle (h^\pm) modes				
$\phi K^*(1410)^+$	< 4.3	$\times 10^{-6}$	CL=90%	-	$h^\pm = K^\pm \text{ or } \pi^\pm$				
$\phi K_0^*(1430)^+$	$(7.0 \pm 1.6) \times 10^{-6}$			-	$h^+ \pi^0$	$(1.6 \pm 0.7) \times 10^{-5}$			2636
$\phi K_2^*(1430)^+$	$(8.4 \pm 2.1) \times 10^{-6}$			2332	ωh^+	$(1.38 \pm 0.27) \times 10^{-5}$			2580
$\phi K_2^*(1770)^+$	< 1.50	$\times 10^{-5}$	CL=90%	-	$h^+ X^0$ (Familon)	< 4.9	$\times 10^{-5}$	CL=90%	-
$\phi K_2^*(1820)^+$	< 1.63	$\times 10^{-5}$	CL=90%	-	$K^+ X^0, X^0 \rightarrow \mu^+ \mu^-$	< 1	$\times 10^{-7}$	CL=95%	-
$a_1^+ K^{*0}$	< 3.6	$\times 10^{-6}$	CL=90%	-	Baryon modes				
$K^+ \phi$	$(4.2 \pm 0.8) \times 10^{-6}$	S=2.2		2306	$p\bar{p}\pi^+$	$(1.62 \pm 0.20) \times 10^{-6}$			2439
$\eta' \eta' K^+$	< 2.5	$\times 10^{-5}$	CL=90%	2338	$p\bar{p}\pi^+$ nonresonant	< 5.3	$\times 10^{-5}$	CL=90%	2439
$\omega \phi K^+$	< 1.9	$\times 10^{-6}$	CL=90%	2374	$p\bar{p}\pi^+ \pi^0$	$(4.6 \pm 1.3) \times 10^{-6}$			2407
$X(1812) K^+ \times B(X \rightarrow \omega \phi)$	< 3.2	$\times 10^{-7}$	CL=90%	-	$p\bar{p}K^+$	$(5.9 \pm 0.5) \times 10^{-6}$		S=1.5	2348
$K^*(892)^+ \gamma$	$(3.92 \pm 0.22) \times 10^{-5}$	S=1.7		2564	$\Theta(1710)^{++} \bar{p}, \Theta^{++} \rightarrow$ pK^+	$[ppp] < 9.1$	$\times 10^{-8}$	CL=90%	-
$K_1(1270)^+ \gamma$	$(4.4 \pm 0.7) \times 10^{-5}$			2491	$f_J(2220) K^+, f_J \rightarrow p\bar{p}$	$[ppp] < 4.1$	$\times 10^{-7}$	CL=90%	2135
$\eta K^+ \gamma$	$(7.9 \pm 0.9) \times 10^{-6}$			2588	$\rho \bar{\Lambda}(1520)$	$(3.1 \pm 0.6) \times 10^{-7}$			2322
$\eta' K^+ \gamma$	$(2.9 \pm 1.0) \times 10^{-6}$			2528	$\rho \bar{p} K^+$ nonresonant	< 8.9	$\times 10^{-5}$	CL=90%	2348
$\phi K^+ \gamma$	$(2.7 \pm 0.4) \times 10^{-6}$	S=1.2		2516	$\rho \bar{p} K^*(892)^+$	$(3.6 \pm 0.8) \times 10^{-6}$			2215
$K^+ \pi^- \pi^+ \gamma$	$(2.58 \pm 0.15) \times 10^{-5}$	S=1.3		2609	$f_J(2220) K^{*+}, f_J \rightarrow p\bar{p}$	< 7.7	$\times 10^{-7}$	CL=90%	2059
$K^*(892)^0 \pi^+ \gamma$	$(2.33 \pm 0.12) \times 10^{-5}$			2562	$\rho \bar{\Lambda}$	$(2.4 \pm 1.0) \times 10^{-7}$			2430
$K^+ \rho^0 \gamma$	$(8.2 \pm 0.9) \times 10^{-6}$			2559	$\rho \bar{\Lambda} \gamma$	$(2.4 \pm 0.5) \times 10^{-6}$			2430
$(K^+ \pi^-)_{NR} \pi^+ \gamma$	$(9.9 \pm 1.7) \times 10^{-6}$			2609	$\rho \bar{\Lambda} \pi^0$	$(3.0 \pm 0.4) \times 10^{-6}$			2402
$K^0 \pi^+ \pi^0 \gamma$	$(4.6 \pm 0.5) \times 10^{-5}$			2609	$\rho \Sigma(1385)^0$	< 4.7	$\times 10^{-7}$	CL=90%	2362
$K_1(1400)^+ \gamma$	$(10 \pm 5) \times 10^{-6}$			2453	$\Delta^+ \bar{\Lambda}$	< 8.2	$\times 10^{-7}$	CL=90%	-
$K^*(1410)^+ \gamma$	$(2.7 \pm 0.8) \times 10^{-5}$			-	$\rho \Sigma \gamma$	< 4.6	$\times 10^{-6}$	CL=90%	2413
$K_0^*(1430)^0 \pi^+ \gamma$	$(1.32 \pm 0.26) \times 10^{-6}$			2445	$\rho \bar{\Lambda} \pi^+ \pi^-$	$(1.13 \pm 0.13) \times 10^{-5}$			2367
$K_2^*(1430)^+ \gamma$	$(1.4 \pm 0.4) \times 10^{-5}$			2447	$\rho \bar{\Lambda} \pi^+ \pi^-$ nonresonant	$(5.9 \pm 1.1) \times 10^{-6}$			2367
$K^*(1680)^+ \gamma$	$(6.7 \pm 1.7) \times 10^{-5}$			2360	$\rho \bar{\Lambda} \rho^0, \rho^0 \rightarrow \pi^+ \pi^-$	$(4.8 \pm 0.9) \times 10^{-6}$			2214
$K_3^*(1780)^+ \gamma$	< 3.9	$\times 10^{-5}$	CL=90%	2340	$\rho \bar{\Lambda} f_2(1270), f_2 \rightarrow \pi^+ \pi^-$	$(2.0 \pm 0.8) \times 10^{-6}$			2026
$K_4^*(2045)^+ \gamma$	< 9.9	$\times 10^{-3}$	CL=90%	2242	$\rho \bar{\Lambda} K^+ K^-$	$(4.1 \pm 0.7) \times 10^{-6}$			2132
Light unflavored meson modes									
$\rho^+ \gamma$	$(9.8 \pm 2.5) \times 10^{-7}$			2583	$\rho \bar{\Lambda} \phi$	$(8.0 \pm 2.2) \times 10^{-7}$			2119
$\pi^+ \pi^0$	$(5.5 \pm 0.4) \times 10^{-6}$	S=1.2		2636	$\bar{p} \Lambda K^+ K^-$	$(3.7 \pm 0.6) \times 10^{-6}$			2132
$\pi^+ \pi^+ \pi^-$	$(1.52 \pm 0.14) \times 10^{-5}$			2630	$\Lambda \bar{\Lambda} \pi^+$	< 9.4	$\times 10^{-7}$	CL=90%	2358
$\rho^0 \pi^+$	$(8.3 \pm 1.2) \times 10^{-6}$			2581	$\Lambda \bar{\Lambda} K^+$	$(3.4 \pm 0.6) \times 10^{-6}$			2251
$\pi^+ f_0(980), f_0 \rightarrow \pi^+ \pi^-$	< 1.5	$\times 10^{-6}$	CL=90%	2545	$\Lambda \bar{\Lambda} K^{*+}$	$(2.2 \pm 1.2) \times 10^{-6}$			2098
$\pi^+ f_2(1270)$	$(2.2 \pm 0.7) \times 10^{-6}$			2484	$\Lambda(1520) \bar{\Lambda} K^+$	$(2.2 \pm 0.7) \times 10^{-6}$			2126
$\rho(1450)^0 \pi^+, \rho^0 \rightarrow \pi^+ \pi^-$	$(1.4 \pm 0.6) \times 10^{-6}$			2434	$\Lambda \bar{\Lambda}(1520) K^+$	< 2.08	$\times 10^{-6}$		2126
$\rho(1450)^0 \pi^+, \rho^0 \rightarrow K^+ K^-$	$(1.60 \pm 0.14) \times 10^{-6}$			-	$\Delta^0 \rho$	< 1.38	$\times 10^{-6}$	CL=90%	2403
$f_0(1370) \pi^+, f_0 \rightarrow \pi^+ \pi^-$	< 4.0	$\times 10^{-6}$	CL=90%	2460	$\Delta^{++} \bar{p}$	< 1.4	$\times 10^{-7}$	CL=90%	2403
$f_0(500) \pi^+, f_0 \rightarrow \pi^+ \pi^-$	< 4.1	$\times 10^{-6}$	CL=90%	-	$D^+ \rho \bar{p}$	< 1.5	$\times 10^{-5}$	CL=90%	1860
$\pi^+ \pi^- \pi^+$ nonresonant	$(5.3 \pm 1.5) \times 10^{-6}$			2630	$D^*(2010) + p\bar{p}$	< 1.5	$\times 10^{-5}$	CL=90%	1786
$\pi^+ \pi^0 \pi^0$	< 8.9	$\times 10^{-4}$	CL=90%	2631	$\bar{D}^0 p\bar{p}\pi^+$	$(3.72 \pm 0.27) \times 10^{-4}$			1789
$\rho^+ \pi^0$	$(1.09 \pm 0.14) \times 10^{-5}$			2581	$\bar{D}^{*0} p\bar{p}\pi^+$	$(3.73 \pm 0.32) \times 10^{-4}$			1709
$\pi^+ \pi^- \pi^+ \pi^0$	< 4.0	$\times 10^{-3}$	CL=90%	2622	$D^- p\bar{p}\pi^+ \pi^-$	$(1.66 \pm 0.30) \times 10^{-4}$			1705
$\rho^+ \rho^0$	$(2.40 \pm 0.19) \times 10^{-5}$			2523	$D^{*-} p\bar{p}\pi^+ \pi^-$	$(1.86 \pm 0.25) \times 10^{-4}$			1621
$\rho^+ f_0(980), f_0 \rightarrow \pi^+ \pi^-$	< 2.0	$\times 10^{-6}$	CL=90%	2486	$\rho \bar{\Lambda}^0 \bar{D}^0$	$(1.43 \pm 0.32) \times 10^{-5}$			-
$a_1(1260)^+ \pi^0$	$(2.6 \pm 0.7) \times 10^{-5}$			2494	$\rho \bar{\Lambda}^0 \bar{D}^*(2007)^0$	< 5	$\times 10^{-5}$	CL=90%	-
$a_1(1260)^0 \pi^+$	$(2.0 \pm 0.6) \times 10^{-5}$			2494	$\bar{\Lambda}_c^- p \pi^+$	$(2.3 \pm 0.4) \times 10^{-4}$		S=2.2	1980
$\omega \pi^+$	$(6.9 \pm 0.5) \times 10^{-6}$			2580	$\bar{\Lambda}_c^- \Delta(1232)^{++}$	< 1.9	$\times 10^{-5}$	CL=90%	1928
$\omega \rho^+$	$(1.59 \pm 0.21) \times 10^{-5}$			2522	$\bar{\Lambda}_c^- \Delta_X(1600)^{++}$	$(4.7 \pm 1.0) \times 10^{-5}$			-
$\eta \pi^+$	$(4.02 \pm 0.27) \times 10^{-6}$			2609	$\bar{\Lambda}_c^- \Delta_X(2420)^{++}$	$(3.7 \pm 0.8) \times 10^{-5}$			-
$\eta \rho^+$	$(7.0 \pm 2.9) \times 10^{-6}$	S=2.8		2553	$(\bar{\Lambda}_c^- p)_s \pi^+$	$[qqq] (3.1 \pm 0.7) \times 10^{-5}$			-
$\eta' \pi^+$	$(2.7 \pm 0.9) \times 10^{-6}$	S=1.9		2551	$\bar{\Sigma}_c(2520)^0 \rho$	< 3	$\times 10^{-6}$	CL=90%	1904
$\eta' \rho^+$	$(9.7 \pm 2.2) \times 10^{-6}$			2492	$\bar{\Sigma}_c(2800)^0 \rho$	$(2.6 \pm 0.9) \times 10^{-5}$			-
$\phi \pi^+$	$(3.2 \pm 1.5) \times 10^{-8}$			2539	$\bar{\Lambda}_c^- p \pi^+ \pi^0$	$(1.8 \pm 0.6) \times 10^{-3}$			1935
$\phi \rho^+$	< 3.0	$\times 10^{-6}$	CL=90%	2480	$\bar{\Lambda}_c^- p \pi^+ \pi^+ \pi^-$	$(2.2 \pm 0.7) \times 10^{-3}$			1880
$a_0(980)^0 \pi^+, a_0^0 \rightarrow \eta \pi^0$	< 5.8	$\times 10^{-6}$	CL=90%	-	$\bar{\Lambda}_c^- p \pi^+ \pi^+ \pi^- \pi^0$	< 1.34	%	CL=90%	1823
$a_0(980)^+ \pi^0, a_0^+ \rightarrow \eta \pi^+$	< 1.4	$\times 10^{-6}$	CL=90%	-	$\Lambda_c^+ \Lambda_c^- K^+$	$(4.9 \pm 0.7) \times 10^{-4}$			739
$\pi^+ \pi^+ \pi^+ \pi^- \pi^-$	< 8.6	$\times 10^{-4}$	CL=90%	2608	$\Xi_c(2930) \Lambda_c^+, \Xi_c \rightarrow K^+ \Lambda_c^-$	$(1.7 \pm 0.5) \times 10^{-4}$			-
					$\bar{\Sigma}_c(2455)^0 p$	$(2.9 \pm 0.7) \times 10^{-5}$			1938
					$\bar{\Sigma}_c(2455)^0 p \pi^0$	$(3.5 \pm 1.1) \times 10^{-4}$			1896
					$\bar{\Sigma}_c(2455)^0 p \pi^- \pi^+$	$(3.5 \pm 1.1) \times 10^{-4}$			1845
					$\bar{\Sigma}_c(2455)^- p \pi^+ \pi^+$	$(2.37 \pm 0.20) \times 10^{-4}$			1845

Meson Summary Table

$\bar{\Lambda}_c(2593)^- / \bar{\Lambda}_c(2625)^- p \pi^+$	< 1.9	$\times 10^{-4}$	CL=90%	-
$\bar{\Sigma}_c^0 \Lambda_c^+$	(9.5 \pm 2.3)	$\times 10^{-4}$		1144
$\bar{\Sigma}_c^0 \Lambda_c^+, \bar{\Xi}_c^0 \rightarrow \Xi^+ \pi^-$	(1.76 \pm 0.29)	$\times 10^{-5}$		1144
$\bar{\Sigma}_c^0 \Lambda_c^+, \bar{\Xi}_c^0 \rightarrow \Lambda K^+ \pi^-$	(1.14 \pm 0.26)	$\times 10^{-5}$		1144
$\bar{\Sigma}_c^0 \Lambda_c^+, \bar{\Xi}_c^0 \rightarrow p K^- K^- \pi^+$	(5.5 \pm 1.9)	$\times 10^{-6}$		-
$\Lambda_c^+ \bar{\Sigma}_c^0$	< 6.5	$\times 10^{-4}$	CL=90%	1023
$\Lambda_c^+ \bar{\Sigma}_c(2645)^0$	< 7.9	$\times 10^{-4}$	CL=90%	-
$\Lambda_c^+ \bar{\Sigma}_c(2790)^0$	(1.1 \pm 0.4)	$\times 10^{-3}$		-

Lepton Family number (LF) or Lepton number (L) or Baryon number (B) violating modes, or/and $\Delta B = 1$ weak neutral current (BI) modes

$\pi^+ \ell^+ \ell^-$	BI	< 4.9	$\times 10^{-8}$	CL=90%	2638
$\pi^+ e^+ e^-$	BI	< 8.0	$\times 10^{-8}$	CL=90%	2638
$\pi^+ \mu^+ \mu^-$	BI	(1.78 \pm 0.23)	$\times 10^{-8}$		2634
$\pi^+ \nu \bar{\nu}$	BI	< 1.4	$\times 10^{-5}$	CL=90%	2638
$K^+ \ell^+ \ell^-$	BI	[iii] (4.7 \pm 0.5)	$\times 10^{-7}$	S=2.3	2617
$K^+ e^+ e^-$	BI	(5.6 \pm 0.6)	$\times 10^{-7}$		2617
$K^+ \mu^+ \mu^-$	BI	(4.53 \pm 0.35)	$\times 10^{-7}$	S=1.8	2612
$K^+ \mu^+ \mu^-$ nonresonant	BI	(4.37 \pm 0.27)	$\times 10^{-7}$		2612
$K^+ \tau^+ \tau^-$	BI	< 2.25	$\times 10^{-3}$	CL=90%	1687
$K^+ \bar{\nu} \nu$	BI	< 1.6	$\times 10^{-5}$	CL=90%	2617
$\rho^+ \nu \bar{\nu}$	BI	< 3.0	$\times 10^{-5}$	CL=90%	2583
$K^*(892)^+ \ell^+ \ell^-$	BI	[iii] (1.01 \pm 0.11)	$\times 10^{-6}$	S=1.1	2564
$K^*(892)^+ e^+ e^-$	BI	(1.55 \pm 0.40 / 0.31)	$\times 10^{-6}$		2564
$K^*(892)^+ \mu^+ \mu^-$	BI	(9.6 \pm 1.0)	$\times 10^{-7}$		2560
$K^*(892)^+ \nu \bar{\nu}$	BI	< 4.0	$\times 10^{-5}$	CL=90%	2564
$K^+ \pi^+ \pi^- \mu^+ \mu^-$	BI	(4.3 \pm 0.4)	$\times 10^{-7}$		2593
$\phi K^+ \mu^+ \mu^-$	BI	(7.9 \pm 2.1 / 1.7)	$\times 10^{-8}$		2490
$\bar{\Lambda} \rho \nu \bar{\nu}$	< 3.0	$\times 10^{-5}$	CL=90%	2430	
$\pi^+ e^+ \mu^-$	LF	< 6.4	$\times 10^{-3}$	CL=90%	2637
$\pi^+ e^- \mu^+$	LF	< 6.4	$\times 10^{-3}$	CL=90%	2637
$\pi^+ e^\pm \mu^\mp$	LF	< 1.7	$\times 10^{-7}$	CL=90%	2637
$\pi^+ e^+ \tau^-$	LF	< 7.4	$\times 10^{-5}$	CL=90%	2338
$\pi^+ e^- \tau^+$	LF	< 2.0	$\times 10^{-5}$	CL=90%	2338
$\pi^+ e^\pm \tau^\mp$	LF	< 7.5	$\times 10^{-5}$	CL=90%	2338
$\pi^+ \mu^+ \tau^-$	LF	< 6.2	$\times 10^{-5}$	CL=90%	2334
$\pi^+ \mu^- \tau^+$	LF	< 4.5	$\times 10^{-5}$	CL=90%	2334
$\pi^+ \mu^\pm \tau^\mp$	LF	< 7.2	$\times 10^{-5}$	CL=90%	2334
$K^+ e^+ \mu^-$	LF	< 7.0	$\times 10^{-9}$	CL=90%	2616
$K^+ e^- \mu^+$	LF	< 6.4	$\times 10^{-9}$	CL=90%	2616
$K^+ e^\pm \mu^\mp$	LF	< 9.1	$\times 10^{-8}$	CL=90%	2616
$K^+ e^+ \tau^-$	LF	< 4.3	$\times 10^{-5}$	CL=90%	2312
$K^+ e^- \tau^+$	LF	< 1.5	$\times 10^{-5}$	CL=90%	2312
$K^+ e^\pm \tau^\mp$	LF	< 3.0	$\times 10^{-5}$	CL=90%	2312
$K^+ \mu^+ \tau^-$	LF	< 4.5	$\times 10^{-5}$	CL=90%	2298
$K^+ \mu^- \tau^+$	LF	< 2.8	$\times 10^{-5}$	CL=90%	2298
$K^+ \mu^\pm \tau^\mp$	LF	< 4.8	$\times 10^{-5}$	CL=90%	2298
$K^*(892)^+ e^+ \mu^-$	LF	< 1.3	$\times 10^{-6}$	CL=90%	2563
$K^*(892)^+ e^- \mu^+$	LF	< 9.9	$\times 10^{-7}$	CL=90%	2563
$K^*(892)^+ e^\pm \mu^\mp$	LF	< 1.4	$\times 10^{-6}$	CL=90%	2563
$\pi^- e^+ e^+$	L	< 2.3	$\times 10^{-8}$	CL=90%	2638
$\pi^- \mu^+ \mu^+$	L	< 4.0	$\times 10^{-9}$	CL=95%	2634
$\pi^- e^+ \mu^+$	L	< 1.5	$\times 10^{-7}$	CL=90%	2637
$\rho^- e^+ e^+$	L	< 1.7	$\times 10^{-7}$	CL=90%	2583
$\rho^- \mu^+ \mu^+$	L	< 4.2	$\times 10^{-7}$	CL=90%	2578
$\rho^- e^+ \mu^+$	L	< 4.7	$\times 10^{-7}$	CL=90%	2582
$K^- e^+ e^+$	L	< 3.0	$\times 10^{-8}$	CL=90%	2617
$K^- \mu^+ \mu^+$	L	< 4.1	$\times 10^{-8}$	CL=90%	2612
$K^- e^+ \mu^+$	L	< 1.6	$\times 10^{-7}$	CL=90%	2616
$K^*(892)^- e^+ e^+$	L	< 4.0	$\times 10^{-7}$	CL=90%	2564
$K^*(892)^- \mu^+ \mu^+$	L	< 5.9	$\times 10^{-7}$	CL=90%	2560
$K^*(892)^- e^+ \mu^+$	L	< 3.0	$\times 10^{-7}$	CL=90%	2563
$D^- e^+ e^+$	L	< 2.6	$\times 10^{-6}$	CL=90%	2309
$D^- e^+ \mu^+$	L	< 1.8	$\times 10^{-6}$	CL=90%	2307
$D^- \mu^+ \mu^+$	L	< 6.9	$\times 10^{-7}$	CL=95%	2303
$D^* \mu^+ \mu^+$	L	< 2.4	$\times 10^{-6}$	CL=95%	2251
$D_s^- \mu^+ \mu^+$	L	< 5.8	$\times 10^{-7}$	CL=95%	2267
$\bar{D}^0 \pi^- \mu^+ \mu^+$	L	< 1.5	$\times 10^{-6}$	CL=95%	2295
$\Lambda^0 \mu^+$	L,B	< 6	$\times 10^{-8}$	CL=90%	-
$\Lambda^0 e^+$	L,B	< 3.2	$\times 10^{-8}$	CL=90%	-
$\bar{\Lambda}^0 \mu^+$	L,B	< 6	$\times 10^{-8}$	CL=90%	-
$\bar{\Lambda}^0 e^+$	L,B	< 8	$\times 10^{-8}$	CL=90%	-

B⁰

$$I(J^P) = \frac{1}{2}(0^-)$$

I, J, P need confirmation. Quantum numbers shown are quark-model predictions.

$$\text{Mass } m_{B^0} = 5279.66 \pm 0.12 \text{ MeV}$$

$$m_{B^0} - m_{B^\pm} = 0.32 \pm 0.05 \text{ MeV}$$

$$\text{Mean life } \tau_{B^0} = (1.519 \pm 0.004) \times 10^{-12} \text{ s}$$

$$c\tau = 455.4 \text{ } \mu\text{m}$$

$$\tau_{B^+} / \tau_{B^0} = 1.076 \pm 0.004 \quad (\text{direct measurements})$$

B⁰- \bar{B}^0 mixing parameters

$$\chi_d (\text{B}^0\text{-}\bar{\text{B}}^0 \text{ mixing probability}) = 0.1858 \pm 0.0011$$

$$\Delta m_{B^0} = m_{B_H^0} - m_{B_L^0} = (0.5065 \pm 0.0019) \times 10^{12} \text{ } \hbar \text{ s}^{-1} \\ = (3.334 \pm 0.013) \times 10^{-10} \text{ MeV}$$

$$x_d = \Delta m_{B^0} / \Gamma_{B^0} = 0.769 \pm 0.004$$

$$\text{Re}(\lambda_{CP} / |\lambda_{CP}|) \text{Re}(z) = 0.047 \pm 0.022$$

$$\Delta \Gamma \text{Re}(z) = -0.007 \pm 0.004 \text{ ps}^{-1}$$

$$\text{Re}(z) = (-4 \pm 4) \times 10^{-2} \quad (S = 1.4)$$

$$\text{Im}(z) = (-0.8 \pm 0.4) \times 10^{-2}$$

CP violation parameters

$$\text{Re}(\epsilon_{B^0}) / (1 + |\epsilon_{B^0}|^2) = (-0.5 \pm 0.4) \times 10^{-3}$$

$$A_{T/CP}(B^0 \leftrightarrow \bar{B}^0) = 0.005 \pm 0.018$$

$$A_{CP}(B^0 \rightarrow D^*(2010)^+ D^-) = 0.013 \pm 0.014$$

$$A_{CP}(B^0 \rightarrow [K^+ K^-]_D K^*(892)^0) = -0.05 \pm 0.10$$

$$A_{CP}(B^0 \rightarrow [K^+ \pi^-]_D K^*(892)^0) = 0.047 \pm 0.029$$

$$A_{CP}(B^0 \rightarrow [K^+ \pi^- \pi^+ \pi^-]_D K^*(892)^0) = 0.037 \pm 0.034$$

$$A_{CP}(B^0 \rightarrow [K^- \pi^+]_D K^*(892)^0) = 0.19 \pm 0.19$$

$$A_{CP}(B^0 \rightarrow [K^- \pi^+ \pi^+ \pi^-]_D K^*(892)^0) = -0.01 \pm 0.24$$

$$R_d^+ = \Gamma(B^0 \rightarrow [\pi^+ K^-]_D K^*) / \Gamma(B^0 \rightarrow [\pi^- K^+]_D K^*) = 0.064 \pm 0.021$$

$$R_d^- = \Gamma(\bar{B}^0 \rightarrow [\pi^- K^+]_D K^*) / \Gamma(\bar{B}^0 \rightarrow [\pi^+ K^-]_D K^*) = 0.095 \pm 0.021$$

$$A_{CP}(B^0 \rightarrow [\pi^+ \pi^-]_D K^*(892)^0) = -0.18 \pm 0.14$$

$$A_{CP}(B^0 \rightarrow [\pi^+ \pi^- \pi^+ \pi^-]_D K^*(892)^0) = -0.03 \pm 0.15$$

$$R_d^+ = \Gamma(B^0 \rightarrow [\pi^+ K^- \pi^+ \pi^-]_D K^*) / \Gamma(B^0 \rightarrow [\pi^- K^+ \pi^+ \pi^-]_D K^*) = 0.074 \pm 0.026$$

$$R_d^- = \Gamma(\bar{B}^0 \rightarrow [\pi^- K^+ \pi^+ \pi^-]_D K^*) / \Gamma(\bar{B}^0 \rightarrow [\pi^+ K^- \pi^+ \pi^-]_D K^*) = 0.072 \pm 0.025$$

$$A_{CP}(B^0 \rightarrow K^+ \pi^-) = -0.0834 \pm 0.0032$$

$$A_{CP}(B^0 \rightarrow \eta' K^*(892)^0) = -0.07 \pm 0.18$$

$$A_{CP}(B^0 \rightarrow \eta' K_0^*(1430)^0) = -0.19 \pm 0.17$$

$$A_{CP}(B^0 \rightarrow \eta' K_2^*(1430)^0) = 0.14 \pm 0.18$$

$$A_{CP}(B^0 \rightarrow \eta K^*(892)^0) = 0.19 \pm 0.05$$

$$A_{CP}(B^0 \rightarrow \eta K_0^*(1430)^0) = 0.06 \pm 0.13$$

$$A_{CP}(B^0 \rightarrow \eta K_2^*(1430)^0) = -0.07 \pm 0.19$$

$$A_{CP}(B^0 \rightarrow b_1 K^+) = -0.07 \pm 0.12$$

$$A_{CP}(B^0 \rightarrow \omega K^*) = 0.45 \pm 0.25$$

$$A_{CP}(B^0 \rightarrow \omega(K\pi)_0^*) = -0.07 \pm 0.09$$

$$A_{CP}(B^0 \rightarrow \omega K_2^*(1430)^0) = -0.37 \pm 0.17$$

$$A_{CP}(B^0 \rightarrow K^+ \pi^- \pi^0) = (0 \pm 6) \times 10^{-2}$$

$$A_{CP}(B^0 \rightarrow \rho^- K^+) = 0.20 \pm 0.11$$

$$A_{CP}(B^0 \rightarrow \rho(1450)^- K^+) = -0.10 \pm 0.33$$

$$A_{CP}(B^0 \rightarrow \rho(1700)^- K^+) = -0.4 \pm 0.6$$

$$A_{CP}(B^0 \rightarrow K^+ \pi^- \pi^0 \text{ nonresonant}) = 0.10 \pm 0.18$$

$$A_{CP}(B^0 \rightarrow K^0 \pi^+ \pi^-) = -0.01 \pm 0.05$$

$$A_{CP}(B^0 \rightarrow K^*(892)^+ \pi^-) = -0.27 \pm 0.04$$

$$A_{CP}(B^0 \rightarrow (K\pi)_0^{*+} \pi^-) = 0.02 \pm 0.04$$

$$A_{CP}(B^0 \rightarrow K_2^*(1430)^+ \pi^-) = -0.29 \pm 0.24$$

$$A_{CP}(B^0 \rightarrow K^*(1680)^+ \pi^-) = -0.07 \pm 0.14$$

$$A_{CP}(B^0 \rightarrow f_0(980) K_S^0) = 0.28 \pm 0.31$$

$$A_{CP}(B^0 \rightarrow (K\pi)_0^{*0} \pi^0) = -0.15 \pm 0.11$$

$$A_{CP}(B^0 \rightarrow K^* \pi^0) = -0.15 \pm 0.13$$

$$A_{CP}(B^0 \rightarrow K^*(892)^0 \pi^+ \pi^-) = 0.07 \pm 0.05$$

$$A_{CP}(B^0 \rightarrow K^*(892)^0 \rho^0) = -0.06 \pm 0.09$$

$$A_{CP}(B^0 \rightarrow K^* f_0(980)) = 0.07 \pm 0.10$$

$$A_{CP}(B^0 \rightarrow K^{*+} \rho^-) = 0.21 \pm 0.15$$

$$A_{CP}(B^0 \rightarrow K^*(892)^0 K^+ K^-) = 0.01 \pm 0.05$$

$$A_{CP}(B^0 \rightarrow a_1^- K^+) = -0.16 \pm 0.12$$

$$A_{CP}(B^0 \rightarrow K^0 K^0) = -0.6 \pm 0.7$$

$$A_{CP}(B^0 \rightarrow K^*(892)^0 \phi) = 0.00 \pm 0.04$$

$$A_{CP}(B^0 \rightarrow K^*(892)^0 K^- \pi^+) = 0.2 \pm 0.4$$

$$A_{CP}(B^0 \rightarrow \phi(K\pi)_0^*) = 0.12 \pm 0.08$$

Meson Summary Table

$A_{CP}(B^0 \rightarrow \phi K_S^*(1430)^0) = -0.11 \pm 0.10$	$S_{K_S K_S K_S}(B^0 \rightarrow K_S K_S K_S) = -0.82 \pm 0.17$
$A_{CP}(B^0 \rightarrow K^*(892)^0 \gamma) = -0.006 \pm 0.011$	$C_{K_S^0 \pi^0 \gamma}(B^0 \rightarrow K_S^0 \pi^0 \gamma) = 0.36 \pm 0.33$
$A_{CP}(B^0 \rightarrow K_S^*(1430)^0 \gamma) = -0.08 \pm 0.15$	$S_{K_S^0 \pi^0 \gamma}(B^0 \rightarrow K_S^0 \pi^0 \gamma) = -0.8 \pm 0.6$
$A_{CP}(B^0 \rightarrow X_S \gamma) = -0.009 \pm 0.018$	$C_{K_S^0 \pi^+ \pi^- \gamma}(B^0 \rightarrow K_S^0 \pi^+ \pi^- \gamma) = -0.39 \pm 0.20$
$A_{CP}(B^0 \rightarrow \rho^+ \pi^-) = 0.13 \pm 0.06 \quad (S = 1.1)$	$S_{K_S^0 \pi^+ \pi^- \gamma}(B^0 \rightarrow K_S^0 \pi^+ \pi^- \gamma) = 0.14 \pm 0.25$
$A_{CP}(B^0 \rightarrow \rho^- \pi^+) = -0.08 \pm 0.08$	$C_{K^{*0} \gamma}(B^0 \rightarrow K^*(892)^0 \gamma) = -0.04 \pm 0.16 \quad (S = 1.2)$
$A_{CP}(B^0 \rightarrow a_1(1260)^\pm \pi^\mp) = -0.07 \pm 0.06$	$S_{K^{*0} \gamma}(B^0 \rightarrow K^*(892)^0 \gamma) = -0.15 \pm 0.22$
$A_{CP}(B^0 \rightarrow b_1^- \pi^+) = -0.05 \pm 0.10$	$C_{\eta K^0 \gamma}(B^0 \rightarrow \eta K^0 \gamma) = 0.1 \pm 0.4 \quad (S = 1.4)$
$A_{CP}(B^0 \rightarrow \rho \bar{P} K^*(892)^0) = 0.05 \pm 0.12$	$S_{\eta K^0 \gamma}(B^0 \rightarrow \eta K^0 \gamma) = -0.5 \pm 0.5 \quad (S = 1.2)$
$A_{CP}(B^0 \rightarrow \rho \bar{A} \pi^-) = 0.04 \pm 0.07$	$C_{K^0 \phi \gamma}(B^0 \rightarrow K^0 \phi \gamma) = -0.3 \pm 0.6$
$A_{CP}(B^0 \rightarrow K^{*0} \ell^+ \ell^-) = -0.05 \pm 0.10$	$S_{K^0 \phi \gamma}(B^0 \rightarrow K^0 \phi \gamma) = 0.7^{+0.7}_{-1.1}$
$A_{CP}(B^0 \rightarrow K^{*0} e^+ e^-) = -0.21 \pm 0.19$	$C(B^0 \rightarrow K_S^0 \rho^0 \gamma) = -0.05 \pm 0.19$
$A_{CP}(B^0 \rightarrow K^{*0} \mu^+ \mu^-) = -0.034 \pm 0.024$	$S(B^0 \rightarrow K_S^0 \rho^0 \gamma) = -0.04 \pm 0.23$
$C_{D^{*+} D^+}(B^0 \rightarrow D^*(2010)^- D^+) = -0.02 \pm 0.08$	$C(B^0 \rightarrow \rho^0 \gamma) = 0.4 \pm 0.5$
$S_{D^{*+} D^+}(B^0 \rightarrow D^*(2010)^- D^+) = -0.83 \pm 0.09$	$S(B^0 \rightarrow \rho^0 \gamma) = -0.8 \pm 0.7$
$C_{D^{*+} D^-}(B^0 \rightarrow D^*(2010)^+ D^-) = -0.03 \pm 0.09 \quad (S = 1.1)$	$C_{\pi \pi}(B^0 \rightarrow \pi^+ \pi^-) = -0.314 \pm 0.030$
$S_{D^{*+} D^-}(B^0 \rightarrow D^*(2010)^+ D^-) = -0.80 \pm 0.09$	$S_{\pi \pi}(B^0 \rightarrow \pi^+ \pi^-) = -0.670 \pm 0.030$
$C_{D^{*+} D^{*-}}(B^0 \rightarrow D^{*+} D^{*-}) = 0.01 \pm 0.09 \quad (S = 1.6)$	$C_{\pi^0 \pi^0}(B^0 \rightarrow \pi^0 \pi^0) = -0.33 \pm 0.22$
$S_{D^{*+} D^{*-}}(B^0 \rightarrow D^{*+} D^{*-}) = -0.59 \pm 0.14 \quad (S = 1.8)$	$C_{\rho \pi}(B^0 \rightarrow \rho^+ \pi^-) = -0.03 \pm 0.07 \quad (S = 1.2)$
$C_+(B^0 \rightarrow D^{*+} D^{*-}) = 0.00 \pm 0.10 \quad (S = 1.6)$	$S_{\rho \pi}(B^0 \rightarrow \rho^+ \pi^-) = 0.05 \pm 0.07$
$S_+(B^0 \rightarrow D^{*+} D^{*-}) = -0.73 \pm 0.09$	$\Delta C_{\rho \pi}(B^0 \rightarrow \rho^+ \pi^-) = 0.27 \pm 0.06$
$C_-(B^0 \rightarrow D^{*+} D^{*-}) = 0.19 \pm 0.31$	$\Delta S_{\rho \pi}(B^0 \rightarrow \rho^+ \pi^-) = 0.01 \pm 0.08$
$S_-(B^0 \rightarrow D^{*+} D^{*-}) = 0.1 \pm 1.6 \quad (S = 3.5)$	$C_{\rho^0 \pi^0}(B^0 \rightarrow \rho^0 \pi^0) = 0.27 \pm 0.24$
$C(B^0 \rightarrow D^*(2010)^+ D^*(2010)^- K_S^0) = 0.01 \pm 0.29$	$S_{\rho^0 \pi^0}(B^0 \rightarrow \rho^0 \pi^0) = -0.23 \pm 0.34$
$S(B^0 \rightarrow D^*(2010)^+ D^*(2010)^- K_S^0) = 0.1 \pm 0.4$	$C_{a_1 \pi}(B^0 \rightarrow a_1(1260)^+ \pi^-) = -0.05 \pm 0.11$
$C_{D^+ D^-}(B^0 \rightarrow D^+ D^-) = -0.22 \pm 0.24 \quad (S = 2.5)$	$S_{a_1 \pi}(B^0 \rightarrow a_1(1260)^+ \pi^-) = -0.2 \pm 0.4 \quad (S = 3.2)$
$S_{D^+ D^-}(B^0 \rightarrow D^+ D^-) = -0.76^{+0.15}_{-0.13} \quad (S = 1.2)$	$\Delta C_{a_1 \pi}(B^0 \rightarrow a_1(1260)^+ \pi^-) = 0.43 \pm 0.14 \quad (S = 1.3)$
$C_{J/\psi(1S) \pi^0}(B^0 \rightarrow J/\psi(1S) \pi^0) = 0.03 \pm 0.17 \quad (S = 1.5)$	$\Delta S_{a_1 \pi}(B^0 \rightarrow a_1(1260)^+ \pi^-) = -0.11 \pm 0.12$
$S_{J/\psi(1S) \pi^0}(B^0 \rightarrow J/\psi(1S) \pi^0) = -0.88 \pm 0.32 \quad (S = 2.2)$	$C(B^0 \rightarrow b_1^- K^+) = -0.22 \pm 0.24$
$C(B^0 \rightarrow J/\psi(1S) \rho^0) = -0.06 \pm 0.06$	$\Delta C(B^0 \rightarrow b_1^- \pi^+) = -1.04 \pm 0.24$
$S(B^0 \rightarrow J/\psi(1S) \rho^0) = -0.66^{+0.16}_{-0.12}$	$C_{\rho^0 \rho^0}(B^0 \rightarrow \rho^0 \rho^0) = 0.2 \pm 0.9$
$C_{D_{CP}^{(*)} h^0}(B^0 \rightarrow D_{CP}^{(*)} h^0) = -0.02 \pm 0.08$	$S_{\rho^0 \rho^0}(B^0 \rightarrow \rho^0 \rho^0) = 0.3 \pm 0.7$
$S_{D_{CP}^{(*)} h^0}(B^0 \rightarrow D_{CP}^{(*)} h^0) = -0.66 \pm 0.12$	$C_{\rho \rho}(B^0 \rightarrow \rho^+ \rho^-) = 0.00 \pm 0.09$
$C_{K^0 \pi^0}(B^0 \rightarrow K^0 \pi^0) = 0.00 \pm 0.13 \quad (S = 1.4)$	$S_{\rho \rho}(B^0 \rightarrow \rho^+ \rho^-) = -0.14 \pm 0.13$
$S_{K^0 \pi^0}(B^0 \rightarrow K^0 \pi^0) = 0.58 \pm 0.17$	$ \lambda (B^0 \rightarrow J/\psi K^*(892)^0) < 0.25, \text{CL} = 95\%$
$C_{\eta'(958) K_S^0}(B^0 \rightarrow \eta'(958) K_S^0) = -0.04 \pm 0.20 \quad (S = 2.5)$	$\cos 2\beta(B^0 \rightarrow J/\psi K^*(892)^0) = 1.7^{+0.7}_{-0.9} \quad (S = 1.6)$
$S_{\eta'(958) K_S^0}(B^0 \rightarrow \eta'(958) K_S^0) = 0.43 \pm 0.17 \quad (S = 1.5)$	$\cos 2\beta(B^0 \rightarrow [K_S^0 \pi^+ \pi^-]_{D^{(*)} h^0}) = 0.91 \pm 0.25$
$C_{\eta' K^0}(B^0 \rightarrow \eta' K^0) = -0.06 \pm 0.04$	$(S_+ + S_-)/2(B^0 \rightarrow D^{*-} \pi^+) = -0.039 \pm 0.11$
$S_{\eta' K^0}(B^0 \rightarrow \eta' K^0) = 0.63 \pm 0.06$	$(S_- - S_+)/2(B^0 \rightarrow D^{*-} \pi^+) = -0.009 \pm 0.015$
$C_{\omega K_S^0}(B^0 \rightarrow \omega K_S^0) = 0.0 \pm 0.4 \quad (S = 3.0)$	$(S_+ + S_-)/2(B^0 \rightarrow D^- \pi^+) = -0.046 \pm 0.023$
$S_{\omega K_S^0}(B^0 \rightarrow \omega K_S^0) = 0.70 \pm 0.21$	$(S_- - S_+)/2(B^0 \rightarrow D^- \pi^+) = -0.022 \pm 0.021$
$C(B^0 \rightarrow K_S^0 \pi^0 \pi^0) = -0.21 \pm 0.20$	$S_+(B^0 \rightarrow D^- \pi^+) = 0.058 \pm 0.023$
$S(B^0 \rightarrow K_S^0 \pi^0 \pi^0) = 0.89^{+0.27}_{-0.30}$	$S_-(B^0 \rightarrow D^- \pi^+) = 0.038 \pm 0.021$
$C_{\rho^0 K_S^0}(B^0 \rightarrow \rho^0 K_S^0) = -0.04 \pm 0.20$	$(S_+ + S_-)/2(B^0 \rightarrow D^- \rho^+) = -0.024 \pm 0.032$
$S_{\rho^0 K_S^0}(B^0 \rightarrow \rho^0 K_S^0) = 0.50^{+0.17}_{-0.21}$	$(S_- - S_+)/2(B^0 \rightarrow D^- \rho^+) = -0.10 \pm 0.06$
$C_{f_0 K_S^0}(B^0 \rightarrow f_0(980) K_S^0) = 0.29 \pm 0.20$	$C_{\eta_c K_S^0}(B^0 \rightarrow \eta_c K_S^0) = 0.08 \pm 0.13$
$S_{f_0 K_S^0}(B^0 \rightarrow f_0(980) K_S^0) = -0.50 \pm 0.16$	$S_{\eta_c K_S^0}(B^0 \rightarrow \eta_c K_S^0) = 0.93 \pm 0.17$
$S_{f_2 K_S^0}(B^0 \rightarrow f_2(1270) K_S^0) = -0.5 \pm 0.5$	$C_{c \bar{c} K^{(*)0}}(B^0 \rightarrow c \bar{c} K^{(*)0}) = (-0.5 \pm 1.5) \times 10^{-2}$
$C_{f_2 K_S^0}(B^0 \rightarrow f_2(1270) K_S^0) = 0.3 \pm 0.4$	$\sin(2\beta) = 0.699 \pm 0.017$
$S_{f_x K_S^0}(B^0 \rightarrow f_x(1300) K_S^0) = -0.2 \pm 0.5$	$C_{J/\psi(nS) K^0}(B^0 \rightarrow J/\psi(nS) K^0) = (-0.8 \pm 1.7) \times 10^{-2}$
$C_{f_x K_S^0}(B^0 \rightarrow f_x(1300) K_S^0) = 0.13 \pm 0.35$	$S_{J/\psi(nS) K^0}(B^0 \rightarrow J/\psi(nS) K^0) = 0.701 \pm 0.017$
$S_{K^0 \pi^+ \pi^-}(B^0 \rightarrow K^0 \pi^+ \pi^- \text{ nonresonant}) = -0.01 \pm 0.33$	$C_{J/\psi K^{*0}}(B^0 \rightarrow J/\psi K^{*0}) = 0.03 \pm 0.10$
$C_{K^0 \pi^+ \pi^-}(B^0 \rightarrow K^0 \pi^+ \pi^- \text{ nonresonant}) = 0.01 \pm 0.26$	$S_{J/\psi K^{*0}}(B^0 \rightarrow J/\psi K^{*0}) = 0.60 \pm 0.25$
$C_{K_S^0 K_S^0}(B^0 \rightarrow K_S^0 K_S^0) = 0.0 \pm 0.4 \quad (S = 1.4)$	$C_{\chi_{c0} K_S^0}(B^0 \rightarrow \chi_{c0} K_S^0) = -0.3^{+0.5}_{-0.4}$
$S_{K_S^0 K_S^0}(B^0 \rightarrow K_S^0 K_S^0) = -0.8 \pm 0.5$	$S_{\chi_{c0} K_S^0}(B^0 \rightarrow \chi_{c0} K_S^0) = -0.7 \pm 0.5$
$C_{K^+ K^- K_S^0}(B^0 \rightarrow K^+ K^- K_S^0 \text{ nonresonant}) = 0.06 \pm 0.08$	$C_{\chi_{c1} K_S^0}(B^0 \rightarrow \chi_{c1} K_S^0) = 0.06 \pm 0.07$
$S_{K^+ K^- K_S^0}(B^0 \rightarrow K^+ K^- K_S^0 \text{ nonresonant}) = -0.66 \pm 0.11$	$S_{\chi_{c1} K_S^0}(B^0 \rightarrow \chi_{c1} K_S^0) = 0.63 \pm 0.10$
$C_{K^+ K^- K_S^0}(B^0 \rightarrow K^+ K^- K_S^0 \text{ inclusive}) = 0.01 \pm 0.09$	$\sin(2\beta_{\text{eff}})(B^0 \rightarrow \phi K^0) = 0.22 \pm 0.30$
$S_{K^+ K^- K_S^0}(B^0 \rightarrow K^+ K^- K_S^0 \text{ inclusive}) = -0.65 \pm 0.12$	$\sin(2\beta_{\text{eff}})(B^0 \rightarrow \phi K_S^*(1430)^0) = 0.97^{+0.03}_{-0.52}$
$C_{\phi K_S^0}(B^0 \rightarrow \phi K_S^0) = 0.01 \pm 0.14$	$\sin(2\beta_{\text{eff}})(B^0 \rightarrow K^+ K^- K_S^0) = 0.77^{+0.13}_{-0.12}$
$S_{\phi K_S^0}(B^0 \rightarrow \phi K_S^0) = 0.59 \pm 0.14$	$\sin(2\beta_{\text{eff}})(B^0 \rightarrow [K_S^0 \pi^+ \pi^-]_{D^{(*)} h^0}) = 0.80 \pm 0.16$
$C_{K_S K_S K_S}(B^0 \rightarrow K_S K_S K_S) = -0.14 \pm 0.12$	$\beta_{\text{eff}}(B^0 \rightarrow [K_S^0 \pi^+ \pi^-]_{D^{(*)} h^0}) = (22 \pm 5)^\circ$
	$2\beta_{\text{eff}}(B^0 \rightarrow J/\psi \rho^0) = (42^{+10}_{-11})^\circ$
	$ \lambda (B^0 \rightarrow [K_S^0 \pi^+ \pi^-]_{D^{(*)} h^0}) = 1.01 \pm 0.08$
	$ \sin(2\beta + \gamma) > 0.40, \text{CL} = 90\%$

Meson Summary Table

$$2\beta + \gamma = (83 \pm 6)^\circ$$

$$\alpha = (85.2_{-4.3}^{+4.8})^\circ$$

$$x_+(B^0 \rightarrow DK^{*0}) = 0.04 \pm 0.17$$

$$x_-(B^0 \rightarrow DK^{*0}) = -0.16 \pm 0.14$$

$$y_+(B^0 \rightarrow DK^{*0}) = -0.68 \pm 0.22$$

$$y_-(B^0 \rightarrow DK^{*0}) = 0.20 \pm 0.25 \quad (S = 1.2)$$

$$r_{B^0}(B^0 \rightarrow DK^{*0}) = 0.257_{-0.023}^{+0.021}$$

$$\delta_{B^0}(B^0 \rightarrow DK^{*0}) = (194.1_{-8.8}^{+9.6})^\circ$$

\bar{B}^0 modes are charge conjugates of the modes below. Reactions indicate the weak decay vertex and do not include mixing. Modes which do not identify the charge state of the B are listed in the B^\pm/B^0 ADMIXTURE section.

The branching fractions listed below assume 50% $B^0\bar{B}^0$ and 50% B^+B^- production at the $\Upsilon(4S)$. We have attempted to bring older measurements up to date by rescaling their assumed $\Upsilon(4S)$ production ratio to 50:50 and their assumed D, D_s, D^* , and ψ branching ratios to current values whenever this would affect our averages and best limits significantly.

Indentation is used to indicate a subchannel of a previous reaction. All resonant subchannels have been corrected for resonance branching fractions to the final state so the sum of the subchannel branching fractions can exceed that of the final state.

For inclusive branching fractions, e.g., $B \rightarrow D^\pm X$, the values usually are multiplicities, not branching fractions. They can be greater than one.

B^0 DECAY MODES	Fraction (Γ_i/Γ)	Scale factor / Confidence level	ρ (MeV/c)
$\ell^+ \nu_\ell X$	[iii] (10.33 ± 0.28) %	–	–
$e^+ \nu_e X_c$	(10.1 ± 0.4) %	–	–
$\ell^+ \nu_\ell X_u$	(1.51 ± 0.19) × 10 ⁻³	–	–
$D \ell^+ \nu_\ell X$	(9.3 ± 0.8) %	–	–
$D^- \ell^+ \nu_\ell$	[iii] (2.24 ± 0.09) %	2309	–
$D^- \tau^+ \nu_\tau$	(1.05 ± 0.23) %	1909	–
$D^*(2010)^- \ell^+ \nu_\ell$	[iii] (4.97 ± 0.12) %	2257	–
$D^*(2010)^- \tau^+ \nu_\tau$	(1.58 ± 0.09) %	S=1.1 1838	–
$\bar{D}^0 \pi^- \ell^+ \nu_\ell$	(4.1 ± 0.5) × 10 ⁻³	2308	–
$D_0^*(2300)^- \ell^+ \nu_\ell, D_0^{*-} \rightarrow$	(3.0 ± 1.2) × 10 ⁻³	S=1.8 –	–
$\bar{D}^0 \pi^-$	–	–	–
$D_2^*(2460)^- \ell^+ \nu_\ell, D_2^{*-} \rightarrow$	(1.21 ± 0.33) × 10 ⁻³	S=1.8 2065	–
$\bar{D}^0 \pi^-$	–	–	–
$\bar{D}^{(*)} n \pi \ell^+ \nu_\ell (n \geq 1)$	(2.3 ± 0.5) %	–	–
$\bar{D}^{*0} \pi^- \ell^+ \nu_\ell$	(5.8 ± 0.8) × 10 ⁻³	S=1.4 2256	–
$D_1(2420)^- \ell^+ \nu_\ell, D_1^- \rightarrow$	(2.80 ± 0.28) × 10 ⁻³	–	–
$\bar{D}^{*0} \pi^-$	–	–	–
$D_1'(2430)^- \ell^+ \nu_\ell, D_1'^- \rightarrow$	(3.1 ± 0.9) × 10 ⁻³	–	–
$\bar{D}^{*0} \pi^-$	–	–	–
$D_2^*(2460)^- \ell^+ \nu_\ell, D_2^{*-} \rightarrow$	(6.8 ± 1.2) × 10 ⁻⁴	2065	–
$\bar{D}^{*0} \pi^-$	–	–	–
$D^- \pi^+ \pi^- \ell^+ \nu_\ell$	(1.3 ± 0.5) × 10 ⁻³	2299	–
$D^{*-} \pi^+ \pi^- \ell^+ \nu_\ell$	(1.4 ± 0.5) × 10 ⁻³	2247	–
$\rho^- \ell^+ \nu_\ell$	[iii] (2.94 ± 0.21) × 10 ⁻⁴	2583	–
$\pi^- \ell^+ \nu_\ell$	[iii] (1.50 ± 0.06) × 10 ⁻⁴	2638	–
$\pi^- \tau^+ \nu_\tau$	< 2.5 × 10 ⁻⁴	CL=90% 2339	–
Inclusive modes			
$K^\pm X$	(78 ± 8) %	–	–
$D^0 X$	(8.1 ± 1.5) %	–	–
$\bar{D}^0 X$	(47.4 ± 2.8) %	–	–
$D^+ X$	< 3.9 %	CL=90% –	–
$D^- X$	(36.9 ± 3.3) %	–	–
$D_s^+ X$	(10.3 ± 2.1) %	–	–
$D_s^- X$	< 2.6 %	CL=90% –	–
$\Lambda_c^+ X$	< 3.1 %	CL=90% –	–
$\bar{\Lambda}_c^- X$	(5.0 ± 2.1) %	–	–
$\bar{c} X$	(95 ± 5) %	–	–
$c X$	(24.6 ± 3.1) %	–	–
$\bar{c}/c X$	(119 ± 6) %	–	–
D, D*, or D_s modes			
$D^- \pi^+$	(2.51 ± 0.08) × 10 ⁻³	2306	–
$D^- \rho^+$	(7.6 ± 1.2) × 10 ⁻³	2235	–
$D^- K^0 \pi^+$	(4.9 ± 0.9) × 10 ⁻⁴	2259	–
$D^- K^*(892)^+$	(4.5 ± 0.7) × 10 ⁻⁴	2211	–
$D^- \omega \pi^+$	(2.8 ± 0.6) × 10 ⁻³	2204	–
$D^- K^+$	(2.05 ± 0.08) × 10 ⁻⁴	2279	–
$D^- K^+ \pi^+ \pi^-$	(3.5 ± 0.8) × 10 ⁻⁴	2236	–
$D^- K^+ \bar{K}^0$	< 3.1 × 10 ⁻⁴	CL=90% 2188	–

$D^- K^+ \bar{K}^*(892)^0$	(8.8 ± 1.9) × 10 ⁻⁴	2070	–
$\bar{D}^0 \pi^+ \pi^-$	(8.8 ± 0.5) × 10 ⁻⁴	2301	–
$D^*(2010)^- \pi^+$	(2.74 ± 0.13) × 10 ⁻³	2255	–
$\bar{D}^0 K^+ K^-$	(6.1 ± 0.5) × 10 ⁻⁵	2191	–
$D^- \pi^+ \pi^+ \pi^-$	(6.0 ± 0.6) × 10 ⁻³	2287	–
$(D^- \pi^+ \pi^+ \pi^-)$ nonresonant	(3.9 ± 1.9) × 10 ⁻³	2287	–
$D^- \pi^+ \rho^0$	(1.1 ± 1.0) × 10 ⁻³	2206	–
$D^- a_1(1260)^+$	(6.0 ± 3.3) × 10 ⁻³	2121	–
$D^*(2010)^- \pi^+ \pi^0$	(1.5 ± 0.5) %	2248	–
$D^*(2010)^- \rho^+$	(6.8 ± 0.9) × 10 ⁻³	2180	–
$D^*(2010)^- K^+$	(2.12 ± 0.15) × 10 ⁻⁴	2226	–
$D^*(2010)^- K^0 \pi^+$	(3.0 ± 0.8) × 10 ⁻⁴	2205	–
$D^*(2010)^- K^*(892)^+$	(3.3 ± 0.6) × 10 ⁻⁴	2155	–
$D^*(2010)^- K^+ \bar{K}^0$	< 4.7 × 10 ⁻⁴	CL=90% 2131	–
$D^*(2010)^- K^+ \bar{K}^*(892)^0$	(1.29 ± 0.33) × 10 ⁻³	2007	–
$D^*(2010)^- \pi^+ \pi^+ \pi^-$	(7.21 ± 0.29) × 10 ⁻³	2235	–
$(D^*(2010)^- \pi^+ \pi^+ \pi^-)$ non-resonant	(0.0 ± 2.5) × 10 ⁻³	2235	–
$D^*(2010)^- \pi^+ \rho^0$	(5.7 ± 3.2) × 10 ⁻³	2150	–
$D^*(2010)^- a_1(1260)^+$	(1.30 ± 0.27) %	2061	–
$\bar{D}_1(2420)^0 \pi^- \pi^+, \bar{D}_1^0 \rightarrow$	(1.47 ± 0.35) × 10 ⁻⁴	–	–
$D^{*-} \pi^+$	–	–	–
$D^*(2010)^- K^+ \pi^- \pi^+$	(4.7 ± 0.4) × 10 ⁻⁴	2181	–
$D^*(2010)^- \pi^+ \pi^+ \pi^- \pi^0$	(1.76 ± 0.27) %	2218	–
$D^{*-} 3\pi^+ 2\pi^-$	(4.7 ± 0.9) × 10 ⁻³	2195	–
$D^*(2010)^- \omega \pi^+$	(2.46 ± 0.18) × 10 ⁻³	S=1.2 2148	–
$\bar{D}_1(2430)^0 \omega, \bar{D}_1^0 \rightarrow$	(2.7 ± 0.8) × 10 ⁻⁴	1992	–
$D^{*-} \pi^+$	–	–	–
$D^{*-} \rho(1450)^+, \rho^+ \rightarrow \omega \pi^+$	(1.07 ± 0.40) × 10 ⁻³	–	–
$\bar{D}_1(2420)^0 \omega, \bar{D}_1^0 \rightarrow$	(7.0 ± 2.2) × 10 ⁻⁵	1995	–
$D^{*-} \pi^+$	–	–	–
$\bar{D}_2^*(2460)^0 \omega, \bar{D}_2^0 \rightarrow$	(4.0 ± 1.4) × 10 ⁻⁵	1975	–
$D^{*-} \pi^+$	–	–	–
$D^{*-} b_1(1235)^+, b_1^+ \rightarrow$	< 7 × 10 ⁻⁵	CL=90% –	–
$\omega \pi^+$	–	–	–
$\bar{D}^{*-} \pi^+$	[nnn] (1.9 ± 0.9) × 10 ⁻³	–	–
$D_1(2420)^- \pi^+, D_1^- \rightarrow$	(9.9 ± 2.0) × 10 ⁻⁵	–	–
$D^- \pi^+ \pi^-$	–	–	–
$D_1(2420)^- \pi^+, D_1^- \rightarrow$	< 3.3 × 10 ⁻⁵	CL=90% –	–
$D^{*-} \pi^+ \pi^-$	–	–	–
$\bar{D}_2^*(2460)^- \pi^+, (D_2^*)^- \rightarrow$	(2.38 ± 0.16) × 10 ⁻⁴	2062	–
$D^0 \pi^-$	–	–	–
$\bar{D}_0^*(2400)^- \pi^+, (D_0^*)^- \rightarrow$	(7.6 ± 0.8) × 10 ⁻⁵	2090	–
$D^0 \pi^-$	–	–	–
$D_2^*(2460)^- \pi^+, (D_2^*)^- \rightarrow$	< 2.4 × 10 ⁻⁵	CL=90% –	–
$D^{*-} \pi^+ \pi^-$	–	–	–
$\bar{D}_2^*(2460)^- \rho^+$	< 4.9 × 10 ⁻³	CL=90% 1974	–
$D^0 \bar{D}^0$	(1.4 ± 0.7) × 10 ⁻⁵	1868	–
$D^* \bar{D}^0$	< 2.9 × 10 ⁻⁴	CL=90% 1794	–
$D^- D^+$	(2.11 ± 0.18) × 10 ⁻⁴	1864	–
$D^\pm D^{*\mp}$ (CP-averaged)	(6.1 ± 0.6) × 10 ⁻⁴	–	–
$D^- D_s^+$	(7.2 ± 0.8) × 10 ⁻³	1812	–
$D^*(2010)^- D_s^+$	(8.0 ± 1.1) × 10 ⁻³	1735	–
$D^- D_s^{*+}$	(7.4 ± 1.6) × 10 ⁻³	1732	–
$D^*(2010)^- D_s^{*+}$	(1.77 ± 0.14) %	1649	–
$D_{s0}(2317)^- K^+, D_{s0}^- \rightarrow$	(4.2 ± 1.4) × 10 ⁻⁵	2097	–
$D_s^- \pi^0$	–	–	–
$D_{s0}(2317)^- \pi^+, D_{s0}^- \rightarrow$	< 2.5 × 10 ⁻⁵	CL=90% 2128	–
$D_s^- \pi^0$	–	–	–
$D_{sJ}(2457)^- K^+, D_{sJ}^- \rightarrow$	< 9.4 × 10 ⁻⁶	CL=90% –	–
$D_s^- \pi^0$	–	–	–
$D_{sJ}(2457)^- \pi^+, D_{sJ}^- \rightarrow$	< 4.0 × 10 ⁻⁶	CL=90% –	–
$D_s^- \pi^0$	–	–	–
$D_s^- D_s^+$	< 3.6 × 10 ⁻⁵	CL=90% 1759	–
$D_s^- D_s^+$	< 1.3 × 10 ⁻⁴	CL=90% 1674	–
$D_s^- D_s^{*+}$	< 2.4 × 10 ⁻⁴	CL=90% 1583	–
$D_{s0}(2317)^+ D^-, D_{s0}^{*+} \rightarrow$	(1.06 ± 0.16) × 10 ⁻³	S=1.1 1602	–
$D_s^+ \pi^0$	–	–	–
$D_{s0}(2317)^+ D^-, D_{s0}^{*+} \rightarrow$	< 9.5 × 10 ⁻⁴	CL=90% –	–
$D_s^{*+} \gamma$	–	–	–
$D_{s0}(2317)^+ D^*(2010)^-,$	(1.5 ± 0.6) × 10 ⁻³	1509	–
$D_{s0}^+ \rightarrow D_s^+ \pi^0$	–	–	–
$D_{sJ}(2457)^+ D^-$	(3.5 ± 1.1) × 10 ⁻³	–	–

Meson Summary Table

$D_{sJ}(2457)^+ D^-$, $D_{sJ}^+ \rightarrow$	$(6.5 \pm 1.7) \times 10^{-4}$	-	$D^0 K^+ \pi^-$	$(5.3 \pm 3.2) \times 10^{-6}$	2261
$D_s^+ \gamma$			$D^0 K^*(892)^0$	$(3.0 \pm 0.6) \times 10^{-6}$	2213
$D_{sJ}(2457)^+ D^-$, $D_{sJ}^+ \rightarrow$	$< 6.0 \times 10^{-4}$	CL=90%	$\bar{D}^{*0} \gamma$	$< 2.5 \times 10^{-5}$	CL=90% 2258
$D_s^{*+} \gamma$			$\bar{D}^*(2007)^0 \pi^0$	$(2.2 \pm 0.6) \times 10^{-4}$	S=2.6 2256
$D_{sJ}(2457)^+ D^-$, $D_{sJ}^+ \rightarrow$	$< 2.0 \times 10^{-4}$	CL=90%	$\bar{D}^*(2007)^0 \rho^0$	$< 5.1 \times 10^{-4}$	CL=90% 2182
$D_s^+ \pi^+ \pi^-$			$\bar{D}^*(2007)^0 \eta$	$(2.3 \pm 0.6) \times 10^{-4}$	S=2.8 2220
$D_{sJ}(2457)^+ D^-$, $D_{sJ}^+ \rightarrow$	$< 3.6 \times 10^{-4}$	CL=90%	$\bar{D}^*(2007)^0 \eta'$	$(1.40 \pm 0.22) \times 10^{-4}$	2141
$D_s^+ \pi^0$			$\bar{D}^*(2007)^0 \pi^+ \pi^-$	$(6.2 \pm 2.2) \times 10^{-4}$	2249
$D^*(2010)^- D_{sJ}(2457)^+$	$(9.3 \pm 2.2) \times 10^{-3}$	-	$\bar{D}^*(2007)^0 K^0$	$(3.6 \pm 1.2) \times 10^{-5}$	2227
$D_{sJ}(2457)^+ D^*(2010)$, $D_{sJ}^+ \rightarrow$	$(2.3 \pm 0.9) \times 10^{-3}$	-	$\bar{D}^*(2007)^0 K^*(892)^0$	$< 6.9 \times 10^{-5}$	CL=90% 2157
$D_s^+ \gamma$			$D^*(2007)^0 K^*(892)^0$	$< 4.0 \times 10^{-5}$	CL=90% 2157
$D^- D_{s1}(2536)^+$, $D_{s1}^+ \rightarrow$	$(2.8 \pm 0.7) \times 10^{-4}$	1444	$D^*(2007)^0 \pi^+ \pi^+ \pi^- \pi^-$	$(2.7 \pm 0.5) \times 10^{-3}$	2219
$D^{*0} K^+ + D^{*+} K^0$			$D^*(2010)^+ D^*(2010)^-$	$(8.0 \pm 0.6) \times 10^{-4}$	1711
$D^- D_{s1}(2536)^+$, $D_{s1}^+ \rightarrow$	$(1.7 \pm 0.6) \times 10^{-4}$	1444	$\bar{D}^*(2007)^0 \omega$	$(3.6 \pm 1.1) \times 10^{-4}$	S=3.1 2180
$D^{*0} K^+$			$D^*(2010)^+ D^-$	$(6.1 \pm 1.5) \times 10^{-4}$	S=1.6 1790
$D^- D_{s1}(2536)^+$, $D_{s1}^+ \rightarrow$	$(2.6 \pm 1.1) \times 10^{-4}$	1444	$D^*(2007)^0 \bar{D}^*(2007)^0$	$< 9 \times 10^{-5}$	CL=90% 1715
$D^{*+} K^0$			$D^- D^0 K^+$	$(1.07 \pm 0.11) \times 10^{-3}$	1574
$D^*(2010)^- D_{s1}(2536)^+$, $D_{s1}^+ \rightarrow$	$(5.0 \pm 1.4) \times 10^{-4}$	1336	$D^- D^*(2007)^0 K^+$	$(3.5 \pm 0.4) \times 10^{-3}$	1478
$D_{s1}^+ \rightarrow D^{*0} K^+ + D^{*+} K^0$			$D^*(2010)^- D^0 K^+$	$(2.47 \pm 0.21) \times 10^{-3}$	1479
$D^*(2010)^- D_{s1}(2536)^+$, $D_{s1}^+ \rightarrow$	$(3.3 \pm 1.1) \times 10^{-4}$	1336	$D^*(2010)^- D^*(2007)^0 K^+$	$(1.06 \pm 0.09) \%$	1366
$D_{s1}^+ \rightarrow D^{*0} K^+$			$D^- D^+ K^0$	$(7.5 \pm 1.7) \times 10^{-4}$	1568
$D^{*-} D_{s1}(2536)^+$, $D_{s1}^+ \rightarrow$	$(5.0 \pm 1.7) \times 10^{-4}$	1336	$D^*(2010)^- D^+ K^0 + D^- D^*(2010)^+ K^0$	$(6.4 \pm 0.5) \times 10^{-3}$	1473
$D^{*+} K^0$			$D^*(2010)^- D^*(2010)^+ K^0$	$(8.1 \pm 0.7) \times 10^{-3}$	1360
$D^- D_{sJ}(2573)^+$, $D_{sJ}^+ \rightarrow$	$(3.4 \pm 1.8) \times 10^{-5}$	1414	$D^{*-} D_{s1}(2536)^+$, $D_{s1}^+ \rightarrow$	$(8.0 \pm 2.4) \times 10^{-4}$	1336
$D^0 K^+$			$D^{*+} K^0$		
$D^*(2010)^- D_{sJ}(2573)^+$, $D_{sJ}^+ \rightarrow$	$< 2 \times 10^{-4}$	CL=90% 1304	$\bar{D}^0 D^0 K^0$	$(2.7 \pm 1.1) \times 10^{-4}$	1574
$D^- D_{sJ}(2700)^+$, $D_{sJ}^+ \rightarrow$	$(7.1 \pm 1.2) \times 10^{-4}$	-	$D^0 \bar{D}^0 K^+ \pi^-$	$(3.5 \pm 0.5) \times 10^{-4}$	1476
$D^0 K^+$			$\bar{D}^0 D^*(2007)^0 K^0 + \bar{D}^*(2007)^0 D^0 K^0$	$(1.1 \pm 0.5) \times 10^{-3}$	1478
$D^+ \pi^-$	$(7.3 \pm 1.2) \times 10^{-7}$	2306	$\bar{D}^*(2007)^0 D^*(2007)^0 K^0$	$(2.4 \pm 0.9) \times 10^{-3}$	1365
$D_s^+ \pi^-$	$(2.03 \pm 0.18) \times 10^{-5}$	2270	$(\bar{D} + \bar{D}^*)(D + D^*) K$	$(3.68 \pm 0.26) \%$	-
$D_s^{*+} \pi^-$	$(2.1 \pm 0.4) \times 10^{-5}$	S=1.4 2215	Charmonium modes		
$D_s^+ \rho^-$	$< 2.4 \times 10^{-5}$	CL=90% 2197	$\eta_c K^0$	$(8.0 \pm 1.1) \times 10^{-4}$	1751
$D_s^{*+} \rho^-$	$(4.1 \pm 1.3) \times 10^{-5}$	2138	$\eta_c(1S) K^+ \pi^-$	$(6.0 \pm 0.7) \times 10^{-4}$	1722
$D_s^+ a_0^-$	$< 1.9 \times 10^{-5}$	CL=90% -	$\eta_c(1S) K^+ \pi^-$ (NR)	$(6.2 \pm 1.3) \times 10^{-5}$	-
$D_s^{*+} a_0^-$	$< 3.6 \times 10^{-5}$	CL=90% -	$X(4100)^- K^+$, $X^- \rightarrow$	$(2.0 \pm 1.0) \times 10^{-5}$	-
$D_s^+ a_1(1260)^-$	$< 2.1 \times 10^{-3}$	CL=90% 2080	$\eta_c \pi^-$		
$D_s^{*+} a_1(1260)^-$	$< 1.7 \times 10^{-3}$	CL=90% 2015	$\eta_c(1S) K^*(1410)^0$	$(1.9 \pm 1.5) \times 10^{-4}$	1395
$D_s^+ a_2^-$	$< 1.9 \times 10^{-4}$	CL=90% -	$\eta_c(1S) K_0^*(1430)^0$	$(1.6 \pm 0.4) \times 10^{-4}$	1388
$D_s^{*+} a_2^-$	$< 2.0 \times 10^{-4}$	CL=90% -	$\eta_c(1S) K_2^*(1430)^0$	$(5.0 \pm 2.3) \times 10^{-5}$	1386
$D_s^- K^+$	$(2.7 \pm 0.5) \times 10^{-5}$	S=2.7 2242	$\eta_c(1S) K^*(1680)^0$	$(3 \pm 4) \times 10^{-5}$	1166
$D_s^{*-} K^+$	$(2.19 \pm 0.30) \times 10^{-5}$	2185	$\eta_c(1S) K_0^*(1950)^0$	$(4.4 \pm 3.0) \times 10^{-5}$	-
$D_s^- K^*(892)^+$	$(3.5 \pm 1.0) \times 10^{-5}$	2172	$\eta_c K^*(892)^0$	$(5.2 \pm 0.8) \times 10^{-4}$	S=1.6 1646
$D_s^{*-} K^*(892)^+$	$(3.2 \pm 1.5) \times 10^{-5}$	2112	$\eta_c(2S) K_S^0$, $\eta_c \rightarrow \rho \bar{\rho} \pi^+ \pi^-$	$(4.2 \pm 1.4) \times 10^{-7}$	-
$D_s^- \pi^+ K^0$	$(9.7 \pm 1.4) \times 10^{-5}$	2222	$\eta_c(2S) K^*0$	$< 3.9 \times 10^{-4}$	CL=90% 1159
$D_s^{*-} \pi^+ K^0$	$< 1.10 \times 10^{-4}$	CL=90% 2164	$h_c(1P) K_S^0$	$< 1.4 \times 10^{-5}$	1401
$D_s^- K^+ \pi^+ \pi^-$	$(1.7 \pm 0.5) \times 10^{-4}$	2198	$h_c(1P) K^*0$	$< 4 \times 10^{-4}$	CL=90% 1253
$D_s^- \pi^+ K^*(892)^0$	$< 3.0 \times 10^{-3}$	CL=90% 2138	$J/\psi(1S) K^0$	$(8.91 \pm 0.21) \times 10^{-4}$	1683
$D_s^{*-} \pi^+ K^*(892)^0$	$< 1.6 \times 10^{-3}$	CL=90% 2076	$J/\psi(1S) K^+ \pi^-$	$(1.15 \pm 0.05) \times 10^{-3}$	1652
$\bar{D}^0 K^0$	$(5.2 \pm 0.7) \times 10^{-5}$	2280	$J/\psi(1S) K^*(892)^0$	$(1.27 \pm 0.05) \times 10^{-3}$	1572
$\bar{D}^0 K^+ \pi^-$	$(8.8 \pm 1.7) \times 10^{-5}$	2261	$J/\psi(1S) \eta K_S^0$	$(5.4 \pm 0.9) \times 10^{-5}$	1508
$\bar{D}^0 K^*(892)^0$	$(4.5 \pm 0.6) \times 10^{-5}$	2213	$J/\psi(1S) \eta' K_S^0$	$< 2.5 \times 10^{-5}$	CL=90% 1271
$\bar{D}^0 K^*(1410)^0$	$< 6.7 \times 10^{-5}$	CL=90% 2062	$J/\psi(1S) \phi K^0$	$(4.9 \pm 1.0) \times 10^{-5}$	S=1.3 1224
$\bar{D}^0 K_0^*(1430)^0$	$(7 \pm 7) \times 10^{-6}$	2058	$J/\psi(1S) \omega K^0$	$(2.3 \pm 0.4) \times 10^{-4}$	1386
$\bar{D}^0 K_2^*(1430)^0$	$(2.1 \pm 0.9) \times 10^{-5}$	2057	$\chi_{c0}(3915)$, $\chi_{c0} \rightarrow J/\psi \omega$	$(2.1 \pm 0.9) \times 10^{-5}$	1102
$D_0^*(2300)^- K^+$, $D_0^{*-} \rightarrow$	$(1.9 \pm 0.9) \times 10^{-5}$	-	$J/\psi(1S) K(1270)^0$	$(1.3 \pm 0.5) \times 10^{-3}$	1402
$\bar{D}^0 \pi^-$			$J/\psi(1S) \pi^0$	$(1.66 \pm 0.10) \times 10^{-5}$	1728
$D_2^*(2460)^- K^+$, $D_2^{*-} \rightarrow$	$(2.03 \pm 0.35) \times 10^{-5}$	2029	$J/\psi(1S) \eta$	$(1.08 \pm 0.23) \times 10^{-5}$	S=1.5 1673
$\bar{D}^0 \pi^-$			$J/\psi(1S) \pi^+ \pi^-$	$(4.00 \pm 0.15) \times 10^{-5}$	1716
$D_3^*(2760)^- K^+$, $D_3^{*-} \rightarrow$	$< 1.0 \times 10^{-6}$	CL=90% -	$J/\psi(1S) \pi^+ \pi^-$ nonresonant	$< 1.2 \times 10^{-5}$	CL=90% 1716
$\bar{D}^0 \pi^-$			$J/\psi(1S) f_0(500)$, $f_0 \rightarrow \pi \pi$	$(8.8 \pm 1.2) \times 10^{-6}$	-
$\bar{D}^0 K^+ \pi^-$ nonresonant	$< 3.7 \times 10^{-5}$	CL=90% 2261	$J/\psi(1S) f_2$	$(3.3 \pm 0.5) \times 10^{-6}$	S=1.5 -
$[K^+ K^-]_D K^*(892)^0$	$(4.2 \pm 0.7) \times 10^{-5}$	-	$J/\psi(1S) \rho^0$	$(2.55 \pm 0.18) \times 10^{-5}$	1612
$[\pi^+ \pi^-]_D K^*(892)^0$	$(6.0 \pm 1.1) \times 10^{-5}$	-	$J/\psi(1S) f_0(980)$, $f_0 \rightarrow \pi^+ \pi^-$	$< 1.1 \times 10^{-6}$	CL=90% -
$[\pi^+ \pi^- \pi^+ \pi^-]_D K^*0$	$(4.6 \pm 0.9) \times 10^{-5}$	-	$J/\psi(1S) \rho(1450)^0$, $\rho^0 \rightarrow \pi \pi$	$(2.9 \pm 1.6) \times 10^{-6}$	-
$\bar{D}^0 \pi^0$	$(2.63 \pm 0.14) \times 10^{-4}$	2308	$J/\psi(1700)^0$, $\rho^0 \rightarrow \pi^+ \pi^-$	$(2.0 \pm 1.3) \times 10^{-6}$	-
$\bar{D}^0 \rho^0$	$(3.21 \pm 0.21) \times 10^{-4}$	2237	$J/\psi(1S) \omega$	$(1.8 \pm 0.7) \times 10^{-5}$	1609
$\bar{D}^0 f_2$	$(1.56 \pm 0.21) \times 10^{-4}$	-	$J/\psi(1S) K^+ K^-$	$(2.54 \pm 0.35) \times 10^{-6}$	1534
$\bar{D}^0 \eta$	$(2.36 \pm 0.32) \times 10^{-4}$	S=2.5 2274			
$\bar{D}^0 \eta'$	$(1.38 \pm 0.16) \times 10^{-4}$	S=1.3 2198			
$\bar{D}^0 \omega$	$(2.54 \pm 0.16) \times 10^{-4}$	2235			
$D^0 \phi$	$< 2.3 \times 10^{-6}$	CL=95% 2183			

Meson Summary Table

$J/\psi(1S) a_0(980), a_0 \rightarrow K^+ K^-$	$(4.7 \pm 3.4) \times 10^{-7}$	-	$a_0(980)^\pm K^\mp, a_0^\pm \rightarrow \eta\pi^\pm$	$< 1.9 \times 10^{-6}$	CL=90%	-
$J/\psi(1S) \phi$	$< 1.1 \times 10^{-7}$	CL=90%	$b_1^- K^+, b_1^- \rightarrow \omega\pi^-$	$(7.4 \pm 1.4) \times 10^{-6}$	-	-
$J/\psi(1S) \eta'(958)$	$(7.6 \pm 2.4) \times 10^{-6}$	1546	$b_1^0 K^0, b_1^0 \rightarrow \omega\pi^0$	$< 8.0 \times 10^{-6}$	CL=90%	-
$J/\psi(1S) K^0 \pi^+ \pi^-$	$(4.5 \pm 0.4) \times 10^{-4}$	1611	$b_1^- K^{*+}, b_1^- \rightarrow \omega\pi^-$	$< 5.0 \times 10^{-6}$	CL=90%	-
$J/\psi(1S) K^0 K^- \pi^+ + c.c.$	$< 2.1 \times 10^{-5}$	CL=90%	$a_0(1450)^\pm K^\mp, a_0^\pm \rightarrow \eta\pi^\pm$	$< 3.1 \times 10^{-6}$	CL=90%	-
$J/\psi(1S) K^0 K^+ K^-$	$(2.5 \pm 0.7) \times 10^{-5}$	S=1.8	$K_S^0 X^0$ (Familon)	$< 5.3 \times 10^{-5}$	CL=90%	-
$J/\psi(1S) K^0 \rho^0$	$(5.4 \pm 3.0) \times 10^{-4}$	1390	$\omega K^*(892)^0$	$(2.0 \pm 0.5) \times 10^{-6}$	-	2503
$J/\psi(1S) K^*(892)^+ \pi^-$	$(8 \pm 4) \times 10^{-4}$	1515	$\omega(K\pi)_0^0$	$(1.84 \pm 0.25) \times 10^{-5}$	-	-
$J/\psi(1S) \pi^+ \pi^- \pi^+ \pi^-$	$(1.44 \pm 0.12) \times 10^{-5}$	1670	$\omega K_0^*(1430)^0$	$(1.60 \pm 0.34) \times 10^{-5}$	-	2380
$J/\psi(1S) f_1(1285)$	$(8.4 \pm 2.1) \times 10^{-6}$	1385	$\omega K_2^*(1430)^0$	$(1.01 \pm 0.23) \times 10^{-5}$	-	2380
$J/\psi(1S) K^*(892)^0 \pi^+ \pi^-$	$(6.6 \pm 2.2) \times 10^{-4}$	1447	$\omega K^+ \pi^-$ nonresonant	$(5.1 \pm 1.0) \times 10^{-6}$	-	2542
$\eta c_2(1D) K_S^0, \eta c_2 \rightarrow h_c \gamma$	$< 3.5 \times 10^{-5}$	CL=90%	$K^+ \pi^- \pi^0$	$(3.78 \pm 0.32) \times 10^{-5}$	-	2609
$\eta c_2(1D) \pi^- K^+, \eta c_2 \rightarrow h_c \gamma$	$< 1.0 \times 10^{-4}$	CL=90%	$K^+ \rho^-$	$(7.0 \pm 0.9) \times 10^{-6}$	-	2559
$\chi_{c1}(3872)^- K^+$	$< 5 \times 10^{-4}$	CL=90%	$K^+ \rho(1450)^-$	$(2.4 \pm 1.2) \times 10^{-6}$	-	-
$\chi_{c1}(3872)^- K^+, [\text{ooo}] < 4.2 \times 10^{-6}$	CL=90%	-	$K^+ \rho(1700)^-$	$(6 \pm 7) \times 10^{-7}$	-	-
$\chi_{c1}(3872)^- \rightarrow J/\psi(1S) \pi^- \pi^0$	-	-	$(K^+ \pi^- \pi^0)$ nonresonant	$(2.8 \pm 0.6) \times 10^{-6}$	-	2609
$\chi_{c1}(3872) K^0$	$(1.1 \pm 0.4) \times 10^{-4}$	1140	$(K\pi)_0^{*+} \pi^-, (K\pi)_0^{*+} \rightarrow$	$(3.4 \pm 0.5) \times 10^{-5}$	-	-
$\chi_{c1}(3872) K^*(892)^0$	$(1.0 \pm 0.5) \times 10^{-4}$	940	$K^+ \pi^- \pi^0$	-	-	-
$\chi_{c1}(3872) K^+ \pi^-$	$(2.1 \pm 0.8) \times 10^{-4}$	1087	$(K\pi)_0^+ \pi^0, (K\pi)_0^+ \rightarrow$	$(8.6 \pm 1.7) \times 10^{-6}$	-	-
$\chi_{c1}(3872) \gamma$	$< 1.3 \times 10^{-5}$	CL=90%	$K^+ \pi^-$	-	-	-
$Z_c(4430)^\pm K^\mp, Z_c^\pm \rightarrow \psi(2S) \pi^\pm$	$(6.0 \pm 3.0) \times 10^{-5}$	583	$K_2^*(1430)^0 \pi^0$	$< 4.0 \times 10^{-6}$	CL=90%	2445
$Z_c(4430)^\pm K^\mp, Z_c^\pm \rightarrow J/\psi \pi^\pm$	$(5.4 \pm 4.0) \times 10^{-6}$	583	$K^*(1680)^0 \pi^0$	$< 7.5 \times 10^{-6}$	CL=90%	2358
$Z_c(3900)^\pm K^\mp, Z_c^\pm \rightarrow J/\psi \pi^\pm$	$< 9 \times 10^{-7}$	-	$K_x^0 \pi^0$	$[rrr] (6.1 \pm 1.6) \times 10^{-6}$	-	-
$Z_c(4200)^\pm K^\mp, X^\pm \rightarrow J/\psi \pi^\pm$	$(2.2 \pm 1.3) \times 10^{-5}$	-	$K^0 \pi^+ \pi^-$	$(4.97 \pm 0.18) \times 10^{-5}$	-	2609
$J/\psi(1S) \rho \bar{\rho}$	$(4.5 \pm 0.6) \times 10^{-7}$	862	$K^0 \pi^+ \pi^-$ nonresonant	$(1.39 \pm 0.26) \times 10^{-5}$	S=1.6	2609
$J/\psi(1S) \gamma$	$< 1.5 \times 10^{-6}$	CL=90%	$K^0 \rho^0$	$(3.4 \pm 1.1) \times 10^{-6}$	S=2.3	2558
$J/\psi(1S) \bar{D}^0$	$< 1.3 \times 10^{-5}$	CL=90%	$K^*(892)^+ \pi^-$	$(7.5 \pm 0.4) \times 10^{-6}$	-	2563
$\psi(2S) \pi^0$	$(1.17 \pm 0.19) \times 10^{-5}$	1348	$K_0^*(1430)^+ \pi^-$	$(3.3 \pm 0.7) \times 10^{-5}$	S=2.0	-
$\psi(2S) K^0$	$(5.8 \pm 0.5) \times 10^{-4}$	1283	$K_x^{*+} \pi^-$	$[rrr] (5.1 \pm 1.6) \times 10^{-6}$	-	-
$\psi(3770) K^0, \psi \rightarrow \bar{D}^0 D^0$	$< 1.23 \times 10^{-4}$	CL=90%	$K^*(1410)^+ \pi^-, K^{*+} \rightarrow$	$< 3.8 \times 10^{-6}$	CL=90%	-
$\psi(3770) K^0, \psi \rightarrow D^- D^+$	$< 1.88 \times 10^{-4}$	CL=90%	$K^0 \pi^+ \pi^+$	$(1.62 \pm 0.13) \times 10^{-5}$	-	-
$\psi(2S) \pi^+ \pi^-$	$(2.24 \pm 0.35) \times 10^{-5}$	1332	$(K\pi)_0^{*+} \pi^-, (K\pi)_0^{*+} \rightarrow$	-	-	-
$\psi(2S) K^+ \pi^-$	$(5.8 \pm 0.4) \times 10^{-4}$	1239	$K^0 \pi^+$	-	-	-
$\psi(2S) K^*(892)^0$	$(5.9 \pm 0.4) \times 10^{-4}$	1116	$f_0(980) K^0, f_0 \rightarrow \pi^+ \pi^-$	$(8.1 \pm 0.8) \times 10^{-6}$	S=1.3	2522
$\chi_{c0} K^0$	$(1.9 \pm 0.4) \times 10^{-4}$	1477	$K^0 f_0(500)$	$(1.6 \pm 2.5) \times 10^{-7}$	-	-
$\chi_{c0} K^*(892)^0$	$(1.7 \pm 0.4) \times 10^{-4}$	1342	$K^0 f_0(1500)$	$(1.3 \pm 0.8) \times 10^{-6}$	-	2397
$\chi_{c1} \pi^0$	$(1.12 \pm 0.28) \times 10^{-5}$	1468	$f_2(1270) K^0$	$(2.7 \pm 1.3) \times 10^{-6}$	-	2459
$\chi_{c1} K^0$	$(3.95 \pm 0.27) \times 10^{-4}$	1411	$f_x(1300) K^0, f_x \rightarrow \pi^+ \pi^-$	$(1.8 \pm 0.7) \times 10^{-6}$	-	-
$\chi_{c1} \pi^- K^+$	$(4.97 \pm 0.30) \times 10^{-4}$	1371	$K^*(892)^0 \pi^0$	$(3.3 \pm 0.6) \times 10^{-6}$	-	2563
$\chi_{c1} K^*(892)^0$	$(2.38 \pm 0.19) \times 10^{-4}$	S=1.2	$K_2^*(1430)^+ \pi^-$	$(3.65 \pm 0.34) \times 10^{-6}$	-	2445
$X(4051)^- K^+, X^- \rightarrow \chi_{c1} \pi^-$	$(3.0 \pm 4.0) \times 10^{-5}$	-	$K^*(1680)^+ \pi^-$	$(1.41 \pm 0.10) \times 10^{-5}$	-	2358
$X(4248)^- K^+, X^- \rightarrow \chi_{c1} \pi^-$	$(4.0 \pm 20.0) \times 10^{-5}$	-	$K^+ \pi^- \pi^+ \pi^-$	$[sss] < 2.3 \times 10^{-4}$	CL=90%	2600
$\chi_{c1} \pi^+ \pi^- K^0$	$(3.2 \pm 0.5) \times 10^{-4}$	1318	$\rho^0 K^+ \pi^-$	$(2.8 \pm 0.7) \times 10^{-6}$	-	2543
$\chi_{c1} \pi^- \pi^0 K^+$	$(3.5 \pm 0.6) \times 10^{-4}$	1321	$f_0(980) K^+ \pi^-, f_0 \rightarrow \pi\pi$	$(1.4 \pm 0.5) \times 10^{-6}$	-	2506
$\chi_{c2} K^0$	$< 1.5 \times 10^{-5}$	CL=90%	$K^+ \pi^- \pi^+ \pi^-$ nonresonant	$< 2.1 \times 10^{-6}$	CL=90%	2600
$\chi_{c2} K^*(892)^0$	$(4.9 \pm 1.2) \times 10^{-5}$	S=1.1	$K^*(892)^0 \pi^+ \pi^-$	$(5.5 \pm 0.5) \times 10^{-5}$	-	2557
$\chi_{c2} \pi^- K^+$	$(7.2 \pm 1.0) \times 10^{-5}$	1338	$K^*(892)^0 \rho^0$	$(3.9 \pm 1.3) \times 10^{-6}$	S=1.9	2504
$\chi_{c2} \pi^+ \pi^- K^0$	$< 1.70 \times 10^{-4}$	CL=90%	$K^*(892)^0 f_0(980), f_0 \rightarrow \pi\pi$	$(3.9 \pm 2.1) \times 10^{-6}$	S=3.9	2466
$\chi_{c2} \pi^- \pi^0 K^+$	$< 7.4 \times 10^{-5}$	CL=90%	$K_1(1270)^+ \pi^-$	$< 3.0 \times 10^{-5}$	CL=90%	2489
$\psi(4660) K^0, \psi \rightarrow \Lambda_c^+ \Lambda_c^-$	$< 2.3 \times 10^{-4}$	CL=90%	$K_1(1400)^+ \pi^-$	$< 2.7 \times 10^{-5}$	CL=90%	2451
$\psi(4230)^0 K^0, \psi^0 \rightarrow J/\psi \pi^+ \pi^-$	$< 1.7 \times 10^{-5}$	CL=90%	$a_1(1260)^- K^+$	$[sss] (1.6 \pm 0.4) \times 10^{-5}$	-	2471
K or K* modes			$K^*(892)^+ \rho^-$	$(1.03 \pm 0.26) \times 10^{-5}$	-	2504
$K^+ \pi^-$	$(1.96 \pm 0.05) \times 10^{-5}$	2615	$K_0^*(1430)^+ \rho^-$	$(2.8 \pm 1.2) \times 10^{-5}$	-	-
$K^0 \pi^0$	$(9.9 \pm 0.5) \times 10^{-6}$	2615	$K_1^+(1400)^0 \rho^0$	$< 3.0 \times 10^{-3}$	CL=90%	2388
$\eta' K^0$	$(6.6 \pm 0.4) \times 10^{-5}$	S=1.4	$K_0^*(1430)^0 \rho^0$	$(2.7 \pm 0.6) \times 10^{-5}$	-	2381
$\eta' K^*(892)^0$	$(2.8 \pm 0.6) \times 10^{-6}$	2472	$K_0^*(1430)^0 f_0(980), f_0 \rightarrow \pi\pi$	$(2.7 \pm 0.9) \times 10^{-6}$	-	-
$\eta' K_0^*(1430)^0$	$(6.3 \pm 1.6) \times 10^{-6}$	2346	$K_2^*(1430)^0 f_0(980), f_0 \rightarrow \pi\pi$	$(8.6 \pm 2.0) \times 10^{-6}$	-	-
$\eta' K_2^*(1430)^0$	$(1.37 \pm 0.32) \times 10^{-5}$	2346	$K^+ K^-$	$(7.8 \pm 1.5) \times 10^{-8}$	-	2593
ηK^0	$(1.23 \pm 0.27) \times 10^{-6}$	2587	$K^0 \bar{K}^0$	$(1.21 \pm 0.16) \times 10^{-6}$	-	2593
$\eta K^*(892)^0$	$(1.59 \pm 0.10) \times 10^{-5}$	2534	$K^0 K^- \pi^+$	$(6.7 \pm 0.5) \times 10^{-6}$	-	2578
$\eta K_0^*(1430)^0$	$(1.10 \pm 0.22) \times 10^{-5}$	2415	$K^*(892)^\pm K^\mp$	$< 4 \times 10^{-7}$	CL=90%	2540
$\eta K_2^*(1430)^0$	$(9.6 \pm 2.1) \times 10^{-6}$	2414	$\bar{K}^{*0} K^0 + K^{*0} \bar{K}^0$	$< 9.6 \times 10^{-7}$	CL=90%	-
ωK^0	$(4.8 \pm 0.4) \times 10^{-6}$	2557	$K^+ K^- \pi^0$	$(2.2 \pm 0.6) \times 10^{-6}$	-	2579
$a_0(980)^0 K^0, a_0^0 \rightarrow \eta\pi^0$	$< 7.8 \times 10^{-6}$	CL=90%	$K_S^0 K_S^0 \pi^0$	$< 9 \times 10^{-7}$	CL=90%	2578
$b_1^0 K^0, b_1^0 \rightarrow \omega\pi^0$	$< 7.8 \times 10^{-6}$	CL=90%	$K_S^0 K_S^0 \eta$	$< 1.0 \times 10^{-6}$	CL=90%	2515
			$K_S^0 K_S^0 \eta'$	$< 2.0 \times 10^{-6}$	CL=90%	2453
			$K_S^0 K^+ K^-$	$(2.68 \pm 0.11) \times 10^{-5}$	-	2522
			$K^0 \phi$	$(7.3 \pm 0.7) \times 10^{-6}$	-	2516
			$f_0(980) K^0, f_0 \rightarrow K^+ K^-$	$(7.0 \pm 3.5) \times 10^{-6}$	-	-
			$f_0(1500) K^0$	$(1.3 \pm 0.7) \times 10^{-5}$	-	2397
			$f_2'(1525)^0 K^0$	$(3 \pm 5) \times 10^{-7}$	-	-

Meson Summary Table

$f_0(1710) K^0, f_0 \rightarrow K^+ K^-$	$(4.4 \pm 0.9) \times 10^{-6}$	-	$\phi \eta'$	< 5	$\times 10^{-7}$	CL=90%	2448
$K^0 K^+ K^-$ nonresonant	$(3.3 \pm 1.0) \times 10^{-5}$	2522	$\phi \pi^+ \pi^-$	$(1.8 \pm 0.5) \times 10^{-7}$			2533
$K_S^0 K_S^0 K_S^0$	$(6.0 \pm 0.5) \times 10^{-6}$	S=1.1 2521	$\phi \rho^0$	< 3.3	$\times 10^{-7}$	CL=90%	2480
$f_0(980) K^0, f_0 \rightarrow K_S^0 K_S^0$	$(2.7 \pm 1.8) \times 10^{-6}$	-	$\phi f_0(980), f_0 \rightarrow \pi^+ \pi^-$	< 3.8	$\times 10^{-7}$	CL=90%	2441
$f_0(1710) K^0, f_0 \rightarrow K_S^0 K_S^0$	$(5.0 \pm 5.0) \times 10^{-7}$	-	$\phi \omega$	< 7	$\times 10^{-7}$	CL=90%	2479
$f_2(2010) K^0, f_2 \rightarrow K_S^0 K_S^0$	$(5 \pm 6) \times 10^{-7}$	-	$\phi \phi$	< 2.7	$\times 10^{-8}$	CL=90%	2435
$K_S^0 K_S^0 K_S^0$ nonresonant	$(1.33 \pm 0.31) \times 10^{-5}$	2521	$a_0(980)^\pm \pi^\mp, a_0^\pm \rightarrow \eta \pi^\pm$	< 3.1	$\times 10^{-6}$	CL=90%	-
$K_S^0 K_S^0 K_L^0 K^+ K^-$	< 1.6	$\times 10^{-5}$ CL=90%	$a_0(1450)^\pm \pi^\mp, a_0^\pm \rightarrow \eta \pi^\pm$	< 2.3	$\times 10^{-6}$	CL=90%	-
$K^*(892)^0 K^+ K^-$	$(2.75 \pm 0.26) \times 10^{-5}$	2467	$\pi^+ \pi^- \pi^0$	< 7.2	$\times 10^{-4}$	CL=90%	2631
$K^*(892)^0 \phi$	$(1.00 \pm 0.05) \times 10^{-5}$	2460	$\rho^0 \pi^0$	$(2.0 \pm 0.5) \times 10^{-6}$			2581
$K^+ K^- \pi^+ \pi^-$ nonresonant	< 7.17	$\times 10^{-5}$ CL=90%	$\rho^\mp \pi^\pm$	[aa] $(2.30 \pm 0.23) \times 10^{-5}$			2581
$K^*(892)^0 K^- \pi^+$	$(4.5 \pm 1.3) \times 10^{-6}$	2524	$\pi^+ \pi^- \pi^+ \pi^-$	< 1.12	$\times 10^{-5}$	CL=90%	2621
$K^*(892)^0 \bar{K}^*(892)^0$	$(8.3 \pm 2.4) \times 10^{-7}$	S=1.5 2485	$\rho^0 \pi^+ \pi^-$	< 8.8	$\times 10^{-6}$	CL=90%	2575
$K^+ K^+ \pi^- \pi^-$ nonresonant	< 6.0	$\times 10^{-6}$ CL=90%	$\rho^0 \rho^0$	$(9.6 \pm 1.5) \times 10^{-7}$			2523
$K^*(892)^0 K^+ \pi^-$	< 2.2	$\times 10^{-6}$ CL=90%	$f_0(980) \pi^+ \pi^-, f_0 \rightarrow$	< 3.0	$\times 10^{-6}$	CL=90%	-
$K^*(892)^0 K^*(892)^0$	< 2	$\times 10^{-7}$ CL=90%	$\pi^+ \pi^-$				2486
$K^*(892)^+ K^*(892)^-$	< 2.0	$\times 10^{-6}$ CL=90%	$\rho^0 f_0(980), f_0 \rightarrow \pi^+ \pi^-$	$(7.8 \pm 2.5) \times 10^{-7}$			2447
$K_1(1400)^0 \phi$	< 5.0	$\times 10^{-3}$ CL=90%	$f_0(980) f_0(980), f_0 \rightarrow$	< 1.9	$\times 10^{-7}$	CL=90%	2447
$\phi(K\pi)_0^*$	$(4.3 \pm 0.4) \times 10^{-6}$	-	$\pi^+ \pi^-, f_0 \rightarrow \pi^+ \pi^-$	< 2.3	$\times 10^{-7}$	CL=90%	2447
$\phi(K\pi)_0^{*0} (1.60 < m_{K\pi} < 2.15) [ttt]$	< 1.7	$\times 10^{-6}$ CL=90%	$f_0 \rightarrow K^+ K^-$				2494
$K_0^*(1430)^0 K^- \pi^+$	< 3.18	$\times 10^{-5}$ CL=90%	$a_1(1260)^\mp \pi^\pm$	[aa] $(2.6 \pm 0.5) \times 10^{-5}$	S=1.9		2494
$K_0^*(1430)^0 \bar{K}^*(892)^0$	< 3.3	$\times 10^{-6}$ CL=90%	$a_2(1320)^\mp \pi^\pm$	[aa] < 6.3	$\times 10^{-6}$	CL=90%	2473
$K_0^*(1430)^0 \bar{K}_0^*(1430)^0$	< 8.4	$\times 10^{-6}$ CL=90%	$\pi^+ \pi^- \pi^0 \pi^0$	< 3.1	$\times 10^{-3}$	CL=90%	2622
$K_0^*(1430)^0 \phi$	$(3.9 \pm 0.8) \times 10^{-6}$	2333	$\rho^+ \rho^-$	$(2.77 \pm 0.19) \times 10^{-5}$			2523
$K_0^*(1430)^0 K^*(892)^0$	< 1.7	$\times 10^{-6}$ CL=90%	$a_1(1260)^0 \pi^0$	< 1.1	$\times 10^{-3}$	CL=90%	2495
$K_0^*(1430)^0 K_0^*(1430)^0$	< 4.7	$\times 10^{-6}$ CL=90%	$\omega \pi^0$	< 5	$\times 10^{-7}$	CL=90%	2580
$K^*(1680)^0 \phi$	< 3.5	$\times 10^{-6}$ CL=90%	$\pi^+ \pi^+ \pi^- \pi^- \pi^0$	< 9.0	$\times 10^{-3}$	CL=90%	2609
$K^*(1780)^0 \phi$	< 2.7	$\times 10^{-6}$ CL=90%	$a_1(1260)^+ \rho^-$	< 6.1	$\times 10^{-5}$	CL=90%	2433
$K^*(2045)^0 \phi$	< 1.53	$\times 10^{-5}$ CL=90%	$a_1(1260)^0 \rho^0$	< 2.4	$\times 10^{-3}$	CL=90%	2433
$K_2^*(1430)^0 \rho^0$	< 1.1	$\times 10^{-3}$ CL=90%	$b_1^\mp \pi^\pm, b_1^\mp \rightarrow \omega \pi^\mp$	$(1.09 \pm 0.15) \times 10^{-5}$			-
$K_2^*(1430)^0 \phi$	$(6.8 \pm 0.9) \times 10^{-6}$	S=1.2 2332	$b_1^0 \pi^0, b_1^0 \rightarrow \omega \pi^0$	< 1.9	$\times 10^{-6}$	CL=90%	-
$K_0^0 \phi \phi$	$(3.7 \pm 0.7) \times 10^{-6}$	S=1.3 2305	$b_1^- \rho^+, b_1^- \rightarrow \omega \pi^-$	< 1.4	$\times 10^{-6}$	CL=90%	-
$\eta' \eta' K^0$	< 3.1	$\times 10^{-5}$ CL=90%	$b_1^0 \rho^0, b_1^0 \rightarrow \omega \pi^0$	< 3.4	$\times 10^{-6}$	CL=90%	-
$\eta K^0 \gamma$	$(7.6 \pm 1.8) \times 10^{-6}$	2587	$\pi^+ \pi^+ \pi^+ \pi^- \pi^- \pi^-$	< 3.0	$\times 10^{-3}$	CL=90%	2592
$\eta' K^0 \gamma$	< 6.4	$\times 10^{-6}$ CL=90%	$a_1(1260)^+ a_1(1260)^-, a_1^\pm \rightarrow$	$(1.18 \pm 0.31) \times 10^{-5}$			2336
$\eta' \phi \gamma$	$(2.7 \pm 0.7) \times 10^{-6}$	2516	$2\pi^+ \pi^-, a_1^- \rightarrow 2\pi^- \pi^+$				2572
$K^+ \pi^- \gamma$	$(4.6 \pm 1.4) \times 10^{-6}$	2615	$\pi^+ \pi^+ \pi^+ \pi^- \pi^- \pi^- \pi^0$	< 1.1	%	CL=90%	2572
$K^*(892)^0 \gamma$	$(4.18 \pm 0.25) \times 10^{-5}$	S=2.1 2565					
$K^*(1410) \gamma$	< 1.3	$\times 10^{-4}$ CL=90%					
$K^+ \pi^- \gamma$ nonresonant	< 2.6	$\times 10^{-6}$ CL=90%					
$K^*(892)^0 X(214), X \rightarrow$	[uuu] < 2.26	$\times 10^{-8}$ CL=90%					
$\mu^+ \mu^-$							
$K^0 \pi^+ \pi^- \gamma$	$(1.99 \pm 0.18) \times 10^{-5}$	2609					
$K^+ \pi^- \pi^0 \gamma$	$(4.1 \pm 0.4) \times 10^{-5}$	2609					
$K_1(1270)^0 \gamma$	< 5.8	$\times 10^{-5}$ CL=90%					
$K_1(1400)^0 \gamma$	< 1.2	$\times 10^{-5}$ CL=90%					
$K_2^*(1430)^0 \gamma$	$(1.24 \pm 0.24) \times 10^{-5}$	2447					
$K^*(1680)^0 \gamma$	< 2.0	$\times 10^{-3}$ CL=90%					
$K_3^*(1780)^0 \gamma$	< 8.3	$\times 10^{-5}$ CL=90%					
$K_4^*(2045)^0 \gamma$	< 4.3	$\times 10^{-3}$ CL=90%					
Light unflavored meson modes							
$\rho^0 \gamma$	$(8.6 \pm 1.5) \times 10^{-7}$	2583					
$\rho^0 X(214), X \rightarrow \mu^+ \mu^-$	[uuu] < 1.73	$\times 10^{-8}$ CL=90%					
$\omega \gamma$	$(4.4 \pm 1.8) \times 10^{-7}$	2582					
$\phi \gamma$	< 1.0	$\times 10^{-7}$ CL=90%					
$\pi^+ \pi^-$	$(5.12 \pm 0.19) \times 10^{-6}$	2636					
$\pi^0 \pi^0$	$(1.59 \pm 0.26) \times 10^{-6}$	S=1.4 2636					
$\eta \pi^0$	$(4.1 \pm 1.7) \times 10^{-7}$	2610					
$\eta \eta$	< 1.0	$\times 10^{-6}$ CL=90%					
$\eta' \pi^0$	$(1.2 \pm 0.6) \times 10^{-6}$	S=1.7 2551					
$\eta' \eta'$	< 1.7	$\times 10^{-6}$ CL=90%					
$\eta' \eta$	< 1.2	$\times 10^{-6}$ CL=90%					
$\eta' \rho^0$	< 1.3	$\times 10^{-6}$ CL=90%					
$\eta' f_0(980), f_0 \rightarrow \pi^+ \pi^-$	< 9	$\times 10^{-7}$ CL=90%					
$\eta \rho^0$	< 1.5	$\times 10^{-6}$ CL=90%					
$\eta f_0(980), f_0 \rightarrow \pi^+ \pi^-$	< 4	$\times 10^{-7}$ CL=90%					
$\omega \eta$	$(9.4 \pm 4.0) \times 10^{-7}$	2552					
$\omega \eta'$	$(1.0 \pm 0.5) \times 10^{-6}$	2491					
$\omega \rho^0$	< 1.6	$\times 10^{-6}$ CL=90%					
$\omega f_0(980), f_0 \rightarrow \pi^+ \pi^-$	< 1.5	$\times 10^{-6}$ CL=90%					
$\omega \omega$	$(1.2 \pm 0.4) \times 10^{-6}$	2521					
$\phi \pi^0$	< 1.5	$\times 10^{-7}$ CL=90%					
$\phi \eta$	< 5	$\times 10^{-7}$ CL=90%					
			$\phi \eta'$	< 5	$\times 10^{-7}$	CL=90%	2448
			$\phi \pi^+ \pi^-$	$(1.8 \pm 0.5) \times 10^{-7}$			2533
			$\phi \rho^0$	< 3.3	$\times 10^{-7}$	CL=90%	2480
			$\phi f_0(980), f_0 \rightarrow \pi^+ \pi^-$	< 3.8	$\times 10^{-7}$	CL=90%	2441
			$\phi \omega$	< 7	$\times 10^{-7}$	CL=90%	2479
			$\phi \phi$	< 2.7	$\times 10^{-8}$	CL=90%	2435
			$a_0(980)^\pm \pi^\mp, a_0^\pm \rightarrow \eta \pi^\pm$	< 3.1	$\times 10^{-6}$	CL=90%	-
			$a_0(1450)^\pm \pi^\mp, a_0^\pm \rightarrow \eta \pi^\pm$	< 2.3	$\times 10^{-6}$	CL=90%	-
			$\pi^+ \pi^- \pi^0$	< 7.2	$\times 10^{-4}$	CL=90%	2631
			$\rho^0 \pi^0$	$(2.0 \pm 0.5) \times 10^{-6}$			2581
			$\rho^\mp \pi^\pm$	[aa] $(2.30 \pm 0.23) \times 10^{-5}$			2581
			$\pi^+ \pi^- \pi^+ \pi^-$	< 1.12	$\times 10^{-5}$	CL=90%	2621
			$\rho^0 \pi^+ \pi^-$	< 8.8	$\times 10^{-6}$	CL=90%	2575
			$\rho^0 \rho^0$	$(9.6 \pm 1.5) \times 10^{-7}$			2523
			$f_0(980) \pi^+ \pi^-, f_0 \rightarrow$	< 3.0	$\times 10^{-6}$	CL=90%	-
			$\pi^+ \pi^-$				2486
			$\rho^0 f_0(980), f_0 \rightarrow \pi^+ \pi^-$	$(7.8 \pm 2.5) \times 10^{-7}$			2447
			$f_0(980) f_0(980), f_0 \rightarrow$	< 1.9	$\times 10^{-7}$	CL=90%	2447
			$\pi^+ \pi^-, f_0 \rightarrow \pi^+ \pi^-$	< 2.3	$\times 10^{-7}$	CL=90%	2447
			$f_0(980) f_0(980), f_0 \rightarrow \pi^+ \pi^-$	< 2.3	$\times 10^{-7}$	CL=90%	2447
			$f_0 \rightarrow K^+ K^-$				2494
			$a_1(1260)^\mp \pi^\pm$	[aa] $(2.6 \pm 0.5) \times 10^{-5}$	S=1.9		2494
			$a_2(1320)^\mp \pi^\pm$	[aa] < 6.3	$\times 10^{-6}$	CL=90%	2473
			$\pi^+ \pi^- \pi^0 \pi^0$	< 3.1	$\times 10^{-3}$	CL=90%	2622
			$\rho^+ \rho^-$	$(2.77 \pm 0.19) \times 10^{-5}$			2523
			$a_1(1260)^0 \pi^0$	< 1.1	$\times 10^{-3}$	CL=90%	2495
			$\omega \pi^0$	< 5	$\times 10^{-7}$	CL=90%	2580
			$\pi^+ \pi^+ \pi^- \pi^- \pi^0$	< 9.0	$\times 10^{-3}$	CL=90%	2609
			$a_1(1260)^+ \rho^-$	< 6.1	$\times 10^{-5}$	CL=90%	2433
			$a_1(1260)^0 \rho^0$	< 2.4	$\times 10^{-3}$	CL=90%	2433
			$b_1^\mp \pi^\pm, b_1^\mp \rightarrow \omega \pi^\mp$	$(1.09 \pm 0.15) \times 10^{-5}$			-
			$b_1^0 \pi^0, b_1^0 \rightarrow \omega \pi^0$	< 1.9	$\times 10^{-6}$	CL=90%	-
			$b_1^- \rho^+, b_1^- \rightarrow \omega \pi^-$	< 1.4	$\times 10^{-6}$	CL=90%	-
			$b_1^0 \rho^0, b_1^0 \rightarrow \omega \pi^0$	< 3.4	$\times 10^{-6}$	CL=90%	-
			$\pi^+ \pi^+ \pi^+ \pi^- \pi^- \pi^-$	< 3.0	$\times 10^{-3}$	CL=90%	2592
			$a_1(1260)^+ a_1(1260)^-, a_1^\pm \rightarrow$	$(1.18 \pm 0.31) \times 10^{-5}$			2336
			$2\pi^+ \pi^-, a_1^- \rightarrow 2\pi^- \pi^+$				2572
			$\pi^+ \pi^+ \pi^+ \pi^- \pi^- \pi^- \pi^0$	< 1.1	%	CL=90%	2572
			Baryon modes				
			$p \bar{p}$	$(1.25 \pm 0.32) \times 10^{-8}$			2467
			$p \bar{p} \pi^+ \pi^-$	$(2.87 \pm 0.19) \times 10^{-6}$			2406
			$p \bar{p} K^+ \pi^-$	$(6.3 \pm 0.5) \times 10^{-6}$	</		

Meson Summary Table

$\Theta_c \bar{p}\pi^+, \Theta_c \rightarrow D^- p$	< 9	$\times 10^{-6}$	CL=90%	-
$\Theta_c \bar{p}\pi^+, \Theta_c \rightarrow D^{*-} p$	< 1.4	$\times 10^{-5}$	CL=90%	-
$\bar{\Sigma}_c^{--} \Delta^{++}$	< 8	$\times 10^{-4}$	CL=90%	1839
$\bar{\Lambda}_c^- p\pi^+\pi^-$	(1.02 ± 0.14)	$\times 10^{-3}$	S=1.3	1934
$\bar{\Lambda}_c^- p$	(1.54 ± 0.18)	$\times 10^{-5}$		2021
$\bar{\Lambda}_c^- p\pi^0$	(1.55 ± 0.19)	$\times 10^{-4}$		1982
$\bar{\Sigma}_c(2455)^- p$	< 2.4	$\times 10^{-5}$		-
$\bar{\Lambda}_c^- p\pi^+\pi^-\pi^0$	< 5.07	$\times 10^{-3}$	CL=90%	1883
$\bar{\Lambda}_c^- p\pi^+\pi^-\pi^+\pi^-$	< 2.74	$\times 10^{-3}$	CL=90%	1821
$\bar{\Lambda}_c^- p\pi^+\pi^-$ (nonresonant)	(5.5 ± 1.0)	$\times 10^{-4}$	S=1.3	1934
$\bar{\Sigma}_c(2520)^- p\pi^+$	(1.02 ± 0.18)	$\times 10^{-4}$		1860
$\bar{\Sigma}_c(2520)^0 p\pi^-$	< 3.1	$\times 10^{-5}$	CL=90%	1860
$\bar{\Sigma}_c(2455)^0 p\pi^-$	(1.08 ± 0.16)	$\times 10^{-4}$		1895
$\bar{\Sigma}_c(2455)^0 N^0, N^0 \rightarrow$	(6.4 ± 1.7)	$\times 10^{-5}$		-
$\bar{\Sigma}_c(2455)^- p\pi^+$	(1.83 ± 0.24)	$\times 10^{-4}$		1895
$\bar{\Lambda}_c^- pK^+\pi^-$	(3.4 ± 0.7)	$\times 10^{-5}$		1786
$\bar{\Sigma}_c(2455)^- pK^+, \bar{\Sigma}_c^{--} \rightarrow$	(8.8 ± 2.5)	$\times 10^{-6}$		1754
$\bar{\Lambda}_c^- \pi^-$				
$\bar{\Lambda}_c^- pK^*(892)^0$	< 2.42	$\times 10^{-5}$	CL=90%	1647
$\bar{\Lambda}_c^- pK^+K^-$	(2.0 ± 0.4)	$\times 10^{-5}$		1588
$\bar{\Lambda}_c^- p\phi$	< 1.0	$\times 10^{-5}$	CL=90%	1567
$\bar{\Lambda}_c^- p\bar{p}p$	< 2.8	$\times 10^{-6}$		677
$\bar{\Lambda}_c^- \Lambda K^+$	(4.8 ± 1.1)	$\times 10^{-5}$		1767
$\bar{\Lambda}_c^- \Lambda_c^+$	< 1.6	$\times 10^{-5}$	CL=95%	1319
$\bar{\Lambda}_c^-(2593)^- / \bar{\Lambda}_c(2625)^- p$	< 1.1	$\times 10^{-4}$	CL=90%	-
$\bar{\Xi}_c^- \Lambda_c^+$	(1.2 ± 0.8)	$\times 10^{-3}$		1147
$\bar{\Xi}_c^- \Lambda_c^+, \bar{\Xi}_c^- \rightarrow \Xi^{*+} \pi^- \pi^-$	(2.4 ± 1.1)	$\times 10^{-5}$	S=1.8	1147
$\bar{\Xi}_c^- \Lambda_c^+, \bar{\Xi}_c^- \rightarrow \bar{p}K^+ \pi^-$	(5.3 ± 1.7)	$\times 10^{-6}$		-
$\bar{\Lambda}_c^+ \Lambda_c^- K^0$	(4.0 ± 0.9)	$\times 10^{-4}$		732
$\bar{\Xi}_c^-(2930)^- \Lambda_c^+, \bar{\Xi}_c^- \rightarrow \bar{\Lambda}_c^- K^0$	(2.4 ± 0.6)	$\times 10^{-4}$		-

Lepton Family number (LF) or Lepton number (L) or Baryon number (B) violating modes, or/and $\Delta B = 1$ weak neutral current (BI) modes

$\gamma\gamma$	BI	< 3.2	$\times 10^{-7}$	CL=90%	2640
e^+e^-	BI	< 2.5	$\times 10^{-9}$	CL=90%	2640
$e^+e^-\gamma$	BI	< 1.2	$\times 10^{-7}$	CL=90%	2640
$\mu^+\mu^-$	BI	(7 $^{+13}_{-11}$)	$\times 10^{-11}$	S=1.8	2638
$\mu^+\mu^-\gamma$	BI	< 2.0	$\times 10^{-9}$	CL=95%	2638
$\mu^+\mu^-\mu^+\mu^-$	BI	< 6.9	$\times 10^{-10}$	CL=95%	2629
$SP, S \rightarrow \mu^+\mu^-,$ $P \rightarrow \mu^+\mu^-$	BI [xxx]	< 6.0	$\times 10^{-10}$	CL=95%	-
$\tau^+\tau^-$	BI	< 2.1	$\times 10^{-3}$	CL=95%	1952
$\pi^0 \ell^+ \ell^-$	BI	< 5.3	$\times 10^{-8}$	CL=90%	2638
$\pi^0 e^+ e^-$	BI	< 8.4	$\times 10^{-8}$	CL=90%	2638
$\pi^0 \mu^+ \mu^-$	BI	< 6.9	$\times 10^{-8}$	CL=90%	2634
$\eta \ell^+ \ell^-$	BI	< 6.4	$\times 10^{-8}$	CL=90%	2611
$\eta e^+ e^-$	BI	< 1.08	$\times 10^{-7}$	CL=90%	2611
$\eta \mu^+ \mu^-$	BI	< 1.12	$\times 10^{-7}$	CL=90%	2607
$\pi^0 \nu \bar{\nu}$	BI	< 9	$\times 10^{-6}$	CL=90%	2638
$K^0 \ell^+ \ell^-$	BI [iii]	(3.3 ± 0.6)	$\times 10^{-7}$		2616
$K^0 e^+ e^-$	BI	(2.5 $^{+1.1}_{-0.9}$)	$\times 10^{-7}$	S=1.3	2616
$K^0 \mu^+ \mu^-$	BI	(3.39 ± 0.35)	$\times 10^{-7}$	S=1.1	2612
$K^0 \nu \bar{\nu}$	BI	< 2.6	$\times 10^{-5}$	CL=90%	2616
$\rho^0 \nu \bar{\nu}$	BI	< 4.0	$\times 10^{-5}$	CL=90%	2583
$K^*(892)^0 \ell^+ \ell^-$	BI [iii]	(9.9 $^{+1.2}_{-1.1}$)	$\times 10^{-7}$		2565
$K^*(892)^0 e^+ e^-$	BI	(1.03 $^{+0.19}_{-0.17}$)	$\times 10^{-6}$		2565
$K^*(892)^0 \mu^+ \mu^-$	BI	(9.4 ± 0.5)	$\times 10^{-7}$		2560
$\pi^+ \pi^- \mu^+ \mu^-$	BI	(2.1 ± 0.5)	$\times 10^{-8}$		2626
$K^*(892)^0 \nu \bar{\nu}$	BI	< 1.8	$\times 10^{-5}$	CL=90%	2565
invisible	BI	< 2.4	$\times 10^{-5}$	CL=90%	-
$\nu \bar{\nu} \gamma$	BI	< 1.6	$\times 10^{-5}$	CL=90%	2640
$\phi \nu \bar{\nu}$	BI	< 1.27	$\times 10^{-4}$	CL=90%	2541
$e^\pm \mu^\mp$	LF [aa]	< 1.0	$\times 10^{-9}$	CL=90%	2639
$\pi^0 e^\pm \mu^\mp$	LF	< 1.4	$\times 10^{-7}$	CL=90%	2637
$K^0 e^\pm \mu^\mp$	LF	< 3.8	$\times 10^{-8}$	CL=90%	2615
$K^*(892)^0 e^+ \mu^-$	LF	< 1.6	$\times 10^{-7}$	CL=90%	2563
$K^*(892)^0 e^- \mu^+$	LF	< 1.2	$\times 10^{-7}$	CL=90%	2563
$K^*(892)^0 e^\pm \mu^\mp$	LF	< 1.8	$\times 10^{-7}$	CL=90%	2563
$e^\pm \tau^\mp$	LF [aa]	< 1.6	$\times 10^{-5}$	CL=90%	2341
$\mu^\pm \tau^\mp$	LF [aa]	< 1.4	$\times 10^{-5}$	CL=95%	2340

$\Lambda_c^+ \mu^-$	L,B	< 1.4	$\times 10^{-6}$	CL=90%	2143
$\Lambda_c^+ e^-$	L,B	< 4	$\times 10^{-6}$	CL=90%	2145

B^\pm/B^0 ADMIXTURE

CP violation

$$\begin{aligned}
 A_{CP}(B \rightarrow K^*(892)\gamma) &= -0.003 \pm 0.011 \\
 A_{CP}(B \rightarrow s\gamma) &= 0.015 \pm 0.011 \\
 A_{CP}(B \rightarrow (s+d)\gamma) &= 0.010 \pm 0.031 \\
 A_{CP}(B \rightarrow X_s \ell^+ \ell^-) &= 0.04 \pm 0.11 \\
 A_{CP}(B \rightarrow X_s \ell^+ \ell^-) &(1.0 < q^2 < 6.0 \text{ GeV}^2/c^4) = -0.06 \pm 0.22 \\
 A_{CP}(B \rightarrow X_s \ell^+ \ell^-) &(10.1 < q^2 < 12.9 \text{ or } q^2 > 14.2 \text{ GeV}^2/c^4) \\
 &= 0.19 \pm 0.18 \\
 A_{CP}(B \rightarrow K^* e^+ e^-) &= -0.18 \pm 0.15 \\
 A_{CP}(B \rightarrow K^* \mu^+ \mu^-) &= -0.03 \pm 0.13 \\
 A_{CP}(B \rightarrow K^* \ell^+ \ell^-) &= -0.04 \pm 0.07 \\
 A_{CP}(B \rightarrow \eta \text{ anything}) &= -0.13 $^{+0.04}_{-0.05}$ \\
 \Delta A_{CP}(X_s \gamma) &= A_{CP}(B^\pm \rightarrow X_s \gamma) - A_{CP}(B^0 \rightarrow X_s \gamma) = \\
 &0.041 \pm 0.023 \\
 \bar{A}_{CP}(B \rightarrow X_s \gamma) &= (A_{CP}(B^+ \rightarrow X_s \gamma) + A_{CP}(B^0 \rightarrow \\
 &X_s \gamma))/2 = 0.009 \pm 0.012 \\
 \Delta A_{CP}(B \rightarrow K^* \gamma) &= A_{CP}(B^+ \rightarrow K^{*+} \gamma) - A_{CP}(B^0 \rightarrow \\
 &K^{*0} \gamma) = 0.024 \pm 0.028 \\
 \bar{A}_{CP}(B \rightarrow K^* \gamma) &= (A_{CP}(B^+ \rightarrow K^{*+} \gamma) + A_{CP}(B^0 \rightarrow \\
 &K^{*0} \gamma))/2 = -0.001 \pm 0.014
 \end{aligned}$$

The branching fraction measurements are for an admixture of B mesons at the $\Upsilon(4S)$. The values quoted assume that $B(\Upsilon(4S) \rightarrow B\bar{B}) = 100\%$.

For inclusive branching fractions, e.g., $B \rightarrow D^\pm$ anything, the treatment of multiple D 's in the final state must be defined. One possibility would be to count the number of events with one-or-more D 's and divide by the total number of B 's. Another possibility would be to count the total number of D 's and divide by the total number of B 's, which is the definition of average multiplicity. The two definitions are identical if only one D is allowed in the final state. Even though the "one-or-more" definition seems sensible, for practical reasons inclusive branching fractions are almost always measured using the multiplicity definition. For heavy final state particles, authors call their results inclusive branching fractions while for light particles some authors call their results multiplicities. In the B sections, we list all results as inclusive branching fractions, adopting a multiplicity definition. This means that inclusive branching fractions can exceed 100% and that inclusive partial widths can exceed total widths, just as inclusive cross sections can exceed total cross section.

\bar{B} modes are charge conjugates of the modes below. Reactions indicate the weak decay vertex and do not include mixing.

B DECAY MODES	Fraction (Γ_i/Γ)	Scale factor/ Confidence level (MeV/c)	ρ
Semileptonic and leptonic modes			
$\ell^+ \nu_\ell$ anything	[iii,yyy] (10.84 ± 0.16) %		-
$D^- \ell^+ \nu_\ell$ anything	[iii] (2.6 ± 0.5) %		-
$\bar{D}^0 \ell^+ \nu_\ell$ anything	[iii] (7.3 ± 1.5) %		-
$\bar{D} \ell^+ \nu_\ell$	(2.42 ± 0.12) %		2310
$D^{*-} \ell^+ \nu_\ell$ anything	[zzz] (6.7 ± 1.3) $\times 10^{-3}$		-
$\bar{D}^* \ell^+ \nu_\ell$	[aaaa] (4.95 ± 0.11) %		2257
$\bar{D}^{**} \ell^+ \nu_\ell$	[iii,bbaa] (2.7 ± 0.7) %		-
$\bar{D}_1(2420) \ell^+ \nu_\ell$ anything	(3.8 ± 1.3) $\times 10^{-3}$	S=2.4	-
$\bar{D} \pi \ell^+ \nu_\ell$ anything + $\bar{D}^* \pi \ell^+ \nu_\ell$ anything	(2.6 ± 0.5) %	S=1.5	-
$\bar{D} \pi \ell^+ \nu_\ell$ anything	(1.5 ± 0.6) %		-
$\bar{D}^* \pi \ell^+ \nu_\ell$ anything	(1.9 ± 0.4) %		-
$\bar{D}_2^*(2460) \ell^+ \nu_\ell$ anything	(4.4 ± 1.6) $\times 10^{-3}$		-
$D^{*-} \pi^+ \ell^+ \nu_\ell$ anything	(1.00 ± 0.34) %		-
$\bar{D} \pi^+ \pi^- \ell^+ \nu_\ell$	(1.62 ± 0.32) $\times 10^{-3}$		2301
$\bar{D}^* \pi^+ \pi^- \ell^+ \nu_\ell$	(9.4 ± 3.2) $\times 10^{-4}$		2247
$D_s^- \ell^+ \nu_\ell$ anything	[iii] < 7	$\times 10^{-3}$	CL=90%
$D_s^- \ell^+ \nu_\ell K^+$ anything	[iii] < 5	$\times 10^{-3}$	CL=90%
$D_s^- \ell^+ \nu_\ell K^0$ anything	[iii] < 7	$\times 10^{-3}$	CL=90%
$X_c \ell^+ \nu_\ell$	(10.65 ± 0.16) %		-
$X_u \ell^+ \nu_\ell$	(1.91 ± 0.27) $\times 10^{-3}$		-
$X_u e^+ \nu_e$	(1.57 ± 0.19) $\times 10^{-3}$		-
$X_u \mu^+ \nu_\mu$	(1.62 ± 0.21) $\times 10^{-3}$		-
$K^+ \ell^+ \nu_\ell$ anything	[iii] (6.3 ± 0.6) %		-
$K^- \ell^+ \nu_\ell$ anything	[iii] (10 ± 4) $\times 10^{-3}$		-
$K^0 / \bar{K}^0 \ell^+ \nu_\ell$ anything	[iii] (4.6 ± 0.5) %		-
$\bar{D} \tau^+ \nu_\tau$	(8.2 ± 0.8) $\times 10^{-3}$		1911
$\bar{D}^* \tau^+ \nu_\tau$	(1.46 ± 0.08) %		1838

Meson Summary Table

D, D*, or D_s modes				Baryon modes			
D^\pm anything	(23.1 ± 1.2) %	-	-	$\phi K^*(892)$	< 2.2	$\times 10^{-5}$	CL=90% 2460
D^0/\bar{D}^0 anything	(61.6 ± 2.9) %	S=1.3	-	π^+ gluon (charmless)	(3.7 ± 0.8)	$\times 10^{-4}$	-
$D^*(2010)^\pm$ anything	(22.5 ± 1.5) %	-	-	$\Lambda_c^+ / \bar{\Lambda}_c^-$ anything	(3.6 ± 0.4)	%	-
$\bar{D}^*(2007)^0$ anything	(26.0 ± 2.7) %	-	-	Λ_c^+ anything	< 1.3	%	CL=90% -
D_s^\pm anything	[aa] (8.3 ± 0.8) %	-	-	$\bar{\Lambda}_c^-$ anything	< 7	%	CL=90% -
$D_s^{*\pm}$ anything	(6.3 ± 1.0) %	-	-	$\bar{\Lambda}_c^- \ell^+$ anything	< 9	$\times 10^{-4}$	CL=90% -
$D_s^\pm \bar{D}^*(*)$	(3.4 ± 0.6) %	-	-	$\bar{\Lambda}_c^- e^+$ anything	< 1.8	$\times 10^{-3}$	CL=90% -
$\bar{D} D_{s0}(2317)$	seen	1605	-	$\bar{\Lambda}_c^- \mu^+$ anything	< - 1.4	$\times 10^{-3}$	CL=90% -
$\bar{D} D_{sJ}(2457)$	seen	-	-	$\bar{\Lambda}_c^- p$ anything	(2.04 ± 0.33)	%	-
$D^*(\bar{D}^*(*) K^0 + D^*(\bar{D}^*(*) K^\pm)$	[aa,ccaa] (7.1 ± 2.7 / -1.7) %	-	-	$\bar{\Lambda}_c^- p e^+ \nu_e$	< 8	$\times 10^{-4}$	CL=90% 2021
$b \rightarrow c \bar{c} s$	(22 ± 4) %	-	-	Σ_c^{--} anything	(3.3 ± 1.7)	$\times 10^{-3}$	-
$D_s^*(*) \bar{D}^*(*)$	[aa,ccaa] (3.9 ± 0.4) %	-	-	Σ_c^- anything	< 8	$\times 10^{-3}$	CL=90% -
$D^* D^*(2010)^\pm$	[aa] < 5.9	$\times 10^{-3}$	CL=90% 1711	Σ_c^0 anything	(3.7 ± 1.7)	$\times 10^{-3}$	-
$D^* D^*(2010)^\pm + D^* D^\pm$	[aa] < 5.5	$\times 10^{-3}$	CL=90% -	$\Sigma_c^0 N(N = p \text{ or } n)$	< 1.2	$\times 10^{-3}$	CL=90% 1938
DD^\pm	[aa] < 3.1	$\times 10^{-3}$	CL=90% 1866	Ξ_c^0 anything, $\Xi_c^0 \rightarrow \Xi^- \pi^+$	(1.93 ± 0.30)	$\times 10^{-4}$	S=1.1 -
$D_s^*(*)^\pm \bar{D}^*(*) X(n\pi^\pm)$	[aa,ccaa] (9 ± 5 / -4) %	-	-	$\Xi_c^+, \Xi_c^+ \rightarrow \Xi^- \pi^+ \pi^+$	(4.5 ± 1.3 / -1.2)	$\times 10^{-4}$	-
$\bar{D}^*(2010)\gamma$	< 1.1	$\times 10^{-3}$	CL=90% 2257	p/\bar{p} anything	[aa] (8.0 ± 0.4) %	-	-
$D_s^+ \pi^-, D_s^{*+} \pi^-, D_s^+ \rho^-, D_s^{*+} \rho^-, D_s^+ \pi^0, D_s^{*+} \pi^0, D_s^+ \eta, D_s^{*+} \eta, D_s^+ \rho^0, D_s^{*+} \rho^0, D_s^+ \omega, D_s^{*+} \omega$	[aa] < 4	$\times 10^{-4}$	CL=90% -	p/\bar{p} (direct) anything	[aa] (5.5 ± 0.5) %	-	-
$D_{s1}(2536)^+$ anything	< 9.5	$\times 10^{-3}$	CL=90% -	$\bar{p} e^+ \nu_e$ anything	< 5.9	$\times 10^{-4}$	CL=90% -
Charmonium modes				$\Lambda/\bar{\Lambda}$ anything	[aa] (4.0 ± 0.5) %	-	-
$J/\psi(1S)$ anything	(1.094 ± 0.032) %	S=1.1	-	Λ anything	seen	-	-
$J/\psi(1S)$ (direct) anything	(7.8 ± 0.4) $\times 10^{-3}$	S=1.1	-	$\bar{\Lambda}$ anything	seen	-	-
$\psi(2S)$ anything	(3.07 ± 0.21) $\times 10^{-3}$	-	-	$\Xi^- / \bar{\Xi}^+$ anything	[aa] (2.7 ± 0.6)	$\times 10^{-3}$	-
$\chi_{c1}(1P)$ anything	(3.55 ± 0.27) $\times 10^{-3}$	S=1.3	-	baryons anything	(6.8 ± 0.6) %	-	-
$\chi_{c1}(1P)$ (direct) anything	(3.08 ± 0.19) $\times 10^{-3}$	-	-	$p\bar{p}$ anything	(2.47 ± 0.23) %	-	-
$\chi_{c2}(1P)$ anything	(10.0 ± 1.7) $\times 10^{-4}$	S=1.6	-	$\Lambda\bar{p}/\bar{\Lambda}p$ anything	[aa] (2.5 ± 0.4) %	-	-
$\chi_{c2}(1P)$ (direct) anything	(7.5 ± 1.1) $\times 10^{-4}$	-	-	$\Lambda\bar{\Lambda}$ anything	< 5	$\times 10^{-3}$	CL=90% -
$\eta_c(1S)$ anything	< 9	$\times 10^{-3}$	CL=90% -	Lepton Family number (LF) violating modes or $\Delta B = 1$ weak neutral current (B1) modes			
$K\chi_{c1}(3872)$	(2.3 ± 0.7) $\times 10^{-4}$	1141	-	se^+e^-	B1 (6.7 ± 1.7)	$\times 10^{-6}$	S=2.0 -
$KX(3940), X \rightarrow D^{*0}D^0$	< 6.7	$\times 10^{-5}$	CL=90% 1084	$s\mu^+\mu^-$	B1 (4.3 ± 1.0)	$\times 10^{-6}$	-
$K\chi_{c0}(3915), \chi_{c0} \rightarrow \omega J/\psi[ddaa]$	(7.1 ± 3.4) $\times 10^{-5}$	1103	-	$s\ell^+\ell^-$	B1 [iii] (5.8 ± 1.3)	$\times 10^{-6}$	S=1.8 -
K or K* modes				$\pi\ell^+\ell^-$	B1 < 5.9	$\times 10^{-8}$	CL=90% 2638
K^\pm anything	[aa] (78.9 ± 2.5) %	-	-	πe^+e^-	B1 < 1.10	$\times 10^{-7}$	CL=90% 2638
K^+ anything	(66 ± 5) %	-	-	$\pi\mu^+\mu^-$	B1 < 5.0	$\times 10^{-8}$	CL=90% 2634
K^- anything	(13 ± 4) %	-	-	Ke^+e^-	B1 (4.4 ± 0.6)	$\times 10^{-7}$	2617
K^0/\bar{K}^0 anything	[aa] (64 ± 4) %	-	-	$K^*(892)e^+e^-$	B1 (1.19 ± 0.20)	$\times 10^{-6}$	S=1.2 2565
$K^*(892)^\pm$ anything	(18 ± 6) %	-	-	$K\mu^+\mu^-$	B1 (4.4 ± 0.4)	$\times 10^{-7}$	2612
$K^*(892)^0/\bar{K}^*(892)^0$ anything	[aa] (14.6 ± 2.6) %	-	-	$K^*(892)\mu^+\mu^-$	B1 (1.06 ± 0.09)	$\times 10^{-6}$	2560
$K^*(892)\gamma$	(4.2 ± 0.6) $\times 10^{-5}$	2565	-	$K\ell^+\ell^-$	B1 (4.8 ± 0.4)	$\times 10^{-7}$	2617
$\eta K\gamma$	(8.5 ± 1.8 / -1.6) $\times 10^{-6}$	2588	-	$K^*(892)\ell^+\ell^-$	B1 (1.05 ± 0.10)	$\times 10^{-6}$	2565
$K_1(1400)\gamma$	< 1.27	$\times 10^{-4}$	CL=90% 2454	$K\nu\bar{\nu}$	B1 < 1.6	$\times 10^{-5}$	CL=90% 2617
$K_2^*(1430)\gamma$	(1.7 ± 0.6 / -0.5) $\times 10^{-5}$	2447	-	$K^*\nu\bar{\nu}$	B1 < 2.7	$\times 10^{-5}$	CL=90% -
$K_2(1770)\gamma$	< 1.2	$\times 10^{-3}$	CL=90% 2342	$\pi\nu\bar{\nu}$	B1 < 8	$\times 10^{-6}$	CL=90% 2638
$K_3^*(1780)\gamma$	< 3.7	$\times 10^{-5}$	CL=90% 2340	$\rho\nu\bar{\nu}$	B1 < 2.8	$\times 10^{-5}$	CL=90% 2583
$K_4^*(2045)\gamma$	< 1.0	$\times 10^{-3}$	CL=90% 2243	$se^\pm\mu^\mp$	LF [aa] < 2.2	$\times 10^{-5}$	CL=90% -
$K\eta'(958)$	(8.3 ± 1.1) $\times 10^{-5}$	2528	-	$\pi e^\pm\mu^\mp$	LF < 9.2	$\times 10^{-8}$	CL=90% 2637
$K^*(892)\eta'(958)$	(4.1 ± 1.1) $\times 10^{-6}$	2472	-	$\rho e^\pm\mu^\mp$	LF < 3.2	$\times 10^{-6}$	CL=90% 2582
$K\eta$	< 5.2	$\times 10^{-6}$	CL=90% 2588	$Ke^\pm\mu^\mp$	LF < 3.8	$\times 10^{-8}$	CL=90% 2616
$K^*(892)\eta$	(1.8 ± 0.5) $\times 10^{-5}$	2534	-	$K^*(892)e^\pm\mu^\mp$	LF < 5.1	$\times 10^{-7}$	CL=90% 2563
$K\phi\phi$	(2.3 ± 0.9) $\times 10^{-6}$	2306	-	$B^\pm/B^0/B_s^0/b$-baryon ADMIXTURE			
$\bar{b} \rightarrow \bar{s}\gamma$	(3.49 ± 0.19) $\times 10^{-4}$	-	-	These measurements are for an admixture of bottom particles at high energy (LHC, LEP, Tevatron, $Spp\bar{S}$).			
$\bar{b} \rightarrow \bar{d}\gamma$	(9.2 ± 3.0) $\times 10^{-6}$	-	-	Mean life $\tau = (1.5672 \pm 0.0029) \times 10^{-12}$ s			
$\bar{b} \rightarrow \bar{s}$ gluon	< 6.8	%	CL=90% -	Mean life $\tau = (1.72 \pm 0.10) \times 10^{-12}$ s Charged b -hadron admixture			
η anything	(2.6 ± 0.5 / -0.8) $\times 10^{-4}$	-	-	Mean life $\tau = (1.58 \pm 0.14) \times 10^{-12}$ s Neutral b -hadron admixture			
η' anything	(4.2 ± 0.9) $\times 10^{-4}$	-	-	$\tau_{\text{charged } b\text{-hadron}}/\tau_{\text{neutral } b\text{-hadron}} = 1.09 \pm 0.13$			
K^+ gluon (charmless)	< 1.87	$\times 10^{-4}$	CL=90% -	$ \Delta\tau_b /\tau_{b,\bar{b}} = -0.001 \pm 0.014$			
K^0 gluon (charmless)	(1.9 ± 0.7) $\times 10^{-4}$	-	-	The branching fraction measurements are for an admixture of B mesons and baryons at energies above the $T(4S)$. Only the highest energy results (LHC, LEP, Tevatron, $Spp\bar{S}$) are used in the branching fraction averages. In the following, we assume that the production fractions are the same at the LHC, LEP, and at the Tevatron.			
Light unflavored meson modes				For inclusive branching fractions, e.g., $B \rightarrow D^\pm$ anything, the values usually are multiplicities, not branching fractions. They can be greater than one.			
$\rho\gamma$	(1.39 ± 0.25) $\times 10^{-6}$	S=1.2 2583	-				
$\rho/\omega\gamma$	(1.30 ± 0.23) $\times 10^{-6}$	S=1.2 -	-				
π^\pm anything	[aa,eeaa] (358 ± 7) %	-	-				
π^0 anything	(235 ± 11) %	-	-				
η anything	(17.6 ± 1.6) %	-	-				
ρ^0 anything	(21 ± 5) %	-	-				
ω anything	< 81	%	CL=90% -				
ϕ anything	(3.43 ± 0.12) %	-	-				

Meson Summary Table

$B_1(5721)$	$I(J^P) = \frac{1}{2}(1^+)$ I, J, P need confirmation.
$B_1(5721)^+$ mass = $5725.9^{+2.5}_{-2.7}$ MeV	
$m_{B_1^+} - m_{B^0} = 401.2^{+2.4}_{-2.7}$ MeV	
$B_1(5721)^0$ mass = 5726.1 ± 1.3 MeV ($S = 1.2$)	
$m_{B_1^0} - m_{B^+} = 446.7 \pm 1.3$ MeV ($S = 1.2$)	
$m_{B_1^0} - m_{B^{*+}} = 401.4 \pm 1.2$ MeV ($S = 1.2$)	
Full width $\Gamma(B_1(5721)^+) = 31 \pm 6$ MeV ($S = 1.1$)	
Full width $\Gamma(B_1(5721)^0) = 27.5 \pm 3.4$ MeV ($S = 1.1$)	

$B_1(5721)$ DECAY MODES	Fraction (Γ_i/Γ)	ρ (MeV/c)
$B^* \pi$	seen	365

$B_2^*(5747)$	$I(J^P) = \frac{1}{2}(2^+)$ I, J, P need confirmation.
$B_2^*(5747)^+$ mass = 5737.2 ± 0.7 MeV	
$m_{B_2^{*+}} - m_{B^0} = 457.5 \pm 0.7$ MeV	
$B_2^*(5747)^0$ mass = 5739.5 ± 0.7 MeV ($S = 1.4$)	
$m_{B_2^{*0}} - m_{B^0} = 13.4 \pm 1.4$ MeV ($S = 1.3$)	
$m_{B_2^{*0}} - m_{B^+} = 460.2 \pm 0.6$ MeV ($S = 1.4$)	
Full width $\Gamma(B_2^*(5747)^+) = 20 \pm 5$ MeV ($S = 2.2$)	
Full width $\Gamma(B_2^*(5747)^0) = 24.2 \pm 1.7$ MeV	

$B_2^*(5747)$ DECAY MODES	Fraction (Γ_i/Γ)	ρ (MeV/c)
$B \pi$	seen	420
$B^* \pi$	seen	376

$B_J(5970)$	$I(J^P) = \frac{1}{2}(2^?)$ I, J, P need confirmation.
$B_J(5970)^+$ mass $m = 5964 \pm 5$ MeV	
$m_{B_J(5970)^+} - m_{B^0} = 685 \pm 5$ MeV	
$B_J(5970)^0$ mass $m = 5971 \pm 5$ MeV	
$m_{B_J(5970)^0} - m_{B^+} = 691 \pm 5$ MeV	
$B_J(5970)^+$ full width $\Gamma = 62 \pm 20$ MeV	
$B_J(5970)^0$ full width $\Gamma = 81 \pm 12$ MeV	

$B_J(5970)$ DECAY MODES	Fraction (Γ_i/Γ)	ρ (MeV/c)
$B \pi$	possibly seen	633
$B^* \pi$	seen	592

BOTTOM, STRANGE MESONS ($B = \pm 1, S = \mp 1$)

$$B_s^0 = s\bar{b}, \bar{B}_s^0 = \bar{s}b, \text{ similarly for } B_s^{*+} \text{'s}$$

B_s^0	$I(J^P) = 0(0^-)$
I, J, P need confirmation. Quantum numbers shown are quark-model predictions.	
Mass $m_{B_s^0} = 5366.92 \pm 0.10$ MeV	
$m_{B_s^0} - m_B = 87.42 \pm 0.14$ MeV	
Mean life $\tau = (1.520 \pm 0.005) \times 10^{-12}$ s	
$c\tau = 455.7 \mu\text{m}$	
$\Delta\Gamma_{B_s^0} = \Gamma_{B_s^0} - \Gamma_{B_s^0} = (0.084 \pm 0.005) \times 10^{12} \text{ s}^{-1}$ ($S = 1.7$)	
B_s^0-\bar{B}_s^0 mixing parameters	
$\Delta m_{B_s^0} = m_{B_s^0} - m_{\bar{B}_s^0} = (17.765 \pm 0.006) \times 10^{12} \hbar \text{ s}^{-1}$	
$= (1.1693 \pm 0.0004) \times 10^{-8}$ MeV	
$x_s = \Delta m_{B_s^0}/\Gamma_{B_s^0} = 27.01 \pm 0.10$	
χ_s (B_s^0 - \bar{B}_s^0 mixing parameter) = 0.499318 ± 0.000005	

CP violation parameters in B_s^0

$$\text{Re}(\epsilon_{B_s^0}) / (1 + |\epsilon_{B_s^0}|^2) = (-0.15 \pm 0.70) \times 10^{-3}$$

$$C_{KK}(B_s^0 \rightarrow K^+ K^-) = 0.162 \pm 0.035$$

$$S_{KK}(B_s^0 \rightarrow K^+ K^-) = 0.14 \pm 0.05 \quad (S = 1.3)$$

$$r_B(B_s^0 \rightarrow D_s^\mp K^\pm) = 0.37^{+0.10}_{-0.09}$$

$$r_B(B_s^0 \rightarrow D_s^\mp K^\pm \pi^\pm \pi^\mp) = 0.47 \pm 0.08$$

$$\delta_B(B_s^0 \rightarrow D_s^\pm K^\mp) = (358 \pm 14)^\circ$$

$$\delta_B(B_s^0 \rightarrow D_s^\pm K^\mp \pi^\pm \pi^\mp) = (-6^{+10}_{-13})^\circ$$

$$\text{CP Violation phase } \beta_s = (2.5 \pm 1.0) \times 10^{-2} \text{ rad}$$

$$|\lambda| (B_s^0 \rightarrow J/\psi(1S)\phi) = 1.001 \pm 0.018 \quad (S = 1.2)$$

$$|\lambda| = 0.999 \pm 0.017$$

$$A, \text{ CP violation parameter} = -0.79 \pm 0.08$$

$$C, \text{ CP violation parameter} = 0.19 \pm 0.06$$

$$S, \text{ CP violation parameter} = 0.17 \pm 0.06$$

$$A_{CP}^L(B_s \rightarrow J/\psi \bar{K}^*(892)^0) = -0.05 \pm 0.06$$

$$A_{CP}^L(B_s \rightarrow J/\psi \bar{K}^*(892)^0) = 0.17 \pm 0.15$$

$$A_{CP}^L(B_s \rightarrow J/\psi \bar{K}^*(892)^0) = -0.05 \pm 0.10$$

$$\text{ACP}(B_s \rightarrow \pi^+ K^-) = 0.224 \pm 0.012$$

$$A_{CP}(B_s^0 \rightarrow [K^+ K^-]_D \bar{K}^*(892)^0) = -0.04 \pm 0.07$$

$$A_{CP}(B_s^0 \rightarrow [\pi^+ K^-]_D K^*(892)^0) = -0.01 \pm 0.04$$

$$A_{CP}(B_s^0 \rightarrow [\pi^+ \pi^-]_D K^*(892)^0) = 0.06 \pm 0.13$$

$$S(B_s^0 \rightarrow \phi\gamma) = 0.43 \pm 0.32$$

$$C(B_s^0 \rightarrow \phi\gamma) = 0.11 \pm 0.31$$

$$A^\Delta(B_s^0 \rightarrow \phi\gamma) = -0.7 \pm 0.4$$

$$\Delta a_\perp < 1.2 \times 10^{-12} \text{ GeV, CL} = 95\%$$

$$\Delta a_\parallel = (-0.9 \pm 1.5) \times 10^{-14} \text{ GeV}$$

$$\Delta a_X = (1.0 \pm 2.2) \times 10^{-14} \text{ GeV}$$

$$\Delta a_Y = (-3.8 \pm 2.2) \times 10^{-14} \text{ GeV}$$

$$\text{Re}(\xi) = -0.022 \pm 0.033$$

$$\text{Im}(\xi) = 0.004 \pm 0.011$$

These branching fractions all scale with $B(\bar{b} \rightarrow B_s^0)$.

The branching fraction $B(B_s^0 \rightarrow D_s^- \ell^+ \nu_\ell \text{ anything})$ is not a pure measurement since the measured product branching fraction $B(\bar{b} \rightarrow B_s^0) \times B(B_s^0 \rightarrow D_s^- \ell^+ \nu_\ell \text{ anything})$ was used to determine $B(\bar{b} \rightarrow B_s^0)$, as described in the note on " B^0 - \bar{B}^0 Mixing"

For inclusive branching fractions, e.g., $B \rightarrow D^\pm \text{ anything}$, the values usually are multiplicities, not branching fractions. They can be greater than one.

B_s^0 DECAY MODES	Fraction (Γ_i/Γ)	Scale factor/ Confidence level	ρ (MeV/c)
$D_s^- \text{ anything}$	$(62 \pm 6) \%$		-
$\ell \nu_\ell X$	$(9.6 \pm 0.8) \%$		-
$e^+ \nu X^-$	$(9.1 \pm 0.8) \%$		-
$\mu^+ \nu X^-$	$(10.2 \pm 1.0) \%$		-
$D_s^- \ell^+ \nu_\ell \text{ anything}$	$[ggaa] (8.1 \pm 1.3) \%$		-
$D_s^{*-} \ell^+ \nu_\ell \text{ anything}$	$(5.4 \pm 1.1) \%$		-
$D_s^- \mu^+ \nu_\mu$	$(2.44 \pm 0.23) \%$		2321
$D_s^- \mu^+ \nu_\mu$	$(5.3 \pm 0.5) \%$		2266
$D_{s1}(2536)^- \mu^+ \nu_\mu, D_{s1}^- \rightarrow D_s^{*-} K_S^0$	$(2.7 \pm 0.7) \times 10^{-3}$		-
$D_{s1}(2536)^- X \mu^+ \nu, D_{s1}^- \rightarrow \bar{D}^0 K^+$	$(4.4 \pm 1.3) \times 10^{-3}$		-
$D_{s2}(2573)^- X \mu^+ \nu, D_{s2}^- \rightarrow \bar{D}^0 K^+$	$(2.7 \pm 1.0) \times 10^{-3}$		-
$K^- \mu^+ \nu_\mu$	$(1.06 \pm 0.09) \times 10^{-4}$		2660
$D_s^- \pi^+$	$(2.98 \pm 0.14) \times 10^{-3}$		2320
$D_s^- \rho^+$	$(6.8 \pm 1.4) \times 10^{-3}$		2249
$D_s^- \pi^+ \pi^+ \pi^-$	$(6.1 \pm 1.0) \times 10^{-3}$		2301
$D_{s1}(2536)^- \pi^+, D_{s1}^- \rightarrow D_s^- \pi^+ \pi^-$	$(2.4 \pm 0.8) \times 10^{-5}$		-
$D_s^\mp K^\pm$	$(2.25 \pm 0.12) \times 10^{-4}$		2293
$D_s^- K^+ \pi^+ \pi^-$	$(3.2 \pm 0.6) \times 10^{-4}$		2249
$D_s^- D_s^-$	$(4.4 \pm 0.5) \times 10^{-3}$		1824
$D_s^- D^+$	$(2.8 \pm 0.5) \times 10^{-4}$		1875
$D^+ D^-$	$(2.2 \pm 0.6) \times 10^{-4}$		1925
$D^0 \bar{D}^0$	$(1.9 \pm 0.5) \times 10^{-4}$		1930
$D_s^{*-} \pi^+$	$(1.9 \pm 0.4) \times 10^{-3}$		2265

Meson Summary Table

$D_s^{*+} K^\pm$	$(1.32^{+0.40}_{-0.32}) \times 10^{-4}$	-	$J/\psi(1S) \pi^+ \pi^- \pi^+ \pi^-$	$(7.5 \pm 0.8) \times 10^{-5}$	1731
$D_s^{*-} \rho^+$	$(9.5 \pm 2.0) \times 10^{-3}$	2191	$J/\psi(1S) f_1(1285)$	$(7.2 \pm 1.4) \times 10^{-5}$	1460
$D_s^{*+} D_s^- + D_s^{*-} D_s^+$	$(1.39 \pm 0.17) \%$	1742	$\psi(2S) \eta$	$(3.3 \pm 0.9) \times 10^{-4}$	1338
$D_s^{*+} D_s^{*-}$	$(1.44 \pm 0.21) \%$	S=1.1 1655	$\psi(2S) \eta'$	$(1.29 \pm 0.35) \times 10^{-4}$	1158
$D_s^{(*)+} D_s^{(*)-}$	$(4.5 \pm 1.4) \%$	-	$\psi(2S) \pi^+ \pi^-$	$(6.9 \pm 1.2) \times 10^{-5}$	1397
$D_s^{*-} D^+$	$(3.9 \pm 0.8) \times 10^{-4}$	1801	$\psi(2S) \phi$	$(5.2 \pm 0.4) \times 10^{-4}$	1120
$\bar{D}^{*0} \bar{K}^0$	$(2.8 \pm 1.1) \times 10^{-4}$	2278	$\psi(2S) K^- \pi^+$	$(3.1 \pm 0.4) \times 10^{-5}$	1310
$\bar{D}^0 \bar{K}^0$	$(4.3 \pm 0.9) \times 10^{-4}$	2330	$\psi(2S) \bar{K}^*(892)^0$	$(3.3 \pm 0.5) \times 10^{-5}$	1196
$\bar{D}^0 K^- \pi^+$	$(1.04 \pm 0.13) \times 10^{-3}$	2312	$\chi_{c1} \phi$	$(1.97 \pm 0.25) \times 10^{-4}$	1274
$\bar{D}^0 \bar{K}^*(892)^0$	$(4.4 \pm 0.6) \times 10^{-4}$	2264	$\chi_{c1}(3872) \phi$	$(1.1 \pm 0.4) \times 10^{-4}$	936
$\bar{D}^0 \bar{K}^*(1410)$	$(3.9 \pm 3.5) \times 10^{-4}$	2117	$\chi_{c1}(3872) (K^+ K^-)_{non-\phi}$	$(8.6 \pm 3.5) \times 10^{-5}$	961
$\bar{D}^0 \bar{K}_0^0(1430)$	$(3.0 \pm 0.7) \times 10^{-4}$	2113	$\pi^+ \pi^-$	$(7.0 \pm 1.0) \times 10^{-7}$	2680
$\bar{D}^0 \bar{K}_2^0(1430)$	$(1.1 \pm 0.4) \times 10^{-4}$	2112	$\pi^0 \pi^0$	$< 2.1 \times 10^{-4}$	CL=90% 2680
$\bar{D}^0 \bar{K}^*(1680)$	$< 7.8 \times 10^{-5}$	CL=90% 1997	$\eta \pi^0$	$< 1.0 \times 10^{-3}$	CL=90% 2654
$\bar{D}^0 \bar{K}_0^0(1950)$	$< 1.1 \times 10^{-4}$	CL=90% 1890	$\eta \eta$	$< 1.43 \times 10^{-4}$	CL=90% 2627
$\bar{D}^0 \bar{K}_3^*(1780)$	$< 2.6 \times 10^{-5}$	CL=90% 1970	$\rho^0 \rho^0$	$< 3.20 \times 10^{-4}$	CL=90% 2569
$\bar{D}^0 \bar{K}_4^*(2045)$	$< 3.1 \times 10^{-5}$	CL=90% 1835	$\eta' \eta$	$< 6.5 \times 10^{-5}$	CL=90% 2568
$\bar{D}^0 K^- \pi^+$ (non-resonant)	$(2.1 \pm 0.8) \times 10^{-4}$	2312	$\eta' \eta'$	$(3.3 \pm 0.7) \times 10^{-5}$	2507
$D_{s_2}^{*+}(2573) \pi^+, D_{s_2}^{*+} \rightarrow$	$(2.6 \pm 0.4) \times 10^{-4}$	-	$\eta' \phi$	$< 8.2 \times 10^{-7}$	CL=90% 2495
$\bar{D}^0 K^-$	-	-	$\phi f_0(980), f_0(980) \rightarrow \pi^+ \pi^-$	$(1.12 \pm 0.21) \times 10^{-6}$	-
$D_{s_1}^{*+}(2700) \pi^+, D_{s_1}^{*+} \rightarrow$	$(1.6 \pm 0.8) \times 10^{-5}$	-	$\phi f_2(1270), f_2(1270) \rightarrow$	$(6.1 \pm 1.8) \times 10^{-7}$	-
$\bar{D}^0 K^-$	-	-	$\pi^+ \pi^-$	-	-
$D_{s_1}^{*+}(2860) \pi^+, D_{s_1}^{*+} \rightarrow$	$(5 \pm 4) \times 10^{-5}$	-	$\phi \rho^0$	$(2.7 \pm 0.8) \times 10^{-7}$	2526
$\bar{D}^0 K^-$	-	-	$\phi \pi^+ \pi^-$	$(3.5 \pm 0.5) \times 10^{-6}$	2579
$D_{s_3}^{*+}(2860) \pi^+, D_{s_3}^{*+} \rightarrow$	$(2.2 \pm 0.6) \times 10^{-5}$	-	$\phi \phi$	$(1.85 \pm 0.14) \times 10^{-5}$	2482
$\bar{D}^0 K^-$	-	-	$\phi \phi \phi$	$(2.2 \pm 0.6) \times 10^{-6}$	2165
$\bar{D}^0 K^+ K^-$	$(5.6 \pm 0.9) \times 10^{-5}$	2243	$\pi^+ K^-$	$(5.8 \pm 0.7) \times 10^{-6}$	2659
$\bar{D}^0 f_0(980)$	$< 3.1 \times 10^{-6}$	CL=90% 2242	$K^+ K^-$	$(2.66 \pm 0.22) \times 10^{-5}$	2638
$\bar{D}^0 \phi$	$(3.0 \pm 0.5) \times 10^{-5}$	2235	$K^0 \bar{K}^0$	$(1.76 \pm 0.31) \times 10^{-5}$	2637
$\bar{D}^{*0} \phi$	$(3.7 \pm 0.6) \times 10^{-5}$	2178	$K^0 \pi^+ \pi^-$	$(9.5 \pm 2.1) \times 10^{-6}$	2653
$D^{*+} \pi^\pm$	$< 6.1 \times 10^{-6}$	CL=90% -	$K^0 K^\pm \pi^\mp$	$(8.4 \pm 0.9) \times 10^{-5}$	2622
$\eta_c \phi$	$(5.0 \pm 0.9) \times 10^{-4}$	1663	$K^*(892)^- \pi^+$	$(2.9 \pm 1.1) \times 10^{-6}$	2607
$\eta_c \pi^+ \pi^-$	$(1.8 \pm 0.7) \times 10^{-4}$	1840	$K^*(892)^0 \pi^\mp$	$(1.9 \pm 0.5) \times 10^{-5}$	2585
$J/\psi(1S) \phi$	$(1.04 \pm 0.04) \times 10^{-3}$	1588	$K_0^*(1430)^\pm K^\mp$	$(3.1 \pm 2.5) \times 10^{-5}$	-
$J/\psi(1S) \phi \phi$	$(1.20 \pm 0.14) \times 10^{-5}$	764	$K_2^*(1430)^\pm K^\mp$	$(1.0 \pm 1.7) \times 10^{-5}$	-
$J/\psi(1S) \pi^0$	$< 1.2 \times 10^{-3}$	CL=90% 1787	$K^*(892)^0 \bar{K}^0 + c.c.$	$(2.0 \pm 0.6) \times 10^{-5}$	2585
$J/\psi(1S) \eta$	$(4.0 \pm 0.7) \times 10^{-4}$	S=1.4 1733	$K_0^*(1430) \bar{K}^0 + c.c.$	$(3.3 \pm 1.0) \times 10^{-5}$	2468
$J/\psi(1S) K_S^0$	$(1.92 \pm 0.14) \times 10^{-5}$	1743	$K_2^*(1430) \bar{K}^0 + c.c.$	$(1.7 \pm 2.2) \times 10^{-5}$	2467
$J/\psi(1S) \bar{K}^*(892)^0$	$(4.1 \pm 0.4) \times 10^{-5}$	1637	$K_S^0 \bar{K}^*(892)^0 + c.c.$	$(1.6 \pm 0.4) \times 10^{-5}$	2585
$J/\psi(1S) \eta'$	$(3.3 \pm 0.4) \times 10^{-4}$	1612	$K^0 K^+ K^-$	$(1.3 \pm 0.6) \times 10^{-6}$	2568
$J/\psi(1S) \pi^+ \pi^-$	$(2.02 \pm 0.17) \times 10^{-4}$	S=1.7 1775	$\bar{K}^*(892)^0 \rho^0$	$< 7.67 \times 10^{-4}$	CL=90% 2550
$J/\psi(1S) f_0(500), f_0 \rightarrow$	$< 4 \times 10^{-6}$	CL=90% -	$\bar{K}^*(892)^0 K^*(892)^0$	$(1.11 \pm 0.27) \times 10^{-5}$	2531
$\pi^+ \pi^-$	-	-	$\phi K^*(892)^0$	$(1.14 \pm 0.30) \times 10^{-6}$	2507
$J/\psi(1S) \rho, \rho \rightarrow \pi^+ \pi^-$	$< 3.4 \times 10^{-6}$	CL=90% -	$p \bar{p}$	$< 1.5 \times 10^{-8}$	CL=90% 2514
$J/\psi(1S) f_0(980), f_0 \rightarrow$	$(1.24 \pm 0.15) \times 10^{-4}$	S=2.1 -	$p \bar{p} K^+ K^-$	$(4.5 \pm 0.5) \times 10^{-6}$	2231
$\pi^+ \pi^-$	-	-	$p \bar{p} K^+ \pi^-$	$(1.39 \pm 0.26) \times 10^{-6}$	2355
$J/\psi(1S) f_2(1270), f_2 \rightarrow$	$(1.0 \pm 0.4) \times 10^{-6}$	-	$p \bar{p} \pi^+ \pi^-$	$(4.3 \pm 2.0) \times 10^{-7}$	2454
$\pi^+ \pi^-$	-	-	$p \bar{p} K^- + c.c.$	$(5.5 \pm 1.0) \times 10^{-6}$	2358
$J/\psi(1S) f_2(1270)_0, f_2 \rightarrow$	$(7.3 \pm 1.7) \times 10^{-7}$	-	$\Lambda_c^- \Lambda \pi^+$	$(3.6 \pm 1.6) \times 10^{-4}$	1979
$\pi^+ \pi^-$	-	-	$\Lambda_c^- \Lambda_c^+$	$< 8.0 \times 10^{-5}$	CL=95% 1405
$J/\psi(1S) f_2(1270)_\parallel, f_2 \rightarrow$	$(1.05 \pm 0.33) \times 10^{-6}$	-	Lepton Family number (LF) violating modes or $\Delta B = 1$ weak neutral current (BI) modes		
$\pi^+ \pi^-$	-	-	$\gamma \gamma$	BI $< 3.1 \times 10^{-6}$	CL=90% 2683
$J/\psi(1S) f_2(1270)_\perp, f_2 \rightarrow$	$(1.3 \pm 0.7) \times 10^{-6}$	-	$\phi \gamma$	BI $(3.4 \pm 0.4) \times 10^{-5}$	2587
$\pi^+ \pi^-$	-	-	$\mu^+ \mu^-$	BI $(3.01 \pm 0.35) \times 10^{-9}$	2681
$J/\psi(1S) f_0(1370), f_0 \rightarrow$	$(4.4 \pm 0.6) \times 10^{-5}$	-	$e^+ e^-$	BI $< 9.4 \times 10^{-9}$	CL=90% 2683
$\pi^+ \pi^-$	-	-	$\tau^+ \tau^-$	BI $< 6.8 \times 10^{-3}$	CL=95% 2011
$J/\psi(1S) f_0(1500), f_0 \rightarrow$	$(2.04 \pm 0.32) \times 10^{-5}$	-	$\mu^+ \mu^- \mu^+ \mu^-$	BI $< 2.5 \times 10^{-9}$	CL=95% 2673
$\pi^+ \pi^-$	-	-	$S P, S \rightarrow \mu^+ \mu^-, P \rightarrow \mu^+ \mu^-$	BI [xxx] $< 2.2 \times 10^{-9}$	CL=95% -
$J/\psi(1S) f_2'(1525)_0, f_2' \rightarrow$	$(1.03 \pm 0.22) \times 10^{-6}$	-	$\phi(1020) \mu^+ \mu^-$	BI $(8.4 \pm 0.4) \times 10^{-7}$	2582
$\pi^+ \pi^-$	-	-	$f_2'(1525) \mu^+ \mu^-$	BI $(1.62 \pm 0.22) \times 10^{-7}$	2464
$J/\psi(1S) f_2'(1525)_\parallel, f_2' \rightarrow$	$(1.2 \pm 2.6) \times 10^{-7}$	-	$\bar{K}^*(892)^0 \mu^+ \mu^-$	BI $(2.9 \pm 1.1) \times 10^{-8}$	2605
$\pi^+ \pi^-$	-	-	$\pi^+ \pi^- \mu^+ \mu^-$	BI $(8.4 \pm 1.7) \times 10^{-8}$	2670
$J/\psi(1S) f_2'(1525)_\perp, f_2' \rightarrow$	$(5 \pm 4) \times 10^{-7}$	-	$\phi \nu \bar{\nu}$	BI $< 5.4 \times 10^{-3}$	CL=90% 2587
$\pi^+ \pi^-$	-	-	$e^\pm \mu^\mp$	LF [aa] $< 5.4 \times 10^{-9}$	CL=90% 2682
$J/\psi(1S) f_0(1790), f_0 \rightarrow$	$(4.9 \pm 10.0) \times 10^{-6}$	-	$\mu^\pm \tau^\mp$	LF $< 4.2 \times 10^{-5}$	CL=95% 2388
$\pi^+ \pi^-$	-	-	B_s^*		
$J/\psi(1S) \pi^+ \pi^-$ (nonresonant)	$(1.74 \pm 1.10) \times 10^{-5}$	1775	$I(J^P) = 0(1^-)$		
$J/\psi(1S) \bar{K}^0 \pi^+ \pi^-$	$< 4.4 \times 10^{-5}$	CL=90% 1675	<p>I, J, P need confirmation. Quantum numbers shown are quark-model predictions.</p> <p>Mass $m = 5415.4^{+1.8}_{-1.5}$ MeV (S = 2.9)</p> <p>$m_{B_s^*} - m_{B_s} = 48.5^{+1.8}_{-1.5}$ MeV (S = 2.9)</p>		
$J/\psi(1S) K^+ K^-$	$(7.9 \pm 0.7) \times 10^{-4}$	1601			
$J/\psi(1S) K^0 K^- \pi^+ + c.c.$	$(9.5 \pm 1.3) \times 10^{-4}$	1538			
$J/\psi(1S) \bar{K}^0 K^+ K^-$	$< 1.2 \times 10^{-5}$	CL=90% 1333			
$J/\psi K^*(892)^0 \bar{K}^*(892)^0$	$(1.10 \pm 0.09) \times 10^{-4}$	1083			
$J/\psi(1S) f_2'(1525)$	$(2.6 \pm 0.6) \times 10^{-4}$	1310			
$J/\psi(1S) p \bar{p}$	$(3.6 \pm 0.4) \times 10^{-6}$	982			
$J/\psi(1S) \gamma$	$< 7.3 \times 10^{-6}$	CL=90% 1790			

Meson Summary Table

B_s^* DECAY MODES	Fraction (Γ_i/Γ)	ρ (MeV/c)
$B_s \gamma$	seen	48

$B_{s1}(5830)^0$ $I(J^P) = 0(1^+)$
 I, J, P need confirmation.

Mass $m = 5828.70 \pm 0.20$ MeV
 $m_{B_{s1}^0} - m_{B^{*+}} = 503.99 \pm 0.17$ MeV
 Full width $\Gamma = 0.5 \pm 0.4$ MeV

$B_{s1}(5830)^0$ DECAY MODES	Fraction (Γ_i/Γ)	ρ (MeV/c)
$B^{*+} K^-$	seen	97

$B_{s2}^*(5840)^0$ $I(J^P) = 0(2^+)$
 I, J, P need confirmation.

Mass $m = 5839.86 \pm 0.12$ MeV
 $m_{B_{s2}^0} - m_{B^+} = 560.52 \pm 0.14$ MeV
 Full width $\Gamma = 1.49 \pm 0.27$ MeV

Branching fractions are given relative to the one **DEFINED AS 1**.

$B_{s2}^*(5840)^0$ DECAY MODES	Fraction (Γ_i/Γ)	ρ (MeV/c)
$B^+ K^-$	DEFINED AS 1	252
$B^{*+} K^-$	0.093 ± 0.018	141
$B^0 K_S^0$	0.43 ± 0.11	245
$B^{*0} K_S^0$	0.04 ± 0.04	-

BOTTOM, CHARMED MESONS ($B = C = \pm 1$)

$B_c^+ = c\bar{b}, B_c^- = \bar{c}b,$ similarly for B_c^* 's

B_c^+ $I(J^P) = 0(0^-)$
 I, J, P need confirmation.

Quantum numbers shown are quark-model predictions.

Mass $m = 6274.47 \pm 0.32$ MeV
 $m_{B_c^+} - m_{B_S^0} = 907.8 \pm 0.5$ MeV
 Mean life $\tau = (0.510 \pm 0.009) \times 10^{-12}$ s

B_c^- modes are charge conjugates of the modes below.

B_c^+ DECAY MODES $\times B(\bar{b} \rightarrow B_c)$	Fraction (Γ_i/Γ)	Confidence level	ρ (MeV/c)
$J/\psi(1S) \ell^+ \nu_\ell$ anything	seen	-	-
$J/\psi(1S) \mu^+ \nu_\mu$	seen	2372	
$J/\psi(1S) \tau^+ \nu_\tau$	seen	1932	
$J/\psi(1S) \pi^+$	seen	2370	
$J/\psi(1S) K^+$	seen	2341	
$J/\psi(1S) \pi^+ \pi^+ \pi^-$	seen	2350	
$J/\psi(1S) a_1(1260)$	not seen	2169	
$J/\psi(1S) K^+ K^- \pi^+$	seen	2203	
$J/\psi(1S) \pi^+ \pi^+ \pi^+ \pi^- \pi^-$	seen	2309	
$\psi(2S) \pi^+$	seen	2051	
$J/\psi(1S) D^0 K^+$	seen	1539	
$J/\psi(1S) D^*(2007)^0 K^+$	seen	1411	
$J/\psi(1S) D^*(2010)^+ K^{*0}$	seen	919	
$J/\psi(1S) D^+ K^{*0}$	seen	1122	
$J/\psi(1S) D_s^+$	seen	1821	
$J/\psi(1S) D_s^{*+}$	seen	1727	
$J/\psi(1S) p\bar{p}\pi^+$	seen	1791	
$\chi_c^0 \pi^+$	$(2.4^{+0.9}_{-0.8}) \times 10^{-5}$	2205	
$p\bar{p}\pi^+$	not seen	2970	
$D^0 K^+$	seen	2837	
$D^0 \pi^+$	not seen	2858	
$D^{*0} \pi^+$	not seen	2814	
$D^{*0} K^+$	not seen	2792	
$D_s^+ \bar{D}^0$	$< 7.2 \times 10^{-4}$	90%	2483

$D_s^+ D^0$	$< 3.0 \times 10^{-4}$	90%	2483
$D^+ \bar{D}^0$	$< 1.9 \times 10^{-4}$	90%	2521
$D^+ D^0$	$< 1.4 \times 10^{-4}$	90%	2521
$D_s^{*+} \bar{D}^0$	$< 5.3 \times 10^{-4}$	90%	2425
$D_s^+ \bar{D}^*(2007)^0$	$< 4.6 \times 10^{-4}$	90%	2427
$D_s^{*+} D^0$	$< 9 \times 10^{-4}$	90%	2425
$D_s^+ D^*(2007)^0$	$< 6.6 \times 10^{-4}$	90%	2427
$D^*(2010)^+ \bar{D}^0$	$< 3.8 \times 10^{-4}$	90%	2467
$D^*(2010)^+ \bar{D}^0, D^{*+} \rightarrow D^+ \pi^0 / \gamma$	not seen	-	-
$D^+ \bar{D}^*(2007)^0$	$< 6.5 \times 10^{-4}$	90%	2466
$D^*(2007)^+ D^0$	$< 2.0 \times 10^{-4}$	90%	-
$D^*(2010)^+ D^0, D^{*+} \rightarrow D^+ \pi^0 / \gamma$	not seen	2467	
$D^+ D^*(2007)^0$	$< 3.7 \times 10^{-4}$	90%	2466
$D_s^{*+} \bar{D}^*(2007)^0$	$< 1.3 \times 10^{-3}$	90%	2366
$D_s^+ D^*(2007)^0$	$< 1.3 \times 10^{-3}$	90%	2366
$D^*(2010)^+ \bar{D}^*(2007)^0$	$< 1.0 \times 10^{-3}$	90%	2410
$D^*(2010)^+ D^*(2007)^0$	$< 7.7 \times 10^{-4}$	90%	2410
$D^+ K^{*0}$	not seen	2783	
$D^+ \bar{K}^{*0}$	not seen	2783	
$D^+ K^{*0}$	not seen	2751	
$D_s^+ \bar{K}^{*0}$	not seen	2751	
$D_s^+ \phi$	not seen	2727	
$K^+ K^0$	not seen	3098	
$B_S^0 \pi^+ / B(\bar{b} \rightarrow B_S)$	seen	-	-

$B_c(2S)^\pm$ $I(J^P) = 0(0^-)$

Mass $m = 6871.2 \pm 1.0$ MeV

$B_c(2S)^\pm$ DECAY MODES	Fraction (Γ_i/Γ)	ρ (MeV/c)
$B_c^+ \pi^+ \pi^-$	seen	504

$c\bar{c}$ MESONS (including possibly non- $q\bar{q}$ states)

$\eta_c(1S)$ $I^G(J^PC) = 0^+(0^-)$

Mass $m = 2983.9 \pm 0.4$ MeV ($S = 1.2$)
 Full width $\Gamma = 32.0 \pm 0.7$ MeV

$\eta_c(1S)$ DECAY MODES	Fraction (Γ_i/Γ)	Confidence level	ρ (MeV/c)
Decays involving hadronic resonances			
$\eta'(958) \pi \pi$	$(4.1 \pm 1.7) \%$		1323
$\eta'(958) K \bar{K}$	$(3.5 \pm 1.5) \%$		1131
$\rho \rho$	$(1.8 \pm 0.5) \%$		1275
$K^*(892)^0 K^- \pi^+ + c.c.$	$(2.0 \pm 0.7) \%$		1278
$K^*(892) \bar{K}^*(892)$	$(6.9 \pm 1.3) \times 10^{-3}$		1196
$K^*(892)^0 \bar{K}^*(892)^0 \pi^+ \pi^-$	$(1.1 \pm 0.5) \%$		1073
$\phi K^+ K^-$	$(2.9 \pm 1.4) \times 10^{-3}$		1104
$\phi \phi$	$(1.74 \pm 0.19) \times 10^{-3}$		1089
$\phi 2(\pi^+ \pi^-)$	$< 4 \times 10^{-3}$	90%	1251
$a_0(980) \pi$	seen		1327
$a_2(1320) \pi$	$< 2 \%$	90%	1196
$K^*(892) \bar{K} + c.c.$	$< 1.28 \%$	90%	1310
$f_2(1270) \eta$	$< 1.1 \%$	90%	1145
$f_2(1270) \eta'$	seen		984
$\omega \omega$	$(2.9 \pm 0.8) \times 10^{-3}$		1270
$\omega \phi$	$< 2.5 \times 10^{-4}$	90%	1185
$f_2(1270) f_2(1270)$	$(9.8 \pm 2.5) \times 10^{-3}$		774
$f_2(1270) f_2'(1525)$	$(9.5 \pm 3.2) \times 10^{-3}$		524
$f_0(500) \eta$	seen		-
$f_0(500) \eta'$	seen		-
$f_0(980) \eta$	seen		1264
$f_0(980) \eta'$	seen		1130
$f_0(1500) \eta$	seen		1025
$f_0(1710) \eta'$	seen		653
$f_0(2100) \eta'$	seen		†

Meson Summary Table

$K_4^*(2045)^+ K^- + c.c. \rightarrow$	$(6.2 \pm 2.9 \pm 1.6) \times 10^{-6}$	–	$2(\pi^+ \pi^- \pi^0) \eta$	$(1.6 \pm 0.5) \times 10^{-3}$	1381
$K_1(1270)^\pm K^\mp$	$< 3.0 \times 10^{-3}$	CL=90%	$\pi^+ \pi^- \pi^0 \pi^0 \eta$	$(2.4 \pm 0.5) \times 10^{-3}$	1448
$K_1(1270) K_S^0 \rightarrow \gamma K_S^0 K_S^0$	$(8.5 \pm 2.5) \times 10^{-7}$	–	$\rho^\pm \pi^\mp \pi^0 \eta$	$(1.9 \pm 0.8) \times 10^{-3}$	1326
$a_2(1320)^\pm \pi^\mp$	$[aa] < 4.3 \times 10^{-3}$	CL=90%	$K^+ K^-$	$(2.86 \pm 0.21) \times 10^{-4}$	1468
$\phi \pi^0$	3×10^{-6} or 1×10^{-7}	1377	$K_S^0 K_L^0$	$(1.95 \pm 0.11) \times 10^{-4}$	S=2.4 1466
$\phi \pi^+ \pi^-$	$(9.4 \pm 1.5) \times 10^{-4}$	S=1.7	$K_S^0 K_S^0$	$< 1.4 \times 10^{-8}$	CL=95% 1466
$\phi \pi^0 \pi^0$	$(5.0 \pm 1.0) \times 10^{-4}$	1366	$K \bar{K} \pi$	$(6.1 \pm 1.0) \times 10^{-3}$	1442
$\phi 2(\pi^+ \pi^-)$	$(1.60 \pm 0.32) \times 10^{-3}$	1318	$K^+ K^- \pi^0$	$(2.88 \pm 0.12) \times 10^{-3}$	1442
$\phi \eta$	$(7.4 \pm 0.8) \times 10^{-4}$	S=1.5	$K_S^0 K_L^0 \pi^\mp$	$(5.6 \pm 0.5) \times 10^{-3}$	1440
$\phi \eta'(958)$	$(4.6 \pm 0.5) \times 10^{-4}$	S=2.2	$K_S^0 K_L^0 \pi^0$	$(2.06 \pm 0.26) \times 10^{-3}$	1440
$\phi \eta \eta'$	$(2.32 \pm 0.17) \times 10^{-4}$	885	$K^*(892)^0 \bar{K}^0 + c.c. \rightarrow$	$(1.21 \pm 0.18) \times 10^{-3}$	–
$\phi f_0(980)$	$(3.2 \pm 0.9) \times 10^{-4}$	S=1.9	$K_S^0 K_L^0 \pi^0$	–	–
$\phi f_0(980) \rightarrow \phi \pi^+ \pi^-$	$(2.60 \pm 0.34) \times 10^{-4}$	–	$K_2^*(1430)^0 \bar{K}^0 + c.c. \rightarrow$	$(4.3 \pm 1.3) \times 10^{-4}$	–
$\phi f_0(980) \rightarrow \phi \pi^0 \pi^0$	$(1.8 \pm 0.5) \times 10^{-4}$	–	$K_S^0 K_L^0 \pi^0$	–	–
$\phi \pi^0 f_0(980) \rightarrow \phi \pi^0 \pi^+ \pi^-$	$(4.5 \pm 1.0) \times 10^{-6}$	–	$K^+ K^- \pi^+ \pi^-$	$(6.86 \pm 0.28) \times 10^{-3}$	1407
$\phi \pi^0 f_0(980) \rightarrow \phi \pi^0 \rho^0 \pi^0$	$(1.7 \pm 0.6) \times 10^{-6}$	1045	$K^+ K^- \pi^0 \pi^0$	$(2.13 \pm 0.22) \times 10^{-3}$	1410
$\phi f_0(980) \eta \rightarrow \eta \phi \pi^+ \pi^-$	$(3.2 \pm 1.0) \times 10^{-4}$	–	$K_S^0 K_L^0 \pi^+ \pi^-$	$(3.8 \pm 0.6) \times 10^{-3}$	1406
$\phi a_0(980)^0 \rightarrow \phi \eta \pi^0$	$(4.4 \pm 1.4) \times 10^{-6}$	–	$K_S^0 K_L^0 \pi^0 \pi^0$	$(1.9 \pm 0.4) \times 10^{-3}$	1408
$\phi f_2(1270)$	$(3.2 \pm 0.6) \times 10^{-4}$	1036	$K_S^0 K_L^0 \eta$	$(1.45 \pm 0.33) \times 10^{-3}$	1328
$\phi f_1(1285)$	$(2.6 \pm 0.5) \times 10^{-4}$	1032	$K_S^0 K_S^0 \pi^+ \pi^-$	$(1.68 \pm 0.19) \times 10^{-3}$	1406
$\phi f_1(1285) \rightarrow$	$(9.4 \pm 2.8) \times 10^{-7}$	952	$K^\mp K_S^0 \pi^\pm \pi^0$	$(5.7 \pm 0.5) \times 10^{-3}$	1408
$\phi \pi^0 f_0(980) \rightarrow$	–	–	$K^+ K^- 2(\pi^+ \pi^-)$	$(3.1 \pm 1.3) \times 10^{-3}$	1320
$\phi \pi^0 \pi^+ \pi^-$	–	–	$K^+ K^- \pi^+ \pi^- \eta$	$(4.7 \pm 0.7) \times 10^{-3}$	1221
$\phi f_1(1285) \rightarrow$	$(2.1 \pm 2.2) \times 10^{-7}$	955	$2(K^+ K^-)$	$(7.2 \pm 0.8) \times 10^{-4}$	1131
$\phi \pi^0 f_0(980) \rightarrow \phi 3\pi^0$	–	–	$K^+ K^- K_S^0 K_S^0$	$(4.2 \pm 0.7) \times 10^{-4}$	1127
$\phi \eta(1405) \rightarrow \phi \eta \pi^+ \pi^-$	$(2.0 \pm 1.0) \times 10^{-5}$	946	$p \bar{p}$	$(2.120 \pm 0.029) \times 10^{-3}$	1232
$\phi f_2'(1525)$	$(8 \pm 4) \times 10^{-4}$	S=2.7	$p \bar{p} \pi^0$	$(1.19 \pm 0.08) \times 10^{-3}$	S=1.1 1176
$\phi X(1835) \rightarrow \phi p \bar{p}$	$< 2.1 \times 10^{-7}$	CL=90%	$p \bar{p} \pi^+ \pi^-$	$(6.0 \pm 0.5) \times 10^{-3}$	S=1.3 1107
$\phi X(1835) \rightarrow \phi \eta \pi^+ \pi^-$	$< 2.8 \times 10^{-4}$	CL=90%	$p \bar{p} \pi^+ \pi^- \pi^0$	$[j\bar{a}a] (2.3 \pm 0.9) \times 10^{-3}$	S=1.9 1033
$\phi X(1870) \rightarrow \phi \eta \pi^+ \pi^-$	$< 6.13 \times 10^{-5}$	CL=90%	$p \bar{p} \eta$	$(2.00 \pm 0.12) \times 10^{-3}$	948
$\phi K \bar{K}$	$(1.77 \pm 0.16) \times 10^{-3}$	S=1.3	$p \bar{p} \rho$	$< 3.1 \times 10^{-4}$	CL=90% 774
$\phi f_0(1710) \rightarrow \phi K \bar{K}$	$(3.6 \pm 0.6) \times 10^{-4}$	875	$p \bar{p} \omega$	$(9.8 \pm 1.0) \times 10^{-4}$	S=1.3 768
$\phi K^+ K^-$	$(8.3 \pm 1.1) \times 10^{-4}$	1179	$p \bar{p} \eta'(958)$	$(1.29 \pm 0.14) \times 10^{-4}$	S=2.0 596
$\phi K_S^0 K_S^0$	$(5.9 \pm 1.5) \times 10^{-4}$	1176	$p \bar{p} a_0(980) \rightarrow p \bar{p} \pi^0 \eta$	$(6.8 \pm 1.8) \times 10^{-5}$	–
$\phi K^\pm K_S^0 \pi^\mp$	$[aa] (7.2 \pm 0.8) \times 10^{-4}$	1114	$p \bar{p} \phi$	$(5.19 \pm 0.33) \times 10^{-5}$	527
$\phi K^*(892) \bar{K}^+ + c.c.$	$(2.18 \pm 0.23) \times 10^{-3}$	969	$p \bar{p} \pi^-$	$(2.12 \pm 0.09) \times 10^{-3}$	1174
$b_1(1235)^\pm \pi^\mp$	$[aa] (3.0 \pm 0.5) \times 10^{-3}$	1300	$n \bar{n}$	$(2.09 \pm 0.16) \times 10^{-3}$	1231
$b_1(1235)^0 \pi^0$	$(2.3 \pm 0.6) \times 10^{-3}$	1300	$n \bar{n} \pi^+ \pi^-$	$(4 \pm 4) \times 10^{-3}$	1106
$f_2'(1525) K^+ K^-$	$(1.06 \pm 0.35) \times 10^{-3}$	897	$n N(1440)$	seen	978
$\Delta(1232) \bar{p}$	$< 1 \times 10^{-4}$	CL=90%	$n N(1520)$	seen	928
$\Delta(1232) \bar{p} \pi^-$	$(1.6 \pm 0.5) \times 10^{-3}$	1030	$n N(1535)$	seen	917
$\Delta(1232) \bar{p} \Delta(1232) \bar{p}$	$(1.10 \pm 0.29) \times 10^{-3}$	938	$\Lambda \bar{\Lambda}$	$(1.89 \pm 0.09) \times 10^{-3}$	S=2.8 1074
$\Sigma(1385)^0 p K^-$	$(5.1 \pm 3.2) \times 10^{-4}$	646	$\Lambda \bar{\Lambda} \pi^0$	$(3.8 \pm 0.4) \times 10^{-5}$	998
$\Sigma(1385)^0 \bar{\Lambda} + c.c.$	$< 8.2 \times 10^{-6}$	CL=90%	$\Lambda \bar{\Lambda} \pi^+ \pi^-$	$(4.3 \pm 1.0) \times 10^{-3}$	903
$\Sigma(1385) \bar{\Sigma}^+ (or c.c.)$	$[aa] (3.1 \pm 0.5) \times 10^{-4}$	855	$\Lambda \bar{\Lambda} \eta$	$(1.62 \pm 0.17) \times 10^{-4}$	672
$\Sigma(1385) \bar{\Sigma}^-(1385)^+ (or c.c.)$	$[aa] (1.16 \pm 0.05) \times 10^{-3}$	697	$\Lambda \bar{\Sigma}^- \pi^+ (or c.c.)$	$[aa] (8.3 \pm 0.7) \times 10^{-4}$	S=1.2 950
$\Sigma(1385)^0 \bar{\Sigma}^-(1385)^0$	$(1.07 \pm 0.08) \times 10^{-3}$	697	$p K^- \bar{\Sigma}^0 + c.c.$	$(8.6 \pm 1.1) \times 10^{-4}$	876
$\Lambda(1520) \bar{\Lambda} + c.c. \rightarrow \gamma \Lambda \bar{\Lambda}$	$< 4.1 \times 10^{-6}$	CL=90%	$p K^- \bar{\Sigma}^0$	$(2.9 \pm 0.8) \times 10^{-4}$	819
$\bar{\Lambda}(1520) \Lambda + c.c.$	$< 1.80 \times 10^{-3}$	CL=90%	$\bar{\Lambda} n K_S^0 + c.c.$	$(6.5 \pm 1.1) \times 10^{-4}$	872
$\Xi^0 \Xi^0$	$(1.17 \pm 0.04) \times 10^{-3}$	818	$\Lambda \bar{\Sigma}^+ + c.c.$	$(2.83 \pm 0.23) \times 10^{-5}$	1034
$\Xi(1530) \bar{\Xi}^+ + c.c.$	$(3.18 \pm 0.08) \times 10^{-4}$	600	$\Sigma^+ \bar{\Sigma}^-$	$(1.07 \pm 0.04) \times 10^{-3}$	992
$\Xi(1530)^0 \Xi^0$	$(3.2 \pm 1.4) \times 10^{-4}$	608	$\Sigma^0 \bar{\Sigma}^0$	$(1.172 \pm 0.032) \times 10^{-3}$	S=1.4 988
$\Theta(1540) \bar{\Theta}(1540) \rightarrow$	$[i\bar{a}a] < 1.1 \times 10^{-5}$	CL=90%	$\Xi^- \bar{\Xi}^+$	$(9.7 \pm 0.8) \times 10^{-4}$	S=1.4 807
$K_S^0 p K^- \bar{n} + c.c.$	–	–	Radiative decays		
$\Theta(1540) K^- \bar{n} \rightarrow K_S^0 p K^- \bar{n}$	$[i\bar{a}a] < 2.1 \times 10^{-5}$	CL=90%	$\gamma \eta_c(1S)$	$(1.7 \pm 0.4) \%$	S=1.5 111
$\Theta(1540) K_S^0 \bar{p} \rightarrow K_S^0 \bar{p} K^+ n$	$[i\bar{a}a] < 1.6 \times 10^{-5}$	CL=90%	$\gamma \eta_c(1S) \rightarrow 3\gamma$	$(3.8 \pm 1.3 \pm 1.0) \times 10^{-6}$	S=1.1 –
$\bar{\Theta}(1540) K^+ n \rightarrow K_S^0 \bar{p} K^+ n$	$[i\bar{a}a] < 5.6 \times 10^{-5}$	CL=90%	$\gamma \eta_c(1S) \rightarrow \gamma \eta \eta'$	$(4.9 \pm 0.8) \times 10^{-5}$	–
$\bar{\Theta}(1540) K_S^0 p \rightarrow K_S^0 p K^- \bar{n}$	$[i\bar{a}a] < 1.1 \times 10^{-5}$	CL=90%	3γ	$(1.16 \pm 0.22) \times 10^{-5}$	1548
Decays into stable hadrons					
$2(\pi^+ \pi^-) \pi^0$	$(3.71 \pm 0.28) \%$	S=1.3	4γ	$< 9 \times 10^{-6}$	CL=90% 1548
$3(\pi^+ \pi^-) \pi^0$	$(2.9 \pm 0.6) \%$	1433	5γ	$< 1.5 \times 10^{-5}$	CL=90% 1548
$\pi^+ \pi^- 3\pi^0$	$(1.9 \pm 0.9) \%$	1497	$\gamma \pi^0$	$(3.56 \pm 0.17) \times 10^{-5}$	1546
$\pi^+ \pi^- 4\pi^0$	$(6.5 \pm 1.3) \times 10^{-3}$	1470	$\gamma \pi^0 \pi^0$	$(1.15 \pm 0.05) \times 10^{-3}$	1543
$\rho^+ \pi^\mp \pi^0 \pi^0$	$(1.41 \pm 0.22) \%$	1421	$\gamma 2\pi^+ 2\pi^-$	$(2.8 \pm 0.5) \times 10^{-3}$	S=1.9 1517
$\rho^+ \rho^- \pi^0$	$(6.0 \pm 1.1) \times 10^{-3}$	1298	$\gamma f_2(1270) f_2(1270)$	$(9.5 \pm 1.7) \times 10^{-4}$	878
$\pi^+ \pi^- \pi^0$	$(2.10 \pm 0.08) \%$	S=1.6	$\gamma f_2(1270) f_2(1270) (non\ reso-nant)$	$(8.2 \pm 1.9) \times 10^{-4}$	–
$2(\pi^+ \pi^- \pi^0)$	$(1.61 \pm 0.20) \%$	1468	$\gamma \pi^+ \pi^- 2\pi^0$	$(8.3 \pm 3.1) \times 10^{-3}$	1518
$\pi^+ \pi^- \pi^0 K^+ K^-$	$(1.20 \pm 0.30) \%$	1368	$\gamma K_S^0 K_S^0$	$(8.1 \pm 0.4) \times 10^{-4}$	1466
$\pi^+ \pi^-$	$(1.47 \pm 0.14) \times 10^{-4}$	1542	$\gamma (K \bar{K} \pi) [J^{PC} = 0^{-+}]$	$(7 \pm 4) \times 10^{-4}$	S=2.1 1442
$2(\pi^+ \pi^-)$	$(3.57 \pm 0.30) \times 10^{-3}$	1517	$\gamma K^+ K^- \pi^+ \pi^-$	$(2.1 \pm 0.6) \times 10^{-3}$	1407
$3(\pi^+ \pi^-)$	$(4.3 \pm 0.4) \times 10^{-3}$	1466	$\gamma K^*(892) \bar{K}^*(892)$	$(4.0 \pm 1.3) \times 10^{-3}$	1266
$2(\pi^+ \pi^-) 3\pi^0$	$(6.2 \pm 0.9) \%$	1435	$\gamma \eta$	$(1.085 \pm 0.018) \times 10^{-3}$	1500
$4(\pi^+ \pi^-) \pi^0$	$(9.0 \pm 3.0) \times 10^{-3}$	1345	$\gamma \eta \pi^0$	$(2.14 \pm 0.31) \times 10^{-5}$	1497
$2(\pi^+ \pi^-) \eta$	$(2.29 \pm 0.28) \times 10^{-3}$	1446	$\gamma a_0(980)^0 \rightarrow \gamma \eta \pi^0$	$< 2.5 \times 10^{-6}$	CL=95% –
$3(\pi^+ \pi^-) \eta$	$(7.2 \pm 1.5) \times 10^{-4}$	1379	$\gamma a_2(1320)^0 \rightarrow \gamma \eta \pi^0$	$< 6.6 \times 10^{-6}$	CL=95% –

Meson Summary Table

$\gamma\eta\pi\pi$	$(6.1 \pm 1.0) \times 10^{-3}$	1487	$\gamma\Lambda\bar{\Lambda}$	< 1.3	$\times 10^{-4}$	CL=90%	1074
$\gamma\eta_2(1870) \rightarrow \gamma\eta\pi^+\pi^-$	$(6.2 \pm 2.4) \times 10^{-4}$	—	$\gamma A \rightarrow \gamma$ invisible	$[kkaa] < 1.7$	$\times 10^{-6}$	CL=90%	—
$\gamma\eta'(958)$	$(5.25 \pm 0.07) \times 10^{-3}$	S=1.3 1400	$\gamma A^0 \rightarrow \gamma\mu^+\mu^-$	$[l\bar{l}aa] < 5$	$\times 10^{-6}$	CL=90%	—
$\gamma\rho\rho$	$(4.5 \pm 0.8) \times 10^{-3}$	1340	Dalitz decays				
$\gamma\rho\omega$	< 5.4	CL=90% 1338	$\pi^0 e^+ e^-$	$(7.6 \pm 1.4) \times 10^{-7}$			1546
$\gamma\rho\phi$	< 8.8	CL=90% 1258	$\eta e^+ e^-$	$(1.42 \pm 0.08) \times 10^{-5}$			1500
$\gamma\omega\omega$	$(1.61 \pm 0.33) \times 10^{-3}$	1336	$\eta'(958) e^+ e^-$	$(6.59 \pm 0.18) \times 10^{-5}$			1400
$\gamma\phi\phi$	$(4.0 \pm 1.2) \times 10^{-4}$	S=2.1 1166	$\eta U \rightarrow \eta e^+ e^-$	$[nnaa] < 9.11$	$\times 10^{-7}$	CL=90%	—
$\gamma\eta(1405/1475) \rightarrow \gamma K\bar{K}\pi$	$(2.8 \pm 0.6) \times 10^{-3}$	S=1.6 1223	$\eta'(958) U \rightarrow \eta'(958) e^+ e^-$	$[nnaa] < 2.0$	$\times 10^{-7}$	CL=90%	—
$\gamma\eta(1405/1475) \rightarrow \gamma\gamma\rho^0$	$(7.8 \pm 2.0) \times 10^{-5}$	S=1.8 1223	$\phi e^+ e^-$	< 1.2	$\times 10^{-7}$	CL=90%	1381
$\gamma\eta(1405/1475) \rightarrow \gamma\eta\pi^+\pi^-$	$(3.0 \pm 0.5) \times 10^{-4}$	—	Weak decays				
$\gamma\eta(1405/1475) \rightarrow \gamma\rho^0\rho^0$	$(1.7 \pm 0.4) \times 10^{-3}$	S=1.3 1223	$D^- e^+ \nu_e + c.c.$	< 7.1	$\times 10^{-8}$	CL=90%	984
$\gamma\eta(1405/1475) \rightarrow \gamma\gamma\phi$	< 8.2	CL=95% —	$\bar{D}^0 e^+ e^- + c.c.$	< 8.5	$\times 10^{-8}$	CL=90%	987
$\gamma\eta(1405) \rightarrow \gamma\gamma\gamma$	< 2.63	CL=90% —	$D_s^- e^+ \nu_e + c.c.$	< 1.3	$\times 10^{-6}$	CL=90%	923
$\gamma\eta(1475) \rightarrow \gamma\gamma\gamma$	< 1.86	CL=90% —	$D_s^{*-} e^+ \nu_e + c.c.$	< 1.8	$\times 10^{-6}$	CL=90%	828
$\gamma\eta(1760) \rightarrow \gamma\rho^0\rho^0$	$(1.3 \pm 0.9) \times 10^{-4}$	1048	$D^- \pi^+ + c.c.$	< 7.5	$\times 10^{-5}$	CL=90%	977
$\gamma\eta(1760) \rightarrow \gamma\omega\omega$	$(1.98 \pm 0.33) \times 10^{-3}$	—	$\bar{D}^0 \bar{K}^0 + c.c.$	< 1.7	$\times 10^{-4}$	CL=90%	898
$\gamma\eta(1760) \rightarrow \gamma\gamma\gamma$	< 4.80	CL=90% —	$\bar{D}^0 \bar{K}^{*0} + c.c.$	< 2.5	$\times 10^{-6}$	CL=90%	670
$\gamma\eta(2225)$	$(3.14 \pm 0.50) \times 10^{-4}$	752	$D_s^- \pi^+ + c.c.$	< 1.3	$\times 10^{-4}$	CL=90%	915
$\gamma f_2(1270)$	$(1.64 \pm 0.12) \times 10^{-3}$	S=1.3 1286	$D_s^- \rho^+ + c.c.$	< 1.3	$\times 10^{-5}$	CL=90%	663
$\gamma f_2(1270) \rightarrow \gamma K_S^0 K_S^0$	$(2.58 \pm 0.60) \times 10^{-5}$	—	Charge conjugation (C), Parity (P), Lepton Family number (LF) violating modes				
$\gamma f_1(1285)$	$(6.1 \pm 0.8) \times 10^{-4}$	1283	$\gamma\gamma$	C	< 2.7	$\times 10^{-7}$	CL=90% 1548
$\gamma f_0(1370) \rightarrow \gamma K\bar{K}$	$(4.2 \pm 1.5) \times 10^{-4}$	—	$\gamma\phi$	C	< 1.4	$\times 10^{-6}$	CL=90% 1381
$\gamma f_0(1370) \rightarrow \gamma K_S^0 K_S^0$	$(1.1 \pm 0.4) \times 10^{-5}$	—	$e^\pm \mu^\mp$	LF	< 1.6	$\times 10^{-7}$	CL=90% 1547
$\gamma f_1(1420) \rightarrow \gamma K\bar{K}\pi$	$(7.9 \pm 1.3) \times 10^{-4}$	1220	$e^\pm \tau^\mp$	LF	< 7.5	$\times 10^{-8}$	CL=90% 1039
$\gamma f_0(1500) \rightarrow \gamma\pi\pi$	$(1.09 \pm 0.24) \times 10^{-4}$	1183	$\mu^\pm \tau^\mp$	LF	< 2.0	$\times 10^{-6}$	CL=90% 1035
$\gamma f_0(1500) \rightarrow \gamma\eta\eta$	$(1.7 \pm 0.6) \times 10^{-5}$	—	$\Lambda_c^+ e^- + c.c.$		< 6.9	$\times 10^{-8}$	CL=90% —
$\gamma f_0(1500) \rightarrow \gamma K_S^0 K_S^0$	$(1.59 \pm 0.24) \times 10^{-5}$	—	Other decays				
$\gamma f_1(1510) \rightarrow \gamma\eta\pi^+\pi^-$	$(4.5 \pm 1.2) \times 10^{-4}$	—	invisible	< 7	$\times 10^{-4}$	CL=90%	—
$\gamma f_2'(1525)$	$(5.7 \pm 0.5) \times 10^{-4}$	S=1.5 1177	$\chi_{c0}(1P)$				
$\gamma f_2'(1525) \rightarrow \gamma K_S^0 K_S^0$	$(8.0 \pm 0.7) \times 10^{-5}$	—	$I(G_{JPC}) = 0^+(0^+ +)$				
$\gamma f_2'(1525) \rightarrow \gamma\eta\eta$	$(3.4 \pm 1.4) \times 10^{-5}$	—	Mass $m = 3414.71 \pm 0.30$ MeV				
$\gamma f_2(1640) \rightarrow \gamma\omega\omega$	$(2.8 \pm 1.8) \times 10^{-4}$	—	Full width $\Gamma = 10.8 \pm 0.6$ MeV				
$\gamma f_0(1710) \rightarrow \gamma\pi\pi$	$(3.8 \pm 0.5) \times 10^{-4}$	—	$\chi_{c0}(1P)$ DECAY MODES				
$\gamma f_0(1710) \rightarrow \gamma K\bar{K}$	$(9.5 \pm 1.0) \times 10^{-4}$	S=1.5 1075	Hadronic decays				
$\gamma f_0(1710) \rightarrow \gamma\omega\omega$	$(3.1 \pm 1.0) \times 10^{-4}$	—	$2(\pi^+\pi^-)$	$(2.34 \pm 0.18) \%$			1679
$\gamma f_0(1710) \rightarrow \gamma\eta\eta$	$(2.4 \pm 1.2) \times 10^{-4}$	—	$\rho^0\pi^+\pi^-$	$(9.1 \pm 2.9) \times 10^{-3}$			1607
$\gamma f_0(1710) \rightarrow \gamma\omega\phi$	$(2.5 \pm 0.6) \times 10^{-4}$	—	$f_0(980)f_0(980)$	$(6.6 \pm 2.1) \times 10^{-4}$			1391
$\gamma f_0(1750) \rightarrow \gamma K_S^0 K_S^0$	$(1.11 \pm 0.33) \times 10^{-5}$	—	$\pi^+\pi^-\pi^0\pi^0$	$(3.3 \pm 0.4) \%$			1680
$\gamma f_2(1810) \rightarrow \gamma\eta\eta$	$(5.4 \pm 3.5) \times 10^{-5}$	—	$\rho^+\pi^-\pi^0 + c.c.$	$(2.9 \pm 0.4) \%$			1607
$\gamma f_2(1910) \rightarrow \gamma\omega\omega$	$(2.0 \pm 1.4) \times 10^{-4}$	—	$4\pi^0$	$(3.3 \pm 0.4) \times 10^{-3}$			1681
$\gamma f_2(1950) \rightarrow$	$(7.0 \pm 2.2) \times 10^{-4}$	—	$\pi^+\pi^- K^+ K^-$	$(1.81 \pm 0.14) \%$			1580
$\gamma K^*(892)\bar{K}^*(892)$	—	—	$K_0^*(1430)^0 \bar{K}_0^*(1430)^0 \rightarrow$	$(9.8 \pm 4.0) \times 10^{-4}$			—
$\gamma f_4(2050)$	$(2.7 \pm 0.7) \times 10^{-3}$	891	$\pi^+\pi^- K^+ K^-$	$(8.0 \pm 2.0) \times 10^{-4}$			—
$\gamma f_0(2100) \rightarrow \gamma\eta\eta$	$(1.13 \pm 0.60) \times 10^{-4}$	—	$K_1(1270)^+ K^- + c.c. \rightarrow$	$(6.3 \pm 1.9) \times 10^{-3}$			—
$\gamma f_0(2100) \rightarrow \gamma\pi\pi$	$(6.2 \pm 1.0) \times 10^{-4}$	—	$\pi^+\pi^- K^+ K^-$	< 2.7	$\times 10^{-3}$	CL=90%	—
$\gamma f_0(2200) \rightarrow \gamma K\bar{K}$	$(5.9 \pm 1.3) \times 10^{-4}$	—	$K_1(1400)^+ K^- + c.c. \rightarrow$	$(1.6 \pm 1.0) \times 10^{-4}$			1391
$\gamma f_0(2200) \rightarrow \gamma K_S^0 K_S^0$	$(2.72 \pm 0.19) \times 10^{-4}$	—	$\pi^+\pi^- K^+ K^-$	$(7.9 \pm 2.0) \times 10^{-4}$			586
$\gamma f_J(2220) \rightarrow \gamma\pi\pi$	< 3.9	CL=90% —	$f_0(980)f_0(2200)$	< 2.7	$\times 10^{-4}$	CL=90%	1019
$\gamma f_J(2220) \rightarrow \gamma K\bar{K}$	< 4.1	CL=90% —	$f_0(1370)f_0(1370)$	< 1.7	$\times 10^{-4}$	CL=90%	920
$\gamma f_J(2220) \rightarrow \gamma\rho\bar{\rho}$	$(1.5 \pm 0.8) \times 10^{-5}$	—	$f_0(1370)f_0(1500)$	$(6.7 \pm 3.5) \times 10^{-4}$			740
$\gamma f_0(2330) \rightarrow \gamma K_S^0 K_S^0$	$(4.9 \pm 0.7) \times 10^{-5}$	—	$f_0(1500)f_0(1370)$	< 1.3	$\times 10^{-4}$	CL=90%	920
$\gamma f_2(2340) \rightarrow \gamma\eta\eta$	$(5.6 \pm 2.4) \times 10^{-5}$	—	$f_0(1500)f_0(1500)$	< 5	$\times 10^{-5}$	CL=90%	804
$\gamma f_2(2340) \rightarrow \gamma K_S^0 K_S^0$	$(5.5 \pm 4.0) \times 10^{-5}$	—	$f_0(1500)f_0(1710)$	< 7	$\times 10^{-5}$	CL=90%	581
$\gamma X(1835) \rightarrow \gamma\pi^+\pi^-\eta'$	$(2.7 \pm 0.6) \times 10^{-4}$	S=1.6 1006	$K^+ K^- \pi^+ \pi^- \pi^0$	$(8.6 \pm 0.9) \times 10^{-3}$			1545
$\gamma X(1835) \rightarrow \gamma\rho\bar{\rho}$	$(7.7 \pm 1.5) \times 10^{-5}$	—	$K_S^0 K^\pm \pi^\mp \pi^+ \pi^-$	$(4.2 \pm 0.4) \times 10^{-3}$			1543
$\gamma X(1835) \rightarrow \gamma K_S^0 K_S^0 \eta$	$(3.3 \pm 2.0) \times 10^{-5}$	—	$K^+ K^- \pi^0 \pi^0$	$(5.6 \pm 0.9) \times 10^{-3}$			1582
$\gamma X(1835) \rightarrow \gamma\gamma\gamma$	< 3.56	CL=90% —	$K^+ \pi^- \bar{K}^0 \pi^0 + c.c.$	$(2.49 \pm 0.33) \%$			1581
$\gamma X(1835) \rightarrow \gamma 3(\pi^+\pi^-)$	$(2.4 \pm 0.7) \times 10^{-5}$	—	$\rho^+ K^- K^0 + c.c.$	$(1.21 \pm 0.21) \%$			1458
$\gamma X(2370) \rightarrow \gamma K^+ K^- \eta'$	$(1.8 \pm 0.7) \times 10^{-5}$	—	$K^*(892)^- K^+ \pi^0 \rightarrow$	$(4.6 \pm 1.2) \times 10^{-3}$			—
$\gamma X(2370) \rightarrow \gamma K_S^0 K_S^0 \eta'$	$(1.2 \pm 0.5) \times 10^{-5}$	—	$K^+ \pi^- \bar{K}^0 \pi^0 + c.c.$				—
$\gamma X(2370) \rightarrow \gamma\eta\eta\eta'$	< 9.2	CL=90% —	$K_S^0 K_S^0 \pi^+ \pi^-$	$(5.7 \pm 1.1) \times 10^{-3}$			1579
$\gamma\rho\bar{\rho}$	$(3.8 \pm 1.0) \times 10^{-4}$	1232	$K^+ K^- \eta\pi^0$	$(3.0 \pm 0.7) \times 10^{-3}$			1468
$\gamma\rho\bar{\rho}\pi^+\pi^-$	< 7.9	CL=90% 1107	$3(\pi^+\pi^-)$	$(1.20 \pm 0.18) \%$			1633

Meson Summary Table

$K^+ \bar{K}^*(892)^0 \pi^- + c.c.$	$(7.5 \pm 1.6) \times 10^{-3}$		1523
$K^*(892)^0 \bar{K}^*(892)^0$	$(1.7 \pm 0.6) \times 10^{-3}$		1456
$\pi \pi$	$(8.51 \pm 0.33) \times 10^{-3}$		1702
$\pi^0 \eta$	$< 1.8 \times 10^{-4}$		1661
$\pi^0 \eta'$	$< 1.1 \times 10^{-3}$		1570
$\pi^0 \eta_c$	$< 1.6 \times 10^{-3}$	CL=90%	383
$\eta \eta$	$(3.01 \pm 0.19) \times 10^{-3}$		1617
$\eta \eta'$	$(9.1 \pm 1.1) \times 10^{-5}$		1521
$\eta' \eta'$	$(2.17 \pm 0.12) \times 10^{-3}$		1413
$\omega \omega$	$(9.7 \pm 1.1) \times 10^{-4}$		1517
$\omega \phi$	$(1.41 \pm 0.13) \times 10^{-4}$		1447
$\omega K^+ K^-$	$(1.94 \pm 0.21) \times 10^{-3}$		1457
$K^+ K^-$	$(6.05 \pm 0.31) \times 10^{-3}$		1634
$K_S^0 K_S^0$	$(3.16 \pm 0.17) \times 10^{-3}$		1633
$\pi^+ \pi^- \eta$	$< 2.0 \times 10^{-4}$	CL=90%	1651
$\pi^+ \pi^- \eta'$	$< 4 \times 10^{-4}$	CL=90%	1560
$\bar{K}^0 K^+ \pi^- + c.c.$	$< 9 \times 10^{-5}$	CL=90%	1610
$K^+ K^- \pi^0$	$< 6 \times 10^{-5}$	CL=90%	1611
$K^+ K^- \eta$	$< 2.3 \times 10^{-4}$	CL=90%	1512
$K^+ K^- K_S^0 K_S^0$	$(1.4 \pm 0.5) \times 10^{-3}$		1331
$K_S^0 K_S^0 K_S^0 K_S^0$	$(5.8 \pm 0.5) \times 10^{-4}$		1327
$K^+ K^- K^+ K^-$	$(2.82 \pm 0.29) \times 10^{-3}$		1333
$K^+ K^- \phi$	$(9.7 \pm 2.5) \times 10^{-4}$		1381
$\bar{K}^0 K^+ \pi^- \phi + c.c.$	$(3.7 \pm 0.6) \times 10^{-3}$		1326
$K^+ K^- \pi^0 \phi$	$(1.90 \pm 0.35) \times 10^{-3}$		1329
$\phi \pi^+ \pi^- \pi^0$	$(1.18 \pm 0.15) \times 10^{-3}$		1525
$\phi \phi$	$(8.0 \pm 0.7) \times 10^{-4}$		1370
$\phi \phi \eta$	$(8.4 \pm 1.0) \times 10^{-4}$		1100
$p \bar{p}$	$(2.21 \pm 0.08) \times 10^{-4}$		1426
$p \bar{p} \pi^0$	$(7.0 \pm 0.7) \times 10^{-4}$	S=1.3	1379
$p \bar{p} \eta$	$(3.5 \pm 0.4) \times 10^{-4}$		1187
$p \bar{p} \omega$	$(5.2 \pm 0.6) \times 10^{-4}$		1043
$p \bar{p} \phi$	$(6.0 \pm 1.4) \times 10^{-5}$		876
$p \bar{p} \pi^+ \pi^-$	$(2.1 \pm 0.7) \times 10^{-3}$	S=1.4	1320
$p \bar{p} \pi^0 \pi^0$	$(1.04 \pm 0.28) \times 10^{-3}$		1324
$p \bar{p} K^+ K^-$ (non-resonant)	$(1.22 \pm 0.26) \times 10^{-4}$		890
$p \bar{p} K_S^0 K_S^0$	$< 8.8 \times 10^{-4}$	CL=90%	884
$p \bar{n} \pi^-$	$(1.27 \pm 0.11) \times 10^{-3}$		1376
$\bar{p} n \pi^+$	$(1.37 \pm 0.12) \times 10^{-3}$		1376
$p \bar{n} \pi^- \pi^0$	$(2.34 \pm 0.21) \times 10^{-3}$		1321
$\bar{p} n \pi^+ \pi^0$	$(2.21 \pm 0.18) \times 10^{-3}$		1321
$\Lambda \bar{\Lambda}$	$(3.59 \pm 0.15) \times 10^{-4}$		1292
$\Lambda \bar{\Lambda} \pi^+ \pi^-$	$(1.18 \pm 0.13) \times 10^{-3}$		1153
$\Lambda \bar{\Lambda} \pi^+ \pi^-$ (non-resonant)	$< 5 \times 10^{-4}$	CL=90%	1153
$\Sigma(1385)^+ \bar{\Lambda} \pi^- + c.c.$	$< 5 \times 10^{-4}$	CL=90%	1083
$\Sigma(1385)^- \bar{\Lambda} \pi^+ + c.c.$	$< 5 \times 10^{-4}$	CL=90%	1083
$K^+ \bar{p} \Lambda + c.c.$	$(1.25 \pm 0.12) \times 10^{-3}$	S=1.3	1132
$n K_S^0 \bar{\Lambda} + c.c.$	$(6.6 \pm 0.5) \times 10^{-4}$		1129
$K^*(892)^+ \bar{p} \Lambda + c.c.$	$(4.8 \pm 0.9) \times 10^{-4}$		845
$K^+ \bar{p} \Lambda(1520) + c.c.$	$(2.9 \pm 0.7) \times 10^{-4}$		859
$\Lambda(1520) \bar{\Lambda}(1520)$	$(3.1 \pm 1.2) \times 10^{-4}$		780
$\Sigma^0 \bar{\Sigma}^0$	$(4.68 \pm 0.32) \times 10^{-4}$		1222
$\Sigma^+ \bar{p} K_S^0 + c.c.$	$(3.52 \pm 0.27) \times 10^{-4}$		1089
$\Sigma^0 \bar{p} K^+ + c.c.$	$(3.03 \pm 0.20) \times 10^{-4}$		1090
$\Sigma^+ \bar{\Sigma}^-$	$(4.6 \pm 0.8) \times 10^{-4}$	S=2.6	1225
$\Sigma^- \bar{\Sigma}^+$	$(5.1 \pm 0.5) \times 10^{-4}$		1217
$\Sigma(1385)^+ \bar{\Sigma}(1385)^-$	$(1.6 \pm 0.6) \times 10^{-4}$		1001
$\Sigma(1385)^- \bar{\Sigma}(1385)^+$	$(2.3 \pm 0.7) \times 10^{-4}$		1001
$K^- \Lambda \bar{\Xi}^+ + c.c.$	$(1.94 \pm 0.35) \times 10^{-4}$		873
$\Xi^0 \bar{\Xi}^0$	$(3.1 \pm 0.8) \times 10^{-4}$		1089
$\Xi^- \bar{\Xi}^+$	$(4.8 \pm 0.7) \times 10^{-4}$		1081
$\eta_c \pi^+ \pi^-$	$< 7 \times 10^{-4}$	CL=90%	307

Radiative decays

$\gamma J/\psi(1S)$	$(1.40 \pm 0.05) \%$		303
$\gamma \rho^0$	$< 9 \times 10^{-6}$	CL=90%	1619
$\gamma \omega$	$< 8 \times 10^{-6}$	CL=90%	1618
$\gamma \phi$	$< 6 \times 10^{-6}$	CL=90%	1555
$\gamma \gamma$	$(2.04 \pm 0.09) \times 10^{-4}$		1707
$e^+ e^- J/\psi(1S)$	$(1.33 \pm 0.29) \times 10^{-4}$		303
$\mu^+ \mu^- J/\psi(1S)$	$< 1.9 \times 10^{-5}$	CL=90%	226

 $\chi_{c1}(1P)$

$$J^G(J^{PC}) = 0^+(1^{++})$$

Mass $m = 3510.67 \pm 0.05$ MeV ($S = 1.2$)
 Full width $\Gamma = 0.84 \pm 0.04$ MeV

$\chi_{c1}(1P)$ DECAY MODES	Fraction (Γ_i/Γ)	Scale factor/ Confidence level	p (MeV/c)
Hadronic decays			
$3(\pi^+ \pi^-)$	$(5.8 \pm 1.4) \times 10^{-3}$	S=1.2	1683
$2(\pi^+ \pi^-)$	$(7.6 \pm 2.6) \times 10^{-3}$		1728
$\pi^+ \pi^- \pi^0 \pi^0$	$(1.19 \pm 0.15) \%$		1729
$\rho^+ \pi^- \pi^0 + c.c.$	$(1.45 \pm 0.24) \%$		1658
$\rho^0 \pi^+ \pi^-$	$(3.9 \pm 3.5) \times 10^{-3}$		1657
$4\pi^0$	$(5.4 \pm 0.8) \times 10^{-4}$		1729
$\pi^+ \pi^- K^+ K^-$	$(4.5 \pm 1.0) \times 10^{-3}$		1632
$K^+ K^- \pi^0 \pi^0$	$(1.12 \pm 0.27) \times 10^{-3}$		1634
$K^+ K^- \pi^+ \pi^- \pi^0$	$(1.15 \pm 0.13) \%$		1598
$K_S^0 K_S^0 \pi^+ \pi^- \pi^0$	$(7.5 \pm 0.8) \times 10^{-3}$		1596
$K^+ \pi^- \bar{K}^0 \pi^0 + c.c.$	$(8.6 \pm 1.4) \times 10^{-3}$		1632
$\rho^- K^+ \bar{K}^0 + c.c.$	$(5.0 \pm 1.2) \times 10^{-3}$		1514
$K^*(892)^0 \bar{K}^0 \pi^0 \rightarrow$ $K^+ \pi^- \bar{K}^0 \pi^0 + c.c.$	$(2.3 \pm 0.6) \times 10^{-3}$		-
$K^+ K^- \eta \pi^0$	$(1.12 \pm 0.34) \times 10^{-3}$		1523
$\pi^+ \pi^- K_S^0 K_S^0$	$(6.9 \pm 2.9) \times 10^{-4}$		1630
$K^+ K^- \eta$	$(3.2 \pm 1.0) \times 10^{-4}$		1566
$\bar{K}^0 K^+ \pi^- + c.c.$	$(7.0 \pm 0.6) \times 10^{-3}$		1661
$K^*(892)^0 \bar{K}^0 + c.c.$	$(10 \pm 4) \times 10^{-4}$		1602
$K^*(892)^+ K^- + c.c.$	$(1.4 \pm 0.6) \times 10^{-3}$		1602
$K_J^*(1430)^0 \bar{K}^0 + c.c. \rightarrow$ $K_S^0 K^+ \pi^- + c.c.$	$< 8 \times 10^{-4}$	CL=90%	-
$K_J^*(1430)^+ K^- + c.c. \rightarrow$ $K_S^0 K^+ \pi^- + c.c.$	$< 2.1 \times 10^{-3}$	CL=90%	-
$K^+ K^- \pi^0$	$(1.81 \pm 0.24) \times 10^{-3}$		1662
$\eta \pi^+ \pi^-$	$(4.62 \pm 0.23) \times 10^{-3}$		1701
$a_0(980)^+ \pi^- + c.c. \rightarrow \eta \pi^+ \pi^-$	$(3.2 \pm 0.4) \times 10^{-3}$	S=2.2	-
$a_2(1320)^+ \pi^- + c.c. \rightarrow \eta \pi^+ \pi^-$	$(1.76 \pm 0.24) \times 10^{-4}$		-
$a_2(1700)^+ \pi^- + c.c. \rightarrow \eta \pi^+ \pi^-$	$(4.6 \pm 0.7) \times 10^{-5}$		-
$f_2(1270) \eta \rightarrow \eta \pi^+ \pi^-$	$(3.5 \pm 0.6) \times 10^{-4}$		-
$f_4(2050) \eta \rightarrow \eta \pi^+ \pi^-$	$(2.5 \pm 0.9) \times 10^{-5}$		-
$\pi_1(1400)^+ \pi^- + c.c. \rightarrow$ $\eta \pi^+ \pi^-$	$< 5 \times 10^{-5}$	CL=90%	-
$\pi_1(1600)^+ \pi^- + c.c. \rightarrow$ $\eta \pi^+ \pi^-$	$< 1.5 \times 10^{-5}$	CL=90%	-
$\pi_1(2015)^+ \pi^- + c.c. \rightarrow$ $\eta \pi^+ \pi^-$	$< 8 \times 10^{-6}$	CL=90%	-
$f_2(1270) \eta$	$(6.7 \pm 1.1) \times 10^{-4}$		1467
$\pi^+ \pi^- \eta'$	$(2.2 \pm 0.4) \times 10^{-3}$		1612
$K^+ K^- \eta'(958)$	$(8.8 \pm 0.9) \times 10^{-4}$		1461
$K_0^*(1430)^+ K^- + c.c.$	$(6.4 \pm 2.2) \times 10^{-4}$		-
$f_0(980) \eta'(958)$	$(1.6 \pm 1.4) \times 10^{-4}$		1460
$f_0(1710) \eta'(958)$	$(7 \pm 5) \times 10^{-5}$		1118
$f_2'(1525) \eta'(958)$	$(9 \pm 6) \times 10^{-5}$		1229
$\pi^0 f_0(980) \rightarrow \pi^0 \pi^+ \pi^-$	$(3.5 \pm 0.9) \times 10^{-7}$		-
$K^+ \bar{K}^*(892)^0 \pi^- + c.c.$	$(3.2 \pm 2.1) \times 10^{-3}$		1577
$K^*(892)^0 \bar{K}^*(892)^0$	$(1.4 \pm 0.4) \times 10^{-3}$		1512
$K^+ K^- K_S^0 K_S^0$	$< 4 \times 10^{-4}$	CL=90%	1390
$K_S^0 K_S^0 K_S^0 K_S^0$	$(3.5 \pm 1.0) \times 10^{-5}$		1387
$K^+ K^- K^+ K^-$	$(5.4 \pm 1.1) \times 10^{-4}$		1393
$K^+ K^- \phi$	$(4.1 \pm 1.5) \times 10^{-4}$		1440
$\bar{K}^0 K^+ \pi^- \phi + c.c.$	$(3.3 \pm 0.5) \times 10^{-3}$		1387
$K^+ K^- \pi^0 \phi$	$(1.62 \pm 0.30) \times 10^{-3}$		1390
$\phi \pi^+ \pi^- \pi^0$	$(7.5 \pm 1.0) \times 10^{-4}$		1578
$\omega \omega$	$(5.7 \pm 0.7) \times 10^{-4}$		1571
$\omega K^+ K^-$	$(7.8 \pm 0.9) \times 10^{-4}$		1513
$\omega \phi$	$(2.7 \pm 0.4) \times 10^{-5}$		1503
$\phi \phi$	$(4.2 \pm 0.5) \times 10^{-4}$		1429
$\phi \phi \eta$	$(3.0 \pm 0.5) \times 10^{-4}$		1172
$p \bar{p}$	$(7.60 \pm 0.34) \times 10^{-5}$		1484
$p \bar{p} \pi^0$	$(1.55 \pm 0.18) \times 10^{-4}$		1438
$p \bar{p} \eta$	$(1.45 \pm 0.25) \times 10^{-4}$		1254
$p \bar{p} \omega$	$(2.12 \pm 0.31) \times 10^{-4}$		1117
$p \bar{p} \phi$	$< 1.7 \times 10^{-5}$	CL=90%	962
$p \bar{p} \pi^+ \pi^-$	$(5.0 \pm 1.9) \times 10^{-4}$		1381
$p \bar{p} \pi^0 \pi^0$	$< 5 \times 10^{-4}$	CL=90%	1385
$p \bar{p} K^+ K^-$ (non-resonant)	$(1.27 \pm 0.22) \times 10^{-4}$		974
$p \bar{p} K_S^0 K_S^0$	$< 4.5 \times 10^{-4}$	CL=90%	968
$p \bar{n} \pi^-$	$(3.8 \pm 0.5) \times 10^{-4}$		1435
$\bar{p} n \pi^+$	$(3.9 \pm 0.5) \times 10^{-4}$		1435
$p \bar{n} \pi^- \pi^0$	$(1.03 \pm 0.12) \times 10^{-3}$		1383

Meson Summary Table

$\bar{p}n\pi^+\pi^0$	$(1.01 \pm 0.12) \times 10^{-3}$		1383
$\Lambda\bar{\Lambda}$	$(1.27 \pm 0.08) \times 10^{-4}$		1355
$\Lambda\bar{\Lambda}\pi^+\pi^-$	$(2.9 \pm 0.5) \times 10^{-4}$		1223
$\Lambda\bar{\Lambda}\pi^+\pi^-$ (non-resonant)	$(2.5 \pm 0.6) \times 10^{-4}$		1223
$\Sigma(1385)^+\bar{\Lambda}\pi^- + \text{c.c.}$	$< 1.3 \times 10^{-4}$	CL=90%	1157
$\Sigma(1385)^-\bar{\Lambda}\pi^+ + \text{c.c.}$	$< 1.3 \times 10^{-4}$	CL=90%	1157
$K^+\bar{p}\Lambda + \text{c.c.}$	$(4.2 \pm 0.4) \times 10^{-4}$	S=1.2	1203
$nK_S^0\bar{\Lambda} + \text{c.c.}$	$(1.66 \pm 0.17) \times 10^{-4}$		1200
$K^*(892)^+\bar{p}\Lambda + \text{c.c.}$	$(4.9 \pm 0.7) \times 10^{-4}$		935
$K^+\bar{p}\Lambda(1520) + \text{c.c.}$	$(1.7 \pm 0.4) \times 10^{-4}$		951
$\Lambda(1520)\bar{\Lambda}(1520)$	$< 9 \times 10^{-5}$	CL=90%	880
$\Sigma^0\bar{\Sigma}^0$	$(4.2 \pm 0.6) \times 10^{-5}$		1288
$\Sigma^+\bar{p}K_S^0 + \text{c.c.}$	$(1.53 \pm 0.12) \times 10^{-4}$		1163
$\Sigma^0\bar{p}K^+ + \text{c.c.}$	$(1.46 \pm 0.10) \times 10^{-4}$		1163
$\Sigma^+\bar{\Sigma}^-$	$(3.6 \pm 0.7) \times 10^{-5}$		1291
$\Sigma^-\bar{\Sigma}^+$	$(5.7 \pm 1.5) \times 10^{-5}$		1283
$\Sigma(1385)^+\bar{\Sigma}(1385)^-$	$< 9 \times 10^{-5}$	CL=90%	1081
$\Sigma(1385)^-\bar{\Sigma}(1385)^+$	$< 5 \times 10^{-5}$	CL=90%	1081
$K^-\Lambda\bar{\Sigma}^+ + \text{c.c.}$	$(1.35 \pm 0.24) \times 10^{-4}$		963
$\Xi^0\bar{\Xi}^0$	$< 6 \times 10^{-5}$	CL=90%	1163
$\Xi^-\bar{\Xi}^+$	$(8.0 \pm 2.1) \times 10^{-5}$		1155
$\pi^+\pi^-\pi^+ + K^+K^-$	$< 2.1 \times 10^{-3}$		-
$K_S^0 K_S^0$	$< 6 \times 10^{-5}$	CL=90%	1683
$\eta_c\pi^+\pi^-$	$< 3.2 \times 10^{-3}$	CL=90%	413

Radiative decays

$\gamma J/\psi(1S)$	$(34.3 \pm 1.0) \%$		389
$\gamma\rho^0$	$(2.16 \pm 0.17) \times 10^{-4}$		1670
$\gamma\omega$	$(6.8 \pm 0.8) \times 10^{-5}$		1668
$\gamma\phi$	$(2.4 \pm 0.5) \times 10^{-5}$		1607
$\gamma\gamma$	$< 6.3 \times 10^{-6}$	CL=90%	1755
$e^+e^-J/\psi(1S)$	$(3.46 \pm 0.22) \times 10^{-3}$		389
$\mu^+\mu^-J/\psi(1S)$	$(2.33 \pm 0.29) \times 10^{-4}$		335

 $h_c(1P)$

$$J^G(J^{PC}) = 0^-(1^-)$$

Mass $m = 3525.38 \pm 0.11$ MeVFull width $\Gamma = 0.7 \pm 0.4$ MeV

$h_c(1P)$ DECAY MODES	Fraction (Γ_i/Γ)	Confidence level	p (MeV/c)
$J/\psi(1S)\pi\pi$	not seen		312
$J/\psi(1S)\pi^+\pi^-$	$< 2.3 \times 10^{-3}$	90%	305
$p\bar{p}$	$< 1.5 \times 10^{-4}$	90%	1492
$p\bar{p}\pi^+\pi^-$	$(2.9 \pm 0.6) \times 10^{-3}$		1390
$p\bar{p}\pi^0\pi^0$	$< 5 \times 10^{-4}$	90%	1394
$\pi^+\pi^-\pi^0$	$(1.6 \pm 0.5) \times 10^{-3}$		1749
$\pi^+\pi^-\pi^0\eta$	$(7.2 \pm 2.3) \times 10^{-3}$		1695
$2\pi^+2\pi^-\pi^0$	$(8.1 \pm 1.8) \times 10^{-3}$		1716
$3\pi^+3\pi^-\pi^0$	$< 9 \times 10^{-3}$	90%	1661
$K^+K^-\pi^+\pi^-$	$< 6 \times 10^{-4}$	90%	1640
$K^+K^-\pi^+\pi^-\pi^0$	$(3.2 \pm 0.8) \times 10^{-3}$		1606
$K^+K^-\pi^+\pi^-\eta$	$< 2.3 \times 10^{-3}$	90%	1480
$K^+K^-\pi^0$	$< 6 \times 10^{-4}$	90%	1670
$K^+K^-\pi^0\eta$	$< 2.1 \times 10^{-3}$	90%	1532
$K^+K^-\eta$	$< 9 \times 10^{-4}$	90%	1574
$2K^+2K^-\pi^0$	$< 2.4 \times 10^{-4}$	90%	1339
$K_S^0 K_S^0$	$< 6 \times 10^{-4}$	90%	1668
$K_S^0 K_S^0 \pi^+\pi^-$	$(2.8 \pm 1.0) \times 10^{-3}$		1604
Radiative decays			
$\gamma\eta$	$(4.7 \pm 2.1) \times 10^{-4}$		1720
$\gamma\eta'(958)$	$(1.5 \pm 0.4) \times 10^{-3}$		1633
$\gamma\eta_c(1S)$	$(50 \pm 9) \%$		500

 $\chi_{c2}(1P)$

$$J^G(J^{PC}) = 0^+(2^+)$$

Mass $m = 3556.17 \pm 0.07$ MeVFull width $\Gamma = 1.97 \pm 0.09$ MeV

$\chi_{c2}(1P)$ DECAY MODES	Fraction (Γ_i/Γ)	Confidence level	p (MeV/c)
Hadronic decays			
$2(\pi^+\pi^-)$	$(1.02 \pm 0.09) \%$		1751
$\pi^+\pi^-\pi^0\pi^0$	$(1.83 \pm 0.23) \%$		1752
$\rho^+\pi^-\pi^0 + \text{c.c.}$	$(2.19 \pm 0.34) \%$		1682
$4\pi^0$	$(1.11 \pm 0.15) \times 10^{-3}$		1752

$K^+K^-\pi^0\pi^0$	$(2.1 \pm 0.4) \times 10^{-3}$		1658
$K^+\pi^-\bar{K}^0\pi^0 + \text{c.c.}$	$(1.38 \pm 0.20) \%$		1657
$\rho^-K^+\bar{K}^0 + \text{c.c.}$	$(4.1 \pm 1.2) \times 10^{-3}$		1540
$K^*(892)^0 K^-\pi^+ \rightarrow$	$(2.9 \pm 0.8) \times 10^{-3}$		-
$K^-\pi^+K^0\pi^0 + \text{c.c.}$			
$K^*(892)^0 \bar{K}^0\pi^0 \rightarrow$	$(3.8 \pm 0.9) \times 10^{-3}$		-
$K^+\pi^-\bar{K}^0\pi^0 + \text{c.c.}$			
$K^*(892)^- K^+\pi^0 \rightarrow$	$(3.7 \pm 0.8) \times 10^{-3}$		-
$K^+\pi^-\bar{K}^0\pi^0 + \text{c.c.}$			
$K^*(892)^+ \bar{K}^0\pi^0 \rightarrow$	$(2.9 \pm 0.8) \times 10^{-3}$		-
$K^+\pi^-\bar{K}^0\pi^0 + \text{c.c.}$			
$K^+K^-\eta\pi^0$	$(1.3 \pm 0.4) \times 10^{-3}$		1549
$K^+K^-\pi^+\pi^-$	$(8.4 \pm 0.9) \times 10^{-3}$		1656
$K^+K^-\pi^+\pi^-\pi^0$	$(1.17 \pm 0.13) \%$		1623
$K_S^0 K_S^0 \pi^+\pi^-\pi^+$	$(7.3 \pm 0.8) \times 10^{-3}$		1621
$K^+\bar{K}^*(892)^0 \pi^+ + \text{c.c.}$	$(2.1 \pm 1.1) \times 10^{-3}$		1602
$K^*(892)^0 \bar{K}^*(892)^0$	$(2.3 \pm 0.4) \times 10^{-3}$		1538
$3(\pi^+\pi^-)$	$(8.6 \pm 1.8) \times 10^{-3}$		1707
$\phi\phi$	$(1.06 \pm 0.09) \times 10^{-3}$		1457
$\phi\phi\eta$	$(5.3 \pm 0.6) \times 10^{-4}$		1206
$\omega\omega$	$(8.4 \pm 1.0) \times 10^{-4}$		1597
ωK^+K^-	$(7.3 \pm 0.9) \times 10^{-4}$		1540
$\omega\phi$	$(9.6 \pm 2.7) \times 10^{-6}$		1529
$\pi\pi$	$(2.23 \pm 0.09) \times 10^{-3}$		1773
$\rho^0\pi^+\pi^-$	$(3.7 \pm 1.6) \times 10^{-3}$		1682
$\pi^+\pi^-\pi^0$ (non-resonant)	$(2.0 \pm 0.4) \times 10^{-5}$		1765
$\rho(770)^\pm\pi^\mp$	$(6 \pm 4) \times 10^{-6}$		-
$\pi^+\pi^-\eta$	$(4.8 \pm 1.3) \times 10^{-4}$		1724
$\pi^+\pi^-\eta'$	$(5.0 \pm 1.8) \times 10^{-4}$		1636
$\eta\eta$	$(5.4 \pm 0.4) \times 10^{-4}$		1692
K^+K^-	$(1.01 \pm 0.06) \times 10^{-3}$		1708
$K_S^0 K_S^0$	$(5.2 \pm 0.4) \times 10^{-4}$		1707
$K^*(892)^\pm K^\mp$	$(1.44 \pm 0.21) \times 10^{-4}$		1627
$K^*(892)^0 \bar{K}^0 + \text{c.c.}$	$(1.24 \pm 0.27) \times 10^{-4}$		1627
$K_2^*(1430)^\pm K^\mp$	$(1.48 \pm 0.12) \times 10^{-3}$		-
$K_2^*(1430)^0 \bar{K}^0 + \text{c.c.}$	$(1.24 \pm 0.17) \times 10^{-3}$		1443
$K_3^*(1780)^\pm K^\mp$	$(5.2 \pm 0.8) \times 10^{-4}$		-
$K_3^*(1780)^0 \bar{K}^0 + \text{c.c.}$	$(5.6 \pm 2.1) \times 10^{-4}$		1274
$a_2(1320)^0 \pi^0$	$(1.29 \pm 0.34) \times 10^{-3}$		-
$a_2(1320)^\pm \pi^\mp$	$(1.8 \pm 0.6) \times 10^{-3}$		1530
$\bar{K}^0 K^+\pi^- + \text{c.c.}$	$(1.28 \pm 0.18) \times 10^{-3}$		1685
$K^+K^-\pi^0$	$(3.0 \pm 0.8) \times 10^{-4}$		1686
$K^+K^-\eta$	$< 3.2 \times 10^{-4}$	90%	1592
$K^+K^-\eta'(958)$	$(1.94 \pm 0.34) \times 10^{-4}$		1488
$\eta\eta'$	$(2.2 \pm 0.5) \times 10^{-5}$		1600
$\eta'\eta'$	$(4.6 \pm 0.6) \times 10^{-5}$		1498
$\pi^+\pi^-K_S^0 K_S^0$	$(2.2 \pm 0.5) \times 10^{-3}$		1655
$K^+K^-K_S^0 K_S^0$	$< 4 \times 10^{-4}$	90%	1418
$K_S^0 K_S^0 K_S^0 K_S^0$	$(1.13 \pm 0.18) \times 10^{-4}$		1415
$K^+K^-K^+K^-$	$(1.65 \pm 0.20) \times 10^{-3}$		1421
$K^+K^-\phi$	$(1.42 \pm 0.29) \times 10^{-3}$		1468
$\bar{K}^0 K^+\pi^-\phi + \text{c.c.}$	$(4.8 \pm 0.7) \times 10^{-3}$		1416
$K^+K^-\pi^0\phi$	$(2.7 \pm 0.5) \times 10^{-3}$		1419
$\phi\pi^+\pi^-\pi^0$	$(9.3 \pm 1.2) \times 10^{-4}$		1603
$p\bar{p}$	$(7.33 \pm 0.33) \times 10^{-5}$		1510
$p\bar{p}\pi^0$	$(4.7 \pm 0.4) \times 10^{-4}$		1465
$p\bar{p}\eta$	$(1.74 \pm 0.25) \times 10^{-4}$		1285
$p\bar{p}\omega$	$(3.6 \pm 0.4) \times 10^{-4}$		1152
$p\bar{p}\phi$	$(2.8 \pm 0.9) \times 10^{-5}$		1002
$p\bar{p}\pi^+\pi^-$	$(1.32 \pm 0.34) \times 10^{-3}$		1410
$p\bar{p}\pi^0\pi^0$	$(7.8 \pm 2.3) \times 10^{-4}$		1414
$p\bar{p}K^+K^-$ (non-resonant)	$(1.91 \pm 0.32) \times 10^{-4}$		1013
$p\bar{p}K_S^0 K_S^0$	$< 7.9 \times 10^{-4}$	90%	1007
$p\bar{p}\pi^-$	$(8.5 \pm 0.9) \times 10^{-4}$		1463
$\bar{p}n\pi^+$	$(8.9 \pm 0.8) \times 10^{-4}$		1463
$p\bar{p}\pi^-\pi^0$	$(2.17 \pm 0.18) \times 10^{-3}$		1411
$\bar{p}n\pi^+\pi^0$	$(2.11 \pm 0.18) \times 10^{-3}$		1411
$\Lambda\bar{\Lambda}$	$(1.83 \pm 0.16) \times 10^{-4}$		1384
$\Lambda\bar{\Lambda}\pi^+\pi^-$	$(1.25 \pm 0.15) \times 10^{-3}$		1255
$\Lambda\bar{\Lambda}\pi^+\pi^-$ (non-resonant)	$(6.6 \pm 1.5) \times 10^{-4}$		1255
$\Sigma(1385)^+\bar{\Lambda}\pi^- + \text{c.c.}$	$< 4 \times 10^{-4}$	90%	1192
$\Sigma(1385)^-\bar{\Lambda}\pi^+ + \text{c.c.}$	$< 6 \times 10^{-4}$	90%	1192
$K^+\bar{p}\Lambda + \text{c.c.}$	$(7.8 \pm 0.5) \times 10^{-4}$		1236
$nK_S^0\bar{\Lambda} + \text{c.c.}$	$(3.58 \pm 0.28) \times 10^{-4}$		1233
$K^*(892)^+\bar{p}\Lambda + \text{c.c.}$	$(8.2 \pm 1.1) \times 10^{-4}$		976
$K^+\bar{p}\Lambda(1520) + \text{c.c.}$	$(2.8 \pm 0.7) \times 10^{-4}$		992
$\Lambda(1520)\bar{\Lambda}(1520)$	$(4.6 \pm 1.5) \times 10^{-4}$		924

Meson Summary Table

$\Sigma^0 \bar{\Sigma}^0$	$(3.7 \pm 0.6) \times 10^{-5}$		1319
$\Sigma^+ \bar{p} K_S^0 + \text{c.c.}$	$(8.2 \pm 0.9) \times 10^{-5}$		1197
$\Sigma^0 \bar{p} K^+ + \text{c.c.}$	$(9.1 \pm 0.8) \times 10^{-5}$		1197
$\Sigma^+ \bar{\Sigma}^-$	$(3.4 \pm 0.7) \times 10^{-5}$		1322
$\Sigma^- \bar{\Sigma}^+$	$(4.4 \pm 1.8) \times 10^{-5}$		1314
$\Sigma(1385)^+ \bar{\Sigma}(1385)^-$	$< 1.6 \times 10^{-4}$	90%	1118
$\Sigma(1385)^- \bar{\Sigma}(1385)^+$	$< 8 \times 10^{-5}$	90%	1118
$K^- \Lambda \bar{\Xi}^+ + \text{c.c.}$	$(1.76 \pm 0.32) \times 10^{-4}$		1004
$\Xi^0 \bar{\Xi}^0$	$< 1.0 \times 10^{-4}$	90%	1197
$\Xi^- \bar{\Xi}^+$	$(1.42 \pm 0.32) \times 10^{-4}$		1189
$J/\psi(1S) \pi^+ \pi^- \pi^0$	$< 1.5 \%$	90%	185
$\pi^0 \eta_c$	$< 3.2 \times 10^{-3}$	90%	511
$\eta_c(1S) \pi^+ \pi^-$	$< 5.4 \times 10^{-3}$	90%	459

Radiative decays

$\gamma J/\psi(1S)$	$(19.0 \pm 0.5) \%$		430
$\gamma \rho^0$	$< 1.9 \times 10^{-5}$	90%	1694
$\gamma \omega$	$< 6 \times 10^{-6}$	90%	1692
$\gamma \phi$	$< 7 \times 10^{-6}$	90%	1632
$\gamma \gamma$	$(2.85 \pm 0.10) \times 10^{-4}$		1778
$e^+ e^- J/\psi(1S)$	$(2.15 \pm 0.14) \times 10^{-3}$		430
$\mu^+ \mu^- J/\psi(1S)$	$(2.02 \pm 0.33) \times 10^{-4}$		381

 $\eta_c(2S)$

$$J^G(J^{PC}) = 0^+(0^{-+})$$

Quantum numbers are quark model predictions.

$$\text{Mass } m = 3637.5 \pm 1.1 \text{ MeV} \quad (S = 1.2)$$

$$\text{Full width } \Gamma = 11.3^{+3.2}_{-2.9} \text{ MeV}$$

$\eta_c(2S)$ DECAY MODES	Fraction (Γ_i/Γ)	Confidence level	p (MeV/c)
hadrons	not seen		—
$K \bar{K} \pi$	$(1.9 \pm 1.2) \%$		1729
$K \bar{K} \eta$	$(5 \pm 4) \times 10^{-3}$		1637
$2\pi^+ 2\pi^-$	not seen		1792
$\rho^0 \rho^0$	not seen		1645
$3\pi^+ 3\pi^-$	not seen		1749
$K^+ K^- \pi^+ \pi^-$	not seen		1700
$K^* 0 \bar{K}^* 0$	not seen		1585
$K^+ K^- \pi^+ \pi^- \pi^0$	$(1.4 \pm 1.0) \%$		1667
$K^+ K^- 2\pi^+ 2\pi^-$	not seen		1627
$K_S^0 K_L^0 2\pi^+ \pi^- + \text{c.c.}$	seen		1666
$2K^+ 2K^-$	not seen		1470
$\phi \phi$	not seen		1506
$p \bar{p}$	seen		1558
$p \bar{p} \pi^+ \pi^-$	seen		1461
$\gamma \gamma$	$(1.9 \pm 1.3) \times 10^{-4}$		1819
$\gamma J/\psi(1S)$	$< 1.4 \%$	90%	500
$\pi^+ \pi^- \eta$	not seen		1766
$\pi^+ \pi^- \eta'$	not seen		1680
$\pi^+ \pi^- \eta_c(1S)$	$< 25 \%$	90%	537

 $\psi(2S)$

$$J^G(J^{PC}) = 0^-(1^{--})$$

$$\text{Mass } m = 3686.10 \pm 0.06 \text{ MeV} \quad (S = 5.9)$$

$$\text{Full width } \Gamma = 294 \pm 8 \text{ keV}$$

$\psi(2S)$ DECAY MODES	Fraction (Γ_i/Γ)	Scale factor/ Confidence level	p (MeV/c)
hadrons	$(97.85 \pm 0.13) \%$		—
virtual $\gamma \rightarrow$ hadrons	$(1.73 \pm 0.14) \%$	S=1.5	—
$g g g$	$(10.6 \pm 1.6) \%$		—
$\gamma g g$	$(1.03 \pm 0.29) \%$		—
light hadrons	$(15.4 \pm 1.5) \%$		—
K_S^0 anything	$(16.0 \pm 1.1) \%$		—
$e^+ e^-$	$(7.93 \pm 0.17) \times 10^{-3}$		1843
$\mu^+ \mu^-$	$(8.0 \pm 0.6) \times 10^{-3}$		1840
$\tau^+ \tau^-$	$(3.1 \pm 0.4) \times 10^{-3}$		489

Decays into $J/\psi(1S)$ and anything

$J/\psi(1S)$ anything	$(61.4 \pm 0.6) \%$		—
$J/\psi(1S)$ neutrals	$(25.38 \pm 0.32) \%$		—
$J/\psi(1S) \pi^+ \pi^-$	$(34.68 \pm 0.30) \%$		477
$J/\psi(1S) \pi^0 \pi^0$	$(18.24 \pm 0.31) \%$		481
$J/\psi(1S) \eta$	$(3.37 \pm 0.05) \%$		199
$J/\psi(1S) \pi^0$	$(1.268 \pm 0.032) \times 10^{-3}$		528

Hadronic decays

$\pi^+ \pi^-$	$(7.8 \pm 2.6) \times 10^{-6}$		1838
$\pi^+ \pi^- \pi^0$	$(2.01 \pm 0.17) \times 10^{-4}$	S=1.7	1830
$\rho(770) \pi \rightarrow \pi^+ \pi^- \pi^0$	$(3.2 \pm 1.2) \times 10^{-5}$	S=1.8	—
$\rho(2150) \pi \rightarrow \pi^+ \pi^- \pi^0$	$(1.9 \pm 1.2_{-0.4}) \times 10^{-4}$		—
$2(\pi^+ \pi^-)$	$(2.4 \pm 0.6) \times 10^{-4}$	S=2.2	1817
$\rho^0 \pi^+ \pi^-$	$(2.2 \pm 0.6) \times 10^{-4}$	S=1.4	1750
$2(\pi^+ \pi^-) \pi^0$	$(2.9 \pm 1.0) \times 10^{-3}$	S=4.7	1799
$\rho a_2(1320)$	$(2.6 \pm 0.9) \times 10^{-4}$		1500
$\pi^+ \pi^- \pi^0 \pi^0 \pi^0$	$(5.3 \pm 0.9) \times 10^{-3}$		1800
$\pi^+ \pi^- 4\pi^0$	$(1.4 \pm 1.0) \times 10^{-3}$		1778
$\rho^\pm \pi^\mp \pi^0 \pi^0$	$< 2.7 \times 10^{-3}$	CL=90%	1737
$3(\pi^+ \pi^-)$	$(3.5 \pm 2.0) \times 10^{-4}$	S=2.8	1774
$2(\pi^+ \pi^- \pi^0)$	$(4.8 \pm 1.5) \times 10^{-3}$		1776
$3(\pi^+ \pi^-) \pi^0$	$(3.5 \pm 1.6) \times 10^{-3}$		1746
$2(\pi^+ \pi^-) 3\pi^0$	$(1.42 \pm 0.31) \%$		1748
$\eta \pi^+ \pi^-$	$< 1.6 \times 10^{-4}$	CL=90%	1791
$\eta \pi^+ \pi^- \pi^0$	$(9.5 \pm 1.7) \times 10^{-4}$		1778
$\eta 2(\pi^+ \pi^-)$	$(1.2 \pm 0.6) \times 10^{-3}$		1758
$\eta \pi^+ \pi^- \pi^0 \pi^0$	$< 4 \times 10^{-4}$	CL=90%	1760
$\eta \pi^+ \pi^- 3\pi^0$	$< 2.1 \times 10^{-3}$	CL=90%	1736
$\eta 2(\pi^+ \pi^-) \pi^0$	$< 2.1 \times 10^{-3}$	CL=90%	1705
$\rho \eta$	$(2.2 \pm 0.6) \times 10^{-5}$	S=1.1	1717
$\eta' \pi^+ \pi^- \pi^0$	$(4.5 \pm 2.1) \times 10^{-4}$		1692
$\eta' \rho$	$(1.9 \pm 1.7_{-1.2}) \times 10^{-5}$		1625
$\omega \pi^0$	$(2.1 \pm 0.6) \times 10^{-5}$		1757
$\omega \pi^+ \pi^-$	$(7.3 \pm 1.2) \times 10^{-4}$	S=2.1	1748
$\omega \pi^+ \pi^- 2\pi^0$	$(8.7 \pm 2.4) \times 10^{-3}$		1715
$b_1^\pm \pi^\mp$	$(4.0 \pm 0.6) \times 10^{-4}$	S=1.1	1635
$\omega f_2(1270)$	$(2.2 \pm 0.4) \times 10^{-4}$		1515
$\omega \pi^0 \pi^0$	$(1.11 \pm 0.35) \times 10^{-3}$		1749
$\omega 3\pi^0$	$< 8 \times 10^{-4}$	CL=90%	1736
$b_1^0 \pi^0$	$(2.4 \pm 0.6) \times 10^{-4}$		—
$\omega \eta$	$< 1.1 \times 10^{-5}$	CL=90%	1715
$\omega \eta'$	$(3.2 \pm 2.5_{-2.1}) \times 10^{-5}$		1623
$\phi \pi^0$	$< 4 \times 10^{-7}$	CL=90%	1699
$\phi \pi^+ \pi^-$	$(1.18 \pm 0.26) \times 10^{-4}$	S=1.5	1690
$\phi f_0(980) \rightarrow \pi^+ \pi^-$	$(7.5 \pm 3.3) \times 10^{-5}$	S=1.6	—
$\phi \eta$	$(3.10 \pm 0.31) \times 10^{-5}$		1654
$\eta \phi(2170), \phi(2170) \rightarrow$ $\phi f_0(980), f_0 \rightarrow \pi^+ \pi^-$	$< 2.2 \times 10^{-6}$	CL=90%	—
$\phi \eta'$	$(1.54 \pm 0.20) \times 10^{-5}$		1555
$\phi f_1(1285)$	$(3.0 \pm 1.3) \times 10^{-5}$		1436
$\phi \eta(1405) \rightarrow \phi \pi^+ \pi^- \eta$	$(8.5 \pm 1.7) \times 10^{-6}$		—
$\phi f_2'(1525)$	$(4.4 \pm 1.6) \times 10^{-5}$		1325
$K^+ K^-$	$(7.5 \pm 0.5) \times 10^{-5}$		1776
$K^+ K^- \pi^+$	$(7.3 \pm 0.5) \times 10^{-4}$		1754
$K^+ K^- \pi^0$	$(4.07 \pm 0.31) \times 10^{-5}$		1754
$K_S^0 K_S^0$	$< 4.6 \times 10^{-6}$		1775
$K_S^0 K_L^0$	$(5.34 \pm 0.33) \times 10^{-5}$		1775
$K_S^0 K_L^0 \pi^0$	$< 3.0 \times 10^{-4}$	CL=90%	1753
$K^+ K^- \pi^0 \pi^0$	$(2.6 \pm 1.3) \times 10^{-4}$		1728
$K^+ K^- \pi^+ \pi^- \pi^0$	$(1.26 \pm 0.09) \times 10^{-3}$		1694
$\omega f_0(1710) \rightarrow \omega K^+ K^-$	$(5.9 \pm 2.2) \times 10^{-5}$		—
$K^*(892)^0 K^- \pi^+ \pi^0 + \text{c.c.}$	$(8.6 \pm 2.2) \times 10^{-4}$		—
$K^*(892)^+ K^- \pi^+ \pi^- + \text{c.c.}$	$(9.6 \pm 2.8) \times 10^{-4}$		—
$K^*(892)^+ K^- \rho^0 + \text{c.c.}$	$(7.3 \pm 2.6) \times 10^{-4}$		—
$K^*(892)^0 K^- \rho^+ + \text{c.c.}$	$(6.1 \pm 1.8) \times 10^{-4}$		—
$K_S^0 K_S^0 \pi^+ \pi^-$	$(2.2 \pm 0.4) \times 10^{-4}$		1724
$K_S^0 K_L^0 \pi^0 \pi^0$	$(1.3 \pm 0.6) \times 10^{-3}$		1726
$K_S^0 K_L^0 \eta$	$(1.3 \pm 0.5) \times 10^{-3}$		1661
$K^+ K^- \rho^0$	$(2.2 \pm 0.4) \times 10^{-4}$		1616
$K^*(892)^0 \bar{K}_2^0(1430)^0$	$(1.9 \pm 0.5) \times 10^{-4}$		1417
$K^+ K^- \pi^+ \pi^- \eta$	$(1.3 \pm 0.7) \times 10^{-3}$		1574
$K^+ K^- 2(\pi^+ \pi^-)$	$(1.9 \pm 0.9) \times 10^{-3}$		1654
$K^+ K^- 2(\pi^+ \pi^-) \pi^0$	$(1.00 \pm 0.31) \times 10^{-3}$		1611
$K^+ K^*(892)^- + \text{c.c.}$	$(2.9 \pm 0.4) \times 10^{-5}$	S=1.2	1698
$2(K^+ K^-)$	$(6.3 \pm 1.3) \times 10^{-5}$		1499
$2(K^+ K^-) \pi^0$	$(1.10 \pm 0.28) \times 10^{-4}$		1440
$K^+ K^- \phi$	$(7.0 \pm 1.6) \times 10^{-5}$		1546
$K_1^+(1270)^\pm K^\mp$	$(1.00 \pm 0.28) \times 10^{-3}$		1588
$K^+ \bar{K}^*(892)^0 \pi^- + \text{c.c.}$	$(6.7 \pm 2.5) \times 10^{-4}$		1674
$\eta K^+ K^-, \text{ no } \eta \phi$	$(3.49 \pm 0.17) \times 10^{-5}$		1664
$X(1750) \eta \rightarrow K^+ K^- \eta$	$(4.8 \pm 2.8) \times 10^{-6}$		—
$K_1^+(1400)^\pm K^\mp$	$< 3.1 \times 10^{-4}$	CL=90%	1532

Meson Summary Table

$K_2^*(1430)^\pm K^\mp$	$(7.1 \pm_{-0.9}^{+1.3}) \times 10^{-5}$	-	$\Theta(1540) K^- \bar{\pi} \rightarrow K_S^0 p K^- \bar{\pi}$	$[iiaa] < 1.0$	$\times 10^{-5}$	CL=90%	-
$K^*(892)^0 \bar{K}^0 + c.c.$	$(1.09 \pm 0.20) \times 10^{-4}$	1697	$\Theta(1540) K_S^0 \bar{p} \rightarrow K_S^0 \bar{p} K^+ n$	$[iiaa] < 7.0$	$\times 10^{-6}$	CL=90%	-
$\omega K^+ K^-$	$(1.62 \pm 0.11) \times 10^{-4}$	S=1.1 1614	$\bar{\Theta}(1540) K^+ n \rightarrow K_S^0 \bar{p} K^+ n$	$[iiaa] < 2.6$	$\times 10^{-5}$	CL=90%	-
$\omega K_S^0 K_S^0$	$(7.0 \pm 0.5) \times 10^{-5}$	1612	$\bar{\Theta}(1540) K_S^0 p \rightarrow K_S^0 p K^- \bar{\pi}$	$[iiaa] < 6.0$	$\times 10^{-6}$	CL=90%	-
$\omega K^*(892)^+ K^- + c.c.$	$(2.07 \pm 0.26) \times 10^{-4}$	1482	Radiative decays				
$\omega K_2^*(1430)^+ K^- + c.c.$	$(6.1 \pm 1.2) \times 10^{-5}$	1252	$\gamma \chi_{c0}(1P)$	$(9.79 \pm 0.20) \%$			261
$\omega \bar{K}^*(892)^0 K^0$	$(1.68 \pm 0.30) \times 10^{-4}$	1481	$\gamma \chi_{c1}(1P)$	$(9.75 \pm 0.24) \%$			171
$\omega \bar{K}_2^*(1430)^0 K^0$	$(5.8 \pm 2.2) \times 10^{-5}$	1250	$\gamma \chi_{c2}(1P)$	$(9.52 \pm 0.20) \%$			128
$\omega X(1440) \rightarrow \omega K_S^0 K^- \pi^+ + c.c.$	$(1.6 \pm 0.4) \times 10^{-5}$	-	$\gamma \eta_c(1S)$	$(3.4 \pm 0.5) \times 10^{-3}$	S=1.3		635
$\omega X(1440) \rightarrow \omega K^+ K^- \pi^0$	$(1.09 \pm 0.26) \times 10^{-5}$	-	$\gamma \eta_c(2S)$	$(7 \pm 5) \times 10^{-4}$			48
$\omega f_1(1285) \rightarrow \omega K_S^0 K^- \pi^+ + c.c.$	$(3.0 \pm 1.0) \times 10^{-6}$	-	$\gamma \pi^0$	$(1.04 \pm 0.22) \times 10^{-6}$	S=1.4		1841
$\omega f_1(1285) \rightarrow \omega K^+ K^- \pi^0$	$(1.2 \pm 0.7) \times 10^{-6}$	-	$\gamma 2(\pi^+ \pi^-)$	$(4.0 \pm 0.6) \times 10^{-4}$			1817
$p \bar{p}$	$(2.94 \pm 0.08) \times 10^{-4}$	1586	$\gamma 3(\pi^+ \pi^-)$	$< 1.7 \times 10^{-4}$	CL=90%		1774
$n \bar{n}$	$(3.06 \pm 0.15) \times 10^{-4}$	1586	$\gamma \eta'(958)$	$(1.24 \pm 0.04) \times 10^{-4}$			1719
$p \bar{p} \pi^0$	$(1.53 \pm 0.07) \times 10^{-4}$	1543	$\gamma f_2(1270)$	$(2.73 \pm_{-0.25}^{+0.29}) \times 10^{-4}$	S=1.8		1622
$N(940) \bar{p} + c.c. \rightarrow p \bar{p} \pi^0$	$(6.4 \pm_{-1.3}^{+1.8}) \times 10^{-5}$	-	$\gamma f_0(1370) \rightarrow \gamma K \bar{K}$	$(3.1 \pm 1.7) \times 10^{-5}$			1588
$N(1440) \bar{p} + c.c. \rightarrow p \bar{p} \pi^0$	$(7.3 \pm_{-1.5}^{+1.7}) \times 10^{-5}$	S=2.5 -	$\gamma f_0(1500)$	$(9.3 \pm 1.9) \times 10^{-5}$			1535
$N(1520) \bar{p} + c.c. \rightarrow p \bar{p} \pi^0$	$(6.4 \pm_{-1.8}^{+2.3}) \times 10^{-6}$	-	$\gamma f_2'(1525)$	$(3.3 \pm 0.8) \times 10^{-5}$			1531
$N(1535) \bar{p} + c.c. \rightarrow p \bar{p} \pi^0$	$(2.5 \pm 1.0) \times 10^{-5}$	-	$\gamma f_0(1710) \rightarrow \gamma \pi \pi$	$(3.5 \pm 0.6) \times 10^{-5}$			-
$N(1650) \bar{p} + c.c. \rightarrow p \bar{p} \pi^0$	$(3.8 \pm_{-1.7}^{+1.4}) \times 10^{-5}$	-	$\gamma f_0(1710) \rightarrow \gamma K \bar{K}$	$(6.6 \pm 0.7) \times 10^{-5}$			-
$N(1720) \bar{p} + c.c. \rightarrow p \bar{p} \pi^0$	$(1.79 \pm_{-0.70}^{+0.26}) \times 10^{-5}$	-	$\gamma f_0(2100) \rightarrow \gamma \pi \pi$	$(4.8 \pm 1.0) \times 10^{-6}$			1244
$N(2300) \bar{p} + c.c. \rightarrow p \bar{p} \pi^0$	$(2.6 \pm_{-0.7}^{+1.2}) \times 10^{-5}$	-	$\gamma f_0(2200) \rightarrow \gamma K \bar{K}$	$(3.2 \pm 1.0) \times 10^{-6}$			1193
$N(2570) \bar{p} + c.c. \rightarrow p \bar{p} \pi^0$	$(2.13 \pm_{-0.31}^{+0.40}) \times 10^{-5}$	-	$\gamma f_2(2220) \rightarrow \gamma \pi \pi$	$< 5.8 \times 10^{-6}$	CL=90%		1168
$p \bar{p} \pi^+ \pi^-$	$(6.0 \pm 0.4) \times 10^{-4}$	1491	$\gamma f_2(2220) \rightarrow \gamma K \bar{K}$	$< 9.5 \times 10^{-6}$	CL=90%		1168
$p \bar{p} K^+ K^-$	$(2.7 \pm 0.7) \times 10^{-5}$	1118	$\gamma \eta$	$(9.2 \pm 1.8) \times 10^{-7}$			1802
$p \bar{p} \eta$	$(6.0 \pm 0.4) \times 10^{-5}$	1373	$\gamma \eta \pi^+ \pi^-$	$(8.7 \pm 2.1) \times 10^{-4}$			1791
$N(1535) \bar{p} + c.c. \rightarrow p \bar{p} \eta$	$(4.5 \pm_{-0.6}^{+0.7}) \times 10^{-5}$	-	$\gamma \eta(1405) \rightarrow \gamma K \bar{K} \pi$	$< 9 \times 10^{-5}$	CL=90%		1569
$p \bar{p} \pi^+ \pi^- \pi^0$	$(7.3 \pm 0.7) \times 10^{-4}$	1435	$\gamma \eta(1405) \rightarrow \gamma \eta \pi^+ \pi^-$	$(3.6 \pm 2.5) \times 10^{-5}$			-
$p \bar{p} \rho^0$	$(5.0 \pm 2.2) \times 10^{-5}$	1252	$\gamma \eta(1405) \rightarrow \gamma f_0(980) \pi^0 \rightarrow \gamma \pi^+ \pi^- \pi^0$	$< 5.0 \times 10^{-7}$	CL=90%		-
$p \bar{p} \omega$	$(6.9 \pm 2.1) \times 10^{-5}$	1247	$\gamma \eta(1475) \rightarrow \gamma K \bar{K} \pi$	$< 1.4 \times 10^{-4}$	CL=90%		-
$p \bar{p} \eta'$	$(1.10 \pm 0.13) \times 10^{-5}$	1141	$\gamma \eta(1475) \rightarrow \gamma \eta \pi^+ \pi^-$	$< 8.8 \times 10^{-5}$	CL=90%		-
$p \bar{p} \phi$	$(6.1 \pm 0.6) \times 10^{-6}$	1109	$\gamma K^{*0} K^+ \pi^- + c.c.$	$(3.7 \pm 0.9) \times 10^{-4}$			1674
$\phi X(1835) \rightarrow p \bar{p} \phi$	$< 1.82 \times 10^{-7}$	CL=90%	$\gamma K^{*0} \bar{K}^{*0}$	$(2.4 \pm 0.7) \times 10^{-4}$			1613
$p \bar{p} \pi^-$ or c.c.	$(2.48 \pm 0.17) \times 10^{-4}$	-	$\gamma K_S^0 K^+ \pi^- + c.c.$	$(2.6 \pm 0.5) \times 10^{-4}$			1753
$p \bar{p} \pi^- \pi^0$	$(3.2 \pm 0.7) \times 10^{-4}$	1492	$\gamma K^+ K^- \pi^+ \pi^-$	$(1.9 \pm 0.5) \times 10^{-4}$			1726
$\Lambda \bar{\Lambda}$	$(3.81 \pm 0.13) \times 10^{-4}$	S=1.4 1467	$\gamma K^+ K^- 2(\pi^+ \pi^-)$	$< 2.2 \times 10^{-4}$	CL=90%		1654
$\Lambda \bar{\Lambda} \pi^0$	$< 2.9 \times 10^{-6}$	CL=90% 1412	$\gamma 2(K^+ K^-)$	$< 4 \times 10^{-5}$	CL=90%		1499
$\Lambda \bar{\Lambda} \eta$	$(2.5 \pm 0.4) \times 10^{-5}$	1197	$\gamma \rho \bar{\rho}$	$(3.9 \pm 0.5) \times 10^{-5}$	S=2.0		1586
$\Lambda \bar{\Lambda} \pi^+ \pi^-$	$(2.8 \pm 0.6) \times 10^{-4}$	1346	$\gamma f_2(1950) \rightarrow \gamma p \bar{p}$	$(1.20 \pm 0.22) \times 10^{-5}$			-
$\Lambda \bar{p} K^+$	$(1.00 \pm 0.14) \times 10^{-4}$	1327	$\gamma f_2(2150) \rightarrow \gamma p \bar{p}$	$(7.2 \pm 1.8) \times 10^{-6}$			-
$\Lambda \bar{p} K^*(892)^+ + c.c.$	$(6.3 \pm 0.7) \times 10^{-5}$	1087	$\gamma X(1835) \rightarrow \gamma p \bar{p}$	$(4.6 \pm_{-4.0}^{+1.8}) \times 10^{-6}$			-
$\Lambda \bar{p} K^+ \pi^+ \pi^-$	$(1.8 \pm 0.4) \times 10^{-4}$	1167	$\gamma X \rightarrow \gamma \rho \bar{\rho}$	$[oaaa] < 2 \times 10^{-6}$	CL=90%		-
$\bar{\Lambda} n K_S^0 + c.c.$	$(8.1 \pm 1.8) \times 10^{-5}$	1324	$\gamma p \bar{p} \pi^+ \pi^-$	$(2.8 \pm 1.4) \times 10^{-5}$			1491
$\Delta^{++} \bar{\Delta}^{--}$	$(1.28 \pm 0.35) \times 10^{-4}$	1371	$\gamma \gamma$	$< 1.5 \times 10^{-4}$	CL=90%		1843
$\Lambda \bar{\Sigma}^+ \pi^- + c.c.$	$(1.40 \pm 0.13) \times 10^{-4}$	1376	$\gamma \gamma J/\psi$	$(3.1 \pm_{-1.2}^{+1.0}) \times 10^{-4}$			542
$\Lambda \bar{\Sigma}^- \pi^+ + c.c.$	$(1.54 \pm 0.14) \times 10^{-4}$	1379	$e^+ e^- \eta'$	$(1.90 \pm 0.26) \times 10^{-6}$			1719
$\Lambda \bar{\Sigma}^0 + c.c.$	$(1.6 \pm 0.7) \times 10^{-6}$	1437	$e^+ e^- \chi_{c0}(1P)$	$(1.06 \pm 0.24) \times 10^{-3}$			261
$\Sigma^0 \bar{p} K^+ + c.c.$	$(1.67 \pm 0.18) \times 10^{-5}$	1291	$e^+ e^- \chi_{c1}(1P)$	$(8.5 \pm 0.6) \times 10^{-4}$			171
$\Sigma^+ \bar{\Sigma}^-$	$(2.43 \pm 0.10) \times 10^{-4}$	S=1.4 1408	$e^+ e^- \chi_{c2}(1P)$	$(7.0 \pm 0.8) \times 10^{-4}$			128
$\Sigma^0 \bar{\Sigma}^0$	$(2.35 \pm 0.09) \times 10^{-4}$	S=1.1 1405	Weak decays				
$\Sigma(1385)^+ \bar{\Sigma}(1385)^-$	$(8.5 \pm 0.7) \times 10^{-5}$	1218	$D^0 e^+ e^- + c.c.$	$< 1.4 \times 10^{-7}$	CL=90%		1371
$\Sigma(1385)^0 \bar{\Sigma}(1385)^0$	$(8.5 \pm 0.8) \times 10^{-5}$	1218	Other decays				
$\Xi^- \bar{\Xi}^+$	$(2.87 \pm 0.11) \times 10^{-4}$	S=1.1 1284	invisible	$< 1.6 \%$	CL=90%		-
$\Xi^0 \bar{\Xi}^0$	$(2.3 \pm 0.4) \times 10^{-4}$	S=4.2 1291	$\psi(3770)$				
$\Xi(1530)^0 \bar{\Xi}(1530)^0$	$(6.8 \pm 0.4) \times 10^{-5}$	1025	$J^{PC} = 0^-(1^{--})$				
$\Lambda \Xi^+ K^- + c.c.$	$(3.9 \pm 0.4) \times 10^{-5}$	1114	Mass $m = 3773.7 \pm 0.4$ MeV (S = 1.4)				
$\Xi(1530)^- \bar{\Xi}(1530)^+$	$(1.15 \pm 0.07) \times 10^{-4}$	1025	Full width $\Gamma = 27.2 \pm 1.0$ MeV				
$\Xi(1530)^- \bar{\Xi}^+$	$(7.0 \pm 1.2) \times 10^{-6}$	1165	$\psi(3770)$ DECAY MODES				
$\Xi(1530)^0 \bar{\Xi}^0$	$(5.3 \pm 0.5) \times 10^{-6}$	1169	Fraction (Γ_i/Γ)	Scale factor/ Confidence level	p (MeV/c)		
$\Xi(1690)^- \bar{\Xi}^+ \rightarrow K^- \Lambda \Xi^+ + c.c.$	$(5.2 \pm 1.6) \times 10^{-6}$	-	$D \bar{D}$	$(93 \pm_8^+)$ %	S=2.0	287	
$\Xi(1820)^- \bar{\Xi}^+ \rightarrow K^- \Lambda \Xi^+ + c.c.$	$(1.20 \pm 0.32) \times 10^{-5}$	-	$D^0 \bar{D}^0$	$(52 \pm_5^+)$ %	S=2.0	287	
$\Sigma^0 \bar{\Xi}^+ K^- + c.c.$	$(3.7 \pm 0.4) \times 10^{-5}$	1060	$D^+ D^-$	(41 ± 4) %	S=2.0	254	
$\Omega^- \bar{\Omega}^+$	$(5.66 \pm 0.30) \times 10^{-5}$	S=1.3 774	$J/\psi X$	$(5.0 \pm 2.2) \times 10^{-3}$		-	
$\eta_c \pi^+ \pi^- \pi^0$	$< 1.0 \times 10^{-3}$	CL=90% 512	$J/\psi \pi^+ \pi^-$	$(1.93 \pm 0.28) \times 10^{-3}$		561	
$h_c(1P) \pi^0$	$(8.6 \pm 1.3) \times 10^{-4}$	85	$J/\psi \pi^0 \pi^0$	$(8.0 \pm 3.0) \times 10^{-4}$		565	
$\Lambda_c^+ \bar{p} e^+ e^- + c.c.$	$< 1.7 \times 10^{-6}$	CL=90% 830	$J/\psi \eta$	$(9 \pm 4) \times 10^{-4}$		361	
$\Theta(1540) \bar{\Theta}(1540) \rightarrow K_S^0 p K^- \bar{\pi} + c.c.$	$[iiaa] < 8.8 \times 10^{-6}$	CL=90%	$J/\psi \pi^0$	$< 2.8 \times 10^{-4}$	CL=90%	604	
			$e^+ e^-$	$(9.6 \pm 0.7) \times 10^{-6}$	S=1.3	1887	

Meson Summary Table

Decays to light hadrons			
$b_1(1235)\pi$	< 1.4	$\times 10^{-5}$	CL=90% 1684
$\phi\eta'$	< 7	$\times 10^{-4}$	CL=90% 1607
$\omega\eta'$	< 4	$\times 10^{-4}$	CL=90% 1672
$\rho^0\eta'$	< 6	$\times 10^{-4}$	CL=90% 1674
$\phi\eta$	(3.1 \pm 0.7)	$\times 10^{-4}$	1703
$\omega\eta$	< 1.4	$\times 10^{-5}$	CL=90% 1762
$\rho^0\eta$	< 5	$\times 10^{-4}$	CL=90% 1764
$\phi\pi^0$	< 3	$\times 10^{-5}$	CL=90% 1746
$\omega\pi^0$	< 6	$\times 10^{-4}$	CL=90% 1803
$\pi^+\pi^-\pi^0$	< 5	$\times 10^{-6}$	CL=90% 1874
$\rho\pi$	< 5	$\times 10^{-6}$	CL=90% 1805
$K^*(892)^+K^- + c.c.$	< 1.4	$\times 10^{-5}$	CL=90% 1745
$K^*(892)^0\bar{K}^0 + c.c.$	< 1.2	$\times 10^{-3}$	CL=90% 1745
$K_S^0 K_L^0$	< 1.2	$\times 10^{-5}$	CL=90% 1820
$2(\pi^+\pi^-)$	< 1.12	$\times 10^{-3}$	CL=90% 1861
$2(\pi^+\pi^-)\pi^0$	< 1.06	$\times 10^{-3}$	CL=90% 1844
$2(\pi^+\pi^-\pi^0)$	< 5.85	%	CL=90% 1821
$\omega\pi^+\pi^-$	< 6.0	$\times 10^{-4}$	CL=90% 1794
$3(\pi^+\pi^-)$	< 9.1	$\times 10^{-3}$	CL=90% 1820
$3(\pi^+\pi^-)\pi^0$	< 1.37	%	CL=90% 1792
$3(\pi^+\pi^-)2\pi^0$	< 11.74	%	CL=90% 1760
$\eta\pi^+\pi^-$	< 1.24	$\times 10^{-3}$	CL=90% 1836
$\pi^+\pi^-2\pi^0$	< 8.9	$\times 10^{-3}$	CL=90% 1862
$\rho^0\pi^+\pi^-$	< 6.9	$\times 10^{-3}$	CL=90% 1796
$\eta3\pi$	< 1.34	$\times 10^{-3}$	CL=90% 1824
$\eta2(\pi^+\pi^-)$	< 2.43	%	CL=90% 1804
$\eta\rho^0\pi^+\pi^-$	< 1.45	%	CL=90% 1708
$\eta'3\pi$	< 2.44	$\times 10^{-3}$	CL=90% 1741
$K^+K^-\pi^+\pi^-$	< 9.0	$\times 10^{-4}$	CL=90% 1773
$\phi\pi^+\pi^-$	< 4.1	$\times 10^{-4}$	CL=90% 1737
$K^+K^-2\pi^0$	< 4.2	$\times 10^{-3}$	CL=90% 1774
$4(\pi^+\pi^-)$	< 1.67	%	CL=90% 1757
$4(\pi^+\pi^-)\pi^0$	< 3.06	%	CL=90% 1720
$\phi f_0(980)$	< 4.5	$\times 10^{-4}$	CL=90% 1597
$K^+K^-\pi^+\pi^-\pi^0$	< 2.36	$\times 10^{-3}$	CL=90% 1741
$K^+K^-\rho^0\pi^0$	< 8	$\times 10^{-4}$	CL=90% 1624
$K^+K^-\rho^+\pi^-$	< 1.46	%	CL=90% 1623
ωK^+K^-	< 3.4	$\times 10^{-4}$	CL=90% 1664
$\phi\pi^+\pi^-\pi^0$	< 3.8	$\times 10^{-3}$	CL=90% 1723
$K^{*0}K^-\pi^+\pi^0 + c.c.$	< 1.62	%	CL=90% 1694
$K^{*+}K^-\pi^+\pi^- + c.c.$	< 3.23	%	CL=90% 1693
$K^+K^-\pi^+\pi^-2\pi^0$	< 2.67	%	CL=90% 1705
$K^+K^-2(\pi^+\pi^-)$	< 1.03	%	CL=90% 1702
$K^+K^-2(\pi^+\pi^-)\pi^0$	< 3.60	%	CL=90% 1661
ηK^+K^-	< 4.1	$\times 10^{-4}$	CL=90% 1712
$\eta K^+K^-\pi^+\pi^-$	< 1.24	%	CL=90% 1624
$\rho^0 K^+K^-$	< 5.0	$\times 10^{-3}$	CL=90% 1666
$2(K^+K^-)$	< 6.0	$\times 10^{-4}$	CL=90% 1552
ϕK^+K^-	< 7.5	$\times 10^{-4}$	CL=90% 1598
$2(K^+K^-)\pi^0$	< 2.9	$\times 10^{-4}$	CL=90% 1494
$2(K^+K^-)\pi^+\pi^-$	< 3.2	$\times 10^{-3}$	CL=90% 1426
$K_S^0 K^-\pi^+$	< 3.2	$\times 10^{-3}$	CL=90% 1799
$K_S^0 K^-\pi^+\pi^0$	< 1.33	%	CL=90% 1773
$K_S^0 K^-\rho^+$	< 6.6	$\times 10^{-3}$	CL=90% 1665
$K_S^0 K^-2\pi^+\pi^-$	< 8.7	$\times 10^{-3}$	CL=90% 1740
$K_S^0 K^-\pi^+\rho^0$	< 1.6	%	CL=90% 1621
$K_S^0 K^-\pi^+\eta$	< 1.3	%	CL=90% 1670
$K_S^0 K^-2\pi^+\pi^-\pi^0$	< 4.18	%	CL=90% 1703
$K_S^0 K^-2\pi^+\pi^-\eta$	< 4.8	%	CL=90% 1570
$K_S^0 K^-\pi^+2(\pi^+\pi^-)$	< 1.22	%	CL=90% 1658
$K_S^0 K^-\pi^+2\pi^0$	< 2.65	%	CL=90% 1742
$K_S^0 K^-K^+K^-\pi^+$	< 4.9	$\times 10^{-3}$	CL=90% 1491
$K_S^0 K^-K^+K^-\pi^+\pi^0$	< 3.0	%	CL=90% 1427
$K_S^0 K^-K^+K^-\pi^+\eta$	< 2.2	%	CL=90% 1214
$K^{*0}K^-\pi^+ + c.c.$	< 9.7	$\times 10^{-3}$	CL=90% 1722
$\rho\bar{\rho}\pi^0$	< 4	$\times 10^{-5}$	CL=90% 1595
$\rho\bar{\rho}\pi^+\pi^-$	< 5.8	$\times 10^{-4}$	CL=90% 1544
$\Lambda\bar{\Lambda}$	< 1.2	$\times 10^{-4}$	CL=90% 1522
$\rho\bar{\rho}\pi^+\pi^-\pi^0$	< 1.85	$\times 10^{-3}$	CL=90% 1490
$\omega\bar{\rho}\bar{\rho}$	< 2.9	$\times 10^{-4}$	CL=90% 1310
$\Lambda\bar{\Lambda}\pi^0$	< 7	$\times 10^{-5}$	CL=90% 1469
$\rho\bar{\rho}2(\pi^+\pi^-)$	< 2.6	$\times 10^{-3}$	CL=90% 1426
$\eta\rho\bar{\rho}$	< 5.4	$\times 10^{-4}$	CL=90% 1431
$\eta\rho\bar{\rho}\pi^+\pi^-$	< 3.3	$\times 10^{-3}$	CL=90% 1284
$\rho^0\rho\bar{\rho}$	< 1.7	$\times 10^{-3}$	CL=90% 1314

$\rho\bar{\rho}K^+K^-$	< 3.2	$\times 10^{-4}$	CL=90% 1186
$\eta\rho\bar{\rho}K^+K^-$	< 6.9	$\times 10^{-3}$	CL=90% 737
$\pi^0\rho\bar{\rho}K^+K^-$	< 1.2	$\times 10^{-3}$	CL=90% 1094
$\phi\rho\bar{\rho}$	< 1.3	$\times 10^{-4}$	CL=90% 1178
$\Lambda\bar{\Lambda}\pi^+\pi^-$	< 2.5	$\times 10^{-4}$	CL=90% 1405
$\Lambda\bar{\rho}K^+$	< 2.8	$\times 10^{-4}$	CL=90% 1387
$\Lambda\bar{\rho}K^+\pi^+\pi^-$	< 6.3	$\times 10^{-4}$	CL=90% 1234
$\Lambda\bar{\Lambda}\eta$	< 1.9	$\times 10^{-4}$	CL=90% 1263
$\Sigma^+\Sigma^-$	< 1.0	$\times 10^{-4}$	CL=90% 1465
$\Sigma^0\Sigma^0$	< 4	$\times 10^{-5}$	CL=90% 1462
$\Xi^+\Xi^-$	< 1.5	$\times 10^{-4}$	CL=90% 1347
$\Xi^0\Xi^0$	< 1.4	$\times 10^{-4}$	CL=90% 1353

Radiative decays

$\gamma\chi_{c2}$	< 6.4	$\times 10^{-4}$	CL=90% 211
$\gamma\chi_{c1}$	(2.49 \pm 0.23)	$\times 10^{-3}$	254
$\gamma\chi_{c0}$	(6.9 \pm 0.6)	$\times 10^{-3}$	342
$\gamma\eta_c$	< 7	$\times 10^{-4}$	CL=90% 707
$\gamma\eta_c(2S)$	< 9	$\times 10^{-4}$	CL=90% 134
$\gamma\eta'$	< 1.8	$\times 10^{-4}$	CL=90% 1765
$\gamma\eta$	< 1.5	$\times 10^{-4}$	CL=90% 1847
$\gamma\pi^0$	< 2	$\times 10^{-4}$	CL=90% 1884

 $\psi_2(3823)$

$$J^G(J^{PC}) = 0^-(2^{--})$$

I, J, P need confirmation.

was $\psi(3823), X(3823)$

$$\text{Mass } m = 3823.7 \pm 0.5 \text{ MeV } (S = 1.1)$$

$$\text{Full width } \Gamma < 5.2 \text{ MeV, CL} = 90\%$$

Branching fractions are given relative to the one DEFINED AS 1.

$\psi_2(3823)$ DECAY MODES	Fraction (Γ_i/Γ)	Confidence level	ρ (MeV/c)
$J/\psi(1S)\pi^+\pi^-$	< 0.06	90%	607
$J/\psi(1S)\pi^0\pi^0$	< 0.11	90%	610
$J/\psi(1S)\pi^0$	< 0.030	90%	646
$J/\psi(1S)\eta$	< 0.14	90%	431
$\chi_{c0}\gamma$	< 0.24	90%	387
$\chi_{c1}\gamma$	DEFINED AS 1		300
$\chi_{c2}\gamma$	0.28 $^{+0.14}_{-0.11}$		258

 $\psi_3(3842)$

$$J^G(J^{PC}) = 0^-(3^{--})$$

J, P need confirmation.

Seen by a single experiment only.

$$\text{Mass } m = 3842.71 \pm 0.20 \text{ MeV}$$

$$\text{Full width } \Gamma = 2.8 \pm 0.6 \text{ MeV}$$

$\psi_3(3842)$ DECAY MODES	Fraction (Γ_i/Γ)	ρ (MeV/c)
D^+D^-	seen	443
$D^0\bar{D}^0$	seen	463

 $\chi_{c1}(3872)$

$$J^G(J^{PC}) = 0^+(1^{++})$$

also known as $X(3872)$

$$\text{Mass } m = 3871.65 \pm 0.06 \text{ MeV}$$

$$m_{\chi_{c1}(3872)} - m_{J/\psi} = 775 \pm 4 \text{ MeV}$$

$$\text{Full width } \Gamma = 1.19 \pm 0.21 \text{ MeV } (S = 1.1)$$

$\chi_{c1}(3872)$ DECAY MODES	Fraction (Γ_i/Γ)	Confidence level	ρ (MeV/c)
e^+e^-	< 2.8	$\times 10^{-6}$	90% 1936
$\pi^+\pi^-J/\psi(1S)$	(3.8 \pm 1.2) %		650
$\pi^+\pi^-\pi^0J/\psi(1S)$	not seen		588
$\omega\eta_c(1S)$	< 33	%	90% 368
$\omega J/\psi(1S)$	(4.3 \pm 2.1) %		†
$\phi\phi$	not seen		1646
$D^0\bar{D}^0\pi^0$	(49 $^{+18}_{-20}$) %		116
$\bar{D}^{*0}D^0$	(37 \pm 9) %		†
$\gamma\gamma$	< 11	%	90% 1936
$D^0\bar{D}^0$	< 29	%	90% 519
D^+D^-	< 19	%	90% 502
$\pi^0\chi_{c2}$	< 4	%	90% 273
$\pi^0\chi_{c1}$	(3.4 \pm 1.6) %		319
$\pi^0\chi_{c0}$	< 70	%	90% -

Meson Summary Table

$\pi^+ \pi^- \eta_c(1S)$	< 14	%	90%	745
$\pi^+ \pi^- \chi_{c1}$	< 7	$\times 10^{-3}$	90%	218
$\rho \bar{\rho}$	< 2.4	$\times 10^{-5}$	95%	1693

Radiative decays

$\gamma D^+ D^-$	< 4	%	90%	502
$\gamma \bar{D}^0 D^0$	< 6	%	90%	519
$\gamma J/\psi$	$(8 \pm 4) \times 10^{-3}$			697
$\gamma \chi_{c1}$	< 9	$\times 10^{-3}$	90%	344
$\gamma \chi_{c2}$	< 3.2	%	90%	303
$\gamma \psi(2S)$	(4.5 ± 2.0)	%		181

C-violating decays

$\eta J/\psi$	< 1.8	%	90%	491
---------------	-------	---	-----	-----

Z_c(3900)

$$I^G(J^{PC}) = 1^+(1^-)$$

was X(3900)

Mass $m = 3887.1 \pm 2.6$ MeV (S = 1.7)
Full width $\Gamma = 28.4 \pm 2.6$ MeV

Z _c (3900) DECAY MODES	Fraction (Γ_i/Γ)	ρ (MeV/c)
$J/\psi \pi$	seen	699
$h_c \pi^\pm$	not seen	318
$\eta_c \pi^+ \pi^-$	not seen	759
$(D \bar{D}^*)^\pm$	seen	—
$D^0 D^{*-} + c.c.$	seen	152
$D^- D^{*0} + c.c.$	seen	143
$\omega \pi^\pm$	not seen	1862
$J/\psi \eta$	not seen	510
$D^+ D^{*-} + c.c.$	seen	—
$D^0 \bar{D}^{*0} + c.c.$	seen	—

χ_{c0}(3915)

$$I^G(J^{PC}) = 0^+(0^{++})$$

was X(3915)

Mass $m = 3921.7 \pm 1.8$ MeV (S = 1.5)
Full width $\Gamma = 18.8 \pm 3.5$ MeV

χ _{c0} (3915) DECAY MODES	Fraction (Γ_i/Γ)	ρ (MeV/c)
$\omega J/\psi$	seen	231
$\bar{D}^{*0} D^0$	not seen	312
$D^+ D^-$	seen	591
$\pi^+ \pi^- \eta_c(1S)$	not seen	788
$\eta_c \eta$	not seen	668
$\eta_c \pi^0$	not seen	817
$K \bar{K}$	not seen	1898
$\gamma \gamma$	seen	1961
$\pi^0 \chi_{c1}$	not seen	368

χ_{c2}(3930)

$$I^G(J^{PC}) = 0^+(2^{++})$$

Mass $m = 3922.5 \pm 1.0$ MeV (S = 1.7)
Full width $\Gamma = 35.2 \pm 2.2$ MeV (S = 1.2)

χ _{c2} (3930) DECAY MODES	Fraction (Γ_i/Γ)	ρ (MeV/c)
$\gamma \gamma$	seen	1961
$D \bar{D}$	seen	607
$D^+ D^-$	seen	592
$D^0 \bar{D}^0$	seen	607
$\pi^+ \pi^- \eta_c(1S)$	not seen	788
$K \bar{K}$	not seen	1898

X(4020)[±]

$$I^G(J^{PC}) = 1^+(?^{?})$$

Mass $m = 4024.1 \pm 1.9$ MeV
Full width $\Gamma = 13 \pm 5$ MeV (S = 1.7)

X(4020) [±] DECAY MODES	Fraction (Γ_i/Γ)	ρ (MeV/c)
$h_c(1P) \pi$	seen	450
$D^* \bar{D}^*$	seen	85

$D \bar{D}^* + c.c.$	not seen	542
$\eta_c \pi^+ \pi^-$	not seen	872
$J/\psi(1S) \pi^\pm$	not seen	811

ψ(4040) [ppaa]

$$I^G(J^{PC}) = 0^-(1^{--})$$

Mass $m = 4039 \pm 1$ MeV
Full width $\Gamma = 80 \pm 10$ MeV

Due to the complexity of the $c\bar{c}$ threshold region, in this listing, "seen" ("not seen") means that a cross section for the mode in question has been measured at effective \sqrt{s} near this particle's central mass value, more (less) than 2σ above zero, without regard to any peaking behavior in \sqrt{s} or absence thereof. See mode listing(s) for details and references.

ψ(4040) DECAY MODES	Fraction (Γ_i/Γ)	Confidence level	ρ (MeV/c)
$e^+ e^-$	$(1.07 \pm 0.16) \times 10^{-5}$		2019
$D \bar{D}$	seen		775
$D^0 \bar{D}^0$	seen		775
$D^+ D^-$	seen		763
$D^* \bar{D}^* + c.c.$	seen		569
$D^*(2007)^0 \bar{D}^0 + c.c.$	seen		575
$D^*(2010)^+ D^- + c.c.$	seen		561
$D^* \bar{D}^*$	seen		193
$D^*(2007)^0 \bar{D}^*(2007)^0$	seen		226
$D^*(2010)^+ D^*(2010)^-$	seen		193
$D^0 D^- \pi^+ + c.c. (excl.)$	not seen		—
$D^*(2007)^0 \bar{D}^0 + c.c.$			
$D^*(2010)^+ D^- + c.c.$			
$D \bar{D}^* \pi (excl. D^* \bar{D}^*)$	not seen		—
$D^0 \bar{D}^{*-} \pi^+ + c.c. (excl.)$	seen		—
$D^*(2010)^+ D^*(2010)^-$			
$D_s^+ D_s^-$	seen		452
$J/\psi \pi^+ \pi^-$	< 4	$\times 10^{-3}$	90%
$J/\psi \pi^0 \pi^0$	< 2	$\times 10^{-3}$	90%
$J/\psi \eta$	$(5.2 \pm 0.7) \times 10^{-3}$		675
$J/\psi \pi^0$	< 2.8	$\times 10^{-4}$	90%
$J/\psi \pi^+ \pi^- \pi^0$	< 2	$\times 10^{-3}$	90%
$\chi_{c1} \gamma$	< 3.4	$\times 10^{-3}$	90%
$\chi_{c2} \gamma$	< 5	$\times 10^{-3}$	90%
$\chi_{c1} \pi^+ \pi^- \pi^0$	< 1.1	%	90%
$\chi_{c2} \pi^+ \pi^- \pi^0$	< 3.2	%	90%
$h_c(1P) \pi^+ \pi^-$	< 3	$\times 10^{-3}$	90%
$\phi \pi^+ \pi^-$	< 3	$\times 10^{-3}$	90%
$\Lambda \bar{\Lambda} \pi^+ \pi^-$	< 2.9	$\times 10^{-4}$	90%
$\Lambda \bar{\Lambda} \pi^0$	< 9	$\times 10^{-5}$	90%
$\Lambda \bar{\Lambda} \eta$	< 3.0	$\times 10^{-4}$	90%
$\Lambda \bar{\Lambda}$	< 6	$\times 10^{-6}$	90%
$\Sigma^+ \bar{\Sigma}^-$	< 1.3	$\times 10^{-4}$	90%
$\Sigma^0 \bar{\Sigma}^0$	< 7	$\times 10^{-5}$	90%
$\Xi^+ \bar{\Xi}^-$	< 1.6	$\times 10^{-4}$	90%
$\Xi^0 \bar{\Xi}^0$	< 1.8	$\times 10^{-4}$	90%
$\mu^+ \mu^-$	$(9 \pm 6) \times 10^{-6}$		2017

χ_{c1}(4140)

$$I^G(J^{PC}) = 0^+(1^{++})$$

was X(4140)

Mass $m = 4146.5 \pm 3.0$ MeV (S = 1.3)
Full width $\Gamma = 19_{-5}^{+7}$ MeV

χ _{c1} (4140) DECAY MODES	Fraction (Γ_i/Γ)	ρ (MeV/c)
$J/\psi \phi$	seen	216
$\gamma \gamma$	not seen	2073

ψ(4160) [ppaa]

$$I^G(J^{PC}) = 0^-(1^{--})$$

Mass $m = 4191 \pm 5$ MeV
Full width $\Gamma = 70 \pm 10$ MeV

Due to the complexity of the $c\bar{c}$ threshold region, in this listing, "seen" ("not seen") means that a cross section for the mode in question has been measured at effective \sqrt{s} near this particle's central mass value, more (less) than 2σ above zero, without regard to any peaking behavior in \sqrt{s} or absence thereof. See mode listing(s) for details and references.

Meson Summary Table

$\psi(4160)$ DECAY MODES	Fraction (Γ_i/Γ)	Confidence level	ρ (MeV/c)
e^+e^-	$(6.9 \pm 3.3) \times 10^{-6}$		2096
$\mu^+\mu^-$	seen		2093
$D\bar{D}$	seen		956
$D^0\bar{D}^0$	seen		956
D^+D^-	seen		947
$D^*\bar{D}^+$ + c.c.	seen		798
$D^*(2007)^0\bar{D}^0$ + c.c.	seen		802
$D^*(2010)^+D^-$ + c.c.	seen		792
$D^*\bar{D}^*$	seen		592
$D^*(2007)^0\bar{D}^*(2007)^0$	seen		604
$D^*(2010)^+D^*(2010)^-$	seen		592
$D^0D^-\pi^+$ + c.c. (excl. $D^*(2007)^0\bar{D}^0$ + c.c., $D^*(2010)^+D^-$ + c.c.)	not seen		—
$D\bar{D}^*\pi$ + c.c. (excl. $D^*\bar{D}^*$)	seen		—
$D^0D^*\pi^-$ + c.c. (excl. $D^*(2010)^+D^*(2010)^-$)	not seen		—
$D_s^+D_s^-$	not seen		719
$D_s^+D_s^-$ + c.c.	seen		385
$J/\psi\pi^+\pi^-$	$< 3 \times 10^{-3}$	90%	919
$J/\psi\pi^0\pi^0$	$< 3 \times 10^{-3}$	90%	922
$J/\psi K^+K^-$	$< 2 \times 10^{-3}$	90%	407
$J/\psi\eta$	$< 8 \times 10^{-3}$	90%	822
$J/\psi\pi^0$	$< 1 \times 10^{-3}$	90%	944
$J/\psi\eta'$	$< 5 \times 10^{-3}$	90%	457
$J/\psi\pi^+\pi^-\pi^0$	$< 1 \times 10^{-3}$	90%	879
$\psi(2S)\pi^+\pi^-$	$< 4 \times 10^{-3}$	90%	396
$\chi_{c1}\gamma$	$< 5 \times 10^{-3}$	90%	625
$\chi_{c2}\gamma$	$< 1.3\%$	90%	587
$\chi_{c1}\pi^+\pi^-\pi^0$	$< 2 \times 10^{-3}$	90%	496
$\chi_{c2}\pi^+\pi^-\pi^0$	$< 8 \times 10^{-3}$	90%	445
$h_c(1P)\pi^+\pi^-$	$< 5 \times 10^{-3}$	90%	556
$h_c(1P)\pi^0\pi^0$	$< 2 \times 10^{-3}$	90%	560
$h_c(1P)\eta$	$< 2 \times 10^{-3}$	90%	348
$h_c(1P)\pi^0$	$< 4 \times 10^{-4}$	90%	600
$\phi\pi^+\pi^-$	$< 2 \times 10^{-3}$	90%	1961
$\gamma\chi_{c1}(3872)$	$< 1.8 \times 10^{-3}$	90%	308
$\gamma\chi_{c0}(3915) \rightarrow \gamma J/\psi\pi^+\pi^-$	$< 1.36 \times 10^{-4}$	90%	—
$\gamma X(3930) \rightarrow \gamma J/\psi\pi^+\pi^-$	$< 1.18 \times 10^{-4}$	90%	—
$\gamma X(3940) \rightarrow \gamma J/\psi\pi^+\pi^-$	$< 1.47 \times 10^{-4}$	90%	—
$\gamma\chi_{c0}(3915) \rightarrow \gamma\gamma J/\psi$	$< 1.26 \times 10^{-4}$	90%	—
$\gamma X(3930) \rightarrow \gamma\gamma J/\psi$	$< 8.8 \times 10^{-5}$	90%	—
$\gamma X(3940) \rightarrow \gamma\gamma J/\psi$	$< 1.79 \times 10^{-4}$	90%	—
$\rho\bar{\rho}\rho\bar{\rho}$	not seen		834
$\Lambda\bar{\Lambda}$	$< 1.5 \times 10^{-6}$	90%	1774

 $\psi(4230)$

$$I^G(J^{PC}) = 0^-(1^{--})$$

also known as $Y(4230)$; was $\psi(4260)$

Mass $m = 4222.7 \pm 2.6$ MeV ($S = 1.7$)

Full width $\Gamma = 49 \pm 8$ MeV ($S = 3.5$)

$\psi(4230)$ DECAY MODES	Fraction (Γ_i/Γ)	ρ (MeV/c)
$\mu^+\mu^-$	$(3.1 \pm 2.8) \times 10^{-5}$	2107
$\eta_c(1S)\pi^+\pi^-$	not seen	1027
$\eta_c(1S)\pi^+\pi^-\pi^0$	seen	992
$J/\psi\pi^+\pi^-$	seen	942
$J/\psi f_0(980), f_0(980) \rightarrow \pi^+\pi^-$	seen	—
$Z_c(3900)^\pm\pi^\mp, Z_c^\pm \rightarrow J/\psi\pi^\pm$	seen	—
$J/\psi\pi^0\pi^0$	seen	944
$J/\psi K^+K^-$	seen	460
$J/\psi K_S^0 K_S^0$	not seen	447
$J/\psi\eta$	seen	848
$J/\psi\pi^0$	not seen	966
$J/\psi\eta'$	seen	504
$J/\psi\pi^+\pi^-\pi^0$	not seen	904
$J/\psi\eta\pi^0$	not seen	770
$J/\psi\eta\eta$	not seen	211
$\psi(2S)\pi^+\pi^-$	seen	426
$\psi(2S)\eta$	not seen	†
$\chi_{c0}\omega$	seen	171
$\chi_{c1}\pi^+\pi^-\pi^0$	not seen	527

$\chi_{c2}\pi^+\pi^-\pi^0$	not seen	477
$h_c(1P)\pi^+\pi^-$	seen	583
$\phi\pi^+\pi^-$	not seen	1976
$\phi f_0(980) \rightarrow \phi\pi^+\pi^-$	not seen	—
$D\bar{D}$	not seen	987
$D^0\bar{D}^0$	not seen	987
D^+D^-	not seen	978
$D^*\bar{D}^+$ + c.c.	not seen	887
$D^*(2007)^0\bar{D}^0$ + c.c.	not seen	—
$D^*(2010)^+D^-$ + c.c.	not seen	—
$D^*(2007)^0\bar{D}^*(2007)^0$	not seen	652
$D^*(2010)^+D^*(2010)^-$	not seen	641
$D^0D^-\pi^+$ + c.c. (excl. $D^*(2007)^0\bar{D}^0$ + c.c., $D^*(2010)^+D^-$ + c.c.)	not seen	—
$D\bar{D}^*\pi$ + c.c. (excl. $D^*\bar{D}^*$)	not seen	723
$D^0D^*\pi^-$ + c.c. (excl. $D^*(2010)^+D^*(2010)^-$)	not seen	—
$D^0D^*(2010)^-\pi^+$ + c.c.	seen	716
$D_1(2420)\bar{D}^+$ + c.c.	not seen	†
$D^*\bar{D}^*\pi$	not seen	367
$D_s^+D_s^-$	not seen	760
$D_s^+D_s^-$ + c.c.	not seen	615
$D_s^+D_s^{*-}$	not seen	†
$\rho\bar{\rho}$	not seen	1890
$\rho\bar{\rho}\pi^0$	not seen	1854
$\rho\bar{\rho}\eta$	not seen	1712
$\rho\bar{\rho}\omega$	not seen	1610
$\Xi^-\Xi^+$	not seen	1645
$\pi^+\pi^+\pi^-\pi^-$	not seen	2087
$\pi^+\pi^+\pi^-\pi^-\pi^0$	not seen	2071
$K_S^0 K^\pm\pi^\mp$	not seen	2032
$K_S^0 K^\pm\pi^\mp\pi^0$	not seen	2009
$K_S^0 K^\pm\pi^\mp\eta$	not seen	1917
$K^+K^-\pi^0$	not seen	2033
$K^+K^-\pi^+\pi^-$	not seen	2008
$K^+K^-\pi^+\pi^-\pi^0$	not seen	1981
$K^+K^+K^-K^-$	not seen	1813
$K^+K^+K^-K^-\pi^0$	not seen	1762
$\rho\bar{\rho}\pi^+\pi^-$	not seen	1810
$\rho\bar{\rho}\pi^+\pi^-\pi^0$	not seen	1764
$\rho\bar{\rho}\rho\bar{\rho}$	not seen	864
$\Lambda\bar{\Lambda}$	not seen	1791
Radiative decays		
$\eta_c(1S)\gamma$	possibly seen	1055
$\eta_c(1S)\pi^0\gamma$	not seen	1049
$\chi_{c1}\gamma$	not seen	650
$\chi_{c2}\gamma$	not seen	612
$\chi_{c1}(3872)\gamma$	seen	334

 $\chi_{c1}(4274)$

$$I^G(J^{PC}) = 0^+(1^{++})$$

was $X(4274)$

Mass $m = 4286^{+8}_{-9}$ MeV ($S = 1.7$)

Full width $\Gamma = 51 \pm 7$ MeV

$\chi_{c1}(4274)$ DECAY MODES	Fraction (Γ_i/Γ)	ρ (MeV/c)
$J/\psi\phi$	seen	522

 $\psi(4360)$

$$I^G(J^{PC}) = 0^-(1^{--})$$

also known as $Y(4360)$; was $X(4360)$

$$\psi(4360) \text{ MASS} = 4372 \pm 9 \text{ MeV} \quad (S = 2.9)$$

$$\psi(4360) \text{ WIDTH} = 115 \pm 13 \text{ MeV} \quad (S = 2.2)$$

$\psi(4360)$ DECAY MODES	Fraction (Γ_i/Γ)	ρ (MeV/c)
$h_c\pi^+\pi^-$	seen	721
$\psi(2S)\pi^+\pi^-$	seen	577
$\psi(3770)\pi^+\pi^-$	possibly seen	493
$\psi_2(3823)\pi^+\pi^-$	possibly seen	442
$J/\psi\eta$	seen	981
$D_1(2420)\bar{D}^+$ + c.c.	possibly seen	426
$\rho\bar{\rho}\eta$	not seen	1805
$\rho\bar{\rho}\omega$	not seen	1707

Meson Summary Table

 $\psi(4415)$ [*ppaa*]

$$J^G(J^{PC}) = 0^-(1^{--})$$

Mass $m = 4421 \pm 4$ MeV
 Full width $\Gamma = 62 \pm 20$ MeV

Due to the complexity of the $c\bar{c}$ threshold region, in this listing, "seen" ("not seen") means that a cross section for the mode in question has been measured at effective \sqrt{s} near this particle's central mass value, more (less) than 2σ above zero, without regard to any peaking behavior in \sqrt{s} or absence thereof. See mode listing(s) for details and references.

$\psi(4415)$ DECAY MODES	Fraction (Γ_i/Γ)	Confidence level	ρ (MeV/c)
$D\bar{D}$	seen		1187
$D^0\bar{D}^0$	seen		1187
D^+D^-	seen		1179
$D^*\bar{D}^+$ c.c.	seen		1063
$D^*(2007)^0\bar{D}^0$ + c.c.	seen		1067
$D^*(2010)^+D^-$ + c.c.	seen		1059
$D^*\bar{D}^*$	seen		919
$D^*(2007)^0\bar{D}^*(2007)^0$ + c.c.	seen		927
$D^*(2010)^+D^*(2010)^-$ + c.c.	seen		919
$D^0D^-\pi^+$ (excl. $D^*(2007)^0\bar{D}^0$) + c.c., $D^*(2010)^+D^-$ + c.c.	< 2.3 %	90%	-
$D\bar{D}_2^*(2460) \rightarrow D^0D^-\pi^+$ + c.c.	(10 \pm 4) %		-
$D^0\bar{D}^{*-}\pi^+$ + c.c.	< 11 %	90%	926
$D_1(2420)\bar{D}^+$ + c.c.	possibly seen		537
$D_s^+D_s^-$	not seen		1006
$\omega\chi_{c2}$	possibly seen		330
$D_s^{*+}D_s^-$ + c.c.	seen		-
$D_s^+D_s^{*-}$	not seen		652
$\psi_2(3823)\pi^+\pi^-$	possibly seen		492
$\psi(3770)\pi^+\pi^-$	possibly seen		541
$J/\psi\eta$	< 6 $\times 10^{-3}$	90%	1022
$\chi_{c1}\gamma$	< 8 $\times 10^{-4}$	90%	817
$\chi_{c2}\gamma$	< 4 $\times 10^{-3}$	90%	780
$\Lambda\bar{\Lambda}$	< 3.1 $\times 10^{-6}$	90%	1908
e^+e^-	(9.4 \pm 3.2) $\times 10^{-6}$		2210
$\mu^+\mu^-$	(2.0 \pm 1.0) $\times 10^{-5}$		2208

 $Z_c(4430)$

$$J^G(J^{PC}) = 1^+(1^{+-})$$

 G, C need confirmation.

was $X(4430)^\pm$

Quantum numbers not established.

Mass $m = 4478_{-18}^{+15}$ MeV
 Full width $\Gamma = 181 \pm 31$ MeV

$Z_c(4430)$ DECAY MODES	Fraction (Γ_i/Γ)	ρ (MeV/c)
$\pi^+\psi(2S)$	seen	711
π^+J/ψ	seen	1162

 $\psi(4660)$

$$J^G(J^{PC}) = 0^-(1^{--})$$

also known as $Y(4660)$; was $X(4660)$

$\psi(4660)$ MASS = 4630 ± 6 MeV ($S = 1.4$)
 $\psi(4660)$ WIDTH = 72_{-12}^{+14} MeV ($S = 1.7$)

$\psi(4660)$ DECAY MODES	Fraction (Γ_i/Γ)	ρ (MeV/c)
e^+e^-	not seen	2315
$\psi(2S)\pi^+\pi^-$	seen	809
$J/\psi\eta$	not seen	1192
$D^0D^{*-}\pi^+$	not seen	1153
$\chi_{c1}\gamma$	not seen	984
$\chi_{c2}\gamma$	not seen	949
$\Lambda_c^+\Lambda_c^-$	seen	363
$D_s^+D_{s1}(2536)^-$	seen	534

$b\bar{b}$ MESONS
 (including possibly non- $q\bar{q}$ states)

 $\eta_b(1S)$

$$J^G(J^{PC}) = 0^+(0^{-+})$$

Mass $m = 9398.7 \pm 2.0$ MeV ($S = 1.5$)
 Full width $\Gamma = 10_{-4}^{+5}$ MeV

$\eta_b(1S)$ DECAY MODES	Fraction (Γ_i/Γ)	Confidence level	ρ (MeV/c)
hadrons	seen		-
$3h^+3h^-$	not seen		4672
$2h^+2h^-$	not seen		4689
$4h^+4h^-$	not seen		4648
$\gamma\gamma$	not seen		4699
$\mu^+\mu^-$	< 9×10^{-3}	90%	4698
$\tau^+\tau^-$	< 8 %	90%	4350

 $\Upsilon(1S)$

$$J^G(J^{PC}) = 0^-(1^{--})$$

Mass $m = 9460.30 \pm 0.26$ MeV ($S = 3.3$)
 Full width $\Gamma = 54.02 \pm 1.25$ keV

$\Upsilon(1S)$ DECAY MODES	Fraction (Γ_i/Γ)	Scale factor/ Confidence level	ρ (MeV/c)
$\tau^+\tau^-$	(2.60 \pm 0.10) %		4384
e^+e^-	(2.38 \pm 0.11) %		4730
$\mu^+\mu^-$	(2.48 \pm 0.05) %		4729

Hadronic decays

ggg	(81.7 \pm 0.7) %		-
γgg	(2.2 \pm 0.6) %		-
$\eta'(958)$ anything	(2.94 \pm 0.24) %		-
$J/\psi(1S)$ anything	(5.4 \pm 0.4) $\times 10^{-4}$	$S=1.4$	4223
$J/\psi(1S)\eta_c$	< 2.2 $\times 10^{-6}$	CL=90%	3623
$J/\psi(1S)\chi_{c0}$	< 3.4 $\times 10^{-6}$	CL=90%	3429
$J/\psi(1S)\chi_{c1}$	(3.9 \pm 1.2) $\times 10^{-6}$		3382
$J/\psi(1S)\chi_{c2}$	< 1.4 $\times 10^{-6}$	CL=90%	3359
$J/\psi(1S)\eta_c(2S)$	< 2.2 $\times 10^{-6}$	CL=90%	3317
$J/\psi(1S)X(3940)$	< 5.4 $\times 10^{-6}$	CL=90%	3148
$J/\psi(1S)X(4160)$	< 5.4 $\times 10^{-6}$	CL=90%	3020
$X(4350)$ anything, $X \rightarrow J/\psi(1S)\phi$	< 8.1 $\times 10^{-6}$	CL=90%	-
$Z_c(3900)^\pm$ anything, $Z_c \rightarrow J/\psi(1S)\pi^\pm$	< 1.3 $\times 10^{-5}$	CL=90%	-
$Z_c(4200)^\pm$ anything, $Z_c \rightarrow J/\psi(1S)\pi^\pm$	< 6.0 $\times 10^{-5}$	CL=90%	-
$Z_c(4430)^\pm$ anything, $Z_c \rightarrow J/\psi(1S)\pi^\pm$	< 4.9 $\times 10^{-5}$	CL=90%	-
X_{cs}^\pm anything, $X \rightarrow J/\psi K^\pm$	< 5.7 $\times 10^{-6}$	CL=90%	-
$\psi(4230)$ anything, $\psi \rightarrow J/\psi(1S)\pi^+\pi^-$	< 3.8 $\times 10^{-5}$	CL=90%	-
$\psi(4230)$ anything, $\psi \rightarrow J/\psi(1S)K^+K^-$	< 7.5 $\times 10^{-6}$	CL=90%	-
$\chi_{c1}(4140)$ anything, $\chi_{c1} \rightarrow J/\psi(1S)\phi$	< 5.2 $\times 10^{-6}$	CL=90%	-
χ_{c0} anything	< 4 $\times 10^{-3}$	CL=90%	-
χ_{c1} anything	(1.90 \pm 0.35) $\times 10^{-4}$		-
$\chi_{c1}(1P)X_{tetra}$	< 3.78 $\times 10^{-5}$	CL=90%	-
χ_{c2} anything	(2.8 \pm 0.8) $\times 10^{-4}$		-
$\psi(2S)$ anything	(1.23 \pm 0.20) $\times 10^{-4}$		-
$\psi(2S)\eta_c$	< 3.6 $\times 10^{-6}$	CL=90%	3345
$\psi(2S)\chi_{c0}$	< 6.5 $\times 10^{-6}$	CL=90%	3124
$\psi(2S)\chi_{c1}$	< 4.5 $\times 10^{-6}$	CL=90%	3070
$\psi(2S)\chi_{c2}$	< 2.1 $\times 10^{-6}$	CL=90%	3043
$\psi(2S)\eta_c(2S)$	< 3.2 $\times 10^{-6}$	CL=90%	2994
$\psi(2S)X(3940)$	< 2.9 $\times 10^{-6}$	CL=90%	2797
$\psi(2S)X(4160)$	< 2.9 $\times 10^{-6}$	CL=90%	2645
$\psi(4230)$ anything, $\psi \rightarrow \psi(2S)\pi^+\pi^-$	< 7.9 $\times 10^{-5}$	CL=90%	-
$\psi(4360)$ anything, $\psi \rightarrow \psi(2S)\pi^+\pi^-$	< 5.2 $\times 10^{-5}$	CL=90%	-
$\psi(4660)$ anything, $\psi \rightarrow \psi(2S)\pi^+\pi^-$	< 2.2 $\times 10^{-5}$	CL=90%	-

Meson Summary Table

$X(4050)^\pm$ anything, $X \rightarrow \psi(2S)\pi^\pm$	< 8.8	$\times 10^{-5}$	CL=90%	-
$Z_c(4430)^\pm$ anything, $Z_c \rightarrow \psi(2S)\pi^\pm$	< 6.7	$\times 10^{-5}$	CL=90%	-
$\chi_{c1}(3872)$ anything	< 2.5	$\times 10^{-4}$	CL=90%	-
$Z_c(4200)^+ Z_c(4200)^-$	< 2.23	$\times 10^{-5}$	CL=90%	-
$Z_c(3900)^\pm Z_c(4200)^\mp$	< 8.1	$\times 10^{-6}$	CL=90%	-
$Z_c(3900)^+ Z_c(3900)^-$	< 1.8	$\times 10^{-6}$	CL=90%	-
$X(4050)^+ X(4050)^-$	< 1.58	$\times 10^{-5}$	CL=90%	-
$X(4250)^+ X(4250)^-$	< 2.66	$\times 10^{-5}$	CL=90%	-
$X(4050)^\pm X(4250)^\mp$	< 4.42	$\times 10^{-5}$	CL=90%	-
$Z_c(4430)^+ Z_c(4430)^-$	< 2.03	$\times 10^{-5}$	CL=90%	-
$X(4055)^\pm X(4055)^\mp$	< 2.33	$\times 10^{-5}$	CL=90%	-
$X(4055)^\pm Z_c(4430)^\mp$	< 4.55	$\times 10^{-5}$	CL=90%	-
$\rho\pi$	< 3.68	$\times 10^{-6}$	CL=90%	4697
$\omega\pi^0$	< 3.90	$\times 10^{-6}$	CL=90%	4697
$\pi^+\pi^-$	< 5	$\times 10^{-4}$	CL=90%	4728
K^+K^-	< 5	$\times 10^{-4}$	CL=90%	4704
$p\bar{p}$	< 5	$\times 10^{-4}$	CL=90%	4636
$\pi^+\pi^-\pi^0$	(2.1 \pm 0.8)	$\times 10^{-6}$		4725
ϕK^+K^-	(2.4 \pm 0.5)	$\times 10^{-6}$		4622
$\omega\pi^+\pi^-$	(4.5 \pm 1.0)	$\times 10^{-6}$		4694
$K^*(892)^0 K^-\pi^+ + c.c.$	(4.4 \pm 0.8)	$\times 10^{-6}$		4667
$\phi f_2'(1525)$	< 1.63	$\times 10^{-6}$	CL=90%	4551
$\omega f_2'(1270)$	< 1.79	$\times 10^{-6}$	CL=90%	4611
$\rho(770)\rho_2(1320)$	< 2.24	$\times 10^{-6}$	CL=90%	4605
$K^*(892)^0 K_2^*(1430)^0 + c.c.$	(3.0 \pm 0.8)	$\times 10^{-6}$		4578
$K_1(1270)^\pm K^\mp$	< 2.41	$\times 10^{-6}$	CL=90%	4634
$K_1(1400)^\pm K^\mp$	(1.0 \pm 0.4)	$\times 10^{-6}$		4613
$b_1(1235)^\pm \pi^\mp$	< 1.25	$\times 10^{-6}$	CL=90%	4649
$\pi^+\pi^-\pi^0$	(1.28 \pm 0.30)	$\times 10^{-5}$		4720
$K_S^0 K^+\pi^- + c.c.$	(1.6 \pm 0.4)	$\times 10^{-6}$		4696
$K^*(892)^0 K^+\pi^- + c.c.$	(2.9 \pm 0.9)	$\times 10^{-6}$		4675
$K^*(892)^- K^+ + c.c.$	< 1.11	$\times 10^{-6}$	CL=90%	4675
$f_1(1285)$ anything	(4.6 \pm 3.1)	$\times 10^{-3}$		-
$D^*(2010)^\pm$ anything	(2.52 \pm 0.20)	%		-
$f_1(1285) X_{tetra}$	< 6.24	$\times 10^{-5}$	CL=90%	-
2H anything	(2.85 \pm 0.25)	$\times 10^{-5}$		-
Sum of 100 exclusive modes	(1.200 \pm 0.017)	%		-
Radiative decays				
$\gamma\pi^+\pi^-$	(6.3 \pm 1.8)	$\times 10^{-5}$		4728
$\gamma\pi^0\pi^0$	(1.7 \pm 0.7)	$\times 10^{-5}$		4728
$\gamma\pi\pi$ (S-wave)	(4.6 \pm 0.7)	$\times 10^{-5}$		4728
$\gamma\pi^0\eta$	< 2.4	$\times 10^{-6}$	CL=90%	4713
γK^+K^-	[qqaa] (1.14 \pm 0.13)	$\times 10^{-5}$		4704
$\gamma p\bar{p}$	[rraa] < 6	$\times 10^{-6}$	CL=90%	4636
$\gamma 2h^+2h^-$	(7.0 \pm 1.5)	$\times 10^{-4}$		4720
$\gamma 3h^+3h^-$	(5.4 \pm 2.0)	$\times 10^{-4}$		4703
$\gamma 4h^+4h^-$	(7.4 \pm 3.5)	$\times 10^{-4}$		4679
$\gamma\pi^+\pi^-K^+K^-$	(2.9 \pm 0.9)	$\times 10^{-4}$		4686
$\gamma 2\pi^+2\pi^-$	(2.5 \pm 0.9)	$\times 10^{-4}$		4720
$\gamma 3\pi^+3\pi^-$	(2.5 \pm 1.2)	$\times 10^{-4}$		4703
$\gamma 2\pi^+2\pi^-K^+K^-$	(2.4 \pm 1.2)	$\times 10^{-4}$		4658
$\gamma\pi^+\pi^-p\bar{p}$	(1.5 \pm 0.6)	$\times 10^{-4}$		4604
$\gamma 2\pi^+2\pi^-p\bar{p}$	(4 \pm 6)	$\times 10^{-5}$		4563
$\gamma 2K^+2K^-$	(2.0 \pm 2.0)	$\times 10^{-5}$		4601
$\gamma\eta(958)$	< 1.9	$\times 10^{-6}$	CL=90%	4682
$\gamma\eta$	< 1.0	$\times 10^{-6}$	CL=90%	4714
$\gamma f_0(980)$	< 3	$\times 10^{-5}$	CL=90%	4678
$\gamma f_2'(1525)$	(2.9 \pm 0.6)	$\times 10^{-5}$		4608
$\gamma f_2(1270)$	(1.01 \pm 0.06)	$\times 10^{-4}$		4644
$\gamma\eta(1405)$	< 8.2	$\times 10^{-5}$	CL=90%	4625
$\gamma f_0(1500)$	< 1.5	$\times 10^{-5}$	CL=90%	4610
$\gamma f_0(1500) \rightarrow \gamma K^+K^-$	(1.0 \pm 0.4)	$\times 10^{-5}$		-
$\gamma f_0(1710)$	< 2.6	$\times 10^{-4}$	CL=90%	4577
$\gamma f_0(1710) \rightarrow \gamma K^+K^-$	(1.01 \pm 0.32)	$\times 10^{-5}$		-
$\gamma f_0(1710) \rightarrow \gamma\pi^+\pi^-$	(5.3 \pm 2.0)	$\times 10^{-6}$		-
$\gamma f_0(1710) \rightarrow \gamma\pi^0\pi^0$	< 1.4	$\times 10^{-6}$	CL=90%	-
$\gamma f_0(1710) \rightarrow \gamma\eta\eta$	< 1.8	$\times 10^{-6}$	CL=90%	-
$\gamma f_0(2050)$	< 5.3	$\times 10^{-5}$	CL=90%	4515
$\gamma f_0(2200) \rightarrow \gamma K^+K^-$	< 2	$\times 10^{-4}$	CL=90%	4475
$\gamma f_2(2220) \rightarrow \gamma K^+K^-$	< 8	$\times 10^{-7}$	CL=90%	4469
$\gamma f_2(2220) \rightarrow \gamma\pi^+\pi^-$	< 6	$\times 10^{-7}$	CL=90%	-
$\gamma f_2(2220) \rightarrow \gamma p\bar{p}$	< 1.1	$\times 10^{-6}$	CL=90%	-
$\gamma\eta(2225) \rightarrow \gamma\phi\phi$	< 3	$\times 10^{-3}$	CL=90%	4469
$\gamma\eta_c(1S)$	< 2.9	$\times 10^{-5}$	CL=90%	4260

$\gamma\eta_c(2S)$	< 4	$\times 10^{-4}$	CL=90%	4031
$\gamma\chi_{c0}$	< 6.6	$\times 10^{-5}$	CL=90%	4114
$\gamma\chi_{c1}$	(4.7 $^{+2.4}_{-1.9}$)	$\times 10^{-5}$		4079
$\gamma\chi_{c2}$	< 7.6	$\times 10^{-6}$	CL=90%	4062
$\gamma\chi_{c1}(3872)$	< 4	$\times 10^{-5}$	CL=90%	3938
$\gamma\chi_{c1}(3872), \chi_{c1} \rightarrow \pi^+\pi^-\pi^0 J/\psi$	< 2.8	$\times 10^{-6}$	CL=90%	-
$\gamma\chi_{c0}(3915) \rightarrow \omega J/\psi$	< 3.0	$\times 10^{-6}$	CL=90%	-
$\gamma\chi_{c1}(4140) \rightarrow \phi J/\psi$	< 2.2	$\times 10^{-6}$	CL=90%	-
γX	[ssaa] < 4.5	$\times 10^{-6}$	CL=90%	-
$\gamma X \bar{X} (m_X < 3.1 \text{ GeV})$	[ttaa] < 1	$\times 10^{-3}$	CL=90%	-
$\gamma X \bar{X} (m_X < 4.5 \text{ GeV})$	[uuaa] < 2.4	$\times 10^{-4}$	CL=90%	-
$\gamma X \rightarrow \gamma + \geq 4 \text{ prongs}$	[vva] < 1.78	$\times 10^{-4}$	CL=95%	-
$\gamma a_1^0 \rightarrow \gamma\mu^+\mu^-$	[xxaa] < 9	$\times 10^{-6}$	CL=90%	-
$\gamma a_1^0 \rightarrow \gamma\tau^+\tau^-$	[qqaa] < 1.30	$\times 10^{-4}$	CL=90%	-
$\gamma a_1^0 \rightarrow \gamma g g$	[yyaa] < 1	%	CL=90%	-
$\gamma a_1^0 \rightarrow \gamma s\bar{s}$	[yyaa] < 1	$\times 10^{-3}$	CL=90%	-

Lepton Family number (LF) violating modes

$\mu^\pm\tau^\mp$	LF	< 6.0	$\times 10^{-6}$	CL=95%	4563
-------------------	----	-------	------------------	--------	------

Other decays

invisible	< 3.0	$\times 10^{-4}$	CL=90%	-
hadrons	(97 \pm 5)	%		-

 $\chi_{b0}(1P)$ [zzaa]

$$I^G(J^{PC}) = 0^+(0^{++})$$

J needs confirmation.

$$\text{Mass } m = 9859.44 \pm 0.42 \pm 0.31 \text{ MeV}$$

$\chi_{b0}(1P)$ DECAY MODES	Fraction (Γ_i/Γ)	Confidence level	ρ (MeV/c)	
$\gamma T(1S)$	(1.94 \pm 0.27) %		391	
$D^0 X$	< 10.4	%	90%	-
$\pi^+\pi^-K^+K^-\pi^0$	< 1.6	$\times 10^{-4}$	90%	4875
$2\pi^+\pi^-K^-K_S^0$	< 5	$\times 10^{-5}$	90%	4875
$2\pi^+\pi^-K^-K_S^0 2\pi^0$	< 5	$\times 10^{-4}$	90%	4846
$2\pi^+2\pi^-2\pi^0$	< 2.1	$\times 10^{-4}$	90%	4905
$2\pi^+2\pi^-K^+K^-$	(1.1 \pm 0.6)	$\times 10^{-4}$		4861
$2\pi^+2\pi^-K^+K^-\pi^0$	< 2.7	$\times 10^{-4}$	90%	4846
$2\pi^+2\pi^-K^+K^-\pi^0$	< 5	$\times 10^{-4}$	90%	4828
$3\pi^+2\pi^-K^-K_S^0\pi^0$	< 1.6	$\times 10^{-4}$	90%	4827
$3\pi^+3\pi^-$	< 8	$\times 10^{-5}$	90%	4904
$3\pi^+3\pi^-2\pi^0$	< 6	$\times 10^{-4}$	90%	4881
$3\pi^+3\pi^-K^+K^-$	(2.4 \pm 1.2)	$\times 10^{-4}$		4827
$3\pi^+3\pi^-K^+K^-\pi^0$	< 1.0	$\times 10^{-3}$	90%	4808
$4\pi^+4\pi^-$	< 8	$\times 10^{-5}$	90%	4880
$4\pi^+4\pi^-2\pi^0$	< 2.1	$\times 10^{-3}$	90%	4850
$J/\psi J/\psi$	< 7	$\times 10^{-5}$	90%	3836
$J/\psi\psi(2S)$	< 1.2	$\times 10^{-4}$	90%	3571
$\psi(2S)\psi(2S)$	< 3.1	$\times 10^{-5}$	90%	3273
$J/\psi(1S)$ anything	< 2.3	$\times 10^{-3}$	90%	-

 $\chi_{b1}(1P)$ [zzaa]

$$I^G(J^{PC}) = 0^+(1^{++})$$

J needs confirmation.

$$\text{Mass } m = 9892.78 \pm 0.26 \pm 0.31 \text{ MeV}$$

$\chi_{b1}(1P)$ DECAY MODES	Fraction (Γ_i/Γ)	Confidence level	ρ (MeV/c)	
$\gamma T(1S)$	(35.2 \pm 2.0) %		423	
$D^0 X$	(12.6 \pm 2.2) %		-	
$\pi^+\pi^-K^+K^-\pi^0$	(2.0 \pm 0.6) $\times 10^{-4}$		4892	
$2\pi^+\pi^-K^-K_S^0$	(1.3 \pm 0.5) $\times 10^{-4}$		4892	
$2\pi^+\pi^-K^-K_S^0 2\pi^0$	< 6	$\times 10^{-4}$	90%	4863
$2\pi^+2\pi^-2\pi^0$	(8.0 \pm 2.5) $\times 10^{-4}$		4921	
$2\pi^+2\pi^-K^+K^-$	(1.5 \pm 0.5) $\times 10^{-4}$		4878	
$2\pi^+2\pi^-K^+K^-\pi^0$	(3.5 \pm 1.2) $\times 10^{-4}$		4863	
$2\pi^+2\pi^-K^+K^-\pi^0$	(8.6 \pm 3.2) $\times 10^{-4}$		4845	
$3\pi^+2\pi^-K^-K_S^0\pi^0$	(9.3 \pm 3.3) $\times 10^{-4}$		4844	
$3\pi^+3\pi^-$	(1.9 \pm 0.6) $\times 10^{-4}$		4921	
$3\pi^+3\pi^-2\pi^0$	(1.7 \pm 0.5) $\times 10^{-3}$		4898	
$3\pi^+3\pi^-K^+K^-$	(2.6 \pm 0.8) $\times 10^{-4}$		4844	
$3\pi^+3\pi^-K^+K^-\pi^0$	(7.5 \pm 2.6) $\times 10^{-4}$		4825	
$4\pi^+4\pi^-$	(2.6 \pm 0.9) $\times 10^{-4}$		4897	
$4\pi^+4\pi^-2\pi^0$	(1.4 \pm 0.6) $\times 10^{-3}$		4867	
ω anything	(4.9 \pm 1.4) %		-	
ωX_{tetra}	< 4.44	$\times 10^{-4}$	90%	-

Meson Summary Table

$J/\psi J/\psi$	< 2.7	$\times 10^{-5}$	90%	3857
$J/\psi \psi(2S)$	< 1.7	$\times 10^{-5}$	90%	3594
$\psi(2S) \psi(2S)$	< 6	$\times 10^{-5}$	90%	3298
$J/\psi(1S)$ anything	< 1.1	$\times 10^{-3}$	90%	–
$J/\psi(1S) X_{tetra}$	< 2.27	$\times 10^{-4}$	90%	–

 $h_b(1P)$

$$I^G(J^{PC}) = 0^-(1^+ -)$$

Mass $m = 9899.3 \pm 0.8$ MeV

$h_b(1P)$ DECAY MODES	Fraction (Γ_i/Γ)	p (MeV/c)
$\eta_b(1S) \gamma$	$(52_{-5}^{+6})\%$	488

 $\chi_{b2}(1P)$ ^[zzaa]

$$I^G(J^{PC}) = 0^+(2^+ +)$$

 J needs confirmation.

Mass $m = 9912.21 \pm 0.26 \pm 0.31$ MeV

$\chi_{b2}(1P)$ DECAY MODES	Fraction (Γ_i/Γ)	Confidence level	p (MeV/c)
$\gamma T(1S)$	$(18.0 \pm 1.0)\%$		442
$D^0 X$	< 7.9 %	90%	–
$\pi^+ \pi^- K^+ K^- \pi^0$	$(8 \pm 5) \times 10^{-5}$		4902
$2\pi^+ \pi^- K^- K_S^0$	< 1.0 $\times 10^{-4}$	90%	4901
$2\pi^+ \pi^- K^- K_S^0 2\pi^0$	$(5.3 \pm 2.4) \times 10^{-4}$		4873
$2\pi^+ 2\pi^- 2\pi^0$	$(3.5 \pm 1.4) \times 10^{-4}$		4931
$2\pi^+ 2\pi^- K^+ K^-$	$(1.1 \pm 0.4) \times 10^{-4}$		4888
$2\pi^+ 2\pi^- K^+ K^- \pi^0$	$(2.1 \pm 0.9) \times 10^{-4}$		4872
$2\pi^+ 2\pi^- K^+ K^- 2\pi^0$	$(3.9 \pm 1.8) \times 10^{-4}$		4855
$3\pi^+ 2\pi^- K^- K_S^0 \pi^0$	< 5 $\times 10^{-4}$	90%	4854
$3\pi^+ 3\pi^-$	$(7.0 \pm 3.1) \times 10^{-5}$		4931
$3\pi^+ 3\pi^- 2\pi^0$	$(1.0 \pm 0.4) \times 10^{-3}$		4908
$3\pi^+ 3\pi^- K^+ K^-$	< 8 $\times 10^{-5}$	90%	4854
$3\pi^+ 3\pi^- K^+ K^- \pi^0$	$(3.6 \pm 1.5) \times 10^{-4}$		4835
$4\pi^+ 4\pi^-$	$(8 \pm 4) \times 10^{-5}$		4907
$4\pi^+ 4\pi^- 2\pi^0$	$(1.8 \pm 0.7) \times 10^{-3}$		4877
$J/\psi J/\psi$	< 4 $\times 10^{-5}$	90%	3869
$J/\psi \psi(2S)$	< 5 $\times 10^{-5}$	90%	3608
$\psi(2S) \psi(2S)$	< 1.6 $\times 10^{-5}$	90%	3313
$J/\psi(1S)$ anything	$(1.5 \pm 0.4) \times 10^{-3}$		–

 $T(2S)$

$$I^G(J^{PC}) = 0^-(1^- -)$$

Mass $m = 10023.26 \pm 0.31$ MeV $m_{T(3S)} - m_{T(2S)} = 331.50 \pm 0.13$ MeVFull width $\Gamma = 31.98 \pm 2.63$ keV

$T(2S)$ DECAY MODES	Fraction (Γ_i/Γ)	Scale factor / Confidence level	p (MeV/c)
$T(1S) \pi^+ \pi^-$	$(17.85 \pm 0.26)\%$		475
$T(1S) \pi^0 \pi^0$	$(8.6 \pm 0.4)\%$		480
$\tau^+ \tau^-$	$(2.00 \pm 0.21)\%$		4686
$\mu^+ \mu^-$	$(1.93 \pm 0.17)\%$	S=2.2	5011
$e^+ e^-$	$(1.91 \pm 0.16)\%$		5012
$T(1S) \pi^0$	< 4 $\times 10^{-5}$	CL=90%	531
$T(1S) \eta$	$(2.9 \pm 0.4) \times 10^{-4}$	S=2.0	126
$J/\psi(1S)$ anything	< 6 $\times 10^{-3}$	CL=90%	4533
$J/\psi(1S) \eta_c$	< 5.4 $\times 10^{-6}$	CL=90%	3984
$J/\psi(1S) \chi_{c0}$	< 3.4 $\times 10^{-6}$	CL=90%	3808
$J/\psi(1S) \chi_{c1}$	< 1.2 $\times 10^{-6}$	CL=90%	3765
$J/\psi(1S) \chi_{c2}$	< 2.0 $\times 10^{-6}$	CL=90%	3744
$J/\psi(1S) \eta_c(2S)$	< 2.5 $\times 10^{-6}$	CL=90%	3707
$J/\psi(1S) X(3940)$	< 2.0 $\times 10^{-6}$	CL=90%	3555
$J/\psi(1S) X(4160)$	< 2.0 $\times 10^{-6}$	CL=90%	3442
χ_{c1} anything	$(2.2 \pm 0.5) \times 10^{-4}$		–
$\chi_{c1}(1P)^0 X_{tetra}$	< 3.67 $\times 10^{-5}$	CL=90%	–
χ_{c2} anything	$(2.3 \pm 0.8) \times 10^{-4}$		–
$\psi(2S) \eta_c$	< 5.1 $\times 10^{-6}$	CL=90%	3732
$\psi(2S) \chi_{c0}$	< 4.7 $\times 10^{-6}$	CL=90%	3536
$\psi(2S) \chi_{c1}$	< 2.5 $\times 10^{-6}$	CL=90%	3488
$\psi(2S) \chi_{c2}$	< 1.9 $\times 10^{-6}$	CL=90%	3464
$\psi(2S) \eta_c(2S)$	< 3.3 $\times 10^{-6}$	CL=90%	3422
$\psi(2S) X(3940)$	< 3.9 $\times 10^{-6}$	CL=90%	3250
$\psi(2S) X(4160)$	< 3.9 $\times 10^{-6}$	CL=90%	3120
$Z_c(3900)^+ Z_c(3900)^-$	< 1.0 $\times 10^{-6}$	CL=90%	–

$Z_c(4200)^+ Z_c(4200)^-$	< 1.67	$\times 10^{-5}$	CL=90%	–
$Z_c(3900)^\pm Z_c(4200)^\mp$	< 7.3	$\times 10^{-6}$	CL=90%	–
$X(4050)^+ X(4050)^-$	< 1.35	$\times 10^{-5}$	CL=90%	–
$X(4250)^+ X(4250)^-$	< 2.67	$\times 10^{-5}$	CL=90%	–
$X(4050)^\pm X(4250)^\mp$	< 2.72	$\times 10^{-5}$	CL=90%	–
$Z_c(4430)^+ Z_c(4430)^-$	< 2.03	$\times 10^{-5}$	CL=90%	–
$X(4055)^\pm X(4055)^\mp$	< 1.11	$\times 10^{-5}$	CL=90%	–
$X(4055)^\pm Z_c(4430)^\mp$	< 2.11	$\times 10^{-5}$	CL=90%	–
$\bar{2}H$ anything	$(2.78_{-0.26}^{+0.30}) \times 10^{-5}$	S=1.2		–
hadrons	$(94 \pm 11)\%$			–
ggg	$(58.8 \pm 1.2)\%$			–
$\gamma g g$	$(1.87 \pm 0.28)\%$			–
$\phi K^+ K^-$	$(1.6 \pm 0.4) \times 10^{-6}$			4910
$\omega \pi^+ \pi^-$	< 2.58 $\times 10^{-6}$	CL=90%		4977
$K^*(892)^0 K^- \pi^+ + c.c.$	$(2.3 \pm 0.7) \times 10^{-6}$			4952
$\phi f_2'(1525)$	< 1.33 $\times 10^{-6}$	CL=90%		4842
$\omega f_2'(1270)$	< 5.7 $\times 10^{-7}$	CL=90%		4899
$\rho(770) a_2(1320)$	< 8.8 $\times 10^{-7}$	CL=90%		4894
$K^*(892)^0 K_2^*(1430)^0 + c.c.$	$(1.5 \pm 0.6) \times 10^{-6}$			4869
$K_1(1270)^\pm K^\mp$	< 3.22 $\times 10^{-6}$	CL=90%		4921
$K_1(1400)^\pm K^\mp$	< 8.3 $\times 10^{-7}$	CL=90%		4901
$b_1(1235)^\pm \pi^\mp$	< 4.0 $\times 10^{-7}$	CL=90%		4935
$\rho \pi$	< 1.16 $\times 10^{-6}$	CL=90%		4981
$\pi^+ \pi^- \pi^0$	< 8.0 $\times 10^{-7}$	CL=90%		5007
$\omega \pi^0$	< 1.63 $\times 10^{-6}$	CL=90%		4980
$\pi^+ \pi^- \pi^0 \pi^0$	$(1.30 \pm 0.28) \times 10^{-5}$			5002
$K_S^0 K^+ \pi^- + c.c.$	$(1.14 \pm 0.33) \times 10^{-6}$			4979
$K^*(892)^0 \bar{K}^0 + c.c.$	< 4.22 $\times 10^{-6}$	CL=90%		4959
$K^*(892)^- K^+ + c.c.$	< 1.45 $\times 10^{-6}$	CL=90%		4960
$f_1(1285)$ anything	$(2.2 \pm 1.6) \times 10^{-3}$			–
$f_1(1285) X_{tetra}$	< 6.47 $\times 10^{-5}$	CL=90%		–
Sum of 100 exclusive modes	$(2.90 \pm 0.30) \times 10^{-3}$			–

Radiative decays

$\gamma \chi_{b1}(1P)$	$(6.9 \pm 0.4)\%$			130
$\gamma \chi_{b2}(1P)$	$(7.15 \pm 0.35)\%$			110
$\gamma \chi_{b0}(1P)$	$(3.8 \pm 0.4)\%$			162
$\gamma f_0(1710)$	< 5.9 $\times 10^{-4}$	CL=90%		4867
$\gamma f_2'(1525)$	< 5.3 $\times 10^{-4}$	CL=90%		4897
$\gamma f_2'(1270)$	< 2.41 $\times 10^{-4}$	CL=90%		4930
$\gamma \eta_c(1S)$	< 2.7 $\times 10^{-5}$	CL=90%		4567
$\gamma \chi_{c0}$	< 1.0 $\times 10^{-4}$	CL=90%		4430
$\gamma \chi_{c1}$	< 3.6 $\times 10^{-6}$	CL=90%		4397
$\gamma \chi_{c2}$	< 1.5 $\times 10^{-5}$	CL=90%		4381
$\gamma \chi_{c1}(3872)$	< 2.1 $\times 10^{-5}$	CL=90%		4264
$\gamma \chi_{c1}(3872), \chi_{c1} \rightarrow \pi^+ \pi^- \pi^0 J/\psi$	< 2.4 $\times 10^{-6}$	CL=90%		–
$\gamma \chi_{c0}(3915) \rightarrow \omega J/\psi$	< 2.8 $\times 10^{-6}$	CL=90%		–
$\gamma \chi_{c1}(4140) \rightarrow \phi J/\psi$	< 1.2 $\times 10^{-6}$	CL=90%		–
$\gamma X(4350) \rightarrow \phi J/\psi$	< 1.3 $\times 10^{-6}$	CL=90%		–
$\gamma \eta_b(1S)$	$(5.5_{-0.9}^{+1.1}) \times 10^{-4}$	S=1.2		605
$\gamma \eta_b(1S) \rightarrow \gamma$ Sum of 26 exclusive modes	< 3.7 $\times 10^{-6}$	CL=90%		–
$\gamma X_{b\bar{B}} \rightarrow \gamma$ Sum of 26 exclusive modes	< 4.9 $\times 10^{-6}$	CL=90%		–
$\gamma X \rightarrow \gamma + \geq 4$ prongs	[$aabb$] < 1.95 $\times 10^{-4}$	CL=95%		–
$\gamma A^0 \rightarrow \gamma$ hadrons	< 8 $\times 10^{-5}$	CL=90%		–
$\gamma a_1^0 \rightarrow \gamma \mu^+ \mu^-$	< 8.3 $\times 10^{-6}$	CL=90%		–

Lepton Family number (LF) violating modes

$e^\pm \tau^\mp$	LF	< 3.2 $\times 10^{-6}$	CL=90%	4854
$\mu^\pm \tau^\mp$	LF	< 3.3 $\times 10^{-6}$	CL=90%	4854

 $T_2(1D)$

$$I^G(J^{PC}) = 0^-(2^- -)$$

was $T(1D)$ Mass $m = 10163.7 \pm 1.4$ MeV (S = 1.7)

$T_2(1D)$ DECAY MODES	Fraction (Γ_i/Γ)	p (MeV/c)
$\gamma \gamma T(1S)$	seen	679
$\gamma \chi_{bJ}(1P)$	seen	300
$\eta T(1S)$	not seen	426
$\pi^+ \pi^- T(1S)$	$(6.6 \pm 1.6) \times 10^{-3}$	623

Meson Summary Table

$\chi_{b0}(2P)$ ^[zzaa]		$J^G(J^{PC}) = 0^+(0^{++})$ J needs confirmation.	
Mass $m = 10232.5 \pm 0.4 \pm 0.5$ MeV			
$\chi_{b0}(2P)$ DECAY MODES	Fraction (Γ_i/Γ)	Confidence level	ρ (MeV/c)
$\gamma T(2S)$	(1.38 ± 0.30) %		207
$\gamma T(1S)$	(3.8 ± 1.7) × 10 ⁻³		743
$D^0 X$	< 8.2 %	90%	–
$\pi^+ \pi^- K^+ K^- \pi^0$	< 3.4 × 10 ⁻⁵	90%	5064
$2\pi^+ \pi^- K^- K^0_S$	< 5 × 10 ⁻⁵	90%	5063
$2\pi^+ \pi^- K^- K^0_S 2\pi^0$	< 2.2 × 10 ⁻⁴	90%	5036
$2\pi^+ 2\pi^- 2\pi^0$	< 2.4 × 10 ⁻⁴	90%	5092
$2\pi^+ 2\pi^- K^+ K^-$	< 1.5 × 10 ⁻⁴	90%	5050
$2\pi^+ 2\pi^- K^+ K^- \pi^0$	< 2.2 × 10 ⁻⁴	90%	5035
$2\pi^+ 2\pi^- K^+ K^- 2\pi^0$	< 1.1 × 10 ⁻³	90%	5019
$3\pi^+ 2\pi^- K^- K^0_S \pi^0$	< 7 × 10 ⁻⁴	90%	5018
$3\pi^+ 3\pi^-$	< 7 × 10 ⁻⁵	90%	5091
$3\pi^+ 3\pi^- 2\pi^0$	< 1.2 × 10 ⁻³	90%	5070
$3\pi^+ 3\pi^- K^+ K^-$	< 1.5 × 10 ⁻⁴	90%	5017
$3\pi^+ 3\pi^- K^+ K^- \pi^0$	< 7 × 10 ⁻⁴	90%	4999
$4\pi^+ 4\pi^-$	< 1.7 × 10 ⁻⁴	90%	5069
$4\pi^+ 4\pi^- 2\pi^0$	< 6 × 10 ⁻⁴	90%	5039

$\chi_{b1}(2P)$ ^[zzaa]		$J^G(J^{PC}) = 0^+(1^{++})$ J needs confirmation.	
Mass $m = 10255.46 \pm 0.22 \pm 0.50$ MeV			
$m_{\chi_{b1}(2P)} - m_{\chi_{b0}(2P)} = 23.5 \pm 1.0$ MeV			
$\chi_{b1}(2P)$ DECAY MODES	Fraction (Γ_i/Γ)		ρ (MeV/c)
$\omega T(1S)$	(1.63 ^{+0.40} _{-0.34}) %		135
$\gamma T(2S)$	(18.1 ± 1.9) %		230
$\gamma T(1S)$	(9.9 ± 1.0) %		764
$\pi\pi\chi_{b1}(1P)$	(9.1 ± 1.3) × 10 ⁻³		238
$D^0 X$	(8.8 ± 1.7) %		–
$\pi^+ \pi^- K^+ K^- \pi^0$	(3.1 ± 1.0) × 10 ⁻⁴		5075
$2\pi^+ \pi^- K^- K^0_S$	(1.1 ± 0.5) × 10 ⁻⁴		5075
$2\pi^+ \pi^- K^- K^0_S 2\pi^0$	(7.7 ± 3.2) × 10 ⁻⁴		5047
$2\pi^+ 2\pi^- 2\pi^0$	(5.9 ± 2.0) × 10 ⁻⁴		5104
$2\pi^+ 2\pi^- K^+ K^-$	(10 ± 4) × 10 ⁻⁵		5062
$2\pi^+ 2\pi^- K^+ K^- \pi^0$	(5.5 ± 1.8) × 10 ⁻⁴		5047
$2\pi^+ 2\pi^- K^+ K^- 2\pi^0$	(10 ± 4) × 10 ⁻⁴		5030
$3\pi^+ 2\pi^- K^- K^0_S \pi^0$	(6.7 ± 2.6) × 10 ⁻⁴		5029
$3\pi^+ 3\pi^-$	(1.2 ± 0.4) × 10 ⁻⁴		5103
$3\pi^+ 3\pi^- 2\pi^0$	(1.2 ± 0.4) × 10 ⁻³		5081
$3\pi^+ 3\pi^- K^+ K^-$	(2.0 ± 0.8) × 10 ⁻⁴		5029
$3\pi^+ 3\pi^- K^+ K^- \pi^0$	(6.1 ± 2.2) × 10 ⁻⁴		5011
$4\pi^+ 4\pi^-$	(1.7 ± 0.6) × 10 ⁻⁴		5080
$4\pi^+ 4\pi^- 2\pi^0$	(1.9 ± 0.7) × 10 ⁻³		5051

$h_b(2P)$		$J^G(J^{PC}) = 0^-(1^{+-})$	
Mass $m = 10259.8 \pm 1.2$ MeV			
$h_b(2P)$ DECAY MODES	Fraction (Γ_i/Γ)		ρ (MeV/c)
hadrons	not seen		–
$\eta_b(1S)\gamma$	(22 ± 5) %		825
$\eta_b(2S)\gamma$	(48 ± 13) %		257

$\chi_{b2}(2P)$ ^[zzaa]		$J^G(J^{PC}) = 0^+(2^{++})$ J needs confirmation.	
Mass $m = 10268.65 \pm 0.22 \pm 0.50$ MeV			
$m_{\chi_{b2}(2P)} - m_{\chi_{b1}(2P)} = 13.10 \pm 0.24$ MeV			
$\chi_{b2}(2P)$ DECAY MODES	Fraction (Γ_i/Γ)	Confidence level	ρ (MeV/c)
$\omega T(1S)$	(1.10 ^{+0.34} _{-0.30}) %		194
$\gamma T(2S)$	(8.9 ± 1.2) %		242
$\gamma T(1S)$	(6.6 ± 0.8) %		777

$\pi\pi\chi_{b2}(1P)$	(5.1 ± 0.9) × 10 ⁻³		229
$D^0 X$	< 2.4 %		–
$\pi^+ \pi^- K^+ K^- \pi^0$	< 1.1 × 10 ⁻⁴	90%	5082
$2\pi^+ \pi^- K^- K^0_S$	< 9 × 10 ⁻⁵	90%	5082
$2\pi^+ \pi^- K^- K^0_S 2\pi^0$	< 7 × 10 ⁻⁴	90%	5054
$2\pi^+ 2\pi^- 2\pi^0$	(3.9 ± 1.6) × 10 ⁻⁴		5110
$2\pi^+ 2\pi^- K^+ K^-$	(9 ± 4) × 10 ⁻⁵		5068
$2\pi^+ 2\pi^- K^+ K^- \pi^0$	(2.4 ± 1.1) × 10 ⁻⁴		5054
$2\pi^+ 2\pi^- K^+ K^- 2\pi^0$	(4.7 ± 2.3) × 10 ⁻⁴		5037
$3\pi^+ 2\pi^- K^- K^0_S \pi^0$	< 4 × 10 ⁻⁴	90%	5036
$3\pi^+ 3\pi^-$	(9 ± 4) × 10 ⁻⁵		5110
$3\pi^+ 3\pi^- 2\pi^0$	(1.2 ± 0.4) × 10 ⁻³		5088
$3\pi^+ 3\pi^- K^+ K^-$	(1.4 ± 0.7) × 10 ⁻⁴		5036
$3\pi^+ 3\pi^- K^+ K^- \pi^0$	(4.2 ± 1.7) × 10 ⁻⁴		5017
$4\pi^+ 4\pi^-$	(9 ± 5) × 10 ⁻⁵		5087
$4\pi^+ 4\pi^- 2\pi^0$	(1.3 ± 0.5) × 10 ⁻³		5058

$T(3S)$		$J^G(J^{PC}) = 0^-(1^{--})$	
Mass $m = 10355.2 \pm 0.5$ MeV			
$m_{T(3S)} - m_{T(2S)} = 331.50 \pm 0.13$ MeV			
Full width $\Gamma = 20.32 \pm 1.85$ keV			
$T(3S)$ DECAY MODES	Fraction (Γ_i/Γ)	Scale factor/ Confidence level	ρ (MeV/c)
$T(2S)$ anything	(10.6 ± 0.8) %		296
$T(2S)\pi^+\pi^-$	(2.82 ± 0.18) %	S=1.6	177
$T(2S)\pi^0\pi^0$	(1.85 ± 0.14) %		190
$T(2S)\gamma\gamma$	(5.0 ± 0.7) %		327
$T(2S)\pi^0$	< 5.1 × 10 ⁻⁴	CL=90%	298
$T(1S)\pi^+\pi^-$	(4.37 ± 0.08) %		813
$T(1S)\pi^0\pi^0$	(2.20 ± 0.13) %		816
$T(1S)\eta$	< 1 × 10 ⁻⁴	CL=90%	677
$T(1S)\pi^0$	< 7 × 10 ⁻⁵	CL=90%	846
$h_b(1P)\pi^0$	< 1.2 × 10 ⁻³	CL=90%	426
$h_b(1P)\pi^0 \rightarrow \gamma\eta_b(1S)\pi^0$	(4.3 ± 1.4) × 10 ⁻⁴		–
$h_b(1P)\pi^+\pi^-$	< 1.2 × 10 ⁻⁴	CL=90%	353
$\tau^+\tau^-$	(2.29 ± 0.30) %		4863
$\mu^+\mu^-$	(2.18 ± 0.21) %	S=2.1	5177
e^+e^-	(2.18 ± 0.20) %		5178
hadrons	(93 ± 12) %		–
ggg	(35.7 ± 2.6) %		–
γgg	(9.7 ± 1.8) × 10 ⁻³		–
2H anything	(2.33 ± 0.33) × 10 ⁻⁵		–

Radiative decays

$\gamma\chi_{b2}(2P)$	(13.1 ± 1.6) %	S=3.4	86
$\gamma\chi_{b1}(2P)$	(12.6 ± 1.2) %	S=2.4	99
$\gamma\chi_{b0}(2P)$	(5.9 ± 0.6) %	S=1.4	122
$\gamma\chi_{b2}(1P)$	(10.0 ± 1.0) × 10 ⁻³	S=1.7	434
$\gamma\chi_{b1}(1P)$	(9 ± 5) × 10 ⁻⁴	S=1.8	452
$\gamma\chi_{b0}(1P)$	(2.7 ± 0.4) × 10 ⁻³		484
$\gamma\eta_b(2S)$	< 6.2 × 10 ⁻⁴	CL=90%	350
$\gamma\eta_b(1S)$	(5.1 ± 0.7) × 10 ⁻⁴		912
$\gamma A^0 \rightarrow \gamma$ hadrons	< 8 × 10 ⁻⁵	CL=90%	–
$\gamma X \rightarrow \gamma + \geq 4$ prongs	[bbbb] < 2.2 × 10 ⁻⁴	CL=95%	–
$\gamma a_1^0 \rightarrow \gamma\mu^+\mu^-$	< 5.5 × 10 ⁻⁶	CL=90%	–
$\gamma a_1^0 \rightarrow \gamma\tau^+\tau^-$	[ccbb] < 1.6 × 10 ⁻⁴	CL=90%	–

Lepton Family number (LF) violating modes

$e^\pm\tau^\mp$	LF	< 4.2 × 10 ⁻⁶	CL=90%	5025
$\mu^\pm\tau^\mp$	LF	< 3.1 × 10 ⁻⁶	CL=90%	5025

$\chi_{b1}(3P)$ ^[zzaa]		$J^G(J^{PC}) = 0^+(1^{++})$	
J needs confirmation.			
Mass $m = 10513.4 \pm 0.7$ MeV			
$\chi_{b1}(3P)$ DECAY MODES	Fraction (Γ_i/Γ)		ρ (MeV/c)
$T(1S)\gamma$	seen		1000
$T(2S)\gamma$	seen		479
$T(3S)\gamma$	seen		157

Meson Summary Table

 $\chi_{b2}(3P)$ [zzaa]

$$I^G(J^{PC}) = 0^+(2^{++})$$

 J needs confirmation.

Mass $m = 10524.0 \pm 0.8$ MeV

$\chi_{b2}(3P)$ DECAY MODES	Fraction (Γ_i/Γ)	ρ (MeV/c)
$\Upsilon(3S)\gamma$	seen	167

 $\Upsilon(4S)$

$$I^G(J^{PC}) = 0^-(1^{--})$$

also known as $\Upsilon(10580)$

Mass $m = 10579.4 \pm 1.2$ MeV

Full width $\Gamma = 20.5 \pm 2.5$ MeV

$\Upsilon(4S)$ DECAY MODES	Fraction (Γ_i/Γ)	Confidence level	ρ (MeV/c)
$B\bar{B}$	> 96 %	95%	326
$B^+ B^-$	(51.4 ± 0.6) %		331
D^+ anything + c.c.	(17.8 ± 2.6) %		–
$B^0 \bar{B}^0$	(48.6 ± 0.6) %		326
$J/\psi K_S^0 + (J/\psi, \eta_c) K_S^0$	< 4 × 10 ⁻⁷	90%	–
non- $B\bar{B}$	< 4 %	95%	–
$e^+ e^-$	(1.57 ± 0.08) × 10 ⁻⁵		5290
$\rho^+ \rho^-$	< 5.7 × 10 ⁻⁶	90%	5233
$K^*(892)^0 \bar{K}^0$	< 2.0 × 10 ⁻⁶	90%	5240
$J/\psi(1S)$ anything	< 1.9 × 10 ⁻⁴	95%	–
D^{*+} anything + c.c.	< 7.4 %	90%	5099
ϕ anything	(7.1 ± 0.6) %		5240
$\phi \eta$	< 1.8 × 10 ⁻⁶	90%	5226
$\phi \eta'$	< 4.3 × 10 ⁻⁶	90%	5196
$\rho \eta$	< 1.3 × 10 ⁻⁶	90%	5247
$\rho \eta'$	< 2.5 × 10 ⁻⁶	90%	5217
$\Upsilon(1S)$ anything	< 4 × 10 ⁻³	90%	1053
$\Upsilon(1S)\pi^+ \pi^-$	(8.2 ± 0.4) × 10 ⁻⁵		1026
$\Upsilon(1S)\eta$	(1.81 ± 0.18) × 10 ⁻⁴		924
$\Upsilon(1S)\eta'$	(3.4 ± 0.9) × 10 ⁻⁵		–
$\Upsilon(2S)\pi^+ \pi^-$	(8.2 ± 0.8) × 10 ⁻⁵		468
$h_b(1P)\pi^+ \pi^-$	not seen		600
$h_b(1P)\eta$	(2.18 ± 0.21) × 10 ⁻³		390
$\eta_b(1S)\omega$	< 1.8 × 10 ⁻⁴	90%	–
2H anything	< 1.3 × 10 ⁻⁵	90%	–
Double Radiative Decays			
$\gamma\gamma \Upsilon(D) \rightarrow \gamma\gamma\eta \Upsilon(1S)$	< 2.3 × 10 ⁻⁵	90%	–

 $Z_b(10610)$

$$I^G(J^{PC}) = 1^+(1^{+-})$$

was $X(10610)$

Mass $m = 10607.2 \pm 2.0$ MeV

Full width $\Gamma = 18.4 \pm 2.4$ MeV

$Z_b(10610)$ DECAY MODES	Fraction (Γ_i/Γ)	ρ (MeV/c)
$\Upsilon(1S)\pi^+$	(5.4 ± 1.9) _{-1.5} × 10 ⁻³	1077
$\Upsilon(1S)\pi^0$	not seen	1077
$\Upsilon(2S)\pi^+$	(3.6 ± 1.1) _{-0.8} %	551
$\Upsilon(2S)\pi^0$	seen	552
$\Upsilon(3S)\pi^+$	(2.1 ± 0.8) _{-0.6} %	207
$\Upsilon(3S)\pi^0$	seen	210
$h_b(1P)\pi^+$	(3.5 ± 1.2) _{-0.9} %	671
$h_b(2P)\pi^+$	(4.7 ± 1.7) _{-1.3} %	313
$B^+ \bar{B}^0$	not seen	505
$B^+ \bar{B}^{*0} + B^{*+} \bar{B}^0$	(85.6 ± 2.1) _{-2.9} %	–

 $Z_b(10650)$

$$I^G(J^{PC}) = 1^+(1^{+-})$$

 I, G, C need confirmation.was $X(10650)^\pm$

Mass $m = 10652.2 \pm 1.5$ MeV

Full width $\Gamma = 11.5 \pm 2.2$ MeV

 $Z_b(10650)^-$ decay modes are charge conjugates of the modes below.

$Z_b(10650)^+$ DECAY MODES	Fraction (Γ_i/Γ)	ρ (MeV/c)
$\Upsilon(1S)\pi^+$	(1.7 ± 0.8) _{-0.6} × 10 ⁻³	1117
$\Upsilon(2S)\pi^+$	(1.4 ± 0.6) _{-0.4} %	595
$\Upsilon(3S)\pi^+$	(1.6 ± 0.7) _{-0.5} %	259
$h_b(1P)\pi^+$	(8.4 ± 2.9) _{-2.4} %	714
$h_b(2P)\pi^+$	(15 ± 4) %	360
$B^+ \bar{B}^0$	not seen	703
$B^+ \bar{B}^{*0} + B^{*+} \bar{B}^0$	not seen	–
$B^{*+} \bar{B}^{*0}$	(74 ± 4) ₋₆ %	122

 $\Upsilon(10860)$

$$I^G(J^{PC}) = 0^-(1^{--})$$

Mass $m = 10885.2 \pm 2.6$ MeV

Full width $\Gamma = 37 \pm 4$ MeV

$\Upsilon(10860)$ DECAY MODES	Fraction (Γ_i/Γ)	Confidence level	ρ (MeV/c)
$B\bar{B}X$	(76.2 ± 2.7) _{-4.0} %		–
$B\bar{B}$	(5.5 ± 1.0) %		1322
$B\bar{B}^* + c.c.$	(13.7 ± 1.6) %		–
$B^* \bar{B}^*$	(38.1 ± 3.4) %		1127
$B\bar{B}^{(*)}\pi$	< 19.7 %	90%	1015
$B\bar{B}\pi$	(0.0 ± 1.2) %		1015
$B^* \bar{B}\pi + B\bar{B}^*\pi$	(7.3 ± 2.3) %		–
$B^* \bar{B}^*\pi$	(1.0 ± 1.4) %		739
$B\bar{B}\pi\pi$	< 8.9 %	90%	551
$B_s^{(*)} \bar{B}_s^{(*)}$	(20.1 ± 3.1) %		905
$B_s \bar{B}_s$	(5 ± 5) × 10 ⁻³		905
$B_s \bar{B}_s^* + c.c.$	(1.35 ± 0.32) %		–
$B_s^* \bar{B}_s^*$	(17.6 ± 2.7) %		543
no open-bottom	(3.8 ± 5.0) _{-0.5} %		–
$e^+ e^-$	(8.3 ± 2.1) × 10 ⁻⁶		5443
$K^*(892)^0 \bar{K}^0$	< 1.0 × 10 ⁻⁵	90%	5395
$\Upsilon(1S)\pi^+ \pi^-$	(5.3 ± 0.6) × 10 ⁻³		1306
$\Upsilon(1S)\eta$	(8.5 ± 1.7) × 10 ⁻⁴		1229
$\Upsilon(1S)\eta'$	< 6.9 × 10 ⁻⁵	90%	985
$\Upsilon(2S)\pi^+ \pi^-$	(7.8 ± 1.3) × 10 ⁻³		783
$\Upsilon(2S)\eta$	(4.1 ± 0.6) × 10 ⁻³		639
$\Upsilon(3S)\pi^+ \pi^-$	(4.8 ± 1.9) _{-1.7} × 10 ⁻³		440
$\Upsilon(1S)K^+ K^-$	(6.1 ± 1.8) × 10 ⁻⁴		959
$\eta \Upsilon(1D)$	(4.8 ± 1.1) × 10 ⁻³		–
$h_b(1P)\pi^+ \pi^-$	(3.5 ± 1.0) _{-1.3} × 10 ⁻³		903
$h_b(2P)\pi^+ \pi^-$	(5.7 ± 1.7) _{-2.1} × 10 ⁻³		544
$\chi_{bj}(1P)\pi^+ \pi^- \pi^0$	(2.5 ± 2.3) × 10 ⁻³		894
$\chi_{b0}(1P)\pi^+ \pi^- \pi^0$	< 6.3 × 10 ⁻³	90%	894
$\chi_{b0}(1P)\omega$	< 3.9 × 10 ⁻³	90%	631
$\chi_{b0}(1P)(\pi^+ \pi^- \pi^0)_{\text{non-}\omega}$	< 4.8 × 10 ⁻³	90%	–
$\chi_{b1}(1P)\pi^+ \pi^- \pi^0$	(1.85 ± 0.33) × 10 ⁻³		861
$\chi_{b1}(1P)\omega$	(1.57 ± 0.30) × 10 ⁻³		582
$\chi_{b1}(1P)(\pi^+ \pi^- \pi^0)_{\text{non-}\omega}$	(5.2 ± 1.9) × 10 ⁻⁴		–
$\chi_{b2}(1P)\pi^+ \pi^- \pi^0$	(1.17 ± 0.30) × 10 ⁻³		841
$\chi_{b2}(1P)\omega$	(6.0 ± 2.7) × 10 ⁻⁴		552
$\chi_{b2}(1P)(\pi^+ \pi^- \pi^0)_{\text{non-}\omega}$	(6 ± 4) × 10 ⁻⁴		–
$\gamma X_b \rightarrow \gamma \Upsilon(1S)\omega$	< 3.8 × 10 ⁻⁵	90%	–
$\eta_b(1S)\omega$	< 1.3 × 10 ⁻³	90%	1177
$\eta_b(2S)\omega$	< 5.6 × 10 ⁻³	90%	399

Inclusive Decays.

These decay modes are submodes of one or more of the decay modes above.

ϕ anything	(13.8 ± 2.4) _{-1.7} %	–
D^0 anything + c.c.	(108 ± 8) %	–
D_s anything + c.c.	(46 ± 6) %	–
J/ψ anything	(2.06 ± 0.21) %	–
B^0 anything + c.c.	(77 ± 8) %	–
B^+ anything + c.c.	(72 ± 6) %	–

Meson Summary Table

$T(11020)$		
$J^{PC} = 0^{-}(1^{-}-)$		
Mass $m = 11000 \pm 4$ MeV		
Full width $\Gamma = 24^{+8}_{-6}$ MeV		
$T(11020)$ DECAY MODES	Fraction (Γ_i/Γ)	p (MeV/c)
$e^+ e^-$	$(5.4^{+1.9}_{-2.1}) \times 10^{-6}$	5500
$\chi_{bJ}(1P)\pi^+\pi^-\pi^0$	$(9^{+9}_{-8}) \times 10^{-3}$	1007
$\chi_{b1}(1P)\pi^+\pi^-\pi^0$	seen	975
$\chi_{b2}(1P)\pi^+\pi^-\pi^0$	seen	956

NOTES

In this Summary Table:

When a quantity has “(S = ...)” to its right, the error on the quantity has been enlarged by the “scale factor” S, defined as $S = \sqrt{\chi^2/(N-1)}$, where N is the number of measurements used in calculating the quantity. We do this when $S > 1$, which often indicates that the measurements are inconsistent. When $S > 1.25$, we also show in the Particle Listings an ideogram of the measurements. For more about S, see the Introduction.

A decay momentum p is given for each decay mode. For a 2-body decay, p is the momentum of each decay product in the rest frame of the decaying particle. For a 3-or-more-body decay, p is the largest momentum any of the products can have in this frame.

- [a] See the review on “Form Factors for Radiative Pion and Kaon Decays” for definitions and details.
- [b] Measurements of $\Gamma(e^+ \nu_e)/\Gamma(\mu^+ \nu_\mu)$ always include decays with γ 's, and measurements of $\Gamma(e^+ \nu_e \gamma)$ and $\Gamma(\mu^+ \nu_\mu \gamma)$ never include low-energy γ 's. Therefore, since no clean separation is possible, we consider the modes with γ 's to be subreactions of the modes without them, and let $[\Gamma(e^+ \nu_e) + \Gamma(\mu^+ \nu_\mu)]/\Gamma_{\text{total}} = 100\%$.
- [c] See the π^\pm Particle Listings for the energy limits used in this measurement; low-energy γ 's are not included.
- [d] Derived from an analysis of neutrino-oscillation experiments.
- [e] Astrophysical and cosmological arguments give limits of order 10^{-13} , but they are model dependent and for the summary value we use the best laboratory limit, which includes any final state of invisible particles.
- [f] Forbidden by angular momentum conservation.
- [g] C parity forbids this to occur as a single-photon process.
- [h] The $\omega\rho$ interference is then due to $\omega\rho$ mixing only, and is expected to be small. If $e\mu$ universality holds, $\Gamma(\rho^0 \rightarrow \mu^+ \mu^-) = \Gamma(\rho^0 \rightarrow e^+ e^-) \times 0.99785$.
- [i] Our estimate. See the Particle Listings for details.
- [j] See the “Note on $a_1(1260)$ ” in the $a_1(1260)$ Particle Listings in PDG 06, Journal of Physics **G33** 1 (2006).
- [k] See also the $\omega(1650)$.
- [l] See also the $\omega(1420)$.
- [n] See the note in the K^\pm Particle Listings.
- [o] Neglecting photon channels. See, e.g., A. Pais and S.B. Treiman, Phys. Rev. **D12**, 2744 (1975).
- [p] The definition of the slope parameters of the $K \rightarrow 3\pi$ Dalitz plot is as follows (see also “Note on Dalitz Plot Parameters for $K \rightarrow 3\pi$ Decays” in the K^\pm Particle Listings):

$$|M|^2 = 1 + g(s_3 - s_0)/m_{\pi^+}^2 + \dots$$
- [q] For more details and definitions of parameters see the Particle Listings.
- [r] See the K^\pm Particle Listings for the energy limits used in this measurement.
- [s] Most of this radiative mode, the low-momentum γ part, is also included in the parent mode listed without γ 's.
- [t] Structure-dependent part.
- [u] Direct-emission branching fraction.
- [v] Violates angular-momentum conservation.
- [x] Derived from measured values of ϕ_{+-} , ϕ_{00} , $|\eta|$, $|m_{K_L^0} - m_{K_S^0}|$, and $\tau_{K_S^0}$, as described in the introduction to “Tests of Conservation Laws.”
- [y] The CP -violation parameters are defined as follows (see also “Note on CP Violation in $K_S \rightarrow 3\pi$ ” and “Note on CP Violation in K_L^0 Decay” in the Particle Listings):

$$\eta_{+-} = |\eta_{+-}|e^{i\phi_{+-}} = \frac{A(K_L^0 \rightarrow \pi^+ \pi^-)}{A(K_S^0 \rightarrow \pi^+ \pi^-)} = \epsilon + \epsilon'$$

$$\eta_{00} = |\eta_{00}|e^{i\phi_{00}} = \frac{A(K_L^0 \rightarrow \pi^0 \pi^0)}{A(K_S^0 \rightarrow \pi^0 \pi^0)} = \epsilon - 2\epsilon'$$

$$\delta = \frac{\Gamma(K_L^0 \rightarrow \pi^- \ell^+ \nu) - \Gamma(K_L^0 \rightarrow \pi^+ \ell^- \nu)}{\Gamma(K_L^0 \rightarrow \pi^- \ell^+ \nu) + \Gamma(K_L^0 \rightarrow \pi^+ \ell^- \nu)},$$

$$\text{Im}(\eta_{+-0})^2 = \frac{\Gamma(K_S^0 \rightarrow \pi^+ \pi^- \pi^0)^{CP \text{ viol.}}}{\Gamma(K_L^0 \rightarrow \pi^+ \pi^- \pi^0)},$$

$$\text{Im}(\eta_{000})^2 = \frac{\Gamma(K_S^0 \rightarrow \pi^0 \pi^0 \pi^0)}{\Gamma(K_L^0 \rightarrow \pi^0 \pi^0 \pi^0)},$$

where for the last two relations CPT is assumed valid, i.e., $\text{Re}(\eta_{+-0}) \simeq 0$ and $\text{Re}(\eta_{000}) \simeq 0$.

- [z] See the K_S^0 Particle Listings for the energy limits used in this measurement.
- [aa] The value is for the sum of the charge states or particle/antiparticle states indicated.
- [bb] $\text{Re}(\epsilon'/\epsilon) = \epsilon'/\epsilon$ to a very good approximation provided the phases satisfy CPT invariance.
- [cc] This mode includes gammas from inner bremsstrahlung but not the direct emission mode $K_L^0 \rightarrow \pi^+ \pi^- \gamma(\text{DE})$.
- [dd] See the K_L^0 Particle Listings for the energy limits used in this measurement.
- [ee] Allowed by higher-order electroweak interactions.
- [ff] Violates CP in leading order. Test of direct CP violation since the indirect CP -violating and CP -conserving contributions are expected to be suppressed.
- [gg] See our minireview under the $K_2(1770)$ in the 2004 edition of this *Review*.
- [hh] This result applies to $Z^0 \rightarrow c\bar{c}$ decays only. Here ℓ^+ is an average (not a sum) of e^+ and μ^+ decays.
- [ii] See the Particle Listings for the (complicated) definition of this quantity.
- [jj] The branching fraction for this mode may differ from the sum of the submodes that contribute to it, due to interference effects. See the relevant papers in the Particle Listings.
- [kk] These subfractions of the $K^- 2\pi^+$ mode are uncertain: see the Particle Listings.
- [ll] Submodes of the $D^+ \rightarrow K^- 2\pi^+ \pi^0$ and $K_S^0 2\pi^+ \pi^-$ modes were studied by ANJOS 92C and COFFMAN 92B, but with at most 142 events for the first mode and 229 for the second – not enough for precise results. With nothing new for 18 years, we refer to our 2008 edition, Physics Letters **B667** 1 (2008), for those results.
- [nn] The unseen decay modes of the resonances are included.
- [oo] This is *not* a test for the $\Delta C=1$ weak neutral current, but leads to the $\pi^+ \ell^+ \ell^-$ final state.
- [pp] This mode is not a useful test for a $\Delta C=1$ weak neutral current because both quarks must change flavor in this decay.
- [qq] In the 2010 *Review*, the values for these quantities were given using a measure of the asymmetry that was inconsistent with the usual definition.
- [rr] This value is obtained by subtracting the branching fractions for 2-, 4- and 6-prongs from unity.
- [ss] This is the sum of our $K^- 2\pi^+ \pi^-$, $K^- 2\pi^+ \pi^- \pi^0$, $\bar{K}^0 2\pi^+ 2\pi^-$, $K^+ 2K^- \pi^+$, $2\pi^+ 2\pi^-$, $2\pi^+ 2\pi^- \pi^0$, $K^+ K^- \pi^+ \pi^-$, and $K^+ K^- \pi^+ \pi^- \pi^0$, branching fractions.
- [tt] This is the sum of our $K^- 3\pi^+ 2\pi^-$ and $3\pi^+ 3\pi^-$ branching fractions.
- [uu] The branching fractions for the $K^- e^+ \nu_e$, $K^*(892)^- e^+ \nu_e$, $\pi^- e^+ \nu_e$, and $\rho^- e^+ \nu_e$ modes add up to $6.17 \pm 0.17\%$.
- [vv] This is a doubly Cabibbo-suppressed mode.
- [xx] Submodes of the $D^0 \rightarrow K_S^0 \pi^+ \pi^- \pi^0$ mode with a K^* and/or ρ were studied by COFFMAN 92B, but with only 140 events. With nothing new for 18 years, we refer to our 2008 edition, Physics Letters **B667** 1 (2008), for those results.
- [yy] This branching fraction includes all the decay modes of the resonance in the final state.
- [zz] This limit is for either D^0 or \bar{D}^0 to $p e^-$.

Meson Summary Table

- [aaa] This limit is for either D^0 or \bar{D}^0 to $\bar{p}e^+$.
- [bbb] This is the purely e^+ semileptonic branching fraction; the e^+ fraction from τ^+ decays has been subtracted off. The sum of our (non- τ) e^+ exclusive fractions — an $e^+ \nu_e$ with an η , η' , ϕ , K^0 , or K^{*0} — is $5.99 \pm 0.31\%$.
- [ccc] This fraction includes η from η' decays.
- [ddd] The sum of our exclusive η' fractions — $\eta' e^+ \nu_e$, $\eta' \mu^+ \nu_\mu$, $\eta' \pi^+$, $\eta' \rho^+$, and $\eta' K^+$ — is $11.8 \pm 1.6\%$.
- [eee] This branching fraction includes all the decay modes of the final-state resonance.
- [fff] A test for $u\bar{u}$ or $d\bar{d}$ content in the D_s^+ . Neither Cabibbo-favored nor Cabibbo-suppressed decays can contribute, and $\omega - \phi$ mixing is an unlikely explanation for any fraction above about 2×10^{-4} .
- [ggg] We decouple the $D_s^+ \rightarrow \phi \pi^+$ branching fraction obtained from mass projections (and used to get some of the other branching fractions) from the $D_s^+ \rightarrow \phi \pi^+$, $\phi \rightarrow K^+ K^-$ branching fraction obtained from the Dalitz-plot analysis of $D_s^+ \rightarrow K^+ K^- \pi^+$. That is, the ratio of these two branching fractions is not exactly the $\phi \rightarrow K^+ K^-$ branching fraction 0.491.
- [hhh] This is the average of a model-independent and a K -matrix parametrization of the $\pi^+ \pi^- S$ -wave and is a sum over several f_0 mesons.
- [iii] An ℓ indicates an e or a μ mode, not a sum over these modes.
- [jjj] An $CP(\pm 1)$ indicates the $CP=+1$ and $CP=-1$ eigenstates of the D^0 - \bar{D}^0 system.
- [kkk] D denotes D^0 or \bar{D}^0 .
- [lll] $D_{CP^+}^{*0}$ decays into $D^0 \pi^0$ with the D^0 reconstructed in CP -even eigenstates $K^+ K^-$ and $\pi^+ \pi^-$.
- [nnn] \bar{D}^{*0} represents an excited state with mass $2.2 < M < 2.8$ GeV/ c^2 .
- [ooo] $\chi_{c1}(3872)^+$ is a hypothetical charged partner of the $\chi_{c1}(3872)$.
- [ppp] $\Theta(1710)^{++}$ is a possible narrow pentaquark state and $G(2220)$ is a possible glueball resonance.
- [qqq] $(\bar{A}_c^- p)_s$ denotes a low-mass enhancement near 3.35 GeV/ c^2 .
- [rrr] Stands for the possible candidates of $K^*(1410)$, $K_0^*(1430)$ and $K_2^*(1430)$.
- [sss] B^0 and B_s^0 contributions not separated. Limit is on weighted average of the two decay rates.
- [ttt] This decay refers to the coherent sum of resonant and nonresonant $J^P = 0^+ K \pi$ components with $1.60 < m_{K\pi} < 2.15$ GeV/ c^2 .
- [uuu] $X(214)$ is a hypothetical particle of mass 214 MeV/ c^2 reported by the HyperCP experiment, Physical Review Letters **94** 021801 (2005)
- [vvv] $\Theta(1540)^+$ denotes a possible narrow pentaquark state.
- [xxx] Here S and P are the hypothetical scalar and pseudoscalar particles with masses of 2.5 GeV/ c^2 and 214.3 MeV/ c^2 , respectively.
- [yyy] These values are model dependent.
- [zzz] Here “anything” means at least one particle observed.
- [aaaa] This is a $B(B^0 \rightarrow D^{*-} \ell^+ \nu_\ell)$ value.
- [bbba] D^{**} stands for the sum of the $D(1^1P_1)$, $D(1^3P_0)$, $D(1^3P_1)$, $D(1^3P_2)$, $D(2^1S_0)$, and $D(2^1S_1)$ resonances.
- [ccaa] $D^{(*)} \bar{D}^{(*)}$ stands for the sum of $D^* \bar{D}^*$, $D^* \bar{D}$, $D \bar{D}^*$, and $D \bar{D}$.
- [ddaa] $X(3915)$ denotes a near-threshold enhancement in the $\omega J/\psi$ mass spectrum.
- [eeaa] Inclusive branching fractions have a multiplicity definition and can be greater than 100%.
- [ffaa] D_J represents an unresolved mixture of pseudoscalar and tensor D^{**} (P -wave) states.
- [ggaa] Not a pure measurement. See note at head of B_s^0 Decay Modes.
- [hhaa] For $E_\gamma > 100$ MeV.
- [iiaa] $\Theta(1540)$ is a hypothetical pentaquark state of 1.54 GeV/ c^2 mass and a width of less than 25 MeV/ c^2 .
- [jjaa] Includes $p\bar{p}\pi^+\pi^-\gamma$ and excludes $p\bar{p}\eta$, $p\bar{p}\omega$, $p\bar{p}\eta'$.
- [kkaa] For a narrow state A with mass less than 960 MeV.
- [llaa] For a narrow scalar or pseudoscalar A^0 with mass 0.21–3.0 GeV.
- [nnaa] For a dark photon U with mass between 100 and 2100 MeV.
- [ooaa] For a narrow resonance in the range $2.2 < M(X) < 2.8$ GeV.
- [ppaa] J^{PC} known by production in e^+e^- via single photon annihilation. IG is not known; interpretation of this state as a single resonance is unclear because of the expectation of substantial threshold effects in this energy region.
- [qqaa] $2m_\tau < M(\tau^+\tau^-) < 9.2$ GeV
- [rraa] $2 \text{ GeV} < m_{K^+K^-} < 3$ GeV
- [ssaa] $X = \text{scalar with } m < 8.0$ GeV
- [ttaa] $X \bar{X} = \text{vectors with } m < 3.1$ GeV
- [uuaa] X and $\bar{X} = \text{zero spin with } m < 4.5$ GeV
- [vvaa] $1.5 \text{ GeV} < m_X < 5.0$ GeV
- [xxaa] $201 \text{ MeV} < M(\mu^+\mu^-) < 3565$ MeV
- [yyaa] $0.5 \text{ GeV} < m_X < 9.0$ GeV, where m_X is the invariant mass of the hadronic final state.
- [zzaa] Spectroscopic labeling for these states is theoretical, pending experimental information.
- [aabb] $1.5 \text{ GeV} < m_X < 5.0$ GeV
- [bbbb] $1.5 \text{ GeV} < m_X < 5.0$ GeV
- [ccbb] For $m_{\tau^+\tau^-}$ in the ranges 4.03–9.52 and 9.61–10.10 GeV.

Meson Summary Table

See also the table of suggested $q\bar{q}$ quark-model assignments in the Quark Model section.

• Indicates particles that appear in the preceding Meson Summary Table. We do not regard the other entries as being established.

LIGHT UNFLAVORED ($S = C = B = 0$)		STRANGE ($S = \pm 1, C = B = 0$)		CHARMED, STRANGE ($C = \pm 1, S = \pm 1$) (+ possibly non- $q\bar{q}$ states)		$c\bar{c}$ continued $J^G(J^{PC})$			
$J^G(J^{PC})$	$J^G(J^{PC})$		$J(J^P)$	$J(J^P)$	$J(J^P)$				
• π^\pm	$1^-(0^-)$	• $\pi_2(1670)$	$1^-(2^-+)$	• K^\pm	$1/2(0^-)$	• D_s^\pm	$0(0^-)$	• $\psi_2(3823)$	$0^-(2^-)$
• π^0	$1^-(0^-)$	• $\phi(1680)$	$0^-(1^-)$	• K^0	$1/2(0^-)$	• $D_s^{*\pm}$	$0(0^-)$	• $\psi_3(3842)$	$0^-(3^-)$
• η	$0^+(0^-)$	• $\rho_3(1690)$	$1^+(3^-)$	• K_S^0	$1/2(0^-)$	• D_{s0}^*	$0(0^+)$	• $\chi_{c0}(3860)$	$0^+(0^+)$
• $f_0(500)$	$0^+(0^+)$	• $\rho(1700)$	$1^+(1^-)$	• K_L^0	$1/2(0^-)$	• D_{s1}^*	$0(0^+)$	• $\chi_{c1}(3872)$	$0^+(1^+)$
• $\rho(770)$	$1^+(1^-)$	• $a_2(1700)$	$1^-(2^+)$	• $K_0^*(700)$	$1/2(0^+)$	• D_{s1}	$0(1^+)$	• $Z_c(3900)$	$1^+(1^+)$
• $\omega(782)$	$0^-(1^-)$	• $f_0(1710)$	$0^+(0^+)$	• $K^*(892)$	$1/2(1^-)$	• D_{s1}	$0(1^+)$	• $\chi_{c2}(3915)$	$0^+(0^+)$
• $\eta'(958)$	$0^+(0^-)$	• $X(1750)$	$?^-(1^-)$	• $K_1(1270)$	$1/2(1^+)$	• D_{s2}^*	$0(2^+)$	• $\chi_{c2}(3930)$	$0^+(2^+)$
• $f_0(980)$	$0^+(0^+)$	• $\eta(1760)$	$0^+(0^-)$	• $K_1(1400)$	$1/2(1^+)$	D_{s0}	$0(0^-)$	• $X(3940)$	$?^?(?^?)$
• $a_0(980)$	$1^-(0^+)$	• $\pi(1800)$	$1^-(0^-)$	• $K^*(1410)$	$1/2(1^-)$	• D_{s1}^*	$0(1^-)$	• $X(4020)^\pm$	$1^+(?^-)$
• $\phi(1020)$	$0^-(1^-)$	• $f_2(1810)$	$0^+(2^+)$	• $K_0^*(1430)$	$1/2(0^+)$	• D_{s1}^*	$0(1^-)$	• $\psi(4040)$	$0^-(1^-)$
• $h_1(1170)$	$0^-(1^+)$	• $X(1835)$	$?^?(0^-)$	• $K_2^*(1430)$	$1/2(2^+)$	• D_{s1}^*	$0(1^-)$	• $X(4050)^\pm$	$1^-(?^+)$
• $b_1(1235)$	$1^+(1^+)$	• $\phi_3(1850)$	$0^-(3^-)$	• $K(1460)$	$1/2(0^-)$	• D_{s3}^*	$0(3^-)$	• $X(4055)^\pm$	$1^+(?^-)$
• $a_1(1260)$	$1^-(1^+)$	• $\eta_2(1870)$	$0^+(2^-)$	$K_2(1580)$	$1/2(2^-)$	$X_0(2900)$	$? (0^+)$	• $X(4100)^\pm$	$1^-(?^?)$
• $f_2(1270)$	$0^+(2^+)$	• $\pi_2(1880)$	$1^-(2^-)$	$K(1630)$	$1/2(?^?)$	$X_1(2900)$	$? (1^-)$	• $\chi_{c1}(4140)$	$0^+(1^+)$
• $f_1(1285)$	$0^+(1^+)$	• $\rho(1900)$	$1^+(1^-)$	• $K_1(1650)$	$1/2(1^+)$	$D_{s,J}(3040)^\pm$	$0(?^?)$	• $\psi(4160)$	$0^-(1^-)$
• $\eta(1295)$	$0^+(0^-)$	• $f_2(1910)$	$0^+(2^+)$	• $K^*(1680)$	$1/2(1^-)$	BOTTOM ($B = \pm 1$)		• $Z_c(4200)$	$1^+(1^+)$
• $\pi(1300)$	$1^-(0^-)$	• $a_0(1950)$	$1^-(0^+)$	• $K_2(1770)$	$1/2(2^-)$	• B^\pm	$1/2(0^-)$	• $\psi(4230)$	$0^-(1^-)$
• $a_2(1320)$	$1^-(2^+)$	• $f_2(1950)$	$0^+(2^+)$	• $K_3^*(1780)$	$1/2(3^-)$	• B^0	$1/2(0^-)$	• $R_{c0}(4240)$	$1^+(0^-)$
• $f_0(1370)$	$0^+(0^+)$	• $a_4(1970)$	$1^-(4^+)$	• $K_2(1820)$	$1/2(2^-)$	• B^\pm/B^0 ADMIXTURE		• $X(4250)^\pm$	$1^-(?^+)$
• $\pi_1(1400)$	$1^-(1^+)$	• $\rho_3(1990)$	$1^+(3^-)$	• $K(1830)$	$1/2(0^-)$	• $B^\pm/B^0/B_s^0/b$ -baryon		• $\chi_{c1}(4274)$	$0^+(1^+)$
• $\eta(1405)$	$0^+(0^-)$	• $\pi_2(2005)$	$1^-(2^-)$	• $K_0^*(1950)$	$1/2(0^+)$	ADMIXTURE		• $X(4350)$	$0^+(?^+)$
• $h_1(1415)$	$0^-(1^+)$	• $f_2(2010)$	$0^+(2^+)$	• $K_2^*(1980)$	$1/2(2^+)$	V_{cb} and V_{ub} CKM Matrix Elements		• $\psi(4360)$	$0^-(1^-)$
• $f_1(1420)$	$0^+(1^+)$	• $f_0(2020)$	$0^+(0^+)$	• $K_4^*(2045)$	$1/2(4^+)$	• B^*	$1/2(1^-)$	• $\psi(4415)$	$0^-(1^-)$
• $\omega(1420)$	$0^-(1^-)$	• $f_4(2050)$	$0^+(4^+)$	$K_2(2250)$	$1/2(2^-)$	• $B_1(5721)$	$1/2(1^+)$	• $Z_c(4430)$	$1^+(1^+)$
• $f_2(1430)$	$0^+(2^+)$	• $\pi_2(2100)$	$1^-(2^-)$	$K_3(2320)$	$1/2(3^+)$	• $B_2^*(5732)$	$? (?^?)$	• $\chi_{c0}(4500)$	$0^+(0^+)$
• $a_0(1450)$	$1^-(0^+)$	• $f_0(2100)$	$0^+(0^+)$	• $K_5^*(2380)$	$1/2(5^-)$	• $B_2^*(5747)$	$1/2(2^+)$	• $X(4630)$	$0^+(?^+)$
• $\rho(1450)$	$1^+(1^-)$	• $f_2(2150)$	$0^+(2^+)$	$K_4(2500)$	$1/2(4^-)$	• $B_{J(5840)}$	$1/2(?^?)$	• $\psi(4660)$	$0^-(1^-)$
• $\eta(1475)$	$0^+(0^-)$	• $\rho(2150)$	$1^+(1^-)$	$K(3100)$	$?^?(?^?)$	• $B_{J(5970)}$	$1/2(?^?)$	• $\chi_{c1}(4685)$	$0^+(1^+)$
• $f_0(1500)$	$0^+(0^+)$	• $\phi(2170)$	$0^-(1^-)$	CHARMED ($C = \pm 1$)				• $\chi_{c0}(4700)$	$0^+(0^+)$
• $f_1(1510)$	$0^+(1^+)$	• $f_0(2200)$	$0^+(0^+)$	• D^\pm	$1/2(0^-)$	BOTTOM, STRANGE ($B = \pm 1, S = \mp 1$)		$b\bar{b}$ (+ possibly non- $q\bar{q}$ states)	
• $f_2'(1525)$	$0^+(2^+)$	• $f_j(2220)$	$0^+(2^+)$ or $4^+ +$	• D^0	$1/2(0^-)$	• B_s^0	$0(0^-)$	• $\eta_b(1S)$	$0^+(0^-)$
• $f_2(1565)$	$0^+(2^+)$			• D^*	$1/2(1^-)$	• B_s^*	$0(1^-)$	• $\Upsilon(1S)$	$0^-(1^-)$
• $\rho(1570)$	$1^+(1^-)$	• $\eta(2225)$	$0^+(0^-)$	• $D^*(2007)^0$	$1/2(1^-)$	$X(5568)^\pm$	$? (?^?)$	• $\chi_{b0}(1P)$	$0^+(0^+)$
• $h_1(1595)$	$0^-(1^+)$	• $\rho_3(2250)$	$1^+(3^-)$	• $D^*(2010)^\pm$	$1/2(1^-)$	• $B_{s1}(5830)^0$	$0(1^+)$	• $\chi_{b1}(1P)$	$0^+(1^+)$
• $\pi_1(1600)$	$1^-(1^+)$	• $f_2(2300)$	$0^+(2^+)$	• $D_0^*(2300)$	$1/2(0^+)$	• $B_{s2}^*(5840)^0$	$0(2^+)$	• $h_b(1P)$	$0^-(1^+)$
• $a_1(1640)$	$1^-(1^+)$	• $f_4(2300)$	$0^+(4^+)$	• $D_1(2420)$	$1/2(1^+)$	• $B_{s,J}^*(5850)$	$? (?^?)$	• $\chi_{b2}(1P)$	$0^-(1^+)$
• $f_2(1640)$	$0^+(2^+)$	• $f_0(2330)$	$0^+(0^+)$	• $D_1(2430)^0$	$1/2(1^+)$	• $B_{s,J}(6063)^0$	$0(?^?)$	• $\eta_b(2S)$	$0^+(0^+)$
• $\eta_2(1645)$	$0^+(2^-)$	• $f_2(2340)$	$0^+(2^+)$	• $D_2^*(2460)$	$1/2(2^+)$	• $B_{s,J}(6114)^0$	$0(?^?)$	• $\Upsilon(2S)$	$0^-(1^-)$
• $\omega(1650)$	$0^-(1^-)$	• $\rho_5(2350)$	$1^+(5^-)$	• $D_0(2550)^0$	$1/2(0^-)$	BOTTOM, CHARMED ($B = C = \pm 1$)		• $\Upsilon_2(1D)$	$0^-(2^-)$
• $\omega_3(1670)$	$0^-(3^-)$	• $X(2370)$	$?^?(?^?)$	• $D_1^*(2600)^0$	$1/2(1^-)$	• B_c^+	$0(0^-)$	• $\chi_{b0}(2P)$	$0^+(0^+)$
		• $f_6(2510)$	$0^+(6^+)$	• $D^*(2640)^\pm$	$1/2(?^?)$	• $B_c(2S)^\pm$	$0(0^-)$	• $\chi_{b1}(2P)$	$0^+(1^+)$
				• $D_2(2740)^0$	$1/2(2^-)$	$c\bar{c}$ (+ possibly non- $q\bar{q}$ states)		• $h_b(2P)$	$0^-(1^+)$
				• $D_3^*(2750)$	$1/2(3^-)$	• $\eta_c(1S)$	$0^+(0^-)$	• $\chi_{b2}(2P)$	$0^+(2^+)$
				• $D_1^*(2760)^0$	$1/2(1^-)$	• $J/\psi(1S)$	$0^-(1^-)$	• $\Upsilon(3S)$	$0^-(1^-)$
				• $D(3000)^0$	$1/2(?^?)$	• $\chi_{c0}(1P)$	$0^+(0^+)$	• $\chi_{b1}(3P)$	$0^+(1^+)$
						• $\chi_{c1}(1P)$	$0^+(1^+)$	• $\chi_{b2}(3P)$	$0^+(2^+)$
						• $h_c(1P)$	$0^-(1^+)$	• $\Upsilon(4S)$	$0^-(1^-)$
						• $\chi_{c2}(1P)$	$0^+(2^+)$	• $Z_b(10610)$	$1^+(1^+)$
						• $\eta_c(2S)$	$0^+(0^-)$	• $Z_b(10650)$	$1^+(1^+)$
						• $\psi(2S)$	$0^-(1^-)$	• $\Upsilon(10753)$	$?^?(1^-)$
						• $\psi(3770)$	$0^-(1^-)$	• $\Upsilon(10860)$	$0^-(1^-)$
								• $\Upsilon(11020)$	$0^-(1^-)$
								OTHER	
								Further States	

Baryon Summary Table

This short table gives the name, the quantum numbers (where known), and the status of baryons in the Review. Only the baryons with 3- or 4-star status are included in the Baryon Summary Table. Due to insufficient data or uncertain interpretation, the other entries in the table are not established baryons. The names with masses are of baryons that decay strongly. The spin-parity J^P (when known) is given with each particle. For the strongly decaying particles, the J^P values are considered to be part of the names.

p	$1/2^+$	****	$\Delta(1232)$	$3/2^+$	****	Σ^+	$1/2^+$	****	Λ_c^+	$1/2^+$	****	Λ_b^0	$1/2^+$	***
n	$1/2^+$	****	$\Delta(1600)$	$3/2^+$	****	Σ^0	$1/2^+$	****	$\Lambda_c(2595)^+$	$1/2^-$	***	$\Lambda_b(5912)^0$	$1/2^-$	***
$N(1440)$	$1/2^+$	****	$\Delta(1620)$	$1/2^-$	****	Σ^-	$1/2^+$	****	$\Lambda_c(2625)^+$	$3/2^-$	***	$\Lambda_b(5920)^0$	$3/2^-$	***
$N(1520)$	$3/2^-$	****	$\Delta(1700)$	$3/2^-$	****	$\Sigma(1385)$	$3/2^+$	****	$\Lambda_c(2765)^+$	*		$\Lambda_b(6070)^0$	$1/2^+$	***
$N(1535)$	$1/2^-$	****	$\Delta(1750)$	$1/2^+$	*	$\Sigma(1580)$	$3/2^-$	*	$\Lambda_c(2860)^+$	$3/2^+$	***	$\Lambda_b(6146)^0$	$3/2^+$	***
$N(1650)$	$1/2^-$	****	$\Delta(1900)$	$1/2^-$	***	$\Sigma(1620)$	$1/2^-$	*	$\Lambda_c(2880)^+$	$5/2^+$	***	$\Lambda_b(6152)^0$	$5/2^+$	***
$N(1675)$	$5/2^-$	****	$\Delta(1905)$	$5/2^+$	****	$\Sigma(1660)$	$1/2^+$	***	$\Lambda_c(2940)^+$	$3/2^-$	***	Σ_b	$1/2^+$	***
$N(1680)$	$5/2^+$	****	$\Delta(1910)$	$1/2^+$	****	$\Sigma(1670)$	$3/2^-$	****	$\Sigma_c(2455)$	$1/2^+$	****	Σ_b^*	$3/2^+$	***
$N(1700)$	$3/2^-$	***	$\Delta(1920)$	$3/2^+$	***	$\Sigma(1750)$	$1/2^-$	***	$\Sigma_c(2520)$	$3/2^+$	***	$\Sigma_b(6097)^+$		***
$N(1710)$	$3/2^+$	****	$\Delta(1930)$	$5/2^-$	***	$\Sigma(1775)$	$5/2^-$	****	$\Sigma_c(2800)$		***	$\Sigma_b(6097)^-$		***
$N(1720)$	$3/2^+$	****	$\Delta(1940)$	$3/2^-$	**	$\Sigma(1780)$	$3/2^+$	*	Ξ_c^+	$1/2^+$	***	Ξ_b^-	$1/2^+$	***
$N(1860)$	$5/2^+$	**	$\Delta(1950)$	$7/2^+$	****	$\Sigma(1880)$	$1/2^+$	**	Ξ_c^0	$1/2^+$	****	Ξ_b^0	$1/2^+$	***
$N(1875)$	$3/2^-$	***	$\Delta(2000)$	$5/2^+$	**	$\Sigma(1900)$	$1/2^-$	**	$\Xi_c^{'+}$	$1/2^+$	***	$\Xi_b'(5935)^-$	$1/2^+$	***
$N(1880)$	$1/2^+$	***	$\Delta(2150)$	$1/2^-$	*	$\Sigma(1910)$	$3/2^-$	***	Ξ_c^0	$1/2^+$	***	$\Xi_b(5945)^0$	$3/2^+$	***
$N(1895)$	$1/2^-$	****	$\Delta(2200)$	$7/2^-$	***	$\Sigma(1915)$	$5/2^+$	****	Ξ_c^0	$1/2^+$	***	$\Xi_b(5955)^-$	$3/2^+$	***
$N(1900)$	$3/2^+$	****	$\Delta(2300)$	$9/2^+$	**	$\Sigma(1940)$	$3/2^+$	*	$\Xi_c(2645)$	$3/2^+$	***	$\Xi_b(6100)^-$	$3/2^-$	***
$N(1990)$	$7/2^+$	**	$\Delta(2350)$	$5/2^-$	*	$\Sigma(2010)$	$3/2^-$	*	$\Xi_c(2790)$	$1/2^-$	***	$\Xi_b(6227)^-$		***
$N(2000)$	$5/2^+$	**	$\Delta(2390)$	$7/2^+$	*	$\Sigma(2030)$	$7/2^+$	****	$\Xi_c(2815)$	$3/2^-$	***	$\Xi_b(6227)^0$		***
$N(2040)$	$3/2^+$	*	$\Delta(2400)$	$9/2^-$	**	$\Sigma(2070)$	$5/2^+$	*	$\Xi_c(2923)$		**	Ω_b^-	$1/2^+$	***
$N(2060)$	$5/2^-$	***	$\Delta(2420)$	$11/2^+$	****	$\Sigma(2080)$	$3/2^+$	*	$\Xi_c(2930)$		**	$\Omega_b(6316)^-$		*
$N(2100)$	$1/2^+$	***	$\Delta(2475)$	$13/2^-$	**	$\Sigma(2100)$	$7/2^-$	*	$\Xi_c(2970)$	$1/2^+$	***	$\Omega_b(6330)^-$		*
$N(2120)$	$3/2^-$	***	$\Delta(2950)$	$15/2^+$	**	$\Sigma(2110)$	$1/2^-$	*	$\Xi_c(3055)$		***	$\Omega_b(6340)^-$		*
$N(2190)$	$7/2^-$	****				$\Sigma(2230)$	$3/2^+$	*	$\Xi_c(3080)$		***	$\Omega_b(6350)^-$		*
$N(2220)$	$9/2^+$	****	Λ	$1/2^+$	****	$\Sigma(2250)$		**	$\Xi_c(3123)$		*			*
$N(2250)$	$9/2^-$	****	$\Lambda(1380)$	$1/2^-$	**	$\Sigma(2455)$		*	Ω_c^0	$1/2^+$	***	$P_c(4312)^+$		*
$N(2300)$	$1/2^+$	**	$\Lambda(1405)$	$1/2^-$	****	$\Sigma(2620)$		*	$\Omega_c(2770)^0$	$3/2^+$	***	$P_c(4380)^+$		*
$N(2570)$	$5/2^-$	**	$\Lambda(1520)$	$3/2^-$	****	$\Sigma(3000)$		*	$\Omega_c(3000)^0$		***	$P_c(4440)^+$		*
$N(2600)$	$11/2^-$	***	$\Lambda(1600)$	$1/2^+$	****	$\Sigma(3170)$		*	$\Omega_c(3050)^0$		***	$P_c(4457)^+$		*
$N(2700)$	$13/2^+$	**	$\Lambda(1670)$	$1/2^-$	****				$\Omega_c(3065)^0$		***			*
			$\Lambda(1690)$	$3/2^-$	****	Ξ^0	$1/2^+$	****	$\Omega_c(3090)^0$		***			*
			$\Lambda(1710)$	$1/2^+$	*	Ξ^-	$1/2^+$	****	$\Omega_c(3120)^0$		***			*
			$\Lambda(1800)$	$1/2^-$	***	$\Xi(1530)$	$3/2^+$	****						*
			$\Lambda(1810)$	$1/2^+$	***	$\Xi(1620)$		*	Ξ_{cc}^+		*			***
			$\Lambda(1820)$	$5/2^+$	****	$\Xi(1690)$		***	Ξ_{cc}^{++}		***			*
			$\Lambda(1830)$	$5/2^-$	****	$\Xi(1820)$	$3/2^-$	***						*
			$\Lambda(1890)$	$3/2^+$	****	$\Xi(1950)$		***						*
			$\Lambda(2000)$	$1/2^-$	*	$\Xi(2030)$	$\geq \frac{5}{2}^?$	***						*
			$\Lambda(2050)$	$3/2^-$	*	$\Xi(2120)$		*						*
			$\Lambda(2070)$	$3/2^+$	*	$\Xi(2250)$		**						*
			$\Lambda(2080)$	$5/2^-$	*	$\Xi(2370)$		**						*
			$\Lambda(2085)$	$7/2^+$	**	$\Xi(2500)$		*						*
			$\Lambda(2100)$	$7/2^-$	****									*
			$\Lambda(2110)$	$5/2^+$	***	Ω^-	$3/2^+$	****						*
			$\Lambda(2325)$	$3/2^-$	*	$\Omega(2012)^-$	$?^-$	***						*
			$\Lambda(2350)$	$9/2^+$	***	$\Omega(2250)^-$		***						*
			$\Lambda(2585)$		*	$\Omega(2380)^-$		**						*
						$\Omega(2470)^-$		**						*

**** Existence is certain, and properties are at least fairly well explored.

*** Existence ranges from very likely to certain, but further confirmation is desirable and/or quantum numbers, branching fractions, etc. are not well determined.

** Evidence of existence is only fair.

* Evidence of existence is poor.

Baryon Summary Table

N BARYONS
 $(S = 0, I = 1/2)$
 $p, N^+ = uud; \quad n, N^0 = udd$

p $I(J^P) = \frac{1}{2}(\frac{1}{2}^+)$

Mass $m = 1.007276466621 \pm 0.000000000053$ u
 Mass $m = 938.27208816 \pm 0.00000029$ MeV ^[a]
 $|m_p - m_{\bar{p}}|/m_p < 7 \times 10^{-10}$, CL = 90% ^[b]
 $|\frac{q_{\bar{p}}}{m_{\bar{p}}}|/(\frac{q_p}{m_p}) = 1.000000000003 \pm 0.000000000016$
 $|q_p + q_{\bar{p}}|/e < 7 \times 10^{-10}$, CL = 90% ^[b]
 $|q_p + q_e|/e < 1 \times 10^{-21}$ [c]
 Magnetic moment $\mu = 2.7928473446 \pm 0.0000000008$ μ_N
 $(\mu_p + \mu_{\bar{p}}) / \mu_p = (0.002 \pm 0.004) \times 10^{-6}$
 Electric dipole moment $d < 0.021 \times 10^{-23}$ e cm
 Electric polarizability $\alpha = (11.2 \pm 0.4) \times 10^{-4}$ fm³
 Magnetic polarizability $\beta = (2.5 \pm 0.4) \times 10^{-4}$ fm³ ($S = 1.2$)
 Charge radius, μp Lamb shift = 0.84087 ± 0.00039 fm ^[d]
 Charge radius = 0.8409 ± 0.0004 fm ^[d]
 Magnetic radius = 0.851 ± 0.026 fm ^[e]
 Mean life $\tau > 3.6 \times 10^{29}$ years, CL = 90% ^[f] ($p \rightarrow$ invisible mode)
 Mean life $\tau > 10^{31}$ to 10^{33} years ^[f] (mode dependent)

See the "Note on Nucleon Decay" in our 1994 edition (Phys. Rev. **D50**, 1173) for a short review.

The "partial mean life" limits tabulated here are the limits on τ/B_j , where τ is the total mean life and B_j is the branching fraction for the mode in question. For N decays, p and n indicate proton and neutron partial lifetimes.

p DECAY MODES	Partial mean life (10 ³⁰ years)	Confidence level	p (MeV/c)
Antilepton + meson			
$N \rightarrow e^+ \pi$	> 5300 (n), > 16000 (p)	90%	459
$N \rightarrow \mu^+ \pi$	> 3500 (n), > 7700 (p)	90%	453
$N \rightarrow \nu \pi$	> 1100 (n), > 390 (p)	90%	459
$p \rightarrow e^+ \eta$	> 10000	90%	309
$p \rightarrow \mu^+ \eta$	> 4700	90%	297
$n \rightarrow \nu \eta$	> 158	90%	310
$N \rightarrow e^+ \rho$	> 217 (n), > 720 (p)	90%	149
$N \rightarrow \mu^+ \rho$	> 228 (n), > 570 (p)	90%	113
$N \rightarrow \nu \rho$	> 19 (n), > 162 (p)	90%	149
$p \rightarrow e^+ \omega$	> 1600	90%	143
$p \rightarrow \mu^+ \omega$	> 2800	90%	105
$n \rightarrow \nu \omega$	> 108	90%	144
$N \rightarrow e^+ K$	> 17 (n), > 1000 (p)	90%	339
$N \rightarrow \mu^+ K$	> 26 (n), > 1600 (p)	90%	329
$N \rightarrow \nu K$	> 86 (n), > 5900 (p)	90%	339
$n \rightarrow \nu K_S^0$	> 260	90%	338
$p \rightarrow e^+ K^*(892)^0$	> 84	90%	45
$N \rightarrow \nu K^*(892)$	> 78 (n), > 51 (p)	90%	45
Antilepton + mesons			
$p \rightarrow e^+ \pi^+ \pi^-$	> 82	90%	448
$p \rightarrow e^+ \pi^0 \pi^0$	> 147	90%	449
$n \rightarrow e^+ \pi^- \pi^0$	> 52	90%	449
$p \rightarrow \mu^+ \pi^+ \pi^-$	> 133	90%	425
$p \rightarrow \mu^+ \pi^0 \pi^0$	> 101	90%	427
$n \rightarrow \mu^+ \pi^- \pi^0$	> 74	90%	427
$n \rightarrow e^+ K^0 \pi^-$	> 18	90%	319
Lepton + meson			
$n \rightarrow e^- \pi^+$	> 65	90%	459
$n \rightarrow \mu^- \pi^+$	> 49	90%	453
$n \rightarrow e^- \rho^+$	> 62	90%	150
$n \rightarrow \mu^- \rho^+$	> 7	90%	115
$n \rightarrow e^- K^+$	> 32	90%	340
$n \rightarrow \mu^- K^+$	> 57	90%	330
Lepton + mesons			
$p \rightarrow e^- \pi^+ \pi^+$	> 30	90%	448
$n \rightarrow e^- \pi^+ \pi^0$	> 29	90%	449
$p \rightarrow \mu^- \pi^+ \pi^+$	> 17	90%	425
$n \rightarrow \mu^- \pi^+ \pi^0$	> 34	90%	427
$p \rightarrow e^- \pi^+ K^+$	> 75	90%	320
$p \rightarrow \mu^- \pi^+ K^+$	> 245	90%	279

Antilepton + photon(s)			
$p \rightarrow e^+ \gamma$	> 670	90%	469
$p \rightarrow \mu^+ \gamma$	> 478	90%	463
$n \rightarrow \nu \gamma$	> 550	90%	470
$p \rightarrow e^+ \gamma \gamma$	> 100	90%	469
$n \rightarrow \nu \gamma \gamma$	> 219	90%	470

Antilepton + single massless			
$p \rightarrow e^+ X$	> 790	90%	—
$p \rightarrow \mu^+ X$	> 410	90%	—

Three (or more) leptons			
$p \rightarrow e^+ e^+ e^-$	> 793	90%	469
$p \rightarrow e^+ \mu^+ \mu^-$	> 359	90%	457
$p \rightarrow e^+ \nu \nu$	> 170	90%	469
$n \rightarrow e^+ e^- \nu$	> 257	90%	470
$n \rightarrow \mu^+ e^- \nu$	> 83	90%	464
$n \rightarrow \mu^+ \mu^- \nu$	> 79	90%	458
$p \rightarrow \mu^+ e^+ e^-$	> 529	90%	463
$p \rightarrow \mu^- e^+ e^+$	$> 1.90 \times 10^{34}$	90%	463
$p \rightarrow \mu^+ \mu^+ \mu^-$	> 675	90%	439
$p \rightarrow \mu^+ \nu \nu$	> 220	90%	463
$p \rightarrow e^- \mu^+ \mu^+$	> 6	90%	457
$n \rightarrow 3\nu$	$> 5 \times 10^{-4}$	90%	470

Inclusive modes			
$N \rightarrow e^+$ anything	> 0.6 (n, p)	90%	—
$N \rightarrow \mu^+$ anything	> 12 (n, p)	90%	—
$N \rightarrow e^+ \pi^0$ anything	> 0.6 (n, p)	90%	—

$\Delta B = 2$ dinucleon modes			
The following are lifetime limits per iron nucleus.			
$pp \rightarrow \pi^+ \pi^+$	> 72.2	90%	—
$pn \rightarrow \pi^+ \pi^0$	> 170	90%	—
$nn \rightarrow \pi^+ \pi^-$	> 0.7	90%	—
$nn \rightarrow \pi^0 \pi^0$	> 404	90%	—
$pp \rightarrow K^+ K^+$	> 170	90%	—
$pp \rightarrow e^+ e^+$	> 5.8	90%	—
$pp \rightarrow e^+ \mu^+$	> 3.6	90%	—
$pp \rightarrow \mu^+ \mu^+$	> 1.7	90%	—
$pn \rightarrow e^+ \bar{\nu}$	> 260	90%	—
$pn \rightarrow \mu^+ \bar{\nu}$	> 200	90%	—
$pn \rightarrow \tau^+ \bar{\nu}_\tau$	> 29	90%	—
$nn \rightarrow \nu_e \bar{\nu}_e$	> 1.4	90%	—
$nn \rightarrow \nu_\mu \bar{\nu}_\mu$	> 1.4	90%	—
$pn \rightarrow$ invisible	$> 2.1 \times 10^{-5}$	90%	—
$pp \rightarrow$ invisible	$> 5 \times 10^{-5}$	90%	—

\bar{p} DECAY MODES			
\bar{p} DECAY MODES	Partial mean life (years)	Confidence level	p (MeV/c)
$\bar{p} \rightarrow e^- \gamma$	$> 7 \times 10^5$	90%	469
$\bar{p} \rightarrow \mu^- \gamma$	$> 5 \times 10^4$	90%	463
$\bar{p} \rightarrow e^- \pi^0$	$> 4 \times 10^5$	90%	459
$\bar{p} \rightarrow \mu^- \pi^0$	$> 5 \times 10^4$	90%	453
$\bar{p} \rightarrow e^- \eta$	$> 2 \times 10^4$	90%	309
$\bar{p} \rightarrow \mu^- \eta$	$> 8 \times 10^3$	90%	297
$\bar{p} \rightarrow e^- K_S^0$	> 900	90%	337
$\bar{p} \rightarrow \mu^- K_S^0$	$> 4 \times 10^3$	90%	326
$\bar{p} \rightarrow e^- K_L^0$	$> 9 \times 10^3$	90%	337
$\bar{p} \rightarrow \mu^- K_L^0$	$> 7 \times 10^3$	90%	326
$\bar{p} \rightarrow e^- \gamma \gamma$	$> 2 \times 10^4$	90%	469
$\bar{p} \rightarrow \mu^- \gamma \gamma$	$> 2 \times 10^4$	90%	463
$\bar{p} \rightarrow e^- \omega$	> 200	90%	143

n $I(J^P) = \frac{1}{2}(\frac{1}{2}^+)$

Mass $m = 1.0086649160 \pm 0.0000000005$ u
 Mass $m = 939.5654205 \pm 0.0000005$ MeV ^[a]
 $(m_n - m_{\bar{n}}) / m_n = (9 \pm 6) \times 10^{-5}$
 $m_n - m_p = 1.2933324 \pm 0.0000005$ MeV
 $= 0.00138844919(45)$ u
 Mean life $\tau = 878.4 \pm 0.5$ s ($S = 1.8$)
 $c\tau = 2.6335 \times 10^8$ km
 Magnetic moment $\mu = -1.9130427 \pm 0.0000005$ μ_N
 Electric dipole moment $d < 0.18 \times 10^{-25}$ e cm, CL = 90%
 Mean-square charge radius $\langle r_n^2 \rangle = -0.1155 \pm 0.0017$ fm²

Baryon Summary Table

Magnetic radius $\sqrt{\langle r_M^2 \rangle} = 0.864^{+0.009}_{-0.008}$ fm
 Electric polarizability $\alpha = (11.8 \pm 1.1) \times 10^{-4}$ fm³
 Magnetic polarizability $\beta = (3.7 \pm 1.2) \times 10^{-4}$ fm³
 Charge $q = (-0.2 \pm 0.8) \times 10^{-21}$ e
 Mean $n\bar{n}$ -oscillation time $> 8.6 \times 10^7$ s, CL = 90% (free n)
 Mean $n\bar{n}$ -oscillation time $> 4.7 \times 10^8$ s, CL = 90% [8] (bound n)
 Mean $n n'$ -oscillation time > 448 s, CL = 90% [h]

 $p e^- \nu_e$ decay parameters [i]

$\lambda \equiv g_A / g_V = -1.2754 \pm 0.0013$ (S = 2.7)
 $A = -0.11958 \pm 0.00021$ (S = 1.2)
 $B = 0.9807 \pm 0.0030$
 $C = -0.2377 \pm 0.0026$
 $a = -0.1049 \pm 0.0013$ (S = 1.8)
 $\phi_{AV} = (180.017 \pm 0.026)^\circ$ [j]
 $D = (-1.2 \pm 2.0) \times 10^{-4}$ [k]
 $R = 0.004 \pm 0.013$ [k]
 FIERZ INTERFERENCE TERM $b = 0.017 \pm 0.020$

n DECAY MODES	Fraction (Γ_i/Γ)	Confidence level	ρ (MeV/c)
$p e^- \bar{\nu}_e$	100 %		1
$p e^- \bar{\nu}_e \gamma$	[i] $(9.2 \pm 0.7) \times 10^{-3}$		1
hydrogen-atom $\bar{\nu}_e$	$< 2.7 \times 10^{-3}$	95%	1.19

Charge conservation (Q) violating mode

$p \nu_e \bar{\nu}_e$	Q $< 8 \times 10^{-27}$	68%	1
-----------------------	-------------------------	-----	---

 $N(1440) 1/2^+$

$$I(J^P) = \frac{1}{2}(\frac{1}{2}^+)$$

Re(pole position) = 1360 to 1380 (≈ 1370) MeV
 $-2\text{Im}(\text{pole position}) = 160$ to 190 (≈ 175) MeV
 Breit-Wigner mass = 1410 to 1470 (≈ 1440) MeV
 Breit-Wigner full width = 250 to 450 (≈ 350) MeV

$N(1440)$ DECAY MODES	Fraction (Γ_i/Γ)	ρ (MeV/c)
$N\pi$	55–75 %	398
$N\eta$	< 1 %	†
$N\pi\pi$	17–50 %	347
$\Delta(1232)\pi$, P-wave	6–27 %	147
$N\sigma$	11–23 %	–
$p\gamma$, helicity=1/2	0.035–0.048 %	414
$n\gamma$, helicity=1/2	0.02–0.04 %	413

 $N(1520) 3/2^-$

$$I(J^P) = \frac{1}{2}(\frac{3}{2}^-)$$

Re(pole position) = 1505 to 1515 (≈ 1510) MeV
 $-2\text{Im}(\text{pole position}) = 105$ to 120 (≈ 110) MeV
 Breit-Wigner mass = 1510 to 1520 (≈ 1515) MeV
 Breit-Wigner full width = 100 to 120 (≈ 110) MeV

$N(1520)$ DECAY MODES	Fraction (Γ_i/Γ)	ρ (MeV/c)
$N\pi$	55–65 %	453
$N\eta$	0.07–0.09 %	142
$N\pi\pi$	25–35 %	410
$\Delta(1232)\pi$	22–34 %	225
$\Delta(1232)\pi$, S-wave	15–23 %	225
$\Delta(1232)\pi$, D-wave	7–11 %	225
$N\rho$	10–16 %	†
$N\rho$, S=3/2, S-wave	10–16 %	†
$N\rho$, S=1/2, D-wave	0.2–0.4 %	†
$N\sigma$	< 10 %	–
$p\gamma$	0.31–0.52 %	467
$p\gamma$, helicity=1/2	0.01–0.02 %	467
$p\gamma$, helicity=3/2	0.30–0.50 %	467
$n\gamma$	0.30–0.53 %	466
$n\gamma$, helicity=1/2	0.04–0.10 %	466
$n\gamma$, helicity=3/2	0.25–0.45 %	466

 $N(1535) 1/2^-$

$$I(J^P) = \frac{1}{2}(\frac{1}{2}^-)$$

Re(pole position) = 1500 to 1520 (≈ 1510) MeV
 $-2\text{Im}(\text{pole position}) = 110$ to 150 (≈ 130) MeV
 Breit-Wigner mass = 1515 to 1545 (≈ 1530) MeV
 Breit-Wigner full width = 125 to 175 (≈ 150) MeV

$N(1535)$ DECAY MODES	Fraction (Γ_i/Γ)	ρ (MeV/c)
$N\pi$	32–52 %	464
$N\eta$	30–55 %	176
$N\pi\pi$	4–31 %	422
$\Delta(1232)\pi$, D-wave	1–4 %	240
$N\rho$	2–17 %	†
$N\rho$, S=1/2, S-wave	2–16 %	†
$N\rho$, S=3/2, D-wave	< 1 %	†
$N\sigma$	2–10 %	–
$N(1440)\pi$	5–12 %	†
$p\gamma$, helicity=1/2	0.15–0.30 %	477
$n\gamma$, helicity=1/2	0.01–0.25 %	477

 $N(1650) 1/2^-$

$$I(J^P) = \frac{1}{2}(\frac{1}{2}^-)$$

Re(pole position) = 1640 to 1670 (≈ 1655) MeV
 $-2\text{Im}(\text{pole position}) = 100$ to 170 (≈ 135) MeV
 Breit-Wigner mass = 1635 to 1665 (≈ 1650) MeV
 Breit-Wigner full width = 100 to 150 (≈ 125) MeV

$N(1650)$ DECAY MODES	Fraction (Γ_i/Γ)	ρ (MeV/c)
$N\pi$	50–70 %	547
$N\eta$	15–35 %	348
ΛK	5–15 %	169
$N\pi\pi$	20–58 %	514
$\Delta(1232)\pi$, D-wave	6–18 %	345
$N\rho$	12–22 %	†
$N\rho$, S=1/2, S-wave	< 4 %	†
$N\rho$, S=3/2, D-wave	12–18 %	†
$N\sigma$	2–18 %	–
$N(1440)\pi$	6–26 %	150
$p\gamma$, helicity=1/2	0.04–0.20 %	558
$n\gamma$, helicity=1/2	0.003–0.17 %	557

 $N(1675) 5/2^-$

$$I(J^P) = \frac{1}{2}(\frac{5}{2}^-)$$

Re(pole position) = 1655 to 1665 (≈ 1660) MeV
 $-2\text{Im}(\text{pole position}) = 125$ to 150 (≈ 135) MeV
 Breit-Wigner mass = 1665 to 1680 (≈ 1675) MeV
 Breit-Wigner full width = 130 to 160 (≈ 145) MeV

$N(1675)$ DECAY MODES	Fraction (Γ_i/Γ)	ρ (MeV/c)
$N\pi$	38–42 %	564
$N\eta$	< 1 %	376
ΛK	< 0.04 %	216
$N\pi\pi$	25–45 %	532
$\Delta(1232)\pi$, D-wave	23–37 %	366
$N\rho$	0.1–0.9 %	†
$N\rho$, S=1/2	< 0.2 %	†
$N\rho$, S=3/2, D-wave	0.1–0.7 %	†
$N\sigma$	3–7 %	–
$p\gamma$	0–0.02 %	575
$p\gamma$, helicity=1/2	0–0.01 %	575
$p\gamma$, helicity=3/2	0–0.01 %	575
$n\gamma$	0–0.15 %	574
$n\gamma$, helicity=1/2	0–0.05 %	574
$n\gamma$, helicity=3/2	0–0.10 %	574

 $N(1680) 5/2^+$

$$I(J^P) = \frac{1}{2}(\frac{5}{2}^+)$$

Re(pole position) = 1665 to 1680 (≈ 1675) MeV
 $-2\text{Im}(\text{pole position}) = 110$ to 135 (≈ 120) MeV
 Breit-Wigner mass = 1680 to 1690 (≈ 1685) MeV
 Breit-Wigner full width = 115 to 130 (≈ 120) MeV

$N(1680)$ DECAY MODES	Fraction (Γ_i/Γ)	ρ (MeV/c)
$N\pi$	60–70 %	571
$N\eta$	< 1 %	386
$N\pi\pi$	28–53 %	539
$\Delta(1232)\pi$	11–23 %	374
$\Delta(1232)\pi$, P-wave	4–10 %	374
$\Delta(1232)\pi$, F-wave	1–13 %	374
$N\rho$	8–11 %	†

Baryon Summary Table

$N\rho, S=3/2, P\text{-wave}$	6–8 %	†
$N\rho, S=3/2, F\text{-wave}$	2–3 %	†
$N\sigma$	9–19 %	–
$\rho\gamma$	0.21–0.32 %	581
$\rho\gamma, \text{helicity}=1/2$	0.001–0.011 %	581
$\rho\gamma, \text{helicity}=3/2$	0.20–0.32 %	581
$n\gamma$	0.021–0.046 %	581
$n\gamma, \text{helicity}=1/2$	0.004–0.029 %	581
$n\gamma, \text{helicity}=3/2$	0.01–0.024 %	581

 $N(1700) 3/2^-$

$$I(J^P) = \frac{1}{2}(\frac{3}{2}^-)$$

Re(pole position) = 1650 to 1750 (≈ 1700) MeV
 $-2\text{Im}(\text{pole position}) = 100$ to 300 (≈ 200) MeV
 Breit-Wigner mass = 1650 to 1800 (≈ 1720) MeV
 Breit-Wigner full width = 100 to 300 (≈ 200) MeV

$N(1700)$ DECAY MODES	Fraction (Γ_i/Γ)	ρ (MeV/c)
$N\pi$	7–17 %	594
$N\eta$	1–2 %	422
$N\omega$	10–34 %	†
ΛK	1–2 %	283
$N\pi\pi$	>89 %	564
$\Delta(1232)\pi$	55–85 %	402
$\Delta(1232)\pi, S\text{-wave}$	50–80 %	402
$\Delta(1232)\pi, D\text{-wave}$	4–14 %	402
$N\rho, S=3/2, S\text{-wave}$	32–44 %	74
$N\sigma$	2–14 %	–
$N(1440)\pi$	3–11 %	225
$N(1520)\pi$	<4 %	145
$\rho\gamma$	0.01–0.05 %	604
$\rho\gamma, \text{helicity}=1/2$	0.0–0.024 %	604
$\rho\gamma, \text{helicity}=3/2$	0.002–0.026 %	604
$n\gamma$	0.01–0.13 %	603
$n\gamma, \text{helicity}=1/2$	0.0–0.09 %	603
$n\gamma, \text{helicity}=3/2$	0.01–0.05 %	603

 $N(1710) 1/2^+$

$$I(J^P) = \frac{1}{2}(\frac{1}{2}^+)$$

Re(pole position) = 1680 to 1720 (≈ 1700) MeV
 $-2\text{Im}(\text{pole position}) = 80$ to 160 (≈ 120) MeV
 Breit-Wigner mass = 1680 to 1740 (≈ 1710) MeV
 Breit-Wigner full width = 80 to 200 (≈ 140) MeV

$N(1710)$ DECAY MODES	Fraction (Γ_i/Γ)	ρ (MeV/c)
$N\pi$	5–20 %	588
$N\eta$	10–50 %	412
$N\omega$	1–5 %	†
ΛK	5–25 %	269
ΣK	seen	138
$N\pi\pi$	14–48 %	557
$\Delta(1232)\pi, P\text{-wave}$	3–9 %	394
$N\rho, S=1/2, P\text{-wave}$	11–23 %	†
$N\sigma$	<16 %	–
$N(1535)\pi$	9–21 %	113
$\rho\gamma, \text{helicity}=1/2$	0.002–0.08 %	598
$n\gamma, \text{helicity}=1/2$	0.0–0.02 %	597

 $N(1720) 3/2^+$

$$I(J^P) = \frac{1}{2}(\frac{3}{2}^+)$$

Re(pole position) = 1660 to 1690 (≈ 1675) MeV
 $-2\text{Im}(\text{pole position}) = 150$ to 400 (≈ 250) MeV
 Breit-Wigner mass = 1680 to 1750 (≈ 1720) MeV
 Breit-Wigner full width = 150 to 400 (≈ 250) MeV

$N(1720)$ DECAY MODES	Fraction (Γ_i/Γ)	ρ (MeV/c)
$N\pi$	8–14 %	594
$N\eta$	1–5 %	422
$N\omega$	12–40 %	†
ΛK	4–19 %	283
$N\pi\pi$	>50 %	564
$\Delta(1232)\pi$	47–89 %	402
$\Delta(1232)\pi, P\text{-wave}$	47–77 %	402
$\Delta(1232)\pi, F\text{-wave}$	<12 %	402

$N\rho, S=1/2, P\text{-wave}$	1–2 %	74
$N\sigma$	2–14 %	–
$N(1440)\pi$	<2 %	225
$N(1520)\pi, S\text{-wave}$	1–5 %	145
$\rho\gamma$	0.05–0.25 %	604
$\rho\gamma, \text{helicity}=1/2$	0.05–0.15 %	604
$\rho\gamma, \text{helicity}=3/2$	0.002–0.16 %	604
$n\gamma$	0.0–0.016 %	603
$n\gamma, \text{helicity}=1/2$	0.0–0.01 %	603
$n\gamma, \text{helicity}=3/2$	0.0–0.015 %	603

 $N(1875) 3/2^-$

$$I(J^P) = \frac{1}{2}(\frac{3}{2}^-)$$

Re(pole position) = 1850 to 1950 (≈ 1900) MeV
 $-2\text{Im}(\text{pole position}) = 100$ to 220 (≈ 160) MeV
 Breit-Wigner mass = 1850 to 1920 (≈ 1875) MeV
 Breit-Wigner full width = 120 to 250 (≈ 200) MeV

$N(1875)$ DECAY MODES	Fraction (Γ_i/Γ)	ρ (MeV/c)
$N\pi$	3–11 %	695
$N\eta$	3–16 %	559
$N\omega$	15–25 %	371
ΛK	1–2 %	454
ΣK	0.3–1.1 %	384
$N\pi\pi$	>56 %	670
$\Delta(1232)\pi$	4–44 %	520
$\Delta(1232)\pi, S\text{-wave}$	2–21 %	520
$\Delta(1232)\pi, D\text{-wave}$	2–23 %	520
$N\rho, S=3/2, S\text{-wave}$	36–56 %	379
$N\sigma$	16–60 %	–
$N(1440)\pi$	2–8 %	365
$N(1520)\pi$	<2 %	301
$\Lambda K^*(892)$	<0.2 %	†
$\rho\gamma$	0.001–0.025 %	703
$\rho\gamma, \text{helicity}=1/2$	0.001–0.021 %	703
$\rho\gamma, \text{helicity}=3/2$	<0.003 %	703
$n\gamma$	<0.040 %	702
$n\gamma, \text{helicity}=1/2$	<0.007 %	702
$n\gamma, \text{helicity}=3/2$	<0.033 %	702

 $N(1880) 1/2^+$

$$I(J^P) = \frac{1}{2}(\frac{1}{2}^+)$$

Re(pole position) = 1820 to 1900 (≈ 1860) MeV
 $-2\text{Im}(\text{pole position}) = 180$ to 280 (≈ 230) MeV
 Breit-Wigner mass = 1830 to 1930 (≈ 1880) MeV
 Breit-Wigner full width = 200 to 400 (≈ 300) MeV

$N(1880)$ DECAY MODES	Fraction (Γ_i/Γ)	ρ (MeV/c)
$N\pi$	3–31 %	698
$N\eta$	1–55 %	563
$N\omega$	12–28 %	377
ΛK	1–3 %	459
ΣK	10–24 %	389
$N\pi\pi$	>32 %	673
$\Delta(1232)\pi$	5–42 %	524
$N\rho, S=1/2, P\text{-wave}$	19–45 %	385
$N\sigma$	8–40 %	539
$N(1535)\pi$	4–12 %	293
$N_{a0}(980)$	1–5 %	†
$\Lambda K^*(892)$	0.5–1.1 %	†
$\rho\gamma, \text{helicity}=1/2$	seen	706
$n\gamma, \text{helicity}=1/2$	0.002–0.63 %	705

 $N(1895) 1/2^-$

$$I(J^P) = \frac{1}{2}(\frac{1}{2}^-)$$

Re(pole position) = 1890 to 1930 (≈ 1910) MeV
 $-2\text{Im}(\text{pole position}) = 80$ to 140 (≈ 110) MeV
 Breit-Wigner mass = 1870 to 1920 (≈ 1895) MeV
 Breit-Wigner full width = 80 to 200 (≈ 120) MeV

$N(1895)$ DECAY MODES	Fraction (Γ_i/Γ)	ρ (MeV/c)
$N\pi$	2–18 %	707
$N\eta$	15–45 %	575

Baryon Summary Table

$N\eta'$	10–40 %	†
$N\omega$	16–40 %	395
ΛK	3–23 %	473
ΣK	6–20 %	405
$N\pi\pi$	17–74 %	683
$\Delta(1232)\pi$, <i>D</i> -wave	3–11 %	535
$N\rho$	14–50 %	403
$N\rho$, <i>S</i> =1/2, <i>S</i> -wave	<18 %	403
$N\rho$, <i>S</i> =3/2, <i>D</i> -wave	14–32 %	403
$N\sigma$	<13 %	–
$N(1440)\pi$	2–12 %	382
$\Lambda K^*(892)$	4–9 %	†
$p\gamma$, helicity=1/2	0.01–0.06 %	715
$n\gamma$, helicity=1/2	0.003–0.05 %	715

 $N(1900) 3/2^+$

$$I(J^P) = \frac{1}{2}(\frac{3}{2}^+)$$

Re(pole position) = 1900 to 1940 (\approx 1920) MeV
 $-2\text{Im}(\text{pole position}) = 100$ to 200 (\approx 150) MeV
 Breit-Wigner mass = 1890 to 1950 (\approx 1920) MeV
 Breit-Wigner full width = 100 to 320 (\approx 200) MeV

$N(1900)$ DECAY MODES	Fraction (Γ_i/Γ)	ρ (MeV/c)
$N\pi$	1–20 %	723
$N\eta$	2–14 %	595
$N\eta'$	4–8 %	151
$N\omega$	7–13 %	424
ΛK	2–20 %	495
ΣK	3–7 %	431
$N\pi\pi$	>56 %	699
$\Delta(1232)\pi$	30–70 %	553
$\Delta(1232)\pi$, <i>P</i> -wave	9–25 %	553
$\Delta(1232)\pi$, <i>F</i> -wave	21–45 %	553
$N\rho$, <i>S</i> =1/2	25–40 %	432
$N\sigma$	1–7 %	–
$N(1520)\pi$	7–23 %	341
$N(1535)\pi$	4–10 %	328
$\Lambda K^*(892)$	< 0.2 %	†
$p\gamma$	0.001–0.025 %	731
$p\gamma$, helicity=1/2	0.001–0.021 %	731
$p\gamma$, helicity=3/2	<0.003 %	731
$n\gamma$	<0.040 %	730
$n\gamma$, helicity=1/2	<0.007 %	730
$n\gamma$, helicity=3/2	<0.033 %	730

 $N(2060) 5/2^-$

$$I(J^P) = \frac{1}{2}(\frac{5}{2}^-)$$

Re(pole position) = 2020 to 2130 (\approx 2070) MeV
 $-2\text{Im}(\text{pole position}) = 350$ to 430 (\approx 400) MeV
 Breit-Wigner mass = 2030 to 2200 (\approx 2100) MeV
 Breit-Wigner full width = 300 to 450 (\approx 400) MeV

$N(2060)$ DECAY MODES	Fraction (Γ_i/Γ)	ρ (MeV/c)
$N\pi$	7–12 %	834
$N\eta$	2–38 %	729
$N\omega$	1–7 %	600
ΛK	10–20 %	644
ΣK	1–5 %	593
$N\pi\pi$	12–52 %	814
$\Delta(1232)\pi$, <i>D</i> -wave	4–10 %	680
$N\rho$	5–33 %	605
$N\rho$, <i>S</i> =1/2, <i>P</i> -wave	<10 %	605
$N\rho$, <i>S</i> =3/2, <i>D</i> -wave	5–23 %	605
$N\sigma$	3–9 %	–
$N(1440)\pi$	4–14 %	544
$N(1520)\pi$, <i>P</i> -wave	9–21 %	490
$N(1680)\pi$, <i>S</i> -wave	8–22 %	353
$\Lambda K^*(892)$	0.3–1.3 %	307
$p\gamma$	0.03–0.19 %	840
$p\gamma$, helicity=1/2	0.02–0.08 %	840
$p\gamma$, helicity=3/2	0.01–0.10 %	840
$n\gamma$	0.003–0.07 %	840
$n\gamma$, helicity=1/2	0.001–0.02 %	840
$n\gamma$, helicity=3/2	0.002–0.05 %	840

 $N(2100) 1/2^+$

$$I(J^P) = \frac{1}{2}(\frac{1}{2}^+)$$

Re(pole position) = 2050 to 2150 (\approx 2100) MeV
 $-2\text{Im}(\text{pole position}) = 240$ to 340 (\approx 300) MeV
 Breit-Wigner mass = 2050 to 2150 (\approx 2100) MeV
 Breit-Wigner full width = 200 to 320 (\approx 260) MeV

$N(2100)$ DECAY MODES	Fraction (Γ_i/Γ)	ρ (MeV/c)
$N\pi$	8–32 %	834
$N\eta$	5–45 %	729
$N\eta'$	5–11 %	451
$N\omega$	10–25 %	600
ΛK	>55 %	644
$N\pi\pi$	6–14 %	814
$\Delta(1232)\pi$, <i>P</i> -wave	6–14 %	680
$N\rho$, <i>S</i> =1/2, <i>P</i> -wave	35–70 %	605
$N\sigma$	14–35 %	–
$N(1535)\pi$	26–34 %	478
$\Lambda K^*(892)$	3–11 %	307
$p\gamma$, helicity=1/2	0.001–0.13 %	840
$n\gamma$, helicity=1/2	0.004–0.09 %	840

 $N(2120) 3/2^-$

$$I(J^P) = \frac{1}{2}(\frac{3}{2}^-)$$

Re(pole position) = 2050 to 2150 (\approx 2100) MeV
 $-2\text{Im}(\text{pole position}) = 200$ to 360 (\approx 280) MeV
 Breit-Wigner mass = 2060 to 2160 (\approx 2120) MeV
 Breit-Wigner full width = 260 to 360 (\approx 300) MeV

$N(2120)$ DECAY MODES	Fraction (Γ_i/Γ)	ρ (MeV/c)
$N\pi$	5–15 %	846
$N\eta$	1–5 %	743
$N\eta'$	2–6 %	474
$N\omega$	4–20 %	617
ΛK	6–11 %	660
$N\pi\pi$	>23 %	827
$\Delta(1232)\pi$	>27 %	693
$\Delta(1232)\pi$, <i>S</i> -wave	15–70 %	693
$\Delta(1232)\pi$, <i>D</i> -wave	8–45 %	693
$N\rho$, <i>S</i> =3/2, <i>S</i> -wave	< 3 %	622
$N\sigma$	4–15 %	–
$N(1535)\pi$	7–23 %	494
$\Lambda K^*(892)$	< 0.2 %	339
$p\gamma$	0.16–2.1 %	852
$p\gamma$, helicity=1/2	0.07–0.80 %	852
$p\gamma$, helicity=3/2	0.09–1.3 %	852
$n\gamma$	0.04–0.72 %	852
$n\gamma$, helicity=1/2	0.04–0.60 %	852
$n\gamma$, helicity=3/2	0.001–0.12 %	852

 $N(2190) 7/2^-$

$$I(J^P) = \frac{1}{2}(\frac{7}{2}^-)$$

Re(pole position) = 2050 to 2150 (\approx 2100) MeV
 $-2\text{Im}(\text{pole position}) = 300$ to 500 (\approx 400) MeV
 Breit-Wigner mass = 2140 to 2220 (\approx 2180) MeV
 Breit-Wigner full width = 300 to 500 (\approx 400) MeV

$N(2190)$ DECAY MODES	Fraction (Γ_i/Γ)	ρ (MeV/c)
$N\pi$	10–20 %	882
$N\eta$	1–5 %	785
$N\omega$	8–20 %	667
ΛK	0.2–0.8 %	705
$N\pi\pi$	22–51 %	864
$\Delta(1232)\pi$, <i>D</i> -wave	19–31 %	734
$N\rho$, <i>S</i> =3/2, <i>D</i> -wave	<11 %	672
$N\sigma$	3–9 %	–
$\Lambda K^*(892)$	0.2–0.8 %	423
$p\gamma$	<0.08 %	888
$p\gamma$, helicity=1/2	<0.06 %	888
$p\gamma$, helicity=3/2	<0.02 %	888
$n\gamma$	<0.04 %	888
$n\gamma$, helicity=1/2	<0.01 %	888
$n\gamma$, helicity=3/2	<0.03 %	888

Baryon Summary Table

 $N(2220) 9/2^+$

$$I(J^P) = \frac{1}{2}(\frac{9}{2}^+)$$

Re(pole position) = 2130 to 2200 (≈ 2170) MeV
 $-2\text{Im}(\text{pole position}) = 360$ to 480 (≈ 400) MeV
 Breit-Wigner mass = 2200 to 2300 (≈ 2250) MeV
 Breit-Wigner full width = 350 to 500 (≈ 400) MeV

$N(2220)$ DECAY MODES	Fraction (Γ_i/Γ)	ρ (MeV/c)
$N\pi$	15–30 %	924

 $N(2250) 9/2^-$

$$I(J^P) = \frac{1}{2}(\frac{9}{2}^-)$$

Re(pole position) = 2150 to 2250 (≈ 2200) MeV
 $-2\text{Im}(\text{pole position}) = 350$ to 500 (≈ 420) MeV
 Breit-Wigner mass = 2250 to 2320 (≈ 2280) MeV
 Breit-Wigner full width = 300 to 600 (≈ 500) MeV

$N(2250)$ DECAY MODES	Fraction (Γ_i/Γ)	ρ (MeV/c)
$N\pi$	5–15 %	941
$N\eta$	<5 %	852
ΛK	1–3 %	777

 $N(2600) 11/2^-$

$$I(J^P) = \frac{1}{2}(\frac{11}{2}^-)$$

Breit-Wigner mass = 2550 to 2750 (≈ 2600) MeV
 Breit-Wigner full width = 500 to 800 (≈ 650) MeV

$N(2600)$ DECAY MODES	Fraction (Γ_i/Γ)	ρ (MeV/c)
$N\pi$	3–8 %	1126

Δ BARYONS ($S = 0, I = 3/2$)

$$\Delta^{++} = uuu, \Delta^+ = uud, \Delta^0 = udd, \Delta^- = ddd$$

 $\Delta(1232) 3/2^+$

$$I(J^P) = \frac{3}{2}(\frac{3}{2}^+)$$

Re(pole position) = 1209 to 1211 (≈ 1210) MeV
 $-2\text{Im}(\text{pole position}) = 98$ to 102 (≈ 100) MeV
 Breit-Wigner mass (mixed charges) = 1230 to 1234 (≈ 1232) MeV
 Breit-Wigner full width (mixed charges) = 114 to 120 (≈ 117) MeV

$\Delta(1232)$ DECAY MODES	Fraction (Γ_i/Γ)	ρ (MeV/c)
$N\pi$	99.4 %	229
$N\gamma$	0.55–0.65 %	259
$N\gamma$, helicity=1/2	0.11–0.13 %	259
$N\gamma$, helicity=3/2	0.44–0.52 %	259
$p e^+ e^-$	$(4.2 \pm 0.7) \times 10^{-5}$	259

 $\Delta(1600) 3/2^+$

$$I(J^P) = \frac{3}{2}(\frac{3}{2}^+)$$

Re(pole position) = 1460 to 1560 (≈ 1510) MeV
 $-2\text{Im}(\text{pole position}) = 200$ to 340 (≈ 270) MeV
 Breit-Wigner mass = 1500 to 1640 (≈ 1570) MeV
 Breit-Wigner full width = 200 to 300 (≈ 250) MeV

$\Delta(1600)$ DECAY MODES	Fraction (Γ_i/Γ)	ρ (MeV/c)
$N\pi$	8–24%	492
$N\pi\pi$	58–84 %	454
$\Delta(1232)\pi$	58–82 %	276
$\Delta(1232)\pi$, P-wave	72–82%	276
$\Delta(1232)\pi$, F-wave	<2%	276
$N(1440)\pi$	17–27%	†
$N\gamma$	0.001–0.035 %	505
$N\gamma$, helicity=1/2	0.0–0.02 %	505
$N\gamma$, helicity=3/2	0.001–0.015 %	505

 $\Delta(1620) 1/2^-$

$$I(J^P) = \frac{3}{2}(\frac{1}{2}^-)$$

Re(pole position) = 1590 to 1610 (≈ 1600) MeV
 $-2\text{Im}(\text{pole position}) = 100$ to 140 (≈ 120) MeV
 Breit-Wigner mass = 1590 to 1630 (≈ 1610) MeV
 Breit-Wigner full width = 110 to 150 (≈ 130) MeV

$\Delta(1620)$ DECAY MODES	Fraction (Γ_i/Γ)	ρ (MeV/c)
$N\pi$	25–35 %	520
$N\pi\pi$	>67 %	484
$\Delta(1232)\pi$, D-wave	44–72 %	311
$N\rho$	23–32%	†
$N\rho$, S=1/2, S-wave	23–32%	†
$N\rho$, S=3/2, D-wave	<0.04%	†
$N(1440)\pi$	<9 %	98
$N\gamma$, helicity=1/2	0.03–0.10 %	532

 $\Delta(1700) 3/2^-$

$$I(J^P) = \frac{3}{2}(\frac{3}{2}^-)$$

Re(pole position) = 1640 to 1690 (≈ 1665) MeV
 $-2\text{Im}(\text{pole position}) = 200$ to 300 (≈ 250) MeV
 Breit-Wigner mass = 1690 to 1730 (≈ 1710) MeV
 Breit-Wigner full width = 220 to 380 (≈ 300) MeV

$\Delta(1700)$ DECAY MODES	Fraction (Γ_i/Γ)	ρ (MeV/c)
$N\pi$	10–20 %	588
$N\pi\pi$	>31 %	557
$\Delta(1232)\pi$	9–70 %	394
$\Delta(1232)\pi$, S-wave	5–54 %	394
$\Delta(1232)\pi$, D-wave	4–16 %	394
$N\rho$, S=3/2, S-wave	22–32%	†
$N(1520)\pi$, P-wave	1–5 %	133
$N(1535)\pi$	0.5–1.5 %	113
$\Delta(1232)\eta$	3–7 %	†
$N\gamma$	0.22–0.60 %	598
$N\gamma$, helicity=1/2	0.12–0.30 %	598
$N\gamma$, helicity=3/2	0.10–0.30 %	598

 $\Delta(1900) 1/2^-$

$$I(J^P) = \frac{3}{2}(\frac{1}{2}^-)$$

Re(pole position) = 1830 to 1900 (≈ 1865) MeV
 $-2\text{Im}(\text{pole position}) = 180$ to 300 (≈ 240) MeV
 Breit-Wigner mass = 1840 to 1920 (≈ 1860) MeV
 Breit-Wigner full width = 180 to 320 (≈ 250) MeV

$\Delta(1900)$ DECAY MODES	Fraction (Γ_i/Γ)	ρ (MeV/c)
$N\pi$	4–12%	685
ΣK	seen	367
$N\pi\pi$	> 5.2%	660
$\Delta(1232)\pi$, D-wave	30–70%	509
$N\rho$	22–60 %	360
$N\rho$, S=1/2, S-wave	11–35%	360
$N\rho$, S=3/2, D-wave	11–25%	360
$N(1440)\pi$	3–32%	353
$N(1520)\pi$	2–10%	288
$\Delta(1232)\eta$	< 2%	251
$N\gamma$, helicity=1/2	0.06–0.43 %	693

 $\Delta(1905) 5/2^+$

$$I(J^P) = \frac{3}{2}(\frac{5}{2}^+)$$

Re(pole position) = 1770 to 1830 (≈ 1800) MeV
 $-2\text{Im}(\text{pole position}) = 260$ to 340 (≈ 300) MeV
 Breit-Wigner mass = 1855 to 1910 (≈ 1880) MeV
 Breit-Wigner full width = 270 to 400 (≈ 330) MeV

$\Delta(1905)$ DECAY MODES	Fraction (Γ_i/Γ)	ρ (MeV/c)
$N\pi$	9–15%	698
$N\pi\pi$	>65%	673
$\Delta(1232)\pi$	>48%	524
$\Delta(1232)\pi$, P-wave	8–43%	524
$\Delta(1232)\pi$, F-wave	40–58%	524

Baryon Summary Table

$N\rho, S=3/2, P\text{-wave}$	17–35%	385
$N(1535)\pi$	< 1%	293
$N(1680)\pi, P\text{-wave}$	5–15%	133
$\Delta(1232)\eta$	2–6%	282
$N\gamma$	0.012–0.036%	706
$N\gamma, \text{helicity}=1/2$	0.002–0.006%	706
$N\gamma, \text{helicity}=3/2$	0.01–0.03%	706

 $\Delta(1910) 1/2^+$

$$I(J^P) = \frac{3}{2}(\frac{1}{2}^+)$$

Re(pole position) = 1830 to 1890 (\approx 1860) MeV
 $-2\text{Im}(\text{pole position}) = 200$ to 400 (\approx 300) MeV
 Breit-Wigner mass = 1850 to 1950 (\approx 1900) MeV
 Breit-Wigner full width = 200 to 400 (\approx 300) MeV

$\Delta(1910)$ DECAY MODES	Fraction (Γ_i/Γ)	ρ (MeV/c)
$N\pi$	10–30%	710
ΣK	4–14%	410
$\Delta(1232)\pi$	34–66%	539
$N(1440)\pi$	3–45%	386
$\Delta(1232)\eta$	5–13%	310
$N\gamma, \text{helicity}=1/2$	0.0–0.02%	718

 $\Delta(1920) 3/2^+$

$$I(J^P) = \frac{3}{2}(\frac{3}{2}^+)$$

Re(pole position) = 1850 to 1950 (\approx 1900) MeV
 $-2\text{Im}(\text{pole position}) = 200$ to 400 (\approx 300) MeV
 Breit-Wigner mass = 1870 to 1970 (\approx 1920) MeV
 Breit-Wigner full width = 240 to 360 (\approx 300) MeV

$\Delta(1920)$ DECAY MODES	Fraction (Γ_i/Γ)	ρ (MeV/c)
$N\pi$	5–20%	723
ΣK	2–6%	431
$N\pi\pi$	>46%	699
$\Delta(1232)\pi$	>46%	553
$\Delta(1232)\pi, P\text{-wave}$	2–28%	553
$\Delta(1232)\pi, F\text{-wave}$	44–72%	553
$N(1440)\pi, P\text{-wave}$	4–86%	403
$N(1520)\pi, S\text{-wave}$	<5%	341
$N(1535)\pi$	<2%	328
$N\pi_0(980)$	seen	41
$\Delta(1232)\eta$	5–17%	336
$N\gamma$	0.01–0.84%	731
$N\gamma, \text{helicity}=1/2$	0.0–0.42%	731
$N\gamma, \text{helicity}=3/2$	0.01–0.42%	731

 $\Delta(1930) 5/2^-$

$$I(J^P) = \frac{3}{2}(\frac{5}{2}^-)$$

Re(pole position) = 1840 to 1920 (\approx 1880) MeV
 $-2\text{Im}(\text{pole position}) = 230$ to 330 (\approx 280) MeV
 Breit-Wigner mass = 1900 to 2000 (\approx 1950) MeV
 Breit-Wigner full width = 200 to 400 (\approx 300) MeV

$\Delta(1930)$ DECAY MODES	Fraction (Γ_i/Γ)	ρ (MeV/c)
$N\pi$	5–15%	742
$N\gamma$	0.0–0.01%	749
$N\gamma, \text{helicity}=1/2$	0.0–0.005%	749
$N\gamma, \text{helicity}=3/2$	0.0–0.004%	749

 $\Delta(1950) 7/2^+$

$$I(J^P) = \frac{3}{2}(\frac{7}{2}^+)$$

Re(pole position) = 1870 to 1890 (\approx 1880) MeV
 $-2\text{Im}(\text{pole position}) = 220$ to 260 (\approx 240) MeV
 Breit-Wigner mass = 1915 to 1950 (\approx 1930) MeV
 Breit-Wigner full width = 235 to 335 (\approx 285) MeV

$\Delta(1950)$ DECAY MODES	Fraction (Γ_i/Γ)	ρ (MeV/c)
$N\pi$	35–45%	729
ΣK	0.3–0.5%	441
$N\pi\pi$	37–77%	706

$\Delta(1232)\pi, F\text{-wave}$	1–9%	560
$N(1680)\pi, P\text{-wave}$	3–9%	191
$\Delta(1232)\eta$	< 0.6%	349
$N\gamma$	0.06–0.14%	737
$N\gamma, \text{helicity}=1/2$	0.03–0.05%	737
$N\gamma, \text{helicity}=3/2$	0.04–0.09%	737

 $\Delta(2200) 7/2^-$

$$I(J^P) = \frac{3}{2}(\frac{7}{2}^-)$$

Re(pole position) = 2050 to 2150 (\approx 2100) MeV
 $-2\text{Im}(\text{pole position}) = 260$ to 420 (\approx 340) MeV
 Breit-Wigner mass = 2150 to 2250 (\approx 2200) MeV
 Breit-Wigner full width = 200 to 500 (\approx 350) MeV

$\Delta(2200)$ DECAY MODES	Fraction (Γ_i/Γ)	ρ (MeV/c)
$N\pi$	2–8%	894
ΣK	1–7%	672
$N\pi\pi$	>45%	876
$\Delta\pi$	>45%	747
$\Delta\pi, D\text{-wave}$	>40%	747
$\Delta\pi, G\text{-wave}$	5–25%	747
$\Delta\eta, D\text{-wave}$	seen	614

 $\Delta(2420) 11/2^+$

$$I(J^P) = \frac{3}{2}(\frac{11}{2}^+)$$

Re(pole position) = 2300 to 2500 (\approx 2400) MeV
 $-2\text{Im}(\text{pole position}) = 350$ to 550 (\approx 450) MeV
 Breit-Wigner mass = 2300 to 2600 (\approx 2450) MeV
 Breit-Wigner full width = 300 to 700 (\approx 500) MeV

$\Delta(2420)$ DECAY MODES	Fraction (Γ_i/Γ)	ρ (MeV/c)
$N\pi$	5–10%	1040

Λ BARYONS

$(S = -1, I = 0)$

$$\Lambda^0 = uds$$

 Λ

$$I(J^P) = 0(\frac{1}{2}^+)$$

Mass $m = 1115.683 \pm 0.006$ MeV
 $(m_\Lambda - m_\pi) / m_\Lambda = (-0.1 \pm 1.1) \times 10^{-5}$ ($S = 1.6$)
 Mean life $\tau = (2.632 \pm 0.020) \times 10^{-10}$ s ($S = 1.6$)
 $(\tau_\Lambda - \tau_\pi) / \tau_\Lambda = -0.001 \pm 0.009$
 $c\tau = 7.89$ cm
 Magnetic moment $\mu = -0.613 \pm 0.004 \mu_N$
 Electric dipole moment $d < 1.5 \times 10^{-16}$ e cm, CL = 95%

Decay parameters

$p\pi^-$ $\alpha_- = 0.732 \pm 0.014$ ($S = 2.3$)
 $\bar{p}\pi^+$ $\alpha_+ = -0.758 \pm 0.012$
 $\bar{\alpha}_0$ FOR $\bar{\Lambda} \rightarrow \bar{n}\pi^0 = -0.692 \pm 0.017$
 $p\pi^-$ $\phi_- = (-6.5 \pm 3.5)^\circ$
 " $\gamma_- = 0.76$ [n]
 " $\Delta_- = (8 \pm 4)^\circ$ [n]
 $\bar{\alpha}_0 / \alpha_+$ in $\bar{\Lambda} \rightarrow \bar{n}\pi^0, \bar{\Lambda} \rightarrow \bar{p}\pi^+ = 0.913 \pm 0.030$
 $R = |\mathcal{G}_E/\mathcal{G}_M|$ in $\Lambda \rightarrow p\pi^-, \bar{\Lambda} \rightarrow \bar{p}\pi^+ = 0.96 \pm 0.14$
 $\Delta\Phi = \Phi_E - \Phi_M$ in $\Lambda \rightarrow p\pi^-, \bar{\Lambda} \rightarrow \bar{p}\pi^+ = 37 \pm 13$ degrees
 $n\pi^0$ $\alpha_0 = 0.74 \pm 0.05$
 $p e^- \bar{\nu}_e$ $g_A/g_V = -0.718 \pm 0.015$ [l]

Λ DECAY MODES	Fraction (Γ_i/Γ)	Confidence level	ρ (MeV/c)
$p\pi^-$	(63.9 \pm 0.5) %		101
$n\pi^0$	(35.8 \pm 0.5) %		104
$n\gamma$	(1.75 \pm 0.15) $\times 10^{-3}$		162
$p\pi^-\gamma$	[0] (8.4 \pm 1.4) $\times 10^{-4}$		101
$p e^- \bar{\nu}_e$	(8.32 \pm 0.14) $\times 10^{-4}$		163
$p\mu^- \bar{\nu}_\mu$	(1.57 \pm 0.35) $\times 10^{-4}$		131

Baryon Summary Table

Lepton (L) and/or Baryon (B) number violating decay modes

$\pi^+ e^-$	L, B	< 6	$\times 10^{-7}$	90%	549
$\pi^+ \mu^-$	L, B	< 6	$\times 10^{-7}$	90%	544
$\pi^- e^+$	L, B	< 4	$\times 10^{-7}$	90%	549
$\pi^- \mu^+$	L, B	< 6	$\times 10^{-7}$	90%	544
$K^+ e^-$	L, B	< 2	$\times 10^{-6}$	90%	449
$K^+ \mu^-$	L, B	< 3	$\times 10^{-6}$	90%	441
$K^- e^+$	L, B	< 2	$\times 10^{-6}$	90%	449
$K^- \mu^+$	L, B	< 3	$\times 10^{-6}$	90%	441
$K_S^0 \nu$	L, B	< 2	$\times 10^{-5}$	90%	447
$\bar{p} \pi^+$	B	< 9	$\times 10^{-7}$	90%	101

 $\Lambda(1405) 1/2^-$

$I(J^P) = 0(\frac{1}{2}^-)$

Mass $m = 1405.1^{+1.3}_{-1.0}$ MeV
Full width $\Gamma = 50.5 \pm 2.0$ MeV
Below $\bar{K}N$ threshold

$\Lambda(1405)$ DECAY MODES	Fraction (Γ_i/Γ)	ρ (MeV/c)
$\Sigma \pi$	100 %	155

 $\Lambda(1520) 3/2^-$

$I(J^P) = 0(\frac{3}{2}^-)$

Mass $m = 1518$ to 1520 (≈ 1519) MeV [p]
Full width $\Gamma = 15$ to 17 (≈ 16) MeV [p]

$\Lambda(1520)$ DECAY MODES	Fraction (Γ_i/Γ)	ρ (MeV/c)
$N\bar{K}$	(45 ± 1) %	242
$\Sigma \pi$	(42 ± 1) %	268
$\Lambda \pi \pi$	(10 ± 1) %	259
$\Sigma \pi \pi$	(0.9 ± 0.1) %	168
$\Lambda \gamma$	(0.85 ± 0.15) %	350

 $\Lambda(1600) 1/2^+$

$I(J^P) = 0(\frac{1}{2}^+)$

Mass $m = 1570$ to 1630 (≈ 1600) MeV
Full width $\Gamma = 150$ to 250 (≈ 200) MeV

$\Lambda(1600)$ DECAY MODES	Fraction (Γ_i/Γ)	ρ (MeV/c)
$N\bar{K}$	15–30 %	343
$\Sigma \pi$	10–60 %	338
$\Lambda \sigma$	(19 ± 4) %	–
$\Sigma(1385) \pi$	(9 ± 4) %	158

 $\Lambda(1670) 1/2^-$

$I(J^P) = 0(\frac{1}{2}^-)$

Mass $m = 1670$ to 1678 (≈ 1674) MeV
Full width $\Gamma = 25$ to 35 (≈ 30) MeV

$\Lambda(1670)$ DECAY MODES	Fraction (Γ_i/Γ)	ρ (MeV/c)
$N\bar{K}$	20–30 %	418
$\Sigma \pi$	25–55 %	398
$\Lambda \eta$	10–25 %	88
$\Sigma(1385) \pi, D$ -wave	(6.0 ± 2.0) %	235
$N\bar{K}^*(892), S=3/2, D$ -wave	(5 ± 4) %	†
$\Lambda \sigma$	(20 ± 8) %	–

 $\Lambda(1690) 3/2^-$

$I(J^P) = 0(\frac{3}{2}^-)$

Mass $m = 1685$ to 1695 (≈ 1690) MeV
Full width $\Gamma = 60$ to 80 (≈ 70) MeV

$\Lambda(1690)$ DECAY MODES	Fraction (Γ_i/Γ)	ρ (MeV/c)
$N\bar{K}$	20–30 %	433
$\Sigma \pi$	20–40 %	410
$\Lambda \sigma$	(5.0 ± 2.0) %	–
$\Lambda \pi \pi$	~ 25 %	419
$\Sigma \pi \pi$	~ 20 %	358
$\Sigma(1385) \pi, S$ -wave	(9 ± 5) %	251
$\Sigma(1385) \pi, D$ -wave	(3.0 ± 2.0) %	251

 $\Lambda(1800) 1/2^-$

$I(J^P) = 0(\frac{1}{2}^-)$

Mass $m = 1750$ to 1850 (≈ 1800) MeV
Full width $\Gamma = 150$ to 250 (≈ 200) MeV

$\Lambda(1800)$ DECAY MODES	Fraction (Γ_i/Γ)	ρ (MeV/c)
$N\bar{K}$	25–40 %	528
$\Sigma \pi$	seen	494
$\Lambda \sigma$	(15 ± 4) %	–
$\Sigma(1385) \pi$	seen	349
$\Lambda \eta$	0.01 to 0.10	326
$N\bar{K}^*(892)$	seen	†

 $\Lambda(1810) 1/2^+$

$I(J^P) = 0(\frac{1}{2}^+)$

Mass $m = 1740$ to 1840 (≈ 1790) MeV
Full width $\Gamma = 50$ to 170 (≈ 110) MeV

$\Lambda(1810)$ DECAY MODES	Fraction (Γ_i/Γ)	ρ (MeV/c)
$N\bar{K}$	0.05 to 0.35	520
$\Sigma \pi$	(16 ± 5) %	487
$\Sigma(1385) \pi$	(40 ± 15) %	340
$N\bar{K}^*(892)$	30–60 %	†

 $\Lambda(1820) 5/2^+$

$I(J^P) = 0(\frac{5}{2}^+)$

Mass $m = 1815$ to 1825 (≈ 1820) MeV
Full width $\Gamma = 70$ to 90 (≈ 80) MeV

$\Lambda(1820)$ DECAY MODES	Fraction (Γ_i/Γ)	ρ (MeV/c)
$N\bar{K}$	55–65 %	545
$\Sigma \pi$	8–14 %	509
$\Sigma(1385) \pi$	5–10 %	366
$N\bar{K}^*(892), S=3/2, P$ -wave	(3.0 ± 1.0) %	†

 $\Lambda(1830) 5/2^-$

$I(J^P) = 0(\frac{5}{2}^-)$

Mass $m = 1820$ to 1830 (≈ 1825) MeV
Full width $\Gamma = 60$ to 120 (≈ 90) MeV

$\Lambda(1830)$ DECAY MODES	Fraction (Γ_i/Γ)	Scale factor	ρ (MeV/c)
$N\bar{K}$	0.04 to 0.08		549
$\Sigma \pi$	35–75 %		512
$\Sigma(1385) \pi$	>15 %		370
$\Sigma(1385) \pi, D$ -wave	(40 ± 15) %	3.2	370

 $\Lambda(1890) 3/2^+$

$I(J^P) = 0(\frac{3}{2}^+)$

Mass $m = 1870$ to 1910 (≈ 1890) MeV
Full width $\Gamma = 80$ to 160 (≈ 120) MeV

$\Lambda(1890)$ DECAY MODES	Fraction (Γ_i/Γ)	ρ (MeV/c)
$N\bar{K}$	0.24 to 0.36	599
$\Sigma \pi$	3–10 %	560
$\Sigma(1385) \pi$	seen	423
$\Sigma(1385) \pi, P$ -wave	(6.0 ± 3.0) %	423
$\Sigma(1385) \pi, F$ -wave	(4.0 ± 2.0) %	423
$N\bar{K}^*(892)$	seen	236

 $\Lambda(2100) 7/2^-$

$I(J^P) = 0(\frac{7}{2}^-)$

Mass $m = 2090$ to 2110 (≈ 2100) MeV
Full width $\Gamma = 100$ to 250 (≈ 200) MeV

$\Lambda(2100)$ DECAY MODES	Fraction (Γ_i/Γ)	ρ (MeV/c)
$N\bar{K}$	25–35 %	751
$\Sigma \pi$	~ 5 %	705
$\Lambda \eta$	<3 %	617

Baryon Summary Table

ΞK	<3 %	491
$\Lambda\omega$	<8 %	443
$\Sigma(1385)\pi$, <i>G</i> -wave	(1.0±1.0) %	584
$N\bar{K}^*(892)$	10–20 %	515
$N\bar{K}^*(892)$, <i>S</i> =3/2, <i>D</i> -wave	(4.0±2.0) %	515

 $\Lambda(2110) 5/2^+$

$$I(J^P) = 0(\frac{5}{2}^+)$$

Mass $m = 2050$ to 2130 (≈ 2090) MeV
Full width $\Gamma = 200$ to 300 (≈ 250) MeV

$\Lambda(2110)$ DECAY MODES	Fraction (Γ_i/Γ)	ρ (MeV/c)
$N\bar{K}$	5–25 %	744
$\Sigma\pi$	10–40 %	698
$\Lambda\omega$	seen	432
$\Lambda\omega$, <i>S</i> =3/2, <i>P</i> -wave	(5.0±2.0) %	432
$\Sigma(1385)\pi$	seen	576
$N\bar{K}^*(892)$	10–60 %	505

 $\Lambda(2350) 9/2^+$

$$I(J^P) = 0(\frac{9}{2}^+)$$

Mass $m = 2340$ to 2370 (≈ 2350) MeV
Full width $\Gamma = 100$ to 250 (≈ 150) MeV

$\Lambda(2350)$ DECAY MODES	Fraction (Γ_i/Γ)	ρ (MeV/c)
$N\bar{K}$	~ 12 %	915
$\Sigma\pi$	~ 10 %	867

Σ BARYONS (*S* = −1, *I* = 1)

$$\Sigma^+ = uus, \quad \Sigma^0 = uds, \quad \Sigma^- = dds$$

 Σ^+

$$I(J^P) = 1(\frac{1}{2}^+)$$

Mass $m = 1189.37 \pm 0.07$ MeV (*S* = 2.2)
Mean life $\tau = (0.8018 \pm 0.0026) \times 10^{-10}$ s
 $c\tau = 2.404$ cm
 $(\tau_{\Sigma^+} - \tau_{\Sigma^-}) / \tau_{\Sigma^+} = -0.0006 \pm 0.0012$
Magnetic moment $\mu = 2.458 \pm 0.010 \mu_N$ (*S* = 2.1)
 $(\mu_{\Sigma^+} + \mu_{\Sigma^-}) / \mu_{\Sigma^+} = 0.014 \pm 0.015$
 $\Gamma(\Sigma^+ \rightarrow n\ell^+\nu) / \Gamma(\Sigma^- \rightarrow n\ell^-\bar{\nu}_\ell) < 0.043$

Decay parameters

$\rho\pi^0$	$\alpha_0 = -0.982 \pm 0.014$
$\bar{\alpha}_0$ FOR $\Sigma^- \rightarrow \bar{p}\pi^0$	$\alpha_0 = 0.99 \pm 0.04$
$(\alpha_0 + \bar{\alpha}_0) / (\alpha_0 - \bar{\alpha}_0)$	$= 0.00 \pm 0.04$
"	$\phi_0 = (36 \pm 34)^\circ$
"	$\gamma_0 = 0.16 [n]$
"	$\Delta_0 = (187 \pm 6)^\circ [n]$
$n\pi^+$	$\alpha_+ = 0.068 \pm 0.013$
"	$\phi_+ = (167 \pm 20)^\circ$ (<i>S</i> = 1.1)
"	$\gamma_+ = -0.97 [n]$
"	$\Delta_+ = (-73^{+133}_{-10})^\circ [n]$
$\rho\gamma$	$\alpha_\gamma = -0.76 \pm 0.08$

Σ^+ DECAY MODES	Fraction (Γ_i/Γ)	Confidence level	ρ (MeV/c)
$\rho\pi^0$	(51.57±0.30) %		189
$n\pi^+$	(48.31±0.30) %		185
$\rho\gamma$	(1.23±0.05) × 10 ⁻³		225
$n\pi^+\gamma$	[o] (4.5 ± 0.5) × 10 ⁻⁴		185
$\Lambda e^+\nu_e$	(2.0 ± 0.5) × 10 ⁻⁵		71

Δ*S* = Δ*Q* (*SQ*) violating modes or Δ*S* = 1 weak neutral current (*S1*) modes

$n e^+ \nu_e$	<i>SQ</i>	< 5	× 10 ⁻⁶	90%	224
$n \mu^+ \nu_\mu$	<i>SQ</i>	< 3.0	× 10 ⁻⁵	90%	202
$p e^+ e^-$	<i>S1</i>	< 7	× 10 ⁻⁶		225
$\rho \mu^+ \mu^-$	<i>S1</i>	(2.4 \pm 1.7 \pm 1.3)	× 10 ⁻⁸		121

 Σ^0

$$I(J^P) = 1(\frac{1}{2}^+)$$

Mass $m = 1192.642 \pm 0.024$ MeV
 $m_{\Sigma^-} - m_{\Sigma^0} = 4.807 \pm 0.035$ MeV (*S* = 1.1)
 $m_{\Sigma^0} - m_\Lambda = 76.959 \pm 0.023$ MeV
Mean life $\tau = (7.4 \pm 0.7) \times 10^{-20}$ s
 $c\tau = 2.22 \times 10^{-11}$ m
Transition magnetic moment $|\mu_{\Sigma\Lambda}| = 1.61 \pm 0.08 \mu_N$

 Σ^0 DECAY MODES

DECAY MODES	Fraction (Γ_i/Γ)	Confidence level	ρ (MeV/c)
$\Lambda\gamma$	100 %		74
$\Lambda\gamma\gamma$	< 3 %	90%	74
$\Lambda e^+ e^-$	[q] 5 × 10 ⁻³		74

 Σ^-

$$I(J^P) = 1(\frac{1}{2}^+)$$

Mass $m = 1197.449 \pm 0.030$ MeV (*S* = 1.2)
 $m_{\Sigma^-} - m_{\Sigma^+} = 8.08 \pm 0.08$ MeV (*S* = 1.9)
 $m_{\Sigma^-} - m_\Lambda = 81.766 \pm 0.030$ MeV (*S* = 1.2)
Mean life $\tau = (1.479 \pm 0.011) \times 10^{-10}$ s (*S* = 1.3)
 $c\tau = 4.434$ cm
Magnetic moment $\mu = -1.160 \pm 0.025 \mu_N$ (*S* = 1.7)
 Σ^- charge radius = 0.78 ± 0.10 fm

Decay parameters

$n\pi^-$	$\alpha_- = -0.068 \pm 0.008$
"	$\phi_- = (10 \pm 15)^\circ$
"	$\gamma_- = 0.98 [n]$
"	$\Delta_- = (249^{+12}_{-120})^\circ [n]$
$n e^- \bar{\nu}_e$	$g_A/g_V = 0.340 \pm 0.017 [I]$
"	$f_2(0)/f_1(0) = 0.97 \pm 0.14$
"	$D = 0.11 \pm 0.10$
$\Lambda e^- \bar{\nu}_e$	$g_V/g_A = 0.01 \pm 0.10 [I]$ (<i>S</i> = 1.5)
"	$g_{WM}/g_A = 2.4 \pm 1.7 [I]$

 Σ^- DECAY MODES

DECAY MODES	Fraction (Γ_i/Γ)	Confidence level	ρ (MeV/c)
$n\pi^-$	(99.848±0.005) %		193
$n\pi^-\gamma$	[o] (4.6 ± 0.6) × 10 ⁻⁴		193
$n e^- \bar{\nu}_e$	(1.017±0.034) × 10 ⁻³		230
$n \mu^- \bar{\nu}_\mu$	(4.5 ± 0.4) × 10 ⁻⁴		210
$\Lambda e^- \bar{\nu}_e$	(5.73 ± 0.27) × 10 ⁻⁵		79
$\Sigma^+ X$	< 1.2 × 10 ⁻⁴	90%	-

Lepton number (*L*) violating modes

$p e^- e^-$	<i>L</i>	< 6.7 × 10 ⁻⁵	90%	231
-------------	----------	--------------------------	-----	-----

 $\Sigma(1385) 3/2^+$

$$I(J^P) = 1(\frac{3}{2}^+)$$

$\Sigma(1385)^+$ mass $m = 1382.83 \pm 0.34$ MeV (*S* = 1.9)
 $\Sigma(1385)^0$ mass $m = 1383.7 \pm 1.0$ MeV (*S* = 1.4)
 $\Sigma(1385)^-$ mass $m = 1387.2 \pm 0.5$ MeV (*S* = 2.2)
 $\Sigma(1385)^+$ full width $\Gamma = 36.2 \pm 0.7$ MeV
 $\Sigma(1385)^0$ full width $\Gamma = 36 \pm 5$ MeV
 $\Sigma(1385)^-$ full width $\Gamma = 39.4 \pm 2.1$ MeV (*S* = 1.7)
Below $\bar{K}N$ threshold

 $\Sigma(1385)$ DECAY MODES

DECAY MODES	Fraction (Γ_i/Γ)	Confidence level	ρ (MeV/c)
$\Lambda\pi$	(87.0 ± 1.5) %		208
$\Sigma\pi$	(11.7 ± 1.5) %		129
$\Lambda\gamma$	(1.25 \pm 0.13 \pm 0.12) %		241
$\Sigma^+\gamma$	(7.0 ± 1.7) × 10 ⁻³		180
$\Sigma^-\gamma$	< 2.4 × 10 ⁻⁴	90%	173

 $\Sigma(1660) 1/2^+$

$$I(J^P) = 1(\frac{1}{2}^+)$$

Re(pole position) = 1585 ± 20 MeV
 $-2\text{Im}(\text{pole position}) = 290 \pm 140$ MeV
Mass $m = 1640$ to 1680 (≈ 1660) MeV
Full width $\Gamma = 100$ to 300 (≈ 200) MeV

Baryon Summary Table

$\Sigma(1660)$ DECAY MODES	Fraction (Γ_i/Γ)	ρ (MeV/c)
$N\bar{K}$	0.05 to 0.15 (≈ 010)	405
$\Lambda\pi$	(35 ± 12) %	440
$\Sigma\pi$	(37 ± 10) %	387
$\Sigma\sigma$	(20 ± 8) %	–
$\Lambda(1405)\pi$	(4.0 ± 2.0) %	199

 $\Sigma(1670) 3/2^-$

$$I(J^P) = 1(\frac{3}{2}^-)$$

Mass $m = 1665$ to 1685 (≈ 1675) MeV
 Full width $\Gamma = 40$ to 100 (≈ 70) MeV

$\Sigma(1670)$ DECAY MODES	Fraction (Γ_i/Γ)	ρ (MeV/c)
$N\bar{K}$	0.06 to 0.12	419
$\Lambda\pi$	5–15 %	452
$\Sigma\pi$	30–60 %	398
$\Sigma\sigma$	(7.0 ± 3.0) %	–

 $\Sigma(1750) 1/2^-$

$$I(J^P) = 1(\frac{1}{2}^-)$$

Mass $m = 1700$ to 1800 (≈ 1750) MeV
 Full width $\Gamma = 100$ to 200 (≈ 150) MeV

$\Sigma(1750)$ DECAY MODES	Fraction (Γ_i/Γ)	ρ (MeV/c)
$N\bar{K}$	0.06 to 0.12	486
$\Lambda\pi$	(14 ± 5) %	507
$\Sigma\pi$	(16 ± 4) %	456
$\Sigma\eta$	15–55 %	98
$\Sigma(1385)\pi$, D -wave	< 1 %	305
$\Lambda(1520)\pi$	(2.0 ± 1.0) %	175
$N\bar{K}^*(892)$, $S=1/2$	(8 ± 4) %	†

 $\Sigma(1775) 5/2^-$

$$I(J^P) = 1(\frac{5}{2}^-)$$

Mass $m = 1770$ to 1780 (≈ 1775) MeV
 Full width $\Gamma = 105$ to 135 (≈ 120) MeV

$\Sigma(1775)$ DECAY MODES	Fraction (Γ_i/Γ)	ρ (MeV/c)
$N\bar{K}$	37–43%	508
$\Lambda\pi$	14–20%	525
$\Sigma\pi$	2–5%	475
$\Sigma(1385)\pi$	8–12%	327
$\Lambda(1520)\pi$, P -wave	17–23%	202

 $\Sigma(1910) 3/2^-$

$$I(J^P) = 1(\frac{3}{2}^-)$$

was $\Sigma(1940)$

Mass $m = 1870$ to 1950 (≈ 1910) MeV
 Full width $\Gamma = 150$ to 300 (≈ 220) MeV

$\Sigma(1910)$ DECAY MODES	Fraction (Γ_i/Γ)	ρ (MeV/c)
$N\bar{K}$	0.01 to 0.05 (≈ 0.02)	615
$\Lambda\pi$	(6 ± 4) %	619
$\Sigma\pi$	(86 ± 21) %	574
$\Sigma(1385)\pi$	seen	439
$\Lambda(1520)\pi$	seen	329
$\Delta(1232)\bar{K}$	(3.0 ± 1.0) %	377
$N\bar{K}^*(892)$	seen	274
$N\bar{K}^*(892)$, $S=1/2$, D -wave	(1.0 ± 1.0) %	274

 $\Sigma(1915) 5/2^+$

$$I(J^P) = 1(\frac{5}{2}^+)$$

Mass $m = 1900$ to 1935 (≈ 1915) MeV
 Full width $\Gamma = 80$ to 160 (≈ 120) MeV

$\Sigma(1915)$ DECAY MODES	Fraction (Γ_i/Γ)	ρ (MeV/c)
$N\bar{K}$	0.05 to 0.15	618
$\Lambda\pi$	(6.0 ± 2.0) %	623

$\Sigma\pi$	(10.0 ± 2.0) %	577
$\Sigma(1385)\pi$, P -wave	(2.0 ± 2.0) %	443
$\Sigma(1385)\pi$, F -wave	(4.0 ± 2.0) %	443
$\Lambda(1520)\pi$, D -wave	(8.0 ± 2.0) %	334
$N\bar{K}^*(892)$, $S=1/2$, F -wave	(5.0 ± 3.0) %	282
$N\bar{K}^*(892)$, $S=3/2$, F -wave	(5.0 ± 2.0) %	282
$\Delta\bar{K}$, P -wave	(16 ± 5) %	383
$\Delta\bar{K}$, F -wave	(5.0 ± 3.0) %	383

 $\Sigma(2030) 7/2^+$

$$I(J^P) = 1(\frac{7}{2}^+)$$

Mass $m = 2025$ to 2040 (≈ 2030) MeV
 Full width $\Gamma = 150$ to 200 (≈ 180) MeV

$\Sigma(2030)$ DECAY MODES	Fraction (Γ_i/Γ)	ρ (MeV/c)
$N\bar{K}$	17–23 %	702
$\Lambda\pi$	17–23 %	700
$\Sigma\pi$	5–10 %	657
ΞK	<2 %	422
$\Sigma(1385)\pi$	5–15 %	532
$\Sigma(1385)\pi$, F -wave	(1.0 ± 1.0) %	532
$\Lambda(1520)\pi$	10–20 %	431
$\Delta(1232)\bar{K}$	10–20 %	498
$\Delta(1232)\bar{K}$, F -wave	(15 ± 5) %	498
$\Delta(1232)\bar{K}$, H -wave	(1.0 ± 1.0) %	498
$N\bar{K}^*(892)$, $S=3/2$, F -wave	(14 ± 8) %	439

 Ξ BARYONS
($S = -2$, $I = 1/2$)

$$\Xi^0 = u s s, \quad \Xi^- = d s s$$

 Ξ^0

$$I(J^P) = \frac{1}{2}(\frac{1}{2}^+)$$

P is not yet measured; + is the quark model prediction.

Mass $m = 1314.86 \pm 0.20$ MeV
 $m_{\Xi^-} - m_{\Xi^0} = 6.85 \pm 0.21$ MeV
 Mean life $\tau = (2.90 \pm 0.09) \times 10^{-10}$ s
 $c\tau = 8.71$ cm
 Magnetic moment $\mu = -1.250 \pm 0.014 \mu_N$

Decay parameters

$\Lambda\pi^0$	$\alpha = -0.356 \pm 0.011$
"	$\phi = (21 \pm 12)^\circ$
"	$\gamma = 0.85 [n]$
"	$\Delta = (218^{+12}_{-19})^\circ [n]$
$\Lambda\gamma$	$\alpha = -0.70 \pm 0.07$
$\Lambda e^+ e^-$	$\alpha = -0.8 \pm 0.2$
$\Sigma^0\gamma$	$\alpha = -0.69 \pm 0.06$
$\Sigma^+ e^- \bar{\nu}_e$	$g_1(0)/f_1(0) = 1.22 \pm 0.05$
$\Sigma^+ e^- \bar{\nu}_e$	$f_2(0)/f_1(0) = 2.0 \pm 0.9$

Ξ^0 DECAY MODES	Fraction (Γ_i/Γ)	Confidence level	ρ (MeV/c)
$\Lambda\pi^0$	(99.524 ± 0.012) %		135
$\Lambda\gamma$	(1.17 ± 0.07) $\times 10^{-3}$		184
$\Lambda e^+ e^-$	(7.6 ± 0.6) $\times 10^{-6}$		184
$\Sigma^0\gamma$	(3.33 ± 0.10) $\times 10^{-3}$		117
$\Sigma^+ e^- \bar{\nu}_e$	(2.52 ± 0.08) $\times 10^{-4}$		120
$\Sigma^+ \mu^- \bar{\nu}_\mu$	(2.33 ± 0.35) $\times 10^{-6}$		64

 $\Delta S = \Delta Q$ (SQ) violating modes or
 $\Delta S = 2$ forbidden ($S2$) modes

$\Sigma^- e^+ \nu_e$	$SQ < 9$	$\times 10^{-4}$	90%	112
$\Sigma^- \mu^+ \nu_\mu$	$SQ < 9$	$\times 10^{-4}$	90%	49
$p\pi^-$	$S2 < 8$	$\times 10^{-6}$	90%	299
$p e^- \bar{\nu}_e$	$S2 < 1.3$	$\times 10^{-3}$		323
$p \mu^- \bar{\nu}_\mu$	$S2 < 1.3$	$\times 10^{-3}$		309

Baryon Summary Table

 Ξ^-

$$I(J^P) = \frac{1}{2}(\frac{1}{2}^+)$$

 P is not yet measured; + is the quark model prediction.

Mass $m = 1321.71 \pm 0.07$ MeV
 $(m_{\Xi^-} - m_{\Xi^+}) / m_{\Xi^-} = (-3 \pm 9) \times 10^{-5}$
 Mean life $\tau = (1.639 \pm 0.015) \times 10^{-10}$ s
 $c\tau = 4.91$ cm
 $(\tau_{\Xi^-} - \tau_{\Xi^+}) / \tau_{\Xi^-} = -0.01 \pm 0.07$
 Magnetic moment $\mu = -0.6507 \pm 0.0025 \mu_N$
 $(\mu_{\Xi^-} + \mu_{\Xi^+}) / |\mu_{\Xi^-}| = +0.01 \pm 0.05$

Decay parameters

$\Lambda\pi^-$ $\alpha = -0.401 \pm 0.010$
 $[\alpha(\Xi^-)\alpha_-(\Lambda) - \alpha(\Xi^+)\alpha_+(\bar{\Lambda})] / [\text{sum}] = (0 \pm 7) \times 10^{-4}$
 " $\phi = (-2.1 \pm 0.8)^\circ$
 " $\gamma = 0.89$ [n]
 " $\Delta = (175.9 \pm 1.5)^\circ$ [n]
 $\Lambda e^- \bar{\nu}_e$ $g_A/g_V = -0.25 \pm 0.05$ [l]

Ξ^- DECAY MODES	Fraction (Γ_i/Γ)	Confidence level	ρ (MeV/c)
$\Lambda\pi^-$	$(99.887 \pm 0.035) \%$		140
$\Sigma^- \gamma$	$(1.27 \pm 0.23) \times 10^{-4}$		118
$\Lambda e^- \bar{\nu}_e$	$(5.63 \pm 0.31) \times 10^{-4}$		190
$\Lambda\mu^- \bar{\nu}_\mu$	$(3.5^{+3.5}_{-2.2}) \times 10^{-4}$		163
$\Sigma^0 e^- \bar{\nu}_e$	$(8.7 \pm 1.7) \times 10^{-5}$		123
$\Sigma^0 \mu^- \bar{\nu}_\mu$	$< 8 \times 10^{-4}$	90%	70
$\Xi^0 e^- \bar{\nu}_e$	$< 2.59 \times 10^{-4}$	90%	7

 $\Delta S = 2$ forbidden (S_2) modes

$n\pi^-$	$S_2 < 1.9 \times 10^{-5}$	90%	304
$n e^- \bar{\nu}_e$	$S_2 < 3.2 \times 10^{-3}$	90%	327
$n\mu^- \bar{\nu}_\mu$	$S_2 < 1.5 \%$	90%	314
$p\pi^- \pi^-$	$S_2 < 4 \times 10^{-4}$	90%	223
$p\pi^- e^- \bar{\nu}_e$	$S_2 < 4 \times 10^{-4}$	90%	305
$p\pi^- \mu^- \bar{\nu}_\mu$	$S_2 < 4 \times 10^{-4}$	90%	251
$p\mu^- \mu^-$	$L < 4 \times 10^{-8}$	90%	272

 $\Xi(1530) 3/2^+$

$$I(J^P) = \frac{1}{2}(\frac{3}{2}^+)$$

$\Xi(1530)^0$ mass $m = 1531.80 \pm 0.32$ MeV ($S = 1.3$)
 $\Xi(1530)^-$ mass $m = 1535.0 \pm 0.6$ MeV
 $\Xi(1530)^0$ full width $\Gamma = 9.1 \pm 0.5$ MeV
 $\Xi(1530)^-$ full width $\Gamma = 9.9^{+1.7}_{-1.9}$ MeV

$\Xi(1530)$ DECAY MODES	Fraction (Γ_i/Γ)	Confidence level	ρ (MeV/c)
$\Xi\pi$	100 %		158
$\Xi\gamma$	$< 3.7 \%$	90%	202

 $\Xi(1690)$

$$I(J^P) = \frac{1}{2}(\frac{1}{2}^?)$$

Mass $m = 1690 \pm 10$ MeV [p]
 Full width $\Gamma = 20 \pm 15$ MeV

$\Xi(1690)$ DECAY MODES	Fraction (Γ_i/Γ)	ρ (MeV/c)
$\Lambda\bar{K}$	seen	240
$\Sigma\bar{K}$	seen	70
$\Xi\pi$	seen	311
$\Xi^- \pi^+ \pi^-$	possibly seen	213

 $\Xi(1820) 3/2^-$

$$I(J^P) = \frac{1}{2}(\frac{3}{2}^-)$$

Mass $m = 1823 \pm 5$ MeV [p]
 Full width $\Gamma = 24^{+15}_{-10}$ MeV [p]

$\Xi(1820)$ DECAY MODES	Fraction (Γ_i/Γ)	ρ (MeV/c)
$\Lambda\bar{K}$	large	402
$\Sigma\bar{K}$	small	324
$\Xi\pi$	small	421
$\Xi(1530)\pi$	small	237

 $\Xi(1950)$

$$I(J^P) = \frac{1}{2}(\frac{1}{2}^?)$$

Mass $m = 1950 \pm 15$ MeV [p]
 Full width $\Gamma = 60 \pm 20$ MeV [p]

$\Xi(1950)$ DECAY MODES	Fraction (Γ_i/Γ)	ρ (MeV/c)
$\Lambda\bar{K}$	seen	522
$\Sigma\bar{K}$	possibly seen	460
$\Xi\pi$	seen	519

 $\Xi(2030)$

$$I(J^P) = \frac{1}{2}(\geq \frac{5}{2}^?)$$

Mass $m = 2025 \pm 5$ MeV [p]
 Full width $\Gamma = 20^{+15}_{-5}$ MeV [p]

$\Xi(2030)$ DECAY MODES	Fraction (Γ_i/Γ)	ρ (MeV/c)
$\Lambda\bar{K}$	$\sim 20 \%$	585
$\Sigma\bar{K}$	$\sim 80 \%$	529
$\Xi\pi$	small	574
$\Xi(1530)\pi$	small	416
$\Lambda\bar{K}\pi$	small	499
$\Sigma\bar{K}\pi$	small	428

 Ω BARYONS
($S = -3, I = 0$)

$$\Omega^- = sss$$

 Ω^-

$$I(J^P) = 0(\frac{3}{2}^+)$$

 $J^P = \frac{3}{2}^+$ is the quark-model prediction; and $J = 3/2$ is fairly well established.

Mass $m = 1672.45 \pm 0.29$ MeV
 $(m_{\Omega^-} - m_{\bar{\Omega}^+}) / m_{\Omega^-} = (-1 \pm 8) \times 10^{-5}$
 Mean life $\tau = (0.821 \pm 0.011) \times 10^{-10}$ s
 $c\tau = 2.461$ cm
 $(\tau_{\Omega^-} - \tau_{\bar{\Omega}^+}) / \tau_{\Omega^-} = 0.00 \pm 0.05$
 Magnetic moment $\mu = -2.02 \pm 0.05 \mu_N$

Decay parameters

$\alpha(\Omega^-)\alpha_-(\Lambda)$ FOR $\Omega^- \rightarrow \Lambda K^- = 0.0115 \pm 0.0015$
 ΛK^- $\alpha = 0.0157 \pm 0.0021$
 $\Lambda K^-, \bar{\Lambda} K^+$ $(\alpha + \bar{\alpha}) / (\alpha - \bar{\alpha}) = -0.02 \pm 0.13$
 $\Xi^0 \pi^-$ $\alpha = 0.09 \pm 0.14$
 $\Xi^- \pi^0$ $\alpha = 0.05 \pm 0.21$

Ω^- DECAY MODES	Fraction (Γ_i/Γ)	Confidence level	ρ (MeV/c)
ΛK^-	$(67.8 \pm 0.7) \%$		211
$\Xi^0 \pi^-$	$(23.6 \pm 0.7) \%$		294
$\Xi^- \pi^0$	$(8.6 \pm 0.4) \%$		289
$\Xi^- \pi^+ \pi^-$	$(3.7^{+0.7}_{-0.6}) \times 10^{-4}$		189
$\Xi(1530)^0 \pi^-$	$< 7 \times 10^{-5}$	90%	17
$\Xi^0 e^- \bar{\nu}_e$	$(5.6 \pm 2.8) \times 10^{-3}$		319
$\Xi^- \gamma$	$< 4.6 \times 10^{-4}$	90%	314

 $\Delta S = 2$ forbidden (S_2) modes

$\Lambda\pi^-$	$S_2 < 2.9 \times 10^{-6}$	90%	449
----------------	----------------------------	-----	-----

 $\Omega(2012)^-$

$$I(J^P) = 0(\frac{1}{2}^-)$$

Mass $m = 2012.4 \pm 0.9$ MeV
 Full width $\Gamma = 6.4^{+3.0}_{-2.6}$ MeV

Branching fractions are given relative to the one DEFINED AS 1.

$\Omega(2012)^-$ DECAY MODES	Fraction (Γ_i/Γ)	Confidence level	ρ (MeV/c)
$\Xi^0 K^-$	DEFINED AS 1		403
$\Xi^- \bar{K}^0$	0.83 ± 0.21		392
$\Xi^0 \pi^0 K^-$	< 0.30	90%	245

Baryon Summary Table

$\Xi^0 \pi^- \bar{K}^0$	<0.21	90%	230
$\Xi^- \pi^0 \bar{K}^0$	<0.7	90%	226
$\Xi^- \pi^+ K^-$	<0.08	90%	224

$\Omega(2250)^-$	$I(J^P) = 0(?^?)$
Mass $m = 2252 \pm 9$ MeV	
Full width $\Gamma = 55 \pm 18$ MeV	

$\Omega(2250)^-$ DECAY MODES	Fraction (Γ_i/Γ)	ρ (MeV/c)
$\Xi^- \pi^+ K^-$	seen	532
$\Xi(1530)^0 K^-$	seen	437

CHARMED BARYONS ($C = +1$)

$$\Lambda_c^+ = udc, \quad \Sigma_c^{++} = uuc, \quad \Sigma_c^+ = udc, \quad \Sigma_c^0 = ddc,$$

$$\Xi_c^+ = usc, \quad \Xi_c^0 = dsc, \quad \Omega_c^0 = ssc$$

Λ_c^+	$I(J^P) = 0(\frac{1}{2}^+)$
Mass $m = 2286.46 \pm 0.14$ MeV	
Mean life $\tau = (201.5 \pm 2.7) \times 10^{-15}$ s ($S = 1.6$)	
$c\tau = 60.4$ μ m	

Decay asymmetry parameters

$\Lambda_c^+ \rightarrow \Sigma^+ \pi^0$	$\alpha = -0.84 \pm 0.09$
$\Sigma^+ \pi^0$	$\alpha = -0.55 \pm 0.11$
α FOR $\Lambda_c^+ \rightarrow \Sigma^0 \pi^+$	$\alpha = -0.73 \pm 0.18$
$\Lambda_c^+ \rightarrow \rho^+ \pi^0$	$\alpha = -0.86 \pm 0.04$
α FOR $\Lambda_c^+ \rightarrow \rho^+ K^0$	$\alpha = 0.2 \pm 0.5$
$(\alpha + \bar{\alpha})/(\alpha - \bar{\alpha})$ in $\Lambda_c^+ \rightarrow \Lambda \pi^+, \bar{\Lambda}_c^- \rightarrow \bar{\Lambda} \pi^-$	$= -0.07 \pm 0.31$
$(\alpha + \bar{\alpha})/(\alpha - \bar{\alpha})$ in $\Lambda_c^+ \rightarrow \Lambda e^+ \nu_e, \bar{\Lambda}_c^- \rightarrow \bar{\Lambda} e^- \bar{\nu}_e$	$= 0.00 \pm 0.04$
$A_{CP}(\Lambda X)$ in $\Lambda_c^+ \rightarrow \Lambda X, \bar{\Lambda}_c^- \rightarrow \bar{\Lambda} X = (2 \pm 7)\%$	
$\Delta A_{CP} = A_{CP}(\Lambda_c^+ \rightarrow \rho^+ K^+ K^-) - A_{CP}(\Lambda_c^+ \rightarrow \rho^+ \pi^+ \pi^-) =$	$(0.3 \pm 1.1)\%$

Branching fractions marked with a footnote, e.g. [a], have been corrected for decay modes not observed in the experiments. For example, the sub-mode fraction $\Lambda_c^+ \rightarrow p \bar{K}^*(892)^0 \rightarrow p K^- \pi^+$ has been multiplied up to include $\bar{K}^*(892)^0 \rightarrow \bar{K}^0 \pi^0$ decays.

Λ_c^+ DECAY MODES	Fraction (Γ_i/Γ)	Scale factor/ Confidence level	ρ (MeV/c)
---------------------------	--------------------------------	-----------------------------------	-------------------

Hadronic modes with a ρ or n : $S = -1$ final states

ρK_S^0	$(1.59 \pm 0.08)\%$	$S=1.1$	873
$\rho K^- \pi^+$	$(6.28 \pm 0.32)\%$	$S=1.4$	823
$\rho \bar{K}^*(892)^0$	[r] $(1.96 \pm 0.27)\%$		685
$\Delta(1232)^{++} K^-$	$(1.08 \pm 0.25)\%$		710
$\Lambda(1520) \pi^+$	[r] $(2.2 \pm 0.5)\%$		628
$\rho K^- \pi^+$ nonresonant	$(3.5 \pm 0.4)\%$		823
$\rho K_S^0 \pi^0$	$(1.97 \pm 0.13)\%$	$S=1.1$	823
$n K_S^0 \pi^+$	$(1.82 \pm 0.25)\%$		821
$\rho \bar{K}^0 \eta$	$(8.3 \pm 1.8) \times 10^{-3}$		568
$\rho K_S^0 \pi^+ \pi^-$	$(1.60 \pm 0.12)\%$	$S=1.1$	754
$\rho K^- \pi^+ \pi^0$	$(4.46 \pm 0.30)\%$	$S=1.5$	759
$\rho K^*(892)^- \pi^+$	[r] $(1.4 \pm 0.5)\%$		580
$\rho(K^- \pi^+)_{\text{nonresonant}} \pi^0$	$(4.6 \pm 0.8)\%$		759
$\Delta(1232) \bar{K}^*(892)$	seen		419
$\rho K^- 2\pi^+ \pi^-$	$(1.4 \pm 0.9) \times 10^{-3}$		671
$\rho K^- \pi^+ 2\pi^0$	$(1.0 \pm 0.5)\%$		678

Hadronic modes with a ρ : $S = 0$ final states

$\rho \pi^0$	< 8	$\times 10^{-5}$	CL=90%	945
$\rho \eta$	$(1.42 \pm 0.12) \times 10^{-3}$			856
$\rho \omega(782)^0$	$(8.3 \pm 1.1) \times 10^{-4}$			751
$\rho \pi^+ \pi^-$	$(4.61 \pm 0.28) \times 10^{-3}$			927
$\rho f_0(980)$	[r] $(3.5 \pm 2.3) \times 10^{-3}$			614
$\rho 2\pi^+ 2\pi^-$	$(2.3 \pm 1.4) \times 10^{-3}$			852
$\rho K^+ K^-$	$(1.06 \pm 0.06) \times 10^{-3}$			616
$\rho \phi$	[r] $(1.06 \pm 0.14) \times 10^{-3}$			590
$\rho K^+ K^-$ non- ϕ	$(5.3 \pm 1.2) \times 10^{-4}$			616
$\rho \phi \pi^0$	$(10 \pm 4) \times 10^{-5}$			460
$\rho K^+ K^- \pi^0$ nonresonant	< 6.3	$\times 10^{-5}$	CL=90%	494

Hadronic modes with a hyperon: $S = -1$ final states

$\Lambda \pi^+$	$(1.30 \pm 0.07)\%$	$S=1.1$	864	
$\Lambda(1670) \pi^+, \Lambda(1670) \rightarrow \eta \Lambda$	$(3.5 \pm 0.5) \times 10^{-3}$		-	
$\Lambda \pi^+ \pi^0$	$(7.1 \pm 0.4)\%$	$S=1.1$	844	
$\Lambda \rho^+$	< 6	CL=95%	636	
$\Lambda \pi^- 2\pi^+$	$(3.64 \pm 0.29)\%$	$S=1.4$	807	
$\Sigma(1385)^+ \pi^+ \pi^-, \Sigma^{*+} \rightarrow \Lambda \pi^+$	$(1.0 \pm 0.5)\%$		688	
$\Sigma(1385)^- 2\pi^+, \Sigma^{*-} \rightarrow \Lambda \pi^+$	$(7.6 \pm 1.4) \times 10^{-3}$		688	
$\Lambda \pi^+ \rho^0$	$(1.5 \pm 0.6)\%$		524	
$\Sigma(1385)^+ \rho^0, \Sigma^{*+} \rightarrow \Lambda \pi^+$	$(5 \pm 4) \times 10^{-3}$		363	
$\Lambda \pi^- 2\pi^+$ nonresonant	< 1.1	CL=90%	807	
$\Lambda \pi^- \pi^0 2\pi^+$ total	$(2.3 \pm 0.8)\%$		757	
$\Lambda \pi^+ \eta$	[r] $(1.84 \pm 0.26)\%$		691	
$\Sigma(1385)^+ \eta$	[r] $(9.1 \pm 2.0) \times 10^{-3}$		570	
$\Lambda \pi^+ \omega$	[r] $(1.5 \pm 0.5)\%$		517	
$\Lambda \pi^- \pi^0 2\pi^+$, no η or ω	< 8	$\times 10^{-3}$	CL=90%	757
$\Lambda K^+ \bar{K}^0$	$(5.7 \pm 1.1) \times 10^{-3}$	$S=1.9$	443	
$\Xi(1690)^0 K^+, \Xi^{*0} \rightarrow \Lambda \bar{K}^0$	$(1.6 \pm 0.5) \times 10^{-3}$		286	
$\Sigma^0 \pi^+$	$(1.29 \pm 0.07)\%$	$S=1.1$	825	
$\Sigma^0 \pi^+ \eta$	$(7.5 \pm 0.8) \times 10^{-3}$		635	
$\Sigma^+ \pi^0$	$(1.25 \pm 0.10)\%$		827	
$\Sigma^+ \eta$	$(4.4 \pm 2.0) \times 10^{-3}$		713	
$\Sigma^+ \eta'$	$(1.5 \pm 0.6)\%$		391	
$\Sigma^+ \pi^+ \pi^-$	$(4.50 \pm 0.25)\%$	$S=1.3$	804	
$\Sigma^+ \rho^0$	< 1.7	CL=95%	575	
$\Sigma^- 2\pi^+$	$(1.87 \pm 0.18)\%$		799	
$\Sigma^0 \pi^+ \pi^0$	$(3.5 \pm 0.4)\%$		803	
$\Sigma^+ \pi^0 \pi^0$	$(1.55 \pm 0.15)\%$		806	
$\Sigma^0 \pi^- 2\pi^+$	$(1.11 \pm 0.30)\%$		763	
$\Sigma^+ \pi^+ \pi^- \pi^0$	-		767	
$\Sigma^+ \omega$	[r] $(1.70 \pm 0.21)\%$		569	
$\Sigma^- \pi^0 2\pi^+$	$(2.1 \pm 0.4)\%$		762	
$\Sigma^+ K^+ K^-$	$(3.5 \pm 0.4) \times 10^{-3}$	$S=1.1$	349	
$\Sigma^+ \phi$	[r] $(3.9 \pm 0.6) \times 10^{-3}$	$S=1.1$	295	
$\Xi(1690)^0 K^+, \Xi^{*0} \rightarrow \Sigma^+ K^-$	$(1.02 \pm 0.25) \times 10^{-3}$		286	
$\Sigma^+ K^+ K^-$ nonresonant	< 8	$\times 10^{-4}$	CL=90%	349
$\Xi^0 K^+$	$(5.5 \pm 0.7) \times 10^{-3}$		653	
$\Xi^- K^+ \pi^+$	$(6.2 \pm 0.6) \times 10^{-3}$	$S=1.1$	565	
$\Xi(1530)^0 K^+$	$(4.3 \pm 0.9) \times 10^{-3}$	$S=1.1$	473	

Hadronic modes with a hyperon: $S = 0$ final states

ΛK^+	$(6.1 \pm 1.2) \times 10^{-4}$		781	
$\Lambda K^+ \pi^+ \pi^-$	< 5	$\times 10^{-4}$	CL=90%	637
$\Sigma^0 K^+$	$(5.2 \pm 0.8) \times 10^{-4}$		735	
$\Sigma^0 K^+ \pi^+ \pi^-$	< 2.6	$\times 10^{-4}$	CL=90%	574
$\Sigma^+ K^+ \pi^-$	$(2.1 \pm 0.6) \times 10^{-3}$		670	
$\Sigma^+ K^*(892)^0$	[r] $(3.5 \pm 1.0) \times 10^{-3}$		470	
$\Sigma^- K^+ \pi^+$	< 1.2	$\times 10^{-3}$	CL=90%	664

Doubly Cabibbo-suppressed modes

$\rho K^+ \pi^-$	$(1.11 \pm 0.18) \times 10^{-4}$		823
------------------	----------------------------------	--	-----

Semileptonic modes

$\Lambda e^+ \nu_e$	$(3.6 \pm 0.4)\%$		871
$\Lambda \mu^+ \nu_\mu$	$(3.5 \pm 0.5)\%$		867

Inclusive modes

e^+ anything	$(3.95 \pm 0.35)\%$		-
p anything	$(50 \pm 16)\%$		-
n anything	$(50 \pm 16)\%$		-
Λ anything	$(38.2 \pm 2.9) \pm 2.4\%$		-
K_S^0 anything	$(9.9 \pm 0.7)\%$		-
3prongs	$(24 \pm 8)\%$		-

 $\Delta C = 1$ weak neutral current ($C1$) modes, or Lepton Family number (LF), or Lepton number (L), or Baryon number (B) violating modes

$pe^+ e^-$	$C1$	< 5.5	$\times 10^{-6}$	CL=90%	951
$p\mu^+ \mu^-$ non-resonant	$C1$	< 7.7	$\times 10^{-8}$	CL=90%	937
$pe^+ \mu^-$	LF	< 9.9	$\times 10^{-6}$	CL=90%	947
$pe^- \mu^+$	LF	< 1.9	$\times 10^{-5}$	CL=90%	947
$\bar{p} 2e^+$	L, B	< 2.7	$\times 10^{-6}$	CL=90%	951
$\bar{p} 2\mu^+$	L, B	< 9.4	$\times 10^{-6}$	CL=90%	937
$\bar{p} e^+ \mu^+$	L, B	< 1.6	$\times 10^{-5}$	CL=90%	947
$\Sigma^- \mu^+ \mu^+$	L	< 7.0	$\times 10^{-4}$	CL=90%	812

Baryon Summary Table

 $\Lambda_c(2595)^+$

$$I(J^P) = 0(\frac{1}{2}^-)$$

The spin-parity follows from the fact that $\Sigma_c(2455)\pi$ decays, with little available phase space, are dominant. This assumes that $J^P = 1/2^+$ for the $\Sigma_c(2455)$.

$$\text{Mass } m = 2592.25 \pm 0.28 \text{ MeV}$$

$$m - m_{\Lambda_c^+} = 305.79 \pm 0.24 \text{ MeV}$$

$$\text{Full width } \Gamma = 2.6 \pm 0.6 \text{ MeV}$$

$\Lambda_c^+ \pi \pi$ and its submode $\Sigma_c(2455)\pi$ — the latter just barely — are the only strong decays allowed to an excited Λ_c^+ having this mass; and the submode seems to dominate.

$\Lambda_c(2595)^+$ DECAY MODES	Fraction (Γ_i/Γ)	ρ (MeV/c)
$\Lambda_c^+ \pi^+ \pi^-$	[s] —	117
$\Sigma_c(2455)^{++} \pi^-$	24 \pm 7 %	3
$\Sigma_c(2455)^0 \pi^+$	24 \pm 7 %	3
$\Lambda_c^+ \pi^+ \pi^-$ 3-body	18 \pm 10 %	117
$\Lambda_c^+ \pi^0$	[t] not seen	258
$\Lambda_c^+ \gamma$	not seen	288

 $\Lambda_c(2625)^+$

$$I(J^P) = 0(\frac{3}{2}^-)$$

J^P has not been measured; $\frac{3}{2}^-$ is the quark-model prediction.

$$\text{Mass } m = 2628.11 \pm 0.19 \text{ MeV} \quad (S = 1.1)$$

$$m - m_{\Lambda_c^+} = 341.65 \pm 0.13 \text{ MeV} \quad (S = 1.1)$$

$$\text{Full width } \Gamma < 0.97 \text{ MeV, CL} = 90\%$$

$\Lambda_c^+ \pi \pi$ and its submode $\Sigma(2455)\pi$ are the only strong decays allowed to an excited Λ_c^+ having this mass.

$\Lambda_c(2625)^+$ DECAY MODES	Fraction (Γ_i/Γ)	Confidence level	ρ (MeV/c)
$\Lambda_c^+ \pi^+ \pi^-$	$\approx 67\%$		184
$\Sigma_c(2455)^{++} \pi^-$	< 5	90%	103
$\Sigma_c(2455)^0 \pi^+$	< 5	90%	103
$\Lambda_c^+ \pi^+ \pi^-$ 3-body	large		184
$\Lambda_c^+ \pi^0$	[t] not seen		293
$\Lambda_c^+ \gamma$	not seen		319

 $\Lambda_c(2860)^+$

$$I(J^P) = 0(\frac{3}{2}^+)$$

$$\text{Mass } m = 2856.1^{+2.3}_{-6.0} \text{ MeV}$$

$$\text{Full width } \Gamma = 68^{+12}_{-22} \text{ MeV}$$

$\Lambda_c(2860)^+$ DECAY MODES	Fraction (Γ_i/Γ)	ρ (MeV/c)
$D^0 p$	seen	259

 $\Lambda_c(2880)^+$

$$I(J^P) = 0(\frac{5}{2}^+)$$

$$\text{Mass } m = 2881.63 \pm 0.24 \text{ MeV}$$

$$m - m_{\Lambda_c^+} = 595.17 \pm 0.28 \text{ MeV}$$

$$\text{Full width } \Gamma = 5.6^{+0.8}_{-0.6} \text{ MeV}$$

$\Lambda_c(2880)^+$ DECAY MODES	Fraction (Γ_i/Γ)	ρ (MeV/c)
$\Lambda_c^+ \pi^+ \pi^-$	seen	471
$\Sigma_c(2455)^0, ++ \pi^\pm$	seen	376
$\Sigma_c(2520)^0, ++ \pi^\pm$	seen	317
$p D^0$	seen	316

 $\Lambda_c(2940)^+$

$$I(J^P) = 0(\frac{3}{2}^-)$$

$J^P = 3/2^-$ is favored, but is not certain

$$\text{Mass } m = 2939.6^{+1.3}_{-1.5} \text{ MeV}$$

$$\text{Full width } \Gamma = 20^{+6}_{-5} \text{ MeV}$$

 $\Lambda_c(2940)^+$ DECAY MODESFraction (Γ_i/Γ) ρ (MeV/c)

$p D^0$	seen	420
$\Sigma_c(2455)^0, ++ \pi^\pm$	seen	—

 $\Sigma_c(2455)$

$$I(J^P) = 1(\frac{1}{2}^+)$$

$$\Sigma_c(2455)^{++} \text{ mass } m = 2453.97 \pm 0.14 \text{ MeV}$$

$$\Sigma_c(2455)^+ \text{ mass } m = 2452.65^{+0.22}_{-0.16} \text{ MeV}$$

$$\Sigma_c(2455)^0 \text{ mass } m = 2453.75 \pm 0.14 \text{ MeV}$$

$$m_{\Sigma_c(2455)^{++}} - m_{\Lambda_c^+} = 167.510 \pm 0.017 \text{ MeV}$$

$$m_{\Sigma_c(2455)^+} - m_{\Lambda_c^+} = 166.19^{+0.16}_{-0.08} \text{ MeV}$$

$$m_{\Sigma_c(2455)^0} - m_{\Lambda_c^+} = 167.290 \pm 0.017 \text{ MeV}$$

$$m_{\Sigma_c(2455)^{++}} - m_{\Sigma_c(2455)^0} = 0.220 \pm 0.013 \text{ MeV}$$

$$m_{\Sigma_c(2455)^+} - m_{\Sigma_c(2455)^0} = -1.10^{+0.16}_{-0.08} \text{ MeV}$$

$$\Sigma_c(2455)^{++} \text{ full width } \Gamma = 1.89^{+0.09}_{-0.18} \text{ MeV} \quad (S = 1.1)$$

$$\Sigma_c(2455)^+ \text{ full width } \Gamma = 2.3 \pm 0.4 \text{ MeV}$$

$$\Sigma_c(2455)^0 \text{ full width } \Gamma = 1.83^{+0.11}_{-0.19} \text{ MeV} \quad (S = 1.2)$$

$\Lambda_c^+ \pi$ is the only strong decay allowed to a Σ_c having this mass.

 $\Sigma_c(2455)$ DECAY MODESFraction (Γ_i/Γ) ρ (MeV/c)

$\Lambda_c^+ \pi$	$\approx 100\%$	94
-------------------	-----------------	----

 $\Sigma_c(2520)$

$$I(J^P) = 1(\frac{3}{2}^+)$$

J^P has not been measured; $\frac{3}{2}^+$ is the quark-model prediction.

$$\Sigma_c(2520)^{++} \text{ mass } m = 2518.41^{+0.22}_{-0.18} \text{ MeV} \quad (S = 1.1)$$

$$\Sigma_c(2520)^+ \text{ mass } m = 2517.4^{+0.7}_{-0.5} \text{ MeV}$$

$$\Sigma_c(2520)^0 \text{ mass } m = 2518.48 \pm 0.20 \text{ MeV} \quad (S = 1.1)$$

$$m_{\Sigma_c(2520)^{++}} - m_{\Lambda_c^+} = 231.95^{+0.18}_{-0.12} \text{ MeV} \quad (S = 1.3)$$

$$m_{\Sigma_c(2520)^+} - m_{\Lambda_c^+} = 230.9^{+0.7}_{-0.5} \text{ MeV}$$

$$m_{\Sigma_c(2520)^0} - m_{\Lambda_c^+} = 232.02^{+0.16}_{-0.14} \text{ MeV} \quad (S = 1.3)$$

$$m_{\Sigma_c(2520)^{++}} - m_{\Sigma_c(2520)^0} = 0.01 \pm 0.15 \text{ MeV}$$

$$\Sigma_c(2520)^{++} \text{ full width } \Gamma = 14.78^{+0.30}_{-0.40} \text{ MeV}$$

$$\Sigma_c(2520)^+ \text{ full width } \Gamma = 17.2^{+4.0}_{-2.2} \text{ MeV}$$

$$\Sigma_c(2520)^0 \text{ full width } \Gamma = 15.3^{+0.4}_{-0.5} \text{ MeV}$$

$\Lambda_c^+ \pi$ is the only strong decay allowed to a Σ_c having this mass.

 $\Sigma_c(2520)$ DECAY MODESFraction (Γ_i/Γ) ρ (MeV/c)

$\Lambda_c^+ \pi$	$\approx 100\%$	179
-------------------	-----------------	-----

 $\Sigma_c(2800)$

$$I(J^P) = 1(?^?)$$

$$\Sigma_c(2800)^{++} \text{ mass } m = 2801^{+4}_{-6} \text{ MeV}$$

$$\Sigma_c(2800)^+ \text{ mass } m = 2792^{+14}_{-5} \text{ MeV}$$

$$\Sigma_c(2800)^0 \text{ mass } m = 2806^{+5}_{-7} \text{ MeV} \quad (S = 1.3)$$

$$m_{\Sigma_c(2800)^{++}} - m_{\Lambda_c^+} = 514^{+4}_{-6} \text{ MeV}$$

$$m_{\Sigma_c(2800)^+} - m_{\Lambda_c^+} = 505^{+14}_{-5} \text{ MeV}$$

$$m_{\Sigma_c(2800)^0} - m_{\Lambda_c^+} = 519^{+5}_{-7} \text{ MeV} \quad (S = 1.3)$$

$$\Sigma_c(2800)^{++} \text{ full width } \Gamma = 75^{+22}_{-17} \text{ MeV}$$

$$\Sigma_c(2800)^+ \text{ full width } \Gamma = 62^{+60}_{-40} \text{ MeV}$$

$$\Sigma_c(2800)^0 \text{ full width } \Gamma = 72^{+22}_{-15} \text{ MeV}$$

 $\Sigma_c(2800)$ DECAY MODESFraction (Γ_i/Γ) ρ (MeV/c)

$\Lambda_c^+ \pi$	seen	443
-------------------	------	-----

 Ξ_c^+

$$I(J^P) = \frac{1}{2}(\frac{1}{2}^+)$$

J^P has not been measured; $\frac{1}{2}^+$ is the quark-model prediction.

$$\text{Mass } m = 2467.71 \pm 0.23 \text{ MeV} \quad (S = 1.3)$$

$$\text{Mean life } \tau = (453 \pm 5) \times 10^{-15} \text{ s}$$

$$c\tau = 135.8 \mu\text{m}$$

Baryon Summary Table

Branching fractions marked with a footnote, e.g. [a], have been corrected for decay modes not observed in the experiments. For example, the sub-mode fraction $\Xi_c^+ \rightarrow \Sigma^+ \bar{K}^*(892)^0$ seen in $\Xi_c^+ \rightarrow \Sigma^+ K^- \pi^+$ has been multiplied up to include $\bar{K}^*(892)^0 \rightarrow \bar{K}^0 \pi^0$ decays.

Ξ_c^+ DECAY MODES	Fraction (Γ_i/Γ)	Scale factor / Confidence level	ρ (MeV/c)
Cabibbo-favored ($S = -2$) decays			
$p 2K_S^0$	$(2.5 \pm 1.3) \times 10^{-3}$		766
$\Lambda \bar{K}^0 \pi^+$	—		852
$\Sigma(1385)^+ \bar{K}^0$	[r] $(2.9 \pm 2.0) \%$		746
$\Lambda K^- 2\pi^+$	$(9 \pm 4) \times 10^{-3}$		787
$\Lambda \bar{K}^*(892)^0 \pi^+$	[r] $< 5 \times 10^{-3}$	CL=90%	608
$\Sigma(1385)^+ K^- \pi^+$	[r] $< 6 \times 10^{-3}$	CL=90%	678
$\Sigma^+ K^- \pi^+$	$(2.7 \pm 1.2) \%$		810
$\Sigma^+ \bar{K}^*(892)^0$	[r] $(2.3 \pm 1.1) \%$		658
$\Sigma^0 K^- 2\pi^+$	$(8 \pm 5) \times 10^{-3}$		735
$\Xi^0 \pi^+$	$(1.6 \pm 0.8) \%$		876
$\Xi^- 2\pi^+$	$(2.9 \pm 1.3) \%$		851
$\Xi(1530)^0 \pi^+$	[r] $< 2.9 \times 10^{-3}$	CL=90%	749
$\Xi(1620)^0 \pi^+$	seen		—
$\Xi(1690)^0 \pi^+$	seen		644
$\Xi^0 \pi^+ \pi^0$	$(6.7 \pm 3.5) \%$		856
$\Xi^0 \pi^- 2\pi^+$	$(5.0 \pm 2.6) \%$		818
$\Xi^0 e^+ \nu_e$	$(7 \pm 4) \%$		884
$\Omega^- K^+ \pi^+$	$(2.0 \pm 1.5) \times 10^{-3}$		399
Cabibbo-suppressed decays			
$p K^- \pi^+$	$(6.2 \pm 3.0) \times 10^{-3}$	S=1.5	944
$p \bar{K}^*(892)^0$	[r] $(3.3 \pm 1.7) \times 10^{-3}$		828
$\Sigma^+ \pi^+ \pi^-$	$(1.4 \pm 0.8) \%$		922
$\Sigma^- 2\pi^+$	$(5.1 \pm 3.4) \times 10^{-3}$		918
$\Sigma^+ K^+ K^-$	$(4.3 \pm 2.5) \times 10^{-3}$		579
$\Sigma^+ \phi$	[r] $< 3.2 \times 10^{-3}$	CL=90%	549
$\Xi(1690)^0 K^+, \Xi^0 \rightarrow \Sigma^+ K^-$	$< 1.3 \times 10^{-3}$	CL=90%	501
$p \phi(1020)$	$(1.2 \pm 0.6) \times 10^{-4}$		751

Ξ_c^0

$$I(J^P) = \frac{1}{2}(\frac{1}{2}^+)$$

J^P has not been measured; $\frac{1}{2}^+$ is the quark-model prediction.

$$\text{Mass } m = 2470.44 \pm 0.28 \text{ MeV} \quad (S = 1.2)$$

$$m_{\Xi_c^0} - m_{\Xi_c^+} = 2.72 \pm 0.23 \text{ MeV} \quad (S = 1.1)$$

$$\text{Mean life } \tau = (151.9 \pm 2.4) \times 10^{-15} \text{ s}$$

$$c\tau = 45.5 \mu\text{m}$$

Decay asymmetry parameters

$$\Xi^- \pi^+ \quad \alpha = -0.64 \pm 0.05$$

$$\alpha \text{ FOR } \Xi_c^0 \rightarrow \Xi^+ \pi^- = 0.61 \pm 0.05$$

$$\alpha \text{ FOR } \Xi_c^0 \rightarrow \Lambda \bar{K}^*(892)^0 = 0.15 \pm 0.22$$

$$\alpha \text{ FOR } \Xi_c^0 \rightarrow \Sigma^+ K^*(892)^- = -0.52 \pm 0.30$$

Ξ_c^0 DECAY MODES	Fraction (Γ_i/Γ)	Scale factor	ρ (MeV/c)
Cabibbo-favored decays			
$p K^- K^- \pi^+$	$(4.8 \pm 1.2) \times 10^{-3}$	1.1	676
$p K^- \bar{K}^*(892)^0, \bar{K}^{*0} \rightarrow K^- \pi^+$	$(2.0 \pm 0.6) \times 10^{-3}$		413
$p K^- K^- \pi^+$ (no \bar{K}^{*0})	$(3.0 \pm 0.9) \times 10^{-3}$		676
ΛK_S^0	$(3.2 \pm 0.7) \times 10^{-3}$		906
$\Lambda K^- \pi^+$	$(1.45 \pm 0.33) \%$	1.1	856
$\Lambda \bar{K}^*(892)^0$	$(2.6 \pm 0.7) \times 10^{-3}$		717
$\Lambda \bar{K}^0 \pi^+ \pi^-$	seen		786
$\Lambda K^- \pi^+ \pi^+ \pi^-$	seen		703
$\Sigma^0 K_S^0$	$(5.4 \pm 1.6) \times 10^{-4}$		864
$\Sigma^+ K^-$	$(1.8 \pm 0.4) \times 10^{-3}$		868
$\Sigma^0 \bar{K}^*(892)^0$	$(9.8 \pm 2.3) \times 10^{-3}$		658
$\Sigma^+ K^*(892)^-$	$(4.9 \pm 1.4) \times 10^{-3}$		661
$\Xi^- \pi^+$	$(1.43 \pm 0.32) \%$	1.1	875
$\Xi^- \pi^+ \pi^+ \pi^-$	$(4.8 \pm 2.3) \%$		816
$\Xi^0 \phi, \phi \rightarrow K^+ K^-$	$(5.1 \pm 1.3) \times 10^{-4}$		—
$\Xi^0 K^+ K^-$ nonresonant	$(5.6 \pm 1.4) \times 10^{-4}$		444
$\Omega^- K^+$	$(4.2 \pm 1.0) \times 10^{-3}$		522

$\Xi^- e^+ \nu_e$	$(1.04 \pm 0.24) \%$	882
$\Xi^- \mu^+ \nu_\mu$	$(1.01 \pm 0.25) \%$	878

Cabibbo-suppressed decays

$\Lambda_c^+ \pi^-$	$(5.5 \pm 1.8) \times 10^{-3}$	115
$\Xi^- K^+$	$(3.9 \pm 1.2) \times 10^{-4}$	789
$\Lambda K^+ K^-$ (no ϕ)	$(4.1 \pm 1.4) \times 10^{-4}$	648
$\Lambda \phi$	$(4.9 \pm 1.5) \times 10^{-4}$	621

$\Xi_c^{'+}$

$$I(J^P) = \frac{1}{2}(\frac{1}{2}^+)$$

J^P has not been measured; $\frac{1}{2}^+$ is the quark-model prediction.

$$\text{Mass } m = 2578.2 \pm 0.5 \text{ MeV} \quad (S = 1.1)$$

$$m_{\Xi_c^{'+}} - m_{\Xi_c^+} = 110.5 \pm 0.4 \text{ MeV}$$

$$m_{\Xi_c^{'+}} - m_{\Xi_c^0} = -0.5 \pm 0.6 \text{ MeV}$$

The $\Xi_c^{'+} - \Xi_c^+$ mass difference is too small for any strong decay to occur.

$\Xi_c^{'+}$ DECAY MODES	Fraction (Γ_i/Γ)	ρ (MeV/c)
$\Xi_c^{'+} \gamma$	seen	108

$\Xi_c^{'0}$

$$I(J^P) = \frac{1}{2}(\frac{1}{2}^+)$$

J^P has not been measured; $\frac{1}{2}^+$ is the quark-model prediction.

$$\text{Mass } m = 2578.7 \pm 0.5 \text{ MeV}$$

$$m_{\Xi_c^{'0}} - m_{\Xi_c^0} = 108.3 \pm 0.4 \text{ MeV}$$

The $\Xi_c^{'0} - \Xi_c^0$ mass difference is too small for any strong decay to occur.

$\Xi_c^{'0}$ DECAY MODES	Fraction (Γ_i/Γ)	ρ (MeV/c)
$\Xi_c^{'0} \gamma$	seen	106

$\Xi_c(2645)$

$$I(J^P) = \frac{1}{2}(\frac{3}{2}^+)$$

J^P has not been measured; $\frac{3}{2}^+$ is the quark-model prediction.

$$\Xi_c(2645)^+ \text{ mass } m = 2645.10 \pm 0.30 \text{ MeV} \quad (S = 1.2)$$

$$\Xi_c(2645)^0 \text{ mass } m = 2646.16 \pm 0.25 \text{ MeV} \quad (S = 1.3)$$

$$m_{\Xi_c(2645)^+} - m_{\Xi_c^0} = 174.67 \pm 0.09 \text{ MeV}$$

$$m_{\Xi_c(2645)^0} - m_{\Xi_c^+} = 178.45 \pm 0.10 \text{ MeV}$$

$$m_{\Xi_c(2645)^+} - m_{\Xi_c(2645)^0} = -1.06 \pm 0.27 \text{ MeV} \quad (S = 1.1)$$

$$\Xi_c(2645)^+ \text{ full width } \Gamma = 2.14 \pm 0.19 \text{ MeV} \quad (S = 1.1)$$

$$\Xi_c(2645)^0 \text{ full width } \Gamma = 2.35 \pm 0.22 \text{ MeV}$$

$\Xi_c \pi$ is the only strong decay allowed to a Ξ_c resonance having this mass.

$\Xi_c(2645)$ DECAY MODES	Fraction (Γ_i/Γ)	ρ (MeV/c)
$\Xi_c^0 \pi^+$	seen	102
$\Xi_c^+ \pi^-$	seen	106

$\Xi_c(2790)$

$$I(J^P) = \frac{1}{2}(\frac{1}{2}^-)$$

J^P has not been measured; $\frac{1}{2}^-$ is the quark-model prediction.

$$\Xi_c(2790)^+ \text{ mass } = 2791.9 \pm 0.5 \text{ MeV}$$

$$\Xi_c(2790)^0 \text{ mass } = 2793.9 \pm 0.5 \text{ MeV}$$

$$m_{\Xi_c(2790)^+} - m_{\Xi_c^0} = 213.20 \pm 0.22 \text{ MeV}$$

$$m_{\Xi_c(2790)^0} - m_{\Xi_c^+} = 215.70 \pm 0.22 \text{ MeV}$$

$$m_{\Xi_c(2790)^+} - m_{\Xi_c(2790)^0} = -2.0 \pm 0.7 \text{ MeV}$$

$$\Xi_c(2790)^+ \text{ width } = 8.9 \pm 1.0 \text{ MeV}$$

$$\Xi_c(2790)^0 \text{ width } = 10.0 \pm 1.1 \text{ MeV}$$

$\Xi_c(2790)$ DECAY MODES	Fraction (Γ_i/Γ)	ρ (MeV/c)
$\Xi_c^- \pi$	seen	159

Baryon Summary Table

 $\Xi_c(2815)$

$$I(J^P) = \frac{1}{2}(\frac{3}{2}^-)$$

J^P has not been measured; $\frac{3}{2}^-$ is the quark-model prediction.

$$\begin{aligned} \Xi_c(2815)^+ \text{ mass } m &= 2816.51 \pm 0.25 \text{ MeV} \quad (S = 1.2) \\ \Xi_c(2815)^0 \text{ mass } m &= 2819.79 \pm 0.30 \text{ MeV} \quad (S = 1.1) \\ m_{\Xi_c(2815)^+} - m_{\Xi_c^+} &= 348.80 \pm 0.10 \text{ MeV} \\ m_{\Xi_c(2815)^0} - m_{\Xi_c^0} &= 349.35 \pm 0.11 \text{ MeV} \\ m_{\Xi_c(2815)^+} - m_{\Xi_c(2815)^0} &= -3.27 \pm 0.27 \text{ MeV} \\ \Xi_c(2815)^+ \text{ full width } \Gamma &= 2.43 \pm 0.26 \text{ MeV} \\ \Xi_c(2815)^0 \text{ full width } \Gamma &= 2.54 \pm 0.25 \text{ MeV} \end{aligned}$$

The $\Xi_c \pi \pi$ modes are consistent with being entirely via $\Xi_c(2645) \pi$.

$\Xi_c(2815)$ DECAY MODES	Fraction (Γ_i/Γ)	ρ (MeV/c)
$\Xi_c^+ \pi$	seen	188
$\Xi_c(2645) \pi$	seen	102
$\Xi_c^0 \gamma$	seen	325

 $\Xi_c(2970)$

$$I(J^P) = \frac{1}{2}(\frac{1}{2}^+)$$

was $\Xi_c(2980)$

$$\begin{aligned} \Xi_c(2970)^+ m &= 2964.3 \pm 1.5 \text{ MeV} \quad (S = 3.9) \\ \Xi_c(2970)^0 m &= 2967.1 \pm 1.7 \text{ MeV} \quad (S = 6.7) \\ m_{\Xi_c(2970)^+} - m_{\Xi_c^+} &= 496.6 \pm 1.5 \text{ MeV} \quad (S = 3.7) \\ m_{\Xi_c(2970)^0} - m_{\Xi_c^0} &= 496.7 \pm 1.8 \text{ MeV} \quad (S = 5.3) \\ m_{\Xi_c(2970)^+} - m_{\Xi_c(2970)^0} &= -2.8 \pm 1.9 \text{ MeV} \quad (S = 4.8) \\ \Xi_c(2970)^+ \text{ width } \Gamma &= 20.9_{-3.5}^{+2.4} \text{ MeV} \quad (S = 1.2) \end{aligned}$$

$\Xi_c(2970)$ DECAY MODES	Fraction (Γ_i/Γ)	ρ (MeV/c)
$\Lambda_c^+ \bar{K} \pi$	seen	223
$\Sigma_c(2455) \bar{K}$	seen	122
$\Lambda_c^+ \bar{K}$	not seen	410
$\Lambda_c^+ K^-$	seen	410
$\Xi_c 2\pi$	seen	381
$\Xi_c^+ \pi$	seen	-
$\Xi_c(2645) \pi$	seen	274

 $\Xi_c(3055)$

$$I(J^P) = ?(??)$$

$$\begin{aligned} \text{Mass } m &= 3055.9 \pm 0.4 \text{ MeV} \\ \text{Full width } \Gamma &= 7.8 \pm 1.9 \text{ MeV} \end{aligned}$$

$\Xi_c(3055)$ DECAY MODES	Fraction (Γ_i/Γ)	ρ (MeV/c)
$\Sigma^{++} K^-$	seen	-
ΛD^+	seen	316

 $\Xi_c(3080)$

$$I(J^P) = \frac{1}{2}(??)$$

$$\begin{aligned} \Xi_c(3080)^+ m &= 3077.2 \pm 0.4 \text{ MeV} \\ \Xi_c(3080)^0 m &= 3079.9 \pm 1.4 \text{ MeV} \quad (S = 1.3) \\ \Xi_c(3080)^+ \text{ width } \Gamma &= 3.6 \pm 1.1 \text{ MeV} \quad (S = 1.5) \\ \Xi_c(3080)^0 \text{ width } \Gamma &= 5.6 \pm 2.2 \text{ MeV} \end{aligned}$$

$\Xi_c(3080)$ DECAY MODES	Fraction (Γ_i/Γ)	ρ (MeV/c)
$\Lambda_c^+ \bar{K} \pi$	seen	415
$\Sigma_c(2455) \bar{K}$	seen	342
$\Sigma_c(2455)^{++} K^-$	seen	342
$\Sigma_c(2520)^{++} K^-$	seen	239
$\Sigma_c(2455) \bar{K} + \Sigma_c(2520) \bar{K}$	seen	-
$\Lambda_c^+ \bar{K}$	not seen	536
$\Lambda_c^+ \bar{K} \pi^+ \pi^-$	not seen	144
ΛD^+	seen	362

 Ω_c^0

$$I(J^P) = 0(\frac{1}{2}^+)$$

J^P has not been measured; $\frac{1}{2}^+$ is the quark-model prediction.

$$\begin{aligned} \text{Mass } m &= 2695.2 \pm 1.7 \text{ MeV} \quad (S = 1.3) \\ \text{Mean life } \tau &= (268 \pm 26) \times 10^{-15} \text{ s} \\ c\tau &= 80 \mu\text{m} \end{aligned}$$

No absolute branching fractions have been measured. The following are branching ratios relative to $\Omega^- \pi^+$.

Ω_c^0 DECAY MODES	Fraction (Γ_i/Γ)	Confidence level	ρ (MeV/c)
Cabibbo-favored ($S = -3$) decays — relative to $\Omega^- \pi^+$			
$\Omega^- \pi^+$			DEFINED AS 1
$\Omega^- \pi^+ \pi^0$	1.80 ± 0.33		821
$\Omega^- \rho^+$	> 1.3	90%	532
$\Omega^- \pi^- 2\pi^+$	0.31 ± 0.05		753
$\Omega^- e^+ \nu_e$	2.4 ± 1.2		829
$\Xi^0 \bar{K}^0$	1.64 ± 0.29		950
$\Xi^0 K^- \pi^+$	1.20 ± 0.18		901
$\Xi^0 \bar{K}^{*0}, \bar{K}^{*0} \rightarrow K^- \pi^+$	0.68 ± 0.16		764
$\Omega(2012)^- \pi^+, \Omega(2012)^- \rightarrow \Xi^0 K^-$	0.12 ± 0.05		-
$\Xi^- \bar{K}^0 \pi^+$	2.12 ± 0.28		895
$\Omega(2012)^- \pi^+, \Omega(2012)^- \rightarrow \Xi^- \bar{K}^0$	0.12 ± 0.06		-
$\Xi^- K^- 2\pi^+$	0.63 ± 0.09		830
$\Xi(1530)^0 K^- \pi^+, \Xi^{*0} \rightarrow \Xi^- \bar{K}^{*0} \pi^+$	0.21 ± 0.06		757
$\Xi^- \bar{K}^{*0} \pi^+$	0.34 ± 0.11		653
$p K^- K^- \pi^+$	seen		864
$\Sigma^+ K^- K^- \pi^+$	< 0.32	90%	689
$\Lambda \bar{K}^0 \bar{K}^0$	1.72 ± 0.35		837

 $\Omega_c(2770)^0$

$$I(J^P) = 0(\frac{3}{2}^+)$$

J^P has not been measured; $\frac{3}{2}^+$ is the quark-model prediction.

$$\begin{aligned} \text{Mass } m &= 2765.9 \pm 2.0 \text{ MeV} \quad (S = 1.2) \\ m_{\Omega_c(2770)^0} - m_{\Omega_c^0} &= 70.7_{-0.9}^{+0.8} \text{ MeV} \end{aligned}$$

The $\Omega_c(2770)^0 - \Omega_c^0$ mass difference is too small for any strong decay to occur.

$\Omega_c(2770)^0$ DECAY MODES	Fraction (Γ_i/Γ)	ρ (MeV/c)
$\Omega_c^0 \gamma$	presumably 100%	70

 $\Omega_c(3000)^0$

$$I(J^P) = ?(??)$$

$$\begin{aligned} \text{Mass } m &= 3000.41 \pm 0.22 \text{ MeV} \\ \text{Full width } \Gamma &= 4.5 \pm 0.7 \text{ MeV} \end{aligned}$$

$\Omega_c(3000)^0$ DECAY MODES	Fraction (Γ_i/Γ)	ρ (MeV/c)
$\Xi_c^+ K^-$	seen	182

 $\Omega_c(3050)^0$

$$I(J^P) = ?(??)$$

$$\begin{aligned} \text{Mass } m &= 3050.19 \pm 0.13 \text{ MeV} \\ \text{Full width } \Gamma &< 1.2 \text{ MeV, CL} = 95\% \end{aligned}$$

$\Omega_c(3050)^0$ DECAY MODES	Fraction (Γ_i/Γ)	ρ (MeV/c)
$\Xi_c^+ K^-$	seen	278

 $\Omega_c(3065)^0$

$$I(J^P) = ?(??)$$

$$\begin{aligned} \text{Mass } m &= 3065.54 \pm 0.26 \text{ MeV} \\ \text{Full width } \Gamma &= 3.3 \pm 0.6 \text{ MeV} \quad (S = 1.5) \end{aligned}$$

$\Omega_c(3065)^0$ DECAY MODES	Fraction (Γ_i/Γ)	ρ (MeV/c)
$\Xi_c^+ K^-$	seen	303

 $\Omega_c(3090)^0$

$$I(J^P) = ?(??)$$

$$\begin{aligned} \text{Mass } m &= 3090.1 \pm 0.5 \text{ MeV} \\ \text{Full width } \Gamma &= 8.7 \pm 1.3 \text{ MeV} \end{aligned}$$

$\Omega_c(3090)^0$ DECAY MODES	Fraction (Γ_i/Γ)	ρ (MeV/c)
$\Xi_c^+ K^-$	seen	340

Baryon Summary Table

 $\Omega_c(3120)^0$ $I(J^P) = ?(??)$ Mass $m = 3119.1 \pm 1.0$ MeVFull width $\Gamma < 2.6$ MeV, CL = 95%

$\Omega_c(3120)^0$ DECAY MODES	Fraction (Γ_i/Γ)	ρ (MeV/c)
$\Xi_c^+ K^-$	seen	379

DOUBLY CHARMED BARYONS
($C = +2$) $\Xi_{cc}^{++} = ucc, \Xi_{cc}^+ = dcc, \Omega_{cc}^+ = scc$ Ξ_{cc}^{++} $I(J^P) = ?(??)$ Mass $m = 3621.6 \pm 0.4$ MeVMean life $\tau = (256 \pm 27) \times 10^{-15}$ s

Ξ_{cc}^{++} DECAY MODES	Fraction (Γ_i/Γ)	ρ (MeV/c)
$\Lambda_c^+ K^- \pi^+ \pi^+$	seen	880
$\Xi_c^+ \pi^+, \Xi_c^+ \rightarrow pK^- \pi^+$	seen	-

BOTTOM BARYONS
($B = -1$) $\Lambda_b^0 = udb, \Xi_b^0 = usb, \Xi_b^- = dsb, \Omega_b^- = ssb$ Λ_b^0 $I(J^P) = 0(\frac{1}{2}^+)$ $I(J^P)$ not yet measured; $0(\frac{1}{2}^+)$ is the quark model prediction.Mass $m = 5619.60 \pm 0.17$ MeV $m_{\Lambda_b^0} - m_{B^0} = 339.2 \pm 1.4$ MeV $m_{\Lambda_b^0} - m_{B^+} = 339.72 \pm 0.28$ MeVMean life $\tau = (1.471 \pm 0.009) \times 10^{-12}$ s $c\tau = 441.0$ μm $A_{CP}(\Lambda_b \rightarrow p\pi^-) = -0.025 \pm 0.029$ ($S = 1.2$) $A_{CP}(\Lambda_b \rightarrow pK^-) = -0.025 \pm 0.022$ $A_{CP}(\Lambda_b \rightarrow DpK^-) = 0.12 \pm 0.09$ $\Delta A_{CP}(pK^-/\pi^-) = 0.014 \pm 0.024$ $A_{CP}(\Lambda_b \rightarrow p\bar{K}^0\pi^-) = 0.22 \pm 0.13$ $\Delta A_{CP}(J/\psi p\pi^-/K^-) = (5.7 \pm 2.7) \times 10^{-2}$ $A_{CP}(\Lambda_b \rightarrow \Lambda K^+\pi^-) = -0.53 \pm 0.25$ $A_{CP}(\Lambda_b \rightarrow \Lambda K^+K^-) = -0.28 \pm 0.12$ $\Delta A_{CP}(\Lambda_b^0 \rightarrow pK^- \mu^+ \mu^-) = (-4 \pm 5) \times 10^{-2}$ $\Delta A_{CP}(\Lambda_b^0 \rightarrow p\pi^- \pi^+ \pi^-) = (1.1 \pm 2.6) \times 10^{-2}$ $\Delta A_{CP}(\Lambda_b^0 \rightarrow (p\pi^- \pi^+ \pi^-)_{LBM}) = (4 \pm 4) \times 10^{-2}$ $\Delta A_{CP}(\Lambda_b^0 \rightarrow p a_1(1260)^-) = (-1 \pm 4) \times 10^{-2}$ $\Delta A_{CP}(\Lambda_b^0 \rightarrow N(1520)^0 \rho(770)^0) = (2 \pm 5) \times 10^{-2}$ $\Delta A_{CP}(\Lambda_b^0 \rightarrow \Delta(1232)^{++} \pi^- \pi^-) = (0.1 \pm 3.3) \times 10^{-2}$ $\Delta A_{CP}(\Lambda_b^0 \rightarrow pK^- \pi^+ \pi^-) = (3.2 \pm 1.3) \times 10^{-2}$ $\Delta A_{CP}(\Lambda_b^0 \rightarrow (pK^- \pi^+ \pi^-)_{LBM}) = (3.5 \pm 1.6) \times 10^{-2}$ $\Delta A_{CP}(\Lambda_b^0 \rightarrow N(1520)^0 K^*(892)^0) = (5.5 \pm 2.5) \times 10^{-2}$ $\Delta A_{CP}(\Lambda_b^0 \rightarrow \Lambda(1520) \rho(770)^0) = (1 \pm 6) \times 10^{-2}$ $\Delta A_{CP}(\Lambda_b^0 \rightarrow \Delta(1232)^{++} K^- \pi^-) = (4.4 \pm 2.7) \times 10^{-2}$ $\Delta A_{CP}(\Lambda_b^0 \rightarrow pK_1(1410)^-) = (5 \pm 4) \times 10^{-2}$ $\Delta A_{CP}(\Lambda_b^0 \rightarrow pK^- K^+ \pi^-) = (-7 \pm 5) \times 10^{-2}$ $\Delta A_{CP}(\Lambda_b^0 \rightarrow pK^- K^+ K^-) = (0.2 \pm 1.9) \times 10^{-2}$ $\Delta A_{CP}(\Lambda_b^0 \rightarrow \Lambda(1520) \phi(1020)) = (4 \pm 6) \times 10^{-2}$ $\Delta A_{CP}(\Lambda_b^0 \rightarrow (pK^-)_{highmass} \phi(1020)) = (-0.7 \pm 3.4) \times 10^{-2}$ $\Delta A_{CP}(\Lambda_b^0 \rightarrow (pK^- K^+ K^-)_{LBM}) = (2.7 \pm 2.4) \times 10^{-2}$ $A_{FB}^{\ell}(\mu\mu)$ in $\Lambda_b \rightarrow \Lambda \mu^+ \mu^- = -0.39 \pm 0.04$ $\Delta(A_{FB}^{\ell}(\mu\mu))$ in $\Lambda_b \rightarrow \Lambda \mu^+ \mu^- = -0.05 \pm 0.09$ $A_{FB}^h(p\pi)$ in $\Lambda_b \rightarrow \Lambda(p\pi) \mu^+ \mu^- = -0.30 \pm 0.05$ $A_{FB}^{\ell h}$ in $\Lambda_b \rightarrow \Lambda \mu^+ \mu^- = 0.25 \pm 0.04$

The branching fractions $B(b\text{-baryon} \rightarrow \Lambda \ell^- \bar{\nu}_\ell \text{anything})$ and $B(\Lambda_b^0 \rightarrow \Lambda_c^+ \ell^- \bar{\nu}_\ell \text{anything})$ are not pure measurements because the underlying measured products of these with $B(b \rightarrow b\text{-baryon})$ were used to determine $B(b \rightarrow b\text{-baryon})$, as described in the note "Production and Decay of b -Flavored Hadrons."

For inclusive branching fractions, e.g., $\Lambda_b \rightarrow \bar{\Lambda}_c \text{anything}$, the values usually are multiplicities, not branching fractions. They can be greater than one.

 Λ_b^0 DECAY MODES

DECAY MODES	Fraction (Γ_i/Γ)	Scale factor / Confidence level	ρ (MeV/c)
$J/\psi(1S) \Lambda \times B(b \rightarrow \Lambda_b^0)$	$(5.8 \pm 0.8) \times 10^{-5}$		1740
$pD^0 \pi^-$	$(6.3 \pm 0.6) \times 10^{-4}$		2370
$pD^0 K^-$	$(4.6 \pm 0.8) \times 10^{-5}$		2269
$pJ/\psi \pi^-$	$(2.6 \pm_{-0.4}^{+0.5}) \times 10^{-5}$		1755
$p\pi^- J/\psi, J/\psi \rightarrow \mu^+ \mu^-$	$(1.6 \pm 0.8) \times 10^{-6}$		-
$pJ/\psi K^-$	$(3.2 \pm_{-0.5}^{+0.6}) \times 10^{-4}$		1589
$p\eta_c(1S) K^-$	$(1.06 \pm 0.26) \times 10^{-4}$		1670
$P_c(4312)^+ K^-, P_c(4312)^+ \rightarrow p\eta_c(1S)$	$< 2.5 \times 10^{-5}$	CL=95%	-
$P_c(4380)^+ K^-, P_c \rightarrow pJ/\psi$	[u] $(2.7 \pm 1.4) \times 10^{-5}$		-
$P_c(4450)^+ K^-, P_c \rightarrow pJ/\psi$	[u] $(1.3 \pm 0.4) \times 10^{-5}$		-
$\chi_{c1}(1P) pK^-$	$(7.6 \pm_{-1.3}^{+1.5}) \times 10^{-5}$		1242
$\chi_{c1}(1P) p\pi^-$	$(5.0 \pm_{-1.1}^{+1.3}) \times 10^{-6}$		1462
$\chi_{c2}(1P) pK^-$	$(7.9 \pm_{-1.4}^{+1.6}) \times 10^{-5}$		1198
$\chi_{c2}(1P) p\pi^-$	$(4.8 \pm 1.9) \times 10^{-6}$		1427
$pJ/\psi(1S) \pi^+ \pi^- K^-$	$(6.6 \pm_{-1.1}^{+1.3}) \times 10^{-5}$		1410
$p\psi(2S) K^-$	$(6.6 \pm_{-1.0}^{+1.2}) \times 10^{-5}$		1063
$\chi_{c1}(3872) pK^-$	$(3.2 \pm 1.4) \times 10^{-5}$		837
$\chi_{c1}(3872) \Lambda(1520)$	$(1.9 \pm 0.9) \times 10^{-5}$		721
$\psi(2S) p\pi^-$	$(7.5 \pm_{-1.4}^{+1.6}) \times 10^{-6}$		1320
$p\bar{K}^0 \pi^-$	$(1.3 \pm 0.4) \times 10^{-5}$		2693
$pK^0 K^-$	$< 3.5 \times 10^{-6}$	CL=90%	2639
$\Lambda_c^+ \pi^-$	$(4.9 \pm 0.4) \times 10^{-3}$	S=1.2	2342
$\Lambda_c^+ K^-$	$(3.56 \pm 0.28) \times 10^{-4}$	S=1.2	2314
$\Lambda_c^+ a_1(1260)^-$	seen		2153
$\Lambda_c^+ D^-$	$(4.6 \pm 0.6) \times 10^{-4}$		1886
$\Lambda_c^+ D_s^-$	$(1.10 \pm 0.10) \%$		1833
$\Lambda_c^+ \pi^+ \pi^- \pi^-$	$(7.6 \pm 1.1) \times 10^{-3}$	S=1.1	2323
$\Lambda_c(2595)^+ \pi^-, \Lambda_c(2595)^+ \rightarrow \Lambda_c^+ \pi^+ \pi^-$	$(3.4 \pm 1.4) \times 10^{-4}$		2210
$\Lambda_c(2625)^+ \pi^-, \Lambda_c(2625)^+ \rightarrow \Lambda_c^+ \pi^+ \pi^-$	$(3.3 \pm 1.3) \times 10^{-4}$		2193
$\Sigma_c(2455)^0 \pi^+ \pi^-, \Sigma_c^0 \rightarrow \Lambda_c^+ \pi^-$	$(5.7 \pm 2.2) \times 10^{-4}$		2265
$\Sigma_c(2455)^{++} \pi^- \pi^-, \Sigma_c^{++} \rightarrow \Lambda_c^+ \pi^+$	$(3.2 \pm 1.5) \times 10^{-4}$		2265
$\Lambda_c^+ K^+ K^- \pi^-$	$(1.02 \pm 0.11) \times 10^{-3}$		2184
$\Lambda_c^+ p\bar{p} \pi^-$	$(2.63 \pm 0.27) \times 10^{-4}$		1805
$\Sigma_c(2455)^0 p\bar{p}, \Sigma_c^0 \rightarrow \Lambda_c^+ \pi^-$	$(2.3 \pm 0.5) \times 10^{-5}$		-
$\Sigma_c(2520)^0 p\bar{p}, \Sigma_c(2520)^0 \rightarrow \Lambda_c^+ \pi^-$	$(3.1 \pm 0.7) \times 10^{-5}$		-
$\Lambda_c^+ \ell^- \bar{\nu}_\ell \text{anything}$	[v] $(10.9 \pm 2.2) \%$		-
$\Lambda_c^+ \ell^- \bar{\nu}_\ell$	$(6.2 \pm_{-1.3}^{+1.4}) \%$		2345
$\Lambda_c^+ \pi^+ \pi^- \ell^- \bar{\nu}_\ell$	$(5.6 \pm 3.1) \%$		2335
$\Lambda_c(2595)^+ \ell^- \bar{\nu}_\ell$	$(7.9 \pm_{-3.5}^{+4.0}) \times 10^{-3}$		2212
$\Lambda_c(2625)^+ \ell^- \bar{\nu}_\ell$	$(1.3 \pm_{-0.5}^{+0.6}) \%$		2195
$p h^-$	[x] $< 2.3 \times 10^{-5}$	CL=90%	2730
$p\pi^-$	$(4.5 \pm 0.8) \times 10^{-6}$		2730
pK^-	$(5.4 \pm 1.0) \times 10^{-6}$		2709
pD_s^-	$< 4.8 \times 10^{-4}$	CL=90%	2364
$p\mu^- \bar{\nu}_\mu$	$(4.1 \pm 1.0) \times 10^{-4}$		2730
$\Lambda \mu^+ \mu^-$	$(1.08 \pm 0.28) \times 10^{-6}$		2695
$p\pi^- \mu^+ \mu^-$	$(6.9 \pm 2.5) \times 10^{-8}$		2720
$pK^- e^+ e^-$	$(3.1 \pm 0.6) \times 10^{-7}$		2708

Baryon Summary Table

$\rho K^- \mu^+ \mu^-$	$(2.6^{+0.5}_{-0.4}) \times 10^{-7}$	2685
$\Lambda \gamma$	$(7.1 \pm 1.7) \times 10^{-6}$	2699
$\Lambda \eta$	$(9^{+7}_{-5}) \times 10^{-6}$	2670
$\Lambda \eta'(958)$	$< 3.1 \times 10^{-6}$	CL=90% 2611
$\Lambda \pi^+ \pi^-$	$(4.6 \pm 1.9) \times 10^{-6}$	2692
$\Lambda K^+ \pi^-$	$(5.6 \pm 1.2) \times 10^{-6}$	2660
$\Lambda K^+ K^-$	$(1.60 \pm 0.22) \times 10^{-5}$	2605
$\Lambda \phi$	$(9.8 \pm 2.6) \times 10^{-6}$	2599
$\rho \pi^- \pi^+ \pi^-$	$(2.10 \pm 0.22) \times 10^{-5}$	2715
$\rho K^- K^+ \pi^-$	$(4.0 \pm 0.6) \times 10^{-6}$	2612
$\rho K^- \pi^+ \pi^-$	$(5.0 \pm 0.5) \times 10^{-5}$	2675
$\rho K^- K^+ K^-$	$(1.26 \pm 0.13) \times 10^{-5}$	2524

$\Lambda_b(5912)^0$	$J^P = \frac{1}{2}^-$
Mass $m = 5912.19 \pm 0.17$ MeV	
Full width $\Gamma < 0.25$ MeV, CL = 90%	
$\Lambda_b(5912)^0$ DECAY MODES	Fraction (Γ_i/Γ)
$\Lambda_b^0 \pi^+ \pi^-$	seen
	86

$\Lambda_b(5920)^0$	$J^P = \frac{3}{2}^-$
Mass $m = 5920.09 \pm 0.17$ MeV	
Full width $\Gamma < 0.19$ MeV, CL = 90%	
$\Lambda_b(5920)^0$ DECAY MODES	Fraction (Γ_i/Γ)
$\Lambda_b^0 \pi^+ \pi^-$	seen
	108

$\Lambda_b(6070)^0$	$J^P = \frac{1}{2}^+$
Quantum numbers based on quark model expectations.	
Mass $m = 6072.3 \pm 2.9$ MeV	
Full width $\Gamma = 72 \pm 11$ MeV	
$\Lambda_b(6070)^0$ DECAY MODES	Fraction (Γ_i/Γ)
$\Lambda_b^0 \pi^+ \pi^-$	seen
	343

$\Lambda_b(6146)^0$	$J^P = \frac{3}{2}^+$
Mass $m = 6146.2 \pm 0.4$ MeV	
$m_{\Lambda_b(6146)^0} - m_{\Lambda_b^0} = 526.55 \pm 0.34$ MeV	
Full width $\Gamma = 2.9 \pm 1.3$ MeV	
$\Lambda_b(6146)^0$ DECAY MODES	Fraction (Γ_i/Γ)
$\Lambda_b^0 \pi^+ \pi^-$	seen
	427

$\Lambda_b(6152)^0$	$J^P = \frac{5}{2}^+$
Mass $m = 6152.5 \pm 0.4$ MeV	
$m_{\Lambda_b(6152)^0} - m_{\Lambda_b^0} = 532.89 \pm 0.28$ MeV	
$m_{\Lambda_b(6152)^0} - m_{\Lambda_b(6146)^0} = 6.34 \pm 0.32$ MeV	
Full width $\Gamma = 2.1 \pm 0.9$ MeV	
$\Lambda_b(6152)^0$ DECAY MODES	Fraction (Γ_i/Γ)
$\Lambda_b^0 \pi^+ \pi^-$	seen
	434

Σ_b	$I(J^P) = 1(\frac{1}{2}^+)$
I, J, P need confirmation.	
Mass $m(\Sigma_b^+) = 5810.56 \pm 0.25$ MeV	
Mass $m(\Sigma_b^-) = 5815.64 \pm 0.27$ MeV	
$m_{\Sigma_b^+} - m_{\Sigma_b^-} = -5.06 \pm 0.18$ MeV	
$\Gamma(\Sigma_b^+) = 5.0 \pm 0.5$ MeV	
$\Gamma(\Sigma_b^-) = 5.3 \pm 0.5$ MeV	
Σ_b DECAY MODES	Fraction (Γ_i/Γ)
$\Lambda_b^0 \pi$	dominant
	133

Σ_b^*	$I(J^P) = 1(\frac{3}{2}^+)$
I, J, P need confirmation.	
Mass $m(\Sigma_b^{*+}) = 5830.32 \pm 0.27$ MeV	
Mass $m(\Sigma_b^{*-}) = 5834.74 \pm 0.30$ MeV	
$m_{\Sigma_b^{*+}} - m_{\Sigma_b^{*-}} = -4.37 \pm 0.33$ MeV ($S = 1.6$)	
$m_{\Sigma_b^{*+}} - m_{\Sigma_b^+} = 19.73 \pm 0.18$	
$m_{\Sigma_b^{*-}} - m_{\Sigma_b^-} = 19.09 \pm 0.22$	
$\Gamma(\Sigma_b^{*+}) = 9.4 \pm 0.5$ MeV	
$\Gamma(\Sigma_b^{*-}) = 10.4 \pm 0.8$ MeV ($S = 1.3$)	
$m_{\Sigma_b^+} - m_{\Sigma_b^-} = 21.2 \pm 2.0$ MeV	

Σ_b^* DECAY MODES	Fraction (Γ_i/Γ)	ρ (MeV/c)
$\Lambda_b^0 \pi$	dominant	159

$\Sigma_b(6097)^+$	$J^P = ?$
Mass $m = 6095.8 \pm 1.7$ MeV	
Full width $\Gamma = 31 \pm 6$ MeV	

$\Sigma_b(6097)^+$ DECAY MODES	Fraction (Γ_i/Γ)	ρ (MeV/c)
$\Lambda_b \pi^+ \times B(b \rightarrow \Sigma_b(6097)^+)$	seen	-

$\Sigma_b(6097)^-$	$J^P = ?$
Mass $m = 6098.0 \pm 1.8$ MeV	
Full width $\Gamma = 29 \pm 4$ MeV	

$\Sigma_b(6097)^-$ DECAY MODES	Fraction (Γ_i/Γ)	ρ (MeV/c)
$\Lambda_b \pi^- \times B(b \rightarrow \Sigma_b(6097)^-)$	seen	-

Ξ_b^-	$I(J^P) = \frac{1}{2}(\frac{1}{2}^+)$
I, J, P need confirmation.	
$m(\Xi_b^-) = 5797.0 \pm 0.6$ MeV ($S = 1.7$)	
$m_{\Xi_b^-} - m_{\Lambda_b^0} = 177.46 \pm 0.31$ MeV ($S = 1.3$)	
$m_{\Xi_b^-} - m_{\Xi_b^0} = 5.9 \pm 0.6$ MeV	
Mean life $\tau_{\Xi_b^-} = (1.572 \pm 0.040) \times 10^{-12}$ s	

Ξ_b^- DECAY MODES	Fraction (Γ_i/Γ)	ρ (MeV/c)
$J/\psi \Xi^- \times B(b \rightarrow \Xi_b^-)$	$(1.02^{+0.26}_{-0.21}) \times 10^{-5}$	1782
$J/\psi \Lambda K^- \times B(b \rightarrow \Xi_b^-)$	$(2.5 \pm 0.4) \times 10^{-6}$	1631
$\rho K^- K^- \times B(b \rightarrow \Xi_b^-)$	$(3.7 \pm 0.8) \times 10^{-8}$	2731
$\rho K^- K^-$	seen	2731
$\rho K^- \pi^-$	seen	2783
$\Lambda_b^0 \pi^- \times B(b \rightarrow \Xi_b^-)/B(b \rightarrow \Lambda_b^0)$	$(5.7 \pm 2.0) \times 10^{-4}$	99
$\Xi_c^0 \pi^-$	seen	2367
$\Sigma(1385) K^-$	$(2.6 \pm 2.3) \times 10^{-7}$	2707
$\Lambda(1405) K^-$	$(1.9 \pm 1.2) \times 10^{-7}$	2702
$\Lambda(1520) K^-$	$(7.6 \pm 3.2) \times 10^{-7}$	2673
$\Lambda(1670) K^-$	$(4.5 \pm 2.3) \times 10^{-7}$	2629
$\Sigma(1775) K^-$	$(2.2 \pm 1.5) \times 10^{-7}$	2599
$\Sigma(1915) K^-$	$(2.6 \pm 2.5) \times 10^{-7}$	2553

Ξ_b^0	$I(J^P) = \frac{1}{2}(\frac{1}{2}^+)$
I, J, P need confirmation.	
$m(\Xi_b^0) = 5791.9 \pm 0.5$ MeV	
$m_{\Xi_b^0} - m_{\Lambda_b^0} = 172.5 \pm 0.4$ MeV	
Mean life $\tau_{\Xi_b^0} = (1.480 \pm 0.030) \times 10^{-12}$ s	

Ξ_b^0 DECAY MODES	Fraction (Γ_i/Γ)	Confidence level	ρ (MeV/c)
$\rho D^0 K^- \times B(b \rightarrow \Xi_b^0)$	$(1.7 \pm 0.5) \times 10^{-6}$		2374
$\rho K^0 \pi^- \times B(b \rightarrow \Xi_b^0)/B(\bar{b} \rightarrow B^0)$	$< 1.6 \times 10^{-6}$	90%	2783
$\rho K^0 K^- \times B(b \rightarrow \Xi_b^0)/B(\bar{b} \rightarrow B^0)$	$< 1.1 \times 10^{-6}$	90%	2730
$\Lambda \pi^+ \pi^- \times B(b \rightarrow \Xi_b^0)/B(b \rightarrow \Lambda_b^0)$	$< 1.7 \times 10^{-6}$	90%	2781

Baryon Summary Table

$\Lambda K^- \pi^+ \times B(b \rightarrow \Xi_b^0)/B(b \rightarrow \Lambda_b^0)$	< 8	$\times 10^{-7}$	90%	2751
$\Lambda K^+ K^- \times B(b \rightarrow \Xi_b^0)/B(b \rightarrow \Lambda_b^0)$	< 3	$\times 10^{-7}$	90%	2698
$J/\psi \Lambda$	seen			1868
$J/\psi \Xi^0$	seen			1785
$\Lambda_c^+ K^- \times B(b \rightarrow \Xi_b^0)$	(6 ± 4)	$\times 10^{-7}$		2416
$p K^- \pi^+ \pi^- \times B(b \rightarrow \Xi_b^0)/B(b \rightarrow \Lambda_b^0)$	(1.9 ± 0.4)	$\times 10^{-6}$		2766
$p K^- K^- \pi^+ \times B(b \rightarrow \Xi_b^0)/B(b \rightarrow \Lambda_b^0)$	(1.71 ± 0.31)	$\times 10^{-6}$		2704
$p K^- K^+ K^- \times B(b \rightarrow \Xi_b^0)/B(b \rightarrow \Lambda_b^0)$	(1.7 ± 1.0)	$\times 10^{-7}$		2620

$\Xi_b'(5935)^-$	$J^P = \frac{1}{2}^+$
Mass $m = 5935.02 \pm 0.05$ MeV	
$m_{\Xi_b'(5935)^-} - m_{\Xi_b^0} - m_{\pi^-} = 3.653 \pm 0.019$ MeV	
Full width $\Gamma < 0.08$ MeV, CL = 95%	

$\Xi_b'(5935)^-$ DECAY MODES	Fraction (Γ_i/Γ)	ρ (MeV/c)
$\Xi_b^0 \pi^- \times B(\bar{b} \rightarrow \Xi_b^0)$	$(11.8 \pm 1.8)\%$	31
$\Xi_b'(5935)^-/B(\bar{b} \rightarrow \Xi_b^0)$		

$\Xi_b(5945)^0$	$J^P = \frac{3}{2}^+$
Mass $m = 5952.3 \pm 0.6$ MeV	
Full width $\Gamma = 0.90 \pm 0.18$ MeV	

$\Xi_b(5945)^0$ DECAY MODES	Fraction (Γ_i/Γ)	ρ (MeV/c)
$\Xi_b^- \pi^+$	seen	78

$\Xi_b(5955)^-$	$J^P = \frac{3}{2}^+$
Mass $m = 5955.33 \pm 0.13$ MeV	
$m_{\Xi_b(5955)^-} - m_{\Xi_b^0} - m_{\pi^-} = 23.96 \pm 0.13$ MeV	
Full width $\Gamma = 1.65 \pm 0.33$ MeV	

$\Xi_b(5955)^-$ DECAY MODES	Fraction (Γ_i/Γ)	ρ (MeV/c)
$\Xi_b^0 \pi^- \times B(\bar{b} \rightarrow \Xi_b^0)$	$(20.7 \pm 3.5)\%$	84
$\Xi_b^*(5955)^-/B(\bar{b} \rightarrow \Xi_b^0)$		

$\Xi_b(6100)^-$	$J^P = \frac{3}{2}^-$ J, P need confirmation.
Mass $m = 6100.3 \pm 0.6$ MeV	
$m_{\Xi_b(6100)^-} - m_{\Xi_b^-} - 2 m_{\pi^\pm} = 24.14 \pm 0.24$ MeV	
Full width $\Gamma < 1.9$ MeV, CL = 95%	

$\Xi_b(6100)^-$ DECAY MODES	Fraction (Γ_i/Γ)	ρ (MeV/c)
$\Xi_b^- \pi^+ \pi^-$	seen	128

$\Xi_b(6227)^-$	$J^P = ?^?$
Mass $m = 6227.9 \pm 0.9$ MeV	
Full width $\Gamma = 19.9 \pm 2.6$ MeV	

$\Xi_b(6227)^-$ DECAY MODES	Fraction (Γ_i/Γ)	Scale factor	ρ (MeV/c)
$\Lambda_b^0 K^- \times B(b \rightarrow \Xi_b(6227)^-)/B(b \rightarrow \Lambda_b^0)$	$(3.20 \pm 0.35) \times 10^{-3}$		336
$\Xi_b^0 \pi^- \times B(b \rightarrow \Xi_b(6227)^-)/B(b \rightarrow \Xi_b^0)$	$(2.8 \pm 1.1)\%$	1.8	398

$\Xi_b(6227)^0$	$J^P = ?^?$
Mass $m = 6226.8 \pm 1.6$ MeV	
Full width $\Gamma = 19_{-4}^{+5}$ MeV	

$\Xi_b(6227)^0$ DECAY MODES	Fraction (Γ_i/Γ)	ρ (MeV/c)
$\Xi_b^- \pi^+ \times B(b \rightarrow \Xi_b(6227)^0)/B(b \rightarrow \Xi_b^-)$	$(4.5 \pm 0.9)\%$	398

Ω_b^-	$I(J^P) = 0(\frac{1}{2}^+)$ I, J, P need confirmation.
Mass $m = 6045.2 \pm 1.2$ MeV	
$m_{\Omega_b^-} - m_{\Lambda_b^0} = 426.4 \pm 2.2$ MeV	
$m_{\Omega_b^-} - m_{\Xi_b^-} = 247.3 \pm 3.2$ MeV	
Mean life $\tau = (1.64_{-0.17}^{+0.18}) \times 10^{-12}$ s	
$\tau(\Omega_b^-)/\tau(\Xi_b^-)$ mean life ratio = 1.11 ± 0.16	

Ω_b^- DECAY MODES	Fraction (Γ_i/Γ)	Confidence level	ρ (MeV/c)
$J/\psi \Omega^- \times B(b \rightarrow \Omega_b)$	$(2.9_{-0.8}^{+1.1}) \times 10^{-6}$		1805
$p K^- K^- \times B(\bar{b} \rightarrow \Omega_b)$	$< 2.3 \times 10^{-9}$	90%	2865
$p \pi^- \pi^- \times B(\bar{b} \rightarrow \Omega_b)$	$< 1.5 \times 10^{-8}$	90%	2943
$p K^- \pi^- \times B(\bar{b} \rightarrow \Omega_b)$	$< 7 \times 10^{-9}$	90%	2915
$\Omega_c^0 \pi^-$	seen		2419
$\Omega_c^0 \pi^-, \Omega_c^0 \rightarrow p K^- K^- \pi^+$	seen		-
$\Xi_c^+ K^- \pi^-$	seen		2472

b-baryon ADMIXTURE ($\Lambda_b, \Xi_b, \Omega_b$)

These branching fractions are actually an average over weakly decaying b -baryons weighted by their production rates at the LHC, LEP, and Tevatron, branching ratios, and detection efficiencies. They scale with the b -baryon production fraction $B(b \rightarrow b\text{-baryon})$.

The branching fractions $B(b\text{-baryon} \rightarrow \Lambda \ell^- \bar{\nu}_\ell \text{ anything})$ and $B(\Lambda_b^0 \rightarrow \Lambda_c^+ \ell^- \bar{\nu}_\ell \text{ anything})$ are not pure measurements because the underlying measured products of these with $B(b \rightarrow b\text{-baryon})$ were used to determine $B(b \rightarrow b\text{-baryon})$, as described in the note "Production and Decay of b -Flavored Hadrons."

For inclusive branching fractions, e.g., $B \rightarrow D^\pm \text{ anything}$, the values usually are multiplicities, not branching fractions. They can be greater than one.

b-baryon ADMIXTURE DECAY MODES ($\Lambda_b, \Xi_b, \Omega_b$)	Fraction (Γ_i/Γ)	Scale factor	ρ (MeV/c)
$p \mu^- \bar{\nu}$ anything	$(5.8_{-2.0}^{+2.3})\%$		-
$p \ell \bar{\nu}_\ell$ anything	$(5.6 \pm 1.2)\%$		-
p anything	$(70 \pm 22)\%$		-
$\Lambda \ell^- \bar{\nu}_\ell$ anything	$(3.8 \pm 0.6)\%$		-
$\Lambda \ell^+ \nu_\ell$ anything	$(3.2 \pm 0.8)\%$		-
Λ anything	$(39 \pm 7)\%$		-
$\Xi^- \ell^- \bar{\nu}_\ell$ anything	$(4.6 \pm 1.4) \times 10^{-3}$	1.2	-

EXOTIC BARYONS

$P_c(4312)^+$	Mass $m = 4311.9_{-0.9}^{+7.0}$ MeV Full width $\Gamma = 10 \pm 5$ MeV
---------------------------------	---

$P_c(4312)^+$ DECAY MODES	Fraction (Γ_i/Γ)	ρ (MeV/c)
$J/\psi p$	seen	658

$P_c(4380)^+$	Mass $m = 4380 \pm 30$ MeV Full width $\Gamma = 205 \pm 90$ MeV
---------------------------------	--

$P_c(4380)^+$ DECAY MODES	Fraction (Γ_i/Γ)	ρ (MeV/c)
$J/\psi p$	seen	741

Baryon Summary Table

 $P_c(4440)^+$

Mass $m = 4440_{-5}^{+4}$ MeV
 Full width $\Gamma = 21_{-11}^{+10}$ MeV

$P_c(4440)^+$ DECAY MODES	Fraction (Γ_i/Γ)	ρ (MeV/c)
$J/\psi p$	seen	810

 $P_c(4457)^+$

was $P_c(4450)$

Mass $m = 4457.3_{-1.8}^{+4.0}$ MeV
 Full width $\Gamma = 6.4_{-2.8}^{+6.0}$ MeV

$P_c(4457)^+$ DECAY MODES	Fraction (Γ_i/Γ)	ρ (MeV/c)
$J/\psi p$	seen	828

NOTES

This Summary Table only includes established baryons. The Particle Listings include evidence for other baryons. The masses, widths, and branching fractions for the resonances in this Table are Breit-Wigner parameters, but pole positions are also given for most of the N and Δ resonances.

For most of the resonances, the parameters come from various partial-wave analyses of more or less the same sets of data, and it is not appropriate to treat the results of the analyses as independent or to average them together. Furthermore, the systematic errors on the results are not well understood. Thus, we usually only give ranges for the parameters. We then also give a best guess for the mass (as part of the name of the resonance) and for the width. The *Note on N and Δ Resonances* and the *Note on Λ and Σ Resonances* in the Particle Listings review the partial-wave analyses.

When a quantity has "(S = ...)" to its right, the error on the quantity has been enlarged by the "scale factor" S, defined as $S = \sqrt{\chi^2/(N-1)}$, where N is the number of measurements used in calculating the quantity. We do this when $S > 1$, which often indicates that the measurements are inconsistent. When $S > 1.25$, we also show in the Particle Listings an ideogram of the measurements. For more about S, see the Introduction.

A decay momentum p is given for each decay mode. For a 2-body decay, p is the momentum of each decay product in the rest frame of the decaying particle. For a 3-or-more-body decay, p is the largest momentum any of the products can have in this frame. For any resonance, the *nominal* mass is used in calculating p . A dagger ("†") in this column indicates that the mode is forbidden when the nominal masses of resonances are used, but is in fact allowed due to the nonzero widths of the resonances.

[a] The masses of the p and n are most precisely known in u (unified atomic mass units). The conversion factor to MeV, $1 u = 931.494061(21)$ MeV, is less well known than are the masses in u .

[b] The $|m_p - m_{\bar{p}}|/m_p$ and $|q_p + q_{\bar{p}}|/e$ are not independent, and both use the more precise measurement of $|q_{\bar{p}}/m_{\bar{p}}|/(q_p/m_p)$.

[c] The limit is from neutrality-of-matter experiments; it assumes $q_n = q_p + q_e$. See also the charge of the neutron.

[d] The μp and $e p$ values for the charge radius are much too different to average them. The disagreement is not yet understood.

[e] There is a lot of disagreement about the value of the proton magnetic charge radius. See the Listings.

[f] The first limit is for $p \rightarrow$ anything or "disappearance" modes of a bound proton. The second entry, a rough range of limits, assumes the dominant decay modes are among those investigated. For antiprotons the best limit, inferred from the observation of cosmic ray \bar{p} 's is $\tau_{\bar{p}} > 10^7$ yr, the cosmic-ray storage time, but this limit depends on a number of assumptions. The best direct observation of stored antiprotons gives $\tau_{\bar{p}}/B(\bar{p} \rightarrow e^- \gamma) > 7 \times 10^5$ yr.

[g] There is some controversy about whether nuclear physics and model dependence complicate the analysis for bound neutrons (from which the best limit comes). The first limit here is from reactor experiments with free neutrons.

[h] Lee and Yang in 1956 proposed the existence of a mirror world in an attempt to restore global parity symmetry—thus a search for oscillations between the two worlds. Oscillations between the worlds would be maximal when the magnetic fields B and B' were equal. The limit for any B' in the range 0 to 12.5 μ T is >12 s (95% CL).

[i] The parameters g_A , g_V , and g_{WM} for semileptonic modes are defined by $\bar{B}_i[\gamma_\lambda(g_V + g_A\gamma_5) + i(g_{WM}/m_{B_i})\sigma_{\lambda\nu}q^\nu]B_j$, and ϕ_{AV} is defined by $g_A/g_V = |g_A/g_V|e^{i\phi_{AV}}$. See the "Note on Baryon Decay Parameters" in the neutron Particle Listings.

[j] Time-reversal invariance requires this to be 0° or 180° .

[k] This coefficient is zero if time invariance is not violated.

[l] This limit is for γ energies between 0.4 and 782 keV.

[n] The decay parameters γ and Δ are calculated from α and ϕ using

$$\gamma = \sqrt{1-\alpha^2} \cos\phi, \quad \tan\Delta = -\frac{1}{\alpha} \sqrt{1-\alpha^2} \sin\phi.$$

See the "Note on Baryon Decay Parameters" in the neutron Particle Listings.

[o] See the Listings for the pion momentum range used in this measurement.

[p] Our estimate. See the Particle Listings for details.

[q] A theoretical value using QED.

[r] This branching fraction includes all the decay modes of the final-state resonance.

[s] See AALTONEN 11H, Fig. 8, for the calculated ratio of $\Lambda_c^+ \pi^0 \pi^0$ and $\Lambda_c^+ \pi^+ \pi^-$ partial widths as a function of the $\Lambda_c(2595)^+ - \Lambda_c^+$ mass difference. At our value of the mass difference, the ratio is about 4.

[t] A test that the isospin is indeed 0, so that the particle is indeed a Λ_c^+ .

[u] P_c^+ is a pentaquark-charmonium state.

[v] Not a pure measurement. See note at head of Λ_b^0 Decay Modes.

[x] Here h^- means π^- or K^- .

Searches Summary Table

SEARCHES not in other sections

Magnetic Monopole Searches

The most sensitive experiments obtain negative results.
Best cosmic-ray supermassive monopole flux limit:
 $< 1.4 \times 10^{-16} \text{ cm}^{-2} \text{sr}^{-1} \text{s}^{-1}$ for $1.1 \times 10^{-4} < \beta < 1$

Supersymmetric Particle Searches

All supersymmetric mass bounds here are model dependent.

The limits assume:

1) $\tilde{\chi}_1^0$ is the lightest supersymmetric particle; 2) R -parity is conserved, unless stated otherwise;

See the Particle Listings for a Note giving details of supersymmetry.

$\tilde{\chi}_i^0$ — neutralinos (mixtures of $\tilde{\gamma}$, \tilde{Z}^0 , and \tilde{H}_i^0)

Mass $m_{\tilde{\chi}_1^0} > 0 \text{ GeV}$, CL = 95%
[general MSSM, non-universal gaugino masses]

Mass $m_{\tilde{\chi}_1^0} > 46 \text{ GeV}$, CL = 95%

[all $\tan\beta$, all m_0 , all $m_{\tilde{\chi}_2^0} - m_{\tilde{\chi}_1^0}$]

Mass $m_{\tilde{\chi}_2^0} > 62.4 \text{ GeV}$, CL = 95%

[$1 < \tan\beta < 40$, all m_0 , all $m_{\tilde{\chi}_2^0} - m_{\tilde{\chi}_1^0}$]

Mass $m_{\tilde{\chi}_3^0} > 99.9 \text{ GeV}$, CL = 95%

[$1 < \tan\beta < 40$, all m_0 , all $m_{\tilde{\chi}_2^0} - m_{\tilde{\chi}_1^0}$]

Mass $m_{\tilde{\chi}_4^0} > 116 \text{ GeV}$, CL = 95%

[$1 < \tan\beta < 40$, all m_0 , all $m_{\tilde{\chi}_2^0} - m_{\tilde{\chi}_1^0}$]

$\tilde{\chi}_i^\pm$ — charginos (mixtures of \tilde{W}^\pm and \tilde{H}_i^\pm)

Mass $m_{\tilde{\chi}_1^\pm} > 94 \text{ GeV}$, CL = 95%
[$\tan\beta < 40$, $m_{\tilde{\chi}_1^\pm} - m_{\tilde{\chi}_1^0} > 3 \text{ GeV}$, all m_0]

Mass $m_{\tilde{\chi}_1^\pm} > 1000 \text{ GeV}$, CL = 95%

[$2\ell + \cancel{E}_T$, Tchi1chi1C, $m_{\tilde{\chi}_1^0} = 0 \text{ GeV}$]

$\tilde{\chi}^\pm$ — long-lived chargino

Mass $m_{\tilde{\chi}^\pm} > 620 \text{ GeV}$, CL = 95% [stable $\tilde{\chi}^\pm$]

$\tilde{\nu}$ — sneutrino

Mass $m > 41 \text{ GeV}$, CL = 95% [model independent]

Mass $m > 94 \text{ GeV}$, CL = 95%

[CMSSM, $1 \leq \tan\beta \leq 40$, $m_{\tilde{\nu}_R} - m_{\tilde{\chi}_1^0} > 10 \text{ GeV}$]

Mass $m > 3400 \text{ GeV}$, CL = 95% [R-Parity Violating]

[$\tilde{\nu}_\tau \rightarrow e\mu$, $\lambda_{312} = \lambda_{321} = 0.07$, $\lambda_{311}^V = 0.11$]

\tilde{e} — scalar electron (selectron)

Mass $m > 107 \text{ GeV}$, CL = 95% [all $m_{\tilde{e}_L} - m_{\tilde{\chi}_1^0}$]

Mass $m > 700 \text{ GeV}$, CL = 95%

[$2\ell + \cancel{E}_T$, $m_{\tilde{e}_R} = m_{\tilde{e}_L}$ and $\tilde{\ell} = \tilde{e}, \tilde{\mu}, m_{\tilde{\chi}_1^0} = 0 \text{ GeV}$]

Mass $m > 250 \text{ GeV}$, CL = 95%

[$\ell^\pm \ell^\mp + \cancel{E}_T$, \tilde{e}_R , $m_{\tilde{\chi}_1^0} = 0 \text{ GeV}$]

Mass $m > 410 \text{ GeV}$, CL = 95% [R-Parity Violating]

[$\geq 4\ell^\pm$, $\tilde{\ell} \rightarrow I\tilde{\chi}_1^0, \tilde{\chi}_1^0 \rightarrow \ell^\pm \ell^\mp \nu$]

$\tilde{\mu}$ — scalar muon (smuon)

Mass $m > 700 \text{ GeV}$, CL = 95%

[$2\ell + \cancel{E}_T$, $m_{\tilde{\mu}_R} = m_{\tilde{\mu}_L}$ and $\tilde{\ell} = \tilde{e}, \tilde{\mu}, m_{\tilde{\chi}_1^0} = 0 \text{ GeV}$]

Mass $m > 210 \text{ GeV}$, CL = 95%

[$\ell^\pm \ell^\mp + \cancel{E}_T$, $\tilde{\mu}_R$, $m_{\tilde{\chi}_1^0} = 0 \text{ GeV}$]

Mass $m > 94 \text{ GeV}$, CL = 95%

[CMSSM, $1 \leq \tan\beta \leq 40$, $m_{\tilde{\mu}_R} - m_{\tilde{\chi}_1^0} > 10 \text{ GeV}$]

Mass $m > 410 \text{ GeV}$, CL = 95% [R-Parity Violating]

[$\geq 4\ell^\pm$, $\tilde{\ell} \rightarrow I\tilde{\chi}_1^0, \tilde{\chi}_1^0 \rightarrow \ell^\pm \ell^\mp \nu$]

$\tilde{\tau}$ — scalar tau (stau)

Mass $m > 81.9 \text{ GeV}$, CL = 95%

[$m_{\tilde{\tau}_R} - m_{\tilde{\chi}_1^0} > 15 \text{ GeV}$, all θ_τ , $B(\tilde{\tau} \rightarrow \tau\tilde{\chi}_1^0) = 100\%$]

Mass $m > 90 \text{ GeV}$, CL = 95%

[RPV, $\tilde{\tau}_R$, indirect, $\Delta m > 5 \text{ GeV}$]

Mass $m > 286 \text{ GeV}$, CL = 95% [long-lived $\tilde{\tau}$]

\tilde{q} — squarks of the first two quark generations

Mass $m > 1.220 \times 10^3 \text{ GeV}$, CL = 95%

[jets + \cancel{E}_T , Tsqk1, 1 non-degenerate \tilde{q} , $m_{\tilde{\chi}_1^0} = 0 \text{ GeV}$]

Mass $m > 1.600 \times 10^3 \text{ GeV}$, CL = 95% [R-Parity Violating]

[$\tilde{q} \rightarrow q\tilde{\chi}_1^0, \tilde{\chi}_1^0 \rightarrow \ell\ell\nu, \lambda_{121}, \lambda_{122} \neq 0, m_{\tilde{g}} = 2400 \text{ GeV}$]

\tilde{q} — long-lived squark

Mass $m > 1340$, CL = 95% [\tilde{t} R-hadrons]

Mass $m > 1250$, CL = 95% [\tilde{b} R-hadrons]

\tilde{b} — scalar bottom (sbottom)

Mass $m > 1.270 \times 10^3 \text{ GeV}$, CL = 95%

[b -jets + \cancel{E}_T , Tsb01, $m_{\tilde{\chi}_1^0} = 0 \text{ GeV}$]

Mass $m > 307 \text{ GeV}$, CL = 95% [R-Parity Violating]

[$\tilde{b} \rightarrow td$ or $ts, \lambda_{332}^{\prime\prime}$ or $\lambda_{331}^{\prime\prime}$ coupling]

\tilde{t} — scalar top (stop)

Mass $m > 1.310 \times 10^3 \text{ GeV}$, CL = 95%

[jets + \cancel{E}_T , Tstop1, $m_{\tilde{\chi}_1^0} < 300 \text{ GeV}$]

Mass $m > 1100 \text{ GeV}$, CL = 95% [R-Parity Violating]

[$\tilde{t} \rightarrow b e, Tstop2RPV$, prompt]

\tilde{g} — gluino

Mass $m > 2.300 \times 10^3 \text{ GeV}$, CL = 95%

[jets + \cancel{E}_T , Tglu1A, $m_{\tilde{\chi}_1^0} < 200 \text{ GeV}$]

Mass $m > 2.260 \times 10^3 \text{ GeV}$, CL = 95% [R-Parity Violating]

[$\geq 4\ell, \lambda_{12k} \neq 0, m_{\tilde{\chi}_1^0} > 1000 \text{ GeV}$]

Technicolor

The limits for technicolor (and top-color) particles are quite varied depending on assumptions. See the Technicolor section of the full Review (the data listings).

Quark and Lepton Compositeness, Searches for

Scale Limits Λ for Contact Interactions (the lowest dimensional interactions with four fermions)

If the Lagrangian has the form

$$\pm \frac{g^2}{2\Lambda^2} \bar{\psi}_L \gamma_\mu \psi_L \bar{\psi}_L \gamma^\mu \psi_L$$

(with $g^2/4\pi$ set equal to 1), then we define $\Lambda \equiv \Lambda_{LL}^\pm$. For the full definitions and for other forms, see the Note in the Listings on Searches for Quark and Lepton Compositeness in the full Review and the original literature.

$$\Lambda_{LL}^+(eeee) > 8.3 \text{ TeV, CL} = 95\%$$

$$\Lambda_{LL}^-(eeee) > 10.3 \text{ TeV, CL} = 95\%$$

$$\Lambda_{LL}^+(ee\mu\mu) > 8.5 \text{ TeV, CL} = 95\%$$

$$\Lambda_{LL}^-(ee\mu\mu) > 9.5 \text{ TeV, CL} = 95\%$$

$$\Lambda_{LL}^+(ee\tau\tau) > 7.9 \text{ TeV, CL} = 95\%$$

$$\Lambda_{LL}^-(ee\tau\tau) > 7.2 \text{ TeV, CL} = 95\%$$

$$\Lambda_{LL}^+(\ell\ell\ell\ell) > 9.1 \text{ TeV, CL} = 95\%$$

$$\Lambda_{LL}^-(\ell\ell\ell\ell) > 10.3 \text{ TeV, CL} = 95\%$$

$$\Lambda_{LL}^+(eeqq) > 24 \text{ TeV, CL} = 95\%$$

$$\Lambda_{LL}^-(eeqq) > 37 \text{ TeV, CL} = 95\%$$

$$\Lambda_{LL}^+(eeuu) > 23.3 \text{ TeV, CL} = 95\%$$

$$\Lambda_{LL}^-(eeuu) > 12.5 \text{ TeV, CL} = 95\%$$

$$\Lambda_{LL}^+(eedd) > 11.1 \text{ TeV, CL} = 95\%$$

$$\Lambda_{LL}^-(eedd) > 26.4 \text{ TeV, CL} = 95\%$$

$$\Lambda_{LL}^+(eecc) > 9.4 \text{ TeV, CL} = 95\%$$

$$\Lambda_{LL}^-(eecc) > 5.6 \text{ TeV, CL} = 95\%$$

$$\Lambda_{LL}^+(eebb) > 9.4 \text{ TeV, CL} = 95\%$$

$$\Lambda_{LL}^-(eebb) > 10.2 \text{ TeV, CL} = 95\%$$

$$\Lambda_{LL}^+(\mu\mu qq) > 22.3 \text{ TeV, CL} = 95\%$$

$$\Lambda_{LL}^-(\mu\mu qq) > 40.0 \text{ TeV, CL} = 95\%$$

$$\Lambda(\ell\nu\ell\nu) > 3.10 \text{ TeV, CL} = 90\%$$

$$\Lambda(e\nu qq) > 2.81 \text{ TeV, CL} = 95\%$$

$$\Lambda_{LL}^+(qqqq) > 13.1 \text{ none } 17.4\text{--}29.5 \text{ TeV, CL} = 95\%$$

$$\Lambda_{LL}^-(qqqq) > 21.8 \text{ TeV, CL} = 95\%$$

$$\Lambda_{LL}^+(\nu\nu qq) > 5.0 \text{ TeV, CL} = 95\%$$

$$\Lambda_{LL}^-(\nu\nu qq) > 5.4 \text{ TeV, CL} = 95\%$$
Excited Leptons

The limits from $\ell^{*+}\ell^{*-}$ do not depend on λ (where λ is the $\ell\ell^*$ transition coupling). The λ -dependent limits assume chiral coupling.

$e^{*\pm}$ — excited electron

- Mass $m > 103.2 \text{ GeV, CL} = 95\%$ (from e^*e^*)
 Mass $m > 5.600 \times 10^3 \text{ GeV, CL} = 95\%$ (from ee^*)
 Mass $m > 356 \text{ GeV, CL} = 95\%$ (if $\lambda_\gamma = 1$)

$\mu^{*\pm}$ — excited muon

- Mass $m > 103.2 \text{ GeV, CL} = 95\%$ (from $\mu^*\mu^*$)
 Mass $m > 5.700 \times 10^3 \text{ GeV, CL} = 95\%$ (from $\mu\mu^*$)

$\tau^{*\pm}$ — excited tau

- Mass $m > 103.2 \text{ GeV, CL} = 95\%$ (from $\tau^*\tau^*$)
 Mass $m > 2.500 \times 10^3 \text{ GeV, CL} = 95\%$ (from $\tau\tau^*$)

ν^* — excited neutrino

- Mass $m > 1.600 \times 10^3 \text{ GeV, CL} = 95\%$ (from $\nu^*\nu^*$)
 Mass $m > 213 \text{ GeV, CL} = 95\%$ (from ν^*X)

q^* — excited quark

- Mass $m > 338 \text{ GeV, CL} = 95\%$ (from q^*q^*)
 Mass $m > 6700 \text{ GeV, CL} = 95\%$ (from q^*X)

Color Sextet and Octet Particles

Color Sextet Quarks (q_6)

$$\text{Mass } m > 84 \text{ GeV, CL} = 95\% \quad (\text{Stable } q_6)$$

Color Octet Charged Leptons (ℓ_8)

$$\text{Mass } m > 86 \text{ GeV, CL} = 95\% \quad (\text{Stable } \ell_8)$$

Color Octet Neutrinos (ν_8)

$$\text{Mass } m > 110 \text{ GeV, CL} = 90\% \quad (\nu_8 \rightarrow \nu g)$$

Extra Dimensions

Please refer to the Extra Dimensions section of the full *Review* for a discussion of the model-dependence of these bounds, and further constraints.

Constraints on the radius of the extra dimensions, for the case of two-flat dimensions of equal radii

(direct tests of Newton's law)

$$R < 3.8 \mu\text{m, CL} = 95\% \quad (pp \rightarrow jG)$$

$$R < 0.16\text{--}916 \text{ nm} \quad (\text{astrophysics; limits depend on technique and assumptions})$$

Constraints on the fundamental gravity scale

$$M_{TT} > 9.02 \text{ TeV, CL} = 95\% \quad (pp \rightarrow \text{dijet, angular distribution})$$

$$M_c > 4.16 \text{ TeV, CL} = 95\% \quad (pp \rightarrow \ell\bar{\ell})$$

Constraints on the Kaluza-Klein graviton in warped extra dimensions

$$M_G > 4.78 \text{ TeV, CL} = 95\% \quad (pp \rightarrow e^+e^-, \mu^+\mu^-)$$

Constraints on the Kaluza-Klein gluon in warped extra dimensions

$$M_{g_{KK}} > 3.8 \text{ TeV, CL} = 95\% \quad (g_{KK} \rightarrow t\bar{t})$$

WIMP and Dark Matter Searches

No confirmed evidence found for galactic WIMPs from the GeV to the TeV mass scales and down to 1×10^{-10} pb spin independent cross section at $M = 100 \text{ GeV}$.

Tests of Conservation Laws

Revised May 2022 by A. Pich (IFIC, Valencia) and M. Ramsey-Musolf (Tsung-Dao Lee Inst.; SJTU; U. Massachusetts).

In keeping with the current interest in tests of conservation laws, we collect together a Table of experimental limits on all weak and electromagnetic decays, mass differences, and moments, and on a few reactions, whose observation would violate conservation laws. The Table is given only in the full Review of Particle Physics (RPP), not in the Particle Physics Booklet, and organizes the data in two main sections: “Discrete Space-Time Symmetries”, *i.e.*, C , P , T , CP and CPT ; and “Number Conservation Laws”, *i.e.*, lepton, baryon, flavor and charge conservation. The references for these data can be found in the Particle Listings. The following text discusses the best limits among those included in the Table and gives a brief overview of the current status. For some topics, a more extensive discussion of the framework for theoretical interpretation is provided, particularly where the analogous discussion does not appear elsewhere in the RPP. References to more extensive review articles are also included where appropriate. Unless otherwise specified, all limits quoted in this review are given at a C.L. of 90%.

DISCRETE SPACE-TIME SYMMETRIES

Charge conjugation (C), parity (P) and time reversal (T) are empirically exact symmetries of the electromagnetic (QED) and strong (QCD) interactions, but they are violated by the weak forces. Owing to the left-handed nature of the $SU(2)_L \otimes U(1)_Y$ electroweak theory, C and P are maximally violated in the fermionic couplings of the W^\pm and (up to $\sin^2 \theta_W$ corrections) the Z . However, their product CP is still an exact symmetry when only one or two fermion families are considered. With three generations of fermions, CP is violated through the single complex phase present in the Cabibbo-Kobayashi-Maskawa (CKM) quark mixing matrix. An analogous CP -violating (CPV) phase appears in the lepton sector when non-vanishing neutrino masses are taken into account (plus two additional phases if neutrinos are Majorana particles). The product of the three discrete symmetries, CPT , is an exact symmetry of any local and Lorentz-invariant quantum field theory with a positive-definite hermitian Hamiltonian that preserves micro-causality [1, 2]. Therefore, the breaking of CP implies a corresponding violation of T .

Violations of charge-conjugation symmetry have never been observed in electromagnetic and strong phenomena. The most stringent limits are extracted from C -violating transitions of neutral (self-conjugate) particles such as $\text{Br}(\pi^0 \rightarrow 3\gamma) < 3.1 \times 10^{-8}$ [3] and $\text{Br}(J/\psi \rightarrow 2\gamma) < 2.7 \times 10^{-7}$ [4]. P (and CP) conservation has been also precisely tested through forbidden decays such as $\text{Br}(\eta \rightarrow 4\pi^0) < 6.9 \times 10^{-7}$ [5], but the best limits on P and T are set by the non-observation of electric dipole moments (see section 2). Obviously, the interplay of the weak interaction puts a lower bound in sensitivity for this type of tests, beyond which violations of the corresponding conservation laws should be detected.

1 Violations of CP and T

The first evidence of CP non-invariance in particle physics was the observation in 1964 of $K_L^0 \rightarrow \pi^+\pi^-$ decays [6]. For many years afterwards, the non-zero ratio

$$\begin{aligned} |\eta_{+-}| &\equiv |\mathcal{M}(K_L^0 \rightarrow \pi^+\pi^-)/\mathcal{M}(K_S^0 \rightarrow \pi^+\pi^-)| \\ &= (2.232 \pm 0.011) \times 10^{-3} \end{aligned} \quad (1)$$

could be explained as a K^0 - \bar{K}^0 mixing effect, $\eta_{+-} = \epsilon$ (superweak CP violation), which would imply an identical ratio $\eta_{00} \equiv \mathcal{M}(K_L^0 \rightarrow \pi^0\pi^0)/\mathcal{M}(K_S^0 \rightarrow \pi^0\pi^0)$ in the neutral decay mode and successfully predicts the observed CPV semileptonic asymmetry ($A_L(e) \approx 2 \text{Re } \epsilon$)

$$\begin{aligned} A_L(e) &\equiv \frac{\Gamma(K_L^0 \rightarrow \pi^- e^+ \nu_e) - \Gamma(K_L^0 \rightarrow \pi^+ e^- \bar{\nu}_e)}{\Gamma(K_L^0 \rightarrow \pi^- e^+ \nu_e) + \Gamma(K_L^0 \rightarrow \pi^+ e^- \bar{\nu}_e)} \\ &= (3.34 \pm 0.07) \times 10^{-3}. \end{aligned} \quad (2)$$

A tiny difference between η_{+-} and η_{00} was reported for the first time in 1988 by the CERN NA31 collaboration [7], and later es-

tablished at the 7.2σ level with the full data samples from the NA31 [8], E731 [9], NA48 [10] and KTeV [11] experiments:

$$\text{Re}(\epsilon'/\epsilon) = \frac{1}{3} (1 - |\eta_{00}/\eta_{+-}|) = (1.66 \pm 0.23) \times 10^{-3}. \quad (3)$$

This important measurement confirmed that CP violation is associated with a $\Delta S = 1$ transition, as predicted by the CKM mechanism. The Standard Model (SM) prediction, $\text{Re}(\epsilon'/\epsilon) = (1.4 \pm 0.5) \times 10^{-3}$ [12–14], is in good agreement with the measured ratio, although the theoretical uncertainty is unfortunately large.

Much larger CP asymmetries have been later measured in B meson decays, many of them involving the interference between B^0 - \bar{B}^0 mixing and the decay amplitude. They provide many successful tests of the CKM unitarity structure, validating the SM mechanism of CP violation (see the review on CP violation in the quark sector). Prominent signals of direct CP violation have been also clearly established in several B^\pm , B_d^0 and B_s^0 decays, and, very recently, in charm decays [15]:

$$\begin{aligned} \Delta a_{CP}^{\text{dir}} &\equiv a_{CP}^{\text{dir}}(D^0 \rightarrow K^+K^-) - a_{CP}^{\text{dir}}(D^0 \rightarrow \pi^+\pi^-) \\ &= (-15.7 \pm 2.9) \times 10^{-4}. \end{aligned} \quad (4)$$

These direct CP asymmetries necessarily involve the presence of a strong phase-shift difference between (at least) two interfering amplitudes, which makes very challenging to perform reliable SM predictions for heavy-flavored mesons.

Global fits to neutrino oscillation data provide some hints of a non-zero mixing phase [16, 17]. Although the statistical significance is not yet compelling, they suggest that CP -violation effects in neutrino oscillations could be large (see the review on neutrino masses, mixings and oscillations). The future DUNE and Hyper-Kamiokande experiments are expected to confirm the presence of CP violation in the lepton sector or constrain the phase in the leptonic mixing matrix to be smaller than $O(10^\circ)$.

While CP violation implies a breaking of time-reversal symmetry, direct tests of T violation are much more difficult. The CPLEAR experiment observed longtime ago a non-zero difference between the oscillation probabilities of $K^0 \rightarrow \bar{K}^0$ and $\bar{K}^0 \rightarrow K^0$ [18]. Initial neutral kaons with defined strangeness were produced from proton-antiproton annihilations at rest, $p\bar{p} \rightarrow K^-\pi^+K^0, K^+\pi^-K^0$, and tagged by the accompanying charged kaon, while the strangeness of the final neutral kaon was identified through its semileptonic decay: $K^0 \rightarrow e^+\pi^-\nu_e$, $\bar{K}^0 \rightarrow e^-\pi^+\bar{\nu}_e$. The average asymmetry over the time interval from 1 to 20 K_S^0 lifetimes was found to be different from zero at 4σ [18]:

$$\begin{aligned} \frac{R[\bar{K}^0(t=0) \rightarrow e^+\pi^-\nu_e(t)] - R[K^0(t=0) \rightarrow e^-\pi^+\bar{\nu}_e(t)]}{R[\bar{K}^0(t=0) \rightarrow e^+\pi^-\nu_e(t)] + R[K^0(t=0) \rightarrow e^-\pi^+\bar{\nu}_e(t)]} &= \\ &= (6.6 \pm 1.3 \pm 1.0) \times 10^{-3}. \end{aligned} \quad (5)$$

Since this asymmetry violates also CP , its interpretation as direct evidence of T violation requires a detailed analysis of the underlying K^0 - \bar{K}^0 mixing process [19–21].

More recently, the exchange of initial and final states has been made possible in B decays, taking advantage of the entanglement of the two daughter mesons produced in the decay $\Upsilon(4S) \rightarrow B\bar{B}$ which allows for both flavor ($B^0 \rightarrow \ell^+X, \bar{B}^0 \rightarrow \ell^-X$) and CP ($B_+ \rightarrow J/\psi K_L^0, B_- \rightarrow J/\psi K_S^0$) tagging. Selecting events where one B candidate is reconstructed in a CP eigenstate and the flavor of the other B is identified, one can compare the rates of the $\bar{B}^0 \rightarrow B_\pm$ and $B^0 \rightarrow B_\pm$ transitions with their T -reversed $B_\pm \rightarrow \bar{B}^0$ and $B_\pm \rightarrow B^0$ processes, as a function of the time difference Δt between the two B decays [22–24]. Neglecting the small width difference between the two B_d^0 mass eigenstates, each of these eight transitions has a time-dependent decay rate of the form $e^{-\Gamma_d \Delta t} \{1 + S_{\alpha,\beta}^\pm \sin(\Delta m_d \Delta t) + C_{\alpha,\beta}^\pm \cos(\Delta m_d \Delta t)\}$, where Γ_d is the average decay width, Δm_d the B_d^0 mass difference, the subindices $\alpha = \ell^+, \ell^-$ and $\beta = K_S^0, K_L^0$ stand for the reconstructed final states of the two B mesons and the superindex +

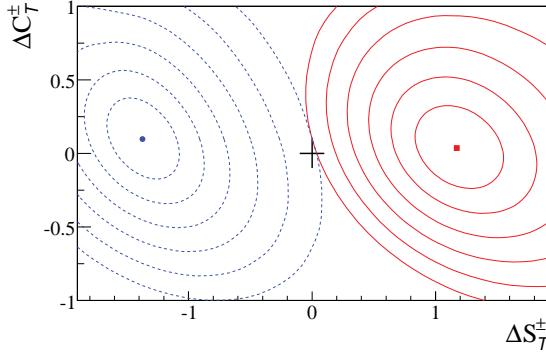


Figure 1: Measured values of ΔS_T^+ , ΔC_T^+ (blue point, dashed lines) and ΔS_T^- , ΔC_T^- (red square, solid lines) [25]. The two-dimensional contours correspond to $1 - \text{CL} = 0.317, 4.55 \times 10^{-2}, 2.70 \times 10^{-3}, 6.33 \times 10^{-5}, 5.73 \times 10^{-7},$ and 1.97×10^{-9} . The + sign indicates the T -invariant point.

or $-$ indicates whether the decay to the flavor final state α occurs before or after the decay to the CP final state β . Figure 1 shows confidence-level contours for the T -asymmetry parameters $\Delta S_T^\pm \equiv S_{\ell^-, K_L^0}^\mp - S_{\ell^+, K_S^0}^\pm$ and $\Delta C_T^\pm \equiv C_{\ell^-, K_L^0}^\mp - C_{\ell^+, K_S^0}^\pm$, reported by the BABAR experiment [25], which clearly demonstrate a violation of T in ΔS_T^\pm , with a significance of 14σ .

2 Electric dipole moments

Among the most powerful tests of CP invariance is the search for a permanent electric dipole moment (EDM) of an elementary fermion or non-degenerate quantum system. The EDM of an elementary spin-1/2 fermion f is defined by the effective, non-renormalizable interaction

$$\mathcal{L}_{\text{EDM}} = -\frac{i}{2} d_f \bar{f} \sigma_{\mu\nu} \gamma_5 f F^{\mu\nu} \quad (6)$$

where $F^{\mu\nu}$ is the QED field strength tensor. The values for d_f are conventionally expressed in units of e cm. The interaction (6) is separately odd under T and P . In the non-relativistic limit, Eq. (6) reduces to

$$\mathcal{L}_{\text{EDM}} \rightarrow d_f \chi_f^\dagger \vec{\sigma} \chi_f \cdot \vec{E} \quad (7)$$

where χ is a two-component Pauli spinor and \vec{E} is the electric field. Note the interaction (7) is manifestly T -odd and carries no direct information on CP . The observation of a non-zero EDM of a non-relativistic (and non-degenerate) quantum system, such as the mercury atom (see below) would imply CP violation under the assumption of CPT invariance.

To date, no experimental observation of an EDM of an elementary particle or non-degenerate bound quantum system has been observed. The most stringent limits have been obtained for the EDMs of the electron, mercury atom, and neutron. A selection of the representative, most stringent limits is given in Table 1. The limits on the electron EDM are inferred from experiments involving polar molecules, paramagnetic systems with an unpaired electron spin. In contrast, the neutron and ^{199}Hg atom are diamagnetic. A variety of experimental efforts aimed at improved sensitivities are underway. For reviews of the experimental and theoretical situation, see, *e.g.* [26–29].

EDMs in the Standard Model

The SM provides two sources of d_f : the CPV phase in the CKM matrix and the P - and T -odd ‘ θ term’ in the QCD Lagrangian. The former is characterized by the Jarlskog invariant [36]

$$\mathcal{J} = \text{Im}(V_{us} V_{cs}^* V_{cb} V_{ub}^*) \sim A^2 \lambda^6 \eta < 10^{-4}, \quad (8)$$

while the latter is given by

$$\mathcal{L}_\theta = -\frac{g_3^2}{16\pi^2} \bar{\theta} \text{Tr} (G^{\mu\nu} \tilde{G}_{\mu\nu}), \quad (9)$$

Table 1: Most stringent limits on electric dipole moments.

EDM	Limit (e cm)	Source
Electron	1.1×10^{-29} (90% C.L.)	ThO [30]
	1.3×10^{-28} (90% C.L.)	HfF ⁺ [31]
Muon	1.8×10^{-19} (95% C.L.)	[32]
Neutron	1.8×10^{-26} (90% C.L.)	[33]
^{199}Hg Atom	7.4×10^{-30} (95% C.L.)	[34]
^{129}Xe Atom	1.5×10^{-27} (95% C.L.)	[35]

where $G_{\mu\nu}$ ($\tilde{G}_{\mu\nu} = \epsilon_{\mu\nu\alpha\beta} G^{\alpha\beta}/2$) is the QCD field strength tensor (dual).

The CKM-induced EDMs of quarks and charged leptons arise at three- and four-loop orders, respectively [37–40]. The resulting numerical impact for the experimental observables (see below) falls well below present and prospective experimental sensitivities. The most important impact of \mathcal{J} for the EDMs of the neutron and diamagnetic atoms arise via induced hadronic interactions. The resulting theoretical expectations for the electron, neutron and ^{199}Hg EDMs are

$$|d_e|_{\text{CKM}} \approx 10^{-44} e \text{ cm} \quad [40], \quad (10a)$$

$$|d_n|_{\text{CKM}} \approx (1 - 6) \times 10^{-32} e \text{ cm} \quad [41], \quad (10b)$$

$$|d_A(^{199}\text{Hg})|_{\text{CKM}} \lesssim 4 \times 10^{-34} e \text{ cm} \quad [26]. \quad (10c)$$

For d_n and $d_A(^{199}\text{Hg})$, the dominant CKM contributions arise from four-quark operators (generated after integrating out the electroweak gauge bosons) rather than from the EDMs of the individual quarks. The corresponding sensitivities to the QCD $\bar{\theta}$ parameter are given by

$$|d_n|_{\bar{\theta}} \approx (0.9 - 1.2) \times 10^{-16} \bar{\theta} e \text{ cm} \quad [41], \quad (11a)$$

$$|d_A(^{199}\text{Hg})|_{\bar{\theta}} \approx (0.07 - 8) \times 10^{-20} \bar{\theta} e \text{ cm} \quad [26, 27], \quad (11b)$$

where the ranges quoted include the impacts of hadronic, nuclear, and atomic theory uncertainties. The neutron EDM puts then a stringent limit on ‘strong’ CP violation: $\bar{\theta} \lesssim 2 \times 10^{-10}$. The corresponding limit from $d_A(^{199}\text{Hg})$ is weaker due to the large theoretical uncertainty.

EDMs Beyond the Standard Model

It is possible that the next generation of EDM searches will yield a non-zero result, arising from the θ -term interaction and/or physics beyond the SM (BSM). Most of the considered BSM scenarios involve new particles with masses well above the electroweak scale. At energies much lower than the BSM mass scale Λ , the dynamics can be described through an effective field theory (SMEFT) involving an infinite set of non-renormalizable operators $\mathcal{O}_k^{(d)}$, with dimensions $d > 4$, that are invariant under the SM gauge group:

$$\mathcal{L}_{\text{SMEFT}} = \mathcal{L}_{\text{SM}} + \sum_{k,d} \alpha_k^{(d)} \left(\frac{1}{\Lambda}\right)^{d-4} \mathcal{O}_k^{(d)}. \quad (12)$$

The operators contain only SM fields, while all short-distance information on the BSM physics is encoded in their Wilson coefficients $\alpha_k^{(d)}$. The $d = 4$ term corresponds to the SM Lagrangian.

For the systems of Table 1 and for many BSM scenarios of recent interest, it suffices to consider the leading contributions from $d = 6$ operators. Considering only the first-generation SM fermions, there exist 12 independent CPV pertinent operators. For a complete listing, see *e.g.*, Refs. [27, 42]. For a given elementary fermion f , two of these operators reduce to the EDM interaction in Eq. (6). Of the remaining, the most relevant include the chromo-electric dipole moments (cEDMs) of the quarks; a CP -odd three gluon operator; three semileptonic, four-fermion operators; two four-quark operators; and a CPV interaction involving two Higgs fields and a right-handed quark current. For the dipole operators, it is useful to define a rescaled Wilson coefficient $\alpha_{fV_j}^{(6)} \equiv g_j C_{fV_j}$, where V_j ($j = 1, 2, 3$) denote the gauge bosons for

Table 2: Pertinent dimension-six EDM and cEDM sources (first generation fermions only).

System	$d = 6$ Source	Wilson Coefficient
Paramagnetic	Electron EDM	$\text{Im } C_{e\gamma}$
	Electron-quark	$C_{eq}^{(\pm)}$
Diamagnetic	Quark EDM	$\text{Im } C_{q\gamma}$
	Quark cEDM	$\text{Im } C_{qG}$
	Three gluon	$C_{\bar{G}}$
	Four quark	$\text{Im } C_{\gamma^{(1,8)}}$
	Quark-Higgs	$\text{Im } C_{\varphi ud}$
	Electron-quark tensor*	$\text{Im } C_{lequ}^{(3)}$

* Applicable only to atoms.

the three SM gauge groups with corresponding couplings g_j ; for all other $d = 6$ operators we correspondingly identify $\alpha_k^{(6)} \equiv C_k$. In this case, one has for the EDM (d_f) and cEDM (\tilde{d}_q)

$$d_f = -(1.13 \times 10^{-16} \text{ e cm}) \left(\frac{v}{\Lambda}\right)^2 \text{Im } C_{f\gamma}, \quad (13a)$$

$$\tilde{d}_q = -(1.13 \times 10^{-16} \text{ cm}) \left(\frac{v}{\Lambda}\right)^2 \text{Im } C_{qG}, \quad (13b)$$

with $\text{Im } C_{f\gamma} = \text{Im } C_{fB} + 3I_3^f \text{Im } C_{fW}$. As the expressions (13a,13b) illustrate, the magnitude of the BSM contributions scales with two inverse powers of the scale Λ . A similar conclusion holds for the contributions from the other $d = 6$ operators to the EDMs of Table 1.

It is important to emphasize that if the BSM mediators are light, with masses below the weak scale, the effective field theory description of Eq. (12) does not apply. For recent studies along these lines, see, *e.g.* [43, 44].

EDM Interpretation: From Short Distances to the Atomic Scale

The EDM limits in Table 1 are obtained using composite quantum systems, wherein the relevant dynamics involve physics at the hadronic, nuclear, atomic and molecular scales. The manifestation of a given CPV source (CKM, θ term, BSM) involves an interplay of these dynamics. In all cases, one must first evolve the Wilson coefficients from the weak scale to the hadronic scale, then match onto the relevant low-energy degrees of freedom (electrons, nucleons, pions, *etc.*). At this level, the most straightforward interpretation involves the paramagnetic systems, for which two sources dominate: the electron EDM and the electron spin-dependent semileptonic interaction $\bar{e}\gamma_5 e \bar{q}q$. The latter gives rise to a spin-independent Hamiltonian, for an atom with Z electrons/protons and N neutrons,

$$\hat{H}_S = \frac{iG_F}{\sqrt{2}} \delta(\vec{r}) \left[(Z + N) C_S^{(0)} + (Z - N) C_S^{(1)} \right] \gamma_0 \gamma_5, \quad (14)$$

where $C_S^{(0)}$ ($C_S^{(1)}$) is proportional to $C_{eq}^{(+)}$ ($C_{eq}^{(-)}$). The computation of $C_S^{(0,1)}$ is relatively free from theoretical uncertainty since the operator $\bar{q}q$ essentially counts the number of quarks of flavor q in the nucleus. Experimental results for paramagnetic systems, thus, often quote bounds on

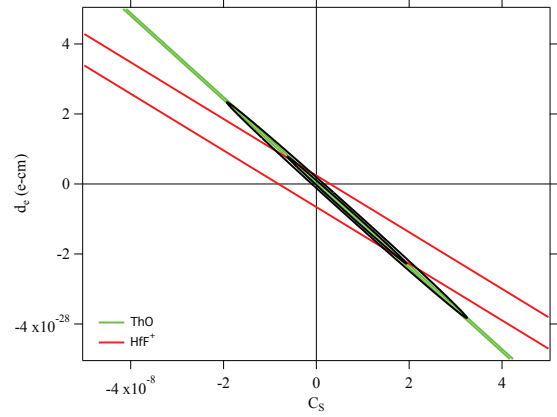
$$C_S \equiv C_S^{(0)} + \left(\frac{Z - N}{Z + N} \right) C_S^{(1)} \quad (15)$$

as well as on d_e , assuming only one of these two sources is non-vanishing. Combining results from ThO and HfF⁺ (see Figure 2) allows one to obtain the global, 90% C.L. bounds

$$|d_e| < 1.8 \times 10^{-28} \text{ e cm}, \quad |C_S| < 9.8 \times 10^{-9}. \quad (16)$$

Note that the limits on d_e given in Table 1 have been obtained assuming $C_S = 0$.

For the diamagnetic systems, the situation is considerably more involved. For the neutron, a variety of approaches – including

**Figure 2:** Constraints on d_e and C_S from EDM searches using polar molecules (updated by [45] from Ref. [26]).

lattice QCD, chiral perturbation theory, QCD sum rules, and the quark model – have been employed to compute the relevant hadronic matrix elements of the CPV sources (see, *e.g.*, [27, 28, 46, 47]). For diamagnetic atoms, the non-leptonic sources of Table 2 give rise to the EDM of the nucleus as well as other P - and T -odd nuclear moments, as allowed by the nuclear spin. However, according to a theorem by Schiff [48], the nuclear EDM generates no contribution to the neutral-atom EDM due to screening by atomic electrons. The leading contribution from these sources, instead, arises via the nuclear Schiff moment, \vec{S} , an r^3 -weighted moment of the T - and P -odd component of the nuclear charge density. The resulting effective atomic Hamiltonian is

$$\hat{H}_{\text{Schiff}} = -4\pi \vec{\nabla} \rho_e(0) \cdot \vec{S}, \quad (17)$$

where $\vec{\nabla} \rho_e(0)$ is the gradient of the electron density at the nucleus. To date, computations of the nuclear Schiff moment have assumed that the leading contribution arises from a pion-exchange induced nuclear force, with the P - and T -odd πN interaction given by

$$\mathcal{L}_{\pi N}^{T,P} = \bar{N} \left[\bar{g}_\pi^{(0)} \vec{\tau} \cdot \vec{\pi} + \bar{g}_\pi^{(1)} \pi^0 + \bar{g}_\pi^{(2)} (3\tau_3 \pi^0 - \vec{\tau} \cdot \vec{\pi}) \right] N. \quad (18)$$

Chiral effective field theory power counting implies that in general the magnitude of $\bar{g}_\pi^{(2)}$ is suppressed with respect to the isoscalar and isovector couplings. The CPV sources then generate a diamagnetic atom EDM d_A via the sequence

$$CPV \text{ source} \longrightarrow \bar{g}_\pi^{(i)} \longrightarrow \vec{S} \longrightarrow d_A. \quad (19)$$

The steps in this sequence involve dynamics at the hadronic, nuclear, and atomic scales, respectively. In addition, d_A may receive contributions from the nuclear spin-dependent interaction generated by the semileptonic tensor interaction listed in Table 2, with the corresponding atomic Hamiltonian

$$\hat{H}_T = \frac{2iG_F}{\sqrt{2}} \delta(\vec{r}) \sum_N \left[C_T^{(0)} + C_T^{(1)} \tau_3 \right] \vec{\sigma}_N \cdot \vec{\gamma}, \quad (20)$$

where σ_N is the nucleon spin Pauli matrix and $C_T^{(0,1)} \propto \text{Im } C_{lequ}^{(3)}$.

Given the large number of CPV sources and existing diamagnetic EDM limits, it is not possible to obtain a set of global constraints on the former. One may, however, do so for the low-energy effective parameters $\bar{g}_\pi^{(0,1)}$, $C_T^{(0,1)}$ and \bar{d}_n^{sr} , where the latter denotes a ‘short-range’ contribution to the neutron EDM [26, 49]. In this context, the dominant source of theoretical uncertainty involves computations of the nuclear Schiff moment. From the bounds on the low-energy parameters, one may then derive constraints on the CPV sources by utilizing computations of the hadronic matrix elements. Reducing the degree of theoretical hadronic and nuclear physics uncertainty is an area of active effort.

3 Tests of CPT

CPT symmetry implies the equality of the masses and widths of a particle and its antiparticle. The most constraining limits are extracted from the neutral kaons [50, 51]:

$$\begin{aligned} 2 \frac{|m_{K^0} - m_{\bar{K}^0}|}{(m_{K^0} + m_{\bar{K}^0})} &< 6 \times 10^{-19}, \\ 2 \frac{|\Gamma_{K^0} - \Gamma_{\bar{K}^0}|}{(\Gamma_{K^0} + \Gamma_{\bar{K}^0})} &= (8 \pm 8) \times 10^{-18}. \end{aligned} \quad (21)$$

The limit on the $K^0 - \bar{K}^0$ mass difference assumes that there is no other source of CPT violation. An upper bound on CPT breaking in $K_L^0 \rightarrow 2\pi$ has been also set through the measured phase difference of the CPV ratios η_{00} and η_{+-} , $\phi_{00} - \phi_{+-} = (0.34 \pm 0.32)^\circ$, thanks to the small value of $(1 - |\eta_{00}/\eta_{+-}|)$ (see the review on CP violation in K_L^0 decays).

The measured masses and electric charges of the electron, the proton and their antiparticles provide also strong limits on CPT violation [52–54]:

$$\begin{aligned} 2 \frac{|m_{e^+} - m_{e^-}|}{m_{e^+} + m_{e^-}} &< 8 \times 10^{-9}, \quad \frac{|q_{e^+} + q_{e^-}|}{e} < 4 \times 10^{-8}, \\ \left| \frac{q_{\bar{p}}/m_{\bar{p}}}{q_p/m_p} - 1 \right| &= (0.1 \pm 6.9) \times 10^{-11}. \end{aligned} \quad (22)$$

Worth mentioning are also the tight constraints derived from the lepton and antilepton magnetic moments [55, 56],

$$\begin{aligned} 2 \frac{g_{e^+} - g_{e^-}}{g_{e^+} + g_{e^-}} &= (-0.5 \pm 2.1) \times 10^{-12}, \\ 2 \frac{g_{\mu^+} - g_{\mu^-}}{g_{\mu^+} + g_{\mu^-}} &= (-0.11 \pm 0.12) \times 10^{-8}, \end{aligned} \quad (23)$$

those of the proton and antiproton [57],

$$(\mu_p + \mu_{\bar{p}})/\mu_p = (2 \pm 4) \times 10^{-9}, \quad (24)$$

and the recent measurement of the 1S-2S atomic transition in anti-hydrogen which agrees with the corresponding frequency spectral line in hydrogen at a relative precision of 2×10^{-12} [58].

A violation of CPT in an interacting local quantum field theory would imply that Lorentz symmetry is also violated [59]. Signatures of Lorentz-invariance violation have been searched for with atomic clocks, penning traps, matter and antimatter spectroscopy, colliders and astroparticle experiments, with so far negative results [60]. A compilation of experimental bounds is given in Ref. [61], parametrized through the coefficients of the so-called Standard Model Extension (SME) Lagrangian which contains all possible Lorentz- and CPT -violating operators preserving gauge invariance, renormalizability, locality and observer causality [62].

QUANTUM-NUMBER CONSERVATION LAWS

Conservation laws of several quantum numbers have been empirically established with a very high degree of confidence. They are usually associated with some global phase symmetry. However, while some of them are deeply rooted in basic principles such as gauge invariance (charge conservation; local symmetry implies global symmetry) or Lorentz symmetry (fermion number conservation), others appear to be accidental symmetries of the SM Lagrangian and could be broken by new physics interactions.

In fact, if one only assumes the SM gauge symmetries and particle content, the most general dynamics at energies below the BSM mass scale is described by the SMEFT Lagrangian in Eq. (12). All $d = 4$ operators (*i.e.*, the SM) happen to preserve the B and L quantum numbers, but this is no-longer true for the gauge-invariant structures of higher dimensionality. There is only one operator with $d = 5$ (up to hermitian conjugation and flavor assignments), and it violates lepton number by two units [63], giving rise to Majorana neutrino masses after the electroweak spontaneous symmetry breaking. With $d = 6$, there are five operators

that violate B and L [64, 65]. Thus, violations of these quantum numbers can be generically expected, unless there is an explicit symmetry protecting them.

4 Electric charge

The conservation of electric charges is associated with the QED gauge symmetry. The most precise tests are the non-observation of the decays $e \rightarrow \nu_e \gamma$ (lifetime larger than 6.6×10^{28} yr [66]) and $n \rightarrow p \nu_e \bar{\nu}_e$ ($\text{Br} < 8 \times 10^{-27}$, 68% C.L. [67]). The neutrality of matter can be also interpreted as a test of electric charge conservation. Worth mentioning are the experimental limits on the electric charge of the neutron, $q_n/e = (-0.2 \pm 0.8) \times 10^{-21}$, and on the sum of the proton and electron charges, $|q_p + q_e|/e < 1 \times 10^{-21}$ [68].

The isotropy of the cosmic microwave background has been used to set stringent limits on a possible charge asymmetry of the Universe [69]. Assuming that charge asymmetries produced by different particles are not anticorrelated, this implies upper bounds on the photon ($|q_\gamma|/e < 1 \times 10^{-35}$) and neutrino ($|q_\nu|/e < 4 \times 10^{-35}$) electric charges. A much stronger upper bound on the photon charge ($|q_\gamma|/e < 1 \times 10^{-46}$) has been derived from the non-observation of Aharonov-Bohm phase differences in interferometric experiments with photons that have traversed cosmological distances, under the assumption that both positive and negative charged photons exist [70].

5 Lepton family numbers

In the SM with massless left-handed neutrinos there is a separate conservation number for each lepton family. However, neutrino oscillations show that neutrinos have tiny masses and there are sizable mixings among the different lepton flavors. Compelling evidence from solar, atmospheric, accelerator and reactor neutrino experiments has established a quite solid pattern of neutrino mass differences and mixing angles [16, 17]. (see the review on neutrino masses, mixings and oscillations). Nevertheless, flavor mixing among the different charged leptons has never been observed.

If neutrino masses and mixings among the three active neutrinos were the only sources of lepton-flavor violation (LFV), neutrinoless transitions from one charged lepton flavor to another would be heavily suppressed by powers of m_{ν_i} (GIM mechanism), leading to un-observably small rates; for instance [73–78],

$$\text{Br}(\mu \rightarrow e \gamma) = \frac{3\alpha}{32\pi} \left| \sum_i U_{\mu i}^* U_{e i} \frac{m_{\nu_i}^2 - m_{\nu_1}^2}{M_W^2} \right|^2 < 10^{-54}, \quad (25)$$

where U_{ia} are the relevant elements of the PMNS mixing matrix. This contribution is clearly too small to be observed in any realistic experiment, so any experimentally accessible effect would arise from BSM physics with sources of LFV not related to m_{ν_i} . The search for charged LFV (CLFV) remains an area of active interest, which has the potential to probe physics at scales much higher than the TeV.

Among the most sensitive probes are searches for the CLFV decays of the muon, $\mu \rightarrow e \gamma$ and $\mu \rightarrow 3e$, as well as the conversion process $\mu^- + A(N, Z) \rightarrow e^- + A(N, Z)$, where $A(N, Z)$ denotes a nucleus with N neutrons and Z protons. Searches for rare τ decays such as $\tau \rightarrow \ell \gamma$ ($\ell = e, \mu$) also provide interesting probes of CLFV. A variety of BSM scenarios predict that rates for these CLFV processes could be sufficiently large to be observed in the present or planned searches. To date, no observation has been reported, and the resulting null results place strong constraints on BSM scenarios. For extensive reviews of the experimental and theoretical status and prospects, see Refs. [72, 79, 80].

A detailed set of upper bounds on CLFV branching ratios is given in the listings for the muon and tau leptons. Here we emphasize those with the strongest limits:

$$\begin{aligned} \text{Br}(\mu \rightarrow e \gamma) &< 4.2 \times 10^{-13} \quad [81], \\ \text{Br}(\mu \rightarrow 3e) &< 1.0 \times 10^{-12} \quad [82] \end{aligned} \quad (26)$$

and

$$B_{\mu \rightarrow e} \equiv \frac{\Gamma(\mu^- + A(N, Z) \rightarrow e^- + A(N, Z))}{\Gamma(\mu^- + A(N, Z) \rightarrow \nu + A(N+1, Z-1))} \quad (27)$$

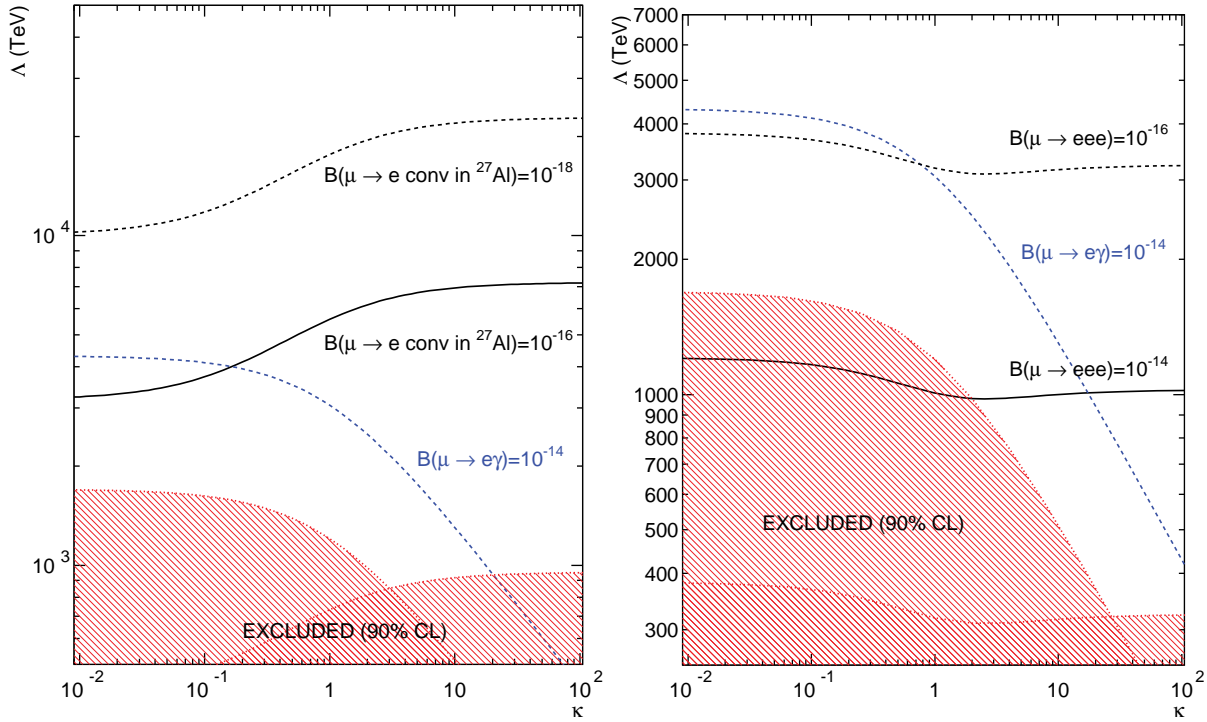


Figure 3: Model-independent CLFV sensitivities based on Eq (31). Left panel shows the comparison of present constraints with prospective future sensitivities for $\mu \rightarrow e\gamma$ and $\mu \rightarrow e$ conversion. Right panel gives analogous comparison for $\mu \rightarrow e\gamma$ and $\mu \rightarrow 3e$. Updated by [71] from Ref. [72].

with the best limit so far, $B_{\mu \rightarrow e} < 7 \times 10^{-13}$ [83], obtained with gold. Several proposed experiments aim to improve these limits by several orders of magnitude with different atoms.

One may interpret both $\mu \rightarrow e\gamma$ and $\mu \rightarrow e$ conversion in terms of the amplitudes to emit a real or virtual photon:

$$\begin{aligned} \mathcal{M}_{\mu \rightarrow e\gamma^{(*)}} = & eG_{\mu} \varepsilon^{\alpha\beta} \bar{e}(p-q) \left[(q^2 \gamma_{\alpha} - \not{q} q_{\alpha}) (\tilde{A}_1^R P_R + \tilde{A}_1^L P_L) \right. \\ & \left. + im_{\mu} \sigma_{\alpha\beta} q^{\beta} (\tilde{A}_2^R P_R + \tilde{A}_2^L P_L) \right] \mu(p), \end{aligned} \quad (28)$$

where it is conventional to normalize the amplitude to the Fermi constant. One then has

$$\text{Br}(\mu \rightarrow e\gamma) = 48\pi^3 \alpha (|\tilde{A}_2^R|^2 + |\tilde{A}_2^L|^2). \quad (29)$$

For the conversion process, the virtual photon is absorbed by the quarks in the nucleus, yielding an effective four-fermion operator. In general, the exchange of other particles could lead to similar or alternate Lorentz structures, and it is not possible to distinguish between the exchange of a virtual photon or other particle. It is conventional to write the most general four-fermion amplitude, valid for energies below the electroweak scale as (adapted from Ref. [88])

$$\mathcal{M}_{\mu \rightarrow e} = G_{\mu} \sum_{n,a,q} a_{a,q}^{(n)} \bar{e} \Gamma^n P_a \mu \bar{q} \Gamma_n q, \quad (30)$$

where P_a ($a = L, R$) denote the left and right-handed projectors and Γ^n denotes $1, \gamma_5, \gamma^{\mu}, \gamma^{\mu} \gamma_5$, and $\sigma_{\mu\nu}$. If any of the coefficients $a_{a,q}^{(n)}$ are generated by physics at a scale $\Lambda > v$, then their effects would be encoded in the SMEFT Lagrangian (12). For scenarios in which the leading CLFV operators occur at $d = 6$, the $a_{a,q}^{(n)}$ will scale as $(v/\Lambda)^2$. The corresponding decay and conversion rates will then scale as $(v/\Lambda)^4$. Note that the scalar and time component of the vector interactions are coherent over the nucleus, essentially counting the number of quarks. Consequently,

these interactions typically yield the greatest sensitivities to high BSM mass scales.

It is sometimes convenient to compare the relative sensitivities of the decay and conversion processes using the following simplified effective Lagrangian [72]:

$$\begin{aligned} \mathcal{L}_{\text{eff}}^{\text{CLFV}} = & \frac{m_{\mu}}{(\kappa+1)\Lambda^2} \bar{\mu}_R \sigma_{\mu\nu} e_L F^{\mu\nu} \\ & + \frac{\kappa}{(\kappa+1)\Lambda^2} \bar{\mu} \gamma_{\mu} e \sum_q \bar{q} \gamma^{\mu} q + \text{h.c.} \end{aligned} \quad (31)$$

Note that one may replace the second term in Eq. (31) by any one of the other four-fermion interactions given in Eq. (30). An analogous expression applies to the process $\mu \rightarrow 3e$ when replacing the sum over quarks by the corresponding electron bilinear. A comparison of the present and prospective sensitivities for various muon CLFV searches in this framework is shown in Figure 3.

Stringent limits have been also set on the LFV decay modes of the τ lepton [89]. As shown in Figure 4, the large τ data samples collected at the B factories have made possible to reach a 10^{-8} sensitivity for many of its leptonic ($\tau \rightarrow \ell\gamma, \tau \rightarrow \ell'\ell^+\ell^-$) and semileptonic ($\tau \rightarrow \ell P^0, \tau \rightarrow \ell V^0, \tau \rightarrow \ell P^0 P^0, \tau \rightarrow \ell P^+ P'^-$) neutrinoless LFV decays, and BELLE-II is expected to push these limits beyond the 10^{-9} level [85]. Being a third generation lepton, the τ could be more sensitive to heavier new-physics scales, which makes his LFV decays particularly interesting. Compared to the muon, the τ decay amplitudes could be enhanced by a chirality ratio $(m_{\tau}/m_{\mu})^2 \sim 280$ and/or by lepton-mixing factors such as $|U_{\tau 3}/U_{e 3}|^2 \sim 20$, but the exact relation is model dependent. In any case, the τ LFV decays provide a rich data set that is very complementary to the μ bounds. If LFV is finally observed, the correlations between μ and τ data, and among different LFV τ decays will allow to probe the underlying mechanism of lepton flavor breaking.

Interesting limits on LFV are also obtained in meson decays. The best bounds come from kaon experiments, e.g., $\text{Br}(K_L^0 \rightarrow e^{\pm} \mu^{\mp}) < 4.7 \times 10^{-12}$ [90], $\text{Br}(K^+ \rightarrow \pi^+ \mu^+ e^-) < 1.3 \times 10^{-11}$ [91]. Quite strong limits have also been set in decays of B and D mesons, the best upper bounds being $\text{Br}(B^0 \rightarrow e^{\pm} \mu^{\mp}) < 1.0 \times$

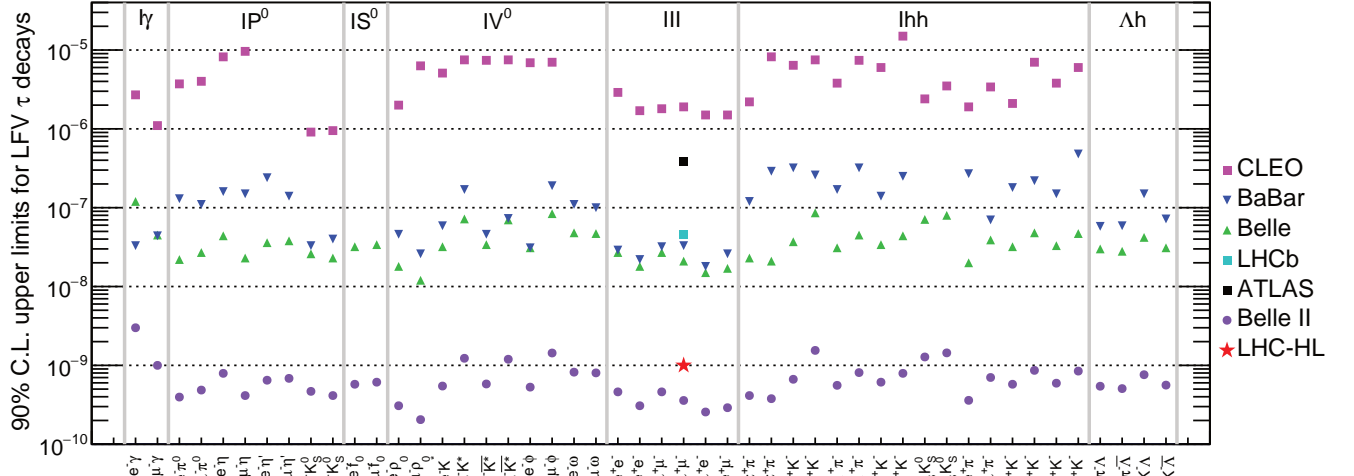


Figure 4: Current experimental limits on neutrinoless LFV τ decays [84]. Also shown are the future projections at Belle-II [85] and at the HL-LHC [86].

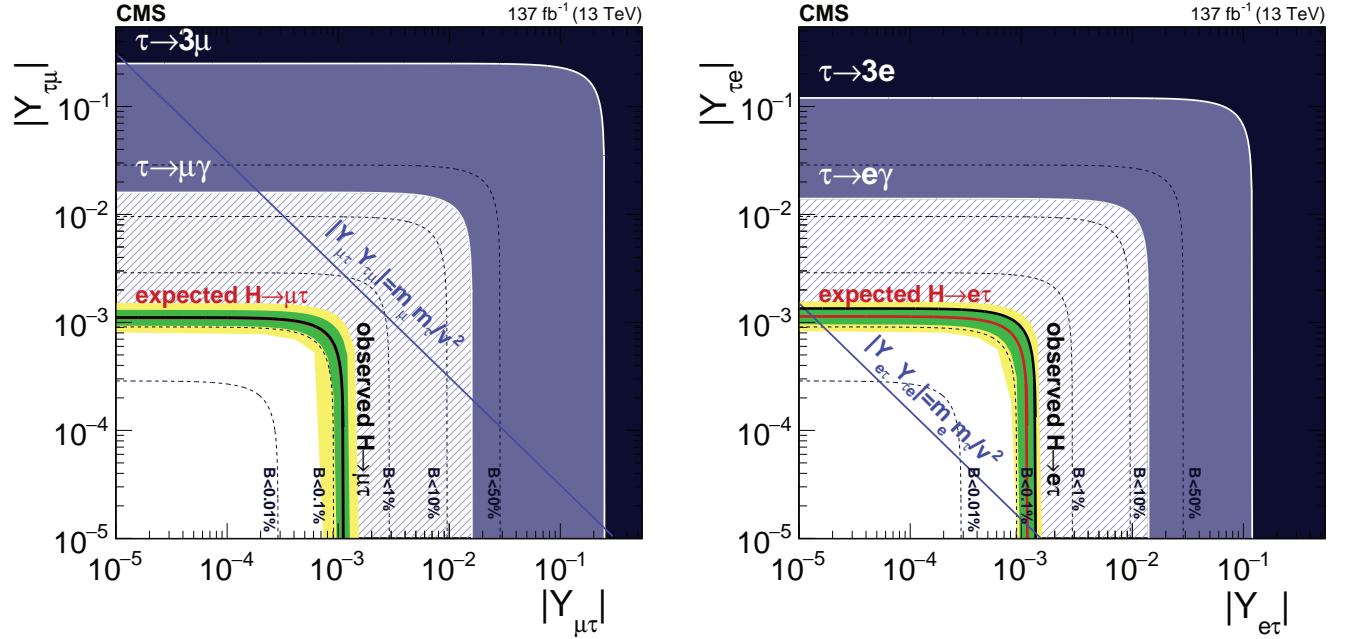


Figure 5: Current limits on the Higgs LFV τ Yukawas from direct $H^0 \rightarrow \ell^\pm \tau^\mp$ decays ($\ell = e, \mu$), and indirect constraints from τ decays [87].

10^{-9} [92] and $\text{Br}(D^0 \rightarrow e^\pm \mu^\mp) < 1.3 \times 10^{-8}$ [93].

The LFV decays of the Z boson were probed at LEP at the 10^{-5} to 10^{-6} level. Stronger (95% C.L.) limits have been set recently by the LHC ATLAS collaboration [94, 95]:

$$\begin{aligned} \text{Br}(Z \rightarrow e^\pm \mu^\mp) < 7.5 \times 10^{-7}, \quad \text{Br}(Z \rightarrow e^\pm \tau^\mp) < 5.0 \times 10^{-6}, \\ \text{Br}(Z \rightarrow \mu^\pm \tau^\mp) < 6.5 \times 10^{-6}. \end{aligned} \quad (32)$$

LHC is now starting to test LFV in Higgs decays, within the available statistics. From the current (95% C.L.) experimental upper bounds [87, 96–98],

$$\begin{aligned} \text{Br}(H^0 \rightarrow e^\pm \mu^\mp) < 6.1 \times 10^{-5}, \quad \text{Br}(H^0 \rightarrow e^\pm \tau^\mp) < 0.22\%, \\ \text{Br}(H^0 \rightarrow \mu^\pm \tau^\mp) < 0.15\%, \end{aligned} \quad (33)$$

one can derive direct limits on the LFV Yukawa couplings of the

Higgs boson,

$$\mathcal{L}_Y = -H^0 \sum_{i \neq j} (Y_{\ell_i \ell_j} \bar{\ell}_L^i \ell_R^j + \text{h.c.}). \quad (34)$$

From $H^0 \rightarrow e^\pm \mu^\mp$, one obtains $\sqrt{Y_{\mu e}^2 + Y_{e\mu}^2} < 2.2 \times 10^{-4}$, which is not yet competitive with the indirect limit set by $\mu \rightarrow e\gamma$ through a (one-loop) virtual Higgs exchange:

$$\sqrt{Y_{\mu e}^2 + Y_{e\mu}^2} < 3.6 \times 10^{-6}. \quad (35)$$

However, the LHC data provide at present the strongest bounds on the LFV τ Yukawas [87]:

$$\sqrt{Y_{e\tau}^2 + Y_{\tau e}^2} < 1.35 \times 10^{-3}, \quad \sqrt{Y_{\mu\tau}^2 + Y_{\tau\mu}^2} < 1.11 \times 10^{-3}. \quad (36)$$

Figure 5 compares the Higgs exclusion limits on the τ Yukawas with the current indirect constraints from LFV τ decays.

6 Baryon and Lepton Number

The transitions discussed in the previous section preserve the total lepton number $L = L_e + L_\mu + L_\tau$. In the SM, conservation of $B - L$ is an accidental symmetry of the Lagrangian. At the classical level, $B + L$ is also conserved, though it is violated at the loop level by the anomaly. The latter is a topological effect that is highly suppressed at zero temperature and, moreover, does not contribute to the processes discussed in the review. Going beyond renormalizable interactions, there exists a tower of operators in the SMEFT Lagrangian (12), containing only SM fields, that break one or both of these symmetries. We briefly review these possibilities in turn.

Lepton Number

The lowest-dimension operator containing only SM fields that breaks baryon or lepton number is the $d = 5$, lepton-number-violating (LNV) ‘Weinberg’ neutrino-mass operator [63]:

$$\mathcal{L}^{\text{LNV}} = \frac{y}{\Lambda} \bar{L}^C H H^T L. \quad (37)$$

When the neutral component of the Higgs field obtains its vacuum expectation value, this $\Delta L = 2$ interaction yields a Majorana mass for the light, active neutrinos. The most comprehensive approach for probing this effect is the search for neutrinoless double-beta decay ($0\nu\beta\beta$) of atomic nuclei, $(Z, A) \rightarrow (Z + 2, A) + e^- + e^-$ [99, 100] (see the review on neutrinoless double- β decay). The detection of a non-zero $0\nu\beta\beta$ signal could represent a spectacular evidence of Majorana neutrinos. The current best limit, $\tau_{1/2} > 1.07 \times 10^{26}$ yr, was obtained by the KamLAND-Zen experiment with ^{136}Xe [101].

Theoretically, the interaction (37) can arise from BSM interactions in the well-known see-saw mechanism for neutrino mass (for a review, see [102]). In this context, the conventional choice for the scale Λ is of order the GUT scale, yielding light neutrino masses of order eV and below when the couplings y are of order the charged elementary fermion Yukawa couplings. BSM theories may also give rise to LNV observables in other contexts. In these scenarios, if the LNV scale is of order 1 TeV, one may observe signatures of LNV not only in $0\nu\beta\beta$ but also in collider searches for final states containing same sign dileptons. Searches for same sign dileptons plus a di-jet pair at the LHC have placed constraints on TeV-scale LNV [103, 104] that in some cases complement those obtained from $0\nu\beta\beta$.

Stringent constraints on violations of L have been also set in $\mu^- \rightarrow e^+$ conversion in muonic atoms, the best limit being $\sigma(\mu^- \text{Ti} \rightarrow e^+ \text{Ca}) / \sigma(\mu^- \text{Ti} \rightarrow \text{all}) < 3.6 \times 10^{-11}$ [105], and at the flavor factories through L -violating decays of the τ lepton and K , D and B mesons. Some representative examples are $\text{Br}(\tau^- \rightarrow e^+ \pi^- \pi^-) < 2.0 \times 10^{-8}$ [106], $\text{Br}(K^+ \rightarrow \pi^- \mu^+ \mu^+) < 4.2 \times 10^{-11}$ [107], $\text{Br}(D^+ \rightarrow \pi^- \mu^+ \mu^+) < 1.4 \times 10^{-8}$ [108] and $\text{Br}(B^- \rightarrow \pi^+ \mu^- \mu^-) < 4.0 \times 10^{-9}$ (95% CL) [109]. All these $|\Delta L| = 2$ processes could be mediated by a massive Majorana neutrino. They provide useful bounds on the effective Majorana neutrino mass matrix $m_{\ell\ell'} \sim \sum_i U_{\ell i} U_{\ell' i} m_{\nu_i}$ [110], although not as strong as the $0\nu\beta\beta$ constraint on m_{ee} .

Baryon Number

Grand Unified Theories (GUTs) combine leptons and quarks in the same symmetry multiplets and, therefore, predict the violation of the baryon and lepton quantum numbers. Many experiments have searched for B -violating transitions, but no positive signal has been identified so far. Proton decay would be the most relevant violation of B , as it would imply the instability of matter. The current lower bound on the proton lifetime is 3.6×10^{29} yr [111]. Stronger limits have been set for particular decay modes, such as $\tau(p \rightarrow e^+ \pi^0) > 1.6 \times 10^{34}$ yr [112]. For a discussion of proton decay in the context of GUTs, see the review on Grand Unified Theories.

Another spectacular signal would be neutron-antineutron oscillations. Searches have been performed for quasi-free $n-\bar{n}$ oscillations and for $n\bar{n}$ annihilation products in a nucleus. The latter would arise when the \bar{n} produced through oscillations annihilates with another neutron in the nuclear medium. The corresponding best limits, expressed in terms of the free and bound oscillation

times, $\tau_{n\bar{n}}$ and τ_m , respectively, are:

$$\tau_{n\bar{n}} > 0.86 \times 10^8 \text{ s} \quad [113], \quad (38a)$$

$$\tau_m > 1.9 \times 10^{32} \text{ yr} \quad [114]. \quad (38b)$$

From the latter, one may infer a bound $\tau_{n\bar{n}} > 2.7 \times 10^8$ s, as discussed below. See Ref. [115] for a recent review.

The theoretical interpretation of these bounds starts with an assumed, effective Hamiltonian for the free (anti-)neutron, \mathcal{H}_{eff} that contains a B -violating part, yielding matrix elements

$$\langle n | \mathcal{H}_{\text{eff}} | n \rangle = \langle \bar{n} | \mathcal{H}_{\text{eff}} | \bar{n} \rangle = m - i \frac{\lambda}{2}, \quad (39a)$$

$$\langle n | \mathcal{H}_{\text{eff}} | \bar{n} \rangle = \langle \bar{n} | \mathcal{H}_{\text{eff}} | n \rangle \equiv \delta m, \quad (39b)$$

where CPT is assumed to be conserved, the neutron lifetime $\tau_n = 1/\lambda$ and $\tau_{n\bar{n}} = 1/|\delta m|$. The rate for a neutron to oscillate into an antineutron after a time t is given by

$$\mathcal{P}_{n\bar{n}}(t) = \sin^2 \left(\frac{t}{\tau_{n\bar{n}}} \right) e^{-\lambda t}. \quad (40)$$

For $t \ll \tau_n \ll \tau_{n\bar{n}}$, one has

$$\mathcal{P}_{n\bar{n}}(t) \rightarrow (t/\tau_{n\bar{n}})^2. \quad (41)$$

In realistic experiments, there exist effects, such as background magnetic fields, that split the energies of the neutron and antineutron. One must ensure that the observation time is sufficiently short so that these effects do not overwhelm the small B -violating term δm and that Eq. (40) applies.

In nuclei, the interactions of neutrons and antineutrons with the surrounding medium are sufficiently distinct that one must take the corresponding matter potentials into account. In particular, the matrix elements in Eq. (39a) become

$$\langle n | \mathcal{H}_{\text{eff}} | n \rangle = m + V_n, \quad \langle \bar{n} | \mathcal{H}_{\text{eff}} | \bar{n} \rangle = m + V_{\bar{n}}, \quad (42)$$

with V_n being essentially real ($V_n \equiv V_{nR}$) and $V_{\bar{n}} = V_{\bar{n}R} - iV_{\bar{n}I}$. The imaginary part $V_{\bar{n}I}$ characterizes the annihilation of the antineutron with bound nucleons into secondary hadrons. The rate for a bound neutron to disappear is given by

$$\Gamma_m = \frac{2(\delta m)^2 |V_{\bar{n}I}|}{(V_{nR} - V_{\bar{n}R})^2 + V_{\bar{n}I}^2} \equiv (R \tau_{n\bar{n}}^2)^{-1}. \quad (43)$$

For the nuclei of experimental interest, nuclear theory computations yield $R \sim 10^{23} \text{ s}^{-1}$. Null results of bound $n-\bar{n}$ oscillation searches thus allow one to infer a bound on $\tau_{n\bar{n}}$ via Eq. (43).

From an elementary particle standpoint, $n-\bar{n}$ oscillations involve the conversion of three quarks into three antiquarks (and vice-versa). The lowest-dimension operators mediating such process arise at dimension nine in the SMEFT:

$$\mathcal{L}_{n-\bar{n}} = \frac{1}{\Lambda^5} \sum_j \alpha_j^{(9)} \mathcal{O}_j^{\text{BNV}}. \quad (44)$$

Consequently, one expects

$$\delta m \sim \alpha_j^{(9)} \frac{\Lambda_{\text{HAD}}^6}{\Lambda^5}, \quad (45)$$

where Λ_{HAD} is a hadronic scale set by the $n-\bar{n}$ matrix elements in Eq. (39b). Taking Λ_{HAD} to be of order the QCD scale and using the present bounds on $\tau_{n\bar{n}}$ yields a lower bound on the B -violating mass scale of ~ 100 TeV.

The search for B -violating decays of short-lived particles such as Z bosons, τ leptons and B mesons provides also relevant constraints. The best limits are $\text{Br}(Z \rightarrow pe, p\mu) < 1.8 \times 10^{-6}$ (95% C.L.) [116], $\text{Br}(\tau^- \rightarrow \bar{p}\mu^- \mu^+) < 1.8 \times 10^{-8}$ [117] and $\text{Br}(B^+ \rightarrow Ae^+) < 3.2 \times 10^{-8}$ [118].

7 Quark flavors

While strong and electromagnetic forces preserve the quark flavor, the charged-current weak interactions generate transitions among the different quark species (see the review on the CKM quark-mixing matrix). Since the SM flavor-changing mechanism is associated with the W^\pm fermionic vertices, the tree-level transitions satisfy a $\Delta F = \Delta Q$ rule where ΔQ denotes the change in charge of the relevant hadrons. Remember that the flavor quantum number F is defined to be +1 for positively charged quarks ($F = U, C, T$) and -1 for quarks with negative charges ($F = D, S, B$). The strongest tests on this conservation law have been obtained in kaon decays such as $\text{Br}(K^+ \rightarrow \pi^+ \pi^+ e^- \bar{\nu}_e) < 1.3 \times 10^{-8}$ [119], and $(\text{Re } x, \text{Im } x) = (-0.002 \pm 0.006, 0.0012 \pm 0.0021)$ [120, 121] where $x \equiv \mathcal{M}(K^0 \rightarrow \pi^- \ell^+ \nu) / \mathcal{M}(K^0 \rightarrow \pi^- \ell^+ \nu)$.

The $\Delta F = \Delta Q$ rule can be violated through quantum loop contributions giving rise to flavor-changing neutral-current transitions (FCNCs). Owing to the GIM mechanism, processes of this type are very suppressed in the SM, which makes them a superb tool in the search for new physics associated with the flavor dynamics. Within the SM itself, these transitions are also sensitive to the heavy-quark mass scales and have played a crucial role identifying the size of the charm (K^0 - \bar{K}^0 mixing) and top (B^0 - \bar{B}^0 mixing) masses before the discovery of those quarks. In addition to the well-established $\Delta F = 2$ mixings in neutral K and B mesons, $\Delta M_{K^0} \equiv M_{K_L^0} - M_{K_S^0} = (0.5293 \pm 0.0009) \times 10^{10} \text{ s}^{-1}$, $\Delta M_{B^0} \equiv M_{B_H^0} - M_{B_L^0} = (0.5065 \pm 0.0019) \times 10^{12} \text{ s}^{-1}$ and $\Delta M_{B_s^0} \equiv M_{B_{sH}^0} - M_{B_{sL}^0} = (17.765 \pm 0.006) \times 10^{12} \text{ s}^{-1}$, the mixing of the D^0 meson and its antiparticle has been recently observed with a significance of more than seven standard deviations [122], showing that there is a nonzero mass difference between the two neutral charm-meson eigenstates, of the expected size:

$$M_{D_H^0} - M_{D_L^0} = (0.997 \pm 0.116) \times 10^{10} \text{ s}^{-1}. \quad (46)$$

The SM prediction of the D_H^0 - D_L^0 mass difference is dominated by long-distance physics, because it involves virtual loops with down-type light quarks, and has unfortunately quite large uncertainties [123].

The FCNC kaon decays into lepton-antilepton pairs put stringent constraints on new flavor-changing interactions. The measured $K_L^0 \rightarrow \mu^+ \mu^-$ rate, $\text{Br}(K_L^0 \rightarrow \mu^+ \mu^-) = (6.84 \pm 0.11) \times 10^{-9}$, is completely dominated by the known 2γ absorptive contribution, leaving very little room for new-physics, and $\text{Br}(K_L^0 \rightarrow e^+ e^-) = (9_{-4}^{+6}) \times 10^{-12}$ [124] (the tiniest branching ratio ever measured) also agrees with the SM expectation [125]. The experimental K_S^0 upper bounds on the electron, $\text{Br}(K_S^0 \rightarrow e^+ e^-) < 9 \times 10^{-9}$ [126], and muon, $\text{Br}(K_S^0 \rightarrow \mu^+ \mu^-) < 2.1 \times 10^{-10}$ [127], modes are still five and two orders of magnitude, respectively, larger than their SM predictions [125]. Another very clean test of FCNCs is provided by the decay $K^+ \rightarrow \pi^+ \nu \bar{\nu}$. The CERN NA62 experiment has already observed 20 signal candidates, providing the first evidence of this decay [128]. This leads to $\text{Br}(K^+ \rightarrow \pi^+ \nu \bar{\nu}) = (1.14_{-0.33}^{+0.40}) \times 10^{-10}$, in agreement with the predicted SM branching fraction of $(7.73 \pm 0.61) \times 10^{-11}$ [129, 130]. Even more interesting is the CP -violating neutral mode $K_L^0 \rightarrow \pi^0 \nu \bar{\nu}$, expected at a rate of $(2.59 \pm 0.29) \times 10^{-11}$ [129, 130] that is still far away from the current upper bound of 3.0×10^{-9} [131]. The KOTO experiment at KEK is expected to substantially increase the sensitivity to this mode.

The strongest bound on FCNC transitions in charm decays is $\text{Br}(D^0 \rightarrow \mu^+ \mu^-) < 6.2 \times 10^{-9}$ [132], while in B decays the LHC experiments have recently reached the SM sensitivity: $\text{Br}(B_d^0 \rightarrow \mu^+ \mu^-) = (0.07_{-0.11}^{+0.13}) \times 10^{-9}$ and $\text{Br}(B_s^0 \rightarrow \mu^+ \mu^-) = (3.01 \pm 0.35) \times 10^{-9}$. At present, there is a lot of interest on the decays $B \rightarrow K^{(*)} \ell^+ \ell^-$ where sizable discrepancies between the measured data and the SM predictions have been reported [133]. In particular, the LHCb experiment has found the ratios of produced muons versus electrons to be below the SM predictions (for dilepton invariant-masses squared in the range $q^2 \leq 6 \text{ GeV}^2$), with a significance of 3.1σ in $B^+ \rightarrow K^+ \ell^+ \ell^-$ [134, 135] and 2.4σ in $B \rightarrow K^* \ell^+ \ell^-$ [136], suggesting a significant violation of lep-

ton universality. The current Belle-II measurements of these ratios [137, 138] are consistent with the SM, but they are also compatible with the LHCb results. Future analyses from LHCb and Belle-II are expected to clarify the situation.

References

- [1] G. Luders, Kong. Dan. Vid. Sel. Mat. Fys. Med. **28N5**, 5, 1 (1954).
- [2] W. Pauli, in L. Rosenfeld and V. Weisskopf, editors, “Niels Bohr and the Development of Physics,” 30–51, McGraw-Hill, New York (1955).
- [3] J. McDonough *et al.*, Phys. Rev. **D38**, 2121 (1988).
- [4] M. Ablikim *et al.* (BESIII), Phys. Rev. **D90**, 9, 092002 (2014), [arXiv:1409.4040].
- [5] S. Prakhov *et al.* (Crystal Ball), Phys. Rev. Lett. **84**, 4802 (2000).
- [6] J. H. Christenson *et al.*, Phys. Rev. Lett. **13**, 138 (1964).
- [7] H. Burkhardt *et al.* (NA31), Phys. Lett. **B206**, 169 (1988).
- [8] G. D. Barr *et al.* (NA31), Phys. Lett. **B317**, 233 (1993).
- [9] L. K. Gibbons *et al.*, Phys. Rev. Lett. **70**, 1203 (1993).
- [10] J. R. Batley *et al.* (NA48), Phys. Lett. **B544**, 97 (2002), [hep-ex/0208009].
- [11] E. Abouzaid *et al.* (KTeV), Phys. Rev. **D83**, 092001 (2011), [arXiv:1011.0127].
- [12] H. Gisbert and A. Pich, Rept. Prog. Phys. **81**, 7, 076201 (2018), [arXiv:1712.06147].
- [13] V. Cirigliano *et al.*, JHEP **02**, 032 (2020), [arXiv:1911.01359].
- [14] R. Abbott *et al.* (RBC, UKQCD), Phys. Rev. D **102**, 5, 054509 (2020), [arXiv:2004.09440].
- [15] R. Aaij *et al.* (LHCb), Phys. Rev. Lett. **122**, 21, 211803 (2019), [arXiv:1903.08726].
- [16] P. F. de Salas *et al.*, JHEP **02**, 071 (2021), [arXiv:2006.11237].
- [17] M. C. Gonzalez-Garcia, M. Maltoni and T. Schwetz, Universe **7**, 12, 459 (2021), [arXiv:2111.03086].
- [18] A. Angelopoulos *et al.* (CLEAR), Phys. Lett. **B444**, 43 (1998).
- [19] L. Wolfenstein, Phys. Rev. Lett. **83**, 911 (1999).
- [20] L. Alvarez-Gaume *et al.*, Phys. Lett. **B458**, 347 (1999), [hep-ph/9812326].
- [21] H. J. Gerber, Eur. Phys. J. **C35**, 195 (2004).
- [22] M. C. Bañuls and J. Bernabeu, Phys. Lett. **B464**, 117 (1999), [hep-ph/9908353].
- [23] M. C. Bañuls and J. Bernabeu, Nucl. Phys. **B590**, 19 (2000), [hep-ph/0005323].
- [24] J. Bernabeu, F. Martinez-Vidal and P. Villanueva-Perez, JHEP **08**, 064 (2012), [arXiv:1203.0171].
- [25] J. P. Lees *et al.* (BaBar), Phys. Rev. Lett. **109**, 211801 (2012), [arXiv:1207.5832].
- [26] T. Chupp *et al.*, Rev. Mod. Phys. **91**, 1, 015001 (2019), [arXiv:1710.02504].
- [27] J. Engel, M. J. Ramsey-Musolf and U. van Kolck, Prog. Part. Nucl. Phys. **71**, 21 (2013), [arXiv:1303.2371].
- [28] M. Pospelov and A. Ritz, Annals Phys. **318**, 119 (2005), [hep-ph/0504231].
- [29] J. S. M. Ginges and V. V. Flambaum, Phys. Rept. **397**, 63 (2004), [arXiv:physics/0309054].
- [30] V. Andreev *et al.* (ACME), Nature **562**, 7727, 355 (2018).
- [31] W. B. Cairncross *et al.*, Phys. Rev. Lett. **119**, 15, 153001 (2017), [arXiv:1704.07928].
- [32] G. W. Bennett *et al.* (Muon (g-2)), Phys. Rev. **D80**, 052008 (2009), [arXiv:0811.1207].
- [33] C. Abel *et al.* (nEDM), Phys. Rev. Lett. **124**, 8, 081803 (2020), [arXiv:2001.11966].

- [34] B. Graner *et al.*, Phys. Rev. Lett. **116**, 16, 161601 (2016), [Erratum: Phys. Rev. Lett.119,no.11,119901(2017)], [arXiv:1601.04339].
- [35] F. Allmendinger *et al.*, Phys. Rev. **A100**, 2, 022505 (2019), [arXiv:1904.12295].
- [36] C. Jarlskog, Phys. Rev. Lett. **55**, 1039 (1985); C. Jarlskog, Z. Phys. **C29**, 491 (1985).
- [37] E. P. Shabalin, Sov. J. Nucl. Phys. **28**, 75 (1978), [Yad. Fiz.28,151(1978)].
- [38] E. P. Shabalin, Sov. Phys. Usp. **26**, 297 (1983), [Usp. Fiz. Nauk139,561(1983)].
- [39] W. Bernreuther and M. Suzuki, Rev. Mod. Phys. **63**, 313 (1991), [Erratum: Rev. Mod. Phys.64,633(1992)].
- [40] M. Pospelov and A. Ritz, Phys. Rev. **D89**, 5, 056006 (2014), [arXiv:1311.5537].
- [41] C.-Y. Seng, Phys. Rev. **C91**, 2, 025502 (2015), [arXiv:1411.1476].
- [42] B. Grzadkowski *et al.*, JHEP **10**, 085 (2010), [arXiv:1008.4884].
- [43] S. Mantry, M. Pitschmann and M. J. Ramsey-Musolf, Phys. Rev. **D90**, 5, 054016 (2014), [arXiv:1401.7339].
- [44] B. K. Sahoo, Phys. Rev. **D95**, 1, 013002 (2017), [arXiv:1612.09371].
- [45] T. Chupp, Private Communication (2019).
- [46] J. Bsaisou *et al.*, Annals Phys. **359**, 317 (2015), [arXiv:1412.5471].
- [47] J. de Vries *et al.*, Annals Phys. **338**, 50 (2013), [arXiv:1212.0990].
- [48] L. I. Schiff, Phys. Rev. **132**, 2194 (1963).
- [49] T. Chupp and M. Ramsey-Musolf, Phys. Rev. **C91**, 3, 035502 (2015), [arXiv:1407.1064].
- [50] J. Beringer *et al.* (Particle Data Group), Phys. Rev. **D86**, 010001 (2012).
- [51] A. Angelopoulos *et al.* (CPLEAR), Phys. Lett. **B471**, 332 (1999).
- [52] M. S. Fee *et al.*, Phys. Rev. **A48**, 192 (1993).
- [53] R. J. Hughes and B. I. Deutch, Phys. Rev. Lett. **69**, 578 (1992).
- [54] S. Ulmer *et al.* (BASE), Nature **524**, 7564, 196 (2015).
- [55] R. S. Van Dyck, P. B. Schwinberg and H. G. Dehmelt, Phys. Rev. Lett. **59**, 26 (1987).
- [56] G. W. Bennett *et al.* (Muon g-2), Phys. Rev. Lett. **92**, 161802 (2004), [hep-ex/0401008].
- [57] C. Smorra *et al.* (BASE), Nature **550**, 7676, 371 (2017).
- [58] M. Ahmadi *et al.*, Nature **557**, 7703, 71 (2018).
- [59] O. W. Greenberg, Phys. Rev. Lett. **89**, 231602 (2002), [hep-ph/0201258].
- [60] S. Liberati, Class. Quant. Grav. **30**, 133001 (2013), [arXiv:1304.5795].
- [61] V. A. Kostelecky and N. Russell, Rev. Mod. Phys. **83**, 11 (2011), [arXiv:0801.0287].
- [62] D. Colladay and V. A. Kostelecky, Phys. Rev. **D58**, 116002 (1998), [hep-ph/9809521].
- [63] S. Weinberg, Phys. Rev. Lett. **43**, 1566 (1979).
- [64] F. Wilczek and A. Zee, Phys. Rev. Lett. **43**, 1571 (1979).
- [65] L. F. Abbott and M. B. Wise, Phys. Rev. **D22**, 2208 (1980).
- [66] M. Agostini *et al.* (Borexino), Phys. Rev. Lett. **115**, 231802 (2015), [arXiv:1509.01223].
- [67] E. B. Norman, J. N. Bahcall and M. Goldhaber, Phys. Rev. **D53**, 4086 (1996).
- [68] G. Bressi *et al.*, Phys. Rev. **A83**, 5, 052101 (2011), [arXiv:1102.2766].
- [69] C. Caprini, S. Biller and P. G. Ferreira, JCAP **0502**, 006 (2005), [hep-ph/0310066].
- [70] B. Altschul, Phys. Rev. Lett. **98**, 261801 (2007), [hep-ph/0703126].
- [71] A. de Gouvea, Private Communication (2019).
- [72] A. de Gouvea and P. Vogel, Prog. Part. Nucl. Phys. **71**, 75 (2013), [arXiv:1303.4097].
- [73] S. T. Petcov, Sov. J. Nucl. Phys. **25**, 340 (1977), [Erratum: Yad. Fiz.25,1336(1977)].
- [74] W. J. Marciano and A. I. Sanda, Phys. Lett. **67B**, 303 (1977).
- [75] S. M. Bilenky, S. T. Petcov and B. Pontecorvo, Phys. Lett. **67B**, 309 (1977).
- [76] T.-P. Cheng and L.-F. Li, Phys. Rev. **D16**, 1425 (1977).
- [77] B. W. Lee and R. E. Shrock, Phys. Rev. **D16**, 1444 (1977).
- [78] B. W. Lee *et al.*, Phys. Rev. Lett. **38**, 937 (1977), [Erratum: Phys. Rev. Lett.38,1230(1977)].
- [79] R. H. Bernstein and P. S. Cooper, Phys. Rept. **532**, 27 (2013), [arXiv:1307.5787].
- [80] L. Calibbi and G. Signorelli, Riv. Nuovo Cim. **41**, 2, 71 (2018), [arXiv:1709.00294].
- [81] A. M. Baldini *et al.* (MEG), Eur. Phys. J. **C76**, 8, 434 (2016), [arXiv:1605.05081].
- [82] U. Bellgardt *et al.* (SINDRUM), Nucl. Phys. **B299**, 1 (1988).
- [83] W. H. Bertl *et al.* (SINDRUM II), Eur. Phys. J. **C47**, 337 (2006).
- [84] Y. S. Amhis *et al.* (HFLAV), Eur. Phys. J. C **81**, 3, 226 (2021), [arXiv:1909.12524].
- [85] W. Altmannshofer *et al.* (Belle-II), PTEP **2019**, 12, 123C01 (2019), [arXiv:1808.10567].
- [86] A. Cerri *et al.*, CERN Yellow Rep. Monogr. **7**, 867 (2019), [arXiv:1812.07638].
- [87] A. M. Sirunyan *et al.* (CMS), Phys. Rev. D **104**, 3, 032013 (2021), [arXiv:2105.03007].
- [88] R. Kitano, M. Koike and Y. Okada, Phys. Rev. **D66**, 096002 (2002), [Erratum: Phys. Rev.D76,059902(2007)], [hep-ph/0203110].
- [89] A. Pich, Prog. Part. Nucl. Phys. **75**, 41 (2014), [arXiv:1310.7922].
- [90] D. Ambrose *et al.* (BNL), Phys. Rev. Lett. **81**, 5734 (1998), [hep-ex/9811038].
- [91] A. Sher *et al.*, Phys. Rev. **D72**, 012005 (2005), [hep-ex/0502020].
- [92] R. Aaij *et al.* (LHCb), JHEP **03**, 078 (2018), [arXiv:1710.04111].
- [93] R. Aaij *et al.* (LHCb), Phys. Lett. **B754**, 167 (2016), [arXiv:1512.00322].
- [94] G. Aad *et al.* (ATLAS), Phys. Rev. **D90**, 7, 072010 (2014), [arXiv:1408.5774].
- [95] G. Aad *et al.* (ATLAS), Nature Phys. **17**, 7, 819 (2021), [arXiv:2105.12491].
- [96] G. Aad *et al.* (ATLAS), Phys. Lett. **B801**, 135148 (2020), [arXiv:1909.10235].
- [97] G. Aad *et al.* (ATLAS), Phys. Lett. **B800**, 135069 (2020), [arXiv:1907.06131].
- [98] A. M. Sirunyan *et al.* (CMS), JHEP **06**, 001 (2018), [arXiv:1712.07173].
- [99] S. Dell’Oro *et al.*, Adv. High Energy Phys. **2016**, 2162659 (2016), [arXiv:1601.07512].
- [100] J. Engel and J. Menéndez, Rept. Prog. Phys. **80**, 4, 046301 (2017), [arXiv:1610.06548].

- [101] A. Gando *et al.* (KamLAND-Zen), Phys. Rev. Lett. **117**, 8, 082503 (2016), [Addendum: Phys. Rev. Lett.117,no.10,109903(2016)], [arXiv:1605.02889].
- [102] P. Fileviez Perez, Phys. Rept. **597**, 1 (2015), [arXiv:1501.01886].
- [103] M. Aaboud *et al.* (ATLAS), JHEP **01**, 016 (2019), [arXiv:1809.11105].
- [104] A. M. Sirunyan *et al.* (CMS), JHEP **05**, 05, 148 (2018), [arXiv:1803.11116].
- [105] J. Kaulard *et al.* (SINDRUM II), Phys. Lett. **B422**, 334 (1998).
- [106] Y. Miyazaki *et al.* (Belle), Phys. Lett. **B719**, 346 (2013), [arXiv:1206.5595].
- [107] E. Cortina Gil *et al.* (NA62), Phys. Lett. **B797**, 134794 (2019), [arXiv:1905.07770].
- [108] R. Aaij *et al.* (LHCb), JHEP **06**, 044 (2021), [arXiv:2011.00217].
- [109] R. Aaij *et al.* (LHCb), Phys. Rev. Lett. **112**, 13, 131802 (2014), [arXiv:1401.5361].
- [110] A. Abada *et al.*, JHEP **02**, 169 (2018), [arXiv:1712.03984].
- [111] M. Anderson *et al.* (SNO+), Phys. Rev. D **99**, 3, 032008 (2019), [arXiv:1812.05552].
- [112] K. Abe *et al.* (Super-Kamiokande), Phys. Rev. **D95**, 1, 012004 (2017), [arXiv:1610.03597].
- [113] M. Baldo-Ceolin *et al.*, Z. Phys. **C63**, 409 (1994).
- [114] K. Abe *et al.* (Super-Kamiokande), Phys. Rev. **D91**, 072006 (2015), [arXiv:1109.4227].
- [115] D. G. Phillips, II *et al.*, Phys. Rept. **612**, 1 (2016), [arXiv:1410.1100].
- [116] G. Abbiendi *et al.* (OPAL), Phys. Lett. **B447**, 157 (1999), [hep-ex/9901011].
- [117] D. Sahoo *et al.* (Belle), Phys. Rev. D **102**, 111101 (2020), [arXiv:2010.15361].
- [118] P. del Amo Sanchez *et al.* (BaBar), Phys. Rev. **D83**, 091101 (2011), [arXiv:1101.3830].
- [119] P. Bloch *et al.* (Geneva-Saclay), Phys. Lett. **60B**, 393 (1976).
- [120] A. Angelopoulos *et al.* (CPLEAR), Phys. Lett. **B444**, 38 (1998).
- [121] A. Angelopoulos *et al.* (CPLEAR), Eur. Phys. J. **C22**, 55 (2001).
- [122] R. Aaij *et al.* (LHCb), Phys. Rev. Lett. **127**, 11, 111801 (2021), [arXiv:2106.03744].
- [123] A. A. Petrov, Int. J. Mod. Phys. **A21**, 5686 (2006), [hep-ph/0611361].
- [124] D. Ambrose *et al.* (BNL E871), Phys. Rev. Lett. **81**, 4309 (1998), [hep-ex/9810007].
- [125] V. Cirigliano *et al.*, Rev. Mod. Phys. **84**, 399 (2012), [arXiv:1107.6001].
- [126] F. Ambrosino *et al.* (KLOE), Phys. Lett. **B672**, 203 (2009), [arXiv:0811.1007].
- [127] R. Aaij *et al.* (LHCb), Phys. Rev. Lett. **125**, 23, 231801 (2020), [arXiv:2001.10354].
- [128] E. Cortina Gil *et al.* (NA62), JHEP **06**, 093 (2021), [arXiv:2103.15389].
- [129] J. Brod, M. Gorbahn and E. Stamou, Phys. Rev. **D83**, 034030 (2011), [arXiv:1009.0947].
- [130] J. Brod, M. Gorbahn and E. Stamou, in “19th International Conference on B-Physics at Frontier Machines,” (2021), [arXiv:2105.02868].
- [131] J. K. Ahn *et al.* (KOTO), Phys. Rev. Lett. **122**, 2, 021802 (2019), [arXiv:1810.09655].
- [132] R. Aaij *et al.* (LHCb), Phys. Lett. **B725**, 15 (2013), [arXiv:1305.5059].
- [133] S. Bifani *et al.*, J. Phys. **G46**, 2, 023001 (2019), [arXiv:1809.06229].
- [134] R. Aaij *et al.* (LHCb), Phys. Rev. Lett. **122**, 19, 191801 (2019), [arXiv:1903.09252].
- [135] R. Aaij *et al.* (LHCb), Nature Phys. **18**, 3, 277 (2022), [arXiv:2103.11769].
- [136] R. Aaij *et al.* (LHCb), JHEP **08**, 055 (2017), [arXiv:1705.05802].
- [137] A. Abdesselam *et al.* (Belle), Phys. Rev. Lett. **126**, 16, 161801 (2021), [arXiv:1904.02440].
- [138] S. Choudhury *et al.* (BELLE), JHEP **03**, 105 (2021), [arXiv:1908.01848].

TESTS OF DISCRETE SPACE-TIME SYMMETRIES

CHARGE CONJUGATION (C) INVARIANCE

$\Gamma(\pi^0 \rightarrow 3\gamma)/\Gamma_{\text{total}}$	$<3.1 \times 10^{-8}$, CL = 90%
η C-nonconserving decay parameters	
$\pi^+ \pi^- \pi^0$ left-right asymmetry	$(0.09 \pm 0.11) \times 10^{-2}$
$\pi^+ \pi^- \pi^0$ sextant asymmetry	$(0.12 \pm 0.10) \times 10^{-2}$
$\pi^+ \pi^- \pi^0$ quadrant asymmetry	$(-0.09 \pm 0.09) \times 10^{-2}$
$\pi^+ \pi^- \gamma$ left-right asymmetry	$(0.9 \pm 0.4) \times 10^{-2}$
$\pi^+ \pi^- \gamma$ parameter β (D -wave)	-0.02 ± 0.07 ($S = 1.3$)
$\Gamma(\eta \rightarrow \pi^0 \gamma)/\Gamma_{\text{total}}$	[a] $<9 \times 10^{-5}$, CL = 90%
$\Gamma(\eta \rightarrow 2\pi^0 \gamma)/\Gamma_{\text{total}}$	$<5 \times 10^{-4}$, CL = 90%
$\Gamma(\eta \rightarrow 3\pi^0 \gamma)/\Gamma_{\text{total}}$	$<6 \times 10^{-5}$, CL = 90%
$\Gamma(\eta \rightarrow 3\gamma)/\Gamma_{\text{total}}$	$<1.6 \times 10^{-5}$, CL = 90%
$\Gamma(\eta \rightarrow \pi^0 e^+ e^-)/\Gamma_{\text{total}}$	[b] $<8 \times 10^{-6}$, CL = 90%
$\Gamma(\eta \rightarrow \pi^0 \mu^+ \mu^-)/\Gamma_{\text{total}}$	[b] $<5 \times 10^{-6}$, CL = 90%
$\Gamma(\omega(782) \rightarrow \eta \pi^0)/\Gamma_{\text{total}}$	$<2.1 \times 10^{-4}$, CL = 90%
$\Gamma(\omega(782) \rightarrow 2\pi^0)/\Gamma_{\text{total}}$	$<2.2 \times 10^{-4}$, CL = 90%
$\Gamma(\omega(782) \rightarrow 3\pi^0)/\Gamma_{\text{total}}$	$<2.3 \times 10^{-4}$, CL = 90%
$\eta'(958) \rightarrow \pi^+ \pi^- \gamma$ decay asymmetry parameter	-0.03 ± 0.04
$\Gamma(\eta'(958) \rightarrow \pi^0 e^+ e^-)/\Gamma_{\text{total}}$	[b] $<1.4 \times 10^{-3}$, CL = 90%
$\Gamma(\eta'(958) \rightarrow \eta e^+ e^-)/\Gamma_{\text{total}}$	[b] $<2.4 \times 10^{-3}$, CL = 90%
$\Gamma(\eta'(958) \rightarrow 3\gamma)/\Gamma_{\text{total}}$	$<1.0 \times 10^{-4}$, CL = 90%
$\Gamma(\eta'(958) \rightarrow \mu^+ \mu^- \pi^0)/\Gamma_{\text{total}}$	[b] $<6.0 \times 10^{-5}$, CL = 90%
$\Gamma(\eta'(958) \rightarrow \mu^+ \mu^- \eta)/\Gamma_{\text{total}}$	[b] $<1.5 \times 10^{-5}$, CL = 90%
$\Gamma(J/\psi(1S) \rightarrow \gamma \gamma)/\Gamma_{\text{total}}$	$<2.7 \times 10^{-7}$, CL = 90%
$\Gamma(J/\psi(1S) \rightarrow \gamma \phi)/\Gamma_{\text{total}}$	$<1.4 \times 10^{-6}$, CL = 90%

PARITY (P) INVARIANCE

e electric dipole moment	$<0.11 \times 10^{-28}$ e cm, CL = 90%
μ electric dipole moment [d]	$<1.8 \times 10^{-19}$ e cm, CL = 95%
$\text{Re}(d_\tau = \tau$ electric dipole moment)	-0.220 to 0.45×10^{-16} e cm, CL = 95%
$\Gamma(\eta \rightarrow \pi^+ \pi^-)/\Gamma_{\text{total}}$	$<4.4 \times 10^{-6}$, CL = 90%
$\Gamma(\eta \rightarrow 2\pi^0)/\Gamma_{\text{total}}$	$<3.5 \times 10^{-4}$, CL = 90%
$\Gamma(\eta \rightarrow 4\pi^0)/\Gamma_{\text{total}}$	$<6.9 \times 10^{-7}$, CL = 90%
$\Gamma(\eta'(958) \rightarrow \pi^+ \pi^-)/\Gamma_{\text{total}}$	$<1.8 \times 10^{-5}$, CL = 90%
$\Gamma(\eta'(958) \rightarrow \pi^0 \pi^0)/\Gamma_{\text{total}}$	$<4 \times 10^{-4}$, CL = 90%
$\Gamma(\eta_C(1S) \rightarrow \pi^+ \pi^-)/\Gamma_{\text{total}}$	$<1.1 \times 10^{-4}$, CL = 90%
$\Gamma(\eta_C(1S) \rightarrow \pi^0 \pi^0)/\Gamma_{\text{total}}$	$<4 \times 10^{-5}$, CL = 90%
$\Gamma(\eta_C(1S) \rightarrow K^+ K^-)/\Gamma_{\text{total}}$	$<6 \times 10^{-4}$, CL = 90%
$\Gamma(\eta_C(1S) \rightarrow K_S^0 K_S^0)/\Gamma_{\text{total}}$	$<3.1 \times 10^{-4}$, CL = 90%
p electric dipole moment	$<0.021 \times 10^{-23}$ e cm
n electric dipole moment	$<0.18 \times 10^{-25}$ e cm, CL = 90%
Λ electric dipole moment	$<1.5 \times 10^{-16}$ e cm, CL = 95%
$a_P(\Lambda_b^0 \rightarrow p \pi^- \pi^+ \pi^-)$	$(-4.0 \pm 0.7)\%$
$a_P(\Lambda_b^0 \rightarrow p K^- \pi^+ \pi^-)$	$(-0.6 \pm 0.9)\%$
$a_P(\Lambda_b^0 \rightarrow p K^- K^+ \pi^-)$	$(4 \pm 5)\%$
$a_P(\Lambda_b^0 \rightarrow p K^- K^+ K^-)$	$(-1.6 \pm 1.5)\%$
$a_P(\Lambda_b^0 \rightarrow p K^- \mu^+ \mu^-)$	$(-5 \pm 5)\%$

TIME REVERSAL (T) INVARIANCE

e electric dipole moment	$<0.11 \times 10^{-28}$ e cm, CL = 90%
μ electric dipole moment [d]	$<1.8 \times 10^{-19}$ e cm, CL = 95%
μ decay parameters	
transverse e^+ polarization normal to plane of μ spin, e^+ momentum	$(-2 \pm 8) \times 10^{-3}$
α'/A	$(-10 \pm 20) \times 10^{-3}$
β'/A	$(2 \pm 7) \times 10^{-3}$
$\text{Re}(d_\tau = \tau$ electric dipole moment)	-0.220 to 0.45×10^{-16} e cm, CL = 95%
P_T in $K^+ \rightarrow \pi^0 \mu^+ \nu_\mu$	$(-1.7 \pm 2.5) \times 10^{-3}$
P_T in $K^+ \rightarrow \mu^+ \nu_\mu \gamma$	$(-0.6 \pm 1.9) \times 10^{-2}$
$\text{Im}(\xi)$ in $K^+ \rightarrow \pi^0 \mu^+ \nu_\mu$ decay (from transverse μ pol.)	-0.006 ± 0.008
asymmetry A_T in K^0, \bar{K}^0 mixing	$(6.6 \pm 1.6) \times 10^{-3}$
$\text{Im}(\xi)$ in $K_{\mu 3}^0$ decay (from transverse μ pol.)	-0.007 ± 0.026

$A_T(D^\pm \rightarrow K_S^0 K^\pm \pi^\mp \pi^\mp)$	[c] $(-12 \pm 11) \times 10^{-3}$
$A_T(D^0 \rightarrow K^+ K^- \pi^+ \pi^-)$	[c] $(2.9 \pm 2.2) \times 10^{-3}$
$A_T(D_S^\pm \rightarrow K_S^0 K^\pm \pi^\mp \pi^\mp)$	[c] $(-14 \pm 8) \times 10^{-3}$
$\Delta S_T^+(S_{\ell^-, K_S^0}^- - S_{\ell^+, K_S^0}^+)$	-1.37 ± 0.15
$\Delta S_T^-(S_{\ell^-, K_S^0}^+ - S_{\ell^+, K_S^0}^-)$	1.17 ± 0.21
$\Delta C_T^+(C_{\ell^-, K_S^0}^- - C_{\ell^+, K_S^0}^+)$	0.10 ± 0.16
$\Delta C_T^-(C_{\ell^-, K_S^0}^+ - C_{\ell^+, K_S^0}^-)$	0.04 ± 0.16
p electric dipole moment	$<0.021 \times 10^{-23}$ e cm
n electric dipole moment	$<0.18 \times 10^{-25}$ e cm, CL = 90%
$n \rightarrow p e^- \bar{\nu}_e$ decay parameters	
ϕ_{AV} , Phase of g_A relative to g_V	[d] $(180.017 \pm 0.026)^\circ$
triple correlation coefficient D	[e] $(-1.2 \pm 2.0) \times 10^{-4}$
triple correlation coefficient R	[e] 0.004 ± 0.013
Λ electric dipole moment	$<1.5 \times 10^{-16}$ e cm, CL = 95%
triple correlation coefficient D for $\Sigma^- \rightarrow n e^- \bar{\nu}_e$	0.11 ± 0.10

CP INVARIANCE

$\text{Re}(d_T^W)$	$<0.50 \times 10^{-17}$ e cm, CL = 95%
$\text{Im}(d_T^W)$	$<1.1 \times 10^{-17}$ e cm, CL = 95%
δ (CP violating phase in neutrino mixing)	1.36 ± 0.20 to 0.16 π rad
$\eta \rightarrow \pi^+ \pi^- e^+ e^-$ decay-plane asymmetry	$(-0.6 \pm 3.1) \times 10^{-2}$
$\Gamma(\eta \rightarrow \pi^+ \pi^-)/\Gamma_{\text{total}}$	$<4.4 \times 10^{-6}$, CL = 90%
$\Gamma(\eta \rightarrow 2\pi^0)/\Gamma_{\text{total}}$	$<3.5 \times 10^{-4}$, CL = 90%
$\Gamma(\eta \rightarrow 4\pi^0)/\Gamma_{\text{total}}$	$<6.9 \times 10^{-7}$, CL = 90%
$\Gamma(\eta'(958) \rightarrow \pi^+ \pi^-)/\Gamma_{\text{total}}$	$<1.8 \times 10^{-5}$, CL = 90%
$\Gamma(\eta'(958) \rightarrow \pi^0 \pi^0)/\Gamma_{\text{total}}$	$<4 \times 10^{-4}$, CL = 90%
$K^\pm \rightarrow \pi^\pm e^+ e^-$ rate difference/sum	$(-2.2 \pm 1.6) \times 10^{-2}$
$K^\pm \rightarrow \pi^\pm \mu^+ \mu^-$ rate difference/sum	0.010 ± 0.023
$K^\pm \rightarrow \pi^\pm \pi^0 \gamma$ rate difference/sum	$(0.0 \pm 1.2) \times 10^{-3}$
$K^\pm \rightarrow \pi^\pm \pi^+ \pi^-$ rate difference/sum	$(0.04 \pm 0.06)\%$
$K^\pm \rightarrow \pi^\pm \pi^0 \pi^0$ rate difference/sum	$(-0.02 \pm 0.28)\%$
$K^\pm \rightarrow \pi^\pm \pi^+ \pi^- (g_+ - g_-) / (g_+ + g_-)$	$(-1.5 \pm 2.2) \times 10^{-4}$
$K^\pm \rightarrow \pi^\pm \pi^0 \pi^0 (g_+ - g_-) / (g_+ + g_-)$	$(1.8 \pm 1.8) \times 10^{-4}$
$A_S = [\Gamma(K_S^0 \rightarrow \pi^- e^+ \nu_e) - \Gamma(K_S^0 \rightarrow \pi^+ e^- \bar{\nu}_e)] / \text{SUM}$	$(-4 \pm 6) \times 10^{-3}$
$\text{Im}(\eta_{+-0}) = \text{Im}(A(K_S^0 \rightarrow \pi^+ \pi^- \pi^0, CP\text{-violating}) / A(K_L^0 \rightarrow \pi^+ \pi^- \pi^0))$	-0.002 ± 0.009
$\text{Im}(\eta_{000}) = \text{Im}(A(K_S^0 \rightarrow \pi^0 \pi^0 \pi^0) / A(K_L^0 \rightarrow \pi^0 \pi^0 \pi^0))$	-0.001 ± 0.016
$ \eta_{000} = A(K_S^0 \rightarrow 3\pi^0) / A(K_L^0 \rightarrow 3\pi^0) $	<0.0088 , CL = 90%
CP asymmetry A in $K_S^0 \rightarrow \pi^+ \pi^- e^+ e^-$	$(-0.4 \pm 0.8)\%$
$\Gamma(K_S^0 \rightarrow 3\pi^0)/\Gamma_{\text{total}}$	$<2.6 \times 10^{-8}$, CL = 90%
linear coefficient j for $K_L^0 \rightarrow \pi^+ \pi^- \pi^0$	0.0012 ± 0.0008
quadratic coefficient f for $K_L^0 \rightarrow \pi^+ \pi^- \pi^0$	0.004 ± 0.006
$ \epsilon_{+-\gamma}' /\epsilon$ for $K_L^0 \rightarrow \pi^+ \pi^- \gamma$	<0.3 , CL = 90%
$ \mathcal{B}_{E1} $ for $K_L^0 \rightarrow \pi^+ \pi^- \gamma$	<0.21 , CL = 90%
$\Gamma(K_L^0 \rightarrow \pi^0 \mu^+ \mu^-)/\Gamma_{\text{total}}$	[f] $<3.8 \times 10^{-10}$, CL = 90%
$\Gamma(K_L^0 \rightarrow \pi^0 e^+ e^-)/\Gamma_{\text{total}}$	[f] $<2.8 \times 10^{-10}$, CL = 90%
$\Gamma(K_L^0 \rightarrow \pi^0 \nu \bar{\nu})/\Gamma_{\text{total}}$	[g] $<3.0 \times 10^{-9}$, CL = 90%
$A_{CP}(D^\pm \rightarrow \mu^\pm \nu)$	$(8 \pm 8)\%$
$A_{CP}(D^\pm \rightarrow K_L^0 e^\pm \nu)$	$(-0.6 \pm 1.6)\%$
$A_{CP}(D^\pm \rightarrow K_S^0 \pi^\pm)$	$(-0.41 \pm 0.09)\%$
$A_{CP}(D^\pm \rightarrow K^\mp 2\pi^\pm)$	$(-0.18 \pm 0.16)\%$
$A_{CP}(D^\pm \rightarrow K^\mp \pi^\pm \pi^\pm \pi^0)$	$(-0.3 \pm 0.7)\%$
$A_{CP}(D^\pm \rightarrow K_S^0 \pi^\pm \pi^0)$	$(-0.1 \pm 0.7)\%$
$A_{CP}(D^\pm \rightarrow K_S^0 \pi^\pm \pi^+ \pi^-)$	$(0.0 \pm 1.2)\%$
$A_{CP}(D^\pm \rightarrow \pi^\pm \pi^0)$	$(0.4 \pm 1.3)\%$ ($S = 1.7$)
$A_{CP}(D^\pm \rightarrow \pi^\pm \eta)$	$(0.3 \pm 0.8)\%$ ($S = 1.2$)
$A_{CP}(D^\pm \rightarrow \pi^\pm \eta'(958))$	$(-0.6 \pm 0.7)\%$
$A_{CP}(D^\pm \rightarrow \bar{K}^0 / K^0 K^\pm)$	$(0.11 \pm 0.17)\%$
$A_{CP}(D^\pm \rightarrow K_S^0 K^\pm)$	$(-0.01 \pm 0.07)\%$
$A_{CP}(D^\pm \rightarrow K^+ K^- \pi^\pm)$	$(0.37 \pm 0.29)\%$
$A_{CP}(D^\pm \rightarrow K^\pm K^* 0)$	$(-0.3 \pm 0.4)\%$
$A_{CP}(D^\pm \rightarrow \phi \pi^\pm)$	$(0.01 \pm 0.09)\%$ ($S = 1.8$)
$A_{CP}(D^\pm \rightarrow K^\pm K_0^*(1430)^0)$	$(8 \pm 7)\%$
$A_{CP}(D^\pm \rightarrow K^\pm K_2^*(1430)^0)$	$(43 \pm 20)\%$

Tests of Conservation Laws

$ACP(D^\pm \rightarrow K^\pm K_S^0(700))$	$(-12 \pm 13)\%$	$ACP(D^0 \rightarrow K^+ \pi^- \pi^0)$	$(0 \pm 5)\%$
$ACP(D^\pm \rightarrow a_0(1450)^0 \pi^\pm)$	$(-19 \pm 14)\%$	$ACP(D^0 \rightarrow K_S^0 \pi^+ \pi^-)$	$(-0.1 \pm 0.8)\%$
$ACP(D^\pm \rightarrow \phi(1680) \pi^\pm)$	$(-9 \pm 26)\%$	$ACP(D^0 \rightarrow K^*(892)^- \pi^+ \rightarrow K_S^0 \pi^+ \pi^-)$	$(0.4 \pm 0.5)\%$
$ACP(D^\pm \rightarrow \pi^+ \pi^- \pi^\pm)$	$(-2 \pm 4)\%$	$ACP(D^0 \rightarrow K^*(892)^+ \pi^- \rightarrow K_S^0 \pi^+ \pi^-)$	$(1 \pm 6)\%$
$ACP(D^\pm \rightarrow K_S^0 K^\pm \pi^+ \pi^-)$	$(-4 \pm 7)\%$	$ACP(D^0 \rightarrow K_S^0 \rho^0 \rightarrow K_S^0 \pi^+ \pi^-)$	$(-0.1 \pm 0.5)\%$
$ACP(D^\pm \rightarrow K^\pm \pi^0)$	$(-3 \pm 5)\%$	$ACP(D^0 \rightarrow K_S^0 \omega \rightarrow K_S^0 \pi^+ \pi^-)$	$(-13 \pm 7)\%$
Local CPV in $D^\pm \rightarrow \pi^+ \pi^- \pi^\pm$	78.1%	$ACP(D^0 \rightarrow K_S^0 f_0(980) \rightarrow K_S^0 \pi^+ \pi^-)$	$(-0.4 \pm 2.7)\%$
Local CPV in $D^\pm \rightarrow K^+ K^- \pi^\pm$	31%	$ACP(D^0 \rightarrow K_S^0 f_2(1270) \rightarrow K_S^0 \pi^+ \pi^-)$	$(-4 \pm 5)\%$
$ q/p $ of $D^0-\bar{D}^0$ mixing	0.995 ± 0.016	$ACP(D^0 \rightarrow K_S^0 f_0(1370) \rightarrow K_S^0 \pi^+ \pi^-)$	$(-1 \pm 9)\%$
A_Γ of $D^0-\bar{D}^0$ mixing	$(0.089 \pm 0.113) \times 10^{-3}$	$ACP(D^0 \rightarrow \bar{K}^0 \rho^0(1450) \rightarrow K_S^0 \pi^+ \pi^-)$	$(-4 \pm 10)\%$
Where there is ambiguity, the CP test is labelled by the D^0 decay mode.		$ACP(D^0 \rightarrow \bar{K}^0 f_0(600) \rightarrow K_S^0 \pi^+ \pi^-)$	$(-3 \pm 5)\%$
$ACP(D^0 \rightarrow K^+ K^-)$	$(-0.07 \pm 0.11)\%$	$ACP(D^0 \rightarrow K^*(1410)^- \pi^+ \rightarrow K_S^0 \pi^+ \pi^-)$	$(-2 \pm 9)\%$
$ACP(D^0 \rightarrow K_S^0 K_S^0)$	$(-1.9 \pm 1.1)\%$ ($S = 1.1$)	$ACP(D^0 \rightarrow K_S^0(1430)^- \pi^+ \rightarrow K_S^0 \pi^+ \pi^-)$	$(4 \pm 4)\%$
$ACP(D^0 \rightarrow \pi^+ \pi^-)$	$(0.13 \pm 0.14)\%$	$ACP(D^0 \rightarrow K_S^0(1430)^- \pi^+ \rightarrow K_S^0 \pi^+ \pi^-)$	$(12 \pm 15)\%$
$ACP(D^0 \rightarrow \pi^0 \pi^0)$	$(0.0 \pm 0.6)\%$	$ACP(D^0 \rightarrow K_S^0(1430)^- \pi^+ \rightarrow K_S^0 \pi^+ \pi^-)$	$(3 \pm 6)\%$
$ACP(D^0 \rightarrow \rho \gamma)$	$(6 \pm 15) \times 10^{-2}$	$ACP(D^0 \rightarrow K_S^0(1430)^+ \pi^- \rightarrow K_S^0 \pi^+ \pi^-)$	$(-10 \pm 32)\%$
$ACP(D^0 \rightarrow \phi \gamma)$	$(-9 \pm 7) \times 10^{-2}$	$ACP(D^0 \rightarrow K^* \pi^+ \pi^+ \pi^-)$	$(0.2 \pm 0.5)\%$
$ACP(D^0 \rightarrow \bar{K}^*(892)^0 \gamma)$	$(-0.3 \pm 2.0) \times 10^{-2}$	$ACP(D^0 \rightarrow K^+ \pi^- \pi^+ \pi^-)$	$(-2 \pm 4)\%$
$ACP(D^0 \rightarrow \pi^+ \pi^- \pi^0)$	$(0.3 \pm 0.4)\%$	$ACP(D^0 \rightarrow K^+ K^- \pi^+ \pi^-)$	$(1.3 \pm 1.7)\%$
$ACP(D^0 \rightarrow \rho(770)^+ \pi^- \rightarrow \pi^+ \pi^- \pi^0)$	[h] $(1.2 \pm 0.9)\%$	$ACP(D^0 \rightarrow K_S^0(1270)^+ K^- \rightarrow K^* \pi^+ K^-)$	$(-1 \pm 10)\%$
$ACP(D^0 \rightarrow \rho(770)^0 \pi^0 \rightarrow \pi^+ \pi^- \pi^0)$	[h] $(-3.1 \pm 3.0)\%$	$ACP(D^0 \rightarrow K_S^0(1270)^- K^+ \rightarrow \bar{K}^* \pi^- K^+)$	$(-10 \pm 32)\%$
$ACP(D^0 \rightarrow \rho(770)^- \pi^+ \rightarrow \pi^+ \pi^- \pi^0)$	[h] $(-1.0 \pm 1.7)\%$	$ACP(D^0 \rightarrow K_S^0(1270)^- K^+ \rightarrow K^+ K^- \pi^+ \pi^-)$	$(1.7 \pm 3.5)\%$
$ACP(D^0 \rightarrow \rho(1450)^+ \pi^- \rightarrow \pi^+ \pi^- \pi^0)$	[h] $(0 \pm 70)\%$	$ACP(D^0 \rightarrow K_S^0(1270)^- K^+ \rightarrow K^+ K^- \pi^+ \pi^-)$	$(-7 \pm 17)\%$
$ACP(D^0 \rightarrow \rho(1450)^0 \pi^0 \rightarrow \pi^+ \pi^- \pi^0)$	[h] $(-20 \pm 40)\%$	$ACP(D^0 \rightarrow K_S^0(1270)^+ K^- \rightarrow \rho^0 K^+ K^-)$	$(10 \pm 13)\%$
$ACP(D^0 \rightarrow \rho(1450)^- \pi^+ \rightarrow \pi^+ \pi^- \pi^0)$	[h] $(6 \pm 9)\%$	$ACP(D^0 \rightarrow K_S^0(1270)^- K^+ \rightarrow \rho^0 K^- K^+)$	$(-4.4 \pm 2.1)\%$
$ACP(D^0 \rightarrow \rho(1700)^+ \pi^- \rightarrow \pi^+ \pi^- \pi^0)$	[h] $(-5 \pm 14)\%$	$ACP(D^0 \rightarrow K^*(1410)^+ K^- \rightarrow K^* \pi^+ K^-)$	$(-20 \pm 17)\%$
$ACP(D^0 \rightarrow \rho(1700)^0 \pi^0 \rightarrow \pi^+ \pi^- \pi^0)$	[h] $(13 \pm 9)\%$	$ACP(D^0 \rightarrow K^*(1410)^- K^+ \rightarrow \bar{K}^* \pi^- K^+)$	$(-1 \pm 14)\%$
$ACP(D^0 \rightarrow \rho(1700)^- \pi^+ \rightarrow \pi^+ \pi^- \pi^0)$	[h] $(8 \pm 11)\%$	$ACP(D^0 \rightarrow K^*(1680)^+ K^- \rightarrow K^+ K^- \pi^+ \pi^-)$	$(-17 \pm 29)\%$
$ACP(D^0 \rightarrow f_0(980) \pi^0 \rightarrow \pi^+ \pi^- \pi^0)$	[h] $(0 \pm 35)\%$	$ACP(K^* \bar{K}^* \text{ in } D^0, \bar{D}^0 \rightarrow K^* \bar{K}^* \text{ S-wave})$	$(-5 \pm 14)\%$
$ACP(D^0 \rightarrow f_0(1370) \pi^0 \rightarrow \pi^+ \pi^- \pi^0)$	[h] $(25 \pm 18)\%$	$ACP(D^0 \rightarrow K^* \bar{K}^* \text{ S-wave})$	$(-3.9 \pm 2.2)\%$
$ACP(D^0 \rightarrow f_0(1500) \pi^0 \rightarrow \pi^+ \pi^- \pi^0)$	[h] $(0 \pm 18)\%$	$ACP(\phi \rho^0 \text{ in } D^0, \bar{D}^0 \rightarrow \phi \rho^0)$	$(1 \pm 9)\%$
$ACP(D^0 \rightarrow f_0(1710) \pi^0 \rightarrow \pi^+ \pi^- \pi^0)$	[h] $(0 \pm 24)\%$	$ACP(D^0 \rightarrow \phi \rho^0 \text{ S-wave})$	$(-3 \pm 5)\%$
$ACP(D^0 \rightarrow f_2(1270) \pi^0 \rightarrow \pi^+ \pi^- \pi^0)$	[h] $(-4 \pm 6)\%$	$ACP(D^0 \rightarrow \phi \rho^0 \text{ D-wave})$	$(-37 \pm 19)\%$
$ACP(D^0 \rightarrow \sigma(400) \pi^0 \rightarrow \pi^+ \pi^- \pi^0)$	[h] $(6 \pm 8)\%$	$ACP(D^0 \rightarrow \phi(\pi^+ \pi^-) \text{ S-wave})$	$(6 \pm 6)\%$
$ACP(\text{nonresonant } D^0 \rightarrow \pi^+ \pi^- \pi^0)$	[h] $(-13 \pm 23)\%$	$ACP(D^0 \rightarrow K^*(892)^0 (K^- \pi^+) \text{ S-wave})$	$(-10 \pm 40)\%$
$ACP(D^0, \bar{D}^0 \rightarrow 2\pi^+ 2\pi^-)$	$(0.5 \pm 1.2)\%$	$ACP(D^0 \rightarrow K^+ K^- \pi^+ \pi^- \text{ non-resonant})$	$(8 \pm 20)\%$
$ACP(D^0 \rightarrow a_1(1260)^+ \pi^- \rightarrow 2\pi^+ 2\pi^-)$	$(5 \pm 6)\%$	$ACP(D^0 \rightarrow K^*(1410)^- K^+ \rightarrow \bar{K}^* \pi^- K^+)$	$(3 \pm 11)\%$
$ACP(D^0 \rightarrow a_1(1260)^- \pi^+ \rightarrow 2\pi^+ 2\pi^-)$	$(14 \pm 18)\%$	$CP\text{-even fraction in } D^0 \rightarrow \pi^+ \pi^- \pi^0 \text{ decays}$	$(97.3 \pm 1.7)\%$
$ACP(D^0 \rightarrow \pi(1300)^+ \pi^- \rightarrow 2\pi^+ 2\pi^-)$	$(-2 \pm 15)\%$	$CP\text{-even fraction in } D^0 \rightarrow K^+ K^- \pi^0 \text{ decays}$	$(73 \pm 6)\%$
$ACP(D^0 \rightarrow \pi(1300)^- \pi^+ \rightarrow 2\pi^+ 2\pi^-)$	$(-6 \pm 30)\%$	$Local CPV p\text{-value in } D^0, \bar{D}^0 \rightarrow \pi^+ \pi^- \pi^0$	4.9%
$ACP(D^0 \rightarrow a_1(1640)^+ \pi^- \rightarrow 2\pi^+ 2\pi^-)$	$(9 \pm 26)\%$	$Local CPV p\text{-value in } D^0, \bar{D}^0 \rightarrow \pi^+ \pi^- \pi^+ \pi^-$	$(0.6 \pm 0.2)\%$
$ACP(D^0 \rightarrow \pi_2(1670)^+ \pi^- \rightarrow 2\pi^+ 2\pi^-)$	$(7 \pm 18)\%$	$Local CPV p\text{-value in } D^0, \bar{D}^0 \rightarrow K_S^0 \pi^+ \pi^-$	96%
$ACP(D^0 \rightarrow \sigma f_0(1370) \rightarrow 2\pi^+ 2\pi^-)$	$(-15 \pm 19)\%$	$Local CPV p\text{-value in } D^0, \bar{D}^0 \rightarrow K^+ K^- \pi^0$	16.6%
$ACP(D^0 \rightarrow \sigma \rho(770)^0 \rightarrow 2\pi^+ 2\pi^-)$	$(3 \pm 27)\%$	$Local CPV p\text{-value in } D^0, \bar{D}^0 \rightarrow K^+ K^- \pi^+ \pi^-$	9.1%
$ACP(D^0 \rightarrow 2\rho(770)^0 \rightarrow 2\pi^+ 2\pi^-)$	$(-6 \pm 6)\%$	$ACP(D_S^\pm \rightarrow \mu^\pm \nu)$	$(-0.2 \pm 2.5)\%$
$ACP(D^0 \rightarrow 2f_2(1270) \rightarrow 2\pi^+ 2\pi^-)$	$(-28 \pm 24)\%$	$ACP(D_S^\pm \rightarrow K^\pm K_S^0)$	$(0.09 \pm 0.26)\%$
$ACP(D^0 \rightarrow K^+ K^- \pi^0)$	$(-1.0 \pm 1.7)\%$	$ACP(D_S^\pm \rightarrow K^+ K^- \pi^\pm)$	$(-0.5 \pm 0.9)\%$
$ACP(D^0 \rightarrow K^*(892)^+ K^- \rightarrow K^+ K^- \pi^0)$	[h] $(-0.9 \pm 1.3)\%$	$ACP(D_S^\pm \rightarrow \phi \pi^\pm)$	$(-0.38 \pm 0.27)\%$
$ACP(D^0 \rightarrow K^*(1410)^+ K^- \rightarrow K^+ K^- \pi^0)$	[h] $(-21 \pm 24)\%$		
$ACP(D^0 \rightarrow (K^+ \pi^0)_S K^- \rightarrow K^+ K^- \pi^0)$	[h] $(7 \pm 15)\%$		
$ACP(D^0 \rightarrow \phi(1020) \pi^0 \rightarrow K^+ K^- \pi^0)$	[h] $(1.1 \pm 2.2)\%$		
$ACP(D^0 \rightarrow f_0(980) \pi^0 \rightarrow K^+ K^- \pi^0)$	[h] $(-3 \pm 19)\%$		
$ACP(D^0 \rightarrow a_0(980)^0 \pi^0 \rightarrow K^+ K^- \pi^0)$	[h] $(-5 \pm 16)\%$		
$ACP(D^0 \rightarrow f_2'(1525) \pi^0 \rightarrow K^+ K^- \pi^0)$	[h] $(0 \pm 160)\%$		
$ACP(D^0 \rightarrow K^*(892)^- K^+ \rightarrow K^+ K^- \pi^0)$	[h] $(-5 \pm 4)\%$		
$ACP(D^0 \rightarrow K^*(1410)^- K^+ \rightarrow K^+ K^- \pi^0)$	[h] $(-17 \pm 29)\%$		
$ACP(D^0 \rightarrow (K^- \pi^0)_S \text{ S-wave } K^+ \rightarrow K^+ K^- \pi^0)$	[h] $(-10 \pm 40)\%$		
$ACP(D^0 \rightarrow K_S^0 \pi^0)$	$(-0.20 \pm 0.17)\%$		
$ACP(D^0 \rightarrow K_S^0 \eta)$	$(0.5 \pm 0.5)\%$		
$ACP(D^0 \rightarrow K_S^0 \eta')$	$(1.0 \pm 0.7)\%$		
$ACP(D^0 \rightarrow K_S^0 \phi)$	$(-3 \pm 9)\%$		
$ACP(D^0 \rightarrow K^- \pi^+)$	$(0.2 \pm 0.5)\%$		
$ACP(D^0 \rightarrow K^+ \pi^-)$	$(-0.9 \pm 1.4)\%$		
$ACP(D_{CP}(\pm 1) \rightarrow K^\mp \pi^\pm)$	$(12.7 \pm 1.5)\%$		
$ACP(D^0 \rightarrow K^- \pi^+ \pi^0)$	$(0.1 \pm 0.5)\%$		

Unless otherwise stated, limits are given at the 90% confidence level, while errors are given as ± 1 standard deviation.

Tests of Conservation Laws

$A_{CP}(D_S^{\pm} \rightarrow K^{\pm} K_S^0 \pi^0)$	$(-2 \pm 6)\%$	$A_{CP}(B^+ \rightarrow [K^+ K^-]_D K^+ \pi^- \pi^+)$	-0.04 ± 0.06
$A_{CP}(D_S^{\pm} \rightarrow 2K_S^0 \pi^{\pm})$	$(3 \pm 5)\%$	$A_{CP}(B^+ \rightarrow [\pi^+ \pi^-]_D K^+ \pi^- \pi^+)$	-0.05 ± 0.10
$A_{CP}(D_S^{\pm} \rightarrow K^+ K^- \pi^{\pm} \pi^0)$	$(0.0 \pm 3.0)\%$	$A_{CP}(B^+ \rightarrow [K^- \pi^+]_D K^+ \pi^- \pi^+)$	0.013 ± 0.023
$A_{CP}(D_S^{\pm} \rightarrow K^{\pm} K_S^0 \pi^+ \pi^-)$	$(-6 \pm 5)\%$	$A_{CP}(B^+ \rightarrow [K^+ K^-]_D \pi^+ \pi^- \pi^+)$	-0.019 ± 0.015
$A_{CP}(D_S^{\pm} \rightarrow K_S^0 K^{\mp} 2\pi^{\pm})$	$(4.1 \pm 2.8)\%$	$A_{CP}(B^+ \rightarrow [\pi^+ \pi^-]_D \pi^+ \pi^- \pi^+)$	-0.013 ± 0.019
$A_{CP}(D_S^{\pm} \rightarrow \pi^+ \pi^- \pi^{\pm})$	$(-0.7 \pm 3.1)\%$	$A_{CP}(B^+ \rightarrow [K^- \pi^+]_D \pi^+ \pi^- \pi^+)$	-0.002 ± 0.011
$A_{CP}(D_S^{\pm} \rightarrow \pi^{\pm} \eta)$	$(0.3 \pm 0.4)\%$	$A_{CP}(B^+ \rightarrow \bar{D}^{*0} \pi^+)$	-0.0004 ± 0.0021 ($S = 1.1$)
$A_{CP}(D_S^{\pm} \rightarrow \pi^{\pm} \eta')$	$(-0.9 \pm 0.5)\%$	$A_{CP}(B^+ \rightarrow (D_{CP(+1)}^*)^0 \pi^+)$	0.010 ± 0.007
$A_{CP}(D_S^{\pm} \rightarrow \eta \pi^{\pm} \pi^0)$	$(-1 \pm 4)\%$	$A_{CP}(B^+ \rightarrow (D_{CP(-1)}^*)^0 \pi^+)$	-0.09 ± 0.05
$A_{CP}(D_S^{\pm} \rightarrow \eta' \pi^{\pm} \pi^0)$	$(0 \pm 8)\%$	$A_{CP}(B^+ \rightarrow D^{*0} K^+)$	0.012 ± 0.010 ($S = 1.5$)
$A_{CP}(D_S^{\pm} \rightarrow \eta' \pi^{\pm} \pi^0)$	$(2 \pm 4)\%$ ($S = 1.2$)	$A_{CP}(B^+ \rightarrow D_{CP(+1)}^{*0} K^+)$	-0.09 ± 0.05 ($S = 2.6$)
$A_{CP}(D_S^{\pm} \rightarrow \bar{K}^0 / K^0 \pi^{\pm})$	$(0.4 \pm 0.5)\%$	$A_{CP}(B^+ \rightarrow D_{CP(-1)}^{*0} K^+)$	0.07 ± 0.10
$A_{CP}(D_S^{\pm} \rightarrow K_S^0 \pi^{\pm})$	$(0.20 \pm 0.18)\%$	$A_{CP}(B^+ \rightarrow D_{CP(+1)} K^*(892)^+)$	0.08 ± 0.06
$A_{CP}(D_S^{\pm} \rightarrow K^{\pm} \pi^+ \pi^-)$	$(4 \pm 5)\%$	$A_{CP}(B^+ \rightarrow D_{CP(-1)} K^*(892)^+)$	-0.23 ± 0.22
$A_{CP}(D_S^{\pm} \rightarrow K^{\pm} \eta)$	$(1.8 \pm 1.9)\%$	$A_{CP}(B^+ \rightarrow D_S^+ \phi)$	0.0 ± 0.4
$A_{CP}(D_S^{\pm} \rightarrow K^{\pm} \eta'(958))$	$(6 \pm 19)\%$	$A_{CP}(B^+ \rightarrow D_S^+ \bar{D}^0)$	$(-0.4 \pm 0.7)\%$
$A_{CP}(B^+ \rightarrow J/\psi(1S) K^+)$	$(1.8 \pm 3.0) \times 10^{-3}$ ($S = 1.5$)	$A_{CP}(B^+ \rightarrow D^{*+} \bar{D}^{*0})$	-0.15 ± 0.11
$A_{CP}(B^+ \rightarrow J/\psi(1S) \pi^+)$	$(1.8 \pm 1.2) \times 10^{-2}$ ($S = 1.3$)	$A_{CP}(B^+ \rightarrow D^{*+} \bar{D}^0)$	-0.06 ± 0.13
$A_{CP}(B^+ \rightarrow J/\psi \rho^+)$	-0.05 ± 0.05	$A_{CP}(B^+ \rightarrow D^+ \bar{D}^{*0})$	0.13 ± 0.18
$A_{CP}(B^+ \rightarrow J/\psi K^*(892)^+)$	-0.048 ± 0.033	$A_{CP}(B^+ \rightarrow D^+ \bar{D}^0)$	0.016 ± 0.025
$A_{CP}(B^+ \rightarrow \eta_c K^+)$	0.01 ± 0.07 ($S = 2.2$)	$A_{CP}(B^+ \rightarrow K_S^0 \pi^+)$	-0.017 ± 0.016
$A_{CP}(B^+ \rightarrow \psi(2S) \pi^+)$	0.03 ± 0.06	$A_{CP}(B^+ \rightarrow K^+ \pi^0)$	0.030 ± 0.013
$A_{CP}(B^+ \rightarrow \psi(2S) K^+)$	0.012 ± 0.020 ($S = 1.5$)	$A_{CP}(B^+ \rightarrow \eta' K^+)$	0.004 ± 0.011
$A_{CP}(B^+ \rightarrow \psi(2S) K^*(892)^+)$	0.08 ± 0.21	$A_{CP}(B^+ \rightarrow \eta' K^*(892)^+)$	-0.26 ± 0.27
$A_{CP}(B^+ \rightarrow \chi_{c1}(1P) \pi^+)$	0.07 ± 0.18	$A_{CP}(B^+ \rightarrow \eta' K_0^*(1430)^+)$	0.06 ± 0.20
$A_{CP}(B^+ \rightarrow \chi_{c0} K^+)$	-0.20 ± 0.18 ($S = 1.5$)	$A_{CP}(B^+ \rightarrow \eta' K_2^*(1430)^+)$	0.15 ± 0.13
$A_{CP}(B^+ \rightarrow \chi_{c1} K^+)$	-0.009 ± 0.033	$A_{CP}(B^+ \rightarrow \eta K^*(892)^+)$	0.02 ± 0.06
$A_{CP}(B^+ \rightarrow \chi_{c1} K^*(892)^+)$	0.5 ± 0.5	$A_{CP}(B^+ \rightarrow \eta K_0^*(1430)^+)$	0.05 ± 0.13
$A_{CP}(B^+ \rightarrow \bar{D}^0 \pi^+)$	-0.007 ± 0.007	$A_{CP}(B^+ \rightarrow \eta K_2^*(1430)^+)$	-0.45 ± 0.30
$A_{CP}(B^+ \rightarrow D_{CP(+1)} \pi^+)$	-0.0080 ± 0.0024	$A_{CP}(B^+ \rightarrow \omega K^+)$	-0.02 ± 0.04
$A_{CP}(B^+ \rightarrow D_{CP(-1)} \pi^+)$	0.017 ± 0.026	$A_{CP}(B^+ \rightarrow \omega K^{*+})$	0.29 ± 0.35
$A_{CP}([K^{\mp} \pi^{\pm} \pi^+ \pi^-]_D \pi^+)$	0.02 ± 0.05	$A_{CP}(B^+ \rightarrow \omega(K\pi)_0^{*+})$	-0.10 ± 0.09
$A_{CP}(B^+ \rightarrow [\pi^+ \pi^+ \pi^- \pi^-]_D K^+)$	0.10 ± 0.04	$A_{CP}(B^+ \rightarrow \omega K_2^*(1430)^+)$	0.14 ± 0.15
$A_{CP}(B^+ \rightarrow [\pi^+ \pi^- \pi^+ \pi^-]_D K^*(892)^+)$	0.02 ± 0.11	$A_{CP}(B^+ \rightarrow K^{*0} \pi^+)$	-0.04 ± 0.09 ($S = 2.1$)
$A_{CP}(B^+ \rightarrow \bar{D}^0 K^+)$	-0.017 ± 0.005	$A_{CP}(B^+ \rightarrow K^*(892)^+ \pi^0)$	-0.39 ± 0.21 ($S = 1.6$)
$A_{CP}([K^{\mp} \pi^{\pm} \pi^+ \pi^-]_D K^+)$	-0.31 ± 0.11	$A_{CP}(B^+ \rightarrow K^+ \pi^- \pi^+)$	0.027 ± 0.008
$A_{CP}(B^+ \rightarrow [\pi^+ \pi^+ \pi^- \pi^-]_D \pi^+)$	$(-4 \pm 8) \times 10^{-3}$	$A_{CP}(B^+ \rightarrow K^+ K^- K^+ \text{ nonresonant})$	0.06 ± 0.05
$A_{CP}(B^+ \rightarrow [K^- \pi^+]_D K^+)$	-0.58 ± 0.21	$A_{CP}(B^+ \rightarrow f(980)^0 K^+)$	-0.08 ± 0.09
$A_{CP}(B^+ \rightarrow [K^- \pi^+ \pi^0]_D K^+)$	0.07 ± 0.30 ($S = 1.5$)	$A_{CP}(B^+ \rightarrow f_0(1500) K^+)$	0.28 ± 0.30
$A_{CP}(B^+ \rightarrow [K^+ K^- \pi^0]_D K^+)$	0.30 ± 0.20	$A_{CP}(B^+ \rightarrow f_2'(1525)^0 K^+)$	$-0.08^{+0.05}_{-0.04}$
$A_{CP}(B^+ \rightarrow [\pi^+ \pi^- \pi^0]_D K^+)$	0.05 ± 0.09	$A_{CP}(B^+ \rightarrow K_0^*(1430)^0 \pi^+)$	0.061 ± 0.032
$A_{CP}(B^+ \rightarrow \bar{D}^0 K^*(892)^+)$	-0.007 ± 0.019	$A_{CP}(B^+ \rightarrow K_0^*(1430)^+ \pi^0)$	$0.26^{+0.18}_{-0.14}$
$A_{CP}(B^+ \rightarrow [K^- \pi^+ \pi^- \pi^+]_D K^*(892)^+)$	-0.45 ± 0.25	$A_{CP}(B^+ \rightarrow K_2^*(1430)^0 \pi^+)$	$0.05^{+0.29}_{-0.24}$
$A_{CP}(B^+ \rightarrow [K^- \pi^+]_D \pi^+)$	0.00 ± 0.09	$A_{CP}(B^+ \rightarrow K^+ \pi^0 \pi^0)$	-0.06 ± 0.07
$A_{CP}(B^+ \rightarrow [K^- \pi^+ \pi^0]_D \pi^+)$	0.35 ± 0.16	$A_{CP}(B^+ \rightarrow K^0 \rho^+)$	-0.03 ± 0.15
$A_{CP}(B^+ \rightarrow [K^+ K^- \pi^0]_D \pi^+)$	-0.03 ± 0.04	$A_{CP}(B^+ \rightarrow K^{*+} \pi^+ \pi^-)$	0.07 ± 0.08
$A_{CP}(B^+ \rightarrow [\pi^+ \pi^- \pi^0]_D \pi^+)$	-0.016 ± 0.020	$A_{CP}(B^+ \rightarrow \rho^0 K^*(892)^+)$	0.31 ± 0.13
$A_{CP}(B^+ \rightarrow [K^- \pi^+]_D \pi^+)$	-0.09 ± 0.27	$A_{CP}(B^+ \rightarrow K^*(892)^+ f_0(980))$	-0.15 ± 0.12
$A_{CP}(B^+ \rightarrow [K^- \pi^+]_D \gamma \pi^+)$	-0.7 ± 0.6	$A_{CP}(B^+ \rightarrow a_1^+ K^0)$	0.12 ± 0.11
$A_{CP}(B^+ \rightarrow [K^- \pi^+]_D \pi K^+)$	0.8 ± 0.4	$A_{CP}(B^+ \rightarrow b_1^+ K^0)$	-0.03 ± 0.15
$A_{CP}(B^+ \rightarrow [K^- \pi^+]_D \gamma K^+)$	0.4 ± 1.0	$A_{CP}(B^+ \rightarrow K^*(892)^0 \rho^+)$	-0.01 ± 0.16
$A_{CP}(B^+ \rightarrow [\pi^+ \pi^- \pi^0]_D K^+)$	-0.02 ± 0.15	$A_{CP}(B^+ \rightarrow b_1^0 K^+)$	-0.46 ± 0.20
$A_{CP}(B^+ \rightarrow [K_S^0 K^+ \pi^-]_D K^+)$	0.10 ± 0.09	$A_{CP}(B^+ \rightarrow K^0 K^+)$	0.04 ± 0.14
$A_{CP}(B^+ \rightarrow [K_S^0 K^- \pi^+]_D K^+)$	-0.04 ± 0.08	$A_{CP}(B^+ \rightarrow K^+ K_S^0 K_S^0)$	0.025 ± 0.031
$A_{CP}(B^+ \rightarrow [K_S^0 K^- \pi^+]_D \pi^+)$	0.003 ± 0.015	$A_{CP}(B^+ \rightarrow \phi K^+)$	0.024 ± 0.028 ($S = 2.3$)
$A_{CP}(B^+ \rightarrow [K_S^0 K^+ \pi^-]_D \pi^+)$	-0.034 ± 0.020	$A_{CP}(B^+ \rightarrow X_0(1550) K^+)$	-0.04 ± 0.07
$A_{CP}(B^+ \rightarrow [K^*(892)^- K^+]_D K^+)$	0.08 ± 0.05	$A_{CP}(B^+ \rightarrow K^{*+} K^+ K^-)$	0.11 ± 0.09
$A_{CP}(B^+ \rightarrow [K^*(892)^+ K^-]_D K^+)$	0.02 ± 0.10	$A_{CP}(B^+ \rightarrow \phi K^*(892)^+)$	-0.01 ± 0.08
$A_{CP}(B^+ \rightarrow [K^*(892)^+ K^-]_D \pi^+)$	0.007 ± 0.017	$A_{CP}(B^+ \rightarrow \phi(K\pi)_0^{*+})$	0.04 ± 0.16
$A_{CP}(B^+ \rightarrow [K^*(892)^- K^+]_D \pi^+)$	-0.020 ± 0.011	$A_{CP}(B^+ \rightarrow \phi K_1(1270)^+)$	0.15 ± 0.20
$A_{ADS}(B^+ \rightarrow D \pi^+)$	0.129 ± 0.014	$A_{CP}(B^+ \rightarrow \phi K_2^*(1430)^+)$	-0.23 ± 0.20
$A_{ADS}(B^+ \rightarrow D^*(D \gamma) K^+)$	-0.6 ± 1.3	$A_{CP}(B^+ \rightarrow K^+ \phi \phi)$	-0.08 ± 0.07
$A_{ADS}(B^+ \rightarrow D^*(D \pi^0) K^+)$	0.72 ± 0.29	$A_{CP}(B^+ \rightarrow K^+ [\phi \phi]_{\eta_c})$	0.10 ± 0.08
$A_{ADS}(B^+ \rightarrow D^*(D \gamma) \pi^+)$	0.08 ± 0.13	$A_{CP}(B^+ \rightarrow K^*(892)^+ \gamma)$	0.014 ± 0.018
$A_{ADS}(B^+ \rightarrow D^*(D \pi^0) \pi^+)$	-0.14 ± 0.06	$A_{CP}(B^+ \rightarrow X_S \gamma)$	0.028 ± 0.019
$A_{ADS}(B^+ \rightarrow [K^- \pi^+]_D K^+ \pi^- \pi^+)$	-0.33 ± 0.35	$A_{CP}(B^+ \rightarrow \eta K^+ \gamma)$	-0.12 ± 0.07
$A_{ADS}(B^+ \rightarrow [K^- \pi^+]_D \pi^+ \pi^- \pi^+)$	-0.01 ± 0.09	$A_{CP}(B^+ \rightarrow \phi K^+ \gamma)$	-0.13 ± 0.11 ($S = 1.1$)
$A_{CP}(B^+ \rightarrow D_{CP(-1)} K^+)$	-0.10 ± 0.07		

Unless otherwise stated, limits are given at the 90% confidence level, while errors are given as ± 1 standard deviation.

Tests of Conservation Laws

$A_{CP}(B^+ \rightarrow \rho^+ \gamma)$	-0.11 ± 0.33	$A_{CP}(B^0 \rightarrow b_1^- \pi^+)$	-0.05 ± 0.10
$A_{CP}(B^+ \rightarrow \pi^+ \pi^0)$	0.03 ± 0.04	$A_{CP}(B^0 \rightarrow p \bar{p} K^*(892)^0)$	0.05 ± 0.12
$A_{CP}(B^+ \rightarrow \rho^0 \pi^+)$	0.009 ± 0.019	$A_{CP}(B^0 \rightarrow p \bar{p} \pi^-)$	0.04 ± 0.07
$A_{CP}(B^+ \rightarrow \rho^0(1450) \pi^+)$	-0.11 ± 0.05	$A_{CP}(B^0 \rightarrow K^{*0} \ell^+ \ell^-)$	-0.05 ± 0.10
$A_{CP}(B^+ \rightarrow \pi^+ \pi^- \pi^+ \text{ nonresonant})$	$-0.14^{+0.23}_{-0.16}$	$A_{CP}(B^0 \rightarrow K^{*0} e^+ e^-)$	-0.21 ± 0.19
$A_{CP}(B^+ \rightarrow \rho^+ \pi^0)$	0.02 ± 0.11	$A_{CP}(B^0 \rightarrow K^{*0} \mu^+ \mu^-)$	-0.034 ± 0.024
$A_{CP}(B^+ \rightarrow \rho^+ \rho^0)$	-0.05 ± 0.05	$C_{D^*(2010)^- D^+} (B^0 \rightarrow D^*(2010)^- D^+)$	-0.02 ± 0.08
$A_{CP}(B^+ \rightarrow \omega \pi^+)$	-0.04 ± 0.05	$C_{D^*(2010)^+ D^-} (B^0 \rightarrow D^*(2010)^+ D^-)$	$-0.03 \pm 0.09 (S = 1.1)$
$A_{CP}(B^+ \rightarrow \omega \rho^+)$	-0.20 ± 0.09	$C_{D^{*+} D^{*-}} (B^0 \rightarrow D^{*+} D^{*-})$	$0.01 \pm 0.09 (S = 1.6)$
$A_{CP}(B^+ \rightarrow \eta \pi^+)$	$-0.14 \pm 0.07 (S = 1.4)$	$C_+ (B^0 \rightarrow D^{*+} D^{*-})$	$0.00 \pm 0.10 (S = 1.6)$
$A_{CP}(B^+ \rightarrow \eta \rho^+)$	0.11 ± 0.11	$C_- (B^0 \rightarrow D^{*+} D^{*-})$	0.19 ± 0.31
$A_{CP}(B^+ \rightarrow \eta' \pi^+)$	0.06 ± 0.16	$S_- (B^0 \rightarrow D^{*+} D^{*-})$	$0.1 \pm 1.6 (S = 3.5)$
$A_{CP}(B^+ \rightarrow \eta' \rho^+)$	0.26 ± 0.17	$C (B^0 \rightarrow D^*(2010)^+ D^*(2010)^- K_S^0)$	0.01 ± 0.29
$A_{CP}(B^+ \rightarrow b_1^0 \pi^+)$	0.05 ± 0.16	$S (B^0 \rightarrow D^*(2010)^+ D^*(2010)^- K_S^0)$	0.1 ± 0.4
$A_{CP}(B^+ \rightarrow p \bar{p} \pi^+)$	0.00 ± 0.04	$C_{D^+ D^-} (B^0 \rightarrow D^+ D^-)$	$-0.22 \pm 0.24 (S = 2.5)$
$A_{CP}(B^+ \rightarrow p \bar{p} K^+(892)^+)$	$0.00 \pm 0.04 (S = 2.2)$	$C_{J/\psi(1S) \pi^0} (B^0 \rightarrow J/\psi(1S) \pi^0)$	$0.03 \pm 0.17 (S = 1.5)$
$A_{CP}(B^+ \rightarrow p \bar{p} K^*(892)^+)$	$0.21 \pm 0.16 (S = 1.4)$	$C(B^0 \rightarrow J/\psi(1S) \rho^0)$	-0.06 ± 0.06
$A_{CP}(B^+ \rightarrow p \bar{p} \gamma)$	0.17 ± 0.17	$C_{D_{CP}^* h^0} (B^0 \rightarrow D_{CP}^* h^0)$	-0.02 ± 0.08
$A_{CP}(B^+ \rightarrow p \bar{p} \pi^0)$	0.01 ± 0.17	$S_{D_{CP}^* h^0} (B^0 \rightarrow D_{CP}^* h^0)$	-0.66 ± 0.12
$A_{CP}(B^+ \rightarrow K^+ \ell^+ \ell^-)$	-0.02 ± 0.08	$C_{K^0 \pi^0} (B^0 \rightarrow K^0 \pi^0)$	$0.00 \pm 0.13 (S = 1.4)$
$A_{CP}(B^+ \rightarrow K^+ e^+ e^-)$	0.14 ± 0.14	$C_{\eta'(958) K_S^0} (B^0 \rightarrow \eta'(958) K_S^0)$	$-0.04 \pm 0.20 (S = 2.5)$
$A_{CP}(B^+ \rightarrow K^+ \mu^+ \mu^-)$	0.011 ± 0.017	$S_{\eta'(958) K_S^0} (B^0 \rightarrow \eta'(958) K_S^0)$	$0.43 \pm 0.17 (S = 1.5)$
$A_{CP}(B^+ \rightarrow K^{*+} \ell^+ \ell^-)$	-0.09 ± 0.14	$C_{\eta' K^0} (B^0 \rightarrow \eta' K^0)$	-0.06 ± 0.04
$A_{CP}(B^+ \rightarrow K^{*+} e^+ e^-)$	-0.14 ± 0.23	$C_{\omega K_S^0} (B^0 \rightarrow \omega K_S^0)$	$0.0 \pm 0.4 (S = 3.0)$
$A_{CP}(B^+ \rightarrow K^{*+} \mu^+ \mu^-)$	-0.12 ± 0.24	$S_{\omega K_S^0} (B^0 \rightarrow \omega K_S^0)$	0.70 ± 0.21
$\text{Re}(\epsilon_{B^0})/(1+ \epsilon_{B^0} ^2)$	$(-0.5 \pm 0.4) \times 10^{-3}$	$C (B^0 \rightarrow K_S^0 \pi^0 \pi^0)$	-0.21 ± 0.20
$A_{T/CP}(B^0 \leftrightarrow \bar{B}^0)$	0.005 ± 0.018	$S (B^0 \rightarrow K_S^0 \pi^0 \pi^0)$	$0.89^{+0.27}_{-0.30}$
$A_{CP}(B^0 \rightarrow D^*(2010)^+ D^-)$	0.013 ± 0.014	$C_{\rho^0 K_S^0} (B^0 \rightarrow \rho^0 K_S^0)$	-0.04 ± 0.20
$A_{CP}(B^0 \rightarrow [K^+ K^-]_D K^*(892)^0)$	-0.05 ± 0.10	$S_{\rho^0 K_S^0} (B^0 \rightarrow \rho^0 K_S^0)$	$0.50^{+0.17}_{-0.21}$
$A_{CP}(B^0 \rightarrow [K^+ \pi^-]_D K^*(892)^0)$	0.047 ± 0.029	$C_{f_0(980) K_S^0} (B^0 \rightarrow f_0(980) K_S^0)$	0.29 ± 0.20
$A_{CP}(B^0 \rightarrow [\pi^+ \pi^-]_D K^*(892)^0)$	-0.18 ± 0.14	$S_{f_0(980) K_S^0} (B^0 \rightarrow f_0(980) K_S^0)$	-0.50 ± 0.16
$A_{CP}(B^0 \rightarrow \eta' K^*(892)^0)$	-0.07 ± 0.18	$S_{f_2(1270) K_S^0} (B^0 \rightarrow f_2(1270) K_S^0)$	-0.5 ± 0.5
$A_{CP}(B^0 \rightarrow \eta' K_S^0(1430)^0)$	-0.19 ± 0.17	$C_{f_2(1270) K_S^0} (B^0 \rightarrow f_2(1270) K_S^0)$	0.3 ± 0.4
$A_{CP}(B^0 \rightarrow \eta' K_S^0(1430)^0)$	0.14 ± 0.18	$S_{f_x(1300) K_S^0} (B^0 \rightarrow f_x(1300) K_S^0)$	-0.2 ± 0.5
$A_{CP}(B^0 \rightarrow \eta K_S^0(1430)^0)$	0.06 ± 0.13	$C_{f_x(1300) K_S^0} (B^0 \rightarrow f_x(1300) K_S^0)$	0.13 ± 0.35
$A_{CP}(B^0 \rightarrow \eta K_S^0(1430)^0)$	-0.07 ± 0.19	$S_{K^0 \pi^+ \pi^-} (B^0 \rightarrow K^0 \pi^+ \pi^- \text{ nonresonant})$	-0.01 ± 0.33
$A_{CP}(B^0 \rightarrow b_1 K^+)$	-0.07 ± 0.12	$C_{K^0 \pi^+ \pi^-} (B^0 \rightarrow K^0 \pi^+ \pi^- \text{ nonresonant})$	0.01 ± 0.26
$A_{CP}(B^0 \rightarrow \omega K^0)$	0.45 ± 0.25	$C_{K_S^0 K_S^0} (B^0 \rightarrow K_S^0 K_S^0)$	$0.0 \pm 0.4 (S = 1.4)$
$A_{CP}(B^0 \rightarrow \omega(K\pi)_0^0)$	-0.07 ± 0.09	$S_{K_S^0 K_S^0} (B^0 \rightarrow K_S^0 K_S^0)$	-0.8 ± 0.5
$A_{CP}(B^0 \rightarrow \omega K_S^0(1430)^0)$	-0.37 ± 0.17	$C_{K^+ K^- K_S^0} (B^0 \rightarrow K^+ K^- K_S^0)$	0.06 ± 0.08
$A_{CP}(B^0 \rightarrow K^+ \pi^- \pi^0)$	$(0 \pm 6) \times 10^{-2}$	nonresonant	
$A_{CP}(B^0 \rightarrow \rho^- K^+)$	0.20 ± 0.11	$C_{K^+ K^- K_S^0} (B^0 \rightarrow K^+ K^- K_S^0 \text{ inclusive})$	0.01 ± 0.09
$A_{CP}(B^0 \rightarrow \rho(1450)^- K^+)$	-0.10 ± 0.33	$C_{\phi K_S^0} (B^0 \rightarrow \phi K_S^0)$	0.01 ± 0.14
$A_{CP}(B^0 \rightarrow \rho(1700)^- K^+)$	-0.4 ± 0.6	$S_{\phi K_S^0} (B^0 \rightarrow \phi K_S^0)$	0.59 ± 0.14
$A_{CP}(B^0 \rightarrow K^+ \pi^- \pi^0 \text{ nonresonant})$	0.10 ± 0.18	$C_{K_S K_S K_S} (B^0 \rightarrow K_S K_S K_S)$	-0.14 ± 0.12
$A_{CP}(B^0 \rightarrow K^0 \pi^+ \pi^-)$	-0.01 ± 0.05	$S_{K_S K_S K_S} (B^0 \rightarrow K_S K_S K_S)$	-0.82 ± 0.17
$A_{CP}(B^0 \rightarrow (K\pi)_0^{*+} \pi^-)$	0.02 ± 0.04	$C_{K_S^0 \pi^0 \gamma} (B^0 \rightarrow K_S^0 \pi^0 \gamma)$	0.36 ± 0.33
$A_{CP}(B^0 \rightarrow K_S^0(1430)^+ \pi^-)$	-0.29 ± 0.24	$S_{K_S^0 \pi^0 \gamma} (B^0 \rightarrow K_S^0 \pi^0 \gamma)$	-0.8 ± 0.6
$A_{CP}(B^0 \rightarrow K^*(1680)^+ \pi^-)$	-0.07 ± 0.14	$C_{K^*(892)^0 \gamma} (B^0 \rightarrow K^*(892)^0 \gamma)$	$-0.04 \pm 0.16 (S = 1.2)$
$A_{CP}(B^0 \rightarrow f_0(980) K_S^0)$	0.28 ± 0.31	$S_{K^*(892)^0 \gamma} (B^0 \rightarrow K^*(892)^0 \gamma)$	-0.15 ± 0.22
$A_{CP}(B^0 \rightarrow (K\pi)_0^0 \pi^0)$	-0.15 ± 0.11	$C_{\eta K^0 \gamma} (B^0 \rightarrow \eta K^0 \gamma)$	$0.1 \pm 0.4 (S = 1.4)$
$A_{CP}(B^0 \rightarrow K^{*0} \pi^0)$	-0.15 ± 0.13	$S_{\eta K^0 \gamma} (B^0 \rightarrow \eta K^0 \gamma)$	$-0.5 \pm 0.5 (S = 1.2)$
$A_{CP}(B^0 \rightarrow K^*(892)^0 \pi^+ \pi^-)$	0.07 ± 0.05	$C_{K^0 \phi \gamma} (B^0 \rightarrow K^0 \phi \gamma)$	-0.3 ± 0.6
$A_{CP}(B^0 \rightarrow K^*(892)^0 \rho^0)$	-0.06 ± 0.09	$S_{K^0 \phi \gamma} (B^0 \rightarrow K^0 \phi \gamma)$	$0.7^{+0.7}_{-1.1}$
$A_{CP}(B^0 \rightarrow K^{*0} f_0(980))$	0.07 ± 0.10	$C(B^0 \rightarrow K_S^0 \rho^0 \gamma)$	-0.05 ± 0.19
$A_{CP}(B^0 \rightarrow K^{*+} \rho^-)$	0.21 ± 0.15	$S(B^0 \rightarrow K_S^0 \rho^0 \gamma)$	-0.04 ± 0.23
$A_{CP}(B^0 \rightarrow K^*(892)^0 K^+ K^-)$	0.01 ± 0.05	$C(B^0 \rightarrow \rho^0 \gamma)$	0.4 ± 0.5
$A_{CP}(B^0 \rightarrow a_1^- K^+)$	-0.16 ± 0.12		
$A_{CP}(B^0 \rightarrow K^0 K^0)$	-0.6 ± 0.7		
$A_{CP}(B^0 \rightarrow K^*(892)^0 \phi)$	0.00 ± 0.04		
$A_{CP}(B^0 \rightarrow K^*(892)^0 K^- \pi^+)$	0.2 ± 0.4		
$A_{CP}(B^0 \rightarrow \phi(K\pi)_0^0)$	0.12 ± 0.08		
$A_{CP}(B^0 \rightarrow \phi K_S^0(1430)^0)$	-0.11 ± 0.10		
$A_{CP}(B^0 \rightarrow K^*(892)^0 \gamma)$	-0.006 ± 0.011		
$A_{CP}(B^0 \rightarrow K_S^0(1430)^0 \gamma)$	-0.08 ± 0.15		
$A_{CP}(B^0 \rightarrow X_S \gamma)$	-0.009 ± 0.018		
$A_{CP}(B^0 \rightarrow \rho^+ \pi^-)$	$0.13 \pm 0.06 (S = 1.1)$		
$A_{CP}(B^0 \rightarrow \rho^- \pi^+)$	-0.08 ± 0.08		
$A_{CP}(B^0 \rightarrow a_1(1260) \pm \pi \mp)$	-0.07 ± 0.06		

Unless otherwise stated, limits are given at the 90% confidence level, while errors are given as ± 1 standard deviation.

Tests of Conservation Laws

$S(B^0 \rightarrow \rho^0 \gamma)$	-0.8 ± 0.7
$C_{\rho^0 \pi^0}(B^0 \rightarrow \pi^0 \pi^0)$	-0.33 ± 0.22
$C_{\rho^+ \pi^-}(B^0 \rightarrow \rho^+ \pi^-)$	-0.03 ± 0.07 ($S = 1.2$)
$S_{\rho^+ \pi^-}(B^0 \rightarrow \rho^+ \pi^-)$	0.05 ± 0.07
$\Delta S_{\rho^+ \pi^-}(B^0 \rightarrow \rho^+ \pi^-)$	0.01 ± 0.08
$C_{\rho^0 \pi^0}(B^0 \rightarrow \rho^0 \pi^0)$	0.27 ± 0.24
$S_{\rho^0 \pi^0}(B^0 \rightarrow \rho^0 \pi^0)$	-0.23 ± 0.34
$C_{a_1 \pi}(B^0 \rightarrow a_1(1260)^+ \pi^-)$	-0.05 ± 0.11
$S_{a_1 \pi}(B^0 \rightarrow a_1(1260)^+ \pi^-)$	-0.2 ± 0.4 ($S = 3.2$)
$\Delta C_{a_1 \pi}(B^0 \rightarrow a_1(1260)^+ \pi^-)$	0.43 ± 0.14 ($S = 1.3$)
$\Delta S_{a_1 \pi}(B^0 \rightarrow a_1(1260)^+ \pi^-)$	-0.11 ± 0.12
$C(B^0 \rightarrow b_1^- K^+)$	-0.22 ± 0.24
$\Delta C(B^0 \rightarrow b_1^- \pi^+)$	-1.04 ± 0.24
$C_{\rho^0 \rho^0}(B^0 \rightarrow \rho^0 \rho^0)$	0.2 ± 0.9
$S_{\rho^0 \rho^0}(B^0 \rightarrow \rho^0 \rho^0)$	0.3 ± 0.7
$C_{\rho^+ \rho^-}(B^0 \rightarrow \rho^+ \rho^-)$	0.00 ± 0.09
$S_{\rho^+ \rho^-}(B^0 \rightarrow \rho^+ \rho^-)$	-0.14 ± 0.13
$ \lambda (B^0 \rightarrow J/\psi K^*(892)^0)$	< 0.25 , CL = 95%
$\cos 2\beta(B^0 \rightarrow J/\psi K^*(892)^0)$	$1.7^{+0.7}_{-0.9}$ ($S = 1.6$)
$\cos 2\beta(B^0 \rightarrow [K_S^0 \pi^+ \pi^-]_{D^{(*)}} h^0)$	0.91 ± 0.25
$(S_+ + S_-)/2(B^0 \rightarrow D^{*+} \pi^-)$	-0.039 ± 0.011
$(S_- - S_+)/2(B^0 \rightarrow D^{*+} \pi^-)$	-0.009 ± 0.015
$(S_+ + S_-)/2(B^0 \rightarrow D^- \pi^+)$	-0.046 ± 0.023
$(S_- - S_+)/2(B^0 \rightarrow D^- \pi^+)$	-0.022 ± 0.021
$S_+(B^0 \rightarrow D^- \pi^+)$	0.058 ± 0.023
$S_-(B^0 \rightarrow D^+ \pi^-)$	0.038 ± 0.021
$(S_+ + S_-)/2(B^0 \rightarrow D^- \rho^+)$	-0.024 ± 0.032
$(S_- - S_+)/2(B^0 \rightarrow D^- \rho^+)$	-0.10 ± 0.06
$C_{\eta_c K_S^0}(B^0 \rightarrow \eta_c K_S^0)$	0.08 ± 0.13
$C_{c\bar{c}K^{(*)0}}(B^0 \rightarrow c\bar{c}K^{(*)0})$	$(-0.5 \pm 1.5) \times 10^{-2}$
$C_{J/\psi(nS)K^0}(B^0 \rightarrow J/\psi(nS)K^0)$	$(-0.8 \pm 1.7) \times 10^{-2}$
$C_{J/\psi K^{*0}}(B^0 \rightarrow J/\psi K^{*0})$	0.03 ± 0.10
$S_{J/\psi K^{*0}}(B^0 \rightarrow J/\psi K^{*0})$	0.60 ± 0.25
$C_{\chi_{c0} K_S^0}(B^0 \rightarrow \chi_{c0} K_S^0)$	$-0.3^{+0.5}_{-0.4}$
$S_{\chi_{c0} K_S^0}(B^0 \rightarrow \chi_{c0} K_S^0)$	-0.7 ± 0.5
$C_{\chi_{c1} K_S^0}(B^0 \rightarrow \chi_{c1} K_S^0)$	0.06 ± 0.07
$\sin(2\beta_{\text{eff}})(B^0 \rightarrow \phi K^0)$	0.22 ± 0.30
$\sin(2\beta_{\text{eff}})(B^0 \rightarrow \phi K_0^*(1430)^0)$	$0.97^{+0.03}_{-0.52}$
$\sin(2\beta_{\text{eff}})(B^0 \rightarrow [K_S^0 \pi^+ \pi^-]_{D^{(*)}} h^0)$	0.80 ± 0.16
$ \lambda (B^0 \rightarrow [K_S^0 \pi^+ \pi^-]_{D^{(*)}} h^0)$	1.01 ± 0.08
$ \sin(2\beta + \gamma) $	> 0.40 , CL = 90%
$2\beta + \gamma$	$(83 \pm 60)^\circ$
$x_+(B^0 \rightarrow D K^{*0})$	0.04 ± 0.17
$x_-(B^0 \rightarrow D K^{*0})$	-0.16 ± 0.14
$y_-(B^0 \rightarrow D K^{*0})$	0.20 ± 0.25 ($S = 1.2$)
$A_{CP}(B \rightarrow K^*(892)\gamma)$	-0.003 ± 0.011
$A_{CP}(B \rightarrow s\gamma)$	0.015 ± 0.011
$A_{CP}(B \rightarrow (s+d)\gamma)$	0.010 ± 0.031
$A_{CP}(B \rightarrow X_S \ell^+ \ell^-)$	0.04 ± 0.11
$A_{CP}(B \rightarrow K^* e^+ e^-)$	-0.18 ± 0.15
$A_{CP}(B \rightarrow K^* \mu^+ \mu^-)$	-0.03 ± 0.13
$A_{CP}(B \rightarrow K^* \ell^+ \ell^-)$	-0.04 ± 0.07
$A_{CP}(B \rightarrow \eta \text{ anything})$	$-0.13^{+0.04}_{-0.05}$
$\Delta A_{CP}(X_S \gamma) = A_{CP}(B^\pm \rightarrow X_S \gamma) - A_{CP}(B^0 \rightarrow X_S \gamma)$	0.041 ± 0.023
$\bar{A}_{CP}(B \rightarrow X_S \gamma) = (A_{CP}(B^+ \rightarrow X_S \gamma) + A_{CP}(B^0 \rightarrow X_S \gamma))/2$	0.009 ± 0.012
$\bar{A}_{CP}(B \rightarrow K^* \gamma) = (A_{CP}(B^+ \rightarrow K^* \gamma) + A_{CP}(B^0 \rightarrow K^* \gamma))/2$	-0.001 ± 0.014
$\text{Re}(\epsilon_{B^0}) / (1 + \epsilon_{B^0} ^2)$	$(-0.15 \pm 0.70) \times 10^{-3}$
$S_{KK}(B_S^0 \rightarrow K^+ K^-)$	0.14 ± 0.05 ($S = 1.3$)
$\delta_B(B_S^0 \rightarrow D_S^\pm K^\mp \pi^\pm \pi^\mp)$	$(-6^{+10}_{-13})^\circ$
CP Violation phase β_s	$(2.5 \pm 1.0) \times 10^{-2}$ rad
$A_{CP}^L(B_S \rightarrow J/\psi \bar{K}^*(892)^0)$	-0.05 ± 0.06

$A_{CP}^{\parallel}(B_S \rightarrow J/\psi \bar{K}^*(892)^0)$	0.17 ± 0.15
$A_{CP}^{\perp}(B_S \rightarrow J/\psi \bar{K}^*(892)^0)$	-0.05 ± 0.10
$A_{CP}(B_S^0 \rightarrow [K^+ K^-]_D \bar{K}^*(892)^0)$	-0.04 ± 0.07
$A_{CP}(B_S^0 \rightarrow [\pi^+ K^-]_D K^*(892)^0)$	-0.01 ± 0.04
$A_{CP}(B_S^0 \rightarrow [\pi^+ \pi^-]_D K^*(892)^0)$	0.06 ± 0.13
$\Gamma(\eta_c(1S) \rightarrow \pi^+ \pi^-) / \Gamma_{\text{total}}$	$< 1.1 \times 10^{-4}$, CL = 90%
$\Gamma(\eta_c(1S) \rightarrow \pi^0 \pi^0) / \Gamma_{\text{total}}$	$< 4 \times 10^{-5}$, CL = 90%
$\Gamma(\eta_c(1S) \rightarrow K^+ K^-) / \Gamma_{\text{total}}$	$< 6 \times 10^{-4}$, CL = 90%
$\Gamma(\eta_c(1S) \rightarrow K_S^0 K_S^0) / \Gamma_{\text{total}}$	$< 3.1 \times 10^{-4}$, CL = 90%
n electric dipole moment	$< 0.18 \times 10^{-25}$ ecm, CL = 90%
$(\alpha + \bar{\alpha}) / (\alpha - \bar{\alpha})$ in $\Lambda \rightarrow p \pi^-, \bar{\Lambda} \rightarrow \bar{p} \pi^+$	-0.002 ± 0.012
$\frac{[\alpha(\Xi^-) - \alpha(\Lambda) - \alpha(\Xi^+) + \alpha(\bar{\Lambda})]}{[\alpha(\Xi^-) - \alpha(\Lambda) + \alpha(\Xi^+) + \alpha(\bar{\Lambda})]}$	$(0 \pm 7) \times 10^{-4}$
$(\alpha + \bar{\alpha}) / (\alpha - \bar{\alpha})$ in $\Omega^- \rightarrow \Lambda K^-, \bar{\Omega}^+ \rightarrow \bar{\Lambda} K^+$	-0.02 ± 0.13
$(\alpha + \bar{\alpha}) / (\alpha - \bar{\alpha})$ in $\Lambda_c^+ \rightarrow \Lambda \pi^+, \bar{\Lambda}_c^- \rightarrow \bar{\Lambda} \pi^-$	-0.07 ± 0.31
$(\alpha + \bar{\alpha}) / (\alpha - \bar{\alpha})$ in $\Lambda_c^+ \rightarrow \Lambda e^+ \nu_e, \bar{\Lambda}_c^- \rightarrow \bar{\Lambda} e^- \bar{\nu}_e$	0.00 ± 0.04
$A_{CP}(\Lambda_b \rightarrow p \pi^-)$	-0.025 ± 0.029 ($S = 1.2$)
$A_{CP}(\Lambda_b \rightarrow p K^-)$	-0.025 ± 0.022
$A_{CP}(\Lambda_b \rightarrow D p K^-)$	0.12 ± 0.09
$\Delta A_{CP}(p K^- / \pi^-)$	0.014 ± 0.024
$A_{CP}(\Lambda_b \rightarrow p \bar{K}^0 \pi^-)$	0.22 ± 0.13
$\Delta A_{CP}(J/\psi p \pi^- / K^-)$	$(5.7 \pm 2.7) \times 10^{-2}$
$A_{CP}(\Lambda_b \rightarrow \Lambda K^+ \pi^-)$	-0.53 ± 0.25
$A_{CP}(\Lambda_b \rightarrow \Lambda K^+ K^-)$	-0.28 ± 0.12
$\Delta A_{CP}(\Lambda_b^0 \rightarrow p K^- \mu^+ \pi^-)$	$(-4 \pm 5) \times 10^{-2}$
$\Delta A_{CP}(\Lambda_b^0 \rightarrow p \pi^- \pi^+ \pi^-)$	$(1.1 \pm 2.6) \times 10^{-2}$
$\Delta A_{CP}(\Lambda_b^0 \rightarrow (p \pi^- \pi^+ \pi^-)_{LBM})$	$(4 \pm 4) \times 10^{-2}$
$\Delta A_{CP}(\Lambda_b^0 \rightarrow p a_1(1260)^-)$	$(-1 \pm 4) \times 10^{-2}$
$\Delta A_{CP}(\Lambda_b^0 \rightarrow N(1520)^0 \rho(770)^0)$	$(2 \pm 5) \times 10^{-2}$
$\Delta A_{CP}(\Lambda_b^0 \rightarrow \Delta(1232)^+ \pi^- \pi^-)$	$(0.1 \pm 3.3) \times 10^{-2}$
$\Delta A_{CP}(\Lambda_b^0 \rightarrow p K^- \pi^+ \pi^-)$	$(3.2 \pm 1.3) \times 10^{-2}$
$\Delta A_{CP}(\Lambda_b^0 \rightarrow (p K^- \pi^+ \pi^-)_{LBM})$	$(3.5 \pm 1.6) \times 10^{-2}$
$\Delta A_{CP}(\Lambda_b^0 \rightarrow N(1520)^0 K^*(892)^0)$	$(5.5 \pm 2.5) \times 10^{-2}$
$\Delta A_{CP}(\Lambda_b^0 \rightarrow \Lambda(1520) \rho(770)^0)$	$(1 \pm 6) \times 10^{-2}$
$\Delta A_{CP}(\Lambda_b^0 \rightarrow \Delta(1232)^+ K^- \pi^-)$	$(4.4 \pm 2.7) \times 10^{-2}$
$\Delta A_{CP}(\Lambda_b^0 \rightarrow p K_1(1410)^-)$	$(5 \pm 4) \times 10^{-2}$
$\Delta A_{CP}(\Lambda_b^0 \rightarrow p K^- K^+ \pi^-)$	$(-7 \pm 5) \times 10^{-2}$
$\Delta A_{CP}(\Lambda_b^0 \rightarrow p K^- K^+ K^-)$	$(0.2 \pm 1.9) \times 10^{-2}$
$\Delta A_{CP}(\Lambda_b^0 \rightarrow \Lambda(1520) \phi(1020))$	$(4 \pm 6) \times 10^{-2}$
$\Delta A_{CP}(\Lambda_b^0 \rightarrow (p K^-)_{\text{highmass}} \phi(1020))$	$(-0.7 \pm 3.4) \times 10^{-2}$
$\Delta A_{CP}(\Lambda_b^0 \rightarrow (p K^- K^+ K^-)_{LBM})$	$(2.7 \pm 2.4) \times 10^{-2}$
$A_c(\Lambda)$	-0.22 ± 0.13
$A_s(\Lambda)$	0.13 ± 0.13
$A_c(\phi)$	-0.01 ± 0.12
$A_s(\phi)$	-0.07 ± 0.12
$a_{CP}(\Lambda_b^0 \rightarrow p \pi^- \pi^+ \pi^-)$	$(-0.7 \pm 0.7)\%$
$a_{CP}(\Lambda_b^0 \rightarrow p K^- \pi^+ \pi^-)$	$(-0.8 \pm 0.9)\%$
$a_{CP}(\Lambda_b^0 \rightarrow p K^- K^+ \pi^-)$	$(-1 \pm 5)\%$
$a_{CP}(\Lambda_b^0 \rightarrow p K^- K^+ K^-)$	$(1.1 \pm 1.5)\%$
$a_{CP}(\Lambda_b^0 \rightarrow p K^- \mu^+ \mu^-)$	$(1 \pm 5)\%$

CP VIOLATION OBSERVED

$\text{Re}(\epsilon)$	$(1.596 \pm 0.013) \times 10^{-3}$
charge asymmetry in K_{L3}^0 decays	
$A_L =$ weighted average of $A_L(\mu)$ and $A_L(e)$	$(0.332 \pm 0.006)\%$
$A_L(\mu) = [\Gamma(\pi^- \mu^+ \nu_\mu) - \Gamma(\pi^+ \mu^- \bar{\nu}_\mu)] / \text{sum}$	$(0.304 \pm 0.025)\%$
$A_L(e) = [\Gamma(\pi^- e^+ \nu_e) - \Gamma(\pi^+ e^- \bar{\nu}_e)] / \text{sum}$	$(0.334 \pm 0.007)\%$
parameters for $K_L^0 \rightarrow 2\pi$ decay	
$ \eta_{00} = A(K_L^0 \rightarrow 2\pi^0) / A(K_S^0 \rightarrow 2\pi^0) $	$(2.220 \pm 0.011) \times 10^{-3}$ ($S = 1.8$)
$ \eta_{+-} = A(K_L^0 \rightarrow \pi^+ \pi^-) / A(K_S^0 \rightarrow \pi^+ \pi^-) $	$(2.232 \pm 0.011) \times 10^{-3}$ ($S = 1.8$)

$ \epsilon = (2 \eta_{+-} + \eta_{00})/3$	$(2.228 \pm 0.011) \times 10^{-3}$ (S = 1.8)
$ \eta_{00}/\eta_{+-} $	[i] 0.9950 ± 0.0007 (S = 1.6)
$\text{Re}(\epsilon'/\epsilon) = (1 - \eta_{00}/\eta_{+-})/3$	[i] $(1.66 \pm 0.23) \times 10^{-3}$ (S = 1.6)
Assuming <i>CPT</i>	
ϕ_{+-} , phase of η_{+-}	$(43.51 \pm 0.05)^\circ$ (S = 1.2)
ϕ_{00} , phase of η_{00}	$(43.52 \pm 0.05)^\circ$ (S = 1.3)
$\phi_e = (2\phi_{+-} + \phi_{00})/3$	$(43.52 \pm 0.05)^\circ$ (S = 1.2)
Not assuming <i>CPT</i>	
ϕ_{+-} , phase of η_{+-}	$(43.4 \pm 0.5)^\circ$ (S = 1.2)
ϕ_{00} , phase of η_{00}	$(43.7 \pm 0.6)^\circ$ (S = 1.2)
$\phi_e = (2\phi_{+-} + \phi_{00})/3$	$(43.5 \pm 0.5)^\circ$ (S = 1.3)
<i>CP</i> asymmetry A in $K_L^0 \rightarrow \pi^+ \pi^- e^+ e^-$	
β_{CP} from $K_L^0 \rightarrow e^+ e^- e^+ e^-$	$(13.7 \pm 1.5)\%$
γ_{CP} from $K_L^0 \rightarrow e^+ e^- e^+ e^-$	-0.19 ± 0.07
parameters for $K_L^0 \rightarrow \pi^+ \pi^- \gamma$ decay	
$ \eta_{+-\gamma} = A(K_L^0 \rightarrow \pi^+ \pi^- \gamma, CP \text{ violating})/A(K_S^0 \rightarrow \pi^+ \pi^- \gamma) $	$(2.35 \pm 0.07) \times 10^{-3}$
$\phi_{+-\gamma} = \text{phase of } \eta_{+-\gamma}$	$(44 \pm 4)^\circ$
$\Gamma(K_L^0 \rightarrow \pi^+ \pi^-)/\Gamma_{\text{total}}$	[j] $(1.967 \pm 0.010) \times 10^{-3}$ (S = 1.5)
$\Gamma(K_L^0 \rightarrow \pi^0 \pi^0)/\Gamma_{\text{total}}$	$(8.64 \pm 0.06) \times 10^{-4}$ (S = 1.8)
$\Delta A_{CP}^D = A_{CP}(K^+ K^-) - A_{CP}(\pi^+ \pi^-)$	$(-0.154 \pm 0.029)\%$
$A_{CP}(B^+ \rightarrow [K^- \pi^+]_{\overline{D}} K^*(892)^+)$	-0.75 ± 0.16
$A_{CP}(B^+ \rightarrow D_{CP(+1)} K^+)$	0.132 ± 0.015 (S = 1.8)
$A_{ADS}(B^+ \rightarrow D K^+)$	-0.451 ± 0.026
$A_{CP}(B^+ \rightarrow \eta K^+)$	-0.37 ± 0.08
$A_{CP}(B^+ \rightarrow f_2(1270) K^+)$	$-0.68^{+0.19}_{-0.17}$
$A_{CP}(B^+ \rightarrow \rho^0 K^+)$	0.37 ± 0.10
$A_{CP}(B^+ \rightarrow K^+ K^- \pi^+)$	-0.122 ± 0.021
$A_{CP}(B^+ \rightarrow K^+ K^- K^+)$	-0.033 ± 0.008
$A_{CP}(B^+ \rightarrow \pi^+ \pi^- \pi^+)$	0.057 ± 0.013
$A_{CP}(B^+ \rightarrow f_2(1270) \pi^+)$	0.40 ± 0.06
$A_{CP}(B^+ \rightarrow f_0(1370) \pi^+)$	0.72 ± 0.22
γ	$(65.9^{+3.3}_{-3.5})^\circ$
$r_B(B^+ \rightarrow D^0 K^+)$	0.0994 ± 0.0026
$\delta_B(B^+ \rightarrow D^0 K^+)$	$(127.7^{+3.6}_{-3.9})^\circ$
$r_B(B^+ \rightarrow D^0 K^{*+})$	$0.101^{+0.016}_{-0.034}$
$\delta_B(B^+ \rightarrow D^0 K^{*+})$	$(48^{+59}_{-16})^\circ$
$r_B(B^+ \rightarrow D^{*0} K^+)$	$0.104^{+0.013}_{-0.014}$
$\delta_B(B^+ \rightarrow D^{*0} K^+)$	$(314.8^{+7.9}_{-9.9})^\circ$
$A_{CP}(B^0 \rightarrow K^+ \pi^-)$	-0.0834 ± 0.0032
$A_{CP}(B^0 \rightarrow \eta K^*(892)^0)$	0.19 ± 0.05
$A_{CP}(B^0 \rightarrow K^*(892)^+ \pi^-)$	-0.27 ± 0.04
$S_{D^*(2010)-D^+}(B^0 \rightarrow D^*(2010)^- D^+)$	-0.83 ± 0.09
$S_{D^*(2010)+D^-}(B^0 \rightarrow D^*(2010)^+ D^-)$	-0.80 ± 0.09
$S_{D^{*+}D^{*-}}(B^0 \rightarrow D^{*+} D^{*-})$	-0.59 ± 0.14 (S = 1.8)
$S_{\pm}(B^0 \rightarrow D^{*+} D^{*-})$	-0.73 ± 0.09
$S_{D^+D^-}(B^0 \rightarrow D^+ D^-)$	$-0.76^{+0.15}_{-0.13}$ (S = 1.2)
$S_{J/\psi(1S)\pi^0}(B^0 \rightarrow J/\psi(1S)\pi^0)$	-0.88 ± 0.32 (S = 2.2)
$S(B^0 \rightarrow J/\psi(1S)\rho^0)$	$-0.66^{+0.16}_{-0.12}$
$S_{K^0\pi^0}(B^0 \rightarrow K^0\pi^0)$	0.58 ± 0.17
$S_{\eta'K^0}(B^0 \rightarrow \eta'K^0)$	0.63 ± 0.06
$S_{K^+K^-K_S^0}(B^0 \rightarrow K^+K^-K_S^0)$	-0.66 ± 0.11
nonresonant)	
$S_{K^+K^-K_S^0}(B^0 \rightarrow K^+K^-K_S^0 \text{ inclusive})$	-0.65 ± 0.12
$C_{\pi\pi}(B^0 \rightarrow \pi^+ \pi^-)$	-0.314 ± 0.030
$S_{\pi\pi}(B^0 \rightarrow \pi^+ \pi^-)$	-0.670 ± 0.030
$\Delta C_{\rho\pi}(B^0 \rightarrow \rho^+ \pi^-)$	0.27 ± 0.06
$S_{\eta_c K_S^0}(B^0 \rightarrow \eta_c K_S^0)$	0.93 ± 0.17
$\sin(2\beta)(B^0 \rightarrow J/\psi K_S^0)$	0.699 ± 0.017
$S_{J/\psi(nS)K^0}(B^0 \rightarrow J/\psi(nS)K^0)$	0.701 ± 0.017
$S_{\chi_{c1} K_S^0}(B^0 \rightarrow \chi_{c1} K_S^0)$	0.63 ± 0.10
$\sin(2\beta_{\text{eff}})(B^0 \rightarrow K^+ K^- K_S^0)$	$0.77^{+0.13}_{-0.12}$
α	$(85.2^{+4.8}_{-4.3})^\circ$
$r_{B^0}(B^0 \rightarrow D K^{*0})$	$0.257^{+0.021}_{-0.023}$
$\delta_{B^0}(B^0 \rightarrow D K^{*0})$	$(194.1^{+9.6}_{-8.8})^\circ$

Unless otherwise stated, limits are given at the 90% confidence level, while errors are given as ± 1 standard deviation.

$C_{KK}(B_S^0 \rightarrow K^+ K^-)$	0.162 ± 0.035
$r_B(B_S^0 \rightarrow D_S^\mp K^\pm)$	$0.37^{+0.10}_{-0.09}$
$r_B(B_S^0 \rightarrow D_S^\mp K^\pm \pi^\pm \pi^\mp)$	0.47 ± 0.08
$\delta_B(B_S^0 \rightarrow D_S^\mp K^\mp)$	$(358 \pm 14)^\circ$
$A_{CP}(B_S \rightarrow \pi^+ K^-)$	0.224 ± 0.012

CPT INVARIANCE

$(m_{W^+} - m_{W^-}) / m_{\text{average}}$	$(-3.7 \pm 3.5) \times 10^{-4}$
$(m_{e^+} - m_{e^-}) / m_{\text{average}}$	$< 8 \times 10^{-9}$, CL = 90%
$ q_{e^+} + q_{e^-} /e$	$< 4 \times 10^{-8}$
$(g_{e^+} - g_{e^-}) / g_{\text{average}}$	$(-0.5 \pm 2.1) \times 10^{-12}$
$(\tau_{\mu^+} - \tau_{\mu^-}) / \tau_{\text{average}}$	$(2 \pm 8) \times 10^{-5}$
$(g_{\mu^+} - g_{\mu^-}) / g_{\text{average}}$	$(-0.11 \pm 0.12) \times 10^{-8}$
$(m_{\tau^+} - m_{\tau^-}) / m_{\text{average}}$	$< 2.8 \times 10^{-4}$, CL = 90%
$\langle \Delta m_{21}^2 - \Delta \overline{m}_{21}^2 \rangle$ in neutrino mixing	$< 1.1 \times 10^{-4} \text{ eV}^2$, CL = 99.7%
$\langle \Delta m_{32}^2 - \Delta \overline{m}_{32}^2 \rangle$ in neutrino mixing	$(-0.12 \pm 0.25) \times 10^{-3} \text{ eV}^2$
$m_t - m_{\overline{t}}$	$-0.15 \pm 0.20 \text{ GeV}$ (S = 1.1)
$(m_{\pi^+} - m_{\pi^-}) / m_{\text{average}}$	$(2 \pm 5) \times 10^{-4}$
$(\tau_{\pi^+} - \tau_{\pi^-}) / \tau_{\text{average}}$	$(6 \pm 7) \times 10^{-4}$
$(m_{K^+} - m_{K^-}) / m_{\text{average}}$	$(-0.6 \pm 1.8) \times 10^{-4}$
$(\tau_{K^+} - \tau_{K^-}) / \tau_{\text{average}}$	$(0.10 \pm 0.09)\%$ (S = 1.2)
$K^\pm \rightarrow \mu^\pm \nu_\mu$ rate difference/sum	$(-0.27 \pm 0.21)\%$
$K^\pm \rightarrow \pi^\pm \pi^0$ rate difference/sum	[k] $(0.4 \pm 0.6)\%$
δ in $K^0 - \overline{K}^0$ mixing	
real part of δ	$(2.5 \pm 2.3) \times 10^{-4}$
imaginary part of δ	$(-1.5 \pm 1.6) \times 10^{-5}$
$\text{Re}(y)$, K_{e3} parameter	$(0.4 \pm 2.5) \times 10^{-3}$
$\text{Re}(x_-)$, K_{e3} parameter	$(-2.9 \pm 2.0) \times 10^{-3}$
$ m_{K^0} - m_{\overline{K}^0} / m_{\text{average}}$	[l] $< 6 \times 10^{-19}$, CL = 90%
$(\Gamma_{K^0} - \Gamma_{\overline{K}^0}) / m_{\text{average}}$	$(8 \pm 8) \times 10^{-18}$
phase difference $\phi_{00} - \phi_{+-}$	$(0.34 \pm 0.32)^\circ$
$\text{Re}(\frac{2}{3}\eta_{+-} + \frac{1}{3}\eta_{00}) - \frac{A_{\pi^+}}{2}$	$(-3 \pm 35) \times 10^{-6}$
$A_{CPT}(D^0 \rightarrow K^- \pi^+)$	0.008 ± 0.008
$\Delta S_{CPT}^+(S_{\ell^+, K_S^0}^- - S_{\ell^+, K_S^0}^+)$	0.16 ± 0.23
$\Delta S_{CPT}^-(S_{\ell^+, K_S^0}^+ - S_{\ell^+, K_S^0}^-)$	-0.03 ± 0.14
$\Delta C_{CPT}^+(C_{\ell^+, K_S^0}^- - C_{\ell^+, K_S^0}^+)$	0.14 ± 0.17
$\Delta C_{CPT}^-(C_{\ell^+, K_S^0}^+ - C_{\ell^+, K_S^0}^-)$	0.03 ± 0.14
$ m_{\rho^-} - m_{\overline{\rho}^-} / m_{\rho^-}$	[n] $< 7 \times 10^{-10}$, CL = 90%
$(\frac{q_{\rho^-}}{m_{\rho^-}} - \frac{q_{\overline{\rho}^-}}{m_{\overline{\rho}^-}}) / \frac{q_{\rho^-}}{m_{\rho^-}}$	$(0.1 \pm 6.9) \times 10^{-11}$
$ q_{\rho^-} + q_{\overline{\rho}^-} /e$	[n] $< 7 \times 10^{-10}$, CL = 90%
$(\mu_{\rho^-} + \mu_{\overline{\rho}^-}) / \mu_{\rho^-}$	$(0.002 \pm 0.004) \times 10^{-6}$
$(m_n - m_{\overline{n}}) / m_n$	$(9 \pm 6) \times 10^{-5}$
$(m_\Lambda - m_{\overline{\Lambda}}) / m_\Lambda$	$(-0.1 \pm 1.1) \times 10^{-5}$ (S = 1.6)
$(\tau_\Lambda - \tau_{\overline{\Lambda}}) / \tau_\Lambda$	-0.001 ± 0.009
$(\tau_{\Sigma^+} - \tau_{\overline{\Sigma}^-}) / \tau_{\Sigma^+}$	-0.0006 ± 0.0012
$(\mu_{\Sigma^+} + \mu_{\overline{\Sigma}^-}) / \mu_{\Sigma^+}$	0.014 ± 0.015
$(m_{\Xi^-} - m_{\overline{\Xi}^+}) / m_{\Xi^-}$	$(-3 \pm 9) \times 10^{-5}$
$(\tau_{\Xi^-} - \tau_{\overline{\Xi}^+}) / \tau_{\Xi^-}$	-0.01 ± 0.07
$(\mu_{\Xi^-} + \mu_{\overline{\Xi}^+}) / \mu_{\Xi^-} $	$+0.01 \pm 0.05$
$(m_{\Omega^-} - m_{\overline{\Omega}^+}) / m_{\Omega^-}$	$(-1 \pm 8) \times 10^{-5}$
$(\tau_{\Omega^-} - \tau_{\overline{\Omega}^+}) / \tau_{\Omega^-}$	0.00 ± 0.05

TESTS OF NUMBER CONSERVATION LAWS

LEPTON FAMILY NUMBER

Lepton family number conservation means separate conservation of each of L_e, L_μ, L_τ .

$\Gamma(Z \rightarrow e^\pm \mu^\mp) / \Gamma_{\text{total}}$	[o] $< 7.5 \times 10^{-7}$, CL = 95%
$\Gamma(Z \rightarrow e^\pm \tau^\mp) / \Gamma_{\text{total}}$	[o] $< 5.0 \times 10^{-6}$, CL = 95%
$\Gamma(Z \rightarrow \mu^\pm \tau^\mp) / \Gamma_{\text{total}}$	[o] $< 6.5 \times 10^{-6}$, CL = 95%

Tests of Conservation Laws

$\Gamma(H^0 \rightarrow e\mu)/\Gamma_{\text{total}}$	$<6.1 \times 10^{-5}$, CL = 95%	Δm_{32}^2 (Inverted order)	$(-2.536 \pm 0.034) \times 10^{-3} \text{ eV}^2$
$\Gamma(H^0 \rightarrow e\tau)/\Gamma_{\text{total}}$	$<2.2 \times 10^{-3}$, CL = 95%	Δm_{32}^2 (Normal order)	$(2.453 \pm 0.033) \times 10^{-3} \text{ eV}^2$
$\Gamma(H^0 \rightarrow \mu\tau)/\Gamma_{\text{total}}$	$<1.5 \times 10^{-3}$, CL = 95%	$\sin^2(\theta_{13})$	$(2.20 \pm 0.07) \times 10^{-2}$
$\sigma(e^+e^- \rightarrow e^\pm\tau^\mp) / \sigma(e^+e^- \rightarrow \mu^\pm\mu^-)$	$<8.9 \times 10^{-6}$, CL = 95%	$\Gamma(\pi^+ \rightarrow \mu^+\nu_e)/\Gamma_{\text{total}}$	[q] $<8.0 \times 10^{-3}$, CL = 90%
$\sigma(e^+e^- \rightarrow \mu^\pm\tau^\mp) / \sigma(e^+e^- \rightarrow \mu^\pm\mu^-)$	$<4.0 \times 10^{-6}$, CL = 95%	$\Gamma(\pi^+ \rightarrow \mu^-e^+e^+\nu)/\Gamma_{\text{total}}$	$<1.6 \times 10^{-6}$, CL = 90%
limit on $\mu^- \rightarrow e^-$ conversion		$\Gamma(\pi^0 \rightarrow \mu^+e^-)/\Gamma_{\text{total}}$	$<3.8 \times 10^{-10}$, CL = 90%
$\sigma(\mu^- 32\text{S} \rightarrow e^- 32\text{S}) / \sigma(\mu^- 32\text{S} \rightarrow \nu_\mu 32\text{P}^*)$	$<7 \times 10^{-11}$, CL = 90%	$\Gamma(\pi^0 \rightarrow \mu^-e^+)/\Gamma_{\text{total}}$	$<3.2 \times 10^{-10}$, CL = 90%
$\sigma(\mu^- \text{Ti} \rightarrow e^- \text{Ti}) / \sigma(\mu^- \text{Ti} \rightarrow \text{capture})$	$<4.3 \times 10^{-12}$, CL = 90%	$\Gamma(\pi^0 \rightarrow \mu^+e^- + \mu^-e^+)/\Gamma_{\text{total}}$	$<3.6 \times 10^{-10}$, CL = 90%
$\sigma(\mu^- \text{Pb} \rightarrow e^- \text{Pb}) / \sigma(\mu^- \text{Pb} \rightarrow \text{capture})$	$<4.6 \times 10^{-11}$, CL = 90%	$\Gamma(\eta(958) \rightarrow e\mu)/\Gamma_{\text{total}}$	$<6 \times 10^{-6}$, CL = 90%
$\sigma(\mu^- \text{Au} \rightarrow e^- \text{Au}) / \sigma(\mu^- \text{Au} \rightarrow \text{capture})$	$<7 \times 10^{-13}$, CL = 90%	$\Gamma(\phi(1020) \rightarrow e^\pm\mu^\mp)/\Gamma_{\text{total}}$	$<4.7 \times 10^{-4}$, CL = 90%
limit on muonium \rightarrow antimuonium conversion $R_g = G_C / G_F$	<0.0030 , CL = 90%	$\Gamma(K^+ \rightarrow \mu^- \nu e^+ e^+)/\Gamma_{\text{total}}$	$<2 \times 10^{-6}$, CL = 90%
$\Gamma(\mu^- \rightarrow e^- \nu_e \bar{\nu}_\mu)/\Gamma_{\text{total}}$	[p] $<1.2 \times 10^{-2}$, CL = 90%	$\Gamma(K^+ \rightarrow \mu^+ \nu_e)/\Gamma_{\text{total}}$	[q] $<4 \times 10^{-3}$, CL = 90%
$\Gamma(\mu^- \rightarrow e^- \gamma)/\Gamma_{\text{total}}$	$<4.2 \times 10^{-13}$, CL = 90%	$\Gamma(K^+ \rightarrow \pi^+ \mu^+ e^-)/\Gamma_{\text{total}}$	$<1.3 \times 10^{-11}$, CL = 90%
$\Gamma(\mu^- \rightarrow e^- e^+ e^-)/\Gamma_{\text{total}}$	$<1.0 \times 10^{-12}$, CL = 90%	$\Gamma(K^+ \rightarrow \pi^+ \mu^- e^+)/\Gamma_{\text{total}}$	$<6.6 \times 10^{-11}$, CL = 90%
$\Gamma(\mu^- \rightarrow e^- 2\gamma)/\Gamma_{\text{total}}$	$<7.2 \times 10^{-11}$, CL = 90%	$\Gamma(K_L^0 \rightarrow e^\pm \mu^\mp)/\Gamma_{\text{total}}$	[o] $<4.7 \times 10^{-12}$, CL = 90%
$\Gamma(\tau^- \rightarrow e^- \gamma)/\Gamma_{\text{total}}$	$<3.3 \times 10^{-8}$, CL = 90%	$\Gamma(K_L^0 \rightarrow e^\pm e^\pm \mu^\mp \mu^\mp)/\Gamma_{\text{total}}$	[o] $<4.12 \times 10^{-11}$, CL = 90%
$\Gamma(\tau^- \rightarrow \mu^- \gamma)/\Gamma_{\text{total}}$	$<4.2 \times 10^{-8}$, CL = 90%	$\Gamma(K_L^0 \rightarrow \pi^0 \mu^\pm e^\mp)/\Gamma_{\text{total}}$	[o] $<7.6 \times 10^{-11}$, CL = 90%
$\Gamma(\tau^- \rightarrow e^- \pi^0)/\Gamma_{\text{total}}$	$<8.0 \times 10^{-8}$, CL = 90%	$\Gamma(K_L^0 \rightarrow \pi^0 \pi^0 \mu^\pm e^\mp)/\Gamma_{\text{total}}$	$<1.7 \times 10^{-10}$, CL = 90%
$\Gamma(\tau^- \rightarrow \mu^- \pi^0)/\Gamma_{\text{total}}$	$<1.1 \times 10^{-7}$, CL = 90%	$\Gamma(D^+ \rightarrow \pi^+ e^+ \mu^-)/\Gamma_{\text{total}}$	$<2.1 \times 10^{-7}$, CL = 90%
$\Gamma(\tau^- \rightarrow e^- K_S^0)/\Gamma_{\text{total}}$	$<2.6 \times 10^{-8}$, CL = 90%	$\Gamma(D^+ \rightarrow \pi^+ e^- \mu^+)/\Gamma_{\text{total}}$	$<2.2 \times 10^{-7}$, CL = 90%
$\Gamma(\tau^- \rightarrow \mu^- K_S^0)/\Gamma_{\text{total}}$	$<2.3 \times 10^{-8}$, CL = 90%	$\Gamma(D^+ \rightarrow K^+ e^+ \mu^-)/\Gamma_{\text{total}}$	$<7.5 \times 10^{-8}$, CL = 90%
$\Gamma(\tau^- \rightarrow e^- \eta)/\Gamma_{\text{total}}$	$<9.2 \times 10^{-8}$, CL = 90%	$\Gamma(D^+ \rightarrow K^+ e^- \mu^+)/\Gamma_{\text{total}}$	$<1.0 \times 10^{-7}$, CL = 90%
$\Gamma(\tau^- \rightarrow \mu^- \eta)/\Gamma_{\text{total}}$	$<6.5 \times 10^{-8}$, CL = 90%	$\Gamma(D^0 \rightarrow \mu^\pm e^\mp)/\Gamma_{\text{total}}$	[o] $<1.3 \times 10^{-8}$, CL = 90%
$\Gamma(\tau^- \rightarrow e^- \rho^0)/\Gamma_{\text{total}}$	$<1.8 \times 10^{-8}$, CL = 90%	$\Gamma(D^0 \rightarrow \pi^0 e^\pm \mu^\mp)/\Gamma_{\text{total}}$	[o] $<8.0 \times 10^{-7}$, CL = 90%
$\Gamma(\tau^- \rightarrow \mu^- \rho^0)/\Gamma_{\text{total}}$	$<1.2 \times 10^{-8}$, CL = 90%	$\Gamma(D^0 \rightarrow \eta e^\pm \mu^\mp)/\Gamma_{\text{total}}$	[o] $<2.25 \times 10^{-6}$, CL = 90%
$\Gamma(\tau^- \rightarrow e^- \omega)/\Gamma_{\text{total}}$	$<4.8 \times 10^{-8}$, CL = 90%	$\Gamma(D^0 \rightarrow \pi^+ \pi^- e^\pm \mu^\mp)/\Gamma_{\text{total}}$	[o] $<1.71 \times 10^{-6}$, CL = 90%
$\Gamma(\tau^- \rightarrow \mu^- \omega)/\Gamma_{\text{total}}$	$<4.7 \times 10^{-8}$, CL = 90%	$\Gamma(D^0 \rightarrow \rho^0 e^\pm \mu^\mp)/\Gamma_{\text{total}}$	[o] $<5.0 \times 10^{-7}$, CL = 90%
$\Gamma(\tau^- \rightarrow e^- K^*(892)^0)/\Gamma_{\text{total}}$	$<3.2 \times 10^{-8}$, CL = 90%	$\Gamma(D^0 \rightarrow \omega e^\pm \mu^\mp)/\Gamma_{\text{total}}$	[o] $<1.71 \times 10^{-6}$, CL = 90%
$\Gamma(\tau^- \rightarrow \mu^- K^*(892)^0)/\Gamma_{\text{total}}$	$<5.9 \times 10^{-8}$, CL = 90%	$\Gamma(D^0 \rightarrow K^- K^+ e^\pm \mu^\mp)/\Gamma_{\text{total}}$	[o] $<1.00 \times 10^{-6}$, CL = 90%
$\Gamma(\tau^- \rightarrow e^- \bar{K}^*(892)^0)/\Gamma_{\text{total}}$	$<3.4 \times 10^{-8}$, CL = 90%	$\Gamma(D^0 \rightarrow \phi e^\pm \mu^\mp)/\Gamma_{\text{total}}$	[o] $<5.1 \times 10^{-7}$, CL = 90%
$\Gamma(\tau^- \rightarrow \mu^- \bar{K}^*(892)^0)/\Gamma_{\text{total}}$	$<7.0 \times 10^{-8}$, CL = 90%	$\Gamma(D^0 \rightarrow \bar{K}^0 e^\pm \mu^\mp)/\Gamma_{\text{total}}$	[o] $<1.74 \times 10^{-6}$, CL = 90%
$\Gamma(\tau^- \rightarrow e^- \eta'(958))/\Gamma_{\text{total}}$	$<1.6 \times 10^{-7}$, CL = 90%	$\Gamma(D^0 \rightarrow K^- \pi^+ e^\pm \mu^\mp)/\Gamma_{\text{total}}$	[o] $<1.90 \times 10^{-6}$, CL = 90%
$\Gamma(\tau^- \rightarrow \mu^- \eta'(958))/\Gamma_{\text{total}}$	$<1.3 \times 10^{-7}$, CL = 90%	$\Gamma(D^0 \rightarrow \bar{K}^*(892)^0 e^\pm \mu^\mp)/\Gamma_{\text{total}}$	[o] $<1.25 \times 10^{-6}$, CL = 90%
$\Gamma(\tau^- \rightarrow e^- f_0(980) \rightarrow e^- \pi^+ \pi^-)/\Gamma_{\text{total}}$	$<3.2 \times 10^{-8}$, CL = 90%	$\Gamma(D_S^+ \rightarrow \pi^+ e^+ \mu^-)/\Gamma_{\text{total}}$	$<1.1 \times 10^{-6}$, CL = 90%
$\Gamma(\tau^- \rightarrow \mu^- f_0(980) \rightarrow \mu^- \pi^+ \pi^-)/\Gamma_{\text{total}}$	$<3.4 \times 10^{-8}$, CL = 90%	$\Gamma(D_S^+ \rightarrow \pi^+ e^- \mu^+)/\Gamma_{\text{total}}$	$<9.4 \times 10^{-7}$, CL = 90%
$\Gamma(\tau^- \rightarrow e^- \phi)/\Gamma_{\text{total}}$	$<3.1 \times 10^{-8}$, CL = 90%	$\Gamma(D_S^+ \rightarrow K^+ e^+ \mu^-)/\Gamma_{\text{total}}$	$<7.9 \times 10^{-7}$, CL = 90%
$\Gamma(\tau^- \rightarrow \mu^- \phi)/\Gamma_{\text{total}}$	$<8.4 \times 10^{-8}$, CL = 90%	$\Gamma(D_S^+ \rightarrow K^+ e^- \mu^+)/\Gamma_{\text{total}}$	$<5.6 \times 10^{-7}$, CL = 90%
$\Gamma(\tau^- \rightarrow e^- e^+ e^-)/\Gamma_{\text{total}}$	$<2.7 \times 10^{-8}$, CL = 90%	$\Gamma(B^+ \rightarrow \pi^+ e^+ \mu^-)/\Gamma_{\text{total}}$	$<6.4 \times 10^{-3}$, CL = 90%
$\Gamma(\tau^- \rightarrow e^- \mu^+ \mu^-)/\Gamma_{\text{total}}$	$<2.7 \times 10^{-8}$, CL = 90%	$\Gamma(B^+ \rightarrow \pi^+ e^- \mu^+)/\Gamma_{\text{total}}$	$<6.4 \times 10^{-3}$, CL = 90%
$\Gamma(\tau^- \rightarrow e^+ \mu^- \mu^-)/\Gamma_{\text{total}}$	$<1.7 \times 10^{-8}$, CL = 90%	$\Gamma(B^+ \rightarrow \pi^+ e^\pm \mu^\mp)/\Gamma_{\text{total}}$	$<1.7 \times 10^{-7}$, CL = 90%
$\Gamma(\tau^- \rightarrow \mu^- e^+ e^-)/\Gamma_{\text{total}}$	$<1.8 \times 10^{-8}$, CL = 90%	$\Gamma(B^+ \rightarrow \pi^+ e^+ \tau^-)/\Gamma_{\text{total}}$	$<7.4 \times 10^{-5}$, CL = 90%
$\Gamma(\tau^- \rightarrow \mu^+ e^- e^-)/\Gamma_{\text{total}}$	$<1.5 \times 10^{-8}$, CL = 90%	$\Gamma(B^+ \rightarrow \pi^+ e^- \tau^+)/\Gamma_{\text{total}}$	$<2.0 \times 10^{-5}$, CL = 90%
$\Gamma(\tau^- \rightarrow \mu^- \mu^+ \mu^-)/\Gamma_{\text{total}}$	$<2.1 \times 10^{-8}$, CL = 90%	$\Gamma(B^+ \rightarrow \pi^+ e^\pm \tau^\mp)/\Gamma_{\text{total}}$	$<7.5 \times 10^{-5}$, CL = 90%
$\Gamma(\tau^- \rightarrow e^- \pi^+ \pi^-)/\Gamma_{\text{total}}$	$<2.3 \times 10^{-8}$, CL = 90%	$\Gamma(B^+ \rightarrow \pi^+ \mu^+ \tau^-)/\Gamma_{\text{total}}$	$<6.2 \times 10^{-5}$, CL = 90%
$\Gamma(\tau^- \rightarrow \mu^- \pi^+ \pi^-)/\Gamma_{\text{total}}$	$<2.1 \times 10^{-8}$, CL = 90%	$\Gamma(B^+ \rightarrow \pi^+ \mu^\pm \tau^\mp)/\Gamma_{\text{total}}$	$<7.2 \times 10^{-5}$, CL = 90%
$\Gamma(\tau^- \rightarrow e^- \pi^+ K^-)/\Gamma_{\text{total}}$	$<3.7 \times 10^{-8}$, CL = 90%	$\Gamma(B^+ \rightarrow K^+ e^+ \mu^-)/\Gamma_{\text{total}}$	$<7.0 \times 10^{-9}$, CL = 90%
$\Gamma(\tau^- \rightarrow e^- \pi^- K^+)/\Gamma_{\text{total}}$	$<3.1 \times 10^{-8}$, CL = 90%	$\Gamma(B^+ \rightarrow K^+ e^- \mu^+)/\Gamma_{\text{total}}$	$<6.4 \times 10^{-9}$, CL = 90%
$\Gamma(\tau^- \rightarrow e^- K_S^0 K_S^0)/\Gamma_{\text{total}}$	$<7.1 \times 10^{-8}$, CL = 90%	$\Gamma(B^+ \rightarrow K^+ e^\pm \mu^\mp)/\Gamma_{\text{total}}$	$<9.1 \times 10^{-8}$, CL = 90%
$\Gamma(\tau^- \rightarrow e^- K^+ K^-)/\Gamma_{\text{total}}$	$<3.4 \times 10^{-8}$, CL = 90%	$\Gamma(B^+ \rightarrow K^+ e^+ \tau^-)/\Gamma_{\text{total}}$	$<4.3 \times 10^{-5}$, CL = 90%
$\Gamma(\tau^- \rightarrow \mu^- \pi^+ K^-)/\Gamma_{\text{total}}$	$<8.6 \times 10^{-8}$, CL = 90%	$\Gamma(B^+ \rightarrow K^+ e^- \tau^+)/\Gamma_{\text{total}}$	$<1.5 \times 10^{-5}$, CL = 90%
$\Gamma(\tau^- \rightarrow \mu^- \pi^- K^+)/\Gamma_{\text{total}}$	$<4.5 \times 10^{-8}$, CL = 90%	$\Gamma(B^+ \rightarrow K^+ \mu^\pm \tau^\mp)/\Gamma_{\text{total}}$	$<3.0 \times 10^{-5}$, CL = 90%
$\Gamma(\tau^- \rightarrow \mu^- K_S^0 K_S^0)/\Gamma_{\text{total}}$	$<8.0 \times 10^{-8}$, CL = 90%	$\Gamma(B^+ \rightarrow K^+ \mu^+ \tau^-)/\Gamma_{\text{total}}$	$<4.5 \times 10^{-5}$, CL = 90%
$\Gamma(\tau^- \rightarrow \mu^- K^+ K^-)/\Gamma_{\text{total}}$	$<4.4 \times 10^{-8}$, CL = 90%	$\Gamma(B^+ \rightarrow K^+ \mu^- \tau^+)/\Gamma_{\text{total}}$	$<2.8 \times 10^{-5}$, CL = 90%
$\Gamma(\tau^- \rightarrow e^- \pi^0 \pi^0)/\Gamma_{\text{total}}$	$<6.5 \times 10^{-6}$, CL = 90%	$\Gamma(B^+ \rightarrow K^+ \mu^\pm \tau^\mp)/\Gamma_{\text{total}}$	$<4.8 \times 10^{-5}$, CL = 90%
$\Gamma(\tau^- \rightarrow \mu^- \pi^0 \pi^0)/\Gamma_{\text{total}}$	$<1.4 \times 10^{-5}$, CL = 90%	$\Gamma(B^+ \rightarrow K^*(892)^+ e^+ \mu^-)/\Gamma_{\text{total}}$	$<1.3 \times 10^{-6}$, CL = 90%
$\Gamma(\tau^- \rightarrow e^- \eta)/\Gamma_{\text{total}}$	$<3.5 \times 10^{-5}$, CL = 90%	$\Gamma(B^+ \rightarrow K^*(892)^+ e^- \mu^+)/\Gamma_{\text{total}}$	$<9.9 \times 10^{-7}$, CL = 90%
$\Gamma(\tau^- \rightarrow \mu^- \eta)/\Gamma_{\text{total}}$	$<6.0 \times 10^{-5}$, CL = 90%	$\Gamma(B^+ \rightarrow K^*(892)^+ e^\pm \mu^\mp)/\Gamma_{\text{total}}$	$<1.4 \times 10^{-6}$, CL = 90%
$\Gamma(\tau^- \rightarrow e^- \pi^0 \eta)/\Gamma_{\text{total}}$	$<2.4 \times 10^{-5}$, CL = 90%	$\Gamma(B^0 \rightarrow e^\pm \mu^\mp)/\Gamma_{\text{total}}$	[o] $<1.0 \times 10^{-9}$, CL = 90%
$\Gamma(\tau^- \rightarrow \mu^- \pi^0 \eta)/\Gamma_{\text{total}}$	$<2.2 \times 10^{-5}$, CL = 90%	$\Gamma(B^0 \rightarrow \pi^0 e^\pm \mu^\mp)/\Gamma_{\text{total}}$	$<1.4 \times 10^{-7}$, CL = 90%
$\Gamma(\tau^- \rightarrow e^- \text{light boson})/\Gamma_{\text{total}}$	$<2.7 \times 10^{-3}$, CL = 95%	$\Gamma(B^0 \rightarrow K^0 e^\pm \mu^\mp)/\Gamma_{\text{total}}$	$<3.8 \times 10^{-8}$, CL = 90%
$\Gamma(\tau^- \rightarrow \mu^- \text{light boson})/\Gamma_{\text{total}}$	$<5 \times 10^{-3}$, CL = 95%	$\Gamma(B^0 \rightarrow K^*(892)^0 e^+ \mu^-)/\Gamma_{\text{total}}$	$<1.6 \times 10^{-7}$, CL = 90%
LEPTON FAMILY NUMBER VIOLATION IN NEUTRINOS		$\Gamma(B^0 \rightarrow K^*(892)^0 e^- \mu^+)/\Gamma_{\text{total}}$	$<1.2 \times 10^{-7}$, CL = 90%
$\sin^2(\theta_{12})$	0.307 ± 0.013	$\Gamma(B^0 \rightarrow K^*(892)^0 e^\pm \mu^\mp)/\Gamma_{\text{total}}$	$<1.8 \times 10^{-7}$, CL = 90%
Δm_{21}^2	$(7.53 \pm 0.18) \times 10^{-5} \text{ eV}^2$	$\Gamma(B^0 \rightarrow e^\pm \tau^\mp)/\Gamma_{\text{total}}$	[o] $<1.6 \times 10^{-5}$, CL = 90%
$\sin^2(\theta_{23})$ (Normal order)	0.546 ± 0.021	$\Gamma(B^0 \rightarrow \mu^\pm \tau^\mp)/\Gamma_{\text{total}}$	[o] $<1.4 \times 10^{-5}$, CL = 95%
		$\Gamma(B \rightarrow s e^\pm \mu^\mp)/\Gamma_{\text{total}}$	[o] $<2.2 \times 10^{-5}$, CL = 90%
		$\Gamma(B \rightarrow \pi e^\pm \mu^\mp)/\Gamma_{\text{total}}$	$<9.2 \times 10^{-8}$, CL = 90%
		$\Gamma(B \rightarrow \rho e^\pm \mu^\mp)/\Gamma_{\text{total}}$	$<3.2 \times 10^{-6}$, CL = 90%

Unless otherwise stated, limits are given at the 90% confidence level, while errors are given as ± 1 standard deviation.

Tests of Conservation Laws

$\Gamma(B \rightarrow K e^\pm \mu^\mp)/\Gamma_{\text{total}}$	$<3.8 \times 10^{-8}$, CL = 90%
$\Gamma(B \rightarrow K^*(892) e^\pm \mu^\mp)/\Gamma_{\text{total}}$	$<5.1 \times 10^{-7}$, CL = 90%
$\Gamma(B_S^0 \rightarrow e^\pm \mu^\mp)/\Gamma_{\text{total}}$	[o] $<5.4 \times 10^{-9}$, CL = 90%
$\Gamma(B_S^0 \rightarrow \mu^\pm \tau^\mp)/\Gamma_{\text{total}}$	$<4.2 \times 10^{-5}$, CL = 95%
$\Gamma(J/\psi(1S) \rightarrow e^\pm \mu^\mp)/\Gamma_{\text{total}}$	$<1.6 \times 10^{-7}$, CL = 90%
$\Gamma(J/\psi(1S) \rightarrow e^\pm \tau^\mp)/\Gamma_{\text{total}}$	$<7.5 \times 10^{-8}$, CL = 90%
$\Gamma(J/\psi(1S) \rightarrow \mu^\pm \tau^\mp)/\Gamma_{\text{total}}$	$<2.0 \times 10^{-6}$, CL = 90%
$\Gamma(\Upsilon(1S) \rightarrow \mu^\pm \tau^\mp)/\Gamma_{\text{total}}$	$<6.0 \times 10^{-6}$, CL = 95%
$\Gamma(\Upsilon(2S) \rightarrow e^\pm \tau^\mp)/\Gamma_{\text{total}}$	$<3.2 \times 10^{-6}$, CL = 90%
$\Gamma(\Upsilon(2S) \rightarrow \mu^\pm \tau^\mp)/\Gamma_{\text{total}}$	$<3.3 \times 10^{-6}$, CL = 90%
$\Gamma(\Upsilon(3S) \rightarrow e^\pm \tau^\mp)/\Gamma_{\text{total}}$	$<4.2 \times 10^{-6}$, CL = 90%
$\Gamma(\Upsilon(3S) \rightarrow \mu^\pm \tau^\mp)/\Gamma_{\text{total}}$	$<3.1 \times 10^{-6}$, CL = 90%
$\Gamma(\Lambda_C^+ \rightarrow p e^+ \mu^-)/\Gamma_{\text{total}}$	$<9.9 \times 10^{-6}$, CL = 90%
$\Gamma(\Lambda_C^+ \rightarrow p e^- \mu^+)/\Gamma_{\text{total}}$	$<1.9 \times 10^{-5}$, CL = 90%

TOTAL LEPTON NUMBER

Violation of total lepton number conservation also implies violation of lepton family number conservation.

$\Gamma(Z \rightarrow p e)/\Gamma_{\text{total}}$	$<1.8 \times 10^{-6}$, CL = 95%
$\Gamma(Z \rightarrow p \mu)/\Gamma_{\text{total}}$	$<1.8 \times 10^{-6}$, CL = 95%
limit on $\mu^- \rightarrow e^+$ conversion	
$\sigma(\mu^- 32S \rightarrow e^+ 32Si^*) / \sigma(\mu^- 32S \rightarrow \nu_\mu 32P^*)$	$<9 \times 10^{-10}$, CL = 90%
$\sigma(\mu^- 127I \rightarrow e^+ 127Sb^*) / \sigma(\mu^- 127I \rightarrow \text{anything})$	$<3 \times 10^{-10}$, CL = 90%
$\sigma(\mu^- Ti \rightarrow e^+ Ca) / \sigma(\mu^- Ti \rightarrow \text{capture})$	$<3.6 \times 10^{-11}$, CL = 90%
$\Gamma(\tau^- \rightarrow e^+ \pi^- \pi^-)/\Gamma_{\text{total}}$	$<2.0 \times 10^{-8}$, CL = 90%
$\Gamma(\tau^- \rightarrow \mu^+ \pi^- \pi^-)/\Gamma_{\text{total}}$	$<3.9 \times 10^{-8}$, CL = 90%
$\Gamma(\tau^- \rightarrow e^+ \pi^- K^-)/\Gamma_{\text{total}}$	$<3.2 \times 10^{-8}$, CL = 90%
$\Gamma(\tau^- \rightarrow e^+ K^- K^-)/\Gamma_{\text{total}}$	$<3.3 \times 10^{-8}$, CL = 90%
$\Gamma(\tau^- \rightarrow \mu^+ \pi^- K^-)/\Gamma_{\text{total}}$	$<4.8 \times 10^{-8}$, CL = 90%
$\Gamma(\tau^- \rightarrow \mu^+ K^- K^-)/\Gamma_{\text{total}}$	$<4.7 \times 10^{-8}$, CL = 90%
$\Gamma(\tau^- \rightarrow p e^- e^-)/\Gamma_{\text{total}}$	$<3.0 \times 10^{-8}$, CL = 90%
$\Gamma(\tau^- \rightarrow \bar{p} e^+ e^-)/\Gamma_{\text{total}}$	$<3.0 \times 10^{-8}$, CL = 90%
$\Gamma(\tau^- \rightarrow \bar{p} e^+ \mu^-)/\Gamma_{\text{total}}$	$<2.0 \times 10^{-8}$, CL = 90%
$\Gamma(\tau^- \rightarrow \bar{p} e^- \mu^+)/\Gamma_{\text{total}}$	$<1.8 \times 10^{-8}$, CL = 90%
$\Gamma(\tau^- \rightarrow p \mu^- \mu^-)/\Gamma_{\text{total}}$	$<4.0 \times 10^{-8}$, CL = 90%
$\Gamma(\tau^- \rightarrow \bar{p} \mu^+ \mu^-)/\Gamma_{\text{total}}$	$<1.8 \times 10^{-8}$, CL = 90%
$\Gamma(\tau^- \rightarrow \bar{p} \gamma)/\Gamma_{\text{total}}$	$<3.5 \times 10^{-6}$, CL = 90%
$\Gamma(\tau^- \rightarrow \bar{p} \pi^0)/\Gamma_{\text{total}}$	$<1.5 \times 10^{-5}$, CL = 90%
$\Gamma(\tau^- \rightarrow \bar{p} 2\pi^0)/\Gamma_{\text{total}}$	$<3.3 \times 10^{-5}$, CL = 90%
$\Gamma(\tau^- \rightarrow \bar{p} \eta)/\Gamma_{\text{total}}$	$<8.9 \times 10^{-6}$, CL = 90%
$\Gamma(\tau^- \rightarrow \bar{p} \pi^0 \eta)/\Gamma_{\text{total}}$	$<2.7 \times 10^{-5}$, CL = 90%
$\Gamma(\tau^- \rightarrow \Lambda \pi^-)/\Gamma_{\text{total}}$	$<7.2 \times 10^{-8}$, CL = 90%
$\Gamma(\tau^- \rightarrow \bar{\Lambda} \pi^-)/\Gamma_{\text{total}}$	$<1.4 \times 10^{-7}$, CL = 90%
$t_{1/2}(^{76}\text{Ge} \rightarrow ^{76}\text{Se} + 2 e^-)$	$>9.0 \times 10^{25}$ yr, CL = 90%
$t_{1/2}(^{136}\text{Xe} \rightarrow ^{136}\text{Ba} + 2 e^-)$	$>10.7 \times 10^{25}$ yr, CL = 90%
$t_{1/2}(^{130}\text{Te} \rightarrow ^{130}\text{Xe} + 2 e^-)$	$>1.5 \times 10^{25}$ yr, CL = 90%
$\Gamma(\pi^+ \rightarrow \mu^+ \bar{\nu}_e)/\Gamma_{\text{total}}$	[q] $<1.5 \times 10^{-3}$, CL = 90%
$\Gamma(K^+ \rightarrow \pi^- \mu^+ e^+)/\Gamma_{\text{total}}$	$<4.2 \times 10^{-11}$, CL = 90%
$\Gamma(K^+ \rightarrow \pi^- e^+ e^+)/\Gamma_{\text{total}}$	$<2.2 \times 10^{-10}$, CL = 90%
$\Gamma(K^+ \rightarrow \pi^- \mu^+ \mu^+)/\Gamma_{\text{total}}$	$<4.2 \times 10^{-11}$, CL = 90%
$\Gamma(K^+ \rightarrow \mu^+ \bar{\nu}_e)/\Gamma_{\text{total}}$	[q] $<3.3 \times 10^{-3}$, CL = 90%
$\Gamma(K^+ \rightarrow \pi^0 e^+ \bar{\nu}_e)/\Gamma_{\text{total}}$	$<3 \times 10^{-3}$, CL = 90%
$\Gamma(D^+ \rightarrow \pi^- 2e^+)/\Gamma_{\text{total}}$	$<5.3 \times 10^{-7}$, CL = 90%
$\Gamma(D^+ \rightarrow \pi^- 2\mu^+)/\Gamma_{\text{total}}$	$<1.4 \times 10^{-8}$, CL = 90%
$\Gamma(D^+ \rightarrow \pi^+ e^+ \mu^+)/\Gamma_{\text{total}}$	$<1.3 \times 10^{-7}$, CL = 90%
$\Gamma(D^+ \rightarrow \rho^- 2\mu^+)/\Gamma_{\text{total}}$	$<5.6 \times 10^{-4}$, CL = 90%
$\Gamma(D^+ \rightarrow K^- 2e^+)/\Gamma_{\text{total}}$	$<9 \times 10^{-7}$, CL = 90%
$\Gamma(D^+ \rightarrow K^- 2\mu^+)/\Gamma_{\text{total}}$	$<1.0 \times 10^{-5}$, CL = 90%
$\Gamma(D^+ \rightarrow K^- e^+ \mu^+)/\Gamma_{\text{total}}$	$<1.9 \times 10^{-6}$, CL = 90%
$\Gamma(D^+ \rightarrow K^*(892)^- 2\mu^+)/\Gamma_{\text{total}}$	$<8.5 \times 10^{-4}$, CL = 90%
$\Gamma(D^+ \rightarrow \Lambda e^+)/\Gamma_{\text{total}}$	$<1.1 \times 10^{-6}$, CL = 90%
$\Gamma(D^+ \rightarrow \bar{\Lambda} e^+)/\Gamma_{\text{total}}$	$<6.5 \times 10^{-7}$, CL = 90%
$\Gamma(D^+ \rightarrow \Sigma^0 e^+)/\Gamma_{\text{total}}$	$<1.7 \times 10^{-6}$, CL = 90%
$\Gamma(D^+ \rightarrow \bar{\Sigma}^0 e^+)/\Gamma_{\text{total}}$	$<1.3 \times 10^{-6}$, CL = 90%
$\Gamma(D^0 \rightarrow 2\pi^- 2e^+)/\Gamma_{\text{total}}$	$<9.1 \times 10^{-7}$, CL = 90%

$\Gamma(D^0 \rightarrow 2\pi^- 2\mu^+)/\Gamma_{\text{total}}$	$<1.52 \times 10^{-6}$, CL = 90%
$\Gamma(D^0 \rightarrow K^- \pi^- 2e^+)/\Gamma_{\text{total}}$	$<5.0 \times 10^{-7}$, CL = 90%
$\Gamma(D^0 \rightarrow K^- \pi^- 2\mu^+)/\Gamma_{\text{total}}$	$<5.3 \times 10^{-7}$, CL = 90%
$\Gamma(D^0 \rightarrow 2K^- 2e^+)/\Gamma_{\text{total}}$	$<3.4 \times 10^{-7}$, CL = 90%
$\Gamma(D^0 \rightarrow 2K^- 2\mu^+)/\Gamma_{\text{total}}$	$<1.0 \times 10^{-7}$, CL = 90%
$\Gamma(D^0 \rightarrow \pi^- \pi^- e^+ \mu^+)/\Gamma_{\text{total}}$	$<3.06 \times 10^{-6}$, CL = 90%
$\Gamma(D^0 \rightarrow K^- \pi^- e^+ \mu^+)/\Gamma_{\text{total}}$	$<2.10 \times 10^{-6}$, CL = 90%
$\Gamma(D^0 \rightarrow 2K^- e^+ \mu^+)/\Gamma_{\text{total}}$	$<5.8 \times 10^{-7}$, CL = 90%
$\Gamma(D^0 \rightarrow p e^-)/\Gamma_{\text{total}}$	[r] $<1.0 \times 10^{-5}$, CL = 90%
$\Gamma(D^0 \rightarrow \bar{p} e^+)/\Gamma_{\text{total}}$	[s] $<1.1 \times 10^{-5}$, CL = 90%
$\Gamma(D_S^+ \rightarrow \pi^- 2e^+)/\Gamma_{\text{total}}$	$<1.4 \times 10^{-6}$, CL = 90%
$\Gamma(D_S^+ \rightarrow \pi^- 2\mu^+)/\Gamma_{\text{total}}$	$<8.6 \times 10^{-8}$, CL = 90%
$\Gamma(D_S^+ \rightarrow \pi^- e^+ \mu^+)/\Gamma_{\text{total}}$	$<6.3 \times 10^{-7}$, CL = 90%
$\Gamma(D_S^+ \rightarrow K^- 2e^+)/\Gamma_{\text{total}}$	$<7.7 \times 10^{-7}$, CL = 90%
$\Gamma(D_S^+ \rightarrow K^- 2\mu^+)/\Gamma_{\text{total}}$	$<2.6 \times 10^{-8}$, CL = 90%
$\Gamma(D_S^+ \rightarrow K^- e^+ \mu^+)/\Gamma_{\text{total}}$	$<2.6 \times 10^{-7}$, CL = 90%
$\Gamma(D_S^+ \rightarrow K^*(892)^- 2\mu^+)/\Gamma_{\text{total}}$	$<1.4 \times 10^{-3}$, CL = 90%
$\Gamma(B^+ \rightarrow \pi^- e^+ e^+)/\Gamma_{\text{total}}$	$<2.3 \times 10^{-8}$, CL = 90%
$\Gamma(B^+ \rightarrow \pi^- \mu^+ \mu^+)/\Gamma_{\text{total}}$	$<4.0 \times 10^{-9}$, CL = 95%
$\Gamma(B^+ \rightarrow \pi^- e^+ \mu^+)/\Gamma_{\text{total}}$	$<1.5 \times 10^{-7}$, CL = 90%
$\Gamma(B^+ \rightarrow \rho^- e^+ e^+)/\Gamma_{\text{total}}$	$<1.7 \times 10^{-7}$, CL = 90%
$\Gamma(B^+ \rightarrow \rho^- \mu^+ \mu^+)/\Gamma_{\text{total}}$	$<4.2 \times 10^{-7}$, CL = 90%
$\Gamma(B^+ \rightarrow \rho^- e^+ \mu^+)/\Gamma_{\text{total}}$	$<4.7 \times 10^{-7}$, CL = 90%
$\Gamma(B^+ \rightarrow K^- e^+ e^+)/\Gamma_{\text{total}}$	$<3.0 \times 10^{-8}$, CL = 90%
$\Gamma(B^+ \rightarrow K^- \mu^+ \mu^+)/\Gamma_{\text{total}}$	$<4.1 \times 10^{-8}$, CL = 90%
$\Gamma(B^+ \rightarrow K^- e^+ \mu^+)/\Gamma_{\text{total}}$	$<1.6 \times 10^{-7}$, CL = 90%
$\Gamma(B^+ \rightarrow K^*(892)^- e^+ e^+)/\Gamma_{\text{total}}$	$<4.0 \times 10^{-7}$, CL = 90%
$\Gamma(B^+ \rightarrow K^*(892)^- \mu^+ \mu^+)/\Gamma_{\text{total}}$	$<5.9 \times 10^{-7}$, CL = 90%
$\Gamma(B^+ \rightarrow K^*(892)^- e^+ \mu^+)/\Gamma_{\text{total}}$	$<3.0 \times 10^{-7}$, CL = 90%
$\Gamma(B^+ \rightarrow D^- e^+ e^+)/\Gamma_{\text{total}}$	$<2.6 \times 10^{-6}$, CL = 90%
$\Gamma(B^+ \rightarrow D^- e^+ \mu^+)/\Gamma_{\text{total}}$	$<1.8 \times 10^{-6}$, CL = 90%
$\Gamma(B^+ \rightarrow D^- \mu^+ \mu^+)/\Gamma_{\text{total}}$	$<6.9 \times 10^{-7}$, CL = 95%
$\Gamma(B^+ \rightarrow D^{*-} \mu^+ \mu^+)/\Gamma_{\text{total}}$	$<2.4 \times 10^{-6}$, CL = 95%
$\Gamma(B^+ \rightarrow D_S^- \mu^+ \mu^+)/\Gamma_{\text{total}}$	$<5.8 \times 10^{-7}$, CL = 95%
$\Gamma(B^+ \rightarrow \bar{D}^0 \pi^- \mu^+ \mu^+)/\Gamma_{\text{total}}$	$<1.5 \times 10^{-6}$, CL = 95%
$\Gamma(B^+ \rightarrow \Lambda^0 \mu^+)/\Gamma_{\text{total}}$	$<6 \times 10^{-8}$, CL = 90%
$\Gamma(B^+ \rightarrow \Lambda^0 e^+)/\Gamma_{\text{total}}$	$<3.2 \times 10^{-8}$, CL = 90%
$\Gamma(B^+ \rightarrow \bar{\Lambda}^0 \mu^+)/\Gamma_{\text{total}}$	$<6 \times 10^{-8}$, CL = 90%
$\Gamma(B^+ \rightarrow \bar{\Lambda}^0 e^+)/\Gamma_{\text{total}}$	$<8 \times 10^{-8}$, CL = 90%
$\Gamma(B^0 \rightarrow \Lambda_C^+ \mu^-)/\Gamma_{\text{total}}$	$<1.4 \times 10^{-6}$, CL = 90%
$\Gamma(B^0 \rightarrow \Lambda_C^+ e^-)/\Gamma_{\text{total}}$	$<4 \times 10^{-6}$, CL = 90%
$\Gamma(\Lambda \rightarrow \pi^+ e^-)/\Gamma_{\text{total}}$	$<6 \times 10^{-7}$, CL = 90%
$\Gamma(\Lambda \rightarrow \pi^+ \mu^-)/\Gamma_{\text{total}}$	$<6 \times 10^{-7}$, CL = 90%
$\Gamma(\Lambda \rightarrow \pi^- e^+)/\Gamma_{\text{total}}$	$<4 \times 10^{-7}$, CL = 90%
$\Gamma(\Lambda \rightarrow \pi^- \mu^+)/\Gamma_{\text{total}}$	$<6 \times 10^{-7}$, CL = 90%
$\Gamma(\Lambda \rightarrow K^+ e^-)/\Gamma_{\text{total}}$	$<2 \times 10^{-6}$, CL = 90%
$\Gamma(\Lambda \rightarrow K^+ \mu^-)/\Gamma_{\text{total}}$	$<3 \times 10^{-6}$, CL = 90%
$\Gamma(\Lambda \rightarrow K^- e^+)/\Gamma_{\text{total}}$	$<2 \times 10^{-6}$, CL = 90%
$\Gamma(\Lambda \rightarrow K^- \mu^+)/\Gamma_{\text{total}}$	$<3 \times 10^{-6}$, CL = 90%
$\Gamma(\Lambda \rightarrow K_S^0 \nu)/\Gamma_{\text{total}}$	$<2 \times 10^{-5}$, CL = 90%
$\Gamma(\Sigma^- \rightarrow p e^- e^-)/\Gamma_{\text{total}}$	$<6.7 \times 10^{-5}$, CL = 90%
$\Gamma(\Xi^- \rightarrow p \mu^- \mu^-)/\Gamma_{\text{total}}$	$<4 \times 10^{-8}$, CL = 90%
$\Gamma(\Lambda_C^+ \rightarrow \bar{p} 2e^+)/\Gamma_{\text{total}}$	$<2.7 \times 10^{-6}$, CL = 90%
$\Gamma(\Lambda_C^+ \rightarrow \bar{p} 2\mu^+)/\Gamma_{\text{total}}$	$<9.4 \times 10^{-6}$, CL = 90%
$\Gamma(\Lambda_C^+ \rightarrow \bar{p} e^+ \mu^+)/\Gamma_{\text{total}}$	$<1.6 \times 10^{-5}$, CL = 90%
$\Gamma(\Lambda_C^+ \rightarrow \Sigma^- \mu^+ \mu^+)/\Gamma_{\text{total}}$	$<7.0 \times 10^{-4}$, CL = 90%

BARYON NUMBER

$\Gamma(Z \rightarrow p e)/\Gamma_{\text{total}}$	$<1.8 \times 10^{-6}$, CL = 95%
$\Gamma(Z \rightarrow p \mu)/\Gamma_{\text{total}}$	$<1.8 \times 10^{-6}$, CL = 95%
$\Gamma(\tau^- \rightarrow p e^- e^-)/\Gamma_{\text{total}}$	$<3.0 \times 10^{-8}$, CL = 90%
$\Gamma(\tau^- \rightarrow \bar{p} e^+ e^-)/\Gamma_{\text{total}}$	$<3.0 \times 10^{-8}$, CL = 90%
$\Gamma(\tau^- \rightarrow \bar{p} e^+ \mu^-)/\Gamma_{\text{total}}$	$<2.0 \times 10^{-8}$, CL = 90%
$\Gamma(\tau^- \rightarrow \bar{p} e^- \mu^+)/\Gamma_{\text{total}}$	$<1.8 \times 10^{-8}$, CL = 90%
$\Gamma(\tau^- \rightarrow p \mu^- \mu^-)/\Gamma_{\text{total}}$	$<4.0 \times 10^{-8}$, CL = 90%
$\Gamma(\tau^- \rightarrow \bar{p} \mu^+ \mu^-)/\Gamma_{\text{total}}$	$<1.8 \times 10^{-8}$, CL = 90%
$\Gamma(\tau^- \rightarrow \bar{p} \gamma)/\Gamma_{\text{total}}$	$<3.5 \times 10^{-6}$, CL = 90%
$\Gamma(\tau^- \rightarrow \bar{p} \pi^0)/\Gamma_{\text{total}}$	$<1.5 \times 10^{-5}$, CL = 90%

Tests of Conservation Laws

$\Gamma(\tau^- \rightarrow \bar{p}2\pi^0)/\Gamma_{\text{total}}$	$<3.3 \times 10^{-5}$, CL = 90%
$\Gamma(\tau^- \rightarrow \bar{p}\eta)/\Gamma_{\text{total}}$	$<8.9 \times 10^{-6}$, CL = 90%
$\Gamma(\tau^- \rightarrow \bar{p}\pi^0\eta)/\Gamma_{\text{total}}$	$<2.7 \times 10^{-5}$, CL = 90%
$\Gamma(\tau^- \rightarrow \Lambda\pi^-)/\Gamma_{\text{total}}$	$<7.2 \times 10^{-8}$, CL = 90%
$\Gamma(\tau^- \rightarrow \bar{\Lambda}\pi^-)/\Gamma_{\text{total}}$	$<1.4 \times 10^{-7}$, CL = 90%
$\Gamma(D^+ \rightarrow \Lambda e^+)/\Gamma_{\text{total}}$	$<1.1 \times 10^{-6}$, CL = 90%
$\Gamma(D^+ \rightarrow \bar{\Lambda}e^+)/\Gamma_{\text{total}}$	$<6.5 \times 10^{-7}$, CL = 90%
$\Gamma(D^+ \rightarrow \Sigma^0 e^+)/\Gamma_{\text{total}}$	$<1.7 \times 10^{-6}$, CL = 90%
$\Gamma(D^+ \rightarrow \bar{\Sigma}^0 e^+)/\Gamma_{\text{total}}$	$<1.3 \times 10^{-6}$, CL = 90%
$\Gamma(D^0 \rightarrow p e^-)/\Gamma_{\text{total}}$	[r] $<1.0 \times 10^{-5}$, CL = 90%
$\Gamma(D^0 \rightarrow \bar{p} e^+)/\Gamma_{\text{total}}$	[s] $<1.1 \times 10^{-5}$, CL = 90%
$\Gamma(B^+ \rightarrow \Lambda^0 \mu^+)/\Gamma_{\text{total}}$	$<6 \times 10^{-8}$, CL = 90%
$\Gamma(B^+ \rightarrow \Lambda^0 e^+)/\Gamma_{\text{total}}$	$<3.2 \times 10^{-8}$, CL = 90%
$\Gamma(B^+ \rightarrow \bar{\Lambda}^0 \mu^+)/\Gamma_{\text{total}}$	$<6 \times 10^{-8}$, CL = 90%
$\Gamma(B^+ \rightarrow \bar{\Lambda}^0 e^+)/\Gamma_{\text{total}}$	$<8 \times 10^{-8}$, CL = 90%
$\Gamma(B^0 \rightarrow \Lambda_c^+ \mu^-)/\Gamma_{\text{total}}$	$<1.4 \times 10^{-6}$, CL = 90%
$\Gamma(B^0 \rightarrow \Lambda_c^+ e^-)/\Gamma_{\text{total}}$	$<4 \times 10^{-6}$, CL = 90%

p mean life [t] $>3.6 \times 10^{29}$ years, CL = 90%

A few examples of proton or bound neutron decay follow. For limits on many other nucleon decay channels, see the Baryon Summary Table.

$\tau(N \rightarrow e^+ \pi)$	> 5300 (n), > 16000 (p) $\times 10^{30}$ years, CL = 90%
$\tau(N \rightarrow \mu^+ \pi)$	> 3500 (n), > 7700 (p) $\times 10^{30}$ years, CL = 90%
$\tau(N \rightarrow e^+ K)$	> 17 (n), > 1000 (p) $\times 10^{30}$ years, CL = 90%
$\tau(N \rightarrow \mu^+ K)$	> 26 (n), > 1600 (p) $\times 10^{30}$ years, CL = 90%

limit on $n\bar{n}$ oscillations (free n) $>0.86 \times 10^8$ s, CL = 90%

limit on $n\bar{n}$ oscillations (bound n) [u] $>2.7 \times 10^8$ s, CL = 90%

$\Gamma(\Lambda \rightarrow \pi^+ e^-)/\Gamma_{\text{total}}$	$<6 \times 10^{-7}$, CL = 90%
$\Gamma(\Lambda \rightarrow \pi^+ \mu^-)/\Gamma_{\text{total}}$	$<6 \times 10^{-7}$, CL = 90%
$\Gamma(\Lambda \rightarrow \pi^- e^+)/\Gamma_{\text{total}}$	$<4 \times 10^{-7}$, CL = 90%
$\Gamma(\Lambda \rightarrow \pi^- \mu^+)/\Gamma_{\text{total}}$	$<6 \times 10^{-7}$, CL = 90%
$\Gamma(\Lambda \rightarrow K^+ e^-)/\Gamma_{\text{total}}$	$<2 \times 10^{-6}$, CL = 90%
$\Gamma(\Lambda \rightarrow K^+ \mu^-)/\Gamma_{\text{total}}$	$<3 \times 10^{-6}$, CL = 90%
$\Gamma(\Lambda \rightarrow K^- e^+)/\Gamma_{\text{total}}$	$<2 \times 10^{-6}$, CL = 90%
$\Gamma(\Lambda \rightarrow K^- \mu^+)/\Gamma_{\text{total}}$	$<3 \times 10^{-6}$, CL = 90%
$\Gamma(\Lambda \rightarrow K_S^0 \nu)/\Gamma_{\text{total}}$	$<2 \times 10^{-5}$, CL = 90%
$\Gamma(\Lambda \rightarrow \bar{p}\pi^+)/\Gamma_{\text{total}}$	$<9 \times 10^{-7}$, CL = 90%
$\Gamma(\Lambda_c^+ \rightarrow \bar{p}2e^+)/\Gamma_{\text{total}}$	$<2.7 \times 10^{-6}$, CL = 90%
$\Gamma(\Lambda_c^+ \rightarrow \bar{p}2\mu^+)/\Gamma_{\text{total}}$	$<9.4 \times 10^{-6}$, CL = 90%
$\Gamma(\Lambda_c^+ \rightarrow \bar{p}e^+ \mu^+)/\Gamma_{\text{total}}$	$<1.6 \times 10^{-5}$, CL = 90%

ELECTRIC CHARGE (Q)

γ charge (mixed)	$<1 \times 10^{-46} e$
γ charge (single)	$<1 \times 10^{-35} e$
$e \rightarrow \nu_e \gamma$ and astrophysical limits	[v] $>6.6 \times 10^{28}$ yr, CL = 90%
ν charge	$<4 \times 10^{-35} e$, CL = 95%
$ q_p + q_e /e$	[x] $<1 \times 10^{-21}$
n charge	$(-0.2 \pm 0.8) \times 10^{-21} e$
$\Gamma(n \rightarrow p\nu_e \bar{\nu}_e)/\Gamma_{\text{total}}$	$<8 \times 10^{-27}$, CL = 68%

$\Delta S = \Delta Q$ RULE

Violations allowed in second-order weak interactions.

$\Gamma(K^+ \rightarrow \pi^+ \pi^+ e^- \bar{\nu}_e)/\Gamma_{\text{total}}$	$<1.3 \times 10^{-8}$, CL = 90%
$\Gamma(K^+ \rightarrow \pi^+ \pi^+ \mu^- \bar{\nu}_\mu)/\Gamma_{\text{total}}$	$<3.0 \times 10^{-6}$, CL = 95%
Re(X_+), K_{e3} parameter	$(-0.9 \pm 3.0) \times 10^{-3}$
$x = A(\bar{K}^0 \rightarrow \pi^- \ell^+ \nu)/A(K^0 \rightarrow \pi^- \ell^+ \nu) = A(\Delta S = -\Delta Q)/A(\Delta S = \Delta Q)$	
real part of x	-0.002 ± 0.006
imaginary part of x	0.0012 ± 0.0021
$\Gamma(\Sigma^+ \rightarrow n\ell^+ \nu)/\Gamma(\Sigma^- \rightarrow n\ell^- \bar{\nu}_\ell)$	<0.043
$\Gamma(\Sigma^+ \rightarrow n e^+ \nu_e)/\Gamma_{\text{total}}$	$<5 \times 10^{-6}$, CL = 90%
$\Gamma(\Sigma^+ \rightarrow n \mu^+ \nu_\mu)/\Gamma_{\text{total}}$	$<3.0 \times 10^{-5}$, CL = 90%
$\Gamma(\Xi^0 \rightarrow \Sigma^- e^+ \nu_e)/\Gamma_{\text{total}}$	$<9 \times 10^{-4}$, CL = 90%
$\Gamma(\Xi^0 \rightarrow \Sigma^- \mu^+ \nu_\mu)/\Gamma_{\text{total}}$	$<9 \times 10^{-4}$, CL = 90%

$\Delta S = 2$ FORBIDDEN

Allowed in second-order weak interactions.

$\Gamma(\Xi^0 \rightarrow p\pi^-)/\Gamma_{\text{total}}$	$<8 \times 10^{-6}$, CL = 90%
$\Gamma(\Xi^0 \rightarrow p e^- \bar{\nu}_e)/\Gamma_{\text{total}}$	$<1.3 \times 10^{-3}$
$\Gamma(\Xi^0 \rightarrow p \mu^- \bar{\nu}_\mu)/\Gamma_{\text{total}}$	$<1.3 \times 10^{-3}$
$\Gamma(\Xi^- \rightarrow n\pi^-)/\Gamma_{\text{total}}$	$<1.9 \times 10^{-5}$, CL = 90%
$\Gamma(\Xi^- \rightarrow n e^- \bar{\nu}_e)/\Gamma_{\text{total}}$	$<3.2 \times 10^{-3}$, CL = 90%
$\Gamma(\Xi^- \rightarrow n \mu^- \bar{\nu}_\mu)/\Gamma_{\text{total}}$	$<1.5 \times 10^{-2}$, CL = 90%
$\Gamma(\Xi^- \rightarrow p\pi^- \pi^-)/\Gamma_{\text{total}}$	$<4 \times 10^{-4}$, CL = 90%
$\Gamma(\Xi^- \rightarrow p\pi^- e^- \bar{\nu}_e)/\Gamma_{\text{total}}$	$<4 \times 10^{-4}$, CL = 90%
$\Gamma(\Xi^- \rightarrow p\pi^- \mu^- \bar{\nu}_\mu)/\Gamma_{\text{total}}$	$<4 \times 10^{-4}$, CL = 90%
$\Gamma(\Omega^- \rightarrow \Lambda\pi^-)/\Gamma_{\text{total}}$	$<2.9 \times 10^{-6}$, CL = 90%

$\Delta S = 2$ VIA MIXING

Allowed in second-order weak interactions, e.g. mixing.

$m_{K_L^0} - m_{K_S^0}$	$(0.5293 \pm 0.0009) \times 10^{10} \hbar s^{-1}$ (S = 1.3)
$m_{K_L^0} - m_{K_S^0}$	$(3.484 \pm 0.006) \times 10^{-12}$ MeV

$\Delta C = 2$ VIA MIXING

Allowed in second-order weak interactions, e.g. mixing.

$ m_{D_1^0} - m_{D_2^0} = x\Gamma$	$(0.997 \pm 0.116) \times 10^{10} \hbar s^{-1}$
$(\Gamma_{D_1^0} - \Gamma_{D_2^0})/\Gamma = 2y$	$(1.23 \pm 0.11) \times 10^{-2}$

$\Delta B = 2$ VIA MIXING

Allowed in second-order weak interactions, e.g. mixing.

χ_d (B^0 - \bar{B}^0 mixing probability)	0.1858 ± 0.0011
$\Delta m_{B^0} = m_{B_H^0} - m_{B_L^0}$	$(0.5065 \pm 0.0019) \times 10^{12} \hbar s^{-1}$
$\chi_d = \Delta m_{B^0}/\Gamma_{B^0}$	0.769 ± 0.004
$\Delta m_{B_S^0} = m_{B_{SH}^0} - m_{B_{SL}^0}$	$(17.765 \pm 0.006) \times 10^{12} \hbar s^{-1}$
$\chi_s = \Delta m_{B_S^0}/\Gamma_{B_S^0}$	27.01 ± 0.10
χ_s (B_S^0 - \bar{B}_S^0 mixing parameter)	0.499318 ± 0.000005

$\Delta S = 1$ WEAK NEUTRAL CURRENT FORBIDDEN

Allowed by higher-order electroweak interactions.

$\Gamma(K^+ \rightarrow \pi^+ e^+ e^-)/\Gamma_{\text{total}}$	$(3.00 \pm 0.09) \times 10^{-7}$
$\Gamma(K^+ \rightarrow \pi^+ \mu^+ \mu^-)/\Gamma_{\text{total}}$	$(9.4 \pm 0.6) \times 10^{-8}$ (S = 2.6)
$\Gamma(K^+ \rightarrow \pi^+ \nu \bar{\nu})/\Gamma_{\text{total}}$	$(1.14 \pm_{-0.33}^{0.40}) \times 10^{-10}$
$\Gamma(K^+ \rightarrow \pi^+ \pi^0 \nu \bar{\nu})/\Gamma_{\text{total}}$	$<4.3 \times 10^{-5}$, CL = 90%
$\Gamma(K_S^0 \rightarrow \mu^+ \mu^-)/\Gamma_{\text{total}}$	$<2.1 \times 10^{-10}$, CL = 90%
$\Gamma(K_S^0 \rightarrow e^+ e^-)/\Gamma_{\text{total}}$	$<9 \times 10^{-9}$, CL = 90%
$\Gamma(K_S^0 \rightarrow \pi^0 e^+ e^-)/\Gamma_{\text{total}}$	[y] $(3.0 \pm_{-1.2}^{1.5}) \times 10^{-9}$
$\Gamma(K_S^0 \rightarrow \pi^0 \mu^+ \mu^-)/\Gamma_{\text{total}}$	$(2.9 \pm_{-1.2}^{1.5}) \times 10^{-9}$
$\Gamma(K_L^0 \rightarrow \mu^+ \mu^-)/\Gamma_{\text{total}}$	$(6.84 \pm 0.11) \times 10^{-9}$
$\Gamma(K_L^0 \rightarrow e^+ e^-)/\Gamma_{\text{total}}$	$(9 \pm_4^6) \times 10^{-12}$
$\Gamma(K_L^0 \rightarrow \pi^+ \pi^- e^+ e^-)/\Gamma_{\text{total}}$	[z] $(3.11 \pm 0.19) \times 10^{-7}$
$\Gamma(K_L^0 \rightarrow \pi^0 \pi^0 e^+ e^-)/\Gamma_{\text{total}}$	$<6.6 \times 10^{-9}$, CL = 90%
$\Gamma(K_L^0 \rightarrow \pi^0 \pi^0 \mu^+ \mu^-)/\Gamma_{\text{total}}$	$<9.2 \times 10^{-11}$, CL = 90%
$\Gamma(K_L^0 \rightarrow \mu^+ \mu^- e^+ e^-)/\Gamma_{\text{total}}$	$(2.69 \pm 0.27) \times 10^{-9}$
$\Gamma(K_L^0 \rightarrow e^+ e^- e^+ e^-)/\Gamma_{\text{total}}$	$(3.56 \pm 0.21) \times 10^{-8}$
$\Gamma(K_L^0 \rightarrow \pi^0 \mu^+ \mu^-)/\Gamma_{\text{total}}$	$<3.8 \times 10^{-10}$, CL = 90%
$\Gamma(K_L^0 \rightarrow \pi^0 e^+ e^-)/\Gamma_{\text{total}}$	$<2.8 \times 10^{-10}$, CL = 90%
$\Gamma(K_L^0 \rightarrow \pi^0 \nu \bar{\nu})/\Gamma_{\text{total}}$	$<3.0 \times 10^{-9}$, CL = 90%
$\Gamma(K_L^0 \rightarrow \pi^0 \pi^0 \nu \bar{\nu})/\Gamma_{\text{total}}$	$<8.1 \times 10^{-7}$, CL = 90%
$\Gamma(\Sigma^+ \rightarrow p e^+ e^-)/\Gamma_{\text{total}}$	$<7 \times 10^{-6}$
$\Gamma(\Sigma^+ \rightarrow p \mu^+ \mu^-)/\Gamma_{\text{total}}$	$(2.4 \pm_{-1.3}^{1.7}) \times 10^{-8}$

$\Delta C = 1$ WEAK NEUTRAL CURRENT FORBIDDEN

Allowed by higher-order electroweak interactions.

$\Gamma(D^+ \rightarrow \pi^+ e^+ e^-)/\Gamma_{\text{total}}$	$<1.1 \times 10^{-6}$, CL = 90%
$\Gamma(D^+ \rightarrow \pi^+ \mu^+ \mu^-)/\Gamma_{\text{total}}$	$<6.7 \times 10^{-8}$, CL = 90%
$\Gamma(D^+ \rightarrow \rho^+ \mu^+ \mu^-)/\Gamma_{\text{total}}$	$<5.6 \times 10^{-4}$, CL = 90%
$\Gamma(D^0 \rightarrow \gamma\gamma)/\Gamma_{\text{total}}$	$<8.5 \times 10^{-7}$, CL = 90%
$\Gamma(D^0 \rightarrow e^+ e^-)/\Gamma_{\text{total}}$	$<7.9 \times 10^{-8}$, CL = 90%
$\Gamma(D^0 \rightarrow \mu^+ \mu^-)/\Gamma_{\text{total}}$	$<6.2 \times 10^{-9}$, CL = 90%
$\Gamma(D^0 \rightarrow \pi^0 e^+ e^-)/\Gamma_{\text{total}}$	$<4 \times 10^{-6}$, CL = 90%
$\Gamma(D^0 \rightarrow \pi^0 \mu^+ \mu^-)/\Gamma_{\text{total}}$	$<1.8 \times 10^{-4}$, CL = 90%
$\Gamma(D^0 \rightarrow \eta e^+ e^-)/\Gamma_{\text{total}}$	$<3 \times 10^{-6}$, CL = 90%
$\Gamma(D^0 \rightarrow \eta \mu^+ \mu^-)/\Gamma_{\text{total}}$	$<5.3 \times 10^{-4}$, CL = 90%
$\Gamma(D^0 \rightarrow \pi^+ \pi^- e^+ e^-)/\Gamma_{\text{total}}$	$<7 \times 10^{-6}$, CL = 90%
$\Gamma(D^0 \rightarrow \rho^0 e^+ e^-)/\Gamma_{\text{total}}$	$<1.0 \times 10^{-4}$, CL = 90%
$\Gamma(D^0 \rightarrow \pi^+ \pi^- \mu^+ \mu^-)/\Gamma_{\text{total}}$	$(9.6 \pm 1.2) \times 10^{-7}$
$\Gamma(D^0 \rightarrow \rho^0 \mu^+ \mu^-)/\Gamma_{\text{total}}$	$<2.2 \times 10^{-5}$, CL = 90%
$\Gamma(D^0 \rightarrow \omega e^+ e^-)/\Gamma_{\text{total}}$	$<6 \times 10^{-6}$, CL = 90%
$\Gamma(D^0 \rightarrow \omega \mu^+ \mu^-)/\Gamma_{\text{total}}$	$<8.3 \times 10^{-4}$, CL = 90%
$\Gamma(D^0 \rightarrow K^- K^+ e^+ e^-)/\Gamma_{\text{total}}$	$<1.1 \times 10^{-5}$, CL = 90%
$\Gamma(D^0 \rightarrow \phi e^+ e^-)/\Gamma_{\text{total}}$	$<5.2 \times 10^{-5}$, CL = 90%
$\Gamma(D^0 \rightarrow K^- K^+ \mu^+ \mu^-)/\Gamma_{\text{total}}$	$(1.54 \pm 0.32) \times 10^{-7}$
$\Gamma(D^0 \rightarrow \phi \mu^+ \mu^-)/\Gamma_{\text{total}}$	$<3.1 \times 10^{-5}$, CL = 90%
$\Gamma(D^0 \rightarrow K^- \pi^+ \mu^+ \mu^-)/\Gamma_{\text{total}}$	$<3.59 \times 10^{-4}$, CL = 90%
$\Gamma(D^0 \rightarrow \pi^+ \pi^- \pi^0 \mu^+ \mu^-)/\Gamma_{\text{total}}$	$<8.1 \times 10^{-4}$, CL = 90%
$\Gamma(D_S^+ \rightarrow K^+ e^+ e^-)/\Gamma_{\text{total}}$	$<3.7 \times 10^{-6}$, CL = 90%
$\Gamma(D_S^+ \rightarrow K^+ \mu^+ \mu^-)/\Gamma_{\text{total}}$	$<1.4 \times 10^{-7}$, CL = 90%
$\Gamma(D_S^+ \rightarrow K^*(892)^+ \mu^+ \mu^-)/\Gamma_{\text{total}}$	$<1.4 \times 10^{-3}$, CL = 90%
$\Gamma(\Lambda_C^+ \rightarrow p e^+ e^-)/\Gamma_{\text{total}}$	$<5.5 \times 10^{-6}$, CL = 90%
$\Gamma(\Lambda_C^+ \rightarrow p \mu^+ \mu^- \text{ non-resonant})/\Gamma_{\text{total}}$	$<7.7 \times 10^{-8}$, CL = 90%

 $\Delta B = 1$ WEAK NEUTRAL CURRENT FORBIDDEN

Allowed by higher-order electroweak interactions.

$\Gamma(B^+ \rightarrow \pi^+ \ell^+ \ell^-)/\Gamma_{\text{total}}$	$<4.9 \times 10^{-8}$, CL = 90%
$\Gamma(B^+ \rightarrow \pi^+ e^+ e^-)/\Gamma_{\text{total}}$	$<8.0 \times 10^{-8}$, CL = 90%
$\Gamma(B^+ \rightarrow \pi^+ \mu^+ \mu^-)/\Gamma_{\text{total}}$	$(1.78 \pm 0.23) \times 10^{-8}$
$\Gamma(B^+ \rightarrow \pi^+ \nu\bar{\nu})/\Gamma_{\text{total}}$	$<1.4 \times 10^{-5}$, CL = 90%
$\Gamma(B^+ \rightarrow K^+ \ell^+ \ell^-)/\Gamma_{\text{total}}$	[a \bar{a}] $(4.7 \pm 0.5) \times 10^{-7}$ (S = 2.3)
$\Gamma(B^+ \rightarrow K^+ e^+ e^-)/\Gamma_{\text{total}}$	$(5.6 \pm 0.6) \times 10^{-7}$
$\Gamma(B^+ \rightarrow K^+ \mu^+ \mu^-)/\Gamma_{\text{total}}$	$(4.53 \pm 0.35) \times 10^{-7}$ (S = 1.8)
$\Gamma(B^+ \rightarrow K^+ \mu^+ \mu^- \text{ nonresonant})/\Gamma_{\text{total}}$	$(4.37 \pm 0.27) \times 10^{-7}$
$\Gamma(B^+ \rightarrow K^+ \tau^+ \tau^-)/\Gamma_{\text{total}}$	$<2.25 \times 10^{-3}$, CL = 90%
$\Gamma(B^+ \rightarrow K^+ \nu\bar{\nu})/\Gamma_{\text{total}}$	$<1.6 \times 10^{-5}$, CL = 90%
$\Gamma(B^+ \rightarrow \rho^+ \nu\bar{\nu})/\Gamma_{\text{total}}$	$<3.0 \times 10^{-5}$, CL = 90%
$\Gamma(B^+ \rightarrow K^*(892)^+ \ell^+ \ell^-)/\Gamma_{\text{total}}$	[a \bar{a}] $(1.01 \pm 0.11) \times 10^{-6}$ (S = 1.1)
$\Gamma(B^+ \rightarrow K^*(892)^+ e^+ e^-)/\Gamma_{\text{total}}$	$(1.55^{+0.40}_{-0.31}) \times 10^{-6}$
$\Gamma(B^+ \rightarrow K^*(892)^+ \mu^+ \mu^-)/\Gamma_{\text{total}}$	$(9.6 \pm 1.0) \times 10^{-7}$
$\Gamma(B^+ \rightarrow K^*(892)^+ \nu\bar{\nu})/\Gamma_{\text{total}}$	$<4.0 \times 10^{-5}$, CL = 90%
$\Gamma(B^+ \rightarrow K^+ \pi^+ \pi^- \mu^+ \mu^-)/\Gamma_{\text{total}}$	$(4.3 \pm 0.4) \times 10^{-7}$
$\Gamma(B^+ \rightarrow \phi K^+ \mu^+ \mu^-)/\Gamma_{\text{total}}$	$(7.9^{+2.1}_{-1.7}) \times 10^{-8}$
$\Gamma(B^0 \rightarrow \gamma\gamma)/\Gamma_{\text{total}}$	$<3.2 \times 10^{-7}$, CL = 90%
$\Gamma(B^0 \rightarrow e^+ e^-)/\Gamma_{\text{total}}$	$<2.5 \times 10^{-9}$, CL = 90%
$\Gamma(B^0 \rightarrow e^+ e^- \gamma)/\Gamma_{\text{total}}$	$<1.2 \times 10^{-7}$, CL = 90%
$\Gamma(B^0 \rightarrow \mu^+ \mu^-)/\Gamma_{\text{total}}$	$(7^{+13}_{-11}) \times 10^{-11}$ (S = 1.8)
$\Gamma(B^0 \rightarrow \mu^+ \mu^- \gamma)/\Gamma_{\text{total}}$	$<2.0 \times 10^{-9}$, CL = 95%
$\Gamma(B^0 \rightarrow \mu^+ \mu^- \mu^+ \mu^-)/\Gamma_{\text{total}}$	$<6.9 \times 10^{-10}$, CL = 95%
$\Gamma(B^0 \rightarrow SP, S \rightarrow \mu^+ \mu^-, P \rightarrow \mu^+ \mu^-)/\Gamma_{\text{total}}$	[bb] $<6.0 \times 10^{-10}$, CL = 95%
$\Gamma(B^0 \rightarrow \tau^+ \tau^-)/\Gamma_{\text{total}}$	$<2.1 \times 10^{-3}$, CL = 95%
$\Gamma(B^0 \rightarrow \pi^0 \ell^+ \ell^-)/\Gamma_{\text{total}}$	$<5.3 \times 10^{-8}$, CL = 90%
$\Gamma(B^0 \rightarrow \pi^0 e^+ e^-)/\Gamma_{\text{total}}$	$<8.4 \times 10^{-8}$, CL = 90%
$\Gamma(B^0 \rightarrow \pi^0 \mu^+ \mu^-)/\Gamma_{\text{total}}$	$<6.9 \times 10^{-8}$, CL = 90%
$\Gamma(B^0 \rightarrow \eta \ell^+ \ell^-)/\Gamma_{\text{total}}$	$<6.4 \times 10^{-8}$, CL = 90%
$\Gamma(B^0 \rightarrow \eta e^+ e^-)/\Gamma_{\text{total}}$	$<1.08 \times 10^{-7}$, CL = 90%
$\Gamma(B^0 \rightarrow \eta \mu^+ \mu^-)/\Gamma_{\text{total}}$	$<1.12 \times 10^{-7}$, CL = 90%
$\Gamma(B^0 \rightarrow \pi^0 \nu\bar{\nu})/\Gamma_{\text{total}}$	$<9 \times 10^{-6}$, CL = 90%
$\Gamma(B^0 \rightarrow K^0 \ell^+ \ell^-)/\Gamma_{\text{total}}$	[a \bar{a}] $(3.3 \pm 0.6) \times 10^{-7}$
$\Gamma(B^0 \rightarrow K^0 e^+ e^-)/\Gamma_{\text{total}}$	$(2.5^{+1.1}_{-0.9}) \times 10^{-7}$ (S = 1.3)

$\Gamma(B^0 \rightarrow K^0 \mu^+ \mu^-)/\Gamma_{\text{total}}$	$(3.39 \pm 0.35) \times 10^{-7}$ (S = 1.1)
$\Gamma(B^0 \rightarrow K^0 \nu\bar{\nu})/\Gamma_{\text{total}}$	$<2.6 \times 10^{-5}$, CL = 90%
$\Gamma(B^0 \rightarrow \rho^0 \nu\bar{\nu})/\Gamma_{\text{total}}$	$<4.0 \times 10^{-5}$, CL = 90%
$\Gamma(B^0 \rightarrow K^*(892)^0 \ell^+ \ell^-)/\Gamma_{\text{total}}$	[a \bar{a}] $(9.9^{+1.2}_{-1.1}) \times 10^{-7}$
$\Gamma(B^0 \rightarrow K^*(892)^0 e^+ e^-)/\Gamma_{\text{total}}$	$(1.03^{+0.19}_{-0.17}) \times 10^{-6}$
$\Gamma(B^0 \rightarrow K^*(892)^0 \mu^+ \mu^-)/\Gamma_{\text{total}}$	$(9.4 \pm 0.5) \times 10^{-7}$
$\Gamma(B^0 \rightarrow \pi^+ \pi^- \mu^+ \mu^-)/\Gamma_{\text{total}}$	$(2.1 \pm 0.5) \times 10^{-8}$
$\Gamma(B^0 \rightarrow K^*(892)^0 \nu\bar{\nu})/\Gamma_{\text{total}}$	$<1.8 \times 10^{-5}$, CL = 90%
$\Gamma(B^0 \rightarrow \text{invisible})/\Gamma_{\text{total}}$	$<2.4 \times 10^{-5}$, CL = 90%
$\Gamma(B^0 \rightarrow \nu\bar{\nu}\gamma)/\Gamma_{\text{total}}$	$<1.6 \times 10^{-5}$, CL = 90%
$\Gamma(B^0 \rightarrow \phi \nu\bar{\nu})/\Gamma_{\text{total}}$	$<1.27 \times 10^{-4}$, CL = 90%
$\Gamma(B \rightarrow s e^+ e^-)/\Gamma_{\text{total}}$	$(6.7 \pm 1.7) \times 10^{-6}$ (S = 2.0)
$\Gamma(B \rightarrow s \mu^+ \mu^-)/\Gamma_{\text{total}}$	$(4.3 \pm 1.0) \times 10^{-6}$
$\Gamma(B \rightarrow s \ell^+ \ell^-)/\Gamma_{\text{total}}$	[a \bar{a}] $(5.8 \pm 1.3) \times 10^{-6}$ (S = 1.8)
$\Gamma(B \rightarrow \pi \ell^+ \ell^-)/\Gamma_{\text{total}}$	$<5.9 \times 10^{-8}$, CL = 90%
$\Gamma(B \rightarrow \pi e^+ e^-)/\Gamma_{\text{total}}$	$<1.10 \times 10^{-7}$, CL = 90%
$\Gamma(B \rightarrow \pi \mu^+ \mu^-)/\Gamma_{\text{total}}$	$<5.0 \times 10^{-8}$, CL = 90%
$\Gamma(B \rightarrow K e^+ e^-)/\Gamma_{\text{total}}$	$(4.4 \pm 0.6) \times 10^{-7}$
$\Gamma(B \rightarrow K^*(892) e^+ e^-)/\Gamma_{\text{total}}$	$(1.19 \pm 0.20) \times 10^{-6}$ (S = 1.2)
$\Gamma(B \rightarrow K \mu^+ \mu^-)/\Gamma_{\text{total}}$	$(4.4 \pm 0.4) \times 10^{-7}$
$\Gamma(B \rightarrow K^*(892) \mu^+ \mu^-)/\Gamma_{\text{total}}$	$(1.06 \pm 0.09) \times 10^{-6}$
$\Gamma(B \rightarrow K \ell^+ \ell^-)/\Gamma_{\text{total}}$	$(4.8 \pm 0.4) \times 10^{-7}$
$\Gamma(B \rightarrow K^*(892) \ell^+ \ell^-)/\Gamma_{\text{total}}$	$(1.05 \pm 0.10) \times 10^{-6}$
$\Gamma(B \rightarrow K \nu\bar{\nu})/\Gamma_{\text{total}}$	$<1.6 \times 10^{-5}$, CL = 90%
$\Gamma(B \rightarrow K^* \nu\bar{\nu})/\Gamma_{\text{total}}$	$<2.7 \times 10^{-5}$, CL = 90%
$\Gamma(B \rightarrow \pi \nu\bar{\nu})/\Gamma_{\text{total}}$	$<8 \times 10^{-6}$, CL = 90%
$\Gamma(B \rightarrow \rho \nu\bar{\nu})/\Gamma_{\text{total}}$	$<2.8 \times 10^{-5}$, CL = 90%
$\Gamma(\bar{B} \rightarrow \bar{s} \nu\bar{\nu})/\Gamma_{\text{total}}$	$<6.4 \times 10^{-4}$, CL = 90%
$\Gamma(\bar{B} \rightarrow \mu^+ \mu^- \text{ anything})/\Gamma_{\text{total}}$	$<3.2 \times 10^{-4}$, CL = 90%
$\Gamma(B_S^0 \rightarrow \gamma\gamma)/\Gamma_{\text{total}}$	$<3.1 \times 10^{-6}$, CL = 90%
$\Gamma(B_S^0 \rightarrow \phi\gamma)/\Gamma_{\text{total}}$	$(3.4 \pm 0.4) \times 10^{-5}$
$\Gamma(B_S^0 \rightarrow \mu^+ \mu^-)/\Gamma_{\text{total}}$	$(3.01 \pm 0.35) \times 10^{-9}$
$\Gamma(B_S^0 \rightarrow e^+ e^-)/\Gamma_{\text{total}}$	$<9.4 \times 10^{-9}$, CL = 90%
$\Gamma(B_S^0 \rightarrow \tau^+ \tau^-)/\Gamma_{\text{total}}$	$<6.8 \times 10^{-3}$, CL = 95%
$\Gamma(B_S^0 \rightarrow \mu^+ \mu^- \mu^+ \mu^-)/\Gamma_{\text{total}}$	$<2.5 \times 10^{-9}$, CL = 95%
$\Gamma(B_S^0 \rightarrow SP, S \rightarrow \mu^+ \mu^-, P \rightarrow \mu^+ \mu^-)/\Gamma_{\text{total}}$	[bb] $<2.2 \times 10^{-9}$, CL = 95%
$\Gamma(B_S^0 \rightarrow \phi(1020) \mu^+ \mu^-)/\Gamma_{\text{total}}$	$(8.4 \pm 0.4) \times 10^{-7}$
$\Gamma(B_S^0 \rightarrow \bar{K}^*(892)^0 \mu^+ \mu^-)/\Gamma_{\text{total}}$	$(2.9 \pm 1.1) \times 10^{-8}$
$\Gamma(B_S^0 \rightarrow \pi^+ \pi^- \mu^+ \mu^-)/\Gamma_{\text{total}}$	$(8.4 \pm 1.7) \times 10^{-8}$
$\Gamma(B_S^0 \rightarrow \phi \nu\bar{\nu})/\Gamma_{\text{total}}$	$<5.4 \times 10^{-3}$, CL = 90%

 $\Delta T = 1$ WEAK NEUTRAL CURRENT FORBIDDEN

Allowed by higher-order electroweak interactions.

$\Gamma(t \rightarrow Zq(q=u,c))/\Gamma_{\text{total}}$	[cc] $<5 \times 10^{-4}$, CL = 95%
$\Gamma(t \rightarrow Hq)/\Gamma_{\text{total}}$	$<1.2 \times 10^{-3}$, CL = 95%
$\Gamma(t \rightarrow Hc)/\Gamma_{\text{total}}$	$<1.1 \times 10^{-3}$, CL = 95%
$\Gamma(t \rightarrow \ell^+ \bar{q} q' (q=d,s,b; q'=u,c))/\Gamma_{\text{total}}$	$<1.6 \times 10^{-3}$, CL = 95%

NOTES

In this Summary Table:

When a quantity has (“S = ...”) to its right, the error on the quantity has been enlarged by the “scale factor” S, defined as $S = \sqrt{\chi^2/(N-1)}$, where N is the number of measurements used in calculating the quantity. We do this when $S > 1$, which often indicates that the measurements are inconsistent. When $S > 1.25$, we also show in the Particle Listings an ideogram of the measurements. For more about S, see the Introduction.

[a] Forbidden by angular momentum conservation.

[b] C parity forbids this to occur as a single-photon process.

[c] See the Particle Listings for the (complicated) definition of this quantity.

[d] Time-reversal invariance requires this to be 0° or 180° .

[e] This coefficient is zero if time invariance is not violated.

[f] Allowed by higher-order electroweak interactions.

Tests of Conservation Laws

- [g] Violates CP in leading order. Test of direct CP violation since the indirect CP -violating and CP -conserving contributions are expected to be suppressed.
- [h] In the 2010 *Review*, the values for these quantities were given using a measure of the asymmetry that was inconsistent with the usual definition.
- [i] $\text{Re}(\epsilon'/\epsilon) = \epsilon'/\epsilon$ to a very good approximation provided the phases satisfy CPT invariance.
- [j] This mode includes gammas from inner bremsstrahlung but not the direct emission mode $K_L^0 \rightarrow \pi^+ \pi^- \gamma$ (DE).
- [k] Neglecting photon channels. See, e.g., A. Pais and S.B. Treiman, *Phys. Rev. D* **12**, 2744 (1975).
- [l] Derived from measured values of ϕ_{+-} , ϕ_{00} , $|\eta|$, $|m_{K_L^0} - m_{K_S^0}|$, and $\tau_{K_S^0}$, as described in the introduction to "Tests of Conservation Laws."
- [n] The $|m_p - m_{\bar{p}}|/m_p$ and $|q_p + q_{\bar{p}}|/e$ are not independent, and both use the more precise measurement of $|q_{\bar{p}}/m_{\bar{p}}|/(q_p/m_p)$.
- [o] The value is for the sum of the charge states or particle/antiparticle states indicated.
- [p] A test of additive vs. multiplicative lepton family number conservation.
- [q] Derived from an analysis of neutrino-oscillation experiments.
- [r] This limit is for either D^0 or \bar{D}^0 to $p e^-$.
- [s] This limit is for either D^0 or \bar{D}^0 to $\bar{p} e^+$.
- [t] The first limit is for $p \rightarrow$ anything or "disappearance" modes of a bound proton. The second entry, a rough range of limits, assumes the dominant decay modes are among those investigated. For antiprotons the best limit, inferred from the observation of cosmic ray \bar{p} 's is $\tau_{\bar{p}} > 10^7$ yr, the cosmic-ray storage time, but this limit depends on a number of assumptions. The best direct observation of stored antiprotons gives $\tau_{\bar{p}}/B(\bar{p} \rightarrow e^- \gamma) > 7 \times 10^5$ yr.
- [u] There is some controversy about whether nuclear physics and model dependence complicate the analysis for bound neutrons (from which the best limit comes). The first limit here is from reactor experiments with free neutrons.
- [v] This is the best limit for the mode $e^- \rightarrow \nu \gamma$. The best limit for Nuclear de-excitation experiments is 6.4×10^{24} yr.
- [x] The limit is from neutrality-of-matter experiments; it assumes $q_n = q_p + q_e$. See also the charge of the neutron.
- [y] See the K_S^0 Particle Listings for the energy limits used in this measurement.
- [z] See the K_L^0 Particle Listings for the energy limits used in this measurement.
- [aa] An ℓ indicates an e or a μ mode, not a sum over these modes.
- [bb] Here S and P are the hypothetical scalar and pseudoscalar particles with masses of $2.5 \text{ GeV}/c^2$ and $214.3 \text{ MeV}/c^2$, respectively.
- [cc] This limit is for $\Gamma(t \rightarrow Z q)/\Gamma(t \rightarrow W b)$.

REVIEWS, TABLES, AND PLOTS

Constants, Units, Atomic and Nuclear Properties

1. Physical constants (rev.)	133
2. Astrophysical constants and parameters (rev.)	134
3. International system of units (SI) (rev.)	136
4. Periodic table of the elements (rev.)	137
5. Electronic structure of the elements	138
6. Atomic and nuclear properties of materials (rev.)	140
7. Electromagnetic relations	142
8. Naming scheme for hadrons (rev.)	144



1. Physical Constants

Table 1.1: Revised 2021 by D. Robinson (LBNL). Reviewed by P. Mohr (NIST). Mainly from “CODATA Recommended Values of the Fundamental Physical Constants: 2018,” E. Tiesinga, D.B. Newell, P.J. Mohr, and B.N. Taylor, NIST SP961 (May 2019) [1]. The electron charge magnitude e , and the Planck, Boltzmann, and Avogadro constants h , k , and N_A , now join c as having defined values; the free-space permittivity and permeability constants ϵ_0 and μ_0 are no longer exact. These changes affect practically everything else in the Table. Figures in parentheses after the values are the 1-standard-deviation uncertainties in the last digits; the fractional uncertainties in parts per 10^9 (ppb) are in the last column. The full 2018 CODATA Committee on Data for Science and Technology set of constants are found at <https://physics.nist.gov/constants>. The last set of constants (beginning with the Fermi coupling constant) comes from the Particle Data Group. See also “The International System of Units (SI),” 9th ed. (2019) of the International Bureau of Weights and Measures (BIPM), <https://www.bipm.org/utis/common/pdf/si-brochure/SI-Brochure-9-EN.pdf>.

Quantity	Symbol, equation	Value	Uncertainty (ppb)
speed of light in vacuum	c	299 792 458 m s ⁻¹	exact
Planck constant	h	6.626 070 15×10 ⁻³⁴ J s (or J/Hz) §	exact
Planck constant, reduced	$\hbar \equiv h/2\pi$	1.054 571 817... × 10 ⁻³⁴ J s = 6.582 119 569... × 10 ⁻²² MeV s	exact* exact*
electron charge magnitude	e	1.602 176 634×10 ⁻¹⁹ C	exact
conversion constant	$\hbar c$	197.326 980 4... MeV fm	exact*
conversion constant	$(\hbar c)^2$	0.389 379 372 1... GeV ² mbarn	exact*
electron mass	m_e	0.510 998 950 00(15) MeV/c ² = 9.109 383 7015(28)×10 ⁻³¹ kg	0.30
proton mass	m_p	938.272 088 16(29) MeV/c ² = 1.672 621 923 69(51)×10 ⁻²⁷ kg = 1.007 276 466 621(53) u = 1836.152 673 43(11) m_e	0.31 0.053, 0.060
neutron mass	m_n	939.565 420 52(54) MeV/c ² = 1.008 664 915 95(49) u	0.57, 0.48
deuteron mass	m_d	1875.612 942 57(57) MeV/c ²	0.30
unified atomic mass unit**	$u = (\text{mass } ^{12}\text{C atom})/12$	931.494 102 42(28) MeV/c ² = 1.660 539 066 60(50)×10 ⁻²⁷ kg	0.30
permittivity of free space	$\epsilon_0 = 1/\mu_0 c^2$	8.854 187 8128(13) × 10 ⁻¹² F m ⁻¹	0.15
permeability of free space	$\mu_0/(4\pi \times 10^{-7})$	1.000 000 000 55(15) N A ⁻²	0.15
fine-structure constant	$\alpha = e^2/4\pi\epsilon_0\hbar c$	7.297 352 5693(11)×10 ⁻³ = 1/137.035 999 084(21)† ‡‡	0.15
classical electron radius	$r_e = e^2/4\pi\epsilon_0 m_e c^2$	2.817 940 3262(13)×10 ⁻¹⁵ m	0.45
(e^- Compton wavelength)/2π	$\lambda_e = \hbar/m_e c = r_e \alpha^{-1}$	3.861 592 6796(12)×10 ⁻¹³ m	0.30
Bohr radius ($m_{\text{nucleus}} = \infty$)	$a_\infty = 4\pi\epsilon_0\hbar^2/m_e e^2 = r_e \alpha^{-2}$	0.529 177 210 903(80)×10 ⁻¹⁰ m	0.15
wavelength of 1 eV/c particle	$hc/(1 \text{ eV})$	1.239 841 984... × 10 ⁻⁶ m	exact*
Rydberg energy	$hcR_\infty = m_e e^4/2(4\pi\epsilon_0)^2 \hbar^2 = m_e c^2 \alpha^2/2$	13.605 693 122 994(26) eV	1.9×10 ⁻³
Thomson cross section	$\sigma_T = 8\pi r_e^2/3$	0.665 245 873 21(60) barn	0.91
Bohr magneton	$\mu_B = e\hbar/2m_e$	5.788 381 8060(17)×10 ⁻¹¹ MeV T ⁻¹	0.30
nuclear magneton	$\mu_N = e\hbar/2m_p$	3.152 451 258 44(96)×10 ⁻¹⁴ MeV T ⁻¹	0.31
electron cyclotron freq./field	$\omega_{\text{cycl}}^e/B = e/m_e$	1.758 820 010 76(53)×10 ¹¹ rad s ⁻¹ T ⁻¹	0.30
proton cyclotron freq./field	$\omega_{\text{cycl}}^p/B = e/m_p$	9.578 833 1560(29)×10 ⁷ rad s ⁻¹ T ⁻¹	0.31
gravitational constant‡	G_N	6.674 30(15)×10 ⁻¹¹ m ³ kg ⁻¹ s ⁻² = 6.708 83(15)×10 ⁻³⁹ $\hbar c$ (GeV/c ²) ⁻²	2.2 × 10 ⁴ 2.2 × 10 ⁴
standard gravitational accel.	g_N	9.806 65 m s ⁻²	exact
Avogadro constant	N_A	6.022 140 76×10 ²³ mol ⁻¹	exact
Boltzmann constant	k	1.380 649×10 ⁻²³ J K ⁻¹ = 8.617 333 262... × 10 ⁻⁵ eV K ⁻¹	exact* exact*
molar volume, ideal gas at STP	$N_A k$ (273.15 K)/(101 325 Pa)	22.413 969 54... × 10 ⁻³ m ³ mol ⁻¹	exact*
Wien displacement law constant	$b = \lambda_{\text{max}} T$	2.897 771 955... × 10 ⁻³ m K	exact*
Stefan-Boltzmann constant	$\sigma = \pi^2 k^4/60\hbar^3 c^2$	5.670 374 419... × 10 ⁻⁸ W m ⁻² K ⁻⁴	exact*
Fermi coupling constant‡‡	$G_F/(\hbar c)^3$	1.166 378 8(6)×10 ⁻⁵ GeV ⁻²	510
weak-mixing angle	$\sin^2 \theta(M_Z)$ ($\overline{\text{MS}}$)	0.231 21(4)††	1.7 × 10 ⁵
W^\pm boson mass	m_W	80.377(12) GeV/c ² ¶	1.5 × 10 ⁵
Z^0 boson mass	m_Z	91.1876(21) GeV/c ²	2.3 × 10 ⁴
strong coupling constant	$\alpha_s(m_Z)$	0.1179(9)	7.6 × 10 ⁶
$\pi = 3.141 592 653 589 793 238 \dots$ $e = 2.718 281 828 459 045 235 \dots$ $\gamma = 0.577 215 664 901 532 860 \dots$			
1 in \equiv 0.0254 m	1 G \equiv 10 ⁻⁴ T	1 eV = 1.602 176 634 × 10 ⁻¹⁹ J (exact)	kT at 300 K = [38.681 727 0718...] ⁻¹ eV (exact*)
1 Å \equiv 0.1 nm	1 dyne \equiv 10 ⁻⁵ N	(1 kg)c ² = 5.609 588 603... × 10 ³⁵ eV(exact*)	0 °C \equiv 273.15K
1 barn \equiv 10 ⁻²⁸ m ²	1 erg \equiv 10 ⁻⁷ J	1 C = 2.997 924 58 × 10 ⁹ esu	1 atmosphere \equiv 760 Torr \equiv 101 325Pa

§CODATA recommends that the unit be J/Hz to stress that in $h = E/\nu$ the frequency ν is in cycles/sec (Hz), not radians/sec.

*These are calculated from exact values and are exact to the number of places given (*i.e.* no rounding).

**The molar mass of ¹²C is 11.999 999 9958(36) g.

†At $Q^2 = 0$. At $Q^2 \approx m_W^2$ the value is $\sim 1/128$.

‡Absolute laboratory measurements of G_N have been made only on scales of about 1 cm to 1 m.

‡‡See the discussion in Ch. 10, “Electroweak model and constraints on new physics.”

††The corresponding $\sin^2 \theta$ for the effective angle is 0.23153(4).

¶See the “Mass and width of the W boson” review.

References

[1] E. Tiesinga *et al.*, Rev. Mod. Phys. **93**, 025010 (2021).

2. Astrophysical Constants and Parameters

Table 2.1: Revised August 2021 by D.E. Groom (LBNL) and D. Scott (U. of British Columbia). The figures in parentheses after some values give the $1\text{-}\sigma$ uncertainties in the last digit(s). Physical constants are from Ref. [1]. While every effort has been made to obtain the most accurate current values of the listed quantities, this table does not represent a critical review or adjustment of the constants, and is not intended as a primary reference. The values and uncertainties for the cosmological parameters depend on the exact data sets, priors, and basis parameters used in the fit. Many of the derived parameters reported in this table have non-Gaussian likelihoods and parameters may be highly correlated, so care must be taken in propagating errors. Unless otherwise specified, cosmological parameters are derived from a 6-parameter Λ CDM cosmology fit to *Planck* cosmic microwave background 2018 temperature (TT) + polarization (TE,EE+lowE) + lensing data [2]. For more information see Ref. [3] and the original papers.

Quantity	Symbol, equation	Value	Reference, footnote
Newtonian constant of gravitation	G_N	$6.674\,30(15) \times 10^{-11} \text{ m}^3 \text{ kg}^{-1} \text{ s}^{-2}$	[1]
Planck mass	$M_P = \sqrt{\hbar c/G_N}$	$1.220\,890(14) \times 10^{19} \text{ GeV}/c^2 = 2.176\,434(24) \times 10^{-8} \text{ kg}$	[1]
Planck length	$l_P = \sqrt{\hbar G_N/c^3}$	$1.616\,255(18) \times 10^{-35} \text{ m}$	[1]
tropical year (equinox to equinox, 2020)	yr	$31\,556\,925.1 \text{ s} = 365.242\,189 \text{ days}$	[4]
sidereal year (period of Earth around Sun relative to stars)		$31\,558\,149.8 \text{ s} \approx \pi \times 10^7 \text{ s}$	[4]
mean sidereal day (Earth rotation period relative to stars)		$23^{\text{h}}\,56^{\text{m}}\,04^{\text{s}}.090\,53$	[4]
astronomical unit	au	$149\,597\,870\,700 \text{ m}$	exact [5]
parsec (1 au/1 arc sec)	pc	$3.085\,677\,581\,49 \dots \times 10^{16} \text{ m} = 3.261\,56 \dots \text{ ly}$	exact [6]
light year (deprecated unit)	ly	$0.306\,601 \dots \text{ pc} = 0.946\,073 \dots \times 10^{16} \text{ m}$	[7]
solid angle	deg ²	$(\pi/180)^2 \text{ sr} = 3.046\,17 \dots \times 10^{-4} \text{ sr}$	[8]
Schwarzschild radius of the Sun	$2G_N M_\odot/c^2$	$2.953\,250\,1 \text{ km}$	[9]
Solar mass	M_\odot	$1.988\,41(4) \times 10^{30} \text{ kg}$	[10]
nominal Solar equatorial radius	R_\odot	$6.957 \times 10^8 \text{ m}$	exact [11]
nominal Solar constant	S_\odot	1361 W m^{-2}	exact [11, 12]
nominal Solar photosphere temperature	T_\odot	5772 K	exact [11]
nominal Solar luminosity	L_\odot	$3.828 \times 10^{26} \text{ W}$	exact [11, 13]
Schwarzschild radius of the Earth	$2G_N M_\oplus/c^2$	$8.870\,056 \text{ mm}$	[9]
Earth mass	M_\oplus	$5.972\,17(13) \times 10^{24} \text{ kg}$	[10]
nominal Earth equatorial radius	R_\oplus	$6.3781 \times 10^6 \text{ m}$	exact [11]
Chandrasekhar mass	M_{Ch}	$3.097\,972 \mu^{-2} M_P^3/m_H^2 = 1.433\,77(6) (\mu/2)^{-2} M_\odot$	[14, 15]
Eddington luminosity	L_{Ed}	$1.257\,065\,179\,8(12) \times 10^{31} (M/M_\odot) \text{ W}$ $= 3.283\,869\,330\,8(31) \times 10^4 (M/M_\odot) L_\odot$	[16, 17]
jansky (flux density)	Jy	$10^{-26} \text{ W m}^{-2} \text{ Hz}^{-1}$	definition
luminosity conversion	f_0	$3.0128 \times 10^{28} \times 10^{-0.4 M_{\text{Bol}}} \text{ W}$ (M_{Bol} = absolute bolometric magnitude = bolometric magnitude at 10 pc)	exact [18]
flux conversion	\mathcal{F}	$2.518\,021\,002 \times 10^{-8} \times 10^{-0.4 m_{\text{Bol}}} \text{ W m}^{-2}$ (m_{Bol} = apparent bolometric magnitude)	exact [18]
ABsolute monochromatic magnitude	AB	$-2.5 \log_{10} f_\nu - 56.10$ (for f_ν in $\text{W m}^{-2} \text{ Hz}^{-1}$) $= -2.5 \log_{10} f_\nu + 8.90$ (for f_ν in Jy)	[19]
Solar angular velocity around Galactic center	Θ_0/R_0	$27.1(5) \text{ km s}^{-1} \text{ kpc}^{-1}$	[20]
Solar distance from Galactic center	R_0	$8.178 \pm 0.013(\text{stat.}) \pm 0.022(\text{sys.}) \text{ kpc}$	[21, 22]
circular velocity at R_0	v_0 or Θ_0	$240(8) \text{ km s}^{-1}$	[22, 23]
escape velocity from the Galaxy	v_{esc}	$492 \text{ km s}^{-1} < v_{\text{esc}} < 587 \text{ km s}^{-1}$ (90%)	[24]
local disk density	ρ_{disk}	$6.6(9) \times 10^{-24} \text{ g cm}^{-3} = 3.7(5) \text{ GeV}/c^2 \text{ cm}^{-3}$	[25]
local dark matter density	ρ_χ	canonical value $0.3 \text{ GeV}/c^2 \text{ cm}^{-3}$ within factor 2–3	[26]
present-day CMB temperature	T_0	$2.7255(6) \text{ K}$	[27, 28]
present-day CMB dipole amplitude	d	$3.3621(10) \text{ mK}$	[27, 29]
Solar velocity with respect to CMB	v_\odot	$369.82(11) \text{ km s}^{-1}$ towards $(l, b) = (264.021(11)^\circ, 48.253(5)^\circ)$	[29]
Local Group velocity with respect to CMB	v_{LG}	$620(15) \text{ km s}^{-1}$ towards $(l, b) = (271.9(20)^\circ, 29.6(14)^\circ)$	[29]
number density of CMB photons	n_γ	$410.73(27) (T/2.7255 \text{ K})^3 \text{ cm}^{-3}$	[30]
density of CMB photons	ρ_γ	$4.645(4) (T/2.7255 \text{ K})^4 \times 10^{-34} \text{ g cm}^{-3} \approx 0.260 \text{ eV cm}^{-3}$	[30]
entropy density/Boltzmann constant	s/k	$2.891.2 (T/2.7255 \text{ K})^3 \text{ cm}^{-3}$	[30]
present-day Hubble expansion rate	H_0	$100 \text{ h km s}^{-1} \text{ Mpc}^{-1} = h \times (9.777\,752 \text{ Gyr})^{-1}$	[31]
scaling factor for Hubble expansion rate	h	$0.674(5)$	[2, 32]
Hubble length	c/H_0	$0.925\,0629 \times 10^{26} \text{ h}^{-1} \text{ m} = 1.372(10) \times 10^{26} \text{ m}$	
scaling for cosmological constant	$c^2/3H_0^2$	$2.85247 \times 10^{51} \text{ h}^{-2} \text{ m}^2 = 6.28(9) \times 10^{51} \text{ m}^2$	
critical density of the Universe	$\rho_{\text{crit}} = 3H_0^2/8\pi G_N$	$1.878\,34(4) \times 10^{-29} \text{ h}^2 \text{ g cm}^{-3}$ $= 1.053\,672(24) \times 10^{-5} \text{ h}^2 (\text{GeV}/c^2) \text{ cm}^{-3}$ $= 2.77536627 \times 10^{11} \text{ h}^2 M_\odot \text{ Mpc}^{-3}$	
baryon-to-photon ratio (from BBN)	$\eta = n_b/n_\gamma$	$6.14(19) \times 10^{-10}$	[33, 34]
number density of baryons	n_b	$2.515(17) \times 10^{-7} \text{ cm}^{-3}$ (from CMB) $2.52(8) \times 10^{-7} \text{ cm}^{-3}$ (from BBN, $\eta \times n_\gamma$)	[2, 35] [3, 33]
CMB radiation density of the Universe	$\Omega_\gamma = \rho_\gamma/\rho_{\text{crit}}$	$2.473 \times 10^{-5} (T/2.7255 \text{ K})^4 \text{ h}^{-2} = 5.38(15) \times 10^{-5}$	[30]
- - - <i>Planck</i> 2018 6-parameter fit to flat Λ CDM cosmology - - -			
baryon density of the Universe	$\Omega_b = \rho_b/\rho_{\text{crit}}$	$\ddagger 0.02237(15) \text{ h}^{-2} = \dagger 0.0493(6)$	[2, 3, 27]
cold dark matter density of the Universe	$\Omega_c = \rho_c/\rho_{\text{crit}}$	$\ddagger 0.1200(12) \text{ h}^{-2} = \dagger 0.265(7)$	[2, 3, 27]
100 \times approximation to r_*/D_A	$100 \times \theta_{\text{MC}}$	$\ddagger 1.04092(31)$	[2, 3, 27]
reionization optical depth	τ	$\ddagger 0.054(7)$	[2, 3, 27]
ln(power prim. curv. pert.) ($k_0 = 0.05 \text{ Mpc}^{-1}$)	$\ln(10^{10} \Delta_{\mathcal{R}}^2)$	$\ddagger 3.044(14)$	[2, 3, 27]
scalar spectral index	n_s	$\ddagger 0.965(4)$	[2, 3, 27]
pressureless matter parameter	$\Omega_m = \Omega_c + \Omega_b$	$\dagger 0.315(7)$	[2, 3]
dark energy density parameter	Ω_Λ	$\dagger 0.685(7)$	[2, 3]
energy density of dark energy	ρ_Λ	$\dagger 5.83(16) \times 10^{-30} \text{ g cm}^{-3}$	[2]
cosmological constant	Λ	$\dagger 1.088(30) \times 10^{-56} \text{ cm}^{-2}$	[2]
fluctuation amplitude at $8 \text{ h}^{-1} \text{ Mpc}$ scale	σ_8	$\dagger 0.811(6)$	[2, 3]

Quantity	Symbol, equation.	Value	Reference, footnote
redshift of matter-radiation equality	z_{eq}	$\dagger 3402(26)$	[2, 36]
age at matter-radiation equality	t_{eq}	$\dagger 51.1(8)$ kyr	[2, 37]
redshift at which optical depth equals unity	z_*	$\dagger 1089.92(25)$	[2]
comoving size of sound horizon at z_*	r_*	$\dagger 144.43(26)$ Mpc	[2, 38]
age when optical depth equals unity	t_*	$\dagger 372.9(10)$ kyr	[2, 37]
redshift at half reionization	z_i	$\dagger 7.7(7)$	[2, 39]
age at half reionization	t_i	$\dagger 690(90)$ Myr	[2]
redshift when acceleration was zero	z_q	$\dagger 0.636(18)$	[2, 37]
age when acceleration was zero	t_q	$\dagger 7.70(10)$ Gyr	[2]
age of the Universe today	t_0	$\dagger 13.797(23)$ Gyr	[2]
effective number of neutrinos	N_{eff}	$\# 2.99(17)$	[2, 40, 41]
sum of neutrino masses	Σm_ν	$\# < 0.12$ eV (95%, CMB + BAO); ≥ 0.06 eV (mixing)	[2, 41–43]
neutrino density of the Universe	$\Omega_\nu = h^{-2} \Sigma m_\nu / 93.14 \text{ eV}$	$\# < 0.003$ (95%, CMB + BAO); ≥ 0.0012 (mixing)	[2, 42, 43]
curvature	Ω_K	$\# 0.0007(19)$	[2]
running spectral index, $k_0 = 0.05 \text{ Mpc}^{-1}$	$dn_s/d \ln k$	$\# -0.004(7)$	[2]
tensor-to-scalar perturbation ratio	$r_{0.05} = T/S$	$\# < 0.036$ (95% CL, $k_0 = 0.05 \text{ Mpc}^{-1}$)	[2, 44–47]
dark energy equation of state parameter	w	$\# -1.028(31)$	[2, 48]
primordial helium fraction	Y_p	$\# 0.2453(34)$	[49]

\dagger Parameter in 6-parameter Λ CDM fit; \ddagger derived parameter in 6-parameter Λ CDM fit; $\#$ extended model parameter, *Planck* + BAO data [2].

References

- [1] CODATA recommended 2018 values of the fundamental physical constants: physics.nist.gov/cuu/Constants/index.html.
- [2] Planck Collab. 2018 Results VI, *Astron. Astrophys.* **641**, A6 (2020), [arXiv:1807.06209].
- [3] O. Lahav and A. R. Liddle, “The Cosmological Parameters,” Sec. 25.1 in this *Review*.
- [4] *The Astronomical Almanac for the year 2020*.
- [5] The astronomical unit of length (au) in meters is re-defined (IAU XXVIII General Assembly 2012, Resolution B2) to be a conventional unit of length in agreement with the value adopted in IAU XXVII 2009 Resolution B2. It is to be used with all time scales.
- [6] The distance at which 1 au subtends 1 arc sec: 1 au divided by $\pi/648000$.
- [7] IAU XVI GA 1976, Recommendations.
- [8] The number of square degrees on a sphere is $360^2/\pi = 41259.9\dots$
- [9] Observationally determined mass parameter $G_N M \times 2/c^2$ [1] for either the Sun or the Earth, using the nominal values $\mathcal{G}M_\odot = 1.3271244 \times 10^{20} \text{ m}^3 \text{ s}^{-2}$ and $\mathcal{G}M_\oplus = 3.986004 \times 10^{14} \text{ m}^3 \text{ s}^{-2}$ [50]. The combination $G_N M$ is known much more precisely than either G_N or M individually. The digits are truncated here at the point where one would need to distinguish between Barycentric Coordinate Time (TCB) and Barycentric Dynamical Time (TDB).
- [10] $G_N M \div G_N$ [1].
- [11] IAU XXIX GA, 2015, Resolution B3, “on recommended nominal conversion constants . . .” The calligraphic symbol indicates the recommended nominal value.
- [12] See also G. Kopp and J. L. Lean, *Geophys. Res. Lett.* **38**, L01706 (2011), who give $(1360.8 \pm 0.6) \text{ W m}^{-2}$; see paper for caveats and other measurements.
- [13] $4\pi (1 \text{ au})^2 \times \mathcal{S}_\odot$, assuming isotropic irradiance.
- [14] S. Chandrasekhar, *Astrophys. J.* **74**, 81 (1931).
- [15] This value assumes an ideal Fermi gas, using a numerical constant from the Lane-Emden equation [51], and with μ the average molecular weight per electron, defined relative to the mass of the single-proton hydrogen atom.
- [16] A. S. Eddington, *Mon. Not. Roy. Astron. Soc.* **77**, 16 (1916).
- [17] The maximum luminosity assuming pure electron scattering for the outward force arising from radiation pressure: $4\pi G_N M m_p c / \sigma_T$.
- [18] IAU XXIX GA, 2015, Resolution B2, “on recommended zero points for the absolute and apparent bolometric magnitude scales”.
- [19] J. B. Oke and J. E. Gunn, *Astrophys. J.* **266**, 713 (1983).
- [20] J. Bovy, *Mon. Not. Roy. Astron. Soc.* **468**, 1, L63 (2017), [arXiv:1610.07610].
- [21] R. Abuter *et al.*, *Astron., Astrophys.* **625**, L10 (2019), [arXiv:1904.05721].
- [22] IAU XIX GA (1985) suggested that “in cases where standardization on a common set of galactic parameters is desirable” that the values $R_0 = (8.5 \pm 1.0) \text{ kpc}$ and $\theta_0 = (220 \pm 20) \text{ km s}^{-1}$ should be used.
- [23] M. J. Reid *et al.*, *Astrophys. J.* **783**, 130 (2014), [arXiv:1401.5377].
- [24] T. Piffl *et al.*, *Astron. Astrophys.* **562**, A91 (2014), [arXiv:1309.4293].
- [25] C. F. McKee, A. Parravano and D. J. Hollenbach, *Astrophys. J.* **814**, 1, 13 (2015), [arXiv:1509.05334]; this is representative of other published estimates.
- [26] J. I. Read, *J. Phys.* **G41**, 063101 (2014), [arXiv:1404.1938]; A. M. Green, *J. Phys.* **G44**, 8, 084001 (2017), [arXiv:1703.10102]; the conclusion is $\rho_{\text{DM}}^{\text{local}} = 0.39 \pm 0.03 \text{ GeV cm}^{-3}$.
- [27] D. Scott and G. F. Smoot, “Cosmic Microwave Background,” Sec. 29 in this *Review*.
- [28] D. J. Fixsen, *Astrophys. J.* **707**, 916 (2009), [arXiv:0911.1955].
- [29] Planck Collab. 2018 Results I, *Astron. Astrophys.* **641**, A1 (2020), [arXiv:1807.06205].
- [30] $n_\gamma = \frac{2\zeta(3)}{\pi^2} \left(\frac{kT}{hc}\right)^3$; $\rho_\gamma = \frac{\pi^2 kT}{15 c^2} \left(\frac{kT}{hc}\right)^3$; $s/k = \frac{2.43 \cdot \pi^2}{11.45} \left(\frac{kT}{hc}\right)^3$; $kT/hc = 11.90235(T/2.7255)/\text{cm}$.
- [31] Conversion using length of sidereal year.
- [32] Distance-ladder estimates of H_0 tend to give higher values than derived from the CMB, *e.g.* Riess *et al.*, *Astrophys. J.* **908**, L6 (2021) give $h = 0.732 \pm 0.013$; for discussion see O. Lahav and A. R. Liddle, “The Cosmological Parameters,” Sec. 25.1 in this *Review*.
- [33] B. D. Fields *et al.*, *JCAP* **03**, 010 (2020), [Erratum: *JCAP* 11, E02 (2020)], [arXiv:1912.01132].
- [34] B. D. Fields, P. Molaro and S. Sarkar, “Big-Bang Nucleosynthesis,” Sec. 24 in this *Review*.
- [35] n_b depends only upon the measured $\Omega_b h^2$, the average baryon mass at the present epoch (G. Steigman, *J. Cosmol. Astropart. Phys.*, **0610**, 016 (2006), [astro-ph/0606206]), and G_N : $n_b = (\Omega_b h^2)(h^{-2} \rho_{\text{crit}})/(0.93711 \text{ GeV}/c^2 \text{ per baryon})$.
- [36] Here “radiation” includes three species of light neutrinos as well as photons.
- [37] D. Scott, A. Narimani and D. N. Page, *Phys. Canada* **70**, 258 (2014), [arXiv:1309.2381].
- [38] D. H. Weinberg and M. White, “Dark Energy,” Sec. 28 in this *Review*.
- [39] Planck Collab. Interm. Results XLVI, *Astron. Astrophys.*, **596**, A108 (2016) extend the range by $\Delta z \approx 1$, depending on the reionization model.
- [40] Summary Tables in this *Review* list $N_\nu = 2.984(8)$ (Standard Model fits to LEP-SLC data). Because neutrinos are not completely decoupled at e^\pm annihilation, the effective number of massless neutrino species is 3.044, rather than 3.
- [41] J. Lesgourgues and L. Verde, “Neutrinos in Cosmology,” Sec. 26 in this *Review*.
- [42] The sum is over all neutrino mass eigenstates, the lower limit following from neutrino mixing results reported in this *Review* combined with the assumptions that there are three light neutrinos and that the lightest neutrino is substantially less massive than the others.
- [43] Astrophysical determinations of Σm_ν , reported in the Full Listings of this *Review* under “Sum of the neutrino masses,” range from $< 0.17 \text{ eV}$ to $< 2.3 \text{ eV}$ in papers published since 2003.
- [44] P. A. R. Ade *et al.* (BICEP2, Keck Array), *Phys. Rev. Lett.* **121**, 221301 (2018), [arXiv:1810.05216].
- [45] M. Tristram *et al.*, *Astron. Astrophys.* **647**, A128 (2021), [arXiv:2010.01139].
- [46] BICEP/Keck Collaboration, *Phys. Rev. Lett.* **127**, 151301 (2021), [arXiv:2110.00483].
- [47] *Planck* data alone give $r < 0.056$, using all power spectra; the currently tightest constraint comes from BICEP/Keck data, using *WMAP* and *Planck* to remove foregrounds.
- [48] This constraint uses BAO and SNe data, as described in Ref. [2]; see discussion in D. H. Weinberg and M. White, “Dark Energy,” Sec. 28 in this *Review*.
- [49] E. Aver *et al.*, *JCAP* **03**, 027 (2021), [arXiv:2010.04180].
- [50] IAU XXIX GA 2015, Resolution B2.
- [51] G. P. Horedt, *Astrophys. Space Sci.* **126**, 2, 357 (1986).

3. International System of Units (SI)

See D.B. Newell and E. Tiesinga, ed. (2019), “The International System of Units (SI)” (National Institute of Standards and Technology, Gaithersburg, MD), NIST Special Publication **330**, 2019 edition, <https://doi.org/10.6028/NIST.SP.330-2019>; and A. Thompson and B.N. Taylor (2008), “Guide for the Use of the International System of Units (SI)” (National Institute of Standards and Technology, Gaithersburg, MD), NIST Special Publication **811**, 2008 edition, <https://doi.org/10.6028/NIST.SP.811e2008>.

SI prefixes		
10^{24}	yotta	(Y)
10^{21}	zetta	(Z)
10^{18}	exa	(E)
10^{15}	peta	(P)
10^{12}	tera	(T)
10^9	giga	(G)
10^6	mega	(M)
10^3	kilo	(k)
10^2	hecto	(h)
10	deca	(da)
10^{-1}	deci	(d)
10^{-2}	centi	(c)
10^{-3}	milli	(m)
10^{-6}	micro	(μ)
10^{-9}	nano	(n)
10^{-12}	pico	(p)
10^{-15}	femto	(f)
10^{-18}	atto	(a)
10^{-21}	zepto	(z)
10^{-24}	yocto	(y)

Physical quantity	Name of unit	Symbol
<i>Base units</i>		
length	meter	m
mass	kilogram	kg
time	second	s
electric current	ampere	A
thermodynamic temperature	kelvin	K
amount of substance	mole	mol
luminous intensity	candela	cd
<i>Derived units with special names</i>		
plane angle	radian	rad
solid angle	steradian	sr
frequency	hertz	Hz
energy	joule	J
force	newton	N
pressure	pascal	Pa
power	watt	W
electric charge	coulomb	C
electric potential	volt	V
electric resistance	ohm	Ω
electric conductance	siemens	S
electric capacitance	farad	F
magnetic flux	weber	Wb
inductance	henry	H
magnetic flux density	tesla	T
luminous flux	lumen	lm
illuminance	lux	lx
celsius temperature	degree celsius	$^{\circ}\text{C}$
activity (of a radioactive source)*	becquerel	Bq
absorbed dose (of ionizing radiation)*	gray	Gy
dose equivalent*	sievert	Sv

* See our section 37, on “Radioactivity and radiation protection.”

Table 4.1. Revised June 2021 by D.E. Groom (LBNL). The atomic number (top left) is the number of protons in the nucleus. The atomic masses (bottom) of stable elements are weighted by isotopic abundances in the Earth's surface. Atomic masses are relative to the mass of ^{12}C , defined to be exactly 12 unified atomic mass units (u). The exceptions are Th, Pa, and U, which have no stable isotopes but do have characteristic terrestrial compositions. Relative isotopic abundances often vary considerably, both in natural and commercial samples; this is reflected in the number of significant figures given for the mass. Masses may be found at https://physics.nist.gov/cgi-bin/Compositions/stand_alone.pl. If there is no stable isotope, the atomic mass of the most stable isotope known as of June 2019 is given in parentheses.

IUPAC announced verification of the discoveries of elements 113, 115, 117, and 118 in December 2015. The names were approved November 2016. The 7th period of the periodic table is now complete. Attempts to synthesize elements with $Z > 118$ are under way, but as of July 2021 no discoveries have been announced.

1 IA																		18 VIIIA																	
1 H hydrogen 1.008																	2 He helium 4.002602																		
3 Li lithium 6.94	4 Be beryllium 9.012182	PERIODIC TABLE OF THE ELEMENTS														5 B boron 10.81	6 C carbon 12.0107	7 N nitrogen 14.007	8 O oxygen 15.999	9 F fluorine 18.998403163	10 Ne neon 20.1797														
11 Na sodium 22.98976928	12 Mg magnesium 24.305	3 IIIB	4 IVB	5 VB	6 VIB	7 VIIB	8	9 VIII	10	11 IB	12 IIB	13 Al aluminum 26.9815385	14 Si silicon 28.085	15 P phosphorus 30.973761998	16 S sulfur 32.06	17 Cl chlorine 35.45	18 Ar argon 39.948																		
19 K potassium 39.0983	20 Ca calcium 40.078	21 Sc scandium 44.955908	22 Ti titanium 47.867	23 V vanadium 50.9415	24 Cr chromium 51.9961	25 Mn manganese 54.938044	26 Fe iron 55.845	27 Co cobalt 58.933195	28 Ni nickel 58.6934	29 Cu copper 63.546	30 Zn zinc 65.38	31 Ga gallium 69.723	32 Ge germanium 72.630	33 As arsenic 74.921595	34 Se selenium 78.971	35 Br bromine 79.904	36 Kr krypton 83.798																		
37 Rb rubidium 85.4678	38 Sr strontium 87.62	39 Y yttrium 88.90584	40 Zr zirconium 91.224	41 Nb niobium 92.90637	42 Mo molybdenum 95.95	43 Tc technetium (97.907212)	44 Ru ruthenium 101.07	45 Rh rhodium 102.90550	46 Pd palladium 106.42	47 Ag silver 107.8682	48 Cd cadmium 112.414	49 In indium 114.818	50 Sn tin 118.710	51 Sb antimony 121.760	52 Te tellurium 127.60	53 I iodine 126.90447	54 Xe xenon 131.293																		
55 Cs caesium 132.90545196	56 Ba barium 137.327	57–71 LANTHANIDES	72 Hf hafnium 178.49	73 Ta tantalum 180.94788	74 W tungsten 183.84	75 Re rhenium 186.207	76 Os osmium 190.23	77 Ir iridium 192.217	78 Pt platinum 195.084	79 Au gold 196.966569	80 Hg mercury 200.592	81 Tl thallium 204.38	82 Pb lead 207.2	83 Bi bismuth 208.98040	84 Po polonium (208.98243)	85 At astatine (209.98715)	86 Rn radon (222.01758)																		
87 Fr francium (223.01974)	88 Ra radium (226.02541)	89–103 ACTINIDES	104 Rf rutherford. (267.12169)	105 Db dubnium (268.12567)	106 Sg seaborgium (269.12863)	107 Bh bohrium (270.13336)	108 Hs hassium (269.13375)	109 Mt meitnerium (278.15631)	110 Ds darmstadt. (281.16451)	111 Rg roentgen. (282.16912)	112 Cn copernicium (285.17712)	113 Nh nihonium (286.18221)	114 Fl flerovium (289.19042)	115 Mc moscovium (290.19598)	116 Lv livermorium (293.20449)	117 Ts tennessine (294.21046)	118 Og oganesson (294.21392)																		

Lanthanide series

57 La lanthanum 138.90547	58 Ce cerium 140.116	59 Pr praseodym. 140.90766	60 Nd neodymium 144.242	61 Pm promethium (144.91276)	62 Sm samarium 150.36	63 Eu europium 151.964	64 Gd gadolinum 157.25	65 Tb terbium 158.92535	66 Dy dysprosium 162.500	67 Ho holmium 164.93033	68 Er erbium 167.259	69 Tm thulium 168.93422	70 Yb ytterbium 173.054	71 Lu lutetium 174.9668
------------------------------------	-------------------------------	-------------------------------------	----------------------------------	---------------------------------------	--------------------------------	---------------------------------	---------------------------------	----------------------------------	-----------------------------------	----------------------------------	-------------------------------	----------------------------------	----------------------------------	----------------------------------

Actinide series

89 Ac actinium (227.02775)	90 Th thorium 232.0377	91 Pa protactinium 231.03588	92 U uranium 238.02891	93 Np neptunium (237.04817)	94 Pu plutonium (244.06420)	95 Am americium (243.06138)	96 Cm curium (247.07035)	97 Bk berkelium (247.07031)	98 Cf californium (251.07959)	99 Es einsteinium (252.08298)	100 Fm fermium (257.09511)	101 Md mendelevium (258.09844)	102 No nobelium (259.10103)	103 Lr lawrencium (262.10961)
-------------------------------------	---------------------------------	---------------------------------------	---------------------------------	--------------------------------------	--------------------------------------	--------------------------------------	-----------------------------------	--------------------------------------	--	--	-------------------------------------	---	--------------------------------------	--

5. Electronic Structure of the Elements

Table 5.1: Reviewed 2011 by J.E. Sansonetti (NIST). The electronic configurations and the ionization energies are from the NIST database, "Ground Levels and Ionization Energies for the Neutral Atoms," W.C. Martin, A. Musgrove, S. Kotochigova, and J.E. Sansonetti, https://www.nist.gov/pml/data/ion_energy.cfm. The electron configuration for, say, iron indicates an argon electronic core (see argon) plus six 3d electrons and two 4s electrons.

	Element	Electron configuration ($3d^5 =$ five 3d electrons, etc.)	Ground state $2S+1L_J$	Ionization energy (eV)	
1	H	Hydrogen	1s	$^2S_{1/2}$	13.5984
2	He	Helium	$1s^2$	1S_0	24.5874
3	Li	Lithium	(He) 2s	$^2S_{1/2}$	5.3917
4	Be	Beryllium	(He) $2s^2$	1S_0	9.3227
5	B	Boron	(He) $2s^2 2p$	$^2P_{1/2}$	8.2980
6	C	Carbon	(He) $2s^2 2p^2$	3P_0	11.2603
7	N	Nitrogen	(He) $2s^2 2p^3$	$^4S_{3/2}$	14.5341
8	O	Oxygen	(He) $2s^2 2p^4$	3P_2	13.6181
9	F	Fluorine	(He) $2s^2 2p^5$	$^2P_{3/2}$	17.4228
10	Ne	Neon	(He) $2s^2 2p^6$	1S_0	21.5645
11	Na	Sodium	(Ne) 3s	$^2S_{1/2}$	5.1391
12	Mg	Magnesium	(Ne) $3s^2$	1S_0	7.6462
13	Al	Aluminum	(Ne) $3s^2 3p$	$^2P_{1/2}$	5.9858
14	Si	Silicon	(Ne) $3s^2 3p^2$	3P_0	8.1517
15	P	Phosphorus	(Ne) $3s^2 3p^3$	$^4S_{3/2}$	10.4867
16	S	Sulfur	(Ne) $3s^2 3p^4$	3P_2	10.3600
17	Cl	Chlorine	(Ne) $3s^2 3p^5$	$^2P_{3/2}$	12.9676
18	Ar	Argon	(Ne) $3s^2 3p^6$	1S_0	15.7596
19	K	Potassium	(Ar) 4s	$^2S_{1/2}$	4.3407
20	Ca	Calcium	(Ar) $4s^2$	1S_0	6.1132
21	Sc	Scandium	(Ar) 3d 4s ²	T $^2D_{3/2}$	6.5615
22	Ti	Titanium	(Ar) $3d^2 4s^2$	r e 3F_2	6.8281
23	V	Vanadium	(Ar) $3d^3 4s^2$	a l $^4F_{3/2}$	6.7462
24	Cr	Chromium	(Ar) $3d^5 4s$	n e 7S_3	6.7665
25	Mn	Manganese	(Ar) $3d^5 4s^2$	s m $^6S_{5/2}$	7.4340
26	Fe	Iron	(Ar) $3d^6 4s^2$	i e 5D_4	7.9024
27	Co	Cobalt	(Ar) $3d^7 4s^2$	t n $^4F_{9/2}$	7.8810
28	Ni	Nickel	(Ar) $3d^8 4s^2$	i t 3F_4	7.6399
29	Cu	Copper	(Ar) $3d^{10} 4s$	o s $^2S_{1/2}$	7.7264
30	Zn	Zinc	(Ar) $3d^{10} 4s^2$	n 1S_0	9.3942
31	Ga	Gallium	(Ar) $3d^{10} 4s^2 4p$	$^2P_{1/2}$	5.9993
32	Ge	Germanium	(Ar) $3d^{10} 4s^2 4p^2$	3P_0	7.8994
33	As	Arsenic	(Ar) $3d^{10} 4s^2 4p^3$	$^4S_{3/2}$	9.7886
34	Se	Selenium	(Ar) $3d^{10} 4s^2 4p^4$	3P_2	9.7524
35	Br	Bromine	(Ar) $3d^{10} 4s^2 4p^5$	$^2P_{3/2}$	11.8138
36	Kr	Krypton	(Ar) $3d^{10} 4s^2 4p^6$	1S_0	13.9996
37	Rb	Rubidium	(Kr) 5s	$^2S_{1/2}$	4.1771
38	Sr	Strontium	(Kr) $5s^2$	1S_0	5.6949
39	Y	Yttrium	(Kr) 4d 5s ²	T $^2D_{3/2}$	6.2173
40	Zr	Zirconium	(Kr) $4d^2 5s^2$	r e 3F_2	6.6339
41	Nb	Niobium	(Kr) $4d^4 5s$	a l $^6D_{1/2}$	6.7589
42	Mo	Molybdenum	(Kr) $4d^5 5s$	n e 7S_3	7.0924
43	Tc	Technetium	(Kr) $4d^5 5s^2$	s m $^6S_{5/2}$	7.28
44	Ru	Ruthenium	(Kr) $4d^7 5s$	i e 5F_5	7.3605
45	Rh	Rhodium	(Kr) $4d^8 5s$	t n $^4F_{9/2}$	7.4589
46	Pd	Palladium	(Kr) $4d^{10}$	i t 1S_0	8.3369
47	Ag	Silver	(Kr) $4d^{10} 5s$	o s $^2S_{1/2}$	7.5762
48	Cd	Cadmium	(Kr) $4d^{10} 5s^2$	n 1S_0	8.9938

Element			Electron configuration ($3d^5 =$ five $3d$ electrons, etc.)				Ground state $2S+1L_J$	Ionization energy (eV)
49	In	Indium	(Kr)	$4d^{10}$	$5s^2$	$5p$	$^2P_{1/2}$	5.7864
50	Sn	Tin	(Kr)	$4d^{10}$	$5s^2$	$5p^2$	3P_0	7.3439
51	Sb	Antimony	(Kr)	$4d^{10}$	$5s^2$	$5p^3$	$^4S_{3/2}$	8.6084
52	Te	Tellurium	(Kr)	$4d^{10}$	$5s^2$	$5p^4$	3P_2	9.0096
53	I	Iodine	(Kr)	$4d^{10}$	$5s^2$	$5p^5$	$^2P_{3/2}$	10.4513
54	Xe	Xenon	(Kr)	$4d^{10}$	$5s^2$	$5p^6$	1S_0	12.1298
55	Cs	Cesium	(Xe)			$6s$	$^2S_{1/2}$	3.8939
56	Ba	Barium	(Xe)			$6s^2$	1S_0	5.2117
57	La	Lanthanum	(Xe)		$5d$	$6s^2$	$^2D_{3/2}$	5.5769
58	Ce	Cerium	(Xe)	$4f$	$5d$	$6s^2$	1G_4	5.5387
59	Pr	Praseodymium	(Xe)	$4f^3$		$6s^2$	$^4I_{9/2}$	5.473
60	Nd	Neodymium	(Xe)	$4f^4$		$6s^2$	5I_4	5.5250
61	Pm	Promethium	(Xe)	$4f^5$		$6s^2$	$^6H_{5/2}$	5.582
62	Sm	Samarium	(Xe)	$4f^6$		$6s^2$	7F_0	5.6437
63	Eu	Europium	(Xe)	$4f^7$		$6s^2$	$^8S_{7/2}$	5.6704
64	Gd	Gadolinium	(Xe)	$4f^7$	$5d$	$6s^2$	9D_2	6.1498
65	Tb	Terbium	(Xe)	$4f^9$		$6s^2$	$^6H_{15/2}$	5.8638
66	Dy	Dysprosium	(Xe)	$4f^{10}$		$6s^2$	5I_8	5.9389
67	Ho	Holmium	(Xe)	$4f^{11}$		$6s^2$	$^4I_{15/2}$	6.0215
68	Er	Erbium	(Xe)	$4f^{12}$		$6s^2$	3H_6	6.1077
69	Tm	Thulium	(Xe)	$4f^{13}$		$6s^2$	$^2F_{7/2}$	6.1843
70	Yb	Ytterbium	(Xe)	$4f^{14}$		$6s^2$	1S_0	6.2542
71	Lu	Lutetium	(Xe)	$4f^{14}$	$5d$	$6s^2$	$^2D_{3/2}$	5.4259
72	Hf	Hafnium	(Xe)	$4f^{14}$	$5d^2$	$6s^2$	3F_2	6.8251
73	Ta	Tantalum	(Xe)	$4f^{14}$	$5d^3$	$6s^2$	$^4F_{3/2}$	7.5496
74	W	Tungsten	(Xe)	$4f^{14}$	$5d^4$	$6s^2$	5D_0	7.8640
75	Re	Rhenium	(Xe)	$4f^{14}$	$5d^5$	$6s^2$	$^6S_{5/2}$	7.8335
76	Os	Osmium	(Xe)	$4f^{14}$	$5d^6$	$6s^2$	5D_4	8.4382
77	Ir	Iridium	(Xe)	$4f^{14}$	$5d^7$	$6s^2$	$^4F_{9/2}$	8.9670
78	Pt	Platinum	(Xe)	$4f^{14}$	$5d^9$	$6s$	3D_3	8.9588
79	Au	Gold	(Xe)	$4f^{14}$	$5d^{10}$	$6s$	$^2S_{1/2}$	9.2255
80	Hg	Mercury	(Xe)	$4f^{14}$	$5d^{10}$	$6s^2$	1S_0	10.4375
81	Tl	Thallium	(Xe)	$4f^{14}$	$5d^{10}$	$6s^2$	$^2P_{1/2}$	6.1082
82	Pb	Lead	(Xe)	$4f^{14}$	$5d^{10}$	$6s^2$	3P_0	7.4167
83	Bi	Bismuth	(Xe)	$4f^{14}$	$5d^{10}$	$6s^2$	$^4S_{3/2}$	7.2855
84	Po	Polonium	(Xe)	$4f^{14}$	$5d^{10}$	$6s^2$	3P_2	8.414
85	At	Astatine	(Xe)	$4f^{14}$	$5d^{10}$	$6s^2$	$^2P_{3/2}$	
86	Rn	Radon	(Xe)	$4f^{14}$	$5d^{10}$	$6s^2$	1S_0	10.7485
87	Fr	Francium	(Rn)			$7s$	$^2S_{1/2}$	4.0727
88	Ra	Radium	(Rn)			$7s^2$	1S_0	5.2784
89	Ac	Actinium	(Rn)		$6d$	$7s^2$	$^2D_{3/2}$	5.3807
90	Th	Thorium	(Rn)		$6d^2$	$7s^2$	3F_2	6.3067
91	Pa	Protactinium	(Rn)	$5f^2$	$6d$	$7s^2$	$^4K_{11/2}^*$	5.89
92	U	Uranium	(Rn)	$5f^3$	$6d$	$7s^2$	$^5L_6^*$	6.1939
93	Np	Neptunium	(Rn)	$5f^4$	$6d$	$7s^2$	$^6L_{11/2}^*$	6.2657
94	Pu	Plutonium	(Rn)	$5f^6$		$7s^2$	7F_0	6.0260
95	Am	Americium	(Rn)	$5f^7$		$7s^2$	$^8S_{7/2}$	5.9738
96	Cm	Curium	(Rn)	$5f^7$	$6d$	$7s^2$	9D_2	5.9914
97	Bk	Berkelium	(Rn)	$5f^9$		$7s^2$	$^6H_{15/2}$	6.1979
98	Cf	Californium	(Rn)	$5f^{10}$		$7s^2$	5I_8	6.2817
99	Es	Einsteinium	(Rn)	$5f^{11}$		$7s^2$	$^4I_{15/2}$	6.3676
100	Fm	Fermium	(Rn)	$5f^{12}$		$7s^2$	3H_6	6.50
101	Md	Mendelevium	(Rn)	$5f^{13}$		$7s^2$	$^2F_{7/2}$	6.58
102	No	Nobelium	(Rn)	$5f^{14}$		$7s^2$	1S_0	6.65
103	Lr	Lawrencium	(Rn)	$5f^{14}$		$7s^2$	$^2P_{1/2}?$	4.9?
104	Rf	Rutherfordium	(Rn)	$5f^{14}$	$6d^2$	$7s^2?$	$^3F_2?$	6.0?

* The usual LS coupling scheme does not apply for these three elements.
See the introductory note to the NIST table from which this table is taken.

6. Atomic and Nuclear Properties of Materials

Table 6.1: Abridged from <https://pdg.lbl.gov/current/AtomicNuclearProperties> by D.E. Groom (2021). See web pages for more detail about entries in this table and for several hundred others. Parentheses in the dE/dx and density columns indicate gases at 20° C and 1 atm. Boiling points are at 1 atm. Refractive indices n are evaluated at the sodium D line blend (589.2 nm); values $\gg 1$ in brackets indicate $(n - 1) \times 10^6$ for gases at 0° C and 1 atm.

Material	Z	A	$\langle Z/A \rangle$	Nucl.coll. length λ_T {g cm ⁻² }	Nucl.inter. length λ_I {g cm ⁻² }	Rad.len. $dE/dx _{\min}$ X_0 {g cm ⁻² }	Density {g cm ⁻³ }	Melting point (K)	Boiling point (K)	Refract. index @ Na D
H ₂	1	1.008(7)	0.99212	42.8	52.0	63.05 (4.103)	0.071(0.084)	13.81	20.28	1.11[132.]
D ₂	1	2.014101764(8)	0.49650	51.3	71.8	125.97 (2.053)	0.169(0.168)	18.7	23.65	1.11[138.]
He	2	4.002602(2)	0.49967	51.8	71.0	94.32 (1.937)	0.125(0.166)		4.220	1.02[35.0]
Li	3	6.94(2)	0.43221	52.2	71.3	82.78 1.639	0.534	453.6	1615.	
Be	4	9.0121831(5)	0.44384	55.3	77.8	65.19 1.595	1.848	1560.	2744.	
C diamond	6	12.0107(8)	0.49955	59.2	85.8	42.70 1.725	3.520			2.419
C graphite	6	12.0107(8)	0.49955	59.2	85.8	42.70 1.742	2.210	Sublimes at 4098. K		
N ₂	7	14.007(2)	0.49976	61.1	89.7	37.99 (1.825)	0.807(1.165)	63.15	77.29	1.20[298.]
O ₂	8	15.999(3)	0.50002	61.3	90.2	34.24 (1.801)	1.141(1.332)	54.36	90.20	1.22[271.]
F ₂	9	18.998403163(6)	0.47372	65.0	97.4	32.93 (1.676)	1.507(1.580)	53.53	85.03	[195.]
Ne	10	20.1797(6)	0.49555	65.7	99.0	28.93 (1.724)	1.204(0.839)	24.56	27.07	1.09[67.1]
Al	13	26.9815385(7)	0.48181	69.7	107.2	24.01 1.615	2.699	933.5	2792.	
Si	14	28.0855(3)	0.49848	70.2	108.4	21.82 1.664	2.329	1687.	3538.	
Cl ₂	17	35.453(2)	0.47951	73.8	115.7	19.28 (1.630)	1.574(2.980)	171.6	239.1	[773.]
Ar	18	39.948(1)	0.45059	75.7	119.7	19.55 (1.519)	1.396(1.662)	83.81	87.26	1.23[281.]
Ti	22	47.867(1)	0.45961	78.8	126.2	16.16 1.477	4.540	1941.	3560.	
Fe	26	55.845(2)	0.46557	81.7	132.1	13.84 1.451	7.874	1811.	3134.	
Cu	29	63.546(3)	0.45636	84.2	137.3	12.86 1.403	8.960	1358.	2835.	
Ge	32	72.630(1)	0.44053	86.9	143.0	12.25 1.370	5.323	1211.	3106.	
Sn	50	118.710(7)	0.42119	98.2	166.7	8.82 1.263	7.310	505.1	2875.	
Xe	54	131.293(6)	0.41129	100.8	172.1	8.48 (1.255)	2.953(5.483)	161.4	165.1	1.39[701.]
W	74	183.84(1)	0.40252	110.4	191.9	6.76 1.145	19.300	3695.	5828.	
Pt	78	195.084(9)	0.39983	112.2	195.7	6.54 1.128	21.450	2042.	4098.	
Au	79	196.966569(5)	0.40108	112.5	196.3	6.46 1.134	19.320	1337.	3129.	
Pb	82	207.2(1)	0.39575	114.1	199.6	6.37 1.122	11.350	600.6	2022.	
U	92	[238.02891(3)]	0.38651	118.6	209.0	6.00 1.081	18.950	1408.	4404.	
Air (dry, 1 atm)			0.49919	61.3	90.1	36.62 (1.815)	(1.205)		78.80	[289]
Shielding concrete			0.50274	65.1	97.5	26.57 1.711	2.300			
Borosilicate glass (Pyrex)			0.49707	64.6	96.5	28.17 1.696	2.230			
Lead glass			0.42101	95.9	158.0	7.87 1.255	6.220			
Standard rock			0.50000	66.8	101.3	26.54 1.688	2.650			
Methane (CH ₄)			0.62334	54.0	73.8	46.47 (2.417)	(0.667)	90.68	111.7	[444.]
Ethane (C ₂ H ₆)			0.59861	55.0	75.9	45.66 (2.304)	(1.263)	90.36	184.5	
Propane (C ₃ H ₈)			0.58962	55.3	76.7	45.37 (2.262)	0.493(1.868)	85.52	231.0	
Butane (C ₄ H ₁₀)			0.59497	55.5	77.1	45.23 (2.278)	(2.489)	134.9	272.6	
Octane (C ₈ H ₁₈)			0.57778	55.8	77.8	45.00 2.123	0.703	214.4	398.8	
Paraffin (CH ₃ (CH ₂) _n ≈23CH ₃)			0.57275	56.0	78.3	44.85 2.088	0.930			
Nylon (type 6, 6/6)			0.54790	57.5	81.6	41.92 1.973	1.18			
Polycarbonate (Lexan)			0.52697	58.3	83.6	41.50 1.886	1.20			
Polyethylene ([CH ₂ CH ₂] _n)			0.57034	56.1	78.5	44.77 2.079	0.89			
Polyethylene terephthalate (Mylar)			0.52037	58.9	84.9	39.95 1.848	1.40			
Polyimide film (Kapton)			0.51264	59.2	85.5	40.58 1.820	1.42			
Polymethylmethacrylate (acrylic)			0.53937	58.1	82.8	40.55 1.929	1.19			1.49
Polypropylene			0.55998	56.1	78.5	44.77 2.041	0.90			
Polystyrene ([C ₆ H ₅ CHCH ₂] _n)			0.53768	57.5	81.7	43.79 1.936	1.06			1.59
Polytetrafluoroethylene (Teflon)			0.47992	63.5	94.4	34.84 1.671	2.20			
Polyvinyltoluene			0.54141	57.3	81.3	43.90 1.956	1.03			1.58
Aluminum oxide (sapphire)			0.49038	65.5	98.4	27.94 1.647	3.970	2327.	3273.	1.77
Barium fluoride (BaF ₂)			0.42207	90.8	149.0	9.91 1.303	4.893	1641.	2533.	1.47
Bismuth germanate (BGO)			0.42065	96.2	159.1	7.97 1.251	7.130	1317.		2.15
Carbon dioxide gas (CO ₂)			0.49989	60.7	88.9	36.20 1.819	(1.842)			[449.]
Solid carbon dioxide (dry ice)			0.49989	60.7	88.9	36.20 1.787	1.563	Sublimes at 194.7 K		
Cesium iodide (CsI)			0.41569	100.6	171.5	8.39 1.243	4.510	894.2	1553.	1.79
Lithium fluoride (LiF)			0.46262	61.0	88.7	39.26 1.614	2.635	1121.	1946.	1.39
Lithium hydride (LiH)			0.50321	50.8	68.1	79.62 1.897	0.820	965.		
Lead tungstate (PbWO ₄)			0.41315	100.6	168.3	7.39 1.229	8.300	1403.		2.20
Silicon dioxide (SiO ₂ , fused quartz)			0.49930	65.2	97.8	27.05 1.699	2.200	1986.	3223.	1.46
Sodium chloride (NaCl)			0.47910	71.2	110.1	21.91 1.847	2.170	1075.	1738.	1.54
Sodium iodide (NaI)			0.42697	93.1	154.6	9.49 1.305	3.667	933.2	1577.	1.77
Water (H ₂ O)			0.55509	58.5	83.3	36.08 1.992	1.000	273.1	373.1	1.33
Silica aerogel			0.50093	65.0	97.3	27.25 1.740	0.200	(0.03 H ₂ O, 0.97 SiO ₂)		
Epoxy (Epotek-301-1)			0.53409	58.1	83.0	41.22 1.925	1.190			

Material	Dielectric constant ($\kappa = \epsilon/\epsilon_0$) () is $(\kappa-1)\times 10^6$ for gas	Young's modulus [10^6 psi]	Coeff. of thermal expansion [10^{-6} cm/cm- $^\circ$ C]	Specific heat [cal/g- $^\circ$ C]	Electrical resistivity [$\mu\Omega$ cm(@ $^\circ$ C)]	Thermal conductivity [cal/cm- $^\circ$ C-sec]
H ₂	(253.9)	—	—	—	—	—
He	(64)	—	—	—	—	—
Li	—	—	56	0.86	8.55(0 $^\circ$)	0.17
Be	—	37	12.4	0.436	5.885(0 $^\circ$)	0.38
C	—	0.7	0.6–4.3	0.165	1375(0 $^\circ$)	0.057
N ₂	(548.5)	—	—	—	—	—
O ₂	(495)	—	—	—	—	—
Ne	(127)	—	—	—	—	—
Al	—	10	23.9	0.215	2.65(20 $^\circ$)	0.53
Si	11.9	16	2.8–7.3	0.162	—	0.20
Ar	(517)	—	—	—	—	—
Ti	—	16.8	8.5	0.126	50(0 $^\circ$)	—
Fe	—	28.5	11.7	0.11	9.71(20 $^\circ$)	0.18
Cu	—	16	16.5	0.092	1.67(20 $^\circ$)	0.94
Ge	16.0	—	5.75	0.073	—	0.14
Sn	—	6	20	0.052	11.5(20 $^\circ$)	0.16
Xe	—	—	—	—	—	—
W	—	50	4.4	0.032	5.5(20 $^\circ$)	0.48
Pt	—	21	8.9	0.032	9.83(0 $^\circ$)	0.17
Pb	—	2.6	29.3	0.038	20.65(20 $^\circ$)	0.083
U	—	—	36.1	0.028	29(20 $^\circ$)	0.064

7. Electromagnetic Relations

Revised September 2005 by H.G. Spieler (LBNL).

Quantity	Gaussian CGS	SI
Conversion factors:		
Charge:	$2.997\,924\,58 \times 10^9$ esu	$= 1\text{ C} = 1\text{ A s}$
Potential:	$(1/299.792\,458)$ statvolt (ergs/esu)	$= 1\text{ V} = 1\text{ J C}^{-1}$
Magnetic field:	10^4 gauss $= 10^4$ dyne/esu	$= 1\text{ T} = 1\text{ N A}^{-1}\text{m}^{-1}$
	$\mathbf{F} = q(\mathbf{E} + \frac{\mathbf{v}}{c} \times \mathbf{B})$	$\mathbf{F} = q(\mathbf{E} + \mathbf{v} \times \mathbf{B})$
	$\nabla \cdot \mathbf{D} = 4\pi\rho$ $\nabla \times \mathbf{H} - \frac{1}{c} \frac{\partial \mathbf{D}}{\partial t} = \frac{4\pi}{c} \mathbf{J}$ $\nabla \cdot \mathbf{B} = 0$ $\nabla \times \mathbf{E} + \frac{1}{c} \frac{\partial \mathbf{B}}{\partial t} = 0$	$\nabla \cdot \mathbf{D} = \rho$ $\nabla \times \mathbf{H} - \frac{\partial \mathbf{D}}{\partial t} = \mathbf{J}$ $\nabla \cdot \mathbf{B} = 0$ $\nabla \times \mathbf{E} + \frac{\partial \mathbf{B}}{\partial t} = 0$
Constitutive relations:	$\mathbf{D} = \mathbf{E} + 4\pi\mathbf{P}$, $\mathbf{H} = \mathbf{B} - 4\pi\mathbf{M}$	$\mathbf{D} = \epsilon_0\mathbf{E} + \mathbf{P}$, $\mathbf{H} = \mathbf{B}/\mu_0 - \mathbf{M}$
Linear media:	$\mathbf{D} = \epsilon\mathbf{E}$, $\mathbf{H} = \mathbf{B}/\mu$ 1 1	$\mathbf{D} = \epsilon\mathbf{E}$, $\mathbf{H} = \mathbf{B}/\mu$ $\epsilon_0 = 8.854\,187\dots \times 10^{-12}$ F m ⁻¹ $\mu_0 = 4\pi \times 10^{-7}$ N A ⁻²
	$\mathbf{E} = -\nabla V - \frac{1}{c} \frac{\partial \mathbf{A}}{\partial t}$ $\mathbf{B} = \nabla \times \mathbf{A}$	$\mathbf{E} = -\nabla V - \frac{\partial \mathbf{A}}{\partial t}$ $\mathbf{B} = \nabla \times \mathbf{A}$
	$V = \sum_{\text{charges}} \frac{q_i}{r_i} = \int \frac{\rho(\mathbf{r}')}{ \mathbf{r} - \mathbf{r}' } d^3x'$ $\mathbf{A} = \frac{1}{c} \oint \frac{I d\boldsymbol{\ell}}{ \mathbf{r} - \mathbf{r}' } = \frac{1}{c} \int \frac{\mathbf{J}(\mathbf{r}')}{ \mathbf{r} - \mathbf{r}' } d^3x'$	$V = \frac{1}{4\pi\epsilon_0} \sum_{\text{charges}} \frac{q_i}{r_i} = \frac{1}{4\pi\epsilon_0} \int \frac{\rho(\mathbf{r}')}{ \mathbf{r} - \mathbf{r}' } d^3x'$ $\mathbf{A} = \frac{\mu_0}{4\pi} \oint \frac{I d\boldsymbol{\ell}}{ \mathbf{r} - \mathbf{r}' } = \frac{\mu_0}{4\pi} \int \frac{\mathbf{J}(\mathbf{r}')}{ \mathbf{r} - \mathbf{r}' } d^3x'$
	$\mathbf{E}'_{\parallel} = \mathbf{E}_{\parallel}$ $\mathbf{E}'_{\perp} = \gamma(\mathbf{E}_{\perp} + \frac{1}{c} \mathbf{v} \times \mathbf{B})$ $\mathbf{B}'_{\parallel} = \mathbf{B}_{\parallel}$ $\mathbf{B}'_{\perp} = \gamma(\mathbf{B}_{\perp} - \frac{1}{c} \mathbf{v} \times \mathbf{E})$	$\mathbf{E}'_{\parallel} = \mathbf{E}_{\parallel}$ $\mathbf{E}'_{\perp} = \gamma(\mathbf{E}_{\perp} + \mathbf{v} \times \mathbf{B})$ $\mathbf{B}'_{\parallel} = \mathbf{B}_{\parallel}$ $\mathbf{B}'_{\perp} = \gamma(\mathbf{B}_{\perp} - \frac{1}{c^2} \mathbf{v} \times \mathbf{E})$
$\frac{1}{4\pi\epsilon_0} = c^2 \times 10^{-7}$ N A ⁻² $= 8.987\,55\dots \times 10^9$ m F ⁻¹ ; $\frac{\mu_0}{4\pi} = 10^{-7}$ N A ⁻² ; $c = \frac{1}{\sqrt{\mu_0\epsilon_0}} = 2.997\,924\,58 \times 10^8$ m s ⁻¹		

7.1 Impedances (SI units)

ρ = resistivity at room temperature in $10^{-8}\Omega\text{ m}$:

- ~ 1.7 for Cu ~ 5.5 for W
- ~ 2.4 for Au ~ 73 for SS 304
- ~ 2.8 for Al ~ 100 for Nichrome

(Al alloys may have double the Al value.)

For alternating currents, instantaneous current I , voltage V , angular frequency ω :

$$V = V_0 e^{j\omega t} = ZI \tag{7.1}$$

Impedance of self-inductance L : $Z = j\omega L$.

Impedance of capacitance C : $Z = 1/j\omega C$.

Impedance of free space: $Z = \sqrt{\mu_0/\epsilon_0} = 376.7\Omega$.

High-frequency surface impedance of a good conductor:

$$Z = \frac{(1+j)\rho}{\delta}, \quad \text{where } \delta = \text{skin depth}; \tag{7.2}$$

$$\delta = \sqrt{\frac{\rho}{\pi\nu\mu}} \approx \frac{6.6\text{ cm}}{\sqrt{\nu(\text{Hz})}} \text{ for Cu.} \tag{7.3}$$

7.2 Capacitors, inductors, and transmission Lines

The capacitance between two parallel plates of area A spaced by the distance d and enclosing a medium with the dielectric constant ϵ is

$$C = K\epsilon A/d, \tag{7.4}$$

where the correction factor K depends on the extent of the fringing field. If the dielectric fills the capacitor volume without extending beyond the electrodes. The correction factor $K \approx 0.8$ for capacitors of typical geometry.

The inductance at high frequencies of a straight wire whose length ℓ is much greater than the wire diameter d is

$$L \approx 2.0 \left[\frac{\text{nH}}{\text{cm}} \right] \cdot \ell \left(\ln \left(\frac{4\ell}{d} \right) - 1 \right). \tag{7.5}$$

For very short wires, representative of vias in a printed circuit board, the inductance is

$$L(\text{in nH}) \approx \ell/d. \tag{7.6}$$

A transmission line is a pair of conductors with inductance L and capacitance C . The characteristic impedance $Z = \sqrt{L/C}$ and the phase velocity $v_p = 1/\sqrt{LC} = 1/\sqrt{\mu\epsilon}$, which decreases with the inverse square root of the dielectric constant of the medium. Typical coaxial and ribbon cables have a propagation delay of about 5 ns/cm.

The impedance of a coaxial cable with outer diameter D and inner diameter d is

$$Z = 60 \Omega \cdot \frac{1}{\sqrt{\epsilon_r}} \ln \frac{D}{d}, \quad (7.7)$$

where the relative dielectric constant $\epsilon_r = \epsilon/\epsilon_0$. A pair of parallel wires of diameter d and spacing $a > 2.5d$ has the impedance

$$Z = 120 \Omega \cdot \frac{1}{\sqrt{\epsilon_r}} \ln \frac{2a}{d}. \quad (7.8)$$

This yields the impedance of a wire at a spacing h above a ground plane,

$$Z = 60 \Omega \cdot \frac{1}{\sqrt{\epsilon_r}} \ln \frac{4h}{d}. \quad (7.9)$$

A common configuration utilizes a thin rectangular conductor above a ground plane with an intermediate dielectric (microstrip). Detailed calculations for this and other transmission line configurations are given by Gunston [1].

7.3 Synchrotron radiation (CGS units)

For a particle of charge e , velocity $v = \beta c$, and energy $E = \gamma mc^2$, traveling in a circular orbit of radius R , the classical energy loss per revolution δE is

$$\delta E = \frac{4\pi}{3} \frac{e^2}{R} \beta^3 \gamma^4. \quad (7.10)$$

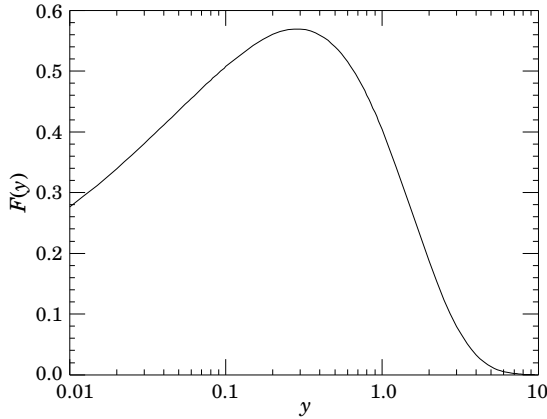


Figure 7.1: The normalized synchrotron radiation spectrum $F(y)$.

For high-energy electrons or positrons ($\beta \approx 1$), this becomes

$$\delta E \text{ (in MeV)} \approx 0.0885 [E \text{ (in GeV)}]^4 / R \text{ (in m)}. \quad (7.11)$$

For $\gamma \gg 1$, the energy radiated per revolution into the photon energy interval $d(\hbar\omega)$ is

$$dI = \frac{8\pi}{9} \alpha \gamma F(\omega/\omega_c) d(\hbar\omega), \quad (7.12)$$

where $\alpha = e^2/\hbar c$ is the fine-structure constant and

$$\omega_c = \frac{3\gamma^3 c}{2R} \quad (7.13)$$

is the critical frequency. The normalized function $F(y)$ is

$$F(y) = \frac{9}{8\pi} \sqrt{3} y \int_y^\infty K_{5/3}(x) dx, \quad (7.14)$$

where $K_{5/3}(x)$ is a modified Bessel function of the third kind. For electrons or positrons,

$$\hbar\omega_c \text{ (in keV)} \approx 2.22 [E \text{ (in GeV)}]^3 / R \text{ (in m)}. \quad (7.15)$$

For $\gamma \gg 1$ and $\omega \ll \omega_c$,

$$\frac{dI}{d(\hbar\omega)} \approx 3.3\alpha (\omega R/c)^{1/3}, \quad (7.16)$$

whereas for

$$\gamma \gg 1 \text{ and } \omega \gtrsim 3\omega_c,$$

$$\frac{dI}{d(\hbar\omega)} \approx \sqrt{\frac{3\pi}{2}} \alpha \gamma \left(\frac{\omega}{\omega_c}\right)^{1/2} e^{-\omega/\omega_c} \left[1 + \frac{55}{72} \frac{\omega_c}{\omega} + \dots\right]. \quad (7.17)$$

The radiation is confined to angles $\lesssim 1/\gamma$ relative to the instantaneous direction of motion. For $\gamma \gg 1$, where Eq. (7.12) applies, the mean number of photons emitted per revolution is

$$N_\gamma = \frac{5\pi}{\sqrt{3}} \alpha \gamma, \quad (7.18)$$

and the mean energy per photon is

$$\langle \hbar\omega \rangle = \frac{8}{15\sqrt{3}} \hbar\omega_c. \quad (7.19)$$

When $\langle \hbar\omega \rangle \gtrsim O(E)$, quantum corrections are important [2].¹

References

- [1] M.A.R. Gunston. *Microwave Transmission Line Data*, Noble Publishing Corp., Atlanta (1997) ISBN 1-884932-57-6, TK6565.T73G85.
- [2] J.D. Jackson, *Classical Electrodynamics*, 3rd edition (John Wiley & Sons, New York, 1998) for more formulae and details.

¹Note that earlier editions of Ref. [2] had ω_c twice as large as Eq. (7.13).

8. Naming Scheme for Hadrons

Revised August 2021 by V.D. Burkert (Jefferson Lab), C. Hanhart (Jülich), R.E. Mitchell (Indiana U.), C. Patrignani (Bologna U.), U. Thoma (Bonn U.), L. Tiator (KPH, JGU Mainz) and R.L. Workman (George Washington U.).

In the 1986 edition [1], the Particle Data Group extended and systematized the naming scheme for mesons and baryons. The extensions were necessary in order to name the new particles containing c or b quarks that were rapidly being discovered. With the discoveries of particles that are candidates for states with more complicated structures than just $q\bar{q}$ or qqq , it is necessary to extend the naming scheme again.

8.1 “Neutral-flavor” mesons

The naming of mesons is based on their quantum numbers. Although wherever possible we use names established within the naive quark model, the name does *not* necessarily designate a (predominantly) $q\bar{q}$ state. In other words, the name provides information on the quantum numbers of a given state and not about its dominant component, which might well be $q\bar{q}$ (if allowed) or tetraquark, molecule, etc. In many cases, exotic states will be difficult to distinguish from $q\bar{q}$ states and will likely mix with them, and we make no attempt to, e.g., distinguish those that are “mostly gluonium” from those that are “mostly $q\bar{q}$.”

Table 8.1: Symbols for mesons with strangeness and heavy-flavor quantum numbers equal to zero. States that do not (yet?) appear in the RPP are listed in parentheses.

$J^{PC} = \left\{ \begin{array}{cccc} 0^{-+} & 1^{+-} & 1^{--} & 0^{++} \\ 2^{-+} & 3^{+-} & 2^{--} & 1^{++} \\ \vdots & \vdots & \vdots & \vdots \end{array} \right.$				
Minimal quark content				
$u\bar{d}, u\bar{u} - d\bar{d}, d\bar{u}$ ($I = 1$)	π	b	ρ	a
$d\bar{d} + u\bar{u}$ and/or $s\bar{s}$ ($I = 0$)	η, η'	h, h'	ω, ϕ	f, f'
$c\bar{c}$	η_c	h_c	ψ^*	χ_c
$b\bar{b}$	η_b	h_b	Υ	χ_b
$I = 1$ with $c\bar{c}$	(H_c)	Z_c	R_c	(W_c)
$I = 1/2$ with $sc\bar{c}$	(H_{cs})	Z_{cs}	(R_{cs})	(W_{cs})
$I = 1$ with $b\bar{b}$	(H_b)	Z_b	(R_b)	(W_b)
$I = 1/2$ with $sb\bar{b}$	(H_{bs})	(Z_{bs})	(R_{bs})	(W_{bs})

*The J/ψ remains the J/ψ .

Table 8.1 shows the names for mesons having strangeness and all heavy-flavor quantum numbers equal to zero. The rows of Table 8.1 give the minimal $q\bar{q}$ content. The columns give the possible parity/charge-conjugation states,

$$PC = ++, +-, --, \text{ and } ++.$$

Within the naive quark model, these combinations correspond one-to-one to the angular-momentum state ${}^{2S+1}L_J$ of the $q\bar{q}$ system being

$${}^1(L \text{ even})_J, {}^1(L \text{ odd})_J, {}^3(L \text{ even})_J, \text{ or } {}^3(L \text{ odd})_J,$$

respectively. Here S , L , and J are the spin, orbital, and total angular momenta of the $q\bar{q}$ system. Within the naive quark model, the quantum numbers are related by $P = (-1)^{L+1}$, $C = (-1)^{L+S}$, and G parity $= (-1)^{L+S+I}$, where the quantum number C is only relevant to neutral mesons with neutral-flavor quantum numbers and G extends to isovector mesons; see the review on the quark model. These expressions impose restrictions on the quantum numbers that are allowed for $q\bar{q}$ states. However, they do not apply to more complicated structures such as tetraquarks.

The spin J is added as a subscript in the name except for pseudoscalar, vector, and axial vector mesons when there is no risk of ambiguity. Moreover, the mass is added in parentheses for mesons that decay strongly. However, for some of the familiar mesons (e.g. η' , ϕ , ω), we omit the mass.

Measurements of the mass, quark content (where relevant), and quantum numbers I , J , P , and C (or G) of a meson thus determine its symbol. Conversely, these properties may be inferred unambiguously from the symbol. The name X is used for states with still unknown quantum numbers.

The mass label used in particle names is chosen using the best information available when a name is assigned. A more accurate value of a particle mass may become available at a later time. PDG will decide on a case-by-case basis whether to revise the mass label, taking into account the updated information.

With u , d , and s quarks, there are two isospin-0 mesons. A prime is used to distinguish one from the other (e.g. η and η'). Vector mesons decoupling to $u\bar{u} + d\bar{d}$ and $s\bar{s}$ (ideal mixing) are labeled ω and ϕ , respectively. As usual, we assign the spectroscopic name (e.g. $\Upsilon(1S)$) as the primary name to most of those ψ , Υ , and χ states whose spectroscopic identity is known. We use the form $\Upsilon(9460)$ as an alternative, and as the primary name when the spectroscopic identity is not known.

Since the top quark is so heavy that it decays too rapidly to form bound states, no name is assigned to structures like $t\bar{t}$.

Mesons with quantum numbers $J^{PC} = 0^{-+}, 0^{+-}, 1^{-+}, 2^{+-}, 3^{-+}$, etc. cannot be $q\bar{q}$. For such a “manifestly exotic” meson, we use the same symbol as for a $q\bar{q}$ meson; the exotic nature of the meson can be inferred from the values of the P and C quantum numbers (given by the symbol), and the spin J (given by the subscript). For example, an isospin-0 1^{-+} meson containing only u , d , and s quarks and antiquarks would be denoted η_1 and an isospin-1 0^{-+} meson containing only u , d , and s quarks and antiquarks would be denoted ρ_0 .

The last two lines of Table 8.1 list isospin-1 states that also contain hidden heavy flavor, i.e. whose minimal quark content includes $c\bar{c}$ or $b\bar{b}$. We have assigned new names to these states, in keeping with the practice in the light-quark sector, where the $I = 0$ and $I = 1$ states have distinct names. The currently established $I = 1$ states in the heavy-quark sector have quantum numbers $J^{PC} = 1^{+-}$ and the proposed scheme keeps their original names Z .

Recently two experiments claimed evidence for states with 1^{+-} decaying into final states containing $sc\bar{c}$ and a light quark calling them Z_{cs} . We therefore extended Tab. 8.1 by allowing also for multiquarks containing strangeness.

8.2 Remarks on “neutral-flavor” mesons with hidden charm or bottom not classified as $q\bar{q}$

In the heavy-quark sector, there are several states with properties – such as masses, decay patterns, and widths – that are in disagreement with predictions from the naive quark model. For example, the vector state at 4230 MeV does not decay into $D\bar{D}$, although within the naive quark model its quantum numbers would call for this decay channel to be dominant. In recent literature, these states have been called X , Y , or Z , with their masses added in parentheses. This nomenclature conflicts with the rules outlined in the previous section, since the meson names are not related to their quantum numbers. However, these states have properties in conflict with the naive quark model and therefore deserve some special labeling.

Therefore in the Review of Particle Physics we will keep two names, one that carries the quantum number information and the other the original name. However, the former name will be given priority. In particular, it will be used when the particle appears as a decay product. Thus, in the Listings as well as Summary Tables from the 2018 edition onwards (listed are only some examples of the particles that appear in the Summary Tables),

- $X(3872)$ will appear as ‘ $\chi_{c1}(3872)$ also known as $X(3872)$ ’;
- $X(3900)^\pm$ will appear as ‘ $Z_c(3900)^\pm$ ’;
- $X(4260)$ will appear as ‘ $\psi(4230)$ also known as $Y(4230)$ ’¹;

In addition, states with quantum numbers allowed by the naive quark model but showing some peculiarities, such as an unusual decay pattern, will have the following information in the header:

¹This is one example where the mass label needed to be shifted given improved experimental information

This state shows properties different from a conventional $q\bar{q}$ state. A candidate for an exotic structure. See the review on (name of the proper review).

The states that cannot be classified as $q\bar{q}$ states (such as charged states with strong decays to heavy quarkonia) will have in the header:

Properties incompatible with a $q\bar{q}$ structure (exotic state). See the review on (name of the proper review).

The names Z_c and Z_b used in the literature for isovector states in the $c\bar{c}$ and $b\bar{b}$ sector, respectively, will now also be the official PDG names. No heavy isovector $PC = -, -, \text{ or } ++$ states have yet been confirmed, but provisional names for such states – Π , R , and W , respectively – are listed in Table 8.1. Note that the heavy isovector $PC = ++$ states were predicted to exist as spin partners of the Z states in [2], where the name W was also introduced.

By analogy to the light-quark sector, states with quantum numbers that are in conflict with the naive quark model are labeled according to their I , P , C , and spin J . The exotic nature can be inferred from the quantum numbers.

Table 8.2 maps the names now used in the PDG to former commonly used names.

Table 8.2: A comparison of current PDG names to former names commonly used in the literature.

Mesons with complete $I^G J^{PC}$ assignment	
PDG Name	Former Common Name(s)
$\psi_2(3823)^*$	$X(3823)$
$\chi_{c1}(3872)$	$X(3872)$
$Z_c(3900)$	$Z_c(3900)$
$\chi_{c2}(3930)^\dagger$	$\chi_{c2}(2P)$, $Z(3930)$
$\chi_{c1}(4140)$	$Y(4140)$
$Z_c(4200)$	$Z_c(4200)$
$\psi(4230)$	$Y(4230)$, $Y(4260)$
$R_{c0}(4240)$	$Z_c(4240)$
$\chi_{c1}(4274)$	$Y(4274)$
$\psi(4360)$	$Y(4360)$
$Z_c(4430)$	$Z_c(4430)$
$\chi_{c0}(4500)$	$X(4500)$
$\psi(4660)$	$X(4630)$, $Y(4660)$
$\chi_{c0}(4700)$	$X(4700)$
$Z_b(10610)$	$Z_b(10610)$
$Z_b(10650)$	$Z_b^{(\prime)}(10650)$
Mesons with incomplete $I^G J^{PC}$ assignment	
PDG Name	Former Common Name(s)
$X(3915)^\ddagger$	$\chi_{c0}(3915)$, $X(3915)$, $Y(3940)$
$X(3940)$	$X(3940)$
$X(4020)$	$Z_c^{(\prime)}(4020)$
$X(4050)^\pm$	$Z_1(4050)$
$X(4055)^\pm$	$Z_c(4055)$
$X(4160)$	$X(4160)$
$X(4250)^\pm$	$Z_2(4250)$
$X(4350)$	$X(4350)$

*The 2016 edition used $\psi(3823)$.

†The 2016 edition used $\chi_{c2}(2P)$. The mass is now used in the name following the current prescription.

‡The 2016 edition used $\chi_{c0}(3915)$. The J^{PC} have since been questioned.

8.3 Mesons with nonzero S , C and/or B

Mesons with nonzero strangeness S or heavy flavor C and/or B are not eigenstates of charge conjugation, and in each of them one of the quarks is heavier than the other (as above, states containing top quarks are not considered). The rules have been and remain:

1. The main symbol is an upper-case italic letter indicating the heavier quark as follows:

$$s \rightarrow \bar{K} \quad c \rightarrow D \quad b \rightarrow \bar{B},$$

We use the convention that *the flavor quantum number and the charge of a quark have the same sign*. Thus the strangeness of the s quark is negative, the charm of the c quark is positive, and the bottomness of the b quark is negative. The effect of this convention is as follows: *any flavor carried by a charged meson has the same sign as its charge*. Thus the K^+ , D^+ , and B^+ have positive strangeness, charm, and bottomness, respectively, and all have positive I_3 . The D_s^+ has positive charm *and* strangeness. Furthermore, the $\Delta(\text{flavor}) = \Delta Q$ rule, best known for the strange kaons, applies to every flavor.

2. If the lighter quark is not a u or a d quark, its identity is given by a subscript. The D_s^+ is an example.
3. When the spin-parity is in the natural series, $J^P = 0^+, 1^-, 2^+, \dots$, a superscript “*” is added.
4. The spin is added as a subscript except for pseudoscalar or vector mesons.

8.4 Baryons with ordinary quantum numbers

All baryons having quantum numbers consistent with a minimal quark content of three quarks are denoted by the symbols N , Δ , Λ , Σ , Ξ , and Ω introduced more than 50 years ago. These symbols are followed by J^P signifying their spin J and parity P . For those where the minimal content involves one or more heavier quarks than the light (u , d , and s) quarks, subscripts are added to their symbols, (c and b) as appropriate. The rules are:

1. Baryons with minimal content of *three* u and/or d quarks are N 's (isospin 1/2) or Δ 's (isospin 3/2).
2. Baryons with *two* u and/or d quarks are Λ 's (isospin 0) or Σ 's (isospin 1). If the third quark is a c or b quark, its identity is given by a subscript.
3. Baryons with *one* u or d quark are Ξ 's (isospin 1/2). One or two subscripts are used if one or both of the remaining quarks are heavy: thus Ξ_c , Ξ_{cc} , Ξ_b , etc.*
4. Baryons with *no* u or d quarks are Ω 's (isospin 0), and subscripts indicate any heavy-quark content.
5. A baryon that decays strongly has its mass in parentheses. Examples are the $\Delta(1232)$ $3/2^+$, $\Sigma(1385)$ $3/2^+$, $N(1440)$ $1/2^+$, $\Xi_c(2645)$ $3/2^+$.
6. If individual states of isospin multiplets are addressed, the electric charge is specified as a superscript. The electric charge is not necessary for isospin-0 states (Λ and Ω), as there is no ambiguity, but may still be included.
7. Antibaryons are labeled by an overline (bar) (e.g. \bar{p} for the antiproton). Alternatively, particle and antiparticle can be distinguished by including a charge-label superscript. For example using Λ_c and $\bar{\Lambda}_c$ is equivalent to Λ_c^+ and Λ_c^- .

In short, the minimal number of u plus d quarks together with the isospin determine the main symbol, and subscripts indicate any content of heavy quarks. A Σ always has isospin 1, an Ω always has isospin 0, etc.

8.5 Exotic baryons

In 2003, several experiments reported finding a strangeness $S = +1$, charge $Q = +1$ baryon, and one experiment reported finding an $S = -2$, $Q = -2$ baryon. Baryons with such quantum numbers cannot be made from three quarks, and thus they are exotic with respect to the naive quark model. However, these “discoveries” were then ruled out by many experiments with far larger statistics: See our 2008 *Review* [3].

More recently, the LHCb collaboration found a series of candidates for pentaquark states in the $J/\psi p$ system extracted from data on $\Lambda_b^0 \rightarrow J/\psi K^- p$ [4, 5]**. These have the quantum numbers of excited nucleons, but have a minimal quark content of $c\bar{c}uud$. Following the name established by the LHCb collaboration, we label these $P_c^+(\text{mass})J^P$, with the mass given in parentheses.

Footnotes:

* See the “Note on Charmed Baryons” in the Charmed Baryon Listings.

** See our review “Pentaquarks” in the 2016 Edition.

References

- [1] M. Aguilar-Benitez *et al.* (Particle Data Group), Phys. Lett. **170B**, 1 (1986).
- [2] M. B. Voloshin, Phys. Rev. **D84**, 031502 (2011), [arXiv:1105.5829].
- [3] C. Amsler *et al.* (Particle Data Group), Phys. Lett. **B667**, 1 (2008).
- [4] R. Aaij *et al.* (LHCb), Phys. Rev. Lett. **115**, 072001 (2015), [arXiv:1507.03414].
- [5] R. Aaij *et al.* (LHCb), Phys. Rev. Lett. **122**, 22, 222001 (2019), [arXiv:1904.03947].

Standard Model and Related Topics

9. Quantum chromodynamics (rev.)	149
10. Electroweak model and constraints on new physics (rev.)	177
11. Higgs boson physics, status of (rev.)	201
12. CKM quark-mixing matrix (rev.)	261
13. <i>CP</i> violation in the quark sector (rev.)	271
14. Neutrino masses, mixing, and oscillations (rev.)	285
15. Quark model (rev.)	312
16. Heavy-quark & soft-collinear effective theory	329
17. Lattice quantum chromodynamics (rev.)	337
18. Structure functions (rev.)	353
19. Fragmentation functions in e^+e^- , ep and pp collisions (rev.)	375
20. High Energy Soft QCD and Diffraction	392

9. Quantum Chromodynamics

Revised August 2021 by J. Huston (Michigan State U.), K. Rabbertz (KIT) and G. Zanderighi (MPI Munich).

9.1	Basics	149
9.1.1	Running coupling	149
9.1.2	Quark masses	150
9.2	Structure of QCD predictions	150
9.2.1	Fully inclusive cross sections	150
9.2.2	Processes with initial-state hadrons	151
9.2.3	Cross sections with phase-space restrictions	153
9.2.4	Accuracy of predictions	156
9.3	Experimental studies of QCD	157
9.3.1	Hadronic final-state observables	157
9.3.2	QCD measurements at colliders	159
9.4	Determinations of the strong coupling constant	162
9.4.1	Hadronic τ decays and low Q^2 continuum:	163
9.4.2	Heavy quarkonia decays:	164
9.4.3	PDF fits:	164
9.4.4	Hadronic final states of e^+e^- annihilations:	164
9.4.5	Observables from hadron-induced collisions:	165
9.4.6	Electroweak precision fit:	165
9.4.7	Lattice QCD:	166
9.4.8	Determination of the world average value of $\alpha_s(M_Z^2)$:	166

9.1 Basics

Quantum Chromodynamics (QCD), the gauge field theory that describes the strong interactions of colored quarks and gluons, is the SU(3) component of the SU(3)×SU(2)×U(1) Standard Model of Particle Physics. The Lagrangian of QCD is given by

$$\mathcal{L} = \sum_q \bar{\psi}_{q,a} (i\gamma^\mu \partial_\mu \delta_{ab} - g_s \gamma^\mu t_{ab}^C \mathcal{A}_\mu^C - m_q \delta_{ab}) \psi_{q,b} - \frac{1}{4} F_{\mu\nu}^A F^{A\mu\nu}, \quad (9.1)$$

where repeated indices are summed over. The γ^μ are the Dirac γ -matrices. The $\psi_{q,a}$ are quark-field spinors for a quark of flavor q and mass m_q , with a color-index a that runs from $a = 1$ to $N_c = 3$, *i.e.* quarks come in three “colors.” Quarks are said to be in the fundamental representation of the SU(3) color group.

The \mathcal{A}_μ^C correspond to the gluon fields, with C running from 1 to $N_c^2 - 1 = 8$, *i.e.* there are eight kinds of gluon. Gluons transform under the adjoint representation of the SU(3) color group. The t_{ab}^C correspond to eight 3×3 matrices and are the generators of the SU(3) group (*cf.* the section on “SU(3) isoscalar factors and representation matrices” in this *Review*, with $t_{ab}^C \equiv \lambda_{ab}^C/2$). They encode the fact that a gluon’s interaction with a quark rotates the quark’s color in SU(3) space. The quantity g_s (or $\alpha_s = \frac{g_s^2}{4\pi}$) is the QCD coupling constant. Besides quark masses, which have electroweak origin, it is the only fundamental parameter of QCD. Finally, the field tensor $F_{\mu\nu}^A$ is given by

$$F_{\mu\nu}^A = \partial_\mu \mathcal{A}_\nu^A - \partial_\nu \mathcal{A}_\mu^A - g_s f_{ABC} \mathcal{A}_\mu^B \mathcal{A}_\nu^C, \quad [t^A, t^B] = if_{ABC} t^C, \quad (9.2)$$

where the f_{ABC} are the structure constants of the SU(3) group.

Neither quarks nor gluons are observed as free particles. Hadrons are color-singlet (*i.e.* color-neutral) combinations of quarks, anti-quarks, and gluons.

Ab-initio predictive methods for QCD include lattice gauge theory and perturbative expansions in the coupling. The Feynman rules of QCD involve a quark-antiquark-gluon ($q\bar{q}g$) vertex, a 3-gluon vertex (both proportional to g_s), and a 4-gluon vertex (proportional to g_s^2). A full set of Feynman rules is to be found for example in Refs. [1, 2].

Adopting a standard notation where repeated indices are summed over, useful color-algebra relations include: $t_{ab}^A t_{bc}^A = C_F \delta_{ac}$, where $C_F \equiv (N_c^2 - 1)/(2N_c) = 4/3$ is the color factor (“Casimir”) associated with gluon emission from a quark; $f_{ACD} f_{BCD} = C_A \delta_{AB}$, where $C_A \equiv N_c = 3$ is the color factor

associated with gluon emission from a gluon; $t_{ab}^A t_{ab}^B = T_R \delta_{AB}$, where $T_R = 1/2$ is the color factor for a gluon to split to a $q\bar{q}$ pair.

There is freedom for an additional CP -violating term to be present in the QCD Lagrangian, $\theta \frac{\alpha_s}{8\pi} F_{\mu\nu}^A \tilde{F}^{A\mu\nu}$, where θ is an additional free parameter, and $\tilde{F}^{A\mu\nu}$ is the dual of the gluon field tensor, $\frac{1}{2} \epsilon_{\mu\nu\sigma\rho} F^{A\sigma\rho}$, with $\epsilon_{\mu\nu\sigma\rho}$ being the fully antisymmetric Levi-Civita symbol. Experimental limits on ultracold neutrons [3, 4] and atomic mercury [5] constrain the QCD vacuum angle to satisfy $|\theta| \lesssim 10^{-10}$. Further discussion is to be found in Ref. [6] and in the Axions section in the Listings of this *Review*.

This section will concentrate mainly on perturbative aspects of QCD as they relate to collider physics. Related textbooks and lecture notes include Refs. [1, 2, 7–9]. Aspects specific to Monte Carlo event generators are reviewed in the dedicated section 43. Lattice QCD is also reviewed in a section of its own, Sec. 17, with further discussion of perturbative and non-perturbative aspects to be found in the sections on “Quark Masses”, “The CKM quark-mixing matrix”, “Structure Functions”, “Fragmentation Functions”, “Passage of Particles Through Matter” and “Heavy-Quark and Soft-Collinear Effective Theory” in this *Review*.

9.1.1 Running coupling

In the framework of perturbative QCD (pQCD), predictions for observables are expressed in terms of the renormalized coupling $\alpha_s(\mu_R^2)$, a function of an (unphysical) renormalization scale μ_R . When one takes μ_R close to the scale of the momentum transfer Q in a given process, then $\alpha_s(\mu_R^2 \simeq Q^2)$ is indicative of the effective strength of the strong interaction in that process.

The coupling satisfies the following renormalization group equation (RGE):

$$\mu_R^2 \frac{d\alpha_s}{d\mu_R^2} = \beta(\alpha_s) = -(b_0 \alpha_s^2 + b_1 \alpha_s^3 + b_2 \alpha_s^4 + \dots), \quad (9.3)$$

where $b_0 = (11C_A - 4n_f T_R)/(12\pi) = (33 - 2n_f)/(12\pi)$ is referred to as the 1-loop β -function coefficient, the 2-loop coefficient is $b_1 = (17C_A^2 - n_f T_R(10C_A + 6C_F))/(24\pi^2) = (153 - 19n_f)/(24\pi^2)$, and the 3-loop coefficient is $b_2 = (2857 - \frac{5033}{9} n_f + \frac{325}{27} n_f^2)/(128\pi^3)$ for the SU(3) values of C_A and C_F . Here n_f is the number of quark flavours. The 4-loop coefficient, b_3 , is to be found in Refs. [10, 11], while the 5-loop coefficient, b_4 , is in Refs. [12–16]. The coefficients b_2 and b_3 (and beyond) are renormalization-scheme-dependent and given here in the modified minimal subtraction scheme ($\overline{\text{MS}}$) [17], by far the most widely used scheme in QCD and the one adopted in the following.

The minus sign in Eq. (9.3) is the origin of “asymptotic freedom” [18, 19], *i.e.* the fact that the strong coupling becomes weak for processes involving large momentum transfers (“hard processes”). For momentum transfers in the 0.1–1 TeV range, $\alpha_s \sim 0.1$, while the theory is strongly interacting for scales around and below 1 GeV.

The β -function coefficients, the b_i , are given for the coupling of an *effective theory* in which n_f of the quark flavors are considered light ($m_q \ll \mu_R$), and in which the remaining heavier quark flavors decouple from the theory. One may relate the coupling for the theory with $n_f + 1$ light flavors to that with n_f flavors through an equation of the form

$$\alpha_s^{(n_f+1)}(\mu_R^2) = \alpha_s^{(n_f)}(\mu_R^2) \times \left(1 + \sum_{n=1}^{\infty} \sum_{\ell=0}^n c_{n\ell} [\alpha_s^{(n_f)}(\mu_R^2)]^n \ln^\ell \frac{\mu_R^2}{m_h^2} \right), \quad (9.4)$$

where m_h is the mass of the $(n_f + 1)$ th flavor, and the first few $c_{n\ell}$ coefficients are $c_{11} = \frac{1}{6\pi}$, $c_{10} = 0$, $c_{22} = c_{11}^2$, $c_{21} = \frac{11}{24\pi^2}$, and $c_{20} = -\frac{11}{72\pi^2}$ when m_h is the $\overline{\text{MS}}$ mass at scale m_h , while $c_{20} = \frac{7}{24\pi^2}$ when m_h is the pole mass (mass definitions are discussed below in Sec. (9.1.2) and in the review on “Quark Masses”). Terms up to $c_{4\ell}$ with $0 \leq \ell \leq 4$ are to be found in Refs. [20, 21].

Numerically, when one chooses $\mu_R = m_h$, the matching is a modest effect, owing to the zero value for the c_{10} coefficient. Relations between n_f and (n_f+2) flavors where the two heavy flavors are close in mass are given to three loops in Ref. [22].

Working in an energy range where the number of flavors is taken constant, a simple exact analytic solution exists for Eq. (9.3) only if one neglects all but the b_0 term, giving $\alpha_s(\mu_R^2) = (b_0 \ln(\mu_R^2/\Lambda^2))^{-1}$. Here Λ is a constant of integration, which corresponds to the scale where the perturbatively-defined coupling would diverge. Its value is indicative of the energy range where non-perturbative dynamics dominates. A convenient approximate analytic solution to the RGE that includes terms up to b_4 is given by solving iteratively Eq. (9.3)

$$\alpha_s(\mu_R^2) \simeq \frac{1}{b_0 t} \left(1 - \frac{b_1 \ell}{b_0^2 t} + \frac{b_1^2(\ell^2 - \ell - 1) + b_0 b_2}{b_0^4 t^2} + \frac{b_1^3(-2\ell^3 + 5\ell^2 + 4\ell - 1) - 6b_0 b_2 b_1 \ell + b_0^2 b_3}{2b_0^6 t^3} + \frac{18b_0 b_2 b_1^2(2\ell^2 - \ell - 1) + b_1^4(6\ell^4 - 26\ell^3 - 9\ell^2 + 24\ell + 7)}{6b_0^8 t^4} + \frac{-b_0^2 b_3 b_1(12\ell + 1) + 2b_0^2(5b_2^2 + b_0 b_4)}{6b_0^8 t^4} \right), \quad (9.5)$$

with $t \equiv \ln \frac{\mu_R^2}{\Lambda^2}$ and $\ell = \ln t$, again parametrized in terms of a constant Λ . Note that Eq. (9.5) is one of several possible approximate 4-loop solutions for $\alpha_s(\mu_R^2)$, and that a value for Λ only defines $\alpha_s(\mu_R^2)$ once one knows which particular approximation is being used. An alternative to the use of formulas such as Eq. (9.5) is to solve the RGE exactly, numerically (including the discontinuities, Eq. (9.4), at flavor thresholds). In such cases the quantity Λ does not directly arise (though it can be defined, *cf.* Eqs. (1–3) of Ref. [23]). For these reasons, in determinations of the coupling, it has become standard practice to quote the value of α_s at a given scale (typically the mass of the Z boson, M_Z) rather than to quote a value for Λ .

A discussion of determinations of the coupling and a graph illustrating its scale dependence (“running”) are to be found in Section 9.4.

9.1.2 Quark masses

Free quarks have never been observed, which is understood as a result of a long-distance, confining property of the strong QCD force: up, down, strange, charm, and bottom quarks all *hadronize*, *i.e.* become part of a meson or baryon, on a timescale $\sim 1/\Lambda$; the top quark instead decays before it has time to hadronize. This means that the question of what one means by the quark mass is a complex one, which requires one to adopt a specific prescription. A perturbatively defined prescription is the pole mass, m_q , which corresponds to the position of the divergence of the propagator. This is close to one’s physical picture of mass. However, when relating it to observable quantities, it suffers from a badly behaved perturbative series which makes it ambiguous to an amount related to Λ (see *e.g.* Ref. [24–26]). An alternative is the $\overline{\text{MS}}$ mass, $\overline{m}_q(\mu_R^2)$, which depends on the renormalization scale μ_R .

Results for the masses of heavier quarks are often quoted either as the pole mass or as the $\overline{\text{MS}}$ mass evaluated at a scale equal to the mass, $\overline{m}_q(\overline{m}_q^2)$; light quark masses are often quoted in the $\overline{\text{MS}}$ scheme at a scale $\mu_R \sim 2 \text{ GeV}$. The pole and $\overline{\text{MS}}$ masses are related by a series that starts as $m_q = \overline{m}_q(\overline{m}_q^2) \left(1 + \frac{4\alpha_s(\overline{m}_q^2)}{3\pi} + \mathcal{O}(\alpha_s^2) \right)$, while the scale-dependence of $\overline{\text{MS}}$ masses is given at lowest order by

$$\mu_R^2 \frac{d\overline{m}_q(\mu_R^2)}{d\mu_R^2} = \left[-\frac{\alpha_s(\mu_R^2)}{\pi} + \mathcal{O}(\alpha_s^2) \right] \overline{m}_q(\mu_R^2). \quad (9.6)$$

A more detailed discussion is to be found in a dedicated section of the *Review*, “Quark Masses”, with detailed formulas also in Ref. [27] and references therein.

In perturbative QCD calculations of scattering processes, it is common to work in an approximation in which one neglects (*i.e.* sets to zero) the masses of all quarks, whose mass is significantly smaller than the momentum transfer in the process.

9.2 Structure of QCD predictions

9.2.1 Fully inclusive cross sections

The simplest observables in perturbative QCD are those that do not involve initial-state hadrons and that are fully inclusive with respect to details of the final state. One example is the total cross section for $e^+e^- \rightarrow$ hadrons at center-of-mass energy Q , for which one can write

$$\frac{\sigma(e^+e^- \rightarrow \text{hadrons}, Q)}{\sigma(e^+e^- \rightarrow \mu^+\mu^-, Q)} \equiv R(Q) = R_{\text{EW}}(Q)(1 + \delta_{\text{QCD}}(Q)), \quad (9.7)$$

where $R_{\text{EW}}(Q)$ is the purely electroweak prediction for the ratio and $\delta_{\text{QCD}}(Q)$ is the correction due to QCD effects. To keep the discussion simple, we can restrict our attention to energies $Q \ll M_Z$, where the process is dominated by photon exchange (neglecting electroweak and finite-quark-mass corrections $R_{\text{EW}} = N_c \sum_q e_q^2$, where the e_q are the electric charges of the quarks) and

$$\delta_{\text{QCD}}(Q) = \sum_{n=1}^{\infty} c_n \cdot \left(\frac{\alpha_s(Q^2)}{\pi} \right)^n + \mathcal{O}\left(\frac{\Lambda^4}{Q^4}\right). \quad (9.8)$$

The first four terms in the α_s series expansion are then to be found in Ref. [28],

$$c_1 = 1, \quad c_2 = 1.9857 - 0.1152n_f, \quad (9.9a)$$

$$c_3 = -6.63694 - 1.20013n_f - 0.00518n_f^2 - 1.240\eta, \quad (9.9b)$$

$$c_4 = -156.61 + 18.775n_f - 0.7974n_f^2 + 0.0215n_f^3 - (17.828 - 0.575n_f)\eta, \quad (9.9c)$$

with $\eta = (\sum e_q)^2 / (N_c \sum e_q^2)$ and $N_c = 3$. For corresponding expressions including also Z exchange and finite-quark-mass effects, see Refs. [29–31].

A related series holds also for the QCD corrections to the hadronic decay width of the τ lepton, which essentially involves an integral of $R(Q)$ over the allowed range of invariant masses of the hadronic part of the τ decay (see *e.g.* Ref. [32]). The series expansions for QCD corrections to Higgs-boson hadronic (partial) decay widths in the limit of heavy top quark and massless light flavours at N⁴LO are given in Ref. [33].

One characteristic feature of Eqs. (9.8) and (9.9) is that the coefficients of α_s^n increase order by order: calculations in perturbative QCD tend to converge more slowly than would be expected based just on the size of α_s . The situation is significantly worse near thresholds or in the presence of tight kinematic cuts. Another feature is the existence of an extra “power-correction” term $\mathcal{O}(\Lambda^4/Q^4)$ in Eq. (9.8), which accounts for contributions that are fundamentally non-perturbative. All high-energy QCD predictions involve power corrections $(\Lambda/Q)^p$, although typically the suppression of these corrections with Q is smaller than given in Eq. (9.8), where $p = 4$. The exact power p depends on the observable and, for many processes and observables, it is possible to introduce an operator product expansion and associate power-suppressed terms with specific higher-dimension (non-perturbative) operators [34].

Scale dependence. In Eq. (9.8) the renormalization scale for α_s has been chosen equal to Q . The result can also be expressed in terms of the coupling at an arbitrary renormalization scale μ_R ,

$$\delta_{\text{QCD}}(Q) = \sum_{n=1}^{\infty} \bar{c}_n \left(\frac{\mu_R^2}{Q^2} \right) \cdot \left(\frac{\alpha_s(\mu_R^2)}{\pi} \right)^n + \mathcal{O}\left(\frac{\Lambda^4}{Q^4}\right), \quad (9.10)$$

where $\bar{c}_1(\mu_R^2/Q^2) \equiv c_1$, $\bar{c}_2(\mu_R^2/Q^2) = c_2 + \pi b_0 c_1 \ln(\mu_R^2/Q^2)$, $\bar{c}_3(\mu_R^2/Q^2) = c_3 + (2b_0 c_2 \pi + b_1 c_1 \pi^2) \times \ln(\mu_R^2/Q^2) +$

$b_0^2 c_1 \pi^2 \ln^2(\mu_R^2/Q^2)$, etc. Given an infinite number of terms in the α_s expansion, the μ_R dependence of the $\bar{c}_n(\mu_R^2/Q^2)$ coefficients will exactly cancel that of $\alpha_s(\mu_R^2)$, and the final result will be independent of the choice of μ_R : physical observables do not depend on unphysical scales.¹

With just terms up to some finite $n = N$, a residual μ_R dependence will remain, which implies an uncertainty on the prediction of $R(Q)$ due to the arbitrariness of the scale choice. This uncertainty will be $\mathcal{O}(\alpha_s^{N+1})$, i.e. of the same order as the neglected higher-order terms. For this reason it is customary to use the scale dependence of QCD predictions as an estimate of the uncertainties due to neglected terms. One usually takes a central value for $\mu_R \sim Q$, in order to avoid the poor convergence of the perturbative series that results from the large $\ln^{n-1}(\mu_R^2/Q^2)$ terms in the \bar{c}_n coefficients when $\mu_R \ll Q$ or $\mu_R \gg Q$. Uncertainties are then commonly determined by varying μ_R by a factor of two up and down around the central scale choice. This is not a rigorous prescription for determining the uncertainty, but is motivated by the requirement that there should not be large logarithms introduced into a calculation by large ratios of scales. A more detailed discussion on the accuracy of theoretical predictions and on ways to estimate the theoretical uncertainties can be found in Section 9.2.4.

9.2.2 Processes with initial-state hadrons

Deep-Inelastic Scattering. To illustrate the key features of QCD cross sections in processes with initial-state hadrons, let us consider deep-inelastic scattering (DIS), $e + p \rightarrow e + X$, where an electron e with four-momentum k emits a highly off-shell photon (momentum q) that interacts with the proton (momentum p). For photon virtualities $Q^2 \equiv -q^2$ far above the squared proton mass (but far below the squared Z mass), the differential cross section in terms of the kinematic variables Q^2 , $x = Q^2/(2p \cdot q)$ and $y = (q \cdot p)/(k \cdot p)$ is

$$\frac{d^2\sigma}{dx dQ^2} = \frac{4\pi\alpha^2}{2xQ^4} \left[(1 + (1-y)^2)F_2(x, Q^2) - y^2 F_L(x, Q^2) \right], \quad (9.11)$$

where α is the electromagnetic coupling and $F_2(x, Q^2)$ and $F_L(x, Q^2)$ are proton structure functions, which encode the interaction between the photon (in given polarization states) and the proton. In the presence of parity-violating interactions (e.g. νp scattering) an additional F_3 structure function is present. For an extended review, including equations for the full electroweak and polarized cases, see Sec. 18 of this *Review*.

Structure functions are not calculable in perturbative QCD, nor is any other cross section that involves QCD interactions and initial-state hadrons. To zeroth order in α_s , the structure functions are given directly in terms of non-perturbative parton (quark or gluon) distribution functions (PDFs),

$$F_2(x, Q^2) = x \sum_q e_q^2 f_{q/p}(x), \quad F_L(x, Q^2) = 0, \quad (9.12)$$

where $f_{q/p}(x)$ is the non-perturbative PDF for quarks of type q inside the proton, i.e. the number density of quarks of type q inside a fast-moving proton that carry a fraction x of its longitudinal momentum (the quark flavor index q , here, is not to be confused with the photon momentum q in the lines preceding Eq. (9.11)). Recently, some first determinations using lattice started to appear [35–44] but there is also some debate about the underlying methods [45]. Accordingly, for all practical uses, PDFs are currently determined from data (cf. Sec. 18 of this *Review* and also Refs. [46, 47])².

¹With respect to pQCD there is an important caveat to this statement: at sufficiently high orders, perturbative series generally suffer from “renormalon” divergences $\alpha_s^n n!$ (reviewed in Ref. [24]). This phenomenon is not usually visible with the limited number of perturbative terms available today. However, it is closely connected with non-perturbative contributions and sets a limit on the possible precision of perturbative predictions. The cancellation of scale dependence will also ultimately be affected by this renormalon-induced breakdown of perturbation theory.

²PDFs can be determined from data in a global fit at LO, NLO and NNLO, depending on the order of the matrix elements used to describe

The above result, with PDFs $f_{q/p}(x)$ that are independent of the scale Q , corresponds to the “quark-parton model” picture, in which the photon interacts with point-like free quarks, or equivalently, one has incoherent elastic scattering between the electron and individual constituents of the proton. As a consequence, in this picture also F_2 and F_L are independent of Q [51]. When including higher orders in pQCD, one has

$$F_2(x, Q^2) = x \sum_{n=0}^{\infty} \frac{\alpha_s^n(\mu_R^2)}{(2\pi)^n} \times \sum_{i=q,g} \int_x^1 \frac{dz}{z} C_{2,i}^{(n)}(z, Q^2, \mu_R^2, \mu_F^2) f_{i/p}\left(\frac{x}{z}, \mu_F^2\right) + \mathcal{O}\left(\frac{\Lambda^2}{Q^2}\right). \quad (9.13)$$

Just as in Eq. (9.10), we have a series in powers of $\alpha_s(\mu_R^2)$, each term involving a coefficient $C_{2,i}^{(n)}$ that can be calculated using Feynman graphs. At variance with the parton model, the PDFs in pQCD depend on an additional scale, the factorization scale μ_F , whose significance will be discussed in the following. Another important difference is the additional integral over z . The parton that comes from the proton can undergo a splitting before it interacts with the photon. As a result, the $C_{2,i}^{(n)}$ coefficients are functions that depend on the ratio, z , of the parton’s momentum before and after radiation, and one must integrate over that ratio. For the electromagnetic component of DIS with light quarks and gluons, the zeroth order coefficient functions are $C_{2,q}^{(0)} = e_q^2 \delta(1-z)$ and $C_{2,g}^{(0)} = 0$. Corrections are known up to $\mathcal{O}(\alpha_s^3)$ (next-to-next-to-next-to-leading order, N³LO) for both electromagnetic [52] and weak currents [53, 54]. For heavy-quark production they are known to $\mathcal{O}(\alpha_s^2)$ [55, 56] (next-to-leading order, NLO, insofar as the series starts at $\mathcal{O}(\alpha_s)$). For precise comparisons of LHC cross sections with theoretical predictions, the photon PDF of the proton is also needed. It has been computed precisely in Ref. [57] and has now been implemented in most global PDF fits. More recently, the PDF for leptons has also been computed [58].

The majority of the emissions that modify a parton’s momentum are collinear (parallel) to that parton, and do not depend on the fact that the parton is destined to interact with a photon. It is natural to view these emissions as modifying the proton’s structure rather than being part of the coefficient function for the parton’s interaction with the photon. Technically, one uses a procedure known as *collinear factorization* to give a well-defined meaning to this distinction, most commonly through the $\overline{\text{MS}}$ factorization scheme, defined in the context of dimensional regularization. The $\overline{\text{MS}}$ factorization scheme involves an arbitrary choice of *factorization scale*, μ_F , whose meaning can be understood roughly as follows: emissions with transverse momenta above μ_F are included in the $C_{2,q}^{(n)}(z, Q^2, \mu_R^2, \mu_F^2)$; emissions with transverse momenta below μ_F are accounted for within the PDFs, $f_{i/p}(x, \mu_F^2)$. While collinear factorization is generally believed to be valid for suitable (sufficiently inclusive) observables in processes with hard scales, Ref. [59], which reviews the factorization proofs in detail, is cautious in the statements it makes about their exhaustivity, notably for the hadron-collider processes which we shall discuss below. The transverse degrees of freedom have been integrated over for collinear PDFs. It is also possible to produce transverse-momentum dependent (or unintegrated) PDFs where

the data. In modern global PDF fits, data are included from DIS, Drell-Yan (DY), jets and $t\bar{t}$ processes, and more LHC collider data, with the global PDF fits using 3000-4000 data points. There is a large change in the PDFs from LO to NLO, with a much smaller change from NLO to NNLO. LO PDFs can be unreliable for collider predictions, especially at low and high x . The uncertainties for the resulting PDFs are determined primarily from the experimental uncertainties of the data that serves as input to the global PDF fits. There is also a component due to the limitations of the parametrizations used, although this may be reduced with the use of more flexible forms. The PDF uncertainties can either be determined through a Hessian approach or through the use of Monte Carlo replicas. It is now relatively straightforward to convert results from one approach to the other. Recently, theoretical uncertainties related to missing higher orders have been included in global PDF determinations but so far only at NLO [48–50].

these degrees of freedom remain. Further discussion is to be found in Refs. [60, 61].

The PDFs' resulting dependence on μ_F is described by the Dokshitzer-Gribov-Lipatov-Altarelli-Parisi (DGLAP) equations [62], which to leading order (LO) read³

$$\mu_F^2 \frac{\partial f_{i/p}(x, \mu_F^2)}{\partial \mu_F^2} = \sum_j \frac{\alpha_s(\mu_F^2)}{2\pi} \int_x^1 \frac{dz}{z} P_{i \leftarrow j}^{(1)}(z) f_{j/p}\left(\frac{x}{z}, \mu_F^2\right), \quad (9.14)$$

with, for example, $P_{q \leftarrow g}^{(1)}(z) = T_R(z^2 + (1-z)^2)$. The other LO splitting functions are listed in Sec. 18 of this *Review*, while results up to NLO, α_s^2 , and NNLO, α_s^3 , are given in Refs. [63] and [64] respectively. At N³LO accuracy, only partial results are currently available in Refs. [65–67]. Splitting functions for PDFs in the helicity dependent case are given in Ref. [68].

Beyond LO, the coefficient functions are also μ_F dependent, for example $C_{2,i}^{(1)}(x, Q^2, \mu_R^2, \mu_F^2) = C_{2,i}^{(1)}(x, Q^2, \mu_R^2, Q^2) - \ln\left(\frac{\mu_F^2}{Q^2}\right) \sum_j \int_x^1 \frac{dz}{z} \times C_{2,j}^{(0)}\left(\frac{x}{z}\right) P_{j \leftarrow i}^{(1)}(z)$. In certain contexts, higher-order QED and mixed QED-QCD corrections to the splitting functions are also needed [69].

As with the renormalization scale, the choice of factorization scale is arbitrary, but if one has an infinite number of terms in the perturbative series, the μ_F -dependencies of the coefficient functions and PDFs will compensate each other fully. Given only N terms of the series, a residual $\mathcal{O}(\alpha_s^{N+1})$ uncertainty is associated with the ambiguity in the choice of μ_F . As with μ_R , varying μ_F provides an input in estimating uncertainties on predictions. In inclusive DIS predictions, the default choice for the scales is usually $\mu_R = \mu_F = Q$.

As is the case for the running coupling, in DGLAP evolution one can introduce flavor thresholds near the heavy quark masses: below a given heavy quark's mass, that quark is not considered to be part of the proton's structure, while above it is considered to be part of the proton's structure and evolves with massless DGLAP splitting kernels. With appropriate parton distribution matching terms at threshold, such a variable flavor number scheme (VFNS), when used with massless coefficient functions, gives the full heavy-quark contributions at high Q^2 scales. For scales near the threshold, it is instead necessary to appropriately adapt the standard massive coefficient functions to account for the heavy-quark contribution already included in the PDFs [70–72].

At sufficiently small x and Q^2 in inclusive DIS, resummation of small x logarithms may be necessary [73, 74]. This may in fact have been observed in Refs. [75] based on HERA data [76], in a kinematic region where useful information for PDFs for collider predictions is present. A better description of the data in this region can be gained by small x resummation matched to NNLO [75, 77], or by the inclusion of power-suppressed contributions [78] or by using an x -dependent factorization scale in the NNLO DIS predictions [79].

In situations in which the total center-of-mass energy \sqrt{s} is much larger than all other momentum-transfer scales in the problem (*e.g.* Q in DIS, m_b for $b\bar{b}$ production in pp collisions, *etc.*), each power of α_s beyond LO can be accompanied by a power of $\ln(s/Q^2)$ (or $\ln(s/m_b^2)$, *etc.*). This is variously referred to as the high-energy, small- x or Balitsky-Fadin-Kuraev-Lipatov (BFKL) limit [74, 80, 81]. Currently it is possible to account for the dominant and first sub-dominant [82, 83] power of such logarithms at each order of α_s , and also to estimate further sub-dominant contributions that are numerically large (see Refs. [84–87] and references therein). Progress towards NNLO is discussed in Ref. [88].

Physically, the summation of all orders in α_s can be understood as leading to a growth with s of the gluon density in the proton. At sufficiently high energies this implies non-linear effects (commonly referred to as parton saturation), whose treatment has been the subject of intense study (see for example Refs. [89–91] and references thereto).

Hadron-hadron collisions.

The extension to processes with two initial-state hadrons can be illustrated with the example of the total (inclusive) cross section for W boson production in collisions of hadrons h_1 and h_2 , which can be written as

$$\begin{aligned} \sigma(h_1 h_2 \rightarrow W + X) &= \sum_{n=0}^{\infty} \alpha_s^n(\mu_R^2) \\ &\times \sum_{i,j} \int dx_1 dx_2 f_{i/h_1}\left(x_1, \mu_F^2\right) f_{j/h_2}\left(x_2, \mu_F^2\right) \\ &\times \hat{\sigma}_{ij \rightarrow W+X}^{(n)}\left(x_1 x_2 s, \mu_R^2, \mu_F^2\right) + \mathcal{O}\left(\frac{\Lambda^2}{M_W^4}\right), \end{aligned} \quad (9.15)$$

where s is the squared center-of-mass energy of the collision. At LO, $n = 0$, the hard (partonic) cross section $\hat{\sigma}_{ij \rightarrow W+X}^{(0)}(x_1 x_2 s, \mu_R^2, \mu_F^2)$ is simply proportional to $\delta(x_1 x_2 s - M_W^2)$, in the narrow W -boson width approximation (see Sec. 51 of this *Review* for detailed expressions for this and other hard scattering cross sections). It is non-zero only for choices of i, j that can directly give a W , such as $i = u, j = \bar{d}$. At higher orders, $n \geq 1$, new partonic channels contribute, such as gg , and $x_1 x_2 s \geq M_W^2$ in the narrow W -boson width approximation.

Equation (9.15) involves a collinear factorization between the hard cross section and the PDFs, just like Eq. (9.13). As long as the same factorization scheme is used in DIS and pp or $p\bar{p}$ (usually the $\overline{\text{MS}}$ scheme), then PDFs extracted in DIS can be directly used in pp and $p\bar{p}$ predictions [59, 92] (with the anti-quark distributions in an anti-proton being the same as the quark distributions in a proton).

A number of fully inclusive cross-sections have been computed up to N³LO, *i.e.* including corrections up to relative order α_s^3 , in recent years. These include inclusive Higgs production through gluon fusion in the large m_t limit, calculated at N³LO in Refs. [93, 94]. Higgs boson pair production via gluon fusion in the same approximation was computed at N³LO in Ref. [95]. Calculations at this order, differential in the Higgs rapidity [96, 97] and fully differential [98] have been presented recently. Vector-boson fusion single- [99] and double-pair [100] production is also known to N³LO [99] in the factorized approximation. Neutral [101, 102] and charged [103] Drell-Yan processes have also been computed at N³LO. Differential rapidity distributions are available, but not yet with fiducial cuts. The uncertainty band derived from scale variation is not contained in the uncertainty band of the previous order, as might be expected from a well-behaved process. This has been ascribed to cancellations between channels at NNLO that lead to underestimates of the uncertainty at that order. This effect does not seem to be present in other processes, such as Higgs boson production through gluon-gluon fusion. Note that there is currently a mis-match in N³LO calculations in that PDFs at the same order are not yet available. The fully inclusive hard cross sections for several other processes are known to NNLO⁴. For instance, Higgs-boson production in association with a vector boson [104], Higgs-pair production in the large m_t approximation [105], and with full m_t dependence [106], top-antitop production [107, 108] and vector-boson pair production [109–111]. For a comprehensive overview on other recent NNLO calculations see Ref. [112].

Photoproduction. γp (and $\gamma\gamma$) collisions are similar to pp collisions, with the subtlety that the photon can behave in two ways: there is “direct” photoproduction, in which the photon behaves as a point-like particle and takes part directly in the hard collision, with hard subprocesses such as $\gamma g \rightarrow q\bar{q}$; there is also resolved photoproduction, in which the photon behaves like a hadron, with non-perturbative partonic substructure and a corresponding PDF for its quark and gluon content, $f_{i/\gamma}(x, Q^2)$. While useful to understand the general structure of γp collisions, the distinction between direct and resolved photoproduction is not well defined beyond leading order, as discussed for example in Ref. [113].

³ LO is generally taken to mean the lowest order at which a quantity is non-zero.

⁴ Processes with jets or photons in the final state have divergent cross sections unless one places a cut on the jet or photon momentum. Accordingly, they are discussed below in Section 9.2.3.2.

9.2.3 Cross sections with phase-space restrictions

QCD final states always consist of hadrons, while perturbative QCD calculations deal with partons. Physically, an energetic parton fragments (“showers”) into many further partons, which then, on later timescales, undergo a transition to hadrons (“hadronization”). Fixed-order perturbation theory captures only a small part of these dynamics. This does not matter for the fully inclusive cross sections discussed above: the showering and hadronization stages are approximately unitary, *i.e.* they do not substantially change the overall probability of hard scattering, because they occur long after it has taken place (they introduce at most a correction proportional to a power of the ratio of timescales involved, *i.e.* a power of Λ/Q , where Q is the hard scattering scale).

Less inclusive measurements, in contrast, may be affected by the extra dynamics. For those sensitive just to the main directions of energy flow (jet rates, event shapes, *cf.* Sec. 9.3.1) fixed-order perturbation theory is often still adequate, because showering and hadronization do not substantially change the overall energy flow. This means that one can make a prediction using just a small number of partons, which should correspond well to a measurement of the same observable carried out on hadrons. For observables that instead depend on distributions of individual hadrons (which, *e.g.*, are the inputs to detector simulations), it is mandatory to account for showering and hadronization. The range of predictive techniques available for QCD final states reflects this diversity of needs of different measurements.

While illustrating the different methods, we shall for simplicity mainly use expressions that hold for e^+e^- scattering. The extension to cases with initial-state partons will be mostly straightforward (space constraints unfortunately prevent us from addressing diffraction and exclusive hadron-production processes; extensive discussion is to be found in Sec. 20 of this *Review* and in Refs. [114, 115]).

9.2.3.1 Soft and collinear limits

Before examining specific predictive methods, it is useful to be aware of a general property of QCD matrix elements in the soft and collinear limits. Consider a squared tree-level matrix element $|M_n^2(p_1, \dots, p_n)|$ for the process $e^+e^- \rightarrow n$ partons with momenta p_1, \dots, p_n , and a corresponding phase-space integration measure $d\Phi_n$. If particle n is a gluon, which becomes collinear (parallel) to another particle i and additionally its momentum tends to zero (is “soft”), the matrix element simplifies as follows,

$$\begin{aligned} & \lim_{\theta_{in} \rightarrow 0, E_n \rightarrow 0} d\Phi_n |M_n^2(p_1, \dots, p_n)| \\ &= d\Phi_{n-1} |M_{n-1}^2(p_1, \dots, p_{n-1})| \frac{\alpha_s C_i}{\pi} \frac{d\theta_{in}^2}{\theta_{in}^2} \frac{dE_n}{E_n}, \end{aligned} \quad (9.16)$$

where $C_i = C_F$ (C_A) if i is a quark (gluon). This formula has non-integrable divergences both for the inter-parton angle $\theta_{in} \rightarrow 0$ and for the gluon energy $E_n \rightarrow 0$, which are mirrored also in the structure of divergences in loop diagrams. These divergences are important for at least two reasons: firstly, they govern the typical structure of events (inducing many emissions either with low energy or at small angle with respect to hard partons); secondly, they will determine which observables can be calculated within perturbative QCD.

9.2.3.2 Fixed-order predictions

Let us consider an observable \mathcal{O} that is a function $\mathcal{O}_n(p_1, \dots, p_n)$ of the four-momenta of the n final-state particles in an event (either partons or hadrons). In what follows, we shall consider the cross section for events weighted with the value of the observable, $\sigma_{\mathcal{O}}$. As examples, if $\mathcal{O}_n \equiv 1$ for all n , then $\sigma_{\mathcal{O}}$ is just the total cross section; if $\mathcal{O}_n \equiv \hat{\tau}(p_1, \dots, p_n)$ where $\hat{\tau}$ is the value of the Thrust for that event (see Eq. (9.22) in Sec. 9.3.1.2), then the average value of the Thrust is $\langle \tau \rangle = \sigma_{\mathcal{O}}/\sigma_{\text{tot}}$; if $\mathcal{O}_n \equiv \delta(\tau - \hat{\tau}(p_1, \dots, p_n))$ then one gets the differential cross section as a function of the Thrust, $\sigma_{\mathcal{O}} \equiv d\sigma/d\tau$.

In the expressions below, we shall omit to write the non-perturbative power correction term, which for most common observables is proportional to a single power of Λ/Q .

Leading Order. If the observable \mathcal{O} is non-zero only for events with at least n final-state particles, then the LO QCD prediction

for the weighted cross section in e^+e^- annihilation is

$$\sigma_{\mathcal{O}}^{\text{LO}} = \alpha_s^{n-2}(\mu_R^2) \int d\Phi_n |M_n^2(p_1, \dots, p_n)| \mathcal{O}_n(p_1, \dots, p_n), \quad (9.17)$$

where the squared tree-level matrix element, $|M_n^2(p_1, \dots, p_n)|$, including relevant symmetry factors, has been summed over all subprocesses (*e.g.* $e^+e^- \rightarrow q\bar{q}q\bar{q}$, $e^+e^- \rightarrow q\bar{q}gg$) and has had all factors of α_s extracted in front. In processes other than e^+e^- collisions, the center-of-mass energy of the LO process is generally not fixed, and so the powers of the coupling are often brought inside the integrals, with the scale μ_R chosen event by event, as a function of the event kinematics.

Other than in the simplest cases (see the review on Cross Sections in this *Review*), the matrix elements in Eq. (9.17) are usually calculated automatically with programs such as CompHEP [116], MADGRAPH [117], ALPGEN [118], COMIX/SHERPA [119], and HELAC/PHEGAS [120]. Some of these (CompHEP, MADGRAPH) use formulas obtained from direct evaluations of Feynman diagrams. Others (ALPGEN, HELAC/PHEGAS and COMIX/SHERPA) use methods designed to be particularly efficient at high multiplicities, such as Berends-Giele recursion [121], which builds up amplitudes for complex processes from simpler ones (see also Refs. [122–124] for other tree-level calculational methods).

The phase-space integration is usually carried out by Monte Carlo sampling, because of the high dimensionality of the integration and in order to deal with the possibly involved kinematic cuts that are used in the corresponding experimental measurements. Perturbatively calculable observables should be insensitive to the emission of soft and collinear radiation. Because of the divergences in the matrix element, Eq. (9.16), at lowest order the integral converges only if the observable vanishes for kinematic configurations in which one of the n particles is arbitrarily soft or it is collinear to another particle. As an example, the cross section for producing any configuration of n partons will lead to an infinite integral, whereas a finite result will be obtained for the cross section for producing n deposits of energy (or jets, see Sec. 9.3.1.1), each above some energy threshold and well separated from each other in angle.

At a practical level, LO calculations can be carried out for $2 \rightarrow n$ processes with $n \lesssim 6 - 10$. The exact upper limit depends on the process, the method used to evaluate the matrix elements (recursive methods are more efficient), and the extent to which the phase-space integration can be optimized to work around the large variations in the values of the matrix elements.

NLO. Given an observable that is non-zero starting from n final-state particles, its prediction at NLO involves supplementing the LO result, Eq. (9.17), with the $2 \rightarrow (n+1)$ -particle squared tree-level matrix element ($|M_{n+1}^2|$), and the interference of a $2 \rightarrow n$ tree-level and $2 \rightarrow n$ 1-loop amplitude ($2\text{Re}(M_n M_{n,1\text{-loop}}^*)$),

$$\begin{aligned} \sigma_{\mathcal{O}}^{\text{NLO}} &= \sigma_{\mathcal{O}}^{\text{LO}} + \alpha_s^{n-1}(\mu_R^2) \int d\Phi_{n+1} |M_{n+1}^2(p_1, \dots, p_{n+1})| \\ &\quad \times \mathcal{O}_{n+1}(p_1, \dots, p_{n+1}) + \alpha_s^{n-1}(\mu_R^2) \\ &\quad \times \int d\Phi_n 2\text{Re} [M_n(p_1, \dots, p_n) M_{n,1\text{-loop}}^*(p_1, \dots, p_n)] \\ &\quad \times \mathcal{O}_n(p_1, \dots, p_n). \end{aligned} \quad (9.18)$$

Relative to LO calculations, two important issues appear in the NLO calculations. Firstly, the extra complexity of loop-calculations relative to tree-level calculations means that automated calculations started to appear only about fifteen years ago (see below). Secondly, loop amplitudes are infinite in four dimensions, while tree-level amplitudes are finite, but their *integrals over the phase space* are infinite, due to the divergences of Eq. (9.16). These two sources of infinities have the same soft and collinear origins and cancel after the integration only if the observable \mathcal{O} satisfies the property of infrared and collinear safety, which means that the observable is non-sensitive to soft emissions

or to collinear splittings, *i.e.*

$$\begin{aligned} \mathcal{O}_{n+1}(p_1, \dots, p_s, \dots, p_n) &\rightarrow \mathcal{O}_n(p_1, \dots, p_{s-1}, p_{s+1}, \dots, p_n) \\ &\text{if } p_s \rightarrow 0 \\ \mathcal{O}_{n+1}(p_1, \dots, p_a, p_b, \dots, p_n) &\rightarrow \mathcal{O}_n(p_1, \dots, p_a + p_b, \dots, p_n) \\ &\text{if } p_a \parallel p_b. \end{aligned} \quad (9.19)$$

Examples of infrared-safe quantities include event-shape distributions and jet cross sections (with appropriate jet algorithms, see below). Unsafe quantities include the distribution of the momentum of the hardest QCD particle (which is not conserved under collinear splitting), observables that require the complete absence of radiation in some region of phase space (*e.g.* rapidity gaps or 100% isolation cuts, which are affected by soft emissions), or the particle multiplicity (affected by both soft and collinear emissions). The non-cancellation of divergences at NLO due to infrared or collinear unsafety compromises the usefulness not only of the NLO calculation, but also that of a LO calculation, since LO is only an acceptable approximation if one can prove that higher-order terms are smaller. Infrared and collinear unsafety usually also implies large non-perturbative effects.

As with LO calculations, the phase-space integrals in Eq. (9.18) are usually carried out by Monte Carlo integration, so as to facilitate the study of arbitrary observables. Various methods exist to obtain numerically efficient cancellation among the different infinities. These include notably dipole [125], FKS [126] and antenna [127] subtraction.

Thanks to new ideas like the OPP method [128], generalised [129] and D -dimensional [130] unitarity, onshell methods [131], and on-the-fly reduction algorithms [132], recent years have seen a breakthrough in the calculation of one-loop matrix elements (for reviews on unitarity based method see Ref. [133, 134]). Thanks to these innovative methods, automated tools for NLO calculations have been developed and a number of programs are available publicly: MADGRAPH5_aMC@NLO [117] and HELAC-NLO [135] provide full frameworks for NLO calculations; GoSAM [136], NJET [137], OPENLOOPS [138] and RECOLA [139] calculate just the 1-loop part and are typically interfaced with an external tool such as SHERPA [140] for a combination with the appropriate tree-level amplitudes. Other tools such as NLOJET++ [141], MCFM [142], VBFNLO [143], the PHOX family [144] or BLACKHAT [145] implement analytic calculations for a selected class of processes.

Recently, a lot of attention has also been paid to the calculation of NLO electroweak corrections. Electroweak corrections are especially important for transverse momenta significantly above the W and Z masses, because they are enhanced by two powers of $\ln p_t/M_W$ for each power of the electroweak coupling, and close to Sudakov peaks, where most of the data lie and the best experimental precision can be achieved. In some cases the above programs (or development versions of them) can be used to calculate also NLO electroweak or beyond-standard-model corrections [146–152].

Given the progress in QCD and EW fixed-order computations, the largest unknown from fixed-order corrections is often given by the mixed QCD-electroweak corrections of $\mathcal{O}(\alpha_s\alpha)$. These mixed two-loop corrections are often available in an approximate form [153–162]. The first complete computation of the mixed QCD–EW corrections to the neutral-current Drell–Yan process appeared recently [163]. For a review on EW corrections to collider processes see Ref. [164].

NNLO. NNLO is considerably more complicated than NLO as it involves a further order in α_s , consisting of: the squared $(n+2)$ -parton tree-level amplitude, the interference of the $(n+1)$ -parton tree-level and 1-loop amplitudes, the interference of the n -parton tree-level and 2-loop amplitudes, and the squared n -parton 1-loop amplitude.

Each of these elements involves large numbers of soft and collinear divergences, satisfying relations analogous to Eq. (9.16) which now involve multiple collinear or soft particles and higher loop orders (see *e.g.* Refs. [165–167]). Arranging for the cancellation of the divergences after numerical Monte Carlo integration has been one of the significant challenges of NNLO calculations, as

has been the determination of the relevant 2-loop amplitudes. For the cancellations of divergences a wide range of methods has been developed. Some of them [168–174] retain the approach, inherent in NLO methods, of directly combining the separate loop and tree-level amplitudes. Others combine a suitably chosen, partially inclusive $2 \rightarrow n$ NNLO calculation with a fully differential $2 \rightarrow n+1$ NLO calculation [175–180]. The q_T -subtraction method was extended to deal with mixed QCD–QED corrections at NNLO [181]. For an overview of NNLO subtraction methods see Ref [182].

Quite a number of processes have been calculated differentially at NNLO so far. The state of the art for e^+e^- collisions is $e^+e^- \rightarrow 3$ jets [183–185]. For DIS, dijet production is known at NNLO [186] and the description jet production has been recently pushed even to N³LO using the Projection-to-Born method [187, 188]. For hadron colliders, all $2 \rightarrow 1$ processes are known, specifically vector boson [189, 190] and Higgs boson production in the large m_t limit [175, 191]. Recently, the finite top-mass corrections at this order have also been computed [192]. This calculation eliminates one important source of theoretical uncertainty to inclusive Higgs production at the LHC. For most of the above calculations there exist public codes (EERAD3 for e^+e^- , DYNLO, FEWZ and MATRIX for W and Z production, Fehipro and HNNLO for Higgs production), links to which are to be found among the above references. Substantial progress has been made in the years for hadron-collider $2 \rightarrow 2$ processes, with calculations having been performed for nearly all relevant processes: ZZ [110] WW [109] and WZ [193], $\gamma\gamma$ [194, 195], $Z\gamma$ [196] and $W\gamma$ [197] (many of these colour singlet processes are available also in MCFM [198] or MATRIX [111]), inclusive photon [199, 200], γ +jet [200, 201], W +jet [177, 202], Z +jet [201, 203, 204] H +jet [205–208], WH [209] and ZH [210], t -channel single-top [211, 212], $t\bar{t}$ production [213], dijet production [214], W production in association with a c -jet [215] and HH [105] (in large-top-mass approximation, see also the exact (two-loop) NLO result [106]). Recently, also the NNLO corrections to identified B -hadron production have been computed [216]. The frontier of NNLO calculation has now reached the complexity of $2 \rightarrow 3$ processes. The first $2 \rightarrow 3$ process known at NNLO has been Higgs production through vector-boson fusion, using an approximation in which the two underlying DIS-like $q \rightarrow qV$ scatterings are factorised, the so-called structure function approximation [180, 217]. Corrections beyond the structure function approximation are expected to be small, on the order of a percent or less [218]. More recently, first genuine $2 \rightarrow 3$ LHC processes have been described at NNLO accuracy, including three photon [219, 220], two photons and one jet [221], and three-jets [222]. The last calculation will be relevant for future extractions of $\alpha_s(M_Z^2)$ from three-jet observables at the LHC.

Cross sections at the LHC are most often measured with fiducial cuts, for example on the transverse momenta and rapidities of the measured objects, restricting the measurement to regions where the objects have a good efficiency to be detected and are well-reconstructed. Ideally, the theoretical predictions should also be constructed at the same fiducial level; the other possibility is to extrapolate the experimental fiducial results to the full phase space. Such an extrapolation, however, requires the extrapolation (typically using a parton shower Monte Carlo) to be accurate over the full phase space.

Comparisons of fixed order predictions to fiducial measurements can sometimes result in the presence of large logarithms which degrade the accuracy of the prediction. Such is the case, for example, in the calculation of the Higgs rapidity distribution, in the diphoton final state. The imposition of transverse momenta and rapidity cuts on the two photons leads to an uncertainty notably greater at N³LO than at NNLO, due to the presence of these logs. One possible solution is to change the form of the kinematic cut on the photons, to a product of the two photon transverse momenta [223], reducing the impact of the logs; another solution is to perform a resummation of the logs, restoring the expected precision [224].

The Les Houches precision wishlist compiles predictions needed to fully exploit the data that will be taken at the High Luminosity LHC [225]. Most of the needed calculations require accuracy of at

least NNLO QCD and NLO EW, and many require the prediction of $2 \rightarrow 3$ processes, such as $W/Z + \geq 2$ jets, $H + \geq 2$ jets, and $t\bar{t}H$ to NNLO.

As discussed in this section, calculations at NLO can now be relatively easily generated by non-experts using the programs described. However, many NNLO calculations can be too complex and CPU-intensive to allow such an approach. In these cases, the relevant matrix element information for a specific observable can be stored by means of interpolation grids developed originally for cross sections at NLO [226–228] and recently extended to include electroweak corrections [229]. The application to NNLO has been demonstrated for $t\bar{t}$ and for DIS jet cross sections in Refs. [230, 231]. Each such interpolation grid corresponds to one fixed observable with specific selection criteria and binning, but is flexible with respect to the renormalization or factorization scale, the PDF, or the α_s evolution chosen for the cross-section computation.

An even more flexible method, at the cost of requiring large amounts of storage space, saves huge numbers of partonic events in the form of ROOT ntuples, which allow predictions to be generated on-the-fly for many observables of a particular process [232, 233]. Recent developments of both techniques for pp collisions at NNLO are described in Ref. [225].

9.2.3.3 Resummation

Many experimental measurements place tight constraints on emissions in the final state. For example, in e^+e^- events, that (one minus) the Thrust should be less than some value $\tau \ll 1$, or, in $pp \rightarrow Z$, events that the Z -boson transverse momentum or the transverse momentum of the accompanying jet should be much smaller than the Z -boson mass. A further example is the production of heavy particles or jets near threshold (so that little energy is left over for real emissions) in DIS and pp collisions.

In such cases, the constraint vetoes a significant part of the integral over the soft and collinear divergence of Eq. (9.16). As a result, there is only a partial cancellation between real emission terms (subject to the constraint) and loop (virtual) contributions (not subject to the constraint), causing each order of α_s to be accompanied by a large coefficient $\sim L^2$, where *e.g.* $L = \ln \tau$ or $L = \ln(M_Z/p_t^2)$. One ends up with a perturbative series, whose terms go as $\sim (\alpha_s L^2)^n$. It is not uncommon that $\alpha_s L^2 \gg 1$, so that the perturbative series converges very poorly if at all.⁵ In such cases one may carry out a “resummation”, which accounts for the dominant logarithmically enhanced terms to all orders in α_s , by making use of known properties of matrix elements for multiple soft and collinear emissions, and of the all-orders properties of the divergent parts of virtual corrections, following original works such as Refs. [234–243] and also through soft-collinear effective theory [244, 245] (*cf.* also the section on “Heavy-Quark and Soft-Collinear Effective Theory” in this *Review*, as well as Ref. [246]).

For cases with double logarithmic enhancements (two powers of logarithm per power of α_s), there are two classification schemes for resummation accuracy. Writing the cross section including the constraint as $\sigma(L)$ and the unconstrained (total) cross section as σ_{tot} , the series expansion takes the form

$$\sigma(L) \simeq \sigma_{\text{tot}} \sum_{n=0}^{\infty} \sum_{k=0}^{2n} R_{nk} \alpha_s^n (\mu_R^2) L^k, \quad L \gg 1, \quad (9.20)$$

and leading log (LL) resummation means that one accounts for all terms with $k = 2n$, next-to-leading-log (NLL) includes additionally all terms with $k = 2n - 1$, *etc.* Often $\sigma(L)$ (or its Fourier

⁵ To be precise one should be aware of two causes of the divergence of perturbative series. That which interests us here is associated with the presence of a new large parameter (*e.g.* ratio of scales). It is distinct from the “renormalon” induced factorial divergences of perturbation theory which were discussed above.

or Mellin transform) *exponentiates*⁶,

$$\sigma(L) \simeq \sigma_{\text{tot}} \exp \left[\sum_{n=1}^{\infty} \sum_{k=0}^{n+1} G_{nk} \alpha_s^n (\mu_R^2) L^k \right], \quad L \gg 1, \quad (9.21)$$

where one notes the different upper limit on k ($\leq n+1$) compared to Eq. (9.20). This is a more powerful form of resummation: the G_{12} term alone reproduces the full LL series in Eq. (9.20). With the form Eq. (9.21) one still uses the nomenclature LL, but this now means that all terms with $k = n+1$ are included, and NLL implies all terms with $k = n$, *etc.*

For a large number of observables, NLL resummations are available in the sense of Eq. (9.21) (see Refs. [250–252] and references therein). NNLL has been achieved for the DY and Higgs-boson p_t distributions [253–256] (also available in the CuTe [257], HRes [258] and ResBos [259] families of programs and also differentially in vector-boson decay products [260]) and related variables [261], for the p_t of vector-boson pairs [262], for the back-to-back energy-energy correlation in e^+e^- [263], the jet broadening in e^+e^- collisions [264], the jet-veto survival probability in Higgs and Z boson production in pp collisions [265, 266]⁷, an event-shape type observable known as the beam Thrust [267], hadron-collider jet masses in specific limits [268] (see also Ref. [269]), the production of top anti-top pairs near threshold [270–272] (and references therein), and high- p_t W and Z production [273]. Automation of NNLL jet-veto resummations for different processes has been achieved in Ref. [274] (*cf.* also the NLL automation in Ref. [275]), while automation for a certain class of e^+e^- observables has been achieved in Ref. [276]. N³LL resummations are available for the Thrust variable, C -parameter and heavy-jet mass in e^+e^- annihilations [277–279] (confirmed for Thrust at NNLL in Ref. [280]), for p_t distribution of the Higgs boson [281] and weak gauge bosons [282] and for Higgs- and vector-boson production near threshold [283]. In order to make better contact with experimental measurements, recent years have seen an increasing interest in resummations in exclusive phase-space regions and joint resummations [284–291]. Finally, there has also been considerable progress in resummed calculations for jet substructure, whose observables involve more complicated definitions than is the case for standard resummations [292–299], see also Refs. [300–302].

9.2.3.4 Fragmentation functions

Since the parton-hadron transition is non-perturbative, it is not possible to perturbatively calculate quantities such as the energy-spectra of specific hadrons in high-energy collisions. However, one can factorize perturbative and non-perturbative contributions via the concept of fragmentation functions. These are the final-state analogue of the parton distribution functions which are used for initial-state hadrons. Like parton distribution functions, they depend on a (fragmentation) factorization scale and satisfy a DGLAP evolution equation.

It should be added that if one ignores the non-perturbative difficulties and just calculates the energy and angular spectrum of partons in perturbative QCD with some low cutoff scale $\sim \Lambda$ (using resummation to sum large logarithms of \sqrt{s}/Λ), then this reproduces many features of the corresponding hadron spectra [303]. This is often taken to suggest that hadronization is “local”, in this sense it mainly involves partons that are close both in position and in momentum.

Section 19 of this *Review* provides further information (and references) on these topics, including also the question of heavy-quark fragmentation.

⁶ Whether or not this happens depends on the quantity being resummed. A classic example involves two-jet rate in e^+e^- collisions as a function of a jet-resolution parameter y_{cut} . The logarithms of $1/y_{\text{cut}}$ exponentiate for the k_t (Durham) jet algorithm [247], but not [248] for the JADE algorithm [249] (both are discussed below in Sec. 9.3.1.1).

⁷ A veto on the jet phase space can be severe, for example by requiring exactly zero jets above a given transverse momentum cut accompanying a Higgs boson, or relatively mild, for example by placing a transverse momentum cut of 30 GeV on the measurement of the production of a Higgs boson with one or more jets. In general, inclusive cross sections are preferable, as uncertainties on both the theoretical and experimental sides are smaller.

9.2.3.5 Parton-shower Monte Carlo event generators

Parton-shower Monte Carlo (MC) event generators like PYTHIA [304–306], HERWIG [307–309], and SHERPA [140]⁸ provide fully exclusive simulations of QCD events at the level of measurable particles, the so-called “particle level” or “hadron level”. Here, “measurable” refers to colour-neutral particles with mean lifetimes τ long enough to be associated with tracks or decay vertices in particle detectors. Usually, this requires mean decay lengths $c\tau$ of around 10 nm. As such the MC event generators are a crucial tool for all applications that involve simulating the response of detectors to QCD events. Here we give only a brief outline of how they work and refer the reader to Sec. 43 and Ref. [311] for a full overview.

The MC generation of an event involves several stages. It starts with the random generation of the kinematics and partonic channels of whatever *hard scattering process* the user has requested at some high scale Q_0 (for complex processes, this may be carried out by an external program). This is followed by a *parton shower*, usually based on the successive random generation of gluon emissions (or $g \rightarrow q\bar{q}$ splittings). Leading contributions to the shower have emissions that are ordered according to some ordering variable. Common choices of scale for the ordering of emissions are virtuality, transverse momentum or angle. Each emission is generated at a scale lower than the previous emission, following a (soft and collinear resummed) perturbative QCD distribution, which depends on the momenta of all previous emissions. Parton showering stops at a scale of order 1 GeV, at which point a *hadronization model* is used to convert the resulting partons into hadrons. One widely-used model involves stretching a color “string” across quarks and gluons, and breaking it up into hadrons [312, 313]. Another breaks each gluon into a $q\bar{q}$ pair and then groups quarks and anti-quarks into colorless “clusters”, which then give the hadrons [307]. As both models are tuned primarily to LEP data, the cluster and string models provide similar results for most observables [314]. For pp and γp processes, modeling is also needed to treat the collision between the two hadron remnants, which generates an *underlying event* (UE), usually implemented via additional $2 \rightarrow 2$ scatterings (“multiple parton interactions”, MPI) at a scale of a few GeV, following Ref. [315]. The parameter values for the MPI models must be determined from fits to underlying-event observables of LHC collision data. As the different MC event generators are adapted to essentially the same measurements, ideally the respective MPI implementations should lead to similar predictions for each program. One complication, however, is the non-universality of the underlying event for different physics processes.

A deficiency of the soft and collinear approximations that underlie parton showers is that they may fail to reproduce the full pattern of hard wide-angle emissions, important, for example, in many new physics searches. It is therefore common to use LO multi-parton matrix elements to generate hard high-multiplicity partonic configurations as additional starting points for the showering, supplemented with some prescription (CKKW [316], MLM [317]) for consistently merging samples with different initial multiplicities. Monte Carlo generators, as described above, compute cross sections for the requested hard process that are correct at LO.

A wide variety of processes are available in MC implementations that are correct also to NLO, using the MC@NLO [318] or POWHEG [319] prescriptions, notably through the MADGRAPH5_aMC@NLO [117], POWHEG-BOX [320] and SHERPA [119] programs. Techniques have also been developed to combine NLO plus shower accuracy for different multiplicities of final-state jets [321]. Building in part on some of that work, several groups have also obtained NNLO plus shower accuracy for Drell-Yan and Higgs production [322, 323], as well as for a handful of $2 \rightarrow 2$ processes [324–332].

It is important to understand/verify the accuracy of the parton shower predictions in the Monte Carlo programs. In the limit of large center-of-mass energy, parton showers and analytic re-

summation must yield the same prediction for physical observables. The expected agreement has been established at next-to-leading logarithmic order for a certain class of algorithms, and for both global [333–336] and non-global observables [337]. A general framework for assessing the logarithmic accuracy of parton-shower algorithms has been formulated, based on their ability to reproduce the singularity structure of multi-parton matrix elements, and their ability to reproduce logarithmic resummation results [338]. The dominant contributions relevant for the extension of parton showers to higher logarithmic accuracy have been computed [339–343] and included in some algorithms, although a parton shower at full next-to-next-to-leading logarithmic accuracy is still missing. There exist ways to improve on current parton-shower algorithms [336, 337] and to demonstrate the shower accuracy through a comparison to analytic next-to-leading logarithmic calculations for a range of observables [337].

Parton showers are typically based on the leading color approximation, but sub-leading color effects arising from real emissions can be included on average [344, 345]. There are limitations of some routinely used parton shower algorithms, both in terms of leading (double) logarithms at subleading N_c and next-to-leading (single) logarithms at leading N_c [338].

In general, we expect parton-shower matched predictions to differ from the underlying fixed-order results in regions where (1) there is a large sensitivity to jet shapes (for instance small R jets), (2) there is a restriction in phase space such that soft gluon resummation effects become important, (3) the observable contains multiple disparate scales, (4) there are perturbative instabilities at fixed order, *e.g.* related to kinematical cuts, and (5) the observable is sensitive to higher multiplicity states than those described by the fixed-order calculation [314].

9.2.4 Accuracy of predictions

Estimating the accuracy of perturbative QCD predictions is not an exact science. It is often said that LO calculations are accurate to within a factor of two. This is based on experience with NLO corrections in the cases where these are available. In processes involving new partonic scattering channels at NLO and/or large ratios of scales (such as jet observables in processes with vector bosons, or the production of high- p_t jets containing B -hadrons), the ratio of the NLO to LO predictions, commonly called the “ K factor”, can be substantially larger than two. NLO corrections tend to be large for processes for which there is a great deal of color annihilation in the interaction. In addition, NLO corrections tend to decrease as more final state legs are added.

For calculations beyond LO, one approach to estimate the perturbative uncertainty is to base it on the last known perturbative correction; this may lead to misleading results if new sub-processes are present at the next-higher order. A more widely used method is to estimate it from the change in the prediction when varying the renormalization and factorization scales around a central value Q that is taken close to the physical scale of the process. A conventional range of variation is $Q/2 < \mu_R, \mu_F < 2Q$, varying the two scales independently with the restriction $\frac{1}{2}\mu_R < \mu_F < 2\mu_R$ [346]. This constraint limits the risk of misleadingly small uncertainties due to fortuitous cancellations between the μ_F and μ_R dependence when both are varied together, while avoiding the appearance of large logarithms of μ_R^2/μ_F^2 when both are varied completely independently. Where possible, it can be instructive to examine the two-dimensional scale distributions (μ_R vs. μ_F) to obtain a better understanding of the interplay between μ_R and μ_F . This procedure should not be assumed to always estimate the full uncertainty from missing higher orders, but it does indicate the size of one important known source of higher-order ambiguity.⁹

Calculations that involve resummations usually have an additional source of uncertainty associated with the choice of argument of the logarithms being resummed, *e.g.* $\ln(2\frac{p_Z^2}{M_Z^2})$ as opposed to

⁸The program ARIADNE [310] has also been widely used for simulating e^+e^- and DIS collisions.

⁹A number of prescriptions also exist for setting the scale automatically, *e.g.* Refs. [347–351], eliminating uncertainties from scale variation, though not from the truncation of the perturbative series itself. Various studies have been carried out on how to estimate uncertainties from missing higher orders that go beyond scale variations [352–355].

$\ln(\frac{1}{2} \frac{p_T^Z}{M_Z})$. In addition to varying renormalization and factorization scales, it is therefore also advisable to vary the argument of the logarithm by a suitable factor in either direction with respect to the “natural” argument.

The accuracy of QCD predictions is limited also by non-perturbative (or hadronization) corrections, which typically scale as a power of Λ/Q .¹⁰ For measurements that are directly sensitive to the structure of the hadronic final state, the corrections are usually linear in Λ/Q . The non-perturbative corrections are further enhanced in processes with a significant underlying event (*i.e.* in pp and $p\bar{p}$ collisions) and in cases where the perturbative cross sections fall steeply as a function of p_T or some other kinematic variable, for example in inclusive jet p_T or dijet mass spectra. In general, the underlying event for a hard scattering process, such as dijet production, is of a similar order, but somewhat harder, than the average energy density in a minimum-bias event [356]. Under high-luminosity running conditions, such as 13 TeV at the LHC, there can be on the order of 50 minimum-bias interactions occurring at each beam-beam crossing. This additional energy needs to be subtracted, and is typically removed by means of a rapidity-dependent transverse energy density determined on an event-by-event basis [357]. This subtraction, of necessity, also removes the underlying event, which must be added back in by means of MC event generator modelling to restore the measured event to the particle level.

Non-perturbative corrections are commonly estimated from the difference between Monte Carlo events at the “parton level” and at particle level. Parton level refers to the stage of the parton shower, where the evolution is stopped at an energy scale of typical hadron masses of a few GeV. An issue to be aware of is that “parton level” is not a uniquely defined concept. For example, in a MC event generator such a procedure depends on an arbitrary and tunable internal cutoff scale that separates the parton showering from the hadronization. In contrast, no such cutoff scale exists in an NLO or NNLO partonic calculation. The uncertainties in these corrections are often estimated by comparing different tunes of the various MC event generators. It should be noted that such estimates are not guaranteed to fully cover the true uncertainties.

Alternative methods exist for estimating hadronization corrections, that attempt to analytically deduce non-perturbative effects in one observable based on measurements of other observables (see the reviews [24,358]). While they directly address the problem of different possible definitions of parton level, it should also be said that they are far less flexible than Monte Carlo programs and not always able to provide equally good descriptions of the data.

One of the main issues is whether the fixed-order partonic final state of a NLO or NNLO prediction can match the parton shower in its ability to describe the experimental jet shape (minus any underlying event). Calculations at NNLO provide a better match to the parton shower predictions than do NLO ones, as might be expected from the additional gluon available to describe the jet shape. The hadronization predictions appear to work for both orders, but at an unknown accuracy. The impact of hadronization should fall as a power correction [1].

9.3 Experimental studies of QCD

Since we are not able to directly measure partons (quarks or gluons), but only hadrons and their decay products, a central issue for every experimental study of perturbative QCD is establishing a correspondence between observables obtained at the parton and the hadron level. The only theoretically sound correspondence is achieved by means of *infrared and collinear safe* quantities, which allow one to obtain finite predictions at any order of perturbative QCD.

As stated above, the simplest case of infrared- and collinear-safe observables are total cross sections. More generally, when measuring fully inclusive observables, the final state is not analyzed at all regarding its (topological, kinematical) structure or its composition. Basically the relevant information consists in the rate of a process ending up in a partonic or hadronic final state. In e^+e^- annihilation, widely used examples are the ratios of partial

widths or branching ratios for the electroweak decay of particles into hadrons or leptons, such as Z or τ decays, (*cf.* Sec. 9.2.1). Such ratios are often favored over absolute cross sections or partial widths because of large cancellations of experimental and theoretical systematic uncertainties. The strong suppression of non-perturbative effects, $\mathcal{O}(\Lambda^4/Q^4)$, is one of the attractive features of such observables, however, at the same time, the sensitivity to radiative QCD corrections is small, which for example affects the statistical uncertainty when using them for the determination of the strong coupling constant. In the case of τ decays not only the hadronic branching ratio is of interest, but also moments of the spectral functions of hadronic tau decays, which sample different parts of the decay spectrum and thus provide additional information. Other examples of fully inclusive observables are structure functions (and related sum rules) in DIS. These are extensively discussed in Sec. 18 of this *Review*.

On the other hand, often the structure or composition of the final state are analyzed and cross sections differential in one or more variables characterizing this structure are of interest. Examples are jet rates, jet substructure, event shapes or transverse momentum distributions of jets or vector bosons in hadron collisions. The case of fragmentation functions, *i.e.* the measurement of hadron production as a function of the hadron momentum relative to some hard scattering scale, is discussed in Sec. 19 of this *Review*.

It is worth mentioning that, besides the correspondence between the parton and hadron level, also a correspondence between the hadron level and the actually measured quantities in the detector has to be established. The simplest examples are corrections for finite experimental acceptance and efficiencies. Whereas acceptance corrections essentially are of theoretical nature, since they involve extrapolations from the measurable (partial) to the full phase space, other corrections such as for efficiency, resolution and response are of experimental nature. For example, measurements of differential cross sections such as jet rates require corrections in order to relate, *e.g.*, the energy deposits in a calorimeter to the jets at the hadron level. Typically detector simulations and/or data-driven methods are used in order to obtain these corrections. Care should be taken here in order to have a clear separation between the parton-to-hadron level and hadron-to-detector level corrections. Finally, for the sake of an easy comparison to the results of other experiments and/or theoretical calculations, it is suggested to provide, whenever possible, measurements corrected for detector effects and/or all necessary information related to the detector response (*e.g.*, the detector response matrix). Any fiducial phase space for measurements should be defined as close as possible to the detector-level selection in order to minimize model-dependent extrapolations.

9.3.1 Hadronic final-state observables

9.3.1.1 Jets

In hard interactions, final-state partons and hadrons appear predominantly in collimated bunches, which are generically called *jets*. To a first approximation, a jet can be thought of as a hard parton that has undergone soft and collinear showering and then hadronization. Jets are used both for testing our understanding and predictions of high-energy QCD processes, and also for identifying the hard partonic structure of decays of massive particles such as top quarks and W , Z and Higgs bosons.

In order to map observed hadrons onto a set of jets, one uses a *jet definition*. The mapping involves explicit choices: for example when a gluon is radiated from a quark, for what range of kinematics should the gluon be part of the quark jet, or instead form a separate jet? Good jet definitions are infrared and collinear safe, simple to use in theoretical and experimental contexts, applicable to any type of inputs (parton or hadron momenta, charged particle tracks, and/or energy deposits in the detectors) and lead to jets that are not too sensitive to non-perturbative effects.

An extensive treatment of the topic of jet definitions is given in Ref. [359] (for e^+e^- collisions) and Refs. [360–362]. Here we briefly review the two main classes: cone algorithms, extensively used at older hadron colliders, and sequential recombination al-

¹⁰In some circumstances, the scale in the denominator could be a smaller kinematic or physical scale that depends on the observable.

gorithms, more widespread in e^+e^- and ep colliders and at the LHC.

Very generically, most (iterative) cone algorithms start with some seed particle i , sum the momenta of all particles j within a cone of opening-angle R , typically defined in terms of rapidity and azimuthal angle. They then take the direction of this sum as a new seed and repeat until the direction of the cone is stable, and call the contents of the resulting stable cone a jet if its transverse momentum is above some threshold $p_{t,\min}$. The parameters R and $p_{t,\min}$ should be chosen according to the needs of a given analysis.

There are many variants of the cone algorithm, and they differ in the set of seeds they use and the manner in which they ensure a one-to-one mapping of particles to jets, given that two stable cones may share particles (“overlap”). The use of seed particles is a problem w.r.t. infrared and collinear safety. Seeded algorithms are generally not compatible with higher-order (or sometimes even leading-order) QCD calculations, especially in multi-jet contexts, as well as potentially subject to large non-perturbative corrections and instabilities. Seeded algorithms (JetCLU, MidPoint, and various other experiment-specific iterative cone algorithms) are therefore to be deprecated. Such algorithms are not used at the LHC, but were at the Fermilab Tevatron, where data still provide useful information, for example for global PDF fits. A modern alternative is to use a seedless variant, SIScone [363].

Sequential recombination algorithms at hadron colliders (and in DIS) are characterized by a distance $d_{ij} = \min(k_{t,i}^{2p}, k_{t,j}^{2p}) \Delta_{ij}^2 / R^2$ between all pairs of particles i, j , where Δ_{ij} is their separation in the rapidity-azimuthal plane, $k_{t,i}$ is the transverse momentum w.r.t. the incoming beams, and R is a free parameter. At the LHC, R is typically in the range from 0.4 to 0.8, although analyses can also use jet sizes up to 1.0–1.2. They also involve a “beam” distance $d_{iB} = k_{t,i}^{2p}$. One identifies the smallest of all the d_{ij} and d_{iB} , and if it is a d_{ij} , then i and j are merged into a new pseudo-particle (with some prescription, a recombination scheme, for the definition of the merged four-momentum). If the smallest distance is a d_{iB} , then i is removed from the list of particles and called a jet. As with cone algorithms, one usually considers only jets above some transverse-momentum threshold $p_{t,\min}$. The parameter p determines the kind of algorithm: $p = 1$ corresponds to the (inclusive-) k_t algorithm [247, 364, 365], $p = 0$ defines the *Cambridge-Aachen* algorithm [366, 367], while for the *anti- k_t* algorithm $p = -1$ [368]. All these variants are infrared and collinear safe. Whereas the former two lead to irregularly shaped jet boundaries, the latter results in cone-like boundaries, except in situations where there are nearby jets. The *anti- k_t* algorithm has become the de-facto standard for the LHC experiments.

In e^+e^- annihilation the k_t algorithm [247] uses $y_{ij} = 2 \min(E_i^2, E_j^2) (1 - \cos \theta_{ij}) / Q^2$ as distance measure between two particles/partons i and j and repeatedly merges the pair with smallest y_{ij} , until all y_{ij} distances are above some threshold y_{cut} , the jet resolution parameter. Q is a measure of the overall hardness of the event. The (pseudo)-particles that remain at this point are called the jets. Here it is y_{cut} (rather than R and $p_{t,\min}$) that should be chosen according to the needs of the analysis. The two-jet rate in the k_t algorithm has the property that logarithms $\ln(1/y_{\text{cut}})$ exponentiate. This is one reason why it is preferred over the earlier JADE algorithm [249], which uses the distance measure $y_{ij} = 2 E_i E_j (1 - \cos \theta_{ij}) / Q^2$. Note that other variants of sequential recombination algorithms for e^+e^- annihilations, using different definitions of the resolution measure y_{ij} , exhibit much larger sensitivities to fragmentation and hadronization effects than the k_t and JADE algorithms [369]. Efficient implementations of the above algorithms are available through the *FastJet* package [370].

9.3.1.2 Event Shapes

Event-shape variables are functions of the four momenta of the particles in the final state and characterize the topology of an event’s energy flow. They are sensitive to QCD radiation (and correspondingly to the strong coupling) insofar as gluon emission changes the shape of the energy flow.

The classic example of an event shape is the *Thrust* [371, 372]

in e^+e^- annihilations, defined as

$$\hat{\tau} = \max_{\vec{n}_\tau} \frac{\sum_i |\vec{p}_i \cdot \vec{n}_\tau|}{\sum_i |\vec{p}_i|}, \quad (9.22)$$

where \vec{p}_i are the momenta of the particles or the jets in the final-state and the maximum is obtained for the Thrust axis \vec{n}_τ . In the Born limit of the production of a perfect back-to-back $q\bar{q}$ pair, the limit $\hat{\tau} \rightarrow 1$ is obtained, whereas a perfectly spherical many-particle configuration leads to $\hat{\tau} \rightarrow 1/2$. Further event shapes of similar nature have been extensively measured at LEP and at HERA, and for their definitions and reviews we refer to Refs. [1, 7, 358, 373, 374]. The energy-energy correlation function [375], namely the energy-weighted angular distribution of produced hadron pairs, and its associated asymmetry are further shape variables which have been studied in detail at e^+e^- colliders. For hadron colliders the appropriate modification consists in only taking the transverse momentum component [376]. More recently, the event shape *N-jettiness* has been proposed [377], that measures the degree to which the hadrons in the final state are aligned along N jet axes or the beam direction. It vanishes in the limit of exactly N infinitely narrow jets.

Phenomenological discussions of event shapes at hadron colliders can be found in Refs. [377–381]. Measurements of hadronic event-shape distributions have been published by CDF [382], ATLAS [383–388] and CMS [389–392].

Event shapes are used for many purposes. These include measuring the strong coupling, tuning the parameters of Monte Carlo programs, investigating analytical models of hadronization and distinguishing QCD events from events that might involve decays of new particles (giving event-shape values closer to the spherical limit).

9.3.1.3 Jet substructure, quark vs. gluon jets

Jet substructure, which can be resolved by finding subjets or by measuring jet shapes, is sensitive to the details of QCD radiation in the shower development inside a jet and has been extensively used to study differences in the properties of quark and gluon induced jets, strongly related to their different color charges. In general, there is clear experimental evidence that gluon jets have a softer particle spectrum and are “broader” than (light-) quark jets (as expected from perturbative QCD) when looking at observables such as the jet shape $\Psi(r/R)$ [393]. This is the fraction of transverse momentum contained within a sub-cone of cone-size r for jets of cone-size R . It is sensitive to the relative fractions of quark and gluon jets in an inclusive jet sample and receives contributions from soft-gluon initial-state radiation and the underlying event. Therefore, it has been widely employed for validation and tuning of Monte Carlo parton-shower models. Furthermore, this quantity turns out to be sensitive to the modification of the gluon radiation pattern in heavy ion collisions (see *e.g.* Ref. [394]).

The most recent jet shape measurements using proton-proton collision data have been presented for inclusive jet samples [395–397] and for top-quark production [398]. Further discussions, references and summaries can be found in Refs. [374, 399, 400] and Sec. 4 of Ref. [401].

The use of jet substructure has also been investigated in order to distinguish QCD jets from jets that originate from hadronic decays of boosted massive particles (high- p_t electroweak bosons, top quarks and hypothesized new particles). A considerable number of experimental studies have been carried out with Tevatron and LHC data, in order to investigate the performance of the proposed algorithms for resolving jet substructure and to apply them to searches for new physics, as well as to the reconstruction of boosted top quarks, vector bosons and the Higgs boson. For reviews of this rapidly growing field, see sec. 5.3 of Ref. [360], Ref. [402] and Refs. [401, 403–406].

Neural network techniques and deep learning methods have also been applied to jet physics and jet substructure, see *e.g.* Refs. [407, 408]. Perhaps no other sub-field has benefited as much from machine learning techniques as the study of jet substructure. As a jet can have $\mathcal{O}(100)$ constituents each with kinematic and other information, jet substructure analysis is naturally a highly multivariate problem. Deep learning techniques can use all of the

available information to study jets in their natural high dimensionality. Such techniques have not only improved discrimination between different final states/types of jets, but have also improved our understanding of perturbative QCD. See for example the review in Ref. [300].

9.3.2 QCD measurements at colliders

There exists a wealth of data on QCD-related measurements in e^+e^- , ep , pp , and $p\bar{p}$ collisions, to which a short overview like this would not be able to do any justice. Extensive reviews of the subject have been published in Refs. [373,374] for e^+e^- colliders and in Ref. [409] for ep scattering, whereas for hadron colliders comprehensive overviews are given in, *e.g.*, Refs. [361,400] and Refs. [2,410–412].

Below we concentrate our discussion on measurements that are most sensitive to hard QCD processes with focus on jet production.

9.3.2.1 e^+e^- colliders

Analyses of jet production in e^+e^- collisions are mostly based on data from the JADE experiment at center-of-mass energies between 14 and 44 GeV, as well as on LEP collider data at the Z resonance and up to 209 GeV. The analyses cover the measurements of (differential or exclusive) jet rates (with multiplicities typically up to 4, 5 or 6 jets), the study of 3-jet events and particle production between the jets, as well as 4-jet production and angular correlations in 4-jet events.

Event-shape distributions from e^+e^- data have been an important input to the tuning of parton shower MC models, typically matched to matrix elements for 3-jet production. In general these models provide good descriptions of the available, highly precise data. Especially for the large LEP data sample at the Z peak, the statistical uncertainties are mostly negligible and the experimental systematic uncertainties are at the percent level or even below. These are usually dominated by the uncertainties related to the MC model dependence of the efficiency and acceptance corrections (often referred to as “detector corrections”).

Observables measured in e^+e^- collisions have been used for determinations of the strong coupling constant (*cf.* Section 9.4 below) and for putting constraints on the QCD color factors (*cf.* Sec. 9.1 for their definitions), thus probing the non-Abelian nature of QCD. Angular correlations in 4-jet events give sensitivity at leading order. Some sensitivity to these color factors, although only at NLO, is also obtained from event-shape distributions. Scaling violations of fragmentation functions and the different subjet structure in quark and gluon induced jets also give access to these color factors. A compilation of results [374] quotes world average values of $C_A = 2.89 \pm 0.03(\text{stat}) \pm 0.21(\text{syst})$ and $C_F = 1.30 \pm 0.01(\text{stat}) \pm 0.09(\text{syst})$, with a correlation coefficient of 82%. These results are in perfect agreement with the expectations from $SU(3)$ of $C_A = 3$ and $C_F = 4/3$.

9.3.2.2 DIS and photoproduction

Jet measurements in ep collisions, both in the DIS and photoproduction regimes, allow for tests of QCD factorization (as they involve only one initial state proton and thus one PDF function), and provide sensitivity to both the gluon PDF and to the strong coupling constant. Calculations are available at NNLO in both regimes [413,414]. Experimental uncertainties of the order of 5–10% have been achieved, mostly dominated by the jet energy scale uncertainty, whereas statistical uncertainties are negligible to a large extent. For comparison to theoretical predictions, at large jet p_t the PDF uncertainty dominates the theoretical uncertainty (typically of order 5–10%, in some regions of phase space up to 20%), therefore jet observables become useful inputs for PDF fits.

In general, the data are well described by the NLO and NNLO matrix-element calculations, combined with DGLAP evolution equations, in particular at large Q^2 and central values of jet pseudo-rapidity. At low values of Q^2 and x , in particular for large jet pseudo-rapidities, certain features of the data have been interpreted as requiring BFKL-type evolution, though the predictions for such schemes are still limited. It is worth noting that there is no indication that the BKFL approximation is needed in the currently probed x, Q^2 values, and an alternative approach [415], which implements the merging of LO matrix-element based event

generation with a parton shower (using the SHERPA framework), successfully describes the data in all kinematical regions, including the low Q^2 , low x domain. At moderately small x values, it should perhaps not be surprising that the BFKL approach and fixed-order matrix-element merging with parton showers may both provide adequate descriptions of the data, because some part of the multi-parton phase space that they model is common to both approaches.

In the case of photoproduction, a wealth of measurements with low p_t jets were performed in order to constrain the photon content of the proton. The uncertainties related to such photon PDFs play a minor role at high jet p_t , which has allowed for precise tests of pQCD calculations.

A few examples of recent measurements can be found in Refs. [416–420] for photoproduction and in Refs. [421–430] for DIS.

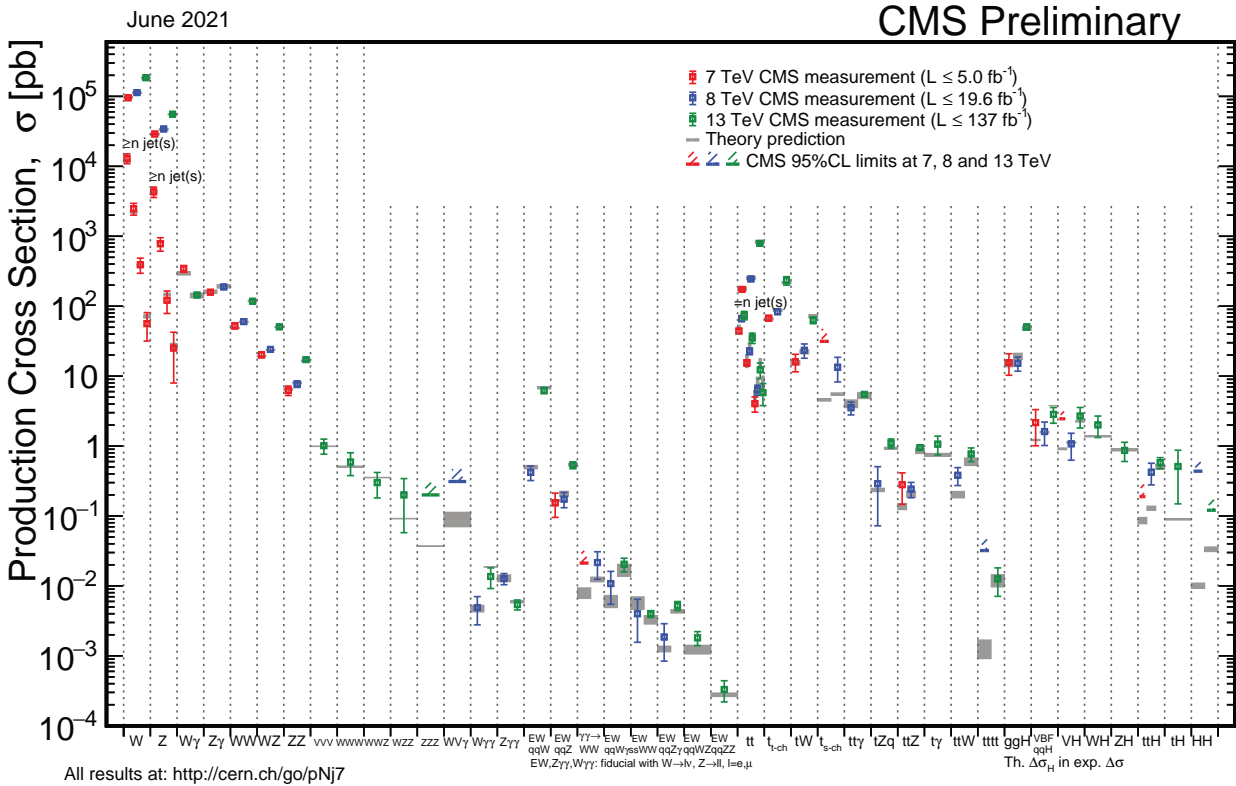
9.3.2.3 Hadron-hadron colliders

The spectrum of observables and the number of measurements performed at hadron colliders is enormous, probing many regions of phase space and covering a huge range of cross sections, as illustrated in Fig. 9.1 for the case of the ATLAS and CMS experiments at the LHC. In general, the theory agreement with data is excellent for a wide variety of processes, indicating the success of perturbative QCD with the PDF and strong coupling inputs. For the sake of brevity, in the following only certain classes of those measurements will be discussed, which permit various aspects of the QCD studies to be addressed. Most of our discussion will focus on LHC results, which are available for center-of-mass energies of 2.76, 5, 7, 8 and 13 TeV with integrated luminosities of up to 140 fb^{-1} . Generally speaking, besides representing precision tests of the standard model and QCD in particular, these measurements serve several purposes, such as: (i) probing pQCD and its various approximations and implementations in MC models, in order to quantify the order of magnitude of not yet calculated contributions, and to gauge their precision when used as background predictions, or (ii) extracting/constraining model parameters such as the strong coupling constant or PDFs. Indeed, data from the LHC are becoming increasingly important for the determination of both PDFs and the strong coupling constant.

The final states measured at the LHC include single, double and triple gauge boson production, top production (single top, top pair and four top production), Higgs boson production, alone and in conjunction with a W or Z boson, and with a top quark pair. Many/most of these events are accompanied by additional jets. So far only relatively loose limits have been placed on double Higgs production. The volume of LHC results prohibits a comprehensive description in this *Review*; hence, only a few highlights will be presented.

Among the most important cross sections measured, and the one with the largest dynamic range, is the inclusive jet spectrum as a function of the jet transverse momentum (p_t), for several rapidity regions and for p_t up to 700 GeV at the Tevatron and $\sim 3.5 \text{ TeV}$ at the LHC. It is worth noting that this upper limit in p_t corresponds to a distance scale of $\sim 10^{-19} \text{ m}$: no other experiment so far is able to directly probe smaller distance scales of nature than this measurement. The Tevatron inclusive jet measurements in Run 2 (Refs. [433–436]) were carried out with the MidPoint jet clustering algorithm (or its equivalent) and with the k_t jet clustering algorithm. Most of the LHC measurements use the *anti- k_t* algorithm, with a variety of jet radii. The use of multiple jet radii in the same analysis allows a better understanding of the underlying QCD dynamics. Measurements by ALICE, ATLAS and CMS have been published in Refs. [437–446].

In general, we observe a good description of the data by the NLO and NNLO QCD predictions over about 11 orders of magnitude in cross section, as long as care is taken for the form of the central scale choice [447]. The experimental systematic uncertainties are dominated by the jet energy scale uncertainty, quoted to be in the range of a few percent (see for instance the review in Ref. [448]), leading to uncertainties of $\sim 5 - 30\%$ on the cross section, increasing with p_t and rapidity. The PDF uncertainties dominate the theoretical uncertainty at large p_t and rapidity. In fact, inclusive jet data are one of the most important inputs to



Standard Model Production Cross Section Measurements

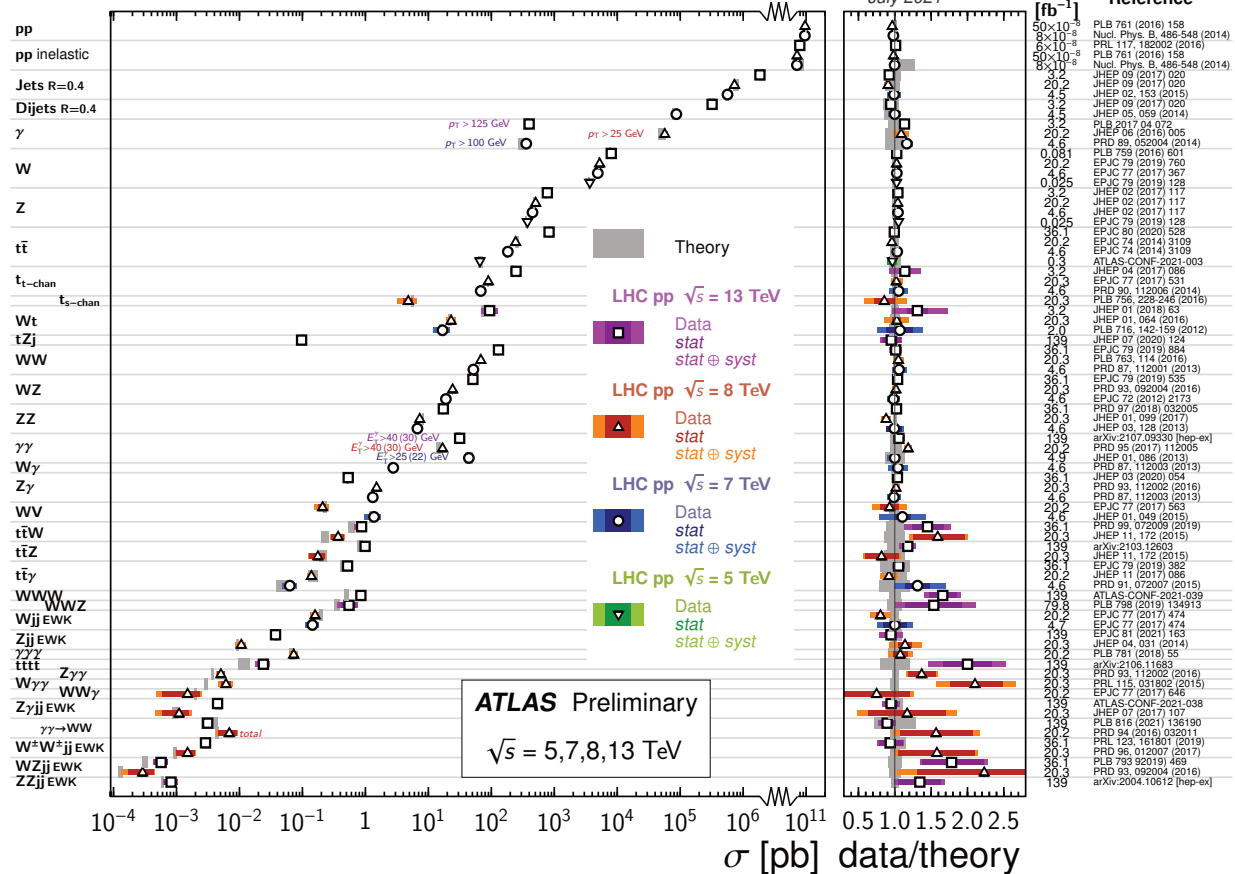


Figure 9.1: Overview of cross section measurements for a wide class of processes and observables, as obtained by the CMS [431] and ATLAS [432] experiments at the LHC, for centre-of-mass energies of 5, 7, 8 and 13 TeV. Also shown are the theoretical predictions and their uncertainties.

global PDF fits, in particular for constraining the high- x gluon PDF [79, 449]. Constraints on the PDFs can also be obtained from ratios of inclusive cross sections at different center-of-mass energies [438, 443]. In general, ratios of jet cross sections are a means to (at least partially) cancel the jet energy scale uncertainties and thus provide jet observables with significantly improved precision.

Dijet events are typically analyzed in terms of their invariant mass or average dijet p_t and angular distributions, which allows for tests of NLO and NNLO QCD predictions (see *e.g.* Refs. [442, 450, 451] for recent LHC results), and for setting stringent limits on deviations from the Standard Model, such as quark compositeness or contact interactions (some examples can be found in Refs. [445, 452–458]). Furthermore, dijet azimuthal correlations between the two leading jets, normalized to the total dijet cross section, are an extremely valuable tool for studying the spectrum of gluon radiation in the event. The azimuthal separation of the two leading jets is sensitive to multi-jet production, avoiding at the same time large systematic uncertainties from the jet energy calibration. For example, results from the Tevatron [459, 460] and the LHC [388, 461–465] show that the LO (non-trivial) prediction for this observable, with at most three partons in the final state, is not able to describe the data for an azimuthal separation below $2\pi/3$, where NLO contributions (with 4 partons) restore the agreement with data. In addition, this observable can be employed to tune Monte Carlo predictions of soft gluon radiation. Further examples of dijet observables that probe special corners of phase space are those that involve forward (large rapidity) jets and where a large rapidity separation, possibly also a rapidity gap, is required between the two jets. Reviews of such measurements can be found in Ref. [400], showing that no single prediction is capable of describing the data in all phase-space regions. In particular, no conclusive evidence for BFKL effects in these observables has been established so far.

Beyond dijet final states, measurements of the production of three or more jets, including cross section ratios, have been performed (see Refs. [400, 466] for recent reviews), as a means of testing perturbative QCD predictions, determining the strong coupling constant (at NLO precision so far), and probing/tuning MC models, in particular those combining multi-parton matrix elements with parton showers. The calculation of 3-jet production to NNLO [222] will allow more precise predictions of the 3-jet to 2-jet ratio, and thus the extraction of $\alpha_s(M_Z^2)$ from this observable.

W and Z production serve as benchmark cross sections at the LHC. The large boson mass provides a stability for the perturbative predictions which results in better theoretical precision. In terms of experimental precision, measurements of inclusive vector boson (W, Z) production provide the most precisely determined observables at hadron colliders so far. This is because the experimental signatures are based on leptons which are measured much more accurately than jets or photons. At the LHC [467–474], the dominant uncertainty stems from the luminosity determination ($\leq 2\text{--}4\%$), while other uncertainties (*e.g.* statistical or from lepton efficiencies) are controlled at the $\sim 0.5\text{--}3\%$ level. The uncertainty from the acceptance correction of about $\sim 1\text{--}2\%$ can be reduced by measuring so-called fiducial cross sections, *i.e.* by applying kinematic cuts also to the particle level of the theoretical predictions. A further reduction or even complete elimination of particular uncertainties (*e.g.* luminosity) is achieved by measuring cross section ratios (W/Z or W^+/W^-) or differential distributions that are normalised to the inclusive cross section. On the theory side, as discussed earlier in this *Review*, the production of these color-singlet states has been calculated to N³LO [101–103]. Since the dominant theoretical uncertainty is related to the choice of PDFs, these high-precision data provide useful handles for PDF determinations.

Further insights are obtained from measurements of differential vector boson production, as a function of the invariant dilepton mass, the boson's rapidity or its transverse momentum. For example, the dilepton invariant mass distribution has been measured [475–480] for masses between 15 and 3000 GeV, covering more than 8 orders of magnitude in cross section. NNLO QCD

predictions, together with modern PDF sets and including higher-order electroweak and QED final-state radiation corrections, describe the data to within 5–10% over this large range, whereas NLO predictions show larger deviations, unless matched to a parton shower.

Similar conclusions can be drawn from the observed rapidity distribution of the dilepton system (see *e.g.* Refs. [467, 476, 481]) or, in the case of W production, from the observed charged lepton rapidity distribution and its charge asymmetry. The latter is particularly sensitive to differences among PDF sets [467, 482–484], also thanks to the high precision achieved by the ATLAS and CMS experiments for central rapidity ranges. These measurements are extended to the very forward region, up to 4.5 in lepton rapidity, by the LHCb experiment [473, 474, 485].

An overview of these kinds of measurement can be found in Ref. [400]. There one can also find a discussion of and references to LHC results from studies of the vector boson's transverse momentum distribution, p_t^V (see also Refs. [486–488]). This observable covers a wide kinematic range and probes different aspects of higher-order QCD effects. It is sensitive to jet production in association with the vector boson, without suffering from the large jet energy scale uncertainties. In the p_t^V region of several tens of GeV to over 1 TeV, the NNLO predictions for V+jet can be used to predict the high- p_t boson production cross section.¹¹ The NNLO predictions agree with the data to within about 10%, and agree somewhat better at high transverse momentum than do the NLO predictions [489]. At transverse momenta below ~ 20 GeV, the fixed-order predictions fail and soft-gluon resummation is needed to restore the agreement with data. The soft gluon resummation can either be performed analytically, or effectively using parton showering implemented in Monte Carlo programs. While analytic approaches reach a higher perturbative precision, they typically refer to inclusive measurements without fiducial cuts. The addition of further jets to the final state extends the kinematic range as well as increasing the complexity of the calculation/measurements. The number of results obtained both at the Tevatron and at the LHC is extensive, summaries can be found in Refs. [400, 490], and more recent results can be found in Refs. [489, 491–494]. The measurements cover a very large phase space, *e.g.* with jet transverse momenta between 30 GeV and ~ 1.5 TeV and jet rapidities up to $|y| < 4.4$ [489]. Jet multiplicities as high as seven jets accompanying the vector boson have already been probed at the LHC, together with a substantial number of other kinematical observables, such as angular correlations among the various jets or among the jets and the vector boson, or the sum of jet transverse momenta, H_T . Whereas the jet p_t and H_T distributions are dominated by jet energy scale uncertainties at levels similar to those discussed above for inclusive jet production, angular correlations and jet multiplicity ratios have been measured with a precision of $\sim 10\%$, see *e.g.* Refs. [390, 495].

NLO calculations for up to five jets [496] in addition to the vector boson are in good agreement with the data over that phase space, where the calculations are applicable. Predictions for V+jet at NNLO improve the description of the data for distributions involving the vector boson or the leading jet. MC models that implement parton shower matching to matrix elements (*either* at LO or NLO) have mixed results.

The challenges get even more severe in the case of vector boson plus heavy quark (b, c) production: on the theory side because an additional scale is introduced by the heavy quark mass, and different schemes exist for the handling of heavy quarks and their mass effects in the initial and/or final state; and on the experimental side because additional uncertainties related to the heavy-flavour tagging must be considered. A review of heavy quark production at the LHC is presented in Ref. [497], where the di- b -jet p_t and mass spectra are found to be well modeled within uncertainties by most generators for b -jet production with or without associated W and Z bosons. However, sizable differences between data and predictions are seen in the modeling of events with single b jets, particularly at large b -jet p_t , where gluon splitting processes

¹¹For these calculations, there is a requirement of the presence of a jet, but the p_t cut is typically small (30 GeV) compared to the high p_t region being discussed here.

become dominant, as also confirmed by studies of b -hadron and b -jet angular correlations.

The precision reached in photon measurements is in between that for lepton and jet measurements. The photon energy and angles can be measured at about the same precision as the lepton energy and angles in Drell-Yan production, but there are greater challenges encountered in photon reconstruction (for example isolation) and in purity determination. Note, though, that the photon purity approaches unity as the photon p_t increases. At high p_t , it becomes increasingly difficult for a jet to fragment into an isolated neutral electromagnetic cluster which mimics the photon signature. The inclusive photon cross section can be measured [450, 498–501], as well as the production of a photon accompanied by one or more jets [501–503, 503–506]. The kinematic range for photon production is less than that for jet production because of the presence of the electromagnetic coupling, but still reaches about 2 TeV. Better agreement is obtained with NNLO predictions for photon production than for NLO predictions, except when the latter are matched to matrix element plus parton shower predictions. Photon production in association with a heavy-flavor jet is a useful input for the determination of the b and c quark PDFs [507].

Electroweak corrections are expected to become more and more relevant now that the TeV energy range starts to be explored. For example, such corrections were found [508] to be sizable (tens of percent) when studying the ratio $(d\sigma^\gamma/dp_t)/(d\sigma^Z/dp_t)$ in $\gamma(Z)$ +jet production, p_t being the boson's transverse momentum, and might account for (some of) the differences observed in a CMS measurement [509] of this quantity.

A number of interesting developments, in terms of probing higher-order QCD effects, have occurred in the sector of diboson production, in particular for the WW and $\gamma\gamma$ cases. Regarding the former, an early disagreement of about 10% between the LHC measurements and the NLO predictions had led to a number of speculations of possible new physics effects in this channel. However, more recent ATLAS and CMS measurements [510–513] are in agreement with the NNLO prediction [109]. The statistical reach of the LHC has resulted in evidence for triple massive gauge boson production [514].

In the case of diphoton production, ATLAS [515, 516] and CMS [517] have provided accurate measurements, in particular for phase-space regions that are sensitive to radiative QCD corrections (multi-jet production), such as small azimuthal photon separation. While there are large deviations between data and NLO predictions in this region, a calculation [194] at NNLO accuracy manages to mostly fill this gap. This is an interesting example where scale variations can not provide a reliable estimate of missing contributions beyond NLO, since at NNLO new channels appear in the initial state (gluon fusion in this case). These missing channels can be included in a matrix element plus parton shower calculation in which two additional jets are included at NLO. The result exhibits a similar level of agreement as that obtained at NNLO. Three-photon production has also been measured [518] and is in good agreement with NNLO theory predictions [219, 220].

In terms of heaviest particle involved, top-quark production at the LHC has become an important tool for probing higher-order QCD calculations, thanks to very impressive achievements both on the experimental and theoretical side, as extensively summarized in Ref. [519]. Regarding $t\bar{t}$ production, the most precise inclusive cross section measurements are achieved using the dilepton ($e\mu$) final state, with a total uncertainty of 4% [520–523]. This is of about the same size as the uncertainty on the most advanced theoretical predictions [107, 108, 524, 525], obtained at NNLO with additional soft-gluon resummation at NNLL accuracy [526]. There is excellent agreement between data and the QCD predictions.

The $t\bar{t}$ final state allows multiple observables to be measured. A large number of differential cross section measurements have been performed at 7, 8 and 13 TeV centre-of-mass energy, studying distributions such as the top-quark p_t and rapidity, the transverse momentum and invariant mass of the $t\bar{t}$ system (probing the TeV range), or the number of additional jets. These measurements

have been compared to a wide range of predictions, at fixed order up to NNLO as well as using LO or NLO matrix elements matched to parton showers. Each of the observables provides information on the high x gluon. However, there are tensions among the multiple observables that can lead to difficulties in PDF fits.

Thanks to both the precise measurements of, and predictions for, the inclusive top-pair cross section, which is sensitive to the strong coupling constant and the top-quark mass, this observable has been used to measure the strong coupling constant at NNLO accuracy from hadron collider data [527, 528] (*cf.* Section 9.4 below), as well as to obtain a measurement of the top-quark's pole mass without employing direct reconstruction methods [527, 529, 530].

The Higgs boson provides a tool for QCD studies, especially as the dominant production mechanism is gg fusion, which is subject to very large QCD corrections. Higgs boson production has been measured in the ZZ , $\gamma\gamma$, $b\bar{b}$, WW and $\tau\tau$ decay channels. The experimental cross section is now known with a precision approaching 10% [531, 532], similar to the size of the theoretical uncertainty [533], of which the PDF+ α_s uncertainty is the largest component. The experimental precision has allowed detailed fiducial and differential cross section measurements. For example, with the diphoton final state, the transverse momentum of the Higgs boson can be measured out to the order of 650 GeV [534, 535], where top quark mass effects become important. The production of a Higgs boson with up to 4 jets has been measured [534, 536]. The experimental cross sections have been compared to NNLO predictions (for $H+\geq 1$ jet), NLO for 2 and 3 jets, and NNLO+NNLL for the transverse momentum distribution. In addition, finite top quark mass effects have been taken into account at NLO. The use of the boosted $H \rightarrow b\bar{b}$ topology allows probes of Higgs boson transverse momenta on the order of 600 GeV and greater [536]. So far the agreement with the perturbative QCD corrections is good.

9.4 Determinations of the strong coupling constant

Beside the quark masses, the only free parameter in the QCD Lagrangian is the strong coupling constant α_s . The coupling constant in itself is not a physical observable, but rather a quantity defined in the context of perturbation theory, which enters predictions for experimentally measurable observables, such as R in Eq. (9.7). The value of the strong coupling constant must be inferred from such measurements and is subject to experimental and theoretical uncertainties. The incomplete knowledge of α_s propagates into uncertainties in numerous precision tests of the Standard Model. Here, we present an update of the 2020 PDG average value of $\alpha_s(M_Z^2)$ and its uncertainty [537].

Many experimental observables are used to determine α_s . A number of recent determinations are collected in Ref. [538]. Further discussions and considerations on determinations of α_s can also be found in Refs. [539–541]. Such considerations include:

- The observable's sensitivity to α_s as compared to the experimental precision. For example, for the e^+e^- cross section to hadrons (*cf.* R in Sec. 9.2.1), QCD effects are only a small correction, since the perturbative series starts at order α_s^0 ; 3-jet production or event shapes in e^+e^- annihilations are directly sensitive to α_s since they start at order α_s ; the hadronic decay width of heavy quarkonia, $\Gamma(\mathcal{T} \rightarrow \text{hadrons})$, is very sensitive to α_s since its leading order term is $\propto \alpha_s^3$.
- The accuracy of the perturbative prediction, or equivalently of the relation between α_s and the value of the observable. The minimal requirement is generally considered to be an NLO prediction. Several observables have been known to NNLO for quite some time. These include, for instance, inclusive observables, as well as 3-jet rates and event shapes in e^+e^- collisions, inclusive jet and dijet production in DIS, and inclusive jet, dijet, $t\bar{t}$, W/Z +jet and three-jet production cross sections in pp or $p\bar{p}$ collisions. The e^+e^- hadronic cross section and τ branching fraction to hadrons are even known to N³LO, if one denotes the LO as the first non-trivial term. In certain cases, fixed-order predictions are supplemented with resummation. The precise magnitude of the associated theory uncertainties

usually is estimated as discussed in Sec. 9.2.4.

- The size of non-perturbative effects. Sufficiently inclusive quantities, like the e^+e^- cross section to hadrons, have small non-perturbative contributions $\sim \Lambda^4/Q^4$. Others, such as event-shape distributions, have typically contributions $\sim \Lambda/Q$.
- The scale at which the measurement is performed. An uncertainty δ on a measurement of $\alpha_s(Q^2)$, at a scale Q , translates to an uncertainty $\delta' = (\alpha_s^2(M_Z^2)/\alpha_s^2(Q^2)) \cdot \delta$ on $\alpha_s(M_Z^2)$. For example, this enhances the already important impact of precise low- Q measurements, such as from τ decays, in combinations performed at the M_Z scale.

The selection of results from which to determine the world average value of $\alpha_s(M_Z^2)$ is restricted to those that are

- published in a peer-reviewed journal at the time of writing this report,
- based on the most complete perturbative QCD predictions of at least NNLO accuracy,
- accompanied by reliable estimates of all experimental and theoretical uncertainties.

Numerous measurements from jet production in DIS and at hadron colliders are still excluded from the average presented here, because the determination of $\alpha_s(M_Z^2)$ from those data sets has not yet been upgraded to NNLO. We expect that this will change in the near future. Still, the NLO analyses will be discussed in this *Review*, as they are important ingredients for the experimental evidence of the energy dependence of α_s , *i.e.* for asymptotic freedom, one of the key features of QCD.

In order to calculate the world average value of $\alpha_s(M_Z^2)$, we apply, as in earlier editions, an intermediate step of pre-averaging results within the sub-fields now labeled “Hadronic τ decays and low Q^2 continuum” (τ decays and low Q^2), “Heavy quarkonia decays” ($Q\bar{Q}$ bound states), “PDF fits” (PDF fits), “Hadronic final states of e^+e^- annihilations” (e^+e^- jets & shapes), “Observables from hadron-induced collisions” (hadron colliders), and “Electroweak precision fit” (electroweak) as explained in the following sections. For each sub-field, the *unweighted average* of all selected results is taken as the pre-average value of $\alpha_s(M_Z^2)$, and the unweighted average of the quoted uncertainties is assigned to be the respective overall error of this pre-average. For the “Lattice QCD” (lattice) sub-field we do not perform a pre-averaging; instead, we adopt for this sub-field the average value and uncertainty derived by the Flavour Lattice Averaging Group (FLAG) in Ref. [542].

Assuming that the six sub-fields (excluding lattice) are largely independent of each other, we determine a non-lattice world average value using a ‘ χ^2 averaging’ method. In a last step we perform an unweighted average of the values and uncertainties of $\alpha_s(M_Z^2)$ from our non-lattice result and the lattice result presented in the FLAG2019 report [542].

9.4.1 Hadronic τ decays and low Q^2 continuum:

Based on complete N³LO predictions [32], analyses of the τ hadronic decay width and spectral functions have been performed, *e.g.* in Refs. [32,543–548], and lead to precise determinations of α_s at the energy scale of M_τ^2 . They are based on different approaches to treat perturbative and non-perturbative contributions, the impacts of which have been a matter of intense discussions for a long time, see *e.g.* Refs. [547–550]. In particular, in τ decays there is a significant difference between results obtained using fixed-order (FOPT) or contour-improved perturbation theory (CIPT),

such that analyses based on CIPT generally arrive at larger values of $\alpha_s(M_\tau^2)$ than those based on FOPT. In addition, some results show differences in $\alpha_s(M_\tau^2)$ between different groups using the same data sets and perturbative calculations, most likely due to different treatments of the non-perturbative contributions, *cf.* Ref. [548] with Refs. [547,551]. References [552,553] question the validity of using a truncated OPE at $Q^2 = m_\tau^2$ based on the disagreement found between experimental values of the spectral moments and the theory representations based on the truncated OPE fits at $Q^2 > m_\tau^2$.

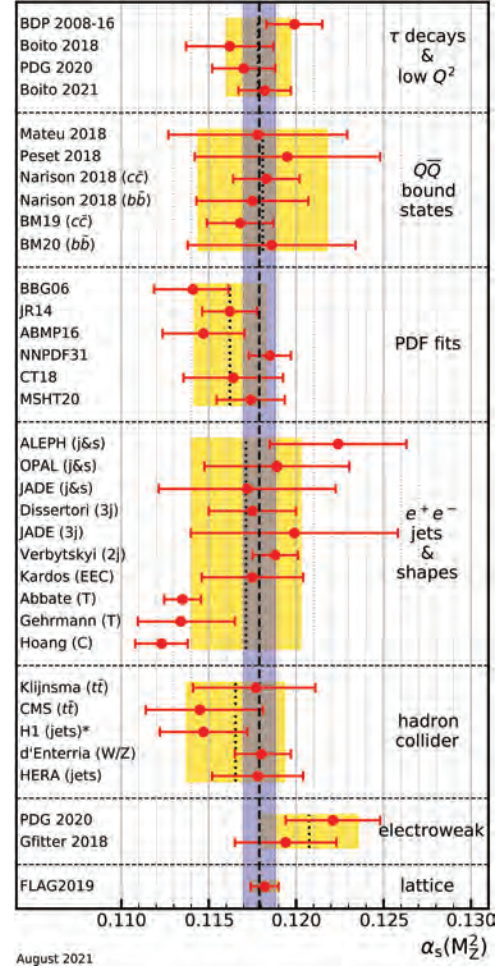


Figure 9.2: Summary of determinations of $\alpha_s(M_Z^2)$ from the seven sub-fields discussed in the text. The yellow (light shaded) bands and dotted lines indicate the pre-average values of each sub-field. The dashed line and blue (dark shaded) band represent the final world average value of $\alpha_s(M_Z^2)$. The “*” symbol within the “hadron colliders” sub-field indicates a determination including a simultaneous fit of PDFs.

We determine the pre-average value of $\alpha_s(M_Z^2)$ for this sub-field from studies that employ both FOPT and CIPT expansions, and that account for the difference among these in the quoted overall uncertainty. If necessary, we perform ourselves the averaging of FOPT and CIPT numbers and the quadratic addition of half their difference to the uncertainty. As the results from Refs. [32,550,551] are not totally independent, we pre-average as a first step the three results $\alpha_s(M_Z^2) = 0.1202 \pm 0.0019$ [32], $\alpha_s(M_Z^2) = 0.1199 \pm 0.0015$ [551], and $\alpha_s(M_Z^2) = 0.1197 \pm 0.0015$ [550] to $\alpha_s(M_Z^2) = 0.1199 \pm 0.0016$ (summarized as BDP2008-16 in Fig. 9.2). Subsequently, this is combined with $\alpha_s(M_Z^2) = 0.1162 \pm 0.0025$ [554], and $\alpha_s(M_Z^2) = 0.1182 \pm 0.0015$ [555], which replaces the previous result from Ref. [548]. We also include the result from τ decay and lifetime measurements, obtained in Sec. *Electroweak Model and constraints on New Physics* of the 2020 edition of this *Review* [537], $\alpha_s(M_Z^2) = 0.1170_{-0.0017}^{+0.0019}$. The latter result, being a global fit of τ data, involves some correlations with the other extractions of this category. However, since we perform an unweighted average of the central value and uncertainty, the effects of the potential correlations are reduced.

All these results are summarized in Fig. 9.2. Determining the unweighted average of the central values and their overall uncertainties, we arrive at $\alpha_s(M_Z^2) = 0.1178 \pm 0.0019$, which we will use as the first input for determining the world average value of

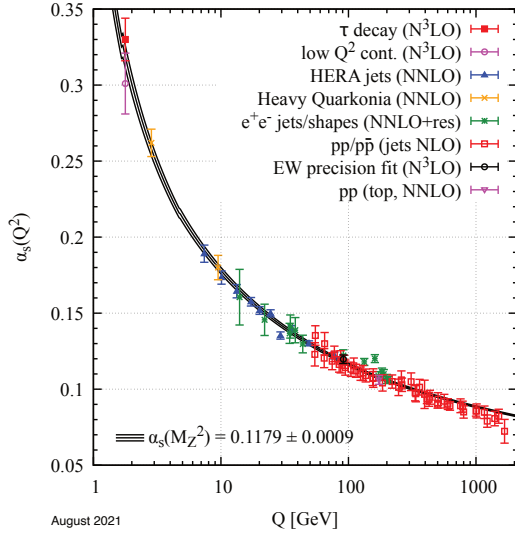


Figure 9.3: Summary of measurements of α_s as a function of the energy scale Q . The respective degree of QCD perturbation theory used in the extraction of α_s is indicated in brackets (NLO: next-to-leading order; NNLO: next-to-next-to-leading order; NNLO+res.: NNLO matched to a resummed calculation; N³LO: next-to-NNLO).

$\alpha_s(M_Z^2)$. This corresponds to $\alpha_s(M_Z^2) = 0.312 \pm 0.015$.

9.4.2 Heavy quarkonia decays:

Recently, two determinations have been performed [556, 557] that are based on N³LO accurate predictions. Reference [556] performs a simultaneous fit of the strong coupling and the bottom mass \overline{m}_b , including states with principal quantum number up to $n \leq 2$ in order to break the degeneracy between α_s and \overline{m}_b , finding $\alpha_s(M_Z^2) = 0.1178 \pm 0.0051$. Reference [557] instead uses as input of the fit the renormalon-free combination of masses of the meson B_c , the bottomonium η_b and the charmonium η_c , $M_{B_c} - M_{\eta_b}/2 - M_{\eta_c}/2$, which is weakly dependent on the heavy quark masses, but shows a good dependence on α_s . Using this observable, they obtain $\alpha_s(M_Z^2) = 0.1195 \pm 0.0053$. Two further values are derived at NNLO in Ref. [558, 559] from mass splittings and sum rules giving $\alpha_s(M_Z^2) = 0.1183 \pm 0.0019$ and $\alpha_s(M_Z^2) = 0.1175 \pm 0.0032$ when evolved from the relevant charmonium respectively bottomonium mass scales to M_Z^2 . Finally, by means of quarkonium sum rules, Refs. [560, 561] quote $\alpha_s(M_Z^2) = 0.1168 \pm 0.0019$ and $\alpha_s(M_Z^2) = 0.1186 \pm 0.0048$ for charmonium and bottomonium respectively. These six determinations satisfy our criteria to be included in the heavy-quarkonia category of the world average. Their unweighted combination leads to the pre-average for this category of $\alpha_s(M_Z^2) = 0.1181 \pm 0.0037$.

9.4.3 PDF fits:

Another class of studies, analyzing structure functions at NNLO QCD (and partly beyond), provide results that serve as relevant inputs for the world average of α_s . Most of these studies do *not*, however, explicitly include estimates of theoretical uncertainties when quoting fit results of α_s . In such cases we add, in quadrature, half of the difference between the results obtained in NNLO and NLO to the quoted errors.

A combined analysis of non-singlet structure functions from DIS [562], based on QCD predictions up to N³LO in some of its parts, results in $\alpha_s(M_Z^2) = 0.1141 \pm 0.0022$ (BBG). Studies of singlet and non-singlet structure functions, based on NNLO predictions, result in $\alpha_s(M_Z^2) = 0.1162 \pm 0.0017$ [563] (JR14). The AMBP group [564, 565] determined a set of parton distribution functions using data from HERA, NOMAD, CHORUS, from the Tevatron and the LHC using the Drell-Yan process and the hadro-production of single-top and top-quark pairs, and determined $\alpha_s(M_Z^2) = 0.1147 \pm 0.0024$ [564].

The MSHT group [566], also including hadron collider data, determined a new set of parton density functions (MSHT20) together with $\alpha_s(M_Z^2) = 0.1174 \pm 0.0013$. Similarly, the CT group [567] determined the CT18 parton density set together with $\alpha_s(M_Z^2) = 0.1164 \pm 0.0026$. The NNPDF group [568] presented NNPDF3.1 parton distribution functions together with $\alpha_s(M_Z^2) = 0.1185 \pm 0.0012$.

We note that criticism has been expressed on some of the above extractions. Among the issues raised, we mention the neglect of singlet contributions at $x \geq 0.3$ in pure non-singlet fits [569], the impact and detailed treatment of particular classes of data in the fits [569, 570], possible biases due to insufficiently flexible parametrizations of the PDFs [571] and the use of a fixed-flavor number scheme [572, 573].

Summarizing the results from world data on structure functions, taking the *unweighted average* of the central values and errors of all selected results, leads to a pre-average value of $\alpha_s(M_Z^2) = 0.1162 \pm 0.0020$, see Fig. 9.2.

9.4.4 Hadronic final states of e^+e^- annihilations:

Re-analyses of jets and event shapes in e^+e^- annihilation (j&es), measured around the Z peak and at LEP2 center-of-mass energies up to 209 GeV, using NNLO predictions matched to NLL resummation and Monte Carlo models to correct for hadronization effects, resulted in $\alpha_s(M_Z^2) = 0.1224 \pm 0.0039$ (ALEPH) [574], and in $\alpha_s(M_Z^2) = 0.1189 \pm 0.0043$ (OPAL) [575]. Similarly, an analysis of JADE data [576] at center-of-mass energies between 14 and 46 GeV gives $\alpha_s(M_Z^2) = 0.1172 \pm 0.0051$, with contributions from the hadronization model and from perturbative QCD uncertainties of 0.0035 and 0.0030, respectively. Precise determinations of α_s from 3-jet production alone (3j), at NNLO, resulted in $\alpha_s(M_Z^2) = 0.1175 \pm 0.0025$ [577] from ALEPH data and in $\alpha_s(M_Z^2) = 0.1199 \pm 0.0059$ [578] from JADE. A recent determination is based on an NNLO+NNLL accurate calculation that allows to fit the region of lower 3-jet rate (2j) using data collected at LEP and PETRA at different energies. This fit gives $\alpha_s(M_Z^2) = 0.1188 \pm 0.0013$ [579], where the dominant uncertainty is the hadronization uncertainty, which is estimated from Monte Carlo simulations. A fit of energy-energy-correlation (EEC) also based on an NNLO+NNLL calculation together with a Monte Carlo based modeling of hadronization corrections gives $\alpha_s(M_Z^2) = 0.1175 \pm 0.0029$ [580]. These results are summarized in the upper seven rows of the e^+e^- sector of Fig. 9.2.

Another class of α_s determinations is based on analytic modeling of non-perturbative and hadronization effects, rather than on Monte Carlo models [581–584], using methods like power corrections, factorization of soft-collinear effective field theory, dispersive models and low scale QCD effective couplings. In these studies, the world data on Thrust distributions (T), or - most recently - C-parameter distributions (C), are analysed and fitted to perturbative QCD predictions at NNLO matched with resummation of leading logs up to N³LL accuracy, see Sec. 9.2.3.3. The results are $\alpha_s(M_Z^2) = 0.1135 \pm 0.0011$ [582] and $\alpha_s(M_Z^2) = 0.1134^{+0.0031}_{-0.0025}$ [583] from Thrust, and $\alpha_s(M_Z^2) = 0.1123 \pm 0.0015$ [584] from C-parameter. They are displayed in the lower three rows of the e^+e^- sector of Fig. 9.2. A recent calculation has determined the leading non-perturbative contribution to the C-parameter in the three-jet limit, and has found that it differs by a factor of two from the two-jet limit [585]. Taking this result into account in analyses of the C-parameter would increase the value of the extracted α_s parameter, leaving it more in keeping with the world average.

The determination of Ref. [581], $\alpha_s(M_Z^2) = 0.1164^{+0.0028}_{-0.0024}$, is no longer included in the average as it is superseded by other determinations that use the same Thrust data but rely on more accurate theoretical predictions. Not included in the computation of the world average but worth mentioning are a computation of the NLO corrections to 5-jet production and comparison to the measured 5-jet rates at LEP [586], giving $\alpha_s(M_Z^2) = 0.1156^{+0.0041}_{-0.0034}$, and a computation of non-perturbative and perturbative QCD contributions to the scale evolution of quark and gluon jet multiplicities, including resummation, resulting in $\alpha_s(M_Z^2) = 0.1199 \pm 0.0026$ [587].

We note that there is criticism on both classes of α_s extractions

described above: those based on corrections of non-perturbative hadronization effects using QCD-inspired Monte Carlo generators (since the parton level of a Monte Carlo simulation is not defined in a manner equivalent to that of a fixed-order calculation), as well as studies based on non-perturbative analytic modeling, as their systematics have not yet been fully verified. For the latter case, Refs. [582, 584] quote surprisingly small overall experimental, hadronization, and theoretical uncertainties of only 2, 5, and 9 per-mille, respectively, which calls for an independent confirmation.

A recent comparison of the non-perturbative corrections, using both Monte Carlo and analytic techniques, for both Thrust and the C-parameter, can be found in Ref. [588].

In view of these open questions, the determination of the *unweighted average* and uncertainties is intended to provide the most appropriate and unbiased estimate of the average value of $\alpha_s(M_Z^2)$ for this sub-field, which results in $\alpha_s(M_Z^2) = 0.1171 \pm 0.0031$.

9.4.5 Observables from hadron-induced collisions:

Until recently, determinations of α_s using hadron collider data, mostly from jet or $t\bar{t}$ production processes, could be performed at NLO only. NNLO calculations have now become available for $t\bar{t}$ [107, 524, 525] and for inclusive jet and dijet production [214, 589, 590]. For $t\bar{t}$ production, in addition, logarithms to NNLL have been resummed [526]. Both should be supplemented by electroweak corrections [591–593], which become important for high- p_T collisions at the LHC. Z +jet production, studied with respect to an α_s determination at NLO from multi-jet events in Ref. [594], is also known at NNLO for the 1-jet case [204, 595]. Determinations of α_s from production cross sections at hadron colliders also require a knowledge of the relevant PDFs for those α_s values. Two strategies are pursued for the extraction of α_s , one using pre-determined PDFs as input and a second strategy fitting the proton PDFs together with the strong coupling constant. Each global PDF group produces PDF sets not only for the world average value of 0.118, but also for a wide range above and below that value, in increments of 0.001, that can be used in such determinations. The latter technique of simultaneously fitting α_s and the PDFs is technically more accurate, given that the new data used in the determination of α_s may modify the PDFs in a manner not taken into account by the α_s -variation PDFs provided by the fitting collaborations. The former technique may result in a bias of unknown magnitude [596]. As the LHC experiments have the ability to combine a PDF fit with the α_s determination, for example with tools like described in Ref. [597], we expect more experimental joint determinations of PDFs and of α_s for future iterations of this review.

The first determination of α_s at NNLO accuracy in QCD has been reported by CMS from the $t\bar{t}$ production cross section at $\sqrt{s} = 7$ TeV [527]. In recent *Reviews* this opened up a new sub-field on its own. In the meantime, multiple datasets on $t\bar{t}$ production from Tevatron at $\sqrt{s} = 1.96$ TeV and from LHC at $\sqrt{s} = 7, 8, \text{ and } 13$ TeV have been analyzed simultaneously to determine α_s [528] to

$$\alpha_s(M_Z^2) = 0.1177_{-0.0036}^{+0.0034},$$

where the largest uncertainties are associated with missing higher orders and with PDFs, and where an additional complication arises from the top-mass dependence. Since this combined analysis contains among other things an updated measurement as compared to the dataset used by CMS, the latter is replaced in the averaging by the new combined result. A second entry into this sub-field is given by an analysis of $t\bar{t}$ production data at $\sqrt{s} = 13$ TeV from the CMS Collaboration [522]. From the four values derived for different PDF sets, the unweighted average is taken:

$$\alpha_s(M_Z^2) = 0.1145_{-0.0031}^{+0.0036}.$$

A second analysis by CMS using differential distributions of $t\bar{t}$ production [598] has been performed at NLO only and is not further considered.

From jet production, the α_s determination at NNLO using DIS data of the H1 Collaboration [430] has been corrected for an issue with the theory prediction reported in Ref. [413]. We choose the

result

$$\alpha_s(M_Z^2) = 0.1147 \pm 0.0025$$

that is derived from a simultaneous fit of the strong coupling constant together with proton PDFs. We note that results of this section derived from such a simultaneous fit will be marked with a “*” in the corresponding figures.

Two new determinations without simultaneous PDF fit are considered for the unweighted pre-average of this sub-field. Reference [599] extracts the strong coupling constant from a fit at NNLO to measurements of inclusive Z and W boson production by experiments at the LHC and Tevatron colliders. From the four values quoted for different PDF sets we include the unweighted average for the CT14 and MMHT14 PDFs

$$\alpha_s(M_Z^2) = 0.1180_{-0.0015}^{+0.0017}.$$

The other two results suffer from either a bad fit quality or $\alpha_s(M_Z^2)$ values outside the range of validity for the PDF set.

The second determination [231] combines multiple datasets on inclusive jet production of the H1 and ZEUS collaborations at the HERA collider into one fit using interpolation grids at NNLO. The result of

$$\alpha_s(M_Z^2) = 0.1178 \pm 0.0026$$

has been updated for the same issue reported above [413].

As unweighted pre-average for this sub-field we obtain: $\alpha_s(M_Z^2) = 0.1165 \pm 0.0028$. If the stricter requirement of simultaneous fits with PDFs is imposed, then only the H1 result is left in this sub-field. In sect. 9.4.8 below, we will also report the outcome for this choice.

Many further α_s determinations from jet measurements either could not be advanced to NNLO accuracy yet, or the NNLO predictions are not yet available as is the case for observables requiring more than three jets in the final state. A selection of results from inclusive jet [429, 443, 600–605], dijet [451], and multi-jet measurements [385, 387, 388, 429, 606–610] is presented in Fig. 9.4, where the uncertainty in most cases is dominated by the impact of missing higher orders estimated through scale variations. From the CMS Collaboration we quote for the inclusive jet production at $\sqrt{s} = 7$ and 8 TeV, and for dijet production at TeV the values that have been derived in a simultaneous fit with the PDFs and marked with “*” in the figure. The last point of the inclusive jet sub-field from Ref. [605] is derived from a simultaneous fit to six datasets from different experiments and partially includes data used already for the other data points, e.g. the CMS result at 7 TeV.

The multi-jet α_s determinations are based on 3-jet cross sections (m3j), 3- to 2-jet cross-section ratios (R32), dijet angular decorrelations (RdR, RdPhi), and transverse energy-energy-correlations and their asymmetry (TEEC, ATEEC). The H1 result is extracted from a fit to inclusive 1-, 2-, and 3-jet cross sections (n_j) simultaneously.

All NLO results are within their large uncertainties in agreement with the world average and the associated analyses provide valuable new values for the scale dependence of α_s at energy scales now extending up to almost 2.0 TeV as shown in Fig. 9.3.

9.4.6 Electroweak precision fit:

For this category, we take the global electroweak fit of Ref. [611], which includes kinematic top quark and W boson mass measurements from the LHC, recent determinations of the effective leptonic electroweak mixing angles from the Tevatron, a Higgs mass measurement from ATLAS and CMS, and a new evaluation of the hadronic contribution to the running of the electromagnetic coupling at the Z -boson mass. In addition, we use the newer results of the electroweak fit at the Z mass pole from LEP and SLC data presented in Sec. *Electroweak Model and constraints on New Physics* of the 2020 edition of this *Review*. Both very similar results, $\alpha_s(M_Z^2) = 0.1221 \pm 0.0027$ [537], $\alpha_s(M_Z^2) = 0.1194 \pm 0.0029$ [611], are also in perfect agreement with the original result obtained from LEP and SLD data [612]. Our pre-averaging gives $\alpha_s(M_Z^2) = 0.1208 \pm 0.0028$.

We note, however, that results from electroweak precision data strongly depend on the strict validity of Standard Model predictions and the existence of the minimal Higgs mechanism to

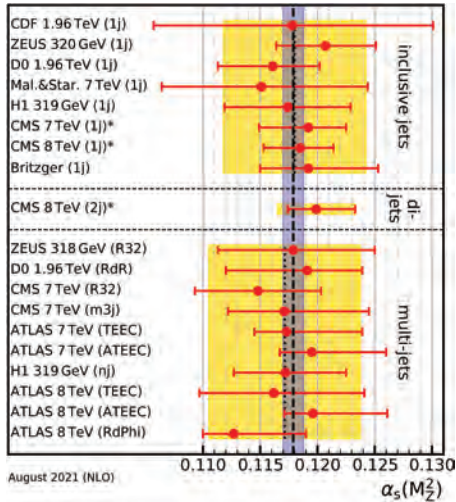


Figure 9.4: Summary of determinations of $\alpha_s(M_Z^2)$ at NLO from inclusive jet, dijet, and multi-jet measurements at hadron colliders. The uncertainty is dominated by estimates of the impact of missing higher orders. The yellow (light shaded) bands and dotted lines indicate average values for the two sub-fields. The dashed line and blue (dark shaded) band represent the final world average value of $\alpha_s(M_Z^2)$. The “*” symbol indicates determinations including a simultaneous fit of PDFs.

implement electroweak symmetry breaking. Any - even small - deviation of nature from this model could strongly influence this extraction of α_s .

9.4.7 Lattice QCD:

Several methods exist to extract the strong coupling constant from lattice QCD, as reviewed also in Sec. *Lattice QCD* of this *Review*. The Flavour Lattice Averaging Group has considered the most up-to-date determinations and combined them to produce an update of their average α_s [542]. Their final result is obtained by considering a multitude of possible input calculations [613–630] and by retaining in their final average only those eight [614–616, 622–624, 626] that fulfill their predefined quality criteria. These determinations, together with their uncertainties, are displayed in Fig. 9.5. The yellow (light shaded) band and dotted line indicate the FLAG2019 average, while the dashed line and blue (dark shaded) band represent the world average (see later). The level of agreement of individual results to the world average, or to the non-lattice world average is very similar. The criteria applied are detailed in the Sec. 9.2.1 of Ref. [542]. We note that, as in our case, the calculation must be published in a peer-reviewed journal for it to be eligible to be included in the FLAG average. We also note that the criteria applied now are considered relatively loose by the FLAG Collaboration and they have already formulated more stringent criteria. It is likely that in future FLAG averages only results satisfying these stricter criteria will be included in their averaging.

Similarly to what is done here, the FLAG Collaboration built pre-averages of results that belong to different classes. The four categories that contribute to the average are: step-scaling methods ($\alpha_s(M_Z^2) = 0.11848_{-0.00081}^{+0.00081}$), the potential at short distances ($\alpha_s(M_Z^2) = 0.11660_{-0.00160}^{+0.00160}$), Wilson loops ($\alpha_s(M_Z^2) = 0.11871_{-0.00128}^{+0.00128}$), and heavy-quark current two-point functions ($\alpha_s(M_Z^2) = 0.11818_{-0.00156}^{+0.00156}$). Other categories like the vacuum polarization at short distances, the calculation of QCD vertices, or of the eigenvalue spectrum of the Dirac operator have not yet published results that fulfill all requirements to be included in the average. Reference [631] has been completed after the publication of Ref. [542], hence these results have not been considered in the last FLAG average.

The final value is obtained by performing a weighted average of the pre-averages. The final uncertainty however is not the com-

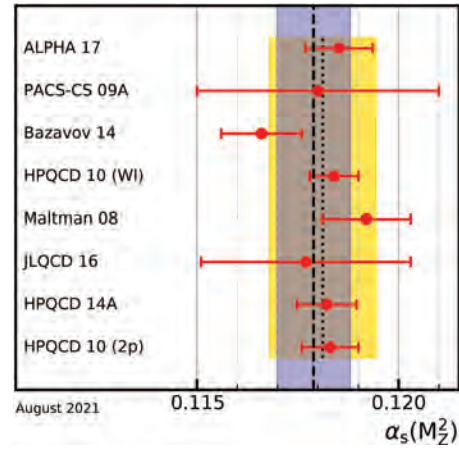


Figure 9.5: Lattice determinations that enter the FLAG2019 average. The yellow (light shaded) band and dotted line indicates the average value for this sub-field. The dashed line and blue (dark shaded) band represent the final world average value of $\alpha_s(M_Z^2)$.^a

^aIn the previous edition, the JLQCD result was incorrectly labelled as “JLQCD17” and had a wrong (too small) uncertainty.

bined uncertainty of the pre-averages. Instead the smallest uncertainty of the pre-averages is taken, which is the one of the step-scaling category and which is dominated by the ALPHA 17 result [626]. The final FLAG average (rounded to four digits) is

$$\alpha_s(M_Z^2) = 0.1182 \pm 0.0008, \quad (\text{lattice}). \quad (9.23)$$

We believe that this result expresses to a large extent the consensus of the lattice community and that the imposed criteria and the rigorous assessment of systematic uncertainties qualify for a direct inclusion of this FLAG average here. As in the previous review, we therefore adopt the FLAG average with its uncertainty as our value of α_s for the lattice category. Moreover, this lattice result will not be directly combined with any other sub-field average, but with our non-lattice average to give our final world average value for α_s .

9.4.8 Determination of the world average value of $\alpha_s(M_Z^2)$:

Obtaining a world average value for $\alpha_s(M_Z^2)$ is a non-trivial exercise. A certain arbitrariness and subjective component is inevitable because of the choice of measurements to be included in the average, the treatment of (non-Gaussian) systematic uncertainties of mostly theoretical nature, as well as the treatment of correlations among the various inputs, of theoretical as well as experimental origin.

We have chosen to determine pre-averages for sub-fields of measurements that are considered to exhibit a maximum degree of independence among each other, considering experimental as well as theoretical issues. The seven pre-averages are summarized in Fig. 9.2. We recall that these are exclusively obtained from extractions that are based on (at least) full NNLO QCD predictions, and are published in peer-reviewed journals at the time of completing this *Review*. To obtain our final world average, we first combine six pre-averages, excluding the lattice result, using a χ^2 averaging method. This gives

$$0.1176 \pm 0.0010, \quad (\text{without lattice}). \quad (9.24)$$

This result is fully compatible with the lattice pre-average Eq. (9.23) and has a comparable error. To avoid a possible over-reduction, we combine these two numbers using an unweighted average and take as an uncertainty the average between these two uncertainties. This gives our final world average value

$$\alpha_s(M_Z^2) = 0.1179 \pm 0.0009. \quad (9.25)$$

If for the sub-field of hadron colliders we are more restrictive instead and only accept results from a simultaneous fit of PDFs, we arrive at 0.1173 ± 0.0010 (without lattice) and $\alpha_s(M_Z^2) = 0.1177 \pm 0.0009$ for the final average.

Both the new world average value and the restricted result are in very good agreement with the last version of this *Review*, which was $\alpha_s(M_Z^2) = 0.1179 \pm 0.0010$, with a slightly larger overall uncertainty. Performing a weighted average of all seven categories gives $\alpha_s(M_Z^2) = 0.1180 \pm 0.0006$. Our uncertainty instead is 50% larger.

Notwithstanding the many open issues still present within each of the sub-fields summarized in this *Review*, the wealth of available results provides a rather precise and reasonably stable world average value of $\alpha_s(M_Z^2)$, as well as a clear signature and proof of the energy dependence of α_s , in full agreement with the QCD prediction of asymptotic freedom. This is demonstrated in Fig. 9.3, where results of $\alpha_s(Q^2)$ obtained at discrete energy scales Q , now also including those based just on NLO QCD, are summarized. Thanks to the results from the Tevatron and from the LHC, the energy scales, at which α_s is determined, now extend up to almost 2 TeV.¹²

In this combination, as in past combinations, we have considered lattice QCD calculations of α_s independently of experimental/phenomenological determinations. In the future, when the lattice continuum extrapolations are under better control, it may be useful to group lattice QCD determinations of α_s with experimental determinations of α_s that have systematics of similar origin, in a similar manner as we currently group, for example, hadron collider results together [632].

References

- [1] R. K. Ellis, W. J. Stirling and B. R. Webber, *Camb. Monogr. Part. Phys. Nucl. Phys. Cosmol.* **8**, 1 (1996).
- [2] J. Campbell, J. Huston, F. Krauss “*The Black Book of Quantum Chromodynamics, a Primer for the QCD Era*,” Oxford University Press, UK (2017).
- [3] C. A. Baker *et al.*, *Phys. Rev. Lett.* **97**, 131801 (2006), [hep-ex/0602020].
- [4] J. M. Pendlebury *et al.*, *Phys. Rev.* **D92**, 9, 092003 (2015), [arXiv:1509.04411].
- [5] B. Graner *et al.*, *Phys. Rev. Lett.* **116**, 16, 161601 (2016), [Erratum: *Phys. Rev. Lett.* 119, no.11, 119901 (2017)], [arXiv:1601.04339].
- [6] J. E. Kim and G. Carosi, *Rev. Mod. Phys.* **82**, 557 (2010), [arXiv:0807.3125].
- [7] G. Dissertori, I. G. Knowles and M. Schmelling, *High energy experiments and theory*, Oxford, UK: Clarendon (2003).
- [8] R. Brock *et al.* (CTEQ), *Rev. Mod. Phys.* **67**, 157 (1995); See also <https://www.phys.psu.edu/~cteq/handbook/v1.1/handbook.pdf/>.
- [9] K. Melnikov, CERN Yellow Rep. School Proc. **3**, 37 (2018).
- [10] T. van Ritbergen, J. A. M. Vermaseren and S. A. Larin, *Phys. Lett.* **B400**, 379 (1997), [hep-ph/9701390].
- [11] M. Czakon, *Nucl. Phys.* **B710**, 485 (2005), [hep-ph/0411261].
- [12] P. A. Baikov, K. G. Chetyrkin and J. H. Kühn, *Phys. Rev. Lett.* **118**, 8, 082002 (2017), [arXiv:1606.08659].
- [13] T. Luthe *et al.*, *JHEP* **07**, 127 (2016), [arXiv:1606.08662].
- [14] F. Herzog *et al.*, *JHEP* **02**, 090 (2017), [arXiv:1701.01404].
- [15] T. Luthe *et al.*, *JHEP* **10**, 166 (2017), [arXiv:1709.07718].
- [16] K. G. Chetyrkin *et al.*, *JHEP* **10**, 179 (2017), [Addendum: *JHEP*12,006(2017)], [arXiv:1709.08541].
- [17] W. A. Bardeen *et al.*, *Phys. Rev.* **D18**, 3998 (1978).
- [18] D. J. Gross and F. Wilczek, *Phys. Rev. Lett.* **30**, 1343 (1973), [,271(1973)].
- [19] H. D. Politzer, *Phys. Rev. Lett.* **30**, 1346 (1973), [,274(1973)].
- [20] Y. Schroder and M. Steinhauser, *JHEP* **01**, 051 (2006), [hep-ph/0512058].
- [21] K. G. Chetyrkin, J. H. Kuhn and C. Sturm, *Nucl. Phys.* **B744**, 121 (2006), [hep-ph/0512060].
- [22] A. G. Grozin *et al.*, *JHEP* **09**, 066 (2011), [arXiv:1107.5970].
- [23] M. Dalla Brida *et al.* (ALPHA), *Phys. Rev. Lett.* **117**, 18, 182001 (2016), [arXiv:1604.06193].
- [24] M. Beneke, *Phys. Rept.* **317**, 1 (1999), [hep-ph/9807443].
- [25] M. Beneke *et al.*, *Phys. Lett.* **B775**, 63 (2017), [arXiv:1605.03609].
- [26] A. H. Hoang, C. Lepenik and M. Preisser, *JHEP* **09**, 099 (2017), [arXiv:1706.08526].
- [27] P. Marquard *et al.*, *Phys. Rev. Lett.* **114**, 14, 142002 (2015), [arXiv:1502.01030].
- [28] P. A. Baikov *et al.*, *Phys. Lett.* **B714**, 62 (2012), [arXiv:1206.1288].
- [29] K. G. Chetyrkin, J. H. Kuhn and A. Kwiatkowski (1996), [*Phys. Rept.* 277,189(1996)], [hep-ph/9503396].
- [30] Y. Kiyo *et al.*, *Nucl. Phys.* **B823**, 269 (2009), [arXiv:0907.2120].
- [31] P. A. Baikov *et al.*, *Phys. Rev. Lett.* **108**, 222003 (2012), [arXiv:1201.5804].
- [32] P. A. Baikov, K. G. Chetyrkin and J. H. Kuhn, *Phys. Rev. Lett.* **101**, 012002 (2008), [arXiv:0801.1821].
- [33] F. Herzog *et al.*, *JHEP* **08**, 113 (2017), [arXiv:1707.01044].
- [34] V. A. Novikov *et al.*, *Nucl. Phys.* **B174**, 378 (1980).
- [35] H.-W. Lin *et al.*, *Phys. Rev.* **D91**, 054510 (2015), [arXiv:1402.1462]; C. Alexandrou *et al.*, *Phys. Rev.* **D92**, 014502 (2015), [arXiv:1504.07455].
- [36] H.-W. Lin *et al.*, *Prog. Part. Nucl. Phys.* **100**, 107 (2018), [arXiv:1711.07916].
- [37] C. Alexandrou *et al.*, *Phys. Rev. Lett.* **121**, 11, 112001 (2018), [arXiv:1803.02685].
- [38] J.-W. Chen *et al.* (2018), [arXiv:1803.04393].
- [39] K. Cichy, L. Del Debbio and T. Giani (2019), [arXiv:1907.06037].
- [40] K. Cichy and M. Constantinou, *Adv. High Energy Phys.* **2019**, 3036904 (2019), [arXiv:1811.07248].
- [41] M. A. Ebert, I. W. Stewart and Y. Zhao, *JHEP* **09**, 037 (2019), [arXiv:1901.03685].
- [42] L. Del Debbio, T. Giani and C. J. Monahan, *JHEP* **09**, 021 (2020), [arXiv:2007.02131].
- [43] M. Constantinou, *Eur. Phys. J. A* **57**, 2, 77 (2021), [arXiv:2010.02445].
- [44] M. Constantinou *et al.* (2020), [arXiv:2006.08636].
- [45] G. C. Rossi and M. Testa, *Phys. Rev.* **D96**, 1, 014507 (2017), [arXiv:1706.04428].
- [46] J. Gao, L. Harland-Lang and J. Rojo, *Phys. Rept.* **742**, 1 (2018), [arXiv:1709.04922].
- [47] K. Kovarik, P. M. Nadolsky and D. E. Soper, *Rev. Mod. Phys.* **92**, 4, 045003 (2020), [arXiv:1905.06957].
- [48] R. Abdul Khalek *et al.* (NNPDF), *Eur. Phys. J. C*, **79**:838 (2019), [arXiv:1905.04311].
- [49] R. Abdul Khalek *et al.* (NNPDF), *Eur. Phys. J. C* **79**, 11, 931 (2019), [arXiv:1906.10698].
- [50] R. D. Ball and R. L. Pearson (2021), [arXiv:2105.05114].
- [51] J. D. Bjorken and E. A. Paschos, *Phys. Rev.* **185**, 1975 (1969).

¹²We note, however, that in many such studies, like those based on exclusive states of jet multiplicities, the relevant energy scale of the measurement is not uniquely defined. For instance, in studies of the ratio of 3- to 2-jet cross sections at the LHC, the relevant scale was taken to be the average of the transverse momenta of the two leading jets [607], but could alternatively have been chosen to be the transverse momentum of the 3rd jet.

- [52] J. A. M. Vermaseren, A. Vogt and S. Moch, Nucl. Phys. **B724**, 3 (2005), [hep-ph/0504242].
- [53] S. Moch, J. A. M. Vermaseren and A. Vogt, Nucl. Phys. **B813**, 220 (2009), [arXiv:0812.4168].
- [54] J. Davies *et al.*, PoS **DIS2016**, 059 (2016), [arXiv:1606.08907].
- [55] E. Laenen *et al.*, Nucl. Phys. **B392**, 162 (1993); S. Riemersma, J. Smith and W. L. van Neerven, Phys. Lett. **B347**, 143 (1995), [hep-ph/9411431].
- [56] J. Blümlein *et al.* (2019), [arXiv:1903.06155].
- [57] A. Manohar *et al.*, Phys. Rev. Lett. **117**, 24, 242002 (2016), [arXiv:1607.04266].
- [58] L. Buonocore *et al.*, JHEP **08**, 08, 019 (2020), [arXiv:2005.06477].
- [59] J. C. Collins, D. E. Soper and G. F. Sterman, Adv. Ser. Direct. High Energy Phys. **5**, 1 (1989), [hep-ph/0409313].
- [60] J.C. Collins, *Foundations of Perturbative QCD*, Cambridge University Press, 2011.
- [61] G. C. Nayak, J.-W. Qiu and G. F. Sterman, Phys. Rev. **D72**, 114012 (2005), [hep-ph/0509021].
- [62] V. N. Gribov and L. N. Lipatov, Sov. J. Nucl. Phys. **15**, 438 (1972), [Yad. Fiz.15,781(1972)]; L. N. Lipatov, Sov. J. Nucl. Phys. **20**, 94 (1975), [Yad. Fiz.20,181(1974)]; G. Altarelli and G. Parisi, Nucl. Phys. **B126**, 298 (1977); Y. L. Dokshitzer, Sov. Phys. JETP **46**, 641 (1977), [Zh. Eksp. Teor. Fiz.73,1216(1977)].
- [63] G. Curci, W. Furmanski and R. Petronzio, Nucl. Phys. **B175**, 27 (1980); W. Furmanski and R. Petronzio, Phys. Lett. **97B**, 437 (1980).
- [64] A. Vogt, S. Moch and J. A. M. Vermaseren, Nucl. Phys. **B691**, 129 (2004), [hep-ph/0404111]; S. Moch, J. A. M. Vermaseren and A. Vogt, Nucl. Phys. **B688**, 101 (2004), [hep-ph/0403192].
- [65] S. Moch *et al.*, JHEP **10**, 041 (2017), [arXiv:1707.08315].
- [66] A. Vogt *et al.*, PoS **RADCOR2017**, 046 (2018), [arXiv:1801.06085].
- [67] A. Vogt *et al.*, PoS **LL2018**, 050 (2018), [arXiv:1808.08981].
- [68] S. Moch, J. A. M. Vermaseren and A. Vogt, Nucl. Phys. **B889**, 351 (2014), [arXiv:1409.5131].
- [69] D. de Florian, G. F. R. Sborlini and G. Rodrigo, Eur. Phys. J. **C76**, 5, 282 (2016), [arXiv:1512.00612]; D. de Florian, G. F. R. Sborlini and G. Rodrigo, JHEP **10**, 056 (2016), [arXiv:1606.02887].
- [70] R. S. Thorne, Phys. Rev. **D73**, 054019 (2006), [hep-ph/0601245].
- [71] S. Forte *et al.*, Nucl. Phys. **B834**, 116 (2010), [arXiv:1001.2312].
- [72] M. Guzzi *et al.*, Phys. Rev. **D86**, 053005 (2012), [arXiv:1108.5112].
- [73] V. S. Fadin, E. A. Kuraev and L. N. Lipatov, Phys. Lett. **60B**, 50 (1975).
- [74] I. I. Balitsky and L. N. Lipatov, Sov. J. Nucl. Phys. **28**, 822 (1978), [Yad. Fiz.28,1597(1978)].
- [75] R. D. Ball *et al.*, Eur. Phys. J. **C78**, 4, 321 (2018), [arXiv:1710.05935].
- [76] H. Abramowicz *et al.* (H1, ZEUS), Eur. Phys. J. **C75**, 12, 580 (2015), [arXiv:1506.06042].
- [77] H. Abdolmaleki *et al.* (xFitter Developers' Team), Eur. Phys. J. **C78**, 8, 621 (2018), [arXiv:1802.00064].
- [78] L. A. Harland-Lang *et al.*, Eur. Phys. J. **C76**, 4, 186 (2016), [arXiv:1601.03413].
- [79] T.-J. Hou *et al.* (2019), [arXiv:1908.11238].
- [80] L. N. Lipatov, Sov. J. Nucl. Phys. **23**, 338 (1976), [Yad. Fiz.23,642(1976)].
- [81] E. A. Kuraev, L. N. Lipatov and V. S. Fadin, Sov. Phys. JETP **45**, 199 (1977), [Zh. Eksp. Teor. Fiz.72,377(1977)].
- [82] V. S. Fadin and L. N. Lipatov, Phys. Lett. **B429**, 127 (1998), [hep-ph/9802290].
- [83] M. Ciafaloni and G. Camici, Phys. Lett. **B430**, 349 (1998), [hep-ph/9803389].
- [84] G. Altarelli, R. D. Ball and S. Forte, Nucl. Phys. **B799**, 199 (2008), [arXiv:0802.0032].
- [85] M. Ciafaloni *et al.*, JHEP **08**, 046 (2007), [arXiv:0707.1453].
- [86] C. D. White and R. S. Thorne, Phys. Rev. **D75**, 034005 (2007), [hep-ph/0611204].
- [87] E. Iancu *et al.*, Phys. Lett. **B744**, 293 (2015), [arXiv:1502.05642].
- [88] N. Gromov, F. Levkovich-Maslyuk and G. Sizov, Phys. Rev. Lett. **115**, 25, 251601 (2015), [arXiv:1507.04010]; V. N. Velizhanin (2015), [arXiv:1508.02857]; S. Caron-Huot and M. Herranen, JHEP **02**, 058 (2018), [arXiv:1604.07417].
- [89] I. Balitsky, Nucl. Phys. **B463**, 99 (1996), [hep-ph/9509348].
- [90] Y. V. Kovchegov, Phys. Rev. **D60**, 034008 (1999), [hep-ph/9901281].
- [91] M. Davier *et al.*, Eur. Phys. J. C **56**, 305 (2008), [arXiv:0803.0979].
- [92] J. C. Collins, D. E. Soper and G. F. Sterman, Nucl. Phys. **B261**, 104 (1985).
- [93] C. Anastasiou *et al.*, Phys. Rev. Lett. **114**, 212001 (2015), [arXiv:1503.06056]; C. Anastasiou *et al.*, JHEP **05**, 058 (2016), [arXiv:1602.00695].
- [94] B. Mistlberger, JHEP **05**, 028 (2018), [arXiv:1802.00833].
- [95] L.-B. Chen *et al.*, Phys. Lett. B **803**, 135292 (2020), [arXiv:1909.06808].
- [96] F. Dulat, B. Mistlberger and A. Pelloni, Phys. Rev. **D99**, 3, 034004 (2019), [arXiv:1810.09462].
- [97] L. Cieri *et al.*, JHEP **02**, 096 (2019), [arXiv:1807.11501].
- [98] X. Chen *et al.* (2021), [arXiv:2102.07607].
- [99] F. A. Dreyer and A. Karlberg, Phys. Rev. Lett. **117**, 7, 072001 (2016), [arXiv:1606.00840].
- [100] F. A. Dreyer and A. Karlberg, Phys. Rev. D **98**, 11, 114016 (2018), [arXiv:1811.07906].
- [101] C. Duhr, F. Dulat and B. Mistlberger, Phys. Rev. Lett. **125**, 17, 172001 (2020), [arXiv:2001.07717].
- [102] X. Chen *et al.* (2021), [arXiv:2107.09085].
- [103] C. Duhr, F. Dulat and B. Mistlberger, JHEP **11**, 143 (2020), [arXiv:2007.13313].
- [104] O. Brein, A. Djouadi and R. Harlander, Phys. Lett. **B579**, 149 (2004), [hep-ph/0307206].
- [105] D. de Florian and J. Mazzitelli, Phys. Rev. Lett. **111**, 201801 (2013), [arXiv:1309.6594].
- [106] S. Borowka *et al.*, Phys. Rev. Lett. **117**, 1, 012001 (2016), [Erratum: Phys. Rev. Lett.117,no.7,079901(2016)], [arXiv:1604.06447].
- [107] M. Czakon, P. Fiedler and A. Mitov, Phys. Rev. Lett. **110**, 252004 (2013), [arXiv:1303.6254].
- [108] S. Catani *et al.*, Phys. Rev. **D99**, 5, 051501 (2019), [arXiv:1901.04005].
- [109] T. Gehrmann *et al.*, Phys. Rev. Lett. **113**, 21, 212001 (2014), [arXiv:1408.5243].
- [110] F. Cascioli *et al.*, Phys. Lett. **B735**, 311 (2014), [arXiv:1405.2219].
- [111] M. Grazzini, S. Kallweit and M. Wiesemann, Eur. Phys. J. **C78**, 7, 537 (2018), [arXiv:1711.06631].
- [112] G. Heinrich, Phys. Rept. **922**, 1 (2021), [arXiv:2009.00516].
- [113] M. Greco and A. Vicini, Nucl. Phys. **B415**, 386 (1994).
- [114] A. Hebecker, Phys. Rept. **331**, 1 (2000), [hep-ph/9905226].

- [115] A. V. Belitsky and A. V. Radyushkin, Phys. Rept. **418**, 1 (2005), [hep-ph/0504030].
- [116] E. Boos *et al.* (CompHEP), Nucl. Instrum. Meth. **A534**, 250 (2004), [hep-ph/0403113]; <http://compep.sinp.su.ru/>.
- [117] J. Alwall *et al.*, JHEP **07**, 079 (2014), [arXiv:1405.0301]; <https://launchpad.net/mg5amcnlo>.
- [118] M. L. Mangano *et al.*, JHEP **07**, 001 (2003), [hep-ph/0206293]; <http://cern.ch/mlm/alpgen/>.
- [119] T. Gleisberg and S. Hoeche, JHEP **12**, 039 (2008), [arXiv:0808.3674]; <https://sherpa.hepforge.org/trac/wiki>.
- [120] A. Cafarella, C. G. Papadopoulos and M. Worek, Comput. Phys. Commun. **180**, 1941 (2009), [arXiv:0710.2427]; <http://cern.ch/helac-phegas/>.
- [121] F. A. Berends and W. T. Giele, Nucl. Phys. **B306**, 759 (1988).
- [122] L. J. Dixon, in "QCD and beyond. Proceedings, Theoretical Advanced Study Institute in Elementary Particle Physics, TASI-95, Boulder, USA, June 4-30, 1995," 539-584 (1996), [hep-ph/9601359], URL <http://www-public.slac.stanford.edu/sciDoc/docMeta.aspx?slacPubNumber=SLAC-PUB-7106>.
- [123] R. Britto, F. Cachazo and B. Feng, Nucl. Phys. **B715**, 499 (2005), [hep-th/0412308].
- [124] F. Cachazo, P. Svrcek and E. Witten, JHEP **09**, 006 (2004), [hep-th/0403047].
- [125] S. Catani and M. H. Seymour, Nucl. Phys. **B485**, 291 (1997), [Erratum: Nucl. Phys. **B510**, 503 (1998)], [hep-ph/9605323].
- [126] S. Frixione, Z. Kunszt and A. Signer, Nucl. Phys. **B467**, 399 (1996), [hep-ph/9512328].
- [127] D. A. Kosower, Phys. Rev. **D57**, 5410 (1998), [hep-ph/9710213]; J. M. Campbell, M. A. Cullen and E. W. N. Glover, Eur. Phys. J. **C9**, 245 (1999), [hep-ph/9809429]; D. A. Kosower, Phys. Rev. **D71**, 045016 (2005), [hep-ph/0311272].
- [128] G. Ossola, C. G. Papadopoulos and R. Pittau, Nucl. Phys. **B763**, 147 (2007), [hep-ph/0609007].
- [129] R. Britto, F. Cachazo and B. Feng, Nucl. Phys. **B725**, 275 (2005), [hep-th/0412103].
- [130] R. K. Ellis *et al.*, Nucl. Phys. **B822**, 270 (2009), [arXiv:0806.3467].
- [131] C. F. Berger and D. Forde, Ann. Rev. Nucl. Part. Sci. **60**, 181 (2010), [arXiv:0912.3534].
- [132] F. Cascioli, P. Maierhofer and S. Pozzorini, Phys. Rev. Lett. **108**, 111601 (2012), [arXiv:1111.5206].
- [133] Z. Bern, L. J. Dixon and D. A. Kosower, Annals Phys. **322**, 1587 (2007), [arXiv:0704.2798].
- [134] R. K. Ellis *et al.*, Phys. Rept. **518**, 141 (2012), [arXiv:1105.4319].
- [135] G. Bevilacqua *et al.*, Comput. Phys. Commun. **184**, 986 (2013), [arXiv:1110.1499]; <http://cern.ch/helax-phegas/>.
- [136] G. Cullen *et al.*, Eur. Phys. J. **C74**, 8, 3001 (2014), [arXiv:1404.7096]; <http://gosam.hepforge.org/>.
- [137] S. Badger *et al.*, Comput. Phys. Commun. **184**, 1981 (2013), [arXiv:1209.0100]; <https://bitbucket.org/njet/wiki/Home/>.
- [138] F. Buccioni, S. Pozzorini and M. Zoller, Eur. Phys. J. **C78**, 1, 70 (2018), [arXiv:1710.11452]; <https://openloops.hepforge.org/>.
- [139] S. Actis *et al.*, Comput. Phys. Commun. **214**, 140 (2017), [arXiv:1605.01090].
- [140] T. Gleisberg *et al.*, JHEP **02**, 007 (2009), [arXiv:0811.4622]; <http://projects.hepforge.org/sherpa>.
- [141] Z. Nagy, Phys. Rev. **D68**, 094002 (2003), [hep-ph/0307268]; <http://www.desy.de/~znagy/Site/NLOJet++.html>.
- [142] J. M. Campbell and R. K. Ellis, Phys. Rev. **D62**, 114012 (2000), [hep-ph/0006304].
- [143] J. Baglio *et al.* (2011), [arXiv:1107.4038]; <http://www-itp.particle.uni-karlsruhe.de/~vbfollowe>.
- [144] T. Binoth *et al.*, Eur. Phys. J. **C16**, 311 (2000), [hep-ph/9911340]; http://laph.in2p3.fr/PHOX_FAMILY/.
- [145] Z. Bern *et al.*, PoS **LL2012**, 018 (2012), [arXiv:1210.6684].
- [146] G. Cullen, N. Greiner and G. Heinrich, Eur. Phys. J. **C73**, 4, 2388 (2013), [arXiv:1212.5154].
- [147] S. Kallweit *et al.*, JHEP **04**, 012 (2015), [arXiv:1412.5157].
- [148] A. Denner *et al.*, JHEP **04**, 018 (2015), [arXiv:1412.7421].
- [149] M. Chiesa, N. Greiner and F. Tramontano, J. Phys. **G43**, 1, 013002 (2016), [arXiv:1507.08579].
- [150] S. Frixione *et al.*, JHEP **06**, 184 (2015), [arXiv:1504.03446].
- [151] B. Biedermann *et al.*, Eur. Phys. J. **C77**, 492 (2017), [arXiv:1704.05783].
- [152] R. Frederix *et al.*, JHEP **07**, 185 (2018), [arXiv:1804.10017].
- [153] C. Anastasiou, R. Boughezal and F. Petriello, JHEP **04**, 003 (2009), [arXiv:0811.3458].
- [154] S. Dittmaier, A. Huss and C. Schwinn, Nucl. Phys. **B885**, 318 (2014), [arXiv:1403.3216].
- [155] S. Dittmaier, A. Huss and C. Schwinn, Nucl. Phys. **B904**, 216 (2016), [arXiv:1511.08016].
- [156] D. de Florian, M. Der and I. Fabre, Phys. Rev. **D98**, 9, 094008 (2018), [arXiv:1805.12214].
- [157] M. Bonetti, K. Melnikov and L. Tancredi, Phys. Rev. **D97**, 3, 034004 (2018), [arXiv:1711.11113].
- [158] M. Bonetti, K. Melnikov and L. Tancredi, Phys. Rev. **D97**, 5, 056017 (2018), [Erratum: Phys. Rev. **D97**, no.9, 099906 (2018)], [arXiv:1801.10403].
- [159] C. Anastasiou *et al.*, JHEP **03**, 162 (2019), [arXiv:1811.11211].
- [160] V. Hirschi, S. Lionetti and A. Schweitzer, JHEP **05**, 002 (2019), [arXiv:1902.10167].
- [161] M. Becchetti *et al.*, Phys. Rev. D **103**, 5, 054037 (2021), [arXiv:2010.09451].
- [162] M. Bonetti *et al.*, JHEP **11**, 045 (2020), [arXiv:2007.09813].
- [163] R. Bonciani *et al.* (2021), [arXiv:2106.11953].
- [164] A. Denner and S. Dittmaier, Phys. Rept. **864**, 1 (2020), [arXiv:1912.06823].
- [165] Z. Bern *et al.*, Nucl. Phys. **B425**, 217 (1994), [hep-ph/9403226].
- [166] J. M. Campbell and E. W. N. Glover, Nucl. Phys. **B527**, 264 (1998), [hep-ph/9710255].
- [167] S. Catani and M. Grazzini, Phys. Lett. **B446**, 143 (1999), [hep-ph/9810389].
- [168] T. Binoth and G. Heinrich, Nucl. Phys. **B585**, 741 (2000), [hep-ph/0004013].
- [169] C. Anastasiou, K. Melnikov and F. Petriello, Phys. Rev. **D69**, 076010 (2004), [hep-ph/0311311].
- [170] A. Gehrmann-De Ridder, T. Gehrmann and E. W. N. Glover, JHEP **09**, 056 (2005), [hep-ph/0505111].
- [171] G. Somogyi, Z. Trocsanyi and V. Del Duca, JHEP **01**, 070 (2007), [hep-ph/0609042].
- [172] M. Czakon, Phys. Lett. **B693**, 259 (2010), [arXiv:1005.0274].
- [173] F. Caola, K. Melnikov and R. Rötsch, Eur. Phys. J. C **77**, 4, 248 (2017), [arXiv:1702.01352].
- [174] L. Magnea *et al.*, JHEP **12**, 107 (2018), [Erratum: JHEP **06**, 013 (2019)], [arXiv:1806.09570].
- [175] S. Catani and M. Grazzini, Phys. Rev. Lett. **98**, 222002 (2007), [hep-ph/0703012]; <http://theory.fi.infn.it/grazzini/codes.html>.

- [176] R. Bonciani *et al.*, Eur. Phys. J. C **75**, 12, 581 (2015), [arXiv:1508.03585].
- [177] R. Boughezal *et al.*, Phys. Rev. Lett. **115**, 6, 062002 (2015), [arXiv:1504.02131].
- [178] R. Boughezal, X. Liu and F. Petriello, Phys. Rev. D **91**, 9, 094035 (2015), [arXiv:1504.02540].
- [179] J. Gaunt *et al.*, JHEP **09**, 058 (2015), [arXiv:1505.04794].
- [180] M. Cacciari *et al.*, Phys. Rev. Lett. **115**, 8, 082002 (2015), [Erratum: Phys. Rev. Lett.120,no.13,139901(2018)], [arXiv:1506.02660].
- [181] L. Cieri *et al.*, JHEP **09**, 155 (2020), [arXiv:2005.01315].
- [182] W. J. Torres Bobadilla *et al.*, Eur. Phys. J. C **81**, 3, 250 (2021), [arXiv:2012.02567].
- [183] A. Gehrmann-De Ridder *et al.*, Phys. Rev. Lett. **99**, 132002 (2007), [arXiv:0707.1285]; A. Gehrmann-De Ridder *et al.*, JHEP **12**, 094 (2007), [arXiv:0711.4711]; A. Gehrmann-De Ridder *et al.*, Phys. Rev. Lett. **100**, 172001 (2008), [arXiv:0802.0813].
- [184] A. Gehrmann-De Ridder *et al.*, Comput. Phys. Commun. **185**, 3331 (2014), [arXiv:1402.4140]; <https://eeraad3.epforge.org/>.
- [185] S. Weinzierl, Phys. Rev. Lett. **101**, 162001 (2008), [arXiv:0807.3241]; S. Weinzierl, JHEP **06**, 041 (2009), [arXiv:0904.1077].
- [186] J. Currie, T. Gehrmann and J. Niehues, Phys. Rev. Lett. **117**, 4, 042001 (2016), [arXiv:1606.03991].
- [187] J. Currie *et al.*, JHEP **05**, 209 (2018), [arXiv:1803.09973].
- [188] T. Gehrmann *et al.*, Phys. Lett. **B792**, 182 (2019), [arXiv:1812.06104].
- [189] K. Melnikov and F. Petriello, Phys. Rev. **D74**, 114017 (2006), [hep-ph/0609070]; <http://gate.hep.anl.gov/fpetriello/FEWZ.html>.
- [190] S. Catani *et al.*, Phys. Rev. Lett. **103**, 082001 (2009), [arXiv:0903.2120]; <http://theory.fi.infn.it/gazzani/dy.html>.
- [191] C. Anastasiou, K. Melnikov and F. Petriello, Nucl. Phys. **B724**, 197 (2005), [hep-ph/0501130]; <http://www.phys.ethz.ch/~pheno/fehipro/>.
- [192] M. Czakon *et al.* (2021), [arXiv:2105.04436].
- [193] M. Grazzini *et al.*, JHEP **05**, 139 (2017), [arXiv:1703.09065].
- [194] S. Catani *et al.*, Phys. Rev. Lett. **108**, 072001 (2012), [Erratum: Phys. Rev. Lett.117,no.8,089901(2016)], [arXiv:1110.2375].
- [195] J. M. Campbell *et al.*, JHEP **07**, 148 (2016), [arXiv:1603.02663].
- [196] M. Grazzini *et al.*, Phys. Lett. **B731**, 204 (2014), [arXiv:1309.7000].
- [197] M. Grazzini, S. Kallweit and D. Rathlev, JHEP **07**, 085 (2015), [arXiv:1504.01330].
- [198] R. Boughezal *et al.*, Eur. Phys. J. **C77**, 1, 7 (2017), [arXiv:1605.08011].
- [199] J. M. Campbell, R. K. Ellis and C. Williams, Phys. Rev. Lett. **118**, 22, 222001 (2017), [arXiv:1612.04333].
- [200] X. Chen *et al.*, Submitted to: J. High Energy Phys. (2019), [arXiv:1904.01044].
- [201] J. M. Campbell, R. K. Ellis and C. Williams, Phys. Rev. **D96**, 1, 014037 (2017), [arXiv:1703.10109].
- [202] A. Gehrmann-De Ridder *et al.*, Phys. Rev. Lett. **120**, 12, 122001 (2018), [arXiv:1712.07543].
- [203] A. Gehrmann-De Ridder *et al.*, Phys. Rev. Lett. **117**, 2, 022001 (2016), [arXiv:1507.02850].
- [204] R. Boughezal *et al.*, Phys. Rev. Lett. **116**, 15, 152001 (2016), [arXiv:1512.01291].
- [205] R. Boughezal *et al.*, Phys. Rev. Lett. **115**, 8, 082003 (2015), [arXiv:1504.07922].
- [206] R. Boughezal *et al.*, Phys. Lett. **B748**, 5 (2015), [arXiv:1505.03893].
- [207] F. Caola, K. Melnikov and M. Schulze, Phys. Rev. **D92**, 7, 074032 (2015), [arXiv:1508.02684].
- [208] X. Chen *et al.*, JHEP **10**, 066 (2016), [arXiv:1607.08817].
- [209] G. Ferrera, M. Grazzini and F. Tramontano, Phys. Rev. Lett. **107**, 152003 (2011), [arXiv:1107.1164].
- [210] G. Ferrera, M. Grazzini and F. Tramontano, Phys. Lett. **B740**, 51 (2015), [arXiv:1407.4747].
- [211] M. Brucherseifer, F. Caola and K. Melnikov, Phys. Lett. **B736**, 58 (2014), [arXiv:1404.7116].
- [212] E. L. Berger *et al.*, Phys. Rev. **D94**, 7, 071501 (2016), [arXiv:1606.08463].
- [213] M. Czakon, P. Fiedler and A. Mitov, Phys. Rev. Lett. **115**, 5, 052001 (2015), [arXiv:1411.3007].
- [214] J. Currie, E. W. N. Glover and J. Pires, Phys. Rev. Lett. **118**, 7, 072002 (2017), [arXiv:1611.01460].
- [215] M. Czakon *et al.* (2020), [arXiv:2011.01011].
- [216] M. L. Czakon *et al.* (2021), [arXiv:2102.08267].
- [217] J. Cruz-Martinez *et al.*, Phys. Lett. **B781**, 672 (2018), [arXiv:1802.02445].
- [218] T. Liu, K. Melnikov and A. A. Penin (2019), [arXiv:1906.10899].
- [219] H. A. Chawdhry *et al.*, JHEP **02**, 057 (2020), [arXiv:1911.00479].
- [220] S. Kallweit, V. Sotnikov and M. Wiesemann, Phys. Lett. B **812**, 136013 (2021), [arXiv:2010.04681].
- [221] H. A. Chawdhry *et al.* (2021), [arXiv:2105.06940].
- [222] M. Czakon, A. Mitov and R. Poncelet (2021), [arXiv:2106.05331].
- [223] G. P. Salam and E. Slade (2021), [arXiv:2106.08329].
- [224] M. A. Ebert *et al.*, JHEP **04**, 102 (2021), [arXiv:2006.11382].
- [225] S. Amoroso *et al.*, in “11th Les Houches Workshop on Physics at TeV Colliders: PhysTeV Les Houches,” (2020), [arXiv:2003.01700].
- [226] T. Carli *et al.*, Eur. Phys. J. C **66**, 503 (2010), [arXiv:0911.2985].
- [227] T. Kluge, K. Rabbertz and M. Wobisch, in “14th International Workshop on Deep Inelastic Scattering (DIS 2006),” 483, Tsukuba, Japan, April 20-24 (2006), [hep-ph/0609285].
- [228] D. Britzger *et al.*, in “Proceedings, XX. International Workshop on Deep-Inelastic Scattering and Related Subjects (DIS 2012),” 217, Bonn, Germany, March 26-30 (2012), [arXiv:1208.3641].
- [229] S. Carrazza *et al.*, JHEP **12**, 108 (2020), [arXiv:2008.12789].
- [230] M. Czakon, D. Heymes and A. Mitov (2017), [arXiv:1704.08551].
- [231] D. Britzger *et al.*, Eur. Phys. J. C **79**, 10, 845 (2019), [Erratum: arXiv:1906.05303v3], [arXiv:1906.05303].
- [232] D. Maître, J. Phys. Conf. Ser. **1525**, 1, 012014 (2020).
- [233] D. Maître, G. Heinrich and M. Johnson, PoS **LL2016**, 016 (2016), [arXiv:1607.06259].
- [234] Y. L. Dokshitzer, D. Diakonov and S. I. Troian, Phys. Rept. **58**, 269 (1980).
- [235] G. Parisi and R. Petronzio, Nucl. Phys. **B154**, 427 (1979).
- [236] G. Curci, M. Greco and Y. Srivastava, Nucl. Phys. **B159**, 451 (1979).
- [237] A. Bassetto, M. Ciafaloni and G. Marchesini, Nucl. Phys. **B163**, 477 (1980).
- [238] J. C. Collins and D. E. Soper, Nucl. Phys. **B193**, 381 (1981), [Erratum: Nucl. Phys.B213,545(1983)].

- [239] J. C. Collins and D. E. Soper, Nucl. Phys. **B197**, 446 (1982).
- [240] J. Kodaira and L. Trentadue, Phys. Lett. **112B**, 66 (1982).
- [241] J. Kodaira and L. Trentadue, Phys. Lett. **123B**, 335 (1983).
- [242] J. C. Collins, D. E. Soper and G. F. Sterman, Nucl. Phys. **B250**, 199 (1985).
- [243] S. Catani *et al.*, Nucl. Phys. **B407**, 3 (1993).
- [244] C. W. Bauer *et al.*, Phys. Rev. **D63**, 114020 (2001), [hep-ph/0011336].
- [245] C. W. Bauer, D. Pirjol and I. W. Stewart, Phys. Rev. **D65**, 054022 (2002), [hep-ph/0109045].
- [246] T. Becher, A. Broggio and A. Ferroglia, Lect. Notes Phys. **896**, pp.1 (2015), [arXiv:1410.1892].
- [247] S. Catani *et al.*, Phys. Lett. **B269**, 432 (1991).
- [248] N. Brown and W. J. Stirling, Phys. Lett. **B252**, 657 (1990).
- [249] W. Bartel *et al.* (JADE), Z. Phys. **C33**, 23 (1986), [53(1986)].
- [250] N. Kidonakis, G. Oderda and G. F. Sterman, Nucl. Phys. **B531**, 365 (1998), [hep-ph/9803241].
- [251] R. Bonciani *et al.*, Phys. Lett. **B575**, 268 (2003), [hep-ph/0307035].
- [252] A. Banfi, G. P. Salam and G. Zanderighi, JHEP **03**, 073 (2005), [hep-ph/0407286].
- [253] D. de Florian and M. Grazzini, Phys. Rev. Lett. **85**, 4678 (2000), [hep-ph/0008152].
- [254] G. Bozzi *et al.*, Nucl. Phys. **B737**, 73 (2006), [hep-ph/0508068]; <http://theory.fi.infn.it/grazzini/codes.html>.
- [255] G. Bozzi *et al.*, Phys. Lett. **B696**, 207 (2011), [arXiv:1007.2351].
- [256] T. Becher and M. Neubert, Eur. Phys. J. **C71**, 1665 (2011), [arXiv:1007.4005].
- [257] T. Becher, M. Neubert, and D. Wilhelm, <http://cute.hepforge.org/>.
- [258] D. de Florian *et al.*, JHEP **06**, 132 (2012), [arXiv:1203.6321]; <http://theory.fi.infn.it/grazzini/codes.html>.
- [259] C. Balazs and C. P. Yuan, Phys. Rev. **D56**, 5558 (1997), [hep-ph/9704258].
- [260] S. Catani *et al.*, JHEP **12**, 047 (2015), [arXiv:1507.06937].
- [261] A. Banfi *et al.*, Phys. Lett. **B715**, 152 (2012), [arXiv:1205.4760].
- [262] M. Grazzini *et al.*, JHEP **08**, 154 (2015), [arXiv:1507.02565].
- [263] D. de Florian and M. Grazzini, Nucl. Phys. **B704**, 387 (2005), [hep-ph/0407241].
- [264] T. Becher and G. Bell, JHEP **11**, 126 (2012), [arXiv:1210.0580].
- [265] A. Banfi *et al.*, Phys. Rev. Lett. **109**, 202001 (2012), [arXiv:1206.4998]; T. Becher, M. Neubert and L. Rothen, JHEP **10**, 125 (2013), [arXiv:1307.0025].
- [266] I. W. Stewart *et al.*, Phys. Rev. **D89**, 5, 054001 (2014), [arXiv:1307.1808].
- [267] I. W. Stewart, F. J. Tackmann and W. J. Waalewijn, Phys. Rev. Lett. **106**, 032001 (2011), [arXiv:1005.4060].
- [268] Y.-T. Chien *et al.*, Phys. Rev. **D87**, 1, 014010 (2013), [arXiv:1208.0010]; T. T. Jouttenus *et al.*, Phys. Rev. **D88**, 5, 054031 (2013), [arXiv:1302.0846].
- [269] M. Dasgupta *et al.*, JHEP **10**, 126 (2012), [arXiv:1207.1640].
- [270] V. Ahrens *et al.*, JHEP **09**, 097 (2010), [arXiv:1003.5827].
- [271] M. Aliev *et al.*, Comput. Phys. Commun. **182**, 1034 (2011), [arXiv:1007.1327].
- [272] N. Kidonakis, Phys. Rev. **D82**, 114030 (2010), [arXiv:1009.4935].
- [273] T. Becher, C. Lorentzen and M. D. Schwartz, Phys. Rev. Lett. **108**, 012001 (2012), [arXiv:1106.4310].
- [274] T. Becher *et al.*, Eur. Phys. J. **C75**, 4, 154 (2015), [arXiv:1412.8408].
- [275] E. Gerwick *et al.*, JHEP **02**, 106 (2015), [arXiv:1411.7325].
- [276] A. Banfi *et al.*, JHEP **05**, 102 (2015), [arXiv:1412.2126].
- [277] T. Becher and M. D. Schwartz, JHEP **07**, 034 (2008), [arXiv:0803.0342].
- [278] A. H. Hoang *et al.*, Phys. Rev. **D91**, 9, 094017 (2015), [arXiv:1411.6633].
- [279] Y.-T. Chien and M. D. Schwartz, JHEP **08**, 058 (2010), [arXiv:1005.1644].
- [280] P. F. Monni, T. Gehrmann and G. Luisoni, JHEP **08**, 010 (2011), [arXiv:1105.4560].
- [281] W. Bizon *et al.*, JHEP **02**, 108 (2018), [arXiv:1705.09127].
- [282] W. Bizon *et al.*, Eur. Phys. J. **C 79**, 10, 868 (2019), [arXiv:1905.05171].
- [283] S. Catani *et al.*, Nucl. Phys. **B888**, 75 (2014), [arXiv:1405.4827].
- [284] A. Banfi *et al.*, JHEP **04**, 049 (2016), [arXiv:1511.02886].
- [285] A. J. Larkoski and I. Moult, Phys. Rev. **D93**, 014017 (2016), [arXiv:1510.08459].
- [286] G. Lustermsans, W. J. Waalewijn and L. Zeune, Phys. Lett. **B762**, 447 (2016), [arXiv:1605.02740].
- [287] C. Muselli, S. Forte and G. Ridolfi, JHEP **03**, 106 (2017), [arXiv:1701.01464].
- [288] M. Bonvini and S. Marzani, Phys. Rev. Lett. **120**, 202003 (2018), [arXiv:1802.07758].
- [289] M. Procura, W. J. Waalewijn and L. Zeune, JHEP **10**, 098 (2018), [arXiv:1806.10622].
- [290] G. Lustermsans *et al.*, JHEP **03**, 124 (2019), [arXiv:1901.03331].
- [291] P. F. Monni, L. Rottoli and P. Torrielli, Phys. Rev. Lett. **124**, 25, 252001 (2020), [arXiv:1909.04704].
- [292] I. Feige *et al.*, Phys. Rev. Lett. **109**, 092001 (2012), [arXiv:1204.3898].
- [293] M. Dasgupta *et al.*, JHEP **09**, 029 (2013), [arXiv:1307.0007].
- [294] A. J. Larkoski *et al.*, JHEP **05**, 146 (2014), [arXiv:1402.2657].
- [295] M. Dasgupta, A. Powling and A. Siodmok, JHEP **08**, 079 (2015), [arXiv:1503.01088].
- [296] A. J. Larkoski, I. Moult and D. Neill, JHEP **05**, 117 (2016), [arXiv:1507.03018].
- [297] C. Frye *et al.*, JHEP **07**, 064 (2016), [arXiv:1603.09338].
- [298] A. J. Larkoski, I. Moult and D. Neill, JHEP **02**, 144 (2018), [arXiv:1710.00014].
- [299] F. A. Dreyer *et al.*, JHEP **06**, 093 (2018), [arXiv:1804.03657].
- [300] A. J. Larkoski, I. Moult and B. Nachman, Phys. Rept. **841**, 1 (2020), [arXiv:1709.04464].
- [301] S. Marzani, G. Soyez and M. Spannowsky (2019), [Lect. Notes Phys.958,pp.(2019)], [arXiv:1901.10342].
- [302] R. Kogler *et al.*, Rev. Mod. Phys. **91**, 4, 045003 (2019), [arXiv:1803.06991].
- [303] Yu.L. Dokshitzer *et al.*, "Basics of perturbative QCD," Gif-sur-Yvette, France: Éditions frontières (1991), see also <http://www.lpthe.jussieu.fr/~yuri/BPQCD/cover.html>.
- [304] T. Sjostrand *et al.*, Comput. Phys. Commun. **135**, 238 (2001), [hep-ph/0010017].
- [305] T. Sjostrand, S. Mrenna and P. Z. Skands, JHEP **05**, 026 (2006), [hep-ph/0603175]; <http://projects.hepforge.org/pythia6/>.

- [306] T. Sjostrand *et al.*, *Comput. Phys. Commun.* **191**, 159 (2015), [arXiv:1410.3012]; <http://home.thep.lu.se/~torbjorn/Pythia.html>.
- [307] B. R. Webber, *Nucl. Phys.* **B238**, 492 (1984).
- [308] G. Corcella *et al.*, *JHEP* **01**, 010 (2001), [hep-ph/0011363]; <http://www.hep.phy.cam.ac.uk/theory/webber/Herwig/>.
- [309] M. Bahr *et al.*, *Eur. Phys. J.* **C58**, 639 (2008), [arXiv:0803.0883]; <http://projects.hepforge.org/herwig/>.
- [310] L. Lonnblad, *Comput. Phys. Commun.* **71**, 15 (1992).
- [311] A. Buckley *et al.*, *Phys. Rept.* **504**, 145 (2011), [arXiv:1101.2599].
- [312] B. Andersson *et al.*, *Phys. Rept.* **97**, 31 (1983).
- [313] T. Sjostrand, *Nucl. Phys.* **B248**, 469 (1984).
- [314] J. Bellm *et al.*, *Eur. Phys. J. C* **80**, 2, 93 (2020), [arXiv:1903.12563].
- [315] T. Sjostrand and M. van Zijl, *Phys. Rev.* **D36**, 2019 (1987).
- [316] S. Catani *et al.*, *JHEP* **11**, 063 (2001), [hep-ph/0109231].
- [317] J. Alwall *et al.*, *Eur. Phys. J.* **C53**, 473 (2008), [arXiv:0706.2569].
- [318] S. Frixione and B. R. Webber, *JHEP* **06**, 029 (2002), [hep-ph/0204244].
- [319] P. Nason, *JHEP* **11**, 040 (2004), [hep-ph/0409146].
- [320] S. Alioli *et al.*, *JHEP* **06**, 043 (2010), [arXiv:1002.2581]; <http://powhegbox.mib.infn.it/>.
- [321] S. Plätzer, *JHEP* **08**, 114 (2013), [arXiv:1211.5467]; R. Frederix and S. Frixione, *JHEP* **12**, 061 (2012), [arXiv:1209.6215]; K. Hamilton *et al.*, *JHEP* **05**, 082 (2013), [arXiv:1212.4504].
- [322] K. Hamilton *et al.*, *JHEP* **10**, 222 (2013), [arXiv:1309.0017]; A. Karlberg, E. Re and G. Zanderighi, *JHEP* **09**, 134 (2014), [arXiv:1407.2940]; S. Höche, Y. Li and S. Prestel, *Phys. Rev.* **D91**, 7, 074015 (2015), [arXiv:1405.3607]; S. Höche, Y. Li and S. Prestel, *Phys. Rev.* **D90**, 5, 054011 (2014), [arXiv:1407.3773]; S. Alioli *et al.*, *Phys. Rev.* **D92**, 9, 094020 (2015), [arXiv:1508.01475]; P. F. Monni *et al.*, *JHEP* **05**, 143 (2020), [arXiv:1908.06987].
- [323] S. Alioli *et al.* (2021), [arXiv:2102.08390].
- [324] W. Astill *et al.*, *JHEP* **06**, 154 (2016), [arXiv:1603.01620].
- [325] W. Astill *et al.*, *JHEP* **11**, 157 (2018), [arXiv:1804.08141].
- [326] E. Re, M. Wiesemann and G. Zanderighi, *JHEP* **12**, 121 (2018), [arXiv:1805.09857].
- [327] S. Alioli *et al.*, *Phys. Rev. D* **100**, 9, 096016 (2019), [arXiv:1909.02026].
- [328] J. Mazzitelli *et al.* (2020), [arXiv:2012.14267].
- [329] D. Lombardi, M. Wiesemann and G. Zanderighi (2020), [arXiv:2010.10478].
- [330] S. Alioli *et al.*, *JHEP* **04**, 041 (2021), [arXiv:2010.10498].
- [331] D. Lombardi, M. Wiesemann and G. Zanderighi (2021), [arXiv:2103.12077].
- [332] S. Alioli *et al.*, *Phys. Lett. B* **818**, 136380 (2021), [arXiv:2103.01214].
- [333] G. Marchesini and B. R. Webber, *Nucl. Phys. B* **238**, 1 (1984).
- [334] G. Marchesini and B. R. Webber, *Nucl. Phys. B* **310**, 461 (1988).
- [335] S. Catani, B. R. Webber and G. Marchesini, *Nucl. Phys. B* **349**, 635 (1991).
- [336] G. Bewick *et al.*, *JHEP* **04**, 019 (2020), [arXiv:1904.11866].
- [337] M. Dasgupta *et al.*, *Phys. Rev. Lett.* **125**, 5, 052002 (2020), [arXiv:2002.11114].
- [338] M. Dasgupta *et al.*, *JHEP* **09**, 033 (2018), [Erratum: *JHEP* **03**, 083 (2020)], [arXiv:1805.09327].
- [339] L. Hartgring, E. Laenen and P. Skands, *JHEP* **10**, 127 (2013), [arXiv:1303.4974].
- [340] H. T. Li and P. Skands, *Phys. Lett. B* **771**, 59 (2017), [arXiv:1611.00013].
- [341] S. Höche and S. Prestel, *Phys. Rev. D* **96**, 7, 074017 (2017), [arXiv:1705.00742].
- [342] F. Dulat, S. Höche and S. Prestel, *Phys. Rev. D* **98**, 7, 074013 (2018), [arXiv:1805.03757].
- [343] A. Banfi, B. K. El-Menoufi and P. F. Monni, *JHEP* **01**, 083 (2019), [arXiv:1807.11487].
- [344] G. Gustafson, *Nucl. Phys. B* **392**, 251 (1993).
- [345] K. Hamilton *et al.* (2020), [arXiv:2011.10054].
- [346] M. Cacciari *et al.*, *JHEP* **04**, 068 (2004), [hep-ph/0303085].
- [347] P. M. Stevenson, *Phys. Lett.* **100B**, 61 (1981).
- [348] P. M. Stevenson, *Phys. Rev.* **D23**, 2916 (1981).
- [349] G. Grunberg, *Phys. Rev.* **D29**, 2315 (1984).
- [350] S. J. Brodsky, G. P. Lepage and P. B. Mackenzie, *Phys. Rev.* **D28**, 228 (1983).
- [351] S.-Q. Wang *et al.* (2019), [arXiv:1908.00060].
- [352] M. Cacciari and N. Houdeau, *JHEP* **09**, 039 (2011), [arXiv:1105.5152].
- [353] A. David and G. Passarino, *Phys. Lett.* **B726**, 266 (2013), [arXiv:1307.1843].
- [354] E. Bagnaschi *et al.*, *JHEP* **02**, 133 (2015), [arXiv:1409.5036].
- [355] C. Duhr *et al.* (2021), [arXiv:2106.04585].
- [356] D. Acosta *et al.* (CDF), *Phys. Rev. D* **70**, 072002 (2004), [hep-ex/0404004].
- [357] G. Soyez *et al.*, *Phys. Rev. Lett.* **110**, 16, 162001 (2013), [arXiv:1211.2811].
- [358] M. Dasgupta and G. P. Salam, *J. Phys.* **G30**, R143 (2004), [hep-ph/0312283].
- [359] S. Moretti, L. Lonnblad and T. Sjostrand, *JHEP* **08**, 001 (1998), [hep-ph/9804296].
- [360] G. P. Salam, *Eur. Phys. J.* **C67**, 637 (2010), [arXiv:0906.1833].
- [361] S. D. Ellis *et al.*, *Prog. Part. Nucl. Phys.* **60**, 484 (2008), [arXiv:0712.2447].
- [362] M. Cacciari, *Int. J. Mod. Phys.* **A30**, 31, 1546001 (2015), [arXiv:1509.02272].
- [363] G. P. Salam and G. Soyez, *JHEP* **05**, 086 (2007), [arXiv:0704.0292].
- [364] S. Catani *et al.*, *Nucl. Phys.* **B406**, 187 (1993).
- [365] S. D. Ellis and D. E. Soper, *Phys. Rev.* **D48**, 3160 (1993), [hep-ph/9305266].
- [366] Y. L. Dokshitzer *et al.*, *JHEP* **08**, 001 (1997), [hep-ph/9707323].
- [367] M. Wobisch and T. Wengler, in “Monte Carlo generators for HERA physics. Proceedings, Workshop, Hamburg, Germany, 1998-1999,” 270–279 (1998), [hep-ph/9907280].
- [368] M. Cacciari, G. P. Salam and G. Soyez, *JHEP* **04**, 063 (2008), [arXiv:0802.1189].
- [369] S. Bethke *et al.*, *Nucl. Phys.* **B370**, 310 (1992), [Erratum: *Nucl. Phys.* **B523**, 681 (1998)].
- [370] M. Cacciari and G. P. Salam, *Phys. Lett.* **B641**, 57 (2006), [hep-ph/0512210]; M. Cacciari, G. P. Salam and G. Soyez, *Eur. Phys. J.* **C72**, 1896 (2012), [arXiv:1111.6097].
- [371] S. Brandt *et al.*, *Phys. Lett.* **12**, 57 (1964).
- [372] E. Farhi, *Phys. Rev. Lett.* **39**, 1587 (1977).
- [373] O. Biebel, *Phys. Rept.* **340**, 165 (2001).
- [374] S. Kluth, *Rept. Prog. Phys.* **69**, 1771 (2006), [hep-ex/0603011].
- [375] C. L. Basham *et al.*, *Phys. Rev. Lett.* **41**, 1585 (1978).

- [376] A. Ali, E. Pietarinen and W. J. Stirling, Phys. Lett. **141B**, 447 (1984).
- [377] I. W. Stewart, F. J. Tackmann and W. J. Waalewijn, Phys. Rev. Lett. **105**, 092002 (2010), [arXiv:1004.2489].
- [378] A. Banfi, G. P. Salam and G. Zanderighi, JHEP **08**, 062 (2004), [hep-ph/0407287].
- [379] A. Banfi, G. P. Salam and G. Zanderighi, JHEP **06**, 038 (2010), [arXiv:1001.4082].
- [380] T. Becher, X. Garcia i Tormo and J. Piclum, Phys. Rev. **D93**, 5, 054038 (2016), [Erratum: Phys. Rev.D93,no.7,079905(2016)], [arXiv:1512.00022].
- [381] A. Gao *et al.*, Phys. Rev. Lett. **123**, 6, 062001 (2019), [arXiv:1901.04497].
- [382] T. Aaltonen *et al.* (CDF), Phys. Rev. **D83**, 112007 (2011), [arXiv:1103.5143].
- [383] G. Aad *et al.* (ATLAS), Eur. Phys. J. **C72**, 2211 (2012), [arXiv:1206.2135].
- [384] G. Aad *et al.* (ATLAS), Phys. Rev. **D88**, 3, 032004 (2013), [arXiv:1207.6915].
- [385] G. Aad *et al.* (ATLAS), Phys. Lett. **B750**, 427 (2015), [arXiv:1508.01579].
- [386] G. Aad *et al.* (ATLAS), Eur. Phys. J. **C76**, 7, 375 (2016), [arXiv:1602.08980].
- [387] M. Aaboud *et al.* (ATLAS), Eur. Phys. J. **C77**, 12, 872 (2017), [arXiv:1707.02562].
- [388] M. Aaboud *et al.* (ATLAS), Phys. Rev. **D98**, 9, 092004 (2018), [arXiv:1805.04691].
- [389] V. Khachatryan *et al.* (CMS), Phys. Lett. **B699**, 48 (2011), [arXiv:1102.0068].
- [390] S. Chatrchyan *et al.* (CMS), Phys. Lett. **B722**, 238 (2013), [arXiv:1301.1646].
- [391] V. Khachatryan *et al.* (CMS), JHEP **10**, 87 (2014), [arXiv:1407.2856].
- [392] A. M. Sirunyan *et al.* (CMS), JHEP **12**, 117 (2018), [arXiv:1811.00588].
- [393] A. Ali and G. Kramer, Eur. Phys. J. H **36**, 245 (2011), [arXiv:1012.2288].
- [394] S. Chatrchyan *et al.* (CMS), Phys. Lett. **B730**, 243 (2014), [arXiv:1310.0878].
- [395] G. Aad *et al.* (ATLAS), Phys. Rev. **D83**, 052003 (2011), [arXiv:1101.0070].
- [396] S. Chatrchyan *et al.* (CMS), JHEP **06**, 160 (2012), [arXiv:1204.3170].
- [397] B. B. Abelev *et al.* (ALICE), Phys. Rev. **D91**, 11, 112012 (2015), [arXiv:1411.4969].
- [398] G. Aad *et al.* (ATLAS), Eur. Phys. J. **C73**, 12, 2676 (2013), [arXiv:1307.5749].
- [399] C. Glasman (H1, ZEUS), Nucl. Phys. Proc. Suppl. **191**, 121 (2009), [arXiv:0812.0757].
- [400] T. Carli, K. Rabbertz and S. Schumann, in T. Schörner-Sadenius, editor, “The Large Hadron Collider: Harvest of Run 1,” 139–194 (2015), [arXiv:1506.03239].
- [401] A. Abdesselam *et al.*, Eur. Phys. J. **C71**, 1661 (2011), [arXiv:1012.5412].
- [402] D. Krohn, J. Thaler and L.-T. Wang, JHEP **02**, 084 (2010), [arXiv:0912.1342].
- [403] A. Altheimer *et al.*, J. Phys. **G39**, 063001 (2012), [arXiv:1201.0008].
- [404] A. Altheimer *et al.*, Eur. Phys. J. **C74**, 3, 2792 (2014), [arXiv:1311.2708].
- [405] P. C. Stichel and W. J. Zakrzewski, Eur. Phys. J. **C75**, 1, 9 (2015), [arXiv:1409.1363].
- [406] D. Adams *et al.*, Eur. Phys. J. **C75**, 9, 409 (2015), [arXiv:1504.00679].
- [407] G. Louppe *et al.*, JHEP **01**, 057 (2019), [arXiv:1702.00748].
- [408] D. Guest, K. Cranmer and D. Whiteson, Ann. Rev. Nucl. Part. Sci. **68**, 161 (2018), [arXiv:1806.11484].
- [409] T. Schorner-Sadenius, Eur. Phys. J. **C72**, 2060 (2012), [Erratum: Eur. Phys. J.C72,2133(2012)].
- [410] J. M. Campbell, J. W. Huston and W. J. Stirling, Rept. Prog. Phys. **70**, 89 (2007), [hep-ph/0611148].
- [411] M. L. Mangano, Phys. Usp. **53**, 109 (2010), [Usp. Fiz. Nauk180,113(2010)].
- [412] J. M. Butterworth, G. Dissertori and G. P. Salam, Ann. Rev. Nucl. Part. Sci. **62**, 387 (2012), [arXiv:1202.0583].
- [413] J. Currie *et al.*, JHEP **07**, 018 (2017), [Erratum: JHEP 12, 042 (2020)], [arXiv:1703.05977].
- [414] M. Klasen, G. Kramer and M. Michael, Phys. Rev. **D89**, 7, 074032 (2014), [arXiv:1310.1724].
- [415] T. Carli, T. Gehrman and S. Hoeche, Eur. Phys. J. **C67**, 73 (2010), [arXiv:0912.3715].
- [416] S. Chekanov *et al.* (ZEUS), Nucl. Phys. **B792**, 1 (2008), [arXiv:0707.3749].
- [417] S. Chekanov *et al.* (ZEUS), Phys. Rev. **D76**, 072011 (2007), [arXiv:0706.3809].
- [418] A. Aktas *et al.* (H1), Phys. Lett. **B639**, 21 (2006), [hep-ex/0603014].
- [419] H. Abramowicz *et al.* (ZEUS), Eur. Phys. J. **C71**, 1659 (2011), [arXiv:1104.5444].
- [420] H. Abramowicz *et al.* (ZEUS), Nucl. Phys. **B864**, 1 (2012), [arXiv:1205.6153].
- [421] F. D. Aaron *et al.* (H1), Eur. Phys. J. **C65**, 363 (2010), [arXiv:0904.3870].
- [422] F. D. Aaron *et al.* (H1), Eur. Phys. J. **C54**, 389 (2008), [arXiv:0711.2606].
- [423] S. Chekanov *et al.* (ZEUS), Eur. Phys. J. **C52**, 515 (2007), [arXiv:0707.3093].
- [424] S. Chekanov *et al.* (ZEUS), Phys. Rev. **D78**, 032004 (2008), [arXiv:0802.3955].
- [425] H. Abramowicz *et al.* (ZEUS), Eur. Phys. J. **C70**, 965 (2010), [arXiv:1010.6167].
- [426] H. Abramowicz *et al.* (ZEUS), Phys. Lett. **B691**, 127 (2010), [arXiv:1003.2923].
- [427] S. Chekanov *et al.* (ZEUS), Phys. Rev. **D85**, 052008 (2012), [arXiv:0808.3783].
- [428] F. D. Aaron *et al.* (H1), Eur. Phys. J. **C67**, 1 (2010), [arXiv:0911.5678].
- [429] V. Andreev *et al.* (H1), Eur. Phys. J. **C75**, 2, 65 (2015), [arXiv:1406.4709].
- [430] V. Andreev *et al.* (H1), Eur. Phys. J. **C77**, 11, 791 (2017), [Erratum: Eur. Phys. J. **C81**, 8, 738 (2021)], [arXiv:1709.07251].
- [431] <http://twiki.cern.ch/twiki/bin/view/CMSPublic/PhysicsResultsCombined>.
- [432] <http://atlas.web.cern.ch/Atlas/GROUPS/PHYSICS/CombinedSummaryPlots/SM>.
- [433] A. Abulencia *et al.* (CDF), Phys. Rev. **D75**, 092006 (2007), [Erratum: Phys. Rev.D75,119901(2007)], [hep-ex/0701051].
- [434] T. Aaltonen *et al.* (CDF), Phys. Rev. **D78**, 052006 (2008), [Erratum: Phys. Rev.D79,119902(2009)], [arXiv:0807.2204].
- [435] V. M. Abazov *et al.* (D0), Phys. Rev. Lett. **101**, 062001 (2008), [arXiv:0802.2400].
- [436] V. M. Abazov *et al.* (D0), Phys. Rev. **D85**, 052006 (2012), [arXiv:1110.3771].
- [437] B. Abelev *et al.* (ALICE), Phys. Lett. **B722**, 262 (2013), [arXiv:1301.3475].
- [438] G. Aad *et al.* (ATLAS), Eur. Phys. J. **C73**, 8, 2509 (2013), [arXiv:1304.4739].

- [439] G. Aad *et al.* (ATLAS), JHEP **02**, 153 (2015), [Erratum: JHEP09,141(2015)], [arXiv:1410.8857].
- [440] M. Aaboud *et al.* (ATLAS), JHEP **09**, 020 (2017), [arXiv:1706.03192].
- [441] V. Khachatryan *et al.* (CMS), Eur. Phys. J. **C76**, 5, 265 (2016), [arXiv:1512.06212].
- [442] S. Chatrchyan *et al.* (CMS), Phys. Rev. **D87**, 11, 112002 (2013), [Erratum: Phys. Rev.D87,no.11,119902(2013)], [arXiv:1212.6660].
- [443] V. Khachatryan *et al.* (CMS), JHEP **03**, 156 (2017), [arXiv:1609.05331].
- [444] V. Khachatryan *et al.* (CMS), Eur. Phys. J. **C76**, 8, 451 (2016), [arXiv:1605.04436].
- [445] M. Aaboud *et al.* (ATLAS), JHEP **05**, 195 (2018), [arXiv:1711.02692].
- [446] A. M. Sirunyan *et al.* (CMS), JHEP **12**, 082 (2020), [arXiv:2005.05159].
- [447] J. Currie *et al.*, JHEP **10**, 155 (2018), [arXiv:1807.03692].
- [448] A. Schwartzman, Int. J. Mod. Phys. **A30**, 31, 1546002 (2015), [arXiv:1509.05459].
- [449] J. Rojo, Int. J. Mod. Phys. **A30**, 1546005 (2015), [arXiv:1410.7728].
- [450] G. Aad *et al.* (ATLAS), JHEP **05**, 059 (2014), [arXiv:1312.3524].
- [451] A. M. Sirunyan *et al.* (CMS), Eur. Phys. J. **C77**, 11, 746 (2017), [arXiv:1705.02628].
- [452] T. Aaltonen *et al.* (CDF), Phys. Rev. **D79**, 112002 (2009), [arXiv:0812.4036].
- [453] V. M. Abazov *et al.* (D0), Phys. Rev. Lett. **103**, 191803 (2009), [arXiv:0906.4819].
- [454] S. Chatrchyan *et al.* (CMS), JHEP **05**, 055 (2012), [arXiv:1202.5535].
- [455] V. Khachatryan *et al.* (CMS), Phys. Lett. **B746**, 79 (2015), [arXiv:1411.2646].
- [456] A. M. Sirunyan *et al.* (CMS), JHEP **07**, 013 (2017), [arXiv:1703.09986].
- [457] G. Aad *et al.* (ATLAS), JHEP **01**, 029 (2013), [arXiv:1210.1718].
- [458] M. Aaboud *et al.* (ATLAS), Phys. Rev. **D96**, 5, 052004 (2017), [arXiv:1703.09127].
- [459] V. M. Abazov *et al.* (D0), Phys. Rev. Lett. **94**, 221801 (2005), [hep-ex/0409040].
- [460] V. M. Abazov *et al.* (D0), Phys. Lett. **B721**, 212 (2013), [arXiv:1212.1842].
- [461] G. Aad *et al.* (ATLAS), Phys. Rev. Lett. **106**, 172002 (2011), [arXiv:1102.2696].
- [462] V. Khachatryan *et al.* (CMS), Phys. Rev. Lett. **106**, 122003 (2011), [arXiv:1101.5029].
- [463] V. Khachatryan *et al.* (CMS), Eur. Phys. J. **C76**, 10, 536 (2016), [arXiv:1602.04384].
- [464] A. M. Sirunyan *et al.* (CMS), Eur. Phys. J. **C78**, 7, 566 (2018), [arXiv:1712.05471].
- [465] A. M. Sirunyan *et al.* (CMS) (2019), [arXiv:1902.04374].
- [466] P. Kokkas, Int. J. Mod. Phys. **A30**, 31, 1546004 (2015), [arXiv:1509.02144].
- [467] M. Aaboud *et al.* (ATLAS), Eur. Phys. J. **C77**, 6, 367 (2017), [arXiv:1612.03016].
- [468] G. Aad *et al.* (ATLAS), Phys. Lett. **B759**, 601 (2016), [arXiv:1603.09222].
- [469] R. Aaij *et al.* (LHCb), JHEP **08**, 039 (2015), [arXiv:1505.07024].
- [470] S. Chatrchyan *et al.* (CMS), JHEP **10**, 132 (2011), [arXiv:1107.4789].
- [471] S. Chatrchyan *et al.* (CMS), Phys. Rev. Lett. **112**, 191802 (2014), [arXiv:1402.0923].
- [472] R. Aaij *et al.* (LHCb), JHEP **06**, 058 (2012), [arXiv:1204.1620].
- [473] R. Aaij *et al.* (LHCb), JHEP **01**, 155 (2016), [arXiv:1511.08039].
- [474] R. Aaij *et al.* (LHCb), JHEP **09**, 136 (2016), [arXiv:1607.06495].
- [475] S. Chatrchyan *et al.* (CMS), JHEP **10**, 007 (2011), [arXiv:1108.0566].
- [476] V. Khachatryan *et al.* (CMS), Eur. Phys. J. **C75**, 4, 147 (2015), [arXiv:1412.1115].
- [477] G. Aad *et al.* (ATLAS), Phys. Lett. **B725**, 223 (2013), [arXiv:1305.4192].
- [478] G. Aad *et al.* (ATLAS), JHEP **06**, 112 (2014), [arXiv:1404.1212].
- [479] G. Aad *et al.* (ATLAS), JHEP **08**, 009 (2016), [arXiv:1606.01736].
- [480] A. M. Sirunyan *et al.* (CMS), Submitted to: JHEP (2018), [arXiv:1812.10529].
- [481] M. Aaboud *et al.* (ATLAS), JHEP **12**, 059 (2017), [arXiv:1710.05167].
- [482] S. Chatrchyan *et al.* (CMS), Phys. Rev. **D90**, 3, 032004 (2014), [arXiv:1312.6283].
- [483] V. Khachatryan *et al.* (CMS), Eur. Phys. J. **C76**, 8, 469 (2016), [arXiv:1603.01803].
- [484] G. Aad *et al.* (ATLAS), Submitted to: Eur. Phys. J. (2019), [arXiv:1904.05631].
- [485] R. Aaij *et al.* (LHCb), JHEP **10**, 030 (2016), [arXiv:1608.01484].
- [486] G. Aad *et al.* (ATLAS), Eur. Phys. J. **C76**, 5, 291 (2016), [arXiv:1512.02192].
- [487] V. Khachatryan *et al.* (CMS), JHEP **02**, 096 (2017), [arXiv:1606.05864].
- [488] A. M. Sirunyan *et al.* (CMS), JHEP **03**, 172 (2018), [arXiv:1710.07955].
- [489] M. Aaboud *et al.* (ATLAS), JHEP **05**, 077 (2018), [arXiv:1711.03296].
- [490] U. Blumenschein, Int. J. Mod. Phys. **A30**, 31, 1546007 (2015), [arXiv:1509.04885].
- [491] G. Aad *et al.* (ATLAS) (2019), [arXiv:1907.06728].
- [492] V. Khachatryan *et al.* (CMS), Phys. Rev. **D95**, 052002 (2017), [arXiv:1610.04222].
- [493] A. M. Sirunyan *et al.* (CMS), Phys. Rev. **D96**, 7, 072005 (2017), [arXiv:1707.05979].
- [494] A. M. Sirunyan *et al.* (CMS), Eur. Phys. J. **C78**, 11, 965 (2018), [arXiv:1804.05252].
- [495] G. Aad *et al.* (ATLAS), JHEP **07**, 032 (2013), [arXiv:1304.7098].
- [496] Z. Bern *et al.*, Phys. Rev. **D88**, 1, 014025 (2013), [arXiv:1304.1253].
- [497] M. Voutilainen, Int. J. Mod. Phys. **A30**, 31, 1546008 (2015), [arXiv:1509.05026].
- [498] G. Aad *et al.* (ATLAS), JHEP **08**, 005 (2016), [arXiv:1605.03495].
- [499] G. Aad *et al.* (ATLAS) (2019), [arXiv:1908.02746].
- [500] S. Chatrchyan *et al.* (CMS), Phys. Rev. **D84**, 052011 (2011), [arXiv:1108.2044].
- [501] S. Chatrchyan *et al.* (CMS), JHEP **06**, 009 (2014), [arXiv:1311.6141].
- [502] G. Aad *et al.* (ATLAS), Phys. Rev. **D89**, 5, 052004 (2014), [arXiv:1311.1440].
- [503] M. Aaboud *et al.* (ATLAS), Phys. Lett. **B780**, 578 (2018), [arXiv:1801.00112].

- [504] M. Aaboud *et al.* (ATLAS), Nucl. Phys. **B918**, 257 (2017), [arXiv:1611.06586].
- [505] A. M. Sirunyan *et al.* (CMS), Eur. Phys. J. **C79**, 1, 20 (2019), [arXiv:1807.00782].
- [506] A. M. Sirunyan *et al.* (CMS) (2019), [arXiv:1907.08155].
- [507] M. Aaboud *et al.* (ATLAS), Phys. Lett. **B776**, 295 (2018), [arXiv:1710.09560].
- [508] J. H. Kuhn *et al.*, JHEP **03**, 059 (2006), [hep-ph/0508253].
- [509] V. Khachatryan *et al.* (CMS), JHEP **10**, 128 (2015), [Erratum: JHEP04,010(2016)], [arXiv:1505.06520].
- [510] G. Aad *et al.* (ATLAS), JHEP **09**, 029 (2016), [arXiv:1603.01702].
- [511] M. Aaboud *et al.* (ATLAS), Phys. Lett. **B773**, 354 (2017), [arXiv:1702.04519].
- [512] M. Aaboud *et al.* (ATLAS) (2019), [arXiv:1905.04242].
- [513] V. Khachatryan *et al.* (CMS), Eur. Phys. J. **C76**, 7, 401 (2016), [arXiv:1507.03268].
- [514] G. Aad *et al.* (ATLAS), Phys. Lett. B **798**, 134913 (2019), [arXiv:1903.10415].
- [515] G. Aad *et al.* (ATLAS), JHEP **01**, 086 (2013), [arXiv:1211.1913].
- [516] M. Aaboud *et al.* (ATLAS), Phys. Rev. **D95**, 11, 112005 (2017), [arXiv:1704.03839].
- [517] S. Chatrchyan *et al.* (CMS), Eur. Phys. J. **C74**, 11, 3129 (2014), [arXiv:1405.7225].
- [518] M. Aaboud *et al.* (ATLAS), Phys. Lett. **B781**, 55 (2018), [arXiv:1712.07291].
- [519] K. Kröninger, A. B. Meyer and P. Uwer, in T. Schörner-Sadenius, editor, “The Large Hadron Collider: Harvest of Run 1,” 259–300 (2015), [arXiv:1506.02800].
- [520] M. Aaboud *et al.* (ATLAS), Phys. Rev. **D94**, 9, 092003 (2016), [arXiv:1607.07281].
- [521] M. Aaboud *et al.* (ATLAS), Eur. Phys. J. **C77**, 5, 292 (2017), [arXiv:1612.05220].
- [522] A. M. Sirunyan *et al.* (CMS), Eur. Phys. J. **C79**, 5, 368 (2019), [arXiv:1812.10505].
- [523] A. M. Sirunyan *et al.* (CMS), Submitted to: Eur. Phys. J. (2019), [arXiv:1904.05237].
- [524] M. Czakon, D. Heymes and A. Mitov, Phys. Rev. Lett. **116**, 8, 082003 (2016), [arXiv:1511.00549].
- [525] S. Catani *et al.*, JHEP **07**, 100 (2019), [arXiv:1906.06535].
- [526] M. Czakon *et al.*, JHEP **05**, 149 (2018), [arXiv:1803.07623].
- [527] S. Chatrchyan *et al.* (CMS), Phys. Lett. **B728**, 496 (2014), [Erratum: Phys. Lett. B738,526(2014)], [arXiv:1307.1907].
- [528] T. Kljinsma *et al.*, Eur. Phys. J. **C77**, 11, 778 (2017), [arXiv:1708.07495].
- [529] G. Aad *et al.* (ATLAS), Eur. Phys. J. **C74**, 10, 3109 (2014), [Addendum: Eur. Phys. J. C76, no.11, 642 (2016)], [arXiv:1406.5375].
- [530] A. M. Sirunyan *et al.* (CMS), JHEP **09**, 051 (2017), [arXiv:1701.06228].
- [531] M. Aaboud *et al.* (ATLAS), Phys. Lett. **B786**, 114 (2018), [arXiv:1805.10197].
- [532] A. M. Sirunyan *et al.* (CMS), Phys. Lett. **B792**, 369 (2019), [arXiv:1812.06504].
- [533] D. de Florian *et al.* (LHC Higgs Cross Section Working Group) (2016), [arXiv:1610.07922].
- [534] M. Aaboud *et al.* (ATLAS), Phys. Rev. **D98**, 052005 (2018), [arXiv:1802.04146].
- [535] A. M. Sirunyan *et al.* (CMS), JHEP **01**, 183 (2019), [arXiv:1807.03825].
- [536] A. M. Sirunyan *et al.* (CMS Collaboration), Phys. Lett. B **792**, arXiv:1812.06504. CMS-HIG-17-028-003, 369, 28 p (2018), submitted to Phys. Lett., URL <http://cds.cern.ch/record/2651932>.
- [537] P. A. Zyla *et al.* (Particle Data Group), PTEP **2020**, 8, 083C01 (2020).
- [538] D. d’Enterria *et al.*, in “Workshop on precision measurements of the QCD coupling constant (alphas-2019) Trento, Trentino, Italy, February 11-15, 2019,” (2019), [arXiv:1907.01435].
- [539] G. P. Salam, in A. Levy, S. Forte and G. Ridolfi, editors, “From My Vast Repertoire ...: Guido Altarelli’s Legacy,” 101–121 (2019), [arXiv:1712.05165].
- [540] A. Pich *et al.*, in “13th Conference on Quark Confinement and the Hadron Spectrum (Confinement XIII) Maynooth, Ireland, July 31-August 6, 2018,” (2018), [arXiv:1811.11801].
- [541] A. Pich, Prog. Part. Nucl. Phys. **117**, 103846 (2021), [arXiv:2012.04716].
- [542] S. Aoki *et al.* (Flavour Lattice Averaging Group), Eur. Phys. J. C **80**, 2, 113 (2020), [arXiv:1902.08191].
- [543] M. Beneke and M. Jamin, JHEP **09**, 044 (2008), [arXiv:0806.3156].
- [544] K. Maltman and T. Yavin, Phys. Rev. **D78**, 094020 (2008), [arXiv:0807.0650].
- [545] S. Narison, Phys. Lett. **B673**, 30 (2009), [arXiv:0901.3823].
- [546] I. Caprini and J. Fischer, Eur. Phys. J. **C64**, 35 (2009), [arXiv:0906.5211].
- [547] A. Pich, Prog. Part. Nucl. Phys. **75**, 41 (2014), [arXiv:1310.7922].
- [548] D. Boito *et al.*, Phys. Rev. **D91**, 3, 034003 (2015), [arXiv:1410.3528].
- [549] G. Altarelli, PoS **Corfu2012**, 002 (2013), [arXiv:1303.6065].
- [550] A. Pich and A. Rodríguez-Sánchez, Phys. Rev. **D94**, 3, 034027 (2016), [arXiv:1605.06830].
- [551] M. Davier *et al.*, Eur. Phys. J. **C74**, 3, 2803 (2014), [arXiv:1312.1501].
- [552] D. Boito *et al.*, Phys. Rev. **D95**, 3, 034024 (2017), [arXiv:1611.03457].
- [553] D. Boito *et al.*, Phys. Rev. **D100**, 7, 074009 (2019), [arXiv:1907.03360].
- [554] D. Boito *et al.*, Phys. Rev. **D98**, 7, 074030 (2018), [arXiv:1805.08176].
- [555] D. Boito *et al.*, Phys. Rev. D **103**, 3, 034028 (2021), [arXiv:2012.10440].
- [556] V. Mateu and P. G. Ortega, JHEP **01**, 122 (2018), [arXiv:1711.05755].
- [557] C. Peset, A. Pineda and J. Segovia, JHEP **09**, 167 (2018), [arXiv:1806.05197].
- [558] S. Narison, Int. J. Mod. Phys. A **33**, 10, 1850045 (2018), [Addendum: Int. J. Mod. Phys. A 33, 1850045 (2018)], [arXiv:1801.00592].
- [559] S. Narison, Int. J. Mod. Phys. A **33**, 33, 1892004 (2018), [arXiv:1812.09360].
- [560] D. Boito and V. Mateu, Phys. Lett. B **806**, 135482 (2020), [arXiv:1912.06237].
- [561] D. Boito and V. Mateu, JHEP **03**, 094 (2020), [arXiv:2001.11041].
- [562] J. Blumlein, H. Bottcher and A. Guffanti, Nucl. Phys. **B774**, 182 (2007), [hep-ph/0607200].
- [563] P. Jimenez-Delgado and E. Reya, Phys. Rev. **D89**, 7, 074049 (2014), [arXiv:1403.1852].
- [564] S. Alekhin *et al.*, Phys. Rev. **D96**, 1, 014011 (2017), [arXiv:1701.05838].
- [565] S. Alekhin, J. Blumlein and S. Moch, Eur. Phys. J. **C78**, 6, 477 (2018), [arXiv:1803.07537].
- [566] T. Cridge *et al.* (2021), [arXiv:2106.10289].

- [567] T.-J. Hou *et al.*, Phys. Rev. D **103**, 1, 014013 (2021), [arXiv:1912.10053].
- [568] R. D. Ball *et al.* (NNPDF), Eur. Phys. J. **C78**, 5, 408 (2018), [arXiv:1802.03398].
- [569] R. S. Thorne and G. Watt, JHEP **08**, 100 (2011), [arXiv:1106.5789].
- [570] S. Alekhin, J. Blumlein and S. Moch, Eur. Phys. J. **C71**, 1723 (2011), [arXiv:1101.5261].
- [571] R. D. Ball *et al.* (NNPDF), Phys. Lett. **B704**, 36 (2011), [arXiv:1102.3182].
- [572] R. D. Ball *et al.* (NNPDF), Phys. Lett. **B723**, 330 (2013), [arXiv:1303.1189].
- [573] R. S. Thorne, PoS **DIS2013**, 042 (2013), [arXiv:1306.3907].
- [574] G. Dissertori *et al.*, JHEP **08**, 036 (2009), [arXiv:0906.3436].
- [575] G. Abbiendi *et al.* (OPAL), Eur. Phys. J. **C71**, 1733 (2011), [arXiv:1101.1470].
- [576] S. Bethke *et al.* (JADE), Eur. Phys. J. **C64**, 351 (2009), [arXiv:0810.1389].
- [577] G. Dissertori *et al.*, Phys. Rev. Lett. **104**, 072002 (2010), [arXiv:0910.4283].
- [578] J. Schieck *et al.* (JADE), Eur. Phys. J. **C73**, 3, 2332 (2013), [arXiv:1205.3714].
- [579] A. Verbytskyi *et al.*, JHEP **08**, 129 (2019), [arXiv:1902.08158].
- [580] A. Kardos *et al.*, Eur. Phys. J. **C78**, 6, 498 (2018), [arXiv:1804.09146].
- [581] R. A. Davison and B. R. Webber, Eur. Phys. J. **C59**, 13 (2009), [arXiv:0809.3326].
- [582] R. Abbate *et al.*, Phys. Rev. **D83**, 074021 (2011), [arXiv:1006.3080].
- [583] T. Gehrmann, G. Luisoni and P. F. Monni, Eur. Phys. J. **C73**, 1, 2265 (2013), [arXiv:1210.6945].
- [584] A. H. Hoang *et al.*, Phys. Rev. **D91**, 9, 094018 (2015), [arXiv:1501.04111].
- [585] G. Luisoni, P. F. Monni and G. P. Salam, Eur. Phys. J. **C81**, 2, 158 (2021), [arXiv:2012.00622].
- [586] R. Frederix *et al.*, JHEP **11**, 050 (2010), [arXiv:1008.5313].
- [587] P. Bolzoni, B. A. Kniehl and A. V. Kotikov, Nucl. Phys. **B875**, 18 (2013), [arXiv:1305.6017].
- [588] A. Kardos, G. Somogyi and A. Verbytskyi, Eur. Phys. J. **C81**, 4, 292 (2021), [arXiv:2009.00281].
- [589] J. Currie *et al.*, Phys. Rev. Lett. **119**, 15, 152001 (2017), [arXiv:1705.10271].
- [590] M. Czakon *et al.* (2019), [arXiv:1907.12911].
- [591] S. Dittmaier, A. Huss and C. Speckner, JHEP **11**, 095 (2012), [arXiv:1210.0438].
- [592] R. Frederix *et al.*, JHEP **04**, 076 (2017), [arXiv:1612.06548].
- [593] M. Czakon *et al.*, JHEP **10**, 186 (2017), [arXiv:1705.04105].
- [594] M. Johnson and D. Maître, Phys. Rev. **D97**, 5, 054013 (2018), [arXiv:1711.01408].
- [595] A. Gehrmann-De Ridder *et al.*, JHEP **07**, 133 (2016), [arXiv:1605.04295].
- [596] S. Forte and Z. Kassabov, Eur. Phys. J. **C80**, 3, 182 (2020), [arXiv:2001.04986].
- [597] S. Alekhin *et al.*, Eur. Phys. J. **C75**, 304 (2015), [arXiv:1410.4412].
- [598] A. M. Sirunyan *et al.* (CMS), Eur. Phys. J. **C80**, 7, 658 (2020), [arXiv:1904.05237].
- [599] D. d'Enterria and A. Poldaru, JHEP **06**, 016 (2020), [arXiv:1912.11733].
- [600] T. Affolder *et al.* (CDF), Phys. Rev. Lett. **88**, 042001 (2002), [hep-ex/0108034].
- [601] S. Chekanov *et al.* (ZEUS), Phys. Lett. **B649**, 12 (2007), [hep-ex/0701039].
- [602] V. M. Abazov *et al.* (D0), Phys. Rev. **D80**, 111107 (2009), [arXiv:0911.2710].
- [603] B. Malaescu and P. Starovoitov, Eur. Phys. J. **C72**, 2041 (2012), [arXiv:1203.5416].
- [604] V. Khachatryan *et al.* (CMS), Eur. Phys. J. **C75**, 6, 288 (2015), [arXiv:1410.6765].
- [605] D. Britzger *et al.*, Eur. Phys. J. **C79**, 1, 68 (2019), [arXiv:1712.00480].
- [606] S. Chekanov *et al.* (ZEUS), Eur. Phys. J. **C44**, 183 (2005), [hep-ex/0502007].
- [607] S. Chatrchyan *et al.* (CMS), Eur. Phys. J. **C73**, 10, 2604 (2013), [arXiv:1304.7498].
- [608] V. M. Abazov *et al.* (D0), Phys. Lett. **B718**, 56 (2012), [arXiv:1207.4957].
- [609] V. Khachatryan *et al.* (CMS), Eur. Phys. J. **C75**, 5, 186 (2015), [arXiv:1412.1633].
- [610] V. Andreev *et al.* (H1), Eur. Phys. J. **C77**, 4, 215 (2017), [arXiv:1611.03421].
- [611] J. Haller *et al.*, Eur. Phys. J. **C78**, 8, 675 (2018), [arXiv:1803.01853].
- [612] S. Schael *et al.* (ALEPH, DELPHI, L3, OPAL, SLD, LEP Electroweak Working Group, SLD Electroweak Group, SLD Heavy Flavour Group), Phys. Rept. **427**, 257 (2006), [hep-ex/0509008].
- [613] I. Allison *et al.* (HPQCD), Phys. Rev. **D78**, 054513 (2008), [arXiv:0805.2999].
- [614] K. Maltman *et al.*, Phys. Rev. **D78**, 114504 (2008), [arXiv:0807.2020].
- [615] S. Aoki *et al.* (PACS-CS), JHEP **10**, 053 (2009), [arXiv:0906.3906].
- [616] C. McNeile *et al.*, Phys. Rev. **D82**, 034512 (2010), [arXiv:1004.4285].
- [617] E. Shintani *et al.*, Phys. Rev. **D82**, 7, 074505 (2010), [Erratum: Phys. Rev. **D89**, no. 9, 099903 (2014)], [arXiv:1002.0371].
- [618] B. Blossier *et al.*, Phys. Rev. **D85**, 034503 (2012), [arXiv:1110.5829].
- [619] A. Bazavov *et al.*, Phys. Rev. **D86**, 114031 (2012), [arXiv:1205.6155].
- [620] B. Blossier *et al.*, Phys. Rev. Lett. **108**, 262002 (2012), [arXiv:1201.5770].
- [621] B. Blossier *et al.* (ETM), Phys. Rev. **D89**, 1, 014507 (2014), [arXiv:1310.3763].
- [622] B. Chakraborty *et al.*, Phys. Rev. **D91**, 5, 054508 (2015), [arXiv:1408.4169].
- [623] A. Bazavov *et al.*, Phys. Rev. **D90**, 7, 074038 (2014), [arXiv:1407.8437].
- [624] K. Nakayama, B. Fahy and S. Hashimoto, Phys. Rev. **D94**, 5, 054507 (2016), [arXiv:1606.01002].
- [625] Y. Maezawa and P. Petreczky, Phys. Rev. **D94**, 3, 034507 (2016), [arXiv:1606.08798].
- [626] M. Bruno *et al.* (ALPHA), Phys. Rev. Lett. **119**, 10, 102001 (2017), [arXiv:1706.03821].
- [627] R. J. Hudspith *et al.* (2018), [arXiv:1804.10286].
- [628] H. Takaura *et al.*, Phys. Lett. **B789**, 598 (2019), [arXiv:1808.01632].
- [629] H. Takaura *et al.*, JHEP **04**, 155 (2019), [arXiv:1808.01643].
- [630] K. Nakayama, H. Fukaya and S. Hashimoto, Phys. Rev. **D98**, 1, 014501 (2018), [arXiv:1804.06695].
- [631] A. Bazavov *et al.* (TUMQCD), Phys. Rev. **D100**, 11, 114511 (2019), [arXiv:1907.11747].
- [632] L. Del Debbio and A. Ramos, Physics Reports **920**, 1 (2021), ISSN 0370-1573, [arXiv:2101.04762].

10. Electroweak Model and Constraints on New Physics

Revised March 2022 by J. Erler (KPH, JGU Mainz) and A. Freitas (Pittsburgh U.).

10.1	Introduction	177
10.2	Renormalization and radiative corrections	177
10.2.1	The Fermi constant	178
10.2.2	The electromagnetic coupling	178
10.2.3	Quark masses	179
10.2.4	The weak mixing angle	179
10.2.5	Radiative corrections	180
10.3	Low energy electroweak observables	181
10.3.1	Neutrino scattering	181
10.3.2	Parity violating lepton scattering	182
10.3.3	Atomic parity violation	183
10.4	Precision flavor physics	183
10.4.1	The τ lifetime	184
10.4.2	The muon anomalous magnetic moment	184
10.5	Physics of the massive electroweak bosons	185
10.5.1	Electroweak physics off the Z pole	185
10.5.2	Z pole physics	186
10.5.3	W and Z decays	187
10.6	Global fit results	189
10.7	Constraints on new physics	191

10.1 Introduction

The standard model of the electroweak interactions (SM) [1–4] is based on the gauge group $SU(2) \times U(1)$, with gauge bosons W_μ^i , $i = 1, 2, 3$, and B_μ for the $SU(2)$ and $U(1)$ factors, respectively, and the corresponding gauge coupling constants g and g' . The left-handed fermion fields of the i^{th} fermion family transform as doublets $\Psi_i = \begin{pmatrix} \nu_i \\ \ell_i^- \end{pmatrix}$ and $\begin{pmatrix} u_i \\ d_i^- \end{pmatrix}$ under $SU(2)$, where $d_i^- \equiv \sum_j V_{ij} d_j$, and V is the Cabibbo-Kobayashi-Maskawa mixing [5, 6] matrix. The right-handed fields are $SU(2)$ singlets. From Higgs and electroweak precision data it is known that there are precisely three sequential fermion families. Constraints on V and tests of universality are discussed in Ref. [7] and in the Section on the “CKM Quark-Mixing Matrix” in this *Review*. The extension of the formalism to allow an analogous leptonic mixing matrix is discussed in the Section on “Neutrino Masses, Mixing, and Oscillations” in this *Review*.

A complex scalar Higgs doublet, ϕ , is added to the model for mass generation through spontaneous symmetry breaking with potential¹ given by,

$$V(\phi) = \mu^2 \phi^\dagger \phi + \frac{\lambda^2}{2} (\phi^\dagger \phi)^2, \quad \phi \equiv \begin{pmatrix} \phi^+ \\ \phi^0 \end{pmatrix}. \quad (10.1)$$

For μ^2 negative, ϕ develops a vacuum expectation value, $v/\sqrt{2} = |\mu|/\lambda$, where $v = 246.22$ GeV, breaking part of the electroweak (EW) gauge symmetry, after which only one neutral Higgs scalar, H , remains in the physical particle spectrum. In non-minimal models there are additional charged and neutral scalar Higgs particles. Higgs boson physics is reviewed in the Section on the “Status of Higgs Boson Physics” in this *Review*.

After symmetry breaking the Lagrangian for the fermion fields, ψ_i , is

$$\mathcal{L}_F = \sum_i \bar{\psi}_i \left(i \not{\partial} - m_i - \frac{m_i H}{v} \right) \psi_i \quad (10.2)$$

$$- \frac{g}{2\sqrt{2}} \sum_i \bar{\psi}_i \gamma^\mu (1 - \gamma^5) (T^+ W_\mu^+ + T^- W_\mu^-) \Psi_i$$

$$- e \sum_i Q_i \bar{\psi}_i \gamma^\mu \psi_i A_\mu \quad (10.3)$$

¹There is no generally accepted convention to write the quartic term. Our numerical coefficient simplifies Eq. (10.6a) below and the squared coupling preserves the relation between the number of external legs and the power counting of couplings at a given loop order. This structure also naturally emerges from physics beyond the SM, such as Supersymmetry.

$$- \frac{g}{2 \cos \theta_W} \sum_i \bar{\psi}_i \gamma^\mu (g_V^i - g_A^i \gamma^5) \psi_i Z_\mu. \quad (10.4)$$

Here $\theta_W \equiv \tan^{-1}(g'/g)$ is the weak mixing angle and $e = g \sin \theta_W$ is the positron electric charge. Furthermore,

$$A_\mu \equiv B_\mu \cos \theta_W + W_\mu^3 \sin \theta_W, \quad (10.5a)$$

$$W_\mu^\pm \equiv \frac{W_\mu^1 \mp i W_\mu^2}{\sqrt{2}}, \quad (10.5b)$$

$$Z_\mu \equiv -B_\mu \sin \theta_W + W_\mu^3 \cos \theta_W, \quad (10.5c)$$

are the photon field (γ) and the charged (W^\pm) and neutral (Z) weak boson fields, respectively.

The Yukawa coupling of H to ψ_i in the first term in \mathcal{L}_F , which is flavor diagonal in the minimal model, is $gm_i/2M_W$. The boson masses in the EW sector are given (at tree level, *i.e.*, to lowest order in perturbation theory) by,

$$M_H = \lambda v, \quad (10.6a)$$

$$M_W = \frac{gv}{2} = \frac{ev}{2 \sin \theta_W}, \quad (10.6b)$$

$$M_Z = \sqrt{g^2 + g'^2} \frac{v}{2} = \frac{ev}{2 \sin \theta_W \cos \theta_W}, \quad (10.6c)$$

$$M_\gamma = 0. \quad (10.6d)$$

The second term in \mathcal{L}_F represents the charged-current weak interaction [8–10], where T^+ and T^- are the weak isospin raising and lowering operators. For example, the coupling of a W to an electron and a neutrino is

$$- \frac{e}{2\sqrt{2} \sin \theta_W} \left[W_\mu^- \bar{e} \gamma^\mu (1 - \gamma^5) \nu + W_\mu^+ \bar{\nu} \gamma^\mu (1 - \gamma^5) e \right]. \quad (10.7)$$

For momenta small compared to M_W , this term gives rise to the effective four-fermion interaction with the Fermi constant given by $G_F/\sqrt{2} = 1/2v^2 = g^2/8M_W^2$. CP violation is incorporated into the EW model by a single observable phase in V_{ij} .

The third term in \mathcal{L}_F describes electromagnetic interactions (QED) [11, 12], and the last is the weak neutral-current interaction [9, 10, 13]. The vector and axial-vector couplings are

$$g_V^i \equiv t_{3L}(i) - 2Q_i \sin^2 \theta_W, \quad (10.8a)$$

$$g_A^i \equiv t_{3L}(i), \quad (10.8b)$$

where $t_{3L}(i)$ is the weak isospin of fermion i ($+1/2$ for u_i and ν_i ; $-1/2$ for d_i and e_i) and Q_i is the charge of ψ_i in units of e .

The first term in Eq. (10.4) also gives rise to fermion masses, and in the presence of right-handed neutrinos to Dirac neutrino masses. The possibility of Majorana masses is discussed in the Section on “Neutrino Mass, Mixing, and Oscillations” in this *Review*.

10.2 Renormalization and radiative corrections

In addition to the Higgs boson mass, M_H , the fermion masses and mixings, and the strong coupling constant, α_s , the SM has three parameters. The set with the smallest experimental errors contains the Z mass², the Fermi constant, and the fine structure constant, to be discussed in turn (the numerical values quoted in Sections 10.2–10.4 correspond to the main fit result in Table 10.7).

The Z boson mass, $M_Z = 91.1876 \pm 0.0021$ GeV, has been determined from the Z lineshape scan at LEP 1 [14]. This value of M_Z corresponds to a definition based on a Breit-Wigner shape with an energy-dependent width³ (see the Section on the “ Z Boson” in this *Review*).

²We emphasize that in the fits described in Sec. 10.6 and Sec. 10.7 the values of the SM parameters are affected by all observables that depend on them. This is of no practical consequence for α and G_F , however, since they are very precisely known.

³The theoretically consistent and gauge-invariant definition of the Z -

10.2.1 The Fermi constant

The Fermi constant,

$$G_F = 1.1663788(6) \times 10^{-5} \text{ GeV}^{-2}, \quad (10.9)$$

is derived from the μ lifetime formula⁴,

$$\frac{\hbar}{\tau_\mu} = \frac{G_F^2 m_\mu^5}{192\pi^3} F(\rho) \left[1 + H_1(\rho) \frac{\hat{\alpha}(m_\mu)}{\pi} + H_2(\rho) \frac{\hat{\alpha}^2(m_\mu)}{\pi^2} + H_3 \frac{\hat{\alpha}^3(m_\mu)}{\pi^3} \right], \quad (10.10)$$

where $\rho = m_e^2/m_\mu^2$, and where

$$F(\rho) = 1 - 8\rho + 8\rho^3 - \rho^4 - 12\rho^2 \ln \rho = 0.99981295, \quad (10.11a)$$

$$H_1(\rho) = \frac{25}{8} - \frac{\pi^2}{2} - (9 + 4\pi^2 + 12 \ln \rho) \rho + 16\pi^2 \rho^{3/2} + \mathcal{O}(\rho^2) = -1.80793, \quad (10.11b)$$

$$H_2(\rho) = \frac{156815}{5184} - \frac{518}{81} \pi^2 - \frac{895}{36} \zeta(3) + \frac{67}{720} \pi^4 + \frac{53}{6} \pi^2 \ln 2 - (0.042 \pm 0.002)_{\text{had}} - \frac{5}{4} \pi^2 \sqrt{\rho} + \mathcal{O}(\rho) = 6.64, \quad (10.11c)$$

$$\hat{\alpha}(m_\mu)^{-1} = \alpha^{-1} + \frac{1}{3\pi} \ln \rho + \mathcal{O}(\alpha) = 135.901. \quad (10.11d)$$

H_1 and H_2 capture the QED corrections within the Fermi model. The results for $\rho = 0$ have been obtained in Refs. [16] and [17, 18] for H_1 and H_2 , respectively, where the term in parentheses is from the hadronic vacuum polarization [17]. The mass corrections to H_1 have been known for some time [19], while those to H_2 are more recent [20]. Notice the term linear in m_e whose appearance was unforeseen and can be traced to the use of the muon pole mass in the prefactor [20]. The coefficient $H_3 = -15.3 \pm 2.3$ has been estimated in Refs. [21, 22]. The remaining uncertainty in G_F is mostly experimental and has been reduced by an order of magnitude by the MuLan collaboration [15] at the PSI.

10.2.2 The electromagnetic coupling

The fine structure constant, α , can be extracted from the anomalous magnetic moment of the electron, $a_e = (1159652180.73 \pm 0.28) \times 10^{-12}$ [23], giving the value [24] $\alpha^{-1} = 137.035999150(33)$. Another approach combines measurements of the Rydberg constant and atomic masses with interferometry of atomic recoil kinematics. Applied to ^{87}Rb [25] and ^{133}Cs [26], this method implies the results $\alpha^{-1} = 137.035999206(11)$ and $\alpha^{-1} = 137.035999046(27)$, respectively, which differ by 5.5σ from each other, and when combined would give $\alpha^{-1} = 137.035999183(10)$. Finally, combining the anomalous magnetic moment and atomic interferometry methods, which unlike in the past are now in agreement, leads to the world average of

$$\alpha^{-1} = 137.035999180(10). \quad (10.12)$$

In most EW renormalization schemes, it is convenient to define a running α dependent on the energy scale of the process, with $\alpha^{-1} \approx 137.036$ appropriate at very low energy, *i.e.* close to the Thomson limit. The OPAL [27] and L3 [28] collaborations at LEP could also observe the running directly in small and large angle Bhabha scattering, respectively. For scales above a few hundred MeV the low energy hadronic contribution to vacuum polarization

introduces a theoretical uncertainty in α . In the modified minimal subtraction ($\overline{\text{MS}}$) scheme⁵ [29] (used for this *Review*), and with $\alpha_s(M_Z) = 0.1185 \pm 0.0016$ we have $\hat{\alpha}^{(4)}(m_\tau)^{-1} = 133.471 \pm 0.007$ and $\hat{\alpha}^{(5)}(M_Z)^{-1} = 127.951 \pm 0.009$. The latter corresponds to a quark sector contribution (without the top) to the conventional (on-shell) QED coupling,

$$\alpha(M_Z) = \frac{\alpha}{1 - \Delta\alpha(M_Z)}, \quad (10.13)$$

of $\Delta\alpha_{\text{had}}^{(5)}(M_Z) = 0.02768 \pm 0.00007$. These values are updated from Ref. [30] with $\Delta\alpha_{\text{had}}^{(5)}(M_Z)$ moved downwards and its uncertainty reduced (partly due to a more precise charm quark mass). Its correlation with a_μ , as well as the non-linear α_s dependence of $\hat{\alpha}(M_Z)$ and the resulting correlation with the input variable α_s , are fully taken into account in the fits. This is done by using as actual input (fit constraint) instead of $\Delta\alpha_{\text{had}}^{(5)}(M_Z)$ the low energy contribution by the three light quarks, $\Delta\alpha_{\text{had}}^{(3)}(2.0 \text{ GeV}) = (58.84 \pm 0.51) \times 10^{-4}$ [31], and by calculating the perturbative and heavy quark contributions to $\hat{\alpha}(M_Z)$ in each call of the fits according to [30]. Part of the error ($\pm 0.37 \times 10^{-4}$) is from e^+e^- annihilation data below $\sqrt{s} = 2 \text{ GeV}$, as well as isospin rotated data from τ decays into two- and four-pion final states [32] (including uncertainties from isospin breaking effects [33]), but uncalculated higher order perturbative ($\pm 0.21 \times 10^{-4}$) and non-perturbative ($\pm 0.28 \times 10^{-4}$ [31]) QCD corrections and the $\overline{\text{MS}}$ quark mass values (see below) also contribute. Various evaluations of $\Delta\alpha_{\text{had}}^{(5)}(M_Z)$ are summarized in Table 10.1, where the relation⁶ between the $\overline{\text{MS}}$ and on-shell definitions (obtained using Refs. [37, 38]) is given by,

$$\begin{aligned} & \Delta\hat{\alpha}(M_Z) - \Delta\alpha(M_Z) \\ &= \frac{\alpha}{\pi} \left[\frac{100}{27} - \frac{1}{6} - \frac{7}{4} \ln \frac{M_Z}{M_W} + \frac{\alpha_s(M_Z)}{\pi} \left(\frac{605}{108} - \frac{44}{9} \zeta(3) \right) \right. \\ &+ \frac{\alpha_s^2}{\pi^2} \left(\frac{976481}{23328} - \frac{253}{36} \zeta(2) - \frac{781}{18} \zeta(3) + \frac{275}{27} \zeta(5) \right) \\ &+ \frac{\alpha_s^3}{\pi^3} \left(\frac{1483517111}{3359232} - \frac{22781}{144} \zeta(2) - \frac{3972649}{7776} \zeta(3) - \frac{31}{81} \zeta(2)^2 \right. \\ &\left. \left. + \frac{521255}{7776} \zeta(5) - \frac{7315}{324} \zeta(7) + \frac{5819}{54} \zeta(2)\zeta(3) + \frac{14675}{162} \zeta(3)^2 \right) \right] \\ &= 0.007122(2)(5), \quad (10.14) \end{aligned}$$

and where the first entry of the lowest order term is from fermions and the other two are from W^\pm loops, which are usually excluded from the on-shell definition. Fermion mass effects and corrections of $\mathcal{O}(\alpha^2)$ contributing to Eq. (10.14) are small, partly cancel each other and are not included here. The first error in Eq. (10.14) is parametric (from α_s) and the second is from the truncation of the perturbative expansion. The most recent results on $\Delta\alpha_{\text{had}}^{(5)}(M_Z)$ [31, 39–41] typically assume the validity of perturbative QCD (PQCD) at scales of $\sim 2 \text{ GeV}$ or above and are in good agreement with each other. In regions where PQCD is not trusted, one can use $e^+e^- \rightarrow$ hadrons cross-section data and τ decay spectral functions [42], where the latter derive from OPAL [43], CLEO [44], ALEPH [45], and Belle [46]. Recently, new data for various $e^+e^- \rightarrow$ hadrons channels was obtained from BaBar, BES III, CLEO, the SND and CMD-3 experiments at VEPP-2000, and the KEDR experiments at VEPP-4M (for a list of references see, *e.g.*, Ref. [31]). While VEPP-2000 and VEPP-4M scanned center-of-mass (CM) energies up to 2 GeV and

boson mass through the complex pole of the propagator would instead lead to a Breit-Wigner shape with a constant width. The two definitions differ numerically, and this difference has to be accounted for in theoretical calculations.

⁴In the spirit of the Fermi theory, we incorporated the small propagator correction, $3/5 m_\mu^2/M_W^2$, into Δr (see below). This is also the convention adopted by the MuLan collaboration [15]. While this breaks with historical consistency, the numerical difference was negligible in the past.

⁵In this Section we denote quantities defined in the $\overline{\text{MS}}$ scheme by a caret; the exception is the strong coupling constant, α_s , which will always correspond to the $\overline{\text{MS}}$ definition and where the caret will be dropped. Furthermore, $\alpha^{(n)}$ and $\alpha_s^{(n)}$ denote the running couplings with n quark flavors.

⁶In practice, $\alpha(M_Z)$ is directly evaluated in the $\overline{\text{MS}}$ scheme using the FORTRAN package GAPP [34], including the QED contributions of both leptons and quarks. The leptonic three-loop [35] and four-loop [36] contributions in the on-shell scheme have also been obtained.

between about 3 and 4 GeV, respectively, the BaBar collaboration studied multi-hadron events radiatively returned from the $\Upsilon(4S)$, reconstructing the radiated photon and normalizing to $\mu^\pm\gamma$ final states. The precision of these results generally exceeds those from τ decays. There are significant discrepancies between the older (CMD-2) and newer (CMD-3) measurements of $e^+e^- \rightarrow K^+K^-$, which could be due to difficulties in determining the detection efficiency of low-momentum kaons. The radiative return data from BaBar is expected to be more reliable for this channel owing to an additional boost of the final-state hadrons.

10.2.3 Quark masses

Further free parameters entering into Eq. (10.4) are the quark and lepton masses, where m_i is the mass of the i^{th} fermion ψ_i . For the light quarks, as described in the Section on “Quark Masses” in this Review, $\widehat{m}_u = 2.16^{+0.49}_{-0.26}$ MeV, $\widehat{m}_d = 4.67^{+0.48}_{-0.17}$ MeV, and $\widehat{m}_s = 93^{+11}_{-5}$ MeV. These are running $\overline{\text{MS}}$ masses evaluated at the scale $\mu = 2$ GeV. For the charm mass we use the constraint [55],

$$\widehat{m}_c(\widehat{m}_c) = 1274 \pm 8 + 2616 [\alpha_s(M_Z) - 0.1182] \text{ MeV} , \quad (10.15)$$

which is based on QCD sum rules [56, 57], and recalculate \widehat{m}_c in each call of our fits to account for its α_s dependence. Similarly, for the bottom quark mass we use [58],

$$\widehat{m}_b(\widehat{m}_b) = 4180 \pm 8 - 108 [\alpha_s(M_Z) - 0.1182] \text{ MeV} , \quad (10.16)$$

with a theoretical correlation of about 60% arising from the PQCD truncation uncertainty which is similar for $\widehat{m}_c(\widehat{m}_c)$ and $\widehat{m}_b(\widehat{m}_b)$. To improve the precisions in $\widehat{m}_c(\widehat{m}_c)$ and $\widehat{m}_b(\widehat{m}_b)$ in the future it would help to remeasure the threshold regions of the heavy quarks, as well as the electronic decay widths of the narrow $c\bar{c}$ and $b\bar{b}$ resonances. It would also be important to obtain data on the R -ratio in e^+e^- annihilation for center-of-mass energies $\gtrsim 11.2$ GeV, as in this region QCD perturbation theory cannot be sufficiently relied upon for b quarks [58].

The top quark “pole” mass (the quotation marks are a reminder that the experiments do not strictly measure the pole mass and that quarks do not form asymptotic states), has been kinematically reconstructed by the Tevatron collaborations, CDF and $D\bar{O}$, in leptonic, hadronic, and mixed channels with the result $m_t = 174.30 \pm 0.35_{\text{stat.}} \pm 0.54_{\text{syst.}}$ GeV [59]. Likewise, using data from CM energies $\sqrt{s} = 7$ and 8 TeV (Run 1), ATLAS and CMS (including alternative technique measurements) at the LHC obtained $m_t = 172.69 \pm 0.25_{\text{stat.}} \pm 0.41_{\text{syst.}}$ GeV [60] and $m_t = 172.43 \pm 0.13_{\text{stat.}} \pm 0.46_{\text{syst.}}$ GeV [61], respectively. In addition, there are first results with $\sqrt{s} = 13$ TeV data (Run 2). CMS obtained $m_t = 172.26 \pm 0.07_{\text{mostly stat.}} \pm 0.61_{\text{syst.}}$ GeV [62] in the lepton + jets and all-jets channels, $m_t = 172.33 \pm 0.14_{\text{stat.}} \pm 0.69_{\text{syst.}}$ GeV [63] in the di-lepton channel, and $m_t = 172.13 \pm 0.32_{\text{stat.}} \pm 0.70_{\text{syst.}}$ GeV [64] in t -channel single top events (leptonic decays). Using a leptonic invariant mass and thus featuring reduced correlation with the more traditional analysis approaches, ATLAS quotes $m_t = 174.48 \pm 0.40_{\text{stat.}} \pm 0.67_{\text{syst.}}$ GeV [65] from the lepton + jets channel. While there seems to be generally good agreement between all these measurements, we observe a 2.8σ discrepancy (or more in case of correlated systematics) between the two most precise determinations, 174.98 ± 0.76 GeV [66] (by the $D\bar{O}$ collaboration) and 172.25 ± 0.63 GeV [67] (by the CMS collaboration), both from the lepton + jets channels. In addition, the latter is also 2.2σ lower than the preliminary result of Ref. [65]. Assuming a systematic error component of 0.17 GeV (the QCD, PDF and Monte Carlo type errors at ATLAS at Run 1) is common to all six results, we arrive at the combination,

$$m_t = 172.83 \pm 0.28_{\text{exp.}} \text{ GeV} + \Delta m_{\text{MC}} , \quad (10.17)$$

where Δm_{MC} is defined to account for any difference between the top pole mass, m_t , and the mass parameter implemented in the Monte Carlo event generators employed by the experimental groups. Δm_{MC} is expected to be of order $\alpha_s(Q_0)Q_0$ with a low scale $Q_0 \sim \mathcal{O}(1 \text{ GeV})$ [68], but its value is unknown in hadron collider environments so that we will treat it as an uncertainty

instead⁷, and choose for definiteness $Q_0 = \Gamma_t = 1.42$ GeV to arrive at $\Delta m_{\text{MC}} = 0 \pm 0.52$ GeV. We further assume that an uncertainty [70] of ± 0.32 GeV in the relation [71] between m_t and the $\overline{\text{MS}}$ definition, $\widehat{m}_t(\widehat{m}_t)$, entering electroweak radiative correction libraries, including the renormalon ambiguity [72], is already included in Δm_{MC} , as m_t merely serves as an intermediate book-keeping device in Ref. [68]. A promising future direction to arrive at a competitive independent constraint on m_t is to analyze differential top quark pair production cross-sections at next-to-next-to-leading order (NNLO) [73, 74] as m_t extraction based on them are easier to interpret, and experimentally they have become much more precise recently [75–77]. The combination in Eq. (10.17) differs slightly from the average, $m_t = 172.76 \pm 0.30_{\text{exp.}}$ GeV, which appears in the Top Quark Listings in this Review, and which is based exclusively on published results. For more details and references, see the Section on the “Top Quark” and the Quarks Listings in this Review.

10.2.4 The weak mixing angle

The observables $\sin^2\theta_W$ and M_W can be calculated from M_Z , $\widehat{\alpha}(M_Z)$, and G_F , when values for m_t and M_H are given, or conversely, M_H can be constrained by $\sin^2\theta_W$ and M_W . The value of $\sin^2\theta_W$ is extracted from neutral-current processes (see Sec. 10.3) and Z pole observables (see Sec. 10.5.3) and depends on the renormalization prescription. There are a number of popular schemes [9] leading to values which differ by small factors depending on m_t and M_H . The notation for these schemes is shown in Table 10.2.

- (i) The on-shell scheme [79] promotes the tree-level formula $\sin^2\theta_W = 1 - M_W^2/M_Z^2$ to a definition of the renormalized $\sin^2\theta_W$ to all orders in perturbation theory, *i.e.*,

$$\sin^2\theta_W \rightarrow s_W^2 \equiv 1 - \frac{M_W^2}{M_Z^2} , \quad (10.18a)$$

$$M_W = \frac{A_0}{s_W(1 - \Delta r)^{1/2}} , \quad M_Z = \frac{M_W}{c_W} , \quad (10.18b)$$

where $c_W \equiv \cos\theta_W$, $A_0 = (\pi\alpha/\sqrt{2}G_F)^{1/2} = 37.28038(1)$ GeV, and Δr includes the radiative corrections relating α , $\alpha(M_Z)$, G_F , M_W , and M_Z . One finds $\Delta r \sim \Delta r_0 - \rho_t \tan^{-2}\theta_W$, where $\Delta r_0 = 1 - \alpha/\widehat{\alpha}(M_Z) = 0.06630(7)$ is due to the running of α , and

$$\rho_t = \frac{3G_F m_t^2}{8\sqrt{2}\pi^2} = 0.00936 \times \frac{m_t^2}{(172.83 \text{ GeV})^2} , \quad (10.19)$$

represents the dominant (quadratic) m_t dependence. There are additional contributions to Δr from bosonic loops, including those which depend logarithmically on M_H and higher-order corrections⁸. One has $\Delta r = 0.03657 \mp 0.00021 \pm 0.00007$, where the first uncertainty is from m_t and the second is from $\alpha(M_Z)$. Thus the value of s_W^2 extracted from M_Z includes an uncertainty (∓ 0.00007) from the currently allowed range of m_t . This scheme is simple conceptually. However, the relatively large ($\sim 3\%$) correction from ρ_t causes large spurious contributions in higher orders. s_W^2 depends not only on the gauge couplings but also on the spontaneous-symmetry breaking, and it is awkward in the presence of any extension of the SM which perturbs the value of M_Z (or M_W). Other definitions are motivated by the tree-level coupling constant definition $\theta_W = \tan^{-1}(g'/g)$:

- (ii) In particular, the $\overline{\text{MS}}$ scheme introduces the quantity,

$$\sin^2\widehat{\theta}_W(\mu) \equiv \frac{\widehat{g}'^2(\mu)}{\widehat{g}^2(\mu) + \widehat{g}'^2(\mu)} , \quad (10.20)$$

⁷However, see Ref. [69] for a proposed procedure to calibrate the Monte-Carlo mass parameter at hadron colliders.

⁸All explicit numbers quoted here and below include the two- and three-loop corrections described near the end of Sec. 10.2.

Table 10.1: Evaluations of the on-shell $\Delta\alpha_{\text{had}}^{(5)}(M_Z)$ by different groups (for a more complete list of evaluations see the 2012 edition of this *Review*). For better comparison we adjusted central values and errors to correspond to a common and fixed value of $\alpha_s(M_Z) = 0.120$. References quoting results without the top quark decoupled are converted to the five flavor definition. Ref. [47] uses $A_{\text{QCD}} = 380 \pm 60$ MeV; for the conversion we assumed $\alpha_s(M_Z) = 0.118 \pm 0.003$.

Reference	Result	Comment
Geshkenbein, Morgunov [48]	0.02780 ± 0.00006	$\mathcal{O}(\alpha_s)$ resonance model
Swartz [49]	0.02754 ± 0.00046	use of fitting function
Krasnikov, Rodenberg [50]	0.02737 ± 0.00039	PQCD for $\sqrt{s} > 2.3$ GeV
Kühn & Steinhauser [51]	0.02778 ± 0.00016	full $\mathcal{O}(\alpha_s^2)$ for $\sqrt{s} > 1.8$ GeV
Groote <i>et al.</i> [47]	0.02787 ± 0.00032	use of QCD sum rules
Martin <i>et al.</i> [52]	0.02741 ± 0.00019	incl. new BES data
de Troconiz, Yndurain [53]	0.02754 ± 0.00010	PQCD for $s > 2$ GeV ²
Burkhardt, Pietrzyk [54]	0.02750 ± 0.00033	PQCD for $\sqrt{s} > 12$ GeV
Erlar, Ferro-Hernández [39]	0.02761 ± 0.00010	conv. from $\overline{\text{MS}}$ scheme
Jegerlehner [40]	0.02755 ± 0.00013	Euclidean split technique
Davier <i>et al.</i> [31]	0.02760 ± 0.00010	PQCD for $\sqrt{s} = 1.8\text{--}3.7$ & > 5 GeV
Keshavarzi <i>et al.</i> [41]	0.02761 ± 0.00011	PQCD for $\sqrt{s} > 11.2$ GeV

Table 10.2: Notations used to indicate the various schemes discussed in the text. Each definition of $\sin^2 \theta_W$ leads to values that differ by small factors depending on m_t and M_H . Numerical values and the uncertainties induced by the imperfectly known SM parameters and unknown higher orders [78] are also given for illustration.

Scheme	Notation	Value	Uncertainty
On-shell	s_W^2	0.22339	± 0.00010
$\overline{\text{MS}}$	\widehat{s}_Z^2	0.23122	± 0.00004
$\overline{\text{MS}}$ (ND)	$\widehat{s}_{\text{ND}}^2$	0.23141	± 0.00004
$\overline{\text{MS}}$	\widehat{s}_0^2	0.23863	± 0.00005
Effective angle	\widehat{s}_ℓ^2	0.23155	± 0.00004

where the couplings \widehat{g} and \widehat{g}' are defined by modified minimal subtraction and the scale μ is conveniently chosen to be M_Z for many EW processes. The value of $\widehat{s}_Z^2 \equiv \sin^2 \widehat{\theta}_W(M_Z)$ extracted from M_Z is less sensitive than s_W^2 to m_t (by a factor of $\tan^2 \theta_W$), and is less sensitive to most types of new physics. It is also very useful for comparing with the predictions of grand unification. There are actually several variant definitions of $\sin^2 \widehat{\theta}_W(M_Z)$, differing according to whether or how finite $\alpha \ln(m_t/M_Z)$ terms are decoupled (subtracted from the couplings). One cannot entirely decouple the $\alpha \ln(m_t/M_Z)$ terms from all EW quantities because $m_t \gg m_b$ breaks SU(2) symmetry. The scheme that will be adopted here decouples the $\alpha \ln(m_t/M_Z)$ terms from the γ - Z mixing [29, 80], essentially eliminating any $\ln(m_t/M_Z)$ dependence in the formulae for asymmetries at the Z pole when written in terms of \widehat{s}_Z^2 . (A similar definition is used for $\widehat{\alpha}$.) The on-shell and $\overline{\text{MS}}$ definitions are related by

$$\widehat{s}_Z^2 = c(m_t, M_H) s_W^2 = (1.0351 \pm 0.0003) s_W^2. \quad (10.21)$$

The quadratic m_t dependence is given by $c \sim 1 + \rho_t / \tan^2 \theta_W$. The expressions for M_W and M_Z in the $\overline{\text{MS}}$ scheme are

$$M_W = \frac{A_0}{\widehat{s}_Z (1 - \Delta\widehat{r}_W)^{1/2}}, \quad M_Z = \frac{M_W}{\widehat{\rho}^{1/2} \widehat{c}_Z}, \quad (10.22)$$

and one predicts $\Delta\widehat{r}_W = 0.06922 \pm 0.00007$. $\Delta\widehat{r}_W$ has no quadratic m_t dependence, because shifts in M_W are absorbed into the observed G_F , so that the error in $\Delta\widehat{r}_W$ is almost entirely due to $\Delta r_0 = 1 - \alpha/\widehat{\alpha}(M_Z)$. The quadratic m_t dependence has been shifted into $\widehat{\rho} \sim 1 + \rho_t$, where including bosonic loops, $\widehat{\rho} = 1.01019 \pm 0.00009$.

- (iii) A variant $\overline{\text{MS}}$ quantity $\widehat{s}_{\text{ND}}^2$ (used in the 1992 edition of this *Review*) does not decouple the $\alpha \ln(m_t/M_Z)$ terms [81]. It is related to \widehat{s}_Z^2 by

$$\widehat{s}_Z^2 = \frac{\widehat{s}_{\text{ND}}^2}{1 + \frac{\alpha}{\pi} d}, \quad d = \frac{1}{3} \left(\frac{1}{\widehat{s}_Z^2} - \frac{8}{3} \right) \left[\left(1 + \frac{\alpha_s}{\pi} \right) \ln \frac{m_t}{M_Z} - \frac{15\alpha_s}{8\pi} \right]. \quad (10.23)$$

Thus, $\widehat{s}_Z^2 - \widehat{s}_{\text{ND}}^2 = -0.0002$.

- (iv) Some of the low-energy experiments discussed in the next section are sensitive to the weak mixing angle at almost vanishing momentum transfer [39, 82–84]. Thus, Table 10.2 also includes $\widehat{s}_0^2 \equiv \sin^2 \widehat{\theta}_W(0)$.
- (v) Yet another definition, the effective angle [85, 86], $\widehat{s}_f^2 \equiv \sin^2 \theta_{\text{eff}}^f$, for the Z vector coupling to fermion f , is based on Z pole observables and described in Sec. 10.5.

10.2.5 Radiative corrections

Experiments are at such level of precision [78] that complete one-loop, dominant two-loop, and partial three and four-loop radiative corrections must be applied. For neutral-current and Z pole processes, these corrections are conveniently divided into two classes:

1. QED diagrams involving the emission of real photons or the exchange of virtual photons in loops, but not including vacuum polarization diagrams. These graphs often yield finite and gauge-invariant contributions to observable processes. However, they are dependent on energies, experimental cuts, *etc.*, and must be calculated individually for each experiment.
2. EW corrections, including $\gamma\gamma$, γZ , ZZ , and WW vacuum polarization diagrams, as well as vertex corrections, box graphs, *etc.*, involving virtual W and Z bosons. One-loop corrections [87] are included for all processes, and many two-loop corrections are also important. In particular, two-loop corrections involving the top quark modify ρ_t in $\widehat{\rho}$, Δr , and elsewhere by

$$\rho_t \rightarrow \rho_t \left[1 + R(M_H, m_t) \frac{\rho_t}{3} \right]. \quad (10.24)$$

$R(M_H, m_t)$ can be described as an expansion in M_Z^2/m_t^2 , for which the leading m_t^4/M_Z^4 [88, 89] and next-to-leading m_t^2/M_Z^2 [90, 91] terms are known. The complete two-loop calculation of Δr (without further approximation) has been performed in Refs. [92–96]. More recently, Ref. [97] obtained the $\overline{\text{MS}}$ quantities $\Delta\widehat{r}_W$ and $\widehat{\rho}$ to two-loop accuracy, confirming the prediction of M_W in the on-shell scheme from

Refs. [94, 98] within about 4 MeV. Similarly, the EW two-loop corrections for the relation between $\bar{s}_{\ell,b}^2$ and s_W^2 are known [99–104], as well as for the partial decay and total decay widths and the effective couplings of the Z boson [105–108]. For $\bar{s}_{s,c}$ only two-loop corrections from diagrams with closed fermion loops are available [109], but given the experimental precision this is more than adequate.

The mixed QCD-EW contributions to gauge boson self-energies of order $\alpha\alpha_s m_t^2$ [110, 111], $\alpha\alpha_s^2 m_t^2$ [112, 113], and $\alpha\alpha_s^3 m_t^2$ [114–116] increase the predicted value of m_t by 6%. This is, however, almost entirely an artifact of using the pole mass definition for m_t . The equivalent corrections when using the $\overline{\text{MS}}$ definition $\hat{m}_t(m_t)$ increase m_t by less than 0.5%. The sub-leading $\alpha\alpha_s$ corrections [117–120] are also included. Further three-loop corrections of order $\alpha\alpha_s^2$ [121, 122], $\alpha^3 m_t^6$, and $\alpha^2\alpha_s m_t^4$ [123, 124], are rather small. The same is true for $\alpha^3 M_H^4$ [125] corrections unless M_H approaches 1 TeV. The theoretical uncertainty from unknown higher-order corrections [78] is estimated to amount to 4 MeV for the prediction of M_W [98] and 4.5×10^{-5} for \bar{s}_ℓ^2 [109].

Throughout this *Review* we utilize EW radiative corrections from the program GAPP [34], which works entirely in the $\overline{\text{MS}}$ scheme, and which is independent of the package ZFITTER [126].

10.3 Low energy electroweak observables

In the following we discuss EW precision observables obtained at low momentum transfers [127], *i.e.*, $Q^2 \ll M_Z^2$. It is convenient to write the four-fermion interactions relevant to ν -hadron, ν - e , as well as parity violating e -hadron and e - e neutral-current processes, in a form that is valid in an arbitrary gauge theory (assuming massless left-handed neutrinos). One has⁹,

$$-\mathcal{L}^{\nu e} = \frac{G_F}{\sqrt{2}} \bar{\nu} \gamma_\mu (1 - \gamma^5) \nu \bar{e} \gamma^\mu (g_{LV}^{\nu e} - g_{LA}^{\nu e} \gamma^5) e, \quad (10.25a)$$

$$-\mathcal{L}^{\nu h} = \frac{G_F}{\sqrt{2}} \bar{\nu} \gamma_\mu (1 - \gamma^5) \nu \sum_q \left[g_{LL}^{\nu q} \bar{q} \gamma^\mu (1 - \gamma^5) q + g_{LR}^{\nu q} \bar{q} \gamma^\mu (1 + \gamma^5) q \right], \quad (10.25b)$$

$$-\mathcal{L}^{ee} = -\frac{G_F}{\sqrt{2}} g_{AV}^{ee} \bar{e} \gamma_\mu \gamma^5 e \bar{e} \gamma^\mu e, \quad (10.25c)$$

$$-\mathcal{L}^{eh} = -\frac{G_F}{\sqrt{2}} \sum_q \left[g_{AV}^{eq} \bar{e} \gamma_\mu \gamma^5 e \bar{q} \gamma^\mu q + g_{VA}^{eq} \bar{e} \gamma_\mu e \bar{q} \gamma^\mu \gamma^5 q \right], \quad (10.25d)$$

where one must include the charged-current contribution for ν_e - e and $\bar{\nu}_e$ - e and the parity conserving QED contribution for electron scattering. The SM tree level expressions for the four-Fermi couplings are given in Table 10.3. Note that they differ from the respective products of the gauge couplings in (10.8) in the radiative corrections and in the presence of possible physics beyond the SM.

10.3.1 Neutrino scattering

The cross-section in the laboratory system for $\nu_\mu e \rightarrow \nu_\mu e$ or $\bar{\nu}_\mu e \rightarrow \bar{\nu}_\mu e$ elastic scattering [9, 128] is (in this subsection we drop the redundant index L in the effective neutrino couplings),

$$\frac{d\sigma_{\nu,\bar{\nu}}}{dy} = \frac{G_F^2 m_e E_\nu}{2\pi} \left[(g_V^{\nu e} \pm g_A^{\nu e})^2 + (g_V^{\nu e} \mp g_A^{\nu e})^2 (1 - y)^2 - (g_V^{\nu e 2} - g_A^{\nu e 2}) \frac{y m_e}{E_\nu} \right], \quad (10.26)$$

where the upper (lower) sign refers to ν_μ ($\bar{\nu}_\mu$), and $y \equiv T_e/E_\nu$ (which runs from 0 to $(1 + m_e/2E_\nu)^{-1}$) is the ratio of the kinetic

⁹We use here slightly different definitions (and to avoid confusion also a different notation) for the coefficients of these four-Fermi operators than we did in previous editions of this *Review*. The new couplings [13] are defined in the static limit, $Q^2 \rightarrow 0$, with specific radiative corrections included, while others (more experiment specific ones) are assumed to be removed by the experimentalist. They are convenient in that their determinations from very different types of processes can be straightforwardly combined.

Table 10.3: SM tree level expressions for the neutral-current parameters for ν -hadron, ν - e , and e^- scattering processes. To obtain the SM values in the last column, the tree level expressions have to be multiplied by the low-energy neutral-current ρ parameter, $\rho_{\text{NC}} = 1.00063$, and further vertex and box corrections need to be added as detailed in Ref. [13]. The dominant m_t dependence is again given by $\rho_{\text{NC}} \sim 1 + \rho_e$.

Quantity	SM tree level	SM value
$g_{LV}^{\nu_\mu e}$	$-\frac{1}{2} + 2 \widehat{s}_0^2$	-0.0397
$g_{LA}^{\nu_\mu e}$	$-\frac{1}{2}$	-0.5064
$g_{LL}^{\nu_\mu u}$	$\frac{1}{2} - \frac{2}{3} \widehat{s}_0^2$	0.3457
$g_{LL}^{\nu_\mu d}$	$-\frac{1}{2} + \frac{1}{3} \widehat{s}_0^2$	-0.4288
$g_{LR}^{\nu_\mu u}$	$-\frac{2}{3} \widehat{s}_0^2$	-0.1553
$g_{LR}^{\nu_\mu d}$	$\frac{1}{3} \widehat{s}_0^2$	0.0777
g_{AV}^{ee}	$\frac{1}{2} - 2 \widehat{s}_0^2$	0.0226
g_{AV}^{eu}	$-\frac{1}{2} + \frac{4}{3} \widehat{s}_0^2$	-0.1887
g_{AV}^{ed}	$\frac{1}{2} - \frac{2}{3} \widehat{s}_0^2$	0.3419
g_{VA}^{eu}	$-\frac{1}{2} + 2 \widehat{s}_0^2$	-0.0351
g_{VA}^{ed}	$\frac{1}{2} - 2 \widehat{s}_0^2$	0.0248

energy of the recoil electron to the incident ν or $\bar{\nu}$ energy. For $E_\nu \gg m_e$ this yields a total cross-section

$$\sigma = \frac{G_F^2 m_e E_\nu}{2\pi} \left[(g_V^{\nu e} \pm g_A^{\nu e})^2 + \frac{1}{3} (g_V^{\nu e} \mp g_A^{\nu e})^2 \right]. \quad (10.27)$$

The most accurate measurements of $\sin^2 \theta_W$ from ν -lepton scattering (see Sec. 10.6) are from the ratio $R \equiv \sigma_{\nu_\mu e} / \sigma_{\bar{\nu}_\mu e}$, in which many of the systematic uncertainties cancel. The results are $\sin^2 \theta_W = 0.211 \pm 0.037$ [129], $\sin^2 \theta_W = 0.195 \pm 0.022$ [130], and $\sin^2 \theta_W = 0.2324 \pm 0.0083$ [131], where radiative corrections (other than m_t effects) are small compared to the precision of present experiments and have negligible effect. As shown in Fig. 10.1, one can determine $g_{V,A}^{\nu e}$ from the experimental data as well. The cross-sections for ν_e - e and $\bar{\nu}_e$ - e may be obtained from Eq. (10.26) by replacing $g_{V,A}^{\nu e}$ by $g_{V,A}^{\nu e} + 1$, where the 1 is due to the charged-current contribution.

A precise determination of the on-shell s_W^2 , which depends only very weakly on m_t and M_H , is obtained from deep inelastic scattering (DIS) of neutrinos [128, 135] from (approximately) isoscalar targets. The ratio $R_\nu \equiv \sigma_{\nu N}^{\text{NC}} / \sigma_{\nu N}^{\text{CC}}$ of neutral-to-charged-current cross-sections has been measured to 1% accuracy by CDHS [136] and CHARM [137] at CERN. CCFR [138] at Fermilab has obtained an even more precise result, so it is important to obtain theoretical expressions for R_ν and $R_{\bar{\nu}} \equiv \sigma_{\bar{\nu} N}^{\text{NC}} / \sigma_{\bar{\nu} N}^{\text{CC}}$ to comparable accuracy. Fortunately, many of the uncertainties from the strong interactions and neutrino spectra cancel in the ratio. A large theoretical uncertainty is associated with the c -threshold, which mainly affects σ^{CC} . Using the slow rescaling prescription [139, 140] the central value of $\sin^2 \theta_W$ from CCFR varies as $0.0111(m_c/\text{GeV} - 1.31)$, where m_c is the effective mass which is numerically close to the $\overline{\text{MS}}$ mass $\hat{m}_c(\hat{m}_c)$, but their exact relation is unknown at higher orders. For $m_c = 1.31 \pm 0.24$ GeV, which was determined from ν -induced di-muon production [141], this contributes ± 0.003 to the total uncertainty of $\Delta \sin^2 \theta_W = \pm 0.004$, where the experimental uncertainty was also ± 0.003 . This uncertainty largely cancels, however, in the Paschos-Wolfenstein ratio [142],

$$R^- = \frac{\sigma_{\nu N}^{\text{NC}} - \sigma_{\bar{\nu} N}^{\text{NC}}}{\sigma_{\nu N}^{\text{CC}} - \sigma_{\bar{\nu} N}^{\text{CC}}}. \quad (10.28)$$

It was measured by Fermilab's NuTeV collaboration [143] for the first time, and required a high-intensity and high-energy anti-neutrino beam.

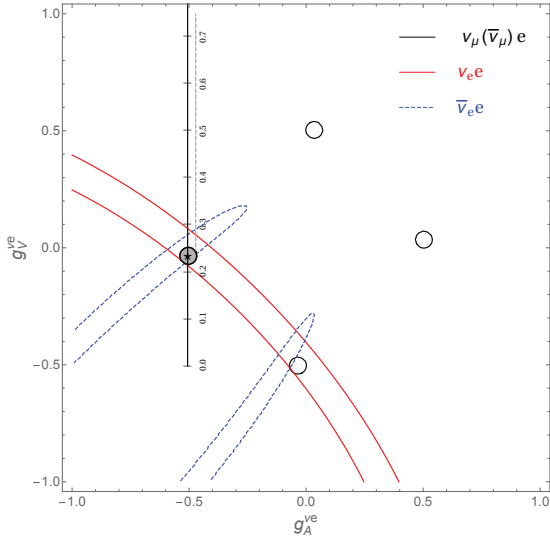


Figure 10.1: Allowed contours in $g_A^{\nu e}$ vs. $g_V^{\nu e}$ from neutrino-electron scattering and the SM prediction as a function of \hat{s}_Z^2 . (The SM best fit value, $\hat{s}_Z^2 = 0.23122$, is also indicated.) The $\nu_e e$ [132, 133] and $\bar{\nu}_e e$ [134] constraints are at 1σ , while each of the four equivalent $\nu_\mu(\bar{\nu}_\mu) e$ [129–131] solutions ($g_{V,A} \rightarrow -g_{V,A}$ and $g_{V,A} \rightarrow g_{A,V}$) are at the 90% CL. The global best fit region (shaded) almost exactly coincides with the corresponding $\nu_\mu(\bar{\nu}_\mu) e$ region. The solution near $g_A = 0$ and $g_V = -0.5$ is eliminated by $e^+e^- \rightarrow \ell^+\ell^-$ data under the weak additional assumption that the neutral current is dominated by the exchange of a single Z boson.

A simple zeroth-order approximation is,

$$R_\nu = g_L^2 + g_R^2 r, \quad R_{\bar{\nu}} = g_L^2 + \frac{g_R^2}{r}, \quad (10.29a)$$

$$R^- = g_L^2 - g_R^2, \quad r \equiv \frac{\sigma_{\bar{\nu}N}^{CC}}{\sigma_{\nu N}^{CC}}, \quad (10.29b)$$

where r is the ratio of $\bar{\nu}$ to ν charged-current cross-sections which can be measured directly¹⁰, and

$$g_L^2 \equiv (g_{LL}^{\nu u})^2 + (g_{LL}^{\nu d})^2 \approx \frac{1}{2} - \sin^2 \theta_W + \frac{5}{9} \sin^4 \theta_W, \quad (10.30a)$$

$$g_R^2 \equiv (g_{LR}^{\nu u})^2 + (g_{LR}^{\nu d})^2 \approx \frac{5}{9} \sin^4 \theta_W. \quad (10.30b)$$

In practice, Eq. (10.29b) must be corrected for quark mixing, quark sea effects, c quark threshold effects, non-isoscalarity, W - Z propagator differences, the finite muon mass, QED and EW radiative corrections. Details of the neutrino spectra, experimental cuts, x and Q^2 dependence of structure functions, and longitudinal structure functions, enter only at the level of these corrections and therefore lead to very small uncertainties. CCFR quotes $s_W^2 = 0.2236 \pm 0.0041$ for the reference values (m_t, M_H) = (175, 150) GeV with very little sensitivity to (m_t, M_H).

The NuTeV collaboration found $s_W^2 = 0.2277 \pm 0.0016$ (for the same reference values), which was 3.0σ higher than the SM prediction [143]. However, since then several groups have raised concerns about the interpretation of the NuTeV result, which could affect the extracted $g_{L,R}^2$ (and thus s_W^2) including their uncertainties and correlation. These include the assumption of symmetric strange and anti-strange sea quark distributions, the electron neutrino contamination from K_{e3} decays, isospin symmetry violation in the parton distribution functions and from QED splitting effects, nuclear shadowing effects, and a more complete treatment

¹⁰In the simple parton model, ignoring hadron energy cuts, $r \approx (1 + 3\epsilon)/(3 + \epsilon)$, where $\epsilon \sim 0.125$ is the ratio of the fraction of the nucleon's momentum carried by anti-quarks to that carried by quarks.

of EW and QCD radiative corrections. A more detailed discussion and a list of references can be found in the 2016 edition of this *Review*. The precise impact of these effects would need to be evaluated carefully by the collaboration, but in the absence of such an effort we do not include the ν DIS constraints in our default set of fits.

Recently, the COHERENT collaboration was the first to observe the coherent elastic neutrino nucleus scattering (CE ν NS) process [144] on a target consisting mostly of ^{133}Cs and ^{127}I , and at the opposite end of the kinematic scale where the momentum transfer is significantly smaller than the inverse of the nuclear radius. Subsequently, COHERENT [145] observed CE ν NS using a liquid ^{40}Ar detector, as well. The coherence enhances the process roughly proportional to the square of the number of neutrons in the nuclei, but the process is difficult to observe as the experimental signature is a mere keV scale nuclear recoil.

10.3.2 Parity violating lepton scattering

Reviews on weak polarized electron scattering may be found in Refs. [9, 146]. The SLAC polarized electron-deuteron DIS (eDIS) experiment [147] measured the parity violating right-left asymmetry,

$$A_{RL} \equiv \frac{\sigma_R - \sigma_L}{\sigma_R + \sigma_L}, \quad (10.31)$$

where $\sigma_{R,L}$ is the cross-section for the deep-inelastic scattering of a right- or left-handed electron, $e_{R,L}N \rightarrow eX$. In the quark parton model,

$$\frac{A_{RL}}{Q^2} = a_1 + a_2 \frac{1 - (1-y)^2}{1 + (1-y)^2}, \quad (10.32)$$

where $Q^2 > 0$ is the momentum transfer and y is the fractional energy transfer from the electron to the hadrons. For the deuteron or other isoscalar targets, one has, neglecting the s quark and anti-quarks,

$$a_1 = \frac{3G_F}{5\sqrt{2}\pi\alpha} \left(g_{AV}^{eu} - \frac{1}{2}g_{AV}^{ed} \right) \approx \frac{3G_F}{5\sqrt{2}\pi\alpha} \left(-\frac{3}{4} + \frac{5}{3}\hat{s}_0^2 \right), \quad (10.33a)$$

$$a_2 = \frac{3G_F}{5\sqrt{2}\pi\alpha} \left(g_{VA}^{eu} - \frac{1}{2}g_{VA}^{ed} \right) \approx \frac{9G_F}{5\sqrt{2}\pi\alpha} \left(\hat{s}_0^2 - \frac{1}{4} \right). \quad (10.33b)$$

The Jefferson Lab Hall A collaboration [148, 149] improved on the SLAC result by measuring A_{RL} at $Q^2 = 1.085 \text{ GeV}^2$ and 1.901 GeV^2 , and determined the weak mixing angle to 2% precision, $\hat{s}^2(161 \text{ MeV}) = 0.2403 \pm 0.0043$. In another polarized electron scattering experiment on deuterons, but in the quasi-elastic kinematic regime, the SAMPLE experiment [150, 151] at MIT-Bates extracted the combination $g_{VA}^{eu} - g_{VA}^{ed}$ at Q^2 values of 0.038 GeV^2 and 0.091 GeV^2 . What was actually determined were nucleon form factors from which the quoted results were obtained by the removal of a multi-quark radiative correction [152]. Other linear combinations of the effective couplings have been determined in polarized lepton scattering at CERN in μ - ^{12}C DIS [153] (the observable was the double charge-helicity cross-section asymmetry), at Mainz in e - ^9Be (quasi-elastic) [154], and at Bates in e - ^{12}C (elastic) [155]. More recent polarized electron scattering experiments, *i.e.*, SAMPLE, the PVA4 experiment at Mainz, and the HAPPEX and G \mathcal{O} experiments at Jefferson Lab, have focussed on the strange quark content of the nucleon [156].

A_{RL} can also be measured in fixed target polarized Møller scattering, $e^-e^- \rightarrow e^-e^-$, and reads [157],

$$\frac{A_{RL}}{Q^2} = -2g_{AV}^{ee} \frac{G_F}{\sqrt{2}\pi\alpha} \frac{1-y}{1+y^4 + (1-y)^4}. \quad (10.34)$$

It has been determined at low $Q^2 = 0.026 \text{ GeV}^2$ in the SLAC E158 experiment [158], with the result, $A_{RL} = (-1.31 \pm 0.14_{\text{stat.}} \pm 0.10_{\text{syst.}}) \times 10^{-7}$. Expressed in terms of the weak mixing angle in the $\overline{\text{MS}}$ scheme this yields $\hat{s}^2(161 \text{ MeV}) = 0.2403 \pm 0.0013$, and as shown in Fig. 10.2 established the scale dependence of the weak mixing angle at the level of 6.4σ . One also extracts the model-independent effective coupling, $g_{AV}^{ee} = 0.0190 \pm 0.0027$ [13].

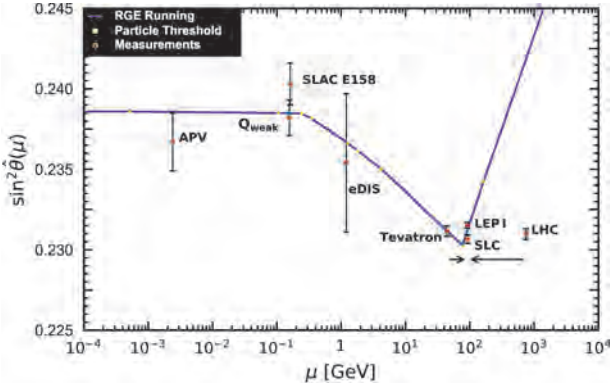


Figure 10.2: Scale dependence of the weak mixing angle defined in the $\overline{\text{MS}}$ scheme [39, 83] (for the scale dependence in a mass-dependent renormalization scheme, see Ref. [82]). The minimum of the curve corresponds to $\mu = M_W$, below which we switch to an effective theory with the W^\pm bosons integrated out, and where the β -function for $\widehat{s}^2(\mu)$ changes sign. At M_W and each fermion mass there are also discontinuities arising from scheme dependent matching terms, which are necessary to ensure that the various effective field theories within a given loop order describe the same physics. However, in the $\overline{\text{MS}}$ scheme these are very small numerically and barely visible in the figure provided one decouples quarks at $\mu = \widehat{m}_q(\widehat{m}_q)$. The width of the curve exceeds the theory uncertainty from strong interaction effects which at low energies is at the level of $\pm 2 \times 10^{-5}$ [39]. The Tevatron and LHC measurements are strongly dominated by invariant masses of the final-state di-lepton pair of $\mathcal{O}(M_Z)$ and can thus be considered as additional Z pole data points. For clarity we displayed the Tevatron and LHC points horizontally to the left and right, respectively.

One-loop radiative corrections and implications are discussed in Ref. [82].

In a similar experiment and at about the same $Q^2 = 0.0248 \text{ GeV}^2$, the Q_{weak} collaboration at Jefferson Lab obtained $A_{RL} = (-2.265 \pm 0.073_{\text{stat.}} \pm 0.058_{\text{sys.}}) \times 10^{-7}$ [159, 160] in elastic $e^-p \rightarrow e^-p$ scattering. To extract the physical quantity of interest, the weak charge of the proton [161], a large ($\approx 30\%$) correction had to be applied to A_{RL} arising from electromagnetic, strange, and axial form factors. This was achieved by performing a global fit [162] including a large number of A_{RL} data points at larger Q^2 , dominated by the HAPPEX result at $Q^2 = 0.109 \text{ GeV}^2$ [163]. Finally, the constraint, $2g_{AV}^{eu} + g_{AV}^{ed} = 0.0356 \pm 0.0023$, which translates into a weak mixing angle measurement of $\widehat{s}^2(157 \text{ MeV}) = 0.2382 \pm 0.0011$, could be deduced, after correcting for a relatively large and uncertain contribution from the γZ box diagram [164–167].

10.3.3 Atomic parity violation

There are precise measurements of atomic parity violation (APV) [9, 168, 169] in ^{133}Cs [170, 171] (at the 0.4% level [170]), ^{205}Tl [172, 173], ^{208}Pb [174], and ^{209}Bi [175]. The EW physics is contained in the nuclear weak charges $Q_W(Z, N)$, where Z and N are the numbers of protons and neutrons in the nucleus. In terms of the nucleon vector couplings,

$$g_{AV}^{ep} \equiv 2g_{AV}^{eu} + g_{AV}^{ed} \approx -\frac{1}{2} + 2\widehat{s}_0^2, \quad (10.35a)$$

$$g_{AV}^{en} \equiv g_{AV}^{eu} + 2g_{AV}^{ed} \approx +\frac{1}{2}, \quad (10.35b)$$

one has,

$$Q_W(Z, N) \equiv -2 \left[Z(g_{AV}^{ep} + 0.00005) + N(g_{AV}^{en} + 0.00006) \right] \left(1 - \frac{\alpha}{2\pi} \right), \quad (10.36)$$

where the numerically small adjustments are discussed in Ref. [13] and include the result of the γZ -box correction from Ref. [176].

E.g., $Q_W(^{133}\text{Cs})$ is extracted by measuring experimentally the ratio of the parity violating amplitude, E_{PNC} , to the Stark vector transition polarizability, β , and by calculating theoretically E_{PNC} in terms of Q_W . One can then write,

$$Q_W(^{133}\text{Cs}) = N \left(\frac{\text{Im } E_{\text{PNC}}}{\beta} \right)_{\text{exp.}} \left(\frac{|e| a_B}{\text{Im } E_{\text{PNC}}} \frac{Q_W}{N} \right)_{\text{th.}} \times \left(\frac{\beta}{a_B^3} \right)_{\text{exp.+th.}} \left(\frac{a_B^2}{|e|} \right), \quad (10.37)$$

where a_B is the Bohr radius. There are currently two semi-empirical approaches to β of similar precision. The ratio of the off-diagonal hyperfine amplitude to the vector polarizability was measured directly by the Boulder group [177]. Combined with the hyperfine amplitude, computed precisely in Ref. [178], one finds $\beta = (26.957 \pm 0.044_{\text{exp.}} \pm 0.027_{\text{th.}}) a_B^3$. Alternatively, one can combine [179] the measurement of the ratio of scalar to vector transition polarizabilities [180] with the recent calculation of the scalar polarizability [181] to obtain $\beta = (27.139 \pm 0.030_{\text{exp.}} \pm 0.030_{\text{th.}}) a_B^3$, in agreement with earlier results [182, 183] based on this approach. The two determinations average to $\beta = (27.064 \pm 0.025_{\text{exp.}} \pm 0.021_{\text{th.}}) a_B^3$, while they differ by 2.7σ .

The uncertainties associated with the atomic wave function calculations are relatively small for cesium [9, 184–186]. State-of-the-art many-body atomic structure computations of the parity non-conserving amplitude, $\text{Im } E_{\text{PNC}} = (0.8977 \pm 0.0040) \times 10^{-11} |e| a_B Q_W / N$ [187–192], together with the measurements [170, 171] which can be combined to give $\text{Im } E_{\text{PNC}} / \beta = -1.5924 \pm 0.0055 \text{ mV/cm}$, imply,

$$Q_W(^{133}\text{Cs}) = -72.82 \pm 0.26_{\text{exp.}} \pm 0.33_{\text{th.}}, \quad (10.38)$$

or equivalently the constraint, $55g_{AV}^{ep} + 78g_{AV}^{en} = 36.46 \pm 0.21$. Within the SM this can also be translated into a determination of the weak mixing angle, $\widehat{s}^2(2.4 \text{ MeV}) = 0.2367 \pm 0.0018$, where the scale setting follows the estimate in Ref. [193] for the typical momentum transfer for parity violation experiments in Cs (the corresponding estimate for Tl amounts to 8 MeV). By comparing different hyperfine transitions, the Boulder experiment in cesium also observed the parity violating weak corrections to the nuclear electromagnetic vertex, called the nuclear anapole moment [194–196].

The theoretical atomic structure uncertainties are 3% for thallium [197] and even larger for the other atoms. However, they mostly cancel if one takes ratios of parity violation in different isotopes [198]. The first result of this type of experiment was announced very recently by the Mainz group [199], who studied APV in ^{100}Yb , ^{102}Yb , ^{104}Yb , and ^{106}Yb , at the 0.5% level. The resulting three ratios can be interpreted as a measurement of $\widehat{s}_0^2 = 0.258 \pm 0.052$, and represent a very complementary approach to search for BSM physics [200]. If the precision increases in the future, one would ultimately face uncertainties from differences in the neutron charge radii [201, 202]. These can be constrained experimentally [203], *e.g.*, by measuring A_{RL} in heavier nuclei as done by the CollaborationsPREX collaboration at Jefferson Lab on ^{208}Pb [204, 205].

10.4 Precision flavor physics

In addition to cross-sections, asymmetries, parity violation, W , Z , Higgs and other collider physics, there is a large number of experiments and observables testing the flavor structure of the SM. These are addressed elsewhere in this *Review*, and are generally not included in this Section. However, we identify three precision observables with sensitivity to similar types of new physics as the other processes discussed here. The branching fraction of the flavor changing transition $b \rightarrow s\gamma$ is of comparatively low precision, but since it is a loop-level process (in the SM) its sensitivity to new physics (and SM parameters, such as heavy quark masses) is enhanced. A discussion can be found in the 2010 edition of this *Review*.

The τ lepton lifetime and leptonic branching ratios are primarily sensitive to α_s and not affected significantly by many types

of new physics. However, having an independent and reliable low energy measurement of α_s in a global analysis allows the comparison with the Z lineshape determination of α_s which shifts easily in the presence of new physics contributions. By far the most precise observable discussed here is the anomalous magnetic moment of the muon. Its combined experimental and theoretical uncertainty is smaller than typical electroweak scale contributions. The electron magnetic moment is measured to even greater precision, and as discussed in Sec. 10.2.2 can be used to determine α . Its new physics sensitivity, however, is suppressed by an additional factor of m_e^2/m_μ^2 , unless there is a new light degree of freedom such as a dark Z [206] boson.

10.4.1 The τ lifetime

The extraction of α_s from the τ lifetime τ_τ [207,208] is standing out from other determinations because of a variety of independent reasons:

- (i) The τ -scale is low, so that upon extrapolation to the Z scale (where it can be compared to the theoretically clean Z lineshape determinations) the α_s error shrinks by about an order of magnitude.
- (ii) Yet, this scale is high enough that perturbation theory and the operator product expansion (OPE) can be applied.
- (iii) These observables are fully inclusive and thus free of fragmentation and hadronization effects that would have to be modeled or measured.
- (iv) Duality violation (DV) effects are most problematic near the branch cut but there they are suppressed by a double zero at $s = m_\tau^2$.
- (v) There are data [43, 45, 209] to constrain non-perturbative effects both within and breaking the OPE.
- (vi) A complete four-loop order QCD calculation is available [210–214] in the massless limit.
- (vii) Large effects associated with the QCD β -function can be re-summed [215] in what has become known as contour improved perturbation theory (CIPT).

However, while CIPT certainly shows faster convergence in the lower (calculable) orders, doubts have been cast on the method by the observation that at least in a specific model [216], which includes the exactly known coefficients and theoretical constraints on the large-order behavior, ordinary fixed order perturbation theory (FOPT) may nevertheless give a better approximation to the full result. We therefore use the expressions [57, 214, 217],

$$\tau_\tau = \hbar \frac{1 - \mathcal{B}_\tau^s}{\Gamma_\tau^e + \Gamma_\tau^\mu + \Gamma_\tau^{ud}} = 290.75 \pm 0.36 \text{ fs}, \quad (10.39)$$

and

$$\Gamma_\tau^{ud} = \frac{G_F^2 m_\tau^5 |V_{ud}|^2}{64\pi^3} S(m_\tau, M_Z) \left(1 + \frac{3}{5} \frac{m_\tau^2 - m_\mu^2}{M_W^2} \right) \times \left[1 + \frac{\alpha_s(m_\tau)}{\pi} + 5.202 \frac{\alpha_s^2}{\pi^2} + 26.37 \frac{\alpha_s^3}{\pi^3} + 127.1 \frac{\alpha_s^4}{\pi^4} + \frac{\hat{\alpha}}{\pi} \left(\frac{85}{24} - \frac{\pi^2}{2} \right) + \delta_{\text{NP}} \right], \quad (10.40)$$

where Γ_τ^e and Γ_τ^μ can be taken from Eq. (10.10) with obvious replacements. The relative fraction of strangeness changing ($\Delta S = -1$) decays, $\mathcal{B}_\tau^s = 0.0292 \pm 0.0004$, is based on experimental data since the value for the strange quark mass, $\hat{m}_s(m_\tau)$, is not well known and the QCD expansion proportional to \hat{m}_s^2 converges poorly and cannot be trusted. $S(m_\tau, M_Z) = 1.01907 \pm 0.0003$ is a logarithmically enhanced EW correction factor [218] with higher orders re-summed [219].

δ_{NP} collects non-perturbative and quark-mass suppressed contributions, including the dimension four, six and eight terms in the OPE, as well as DV effects. We use the average $\delta_{\text{NP}} = 0.0141 \pm 0.0072$ derived from the τ decay spectral functions provided by OPAL [43] and ALEPH [45, 209], which give $\delta_{\text{NP}} = 0.000 \pm 0.012$

and $\delta_{\text{NP}} = 0.022 \pm 0.009$, respectively. These numbers are based on the original analyses in Refs. [220, 221], but are modified to correspond to a strict FOPT analysis as is appropriate for our purpose¹¹ (for alternative analyses, see the Section on “Quantum Chromodynamics” in this Review).

The dominant uncertainty arises from the truncation of the FOPT series and is conservatively taken as the α_s^4 term (this is re-calculated in each call of the fits, leading to an α_s -dependent and thus asymmetric error) until a better understanding of the numerical differences between FOPT and CIPT has been gained. Our perturbative error covers almost the entire range from using CIPT to assuming that the nearly geometric series in Eq. (10.40) continues to higher orders. The experimental uncertainty in Eq. (10.39) is from the combination of the two leptonic branching ratios with the direct τ_τ . Included are also various smaller uncertainties (± 0.15 fs) from other sources. Based on the method of Refs. [57, 222], we obtain in total

$$\alpha_s^{(4)}(m_\tau) = 0.312_{-0.013}^{+0.016}, \quad \alpha_s^{(5)}(M_Z) = 0.1171_{-0.0017}^{+0.0018}, \quad (10.41)$$

which represents a 1.5% determination of $\alpha_s(M_Z)$. For more details, see Refs. [220, 221] where the τ spectral functions themselves and an estimate of the unknown α_s^5 term were used as additional inputs.

10.4.2 The muon anomalous magnetic moment

The world average of the muon anomalous magnetic moment¹²,

$$a_\mu^{\text{exp}} = \frac{g_\mu - 2}{2} = (1165920.61 \pm 0.41) \times 10^{-9}, \quad (10.42)$$

is the combination of the final result of the BNL E821 collaboration [223] and the first result of the Muon $g - 2$ collaboration at Fermilab [224]. The QED contribution has been calculated to five loops [225–227] (fully analytic to three loops [228–232] and semi-analytic to four loops [233]). The estimated SM EW contribution [234–239], $a_\mu^{\text{EW}} = (1.54 \pm 0.01) \times 10^{-9}$, includes two-loop [240–244] and leading three-loop [245, 246] corrections and is at the level of two and a half times the current uncertainty.

The limiting factor in the interpretation of the result are the uncertainties from hadronic effects. The most recent evaluations of the leading-order (two-loop) hadronic vacuum polarization contribution obtained $a_\mu^{\text{had,VP}}(\alpha^2) = (68.81 \pm 0.41) \times 10^{-9}$ [247], $a_\mu^{\text{had,VP}}(\alpha^2) = (69.40 \pm 0.40) \times 10^{-9}$ [31], and $a_\mu^{\text{had,VP}}(\alpha^2) = (69.28 \pm 0.24) \times 10^{-9}$ [41]. These are mainly based on data from $e^+e^- \rightarrow$ hadrons (see, e.g., Ref. [31] for references). Our analysis combines the e^+e^- [31] and τ -decay data [32, 33] for contributions up to $\sqrt{s} = 2$ GeV, $a_\mu^{\text{had,VP}}(\alpha^2, 2 \text{ GeV}) = (64.49 \pm 0.33) \times 10^{-9}$, with analytical PQCD expressions for energies beyond 2 GeV and for the c and b quark contributions [232, 248]. By now there are also precise results for the determination of $a_\mu^{\text{had,VP}}(\alpha^2)$ from lattice QCD calculations, which were averaged in Ref. [249] with the result $a_\mu^{\text{had,VP}}(\alpha^2) = (71.16 \pm 1.84) \times 10^{-9}$. The most recent lattice calculation has a 0.8% quoted uncertainty [250], $a_\mu^{\text{had,VP}}(\alpha^2) = (70.75 \pm 0.55) \times 10^{-9}$, showing a roughly 2 σ conflict with the data-driven evaluations. If confirmed, a more detailed understanding of the numerical differences between data-driven and lattice approaches will be needed.

The other hadronic uncertainty is induced by the three-loop light-by-light scattering amplitude, where a number of independent model calculations yield results which are in reasonable agreement with each other, $a_\mu^{\text{had,\gamma}\times\gamma}(\alpha^3) = (1.36 \pm 0.25) \times 10^{-9}$ [251], $a_\mu^{\text{had,\gamma}\times\gamma}(\alpha^3) = 1.37_{-0.27}^{+0.15} \times 10^{-9}$ [252],

¹¹We are indebted to Diogo Boito, Maarten Golterman, Kim Maltman and Santiago Peris for privately communicating these results to us.

¹²In what follows, we summarize the most important aspects of a_μ and give some details on the evaluation in our fits. For more details and references, see the Section on the “Muon Anomalous Magnetic Moment” in this Review. There are some numerical differences, which are well understood and arise because internal consistency of the fits requires the calculation of all observables from analytical expressions and common inputs and fit parameters, so that an independent evaluation is necessary for this Section. Note, that in the spirit of a global analysis based on all available information we have chosen here to also include τ decay data [32], corrected for isospin breaking effects [33].

$a_\mu^{\text{had},\gamma\times\gamma}(\alpha^3) = (1.05 \pm 0.26) \times 10^{-9}$ [253], and $a_\mu^{\text{had},\gamma\times\gamma}(\alpha^3) = (1.03 \pm 0.29) \times 10^{-9}$ [247], but the sign of this effect is opposite [254] to the one quoted in the 2002 edition of this *Review*. There is also an upper bound given by $a_\mu^{\text{had},\gamma\times\gamma}(\alpha^3) < 1.59 \times 10^{-9}$ [252] but this requires an *ad hoc* assumption, too. Efforts to improve the evaluation by using experimental input where available yield the slightly lower values, $a_\mu^{\text{had},\gamma\times\gamma}(\alpha^3) = (0.87 \pm 0.13) \times 10^{-9}$ [255] and $a_\mu^{\text{had},\gamma\times\gamma}(\alpha^3) = (0.92 \pm 0.19) \times 10^{-9}$ [249]. The first two complete results from lattice simulations, both accounting for all systematic errors, $a_\mu^{\text{had},\gamma\times\gamma}(\alpha^3) = (0.79 \pm 0.35) \times 10^{-9}$ [256] and $a_\mu^{\text{had},\gamma\times\gamma}(\alpha^3) = (1.07 \pm 0.15) \times 10^{-9}$ [257], are consistent with the model and data-driven calculations. For our fits we take the result from Ref. [249], shifted by 1×10^{-11} to correspond to the charm quark treatment of Ref. [252] and with an increased error to also account for the precise constraint in Ref. [257], giving $a_\mu^{\text{had},\gamma\times\gamma}(\alpha^3) = (0.93 \pm 0.29) \times 10^{-9}$.

Sub-leading hadronic vacuum polarization effects at three-loop [258] and four-loop order [259] contribute $a_\mu^{\text{had,VP}}(\alpha^3) = (-0.983 \pm 0.004) \times 10^{-9}$ [41] and $a_\mu^{\text{had,VP}}(\alpha^4) = (0.124 \pm 0.001) \times 10^{-9}$ [259], respectively. The correlations with the two-loop hadronic contribution and with $\Delta\alpha(M_Z)$ (see Sec. 10.2) were considered in Ref. [232]. The contributions with a hadronic light-by-light scattering subgraph have been estimated in Ref. [260] with the result, $a_\mu^{\text{had},\gamma\times\gamma}(\alpha^4) = (0.02 \pm 0.01) \times 10^{-9}$ [249].

Altogether, the SM prediction is

$$a_\mu^{\text{theory}} = (1165918.34 \pm 0.44) \times 10^{-9}, \quad (10.43)$$

where the error is from the hadronic uncertainties excluding parametric ones such as from α_s and the heavy quark masses. We evaluate the correlation of the total (experimental plus theoretical) uncertainty in a_μ with $\Delta\alpha(M_Z)$ to amount to roughly 30%. The overall 3.8σ discrepancy¹³,

$$a_\mu^{\text{exp}} - a_\mu^{\text{theory}} = (2.27 \pm 0.60) \times 10^{-9},$$

could be due to fluctuations (the experimental results are statistics dominated) or underestimates of the theoretical uncertainties. On the other hand, the deviation could also arise from physics beyond the SM, such as supersymmetric models with large $\tan\beta$ and moderately light superparticle masses [261], or a dark Z boson [206].

10.5 Physics of the massive electroweak bosons

If the CM energy \sqrt{s} is large compared to the fermion mass m_f , the unpolarized Born cross-section for $e^+e^- \rightarrow f\bar{f}$ [262] can be written as,

$$\frac{d\sigma}{d\cos\theta} = \frac{\pi\alpha^2(s)}{2s} [F_1(1 + \cos^2\theta) + 2F_2\cos\theta] + B, \quad (10.44a)$$

$$F_1 = Q_e^2 Q_f^2 - 2\chi Q_e Q_f \bar{g}_V^e \bar{g}_V^f \cos\delta_R + \chi^2 (\bar{g}_V^e)^2 + \bar{g}_A^e (\bar{g}_V^f)^2 + \bar{g}_A^e (\bar{g}_A^f)^2, \quad (10.44b)$$

$$F_2 = -2\chi Q_e Q_f \bar{g}_A^e \bar{g}_A^f \cos\delta_R + 4\chi^2 \bar{g}_V^e \bar{g}_A^e \bar{g}_V^f \bar{g}_A^f, \quad (10.44c)$$

where

$$\tan\delta_R = \frac{\bar{M}_Z \bar{\Gamma}_Z}{\bar{M}_Z^2 - s}, \quad \chi = \frac{G_F}{2\sqrt{2}\pi\alpha(s)} \frac{s\bar{M}_Z^2}{\left[(\bar{M}_Z^2 - s)^2 + \bar{M}_Z^2 \bar{\Gamma}_Z^2\right]^{1/2}}. \quad (10.45)$$

B accounts for box graphs involving virtual Z and W bosons, and the $\bar{g}_{V,A}^f$ are defined in Eq. (10.46) below. \bar{M}_Z and $\bar{\Gamma}_Z$ correspond to mass and width definitions based on a Breit-Wigner shape with an energy-independent width (see the Section on the “ Z Boson”

in this *Review*). The differential cross-section receives important corrections from QED effects in the initial and final state, and interference between the two [263]. For $q\bar{q}$ production, there are additional final-state QCD corrections, which are relatively large. Note also that the equations above are written in the CM frame of the incident e^+e^- system, which may be boosted due to the initial-state QED radiation.

Some of the leading virtual EW corrections are captured by the running QED coupling $\alpha(s)$ and the Fermi constant G_F . The remaining corrections to the $Zf\bar{f}$ interactions are absorbed by replacing the tree-level couplings in Eq. (10.8) with the s -dependent *effective couplings* [14],

$$\bar{g}_V^f = \sqrt{\rho_f} (t_{3L}^f - 2Q_f \kappa_f \sin^2\theta_W), \quad (10.46a)$$

$$\bar{g}_A^f = \sqrt{\rho_f} t_{3L}^f. \quad (10.46b)$$

In these equations, the effective couplings are to be taken at the scale \sqrt{s} , but for notational simplicity we do not show this explicitly. At tree-level, $\rho_f = \kappa_f = 1$, but inclusion of EW radiative corrections leads to $\rho_f \neq 1$ and $\kappa_f \neq 1$, which depend on the fermion f and on the renormalization scheme. In the on-shell scheme, the quadratic m_t dependence is given by,

$$\rho_f \sim 1 + \rho_t, \quad \kappa_f \sim 1 + \frac{\rho_t}{\tan^2\theta_W}, \quad (10.47)$$

while in $\overline{\text{MS}}$, $\hat{\rho}_f \sim \hat{\kappa}_f \sim 1$, for $f \neq b$, and

$$\hat{\rho}_b \sim 1 - \frac{4}{3}\rho_t, \quad \hat{\kappa}_b \sim 1 + \frac{2}{3}\rho_t. \quad (10.48)$$

In the $\overline{\text{MS}}$ scheme the normalization is changed according to $G_F M_Z^2 / 2\sqrt{2}\pi \rightarrow \hat{\alpha} / 4s_W^2 c_W^2$ in the second Eq. (10.45).

As reviewed in Sec. 10.2.5, for the high precision Z pole observables discussed below, many additional bosonic and fermionic loop effects, vertex corrections, and higher order contributions, *etc.*, must be included. For example, in the $\overline{\text{MS}}$ scheme one then has $\hat{\rho}_\ell = 0.9977$, $\hat{\kappa}_\ell = 1.0014$, $\hat{\rho}_b = 0.9866$, and $\hat{\kappa}_b = 1.0068$.

To connect to measured quantities, it is convenient to define an effective angle

$$\bar{s}_f^2 \equiv \sin^2\bar{\theta}_{Wf} \equiv \hat{\kappa}_f \hat{s}_Z^2 = \kappa_f s_W^2, \quad (10.49)$$

in terms of which \bar{g}_V^f and \bar{g}_A^f are given by $\sqrt{\rho_f}$ times their tree-level formulae. One finds that the $\hat{\kappa}_f$ ($f \neq b$) are almost independent of m_t and M_H , and thus one can write,

$$\bar{s}_\ell^2 = \hat{s}_Z^2 + 0.00032, \quad (10.50)$$

while the κ_f for the on-shell scheme are m_t dependent.

10.5.1 Electroweak physics off the Z pole

Experiments at PEP, PETRA and TRISTAN have measured the unpolarized forward-backward asymmetry, A_{FB} , and the total cross-section relative to pure QED, R , for $e^+e^- \rightarrow \ell^+\ell^-$, $\ell = \mu$ or τ at CM energies $\sqrt{s} < M_Z$. They are defined as

$$A_{FB} \equiv \frac{\sigma_F - \sigma_B}{\sigma_F + \sigma_B}, \quad R = \frac{\sigma}{\mathcal{R}_{\text{ini}} \otimes \sigma_{\text{QED}}}, \quad (10.51)$$

where σ_F (σ_B) is the cross-section for ℓ^- to travel forward (backward) with respect to the e^- direction, σ_{QED} is the tree-level cross-section from s-channel photon exchange, and $\mathcal{R}_{\text{ini}} \otimes$ denotes convolution with initial-state QED corrections. Neglecting box graph contributions, they are given by,

$$A_{FB} = \frac{3}{4} \frac{F_2}{F_1}, \quad R = F_1. \quad (10.52)$$

For the available data, it is sufficient to approximate the EW corrections through the leading running $\alpha(s)$ and quadratic m_t contributions [264], as described above. Reviews and formulae for $e^+e^- \rightarrow \text{hadrons}$ may be found in [9, 265, 266].

LEP 2 [267] ran at several energies above the Z pole up to ~ 209 GeV. Measurements were made of a number of observables,

¹³Alternatively, if we employ the light-by-light scattering amplitude from Ref. [257] with the charm contribution [252] added, we find $a_\mu^{\text{exp}} - a_\mu^{\text{theory}} = (2.10 \pm 0.55) \times 10^{-9}$, likewise corresponding to a 3.8σ discrepancy.

including the total production cross-sections of $f\bar{f}$ pairs for $f = \mu, \tau$, and q (hadrons), of four-fermion final states, of $\gamma\gamma$, ZZ , WW , $WW\gamma$, and WWZ , as well as of single resonant W and Z bosons. The differential cross-sections for all three lepton flavors, and the leptonic and hadronic W branching ratios were also extracted.

Among the most important LEP 2 results were the measurements [267] of the W boson mass,

$$M_W = 80.376 \pm 0.025_{\text{stat.}} \pm 0.022_{\text{syst.}} \text{ GeV (LEP 2)}, \quad (10.53)$$

which were dominated by kinematic reconstruction, but included the complementary albeit statistics limited and thus much less precise determination from a WW threshold cross section measurement. The kinematic method was also employed at the Tevatron [268] and by ATLAS [270] and LHCb [271] at the LHC. They quote,

$$M_W = 80.387 \pm 0.016 \text{ GeV (Tevatron)}, \quad (10.54a)$$

$$M_W = 80.3695 \pm 0.0068_{\text{stat.}} \pm 0.0106_{\text{syst.}} \pm 0.0136_{\text{th.}} \text{ GeV (ATLAS)}, \quad (10.54b)$$

$$M_W = 80.354 \pm 0.023_{\text{stat.}} \pm 0.010_{\text{syst.}} \pm 0.017_{\text{th.}} \pm 0.009_{\text{PDF}} \text{ GeV (LHCb)}. \quad (10.54c)$$

To arrive at our LHC average, $M_W = 80.366 \pm 0.017$ GeV, we assume the PDF error from LHCb of 9 MeV to be common between the two LHC determinations. Furthermore, we assume an error component of 7 MeV to be common between the Tevatron and the LHC. This is smaller than the 10 MeV (9 MeV) PDF uncertainty quoted by CDF (LHCb), because the larger CM energy at the LHC enhances the sensitivity to second generation quark PDFs, in addition to the greater sea quark PDF dependence of the Drell-Yan process in the pp environment. There may also be some correlation due to other production modeling uncertainties. This implies for the average,

$$M_W = 80.377 \pm 0.012 \text{ GeV (world average)}. \quad (10.55)$$

For details and references, see the Section on the “Mass and Width of the W Boson” in this *Review*.

Strong constraints on anomalous triple and quartic gauge couplings have been obtained at LEP 2, the Tevatron, and the LHC. These are described in detail in the three Sections on the “Extraction of Triple Gauge Couplings (TGCs)”, “Anomalous W/Z Quartic Couplings (QGCs)”, and “Anomalous $ZZ\gamma$, $Z\gamma\gamma$, and ZZV Couplings” in this *Review*.

After their discovery of the Higgs boson [273, 274], the LHC experiments are now performing high precision measurements of its mass. We average the results, $M_H = 124.97 \pm 0.16_{\text{stat.}} \pm 0.18_{\text{syst.}} \text{ GeV}$ from ATLAS [275], and $M_H = 125.38 \pm 0.11_{\text{stat.}} \pm 0.09_{\text{syst.}} \text{ GeV}$ from CMS [276], by conservatively treating the smaller systematic error as common among the two determinations, and arrive at,

$$M_H = 125.30 \pm 0.09_{\text{stat.}} \pm 0.09_{\text{syst.}} \text{ GeV (LHC)}. \quad (10.56)$$

For further references and many more details on Higgs boson properties, see the Section on the “Status of Higgs Boson Physics” in this *Review*. The principal non- Z pole observables discussed here and in Sections 10.2–10.4 are summarized in Table 10.4. Included there is also the first measurement of the Higgs boson width (by CMS [277], assuming equal on- and off-shell effective couplings) and the SM prediction (without electroweak corrections as in Ref. [278]).

10.5.2 Z pole physics

High precision measurements of various Z pole ($\sqrt{s} \approx M_Z$) observables [9, 286, 287] have been performed at LEP 1 and SLC [14, 284, 285, 288, 289], as summarized in Table 10.5. These include the Z mass and total width, Γ_Z , and partial widths $\Gamma_{f\bar{f}}$ for $Z \rightarrow f\bar{f}$, where $f = e, \mu, \tau$, light hadrons, b , and c . It is

convenient to use the variables M_Z, Γ_Z ,

$$\sigma_{\text{had}} \equiv \frac{12\pi\Gamma_{e^+e^-}\Gamma_{\text{had}}}{M_Z^2\Gamma_Z^2}, \quad R_\ell \equiv \frac{\Gamma_{\text{had}}}{\Gamma_{\ell^+\ell^-}}, \quad R_q \equiv \frac{\Gamma_{q\bar{q}}}{\Gamma_{\text{had}}}, \quad (10.57)$$

for $\ell = e, \mu$ or τ , and $q = b$ or c , where Γ_{had} is the partial decay width into hadrons. Most of these are weakly correlated experimentally. The three values for R_ℓ are consistent with lepton universality (although R_τ is somewhat low compared to R_e and R_μ), but we use the general analysis in which the three observables are treated as independent. Similar remarks apply to $A_{FB}^{0,\ell}$ defined through Eq. (10.58) with $P_e = 0$, where $A_{FB}^{0,\tau}$ is somewhat high. Initial-state radiation reduces the peak cross section by more than 25%, where $\mathcal{O}(\alpha^3)$ QED effects induce a large anti-correlation (-30%) between Γ_Z and σ_{had} . The anti-correlation between R_b and R_c amounts to -18% [14]. The R_ℓ are insensitive to m_t except for the $Z \rightarrow b\bar{b}$ vertex, final-state corrections, and the implicit dependence through $\sin^2\theta_W$. Thus, they are especially useful for constraining α_s .

Very important constraints follow from measurements of various Z pole asymmetries. These include the forward-backward asymmetry, A_{FB} , and the polarization or left-right asymmetry, A_{LR} , defined analogously to Eq. (10.31). The latter was measured precisely by the SLD collaboration at the SLC [284], and has the advantages of being very sensitive to \bar{s}_ℓ^2 and that systematic uncertainties largely cancel. After removing initial-state QED corrections and contributions from photon exchange, γ - Z interference, as well as the EW boxes in Eq. (10.44a), one can use the effective tree-level expressions,

$$A_{LR} = A_e P_e, \quad A_{FB} = \frac{3}{4} A_f \frac{A_e + P_e}{1 + P_e A_e}, \quad (10.58)$$

where,

$$A_f \equiv \frac{2\bar{g}_V^f \bar{g}_A^f}{\bar{g}_V^{f2} + \bar{g}_A^{f2}} = \frac{1 - 4|Q_f|\bar{s}_f^2}{1 - 4|Q_f|\bar{s}_f^2 + 8(|Q_f|\bar{s}_f^2)^2}. \quad (10.59)$$

P_e is the initial e^- polarization, so that the second equality in Eq. (10.60) is reproduced for $P_e = 1$, and the Z pole forward-backward asymmetries at LEP 1 ($P_e = 0$) are given by $A_{FB}^{(0,f)} = \frac{3}{4} A_e A_f$ for $f = e, \mu, \tau, b, c, s$ [14], and q , and where $A_{FB}^{(0,q)}$ refers to the hadronic charge asymmetry. Corrections for t -channel exchange and s/t -channel interference cause $A_{FB}^{(0,e)}$ to be strongly anti-correlated with R_e (-37%). Very recently, the m_b -dependence [290] of the $\mathcal{O}(\alpha_s^2)$ QCD correction [291], affecting the reference axis of the b quark asymmetry [292], increased the extracted¹⁴ $A_{FB}^{(0,b)}$ by about 0.2 σ . The correlation between $A_{FB}^{(0,b)}$ and $A_{FB}^{(0,c)}$ amounts to 15%.

In addition, SLD extracted the final-state couplings A_b, A_c [14], A_s [288], A_τ , and A_μ [285], from left-right forward-backward asymmetries, using

$$A_{LR}^{FB}(f) = \frac{\sigma_{LF}^f - \sigma_{LB}^f - \sigma_{RF}^f + \sigma_{RB}^f}{\sigma_{LF}^f + \sigma_{LB}^f + \sigma_{RF}^f + \sigma_{RB}^f} = \frac{3}{4} A_f, \quad (10.60)$$

where, for example, σ_{LF}^f is the cross-section for a left-handed incident electron to produce a fermion f traveling in the forward hemisphere. Similarly, A_τ and A_e were measured at LEP 1 [14] through the τ polarization, \mathcal{P}_τ , as a function of the scattering angle θ , which can be written as,

$$\mathcal{P}_\tau = -\frac{A_\tau(1 + \cos^2\theta) + 2A_e \cos\theta}{(1 + \cos^2\theta) + 2A_\tau A_e \cos\theta}. \quad (10.61)$$

The average polarization, $\langle\mathcal{P}_\tau\rangle$, obtained by integrating over $\cos\theta$ in the numerator and denominator of Eq. (10.61), yields

¹⁴We are grateful to Werner Bernreuther and Long Chen for the recalculation of their result employing the more appropriate $\overline{\text{MS}}$ mixing angle, \bar{s}_Z^2 , instead of the on-shell quantity, s_W^2 .

Table 10.4: Non- Z pole observables, compared with the SM best fit predictions. The first M_W and Γ_W values are from the Tevatron [268, 269], the second ones from LEP 2 [267], while the third M_W is from the LHC [270, 271]. The hadronic branching ratio for W decays combines LEP 2 [267] and CMS [272] and assumes lepton flavor universality. The world averages for $g_{V,A}^{\nu e}$ are dominated by the CHARM II [131] results, $g_V^{\nu e} = -0.035 \pm 0.017$ and $g_A^{\nu e} = -0.503 \pm 0.017$. The τ_τ value is the τ lifetime world average computed by combining the direct measurements with values derived from the leptonic branching ratios [57]; in this case, the theory error is included in the SM prediction. In all other SM predictions, the uncertainty is parametric from M_Z , M_H , m_t , m_b , m_c , $\hat{\alpha}(M_Z)$, and α_s , and theoretical from unknown higher orders [78], where correlations due to both types have been accounted for. The column denoted by Pull gives the standard deviations.

Quantity	Value	Standard Model	Pull
m_t [GeV]	172.83 ± 0.59	173.13 ± 0.56	-0.5
M_H [GeV]	125.30 ± 0.13	125.30 ± 0.13	0.0
Γ_H [MeV]	$3.2^{+2.4}_{-1.7}$	4.12 ± 0.05	-0.4
M_W [GeV]	80.387 ± 0.016	80.360 ± 0.006	1.7
	80.376 ± 0.033		0.5
	80.366 ± 0.017		0.4
Γ_W [GeV]	2.046 ± 0.049	2.089 ± 0.001	-0.9
	2.195 ± 0.083		1.3
$\mathcal{B}(W \rightarrow \text{hadrons})$	0.6736 ± 0.0018	0.6751 ± 0.0001	-0.8
$g_V^{\nu e}$	-0.040 ± 0.015	-0.0397 ± 0.0001	0.0
$g_A^{\nu e}$	-0.507 ± 0.014	-0.5064	0.0
$Q_W(e)$	-0.0403 ± 0.0053	-0.0473 ± 0.0002	1.3
$Q_W(p)$	0.0719 ± 0.0045	0.0709 ± 0.0002	0.2
$Q_W(\text{Cs})$	-72.82 ± 0.42	-73.24 ± 0.01	1.0
$Q_W(\text{Tl})$	-116.4 ± 3.6	-116.90 ± 0.02	0.1
$\hat{s}_Z^2(\text{eDIS})$	0.2299 ± 0.0043	0.23122 ± 0.00004	-0.3
τ_τ [fs]	290.75 ± 0.36	288.90 ± 2.24	0.8
$\frac{1}{2}(g_\mu - 2 - \frac{\alpha}{\pi})$	$(4510.88 \pm 0.60) \times 10^{-9}$	$(4508.61 \pm 0.03) \times 10^{-9}$	3.8

$\langle \mathcal{P}_\tau \rangle = -A_\tau$, and A_e can be extracted from the \mathcal{P}_τ angular distribution. The initial-state coupling, A_e , was also determined through the left-right charge asymmetry [289] and in polarized Bhabha scattering [285] at the SLC. Because \bar{g}_V^ℓ is very small, not only $A_{LR}^0 = A_e$, $A_{FB}^{(0,\ell)}$, and \mathcal{P}_τ , but also $A_{FB}^{(0,q)}$ for $q = b, c$, and s , as well as the hadronic asymmetries are mainly sensitive to \bar{s}_ℓ^2 .

As an example of the precision of the Z pole observables, the values of \bar{g}_A^f and \bar{g}_V^f for $f = e, \mu, \tau$, and ℓ , extracted from the LEP and SLC lineshape and asymmetry data, are shown in Fig. 10.3. It may be compared with Fig. 10.1 as the two sets of parameters coincide at the SM at tree-level.

As for hadron colliders, the forward-backward asymmetry, A_{FB} , for e^+e^- and $\mu^+\mu^-$ final states (with invariant masses restricted to or dominated by values around M_Z) in $p\bar{p}$ collisions has been measured by the CDF [293] and DØ [294] collaborations, and the values $\bar{s}_\ell^2 = 0.23221 \pm 0.00046$ and $\bar{s}_\ell^2 = 0.23095 \pm 0.00040$ were extracted, respectively. The combination of these measurements (which differ by more than 2σ) yields [279],

$$\bar{s}_\ell^2 = 0.23148 \pm 0.00033 \text{ (Tevatron)}. \quad (10.62)$$

By varying the invariant mass and the scattering angle (and assuming the electron couplings), information on the effective Z couplings to light quarks, $\bar{g}_{V,A}^{u,d}$, could also be obtained [295, 296], but with large uncertainties, mutual correlations, and not independently of \bar{s}_ℓ^2 above. Similar analyses have also been reported by the H1 [297] and ZEUS [298] collaborations at HERA and by the LEP collaborations [14]. This kind of measurement is harder in the $p\bar{p}$ environment due to the difficulty to assign the initial quark and antiquark in the underlying Drell-Yan process to the protons, thus requiring excellent control of uncertainties from parton distribution functions. ATLAS obtained $\bar{s}_\ell^2 = 0.2308 \pm 0.0012$ using 7 TeV data [280] and $\bar{s}_\ell^2 = 0.23140 \pm 0.00036$ at 8 TeV [281], while CMS measured $\bar{s}_\ell^2 = 0.23101 \pm 0.00053$ (8 TeV) [282] and LHCb reported $\bar{s}_\ell^2 = 0.23142 \pm 0.00106$ (from both 7 and 8 TeV data, but only analyzing $\mu^+\mu^-$ final state) [283]. Assuming that the smallest theoretical and PDF uncertainty (± 0.00024 from AT-

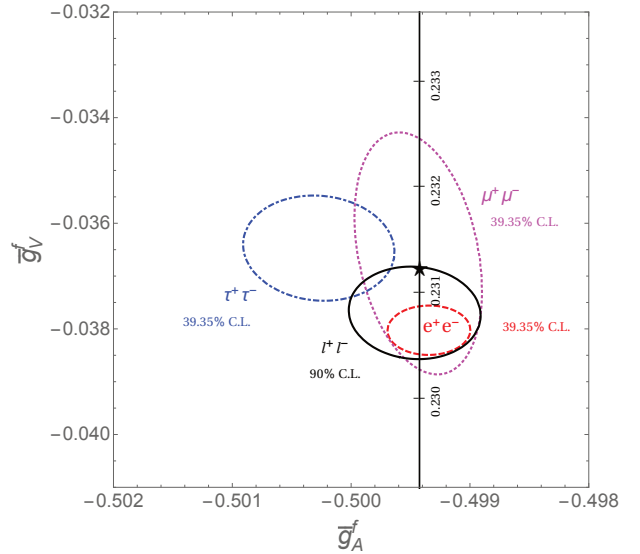


Figure 10.3: 1σ (39.35% CL) contours of the effective couplings \bar{g}_A^f and \bar{g}_V^f for $f = e, \mu$ and τ from LEP and SLC, compared to the SM expectation as a function of \hat{s}_Z^2 . (The SM best fit value $\hat{s}_Z^2 = 0.23122$ is also indicated.) Also shown is the 90% CL allowed region in $\bar{g}_{A,V}^\ell$ obtained assuming lepton universality.

LAS [281]) is fully correlated among the four determinations, they combine to

$$\bar{s}_\ell^2 = 0.23129 \pm 0.00033 \text{ (LHC)}. \quad (10.63)$$

10.5.3 W and Z decays

The partial decay widths for gauge bosons to decay into massless fermions $f_1\bar{f}_2$ (the numerical values include the small EW

Table 10.5: Principal Z pole observables and their SM predictions (*cf.* Table 10.4). The first \bar{s}_ℓ^2 is the effective weak mixing angle extracted from the hadronic charge asymmetry at LEP 1 [14], the second is the combined value from the Tevatron [279], and the third is from the LHC [280–283]. The values of A_e are (i) from A_{LR} for hadronic final states [284]; (ii) from A_{LR} for leptonic final states and from polarized Bhabba scattering [285]; and (iii) from the angular distribution of the τ polarization at LEP 1 [14]. The A_τ values are from SLD [285] and the total τ polarization, respectively. Note that the SM errors in Γ_Z , the R_ℓ , and σ_{had} are largely dominated by the uncertainty in α_s .

Quantity	Value	Standard Model	Pull
M_Z [GeV]	91.1876 ± 0.0021	91.1882 ± 0.0020	−0.3
Γ_Z [GeV]	2.4955 ± 0.0023	2.4941 ± 0.0009	0.6
σ_{had} [nb]	41.481 ± 0.033	41.482 ± 0.008	0.0
R_e	20.804 ± 0.050	20.736 ± 0.010	1.4
R_μ	20.784 ± 0.034	20.736 ± 0.010	1.4
R_τ	20.764 ± 0.045	20.781 ± 0.010	−0.4
R_b	0.21629 ± 0.00066	0.21582 ± 0.00002	0.7
R_c	0.1721 ± 0.0030	0.17221 ± 0.00003	0.0
$A_{FB}^{(0,e)}$	0.0145 ± 0.0025	0.01617 ± 0.00007	−0.7
$A_{FB}^{(0,\mu)}$	0.0169 ± 0.0013		0.6
$A_{FB}^{(0,\tau)}$	0.0188 ± 0.0017		1.5
$A_{FB}^{(0,b)}$	0.0996 ± 0.0016	0.1029 ± 0.0002	−2.0
$A_{FB}^{(0,c)}$	0.0707 ± 0.0035	0.0735 ± 0.0002	−0.8
$A_{FB}^{(0,s)}$	0.0976 ± 0.0114	0.1030 ± 0.0002	−0.4
\bar{s}_ℓ^2	0.2324 ± 0.0012	0.23155 ± 0.00004	0.7
	0.23148 ± 0.00033		−0.2
	0.23129 ± 0.00033		−0.8
A_e	0.15138 ± 0.00216	0.1468 ± 0.0003	2.1
	0.1544 ± 0.0060		1.3
	0.1498 ± 0.0049		0.6
A_μ	0.142 ± 0.015		−0.3
A_τ	0.136 ± 0.015		−0.7
	0.1439 ± 0.0043		−0.7
A_b	0.923 ± 0.020	0.9347	−0.6
A_c	0.670 ± 0.027	0.6677 ± 0.0001	0.1
A_s	0.895 ± 0.091	0.9356	−0.4

Table 10.6: Results derived from Table 10.5 and the corresponding covariance matrices [14, 299], and the SM predictions for the partial and total Z decay widths [in MeV]. In the (second) third column lepton universality is (not) assumed.

Quantity	Value	Value (universal)	Standard Model
$\Gamma_{e^+e^-}$	83.87 ± 0.12	83.942 ± 0.085	83.960 ± 0.009
$\Gamma_{\mu^+\mu^-}$	83.95 ± 0.18	83.941 ± 0.085	83.959 ± 0.009
$\Gamma_{\tau^+\tau^-}$	84.03 ± 0.21	83.759 ± 0.085	83.777 ± 0.009
Γ_{inv}	498.9 ± 2.5	500.5 ± 1.5	501.445 ± 0.047
$\Gamma_{u\bar{u}}$	—	—	299.89 ± 0.20
$\Gamma_{c\bar{c}}$	300.3 ± 5.3	300.0 ± 5.2	299.81 ± 0.20
$\Gamma_{d\bar{d}}, \Gamma_{s\bar{s}}$	—	—	382.77 ± 0.14
$\Gamma_{b\bar{b}}$	377.4 ± 1.3	377.0 ± 1.2	375.73 ± 0.18
Γ_{had}	1744.8 ± 2.6	1743.2 ± 1.9	1740.97 ± 0.85
Γ_Z	2495.5 ± 2.3	2495.5 ± 2.3	2494.11 ± 0.86

radiative corrections and final-state mass effects) are given by,

$$\Gamma(W^+ \rightarrow e^+ \nu_e) = \frac{M_W^3}{12\pi v^2} = 226.33 \pm 0.05 \text{ MeV} , \quad (10.64a)$$

$$\Gamma(W^+ \rightarrow u_i \bar{d}_j) = \frac{M_W^3}{12\pi v^2} |V_{ij}|^2 \mathcal{R}_V^q = (705.4 \pm 0.4 \text{ MeV}) |V_{ij}|^2 , \quad (10.64b)$$

$$\Gamma(Z \rightarrow f \bar{f}) = \frac{M_Z^3}{12\pi v^2} [\mathcal{R}_V^f \bar{g}_V^{f2} + \mathcal{R}_A^f \bar{g}_A^{f2}] , \quad (10.64c)$$

where the result for the latter are shown in Table 10.6. Final-state QED and QCD corrections [300] to the vector and axial-vector form factors are given by,

$$\mathcal{R}_{V,A}^f = N_C \left[1 + \frac{3}{4} \left(Q_f^2 \frac{\alpha(s)}{\pi} + \frac{N_C^2 - 1}{2N_C} \frac{\alpha_s(s)}{\pi} \right) + \dots \right] , \quad (10.65)$$

where $N_C = 3$ (1) is the color factor for quarks (leptons) and the dots indicate finite fermion mass effects proportional to m_f^2/s which are different for \mathcal{R}_V^f and \mathcal{R}_A^f , as well as higher-order QCD corrections [301], which are known to $\mathcal{O}(\alpha_s^4)$ [214]. These include

singlet contributions starting from two-loop order which are large, strongly top quark mass dependent, family universal, and flavor non-universal [302–306]. The $\mathcal{O}(\alpha^2)$ self-energy corrections from Ref. [307] are also taken into account.

For the W decay into quarks, Eq. (10.64b), only the universal massless part (non-singlet and $m_q = 0$) of the final-state QCD radiator function in \mathcal{R}_V from Eq. (10.65) is used, and the QED corrections are modified. Expressing the widths in terms of $G_F M_{W,Z}^3$ incorporates the largest radiative corrections from the running QED coupling. EW corrections to the Z widths are then taken into account through the effective couplings $\bar{g}_{V,A}^i$. Hence, in the on-shell scheme the Z widths are proportional to $\rho_i \sim 1 + \rho_t$. There is additional (negative) quadratic m_t dependence in the $Z \rightarrow b\bar{b}$ vertex corrections [308, 309] which causes $\Gamma_{b\bar{b}}$ to decrease with m_t . The dominant effect is to multiply $\Gamma_{b\bar{b}}$ by the vertex correction $1 + \delta\rho_{b\bar{b}}$, where $\delta\rho_{b\bar{b}} \sim 10^{-2}(-\frac{1}{2}m_t^2/M_Z^2 + \frac{1}{3})$. In practice, the corrections are included in $\hat{\rho}_b$ and $\hat{\kappa}_b$, as discussed in Sec. 10.5.

Starting at $\mathcal{O}(\alpha\alpha_s)$, the factorized form indicated in Eq. (10.64) is violated and corrections need to be included [310–312]. They add coherently, resulting in a sizable effect, and shift $\alpha_s(M_Z)$ when extracted from Z lineshape observables by about +0.0007. Similar non-factorizable corrections are also known for mixed QED-EW corrections [106, 107, 109, 313].

For three fermion families the total widths of the Z [314–318] and W [319, 320] bosons are predicted to be,

$$\Gamma_Z = 2.4941 \pm 0.0009 \text{ GeV}, \quad \Gamma_W = 2.0895 \pm 0.0008 \text{ GeV}. \quad (10.66)$$

The uncertainties in these predictions are almost entirely induced by the parametric error in $\alpha_s(M_Z) = 0.1185 \pm 0.0016$ from the global fit. These predictions can be compared with the experimental results, $\Gamma_Z = 2.4955 \pm 0.0023 \text{ GeV}$ [14, 299] and $\Gamma_W = 2.085 \pm 0.042 \text{ GeV}$ [267, 269] (see the Gauge & Higgs Bosons Particle Listings). The hadronic branching ratio of the W boson, $\mathcal{B}(W \rightarrow \text{hadrons})$ has been measured by both LEP 2 [267] and CMS [272]. The measurements of the total and partial widths are generally in good agreement with the SM. The exception is the branching ratio $W \rightarrow \tau + \nu_\tau$ from LEP 2, which is 2.6 σ larger than the electron-muon average [267]¹⁵.

The invisible decay width, $\Gamma_{\text{inv}} = \Gamma_Z - \Gamma_{e^+e^-} - \Gamma_{\mu^+\mu^-} - \Gamma_{\tau^+\tau^-} - \Gamma_{\text{had}}$, can be used to determine the number of neutrino flavors, N_ν , much lighter than $M_Z/2$. The hadronic peak cross section, and therefore the extracted Γ_{had} , depends strongly on the knowledge of the LEP 1 luminosity derived from small-angle Bhabha scattering. However, the prediction for the Bhabha cross-section was recently found to be overestimated, and consequently the luminosity underestimated [299]. The updated analysis involved an improved Z lineshape fit, significantly reducing σ_{had} , while slightly increasing Γ_Z , with the result, $N_\nu = 2.9963 \pm 0.0074$ [299]. In practice, we determine N_ν by allowing it as an additional fit parameter and obtain,

$$N_\nu = 3.0026 \pm 0.0061, \quad (10.67)$$

which is now in perfect agreement with the observed number of fermion generations and $N_\nu = 3$ (a 1.3 σ deviation was observed in the 2018 edition of this *Review* before including the correction in the luminosity determination).

10.6 Global fit results

In this section, we present the results of global fits, subject to the experimental data and theoretical constraints discussed in Section 10.2–10.5. For earlier analyses, see Refs. [14, 78, 322–325] and previous editions of this *Review*. The values for m_t , M_H [275, 276], Γ_H [277], M_W [267, 268, 270, 271], Γ_W [267, 269], the weak charges of the electron [158], the proton [159], cesium [170, 171] and thallium [172, 173], the weak mixing angle extracted from eDIS [148],

$\nu_\mu(\bar{\nu}_\mu)$ - e scattering [129–131], the τ lifetime, and the μ anomalous magnetic moment [224] are listed in Table 10.4. Likewise, Table 10.5 summarizes the principal Z pole observables, where the LEP 1 averages of the ALEPH, DELPHI, L3, and OPAL results include common systematic uncertainties and correlations [14, 299]. The heavy flavor results [14, 290] of LEP 1 and SLD are based on common inputs, and are thus correlated, as well.

Also shown in both tables are the SM predictions for the values of M_Z , $\alpha_s(M_Z)$, $\Delta\alpha_{\text{had}}^{(3)}$ and the heavy quark masses shown in Table 10.7. The predictions result from a global least-square (χ^2) fit to all data using the minimization package MINUIT [326] and the EW library GAPP [34]. In most cases, we treat all input errors (the uncertainties of the values) as Gaussian. The reason is not that we assume that theoretical and systematic errors are intrinsically bell-shaped (which they are not) but because in most cases the input errors are either dominated by the statistical components or they are combinations of many different (including statistical) error sources, which should yield approximately Gaussian *combined* errors by the large number theorem. An exception is the theory dominated error on the τ lifetime, which we recalculate in each χ^2 -function call since it depends itself on α_s . Sizes and shapes of the output errors (the uncertainties of the predictions and the SM fit parameters) are fully determined by the fit, and 1 σ errors are defined to correspond to $\Delta\chi^2 = \chi^2 - \chi_{\text{min}}^2 = 1$, and do not necessarily correspond to the 68.3% probability range or the 39.3% probability contour (for 2 parameters).

The agreement is generally very good. Despite the few discrepancies addressed in the following, the global electroweak fit describes the data well, with a very good $\chi^2/\text{d.o.f.} = 46.7/43$. The probability of a larger χ^2 is 32%, and only $g_\mu - 2$ is currently showing a larger (3.8 σ) conflict. In addition, A_{LR}^0 (SLD) from hadronic final states and $A_{FB}^{(0,b)}$ (LEP 1) deviate at the 2 σ level. g_L^2 from NuTeV is nominally in conflict with the SM, as well, but the precise status is unresolved (see Sec. 10.3.1). We also emphasize that there are a number of discrepancies among individual measurements of certain quantities, as discussed in previous sections, but that they are not reflected in the overall χ^2 of the fit as only the corresponding combinations are used as constraints.

A_b can be extracted from $A_{FB}^{(0,b)}$ when $A_e = 0.1501 \pm 0.0016$ is taken from a fit to leptonic asymmetries (using lepton universality). The result, $A_b = 0.885 \pm 0.017$, is 2.9 σ below the SM prediction¹⁶ and also 1.4 σ below $A_b = 0.923 \pm 0.020$ obtained from $A_{LR}^{FB}(b)$ at SLD. Thus, it appears that at least some of the problem in A_b is due to a statistical fluctuation or other experimental effect in one of the asymmetries. Note, however, that the uncertainty in $A_{FB}^{(0,b)}$ is strongly statistics dominated. The combined value, $A_b = 0.901 \pm 0.013$ deviates by 2.6 σ .

The left-right asymmetry, $A_{LR}^0 = 0.15138 \pm 0.00216$ [284], from hadronic decays at SLD, differs by 2.1 σ from the SM expectation of 0.1468 ± 0.0003 . The combined value of $A_\ell = 0.1513 \pm 0.0021$ from SLD (using lepton-family universality and including correlations) is also 2.1 σ above the SM prediction; but there is experimental agreement between this SLD value and the LEP 1 value, $A_\ell = 0.1481 \pm 0.0027$, obtained from a fit to $A_{FB}^{(0,\ell)}$, $A_\ell(\mathcal{P}_\tau)$, and $A_\tau(\mathcal{P}_\tau)$, again assuming universality.

The observables in Table 10.4 and Table 10.5, as well as some other less precise observables, are used in the global fits described below. In all fits, the errors include full statistical, systematic, and theoretical uncertainties. The correlations from the LEP 1 lineshape and τ polarization measurements, the LEP/SLD heavy flavor observables, the SLD lepton asymmetries, and the ν - e scattering observables, are included. The theoretical correlations between $\Delta\alpha_{\text{had}}^{(5)}$, s_0^2 , and $g_\mu - 2$, and between the M_W extractions from the LHC and the Tevatron, are also accounted for.

The electroweak data allow a simultaneous determination of M_Z , m_t , and $\alpha_s(M_Z)$. The direct measurements of M_H at the LHC [275, 276] have reached a precision that the global fit result

¹⁵ W -boson branching ratio measurements from CMS and ATLAS are in good agreement with lepton universality and slightly more precise than LEP-2 [272, 321].

¹⁶Alternatively, one can use $A_\ell = 0.1481 \pm 0.0027$, which is from LEP 1 alone and in excellent agreement with the SM, and obtain $A_b = 0.897 \pm 0.022$ which is 1.7 σ low. This illustrates that some of the discrepancy is related to the one in A_{LR} .

Table 10.7: Principal SM fit result including mutual correlations.

M_Z [GeV]	91.1882 ± 0.0020	1.00	-0.07	0.00	0.00	0.02	0.02
$\widehat{m}_t(\widehat{m}_t)$ [GeV]	163.45 ± 0.55	-0.07	1.00	0.00	-0.11	-0.22	0.04
$\widehat{m}_b(\widehat{m}_b)$ [GeV]	4.180 ± 0.008	0.00	0.00	1.00	0.20	-0.02	0.00
$\widehat{m}_c(\widehat{m}_c)$ [GeV]	1.274 ± 0.009	0.00	-0.11	0.20	1.00	0.47	0.00
$\alpha_s(M_Z)$	0.1185 ± 0.0016	0.02	-0.22	-0.02	0.47	1.00	-0.03
$\Delta\alpha_{\text{had}}^{(3)}(2 \text{ GeV})$	0.00593 ± 0.00005	0.02	0.04	0.00	0.00	-0.03	1.00

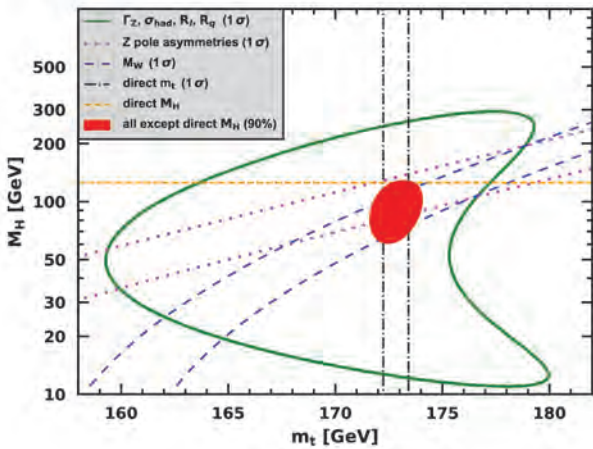


Figure 10.4: Fit result and one-standard-deviation (39.35% for the closed contours and 68% for the others) uncertainties in M_H as a function of m_t for various inputs, and the 90% CL region ($\Delta\chi^2 = 4.605$) allowed by all data. $\alpha_s(M_Z) = 0.1185$ is assumed except for the fits including the Z lineshape. The width of the horizontal dashed band is not visible on the scale of the plot.

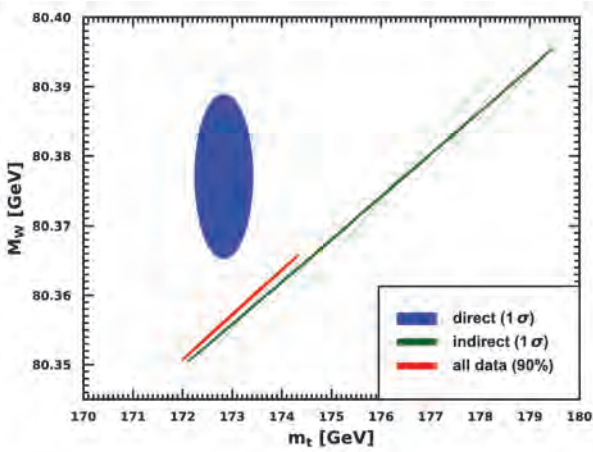


Figure 10.5: One-standard-deviation (39.35%) regions in M_W as a function of m_t for the direct and indirect data, and the 90% CL region ($\Delta\chi^2 = 4.605$) allowed by all data.

for M_H coincides with the constraint in Eq. (10.56) with negligible correlations with the other fit parameters. \widehat{m}_c , \widehat{m}_b , and $\Delta\alpha_{\text{had}}^{(3)}$ are also allowed to float in the fits, subject to the theoretical constraints [30, 55] described in Sec. 10.2, and are correlated with α_s , which in turn is determined mainly through R_ℓ , Γ_Z , σ_{had} , and τ_τ . The global fit to all data, including the hadron collider m_t average in Eq. (10.17), yields the results in Table 10.7, while those for the weak mixing angle in various schemes are summarized in Table 10.2.

Removing the kinematic constraint on M_H from LHC gives the

loop-level determination from the precision data,

$$M_H = 91_{-16}^{+18} \text{ GeV}, \quad (10.68)$$

which is 1.7σ below the value in Eq. (10.56). The latter is also slightly outside the 90% central confidence range,

$$65 \text{ GeV} < M_H < 122 \text{ GeV}. \quad (10.69)$$

This is mostly a reflection of the Tevatron determination of M_W , which is 1.7σ higher than the SM best fit value in Table 10.4. This is shown in Fig. 10.4 where one sees that the precision data together with M_H from the LHC prefer m_t to be closer to the upper end of its 1σ allowed range.

Conversely, one can remove the explicit M_W and Γ_W constraints from the global fit and use $M_H = 125.30 \pm 0.13 \text{ GeV}$ to obtain $M_W = 80.356 \pm 0.006 \text{ GeV}$, which is 1.6σ below the world average in Eq. (10.55). Finally, one can carry out a fit without including the direct constraint, $m_t = 172.83 \pm 0.59 \text{ GeV}$, from the hadron colliders. One obtains $m_t = 176.2 \pm 1.9 \text{ GeV}$, which is 1.7σ higher than the collider average. (The indirect prediction is for the $\overline{\text{MS}}$ mass definition, $\widehat{m}_t(\widehat{m}_t) = 166.4 \pm 1.8 \text{ GeV}$, which is in the end converted to the pole mass.) The situation is summarized in Fig. 10.5 showing the 1σ contours in the $M_W - m_t$ plane from the direct and indirect determinations, as well as the combined 90% CL region.

In view of these tensions it is instructive to study the effect of doubling the uncertainty in $\Delta\alpha_{\text{had}}^{(3)}(2 \text{ GeV}) = (58.84 \pm 0.51) \times 10^{-4}$ (see Sec. 10.2) on the loop-level determination of the Higgs boson mass. The result, $M_H = 88_{-19}^{+16} \text{ GeV}$, deviates even slightly *more* (1.8σ) than Eq. (10.68), and demonstrates that the uncertainty in $\Delta\alpha_{\text{had}}$ is currently of only secondary importance. Note also that an increase of 3×10^{-4} in $\Delta\alpha_{\text{had}}^{(3)}(2 \text{ GeV})$, as favored by the very recent lattice evaluation in Ref. [329], corresponds to a decrease of the indirectly extracted M_H by 13 GeV. The hadronic contribution to $\alpha(M_Z)$ is correlated with $g_\mu - 2$ (see Sec. 10.4). The measurement of the latter is higher than the SM prediction, and its inclusion in the fit favors a larger $\alpha(M_Z)$ and a lower M_H from the precision data (currently by 2.8 GeV).

The weak mixing angle can be determined from Z pole observables, M_W , and a variety of neutral-current processes spanning a very wide Q^2 range. The results (for older low energy neutral-current data see Refs. [322–325], as well as earlier editions of this *Review*) shown in Table 10.8 are in reasonable agreement with each other, indicating the quantitative success of the SM. One of the largest discrepancies is the value $\widehat{s}_Z^2 = 0.23176 \pm 0.00027$ from $A_{FB}^{(0,b)}$ and $A_{FB}^{(0,c)}$, which is 2.0σ above the value 0.23122 ± 0.00004 from the global fit to all data. Similarly, $\widehat{s}_Z^2 = 0.23064 \pm 0.00028$ from the SLD asymmetries (in both cases when combined with M_Z , Γ_Z , and m_t) is 2.1σ low.

The extracted Z pole value of $\alpha_s(M_Z)$ is based on a formula with negligible theoretical uncertainty if one assumes the exact validity of the SM. One should keep in mind, however, that this value, $\alpha_s(M_Z) = 0.1221 \pm 0.0027$, which increased after the updated analysis in Ref. [299], is very sensitive to certain types of new physics such as non-universal vertex corrections. In contrast, the value derived from τ decays, $\alpha_s(M_Z) = 0.1171_{-0.0017}^{+0.0018}$, is theory dominated but less sensitive to new physics. The agreement between the two values is only marginal, but the latter does agree well with the averages deduced from heavy quarkonia spectroscopy (0.1183 ± 0.0039), DIS and global PDF fits

Table 10.8: Values of \widehat{s}_Z^2 , s_W^2 , α_s , m_t and M_H for various data sets. In the fit to the LHC data, the α_s constraint is from a combined NNLO analysis of inclusive electroweak boson production cross-sections at the LHC [327]. Likewise, for the Tevatron fit we use the α_s result from the inclusive jet cross-section at $D\bar{O}$ [328].

data set	\widehat{s}_Z^2	s_W^2	$\alpha_s(M_Z)$	m_t [GeV]	M_H [GeV]
all data	0.23122(4)	0.22339(10)	0.1185(16)	173.1 ± 0.6	125
all data except M_H	0.23109(9)	0.22312(19)	0.1189(17)	172.8 ± 0.6	91_{-16}^{+18}
all data except M_Z	0.23113(6)	0.22335(10)	0.1185(16)	172.8 ± 0.6	125
all data except M_W	0.23125(4)	0.22346(11)	0.1189(17)	172.9 ± 0.6	125
all data except m_t	0.23115(6)	0.22307(21)	0.1190(17)	176.2 ± 1.9	125
$M_{H,Z} + \Gamma_{H,Z} + m_t$	0.23128(8)	0.22353(16)	0.1218(45)	172.8 ± 0.6	125
LHC	0.23116(10)	0.22340(12)	0.1187(16)	172.6 ± 0.6	125
Tevatron + M_Z	0.23103(14)	0.22294(30)	0.1160(45)	174.3 ± 0.8	99_{-27}^{+31}
LEP 1 + LEP 2	0.23137(18)	0.22352(46)	0.1234(29)	178 ± 11	195_{-109}^{+267}
LEP 1 + SLD	0.23116(17)	0.22345(58)	0.1221(27)	169 ± 10	79_{-38}^{+100}
SLD + $M_Z + \Gamma_Z + m_t$	0.23064(28)	0.22226(54)	0.1191(48)	172.8 ± 0.6	36_{-21}^{+29}
$A_{FB}^{(b,c)} + M_Z + \Gamma_Z + m_t$	0.23176(27)	0.22465(66)	0.1267(45)	172.8 ± 0.6	273_{-98}^{+140}
$M_{W,Z} + \Gamma_{W,Z} + m_t$	0.23106(12)	0.22306(25)	0.1201(42)	172.8 ± 0.6	86_{-20}^{+23}
low energy + $M_{H,Z}$	0.23174(94)	0.2253(35)	0.1172(18)	157 ± 29	125

Table 10.9: Values of model-independent neutral-current parameters, compared with the SM predictions, where the uncertainties in the latter are $\lesssim 0.0001$, throughout.

Quantity	Experimental Value	Standard Model	Correlation
$g_{LV}^{\nu e}$	-0.040 ± 0.015	-0.0397	-0.05
$g_{LA}^{\nu e}$	-0.507 ± 0.014	-0.5064	
$g_{AV}^{eU} + 2g_{AV}^{eD}$	0.4927 ± 0.0031	0.4950	-0.88 0.20
$2g_{AV}^{eU} - g_{AV}^{eD}$	-0.7165 ± 0.0068	-0.7193	-0.22
$2g_{VA}^{eU} - g_{VA}^{eD}$	-0.13 ± 0.06	-0.0950	
g_{VA}^{ee}	0.0190 ± 0.0027	0.0226	

(0.1162 ± 0.0020), hadronic final states of e^+e^- annihilations (0.1171 ± 0.0031), hadron colliders (0.1165 ± 0.0028), as well as lattice QCD simulations (0.1182 ± 0.0008). For more details, other determinations, and references, see the Section on ‘‘Quantum Chromodynamics’’ in this *Review*. We also provide the values, computed with five-loop beta functions and four-loop matching,

$$\alpha_s^{(4)}(m_\tau) = 0.324 \pm 0.014, \quad (10.70)$$

$$\alpha_s^{(5)}(M_W) = 0.1208 \pm 0.0017, \quad (10.71)$$

$$\alpha_s^{(5)}(M_H) = 0.1131 \pm 0.0015, \quad (10.72)$$

$$\alpha_s^{(6)}(m_t) = 0.1089 \pm 0.0014, \quad (10.73)$$

to be used in precision calculations.

Using $\alpha(M_Z)$ and \widehat{s}_Z^2 as inputs, one can predict $\alpha_s(M_Z)$ assuming grand unification. One finds $\alpha_s(M_Z) = 0.13 \pm 0.01$ [330, 331] for the simplest theories based on the minimal supersymmetric extension of the SM, where the uncertainty is from the unknown particle thresholds. This is slightly larger, but consistent with $\alpha_s(M_Z) = 0.1185 \pm 0.0016$ from our fit and most other determinations, while minimal non-supersymmetric theories predict much lower and excluded values (see the Section on ‘‘Grand Unified Theories’’ in this *Review*).

Most of the parameters relevant to ν -hadron, ν - e , e -hadron, and e - e processes are determined uniquely and precisely from the data in ‘‘model-independent’’ fits, *i.e.*, fits allowing for an arbitrary EW gauge theory. The values for the parameters defined in Eq. (10.25) are given in Table 10.9 along with the predictions of the SM. The agreement is very good. (The ν -hadron results including NuTeV [143] and other ν -DIS data can be found in the 2006 edition of this *Review*, and fits with modified NuTeV constraints in the 2008 and 2010 editions.)

10.7 Constraints on new physics

The masses and decay properties of the electroweak bosons and low energy data can be used to search for and set limits on deviations from the SM. We will mainly discuss the effects of exotic particles (with heavy masses $M_{\text{new}} \gg M_Z$ in an expansion in M_Z/M_{new}) on the gauge boson self-energies. (Brief remarks are made on new physics which is not of this type.) Most of the effects on precision measurements can be described by three gauge self-energy parameters S , T , and U . We will define these, as well as the related parameters ρ_0 , ϵ_i , and $\widehat{\epsilon}_i$, to arise from new physics only. In other words, they are equal to zero ($\rho_0 = 1$) exactly in the SM, and do not include any (loop induced) contributions that depend on m_t or M_H , which are treated separately. Our treatment differs from most of the original papers.

The dominant effect of many extensions of the SM can be described by the ρ_0 parameter,

$$\rho_0 \equiv \frac{M_W^2}{M_Z^2 \widehat{c}_Z^2 \widehat{\rho}}, \quad (10.74)$$

which describes new sources of $SU(2)$ breaking that cannot be accounted for by the SM Higgs doublet or by m_t effects. $\widehat{\rho}$ is calculated as in Eq. (10.22) assuming the validity of the SM. In the presence of $\rho_0 \neq 1$, Eq. (10.74) generalizes the second Eq. (10.22) while the first remains unchanged. Provided that the new physics which yields $\rho_0 \neq 1$ is a small perturbation which does not significantly affect other radiative corrections, ρ_0 can be regarded as a phenomenological parameter which multiplies G_F in Eqs. (10.25) and (10.45), as well as Γ_Z in Eq. (10.64c). There are enough data to determine ρ_0 , M_H , m_t , and α_s , simultaneously. From the

global fit,

$$\rho_0 = 1.00038 \pm 0.00020, \quad (10.75a)$$

$$\alpha_s(M_Z) = 0.1188 \pm 0.0017, \quad (10.75b)$$

where as before the uncertainty is from the experimental inputs and includes an estimate of the error from unknown higher-order electroweak corrections. The result in Eq. (10.75a) is 2.0σ above the SM expectation, $\rho_0 = 1$. It can be used to constrain higher-dimensional Higgs representations to have vacuum expectation values of less than a few percent of those of the doublets. Indeed, the relation between M_W and M_Z is modified if there are Higgs multiplets with weak isospin $> 1/2$ and significant vacuum expectation values. For a general (charge-conserving) Higgs structure,

$$\rho_0 = \frac{\sum_i [t_i(t_i + 1) - t_{3i}^2] |v_i|^2}{2 \sum_i t_{3i}^2 |v_i|^2}, \quad (10.76)$$

where v_i is the expectation value of the neutral component of a Higgs multiplet with weak isospin t_i and third component t_{3i} . In order to calculate to higher orders in such theories one must define a set of four fundamental renormalized parameters which one may conveniently choose to be α , G_F , M_Z , and M_W , since M_W and M_Z are directly measurable. Then \hat{s}_Z^2 and ρ_0 can be considered dependent parameters.

Eq. (10.75a) can also be used to constrain other types of new physics. For example, non-degenerate multiplets of heavy fermions or scalars break the vector part of weak SU(2) and lead to a decrease in the value of M_Z/M_W . Each non-degenerate SU(2) doublet $\begin{pmatrix} f_1 \\ f_2 \end{pmatrix}$ yields a positive contribution to ρ_0 [332–334] of

$$\frac{N_C G_F}{8\sqrt{2}\pi^2} \Delta m^2, \quad (10.77)$$

where

$$\Delta m^2 \equiv m_1^2 + m_2^2 - \frac{4m_1^2 m_2^2}{m_1^2 - m_2^2} \ln \frac{m_1}{m_2} \geq (m_1 - m_2)^2, \quad (10.78)$$

and $N_C = 1$ (3) for color singlets (triplets). Eq. (10.75a) taken together with Eq. (10.77) implies the following constraint on the mass splitting at the 90% CL,

$$(14 \text{ GeV})^2 < \sum_i \frac{N_C^i}{3} \Delta m_i^2 < (48 \text{ GeV})^2, \quad (10.79)$$

where the sum runs over all new-physics doublets, for example fourth-family quarks or leptons, $\begin{pmatrix} t' \\ b' \end{pmatrix}$ or $\begin{pmatrix} \nu' \\ e' \end{pmatrix}$, vector-like fermion doublets (which contribute to the sum in Eq. (10.79) with an extra factor of 2), and scalar doublets such as $\begin{pmatrix} \tilde{t} \\ \tilde{b} \end{pmatrix}$ in Supersymmetry (in the absence of L - R mixing).

Non-degenerate multiplets usually imply $\rho_0 > 1$. Similarly, heavy Z' bosons decrease the prediction for M_Z due to mixing and generally lead to $\rho_0 > 1$ [335]. On the other hand, extra Higgs doublets participating in spontaneous symmetry breaking [336–338] or heavy lepton doublets involving Majorana neutrinos [339], both of which have more complicated expressions, and the v_i of higher-dimensional Higgs representations can contribute to ρ_0 with either sign.

A number of authors [340–342] have considered the general effects on neutral-current, Z and W boson observables of various types of heavy (*i.e.*, $M_{\text{new}} \gg M_Z$) physics which contribute to the W and Z self-energies but which do not have any direct coupling to the ordinary fermions (an alternative formulation is given by Ref. [343]). In addition to non-degenerate multiplets, which break the vector part of weak SU(2), these include heavy degenerate multiplets of chiral fermions which break the axial generators.

Such effects can be described by just three parameters, S , T , and U [344], at the (EW) one-loop level¹⁷. T is proportional to

the difference between the W and Z self-energies at $Q^2 = 0$ (*i.e.*, vector SU(2)-breaking), while S ($S + U$) is associated with the difference between the Z (W) self-energy at $Q^2 = M_{Z,W}^2$ and $Q^2 = 0$ (axial SU(2)-breaking). Denoting the contributions of new physics to the various self-energies by Π_{ij}^{new} , we have

$$\hat{\alpha}(M_Z)T \equiv \frac{\Pi_{WW}^{\text{new}}(0)}{M_W^2} - \frac{\Pi_{ZZ}^{\text{new}}(0)}{M_Z^2}, \quad (10.80a)$$

$$\frac{\hat{\alpha}(M_Z)}{4\hat{s}_Z^2\hat{c}_Z^2}S \equiv \frac{\Pi_{ZZ}^{\text{new}}(M_Z^2) - \Pi_{ZZ}^{\text{new}}(0)}{M_Z^2} - \frac{\hat{c}_Z^2 - \hat{s}_Z^2}{\hat{c}_Z\hat{s}_Z} \frac{\Pi_{Z\gamma}^{\text{new}}(M_Z^2)}{M_Z^2} - \frac{\Pi_{\gamma\gamma}^{\text{new}}(M_Z^2)}{M_Z^2}, \quad (10.80b)$$

$$\frac{\hat{\alpha}(M_Z)}{4\hat{s}_Z^2}(S+U) \equiv \frac{\Pi_{WW}^{\text{new}}(M_W^2) - \Pi_{WW}^{\text{new}}(0)}{M_W^2} - \frac{\hat{c}_Z}{\hat{s}_Z} \frac{\Pi_{Z\gamma}^{\text{new}}(M_Z^2)}{M_Z^2} - \frac{\Pi_{\gamma\gamma}^{\text{new}}(M_Z^2)}{M_Z^2}. \quad (10.80c)$$

S , T , and U are defined with a factor proportional to $\hat{\alpha}$ removed, so that they are expected to be of order unity in the presence of new physics. In the $\overline{\text{MS}}$ scheme as defined in Ref. [80], the last two terms in Eqs. (10.80b) and (10.80c) can be omitted, as was done in some earlier editions of this *Review*. These parameters are related to other parameter sets, S_i [80], $\hat{\epsilon}_i$ [348], and h_i [349], by

$$T = h_V = \frac{\hat{\epsilon}_1}{\hat{\alpha}(M_Z)}, \quad (10.81a)$$

$$S = h_{AZ} = S_Z = 4\hat{s}_Z^2 \frac{\hat{\epsilon}_3}{\hat{\alpha}(M_Z)}, \quad (10.81b)$$

$$U = h_{AW} - h_{AZ} = S_W - S_Z = -4\hat{s}_Z^2 \frac{\hat{\epsilon}_2}{\hat{\alpha}(M_Z)}. \quad (10.81c)$$

A heavy non-degenerate multiplet of fermions or scalars contributes positively to T as

$$\rho_0 - 1 = \frac{1}{1 - \hat{\alpha}(M_Z)T} - 1 \approx \hat{\alpha}(M_Z)T, \quad (10.82)$$

where $\rho_0 - 1$ is given in Eq. (10.77). The effects of non-standard Higgs representations cannot be separated from heavy non-degenerate multiplets unless the new physics has other consequences, such as vertex corrections. Most of the original papers defined T to include the effects of loops only. However, we will redefine T to include all new sources of SU(2) breaking, including non-standard Higgs, so that T and ρ_0 are equivalent by Eq. (10.82).

A multiplet of heavy degenerate chiral fermions yields

$$S = \frac{N_C}{3\pi} \sum_i \left(t_{3i}^L - t_{3i}^R \right)^2, \quad (10.83)$$

where $t_{3i}^{L,R}$ is the 3rd component of weak isospin of the left-(right-)handed component of fermion i . For example, a heavy degenerate ordinary or mirror family would contribute $2/3\pi$ to S . In models with warped extra dimensions [350], sizeable corrections to the S parameter are generated through mixing between the SM gauge bosons and their Kaluza-Klein (KK) excitations, and one finds $S \approx 30 v^2 M_{KK}^{-2}$ [351], where M_{KK} is the mass scale of the KK gauge bosons. Large positive values of S can also be generated in models with dynamical electroweak symmetry breaking, where the Higgs boson is composite. In simple composite Higgs models, the dominant contribution stems from heavy spin-1 resonances of the strong dynamics leading to $S \approx 4\pi v^2 (M_V^{-2} + M_A^{-2})$, where $M_{V,A}$ are the masses of the lightest vector and axial-vector resonances, respectively [352].

¹⁷Three additional parameters are needed if the new physics scale is comparable to M_Z [345]. Further generalizations, including effects relevant to LEP 2 and Drell-Yan production at the LHC, are described in Refs. [346] and [347], respectively.

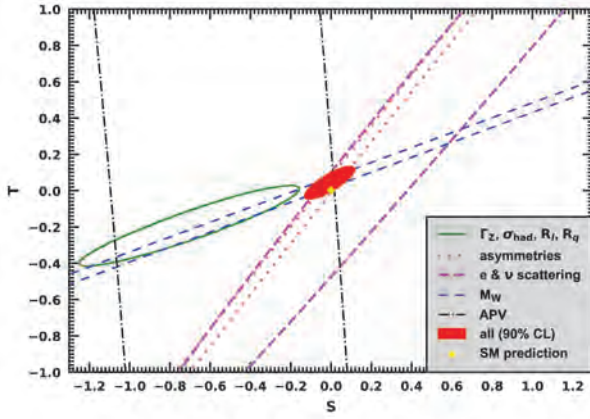


Figure 10.6: 1σ constraints (39.35% for the closed contours and 68% for the others) on S and T (for $U = 0$) from various inputs combined with M_Z . S and T represent the contributions of new physics only. Data sets not involving M_W or Γ_W are insensitive to U . With the exception of the fit to all data, we fix $\alpha_s = 0.1185$. The yellow dot indicates the Standard Model values $S = T = 0$.

Negative values of S are possible, for example, in composite Higgs models [353], or from loops involving scalars or Majorana particles [354–356]. The simplest origin of $S < 0$ would probably be an additional heavy Z' boson [335]. Supersymmetric extensions of the SM [357, 358] generally give very small effects. For more details and references, see Refs. [359–368] and the Sections on “Supersymmetry” in this *Review*. Most simple types of new physics yield $U = 0$, although there are counter-examples, such as the effects of anomalous triple gauge vertices [348].

The SM expressions for observables are replaced by,

$$M_Z^2 = M_{Z0}^2 \frac{1 - \widehat{\alpha}(M_Z)T}{1 - G_F M_{Z0}^2 S / 2\sqrt{2}\pi}, \quad (10.84a)$$

$$M_W^2 = M_{W0}^2 \frac{1}{1 - G_F M_{W0}^2 (S + U) / 2\sqrt{2}\pi}, \quad (10.84b)$$

where M_{Z0} and M_{W0} are the SM expressions (as functions of m_t and M_H) in the $\overline{\text{MS}}$ scheme. Furthermore,

$$\Gamma_Z = \frac{M_Z^3 \beta_Z}{1 - \widehat{\alpha}(M_Z)T}, \quad (10.85a)$$

$$\Gamma_W = M_W^3 \beta_W, \quad (10.85b)$$

$$A_i = \frac{A_{i0}}{1 - \widehat{\alpha}(M_Z)T}, \quad (10.85c)$$

where $\beta_{Z,W}$ are the SM expressions for the reduced widths Γ_{Z0}/M_{Z0}^3 and Γ_{W0}/M_{W0}^3 , M_Z and M_W are the physical masses, and A_i (A_{i0}) is a neutral-current amplitude (in the SM).

The data allows for a simultaneous determination of M_H and m_t (from the hadron colliders), S (from M_Z), T (mainly from Γ_Z), U (from M_W), $\widehat{s}_Z^2 = 0.23112 \pm 0.00013$ (from the Z pole asymmetries), and $\alpha_s(M_Z) = 0.1189 \pm 0.0018$ (from R_ℓ , σ_{had} , and τ_τ), giving,

$$S = -0.02 \pm 0.10, \quad (10.86a)$$

$$T = 0.03 \pm 0.12, \quad (10.86b)$$

$$U = 0.01 \pm 0.11, \quad (10.86c)$$

with little correlation among the SM parameters, where the uncertainties are from unknown higher orders in the SM predictions and the inputs. The parameters in Eq. (10.86), which by definition are due to new physics only, are in excellent agreement with the SM values of zero. Fixing $U = 0$, which is motivated by the

fact that U is suppressed by an additional factor M_{new}^2/M_Z^2 compared to S and T [369], greatly improves the precision on S and particularly T ,

$$S = -0.01 \pm 0.07, \quad (10.87a)$$

$$T = 0.04 \pm 0.06. \quad (10.87b)$$

If only one of the three parameters is allowed, then this parameter would deviate almost at the 2σ level, reflecting the deviation in M_W . Using Eq. (10.82), the value of ρ_0 corresponding to T in Eqs. (10.86) is 1.0002 ± 0.0009 , while the one corresponding to Eqs. (10.87) is 1.0003 ± 0.0005 . Thus, the multi-parameter fits are consistent with $\rho_0 = 1$, in contrast to the fit with $S = U = 0$ in Eq. (10.75a). There is a strong correlation (92%) between the S and T parameters. The U parameter is -80% (-93%) anticorrelated with S (T). The allowed regions in S – T (for $U = 0$) are shown in Fig. 10.6. From Eq. (10.86) one obtains $S < 0.14$ and $T < 0.22$ at 95% CL, where the former puts the constraint $M_{KK} \gtrsim 3.6$ TeV on the masses of KK gauge bosons in warped extra dimensions. In minimal composite Higgs models, the bound on S requires $M_V \gtrsim 4$ TeV [370], but this constraint can be relaxed, *e.g.*, if the fermionic sector is also allowed to be partially composite [371, 372].

The S parameter can also be used to constrain the number of fermion families, *under the assumption* that there are no new contributions to T or U and therefore that any new families are degenerate; then an extra generation of SM fermions is excluded with almost 9σ confidence, corresponding to $N_F = 2.74 \pm 0.15$. This can be compared to the fit to the number of light neutrinos given in Eq. (10.67), $N_\nu = 3.0026 \pm 0.0061$, but the S parameter fits are valid even for a very heavy fourth family neutrino. Allowing T to vary as well, the constraint on a fourth family is weaker [373]. However, a heavy fourth family would increase the Higgs production cross-section through gluon fusion by a factor of about 9 [374], which is in considerable tension with the observed Higgs signal at the LHC [375]. Combining the limits from electroweak precision data with the measured Higgs production rate and limits from direct searches for heavy quarks [376], a fourth family of chiral fermions is now excluded by more than five standard deviations [377, 378]. Similar remarks apply to a heavy mirror family [379] involving right-handed $SU(2)$ doublets and left-handed singlets. In contrast, new doublets that receive most of their mass from a different source than the Higgs vacuum expectation value, such as vector-like fermion doublets or scalar doublets in Supersymmetry, give small or no contribution to S , T , U , and the Higgs production cross-section and are therefore still allowed. Partial or complete vector-like fermion families are predicted in many Grand Unified Theories [380] (see the Section on “Grand Unified Theories” in this *Review*), and many other models including supersymmetric and superstring inspired ones [381–384].

As discussed in Sec. 10.6, there is a 3.6% deviation in the asymmetry parameter A_b . Assuming that this is due to new physics affecting preferentially the third generation, we can perform a fit allowing additional $Z \rightarrow b\bar{b}$ vertex corrections ρ_b and κ_b as in Eq. (10.46) (here defined to be due to new physics only with the SM contributions removed), as well as S , T , U , and the SM parameters, with the result,

$$\rho_b = 0.058 \pm 0.020, \quad (10.88a)$$

$$\kappa_b = 0.186 \pm 0.067, \quad (10.88b)$$

with an almost perfect correlation of 99% (because R_b is much better determined than A_b). The central values of the oblique parameters are consistent with their SM values of zero, and there is little change in the SM parameters, except that the value of $\alpha_s(M_Z)$ is lower by 0.0008 compared to the SM fit. Given that an $\mathcal{O}(20\%)$ correction to κ_b would be necessary, it would be difficult to account for the deviation in A_b by new physics that enters only at the level of radiative corrections. Thus, if it is due to new physics, it is most likely of tree-level type affecting preferentially the third generation. Examples include the decay of a scalar neutrino resonance [385], mixing of the b quark with heavy exotics [386], and

a heavy Z' with family non-universal couplings [387, 388]. It is difficult, however, to simultaneously account for R_b without tuning, which has been measured on the Z peak and off-peak [389] at LEP 1.

There is no simple parametrization to describe the effects of every type of new physics on every possible observable. The S , T , and U formalism describes many types of heavy physics which affect only the gauge self-energies, and it can be applied to all precision observables. However, new physics which couples directly to ordinary fermions cannot be fully parametrized in the S , T , and U framework. Examples include heavy Z' bosons [335], mixing with exotic fermions [9, 390, 391], leptoquark exchange [267, 392, 393], supersymmetric models, strong EW dynamics [371], Little Higgs models [394, 395], and TeV-scale extra spatial dimensions [396–399] (for more details and references, see the Section on “Extra Dimensions” in this *Review*). These types of new physics can be parametrized in a model-independent way by using an effective field theory description [400–403]. Here the SM is extended by a set of higher-dimensional operators, denoted \mathcal{O}_i ,

$$\mathcal{L} = \mathcal{L}_{\text{SM}} + \sum_{d>4} \sum_i \frac{C_i}{\Lambda^{d-4}} \mathcal{O}_i, \quad (10.89)$$

where Λ is the characteristic scale of the new physics sector, which is assumed to satisfy $\Lambda \gg v$. For EW precision observables, the leading new operators enter at dimension $d = 6$. Note that S and T can be identified with two of these operators (or linear combinations thereof, depending on the chosen operator basis), while U corresponds to a dimension-8 operator [369, 404]. With current data on M_W and Z pole observables, Λ is constrained to be larger than $\mathcal{O}(\text{TeV})$ if the Wilson coefficients C_i are of order unity [405–410].

Limits on new four-Fermi operators and on leptoquarks using LEP 2 and lower energy data are given in Refs. [267, 411–413], while constraints on various types of new physics are addressed in Refs. [9, 161, 287, 414, 415]. For a particularly well motivated and explored type of physics beyond the SM, see the Section on “ Z' -Boson Searches” in this *Review*.

Acknowledgments

It is a pleasure to thank Rodolfo Ferro-Hernández for discussions, for performing some of the calculations and checks, and for updating the plots. J.E. is supported by the German–Mexican research collaboration grant SP 778/4–1 (DFG) and 278017 (CONACyT). A.F. is supported in part by the National Science Foundation under grant no. PHY–1820760.

References

- [1] S. Glashow, Nucl. Phys. **22**, 579 (1961).
- [2] S. Weinberg, Phys. Rev. Lett. **19**, 1264 (1967).
- [3] A. Salam, Conf. Proc. C **680519**, 367 (1968).
- [4] S. Glashow, J. Iliopoulos and L. Maiani, Phys. Rev. D **2**, 1285 (1970).
- [5] N. Cabibbo, Phys. Rev. Lett. **10**, 531 (1963).
- [6] M. Kobayashi and T. Maskawa, Prog. Theor. Phys. **49**, 652 (1973).
- [7] S. Descotes-Genon and P. Koppenburg, Ann. Rev. Nucl. Part. Sci. **67**, 97 (2017), [arXiv:1702.08834].
- [8] E. Commins and P. Bucksbaum, *Weak Interactions of Leptons and Quarks*, Cambridge Univ. Pr., Cambridge, USA (1983), ISBN 978-0-521-27370-1.
- [9] P. Langacker, editor, *Precision tests of the standard electroweak model*, volume 14, WSP, Singapore (1996).
- [10] P. Langacker, *The standard model and beyond*, CRC Pr., Boca Raton, USA (2010), ISBN 978-1-4200-7906-7.
- [11] T. Kinoshita, editor, *Quantum electrodynamics*, volume 7, WSP, Singapore (1990).
- [12] S. G. Karshenboim, Phys. Rept. **422**, 1 (2005), [hep-ph/0509010].
- [13] J. Erler and S. Su, Prog. Part. Nucl. Phys. **71**, 119 (2013), [arXiv:1303.5522].
- [14] S. Schael *et al.* (ALEPH, DELPHI, L3, OPAL, SLD, LEP Electroweak Working Group, SLD Electroweak Group, SLD Heavy Flavour Group), Phys. Rept. **427**, 257 (2006), [hep-ex/0509008].
- [15] D. Webber *et al.* (MuLan), Phys. Rev. Lett. **106**, 041803 (2011), [arXiv:1010.0991].
- [16] T. Kinoshita and A. Sirlin, Phys. Rev. **113**, 1652 (1959).
- [17] T. van Ritbergen and R. G. Stuart, Nucl. Phys. B **564**, 343 (2000), [hep-ph/9904240].
- [18] M. Steinhauser and T. Seidensticker, Phys. Lett. B **467**, 271 (1999), [hep-ph/9909436].
- [19] Y. Nir, Phys. Lett. B **221**, 184 (1989).
- [20] A. Pak and A. Czarnecki, Phys. Rev. Lett. **100**, 241807 (2008), [arXiv:0803.0960].
- [21] A. Ferroglia, G. Ossola and A. Sirlin, Nucl. Phys. B **560**, 23 (1999), [hep-ph/9905442].
- [22] B. Ananthanarayan, S. Friot and S. Ghosh, Phys. Rev. D **101**, 11, 116008 (2020), [arXiv:2003.12030].
- [23] D. Hanneke, S. Fogwell and G. Gabrielse, Phys. Rev. Lett. **100**, 120801 (2008), [arXiv:0801.1134].
- [24] T. Aoyama, T. Kinoshita and M. Nio, Atoms **7**, 1, 28 (2019).
- [25] L. Morel *et al.*, Nature **588**, 7836, 61 (2020).
- [26] R. H. Parker *et al.*, Science **360**, 191 (2018), [arXiv:1812.04130].
- [27] G. Abbiendi *et al.* (OPAL), Eur. Phys. J. C **45**, 1 (2006), [hep-ex/0505072].
- [28] P. Achard *et al.* (L3), Phys. Lett. B **623**, 26 (2005), [hep-ex/0507078].
- [29] S. Fanchiotti, B. A. Kniehl and A. Sirlin, Phys. Rev. D **48**, 307 (1993), [hep-ph/9212285].
- [30] J. Erler, Phys. Rev. D **59**, 054008 (1999), [hep-ph/9803453].
- [31] M. Davier *et al.*, Eur. Phys. J. C **80**, 3, 241 (2020), [arXiv:1908.00921].
- [32] F. Jegerlehner, EPJ Web Conf. **118**, 01016 (2016), [arXiv:1511.04473].
- [33] F. Jegerlehner and R. Szafron, Eur. Phys. J. C **71**, 1632 (2011), [arXiv:1101.2872].
- [34] J. Erler (1999), [hep-ph/0005084].
- [35] M. Steinhauser, Phys. Lett. B **429**, 158 (1998), [hep-ph/9803313].
- [36] C. Sturm, Nucl. Phys. B **874**, 698 (2013), [arXiv:1305.0581].
- [37] K. Chetyrkin, J. H. Kuhn and M. Steinhauser, Nucl. Phys. B **482**, 213 (1996), [hep-ph/9606230].
- [38] A. V. Nesterenko, *Strong interactions in spacelike and time-like domains: dispersive approach*, Elsevier (2016), ISBN 978-0-12-803448-4.
- [39] J. Erler and R. Ferro-Hernández, JHEP **03**, 196 (2018), [arXiv:1712.09146].
- [40] A. Blondel *et al.* (2019), [arXiv:1905.05078].
- [41] A. Keshavarzi, D. Nomura and T. Teubner, Phys. Rev. D **101**, 1, 014029 (2020), [arXiv:1911.00367].
- [42] M. Davier *et al.*, Eur. Phys. J. C **71**, 1515 (2011), [Erratum: Eur.Phys.J.C 72, 1874 (2012)], [arXiv:1010.4180].
- [43] K. Ackerstaff *et al.* (OPAL), Eur. Phys. J. C **7**, 571 (1999), [hep-ex/9808019].
- [44] S. Anderson *et al.* (CLEO), Phys. Rev. D **61**, 112002 (2000), [hep-ex/9910046].
- [45] S. Schael *et al.* (ALEPH), Phys. Rept. **421**, 191 (2005), [hep-ex/0506072].
- [46] M. Fujikawa *et al.* (Belle), Phys. Rev. D **78**, 072006 (2008), [arXiv:0805.3773].
- [47] S. Groote *et al.*, Phys. Lett. B **440**, 375 (1998), [hep-ph/9802374].

- [48] B. Geshkenbein and V. Morgunov, Phys. Lett. B **352**, 456 (1995).
- [49] M. L. Swartz, Phys. Rev. D **53**, 5268 (1996), [hep-ph/9509248].
- [50] N. Krasnikov and R. Rodenberg, Nuovo Cim. A **111**, 217 (1998), [hep-ph/9711367].
- [51] J. H. Kuhn and M. Steinhauser, Phys. Lett. B **437**, 425 (1998), [hep-ph/9802241].
- [52] A. D. Martin, J. Outhwaite and M. Ryskin, Phys. Lett. B **492**, 69 (2000), [hep-ph/0008078].
- [53] J. de Troconiz and F. Yndurain, Phys. Rev. D **65**, 093002 (2002), [hep-ph/0107318].
- [54] H. Burkhardt and B. Pietrzyk, Phys. Rev. D **84**, 037502 (2011), [arXiv:1106.2991].
- [55] J. Erler, P. Masjuan and H. Spiesberger, Eur. Phys. J. C **77**, 2, 99 (2017), [arXiv:1610.08531].
- [56] V. Novikov *et al.*, Phys. Rept. **41**, 1 (1978).
- [57] J. Erler and M. Luo, Phys. Lett. B **558**, 125 (2003), [hep-ph/0207114].
- [58] J. Erler, P. Masjuan and H. Spiesberger (2022), [arXiv:2203.02348].
- [59] T. Aaltonen *et al.* (CDF, DØ, Tevatron Electroweak Working Group) (2016), [arXiv:1608.01881].
- [60] M. Aaboud *et al.* (ATLAS), Eur. Phys. J. C **79**, 4, 290 (2019), [arXiv:1810.01772].
- [61] Technical Report CMS-PAS-TOP-15-012, CERN, Geneva (2016), URL <https://cds.cern.ch/record/2235162>.
- [62] A. M. Sirunyan *et al.* (CMS), Eur. Phys. J. C **79**, 4, 313 (2019), [arXiv:1812.10534].
- [63] A. M. Sirunyan *et al.* (CMS), Eur. Phys. J. C **79**, 5, 368 (2019), [arXiv:1812.10505].
- [64] A. Tumasyan *et al.* (CMS), JHEP **12**, 161 (2021), [arXiv:2108.10407].
- [65] Technical Report ATLAS-CONF-2019-046, CERN, Geneva (2019), URL <https://cds.cern.ch/record/2693954>.
- [66] V. M. Abazov *et al.* (DØ), Phys. Rev. Lett. **113**, 032002 (2014), [arXiv:1405.1756].
- [67] A. M. Sirunyan *et al.* (CMS), Eur. Phys. J. C **78**, 11, 891 (2018), [arXiv:1805.01428].
- [68] A. H. Hoang, S. Plätzer and D. Samitz, JHEP **10**, 200 (2018), [arXiv:1807.06617].
- [69] J. Kieseler, K. Lipka and S.-O. Moch, Phys. Rev. Lett. **116**, 16, 162001 (2016), [arXiv:1511.00841].
- [70] M. Beneke *et al.*, Phys. Lett. B **775**, 63 (2017), [arXiv:1605.03609].
- [71] P. Marquard *et al.*, Phys. Rev. Lett. **114**, 14, 142002 (2015), [arXiv:1502.01030].
- [72] M. Beneke, Phys. Rept. **317**, 1 (1999), [hep-ph/9807443].
- [73] S. Catani *et al.*, JHEP **07**, 100 (2019), [arXiv:1906.06535].
- [74] S. Catani *et al.*, Eur. Phys. J. C **81**, 6, 491 (2021), [arXiv:2102.03256].
- [75] A. M. Sirunyan *et al.* (CMS), Eur. Phys. J. C **80**, 7, 658 (2020), [arXiv:1904.05237].
- [76] G. Aad *et al.* (ATLAS), JHEP **11**, 150 (2019), [arXiv:1905.02302].
- [77] A. Tumasyan *et al.* (CMS), JHEP **02**, 142 (2022), [arXiv:2111.10431].
- [78] J. Erler and M. Schott, Prog. Part. Nucl. Phys. **106**, 68 (2019), [arXiv:1902.05142].
- [79] A. Sirlin, Phys. Rev. D **22**, 971 (1980).
- [80] W. J. Marciano and J. L. Rosner, Phys. Rev. Lett. **65**, 2963 (1990), [Erratum: Phys.Rev.Lett. 68, 898 (1992)].
- [81] G. Degrossi, S. Fanchiotti and A. Sirlin, Nucl. Phys. B **351**, 49 (1991).
- [82] A. Czarnecki and W. J. Marciano, Int. J. Mod. Phys. A **15**, 2365 (2000), [hep-ph/0003049].
- [83] J. Erler and M. J. Ramsey-Musolf, Phys. Rev. D **72**, 073003 (2005), [hep-ph/0409169].
- [84] K. Kumar *et al.*, Ann. Rev. Nucl. Part. Sci. **63**, 237 (2013), [arXiv:1302.6263].
- [85] G. Degrossi and A. Sirlin, Nucl. Phys. B **352**, 342 (1991).
- [86] P. Gambino and A. Sirlin, Phys. Rev. D **49**, 1160 (1994), [hep-ph/9309326].
- [87] W. Hollik, Fortsch. Phys. **38**, 165 (1990).
- [88] R. Barbieri *et al.*, Nucl. Phys. B **409**, 105 (1993).
- [89] J. Fleischer, O. Tarasov and F. Jegerlehner, Phys. Lett. B **319**, 249 (1993).
- [90] G. Degrossi, P. Gambino and A. Vicini, Phys. Lett. B **383**, 219 (1996), [hep-ph/9603374].
- [91] G. Degrossi, P. Gambino and A. Sirlin, Phys. Lett. B **394**, 188 (1997), [hep-ph/9611363].
- [92] A. Freitas *et al.*, Phys. Lett. B **495**, 338 (2000), [Erratum: Phys.Lett.B 570, 265 (2003)], [hep-ph/0007091].
- [93] M. Awramik and M. Czakon, Phys. Lett. B **568**, 48 (2003), [hep-ph/0305248].
- [94] A. Freitas *et al.*, Nucl. Phys. B **632**, 189 (2002), [Erratum: Nucl.Phys.B 666, 305–307 (2003)], [hep-ph/0202131].
- [95] M. Awramik and M. Czakon, Phys. Rev. Lett. **89**, 241801 (2002), [hep-ph/0208113].
- [96] A. Onishchenko and O. Veretin, Phys. Lett. B **551**, 111 (2003), [hep-ph/0209010].
- [97] G. Degrossi, P. Gambino and P. P. Giardino, JHEP **05**, 154 (2015), [arXiv:1411.7040].
- [98] M. Awramik *et al.*, Phys. Rev. D **69**, 053006 (2004), [hep-ph/0311148].
- [99] M. Awramik *et al.*, Phys. Rev. Lett. **93**, 201805 (2004), [hep-ph/0407317].
- [100] W. Hollik, U. Meier and S. Uccirati, Nucl. Phys. B **731**, 213 (2005), [hep-ph/0507158].
- [101] M. Awramik, M. Czakon and A. Freitas, Phys. Lett. B **642**, 563 (2006), [hep-ph/0605339].
- [102] W. Hollik, U. Meier and S. Uccirati, Nucl. Phys. B **765**, 154 (2007), [hep-ph/0610312].
- [103] M. Awramik *et al.*, Nucl. Phys. B **813**, 174 (2009), [arXiv:0811.1364].
- [104] I. Dubovyk *et al.*, Phys. Lett. B **762**, 184 (2016), [arXiv:1607.08375].
- [105] A. Freitas, Phys. Lett. B **730**, 50 (2014), [arXiv:1310.2256].
- [106] A. Freitas, JHEP **04**, 070 (2014), [arXiv:1401.2447].
- [107] I. Dubovyk *et al.*, Phys. Lett. B **783**, 86 (2018), [arXiv:1804.10236].
- [108] I. Dubovyk *et al.*, JHEP **08**, 113 (2019), [arXiv:1906.08815].
- [109] M. Awramik, M. Czakon and A. Freitas, JHEP **11**, 048 (2006), [hep-ph/0608099].
- [110] A. Djouadi and C. Verzegnassi, Phys. Lett. B **195**, 265 (1987).
- [111] A. Djouadi, Nuovo Cim. A **100**, 357 (1988).
- [112] K. Chetyrkin, J. H. Kuhn and M. Steinhauser, Phys. Lett. B **351**, 331 (1995), [hep-ph/9502291].
- [113] L. Avdeev *et al.*, Phys. Lett. B **336**, 560 (1994), [Erratum: Phys.Lett.B 349, 597–598 (1995)], [hep-ph/9406363].
- [114] Y. Schroder and M. Steinhauser, Phys. Lett. B **622**, 124 (2005), [hep-ph/0504055].
- [115] K. Chetyrkin *et al.*, Phys. Rev. Lett. **97**, 102003 (2006), [hep-ph/0605201].
- [116] R. Boughezal and M. Czakon, Nucl. Phys. B **755**, 221 (2006), [hep-ph/0606232].

- [117] B. A. Kniehl, J. H. Kuhn and R. Stuart, *Phys. Lett. B* **214**, 621 (1988).
- [118] B. A. Kniehl, *Nucl. Phys. B* **347**, 86 (1990).
- [119] F. Halzen and B. A. Kniehl, *Nucl. Phys. B* **353**, 567 (1991).
- [120] A. Djouadi and P. Gambino, *Phys. Rev. D* **49**, 3499 (1994), [Erratum: *Phys.Rev.D* 53, 4111 (1996)], [hep-ph/9309298].
- [121] A. Anselm, N. Dombey and E. Leader, *Phys. Lett. B* **312**, 232 (1993).
- [122] K. Chetyrkin, J. H. Kuhn and M. Steinhauser, *Phys. Rev. Lett.* **75**, 3394 (1995), [hep-ph/9504413].
- [123] J. van der Bij *et al.*, *Phys. Lett. B* **498**, 156 (2001), [hep-ph/0011373].
- [124] M. Faisst *et al.*, *Nucl. Phys. B* **665**, 649 (2003), [hep-ph/0302275].
- [125] R. Boughezal, J. Tausk and J. van der Bij, *Nucl. Phys. B* **725**, 3 (2005), [hep-ph/0504092].
- [126] A. Arbuzov *et al.*, *Comput. Phys. Commun.* **174**, 728 (2006), [hep-ph/0507146].
- [127] J. Erler and M. J. Ramsey-Musolf, *Prog. Part. Nucl. Phys.* **54**, 351 (2005), [hep-ph/0404291].
- [128] J. Formaggio and G. Zeller, *Rev. Mod. Phys.* **84**, 1307 (2012), [arXiv:1305.7513].
- [129] J. Dorenbosch *et al.* (CHARM), *Z. Phys. C* **41**, 567 (1989), [Erratum: *Z.Phys.C* 51, 142 (1991)].
- [130] L. Ahrens *et al.*, *Phys. Rev. D* **41**, 3297 (1990).
- [131] P. Vilain *et al.* (CHARM-II), *Phys. Lett. B* **335**, 246 (1994).
- [132] R. Allen *et al.*, *Phys. Rev. D* **47**, 11 (1993).
- [133] L. Auerbach *et al.* (LSND), *Phys. Rev. D* **63**, 112001 (2001), [hep-ex/0101039].
- [134] M. Deniz *et al.* (TEXONO), *Phys. Rev. D* **81**, 072001 (2010), [arXiv:0911.1597].
- [135] J. M. Conrad, M. H. Shaevitz and T. Bolton, *Rev. Mod. Phys.* **70**, 1341 (1998), [hep-ex/9707015].
- [136] A. Blondel *et al.*, *Z. Phys. C* **45**, 361 (1990).
- [137] J. Allaby *et al.* (CHARM), *Z. Phys. C* **36**, 611 (1987).
- [138] K. S. McFarland *et al.* (CCFR, E744, E770), *Eur. Phys. J. C* **1**, 509 (1998), [hep-ex/9701010].
- [139] R. Barnett, *Phys. Rev. D* **14**, 70 (1976).
- [140] H. Georgi and H. Politzer, *Phys. Rev. D* **14**, 1829 (1976).
- [141] S. Rabinowitz *et al.*, *Phys. Rev. Lett.* **70**, 134 (1993).
- [142] E. Paschos and L. Wolfenstein, *Phys. Rev. D* **7**, 91 (1973).
- [143] G. Zeller *et al.* (NuTeV), *Phys. Rev. Lett.* **88**, 091802 (2002), [Erratum: *Phys.Rev.Lett.* 90, 239902 (2003)], [hep-ex/0110059].
- [144] D. Akimov *et al.* (COHERENT), *Science* **357**, 6356, 1123 (2017), [arXiv:1708.01294].
- [145] D. Akimov *et al.* (COHERENT), *Phys. Rev. Lett.* **126**, 1, 012002 (2021), [arXiv:2003.10630].
- [146] J. Erler *et al.*, *Ann. Rev. Nucl. Part. Sci.* **64**, 269 (2014), [arXiv:1401.6199].
- [147] C. Prescott *et al.*, *Phys. Lett. B* **84**, 524 (1979).
- [148] D. Wang *et al.* (PVDIS), *Nature* **506**, 7486, 67 (2014).
- [149] D. Wang *et al.*, *Phys. Rev. C* **91**, 4, 045506 (2015), [arXiv:1411.3200].
- [150] R. Hasty *et al.* (SAMPLE), *Science* **290**, 2117 (2000), [arXiv:nucl-ex/0102001].
- [151] E. Beise, M. Pitt and D. Spayde, *Prog. Part. Nucl. Phys.* **54**, 289 (2005), [arXiv:nucl-ex/0412054].
- [152] S.-L. Zhu *et al.*, *Phys. Rev. D* **62**, 033008 (2000), [hep-ph/0002252].
- [153] A. Argento *et al.*, *Phys. Lett. B* **120**, 245 (1983).
- [154] W. Heil *et al.*, *Nucl. Phys. B* **327**, 1 (1989).
- [155] P. Souder *et al.*, *Phys. Rev. Lett.* **65**, 694 (1990).
- [156] D. Armstrong and R. McKeown, *Ann. Rev. Nucl. Part. Sci.* **62**, 337 (2012), [arXiv:1207.5238].
- [157] E. Derman and W. J. Marciano, *Annals Phys.* **121**, 147 (1979).
- [158] P. Anthony *et al.* (SLAC E158), *Phys. Rev. Lett.* **95**, 081601 (2005), [hep-ex/0504049].
- [159] D. Androic *et al.* (Qweak), *Nature* **557**, 7704, 207 (2018), [arXiv:1905.08283].
- [160] R. D. Carlini *et al.*, *Ann. Rev. Nucl. Part. Sci.* **69**, 191 (2019).
- [161] J. Erler, A. Kurylov and M. J. Ramsey-Musolf, *Phys. Rev. D* **68**, 016006 (2003), [hep-ph/0302149].
- [162] R. D. Young *et al.*, *Phys. Rev. Lett.* **99**, 122003 (2007), [arXiv:0704.2618].
- [163] A. Acha *et al.* (HAPPEX), *Phys. Rev. Lett.* **98**, 032301 (2007), [arXiv:nucl-ex/0609002].
- [164] M. Gorchtein and C. Horowitz, *Phys. Rev. Lett.* **102**, 091806 (2009), [arXiv:0811.0614].
- [165] M. Gorchtein, C. Horowitz and M. J. Ramsey-Musolf, *Phys. Rev. C* **84**, 015502 (2011), [arXiv:1102.3910].
- [166] N. Hall *et al.*, *Phys. Lett. B* **753**, 221 (2016), [arXiv:1504.03973].
- [167] J. Erler *et al.*, *Phys. Rev. D* **100**, 5, 053007 (2019), [arXiv:1907.07928].
- [168] M. Bouchiat and C. Bouchiat, *Phys. Lett. B* **48**, 111 (1974).
- [169] M. Safronova *et al.*, *Rev. Mod. Phys.* **90**, 2, 025008 (2018), [arXiv:1710.01833].
- [170] C. Wood *et al.*, *Science* **275**, 1759 (1997).
- [171] J. Guena, M. Lintz and M. Bouchiat, *Phys. Rev. A* **71**, 042108 (2005), [arXiv:physics/0412017].
- [172] N. Edwards *et al.*, *Phys. Rev. Lett.* **74**, 2654 (1995).
- [173] P. Vetter *et al.*, *Phys. Rev. Lett.* **74**, 2658 (1995).
- [174] D. Meekhof *et al.*, *Phys. Rev. Lett.* **71**, 3442 (1993).
- [175] M. Macpherson *et al.*, *Phys. Rev. Lett.* **67**, 20, 2784 (1991).
- [176] P. Blunden, W. Melnitchouk and A. Thomas, *Phys. Rev. Lett.* **109**, 262301 (2012), [arXiv:1208.4310].
- [177] S. Bennett and C. E. Wieman, *Phys. Rev. Lett.* **82**, 2484 (1999), [Erratum: *Phys.Rev.Lett.* 82, 4153 (1999), Erratum: *Phys.Rev.Lett.* 83, 889 (1999)], [hep-ex/9903022].
- [178] V. Dzuba and V. Flambaum., *Phys. Rev. A* **62**, 052101 (2000), [arXiv:physics/0005038].
- [179] V. Dzuba, V. Flambaum and O. Sushkov, *Phys. Rev. A* **56**, 4357 (1997), [hep-ph/9709251].
- [180] D. Cho *et al.*, *Phys. Rev. A* **55**, 1007 (1997).
- [181] G. Toh *et al.*, *Phys. Rev. Lett.* **123**, 7, 073002 (2019), [arXiv:1905.02768].
- [182] A. A. Vasilyev *et al.*, *Phys. Rev. A* **66**, 020101 (2002).
- [183] V. Dzuba, V. Flambaum and J. Ginges, *Phys. Rev. D* **66**, 076013 (2002), [hep-ph/0204134].
- [184] J. Ginges and V. Flambaum, *Phys. Rept.* **397**, 63 (2004), [arXiv:physics/0309054].
- [185] A. Derevianko and S. G. Porsev, *Eur. Phys. J. A* **32**, 4, 517 (2007), [hep-ph/0608178].
- [186] B. Roberts, V. Dzuba and V. Flambaum, *Ann. Rev. Nucl. Part. Sci.* **65**, 63 (2015), [arXiv:1412.6644].
- [187] A. Derevianko, *Phys. Rev. Lett.* **85**, 1618 (2000), [hep-ph/0005274].
- [188] W. Johnson, I. Bednyakov and G. Soff, *Phys. Rev. Lett.* **87**, 233001 (2001), [Erratum: *Phys.Rev.Lett.* 88, 079903 (2002)], [hep-ph/0110262].
- [189] M. Kuchiev and V. Flambaum, *Phys. Rev. Lett.* **89**, 283002 (2002), [hep-ph/0206124].

- [190] A. Milstein, O. Sushkov and I. Terekhov, Phys. Rev. Lett. **89**, 283003 (2002), [hep-ph/0208227].
- [191] S. Porsev, K. Bely and A. Derevianko, Phys. Rev. Lett. **102**, 181601 (2009), [arXiv:0902.0335].
- [192] V. Dzuba *et al.*, Phys. Rev. Lett. **109**, 203003 (2012), [arXiv:1207.5864].
- [193] C. Bouchiat and C. Piketty, Phys. Lett. B **128**, 73 (1983).
- [194] I. Zel'dovich, J. Exp. Theor. Phys. **6**, 1184 (1958).
- [195] V. Flambaum and D. Murray, Phys. Rev. C **56**, 1641 (1997), [arXiv:nucl-th/9703050].
- [196] W. Haxton and C. E. Wieman, Ann. Rev. Nucl. Part. Sci. **51**, 261 (2001), [arXiv:nucl-th/0104026].
- [197] V. Dzuba *et al.*, J. Phys. B **20**, 3297 (1987).
- [198] J. L. Rosner, Phys. Rev. D **53**, 2724 (1996), [hep-ph/9507375].
- [199] D. Antypas *et al.*, Nature Phys. **15**, 2, 120 (2019), [arXiv:1804.05747].
- [200] M. Ramsey-Musolf, Phys. Rev. C **60**, 015501 (1999), [hep-ph/9903264].
- [201] S. Pollock, E. Fortson and L. Wilets, Phys. Rev. C **46**, 2587 (1992), [arXiv:nucl-th/9211004].
- [202] B. Chen and P. Vogel, Phys. Rev. C **48**, 1392 (1993), [arXiv:nucl-th/9303003].
- [203] C. Horowitz *et al.*, Phys. Rev. C **63**, 025501 (2001), [arXiv:nucl-th/9912038].
- [204] S. Abrahamyan *et al.*, Phys. Rev. Lett. **108**, 112502 (2012), [arXiv:1201.2568].
- [205] D. Adhikari *et al.* (PREX), Phys. Rev. Lett. **126**, 17, 172502 (2021), [arXiv:2102.10767].
- [206] H. Davoudiasl, H.-S. Lee and W. J. Marciano, Phys. Rev. D **86**, 095009 (2012), [arXiv:1208.2973].
- [207] E. Braaten, S. Narison and A. Pich, Nucl. Phys. B **373**, 581 (1992).
- [208] A. Pich, Prog. Part. Nucl. Phys. **75**, 41 (2014), [arXiv:1310.7922].
- [209] M. Davier *et al.*, Eur. Phys. J. C **74**, 3, 2803 (2014), [arXiv:1312.1501].
- [210] K. Chetyrkin, A. Kataev and F. Tkachov, Phys. Lett. B **85**, 277 (1979).
- [211] M. Dine and J. Sapiirstein, Phys. Rev. Lett. **43**, 668 (1979).
- [212] S. Gorishnii, A. Kataev and S. Larin, Phys. Lett. B **259**, 144 (1991).
- [213] L. R. Surguladze and M. A. Samuel, Phys. Rev. Lett. **66**, 560 (1991), [Erratum: Phys.Rev.Lett. 66, 2416 (1991)].
- [214] P. Baikov, K. Chetyrkin and J. H. Kuhn, Phys. Rev. Lett. **101**, 012002 (2008), [arXiv:0801.1821].
- [215] F. Le Diberder and A. Pich, Phys. Lett. B **286**, 147 (1992).
- [216] M. Beneke and M. Jamin, JHEP **09**, 044 (2008), [arXiv:0806.3156].
- [217] E. Braaten and C.-S. Li, Phys. Rev. D **42**, 3888 (1990).
- [218] W. Marciano and A. Sirlin, Phys. Rev. Lett. **61**, 1815 (1988).
- [219] J. Erler, Rev. Mex. Fis. **50**, 200 (2004), [hep-ph/0211345].
- [220] D. Boito *et al.*, Phys. Rev. D **85**, 093015 (2012), [arXiv:1203.3146].
- [221] D. Boito *et al.*, Phys. Rev. D **91**, 3, 034003 (2015), [arXiv:1410.3528].
- [222] J. Erler (2011), [arXiv:1102.5520].
- [223] G. Bennett *et al.* (Muon g-2), Phys. Rev. Lett. **92**, 161802 (2004), [hep-ex/0401008].
- [224] B. Abi *et al.* (Muon g-2), Phys. Rev. Lett. **126**, 14, 141801 (2021), [arXiv:2104.03281].
- [225] T. Aoyama *et al.*, Phys. Rev. Lett. **109**, 111808 (2012), [arXiv:1205.5370].
- [226] T. Aoyama *et al.*, PTEP **2012**, 01A107 (2012).
- [227] P. Baikov, A. Maier and P. Marquard, Nucl. Phys. B **877**, 647 (2013), [arXiv:1307.6105].
- [228] G. Li, R. Mendel and M. A. Samuel, Phys. Rev. D **47**, 1723 (1993).
- [229] S. Laporta and E. Remiddi, Phys. Lett. B **301**, 440 (1993).
- [230] S. Laporta and E. Remiddi, Phys. Lett. B **379**, 283 (1996), [hep-ph/9602417].
- [231] A. Czarnecki and M. Skrzypek, Phys. Lett. B **449**, 354 (1999), [hep-ph/9812394].
- [232] J. Erler and M. Luo, Phys. Rev. Lett. **87**, 071804 (2001), [hep-ph/0101010].
- [233] S. Laporta, Phys. Lett. B **772**, 232 (2017), [arXiv:1704.06996].
- [234] S. J. Brodsky and J. D. Sullivan, Phys. Rev. **156**, 1644 (1967).
- [235] T. Burnett and M. Levine, Phys. Lett. B **24**, 467 (1967).
- [236] R. Jackiw and S. Weinberg, Phys. Rev. D **5**, 2396 (1972).
- [237] I. Bars and M. Yoshimura, Phys. Rev. D **6**, 374 (1972).
- [238] K. Fujikawa, B. Lee and A. Sanda, Phys. Rev. D **6**, 2923 (1972).
- [239] W. A. Bardeen, R. Gastmans and B. Lautrup, Nucl. Phys. B **46**, 319 (1972).
- [240] T. Kukhto *et al.*, Nucl. Phys. B **371**, 567 (1992).
- [241] S. Peris, M. Perrottet and E. de Rafael, Phys. Lett. B **355**, 523 (1995), [hep-ph/9505405].
- [242] A. Czarnecki, B. Krause and W. J. Marciano, Phys. Rev. D **52**, 2619 (1995), [hep-ph/9506256].
- [243] A. Czarnecki, B. Krause and W. J. Marciano, Phys. Rev. Lett. **76**, 3267 (1996), [hep-ph/9512369].
- [244] C. Gnendiger, D. Stöckinger and H. Stöckinger-Kim, Phys. Rev. D **88**, 053005 (2013), [arXiv:1306.5546].
- [245] G. Degross and G. Giudice, Phys. Rev. D **58**, 053007 (1998), [hep-ph/9803384].
- [246] A. Czarnecki, W. J. Marciano and A. Vainshtein, Phys. Rev. D **67**, 073006 (2003), [Erratum: Phys.Rev.D 73, 119901 (2006)], [hep-ph/0212229].
- [247] F. Jegerlehner, EPJ Web Conf. **166**, 00022 (2018), [arXiv:1705.00263].
- [248] P. D. Kennedy, J. Erler and H. Spiesberger (2021), [arXiv:2111.13016].
- [249] T. Aoyama *et al.*, Phys. Rept. **887**, 1 (2020), [arXiv:2006.04822].
- [250] S. Borsanyi *et al.*, Nature **593**, 7857, 51 (2021), [arXiv:2002.12347].
- [251] K. Melnikov and A. Vainshtein, Phys. Rev. D **70**, 113006 (2004), [hep-ph/0312226].
- [252] J. Erler and G. Toledo Sanchez, Phys. Rev. Lett. **97**, 161801 (2006), [hep-ph/0605052].
- [253] J. Prades, E. de Rafael and A. Vainshtein **20**, 303 (2009), [arXiv:0901.0306].
- [254] M. Knecht and A. Nyffeler, Phys. Rev. D **65**, 073034 (2002), [hep-ph/0111058].
- [255] I. Danilkin, C. F. Redmer and M. Vanderhaeghen, Prog. Part. Nucl. Phys. **107**, 20 (2019), [arXiv:1901.10346].
- [256] T. Blum *et al.*, Phys. Rev. Lett. **124**, 13, 132002 (2020), [arXiv:1911.08123].
- [257] E.-H. Chao *et al.*, Eur. Phys. J. C **81**, 7, 651 (2021), [arXiv:2104.02632].
- [258] B. Krause, Phys. Lett. B **390**, 392 (1997), [hep-ph/9607259].

- [259] A. Kurz *et al.*, Phys. Lett. B **734**, 144 (2014), [arXiv:1403.6400].
- [260] G. Colangelo *et al.*, Phys. Lett. B **735**, 90 (2014), [arXiv:1403.7512].
- [261] J. L. Lopez, D. V. Nanopoulos and X. Wang, Phys. Rev. D **49**, 366 (1994), [hep-ph/9308336].
- [262] G. Passarino and M. Veltman, Nucl. Phys. B **160**, 151 (1979).
- [263] W. Hollik and G. Duckeck, Springer Tracts Mod. Phys. **162**, 1 (2000).
- [264] B. Lynn and R. Stuart, Nucl. Phys. B **253**, 216 (1985).
- [265] S. L. Wu, Phys. Rept. **107**, 59 (1984).
- [266] R. Marshall, Z. Phys. C **43**, 607 (1989).
- [267] S. Schael *et al.* (ALEPH, DELPHI, L3, OPAL, LEP Electroweak), Phys. Rept. **532**, 119 (2013), [arXiv:1302.3415].
- [268] T. A. Aaltonen *et al.* (CDF, DØ), Phys. Rev. D **88**, 5, 052018 (2013), [arXiv:1307.7627].
- [269] Technical Report TEVEWWG/WZ 2010/01, FERMILAB, Batavia (2010), [arXiv:1003.2826], URL <https://www-d0.fnal.gov/Run2Physics/WWW/results/prelim/EW/E34>.
- [270] M. Aaboud *et al.* (ATLAS), Eur. Phys. J. C **78**, 2, 110 (2018), [Erratum: Eur.Phys.J.C 78, 898 (2018)], [arXiv:1701.07240].
- [271] R. Aaij *et al.* (LHCb), JHEP **01**, 036 (2022), [arXiv:2109.01113].
- [272] A. Tumasyan *et al.* (CMS) (2022), [arXiv:2201.07861].
- [273] G. Aad *et al.* (ATLAS), Phys. Lett. B **716**, 1 (2012), [arXiv:1207.7214].
- [274] S. Chatrchyan *et al.* (CMS), Phys. Lett. B **716**, 30 (2012), [arXiv:1207.7235].
- [275] M. Aaboud *et al.* (ATLAS), Phys. Lett. B **784**, 345 (2018), [arXiv:1806.00242].
- [276] A. M. Sirunyan *et al.* (CMS), Phys. Lett. B **805**, 135425 (2020), [arXiv:2002.06398].
- [277] A. Tumasyan *et al.* (CMS) (2022), [arXiv:2202.06923].
- [278] D. de Florian *et al.* (LHC Higgs Cross Section Working Group) (2016), [arXiv:1610.07922].
- [279] T. A. Aaltonen *et al.* (CDF, DØ), Phys. Rev. D **97**, 11, 112007 (2018), [arXiv:1801.06283].
- [280] G. Aad *et al.* (ATLAS), JHEP **09**, 049 (2015), [arXiv:1503.03709].
- [281] Technical Report ATLAS-CONF-2018-037, CERN, Geneva (2018), URL <https://cds.cern.ch/record/2630340>.
- [282] A. M. Sirunyan *et al.* (CMS), Eur. Phys. J. C **78**, 9, 701 (2018), [arXiv:1806.00863].
- [283] R. Aaij *et al.* (LHCb), JHEP **11**, 190 (2015), [arXiv:1509.07645].
- [284] K. Abe *et al.* (SLD), Phys. Rev. Lett. **84**, 5945 (2000), [hep-ex/0004026].
- [285] K. Abe *et al.* (SLD), Phys. Rev. Lett. **86**, 1162 (2001), [hep-ex/0010015].
- [286] D. Kennedy *et al.*, Nucl. Phys. B **321**, 83 (1989).
- [287] S. Riemann, Rept. Prog. Phys. **73**, 126201 (2010).
- [288] K. Abe *et al.* (SLD), Phys. Rev. Lett. **85**, 5059 (2000), [hep-ex/0006019].
- [289] K. Abe *et al.* (SLD), Phys. Rev. Lett. **78**, 17 (1997), [hep-ex/9609019].
- [290] W. Bernreuther *et al.*, JHEP **01**, 053 (2017), [arXiv:1611.07942].
- [291] S. Catani and M. H. Seymour, JHEP **07**, 023 (1999), [hep-ph/9905424].
- [292] A. Djouadi, J. H. Kuhn and P. Zerwas, Z. Phys. C **46**, 411 (1990).
- [293] T. A. Aaltonen *et al.* (CDF), Phys. Rev. D **93**, 11, 112016 (2016), [Addendum: Phys.Rev.D 95, 119901 (2017)], [arXiv:1605.02719].
- [294] V. M. Abazov *et al.* (DØ), Phys. Rev. Lett. **120**, 24, 241802 (2018), [arXiv:1710.03951].
- [295] V. Abazov *et al.* (DØ), Phys. Rev. D **84**, 012007 (2011), [arXiv:1104.4590].
- [296] D. Acosta *et al.* (CDF), Phys. Rev. D **71**, 052002 (2005), [hep-ex/0411059].
- [297] V. Andreev *et al.* (H1), Eur. Phys. J. C **78**, 9, 777 (2018), [arXiv:1806.01176].
- [298] H. Abramowicz *et al.* (ZEUS), Phys. Rev. D **93**, 9, 092002 (2016), [arXiv:1603.09628].
- [299] P. Janot and S. Jadach, Phys. Lett. B **803**, 135319 (2020), [arXiv:1912.02067].
- [300] D. Albert *et al.*, Nucl. Phys. B **166**, 460 (1980).
- [301] K. Chetyrkin, J. H. Kuhn and A. Kwiatkowski, Phys. Rept. **277**, 189 (1996), [hep-ph/9503396].
- [302] B. A. Kniehl and J. H. Kuhn, Nucl. Phys. B **329**, 547 (1990).
- [303] K. Chetyrkin and A. Kwiatkowski, Phys. Lett. B **319**, 307 (1993), [hep-ph/9310229].
- [304] S. Larin, T. van Ritbergen and J. Vermaseren, Phys. Lett. B **320**, 159 (1994), [hep-ph/9310378].
- [305] K. Chetyrkin and O. Tarasov, Phys. Lett. B **327**, 114 (1994), [hep-ph/9312323].
- [306] P. Baikov *et al.*, Phys. Rev. Lett. **108**, 222003 (2012), [arXiv:1201.5804].
- [307] A. Kataev, Phys. Lett. B **287**, 209 (1992).
- [308] B. W. Lynn and R. G. Stuart, Phys. Lett. B **252**, 676 (1990).
- [309] J. Bernabeu, A. Pich and A. Santamaria, Nucl. Phys. B **363**, 326 (1991).
- [310] A. Czarnecki and J. H. Kuhn, Phys. Rev. Lett. **77**, 3955 (1996), [hep-ph/9608366].
- [311] R. Harlander, T. Seidensticker and M. Steinhauser, Phys. Lett. B **426**, 125 (1998), [hep-ph/9712228].
- [312] J. Fleischer *et al.*, Phys. Lett. B **459**, 625 (1999), [hep-ph/9904256].
- [313] P. A. Grassi, B. A. Kniehl and A. Sirlin, Phys. Rev. Lett. **86**, 389 (2001), [hep-th/0005149].
- [314] A. Akhundov, D. Bardin and T. Riemann, Nucl. Phys. B **276**, 1 (1986).
- [315] F. Jegerlehner, Z. Phys. C **32**, 425 (1986), [Erratum: Z.Phys.C 38, 519 (1988)].
- [316] W. Beenakker and W. Hollik, Z. Phys. C **40**, 141 (1988).
- [317] D. Bardin *et al.*, Z. Phys. C **44**, 493 (1989).
- [318] A. Borrelli *et al.*, Nucl. Phys. B **333**, 357 (1990).
- [319] A. Denner and T. Sack, Z. Phys. C **46**, 653 (1990).
- [320] A. Denner, Fortsch. Phys. **41**, 307 (1993), [arXiv:0709.1075].
- [321] G. Aad *et al.* (ATLAS), Nature Phys. **17**, 7, 813 (2021), [arXiv:2007.14040].
- [322] U. Amaldi *et al.*, Phys. Rev. D **36**, 1385 (1987).
- [323] G. Costa *et al.*, Nucl. Phys. B **297**, 244 (1988).
- [324] P. Langacker and M. Luo, Phys. Rev. D **44**, 817 (1991).
- [325] J. Erler and P. Langacker, Phys. Rev. D **52**, 441 (1995), [hep-ph/9411203].
- [326] F. James and M. Roos, Comput. Phys. Commun. **10**, 343 (1975).
- [327] D. d'Enterrria and A. Poldaru, JHEP **06**, 016 (2020), [arXiv:1912.11733].
- [328] V. Abazov *et al.* (DØ), Phys. Rev. D **80**, 111107 (2009), [arXiv:0911.2710].
- [329] M. Cè *et al.* (2022), [arXiv:2203.08676].

- [330] J. Bagger, K. T. Matchev and D. Pierce, Phys. Lett. B **348**, 443 (1995), [hep-ph/9501277].
- [331] P. Langacker and N. Polonsky, Phys. Rev. D **52**, 3081 (1995), [hep-ph/9503214].
- [332] M. Veltman, Nucl. Phys. B **123**, 89 (1977).
- [333] M. S. Chanowitz, M. Furman and I. Hinchliffe, Phys. Lett. B **78**, 285 (1978).
- [334] J. van der Bij and F. Hoogeveen, Nucl. Phys. B **283**, 477 (1987).
- [335] P. Langacker and M. Luo, Phys. Rev. D **45**, 278 (1992).
- [336] A. Denner, R. Guth and J. H. Kuhn, Phys. Lett. B **240**, 438 (1990).
- [337] W. Grimus *et al.*, J. Phys. G **35**, 075001 (2008), [arXiv:0711.4022].
- [338] H. E. Haber and D. O'Neil, Phys. Rev. D **83**, 055017 (2011), [arXiv:1011.6188].
- [339] S. Bertolini and A. Sirlin, Phys. Lett. B **257**, 179 (1991).
- [340] M. Golden and L. Randall, Nucl. Phys. B **361**, 3 (1991).
- [341] B. Holdom and J. Terning, Phys. Lett. B **247**, 88 (1990).
- [342] M. E. Peskin and T. Takeuchi, Phys. Rev. Lett. **65**, 964 (1990).
- [343] K. Hagiwara *et al.*, Z. Phys. C **64**, 559 (1994), [Erratum: Z.Phys.C 68, 352 (1995)], [hep-ph/9409380].
- [344] M. E. Peskin and T. Takeuchi, Phys. Rev. D **46**, 381 (1992).
- [345] I. Maksymyk, C. Burgess and D. London, Phys. Rev. D **50**, 529 (1994), [hep-ph/9306267].
- [346] R. Barbieri *et al.*, Nucl. Phys. B **703**, 127 (2004), [hep-ph/0405040].
- [347] M. Farina *et al.*, Phys. Lett. B **772**, 210 (2017), [arXiv:1609.08157].
- [348] G. Altarelli and R. Barbieri, Phys. Lett. B **253**, 161 (1991).
- [349] D. Kennedy and P. Langacker, Phys. Rev. D **44**, 1591 (1991).
- [350] L. Randall and R. Sundrum, Phys. Rev. Lett. **83**, 3370 (1999), [hep-ph/9905221].
- [351] M. Carena *et al.*, Nucl. Phys. B **759**, 202 (2006), [hep-ph/0607106].
- [352] R. Contino (2011), [arXiv:1005.4269].
- [353] D. D. Dietrich, F. Sannino and K. Tuominen, Phys. Rev. D **72**, 055001 (2005), [hep-ph/0505059].
- [354] E. Gates and J. Terning, Phys. Rev. Lett. **67**, 1840 (1991).
- [355] H. Georgi, Nucl. Phys. B **363**, 301 (1991).
- [356] M. J. Dugan and L. Randall, Phys. Lett. B **264**, 154 (1991).
- [357] H. E. Haber and G. L. Kane, Phys. Rept. **117**, 75 (1985).
- [358] A. Djouadi, Phys. Rept. **459**, 1 (2008), [hep-ph/0503173].
- [359] R. Barbieri *et al.*, Nucl. Phys. B **341**, 309 (1990).
- [360] R. Barbieri, M. Frigeni and F. Caravaglios, Phys. Lett. B **279**, 169 (1992).
- [361] J. Erler and D. M. Pierce, Nucl. Phys. B **526**, 53 (1998), [hep-ph/9801238].
- [362] G.-C. Cho and K. Hagiwara, Nucl. Phys. B **574**, 623 (2000), [hep-ph/9912260].
- [363] G. Altarelli *et al.*, JHEP **06**, 018 (2001), [hep-ph/0106029].
- [364] S. Heinemeyer, W. Hollik and G. Weiglein, Phys. Rept. **425**, 265 (2006), [hep-ph/0412214].
- [365] S. P. Martin, K. Tobe and J. D. Wells, Phys. Rev. D **71**, 073014 (2005), [hep-ph/0412424].
- [366] M. Ramsey-Musolf and S. Su, Phys. Rept. **456**, 1 (2008), [hep-ph/0612057].
- [367] S. Heinemeyer *et al.*, JHEP **04**, 039 (2008), [arXiv:0710.2972].
- [368] O. Buchmueller *et al.*, Eur. Phys. J. C **72**, 2020 (2012), [arXiv:1112.3564].
- [369] B. Grinstein and M. B. Wise, Phys. Lett. B **265**, 326 (1991).
- [370] A. Pich, I. Rosell and J. Sanz-Cillero, JHEP **01**, 157 (2014), [arXiv:1310.3121].
- [371] C. T. Hill and E. H. Simmons, Phys. Rept. **381**, 235 (2003), [Erratum: Phys.Rept. 390, 553–554 (2004)], [hep-ph/0203079].
- [372] G. Panico and A. Wulzer **913** (2016), [arXiv:1506.01961].
- [373] J. Erler and P. Langacker, Phys. Rev. Lett. **105**, 031801 (2010), [arXiv:1003.3211].
- [374] J. Gunion, D. W. McKay and H. Pois, Phys. Rev. D **53**, 1616 (1996), [hep-ph/9507323].
- [375] A. Lenz, Adv. High Energy Phys. **2013**, 910275 (2013).
- [376] S. Chatrchyan *et al.* (CMS), Phys. Rev. D **86**, 112003 (2012), [arXiv:1209.1062].
- [377] A. Djouadi and A. Lenz, Phys. Lett. B **715**, 310 (2012), [arXiv:1204.1252].
- [378] O. Eberhardt *et al.*, Phys. Rev. Lett. **109**, 241802 (2012), [arXiv:1209.1101].
- [379] J. Maalampi and M. Roos, Phys. Rept. **186**, 53 (1990).
- [380] P. Langacker, Phys. Rept. **72**, 185 (1981).
- [381] J. L. Hewett and T. G. Rizzo, Phys. Rept. **183**, 193 (1989).
- [382] J. Kang, P. Langacker and B. D. Nelson, Phys. Rev. D **77**, 035003 (2008), [arXiv:0708.2701].
- [383] S. P. Martin, Phys. Rev. D **81**, 035004 (2010), [arXiv:0910.2732].
- [384] P. W. Graham *et al.*, Phys. Rev. D **81**, 055016 (2010), [arXiv:0910.3020].
- [385] J. Erler, J. L. Feng and N. Polonsky, Phys. Rev. Lett. **78**, 3063 (1997), [hep-ph/9612397].
- [386] D. Choudhury, T. M. Tait and C. Wagner, Phys. Rev. D **65**, 053002 (2002), [hep-ph/0109097].
- [387] J. Erler and P. Langacker, Phys. Rev. Lett. **84**, 212 (2000), [hep-ph/9910315].
- [388] P. Langacker and M. Plumacher, Phys. Rev. D **62**, 013006 (2000), [hep-ph/0001204].
- [389] P. Abreu *et al.* (DELPHI), Eur. Phys. J. C **10**, 415 (1999).
- [390] P. Langacker and D. London, Phys. Rev. D **38**, 886 (1988).
- [391] F. del Aguila, J. de Blas and M. Perez-Victoria, Phys. Rev. D **78**, 013010 (2008), [arXiv:0803.4008].
- [392] M. Chemtob, Prog. Part. Nucl. Phys. **54**, 71 (2005), [hep-ph/0406029].
- [393] R. Barbieri *et al.*, Phys. Rept. **420**, 1 (2005), [hep-ph/0406039].
- [394] T. Han, H. E. Logan and L.-T. Wang, JHEP **01**, 099 (2006), [hep-ph/0506313].
- [395] M. Perelstein, Prog. Part. Nucl. Phys. **58**, 247 (2007), [hep-ph/0512128].
- [396] I. Antoniadis (2001), [hep-th/0102202].
- [397] M. Carena *et al.*, Phys. Rev. D **68**, 035010 (2003), [hep-ph/0305188].
- [398] K. Agashe *et al.*, JHEP **08**, 050 (2003), [hep-ph/0308036].
- [399] I. Gogoladze and C. Macesanu, Phys. Rev. D **74**, 093012 (2006), [hep-ph/0605207].
- [400] S. Weinberg, Phys. Rev. Lett. **43**, 1566 (1979).
- [401] W. Buchmuller and D. Wyler, Nucl. Phys. B **268**, 621 (1986).
- [402] B. Grzadkowski *et al.*, JHEP **10**, 085 (2010), [arXiv:1008.4884].
- [403] R. Contino *et al.*, JHEP **07**, 035 (2013), [arXiv:1303.3876].
- [404] K. Hagiwara *et al.*, Phys. Rev. D **48**, 2182 (1993).

- [405] A. Falkowski, F. Riva and A. Urbano, JHEP **11**, 111 (2013), [arXiv:1303.1812].
- [406] A. Pomarol and F. Riva, JHEP **01**, 151 (2014), [arXiv:1308.2803].
- [407] J. Ellis, V. Sanz and T. You, JHEP **03**, 157 (2015), [arXiv:1410.7703].
- [408] A. Efrati, A. Falkowski and Y. Soreq, JHEP **07**, 018 (2015), [arXiv:1503.07872].
- [409] J. de Blas *et al.*, PoS **EPS-HEP2017**, 467 (2017), [arXiv:1710.05402].
- [410] S. Dawson and P. P. Giardino, Phys. Rev. D **101**, 1, 013001 (2020), [arXiv:1909.02000].
- [411] G.-C. Cho, K. Hagiwara and S. Matsumoto, Eur. Phys. J. C **5**, 155 (1998), [hep-ph/9707334].
- [412] K. Cheung, Phys. Lett. B **517**, 167 (2001), [hep-ph/0106251].
- [413] Z. Han and W. Skiba, Phys. Rev. D **71**, 075009 (2005), [hep-ph/0412166].
- [414] P. Langacker, M. Luo and A. K. Mann, Rev. Mod. Phys. **64**, 87 (1992).
- [415] P. Langacker, Rev. Mod. Phys. **81**, 1199 (2009), [arXiv:0801.1345].

11. Status of Higgs Boson Physics

Revised October 2021 by M. Carena (FNAL; Chicago U.; Chicago U., Kavli Inst.), C. Grojean (DESY, Hamburg; Physik, Humboldt U.), M. Kado (Rome U. Sapienza; INFN, Rome; U. Paris-Saclay, IJCLab) and V. Sharma (UC San Diego).

11.1	Introduction	201
11.2	The Standard Model and the mechanism of electroweak symmetry breaking	202
11.2.1	The SM Higgs boson mass, couplings and quantum numbers	203
11.2.2	The SM custodial symmetry	203
11.2.3	Stability of the Higgs potential	203
11.2.4	Higgs boson production and decay mechanisms	203
11.3	The experimental profile of the Higgs boson	208
11.3.1	The principal decay channels to vector bosons	208
11.3.2	Decays to third generation fermions ($b\bar{b}$ and $\tau^+\tau^-$)	210
11.3.3	Higgs boson production in association with top quarks or in top decays	212
11.3.4	Higgs boson pair production	214
11.3.5	Searches for rare decays of the Higgs boson	215
11.3.6	Searches for non-SM decay channels	217
11.4	Combining the main channels	219
11.4.1	Principles of the combination	219
11.4.2	Main decay modes	220
11.4.3	Main production modes	222
11.5	Main quantum numbers and width of the Higgs boson	222
11.5.1	Main quantum numbers J^{PC}	222
11.5.2	Off-shell couplings of the Higgs boson	225
11.5.3	The Higgs boson width	226
11.6	Probing the coupling properties of the Higgs boson	227
11.6.1	Effective Lagrangian framework	228
11.6.2	Probing coupling properties	228
11.7	New physics models of EWSB in the light of the Higgs boson discovery	234
11.7.1	Higgs bosons in the minimal supersymmetric standard model (MSSM)	236
11.7.2	Supersymmetry with singlet extensions	238
11.7.3	Supersymmetry with extended gauge sectors	238
11.7.4	Effects of CP violation	239
11.7.5	Non-supersymmetric extensions of the Higgs sector	240
11.7.6	Composite Higgs models	242
11.7.7	Searches for signatures of extended Higgs sectors	245
11.8	Summary and outlook	250

11.1 Introduction

Understanding the mechanism that breaks the electroweak symmetry and generates the masses of the known elementary particles has been one of the fundamental endeavours in particle physics for several decades. The discovery in 2012 by the ATLAS [1] and the CMS [2] collaborations of a new resonance with a mass of approximately 125 GeV and the subsequent studies of its properties with the full data set from Run 1, from 2009 to 2012, with a centre-of-mass energy of 7 TeV and 8 TeV, conclusively provided a first portrait of the Electroweak Symmetry Breaking (EWSB) mechanism. The data collected during the LHC Run 2, from 2015 to 2018, with a higher centre-of-mass energy of 13 TeV and more conspicuous dataset, put in solid grounds the compatibility of the measured resonance with the Higgs boson of the Standard Model (SM) [3] and strongly challenge its contenders. LHC will start its Run 3 in 2022 and is expected to last until 2025. During this period the LHC is expected to deliver proton-proton collision data corresponding to an integrated luminosity of approximately 160 fb^{-1} per experiment.

In the SM, the electroweak interactions are described by a gauge field theory invariant under the $SU(2)_L \times U(1)_Y$ symmetry group. The mechanism of EWSB [4] provides a general framework to keep

untouched the structure of these gauge interactions at high energies and still generate the observed masses of the W and Z gauge bosons. The EWSB mechanism posits a self-interacting complex EW doublet scalar field, whose CP -even neutral component acquires a vacuum expectation value (VEV) $v \approx 246\text{ GeV}$, which sets the scale of the symmetry breaking. Three massless Goldstone bosons are generated and are absorbed to give masses to the W and Z gauge bosons. The remaining component of the complex doublet becomes the Higgs boson – a new, and so far unique, fundamental scalar particle. The masses of all fermions are also a consequence of EWSB since the Higgs doublet is postulated to couple to the fermions through Yukawa interactions. Remarkably, these Yukawa interactions to the heaviest fermions have now been established.

The initial measurements during the LHC Run 1 were accessible mainly through production and decay channels related to the couplings of the Higgs boson to the vector gauge bosons (the mediators of the electroweak interactions, W^\pm , Z and γ , as well as the gluons, g , mediators of the strong interactions). The outstanding performance of the LHC Run 2, made it possible for the ATLAS and CMS experiments to independently and unambiguously establish the couplings of the Higgs boson to the charged fermions of the third generation (the top quark, the bottom quark, and the tau lepton). These observations of fundamental importance were made with partial Run 2 datasets. In all observed production and decay modes measured so far, the rates and differential measurements are found to be consistent, within experimental and theoretical uncertainties, with the SM predictions. In high resolution decay channels, such as the ones with four leptons (electrons or muons) or diphoton final states, the mass of the Higgs boson has been measured at the permill precision level. Nevertheless, several channels are still out of reach experimentally and the couplings of the Higgs boson to light fermions are very challenging and yet to be observed; however, the very recent results of the search for Higgs boson decays to muons by the ATLAS and CMS experiments provide evidence for the Yukawa coupling of the Higgs boson to muons. Moreover, within the current precision, a more complex sector with additional states, although significantly constrained, is not ruled out, nor has it been established whether the Higgs boson is an elementary particle or whether it has an internal structure like any other scalar particle observed before it.

Without the Higgs boson, the calculability of the SM would have been spoiled. In particular, perturbative unitarity [5] would be lost at high energies since the longitudinal W/Z boson scattering amplitude would grow with the centre-of-mass energy. In addition, the radiative corrections to the gauge boson self-energies would exhibit dangerous logarithmic divergences that would be difficult to reconcile with EW precision data. With the discovery of the Higgs boson, the SM is a spontaneously broken gauge theory and, as such, it could a priori be consistently extrapolated well above the masses of the W and Z bosons. Hence, formally there is no need for new physics at the EW scale. However, as the SM Higgs boson is a scalar particle, at the quantum level it has sensitivity to possible new physics scales. Quite generally, the Higgs boson mass is affected by the presence of heavy particles and it receives quantum corrections which destabilise the weak scale barring a large fine-tuning of unrelated parameters. This is known as the Higgs naturalness or hierarchy problem [6]. It has been the prime argument for expecting new physics right at the TeV scale. New theoretical paradigms have been imagined, such as a new fermion-boson symmetry called supersymmetry (SUSY) [7] (for recent reviews, see Refs. [8,9]), or the existence of strong interactions at a scale of the order of a TeV from which the Higgs boson would emerge as a composite state [10] (see Refs. [11,12] for recent reviews). Alternatively, new agents stabilising the weak scale could also be light but elusive, like in models of neutral naturalness [13,14]. Other recent scenarios [15,16], instead, rely on the cosmological evolution of the Universe to drive the Higgs boson mass to a value much smaller than the cutoff of the theory and aim at alleviating the hierarchy problem without the need for TeV scale new physics, even thought there might still be interesting and spectacular signatures [15,17]. This new approach spurs a change in perspective invoking our Universe as part of a

multiverse that should be treated as a quantum statistical system [18]. Beyond the naturalness problem, extensions of the SM Higgs sector without other low-energy particles have been proposed, for example, to provide explanations for the fermion mass hierarchies, see e.g. Ref. [19], to account for the Dark Matter abundance, see e.g. Ref. [20], or to modify the properties of the electroweak phase transition [21]. Such models with additional scalars provide grounds to explore new Higgs boson signals in concrete and complete scenarios, with different types of coupling structure to fermions and gauge bosons.

The Higgs boson is anyway special and, in the nine years since its discovery, it became a powerful tool to explore the manifestations of the SM and to probe the physics landscape beyond it. It might offer direct insights on what comes beyond the weak scale through possible sizeable effects on the Higgs boson properties. The Higgs boson couplings, however, are observed to be in good agreement with their SM predictions. This, together with the strong bounds from precision electroweak and flavour data, leaves open the possibility that the Higgs boson may well be elementary, weakly coupled and solitary up to the Planck scale, rendering the EW vacuum potentially metastable [22].

After completion of the first two runs, the LHC has only gathered approximately 5% of its projected full dataset. LHC is undergoing important upgrades in order to prepare for its high luminosity phase. The foreseen larger datasets to be collected during Run 3 and ultimately during the High Luminosity LHC (HL-LHC), will enable yet more fundamental and challenging measurements to explore new physics.

This review is organised as follows. Section 11.2 is a theoretical review of the SM Higgs boson, its properties, production mechanisms and decay rates. In Section 11.3, the experimental measurements are described. In Section 11.4, the combination of the main Higgs boson production and decay channels is presented. In Section 11.5, measurements of the main quantum numbers and CP properties of the Higgs boson are reported and the bounds on its total width are discussed. In Section 11.6, a general theoretical framework to describe the deviations of the Higgs boson couplings from the SM predictions is introduced and the experimental measurements of these Higgs couplings is reviewed. Measurements of differential cross sections are outlined. Section 11.7 presents, in detail, some interesting models proposed for extensions of the SM Higgs sector, addressing the hierarchy problem or not, and considers their experimental signatures. Section 11.8 provides a short summary and a brief outlook.

11.2 The Standard Model and the mechanism of electroweak symmetry breaking

In the SM [3], electroweak symmetry breaking [4] is responsible for generating mass for the W and Z gauge bosons rendering the weak interactions short ranged. The SM scalar potential reads:

$$V(\Phi) = m^2 \Phi^\dagger \Phi + \lambda (\Phi^\dagger \Phi)^2 \quad (11.1)$$

with the Higgs field Φ being a self-interacting $SU(2)_L$ complex doublet (four real degrees of freedom) with weak hypercharge $Y=1$ (the hypercharge is normalised such that $Q = T_{3L} + Y/2$, Q being the electric charge and T_{3L} the eigenvalue of the diagonal generator of $SU(2)_L$):

$$\Phi = \frac{1}{\sqrt{2}} \begin{pmatrix} \sqrt{2}\phi^+ \\ \phi^0 + ia^0 \end{pmatrix}, \quad (11.2)$$

where ϕ^0 and a^0 are the CP -even and CP -odd neutral components, and ϕ^+ is the complex charged component of the Higgs doublet, respectively. $V(\Phi)$ is the most general renormalisable scalar potential. If the quadratic term is negative, the neutral component of the scalar doublet acquires a non-zero (real) vacuum expectation value (VEV)

$$\langle \Phi \rangle = \frac{1}{\sqrt{2}} \begin{pmatrix} 0 \\ v \end{pmatrix}, \quad (11.3)$$

with $\phi^0 = H + \langle \phi^0 \rangle$ and $\langle \phi^0 \rangle \equiv v$, inducing the spontaneous breaking of the SM gauge symmetry $SU(3)_C \times SU(2)_L \times U(1)_Y$ into $SU(3)_C \times U(1)_{\text{em}}$. The global minimum of the theory defines the

ground state, and spontaneous symmetry breaking implies that there is a (global and/or local) symmetry of the system that is not respected by the ground state. From the four generators of the $SU(2)_L \times U(1)_Y$ SM gauge group, three are spontaneously broken, implying that they lead to non-trivial transformations of the ground state and indicate the existence of three massless Goldstone bosons identified with three of the four Higgs field degrees of freedom. The Higgs field couples to the W_μ and B_μ gauge fields associated with the $SU(2)_L \times U(1)_Y$ local symmetry through the covariant derivative appearing in the kinetic term of the Higgs Lagrangian,

$$\mathcal{L}_{\text{Higgs}} = (D_\mu \Phi)^\dagger (D^\mu \Phi) - V(\Phi), \quad (11.4)$$

where $D_\mu \Phi = (\partial_\mu + ig\sigma^a W_\mu^a/2 + ig'YB_\mu/2)\Phi$, g and g' are the $SU(2)_L$ and $U(1)_Y$ gauge couplings, respectively, and $\sigma^a, a = 1, 2, 3$ are the usual Pauli matrices. As a result, the neutral and the two charged massless Goldstone degrees of freedom mix with the gauge fields corresponding to the broken generators of $SU(2)_L \times U(1)_Y$ and become, in the unitarity gauge, the longitudinal components of the Z and W physical gauge bosons, respectively. The Z and W gauge bosons acquire masses,

$$m_W^2 = \frac{g^2 v^2}{4}, \quad m_Z^2 = \frac{(g'^2 + g^2)v^2}{4}. \quad (11.5)$$

The fourth generator remains unbroken since it is the one associated to the conserved $U(1)_{\text{em}}$ gauge symmetry, and its corresponding gauge field, the photon, remains massless. Similarly, the eight color gauge bosons, the gluons, corresponding to the conserved $SU(3)_C$ gauge symmetry with 8 unbroken generators, also remain massless (though confined inside hadrons and mesons as the result of the asymptotic freedom behaviour of Quantum Chromodynamics (QCD)). Hence, from the initial four degrees of freedom of the Higgs field, two are absorbed by the W^\pm gauge bosons, one by the Z gauge boson, and there is one remaining degree of freedom, H , that is the physical Higgs boson — a new scalar particle first imagined by P. Higgs [4]. The Higgs boson is neutral under the electromagnetic interactions and transforms as a singlet under $SU(3)_C$ and hence does not couple at tree level to the massless photons and gluons.

The fermions of the SM acquire mass through renormalisable interactions between the Higgs field and the fermions: the Yukawa interactions,

$$\mathcal{L}_{\text{Yukawa}} = -\hat{h}_{d_{ij}} \bar{q}_{L_i} \Phi d_{R_j} - \hat{h}_{u_{ij}} \bar{q}_{L_i} \tilde{\Phi} u_{R_j} - \hat{h}_{l_{ij}} \bar{l}_{L_i} \Phi e_{R_j} + h.c., \quad (11.6)$$

which respect the symmetries of the SM but generate fermion masses once EWSB occurs. In the Lagrangian above, $\tilde{\Phi} = i\sigma_2 \Phi^*$ and q_L (l_L) and u_R , d_R (e_R) are the quark (lepton) $SU(2)_L$ doublets and singlets, respectively, while in each term, $\hat{h}_{f_{ij}}$, $f = u, d, l$ is parametrized by a 3×3 matrix in family space. The mass term for neutrinos is omitted, but could be added in an analogous manner to the up-type quarks when right-handed neutrinos are supplementing the SM particle content (neutrinos can also acquire Majorana masses via non-renormalisable dimension-5 interactions with the Higgs field [23]). Once the Higgs field acquires a VEV, and after rotation to the fermion mass eigenstate basis that also diagonalises the Higgs-fermion interactions, $\hat{h}_{f_{ij}} \rightarrow h_{f_i} \delta_{ij}$ (the diagonal Yukawa coupling h_{f_i} is often denoted as y_{f_i}), all fermions acquire a mass given by $m_{f_i} = h_{f_i} v / \sqrt{2}$. The indices $i, j = 1, 2, 3$ refer to the three families in the up-quark, down-quark or charged lepton sectors. Remarkably, if the Yukawa interactions Eq. (11.6) are indeed fully responsible for the fermion masses, the Higgs interactions do not mediate flavour changing neutral currents at tree-level. It should be further noted that the EWSB mechanism provides no additional insight on possible underlying reasons for the large variety of mass values of the fermions, often referred to as the flavour hierarchy. The fermion masses, accounting for a large number of the free parameters of the SM, are simply translated into Yukawa couplings.

11.2.1 The SM Higgs boson mass, couplings and quantum numbers

The SM Higgs boson is a CP -even scalar of spin 0. Its mass is given by $m_H = \sqrt{2\lambda} v$, where λ is the self coupling parameter in $V(\Phi)$. The expectation value of the Higgs field, $v = (\sqrt{2}G_F)^{-1/2} \approx 246$ GeV, is fixed by the Fermi coupling G_F , which is determined with a precision of 0.6 ppm from muon decay measurements [24]. The quartic coupling λ is a free parameter in the SM, and hence, there is no a priori prediction for the Higgs mass. Moreover the sign of the mass parameter $m^2 = -\lambda v^2$ has to be negative for the EW symmetry breaking to take place, but there is no a priori understanding of what decides of this sign. The experimentally measured Higgs boson mass, $m_H = 125.25 \pm 0.17$ GeV [24], implies that $\lambda \simeq 0.13$ and $|m| \simeq 88.4$ GeV.

The Higgs boson couplings to the fundamental particles are set by their masses. This is a new type of interaction; very weak for light particles, such as up and down quarks, and electrons, but strong for heavy particles such as the W and Z bosons and the top quark. More precisely, the SM Higgs couplings to fundamental fermions are linearly proportional to the fermion masses, whereas the couplings to bosons are proportional to the square of the boson masses. The SM Higgs boson couplings to gauge bosons and fermions, as well as the Higgs boson self coupling, are summarized in the following Lagrangian:

$$\mathcal{L} = -g_{Hf\bar{f}}\bar{f}fH + \frac{g_{HHH}}{6}H^3 + \frac{g_{HHHH}}{24}H^4 + \delta_V V_\mu V^\mu \left(g_{HVV}H + \frac{g_{HHVV}}{2}H^2 \right) \quad (11.7)$$

with

$$g_{Hf\bar{f}} \equiv y_f = \frac{m_f}{v}, \quad g_{HVV} = \frac{2m_V^2}{v}, \quad g_{HHVV} = \frac{2m_V^2}{v^2}, \quad (11.8)$$

$$g_{HHH} = \frac{3m_H^2}{v}, \quad g_{HHHH} = \frac{3m_H^2}{v^2},$$

where $V = W^\pm$ or Z and $\delta_W = 1, \delta_Z = 1/2$. As a result, the dominant mechanisms for Higgs boson production and decay involve the coupling of H to W, Z and/or the third generation quarks and leptons. The Higgs boson coupling to gluons [25,26] is induced at leading order by a one-loop process in which H couples to a virtual $t\bar{t}$ pair (with minor contributions from the other lighter quarks). Likewise, the Higgs boson coupling to photons is also generated via loops, although in this case the one-loop graph with a virtual W^+W^- pair provides the dominant contribution [27] and it is interfering destructively with the smaller contribution involving a virtual $t\bar{t}$ pair (as such, the Higgs coupling to photons is sensitive to the relative phase of the interactions between bosons and fermions).

11.2.2 The SM custodial symmetry

The SM Higgs Lagrangian, $\mathcal{L}_{\text{Higgs}} + \mathcal{L}_{\text{Yukawa}}$ of Eq. (11.4) and Eq. (11.6), is, by construction, $SU(2)_L \times U(1)_Y$ gauge invariant, but it also has an approximate global symmetry. In the limit $g' \rightarrow 0$ and $h_f \rightarrow 0$, a global $SU(2)_R$ symmetry emerges. This symmetry is preserved for non-vanishing Yukawa couplings, provided $h_u = h_d$. Once the Higgs acquires a VEV, both the $SU(2)_L$ and $SU(2)_R$ symmetry groups are broken but the diagonal subgroup $SU(2)_{L+R}$ remains unbroken and it is the subgroup that defines the custodial symmetry of the SM [28].

In the limit $g' \rightarrow 0$, the W and Z gauge bosons have equal mass and form a triplet of the $SU(2)_{L+R}$ unbroken global symmetry. Using the expressions for the W and Z gauge boson masses in term of the gauge couplings, one obtains at tree level

$$\frac{m_W^2}{m_Z^2} = \frac{g^2}{g'^2 + g^2} = \cos^2 \theta_W \quad \text{or} \quad \rho \equiv \frac{m_W^2}{m_Z^2 \cos^2 \theta_W} = 1. \quad (11.9)$$

The custodial symmetry protects the above relation from large radiative corrections. All corrections to the ρ parameter are therefore proportional to terms that break the custodial symmetry. For instance, radiative corrections involving the Higgs boson are proportional to $\sin^2 \theta_W, \delta\rho =$

$-11G_F m_Z^2 \sin^2 \theta_W \log(m_H^2/m_Z^2)/(24\sqrt{2}\pi^2)$, and vanish in the limit $g' \rightarrow 0$. Since $m_t \neq m_b$, there are also relevant radiative corrections generated by massive fermions. They are proportional to $m_t^2 + m_b^2 - 2(m_t^2 m_b^2) \log(m_t^2/m_b^2)/(m_t^2 - m_b^2)$ and would indeed vanish for $m_t = m_b$ [29].

11.2.3 Stability of the Higgs potential

The discovery of the Higgs boson with $m_H \approx 125$ GeV has far reaching consequences within the SM framework. In particular, the precise value of m_H determines the value of the quartic coupling λ at the electroweak scale and makes it possible to study its behavior up to high energy scales. A larger value of m_H would have implied that the self coupling λ would become non-perturbative at some scale Λ that could be well below the Planck scale [30].

However, for the value of Higgs boson mass experimentally measured, the EW vacuum of the Higgs potential is most likely metastable [22]. The high-energy evolution of λ shows that it becomes negative at energies $\Lambda = \mathcal{O}(10^{11})$ GeV (even though λ could remain positive till higher energy, maybe all the way to the Planck scale, if the top quark mass exceeds its current measured value by 3σ). When this occurs, the SM Higgs potential develops an instability and the long term existence of the EW vacuum is challenged. This behaviour may call for new physics at an intermediate scale before the instability develops, i.e., below M_{Planck} , even though new physics at M_{Planck} could influence the stability of the EW vacuum and possibly modify this conclusion [31]. The consequences of the instability of the EW vacuum on high-scale inflation have been discussed in Ref. [32]. It was also noticed that Higgs field fluctuations during inflation could seed the formation of primordial black holes, possibly making up the Dark Matter relic abundance [33] or they could produce a stochastic background of gravitational waves with characteristic structures [34], offering a probe of the EW vacuum near criticality.

The lifetime of the EW metastable vacuum is determined by the rate of quantum tunnelling from this vacuum into the true vacuum of the theory (for the most recent computation of the EW vacuum lifetime within the SM, see Ref. [35]). Within the SM, the running of the Higgs self coupling slows down at high energies with a cancellation of its β -function at energies just one to two orders of magnitude below the Planck scale [36]. This slow evolution of the quartic coupling is responsible for saving the EW vacuum from premature collapse. It might also help the Higgs boson to play the role of an inflaton [37] (see, however, Ref. [38] for potential issues with this Higgs-boson-as-an-inflaton idea).

11.2.4 Higgs boson production and decay mechanisms

Comprehensive reviews of the SM Higgs boson's properties and phenomenology, with an emphasis on the impact of loop corrections to the Higgs boson decay rates and cross sections, can be found in Refs. [39–46]. The main results are summarised here.

11.2.4.1 Production mechanisms at hadron colliders

The main production mechanisms at the Tevatron collider and the LHC are gluon fusion (ggF), weak-boson fusion (VBF), associated production with a gauge boson (VH), and associated production with a pair of $t\bar{t}$ quarks ($t\bar{t}H$) or with a single top quark (tHq). Figure 11.1 depicts representative diagrams for these dominant Higgs boson production processes.

The state-of-the-art of the theoretical calculations in the main different production channels is summarized in Table 11.1.

The cross sections for the production of a SM Higgs boson as a function of \sqrt{s} , the center of mass energy, for pp collisions, including bands indicating the theoretical uncertainties, are summarized in Fig. 11.2 (left) [47]. A detailed discussion, including uncertainties in the theoretical calculations due to missing higher-order effects and experimental uncertainties on the determination of SM parameters involved in the calculations, can be found in Refs. [43–46]. These references also contain state-of-the-art discussions on the impact of PDF uncertainties, QCD scale uncertainties and uncertainties due to different procedures for including higher-order corrections matched to parton shower simulations, as well as uncertainties due to hadronisation and parton-shower events.

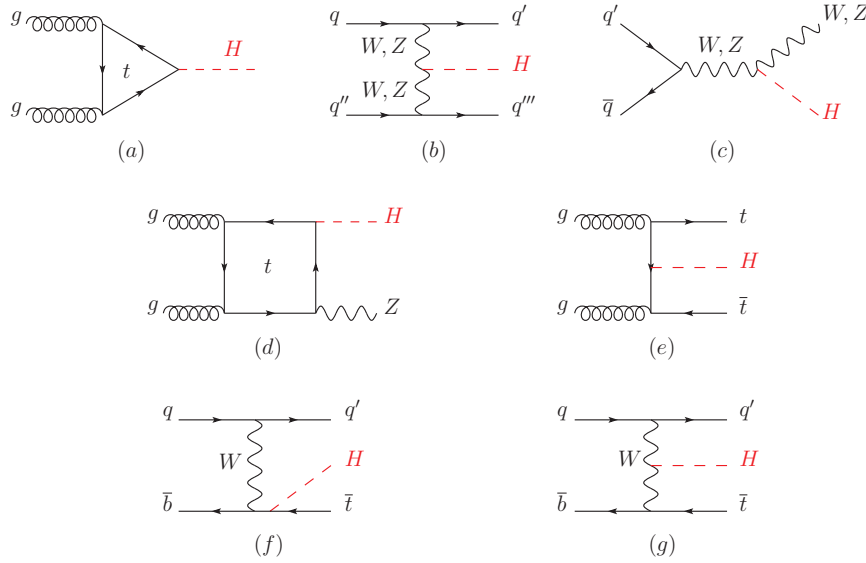


Figure 11.1: Main leading order Feynman diagrams contributing to the Higgs boson production in (a) gluon fusion, (b) Vector-boson fusion, (c) Higgs-strahlung (or associated production with a gauge boson at tree level from a quark-quark interaction), (d) associated production with a gauge boson (at loop level from a gluon-gluon interaction), (e) associated production with a pair of top quarks (there is a similar diagram for the associated production with a pair of bottom quarks), (f-g) production in association with a single top quark

Table 11.1: State-of-the-art of the theoretical calculations in the main Higgs boson production channels in the SM, and the major MC tools used in the simulations

ggF	VBF	VH	ttH
Fixed order: N3LO QCD + NLO EW (HIGLU, iHixs, FeHiPro, HNLO)	Fixed order: NNLO/NLOPS QCD (VBF@NNLO)	Fixed order: NNLO QCD+EW (V2HV and HAWK)	Fixed order: NNLO QCD (Powheg)
Resummed: NNLO + NNLL QCD (HRes)	Fixed order: NLO QCD + NLO EW (HAWK)	Fixed order: NNLO QCD (VH@NNLO)	(MG5_aMC@NLO)
Differential $p_T(H)$: N3LO (HqT, HRes)			
Fiducial: N3LO+N3LL'			

Table 11.2 summarizes the Higgs boson production cross sections and relative uncertainties for a Higgs boson mass of 125 GeV, for $\sqrt{s} = 7, 8, 13$ and 14 TeV.

i. Gluon fusion production mechanism

At high-energy hadron colliders, the Higgs boson production mechanism with the largest cross section is the gluon-fusion process, $gg \rightarrow H + X$, mediated by the exchange of a virtual, heavy top quark [49]. Contributions from lighter quarks propagating in the loop are suppressed proportionally to m_q^2 . QCD radiative corrections to the gluon-fusion process are very important and have been studied in detail. Including the full dependence on the (top, bottom, charm) quark and Higgs boson masses, the cross section has been calculated at the next-to-leading order (NLO) in α_s [50, 51]. To a very good approximation, the leading top-quark contribution can be evaluated in the limit $m_t \rightarrow \infty$ by matching the SM to an effective theory. The gluon-fusion amplitude is then evaluated from an effective Lagrangian containing a local $HG_{\mu\nu}^a G^{a\mu\nu}$ operator [25, 26]. In this approximation, the cross section is known at next-to-next-to-next-to-leading order (N3LO) [52]. The validity of the effective theory with infinite m_t is greatly enhanced by rescaling the result by the exact LO result: $\sigma = (\sigma_{m_t}^{\text{LO}} / \sigma_{m_t=\infty}^{\text{LO}}) \times \sigma_{m_t=\infty}$ [46]. The large top-quark mass approximation, after this rescaling of the cross section, yields a NNLO result that has been established to be at the percent level accuracy [53]. Further progress is made to include full top mass

dependence at NNLO [54].

The LO and NLO QCD corrections [55] amount to about 80% of the total N3LO cross section. The NNLO corrections [56] further enhance the cross section by approximately 30% of the LO plus NLO result (at $\mu_f = \mu_r = m_H/2$). Electroweak radiative corrections have been computed at NLO and increase the LO cross section by about 5% for $m_H \simeq 125$ GeV [57]. Mixed QCD-EW corrections are now being investigated with encouraging results on the computation of the exact 3-loop amplitude [58] complementing the results obtained in either limit of heavy [59] or massless [60] gauge bosons. The mixed QCD-EW corrections still have to be evaluated at large p_T .

At N3LO, the perturbation series is rather stable with a mere enhancement of 3% of the total cross section, with a central value quite insensitive to threshold resummation effects with the scale choice mentioned above ($\mu_f = \mu_r = m_H/2$) [46, 52, 61]. At the LHC with a center-of-mass energy of 13 TeV, the most up-to-date value for the production cross section of a 125.09 GeV Higgs boson amounts to [46]

$$\sigma_{\text{ggF}}^{\text{N3LO}} = 48.5 \pm 1.9 (\pm 3.9\%) (\text{theory}) \pm 1.6 (3.2\%) (\text{PDF} + \alpha_s) \text{ pb.} \quad (11.10)$$

Besides considering the inclusive Higgs boson production cross section at the LHC, it is important to study differential distributions in order to probe the properties of the Higgs boson in a detailed way. Fully-differential N3LO QCD predictions for Higgs production in gluon fusion have been obtained by combin-

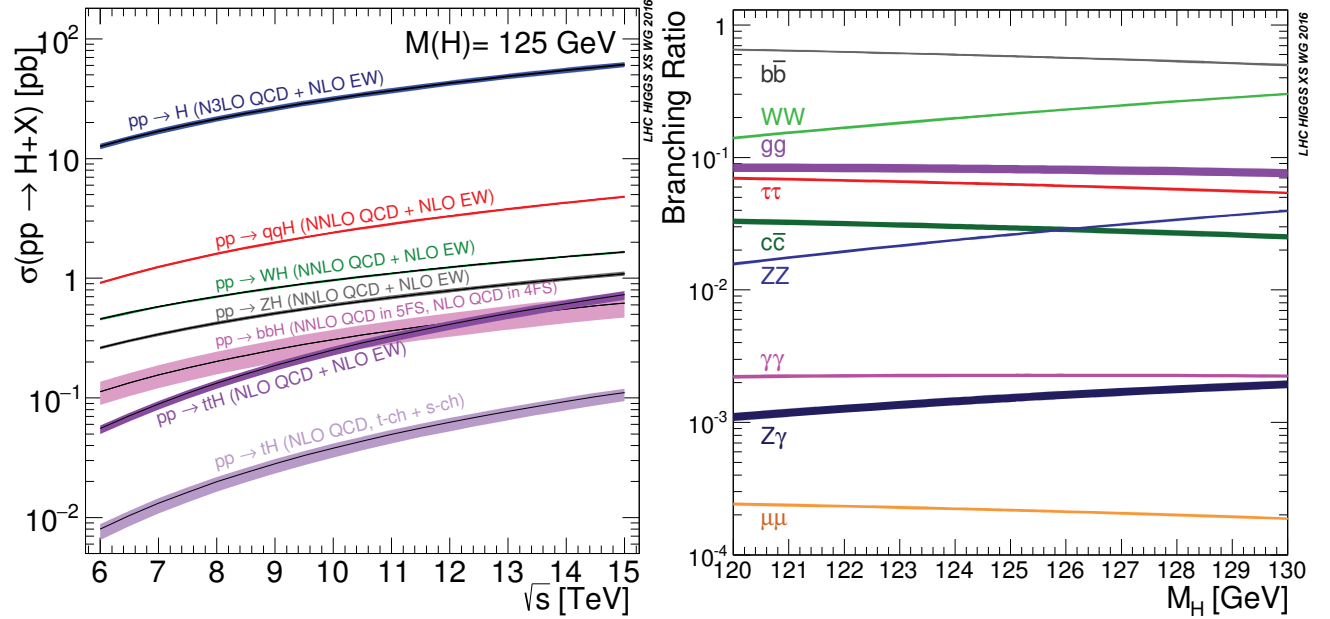


Figure 11.2: (Left) The SM Higgs boson production cross sections as a function of the center of mass energy, \sqrt{s} , for pp collisions [47]. The VBF process is indicated here as qqH . The theoretical uncertainties are indicated as bands. (Right) The branching ratios for the main decays of the SM Higgs boson near $m_H = 125$ GeV [45, 46]. The theoretical uncertainties are indicated as bands.

Table 11.2: The SM Higgs boson production cross sections for $m_H = 125$ GeV in pp collisions (pp collisions at $\sqrt{s} = 1.96$ TeV for the Tevatron), as a function of the center of mass energy, \sqrt{s} . The predictions for the LHC energies are taken from Refs. [43–46], the ones for the Tevatron energy are the ones used in Ref. [48]. The predictions for the ggF channel at the LHC include the latest N3LO results leading to reduced theoretical uncertainties by a factor around 2 compared to the NNLO+NLL results. The total uncertainties are estimated assuming no correlations between α_S and PDF uncertainties.

\sqrt{s} (TeV)	Production cross section (in pb) for $m_H = 125$ GeV					total
	ggF	VBF	WH	ZH	ttH	
1.96	$0.95^{+17\%}_{-17\%}$	$0.065^{+8\%}_{-7\%}$	$0.13^{+8\%}_{-8\%}$	$0.079^{+8\%}_{-8\%}$	$0.004^{+10\%}_{-10\%}$	1.23
7	$16.9^{+5.5\%}_{-7.6\%}$	$1.24^{+2.2\%}_{-2.2\%}$	$0.58^{+2.2\%}_{-2.3\%}$	$0.34^{+3.1\%}_{-3.0\%}$	$0.09^{+5.6\%}_{-10.2\%}$	19.1
8	$21.4^{+5.4\%}_{-7.6\%}$	$1.60^{+2.1\%}_{-2.1\%}$	$0.70^{+2.1\%}_{-2.2\%}$	$0.42^{+3.4\%}_{-2.9\%}$	$0.13^{+5.9\%}_{-10.1\%}$	24.2
13	$48.6^{+5.6\%}_{-7.4\%}$	$3.78^{+2.1\%}_{-2.1\%}$	$1.37^{+2.0\%}_{-2.0\%}$	$0.88^{+4.1\%}_{-3.5\%}$	$0.50^{+6.8\%}_{-9.9\%}$	55.1
14	$54.7^{+5.6\%}_{-7.4\%}$	$4.28^{+2.1\%}_{-2.1\%}$	$1.51^{+1.8\%}_{-1.9\%}$	$0.99^{+4.1\%}_{-3.7\%}$	$0.61^{+6.9\%}_{-9.8\%}$	62.1

ing N3LO QCD predictions for Higgs rapidity distribution with NNLO predictions for H +jet [62]. A more exclusive account of Higgs boson production is also required because experimental analyses often impose cuts on the final states in order to improve the signal-to-background ratio. Using soft-collinear effective theory, large fiducial power corrections induced by fiducial cuts have been resummed at N3LO+N3LL' accuracy [63]. This is the most accurate result that can be directly compared with fiducial measurements. Different fiducial cuts are explored to suppress these fiducial effects. In addition, nice progress is made to improve the calculation of the Higgs boson production cross section with a jet veto (the “0-jet bin” or in the presence of a veto bounding

the transverse momentum of the hardest accompanying jet) [64], reaching N2LL accuracy matched to N3LO. These accurate predictions for the jet-veto cross section are required, e.g., to suppress the $t\bar{t}$ background in the $H \rightarrow WW$ channel [65].

ii. Vector boson fusion production mechanism

The SM Higgs boson production mode with the second-largest cross section at the LHC is vector boson fusion. At the Tevatron collider, VBF also occurred, but for $m_H = 125$ GeV had a smaller cross section than Higgs boson production in association with a W or Z boson. Higgs boson production via VBF, $qq \rightarrow qqH$, proceeds by the scattering of two (anti-)quarks, mediated by t - or u -channel exchange of a W or Z boson, with the Higgs boson radiated off the weak-boson propagator. The scattered quarks give rise to two back-to-back hard jets in the forward and backward regions of the detector [66]. Because of the color-singlet nature of the weak-gauge boson exchange, gluon radiation from the central-rapidity regions is strongly suppressed. These characteristic features of VBF processes can be exploited to distinguish them from overwhelming QCD backgrounds, including gluon-fusion induced Higgs boson + 2 jet production, and from s -channel WH or ZH production with a hadronically decaying weak gauge boson. After the application of specific selection cuts, the VBF channel provides a clean environment, not only for the Higgs boson searches originally performed, but also for the subsequent determination of Higgs boson couplings at the LHC.

The cross-section is known at N3LO at the inclusive level and at N2LO enforcing the VBF cuts [67] with a residual uncertainty of the order of few permill. However, this result is obtained in the DIS/factorized approximation [68] where the fusing gauge bosons are emitted from the two quark legs independently. While, the exact NNLO VBF calculation will remain out-of-reach in the near future, the leading non-factorisable contributions with two forward jets have been estimated [69] and the impact of non-factorizable effects have been studied in Ref. [70]. They give some corrections, also of the order of few permill, to inclusive quantities, but they are an order of magnitude larger for differential observables. Overall, the residual uncertainty is of the order of a few percent but is quite sensitive to the tagging jet cuts and jet radius modelling [71]. Extensive studies on VBF at fixed order and with parton shower matched computations can be found in Ref. [72].

iii. *WH and ZH associated production mechanism*

The next most relevant Higgs boson production mechanisms are associated production with W and Z gauge bosons. The cross sections for the associated production processes, $pp \rightarrow VH + X$, with $V = W^\pm, Z$ receive contributions at NLO given by NLO QCD corrections to the Drell–Yan cross section [73, 74] and from NLO EW corrections. The latter, unlike the QCD corrections, do not respect the factorisation into Drell–Yan production since there are irreducible box contributions already at one loop [75]. At NNLO, the Drell–Yan-like corrections to WH production also give the bulk of the corrections to ZH production [76]. For ZH production there are, however, gluon-gluon induced contributions that do not involve a virtual Z gauge boson but are such that the Z gauge boson and H boson couple to gluons via top-quark loops [77], see diagram (d) in Fig. 11.1. NLO virtual corrections to the partonic cross section for $gg \rightarrow ZH$, in the high-energy and large top mass limits are available in Refs. [78]. In addition, WH and ZH production receive non Drell–Yan-like corrections in the $q\bar{q}'$ and $q\bar{q}$ initiated channels, respectively, at the NNLO level, where the Higgs boson is radiated off top-quark loops [79]. The full QCD corrections up to NNLO order, the NLO EW corrections and the NLO corrections to the gluon-gluon channel are available in VH NNLO [80]. NNLO QCD corrections to $pp \rightarrow WH + \text{jet}$ are important for signal modelling. NLO corrections to cross section inclusive in the number of jets show excellent convergence while NNLO QCD corrections to exclusive single jet cross section are much more significant [81].

As neither the Higgs boson nor the weak gauge bosons are stable particles, their decays also have to be taken into account. Providing full kinematical information for the decay products can furthermore help in the suppression of large QCD backgrounds. Differential distributions for the processes $pp \rightarrow WH \rightarrow \bar{\nu}_\ell \ell H$ and $pp \rightarrow ZH \rightarrow \ell^+ \ell^- H / \nu_\ell \bar{\nu}_\ell H$, including NLO QCD and EW corrections, have been presented in Ref. [82]. The NNLO QCD corrections to differential observables for WH production at the LHC, including the leptonic decays of the W boson and the decay of the Higgs boson into a $b\bar{b}$ pair, are presented in Ref. [83]. Calculations at the same level, including also the ZH process have been performed [84]. The WH production mode has also been matched to a parton shower at NNLO accuracy [85]. Full NNLO results for both the production and decay are available [86] and show a large impact of radiation from the final-state bottoms. The WH and ZH production modes, especially in the boosted regime, provide a relatively clean environment for studying the decay of the Higgs boson into bottom quarks [87]. Bottom mass effects have been computed at NNLO [88, 89] and tend to increase the rates by 6–7%.

iv. *Higgs boson production in association with $t\bar{t}$*

Higgs boson radiation off top quarks, $pp \rightarrow t\bar{t}H$, provides a direct probe of the top-Higgs Yukawa coupling. The LO cross section for this production process was computed in Ref. [90]. Later, the NLO(+NNLL) QCD [91] and NLO EW corrections [92] were evaluated yielding a moderate increase in the total cross section of at most 20%, but significantly reducing the scale dependence of the inclusive cross section. The EW corrections can be enhanced by large electroweak Sudakov logarithms in particular in the boosted regime often used in the phenomenological analyses [93]. The resummation of soft gluon contributions close to the partonic kinematical threshold are considered in Refs. [94]. Full off-shell calculations with decaying top quarks are computed at NLO QCD [95] and NLO QCD plus EW [96] order, respectively. Interfaces between NLO QCD calculations for $t\bar{t}H$ production with parton-shower Monte-Carlo programs have been provided in Refs. [97]. These programs provide the most flexible tools to date for the computation of differential distributions, including experimental selection cuts and vetoes on the final-state particles and their decay products. The fixed-order NLO QCD calculation has been interfaced with the standard Parton Shower Monte-Carlo generators, allowing an accurate description of the $t\bar{t}H$ signal, from the energy scale of the hard scattering to the hadronisation energy scale. The exploitation of this channel requires, however, a

proper description of the background, in particular $t\bar{t}b\bar{b}$, which exhibits a huge k-factor¹ enhancement from shower effects, see Ref. [46] for a detailed discussion. The total theoretical uncertainties, estimated by combining the ones from factorisation and renormalisation scales, strong gauge coupling, and parton distributions, amount to 10–15% of the corresponding inclusive cross section. To match the experimental precision envisioned at the end of HL-LHC, NNLO QCD predictions are required. Using the q_T subtraction formalism for $t\bar{t}H$ production, Ref. [98] presented the first quantitative results at NLO and NNLO. The calculation is accurate at NLO in QCD and agrees with the results obtained using the conventional subtraction methods. The NNLO corrections are computed for the flavour off-diagonal partonic channels but their contribution turn out to be at the permill level. The results for the diagonal channels are still missing. Most recently, the fragmentation and splitting functions for the production of a Higgs boson have been computed at order $y_t^2 \alpha_s$ and they can be used to compute differential cross sections with arbitrary top-quark and Higgs-boson masses directly from the results in the massless limit [99].

v. *Other single Higgs boson production mechanisms at the LHC*

The Higgs boson production in association with a single top quark, though subdominant, can bring valuable information, in particular regarding the sign of the top Yukawa coupling. This is due to an almost totally destructive interference between two large contributions, one where the Higgs boson couples to a space-like W boson and the other where it couples to the top quark. This process has been computed at NLO QCD in a five-flavour scheme [100] and amounts to about 90 fb at $\sqrt{s} = 14$ TeV (with the opposite sign of the top Yukawa coupling, the cross section increases by one order of magnitude while the cross section for associated production with a pair of top quarks is unaffected). Recently, the tHj (and tZj) process has been computed at NLO QCD+EW accuracy [101]. The NLO EW correction is found to be within the NLO QCD theory uncertainties if the 4 vs 5 flavor scheme uncertainty is taken into account. The EW corrections reduce the total cross section by 3–4%.

The Higgs boson production in association with a pair of bottom quarks ($b\bar{b}H$) is known at NNLO in the 5-flavour scheme [102–104]. The coupling of the Higgs boson to a b -quark is suppressed in the SM by the bottom-quark mass over the Higgs VEV, m_b/v , implying that associated production of a SM Higgs boson with b -quarks is small at the LHC. Yet, at high energy, large logarithms are present and need to be resummed, leading to an enhancement of the inclusive cross section. At $\sqrt{s} = 14$ TeV, the $b\bar{b}H$ cross section can be as large as 550 fb, still two orders of magnitude below the ggF production cross section. Furthermore, the overwhelming ZH and VBF backgrounds (at the inclusive but also differential levels) make it challenging to extract genuine bottom Yukawa signal in a traditional cut-based analysis [105] but innovative machine-learning techniques are a promising avenue to obtain information complementary to the ones extracted from $gg \rightarrow h \rightarrow b\bar{b}$, in particular for what concerns the phase of the bottom Yukawa coupling [106]. In a two Higgs doublet model or a SUSY model, which will be discussed in Section 11.7, this coupling is proportional to the ratio of neutral Higgs boson vacuum expectation values, $\tan\beta$, and can be significantly enhanced for large values of this ratio. Consequently, the $b\bar{b}H$ mode can even become the dominant production process for the Higgs boson, unlike in the SM.

The Higgs boson production in association with charm quarks is also known at NNLO and its cross section is approximately 85 fb at $\sqrt{s} = 13$ TeV [46].

vi. *Double Higgs boson production at the LHC*

The main interest in the double Higgs boson production is that it can provide invaluable information on the Higgs potential. In particular, it gives access to the Higgs trilinear self coupling. The

¹the k-factor is defined as the ratio of a physical quantity with and without radiative corrections included.

dominant production is via gluon fusion $gg \rightarrow HH$. It accounts for more than 90% of the total inclusive cross-section, the sub-leading production mechanisms are VBF $HHjj$ (around 1.7 fb at 13 TeV), HHW (0.50 fb), HHZ (0.36 fb) and $t\bar{t}HH$ (0.8 fb). The fixed order QCD corrections, computed in the infinite top mass limit, are large, typically doubling the cross section from LO to NLO [107], further enhancing it by 20% and reducing the scale uncertainty by a factor 2-3 from NLO to NNLO [108], with a milder increase of order 3% at N3LO [109] to finally reach at 13 TeV

$$\sigma(gg \rightarrow HH)_{\text{ggF}}^{\text{N3LO}} = 31.31 \text{ fb}_{-2.8\%}^{+0.66\%}. \quad (11.11)$$

Recently, the complete NLO corrections with all top quark mass effects also became available numerically [110], intriguingly revealing a k -factor much less flat than predicted in the large top mass approximations. The non-trivial dependence of the results on the renormalisation scheme and scale for the top quark mass questions the assessment of the scale uncertainty and would warrant a proper NNLO computation that will however remain out of reach for quite some time. At the differential level, the destructive interference between the box and the triangle contributions complicates the predictions made in the infinite top mass limit for both the HH invariant mass and the leading Higgs boson p_T distributions. With an inclusive cross section of about 35 fb at $\sqrt{s} = 13$ TeV and a difficult signal vs background discrimination, the double Higgs boson production remains a challenging channel to probe and will greatly benefit from the high-luminosity run of the LHC and the combination of various decay modes [111]. The double Higgs channel is definitively a prime target on the Higgs physics agenda and the forthcoming analyses will greatly benefit from the solidification of the fixed order predictions and the detailed uncertainty budget estimate that is underway [112].

11.2.4.2 Production mechanisms at e^+e^- colliders

The dominant Higgs boson production cross sections at an e^+e^- collider are from the Higgs-strahlung process [25, 113], $e^+e^- \rightarrow ZH$, and the WW fusion process [114], $e^+e^- \rightarrow \bar{\nu}_e \nu_e W^* W^* \rightarrow \bar{\nu}_e \nu_e H$. The cross-section for the Higgs-strahlung process scales as s^{-1} and is predominant at low energies, while the cross-section for the WW fusion process scales as $\ln(s/m_H^2)$ and dominates at high energies [115]. The ZZ fusion mechanism, $e^+e^- \rightarrow e^+e^- Z^* Z^* \rightarrow e^+e^- H$, also contributes to the Higgs boson production, with a cross-section suppressed by an order of magnitude with respect to that of WW fusion. The process $e^+e^- \rightarrow t\bar{t}H$ [116] becomes important for $\sqrt{s} \geq 500$ GeV. For a more detailed discussion of Higgs boson production properties at lepton colliders, see for example Refs. [117]. Interesting progress has been made recently [118] to accurately account for beamstrahlung and initial state radiation using the factorisation approach primarily developed for hadron colliders and this method is being implemented in Monte Carlo event generators.

11.2.4.3 SM Higgs boson branching ratios and total width

For the understanding and interpretation of the experimental results, the computation of all relevant Higgs boson decay widths is essential, including an estimate of their uncertainties and, when appropriate, the effects of Higgs boson decays into off-shell particles with successive decays into lighter SM ones. A Higgs boson mass of about 125 GeV allows to explore the Higgs boson couplings to many SM particles. In particular the dominant decay modes are $H \rightarrow b\bar{b}$ and $H \rightarrow WW^*$, followed by $H \rightarrow gg$, $H \rightarrow \tau^+\tau^-$, $H \rightarrow c\bar{c}$ and $H \rightarrow ZZ^*$. With much smaller rates follow the Higgs boson decays into $H \rightarrow \gamma\gamma$, $H \rightarrow \gamma Z$ and $H \rightarrow \mu^+\mu^-$. Since the decays into gluons, diphotons and $Z\gamma$ are loop induced, they provide indirect information on the Higgs boson couplings to WW , ZZ and $t\bar{t}$ in different combinations. The uncertainties in the branching ratios include the missing higher-order corrections in the theoretical calculations as well as the errors in the SM input parameters, in particular fermion masses and the QCD gauge coupling, involved in the decay. In the following the state-of-the-art of the theoretical calculations compiled by the LHC Higgs Working Group [47] will be discussed and the reader is referred to Refs. [43–46, 119] for detail.

The evaluation of the radiative corrections to the fermionic decays of the SM Higgs boson are implemented in HDECAY [120]

at different levels of accuracy. The computations of the $H \rightarrow b\bar{b}$ and $H \rightarrow c\bar{c}$ decays include the complete massless QCD corrections up to N4LO, with a corresponding scale dependence of about 0.1% [121]. Both the electroweak corrections to $H \rightarrow b\bar{b}$, $c\bar{c}$ as well as $H \rightarrow \tau^+\tau^-$ are known at NLO [122] providing predictions with an overall accuracy of about 1–2% for $m_H \simeq 125$ GeV.

The loop induced decays of the SM Higgs boson are known fully at NLO and partially beyond that approximation. For $H \rightarrow gg$, the QCD corrections are known up to N3LO in the limit of heavy top quarks [51, 123] and the uncertainty from the scale dependence is about 3%. For the $H \rightarrow \gamma\gamma$, the full NLO QCD corrections are available [51, 124] and the three-loop QCD corrections have also been evaluated [125]. The NLO electroweak corrections to $H \rightarrow gg$ and $H \rightarrow \gamma\gamma$ have been computed in Ref. [126]. All these corrections are implemented in HDECAY [120]. For $m_H \simeq 125$ GeV, the overall impact of known QCD and EW radiative effects turns out to be well below 1%. In addition, the contribution of the $H \rightarrow \gamma e^+e^-$ decay via virtual photon conversion has been computed in Ref. [127]. The partial decay width $H \rightarrow Z\gamma$ is only implemented at LO in HDECAY, including the virtual W , top-, bottom-, and τ -loop contributions. The QCD corrections have been calculated and are at the percent level [128]. The theoretical uncertainty due to unknown electroweak corrections is estimated to be less than 5%, an accuracy that will be hard to achieve in the measurement of this process at the LHC.

Table 11.3: The branching ratios and the relative uncertainty for a SM Higgs boson with $m_H = 125$ GeV [45, 46].

Decay channel	Branching ratio	Rel. uncertainty
$H \rightarrow \gamma\gamma$	2.27×10^{-3}	2.1%
$H \rightarrow ZZ$	2.62×10^{-2}	$\pm 1.5\%$
$H \rightarrow W^+W^-$	2.14×10^{-1}	$\pm 1.5\%$
$H \rightarrow \tau^+\tau^-$	6.27×10^{-2}	$\pm 1.6\%$
$H \rightarrow b\bar{b}$	5.82×10^{-1}	$+1.2\%$ -1.3%
$H \rightarrow c\bar{c}$	2.89×10^{-2}	$+5.5\%$ -2.0%
$H \rightarrow Z\gamma$	1.53×10^{-3}	$\pm 5.8\%$
$H \rightarrow \mu^+\mu^-$	2.18×10^{-4}	$\pm 1.7\%$

The decays $H \rightarrow WW/ZZ \rightarrow 4f$ can be simulated with the **Prophecy4f** Monte-Carlo generator [129] that includes complete NLO QCD and EW corrections for Higgs decays into any possible four-fermion final state. All calculations are consistently performed with off-shell gauge bosons, without any on-shell approximation. For the SM Higgs boson, the missing higher-order corrections are estimated to be roughly 0.5%. Such uncertainties will have to be combined with the parametric uncertainties, in particular those associated to the bottom-quark mass and the strong gauge coupling, to arrive at the full theory uncertainty. A detailed treatment of the differential distributions for a Higgs boson decay into four charged leptons in the final state is discussed in Refs. [45, 130].

The total width of a 125 GeV SM Higgs boson is $\Gamma_H = 4.07 \times 10^{-3}$ GeV, with a relative uncertainty of $+4.0\%$
 -3.9% . The branching ratios for the most relevant decay modes of the SM Higgs boson as a function of m_H , including the most recent theoretical uncertainties, are shown in Fig. 11.2 (right) and listed for $m_H = 125$ GeV in Table 11.3. Further details of these calculations can be found in the reviews [43–46] and references therein.

11.3 The experimental profile of the Higgs boson

The observation [1, 2] at the LHC of a narrow resonance with a mass of about 125 GeV was an important landmark in the decades-long direct search [48, 131] for the SM Higgs boson. This was followed by a detailed exploration of properties of the Higgs boson at the different runs of the LHC at $\sqrt{s} = 7, 8$ and 13 TeV.

The dataset at $\sqrt{s} = 13$ TeV in the Run 2 phase of the LHC operation corresponds to an integrated luminosity of about 156 fb^{-1} to the ATLAS and CMS experiments, see Table 11.4. The datasets effectively useful for analysis need to take into account the data-taking efficiency with fully operational detectors and the data quality efficiency. The typical total inefficiency for both ATLAS and CMS is approximately 10%, where approximately half is due to the data taking inefficiency and half from data quality.

In this section, most of the references for the Run 1 measurements that have been updated at the Run 2 are given in the previous version of this review [132] and are not repeated herein.

Table 11.4: The LHC pp collision centre-of-mass energies and delivered data samples.

Year	\sqrt{s} (TeV)	$\int \text{L.dt}$ (fb^{-1})	Period
2010	7	0.04	Run 1
2011	7	6.1	Run 1
2012	8	23.3	Run 1
2015	13	4.2	Run 2
2016	13	40.8	Run 2
2017	13	50.2	Run 2
2018	13	60.6	Run 2

11.3.1 The principal decay channels to vector bosons

For a given m_H , the sensitivity of a channel depends on the production cross section of the Higgs boson, its decay branching fraction, the reconstructed mass resolution, the selection efficiency and the level of background in the final state. For a low-mass Higgs boson ($110 \text{ GeV} < m_H < 150 \text{ GeV}$) for which the SM width would be only a few MeV, five decay channels play an important role at the LHC. In the $H \rightarrow \gamma\gamma$ and $H \rightarrow ZZ^* \rightarrow 4\ell$ channels, all final state particles can be very precisely measured and the reconstructed m_H resolution is excellent (typically 1-2%). While the $H \rightarrow W^\pm W^\mp(*) \rightarrow \ell^+ \nu_\ell \ell'^- \bar{\nu}_{\ell'}$ channel has relatively large branching fraction, however, due to the presence of neutrinos which are not reconstructed in the final state, the m_H resolution, obtained through observables sensitive to the Higgs boson mass such as the transverse mass, is poor (approximately 20%). The $H \rightarrow b\bar{b}$ and the $H \rightarrow \tau^+\tau^-$ (with the tau subsequently decaying to electrons or muons and two neutrinos $\tau \rightarrow \ell\nu\nu$ or to hadrons and one neutrino $\tau \rightarrow \text{hadrons}\nu$) channels suffer from large backgrounds and lead to an intermediate mass resolution of about 10% and 15% respectively.

With the increase in the size of datasets, measurements in the most sensitive channels are now carried out differentially or in exclusive modes depending on specific production characteristics. These measurements are discussed in Section 11.6.2.4.

The candidate events in each Higgs boson decay channel are split into several mutually exclusive categories (or event tags) based on the specific topological, kinematic or other features present in the event. The categorization of events increases the sensitivity of the overall analysis and allows a separation of different Higgs boson production processes. Most categories are dominated by signal from one Higgs boson decay mode but contain an admixture of various Higgs boson production processes. For example, a typical VBF selection requires Higgs boson candidates to be accompanied by two energetic jets ($\geq 30 \text{ GeV}$) with a large dijet mass ($\geq 400 \text{ GeV}$) and separated by a large pseudo-rapidity ($\Delta\eta_{jj} \geq 3.5$) [133]. While such a category is enriched in Higgs bosons produced via VBF, the contamination from the ggF production mechanism can be significant. Hence, a measurement of the signal rate in the VBF category does not imply a measurement of VBF production cross section since one cannot resolve the contamination from ggF. Simulations are used to determine the relative contributions of the various Higgs boson production

modes in each specific categories.

An important difference between the Run 1 and Run 2 results, in particular when comparing signal strengths, and therefore in the measurement of the couplings of the Higgs boson as discussed in Section 11.4, is that values and errors of the predicted cross sections have been improved (mostly the scale and PDF uncertainties). The theoretical predictions are however compatible and therefore, the signal strengths can be compared on a sound basis.

11.3.1.1 $H \rightarrow \gamma\gamma$

In the diphoton channel, a search is performed for a narrow peak over a smoothly falling background in the invariant mass distribution of two high p_T photons. The background in this channel is conspicuous and stems from prompt $\gamma\gamma$ processes for the irreducible backgrounds, and the γ +jet and dijet processes for the reducible backgrounds where one jet fragments typically into a leading π^0 . In order to optimise search sensitivity and also to separate the various Higgs boson production modes, ATLAS and CMS split events into several mutually exclusive categories. Diphoton events containing high p_T muons or electrons, or missing energy (E_T^{miss}) consistent with the decay of a W or Z boson, are tagged in the VH production category. Diphoton events containing energetic dijets with a large mass and pseudo-rapidity difference are assigned to the VBF production category, and the remaining events are considered either in the VH category when the two jets are compatible with the hadronic decay of a W or a Z , or in the ggF production category. While the leptonic VH category is relatively pure, the VBF category has significant contamination from the gluon fusion process. Events which are not picked by any of the above selections are further categorised according to their expected $m_{\gamma\gamma}$ resolution and signal-to-background ratio. Categories with good m_H resolution and larger signal-to-background ratio contribute most to the sensitivity of the search.

Both ATLAS and CMS have studied in detail the calibration of the energy response of photons, in particular using $Z \rightarrow e^+e^-$, $Z \rightarrow \mu^+\mu^-\gamma$ and the response of muons in the calorimeter (for ATLAS) from $Z \rightarrow \mu^+\mu^-$ events. This information is used to correct the simulated signal mass line-shapes. In each category, parametric signal models are adjusted to these line-shapes to provide a functional form for the signal. Simple monotonic functional forms of the backgrounds are determined by a fit to the $m_{\gamma\gamma}$ distribution in each category (typically exponential, Bernstein polynomials, Laurent series or power laws). All categories are fitted simultaneously to determine the signal yield at the measured combined Run 1 mass of $125.09 \pm \text{GeV}$ [136] for ATLAS and $m_H = 125.38 \text{ GeV}$ for CMS as discussed in Section 11.3.1.3. The $m_{\gamma\gamma}$ distribution after combining all categories is shown in Fig. 11.3, using the full ATLAS Run 2 dataset.

The signal strength, $\mu = (\sigma \cdot \text{BR})_{\text{obs}} / (\sigma \cdot \text{BR})_{\text{SM}}$, which is the observed product of the Higgs boson production cross section (σ) and its branching ratio (BR) normalised to the corresponding SM values, is 1.17 ± 0.27 for ATLAS in Run 1 and 1.02 ± 0.14 in Run 2 [137] (where this signal strength measurement is estimated from the measured fiducial cross sections and thus neglects acceptance systematic uncertainties, which are not expected to be dominant in particular given that the measurement is inclusive). The signal strengths² measured in Run 1 and Run 2 by the CMS collaboration are $1.18_{-0.23}^{+0.26}$ and 1.12 ± 0.09 [138] respectively.

11.3.1.2 $H \rightarrow ZZ^* \rightarrow \ell^+\ell^-\ell'^+\ell'^-$

In the $H \rightarrow ZZ^* \rightarrow \ell^+\ell^-\ell'^+\ell'^-$ channel, a search is performed for a narrow mass peak over a small continuous background dominated by non-resonant ZZ^* production from $q\bar{q}$ annihilation and gg fusion processes. The contribution and the shape of this irreducible background is taken from simulation. The subdominant and reducible backgrounds stem from $Z+b\bar{b}$, $t\bar{t}$ and Z +jets events. Their contribution is suppressed by requirements on lepton isolation and lepton impact parameter and their yield is estimated from control samples in data.

To help to distinguish the Higgs boson signal from the dominant non-resonant ZZ^* background, both ATLAS and CMS [139]

²The Run 1 results for ATLAS and CMS are at fixed values of $m_H = 125.4 \text{ GeV}$ and 124.7 GeV , respectively.

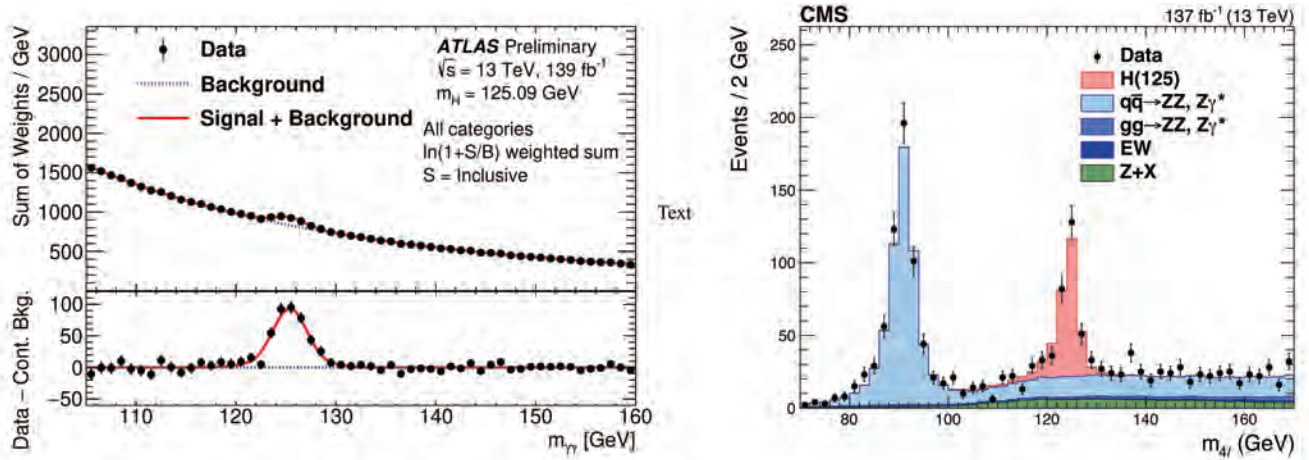


Figure 11.3: (Left) The invariant mass distribution of diphoton candidates, with each event weighted by the ratio of signal-to-background in each event category, observed by ATLAS [134] at Run 2. The residuals of the data with respect to the fitted background are displayed in the lower panel. (Right) The $m_{4\ell}$ distribution from CMS [135] Run 2 data.

use a matrix element likelihood approach to construct a kinematic discriminant built for each 4ℓ event based on the ratio of complete leading-order matrix elements $|\mathcal{M}_{\text{sig}}^2/\mathcal{M}_{\text{bkg}}^2|$ for the signal ($gg \rightarrow H \rightarrow 4\ell$) and background ($q\bar{q} \rightarrow ZZ \rightarrow 4\ell$) hypotheses. To further enhance the sensitivity, experiments also use multivariate techniques.

To improve the sensitivity to more exclusive production processes such as VBF, VH , and $t\bar{t}H$, the experiments divide 4ℓ events into mutually exclusive categories. Events are categorised in terms of the number of reconstructed jets, the number of additional leptons (from the decay of a vector boson in the associated production mode), number of jet tagged as containing a b -hadron, the transverse momentum of the Higgs boson (or e.g. its associated vector boson) and missing transverse momentum. The exclusive processes are also further separated in different kinematic regions in a framework referred to as Simplified Template Cross Sections (see Section 11.6.2.4). Dijets with a large mass and pseudo-rapidity difference populate the VBF category. ATLAS requires the presence of an additional lepton in the VH category. In events with less than two jets, CMS uses the $p_T^{4\ell}$ to distinguish between production via the gluon fusion and the VH/VBF processes.

Since the $m_{4\ell}$ resolutions and the reducible background levels are different in the 4μ , $4e$ and $2e2\mu$ sub-channels, they are analysed separately and the results are then combined. The distribution of the reconstructed invariant mass of the four leptons for CMS [135] is given in Fig. 11.3 (right), showing a clear excess at a mass of approximately $m_H = 125$ GeV. Both experiments also observe a clear peak at $m_{4\ell} = 91$ GeV from the production of a Z boson on-mass-shell and decaying to four leptons due typically to the emission of an off-shell photon from one of the primary leptons from the Z boson decay.

The signal strengths μ for the inclusive $H \rightarrow 4\ell$ production measured by ATLAS and CMS are $1.44^{+0.40}_{-0.33}$ at $m_H = 125.38$ GeV and $0.93^{+0.29}_{-0.25}$ at $m_H = 125.6$ GeV respectively, in Run 1. The signal strengths measured by ATLAS and CMS in Run 2 are 1.01 ± 0.11 [140] and $0.94^{+0.12}_{-0.11}$ [135] respectively (the ATLAS measurement is made at the combined Run 1 Higgs boson mass of $m_H = 125.09$ GeV and $m_H = 125.38$ GeV for the CMS measurement).

11.3.1.3 Measurement of the Higgs boson mass

To measure the mass of the Higgs boson, ATLAS and CMS collaborations rely on the two high mass-resolution and sensitive channels, $\gamma\gamma$ and $ZZ^*/4\ell$. The ATLAS and CMS approaches are very similar in these two analyses with small differences on the usage of categories, additional discriminating variables and percent errors. In these two channels, the mass resolutions range from 1.4 GeV to 2 GeV for ATLAS and from 1.0 GeV to 2.8 GeV

for CMS (see Ref. [136] and the reconstruction-performance references therein). An excellent mass resolution is obtained for both experiments in the diphoton channel for central diphoton pairs (typically for events where both photons are not converted). However, the best precision in this measurement at Run 2 is obtained using the four lepton channel and in particular in the sub-channel of four muons (followed by the two-electrons and two muons channel where the mass resolution is driven by the reconstruction of the lower mass di-lepton pair with typically lower transverse momentum leptons).

Both ATLAS and CMS have produced several Higgs boson mass measurements, including the individual and combined Run 1 measurements [136] and the Run 2 measurements by ATLAS [141, 142] and CMS [139, 143] for both the 4ℓ and the diphoton channels. The current most precise result is obtained by CMS using a partial Run 2 dataset and a combination of Run 1 and Run 2 measurements yielding a measurement of 125.38 ± 0.11 (stat.) ± 0.08 (syst.). The later measurement is used by CMS as reference Higgs boson mass.

The Run 1 combination including both ATLAS and CMS measurements of 125.09 ± 0.21 (stat.) ± 0.11 (syst.) is currently used as a reference for Higgs measurement results by ATLAS. [136].

In the diphoton channel, as discussed in Section 11.5.3.2, a mass shift is expected to be induced by the deformation of the mass line-shape of the signal in presence of background, from the interference between the Higgs boson production and the continuum irreducible background. It is a small but non negligible effect of approximately 35 MeV [144] for a Higgs boson width close to that of the SM. This effect could be larger if the width of the Higgs boson were to be substantially larger. This effect estimated by ATLAS with a full simulation is still relatively small with respect to the total uncertainty on the mass and is therefore neglected.

11.3.1.4 $H \rightarrow W^+W^- \rightarrow \ell^+\nu\ell^-\bar{\nu}$

In this challenging channel, experiments search for an excess of events with two leptons (electrons or muons) of opposite charge accompanied by missing energy and/or jets. A typical event selection is described below in order to give an idea of the main intricacies. Specific selections vary between experiments and between Run 1 and Run 2 analyses. Events are divided into several categories depending on the lepton flavour combination (e^+e^- , $\mu^+\mu^-$ and $e^\pm\mu^\mp$) and the number of accompanying jets ($N_{\text{jet}} = 0, 1, \geq 2$). In the ATLAS analysis, the $N_{\text{jet}} \geq 2$ category is optimised for the VBF production process by selecting two leading jets with a large pseudo-rapidity difference and with a large mass ($m_{jj} > 500$ GeV).

Backgrounds contributing to this channel are numerous and depend on the category of selected events. Reducing them and accurately estimating the remainder is a major challenge in this analysis. For events with opposite-flavour leptons and no ac-

companying high p_T jets, the dominant background stems from non-resonant WW production. Events with same-flavour leptons suffer from large Drell–Yan contamination (note that also the opposite-flavour leptons analysis has Drell–Yan $\tau\bar{\tau}$ background in 0-jet category). The $t\bar{t}$, tW and W +jets (with the jet misidentified as a lepton) events contaminate all categories. Non-resonant WZ , ZZ and $W\gamma$ processes also contribute to the background at a sub-leading level.

A requirement of large missing transverse energy (E_T^{miss}) is used to reduce the Drell–Yan and multijet backgrounds. In the e^+e^- and $\mu^+\mu^-$ categories, events with $m_{\ell\ell}$ consistent with the Z mass are vetoed. The $t\bar{t}$ background is suppressed by a veto against identified b -jets or low p_T muons assumed to be coming from semi-leptonic b -hadron decays within jets (this soft muon veto was not applied anymore in Run 2 analysis) and tight isolation requirements diminish the W +jets background. The scalar nature of the Higgs boson and the $V - A$ nature of the W boson decay implies that the two charged leptons in the final state are preferentially emitted at small angles with respect to each other. Therefore the dilepton invariant mass ($m_{\ell\ell}$) and the azimuthal angle difference between the leptons ($\Delta\phi_{\ell\ell}$) are used to discriminate between the signal and non-resonant WW events [145]. The transverse mass, constructed from the dilepton p_T ($p_T^{\ell\ell}$), E_T^{miss} and the azimuthal angle between E_T^{miss} and $p_T^{\ell\ell}$, is defined as $m_T = \sqrt{2p_T^{\ell\ell}E_T^{\text{miss}}(1 - \cos\Delta\phi_{E_T^{\text{miss}}\ell\ell})}$ and serves as an effective discriminant against backgrounds. The transverse mass variable also tracks the Higgs boson mass but with a poor mass resolution. Background rates except for the small contributions typically from non-resonant WZ , ZZ and $W\gamma$ are evaluated from data control samples with floating normalisation.

At Run 1 ATLAS fitted the m_T distributions and observed an excess at $m_H = 125.38$ GeV with a local significance of 6.1σ similar to that expected from a 125 GeV SM Higgs boson. The measured inclusive signal strength is $\mu = 1.09_{-0.21}^{+0.23}$. In the VBF category, an excess with a significance of 3.2σ corresponding to a signal strength of $\mu = 1.27_{-0.45}^{+0.53}$ is observed. The CMS analysis of 0- and 1-jet categories, using all lepton flavour combinations, shows an excess with an observed significance of 4.3σ , lower than the expected sensitivity of 5.8σ for a 125.6 GeV SM Higgs boson. CMS observes no significant excess in the VBF production mode and sets a 95% CL limit on the signal strength of $\mu_{\text{VBF}} < 1.7$ for $m_H = 125.6$ GeV.

ATLAS and CMS have also searched for the associated Higgs boson production in this channel. The signal consists of up to three (WH) or four (ZH) high p_T isolated leptons with missing transverse energy and low hadronic activity. The major backgrounds stem from triboson and diboson production where each boson decays leptonically. ATLAS observes [146] an excess at $m_H = 125.38$ GeV with a local significance of 2.5σ corresponding to a $\mu_{\text{VH}} = 3.0_{-1.0}^{+1.6}$. CMS instead sets a 95% CL limit of $\mu_{\text{VH}} < 4.7$.

Both ATLAS [147] and CMS [148] have performed this analysis with the full Run 2 dataset. The ATLAS analysis was done with the different flavour $WW \rightarrow e\nu\mu\nu$ decay mode in categories selected according to the numbers of jets with categories aiming specifically at the VBF production mode. The gluon fusion and VBF production cross sections are measured simultaneously. The measured signal strengths are:

$$\begin{aligned} \mu_{\text{ggF}} &= 1.20 \pm 0.05 \text{ (stat.)}_{-0.08}^{+0.09} \text{ (exp.sys.)}_{-0.08}^{+0.10} \text{ (sig.th.)}_{-0.11}^{+0.12} \text{ (bkg.th.)} \\ \mu_{\text{VBF}} &= 0.99 \pm_{-0.12}^{+0.13} \text{ (stat.)}_{-0.06}^{+0.07} \text{ (exp.sys.)}_{-0.12}^{+0.18} \text{ (sig.th.)}_{-0.08}^{+0.10} \text{ (bkg.th.)} \end{aligned}$$

It is interesting to note that the largest uncertainty is from the theoretical prediction of the background in the gluon fusion process and that the statistical uncertainty is sub-dominant. While in the VBF mode the largest uncertainty is from the signal modelling.

With the entire Run 2 dataset CMS performed a fiducial measurement of the inclusive and differential production cross sections

of the Higgs boson in the leptonic modes of its WW decay channel. The results are unfolded to correct for selection efficiency and purity as well as resolution effects. The measured cross section in the fiducial volume is 86.5 ± 9.5 fb, consistent with the Standard Model expectation of 82.5 ± 4.2 fb.

CMS has also performed with the full dataset an analysis of the WH and ZH production modes of the Higgs boson subsequently decaying to WW using both leptonic and hadronic decay modes of the W and Z boson. The selected channels are: (i) two same-sign leptons (electrons or muons) and jets targeting the WH production mode, (ii) 3 leptons targeting the WH production, (iii) 3 leptons to select events from the ZH production mode, and (iv) 4 lepton channels. In the (iii) and (iv) one pair of same flavour and opposite sign leptons are required to be compatible with the mass of the Z boson. The overall measured signal strength is [149]:

$$\mu = 1.85 \pm 0.33 \text{ (stat.)}_{-0.25}^{+0.27} \text{ (exp.)}_{-0.07}^{+0.10} \text{ (th.)}$$

11.3.2 Decays to third generation fermions ($b\bar{b}$ and $\tau^+\tau^-$)

In the SM, fermions acquire a mass through gauge invariant interactions with the Higgs field which is also responsible for the electroweak symmetry breaking and thus for generating the masses of gauge bosons (see Section 11.2 for more details). While this minimal solution is very elegant, there is no fundamental reason for it to be the case, and probing the couplings of the Higgs boson to fermions is therefore of fundamental importance, in particular since BSM physics can largely change the SM predictions.

The discovery of the Higgs boson was made essentially through bosonic final states. These decays probed mostly the couplings of the Higgs boson to vector bosons (the decay of the Higgs boson to photons occurring only through loops is also dominated in the SM by the coupling of the Higgs boson to W bosons). However, the predominant Higgs boson production mode is the gluon fusion, occurring only through loops dominated by the coupling of the Higgs boson to fermions. The observation of the Higgs boson in the two photons or two gluons decay modes is also an indirect evidence for the coupling of the Higgs boson to fermions (and in particular to the top quark). Nevertheless, the observation of either decays to fermions or production modes which unambiguously proceed through fermion couplings provide direct probes of the coupling of the Higgs boson to fermions and is thus of fundamental importance.

At hadron colliders, the most promising channel for probing the coupling of the Higgs field to the quarks and leptons are $H \rightarrow b\bar{b}$ and $H \rightarrow \tau^+\tau^-$, respectively. For a Higgs boson with $m_H \approx 125$ GeV, the branching fraction to $b\bar{b}$ is about 58% and to $\tau^+\tau^-$ is about 6%. Nevertheless, the presence of very large backgrounds makes the isolation of a Higgs boson signal in these channels quite challenging.

One of the most prominent goals of the LHC Run 2 for ATLAS and CMS was the direct observation of the Yukawa coupling of the Higgs boson to fermions of the third generation (bottom quarks, tau leptons and top quarks). This goal has been reached independently by both ATLAS and CMS and with only partial Run 2 datasets.

The Run 2 of the LHC has also delivered beyond expectations as it provided evidence for two new rare decay modes of the Higgs boson in the $H \rightarrow \mu^+\mu^-$ and the $H \rightarrow \ell^+\ell^-\gamma$ channels (where ℓ denotes and electron or a muon).

11.3.2.1 $H \rightarrow \tau^+\tau^-$

In the $H \rightarrow \tau^+\tau^-$ search, τ leptons decaying to electrons (τ_e), muons (τ_μ) and hadrons (τ_{had}) are considered. The $\tau^+\tau^-$ invariant mass ($m_{\tau\tau}$) is reconstructed from a kinematic fit of the visible products from the two τ leptons and the missing energy observed in the event. Due to the presence of missing neutrinos, the $m_{\tau\tau}$ resolution is poor ($\approx 15\%$). As a result, a broad excess over the expected background in the $m_{\tau\tau}$ distribution is searched for. The major sources of background stem from Drell–Yan $Z \rightarrow \tau^+\tau^-$ and $Z \rightarrow e^+e^-$, W +jets, $t\bar{t}$ and multijet production. Events in all sub-channels are divided into categories based on the number and kinematic properties of additional energetic jets in the event and the transverse momentum of the reconstructed Higgs boson and the distance ΔR distance between the two τ 's. The sensitivity

of the search is generally higher for categories with one or more additional jets. The VBF category, consisting of a τ pair with two energetic jets separated by a large pseudo-rapidity, has the best signal-to-background ratio and search sensitivity, followed by the $\tau^+\tau^-+1$ jet category. The signal to background discrimination relies in part on the $m_{\tau\tau}$ resolution, which improves with the boost of the Higgs boson. The non-VBF categories are further subdivided according to the observed boost of the $\tau^+\tau^-$ system. CMS primarily uses the reconstructed $m_{\tau\tau}$ as the final discriminating variable while ATLAS combines various kinematic properties of each event categories with multivariate techniques to build the final discriminant [150].

Searches for $H \rightarrow \tau^+\tau^-$ decays in the VH production mode are also performed in final states where the W or Z boson decays into leptons or jets. The irreducible background in this search arises from non-resonant WZ and ZZ diboson production. The reducible backgrounds originate from W , Z , and $t\bar{t}$ events that contain at least one fake lepton in the final state due to a misidentified jet. The shape and yield of the major backgrounds in each category are estimated from control samples in data. Contributions from non-resonant WZ and ZZ diboson production are estimated from simulations but corrected for reconstruction efficiency using control samples formed from observed data.

For CMS, the significance of the observed excess at $m_H = 125$ GeV in Run 1 is 3.2σ , close to the expected 3.7σ sensitivity, and corresponds to a signal strength of $\mu = 0.86 \pm 0.29$. The observed (expected) deviation from the background-only hypothesis in ATLAS corresponds to a local significance of 4.5σ (3.4σ) and the best fit value of the signal strength is $\mu = 1.43^{+0.43}_{-0.37}$ [150].

When the ATLAS and CMS $H \rightarrow \tau\tau$ Run 1 measurements are combined [151], the significance of the observed excess corresponding to $m_H = 125.09$ GeV is 5.5σ and the combined signal strength is $\mu = 1.11^{+0.24}_{-0.22}$, consistent with the SM expectation.

The Run 1 evidence was strong only through the combination of the two experiments. The Run 2 larger dataset at a greater centre-of-mass energy is essential to further confirm this observation and perform first precision measurements in this important channel.

ATLAS [152] and CMS [153, 154] had analysed an early Run 2 dataset to provide independent observations, with significances of 4.4σ and 4.9σ respectively. These results in combination with the Run 1 results provide an unambiguous observation of this process. ATLAS quantified the combined result yielding a significance of 6.4σ [152].

CMS has also performed the search for Higgs boson decays to taus in the associated production with a vector boson [155] with a larger dataset corresponding to an integrated luminosity of almost 80 fb^{-1} of data.

Both ATLAS [156] and CMS [157, 158] have then completed the analyses of the full Run 2 dataset. ATLAS performed simultaneously measurements not only of the VBF production mode, but also of the gluon fusion channel where the Higgs boson has a sizeable boost, the associated production with a vector boson as well as the associated production with a pair of top quarks. The measured total production cross-section is 2.90 ± 0.21 (stat.) $^{+0.37}_{-0.32}$ (sys.) corresponding to a signal strength of $\mu = 0.92 \pm 0.13$ in excellent agreement with the prediction from the Standard Model. The individual processes measured signal strengths are: (i) for the VBF production mode $\mu_{VBF} = 0.89 \pm 0.18$, (ii) the gluon fusion mode $\mu_{ggF} = 0.95^{+0.34}_{-0.27}$ where the dominant uncertainty is systematic and mainly related to the signal acceptance in the high boost regime, (iii) the associated production with a vector boson where the vector boson decays hadronically $\mu_{VH} = 0.95^{+0.59}_{-0.57}$, and the associated production with a pair of top-quarks $\mu_{t\bar{t}H} = 1.53^{+1.56}_{-1.32}$.

CMS has not yet combined its associated production channels, it has however performed a measurement in both the gluon fusion (boosted) and VBF production modes. The overall measured signal strength is $\mu = 0.85^{+0.12}_{-0.11}$. The gluon fusion signal and VBF signal strengths are $\mu_{ggF} = 0.98^{+0.20}_{-0.19}$ and $\mu_{VBF} = 0.67^{+0.23}_{-0.22}$ respectively. The precision of the former is limited by systematic uncertainties while for the latter the main uncertainty is from the data statistics [157]. The CMS collaboration also reported measurements of inclusive fiducial and differential cross sections,

yielding a fiducial cross section of $426 \pm 102 \text{ fb}$, in agreement with the Standard-Model expectation of $408 \pm 27 \text{ fb}$ [158].

11.3.2.2 $H \rightarrow b\bar{b}$

In the search for the decay of the Higgs boson to a pair of b -quarks, the most sensitive production modes are the associated WH and ZH processes allowing use of the leptonic W and Z decays for triggering, and to purify the signal and reject QCD backgrounds. The W bosons are reconstructed via their leptonic decay $W \rightarrow \ell\bar{\nu}_\ell$ where $\ell = e, \mu$ or τ . The Z bosons are reconstructed via their decay into e^+e^- , $\mu^+\mu^-$ or $\nu\bar{\nu}$. The Higgs boson candidate mass is reconstructed from two b -tagged jets in the event. Backgrounds arise from production of W and Z bosons in association with gluon, light and heavy-flavoured jets (V +jets), $t\bar{t}$, diboson (ZZ and WZ with $Z \rightarrow b\bar{b}$) and QCD multi-jet processes. Due to the limited $m_{b\bar{b}}$ mass resolution, a SM Higgs boson signal is expected to appear as a broad enhancement in the reconstructed dijet mass distribution. The crucial elements in this search are b -jet tagging with high efficiency and low fake rate, accurate estimate of b -jet momentum and estimate of backgrounds from various signal depleted control samples constructed from data.

At the Tevatron, the $H \rightarrow b\bar{b}$ channel contributes the majority of the Higgs boson search sensitivity below $m_H = 130$ GeV. To separate signal from background, CDF and D0 use multivariate analysis (MVA) techniques that combine several discriminating variables into a single final discriminant. Each channel is divided into exclusive sub-channels according to various lepton, jet multiplicity, and b -tagging characteristics in order to group events with similar signal-to-background ratio and thus optimise the overall search sensitivity. The combined CDF and D0 data show [48, 159] an excess of events with respect to the predicted background in the 115–140 GeV mass range in the most sensitive bins of the discriminant distributions suggesting the potential presence of a signal. At $m_H = 125$ GeV, the observed signal strength is $\mu = 1.59^{+0.69}_{-0.72}$.

At the LHC, in order to reduce the dominant V +jets background, following Ref. [87], experiments select a region in the VH production phase space where the vector boson is significantly boosted and recoils from the $H \rightarrow b\bar{b}$ candidate with a large azimuthal angle $\Delta\phi_{VH}$. For each channel, events are categorised into different $p_T(V)$ regions with varying signal/background ratios. Events with higher $p_T(V)$ have smaller backgrounds and better $m_{b\bar{b}}$ resolution. CMS uses MVA classifiers based on kinematic, topological and quality of b -jet tagging and trained on different values of m_H to separate Higgs boson signal in each category from backgrounds. The MVA outputs for all categories are then fitted simultaneously.

The nominal results from ATLAS are also based on a combination of (i) a multivariate analysis of their 8 TeV data, incorporating various kinematic variables in addition to $m_{b\bar{b}}$ and b -tagging information and (ii) a statistical analysis of their 7 TeV data centered on $m_{b\bar{b}}$ as the main discriminant. In both cases, customised control samples devised from data are used to constrain the contributions of the dominant background processes.

The direct observation of the Higgs boson decaying to a pair of b -quarks, a major result of Run 2, was obtained by both ATLAS and CMS independently after the update of their search with similar analyses as those performed at Run 1 but with a larger dataset of approximately 80 fb^{-1} of data collected in 2015, 2016 and 2017. The increase in signal cross sections of nearly a factor of 3 at the centre-of-mass energy of 13 TeV with respect to 7 TeV, has also been instrumental in bringing the two experiments to the required sensitivity to claim an evidence for this decay mode in the VH production mode (in the high transverse momentum of the vector boson fiducial region of interest for this channel). The expected significance for a SM Higgs boson is 4.3σ for ATLAS [160] and 4.9σ for CMS [161]. Both ATLAS and CMS observe significant excesses corresponding to 4.9σ and 4.8σ respectively with Run 2 data only. When combined with results obtained in Run 1, the observed (expected) significance of the excesses are 5.4σ (5.5σ) and 5.6σ (5.5σ) respectively. These results provide direct evidence for the $H \rightarrow b\bar{b}$ decay through the VH production mode.

Since these important observations, ATLAS has completed its

Table 11.5: Summary of the results of measurements for a Higgs boson decaying to a pair of b -quarks by ATLAS and CMS. The results are given in terms of measured signal strength. When available, the statistical and systematic contributions to the total uncertainty are reported separately and in this order.

$H \rightarrow b\bar{b}$	Tevatron	ATLAS Run 1	CMS Run 1	ATLAS Run 2	CMS Run 2
VH	1.6 ± 0.7	$0.52 \pm 0.32 \pm 0.24$	1.0 ± 0.5	$1.02^{+0.12+0.14}_{-0.11-0.13}$	1.01 ± 0.22
VBF (γ)	—	-0.8 ± 2.3	$2.8 \pm 1.4 \pm 0.8$	$0.99^{+0.30+0.18}_{-0.30-0.16}$	1.3 ± 1.2
$t\bar{t}H$	—	$1.4 \pm 0.6 \pm 0.8$	0.7 ± 1.9	$0.79 \pm 0.29 \pm 0.53$	$1.49 \pm 0.21 \pm 0.39$
Inclusive	—	—	—	0.7 ± 3.3	3.7 ± 1.6

analysis of the full dataset using two reconstruction techniques. The first is based on the reconstruction of the Higgs boson with two jets is referred to as *resolved* [162]. The second is based on the reconstruction of the Higgs boson as a large radius jet and is referred to as *boosted* [163]. These measurements expand the range of measurements of the Higgs boson decays to b -quarks in association with a vector boson at higher transverse momentum, above 400 GeV. These results are summarized in Table 11.5. It should be noted that the sensitivity of these analyses are already limited by systematic uncertainties.

Also, the LHCb collaboration has performed a search for the VH production with subsequent decay of the Higgs boson to a pair of b -quarks [164] with 1.98 fb^{-1} of data taken at a centre-of-mass energy of 8 TeV. The final state is required to have two reconstructed b quarks and one lepton in the LHCb acceptance of $2 < \eta < 5$. The sensitivity of this search is an expected 95% CL exclusion of 84 times the SM production rate. This analysis is also used to set a limit on the VH production with the subsequent decay of the Higgs boson in a pair of c quarks with a 95% CL limit at 6.4×10^3 times the SM production rate, while the expected sensitivity corresponds to an exclusion of 7.9×10^3 times the SM production rate.

ATLAS and CMS have also searched for $H \rightarrow b\bar{b}$ in the VBF production mode. The event topology consists of two VBF-tagging energetic light-quark jets in the forward and backward direction relative to the beam direction and two b -tagged jets in the central region of the detector. Due to the electroweak nature of the process, for the signal events, no additional energetic jet activity (excluding that from the Higgs boson) is expected in the rapidity gap between the two VBF-tagging jets. The dominant background in this search stems from QCD production of multi-jet events and the hadronic decays of vector bosons accompanied by additional jets. A contribution of Higgs boson events produced in the ggF process but with two or more associated jets is expected in the signal sample. The signal is expected as a broad enhancement in the $m_{b\bar{b}}$ distribution over the smoothly falling contribution from the SM background processes. Both ATLAS [165] and CMS [166] have produced results in this channel with Run 1 data, but with limited sensitivity. Both experiments performed a similar analysis with Run 2 data [167]. The results are summarized in Table 11.5.

Two of the main difficulties for the VBF production mode are the large QCD background and the difficulty in triggering fully hadronic events. Both difficulties are addressed, by the proposal made in Ref. [168], where the requirement of an additional photon in the final state reduces the background through an interference effect and enhances the possibilities for triggering. This analysis has been carried out by ATLAS at Run 2 [169] and its result combined with the standard VBF channel (see Table 11.5). The sensitivity in this channel is smaller than in the fully hadronic mode.

The sensitivity in the inclusive search for the Higgs boson in the ggF production mode with $H \rightarrow b\bar{b}$ is limited by the overwhelming background from the inclusive production of $pp \rightarrow b\bar{b} + X$ via the strong interaction. For this reason, no meaningful results exist with the Run 1 dataset for this production mode. With the increase in centre-of-mass energy to 13 TeV, and by taking advan-

tage of the harder transverse momentum spectrum of the $gg \rightarrow H$ production mode with respect to the QCD background, a search for high p_T Higgs boson decaying to a pair of b quarks in association with an energetic Initial State Radiation (ISR) jet, has been performed by ATLAS [170] and CMS [171]. For this analysis with the Run 2 data, ATLAS and CMS require jets clustered with the anti- k_T algorithm [172] with a distance parameter of 1.0 and 0.8 respectively, with a transverse momentum in excess of 450 GeV. As in the case of VH production mode, this analysis is sensitive also to the $VZ, Z \rightarrow b\bar{b}$ production, which is an important step in the validation of the analysis chain. The $Z \rightarrow b\bar{b}$ decay is observed with a significance in excess of five standard deviations, in agreement with the expected rate from the Standard Model. CMS provides an expected sensitivity to the observation of a Higgs boson of 0.7σ . This estimate has a non negligible uncertainty from the precise estimate of the fiducial signal cross section in the specific acceptance of this analysis. CMS observes an excesses at $m_H = 125 \text{ GeV}$ of 2.5σ . ATLAS provides measurements in different regions of transverse momentum which are compatible with the Standard Model expectation for a signal, and which are also compatible with the absence of a signal within the current precision. These results are reported in Table 11.5.

Another important production mode sensitive to the decay of the Higgs boson to bottom quarks, is the associated production with a pair of top quarks. The results of the searches for this process have been combined with the channels described above, to provide an additional constraint on the Yukawa coupling of the Higgs boson to bottom quarks. The channels corresponding to this production mode are described in Section 11.3.3. The results are, however, also reported in Table 11.5.

11.3.3 Higgs boson production in association with top quarks or in top decays

11.3.3.1 The associated production with top quark pairs

As discussed in Section 11.2, the coupling of the Higgs boson to top quarks plays a special role in the electroweak symmetry breaking mechanism in the SM, as well as in its possible extensions. Substantial indirect evidence of this coupling is provided by the compatibility of observed rates of the Higgs boson in the principal discovery channels, given that the main production process – the gluon fusion – is dominated by a top quark loop. Direct evidence of this coupling at the LHC and the future e^+e^- colliders will be mainly available through the $t\bar{t}H$ final state and will permit a clean measurement of the top quark-Higgs boson Yukawa coupling. The $t\bar{t}H$ production cross section at the LHC is small in comparison with the ggF or even VH production modes. The production cross section for a 125 GeV Higgs boson in pp collisions at $\sqrt{s} = 8 \text{ TeV}$ of about 130 fb made it challenging to measure the $t\bar{t}H$ process with the LHC Run 1 dataset. However, in Run 2, the increase in cross section at $\sqrt{s} = 13 \text{ TeV}$ is substantial, reaching approximately 500 fb. For a sensitive search, at Run 1, it was important to target as many accessible experimental signatures as possible. The analysis channels for such complex final states can be separated in four classes according to the decays of the Higgs boson. In each of these classes, most of the decay final states of the top quarks are considered (fully hadronic, semi-leptonic and dilepton decay final states).

The first analysis in this ensemble is the search for $t\bar{t}H$ production in the $H \rightarrow \gamma\gamma$ channel. This analysis relies on the search for a narrow mass peak in the $m_{\gamma\gamma}$ distribution. The background is estimated from the $m_{\gamma\gamma}$ sidebands. The sensitivity in this channel is mostly limited by the available statistics. The second analysis is the search for the Higgs boson decaying to ZZ^* and subsequently to four leptons (electrons and/or muons). This channel is currently limited by the low statistics due to the small branching fraction of the Z decays to leptons. The third analysis is the search in the $H \rightarrow b\bar{b}$ channel. This search is intricate due to the large backgrounds, both physical and combinatorial in resolving the $b\bar{b}$ system from the Higgs boson decay, in events with six jets and four b -tagged jets. Already with the Run 1 dataset, the sensitivity of this analysis was strongly impacted by the systematic uncertainties on the background predictions. The fourth analysis channel is a specific search for $\tau^+\tau^-$ where the two tau leptons decay to hadrons. Finally, the W^+W^- , $\tau^+\tau^-$ and ZZ^* final states can be searched for inclusively in multilepton event topologies (not including the resonant $H \rightarrow 4\ell$ channel that is covered in a more specific analysis). The corresponding $t\bar{t}H$ modes can be decomposed in terms of the decays of the Higgs boson and those of the top quarks as having two b -quarks and four W bosons (or two W and two taus, or two W and two Z) in the final state.

ATLAS and CMS have provided a complete set of results in these channels and their combination with the Run 1 data [173, 174].

With the large increase in production cross section for the $t\bar{t}H$ associated production process of a factor of 3.9 from 7 TeV to 13 TeV, an outstanding goal of the Run 2 physics program was the direct observation of the top Yukawa coupling through this production mode. As could be seen in the Run 1 results, the $H \rightarrow b\bar{b}$ channel sensitivity was already dominated by systematic uncertainties and the multilepton channel had already large systematic uncertainties, while channels such as the $H \rightarrow \gamma\gamma$ had very limited sensitivity due to the low statistics. With a conspicuous amount of data, the hierarchy of channels was therefore bound to change.

ATLAS and CMS have analysed Run 2 data in all the sensitive decay channels for this production mode, with datasets of variable size of up to the full Run 2 dataset in the case where it matters the most, i.e., the $t\bar{t}(H \rightarrow \gamma\gamma)$ channel. With this partial analysis of the Run 2 data, ATLAS and CMS were able to independently observe the production of the Higgs boson in association with a pair of top quarks, and therefore the Yukawa coupling of the Higgs boson to the top quark [175, 176]. This observation is particularly important in comparison to the indirect evidence through the gluon fusion production process dominated by the top quark loop.

The observation made independently by the two experiments was based on all the channels that were studied at the Run 1. ATLAS used up to 79.8 fb^{-1} of Run 2 data and CMS has used its 2016 dataset of 35.9 fb^{-1} . ATLAS reached an expected sensitivity of 4.9σ and an observed significance of 5.8σ with the Run 2 partial dataset alone, and 6.3σ (with 5.1σ expected) in combination with the Run 1 results. CMS reached a sensitivity of 4.2σ and observed an excess with respect to the background-only hypothesis of 5.2σ , combining the Run 1 and Run 2 results.

With the larger Run 2 dataset, the dominant mode is the $t\bar{t}(H \rightarrow \gamma\gamma)$ channel, where a narrow peak over a continuous background is searched for. At Run 2, this channel has reached a signal-to-background ratio in excess of 1 in the most signal-like categories. This is in contrast with the inclusive diphoton channel Higgs channels where the signal-to-background ratios are of the order of a few percents. ATLAS and CMS have analysed the entire Run 2 dataset reaching an observed (expected) sensitivity of 5.2σ (4.4σ) and 6.6σ (4.7σ) [177] and [178], providing nearly unambiguous observations in this channel alone. These results are largely dominated by statistical uncertainty and are therefore expected to improve significantly with more data.

The search for the resonant Higgs boson decay to four leptons in the associated production with a pair of top quarks has also been updated in ATLAS [140] with the full Run 2 dataset and reported in Table 11.6, but it is also not included in the combination.

The ATLAS experiment performed a measurement of the Higgs

boson decaying to b -quarks in the $t\bar{t}H$ production mode with the full Run 2 dataset [179]. This analysis was performed in the semi-leptonic and di-leptonic channels, including a resolved mode where the Higgs boson is reconstructed as two standard jets and a *boosted* mode where the Higgs boson is reconstructed as a single large radius jet. This analysis yields the following combined measurement:

$$\mu_{t\bar{t}H} = 0.43^{+0.20}_{-0.19} (\text{stat.})^{+0.30}_{-0.27} (\text{syst.})$$

The precision of this result is already limited by systematic uncertainties. The dominant systematic unknown is the modelling of the top-quark pair production in association with heavy flavour jets [179].

An update of the $H \rightarrow b\bar{b}$ channel made by CMS with a partial Run 2 dataset of 41.5 fb^{-1} [180], using in particular the fully hadronic channel, is not in combination either. It is nevertheless reported in Table 11.5.

For the so-called “multi-lepton” channels which cover mostly the WW , ZZ and $\tau\tau$ decay modes, CMS has analysed the full Run 2 dataset [181] and ATLAS only part of it [182]. Using a dataset corresponding to an integrated luminosity of 36.1 fb^{-1} , the ATLAS experiment obtained an evidence in this channel [183]. In a preliminary release of this analysis using a larger, but not full Run 2 dataset corresponding to an integrated luminosity of approximately 80 fb^{-1} , the ATLAS experiment found that the normalisation of the $t\bar{t}W$ background was larger than expected from Standard Model calculations by factors ranging from 1.3 to 1.7 and modelling issues were observed in analysis regions where the $t\bar{t}W$ process is dominant [182]. It should be noted that a specific search for Higgs boson decays to tau leptons in association with a pair of top quarks was carried out by ATLAS with the full Run 2 dataset and discussed in 11.3.2.1 [156]. This search is orthogonal to the multi-lepton channel approach where the leptons (including taus) are searched for inclusively.

Using the full dataset in this channel CMS obtained an observation of the Higgs boson production in association with top quarks with an observed significance of 4.7 standard deviations (5.2σ expected). The rate of the $t\bar{t}W$ background in this analysis is also high by a factor of approximately 1.4. The combined result in this channel yields [181]:

$$\mu_{t\bar{t}H} = 0.92 \pm 0.19 (\text{stat.})^{+0.17}_{-0.13} (\text{syst.})$$

All results, except the ATLAS update of the $t\bar{t}H(b\bar{b})$ channel reported above [179], are summarized in Table 11.6.

11.3.3.2 The associated production with a single top quark

An additional production mode of the Higgs boson in association with a top quark is the single top associated production mode. There is an interesting similarity between this production mode and the $H \rightarrow \gamma\gamma$ decay mode. Both processes proceed through either the top Yukawa coupling or the interaction of the Higgs boson with the W boson, with a negative interference between the two. Representative Feynman diagrams for this production process are shown in Fig. 11.1. Contrary to the diphoton decay channel, in this production mode the interference occurs at the tree level and is dominant. This process can therefore be used to further discriminate a negative relative sign between the couplings of the Higgs boson to fermions and its couplings to gauge bosons [186].

ATLAS and CMS have produced specific searches for the tH production mode with the Run 1 and Run 2 data exploiting a variety of Higgs boson decay modes resulting in final states with photons, bottom quarks, and multiple charged leptons, including tau leptons. In particular, with the Run 2 data, CMS has searched for multi-leptonic decay signatures from the $H \rightarrow WW^*$, $H \rightarrow \tau^+\tau^-$ and $H \rightarrow ZZ^*$ modes [187]. This analysis restricts values of κ_t , the top-Higgs coupling normalised to its SM value, to $[-1.25, 1.60]$ at 95% CL. CMS has also performed an analysis of the 2015 dataset to search for the $H \rightarrow b\bar{b}$ mode [188], yielding much less stringent constraints.

The diphoton channel has also been used to search specifically for this production mode by ATLAS using Run 1 data, yielding the restricted range of allowed values of κ_t at the 95% CL to $[-1.3, 8]$.

Table 11.6: Summary of the results of searches for a Higgs boson in association with a top quark pair by ATLAS and CMS. The results are given in terms of a measured signal strength. When available, the statistical and systematic contributions to the total uncertainty are reported separately and in this order. The ATLAS [184] and CMS [185] diphoton and four-leptons results indicated by (*) are not included in the overall combinations which include versions of the diphoton analyses with smaller Run 2 datasets. The combination includes the $t\bar{t}(H \rightarrow b\bar{b})$ channels reported in Table 11.5, but does not include the latest update of the multi-lepton channel [181].

$t\bar{t}H$	ATLAS Run 1	CMS Run 1	ATLAS Run 2	CMS Run 2
$H \rightarrow \gamma\gamma$	$1.3^{+2.6}_{-1.7}{}^{+2.5}_{-1.7}$	$1.2^{+2.5}_{-1.7}{}^{+2.6}_{-1.8}$	$1.38^{+0.33}_{-0.31}{}^{+0.26}_{-0.18}$ (*)	$2.27^{+0.86}_{-0.74}$ (*)
$H \rightarrow 4\ell$	—	—	$1.2^{+1.4}_{-0.8}$ (*)	0.0 ± 1.2 (*)
$WW/\tau\tau/ZZ$	$1.4 \pm 0.6 \pm 1.0$	3.3 ± 1.4	$1.56^{+0.30}_{-0.29}{}^{+0.30}_{-0.27}$	$0.92^{+0.26}_{-0.23}$
Combination	$1.7 \pm 0.5 \pm 0.8$	$2.6^{+1.0}_{-0.9}$	$1.32 \pm 0.18^{+0.21}_{-0.19}$	$1.49 \pm 0.16^{+0.27}_{-0.21}$

The strongest constraint on the negative (relative) sign of κ_t was obtained by CMS using the recent analysis of the full dataset [181] in the multilepton ($H \rightarrow WW$, $H \rightarrow ZZ$, $H \rightarrow \tau\tau$) discussed in 11.3.3.1, negative values of κ_t are disfavoured and the only non excluded negative values of κ_t at 95% CL. range between -0.9 and -0.7.

11.3.3.3 Flavour changing neutral current decays of the top quark

The discovery of the Higgs boson at a mass smaller than the top quark mass opened a new decay channel for the top quark. The decays of the top quark to a Higgs boson and a charm or an up quark proceed through a Flavour Changing Neutral Current (FCNC) which are forbidden at tree level and suppressed at higher orders through the Glashow–Iliopoulos–Maiani (GIM) mechanism [3]. The SM prediction for these branching fractions is $\text{BR}(t \rightarrow Hc) = 10^{-15}$ and two orders of magnitude less for the Hu final state. These decay channels of the top quark are, therefore, very interesting to probe possible FCNC interactions in the Yukawa couplings to the quark sector, see Section 11.7.

ATLAS has searched for FCNC top decays specifically in channels involving a Higgs boson with subsequent decays to two photons and a pair of b -quarks [189]. It has also reinterpreted a search for the $t\bar{t}H$ production in the multilepton final state (discussed in Section 11.3.3.1) [174]. The latter channel covers Higgs boson decays to a pair of W bosons and a pair of taus. No significant excess was observed in any of the specific channels (as discussed in Section 11.3.3.1, a slight excess is observed in the $t\bar{t}H$ multilepton channel) and 95% CL upper limits are set on $\text{BR}(t \rightarrow Hc) < 0.46\%$ with an expected sensitivity of 0.25% and $\text{BR}(t \rightarrow Hu) < 0.45\%$ with an expected sensitivity of 0.29%. CMS has performed a search for these FCNC top decays in the diphoton and multi-lepton channels [190], placing a 95% CL upper limit on $\text{BR}(t \rightarrow Hc) < 0.40\%$ with an expected sensitivity of 0.43%.

From these limits on branching fractions, constraints on non-flavour-diagonal Yukawa couplings of a FCNC Lagrangian of the form:

$$\mathcal{L}_{\text{FCNC}} = \lambda_{t\bar{c}H}\bar{t}Hc + \lambda_{t\bar{u}H}\bar{t}Hu + h.c. \quad (11.12)$$

can be derived. The 95% CL observed (expected) upper limits from ATLAS on the $|\lambda_{t\bar{c}H}|$ and $|\lambda_{t\bar{u}H}|$ couplings are 0.13 (0.10) and 0.13 (0.10), respectively.

The results above are derived from the combination of several channels for searches performed with Run 1 data. Both ATLAS and CMS have produced updates of individual channels with Run 2 data. ATLAS has searched for FCNC top decays with subsequent decays of the Higgs boson to a pair of photons [191], yielding a 95% CL upper limit on $\text{BR}(t \rightarrow Hc) < 0.22\%$ with an expected sensitivity of 0.16%. CMS has searched for FCNC top decays with subsequent decays of the Higgs boson to a pair of b -quarks [192], yielding a 95% CL upper limit on $\text{BR}(t \rightarrow Hc) < 0.47\%$ with an expected sensitivity of 0.44%.

11.3.4 Higgs boson pair production

Higgs boson pair production in the SM is a rare but very important mode to measure and search for. The measurement of

Higgs boson pair production is essential to directly constrain the trilinear Higgs boson self coupling and the search for Higgs boson pair resonances is key in a variety of BSM models. The latter searches are discussed in Section 11.7.7.

In the SM, the main non-resonant production mode of two Higgs bosons proceeds through a loop, mainly of top quarks, see Fig. 11.4 (a). Another production mode is via the trilinear coupling of the Higgs boson, see Fig. 11.4 (b), whose amplitude is not negligible compared to the former. These diagrams interfere negatively, making the overall production rate smaller than what would be expected in the absence of a trilinear coupling.

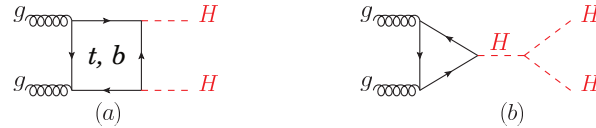


Figure 11.4: Feynman diagrams contributing at leading order to Higgs boson pair production through (a) a top- and bottom-quark loop and (b) through the self coupling of the Higgs boson.

11.3.4.1 Searches for Higgs boson pair production

The searches for Higgs boson pair production both resonant and non-resonant are important probes for a variety of BSM theories, and they can be done in a large number of Higgs boson decay channels. At Run 1, ATLAS and CMS have searched for both resonant and non resonant Higgs boson pair production in the following channels: (i) $HH \rightarrow b\bar{b}\gamma\gamma$; (ii) $HH \rightarrow b\bar{b}\tau^+\tau^-$; (iii) $HH \rightarrow b\bar{b}b\bar{b}$; (iv) $HH \rightarrow b\bar{b}4\ell$; (v) $HH \rightarrow WW^*\gamma\gamma$; (vi) in final states containing multiple leptons (electrons or muons) covering the WW^*WW^* , WW^*ZZ^* , ZZ^*ZZ^* , $ZZ^*\tau^+\tau^-$, $WW^*\tau^+\tau^-$, $ZZ^*b\bar{b}$, $\tau^+\tau^-\tau^+\tau^-$ channels; and (vii) $\gamma\gamma\tau^+\tau^-$ channels.

At Run 2, similarly to the $t\bar{t}H$ production process, the di-Higgs production gains a substantial increase in production cross section of a factor in excess of 3 from 8 TeV to 13 TeV, and most of these channels have been updated both by ATLAS [193] and CMS [194]. The detailed description of the analyses can be found in the following references [193–200] and the references within the combination results published by the collaborations [193–195]. All the results and their combinations are summarised in Table 11.7. The channels (i)–(iii) are the most sensitive to the HH production. These three channels have been updated with the full Run 2 dataset except the $HH \rightarrow b\bar{b}\tau^+\tau^-$ channel by CMS and the $HH \rightarrow b\bar{b}b\bar{b}$ channel by ATLAS which have both been analysed using a partial Run 2 dataset.

In several of these analysis channels the VBF production mode is searched for separately providing sensitivity to the coupling involving two vector bosons and two Higgs bosons HHVV which is an expected coupling in the Standard Model.

The limits obtained on the HHVV coupling modifier denoted κ_{2V} are obtained from the analysis performed by CMS [199] in

Table 11.7: Summary of the final states investigated in the search for Higgs boson pair production by ATLAS and CMS, the results reported in bold are based on the full Run 2 dataset. For ATLAS, the result indicated by (*) uses mostly the $b\bar{b}W^+W^-$ channel. Results are 95% CL upper limits on the observed (expected) SM signal strengths.

Channel	ATLAS	CMS
$b\bar{b}\gamma\gamma$	4.1 (5.5)	7.7 (5.2)
$b\bar{b}b\bar{b}$	12.9 (21)	3.6 (7.3)
$b\bar{b}\tau^+\tau^-$	4.7 (3.9)	31.4 (25.1)
$b\bar{b}4\ell$	-	30 (37)
$W^+W^-W^+W^-$	160 (120)	-
$W^+W^-\gamma\gamma$	230 (170)	-
$b\bar{b}VV$	305 (305)*	79 (89)
Combination	6.9 (10)	22.2 (12.8)

the $b\bar{b}\gamma\gamma$:

$$-1.3 < \kappa_{2V} < 3.5 \text{ (observed)}, \quad -0.9 < \kappa_{2V} < 3.1 \text{ (expected)}$$

11.3.4.2 The Higgs boson self coupling

The Higgs boson self coupling is an extremely important direct probe of the Higgs potential with implications on our understanding of the electroweak phase transition. Constraints on the trilinear self coupling from HH processes is an outstanding long term goal of the LHC and the reach in sensitivity has been reappraised in the light of the recent HH analyses from ATLAS and CMS, shedding a different light on the achievable sensitivity [111]. Constraints from the HHH final state on the quartic Higgs boson self coupling are out of reach at the LHC due mostly to the very small production rates and intricate final states.

In the SM, the Higgs boson pair production through the trilinear Higgs boson self coupling has an on-shell component and a large off-shell component. The on-shell $H \rightarrow H^*H^*$ is strongly disfavoured, requiring two off-shell Higgs bosons in the final state. The sensitivity region to the trilinear coupling production as in Fig. 11.4 (b), is mainly in the kinematic region where the two Higgs boson in the final state are on-shell and the Higgs boson acts as a propagator (off-shell). As discussed in the introduction to this section, this process interferes negatively with the background Higgs boson pair production (Fig. 11.4 (a)).

The measurement of the trilinear coupling requires separating the contributions of the diagram of Fig. 11.4 (b) from the box diagram of Fig. 11.4 (b), and therefore a precise knowledge of the top-Yukawa coupling is needed. Each diagram alone would produce rather distinct m_{HH} distribution. And, for values of the trilinear coupling close to the SM value, an additional discriminating feature of the signal with respect to one obtained with the box contribution alone is a deficit in the number of events. With large variations of the trilinear coupling, an excess of events over the SM prediction would be observed (for a value of the trilinear coupling about 6 times larger than its SM value, the number of events is equal to the SM expectation). Additional sensitivity to the trilinear coupling is also obtained from the kinematical distributions of the signal taking in particular into account the effect of the HH mass distribution which discriminates the main contributions of Fig. 11.4. This further discrimination is instrumental in resolving the degeneracy in the total cross section mentioned above. The bounds obtained by ATLAS [200] and CMS [199] for

the $b\bar{b}\gamma\gamma$ channel alone for are the following:

$$\begin{aligned} \text{(ATLAS)} \quad & -1.5 < \kappa_\lambda < 6.7 \text{ (observed)}, \\ & -2.4 < \kappa_\lambda < 7.7 \text{ (expected)}, \\ \text{(CMS)} \quad & -3.3 < \kappa_\lambda < 8.5 \text{ (observed)}, \\ & -2.5 < \kappa_\lambda < 8.2 \text{ (expected)}, \end{aligned} \quad (11.13)$$

where κ_λ is the ratio between the trilinear coupling value left free in the fit and its expected value in the SM ($\kappa_\lambda = 1$ corresponds to the SM). These results are also illustrated in Fig. 11.5.

The analyses performed at Run 2 bring substantial improvements from those of Run 1, and they were used to reappraise the sensitivity of the LHC in the High Luminosity regime in the framework of the update of the European Strategy for Particle Physics [111]. The result in terms of bounds on the trilinear coupling are shown in Fig. 11.5, indicating that the significance of the observation of the HH process reaches 4σ . It is also apparent that the degeneracy of secondary minimum at intermediate values of κ_λ is resolved by the use of the kinematical discriminants. Indeed, this secondary minimum is expected to be excluded at 99.4% CL. This is very important to allow the measurement in the vicinity of the SM value at one standard deviation and to provide a meaningful confidence interval. At HL-LHC, the foreseen precision on κ_λ is approximately 50%.

Significantly higher precisions can be reached at pp colliders (and e^+e^- colliders) at higher centre-of-mass energies. The foreseen precision for a High-Energy (HE) LHC at a centre-of-mass energy of 27 TeV is expected to be within 10% to 20% [111]. At a very large hadron collider at a centre-of-mass energy of 100 TeV, a 5% sensitivity is expected to be reached, provided that the theoretical and parametric uncertainties are kept at the 1% level.

Indirect constraints on the Higgs boson trilinear coupling from single Higgs boson production processes will be discussed in Section 11.6.2.5.

11.3.5 Searches for rare decays of the Higgs boson

11.3.5.1 $H \rightarrow Z\gamma$ and the first evidence for the Dalitz $H \rightarrow \ell^+\ell^-\gamma$ decay

The search for $H \rightarrow Z\gamma$ is performed in the final states where the Z boson decays into opposite sign and same flavour leptons ($\ell^+\ell^-$), ℓ here refers to e or μ . While the branching fraction for $H \rightarrow Z\gamma$ is comparable to $H \rightarrow \gamma\gamma$ (about 10^{-3}) at $m_H = 125$ GeV, the observable signal yield is brought down by the small branching ratio of $Z \rightarrow (e^+e^- + \mu^+\mu^-) = 6.7 \times 10^{-2}$. In these channels, the $m_{\ell\ell\gamma}$ mass resolution is excellent (1–3%), therefore the analyses search for a narrow mass peak over a continuous background. The major backgrounds arise from the $Z + \gamma$ final state radiation in Drell-Yan decays and from the $Z + \text{jets}$ processes where a jet is misidentified as a photon. The ratio of signal over background in this channel is typically of the order of 0.5%. In a narrow window of a few GeV around 125 GeV, several hundreds of events are expected in a Run 2 dataset corresponding to approximately 36 fb^{-1} .

Events are divided into mutually exclusive categories on the basis either of the expected $m_{Z\gamma}$ resolution or exclusive production mode categories.

No excess of events is observed in either ATLAS or CMS in the Run 1 data. The CMS expected and observed 95% CL upper limits for $m_H = 125$ GeV on the signal strength μ are 10.0 and 9.5 respectively. The ATLAS expected and observed upper limits on the signal strength μ are 9.0 and 11.0 respectively, for $m_H = 125.5$ GeV.

With the full Run 2 dataset, ATLAS observes no significant excess and places a 95% CL observed (expected) upper limit on the signal strength of 3.6 (2.6) [201]. An excess with a significance of 2.2σ is observed. The expected significance of an excess with respect to the background hypothesis sensitivity is 1.2σ . With a partial dataset CMS reports a limit of 4.0 (11.4) times the SM cross section for $H \rightarrow Z\gamma$ [202] process.

Both ATLAS and CMS experiments have extended the search for the so-called Dalitz Higgs boson decays $H \rightarrow \gamma^*\gamma \rightarrow \ell^+\ell^-\gamma$ in the low mass γ^* range of approximately 20–30 GeV. This decay mode has a substantially larger branching fraction compared to

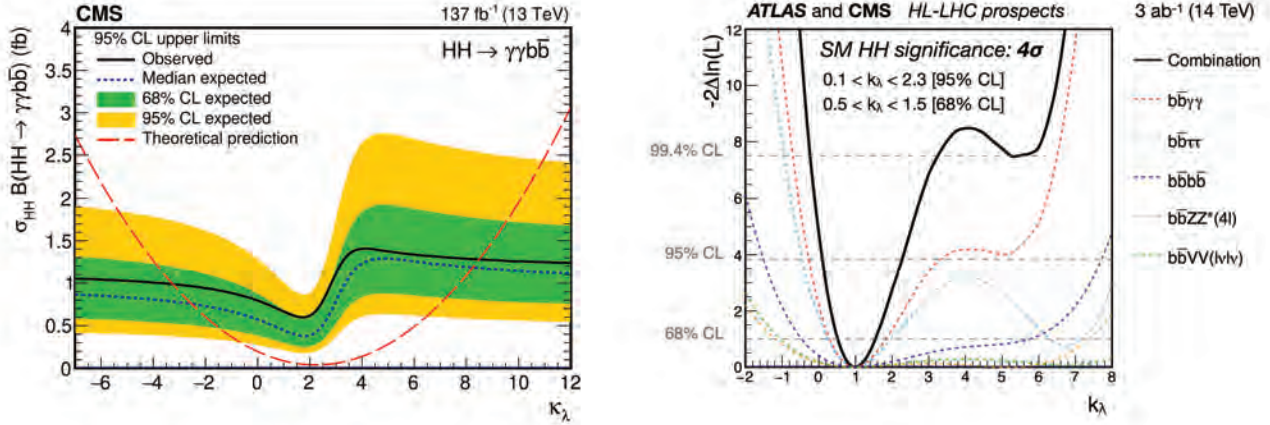


Figure 11.5: (Left) Upper limit obtained by CMS on the total $pp \rightarrow HH$ production cross section as a function of the trilinear coupling modifier κ_λ . The variation of the limit corresponds to variations in the signal acceptance. The expected total production cross section is also illustrated (red). (Right) Expected combined ATLAS and CMS likelihood for the searches for the $pp \rightarrow HH$ production at the High Luminosity LHC. The channels used in the combination are indicated in the figure.

the $Z\gamma$ decay, as $\Gamma(H \rightarrow \gamma^*\gamma \rightarrow e^+e^-\gamma) \sim 3.5\% \times \Gamma(H \rightarrow \gamma\gamma)$ and $\Gamma(H \rightarrow \gamma^*\gamma \rightarrow \mu^+\mu^-\gamma) \sim 1.7\% \times \Gamma(H \rightarrow \gamma\gamma)$, while $\Gamma(H \rightarrow Z\gamma) = 2.3\% \times \Gamma(H \rightarrow \gamma\gamma)$ (which does not account for the subsequent decay of the Z boson to electrons or muons). With the Run 1 dataset, CMS observes an upper limit of 6.7 times the SM branching ratio [203]. With a partial Run 2 dataset, in the $\gamma^*\gamma$ CMS obtained a much more stringent limits on cross section times the corresponding branching fractions of 1.4 (6.1) times the SM cross section [202]. CMS also performed a combination of the two this mode with $H \rightarrow Z\gamma$, obtaining a combined observed (expected) limit of 3.9 (2.0) times the SM branching fractions.

Using the full Run 2 dataset corresponding to 139 fb^{-1} , ATLAS obtained the first evidence for Higgs boson decays to a low-mass dilepton pair and a photon with a significance of 3.2 (2.1) standard deviations (expected) [204]. The invariance mass requirement on the di-lepton is $m_{\ell\ell} < 30 \text{ GeV}$. The corresponding signal strength is $\mu = 1.5 \pm 0.5$, compatible with the expectation from the Standard Model.

11.3.5.2 First evidence of $H \rightarrow \mu^+\mu^-$

The branching fraction in the $H \rightarrow \mu^+\mu^-$ channel for a 125 GeV SM Higgs boson is 2.2×10^{-4} , about ten times smaller than that for $H \rightarrow \gamma\gamma$. The dominant and irreducible background arises from the $Z/\gamma^* \rightarrow \mu^+\mu^-$ process which has a rate several orders of magnitude larger than that from the SM Higgs boson signal. Due to the precise muon momentum measurement achieved by ATLAS and CMS, the $m_{\mu^+\mu^-}$ mass resolution is very good ($\approx 2\text{--}3\%$ for ATLAS and $\approx 1\text{--}3\%$ for CMS depending on the selected categories; a better resolution is expected for CMS due its higher field in the inner detector). A search is performed for a narrow peak over a large but smoothly falling background. For optimal search sensitivity, events are divided into several categories. Either taking advantage of the superior muon momentum measurement in the central region, events can be subdivided by the pseudo-rapidity of the muons, or designing selections aiming at specific production processes such in particular as the vector boson fusion.

No excess in the $m_{\mu^+\mu^-}$ spectrum is observed near 125 GeV. From an analysis of the Run1 data, ATLAS sets an observed (expected) 95% CL upper limit on the signal strength $\mu < 7.0$ (7.2). The CMS analysis of its 7 and 8 TeV data sets an observed (expected) limit of $\mu < 7.4$ (6.5).

ATLAS [205] and CMS [206] have performed a reoptimised analysis using the full Run2 dataset. Both the ATLAS and CMS selections target all the main production modes including gluon fusion, the associated production with a vector boson (VH), the vector boson fusion and the associated production with a top-quark pair and in various cases further use multivariate and deep learning methods to discriminate signal from background in these

categories. The signal in both experiments is extracted from a fit to the di-muon invariant mass spectrum and the background is modelled using an analytical function, except in the case of the most sensitive channel (VBF) in the CMS analysis where the discriminant Deep Neural Network output is used [206]. The reach in sensitivities of the analyses has been significantly improved. With the full dataset ATLAS and CMS have respectively an expected significance of 1.7σ and 2.5σ . Both ATLAS and CMS observe an excess of events respectively with signal strengths of $\mu = 1.2 \pm 0.6$ and $\mu = 1.19 \pm 0.40$ (stat.) ± 0.15 (syst.). In both cases the measurement uncertainties are dominated by the data statistics. The observed significances are 2.0σ and 3.0σ respectively. These results show a first direct evidence for the decay of the Higgs boson to muons and thus of the Yukawa coupling of the Higgs boson to second generation fermions. The significant increase in sensitivity is very encouraging for these important measurements at the LHC Run 3.

11.3.5.3 $H \rightarrow e^+e^-$

A search similar to the $H \rightarrow \mu^+\mu^-$ is performed by CMS in the di-electron channel. In this search channel, the contribution from the peaking background from Higgs boson decays to diphotons mis-identified as di-electrons (when mostly converted photons are faking electrons) needs to be assessed. The sensitivity to the SM Higgs decays is negligible given the extremely small branching fraction to e^+e^- , approximately 40'000 times smaller than the branching fraction to dimuons. It is nevertheless interesting to probe this decay channel to search for potential large anomalous couplings. Assuming a SM Higgs boson production cross section, the observed limit on the branching fraction at the 95% CL is 0.0019, five orders of magnitude larger than the expected SM prediction. It is also important to note that processes not depending on the electron Yukawa coupling such as the $H \rightarrow e^+e^-\gamma$ (where the photon is soft), are sizeably larger than the direct Yukawa coupling process, but also much smaller than the current constraints, making any interpretation in terms of constraint on the electron Yukawa couplings far from straightforward.

At Run2, ATLAS has also performed a search for the $H \rightarrow e^+e^-$ decay mode with the full dataset, improving the current limit by a factor of approximately 5, with a limit of 3.6×10^{-4} on the branching fraction [207].

11.3.5.4 Lepton flavour violating (LFV) Higgs boson decays

Given the Yukawa suppression of the couplings of the Higgs boson to quarks and leptons of the first two generations and the small total width of the Higgs boson, new physics contributions could easily have sizable branching fractions. One very interesting possibility is the Lepton Flavour Violating (LFV) decays of the Higgs boson, in particular in the $\tau\mu$ and τe modes. These

decays are suppressed in the SM but they could easily be enhanced in theories such as two-Higgs-doublet models (discussed in Section 11.7).

There are already constraints on LFV Yukawa couplings $|Y_{\tau\mu}|$ from channels such as the $\tau \rightarrow 3\mu$ or $\tau \rightarrow \mu\gamma$, or a reinterpretation of the search for Higgs boson decays to $\tau^+\tau^-$. A direct search at the LHC, however, complements these indirect limits. The search for LFV decays in the $\tau\mu$ channel have been done with the Run 1 dataset in several channels according to the subsequent decay of the τ . The results from CMS [208] and from ATLAS for the hadronic [209], the leptonic [210] decays of the tau, and their combination [210] are reported in Table 11.8. It is interesting to note that the analysis strategies at Run 1 for the dilepton $\tau_{\text{lep}}\mu$ channel are very different between ATLAS [210] and CMS [208]. The CMS results are obtained using the full Run 2 dataset.

As shown in Table 11.8, an excess was observed in this channel by CMS with a significance of 2.5σ , while in ATLAS analysis, the excess is smaller, about 1σ at Run 1. CMS has performed the search again with the full 2016 Run 2 dataset [211], relying on a multivariate analysis. The observed best fit branching fraction is $(0.00 \pm 0.12)\%$. These limits are reported in Table 11.8.

ATLAS and CMS have also performed a search for the LFV Higgs boson decays in the τe and μe channels [210–212]. No significant excess was observed and 95% CL limits are reported in Table 11.8, for the τe channel only. For the μe channel, the constraints from the $\mu \rightarrow e\gamma$ experiments [213] are much stronger than those from the direct LFV Higgs boson decay search. However these indirect constraints can be relaxed by the cancellation of LFV effects from new physics.

At Run 2, ATLAS has performed searches for LFV decays of the Higgs boson in the $e\tau$ and $\mu\tau$ channels [214] as well as in the $e\mu$ channel [207]. The searches for the $H \rightarrow e\tau$ and $H \rightarrow \mu\tau$ decays were done with the 2016 data only and yielded upper limits on the LFV decay branching fraction of 0.47% (0.34%) and 0.28% (0.37%), respectively.

CMS has also searched for LFV decays with the 2016 dataset at Run 2 and obtained observed (expected) limits on the LFV branching fraction of $\text{BR}(H \rightarrow \mu\tau) < 0.25\%$ (0.25%) and $\text{BR}(H \rightarrow e\tau) < 0.61\%$ (0.37%), at the 95% CL [215]. These limits were also interpreted in terms of constraints on the corresponding off-diagonal Yukawa couplings.

The results obtained by ATLAS and CMS at Run 2 do not confirm the excesses observed at Run 1.

11.3.5.5 Probing charm- and light-quark-Yukawa couplings

Probing the Yukawa couplings to quarks of the second or even the first generation is extremely challenging given the overwhelming backgrounds and very small signal rates.

The possibility of probing the Yukawa coupling to the charm has been discussed in Ref. [216] where indirect bounds are estimated from a combined fit to the Higgs data and the importance of using charm tagging is emphasised. Searches in the VH production mode have been carried out, in the channels very similarly to those aiming at the b -quark Yukawa coupling, by both ATLAS [217] and CMS [218] with Run 2 data. The upper limits obtained (expected) on the VH production cross section times the charm quark decay branching fraction of the Higgs boson are:

$$\text{(ATLAS)} \quad \frac{\sigma(VH) \times \text{BR}(H \rightarrow c\bar{c})}{\sigma(VH)_{SM} \times \text{BR}(H \rightarrow c\bar{c})_{SM}} < 26(31). \quad (11.14)$$

$$\text{(CMS)} \quad \frac{\sigma(VH) \times \text{BR}(H \rightarrow c\bar{c})}{\sigma(VH)_{SM} \times \text{BR}(H \rightarrow c\bar{c})_{SM}} < 70 \quad (37_{-10}^{+16}). \quad (11.15)$$

The ATLAS search [217] was done with the full Run 2 dataset and the cross section times branching fraction upper limit is interpreted in terms of charm yukawa coupling modifier yielding an observed limit of $\kappa_c < 8.5$ (12.4 expected) at the 95% CL. It should be noted that these analyses are sensitive to the diboson VZ where $Z \rightarrow c\bar{c}$ and VW where $W \rightarrow c\bar{q}$. The ATLAS collaboration reported significances of 2.6σ and 3.8σ for these two standard signals respectively, in good agreement with the expectation from the Standard Model.

Another possibility to access the charm Yukawa coupling has been discussed in Ref. [219]. It relies on the decays of the Higgs boson to a final state with charmonium: $H \rightarrow J/\Psi\gamma$. Higgs boson decays in this final state have been searched for by ATLAS [220]. The sensitivity of this analysis is, however, several orders of magnitude above the branching fraction estimated in the SM: $\text{BR}(H \rightarrow J/\Psi\gamma) = (2.8 \pm 0.2) \times 10^{-6}$. ATLAS [220] has also searched for Higgs boson decays to $\Upsilon(nS)\gamma$ where ($n = 1, 2, 3$), a channel with much lower sensitivity than the $H \rightarrow b\bar{b}$ to the Yukawa coupling to b -quarks.

More recently, ATLAS [221] and CMS [222] have searched, for quarkonia in the Higgs decay final state where the Higgs boson decays to $\phi\gamma$ or $\rho\gamma$ at the LHC Run 2 and a center-of-mass energy of 13 TeV. These channels require specific triggers and could probe deviations from the strange-quark or light-quarks Yukawa couplings respectively. Its sensitivity is several orders of magnitude above the SM expectation.

CMS has also performed a search of the decays of the Higgs boson in the $J/\Psi J/\Psi$ and $\Upsilon\Upsilon$ decay to cover the cases where the photon in the $J/\Psi\gamma$ decay is virtual and transforms into a J/Ψ meson. These decays provide an additional channel potentially sensitive to BSM phenomena [223].

11.3.5.6 Rare decays outlook

Rare decays such as those described in the above sections have clearly a limited sensitivity. However, they already deliver interesting messages. For example, if the coupling of the Higgs boson to muons was as strong as it is to top quarks, this mode should have been observed. Therefore, it can be concluded that the observed couplings of the Higgs boson are manifestly non-universal. Further, developing these rare decay modes is an important component of the High Luminosity program of the LHC in order to directly probe the couplings of the Higgs boson, and to potentially measure the Yukawa coupling to the fermions of the second generation, in particular to muons. It is also an integral part of the physics program of the discussed potential future Higgs boson factories.

11.3.6 Searches for non-SM decay channels

The main decay and production properties of the observed Higgs boson are consistent with the SM predictions. The Higgs boson may, however, have other decay channels beyond those anticipated in the SM. Among these, and of great interest, are the invisible decays into stable particles, such as DM particle candidates, that interact very weakly with the detector, and that remain undetected. Other non standard decay channels that have been investigated are the decays of the Higgs particle to hidden valley or dark particles.

11.3.6.1 Invisible decays of the Higgs boson

The discovery of the Higgs boson immediately raised the question of its couplings to DM and how it could be used to reveal at colliders the existence of a dark sector coupled to the SM via the Higgs boson portal, see Ref. [224] and references therein. If kinematically accessible and with a sufficiently large coupling to the Higgs boson, DM particles, such as, e.g., neutralinos in SUSY models, graviscalars in models with extra dimensions or heavy neutrinos in the context of four-generation fermion models, would manifest themselves as invisible decays of the Higgs boson, thus strongly motivating searches for the invisible decays of the Higgs boson.

To identify an invisibly decaying Higgs boson at the LHC, it must be produced in association with other particles. Searches for invisible decays of the Higgs particle at the LHC have been carried out in the three associated production modes of the Higgs boson with the highest SM cross sections and target events with large missing energy.

The ggF production mode has the largest SM cross section but it usually results in the Higgs boson being created alone and hence leaving no characteristic signature in the detector of its invisible decay. One way to search for invisible decays in ggF production mode is to look for events with the monojet topology arising from initial state gluon radiation and containing missing energy. The major irreducible background in such searches stems from $Z + \text{jets}$ events where the Z boson decays into a pair of neutrinos [225].

Table 11.8: Summary of the results of searches for lepton flavour violating decays of the Higgs boson in the $\tau\mu$ and τe channels from ATLAS and CMS. For the result with *, the expected sensitivity was not reported but appears consistent with the observed one. In its Run 2 analysis CMS reports no significant excess (NSE).

	ATLAS (Run 1)	CMS (Run 1)	CMS (Run 2)
$\text{BR}(H \rightarrow \tau\mu)$	$(0.53 \pm 0.51)\%$	$(0.84^{+0.39}_{-0.37})\%$	NSE
95% CL Obs. (Exp.)	1.43% (1.01%)	1.51% (0.75%)	0.15% (0.15%)
$H \rightarrow \tau e$ 95% CL Obs. (Exp.)	1.02% (1.21%)	0.69%*	0.22% (0.16%)

The analysis with the best sensitivity targets the VBF production topology but it suffers from large backgrounds arising from events with two jets and large missing energy. The VH mode has much smaller cross section but the presence of a W or Z boson allows a variety of final states that can be tagged with relatively low background.

ATLAS and CMS have searched for such final states at Run 1 and have observed no significant excess over the predicted backgrounds (for references, see the previous edition of this review [132]). Table 11.9 summarizes the 95% CL limits on the invisible decays of the Higgs boson assuming a SM Higgs boson production cross section and the corresponding detector acceptances.

ATLAS has performed the search for invisible decays of the Higgs boson at Run 2 with the full dataset in the VBF production [226], the ZH associated production where the Z boson subsequently decays to a pair of leptons [227], and in the 2015 and 2016 datasets, corresponding to an integrated luminosity of approximately 36 fb^{-1} in the VH associated production where the vector boson (a W or a Z) subsequently decays hadronically [228]. The most stringent constraint is obtained through the VBF channel. All results and their combination [229] are reported in Table 11.9. Combined with the Run 1 results, the ATLAS limit on the invisible branching fraction reaches 11%, with an expected sensitivity of 11% [229].

CMS has updated the search for invisible decays of the Higgs boson in the vector boson fusion and the associated production with a vector boson channels (both with subsequent leptonic [230] and hadronic decays [231]) using Run 2 data collected in 2016 [232]. It has produced a combination with Run 1 channels, yielding a limit on the invisible branching fraction of 19%, with an expected sensitivity of 15% [232].

ATLAS and CMS have also reinterpreted a search for scalar top quarks in the all-hadronic, semi-leptonic and fully leptonic final state with the 2016 data of Run 2 to set limits on the invisible Higgs decays through the $pp \rightarrow t\bar{t}H$ production mode [229, 233]. The results of the search are reported in Table 11.9.

This constraint can then be further used to probe Higgs portal models to DM [224], where an additional weakly interacting particle χ with mass lower than $m_H/2$ is introduced as DM candidate and where the Higgs boson is considered as the only mediator between the SM particles and DM. In this model, it is interesting to express the limit on the invisible branching fraction in terms of strength of interaction of DM with standard matter, i.e., in terms of its interaction cross section with nucleons $\sigma_{\chi-N}$. In this model, the couplings of the Higgs boson to SM particles are assumed to be those of the SM and the interaction of the Higgs boson with the nucleon is parametrised in a Higgs-Nucleon form factor estimated using lattice QCD calculations [224]. The exclusion limits from the constraints on invisible Higgs boson decays, both direct and indirect from the measurement of the coupling properties of the Higgs boson can be compared to direct detection experiments. For comparison, the limit at 90% CL on the invisible branching fraction of $\text{BR}_{\text{inv}} < 19\%$ [232] is used and converted into limits on $\sigma_{\chi-N}$ under several hypotheses on the nature of DM particles depending mainly on their spin (scalar- or fermion-like). The vector DM hypothesis is not included since (renormalisable) models of vectorial DM require an extended dark sector that could imply modifications of the signal. The results are shown in Fig. 11.6.

11.3.6.2 Exotic Higgs boson decays

The 125 GeV Higgs boson serves not only as a probe for potential DM candidates, but also to search for other exotic particles

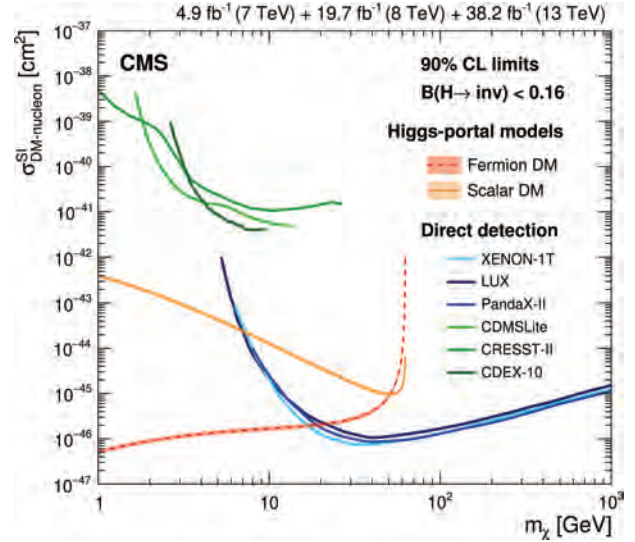


Figure 11.6: 90% CL upper limits on the WIMP-nucleon scattering cross section as a function of the DM particle mass in models where the Higgs boson is a portal between the SM matter and the Dark Sector. Spin-independent results excluded and favoured regions from direct detection experiments are also shown.

arising from fields associated with a low-mass hidden sector. Such hidden sectors are composed of fields that are singlet under the SM gauge group $SU(3) \times SU(2) \times U(1)$. These models are referred to as hidden valley models [234]. Since a light Higgs boson is a particle with a narrow width, even modest couplings to new states can give rise to a significant modification of the Higgs boson phenomenology through exotic decays. Simple hidden valley models exist in which the Higgs boson decays to an invisible fundamental particle, which has a long lifetime to decay back to SM particles through a small mixing with the SM Higgs boson, see Ref. [234] for a concrete example. The Higgs boson may also decay to a pair of hidden valley “v-quarks,” which subsequently hadronise in the hidden sector, forming “v-mesons.” These mesons often prefer to decay to the heaviest state kinematically available, so that a possible signature is $H \rightarrow 4b$. Some of the v-mesons may be stable, implying a mixed missing energy plus heavy flavour final state. In other cases, the v-mesons may decay to leptons, implying the presence of low mass lepton resonances in high- H_T events [235]. Other scenarios have been studied [236] in which the Higgs boson decays predominantly into light hidden sector particles, either directly, or through light SUSY states, and with subsequent cascades that increase the multiplicity of hidden sector particles. In such scenarios, the high-multiplicity hidden-sector particles, after decaying back into the SM, appear in the detector as clusters of collimated leptons known as “lepton jets”.

A variety of models have been investigated searching for final states involving dark photons and hidden valley scalars. The resulting topologies typically have leptons or light hadrons which in some cases can be prompt (i.e., originating from the hard process interaction point) or not and are in some cases collimated and reconstructed as jets [237, 238], and long-lived weakly interacting particles. The latter occur not only in hidden valley scenarios, but

Table 11.9: Summary of the channels searched for and the corresponding 95% CL limits from ATLAS and CMS on the branching fraction for the Higgs boson decay to invisible particles assuming a SM Higgs boson production cross section. The results in parentheses are the expected exclusions.

	ATLAS (Run 1)	ATLAS (Run 2)	CMS (Run 1)	CMS (Run 2)
ggF (monojet); $H \rightarrow \text{inv.}$	–	–	67 (71) %	66 (59)%
VBF; $H \rightarrow \text{inv.}$	28 (31) %	13 (13) %	57 (40) %	33 (25) %
ZH; $Z \rightarrow \ell^+\ell^-$; $H \rightarrow \text{inv.}$	75 (62)%	18 (18) %	75 (91) %	40 (42)%
VH; $Z, W \rightarrow jj$; $H \rightarrow \text{inv.}$	78 (86)%	83 (58) %	–	50 (48)%
ZH; $Z \rightarrow b\bar{b}$; $H \rightarrow \text{inv.}$	–	–	182 (189)%	–
$t\bar{t}H$; $H \rightarrow \text{inv.}$	–	40 (36)%	–	46 (48)%
Combination	25 (27)%	13 (12)%	–	26 (20) %
Run 1 & 2 Combination	11 (11)%		19 (15)%	

also in gauge-mediated extensions of the minimal SUSY standard model (MSSM), the MSSM with R-parity violation, and inelastic DM scenarios [239]. Finally, CMS has performed a search for pair production of light bosons [240]. Such a scenario can occur in SUSY models with additional hidden (or dark) valleys.

11.4 Combining the main channels

The analysis strategy used by the LHC experiments to perform the searches for the Higgs boson has been based on the Higgs boson decay modes. It is a natural choice given that it focusses on the decay products of the object searched for. However, for each channel, exclusive sub-channels have been defined to target different production modes and kinematic regimes, and these sub-channels have been combined. The natural extension of this approach in order to probe further the production and decay modes of the Higgs boson is to combine the analysis channels together. Such a combination is also used in Section 11.6 to further measure the coupling properties of the Higgs boson.

At the LHC, the total cross section cannot be measured in any of the production modes. As a consequence, neither the absolute branching fractions nor the total width of the Higgs boson can be directly measured, at least if the width is of the SM size. However, a combined measurement of the large variety of categories described in Section 11.3, with different sensitivities to various production and decay modes, permits a wide variety of measurements of the production, decay and coupling properties. These measurements require, in general, a limited but nevertheless restrictive number of assumptions.

In this section, three sets of results will be given. The first one is the ATLAS and CMS Run 1 combination [151]. The other two are the individual combinations of ATLAS and CMS independently with partial Run 2 dataset. It is important to note that, between the Run 1 and the Run 2 results, the signal theoretical systematic uncertainties have improved significantly.

The Run 1 full combination results were derived by the two collaborations, taking rigorously into account all correlations in the systematic uncertainties and in the large number of channels and their categories.

At Run 2, ATLAS [241] and CMS [242] have already produced combined measurements of the coupling properties and production cross section ratios of the Higgs boson.

In this section, only the results on the main Higgs boson production and decay modes will be discussed. Only a brief presentation of the combination framework is given here (a more detailed description is given in Ref. [243]). This framework will also be used in Section 11.6 to discuss the measurements of the coupling properties of the Higgs boson.

11.4.1 Principles of the combination

The combination of the Higgs boson analysis channels in each experiment and for the two experiments together was done using a fit of a signal and background model to the data. As described above, the data was made of a large number of categories, aiming at reconstructing exclusive production and decay modes. In the combination of ATLAS and CMS [151], there were approximately 600 categories. The combination was a simultaneous fit to all these categories, using a reduced number of parameters of interest and a Higgs boson mass fixed at its measured value (see

Section 11.3.1.3). The much larger number of categories present in the ATLAS and CMS combination [151] is due to additional separation in terms of finer exclusive production regions, decay channels of the Z and the W bosons, and taus, control regions where little-to-no signal is present, and different center-of-mass energies. It should be noted that the individual combination performed by ATLAS [244] included two additional decay channels: the $\mu^+\mu^-$ and $Z\gamma$. For the sake of simplicity these channels were omitted in the ATLAS–CMS combination due to the very little sensitivity in these channels with this dataset.

In their Run 2 individual combinations, ATLAS and CMS have not considered the $Z\gamma$ channel. Both ATLAS and CMS experiment have included the $\mu\mu$ channel based on a partial Run 2 dataset corresponding to an integrated luminosity of 36 fb^{-1} only.

The key to understand how the combination of channels works relies on the combination master formula, which expresses for each category, indexed by c , of a given channel (typically a category covers mostly one decay mode, but possibly various production modes), the measured number of signal events n_s^c as a function of a limited number of parameters as follows:

$$n_s^c = \left(\sum_{i,f} \mu_i \sigma_i^{\text{SM}} \times A_{if}^c \times \varepsilon_{if}^c \times \mu_f \text{BR}_f^{\text{SM}} \right) \times \mathcal{L}^c. \quad (11.16)$$

The production index is defined as $i \in \{\text{ggF}, \text{VBF}, \text{VH}, \text{t}\bar{t}H, \text{t}H, \dots\}$ (including specific modes and regions of phase space) and the decay index is defined as $f \in \{\gamma\gamma, WW, ZZ, b\bar{b}, \tau\tau\}$, while σ_i^{SM} and BR_f^{SM} are the corresponding production cross sections and decay branching fractions, estimated as described in Section 11.2, assuming that the Higgs boson is that of the SM. A_{if}^c and ε_{if}^c are the signal acceptance and the reconstruction efficiency for the given production and decay modes in the category c . \mathcal{L}^c is the integrated luminosity used for that specific category. For the purpose of this review, these parameters can be considered as fixed³.

The parameters of interest in the master formula are the signal strength parameters μ_i and μ_f . It is important to note that the formula relies on the factorisation of the production cross section and decay branching fraction, which assumes the narrow width approximation. The width of the Higgs boson will be discussed in Section 11.5, however, for the precision needed here, the fact that the Higgs boson has been observed in decay channels with high mass resolution as a resonance is sufficient to validate this hypothesis. It is also manifest in the above equation that the ten parameters for the production modes (μ_i) and decay modes (μ_f) cannot be determined simultaneously. This illustrates that total cross sections or branching fractions cannot be measured without further assumptions in this fit.

The master formula also illustrates an important caveat to the measurement of signal strength parameters. In case these are interpreted as scale factors of the production cross sections or branching fractions, then all the other quantities such as the acceptances and efficiencies, A_{if}^c and ε_{if}^c , need to be assumed as

³In the combination performed by ATLAS and CMS, the systematic uncertainties on these parameters are taken into account by allowing these parameters to vary in the fit.

Table 11.10: Summary, for the main production and decay processes at the LHC, of the observed (and expected) significances with respect to the background only hypothesis. When the observation has been established unambiguously, the measured signal strength is reported together with the total uncertainty or, when available, the statistical (first) and the systematic (last) uncertainties. The results for the gauge boson decays of the Higgs boson for the ATLAS experiment are not reported in the combination and are thus taken from the individual channels results (*) and when needed computed from the ratio of fiducial cross sections (**) discussed in this review. *The Run 2 VH significances reported in this table are obtained from the observation of the Higgs boson decays to b quarks, while the Run 1 combination corresponds to combination of all channels.

	Decay modes			
	ATLAS (Run 1)	CMS (Run 1)	ATLAS (Run 2)	CMS (Run 2)
$\gamma\gamma$	4.6σ (5.3 σ)	5.2σ (4.6 σ)	$1.02 \pm 0.13^{**}$	$1.07^{+0.08+0.08}_{-0.08-0.07}$
ZZ	6.2σ (6.3 σ)	8.1σ (6.5 σ)	$1.01 \pm 0.11^*$	$0.93^{+0.07+0.07}_{-0.07-0.06}$
WW	5.9σ (5.4 σ)	6.5σ (4.7 σ)	$1.05 \pm 0.13^{**}$	$1.20^{+0.09+0.13}_{-0.09-0.12}$
$\tau^+\tau^-$	3.4σ (3.9 σ)	4.5σ (3.8 σ)	6.4σ (5.4 σ)	$0.80^{+0.10+0.14}_{-0.10-0.13}$
	Comb. 5.0σ (5.5 σ)			
$b\bar{b}$	2.6σ (2.5 σ)	1.4σ (2.1 σ)	5.4σ (5.5 σ)	$1.11^{+0.13+0.16}_{-0.13-0.15}$
	Comb. 3.7σ (2.6 σ)			
	Production modes			
	ATLAS and CMS (Run 1)	ATLAS (Run 2)	CMS (Run 2)	
$gg \rightarrow H$ (ggF)	NR	$1.00 \pm 0.05 \pm 0.05$	1.04 ± 0.05	$^{+0.08}_{-0.07}$
$qq \rightarrow qqH$ (VBF)	Comb. 5.4σ (4.6 σ)	$1.15 \pm 0.13^{+0.12}_{-0.10}$	$0.75^{+0.16+0.10}_{-0.15-0.08}$	
$pp \rightarrow WH$	Comb. 3.5σ (4.2 σ)	$1.20^{+0.17+0.15}_{-0.16-0.14}$	$1.46^{+0.29+0.22}_{-0.28-0.21}$	
$pp \rightarrow ZH$		$0.98 \pm 0.16^{+0.15}_{-0.13}$	$0.98^{+0.26+0.17}_{-0.25-0.16}$	
$pp \rightarrow t\bar{t}H$	Comb. 4.4σ (2.2 σ)	$1.10^{+0.16+0.14}_{-0.15-0.13}$	$1.14^{+0.13+0.17}_{-0.13-0.15}$	

independent and fixed to their estimated values for the SM Higgs boson. An additional important caveat to note concerning these combined results is that only the normalisation is varied, while the discriminating variables for the signal are not modified and are still used in the fit. These caveats are of particular importance in the use of the combination to measure the coupling properties of the Higgs boson, as discussed in Section 11.6. For relatively small perturbations of the couplings of the Higgs boson from the SM values, this hypothesis is valid.

However, the products $\mu_i \times \mu_f$ can be considered as free parameters and in principle measurable (if there is sufficient sensitivity from specific categories). Measuring the products of signal strengths can be viewed as measuring the cross sections times the branching fraction, $\sigma \cdot \text{BR}$. An illustration of the results for the Run 2 combinations of ATLAS is presented in Fig. 11.7 and for CMS in Fig. 11.8.

Other fits involving ratios of cross sections, which are less sensitive to theory uncertainties, are performed and reported in Ref. [243].

The most constrained fit in the combination allows for only one single parameter to vary, i.e., $\forall(i, f), \mu_i = \mu_f = \mu$. This global-signal-strength model provides the simplest probe of the compatibility of the signal with the SM Higgs boson. Indeed, it is sensitive to any deviation from the SM Higgs boson couplings provided that these deviations do not cancel overall. The full Run 1 combination determines the global signal strength to be

$$\mu = 1.09 \pm 0.11 = 1.09 \pm 0.07 \text{ (stat.)} \pm 0.04 \text{ (expt.)} \pm 0.03 \text{ (th. bkg.)} \pm 0.07 \text{ (th. sig.)}, \quad (11.17)$$

where the statistical, experimental uncertainties as well as the theoretical uncertainties on the background and on the signal are reported separately. The ATLAS Run 2 combination of the global

signal strength yields [241]:

$$\mu = 1.06 \pm 0.07 = 1.06 \pm 0.04 \text{ (stat.)} \pm 0.03 \text{ (exp.)} \pm 0.02 \text{ (th. bkg.)}^{+0.05}_{-0.04} \text{ (th. sig.)}, \quad (11.18)$$

while the CMS Run 2 combination yields [242]:

$$\mu = 1.02^{+0.07}_{-0.06} = 1.02 \pm 0.04 \text{ (stat.)} \pm 0.04 \text{ (th)} \pm 0.04 \text{ (exp.)}. \quad (11.19)$$

These overall signal strengths are fully compatible with the SM expectation, $\mu = 1$, with a precision of 7%. It is interesting to note that the main uncertainty in these measurements arises from the limited precision in the theoretical predictions for the signal production processes. The precision reached with the individual experiments combinations using partial Run 2 data sets have already exceeded the full Run 1 ATLAS and CMS combination precision.

11.4.2 Main decay modes

Despite the large number of decay channels, since the cross sections cannot be independently measured, from the measurements described in this section it is impossible to measure the decay branching fractions without a loss of generality. The simplest assumption that can be made is that the production cross sections are those of the SM, which is equivalent to assume that, for all i indices, $\mu_i = 1$. All branching fractions μ_f can then be measured in a simple 5 parameter fit. The results of these fits are reported in Table 11.10 in terms of significances to highlight their unambiguous observations: all the measured branching fractions are compatible with the SM values.

As illustrated in Table 11.10, for all channels directly sensitive to the third generation Yukawa couplings (i.e. the $H \rightarrow \tau\tau$ the $VH \rightarrow b\bar{b}$) the Run 2 data made a significant difference. The

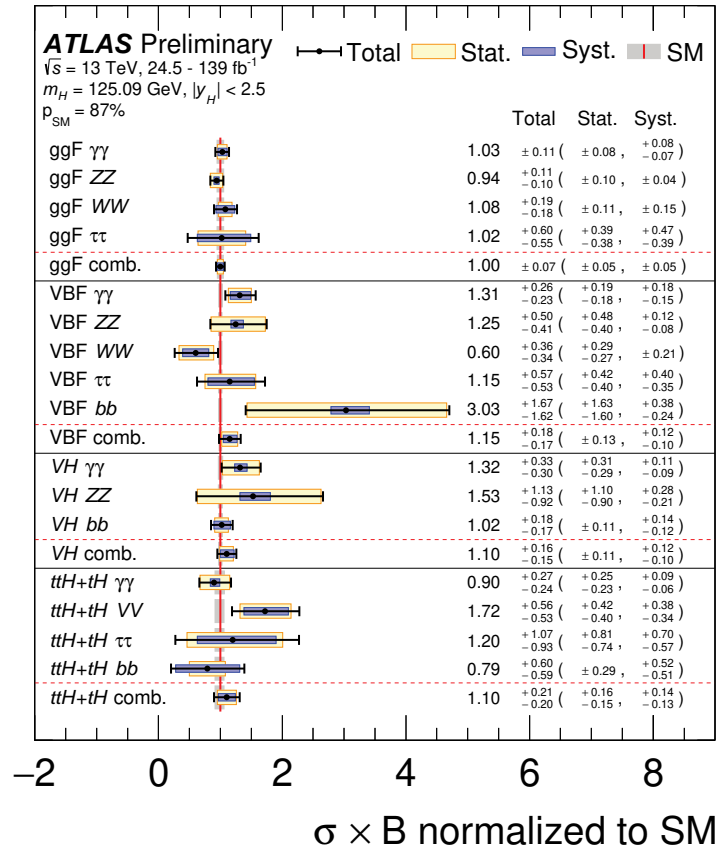


Figure 11.7: Combined measurements by ATLAS of the products $\sigma \cdot BR$, normalised to the SM predictions, for the five main production and five main decay modes.

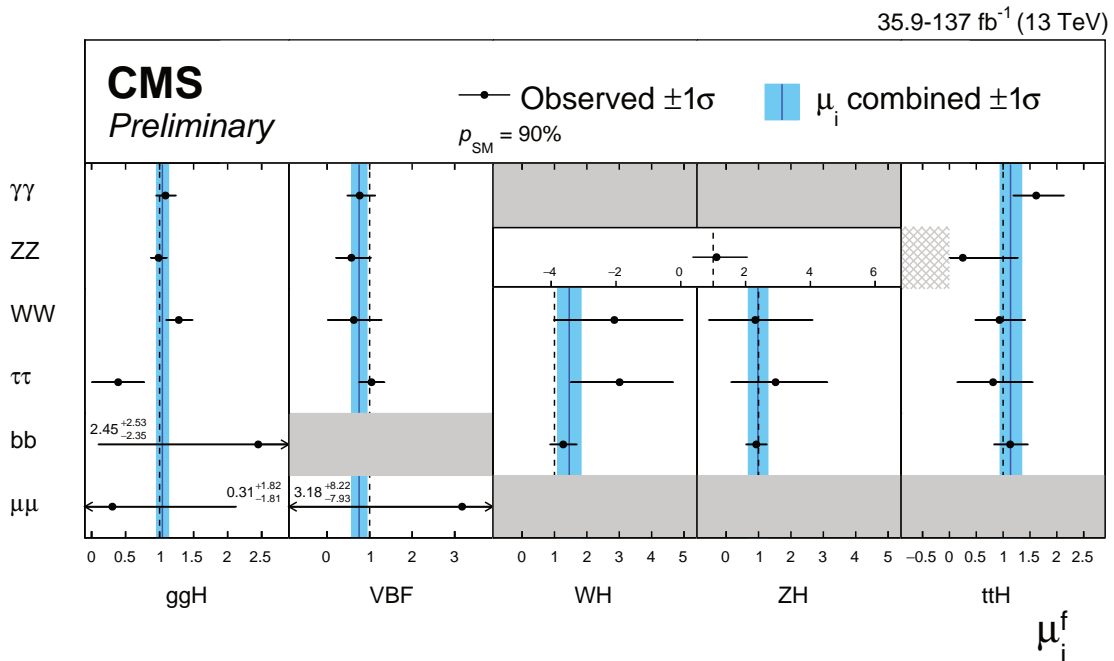


Figure 11.8: Combined measurements by CMS of signal strengths for the five main production and five main decay modes. The hatched combinations require more data for a meaningful confidence interval to be provided.

available sensitivity came mostly from the VH process. The combined significance of 3.7σ at Run 1 was sufficient to suggest ev-

idence, however ATLAS and CMS observations were both low with respect to the rate expected in the SM. At Run2, this channel benefited largely from the increased production cross sections at 13 TeV and the much larger dataset. In this case as well, it is with the addition of the Run2 data that both experiments were able to establish a measurement in this channel (as discussed in Section 11.3.2).

These are major milestones of the LHC physics program.

11.4.3 Main production modes

Most analysis channels are divided into exclusive categories allowing for an increased overall sensitivity and permitting to access the various Higgs boson production modes. The cross sections of the main production modes can be measured assuming that the branching fractions are those of the SM, i.e., for all f indices $\mu_f = 1$. These assumptions lead to a 5 parameter combination. The results are reported in terms of significances of observation of the production modes in Table 11.10.

The gluon fusion production process is the dominant production mode. Although no numerical estimate of combined significance of observation for this process has been given by the experiments, it is considered as established due to the overwhelming evidence from the three main discovery channels. None of the other production modes have been firmly established by the experiments individually. However, the table shows that, for the VBF production mode, the combination had a large sensitivity and produced a combined observation of 5.4σ , therefore establishing this process with a rate compatible with that expected in the SM.

The VH production mode has only very recently been unambiguously observed by ATLAS and CMS independently (as discussed in Section 11.3.2) through the $V(H \rightarrow b\bar{b})$ channel. This is illustrated in the relative contributions of all channels to the VH process shown in Fig. 11.7 and Fig. 11.8.

With the Run 2 data, all production processes have been established, and in particular the $pp \rightarrow t\bar{t}H$ process, which provides direct evidence of the coupling of the Higgs boson to top quarks. This is another milestone in the LHC physics program.

11.5 Main quantum numbers and width of the Higgs boson

11.5.1 Main quantum numbers J^{PC}

Probing the Higgs boson quantum numbers is essential to further unveiling its coupling properties. The measurements of the signal event yields in all the channels discussed in Sections 11.3 and 11.4, and their compatibility with the SM Higgs boson predictions, give a qualitative but, nonetheless, compelling indication of its nature. This qualitative picture is further complemented by the implications of the observation of the particle in the diphoton channel. According to the Landau–Yang theorem [245], the observation made in the diphoton channel excludes the spin-1 hypothesis and restricts possibilities for the spin to 0 or 2.

The Landau–Yang theorem does not apply if the observed state is not decaying to a pair of photons but to a pair of scalars subsequently decaying to two very collimated pairs of photons (as for example in the case of $H \rightarrow a_1 a_1 \rightarrow 4\gamma$). This possibility has not been rigorously excluded but is not experimentally favoured since tight selection criteria are applied on the electromagnetic shower shapes of the reconstructed photons. A more systematic analysis of shower shapes and the fraction of conversions could be performed to further discriminate between the single prompt photon and the two overlapping photons hypotheses. There are also potential theoretical loopholes concerning the applicability of the Landau–Yang theorem, such as off-shell vector boson decays. However, for the observed particle not to be of spin 0 and +1 parity would require an improbable conspiracy of effects. It is nevertheless important to test this hypothesis independently, in particular since the measurements of coupling properties of the Higgs boson assume that it is a CP -even state.

11.5.1.1 Charge conjugation

The charge conjugation quantum number is multiplicative, therefore given that the Higgs-like particle is observed in the $H \rightarrow \gamma\gamma$ channel, and given that photons are C -odd eigenstates, assuming C conservation, the observed neutral particle should be

C -even.

11.5.1.2 Spin and parity

To probe the spin and parity quantum numbers of the discovered particle, a systematic analysis of its production and decay processes is performed in several analyses. These analyses are designed to be independent of the measured event yields and they rely instead on the production and the decay angles, and on the threshold distributions as long as a significant signal is observed, i.e., in situations when an excess over the expected background can be used to further discriminate between signal hypotheses. These analyses are based on probing various alternative models of spin and parity [246]. These models can be expressed in terms of an effective Lagrangian [247] or in terms of helicity amplitudes [248]. The two approaches are equivalent. In the following, the effective Lagrangian formalism is chosen to describe the models considered and a restricted number of models are discussed [247]. In the analysis performed by CMS [248], a larger number of models have been investigated, however, the main channels studied by both experiments are essentially the same and the main conclusions are similar and fully consistent.

i. Spin-0 model

The interaction Lagrangian relevant for the analysis of spin-0 particle interaction with a pair of W or Z bosons with either fixed or mixed SM and BSM CP -even couplings or CP -odd couplings, is the following [249]:

$$\begin{aligned} \mathcal{L}_0^{W,Z} \supset & \left\{ \cos(\alpha)\kappa_{\text{SM}} \left[\frac{1}{2}g_{HZZ}Z_\mu Z^\mu + g_{HWW}W_\mu^+ W^{-\mu} \right] \right. \\ & - \frac{1}{4\Lambda} \left[\cos(\alpha)\kappa_{HZZ}Z_{\mu\nu}Z^{\mu\nu} + \sin(\alpha)\kappa_{AZZ}Z_{\mu\nu}\tilde{Z}^{\mu\nu} \right] \\ & \left. - \frac{1}{2\Lambda} \left[\cos(\alpha)\kappa_{HWW}W_{\mu\nu}^+ W^{-\mu\nu} + \sin(\alpha)\kappa_{AWW}W_{\mu\nu}^+\tilde{W}^{-\mu\nu} \right] \right\} H, \end{aligned} \quad (11.20)$$

where $V^\mu = Z^\mu, W^{+\mu}$ are the vector boson fields, $V^{\pm\mu\nu}$ are the reduced field tensors and $\tilde{V}^{\pm\mu\nu} = 1/2 \varepsilon^{\mu\nu\rho\sigma} V_{\rho\sigma}$ are the dual tensor fields. And Λ defines an effective theory energy scale. The factors $\kappa_{\text{SM}}, \kappa_{HZZ}, \kappa_{HWW}, \kappa_{AZZ}, \kappa_{AWW}$ denote the coupling constants corresponding of the coupling of the SM and BSM CP -even and CP -odd components of the Higgs boson to the W and Z fields. The mixing angle α allows for the production of a CP -mixed state and the CP -symmetry is broken when $\alpha \neq 0, \pi$.

This formalism can be used to probe both CP -mixing for a spin-0 state, as discussed in Section 11.5.1.4 or specific alternative hypotheses, as discussed below in Section 11.5.1.3, such as a pure CP -odd state ($J^P = 0^-$) corresponding to $\alpha = \pi/2$, $\kappa_{\text{SM}} = \kappa_{HVV} = 0$ and $\kappa_{AVV} = 1$. A BSM CP -even state $J^P = 0^+$ corresponds to $\alpha = 0$, $\kappa_{AVV} = 0$, $\kappa_{HVV} = 1$ and κ_{SM} arbitrary. These hypotheses are compared to the SM Higgs boson hypothesis corresponding to $\alpha = 0$ and $\kappa_{HVV} = \kappa_{AVV} = 0$ and $\kappa_{\text{SM}} = 1$. This formalism has been adopted by the ATLAS experiment. The analysis of these benchmarks are illustrated in Fig. 11.9.

A different parametrisation of anomalous couplings of a spin-zero boson with two gauge bosons VV can also be expressed in the general form of the scattering amplitude A :

$$\begin{aligned} A \sim & \left[a_1^{VV} - \frac{\kappa_1^{VV} q_1^2 + \kappa_2^{VV} q_2^2}{(\Lambda_1^{VV})^2} - \frac{\kappa_3^{VV} (q_1 + q_2)^2}{(\Lambda_Q^{VV})^2} \right] m_{V_1}^2 \varepsilon_{V_1}^* \varepsilon_{V_2}^* \\ & + a_2^{VV} f_{\mu\nu}^{*(1)} f^{*(2)\mu\nu} + a_3^{VV} f_{\mu\nu}^{*(1)} \tilde{f}^{*(2)\mu\nu} \end{aligned} \quad (11.21)$$

where ε_i is the polarization vector of the boson V_i , $f_{\mu\nu}^{*(i)} = \varepsilon_i^\mu q^\nu - \varepsilon_i^\nu q^\mu$ is a scalar tensor constructed from the vector boson V_i polarization and four momentum, $\tilde{f}_{\mu\nu}^{*(i)} = \frac{1}{2} \varepsilon_{\mu\nu\rho\sigma} f^{*(i)\rho\sigma}$ is the corresponding pseudo-scalar tensor. Λ_1 and Λ_Q are new physics scales, $a_{1,2,3}$ are coupling strength modifiers and $|\kappa_{(1,2,3)}^{VV}| = 0$ or 1. The custodial symmetry would require that $a^{WW} = a^{ZZ}$ and, at tree-level, the only non-zero contributions would come from the a_1

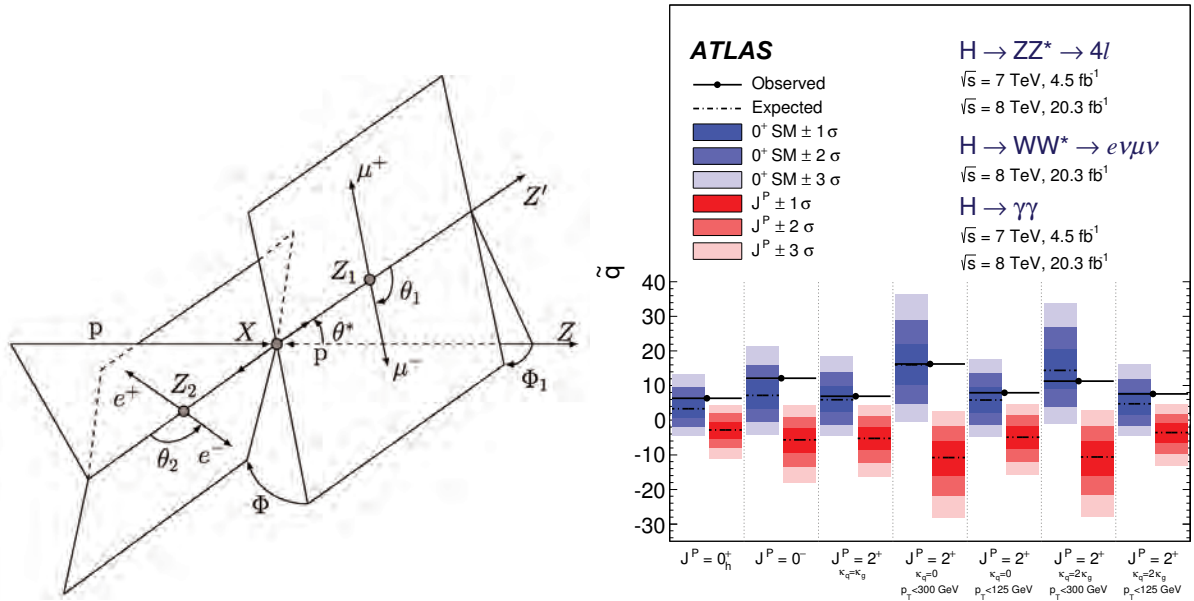


Figure 11.9: (Left) Definition of the production and decay angles defined for the $H \rightarrow ZZ^{(*)} \rightarrow 4l$ final state [248]. (Right) Expected distributions of the test statistic for the SM hypothesis (in blue) and several alternative spin and parity hypotheses (in red).

term. This parametrisation is used by CMS. It is fully equivalent to the interaction Lagrangian approach described above.

ii. Spin-2 model

The graviton-inspired interaction Lagrangian for a spin-2 boson $X^{\mu\nu}$ that does not carry any color, weak and electromagnetic charge and that uniquely interacts with the energy momentum tensor $\mathcal{T}^{V,f}$ of vector bosons V or fermions f , can be written as follows [249]:

$$\mathcal{L}_2 \supset \frac{1}{\Lambda} \left[\sum_V \xi_V \mathcal{T}_{\mu\nu}^V X^{\mu\nu} + \sum_f \xi_f \mathcal{T}_{\mu\nu}^f X^{\mu\nu} \right], \quad (11.22)$$

where the strength of the interaction is determined by the couplings ξ_V and ξ_f . The simplest scenarios, referred to as universal couplings (UC), correspond to $\xi_V = \xi_f$. They predict a large branching ratio to photons (of approximately 5%) and negligible couplings to massive gauge bosons (W and Z). They are therefore disfavoured, and other models are investigated where the couplings of the W , Z and γ are assumed to be independent. Universality of the couplings refers to $\xi_g = \xi_q$. Two other scenarios are considered: $\xi_q = 0$ and $\xi_q = 2\xi_g$. In these scenarios, a large enhancement of the tail of the transverse momentum of the spin-2 state is expected and requires a further selection requirement in order to probe the models within the range of validity of the effective field theory. Two requirements are considered, $p_T^X < 300$ GeV and $p_T^X < 125$ GeV [247]. The analysis of these benchmarks are discussed below and results are illustrated in Fig. 11.9.

11.5.1.3 Probing fixed J^P scenarios

At the LHC, the determination of the spin and CP properties of the Higgs boson is done independently from the total rates measurement, it uses a global angular helicity analysis and, when applicable, the study of threshold effects. The channels used for this analysis, $H \rightarrow \gamma\gamma$, $H \rightarrow WW^{(*)} \rightarrow l\nu l\nu$ and $H \rightarrow ZZ^{(*)} \rightarrow 4l$, are those where the observation of a signal is unambiguous.

At the Tevatron, an analysis using the threshold distribution in the associated production mode VH with subsequent decay to a pair of b quarks was performed by the D0 collaboration.

i. The VH production at D0

The mass of the VH system is a powerful discriminant to distinguish a $J^P = 0^+$, with a threshold behaviour in $d\sigma/dM^2 \sim$

β, β^3, β^5 from a 0^+ , 0^- and 2^+ state, respectively [250]. The VH mass observable not only discriminates signal hypotheses, but also has an increased separation between the 0^- and 2^+ hypotheses with respect to the backgrounds, thus allowing, with a small and not yet significant signal yield, to exclude that the observed state is 0^- at 98% CL [251] and 2^+ at the 99.9% CL [252], assuming a signal produced with their best fit signal strength (which was $\mu = 1.23$).

ii. The $\gamma\gamma$ channel at the LHC

In the $H \rightarrow \gamma\gamma$ channel, the analysis is performed inclusively using the production angle $\cos\theta_{CS}^*$ and the transverse momentum of the diphoton pair [247]. The polar angle in the rest frame is defined with respect to the bisector axis of the momenta of the incoming protons and is referred to as the polar angle in the Collins–Soper frame [253]. The SM Higgs boson signal distribution is expected to be uniform with a cutoff due to the selection requirements on the photons transverse momentum. The $H \rightarrow \gamma\gamma$ channel is mostly sensitive to the gluon-initiated spin-2 production scenarios, which yield a $\cos\theta_{CS}^*$ distribution peaking at values close to 1. The ATLAS limits are derived from a fit of the signal in bins of $\cos\theta_{CS}^*$ and diphoton transverse momentum and are summarized in Fig. 11.9 (right) (only combined results are shown). The data shows a good compatibility with the SM 0^+ hypothesis and contributes strongly to the exclusion of several spin-2 scenarios. The conclusions are the same from CMS results [248].

iii. The $H \rightarrow WW^{(*)} \rightarrow l\nu l\nu$ channel at the LHC

In the $H \rightarrow WW^{(*)} \rightarrow l\nu l\nu$ channel, the production and decay angles cannot be easily reconstructed due to the presence of neutrinos in the final state, however, sensitivity arises from the $V - A$ structure of the decay of the W bosons. A scalar state thus yields a clear spin correlation pattern that implies that the charged leptons e or μ from the decays of the W bosons are produced close to one another in the transverse plane. This feature impacts observables such as the azimuthal angle between the two leptons $\Delta\Phi_{\ell\ell}$ or their invariant mass $m_{\ell\ell}$ in addition to the threshold behaviour of the decay. It can be used to discriminate between various spin and parity hypotheses. The approach adopted by ATLAS uses a multivariate discriminant, whereas CMS uses a 2D-fit of the dilepton mass and the transverse mass. Figure 11.9 (right) summarizes the ATLAS results of the $H \rightarrow WW^{(*)} \rightarrow l\nu l\nu$ analyses alone and in combination with other channels. Spin-1 hypotheses

(1^+ and 1^-) have also been tested in this channel by ATLAS and CMS. ATLAS and CMS exclude the 1^+ and 1^- hypotheses at more than 95% CL.

iv. *The $H \rightarrow ZZ^{(*)} \rightarrow 4\ell$ channel at the LHC*

The $H \rightarrow ZZ^{(*)} \rightarrow 4\ell$ coupling analysis, as described in Section 11.3, also uses a discriminant based on the 0^+ nature of the Higgs boson to further separate signal and background. In this analysis, this feature is used to discriminate between signal hypotheses. The observables sensitive to the spin and parity are [254] the masses of the two Z bosons (due to the threshold dependence of the mass of the off-shell Z boson), two production angle θ^* and Φ_1 , and three decay angles, Φ , θ_1 and θ_2 . The production and decay angles are defined as:

- θ_1 and θ_2 , the angles between the negative final state lepton and the direction of flight of Z_1 and Z_2 in the rest frame.
- Φ , the angle between the decay planes of the four final state leptons expressed in the four lepton rest frame.
- Φ_1 , the angle defined between the decay plane of the leading lepton pair and a plane defined by the vector of the Z_1 in the four lepton rest frame and the positive direction of the proton axis.
- θ^* , the production angle of the Z_1 defined in the four lepton rest frame with respect to the proton axis.

These angles are illustrated in Fig. 11.9 (left). There are two approaches to this analysis. The first, used by CMS, is a matrix element likelihood approach where a kinematic discriminant is defined based on the ratio of the signal and background probabilities. These probabilities are defined using the leading-order matrix elements. A similar approach is also performed by ATLAS as a cross check of their main result. The main approach adopted by ATLAS is the combination of sensitive observables with a Boosted Decision Tree. These analyses are sensitive to various J^P hypotheses and in particular discriminate the 0^+ hypothesis from the 0^- . In all scenarios investigated, and for both ATLAS and CMS, the data is compatible with the 0^+ hypothesis. ATLAS and CMS exclude a pure pseudo-scalar nature of the observed boson at CL_S levels of 98% and 99.8% [248].

11.5.1.4 *Probing CP-mixing and anomalous HVV couplings*

The careful study of the kinematic properties of the events observed in the $H \rightarrow ZZ^{(*)} \rightarrow 4\ell$ and $H \rightarrow WW^{(*)} \rightarrow \ell\nu\ell\nu$ channel, and in particular the angular distributions described above, allows one to further probe the HVV coupling beyond testing fixed hypotheses. Assuming that the observed particle is a spin-0 state, and using several discriminating observables in the $H \rightarrow ZZ^{(*)} \rightarrow 4\ell$ and $H \rightarrow WW^{(*)} \rightarrow \ell\nu\ell\nu$ channels, the anomalous terms in the formalism of Eq. (11.20) can be probed. In the approach of helicity amplitudes used by CMS [248], all terms are essentially equivalent, except for one additional phase which is neglected in Eq. (11.20).

Results are derived in terms of the parameters $\tilde{\kappa}_{HVV} = v\kappa_{HVV}/\Lambda$ and $\tilde{\kappa}_{AVV} = v\kappa_{AVV}/\Lambda$, and, more precisely, as measurements of $\tilde{\kappa}_{HVV}/\kappa_{SM}$ and $\tan\alpha \cdot \tilde{\kappa}_{AVV}/\kappa_{SM}$, as shown in Fig. 11.10. These parameters can be interpreted as mixing parameters of a tensor anomalous CP -even coupling and a CP -odd component. The measurements are made in the $H \rightarrow ZZ^{(*)} \rightarrow 4\ell$ and $H \rightarrow WW^{(*)} \rightarrow \ell\nu\ell\nu$ channels independently and then combined assuming that the $\tilde{\kappa}_{HVV}/\kappa_{SM}$ and $\tan\alpha \cdot \tilde{\kappa}_{AVV}/\kappa_{SM}$ are the same for the W and Z vector bosons. Only the combination of the WW and ZZ channels is shown in Fig. 11.10. The asymmetric shape of the likelihood as a function of $\tilde{\kappa}_{HWW}, HZZ/\kappa_{SM}$ is mainly due to the interference between the BSM and the SM contributions that gives a maximal deviation from the SM predictions for negative relative values of the BSM couplings. In Fig. 11.10, the expected likelihood profiles for a SM Higgs boson are also displayed. While no significant deviation from the SM expectation is observed, the precision of the measurements of the mixing parameters is fairly low. The results and conclusions from the CMS measurements [248] are very similar.

An individual ZZ^* channel measurement has also been carried out with a partial Run2 dataset by ATLAS [255]. CMS has performed a CP -mixing analysis of a partial Run2 dataset of

36 pb $^{-1}$ combined with the full Run1 data using the ZZ^* channel [256]. In this analysis the CMS experiment sets constraints on the following parameters defined in the scattering amplitude parametrisation (11.21):

$$f_{a_i} = \frac{|a_i|^2 \sigma_i}{\sum_{j=1,2,3} |a_j|^2 \sigma_j}, \quad \phi_{a_i} = \arg\left(\frac{a_i}{a_1}\right), \quad (11.23)$$

where σ_i is the cross section for process with $a_i = 1$ and $a_{j \neq i} = 0$. The constraints on these parameters are shown in Fig. 11.11.

CP invariance in the HVV coupling can also be probed with the VBF production process in the $H \rightarrow \tau^+\tau^-$ channel. CMS has performed an analysis in this channel and has combined its results with the aforementioned ZZ^* channel using the same dataset [257].

ATLAS has also performed an analysis using optimal observables [258], defined as the ratio of the interference between the CP -odd and the SM contributions normalised to the SM matrix element squared, using the Run1 data. In this study, the CP -mixing contributions are described in the framework of an effective field theory governed by a single parameter \tilde{d} , found to be consistent with its SM value of $\tilde{d} = 0$ and constrained to the interval $[-0.11, 0.05]$ at the 68% CL.

11.5.1.5 *Probing $Hf\bar{f}$ coupling CP properties in $pp \rightarrow t\bar{t}H$ production*

The CP -properties of the Higgs boson coupling to fermions can be probed with the $p\bar{p} \rightarrow t\bar{t}H$ process. The increased sensitivity to this process in particular in the channels where the Higgs boson decays to a pair of photons provide a good sensitivity to the CP properties of the coupling through kinematics and angular distributions between the Higgs boson and the top quarks produced in the final state. The

$$\mathcal{L} \supset -\frac{m_t}{v} \bar{\psi}_t (\kappa_t + i\gamma_5 \tilde{\kappa}_t) \psi_t$$

To probe the CP properties of the Higgs to fermion couplings, ATLAS [177] and CMS [178] use slightly different observables. ATLAS measures an overall coupling-strength factor denoted κ'_t and a CP -mixing angle α which are related to the above Lagrangian by:

$$\kappa'_t = \frac{\kappa_t}{\cos\alpha} \quad \text{and} \quad \alpha = \arctan \frac{\tilde{\kappa}_t}{\kappa_t}$$

With the full Run 2 dataset, ATLAS [177] excludes CP -mixing angle greater (less) than 43° (-43°) is excluded at 95% confidence level.

CMS provides a measurement of the fraction of CP -odd contribution to the scattering amplitude from the above Lagrangian estimated as:

$$f_{CP} = \frac{|\tilde{\kappa}_t|^2}{|\kappa_t|^2 + |\tilde{\kappa}_t|^2} \times \text{sign}(\tilde{\kappa}_t/\kappa_t)$$

Also using the full Run 2 dataset, CMS [178] measures the CP -odd fraction $f_{CP} = 0.00 \pm 0.33$.

Both the ATLAS and CMS experiments used multivariate analyses in order to maximize the sensitivity to the measurement of the CP properties of the $Hf\bar{f}$ coupling. Both experiments used leptonic and hadronic decays of the top quarks.

11.5.1.6 *Probing $Hf\bar{f}$ coupling CP properties in $H \rightarrow \tau^+\tau^-$ decays*

Another interesting channel to investigate the CP properties of the $Hf\bar{f}$ coupling is the Higgs decay to taus through tau polarisation sensitive variables. Preliminary studies of the sensitivity to CP properties in this channel have been carried out by ATLAS [259]. At HL-LHC this analysis has investigated $H \rightarrow \tau^+\tau^-$ decays where taus decay via the $\tau^\pm \rightarrow \rho^\pm \nu_\tau \rightarrow \pi^0 \pi^\pm \nu_\tau$. This analysis is foreseen to constrain the CP -mixing angle to be measured with a precision between $\pm 18^\circ$ to $\pm 30^\circ$, depending on the precision of the reconstruction of the π^0 .

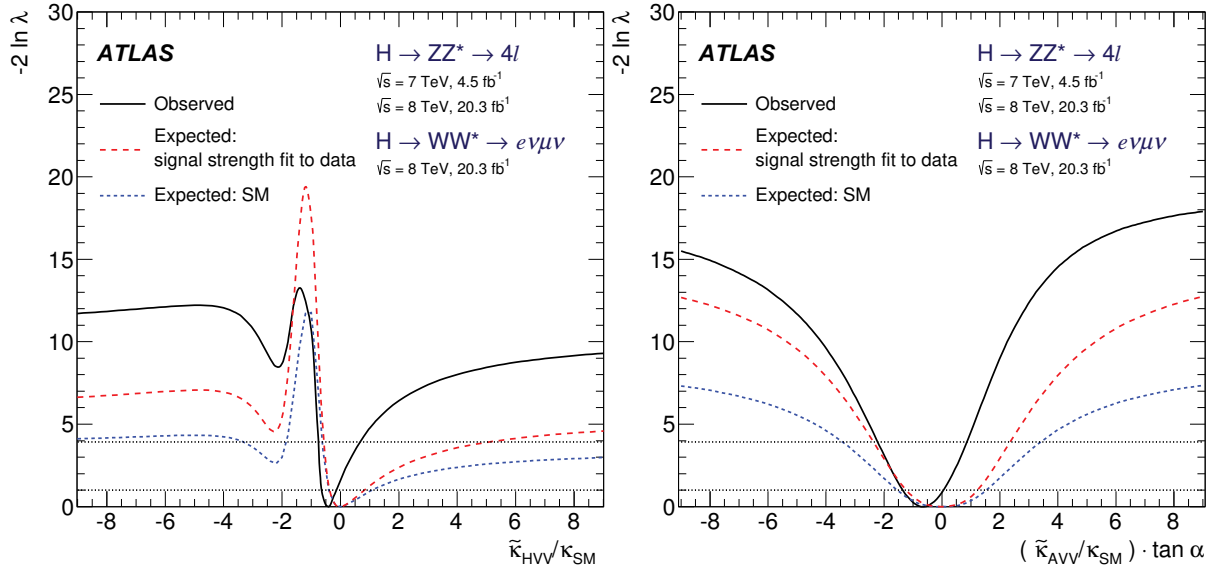


Figure 11.10: Likelihood profiles for the $\tilde{\kappa}_{HV V}$ and $\tilde{\kappa}_{AVV} \cdot \tan \alpha$ parameters, representing respectively CP -even and CP -odd anomalous couplings of the Higgs boson.

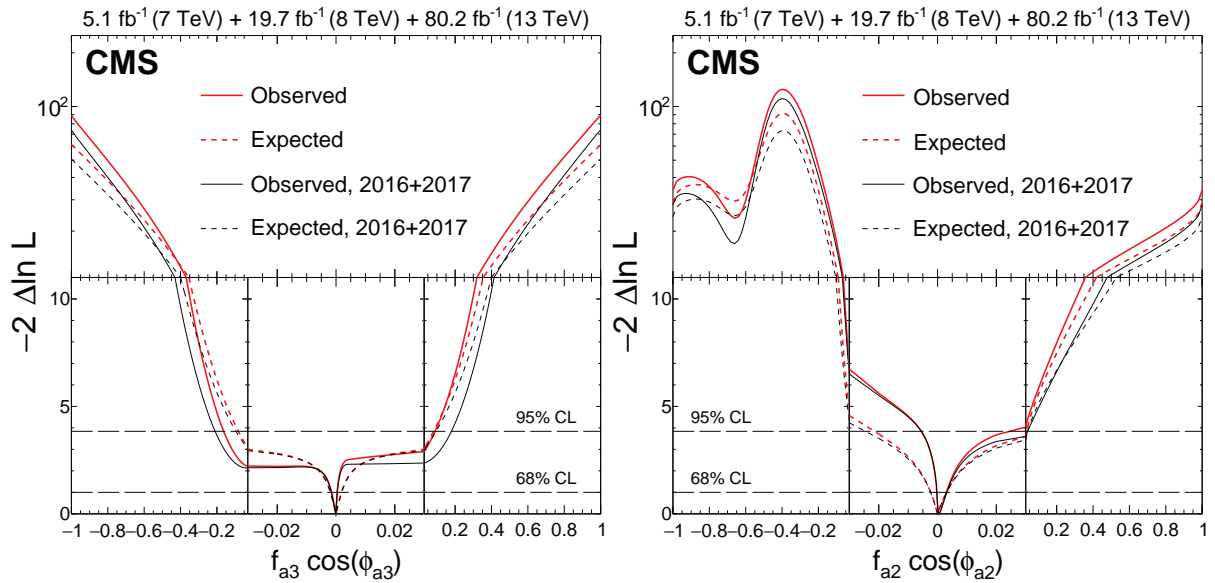


Figure 11.11: Observed (solid) and expected (dashed) likelihoods as a function of $f_{a3} \cos(\phi_{a3})$ (left), $f_{a2} \cos(\phi_{a2})$ (right) for the Run 1 and Run 2 datasets separately and combined.

11.5.2 Off-shell couplings of the Higgs boson

In the dominant ggF production mode with a subsequent decay of the Higgs boson into a pair of Z bosons, the production cross section of an off-shell Higgs boson is known to be sizeable. This follows as a consequence of the enhanced couplings of the Higgs boson to the longitudinal polarization of the massive vector bosons at high energy.

The off-shell to on-shell cross section ratio is approximately 8% in the SM [260]. Still, the Higgs contribution to VV production at large invariant mass remains small compared to the background. It is nevertheless interesting to probe Higgs production in this regime as it is sensitive to new physics beyond the SM.

The difficulty in the off-shell VV analysis, beyond the small signal-to-background ratio, is due to a large negative interference between the signal and the $gg \rightarrow VV$ background.

The resulting presence of a SM Higgs boson signal in the far off-shell domain results in a deficit of events with respect to the expectation from background only events. It is only when the off-shell couplings of the Higgs boson are larger than expected in

the SM that the presence of a signal appears as an excess over the background expectation. One additional intricacy arises from the precision in the prediction of the rate for $gg \rightarrow VV$, a loop process at lowest order, and its interference with the signal. At the time of the publication of the original ATLAS and CMS results, a full NLO prediction had not been computed.

It is interesting to note that, in this regime, the Higgs boson is studied as a propagator and not as a particle. The measurement of its off-shell couplings is therefore absolute and does not rely on the knowledge of the total Higgs boson width. The off-shell coupling constraints can then be used to indirectly constrain the width of the Higgs boson, under specific assumptions detailed in Section 11.5.3.3.

This measurement has been carried out in the $H \rightarrow ZZ \rightarrow 4\ell$, $H \rightarrow ZZ \rightarrow \ell\ell\nu\nu$ and $H \rightarrow WW \rightarrow \ell\nu\ell\nu$ channels. To enhance the sensitivity of the analysis, the knowledge of the full kinematics of the events is important. In particular the signal and the background can be further distinguished by the invariant mass of the VV system, which is more accurately accessible in the

$H \rightarrow ZZ \rightarrow 4\ell$ channel. Angular distributions also play an important role in this analysis. For these reasons, the $H \rightarrow ZZ^{(*)} \rightarrow 4\ell$ channel is significantly more sensitive than $H \rightarrow WW^{(*)} \rightarrow \ell\nu\ell\nu$. The CMS results in Refs. [261] include the VBF and VH processes through the selection of two additional jets in the final state. The ATLAS results do not have a specific selection for the VBF or VH production processes, but their contributions are taken into account.

Limits on the off-shell rates have been reported for the two channels by ATLAS [262] and CMS [261] with Run 1 data. The combined results, assuming that the off-shell rates in the ZZ and WW channels scale equally, are given for two different hypotheses on the VBF production rate: fixing it to its SM value or scaling it as the gluon fusion rate. The observed (expected) limits on the off-shell rate fraction with respect to its SM expectation is 6.7 (9.1) for ATLAS [262] with the VBF rate fixed to its SM value and 2.4 (6.2) for CMS [261] where no assumption is made on the relative production rates of gluon-fusion and VBF. In both cases, the custodial symmetry is assumed and the ratio of the rates in the ZZ and WW decays are fixed to those of the SM. Results without this assumption have also been reported in Ref. [261].

Both ATLAS [263] and CMS [256] have performed off-shell Higgs boson analyses to constrain the off-shell Higgs boson production rates with partial Run 2 datasets, corresponding respectively to luminosities of 36.1 fb^{-1} and 80.2 fb^{-1} . With the increase in centre-of-mass energy and luminosities, significantly better sensitivities are achieved. The ATLAS analysis is based on two decay channels, $H \rightarrow 4\ell$ and $H \rightarrow 2\ell 2\nu$, and the two main ggF and VBF production modes, while the CMS analysis is based on the $H \rightarrow 4\ell$ channel exclusively, but uses the exclusive VH categories. The results obtained have already reached an impressive sensitivity, with 95% CL upper limits on the off shell signal strength $\mu_{\text{off-shell}}$ (the CMS Run 2 results are combined with the measurements made with Run 1 data):

$$\begin{aligned} (\text{ATLAS}) \quad \mu_{\text{off-shell}} &< 3.8 \text{ (obs)} [3.4 \text{ (exp)}], \\ (\text{CMS}) \quad \mu_{\text{off-shell}} &= 0.78_{-0.53}^{+0.72} \text{ (obs)} [1.00_{-0.99}^{+1.20} \text{ (exp)}]. \end{aligned} \quad (11.24)$$

11.5.3 The Higgs boson width

In the SM, the Higgs boson width is very precisely predicted once the Higgs boson mass is known. For a mass of 125 GeV, the Higgs boson has a very narrow width of 4.1 MeV [46]. It is dominated by the fermionic decays partial width at approximately 75%, while the vector boson modes are suppressed and contribute 25% only.

At the LHC or the Tevatron, in all production modes, only the cross sections times branching fractions can be measured. As a consequence, the total width of the Higgs boson cannot be inferred from measurements of Higgs boson rates. Direct constraints on the Higgs boson width are much larger than the expected width of the SM Higgs boson.

11.5.3.1 Direct constraints

Analyses of the reconstructed mass line-shape in the two channels with a good mass resolution, the $H \rightarrow \gamma\gamma$ and $H \rightarrow ZZ^{(*)} \rightarrow 4\ell$ channels, allow for a direct measurement of the width of the SM Higgs boson. The intrinsic mass resolution in these channels is about 1–2 GeV, much larger than the expected width of the SM Higgs boson. As a result, only upper limits on the Higgs boson width have been set by ATLAS [264] and CMS [265]. The two main challenges of direct constraints on the width through the measurement of the line-shape are: (i) the modelling of resolution uncertainties and (ii) the modelling of the interference between the signal and the continuum background which can be sizeable for large widths, in particular in the range where direct constraints are set. Given that these interference effects are small with respect to the individual channels sensitivity, they are neglected in deriving constraints on the total width. The combined constraints, however, being more precise, could be affected by the interference. ATLAS [264] has therefore not combined the constraints on the width from the two channels. The results are reported in Table 11.11. These constraints are still three orders of magnitude larger than the expected SM width and are fully compatible with the SM hypothesis.

Another direct constraint on the Higgs boson width can be obtained, in the $H \rightarrow ZZ^{(*)} \rightarrow 4\ell$ channel, from the measurement of the average lifetime of the Higgs boson calculated from the displacement of the four-lepton vertex from the beam spot. This analysis has been carried out by CMS (see references in Ref. [132]), using the measured decay length. The measured $c\tau_H$ is $2_{-2}^{+25} \mu\text{m}$, yielding an observed (and expected) limit at the 95% CL of $c\tau_H < 57(56) \mu\text{m}$. From this upper limit on the lifetime of the Higgs boson, the 95% CL lower limit on its width is $\Gamma_H > 3.5 \times 10^{-12} \text{ GeV}$.

11.5.3.2 Indirect constraints from mass shift in the diphoton channel

In the diphoton channel, it was noticed in Ref. [266], that the effect of the interference between the main signal $gg \rightarrow H \rightarrow \gamma\gamma$ and the continuum irreducible background $gg \rightarrow \gamma\gamma$, taking into account detector resolution effects, is responsible for a non negligible mass shift. The size of the mass shift depends on the total width of the Higgs boson and it was suggested that measuring this mass shift could provide a constraint on the width [266]. It was further noticed that the mass shift has a dependence also on the diphoton transverse momentum. The total width of the Higgs boson could therefore be constrained using the diphoton channel alone.

Further studies were performed by ATLAS to estimate the size of the expected mass shift [144]. The expected shift in mass in the diphoton channel is $35 \pm 9 \text{ MeV}$ for the SM Higgs boson. Very preliminary studies of the sensitivity of this method to estimate the width of the Higgs boson in the High-Luminosity regime have been made by ATLAS [267] and yield an expected 95% CL upper limit on the total width of approximately 200 MeV from 3 ab^{-1} of 14 TeV data.

11.5.3.3 Indirect constraints from on-shell rate in the diphoton channel

In the diphoton channel, it was noticed in Ref. [268], that the interference between the main signal $gg \rightarrow H \rightarrow \gamma\gamma$ amplitude and the continuum irreducible background $gg \rightarrow \gamma\gamma$ amplitude generates non-negligible change in the on-shell cross sections, as a result of the existence of a relative phase between these amplitudes. The size of this on-shell interference effect depends on the total width of the Higgs boson and it was suggested that measuring this on-shell cross section precisely could provide a constraint on the Higgs total width. This interference effect yields around 2% reduction for the $gg \rightarrow H \rightarrow \gamma\gamma$ cross section measurement. The current evaluation of this interference effect is performed at NLO and has a $^{+50\%}_{-30\%}$ uncertainty, due to the fact that the large relative phase is driven by the two-loop $gg \rightarrow \gamma\gamma$ background amplitude [266, 268]. This on-shell interference effect has a dependence on the p_T of the diphoton system and the photon polar angle in the diphoton rest frame, which can be further exploited to improve the measurement to constrain the Higgs total width.

Taking the ratios of the on-shell cross section of Higgs boson to diphoton channel and the cross section of Higgs boson to four-leptons channel where the interference effect is negligible could put bound on the Higgs boson total width. This ratio is free from many dominant sources of systematic uncertainties for cross section measurements, i.e., PDF uncertainty and luminosity uncertainty, and can be further improved by the accumulation of the LHC data. From this cross section ratio measurement alone, a preliminary estimation of the current limit from this interference effect with current 30% precision puts an upper bound of 800 MeV on the Higgs boson total width and the limit improves to 60 MeV with 3 ab^{-1} of 14 TeV data [268, 269].

11.5.3.4 Indirect constraints from off-shell couplings

Using simultaneously on-shell and off-shell measurements in the VV channels, it was noticed [260, 270] that the total width of the Higgs boson could be constrained. This can be illustrated from the parametrisation of the signal strength measurements both on-shell ($\mu_{\text{on-shell}}$) and off-shell ($\mu_{\text{off-shell}}$) as a function of the couplings modifiers κ_g and κ_V parameterizing the main process $gg \rightarrow H \rightarrow VV$ (see Section 11.6.2 for the definition of these coupling modifiers). The on-shell and off-shell signal strengths can

Table 11.11: Run 1 observed (expected) direct 95% CL constraints on the width of the 125 GeV resonance from fits to the $\gamma\gamma$ and ZZ mass spectra and to the 4ℓ vertex lifetime. *The CMS measurement from the 4ℓ mass line-shape was performed using Run 2 data.

Exp.	$M_{\gamma\gamma}$ mass spectrum	$M_{4\ell}$ spectrum	4ℓ vertex lifetime
ATLAS	< 5.0 (6.2) GeV	< 2.6 (6.2) GeV	—
CMS	< 2.4 (3.1) GeV	< 1.1 (1.6) GeV*	$> 3.5 \times 10^{-12}$ GeV

be written as:

$$\begin{aligned}\mu_{\text{on-shell}} &= \frac{\kappa_{g,\text{on-shell}}^2 \kappa_{V,\text{on-shell}}^2}{\Gamma_H/\Gamma_{\text{SM}}}, \\ \mu_{\text{off-shell}} &= \kappa_{g,\text{off-shell}}^2 \kappa_{V,\text{off-shell}}^2.\end{aligned}\quad (11.25)$$

A bound on the Higgs boson width can then be obtained from the measurements of the on-shell and off-shell signal strengths. This assumes that no new physics alters the Higgs boson couplings in the off-shell regime, i.e., that the running of its couplings is negligible in the off-shell regime [271,272]. Both ATLAS [262] and CMS [261] have used their off-shell production limits to constrain the width of the Higgs boson.

Both ATLAS and CMS analyses use the kinematic event characteristics to further gain in sensitivity to discriminate between the signal and background. The ATLAS analysis assumed that there are no anomalous couplings of the Higgs boson to vector bosons, and obtains 95% CL observed (expected) upper limit on the total width of $5.5 \times \Gamma_{\text{SM}}$ ($8.0 \times \Gamma_{\text{SM}}$) with the Run 1 dataset. In the CMS analysis, the observed (expected) limit on the total width is $6.2 \times \Gamma_{\text{SM}}$ ($9.8 \times \Gamma_{\text{SM}}$) for the ZZ channel only at Run 1.

In addition, in the CMS analysis, results are also derived allowing for anomalous couplings of the Higgs boson, therefore reducing the discriminating power of the kinematic variables used in the analysis but reducing the model dependence. The observed (expected) limit on the total width is $10.9 \times \Gamma_{\text{SM}}$ ($17.4 \times \Gamma_{\text{SM}}$).

CMS has also combined the ZZ and W^+W^- channels while keeping the gluon-fusion and VBF production processes separate. For the gluon fusion mode, the observed (expected) combined upper limit at the 95% CL on the total width of the Higgs boson is $2.4 \times \Gamma_{\text{SM}}$ ($6.2 \times \Gamma_{\text{SM}}$) [261], while for the VBF production mode the exclusion limits are $19.3 \times \Gamma_{\text{SM}}$ ($34.4 \times \Gamma_{\text{SM}}$) [261].

At Run 2, using the ATLAS [263] and CMS [256] analyses described in Section 11.5.2, the following bounds were obtained:

$$\text{(ATLAS)} \quad \Gamma_H/\Gamma_H^{\text{SM}} < 3.5 \quad [3.7 \text{ (exp)}], \quad (11.26)$$

$$\begin{aligned}\text{(CMS)} \quad \Gamma_H &< 9.16 \quad [13.7 \text{ (exp)}] \text{ MeV} \\ \text{or } \Gamma_H &= 3.2_{-2.2}^{+2.8} \quad [4.1_{-4.0}^{+5.0} \text{ (exp)}] \text{ MeV.}\end{aligned}\quad (11.27)$$

The CMS combination includes results obtained with run 1 data. CMS has also performed this analysis considering possible anomalous HZZ couplings as discussed in Section 11.5.1.4. Neither the results nor the sensitivities are significantly affected by allowing specific anomalous coupling parameters to float in the fits.

ATLAS and CMS have also performed a study of the prospects for measuring the Higgs boson width mainly in the four lepton channel. Projecting to a luminosity of 3 ab^{-1} , it was concluded that, within assumptions similar to the ones mentioned above and assuming the SM central value, the observed (expected) combined upper limit at the 95% CL on the total width of the Higgs boson would be $3.8 \times \Gamma_{\text{SM}}$ ($3.4 \times \Gamma_{\text{SM}}$), i.e., the width of the Higgs boson could be constrained with the following precision [111]:

$$\Gamma_H = 4.1_{-0.8}^{+0.7} \text{ MeV.} \quad (11.28)$$

11.6 Probing the coupling properties of the Higgs boson

As discussed in Section 11.2, within the SM, all the Higgs boson couplings are fixed unambiguously once all the particle masses are known. Any deviation in the measurement of the couplings of the Higgs boson could therefore signal BSM physics.

Measuring the Higgs boson couplings without relying on the SM assumption requires a general framework treating deviations from the SM coherently at the quantum level in order to provide theoretical predictions for relevant observables to be confronted

with experimental data. An attempt in that direction has been formalised in the so-called κ -formalism [273], following earlier attempts [274] and initial phenomenological studies of the first hints of the existence of the Higgs boson [275]. In this LO-inspired approach, the SM Higgs boson couplings are rescaled by arbitrary factors, κ 's, keeping the same Lorentz structure of the interactions. This formalism allows for simple interpretation of the signal strengths measured in the various Higgs channels. It has been utilised to test various physics scenarios, like the existence of additional new particles contributing to the radiative Higgs boson production and decays, or to probe various symmetries of the SM itself, as for example the custodial symmetry. It only compares the experimental measurements to their best SM predictions and does not require any new BSM computations per se. And, from a more theoretical perspective, its relevance arises from the fact that it actually fully captures the leading effects in single Higgs processes of well motivated scenarios. Still, the κ -formalism has obvious limitations and certainly does not capture the most general deformations of the SM, even under the assumptions of heavy and decoupling new physics. A particularly acute shortcoming at the time Higgs physics is entering a precision era is the lack of proficiency to assert the richness of kinematical distributions beyond simple signal strength measurements. Several extensions and alternative approaches are being developed as part of the activities of the LHC Higgs Cross Section Working Group [47].

The Higgs Pseudo-Observable (HPO) approach [276] allows one to report the data in terms of a finite set of on-shell form factors parametrising amplitudes of physical processes subject to constraints from Lorentz invariance and other general requirements like analyticity, unitarity, and crossing symmetry. These form factors are expanded in powers of kinematical invariants of the process around the known poles of SM particles, assuming that poles from BSM particles are absent in the relevant energy regime. A set of HPOs have been proposed to characterise both the Higgs boson decays and the EW Higgs boson production channels, thus exploring different kinematical regimes. Prospective studies concluded that these HPOs can be measured/bounded at the percent level at the HL-LHC and could therefore be used to constrain some explicit models of new physics.

Another systematic approach to characterise the possible Higgs boson coupling deviations induced by BSM physics is the use of Effective Field Theories (EFT) [277,278]. This approach assumes again that the new physics degrees of freedom are sufficiently heavy to be integrated out, and they give rise to effective interactions among the light SM particles. By construction, the effective Lagrangians cannot account for deviations in Higgs physics induced by light degrees of freedom, unless they are added themselves as extra fields in the effective Lagrangians. In Section 11.7, several examples of models with light degrees of freedom affecting Higgs boson production and decay rates will be presented. The main advantage of EFTs is their prowess to relate different observables in different sectors and at different energies to constrain a finite set of effective interactions among the SM degrees of freedom. In an EFT, the SM Lagrangian is extended by a set of higher-dimensional operators, and it reproduces the low-energy limit of a more fundamental UV description. It will be assumed that the Higgs boson is part of a CP -even EW doublet, Φ , and that the Lagrangian is an analytic function of the gauge invariant $\Phi^\dagger\Phi$. This scenario is commonly refereed as SMEFT. Even though it is not fully established experimentally, this set-up is motivated by the measurements of the Higgs couplings to the different SM particles that show an alignment with their masses, such an alignment naturally follows under this assumption of a linear realisation of the $SU(2)_L \times U(1)_Y$ symmetry of the SM but would require an ad hoc tuning otherwise. General Lagrangians bypass-

ing this linear assumption have been explicitly written down, see for instance Ref. [279]. They rely on a chiral expansion with a specific power-counting, effectively resumming the expansion in powers of the Higgs field, usually referred as HEFT as opposed to SMEFT.

11.6.1 Effective Lagrangian framework

The SMEFT has the same field content and it respects the same linearly-realised $SU(3)_C \times SU(2)_L \times U(1)_Y$ local symmetry as the SM. The difference is the presence of operators with canonical mass-dimension d larger than 4. These are organised in a systematic expansion in d , where each consecutive term is suppressed by a larger power of a high mass scale. Assuming baryon and lepton number conservation, the most general Lagrangian takes the form

$$\mathcal{L}_{\text{eff}} = \mathcal{L}_{\text{SM}} + \sum_i c_i^{(6)} \mathcal{O}_i^{(6)} + \sum_j c_j^{(8)} \mathcal{O}_j^{(8)} + \dots \quad (11.29)$$

The contribution of the higher order operators of dimension d to physical amplitudes is suppressed by $(E/\Lambda)^{d-4}$, where E is the relevant energy scale of the process and Λ is the energy scale suppressing the higher-dimensional operators. The Wilson coefficients $c_i^{(d)}$ encode the virtual effects of the heavy new physics in low-energy observables. Their precise forms in terms of masses and couplings of the new particles can be obtained via matching with the ultraviolet (UV) completion of the SM, see, e.g., Ref. [280], or inferred using specific power-counting rules [277, 281].

The list of dimension-6 operators was first classified in a systematic way in Ref. [282] after the works of Ref. [283]. Subsequent analyses pointed out the presence of redundant operators, and a minimal and complete list of operators was finally provided in Ref. [284]⁴. For a single family of fermions, there are 76 real ways to deform the SM generated by 59 independent operators. With the 3 families of fermions of the SM, flavour indices can be added to these 59 operators, and furthermore, new operator structures, that have been dismissed by means of Fierz transformations in the single family case, have to be considered, for a total of 2499 real deformations [287]. When considering Higgs data, one can reasonably focus on a relatively small subset of the 2499 operators of dimension 6. In particular the vast subset of 4-fermion operators, whether flavour and CP preserving or not, can be more strongly constrained by other processes. Thus, it makes sense to neglect this whole class, with the exception of one particular four-fermion interaction that contributes to the muon decay and thus directly affects the Fermi constant. The dipole operators, instead do directly affect Higgs boson production, however, under very general and plausible assumptions on the flavour structure of new physics, the coefficients of these operators display the same structure and the same chiral suppression of the Yukawa couplings. The consequence is that, with the possible exception of processes involving the top quark, their effect in Higgs boson production is expected to be negligible. Furthermore, as far as Higgs boson decays are concerned, the dipole operators only contribute to three (or more)-body final states (for instance $H \rightarrow b\bar{b}\gamma$) and as such they can easily be neglected too. Eliminating these two classes, there remain three other classes: 1) purely bosonic operators, 2) generalised Yukawas, 3) Higgs-fermion current operators. Operators in class 2 and 3, per se, can still contain CP - or flavour-violating terms, on which experimental constraints are rather strong. Under the assumption of flavour universality (respectively diagonality), one is left with 12 (14) parameters affecting EW precision measurements, diboson processes and single- and double-Higgs data and 7 (17) other parameters modifying the EW gauge boson couplings to fermions, see Ref. [46] for further technical details. Working in the unitary gauge and performing suitable redefinition of fields and input parameters the effective Lagrangian can be conveniently expressed in the parameterisation of Ref. [288], the so-called *Higgs basis* that conveniently single out these special

less constrained parameters. Such a classification reflects the current experimental situation and the hierarchy in the sensitivity of the experimental measurements in the various sectors of the SM. As the sensitivity of the measurements in the Higgs sector improves, another and more general parametrisation of the SM deformation will have to be retained, in particular a parametrisation more suited for a treatment at the quantum level. In other bases of operators, in particular the so-called Warsaw basis [284] used in some experimental EFT analyses [137, 289, 290], one finds strong correlations among the operators affecting the EW gauge couplings to fermions, leaving 12 (14) linear combinations of operators with weaker constraints.

Section 11.6.2 illustrates how the Higgs data accumulated at the LHC can (partially) constrain the SM deformations, i.e., the dimension-6 operators of the SMEFT Lagrangian. Automatic tools are being developed to analyse the experimental data within an EFT framework, see the report [291] and references therein.

11.6.2 Probing coupling properties

As described in Section 11.3, a framework was developed by ATLAS and CMS [151], individually and together, to combine the very large number of exclusive categories aimed at reconstructing the five main decay modes and the five main production modes of the Higgs boson. The general conclusion of this combination, illustrating the compatibility of the observation with the SM expectations, is given in Section 11.3. The same framework with its master formula, Eq. (11.16), can be used to further measure coupling properties of the Higgs boson under specific additional assumptions.

11.6.2.1 Combined measurements of the Higgs boson coupling properties

i. From effective Lagrangians to Higgs observables

The κ framework, described in detail in Ref. [45, 273], facilitates the characterisation of Higgs coupling properties in terms of a series of Higgs coupling strength modifier parameters κ_i , which are defined as the ratios of the couplings of the Higgs bosons to particles i to their corresponding SM values. The κ framework assumes a single narrow resonance so that the zero-width approximation can be used to decompose the cross section as a product of two factors characterising the production and the decay of the Higgs boson. The κ parameters are introduced by expressing each of these factors as their SM expectation multiplied by the square of a coupling strength modifier for the corresponding process at leading order:

$$\begin{aligned} (\sigma \cdot \text{BR})(i \rightarrow H \rightarrow f) &= \frac{\sigma_i^{SM} \kappa_i^2 \cdot \Gamma_f^{SM} \kappa_f^2}{\Gamma_H^{SM} \kappa_H^2} \rightarrow \\ &\rightarrow \mu_i^f \equiv \frac{\sigma \cdot \text{BR}}{\sigma_{\text{SM}} \cdot \text{BR}_{\text{SM}}} = \frac{\kappa_i^2 \cdot \kappa_f^2}{\kappa_H^2}, \end{aligned} \quad (11.30)$$

where μ_i^f is the rate relative to the SM expectation and κ_H^2 is an expression that adjusts the SM Higgs width to take into account the modifications induced by the deformed Higgs boson couplings. When all κ_i are set to 1, the SM is reproduced. For loop-induced processes, e.g. $H \rightarrow \gamma\gamma$, there is a choice of either resolving the coupling strength modification in its SM expectation, i.e., $\kappa_\gamma(\kappa_t, \kappa_W)$ or keeping κ_γ as an effective coupling strength parameter.

The κ -framework is the simplest parametrisation directly related to experimental measurements of the Higgs boson production and decay modes. For this reason, it has been widely used by the community. It can also be connected to the SMEFT formalism as follows. Restricting to the EFT directions not probed outside Higgs physics [292], the Higgs boson couplings are written

⁴Complete enumerations of $d=8$ operators have been obtained [285] and some preliminary constraints on peculiar subsets of these operators have been derived from experimental measurements [286]. Still, in this review, the EFT Lagrangians will be truncated at the level of dimension-6 operators.

in the unitary gauge as:

$$\begin{aligned} \mathcal{L} = & \kappa_Z \frac{m_Z^2}{v} Z_\mu Z^\mu H + \kappa_W \frac{2m_W^2}{v} W_\mu^+ W^{-\mu} H \\ & + \kappa_{VV} \frac{\alpha}{2\pi v} \left(\cos^2 \theta_W Z_{\mu\nu} Z^{\mu\nu} + 2W_{\mu\nu}^+ W^{-\mu\nu} \right) H \\ & + \kappa_g \frac{\alpha_s}{12\pi v} G_{\mu\nu}^a G^{a\mu\nu} H + \kappa_\gamma \frac{\alpha}{2\pi v} A_{\mu\nu} A^{\mu\nu} H + \kappa_{Z\gamma} \frac{\alpha}{\pi v} A_{\mu\nu} Z^{\mu\nu} H \\ & - \sum_f \kappa_f \frac{m_f}{v} f \bar{f} H + \kappa_3 \frac{m_H^2}{2v} H^3 + \dots \end{aligned} \quad (11.31)$$

The exact correspondence between the effective coefficients of the dimension-6 operators and the κ 's can be found for instance in Ref. [46]. In the SM, the Higgs boson does not couple to massless gauge bosons at tree level, hence $\kappa_g = \kappa_\gamma = \kappa_{Z\gamma} = 0$. Nonetheless, the contact operators are generated radiatively by SM particles loops. In particular, the top quark gives a contribution to the 3 coefficients $\kappa_g, \kappa_\gamma, \kappa_{Z\gamma}$ that does not decouple in the infinite top mass limit. For instance, in that limit $\kappa_\gamma = \kappa_g = 1$ [25, 26, 293].

The coefficient for the contact interactions of the Higgs boson to the W and Z field strengths is not independent but obeys the relation

$$(1 - \cos^4 \theta_W) \kappa_{VV} = \sin 2\theta_W \kappa_{Z\gamma} + \sin^2 \theta_W \kappa_{\gamma\gamma}. \quad (11.32)$$

This relation is a general consequence of the custodial symmetry [294], which also imposes $\kappa_Z = \kappa_W$ at leading order ($\kappa_Z/\kappa_W - 1$ is a measure of custodial symmetry breaking and, as such, is already constrained by electroweak precision data and the bounds on anomalous gauge couplings). When the Higgs boson is part of a $SU(2)_L$ doublet, the custodial symmetry in the bosonic sector could only be broken by the $\mathcal{O}_T = \frac{1}{2} (\Phi^\dagger \overleftrightarrow{D}^\mu \Phi)^2$ operator at the level of dimension-6 operators and it is accidentally realised among the interactions with four derivatives, like the contact interactions considered.

The coefficient κ_3 can be accessed directly only through double Higgs boson production processes, hence it will remain largely unconstrained at the LHC. Before the associated production of a Higgs boson with a pair of top quarks was observed, the Higgs boson coupling to the top quark was only probed indirectly via the one-loop gluon fusion production or the radiative decay into two photons. However, these two processes are only sensitive to the combinations of couplings $(\kappa_t + \kappa_g)$ and $(\kappa_t + \kappa_\gamma)$ and not to the individual couplings. Therefore a deviation in the Higgs boson coupling to the top quark can in principle always be masked by new contact interactions to photons and gluons (and this is precisely what is happening in minimal incarnations of composite Higgs models [295]). The current and still limited sensitivity, of the order of 20%, in the $t\bar{t}H$ channel leaves elongated ellipses in the direction $\kappa_g = \kappa_\gamma = 1 - \kappa_t$.

The operators already bounded by EW precision data and the limits on anomalous gauge couplings modify in general the Lorentz structure of the Higgs couplings and hence induce some modifications of the kinematical differential distributions [296]. A promising way to have a direct access to the effective coefficients of these operators in Higgs physics is to study the VH associated production with a W or a Z at large invariant mass of the VH system [297]. These differential distributions could also be a way to test the hypothesis that the Higgs boson belongs to a $SU(2)_L$ doublet together with the longitudinal components of the massive electroweak gauge bosons.

ii. Interpretations of the experimental data

The measurements of the coupling properties of the Higgs boson are entirely based on the formalism of the effective Lagrangian described above. Measurements of coupling properties in this framework implies assessing the parameters of the model Eq. (11.31) or combinations of these parameters with different sets of assumptions.

These measurements are carried out with the combination framework described in Section 11.4, where the μ_i and μ_f sig-

nal strength parameters are further interpreted in terms of modifiers of the SM couplings κ_k where $k \in \{Z, W, f, g, \gamma, Z\gamma\}$ as in Eq. (11.31). The number of signal events per category for the various production modes are typically estimated at higher orders in the analyses but are scaled by these single LO-inspired factors, thus not taking into account possible intricacies and correlations of these parameters through the higher-order corrections. This approximation is valid within the level of precision of current results and their compatibility with the SM expectation.

In this formalism, further assumptions are explicitly made: (i) the signals observed in the different search channels originate from a single narrow resonance with a mass of 125 GeV; (ii) similarly to the combination described in Section 11.4, the narrow width approximation is assumed (to allow the decomposition of signal yields into products of production and decay signal strengths); (iii) the tensor structure of the couplings is assumed to be the same as that of a SM Higgs boson. This means in particular that the observed state is assumed to be a CP -even scalar as in the SM.

Loop-level couplings such as the $gg \rightarrow H$, $H \rightarrow \gamma\gamma$ and $H \rightarrow Z\gamma$ can either be treated effectively, with κ_g , κ_γ and $\kappa_{Z\gamma}$ as free parameters in the fit or these parameters can be expressed in terms of the known SM field content and as a function of the SM coupling modifiers, in the following way [298]:

$$\begin{aligned} \kappa_g^2(\kappa_t, \kappa_b, \kappa_c) = & 1.042 \kappa_t^2 - 0.040 \kappa_t \kappa_b + 0.002 \kappa_b^2 \\ & - 0.005 \kappa_t \kappa_c + 0.0005 \kappa_b \kappa_c + 0.00002 \kappa_c^2, \\ \kappa_\gamma^2(\kappa_F, \kappa_V) = & 1.59 \kappa_V^2 - 0.66 \kappa_V \kappa_F + 0.07 \kappa_F^2, \\ \kappa_{Z\gamma}^2(\kappa_F, \kappa_V) = & 1.12 \kappa_V^2 - 0.15 \kappa_V \kappa_F + 0.03 \kappa_F^2. \end{aligned} \quad (11.33)$$

The $\kappa_{Z\gamma}$ parametrisation has been used only in the ATLAS Run 1 combined measurements of the coupling properties of the Higgs boson. The $\mu^+ \mu^-$ channels is not included in the CMS and ATLAS-CMS Run 1 combinations, while it is included in the ATLAS [241] and the CMS [242] Run 2 combinations.

The parametrisations are given for a Higgs boson mass hypothesis of 125.09 GeV (and in the last two expressions, all the Higgs-fermion couplings are assumed to be rescaled by an universal multiplicative factor κ_F). It can be noted from the expression of κ_γ that the coupling of the Higgs boson to photons is dominated by the loop of W bosons, and it is affected by the top quark loop mostly through its interference with the W loop. The sensitivity of the current measurements to the relative sign of the fermion and vector boson couplings to the Higgs boson is due to this large negative interference term. The κ_g parameter is expressed in terms of the scaling of production cross sections and therefore also depends on the pp collisions centre-of-mass energy. The parametrisations of κ_γ and $\kappa_{Z\gamma}$ are obtained from the scaling of partial widths and are only dependent on the Higgs boson mass hypothesis. Experiments use a more complete parametrisation with the contributions from the b -quarks, τ -leptons in the loops [45, 273].

The global fit is then performed expressing the μ_i and μ_f parameters in terms of a limited number of κ_k parameters or their ratios, under various assumptions. The parametrisation for the main production modes are: (i) $\mu_{\text{ggF}} = \kappa_g^2$ for the gluon fusion and an effective coupling of the Higgs boson to the gluons; (ii) $\mu_{\text{VBF}, VH} = \kappa_V^2$ for the VBF and VH processes when the W and Z couplings are assumed to scale equally, and $\mu_{\text{VBF}}^2(\kappa_W, \kappa_Z) = (\kappa_W^2 \sigma_{WWH} + \kappa_Z^2 \sigma_{ZZH}) / (\sigma_{WWH} + \sigma_{ZZH})$, when the couplings to the W and Z bosons are varied independently (σ_{WWH} and σ_{ZZH} denote the VBF cross sections via the fusion of a W and a Z boson respectively, the small interference term is neglected); (iii) $\mu_{t\bar{t}H} = \kappa_t^2$ for the $t\bar{t}H$ production mode. Numerically the production modes signal strengths as a function of the coupling modifiers to the SM fields are:

$$\begin{aligned} \mu_{\text{ggF}} = & 1.06 \kappa_t^2 + 0.01 \kappa_b^2 - 0.07 \kappa_t \kappa_b, \quad \text{and} \\ \mu_{\text{VBF}} = & 0.74 \kappa_W^2 + 0.26 \kappa_Z^2. \end{aligned} \quad (11.34)$$

The decay mode signal strengths are parametrised as $\mu_k = \kappa_k^2 / \kappa_H^2$ where $k \in \{Z, W, f, g, \gamma, Z\gamma\}$ denotes the decay mode and κ_H ,

the overall modifier of the total width that affects all the signal yields. κ_H is a priori an independent parameter. However, when it is assumed that the Higgs boson cannot decay to new particles beyond those of the SM, κ_H can also be treated as an effective parameter and expressed in terms of the coupling modifiers to the SM field content. Its general expression is:

$$\begin{aligned} \kappa_H^2 = & 0.57\kappa_b^2 + 0.06\kappa_\tau^2 + 0.03\kappa_c^2 + 0.22\kappa_W^2 + 0.03\kappa_Z^2 + 0.09\kappa_g^2 \\ & + 0.0023\kappa_\gamma^2. \end{aligned} \quad (11.35)$$

The general expression of the total width of the Higgs boson can be written as follows:

$$\Gamma_H = \frac{\kappa_H^2 \Gamma_H^{\text{SM}}}{1 - \text{BR}_{\text{BSM}}} \quad (11.36)$$

where Γ_H^{SM} is the total width of the SM Higgs boson and BR_{BSM} is the branching fraction of the Higgs boson to new particles beyond the SM.

It is worth reminding that the inability to determine BR_{BSM} and Γ_H at the LHC requires some hypotheses in order to extract the Higgs couplings from the measured Higgs signal strengths. In particular, one can assume either (i) no BSM particles in the decay, or (ii) all invisible decays are detectable, or (iii) $|\kappa_V| \leq 1$. These scenarios will be examined below.

Specific parametrisations will be made in order to address the following aspects of the coupling properties of the Higgs boson under different assumptions: (i) the relative couplings of the Higgs boson to fermions and bosons; (ii) the potential impact of the presence of new particles beyond the SM either in the loops or both in the loops and the decay of the H ; and (iii) also, more general models either of coupling modifiers or their ratios, under different assumptions.

iii. Couplings to bosons and fermions

As it will be discussed in Section 11.7.6.3, it is interesting to probe a model where no additional field content is considered in the decay width of the Higgs boson and where the relative couplings of the Higgs boson to W - and Z -bosons is fixed to its SM value, i.e., $\kappa_W = \kappa_Z$, and where all Yukawa couplings scale with one coupling modifier. In this model, only the SM particles are assumed to contribute to the gluon fusion and the diphoton loops, and all fermion couplings modifiers are required to scale simultaneously with a unique factor κ_F while all vector boson couplings modifiers also scale with a common factor κ_V . It is a two-parameter fit with κ_V and κ_F as free variables of interest. The ATLAS-CMS combined results for each channel independently, the combinations of all channels for the two experiments separately and the results of the overall combination are all shown in Fig. 11.12.

The global fit is only sensitive to the relative sign of κ_V and κ_F . By convention, either κ_F or κ_V can be considered positive and negative values of κ_V or κ_F respectively can be considered. Such values are not excluded a priori, but would imply the existence of new physics at a light scale and would also raise questions about the validity of the perturbative treatment of the SM deformations and also about the stability of the vacuum [300]. Among the five main Higgs boson decay channels, only the $\gamma\gamma$ is sensitive to the sign of κ_F (or κ_V) through the interference of the W and t loops as shown in Eq. (11.33). The current global fit disfavors a negative value of κ_F at more than five standard deviations. A specific analysis for the Higgs boson production in association with a single top quark has been proposed in order to more directly probe the sign of κ_F (see references in Ref. [132]). All available experimental data show a fair agreement of the SM prediction of the couplings of the Higgs boson to fermions and gauge bosons. The results shown in Fig. 11.12 assume that $\kappa_F \geq 0$, however, in Ref. [151], a similar combination is done without this assumption. The observed exclusion is fully compatible with the SM expectation. The ATLAS and CMS combined measurements with the Run 1 dataset lead to

$$\kappa_V = 1.03 \pm 0.03 \quad \text{and} \quad \kappa_F = 0.97 \pm 0.07, \quad (11.37)$$

and were already at an impressive 5% level of accuracy for the κ_V parameter. The ATLAS Run 2 combination yielded:

$$\kappa_V = 1.05 \pm 0.04 \quad \text{and} \quad \kappa_F = 1.05 \pm 0.09. \quad (11.38)$$

The ATLAS Run 2 results are also reported as likelihood contours shown in Fig. 11.12.

iv. Probing new physics in the loops (and the decay)

A more constrained model fully focussing on BSM scenarios with new heavy particles contributing to the loops and where all couplings to the SM particles are assumed to be the same as in the SM ($\kappa_W = \kappa_Z = \kappa_t = \kappa_b = \kappa_\tau = 1$) is also used to constrain the κ_g and κ_γ parameters only. In this model, it can be assumed that the new physics affecting the loops are either introducing new decay channels (i.e., BR_{BSM} allowed to vary in the fit) or not (i.e., $\text{BR}_{\text{BSM}} = 0$). In the two cases, the results on the couplings through loops (to gluons and photons) do not change significantly. The constraints on BR_{BSM} will be discussed in the next section, while here the focus will be on the effective couplings of the Higgs boson to gluons and photons. The contours of the combined likelihood in the $(\kappa_\gamma, \kappa_g)$ plane for the ATLAS and CMS experiments and their combination are shown in Fig. 11.13. The measured values of these parameters for the ATLAS and CMS Run 1 combination are:

$$\kappa_g = 0.78_{-0.10}^{+0.13} \quad \text{and} \quad \kappa_\gamma = 0.87_{-0.09}^{+0.14}. \quad (11.39)$$

At Run 2, the ATLAS combination yielded:

$$\kappa_g = 0.98 \pm 0.05 \quad \text{and} \quad \kappa_\gamma = 1.06 \pm 0.05. \quad (11.40)$$

In this model as well, all results are fully compatible with the SM expectations.

v. Coupling measurements and probing BSM physics in loops and in the decay

In the models described above, it was either assumed that no new BSM degree of freedom distorts neither the loop-induced Higgs boson couplings to gluons and photons nor the total Higgs boson width, or that all tree level couplings to SM particles are SM-like. These assumptions can be relaxed.

In order to probe simultaneously the Higgs boson couplings to massive and massless particles, only the assumption $\text{BR}_{\text{BSM}} = 0$ is kept. The couplings to photons and gluons are then parametrised by independent effective couplings, κ_g and κ_γ , and κ_Z , κ_W , κ_t , $|\kappa_\tau|$, and $|\kappa_b|$ are measured simultaneously. The absolute values of certain coupling modifiers only indicate the degeneracy of combined likelihood for the two signs. It can be noted that when the coupling to gluons is not considered effective, there is some sensitivity to the sign of κ_b through the interference between the top- and bottom-quark loops in the gluon fusion process. In this analysis, the constraint on the top quark Yukawa coupling comes from the $t\bar{t}H$ direct search channels only. The complete set of results from this model is given in Table 11.12 for the ATLAS-CMS combination using the full Run 1 dataset [299] and for the ATLAS [241] and CMS [301] individual combinations using partial Run 2 datasets. Figure 11.14 also displays the results of the individual ATLAS and CMS combinations. A negative relative sign is allowed for the κ_W and κ_Z parameters without loss of generality. This convention is used in the ATLAS and CMS Run 1 combination and in the CMS Run 2 combination. Neglecting the very small interference between the W and Z exchanges in the VBF production and when treating the photon and gluon couplings as effective, the sensitivity to the negative signs of the couplings of the Higgs boson to the W and the top quark and that of the Z to the gluon come respectively from the tH and the $ggHZ$ production processes. In the case of the ATLAS Run 2 combination, only a relative negative sign of the coupling of the Higgs boson to the top quark is allowed. The cases reported in Table 11.12 of negative values of the couplings correspond to *quasi*-degenerate cases and the choice of sign is therefore not significant. For instance, the negative value of κ_W obtained by CMS in its Run 2

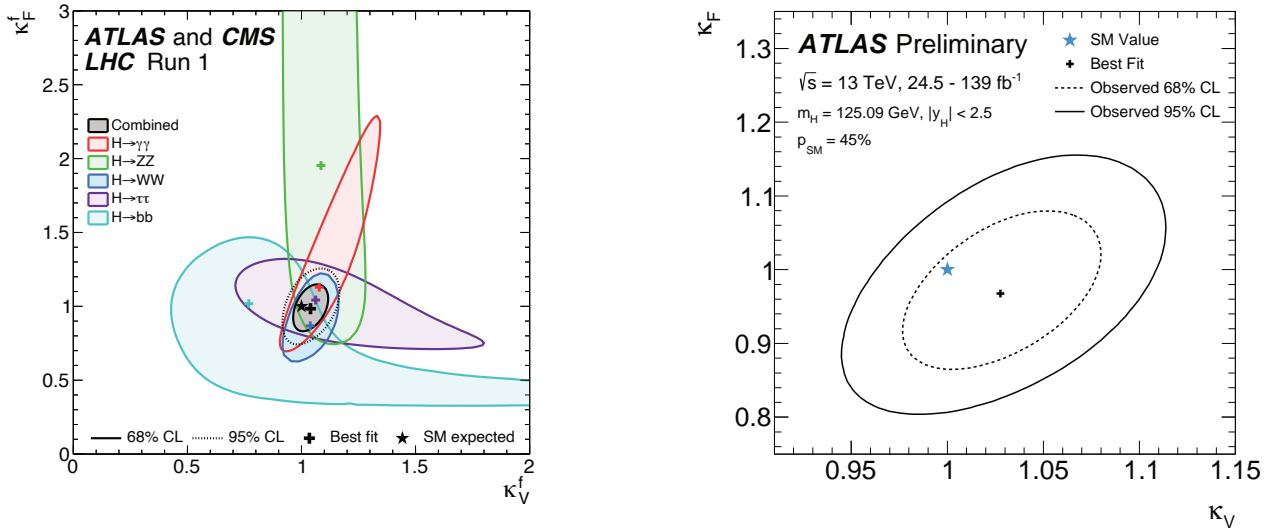


Figure 11.12: Likelihood contours in the (κ_F, κ_V) plane for the ATLAS-CMS Run 1 combination [299] (left) and ATLAS [241] (right) individual Run 2 combinations. These results correspond to a 2-parameter fit assuming a universal rescaling of the Higgs couplings to all fermions and also $\kappa_W = \kappa_Z$.

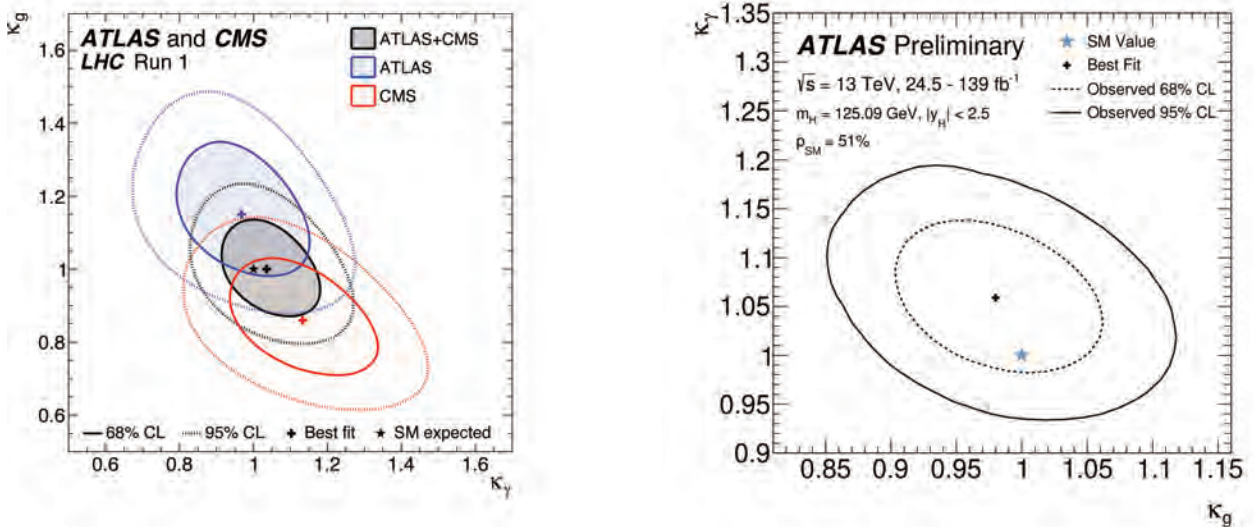


Figure 11.13: Likelihood contours in the $(\kappa_g, \kappa_\gamma)$ plane for the ATLAS-CMS [299] combination (left) and for the ATLAS [241] (right) under the assumption that undetected and invisible branching fractions vanish and that all the couplings to SM particles are those expected from the SM. This model probes new physics in the loops.

combination is due to tH contribution to the $t\bar{t}H$ channels as the specific tH analyses described in Section 11.3.3 are not included in the combination.

It is interesting to note that, with a partial Run 2 dataset, the sensitivity of individual experiments is already better than the one obtained at Run 1. This is in large part due to the improved systematic uncertainties related to the predictions of the Higgs boson production and decay that have been discussed in Section 11.2.

The results above are obtained under the assumption that the Higgs boson decays only to SM particles. This assumption is necessary since the signal rates cannot resolve separately κ_H and the absolute couplings of the Higgs boson to the SM particles. This degeneracy can, however, be resolved using an independent constraint on the Higgs boson width as the one derived from off-shell couplings measurements. This approach was used by the ATLAS experiment (see references in Ref. [132]), thus yielding a priori an absolute measurement of the couplings of the Higgs boson. The validity of the results obtained still relies on assumptions that have been discussed in Section 11.5.2. Another well-motivated assumption to resolve the aforementioned degen-

eracy preventing the determination of κ_H is inspired by unitarity conditions. Requiring that $\kappa_V \leq 1$ allows to free the BR_{BSM} parameter and further probe new physics in the decay of the Higgs boson. An intuitive understanding of how this constraint works can be given by a simple example. In the VBF $H \rightarrow W^+W^-$ channel, the number of signal events compared to the SM prediction is rescaled by $(1 - BR_{BSM})\kappa_W^4/\kappa_H^2$, and, an observed signal close to the SM expectation cannot accommodate a large value of BR_{BSM} since the depletion factor $(1 - BR_{BSM})$ cannot be compensated by an enhanced value $\kappa_W > 1$. Or, in other terms, if $\kappa_W \sim 1$ is preferred from other channels, a low signal in the VBF $H \rightarrow W^+W^-$ channel would be a sign of the presence of BSM physics in the Higgs boson decays. Within this framework, all the Higgs boson couplings to massive and massless SM particles can be measured in addition to BR_{BSM} . The results of this combination are shown in Fig. 11.14 (left). The results for all parameters do not change significantly with respect to the previous fit that assumed $BR_{BSM} = 0$. But a 95%CL bound on this parameter

Table 11.12: Coupling modifier combined measurements assuming the absence of perceptible new physics in the decay of the Higgs boson. No assumption is made for the loop level couplings of the Higgs boson to gluons and photons which are considered as effective. The last column gives the expected precision at the HL-LHC [111].

	LHC Run 1	ATLAS Run 2	CMS Run 2	HL-LHC (expected)
κ_γ	$0.87^{+0.14}_{-0.09}$	$1.06^{+0.08}_{-0.07}$	$1.01^{+0.07+0.06}_{-0.07-0.12}$	1.8%
κ_W	$0.87^{+0.13}_{-0.09}$	1.06 ± 0.07	$-1.11^{+0.13+0.05}_{-0.07-0.06}$	1.7%
κ_Z	-0.98 ± 0.10	1.02 ± 0.06	$0.96^{+0.06+0.04}_{-0.06-0.05}$	1.5%
κ_g	$0.78^{+0.13}_{-0.10}$	$0.96^{+0.09}_{-0.08}$	$1.16^{+0.08+0.08}_{-0.08-0.08}$	2.5%
κ_t	$1.40^{+0.24}_{-0.21}$	1.00 ± 0.12	$1.01^{+0.06+0.09}_{-0.06-0.08}$	3.4%
κ_b	$0.49^{+0.27}_{-0.15}$	$0.98^{+0.14}_{-0.13}$	$1.18^{+0.14+0.13}_{-0.13-0.24}$	3.7%
κ_τ	$0.84^{+0.15}_{-0.11}$	$1.05^{+0.15}_{-0.14}$	$0.94^{+0.08+0.09}_{-0.11-0.06}$	1.9%

can now be obtained:

$$\text{BR}_{\text{BSM}} < 34\% \text{ (ATLAS)}, \quad \text{BR}_{\text{BSM}} < 38\% \text{ (CMS)}. \quad (11.41)$$

Both ATLAS and CMS in their Run 2 combinations have included the search for invisible decays of the Higgs boson [301,302], described in Section 11.3. This allows for a coherent interpretation of the constraints on invisible decays and the measurements in the visible channels as well as simultaneously constraining BR_{inv} and the overall branching fraction to potentially “visible” particles but to which none of the considered measurements are sensitive, as for example Higgs boson decays to light quarks or BSM particles decaying subsequently mainly to light quarks (BR_{und} referred to as branching fraction to undetected particles). The limits obtained on the invisible branching fractions are:

$$\text{BR}_{\text{inv}} < 30\% \text{ (ATLAS)}, \quad \text{BR}_{\text{inv}} < 22\% \text{ (CMS)}. \quad (11.42)$$

Models which are less sensitive to modelling systematic uncertainties and requiring no constraints on the natural width of the Higgs bosons have been considered, either through the ratio of cross section and branching ratios (see results in Ref. [132]) or through a more generic approach to avoid the degeneracy in the measurement of the coupling modifiers, probing the coupling properties of the Higgs boson through ratio of couplings. In the latter model, the cross section times branching fraction of the $gg \rightarrow H \rightarrow ZZ$ process is parametrised as a function of a single coupling modifier:

$$\kappa_{gZ} = \kappa_g \times \frac{\kappa_Z}{\kappa_H} \quad (11.43)$$

Then all combination signals can be parametrised with the following ratios of coupling modifiers: (i) the $\lambda_{Zg} = \kappa_Z/\kappa_g$ ratio which is mainly probed by the measurements of the VBF and ZH production; (ii) the $\lambda_{tg} = \kappa_t/\kappa_g$ ratio constrained by the $t\bar{t}H$ production process; (iii) the $\lambda_{WZ} = \kappa_W/\kappa_Z$ ratio mainly probed by the WW and ZZ decay modes; (iv) the $\lambda_{\tau Z} = \kappa_\tau/\kappa_Z$ ratio constrained by the $\tau^+\tau^-$ channel; (v) the $\lambda_{bZ} = \kappa_b/\kappa_Z$ ratio probed mainly by the $VH(b\bar{b})$ channels; and (vi) the $\lambda_{\gamma Z} = \kappa_\gamma/\kappa_Z$ ratio constrained by the diphoton channel. In this parametrisation, the ZZ channel plays an important normalisation role (the results are discussed in detail in the previous edition of this review [132]).

11.6.2.2 Differential cross sections

To further characterise the production and decay properties of the Higgs boson, with the increase in size of the LHC datasets, measurements of fiducial and differential cross sections are being carried out by ATLAS and CMS both at Run 1 (the references can be found in the previous edition of this review [132]) and Run 2 [289,303] and in several channels: (i) the diphoton, (ii) the four leptons, and (iii) the WW channels.

The definition of a fiducial volume as close as possible to the reconstruction level selection criteria is very important as it will minimise the model dependence from possible variations in the signal reconstruction efficiencies. Minimising model dependence

of unfolded fiducial differential cross section measurements is also key to ensure their usefulness to further probe and tune more accurate models in the future.

As an example in the diphoton channel for the ATLAS Run 1 analysis (similar criteria are used at Run 2 and by CMS), the selection criteria defining the fiducial volume are the following: the two highest transverse momentum (E_T), isolated final state photons, within $|\eta| < 2.37$ and with $105 \text{ GeV} < M_{\gamma\gamma} < 160 \text{ GeV}$ are selected (the transition region between the barrel and end-cap calorimeters is not removed); after the pair is selected, the same cut on $E_T/M_{\gamma\gamma}$ as in the event selection, i.e., in excess of 0.35 (0.25) for the two photons is applied. The requirement of the isolation of the photon to define the fiducial volume is particularly important to avoid potentially large variations of the reconstruction efficiency within this volume for production processes as different as the gluon fusion and $t\bar{t}H$.

While strict fiducial requirements are key to minimise model dependence, these make combinations of decay channels impossible. To gain precision in the measurement of the production properties of the Higgs boson, the fiducial volume defined on the decay products of the Higgs boson can be removed and channels can be combined relying on the extrapolation from the reconstruction acceptance using Monte Carlo simulations. This has been used to combine differential cross section for instance in the transverse momentum of the Higgs boson. Such hybrid approaches are also discussed in Section 11.6.2.4.

A large number of observables have been studied aiming at probing the accuracy of the modelling of the Higgs boson production simulations. Some examples include (i) the transverse momentum and pseudo rapidity of the objects, such as jets or leptons, produced in association with the Higgs boson in several modes, the principal distributions of the Higgs boson decay products such for instance in the diphoton channel; (ii) the production angle in the Collins–Soper frame [253] in the diphoton channel; (iii) the overall distribution of the Higgs boson transverse momentum.

The measured differential cross section in the Higgs boson transverse momentum by ATLAS and CMS using the full Run 2 datasets are illustrated in Fig. 11.15.

11.6.2.3 Constraints on non-SM Higgs boson interactions in an effective Lagrangian

An example of the possible use of differential cross sections in constraining non-SM Higgs boson couplings in an EFT is given by ATLAS [305]. In this analysis, differential cross section measured in the diphoton channel are used to constrain an effective Lagrangian where the SM is supplemented by dimension six CP -even operators of the Strongly Interacting Light Higgs (SILH) formulation [277] and corresponding CP -odd operators. The diphoton differential cross sections are mainly sensitive to the operators that affect the Higgs boson interactions with gauge bosons. CMS has also recently analysed [289] the Higgs boson transverse momentum distribution to constrain the Higgs boson couplings to top, bottom, and charm quarks as well as the effective coupling

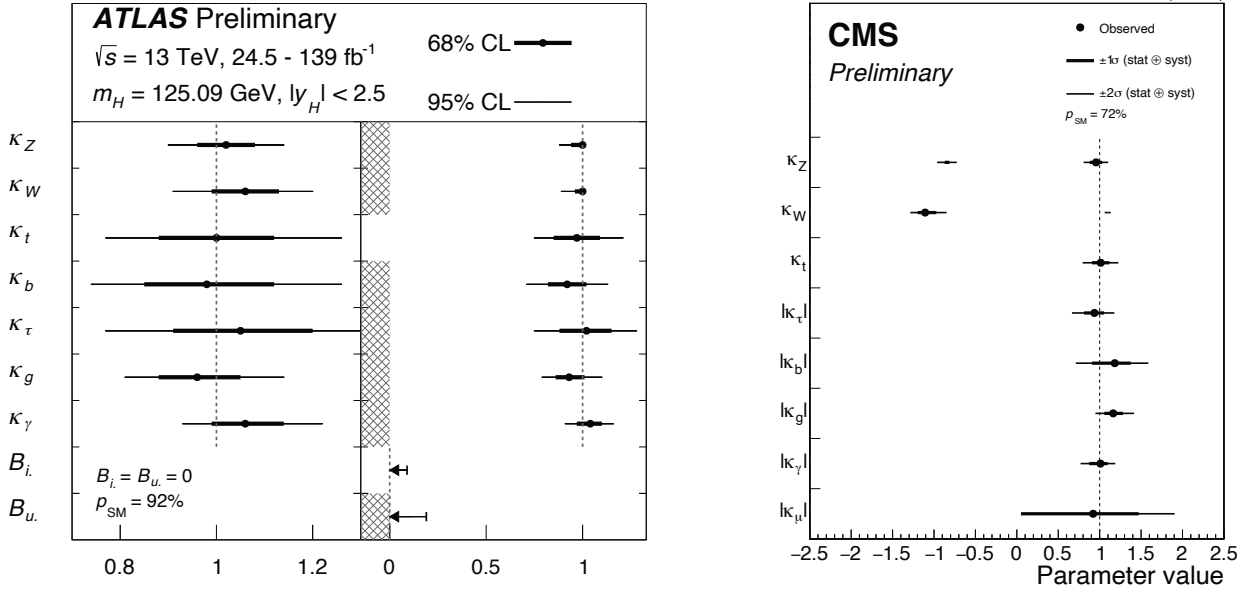


Figure 11.14: ATLAS [241] (left) and CMS [242] (right) combined measurements of coupling modifiers with various assumptions on the $\kappa_V < 1$ scenario, and in the case of the ATLAS measurements with the assumption $\text{BR}_{\text{BSM}} = 0$ and using the off-shell Higgs measurements.

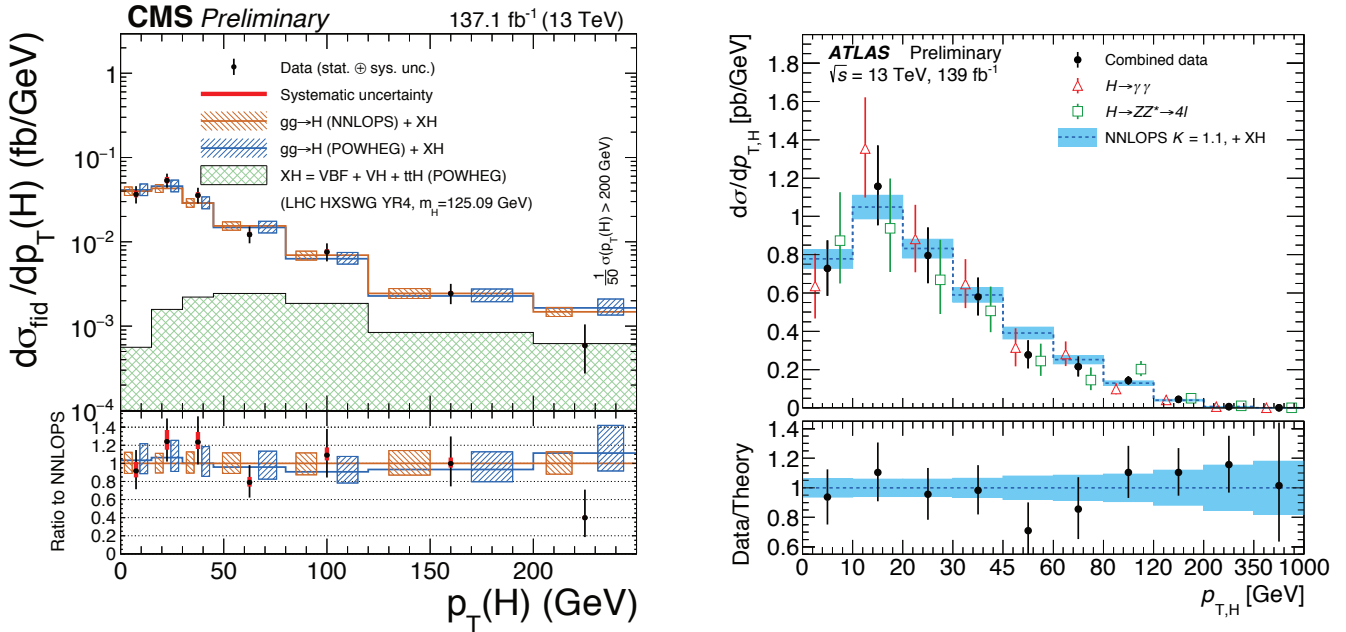


Figure 11.15: (Left) Fiducial differential, closely matching the reconstruction level selections, cross sections in Higgs boson transverse momentum in the $H \rightarrow 4\ell$ channel from the CMS experiment [304]. (Right) Partially fiducial combined cross sections using the $H \rightarrow \gamma\gamma$ and $H \rightarrow 4\ell$ channels from the ATLAS experiment [303].

to gluons. This analysis is, however, not performed in an EFT framework.

The differential distributions used in this combination are: (i) the transverse momentum of the Higgs boson, (ii) the number of reconstructed jets produced in association with the diphoton pair, (iii) the invariant mass of the diphoton system and (iv) the difference in azimuthal angle of the leading and sub-leading jets in events with two or more jets. This analysis shows how differential information significantly improves the sensitivity to dimension-6 operators.

11.6.2.4 Simplified Template Cross Sections (STXS)

An overarching subject of discussion between the theory and experimental communities in the field of Higgs physics has been how experimentalists could best communicate their results for them to be most efficiently used by others for further interpretation. In the field of precision SM measurements, the commonly used practise is that results are given at particle level within a well-defined fiducial volume of phase space. The fiducial volume is usually defined close enough to the experimental reconstruction to minimise the possible variations of the reconstruction efficiency within the particle level fiducial volume. In this way, results minimise their dependence on theoretical uncertainties.

ATLAS and CMS have produced fiducial and unfolded cross sections based on all objects reconstructed in the events. These measurements could be used for further interpretation. However, performing a proper combination of channels taking into account all experimental systematic uncertainties is non trivial. A proposal [46, 306] was made by the LHC Higgs Working Group to produce results in each decay channel with a well defined fiducial phase space of the Higgs boson (and not its decay products) and for other associated objects pertaining to all channels, such as jets and missing transverse momentum (MET). The definition of the fiducial regions is motivated by maximising the experimental sensitivity, isolating possible BSM effects, and minimising the dependence on theoretical uncertainties. The number of regions is also minimised to avoid the loss of experimental sensitivity. The observables that are measured in this approach are still the standard production cross sections (the gluon fusion, the vector boson fusion, the VH and $t\bar{t}H$ associated production modes) within the defined fiducial volumes.

In summary, this approach is hybrid. It is fiducial on specific objects to reduce the theory dependence and inclusive in the Higgs kinematics in order to allow for a more straightforward combination. This approach also allows the use of multivariate techniques to enhance the sensitivity within given fiducial regions, at the expense of a greater extrapolation and therefore increased model dependence.

The currently used Simplified Template Cross Sections (STXS) scheme covers, with a limited number of bins, the ggF process in four categories in number of jets (0, 1, 2 and 2 VBF-like jets, where VBF-like means a selection of two high invariant mass jets with large pseudo rapidity difference) further subdivided in four transverse momentum categories covering the full spectrum with the last bin being inclusive for $p_T > 200$ GeV. The VH process is subdivided two categories depending on the number of reconstructed charged leptons corresponding to the decays of either a W boson or a Z boson, and two bins in transverse momentum. VBF and hadronic VH categories are defined using jet cuts and two bins in transverse momentum.

Measurements in this framework have been made in various decay channels. The first measurements have been performed in the main Higgs boson discovery channels. ATLAS has produced measurements of the diphoton and the 4ℓ channels with Run 2 data [255, 265, 307–309]. And full Run 2 results are available for the $H \rightarrow 4\ell$ channel from ATLAS [310] and CMS [311].

CMS has carried out a measurement of the STXS in the $H \rightarrow \tau^+\tau^-$ decay channel targeting the high transverse momentum of the Higgs boson [154], in particular in the channel where the Higgs boson is produced with one jet of transverse energy in excess of 200 GeV.

ATLAS [312] has made a measurement of the STXS aiming at the VH production mode in the $H \rightarrow b\bar{b}$ decay mode at high transverse momentum of the vector boson above 250 GeV, where the discrimination of the background further increases.

A combination of STXS across decay channels has also been carried out by ATLAS with the full Run 2 dataset [241, 313].

11.6.2.5 Indirect constraints on the Higgs boson couplings

The direct measurements at the LHC provide direct probes of the Higgs boson couplings to the vector bosons (photons, W , Z and gluons) and to a limited number of Yukawa couplings to fermions. Currently these include essentially the third generation fermions – tau leptons, bottom and top quarks. For the High-Luminosity run, prospective studies [111] have shown that a good precision will be reached in the measurement of the coupling of the Higgs boson to muons and an evidence of the Higgs boson trilinear self-coupling with a precision of the order of 50% can be achieved. For the couplings of the Higgs boson to the other light SM fermions, direct evidences will be hard to reach at the LHC. However, from the measurements of the main observed Higgs final states, it is possible to constrain specific couplings through their radiative corrections to dominant processes. Two prime examples are: (i) the trilinear self-coupling can be constrained through loop corrections to the single Higgs boson production [314–316], see the interpretation carried out by ATLAS of the combination of the main decay channels [317]; (ii) the charm Yukawa coupling can

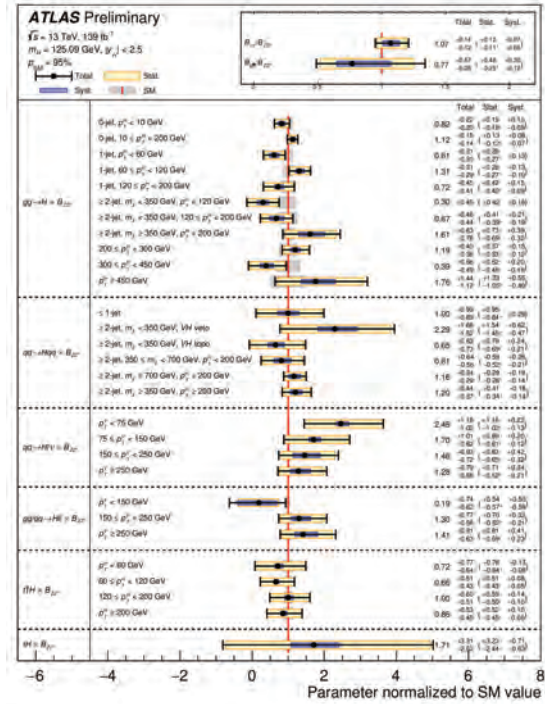


Figure 11.16: Simultaneous measurement of the simplified template cross sections the branching fraction $BR(H \rightarrow ZZ)$ (normalised to their Standard Model expectations) and the ratios of branching fractions $BR(f)/BR(ZZ)$ [241].

be constrained from the differential cross section in Higgs boson transverse momentum [318], see the ATLAS [319] and CMS [289] analyses in the diphoton channel. These indirect constraints, however, require assumptions on the possible variations of all the other couplings.

ATLAS has also performed a preliminary combination of the single Higgs boson production measurements [320], using the approach and parametrisations of Ref. [315], which yield the following constraint:

$$-3.2 < \kappa_\lambda < 11.9. \quad (11.44)$$

When combined with results of the double Higgs boson production searches, the following combined constraint on the Higgs boson trilinear coupling yields:

$$-2.3 < \kappa_\lambda < 10.3 \text{ (obs)} \quad [-5.1 < \kappa_\lambda < 11.2 \text{ (exp)}]. \quad (11.45)$$

The *direct* and *indirect* constraints on the Higgs boson trilinear self-coupling are currently of similar strength. The double Higgs boson measurements are dominated by statistical uncertainties and are expected to improve much more rapidly than the precision on single Higgs boson measurements. Furthermore, it should be stressed that the constraints on the trilinear self-coupling obtained via the NLO fit of single Higgs boson data are less robust and more model-dependent since the NLO effects induced by a shift of the trilinear self-coupling compete with possible LO effects sourced by the deviations of the Higgs boson couplings to the other SM particles. The different effects can be disentangled by the measurements of various kinematical differential distributions in addition to the study of the inclusive rates [321], but the expected sensitivity in such global fits is not as promising as the one obtained when only the Higgs boson self-coupling is allowed to deviate from its SM value [112].

11.7 New physics models of EWSB in the light of the Higgs boson discovery

The discovery of a light scalar with couplings to gauge bosons and fermions that are consistent with SM predictions, together with the slow running of the Higgs boson self-coupling at high

energies allow one to consider the SM as a valid perturbative description of nature all the way to the Planck scale. This picture is admittedly very attractive, but it posits that the Higgs boson is an elementary scalar field, whose mass has quantum sensitivity to possible new physics scales. This EW/Higgs naturalness problem [6] has become much more definite after the Higgs boson discovery.

There are two broad classes of models addressing the naturalness problem⁵. One is based on SUSY [7] (for recent reviews, see Refs. [8, 9]). This is a weakly coupled approach to EWSB, maintaining the perturbativity of the SM, and, the Higgs boson remains elementary and the corrections to its mass are screened at the scale at which SUSY is broken so the value of the weak scale remains insensitive to the details of the physics at higher scales. These theories predict at least three neutral Higgs particles and a pair of charged Higgs particles [27]. One of the neutral Higgs bosons, most often the lightest CP -even one, has properties that can resemble those of the SM Higgs boson (at least in some regions of the parameter space like the so-called decoupling limit). It is referred to as a SM-like Higgs boson, meaning that its couplings are close to the ones predicted in the SM, and one talk of the alignment limit. The other approach invokes the existence of strong interactions at a scale of the order of one TeV or above and these new interactions induce the breaking of the electroweak symmetry [323]. In the original incarnation, dubbed technicolor, the strong interactions themselves trigger EWSB without the need of a Higgs boson. Another possibility, more compatible with the ATLAS and CMS discovery, is that the strong interactions produce four light resonances identified with the Higgs doublet and EWSB proceeds through vacuum misalignment [10] (see Refs. [11, 12] for recent reviews). In that case, the Higgs boson itself has a finite size and thus never feels the UV degrees of freedom that would otherwise have dragged its mass to much higher scales. The Higgs boson could also correspond to the Goldstone boson associated with the spontaneous breaking of scale invariance, see Ref. [324] and references therein. However, this dilaton/radion scenario now requires a jumbled model-building to be consistent with the constraints from the coupling measurements. All these BSM scenarios can have important effects on the phenomenology of the Higgs boson. Also, in each case, the role of the Higgs boson in the unitarisation of scattering amplitudes is shared by other particles which remain targets of experimental searches.

The realisation of SUSY at low energies has many good qualities that render it attractive as a model of new physics. First of all since, for every SM degree of freedom, there is a superpartner of different spin but of equal mass and effective coupling to the SM-like Higgs boson, in the case of exact SUSY, an automatic cancellation of quantum corrections to the Higgs mass parameter holds. In practice, it is known that SUSY must be broken since no superpartners of the SM particles have been observed so far. The mass difference between the precise value of the mass of any particle and that of its corresponding superpartner is proportional to the correlated soft SUSY breaking parameter, generically called M_{SUSY} . The quantum corrections to the Higgs boson mass parameter are proportional to M_{SUSY}^2 , and provided M_{SUSY} is of order of a few TeV, the low energy mass parameters of the Higgs sector become insensitive to physics at the GUT or Planck scale. Another interesting feature of SUSY theories is related to the dynamical generation of EWSB [325]. In the SM, a negative Higgs mass parameter, m^2 , needs to be inserted by hand to induce EWSB, see Eq. (11.1). In SUSY, instead, even if the relevant Higgs mass parameter is positive in the ultraviolet, it may become negative and induce EWSB radiatively through the strong effect of the top quark-Higgs boson coupling in its renormalisation group evolution [325].

In the following, the Higgs sector will be explored in specific SUSY models. In all of them, it is often possible to find regions of the parameter space that accommodate one neutral Higgs boson with properties that resemble those of the SM Higgs boson, whereas additional neutral and charged Higgs bosons are also

predicted and are intensively being sought for at the LHC (see Section 11.7.7). In the simplest SUSY model, accommodating a SM-like Higgs boson mass of about 125 GeV results in constraints on the stop sector, with at least one stop mass in the few TeV mass range. In non-minimal SUSY extensions of the SM (details and related references can be found in the previous edition of this review [132]), a SM-like Higgs boson with mass of 125 GeV can be accommodated with less restrictions on the stop sector. While naturalness dictates relatively light stops and - at the two loop level - also gluinos, the first and second generation of squarks and sleptons couple weakly to the Higgs sector and may be heavy. Moreover, small values of the μ parameter and therefore light Higgsinos, the fermionic superpartners of the Higgs bosons, would be a signature of a natural realization of electroweak symmetry breaking [326]. Such SUSY spectra, consisting of TeV range stop masses and light Higgsinos, continue to be under intense scrutiny by the experimental collaborations [327] in order to understand if such natural SUSY scenarios endure and can explain why the Higgs boson remains light.

In the context of weakly coupled models of EWSB, one can also consider multiple Higgs $SU(2)_L$ doublets as well as additional Higgs singlets, triplets or even more complicated multiplet structures, with or without low energy SUSY. In general, for such models, one needs to take into account experimental constraints from precision measurements and flavour changing neutral currents. The LHC signatures of such extended Higgs sectors are largely shaped by the role of the exotic scalar fields in EWSB.

The idea that the Higgs boson itself could be a composite bound state emerging from a new strongly-coupled sector has been reconsidered thanks to the insights gained from the AdS/CFT duality. The composite Higgs boson idea is an incarnation of EWSB via strong dynamics that smoothly interpolates between the standard technicolor approach and the true SM limit. To avoid the usual conflict with EW data, it is sufficient, if not necessary, that a mass gap separates the Higgs resonance from the other resonances of the strong sector. Such a mass gap can naturally follow from dynamics if the strongly-interacting sector exhibits a global symmetry, G , broken dynamically to a subgroup H at the scale f , such that, in addition to the three Nambu-Goldstone bosons of $SO(4)/SO(3)$ that describe the longitudinal components of the massive W and Z , the coset G/H contains a fourth Nambu-Goldstone boson that can be identified with the physical Higgs boson. Simple examples of such a coset are $SU(3)/SU(2)$ or $SO(5)/SO(4)$, the latter being favoured since it is invariant under the custodial symmetry. It is also possible to have non-minimal custodial cosets with extra Goldstone bosons leading to additional Higgs bosons in the spectrum, see for instance Ref. [328]. Modern incarnations of composite Higgs models have been recently investigated in the framework of 5D warped models where, according to the principles of the AdS/CFT correspondence, the holographic composite Higgs boson then originates from a component of a gauge field along the 5th dimension with appropriate boundary conditions.

A last crucial ingredient in the construction of viable composite Higgs boson models is the concept of partial compositeness [329], i.e., the idea that there are only linear mass mixings between elementary fields and composite states. After diagonalisation of the mass matrices, the SM particles, fermions and gauge bosons, are admixtures of elementary and composite states and thus they interact with the strong sector, and in particular with the Higgs boson, through their composite component. This setup has important consequences on the flavour properties, chiefly the suppression of large flavour changing neutral currents involving light fermions. It also plays an important role in dynamically generating a potential for the would-be Goldstone bosons. Partial compositeness also links the properties of the Higgs boson to the spectrum of the fermionic resonances, i.e., the partners of the top quark. As in the MSSM, these top partners are really the agents that trigger the EWSB and also generate the mass of the Higgs boson that otherwise would remain an exact Goldstone boson and hence massless. The bounds from the direct searches for the top partners, in addition to the usual constraints from EW precision data, force the minimal composite Higgs models into some unnatural corners of their parameter spaces [330].

⁵Another solution to the naturalness problem is to lower the fundamental scale of quantum gravity, like for instance in models with large extra-dimensions, see Ref. [322].

11.7.1 Higgs bosons in the minimal supersymmetric standard model (MSSM)

The particle masses and interactions in a SUSY theory are uniquely defined as a function of the superpotential and the Kähler potential [9]. A fundamental theory of SUSY breaking, however, is unknown at this time. Nevertheless, one can parametrise the low-energy theory in terms of the most general set of soft SUSY-breaking operators [9]. The simplest realistic model of low-energy SUSY is the minimal SUSY extension of the SM (MSSM) [9, 331], that associates a SUSY partner to each gauge boson and chiral fermion of the SM, and provides a realistic model of physics at the weak scale. However, even in this minimal model with the most general set of soft SUSY-breaking terms, more than 100 new parameters are introduced. However, only a subset of these parameters impact the Higgs boson phenomenology either directly at tree-level or through quantum effects.

The MSSM contains the particle spectrum of a two-Higgs-doublet model (2HDM) extension of the SM and the corresponding SUSY partners. Two Higgs doublets, Φ_1 and Φ_2 , with hypercharge $Y = -1$ and $Y = 1$, respectively, are required to ensure an anomaly-free SUSY extension of the SM and to generate mass for down-type quarks/charged leptons (Φ_1) and up-type quarks (Φ_2) [27]. The Higgs potential reads

$$\begin{aligned}
 V = & m_1^2 \Phi_1^\dagger \Phi_1 + m_2^2 \Phi_2^\dagger \Phi_2 - m_3^2 (\Phi_1^T i \sigma_2 \Phi_2 + \text{h.c.}) \\
 & + \frac{1}{2} \lambda_1 (\Phi_1^\dagger \Phi_1)^2 + \frac{1}{2} \lambda_2 (\Phi_2^\dagger \Phi_2)^2 + \lambda_3 (\Phi_1^\dagger \Phi_1) (\Phi_2^\dagger \Phi_2) \\
 & + \lambda_4 |\Phi_1^T i \sigma_2 \Phi_2|^2 + \frac{1}{2} \lambda_5 [(\Phi_1^T i \sigma_2 \Phi_2)^2 + \text{h.c.}] \\
 & + [\lambda_6 (\Phi_1^\dagger \Phi_1) + \lambda_7 (\Phi_2^\dagger \Phi_2)] \Phi_1^T i \sigma_2 \Phi_2 + \text{h.c.},
 \end{aligned} \quad (11.46)$$

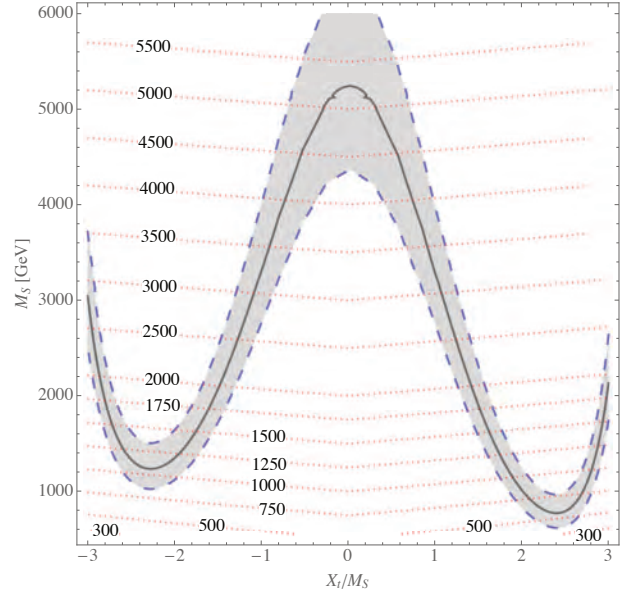
where $m_i^2 = \mu^2 + m_{H_i}^2$ ($i = 1, 2$), with μ being the supersymmetric Higgsino mass parameter and m_{H_i} the soft supersymmetric breaking mass parameters of the two Higgs doublets; $m_3^2 \equiv B\mu$ is associated to the B-term soft SUSY breaking parameter; and λ_i , for $i = 1$ to 7, are all the Higgs quartic couplings.

After the spontaneous breaking of the electroweak symmetry, five physical Higgs particles are left in the MSSM spectrum: one charged Higgs pair, H^\pm , one CP -odd neutral scalar, A , and two CP -even neutral states, H and h , with h being the lightest.⁶ The Higgs sector at tree level depends on the electroweak gauge coupling constants and the vacuum expectation value v – or equivalently the Z gauge boson mass – and is determined by only two free parameters: $\tan\beta$ – the ratio of the two Higgs doublets' vacuum expectation values v_2/v_1 – and one Higgs boson mass, conventionally chosen to be the CP -odd Higgs boson mass, m_A . The other tree-level Higgs boson masses are then given in terms of these parameters. The tree level value of m_h is maximised not only for $m_A \gg m_Z$ but also for $\tan\beta \gg 1$. For $m_A \gg m_Z$ it acquires a maximum value $m_h = m_Z \cos 2\beta$.

Radiative corrections have a significant impact on the values of Higgs boson masses and couplings in the MSSM. The dominant radiative effects to the SM-like Higgs boson mass arise from the incomplete cancellation between top and scalar-top (stop) loops and at large $\tan\beta$ also from sbottom and stau loops. The stop, sbottom and stau masses and mixing angles depend on the SUSY Higgsino mass parameter μ and on the soft-SUSY-breaking parameters [9, 331]: $M_Q, M_U, M_D, M_L, M_E, A_t, A_b, A_\tau$. The first three of these are the left-chiral and the right-chiral top and bottom scalar quark mass parameters. The next two are the left-chiral stau/sneutrino and the right-chiral stau mass parameters, and the last three are the trilinear parameters that enter in the off-diagonal squark/slepton mixing elements: $X_t \equiv A_t - \mu \cot\beta$ and $X_{b,\tau} \equiv A_{b,\tau} - \mu \tan\beta$. At one-loop, the electroweak gauginos yield a small contribution to the Higgs boson mass, and at

⁶Observe that in the SM sections of this review, H denotes the SM Higgs boson, whereas in the sections about SUSY, or extensions of the SM with two Higgs doublets, H is used for the heaviest CP -even Higgs boson, since this is the standard notation in the literature, and the 125 GeV SM-like light Higgs boson will be denoted by h . Generically, in the MSSM, the lightest CP -even Higgs boson is indeed SM-like and thus it is naturally identified with the 125 GeV Higgs boson discovered by ATLAS and CMS, while in 2HDM extensions, with or without SUSY, there could still be lighter scalar states below 125 GeV.

Figure 11.17: Values of the SUSY mass scale $M_{\text{SUSY}} = M_S$ versus the stop mixing parameter normalised by the SUSY mass scale X_t/M_{SUSY} , for fixed $\tan\beta = 20$, $\mu = 200$ GeV and $A_t = A_b = A_\tau$. The solid black line corresponds to $m_h = 125$ GeV while in the grey band m_h varies by ± 1 GeV. The red dotted lines are iso-values of the stop mass. This figure is based on Ref. [333].



the two-loop level, the masses of the gluinos also enter in the calculations. Radiative corrections to the Higgs boson masses have been computed using a number of techniques, with a variety of approximations, see Ref. [332] for a recent review.

The discovered SM-like Higgs boson, if interpreted as the lightest MSSM Higgs boson with a mass of about 125 GeV, provides information on the possible MSSM parameter space, see Fig. 11.17.

The phenomenology of the Higgs sector depends on the couplings of the Higgs bosons to gauge bosons and fermions. At tree-level, the couplings of the two CP -even Higgs bosons to W and Z bosons are given in terms of the angles α , that diagonalises the CP -even Higgs boson squared-mass matrix, and β

$$g_{hVV} = g_V m_V \sin(\beta - \alpha), \quad g_{HVV} = g_V m_V \cos(\beta - \alpha), \quad (11.47)$$

where $g_V \equiv 2m_V/v$, for $V = W$ or Z ($g_V m_V$ is the SM hVV coupling). Observe that in the limit $\cos(\beta - \alpha) \rightarrow 0$, the lightest CP -even Higgs boson h behaves as the SM Higgs boson. This situation is called alignment and is achieved in specific regions of parameter space for $m_A \geq m_Z$ [334] or in the large $m_A \gg m_Z$ limit, in which alignment is achieved through decoupling [334, 335]. There are no tree-level couplings of A or H^\pm to VV . The couplings of the Z boson to two neutral Higgs bosons are given by $g_{\phi AZ}(p_\phi - p_A)$, where $\phi = H$ or h , the momenta p_ϕ and p_A point into the vertex, and

$$g_{hAZ} = g_Z \cos(\beta - \alpha)/2, \quad g_{HAZ} = -g_Z \sin(\beta - \alpha)/2. \quad (11.48)$$

The expressions of the couplings between a charged Higgs boson, a neutral Higgs boson and the W boson as well as the expressions of the four-point couplings of vector bosons and Higgs bosons can be found in Ref. [27].

The tree-level Higgs boson couplings to fermions obey the following property: the neutral components of one Higgs doublet, Φ_1 , couple exclusively to down-type fermion pairs while the neutral components of the other doublet, Φ_2 , couple exclusively to up-type fermion pairs [27]. This Higgs-fermion coupling structure defines the Type-II 2HDM. In the MSSM, fermion masses are generated when both neutral Higgs components acquire a vacuum expectation value, and the relations between Yukawa couplings

and fermion masses are (in third-generation notation)

$$h_{b,\tau} = \sqrt{2} m_{b,\tau} / (v \cos \beta), \quad h_t = \sqrt{2} m_t / (v \sin \beta). \quad (11.49)$$

The couplings of the neutral Higgs bosons to $f\bar{f}$, relative to their SM values, $g m_f / (2m_W)$, are therefore given by

$$\begin{aligned} h\bar{b}b &: -\sin \alpha / \cos \beta, & h\bar{t}t &: \cos \alpha / \sin \beta, \\ H\bar{b}b &: \cos \alpha / \cos \beta, & H\bar{t}t &: \sin \alpha / \sin \beta, \\ A\bar{b}b &: \gamma_5 \tan \beta, & A\bar{t}t &: \gamma_5 \cot \beta. \end{aligned} \quad (11.50)$$

In each relation above, the factor listed for $b\bar{b}$ also pertains to $\tau^+\tau^-$. The charged Higgs boson couplings to fermion pairs, normalised to $g/(\sqrt{2}m_W)$, are given by

$$\begin{aligned} g_{H-t\bar{b}} &: m_t \cot \beta \frac{1+\gamma_5}{2} + m_b \tan \beta \frac{1-\gamma_5}{2}, \\ g_{H-\tau^+\nu} &: m_\tau \tan \beta \frac{1-\gamma_5}{2}. \end{aligned} \quad (11.51)$$

The non-standard neutral Higgs bosons have significantly enhanced couplings to down-type fermions at sizeable $\tan \beta$. Radiative corrections can modify significantly the values of the Higgs boson couplings to fermion pairs and to vector boson pairs, through a radiatively-corrected value for $\cos(\beta - \alpha)$ as well as from the one-loop vertex corrections to tree-level Higgs-fermion Yukawa couplings, see Ref. [9] and references therein, for a detailed discussion.

11.7.1.1 MSSM Higgs boson phenomenology

The MSSM parameters have to be arranged such that the mass, the CP properties, the decay and production properties of one of the neutral Higgs bosons agree with the LHC Higgs data. Given that present data allows only for moderate departures from the SM predictions, it implies that some degree of alignment is necessary.

The SM-like branching ratios of h can be modified if decays into SUSY particles are kinematically allowed, and, in particular, decays into a pair of the lightest SUSY particles – i.e., the lightest neutralinos, $\tilde{\chi}_1^0$ – can become dominant and would be invisible if R -parity is conserved [336]. Moreover, if light superpartners exist and couple to photons and/or gluons, the h loop-induced coupling to gg and $\gamma\gamma$ could deviate sizeably from the corresponding SM predictions (see for instance the review [337]), and would be in conflict with present data (see Section 11.3). For the heavier Higgs states, there are two possibilities to be considered⁷:

- i) Alignment triggered by decoupling, hence $m_A \geq$ several hundred GeV: The HWW and HZZ couplings are very small. The dominant H, A decay branching ratios strongly depend on $\tan \beta$. The decay modes $H, A \rightarrow b\bar{b}, \tau^+\tau^-$ dominate when $\tan \beta$ is large (this holds even away from decoupling). For small $\tan \beta$, the $t\bar{t}$ decay mode dominates above its kinematic threshold. For the charged Higgs boson, $H^\pm \rightarrow t\bar{b}$ dominates.
- ii) Some degree of alignment without decoupling, hence $m_A \leq$ a few hundred GeV: The main difference with the previous case is that, in the low $\tan \beta$ regime ($\tan \beta \leq 5$), additional decay channels may be allowed which involve decays into the lightest SM-like Higgs boson; $A \rightarrow Zh, H \rightarrow hh$ as well as $H \rightarrow WW/ZZ$ decay modes are available (they are suppressed in the strict alignment limit). When kinematically open, the decays $A/H \rightarrow t\bar{t}$ become relevant or even dominant for sufficiently small $\tan \beta$. For the charged Higgs boson, $H^\pm \rightarrow \tau^+\nu_\tau$ dominates below the $t\bar{b}$ threshold, and also $H^\pm \rightarrow W^\pm h$ may be searched for.

In both cases i) and ii), the heavier Higgs states, H, A and H^\pm , are roughly mass degenerate (with masses ± 20 GeV or less apart). If kinematically allowed, the heavy Higgs boson decays into charginos, neutralinos and third-generation squarks and sleptons can be important [340].

At hadron colliders, the dominant neutral Higgs boson production mechanism at moderate values of $\tan \beta$ is gluon fusion, mediated by loops containing heavy top and bottom quarks and the corresponding SUSY partners. The effect of light stops that may contribute to the gluon fusion production can be partially cancelled by mixing effects. Higgs boson radiation off bottom quarks becomes important for large $\tan \beta$, where at least two of the three neutral Higgs bosons have enhanced couplings to bottom-type fermions [341, 342]. Detailed discussions of the impact of radiative corrections in these search modes are presented for instance in Ref. [343]. The vector boson fusion and Higgs-strahlung production of the CP -even Higgs bosons as well as the associated production of neutral Higgs bosons with top quark pairs have lower production cross sections by at least an order of magnitude with respect to the dominant ones, depending on the precise region of MSSM parameter space [43–46]. Higgs boson pair production of non-standard MSSM Higgs bosons has been studied in Ref. [344]. For a discussion of charged Higgs boson production at LHC, see Refs. [44, 45, 345].

Strong production of a heavy neutral Higgs boson followed by its decay into top-quark pairs is a challenging channel, only most recently being searched for by ATLAS and CMS. Interference effects between the signal and the SM $t\bar{t}$ background need to be carefully taken into account [346].

Summarising, the additional Higgs bosons are sought for mainly via the channels:

$$\begin{aligned} pp &\rightarrow A/H \rightarrow \tau^+\tau^- \text{ (inclusive),} \\ b\bar{b}A/H, A/H &\rightarrow \tau^+\tau^- \text{ (with } b\text{-tag),} \\ b\bar{b}A/H, A/H &\rightarrow b\bar{b} \text{ (with } b\text{-tag),} \\ pp &\rightarrow t\bar{t} \rightarrow H^\pm W^\mp b\bar{b}, H^\pm \rightarrow \tau\nu_\tau, \\ g\bar{b} &\rightarrow H^-t \text{ or } g\bar{b} \rightarrow H^+\bar{t}, H^\pm \rightarrow \tau\nu_\tau. \end{aligned} \quad (11.52)$$

After the Higgs boson discovery, updated MSSM benchmark scenarios have been defined to highlight interesting conditions for the MSSM Higgs boson searches [45, 339] and are scrutinised by the LHC Higgs Working Group [347]. The latest benchmark scenarios update [339], partly based in MSSM parameter space discussions in Ref. [348], considers six benchmarks to illustrate different aspects of Higgs phenomenology in the MSSM. They include one case with complex parameters, but they all assume R -parity conservation and no flavour mixing. Each scenario contains one CP -even scalar with mass around 125 GeV and SM-like couplings. These scenarios include a M_h^{125} scenario with relatively heavy superparticles, so the Higgs phenomenology at the LHC resembles that of a 2HDM with MSSM-inspired Higgs boson couplings. Other two scenarios are characterised by some of the superparticles – staus or electroweakinos – being relatively light, that in turn is of relevance for heavy neutral Higgs boson searches. In particular, the traditional $A/H \rightarrow \tau^+\tau^-$ search channel varies depending on the values of μ and M_2 , that may enable the A/H decays into electroweakinos. Another two scenarios are characterised by the phenomenon of alignment without decoupling, in which one of the two neutral CP -even scalars has SM-like couplings independently of the mass spectrum of the remaining Higgs bosons, hence allowing for all the Higgs bosons to have relatively low mass values (about few hundred GeV). Finally, there is one scenario which incorporates CP violation in the Higgs sector and gives rise to a strong admixture of the two heavier neutral states. All the above scenarios assume all parameters in the mass range from 1 to a few TeV, hence they are not applicable for values of $\tan \beta$ of order a few, for which a Higgs boson mass value of 125 GeV is out of reach. An additional study [349], relying on an EFT approach in the MSSM, focusses on two scenarios specifically designed for the low $\tan \beta$ region and ensures a 125 GeV Higgs boson mass in almost the entire parameter space by employing a flexible supersymmetric mass scale, reaching values of up to 10^{16} GeV.

An alternative approach to reduce the large number of parameters relevant to the Higgs sector is to consider that, in the Higgs basis, the only important radiative corrections are those affecting the Higgs boson mass [350]. This approximation is called hMSSM and works well in large regions of parameter space but it breaks

⁷In very special regions of the parameter space, there is still the possibility that the heavier CP -even Higgs state is identified with the 125 GeV Higgs boson discovered by ATLAS and CMS, see for instance the discussion in Ref. [338] and the benchmark M_H^{125} defined in Ref. [339].

down for sizeable values of μ and A_t , and moderate values of $\tan\beta$, for which the radiative corrections to the mixing between the two CP even eigenstates become relevant. The effect of such radiative corrections is to allow for alignment for small to intermediate values of $\tan\beta$, independent of the specific value of m_A [351]. In addition, the hMSSM assumption that the right value of the Higgs boson mass may be obtained for all values of m_A and $\tan\beta$ is in conflict with the MSSM predictions for the Higgs boson mass for small values of m_A and $\tan\beta \simeq \mathcal{O}(1)$. The recent M_h^{125} [339] and EFTMSSM benchmarks [349], are designed to address the limitations of the hMSSM, in particular the low $\tan\beta$ region for the EFTMSSM.

The compatibility between the predicted and measured Higgs boson mass sets stringent constraints on the parameter space of BSM models. The predictions are illustrated in Fig. 11.18 for two concrete scenarios. Note that to use the predicted Higgs boson mass as a constraint (exclusion at nearly constant $\tan\beta$ at high M_A in the $(M_A, \tan\beta)$ plane), it is important to account for the theoretical uncertainty on the prediction which is in excess of an order of magnitude larger than the experimental uncertainty on the measured mass of the Higgs boson. The theoretical uncertainty depends itself on the specific SUSY spectrum for a given MSSM parameter set and should be estimated accordingly, however, a more generic estimate of ± 3 GeV is made and found to be a conservative choice [332].

Reviews of the properties and phenomenology of the Higgs bosons of the MSSM can be found for example in Refs. [9, 41, 337]. Future precision measurements of the Higgs boson couplings to fermions and gauge bosons together with information on heavy Higgs boson searches will provide powerful information on the SUSY parameter space [353].

Improvements in our understanding of B -physics observables put indirect constraints on additional Higgs bosons in mass ranges that would be accessible in direct LHC searches. In particular, $\text{BR}(B_s \rightarrow \mu^+ \mu^-)$, $\text{BR}(b \rightarrow s\gamma)$, and $\text{BR}(B_u \rightarrow \tau\nu)$ play an important role within minimal flavour-violating (MFV) models [354], in which flavor effects proportional to the CKM matrix elements are induced as in the SM.

11.7.2 Supersymmetry with singlet extensions

The Higgs mass parameter μ is a SUSY parameter, and as such, it should naturally be of order M_{GUT} or M_{Planck} . The fact that phenomenologically it is required that μ be at the electroweak/TeV scale is known as the μ problem [355]. SUSY models with additional singlets can provide a solution to the μ problem, by promoting the μ parameter to a dynamical singlet superfield S that only interacts with the MSSM Higgs doublets through a coupling λ_S at the level of the superpotential. An effective μ is generated when the real scalar component of S acquires a vacuum expectation value v_S , yielding $\mu_{eff} = \lambda_S v_S$. After the minimization of the Higgs potential, the vacuum state relates the vacuum expectation values of the three CP -even neutral scalars, v_1 , v_2 and v_S , to the scalar doublet and singlet soft SUSY breaking masses, hence, one expects that these VEVs should all be of order M_{SUSY} and therefore the μ problem is solved.

The addition of a singlet superfield to the MSSM may come along with additional symmetries imposed to the theory. Depending on such symmetries, different models with singlet extensions of the MSSM (xMSSM) have been proposed, see Ref. [356] for a general review. Among the most studied examples are the NMSSM with an additional discrete Z_3 symmetry (first introduced in Ref. [357]), the Nearly-Minimal SUSY SM (nMSSM), with additional discrete Z_5^R , and Z_7^R symmetries [358], and the $U(1)'$ -extended MSSM (UMSSM) [359]. A Secluded $U(1)'$ -extended MSSM (sMSSM) [360] contains three singlets in addition to the standard UMSSM Higgs boson singlet; this model is equivalent to the nMSSM in the limit that the additional singlet VEV's are large, and the trilinear singlet coupling, λ_S , is small [361]. The non-zero neutrino masses provide also a motivation for a particular extension of the MSSM, $\mu\nu$ SMS [362], which also happens to address the address the $-mu$ problem. The computation of the Higgs boson spectrum in these various models has been reviewed in Ref. [332].

A singlet extended SUSY Higgs sector opens new avenues for

discovery. Since the singlet pseudoscalar particle may be identified as the pseudo-Goldstone boson of a spontaneously broken Peccei–Quinn symmetry, it may become naturally light [363]. Generally, there is mixing of the singlet sector with the MSSM Higgs sector, and for a sufficiently light, singlet-dominated scalar or pseudoscalar, h_S or A_S , respectively, the SM-like Higgs boson h may decay to pairs of h_S or A_S . The light scalar and/or pseudoscalar may subsequently decay to $\tau\tau$ or $b\bar{b}$ pairs. Such cascade decays are more difficult to detect than in standard searches due to the potentially soft decay products. There is also a rich phenomenology for the decays of the heavy CP -even and CP -odd doublets, H and A into two lighter Higgs bosons such as $H \rightarrow hh_S$, hh , $h_S h_S$ or $A \rightarrow A_S h_S$, $A_S h$ as well as into a light Higgs boson and a gauge boson: $H \rightarrow A_S Z$; $A \rightarrow h_S Z$, hZ . If kinematically allowed, the heavy Higgs bosons decay into $t\bar{t}$. If the singlet-dominated scalar or pseudoscalar are somewhat heavier, the decays $h_S \rightarrow WW$ or $A_S \rightarrow h_S Z$ will be allowed.

In addition, the light singlet scenario in the NMSSM or nMSSM is typically associated with a light singlino-dominated neutralino. The 125 GeV SM-like Higgs boson can then decay to pairs of this neutralino [364], opening an invisible decay mode that is not excluded by present data. All of the Higgs bosons can decay into electroweakinos depending on kinematics and on the singlino or Higgsino composition of the electroweakinos.

In models with extended singlets, at low $\tan\beta$, it is possible to trade the requirement of a large stop mixing by a sizeable trilinear Higgs-singlet Higgs coupling λ_S , rendering more freedom on the requirements for gluon fusion production. As in the MSSM, mixing in the Higgs sector – additionally triggered by the extra new parameter λ_S – can produce variations in the Higgs- $b\bar{b}$ and Higgs- $\tau^-\tau^+$ couplings that can alter the Higgs to ZZ / WW and to diphoton rates. Light charginos at low $\tan\beta$ can independently contribute to enhance the di-photon rate, without altering any other of the Higgs boson decay rates, see for instance Ref. [365].

There is much activity in exploring the NMSSM phenomenology in the light of the 125 GeV Higgs boson as well as in defining benchmark scenarios with new topologies including Higgs decay chains, see Refs. [46, 366] and references therein. An analytic understanding of the alignment condition in the NMSSM is presented in Ref. [367]. The NMSSM with a Higgs boson of mass 125 GeV can be compatible with stop masses of order of the electroweak/TeV scale, thereby reducing the degree of fine-tuning necessary to achieve electroweak symmetry breaking. Interestingly, the alignment conditions point toward a more natural region of parameter space for electroweak symmetry breaking, while allowing for perturbativity of the theory up to the Planck scale and yielding a rich and interesting Higgs boson phenomenology at the LHC.

11.7.3 Supersymmetry with extended gauge sectors

In the MSSM, the tree-level value of the lightest CP -even Higgs boson mass originates from the D-term dependence of the scalar potential that comes from the SUSY kinetic terms in the Kähler potential. The D-terms lead to tree-level quartic couplings which are governed by the squares of the gauge couplings of the weak interactions, under which the Higgs boson has non-trivial charges. Hence, the lightest Higgs mass is bounded to be smaller than M_Z . In the presence of new gauge interactions at the TeV scale, and if the Higgs fields had non-trivial charges under them, new D-term contributions would lead to an enhancement of the tree-level Higgs boson mass value. Since the low energy gauge interactions reduce to the known $SU(3)_c \times SU(2)_L \times U(1)_Y$ ones, in order for this mechanism to work, the extended gauge and Higgs sectors should be integrated out in a non-SUSY way. This means that there must be SUSY breaking terms that are of the order of, or larger than, the new gauge boson masses. The tree-level quartic couplings would then be enhanced through their dependence on the square of the gauge couplings of the extended Higgs sector. This effect will be suppressed when the heavy gauge boson masses are larger than the SUSY breaking scale and will acquire its full potential only for large values of this scale.

One of the simplest possibilities is to extend the weak interactions to a $SU(2)_1 \times SU(2)_2$ sector, such that the known weak interactions are obtained after the spontaneous breaking of these

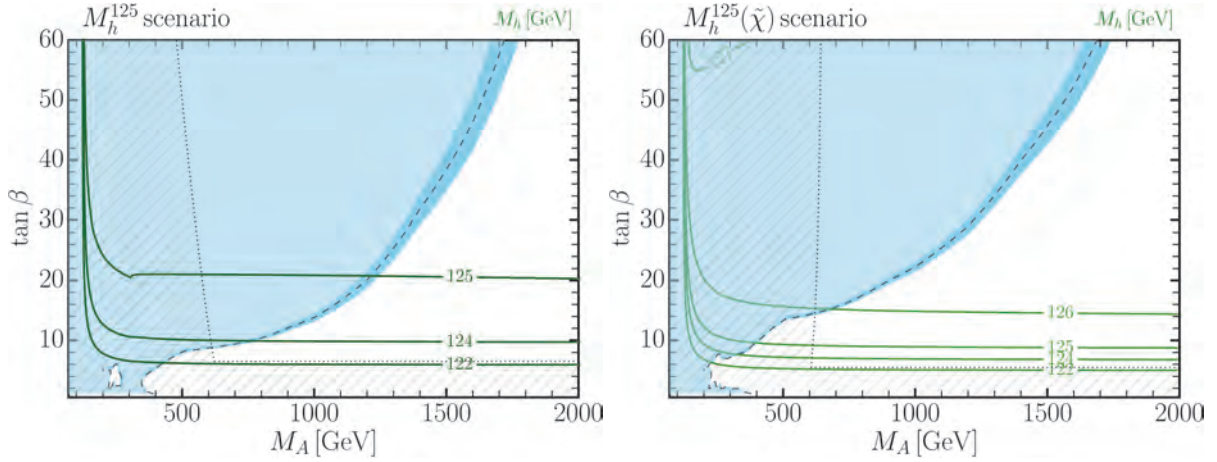


Figure 11.18: The 95% CL exclusion contours in the $(M_A, \tan \beta)$ parameter space for the M_h^{125} (right) and $M_h^{125}(\tilde{\chi})$ (left) benchmark scenarios [352]. The M_h^{125} benchmark assumes that super partners are heavy, so that the phenomenology of the observed Higgs boson is not altered except in its couplings due to the existence of another doublet. The $M_h^{125}(\tilde{\chi})$ scenario on the other hand considers light electroweakinos and therefore the heavy Higgs bosons H and A can have sizeable decay rates to charginos and neutralinos, consequently suppressing the $\tau^+\tau^-$ decay rate. The nearly vertical dotted line illustrates the lower limit on the mass of the A boson and the close-to horizontal dotted line represents the limit on $\tan \beta$ from the compatibility of the measured mass of the observed Higgs boson and the prediction using radiative corrections (mostly from the stop sector).

groups to $SU(2)_L$ [368]. This example is briefly summarized in the previous editions of this review [132]. Assuming SUSY breaking terms of the order of the new gauge boson masses, enhancements of order 50% of the MSSM D-term contribution to the Higgs boson mass may be obtained. Such enhancements are sufficient to obtain the measured Higgs mass value without the need for very heavy stops or large stop mixing parameters. This gauge extension leads to new, heavy gauge and Higgs bosons, as well as new neutralinos and charginos, that depending on the region of parameter space can induce novel phenomenology at the LHC. Gauge extensions including new Abelian gauge groups have also been considered.

Gauge extensions of the MSSM can also lead to an enhancement of the Higgs boson mass value by modifying the renormalisation group evolution of the Higgs quartic coupling to low energies. In the MSSM, the evolution of the quartic coupling is governed by the top-quark Yukawa interactions and depends on the fourth power of the top-quark Yukawa coupling. The neutralino and chargino contributions, which depend on the fourth power of the weak gauge couplings, are small due to the smallness of these couplings. Depending on the values of the soft SUSY breaking parameters in the gaugino and Higgsino sectors, the $SU(2)_1$ gauginos may become light, with masses of the order of the weak scale. Since the $SU(2)_1$ coupling may be significantly larger than the $SU(2)_L$ one, for small values of the Higgsino mass parameter μ , the associated charginos and neutralinos may modify the evolution of the quartic coupling in a significant way [369]. This may lead to a significant increase of the lightest CP -even Higgs boson mass, even for small values of $\tan \beta \simeq 1$ for which the D-term contributions become small. Radiative corrections should be properly taken into account in this scenario as they might modify the tree-level result.

11.7.4 Effects of CP violation

SUSY scenarios with CP -violation (CPV) phases are theoretically appealing, since additional CPV beyond that observed in the K , D , and B meson systems is required to explain the observed cosmic matter-antimatter asymmetry. In the MSSM, CP -violation effects in the Higgs sector appear at the quantum level, while in singlet extensions of the MSSM CP -violation effects can already be effective at tree level. In general, CP -violation effects in the Higgs sector have significant constraints from electric dipole moments data [370].

In the MSSM, the gaugino mass parameters $(M_{1,2,3})$, the Higgsino mass parameter, μ , the bilinear Higgs squared-mass parameter, m_{12}^2 , and the trilinear couplings of the squark and slepton fields to the Higgs fields, A_f , may carry non-trivial

phases. The two parameter combinations $\arg[\mu A_f (m_{12}^2)^*]$ and $\arg[\mu M_i (m_{12}^2)^*]$ are invariant under phase redefinitions of the MSSM fields [371, 372]. Therefore, if one of these quantities is non-zero, there would be new sources of CP -violation affecting the Higgs sector through radiative corrections, see Ref. [373] and references therein. The mixing of the neutral CP -odd and CP -even Higgs boson states is no longer forbidden. Hence, m_A is no longer a physical parameter. However, the charged Higgs boson mass m_{H^\pm} is still physical and can be used as an input for the computation of the neutral Higgs boson spectrum of the theory. For large values of m_{H^\pm} , corresponding to the decoupling limit, the properties of the lightest neutral Higgs boson state approach those of the SM Higgs boson. In particular, the upper bound on the lightest neutral Higgs boson mass takes the same value as in the CP -conserving case [372]. Nevertheless, there still can be significant mixing between the two heavier neutral mass eigenstates. For a detailed study of the Higgs boson mass spectrum and parametric dependence of the associated radiative corrections, see Ref. [373] and references therein.

Major variations to the Higgs boson phenomenology occur in the presence of explicit CPV phases. In the CPV case, vector boson pairs couple to all three neutral Higgs boson mass eigenstates, H_i ($i = 1, 2, 3$), with couplings

$$\begin{aligned} g_{H_i V V} &= \cos \beta \mathcal{O}_{1i} + \sin \beta \mathcal{O}_{2i}, \\ g_{H_i H_j Z} &= \mathcal{O}_{3i} (\cos \beta \mathcal{O}_{2j} - \sin \beta \mathcal{O}_{1j}) \\ &\quad - \mathcal{O}_{3j} (\cos \beta \mathcal{O}_{2i} - \sin \beta \mathcal{O}_{1i}), \end{aligned} \quad (11.53)$$

where the $g_{H_i V V}$ couplings are normalised to the analogous SM coupling and the $g_{H_i H_j Z}$ have been normalised to $g_Z^{\text{SM}}/2$. The orthogonal matrix \mathcal{O}_{ij} , only defined in the $p^2 \rightarrow 0$ limit, is relating the weak eigenstates to the mass eigenstates. It has non-zero off-diagonal entries mixing the CP -even and CP -odd components of the weak eigenstates. Moreover, CPV phases imply that all neutral Higgs bosons can couple to both scalar and pseudoscalar fermion bilinear densities. The couplings of the mass eigenstates H_i to fermions depend on the loop-corrected fermion Yukawa couplings (similarly to the CP conserving (CPC) case), on $\tan \beta$ and on \mathcal{O}_{ji} [374].

The production processes of neutral MSSM Higgs bosons in the CPV scenario are similar to those in the CPC scenario. Regarding the decay properties, the lightest mass eigenstate, H_1 , predominantly decays to $b\bar{b}$ if kinematically allowed, with a smaller fraction decaying to $\tau^+\tau^-$. If kinematically allowed, a SM-like neutral Higgs boson, H_2 or H_3 can decay predominantly to $H_1 H_1$

leading to many new interesting signals both at lepton and hadron colliders; otherwise it will decay preferentially to $b\bar{b}$.

The discovery of a 125 GeV Higgs boson has put strong constraints on the realisation of the CPV scenario within the MSSM. This is partly due to the fact that the observed Higgs boson rates are close to the SM values, and a large CP -violating component would necessarily induce a large variation in the rate of the SM-like Higgs boson decays into the weak gauge bosons W^\pm and Z . The measured Higgs mass imposes additional constraints on the realisation of this scenario. Once all effects are considered, the CP -odd Higgs boson A component of the lightest Higgs boson tends to be smaller than about 10% [375]. This restriction can be alleviated in the NMSSM or more general two Higgs doublet models. CP -violating effects can still be significant in the heavy Higgs sector. For instance, the Higgs bosons H_2 and H_3 may be admixtures of CP -even and CP -odd scalars, and therefore both may be able to decay into pairs of weak gauge bosons. The observation of such decays would be a clear signal of CP -violation. In the MSSM, the proximity of the masses of H_2 and H_3 makes the measurement of such effect quite challenging, but in generic two Higgs doublet models, the mass splitting between the two heavy mass eigenstates may become larger, facilitating the detection of CP -violating effects at collider experiments [376].

11.7.5 Non-supersymmetric extensions of the Higgs sector

There are many ways to extend the minimal Higgs sector of the SM. In the preceding sections the phenomenology of SUSY Higgs sectors is considered, which at tree level implies a constrained type-II 2HDM (with restrictions on the Higgs boson masses and couplings). In the following discussion, more generic 2HDM's are presented (for some comprehensive reviews, see the reviews [377]). These models are theoretically less compelling since they do not provide an explanation for the SM Higgs naturalness problem, but can lead to different patterns of Higgs-fermion couplings, hence, to different phenomenology. It is also possible to consider models with a SM Higgs boson and one or more additional scalar $SU(2)$ doublets that acquire no VEV and hence play no role in the EWSB mechanism. Such models are dubbed Inert Higgs Doublet Models (IHD) [378]. Without a VEV associated to it, a Higgs boson from an inert doublet has no tree-level coupling to gauge bosons and hence cannot decay into a pair of them. Moreover, imposing a Z_2 symmetry that prevents them from coupling to the fermions, it follows that, if the lightest inert Higgs boson is neutral, it becomes a good DM candidate with interesting associated collider signals. Various studies of IHD models in the light of a 125 GeV Higgs boson have been performed, see for instance Ref. [379], showing an interesting interplay between collider and direct DM detection signals.

An interesting type of 2HDMs are those in which an Abelian flavour symmetry broken at the electroweak scales creates the fermion mass hierarchies and mixing angles [19]. This idea is based on the Froggatt–Nielsen model [380], where a flavon field couples differently to the SM fermions of different flavour charges. Such flavon acquires a vacuum expectation value, breaking the flavour symmetry but leaving both the flavour breaking and the new physics scales undetermined. In Refs. [381], it was proposed to relate the flavour breaking scale to the electroweak scale by identifying the flavon with the modulus square of the Higgs field. A 2HDM, however, provides a more compelling realisation of the electroweak scale flavour breaking idea. In the most ambitious constructions of two Higgs doublet flavour models (2HDFM), the textures of the Yukawa couplings are a result of an Abelian flavour symmetry that only allows renormalisable Yukawa couplings of the top quark to the Higgs bosons. All other Yukawa couplings are generated by higher dimensional operators that produce hierarchical entries of the Yukawa matrices, explaining the observed quark masses and mixing angles. Flavour observables, LHC Higgs signal strength measurements, electroweak precision measurements, unitarity and perturbativity bounds, as well as collider searches for new scalar resonances result in precise predictions for the parameters of these 2HDFMs. In particular, correlated departures from SM Higgs boson couplings, as well as additional Higgs bosons with masses < 700 GeV must be observed at the LHC. Other incarnations of 2HDFMs can aim at only partially explaining the fermion

mass hierarchies but are therefore less restrictive.

Other extensions of the Higgs sector can include multiple copies of $SU(2)_L$ doublets [382], additional Higgs singlets [383], triplets or more complicated combinations of Higgs multiplets. It is also possible to enlarge the gauge symmetry beyond $SU(2)_L \times U(1)_Y$ along with the necessary Higgs field structure to generate gauge boson and fermion masses. There are two main experimental constraints on these extensions: (i) precision measurements which constrain $\rho = m_W^2/(m_Z^2 \cos^2 \theta_W)$ to be very close to 1 and (ii) flavour changing neutral current (FCNC) effects. In electroweak models based on the SM gauge group, the tree-level value of ρ is determined by the Higgs multiplet structure. By suitable choices for the hypercharges, and in some cases the mass splitting between the charged and neutral Higgs sector or the vacuum expectation values of the Higgs fields, it is possible to obtain a richer combination of singlets, doublets, triplets and higher multiplets compatible with precision measurements. Concerning the constraints coming from FCNC effects, the Glashow–Weinberg (GW) criterion [384] states that, in the presence of multiple Higgs doublets, the tree-level FCNC's mediated by neutral Higgs bosons will be absent if all fermions of a given electric charge couple to no more than one Higgs doublet. An alternative way of suppressing FCNC in a two Higgs doublet model has been considered in Ref. [385], where it is shown that it is possible to have tree level FCNC completely fixed by the CKM matrix, as a result of an Abelian symmetry.

There is a lot of activity on the study of non-supersymmetric models with an extended Higgs sector with an intense collaboration between theorists and experimentalists, in particular inside the LHC Higgs Working Group [347].

11.7.5.1 Two-Higgs-doublet models

General two Higgs doublet models [377] can have a more diverse Higgs-fermion coupling structure than in SUSY, and can be viewed as a simple extension of the SM to realise the spontaneous breakdown of $SU(2)_L \times U(1)_Y$ to $U(1)_{em}$. Quite generally, if the two Higgs doublets contain opposite hypercharges, the scalar potential will contain mixing mass parameters of the kind $m_{12}^2 \Phi_1^\dagger i\sigma_2 \Phi_2 + h.c.$. In the presence of such terms, both Higgs doublets will acquire vacuum expectation values, $v_1/\sqrt{2}$ and $v_2/\sqrt{2}$, respectively, and the gauge boson masses will keep their SM expressions with the Higgs VEV v replaced by $\sqrt{v_1^2 + v_2^2}$. Apart from the mass terms, the most generic renormalisable and gauge invariant scalar potential for two Higgs doublets with opposite hypercharges contains seven quartic couplings, as presented in Eq. (11.46).

Just as in the MSSM case, after electroweak symmetry breaking and in the absence of CP -violation, the physical spectrum contains a pair of charged Higgs bosons H^\pm , a CP -odd Higgs boson A and two neutral CP -even Higgs bosons, h and H . The angles α and β diagonalise the CP -even, and the CP -odd and charged Higgs sectors, respectively. The complete 2HDM is defined only after considering the interactions of the Higgs fields to fermions. Yukawa couplings of the generic form

$$- h_{ij}^a \bar{\Psi}_L^i H_a \Psi_R^j + h.c. \quad (11.54)$$

may be added to the renormalisable Lagrangian of the theory. Contrary to the SM, the two Higgs doublet structure does not ensure the alignment of the fermion mass terms $m_{ij} = h_{ij}^a v_a/\sqrt{2}$ with the Yukawa couplings h_{ij}^a . This implies that quite generally the neutral Higgs boson will mediate flavour changing interactions between the different mass eigenstates of the fermion fields. Such flavour changing interactions should be suppressed in order to describe properly the Kaon, D and B meson phenomenology. Based on the Glashow–Weinberg criterion, it is clear that the simplest way of avoiding such transitions is to assume the existence of a symmetry that ensures the couplings of the fermions of each given quantum number (up-type and down-type quarks, charged and neutral leptons) to only one of the two Higgs doublets. Different models may be defined depending on which of these fermion fields couple to a given Higgs boson, see Table 11.13. Models of type-I are those in which all SM fermions couple to a single Higgs field. In type-II models, down-type quarks and charged leptons

couple to a common Higgs field, while the up-type quarks and neutral leptons couple to the other. In models of type-III (lepton-specific), quarks couple to one of the Higgs bosons, while leptons couple to the other. Finally, in models of type-IV (flipped), up-type quarks and charged leptons couple to one of the Higgs fields while down-quarks and neutral leptons couple to the other.

Table 11.13: Higgs boson couplings to up, down and charged lepton-type $SU(2)_L$ singlet fermions in the four discrete types of 2HDM models that satisfy the Glashow–Weinberg criterion.

Model	2HDM I	2HDM II	2HDM III	2HDM IV
u	Φ_2	Φ_2	Φ_2	Φ_2
d	Φ_2	Φ_1	Φ_2	Φ_1
e	Φ_2	Φ_1	Φ_1	Φ_2

The two Higgs doublet model phenomenology depends strongly on the size of the mixing angle α and therefore on the quartic couplings. For large values of m_A , $\sin \alpha \rightarrow -\cos \beta$, $\cos \alpha \rightarrow \sin \beta$, $\cos(\beta - \alpha) \rightarrow 0$, and the lightest CP -even Higgs boson h behaves as the SM Higgs boson. The same behaviour is obtained if the quartic couplings are such that $\mathcal{M}_{12}^2 \sin \beta = -(\mathcal{M}_{11}^2 - m_h^2) \cos \beta$. The latter condition represents a situation in which the couplings of h to fermions and weak gauge bosons become the same as in the SM, without decoupling the rest of the non-standard scalars and it is of particular interest due to the fact that the discovered Higgs boson has SM-like properties. This situation will be referred to as alignment, as in the MSSM case.

In analogy to the effects of CP violation in the SUSY 2HDM, some parameters of the Higgs potential can be complex and one has a model that is explicitly CP violating. The three neutral mass eigenstates mixed with each other and the Higgs phenomenology is analogous to the one described for the SUSY case above, with the caveat that when considering the neutral Higgs boson couplings to the scalar and pseudoscalar fermion bilinear densities, the proper weight should be considered for the respective 2HDM's.

In type-II Higgs doublet models, at large values of $\tan \beta$ and moderate values of m_A , the non-standard Higgs bosons H, A and H^\pm couple strongly to bottom quarks and τ leptons. Hence, the decay modes of the non-standard Higgs bosons tend to be dominated by the b -quark and τ -lepton modes, including top quarks or neutrinos in the case of the charged Higgs boson. However, for large and negative values of λ_4 , the charged Higgs boson mass may be sufficiently heavy to allow on-shell decays $H^\pm \rightarrow W^\pm + (H, A)$, via a trilinear coupling

$$g_{H^\pm W^\mp H, A} \simeq \frac{M_W}{v} \sin(\beta - \alpha)(p_{H^\pm} - p_{H, A}), \quad (11.55)$$

where p_{H^\pm} and $p_{H, A}$ are the charged and neutral scalar Higgs boson momenta pointing into the vertex. On the other hand, for large and positive values of λ_5 , the above charged Higgs boson decay into a W^\pm and the CP -odd Higgs boson may be allowed, but the heavy Higgs boson H may be sufficiently heavy to decay into a CP -odd Higgs boson and an on-shell Z , $H \rightarrow Z + A$, via

$$g_{HZ A} \simeq \frac{M_Z}{v} \sin(\beta - \alpha)(p_H - p_A). \quad (11.56)$$

The decay $H^\pm \rightarrow W^\pm + H$, on the other hand may be allowed only if $\lambda_4 < -\lambda_5$. The couplings controlling all the above decay modes are proportional to $\sin(\beta - \alpha)$ and therefore they are unsuppressed in the alignment limit. Moreover, these could still be the dominant decay modes at moderate values of $\tan \beta$, offering a way to evade the current bounds obtained assuming a dominant decay into b -quarks or τ -leptons.

The quartic couplings are restricted by the condition of stability of the effective potential as well as by the restriction of obtaining the proper value of the lightest CP -even Higgs boson mass. Close to the alignment limit, the lightest CP -even Higgs boson mass

becomes

$$m_h^2 \simeq v^2(\lambda_1 \cos^4 \beta + \lambda_2 \sin^4 \beta + 2\tilde{\lambda}_3 v^2 \cos^2 \beta \sin^2 \beta + 4\lambda_6 \cos^3 \beta \sin \beta + 4\lambda_7 \sin^3 \beta \cos \beta), \quad (11.57)$$

where $\tilde{\lambda}_3 = \lambda_3 + \lambda_4 + \lambda_5$.

The stability conditions imply the positiveness of all masses, as well as the avoidance of run-away solutions to large negative values of the fields in the scalar potential. These conditions imply

$$\begin{aligned} \lambda_1 \geq 0, \quad \lambda_2 \geq 0, \quad \lambda_3 + \lambda_4 - |\lambda_5| \geq -\sqrt{\lambda_1 \lambda_2}, \quad \lambda_3 \geq -\sqrt{\lambda_1 \lambda_2}, \\ 2|\lambda_6 + \lambda_7| < \frac{\lambda_1 + \lambda_2}{2} + \tilde{\lambda}_3, \end{aligned} \quad (11.58)$$

where the first four conditions are necessary and sufficient conditions in the case of $\lambda_6 = \lambda_7 = 0$, while the last one is a necessary condition in the case all couplings are non-zero. Therefore, to obtain the conditions that allow the decays $H^\pm \rightarrow W^\pm H, A$ and $H \rightarrow Z A$, λ_3 should take large positive values in order to compensate for the effects of λ_4 and λ_5 . For more detailed discussions about 2HDM phenomenology, see for example Refs. [46, 377].

11.7.5.2 Higgs triplets

Electroweak triplet scalars are the simplest non-doublet extension of the SM that can participate in the spontaneous breakdown of $SU(2)_L \times U(1)_Y$ to $U(1)_{em}$. Two types of model have been developed in enough detail to make a meaningful comparison to LHC data: the Higgs triplet model (HTM) [386] and the Georgi–Machacek model (GM) [387].

The Higgs triplet model extends the SM by the addition of a complex $SU(2)_L$ triplet scalar field Δ with hypercharge $Y = 2$, and a general gauge-invariant renormalisable potential $V(\Phi, \Delta)$ for Δ and the SM Higgs doublet Φ . The components of the triplet field can be parameterised as

$$\Delta = \frac{1}{\sqrt{2}} \begin{pmatrix} \Delta^+ & \sqrt{2}\Delta^{++} \\ v_\Delta + \delta + i\xi & -\Delta^+ \end{pmatrix}. \quad (11.59)$$

where Δ^+ is a singly-charged field, Δ^{++} is a doubly-charged field, δ is a neutral CP -even scalar, ξ is a neutral CP -odd scalar, and v_Δ is the triplet VEV. The general scalar potential mixes the doublet and triplet components. After electroweak symmetry breaking there are seven physical mass eigenstates, denoted $H^{\pm\pm}, H^\pm, A, H$, and h .

A distinguishing feature of the HTM is that it violates the custodial symmetry of the SM; thus the ρ parameter deviates from 1 even at tree level. Letting x denote the ratio of triplet and doublet VEVs, the tree level expression is

$$\rho = \frac{1 + 2x^2}{1 + 4x^2}. \quad (11.60)$$

The measured value of the ρ parameter then limits the triplet VEV to be quite small, $x \lesssim 0.03$, or $v_\Delta < 8 \text{ GeV}$. This constraint severely limits the role of the triplet scalar in the EWSB mechanism.

The small VEV of the Higgs triplet in the HTM is a virtue from the point of view of generating neutrino masses without the necessity for introducing right-handed neutrino fields. The gauge invariant dimension four interaction

$$h_{\nu_{ij}} \ell_i^T C^{-1} i\sigma_2 \Delta \ell_j, \quad (11.61)$$

where ℓ_i are the lepton doublets, C is the charge conjugation matrix, and $h_{\nu_{ij}}$ is a complex symmetric coupling matrix, generates a Majorana mass matrix for the neutrinos:

$$m_{\nu_{ij}} = \sqrt{2} h_{\nu_{ij}} v_\Delta. \quad (11.62)$$

This can be combined with the usual neutrino seesaw to produce what is known as the type-II seesaw [388].

The HTM suggests the exciting possibility of measuring parameters of the neutrino mass matrix at the LHC. If the doubly-charged Higgs boson is light enough and/or its couplings to

W^+W^+ are sufficiently suppressed, then its primary decay is into same-sign lepton pairs: $H^{++} \rightarrow \ell_i^+\ell_j^+$; from Eq. (11.61) and Eq. (11.62), it is apparent that these decays are in general lepton-flavor violating with branchings proportional to elements of the neutrino mass matrix [389].

Precision electroweak data constrain the mass spectrum as well as the triplet VEV of the HTM [390]. These constraints favour a spectrum where H^{++} is the lightest of the exotic bosons, and where the mass difference between H^+ and H^{++} is a few hundred GeV. The favoured triplet VEV is a few GeV, which also favours H^{++} decays into W^+W^+ over same-sign dileptons.

The GM model addresses the ρ parameter constraint directly by building in a custodial symmetry (it was however argued that large corrections to $\rho = 1$ are generated at one-loop [391], requiring some fine-tuning to preserve agreement with EW precision data). Writing the complex scalar doublet of the SM as a $(2, 2)$ under $SU(2)_L \times SU(2)_R$, it is obvious that the next simplest construction respecting custodial symmetry is a scalar transforming like a $(3, 3)$ [392]. These nine real degrees of freedom correspond to a complex electroweak triplet combined with a real triplet, with the scalar potential required to be invariant under $SU(2)_R$. Under the custodial $SU(2)_{L+R}$, they transform as $1 \oplus 3 \oplus 5$, with a CP -even neutral scalar as the custodial singlet (thus matching the SM Higgs boson), a CP -odd neutral scalar in the custodial triplet, and another CP -even neutral scalar in the custodial 5-plet.

The scalar components can be decomposed as

$$\Xi = \begin{pmatrix} \chi_3^* & \xi_1 & \chi_1 \\ -\chi_2^* & \xi_2 & \chi_2 \\ \chi_1^* & -\xi_1^* & \chi_3 \end{pmatrix}, \quad (11.63)$$

where ξ_2 is a real scalar and the others are complex scalars. Linear combinations of these scalars account for the neutral custodial singlet, a neutral and singly-charged field making up the custodial triplet, and neutral, singly-charged, and doubly-charged fields making up the custodial 5-plet.

When combined with the usual SM doublet field Φ , the electroweak scale v is now related to the doublet and triplet VEVs by

$$v^2 = v_\Phi^2 + 8v_\Xi^2. \quad (11.64)$$

Note that the GM triplets by themselves are sufficient to explain electroweak symmetry breaking and the existence of a 125 GeV neutral boson along with a custodial triplet of Goldstone bosons; the complex doublet field in the GM model is required to generate fermion masses via the usual dimension four Yukawa couplings. This raises the question of whether one can rule out the possibility that the 125 GeV boson is the neutral member of a custodial 5-plet rather than a custodial singlet, without invoking decays to fermions. A conclusive answer is given by observing that the ratio of the branching fractions to W versus Z bosons is completely determined by the custodial symmetry properties of the boson. For a custodial 5-plet, the ratio of the signal strength to WW over that to ZZ is predicted to be $1/4$ that of a SM Higgs boson [392], and thus already ruled out by the experimental results presented in Section 11.6.

Another interesting general feature of Higgs triplet models is that, after mixing, the SM-like neutral boson can have stronger couplings to WW and ZZ than predicted by the SM [393]; this is in contrast to mixing with additional doublets and singlet, which can only reduce the WW and ZZ couplings versus the SM. This emphasises that LHC Higgs data cannot extract model independent coupling strengths for the Higgs boson [273].

Because of the built-in custodial symmetry, the triplet VEV in the GM model can be large compared to the doublet VEV. The custodial singlet neutral boson from the triplets mixes with the neutral boson from the doublet. Two interesting special cases are (i) the triplet VEV is small and the 125 GeV boson is SM-like except for small deviations, and (ii) the 125 GeV boson is mostly the custodial singlet neutral boson from the electroweak triplets. The phenomenology of the doubly-charged and singly-charged bosons is similar to that of the HTM. The constraints on the GM model from precision electroweak data, LEP data, and current LHC data are summarised in Ref. [46].

11.7.6 Composite Higgs models

Within the SM, EWSB is posited but has no dynamical origin. Furthermore, the Higgs boson appears to be unnaturally light. A scenario that remedies these two catches is to consider the Higgs boson as a bound state of new dynamics becoming strong around the weak scale. The Higgs boson can be made significantly lighter than the other resonances of the strong sector if it appears as a pseudo-Nambu–Goldstone boson, see Refs. [11] for reviews.

11.7.6.1 Little Higgs models

The idea behind the Little Higgs boson models [394] is to identify the Higgs doublet as a (pseudo) Nambu–Goldstone boson while keeping some sizeable non-derivative interactions, in particular a largish Higgs quartic interaction. By analogy with QCD where the pions $\pi^{\pm,0}$ appear as Nambu–Goldstone bosons associated to the breaking of the chiral symmetry $SU(2)_L \times SU(2)_R/SU(2)$, switching on some interactions that break explicitly the global symmetry will generate masses for the would-be massless Nambu–Goldstone bosons of the order of $g\Lambda_{G/H}/(4\pi)$, where g is the coupling of the symmetry breaking interaction and $\Lambda_{G/H} = 4\pi f_{G/H}$ is the dynamical scale of the global symmetry breaking G/H . In the case of the Higgs boson, the top Yukawa interaction or the gauge interactions themselves will certainly break explicitly (part of) the global symmetry since they act non-linearly on the Higgs boson. Therefore, obtaining a Higgs boson mass around 125 GeV would demand a dynamical scale $\Lambda_{G/H}$ of the order of 1 TeV, which is known to lead to too large oblique corrections. Raising the strong dynamical scale by at least one order of magnitude requires an additional selection rule to ensure that a Higgs boson mass is generated at the 2-loop level only

$$m_H^2 = \frac{g^2}{16\pi^2} \Lambda_{G/H}^2 \rightarrow m_H^2 = \frac{g_1^2 g_2^2}{(16\pi^2)^2} \Lambda_{G/H}^2. \quad (11.65)$$

The way to enforce this selection rule is through a “collective breaking” of the global symmetry:

$$\mathcal{L} = \mathcal{L}_{G/H} + g_1 \mathcal{L}_1 + g_2 \mathcal{L}_2. \quad (11.66)$$

Each interaction \mathcal{L}_1 or \mathcal{L}_2 individually preserves a subset of the global symmetry such that the Higgs boson remains an exact Nambu–Goldstone boson whenever either g_1 or g_2 is vanishing. A mass term for the Higgs boson can be generated only by diagrams involving simultaneously both interactions. At one-loop, such diagrams are not quadratically divergent, so the Higgs boson mass is not UV sensitive. Explicitly, the cancellation of the SM quadratic divergences is achieved by a set of new particles around the Fermi scale: gauge bosons, vector-like quarks, and extra massive scalars, which are related, by the original global symmetry, to the SM particles with the same spin. Contrary to SUSY, the cancellation of the quadratic divergences is achieved by same-spin particles. These new particles, with definite couplings to SM particles as dictated by the global symmetries of the theory, are perfect goals for the LHC.

The simplest incarnation of the collective breaking idea, the so-called littlest Higgs boson model, is based on a non-linear σ -model describing the spontaneous breaking $SU(5)$ down to $SO(5)$. A subgroup $SU(2)_1 \times U(1)_1 \times SU(2)_2 \times U(1)_2$ is weakly gauged. This model contains a weak doublet, that is identified with the Higgs doublet, and a complex weak triplet whose mass is not protected by collective breaking. Other popular little Higgs models are based on different coset spaces: minimal moose ($SU(3)^2/SU(3)$), the simplest little Higgs ($SU(3)^2/SU(2)^2$), the bestest little Higgs ($SO(6)^2/SO(6)$). For comprehensive reviews, see Ref. [395].

Generically, oblique corrections in Little Higgs models are reduced either by increasing the coupling of one of the gauge groups (in the case of product group models) or by increasing the masses of the W and Z partners, leading ultimately to a fine-tuning of the order of a few percents (see for instance Ref. [396] and references therein). The compatibility of Little Higgs models with experimental data is significantly improved when the global symmetry involves a custodial symmetry as well as a T -parity [397] under which, in analogy with R -parity in SUSY models, the SM particles are even and their partners are odd. Such Little Higgs models would therefore appear in colliders as jet(s) with missing

transverse energy [398] and the ATLAS and CMS searches for squarks and gluinos can be recast to obtain limits on the masses of the heavy vector-like quarks. The T -even top partner, with an expected mass below 1 TeV to cancel the top loop quadratic divergence without too much fine-tuning, would decay dominantly into a $t+Z$ pair or into a $b+W$ pair or even into $t+H$. The latest CMS and ATLAS direct searches [399] for vector-like top partners put a lower bound around 1.1–1.3 TeV (for various branching fraction combinations), excluding the most natural region of the parameter space of these models, i.e., imposing a fine-tuning below the percent level.

The motivation for Little Higgs models is to solve the little hierarchy problem, i.e., to push the need for new physics (responsible for the stability of the weak scale) up to around 10 TeV. Per se, Little Higgs models are effective theories valid up to their cut-off scale $\Lambda_{G/H}$. Their UV completions could either be weakly or strongly coupled.

11.7.6.2 Models of partial compositeness

Even in composite models, the Higgs boson cannot appear as a regular resonance of the strong sector without endangering the viability of the setup when confronted to data. The way out is that the Higgs boson appears as a pseudo Nambu–Goldstone boson: the new strongly coupled sector is supposed to be invariant under a global symmetry G spontaneously broken to a subgroup H at the scale f (the typical mass scale of the resonances of the strong sector is $m_\rho \sim g_\rho f$ with g_ρ the characteristic coupling of the strong sector). To avoid conflict with EW precision measurements, the strong interactions themselves should better not break the EW symmetry. Hence the SM gauge symmetry itself should be contained in H . See Table 11.14 for a few examples of coset spaces.

Table 11.14: Global symmetry breaking patterns and the corresponding Goldstone boson contents of the SM, the minimal composite Higgs model, the next to minimal composite Higgs model, and the minimal composite two Higgs doublet model. Note that the SU(3) model does not have a custodial invariance. a denotes a CP -odd scalar while h and H are CP -even scalars.

Model	Symmetry Pattern	Goldstones
SM	SO(4)/SO(3)	W_L, Z_L
–	SU(3)/SU(2)×U(1)	W_L, Z_L, H
MCHM	SO(5)/SO(4)	W_L, Z_L, H
NMCHM	SO(6)/SO(5)	W_L, Z_L, H, a
MC2HM	SO(6)/SO(4)×SO(2)	W_L, Z_L, h, H, H^\pm, a

The SM (light) fermions and gauge bosons cannot be part of the strong sector itself since LEP data have already put stringent bounds on the compositeness scale of these particles far above the TeV scale. The gauge bosons couple to the strong sector by a weak gauging of a SU(2)×U(1) subgroup of the global symmetry G . Inspiration for the construction of such models comes from the AdS/CFT correspondence: the components of a gauge field along an extra warped space dimension can be interpreted as the Goldstone bosons resulting from the breaking of global symmetry of the strong sector. The couplings of the SM fermions to the strong sector could a priori take two different forms:

- (i) a bilinear coupling of two SM fermions to a composite scalar operator, \mathcal{O} , of the form $\mathcal{L} = y \bar{q}_L u_R \mathcal{O} + h.c.$, in simple analogy with the SM Yukawa interactions. This is the way fermion masses were introduced in technicolor theories and it generically comes with severe flavour problems and calls for extended model-building gymnastics [12] to circumvent them;
- (ii) a linear mass mixing with fermionic vector-like operators: $\mathcal{L} = \lambda_L \bar{q}_L Q_R + \lambda_R \bar{U}_L u_R$. Q and U are two fermionic composite operators of mass M_Q and M_U .

Being part of the composite sector, the composite fermionic operators can have a direct coupling of generic order Y_* to the Higgs boson.

In analogy with the photon- ρ mixing in QCD, once the linear mixings are diagonalised, the physical states are a linear combination of elementary and composite fields. Effective Yukawa couplings are generated and read for instance for the up-type quark

$$y = Y_* \sin \theta_L \sin \theta_R \tag{11.67}$$

where $\sin \theta_i = \lambda_i / \sqrt{M_{Q,U}^2 + \lambda_i^2}$, $i = L, R$, measure the amount of compositeness of the SM left- and right-handed up-type quark. If the strong sector is flavour-anarchic, i.e., if the couplings of the Higgs boson to the composite fermions does not exhibit any particular flavour structure, the relation Eq. (11.67) implies that the light fermions are mostly elementary states ($\sin \theta_i \ll 1$), while the third generation quarks need to have a sizable degree of compositeness. The partial compositeness paradigm offers an appealing dynamical explanation of the hierarchies in the fermion masses. In fact, assuming the strong sector to be almost conformal above the confinement scale, the low-energy values of the mass-mixing parameters $\lambda_{L,R}$ are determined by the (constant) anomalous dimension of the composite operator they mix with. If the UV scale at which the linear mixings are generated is large, then $\mathcal{O}(1)$ differences in the anomalous dimensions can generate naturally large hierarchies in the fermion masses via renormalisation group running [400]. While the introduction of partial compositeness greatly ameliorated the flavor problem of the original composite Higgs models, nevertheless, it did not solve the issue completely, at least in the case where the strong sector is assumed to be flavour-anarchic [401]. While the partial compositeness set-up naturally emerges in models built in space-times with extra dimensions, no fully realistic microscopic realisation of partial compositeness has been proposed in the literature.

Another nice aspect of the partial compositeness structure is the dynamical generation of the Higgs potential that is not arbitrary like in the SM. The Higgs boson being a pseudo-Nambu–Goldstone boson, its mass does not receive any contribution from the strong sector itself but it is generated at the one-loop level via the couplings of the SM particles to the strong sector since these interactions are breaking the global symmetries under which the Higgs doublet transforms non-linearly. Obtaining $v \ll f$, as required phenomenologically, requires some degree of tuning, which scales like $\xi \equiv v^2/f^2$. A mild tuning of the order of 10% ($\xi \approx 0.1$) is typically enough to comply with electroweak precision constraints. This is an important point: in partial compositeness models, the entire Higgs potential is generated at one loop, therefore the separation between v and f can only be obtained at a price of a tuning. This marks a difference with respect to the Little Higgs models which realise a parametric hierarchy between the quartic and mass terms through the collective symmetry breaking mechanism. In fact in Little Higgs models, the quartic coupling is a tree-level effect, leading to a potential

$$V(H) \approx \frac{g_{SM}^2}{16\pi^2} m_\rho^2 H^2 + g_{SM}^2 H^4, \tag{11.68}$$

where g_{SM} generically denotes the SM couplings. The minimisation condition reads $v^2/f^2 \sim g_\rho^2/(16\pi^2)$, therefore v is formally loop suppressed with respect to f . This is the major achievement of the Little Higgs constructions, which however comes at the price of the presence of sub-TeV vectors carrying EW quantum numbers and therefore giving rise generically to large oblique corrections to the propagators of the W and the Z gauge bosons.

After minimisation, the dynamically generated potential leads to an estimate of the Higgs boson mass as

$$m_H^2 \approx g_\rho^3 y_t 2\pi^2 v^2. \tag{11.69}$$

It follows that the limit $f \rightarrow \infty$, i.e., $\xi \rightarrow 0$, is a true decoupling limit: all the resonances of the strong sector become heavy but the Higgs boson whose mass is protected by the symmetries of the coset G/H . When compared to the experimentally measured Higgs boson mass, this estimate puts an upper bound on the strength of the strong interactions: $g_\rho \lesssim 2$. In this limit of not so large coupling, the Higgs potential receives additional contributions. In particular, the fermionic resonances in the top

sector which follow from the global symmetry structure of the new physics sector can help raising the Higgs boson mass. Using some dispersion relation techniques, the mass of the Higgs is connected to the resonance masses. In the minimal $SO(5)/SO(4)$ model, it was shown [402] that a 125 GeV mass can be obtained if at least one of the fermionic resonances is lighter than $\sim 1.4f$. As in SUSY scenarios, the top sector is playing a crucial role in the dynamics of EWSB and can provide the first direct signs of new physics. The direct searches for these top partners, in particular the ones with exotic electric charges $5/3$, are already exploring the natural parameter spaces of these models [403].

The main physics properties of a pseudo Nambu–Goldstone Higgs boson can be captured in a model-independent way by a small number of higher-dimensional operators. Indeed, the strong dynamics at the origin of the composite Higgs boson singles out a few operators among the complete list discussed earlier in Section 11.6: these are the operators that involve extra powers of the Higgs doublets, and they are therefore generically suppressed by a factor $1/f^2$ as opposed to the operators that involve extra derivatives or gauge bosons that are suppressed by a factor $1/(g_\rho^2 f^2)$. The relevant effective Lagrangian describing a strongly interacting light Higgs boson is:

$$\begin{aligned} \mathcal{L}_{\text{SILH}} = & \frac{c_H}{2f^2} (\partial_\mu (\Phi^\dagger \Phi))^2 + \frac{c_T}{2f^2} (\Phi^\dagger \overleftrightarrow{D}^\mu \Phi)^2 - \frac{c_6 \lambda}{f^2} (\Phi^\dagger \Phi)^3 \\ & + \left(\sum_f \frac{c_f y_f}{f^2} \Phi^\dagger \Phi \bar{f}_L \Phi f_R + \text{h.c.} \right). \end{aligned} \quad (11.70)$$

Typically, these new interactions induce deviations in the Higgs boson couplings that scale like $\mathcal{O}(v^2/f^2)$. Hence, the measurements of the Higgs boson couplings can be translated into some constraints on the compositeness scale, $4\pi f$, of the Higgs boson. The peculiarity of these composite models is that, due to the Goldstone nature of the Higgs boson, the direct couplings to photons and gluons are further suppressed and generically the coupling modifiers scale like

$$\begin{aligned} \kappa_{W,Z,f} & \sim 1 + \mathcal{O}\left(\frac{v^2}{f^2}\right), \quad \kappa_{Z\gamma} \sim \mathcal{O}\left(\frac{v^2}{f^2}\right), \\ \kappa_{\gamma,g} & \sim \mathcal{O}\left(\frac{v^2}{f^2} \times \frac{y_t^2}{g_\rho^2}\right), \end{aligned} \quad (11.71)$$

where g_ρ denotes the typical coupling strength among the states of the strongly coupled sector and y_t is the top Yukawa coupling, the largest interaction that breaks the Goldstone symmetry. The $\kappa_{Z\gamma,\gamma,g}$ coupling modifiers are not generated by the strong coupling operators of Eq. (11.70) but by some subleading form-factor operator generated by loops of heavy resonances of the strong sector. The coupling modifiers also receive additional contributions from the other resonances of the strong sector, in particular the fermionic resonances of the top sector that are required to be light to generate a 125 GeV Higgs boson mass. Some indirect information on the resonance spectrum could thus be inferred by a precise measurement of the Higgs boson coupling deviations. However, it was realised, see in particular Ref. [295], that the task is actually complicated by the fact that, in the minimal models, these top partners give a contribution to both κ_t (resulting from a modification of the top Yukawa coupling) and κ_γ and κ_g (resulting from new heavy particles running into the loops) and the structure of interactions is such that the net effect vanishes for inclusive quantities like $\sigma(gg \rightarrow H)$ or $\Gamma(H \rightarrow \gamma\gamma)$ as a consequence of the Higgs low energy theorem [25, 26, 293]. So, one would need to rely on differential distribution, like the Higgs boson p_T distribution discussed in Section 11.2.4.1, to see the top partner effects in Higgs data [404]. The off-shell channel $gg \rightarrow H^* \rightarrow 4\ell$ [272] and the double Higgs boson production $gg \rightarrow HH$ [405] can also help to resolve the gluon loop and separate the top and top-partner contributions.

11.7.6.3 Minimal composite Higgs models

The minimal composite Higgs models (MCHM) are concrete examples of the partial compositeness paradigm. The Higgs doublet is described by the coset space $SO(5)/SO(4)$ where a subgroup $SU(2)_L \times U(1)_Y$ is weakly gauged and under which the four Goldstone bosons transform as a doublet of hypercharge 1. There is some freedom on how the global symmetry is acting on the SM fermions: in MCHM4 the quarks and leptons are embedded into spinorial representations of $SO(5)$, while in MCHM5 they are part of fundamental representations (it might also be interesting phenomenologically to consider larger representations like MCHM14 [406] with the SM fermions inside a representation of dimension 14). It is also possible to consider that fermions of different chirality and flavour are in different representations of $SO(5)$, leading to a more varied phenomenology [407]. The non-linearly realised symmetry acting on the Goldstone bosons leads to general predictions of the coupling of the Higgs boson to the EW gauge bosons. For instance, it can be shown that the quadratic terms in the W and Z bosons read

$$m_W^2(H) \left(W_\mu W^\mu + \frac{1}{2 \cos^2 \theta_W} Z_\mu Z^\mu \right), \quad (11.72)$$

with $m_W(H) = \frac{gf}{2} \sin \frac{H}{f}$. Expanding around the EW vacuum, the expression of the weak scale is $v = f \sin(\langle H \rangle / f)$. And the values of the modified Higgs boson couplings to the W and Z become:

$$g_{HVV} = \frac{2m_V^2}{v} \sqrt{1 - v^2/f^2}, \quad g_{HHVV} = \frac{2m_V^2}{v^2} (1 - 2v^2/f^2). \quad (11.73)$$

Note that the Higgs boson couplings to gauge bosons is always suppressed compared to the SM prediction. This is a general result [408] that holds as long as the coset space is compact.

The Higgs boson couplings to the fermions depend on the representation which the SM fermions are embedded into. The most commonly used embeddings consider all fermion doublets and singlets in the same representations. While, in MCHM4 and MCHM5, the modifications of the couplings depend only on the Higgs boson compositeness scale, in MCHM14 the leading corrections depend also on the mass spectrum of the resonances [406]. This is due to the fact that more than one $SO(5)$ invariant gives rise to SM fermion masses. The (κ_V, κ_f) experimental fit of the Higgs boson couplings can be used to derive a lower bound on the Higgs boson compositeness scale $4\pi f \gtrsim 9 \text{ TeV}$, which is less stringent than the indirect bound obtained from EW precision data, $4\pi f \gtrsim 15 \text{ TeV}$ [409] but more robust and less subject on assumptions [410].

11.7.6.4 Twin Higgs models

In all composite models presented above, the particles responsible for canceling the quadratic divergences in the Higgs boson mass are charged under the SM gauge symmetries. In particular, the top partner carries color charge, implying a reasonably large minimal production cross section at the LHC. An alternative scenario, which is experimentally quite challenging and might explain the null result in various new physics searches, is the case nowadays referred to as “neutral naturalness” [13, 14], where the particles canceling the 1-loop quadratic divergences are neutral under the SM. The canonical example for such theories is the Twin Higgs model of Ref. [13]. This is an example of a pseudo-Goldstone boson model with an approximate global $SU(4)$ symmetry broken to $SU(3)$. The Twin Higgs model is obtained by gauging the $SU(2)_A \times SU(2)_B$ subgroup of $SU(4)$, where $SU(2)_A$ is identified with the SM $SU(2)_L$, while $SU(2)_B$ is the twin $SU(2)$ group. Gauging this subgroup breaks the $SU(4)$ symmetry explicitly, but quadratically divergent corrections do not involve the Higgs boson when the gauge couplings of the two $SU(2)$ subgroups are equal, $g_A = g_B$. The $SU(4) \rightarrow SU(3)$ breaking will also result in the breaking of the twin $SU(2)_B$ group and, as a result, three of the seven Goldstone bosons will be eaten, leaving 4 Goldstone bosons corresponding to the SM Higgs doublet. In fact, imposing the Z_2 symmetry on the full model will ensure the cancellation of all 1-loop quadratic divergences to the Higgs boson mass. Logarithmically divergent terms can, however, arise for example from

gauge loops, leading to a Higgs boson mass of order $g^2 f/4\pi$, which is of the order of the physical Higgs boson mass for $f \sim 1$ TeV. The quadratic divergences from the top sector can be eliminated if the Z_2 protecting the Higgs boson mass remains unbroken by the couplings that result in the top Yukawa coupling. This can be achieved by introducing top partners charged under a twin $SU(3)_C$. In this case, the quadratic divergences are cancelled by top partners that are neutral under the SM gauge symmetries.

Twin Higgs models are low-energy effective theories valid up to a cutoff scale of order $\Lambda \sim 4\pi f \sim 5$ –10 TeV, beyond which a UV completion has to be specified. The simplest such possibility is to also make the Higgs boson composite, and to UV complete the twin Higgs model via gauge and top partners at masses of the order of a few TeV. A concrete implementation is the holographic twin Higgs model [411], which also incorporates a custodial symmetry to protect the T -parameter from large corrections. It is based on a warped extra dimensional theory with a bulk $SO(8)$ gauge group, which incorporates the $SU(4)$ global symmetry discussed above enlarged to contain the $SU(2)_L \times SU(2)_R$ custodial symmetry. In addition, the bulk contains either a full $SU(7)$ group or an $SU(3) \times SU(3) \times U(1) \times U(1) \times Z_2$ subgroup of it to incorporate the QCD, its twin, and the hypercharge local symmetries. The breaking on the UV brane is to the SM symmetries and their twin symmetries, while on the IR brane $SO(8) \rightarrow SO(7)$, giving rise to the 7 Goldstone bosons, three of which will be again eaten by the twin W, Z . The main difference compared to ordinary composite Higgs models is that, in composite twin Higgs models, the cancellation of the one-loop quadratic divergences is achieved by the twin partners. They have a mass of order 700 GeV–1 TeV and they are uncharged under the SM gauge group. This allows the IR scale of the warped extra dimension to be raised to the multi-TeV range without reintroducing the hierarchy problem. The role of the composite partners is to UV complete the theory, rather than to cancel the one-loop quadratic divergences. For more details about the composite twin Higgs models, see Refs. [412].

11.7.7 Searches for signatures of extended Higgs sectors

The measurements described in Sections 11.3 to 11.6 have established the existence of one state of the electroweak symmetry breaking sector, compatible with a SM Higgs boson, but not that it is the only one. As was discussed above, several classes of models beyond the SM require extended Higgs sectors. The searches are typically designed to be as model-independent as possible⁸ and can be categorised in the classes summarised as follows:

- (i) the search for an additional CP -even state mostly in the high mass domain decaying to vector bosons, which would correspond either to the heavy CP -even state in a generic 2HDM where the light state would be the discovered Higgs boson at 125 GeV or to a generic additional singlet;
- (ii) the search for a state in the high mass domain decaying to pairs of fermions, which would correspond to the CP -odd A or the heavy CP -even state H in a generic 2HDM;
- (iii) the search for charged Higgs bosons, which also appear in generic 2HDMs;
- (iv) the search for a CP -odd state a in the low mass region which appears in the NMSSM in a variety of final states, e.g., with one or two a bosons decaying to pairs of photons, muons, taus, and b -quarks;
- (v) the search for doubly charged Higgs bosons which are expected in extensions of the Higgs sector with triplets.

Below is a concise description of the most recent searches performed at the LHC and elsewhere. A summary of these searches in terms of final states is given in Table 11.15 where the corresponding references are given for more details.

11.7.7.1 Searches for an additional CP -even state

(a) Exclusion limits from LEP

⁸Still, most non-SUSY models are likely to include further states and dynamics above the weak scale to stabilise the scalar sector and this new and unknown physics may influence the searches described in this section in a way difficult to estimate.

The searches for the SM Higgs boson at LEP provided an absolute lower limit of 114 GeV on its mass. These searches are also relevant for non-SM Higgs bosons. These searches were interpreted as 95% CL upper bounds on the ratio of the coupling g_{HZZ} to its SM prediction as a function of the Higgs boson mass [131, 485]. These results have an impact on MSSM benchmarks such as the low- m_H scenario where the heavy CP -even Higgs boson is the discovered 125 GeV boson [348], which is also nearly ruled out by current direct constraints and charged Higgs boson limits from LHC. These results also impact scenarios of light CP -even Higgs boson of the NMSSM which are constrained to project predominantly onto the EW singlet component. Additional interest for these scenarios is due to the slight excess observed at LEP [131] at a Higgs boson mass hypothesis of approximately 98 GeV, bolstered by a possible excess in the diphoton channel at 96 GeV in Run 2 data of CMS [416].

(b) Searches at the LHC

At the LHC, the searches for the SM Higgs boson before the 2012 discovery covered a wide range of mass hypotheses up to approximately 1 TeV. After the discovery, the SM Higgs boson searches have been reappraised to search for a heavy CP -even state, extending progressively the search mass range beyond 1 TeV. This state could be the heavy CP -even Higgs boson of a 2HDM, or a generic additional singlet. In both cases, the natural width of the additional H state can be very different from that of the SM Higgs boson. To preserve unitarity of the longitudinal vector boson scattering and the longitudinal vector boson scattering into fermion pairs, the couplings of the additional CP -even Higgs boson to gauge bosons and fermions should not be too large and should constrain the natural width to be smaller than that of a unique Higgs boson at high mass with couplings to fermions and gauge bosons as predicted by the SM (and provided that trilinear and quartic couplings are not too large and that no new state affects the heavy state total width). It is therefore reasonable to consider total widths for the high mass CP -even state smaller than the equivalent SM width. Two specific cases have been considered: (i) the SM width using the complex pole scheme (CPS), and (ii) the narrow width approximation. For the sake of generality, these searches are now done as a function of the Higgs boson mass and total width.

Searches for the Higgs boson in the channels $H \rightarrow \gamma\gamma$, $H \rightarrow Z\gamma$, $H \rightarrow WW^{(*)}$ leptonic and semi-leptonic, and in the $H \rightarrow ZZ^{(*)}$ searches in the 4ℓ , $\ell\ell q\bar{q}$ and $\ell\nu\nu$ channels have also been done, but some of them are simple reinterpretations of the SM Higgs boson search in the CPS scheme. References for these searches are summarised in Table 11.15.

(c) Searches for an additional resonance decaying to a pair of Higgs bosons

In addition to the rare and expected Higgs boson pair production mode, high mass CP -even Higgs bosons can be searched for in the resonant double Higgs boson mode. Searches for such processes, where the Higgs boson is used as a tool for searches for BSM phenomena, have been carried out in a variety of distinct modes depending on the subsequent decays of each Higgs boson. ATLAS and CMS have searched for the $H \rightarrow hh \rightarrow b\bar{b}\tau\tau$, $b\bar{b}\gamma\gamma$, $H \rightarrow hh \rightarrow 4b$, $H \rightarrow hh \rightarrow \gamma\gamma WW^*$, $H \rightarrow hh \rightarrow b\bar{b}WW^*$, $H \rightarrow hh \rightarrow WW^* WW^*$ and $H \rightarrow hh \rightarrow b\bar{b}ZZ^*$ final states. For mass hypotheses of an additional Higgs boson below 500 GeV, the two dominant search channels are the $b\bar{b}\gamma\gamma$ and the $b\bar{b}\tau\tau$ channels. For masses above 500 GeV, the most powerful search is with the $4b$ final state. As illustrated in Figure 11.19, these searches provide useful limits in the low $\tan\beta$ and high mass domain. The list of references for these searches is given in Table 11.15.

(d) Searches for an additional state with the presence of the Higgs boson

In the post-discovery era, analyses searching for additional Higgs bosons need to take into account the presence of the 125 GeV Higgs boson. For searches with sufficiently high mass resolution to disentangle the additional states which are not degenerate in mass, the strength of the observed state and limits on the signal

Table 11.15: Summary of references to the searches for additional states from extended Higgs sectors. (BBr) denotes the BaBar experiment and (TeV), the Tevatron experiments. V denotes either the W or the Z boson. Only Run2 searches references are indicated except when searches have been carried out using Run 1 data only. References for Run 1 searches are available in Ref. [132].

	ATLAS	CMS	Other experiments
<i>CP-even H</i>			
$H \rightarrow \gamma\gamma$	[413]	[414]	—
$H \rightarrow \gamma\gamma$ (low mass)	[415]	[416]	—
$H \rightarrow Z\gamma$	[417]	[418]	—
$H \rightarrow ZZ \rightarrow 4\ell$	[419]	[420]	—
$H \rightarrow ZZ \rightarrow \ell\ell\nu\nu$	[419]	[421]	—
$H \rightarrow ZZ \rightarrow \ell\ell q\bar{q}$	[422]	[423, 424]	—
$H \rightarrow ZZ \rightarrow \nu\nu q\bar{q}$	[425]	—	—
$H \rightarrow WW \rightarrow \ell\nu\ell\nu$	[426]	[427]	—
$H \rightarrow WW \rightarrow \ell\nu q\bar{q}'$	[428]	[427]	—
$H \rightarrow VV \rightarrow qq'q\bar{q}'(JJ)$	[429, 430]	—	—
$H \rightarrow VV$ combination	[431]	—	—
$H \rightarrow hh \rightarrow b\bar{b}\tau\tau, b\bar{b}\gamma\gamma, 4b,$ $\gamma\gamma WW^*, bbWW^*, WW^*WW^*, bbZZ^*$	[432, 433]	[424, 434, 435]	—
<i>CP-odd A (and/or CP-even H)</i>			
$H, A \rightarrow \tau^+\tau^-$	[436]	[437]	[438, 439] (TeV) [440] (LHCb)
$A \rightarrow \tau^+\tau^-$ (low mass)	—	[441]	—
$H, A \rightarrow \mu^+\mu^-$	[442]	[443]	—
$H \rightarrow \mu\tau, e\tau$ LFBV	—	[444]	—
$bj\mu^+\mu^-$ (low $\mu^+\mu^-$ mass)	[445]	[446]	—
$H, A \rightarrow t\bar{t}$	[430, 447]	[448]	—
$H, A \rightarrow b\bar{b}$	[449]	[450]	[451, 452] (TeV)
$A \rightarrow hV \rightarrow b\bar{b}q\bar{q}', b\bar{b}\ell\nu, b\bar{b}\ell\ell, \ell\ell\tau\tau, \nu\bar{\nu}b\bar{b}$	[453, 454]	[455, 456]	—
$H \rightarrow ZA \rightarrow b\bar{b}\ell^+\ell^-$	[457]	[458]	—
<i>Charged H^\pm</i>			
$H^\pm \rightarrow \tau^\pm\nu$	[459, 460]	[461]	—
$H^\pm \rightarrow cs$	[462]	[463]	—
$H^\pm \rightarrow tb$	[464]	[465]	—
$H^\pm \rightarrow W^\pm Z$	[466]	[467, 468]	—
$H^\pm \rightarrow W^\pm A$	—	[469]	—
$H^\pm \rightarrow cb$	—	[470]	—
<i>CP-odd NMSSM a</i>			
$a \rightarrow \mu^+\mu^-$	[471]	[472]	—
$h \rightarrow aa \rightarrow 4\mu, 4\tau, 2\mu 2\tau, 4\gamma,$ $aa \rightarrow \mu^+\mu^-\mu^+\mu^-$	[473]	[474-477]	[478] (TeV)
$bb\mu\mu, bb\tau\tau$	—	[479]	—
$\Upsilon_{1s,3s} \rightarrow a\gamma$	—	—	[480] (LEP)
Doubly charged $H^{\pm\pm}$	[483]	[468, 484]	—

strength of a potential additional state can be set independently, as discussed in the next section. However, in some cases where channels do not have a sufficiently fine mass resolution to resolve states nearly degenerate in mass, specific analyses need to be designed. There are two examples of such analyses: (i) the search for an additional state in the $H \rightarrow WW^{(*)} \rightarrow \ell\nu\ell\nu$ channel in ATLAS, and (ii) the search for nearly degenerate states in the $H \rightarrow \gamma\gamma$ channel with the CMS detector.

In the $H \rightarrow WW^{(*)} \rightarrow \ell\nu\ell\nu$ channel, the search for an additional state is done using a boosted decision tree combining several discriminating kinematic characteristics to separate both the signal from the background and a high mass signal H from the lower mass state h [486]. A simultaneous fit of the two states h and H is then made to test the presence of an additional state. In this case, the usual null hypothesis of background includes the SM signal.

The CMS search for nearly degenerate mass states decaying to a pair of photons [487] is more generic and could for instance apply to CP -odd Higgs bosons as well. It consists of a fit to the diphoton mass spectrum using two nearly degenerate mass templates.

(e) Type I 2HDM and fermiophobia

The measurements of coupling properties of the 125 GeV Higgs boson directly establish its couplings to fermions. However, the presence of an additional fermiophobic state, as predicted by Type I 2HDMs, is not excluded. Prior to the discovery, AT-

LAS and CMS have performed searches for a fermiophobic Higgs boson, i.e., produced through couplings with vector bosons only (VBF and VH) and decaying in two photons. CMS has further combined these results with searches in the W^+W^- and ZZ channels, assuming fermiophobic production and decay. This way, CMS excluded a fermiophobic Higgs boson in the range $110 \text{ GeV} < m_H < 188 \text{ GeV}$ at the 95% CL. References for these Run 1 measurements can be found in Ref. [132]

11.7.7.2 Searches for additional neutral states ($\phi \equiv h, H, A$) decaying to fermions

(a) Exclusion limits from LEP

In e^+e^- collisions, around the centre-of-mass energies reached by LEP, the main production mechanisms of the neutral MSSM Higgs bosons were the Higgs-strahlung processes $e^+e^- \rightarrow hZ, HZ$ and the pair production processes $e^+e^- \rightarrow hA, HA$, while the vector boson fusion processes played a marginal role. Higgs boson decays to $b\bar{b}$ and $\tau^+\tau^-$ were used in these searches.

The searches and limits from the four LEP experiments are described in Refs. [488]. The combined LEP data did not contain any excess of events which would imply the production of a Higgs boson. Combined limits were derived [485]. For $m_A \gg M_Z$, the limit on m_h is nearly that of the SM searches, as $\sin^2(\beta - \alpha) \approx 1$. For high values of $\tan\beta$ and low m_A ($m_A \leq m_h^{max}$), the $e^+e^- \rightarrow hA$ searches become the most important, and the lightest

Higgs boson h is non SM-like. In this region, the 95% CL mass bounds are $m_h > 92.8 \text{ GeV}$ and $m_A > 93.4 \text{ GeV}$. In the m_h^{max} scenario [489], values of $\tan\beta$ from 0.7 to 2.0 are excluded taking $m_t = 174.3 \text{ GeV}$, while a much larger $\tan\beta$ region is excluded for other benchmark scenarios such as the no-mixing one.

A flavour-independent limit for Higgs bosons in the Higgs-strahlung process at LEP has also been set at 112 GeV [490].

Neutral Higgs bosons may also be produced by Yukawa processes $e^+e^- \rightarrow f\bar{f}\phi$, where the Higgs particle $\phi \equiv h, H, A$, is radiated off a massive fermion ($f \equiv b$ or τ^\pm). These processes can be dominant at low masses, and whenever the $e^+e^- \rightarrow hZ$ and hA processes are suppressed. The corresponding ratios of the $f\bar{f}h$ and $f\bar{f}A$ couplings to the SM coupling are $-\sin\alpha/\cos\beta$ and $\tan\beta$, respectively. The LEP data have been used to search for $b\bar{b}b\bar{b}$, $b\bar{b}\tau^+\tau^-$, and $\tau^+\tau^-\tau^+\tau^-$ final states [491]. Regions of low mass and high enhancement factors are excluded by these searches.

The searches for the Higgs boson at LEP also included the case where it does not predominantly decay to a pair of b quarks. All four collaborations conducted dedicated searches for the Higgs boson with reduced model dependence, assuming it is produced via the Higgs-strahlung process, and not addressing its flavour of decay, a lower limit on the Higgs boson mass of 112.9 GeV is set by combining the data of all four experiments [490].

Using an effective Lagrangian approach and combining results sensitive to the $h\gamma\gamma$, $hZ\gamma$ and hZZ couplings, an interpretation of several searches for the Higgs boson was made and set a lower limit of 106.7 GeV on the mass of a Higgs boson that can couple anomalously to photons [490].

(b) Searches at the Tevatron and the LHC

The best sensitivity is in the regime with low to moderate m_A and with large $\tan\beta$ which enhances the couplings of the Higgs bosons to down-type fermions. The corresponding limits on the Higgs boson production cross section times the branching ratio of the Higgs boson into down-type fermions can be interpreted in MSSM benchmark scenarios [492]. The most promising channels at the Tevatron are the inclusive $p\bar{p} \rightarrow \phi \rightarrow \tau^+\tau^-$ process ($\phi = A, H, h$), with contributions from both $gg \rightarrow \phi$ and $b\bar{b}\phi$ production, and $b\bar{b}\phi, \phi \rightarrow \tau^+\tau^-$ or $\phi \rightarrow b\bar{b}$, with $b\tau\tau$ or three tagged b -jets in the final state, respectively. Although the Higgs boson production via gluon fusion has a higher cross section in general than via associated production, it cannot be used to study the $\phi \rightarrow b\bar{b}$ decay mode since the signal is overwhelmed by the QCD background.

CDF and D0 have searched for neutral Higgs bosons produced in association with bottom quarks and which decay into $b\bar{b}$ [451, 452], or into $\tau^+\tau^-$ [438, 439]. The most recent searches in the $b\bar{b}\phi$ channel with $\phi \rightarrow b\bar{b}$ analyse approximately 2.6 fb^{-1} (CDF) and 5.2 fb^{-1} (D0) of data, seeking events with at least three b -tagged jets. The cross section is defined such that at least one b quark not from ϕ decay is required to have $p_T > 20 \text{ GeV}$ and $|\eta| < 5$. The invariant mass of the two leading jets as well as b -tagging variables are used to discriminate the signal from the backgrounds. The QCD background rates and shapes are inferred from data control samples, in particular, the sample with two b -tagged jets and a third, untagged jet. Separate-signal hypotheses are tested and limits are placed on $\sigma(p\bar{p} \rightarrow b\bar{b}\phi) \times \text{BR}(\phi \rightarrow b\bar{b})$. A local excess of approximately 2.5σ significance has been observed in the mass range of $130\text{--}160 \text{ GeV}$, but D0's search is more sensitive and sets stronger limits. The D0 result had a $\mathcal{O}(2\sigma)$ local upward fluctuation in the 110 to 125 GeV mass range. These results have been superseded by the LHC searches and the excess seen by D0 has not been confirmed elsewhere.

A substantially larger sensitivity in the search for the $\phi \rightarrow \tau^+\tau^-$ is obtained with the ATLAS and CMS analyses. The higher centre-of-mass energy reached at the Run2 brings a substantial, though not excessively large, increase in sensitivity due to the intermediate masses probed. Both ATLAS and CMS have reported the result of their searches in this important channel with the full 2016 dataset. The searches are performed in categories of the decays of the two tau leptons: $e\tau_{\text{had}}, \mu\tau_{\text{had}}, e\mu$, and $\mu\mu$, where τ_{had} denotes a tau lepton which decays to one or more hadrons plus a

tau neutrino, e denotes $\tau \rightarrow e\nu\nu$, and μ denotes $\tau \rightarrow \mu\nu\nu$. The dominant background comes from $Z \rightarrow \tau^+\tau^-$ decays, although $t\bar{t}$, W +jets and Z +jets events contribute as well. Separating events into categories based on the number of b -tagged jets improves the sensitivity in the MSSM. The $b\bar{b}$ annihilation process and radiation of a Higgs boson from a b quark gives rise to events in which the Higgs boson is accompanied by a $b\bar{b}$ pair in the final state. Requiring the presence of one or more b -jets reduces the background from Z +jets. Data control samples are used to constrain background rates. The rates for jets to be identified as a hadronically decaying tau lepton are measured in dijet samples, and W +jets samples provide a measurement of the rate of events that, with a fake hadronic tau, can pass the signal selection requirements. Lepton fake rates are measured using samples of isolated lepton candidates and same-sign lepton candidates. Constraints from the ATLAS searches are shown in Fig. 11.19 (left) in the hMSSM approximation defined in Ref. [350]. The neutral Higgs boson searches consider the contributions of both the CP -odd and CP -even neutral Higgs bosons with enhanced couplings to bottom quarks, similarly to what was done for the Tevatron results. In Fig. 11.19, decays of the charged Higgs boson into $\tau\nu$ and decays of the heavy Higgs boson into a pair of SM-like Higgs bosons or gauge bosons, or decays of A into hZ are also being constrained. In addition, decays of the neutral Higgs bosons into muon pairs are also being explored. In the $m_h^{\text{mod}+}$ scenario, the region of $\tan\beta$ lower than 5 does not allow for a Higgs boson mass m_h close to 125 GeV . For the hMSSM scenario, instead, the SM-like Higgs boson mass is fixed as an input and hence the requirement that it is close to 125 GeV is always fulfilled, although this may imply other limitations as discussed in Section 11.7.1.1.

A search for $\phi \rightarrow \mu^+\mu^-$ has also been performed by ATLAS [442] and CMS [443] and no significant deviations from the SM expectation were observed, allowing to set model-independent limit on the product of the branching fraction for the decay into a muon pair and the cross section for the production of a scalar neutral boson, either via gluon fusion, or in association with b quarks, in the mass range from 130 to 1000 GeV .

Finally, searches for a resonance decaying to a top quark pair were done by ATLAS [447, 493] and CMS [448, 494]. These searches were interpreted as searches for scalar resonances by ATLAS [447], however, an important component of these searches is an accurate treatment of the interference effects between the signal and the continuum background. These effects can yield a dip and peak structure instead of a simple peak [346]. ATLAS has performed a search for a high mass state decaying to a pair of top quarks taking into account the deformation in mass shape of the signal in the presence of the continuum background [495].

The LHC has the potential to explore a broad range of SUSY parameter space through the search for non-SM-like Higgs bosons. As illustrated in Fig. 11.19, the parameter space corresponding to large $\tan\beta$ values and large masses of the A boson are covered mostly by the searches in the $A, H \rightarrow \tau^+\tau^-$ channel. A projection of the combined sensitivity of ATLAS and CMS at the HL-LHC has been performed in Ref. [111], showing that, compared to the current sensitivity, the full HL-LHC luminosity can expand the exclusion domain by nearly 1 TeV . In the low $\tan\beta$ limit, the parameter space spanning large A boson masses is best excluded indirectly from the observed Higgs boson measurements. This is illustrated in the M_h^{125} scenario by the nearly horizontal exclusion which is due to the compatibility of the Higgs boson mass measurement with its prediction from radiative corrections (mostly from the stop sector). Nevertheless, Fig. 11.19 (right) shows a broad region with intermediate $\tan\beta$ and large values of m_A that is not accessed by current searches, and in which the most promising channel is the very difficult search for $t\bar{t}$ decays with its aforementioned intricacies [353]. In this region of parameter space, it is possible that only the SM-like Higgs boson can be within the LHC's reach. If no other state of the EWSB sector than the 125 GeV state is discovered, it may be challenging to determine only from the Higgs sector whether there is a SUSY extension of the SM in nature.

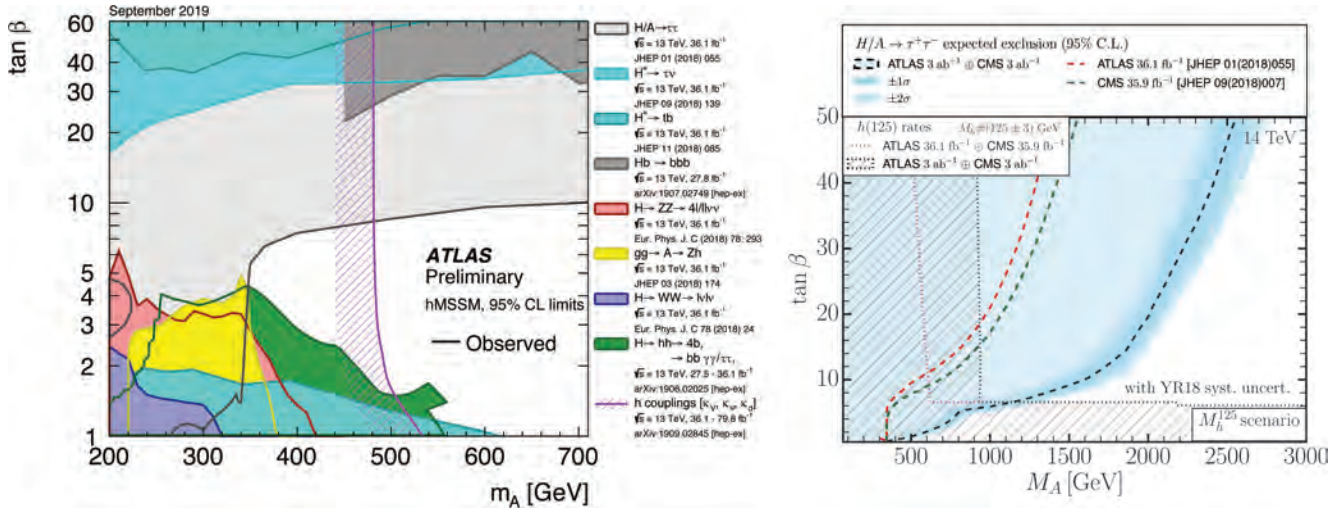


Figure 11.19: The 95% CL exclusion contours in the $(M_A, \tan\beta)$ parameter space for: (left) a summary of ATLAS Run 2 searches in the hMSSM and (right) the projected sensitivity for the combination of ATLAS and CMS searches in the $A, H \rightarrow \tau^+\tau^-$ channel at HL-LHC and the interpretation of the constraints from the measurements of the Higgs boson couplings in the M_h^{125} benchmark [353] (the projected ATLAS sensitivity in the $A, H \rightarrow \tau^+\tau^-$ channel used for this projection was not optimised for high masses, when re-optimised similar sensitivities are obtained between ATLAS and CMS).

11.7.7.3 Searches for a CP -odd state decaying to hZ

Similarly, to the search for a CP -even high mass Higgs boson decaying to a pair of Higgs bosons, the search for a CP -odd states decaying to hZ was carried out at the LHC by ATLAS and CMS in various channels:

- (i) $(Z \rightarrow \ell\ell)(h \rightarrow b\bar{b})$,
- (ii) $(Z \rightarrow \nu\nu)(h \rightarrow b\bar{b})$,
- (iii) $(Z \rightarrow \ell\ell)(h \rightarrow \tau\tau)$,
- (iv) and $(Z \rightarrow \ell\ell)(h \rightarrow \tau\tau)$.

The searches where the A boson decays to a pair of b quarks have been performed both in the regime where both b -jets are resolved and in the boosted regime where the two b -jets are merged in a single larger radius jet. These searches have been used to constrain the parameter space of 2HDMs. In the MSSM, these searches place limits on small values of $\tan\beta$ for masses of A between 220 GeV and 360 GeV.

11.7.7.4 Searches for low mass states

Searches for pseudo-scalar Higgs boson at intermediate to low masses, below the Z mass (in the 25 GeV to 80 GeV mass range) have been performed by CMS both in the $\tau^+\tau^-$ [496] and the $\mu^+\mu^-$ [497] decay channels. A light pseudo-scalar in this mass range is excluded by current direct constraints in the MSSM but not in general 2HDMs [498]. These searches are done in the decay channels where the pseudo-scalar Higgs boson is produced in association with a pair of b -quarks and decays into a pair of taus or muons.

CMS has also reported an anomaly observed in the search for $\mu^+\mu^-$ resonances produced with one jet tagged as containing a b -hadron and a forward jet in the Run 1 data. A mild excess appeared in the di-muon mass distribution at approximately 28 GeV. Another very mild excess was then also found in the 2016 Run 2 data [446]. ATLAS then performed a similar analysis with the full Run 2 dataset corresponding to an integrated luminosity of approximately 139 fb^{-1} , and no significant excess was found [445].

Searches for low mass Higgs bosons were also performed in the diphoton channel by both ATLAS and CMS [499, 500] at Run 1. CMS has updated the results of this search with Run 2 data [416]. A modest excess has been observed by CMS at a mass of 95.3 GeV with a local significance of 2.8σ (the corresponding global significance is 1.3σ). A slight excess was also seen by CMS in the 8 TeV data at a slightly higher mass of 97.6 GeV with a local significance of 2.0σ (1.47σ global). No significant excess has been observed in this region by ATLAS neither in the Run 1 nor Run 2 [413] data. It

should, however, be noted that the ATLAS search does not reach the level of sensitivity to exclude at the 95% CL the excess seen in CMS. This mildly significant excess also coincides in mass with the excess observed at LEP and discussed in Section 11.7.7.1. It has therefore raised interest and speculations on its possible nature, see for instance Ref. [501] and references therein.

11.7.7.5 Searches for charged Higgs bosons H^\pm

At e^+e^- colliders, charged Higgs bosons can be pair produced in the s -channel via γ or Z boson exchange. This process is dominant in the LEP centre-of-mass energies range, i.e., up to 209 GeV. At higher centre-of-mass energies, other processes can play an important role such as the production in top quark decays via $t \rightarrow b + H^\pm$ if $m_{H^\pm} < m_t - m_b$ or via the one-loop process $e^+e^- \rightarrow W^\pm H^\mp$ [502, 503], which allows the production of a charged Higgs boson with $m_{H^\pm} > \sqrt{s}/2$, even when H^+H^- production is kinematically forbidden. Other single charged Higgs boson production mechanisms include $t\bar{b}H^- / \bar{t}bH^+$ production [116], $\tau^+\nu H^- / \tau^-\bar{\nu}H^+$ production [504], and a variety of processes in which H^\pm is produced in association with a one or two other gauge and/or Higgs bosons [505].

At hadron colliders, charged Higgs bosons can be produced in several different modes depending on the value of its mass with respect to the top-quark mass. For light values of the charged Higgs boson mass, defined by Higgs boson masses smaller than the mass of the top quark (with experimental analyses typically considering masses up to $m_{H^\pm} \leq 160$ GeV), the top-quark decay $t \rightarrow Hb$ is allowed and the charged Higgs boson is light enough so that top-quark off-shell effects can be neglected. The cross section for the production of a light charged Higgs boson is simply given by the product of the top-pair production cross section and the branching ratio of a top quark into a charged Higgs boson. The top-pair production cross section is known up to NNLO in perturbative QCD [506], and relevant QCD and SUSY-QCD including NLO corrections to the branching ratio for $t \rightarrow H^+b$ have been computed in the literature, see Refs. [507–509] and references therein. At present, the theoretical accuracy for the production of a light charged Higgs boson is at the few percent level. For the intermediate mass range, values of m_{H^\pm} near m_t , the finite top-width effects as well as the interplay between top-quark resonant and non-resonant diagrams cannot be neglected. Hence, the full process $pp \rightarrow H^\pm W^\mp b\bar{b}$ (with massive b -quarks) must be considered to perform a reliable perturbative calculation of the charged Higgs boson production cross section [509]. For heavy charged Higgs boson scenarios, with charged Higgs boson masses larger than the top-quark mass (typically above 180 GeV), the dominant charged

Higgs boson production channel is the associated production with a top quark/antiquark and a (possibly low transverse momentum) bottom antiquark/quark. Theoretical calculation at NLO have been computed both at the inclusive and fully-differential level in the five-flavour scheme and in the four-flavour scheme, see Ref. [46] and references therein. Charged Higgs bosons can also be produced via associated production with W^\pm bosons through $b\bar{b}$ annihilation and gg -fusion annihilation [510].

For charged Higgs boson production cross section predictions for the Tevatron and the LHC, see Refs. [44, 45, 345].

(a) *Exclusion limits from LEP*

Charged Higgs bosons have been searched for at LEP, where the combined data of the four experiments, ALEPH, DELPHI, L3, and OPAL, were sensitive to masses of up to about 90 GeV [485] in two decay channels, $\tau\nu$ and $c\bar{s}$. The combined LEP data exclude, at 95% CL, charged Higgs bosons with mass below 80 GeV (Type II scenario) or 72.5 GeV (Type I scenario) [511].

(b) *Exclusion limits from Tevatron*

Compared to the mass domain covered by LEP searches, the Tevatron covered a complementary range of charged Higgs boson masses. CDF and D0 have also searched for charged Higgs bosons in top quark decays with subsequent decays to $\tau\nu$ or to $c\bar{s}$ [512]. For the $H^+ \rightarrow c\bar{s}$ channel, the limits on $\text{BR}(t \rightarrow H^+b)$ from CDF and D0 are $\approx 20\%$ in the mass range $90 \text{ GeV} < m_{H^+} < 160 \text{ GeV}$ and assuming a branching fraction of 100% in this specific final state. $H^+ \rightarrow \tau^+\nu_\tau$ channel, D0's limits on $\text{BR}(t \rightarrow H^+b)$ are also $\approx 20\%$ in the same mass range and assuming a branching fraction of 100% in this final state. These limits are valid in general 2HDMs, and they have also been interpreted in terms of the MSSM [512].

(c) *Exclusion limits from LHC*

Similarly, to the Tevatron, at the LHC, light charged Higgs bosons can be searched for in the decays of top quarks. The main initial production mode for light charged Higgs bosons ($m_{H^\pm} < m_t - m_b$) is top pair production. The subsequent decay modes of the charged Higgs boson for these searches are $\tau\nu$ and $c\bar{s}$. More recently, ATLAS and CMS have also searched for higher mass charged Higgs bosons ($m_{H^\pm} > m_t + m_b$) in $H^+ \rightarrow t\bar{b}$. The main production modes are the associated production of a charged Higgs boson in association with a top and a bottom quark or in association with a top quark only.

The decay $H^+ \rightarrow \tau^+\nu_\tau$ is searched typically in three final state topologies:

- (i) lepton+jets: with $t\bar{t} \rightarrow \bar{b}WH^+ \rightarrow \bar{b}\bar{b}(q\bar{q}')(\tau_{\text{lep}}\nu)$, i.e., the W boson decays hadronically and the tau decays into an electron or a muon, with two neutrinos;
- (ii) τ +lepton: with $t\bar{t} \rightarrow \bar{b}WH^+ \rightarrow \bar{b}\bar{b}(\ell\nu)(\tau_{\text{had}}\nu)$, i.e., the W boson decays leptonically (with $\ell = e, \mu$) and the tau decays hadronically;
- (iii) τ +jets: $t\bar{t} \rightarrow \bar{b}WH^+ \rightarrow \bar{b}\bar{b}(q\bar{q}')(\tau_{\text{had}}\nu)$, i.e., both the W boson and the τ decay hadronically.

CMS has also searched for the charged Higgs boson in the decay products of top quark pairs: $t\bar{t} \rightarrow H^\pm W^\mp b\bar{b}$ and $t\bar{t} \rightarrow H^+ H^- b\bar{b}$ as well. Three types of final states with large missing transverse energy and jets originating from b -quark hadronisation have been analysed: the fully-hadronic channel with a hadronically decaying tau in association with jets, the dilepton channel with a hadronically decaying tau in association with an electron or muon and the dilepton channel with an electron-muon pair. The results of the searches at the LHC are illustrated in Figure 11.19.

Both ATLAS and CMS have also searched for high mass charged Higgs bosons decaying to a top and bottom quarks. The main production mode for this search is the associated production with one top quark (5-flavour scheme) or a top quark and a bottom quark (4-flavour scheme) in the final state. The s -channel production mode where the charged Higgs boson is produced alone in the final state at tree level is also considered. This search is particularly intricate and it is sensitive to the modelling of the

top pair production background produced in association with additional partons and in particular b -quarks. No excess was found and the results are expressed in terms of exclusion limits of cross section times branching fractions.

ATLAS and CMS have also searched for charged Higgs bosons in top quark decays assuming $\text{BR}(H^+ \rightarrow c\bar{s}) = 100\%$ [462, 513], and sets limits of $\approx 20\%$ on $\text{BR}(t \rightarrow H^+b)$ in the $90 \text{ GeV} < m_{H^+} < 160 \text{ GeV}$ mass range.

In 2HDMs, the decay of the charged Higgs boson to a W and a Z boson is allowed only at loop level and is therefore suppressed. However the $H^\pm \rightarrow W^\pm Z$ decay channel is allowed in Higgs triplet models. ATLAS [466] has searched for such decays, requiring that the charged Higgs boson is produced through the fusion of vector bosons. No excess with respect to the SM backgrounds has been observed in this channel, and the results are interpreted in the Georgi–Machacek model [387] discussed in Section 11.7.5.2.

At the LHC, various other channels still remain to be explored, in particular searches involving additional neutral scalars in particular in the WH , WA channels (A is the pseudo-scalar MSSM Higgs boson), and in the Wa channel (a is the light CP -odd scalars of the NMSSM).

11.7.7.6 *Interpretation of the measurements of the coupling properties of the Higgs boson*

The 125 GeV Higgs boson being part of any hypothetically extended EWSB sector, it can be used through the compatibility of its measured couplings and mass with those predicted in specific models to provide constraints on these specific models parameters.

As discussed in Section 11.7.1.1, the mass of the Higgs boson limits drastically the MSSM parameter space and can be used to set limits on specific MSSM benchmarks. This is the case for the Mh125 scenario as illustrated in Figure 11.18 and in Figure 11.19, corresponding approximately to a lower limit on $\tan\beta$ in this model [111].

The measurements of the Higgs boson couplings, discussed in Section 11.6, can be interpreted in the framework of a constrained model where the couplings of the Higgs boson to vector bosons, up-type quarks, down-type quarks and leptons, are varied. In 2HDMs, these couplings are functions of the mixing angle α between the observed Higgs boson and the heavy CP -even neutral scalar, and of the ratio of the vacuum expectation values of the two doublets, $\tan\beta$. In the case of the MSSM, the two parameters are the A boson mass and $\tan\beta$ (the sole two parameters needed to describe the MSSM Higgs sector at tree level). The coupling measurements have been interpreted both by ATLAS [514] and CMS [301] in specific MSSM benchmarks and in 2HDMs. The exclusion contour in the hMSSM for the ATLAS combination [514] is illustrated in Figure 11.19.

11.7.7.7 *Searches for a light CP-odd Higgs boson*

A light pseudo-scalar boson a is present in any two Higgs doublet model enhanced with an additional singlet field. A prominent example is the NMSSM. The theoretical motivations for singlet extensions of the MSSM are discussed in Section 11.7.2. There is also a variety of other models with light additional spin-0 bosons such as two Higgs doublet models with a scalar, Little Higgs models or light scalar mediator to a dark sector.

In the framework of the NMSSM, the searches now focus on the low a mass region for several reasons:

- (i) in the NMSSM, the light pseudo-scalar a boson can, as a pseudo-Goldstone boson, be a natural candidate for an axion;
- (ii) scenarios where $m_a > 2m_b$ and a CP -even state h decaying to a pair of a ($m_h > 2m_a$) are excluded by direct searches at LEP in the four b 's channel [478, 485, 515];
- (iii) in the pre-discovery era, LEP limits on a CP -even Higgs boson resulted in fine-tuning MSSM constraints [516] which could be evaded through non standard decays of the Higgs boson to aa ;
- (iv) in the NMSSM, a CP -odd a boson with a mass in the range 9.2–12 GeV can also account for the difference observed between the measured anomalous muon magnetic moment and its prediction [517].

The benchmark scenarios have also changed in the light of the Higgs boson discovery. The 125 GeV state could be the lightest or the next-to-lightest of the three CP -even states of the NMSSM. Light pseudo-scalar scenarios are still very interesting in particular for the potential axion candidate. There are three main types of direct searches for the light a boson:

- (i) for masses below the Υ resonance, the search is for radiative decays $\Upsilon \rightarrow a\gamma$ at B-factories;
- (ii) the inclusive search in high energy pp collisions at the LHC;
- (iii) the search for decays of the observed CP -even Higgs h boson into a pair of a bosons.

Radiative decays $\Upsilon \rightarrow a\gamma$ have been searched for in various colliders, the most recent results are searches for radiative decays of the $\Upsilon(1s)$ to $a\gamma$ with a subsequent decay of the a boson to a pair of taus at CLEO [518], and the radiative decays of the $\Upsilon(1s, 2s, 3s)$ to $a\gamma$ with subsequent decays to a pair of muons or taus by BaBar [481, 482].

Direct inclusive searches for the light pseudo scalar a boson were performed in the $a \rightarrow \mu\mu$ channel at the Tevatron by D0 [478] and by ATLAS [471], CMS [472], and LHCb [165] at the LHC.

Finally, searches for the decays of the Higgs boson to a pair of a bosons were performed with subsequent decays to four photons, in the four muons final state, in the two muons and two taus final state, and in the four taus final state.

No significant excess in the searches for a light CP -odd a boson was found and limits on the production times branching fractions of the a boson have been set.

References for all these searches are summarised in Table 11.15.

11.7.7.8 Searches for doubly charged Higgs bosons $H^{\pm\pm}$

As discussed in Section 11.7.5, the generation of small neutrino masses via the standard EWSB mechanism described in Section 11.2 requires unnaturally small Yukawa couplings, provided that neutrinos are Dirac-type fermions. A Majorana mass term with a see-saw mechanism for neutrinos, would allow for naturally small masses and would also yield a framework for the appealing scenario of leptogenesis. However, within the SM, Majorana mass terms correspond to (non-renormalizable) dimension-5 operators. Such effective interactions can be generated via renormalisable interactions with an electroweak triplet of complex scalar fields (corresponding to a type-II see-saw mechanism). Other models such as the Zee–Babu model, with the introduction of two $SU(2)_L$ singlets, also generate Majorana mass terms. The signature of such models would be the presence of doubly charged Higgs bosons $H^{\pm\pm}$.

The main production mechanisms of $H^{\pm\pm}$ bosons at hadron colliders are the pair production in the s -channel through the exchange of a Z boson or a photon and the associated production with a charged Higgs boson through the exchange of a W boson. Various searches for doubly charged Higgs bosons have been performed by ATLAS and CMS at Run 1 [519] and Run 2 [483, 484]. Typically, these searches aim at low values of the Higgs triplet vacuum expectation for which the doubly charged Higgs boson will decay mostly to leptons (for high values, the decay to W bosons will become predominant). These searches assume that the coupling to W bosons is negligible and that the main production mode is through the Drell–Yan process.

11.7.7.9 Searches for non-standard production processes of the Higgs boson

The discovery of the Higgs boson has also allowed for searches of BSM processes involving standard decays of the Higgs boson. One example directly pertaining to the search for additional states of the EWSB sector is the search for Higgs bosons in the cascade decay of a heavy CP -even Higgs boson decaying to charged Higgs boson and a W boson, and the charged Higgs boson subsequently decaying to H and another W boson. This search has been performed by ATLAS in $b\bar{b}$ decays of the 125 GeV Higgs boson [520].

11.7.7.10 Outlook on searches for additional states

The LHC program of searches for additional states covers a large variety of decay and production channels. Since the Higgs boson discovery, many new channels have been explored at the

LHC, e.g., the searches for additional states decaying into hh or Vh or ZA . The search for charged Higgs bosons has been extended to include the WZ , WA and the very difficult $t\bar{b}$ decay channel.

11.8 Summary and outlook

Summary– The discovery of the Higgs boson is a major milestone in the history of particle physics as well as an extraordinary achievement of the LHC machine and the ATLAS and CMS experiments. Nine years after the discovery, substantial progress in the field of Higgs boson physics has been accomplished and a significant number of measurements probing the nature of this unique particle have been made. They are revealing an increasingly precise profile of the Higgs boson.

The LHC has now concluded its Run 2, delivering a dataset of 13 TeV pp collisions corresponding to an integrated luminosity of approximately 140 fb^{-1} of data collected by ATLAS and CMS. With the substantial increase in production rates at the higher center-of-mass energy and the larger datasets, new landmark results in Higgs physics have been achieved.

Three new results of fundamental importance have been achieved with Run 2 datasets by ATLAS and CMS independently: (i) the clear and unambiguous observation of the Higgs boson decay to taus; (ii) the clear and unambiguous observation of the Higgs boson decay to a pair of b quarks; (iii) the clear and unambiguous observation of the production of the Higgs boson through the $t\bar{t}H$ process. These results provide direct evidence for the Yukawa coupling of the Higgs boson to fermions of the third generation: taus, bottom quarks and top quarks, at rates compatible with those expected in the SM. In addition, with the full Run 2 dataset, a first evidence for the decay of the Higgs boson to muons was achieved. These, and all other experimental measurements, are consistent with the EWSB mechanism of the SM.

New theoretical calculations and developments in Monte-Carlo simulation pertaining to Higgs physics are still occurring at a rapid pace. For example, the theoretical prediction for the dominant gluon fusion production mode now includes the latest N3LO result, which is twice as precise as previous N2LO calculations. With these improvements in the state-of-the-art theory predictions and the increase in luminosity and center-of-mass energy, Higgs physics has definitively entered a precision era. Its impact can already be seen on the latest Run 2 combined measurements of the Higgs boson couplings (see Section 11.6).

Since the discovery of the Higgs boson, new ideas have emerged to probe its rare decays and production modes, as well as to indirectly measure the Higgs boson width through the study of its off-shell couplings, or via on-shell interference effects. The Higgs boson has now become part of the standard toolkit in searches for new physics.

Many extensions of the SM at higher energies call for an enlargement of the EWSB sector. Hence, direct searches for additional scalar states can provide valuable insights on the dynamics of the EWSB mechanism. The ATLAS and CMS experiments have searched for additional Higgs bosons in the Run 2 data, and have imposed constraints in broad ranges of mass and couplings for various scenarios with an extended Higgs sector.

The landscape of Higgs physics has been extended extraordinarily since its discovery. The current precisions on the measurements of the couplings of the Higgs boson to gauge bosons and third generation fermions are typically of the order of 10–20%. The uncertainty on the Higgs boson coupling to the muon shrank below 50%, and the upper limits on the branching fraction to new invisible particles are approximately 10%. The sensitivity to the Higgs boson self-coupling has not reached the SM value yet and there is no information on how the Higgs field acquired its VEV in the early times of the Universe. This situation allows for new challenges to ultimately increase further the reach in precision and it also widens the possibilities of unveiling the true nature and the dynamics of the electroweak symmetry breaking.

Outlook– The unitarisation of the vector boson scattering (VBS) amplitudes, dominated at high energies by their longitudinal polarisation, has been the basis of the *no lose* theorem at the LHC, and was a determining consideration in the building of the accelerator and detectors. It motivated the existence of a Higgs

boson or the observability of manifestations of strong dynamics at the TeV scale. Now that a Higgs boson has been found and its couplings to gauge bosons are consistent with the SM predictions, perturbative unitarity is preserved to a large extent with the sole exchange of the Higgs boson, and without the need for any additional states. VBS is, however, still an important channel to further investigate in order to better understand the nature of the Higgs sector and the possible completion of the SM at the TeV scale. In association with the double Higgs boson production channel by vector boson fusion, VBS could, for instance, confirm that the Higgs boson is part of a weak doublet and also establish whether it is an elementary object or a composite state that could emerge as a pseudo-Nambu–Goldstone boson from a new underlying broken symmetry.

The fermion-Higgs boson couplings are not governed by local gauge symmetry. Thus, in addition to a new particle, the LHC has also discovered a new force, different in nature from the other fundamental interactions since it is non-universal and distinguishes between the three families of quarks and leptons. The existence of the Higgs boson embodies the problem of an unnatural cancellation among the quantum corrections to its mass if new physics is present at scales significantly higher than the EW scale. The non-observation of additional states which could stabilise the Higgs boson mass is a challenge for natural scenarios like SUSY or models with a new strong interaction in which the Higgs boson is not a fundamental particle. This increasingly pressing paradox starts questioning the principle of naturalness or inspires new solutions tied to the cosmological evolution of the Universe.

The search for the Higgs boson has occupied the particle physics community for the last 50 years. Its discovery has shaped and sharpened the physics programs of the LHC and of prospective future accelerators [521]. With the HL-LHC, the precision will improve by a factor 5–10 on all observables with respect to current data. Table 11.12 displays the expected sensitivities in the characterization of the Higgs boson at HL-LHC: in this table, the parameters κ_i specify by how much the coupling of the Higgs boson to a given particle i deviates from the SM expectation. The only channels which are expected to be limited by data statistics are the rare decays to muons and $Z\gamma$. In all other cases, the experimental systematic uncertainties are similar to the statistical uncertainties, but the dominant source of uncertainty arises from theory, and this remains the case even after assuming that, by the end of the HL-LHC run, the theory uncertainties can be reduced by a factor two compared to the current uncertainties, a hypothesis that appears realistic but still requires dedicated and concerted work [111]. For both hadron and lepton colliders, some theoretical progress is crucial to fully exploit and capitalise on the experimental data. In particular, the expected HL-LHC data together with rapid ongoing progress in theoretical calculations are defining a new era of precision Higgs boson measurements.

Acknowledgements

We would like to thank many of our colleagues for proofreading this review, for useful criticism and for their input in general: W. Altmannshofer, J. de Blas, G. Branco, J. Campbell, F. Caola, F. Cerutti, C. Csáki, R. Contino, J. Conway, N. Craig, A. David, S. Dawson, J.B. De Vivie, J. D’Hondt, G. Durieux, C. Englert, J.R. Espinosa, A. Falkowski, L. Fayard, W. Fischer, S. Forte, M. Grazzini, J. Gu, H. Haber, B. Heinemann, S. Heinemeyer, J. Hubisz, A. Korytov, B. Jäger, H. Ji, T. Junk, P. Langacker, J. Lykken, F. Maltoni, M.L. Mangano, B. Mansoulié, M. McCullough, R. Mishra, M. Mühlleitner, B. Murray, M. Neubert, A. Nisati, Y. Paul, G. Perez, G. Petrucciani, A. Pomarol, E. Pontón, R. Rattazzi, D. Rebuszi, F. Riva, R. Salerno, E. Salvioni, N. Shah, G. Shaughnessy, M. Spira, O. Stål, A. Strumia, K. Tackmann, R. Tanaka, J. Terning, A. Vartak, C. Wagner, A. Weiler, A. Wulzer, and G. Zanderighi. We are also most grateful to the ATLAS, CDF, CMS and D0 collaborations for their help with this review.

M.C. is supported by Fermilab, that is operated by Fermi Research Alliance, LLC under Contract No. DE-AC02-07CH11359 with the United States Department of Energy. C.G. is supported by the Helmholtz Association and by the Deutsche Forschungs-

gemeinschaft under Germany’s Excellence Strategy – EXC 2121 “Quantum Universe” – 390833306. V.S. is supported by the grant DE-SC0009919 of the United States Department of Energy.

References

- [1] G. Aad *et al.* (ATLAS), *Phys. Lett.* **B716**, 1 (2012), [arXiv:1207.7214].
- [2] S. Chatrchyan *et al.* (CMS), *Phys. Lett.* **B716**, 30 (2012), [arXiv:1207.7235].
- [3] S.L. Glashow, *Nucl. Phys.* **20**, 579 (1961); S. Weinberg, *Phys. Rev. Lett.* **19**, 1264 (1967); A. Salam, *Elementary Particle Theory*, eds.: Svartholm, Almqvist and Wiksells, Stockholm, 1968; S. L. Glashow, J. Iliopoulos and L. Maiani, *Phys. Rev.* **D2**, 1285 (1970).
- [4] F. Englert and R. Brout, *Phys. Rev. Lett.* **13**, 321 (1964), [157(1964)]; P. W. Higgs, *Phys. Rev.* **145**, 1156 (1966); G. S. Guralnik, C. R. Hagen and T. W. B. Kibble, *Phys. Rev. Lett.* **13**, 585 (1964), [162(1964)].
- [5] J. M. Cornwall, D. N. Levin and G. Tiktopoulos, *Phys. Rev. Lett.* **30**, 1268 (1973), [Erratum: *Phys. Rev. Lett.* **31**, 572 (1973)]; J. M. Cornwall, D. N. Levin and G. Tiktopoulos, *Phys. Rev.* **D10**, 1145 (1974), [Erratum: *Phys. Rev.* **D11**, 972 (1975)]; C. H. Llewellyn Smith, *Phys. Lett.* **46B**, 233 (1973); B. W. Lee, C. Quigg and H. B. Thacker, *Phys. Rev.* **D16**, 1519 (1977).
- [6] K. G. Wilson, *Phys. Rev.* **D3**, 1818 (1971); G. ’t Hooft, in *Proc. of 1979 Cargèse Institute on Recent Developments in Gauge Theories*, p. 135 Press, New York 1980; For a modern discussion, see the GGI Tea Break’s Seminar by G.F. Giudice and R. Rattazzi, <https://is.gd/nUnjAr> (2021).
- [7] J. Wess and B. Zumino, *Phys. Lett.* **49B**, 52 (1974).
- [8] S. P. Martin, *Adv. Ser. Direct. High Energy Phys.* 1–98 (1998), [hep-ph/9709356].
- [9] B.C. Allanach and H.E. Haber, *Supersymmetry, Part I (Theory)*, in this volume.
- [10] D. B. Kaplan and H. Georgi, *Phys. Lett.* **136B**, 183 (1984).
- [11] B. Bellazzini, C. Csaki and J. Serra, *Eur. Phys. J.* **C74**, 5, 2766 (2014), [arXiv:1401.2457]; G. Panico and A. Wulzer, *Lect. Notes Phys.* **913**, pp.1 (2016), [arXiv:1506.01961]; C. Csaki, C. Grojean and J. Terning, *Rev. Mod. Phys.* **88**, 4, 045001 (2016), [arXiv:1512.00468].
- [12] K.M. Black, R.S. Chivukula and M. Narain, *Dynamical Electroweak Symmetry Breaking: Implications of the H0*, in this volume.
- [13] Z. Chacko, H.-S. Goh and R. Harnik, *Phys. Rev. Lett.* **96**, 231802 (2006), [hep-ph/0506256]; Z. Chacko, H.-S. Goh and R. Harnik, *JHEP* **01**, 108 (2006), [hep-ph/0512088].
- [14] N. Craig *et al.*, *JHEP* **07**, 105 (2015), [arXiv:1501.05310]; N. Craig, S. Knapen and P. Longhi, *Phys. Rev. Lett.* **114**, 6, 061803 (2015), [arXiv:1410.6808].
- [15] P. W. Graham, D. E. Kaplan and S. Rajendran, *Phys. Rev. Lett.* **115**, 22, 221801 (2015), [arXiv:1504.07551]; J. R. Espinosa *et al.*, *Phys. Rev. Lett.* **115**, 25, 251803 (2015), [arXiv:1506.09217]; G. Dvali (2019), [arXiv:1908.05984].
- [16] C. Csaki *et al.*, *Phys. Rev. Lett.* **126**, 091801 (2021), [arXiv:2007.14396]; N. Arkani-Hamed, R. Tito D’agnolo and H. D. Kim (2020), [arXiv:2012.04652]; R. Tito D’agnolo and D. Teresi (2021), [arXiv:2106.04591].
- [17] T. Flacke *et al.*, *JHEP* **06**, 050 (2017), [arXiv:1610.02025].
- [18] J. Khoury and O. Parrikar, *JCAP* **12**, 014 (2019), [arXiv:1907.07693]; G. F. Giudice, M. McCullough and T. You (2021), [arXiv:2105.08617].
- [19] M. Bauer, M. Carena and K. Gemmler, *JHEP* **11**, 016 (2015), [arXiv:1506.01719]; M. Bauer, M. Carena and K. Gemmler, *Phys. Rev.* **D94**, 11, 115030 (2016), [arXiv:1512.03458].
- [20] R. Barbieri, L. J. Hall and V. S. Rychkov, *Phys. Rev.* **D74**, 015007 (2006), [hep-ph/0603188].

- [21] D. E. Morrissey and M. J. Ramsey-Musolf, *New J. Phys.* **14**, 125003 (2012), [arXiv:1206.2942].
- [22] G. Degrandi *et al.*, *JHEP* **08**, 098 (2012), [arXiv:1205.6497]; S. Alekhin, A. Djouadi and S. Moch, *Phys. Lett.* **B716**, 214 (2012), [arXiv:1207.0980]; D. Buttazzo *et al.*, *JHEP* **12**, 089 (2013), [arXiv:1307.3536].
- [23] S. Weinberg, *Phys. Rev. Lett.* **43**, 1566 (1979).
- [24] See the particle listing section at <http://pdg.lbl.gov>.
- [25] J. R. Ellis, M. K. Gaillard and D. V. Nanopoulos, *Nucl. Phys.* **B106**, 292 (1976).
- [26] M. A. Shifman *et al.*, *Sov. J. Nucl. Phys.* **30**, 711 (1979), [*Yad. Fiz.*30,1368(1979)].
- [27] J. F. Gunion *et al.*, *The Higgs Hunter's Guide*, Addison-Wesley (1990).
- [28] P. Sikivie *et al.*, *Nucl. Phys.* **B173**, 189 (1980); H. Georgi, *Ann. Rev. Nucl. Part. Sci.* **43**, 209 (1993).
- [29] M. J. G. Veltman, *Nucl. Phys.* **B123**, 89 (1977).
- [30] M. Luscher and P. Weisz, *Nucl. Phys.* **B290**, 25 (1987); M. Luscher and P. Weisz, *Nucl. Phys.* **B295**, 65 (1988).
- [31] V. Branchina, E. Messina and M. Sher, *Phys. Rev.* **D91**, 013003 (2015), [arXiv:1408.5302].
- [32] A. Hook *et al.*, *JHEP* **01**, 061 (2015), [arXiv:1404.5953]; J. Kearney, H. Yoo and K. M. Zurek, *Phys. Rev.* **D91**, 12, 123537 (2015), [arXiv:1503.05193].
- [33] J. R. Espinosa, D. Racco and A. Riotto, *Phys. Rev. Lett.* **120**, 12, 121301 (2018), [arXiv:1710.11196].
- [34] J. R. Espinosa, D. Racco and A. Riotto, *JCAP* **1809**, 09, 012 (2018), [arXiv:1804.07732].
- [35] A. Andreassen, W. Frost and M. D. Schwartz, *Phys. Rev.* **D97**, 5, 056006 (2018), [arXiv:1707.08124]; S. Chigusa, T. Moroi and Y. Shoji, *Phys. Rev. Lett.* **119**, 21, 211801 (2017), [arXiv:1707.09301].
- [36] M. Shaposhnikov and C. Wetterich, *Phys. Lett.* **B683**, 196 (2010), [arXiv:0912.0208]; M. Holthausen, K. S. Lim and M. Lindner, *JHEP* **02**, 037 (2012), [arXiv:1112.2415].
- [37] F. L. Bezrukov and M. Shaposhnikov, *Phys. Lett.* **B659**, 703 (2008), [arXiv:0710.3755]; F. L. Bezrukov, A. Magnin and M. Shaposhnikov, *Phys. Lett.* **B675**, 88 (2009), [arXiv:0812.4950].
- [38] C. P. Burgess, H. M. Lee and M. Trott, *JHEP* **09**, 103 (2009), [arXiv:0902.4465]; J. L. F. Barbón and J. R. Espinosa, *Phys. Rev.* **D79**, 081302 (2009), [arXiv:0903.0355]; M. P. Hertzberg, *JHEP* **11**, 023 (2010), [arXiv:1002.2995].
- [39] B. A. Kniehl, *Phys. Rept.* **240**, 211 (1994).
- [40] M. Spira, *Fortsch. Phys.* **46**, 203 (1998), [hep-ph/9705337].
- [41] M. Carena and H. E. Haber, *Prog. Part. Nucl. Phys.* **50**, 63 (2003), [hep-ph/0208209].
- [42] A. Djouadi, *Phys. Rept.* **457**, 1 (2008), [hep-ph/0503172].
- [43] S. Dittmaier *et al.* (LHC Higgs Cross Section Working Group), CERN Report **2011-002** (2011), [arXiv:1101.0593].
- [44] S. Dittmaier *et al.* (LHC Higgs Cross Section Working Group), CERN Report **2012-002** (2012), [arXiv:1201.3084].
- [45] S. Heinemeyer *et al.* (LHC Higgs Cross Section Working Group), CERN Report **2013-004** (2013), [arXiv:1307.1347].
- [46] D. de Florian *et al.* (LHC Higgs Cross Section Working Group), CERN Report **2017-002** (2016), [arXiv:1610.07922].
- [47] LHC Higgs Working Group, <https://twiki.cern.ch/twiki/bin/view/LHCPhysics/LHCHWG>.
- [48] T. Aaltonen *et al.* (CDF, D0), *Phys. Rev.* **D88**, 5, 052014 (2013), [arXiv:1303.6346].
- [49] H. M. Georgi *et al.*, *Phys. Rev. Lett.* **40**, 692 (1978).
- [50] D. Graudenz, M. Spira and P. M. Zerwas, *Phys. Rev. Lett.* **70**, 1372 (1993).
- [51] M. Spira *et al.*, *Nucl. Phys.* **B453**, 17 (1995), [hep-ph/9504378].
- [52] C. Anastasiou *et al.*, *Phys. Rev. Lett.* **114**, 212001 (2015), [arXiv:1503.06056]; C. Anastasiou *et al.*, *JHEP* **05**, 058 (2016), [arXiv:1602.00695].
- [53] R. V. Harlander and K. J. Ozeren, *JHEP* **11**, 088 (2009), [arXiv:0909.3420]; A. Pak, M. Rogal and M. Steinhauser, *JHEP* **02**, 025 (2010), [arXiv:0911.4662].
- [54] J. Davies *et al.*, *Phys. Rev.* **D100**, 3, 034017 (2019), [arXiv:1906.00982]; M. Czakon *et al.* (2021), [arXiv:2105.04436].
- [55] S. Dawson, *Nucl. Phys.* **B359**, 283 (1991); A. Djouadi, M. Spira and P. M. Zerwas, *Phys. Lett.* **B264**, 440 (1991).
- [56] R. V. Harlander and W. B. Kilgore, *Phys. Rev. Lett.* **88**, 201801 (2002), [hep-ph/0201206]; C. Anastasiou and K. Melnikov, *Nucl. Phys.* **B646**, 220 (2002), [hep-ph/0207004]; V. Ravindran, J. Smith and W. L. van Neerven, *Nucl. Phys.* **B665**, 325 (2003), [hep-ph/0302135].
- [57] A. Djouadi and P. Gambino, *Phys. Rev. Lett.* **73**, 2528 (1994), [hep-ph/9406432]; S. Actis *et al.*, *Phys. Lett.* **B670**, 12 (2008), [arXiv:0809.1301]; U. Aglietti *et al.*, *Phys. Lett.* **B595**, 432 (2004), [hep-ph/0404071]; G. Degrandi and F. Maltoni, *Phys. Lett.* **B600**, 255 (2004), [hep-ph/0407249].
- [58] M. Bonetti, K. Melnikov and L. Tancredi, *Phys. Rev.* **D97**, 5, 056017 (2018), [Erratum: *Phys. Rev.* **D97**, 9, 099906 (2018)], [arXiv:1801.10403]; M. Bonetti *et al.*, *JHEP* **11**, 045 (2020), [arXiv:2007.09813]; M. Becchetti *et al.*, *Phys. Rev. D* **103**, 5, 054037 (2021), [arXiv:2010.09451].
- [59] C. Anastasiou, R. Boughezal and F. Petriello, *JHEP* **04**, 003 (2009), [arXiv:0811.3458].
- [60] C. Anastasiou *et al.*, *JHEP* **03**, 162 (2019), [arXiv:1811.11211].
- [61] M. Bonvini *et al.*, *JHEP* **08**, 105 (2016), [arXiv:1603.08000]; B. Mistlberger, *JHEP* **05**, 028 (2018), [arXiv:1802.00833].
- [62] X. Chen *et al.*, *Phys. Rev. Lett.* **127**, 7, 072002 (2021), [arXiv:2102.07607].
- [63] G. Billis *et al.*, *Phys. Rev. Lett.* **127**, 7, 072001 (2021), [arXiv:2102.08039].
- [64] A. Banfi, G. P. Salam and G. Zanderighi, *JHEP* **06**, 159 (2012), [arXiv:1203.5773]; T. Becher, M. Neubert and D. Wilhelm, *JHEP* **05**, 110 (2013), [arXiv:1212.2621]; A. Banfi *et al.*, *JHEP* **04**, 049 (2016), [arXiv:1511.02886]; J. K. L. Michel, P. Pietrulewicz and F. J. Tackmann, *JHEP* **04**, 142 (2019), [arXiv:1810.12911]; P. F. Monni, L. Rottoli and P. Torrielli, *Phys. Rev. Lett.* **124**, 25, 252001 (2020), [arXiv:1909.04704].
- [65] I. Moutl and I. W. Stewart, *JHEP* **09**, 129 (2014), [arXiv:1405.5534].
- [66] V. D. Barger *et al.*, *Phys. Rev.* **D44**, 1426 (1991).
- [67] M. Cacciari *et al.*, *Phys. Rev. Lett.* **115**, 8, 082002 (2015), [Erratum: *Phys. Rev. Lett.* **120**, 13, 139901 (2018)], [arXiv:1506.02660]; F. A. Dreyer and A. Karlberg, *Phys. Rev. Lett.* **117**, 7, 072001 (2016), [arXiv:1606.00840]; J. Cruz-Martinez *et al.*, *Phys. Lett.* **B781**, 672 (2018), [arXiv:1802.02445].
- [68] T. Han, G. Valencia and S. Willenbrock, *Phys. Rev. Lett.* **69**, 3274 (1992), [hep-ph/9206246].
- [69] T. Liu, K. Melnikov and A. A. Penin, *Phys. Rev. Lett.* **123**, 12, 122002 (2019), [arXiv:1906.10899].
- [70] F. A. Dreyer, A. Karlberg and L. Tancredi, *JHEP* **10**, 131 (2020), [arXiv:2005.11334].
- [71] M. Rauch and D. Zeppenfeld, *Phys. Rev.* **D95**, 11, 114015 (2017), [arXiv:1703.05676].
- [72] A. Buckley *et al.* (2021), [arXiv:2105.11399].

- [73] S. L. Glashow, D. V. Nanopoulos and A. Yildiz, *Phys. Rev. D* **18**, 1724 (1978); T. Han and S. Willenbrock, *Phys. Lett. B* **273**, 167 (1991); T. Han, G. Valencia, and S. Willenbrock, *Phys. Rev. Lett.* **69**, 3274 (1992); H. Baer, B. Bailey and J. F. Owens, *Phys. Rev. D* **47**, 2730 (1993); J. Ohnemus and W. J. Stirling, *Phys. Rev. D* **47**, 2722 (1993).
- [74] A. Stange, W. J. Marciano and S. Willenbrock, *Phys. Rev. D* **49**, 1354 (1994), [hep-ph/9309294]; A. Stange, W. J. Marciano and S. Willenbrock, *Phys. Rev. D* **50**, 4491 (1994), [hep-ph/9404247].
- [75] M. L. Ciccolini, S. Dittmaier and M. Kramer, *Phys. Rev. D* **68**, 073003 (2003), [hep-ph/0306234]; A. Denner *et al.*, *JHEP* **03**, 075 (2012), [arXiv:1112.5142].
- [76] R. Hamberg, W. L. van Neerven and T. Matsuura, *Nucl. Phys. B* **359**, 343 (1991), [Erratum: *Nucl. Phys. B* **644**, 403 (2002)].
- [77] O. Brein, A. Djouadi and R. Harlander, *Phys. Lett. B* **579**, 149 (2004), [hep-ph/0307206]; L. Altenkamp *et al.*, *JHEP* **02**, 078 (2013), [arXiv:1211.5015].
- [78] J. Davies, G. Mishima and M. Steinhauser, *JHEP* **03**, 034 (2021), [arXiv:2011.12314]; L. Chen *et al.*, *JHEP* **03**, 125 (2021), [arXiv:2011.12325].
- [79] O. Brein *et al.*, *Eur. Phys. J. C* **72**, 1868 (2012), [arXiv:1111.0761].
- [80] O. Brein, R. V. Harlander and T. J. E. Zirke, *Comput. Phys. Commun.* **184**, 998 (2013), [arXiv:1210.5347]; R. V. Harlander *et al.*, *JHEP* **05**, 089 (2018), [arXiv:1802.04817].
- [81] R. Gauld *et al.*, *Phys. Lett. B* **817**, 136335 (2021), [arXiv:2009.14209].
- [82] A. Denner *et al.*, *JHEP* **03**, 075 (2012), [arXiv:1112.5142].
- [83] G. Ferrera, M. Grazzini, and F. Tramontano, *Phys. Rev. Lett.* **107**, 152003 (2011).
- [84] G. Ferrera, M. Grazzini and F. Tramontano, *Phys. Lett. B* **740**, 51 (2015), [arXiv:1407.4747]; J. M. Campbell, R. K. Ellis and C. Williams, *JHEP* **06**, 179 (2016), [arXiv:1601.00658].
- [85] W. Astill *et al.*, *JHEP* **06**, 154 (2016), [arXiv:1603.01620].
- [86] F. Caola *et al.*, *Phys. Rev. D* **97**, 7, 074022 (2018), [arXiv:1712.06954]; R. Gauld *et al.*, *JHEP* **10**, 002 (2019), [arXiv:1907.05836].
- [87] J. M. Butterworth *et al.*, *Phys. Rev. Lett.* **100**, 242001 (2008), [arXiv:0802.2470].
- [88] A. Behring *et al.*, *Phys. Rev. D* **101**, 11, 114012 (2020), [arXiv:2003.08321].
- [89] W. Bizon *et al.* (2021), [arXiv:2106.06328].
- [90] R. Raitio and W. W. Wada, *Phys. Rev. D* **19**, 941 (1979); Z. Kunszt, *Nucl. Phys. B* **247**, 339 (1984); J. N. Ng and P. Zakarauskas, *Phys. Rev. D* **29**, 876 (1984); J. F. Gunion, *Phys. Lett. B* **261**, 510 (1991); W. J. Marciano and F. E. Paige, *Phys. Rev. Lett.* **66**, 2433 (1991).
- [91] W. Beenakker *et al.*, *Phys. Rev. Lett.* **87**, 201805 (2001), [hep-ph/0107081]; L. Reina and S. Dawson, *Phys. Rev. Lett.* **87**, 201804 (2001), [hep-ph/0107101]; L. Reina, S. Dawson and D. Wackerroth, *Phys. Rev. D* **65**, 053017 (2002), [hep-ph/0109066]; S. Dawson *et al.*, *Phys. Rev. D* **67**, 071503 (2003), [hep-ph/0211438]; W. Beenakker *et al.*, *Nucl. Phys. B* **653**, 151 (2003), [hep-ph/0211352]; S. Dawson *et al.*, *Phys. Rev. D* **68**, 034022 (2003), [hep-ph/0305087].
- [92] Y. Zhang *et al.*, *Phys. Lett. B* **738**, 1 (2014), [arXiv:1407.1110]; S. Frixione *et al.*, *JHEP* **09**, 065 (2014), [arXiv:1407.0823]; S. Frixione *et al.*, *JHEP* **06**, 184 (2015), [arXiv:1504.03446].
- [93] T. Plehn, G. P. Salam and M. Spannowsky, *Phys. Rev. Lett.* **104**, 111801 (2010), [arXiv:0910.5472].
- [94] A. Kulesza *et al.*, *JHEP* **03**, 065 (2016), [arXiv:1509.02780]; A. Broggio *et al.*, *JHEP* **03**, 124 (2016), [arXiv:1510.01914]; A. Broggio *et al.*, *JHEP* **02**, 126 (2017), [arXiv:1611.00049]; A. Kulesza *et al.*, *Phys. Rev. D* **97**, 11, 114007 (2018), [arXiv:1704.03363]; A. Broggio *et al.*, *JHEP* **08**, 039 (2019), [arXiv:1907.04343]; A. Kulesza *et al.*, *Eur. Phys. J. C* **80**, 5, 428 (2020), [arXiv:2001.03031].
- [95] A. Denner and R. Feger, *JHEP* **11**, 209 (2015), [arXiv:1506.07448].
- [96] A. Denner *et al.*, *JHEP* **02**, 053 (2017), [arXiv:1612.07138].
- [97] R. Frederix *et al.*, *Phys. Lett. B* **701**, 427 (2011), [arXiv:1104.5613]; M. V. Garzelli *et al.*, *EPL* **96**, 1, 11001 (2011), [arXiv:1108.0387].
- [98] S. Catani *et al.*, *Eur. Phys. J. C* **81**, 6, 491 (2021), [arXiv:2102.03256].
- [99] C. Branchiaccio *et al.*, *JHEP* **08**, 145 (2021), [arXiv:2106.06516].
- [100] F. Demartin *et al.*, *Eur. Phys. J. C* **75**, 6, 267 (2015), [arXiv:1504.00611].
- [101] D. Pagani, I. Tsinikos and E. Vryonidou, *JHEP* **08**, 082 (2020), [arXiv:2006.10086].
- [102] K.A. Assamagan *et al.*, [Higgs Working Group, "Physics at TeV Colliders" workshop, Les Houches, 2003], arXiv:hep-ph/0406152 (2004).
- [103] R. V. Harlander and W. B. Kilgore, *Phys. Rev. D* **68**, 013001 (2003), [hep-ph/0304035]; J. M. Campbell *et al.*, *Phys. Rev. D* **67**, 095002 (2003), [hep-ph/0204093]; S. Dawson *et al.*, *Phys. Rev. Lett.* **94**, 031802 (2005), [hep-ph/0408077]; S. Dittmaier, M. Krämer and M. Spira, *Phys. Rev. D* **70**, 074010 (2004), [hep-ph/0309204]; S. Dawson *et al.*, *Phys. Rev. D* **69**, 074027 (2004), [hep-ph/0311067].
- [104] W. J. Stirling and D. J. Summers, *Phys. Lett. B* **283**, 411 (1992); F. Maltoni *et al.*, *Phys. Rev. D* **64**, 094023 (2001), [hep-ph/0106293].
- [105] D. Pagani, H.-S. Shao and M. Zaro, *JHEP* **11**, 036 (2020), [arXiv:2005.10277].
- [106] C. Grojean, A. Paul and Z. Qian, *JHEP* **04**, 139 (2021), [arXiv:2011.13945].
- [107] S. Dawson, S. Dittmaier and M. Spira, *Phys. Rev. D* **58**, 115012 (1998), [hep-ph/9805244].
- [108] D. de Florian and J. Mazzitelli, *Phys. Rev. Lett.* **111**, 201801 (2013), [arXiv:1309.6594].
- [109] L.-B. Chen *et al.*, *Phys. Lett. B* **803**, 135292 (2020), [arXiv:1909.06808].
- [110] S. Borowka *et al.*, *Phys. Rev. Lett.* **117**, 1, 012001 (2016), [Erratum: *Phys. Rev. Lett.* **117**, 7, 079901 (2016)], [arXiv:1604.06447]; J. Baglio *et al.*, *Eur. Phys. J. C* **79**, 6, 459 (2019), [arXiv:1811.05692]; J. Davies *et al.*, *JHEP* **11**, 024 (2019), [arXiv:1907.06408].
- [111] M. Cepeda *et al.* (HL/HE-LHC WG2 group) (2019), [arXiv:1902.00134].
- [112] J. Alison *et al.*, *Rev. Phys.* **5**, 100045 (2020), [arXiv:1910.00012].
- [113] B.L. Ioffe and V.A. Khoze, *Sov. J. Nucl. Phys.* **9**, 50 (1978).
- [114] D. R. T. Jones and S. T. Petcov, *Phys. Lett. B* **84B**, 440 (1979); R. N. Cahn and S. Dawson, *Phys. Lett.* **136B**, 196 (1984), [Erratum: *Phys. Lett.* **138B**, 464 (1984)]; G. L. Kane, W. W. Repko and W. B. Rolnick, *Phys. Lett. B* **148B**, 367 (1984); G. Altarelli, B. Mele and F. Pitolli, *Nucl. Phys. B* **287**, 205 (1987); W. Kilian, M. Kramer and P. M. Zerwas, *Phys. Lett. B* **373**, 135 (1996), [hep-ph/9512355].
- [115] B. A. Kniehl, *Z. Phys.* **C55**, 605 (1992); J. Fleischer and F. Jegerlehner, *Nucl. Phys. B* **216**, 469 (1983); A. Denner *et al.*, *Z. Phys.* **C56**, 261 (1992); B. A. Kniehl, *Int. J. Mod. Phys. A* **17**, 1457 (2002), [hep-ph/0112023].
- [116] K. J. F. Gaemers and G. J. Gounaris, *Phys. Lett.* **77B**, 379 (1978); A. Djouadi, J. Kalinowski and P. M. Zerwas, *Z. Phys.* **C54**, 255 (1992); B. A. Kniehl, F. Madricardo and M. Steinhauser, *Phys. Rev. D* **66**, 054016 (2002), [hep-ph/0205312]; S. Dittmaier *et al.*, *Phys. Lett. B* **441**,

- 383 (1998), [hep-ph/9808433]; S. Dittmaier *et al.*, Phys. Lett. **B478**, 247 (2000), [hep-ph/0002035]; S. Dawson and L. Reina, Phys. Rev. **D59**, 054012 (1999), [hep-ph/9808443].
- [117] A. Arbey *et al.*, Eur. Phys. J. **C75**, 8, 371 (2015), [arXiv:1504.01726]; A. Freitas *et al.* (2019), [arXiv:1906.05379].
- [118] S. Frixione *et al.* (2021), [arXiv:2108.10261].
- [119] A. Denner *et al.*, Eur. Phys. J. **C71**, 1753 (2011), [arXiv:1107.5909].
- [120] A. Djouadi, J. Kalinowski, and M. Spira, Comp. Phys. Comm. **108**, 56 (1998); A. Djouadi *et al.*, arXiv:1003.1643 [hep-ph] (2010).
- [121] S. G. Gorishnii *et al.*, Mod. Phys. Lett. **A5**, 2703 (1990); S. G. Gorishnii *et al.*, Phys. Rev. **D43**, 1633 (1991); A. L. Kataev and V. T. Kim, Mod. Phys. Lett. **A9**, 1309 (1994); L. R. Surguladze, Phys. Lett. **B341**, 60 (1994), [hep-ph/9405325]; S. A. Larin, T. van Ritbergen and J. A. M. Vermaseren, Phys. Lett. **B362**, 134 (1995), [hep-ph/9506465]; K. G. Chetyrkin and A. Kwiatkowski, Nucl. Phys. **B461**, 3 (1996), [hep-ph/9505358]; K. G. Chetyrkin, Phys. Lett. **B390**, 309 (1997), [hep-ph/9608318]; P. A. Baikov, K. G. Chetyrkin and J. H. Kuhn, Phys. Rev. Lett. **96**, 012003 (2006), [hep-ph/0511063].
- [122] J. Fleischer and F. Jegerlehner, Phys. Rev. **D23**, 2001 (1981); D. Yu. Bardin, B. M. Vilensky and P. K. Khristova, Sov. J. Nucl. Phys. **53**, 152 (1991), [Yad. Fiz.53,240(1991)]; A. Dabelstein and W. Hollik, Z. Phys. **C53**, 507 (1992); B. A. Kniehl, Nucl. Phys. **B376**, 3 (1992); A. Djouadi *et al.*, in "In *Munich/Annecy/Hamburg 1991, Proceedings, e+ e- collisions at 500-GeV, pt. A* 11-30," (1991).
- [123] T. Inami, T. Kubota and Y. Okada, Z. Phys. **C18**, 69 (1983); K. G. Chetyrkin, B. A. Kniehl and M. Steinhauser, Phys. Rev. Lett. **79**, 353 (1997), [hep-ph/9705240]; P. A. Baikov and K. G. Chetyrkin, Phys. Rev. Lett. **97**, 061803 (2006), [hep-ph/0604194].
- [124] H.-Q. Zheng and D.-D. Wu, Phys. Rev. **D42**, 3760 (1990); A. Djouadi *et al.*, Phys. Lett. **B257**, 187 (1991); S. Dawson and R. P. Kauffman, Phys. Rev. **D47**, 1264 (1993); A. Djouadi, M. Spira and P. M. Zerwas, Phys. Lett. **B311**, 255 (1993), [hep-ph/9305335]; K. Melnikov and O. I. Yakovlev, Phys. Lett. **B312**, 179 (1993), [hep-ph/9302281]; M. Inoue *et al.*, Mod. Phys. Lett. **A9**, 1189 (1994).
- [125] P. Maierhöfer and P. Marquard, Phys. Lett. **B721**, 131 (2013), [arXiv:1212.6233].
- [126] U. Aglietti *et al.*, Phys. Lett. **B595**, 432 (2004), [hep-ph/0404071]; G. Degrossi and F. Maltoni, Phys. Lett. **B600**, 255 (2004), [hep-ph/0407249]; S. Actis *et al.*, Phys. Lett. **B670**, 12 (2008), [arXiv:0809.1301]; U. Aglietti *et al.*, Phys. Lett. **B600**, 57 (2004), [hep-ph/0407162]; G. Degrossi and F. Maltoni, Nucl. Phys. **B724**, 183 (2005), [hep-ph/0504137]; U. Aglietti *et al.*, FERMILAB-CONF (2006), [hep-ph/0612172].
- [127] A. Abbasabadi *et al.*, Phys. Rev. **D55**, 5647 (1997), [hep-ph/9611209]; A. Abbasabadi and W. W. Repko, Phys. Rev. **D71**, 017304 (2005), [hep-ph/0411152]; A. Abbasabadi and W. W. Repko, JHEP **08**, 048 (2006), [hep-ph/0602087]; D. A. Dicus and W. W. Repko, Phys. Rev. **D87**, 7, 077301 (2013), [arXiv:1302.2159]; L.-B. Chen, C.-F. Qiao and R.-L. Zhu, Phys. Lett. **B726**, 306 (2013), [arXiv:1211.6058]; Y. Sun, H.-R. Chang and D.-N. Gao, JHEP **05**, 061 (2013), [arXiv:1303.2230]; G. Passarino, Phys. Lett. **B727**, 424 (2013), [arXiv:1308.0422].
- [128] M. Spira, A. Djouadi and P. M. Zerwas, Phys. Lett. **B276**, 350 (1992).
- [129] A. Bredenstein *et al.*, Phys. Rev. **D74**, 013004 (2006), [hep-ph/0604011]; A. Bredenstein *et al.*, JHEP **02**, 080 (2007), [hep-ph/0611234]; A. Bredenstein *et al.*, Prophecy4f: A Monte Carlo generator for a proper description of the Higgs decay into 4 fermions, <http://omnibus.uni-freiburg.de/~sd565/programs/prophecy4f/prophecy4f.html>.
- [130] A. Ghinculov, Phys. Lett. **B337**, 137 (1994), [Erratum: Phys. Lett. **B346**, 426 (1995)], [hep-ph/9405394]; L. Durand, B. A. Kniehl and K. Riesselmann, Phys. Rev. **D51**, 5007 (1995), [hep-ph/9412311]; L. Durand, K. Riesselmann and B. A. Kniehl, Phys. Rev. Lett. **72**, 2534 (1994), [Erratum: Phys. Rev. Lett. **74**, 1699 (1995)].
- [131] R. Barate *et al.* (LEP Working Group for Higgs boson searches, ALEPH, DELPHI, L3, OPAL), Phys. Lett. **B565**, 61 (2003), [hep-ex/0306033].
- [132] M. Tanabashi *et al.* (Particle Data Group), Phys. Rev. **D98**, 3, 030001 (2018).
- [133] Y. L. Dokshitzer, S. I. Troian and V. A. Khoze, Sov. J. Nucl. Phys. **46**, 712 (1987), [Yad. Fiz.46,1220(1987)].
- [134] ATLAS Collaboration, ATLAS-CONF-2020-026 (2020).
- [135] A. M. Sirunyan *et al.* (CMS), Eur. Phys. J. C **81**, 6, 488 (2021), [arXiv:2103.04956].
- [136] G. Aad *et al.* (ATLAS, CMS), Phys. Rev. Lett. **114**, 191803 (2015), [arXiv:1503.07589].
- [137] ATLAS Collaboration, ATLAS-CONF-2019-029 (2019).
- [138] A. M. Sirunyan *et al.* (CMS), JHEP **07**, 027 (2021), [arXiv:2103.06956].
- [139] A. M. Sirunyan *et al.* (CMS), JHEP **11**, 047 (2017), [arXiv:1706.09936].
- [140] G. Aad *et al.* (ATLAS), Eur. Phys. J. C **80**, 10, 957 (2020), [Erratum: Eur.Phys.J.C 81, 29 (2021), Erratum: Eur.Phys.J.C 81, 398 (2021)], [arXiv:2004.03447].
- [141] M. Aaboud *et al.* (ATLAS), Phys. Lett. **B784**, 345 (2018), [arXiv:1806.00242].
- [142] ATLAS Collaboration, ATLAS-CONF-2020-005 (2020).
- [143] A. M. Sirunyan *et al.* (CMS), Phys. Lett. B **805**, 135425 (2020), [arXiv:2002.06398].
- [144] ATLAS Collaboration, ATLAS-PHYS-PUB-2016-009 (2016).
- [145] M. Dittmar and H. K. Dreiner, Phys. Rev. **D55**, 167 (1997), [hep-ph/9608317].
- [146] G. Aad *et al.* (ATLAS), JHEP **08**, 137 (2015), [arXiv:1506.06641].
- [147] ATLAS Collaboration, ATLAS-CONF-2021-014 (2021).
- [148] A. M. Sirunyan *et al.* (CMS), JHEP **03**, 003 (2021), [arXiv:2007.01984].
- [149] CMS Collaboration, CMS-PAS-HIG-19-017 (2021).
- [150] G. Aad *et al.* (ATLAS), JHEP **04**, 117 (2015), [arXiv:1501.04943].
- [151] ATLAS and CMS Collaborations, ATLAS-CONF-2015-044 and CMS-PAS-HIG-15-002 (2015).
- [152] M. Aaboud *et al.* (ATLAS), Phys. Rev. **D99**, 072001 (2019), [arXiv:1811.08856].
- [153] A. M. Sirunyan *et al.* (CMS), Phys. Lett. **B779**, 283 (2018), [arXiv:1708.00373].
- [154] CMS Collaboration, CMS-PAS-HIG-18-032 (2019).
- [155] A. M. Sirunyan *et al.* (CMS), JHEP **06**, 093 (2019), [arXiv:1809.03590].
- [156] ATLAS Collaboration, ATLAS-CONF-2021-044 (2021).
- [157] CMS Collaboration, CMS-PAS-HIG-19-010 (2020).
- [158] A. Tumasyan *et al.* (CMS) (2021), [arXiv:2107.11486].
- [159] T. Aaltonen *et al.* (CDF, D0), Phys. Rev. Lett. **109**, 071804 (2012), [arXiv:1207.6436].
- [160] M. Aaboud *et al.* (ATLAS), Phys. Lett. **B786**, 59 (2018), [arXiv:1808.08238].
- [161] A. M. Sirunyan *et al.* (CMS), Phys. Rev. Lett. **121**, 12, 121801 (2018), [arXiv:1808.08242].
- [162] G. Aad *et al.* (ATLAS), Eur. Phys. J. C **81**, 2, 178 (2021), [arXiv:2007.02873].

- [163] G. Aad *et al.* (ATLAS), Phys. Lett. B **816**, 136204 (2021), [arXiv:2008.02508].
- [164] LHCb-CONF-2016-006, CERN-LHCb-CONF-2016-006.
- [165] M. Aaboud *et al.* (ATLAS), JHEP **11**, 112 (2016), [arXiv:1606.02181].
- [166] V. Khachatryan *et al.* (CMS), Phys. Rev. **D92**, 3, 032008 (2015), [arXiv:1506.01010].
- [167] G. Aad *et al.* (ATLAS), Eur. Phys. J. C **81**, 6, 537 (2021), [arXiv:2011.08280]; CMS Collaboration, CMS-PAS-HIG-16-003 (2019).
- [168] E. Gabrielli *et al.*, Nucl. Phys. **B781**, 64 (2007), [hep-ph/0702119].
- [169] G. Aad *et al.* (ATLAS), JHEP **03**, 268 (2021), [arXiv:2010.13651].
- [170] ATLAS Collaboration, ATLAS-CONF-2021-010 (2021).
- [171] A. M. Sirunyan *et al.* (CMS), JHEP **12**, 085 (2020), [arXiv:2006.13251].
- [172] M. Cacciari, G. P. Salam and G. Soyez, JHEP **04**, 063 (2008), [arXiv:0802.1189].
- [173] V. Khachatryan *et al.* (CMS), Eur. Phys. J. **C75**, 6, 251 (2015), [arXiv:1502.02485].
- [174] G. Aad *et al.* (ATLAS), Phys. Lett. **B749**, 519 (2015), [arXiv:1506.05988].
- [175] M. Aaboud *et al.* (ATLAS), Phys. Lett. **B784**, 173 (2018), [arXiv:1806.00425].
- [176] A. M. Sirunyan *et al.* (CMS), Phys. Rev. Lett. **120**, 23, 231801 (2018), [arXiv:1804.02610].
- [177] G. Aad *et al.* (ATLAS), Phys. Rev. Lett. **125**, 6, 061802 (2020), [arXiv:2004.04545].
- [178] A. M. Sirunyan *et al.* (CMS), Phys. Rev. Lett. **125**, 6, 061801 (2020), [arXiv:2003.10866].
- [179] ATLAS Collaboration, ATLAS-CONF-2020-058 (2020).
- [180] CMS Collaboration, CMS-PAS-HIG-18-030 (2019).
- [181] A. M. Sirunyan *et al.* (CMS), Eur. Phys. J. C **81**, 4, 378 (2021), [arXiv:2011.03652].
- [182] ATLAS Collaboration, ATLAS-CONF-2019-045 (2019).
- [183] ATLAS Collaboration, ATLAS-CONF-2017-077 (2017).
- [184] ATLAS Collaboration, ATLAS-CONF-2019-004 (2019).
- [185] CMS Collaboration, CMS-PAS-HIG-18-018 (2019).
- [186] M. Farina *et al.*, JHEP **05**, 022 (2013), [arXiv:1211.3736].
- [187] CMS Collaboration, CMS-PAS-HIG-17-005 (2017).
- [188] CMS Collaboration, CMS-PAS-HIG-16-019 (2016).
- [189] G. Aad *et al.* (ATLAS), JHEP **12**, 061 (2015), [arXiv:1509.06047].
- [190] V. Khachatryan *et al.* (CMS), JHEP **02**, 079 (2017), [arXiv:1610.04857].
- [191] ATLAS Collaboration, JHEP **129**, 010 (2017).
- [192] CMS Collaboration, CMS-PAS-TOP-2017-003 (2017).
- [193] G. Aad *et al.* (ATLAS) (2019), [arXiv:1906.02025].
- [194] A. M. Sirunyan *et al.* (CMS), Phys. Rev. Lett. **122**, 12, 121803 (2019), [arXiv:1811.09689].
- [195] ATLAS Collaboration, ATLAS-CONF-2021-030 (2021).
- [196] CMS Collaboration, CMS-PAS-HIG-20-004 (2020).
- [197] G. Aad *et al.* (ATLAS), JHEP **07**, 108 (2020), [Erratum: JHEP 01, 145 (2021), Erratum: JHEP 05, 207 (2021)], [arXiv:2001.05178].
- [198] CMS Collaboration, CMS-PAS-HIG-20-005 (2021).
- [199] A. M. Sirunyan *et al.* (CMS), JHEP **03**, 257 (2021), [arXiv:2011.12373].
- [200] ATLAS Collaboration, ATLAS-CONF-2021-016 (2021).
- [201] G. Aad *et al.* (ATLAS), Phys. Lett. B **809**, 135754 (2020), [arXiv:2005.05382].
- [202] A. M. Sirunyan *et al.* (CMS), JHEP **11**, 152 (2018), [arXiv:1806.05996].
- [203] V. Khachatryan *et al.* (CMS), Phys. Lett. **B753**, 341 (2016), [arXiv:1507.03031].
- [204] G. Aad *et al.* (ATLAS), Phys. Lett. B **819**, 136412 (2021), [arXiv:2103.10322].
- [205] G. Aad *et al.* (ATLAS), Phys. Lett. B **812**, 135980 (2021), [arXiv:2007.07830].
- [206] A. M. Sirunyan *et al.* (CMS), JHEP **01**, 148 (2021), [arXiv:2009.04363].
- [207] ATLAS Collaboration, ATLAS-CONF-2019-037 (2019).
- [208] A. M. Sirunyan *et al.* (CMS), Phys. Rev. D **104**, 3, 032013 (2021), [arXiv:2105.03007].
- [209] G. Aad *et al.* (ATLAS), JHEP **11**, 211 (2015), [arXiv:1508.03372].
- [210] G. Aad *et al.* (ATLAS), Eur. Phys. J. **C77**, 2, 70 (2017), [arXiv:1604.07730].
- [211] CMS Collaboration, CMS-PAS-HIG-17-001 (2017).
- [212] V. Khachatryan *et al.* (CMS), Phys. Lett. **B763**, 472 (2016), [arXiv:1607.03561].
- [213] R. Harnik, J. Kopp and J. Zupan, JHEP **03**, 026 (2013), [arXiv:1209.1397].
- [214] G. Aad *et al.* (ATLAS) (2019), [arXiv:1907.06131].
- [215] A. M. Sirunyan *et al.* (CMS), JHEP **06**, 001 (2018), [arXiv:1712.07173].
- [216] C. Delaunay *et al.*, Phys. Rev. **D89**, 3, 033014 (2014), [arXiv:1310.7029].
- [217] ATLAS Collaboration, ATLAS-CONF-2021-021 (2021).
- [218] A. M. Sirunyan *et al.* (CMS), JHEP **03**, 131 (2020), [arXiv:1912.01662].
- [219] G. Isidori, A. V. Manohar and M. Trott, Phys. Lett. **B728**, 131 (2014), [arXiv:1305.0663]; G. T. Bodwin *et al.*, Phys. Rev. **D88**, 5, 053003 (2013), [arXiv:1306.5770]; M. König and M. Neubert, JHEP **08**, 012 (2015), [arXiv:1505.03870].
- [220] G. Aad *et al.* (ATLAS), Phys. Rev. Lett. **114**, 12, 121801 (2015), [arXiv:1501.03276].
- [221] M. Aaboud *et al.* (ATLAS), Phys. Rev. Lett. **117**, 11, 111802 (2016), [arXiv:1607.03400].
- [222] A. M. Sirunyan *et al.* (CMS), JHEP **11**, 039 (2020), [arXiv:2007.05122].
- [223] A. M. Sirunyan *et al.* (CMS), Phys. Lett. **B797**, 134811 (2019), [arXiv:1905.10408].
- [224] A. Djouadi *et al.*, Eur. Phys. J. **C73**, 6, 2455 (2013), [arXiv:1205.3169].
- [225] O. J. P. Eboli and D. Zeppenfeld, Phys. Lett. **B495**, 147 (2000), [hep-ph/0009158].
- [226] ATLAS Collaboration, ATLAS-CONF-2020-008 (2020).
- [227] ATLAS Collaboration, ATLAS-CONF-2021-029 (2021).
- [228] M. Aaboud *et al.* (ATLAS), JHEP **10**, 180 (2018), [arXiv:1807.11471].
- [229] ATLAS Collaboration, ATLAS-CONF-2020-052 (2020).
- [230] A. M. Sirunyan *et al.* (CMS), Eur. Phys. J. **C78**, 4, 291 (2018), [arXiv:1711.00431].
- [231] A. M. Sirunyan *et al.* (CMS), Phys. Rev. **D97**, 9, 092005 (2018), [arXiv:1712.02345].
- [232] A. M. Sirunyan *et al.* (CMS), Phys. Lett. **B793**, 520 (2019), [arXiv:1809.05937].
- [233] CMS Collaboration, CMS-PAS-HIG-18-008 (2019).
- [234] M. J. Strassler and K. M. Zurek, Phys. Lett. **B651**, 374 (2007), [hep-ph/0604261]; M. J. Strassler and K. M. Zurek, Phys. Lett. **B661**, 263 (2008), [hep-ph/0605193].
- [235] T. Han *et al.*, JHEP **07**, 008 (2008), [arXiv:0712.2041].

- [236] A. Falkowski *et al.*, Phys. Rev. Lett. **105**, 241801 (2010), [arXiv:1007.3496].
- [237] G. Aad *et al.* (ATLAS), Eur. Phys. J. C **80**, 5, 450 (2020), [arXiv:1909.01246].
- [238] CMS Collaboration, CMS-PAS-EXO-19-007 (2019).
- [239] D. Tucker-Smith and N. Weiner, Phys. Rev. **D64**, 043502 (2001), [hep-ph/0101138].
- [240] S. Chatrchyan *et al.* (CMS), Phys. Lett. **B726**, 564 (2013), [arXiv:1210.7619].
- [241] ATLAS Collaboration, ATLAS-CONF-2020-027 (2020).
- [242] CMS Collaboration, CMS-PAS-HIG-19-005 (2020).
- [243] C. Patrignani *et al.* (Particle Data Group), Chin. Phys. **C40**, 10, 100001 (2016).
- [244] G. Aad *et al.* (ATLAS), Eur. Phys. J. **C76**, 1, 6 (2016), [arXiv:1507.04548].
- [245] L. D. Landau, Dokl. Akad. Nauk Ser. Fiz. **60**, 2, 207 (1948); C.-N. Yang, Phys. Rev. **77**, 242 (1950).
- [246] S. Bolognesi *et al.*, Phys. Rev. **D86**, 095031 (2012), [arXiv:1208.4018].
- [247] G. Aad *et al.* (ATLAS), Eur. Phys. J. **C75**, 10, 476 (2015), [Erratum: Eur. Phys. J. **C76**, 3, 152 (2016)], [arXiv:1506.05669].
- [248] V. Khachatryan *et al.* (CMS), Phys. Rev. **D92**, 1, 012004 (2015), [arXiv:1411.3441]; G. Aad *et al.* (ATLAS), Phys. Lett. **B726**, 120 (2013), [arXiv:1307.1432].
- [249] P. Artoisenet *et al.*, JHEP **11**, 043 (2013), [arXiv:1306.6464].
- [250] J. Ellis *et al.*, JHEP **11**, 134 (2012), [arXiv:1208.6002].
- [251] D0 Collaboration, Note 6387-CONF (2013).
- [252] D0 Collaboration, Note 6406-CONF (2013).
- [253] J. C. Collins and D. E. Soper, Phys. Rev. **D16**, 2219 (1977).
- [254] A. De Rujula *et al.*, Phys. Rev. **D82**, 013003 (2010), [arXiv:1001.5300].
- [255] ATLAS Collaboration, ATLAS-CONF-2017-043 (2017).
- [256] A. M. Sirunyan *et al.* (CMS), Phys. Rev. **D99**, 11, 112003 (2019), [arXiv:1901.00174].
- [257] A. M. Sirunyan *et al.* (CMS), Submitted to: Phys. Rev. (2019), [arXiv:1903.06973].
- [258] G. Aad *et al.* (ATLAS), Eur. Phys. J. **C76**, 12, 658 (2016), [arXiv:1602.04516].
- [259] ATLAS Collaboration, ATL-PHYS-PUB-2019-008 (2019).
- [260] N. Kauer and G. Passarino, JHEP **08**, 116 (2012), [arXiv:1206.4803].
- [261] V. Khachatryan *et al.* (CMS), JHEP **09**, 051 (2016), [arXiv:1605.02329].
- [262] G. Aad *et al.* (ATLAS), Eur. Phys. J. **C75**, 7, 335 (2015), [arXiv:1503.01060].
- [263] M. Aaboud *et al.* (ATLAS), Phys. Lett. **B786**, 223 (2018), [arXiv:1808.01191].
- [264] G. Aad *et al.* (ATLAS), Phys. Rev. **D90**, 5, 052004 (2014), [arXiv:1406.3827].
- [265] CMS Collaboration, CMS-PAS-HIG-16-041 (2017).
- [266] L. J. Dixon and M. S. Siu, Phys. Rev. Lett. **90**, 252001 (2003), [hep-ph/0302233]; S. P. Martin, Phys. Rev. **D86**, 073016 (2012), [arXiv:1208.1533]; L. J. Dixon and Y. Li, Phys. Rev. Lett. **111**, 111802 (2013), [arXiv:1305.3854].
- [267] ATLAS Collaboration, ATL-PHYS-PUB-2013-014 (2013).
- [268] J. Campbell *et al.*, Phys. Rev. Lett. **119**, 18, 181801 (2017), [Addendum: Phys. Rev. Lett. **119**, 19, 199901 (2017)], [arXiv:1704.08259].
- [269] ATLAS Collaboration, ATL-PHYS-PUB-2014-016 (2014).
- [270] F. Caola and K. Melnikov, Phys. Rev. **D88**, 054024 (2013), [arXiv:1307.4935]; J. M. Campbell, R. K. Ellis and C. Williams, JHEP **04**, 060 (2014), [arXiv:1311.3589]; J. M. Campbell, R. K. Ellis and C. Williams, Phys. Rev. **D89**, 5, 053011 (2014), [arXiv:1312.1628].
- [271] C. Englert and M. Spannowsky, Phys. Rev. **D90**, 053003 (2014), [arXiv:1405.0285].
- [272] A. Azatov *et al.*, Zh. Eksp. Teor. Fiz. **147**, 410 (2015), [J. Exp. Theor. Phys. **120**, 354 (2015)], [arXiv:1406.6338]; A. Azatov *et al.*, JHEP **09**, 123 (2016), [arXiv:1608.00977].
- [273] A. David *et al.* (LHC Higgs Cross Section Working Group), “LHC HXSWG interim recommendations to explore the coupling structure of a Higgs-like particle,” (2012), [arXiv:1209.0040].
- [274] M. Dührssen, “Prospects for the measurement of Higgs boson coupling parameters in the mass range from 110–190 GeV,” (2003); M. Dührssen *et al.*, Phys. Rev. **D70**, 113009 (2004), [hep-ph/0406323]; R. Lafaye *et al.*, JHEP **08**, 009 (2009), [arXiv:0904.3866].
- [275] J. R. Espinosa *et al.*, JHEP **05**, 097 (2012), [arXiv:1202.3697]; A. Azatov, R. Contino and J. Galloway, JHEP **04**, 127 (2012), [Erratum: JHEP **04**, 140 (2013)], [arXiv:1202.3415]; D. Carmi *et al.*, JHEP **07**, 136 (2012), [arXiv:1202.3144]; J. R. Espinosa *et al.*, JHEP **12**, 045 (2012), [arXiv:1207.1717].
- [276] M. Gonzalez-Alonso *et al.*, Eur. Phys. J. **C75**, 128 (2015), [arXiv:1412.6038]; A. Greljo *et al.*, Eur. Phys. J. **C76**, 3, 158 (2016), [arXiv:1512.06135].
- [277] G. F. Giudice *et al.*, JHEP **06**, 045 (2007), [hep-ph/0703164].
- [278] S. Willenbrock and C. Zhang, Ann. Rev. Nucl. Part. Sci. **64**, 83 (2014), [arXiv:1401.0470]; I. Brivio and M. Trott, Phys. Rept. **793**, 1 (2019), [arXiv:1706.08945]; S. Dawson, C. Englert and T. Plehn, Phys. Rept. **816**, 1 (2019), [arXiv:1808.01324]; T. Cohen, PoS **TASI2018**, 011 (2019), [arXiv:1903.03622].
- [279] F. Feruglio, Int. J. Mod. Phys. **A8**, 4937 (1993), [hep-ph/9301281]; G. Buchalla, O. Catà and C. Krause, Nucl. Phys. **B880**, 552 (2014), [Erratum: Nucl. Phys. **B913**, 475 (2016)], [arXiv:1307.5017]; R. Alonso *et al.*, Phys. Lett. **B722**, 330 (2013), [Erratum: Phys. Lett. **B726**, 926 (2013)], [arXiv:1212.3305]; A. V. Manohar, in “Les Houches summer school: EFT in Particle Physics and Cosmology Les Houches, Chamonix Valley, France, July 3–28, 2017,” (2018), [arXiv:1804.05863]; I. Brivio *et al.*, JHEP **03**, 024 (2014), [arXiv:1311.1823].
- [280] J. de Blas *et al.*, JHEP **03**, 109 (2018), [arXiv:1711.10391].
- [281] A. Manohar and H. Georgi, Nucl. Phys. **B234**, 189 (1984); M. A. Luty, Phys. Rev. **D57**, 1531 (1998), [hep-ph/9706235]; D. Liu *et al.*, JHEP **11**, 141 (2016), [arXiv:1603.03064].
- [282] W. Buchmüller and D. Wyler, Nucl. Phys. **B268**, 621 (1986).
- [283] C. J. C. Burges and H. J. Schnitzer, Nucl. Phys. **B228**, 464 (1983); C. N. Leung, S. T. Love and S. Rao, Z. Phys. **C31**, 433 (1986).
- [284] B. Grzadkowski *et al.*, JHEP **10**, 085 (2010), [arXiv:1008.4884].
- [285] L. Lehman and A. Martin, JHEP **02**, 081 (2016), [arXiv:1510.00372]; B. Henning *et al.*, JHEP **08**, 016 (2017), [arXiv:1512.03433].
- [286] C. Hays *et al.*, JHEP **02**, 123 (2019), [arXiv:1808.00442].
- [287] R. Alonso *et al.*, JHEP **04**, 159 (2014), [arXiv:1312.2014].
- [288] A. Falkowski, LHCHXSWG-INT-2015-001 (2015); A. Falkowski, Pramana **87**, 3, 39 (2016), [arXiv:1505.00046].
- [289] A. M. Sirunyan *et al.* (CMS), Phys. Lett. **B792**, 369 (2019), [arXiv:1812.06504].

- [290] M. Aaboud *et al.* (ATLAS), Phys. Rev. **D98**, 052005 (2018), [arXiv:1802.04146].
- [291] F. Maltoni *et al.* (2019), [arXiv:1906.12310].
- [292] R. S. Gupta, A. Pomarol and F. Riva, Phys. Rev. **D91**, 3, 035001 (2015), [arXiv:1405.0181].
- [293] B. A. Kniehl and M. Spira, Z. Phys. **C69**, 77 (1995), [hep-ph/9505225].
- [294] R. Contino *et al.*, JHEP **07**, 035 (2013), [arXiv:1303.3876].
- [295] A. Azatov and J. Galloway, Phys. Rev. **D85**, 055013 (2012), [arXiv:1110.5646].
- [296] G. Isidori and M. Trott, JHEP **02**, 082 (2014), [arXiv:1307.4051]; A. Pomarol and F. Riva, JHEP **01**, 151 (2014), [arXiv:1308.2803].
- [297] J. Ellis, V. Sanz and T. You, JHEP **07**, 036 (2014), [arXiv:1404.3667]; A. Biekötter *et al.*, Phys. Rev. **D91**, 055029 (2015), [arXiv:1406.7320].
- [298] LHC Higgs Cross Section Working Group, <https://twiki.cern.ch/twiki/bin/view/LHCPhysics/LHCHWG2KAPPA>.
- [299] ATLAS and CMS Collaborations, CMS-PAS-HIG-15-002 (2015).
- [300] M. Reece, New J. Phys. **15**, 043003 (2013), [arXiv:1208.1765].
- [301] A. M. Sirunyan *et al.* (CMS), Eur. Phys. J. **C79**, 5, 421 (2019), [arXiv:1809.10733].
- [302] G. Aad *et al.* (ATLAS) (2019), [arXiv:1909.02845].
- [303] ATLAS Collaboration, ATLAS-CONF-2019-032 (2019).
- [304] CMS Collaboration, CMS-PAS-HIG-19-001 (2019).
- [305] G. Aad *et al.* (ATLAS), Phys. Lett. **B753**, 69 (2016), [arXiv:1508.02507].
- [306] N. Berger *et al.* (2019), [arXiv:1906.02754].
- [307] ATLAS Collaboration, ATLAS-CONF-2017-045 (2017).
- [308] CMS Collaboration, CMS-PAS-HIG-16-040 (2017).
- [309] ATLAS Collaboration, ATLAS-CONF-2018-028 (2018).
- [310] ATLAS Collaboration, ATLAS-CONF-2019-025 (2019).
- [311] ATLAS Collaboration, CMS-PAS-HIG-19-001 (2019).
- [312] M. Aaboud *et al.* (ATLAS), JHEP **05**, 141 (2019), [arXiv:1903.04618].
- [313] ATLAS Collaboration, ATLAS-CONF-2020-053 (2020).
- [314] M. McCullough, Phys. Rev. **D90**, 1, 015001 (2014), [Erratum: Phys. Rev. **D92**, 3, 039903 (2015)], [arXiv:1312.3322].
- [315] G. Degross *et al.*, JHEP **12**, 080 (2016), [arXiv:1607.04251].
- [316] M. Gorbahn and U. Haisch, JHEP **10**, 094 (2016), [arXiv:1607.03773].
- [317] ATLAS Collaboration, ATL-PHYS-PUB-2019-009 (2019).
- [318] F. Bishara *et al.*, Phys. Rev. Lett. **118**, 12, 121801 (2017), [arXiv:1606.09253].
- [319] ATLAS Collaboration, ATLAS-CONF-2019-029 (2019).
- [320] ATLAS Collaboration, ATLAS-CONF-2019-049 (2019).
- [321] S. Di Vita *et al.*, JHEP **09**, 069 (2017), [arXiv:1704.01953]; F. Maltoni *et al.*, Eur. Phys. J. **C77**, 12, 887 (2017), [arXiv:1709.08649].
- [322] Y. Gershtein, and A. Pomarol, *Extra Dimensions*, in this volume.
- [323] S. Weinberg, Phys. Rev. **D13**, 974 (1976), [Addendum: Phys. Rev. **D19**, 1277 (1979)]; L. Susskind, Phys. Rev. **D20**, 2619 (1979); For a review, see C. T. Hill and E. H. Simmons, Phys. Reports **381**, 235 (2003) [Erratum: 390, 553 (2004)], [arXiv:hep-ph/0203079].
- [324] Z. Chacko, R. Franceschini and R. K. Mishra, JHEP **04**, 015 (2013), [arXiv:1209.3259].
- [325] L. E. Ibanez and G. G. Ross, Phys. Lett. **110B**, 215 (1982); L. E. Ibanez, Phys. Lett. **118B**, 73 (1982); J. R. Ellis, D. V. Nanopoulos and K. Tamvakis, Phys. Lett. **121B**, 123 (1983); L. Alvarez-Gaume, J. Polchinski and M. B. Wise, Nucl. Phys. **B221**, 495 (1983).
- [326] S. Dimopoulos and G. F. Giudice, Phys. Lett. **B357**, 573 (1995), [hep-ph/9507282]; M. Papucci, J. T. Ruderman and A. Weiler, JHEP **09**, 035 (2012), [arXiv:1110.6926].
- [327] ATLAS Collaboration, <https://twiki.cern.ch/twiki/bin/view/AtlasPublic/Publications>; CMS Collaboration, <http://cms-results.web.cern.ch/cms-results/public-results/publications/SUS/STOP.html>.
- [328] J. Mrazek *et al.*, Nucl. Phys. **B853**, 1 (2011), [arXiv:1105.5403].
- [329] D. B. Kaplan, Nucl. Phys. **B365**, 259 (1991).
- [330] G. Panico *et al.*, JHEP **03**, 051 (2013), [arXiv:1210.7114].
- [331] H. E. Haber and G. L. Kane, Phys. Rept. **117**, 75 (1985).
- [332] P. Slavich *et al.*, Eur. Phys. J. C **81**, 5, 450 (2021), [arXiv:2012.15629].
- [333] P. Draper, G. Lee and C. E. M. Wagner, Phys. Rev. **D89**, 5, 055023 (2014), [arXiv:1312.5743].
- [334] J. F. Gunion and H. E. Haber, Phys. Rev. **D67**, 075019 (2003), [hep-ph/0207010].
- [335] H. E. Haber and Y. Nir, Nucl. Phys. **B335**, 363 (1990).
- [336] E. L. Berger *et al.*, Phys. Rev. **D66**, 095001 (2002), [hep-ph/0205342].
- [337] A. Djouadi, Phys. Rept. **459**, 1 (2008), [hep-ph/0503173].
- [338] P. Bechtle *et al.*, Eur. Phys. J. **C77**, 2, 67 (2017), [arXiv:1608.00638].
- [339] E. Bagnaschi *et al.*, Eur. Phys. J. **C79**, 7, 617 (2019), [arXiv:1808.07542].
- [340] A. Djouadi, J. Kalinowski and P. M. Zerwas, Z. Phys. **C57**, 569 (1993).
- [341] G. Lee and C. E. M. Wagner, Phys. Rev. **D92**, 7, 075032 (2015), [arXiv:1508.00576].
- [342] D. Dicus *et al.*, Phys. Rev. **D59**, 094016 (1999), [hep-ph/9811492].
- [343] M. Carena *et al.*, JHEP **07**, 091 (2012), [arXiv:1203.1041].
- [344] A. A. Barrientos Bendezu and B. A. Kniehl, Phys. Rev. **D64**, 035006 (2001), [hep-ph/0103018].
- [345] LHC Higgs Working Group, <https://twiki.cern.ch/twiki/bin/view/LHCPhysics/LHCHWGMSSMCharged>.
- [346] A. Djouadi, J. Ellis and J. Quevillon, JHEP **07**, 105 (2016), [arXiv:1605.00542]; M. Carena and Z. Liu, JHEP **11**, 159 (2016), [arXiv:1608.07282].
- [347] LHC Higgs Working Group for BSM Higgs, <https://twiki.cern.ch/twiki/bin/view/LHCPhysics/LHCHWG3>.
- [348] M. Carena *et al.*, Eur. Phys. J. **C73**, 9, 2552 (2013), [arXiv:1302.7033].
- [349] H. Bahl, S. Liebler and T. Stefaniak, Eur. Phys. J. **C79**, 3, 279 (2019), [arXiv:1901.05933].
- [350] L. Maiani, A. D. Polosa and V. Riquer, Phys. Lett. **B718**, 465 (2012), [arXiv:1209.4816]; A. Djouadi and J. Quevillon, JHEP **10**, 028 (2013), [arXiv:1304.1787]; A. Djouadi *et al.*, Eur. Phys. J. **C73**, 2650 (2013), [arXiv:1307.5205].
- [351] M. Carena *et al.*, Phys. Rev. **D91**, 3, 035003 (2015), [arXiv:1410.4969].
- [352] E. Bagnaschi *et al.*, Eur. Phys. J. C **79**, 7, 617 (2019), [arXiv:1808.07542].
- [353] H. Bahl *et al.*, Eur. Phys. J. C **80**, 10, 916 (2020), [arXiv:2005.14536].
- [354] R. S. Chivukula and H. Georgi, Phys. Lett. **B188**, 99 (1987); L. J. Hall and L. Randall, Phys. Rev. Lett. **65**, 2939 (1990); A. J. Buras *et al.*, Phys. Lett. **B500**, 161 (2001), [hep-ph/0007085]; G. D'Ambrosio *et al.*, Nucl. Phys. **B645**, 155 (2002), [hep-ph/0207036].

- [355] L. J. Hall, J. D. Lykken and S. Weinberg, *Phys. Rev.* **D27**, 2359 (1983); J. E. Kim and H. P. Nilles, *Phys. Lett.* **138B**, 150 (1984); G. F. Giudice and A. Masiero, *Phys. Lett.* **B206**, 480 (1988).
- [356] U. Ellwanger, C. Hugonie and A. M. Teixeira, *Phys. Rept.* **496**, 1 (2010), [arXiv:0910.1785].
- [357] P. Fayet, *Nucl. Phys.* **B90**, 104 (1975).
- [358] C. Panagiotakopoulos and K. Tamvakis, *Phys. Lett.* **B469**, 145 (1999), [hep-ph/9908351]; A. Dedes *et al.*, *Phys. Rev.* **D63**, 055009 (2001), [hep-ph/0009125]; A. Menon, D. E. Morrissey and C. E. M. Wagner, *Phys. Rev.* **D70**, 035005 (2004), [hep-ph/0404184].
- [359] M. Cvetič *et al.*, *Phys. Rev.* **D56**, 2861 (1997), [Erratum: *Phys. Rev.* **D58**, 119905 (1998)], [hep-ph/9703317]; P. Langacker and J. Wang, *Phys. Rev.* **D58**, 115010 (1998), [hep-ph/9804428].
- [360] J. Erler, P. Langacker and T.-j. Li, *Phys. Rev.* **D66**, 015002 (2002), [hep-ph/0205001]; T. Han, P. Langacker and B. McElrath, *Phys. Rev.* **D70**, 115006 (2004), [hep-ph/0405244]; V. Barger *et al.*, *Phys. Rev.* **D73**, 115010 (2006), [hep-ph/0603247].
- [361] V. Barger, P. Langacker and G. Shaughnessy, *Phys. Rev.* **D75**, 055013 (2007), [hep-ph/0611239].
- [362] D. E. Lopez-Fogliani and C. Munoz, *Phys. Rev. Lett.* **97**, 041801 (2006), [hep-ph/0508297].
- [363] B. A. Dobrescu, G. L. Landsberg and K. T. Matchev, *Phys. Rev.* **D63**, 075003 (2001), [hep-ph/0005308]; R. Dermisek and J. F. Gunion, *Phys. Rev. Lett.* **95**, 041801 (2005), [hep-ph/0502105].
- [364] O. J. P. Eboli and D. Zeppenfeld, *Phys. Lett.* **B495**, 147 (2000), [hep-ph/0009158]; H. Davoudiasl, T. Han and H. E. Logan, *Phys. Rev.* **D71**, 115007 (2005), [hep-ph/0412269].
- [365] J.-J. Cao *et al.*, *JHEP* **03**, 086 (2012), [arXiv:1202.5821].
- [366] LHC Higgs Working Group, Beyond the Standard Model Higgs – NMSSM, <https://twiki.cern.ch/twiki/bin/view/LHCPhysics/LHCHWGMSSM>.
- [367] M. Carena *et al.*, *Phys. Rev.* **D93**, 3, 035013 (2016), [arXiv:1510.09137].
- [368] P. Batra *et al.*, *JHEP* **02**, 043 (2004), [hep-ph/0309149].
- [369] R. Huo *et al.*, *Phys. Rev.* **D87**, 5, 055011 (2013), [arXiv:1212.0560].
- [370] J. Engel, M. J. Ramsey-Musolf and U. van Kolck, *Prog. Part. Nucl. Phys.* **71**, 21 (2013), [arXiv:1303.2371].
- [371] S. Dimopoulos and S. D. Thomas, *Nucl. Phys.* **B465**, 23 (1996), [hep-ph/9510220]; S. D. Thomas, *Int. J. Mod. Phys.* **A13**, 2307 (1998), [hep-ph/9803420].
- [372] A. Pilaftsis and C. E. M. Wagner, *Nucl. Phys.* **B553**, 3 (1999), [hep-ph/9902371].
- [373] M. Frank *et al.*, *JHEP* **02**, 047 (2007), [hep-ph/0611326].
- [374] M. Carena *et al.*, *Nucl. Phys.* **B586**, 92 (2000), [hep-ph/0003180].
- [375] B. Li and C. E. M. Wagner, *Phys. Rev.* **D91**, 095019 (2015), [arXiv:1502.02210].
- [376] M. D. Goodsell and F. Staub, *Eur. Phys. J.* **C77**, 1, 46 (2017), [arXiv:1604.05335]; A. Chakraborty *et al.*, *Phys. Rev.* **D90**, 5, 055005 (2014), [arXiv:1301.2745]; M. Carena *et al.*, *JHEP* **02**, 123 (2016), [arXiv:1512.00437].
- [377] J. F. Gunion and H. E. Haber, *Phys. Rev.* **D67**, 075019 (2003), [hep-ph/0207010]; G. C. Branco *et al.*, *Phys. Rept.* **516**, 1 (2012), [arXiv:1106.0034].
- [378] N. G. Deshpande and E. Ma, *Phys. Rev.* **D18**, 2574 (1978).
- [379] A. Goudelis, B. Herrmann and O. Stål, *JHEP* **09**, 106 (2013), [arXiv:1303.3010].
- [380] C. D. Froggatt and H. B. Nielsen, *Nucl. Phys.* **B147**, 277 (1979).
- [381] K. S. Babu and S. Nandi, *Phys. Rev.* **D62**, 033002 (2000), [hep-ph/9907213]; G. F. Giudice and O. Lebedev, *Phys. Lett.* **B665**, 79 (2008), [arXiv:0804.1753].
- [382] E. Accomando *et al.*, CERN Report **2006-009** (2006), [hep-ph/0608079].
- [383] T. Robens and T. Stefaniak, *Eur. Phys. J.* **C75**, 104 (2015), [arXiv:1501.02234].
- [384] S. L. Glashow and S. Weinberg, *Phys. Rev.* **D15**, 1958 (1977); E. A. Paschos, *Phys. Rev.* **D15**, 1966 (1977).
- [385] G. C. Branco, W. Grimus and L. Lavoura, *Phys. Lett.* **B380**, 119 (1996), [hep-ph/9601383]; F. J. Botella, G. C. Branco and M. N. Rebelo, *Phys. Lett.* **B687**, 194 (2010), [arXiv:0911.1753].
- [386] J. Schechter and J. W. F. Valle, *Phys. Rev.* **D22**, 2227 (1980); T. P. Cheng and L.-F. Li, *Phys. Rev.* **D22**, 2860 (1980).
- [387] H. Georgi and M. Machacek, *Nucl. Phys.* **B262**, 463 (1985); M. S. Chanowitz and M. Golden, *Phys. Lett.* **165B**, 105 (1985); J. F. Gunion, R. Vega and J. Wudka, *Phys. Rev.* **D42**, 1673 (1990).
- [388] P. Nath *et al.*, *Nucl. Phys. Proc. Suppl.* **200-202**, 185 (2010), [arXiv:1001.2693].
- [389] J. Garayoa and T. Schwetz, *JHEP* **03**, 009 (2008), [arXiv:0712.1453].
- [390] H. E. Haber and H. E. Logan, *Phys. Rev.* **D62**, 015011 (2000), [hep-ph/9909335]; S. Kanemura and K. Yagyu, *Phys. Rev.* **D85**, 115009 (2012), [arXiv:1201.6287].
- [391] J. F. Gunion, R. Vega and J. Wudka, *Phys. Rev.* **D43**, 2322 (1991).
- [392] I. Low and J. Lykken, *JHEP* **10**, 053 (2010), [arXiv:1005.0872]; I. Low, J. Lykken and G. Shaughnessy, *Phys. Rev.* **D86**, 093012 (2012), [arXiv:1207.1093].
- [393] H. E. Logan and M.-A. Roy, *Phys. Rev.* **D82**, 115011 (2010), [arXiv:1008.4869]; A. Falkowski, S. Rychkov and A. Urbano, *JHEP* **04**, 073 (2012), [arXiv:1202.1532].
- [394] N. Arkani-Hamed *et al.*, *JHEP* **07**, 034 (2002), [hep-ph/0206021]; N. Arkani-Hamed, A. G. Cohen and H. Georgi, *Phys. Lett.* **B513**, 232 (2001), [hep-ph/0105239].
- [395] M. Perelstein, *Prog. Part. Nucl. Phys.* **58**, 247 (2007), [hep-ph/0512128]; M. Schmaltz and D. Tucker-Smith, *Ann. Rev. Nucl. Part. Sci.* **55**, 229 (2005), [hep-ph/0502182].
- [396] J. A. Casas, J. R. Espinosa and I. Hidalgo, *JHEP* **03**, 038 (2005), [hep-ph/0502066].
- [397] H.-C. Cheng and I. Low, *JHEP* **09**, 051 (2003), [hep-ph/0308199].
- [398] M. Carena *et al.*, *Phys. Rev.* **D75**, 091701 (2007), [hep-ph/0610156].
- [399] M. Aaboud *et al.* (ATLAS), *Phys. Rev. Lett.* **121**, 21, 211801 (2018), [arXiv:1808.02343]; A. M. Sirunyan *et al.* (CMS), *Eur. Phys. J.* **C79**, 4, 364 (2019), [arXiv:1812.09768].
- [400] H. Georgi, A. E. Nelson and A. Manohar, *Phys. Lett.* **126B**, 169 (1983); A. E. Nelson and M. J. Strassler, *JHEP* **09**, 030 (2000), [hep-ph/0006251]; S. Davidson, G. Isidori and S. Uhlig, *Phys. Lett.* **B663**, 73 (2008), [arXiv:0711.3376].
- [401] C. Csaki, A. Falkowski and A. Weiler, *JHEP* **09**, 008 (2008), [arXiv:0804.1954]; B. Keren-Zur *et al.*, *Nucl. Phys.* **B867**, 394 (2013), [arXiv:1205.5803].
- [402] O. Matsedonskyi, G. Panico and A. Wulzer, *JHEP* **01**, 164 (2013), [arXiv:1204.6333]; M. Redi and A. Tesi, *JHEP* **10**, 166 (2012), [arXiv:1205.0232]; D. Marzocca, M. Serone and J. Shu, *JHEP* **08**, 013 (2012), [arXiv:1205.0770]; A. Pomarol and F. Riva, *JHEP* **08**, 135 (2012), [arXiv:1205.6434].
- [403] R. Contino and G. Servant, *JHEP* **06**, 026 (2008), [arXiv:0801.1679]; J. Mrazek and A. Wulzer, *Phys. Rev.* **D81**, 075006 (2010), [arXiv:0909.3977]; A. De Simone *et al.*, *JHEP* **04**, 004 (2013), [arXiv:1211.5663]; A. Azatov *et al.*, *Phys. Rev.* **D89**, 7, 075001 (2014), [arXiv:1308.6601].

- [404] A. Banfi, A. Martin and V. Sanz, *JHEP* **08**, 053 (2014), [arXiv:1308.4771]; A. Azatov and A. Paul, *JHEP* **01**, 014 (2014), [arXiv:1309.5273]; C. Grojean *et al.*, *JHEP* **05**, 022 (2014), [arXiv:1312.3317].
- [405] A. Azatov *et al.*, *Phys. Rev.* **D92**, 3, 035001 (2015), [arXiv:1502.00539].
- [406] K. Agashe, R. Contino and A. Pomarol, *Nucl. Phys.* **B719**, 165 (2005), [hep-ph/0412089]; R. Contino, L. Da Rold and A. Pomarol, *Phys. Rev.* **D75**, 055014 (2007), [hep-ph/0612048]; D. Pappadopulo, A. Thamm and R. Torre, *JHEP* **07**, 058 (2013), [arXiv:1303.3062]; M. Montull *et al.*, *Phys. Rev.* **D88**, 095006 (2013), [arXiv:1308.0559].
- [407] M. Carena, L. Da Rold and E. Pontón, *JHEP* **06**, 159 (2014), [arXiv:1402.2987]; D. Liu, I. Low and C. E. M. Wagner, *Phys. Rev.* **D96**, 3, 035013 (2017), [arXiv:1703.07791].
- [408] I. Low, R. Rattazzi and A. Vichi, *JHEP* **04**, 126 (2010), [arXiv:0907.5413].
- [409] M. Ciuchini *et al.*, *JHEP* **08**, 106 (2013), [arXiv:1306.4644].
- [410] C. Grojean, O. Matsedonskyi and G. Panico, *JHEP* **10**, 160 (2013), [arXiv:1306.4655].
- [411] M. Geller and O. Telem, *Phys. Rev. Lett.* **114**, 191801 (2015), [arXiv:1411.2974].
- [412] P. Batra and Z. Chacko, *Phys. Rev.* **D79**, 095012 (2009), [arXiv:0811.0394]; R. Barbieri *et al.*, *JHEP* **08**, 161 (2015), [arXiv:1501.07803]; M. Low, A. Tesi and L.-T. Wang, *Phys. Rev.* **D91**, 095012 (2015), [arXiv:1501.07890].
- [413] G. Aad *et al.* (ATLAS), *Phys. Lett. B* **822**, 136651 (2021), [arXiv:2102.13405].
- [414] CMS Collaboration, CMS-PAS-HIG-17-13 (2017); V. Khachatryan *et al.* (CMS), *Phys. Lett.* **B767**, 147 (2017), [arXiv:1609.02507].
- [415] M. Aaboud *et al.* (ATLAS), *Phys. Lett.* **B775**, 105 (2017), [arXiv:1707.04147].
- [416] A. M. Sirunyan *et al.* (CMS), *Phys. Lett. B* **793**, 320 (2019), [arXiv:1811.08459].
- [417] M. Aaboud *et al.* (ATLAS), *JHEP* **10**, 112 (2017), [arXiv:1708.00212].
- [418] CMS Collaboration, CMS-PAS-HIG-16-014 (2016).
- [419] G. Aad *et al.* (ATLAS), *Eur. Phys. J. C* **81**, 4, 332 (2021), [arXiv:2009.14791].
- [420] CMS Collaboration, CMS-PAS-HIG-16-033 (2016).
- [421] CMS Collaboration, CMS-PAS-HIG-16-023 (2016).
- [422] G. Aad *et al.* (ATLAS), *Eur. Phys. J. C* **80**, 12, 1165 (2020), [arXiv:2004.14636].
- [423] CMS Collaboration, CMS-PAS-HIG-16-034 (2017).
- [424] A. M. Sirunyan *et al.* (CMS), *Phys. Rev. D* **102**, 3, 032003 (2020), [arXiv:2006.06391].
- [425] ATLAS Collaboration, ATLAS-CONF-2016-082 (2016).
- [426] ATLAS Collaboration, ATLAS-CONF-2013-067 (2013).
- [427] A. M. Sirunyan *et al.* (CMS), *JHEP* **03**, 034 (2020), [arXiv:1912.01594].
- [428] ATLAS Collaboration, ATLAS-CONF-2012-018 (2012).
- [429] M. Aaboud *et al.* (ATLAS), *Phys. Lett.* **B777**, 91 (2018), [arXiv:1708.04445].
- [430] G. Aad *et al.* (ATLAS), *JHEP* **09**, 091 (2019), [arXiv:1906.08589].
- [431] M. Aaboud *et al.* (ATLAS), *Phys. Rev.* **D98**, 5, 052008 (2018), [arXiv:1808.02380].
- [432] ATLAS Collaboration, ATLAS-CONF-2016-004 (2016); M. Aaboud *et al.* (ATLAS), *JHEP* **05**, 124 (2019), [arXiv:1811.11028]; M. Aaboud *et al.* (ATLAS), *Eur. Phys. J. C* **78**, 12, 1007 (2018), [arXiv:1807.08567].
- [433] ATLAS Collaboration, ATLAS-CONF-2019-030 (2019); M. Aaboud *et al.* (ATLAS), *Phys. Rev. Lett.* **121**, 19, 191801 (2018), [Erratum: *Phys. Rev. Lett.* **122**, 089901 (2019)], [arXiv:1808.00336]; G. Aad *et al.* (ATLAS) (2019), [arXiv:1908.06765].
- [434] A. M. Sirunyan *et al.* (CMS), *Phys. Lett. B* **788**, 7 (2019), [arXiv:1806.00408].
- [435] V. Khachatryan *et al.* (CMS), *Phys. Lett.* **B755**, 217 (2016), [arXiv:1510.01181].
- [436] G. Aad *et al.* (ATLAS), *Phys. Rev. Lett.* **125**, 5, 051801 (2020), [arXiv:2002.12223].
- [437] A. M. Sirunyan *et al.* (CMS), *JHEP* **09**, 007 (2018), [arXiv:1803.06553].
- [438] V. M. Abazov *et al.* (D0), *Phys. Rev. Lett.* **104**, 151801 (2010), [arXiv:0912.0968].
- [439] D0 Collaboration, D0Note 5974-CONF (2011).
- [440] R. Aaij *et al.* (LHCb), *JHEP* **05**, 132 (2013), [arXiv:1304.2591].
- [441] A. M. Sirunyan *et al.* (CMS), *JHEP* **05**, 210 (2019), [arXiv:1903.10228].
- [442] M. Aaboud *et al.* (ATLAS), *JHEP* **07**, 117 (2019), [arXiv:1901.08144].
- [443] A. M. Sirunyan *et al.* (CMS) (2019), [arXiv:1907.03152].
- [444] A. M. Sirunyan *et al.* (CMS), *JHEP* **03**, 103 (2020), [arXiv:1911.10267].
- [445] ATLAS Collaboration, ATLAS-CONF-2019-036 (2019).
- [446] A. M. Sirunyan *et al.* (CMS), *JHEP* **11**, 161 (2018), [arXiv:1808.01890].
- [447] G. Aad *et al.* (ATLAS), *JHEP* **08**, 148 (2015), [arXiv:1505.07018].
- [448] A. M. Sirunyan *et al.* (CMS), *JHEP* **04**, 171 (2020), [arXiv:1908.01115].
- [449] G. Aad *et al.* (ATLAS), *Phys. Rev. D* **102**, 3, 032004 (2020), [arXiv:1907.02749].
- [450] S. Chatrchyan *et al.* (CMS), *Phys. Lett.* **B722**, 207 (2013), [arXiv:1302.2892]; CMS Collaboration, CMS-PAS-HIG-16-025 (2016); A. M. Sirunyan *et al.* (CMS), *JHEP* **08**, 113 (2018), [arXiv:1805.12191].
- [451] V. M. Abazov *et al.* (D0), *Phys. Lett.* **B698**, 97 (2011), [arXiv:1011.1931].
- [452] T. Aaltonen *et al.* (CDF), *Phys. Rev.* **D85**, 032005 (2012), [arXiv:1106.4782].
- [453] ATLAS Collaboration, ATLAS-CONF-2017-055 (2017).
- [454] G. Aad *et al.* (ATLAS), *Phys. Rev. D* **102**, 11, 112008 (2020), [arXiv:2007.05293]; G. Aad *et al.* (ATLAS), *Phys. Lett.* **B744**, 163 (2015), [arXiv:1502.04478].
- [455] A. M. Sirunyan *et al.* (CMS), *JHEP* **03**, 065 (2020), [arXiv:1910.11634].
- [456] A. M. Sirunyan *et al.* (CMS), *Eur. Phys. J. C* **79**, 7, 564 (2019), [arXiv:1903.00941].
- [457] G. Aad *et al.* (ATLAS), *Phys. Rev. Lett.* **125**, 22, 221802 (2020), [arXiv:2004.01678].
- [458] A. M. Sirunyan *et al.* (CMS), *JHEP* **03**, 055 (2020), [arXiv:1911.03781].
- [459] M. Aaboud *et al.* (ATLAS), *Phys. Lett.* **B759**, 555 (2016), [arXiv:1603.09203].
- [460] M. Aaboud *et al.* (ATLAS), *JHEP* **09**, 139 (2018), [arXiv:1807.07915].
- [461] CMS Collaboration, CMS-PAS-HIG-16-031 (2016); A. M. Sirunyan *et al.* (CMS), *JHEP* **07**, 142 (2019), [arXiv:1903.04560].
- [462] ATLAS Collaboration, ATLAS-CONF-2012-010 (2012).
- [463] A. M. Sirunyan *et al.* (CMS), *Phys. Rev. D* **102**, 7, 072001 (2020), [arXiv:2005.08900].

- [464] G. Aad *et al.* (ATLAS), JHEP **06**, 145 (2021), [arXiv:2102.10076].
- [465] A. M. Sirunyan *et al.* (CMS), JHEP **07**, 126 (2020), [arXiv:2001.07763]; V. Khachatryan *et al.* (CMS), JHEP **11**, 018 (2015), [arXiv:1508.07774]; A. M. Sirunyan *et al.* (CMS) (2019), [arXiv:1908.09206].
- [466] G. Aad *et al.* (ATLAS), Phys. Rev. Lett. **114**, 23, 231801 (2015), [arXiv:1503.04233].
- [467] A. M. Sirunyan *et al.* (CMS), Phys. Rev. Lett. **119**, 14, 141802 (2017), [arXiv:1705.02942].
- [468] A. M. Sirunyan *et al.* (CMS), Eur. Phys. J. C **81**, 8, 723 (2021), [arXiv:2104.04762].
- [469] A. M. Sirunyan *et al.* (CMS), Phys. Rev. Lett. **123**, 13, 131802 (2019), [arXiv:1905.07453].
- [470] A. M. Sirunyan *et al.* (CMS), JHEP **11**, 115 (2018), [arXiv:1808.06575].
- [471] ATLAS Collaboration, ATLAS-CONF-2011-020 (2011).
- [472] A. M. Sirunyan *et al.* (CMS), JHEP **11**, 010 (2017), [arXiv:1707.07283].
- [473] G. Aad *et al.* (ATLAS), Phys. Rev. **D92**, 5, 052002 (2015), [arXiv:1505.01609]; ATLAS Collaboration, ATLAS-CONF-2012-079 (2012).
- [474] CMS Collaboration, CMS-PAS-HIG-21-003 (2021).
- [475] A. Tumasyan *et al.* (CMS), JHEP **11**, 057 (2021), [arXiv:2106.10361].
- [476] CMS Collaboration, CMS-PAS-HIG-16-055 (2016).
- [477] A. M. Sirunyan *et al.* (CMS), JHEP **08**, 139 (2020), [arXiv:2005.08694]; V. Khachatryan *et al.* (CMS), JHEP **10**, 076 (2017), [arXiv:1701.02032]; A. M. Sirunyan *et al.* (CMS), Phys. Lett. **B795**, 398 (2019), [arXiv:1812.06359]; A. M. Sirunyan *et al.* (CMS) (2019), [arXiv:1907.07235]; A. M. Sirunyan *et al.* (CMS), Phys. Lett. **B785**, 462 (2018), [arXiv:1805.10191]; A. M. Sirunyan *et al.* (CMS), JHEP **11**, 018 (2018), [arXiv:1805.04865]; CMS Collaboration, CMS-PAS-HIG-18-015 (2019).
- [478] V. M. Abazov *et al.* (D0), Phys. Rev. Lett. **103**, 061801 (2009), [arXiv:0905.3381].
- [479] A. M. Sirunyan *et al.* (CMS), Phys. Lett. **B796**, 131 (2019), [arXiv:1812.00380].
- [480] S. Schael *et al.* (ALEPH), JHEP **05**, 049 (2010), [arXiv:1003.0705].
- [481] B. Aubert *et al.* (BaBar), Phys. Rev. Lett. **103**, 081803 (2009), [arXiv:0905.4539].
- [482] B. Aubert *et al.* (BaBar), Phys. Rev. Lett. **103**, 181801 (2009), [arXiv:0906.2219].
- [483] ATLAS Collaboration, ATLAS-CONF-2016-051 (2016); ATLAS Collaboration, ATLAS-CONF-2017-053 (2017); M. Aaboud *et al.* (ATLAS), Eur. Phys. J. **C79**, 1, 58 (2019), [arXiv:1808.01899].
- [484] CMS Collaboration, CMS-PAS-HIG-16-036 (2017).
- [485] S. Schael *et al.* (ALEPH, DELPHI, L3, OPAL, LEP Working Group for Higgs Boson Searches), Eur. Phys. J. **C47**, 547 (2006), [hep-ex/0602042].
- [486] ATLAS Collaboration, ATLAS-CONF-2013-027 (2013).
- [487] CMS Collaboration, CMS-PAS-HIG-13-016 (2013).
- [488] A. Heister *et al.* (ALEPH), Phys. Lett. **B526**, 191 (2002), [hep-ex/0201014]; P. Achard *et al.* (L3), Phys. Lett. **B545**, 30 (2002), [hep-ex/0208042].
- [489] M. Carena *et al.* (1999), [hep-ph/9912223].
- [490] M. M. Kado and C. G. Tully, Ann. Rev. Nucl. Part. Sci. **52**, 65 (2002).
- [491] G. Abbiendi *et al.* (OPAL), Eur. Phys. J. **C23**, 397 (2002), [hep-ex/0111010]; J. Abdallah *et al.* (DELPHI), Eur. Phys. J. **C38**, 1 (2004), [hep-ex/0410017].
- [492] M. Carena *et al.*, Eur. Phys. J. **C45**, 797 (2006), [hep-ph/0511023].
- [493] ATLAS Collaboration, ATLAS-CONF-2016-104 (2016).
- [494] S. Chatrchyan *et al.* (CMS), JHEP **09**, 029 (2012), [Erratum: JHEP **03**, 132 (2014)], [arXiv:1204.2488].
- [495] M. Aaboud *et al.* (ATLAS), Phys. Rev. Lett. **119**, 19, 191803 (2017), [arXiv:1707.06025].
- [496] V. Khachatryan *et al.* (CMS), Phys. Lett. **B758**, 296 (2016), [arXiv:1511.03610].
- [497] A. M. Sirunyan *et al.* (CMS), JHEP **11**, 010 (2017), [arXiv:1707.07283].
- [498] J. Bernon *et al.*, Phys. Rev. **D91**, 7, 075019 (2015), [arXiv:1412.3385].
- [499] G. Aad *et al.* (ATLAS), Phys. Rev. Lett. **113**, 17, 171801 (2014), [arXiv:1407.6583].
- [500] CMS Collaboration, CMS-PAS-HIG-14-037 (2015).
- [501] T. Biekötter, M. Chakraborti and S. Heinemeyer, Eur. Phys. J. C **80**, 1, 2 (2020), [arXiv:1903.11661].
- [502] S. H. Zhu, arXiv preprint (1999), [hep-ph/9901221].
- [503] H. E. Logan and S.-f. Su, Phys. Rev. **D66**, 035001 (2002), [hep-ph/0203270].
- [504] A. Gutierrez-Rodriguez and O. A. Sampayo, Phys. Rev. **D62**, 055004 (2000).
- [505] S. Kanemura, S. Moretti and K. Odagiri, JHEP **02**, 011 (2001), [hep-ph/0012030].
- [506] M. Czakon, P. Fiedler and A. Mitov, Phys. Rev. Lett. **110**, 252004 (2013), [arXiv:1303.6254].
- [507] M. Carena *et al.*, Nucl. Phys. **B577**, 88 (2000), [hep-ph/9912516].
- [508] J. M. Campbell, R. K. Ellis and F. Tramontano, Phys. Rev. **D70**, 094012 (2004), [hep-ph/0408158].
- [509] C. Degrande *et al.*, Phys. Lett. **B772**, 87 (2017), [arXiv:1607.05291].
- [510] A. A. Barrientos Bendezu and B. A. Kniehl, Phys. Rev. **D63**, 015009 (2001), [hep-ph/0007336]; A. A. Barrientos Bendezu and B. A. Kniehl, Nucl. Phys. **B568**, 305 (2000), [hep-ph/9908385].
- [511] G. Abbiendi *et al.* (ALEPH, DELPHI, L3, OPAL, LEP), Eur. Phys. J. **C73**, 2463 (2013), [arXiv:1301.6065].
- [512] B. Abbott *et al.* (D0), Phys. Rev. Lett. **82**, 4975 (1999), [hep-ex/9902028]; A. Abulencia *et al.* (CDF), Phys. Rev. Lett. **96**, 042003 (2006), [hep-ex/0510065]; V. M. Abazov *et al.* (D0), Phys. Lett. **B682**, 278 (2009), [arXiv:0908.1811].
- [513] V. Khachatryan *et al.* (CMS), JHEP **12**, 178 (2015), [arXiv:1510.04252].
- [514] G. Aad *et al.* (ATLAS), Phys. Rev. D **101**, 1, 012002 (2020), [arXiv:1909.02845].
- [515] J. Abdallah *et al.* (DELPHI), Eur. Phys. J. **C54**, 1 (2008), [Erratum: Eur. Phys. J. **C56**, 165 (2008)], [arXiv:0801.3586].
- [516] R. Dermisek, Mod. Phys. Lett. **A24**, 1631 (2009), [arXiv:0907.0297].
- [517] J. F. Gunion, JHEP **08**, 032 (2009), [arXiv:0808.2509].
- [518] W. Love *et al.* (CLEO), Phys. Rev. Lett. **101**, 151802 (2008), [arXiv:0807.1427].
- [519] G. Aad *et al.* (ATLAS), Eur. Phys. J. **C72**, 2244 (2012), [arXiv:1210.5070]; S. Chatrchyan *et al.* (CMS), Eur. Phys. J. **C72**, 2189 (2012), [arXiv:1207.2666].
- [520] G. Aad *et al.* (ATLAS), Phys. Rev. **D89**, 3, 032002 (2014), [arXiv:1312.1956].
- [521] J. de Blas *et al.*, JHEP **01**, 139 (2020), [arXiv:1905.03764].

12. CKM Quark-Mixing Matrix

Revised March 2022 by A. Ceccucci (CERN), Z. Ligeti (LBNL) and Y. Sakai (KEK).

12.1 Introduction

The masses and mixings of quarks have a common origin in the Standard Model (SM). They arise from the Yukawa interactions with the Higgs condensate,

$$\mathcal{L}_Y = -Y_{ij}^d \overline{Q_{Li}^I} \phi d_{Rj}^I - Y_{ij}^u \overline{Q_{Li}^I} \epsilon \phi^* u_{Rj}^I + \text{h.c.}, \quad (12.1)$$

where $Y^{u,d}$ are 3×3 complex matrices, ϕ is the Higgs field, i, j are generation labels, and ϵ is the 2×2 antisymmetric tensor. Q_L^I are left-handed quark doublets, and d_R^I and u_R^I are right-handed down- and up-type quark singlets, respectively, in the weak-eigenstate basis. When ϕ acquires a vacuum expectation value, $\langle \phi \rangle = (0, v/\sqrt{2})$, Eq. (12.1) yields mass terms for the quarks. The physical states are obtained by diagonalizing $Y^{u,d}$

by four unitary matrices, $V_{L,R}^{u,d}$, as $M_{\text{diag}}^f = V_L^f Y^f V_R^{f\dagger} (v/\sqrt{2})$, $f = u, d$. As a result, the charged-current W^\pm interactions couple to the physical u_{Lj} and d_{Lk} quarks with couplings given by

$$\frac{-g}{\sqrt{2}} (\overline{u}_L, \overline{c}_L, \overline{t}_L) \gamma^\mu W_\mu^+ V_{\text{CKM}} \begin{pmatrix} d_L \\ s_L \\ b_L \end{pmatrix} + \text{h.c.}, \quad (12.2)$$

$$V_{\text{CKM}} \equiv V_L^u V_L^{d\dagger} = \begin{pmatrix} V_{ud} & V_{us} & V_{ub} \\ V_{cd} & V_{cs} & V_{cb} \\ V_{td} & V_{ts} & V_{tb} \end{pmatrix}.$$

This Cabibbo-Kobayashi-Maskawa (CKM) matrix [1,2] is a 3×3 unitary matrix. It can be parameterized by three mixing angles and the CP -violating KM phase [2]. Of the many possible conventions, a standard choice has become [3]

$$V_{\text{CKM}} = \begin{pmatrix} 1 & 0 & 0 \\ 0 & c_{23} & s_{23} \\ 0 & -s_{23} & c_{23} \end{pmatrix} \begin{pmatrix} c_{13} & 0 & s_{13} e^{-i\delta} \\ 0 & 1 & 0 \\ -s_{13} e^{i\delta} & 0 & c_{13} \end{pmatrix} \begin{pmatrix} c_{12} & s_{12} & 0 \\ -s_{12} & c_{12} & 0 \\ 0 & 0 & 1 \end{pmatrix} \quad (12.3)$$

$$= \begin{pmatrix} c_{12} c_{13} & s_{12} c_{13} & s_{13} e^{-i\delta} \\ -s_{12} c_{23} - c_{12} s_{23} s_{13} e^{i\delta} & c_{12} c_{23} - s_{12} s_{23} s_{13} e^{i\delta} & s_{23} c_{13} \\ s_{12} s_{23} - c_{12} c_{23} s_{13} e^{i\delta} & -c_{12} s_{23} - s_{12} c_{23} s_{13} e^{i\delta} & c_{23} c_{13} \end{pmatrix},$$

where $s_{ij} = \sin \theta_{ij}$, $c_{ij} = \cos \theta_{ij}$, and δ is the phase responsible for all CP -violating phenomena in flavor-changing processes in the SM. The angles θ_{ij} can be chosen to lie in the first quadrant, so $s_{ij}, c_{ij} \geq 0$.

It is known experimentally that $s_{13} \ll s_{23} \ll s_{12} \ll 1$, and it is convenient to exhibit this hierarchy using the Wolfenstein parameterization. We define [4–6]

$$s_{12} = \lambda = \frac{|V_{us}|}{\sqrt{|V_{ud}|^2 + |V_{us}|^2}}, \quad s_{23} = A\lambda^2 = \lambda \left| \frac{V_{cb}}{V_{us}} \right|,$$

$$s_{13} e^{i\delta} = V_{ub}^* = A\lambda^3 (\rho + i\eta) = \frac{A\lambda^3 (\bar{\rho} + i\bar{\eta}) \sqrt{1 - A^2 \lambda^4}}{\sqrt{1 - \lambda^2 [1 - A^2 \lambda^4 (\bar{\rho} + i\bar{\eta})]}}. \quad (12.4)$$

These relations ensure that $\bar{\rho} + i\bar{\eta} = -(V_{ud} V_{ub}^*) / (V_{cd} V_{cb}^*)$ is phase convention independent, and the CKM matrix written in terms of λ , A , $\bar{\rho}$, and $\bar{\eta}$ is unitary to all orders in λ . The definitions of $\bar{\rho}$, $\bar{\eta}$ reproduce all approximate results in the literature; *i.e.*, $\bar{\rho} = \rho(1 - \lambda^2/2 + \dots)$ and $\bar{\eta} = \eta(1 - \lambda^2/2 + \dots)$, and one can write V_{CKM} to $\mathcal{O}(\lambda^4)$ either in terms of $\bar{\rho}$, $\bar{\eta}$ or, traditionally,

$$V_{\text{CKM}} = \begin{pmatrix} 1 - \lambda^2/2 & \lambda & A\lambda^3(\rho - i\eta) \\ -\lambda & 1 - \lambda^2/2 & A\lambda^2 \\ A\lambda^3(1 - \rho - i\eta) & -A\lambda^2 & 1 \end{pmatrix} + \mathcal{O}(\lambda^4). \quad (12.5)$$

The CKM matrix elements are fundamental parameters of the SM, so their precise determination is important. The unitarity of the CKM matrix imposes $\sum_i V_{ij} V_{ik}^* = \delta_{jk}$ and $\sum_j V_{ij} V_{kj}^* = \delta_{ik}$. The six vanishing combinations can be represented as triangles in a complex plane, of which those obtained by taking scalar products of neighboring rows or columns are nearly degenerate. The areas of all triangles are the same, half of the Jarlskog invariant, J [7], which is a phase-convention-independent measure of CP violation, defined by $\text{Im}[V_{ij} V_{kl} V_{il}^* V_{kj}^*] = J \sum_{m,n} \varepsilon_{ikm} \varepsilon_{jln}$.

The most commonly used unitarity triangle arises from

$$V_{ud} V_{ub}^* + V_{cd} V_{cb}^* + V_{td} V_{tb}^* = 0, \quad (12.6)$$

by dividing each side by $V_{cd} V_{cb}^*$ (see Fig. 12.1). Its vertices are exactly $(0, 0)$, $(1, 0)$, and, due to the definition in Eq. (12.4), $(\bar{\rho}, \bar{\eta})$. An important goal of flavor physics is to overconstrain the CKM elements, and many measurements can be conveniently displayed and compared in the $\bar{\rho}, \bar{\eta}$ plane. While the Lagrangian in Eq. (12.1) is renormalized, and the CKM matrix has a well-known

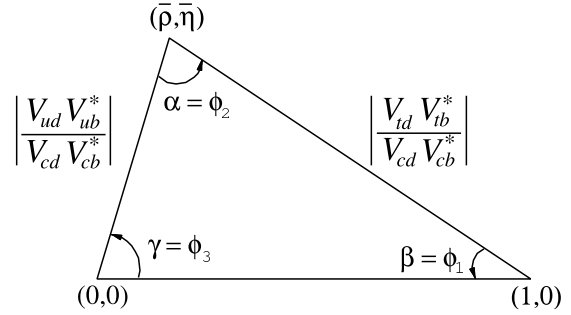


Figure 12.1: Sketch of the unitarity triangle.

scale dependence above the weak scale [8], below $\mu = m_W$ the CKM elements can be treated as constants, with all μ -dependence contained in the running of quark masses and higher-dimension operators.

Unless explicitly stated otherwise, we describe all measurements assuming the SM, to extract magnitudes and phases of CKM elements in Sec. 12.2 and 12.3. Processes dominated by loop-level contributions in the SM are particularly sensitive to new physics beyond the SM (BSM). We give the global fit results for the CKM elements in Sec. 12.4, and discuss some implications for beyond standard model physics in Sec. 12.5.

12.2 Magnitudes of CKM elements

12.2.1 $|V_{ud}|$

The most precise determination of $|V_{ud}|$ comes from the study of superallowed $0^+ \rightarrow 0^+$ nuclear beta decays, which are pure vector transitions. Taking the average of the fifteen most precise determinations [9] yields [10]

$$|V_{ud}| = 0.97373 \pm 0.00031. \quad (12.7)$$

This uncertainty is slightly more than twice larger than that in the previous edition, due to a more conservative estimate of the nuclear structure uncertainties. A less precise determination of $|V_{ud}|$ can be obtained from the measurement of the neutron lifetime. The theoretical uncertainties are very small, but the determination is limited by the knowledge of the ratio of the axial-vector and vector couplings, $g_A = G_A/G_V$ [10]. The PIBETA experiment [11] has improved the measurement of the $\pi^+ \rightarrow \pi^0 e^+ \nu$ branching ratio to 0.6%, and quotes $|V_{ud}| = 0.9739 \pm 0.0029$, in

agreement with the more precise result listed above. The interest in this measurement is that the determination of $|V_{ud}|$ is very clean theoretically, because it is a pure vector transition and is free from nuclear-structure uncertainties.

12.2.2 $|V_{us}|$

The product of $|V_{us}|$ and the form factor at $q^2 = 0$, $|V_{us}| f_+(0)$, has been extracted traditionally from $K_L^0 \rightarrow \pi e \nu$ decays in order to avoid isospin-breaking corrections ($\pi^0 - \eta$ mixing) that affect K^\pm semileptonic decay, and the complications induced by a second (scalar) form factor present in the muonic decays. The last round of measurements has led to enough experimental constraints to justify the comparison between different decay modes. Systematic errors related to the experimental quantities, *e.g.*, the lifetime of neutral or charged kaons, and the form factor determinations for electron and muonic decays, differ among decay modes, and the consistency between different determinations enhances the confidence in the final result. For this reason, we follow the prescription [12] to average $K_L^0 \rightarrow \pi e \nu$, $K_L^0 \rightarrow \pi \mu \nu$, $K^\pm \rightarrow \pi^0 e^\pm \nu$, $K^\pm \rightarrow \pi^0 \mu^\pm \nu$ and $K_S^0 \rightarrow \pi e \nu$. The average of these five decay modes yields $|V_{us}| f_+(0) = 0.21635 \pm 0.00038$. Results obtained from each decay mode, and exhaustive references to the experimental data, are listed for instance in Ref. [10]. The form factor average $f_+(0) = 0.9698 \pm 0.0017$ [13] from $N_f = 2 + 1 + 1$ lattice QCD calculations gives $|V_{us}| = 0.2231 \pm 0.0006$ [10].¹ The broadly used classic calculation of $f_+(0)$ [15] is in good agreement with this value, while other calculations [17] differ by as much as 2%.

The calculation of the ratio of the kaon and pion decay constants enables one to extract $|V_{us}/V_{ud}|$ from $K \rightarrow \mu \nu(\gamma)$ and $\pi \rightarrow \mu \nu(\gamma)$, where (γ) indicates that radiative decays are included [18]. The value of $\Gamma(K \rightarrow \mu \nu(\gamma))$ [10] derived from the KLOE measurement of the corresponding branching ratio [19], combined with the lattice QCD result, $f_K/f_\pi = 1.1932 \pm 0.0021$ [13], leads to $|V_{us}| = 0.2252 \pm 0.0005$, where the accuracy is limited by the knowledge of the ratio of the decay constants. The average of these two determinations, with the error scaled according to the PDG prescription [20] by $\sqrt{\chi^2} = 2.0$, is quoted as [10]

$$|V_{us}| = 0.2243 \pm 0.0008. \quad (12.8)$$

It is important to include both QED and QCD isospin violations in the lattice QCD calculations.

The latest determination from hyperon decays can be found in Ref. [21]. The authors focus on the analysis of the vector form factor, protected from first order $SU(3)$ breaking effects by the Ademollo-Gatto theorem [22], and treat the ratio between the axial and vector form factors g_1/f_1 as experimental input, thus avoiding first order $SU(3)$ breaking effects in the axial-vector contribution. They find $|V_{us}| = 0.2250 \pm 0.0027$, although this does not include an estimate of the theoretical uncertainty due to second-order $SU(3)$ breaking, contrary to Eq. (12.8). Concerning hadronic τ decays to strange particles, averaging the inclusive decay and the exclusive $\tau \rightarrow h \nu$ ($h = \pi, K$) measurements yields $|V_{us}| = 0.2221 \pm 0.0013$ [23].

12.2.3 $|V_{cd}|$

The magnitude of V_{cd} can be extracted from semileptonic charm decays, using theoretical knowledge of the form factors. In semileptonic D decays, lattice QCD calculations have predicted the normalization of the $D \rightarrow \pi \ell \nu$ and $D \rightarrow K \ell \nu$ form factors [13]. The dependence on the invariant mass of the lepton pair, q^2 , is determined from lattice QCD and theoretical constraints from analyticity [14]. Using $N_f = 2 + 1 + 1$ lattice QCD calculations for $D \rightarrow \pi \ell \nu$, $f_+^{D\pi}(0) = 0.612 \pm 0.035$ [13], and the average [23] of the measurements of $D \rightarrow \pi \ell \nu$ decays by *BABAR* [24], BESIII [25, 26], CLEO-c [27], and Belle [28], one obtains $|V_{cd}| = 0.2330 \pm 0.0029 \pm 0.0133$, where the first uncertainty is experimental, and the second is from the theoretical uncertainty of the form factor.

¹For lattice QCD inputs, we use the averages from Ref. [13], unless the minireviews [10, 14] choose different values. We only use unquenched results, and if both $N_f = 2 + 1 + 1$ and $2 + 1$ calculations are available, we use the former.

The determination of $|V_{cd}|$ is also possible from the leptonic decay $D^+ \rightarrow \mu^+ \nu$ and $\tau^+ \nu$. The experimental uncertainties have not decreased significantly recently. Averaging the BESIII [29] and earlier CLEO [30] for $\mu^+ \nu$ and BESIII [31] for $\tau^+ \nu$ measurements, and using the $N_f = 2 + 1 + 1$ lattice QCD result, $f_D = 212.0 \pm 0.7$ MeV [13], yields $|V_{cd}| = 0.2181 \pm 0.0049 \pm 0.0007$ [23, 32].²

Earlier determinations of $|V_{cd}|$ came from neutrino scattering data. The difference of the ratio of double-muon to single-muon production by neutrino and antineutrino beams is proportional to the charm cross section off valence d quarks, and therefore to $|V_{cd}|^2$ times the average semileptonic branching ratio of charm mesons, \mathcal{B}_μ . The method was used first by CDHS [33] and then by CCFR [34, 35] and CHARM II [36]. Averaging these results is complicated, because it requires assumptions about the scale of the QCD corrections, and because \mathcal{B}_μ is an effective quantity, which depends on the specific neutrino beam characteristics. With no recent experimental input available, we quote the average from a past review, $\mathcal{B}_\mu |V_{cd}|^2 = (0.463 \pm 0.034) \times 10^{-2}$ [37]. Analysis cuts make these experiments insensitive to neutrino energies smaller than 30 GeV. Thus, \mathcal{B}_μ should be computed using only neutrino interactions with visible energy larger than 30 GeV. An appraisal [38] based on charm-production fractions measured in neutrino interactions [39, 40] gives $\mathcal{B}_\mu = 0.088 \pm 0.006$. Data from the CHORUS experiment [41] are sufficiently precise to extract \mathcal{B}_μ directly, by comparing the number of charm decays with a muon to the total number of charmed hadrons found in the nuclear emulsions. Requiring the visible energy to be larger than 30 GeV, CHORUS found $\mathcal{B}_\mu = 0.085 \pm 0.009 \pm 0.006$. We use the average of these two determinations, $\mathcal{B}_\mu = 0.087 \pm 0.005$, and obtain $|V_{cd}| = 0.230 \pm 0.011$. Averaging the three determinations above, we find

$$|V_{cd}| = 0.221 \pm 0.004. \quad (12.9)$$

12.2.4 $|V_{cs}|$

The direct determination of $|V_{cs}|$ is possible from semileptonic D or leptonic D_s decays, using lattice QCD calculations of the semileptonic D form factor or the D_s decay constant. For muonic decays, the average of Belle [42], CLEO-c [43], *BABAR* [44], and BESIII [45, 46] is $\mathcal{B}(D_s^+ \rightarrow \mu^+ \nu) = (5.43 \pm 0.16) \times 10^{-3}$ [23]. For decays to τ leptons, the average of CLEO-c [43, 47, 48], *BABAR* [44], Belle [42], and BESIII [45] gives $\mathcal{B}(D_s^+ \rightarrow \tau^+ \nu) = (5.40 \pm 0.23) \times 10^{-2}$ [23]. From each of these values, determinations of $|V_{cs}|$ can be obtained using the PDG values for the mass and lifetime of the D_s , the masses of the leptons, and $f_{D_s} = (249.9 \pm 0.5)$ MeV [13]. The average of these determinations gives $|V_{cs}| = 0.984 \pm 0.012$, where the error is dominated by the experimental uncertainty. In semileptonic D decays, lattice QCD calculations of the $D \rightarrow K \ell \nu$ form factor are available [13]. Using $f_+^{DK}(0) = 0.7385 \pm 0.0044$ and the average [23] of CLEO-c [27], Belle [28], *BABAR* [49], and recent BESIII [25, 50] measurements of $D \rightarrow K \ell \nu$ decays, one obtains $|V_{cs}| = 0.972 \pm 0.007$, where the dominant uncertainty is from the theoretical calculation of the form factor. Averaging the determinations from leptonic and semileptonic decays, we find

$$|V_{cs}| = 0.975 \pm 0.006. \quad (12.10)$$

Measurements of on-shell W^\pm decays sensitive to $|V_{cs}|$ were made by LEP-2. The W branching ratios depend on the six CKM elements involving quarks lighter than m_W . The W branching ratio to each lepton flavor is $1/\mathcal{B}(W \rightarrow \ell \bar{\nu}_\ell) = 3[1 + \sum_{u,c,d,s,b} |V_{ij}|^2 (1 + \alpha_s(m_W)/\pi) + \dots]$. Assuming lepton universality, the measurement $\mathcal{B}(W \rightarrow \ell \bar{\nu}_\ell) = (10.83 \pm 0.07 \pm 0.07)\%$ [51] implies $\sum_{u,c,d,s,b} |V_{ij}|^2 = 2.002 \pm 0.027$. This is a precise test of unitarity; however, only flavor-tagged W -decays determine $|V_{cs}|$ directly, such as DELPHI's tagged $W^+ \rightarrow c \bar{s}$ analysis, yielding $|V_{cs}| = 0.94_{-0.26}^{+0.32} \pm 0.13$ [52].

²Hereafter the first error is statistical and the second is systematic, unless mentioned otherwise.

12.2.5 $|V_{cb}|$

This matrix element can be determined from exclusive and inclusive semileptonic decays of B mesons to charm. The inclusive determinations use the semileptonic decay rate measurement, together with (certain moments of) the lepton energy and the hadronic invariant-mass spectra. The theoretical basis is the operator product expansion [53, 54], which allows calculation of the decay rate and various spectra as expansions in α_s and inverse powers of the heavy-quark mass. The dependence on m_b , m_c , and the parameters that occur at subleading order is different for different moments. The measurements of many moments overconstrain these parameters, and also test the consistency of their determination. The precise extraction of $|V_{cb}|$ requires using a “threshold” quark mass definition [55, 56]. Inclusive measurements have been performed using B mesons from Z^0 decays at LEP, and at e^+e^- colliders operated at the $\Upsilon(4S)$. At LEP, the large boost of B mesons from the Z^0 decay allows the determination of the moments throughout phase space, which is not possible otherwise, but the large statistics available at the B factories lead to more precise determinations. An average of the measurements and a compilation of the references are provided in Ref. [14]: $|V_{cb}| = (42.2 \pm 0.8) \times 10^{-3}$.

Complementary determinations are based on exclusive semileptonic B decays to D and D^* . In the $m_{b,c} \gg \Lambda_{\text{QCD}}$ limit, all form factors are given by a single Isgur-Wise function [57], which depends on the product of the four-velocities of the B and $D^{(*)}$ mesons, $w = v \cdot v'$. Heavy-quark symmetry determines the rate at $w = 1$ (in the symmetry limit), the maximum momentum transfer to the $\ell\bar{\nu}$ pair, and $|V_{cb}|$ is obtained from extrapolating a fit to the spectrum to $w = 1$. The current update of the V_{cb} and V_{ub} mini-review quotes from exclusive decays $|V_{cb}| = (39.4 \pm 0.8) \times 10^{-3}$ [14], based on the only unfolded measurement of $B \rightarrow D^*$ semileptonic decay distributions [58], and using a more general fit [59] than in earlier B factory measurements. With the uncertainty scaled by $\sqrt{\chi^2} = 2.4$, this yields the combination [14],

$$|V_{cb}| = (40.8 \pm 1.4) \times 10^{-3}. \quad (12.11)$$

Determinations of $|V_{cb}|$ that are currently less precise and not included in this average, can be obtained from the measurement of $B_s \rightarrow D_s^{(*)} \mu\bar{\nu}$ decays [60]. In addition, semileptonic decays to τ leptons measured in $B \rightarrow D^{(*)} \tau\bar{\nu}$ and related modes are also sensitive to $|V_{cb}|$. The most precise data involving τ leptons are the $|V_{cb}|$ -independent ratios, $\mathcal{B}(B \rightarrow D^{(*)} \tau\bar{\nu})/\mathcal{B}(B \rightarrow D^{(*)} \ell\bar{\nu})$ measured by BaBar, Belle, and LHCb. If the current, approximately 3σ [23], hint of lepton non-universality prevails, the determination of $|V_{cb}|$ becomes more complicated.

12.2.6 $|V_{ub}|$

The determination of $|V_{ub}|$ from inclusive $B \rightarrow X_u \ell\bar{\nu}$ decay is complicated due to large $B \rightarrow X_c \ell\bar{\nu}$ backgrounds. In most regions of phase space where the charm background is kinematically forbidden, the hadronic physics enters via unknown nonperturbative functions, so-called shape functions. (In contrast, the nonperturbative physics for $|V_{cb}|$ is encoded in a few parameters.) At leading order in Λ_{QCD}/m_b , there is only one shape function, which can be extracted from the photon energy spectrum in $B \rightarrow X_s \gamma$ [61, 62], and applied to several spectra in $B \rightarrow X_u \ell\bar{\nu}$. The subleading shape functions are modeled in the current determinations. Phase space cuts for which the rate has only subleading dependence on the shape function are also possible [63]. The measurements of both the hadronic and the leptonic systems are important for an optimal choice of phase space. A different approach is to make the measurements more inclusive by extending them deeper into the $B \rightarrow X_c \ell\bar{\nu}$ region, and thus reduce the theoretical uncertainties. Analyses of the electron-energy endpoint from CLEO [64], BABAR [65], and Belle [66] quote $B \rightarrow X_u e\bar{\nu}$ partial rates for $|\vec{p}_e| \geq 2.0$ GeV and 1.9 GeV, which are well below the charm endpoint. The large and pure $B\bar{B}$ samples at the B factories permit the selection of $B \rightarrow X_u \ell\bar{\nu}$ decays in events where the other B is fully reconstructed [67]. With this full-reconstruction tag method, the four-momenta of both the leptonic and the hadronic final states can be measured. It also gives access to a wider kinematic region, because of improved signal purity. Ref. [14] quotes

the inclusive average, $|V_{ub}| = (4.13 \pm 0.12_{-0.14}^{+0.13} \pm 0.18) \times 10^{-3}$, where the first error is experimental, the second arises from the model dependence quoted by the individual measurements, and the third is an additional one estimated in Ref. [14].

To extract $|V_{ub}|$ from exclusive decays, the form factors have to be known. Experimentally, better signal-to-background ratios are offset by smaller yields. The $B \rightarrow \pi \ell\bar{\nu}$ branching ratio is now known to 5%. Lattice QCD calculations of the $B \rightarrow \pi \ell\bar{\nu}$ form factor are available [68] for the high q^2 region ($q^2 > 16$ or 18 GeV²). A fit to the experimental partial rates and lattice QCD results versus q^2 yields $|V_{ub}| = (3.70 \pm 0.10 \pm 0.12) \times 10^{-3}$ [23]. Light-cone QCD sum rules are supposed to be applicable for $q^2 < 12$ GeV² [69], yielding a combination, $|V_{ub}| = (3.67 \pm 0.09 \pm 0.12) \times 10^{-3}$ [14, 23].

The uncertainties in extracting $|V_{ub}|$ from inclusive and exclusive decays are different to a large extent. An average of these determinations, with the uncertainty scaled by $\sqrt{\chi^2} = 1.4$, is [14]

$$|V_{ub}| = (3.82 \pm 0.20) \times 10^{-3}. \quad (12.12)$$

A determination of $|V_{ub}|$ not included in this average can be obtained from $\mathcal{B}(B \rightarrow \tau\bar{\nu}) = (1.06 \pm 0.19) \times 10^{-4}$ [23]. Using $f_B = (190.0 \pm 1.3)$ MeV [13] and $\tau_{B^\pm} = (1.638 \pm 0.004)$ ps [70], we find the remarkably consistent result, $|V_{ub}| = (4.05 \pm 0.36) \times 10^{-3}$. This decay is sensitive, for example, to tree-level charged Higgs contributions, and the measured rate is consistent with the SM expectation. The LHCb measurement $|V_{ub}/V_{cb}| = 0.084 \pm 0.007$ [14] from the ratios of $\Lambda_b \rightarrow p^+ \mu^- \bar{\nu}$ and $\Lambda_b \rightarrow \Lambda_c^+ \mu^- \bar{\nu}$ [71] and $B_s^0 \rightarrow K^- \mu^+ \nu$ and $B_s^0 \rightarrow D_s^- \mu^+ \nu$ [72] in different regions of q^2 , provides another complementary determination.

12.2.7 $|V_{td}|$ and $|V_{ts}|$

The CKM elements $|V_{td}|$ and $|V_{ts}|$ are not likely to be precisely measurable in tree-level processes involving top quarks, so one has to rely on determinations from $B-\bar{B}$ oscillations dominated by box diagrams with top quarks, or loop-mediated rare K and B decays. Theoretical uncertainties in hadronic effects limit the accuracy of the current determinations. These can be reduced by taking ratios of processes that are equal in the flavor $SU(3)$ limit to determine $|V_{td}/V_{ts}|$.

The mixing of the two B^0 mesons was discovered by ARGUS [73], and the mass difference is now precisely measured as $\Delta m_d = (0.5065 \pm 0.0019)$ ps⁻¹ [74]. In the B_s^0 system, Δm_s was first measured significantly by CDF [75] and the world average, dominated by an LHCb measurement [76], is $\Delta m_s = (17.765 \pm 0.006)$ ps⁻¹ [74]. Neglecting corrections suppressed by $|V_{tb}| - 1$, and using the lattice QCD results $f_{B_d} \sqrt{\widehat{B}_{B_d}} = (210.6 \pm 5.5)$ MeV and $f_{B_s} \sqrt{\widehat{B}_{B_s}} = (256.1 \pm 5.7)$ MeV [13],

$$|V_{td}| = (8.6 \pm 0.2) \times 10^{-3}, \quad |V_{ts}| = (41.5 \pm 0.9) \times 10^{-3}. \quad (12.13)$$

The uncertainties are dominated by lattice QCD. Several uncertainties are reduced in the calculation of the ratio $\xi = (f_{B_s} \sqrt{\widehat{B}_{B_s}})/(f_{B_d} \sqrt{\widehat{B}_{B_d}}) = 1.216 \pm 0.016$ [13] and therefore the constraint on $|V_{td}/V_{ts}|$ from $\Delta m_d/\Delta m_s$ is more reliable theoretically. These provide a theoretically clean and significantly improved determination,

$$|V_{td}/V_{ts}| = 0.207 \pm 0.001 \pm 0.003. \quad (12.14)$$

The inclusive branching ratio $\mathcal{B}(B \rightarrow X_s \gamma) = (3.32 \pm 0.15) \times 10^{-4}$ extrapolated to $E_\gamma > E_0 = 1.6$ GeV [23] is also sensitive to $|V_{tb}V_{ts}|$. In addition to t -quark penguins, a substantial part of the rate comes from charm contributions proportional to $V_{cb}V_{cs}^*$ via the application of 3×3 CKM unitarity (which is used here). With the NNLO calculation of $\mathcal{B}(B \rightarrow X_s \gamma)_{E_\gamma > E_0}/\mathcal{B}(B \rightarrow X_c e\bar{\nu})$ [77], we obtain $|V_{ts}/V_{cb}| = 0.98 \pm 0.04$. The $B_s \rightarrow \mu^+ \mu^-$ rate is also proportional to $|V_{tb}V_{ts}|^2$ in the SM, and the world average, $\mathcal{B}(B_s \rightarrow \mu^+ \mu^-) = (2.9 \pm 0.4) \times 10^{-9}$ [70], is consistent with the SM, with sizable uncertainties.

A complementary determination of $|V_{td}/V_{ts}|$ is possible from the ratio of $B \rightarrow \rho\gamma$ and $K^* \gamma$ rates. The ratio of the neutral modes

is theoretically cleaner than that of the charged ones, because the poorly known spectator-interaction contribution is expected to be smaller (W -exchange vs. weak annihilation). For now, because of low statistics, we average the charged and neutral rates assuming the isospin symmetry and heavy-quark limit motivated relation, $|V_{td}/V_{ts}|^2/\xi_\gamma^2 = [\Gamma(B^+ \rightarrow \rho^+\gamma) + 2\Gamma(B^0 \rightarrow \rho^0\gamma)]/[\Gamma(B^+ \rightarrow K^{*+}\gamma) + \Gamma(B^0 \rightarrow K^{*0}\gamma)] = (3.37 \pm 0.49)\%$ [23]. Here ξ_γ contains the poorly known hadronic physics. Using $\xi_\gamma = 1.2 \pm 0.2$ [78] gives $|V_{td}/V_{ts}| = 0.220 \pm 0.016 \pm 0.037$, where the first uncertainty is experimental and the second is theoretical.

A theoretically clean determination of $|V_{td}V_{ts}^*|$ is possible from $K^+ \rightarrow \pi^+\nu\bar{\nu}$ decay [79]. Experimentally, more than 20 candidates have been observed [80, 81] and the rate is consistent with the SM within errors. Much more data are needed for a precision measurement.

12.2.8 $|V_{tb}|$

The determination of $|V_{tb}|$ from top decays uses the ratio of branching fractions $R = \mathcal{B}(t \rightarrow Wb)/\mathcal{B}(t \rightarrow Wq) = |V_{tb}|^2/(\sum_q |V_{tq}|^2) = |V_{tb}|^2$, where $q = b, s, d$. The CDF and DØ measurements performed on data collected during Run II of the Tevatron give $|V_{tb}| > 0.78$ [82] and $0.99 > |V_{tb}| > 0.90$ [83], respectively, at 95% CL. CMS measured the same quantity at 8 TeV and obtained $|V_{tb}| > 0.975$ [84] at 95% CL.

The direct determination of $|V_{tb}|$, without assuming unitarity, is possible from the single top quark production cross section. The $(3.30_{-0.40}^{+0.52})$ pb combined cross section [85] of DØ and CDF measurements implies $|V_{tb}| = 1.02_{-0.05}^{+0.06}$. The LHC experiments, ATLAS and CMS, have measured single top quark production cross sections (and extracted $|V_{tb}|$) in t -channel, Wt -channel, and s -channel at 7 TeV, 8 TeV, and 13 TeV [86]. The average of these $|V_{tb}|$ values is calculated to be $|V_{tb}| = 1.014 \pm 0.035$, where all systematic errors and theoretical errors are treated to be fully correlated. The average of Tevatron and LHC values gives

$$|V_{tb}| = 1.014 \pm 0.029. \quad (12.15)$$

The experimental systematic uncertainties dominate, and a dedicated combination would be welcome.

A weak constraint on $|V_{tb}|$ can be obtained from precision electroweak data, where top quarks enter in loops. The sensitivity is best in $\Gamma(Z \rightarrow b\bar{b})$ and yields $|V_{tb}| = 0.77_{-0.24}^{+0.18}$ [87].

12.3 Phases of CKM elements

As can be seen from Fig. 12.1, the angles of the unitarity triangle are

$$\begin{aligned} \beta &= \phi_1 = \arg\left(-\frac{V_{cd}V_{cb}^*}{V_{td}V_{tb}^*}\right), \\ \alpha &= \phi_2 = \arg\left(-\frac{V_{td}V_{tb}^*}{V_{ud}V_{ub}^*}\right), \\ \gamma &= \phi_3 = \arg\left(-\frac{V_{ud}V_{ub}^*}{V_{cd}V_{cb}^*}\right). \end{aligned} \quad (12.16)$$

Since CP violation involves phases of CKM elements, many measurements of CP -violating observables can be used to constrain these angles and the $\bar{\rho}, \bar{\eta}$ parameters.

12.3.1 ϵ and ϵ'

The measurement of CP violation in $K^0-\bar{K}^0$ mixing, $|\epsilon| = (2.228 \pm 0.011) \times 10^{-3}$ [88], provides important information about the CKM matrix. The phase of ϵ is determined by long-distance physics, $\epsilon = \frac{1}{2} e^{i\phi_\epsilon} \sin\phi_\epsilon \arg(-M_{12}/\Gamma_{12})$, where $\phi_\epsilon = \arctan[2\Delta m_K/\Delta\Gamma_K] \simeq 43.5^\circ$. The SM prediction can be written as

$$\begin{aligned} \epsilon &= \kappa_\epsilon e^{i\phi_\epsilon} \frac{G_F^2 m_W^2 m_K}{12\sqrt{2}\pi^2 \Delta m_K} f_K^2 \widehat{B}_K \left\{ \eta_{tt} S(x_t) \text{Im}[(V_{ts}V_{td}^*)^2] \right. \\ &\quad \left. + 2\eta_{ct} S(x_c, x_t) \text{Im}(V_{cs}V_{cd}^*V_{ts}V_{td}^*) + \eta_{cc} x_c \text{Im}[(V_{cs}V_{cd}^*)^2] \right\}, \end{aligned} \quad (12.17)$$

where $\kappa_\epsilon \simeq 0.94 \pm 0.02$ [89] includes the effects of strangeness changing $\Delta s = 1$ operators and additional dependence on $\phi_\epsilon \neq$

$\pi/4$ (see also Ref. [90]). The displayed terms are the short-distance $\Delta s = 2$ contribution to $\text{Im}M_{12}$ in the usual phase convention, S is an Inami-Lim function [91], $x_q = m_q^2/m_W^2$, and η_{ij} are perturbative QCD corrections. The constraint from ϵ in the $\bar{\rho}, \bar{\eta}$ plane is bounded by approximate hyperbolas. Lattice QCD determined the bag parameter $\widehat{B}_K = 0.717 \pm 0.024$ [13] and the main uncertainties are from $(V_{ts}V_{td}^*)^2$ (approximately given by that of $|V_{cb}|^4$ or A^4), the η_{ij} coefficients, and estimates of κ_ϵ .

The measurement of $6 \text{Re}(\epsilon'/\epsilon) = 1 - |\eta_{00}/\eta_{+-}|^2$, where each $\eta_{ij} = \langle \pi^i \pi^j | \mathcal{H} | K_L \rangle / \langle \pi^i \pi^j | \mathcal{H} | K_S \rangle$ violates CP , provides a qualitative test of the CKM mechanism, and strong constraints on many BSM scenarios. Its nonzero value, $\text{Re}(\epsilon'/\epsilon) = (1.67 \pm 0.23) \times 10^{-3}$ [88], demonstrated the existence of direct CP violation, a prediction of the KM ansatz. While $\text{Re}(\epsilon'/\epsilon) \propto \text{Im}(V_{td}V_{ts}^*)$, this quantity cannot easily be used to extract CKM parameters, because cancellations between the electromagnetic and gluonic penguin contributions for large m_t [92] enhance the hadronic uncertainties. Most SM estimates [93] agree with the observed value, indicating that $\bar{\eta}$ is positive. Progress in lattice QCD [94] may yield a precise SM prediction in the future, and trigger new work on assessing the consistency of the SM with the measured value [95, 96].

12.3.2 β / ϕ_1

12.3.2.1 Charmonium modes

CP -violation measurements in B -meson decays provide direct information on the angles of the unitarity triangle, shown in Fig. 12.1. These overconstraining measurements serve to improve the determination of the CKM elements, and to reveal possible effects beyond the SM.

The time-dependent CP asymmetry of neutral B decays to a final state f common to B^0 and \bar{B}^0 is given by [97–99]

$$\begin{aligned} \mathcal{A}_f &= \frac{\Gamma(\bar{B}^0(t) \rightarrow f) - \Gamma(B^0(t) \rightarrow f)}{\Gamma(\bar{B}^0(t) \rightarrow f) + \Gamma(B^0(t) \rightarrow f)}, \\ &= S_f \sin(\Delta m_d t) - C_f \cos(\Delta m_d t), \end{aligned} \quad (12.18)$$

where

$$S_f = \frac{2 \text{Im}\lambda_f}{1 + |\lambda_f|^2}, \quad C_f = \frac{1 - |\lambda_f|^2}{1 + |\lambda_f|^2}, \quad \lambda_f = \frac{q}{p} \frac{\bar{A}_f}{A_f}. \quad (12.19)$$

Here, q/p describes $B^0-\bar{B}^0$ mixing and, to a good approximation in the SM, $q/p = V_{tb}^*V_{td}/V_{tb}V_{td}^* = e^{-2i\beta + \mathcal{O}(\lambda^4)}$ in the usual phase convention. A_f (\bar{A}_f) is the amplitude of the $B^0 \rightarrow f$ ($\bar{B}^0 \rightarrow f$) decay. If f is a CP eigenstate, and amplitudes with one CKM phase dominate the decay, then $|A_f| = |\bar{A}_f|$, $C_f = 0$, and $S_f = \sin(\arg\lambda_f) = \eta_f \sin 2\phi$, where η_f is the CP eigenvalue of f and 2ϕ is the phase difference between the $B^0 \rightarrow f$ and $B^0 \rightarrow \bar{B}^0 \rightarrow f$ decay paths. A contribution of another amplitude to the decay with a different CKM phase makes the value of S_f sensitive to relative strong-interaction phases between the decay amplitudes (it also makes $C_f \neq 0$ possible).

The $b \rightarrow c\bar{c}s$ decays to CP eigenstates ($B^0 \rightarrow$ charmonium $K_{S,L}^0$) give currently the most precise measurements of $S_f = -\eta_f \sin 2\beta$. The $b \rightarrow s$ penguin amplitudes have dominantly the same weak phase as the $b \rightarrow c\bar{c}s$ tree amplitude. Since only λ^2 -suppressed penguin amplitudes introduce a different CP -violating phase, amplitudes with a single weak phase dominate, and we expect $|\bar{A}_\psi/K/A_\psi K| - 1| < 0.01$. The e^+e^- asymmetric-energy B -factory experiments, BABAR [100] and Belle [101], and LHCb [102] provided precise measurements. The world average, including some other measurements, is [23]

$$\sin 2\beta = 0.699 \pm 0.017. \quad (12.20)$$

This measurement has a four-fold ambiguity in β , which can be resolved by a global fit as mentioned in Sec. 12.4. Experimentally, the two-fold ambiguity $\beta \rightarrow \pi/2 - \beta$ (but not $\beta \rightarrow \pi + \beta$) can be resolved by a time-dependent angular analysis of $B^0 \rightarrow J/\psi K^{*0}$ [103, 104], or a time-dependent Dalitz plot analysis of $B^0 \rightarrow \bar{D}^0 h^0$. The time-dependent Dalitz plot analysis of $B^0 \rightarrow \bar{D}^0 h^0$ ($h^0 = \pi^0, \eta, \omega$) with $\bar{D}^0 \rightarrow K_S^0 \pi^+ \pi^-$, jointly performed by Belle and BABAR, excludes the $\pi/2 - \beta$ solution with

7.3 σ confidence level [105]. These results exclude the negative $\cos 2\beta$ solutions, in agreement with the global CKM fit, which is no longer shown in Fig. 12.2.

The $b \rightarrow c\bar{c}d$ mediated transitions, such as $B^0 \rightarrow J/\psi\pi^0$ and $B^0 \rightarrow D^{(*)+}D^{(*)-}$, also measure approximately $\sin 2\beta$. However, the dominant component of the $b \rightarrow d$ penguin amplitude has a different CKM phase ($V_{tb}^*V_{td}$) than the tree amplitude ($V_{cb}^*V_{cd}$), and their magnitudes are of the same order in λ . Therefore, the effect of penguins could be large, resulting in $S_f \neq -\eta_f \sin 2\beta$ and $C_f \neq 0$. Such decay modes have been measured by *BABAR*, *Belle*, and *LHCb*. The world averages [23], $S_{J/\psi\pi^0} = -0.86 \pm 0.14$, $S_{J/\psi\rho^0} = -0.66_{-0.12}^{+0.16}$, $S_{D^+D^-} = -0.84 \pm 0.12$, and $S_{D^{*+}D^{*-}} = -0.71 \pm 0.09$ (where $\eta_f = +1$ for the $J/\psi\pi^0$ and D^+D^- modes, while $J/\psi\rho^0$ and $D^{*+}D^{*-}$ are mixtures of CP even and odd states), are consistent with $\sin 2\beta$ obtained from $B^0 \rightarrow$ charmium K^0 decays, and the C_f 's are consistent with zero, although the uncertainties are sizable.

The $b \rightarrow c\bar{u}d$ decays $B^0 \rightarrow \bar{D}^0(*)h^0$, with $\bar{D}^0 \rightarrow CP$ eigenstates and $\bar{D}^0 \rightarrow K_S^0\pi^+\pi^-$ with Dalitz plot analysis, have no penguin contributions, and provide theoretically clean $\sin 2\beta$ measurements. The average of joint analyses of *BABAR* and *Belle* data [105, 106] give $\sin 2\beta = 0.71 \pm 0.09$ [23, 107].

12.3.2.2 Penguin-dominated modes

The $b \rightarrow s\bar{q}q$ penguin-dominated decays have the same CKM phase as the $b \rightarrow c\bar{c}s$ tree level decays, up to corrections suppressed by λ^2 , since $V_{tb}^*V_{ts} = -V_{cb}^*V_{cs}[1 + \mathcal{O}(\lambda^2)]$. Therefore, decays such as $B^0 \rightarrow \phi K^0$ and $\eta' K^0$ provide $\sin 2\beta$ measurements in the SM. Any BSM contribution to the amplitude with a different weak phase would give rise to $S_f \neq -\eta_f \sin 2\beta$, and possibly $C_f \neq 0$. Therefore, the main interest in these modes is not simply to measure $\sin 2\beta$, but to search for new physics. Measurements of many other decay modes in this category, such as $B \rightarrow \pi^0 K_S^0$, $K_S^0 K_S^0 K_S^0$, *etc.*, have also been performed by *BABAR* and *Belle*. The results and their uncertainties are summarized in Fig. 13.3 and Table 13.1 of Ref. [98]. The comparison of CP violation measurements between tree-dominated and penguin-dominated modes in B_s^0 decays provides similar sensitivity to new physics.

12.3.3 α / ϕ_2

Since α is the phase between $V_{tb}^*V_{td}$ and $V_{ub}^*V_{ud}$, only time-dependent CP asymmetries in decay modes dominated by $b \rightarrow u\bar{u}d$ transitions can directly measure $\sin 2\alpha$, in contrast to $\sin 2\beta$, where several different quark-level transitions can be used. Since $b \rightarrow d$ penguin amplitudes have a different CKM phase than $b \rightarrow u\bar{u}d$ tree amplitudes, and their magnitudes are of the same order in λ , the penguin contribution can be sizable, which makes the determination of α complicated. To date, α has been measured in $B \rightarrow \pi\pi$, $\rho\pi$ and $\rho\rho$ decay modes.

12.3.3.1 $B \rightarrow \pi\pi$

It is well-established from the data that there is a sizable contribution of $b \rightarrow d$ penguin amplitudes in $B \rightarrow \pi\pi$ decays. Thus, $S_{\pi^+\pi^-}$ in the time-dependent $B^0 \rightarrow \pi^+\pi^-$ analysis does not measure $\sin 2\alpha$, but

$$S_{\pi^+\pi^-} = \sqrt{1 - C_{\pi^+\pi^-}^2} \sin(2\alpha + 2\Delta\alpha), \quad (12.21)$$

where $2\Delta\alpha$ is the phase difference between $e^{2i\gamma}\bar{A}_{\pi^+\pi^-}$ and $A_{\pi^+\pi^-}$. The value of $\Delta\alpha$, and hence α , can be extracted using the isospin relation among the amplitudes of $B^0 \rightarrow \pi^+\pi^-$, $B^0 \rightarrow \pi^0\pi^0$, and $B^+ \rightarrow \pi^+\pi^0$ decays [108],

$$\frac{1}{\sqrt{2}} A_{\pi^+\pi^-} + A_{\pi^0\pi^0} - A_{\pi^+\pi^0} = 0, \quad (12.22)$$

and a similar expression for the $\bar{A}_{\pi\pi}$'s. This method utilizes the fact that a pair of pions from $B \rightarrow \pi\pi$ decay must be in a zero angular momentum state, and, because of Bose statistics, they must have even isospin. Consequently, $\pi^\pm\pi^0$ is in a pure isospin-2 state, while the penguin amplitudes only contribute to the isospin-0 final state. The latter does not hold for the electroweak penguin amplitudes, but their effect is expected to be small. The isospin

analysis uses the world averages of *BABAR*, *Belle*, and *LHCb* measurements, $S_{\pi^+\pi^-} = -0.666 \pm 0.029$, $C_{\pi^+\pi^-} = -0.311 \pm 0.030$, the decay widths of all three modes, and the direct CP asymmetry $C_{\pi^0\pi^0} = -0.33 \pm 0.22$ [23]. This analysis leads to 16 mirror solutions for $0 \leq \alpha < 2\pi$. Because of this, and due to the experimental uncertainties, some of these solutions are not well separated [99].

12.3.3.2 $B \rightarrow \rho\rho$

The decay $B^0 \rightarrow \rho^+\rho^-$ contains two vector mesons in the final state, and so in general is a mixture of CP -even and CP -odd components. At the current level of precision, it simplifies the analysis that the longitudinal polarization fractions in $B^+ \rightarrow \rho^+\rho^0$ and $B^0 \rightarrow \rho^+\rho^-$ decays were measured to be close to unity [109], which implies that the final states are almost purely CP -even. Furthermore, $\mathcal{B}(B^0 \rightarrow \rho^0\rho^0) = (0.95 \pm 0.16) \times 10^{-6}$ is much smaller than $\mathcal{B}(B^0 \rightarrow \rho^+\rho^-) = (27.7 \pm 1.9) \times 10^{-6}$ and $\mathcal{B}(B^+ \rightarrow \rho^+\rho^0) = (24.0_{-2.0}^{+1.9}) \times 10^{-6}$ [23], which implies that the effect of the penguin contributions is small. The isospin analysis using the world averages, $S_{\rho^+\rho^-} = -0.14 \pm 0.13$ and $C_{\rho^+\rho^-} = 0.00 \pm 0.09$ [23], together with the time-dependent CP asymmetry, $S_{\rho^0\rho^0} = -0.3 \pm 0.7$ and $C_{\rho^0\rho^0} = -0.2 \pm 0.9$ [110], and the above mentioned branching fractions and longitudinal polarization fractions, gives two solutions (with mirror solutions at $3\pi/2 - \alpha$) [99]. A possible small violation of Eq. (12.22) due to the finite width of the ρ [111] is so far neglected.

12.3.3.3 $B \rightarrow \rho\pi$

The final state in $B^0 \rightarrow \rho^+\pi^-$ decay is not a CP eigenstate, but this decay proceeds via the same quark-level diagrams as $B^0 \rightarrow \pi^+\pi^-$, and both B^0 and \bar{B}^0 can decay to $\rho^+\pi^-$, while the final state in $B^0 \rightarrow \rho^0\pi^0$ is a CP eigenstate. Consequently, mixing-induced CP violation can occur in B^0 and \bar{B}^0 decays to $\rho^\pm\pi^\mp$ and $\rho^0\pi^0$. The time-dependent Dalitz plot analysis of $B^0 \rightarrow \pi^+\pi^-\pi^0$ decays permits the extraction of α with a single discrete ambiguity, $\alpha \rightarrow \alpha + \pi$, since one knows the variation of the strong phases in the interference regions of the $\rho^+\pi^-$, $\rho^-\pi^+$, and $\rho^0\pi^0$ amplitudes in the Dalitz plot [112]. The combination of *Belle* [113] and *BABAR* [114] measurements gives only moderate constraints [99].

Combining the $B \rightarrow \pi\pi$, $\rho\pi$, and $\rho\rho$ decay modes [23, 99], α is constrained as

$$\alpha = (85.2_{-4.3}^{+4.8})^\circ. \quad (12.23)$$

Similar results can be found in Refs. [115, 116].

12.3.4 γ / ϕ_3

By virtue of Eq. (12.16), γ does not depend on CKM elements involving the top quark, so it can be measured in tree-level B decays. This is an important distinction from the measurements of α and β , and implies that measurements of γ are unlikely to be affected by physics beyond the SM.

12.3.4.1 $B_{(s)} \rightarrow D_{(s)}K^{(*)}$

The interference of $B^- \rightarrow D^0K^-$ ($b \rightarrow c\bar{u}s$) and $B^- \rightarrow \bar{D}^0K^-$ ($b \rightarrow u\bar{c}s$) transitions can be studied in final states accessible in both D^0 and \bar{D}^0 decays [97]. In principle, it is possible to extract the B and D decay amplitudes, the relative strong phases, and the weak phase γ from the data [99].

A practical complication is that the precision depends sensitively on the ratio of the interfering amplitudes

$$r_B = \left| A(B^- \rightarrow \bar{D}^0K^-) / A(B^- \rightarrow D^0K^-) \right|, \quad (12.24)$$

which is around 0.1. The original GLW method [117, 118] considers D decays to CP eigenstates, such as $B^\pm \rightarrow D_{CP}^{(*)}(\rightarrow \pi^+\pi^-)K^{(*)\pm}$. To alleviate the smallness of r_B and make the interfering amplitudes (which are products of the B and D decay amplitudes) comparable in magnitude, the ADS method [119] considers final states where Cabibbo-allowed \bar{D}^0 and doubly-Cabibbo-suppressed D^0 decays interfere. Measurements have been made by the B factories, CDF, and *LHCb*, using both methods [23]. The GLW method currently gives only a loose constraint on γ , $13.7^\circ < \gamma < 80.0^\circ$, $100.0^\circ < \gamma < 166.3^\circ$ at 68% CL with 4 solutions at $26^\circ, 72^\circ, 107^\circ$, and 154° ; while the ADS method provides $\gamma = (70_{-33}^{+15})^\circ$ [99, 107].

The BPGGSZ method [120, 121] utilizes the fact that both D^0 and \bar{D}^0 can have large branching fractions to CP self-conjugate three-body final states, such as $K_s^0 \pi^+ \pi^-$, and the analysis can be optimized by studying the Dalitz plot dependence of the interferences. The best present determination of γ comes from this method. Combining the Belle [122], *BABAR* [123], and now dominant LHCb [124] measurements, $\gamma = (69.3 \pm 4.5)^\circ$ is obtained [99, 107]. The uncertainty is sensitive to the central value of the amplitude ratio r_B (and r_B^* for the $D^* K$ mode), for which Belle found somewhat larger central values than *BABAR* and LHCb. The same values of $r_B^{(*)}$ enter the ADS analyses, and the data can be combined to fit for $r_B^{(*)}$ and γ . The effect of D^0 - \bar{D}^0 mixing on γ is either below the present experimental accuracy or can be taken into account in the analysis [125, 126] (even if D^0 - \bar{D}^0 mixing is due to CP -violating new physics [127]).

The amplitude ratio is much larger in the analogous $B_s^0 \rightarrow D_s^\pm K^\mp$ decays, which allows a model-independent extraction of $\gamma - 2\beta_s$ [128] (here $\beta_s = \arg(-V_{ts} V_{tb}^* / V_{cs} V_{cb}^*)$ is related to the phase of B_s mixing). Measurements by LHCb with $B_s^0 \rightarrow D_s^\pm K^\mp$ [129] and $B_s^0 \rightarrow D_s^\pm K^\mp \pi^+ \pi^-$ [130] give $\gamma = (79_{-21}^{+19})^\circ$ using a constraint on $2\beta_s$ (see Sec. 12.5).

Combining all the above measurements [99, 107], γ is constrained as

$$\gamma = (65.9_{-3.5}^{+3.3})^\circ. \quad (12.25)$$

Similar results can be found in Refs. [115, 116].

12.3.4.2 $B^0 \rightarrow D^{(*)} \pi^\mp$

The interference of $b \rightarrow u$ and $b \rightarrow c$ transitions can be studied in $\bar{B}^0 \rightarrow D^{(*)} \pi^-$ ($b \rightarrow \bar{c} u d$) and $\bar{B}^0 \rightarrow B^0 \rightarrow D^{(*)} \pi^-$ ($\bar{b} \rightarrow \bar{u} c d$) decays and their CP conjugates, since both B^0 and \bar{B}^0 decay to $D^{(*)} \pi^\mp$ (or $D^\pm \rho^\mp$, etc.). Since there are only tree and no penguin contributions to these decays, in principle, it is possible to extract from the four time-dependent rates the magnitudes of the two hadronic amplitudes, their relative strong phase, and the weak phase between the two decay paths, which is $2\beta + \gamma$.

A complication is that the ratio of the interfering amplitudes is very small, $r_{D\pi} = A(B^0 \rightarrow D^+ \pi^-) / A(\bar{B}^0 \rightarrow D^+ \pi^-) = \mathcal{O}(0.01)$ (and similarly for $r_{D^* \pi}$ and $r_{D\rho}$), and therefore it has not been possible to measure it. To obtain $2\beta + \gamma$, $SU(3)$ flavor symmetry and dynamical assumptions have been used to relate $A(\bar{B}^0 \rightarrow D^+ \pi^-)$ to $A(\bar{B}^0 \rightarrow D_s^+ \pi^+)$, so this measurement is not model independent at present. Combining the $D^\pm \pi^\mp$, $D^{* \pm} \pi^\mp$ and $D^\pm \rho^\mp$ measurements [131] gives $\sin(2\beta + \gamma) > 0.68$ at 68% CL [115], consistent with the previously discussed results for β and γ .

12.4 Global fit in the Standard Model

Using the independently measured CKM elements mentioned in the previous sections, the unitarity of the CKM matrix can be checked. We obtain $|V_{ud}|^2 + |V_{us}|^2 + |V_{ub}|^2 = 0.9985 \pm 0.0007$ (1st row), $|V_{cd}|^2 + |V_{cs}|^2 + |V_{cb}|^2 = 1.001 \pm 0.012$ (2nd row), $|V_{ud}|^2 + |V_{cd}|^2 + |V_{td}|^2 = 0.9972 \pm 0.0020$ (1st column), and $|V_{us}|^2 + |V_{cs}|^2 + |V_{ts}|^2 = 1.004 \pm 0.012$ (2nd column), respectively. Due to the recent reduction of the value of $|V_{ud}|$, there is a 2.2σ tension with unitarity in the 1st row, leading also to poor consistency of the SM fit below. The uncertainties in the second row and column are dominated by that of $|V_{cs}|$. For the second row, another check is obtained from the measurement of $\sum_{u,c,d,s,b} |V_{ij}|^2$ in Sec. 12.2.4, minus the sum in the first row above: $|V_{cd}|^2 + |V_{cs}|^2 + |V_{cb}|^2 = 1.002 \pm 0.027$. These provide strong tests of the unitarity of the CKM matrix. With the significantly improved direct determination of $|V_{tb}|$, the unitarity checks for the third row and column have also become fairly precise, leaving decreasing room for mixing with other states. The sum of the three angles of the unitarity triangle, $\alpha + \beta + \gamma = (173 \pm 6)^\circ$, is also consistent with the SM expectation.

The CKM matrix elements can be most precisely determined using a global fit to all available measurements and imposing the SM constraints (*i.e.*, three generation unitarity). The fit must also use theory predictions for hadronic matrix elements, which sometimes have significant uncertainties. There are several approaches to combining the experimental data. CKMfitter [6, 115]

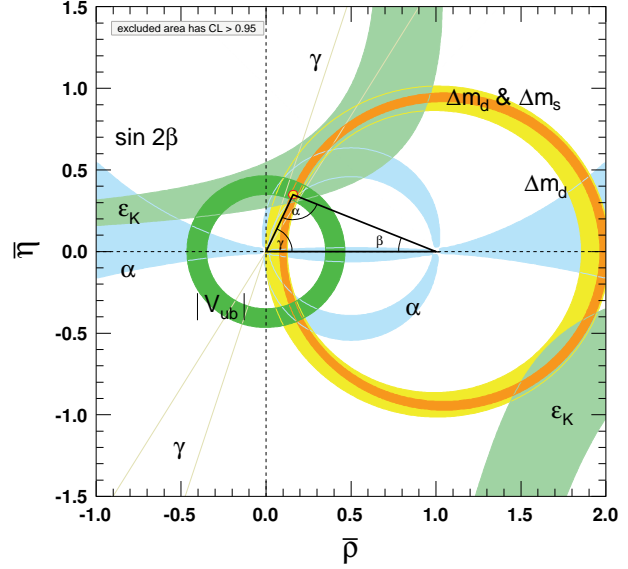


Figure 12.2: Constraints on the $\bar{\rho}$, $\bar{\eta}$ plane. The shaded areas have 95% CL.

and Ref. [132] (which develops [133, 134] further) use frequentist statistics, while UTfit [116, 135] uses a Bayesian approach. These approaches provide similar results.

The constraints implied by the unitarity of the three generation CKM matrix significantly reduce the allowed range of some of the CKM elements. The fit for the Wolfenstein parameters defined in Eq. (12.4) gives

$$\begin{aligned} \lambda &= 0.22500 \pm 0.00067, & A &= 0.826_{-0.015}^{+0.018}, \\ \bar{\rho} &= 0.159 \pm 0.010, & \bar{\eta} &= 0.348 \pm 0.010. \end{aligned} \quad (12.26)$$

These values are obtained using the method of Refs. [6, 115]. The prescription of Refs. [116, 135] gives $\lambda = 0.22499 \pm 0.00067$, $A = 0.833 \pm 0.011$, $\bar{\rho} = 0.159 \pm 0.010$, and $\bar{\eta} = 0.348 \pm 0.009$ [136]; these results are now very close to one another. The fit results for the magnitudes of all nine CKM elements are

$$|V_{\text{CKM}}| = \begin{pmatrix} 0.97435 \pm 0.00016 & 0.22500 \pm 0.00067 & 0.00369 \pm 0.00011 \\ 0.22486 \pm 0.00067 & 0.97349 \pm 0.00016 & 0.04182_{-0.00074}^{+0.00085} \\ 0.00857_{-0.00018}^{+0.00020} & 0.04110_{-0.00072}^{+0.00083} & 0.999118_{-0.000036}^{+0.000031} \end{pmatrix}, \quad (12.27)$$

and the Jarlskog invariant is $J = (3.08_{-0.13}^{+0.15}) \times 10^{-5}$. The parameters in Eq. (12.3) are

$$\begin{aligned} \sin \theta_{12} &= 0.22500 \pm 0.00067, & \sin \theta_{13} &= 0.00369 \pm 0.00011, \\ \sin \theta_{23} &= 0.04182_{-0.00074}^{+0.00085}, & \delta &= 1.144 \pm 0.027. \end{aligned} \quad (12.28)$$

Fig. 12.2 illustrates the constraints on the $\bar{\rho}$, $\bar{\eta}$ plane from various measurements, and the global fit result. The shaded 95% CL regions all overlap consistently around the global fit region. This reverts a change in the 2020 edition, when the shown CL of each region was increased to 99%, because of poor consistency (primarily due to changes in $|V_{ud}|$), which is no longer the case.

If one uses only tree-level inputs (magnitudes of CKM elements not coupling to the top quark and the angle γ), the resulting fit is almost identical for λ in Eq. (12.26), while the other parameters' central values can change by about a sigma and their uncertainties double, yielding $\lambda = 0.22507 \pm 0.00068$, $A = 0.805 \pm 0.028$, $\bar{\rho} = 0.166_{-0.024}^{+0.026}$, and $\bar{\eta} = 0.370_{-0.028}^{+0.029}$. This illustrates how the constraints can be less tight in the presence of BSM physics.

12.5 Implications beyond the SM

The effects in B , B_s , K , and D decays and mixings due to high-scale physics (W , Z , t , H in the SM, and unknown heavier particles) can be parameterized by operators composed of SM fields, obeying the $SU(3) \times SU(2) \times U(1)$ gauge symmetry. Flavor-changing neutral currents, suppressed in the SM, are especially sensitive to beyond SM contributions. Processes studied in great detail, both experimentally and theoretically, include neutral meson mixings, $B_{(s)} \rightarrow X\gamma$, $X\ell^+\ell^-$, $\ell^+\ell^-$, $K \rightarrow \pi\nu\bar{\nu}$, etc. The BSM contributions to these operators are suppressed by powers of the scale at which they are generated. Already at lowest order, there are many dimension-6 operators, and the observable effects of BSM interactions are encoded in their coefficients. In the SM, these coefficients are determined by just the four CKM parameters, and the W , Z , and quark masses. For example, Δm_d , $\Gamma(B \rightarrow \rho\gamma)$, $\Gamma(B \rightarrow \pi\ell^+\ell^-)$, and $\Gamma(B \rightarrow \ell^+\ell^-)$ are all proportional to $|V_{td}V_{tb}|^2$ in the SM, however, they may receive unrelated BSM contributions. These BSM contributions may or may not obey the SM relations. (For example, the flavor sector of the MSSM contains 69 CP -conserving parameters and 41 CP -violating phases, *i.e.*, 40 new ones [137]). Thus, similar to the measurements of $\sin 2\beta$ in tree- and loop-dominated decay modes, overconstraining measurements of the magnitudes and phases of flavor-changing neutral-current amplitudes gives good sensitivity to BSM.

To illustrate the level of suppression required for BSM contributions, consider a class of models in which the unitarity of the CKM matrix is maintained, and the dominant BSM effects modify the neutral meson mixing amplitudes [138] by $(z_{ij}/\Lambda^2)(\bar{q}_i\gamma^\mu P_L q_j)^2$, where z_{ij} is an unknown coefficient and Λ is the scale suppressing this BSM contribution (see, [139, 140]). It is only known since the first measurements of γ and α that the SM gives the leading contribution to $B^0 - \bar{B}^0$ mixing [6, 141]. Nevertheless, new physics with a generic weak phase may still contribute to neutral meson mixings at a significant fraction of the SM [135, 142, 143]. The existing data imply that $\Lambda/|z_{ij}|^{1/2}$ has to exceed about 10^4 TeV for $K^0 - \bar{K}^0$ mixing, 10^3 TeV for $D^0 - \bar{D}^0$ mixing, 500 TeV for $B^0 - \bar{B}^0$ mixing, and 100 TeV for $B_s^0 - \bar{B}_s^0$ mixing [135, 140]. (Some other operators are even better constrained [135].) The constraints are the strongest in the kaon sector, because the CKM suppression is the most severe. Thus, if there is new physics at the TeV scale, $|z_{ij}| \ll 1$ is required. Even if $|z_{ij}|$ are suppressed by a loop factor and $|V_{ti}^*V_{tj}|^2$ (in the down quark sector), similar to the SM, one expects percent-level effects, which may be observable in forthcoming flavor physics experiments. To constrain such extensions of the SM, many measurements irrelevant for the SM-CKM fit, such as the CP asymmetry in semileptonic $B_{d,s}^0$ decays, $A_{SL}^{d,s}$, are important [144]. The current world averages [23] are consistent with the SM, with experimental uncertainties far greater than those of the theory predictions.

There are many key measurements sensitive to BSM physics, which do not constrain the unitarity triangle in Fig. 12.1. For example, a key quantity in the B_s system is $\beta_s = \arg(-V_{ts}V_{tb}^*/V_{cs}V_{cb}^*)$, which is the small, λ^2 -suppressed, angle of a “squashed” unitarity triangle, obtained by taking the scalar product of the second and third columns of the CKM matrix. This angle can be measured via time-dependent CP violation in $B_s^0 \rightarrow J/\psi\phi$, similar to β in $B^0 \rightarrow J/\psi K^0$. Since the $J/\psi\phi$ final state is not a CP eigenstate, an angular analysis of the decay products is needed to separate the CP -even and CP -odd components, which give opposite asymmetries. In the SM, the asymmetry for the CP -even part is $2\beta_s$, when one neglects subdominant amplitudes with a weak phase V_{ub} . (Sometimes the notation $\phi_s = -2\beta_s$ plus a possible BSM contribution to the B_s mixing phase is used.) Testing if the data agree with the SM prediction, $2\beta_s = 0.0369_{-0.0010}^{+0.0011}$ [115], is another sensitive probe of the SM. The current world average, dominated by LHC measurements [145] including the $B_s \rightarrow J/\psi K^+ K^-$ and $J/\psi \pi^+ \pi^-$ decay modes, is $2\beta_s = 0.050 \pm 0.019$ [74]. Since the uncertainty is much larger than that in the SM, a lot will be learned from more precise future measurements. Searches for CP violation in the charm sector, in particular in $D^0 - \bar{D}^0$ mixing, provide complementary sensitivity to BSM.

In the kaon sector, the CP -violating observables, ϵ and ϵ' , are tiny, so models in which all sources of CP violation are small were viable before the B -factory measurements. Since the measurement of $\sin 2\beta$, we know that CP violation can be an $\mathcal{O}(1)$ effect, and only flavor mixing is suppressed between the three quark generations. Thus, many models with spontaneous CP violation were excluded. In the kaon sector, clean tests of the SM can come from measurements of $K^+ \rightarrow \pi^+ \nu\bar{\nu}$ [81] and $K_L^0 \rightarrow \pi^0 \nu\bar{\nu}$ [146]. These loop-induced rare decays are sensitive to BSM, and will allow precise tests [147] of the CKM paradigm, independent of B decays.

The CKM elements are fundamental parameters, so they should be measured as precisely as possible. The overconstraining measurements of CP asymmetries, mixing, semileptonic, and rare decays severely constrain the magnitudes and phases of possible BSM contributions to flavor-changing interactions. If new particles are observed at the LHC, it will be important to explore their flavor parameters as precisely as possible to understand the underlying physics.

References

- [1] N. Cabibbo, Phys. Rev. Lett. **10**, 531 (1963).
- [2] M. Kobayashi and T. Maskawa, Prog. Theor. Phys. **49**, 652 (1973).
- [3] L.-L. Chau and W.-Y. Keung, Phys. Rev. Lett. **53**, 1802 (1984).
- [4] L. Wolfenstein, Phys. Rev. Lett. **51**, 1945 (1983).
- [5] A. J. Buras, M. E. Lautenbacher and G. Ostermaier, Phys. Rev. **D50**, 3433 (1994), [hep-ph/9403384].
- [6] J. Charles *et al.* (CKMfitter Group), Eur. Phys. J. **C41**, 1, 1 (2005), [hep-ph/0406184].
- [7] C. Jarlskog, Phys. Rev. Lett. **55**, 1039 (1985).
- [8] W. J. Marciano and A. Sirlin, Nucl. Phys. **B93**, 303 (1975); K. S. Babu, Z. Phys. **C35**, 69 (1987).
- [9] J. C. Hardy and I. S. Towner, Phys. Rev. C **102**, 4, 045501 (2020).
- [10] E. Blucher and W. J. Marciano, “ V_{ud} , V_{us} , the Cabibbo Angle and CKM Unitarity,” in this *Review*.
- [11] D. Poganic *et al.*, Phys. Rev. Lett. **93**, 181803 (2004), [hep-ex/0312030].
- [12] M. Antonelli *et al.* (FlaviaNet Working Group on Kaon Decays), Eur. Phys. J. **C69**, 399 (2010), [arXiv:1005.2323]; see also <http://www.inf.infn.it/wg/vus>.
- [13] S. Aoki *et al.* (Flavour Lattice Averaging Group) “FLAG Review 2021”, <http://flag.umibe.ch/2021>; The original papers that led to the quoted averages are cited in this reference.
- [14] T. Mannel and P. Urquijo, “Semileptonic b -Hadron Decays, Determination of V_{cb} and V_{ub} ,” in this *Review*.
- [15] H. Leutwyler and M. Roos, Z. Phys. **C25**, 91 (1984); For earlier fits for $|V_{ud}|$ and $|V_{us}|$ in the 3-generation SM, see Ref. [16].
- [16] R. E. Shrock and L.-L. Wang, Phys. Rev. Lett. **41**, 1692 (1978).
- [17] J. Bijnens and P. Talavera, Nucl. Phys. **B669**, 341 (2003), [hep-ph/0303103]; M. Jamin, J. A. Oller and A. Pich, JHEP **02**, 047 (2004), [hep-ph/0401080]; V. Cirigliano *et al.*, JHEP **04**, 006 (2005), [hep-ph/0503108]; C. Dawson *et al.*, PoS **LAT2005**, 337 (2006), [hep-lat/0510018]; N. Tsutsui *et al.* (JLQCD), PoS **LAT2005**, 357 (2006), [hep-lat/0510068]; M. Okamoto (Fermilab Lattice, MILC, HPQCD), in “3rd Conference on Flavor Physics and CP Violation (FPCP 2004) Daegu, Korea, October 4-9, 2004,” (2004), [hep-lat/0412044].
- [18] W. J. Marciano, Phys. Rev. Lett. **93**, 231803 (2004), [hep-ph/0402299].
- [19] F. Ambrosino *et al.* (KLOE), Phys. Lett. **B632**, 76 (2006), [hep-ex/0509045].

- [20] See Sec. 5.2, “Averages and fits,” in the Introduction to this *Review*, <http://pdg.lbl.gov/2019/reviews/rpp2019-rev-rpp-intro.pdf>.
- [21] N. Cabibbo, E. C. Swallow and R. Winston, *Ann. Rev. Nucl. Part. Sci.* **53**, 39 (2003), [hep-ph/0307298]; N. Cabibbo, E. C. Swallow and R. Winston, *Phys. Rev. Lett.* **92**, 251803 (2004), [hep-ph/0307214].
- [22] M. Ademollo and R. Gatto, *Phys. Rev. Lett.* **13**, 264 (1964).
- [23] Y. S. Amhis *et al.* (HFLAV), *Eur. Phys. J. C* **81**, 3, 226 (2021), [arXiv:1908.12524]; and updates at <https://hflav.web.cern.ch/>.
- [24] J. P. Lees *et al.* (BaBar), *Phys. Rev.* **D91**, 5, 052022 (2015), [arXiv:1412.5502].
- [25] M. Ablikim *et al.* (BESIII), *Phys. Rev.* **D92**, 7, 072012 (2015), [arXiv:1508.07560].
- [26] M. Ablikim *et al.* (BESIII), *Phys. Rev.* **D96**, 1, 012002 (2017), [arXiv:1703.09084].
- [27] D. Besson *et al.* (CLEO), *Phys. Rev.* **D80**, 032005 (2009), [arXiv:0906.2983].
- [28] L. Widhalm *et al.* (Belle), *Phys. Rev. Lett.* **97**, 061804 (2006), [hep-ex/0604049].
- [29] M. Ablikim *et al.* (BESIII), *Phys. Rev.* **D89**, 5, 051104 (2014), [arXiv:1312.0374].
- [30] B. I. Eisenstein *et al.* (CLEO), *Phys. Rev.* **D78**, 052003 (2008), [arXiv:0806.2112].
- [31] M. Ablikim *et al.* (BESIII), *Phys. Rev. Lett.* **123**, 21, 211802 (2019), [arXiv:1908.08877].
- [32] Heavy Flavor Averaging Group [23], June 2021 update of Charm Leptonic Decays <https://hflav-eos.web.cern.ch/hflav-eos/charm/Vcd/june21/Vcd-from-leptonic-D-decays.html>.
- [33] H. Abramowicz *et al.*, *Z. Phys.* **C15**, 19 (1982).
- [34] S. A. Rabinowitz *et al.*, *Phys. Rev. Lett.* **70**, 134 (1993).
- [35] A. O. Bazarko *et al.* (CCFR), *Z. Phys.* **C65**, 189 (1995), [hep-ex/9406007].
- [36] P. Vilain *et al.* (CHARM II), *Eur. Phys. J.* **C11**, 19 (1999).
- [37] F. J. Gilman, K. Kleinknecht and B. Renk (2004).
- [38] G. De Lellis, P. Migliozi and P. Santorelli, *Phys. Rept.* **399**, 227 (2004), [Erratum: *Phys. Rept.* 411,323(2005)].
- [39] N. Ushida *et al.* (Fermilab E531), *Phys. Lett.* **B206**, 380 (1988).
- [40] T. Bolton (1997), [hep-ex/9708014].
- [41] A. Kayis-Topaksu *et al.* (CHORUS), *Phys. Lett.* **B626**, 24 (2005).
- [42] A. Zupanc *et al.* (Belle), *JHEP* **09**, 139 (2013), [arXiv:1307.6240].
- [43] J. P. Alexander *et al.* (CLEO), *Phys. Rev.* **D79**, 052001 (2009), [arXiv:0901.1216].
- [44] P. del Amo Sanchez *et al.* (BaBar), *Phys. Rev.* **D82**, 091103 (2010), [Erratum: *Phys. Rev.* D91,no.1,019901(2015)], [arXiv:1008.4080].
- [45] M. Ablikim *et al.* (BESIII), *Phys. Rev.* **D94**, 7, 072004 (2016), [arXiv:1608.06732].
- [46] M. Ablikim *et al.* (BESIII), *Phys. Rev. D* **104**, 5, 052009 (2021), [arXiv:2102.11734].
- [47] P. U. E. Onyisi *et al.* (CLEO), *Phys. Rev.* **D79**, 052002 (2009), [arXiv:0901.1147].
- [48] P. Naik *et al.* (CLEO), *Phys. Rev.* **D80**, 112004 (2009), [arXiv:0910.3602].
- [49] B. Aubert *et al.* (BaBar), *Phys. Rev.* **D76**, 052005 (2007), [arXiv:0704.0020].
- [50] M. Ablikim *et al.* (BESIII), *Phys. Rev. Lett.* **122**, 1, 011804 (2019), [arXiv:1810.03127].
- [51] LEP W branching fraction results for this Review of Particle Physics, LEPEWWG/XSEC/2005-01, <http://lepewwg.web.cern.ch/LEPEWWG/lepww/4f/Winter05>.
- [52] P. Abreu *et al.* (DELPHI), *Phys. Lett.* **B439**, 209 (1998).
- [53] I. I. Y. Bigi *et al.*, *Phys. Rev. Lett.* **71**, 496 (1993), [hep-ph/9304225].
- [54] A. V. Manohar and M. B. Wise, *Phys. Rev.* **D49**, 1310 (1994), [hep-ph/9308246].
- [55] I. I. Y. Bigi *et al.*, *Phys. Rev.* **D56**, 4017 (1997), [hep-ph/9704245].
- [56] A. H. Hoang, Z. Ligeti and A. V. Manohar, *Phys. Rev.* **D59**, 074017 (1999), [hep-ph/9811239]; A. H. Hoang, Z. Ligeti and A. V. Manohar, *Phys. Rev. Lett.* **82**, 277 (1999), [hep-ph/9809423]; A. H. Hoang and T. Teubner, *Phys. Rev.* **D60**, 114027 (1999), [hep-ph/9904468].
- [57] N. Isgur and M. B. Wise, *Phys. Lett.* **B237**, 527 (1990); N. Isgur and M. B. Wise, *Phys. Lett.* **B232**, 113 (1989).
- [58] A. Abdesselam *et al.* (Belle) (2017), [arXiv:1702.01521].
- [59] C. G. Boyd, B. Grinstein and R. F. Lebed, *Phys. Rev.* **D56**, 6895 (1997), [hep-ph/9705252]; C. G. Boyd, B. Grinstein and R. F. Lebed, *Nucl. Phys.* **B461**, 493 (1996), [hep-ph/9508211].
- [60] R. Aaij *et al.* (LHCb), *Phys. Rev. D* **101**, 7, 072004 (2020), [arXiv:2001.03225].
- [61] M. Neubert, *Phys. Rev.* **D49**, 3392 (1994), [hep-ph/9311325]; M. Neubert, *Phys. Rev.* **D49**, 4623 (1994), [hep-ph/9312311].
- [62] I. I. Y. Bigi *et al.*, *Int. J. Mod. Phys.* **A9**, 2467 (1994), [hep-ph/9312359].
- [63] C. W. Bauer, Z. Ligeti and M. E. Luke, *Phys. Lett.* **B479**, 395 (2000), [hep-ph/0002161]; C. W. Bauer, Z. Ligeti and M. E. Luke, *Phys. Rev.* **D64**, 113004 (2001), [hep-ph/0107074].
- [64] A. Bornheim *et al.* (CLEO), *Phys. Rev. Lett.* **88**, 231803 (2002), [hep-ex/0202019].
- [65] B. Aubert *et al.* (BaBar), *Phys. Rev.* **D73**, 012006 (2006), [hep-ex/0509040].
- [66] A. Limosani *et al.* (Belle), *Phys. Lett.* **B621**, 28 (2005), [hep-ex/0504046].
- [67] P. Urquijo *et al.* (Belle), *Phys. Rev. Lett.* **104**, 021801 (2010), [arXiv:0907.0379]; J. P. Lees *et al.* (BaBar), *Phys. Rev.* **D86**, 032004 (2012), [arXiv:1112.0702].
- [68] J. A. Bailey *et al.* (Fermilab Lattice, MILC), *Phys. Rev.* **D92**, 1, 014024 (2015), [arXiv:1503.07839]; J. M. Flynn *et al.*, *Phys. Rev.* **D91**, 7, 074510 (2015), [arXiv:1501.05373]; B. Colquhoun *et al.*, *Phys. Rev.* **D93**, 3, 034502 (2016), [arXiv:1510.07446].
- [69] P. Ball and R. Zwicky, *Phys. Rev.* **D71**, 014015 (2005), [hep-ph/0406232]; A. Khodjamirian *et al.*, *Phys. Rev.* **D83**, 094031 (2011), [arXiv:1103.2655].
- [70] Particle listing, in this *Review*.
- [71] R. Aaij *et al.* (LHCb), *Nature Phys.* **11**, 743 (2015), [arXiv:1504.01568].
- [72] R. Aaij *et al.* (LHCb), *Phys. Rev. Lett.* **126**, 8, 081804 (2021), [arXiv:2012.05143].
- [73] H. Albrecht *et al.* (ARGUS), *Phys. Lett.* **B192**, 245 (1987).
- [74] O. Schneider, “ $B^0-\bar{B}^0$ mixing,” in this *Review*.
- [75] A. Abulencia *et al.* (CDF), *Phys. Rev. Lett.* **97**, 242003 (2006), [hep-ex/0609040].
- [76] R. Aaij *et al.* (LHCb), *Nature Phys.* **18**, 1, 1 (2022), [arXiv:2104.04421].
- [77] M. Misiak *et al.*, *Phys. Rev. Lett.* **114**, 22, 221801 (2015), [arXiv:1503.01789]; M. Czakon *et al.*, *JHEP* **04**, 168 (2015), [arXiv:1503.01791].

- [78] B. Grinstein and D. Pirjol, Phys. Rev. **D62**, 093002 (2000), [hep-ph/0002216]; A. Ali, E. Lunghi and A. Ya. Parkhomenko, Phys. Lett. **B595**, 323 (2004), [hep-ph/0405075]; M. Beneke, T. Feldmann and D. Seidel, Nucl. Phys. **B612**, 25 (2001), [hep-ph/0106067]; S. W. Bosch and G. Buchalla, Nucl. Phys. **B621**, 459 (2002), [hep-ph/0106081]; Z. Ligeti and M. B. Wise, Phys. Rev. **D60**, 117506 (1999), [hep-ph/9905277]; D. Becirevic *et al.*, JHEP **05**, 007 (2003), [hep-lat/0301020]; P. Ball, G. W. Jones and R. Zwicky, Phys. Rev. **D75**, 054004 (2007), [hep-ph/0612081]; W. Wang, R.-H. Li and C.-D. Lu (2007), [arXiv:0711.0432]; C.-D. Lu, W. Wang and Z.-T. Wei, Phys. Rev. **D76**, 014013 (2007), [hep-ph/0701265].
- [79] A. J. Buras *et al.*, Phys. Rev. Lett. **95**, 261805 (2005), [hep-ph/0508165].
- [80] A. V. Artamonov *et al.* (E949), Phys. Rev. Lett. **101**, 191802 (2008), [arXiv:0808.2459]; A. V. Artamonov *et al.* (BNL-E949), Phys. Rev. **D79**, 092004 (2009), [arXiv:0903.0030].
- [81] E. Cortina Gil *et al.* (NA62), JHEP **06**, 093 (2021), [arXiv:2103.15389].
- [82] D. Acosta *et al.* (CDF), Phys. Rev. Lett. **95**, 102002 (2005), [hep-ex/0505091].
- [83] V. M. Abazov *et al.* (D0), Phys. Rev. Lett. **107**, 121802 (2011), [arXiv:1106.5436].
- [84] V. Khachatryan *et al.* (CMS), Phys. Lett. **B736**, 33 (2014), [arXiv:1404.2292].
- [85] T. A. Aaltonen *et al.* (CDF, D0), Phys. Rev. Lett. **115**, 15, 152003 (2015), [arXiv:1503.05027].
- [86] LHC Top Working Group summary plots, single top quark production, Sep. 2021, <https://twiki.cern.ch/twiki/bin/view/LHCPhysics/LHCtopWGSummaryPlots>.
- [87] J. Swain and L. Taylor, Phys. Rev. **D58**, 093006 (1998), [hep-ph/9712420].
- [88] “ K_L^0 meson” particle listing, in this *Review*.
- [89] A. J. Buras, D. Guadagnoli and G. Isidori, Phys. Lett. **B688**, 309 (2010), [arXiv:1002.3612]; For earlier discussions, see Ref. [90].
- [90] E. A. Andriyash, G. G. Ovanesyan and M. I. Vysotsky, Phys. Lett. **B599**, 253 (2004), [hep-ph/0310314]; K. Anikeev *et al.*, in “Workshop on B Physics at the Tevatron: Run II and Beyond Batavia, Illinois, September 23-25, 1999,” (2001), [hep-ph/0201071]; A. J. Buras and D. Guadagnoli, Phys. Rev. **D78**, 033005 (2008), [arXiv:0805.3887].
- [91] T. Inami and C. S. Lim, Prog. Theor. Phys. **65**, 297 (1981), [Erratum: Prog. Theor. Phys.65,1772(1981)].
- [92] J. M. Flynn and L. Randall, Phys. Lett. **B224**, 221 (1989), [Erratum: Phys. Lett.B235,412(1990)]; G. Buchalla, A. J. Buras and M. K. Harlander, Nucl. Phys. **B337**, 313 (1990).
- [93] M. Ciuchini *et al.*, Phys. Lett. **B301**, 263 (1993), [hep-ph/9212203]; A. J. Buras, M. Jamin and M. E. Lautenbacher, Nucl. Phys. **B408**, 209 (1993), [hep-ph/9303284]; T. Hambye *et al.*, Nucl. Phys. **B564**, 391 (2000), [hep-ph/9906434]; S. Bertolini, J. O. Eeg and M. Fabbri-chesi, Phys. Rev. **D63**, 056009 (2001), [hep-ph/0002234]; V. Cirigliano *et al.*, Phys. Rev. Lett. **91**, 162001 (2003), [hep-ph/0307030].
- [94] R. Abbott *et al.* (RBC, UKQCD), Phys. Rev. D **102**, 5, 054509 (2020), [arXiv:2004.09440].
- [95] A. J. Buras *et al.*, JHEP **11**, 202 (2015), [arXiv:1507.06345].
- [96] V. Cirigliano *et al.*, JHEP **02**, 032 (2020), [arXiv:1911.01359].
- [97] A. B. Carter and A. I. Sanda, Phys. Rev. Lett. **45**, 952 (1980); A. B. Carter and A. I. Sanda, Phys. Rev. **D23**, 1567 (1981).
- [98] A more detailed discussion and references can be found in: T. Gershon and Y. Nir, “ CP violation in meson decays,” in this *Review*.
- [99] T. Gershon, M. Kenzie and K. Trabelsi, “Determination of CKM angles from B hadrons,” in this *Review*.
- [100] B. Aubert *et al.* (BaBar), Phys. Rev. **D79**, 072009 (2009), [arXiv:0902.1708].
- [101] I. Adachi *et al.* (Belle), Phys. Rev. Lett. **108**, 171802 (2012), [arXiv:1201.4643].
- [102] R. Aaij *et al.* (LHCb), Phys. Rev. Lett. **115**, 3, 031601 (2015), [arXiv:1503.07089].
- [103] B. Aubert *et al.* (BaBar), Phys. Rev. **D71**, 032005 (2005), [hep-ex/0411016].
- [104] R. Itoh *et al.* (Belle), Phys. Rev. Lett. **95**, 091601 (2005), [hep-ex/0504030].
- [105] I. Adachi *et al.* (BaBar, Belle), Phys. Rev. Lett. **121**, 26, 261801 (2018), [arXiv:1804.06152]; I. Adachi *et al.* (BaBar, Belle), Phys. Rev. **D98**, 11, 112012 (2018), [arXiv:1804.06153].
- [106] A. Abdesselam *et al.* (BaBar, Belle), Phys. Rev. Lett. **115**, 12, 121604 (2015), [arXiv:1505.04147].
- [107] Heavy Flavor Averaging Group [23], Results on Time-Dependent CP Violation and Measurements Related to the Angles of the Unitarity Triangle: Winter conferences (Moriond, etc.) and PDG 2022: <https://hflav-eos.web.cern.ch/hflav-eos/triangle/pdg2022/>.
- [108] M. Gronau and D. London, Phys. Rev. Lett. **65**, 3381 (1990).
- [109] J. Zhang *et al.* (Belle), Phys. Rev. Lett. **91**, 221801 (2003), [hep-ex/0306007]; A. Somov *et al.* (Belle), Phys. Rev. Lett. **96**, 171801 (2006), [hep-ex/0601024]; B. Aubert *et al.* (BaBar), Phys. Rev. Lett. **97**, 261801 (2006), [hep-ex/0607092]; B. Aubert *et al.* (BaBar), Phys. Rev. **D76**, 052007 (2007), [arXiv:0705.2157].
- [110] B. Aubert *et al.* (BaBar), Phys. Rev. **D78**, 071104 (2008), [arXiv:0807.4977].
- [111] A. F. Falk *et al.*, Phys. Rev. **D69**, 011502 (2004), [hep-ph/0310242].
- [112] A. E. Snyder and H. R. Quinn, Phys. Rev. **D48**, 2139 (1993).
- [113] A. Kusaka *et al.* (Belle), Phys. Rev. Lett. **98**, 221602 (2007), [hep-ex/0701015].
- [114] J. P. Lees *et al.* (BaBar), Phys. Rev. **D88**, 1, 012003 (2013), [arXiv:1304.3503].
- [115] A. Hocker *et al.*, Eur. Phys. J. **C21**, 225 (2001), [hep-ph/0104062]; and updates at <http://ckmfitter.in2p3.fr/>.
- [116] M. Bona *et al.* (UTfit), JHEP **07**, 028 (2005), [hep-ph/0501199]; and updates at <http://www.utfit.org>.
- [117] M. Gronau and D. London, Phys. Lett. **B253**, 483 (1991).
- [118] M. Gronau and D. Wyler, Phys. Lett. **B265**, 172 (1991).
- [119] D. Atwood, I. Dunietz and A. Soni, Phys. Rev. Lett. **78**, 3257 (1997), [hep-ph/9612433]; D. Atwood, I. Dunietz and A. Soni, Phys. Rev. **D63**, 036005 (2001), [hep-ph/0008090].
- [120] A. Bondar, talk at the Belle analysis workshop, Novosibirsk, September 2002; A. Poluektov *et al.* (Belle), Phys. Rev. **D70**, 072003 (2004), [hep-ex/0406067].
- [121] A. Giri *et al.*, Phys. Rev. **D68**, 054018 (2003), [hep-ph/0303187].
- [122] A. Poluektov *et al.* (Belle), Phys. Rev. **D81**, 112002 (2010), [arXiv:1003.3360].
- [123] P. del Amo Sanchez *et al.* (BaBar), Phys. Rev. Lett. **105**, 121801 (2010), [arXiv:1005.1096].
- [124] R. Aaij *et al.* (LHCb), JHEP **02**, 169 (2021), [arXiv:2010.08483].
- [125] Y. Grossman, A. Soffer and J. Zupan, Phys. Rev. **D72**, 031501 (2005), [hep-ph/0505270].
- [126] M. Rama, Phys. Rev. D **89**, 1, 014021 (2014), [arXiv:1307.4384].

- [127] A. Amorim, M. G. Santos and J. P. Silva, Phys. Rev. **D59**, 056001 (1999), [hep-ph/9807364].
- [128] R. Aleksan, I. Dunietz and B. Kayser, Z. Phys. **C54**, 653 (1992).
- [129] R. Aaij *et al.* (LHCb), JHEP **03**, 059 (2018), [arXiv:1712.07428].
- [130] R. Aaij *et al.* (LHCb), JHEP **03**, 137 (2021), [arXiv:2011.12041].
- [131] B. Aubert *et al.* (BaBar), Phys. Rev. **D71**, 112003 (2005), [hep-ex/0504035]; B. Aubert *et al.* (BaBar), Phys. Rev. **D73**, 111101 (2006), [hep-ex/0602049]; F. J. Ronga *et al.* (Belle), Phys. Rev. **D73**, 092003 (2006), [hep-ex/0604013]; S. Bahinipati *et al.* (Belle), Phys. Rev. **D84**, 021101 (2011), [arXiv:1102.0888]; R. Aaij *et al.* (LHCb), JHEP **06**, 084 (2018), [arXiv:1805.03448].
- [132] G. P. Dubois-Felsmann *et al.*, *Sensitivity of CKM fits to theoretical uncertainties and their representation* (2003), [hep-ph/0308262]; G. Eigen *et al.*, Phys. Rev. **D89**, 3, 033004 (2014), [arXiv:1301.5867].
- [133] D. Boutigny *et al.* (BaBar), in “Workshop on Physics at an Asymmetric B Factory (BaBar Collaboration Meeting) Pasadena, California, September 22-24, 1997,” (1998), URL <http://www-public.slac.stanford.edu/sciDoc/docMeta.aspx?slacPubNumber=SLAC-R-504>.
- [134] S. Plaszczynski and M.-H. Schune hf8/019 (1999), [PoShf8,019(1999)], [hep-ph/9911280].
- [135] M. Bona *et al.* (UTfit), JHEP **03**, 049 (2008), [arXiv:0707.0636].
- [136] We thank the CKMfitter and UTfit groups for performing fits and preparing plots using input values from this *Review*.
- [137] H. E. Haber, Nucl. Phys. Proc. Suppl. **62**, 469 (1998), [hep-ph/9709450]; Y. Nir, *CP violation: A New era* (2001), [hep-ph/0109090].
- [138] J. M. Soares and L. Wolfenstein, Phys. Rev. **D47**, 1021 (1993); T. Goto *et al.*, Phys. Rev. **D53**, 6662 (1996), [hep-ph/9506311]; J. P. Silva and L. Wolfenstein, Phys. Rev. **D55**, 5331 (1997), [hep-ph/9610208].
- [139] Y. Grossman, Z. Ligeti and Y. Nir, Prog. Theor. Phys. **122**, 125 (2009), [arXiv:0904.4262].
- [140] G. Isidori, Y. Nir and G. Perez, Ann. Rev. Nucl. Part. Sci. **60**, 355 (2010), [arXiv:1002.0900]; G. Isidori, in “Proceedings, 2012 European School of High-Energy Physics (ES-HEP 2012): La Pommeraye, Anjou, France, June 06-19, 2012,” 69–105 (2014), [arXiv:1302.0661].
- [141] Z. Ligeti, Int. J. Mod. Phys. **A20**, 5105 (2005), [hep-ph/0408267].
- [142] J. Charles *et al.*, Phys. Rev. **D89**, 3, 033016 (2014), [arXiv:1309.2293].
- [143] K. Agashe *et al.* (2005), [hep-ph/0509117].
- [144] S. Laplace *et al.*, Phys. Rev. **D65**, 094040 (2002), [hep-ph/0202010].
- [145] R. Aaij *et al.* (LHCb), JHEP **08**, 037 (2017), [arXiv:1704.08217]; G. Aad *et al.* (ATLAS) (2020), [arXiv:2001.07115]; V. Khachatryan *et al.* (CMS), Phys. Lett. **B757**, 97 (2016), [arXiv:1507.07527].
- [146] J. K. Ahn *et al.* (KOTO), Phys. Rev. Lett. **122**, 2, 021802 (2019), [arXiv:1810.09655].
- [147] A. J. Buras *et al.*, JHEP **11**, 033 (2015), [arXiv:1503.02693].

13. CP Violation in the Quark Sector

Revised August 2021 by T. Gershon (Warwick U.) and Y. Nir (Weizmann Inst.).

The CP transformation combines charge conjugation C with parity P . Under C , particles and antiparticles are interchanged, by conjugating all internal quantum numbers, *e.g.*, $Q \rightarrow -Q$ for electromagnetic charge. Under P , the handedness of space is reversed, $\vec{x} \rightarrow -\vec{x}$. Thus, for example, a left-handed electron e_L^- is transformed under CP into a right-handed positron, e_R^+ .

If CP were an exact symmetry, the laws of nature would be the same for matter and for antimatter. We observe that most phenomena are C - and P -symmetric, and therefore, also CP -symmetric. In particular, these symmetries are respected by the electromagnetic and strong interactions. The weak interactions, on the other hand, violate C and P in the strongest possible way. For example, the W bosons couple to left-handed electrons, e_L^- , and to their CP -conjugate right-handed positrons, e_R^+ , but to neither their C -conjugate left-handed positrons, e_L^+ , nor their P -conjugate right-handed electrons, e_R^- . While weak interactions violate C and P separately, CP is still preserved in most weak interaction processes. The CP symmetry is, however, violated in certain processes involving interference effects, as discovered in neutral K decays in 1964 [1], and established later in B (2001) and D (2019) decays. For example, as discovered in 1967, a K_L meson decays more often to $\pi^- e^+ \nu_e$ than to $\pi^+ e^- \bar{\nu}_e$, thus allowing electrons and positrons to be unambiguously distinguished, but the decay-rate asymmetry is only at the 0.003 level. The CP -violating effects observed in the B system are larger: the parameter describing the CP asymmetry in the decay time distribution of B^0/\bar{B}^0 meson transitions to CP eigenstates like $J/\psi K_S$ is about 0.7 [2, 3]. These effects are related to $K^0-\bar{K}^0$ and $B^0-\bar{B}^0$ mixing, but CP violation arising solely from decay amplitudes has also been observed, first in $K \rightarrow \pi\pi$ decays [4–6], subsequently in B^0 [7, 8], B^+ [9–11], and B_s^0 [12] decays, and most recently in charm decays [13]. All of these observed CP asymmetries are consistent with the Standard Model predictions. Similar effects could also occur in decays of baryons, but have not yet been observed. Given that neutrino masses and lepton mixing have been established, it is expected that CP is violated also in the lepton sector [14]. Discovering CP violation in the lepton sector is one of the main goals of current and near-future experiments. CP violation has not yet been observed in processes involving the top quark, nor in flavor-conserving processes such as electric dipole moments; for these, any significant observation would be a clear indication of physics beyond the Standard Model.

In addition to parity and to continuous Lorentz transformations, there is one other spacetime operation that could be a symmetry of the interactions: time reversal T , $t \rightarrow -t$. Violations of T symmetry have been observed in neutral K decays [15]. More recently, T violation has been observed between states that are not CP -conjugate [16], exploiting the fact that for neutral B mesons both flavor tagging and CP tagging can be used [17]. Moreover, T violation is expected as a corollary of CP violation if the combined CPT transformation is a fundamental symmetry of nature [18]. All observations indicate that CPT is indeed a symmetry of nature [15]. Furthermore, one cannot build a locally Lorentz-invariant quantum field theory with a Hermitian Hamiltonian that violates CPT . (At several points in our discussion, we avoid assumptions about CPT , in order to identify cases where evidence for CP violation relies on assumptions about CPT .)

Within the Standard Model, CP symmetry is broken by complex phases in the Yukawa couplings (that is, the couplings of the Higgs scalar to quarks). When all transformations to remove unphysical phases in this model are exhausted, a single CP -violating parameter remains [19]. In the basis of mass eigenstates, this single phase appears in the 3×3 unitary matrix that gives the W -boson couplings to an up-type antiquark and a down-type quark. (If the Standard Model is supplemented with Majorana mass terms for the neutrinos, the analogous mixing matrix for leptons has three CP -violating phases.) The beautifully consistent and economical Standard-Model description of CP violation in terms of Yukawa couplings, known as the Kobayashi-Maskawa (KM) mechanism [19], agrees with all measurements to date. Fur-

thermore, one can fit the data allowing contributions from beyond the Standard Model (referred to subsequently as new physics) to loop processes to compete with, or even dominate over, the Standard Model amplitudes [20, 21]. Such an analysis provides model-independent proof that the KM phase is different from zero, and that the matrix of three-generation quark mixing is the dominant source of CP violation in meson decays.

The current level of experimental accuracy and the theoretical uncertainties involved in the interpretation of the various observations leave room, however, for additional subdominant sources of CP violation from new physics. Indeed, almost all extensions of the Standard Model imply that there are such additional sources. Moreover, CP violation is a necessary condition for baryogenesis, the process of dynamically generating the matter-antimatter asymmetry of the Universe [22]. Despite the phenomenological success of the KM mechanism, it fails (by several orders of magnitude) to accommodate the observed asymmetry [23]. This discrepancy strongly suggests that nature provides additional sources of CP violation beyond the KM mechanism. The evidence for neutrino masses implies that CP can be violated also in the lepton sector. This situation makes leptogenesis [24, 25], a scenario where CP -violating phases in the Yukawa couplings of the neutrinos play a crucial role in the generation of the baryon asymmetry, a very attractive possibility. The expectation of new sources motivates the large ongoing experimental effort to find deviations from the predictions of the KM mechanism.

CP violation can be experimentally searched for in a variety of processes, such as hadron decays, electric dipole moments of neutrons, electrons and nuclei, and neutrino oscillations. Hadron decays via the weak interaction probe flavor-changing CP violation. The search for electric dipole moments may find (or constrain) sources of CP violation that, unlike the KM phase, are not related to flavor-changing couplings. Following the discovery of the Higgs boson [26, 27], searches for CP violation in the Higgs sector are becoming feasible. Future searches for CP violation in neutrino oscillations might provide further input on leptogenesis.

The present measurements of CP asymmetries provide some of the strongest constraints on the weak couplings of quarks. Future measurements of CP violation in K , D , B , and B_s^0 meson decays will provide additional constraints on the flavor parameters of the Standard Model, and can probe new physics. In this review, we give the formalism and basic physics motivations that are relevant to present and near future measurements of CP violation in the quark sector.

13.1 Formalism

The phenomenology of CP violation for neutral flavored mesons is particularly interesting, since many of the observables can be cleanly interpreted. Although the phenomenology is superficially different for K^0 , D^0 , B^0 , and B_s^0 decays, this is primarily because each of these systems is governed by a different balance between decay rates, oscillations, and lifetime splitting. However, the general considerations presented in this section are identical for all flavored neutral pseudoscalar mesons. The phenomenology of CP violation for neutral mesons that do not carry flavor quantum numbers (such as the $\eta^{(l)}$ state) is quite different: such states are their own antiparticles and have definite CP eigenvalues, so the signature of CP violation is simply the decay to a final state with the opposite CP . Such decays are mediated by the electromagnetic or (OZI-suppressed [28–30]) strong interaction, where CP violation is not expected and has not yet been observed. In the remainder of this review, we restrict ourselves to considerations of weakly decaying hadrons.

In this section, we present a general formalism for, and classification of, CP violation in the decay of a weakly decaying hadron, denoted M . We pay particular attention to the case that M is a K^0 , D^0 , B^0 , or B_s^0 meson. Subsequent sections describe the CP -violating phenomenology, approximations, and alternative formalisms that are specific to each system.

13.1.1 Charged- and neutral-hadron decays

We define decay amplitudes of M (which could be charged or neutral) and its CP conjugate \bar{M} to a multi-particle final state f

and its CP conjugate \bar{f} as

$$A_f = \langle f | \mathcal{H} | M \rangle, \quad \bar{A}_f = \langle \bar{f} | \mathcal{H} | \bar{M} \rangle, \quad (13.1a)$$

$$A_{\bar{f}} = \langle \bar{f} | \mathcal{H} | M \rangle, \quad \bar{A}_{\bar{f}} = \langle \bar{f} | \mathcal{H} | \bar{M} \rangle, \quad (13.1b)$$

where \mathcal{H} is the Hamiltonian governing weak interactions. The action of CP on these states introduces phases ξ_M and ξ_f that depend on their flavor content, according to

$$CP|M\rangle = e^{+i\xi_M} |\bar{M}\rangle, \quad CP|f\rangle = e^{+i\xi_f} |\bar{f}\rangle, \quad (13.2a)$$

$$CP|\bar{M}\rangle = e^{-i\xi_M} |M\rangle, \quad CP|\bar{f}\rangle = e^{-i\xi_f} |f\rangle, \quad (13.2b)$$

so that $(CP)^2 = 1$. The phases ξ_M and ξ_f are arbitrary and unobservable because of the flavor symmetry of the strong interaction. If CP is conserved by the dynamics, $[CP, \mathcal{H}] = 0$, then A_f and $\bar{A}_{\bar{f}}$ have the same magnitude and an arbitrary unphysical relative phase

$$\bar{A}_{\bar{f}} = e^{i(\xi_f - \xi_M)} A_f. \quad (13.3)$$

13.1.2 Neutral-meson mixing

A state that is initially a superposition of M^0 and \bar{M}^0 , say

$$|\psi(0)\rangle = a(0)|M^0\rangle + b(0)|\bar{M}^0\rangle, \quad (13.4)$$

will evolve in time acquiring components that describe all possible decay final states $\{f_1, f_2, \dots\}$, that is,

$$|\psi(t)\rangle = a(t)|M^0\rangle + b(t)|\bar{M}^0\rangle + c_1(t)|f_1\rangle + c_2(t)|f_2\rangle + \dots \quad (13.5)$$

If we are interested in computing only the values of $a(t)$ and $b(t)$ (and not the values of all $c_i(t)$), and if the times t under study are much larger than the typical strong interaction scale, then we can use a much simplified formalism [31]. The simplified time evolution is determined by a 2×2 effective Hamiltonian \mathbf{H} that is not Hermitian, since otherwise the mesons would only oscillate and not decay. Any complex matrix, such as \mathbf{H} , can be written in terms of Hermitian matrices \mathbf{M} and $\mathbf{\Gamma}$ as

$$\mathbf{H} = \mathbf{M} - \frac{i}{2} \mathbf{\Gamma}. \quad (13.6)$$

\mathbf{M} and $\mathbf{\Gamma}$ are associated with $(M^0, \bar{M}^0) \leftrightarrow (M^0, \bar{M}^0)$ transitions via off-shell (dispersive), and on-shell (absorptive) intermediate states, respectively. Diagonal elements of \mathbf{M} and $\mathbf{\Gamma}$ are associated with the flavor-conserving transitions $M^0 \rightarrow M^0$ and $\bar{M}^0 \rightarrow \bar{M}^0$, while off-diagonal elements are associated with flavor-changing transitions $M^0 \leftrightarrow \bar{M}^0$.

The eigenvectors of \mathbf{H} have well-defined masses and decay widths. To specify the components of the strong interaction eigenstates, M^0 and \bar{M}^0 , in the light (M_L) and heavy (M_H) mass eigenstates, we introduce three complex parameters: p , q , and, for the case that both CP and CPT are violated in mixing, z . Then

$$|M_L\rangle \propto p\sqrt{1-z}|M^0\rangle + q\sqrt{1+z}|\bar{M}^0\rangle, \quad (13.7a)$$

$$|M_H\rangle \propto p\sqrt{1+z}|M^0\rangle - q\sqrt{1-z}|\bar{M}^0\rangle, \quad (13.7b)$$

with the normalization $|q|^2 + |p|^2 = 1$ when $z = 0$. (Another possible choice of labeling, which is in standard usage for K mesons, defines the mass eigenstates according to their lifetimes: K_S for the short-lived and K_L for the long-lived state. The K_L is experimentally found to be the heavier state. Yet another choice is often used for the D mesons [32]: the eigenstates are labeled according to their dominant CP content.)

The real and imaginary parts of the eigenvalues $\omega_{L,H}$ corresponding to $|M_{L,H}\rangle$ represent their masses and decay widths, respectively. The mass and width splittings are

$$\Delta m \equiv m_H - m_L = \mathcal{R}e(\omega_H - \omega_L), \quad (13.8a)$$

$$\Delta\Gamma \equiv \Gamma_H - \Gamma_L = -2\mathcal{I}m(\omega_H - \omega_L). \quad (13.8b)$$

Note that here Δm is positive by definition, while the sign of $\Delta\Gamma$ must be experimentally determined. The sign of $\Delta\Gamma$ has not yet been established for B^0 mesons, while $\Delta\Gamma < 0$ is established for K

and B_s^0 mesons. The Standard Model predicts $\Gamma_L > \Gamma_H$ for $B_{(s)}^0$ mesons; for this reason, $\Delta\Gamma = \Gamma_L - \Gamma_H$, which is still a signed quantity, is often used in the $B_{(s)}^0$ literature and is the convention used in the PDG experimental summaries.

Solving the eigenvalue problem for \mathbf{H} yields

$$\left(\frac{q}{p}\right)^2 = \frac{\mathbf{M}_{12}^* - (i/2)\mathbf{\Gamma}_{12}^*}{\mathbf{M}_{12} - (i/2)\mathbf{\Gamma}_{12}} \quad (13.9)$$

and

$$z \equiv \frac{\delta m - (i/2)\delta\Gamma}{\Delta m - (i/2)\Delta\Gamma}, \quad (13.10)$$

where

$$\delta m \equiv \mathbf{M}_{11} - \mathbf{M}_{22}, \quad \delta\Gamma \equiv \mathbf{\Gamma}_{11} - \mathbf{\Gamma}_{22} \quad (13.11)$$

are the differences in effective mass and decay-rate expectation values for the strong interaction states M^0 and \bar{M}^0 .

If either CP or CPT is a symmetry of \mathbf{H} (independently of whether T is conserved or violated), then the values of δm and $\delta\Gamma$ are both zero, and hence $z = 0$. We also find that

$$\omega_H - \omega_L = 2\sqrt{\left(\mathbf{M}_{12} - \frac{i}{2}\mathbf{\Gamma}_{12}\right)\left(\mathbf{M}_{12}^* - \frac{i}{2}\mathbf{\Gamma}_{12}^*\right)}. \quad (13.12)$$

If either CP or T is a symmetry of \mathbf{H} (independently of whether CPT is conserved or violated), then $\mathbf{\Gamma}_{12}/\mathbf{M}_{12}$ is real, leading to

$$\left(\frac{q}{p}\right)^2 = e^{2i\xi_M} \Rightarrow \left|\frac{q}{p}\right| = 1, \quad (13.13)$$

where ξ_M is the arbitrary unphysical phase introduced in Eq. (13.2). If, and only if, CP is a symmetry of \mathbf{H} (independently of CPT and T), then both of the above conditions hold, with the result that the mass eigenstates are orthogonal

$$\langle M_H | M_L \rangle = |p|^2 - |q|^2 = 0. \quad (13.14)$$

13.1.3 CP-violating observables

All CP -violating observables in M and \bar{M} decays to final states f and \bar{f} can be expressed in terms of phase-convention-independent combinations of $A_f, \bar{A}_f, A_{\bar{f}},$ and $\bar{A}_{\bar{f}}$, together with, for neutral meson decays only, q/p . CP violation in charged meson and all baryon decays depends only on the combination $|\bar{A}_{\bar{f}}/A_f|$, while CP violation in flavored neutral meson decays is enriched by $M^0 \leftrightarrow \bar{M}^0$ oscillations, and depends, additionally, on $|q/p|$ and on $\lambda_f \equiv (q/p)(\bar{A}_{\bar{f}}/A_f)$.

The decay rates of the two neutral kaon mass eigenstates, K_S and K_L , are different enough ($\Gamma_S/\Gamma_L \sim 500$) that one can, in most cases, actually study their decays independently. For $D^0, B^0,$ and B_s^0 mesons, however, values of $\Delta\Gamma/\Gamma$ (where $\Gamma \equiv (\Gamma_H + \Gamma_L)/2$) are relatively small, and so both mass eigenstates must be considered in their evolution. We denote the state of an initially pure $|M^0\rangle$ or $|\bar{M}^0\rangle$ after an elapsed proper time t as $|M_{\text{phys}}^0(t)\rangle$ or $|\bar{M}_{\text{phys}}^0(t)\rangle$, respectively. Using the effective Hamiltonian approximation, but not assuming CPT to be a good symmetry, we obtain

$$|M_{\text{phys}}^0(t)\rangle = (g_+(t) + z g_-(t)) |M^0\rangle - \sqrt{1-z^2} \frac{q}{p} g_-(t) |\bar{M}^0\rangle, \quad (13.15a)$$

$$|\bar{M}_{\text{phys}}^0(t)\rangle = (g_+(t) - z g_-(t)) |\bar{M}^0\rangle - \sqrt{1-z^2} \frac{p}{q} g_-(t) |M^0\rangle, \quad (13.15b)$$

where

$$g_{\pm}(t) \equiv \frac{1}{2} \left[\exp\left(-im_H t - \frac{1}{2}\Gamma_H t\right) \pm \exp\left(-im_L t - \frac{1}{2}\Gamma_L t\right) \right] \quad (13.16)$$

and $z = 0$ if either CPT or CP is conserved.

Defining $x \equiv \Delta m/\Gamma$ and $y \equiv \Delta\Gamma/(2\Gamma)$, and assuming $z = 0$, one obtains the following time-dependent decay rates:

$$\begin{aligned} \frac{d\Gamma[M_{\text{phys}}^0(t) \rightarrow f]/dt}{e^{-\Gamma t}\mathcal{N}_f} &= (|A_f|^2 + |(q/p)\bar{A}_f|^2) \cosh(y\Gamma t) \\ &+ (|A_f|^2 - |(q/p)\bar{A}_f|^2) \cos(x\Gamma t) \\ &+ 2\mathcal{R}e((q/p)A_f^*\bar{A}_f) \sinh(y\Gamma t) \\ &- 2\mathcal{I}m((q/p)A_f^*\bar{A}_f) \sin(x\Gamma t), \end{aligned} \quad (13.17a)$$

$$\begin{aligned} \frac{d\Gamma[\bar{M}_{\text{phys}}^0(t) \rightarrow \bar{f}]/dt}{e^{-\Gamma t}\mathcal{N}_{\bar{f}}} &= (|(p/q)A_f|^2 + |\bar{A}_f|^2) \cosh(y\Gamma t) \\ &- (|(p/q)A_f|^2 - |\bar{A}_f|^2) \cos(x\Gamma t) \\ &+ 2\mathcal{R}e((p/q)A_f\bar{A}_f^*) \sinh(y\Gamma t) \\ &- 2\mathcal{I}m((p/q)A_f\bar{A}_f^*) \sin(x\Gamma t), \end{aligned} \quad (13.17b)$$

where \mathcal{N}_f is a common, time-independent, normalization factor that can be determined bearing in mind that the range of t is $0 < t < \infty$. Decay rates to the CP -conjugate final state \bar{f} are obtained analogously, with $\mathcal{N}_{\bar{f}} = \mathcal{N}_f$ and the substitutions $A_f \rightarrow \bar{A}_f$ and $\bar{A}_f \rightarrow A_f$ in Eqs. (13.17a) and (13.17b). Terms proportional to $|A_f|^2$ or $|\bar{A}_f|^2$ are associated with decays that occur without any net $M^0 \leftrightarrow \bar{M}^0$ oscillation, while terms proportional to $|(q/p)\bar{A}_f|^2$ or $|(p/q)A_f|^2$ are associated with decays following a net oscillation. The $\sinh(y\Gamma t)$ and $\sin(x\Gamma t)$ terms of Eqs. (13.17a) and (13.17b) are associated with the interference between these two cases. Note that, in multi-body decays such as $D^0 \rightarrow K_S\pi^+\pi^-$ or $B^0 \rightarrow \pi^+\pi^-\pi^+\pi^-$, amplitudes are functions of variables that describe the phase-space of the final state. Interference may be present in some regions but not others, and is strongly influenced by resonant substructure.

When neutral pseudoscalar mesons are produced coherently in pairs from the decay of a vector resonance, $V \rightarrow M^0\bar{M}^0$ (for example, $\Upsilon(4S) \rightarrow B^0\bar{B}^0$, $\psi(3770) \rightarrow D^0\bar{D}^0$ or $\phi \rightarrow K^0\bar{K}^0$), the time-dependence of their subsequent decays to final states f_1 and f_2 has a similar form to Eqs. (13.17a) and (13.17b):

$$\begin{aligned} \frac{d\Gamma[V_{\text{phys}}(t_1, t_2) \rightarrow f_1 f_2]/d(\Delta t)}{e^{-\Gamma|\Delta t|}\mathcal{N}_{f_1 f_2}} &= (|a_+|^2 + |a_-|^2) \cosh(y\Gamma\Delta t) \\ &+ (|a_+|^2 - |a_-|^2) \cos(x\Gamma\Delta t) \\ &- 2\mathcal{R}e(a_+^*a_-) \sinh(y\Gamma\Delta t) \\ &+ 2\mathcal{I}m(a_+^*a_-) \sin(x\Gamma\Delta t), \end{aligned} \quad (13.18)$$

where $\Delta t \equiv t_2 - t_1$ is the difference in the production times, t_1 and t_2 , of f_1 and f_2 , respectively, and the dependence on the average decay time and on decay angles has been integrated out. The normalization factor $\mathcal{N}_{f_1 f_2}$ can be evaluated, noting that the range of Δt is $-\infty < \Delta t < \infty$. The coefficients in Eq. (13.18) are determined by the amplitudes for no net oscillation from $t_1 \rightarrow t_2$, $\bar{A}_{f_1}A_{f_2}$, and $A_{f_1}\bar{A}_{f_2}$, and for a net oscillation, $(q/p)\bar{A}_{f_1}A_{f_2}$ and $(p/q)A_{f_1}\bar{A}_{f_2}$, via

$$a_+ \equiv \bar{A}_{f_1}A_{f_2} - A_{f_1}\bar{A}_{f_2}, \quad (13.19a)$$

$$\begin{aligned} a_- &\equiv -\sqrt{1-z^2} \left(\frac{q}{p}\bar{A}_{f_1}\bar{A}_{f_2} - \frac{p}{q}A_{f_1}A_{f_2} \right) \\ &+ z \left(\bar{A}_{f_1}A_{f_2} + A_{f_1}\bar{A}_{f_2} \right). \end{aligned} \quad (13.19b)$$

Assuming CPT conservation, $z = 0$, and identifying $\Delta t \rightarrow t$ and $f_2 \rightarrow f$, we find that Eqs. (13.18) and (13.19) reduce to Eq. (13.17a) with $A_{f_1} = 0$, $\bar{A}_{f_1} = 1$, or to Eq. (13.17b) with $\bar{A}_{f_1} = 0$, $A_{f_1} = 1$. Indeed, this plays an important role in experiments that exploit the coherence of $V \rightarrow M^0\bar{M}^0$ production. Final states f_1 with $A_{f_1} = 0$ or $\bar{A}_{f_1} = 0$ are called tagging states,

because they identify the decaying pseudoscalar meson as, respectively, \bar{M}^0 or M^0 . Before one of M^0 or \bar{M}^0 decays, they evolve in phase, so that there is always one M^0 and one \bar{M}^0 present. A tagging decay of one meson sets the clock for the time evolution of the other: it starts at t_1 as purely M^0 or \bar{M}^0 , with time evolution that depends only on $t_2 - t_1$.

When f_1 is a state that both M^0 and \bar{M}^0 can decay into, then Eq. (13.18) contains interference terms proportional to $A_{f_1}\bar{A}_{f_1} \neq 0$ that are not present in Eqs. (13.17a) and (13.17b). Even when f_1 is dominantly produced by M^0 decays rather than \bar{M}^0 decays, or vice versa, $A_{f_1}\bar{A}_{f_1}$ can be non-zero owing to doubly-CKM-suppressed decays (with amplitudes suppressed by at least two powers of λ relative to the dominant amplitude, in the language of Section 13.3), and these terms should be considered for precision studies of CP violation in coherent $V \rightarrow M^0\bar{M}^0$ decays [33]. The correlations in $V \rightarrow M^0\bar{M}^0$ decays can also be exploited to determine strong phase differences between favored and suppressed decay amplitudes [34].

13.1.4 Classification of CP-violating effects

We distinguish three types of CP -violating effects that can occur in the quark sector:

- I. CP violation in decay is defined by

$$|\bar{A}_{\bar{f}}/A_f| \neq 1. \quad (13.20)$$

In charged meson (and all baryon) decays, where mixing effects are absent, this is the only possible source of CP asymmetries:

$$A_{f\pm} \equiv \frac{\Gamma(M^- \rightarrow f^-) - \Gamma(M^+ \rightarrow f^+)}{\Gamma(M^- \rightarrow f^-) + \Gamma(M^+ \rightarrow f^+)} = \frac{|\bar{A}_{f-}/A_{f+}|^2 - 1}{|\bar{A}_{f-}/A_{f+}|^2 + 1}. \quad (13.21)$$

Note that the usual sign convention for CP asymmetries of hadrons is for the difference between the rate involving the particle that contains a heavy quark and that which contains an antiquark. Hence, Eq. (13.21) corresponds to the definition for B^\pm mesons, but the opposite sign is used for $D_{(s)}^\pm$ decays.

- II. CP (and T) violation in mixing is defined by

$$|q/p| \neq 1. \quad (13.22)$$

In charged-current semileptonic neutral meson decays $M, \bar{M} \rightarrow \ell^\pm X^\mp$ (taking $|A_{\ell^+ X^-}| = |\bar{A}_{\ell^- X^+}|$ and $A_{\ell^- X^+} = \bar{A}_{\ell^+ X^-} = 0$, as is the case in the Standard Model, to lowest order in G_F , and in most of its extensions), this is the only source of CP violation, and can be measured via the asymmetry of “wrong-sign” decays induced by oscillations:

$$\begin{aligned} A_{\text{SL}}(t) &\equiv \frac{d\Gamma/dt[\bar{M}_{\text{phys}}^0(t) \rightarrow \ell^+ X^-] - d\Gamma/dt[M_{\text{phys}}^0(t) \rightarrow \ell^- X^+]}{d\Gamma/dt[\bar{M}_{\text{phys}}^0(t) \rightarrow \ell^+ X^-] + d\Gamma/dt[M_{\text{phys}}^0(t) \rightarrow \ell^- X^+]}, \end{aligned} \quad (13.23a)$$

$$= \frac{1 - |q/p|^4}{1 + |q/p|^4}. \quad (13.23b)$$

Note that this asymmetry of time-dependent decay rates is actually time-independent.

- III. CP violation in interference between a decay without mixing, $M^0 \rightarrow f$, and a decay with mixing, $M^0 \rightarrow \bar{M}^0 \rightarrow f$ (such an effect occurs only in decays to final states that are common to M^0 and \bar{M}^0 , including all CP eigenstates), is defined by

$$\arg(\lambda_f) + \arg(\lambda_{\bar{f}}) \neq 0, \quad \text{with} \quad \lambda_f \equiv \frac{q}{p} \frac{\bar{A}_f}{A_f}. \quad (13.24)$$

For final CP eigenstates, f_{CP} , the condition Eq. (13.24) simplifies to

$$\mathcal{I}m(\lambda_{f_{CP}}) \neq 0, \quad (13.25)$$

This form of CP violation can be observed, for example, using the asymmetry of neutral meson decay rates into CP eigenstates

$$\begin{aligned} \mathcal{A}_{f_{CP}}(t) &\equiv \\ &\equiv \frac{d\Gamma/dt[\overline{M}_{\text{phys}}^0(t) \rightarrow f_{CP}] - d\Gamma/dt[M_{\text{phys}}^0(t) \rightarrow f_{CP}]}{d\Gamma/dt[\overline{M}_{\text{phys}}^0(t) \rightarrow f_{CP}] + d\Gamma/dt[M_{\text{phys}}^0(t) \rightarrow f_{CP}]} . \end{aligned} \quad (13.26)$$

If $\Delta\Gamma = 0$, as expected to a good approximation for B^0 mesons but not for K^0 and B_s^0 mesons, and $|q/p| = 1$, then $\mathcal{A}_{f_{CP}}$ has a particularly simple form (see Eq. (13.75), below). If, in addition, the decay amplitudes fulfill $|\overline{A}_{f_{CP}}| = |A_{f_{CP}}|$, the interference between decays with and without mixing is the only source of asymmetry and $\mathcal{A}_{f_{CP}}(t) = \mathcal{I}m(\lambda_{f_{CP}}) \sin(x\Gamma t)$.

Examples of these three types of CP violation will be given in Sections 13.4, 13.5, and 13.6.

13.2 Theoretical Interpretation: General Considerations

Consider the $M \rightarrow f$ decay amplitude A_f , and the CP conjugate process, $\overline{M} \rightarrow \overline{f}$, with decay amplitude $\overline{A}_{\overline{f}}$. There are two types of phases that may appear in these decay amplitudes. Complex parameters in any Lagrangian term that contributes to the amplitude will appear in complex conjugate form in the CP -conjugate amplitude. Thus, their phases appear in A_f and $\overline{A}_{\overline{f}}$ with opposite signs. In the Standard Model, these phases occur only in the couplings of the W^\pm bosons, and hence, are often called “weak phases.” The weak phase of any single term is convention-dependent. However, the difference between the weak phases in two different terms in A_f is convention-independent. A second type of phase can appear in scattering or decay amplitudes, even when the Lagrangian is real. This phase originates from the possible contribution from intermediate on-shell states in the decay process. Since such phases are generated by CP -invariant interactions, they are the same in A_f and $\overline{A}_{\overline{f}}$. Usually the dominant rescattering is due to strong interactions; hence the designation “strong phases” for the phase shifts so induced. Again, only the relative strong phases between different terms in the amplitude are physically meaningful.

The “weak” and “strong” phases discussed here appear in addition to the spurious CP -transformation phases of Eq. (13.3). Those spurious phases are due to an arbitrary choice of phase convention, and do not originate from any dynamics or induce any CP violation. For simplicity, we set them to zero from here on.

It is useful to write each contribution a_i to A_f in three parts: its magnitude $|a_i|$, its weak phase ϕ_i , and its strong phase δ_i . If, for example, there are two such contributions, $A_f = a_1 + a_2$, we have

$$A_f = |a_1|e^{i(\delta_1+\phi_1)} + |a_2|e^{i(\delta_2+\phi_2)} , \quad (13.27a)$$

$$\overline{A}_{\overline{f}} = |a_1|e^{i(\delta_1-\phi_1)} + |a_2|e^{i(\delta_2-\phi_2)} . \quad (13.27b)$$

Similarly, for neutral mesons, it is useful to write

$$\mathbf{M}_{12} = |\mathbf{M}_{12}|e^{i\phi_M} , \quad \mathbf{\Gamma}_{12} = |\mathbf{\Gamma}_{12}|e^{i\phi_\Gamma} . \quad (13.28)$$

Each of the phases appearing in Eqs. (13.27) and (13.28) is convention-dependent, but combinations such as $\delta_1 - \delta_2$, $\phi_1 - \phi_2$, $\phi_M - \phi_\Gamma$, and $\phi_M + \phi_1 - \phi_1$ (where ϕ_1 is a weak phase contributing to $\overline{A}_{\overline{f}}$) are physical.

It is now straightforward to evaluate the various asymmetries in terms of the theoretical parameters introduced here. We will do so with approximations that are often relevant to the most interesting measured asymmetries.

1. The CP asymmetry in charged meson and all baryon decays

[Eq. (13.21)] is given by

$$\mathcal{A}_f = - \frac{2|a_1 a_2| \sin(\delta_2 - \delta_1) \sin(\phi_2 - \phi_1)}{|a_1|^2 + |a_2|^2 + 2|a_1 a_2| \cos(\delta_2 - \delta_1) \cos(\phi_2 - \phi_1)} . \quad (13.29)$$

The quantity of most interest to theory is the weak phase difference $\phi_2 - \phi_1$. Its extraction from the asymmetry requires, however, that the amplitude ratio $|a_2/a_1|$ and the strong phase difference $\delta_2 - \delta_1$ are known. Both quantities depend on non-perturbative hadronic parameters that are difficult to calculate, but in some cases can be obtained from experiment.

2. In the approximation that $|\mathbf{\Gamma}_{12}/\mathbf{M}_{12}| \ll 1$ (valid for B^0 and B_s^0 mesons), the CP asymmetry in semileptonic neutral-meson decays [Eq. (13.23)] is given by

$$\mathcal{A}_{\text{SL}} = - \left| \frac{\mathbf{\Gamma}_{12}}{\mathbf{M}_{12}} \right| \sin(\phi_M - \phi_\Gamma) . \quad (13.30)$$

The quantity of most interest to theory is the weak phase $\phi_M - \phi_\Gamma$. Its extraction from the asymmetry requires, however, that $|\mathbf{\Gamma}_{12}/\mathbf{M}_{12}|$ is known. State of the art calculations of this quantity for the B^0 and B_s^0 mesons have uncertainties of around 15–20% [35].

3. In the approximations that only a single weak phase contributes to decay, $A_f = |a_f|e^{i(\delta_f+\phi_f)}$, and that $|\mathbf{\Gamma}_{12}/\mathbf{M}_{12}| = 0$, we obtain $|\lambda_f| = 1$, and the CP asymmetries in decays to a final CP eigenstate f [Eq. (13.26)] with eigenvalue $\eta_f = \pm 1$ are given by

$$\mathcal{A}_{f_{CP}}(t) = \mathcal{I}m(\lambda_f) \sin(\Delta mt) \quad \text{with} \quad \mathcal{I}m(\lambda_f) = \eta_f \sin(\phi_M + 2\phi_f) . \quad (13.31)$$

Note that the phase measured is purely a weak phase, and no hadronic parameters are involved in the extraction of its value from $\mathcal{I}m(\lambda_f)$.

The discussion above allows us to introduce another classification of CP -violating effects:

1. *Indirect CP violation* is consistent with taking $\phi_M \neq 0$ and setting all other CP violating phases to zero. CP violation in mixing (type II) belongs to this class.
2. *Direct CP violation* cannot be accounted for by just $\phi_M \neq 0$. CP violation in decay (type I) belongs to this class.

The historical significance of this classification is related to theory. In superweak models [36], CP violation appears only in diagrams that contribute to \mathbf{M}_{12} , hence predicting no direct CP violation. In most models and, in particular, in the Standard Model, CP violation is both direct and indirect. As concerns type III CP violation, a single observation of such an effect would be consistent with indirect CP violation, but observing $\eta_{f_1} \mathcal{I}m(\lambda_{f_1}) \neq \eta_{f_2} \mathcal{I}m(\lambda_{f_2})$ (for the same decaying meson and two different final CP eigenstates f_1 and f_2) would establish direct CP violation. The experimental observation of $\epsilon' \neq 0$, which was achieved by establishing that $\mathcal{I}m(\lambda_{\pi^+\pi^-}) \neq \mathcal{I}m(\lambda_{\pi^0\pi^0})$ (see Section 13.4), excluded the superweak scenario.

13.3 Theoretical Interpretation: The KM Mechanism

Of all the Standard Model quark parameters, only the Kobayashi-Maskawa (KM) phase is CP -violating. Having a single source of CP violation, the Standard Model is very predictive for CP asymmetries: some vanish, and those that do not are correlated.

To be precise, CP could be violated also by strong interactions. The experimental upper bound on the electric-dipole moment of the neutron [37] implies, however, that θ_{QCD} , the non-perturbative parameter that determines the strength of this type of CP violation, is tiny, if not zero [38]. The smallness of θ_{QCD} constitutes a theoretical puzzle, known as “the strong CP problem.” This, however, is irrelevant to our discussion of hadron decays.

The charged current interactions (that is, the W^\pm interactions) for quarks are given by

$$- \mathcal{L}_{W^\pm} = \frac{g}{\sqrt{2}} \overline{u_{Li}} \gamma^\mu (V_{CKM})_{ij} d_{Lj} W_\mu^\pm + \text{h.c.} \quad (13.32)$$

Here $i, j = 1, 2, 3$ are generation numbers. The Cabibbo-Kobayashi-Maskawa (CKM) mixing matrix for quarks is a 3×3 unitary matrix [39]. Ordering the quarks by their masses, *i.e.*, $(u_1, u_2, u_3) \rightarrow (u, c, t)$ and $(d_1, d_2, d_3) \rightarrow (d, s, b)$, the elements of V_{CKM} are written as follows:

$$V_{\text{CKM}} = \begin{pmatrix} V_{ud} & V_{us} & V_{ub} \\ V_{cd} & V_{cs} & V_{cb} \\ V_{td} & V_{ts} & V_{tb} \end{pmatrix}. \quad (13.33)$$

While a general 3×3 unitary matrix depends on three real angles

$$V_{\text{CKM}} = \begin{pmatrix} 1 - \frac{1}{2}\lambda^2 - \frac{1}{8}\lambda^4 & \lambda & A\lambda^3(\rho - i\eta) \\ -\lambda + \frac{1}{2}A^2\lambda^5[1 - 2(\rho + i\eta)] & 1 - \frac{1}{2}\lambda^2 - \frac{1}{8}\lambda^4(1 + 4A^2) & A\lambda^2 \\ A\lambda^3[1 - (1 - \frac{1}{2}\lambda^2)(\rho + i\eta)] & -A\lambda^2 + \frac{1}{2}A\lambda^4[1 - 2(\rho + i\eta)] & 1 - \frac{1}{2}A^2\lambda^4 \end{pmatrix}. \quad (13.34)$$

Here $\lambda \approx 0.23$ (not to be confused with λ_f), the sine of the Cabibbo angle, plays the role of an expansion parameter, and η represents the CP -violating phase. Terms of $\mathcal{O}(\lambda^6)$ have been neglected.

The unitarity of the CKM matrix, $(VV^\dagger)_{ij} = (V^\dagger V)_{ij} = \delta_{ij}$, leads to twelve distinct complex relations among the matrix elements. The six relations with $i \neq j$ can be represented geometrically as triangles in the complex plane. Two of these,

$$V_{ud}V_{ub}^* + V_{cd}V_{cb}^* + V_{td}V_{tb}^* = 0, \quad (13.35a)$$

$$V_{td}V_{ud}^* + V_{ts}V_{us}^* + V_{tb}V_{ub}^* = 0, \quad (13.35b)$$

have terms of equal order, $\mathcal{O}(A\lambda^3)$, and so have corresponding triangles whose interior angles are all $\mathcal{O}(1)$ physical quantities that can be independently measured. The angles of the first triangle (see Fig. 13.1) are given by

$$\alpha \equiv \varphi_2 \equiv \arg\left(-\frac{V_{td}V_{tb}^*}{V_{ud}V_{ub}^*}\right) \simeq \arg\left(-\frac{1 - \rho - i\eta}{\rho + i\eta}\right), \quad (13.36a)$$

$$\beta \equiv \varphi_1 \equiv \arg\left(-\frac{V_{cd}V_{cb}^*}{V_{td}V_{tb}^*}\right) \simeq \arg\left(\frac{1}{1 - \rho - i\eta}\right), \quad (13.36b)$$

$$\gamma \equiv \varphi_3 \equiv \arg\left(-\frac{V_{ud}V_{ub}^*}{V_{cd}V_{cb}^*}\right) \simeq \arg(\rho + i\eta). \quad (13.36c)$$

The angles of the second triangle are equal to (α, β, γ) up to corrections of $\mathcal{O}(\lambda^2)$. The notations (α, β, γ) and $(\varphi_1, \varphi_2, \varphi_3)$ are both in common usage but, for convenience, we only use the first convention in the following.

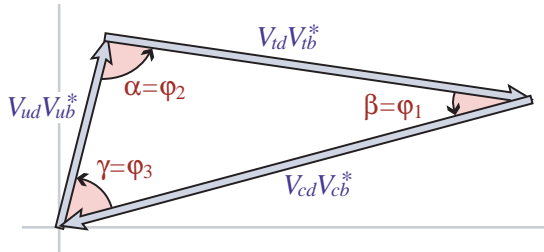


Figure 13.1: Graphical representation of the unitarity constraint $V_{ud}V_{ub}^* + V_{cd}V_{cb}^* + V_{td}V_{tb}^* = 0$ as a triangle in the complex plane.

Another relation that can be represented as a triangle,

$$V_{us}V_{ub}^* + V_{cs}V_{cb}^* + V_{ts}V_{tb}^* = 0, \quad (13.37)$$

and, in particular, its small angle, of $\mathcal{O}(\lambda^2)$,

$$\beta_s \equiv \arg\left(-\frac{V_{ts}V_{tb}^*}{V_{cs}V_{cb}^*}\right), \quad (13.38)$$

is convenient for analyzing CP violation in the B_s^0 sector.

and six phases, the freedom to redefine the phases of the quark mass eigenstates can be used to remove five of the phases, leaving a single physical phase, the Kobayashi-Maskawa phase, that is responsible for all CP violation in the Standard Model.

The fact that one can parameterize V_{CKM} by three real and only one imaginary physical parameters can be made manifest by choosing an explicit parametrization. The Wolfenstein parametrization [40, 41] is particularly useful:

All unitarity triangles have the same area, commonly denoted by $J/2$ [42]. If CP is violated, J is different from zero and can be taken as the single CP -violating parameter. In the Wolfenstein parametrization of Eq. (13.34), $J \simeq \lambda^6 A^2 \eta$.

13.4 Kaons

CP violation was discovered in $K \rightarrow \pi\pi$ decays in 1964 [1]. The same mode provided the first observation of direct CP violation [4–6].

The decay amplitudes actually measured in neutral K decays refer to the mass eigenstates K_L and K_S , rather than to the K and \bar{K} states referred to in Eq. (13.1). The final $\pi^+\pi^-$ and $\pi^0\pi^0$ states are CP -even. In the CP conservation limit, K_S (K_L) would be CP -even (odd), and therefore would (would not) decay to two pions. We define CP -violating amplitude ratios for two-pion final states,

$$\eta_{00} \equiv \frac{\langle \pi^0\pi^0 | \mathcal{H} | K_L \rangle}{\langle \pi^0\pi^0 | \mathcal{H} | K_S \rangle}, \quad \eta_{+-} \equiv \frac{\langle \pi^+\pi^- | \mathcal{H} | K_L \rangle}{\langle \pi^+\pi^- | \mathcal{H} | K_S \rangle}. \quad (13.39)$$

Another important observable is the asymmetry of time-integrated semileptonic decay rates:

$$\delta_L \equiv \frac{\Gamma(K_L \rightarrow \ell^+\nu_\ell\pi^-) - \Gamma(K_L \rightarrow \ell^-\bar{\nu}_\ell\pi^+)}{\Gamma(K_L \rightarrow \ell^+\nu_\ell\pi^-) + \Gamma(K_L \rightarrow \ell^-\bar{\nu}_\ell\pi^+)}. \quad (13.40)$$

CP violation has been observed as an appearance of K_L decays to two-pion final states [43],

$$|\eta_{00}| = (2.220 \pm 0.011) \times 10^{-3}, \quad (13.41a)$$

$$|\eta_{+-}| = (2.232 \pm 0.011) \times 10^{-3}, \quad (13.41b)$$

$$|\eta_{00}/\eta_{+-}| = 0.9950 \pm 0.0007, \quad (13.41c)$$

where the CP -conserving phases ϕ_{ij} of the amplitude ratios η_{ij} have been determined both assuming CPT invariance:

$$\phi_{00} = (43.52 \pm 0.05)^\circ, \quad \phi_{+-} = (43.51 \pm 0.05)^\circ, \quad (13.42)$$

and without assuming CPT invariance:

$$\phi_{00} = (43.7 \pm 0.6)^\circ, \quad \phi_{+-} = (43.4 \pm 0.5)^\circ. \quad (13.43)$$

CP violation has also been observed in semileptonic K_L decays [43]

$$\delta_L = (3.32 \pm 0.06) \times 10^{-3}, \quad (13.44)$$

where δ_L is a weighted average of muon and electron measurements, as well as in K_L decays to $\pi^+\pi^-\gamma$ and $\pi^+\pi^-e^+e^-$ [43]. CP violation in $K \rightarrow 3\pi$ decays has not yet been observed [43, 44].

Historically, CP violation in neutral K decays has been described in terms of the complex parameters ϵ and ϵ' . The observables η_{00} , η_{+-} , and δ_L are related to these parameters, and to

those of Section 13.1, by

$$\eta_{00} = \frac{1 - \lambda_{\pi^0\pi^0}}{1 + \lambda_{\pi^0\pi^0}} = \epsilon - 2\epsilon', \quad (13.45a)$$

$$\eta_{+-} = \frac{1 - \lambda_{\pi^+\pi^-}}{1 + \lambda_{\pi^+\pi^-}} = \epsilon + \epsilon', \quad (13.45b)$$

$$\delta_L = \frac{1 - |q/p|^2}{1 + |q/p|^2} = \frac{2\mathcal{R}e(\epsilon)}{1 + |\epsilon|^2}, \quad (13.45c)$$

where, in the last line, we have assumed that $|A_{\ell^+\nu_\ell\pi^-}| = |\bar{A}_{\ell^-\bar{\nu}_\ell\pi^+}|$ and $|A_{\ell^-\bar{\nu}_\ell\pi^+}| = |\bar{A}_{\ell^+\nu_\ell\pi^-}| = 0$. (The convention-dependent parameter $\tilde{\epsilon} \equiv (1 - q/p)/(1 + q/p)$, sometimes used in the literature, is, in general, different from ϵ but yields a similar expression, $\delta_L = 2\mathcal{R}e(\tilde{\epsilon})/(1 + |\tilde{\epsilon}|^2)$.) A fit to the $K \rightarrow \pi\pi$ data yields [43]

$$|\epsilon| = (2.228 \pm 0.011) \times 10^{-3}, \quad (13.46a)$$

$$\mathcal{R}e(\epsilon'/\epsilon) = (1.66 \pm 0.23) \times 10^{-3}. \quad (13.46b)$$

In discussing two-pion final states, it is useful to express the amplitudes $A_{\pi^0\pi^0}$ and $A_{\pi^+\pi^-}$ in terms of their isospin components via

$$A_{\pi^0\pi^0} = \sqrt{\frac{1}{3}} |A_0| e^{i(\delta_0+\phi_0)} - \sqrt{\frac{2}{3}} |A_2| e^{i(\delta_2+\phi_2)}, \quad (13.47a)$$

$$A_{\pi^+\pi^-} = \sqrt{\frac{2}{3}} |A_0| e^{i(\delta_0+\phi_0)} + \sqrt{\frac{1}{3}} |A_2| e^{i(\delta_2+\phi_2)}, \quad (13.47b)$$

where we parameterize the amplitude $A_I(\bar{A}_I)$ for $K^0(\bar{K}^0)$ decay into two pions with total isospin $I = 0$ or 2 as

$$A_I \equiv \langle (\pi\pi)_I | \mathcal{H} | K^0 \rangle = |A_I| e^{i(\delta_I+\phi_I)}, \quad (13.48a)$$

$$\bar{A}_I \equiv \langle (\pi\pi)_I | \mathcal{H} | \bar{K}^0 \rangle = |A_I| e^{i(\delta_I-\phi_I)}. \quad (13.48b)$$

The smallness of $|\eta_{00}|$ and $|\eta_{+-}|$ allows us to approximate

$$\epsilon \simeq \frac{1}{2}(1 - \lambda_{(\pi\pi)I=0}), \quad \epsilon' \simeq \frac{1}{6}(\lambda_{\pi^0\pi^0} - \lambda_{\pi^+\pi^-}). \quad (13.49)$$

The parameter ϵ represents indirect CP violation, while ϵ' parameterizes direct CP violation: $\mathcal{R}e(\epsilon')$ measures CP violation in decay (type I), $\mathcal{R}e(\epsilon)$ measures CP violation in mixing (type II), and $\mathcal{I}m(\epsilon)$ and $\mathcal{I}m(\epsilon')$ measure the interference between decays with and without mixing (type III).

The following expressions for ϵ and ϵ' are useful for theoretical evaluations:

$$\epsilon \simeq \frac{e^{i\pi/4} \mathcal{I}m(\mathbf{M}_{12})}{\sqrt{2} \Delta m}, \quad \epsilon' = \frac{i}{\sqrt{2}} \left| \frac{A_2}{A_0} \right| e^{i(\delta_2-\delta_0)} \sin(\phi_2 - \phi_0). \quad (13.50)$$

The expression for ϵ is only valid in a phase convention where $\phi_2 = 0$, corresponding to a real $V_{ud}V_{us}^*$, and in the approximation that also $\phi_0 = 0$. The phase of $\tilde{\epsilon}$, $\arg(\tilde{\epsilon}) \approx \arctan(-2\Delta m/\Delta\Gamma)$, is determined by non-perturbative QCD dynamics and is experimentally determined to be about $\pi/4$. The calculation of ϵ benefits from the fact that $\mathcal{I}m(\mathbf{M}_{12})$ is dominated by short distance physics. Consequently, the main sources of uncertainty in theoretical interpretations of ϵ are the values of matrix elements, such as $\langle K^0 | (\bar{s}d)_{V-A}(\bar{s}d)_{V-A} | \bar{K}^0 \rangle$. The expression for ϵ' is valid to first order in $|A_2/A_0| \sim 1/20$. The phase of ϵ' is experimentally determined, $\pi/2 + \delta_2 - \delta_0 \approx \pi/4$, and is independent of the model of electroweak interactions. Note that, accidentally, ϵ'/ϵ is real to a good approximation. Determination of weak phase information from the measurement of $\mathcal{R}e(\epsilon'/\epsilon)$ given in Eq. (13.46) has until now been precluded by uncertainties in the hadronic parameters, but recent advances in lattice QCD calculations [45, 46] suggest that it may become possible [47].

A future measurement of much interest is that of CP violation in the rare $K \rightarrow \pi\nu\bar{\nu}$ decays. The signal for CP violation is simply observing the $K_L \rightarrow \pi^0\nu\bar{\nu}$ decay. The effect here is that

of interference between decays with and without mixing (type III) [48]:

$$\frac{\Gamma(K_L \rightarrow \pi^0\nu\bar{\nu})}{\Gamma(K^+ \rightarrow \pi^+\nu\bar{\nu})} = \frac{1}{2} [1 + |\lambda_{\pi\nu\bar{\nu}}|^2 - 2\mathcal{R}e(\lambda_{\pi\nu\bar{\nu}})] \simeq 1 - \mathcal{R}e(\lambda_{\pi\nu\bar{\nu}}), \quad (13.51)$$

where in the last equation we neglect CP violation in decay and in mixing (expected, model-independently, to be of order 10^{-5} and 10^{-3} , respectively). Such a measurement is experimentally very challenging but would be theoretically very rewarding [49]. Similar to the CP asymmetry in $B^0 \rightarrow J/\psi K_S$, the CP violation in $K \rightarrow \pi\nu\bar{\nu}$ decay is predicted to be large (that is, the ratio in Eq. (13.51) is neither CKM- nor loop-suppressed) and can be very cleanly interpreted. In particular, the independent determinations of the CKM parameters via B -meson and K -meson decays and mixing will over-constrain the unitarity triangle and provide a stringent test of the KM mechanism.

Within the Standard Model, the $K_L \rightarrow \pi^0\nu\bar{\nu}$ decay is dominated by an intermediate top quark contribution and, consequently, can be interpreted in terms of CKM parameters [50]. (For the charged mode, $K^+ \rightarrow \pi^+\nu\bar{\nu}$, the contribution from an intermediate charm quark is not negligible, and constitutes a source of hadronic uncertainty.) In particular, $\mathcal{B}(K_L \rightarrow \pi^0\nu\bar{\nu})$ provides a theoretically clean way to determine the Wolfenstein parameter η [51]:

$$\mathcal{B}(K_L \rightarrow \pi^0\nu\bar{\nu}) = \kappa_L [X(m_t^2/m_W^2)]^2 A^4 \eta^2, \quad (13.52)$$

where the hadronic parameter $\kappa_L \sim 2 \times 10^{-10}$ incorporates the value of the four-fermion matrix element which is deduced, using isospin relations, from $\mathcal{B}(K^+ \rightarrow \pi^0 e^+ \nu_e)$, and $X(m_t^2/m_W^2)$ is a known function of the top mass. An explicit calculation gives $\mathcal{B}(K_L \rightarrow \pi^0\nu\bar{\nu}) = (3.00 \pm 0.30) \times 10^{-11}$ [52].

Currently the most stringent experimental limit is $\mathcal{B}(K_L \rightarrow \pi^0\nu\bar{\nu}) < 3.0 \times 10^{-9}$ [53, 54], which does not yet reach the bound that can be derived from Eq. (13.51), $\mathcal{B}(K_L \rightarrow \pi^0\nu\bar{\nu}) < 4.4 \times \mathcal{B}(K^+ \rightarrow \pi^+\nu\bar{\nu})$ [48], with the most precise result for the charged kaon decay being $\mathcal{B}(K^+ \rightarrow \pi^+\nu\bar{\nu}) = (10.6_{-3.4}^{+4.0} \pm 0.9) \times 10^{-11}$ [55]. Significant further progress is anticipated from experiments searching for $K \rightarrow \pi\nu\bar{\nu}$ decays in the next few years.

13.5 Charm

The existence of $D^0-\bar{D}^0$ mixing is well established [56–60], with the latest experimental constraints giving [61, 62] $x \equiv \Delta m/\Gamma = (0.41 \pm 0.05) \times 10^{-2}$ and $y \equiv \Delta\Gamma/(2\Gamma) = (0.62 \pm 0.06) \times 10^{-2}$. Long-distance contributions make it difficult to calculate Standard Model predictions for the $D^0-\bar{D}^0$ mixing parameters. Therefore, the goal of the search for $D^0-\bar{D}^0$ mixing is not to constrain the CKM parameters, but rather to probe new physics. Here CP violation plays an important role. Within the Standard Model, the CP -violating effects are predicted to be small, since the mixing and the relevant decays are described, to an excellent approximation, by the physics of the first two generations only. The expectation is that the Standard Model size of CP violation in D decays is $\mathcal{O}(10^{-3})$ or less. At present, the most sensitive searches involve the $D^0 \rightarrow K^+K^-$, $D^0 \rightarrow \pi^+\pi^-$ and $D^0 \rightarrow K^\pm\pi^\mp$ modes.

The neutral D mesons decay via a singly-Cabibbo-suppressed transition to the CP eigenstates K^+K^- and $\pi^+\pi^-$. These decays are dominated by Standard-Model tree diagrams. Thus, we can write, for $f = K^+K^-$ or $\pi^+\pi^-$,

$$A_f = A_f^T e^{+i\phi_f^T} [1 + r_f e^{i(\delta_f+\phi_f)}], \quad (13.53a)$$

$$\bar{A}_f = A_f^T e^{-i\phi_f^T} [1 + r_f e^{i(\delta_f-\phi_f)}], \quad (13.53b)$$

where $A_f^T e^{\pm i\phi_f^T}$ is the Standard Model tree-level contribution, ϕ_f^T and ϕ_f are weak, CP violating phases, δ_f is a strong phase difference, and r_f is the ratio between a subleading ($r_f \ll 1$) contribution with a weak phase different from ϕ_f^T and the Standard Model tree-level contribution. Neglecting r_f , λ_f is universal, and

we can define an observable phase ϕ_D via

$$\lambda_f \equiv -|q/p|e^{i\phi_D}. \quad (13.54)$$

(In the limit of CP conservation, choosing $\phi_D = 0$ is equivalent to defining the mass eigenstates by their CP eigenvalue: $|D_{\mp}\rangle = p|D^0\rangle \pm q|\bar{D}^0\rangle$, with D_- (D_+) being the CP -odd (CP -even) state; that is, the state that does not (does) decay into K^+K^- .)

We define the time integrated CP asymmetry for a final CP eigenstate f as follows:

$$a_f \equiv \frac{\int_0^\infty \Gamma(D_{\text{phys}}^0(t) \rightarrow f)dt - \int_0^\infty \Gamma(\bar{D}_{\text{phys}}^0(t) \rightarrow f)dt}{\int_0^\infty \Gamma(D_{\text{phys}}^0(t) \rightarrow f)dt + \int_0^\infty \Gamma(\bar{D}_{\text{phys}}^0(t) \rightarrow f)dt}. \quad (13.55)$$

(This expression corresponds to the D meson being tagged at production, hence the integration goes from 0 to $+\infty$; measurements are also possible with $\psi(3770) \rightarrow D^0\bar{D}^0$, in which case the integration goes from $-\infty$ to $+\infty$ giving slightly different results; see the discussion in Section 13.1.3.) We take $x, y, r_f \ll 1$ and expand to leading order in these parameters. We can then separate the contribution to a_f into three parts [63],

$$a_f = a_f^d + a_f^m + a_f^i, \quad (13.56)$$

with the following underlying mechanisms:

1. a_f^d signals CP violation in decay (similar to Eq. (13.21)):

$$a_f^d = 2r_f \sin \phi_f \sin \delta_f. \quad (13.57)$$

2. a_f^m signals CP violation in mixing (similar to Eq. (13.30)). With our approximations, it is universal:

$$a^m = -\frac{y}{2} \left(\left| \frac{q}{p} \right| - \left| \frac{p}{q} \right| \right) \cos \phi_D. \quad (13.58)$$

3. a_f^i signals CP violation in the interference of mixing and decay (similar to Eq. (13.31)). With our approximations, it is universal:

$$a^i = \frac{x}{2} \left(\left| \frac{q}{p} \right| + \left| \frac{p}{q} \right| \right) \sin \phi_D. \quad (13.59)$$

In the SM, both a^m and a^i are $\mathcal{O}(10^{-5})$ or less, while a^d could be up to two orders of magnitude larger.

One can isolate the effects of direct CP violation by taking the difference between the CP asymmetries in the K^+K^- and $\pi^+\pi^-$ modes:

$$\Delta a_{CP} \equiv a_{K^+K^-} - a_{\pi^+\pi^-} = a_{K^+K^-}^d - a_{\pi^+\pi^-}^d, \quad (13.60)$$

where we neglected a residual, experiment-dependent, contribution from indirect CP violation due to the fact that there may be a decay time-dependent acceptance function that can be different for the K^+K^- and $\pi^+\pi^-$ channels. The current average gives [13, 61]:

$$a_{K^+K^-}^d - a_{\pi^+\pi^-}^d = (-0.164 \pm 0.028) \times 10^{-2}, \quad (13.61)$$

demonstrating CP violation in charm decay. While the asymmetry is somewhat larger than the theoretical predictions that preceded the measurement, it can in principle be explained by non-perturbative QCD effects.

One can also isolate the effects of indirect CP violation in the following way. Consider the time-dependent decay rates in Eq. (13.17a) and Eq. (13.17b). The mixing processes modify the time dependence from a pure exponential. However, given the small values of x and y , the time dependences can be recast, to a good approximation, into purely exponential form, but with modified decay-rate parameters [64, 65] (given here for the K^+K^- final state):

$$\Gamma_{D^0 \rightarrow K^+K^-} = \Gamma \times [1 + |q/p| (y \cos \phi_D - x \sin \phi_D)], \quad (13.62a)$$

$$\Gamma_{\bar{D}^0 \rightarrow K^+K^-} = \Gamma \times [1 + |p/q| (y \cos \phi_D + x \sin \phi_D)]. \quad (13.62b)$$

One can define CP -conserving and CP -violating combinations of these two observables (normalized to the true width Γ):

$$y_{CP} \equiv \frac{\Gamma_{\bar{D}^0 \rightarrow K^+K^-} + \Gamma_{D^0 \rightarrow K^+K^-}}{2\Gamma} - 1 \\ = (y/2) (|q/p| + |p/q|) \cos \phi_D - (x/2) (|q/p| - |p/q|) \sin \phi_D, \quad (13.63a)$$

$$A_\Gamma \equiv \frac{\Gamma_{D^0 \rightarrow K^+K^-} - \Gamma_{\bar{D}^0 \rightarrow K^+K^-}}{2\Gamma} \\ = -(a^m + a^i). \quad (13.63b)$$

In the limit of CP conservation (and, in particular, within the Standard Model), $y_{CP} = (\Gamma_+ - \Gamma_-)/2\Gamma = y$ (where Γ_+ (Γ_-) is the decay width of the CP -even (-odd) mass eigenstate) and $A_\Gamma = 0$. Indeed, present measurements imply that CP violation is small [61],

$$y_{CP} = (+0.72 \pm 0.11) \times 10^{-2}, \quad (13.64a)$$

$$A_\Gamma = (0.009 \pm 0.011) \times 10^{-2}. \quad (13.64b)$$

The $K^\pm\pi^\mp$ states are not CP eigenstates, but they are still common final states for D^0 and \bar{D}^0 decays. Since $D^0(\bar{D}^0) \rightarrow K^-\pi^+$ is a Cabibbo-favored (doubly-Cabibbo-suppressed) process, these processes are particularly sensitive to x and/or $y = \mathcal{O}(\lambda^2)$. Taking into account that $|\lambda_{K^-\pi^+}|, |\lambda_{K^+\pi^-}^{-1}| \ll 1$ and $x, y \ll 1$, assuming that there is no direct CP violation (these are Standard Model tree-level decays dominated by a single weak phase, and there is no contribution from penguin-like and chromomagnetic operators), and expanding the time-dependent rates for $xt, yt \lesssim \Gamma^{-1}$, one obtains

$$\Gamma[D_{\text{phys}}^0(t) \rightarrow K^+\pi^-] = e^{-\Gamma t} |\bar{A}_{K^-\pi^+}|^2 \\ \times \left[r_d^2 + r_d \left| \frac{q}{p} \right| (y' \cos \phi_D - x' \sin \phi_D) \Gamma t + \left| \frac{q}{p} \right|^2 \frac{y^2 + x^2}{4} (\Gamma t)^2 \right], \quad (13.65a)$$

$$\Gamma[\bar{D}_{\text{phys}}^0(t) \rightarrow K^-\pi^+] = e^{-\Gamma t} |\bar{A}_{K^-\pi^+}|^2 \\ \times \left[r_d^2 + r_d \left| \frac{p}{q} \right| (y' \cos \phi_D + x' \sin \phi_D) \Gamma t + \left| \frac{p}{q} \right|^2 \frac{y^2 + x^2}{4} (\Gamma t)^2 \right], \quad (13.65b)$$

where

$$y' \equiv y \cos \delta - x \sin \delta \quad \text{and} \quad x' \equiv x \cos \delta + y \sin \delta. \quad (13.66)$$

The weak phase ϕ_D is the same as that of Eq. (13.54) (a consequence of neglecting direct CP violation) and $r_d = \mathcal{O}(\tan^2 \theta_c)$ is the amplitude ratio, $r_d = |\bar{A}_{K^-\pi^+}/A_{K^-\pi^+}| = |A_{K^+\pi^-}/\bar{A}_{K^+\pi^-}|$, that is, $\lambda_{K^-\pi^+} = r_d|q/p|e^{-i(\delta-\phi_D)}$ and $\lambda_{K^+\pi^-}^{-1} = r_d|p/q|e^{-i(\delta+\phi_D)}$. The parameter δ is a strong-phase difference for these processes, that can be obtained from measurements of quantum correlated $\psi(3770) \rightarrow D^0\bar{D}^0$ decays [66, 67]. By fitting to the six coefficients of the various time-dependences, one can determine r_d , $|q/p|$, $(x^2 + y^2)$, $y' \cos \phi_D$, and $x' \sin \phi_D$. In particular, finding CP violation ($|q/p| \neq 1$ and/or $\sin \phi_D \neq 0$) at a level much higher than 10^{-3} would constitute evidence for new physics. The most stringent constraints to date on CP violation in charm mixing have been obtained with this method [68] and from the A_Γ measurement [69].

A fit to all data [61], including also results from time-dependent analyses of $D^0 \rightarrow K_S\pi^+\pi^-$ decays, from which $x, y, |q/p|$ and ϕ_D can be determined directly, yields no evidence for indirect CP violation:

$$1 - |q/p| = +0.005 \pm 0.016, \quad (13.67a)$$

$$\phi_D = (-2.5 \pm 1.2)^\circ. \quad (13.67b)$$

With the additional assumption of no direct CP violation in doubly-Cabibbo-suppressed D decays [70–72], more stringent con-

straints are obtained:

$$1 - |q/p| = -0.005 \pm 0.007, \quad (13.68a)$$

$$\phi_D = (-0.2 \pm 0.3)^\circ. \quad (13.68b)$$

More details on various theoretical and experimental aspects of D^0 - \bar{D}^0 mixing can be found in Ref. [32].

Searches for CP violation in charged $D_{(s)}$ decays have been performed in many modes. Searches in decays mediated by Cabibbo-suppressed amplitudes are particularly interesting, since in other channels effects are likely to be too small to be observable in current experiments. Examples of relevant two-body modes are $D^+ \rightarrow \pi^+\pi^0$, $K_S K^+$, $\phi\pi^+$ and $D_s^+ \rightarrow K^+\pi^0$, $K_S\pi^+$, ϕK^+ . The most precise results are $\mathcal{A}_{D^+ \rightarrow K_S K^+} = +0.0011 \pm 0.0017$ and $\mathcal{A}_{D_s^+ \rightarrow K_S \pi^+} = +0.0038 \pm 0.0048$ [61]. The precision of experiments is now sufficient that the effect from CP violation in the neutral kaon system can be seen in $D^+ \rightarrow K_S\pi^+$ decays [73, 74].

Three- and four-body final states provide additional possibilities to search for CP violation, since effects may vary over the phase-space [75]. A number of methods have been proposed to exploit this feature and search for CP violation in ways that do not require modelling of the decay distribution [76–79]. Such methods are useful for analysis of charm decays since they are less sensitive to biases from production asymmetries, and are well suited to address the issue of whether or not CP violation effects are present. They can also be applied to tagged neutral D meson as well as to charged $D_{(s)}$ decays (flavor tagging is typically achieved from the charge of the pion produced in $D^{*+} \rightarrow D^0\pi^+$ decays). The results of all searches to date are consistent with the absence of CP violation, with the most significant hint at the level of 2.7σ [80].

13.6 Beauty

13.6.1 CP violation in mixing of B^0 and B_s^0 mesons

The upper bound on the CP asymmetry in semileptonic B decays [81] implies that CP violation in B^0 - \bar{B}^0 mixing is a small effect (we use $\mathcal{A}_{\text{SL}}/2 \approx 1 - |q/p|$, see Eq. (13.23)):

$$\mathcal{A}_{\text{SL}}^d = (-2.1 \pm 1.7) \times 10^{-3} \implies |q/p| = 1.0010 \pm 0.0008. \quad (13.69)$$

The Standard Model prediction is

$$\mathcal{A}_{\text{SL}}^d = \mathcal{O} \left[(m_c^2/m_t^2) \sin \beta \right] \lesssim 0.001. \quad (13.70)$$

An explicit calculation gives $(-4.7 \pm 0.6) \times 10^{-4}$ [35].

The experimental constraint on CP violation in B_s^0 - \bar{B}_s^0 mixing is somewhat weaker than that in the B^0 - \bar{B}^0 system [81]

$$\mathcal{A}_{\text{SL}}^s = (-0.6 \pm 2.8) \times 10^{-3} \implies |q/p| = 1.0003 \pm 0.0014. \quad (13.71)$$

The Standard Model prediction is $\mathcal{A}_{\text{SL}}^s = \mathcal{O} \left[(m_c^2/m_t^2) \sin \beta_s \right] \lesssim 10^{-4}$, with an explicit calculation giving $(2.22 \pm 0.27) \times 10^{-5}$ [35].

The fit to experimental data that results in the averages quoted above has a χ^2 probability of 4.5% indicating some tension between the different measurements [61]. This originates in part from a result from the D0 collaboration for the inclusive same-sign dimuon asymmetry that deviates from the Standard Model prediction by 3.6σ [82]. As yet, this has not been confirmed by independent studies.

In models where $\mathbf{\Gamma}_{12}/\mathbf{M}_{12}$ is approximately real, such as the Standard Model, an upper bound on $\Delta\Gamma/\Delta m \approx \text{Re}(\mathbf{\Gamma}_{12}/\mathbf{M}_{12})$ provides yet another upper bound on the deviation of $|q/p|$ from one. This constraint does not hold if $\mathbf{\Gamma}_{12}/\mathbf{M}_{12}$ is approximately imaginary. (An alternative parameterization uses $q/p = (1 - \tilde{\epsilon}_B)/(1 + \tilde{\epsilon}_B)$, leading to $\mathcal{A}_{\text{SL}} \simeq 4\text{Re}(\tilde{\epsilon}_B)$.)

13.6.2 CP violation in interference of B^0 decays with and without mixing

The small deviation (less than one percent) of $|q/p|$ from 1 implies that, at the present level of experimental precision, CP violation in B^0 mixing is a negligible effect. Thus, for the purpose of analyzing CP asymmetries in hadronic B^0 decays, we can use

$$\lambda_f = e^{-i\phi_{M(B^0)}} (\bar{A}_f/A_f), \quad (13.72)$$

where $\phi_{M(B^0)}$ refers to the phase of \mathbf{M}_{12} appearing in Eq. (13.28) that is appropriate for B^0 - \bar{B}^0 oscillations. Within the Standard Model, the corresponding phase factor is given by

$$e^{-i\phi_{M(B^0)}} = (V_{tb}^* V_{td}) / (V_{tb} V_{td}^*). \quad (13.73)$$

The class of CP violation effects in interference between mixing and decay is studied with final states that are common to B^0 and \bar{B}^0 decays [83–85]. It is convenient to rewrite Eq. (13.26) for B^0 decays as [86–88]

$$\mathcal{A}_f(t) = S_f \sin(\Delta m t) - C_f \cos(\Delta m t), \quad (13.74)$$

$$S_f \equiv \frac{2\text{Im}(\lambda_f)}{1 + |\lambda_f|^2}, \quad C_f \equiv \frac{1 - |\lambda_f|^2}{1 + |\lambda_f|^2}, \quad (13.75)$$

where we assume that $\Delta\Gamma = 0$ and $|q/p| = 1$. An alternative notation in use is $A_f \equiv -C_f$ – this A_f should not be confused with the A_f of Eq. (13.1), but in the limit that $|q/p| = 1$ is equivalent with the A_f of Eq. (13.21).

A large class of interesting processes proceed via quark transitions of the form $\bar{b} \rightarrow \bar{q}q\bar{q}'$ with $q' = s$ or d . For $q = c$ or u , there are contributions from both tree (t) and penguin (p^{qu} , where $qu = u, c, t$ is the quark in the loop) diagrams (see Fig. 13.2) which carry different weak phases:

$$A_f = (V_{qb}^* V_{qq'}) t_f + \sum_{qu=u,c,t} (V_{qu}^* V_{quq'}) p_f^{qu}. \quad (13.76)$$

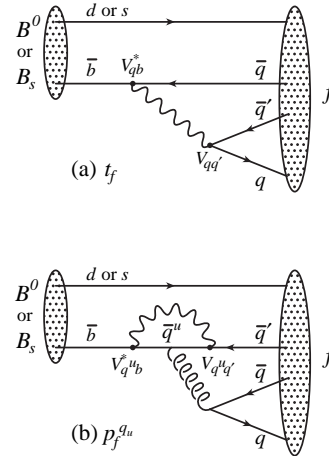


Figure 13.2: Feynman diagrams for (a) tree and (b) penguin amplitudes contributing to $B^0 \rightarrow f$ or $B_s^0 \rightarrow f$ via a $\bar{b} \rightarrow \bar{q}q\bar{q}'$ quark-level process.

(The distinction between tree and penguin contributions is a heuristic one; the separation by the operator that enters is more precise. A more detailed discussion of the operator product expansion approach, which also includes higher order QCD corrections, can be found in Ref. [89, 90] for example.) Using CKM unitarity, the various decay amplitudes can always be written in terms of just two CKM combinations. For example, for $f = \pi\pi$, which proceeds via a $\bar{b} \rightarrow \bar{u}ud$ transition, we can write

$$A_{\pi\pi} = (V_{ub}^* V_{ud}) T_{\pi\pi} + (V_{tb}^* V_{td}) P_{\pi\pi}^t, \quad (13.77)$$

where $T_{\pi\pi} = t_{\pi\pi} + p_{\pi\pi}^c - p_{\pi\pi}^t$ and $P_{\pi\pi}^t = p_{\pi\pi}^t - p_{\pi\pi}^c$. CP -violating phases in Eq. (13.77) appear only in the CKM elements, so that

$$\frac{\bar{A}_{\pi\pi}}{A_{\pi\pi}} = \frac{(V_{ub} V_{ud}^*) T_{\pi\pi} + (V_{tb} V_{td}^*) P_{\pi\pi}^t}{(V_{ub}^* V_{ud}) T_{\pi\pi} + (V_{tb}^* V_{td}) P_{\pi\pi}^t}. \quad (13.78)$$

For $f = J/\psi K$, which proceeds via a $\bar{b} \rightarrow \bar{c}c\bar{s}$ transition, we can write

$$A_{\psi K} = (V_{cb}^* V_{cs}) T_{\psi K} + (V_{ub}^* V_{us}) P_{\psi K}^u, \quad (13.79)$$

where $T_{\psi K} = t_{\psi K} + p_{\psi K}^c - p_{\psi K}^t$ and $P_{\psi K}^u = p_{\psi K}^u - p_{\psi K}^t$. A subtlety arises in this decay that is related to the fact that B^0 decays into a final $J/\psi K^0$ state while \bar{B}^0 decays into a final $J/\psi \bar{K}^0$ state. A common final state, e.g., $J/\psi K_S$, is reached only via $K^0 - \bar{K}^0$ mixing. Consequently, the phase factor (defined in Eq. (13.28)) corresponding to neutral K mixing, $e^{-i\phi_M(K)} = (V_{cd}^* V_{cs}) / (V_{cb}^* V_{cs})$, plays a role:

$$\frac{\bar{A}_{\psi K_S}}{A_{\psi K_S}} = - \frac{(V_{cb}^* V_{cs}^*) T_{\psi K} + (V_{ub}^* V_{us}^*) P_{\psi K}^u}{(V_{cb}^* V_{cs}^*) T_{\psi K} + (V_{ub}^* V_{us}^*) P_{\psi K}^u} \times \frac{V_{cd}^* V_{cs}}{V_{cb}^* V_{cs}}. \quad (13.80)$$

For $q = s$ or d , there are only penguin contributions to A_f , that is, $t_f = 0$ in Eq. (13.76). (The tree $\bar{b} \rightarrow \bar{u}u\bar{q}$ transition followed by $\bar{u}u \rightarrow \bar{q}q$ rescattering is included below in the P^u terms.) Again, CKM unitarity allows us to write A_f in terms of two CKM combinations. For example, for $f = \phi K_S$, which proceeds via a $\bar{b} \rightarrow \bar{s}s\bar{s}$ transition, we can write

$$\frac{\bar{A}_{\phi K_S}}{A_{\phi K_S}} = - \frac{(V_{cb}^* V_{cs}^*) P_{\phi K}^c + (V_{ub}^* V_{us}^*) P_{\phi K}^u}{(V_{cb}^* V_{cs}^*) P_{\phi K}^c + (V_{ub}^* V_{us}^*) P_{\phi K}^u} \times \frac{V_{cd}^* V_{cs}}{V_{cb}^* V_{cs}}, \quad (13.81)$$

where $P_{\phi K}^c = p_{\phi K}^c - p_{\phi K}^t$ and $P_{\phi K}^u = p_{\phi K}^u - p_{\phi K}^t$.

Since in general the amplitude A_f involves two different weak phases, the corresponding decays can exhibit both CP violation in the interference of decays with and without mixing, $S_f \neq 0$, and CP violation in decay, $C_f \neq 0$. (At the present level of experimental precision, the contribution to C_f from CP violation in mixing is negligible, see Eq. (13.69).) If the contribution from a second weak phase is suppressed, then the interpretation of S_f in terms of Lagrangian CP -violating parameters is clean, while C_f is small. If such a second contribution is not suppressed, S_f depends on hadronic parameters and, if the relevant strong phase difference is large, C_f is large.

A summary of $\bar{b} \rightarrow \bar{q}q\bar{q}'$ modes with $q' = s$ or d is given in Table 13.1. The $\bar{b} \rightarrow \bar{d}d\bar{q}$ transitions lead to final states that are similar to those from $\bar{b} \rightarrow \bar{u}u\bar{q}$ transitions and have similar phase dependence. Final states that consist of two vector mesons ($\psi\phi$ and $\phi\phi$) are not CP eigenstates, and angular analysis is needed to separate the CP -even from the CP -odd contributions.

The cleanliness of the theoretical interpretation of S_f can be assessed from the information in the last column of Table 13.1. In case of small uncertainties, the expression for S_f in terms of CKM phases can be deduced from the fourth column of Table 13.1 in combination with Eq. (13.73) (and, for $b \rightarrow q\bar{q}s$ decays, the example in Eq. (13.80)). Here we consider several interesting examples.

For $B^0 \rightarrow J/\psi K_S$ and other $\bar{b} \rightarrow \bar{c}c\bar{s}$ processes, we can neglect the P^u contribution to A_f , in the Standard Model, to an approximation that is better than one percent, giving

$$\lambda_{\psi K_S} = -e^{-2i\beta} \Rightarrow S_{\psi K_S} = \sin(2\beta), \quad C_{\psi K_S} = 0. \quad (13.82)$$

It is important to verify experimentally the level of suppression of the penguin contribution. Methods based on flavor symmetries [91–94] allow limits to be obtained. All are currently consistent with the P^u term being negligible. Explicit calculations [94–97] also support this conclusion.

In the presence of new physics, A_f is still likely to be dominated by the T term, but the mixing amplitude might be modified. Thus, model-independently, $C_f \approx 0$ while S_f cleanly determines the mixing phase ($\phi_M - 2 \arg(V_{cb} V_{cd}^*)$). The experimental measurement [61], $S_{\psi K} = +0.699 \pm 0.017$, gave the first precision test of the Kobayashi-Maskawa mechanism, and its consistency with the predictions for $\sin 2\beta$ makes it very likely that this mechanism is indeed the dominant source of CP violation in the quark sector.

For $B^0 \rightarrow \phi K_S$ and other $\bar{b} \rightarrow \bar{s}s\bar{s}$ processes (as well as some $\bar{b} \rightarrow \bar{u}u\bar{s}$ processes), we can neglect the subdominant contributions, in the Standard Model, to an approximation that is good to the order of a few percent:

$$\lambda_{\phi K_S} = -e^{-2i\beta} \Rightarrow S_{\phi K_S} = \sin 2\beta, \quad C_{\phi K_S} = 0. \quad (13.83)$$

A review of explicit calculations of the effects of subleading amplitudes can be found in Ref. [98]. In the presence of new physics,

both A_f and M_{12} can have contributions that are comparable in size to those of the Standard Model and carry new weak phases. Such a situation gives several interesting consequences for penguin-dominated $\bar{b} \rightarrow \bar{q}q\bar{s}$ decays ($q = u, d, s$) to a final state f :

1. The value of $-\eta_f S_f$ may be different from $S_{\psi K_S}$ by more than a few percent, where η_f is the CP eigenvalue of the final state.
2. The values of $\eta_f S_f$ for different final states f may be different from each other by more than a few percent (for example, $S_{\phi K_S} \neq S_{\eta' K_S}$).
3. The value of C_f may be different from zero by more than a few percent.

While a clear interpretation of such signals in terms of Lagrangian parameters will be difficult because, under these circumstances, hadronic parameters play a role, any of the above three options will clearly signal new physics. In addition, flavor symmetry relations, such as those that relate observables in $B \rightarrow K\pi$ decays [99, 100] can be used to provide further tests of the Standard Model. Fig. 13.3 summarizes the present experimental results: none of the possible signatures listed above is unambiguously established, but there is definitely still room for new physics.

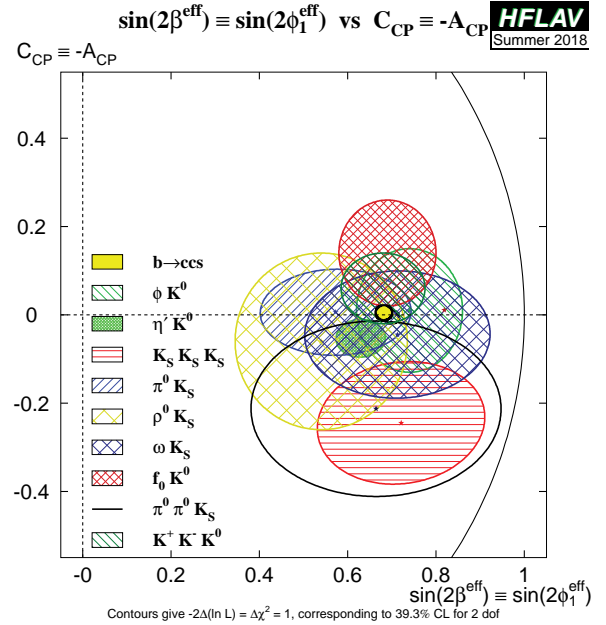


Figure 13.3: Summary of the results [61] of time-dependent analyses of $b \rightarrow \bar{q}q\bar{s}$ decays, which are potentially sensitive to new physics.

For the $\bar{b} \rightarrow \bar{u}u\bar{d}$ process $B \rightarrow \pi\pi$ and other related channels, the penguin-to-tree ratio can be estimated using SU(3) relations and experimental data on related $B \rightarrow K\pi$ decays. The result (for $\pi\pi$) is that the suppression is at the level of 0.2–0.3 and so cannot be neglected. The expressions for $S_{\pi\pi}$ and $C_{\pi\pi}$ to leading order in $R_{PT} \equiv (|V_{tb}V_{td}| P_{\pi\pi}^t) / (|V_{ub}V_{ud}| T_{\pi\pi})$ are:

$$\lambda_{\pi\pi} = e^{2i\alpha} \left[(1 - R_{PT} e^{-i\alpha}) / (1 - R_{PT} e^{+i\alpha}) \right] \Rightarrow \quad (13.84)$$

$$S_{\pi\pi} \approx \sin 2\alpha + 2 \mathcal{R}e(R_{PT}) \cos 2\alpha \sin \alpha, \quad C_{\pi\pi} \approx 2 \mathcal{I}m(R_{PT}) \sin \alpha. \quad (13.85)$$

Note that R_{PT} is mode-dependent and, in particular, could be different for $\pi^+\pi^-$ and $\pi^0\pi^0$. If strong phases can be neglected, then R_{PT} is real, resulting in $C_{\pi\pi} = 0$. The size of $C_{\pi\pi}$ is an indicator of how large the strong phase is. The present experimental average is $C_{\pi^+\pi^-} = -0.31 \pm 0.03$ [61]. As concerns $S_{\pi\pi}$, it is clear from Eq. (13.85) that the relative size or strong phase of the penguin contribution must be known to extract α . The theoretical uncertainty stemming from $|R_{PT}| \ll 1$ is referred to in the literature as penguin pollution.

Table 13.1: Summary of $\bar{b} \rightarrow \bar{q}q\bar{q}'$ modes with $q' = s$ or d . The second and third columns give examples of hadronic final states (usually those which are experimentally most convenient to study). The fourth column gives the CKM dependence of the amplitude A_f , using the notation of Eqs. ((13.77), (13.79), (13.81)), with the dominant term first and the subdominant second. The suppression factor of the second term compared to the first is given in the last column. “Loop” refers to a penguin versus tree-suppression factor (it is mode-dependent and roughly $\mathcal{O}(0.2 - 0.3)$) and $\lambda \simeq 0.23$ is the expansion parameter of Eq. (13.34).

$\bar{b} \rightarrow \bar{q}q\bar{q}'$	$B^0 \rightarrow f$	$B_s^0 \rightarrow f$	CKM dependence of A_f	Suppression
$\bar{b} \rightarrow \bar{c}c\bar{s}$	ψK_S	$\psi\phi$	$(V_{cb}^* V_{cs})T + (V_{ub}^* V_{us})P^u$	loop $\times \lambda^2$
$\bar{b} \rightarrow \bar{s}s\bar{s}$	ϕK_S	$\phi\phi$	$(V_{cb}^* V_{cs})P^c + (V_{ub}^* V_{us})P^u$	λ^2
$\bar{b} \rightarrow \bar{u}u\bar{s}$	$\pi^0 K_S$	$K^+ K^-$	$(V_{cb}^* V_{cs})P^c + (V_{ub}^* V_{us})T$	λ^2/loop
$\bar{b} \rightarrow \bar{c}c\bar{d}$	$D^+ D^-$	ψK_S	$(V_{cb}^* V_{cd})T + (V_{tb}^* V_{td})P^t$	loop
$\bar{b} \rightarrow \bar{s}s\bar{d}$	$K_S K_S$	ϕK_S	$(V_{tb}^* V_{td})P^t + (V_{cb}^* V_{cd})P^c$	$\lesssim 1$
$\bar{b} \rightarrow \bar{u}u\bar{d}$	$\pi^+ \pi^-$	$\rho^0 K_S$	$(V_{ub}^* V_{ud})T + (V_{tb}^* V_{td})P^t$	loop
$\bar{b} \rightarrow \bar{c}c\bar{d}$	$D_{CP}\pi^0$	$D_{CP}K_S$	$(V_{cb}^* V_{ud})T + (V_{ub}^* V_{cd})T'$	λ^2
$\bar{b} \rightarrow \bar{c}u\bar{s}$	$D_{CP}K_S$	$D_{CP}\phi$	$(V_{cb}^* V_{us})T + (V_{ub}^* V_{cs})T'$	$\lesssim 1$

The cleanest solution involves isospin relations among the $B \rightarrow \pi\pi$ amplitudes [101]:

$$\frac{1}{\sqrt{2}}A_{\pi^+\pi^-} + A_{\pi^0\pi^0} = A_{\pi^+\pi^0}. \quad (13.86)$$

The method exploits the fact that the penguin contribution to $P_{\pi\pi}^t$ is pure $\Delta I = 1/2$ (this is not true for the electroweak penguins which, however, are expected to be small), while the tree contribution to $T_{\pi\pi}$ contains amplitudes that are both $\Delta I = 1/2$ and $\Delta I = 3/2$. A simple geometric construction then allows one to find R_{PT} and extract α cleanly from $S_{\pi^+\pi^-}$. The key experimental difficulty is that one must measure accurately the separate rates for B^0 and $\bar{B}^0 \rightarrow \pi^0\pi^0$.

CP asymmetries in $B \rightarrow \rho\pi$ and $B \rightarrow \rho\rho$ can also be used to determine α . In particular, the $B \rightarrow \rho\rho$ measurements are presently very significant in constraining α . The extraction proceeds via isospin analysis similar to that of $B \rightarrow \pi\pi$. There are, however, several important differences. First, due to the finite width of the ρ mesons, a final $(\rho\rho)_{I=1}$ state is possible [102]. The effect is, however, of the order of $(\Gamma_\rho/m_\rho)^2 \sim 0.04$. Second, due to the presence of three helicity states for the two vector mesons, angular analysis is needed to separate the CP -even and CP -odd components. The theoretical expectation is that the CP -odd component is small. This is supported by experiments which find that the $\rho^+\rho^-$ and $\rho^\pm\rho^0$ modes are dominantly longitudinally polarized. Third, an important advantage of the $\rho\rho$ modes is that the penguin contribution is expected to be small due to different hadronic dynamics. This expectation is confirmed by the smallness of $\mathcal{B}(B^0 \rightarrow \rho^0\rho^0) = (0.95 \pm 0.16) \times 10^{-6}$ compared to $\mathcal{B}(B^0 \rightarrow \rho^+\rho^-) = (24.2 \pm 3.1) \times 10^{-6}$ [61]. Thus, $S_{\rho^+\rho^-}$ is not far from $\sin 2\alpha$. Finally, both $S_{\rho^0\rho^0}$ and $C_{\rho^0\rho^0}$ are experimentally accessible, which may allow a precise determination of α . However, a full isospin analysis should allow that the fractions of longitudinal polarization in B and \bar{B} decays may differ, which has not yet been done by the experiments.

Detailed discussion of the determination of α with these methods, and the latest world average, can be found in Refs. [103,104]. The consistency between the range of α determined by the $B \rightarrow \pi\pi$, $\rho\pi$ and $\rho\rho$ measurements and the range allowed by CKM fits (excluding these direct determinations) provides further support to the Kobayashi-Maskawa mechanism.

All modes discussed in this Section so far have possible contributions from penguin amplitudes. As shown in Table 13.1, CP violation can also be studied with final states, typically containing charmed mesons, where no such contribution is possible. The neutral charmed meson must be reconstructed in a final state, such as a CP eigenstate, common to D^0 and \bar{D}^0 so that the amplitudes for the B and \bar{B} meson decays interfere. Although there is a second tree amplitude with a different weak phase, the contributions of the different diagrams can in many cases be separated experimentally (for example by exploiting different decays of the neutral D mesons) making these channels very clean theoretically. The first determination of $\sin(2\beta)$, with significance of CP violation over 5σ , with this method has recently been reported [105]. Moreover, the interference between the two tree diagrams gives

sensitivity to γ , as will be discussed in Section 13.6.4.

13.6.3 CP violation in interference of B_s^0 decays with and without mixing

As discussed in Section 13.6.1, the world average for $|q/p|$ in the B_s^0 system currently deviates from the Standard Model expectation due to an anomalous value of the dimuon asymmetry. Attributing the dimuon asymmetry result to a fluctuation, we again neglect the deviation of $|q/p|$ from 1, and use

$$\lambda_f = e^{-i\phi_M(B_s^0)}(\bar{A}_f/A_f). \quad (13.87)$$

Within the Standard Model,

$$e^{-i\phi_M(B_s^0)} = (V_{tb}^* V_{ts})/(V_{tb} V_{ts}^*). \quad (13.88)$$

Note that $\Delta\Gamma/\Gamma = 0.132 \pm 0.008$ [61] and therefore y should not be put to zero in Eqs. (13.17a) and (13.17b). However, $|q/p| = 1$ is expected to hold to an even better approximation than for B^0 mesons. One therefore obtains

$$A_f(t) = \frac{S_f \sin(\Delta mt) - C_f \cos(\Delta mt)}{\cosh(\Delta\Gamma t/2) - A_f^{\Delta\Gamma} \sinh(\Delta\Gamma t/2)}, \quad (13.89)$$

$$A_f^{\Delta\Gamma} \equiv \frac{-2\mathcal{R}e(\lambda_f)}{1 + |\lambda_f|^2}. \quad (13.90)$$

The presence of the $A_f^{\Delta\Gamma}$ term implies that information on λ_f can be obtained from analyses that do not use tagging of the initial flavor, through so-called effective lifetime measurements [106].

The $B_s^0 \rightarrow J/\psi\phi$ decay proceeds via the $\bar{b} \rightarrow \bar{c}c\bar{s}$ transition. The CP asymmetry in this mode thus determines (with angular analysis to disentangle the CP -even and CP -odd components of the final state) $\sin 2\beta_s$, where β_s is defined in Eq. (13.38) [107]. The $B_s^0 \rightarrow J/\psi\pi^+\pi^-$ decay, which has a large contribution from $J/\psi f_0(980)$ and is assumed to also proceed dominantly via the $\bar{b} \rightarrow \bar{c}c\bar{s}$ transition, has also been used to determine β_s . In this case no angular analysis is necessary, since the final state has been shown to be dominated by the CP -odd component [108]. The combination of measurements yields [61]

$$2\beta_s = 0.050 \pm 0.019, \quad (13.91)$$

consistent with the Standard Model prediction, assuming negligible penguin contributions, $\beta_s = 0.0184 \pm 0.0004$ [20].

A time-dependent CP asymmetry was established in $B_s^0 \rightarrow K^+ K^-$ decay, which proceeds via the $\bar{b} \rightarrow \bar{u}u\bar{s}$ transition [109]:

$$C_{KK} = +0.172 \pm 0.039, \quad S_{KK} = +0.139 \pm 0.032. \quad (13.92)$$

For both C_{KK} and S_{KK} , the hadronic ratio (T/P^c) plays an important role (see Table 13.1), making a clean theoretical interpretation challenging. First results on the $\bar{b} \rightarrow \bar{q}q\bar{s}$ decays $B_s^0 \rightarrow \phi\phi$ and $K^{*0}\bar{K}^{*0}$ have also been reported. Parameters of CP violation have also been determined from the decay-time distributions of $B_s^0 \rightarrow D_s^\mp K^\pm$ and $D_s^\mp K^\pm \pi^+ \pi^-$ decays, involving interference between $\bar{b} \rightarrow \bar{c}u\bar{s}$ and $\bar{b} \rightarrow \bar{u}c\bar{s}$ amplitudes.

13.6.4 Direct CP violation in the B system

An interesting class of decay modes is that of the tree-level decays $B^\pm \rightarrow D^{(*)}K^\pm$, which allow a theoretically pristine determination of the angle γ [110–115]. The method uses the decays $B^+ \rightarrow D^0K^+$, which proceeds via the quark transition $\bar{b} \rightarrow \bar{u}\bar{c}\bar{s}$, and $B^+ \rightarrow \bar{D}^0K^+$, which proceeds via the quark transition $\bar{b} \rightarrow \bar{c}\bar{u}\bar{s}$, with the D^0 and \bar{D}^0 decaying into a common final state. The decays into common final states, such as $(\pi^0 K_S)DK^+$, involve interference effects between the two amplitudes, with sensitivity to the relative phase, $\delta + \gamma$ (δ is the relevant strong phase difference). The CP-conjugate processes are sensitive to $\delta - \gamma$. Measurements of branching ratios and CP asymmetries allow the determination of γ and δ from amplitude triangle relations. The method suffers from discrete ambiguities but, since all hadronic parameters can be determined from the data, has negligible theoretical uncertainty [116].

Unfortunately, the smallness of the CKM-suppressed $b \rightarrow u$ transitions makes it difficult to use the simplest methods alone [110–112] to determine γ . These difficulties are overcome (and the discrete ambiguities are removed) by performing a Dalitz plot analysis for multi-body D decays [113–115]. Detailed discussion of the determination of γ with these methods can be found in Ref. [104].

Constraints on γ from combinations of results on various $B \rightarrow D^{(*)}K^{(*)}$ processes have been obtained by experiments [117,118]. The latest world average is [61,104]

$$\gamma = (66.2^{+3.4}_{-3.6})^\circ. \quad (13.93)$$

The consistency between the range of γ determined by the $B \rightarrow DK$ measurements and the range allowed by CKM fits (excluding these direct determinations) provides further support to the Kobayashi-Maskawa mechanism. As more data become available, determinations of γ from $B_s^0 \rightarrow D_s^\mp K^\pm$ [119,120] and $B^0 \rightarrow DK^{*0}$ [121–124] are expected to also give competitive measurements.

Decays to the final state $K^\mp \pi^\pm$ provided the first observations of direct CP violation in both B^0 and B_s^0 systems. The asymmetry arises due to interference between tree and penguin diagrams [125], similar to the effect discussed in Section 13.6.2. In principle, measurements of $\mathcal{A}_{B^0 \rightarrow K^+ \pi^-}$ and $\mathcal{A}_{B_s^0 \rightarrow K^- \pi^+}$ could be used to determine the weak phase difference γ , but lack of knowledge of the relative magnitude and strong phase of the contributing amplitudes limits the achievable precision. The uncertainties on these hadronic parameters can be reduced by exploiting flavor symmetries, which predict a number of relations between asymmetries in different modes. One such relation is that the partial rate differences for B^0 and B_s^0 decays to $K^\mp \pi^\pm$ are expected to be approximately equal and opposite [126], which is consistent with current data. It is also expected that the partial rate asymmetries for $B^0 \rightarrow K^+ \pi^-$ and $B^+ \rightarrow K^+ \pi^0$ should be approximately equal; however, the experimental results currently show a significant discrepancy [61]:

$$\mathcal{A}_{B^0 \rightarrow K^+ \pi^-} = -0.083 \pm 0.004, \quad \mathcal{A}_{B^+ \rightarrow K^+ \pi^0} = +0.029 \pm 0.013. \quad (13.94)$$

It is therefore of great interest to understand whether this originates from Standard Model QCD corrections, or whether it is a signature of new dynamics. Improved tests of a more precise relation between the partial rate differences of all four $K\pi$ final states [127–130], currently limited by knowledge of the CP asymmetry in $\bar{B}^0 \rightarrow K_S \pi^0$ decays, may help to resolve the situation.

It is also of interest to investigate whether similar patterns appear among the CP violating asymmetries in B meson decays to final states containing one pseudoscalar and one vector meson. Since the vector resonance decays to two particles, such channels can be studied through Dalitz plot analysis of the three-body final state. Model-independent analyses of $B^+ \rightarrow K^+ K^- K^+$, $\pi^+ \pi^- K^+$, $\pi^+ \pi^- \pi^+$ and $K^+ K^- \pi^+$ decays have revealed large CP violation effects in certain regions of phase space [131]. For the $B^+ \rightarrow K^+ K^- \pi^+$ decay, an amplitude analysis has established a large CP violation effect associated with $\pi\pi \leftrightarrow KK$ S-wave rescattering [132]. In $B^+ \rightarrow \pi^+ \pi^- \pi^+$ decays, amplitude analysis has

established CP violation effects in the decay amplitude involving the $f_2(1270)$ resonance, in the $\pi^+ \pi^-$ S-wave at low invariant mass, and in the interference between the $\pi^+ \pi^-$ S-wave and the P-wave $B^+ \rightarrow \rho(770)^0 \pi^+$ amplitude [133,134]. For the other channels it remains to be seen whether the CP violation effects are associated to particular resonances or to interference effects, which will be necessary to understand the underlying dynamics.

13.7 Summary and Outlook

CP violation has been experimentally established in K , D and B meson decays. A full list of CP asymmetries that have been measured at a level higher than 5σ is given in the introduction to this review. In Section 13.1.4 we introduced three types of CP-violating effects. Examples of these three types include the following:

1. All three types of CP violation have been observed in $K \rightarrow \pi\pi$ decays:

$$\begin{aligned} \mathcal{R}e(\epsilon') &= \frac{1}{6} \left(\left| \frac{\bar{A}_{\pi^0 \pi^0}}{A_{\pi^0 \pi^0}} \right| - \left| \frac{\bar{A}_{\pi^+ \pi^-}}{A_{\pi^+ \pi^-}} \right| \right) \\ &= (2.5 \pm 0.4) \times 10^{-6}, \end{aligned} \quad (\text{I}) \quad (13.95a)$$

$$\begin{aligned} \mathcal{R}e(\epsilon) &= \frac{1}{2} \left(1 - \left| \frac{q}{p} \right| \right) \\ &= (1.66 \pm 0.02) \times 10^{-3}, \end{aligned} \quad (\text{II}) \quad (13.95b)$$

$$\begin{aligned} \mathcal{I}m(\epsilon) &= -\frac{1}{2} \mathcal{I}m(\lambda_{(\pi\pi)I=0}) \\ &= (1.57 \pm 0.02) \times 10^{-3}. \end{aligned} \quad (\text{III}) \quad (13.95c)$$

2. For D mesons, CP violation in decay has been established in the difference of asymmetries for $D^0 \rightarrow K^+ K^-$ and $D^0 \rightarrow \pi^+ \pi^-$ decays.

$$\begin{aligned} \Delta a_{CP} &= \frac{|\bar{A}_{K^+ K^-} / A_{K^+ K^-}|^2 - 1}{|\bar{A}_{K^+ K^-} / A_{K^+ K^-}|^2 + 1} - \frac{|\bar{A}_{\pi^+ \pi^-} / A_{\pi^+ \pi^-}|^2 - 1}{|\bar{A}_{\pi^+ \pi^-} / A_{\pi^+ \pi^-}|^2 + 1} \\ &= (-0.164 \pm 0.028) \times 10^{-2}, \end{aligned} \quad (\text{I}) \quad (13.96)$$

3. In the B meson system, CP violation in decay has been observed in, for example, $B^0 \rightarrow K^+ \pi^-$ transitions, while CP violation in interference of decays with and without mixing has been observed in, for example, the $B^0 \rightarrow J/\psi K_S$ channel:

$$\begin{aligned} \mathcal{A}_{K^+ \pi^-} &= \frac{|\bar{A}_{K^- \pi^+} / A_{K^+ \pi^-}|^2 - 1}{|\bar{A}_{K^- \pi^+} / A_{K^+ \pi^-}|^2 + 1} \\ &= -0.083 \pm 0.004, \end{aligned} \quad (\text{I}) \quad (13.97a)$$

$$\begin{aligned} S_{\psi K} &= \mathcal{I}m(\lambda_{\psi K}) \\ &= +0.699 \pm 0.017. \end{aligned} \quad (\text{III}) \quad (13.97b)$$

Based on Standard Model predictions, further observations of CP violation in B^0 , B^+ and B_s^0 decays seem likely in the near future, at both LHCb and its upgrades [135–137] as well as the Belle II experiment [138]. The first observation of CP violation in b baryons is also likely to be within reach of LHCb. Further improvements in the sensitivity to CP violation effects in the charm sector can also be anticipated, though uncertainty in the Standard Model predictions makes it difficult to forecast whether or not additional discoveries will be forthcoming. A number of upcoming experiments have potential to make significant progress on rare kaon decays. Observables that are subject to clean theoretical interpretation, such as β from $S_{\psi K_S}$, β_s from $B_s^0 \rightarrow J/\psi \phi$, $\mathcal{B}(K_L \rightarrow \pi^0 \nu \bar{\nu})$ and γ from CP violation in $B \rightarrow DK$ decays, are of particular value for constraining the values of the CKM parameters and probing the flavor sector of extensions to the Standard Model. Progress in lattice QCD calculations is also needed to complement the anticipated experimental results. Other probes of CP violation now being pursued experimentally include the electric dipole moments of the neutron and electron, and the decays of tau leptons. Additional processes that are likely to play an

important role in future CP studies include top-quark production and decay, Higgs boson decays and neutrino oscillations.

All measurements of CP violation to date are consistent with the predictions of the Kobayashi-Maskawa mechanism of the Standard Model. In fact, it is now established that the KM mechanism plays a dominant role in the CP violation measured in the quark sector. However, a dynamically-generated matter-antimatter asymmetry of the universe requires additional sources of CP violation, and such sources are naturally generated by extensions to the Standard Model. New sources might eventually reveal themselves as small deviations from the predictions of the KM mechanism, or else might not be observable in the quark sector at all, but observable with future probes such as neutrino oscillations or electric dipole moments. The fundamental nature of CP violation demands a vigorous search.

A number of excellent reviews of CP violation are available [139–146], where the interested reader may find a detailed discussion of the various topics that are briefly reviewed here.

We thank David Kirkby for significant contributions to earlier versions of this review.

13.8 Observed CP violation effects

We conclude by listing the observables where CP violation has been observed at a level above 5σ [43, 61, 81]:

- Indirect CP violation in $K \rightarrow \pi\pi$ and $K \rightarrow \pi\ell\nu$ decays, and in the $K_L \rightarrow \pi^+\pi^-e^+e^-$ decay, is given by

$$|\epsilon| = (2.228 \pm 0.011) \times 10^{-3}. \quad (13.98)$$

- Direct CP violation in $K \rightarrow \pi\pi$ decays is given by

$$\mathcal{R}e(\epsilon'/\epsilon) = (1.65 \pm 0.26) \times 10^{-3}. \quad (13.99)$$

- CP violation in the interference of mixing and decay in the tree-dominated $b \rightarrow c\bar{c}s$ transitions, such as $B^0 \rightarrow \psi K^0$, is given by (we use K^0 throughout to denote results that combine K_S and K_L modes, but use the sign appropriate to K_S):

$$S_{\psi K^0} = +0.699 \pm 0.017. \quad (13.100)$$

- CP violation in the interference of mixing and decay in modes governed by the tree-dominated $b \rightarrow c\bar{u}d$ transitions is given by

$$S_{D^{(*)}h^0} = +0.71 \pm 0.09, \quad (13.101)$$

- CP violation in the interference of mixing and decay in various modes related to $b \rightarrow c\bar{c}d$ transitions is given by

$$\begin{aligned} S_{\psi\pi^0} &= -0.86 \pm 0.14, \\ S_{D^+D^-} &= -0.84 \pm 0.12, \\ S_{D^{*+}D^{\mp}} &= -0.81 \pm 0.06, \\ S_{D^{*+}D^{*-}} &= -0.71 \pm 0.09. \end{aligned} \quad (13.102)$$

- CP violation in the interference of mixing and decay in various modes related to $b \rightarrow q\bar{q}s$ (penguin) transitions is given by

$$\begin{aligned} S_{\phi K^0} &= +0.74^{+0.11}_{-0.13}, \\ S_{\eta' K^0} &= +0.63 \pm 0.06, \\ S_{f_0 K^0} &= +0.69^{+0.10}_{-0.12}, \\ S_{K^+K^-K_S} &= +0.68^{+0.09}_{-0.10}. \end{aligned} \quad (13.103)$$

- CP violation in the interference of mixing and decay in the $B^0 \rightarrow \pi^+\pi^-$ mode is given by

$$S_{\pi^+\pi^-} = -0.67 \pm 0.03. \quad (13.104)$$

- Direct CP violation in the $B^0 \rightarrow \pi^+\pi^-$ mode is given by

$$C_{\pi^+\pi^-} = -0.31 \pm 0.03. \quad (13.105)$$

- Direct CP violation in the $B_s^0 \rightarrow K^+K^-$ mode is given by

$$C_{K^+K^-} = 0.17 \pm 0.03. \quad (13.106)$$

- Direct CP violation in $B^+ \rightarrow D_+^{(*)}K^+$ decays ($D_+^{(*)}$ is the CP -even neutral $D^{(*)}$ state) are given by

$$\begin{aligned} \mathcal{A}_{B^+ \rightarrow D_+ K^+} &= +0.139 \pm 0.009 \quad \text{and} \\ \mathcal{A}_{B^+ \rightarrow D_+^* K^+} &= -0.109 \pm 0.019, \end{aligned} \quad (13.107)$$

while the corresponding quantity in the case that the neutral D meson is reconstructed in the suppressed $K^-\pi^+$ final state is

$$\mathcal{A}_{B^+ \rightarrow D_{K^-\pi^+} K^+} = -0.453 \pm 0.026, \quad (13.108)$$

- Direct CP violation has also been observed in $B^+ \rightarrow DK^+$ decays through differences between the Dalitz plot distributions of subsequent $D \rightarrow K_S\pi^+\pi^-$ decays.

- Direct CP violation in the $B^0 \rightarrow K^+\pi^-$ mode is given by

$$\mathcal{A}_{B^0 \rightarrow K^+\pi^-} = -0.083 \pm 0.004. \quad (13.109)$$

- Direct CP violation in the $B_s^0 \rightarrow K^-\pi^+$ mode is given by

$$\mathcal{A}_{B_s^0 \rightarrow K^-\pi^+} = +0.225 \pm 0.012. \quad (13.110)$$

- Direct CP violation in $B^+ \rightarrow K^+K^-\pi^+$ decays is given by

$$\mathcal{A}_{B^+ \rightarrow K^+K^-\pi^+} = -0.118 \pm 0.022. \quad (13.111)$$

- Large CP violation effects have been observed model-independently in certain regions of the phase space of $B^+ \rightarrow K^+K^-K^+$, $K^+K^-\pi^+$, $\pi^+\pi^-K^+$ and $\pi^+\pi^-\pi^+$ decays. An amplitude analysis has established a large CP violation effect associated with $\pi\pi \leftrightarrow KK$ S-wave rescattering in $B^+ \rightarrow K^+K^-\pi^+$ decays. In $B^+ \rightarrow \pi^+\pi^-\pi^+$ decays, amplitude analysis has established CP violation effects in the decay amplitude involving the $f_2(1270)$ resonance, in the $\pi^+\pi^-$ S-wave at low invariant mass, and in the interference between the $\pi^+\pi^-$ S-wave and the P-wave $B^+ \rightarrow \rho(770)^0\pi^+$ amplitude.
- Direct CP violation has been established in the difference of asymmetries for $D^0 \rightarrow K^+K^-$ and $D^0 \rightarrow \pi^+\pi^-$ decays

$$\Delta_{CP} = (-0.164 \pm 0.028) \times 10^{-2}. \quad (13.112)$$

References

- [1] J. H. Christenson *et al.*, Phys. Rev. Lett. **13**, 138 (1964).
- [2] B. Aubert *et al.* (BaBar), Phys. Rev. Lett. **87**, 091801 (2001), [hep-ex/0107013].
- [3] K. Abe *et al.* (Belle), Phys. Rev. Lett. **87**, 091802 (2001), [hep-ex/0107061].
- [4] H. Burkhardt *et al.* (NA31), Phys. Lett. **B206**, 169 (1988).
- [5] V. Fanti *et al.* (NA48), Phys. Lett. **B465**, 335 (1999), [hep-ex/9909022].
- [6] A. Alavi-Harati *et al.* (KTeV), Phys. Rev. Lett. **83**, 22 (1999), [hep-ex/9905060].
- [7] B. Aubert *et al.* (BaBar), Phys. Rev. Lett. **93**, 131801 (2004), [hep-ex/0407057].
- [8] Y. Chao *et al.* (Belle), Phys. Rev. Lett. **93**, 191802 (2004), [hep-ex/0408100].
- [9] A. Poluektov *et al.* (Belle), Phys. Rev. **D81**, 112002 (2010), [arXiv:1003.3360].
- [10] P. del Amo Sanchez *et al.* (BaBar), Phys. Rev. **D82**, 072004 (2010), [arXiv:1007.0504].
- [11] R. Aaij *et al.* (LHCb), Phys. Lett. **B712**, 203 (2012), [Erratum-ibid. **B713**, 351 (2012)], [arXiv:1203.3662].
- [12] R. Aaij *et al.* (LHCb), Phys. Rev. Lett. **110**, 221601 (2013), [arXiv:1304.6173].
- [13] R. Aaij *et al.* (LHCb), Phys. Rev. Lett. **122**, 211803 (2019), [arXiv:1903.08726].
- [14] See the review on “Neutrino Masses, Mixing, and Oscillations,” in this *Review*.

- [15] See the review on “Tests of Conservation Laws,” in this *Review*.
- [16] J. P. Lees *et al.* (BaBar), Phys. Rev. Lett. **109**, 211801 (2012), [arXiv:1207.5832].
- [17] J. Bernabeu, F. Martinez-Vidal and P. Villanueva-Perez, JHEP **08**, 064 (2012), [arXiv:1203.0171].
- [18] See, for example, R. F. Streater and A. S. Wightman, *CPT, Spin and Statistics, and All That*, reprinted by Addison-Wesley, New York (1989).
- [19] M. Kobayashi and T. Maskawa, Prog. Theor. Phys. **49**, 652 (1973).
- [20] J. Charles *et al.* (CKMfitter Group), Eur. Phys. J. **C41**, 1 (2005), updated results and plots available at: <http://ckmfitter.in2p3.fr>, [hep-ph/0406184].
- [21] M. Bona *et al.* (UTfit), JHEP **10**, 081 (2006), updated results and plots available at: <http://www.utfit.org/UTfit>, [hep-ph/0606167].
- [22] A. D. Sakharov, Pisma Zh. Eksp. Teor. Fiz. **5**, 32 (1967), [Usp. Fiz. Nauk161,no.5,61(1991)].
- [23] A. Riotto, in “Proceedings, Summer School in High-energy physics and cosmology: Trieste, Italy, June 29-July 17, 1998,” 326–436 (1998), [hep-ph/9807454].
- [24] M. Fukugita and T. Yanagida, Phys. Lett. **B174**, 45 (1986).
- [25] S. Davidson, E. Nardi and Y. Nir, Phys. Rept. **466**, 105 (2008), [arXiv:0802.2962].
- [26] G. Aad *et al.* (ATLAS), Phys. Lett. **B716**, 1 (2012), [arXiv:1207.7214].
- [27] S. Chatrchyan *et al.* (CMS), Phys. Lett. **B716**, 30 (2012), [arXiv:1207.7235].
- [28] S. Okubo, Phys. Lett. **5**, 165 (1963).
- [29] G. Zweig (1964), *An SU_3 model for strong interaction symmetry and its breaking; Version 2*, CERN-TH-412.
- [30] J. Iizuka, Prog. Theor. Phys. Suppl. **37**, 21 (1966).
- [31] V. Weisskopf and E. P. Wigner, Z. Phys. **63**, 54 (1930).
- [32] See the review on “ D^0 - \bar{D}^0 Mixing” in this *Review*.
- [33] O. Long *et al.*, Phys. Rev. **D68**, 034010 (2003), [hep-ex/0303030].
- [34] M. Gronau, Y. Grossman and J. L. Rosner, Phys. Lett. **B508**, 37 (2001), [hep-ph/0103110].
- [35] M. Artuso, G. Borissov and A. Lenz, Rev. Mod. Phys. **88**, 045002 (2016), [arXiv:1511.09466].
- [36] L. Wolfenstein, Phys. Rev. Lett. **13**, 562 (1964).
- [37] C. Abel *et al.* (nEDM), Phys. Rev. Lett. **124**, 081803 (2020), [arXiv:2001.11966].
- [38] R. J. Crewther *et al.*, Phys. Lett. **B88**, 123 (1979), [Erratum-ibid. **B91**, 487 (1980)].
- [39] See the review on “Cabibbo-Kobayashi-Maskawa Mixing Matrix,” in this *Review*.
- [40] L. Wolfenstein, Phys. Rev. Lett. **51**, 1945 (1983).
- [41] A. J. Buras, M. E. Lautenbacher and G. Ostermaier, Phys. Rev. **D50**, 3433 (1994), [hep-ph/9403384].
- [42] C. Jarlskog, Phys. Rev. Lett. **55**, 1039 (1985).
- [43] See the K -meson Listings in this *Review*.
- [44] See the review on “ CP violation in $K_S \rightarrow 3\pi$,” in this *Review*.
- [45] T. Blum *et al.*, Phys. Rev. **D91**, 074502 (2015), [arXiv:1502.00263].
- [46] Z. Bai *et al.* (RBC, UKQCD), Phys. Rev. Lett. **115**, 212001 (2015), [arXiv:1505.07863].
- [47] A. J. Buras *et al.*, JHEP **11**, 202 (2015), [arXiv:1507.06345].
- [48] Y. Grossman and Y. Nir, Phys. Lett. **B398**, 163 (1997), [hep-ph/9701313].
- [49] L. S. Littenberg, Phys. Rev. **D39**, 3322 (1989).
- [50] A. J. Buras, Phys. Lett. **B333**, 476 (1994), [hep-ph/9405368].
- [51] G. Buchalla and A. J. Buras, Nucl. Phys. **B400**, 225 (1993).
- [52] A. J. Buras *et al.*, JHEP **11**, 033 (2015), [arXiv:1503.02693].
- [53] J. K. Ahn *et al.* (KOTO), Phys. Rev. Lett. **122**, 021802 (2019), [arXiv:1810.09655].
- [54] J. K. Ahn *et al.* (KOTO), Phys. Rev. Lett. **126**, 121801 (2021), [arXiv:2012.07571].
- [55] E. Cortina Gil *et al.* (NA62), JHEP **06**, 093 (2021), [arXiv:2103.15389].
- [56] B. Aubert *et al.* (BaBar), Phys. Rev. Lett. **98**, 211802 (2007), [hep-ex/0703020].
- [57] M. Staric *et al.* (Belle), Phys. Rev. Lett. **98**, 211803 (2007), [hep-ex/0703036].
- [58] T. Aaltonen *et al.* (CDF), Phys. Rev. Lett. **100**, 121802 (2008), [arXiv:0712.1567].
- [59] R. Aaij *et al.* (LHCb), Phys. Rev. Lett. **110**, 101802 (2013), [arXiv:1211.1230].
- [60] R. Aaij *et al.* (LHCb) (2021), to appear in PRL, [arXiv:2106.03744].
- [61] Y. S. Amhis *et al.* (HFLAV), Eur. Phys. J. **C81**, 226 (2021), updated results and plots available at <https://hflav.web.cern.ch/>, [arXiv:1909.12524].
- [62] See the D -meson Listings in this *Review*.
- [63] Y. Grossman, A. L. Kagan and Y. Nir, Phys. Rev. **D75**, 036008 (2007), [hep-ph/0609178].
- [64] S. Bergmann *et al.*, Phys. Lett. **B486**, 418 (2000), [hep-ph/0005181].
- [65] M. Gersabeck *et al.*, J. Phys. **G39**, 045005 (2012), [arXiv:1111.6515].
- [66] D. M. Asner *et al.* (CLEO), Phys. Rev. **D78**, 012001 (2008), [arXiv:0802.2268].
- [67] M. Ablikim *et al.* (BESIII), Phys. Lett. **B734**, 227 (2014), [arXiv:1404.4691].
- [68] R. Aaij *et al.* (LHCb), Phys. Rev. Lett. **111**, 251801 (2013), [arXiv:1309.6534].
- [69] R. Aaij *et al.* (LHCb), Phys. Rev. Lett. **118**, 261803 (2017), [arXiv:1702.06490].
- [70] M. Ciuchini *et al.*, Phys. Lett. **B655**, 162 (2007), [hep-ph/0703204].
- [71] Y. Grossman, Y. Nir and G. Perez, Phys. Rev. Lett. **103**, 071602 (2009), [arXiv:0904.0305].
- [72] A. L. Kagan and M. D. Sokoloff, Phys. Rev. **D80**, 076008 (2009), [arXiv:0907.3917].
- [73] Y. Grossman and Y. Nir, JHEP **04**, 002 (2012), [arXiv:1110.3790].
- [74] B. R. Ko *et al.* (Belle), Phys. Rev. Lett. **109**, 021601 (2012), [Erratum-ibid. **109**, 119903 (2012)], [arXiv:1203.6409].
- [75] See the “Review of Multibody Charm Analyses” in this *Review*.
- [76] B. Aubert *et al.* (BaBar), Phys. Rev. **D78**, 051102 (2008), [arXiv:0802.4035].
- [77] I. Bediaga *et al.*, Phys. Rev. **D80**, 096006 (2009), [arXiv:0905.4233].
- [78] I. Bediaga *et al.*, Phys. Rev. **D86**, 036005 (2012), [arXiv:1205.3036].
- [79] M. Williams, Phys. Rev. **D84**, 054015 (2011), [arXiv:1105.5338].
- [80] R. Aaij *et al.* (LHCb), Phys. Lett. **B769**, 345 (2017), [arXiv:1612.03207].
- [81] See the B -meson Listings in this *Review*.
- [82] V. M. Abazov *et al.* (D0), Phys. Rev. **D82**, 032001 (2010), [arXiv:1005.2757].

- [83] A. B. Carter and A. I. Sanda, Phys. Rev. Lett. **45**, 952 (1980).
- [84] A. B. Carter and A. I. Sanda, Phys. Rev. **D23**, 1567 (1981).
- [85] I. I. Y. Bigi and A. I. Sanda, Nucl. Phys. **B193**, 85 (1981).
- [86] I. Dunietz and J. L. Rosner, Phys. Rev. **D34**, 1404 (1986).
- [87] Y. I. Azimov, N. G. Uraltsev and V. A. Khoze, Sov. J. Nucl. Phys. **45**, 878 (1987), [Yad. Fiz. **45**, 1412 (1987)].
- [88] I. I. Y. Bigi and A. I. Sanda, Nucl. Phys. **B281**, 41 (1987).
- [89] G. Buchalla, A. J. Buras and M. E. Lautenbacher, Rev. Mod. Phys. **68**, 1125 (1996), [hep-ph/9512380].
- [90] A. J. Buras and L. Silvestrini, Nucl. Phys. **B569**, 3 (2000), [hep-ph/9812392].
- [91] R. Fleischer, Eur. Phys. J. **C10**, 299 (1999), [hep-ph/9903455].
- [92] M. Ciuchini, M. Pierini and L. Silvestrini, Phys. Rev. Lett. **95**, 221804 (2005), [hep-ph/0507290].
- [93] S. Faller *et al.*, Phys. Rev. **D79**, 014030 (2009), [arXiv:0809.0842].
- [94] M. Jung, Phys. Rev. **D86**, 053008 (2012), [arXiv:1206.2050].
- [95] H.-n. Li and S. Mishima, JHEP **03**, 009 (2007), [hep-ph/0610120].
- [96] K. De Bruyn and R. Fleischer, JHEP **03**, 145 (2015), [arXiv:1412.6834].
- [97] P. Frings, U. Nierste and M. Wiebusch, Phys. Rev. Lett. **115**, 061802 (2015), [arXiv:1503.00859].
- [98] L. Silvestrini, Ann. Rev. Nucl. Part. Sci. **57**, 405 (2007), [arXiv:0705.1624].
- [99] R. Fleischer *et al.*, Phys. Rev. **D78**, 111501 (2008), [arXiv:0806.2900].
- [100] R. Fleischer *et al.*, Eur. Phys. J. **C78**, 943 (2018), [arXiv:1806.08783].
- [101] M. Gronau and D. London, Phys. Rev. Lett. **65**, 3381 (1990).
- [102] A. F. Falk *et al.*, Phys. Rev. **D69**, 011502 (2004), [hep-ph/0310242].
- [103] J. Charles *et al.*, Eur. Phys. J. **C77**, 574 (2017), [arXiv:1705.02981].
- [104] See the review on “Determination of CKM Angles from B hadrons,” in this *Review*.
- [105] A. Abdesselam *et al.* (BaBar, Belle), Phys. Rev. Lett. **115**, 121604 (2015), [arXiv:1505.04147].
- [106] R. Fleischer and R. Knegjens, Eur. Phys. J. **C71**, 1789 (2011), [arXiv:1109.5115].
- [107] A. S. Dighe, I. Dunietz and R. Fleischer, Eur. Phys. J. **C6**, 647 (1999), [hep-ph/9804253].
- [108] R. Aaij *et al.* (LHCb), Phys. Rev. **D89**, 092006 (2014), [arXiv:1402.6248].
- [109] R. Aaij *et al.* (LHCb), JHEP **03**, 075 (2021), [arXiv:2012.05319].
- [110] M. Gronau and D. London, Phys. Lett. **B253**, 483 (1991).
- [111] M. Gronau and D. Wyler, Phys. Lett. **B265**, 172 (1991).
- [112] D. Atwood, I. Dunietz and A. Soni, Phys. Rev. Lett. **78**, 3257 (1997), [hep-ph/9612433].
- [113] D. Atwood, I. Dunietz and A. Soni, Phys. Rev. **D63**, 036005 (2001), [hep-ph/0008090].
- [114] A. Giri *et al.*, Phys. Rev. **D68**, 054018 (2003), [hep-ph/0303187].
- [115] A. Bondar, *Proceedings of BINP special analysis meeting on Dalitz analysis*, 24-26 Sep. 2002, unpublished.
- [116] J. Brod and J. Zupan, JHEP **01**, 051 (2014), [arXiv:1308.5663].
- [117] J. P. Lees *et al.* (BaBar), Phys. Rev. **D87**, 052015 (2013), [arXiv:1301.1029].
- [118] R. Aaij *et al.* (LHCb), JHEP **12**, 087 (2016), [arXiv:1611.03076].
- [119] R. Aleksan, I. Dunietz and B. Kayser, Z. Phys. **C54**, 653 (1992).
- [120] R. Fleischer, Nucl. Phys. **B671**, 459 (2003), [hep-ph/0304027].
- [121] I. Dunietz, Phys. Lett. **B270**, 75 (1991).
- [122] M. Gronau, Phys. Lett. **B557**, 198 (2003), [hep-ph/0211282].
- [123] T. Gershon, Phys. Rev. **D79**, 051301 (2009), [arXiv:0810.2706].
- [124] T. Gershon and M. Williams, Phys. Rev. **D80**, 092002 (2009), [arXiv:0909.1495].
- [125] M. Bander, D. Silverman and A. Soni, Phys. Rev. Lett. **43**, 242 (1979).
- [126] X.-G. He, Eur. Phys. J. **C9**, 443 (1999), [hep-ph/9810397].
- [127] D. Atwood and A. Soni, Phys. Rev. **D58**, 036005 (1998), [hep-ph/9712287].
- [128] M. Gronau and J. L. Rosner, Phys. Rev. **D59**, 113002 (1999), [hep-ph/9809384].
- [129] H. J. Lipkin, Phys. Lett. **B445**, 403 (1999), [hep-ph/9810351].
- [130] M. Gronau, Phys. Lett. **B627**, 82 (2005), [hep-ph/0508047].
- [131] R. Aaij *et al.* (LHCb), Phys. Rev. **D90**, 112004 (2014), [arXiv:1408.5373].
- [132] R. Aaij *et al.* (LHCb) (2019), [arXiv:1905.09244].
- [133] R. Aaij *et al.* (LHCb), Phys. Rev. Lett. **124**, 031801 (2020), [arXiv:1909.05211].
- [134] R. Aaij *et al.* (LHCb), Phys. Rev. **D101**, 012006 (2020), [arXiv:1909.05212].
- [135] A. A. Alves, Jr. *et al.* (LHCb), JINST **3**, S08005 (2008).
- [136] I. Bediaga *et al.* (LHCb) (2012), CERN-LHCC-2012-007.
- [137] R. Aaij *et al.* (LHCb) (2017), CERN-LHCC-2017-003.
- [138] W. Altmannshofer *et al.* (Belle-II), PTEP **2019**, 123C01 (2019), [Erratum-ibid. **2020**, 029201 (2020)], [arXiv:1808.10567].
- [139] G. C. Branco, L. Lavoura and J. P. Silva, Int. Ser. Monogr. Phys. **103**, 1 (1999).
- [140] I. I. Bigi and A. I. Sanda (2000), [Camb. Monogr. Part. Phys. Nucl. Phys. Cosmol. **9**, 1(2009)].
- [141] A. J. Bevan *et al.* (BaBar, Belle), Eur. Phys. J. **C74**, 3026 (2014), [arXiv:1406.6311].
- [142] H.R. Quinn and Y. Nir, “*The Mystery of the Missing Antimatter*,” Princeton University Press, Princeton (2008).
- [143] T. E. Browder *et al.*, Rev. Mod. Phys. **81**, 1887 (2009), [arXiv:0802.3201].
- [144] M. Ciuchini and A. Stocchi, Ann. Rev. Nucl. Part. Sci. **61**, 491 (2011), [arXiv:1110.3920].
- [145] R. Aaij *et al.* (LHCb), Eur. Phys. J. **C73**, 2373 (2013), [arXiv:1208.3355].
- [146] T. Gershon and V. V. Gligorov, Rept. Prog. Phys. **80**, 046201 (2017), [arXiv:1607.06746].

14. Neutrino Masses, Mixing, and Oscillations

Revised October 2021 by M.C. Gonzalez-Garcia (YITP, Stony Brook; ICREA, Barcelona; ICC, U. of Barcelona) and M. Yokoyama (UTokyo; Kavli IPMU (WPI), UTokyo).

14.1	Neutrinos in the Standard Model: Massless Neutrinos	285
14.2	Extending the Standard Model to Introduce Massive Neutrinos	285
14.2.1	Dirac Neutrinos	286
14.2.2	The See-saw Mechanism	286
14.2.3	Light Sterile Neutrinos	287
14.2.4	Neutrino Masses from Generic New Physics	287
14.3	Lepton Mixing	287
14.4	Mass-Induced Flavour Oscillations in Vacuum	288
14.5	Propagation of Massive Neutrinos in Matter	289
14.5.1	The Mikheyev-Smirnov-Wolfenstein Effect for Solar Neutrinos	291
14.6	Experimental Study of Neutrino Oscillations	291
14.6.1	Solar Neutrinos	292
14.6.2	Atmospheric Neutrinos	293
14.6.3	Accelerator Neutrinos	294
14.6.4	Reactor Antineutrinos	298
14.7	Combined Analysis of Experimental Results: The 3ν Paradigm	300
14.7.1	3ν Oscillation Probabilities	301
14.7.2	3ν Oscillation Analysis	302
14.7.3	Convention-independent Measures of Leptonic CP Violation in 3ν Mixing	302
14.8	Beyond 3ν : Additional Neutrinos at the eV Scale	304
14.9	Laboratory Probes of ν Mass Scale and its Nature	305
14.9.1	Constraints from Kinematics of Weak Decays	305
14.9.2	Dirac vs. Majorana: Neutrinoless Double-beta Decay	307
14.9.3	Experimental Search for Neutrinoless Double-beta Decay	307

14.1 Neutrinos in the Standard Model: Massless Neutrinos

The gauge symmetry principle is one of the pillars of the great success of modern particle physics as it establishes an unambiguous connection between local (gauge) symmetries and forces mediated by spin-1 particles. In the Standard Model (SM) of particle physics the strong, weak, and electromagnetic interactions are connected to gauge symmetry under $SU(3)_C \times SU(2)_L \times U(1)_Y$ where C stands for colour, L for left-handedness, and Y for hypercharge. The SM gauge symmetry is spontaneously broken to $SU(3)_C \times U(1)_{EM}$ where $U(1)_{EM}$ couples to the electromagnetic charge $Q_{EM} = T_{L3} + Y$ (T_{L3} is the weak isospin which is the third generator of $SU(2)_L$). The model explains all the interactions of the known fermions once they are assigned to a well defined representation of the gauge group. The construction and tests of the Standard Model as a gauge theory are covered in Chapter 9 “Quantum chromodynamics” and Chapter 10 “Electroweak model and constraints on new physics” of this *Review*. Here we emphasize that the gauge invariance principle requires that all terms in the Lagrangian, including the mass terms, respect the local symmetry. This has important implications for the neutrino and in particular for the question of the neutrino mass ¹.

In the SM, neutrinos are fermions that do not have strong nor electromagnetic interactions. Consequently, they are singlets of the subgroup $SU(3)_C \times U(1)_{EM}$. They are part of the lepton doublets $L_{L\ell} = \begin{pmatrix} \nu_\ell \\ \ell \end{pmatrix}_L$ where f_L is the left-handed component of the fermion f , $f_L = P_L f \equiv \frac{1-\gamma_5}{2} f$. In what follows we will refer as *active* neutrinos to neutrinos that are part of these lepton doublets. In the SM there is one active neutrino for each charged

leptons, $\ell = e, \mu, \tau$. $SU(2)_L$ gauge invariance dictates the form of weak charged current (CC) interactions between the neutrinos and their corresponding charged leptons and neutral current (NC) among themselves to be:

$$-\mathcal{L}_{CC} = \frac{g}{\sqrt{2}} \sum_{\ell} \bar{\nu}_{L\ell} \gamma^\mu \ell_L^- W_\mu^+ + \text{h.c.}, \quad (14.1)$$

$$-\mathcal{L}_{NC} = \frac{g}{2 \cos \theta_W} \sum_{\ell} \bar{\nu}_{L\ell} \gamma^\mu \nu_{L\ell} Z_\mu^0. \quad (14.2)$$

In the above equations, g is the coupling constant associated with $SU(2)$ and θ_W is the Weinberg angle. Equations(14.1) and (14.2) describe all the neutrino interactions in the SM. In particular, Eq.(14.2) determines the decay width of the Z boson into light ($m_\nu \leq m_Z/2$) left-handed neutrinos states. Thus from the measurement of the total decay width of the Z one can infer the number of such states. At present the measurement implies $N_\nu = 2.984 \pm 0.008$ (see Particle Listing). As a result any extension of the SM should contain three, and only three, light active neutrinos.

Sterile neutrinos are defined as having no SM gauge interactions, that is, they are singlets of the complete SM gauge group. Thus the SM, as the gauge theory able to describe all known particle interactions, contains no sterile neutrinos.

The SM with its gauge symmetry and the particle content required for the gauge interactions, that is, in the absence of SM singlets, respects an accidental global symmetry that is not imposed but appears as a consequence of the gauge symmetry and the representation of the matter fields:

$$G_{SM}^{\text{global}} = U(1)_B \times U(1)_{L_e} \times U(1)_{L_\mu} \times U(1)_{L_\tau}, \quad (14.3)$$

where $U(1)_B$ is the baryon number symmetry, and $U(1)_{L_e, L_\mu, L_\tau}$ are the three lepton flavour symmetries. The total lepton number, $L_e + L_\mu + L_\tau$, is then also an accidental symmetry since it is a subgroup of G_{SM}^{global} . This fact has consequences that are relevant to the question of the neutrino mass as we argue next.

In the SM, the masses of the fermions are generated via a Yukawa coupling of the scalar Higgs doublet ϕ with a fermion right-handed and left-handed component. The former is an $SU(2)_L$ singlet, the latter is part of a doublet. For leptons, we can build such a term coupling the left-handed lepton doublets L_L with the right-handed charged lepton fields E_R :

$$-\mathcal{L}_{\text{Yukawa,lep}} = Y_{ij}^\ell \bar{L}_{Li} \phi E_{Rj} + \text{h.c.} \quad (14.4)$$

After spontaneous symmetry breaking these terms lead to charged lepton masses

$$m_{ij}^\ell = Y_{ij}^\ell \frac{v}{\sqrt{2}}, \quad (14.5)$$

where v is the vacuum expectation value of the Higgs field. However, since the model does not contain right-handed neutrinos, no such Yukawa interaction can be built for the neutrinos, which are consequently massless at the Lagrangian level.

In principle, a neutrino mass term could be generated at loop level. With the particle content of the SM the only possible neutrino mass term that could be constructed is the bilinear $\bar{L}_L L_L^c$, where L_L^c is the charge conjugated field, $L_L^c = C \bar{L}_L^T$ and C is the charge conjugation matrix. However this term is forbidden in the SM because it violates the total lepton symmetry by two units and therefore it cannot be induced by loop corrections because it breaks the accidental symmetry of the model. Also, because $U(1)_{B-L}$ is a non-anomalous subgroup of G_{SM}^{global} , the bilinear $\bar{L}_L L_L^c$, cannot be induced by nonperturbative corrections either since it breaks $B - L$.

We conclude that within the SM neutrinos are precisely massless. Consequently one must go beyond the SM in order to add a mass to the neutrino.

14.2 Extending the Standard Model to Introduce Massive Neutrinos

From the above discussion, we conclude that it is not possible to construct a renormalizable mass term for the neutrinos with the

¹The physics of massive neutrinos has been the subject of excellent books such as [1–5] and multiple review articles. The contents of the present review is built upon the structure and the contents of the review articles [6, 7].

fermionic content and gauge symmetry of the SM. The obvious consequence is that in order to introduce a neutrino mass in the theory one must extend the particle content of the model, depart from gauge invariance and/or renormalizability, or do both.

As a matter of fact, neutrino mass terms can be constructed in different ways. In the following we shall assume to maintain the gauge symmetry and explore the different possibilities to introduce a neutrino mass term adding to the SM an arbitrary number of sterile neutrinos ν_{si} ($i = 1, \dots, m$).

In the SM extended with the addition of m number of sterile neutrinos one can construct two gauge invariant renormalizable operators leading to two types of mass terms

$$-\mathcal{L}_{M_\nu} = M_{Dij} \bar{\nu}_{si} \nu_{Lj} + \frac{1}{2} M_{Nij} \bar{\nu}_{si} \nu_{sj}^c + \text{h.c.}, \quad (14.6)$$

where ν^c is the neutrino charge conjugated field (defined in section 14.1). M_D is a complex matrix of dimension $m \times 3$ and M_N is a symmetric $m \times m$ matrix.

The first term is generated after spontaneous electroweak symmetry breaking from Yukawa interactions,

$$Y_{ij}^\nu \bar{\nu}_{si} \tilde{\phi}^\dagger L_{Lj} \Rightarrow M_{Dij} = Y_{ij}^\nu \frac{v}{\sqrt{2}}, \quad (14.7)$$

in similarity to Eqs.(14.4) and (14.5) for the charged fermion masses. It is correspondingly called a Dirac mass term. It conserves total lepton number but it can break the lepton flavour number symmetries.

The second term in Eq.(14.6) is a Majorana mass term and it differs from the Dirac mass terms in several relevant aspects. First, it is a singlet of the SM gauge group and, as such, it can appear as a bare mass term in the Lagrangian. Second, since it involves two neutrino fields (right-handed in this case), it breaks lepton number by two units. In general, such a term is not allowed if the neutrinos carry any additive conserved charge.

It is possible to rewrite Eq.(14.6) as:

$$-\mathcal{L}_{M_\nu} = \frac{1}{2} (\bar{\nu}_L^c, \bar{\nu}_s^c) \begin{pmatrix} 0 & M_D^T \\ M_D & M_N \end{pmatrix} \begin{pmatrix} \bar{\nu}_L \\ \bar{\nu}_s^c \end{pmatrix} + \text{h.c.} \equiv \bar{\nu}^c M_\nu \bar{\nu} + \text{h.c.}, \quad (14.8)$$

where $\bar{\nu} = (\bar{\nu}_L, \bar{\nu}_s^c)^T$ is a $(3+m)$ -dimensional vector. The matrix M_ν is complex and symmetric². Thus it can be diagonalized by a unitary matrix V^ν of dimension $(3+m)$, so

$$(V^\nu)^T M_\nu V^\nu = \text{diag}(m_1, m_2, \dots, m_{3+m}). \quad (14.9)$$

One can express the original weak eigenstates in terms of the resulting $3+m$ mass eigenstates

$$\bar{\nu}_{\text{mass}} = (V^\nu)^\dagger \bar{\nu}, \quad (14.10)$$

and in terms of the mass eigenstates, Eq.(14.8) takes the form:

$$\begin{aligned} -\mathcal{L}_{M_\nu} &= \frac{1}{2} \sum_{k=1}^{3+m} m_k (\bar{\nu}_{\text{mass},k}^c \nu_{\text{mass},k} + \bar{\nu}_{\text{mass},k} \nu_{\text{mass},k}^c) \\ &= \frac{1}{2} \sum_{k=1}^{3+m} m_k \bar{\nu}_{Mk} \nu_{Mk}, \end{aligned} \quad (14.11)$$

where

$$\nu_{Mk} = \nu_{\text{mass},k} + \nu_{\text{mass},k}^c = (V^\nu)^\dagger \bar{\nu}_k + (V^\nu)^\dagger \bar{\nu}_k^c. \quad (14.12)$$

So these states obey the Majorana condition

$$\nu_M = \nu_M^c, \quad (14.13)$$

and are referred to as Majorana neutrinos. The Majorana condition implies that only one field describes both neutrino and antineutrino states, unlike the case of a charge of which particles and

²Notice that Eq.(14.8) corresponds to the tree-level neutrino mass matrix. Corrections are induced at the loop level, which in particular lead to non-vanishing $\bar{\nu}_L^c \nu_L$ entry [8].

antiparticles are described by two different fields. So a Majorana neutrino can be described by a two-component spinor unlike the charged fermions, which are Dirac particles, and are represented by four-component spinors.

Inverting Eq.(14.12) we can write the weak-doublet components of the neutrino fields as:

$$\nu_{Li} = P_L \sum_{j=1}^{3+m} V_{ij}^\nu \nu_{Mj} \quad i = 1, 2, 3, \quad (14.14)$$

where P_L is the left projector.

In the following, we will discuss some interesting particular cases of this general framework: light Dirac neutrinos in Sec.14.2.1, and light Majorana neutrinos and the see-saw mechanism in Sec.14.2.2. A special case of the second example is the possibility of light-sterile neutrinos discussed in Sec.14.2.3. In Sec.14.2.4 we shall discuss the effective generation of neutrino masses from non-renormalizable operators (of which the see-saw mechanism is a particular realization).

14.2.1 Dirac Neutrinos

Imposing $M_N = 0$ is equivalent to imposing lepton number symmetry on the model. In doing this only the first term in Eq.(14.6), the Dirac mass term, is allowed. If sterile neutrinos are three ($m = 3$), we can identify them with the right-handed component of a four-spinor neutrino field. In this case the Dirac mass term can be diagonalized with two 3×3 unitary matrices, V^ν and V_R^ν as:

$$V_R^{\nu\dagger} M_D V^\nu = \text{diag}(m_1, m_2, m_3). \quad (14.15)$$

The neutrino mass term can be written as:

$$-\mathcal{L}_{M_\nu} = \sum_{k=1}^3 m_k \bar{\nu}_{Dk} \nu_{Dk}, \quad (14.16)$$

where

$$\nu_{Dk} = (V^\nu)^\dagger \bar{\nu}_L)_k + (V_R^{\nu\dagger} \bar{\nu}_s)_k, \quad (14.17)$$

so the weak-doublet components of the neutrino fields are

$$\nu_{Li} = P_L \sum_{j=1}^3 V_{ij}^\nu \nu_{Dj}. \quad i = 1, 2, 3. \quad (14.18)$$

Let us stress that in this case both the low-energy matter content and the assumed symmetries are different from those of the SM. Consequently, the SM is not even a good low-energy effective theory. Furthermore, this scenario does not explain the fact that neutrinos are much lighter than the corresponding charged fermions, because all acquire their mass via the same mechanism.

14.2.2 The See-saw Mechanism

If the mass eigenvalues of M_N are much higher than the scale of electroweak symmetry breaking v , the diagonalization of M_ν leads to three light neutrinos, ν_l , and m heavy neutrinos, N :

$$-\mathcal{L}_{M_\nu} = \frac{1}{2} \bar{\nu}_l M^l \nu_l + \frac{1}{2} \bar{N} M^h N, \quad (14.19)$$

with

$$M^l \simeq -V_l^T M_D^T M_N^{-1} M_D V_l, \quad M^h \simeq V_h^T M_N V_h, \quad (14.20)$$

and

$$V^\nu \simeq \begin{bmatrix} \left(1 - \frac{1}{2} M_D^\dagger M_N^* - 1 M_N^{-1} M_D\right) V_l & M_D^\dagger M_N^* V_h \\ -M_N^{-1} M_D V_l & \left(1 - \frac{1}{2} M_N^{-1} M_D M_D^\dagger M_N^* - 1\right) V_h \end{bmatrix}, \quad (14.21)$$

where V_l and V_h are 3×3 and $m \times m$ unitary matrices respectively. From Eq.(14.20) we see that the masses of the heavier states are proportional to M_N while those of the lighter ones to M_N^{-1} , hence the name *see-saw mechanism* [9–13]. Also, as seen from Eq.(14.21), the heavy states are mostly right-handed while the light ones are mostly left-handed. Both the light and the heavy neutrinos are Majorana particles. Two well-known examples of extensions of the SM leading to a see-saw mechanism for neutrino masses are SO(10) Grand Unified Theories [10, 11] and left-right symmetry [13].

In this case, the SM is a good effective low energy theory. Indeed the see-saw mechanism is a particular example of a full theory whose low energy effective realization is the SM with three light Majorana neutrinos which we describe in Sec.14.2.4.

14.2.3 Light Sterile Neutrinos

If the scale of some $n_s \leq m$ eigenvalues of M_N are not higher than the electroweak scale, the low energy spectrum contains n_s additional light states with a large admixture of sterile component. As in the case with Dirac Neutrinos, the SM is not a good low energy effective theory: there are more than three ($3+n_s$) light neutrinos, and they are admixtures of doublet and singlet fields. As in the general case, both light and heavy neutrinos are Majorana particles.

14.2.4 Neutrino Masses from Generic New Physics

Under the generic hypothesis that new physics (NP) beyond the SM only manifests itself directly above some scale Λ_{NP} , we can consider that the SM is an effective low energy theory which is valid to describe the physical world at energies well below Λ_{NP} with the same gauge group, fermionic spectrum, and the pattern of spontaneous symmetry breaking of the SM. However, this is an effective theory, holding only till energy below Λ_{NP} , and consequently does not need to be renormalizable. In this case, the low energy Lagrangian can contain non-renormalizable higher dimensional terms whose effect will be suppressed by powers $1/\Lambda_{\text{NP}}^{\text{dim}-4}$.

In this approach, the least suppressed NP effects at low energy are expected to come from $\text{dim}=5$ operators. With the SM fields and gauge symmetry one can only construct the following set of dimension-five terms

$$\mathcal{O}_5 = \frac{Z_{ij}^\nu}{\Lambda_{\text{NP}}} (\bar{L}_{Li} \tilde{\phi}) (\tilde{\phi}^T L_{Lj}^C) + \text{h.c.} \quad (14.22)$$

This set violates (14.3), which poses no problem since, in general, there is no reason for the NP to respect the accidental symmetries of the SM. In particular, it violates the total lepton number by two units, and after spontaneous symmetry breaking it generates a bilinear neutrino field term:

$$-\mathcal{L}_{M_\nu} = \frac{Z_{ij}^\nu}{2} \frac{v^2}{\Lambda_{\text{NP}}} \bar{\nu}_{Li} \nu_{Lj}^c + \text{h.c.} \quad (14.23)$$

This is a Majorana mass term (see Eq.(14.8)). It is built with the left-handed neutrino fields and with mass matrix:

$$(M_\nu)_{ij} = Z_{ij}^\nu \frac{v^2}{\Lambda_{\text{NP}}}. \quad (14.24)$$

We conclude that Eq.(14.24) would arise in a generic extension of the SM and that neutrino masses are very likely to appear if there is NP. Comparing Eq.(14.24) and Eq.(14.5), we also find that the scale of neutrino masses is suppressed by v/Λ_{NP} when compared to the scale of charged fermion masses, which provides an explanation for their smallness. Furthermore, both total lepton number and the lepton flavour symmetry $U(1)_e \times U(1)_\mu \times U(1)_\tau$ are broken by Eq.(14.24), which means that, generically, in the absence of additional symmetries on the coefficients Z_{ij} , we can expect lepton flavour mixing and CP violation as we discuss in the next section.

Finally, we notice that, as mentioned in Sec.14.2.2, a theory where the NP is composed of m heavy sterile neutrinos, provides an specific example of a theory which at low energy theory contains three light mass eigenstates with an effective dim-5 interaction of the form (14.22) with $\Lambda_{\text{NP}} = M_N$. In this case, the NP scale is the characteristic mass scale of the heavy sterile neutrinos.

14.3 Lepton Mixing

Let us start by considering $n = 3 + m$ massive neutrino states and denote the neutrino mass eigenstates by $(\nu_1, \nu_2, \nu_3, \dots, \nu_n)$. The neutrino interaction eigenstates are denoted by $\vec{\nu} = (\nu_{Le}, \nu_{L\mu}, \nu_{L\tau}, \nu_{s1}, \dots, \nu_{sm})$. We label the corresponding mass and interaction eigenstates for the charged leptons as (e, μ, τ) and (e^I, μ^I, τ^I) , respectively. The Lagrangian for the leptonic charged current interactions in the mass basis takes the form:

$$-\mathcal{L}_{\text{CC}} = \frac{g}{\sqrt{2}} (\bar{e}_L, \bar{\mu}_L, \bar{\tau}_L) \gamma^\mu U \begin{pmatrix} \nu_1 \\ \nu_2 \\ \nu_3 \\ \vdots \\ \nu_n \end{pmatrix} W_\mu^+ + \text{h.c.}, \quad (14.25)$$

where U is a $3 \times n$ matrix [14–16]. It satisfies the unitary condition

$$UU^\dagger = I_{3 \times 3}. \quad (14.26)$$

However, in general $U^\dagger U \neq I_{n \times n}$.

In the interaction basis, the mass terms for the leptons are:

$$-\mathcal{L}_M = [(\bar{e}_L^I, \bar{\mu}_L^I, \bar{\tau}_L^I) M_\ell \begin{pmatrix} e_R^I \\ \mu_R^I \\ \tau_R^I \end{pmatrix} + \text{h.c.}] - \mathcal{L}_{M_\nu}, \quad (14.27)$$

with \mathcal{L}_{M_ν} given in Eq.(14.8). M_ℓ can be diagonalized with two 3×3 unitary matrices V^ℓ and V_R^ℓ which satisfy

$$V^{\ell\dagger} M_\ell V_R^\ell = \text{diag}(m_e, m_\mu, m_\tau). \quad (14.28)$$

Then for the charged leptons we have

$$-\mathcal{L}_{M_\ell} = \sum_{k=1}^3 m_{\ell_k} \bar{\ell}_k \ell_k, \quad (14.29)$$

with

$$\ell_k = (V^{\ell\dagger} \ell_L^I)_k + (V_R^\ell \ell_R^I)_k. \quad (14.30)$$

Inverting the equation above we find that the weak-doublet components of the charged lepton fields are

$$\ell_{Li}^I = P_L \sum_{j=1}^3 V_{ij}^\ell \ell_j. \quad i = 1, 2, 3 \quad (14.31)$$

From Eqs.(14.14), (14.18) and (14.31) we find that the mixing matrix U can be expressed as:

$$U_{ij} = \mathcal{P}_{\ell,ii} V_{ik}^{\ell\dagger} V_{kj}^\nu (\mathcal{P}_{\nu,jj}). \quad (14.32)$$

The matrix $V^{\ell\dagger} V^\nu$ contains a number of phases that are not physical. Three of them are eliminated by the diagonal 3×3 phase matrix \mathcal{P}_ℓ that absorbs them in the charged lepton mass eigenstates. If neutrinos are Dirac states, further $n - 1$ are similarly eliminated by absorbing them in the neutrino mass eigenstates with the diagonal $n \times n$ phase matrix \mathcal{P}_ν . For Majorana neutrinos, $\mathcal{P}_\nu = I_{n \times n}$ because one cannot rotate by an arbitrary phase a Majorana field without physical effects. If one rotates a Majorana neutrino by a phase, this phase will appear in its mass term, which will no longer be real. Consequently, the number of phases that can be absorbed by redefining the mass eigenstates

depends on whether the neutrinos are Dirac or Majorana particles. Altogether for $n \geq 3$ Majorana [Dirac] neutrinos, the U matrix contains a total of $6(n-2)$ [$5n-11$] real parameters, of which $3(n-2)$ are angles, and $3(n-2)$ [$2n-5$] can be interpreted as physical phases.

The possibility of arbitrary mixing between massive neutrino states was first discussed in the context of two neutrinos introduced in Ref. [17] (the possibility of two mixed massless flavour neutrino states had been previously considered in the literature [18], and the possibility of mixing between neutrino and antineu-

trino states even earlier, in the seminal paper of Pontecorvo [19]). For that case, in which only mixing between two generations is considered with $n=2$ distinct neutrino masses, the U matrix is 2×2 and contains one mixing angle if the neutrinos are Dirac and an additional physical phase if they are Majorana.

If there are only $n=3$ Majorana neutrinos, U is a 3×3 matrix analogous to the CKM matrix for the quarks [20, 21], but due to the Majorana nature of the neutrinos it depends on six independent parameters: three mixing angles and three phases. In this case the mixing matrix can be conveniently parameterized as:

$$U = \begin{pmatrix} 1 & 0 & 0 \\ 0 & c_{23} & s_{23} \\ 0 & -s_{23} & c_{23} \end{pmatrix} \cdot \begin{pmatrix} c_{13} & 0 & s_{13}e^{-i\delta_{\text{CP}}} \\ 0 & 1 & 0 \\ -s_{13}e^{i\delta_{\text{CP}}} & 0 & c_{13} \end{pmatrix} \cdot \begin{pmatrix} c_{12} & s_{12} & 0 \\ -s_{12} & c_{12} & 0 \\ 0 & 0 & 1 \end{pmatrix} \cdot \begin{pmatrix} e^{i\eta_1} & 0 & 0 \\ 0 & e^{i\eta_2} & 0 \\ 0 & 0 & 1 \end{pmatrix}, \quad (14.33)$$

where $c_{ij} \equiv \cos \theta_{ij}$ and $s_{ij} \equiv \sin \theta_{ij}$. The angles θ_{ij} can be taken without loss of generality to lie in the first quadrant, $\theta_{ij} \in [0, \pi/2]$ and the phases $\delta_{\text{CP}}, \eta_i \in [0, 2\pi]$. This is to be compared to the case of three Dirac neutrinos. In this case, the Majorana phases,

η_1 and η_2 , can be absorbed in the neutrino states so the number of physical phases is one (similar to the CKM matrix). Thus we can write U as:

$$U = \begin{pmatrix} c_{12}c_{13} & s_{12}c_{13} & s_{13}e^{-i\delta_{\text{CP}}} \\ -s_{12}c_{23} - c_{12}s_{13}s_{23}e^{i\delta_{\text{CP}}} & c_{12}c_{23} - s_{12}s_{13}s_{23}e^{i\delta_{\text{CP}}} & c_{13}s_{23} \\ s_{12}s_{23} - c_{12}s_{13}c_{23}e^{i\delta_{\text{CP}}} & -c_{12}s_{23} - s_{12}s_{13}c_{23}e^{i\delta_{\text{CP}}} & c_{13}c_{23} \end{pmatrix}. \quad (14.34)$$

This matrix is often called the Pontecorvo-Maki-Nakagawa-Sakata (PMNS) mixing matrix.

Notice that when the charged leptons have no other interactions than the SM ones, one can identify their interaction eigenstates with the corresponding mass eigenstates up to phase redefinition. This implies that, in this case, U is just a $3 \times n$ sub-matrix of the unitary neutrino mass diagonalizing matrix V^ν .

Finally, let us point out that for the case of 3 light Dirac neutrinos, the procedure above leads to a unitary U matrix for the light states. But for three light Majorana neutrinos, this is not the case when the full spectrum contains states which are heavy and are not in the low energy spectrum as seen, for example, in Eq.(14.21). This implies that, strictly speaking, the parametrization in Eq.(14.33) is not valid to describe the flavour mixing of the three light Majorana neutrinos in the see-saw mechanism. The violation of unitarity, however, is rather small, of the order $\mathcal{O}(M_D/M_N)$ as seen in Eq.(14.21). It is also severely constrained experimentally [22, 23]. For all these reasons, for all practical purposes, we will consider the U matrix for the 3ν mixing case to be unitary independently of whether neutrinos are Dirac or Majorana particles.

14.4 Mass-Induced Flavour Oscillations in Vacuum

If neutrinos have masses and lepton flavours are mixed in the weak CC interactions, lepton flavour is not conserved in neutrino propagation [19, 24]. This phenomenon is usually referred to as *neutrino oscillations*. In brief, a weak eigenstates, ν_α , which by default is the state produced in the weak CC interaction of a charged lepton ℓ_α , is the linear combination determined by the mixing matrix U

$$|\nu_\alpha\rangle = \sum_{i=1}^n U_{\alpha i}^* |\nu_i\rangle, \quad (14.35)$$

where ν_i are the mass eigenstates, and here n is the number of light neutrino species (implicit in our definition of the state $|\nu\rangle$ is its energy-momentum and space-time dependence). After traveling a distance L ($L \simeq ct$ for relativistic neutrinos), that state evolves as:

$$|\nu_\alpha(t)\rangle = \sum_{i=1}^n U_{\alpha i}^* |\nu_i(t)\rangle. \quad (14.36)$$

This neutrino can then undergo a charged-current (CC) interaction producing a charge lepton ℓ_β , $\nu_\alpha(t)N' \rightarrow \ell_\beta N$, with a

probability

$$P_{\alpha\beta} = |\langle \nu_\beta | \nu_\alpha(t) \rangle|^2 = \left| \sum_{i=1}^n \sum_{j=1}^n U_{\alpha i}^* U_{\beta j} \langle \nu_j | \nu_i(t) \rangle \right|^2. \quad (14.37)$$

Assuming that $|\nu\rangle$ is a plane wave, $|\nu_i(t)\rangle = e^{-iE_i t} |\nu_i(0)\rangle$,³ with $E_i = \sqrt{p_i^2 + m_i^2}$ and m_i being, respectively, the energy and the mass of the neutrino mass eigenstate ν_i . In all practical cases neutrinos are very relativistic, so $p_i \simeq p_j \equiv p \simeq E$. We can then write

$$E_i = \sqrt{p_i^2 + m_i^2} \simeq p + \frac{m_i^2}{2E}, \quad (14.38)$$

and use the orthogonality of the mass eigenstates, $\langle \nu_j | \nu_i \rangle = \delta_{ij}$, to arrive to the following form for $P_{\alpha\beta}$:

$$P_{\alpha\beta} = \delta_{\alpha\beta} - 4 \sum_{i<j} \text{Re}[U_{\alpha i} U_{\beta i}^* U_{\alpha j}^* U_{\beta j}] \sin^2 X_{ij} + 2 \sum_{i<j} \text{Im}[U_{\alpha i} U_{\beta i}^* U_{\alpha j}^* U_{\beta j}] \sin 2X_{ij}, \quad (14.39)$$

where

$$X_{ij} = \frac{(m_i^2 - m_j^2)L}{4E} = 1.267 \frac{\Delta m_{ij}^2}{\text{eV}^2} \frac{L/E}{\text{m/MeV}}. \quad (14.40)$$

If we had made the same derivation for antineutrino states, we would have ended with a similar expression but with the exchange $U \rightarrow U^*$. Consequently, we conclude that the first term in the right-hand-side of Eq.(14.39) is CP conserving since it is the same for neutrinos and antineutrinos, while the last one is CP violating because it has opposite signs for neutrinos and antineutrinos.

Equation (14.39) is oscillatory in distance with oscillation lengths

$$L_{0,ij}^{\text{osc}} = \frac{4\pi E}{|\Delta m_{ij}^2|}, \quad (14.41)$$

and with amplitudes proportional to products of elements in the mixing matrix. Thus, neutrinos must have different masses

³ For a pedagogical discussion of the quantum mechanical description of flavour oscillations in the wave package approach see for example Ref. [3]. A recent review of the quantum mechanical aspects and subtleties on neutrino oscillations can be found in Ref. [25].

Table 14.1: Characteristic values of L and E for experiments performed using various neutrino sources and the corresponding ranges of $|\Delta m^2|$ to which they can be most sensitive to flavour oscillations in vacuum. SBL stands for Short Baseline, VSBL stands for Very Short Baseline, MBL stands for Medium Baseline, and LBL for Long Baseline.

Experiment		L (m)	E (MeV)	$ \Delta m^2 $ (eV^2)
Solar		10^{10}	1	10^{-10}
Atmospheric		$10^4 - 10^7$	$10^2 - 10^5$	$10^{-1} - 10^{-4}$
Reactor	VSBL-SBL-MBL	$10 - 10^3$	1	$1 - 10^{-3}$
	LBL	$10^4 - 10^5$		$10^{-4} - 10^{-5}$
Accelerator	SBL	10^2	$10^3 - 10^4$	> 0.1
	LBL	$10^5 - 10^6$	$10^3 - 10^4$	$10^{-2} - 10^{-3}$

($\Delta m_{ij}^2 \neq 0$) and they must have not vanishing mixing ($U_{\alpha i} U_{\beta i} \neq 0$) in order to undergo flavour oscillations. Also, from Eq.(14.39) we see that the Majorana phases cancel out in the oscillation probability. This is expected because flavour oscillation is a total lepton number conserving process.

Ideally, a neutrino oscillation experiment would like to measure an oscillation probability over a distance L between the source and the detector, for neutrinos of a definite energy E . In practice, neutrino beams, both from natural or artificial sources, are never monoenergetic but have an energy spectrum $\Phi(E)$. In addition, each detector has a finite energy resolution. Under these circumstances what is measured is an average probability

$$\begin{aligned} \langle P_{\alpha\beta} \rangle &= \frac{\int dE \frac{d\Phi}{dE} \sigma(E) P_{\alpha\beta}(E) \epsilon(E)}{\int dE \frac{d\Phi}{dE} \sigma_{CC}(E) \epsilon(E)} \\ &= \delta_{\alpha\beta} - 4 \sum_{i < j}^n \text{Re}[U_{\alpha i} U_{\beta i}^* U_{\alpha j}^* U_{\beta j}] \langle \sin^2 X_{ij} \rangle \\ &\quad + 2 \sum_{i < j}^n \text{Im}[U_{\alpha i} U_{\beta i}^* U_{\alpha j}^* U_{\beta j}] \langle \sin 2X_{ij} \rangle. \end{aligned} \quad (14.42)$$

σ is the cross-section for the process in which the neutrino flavour is detected, and $\epsilon(E)$ is the detection efficiency. The minimal range of the energy integral is determined by the energy resolution of the experiment.

It is clear from the above expression that if $(E/L) \gg |\Delta m_{ij}^2|$ ($L \ll L_{0,ij}^{\text{osc}}$) so $\sin^2 X_{ij} \ll 1$, the oscillation phase does not give any appreciable effect. Conversely, if $L \gg L_{0,ij}^{\text{osc}}$, many oscillation cycles occur between production and detection, so the oscillating term is averaged to $\langle \sin^2 X_{ij} \rangle = 1/2$.

We summarize in Table 14.1 the typical values of L/E for different types of neutrino sources and experiments and the corresponding ranges of Δm^2 to which they can be most sensitive.

Historically, the results of neutrino oscillation experiments were interpreted assuming two-neutrino states so there is only one oscillating phase; the mixing matrix depends on a single mixing angle θ , and no CP violation effect in oscillations is possible. At present, as we will discuss in Sec.14.7, we need at least the mixing among three-neutrino states to fully describe the bulk of experimental results. However, in many cases, the observed results can be understood in terms of oscillations dominantly driven by one Δm^2 . In this limit $P_{\alpha\beta}$ of Eq.(14.39) takes the form [24]

$$P_{\alpha\beta} = \delta_{\alpha\beta} - (2\delta_{\alpha\beta} - 1) \sin^2 2\theta \sin^2 X. \quad (14.43)$$

In this effective $2 - \nu$ limit, changing the sign of the mass difference, $\Delta m^2 \rightarrow -\Delta m^2$, and changing the octant of the mixing angle, $\theta \rightarrow \frac{\pi}{2} - \theta$, is just redefining the mass eigenstates, $\nu_1 \leftrightarrow \nu_2$: $P_{\alpha\beta}$ must be invariant under such transformation. So the physical parameter space can be covered with either $\Delta m^2 \geq 0$ with $0 \leq \theta \leq \frac{\pi}{2}$, or, alternatively, $0 \leq \theta \leq \frac{\pi}{4}$ with either sign for Δm^2 .

However, from Eq.(14.43) we see that $P_{\alpha\beta}$ is actually invariant under the change of sign of the mass splitting and the change of octant of the mixing angle separately. This implies that there is a two-fold discrete ambiguity since the two different sets of physical parameters, $(\Delta m^2, \theta)$ and $(\Delta m^2, \frac{\pi}{2} - \theta)$, give the same

transition probability in vacuum. In other words, one could not tell from a measurement of, say, $P_{e\mu}$ in vacuum whether the larger component of ν_e resides in the heavier or in the lighter neutrino mass eigenstate. This symmetry is broken when one considers mixing of three or more neutrinos in the flavour evolution and or when the neutrinos traverse regions of dense matter as we describe in Sec.14.7.1 and Sec.14.5, respectively.

14.5 Propagation of Massive Neutrinos in Matter

Neutrinos propagating in a dense medium can interact with the particles in the medium. The probability of an incoherent inelastic scattering is very small. For example the characteristic cross section for ν -proton scattering is of the order

$$\sigma \sim \frac{G_F^2 s}{\pi} \sim 10^{-43} \text{ cm}^2 \left(\frac{E}{\text{MeV}} \right)^2, \quad (14.44)$$

where G_F is the Fermi constant and s is the square of the center of mass energy of the collision.

But when neutrinos propagate in dense matter, they can also interact coherently with the particles in the medium. By definition, in coherent interactions, the medium remains unchanged so it is possible to have interference of the forward scattered and the unscattered neutrino waves which enhances the effect of matter in the neutrino propagation. In this case, the effect of the medium is not on the intensity of the propagating neutrino beam, which remains unchanged, but on the phase velocity of the neutrino wave, and for this reason the effect is proportional to G_F , instead of the G_F^2 dependence of the incoherent scattering. Coherence also allows decoupling the evolution equation of the neutrinos from those of the medium. In this limit, the effect of the medium is introduced in the evolution equation for the neutrinos in the form of an effective potential which depends on the density and composition of the matter [26].

As an example, let us consider the evolution of ν_e in a medium with electrons, protons, and neutrons with corresponding n_e , n_p , and n_n number densities. The effective low-energy Hamiltonian describing the relevant neutrino interactions at point x is given by

$$H_W = \frac{G_F}{\sqrt{2}} \left[J^{(+)\alpha}(x) J_\alpha^{(-)}(x) + \frac{1}{4} J^{(N)\alpha}(x) J_\alpha^{(N)}(x) \right], \quad (14.45)$$

where the J_α 's are the standard fermionic currents

$$J_\alpha^{(+)}(x) = \bar{\nu}_e(x) \gamma_\alpha (1 - \gamma_5) e(x), \quad (14.46)$$

$$J_\alpha^{(-)}(x) = \bar{e}(x) \gamma_\alpha (1 - \gamma_5) \nu_e(x), \quad (14.47)$$

$$\begin{aligned} J_\alpha^{(N)}(x) &= \bar{\nu}_e(x) \gamma_\alpha (1 - \gamma_5) \nu_e(x) \\ &\quad - \bar{e}(x) [\gamma_\alpha (1 - \gamma_5) - 4 \sin^2 \theta_W \gamma_\alpha] e(x) \\ &\quad + \bar{p}(x) [\gamma_\alpha (1 - g_A^{(p)} \gamma_5) - 4 \sin^2 \theta_W \gamma_\alpha] p(x) \\ &\quad - \bar{n}(x) \gamma_\alpha (1 - g_A^{(n)} \gamma_5) n(x), \end{aligned} \quad (14.48)$$

and $g_A^{(n,p)}$ are the axial couplings for neutrons and protons, respectively.

Let us focus first on the effect of the charged current inter-

actions. The effective CC Hamiltonian due to electrons in the medium is

$$\begin{aligned} H_C^{(e)} &= \frac{G_F}{\sqrt{2}} \int d^3 p_e f(E_e, T) \times \left\langle \langle e(s, p_e) | \bar{e}(x) \gamma^\alpha (1 - \gamma_5) \nu_e(x) \bar{\nu}_e(x) \gamma_\alpha (1 - \gamma_5) e(x) | e(s, p_e) \rangle \right\rangle \\ &= \frac{G_F}{\sqrt{2}} \bar{\nu}_e(x) \gamma_\alpha (1 - \gamma_5) \nu_e(x) \int d^3 p_e f(E_e, T) \left\langle \langle e(s, p_e) | \bar{e}(x) \gamma_\alpha (1 - \gamma_5) e(x) | e(s, p_e) \rangle \right\rangle. \end{aligned} \quad (14.49)$$

In the above equation, we denote by s the electron spin, and by p_e its momentum, and $f(E_e, T)$ is the energy distribution function of the electrons in the medium which is assumed to be homogeneous and isotropic and is normalized as

$$\int d^3 p_e f(E_e, T) = 1. \quad (14.50)$$

We denote by $\langle \dots \rangle$ the averaging over electron spinors and summing over all electrons in the medium. Coherence dictates that s, p_e are the same for initial and final electrons. The axial current reduces to the spin in the non-relativistic limit and therefore averages to zero for a background of non-relativistic electrons. The spatial components of the vector current cancel because of isotropy. Therefore, the only non-trivial average is

$$\int d^3 p_e f(E_e, T) \left\langle \langle e(s, p_e) | \bar{e}(x) \gamma_0 e(x) | e(s, p_e) \rangle \right\rangle = n_e(x), \quad (14.51)$$

which gives a contribution to the effective Hamiltonian

$$H_C^{(e)} = \sqrt{2} G_F n_e \bar{\nu}_{eL}(x) \gamma_0 \nu_{eL}(x). \quad (14.52)$$

This can be interpreted as a contribution to the ν_{eL} potential energy

$$V_C = \sqrt{2} G_F n_e. \quad (14.53)$$

Should we have considered antineutrino states, we would have ended up with $V_C = -\sqrt{2} G_F n_e$. For a more detailed derivation of the matter potentials see, for example, Ref. [3].

With an equivalent derivation, we find that for ν_μ and ν_τ , the potential due to its CC interactions is zero for most media since neither μ 's nor τ 's are present, while the effective potential for any active neutrino due to the neutral current interactions is found to be

$$V_{NC} = \frac{\sqrt{2}}{2} G_F [-n_e(1 - 4 \sin^2 \theta_w) + n_p(1 - 4 \sin^2 \theta_w) - n_n]. \quad (14.54)$$

In neutral matter, $n_e = n_p$ and the contribution from electrons and protons cancel each other. So we are left only with the neutron contribution

$$V_{NC} = -1/\sqrt{2} G_F n_n. \quad (14.55)$$

After including these effects, the evolution equation for n ultrarelativistic neutrinos propagating in matter written in the mass basis is (see for instance Ref. [27–29] for the derivation):

$$i \frac{d\vec{\nu}}{dx} = H \vec{\nu}, \quad H = H_m + U^{\nu\dagger} V U^\nu. \quad (14.56)$$

Here $\vec{\nu} \equiv (\nu_1, \nu_2, \dots, \nu_n)^T$, H_m is the kinetic Hamiltonian,

$$H_m = \frac{1}{2E} \text{diag}(m_1^2, m_2^2, \dots, m_n^2), \quad (14.57)$$

and V is the effective neutrino potential in the interaction basis. U^ν is the $n \times n$ submatrix of the unitary V^ν matrix corresponding to the n ultrarelativistic neutrino states. For the three SM active neutrinos with purely SM interactions crossing a neutral medium with electrons, protons and neutrons, the evolution equation takes the form (14.56) with $U^\nu \equiv U$, and the effective potential:

$$V = \text{diag}(\pm\sqrt{2} G_F n_e(x), 0, 0) \equiv \text{diag}(V_e, 0, 0). \quad (14.58)$$

The sign $+$ ($-$) in Eq.(14.58) applies to neutrinos (antineutrinos), and $n_e(x)$ is the electron number density in the medium, which in general is not constant along the neutrino trajectory so the potential is not constant. The characteristic value of the potential at the Earth core is $V_e \sim 10^{-13}$ eV, while at the solar core $V_e \sim 10^{-12}$ eV. Since the neutral current potential Eq.(14.55) is flavour diagonal, it can be eliminated from the evolution equation as it only contributes to an overall unobservable phase.

The instantaneous mass eigenstates in matter, ν_i^m , are the eigenstates of the Hamiltonian H in (14.56) for a fixed value of x , and they are related to the interaction basis by

$$\vec{\nu} = \tilde{U}(x) \nu^{\vec{m}}. \quad (14.59)$$

The corresponding instantaneous eigenvalues of H are $\mu_i(x)^2/(2E)$ with $\mu_i(x)$ being the instantaneous effective neutrino masses.

Let us take for simplicity a neutrino state which is an admixture of only two neutrino species $|\nu_\alpha\rangle$ and $|\nu_\beta\rangle$, so the two instantaneous mass eigenstates in matter ν_1^m and ν_2^m have instantaneous effective neutrino masses

$$\mu_{1,2}^2(x) = \frac{m_1^2 + m_2^2}{2} + E[V_\alpha + V_\beta] \quad (14.60)$$

$$\mp \frac{1}{2} \sqrt{[\Delta m^2 \cos 2\theta - A]^2 + [\Delta m^2 \sin 2\theta]^2},$$

and $\tilde{U}(x)$ is a 2x2 rotation matrix with the instantaneous mixing angle in matter given by

$$\tan 2\theta_m = \frac{\Delta m^2 \sin 2\theta}{\Delta m^2 \cos 2\theta - A}. \quad (14.61)$$

In the Eqs.(14.60) and (14.61) A is

$$A \equiv 2E(V_\alpha - V_\beta), \quad (14.62)$$

and its sign depends on the composition of the medium and on the flavour composition of the neutrino state considered. From the expressions above, we see that for a given sign of A the mixing angle in matter is larger(smaller) than in vacuum if this last one is in the first (second) octant. We see that the symmetry about $\theta = 45^\circ$ which exists in vacuum oscillations between two neutrino states is broken by the matter potential in propagation in a medium. The expressions above show that significant effects are present when A , is close to $\Delta m^2 \cos 2\theta$. In particular, as seen in Eq.(14.61), the tangent of the mixing angle changes sign if, along its path, the neutrino passes by some matter density region satisfying, for its energy, the *resonance condition*

$$A_R = \Delta m^2 \cos 2\theta. \quad (14.63)$$

This implies that if the neutrino is created in a region where the relevant potential satisfies $A_0 > A_R$ (A_0 here is the value of the relevant potential at the production point), then the effective mixing angle in matter at the production point is such that $\text{sgn}(\cos 2\theta_{m,0}) = -\text{sgn}(\cos 2\theta)$. So the flavour component of the mass eigenstates is inverted as compared to their composition in vacuum. In particular, if at the production point we have $A_0 = 2A_R$, then $\theta_{m,0} = \frac{\pi}{2} - \theta$. Asymptotically, for $A_0 \gg A_R$, $\theta_{m,0} \rightarrow \frac{\pi}{2}$. In other words, if in vacuum the lightest (heaviest) mass eigenstate has a larger projection on the flavour α (β), inside a matter with density and composition such that $A > A_R$,

the opposite holds. So if the neutrino system is traveling across a monotonically varying matter potential, the dominant flavour component of a given mass eigenstate changes when crossing the region with $A = A_R$. This phenomenon is known as *level crossing*.

Taking the derivative of Eq.(14.59) with respect to x and using Eq.(14.56), we find that in the instantaneous mass basis the evolution equation reads:

$$i \frac{d\vec{\nu}^m}{dx} = \left[\frac{1}{2E} \text{diag} (\mu_1^2(x), \mu_2^2(x), \dots, \mu_n^2(x)) - i \tilde{U}^\dagger(x) \frac{d\tilde{U}(x)}{dx} \right] \vec{\nu}^m. \quad (14.64)$$

The presence of the last term, Eq.(14.64) implies that this is a system of coupled equations. So, in general, the instantaneous mass eigenstates, ν_i^m are not energy eigenstates. For constant or slowly enough varying matter potential this last term can be neglected and the instantaneous mass eigenstates, ν_i^m , behave approximately as energy eigenstates, and they do not mix in the evolution. This is the *adiabatic* transition approximation. On the contrary, when the last term in Eq.(14.64) cannot be neglected, the instantaneous mass eigenstates mix along the neutrino path. This implies there can be *level-jumping* [30–33], and the evolution is *non-adiabatic*.

For adiabatic evolution in matter, the oscillation probability take a form very similar to the vacuum oscillation expression, Eq.(14.39). For example, neglecting CP violation:

$$P_{\alpha\beta} = \left| \sum_i \tilde{U}_{\alpha i}(0) \tilde{U}_{\beta i}(L) \exp \left(-\frac{i}{2E} \int_0^L \mu_i^2(x') dx' \right) \right|^2. \quad (14.65)$$

To compute $P_{\alpha\beta}$ in a varying potential, one can always solve the evolution equation numerically. Also, several analytic approximations for specific profiles of the matter potential can be found in the literature [34].

14.5.1 The Mikheyev-Smirnov-Wolfenstein Effect for Solar Neutrinos

The matter effects discussed in the previous section are of special relevance for solar neutrinos. As the Sun produces ν_e 's in its core, we consider the propagation of a $\nu_e - \nu_X$ neutrino system (X is some superposition of μ and τ , which is arbitrary because ν_μ and ν_τ have only and equal neutral current interactions) in the matter density of the Sun.

The density of solar matter is a monotonically decreasing function of the distance R from the center of the Sun, and it can be approximated by an exponential for $R < 0.9R_\odot$

$$n_e(R) = n_e(0) \exp(-R/r_0), \quad (14.66)$$

with $r_0 = R_\odot/10.54 = 6.6 \times 10^7 \text{ m} = 3.3 \times 10^{14} \text{ eV}^{-1}$.

As mentioned above, the nuclear reactions in the Sun produce electron neutrinos. After crossing the Sun, the composition of the neutrino state exiting the Sun will depend on the relative size of $\Delta m^2 \cos 2\theta$ versus $A_0 = 2EG_F n_{e,0}$ (where 0 refers to the neutrino production point, which is near but not exactly at the center of the Sun, $R = 0$).

If the relevant matter potential at production is well below the resonant value, $A_R = \Delta m^2 \cos 2\theta \gg A_0$, matter effects are negligible. With the characteristic matter density and energy of the solar neutrinos, this condition is fulfilled for values of Δm^2 such that $\Delta m^2/E \gg L_{\text{Sun-Earth}}$. So the propagation occurs as in vacuum with the oscillating phase averaged to 1/2 and the survival probability at the exposed surface of the Earth is

$$P_{ee}(\Delta m^2 \cos 2\theta \gg A_0) = 1 - \frac{1}{2} \sin^2 2\theta > \frac{1}{2}. \quad (14.67)$$

If the relevant matter potential at production is only slightly below the resonant value, $A_R = \Delta m^2 \cos 2\theta \gtrsim A_0$, the neutrino does not cross a region with resonant density, but matter effects are sizable enough to modify the mixing. The oscillating phase is

averaged in the propagation between the Sun and the Earth. This regime is well described by an adiabatic propagation, Eq.(14.65). Using that $\tilde{U}(0)$ is a 2x2 rotation of angle $\theta_{m,0}$ – the mixing angle in matter at the neutrino production point–, and $\tilde{U}(L)$ is the corresponding rotation with vacuum mixing angle θ , we get

$$P_{ee}(\Delta m^2 \cos 2\theta \geq A_0) = \cos^2 \theta_{m,0} \cos^2 \theta + \sin^2 \theta_{m,0} \sin^2 \theta = \frac{1}{2} [1 + \cos 2\theta_{m,0} \cos 2\theta]. \quad (14.68)$$

This expression reflects that an electron neutrino produced at A_0 is an admixture of ν_1 with fraction $P_{e1,0} = \cos^2 \theta_{m,0}$ and ν_2 with fraction $P_{e2,0} = \sin^2 \theta_{m,0}$. On exiting the Sun, ν_1 consists of ν_e with fraction $P_{1e} = \cos^2 \theta$, and ν_2 consists of ν_e with fraction $P_{2e} = \sin^2 \theta$ so $P_{ee} = P_{e1,0}P_{1e} + P_{e2,0}P_{2e} = \cos^2 \theta_{m,0} \cos^2 \theta + \sin^2 \theta_{m,0} \sin^2 \theta$ [35–37], exactly as given in Eq.(14.68). Since $A_0 < A_R$ the resonance is not crossed so $\cos 2\theta_{m,0}$ has the same sign as $\cos 2\theta$ and still $P_{ee} \geq 1/2$.

Finally, in the case that $A_R = \Delta m^2 \cos 2\theta < A_0$, the neutrino can cross the resonance on its way out. In the convention of $\Delta m^2 > 0$ this occurs if $\cos 2\theta > 0$ ($\theta < \pi/4$). which means that in vacuum ν_e is a combination of ν_1 and ν_2 with a larger ν_1 component, while at the production point ν_e is a combination of ν_1^m and ν_2^m with larger ν_2^m component. In particular, if the density at the production point is much higher than the resonant density, $\Delta m^2 \cos 2\theta \ll A_0$,

$$\theta_{m,0} = \frac{\pi}{2} \Rightarrow \cos 2\theta_{m,0} = -1, \quad (14.69)$$

and the produced ν_e is purely ν_2^m .

In this regime, the evolution of the neutrino ensemble can be adiabatic or non-adiabatic depending on the particular values of Δm^2 and the mixing angle. The oscillation parameters (see Secs.14.6.1 and 14.7) happen to be such that the transition is adiabatic in all ranges of solar neutrino energies. Thus the survival probability at the exposed surface of the Earth is given by Eq.(14.68) but now with mixing angle (14.69) so

$$P_{ee}(\Delta m^2 \cos 2\theta < A_0) = \frac{1}{2} [1 + \cos 2\theta_{m,0} \cos 2\theta] = \sin^2 \theta. \quad (14.70)$$

So, in this case, P_{ee} can be much smaller than 1/2 because $\cos 2\theta_{m,0}$ and $\cos 2\theta$ have opposite signs. This is referred to as the Mikheyev-Smirnov-Wolfenstein (MSW) effect [26, 38], which plays a fundamental role in the interpretation of the solar neutrino data.

The resulting energy dependence of the survival probability of solar neutrinos is shown in Fig.14.3 (together with a compilation of data from solar experiments). The plotted curve corresponds to $\Delta m^2 \sim 7.5 \times 10^{-5} \text{ eV}^2$ and $\sin^2 \theta \sim 0.3$ (the so-called large mixing angle, LMA, solution). The figure illustrates the regimes described above. For these values of the oscillation parameters, neutrinos with $E \ll 1 \text{ MeV}$ are in the regime with $\Delta m^2 \cos 2\theta \gg A_0$ so the curve represents the value of vacuum averaged survival probability, Eq.(14.67), and therefore $P_{ee} > 0.5$. For $E > 10 \text{ MeV}$, on the contrary, $\Delta m^2 \cos 2\theta \ll A_0$ and the survival probability is given by Eq.(14.70), so $P_{ee} = \sin^2 \theta \sim 0.3$. In between, the survival probability is given by Eq.(14.68) with θ_0 changing rapidly from its vacuum value to the asymptotic matter value (14.69), 90° .

14.6 Experimental Study of Neutrino Oscillations

Neutrino flavour transitions, or neutrino oscillations, have been experimentally studied using various neutrino sources and detection techniques. Intense sources and large detectors are mandatory because of a large distance necessary for observable oscillation effects in addition to the tiny cross-sections. Also, the relevant neutrino flux before oscillations should be known with sufficient precision for a definitive measurement. Here, the experimental status of neutrino oscillations with the different neutrino sources: the Sun, Earth's atmosphere, accelerators, and nuclear reactors are reviewed.

14.6.1 Solar Neutrinos

14.6.1.1 Solar neutrino flux

In the Sun, electron neutrinos are produced in the thermonuclear reactions which generate solar energy. These reactions occur via two main chains, the pp chain and the CNO cycle. The pp chain includes reactions $p+p \rightarrow d+e^++\nu$ (pp), $p+e^-+p \rightarrow d+\nu$ (pep), ${}^3\text{He}+p \rightarrow {}^4\text{He}+e^++\nu$ (hep), ${}^7\text{Be}+e^- \rightarrow {}^7\text{Li}+\nu(+\gamma)$ (${}^7\text{Be}$), and ${}^8\text{B} \rightarrow {}^8\text{Be}^*+e^++\nu$ (${}^8\text{B}$). The CNO cycle involves ${}^{13}\text{N} \rightarrow {}^{13}\text{C}+e^++\nu$ (${}^{13}\text{N}$), ${}^{15}\text{O} \rightarrow {}^{15}\text{N}+e^++\nu$ (${}^{15}\text{O}$), and ${}^{17}\text{F} \rightarrow {}^{17}\text{O}+e^++\nu$ (${}^{17}\text{F}$). Those reactions result in the overall fusion of protons into ${}^4\text{He}$, $4p \rightarrow {}^4\text{He}+2e^++2\nu_e$, where the energy released in the reaction, $Q=4m_p-m_{{}^4\text{He}}-2m_e \sim 26$ MeV, is mostly radiated through the photons and only a small fraction is carried by the neutrinos, $(E_{2\nu_e})=0.59$ MeV. In addition, electron capture on ${}^{13}\text{N}$, ${}^{15}\text{O}$, and ${}^{17}\text{F}$ produces line spectra of neutrinos called ecCNO neutrinos. Dividing the solar luminosity by the energy released per neutrino production, the total neutrino flux can be estimated. At Earth, the pp solar neutrino flux is about $6 \times 10^{10} \text{ cm}^{-2}\text{s}^{-1}$.

The solar neutrino flux has been calculated based on the Standard Solar Model (SSM). The SSM describes the structure and evolution of the Sun based on a variety of inputs such as the mass, luminosity, radius, surface temperature, age, and surface elemental abundances. In addition, the knowledge of the absolute nuclear reaction cross sections for relevant fusion reactions and radiative opacities are necessary. John Bahcall and his collaborators continuously updated the SSM calculations over several decades [39,40]. Figure 14.1 shows the solar neutrino fluxes predicted by the SSM calculation in [41] and ecCNO neutrinos in [42].

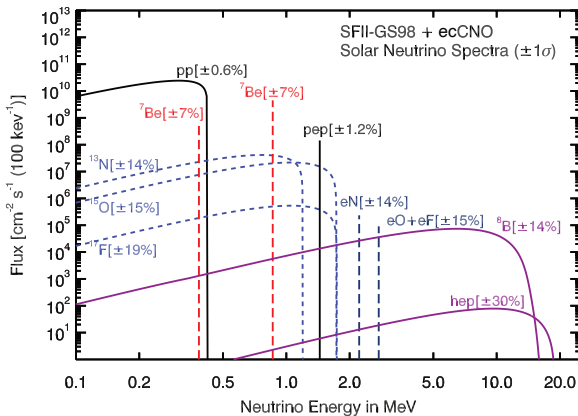


Figure 14.1: Spectrum of solar neutrino fluxes predicted by SSM calculation in [41]. In addition to standard fluxes, ecCNO neutrinos have been added based on [42]. Electron capture fluxes are given in $\text{cm}^{-2}\text{s}^{-1}$. Taken from [43].

14.6.1.2 Detection of solar neutrinos and the solar neutrino problem

Experiments that observed solar neutrinos are summarized in Table 14.2. A pioneering solar neutrino experiment was carried out by R. Davis, Jr. and collaborators at Homestake starting in the late 1960s [44]. The Davis' experiment utilizes the reaction $\nu_e+{}^{37}\text{Cl} \rightarrow e^-+{}^{37}\text{Ar}$. Because this process has an energy threshold of 814 keV, the most relevant fluxes are the ${}^7\text{Be}$ and ${}^8\text{B}$ neutrinos. The detector contained ~ 615 t of C_2Cl_4 . The produced ${}^{37}\text{Ar}$, which has a half-life of 34.8 d, was chemically extracted and introduced into a low-background proportional chamber every few months. The Auger electrons from electron capture of ${}^{37}\text{Ar}$ were counted to determine the reaction rate.

From the beginning, the observed number of neutrinos in the Homestake mine experiment was significantly smaller than the prediction by SSM — it was almost one-third. After thorough checks of both experimental and theoretical work, the discrepancy remained. This became to be known as the solar neutrino problem. The final result from the Homestake experiment is $2.56 \pm 0.16 \pm 0.16$ SNU [45], where SNU (solar neutrino unit)

is a unit of event rate, $1 \text{ SNU} = 10^{-36} \text{ captures}/(\text{s atom})$. On the other hand, prediction based on SSM is $8.46^{+0.87}_{-0.88}$ SNU [46].

The detection of neutrinos from other production processes was recognized as an important input to investigate the origin of the solar neutrino problem. In particular, the pp neutrino is most abundant, and its flux prediction has the smallest uncertainty. Using the radiochemical technique with gallium, the reaction $\nu_e+{}^{71}\text{Ga} \rightarrow e^-+{}^{71}\text{Ge}$ has an energy threshold of 233 keV and can be used for the pp neutrino detection. According to the SSM, more than half of the events on ${}^{71}\text{Ga}$ are due to the pp neutrinos, with the second dominant contribution coming from the ${}^7\text{Be}$ neutrinos. ${}^{71}\text{Ge}$ decays via electron capture with a half-life of 11.4 d. The SAGE experiment in Baksan [47] used about 50 t of liquid metallic gallium as a target. The GALLEX experiment in LNGS [48] used 101 t of GaCl_3 , containing 30.3 t of gallium. Both experiments used natural gallium, containing 39.9% of ${}^{71}\text{Ga}$ isotope. GALLEX was followed by its successor GNO experiment. The measured capture rate is $69.3 \pm 4.1 \pm 3.6$ SNU for GALLEX+GNO [49] and $65.4^{+3.1+2.6}_{-3.0-2.8}$ SNU for SAGE [50]. A SSM prediction is $127.9^{+8.1}_{-8.2}$ SNU [46].

The radiochemical detectors measure the reaction rate integrated between extractions. The real-time measurement of solar neutrinos was realized by the Kamiokande experiment [51]. The Kamiokande detector was a 3,000-t water-Cherenkov detector in the Kamioka mine. Super-Kamiokande, the successor of Kamiokande, started operation in April 1996. It is a large upright cylindrical water Cherenkov detector containing 50 kt of pure water⁴. An inner detector volume corresponding to 32 kt water mass is viewed by more than 11,000 inward-facing 50 cm diameter photomultiplier tubes (PMTs). Kamiokande and Super-Kamiokande can observe solar neutrinos using ν_e -e elastic scattering (ES), $\nu_x+e^- \rightarrow \nu_x+e^-$. The ES reaction occurs via both charged and neutral current interactions. Consequently, it is sensitive to all active neutrino flavours, although the cross-section for ν_e , which is the only flavour to interact via charged current, is about six times larger than that for ν_μ or ν_τ . Because the energy threshold is 6.5 MeV for Kamiokande and 3.5 MeV for the present Super-Kamiokande (for the kinetic energy of recoil electron), these experiments are sensitive to primarily to ${}^8\text{B}$ neutrinos.

The results from Kamiokande [52, 53] and Super-Kamiokande [54, 55] showed significantly smaller numbers of observed solar neutrinos compared to the prediction. The latest ${}^8\text{B}$ neutrino flux measured by Super-Kamiokande is $(2.345 \pm 0.014 \pm 0.036) \times 10^6 \text{ cm}^{-2}\text{s}^{-1}$ [56], while a prediction based on the SSM is $(5.46 \pm 0.66) \times 10^6 \text{ cm}^{-2}\text{s}^{-1}$ [57]. In addition, no significant zenith angle variation nor spectrum distortion were observed in the initial phase of Super-Kamiokande, which placed strong constraints on the solution of the solar neutrino problem [58, 59].

14.6.1.3 Solution of the solar neutrino problem

The SNO experiment in Canada used 1,000 t of heavy water (D_2O) contained in a spherical acrylic vessel which was surrounded by an H_2O shield. An array of PMTs installed on a stainless steel structure detected Cherenkov radiation produced in both the D_2O and H_2O . The SNO detector observed ${}^8\text{B}$ neutrinos via three different reactions. In addition to the ES scattering with an electron, with D_2O target the CC $\nu_e+d \rightarrow e^-+p+p$ and the NC $\nu_x+d \rightarrow \nu_x+p+n$ interactions are possible. The CC reaction is sensitive to only ν_e , while NC reaction is sensitive to all active flavours of neutrinos with equal cross-sections. Therefore, by comparing the measurements of different reactions, SNO could provide a model-independent test of the neutrino flavour change.

In 2001, SNO reported the initial result of CC measurement [62]. Combined with the high statistics measurement of ν_e -e elastic scattering from Super-Kamiokande [58], it provided a direct evidence for the existence of non- ν_e component in solar neutrino flux. The result of the NC measurement in 2002 [63] established it with 5.3σ of statistical significance. Figure 14.2 shows the fluxes of electron neutrinos ($\phi(\nu_e)$) and muon and tau neutrinos ($\phi(\nu_{\mu,\tau})$) with the 68%, 95%, and 99% joint probability contours obtained with the SNO data. Finally, together with

⁴From 2020, gadolinium (0.01% by weight) is loaded in the water.

Table 14.2: List of solar neutrino experiments

Name	Target material	Energy threshold (MeV)	Mass (ton)	Years
Homestake	C ₂ Cl ₄	0.814	615	1970–1994
SAGE	Ga	0.233	50	1989–
GALLEX	GaCl ₃	0.233	100 [30.3 for Ga]	1991–1997
GNO	GaCl ₃	0.233	100 [30.3 for Ga]	1998–2003
Kamiokande	H ₂ O	6.5	3,000	1987–1995
Super-Kamiokande	H ₂ O	3.5	50,000	1996–
SNO	D ₂ O	3.5	1,000	1999–2006
KamLAND	Liquid scintillator	0.5/5.5	1,000	2001–
Borexino	Liquid scintillator	0.19	300	2007–

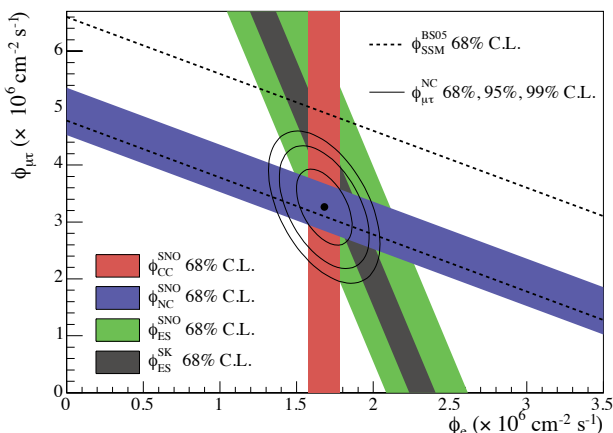


Figure 14.2: Fluxes of ^8B solar neutrinos, $\phi(\nu_e)$, and $\phi(\nu_{\mu,\tau})$, deduced from the SNO's CC, ES, and NC results [60]. The Super-Kamiokande ES flux is from [61]. The BS05(OP) standard solar model prediction [40] is also shown. The bands represent the 1σ error. The contours show the 68%, 95%, and 99% joint probability for $\phi(\nu_e)$ and $\phi(\nu_{\mu,\tau})$. The figure is from [60].

the reactor neutrino experiment KamLAND (see Sec.14.6.4), the solution of solar neutrino problem was found to be the MSW adiabatic flavour transitions in the solar matter, the so-called large mixing angle (LMA) solution. From a combined result of three phases of SNO [64], the total flux of ^8B solar neutrino is found to be $(5.25 \pm 0.16^{+0.11}_{-0.13}) \text{ cm}^{-2}\text{s}^{-1}$, consistent with the SSM prediction. This consistency is one of the major accomplishments of SSM.

In order to understand the SSM as well as to study the MSW effect for the solar neutrino, measurements of solar neutrinos other than ^8B are important. The Borexino experiment at Gran Sasso, Italy, detects solar neutrino via ν -e scattering in real-time with a low energy threshold. The Borexino detector consists of 300 t of ultra-pure liquid scintillator, which achieved 0.19 MeV of energy threshold and 5% energy resolution at 1 MeV. Borexino reported the first real-time detection of ^7Be solar neutrinos [66]. They also measured the fluxes of pep [67], pp [68], and CNO [69] neutrino for the first time. Together with ^8B [70] neutrino measurement, Borexino provides important data to study the MSW effect. The KamLAND experiment also measured ^8B [71] and ^7Be [72] solar neutrinos.

Figure 14.3 shows the survival probability of solar ν_e as a function of neutrino energy. The data points are from the Borexino results [73, 74] and the SNO+SK ^8B data. The theoretical curve shows the prediction of the MSW-LMA solution. All the data shown in this plot are consistent with the theoretically calculated curve. This indicates that these solar neutrino measurements are consistent with the MSW-LMA solution of the solar neutrino problem.

The matter effects can also be relevant to the propagation of solar neutrinos through the Earth. Because solar neutrinos go through the Earth before interaction in the detector during the

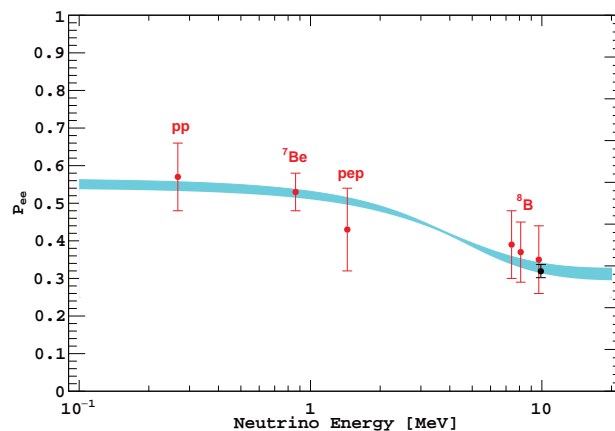


Figure 14.3: Electron neutrino survival probability as a function of neutrino energy. The points represent, from left to right, the Borexino pp , ^7Be , pep , and ^8B data (red points) and the SNO+SK ^8B data (black point). The three Borexino ^8B data points correspond, from left to right, to the low-energy (LE) range, LE+HE range, and the high-energy (HE) range. The electron neutrino survival probabilities from experimental points are determined using a high metallicity SSM from Ref. [57]. The error bars represent the $\pm 1\sigma$ experimental + theoretical uncertainties. The curve corresponds to the $\pm 1\sigma$ prediction of the MSW-LMA solution using the parameter values given in [65]. This figure is provided by A. Ianni.

nighttime, a comparison of measured event rate between daytime and nighttime provides a clean and direct test of matter effects on neutrino oscillations. Super-Kamiokande reported the indication of the day/night asymmetry in ^8B solar neutrinos [75, 76]. The measured asymmetry, defined as the difference of the average day rate and average night rate divided by the average of those two rates, is $(-3.3 \pm 1.0 \pm 0.5)\%$, corresponding to a statistical significance of 2.9σ .

14.6.2 Atmospheric Neutrinos

14.6.2.1 Atmospheric neutrino flux

Atmospheric neutrinos are produced by the decays of pions and kaons generated in the interaction of cosmic rays and nucleons in the Earth's atmosphere. They have a broad range of energy (~ 0.1 GeV to $> \text{TeV}$) and long travel distances before detection (~ 10 to $\sim 10^4$ km), and contain all the flavours of neutrinos and antineutrinos.

Considering their dominant production modes, some generic relations for flux ratios of different flavours of neutrinos can be derived without detailed calculations. From the decay chain of a charged pion $\pi^+ \rightarrow \mu^+ \nu_\mu$ followed by $\mu^+ \rightarrow e^+ \nu_e \bar{\nu}_\mu$ (and the charge conjugate for π^-), the ratio $(\nu_\mu + \bar{\nu}_\mu)/(\nu_e + \bar{\nu}_e)$ is expected to be around 2 at low energies (~ 1 GeV), where most muons decay in the atmosphere. For higher energies, some muons reach the Earth before they decay and the ratio increases. One can also expect that the zenith angle distributions of atmospheric neu-

trinos are symmetric between upward-going and downward-going neutrinos. It is true for the energy above 1 GeV, but at lower energies, the Earth's geomagnetic field induces up-down asymmetries in the primary cosmic ray. The zenith angle corresponds to the flight length of atmospheric neutrinos. Vertically upward-going neutrinos come from the other side of the Earth with flight lengths of $\sim 10^4$ km, while downward-going neutrinos produced just above the experimental site travel ~ 10 km before detection.

The atmospheric neutrino fluxes are calculated in detail based on the energy spectrum and composition of primary cosmic rays and their hadronic interactions in the atmosphere. The effects of solar activity and geomagnetic field are also taken into account. Results of calculations by several groups are available [77–80]. A typical uncertainty of the absolute flux is 10–20%, while the ratio of fluxes between different flavour has much smaller uncertainty ($< 5\%$).

14.6.2.2 Observation of atmospheric neutrino oscillations

The first detection of atmospheric neutrinos was reported in the 1960's by the underground experiments in the Kolar Gold Field experiment in India [81] and in South Africa [82]. In the 1980's, experiments searching for nucleon decays started operation. They used large underground detectors which could also observe atmospheric neutrinos that were studied as backgrounds to nucleon decays. Among the early experiments were Kamiokande [83] and IMB [84] using water Cherenkov detectors, and Frejus [85] and NUSEX [86] using iron tracking calorimeters.

The flavour of an atmospheric neutrino can be identified in charged current interaction with nuclei, which produces the corresponding charged lepton. Those detectors originally designed for nucleon decay search had the capability to distinguish muons and electrons. For example, a water Cherenkov detector can utilize the information from Cherenkov ring patterns for particle identification; e -like particles (e^\pm , γ) produce more diffuse ring than μ -like particles (μ^\pm , π^\pm) because of electromagnetic cascades and multiple Coulomb scattering effects.

To reduce the uncertainty, in early results the flux ratio $\nu_\mu/\nu_e \equiv (\nu_\mu + \bar{\nu}_\mu)/(\nu_e + \bar{\nu}_e)$ was measured, and the double ratio between observation and expectation $(\nu_\mu/\nu_e)_{\text{obs}}/(\nu_\mu/\nu_e)_{\text{exp}}$ was reported. The Kamiokande experiment reported an indication of a deficit of $(\nu_\mu + \bar{\nu}_\mu)$ flux [83]. IMB also observed a similar deficit [84], but measurements by Frejus [85] and NUSEX [86] were consistent with the expectations. This was called the atmospheric neutrino anomaly. Kamiokande reported studies with an increased data set of the sub-GeV (< 1.33 GeV) [87] as well as the multi-GeV (> 1.33 GeV) [88] samples. In the latter, they reported an analysis of zenith angle distributions, which showed an indication that the muon disappearance probability is dependent on the zenith angle, hence the travel length of neutrinos. However, the statistical significance was not sufficient to provide a conclusive interpretation.

The solution to the atmospheric neutrino anomaly was brought by Super-Kamiokande, which reported compelling evidence for neutrino oscillations in atmospheric neutrinos in 1998 [89]. The zenith angle (θ_z , with $\theta_z = 0$ for vertically downward-going) distributions of μ -like events showed a clear deficit of upward-going events, while no significant asymmetry was observed for e -like events. The asymmetry is defined as $A = (U - D)/(U + D)$, where U is the number of upward-going ($-1 < \cos \theta_z < -0.2$) events and D is the number of downward-going ($0.2 < \cos \theta_z < 1.0$) events. With multi-GeV (visible energy > 1.33 GeV) μ -like events alone, the measured asymmetry was $A = -0.296 \pm 0.048 \pm 0.001$, deviating from zero by more than 6σ . The sub-GeV (< 1.33 GeV) μ -like, upward through going, and upward stopping μ samples which correspond to different energy ranges of neutrinos, showed the consistent behaviour which strengthens the credibility of the observation. Super-Kamiokande's results were confirmed by other atmospheric neutrino observations MACRO [90] and Soudan2 [91].

Although the energy and zenith-angle-dependent muon neutrino disappearance observed with atmospheric neutrinos could be consistently explained by the neutrino oscillations predominantly between ν_μ and ν_τ , other exotic explanations such as neutrino decay [92] or decoherence [93] were not initially ruled out. By using a selected sample from Super-Kamiokande's atmospheric data with good L/E resolution, the L/E dependence of the sur-

vival probability was measured [94]. The observed dip in the L/E distribution was consistent with the expectation from neutrino oscillation, while alternative models were strongly disfavored.

As an experimental proof of ν_μ - ν_τ oscillation, an appearance signal of ν_τ was searched for in the atmospheric neutrino data. Because of the high energy threshold (> 3.5 GeV) of ν_τ CC interaction and the short lifetime of τ lepton (0.3 ps), identifying the appearance of ν_τ experimentally is challenging. Super-Kamiokande reported evidence of tau neutrino appearance using atmospheric neutrino data with 4.6σ significance [95]. The definitive observation of ν_τ appearance was made by the long-baseline experiment, OPERA (See Sec.14.6.3.3), and recently IceCube also reported the ν_τ appearance analysis [96] using atmospheric neutrinos.

14.6.2.3 Neutrino oscillation measurements using atmospheric neutrinos

Figure 14.4 shows the zenith angle distributions of atmospheric neutrino data from Super-Kamiokande. For a wide range of neutrino energy and path length, the observed distributions are consistent with the expectation from neutrino oscillation. Atmospheric neutrinos in the energy region of a few to ~ 10 GeV provide information for the determination of the neutrino mass ordering [97].

The neutrino telescopes primarily built for high-energy neutrino astronomy such as ANTARES and IceCube can also measure neutrino oscillations with atmospheric neutrinos. ANTARES consists of a sparse array of PMTs deployed under the Mediterranean Sea at a depth of about 2.5 km to instrument a 10^5 m³ volume. IceCube is a detector deployed in ice in Antarctica at the South Pole, at a depth between 1.45 and 2.45 km. In the bottom center of IceCube there is a region of $\sim 10^7$ m³ volume with denser PMT spacing called DeepCore to extend the observable energies to the lower energy region. By observing the charged current interaction of up-going ν_μ , they measure the ν_μ disappearance. ANTARES reported a measurement of ν_μ disappearance with 20 GeV threshold [98]. With analysis of events with 6–56 GeV energy range, the results on ν_μ disappearance measurements from IceCube DeepCore [99] provided a precision comparable to the measurements by Super-Kamiokande and long-baseline accelerator neutrino experiments.

There are several projects for atmospheric neutrino observations either proposed or under preparation. The atmospheric neutrino observation program is included in the plans for future neutrino telescopes such as ORCA in the KM3NeT project [100] in the Mediterranean Sea and the IceCube Upgrade [101]. In India, a 50 kt magnetized iron tracking calorimeter ICAL is planned at the INO [102]. Future large underground detectors, Hyper-Kamiokande in Japan [103] and DUNE in US [104] can also study the atmospheric neutrinos.

14.6.3 Accelerator Neutrinos

14.6.3.1 Accelerator neutrino beams

A comprehensive description of the accelerator neutrino beams is found in [105]. Conventional neutrino beams from accelerators are produced by colliding high-energy protons onto a target, producing π and K , which then decay into neutrinos. Undecayed mesons and muons are stopped in a beam dump and soil. Because pions are the most abundant product of the high energy collisions, a conventional neutrino beam contains a dominant amount of muon-type neutrinos (or antineutrinos).

Focusing devices called magnetic horns are used to concentrate the neutrino beam flux towards the desired direction [106]. A magnetic horn is a pulsed electromagnet with toroidal magnetic fields to focus charged particles that are parents of neutrinos. One can choose the dominant component of the beam to be either neutrinos or antineutrinos by selecting the direction of current in the magnetic horns. Even with the focusing with horns, *wrong sign* neutrinos contaminate in the beam. Also, there is a small amount of contamination of ν_e and $\bar{\nu}_e$ coming primarily from kaon and muon decays.

In order to maximize the sensitivity of the experiment, the ratio of baseline and neutrino energy (L/E) should be chosen to match the oscillation effects to be studied. In addition to maximizing the flux of neutrinos with relevant energy, neutrinos with irrele-

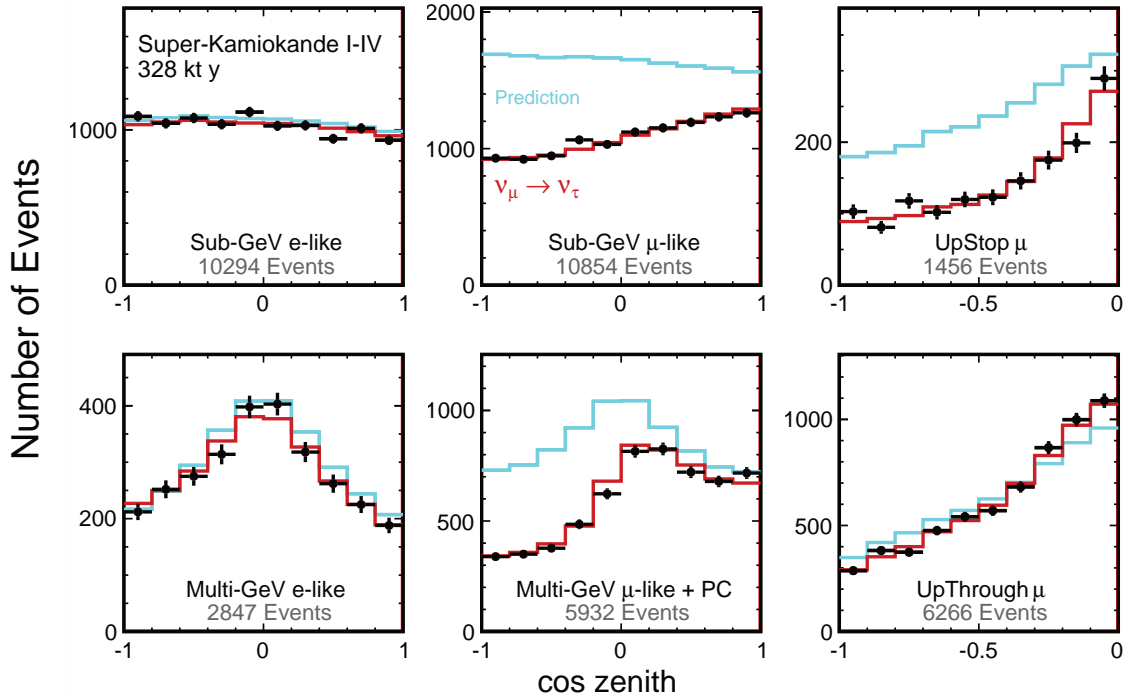


Figure 14.4: The zenith angle distributions of Super-Kamiokande atmospheric neutrino events. A data set corresponding to 328 kton-years of exposure is used. Fully contained 1-ring e -like and μ -like events with visible energy < 1.33 GeV (sub-GeV) and > 1.33 GeV (multi-GeV), as well as upward stopping and upward through going μ samples are shown. Partially contained (PC) events are combined with multi-GeV μ -like events. The blue histograms show the non-oscillated Monte Carlo events, and the red histograms show the best-fit expectations for neutrino oscillations. (This figure is provided by the Super-Kamiokande Collaboration)

vant energy that result in unwanted background process should be suppressed. The energy of a neutrino from a pion decay is

$$E_\nu = \frac{[1 - (m_\mu/m_\pi)^2]E_\pi}{1 + \gamma^2\theta^2}, \quad (14.71)$$

where E_ν and E_π are the energy of neutrino and pion, respectively, θ is the angle between the pion and neutrino direction, and $\gamma = E_\pi/m_\pi$. For $\theta = 0$, the energy of neutrino is linearly proportional to the energy of pion. In this case, a narrow band beam can be made by selecting the momentum of pions. On the other hand, for $\theta \neq 0$, the energy of neutrino is not strongly dependent on the parent energy for a wide range of pion energy, but dependent on the off-axis angle θ . Using this relation, a neutrino beam with narrow energy spectrum, around the energy determined by θ , can be produced. This off-axis beam method was first introduced for BNL E889 proposal [107] and adopted in T2K and NOvA experiments. For a list of neutrino beamlines, see also Chapter 33 of this *Review*, “Neutrino Beam Lines at High-Energy Proton Synchrotrons.”

As indicated in Table 14.1, there are two different scales of baselines for accelerator-based experiments to study different ranges of Δm^2 . The atmospheric mass splitting $\Delta m^2 \sim 2.5 \times 10^{-3} \text{ eV}^2$ gives rise to the first oscillation maximum at $L/E \sim 500 \text{ GeV/km}$. In order to study this parameter region with a $\sim 1 \text{ GeV}$ accelerator neutrino beam, a long baseline of a few hundred to a thousand km is necessary. On the other hand, there have been reports of possible neutrino oscillations at the $\sim 1 \text{ eV}^2$ scale, which can be studied at $\sim 1 \text{ km}$ baseline with neutrinos from accelerators. These experiments are called short-baseline oscillation experiments.

The flux of a neutrino beam is calculated using Monte Carlo simulation based on the configuration of the beamline. An important ingredient of the neutrino flux prediction is the hadron production cross-section. Data from dedicated hadron production experiments [108–110] are used to tune the beam simulation and constrain the uncertainty. The uncertainty of predicted neutrino flux for the most relevant energy region is $\sim 5\text{--}10\%$ with the latest hadron production data [111–113].

14.6.3.2 Near detectors and neutrino interaction cross sections

Many long-baseline experiments use two detectors to reduce the systematic uncertainties arising from neutrino flux and neutrino-nucleus interactions. The near detectors either use the same technology as the far detector or consist of sub-detectors with complementary functions to obtain detailed information of the neutrino beam and interactions. The near detectors provide information for the neutrino flux, energy spectrum, and the interaction cross-sections, which is used as input to make predictions of observables at the far detector. However, even with the two-detector configuration, one should note that the neutrino flux is inevitably different between the near and the far detectors. In addition to the fact that the neutrino source looks like a line source for the near detector while it looks like a point source for the far detector, the neutrino oscillations alter the flavour composition of the neutrino beam quite significantly, as the design of a neutrino oscillation experiment requires.

For the precision measurements of neutrino oscillations with long-baseline experiments, the understanding of the neutrino-nucleus interaction becomes crucial. Because heavy nuclei are used as the interaction target, the nuclear effects complicate the understanding of the neutrino-nucleus interaction. For more information on the neutrino cross-sections, see also Chapter 52 of this *Review*, “Neutrino Cross Section Measurements.”

14.6.3.3 Long-baseline experiments

Long-baseline neutrino oscillation experiments are summarized in Table 14.3. The first long-baseline experiment was the K2K experiment which used a neutrino beam from the KEK 12 GeV proton synchrotron directed towards Super-Kamiokande with a baseline of 250 km. The beam had an average energy of 1.3 GeV. The K2K near detectors, located 300 m downstream of the production target, consisted of a combination of a 1 kt water Cherenkov detector and a set of fine-grained detectors. K2K confirmed the muon neutrino disappearance originally reported by Super-Kamiokande atmospheric neutrino observation [114].

The MINOS experiment used a beam from Fermilab and a de-

Table 14.3: List of long-baseline neutrino oscillation experiments

Name	Beamline	Far Detector	L (km)	E_ν (GeV)	Year
K2K	KEK-PS	Water Cherenkov	250	1.3	1999–2004
MINOS	NuMI	Iron-scintillator	735	3	2005–2013
MINOS+	NuMI	Iron-scintillator	735	7	2013–2016
OPERA	CNGS	Emulsion hybrid	730	17	2008–2012
ICARUS	CNGS	Liquid argon TPC	730	17	2010–2012
T2K	J-PARC	Water Cherenkov	295	0.6	2010–
NOvA	NuMI	Liquid scint. tracking calorimeter	810	2	2014–
DUNE	LBNF	Liquid argon TPC	1300	2–3	
Hyper-Kamiokande	J-PARC	Water Cherenkov	295	0.6	

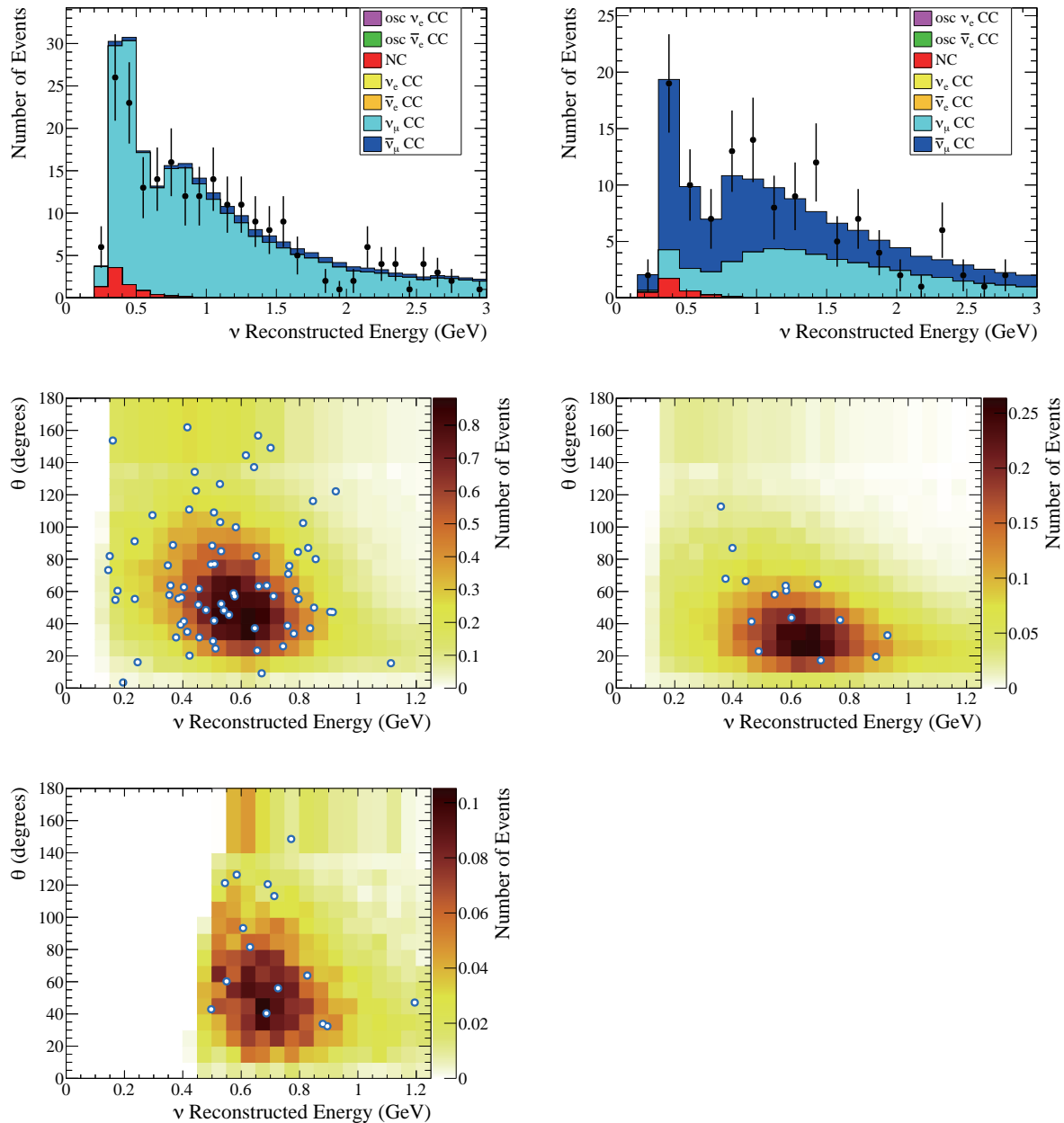


Figure 14.5: Observed kinematic distributions from T2K compared to the expectations assuming neutrino oscillations. Left and right panels correspond to data from neutrino and antineutrino beam mode, respectively. Top: Reconstructed energy distribution of single ring μ -like events. The error bars indicate the statistical uncertainty. Middle: Reconstructed energy vs. angle from beam direction of single ring e -like events with no associated decay electron. Bottom: Reconstructed energy vs. angle from beam direction of single ring e -like events with one associated decay electron for neutrino beam mode data.

tector in the Soudan mine 735 km away. The neutrino beam is produced in the NuMI beamline with a 120 GeV proton beam from the Main Injector. The MINOS detectors are both iron-scintillator tracking calorimeters with toroidal magnetic fields. The far detector was 5.4 kt, while the near detector had a total mass of 0.98 kt and was located 1 km downstream of the production target. The energy spectrum of the NuMI beamline can be varied by changing the relative position of the target and horns. Most of MINOS data were taken with the “low energy” configuration with a peak energy of around 3 GeV. Since 2013, NuMI was operated with a “medium energy” configuration with the peak neutrino energy of around 7 GeV. The experiment for this period was called MINOS+. MINOS and MINOS+ combined accelerator and atmospheric neutrino data in both disappearance and appearance modes to measure oscillation parameters [115–117].

In Europe, the CNGS neutrino beamline provided a beam with mean energy of 17 GeV from CERN to LNGS for long-baseline experiments with about 730 km of baseline. The beam energy was chosen so that CC interaction of ν_τ can occur for direct confirmation of ν_τ appearance. There was no near detector in CNGS because it was not necessary for the ν_τ appearance search. The OPERA experiment used a detector consisting of an emulsion/lead target with about 1.25 kt total mass, complemented by electronic detectors. The excellent spatial resolution of the emulsion enabled the event-by-event identification of τ leptons. OPERA observed ten ν_τ CC candidate events with 2.0 ± 0.4 expected background [118] and confirmed $\nu_\mu \rightarrow \nu_\tau$ oscillation in appearance mode with a statistical significance of 6.1σ . Another neutrino experiment, ICARUS [119], which used 600 t liquid argon time projection chambers (TPCs), was operated in Gran Sasso from 2010 to 2012.

The first generation of long-baseline experiments confirmed the existence of neutrino oscillation. The major initial goal of second-generation experiments was the observation of $\nu_\mu \rightarrow \nu_e$ oscillation. Using this appearance mode, and by comparison of neutrino and antineutrino oscillation probabilities, search for CP violation in the neutrino mixing and measurement of the mass ordering and the octant of θ_{23} become possible.

The T2K experiment started in 2010 using a newly constructed high-intensity proton synchrotron J-PARC and the Super-Kamiokande detector. It is the first long-baseline experiment to employ the off-axis neutrino beam. The off-axis angle of 2.5° was chosen to set the peak of the neutrino energy spectrum at 0.6 GeV, matching the first maximum of oscillation probability at the 295 km baseline for $\Delta m^2 \sim 2.5 \times 10^{-3} \text{ eV}^2$. T2K employs a set of near detectors at about 280 m from the production target. In 2011, T2K reported the first indication of $\nu_\mu \rightarrow \nu_e$ oscillation with a statistical significance of 2.5σ [120]. In the framework of 3ν mixing, it corresponds to detecting non-zero amplitude generated by the mixing angle θ_{13} (see Eq.14.33). Later $\nu_\mu \rightarrow \nu_e$ oscillation was established by T2K with more than 7σ in 2014 [121]. Figure 14.5 shows the observed kinematic distributions from T2K, for neutrino and antineutrino beam mode and also for muon and electron candidates. By a combined analysis of the neutrino and antineutrino data, T2K reported a hint of CP violation at the 2σ level [122, 123].

The NOvA experiment uses the upgraded NuMI beamline with an off-axis configuration. The 14 kt NOvA far detector is located near Ash River, Minnesota, 810 km away from the source. At 14.6 mrad off-axis from the central axis of the NuMI beam, the neutrino energy spectrum at the far detector has a peak of around 2 GeV. The near detector, located around 1 km from the source, has a functionally identical design to the far detector with a total mass of 290 t. Both detectors are tracking calorimeters consisting of planes of polyvinyl chloride cells alternating in vertical and horizontal orientation filled with liquid scintillator. The physics run of NOvA was started in 2014. After confirmation of ν_e appearance from ν_μ beam [124, 125], NOvA started data taking with antineutrino beam in 2016. Using the antineutrino beam data, NOvA has reported the observation of $\bar{\nu}_e$ appearance from $\bar{\nu}_\mu$ beam with 4.4σ significance [126]. Figure 14.6 shows the reconstructed neutrino energy distributions from NOvA. Some values of the CP -violating phase δ_{CP} (see Eq.14.33) have been excluded

for the inverted mass ordering ($m_3 < m_2 < m_1$, see Sec.14.7 for definitions), while no significant limit has been set for the case of normal mass ordering ($m_1 < m_2 < m_3$, see Sec.14.7 for definitions).

Two large-scale long-baseline experiments are under preparation. DUNE [127] will be a 1,300 km long-baseline experiment based in the US. The DUNE far detector will consist of four modules of at least 10 kt fiducial mass liquid argon time projection chambers, located 1.5 km underground at the Sanford Underground Research Facility in South Dakota. The beamline for DUNE, 1.2 MW at start and upgradable to 2.4 MW, as well as the facility for near detectors will be newly constructed at Fermilab. The Hyper-Kamiokande detector [128] in Japan will be the successor of the Super-Kamiokande detector. It will be a water Cherenkov detector with 260 kt total water mass. With upgrades to the existing accelerator and beamline, J-PARC will provide a 1.3 MW neutrino beam to Hyper-Kamiokande with a baseline of 295 km. Both DUNE and Hyper-Kamiokande will have a rich physics program besides the long-baseline experiment, such as searches for nucleon decays and study of supernova neutrinos.

14.6.3.4 Short-baseline experiments

The LSND experiment searched for neutrino oscillation using neutrinos from stopped pions at Los Alamos. A 800 MeV linac was used to produce pions that stopped in the target. Most of π^- s are absorbed by the nuclei inside the target, while π^+ s and their daughter μ^+ s decay and produce neutrinos. Therefore, the produced neutrinos are mostly ν_μ , $\bar{\nu}_\mu$, and ν_e with minimal contamination of $\bar{\nu}_e$. The detector was a tank filled with 167 t of diluted liquid scintillator, located about 30 m from the neutrino source. LSND searched for $\bar{\nu}_\mu \rightarrow \bar{\nu}_e$ appearance using the inverse beta decay process, $\bar{\nu}_e + p \rightarrow e^+ + n$, and found an excess of $87.9 \pm 22.4 \pm 6.0$ events over the expected background [129].

The KARMEN experiment was performed at the neutron spallation facility ISIS of the Rutherford Appleton Laboratory. The KARMEN 2 detector was a segmented liquid scintillation calorimeter with a total volume of 65 m^3 located at a mean distance of 17.7 m from the ISIS target. KARMEN found a number of events consistent with the total background expectation, showing no signal for $\bar{\nu}_\mu \rightarrow \bar{\nu}_e$ oscillations [130]. The resulting limits exclude large regions of the parameter area favored by LSND.

The MiniBooNE experiment at Fermilab used a conventional neutrino beam to search for ν_e and $\bar{\nu}_e$ appearance in the same parameter region as LSND. The booster neutrino beamline (BNB) with a single magnetic horn uses an 8 GeV proton beam from the Fermilab booster to produce a neutrino (antineutrino) beam with an energy spectrum peak of 600 (400) MeV. The MiniBooNE detector consists of a 12.2 m diameter sphere filled with 818 t of mineral and oil located 541 m from the target. MiniBooNE reported ν_e and $\bar{\nu}_e$ event excess in both neutrino and antineutrino running modes. In total, $638.0 \pm 52.1 \pm 122.2$ excess events are observed over the expected backgrounds, corresponding to 4.8σ significance [131].

Both LSND and MiniBooNE are single detector experiments. The reported excess will be further investigated with the multi-detector short-baseline neutrino (SBN) program at Fermilab BNB [132]. The SBN program comprises three liquid argon time projection chambers at different baselines in the same neutrino beamline. The 112 t Short-Baseline Near Detector will be located at 110 m from the target. The 85 t MicroBooNE detector has been operated at 470 m from the target. The ICARUS detector was transported from Europe after refurbishment at CERN and is located at a baseline of 600 m.

JSNS² experiment at J-PARC has started the search for neutrino oscillations with $\Delta m^2 \sim 1 \text{ eV}^2$ [133]. 1MW proton beam from the 3 GeV Rapid Cycling Synchrotron of J-PARC produces neutrinos from muon decay at rest. With a detector filled with a gadolinium-loaded liquid scintillator of 17 t fiducial mass at 24 m from the target, JSNS² is aiming to provide a direct test of the LSND anomaly. The second phase with additional second detector at 48 m is under preparation.

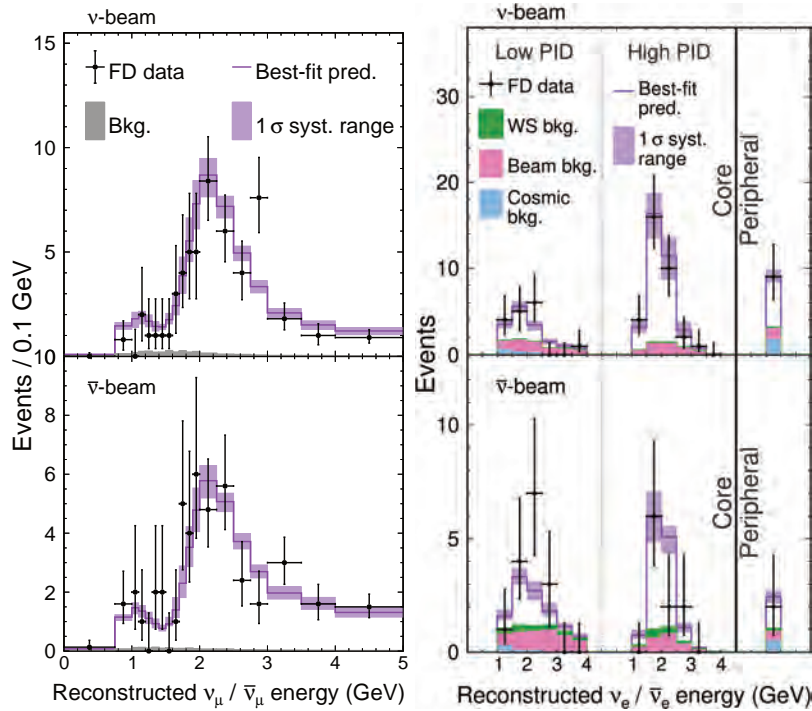


Figure 14.6: Reconstructed neutrino energy distributions from the NOvA far detector [126]. Top plots are for neutrino beam mode, and bottom plots are for antineutrino beam mode. Left: muon-type candidates. Right: electron-type candidates, split into a low and high purity sample as well as the event counts in the peripheral sample which occurred near the edge of the detector.

14.6.4 Reactor Antineutrinos

14.6.4.1 Reactor antineutrino flux

Nuclear reactors are very intense sources of $\bar{\nu}_e$'s in the MeV energy region, which are generated in nuclear fission of heavy isotopes (mainly ^{235}U , ^{238}U , ^{239}Pu , and ^{241}Pu). The $\bar{\nu}_e$ flux from a reactor can be estimated based on the thermal power output and fuel composition as a function of time. On average, about six $\bar{\nu}_e$'s are emitted, and about 200 MeV of energy is released per fission. Therefore, a 1 GW_{th} (thermal power) reactor produces about 2×10^{20} $\bar{\nu}_e$'s per second.

The detailed estimate of $\bar{\nu}_e$ flux and energy spectrum can be obtained by either summing up the spectra of beta decays involved using available nuclear data information of each fission fragment and its decays, or by using measurements of cumulative electron spectra associated with the beta decays of fission fragments. Because the fission of four main fuel isotopes involves thousands of beta-decay branches, a complete *ab initio* calculation is challenging. The cumulative electron spectra for ^{235}U , ^{239}Pu , and ^{241}Pu were measured at the Institut Laue-Langevin (ILL) reactor in Grenoble, France in the 1980s [134–136]. For the prediction of $\bar{\nu}_e$ flux from ^{238}U , a summation calculation in [137] was often used together with the ILL results.

A recent calculation of the reactor $\bar{\nu}_e$ flux [138] uses an improved *ab initio* approach for ^{238}U and combined information from nuclear databases and electron spectra measured at ILL for ^{235}U , ^{239}Pu , and ^{241}Pu . Another calculation [139] is provided for ^{235}U , ^{239}Pu , and ^{241}Pu based on the ILL measurement of electron spectra, taking into account higher-order corrections and minimizing the use of nuclear databases. Both calculations predict a few percent higher normalization for the energy-averaged antineutrino fluxes of ^{235}U , ^{239}Pu , and ^{241}Pu compared to the original analyses of ILL data. However, the reactor antineutrino flux measurement at Daya Bay [140] is consistent with the old flux predictions and the flux measurement results. Also, an excess of $\bar{\nu}_e$ flux around 5 MeV, compared to the prediction, has been observed by recent reactor experiments [141–144].

14.6.4.2 Reactor antineutrino oscillation experiments

Charged current interaction cannot happen if a reactor $\bar{\nu}_e$ changes its flavour to $\bar{\nu}_\mu$ or $\bar{\nu}_\tau$, because its energy is not sufficient to produce heavier charged leptons. Thus, $\bar{\nu}_e$ disappearance is the only channel to study neutrino flavour change with reactor experiments. The inverse beta decay $\bar{\nu}_e + p \rightarrow e^+ + n$ provides a way to detect $\bar{\nu}_e$ in the relevant energy region. The energy of prompt signal from e^+ , E_p , is related to the energy of $\bar{\nu}_e$, $E_{\bar{\nu}} \sim E_p + 0.8$ MeV. The delayed coincidence with the signal from γ ray emitted by neutron capture on nucleus after thermalization very efficiently suppresses the backgrounds. A liquid scintillator is often used to realize large detectors containing hydrogen as the target of inverse beta decay. In order to increase the neutron detection efficiency, a liquid scintillator is sometimes loaded with gadolinium because of a large neutron capture cross-section and higher energy of emitted γ rays, the total energy of about 8 MeV, by gadolinium, in contrast to 2.2 MeV for the capture by hydrogen.

Early reactor experiments that searched for neutrino oscillations at short or intermediate baselines reported negative results. The CHOOZ [145] and Palo Verde [146] experiments in the 1990's searched for neutrino oscillations in the $\Delta m^2 \sim 10^{-2} - 10^{-3}$ eV² range and set a limit on the corresponding mixing angle $\sin^2 2\theta < 0.1$ at 90% CL.

Table 14.4 shows a list of reactor antineutrino experiments measuring neutrino oscillation. As was also shown in Table 14.1, experiments are designed with different baselines because of the different scale of mass splittings found by solar and atmospheric neutrino experiments. Experiments with O(100) km baseline are sensitive to Δm^2 of $10^{-4} - 10^{-5}$ eV², while ~ 1 km of baseline results in a sensitivity in the range of $10^{-2} - 10^{-3}$ eV².

The KamLAND detector consists of 1,000 t of ultra-pure liquid scintillator contained in a 13-m diameter spherical balloon [147]. The detector is located in the original Kamiokande cavern, where the $\bar{\nu}_e$ flux was dominated by a few reactors at an average distance of ~ 180 km until 2011. KamLAND reported the first results in 2002 showing that the ratio of the observed number of $\bar{\nu}_e$ events and expectation without disappearance is $0.611 \pm 0.085 \pm 0.041$, evidence for reactor $\bar{\nu}_e$ disappearance at the 99.95% confidence

Table 14.4: List of reactor antineutrino oscillation experiments

Name	Reactor power (GW _{th})	Baseline (km)	Detector mass (t)	Year
KamLAND	various	180 (ave.)	1,000	2001–
Double Chooz	4.25×2	1.05	8.3	2011–2018
Daya Bay	2.9×6	1.65	20×4	2011–2020
RENO	2.8×6	1.38	16	2011–
JUNO	26.6 (total)	53	20,000	

Table 14.5: List of reactor antineutrino experiments for O(eV^2) oscillations

Name	Reactor power (MW _{th})	Baseline (m)	Detector mass (t)	Detector technology	σ_E/E @1 MeV(%)	S/B
NEOS	2,800	24	1	Gd-LS	5	22
DANSS	3,100	10–13	0.9	Gd-PS	34	~30
STEREO	57	9–11	1.7	Gd-LS	10	0.9
PROSPECT	85	7–9	4	⁶ Li-LS	4.5	1.3
NEUTRINO-4	100	6–12	1.5	Gd-LS	16	0.5
SoLid	80	6–9	1.6	⁶ Li-PS	14	

level [147]. It confirmed a large value of the mixing angle corresponding to the LMA solution, which was reported by solar neutrino experiments. KamLAND also showed the evidence of $\bar{\nu}_e$ spectrum distortion consistent with the expectation from neutrino oscillations [148]. Figure 14.7 shows the ratio of observed $\bar{\nu}_e$ spectrum to the expectation for no-oscillation as a function of L_0/E ($L_0 = 180$ km) for the KamLAND data. A clear oscillatory signature can be seen.

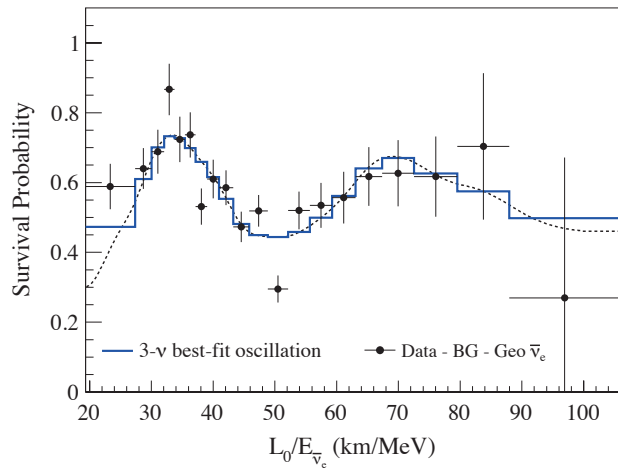


Figure 14.7: Ratio of the observed $\bar{\nu}_e$ spectrum to the expectation for no-oscillation versus L_0/E for the KamLAND data. $L_0 = 180$ km is the flux-weighted average reactor baseline. The 3- ν histogram is the best-fit survival probability curve from the three-flavour unbinned maximum-likelihood analysis using only the KamLAND data. This figure is taken from [149].

Following the establishment of neutrino oscillations with atmospheric, solar, accelerator, and reactor experiments, the measurement of the remaining mixing angle θ_{13} was recognized as the next major milestone. A reactor neutrino experiment with a baseline of ~ 1 km can make an almost pure measurement of $\sin^2 2\theta_{13}$ from the disappearance of $\bar{\nu}_e$. To be sensitive to a small value below the limit set by CHOOZ and Palo Verde, experiments with two detectors were proposed. Among several proposals, three experiments have been realized: Double Chooz in France, Daya Bay in China, and RENO in Korea.

These three experiments employ a similar detector design optimized for the precise measurement of a reactor antineutrino. An antineutrino detector consists of a cylindrical stainless steel vessel

that houses two nested acrylic cylindrical vessels. The innermost vessel is filled with gadolinium-doped liquid scintillator as the primary antineutrino target. It is surrounded by a liquid scintillator layer to contain γ rays from the target volume. A buffer layer of mineral oil is placed outside to shield inner volumes from radioactivity of PMTs and surrounding rock. The light from liquid scintillator is detected by an array of PMTs mounted on the stainless steel vessel. Optically separated by the stainless steel vessel, the outside region is instrumented as a veto detector with either liquid scintillator (Double Chooz) or water Cherenkov (Daya Bay and RENO) detector.

The Double Chooz detector has a gadolinium-doped liquid scintillator with a mass of 8.3 t. The far detector at a baseline of ~ 1050 m from the two 4.25 GW_{th} reactors started physics data taking in 2011. The near detector, located at ~ 400 m from the reactors, was completed in the end of 2014. Double Chooz finished data taking in early 2018. Daya Bay has two near (flux-weighted baseline 470 m and 576 m), and one far (1648 m) underground experimental halls near six reactors with 2.9 GW_{th} each. Daya Bay has eight antineutrino detectors in total; two detectors in each of the near detector halls, and four detectors in the far detector hall. Each detector contains 20 t of gadolinium-loaded liquid scintillator. RENO has two identical detectors located at 294 m and 1383 m from the center of an array of six 2.8 GW_{th} reactors. The mass of the gadolinium-loaded liquid scintillator is 16 t per detector. RENO started data taking with both near and far detectors from August 2011.

All three reactor neutrino experiments published their first results in 2012. First, Double Chooz reported an indication of reactor electron antineutrino disappearance with the ratio of observed to expected events of $R = 0.944 \pm 0.016 \pm 0.04$, ruling out the no-oscillation hypothesis at the 94.6% CL [150]. Daya Bay observed $R = 0.940 \pm 0.011 \pm 0.004$, corresponding to 5.2 σ significance of non-zero value of θ_{13} [151]. RENO also reported $R = 0.920 \pm 0.009 \pm 0.014$, indicating a non-zero value of θ_{13} with a significance of 4.9 σ [152]. These results established a non-zero value of θ_{13} .

Both Daya Bay [141] and RENO [142] report results constraining mass-squared difference as well as the mixing angle by using both relative $\bar{\nu}_e$ rate and energy spectra information. Double Chooz has reported the analysis based on both far and near detectors [143] for the mixing angle, using neutron capture on any elements (primarily gadolinium and hydrogen) to increase the effective target mass. Figure 14.8 shows the energy spectra of the prompt signals observed in the far detector of three experiments.

In all three experiments, as well as in the NEOS experiment [144], an excess of $\bar{\nu}_e$ events over the expected energy spectrum has been observed around 5 MeV, as mentioned earlier. This excess is observed in both near and far detectors and scales with

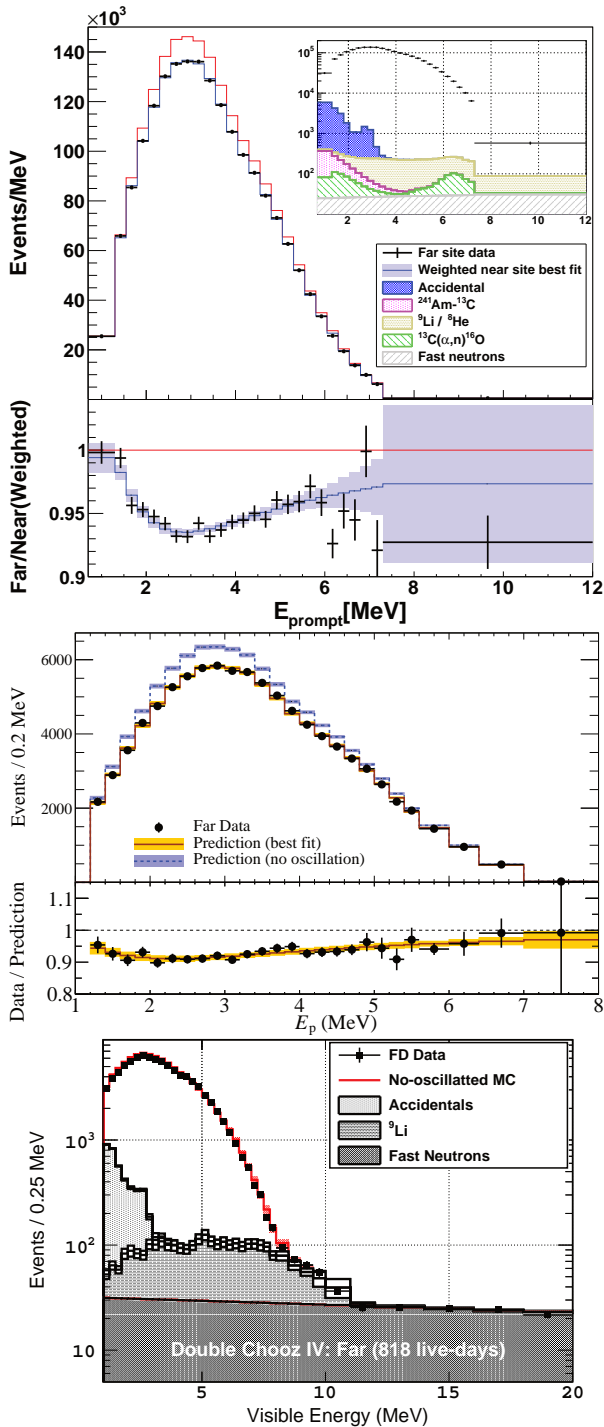


Figure 14.8: Energy spectra for prompt events at the far detectors for Daya Bay [141], RENO [142], and Double Chooz [143].

the reactor power. Thanks to the cancellation between the near and far detectors, the neutrino oscillation measurements are not affected in a multi-detector setup.

With a baseline of ~ 50 km and an excellent energy measurement, reactor antineutrino experiments have significant sensitivity to the mass ordering. The JUNO detector, which is under construction, will consist of a 20 kt liquid scintillator and be located at 53 km from two nuclear power plants in China [153]. The JUNO experiment aims to determine the mass ordering with this technique as its primary goal. It can also provide precision measurements of neutrino mixing parameters as well as a broad

non-oscillation science program.

14.6.4.3 New reactor experiments sensitive to $O(1)$ eV^2 oscillations

Possible hints of neutrino oscillation at a scale of $\Delta m^2 \sim 1$ eV^2 (see Sec.14.8) have motivated reactor experiments at a distance of ~ 10 m from the core. Recent experiments searching for ~ 1 eV^2 oscillation at reactors are summarized in Table 14.5.

As the antineutrino source, some use commercial reactors, which can provide a large flux leading to high statistical precision. On the other hand, though the flux is orders of magnitude smaller, a research reactor could have favorable conditions such as relatively easier access to a short baseline, simpler fuel composition, and compact core size.

The detectors are based on organic scintillators, either liquid scintillator (LS) or solid plastic scintillator (PS), which contain hydrogen as the target for inverse beta decay ($\bar{\nu}_e + p \rightarrow e^+ + n$). To identify the signal, neutron capture on either gadolinium (Gd) or ^6Li is detected with delayed coincidence. When a neutron is captured by Gd, γ rays with a total energy of 8 MeV are emitted. After neutron capture, ^6Li decays into triton and α . The effect of neutrino oscillation appears as a distortion of energy spectrum. To be independent from the reactor neutrino spectrum uncertainties, some experiments compare the spectra at different baselines by using a segmented detector or moving the detector.

NEOS [144] uses about 1 t of gadolinium-loaded liquid scintillator in an unsegmented detector. It is located at 23.7 m from the center of a commercial reactor and covered by an overburden of about 20 meters of water equivalent.

DANSS [154] is another experiment using a commercial reactor. The detector is highly segmented, consisting of 2,500 plastic scintillator strips, each with the size of $1 \times 4 \times 100$ cm^3 and coated with a thin gadolinium-loaded reflective layer. The detector is placed on a movable platform below the reactor core, which varies the distance to the core from 10.7 to 12.7 m.

The STEREO detector [155] has six identical target cells of 37 cm length, $\sim 2\text{m}^3$ of volume in total, filled with gadolinium-loaded liquid scintillator. They are placed from 9.4 to 11.1 m from the compact (80 cm high, 40 cm diameter) core of the ILL research reactor.

The PROSPECT detector [156] consists of a segmented 4 t ^6Li -doped liquid scintillator detector. It covers a baseline range of 7–9 m from the highly ^{235}U enriched reactor core of the High Flux Isotope Reactor (HFIR) at Oak Ridge National Laboratory. Thin reflecting panels divide the LS volume into an 11×14 two-dimensional array of 154 optically isolated rectangular segments ($14.5 \times 14.5 \times 117.6$ cm^3).

NEUTRINO-4 [157, 158] uses a gadolinium-loaded liquid scintillator detector segmented in 10×5 sections with a total volume of 1.8 m^3 . The detector is installed on a movable platform and moved to various positions with baselines of 6–12 m from the SM-3 reactor core in Russia.

The SoLid detector [159] is a finely segmented detector made of $5 \times 5 \times 5$ cm^3 plastic scintillator cubes and $^6\text{LiF}:\text{ZnS}$ sheets. Using the difference of time constant of scintillation between ZnS and the plastic scintillator a n - γ separation capability is achieved. A detector with 1.6 t of active volume is installed at a distance of 6–9 m from the research reactor core in the BR2 reactor, Belgium.

14.7 Combined Analysis of Experimental Results: The 3ν Paradigm

From the experimental situation described in Sec.14.6 we conclude that

- Atmospheric ν_μ and $\bar{\nu}_\mu$ disappear most likely converting to ν_τ and $\bar{\nu}_\tau$. The results show an energy and distance dependence perfectly described by mass-induced oscillations.
- Accelerator ν_μ and $\bar{\nu}_\mu$ disappear over distances of ~ 200 to 800 km. The energy spectrum of the results show a clear oscillatory behavior also in accordance with mass-induced oscillations with a wavelength in agreement with the effect observed in atmospheric neutrinos.
- Accelerator ν_μ and $\bar{\nu}_\mu$ appear as ν_e and $\bar{\nu}_e$ at distances ~ 200 to 800 km.

- Solar ν_e convert to ν_μ and/or ν_τ . The observed energy dependence of the effect is well described by massive neutrino conversion in the Sun matter according to the MSW effect
- Reactor $\bar{\nu}_e$ disappear over distances of ~ 200 km and ~ 1.5 km with different probabilities. The observed energy spectra show two different mass-induced oscillation wavelengths: at short distances in agreement with the one observed in accelerator ν_μ disappearance, and a long-distance compatible with the required parameters for MSW conversion in the Sun.

The minimum scenario to describe these results requires the mixing between the three flavour neutrinos of the standard model in three distinct mass eigenstates. In this case U in Eq. (14.32) is a 3×3 matrix analogous to the CKM matrix for the quarks [21], but due to the possible Majorana nature of the neutrinos it can depend on six independent parameters: three mixing angles and three phases. There are several possible conventions for the ranges of the angles and ordering of the states. The community finally agreed to a parametrization of the leptonic mixing matrix as in Eq. (14.33). The angles θ_{ij} can be taken without loss of generality to lie in the first quadrant, $\theta_{ij} \in [0, \pi/2]$, and the phase $\delta_{CP} \in [0, 2\pi]$. Values of δ_{CP} different from 0 and π imply CP violation in neutrino oscillations in vacuum [160–162]. The Majorana phases η_1 and η_2 play no role in neutrino oscillations [161, 163]. Hence for the study of neutrino oscillations in the 3ν mixing scenario one can use the parametrization in Eq. (14.34) irrespective of whether neutrinos are Dirac or Majorana particles. Indeed, Majorana phases are very hard to measure since they are only physical if neutrino mass is non-zero, and therefore, the amplitude of any process involving them is suppressed by a factor m_ν/E to some power where E is the energy involved in the process, which is typically much larger than the neutrino mass. The most sensitive experimental probe of Majorana phases is the rate of neutrinoless $\beta\beta$ decay discussed in Secs. 14.9.3 and 14.9.2.

In this convention there are two non-equivalent orderings for the spectrum of neutrino masses:

- Spectrum with Normal Ordering (NO) with $m_1 < m_2 < m_3$
- Spectrum Inverted ordering (IO) with $m_3 < m_1 < m_2$.

Furthermore, the data show a hierarchy between the mass splittings, $\Delta m_{21}^2 \ll |\Delta m_{31}^2| \simeq |\Delta m_{32}^2|$ with $\Delta m_{ij}^2 \equiv m_i^2 - m_j^2$.

In this section, we follow the convention used in the listing section of the PDG and discuss the results for both, NO and IO, using Δm_{21}^2 , which is always the smallest mass splitting, and Δm_{32}^2 , which up to a sign, is the largest mass splitting for IO, while for NO the largest mass splitting is $\Delta m_{31}^2 = \Delta m_{32}^2 + \Delta m_{21}^2$.

With what we know of the mass differences (see table 14.7) and the neutrino mass scale (see Sec. 14.9), depending on the value of the lightest neutrino mass, the neutrino mass spectrum can be further classified in:

- Normal Hierarchical Spectrum (NH): $m_1 \ll m_2 < m_3$,
 $\Rightarrow m_2 \simeq \sqrt{\Delta m_{21}^2} \sim 8.6 \times 10^{-3} \text{eV}$, $m_3 \simeq \sqrt{\Delta m_{32}^2 + \Delta m_{21}^2} \sim 0.05 \text{eV}$,
- Inverted Hierarchical Spectrum (IH): $m_3 \ll m_1 < m_2$,
 $\Rightarrow m_1 \simeq \sqrt{|\Delta m_{32}^2 + \Delta m_{21}^2|} \sim 0.0492 \text{eV}$, $m_2 \simeq \sqrt{|\Delta m_{32}^2|} \sim 0.05 \text{eV}$,
- Quasidegenerate Spectrum (QD): $m_1 \simeq m_2 \simeq m_3 \gg \sqrt{|\Delta m_{32}^2|}$.

Sometimes in the literature the determination of the neutrino mass spectrum is referred to as determination of the neutrino hierarchy. However, as described above, with what we know so far of the neutrino mass scale, the neutrino spectrum may or may not be hierarchical. Therefore determination of neutrino mass ordering is a more precise expression, and it is the one used in this review.

In total, the 3ν oscillation analysis of the existing data involves six parameters: 2 mass differences (one of which can be positive

or negative), 3 mixing angles, and the CP phase. The different experiments described in Sec.14.6 provide information on different subsets of these parameters. The precise statistical analysis of the data requires the numerical evaluation of the corresponding oscillation probabilities by solving the evolution equation of the neutrino ensemble from their source to the experiment. Nevertheless, the dominant effects in the different experiments can be qualitatively understood in terms of approximate expressions for the oscillation probabilities which, for convenience, we briefly summarize here.

14.7.1 3ν Oscillation Probabilities

The relevant survival probabilities for solar and KamLAND experiments in the framework of three neutrino oscillations can be written as:

$$P_{ee}^{3\nu} = \sin^4 \theta_{13} + \cos^4 \theta_{13} P_{ee}^{2\nu}(\Delta m_{21}^2, \theta_{12}), \quad (14.72)$$

where we have used the fact that $L_{0,32}^{\text{osc}} = 4\pi E_\nu / \Delta m_{32}^2$ is much shorter than the distance traveled by both solar and KamLAND neutrinos, so that the oscillations related to $L_{0,32}^{\text{osc}}$ are averaged. In the presence of matter effects $P_{ee}^{2\nu}(\Delta m_{21}^2, \theta_{12})$ should be calculated, taking into account the evolution in an effective matter density $n_e^{\text{eff}} = n_e \cos^2 \theta_{13}$. For $10^{-5} \lesssim \Delta m^2 / \text{eV}^2 \lesssim 10^{-4}$, $P_{ee}^{2\nu}(\Delta m_{21}^2, \theta_{12})$ presents the following asymptotic behaviors [164]:

$$P_{ee}^{2\nu, \text{sun}} \simeq 1 - \frac{1}{2} \sin^2(2\theta_{12}) \quad \text{for } E_\nu \lesssim \text{few} \times 100 \text{ keV}, \quad (14.73)$$

$$P_{ee}^{2\nu, \text{sun}} \simeq \sin^2(\theta_{12}) \quad \text{for } E_\nu \gtrsim \text{few} \times 1 \text{ MeV}, \quad (14.74)$$

$$P_{ee}^{2\nu, \text{kam}} = 1 - \sin^2(2\theta_{12}) \sin^2 \frac{\Delta m_{21}^2 L}{4E_\nu}. \quad (14.75)$$

At present most of the precision of the solar analysis is provided by SNO and SK, for which the relevant MSW survival probability provides a direct measurement of $\sin^2 \theta_{12}$, as seen in Eq. (14.74). In the MSW regime, the determination of Δm_{21}^2 in solar experiments comes dominantly from the ratio between the solar potential and the Δm_{21}^2 term required to simultaneously describe the CC/NC data at SNO and the undistorted spectra of ^8B neutrinos as measured in both SK and SNO. Conversely, KamLAND $\bar{\nu}_e$ survival probability proceeds dominantly as vacuum oscillations and provides a most precise determination of Δm_{21}^2 via the strong effect of the oscillating phase in the distortion of the reactor energy spectrum. On the contrary, it yields a weaker constraint on θ_{12} as the vacuum oscillation probability depends on the double-valued and “flatter” function $\sin^2(2\theta_{12})$.

In what respects the interpretation of ν_μ disappearance data, at LBL experiments, the ν_μ survival probability can be expanded in the small parameters $\sin \theta_{13}$ and $\alpha \equiv \Delta m_{21}^2 / \Delta m_{31}^2$ to good accuracy as [165, 166]

$$\begin{aligned} P_{\nu_\mu \rightarrow \nu_\mu} &\approx 1 - \sin^2 2\theta_{\mu\mu} \sin^2 \frac{\Delta m_{\mu\mu}^2 L}{4E_\nu} \\ &\approx 1 - \cos^2 \theta_{13} \sin^2(2\theta_{23}) \sin^2 \frac{\Delta m_{32}^2 L}{4E_\nu} + \mathcal{O}(\alpha, s_{13}^2), \end{aligned} \quad (14.76)$$

with

$$\begin{aligned} \sin^2 \theta_{\mu\mu} &= \cos^2 \theta_{13} \sin^2 \theta_{23}, \\ \Delta m_{\mu\mu}^2 &= \sin^2 \theta_{12} \Delta m_{31}^2 + \cos^2 \theta_{12} \Delta m_{32}^2 \\ &\quad + \cos \delta_{CP} \sin \theta_{13} \sin 2\theta_{12} \tan \theta_{23} \Delta m_{21}^2. \end{aligned}$$

At present ν_μ disappearance results at LBL provide the best determination of $|\Delta m_{32}^2|$ and θ_{23} , but as seen above, the probability is symmetric with respect to the octant of $\theta_{\mu\mu}$, which implies symmetry around $s_{23}^2 = 0.5/c_{13}^2$.

The relevant oscillation probability for ν_e appearance at LBL experiments can be expanded at the second order in the small

parameters $\sin\theta_{13}$ and α , and assuming a constant matter density it takes the form [167–169]:

$$P_{\nu_\mu \rightarrow \nu_e, (\bar{\nu}_\mu \rightarrow \bar{\nu}_e)} \approx 4 \sin^2 \theta_{13} \sin^2 \theta_{23} \frac{\sin^2 \Delta}{(1-A)^2} + \alpha^2 \sin^2 2\theta_{12} \cos^2 \theta_{23} \frac{\sin^2 A\Delta}{A^2} + 8\alpha J_{\text{CP}}^{\text{max}} \cos(\Delta \pm \delta_{\text{CP}}) \frac{\sin \Delta A}{A} \frac{\sin \Delta(1-A)}{1-A}, \quad (14.77)$$

with

$$J_{\text{CP}}^{\text{max}} = \cos\theta_{12} \sin\theta_{12} \cos\theta_{23} \sin\theta_{23} \cos^2\theta_{13} \sin\theta_{13}, \quad (14.78)$$

and

$$\Delta \equiv \frac{\Delta m_{31}^2 L}{4E_\nu}, \quad A \equiv \frac{2E_\nu V}{\Delta m_{31}^2}, \quad (14.79)$$

where V is the effective matter potential in the Earth's crust. Results on ν_e appearance at LBL provide us with the dominant information on leptonic CP violation. Furthermore, α , Δ , and A are sensitive to the sign of Δm_{32}^2 (*i.e.*, the type of the neutrino mass ordering). The plus (minus) sign in Eq. (14.77) applies for neutrinos (antineutrinos), and for antineutrinos $V \rightarrow -V$, which implies $A \rightarrow -A$. Numerically one finds for a typical Earth crust matter density of 3 g/cm^3 that at T2K with $E \sim 0.7 \text{ GeV}$, matter effects cause $\sim \pm 10\%$ differences in the rates, whereas in NOvA with $E \sim 2 \text{ GeV}$, we can have $|A| \sim 0.2$. Also, $\alpha^2 \approx 10^{-3}$, which implies that the second term in the first line of Eq. (14.77) gives a very small contribution compared to the other terms. Also, the first term in Eq. (14.77) (which dominates for large θ_{13}) depends on $\sin^2 \theta_{23}$ and therefore is sensitive to the octant.

The ν_e survival probability relevant for reactor experiments with medium baseline (MBL), $L \sim 1 \text{ km}$, can be approximated as [166, 170]:

$$P_{\nu_e \rightarrow \nu_e} = 1 - \sin^2 2\theta_{13} \sin^2 \frac{\Delta m_{ee}^2 L}{4E_\nu} + \mathcal{O}(\alpha^2), \quad (14.80)$$

where

$$\Delta m_{ee}^2 = \cos^2 \theta_{12} \Delta m_{31}^2 + \sin^2 \theta_{12} \Delta m_{32}^2. \quad (14.81)$$

These MBL reactor experiments provide the most precise determination of θ_{13} . Furthermore there is an additional effect sensitive to the mass ordering when comparing the disappearance of ν_μ at LBL experiments – which is symmetric with respect to the sign of $\Delta m_{\mu\mu}^2$ given in Eq.(14.7.1) – with that of ν_e disappearance at MBL reactors which is symmetric with respect to the slightly different effective mass-squared difference Δm_{ee}^2 given in Eq. (14.81).

Finally, for atmospheric neutrinos, the fluxes contain ν_e , ν_μ , $\bar{\nu}_e$, and $\bar{\nu}_\mu$, and for a good fraction of the events, neutrinos travel through the Earth's matter. In the context of 3ν mixing, the dominant oscillation channel of atmospheric neutrinos is $\nu_\mu \rightarrow \nu_\tau$ driven by $|\Delta m_{32}^2|$ with an amplitude controlled by θ_{23} with sub-leading oscillation modes, triggered by Δm_{21}^2 and/or θ_{13} , which depend on the octant of θ_{23} , on the mass ordering, and on δ_{CP} . In that respect, an interesting observable is the deviation of e -like events relative to the no-oscillation prediction N_e^0 , since in the two-flavour limit one expects $N_e = N_e^0$. Such deviation can be written in the following way (see, *e.g.*, [171]):

$$\frac{N_e}{N_e^0} - 1 \approx (r \sin^2 \theta_{23} - 1) P_{2\nu}(\Delta m_{32}^2, \theta_{13}) + (r \cos^2 \theta_{23} - 1) P_{2\nu}(\Delta m_{21}^2, \theta_{12}) - \sin \theta_{13} \sin 2\theta_{23} r \Re(A_{ee}^* A_{\mu e}). \quad (14.82)$$

Here $r \equiv \Phi_\mu / \Phi_e$ is the flux ratio with $r \approx 2$ in the sub-GeV range and $r \approx 2.6 \rightarrow 4.5$ in the multi-GeV range. $P_{2\nu}(\Delta m^2, \theta)$ is an effective two-flavour oscillation probability, and $A_{ee}, A_{\mu e}$ are elements of a transition amplitude matrix. The three terms appearing in Eq. (14.82) have a well-defined physical interpretation. The first term is important in the multi-GeV range and is controlled by

the mixing angle θ_{13} in $P_{2\nu}(\Delta m_{32}^2, \theta_{13})$. This probability can be strongly affected by resonant matter effects [172–177]. Depending on the mass ordering, the resonance will occur either for neutrinos or antineutrinos. The second term is important for sub-GeV events, and it takes into account the effect of oscillations due to Δm_{21}^2 and θ_{12} [178–181]. Via the pre-factor containing the flux ratio r both, the first and second terms in Eq. (14.82) depend on the octant of θ_{23} , though in opposite directions: the multi-GeV (sub-GeV) excess is suppressed (enhanced) for $\theta_{23} < 45^\circ$. Finally, the last term in Eq. (14.82) is an interference term between θ_{13} and Δm_{21}^2 amplitudes and this term shows also dependence on the CP phase δ_{CP} [171, 181].

Subdominant three neutrino effects can also affect μ -like events. For example, for multi-GeV muon events one can write the excess in μ -like events as [182, 183]

$$\frac{N_\mu}{N_\mu^0} - 1 \approx \sin^2 \theta_{23} \left(\frac{1}{r} - \sin^2 \theta_{23} \right) P_{2\nu}(\Delta m_{32}^2, \theta_{13}) - \frac{1}{2} \sin^2 2\theta_{23} [1 - \Re(A_{33})]. \quad (14.83)$$

The first term is controlled by θ_{13} and is subject to resonant matter effects, similar to the first term in Eq. (14.82), though with a different dependence on θ_{23} and the flux ratio. In the second term, A_{33} is a probability amplitude satisfying $P_{2\nu}(\Delta m_{32}^2, \theta_{13}) = 1 - |A_{33}|^2$. In the limit $\theta_{13} = 0$ we have $\Re(A_{33}) = \cos(\Delta m_{32}^2 L/2E)$, such that the second term in Eq. (14.83) just describes two-flavour $\nu_\mu \rightarrow \nu_\mu$ vacuum oscillations.

14.7.2 3ν Oscillation Analysis

We summarize in Table 14.6 the different experiments which dominantly contribute to the present determination of the different parameters in the chosen convention.

The table illustrates that the determination of the leptonic parameters requires global analyses of the data from the different experiments. Over the years, these analyses have been in the hands of a few phenomenological groups. We show in Table 14.7 the results from the latest analyses in Refs. [184–187]. For the sake of comparison, all results are presented in the convention of the listing section as described above.

The table illustrates the dependence of the present determination of the parameters on variations of the statistical analysis performed by the different groups and on the data samples included. In that last respect, the main difference resides in the results from Super-Kamiokande atmospheric data [97] which, at present, can only be included in this analysis by directly adding the χ^2 tabulated χ^2 map provided by the experiment.

Altogether the different analyses find consistent results, in particular on the better-known parameters, θ_{12} , θ_{13} and Δm_{21}^2 and $|\Delta m_{32}^2|$. The issues which still require clarification are the mass ordering discrimination, the determination of θ_{23} and the leptonic CP phase δ_{CP} :

- In all analyses the best fit is for the normal mass ordering. Inverted ordering is disfavoured with a $\Delta\chi^2$, which ranges from slightly above 2σ – driven by the interplay of long-baseline accelerator and short-baseline reactor data – to 3σ when adding the atmospheric χ^2 table from Ref. [97].
- All analyses find some preference for the second octant of θ_{23} but with statistical significance still well below 3σ .
- The best fit for the complex phase in NO is at $\delta_{\text{CP}} \sim 120^\circ$, but CP conservation (for $\delta_{\text{CP}} \sim 180^\circ$) is still allowed at a confidence level (CL) of $1-2\sigma$. We notice that, at present, the significance of CP violation in the global analysis is reduced with respect to that reported by T2K [188] because NOvA data does not show a significant indication of CP violation.

14.7.3 Convention-independent Measures of Leptonic CP Violation in 3ν Mixing

In the framework of 3ν mixing leptonic CP violation can also be quantified in terms of the leptonic Jarlskog invariant [189],

Table 14.6: Experiments contributing to the present determination of the oscillation parameters.

Experiment	Dominant	Important
Solar Experiments	θ_{12}	$\Delta m_{21}^2, \theta_{13}$
Reactor LBL (KamLAND)	Δm_{21}^2	θ_{12}, θ_{13}
Reactor MBL (Daya-Bay, Reno, D-Chooz)	$\theta_{13}, \Delta m_{31,32}^2 $	
Atmospheric Experiments (SK, IC-DC)		$\theta_{23}, \Delta m_{31,32}^2 , \theta_{13}, \delta_{CP}$
Accel LBL $\nu_\mu, \bar{\nu}_\mu$, Disapp (K2K, MINOS, T2K, NO ν A)	$ \Delta m_{31,32}^2 , \theta_{23}$	
Accel LBL $\nu_e, \bar{\nu}_e$ App (MINOS, T2K, NO ν A)	δ_{CP}	θ_{13}, θ_{23}

Table 14.7: 3ν oscillation parameters obtained from different global analyses of neutrino data. In all cases, the numbers labeled as NO (IO) are obtained assuming NO (IO), *i.e.*, relative to the respective local minimum. SK-ATM makes reference to the tabulated χ^2 map from the Super-Kamiokande analysis of their data in Ref. [97].

Param	Ref. [185] w/o SK-ATM		Ref. [185] w SK-ATM		Ref. [186] w SK-ATM		Ref. [187] w SK-ATM	
	Best Fit Ordering		Best Fit Ordering		Best Fit Ordering		Best Fit Ordering	
	bfp $\pm 1\sigma$	3σ range	bfp $\pm 1\sigma$	3σ range	bfp $\pm 1\sigma$	3σ range	bfp $\pm 1\sigma$	3σ range
$\sin^2 \theta_{12}$	$3.10^{+0.13}_{-0.12}$	$2.75 \rightarrow 3.50$	$3.10^{+0.13}_{-0.12}$	$2.75 \rightarrow 3.50$	$3.04^{+0.14}_{-0.13}$	$2.65 \rightarrow 3.46$	$3.20^{+0.20}_{-0.16}$	$2.73 \rightarrow 3.79$
$\theta_{12}/^\circ$	$33.82^{+0.78}_{-0.76}$	$31.61 \rightarrow 36.27$	$33.82^{+0.78}_{-0.76}$	$31.61 \rightarrow 36.27$	$33.46^{+0.87}_{-0.88}$	$30.98 \rightarrow 36.03$	$34.5^{+1.2}_{-1.0}$	$31.5 \rightarrow 38.0$
$\sin^2 \theta_{23}$	$5.58^{+0.20}_{-0.33}$	$4.27 \rightarrow 6.09$	$5.63^{+0.18}_{-0.24}$	$4.33 \rightarrow 6.09$	$5.51^{+0.19}_{-0.80}$	$4.30 \rightarrow 6.02$	$5.47^{+0.20}_{-0.30}$	$4.45 \rightarrow 5.99$
$\theta_{23}/^\circ$	$48.3^{+1.2}_{-1.9}$	$40.8 \rightarrow 51.3$	$48.6^{+1.0}_{-1.4}$	$41.1 \rightarrow 51.3$	$47.9^{+1.1}_{-4.0}$	$41.0 \rightarrow 50.9$	$47.7^{+1.2}_{-1.7}$	$41.8 \rightarrow 50.7$
$\sin^2 \theta_{13}$	$2.241^{+0.066}_{-0.065}$	$2.046 \rightarrow 2.440$	$2.237^{+0.066}_{-0.065}$	$2.044 \rightarrow 2.435$	$2.14^{+0.09}_{-0.07}$	$1.90 \rightarrow 2.39$	$2.160^{+0.083}_{-0.069}$	$1.96 \rightarrow 2.41$
$\theta_{13}/^\circ$	$8.61^{+0.13}_{-0.13}$	$8.22 \rightarrow 8.99$	$8.60^{+0.13}_{-0.13}$	$8.22 \rightarrow 8.98$	$8.41^{+0.18}_{-0.14}$	$7.9 \rightarrow 8.9$	$8.45^{+0.16}_{-0.14}$	$8.0 \rightarrow 8.9$
$\delta_{CP}/^\circ$	222^{+38}_{-28}	$141 \rightarrow 370$	221^{+39}_{-28}	$144 \rightarrow 357$	238^{+41}_{-33}	$149 \rightarrow 358$	218^{+38}_{-27}	$157 \rightarrow 349$
$\frac{\Delta m_{21}^2}{10^{-5} \text{ eV}^2}$	$7.39^{+0.21}_{-0.20}$	$6.79 \rightarrow 8.01$	$7.39^{+0.21}_{-0.20}$	$6.79 \rightarrow 8.01$	$7.34^{+0.17}_{-0.14}$	$6.92 \rightarrow 7.91$	$7.55^{+0.20}_{-0.16}$	$7.05 \rightarrow 8.24$
$\frac{\Delta m_{32}^2}{10^{-3} \text{ eV}^2}$	$2.449^{+0.032}_{-0.030}$	$2.358 \rightarrow 2.544$	$2.454^{+0.029}_{-0.031}$	$2.362 \rightarrow 2.544$	$2.419^{+0.035}_{-0.032}$	$2.319 \rightarrow 2.521$	2.424 ± 0.03	$2.334 \rightarrow 2.524$
IO	$\Delta\chi^2 = 6.2$		$\Delta\chi^2 = 10.4$		$\Delta\chi^2 = 9.5$		$\Delta\chi^2 = 11.7$	
$\sin^2 \theta_{12}$	$3.10^{+0.13}_{-0.12}$	$2.75 \rightarrow 3.50$	$3.10^{+0.13}_{-0.12}$	$2.75 \rightarrow 3.50$	$3.03^{+0.14}_{-0.13}$	$2.64 \rightarrow 3.45$	$3.20^{+0.20}_{-0.16}$	$2.73 \rightarrow 3.79$
$\theta_{12}/^\circ$	$33.82^{+0.78}_{-0.76}$	$31.61 \rightarrow 36.27$	$33.82^{+0.78}_{-0.75}$	$31.62 \rightarrow 36.27$	$33.40^{+0.87}_{-0.81}$	$30.92 \rightarrow 35.97$	$34.5^{+1.2}_{-1.0}$	$31.5 \rightarrow 38.0$
$\sin^2 \theta_{23}$	$5.63^{+0.19}_{-0.26}$	$4.30 \rightarrow 6.12$	$5.65^{+0.17}_{-0.22}$	$4.36 \rightarrow 6.10$	$5.57^{+0.17}_{-0.24}$	$4.44 \rightarrow 6.03$	$5.51^{+0.18}_{-0.30}$	$4.53 \rightarrow 5.98$
$\theta_{23}/^\circ$	$48.6^{+1.1}_{-1.5}$	$41.0 \rightarrow 51.5$	$48.8^{+1.0}_{-1.2}$	$41.4 \rightarrow 51.3$	$48.2^{+1.0}_{-1.4}$	$41.8 \rightarrow 50.9$	$47.9^{+1.0}_{-1.7}$	$42.3 \rightarrow 50.7$
$\sin^2 \theta_{13}$	$2.261^{+0.067}_{-0.064}$	$2.066 \rightarrow 2.461$	$2.259^{+0.065}_{-0.065}$	$2.064 \rightarrow 2.457$	$2.18^{+0.08}_{-0.07}$	$1.95 \rightarrow 2.43$	$2.220^{+0.074}_{-0.076}$	$1.99 \rightarrow 2.44$
$\theta_{13}/^\circ$	$8.65^{+0.13}_{-0.12}$	$8.26 \rightarrow 9.02$	$8.64^{+0.12}_{-0.13}$	$8.26 \rightarrow 9.02$	$8.49^{+0.15}_{-0.14}$	$8.0 \rightarrow 9.0$	$8.53^{+0.14}_{-0.15}$	$8.1 \rightarrow 9.0$
$\delta_{CP}/^\circ$	285^{+24}_{-26}	$205 \rightarrow 354$	282^{+23}_{-25}	$205 \rightarrow 348$	247^{+26}_{-27}	$193 \rightarrow 346$	281^{+23}_{-27}	$202 \rightarrow 349$
$\frac{\Delta m_{21}^2}{10^{-5} \text{ eV}^2}$	$7.39^{+0.21}_{-0.20}$	$6.79 \rightarrow 8.01$	$7.39^{+0.21}_{-0.20}$	$6.79 \rightarrow 8.01$	$7.34^{+0.17}_{-0.14}$	$6.92 \rightarrow 7.91$	$7.55^{+0.20}_{-0.16}$	$7.05 \rightarrow 8.24$
$\frac{\Delta m_{32}^2}{10^{-3} \text{ eV}^2}$	$-2.509^{+0.032}_{-0.032}$	$-2.603 \rightarrow -2.416$	$-2.510^{+0.030}_{-0.031}$	$-2.601 \rightarrow -2.419$	$-2.478^{+0.035}_{-0.033}$	$-2.577 \rightarrow -2.375$	-2.50 ± 0.04	$-2.59 \rightarrow -2.39$

defined by:

$$\begin{aligned} \Im[U_{\alpha i} U_{\alpha j}^* U_{\beta i} U_{\beta j}] &\equiv \sum_{\gamma=e,\mu,\tau} \sum_{k=1,2,3} J_{CP} \epsilon_{\alpha\beta\gamma} \epsilon_{ijk} \\ &\equiv J_{CP}^{\max} \sin \delta_{CP}. \end{aligned} \quad (14.84)$$

 With the convention in Eq. (14.33) J_{CP}^{\max} is the combination of mixing angles in Eq. (14.78). For example, from the analysis in Ref. [184, 185]

$$J_{CP}^{\max} = 0.03359 \pm 0.0006 (\pm 0.0019), \quad (14.85)$$

 at 1σ (3σ) for both orderings, and the preference of the present data for non-zero δ_{CP} implies a non-zero best fit value $J_{CP}^{\text{best}} = -0.019$.

 The status of the determination of leptonic CP violation can also be graphically displayed by projecting the results of the global analysis in terms of leptonic unitarity triangles [190–192]. Since in the analysis U is unitary by construction, any given pair of rows or columns can be used to define a triangle in the complex plane. There are a total of six possible triangles corresponding to

the unitary conditions

$$\sum_{i=1,2,3} U_{\alpha i} U_{\beta i}^* = 0 \text{ with } \alpha \neq \beta, \quad \sum_{\alpha=e,\mu,\tau} U_{\alpha i} U_{\alpha j}^* = 0 \text{ with } i \neq j. \quad (14.86)$$

 As an illustration we show in Fig. 14.9 the recasting of the allowed regions of the analysis in Ref. [184, 185] in terms of one leptonic unitarity triangle. We show the triangle corresponding to the unitarity conditions on the first and third columns (after the shown rescaling), which is the equivalent to the one usually shown for the quark sector. In this figure, the absence of CP violation would imply a flat triangle, *i.e.*, $\Im(z) = 0$. So the CL at which leptonic CP violation is being observed would be given by the CL at which the region crosses the horizontal axis. Notice however, that this representation is made *under the assumption of a unitary U matrix* and therefore does not provide any test of unitarity in the leptonic sector.

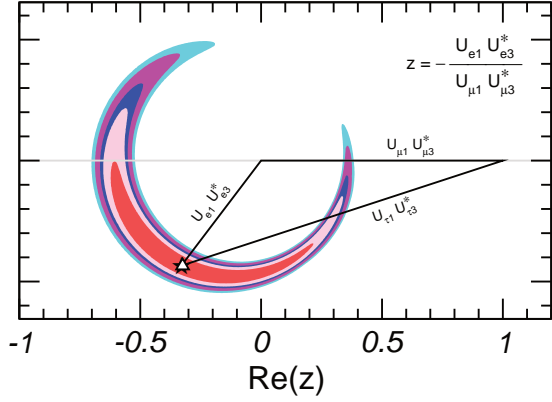


Figure 14.9: Leptonic unitarity triangle for the first and third columns of the mixing matrix. After scaling and rotating the triangle so that two of its vertices always coincide with (0, 0) and (1, 0) the figure shows the 1σ , 90%, 2σ , 99%, 3σ CL (2 dof) allowed regions of the third vertex for the NO from the analysis in Ref. [184, 185].

14.8 Beyond 3ν : Additional Neutrinos at the eV Scale

Besides the huge success of three-flavour oscillations described in Sec.14.7, as mentioned in Secs.14.6.3 and 14.6.4, there are some anomalies which cannot be explained within the 3ν framework and which might point towards the existence of additional neutrino states with masses at the eV scale. In brief:

- the LSND experiment [129] reports evidence for $\bar{\nu}_\mu \rightarrow \bar{\nu}_e$ transitions with $E/L \sim 1 \text{ eV}^2$, where E and L are the neutrino energy and the distance between source and detector, respectively (see *Short Baseline Experiments* subsection of Sec.14.6.3).
- this effect has also been searched for by the MiniBooNE experiment [193], which reports a yet unexplained event excess in the low-energy region of the electron neutrino and antineutrino event spectra. No significant excess is found at higher neutrino energies. Interpreting the data in terms of oscillations, parameter values consistent with the ones from LSND are obtained, but the test is not definitive;
- radioactive source experiments at the Gallium solar neutrino experiments both in SAGE and GALLEX/GNO have obtained an event rate that is somewhat lower than expected. If not due to uncertainties in the interaction cross-section, this effect can be explained by the hypothesis of ν_e disappearance due to oscillations with $\Delta m^2 \gtrsim 1 \text{ eV}^2$ (“Gallium anomaly”) [194, 195];
- new calculations of the neutrino flux emitted by nuclear reactors [138, 139] predict a neutrino rate that is a few percent higher than observed in short-baseline ($L \lesssim 100 \text{ m}$) reactor experiments⁵. If not due to systematic or theoretical uncertainties, a decrease rate at those distances can be explained by assuming $\bar{\nu}_e$ disappearance due to oscillations with $\Delta m^2 \sim 1 \text{ eV}^2$ (“reactor anomaly”) [198]. This reactor anomaly is under study both by the experimental community – with a set of follow-up measurements performed at SBL both at reactors and accelerators (see the corresponding subsections in Sec.14.6.4 and Sec.14.6.3) –, and by the theory community for improvements of the reactor flux calculations.

As mentioned in Sec.14.1, whatever the extension of the SM we want to consider, it must contain only three light active neutrinos. Therefore if we need more than three light massive neutrinos, we must add sterile neutrinos to the particle content of the model.

⁵However, as discussed in Sec.14.6.4, the reactor antineutrino flux measurement at Daya Bay [196, 197] is consistent with the old flux predictions and the flux measurement results in the previous short-baseline reactor neutrino oscillation experiments.

The most immediate question as these anomalies were reported was whether they could all be consistently described in combination with the rest of the neutrino data – in particular with the negative results on the disappearance of ν_μ at short distances – if one adds those additional sterile states. Quantitatively one can start by adding a fourth massive neutrino state to the spectrum and perform a global data analysis to answer this question. Although the answer is always the same, the physical reason behind it depends on ordering assumed for the states. In brief, there are six possible four-neutrino schemes that can, in principle, accommodate the results of solar+KamLAND and atmospheric+LBL neutrino experiments as well as the SBL result. They can be divided into two classes: (2+2) and (3+1). In the (3+1) schemes, there is a group of three close-by neutrino masses (as on the 3ν schemes described in the previous section) that is separated from the fourth one by a gap of the order of 1 eV, which is responsible for the SBL oscillations. In (2+2) schemes, there are two pairs of close masses (one pair responsible for solar results and the other for atmospheric [199]) separated by the $\mathcal{O}(\text{eV})$ gap. The main difference between these two classes is the following: if a (2+2)-spectrum is realized in nature, the transition into the sterile neutrino is a solution of either the solar or the atmospheric neutrino problem, or the sterile neutrino takes part in both. Consequently, a (2+2)-spectrum is easier to test because the required mixing of sterile neutrinos in either solar and/or atmospheric oscillations would modify their effective matter potential in the Sun and in the Earth, giving distinctive effects in the solar and/or atmospheric neutrino observables. Those distinctive effects were not observed so oscillations into sterile neutrinos did not describe well either solar or atmospheric data. Consequently, as soon as the early 2000’s 2+2 spectra could be ruled out already beyond 3-4 σ as seen in the left panel in Fig.14.10 taken from Ref. [200].

On the contrary, for a (3+1)-spectrum (and more generally for a $3+N$ -spectrum with an arbitrary N number of sterile states), the sterile neutrino(s) could be only slightly mixed with the active ones and mainly provide a description of the SBL results. In this case, the oscillation probabilities for experiments working at $E/L \sim 1 \text{ eV}^2$ take a simple form:

$$P_{\alpha\alpha} = 1 - \sin^2 2\theta_{\alpha\alpha} \sin^2 \Delta, \quad P_{\mu e} = \sin^2 2\theta_{\mu e} \sin^2 \Delta, \quad (14.87)$$

where $\Delta \equiv \Delta m_{41}^2 L/4E$ and one can define effective mixing angles

$$\sin^2 2\theta_{\alpha\alpha} \equiv 4|U_{\alpha 4}|^2(1 - |U_{\alpha 4}|^2), \quad \sin^2 2\theta_{\mu e} \equiv 4|U_{\mu 4}|^2|U_{e 4}|^2. \quad (14.88)$$

In here $\alpha = e, \mu$ and $U_{\alpha 4}$ are the elements of the lepton mixing matrix describing the mixing of the 4th neutrino mass state with the electron and muon flavour. In this scenario, there is no sensitivity to CP violation in the Δ driven oscillations, so the relations above are valid for both neutrinos and antineutrinos. At linear order in the mixing elements one can derive a relation between the amplitudes of appearance and disappearance probabilities:

$$4 \sin^2 2\theta_{\mu e} \approx \sin^2 2\theta_{ee} \sin^2 2\theta_{\mu\mu}. \quad (14.89)$$

This relation implies a constraint between the possible results in disappearance and appearance experiments. Consequently, it is not trivial to find a consistent description to all the SBL anomalies. Over the years, different groups have performed a variety of such global analyses leading to different quantitative conclusions on the statistical quality of the global fit (see for example [201–206], see also Refs. [207, 208] for recent reviews on the subject). Generically, the results of the global analysis show that there is significant tension between groups of different data sets – in particular between appearance and disappearance results – and Eq.(14.89) makes it difficult to obtain a good global fit as illustrated in the right panel in Fig.14.10 taken from Ref. [201] which concluded that 3+1 scenario is excluded at 4.7σ level.

A straightforward question to ask is whether the situation improves if more neutrino states at the eV scale are introduced. The simplest extension is the introduction of 2 states with eV mass splittings, ν_4 and ν_5 . The ordering of the states can be such that Δm_{41}^2 and Δm_{51}^2 are both positive (“3+2”), or one of them

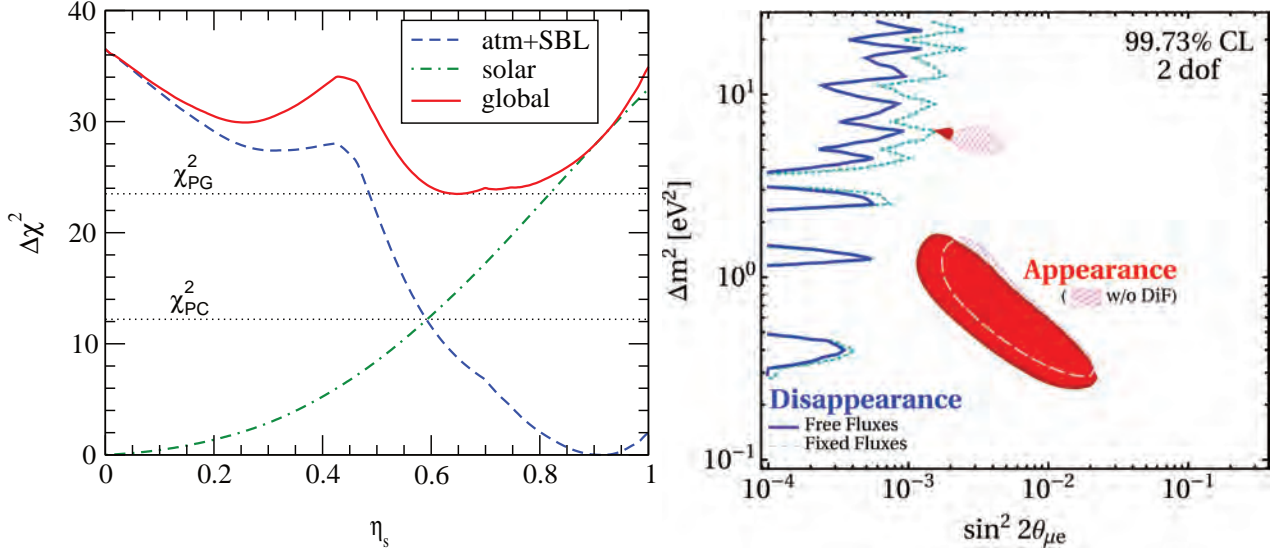


Figure 14.10: *Left:* Status of the 2+2 oscillation scenarios from Ref. [200] ($\eta_s = \sum_i |U_{is}|^2$ where i runs over the two massive states mostly relevant for solar neutrino oscillations). In the figure also shown are the values of χ_{PC}^2 and χ_{PG}^2 relevant for parameter consistency test and parameter goodness of fit, respectively. *Right:* Present status of 3+1 oscillation scenarios from Ref. [201].

is negative (“1+3+1”). From the point of view of the description of the data, the most important new qualitative feature is that now, non-zero CP violation at $E/L \sim eV^2$ is possibly observable [204, 209–211]. This allows some additional freedom in fitting neutrino versus antineutrino data from LSND and MiniBooNE together. However, it still holds that a non-zero $\nu_\mu \rightarrow \nu_e$ appearance at SBL necessarily predicts SBL disappearance for both ν_e and ν_μ . So, generically, the tension between appearance and disappearance results remains, though differences in the methodology of statistical quantification of the degree of agreement/disagreement in these scenarios can lead to different conclusions on whether they can provide a successful description of all the data [201, 207, 208]. Cosmological observations can provide complementary information on the number of relativistic neutrino states in thermal equilibrium in the early Universe and on the sum of their masses, which sets further constraints on light sterile neutrino scenarios (see Chapter 26 of this *Review*, “Neutrinos in cosmology”).

14.9 Laboratory Probes of ν Mass Scale and its Nature

As described in Secs. 14.4 and 14.5, neutrino flavour oscillations in vacuum and flavour transitions in matter only depend on the differences between the neutrino masses-squared, Δm_{ij}^2 , and on the mixing matrix elements, U_{ij} . However, they are insensitive to the absolute mass scale for the neutrinos, m_i . They also give us no information on whether they are Dirac or Majorana particles.

Clearly, the observation of flavour oscillations implies a lower bound on the mass of the heavier neutrino in Δm_{ij}^2 , $|m_i| \geq \sqrt{\Delta m_{ij}^2}$ for $\Delta m_{ij}^2 > 0$. However, there is no upper bound on m_i . In particular, oscillation results allow the neutrino spectrum to be approximately degenerate at a mass scale that is much higher than the $\sqrt{\Delta m_{ij}^2}$ that they determine. Information of the mass scale of the neutrino is provided by other types of experiments. Here we briefly summarize the most sensitive laboratory probes of the neutrino mass scale and on whether they are Dirac or Majorana particles. Cosmological observations provide, albeit indirectly, complementary information on the neutrino mass scale as it is reviewed in Chapter 26 of this *Review*, “Neutrinos in cosmology”.

14.9.1 Constraints from Kinematics of Weak Decays

The only model-independent information on the neutrino masses, rather than mass differences, can be extracted from energy-momentum conservation relation in reactions in which a

neutrino or an antineutrino is involved.

Historically these bounds were labeled as limits on the mass of the flavour neutrino states corresponding to the charged flavour involved in the decay. Fermi proposed in 1933 such a kinematic search for the ν_e neutrino mass (which we will label here as $m_{\nu_e}^{\text{eff}}$) in the end part of the beta spectra in ${}^3\text{H}$ beta decay ${}^3\text{H} \rightarrow {}^3\text{He} + e^- + \bar{\nu}_e$.

Because ${}^3\text{H}$ beta decay is a superallowed transition, the nuclear matrix elements are energy independent, so the electron spectrum is determined exclusively by the phase space

$$\begin{aligned} \frac{dN}{dE} &= C p E (Q - T) \sqrt{(Q - T)^2 - (m_{\nu_e}^{\text{eff}})^2} F(E) \\ &\equiv R(E) \sqrt{(E_0 - E)^2 - (m_{\nu_e}^{\text{eff}})^2}. \end{aligned} \quad (14.90)$$

E_0 is the mass difference between the initial and final nucleus, $E = T + m_e$ is the total electron energy, p its momentum, $Q \equiv E_0 - m_e$ is the maximum kinetic energy of the electron and Final state Coulomb interactions are contained in the Fermi function $F(E)$. $R(E)$ in the second equality contains all the m_{ν_e} -independent factors.

The Kurie function is defined as $K(T) \equiv \sqrt{\frac{dN}{dE} \frac{1}{pEF(E)}}$. From Eq.(14.90), we see that if $m_{\nu_e}^{\text{eff}} = 0$ $K(T)$ would depend linearly on T . A non-vanishing neutrino mass then provokes a distortion from the straight-line T -dependence at the endpoint. So for $m_{\nu_e}^{\text{eff}} = 0$, $T_{\text{max}} = Q$, while for $m_{\nu_e}^{\text{eff}} \neq 0$, $T_{\text{max}} = Q - m_{\nu_e}^{\text{eff}}$. In ${}^3\text{H}$ beta decay $Q = 18.6$ KeV is very small and therefore, this decay is more sensitive to this $m_{\nu_e}^{\text{eff}}$ -induced distortion.

The most recent result on the kinematic search for neutrino mass in tritium decay is from KATRIN [212], an experiment which has found so far no indication of $m_{\nu_e} \neq 0$ and sets an upper limit

$$m_{\nu_e}^{\text{eff}} < 1.1 \text{ eV}, \quad (14.91)$$

at 90% CL improving over the previous bound from the Mainz [213] and Troitsk [214] experiments which constrained $m_{\nu_e}^{\text{eff}} < 2.2$ eV at 95% CL. KATRIN continues running with an estimated sensitivity limit of $m_{\nu_e}^{\text{eff}} \sim 0.2$ eV. Project 8 is exploring a new technique for β -spectrometry based on cyclotron radiation [215].

An alternative isotope to Tritium is ${}^{163}\text{Ho}$ [216] which presents the advantage of a smaller $Q = 2.8$ KeV. It decays via electron capture to ${}^{163}\text{Dy}$. Currently, there are three experiments

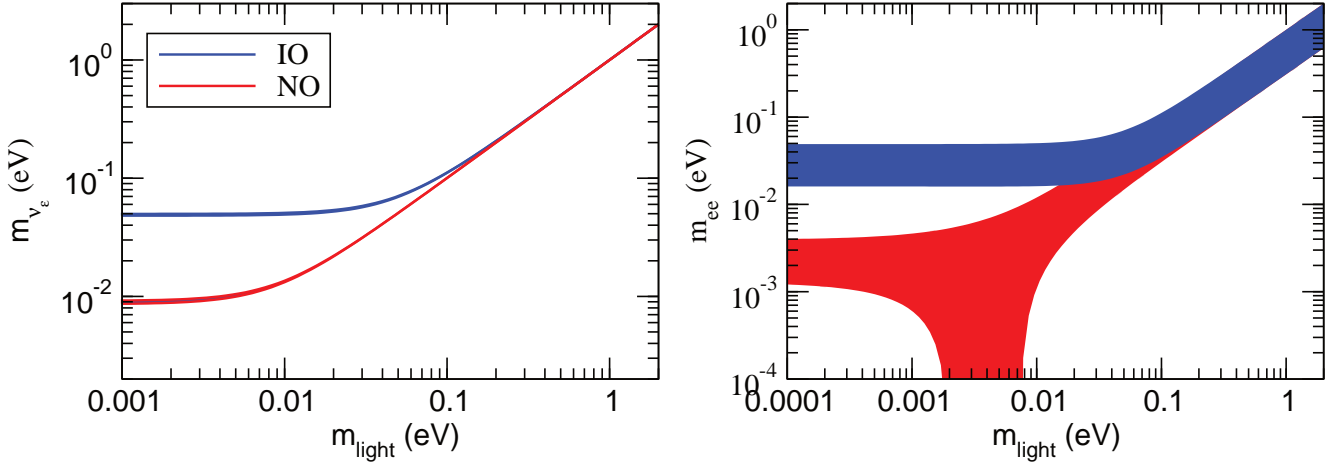


Figure 14.11: Allowed 95% CL ranges (1 dof) for the neutrino mass observable determined in ${}^3\text{H}$ beta decay (left panel) and in $0\nu\beta\beta$ (right panel) in the framework of 3ν mixing as a function of the lightest neutrino mass. The ranges are obtained by projecting the results of the global analysis of oscillation data (w/o SK-atm) in Ref. [184]. The region for each ordering is defined with respect to its local minimum.

exploring this decay to probe the neutrino mass: ECHO [217], HOLMES [218], and NuMECS [219]. These experiments are complementary to tritium-based searches from a technical point of view. Also, the decay of ${}^{163}\text{Ho}$ determines the effective electron neutrino mass as opposed to antineutrino in Tritium.

For the other flavours the present limits compiled in the listing section of the PDG read

$$m_{\nu_\mu}^{\text{eff}} < 190 \text{ keV (90\% CL)} \quad \text{from} \quad \pi^- \rightarrow \mu^- + \bar{\nu}_\mu, \quad (14.92)$$

$$m_{\nu_\tau}^{\text{eff}} < 18.2 \text{ MeV (95\% CL)} \quad \text{from} \quad \tau^- \rightarrow n\pi + \nu_\tau. \quad (14.93)$$

In the presence of mixing and for neutrinos with small mass differences, the distortion of the beta spectrum is given by the sum of the individual spectra generated incoherently by each neutrino massive state weighted with the relevant mixing matrix element squared [220]:

$$\frac{dN}{dE} = R(E) \sum_i |U_{ei}|^2 \sqrt{(E_0 - E)^2 - m_i^2} \Theta(E_0 - E - m_i). \quad (14.94)$$

The step function $\Theta(E_0 - E - m_i)$ arises because a neutrino with a given mass m_i can only be produced if the available energy is larger than its mass. Equation (14.94) shows the two main effects of the neutrino masses and mixings on the electron energy spectrum: First, kinks appear at the electron energies $E_e^{(i)} = E \sim E_0 - m_i$ with sizes that are determined by $|U_{ei}|^2$. Second, the endpoint shifts to $E_{\text{ep}} = E_0 - m_0$, where m_0 is the lightest neutrino mass. Corrections are induced once the energy resolution of the experiment is considered. [221, 222]

In the 3ν mixing scenario, the distortion of the spectrum can still be effectively described by a single parameter – which we will still denote as m_{ν_e} – if for all neutrino states $E_0 - E = Q - T \gg m_i$. In this case, one can expand Eq.(14.94) as:

$$\frac{dN}{dE} \simeq R(E) \sum_i |U_{ei}|^2 \sqrt{(E_0 - E)^2 - (m_{\nu_e}^{\text{eff}})^2}, \quad (14.95)$$

with

$$(m_{\nu_e}^{\text{eff}})^2 = \frac{\sum_i m_i^2 |U_{ei}|^2}{\sum_i |U_{ei}|^2} = \sum_i m_i^2 |U_{ei}|^2, \quad (14.96)$$

where unitarity is assumed in the second equality. In this approximation, the distortion of the endpoint of the spectrum is described by a single parameter, and with the present results from KATRIN,

it is bounded to be

$$1.1 \text{ eV} \geq m_{\nu_e}^{\text{eff}} = \sqrt{\sum_i m_i^2 |U_{ei}|^2} = \begin{cases} \sqrt{m_0^2 + \Delta m_{21}^2 (1 - c_{13}^2 c_{12}^2) + \Delta m_{32}^2 s_{13}^2} & \text{in NO,} \\ \sqrt{m_0^2 + \Delta m_{21}^2 c_{13}^2 c_{12}^2 - \Delta m_{32}^2 c_{13}^2} & \text{in IO,} \end{cases} \quad (14.97)$$

where $m_0 = m_1$ (m_3) is the lightest neutrino mass in the NO (IO) spectrum. Correspondingly the bounds in Eqs.(14.92) and (14.93) apply to the combinations $\sum_i m_i^2 |U_{\alpha i}|^2$ for $\alpha = \mu$ and τ respectively. So with the values known of the mixing matrix elements, the strongest constraint on the absolute value of the neutrino mass comes from Tritium beta decay.

From Eq.(14.97) we see that, given the present knowledge of the neutrino mass differences and their mixing from oscillation experiments, it is possible to translate the experimental information of m_{ν_e} on a corresponding range for the lightest neutrino mass and that such relation depends on the ordering of the states. We plot in Fig.14.11 the recasting of the allowed regions of the analysis in Ref. [184] in terms of the allowed range m_{ν_e} as a function of $m_{\text{light}} \equiv m_0$. In particular, one finds that the results of oscillation experiments imply a lower bound on $m_{\nu_e} > 0.048$ (0.0085) eV for IO (NO) at 95% CL.

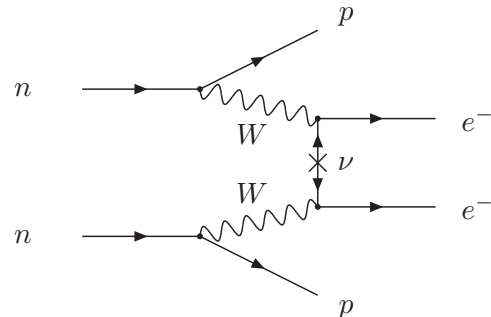


Figure 14.12: Feynman diagram for neutrinoless double-beta decay.

14.9.2 Dirac vs. Majorana: Neutrinoless Double-beta Decay

The most sensitive probe to whether neutrinos are Dirac or Majorana states is the neutrinoless double beta decay ($0\nu\beta\beta$):

$$(A, Z) \rightarrow (A, Z + 2) + e^- + e^-. \quad (14.98)$$

In the presence of neutrino masses and mixing, the process in Eq.(14.98) can be generated at lower order in perturbation theory by the term represented in Fig.14.12. The corresponding amplitude is proportional to the product of the two leptonic currents

$$M_{\alpha\beta} \propto [\bar{e}\gamma_\alpha(1-\gamma_5)\nu_e] [\bar{e}\gamma_\beta(1-\gamma_5)\nu_e] \\ \propto \sum_i (U_{ei})^2 [\bar{e}\gamma_\alpha(1-\gamma_5)\nu_i] [\bar{e}\gamma_\beta(1-\gamma_5)\nu_i]. \quad (14.99)$$

The neutrino propagator in Fig.14.12 can only arise from the contraction $\langle 0 | \nu_i(x)\nu_i(y)^T | 0 \rangle$. However, if the neutrino is a Dirac particle ν_i field annihilates a neutrino state and creates an antineutrino state, and neutrino and antineutrino states are different, so the contraction $\langle 0 | \nu_i(x)\nu_i(y)^T | 0 \rangle = 0$ and $M_{\alpha\beta} = 0$. On

the other hand, if ν_i is a Majorana particle, neutrino and antineutrino are described by the same field and $\langle 0 | \nu_i(x)\nu_i(y)^T | 0 \rangle \neq 0$.

The conclusion is that in order to induce the $0\nu\beta\beta$ decay, neutrinos must be Majorana particles. This is consistent with the fact that the process (14.98) violates the total lepton number by two units. Conversely, if $0\nu\beta\beta$ decay is observed, massive neutrinos cannot be Dirac states [223].

It is important to stress that neutrinoless double-beta decay could be dominantly induced by other new physics effects beyond that of Majorana neutrino masses. Consequently, the connection between the observation or limitation of the neutrinoless double beta decay and the neutrino mass can only be made under some assumption about the source of total lepton number violation in the model.

The observable determined by the experiments is the half-life of the decay. Under the assumption that the Majorana neutrino mass is the only source of lepton number violation at low energies, the decay half-life is given by:

$$(T_{1/2}^{0\nu})^{-1} = G^{0\nu} |M^{0\nu}|^2 \left(\frac{m_{ee}}{m_e}\right)^2, \quad (14.100)$$

where $G^{0\nu}$ is the phase space integral taking into account the final atomic state, $|M^{0\nu}|$ is the nuclear matrix element of the transition, and m_{ee} is the *effective Majorana mass* of ν_e ,

$$m_{ee} = \left| \sum_i m_i U_{ei}^2 \right| \\ = \begin{cases} \left| m_0 c_{12}^2 c_{13}^2 + \sqrt{\Delta m_{21}^2 + m_0^2 s_{12}^2 c_{13}^2} e^{2i(\eta_2 - \eta_1)} + \sqrt{\Delta m_{32}^2 + \Delta m_{21}^2 + m_0^2 s_{13}^2} e^{-2i(\delta_{CP} + \eta_1)} \right| & \text{in NO,} \\ \left| m_0 s_{13}^2 + \sqrt{m_0^2 - \Delta m_{32}^2 s_{12}^2 c_{13}^2} e^{2i(\eta_2 + \delta_{CP})} + \sqrt{m_0^2 - \Delta m_{32}^2 - \Delta m_{21}^2} c_{12}^2 c_{13}^2 e^{2i(\eta_1 + \delta_{CP})} \right| & \text{in IO,} \end{cases}$$

which, in addition to the masses and mixing parameters that affect the tritium beta decay spectrum, also depends on the leptonic CP -violating phases. We plot in Fig.14.11 the recasting of the allowed regions of the analysis in Ref. [184] in terms of the allowed range m_{ee} as a function of $m_{\text{light}} \equiv m_0$ for the two orderings. As a consequence of the dependence on the unknown Majorana phases, the allowed range of m_{ee} for a given value of m_{light} and ordering is substantially broader than that of m_{ν_e} . Nevertheless, the results of oscillation experiments imply a lower bound on the effective Majorana mass for the IO, which at 95%CL reads $m_{ee} > 0.016$ eV.

From Eq.(14.100) we see that nuclear structure details enter relation between the decay rate (or lifetime) and the effective Majorana mass. As a consequence, uncertainties in the nuclear structure calculations result in a spread of m_{ee} values for a given $T_{1/2}^{0\nu}$ by a factor of 2–3 [224].

We present in Sec.14.9.3 a brief description of the experimental searches for neutrinoless double-beta decay. At the time of writing of this review, the strongest bound on $0\nu\beta\beta$ decay lifetimes came for Xenon and Germanium from the KamLAND-Zen [225] and GERDA [226] experiments, respectively. They have set a bound on the corresponding half-lives of $T_{1/2}^{0\nu} > 1.07 \times 10^{26}$ yr, and $T_{1/2}^{0\nu} > 1.8 \times 10^{26}$ yr, at 90% CL. Using a variety of nuclear matrix element calculations, the corresponding upper bounds on the effective Majorana mass are

$$m_{ee} < 61 - 165 \text{ meV} \quad (14.101)$$

$$m_{ee} < 79 - 180 \text{ meV}. \quad (14.102)$$

14.9.3 Experimental Search for Neutrinoless Double-beta Decay

There are 35 candidate nuclei for double-beta decay. Currently, experiments using ^{136}Xe and ^{76}Ge have reported the most sensitive results of $0\nu\beta\beta$ search. Because of the uncertainties related to the nuclear matrix element, the complementarity of technologies, different backgrounds, and the investigation of the mechanism behind the $0\nu\beta\beta$ in case of a positive signal, it is important to pursue

the searches with as many isotopes as possible.

The signature of $0\nu\beta\beta$ is that the sum of the energy of two electrons is equal to the Q -value of the nuclear transition. The energy from electrons is measured with either ionization, scintillation, or through phonons. In some experiments, a combination of two techniques is used to enhance the sensitivity. In the case of background-free measurement, the sensitivity to the half-life is proportional to the product of the detection efficiency of the signal ε , the source mass M , and the measurement time t . If background exists, it is proportional to $\varepsilon \sqrt{\frac{Mt}{b\Delta E}}$, where b is the background rate, and ΔE is the energy resolution.

Among the experiments using ionization detection, ultra-high-purity germanium detector provides the best sensitivity thanks to high energy resolution and low background. GERDA, in its final phase, used a total of 20.0 kg of broad energy germanium (BEGE), 14.6 kg of coaxial detectors, and 9.6 kg of inverted coaxial detectors. A background level of $(5.2^{+1.6}_{-1.3}) \times 10^{-4}$ counts/(keV.kg.year) was achieved [226], which enabled a background-free search. The final result from GERDA for the half-life limit for $0\nu\beta\beta$ decay of ^{76}Ge is $T_{1/2} > 1.8 \times 10^{26}$ years at 90% CL. The Majorana Demonstrator [227] consisted of 44.1 kg of Ge (29.7 kg enriched to 88% in ^{76}Ge) detectors split between two modules. It achieved energy resolution of 2.53 keV FWHM (full width at half maximum) at the Q -value (2.039 MeV). GERDA and Majorana collaborations have united and formed, together with new groups, the LEGEND collaboration. LEGEND has adopted a phased approach toward the deployment of a tonne of enriched Ge detectors [228]. The first phase of LEGEND, based on 200 kg of enriched Ge and using the GERDA infrastructure at LNGS, is expected to start in 2022. The second phase of LEGEND is planned as a one-ton experiment in a new cryostat, reaching a discovery sensitivity of half-life beyond 10^{28} years.

Liquid scintillator detectors have a simple structure and can utilize existing large detectors with low background environments. By adding an inner balloon to contain xenon-loaded liquid scintillator to the KamLAND detector, KamLAND-Zen used 380 kg of xenon with 90.1% enrichment in ^{136}Xe . Reducing the background

level by purification of scintillator, KamLAND-Zen reported the half-life limit above 10^{26} years at 90% CL [225]. KamLAND-Zen has been accumulating more data with about 750 kg of enriched xenon. The SNO detector has also been upgraded to be filled with a liquid scintillator in the SNO+ experiment [229]. The SNO+ detector will be loaded with 0.5% natural tellurium, corresponding to approximately 1.3 t of ^{130}Te , to search for $0\nu\beta\beta$.

With a time projection chamber, one can utilize both ionization and scintillation. EXO-200 used a liquid xenon time projection chamber with enrichment to 80.6%, corresponding to 74.7 kg of ^{136}Xe in the fiducial mass [230]. An energy resolution of 1.15% (σ/E) is achieved at the Q-value of ^{136}Xe $0\nu\beta\beta$. Based on the technology validated by EXO-200, nEXO plans to use 5,000 kg of xenon enriched to 90% in ^{136}Xe to achieve beyond 10^{28} year half-life sensitivity [231,232]. NEXT has been developing a high-pressure xenon gas time projection chamber with electroluminescence amplification and optical readouts. An energy resolution of 1% FWHM at the Q-value of ^{136}Xe $0\nu\beta\beta$ is demonstrated with NEXT-White detector [233]. NEXT proved background suppression by exploiting differences in the spatial ionization patterns of double beta decay and single-electron events [234]. A robust identification of signal is possible by tagging Ba^{2+} ions produced in ^{136}Xe decay. NEXT [235–238] and nEXO [239] have made significant progress in this technology. AXEL develops a cellular readout structure based on electroluminescence for the ^{136}Xe $0\nu\beta\beta$ search using a high-pressure xenon gas time projection chamber [240].

CUORE uses a cryogenic bolometer to measure the energy in a calorimetric way. The detector is located in Gran Sasso and composed of 988 TeO_2 bolometers for a total mass of 742 kg, corresponding to 206 kg of ^{130}Te . An effective energy resolution of (7.0 ± 0.4) keV FWHM is achieved [241]. For further reduction of background towards future search based on the CUORE technology, CUPID proposes to simultaneously measure the calorimetric signal and the scintillation light with a tonne-scale bolometric detector [242]. Using the prototype CUPID-0, the technology is demonstrated, and $0\nu\beta\beta$ is also searched for with ^{82}Se [243] and ^{100}Mo [244].

AMoRE also uses the simultaneous detection of heat and scintillation. Six ^{100}Mo -enriched and ^{48}Ca -depleted CaMoO_4 crystals with a total mass of 1.9 kg (AMoRE-Pilot) are operated in Yangyang underground laboratory located in South Korea, searching for $0\nu\beta\beta$ of ^{100}Mo [245]. Currently, AMoRE-I experiment [246] using 13 enriched CaMoO_4 crystals and 5 enriched Li_2MoO_4 crystals (6 kg total mass) is under operation in Yemilab.

A tracker-calorimeter technique is employed in NEMO. Source isotopes are hosted in thin foils surrounded by a tracking detector, which in turn is surrounded by a calorimeter. Full topological event reconstruction with this configuration enables background rejection and gives additional information after discovery. The NEMO-3 experiment used 7 isotopes, with the largest mass comprised of ^{100}Mo (7 kg) [247]. NEMO-3 also reported the first search for neutrinoless quadruple- β decay of ^{150}Nd [248].

References

- [1] J. N. Bahcall, *NEUTRINO ASTROPHYSICS* (1989), ISBN 9780521379755.
- [2] R. N. Mohapatra and P. B. Pal, World Sci. Lect. Notes Phys. **60**, 1 (1998), [World Sci. Lect. Notes Phys.72,1(2004)].
- [3] C. W. Kim and A. Pevsner, Contemp. Concepts Phys. **8**, 1 (1993).
- [4] B. Kayser, F. Gibrat-Debu and F. Perrier, World Sci. Lect. Notes Phys. **25**, 1 (1989).
- [5] C. Giunti and C. W. Kim, *Fundamentals of Neutrino Physics and Astrophysics* (2007), ISBN 9780198508717.
- [6] M. C. Gonzalez-Garcia and Y. Nir, Rev. Mod. Phys. **75**, 345 (2003), [hep-ph/0202058].
- [7] M. C. Gonzalez-Garcia and M. Maltoni, Phys. Rept. **460**, 1 (2008), [arXiv:0704.1800].
- [8] A. Pilaftsis, Z. Phys. **C55**, 275 (1992), [hep-ph/9901206].
- [9] P. Minkowski, Phys. Lett. **67B**, 421 (1977).
- [10] P. Ramond, in “International Symposium on Fundamentals of Quantum Theory and Quantum Field Theory,” (1979), [hep-ph/9809459].
- [11] M. Gell-Mann, P. Ramond and R. Slansky, Conf. Proc. **C790927**, 315 (1979), [arXiv:1306.4669].
- [12] T. Yanagida, Conf. Proc. C **7902131**, 95 (1979).
- [13] R. N. Mohapatra and G. Senjanovic, Phys. Rev. Lett. **44**, 912 (1980).
- [14] J. Schechter and J. W. F. Valle, Phys. Rev. **D21**, 309 (1980).
- [15] J. Schechter and J. W. F. Valle, Phys. Rev. **D22**, 2227 (1980).
- [16] J. Schechter and J. W. F. Valle, Phys. Rev. **D24**, 1883 (1981), [Erratum: Phys. Rev.D25,283(1982)].
- [17] Z. Maki, M. Nakagawa and S. Sakata, Prog. Theor. Phys. **28**, 870 (1962).
- [18] Y. Katayama *et al.*, Prog. Theor. Phys. **28**, 675 (1962).
- [19] B. Pontecorvo, Zh. Eksp. Teor. Fiz. **53**, 1717 (1967).
- [20] N. Cabibbo, Phys. Rev. Lett. **10**, 531 (1963).
- [21] M. Kobayashi and T. Maskawa, Prog. Theor. Phys. **49**, 652 (1973).
- [22] S. Antusch *et al.*, JHEP **10**, 084 (2006), [hep-ph/0607020].
- [23] S. Antusch and O. Fischer, JHEP **10**, 094 (2014), [arXiv:1407.6607].
- [24] V. N. Gribov and B. Pontecorvo, Phys. Lett. **28B**, 493 (1969).
- [25] E. Akhmedov, in “International Conference on History of the Neutrino: 1930-2018 Paris, France, September 5-7, 2018,” (2019), [arXiv:1901.05232].
- [26] L. Wolfenstein, Phys. Rev. D **17**, 2369 (1978).
- [27] A. Halprin, Phys. Rev. **D34**, 3462 (1986).
- [28] A. J. Baltz and J. Weneser, Phys. Rev. **D37**, 3364 (1988).
- [29] P. D. Mannheim, Phys. Rev. **D37**, 1935 (1988).
- [30] L. Landau, Phys. Z. Sov. **2**, 46 (1932).
- [31] C. Zener, Proc. Roy. Soc. Lond. **A137**, 696 (1932).
- [32] E. Majorana, Nuovo Cim. **9**, 43 (1932).
- [33] E. C. G. Stueckelberg, Helv. Phys. Acta **5**, 369 (1932).
- [34] T.-K. Kuo and J. T. Pantaleone, Rev. Mod. Phys. **61**, 937 (1989).
- [35] S. J. Parke, Phys. Rev. Lett. **57**, 1275 (1986).
- [36] W. C. Haxton, Phys. Rev. Lett. **57**, 1271 (1986).
- [37] S. T. Petcov, Phys. Lett. B **191**, 299 (1987).
- [38] S. P. Mikheyev and A. Y. Smirnov, Sov. J. Nucl. Phys. **42**, 913 (1985).
- [39] J. N. Bahcall *et al.*, Rev. Mod. Phys. **54**, 767 (1982).
- [40] J. N. Bahcall, A. M. Serenelli and S. Basu, Astrophys. J. **621**, L85 (2005), [arXiv:astro-ph/0412440].
- [41] A. M. Serenelli, W. C. Haxton and C. Pena-Garay, Astrophys. J. **743**, 24 (2011), [arXiv:1104.1639].
- [42] F. L. Villante, Phys. Lett. **B742**, 279 (2015), [arXiv:1410.2796].
- [43] A. Serenelli, Eur. Phys. J. **A52**, 4, 78 (2016), [arXiv:1601.07179].
- [44] R. Davis, Jr., D. S. Harmer and K. C. Hoffman, Phys. Rev. Lett. **20**, 1205 (1968).
- [45] B. T. Cleveland *et al.*, Astrophys. J. **496**, 505 (1998).
- [46] C. Pena-Garay and A. Serenelli (2008), [arXiv:0811.2424].
- [47] J. N. Abdurashitov *et al.* (SAGE), J. Exp. Theor. Phys. **95**, 181 (2002), [Zh. Eksp. Teor. Fiz.122,211(2002)], [arXiv:astro-ph/0204245].
- [48] W. Hampel *et al.* (GALLEX), Phys. Lett. **B447**, 127 (1999).
- [49] M. Altmann *et al.* (GNO), Phys. Lett. **B616**, 174 (2005), [hep-ex/0504037].

- [50] J. N. Abdurashitov *et al.* (SAGE), Phys. Rev. **C80**, 015807 (2009), [arXiv:0901.2200].
- [51] K. S. Hirata *et al.* (Kamiokande-II), Phys. Rev. Lett. **63**, 16 (1989).
- [52] K. S. Hirata *et al.* (Kamiokande-II), Phys. Rev. **D44**, 2241 (1991), [Erratum: Phys. Rev. **D45**, 2170 (1992)].
- [53] Y. Fukuda *et al.* (Kamiokande), Phys. Rev. Lett. **77**, 1683 (1996).
- [54] Y. Fukuda *et al.* (Super-Kamiokande), Phys. Rev. Lett. **81**, 1158 (1998), [Erratum: Phys. Rev. Lett. **81**, 4279 (1998)], [hep-ex/9805021].
- [55] Y. Fukuda *et al.* (Super-Kamiokande), Phys. Rev. Lett. **82**, 2430 (1999), [hep-ex/9812011].
- [56] K. Abe *et al.* (Super-Kamiokande), Phys. Rev. **D94**, 5, 052010 (2016), [arXiv:1606.07538].
- [57] N. Vinyoles *et al.*, Astrophys. J. **835**, 2, 202 (2017), [arXiv:1611.09867].
- [58] S. Fukuda *et al.* (Super-Kamiokande), Phys. Rev. Lett. **86**, 5651 (2001), [hep-ex/0103032].
- [59] S. Fukuda *et al.* (Super-Kamiokande), Phys. Rev. Lett. **86**, 5656 (2001), [hep-ex/0103033].
- [60] B. Aharmim *et al.* (SNO), Phys. Rev. **C72**, 055502 (2005), [arXiv:nucl-ex/0502021].
- [61] S. Fukuda *et al.* (Super-Kamiokande), Phys. Lett. **B539**, 179 (2002), [hep-ex/0205075].
- [62] Q. R. Ahmad *et al.* (SNO), Phys. Rev. Lett. **87**, 071301 (2001), [arXiv:nucl-ex/0106015].
- [63] Q. R. Ahmad *et al.* (SNO), Phys. Rev. Lett. **89**, 011301 (2002), [arXiv:nucl-ex/0204008].
- [64] B. Aharmim *et al.* (SNO), Phys. Rev. **C88**, 025501 (2013), [arXiv:1109.0763].
- [65] J. Bergstrom *et al.*, JHEP **03**, 132 (2016), [arXiv:1601.00972].
- [66] C. Arpesella *et al.* (Borexino), Phys. Lett. B **658**, 101 (2008), [arXiv:0708.2251].
- [67] G. Bellini *et al.* (Borexino), Phys. Rev. Lett. **108**, 051302 (2012), [arXiv:1110.3230].
- [68] M. Agostini *et al.* (BOREXINO), Nature **562**, 7728, 505 (2018).
- [69] M. Agostini *et al.* (BOREXINO), Nature **587**, 577 (2020), [arXiv:2006.15115].
- [70] G. Bellini *et al.* (Borexino), Phys. Rev. D **82**, 033006 (2010), [arXiv:0808.2868].
- [71] S. Abe *et al.* (KamLAND), Phys. Rev. **C84**, 035804 (2011), [arXiv:1106.0861].
- [72] A. Gando *et al.* (KamLAND), Phys. Rev. **C92**, 5, 055808 (2015), [arXiv:1405.6190].
- [73] M. Agostini *et al.* (Borexino), Phys. Rev. D **100**, 8, 082004 (2019), [arXiv:1707.09279].
- [74] M. Agostini *et al.* (Borexino), Phys. Rev. D **101**, 6, 062001 (2020), [arXiv:1709.00756].
- [75] A. Renshaw *et al.* (Super-Kamiokande), Phys. Rev. Lett. **112**, 9, 091805 (2014), [arXiv:1312.5176].
- [76] K. Abe *et al.* (Super-Kamiokande), Phys. Rev. D **94**, 5, 052010 (2016), [arXiv:1606.07538].
- [77] M. Honda *et al.*, Phys. Rev. **D92**, 2, 023004 (2015), [arXiv:1502.03916].
- [78] G. D. Barr *et al.*, Phys. Rev. **D74**, 094009 (2006), [arXiv:astro-ph/0611266].
- [79] G. Battistoni *et al.*, Astropart. Phys. **19**, 269 (2003), [Erratum: Astropart. Phys. **19**, 291 (2003)], [hep-ph/0207035].
- [80] J. Evans *et al.*, Phys. Rev. **D95**, 2, 023012 (2017), [arXiv:1612.03219].
- [81] C. V. Achar *et al.*, Phys. Lett. **18**, 196 (1965).
- [82] F. Reines *et al.*, Phys. Rev. Lett. **15**, 429 (1965).
- [83] K. S. Hirata *et al.* (Kamiokande-II), Phys. Lett. B **205**, 416 (1988).
- [84] D. Casper *et al.*, Phys. Rev. Lett. **66**, 2561 (1991).
- [85] K. Daum *et al.* (Frejus), Z. Phys. **C66**, 417 (1995).
- [86] M. Aglietta *et al.* (NUSEX), Europhys. Lett. **8**, 611 (1989).
- [87] K. S. Hirata *et al.* (Kamiokande-II), Phys. Lett. **B280**, 146 (1992).
- [88] Y. Fukuda *et al.* (Kamiokande), Phys. Lett. **B335**, 237 (1994).
- [89] Y. Fukuda *et al.* (Super-Kamiokande), Phys. Rev. Lett. **81**, 1562 (1998), [hep-ex/9807003].
- [90] M. Ambrosio *et al.* (MACRO), Phys. Lett. **B517**, 59 (2001), [hep-ex/0106049].
- [91] M. C. Sanchez *et al.* (Soudan 2), Phys. Rev. **D68**, 113004 (2003), [hep-ex/0307069].
- [92] V. D. Barger *et al.*, Phys. Rev. Lett. **82**, 2640 (1999), [arXiv:astro-ph/9810121].
- [93] E. Lisi, A. Marrone and D. Montanino, Phys. Rev. Lett. **85**, 1166 (2000), [hep-ph/0002053].
- [94] Y. Ashie *et al.* (Super-Kamiokande), Phys. Rev. Lett. **93**, 101801 (2004), [hep-ex/0404034].
- [95] Z. Li *et al.* (Super-Kamiokande), Phys. Rev. **D98**, 5, 052006 (2018), [arXiv:1711.09436].
- [96] M. G. Aartsen *et al.* (IceCube), Phys. Rev. **D99**, 3, 032007 (2019), [arXiv:1901.05366].
- [97] K. Abe *et al.* (Super-Kamiokande), Phys. Rev. **D97**, 7, 072001 (2018), [arXiv:1710.09126].
- [98] A. Albert *et al.* (ANTARES), JHEP **06**, 113 (2019), [arXiv:1812.08650].
- [99] M. G. Aartsen *et al.* (IceCube), Phys. Rev. Lett. **120**, 7, 071801 (2018), [arXiv:1707.07081].
- [100] S. Adrian-Martinez *et al.* (KM3Net), J. Phys. **G43**, 8, 084001 (2016), [arXiv:1601.07459].
- [101] M. G. Aartsen *et al.* (IceCube-Gen2), J. Phys. G **48**, 6, 060501 (2021), [arXiv:2008.04323].
- [102] S. Ahmed *et al.* (ICAL), Pramana **88**, 5, 79 (2017), [arXiv:1505.07380].
- [103] K. Abe *et al.* (Hyper-Kamiokande) (2018), [arXiv:1805.04163].
- [104] B. Abi *et al.* (DUNE) (2018), [arXiv:1807.10334].
- [105] S. E. Kopp, Phys. Rept. **439**, 101 (2007), [arXiv:physics/0609129].
- [106] S. van der Meer (1961), CERN-61-07.
- [107] D. Beavis *et al.* (E899) (1995), BNL-52459.
- [108] M. G. Catanesi *et al.* (HARP), Nucl. Instrum. Meth. **A571**, 527 (2007).
- [109] J. M. Paley *et al.* (MIPP), Phys. Rev. **D90**, 3, 032001 (2014), [arXiv:1404.5882].
- [110] N. Abgrall *et al.* (NA61), JINST **9**, P06005 (2014), [arXiv:1401.4699].
- [111] J. M. Paley *et al.* (MIPP), Phys. Rev. D **90**, 3, 032001 (2014), [arXiv:1404.5882].
- [112] N. Abgrall *et al.* (NA61/SHINE), Phys. Rev. C **84**, 034604 (2011), [arXiv:1102.0983].
- [113] N. Abgrall *et al.* (NA61/SHINE), Eur. Phys. J. C **76**, 11, 617 (2016), [arXiv:1603.06774].
- [114] M. H. Ahn *et al.* (K2K), Phys. Rev. **D74**, 072003 (2006), [hep-ex/0606032].
- [115] P. Adamson *et al.* (MINOS), Phys. Rev. Lett. **110**, 25, 251801 (2013), [arXiv:1304.6335].
- [116] P. Adamson *et al.* (MINOS), Phys. Rev. Lett. **112**, 191801 (2014), [arXiv:1403.0867].

- [117] P. Adamson *et al.* (MINOS+), Phys. Rev. Lett. **125**, 13, 131802 (2020), [arXiv:2006.15208].
- [118] N. Agafonova *et al.* (OPERA), Phys. Rev. Lett. **120**, 21, 211801 (2018), [Erratum: Phys. Rev. Lett.121,no.13,139901(2018)], [arXiv:1804.04912].
- [119] C. Rubbia *et al.*, JINST **6**, P07011 (2011), [arXiv:1106.0975].
- [120] K. Abe *et al.* (T2K), Phys. Rev. Lett. **107**, 041801 (2011), [arXiv:1106.2822].
- [121] K. Abe *et al.* (T2K), Phys. Rev. Lett. **112**, 061802 (2014), [arXiv:1311.4750].
- [122] K. Abe *et al.* (T2K), Nature **580**, 7803, 339 (2020), [Erratum: Nature 583, E16 (2020)], [arXiv:1910.03887].
- [123] K. Abe *et al.* (T2K), Phys. Rev. D **103**, 11, 112008 (2021), [arXiv:2101.03779].
- [124] P. Adamson *et al.* (NOvA), Phys. Rev. Lett. **116**, 15, 151806 (2016), [arXiv:1601.05022].
- [125] P. Adamson *et al.* (NOvA), Phys. Rev. Lett. **118**, 23, 231801 (2017), [arXiv:1703.03328].
- [126] M. A. Acero *et al.* (NOvA), Phys. Rev. Lett. **123**, 15, 151803 (2019), [arXiv:1906.04907].
- [127] B. Abi *et al.* (DUNE), JINST **15**, 08, T08008 (2020), [arXiv:2002.02967].
- [128] K. Abe *et al.* (Hyper-Kamiokande) (2018), [arXiv:1805.04163].
- [129] A. Aguilar-Arevalo *et al.* (LSND), Phys. Rev. **D64**, 112007 (2001), [hep-ex/0104049].
- [130] B. Armbruster *et al.* (KARMEN), Phys. Rev. **D65**, 112001 (2002), [hep-ex/0203021].
- [131] A. A. Aguilar-Arevalo *et al.* (MiniBooNE), Phys. Rev. D **103**, 5, 052002 (2021), [arXiv:2006.16883].
- [132] M. Antonello *et al.* (MicroBooNE, LAr1-ND, ICARUS-WA104) (2015), [arXiv:1503.01520].
- [133] S. Ajimura *et al.* (JSNS2), Nucl. Instrum. Meth. A **1014**, 165742 (2021), [arXiv:2104.13169].
- [134] F. Von Feilitzsch, A. A. Hahn and K. Schreckenbach, Phys. Lett. **118B**, 162 (1982).
- [135] K. Schreckenbach *et al.*, Phys. Lett. **160B**, 325 (1985).
- [136] A. A. Hahn *et al.*, Phys. Lett. **B218**, 365 (1989).
- [137] P. Vogel *et al.*, Phys. Rev. **C24**, 1543 (1981).
- [138] T. A. Mueller *et al.*, Phys. Rev. **C83**, 054615 (2011), [arXiv:1101.2663].
- [139] P. Huber, Phys. Rev. **C84**, 024617 (2011), [Erratum: Phys. Rev. C85,029901(2012)], [arXiv:1106.0687].
- [140] D. Adey *et al.* (Daya Bay), Phys. Rev. **D100**, 5, 052004 (2019), [arXiv:1808.10836].
- [141] D. Adey *et al.* (Daya Bay), Phys. Rev. Lett. **121**, 24, 241805 (2018), [arXiv:1809.02261].
- [142] G. Bak *et al.* (RENO), Phys. Rev. Lett. **121**, 20, 201801 (2018), [arXiv:1806.00248].
- [143] H. de Kerret *et al.* (Double Chooz), Nature Phys. **16**, 5, 558 (2020), [arXiv:1901.09445].
- [144] Y. J. Ko *et al.* (NEOS), Phys. Rev. Lett. **118**, 12, 121802 (2017), [arXiv:1610.05134].
- [145] M. Apollonio *et al.* (CHOOZ), Eur.Phys.J. **C27**, 331 (2003), [hep-ex/0301017].
- [146] F. Boehm *et al.*, Phys. Rev. **D64**, 112001 (2001), [hep-ex/0107009].
- [147] K. Eguchi *et al.* (KamLAND), Phys. Rev. Lett. **90**, 021802 (2003), [hep-ex/0212021].
- [148] T. Araki *et al.* (KamLAND), Phys. Rev. Lett. **94**, 081801 (2005), [hep-ex/0406035].
- [149] A. Gando *et al.* (KamLAND), Phys. Rev. **D88**, 3, 033001 (2013), [arXiv:1303.4667].
- [150] Y. Abe *et al.* (Double Chooz), Phys. Rev. Lett. **108**, 131801 (2012), [arXiv:1112.6353].
- [151] F. P. An *et al.* (Daya Bay), Phys. Rev. Lett. **108**, 171803 (2012), [arXiv:1203.1669].
- [152] J. K. Ahn *et al.* (RENO), Phys. Rev. Lett. **108**, 191802 (2012), [arXiv:1204.0626].
- [153] F. An *et al.* (JUNO), J. Phys. **G43**, 3, 030401 (2016), [arXiv:1507.05613].
- [154] I. Alekseev *et al.* (DANSS), Phys. Lett. **B787**, 56 (2018), [arXiv:1804.04046].
- [155] H. Almázán *et al.* (STEREO), Phys. Rev. D **102**, 5, 052002 (2020), [arXiv:1912.06582].
- [156] M. Andriamirado *et al.* (PROSPECT), Phys. Rev. D **103**, 3, 032001 (2021), [arXiv:2006.11210].
- [157] A. P. Serebrov *et al.* (NEUTRINO-4), Pisma Zh. Eksp. Teor. Fiz. **109**, 4, 209 (2019), [JETP Lett.109,no.4,213(2019)], [arXiv:1809.10561].
- [158] A. P. Serebrov *et al.*, Phys. Rev. D **104**, 3, 032003 (2021), [arXiv:2005.05301].
- [159] Y. Abreu *et al.* (SoLid), JINST **16**, 02, P02025 (2021), [arXiv:2002.05914].
- [160] N. Cabibbo, Phys. Lett. **72B**, 333 (1978).
- [161] S. M. Bilenky, J. Hosek and S. T. Petcov, Phys. Lett. **94B**, 495 (1980).
- [162] V. D. Barger, K. Whisnant and R. J. N. Phillips, Phys. Rev. Lett. **45**, 2084 (1980).
- [163] P. Langacker *et al.*, Nucl. Phys. **B282**, 589 (1987).
- [164] S. Goswami and A. Yu. Smirnov, Phys. Rev. **D72**, 053011 (2005), [hep-ph/0411359].
- [165] N. Okamura, Prog. Theor. Phys. **114**, 1045 (2006), [hep-ph/0411388].
- [166] H. Nunokawa, S. J. Parke and R. Zukanovich Funchal, Phys. Rev. **D72**, 013009 (2005), [hep-ph/0503283].
- [167] A. Cervera *et al.*, Nucl. Phys. **B579**, 17 (2000), [Erratum: Nucl. Phys. B593,731(2001)], [hep-ph/0002108].
- [168] M. Freund, Phys. Rev. **D64**, 053003 (2001), [hep-ph/0103300].
- [169] E. K. Akhmedov *et al.*, JHEP **04**, 078 (2004), [hep-ph/0402175].
- [170] H. Minakata *et al.*, Phys. Rev. **D74**, 053008 (2006), [hep-ph/0607284].
- [171] O. L. G. Peres and A. Yu. Smirnov, Nucl. Phys. **B680**, 479 (2004), [hep-ph/0309312].
- [172] S. Petcov, Phys.Lett. **B434**, 321 (1998), [hep-ph/9805262].
- [173] E. K. Akhmedov *et al.*, Nucl.Phys. **B542**, 3 (1999), [hep-ph/9808270].
- [174] E. K. Akhmedov, Nucl.Phys. **B538**, 25 (1999), [hep-ph/9805272].
- [175] M. Chizhov, M. Maris and S. Petcov (1998), SISSA-53-98-EP, [hep-ph/9810501].
- [176] M. Chizhov and S. Petcov, Phys.Rev.Lett. **83**, 1096 (1999), [hep-ph/9903399].
- [177] E. K. Akhmedov, M. Maltoni and A. Y. Smirnov, JHEP **0705**, 077 (2007), [hep-ph/0612285].
- [178] C. Kim and U. Lee, Phys.Lett. **B444**, 204 (1998), [hep-ph/9809491].
- [179] O. Peres and A. Y. Smirnov, Phys.Lett. **B456**, 204 (1999), [hep-ph/9902312].
- [180] M. Gonzalez-Garcia, M. Maltoni and A. Y. Smirnov, Phys.Rev. **D70**, 093005 (2004), [hep-ph/0408170].
- [181] E. K. Akhmedov, M. Maltoni and A. Y. Smirnov, JHEP **0806**, 072 (2008), [arXiv:0804.1466].
- [182] J. Bernabeu, S. Palomares Ruiz and S. Petcov, Nucl.Phys. **B669**, 255 (2003), [hep-ph/0305152].

- [183] S. Petcov and T. Schwetz, Nucl.Phys. **B740**, 1 (2006), [hep-ph/0511277].
- [184] I. Esteban *et al.*, JHEP **01**, 106 (2019), [arXiv:1811.05487].
- [185] I. Esteban *et al.*, “Nufit4.1 at nufit webpage,” <http://www.nu-fit.org>.
- [186] F. Capozzi *et al.*, Prog. Part. Nucl. Phys. **102**, 48 (2018), [arXiv:1804.09678].
- [187] P. F. de Salas *et al.*, Phys. Lett. **B782**, 633 (2018), [arXiv:1708.01186].
- [188] M. Friend, “Updated Results from the T2K Experiment with 3.13×10^{21} Protons on Target,” (2019), KEK/J-PARC Physics seminar, January 10, 2019, URL <https://t2k.org/docs/talk/335/2019kekseminar>.
- [189] C. Jarlskog, Phys. Rev. Lett. **55**, 1039 (1985).
- [190] M. C. Gonzalez-Garcia, M. Maltoni and T. Schwetz, JHEP **11**, 052 (2014), [arXiv:1409.5439].
- [191] Y. Farzan and A. Yu. Smirnov, Phys. Rev. **D65**, 113001 (2002), [hep-ph/0201105].
- [192] A. Dueck, S. Petcov and W. Rodejohann, Phys. Rev. **D82**, 013005 (2010), [arXiv:1006.0227].
- [193] A. Aguilar-Arevalo *et al.* (MiniBooNE) (2012), [arXiv:1207.4809].
- [194] M. A. Acero, C. Giunti and M. Laveder, Phys. Rev. **D78**, 073009 (2008), [arXiv:0711.4222].
- [195] C. Giunti and M. Laveder, Phys. Rev. **C83**, 065504 (2011), [arXiv:1006.3244].
- [196] F. P. An *et al.* (Daya Bay), Phys. Rev. Lett. **116**, 6, 061801 (2016), [Erratum: Phys. Rev. Lett.118,no.9,099902(2017)], [arXiv:1508.04233].
- [197] F. P. An *et al.* (Daya Bay), Phys. Rev. Lett. **118**, 25, 251801 (2017), [arXiv:1704.01082].
- [198] G. Mention *et al.*, Phys. Rev. **D83**, 073006 (2011), [arXiv:1101.2755].
- [199] J. J. Gomez-Cadenas and M. C. Gonzalez-Garcia, Z. Phys. **C71**, 443 (1996), [hep-ph/9504246].
- [200] M. Maltoni *et al.*, Nucl. Phys. **B643**, 321 (2002), [hep-ph/0207157].
- [201] M. Dentler *et al.*, JHEP **08**, 010 (2018), [arXiv:1803.10661].
- [202] C. Giunti and M. Laveder, Phys. Rev. **D84**, 093006 (2011), [arXiv:1109.4033].
- [203] J. M. Conrad *et al.*, Adv. High Energy Phys. **2013**, 163897 (2013), [arXiv:1207.4765].
- [204] J. Kopp *et al.*, JHEP **05**, 050 (2013), [arXiv:1303.3011].
- [205] G. H. Collin *et al.*, Phys. Rev. Lett. **117**, 22, 221801 (2016), [arXiv:1607.00011].
- [206] S. Gariazzo *et al.*, JHEP **06**, 135 (2017), [arXiv:1703.00860].
- [207] A. Diaz *et al.*, Phys. Rept. **884**, 1 (2020), [arXiv:1906.00045].
- [208] S. Böser *et al.*, Prog. Part. Nucl. Phys. **111**, 103736 (2020), [arXiv:1906.01739].
- [209] G. Karagiorgi *et al.*, Phys. Rev. **D75**, 013011 (2007), [Erratum: Phys. Rev.D80,099902(2009)], [hep-ph/0609177].
- [210] M. Maltoni and T. Schwetz, Phys. Rev. **D76**, 093005 (2007), [arXiv:0705.0107].
- [211] C. Giunti and M. Laveder, Phys. Rev. **D84**, 073008 (2011), [arXiv:1107.1452].
- [212] M. Aker *et al.* (KATRIN) (2019), [arXiv:1909.06048].
- [213] J. Bonn *et al.*, Nucl. Phys. B Proc. Suppl. **91**, 273 (2001).
- [214] V. M. Lobashev *et al.*, Nucl. Phys. B Proc. Suppl. **91**, 280 (2001).
- [215] B. Monreal and J. A. Formaggio, Phys. Rev. **D80**, 051301 (2009), [arXiv:0904.2860].
- [216] A. De Rujula and M. Lusignoli, Phys. Lett. **118B**, 429 (1982).
- [217] L. Gastaldo *et al.*, J. Low Temp. Phys. **176**, 5-6, 876 (2014), [arXiv:1309.5214].
- [218] B. Alpert *et al.*, Eur. Phys. J. **C75**, 3, 112 (2015), [arXiv:1412.5060].
- [219] M. P. Croce *et al.*, J. Low. Temp. Phys. **184**, 3-4, 958 (2016), [arXiv:1510.03874].
- [220] R. E. Shrock, Phys. Lett. **96B**, 159 (1980).
- [221] F. Vissani, Nucl. Phys. B Proc. Suppl. **100**, 273 (2001), [hep-ph/0012018].
- [222] Y. Farzan, O. L. G. Peres and A. Yu. Smirnov, Nucl. Phys. **B612**, 59 (2001), [hep-ph/0105105].
- [223] J. Schechter and J. W. F. Valle, Phys. Rev. D **25**, 2951 (1982).
- [224] J. Engel and J. Menendez, Rept. Prog. Phys. **80**, 4, 046301 (2017), [arXiv:1610.06548].
- [225] A. Gando *et al.* (KamLAND-Zen), Phys. Rev. Lett. **117**, 8, 082503 (2016), [Addendum: Phys.Rev.Lett. 117, 109903 (2016)], [arXiv:1605.02889].
- [226] M. Agostini *et al.* (GERDA), Phys. Rev. Lett. **125**, 25, 252502 (2020), [arXiv:2009.06079].
- [227] S. I. Alvis *et al.* (Majorana), Phys. Rev. C **100**, 2, 025501 (2019), [arXiv:1902.02299].
- [228] N. Abgrall *et al.* (LEGEND) (2021), [arXiv:2107.11462].
- [229] V. Albanese *et al.* (SNO+), JINST **16**, 08, P08059 (2021), [arXiv:2104.11687].
- [230] G. Anton *et al.* (EXO-200), Phys. Rev. Lett. **123**, 16, 161802 (2019), [arXiv:1906.02723].
- [231] S. A. Kharusi *et al.* (nEXO) (2018), [arXiv:1805.11142].
- [232] G. Adhikari *et al.* (nEXO) (2021), [arXiv:2106.16243].
- [233] J. Renner *et al.* (NEXT), JINST **13**, 10, P10020 (2018), [arXiv:1808.01804].
- [234] A. Simón *et al.* (NEXT), JHEP **21**, 146 (2020), [arXiv:2102.11931].
- [235] D. R. Nygren, J. Phys. Conf. Ser. **650**, 1, 012002 (2015).
- [236] B. J. P. Jones, A. D. McDonald and D. R. Nygren, JINST **11**, 12, P12011 (2016), [arXiv:1609.04019].
- [237] A. D. McDonald *et al.*, Phys. Rev. Lett. **120**, 13, 132504 (2018), [arXiv:1711.04782].
- [238] I. Rivilla *et al.*, Nature **583**, 7814, 48 (2020).
- [239] C. Chambers *et al.* (nEXO), Nature **569**, 7755, 203 (2019), [arXiv:1806.10694].
- [240] S. Ban *et al.*, PTEP **2020**, 3, 033H01 (2020), [arXiv:2001.03281].
- [241] D. Q. Adams *et al.* (CUORE), Phys. Rev. Lett. **124**, 12, 122501 (2020), [arXiv:1912.10966].
- [242] W. R. Armstrong *et al.* (CUPID) (2019), [arXiv:1907.09376].
- [243] O. Azzolini *et al.* (CUPID), Phys. Rev. Lett. **123**, 3, 032501 (2019), [arXiv:1906.05001].
- [244] E. Armengaud *et al.* (CUPID), Phys. Rev. Lett. **126**, 18, 181802 (2021), [arXiv:2011.13243].
- [245] V. Alenkov *et al.* (AMoRE), Eur. Phys. J. **C79**, 9, 791 (2019), [arXiv:1903.09483].
- [246] M. H. Lee (AMoRE), JINST **15**, 08, C08010 (2020), [arXiv:2005.05567].
- [247] R. Arnold *et al.* (NEMO-3), Phys. Rev. **D92**, 7, 072011 (2015), [arXiv:1506.05825].
- [248] R. Arnold *et al.* (NEMO-3), Phys. Rev. Lett. **119**, 4, 041801 (2017), [arXiv:1705.08847].

15. Quark Model

Revised August 2021 by C. Amsler (Stefan Meyer Inst.), T. De-Grand (Colorado U., Boulder) and B. Krusche (Basel U.).

- 15.1 Introduction 312
- 15.2 Quantum numbers of the quarks 312
- 15.3 Mesons 312
- 15.4 Exotic mesons 316
- 15.5 Baryons: qqq states 317
 - 15.5.1 Light baryons 317
 - 15.5.2 Charmed and bottom baryons 320
- 15.6 Magnetic moments 321
- 15.7 Dynamics 322
- 15.8 Lattice Calculations of Hadronic Spectroscopy . 323
 - 15.8.1 Spectroscopy of low-lying states 323
 - 15.8.2 Excited state spectroscopy 324
 - 15.8.3 Electromagnetic effects 326

15.1 Introduction

Quantum chromodynamics (QCD) is the theory of strong interactions. QCD is a quantum field theory with an $SU(N_c)$ local “color” gauge symmetry with $N_c = 3$ colors and a collection of N_f “flavors” of colored fermions, the quarks. It involves a set of $N_c^2 - 1 = 8$ non-Abelian gauge fields, the gluons. QCD is believed to confine, that is, its physical states are color singlets with internal quark and gluon degrees of freedom. This review is concerned with the description of the properties (masses and matrix elements for couplings to electromagnetism and the weak interactions) of the low lying bound states of QCD. The shorthand expression for describing this physics is called the “quark model.”

The spectrum of strongly interacting particles consists of a tower of many states, which can be either bosons (labelled as “mesons”) or fermions (labelled as “baryons”). The spectrum of baryons and mesons exhibits a high degree of regularity. The organizational principle which best categorizes this regularity is encoded in the quark model. All descriptions of strongly interacting states use the language of the quark model. At the same time, the language is not precise. The quark model exists on many levels: at the simplest level, it is an almost dynamics-free picture of strongly interacting particles as bound states of quarks and antiquarks. As one refines the description, the quark model can become a framework with more detailed descriptions of dynamics. At its most fundamental level, it might be a description of QCD.

At its heart, the quark model assumes that mesons are bound states of a quark - antiquark pair, and baryons are bound states of three quarks. These are the minimal particle content states which can be color singlets in an $SU(3)$ gauge theory. This approach cannot be justified directly from QCD; however, there is indirect evidence that this description has some fundamental validity from the version of QCD where the number of colors N_c is taken to infinity [1–3]. In that limit, mesons are dominantly narrow (width proportional to $1/N_c$) bound states of a quark - antiquark pair, and baryons have a mass which scales as N_c .

A better justification is that this approach works. Indeed, the quark model is much older (circa 1963-64) than QCD as a theory of the strong interactions (1973-1974). In fact, the principle issue in strong interaction physics before QCD was to justify the success of the quark model in systemizing the properties of mesons and baryons in terms of some more fundamental dynamics (QCD).

Today one knows that this is not the whole story. There are experimentally observed states which either cannot be described, or have an uncomfortable description, as minimal quark number states. Some of them have “exotic” (non- $\bar{q}q$ or qqq) quantum numbers. Given the successes of the quark model, these are classified as “tetraquarks”, “pentaquarks” (or more) or “glueballs” (bound states of the gluonic degrees of freedom in QCD). Of course, such labels are imprecise: bound states with the same overall quantum numbers can mix, regardless of their internal degrees of freedom.

This review has several parts. We start by describing the properties of strongly interacting particles in terms of the properties

of states made of a minimal number of quark fields which can be coupled into a color singlet – two fields (a quark and an antiquark) for the mesons, and three quarks, for a baryon. Quarks come in six flavors. We describe the properties of mesons as $\bar{q}q$ systems and baryons as qqq systems. Along the way we discuss hadronic bound states which do not fit into this classification.

Finally, at the end of this review, we present results from lattice simulations of QCD, a direct approach to the solution of QCD from its Lagrangian, without reference to models. Lattice simulations interact with the quark model in (at least) two ways: first, the interpolating fields which are used in lattice simulations are usually directly based on quark model constructions. That is the simplest way to create states with the desired quantum numbers, which can then be processed by the lattice calculation. The second way that lattice calculations interact with the quark model comes when one wishes to put the lattice calculations into some context: without the quark model, there are simply the results from the lattice calculations, and the results from experiment, and no way to understand why they are similar or different. The quark model is the framework which is almost universally used to generate that context. Of course, that statement is equally valid when one tries to systemize actual experimental data: the context is always some variation of a quark model.

15.2 Quantum numbers of the quarks

As gluons carry no intrinsic quantum numbers beyond color charge, and because color is believed to be permanently confined, the quantum numbers of strongly interacting particles are given by the quantum numbers of their constituent quarks and antiquarks.

Quarks are strongly interacting fermions with spin 1/2 and, by convention, positive parity. Antiquarks have negative parity. Quarks have the additive baryon number 1/3, antiquarks -1/3. Table 15.1 gives the other additive quantum numbers (flavors) for the three generations of quarks. They are related to the charge Q (in units of the elementary charge e) through the generalized Gell-Mann-Nishijima formula

$$Q = I_z + \frac{B + S + C + B + T}{2}, \quad (15.1)$$

where B is the baryon number. The convention is that the quark flavor (I_z , S , C , B , or T) has the same sign as its charge Q . With this convention, any flavor carried by a charged meson has

Table 15.1: Quark quantum numbers.

	d	u	s	c	b	t
Q – electric charge	$-\frac{1}{3}$	$+\frac{2}{3}$	$-\frac{1}{3}$	$+\frac{2}{3}$	$-\frac{1}{3}$	$+\frac{2}{3}$
I – isospin	$\frac{1}{2}$	$\frac{1}{2}$	0	0	0	0
I_z – isospin z -component	$-\frac{1}{2}$	$+\frac{1}{2}$	0	0	0	0
S – strangeness	0	0	-1	0	0	0
C – charm	0	0	0	+1	0	0
B – bottomness	0	0	0	0	-1	0
T – topness	0	0	0	0	0	+1

the same sign as its charge, *e.g.*, the strangeness of the K^+ is +1, the bottomness of the B^+ is +1, and the charm and strangeness of the D_s^- are each -1. Antiquarks have the opposite flavor signs. The hypercharge is defined as

$$Y = B + S - \frac{C - B + T}{3}.$$

Thus Y is equal to $\frac{1}{3}$ for the u and d quarks, $-\frac{2}{3}$ for the s quark, and 0 for all other quarks. More details and derivations on the quark structure of mesons and baryons can be found *e.g.* in Ref. [4].

15.3 Mesons

Mesons have baryon number $B = 0$. In the quark model, they are $q\bar{q}'$ bound states of quarks q and antiquarks \bar{q}' (the flavors of q and q' may be different). If the orbital angular momentum of the $q\bar{q}'$ state is ℓ , then the parity P is $(-1)^{\ell+1}$. The meson spin

J is given by the usual relation $|\ell - s| \leq J \leq |\ell + s|$, where s is 0 (antiparallel quark spins) or 1 (parallel quark spins). The charge conjugation, or C -parity $C = (-1)^{\ell+s}$, is defined only for the $q\bar{q}$ states made of quarks and their own antiquarks. The C -parity can be generalized to the G -parity $G = (-1)^{I+\ell+s}$ for mesons made of quarks and their own antiquarks (isospin $I_z = 0$), and for the charged $u\bar{d}$ and $d\bar{u}$ states (isospin $I = 1$).

The mesons are classified in J^{PC} multiplets. The $\ell = 0$ states are the pseudoscalars (0^{-+}) and the vectors (1^{--}). The orbital excitations $\ell = 1$ are the scalars (0^{++}), the axial vectors (1^{++}) and (1^{+-}), and the tensors (2^{++}). Assignments for many of the known mesons are given in Tables 15.2, 15.3 and 15.4. Radial excitations are denoted by the principal quantum number n . The very short lifetime of the t quark makes it likely that bound-state hadrons containing t quarks and/or antiquarks do not exist.

States in the natural spin-parity series $P = (-1)^J$ must, according to the above, have $s = 1$ and hence, $CP = +1$. Thus, mesons with natural spin-parity and $CP = -1$ (0^{+-} , 1^{-+} , 2^{+-} , 3^{-+} , etc.) are forbidden in the $q\bar{q}$ model. The $J^{PC} = 0^{- -}$ state is forbidden as well. Mesons with such exotic quantum numbers may exist, but would lie outside the $q\bar{q}$ model (see section 15.4 below on exotic mesons).

Following SU(3), the nine possible $q\bar{q}'$ combinations containing the light u , d , and s quarks are grouped into an octet and a singlet of light quark mesons:

$$\mathbf{3} \otimes \bar{\mathbf{3}} = \mathbf{8} \oplus \mathbf{1}. \quad (15.2)$$

A fourth quark such as charm c can be included by extending SU(3) to SU(4). However, SU(4) is badly broken owing to the much heavier c quark. Nevertheless, in an SU(4) classification, the sixteen mesons are grouped into a 15-plet and a singlet:

$$\mathbf{4} \otimes \bar{\mathbf{4}} = \mathbf{15} \oplus \mathbf{1}. \quad (15.3)$$

The weight diagrams for the ground-state pseudoscalar (0^{-+}) and vector (1^{--}) mesons are depicted in Fig. 15.1. The light quark mesons are members of nonets building the middle plane in Fig. 15.1(a) and (b).

Isoscalar states with the same J^{PC} mix, but mixing between the two light quark isoscalar mesons, and the much heavier charmonium and bottomonium states, are generally assumed to be negligible. In the following, we shall use the generic names a for the $I = 1$, K for the $I = 1/2$, and f and f' for the $I = 0$ members of the light quark nonets. Thus, the physical isoscalars are mixtures of the SU(3) wave function ψ_8 and ψ_1 :

$$f' = \psi_8 \cos \theta - \psi_1 \sin \theta, \quad (15.4)$$

$$f = \psi_8 \sin \theta + \psi_1 \cos \theta, \quad (15.5)$$

where θ is the nonet mixing angle and

$$\psi_8 = \frac{1}{\sqrt{6}}(u\bar{u} + d\bar{d} - 2s\bar{s}), \quad (15.6)$$

$$\psi_1 = \frac{1}{\sqrt{3}}(u\bar{u} + d\bar{d} + s\bar{s}). \quad (15.7)$$

The mixing relations are often rewritten to exhibit the $u\bar{u} + d\bar{d}$ and $s\bar{s}$ components which decouple for the “ideal” mixing angle θ_i , such that $\tan \theta_i = 1/\sqrt{2}$ (or $\theta_i = 35.3^\circ$). Defining $\alpha = \theta + 54.7^\circ$, one obtains the physical isoscalar state in the flavor basis

$$f' = \frac{1}{\sqrt{2}}(u\bar{u} + d\bar{d}) \cos \alpha - s\bar{s} \sin \alpha, \quad (15.8)$$

and its orthogonal partner f (replace α by $\alpha - 90^\circ$). Thus for ideal mixing ($\alpha_i = 90^\circ$), the f' becomes pure $s\bar{s}$ and the f pure $u\bar{u} + d\bar{d}$. The mixing angle θ can be derived by diagonalizing the mass matrix

$$\begin{pmatrix} m_8 & m_{81} \\ m_{18} & m_1 \end{pmatrix}.$$

The mass eigenvalues are $m_{f'}$ and m_f . The mixing angle is given by

$$\tan \theta = \frac{m_8 - m_{f'}}{m_{81}}.$$

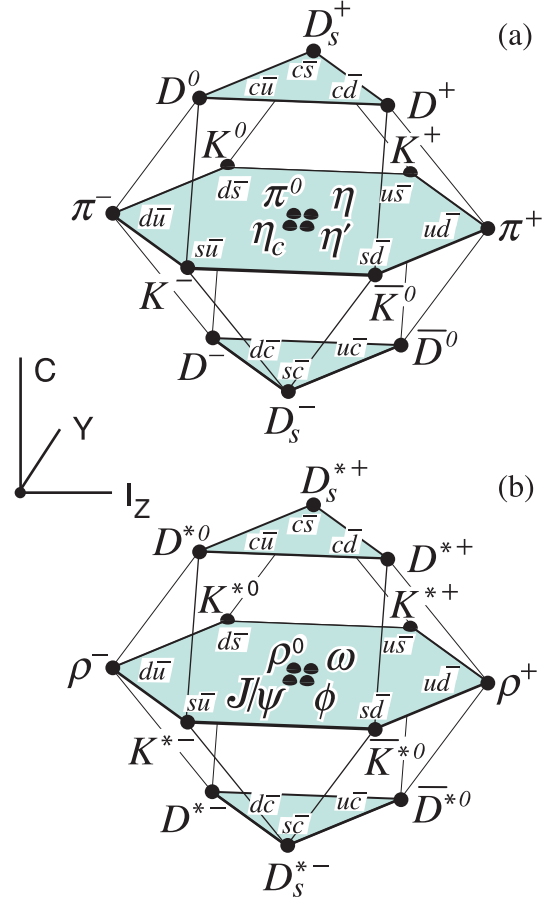


Figure 15.1: SU(4) weight diagram showing the 16-plets for the pseudoscalar (a) and vector mesons (b) made of the u , d , s , and c quarks as a function of isospin I_z , charm C , and hypercharge $Y = B + S - \frac{C}{3}$. The nonets of light mesons occupy the central planes to which the $c\bar{c}$ states have been added.

Calculating m_8 and m_{81} from the wave functions Eq. (15.6) and Eq. (15.7), and expressing the quark masses as a function of the $I = 1/2$ and $I = 1$ meson masses, one obtains

$$\tan \theta = \frac{4m_K - m_a - 3m_{f'}}{2\sqrt{2}(m_a - m_K)}, \quad (15.9)$$

which also determines the sign of θ . Alternatively, one can express the mixing angle as a function of all nonet masses. The octet mass is given by

$$m_8 = m_{f'} \cos^2 \theta + m_f \sin^2 \theta$$

whence

$$\tan^2 \theta = \frac{4m_K - m_a - 3m_{f'}}{-4m_K + m_a + 3m_{f'}}. \quad (15.10)$$

Eliminating θ from Eq. (15.9) and Eq. (15.10) leads to the sum rule [10]

$$(m_f + m_{f'})(4m_K - m_a) - 3m_{f'}m_f = 8m_K^2 - 8m_Km_a + 3m_a^2. \quad (15.11)$$

This relation is verified for the ground-state vector mesons. We identify the $\phi(1020)$ with the f' and the $\omega(783)$ with the f . Thus

$$\phi(1020) = \psi_8 \cos \theta_V - \psi_1 \sin \theta_V, \quad (15.12)$$

$$\omega(783) = \psi_8 \sin \theta_V + \psi_1 \cos \theta_V, \quad (15.13)$$

with the vector mixing angle $\theta_V = 36.5^\circ$ from Eq. (15.10), very close to ideal mixing. Thus $\phi(1020)$ is nearly pure $s\bar{s}$. For ideal mixing, Eq. (15.9) and Eq. (15.10) lead to the relations

$$m_K = \frac{m_f + m_{f'}}{2}, \quad m_a = m_f, \quad (15.14)$$

Table 15.2: Suggested $q\bar{q}$ quark-model assignments for the lightest mesons made of u , d and s quarks. Mesons in boldface are included in the Meson Summary Table. The wave functions f and f' are given in the text (Eq. (15.8)) and the singlet-octet mixing angles in Table 15.5 below for the well established nonets. The classification of the 0^{++} mesons is tentative: (i) the scalars $a_0(980)$, $K_0^*(700)$, $f_0(980)$ and $f_0(500)$, omitted from the table, are often considered to be four-quark states, see Eq. (15.21) below, but are also proposed for the ground state scalar nonet (see the chapter “Scalar Mesons below 1 GeV” in this *Review*); (ii) the isoscalar 0^{++} mesons $f_0(1370)$, $f_0(1500)$ (not shown) and $f_0(1710)$ are expected to mix. The isoscalar assignments in the 2^1S_0 (0^{-+}) nonet are also tentative. Details and alternative schemes can be found in “Spectroscopy of Light Meson Resonances” in this *Review*.

^a The $1^{+\pm}$ and $2^{-\pm}$ isospin $\frac{1}{2}$ states mix. In particular, the K_{1A} and K_{1B} are nearly equal mixtures of the $K_1(1270)$ and $K_1(1400)$ [5].

^b The physical vector mesons are mixtures of 1^3D_1 and 2^3S_1 [6].

^c The $\eta(1475)$ and $\eta(1405)$ (not shown) may be manifestations of a single state [7].

^d This state has also been proposed as a tetraquark state [8].

$n^{2s+1}\ell_J$	J^{PC}	$l = 1$	$l = \frac{1}{2}$	$l = 0$	$l = 0$
		$u\bar{d}, \bar{u}d,$ $\frac{1}{\sqrt{2}}(d\bar{d} - u\bar{u})$	$u\bar{s}, d\bar{s};$ $\bar{d}s, \bar{u}s$	f'	f
1^1S_0	0^{-+}	π	K	η	$\eta'(958)$
1^3S_1	1^{--}	$\rho(770)$	$K^*(892)$	$\phi(1020)$	$\omega(782)$
1^1P_1	1^{+-}	$b_1(1235)$	K_{1B}^a	$h_1(1415)$	$h_1(1170)$
1^3P_0	0^{++}	$a_0(1450)$	$K_0^*(1430)$	$f_0(1710)$	$f_0(1370)$
1^3P_1	1^{++}	$a_1(1260)$	K_{1A}^a	$f_1(1420)$	$f_1(1285)$
1^3P_2	2^{++}	$a_2(1320)$	$K_2^*(1430)$	$f_2'(1525)$	$f_2(1270)$
1^1D_2	2^{-+}	$\pi_2(1670)$	$K_2(1770)^a$	$\eta_2(1870)$	$\eta_2(1645)$
1^3D_1	1^{--}	$\rho(1700)$	$K^*(1680)^b$	$\phi(2170)^d$	$\omega(1650)$
1^3D_2	2^{--}		$K_2(1820)^a$		
1^3D_3	3^{--}	$\rho_3(1690)$	$K_3^*(1780)$	$\phi_3(1850)$	$\omega_3(1670)$
1^3F_4	4^{++}	$a_4(1970)$	$K_4^*(2045)$	$f_4(2300)$	$f_4(2050)$
1^3G_5	5^{-}	$\rho_5(2350)$	$K_5^*(2380)$		
2^1S_0	0^{-+}	$\pi(1300)$	$K(1460)$	$\eta(1475)^c$	$\eta(1295)$
2^3S_1	1^{--}	$\rho(1450)$	$K^*(1410)^b$	$\phi(1680)$	$\omega(1420)$
2^3P_1	1^{++}	$a_1(1640)$			
2^3P_2	2^{++}	$a_2(1700)$	$K_2^*(1980)$	$f_2(1950)$	$f_2(1640)$

Table 15.3: $c\bar{c}$ quark-model assignments for the charmonium mesons with established J^{PC} and their corresponding open charm mesons. Mesons in bold face are included in the Meson Summary Table. The open flavor states in the 1^{+-} and 1^{++} rows are mixtures of the $1^{\pm\pm}$ states.

^a This meson splits into two states. The ground state scalar meson lies around 2100 MeV [9].

^b The masses are considerably smaller than most theoretical predictions. They have also been considered as tetraquark or $D^{(*)}K$ molecular states.

^c Mixtures of the 1^3D_1 and 2^3S_1 states.

$n^{2s+1}\ell_J$	J^{PC}	$l = 0$	$l = \frac{1}{2}$	$l = 0$
		$c\bar{c}$	$c\bar{u}, c\bar{d};$ $\bar{c}u, \bar{c}d$	$c\bar{s};$ $\bar{c}s$
1^1S_0	0^{-+}	$\eta_c(1S)$	D	D_s^\pm
1^3S_1	1^{--}	$J/\psi(1S)$	D^*	$D_s^{*\pm}$
1^3P_0	0^{++}	$\chi_{c0}(1P)$	$D_0^*(2300)^a$	$D_{s0}^*(2317)^{\pm b}$
1^3P_1	1^{++}	$\chi_{c1}(1P)$	$D_1(2430)$	$D_{s1}^*(2460)^{\pm b}$
1^1P_1	1^{+-}	$h_c(1P)$	$D_1(2420)$	$D_{s1}(2536)^\pm$
1^3P_2	2^{++}	$\chi_{c2}(1P)$	$D_2^*(2460)$	$D_{s2}^*(2573)^\pm$
2^1S_0	0^{-+}	$\eta_c(2S)$	$D_0(2500)^0$	$D_{s0}(2590)^+$
2^3S_1	1^{--}	$\psi(2S)$	$D_1^*(2760)^0$	$D_{s1}^*(2700)^{\pm c}$
1^3D_1	1^{--}	$\psi(3770)$		$D_{s1}^*(2860)^{\pm c}$
1^3D_2	2^{--}	$\psi_2(3823)$	$D_2(2740)^0$	
2^3P_J	$0^{++}, 1^{++}$	$\chi_{c0}(3860)$		
	2^{++}	$\chi_{c2}(3930)$		
3^3S_1	1^{--}	$\psi(4040)$		
2^3D_1	1^{--}	$\psi(4160)$		
4^3S_1	1^{--}	$\psi(4415)$		
1^3D_3	3^{--}	$\psi_3(3842)$	$D_3^*(2750)$	$D_{s3}^*(2860)^\pm$

Table 15.4: $b\bar{b}$ quark-model assignments for the bottomonium mesons with established J^{PC} and their corresponding open bottom mesons.

$n^{2s+1}\ell_J$	J^{PC}	$I = 0$ $b\bar{b}$	$I = \frac{1}{2}$ $b\bar{u}, b\bar{d};$ $bu, b\bar{d}$	$I = 0$ $b\bar{s};$ bs	$I = 0$ $b\bar{c};$ bc
1^1S_0	0^{-+}	$\eta_b(1S)$	B	B_s^0	B_c^\pm
1^3S_1	1^{--}	$\Upsilon(1S)$	B^*	B_s^*	
1^3P_0	0^{++}	$\chi_{b0}(1P)$			
1^3P_1	1^{++}	$\chi_{b1}(1P)$			
1^1P_1	1^{+-}	$h_b(1P)$	$B_1(5721)$	$B_{s1}(5830)^0$	
1^3P_2	2^{++}	$\chi_{b2}(1P)$	$B_2^*(5747)$	$B_{s2}^*(5840)^0$	
2^1S_0	0^{-+}	$\eta_b(2S)$			$B_c(2S)^\pm$
2^3S_1	1^{--}	$\Upsilon(2S)$			
1^3D_2	2^{--}	$\Upsilon_2(1D)$			
2^3P_J	$0, 1, 2^{++}$	$\chi_{b0,1,2}(2P)$			
2^1P_1	1^{+-}	$h_b(2P)$			
3^3S_1	1^{--}	$\Upsilon(3S)$			
3^3P_J	$0, 1, 2^{++}$	$\chi_{b1,2}(3P)$			
4^3S_1	1^{--}	$\Upsilon(4S)$			

which are satisfied for the vector mesons.

The situation for the pseudoscalar and scalar mesons is not so clear cut, either theoretically or experimentally. For the pseudoscalars, the mixing angle is small. This can be understood qualitatively via gluon-line counting of the mixing process. The size of the mixing process between the nonstrange and strange mass bases scales as α_s^2 , not α_s^3 , because of two rather than three gluon exchange as it does for the vector mesons. It may also be that the lightest isoscalar pseudoscalars mix more strongly with excited states or with states of substantial non- $q\bar{q}$ content, as will be discussed below.

In fact a large mixing from hadronic loops is expected for scalar mesons, no matter what model is assumed for $q\bar{q}$ pair production [11]. A variety of analysis methods lead to similar results: First, for these states, Eq. (15.11) is satisfied only approximately. Then Eq. (15.9) and Eq. (15.10) lead to somewhat different values for the mixing angle. Identifying the η with the f' one gets

$$\eta = \psi_8 \cos \theta_P - \psi_1 \sin \theta_P, \quad (15.15)$$

$$\eta' = \psi_8 \sin \theta_P + \psi_1 \cos \theta_P. \quad (15.16)$$

Following chiral perturbation theory, the meson masses in the mass formulae (Eq. (15.9) and Eq. (15.10)) might be replaced by their squares. Table 15.5 lists the mixing angle θ_{lin} from Eq. (15.10) (using the neutral members of the nonets) and the corresponding θ_{quad} obtained by replacing the meson masses by their squares throughout. The mixing angles in the 1^{--} , 2^{++} and 3^{--} nonets are not far from ideal, while larger $s\bar{s}$ -($u\bar{u} + d\bar{d}$) mixing is predicted from hadronic loops in the 0^{++} , 0^{-+} and $1^{+\pm}$ nonets [11].

Table 15.5: Singlet-octet mixing angles for the well established nonets from the linear mass formula Eq. (15.10) and its quadratic version in which the masses are squared. The 1^{++} and 1^{+-} nonet mixing angles depend on the mixing angle θ_{K_1} between K_{1A} and K_{1B} . The recommended values are $\sim 23^\circ$ and $\sim 28^\circ$ for 1^{++} and 1^{+-} , respectively, with $\theta_{K_1} \sim 35^\circ$ [5].

$n^{2s+1}\ell_J$	J^{PC}	θ_{quad} [$^\circ$]	θ_{lin} [$^\circ$]
1^1S_0	0^{-+}	-11.3	-24.5
1^3S_1	1^{--}	39.2	36.5
1^3P_2	2^{++}	29.6	28.0
1^3D_3	3^{--}	31.8	30.8

The pseudoscalar mixing angle θ_P can also be measured by comparing the partial widths for radiative J/ψ decay into a vector and a pseudoscalar [12], radiative $\phi(1020)$ decay into η and η' [13],

radiative decays between pseudoscalar and vector mesons [14], or $p\bar{p}$ annihilation at rest into a pair of vector and pseudoscalar or into two pseudoscalars [15, 16]. One obtains a mixing angle between -10° and -20° . More recently, a lattice QCD simulation, Ref. [17], has successfully reproduced the masses of the η and η' , and as a byproduct find a mixing angle $\theta_{\text{lin}} = -14.1(2.8)^\circ$. We return to this point in Sec. 15.8.

The nonet mixing angles can be measured in $\gamma\gamma$ collisions, e.g., for the 0^{-+} , 0^{++} , and 2^{++} nonets. In the quark model, the amplitude for the coupling of neutral mesons to two photons is proportional to $\sum_i Q_i^2$, where Q_i is the charge of the i -th quark. The 2γ partial width of an isoscalar meson with mass m is then given in terms of the mixing angle α by

$$\Gamma_{2\gamma} = C(5 \cos \alpha - \sqrt{2} \sin \alpha)^2 m^3, \quad (15.17)$$

for f' and f ($\alpha \rightarrow \alpha - 90^\circ$). The coupling C may depend on the meson mass. It is often assumed to be a constant in the nonet. For the isovector a , one finds $\Gamma_{2\gamma} = 9 C m^3$. Thus the members of an ideally mixed nonet couple to 2γ with partial widths in the ratios $f : f' : a = 25 : 2 : 9$. For tensor mesons, one finds from the ratios of the measured 2γ partial widths for the $f_2(1270)$ and $f_2'(1525)$ mesons a mixing angle α_T of $(81 \pm 1)^\circ$, or $\theta_T = (27 \pm 1)^\circ$, in accord with the linear mass formula. For the pseudoscalars, one finds from the ratios of partial widths $\Gamma(\eta' \rightarrow 2\gamma)/\Gamma(\eta \rightarrow 2\gamma)$ a mixing angle $\theta_P = (-18 \pm 2)^\circ$, while the ratio $\Gamma(\eta' \rightarrow 2\gamma)/\Gamma(\pi^0 \rightarrow 2\gamma)$ leads to $\sim -24^\circ$. SU(3) breaking effects for pseudoscalars are discussed in [18].

The partial width Γ for the decay of a scalar or a tensor meson into a pair of pseudoscalar mesons is model-dependent. Following Ref. [19],

$$\Gamma = C \times \gamma^2 \times |F(q)|^2 \times q, \quad (15.18)$$

where C is a nonet constant, q the momentum of the decay products, $F(q)$ a form factor, and γ^2 the SU(3) coupling. Details and explicit expressions for γ^2 and $F(q)$ are given in ‘‘Spectroscopy of Light Meson Resonances’’. The decay of a $q\bar{q}$ meson into a pair of mesons involves the creation of a $q\bar{q}$ pair, and SU(3) symmetry assumes that the matrix elements for the creation of $s\bar{s}$, $u\bar{u}$, and $d\bar{d}$ pairs are equal. An excellent fit to the tensor meson decay widths is obtained assuming SU(3) symmetry and a pseudoscalar mixing angle $\theta_P \simeq -17^\circ$ [19].

The analysis of resonances is complicated by the presence of thresholds such as $K\bar{K}$ in $a_0(980) \rightarrow \eta\pi$ or $f_0(980) \rightarrow \pi\pi$, which affect the resonance masses and widths. A particularly nasty kinematic effect is the triangle singularity in which one of the primary decay daughters in turn decays and is emitted backwards, catching up and scattering with the second primary product. This mechanism generates fake peaks in the final state and has been proposed as alternative explanation for several meson (and baryon) signals. Prominent examples are the $\eta(1475) \rightarrow K^*(\rightarrow K\pi)\bar{K}$

and $\eta(1410) \rightarrow a_0(980)(\rightarrow \eta\pi)\pi$ signals which could be due to one single state [7] (see also Table 15.2).

15.4 Exotic mesons

The existence of a light nonet composed of four quarks (tetraquarks) with masses below 1 GeV was suggested a long time ago [20,21]. Coupling two triplets of light quarks $u, d,$ and $s,$ one obtains nine states, of which the six symmetric ($uu, dd, ss, ud + du, us + su, ds + sd$) form the six dimensional representation $\mathbf{6}$, while the three antisymmetric ($ud - du, us - su, ds - sd$) form the three dimensional representation $\mathbf{\bar{3}}$ of SU(3):

$$\mathbf{3} \otimes \mathbf{3} = \mathbf{6} \oplus \mathbf{\bar{3}}. \quad (15.19)$$

Hence for tetraquarks one gets the reduction

$$\begin{aligned} \mathbf{3} \otimes \mathbf{3} \otimes \mathbf{\bar{3}} \otimes \mathbf{\bar{3}} \\ &= \mathbf{6} \oplus \mathbf{\bar{3}} \otimes \mathbf{\bar{6}} \otimes \mathbf{3} \\ &= \mathbf{\bar{3}} \otimes \mathbf{3} \oplus \mathbf{6} \otimes \mathbf{\bar{6}} \oplus \mathbf{6} \otimes \mathbf{3} \oplus \mathbf{\bar{3}} \otimes \mathbf{\bar{6}} \\ &= \mathbf{9} \oplus \mathbf{36} \oplus \mathbf{18} \oplus \mathbf{\bar{18}}. \end{aligned} \quad (15.20)$$

Combining with spin and color and requiring antisymmetry for diquarks and antidiquarks, one finds for ground states (zero angular momenta) that the most deeply bound tetraquarks (and hence the lightest ones) lie in the nonet and are scalar mesons (see also [4]). The average mass is estimated to be around 900 MeV from the mass differences between the ρ and π masses. Letting the strange quark determine the mass splittings one obtains a mass inverted spectrum with a light isosinglet, a medium heavy isodoublet and a heavy isotriplet + isosinglet. It is then tempting to identify these mesons as the lightest scalars

$$\begin{aligned} f_0(500) &= \bar{u}\bar{d}ud, \\ K_0^*(700) &= (\bar{s}\bar{d}ud, \bar{s}\bar{u}ud) \text{ and } (\bar{u}\bar{d}us, \bar{u}\bar{d}ds), \\ a_0(980) &= (us\bar{d}\bar{s}, \frac{1}{\sqrt{2}}[u\bar{u} - d\bar{d}]s\bar{s}, \bar{u}\bar{s}ds), \\ f_0(980) &= \frac{1}{\sqrt{2}}[u\bar{u} + d\bar{d}]s\bar{s}. \end{aligned} \quad (15.21)$$

In alternative schemes these states build the lightest $q\bar{q}$ scalar nonet (for details see “Scalar mesons below 1 GeV” in this “Review”).

A plethora of new states have been reported in the charmonium and bottomonium spectra. The most prominent one is the $\chi_{c1}(3872)$ (formerly $X(3872)$), first observed in 2003 in B -decays in the final state $J/\psi\pi^+\pi^-$ (see Fig. 15.2). Even more remarkable is the observation of isovector (charged) candidates decaying into $c\bar{c}$ plus a charged pion, such as the $Z^\pm(4430)$ decaying into $\psi(2S)\pi^\pm$, which a priori excludes an interpretation as true $c\bar{c}$ (charmonium) state. Similar states are also observed in the bottomonium spectrum. Some of these states may be tetraquarks (e.g. $cq\bar{c}\bar{q}$), molecular structures (e.g. $c\bar{q}\bar{c}q$) made of pairs of mesons such as D, D_s and D^*, D_s^* excitations, or their B and B^* counterparts. They could also be mimicked by kinematical effects such as triangle singularities. Details and references can be found in recent reviews [23], [24] and in the review “Heavy non- $q\bar{q}$ Mesons”.

QCD predicts the existence of extra isoscalar mesons which cannot be addressed by the quark model. In the pure gauge theory they contain only gluons, and are called glueballs. The ground state glueball is predicted by lattice gauge theories to be 0^{++} , the first excited state 2^{++} . Errors on the mass predictions are large. From Ref. [25] one obtains 1750 (50) (80) MeV for the mass of the lightest 0^{++} glueball from quenched QCD. As an example for the glueball mass spectrum, we show in Fig. 15.3 a calculation from Ref. [22]. A mass of 1710 MeV is predicted for the ground state, also with an error of about 100 MeV. Earlier work by other groups produced masses at 1650 MeV [26] and 1550 MeV [27] (see also [28]). The first excited state has a mass of about 2.4 GeV, and the lightest glueball with exotic quantum numbers (2^{+-}) has a mass of about 4 GeV.

These calculations are made in the so-called “quenched approximation” which neglects $q\bar{q}$ loops. However, both glue and $q\bar{q}$ states

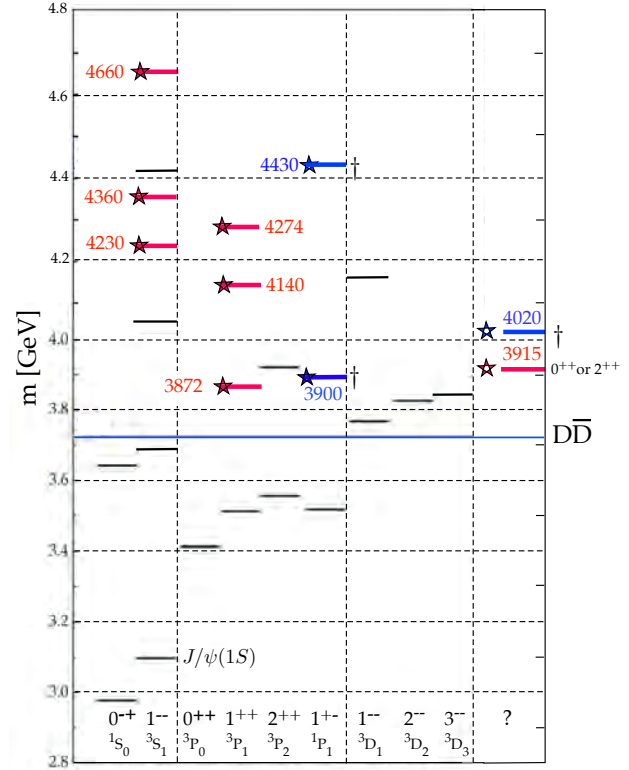


Figure 15.2: Established states populating the charmonium spectrum that are listed in the Summary Tables. The $c\bar{c}$ states are shown in black, the exotic ones are tagged by stars (red for the isoscalars, blue for the isovectors). The quantum numbers of the two states in the right column are not firmly established.

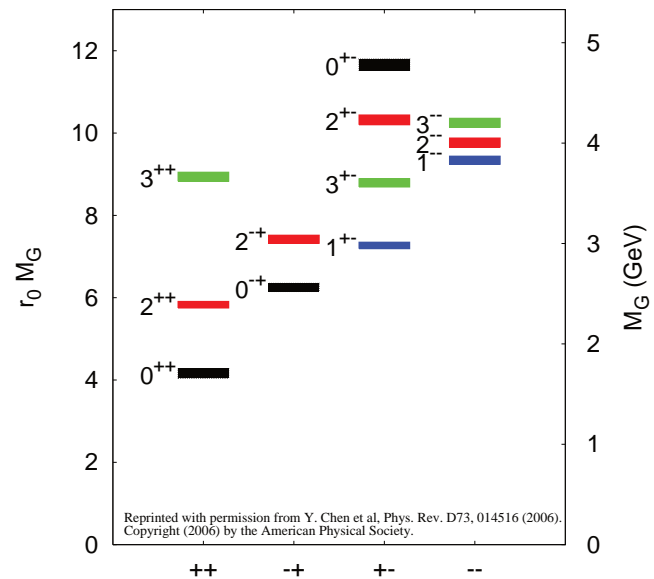


Figure 15.3: Predicted glueball mass spectrum from the lattice in quenched approximation (from [22]).

couple to singlet scalar mesons. Therefore glueballs will mix with nearby $q\bar{q}$ states of the same quantum numbers. For example, the two isoscalar 0^{++} mesons around 1500 MeV will mix with the pure ground state glueball to generate the observed physical states $f_0(1370)$, $f_0(1500)$, and $f_0(1710)$ [19, 29]. The first results from lattice calculations, which include these effects, indicate that the mass shifts are small. We return to a discussion of this point in Sec. 15.8, see also Fig. 15.15.

The existence of three singlet scalar mesons around 1.5 GeV suggests additional degrees of freedom such as glue, since only two mesons are predicted in this mass range. The $f_0(1500)$ [19, 29] or, alternatively, the $f_0(1710)$ [26], have been proposed as candidates for the scalar glueball, both states having considerable mixing also with the $f_0(1370)$. Other mixing schemes, in particular with the $f_0(500)$ and the $f_0(980)$, have also been proposed [30]. According to a holographic model of low-energy QCD scalar glueballs decay strongly into kaons and η mesons, in good agreement with data on the $f_0(1710)$ [31]. Details can be found in the review ‘‘Spectroscopy of Light Meson Resonances’’ and in Ref. [32]. See also the review ‘‘Scalar Mesons below 1 GeV’’ in this *Review*.

Mesons made of $q\bar{q}$ pairs bound by excited gluons g , the hybrid states $q\bar{q}g$, are also predicted. They should lie in the 1.9 GeV mass region, according to gluon flux tube models [33]. Lattice QCD also predicts the lightest hybrid, an exotic 1^{-+} , at a mass of 1.8 to 1.9 GeV [34]. However, the bag model predicts four nonets, among them an exotic 1^{-+} around or above 1.4 GeV [35, 36]. There are so far two candidates for exotic states with quantum numbers 1^{-+} , the $\pi_1(1400)$ and $\pi_1(1600)$, which could be hybrids or four-quark states. However, a recent combined re-analysis of π_1 production in diffractive π^-p interaction and low energy $\bar{p}p$ annihilation leads to a single pole at ~ 1560 MeV with a width of ~ 390 MeV, although a two-pole scenario cannot be excluded [37]. (See the review ‘‘Spectroscopy of Light Meson Resonances’’ in this *Review* and Ref. [32].)

15.5 Baryons: qqq states

Baryons are fermions with baryon number $\mathcal{B} = 1$, *i.e.*, in the most general case, they are composed of three quarks plus any number of quark - antiquark pairs. Until recently, all established baryons were 3-quark (qqq) configurations, which we mainly discuss in this section. However, in 2015 the LHCb collaboration published first evidence for charmed ‘pentaquark’ states of minimal quark content $c\bar{c}uud$ at invariant masses close to 4.4 GeV [38]. More refined LHCb experiments have revealed evidence for three such states called $P_c(4312)^+$, $P_c(4440)^+$, and $P_c(4457)^+$ [39]. These states are located close to the thresholds of the production of ordinary baryon-meson pairs like $\Sigma_c^+ \bar{D}^0$ and $\Sigma_c^+ \bar{D}^{*0}$ and are consistent with the predictions [40, 41] in terms of molecular-like states. A nice overview on the discussion of pentaquark and tetraquark states is given in Ref. [42].

The color part of baryon state functions is an SU(3) singlet, a completely antisymmetric state of the three colors. Since the quarks are fermions, the state function must be antisymmetric under interchange of any two equal-mass quarks (up and down quarks in the limit of isospin symmetry). Thus it can be written as

$$|qqq\rangle_A = |\text{color}\rangle_A \times |\text{space, spin, flavor}\rangle_S, \quad (15.22)$$

where the subscripts S and A indicate symmetry or antisymmetry under interchange of any two equal-mass quarks. Note the contrast with the state function for the three nucleons in ${}^3\text{H}$ or ${}^3\text{He}$:

$$|NNN\rangle_A = |\text{space, spin, isospin}\rangle_A. \quad (15.23)$$

This difference has major implications for internal structure, magnetic moments, *etc.* (For a nice discussion, see Ref. [43].)

15.5.1 Light baryons

The ‘‘ordinary’’ baryons are made up of u , d , and s quarks. The three flavors imply an approximate flavor SU(3), which requires that baryons made of these quarks belong to the multiplets on the right side of

$$\mathbf{3} \otimes \mathbf{3} \otimes \mathbf{3} = \mathbf{10}_S \oplus \mathbf{8}_M \oplus \mathbf{8}_M \oplus \mathbf{1}_A \quad (15.24)$$

(see the section on ‘‘SU(n) Multiplets and Young Diagrams’’ in this *Review*). Here the subscripts indicate symmetric, mixed-symmetry, or antisymmetric states under interchange of any two quarks. The $\mathbf{1}$ is a uds state (Λ_1), and the octet contains a similar state (Λ_8). If these have the same spin and parity, they can mix. The mechanism is the same as for the mesons (see above). In the ground state multiplet, the SU(3) flavor singlet Λ_1 is forbidden by Fermi statistics. The section on ‘‘SU(3) Isoscalar Factors and Representation Matrices,’’ shows how relative decay rates in, say, $\mathbf{10} \rightarrow \mathbf{8} \otimes \mathbf{8}$ decays may be calculated.

For the ‘‘ordinary’’ baryons (no c or b quark), flavor and spin may be combined in an approximate flavor-spin SU(6), in which the six basic states are $d \uparrow$, $d \downarrow$, \dots , $s \downarrow$ (\uparrow , \downarrow = spin up, down). Then the baryons belong to the multiplets on the right side of

$$\mathbf{6} \otimes \mathbf{6} \otimes \mathbf{6} = \mathbf{56}_S \oplus \mathbf{70}_M \oplus \mathbf{70}_M \oplus \mathbf{20}_A. \quad (15.25)$$

These SU(6) multiplets decompose into flavor SU(3) multiplets as follows:

$$\mathbf{56} = {}^4\mathbf{10} \oplus {}^2\mathbf{8} \quad (15.26a)$$

$$\mathbf{70} = {}^2\mathbf{10} \oplus {}^4\mathbf{8} \oplus {}^2\mathbf{8} \oplus {}^2\mathbf{1} \quad (15.26b)$$

$$\mathbf{20} = {}^2\mathbf{8} \oplus {}^4\mathbf{1}, \quad (15.26c)$$

where the superscript ($2S+1$) gives the net spin S of the quarks for each particle in the SU(3) multiplet. The $J^P = 1/2^+$ octet containing the nucleon and the $J^P = 3/2^+$ decuplet containing the $\Delta(1232)$ together make up the ‘‘ground-state’’ 56-plet, in which the orbital angular momenta between the quark pairs are zero (so that the spatial part of the state function is trivially symmetric). The $\mathbf{70}$ and $\mathbf{20}$ require some excitation of the spatial part of the state function in order to make the overall state function symmetric. States with nonzero orbital angular momenta are classified in SU(6) \otimes O(3) supermultiplets.

It is useful to classify the baryons into bands that have the same number N of quanta of excitation. Each band consists of a number of supermultiplets, specified by (D, L_N^P) , where D is the dimensionality of the SU(6) representation, L is the total quark orbital angular momentum, and P is the total parity. Supermultiplets contained in bands up to $N = 12$ are given in Ref. [44]. The $N = 0$ band, which contains the nucleon and $\Delta(1232)$, consists only of the $(56, 0_0^+)$ supermultiplet. The $N = 1$ band consists only of the $(70, 1_1^-)$ multiplet and contains the negative-parity baryons with masses below about 1.9 GeV. The $N = 2$ band contains five supermultiplets: $(56, 0_2^+)$, $(70, 0_2^+)$, $(56, 2_2^+)$, $(70, 2_2^+)$, and $(20, 1_2^+)$.

The wave functions of the non-strange baryons in the harmonic oscillator basis are often labeled by $|X^{2S+1} L_N J^P\rangle$, where S, L, J, P are as above, $X = N$ or Δ , and $\pi = S, M$ or A denotes the symmetry of the spatial wave function. The possible model states for the bands with $N=0, 1, 2$ are given in Table 15.7. The assignment of experimentally observed states is only complete and well established up to the $N=1$ band. Some more tentative assignments for higher multiplets are suggested in [45].

In Table 15.6, quark-model assignments are given for many of the established baryons whose SU(6) \otimes O(3) compositions are relatively unmixed. One must, however, keep in mind that apart from the mixing of the Λ singlet and octet states, states with same J^P but different L, S combinations can also mix. In the quark model with one-gluon exchange motivated interactions, the size of the mixing is determined by the relative strength of the tensor term with respect to the contact term (see below). The mixing is more important for the decay patterns of the states than for their positions. An example are the lowest lying $(70, 1_1^-)$ states with $J^P = 1/2^-$ and $3/2^-$. The physical states are:

$$|N(1535)1/2^-\rangle = \cos(\Theta_S)|N^2 P_M 1/2^-\rangle - \sin(\Theta_S)|N^4 P_M 1/2^-\rangle \quad (15.27)$$

$$|N(1520)3/2^-\rangle = \cos(\Theta_D)|N^2 P_M 3/2^-\rangle - \sin(\Theta_D)|N^4 P_M 3/2^-\rangle \quad (15.28)$$

and the orthogonal combinations for $N(1650)1/2^-$ and $N(1700)3/2^-$. The mixing is large for the $J^P = 1/2^-$ states ($\Theta_S \approx -32^\circ$), but small for the $J^P = 3/2^-$ states ($\Theta_D \approx +6^\circ$) [47–49].

All baryons of the ground state multiplets are known. Many of their properties, in particular their masses, are in good agreement

Table 15.6: Quark-model assignments for some of the known baryons in terms of a flavor-spin SU(6) basis. Only the dominant representation is listed. Assignments for several states, especially for the $\Lambda(1810)$, $\Lambda(2350)$, $\Xi(1820)$, and $\Xi(2030)$, are merely educated guesses. [†] suggestions for assignments and re-assignments from Ref. [46].

J^P	(D, L_N^P)	S	Octet members				Singlets
$1/2^+$	$(56, 0_0^+)$	$1/2$	$N(939)$	$\Lambda(1116)$	$\Sigma(1193)$	$\Xi(1318)$	
$1/2^+$	$(56, 0_2^+)$	$1/2$	$N(1440)$	$\Lambda(1600)$	$\Sigma(1660)$	$\Xi(1690)^\dagger$	
$1/2^-$	$(70, 1_1^-)$	$1/2$	$N(1535)$	$\Lambda(1670)$	$\Sigma(1620)$	$\Xi(?)$	$\Lambda(1405)$
					$\Sigma(1560)^\dagger$		
$3/2^-$	$(70, 1_1^-)$	$1/2$	$N(1520)$	$\Lambda(1690)$	$\Sigma(1670)$	$\Xi(1820)$	$\Lambda(1520)$
$1/2^-$	$(70, 1_1^-)$	$3/2$	$N(1650)$	$\Lambda(1800)$	$\Sigma(1750)$	$\Xi(?)$	
					$\Sigma(1620)^\dagger$		
$3/2^-$	$(70, 1_1^-)$	$3/2$	$N(1700)$	$\Lambda(?)$	$\Sigma(1940)^\dagger$	$\Xi(?)$	
$5/2^-$	$(70, 1_1^-)$	$3/2$	$N(1675)$	$\Lambda(1830)$	$\Sigma(1775)$	$\Xi(1950)^\dagger$	
$1/2^+$	$(70, 0_2^+)$	$1/2$	$N(1710)$	$\Lambda(1810)$	$\Sigma(1880)$	$\Xi(?)$	$\Lambda(1810)^\dagger$
$3/2^+$	$(56, 2_2^+)$	$1/2$	$N(1720)$	$\Lambda(1890)$	$\Sigma(?)$	$\Xi(?)$	
$5/2^+$	$(56, 2_2^+)$	$1/2$	$N(1680)$	$\Lambda(1820)$	$\Sigma(1915)$	$\Xi(2030)$	
$7/2^-$	$(70, 3_3^-)$	$1/2$	$N(2190)$	$\Lambda(?)$	$\Sigma(?)$	$\Xi(?)$	$\Lambda(2100)$
$9/2^-$	$(70, 3_3^-)$	$3/2$	$N(2250)$	$\Lambda(?)$	$\Sigma(?)$	$\Xi(?)$	
$9/2^+$	$(56, 4_4^+)$	$1/2$	$N(2220)$	$\Lambda(2350)$	$\Sigma(?)$	$\Xi(?)$	

Decuplet members						
$3/2^+$	$(56, 0_0^+)$	$3/2$	$\Delta(1232)$	$\Sigma(1385)$	$\Xi(1530)$	$\Omega(1672)$
$3/2^+$	$(56, 0_2^+)$	$3/2$	$\Delta(1600)$	$\Sigma(1690)^\dagger$	$\Xi(?)$	$\Omega(?)$
$1/2^-$	$(70, 1_1^-)$	$1/2$	$\Delta(1620)$	$\Sigma(1750)^\dagger$	$\Xi(?)$	$\Omega(?)$
$3/2^-$	$(70, 1_1^-)$	$1/2$	$\Delta(1700)$	$\Sigma(?)$	$\Xi(?)$	$\Omega(?)$
$5/2^+$	$(56, 2_2^+)$	$3/2$	$\Delta(1905)$	$\Sigma(?)$	$\Xi(?)$	$\Omega(?)$
$7/2^+$	$(56, 2_2^+)$	$3/2$	$\Delta(1950)$	$\Sigma(2030)$	$\Xi(?)$	$\Omega(?)$
$11/2^+$	$(56, 4_4^+)$	$3/2$	$\Delta(2420)$	$\Sigma(?)$	$\Xi(?)$	$\Omega(?)$

Table 15.7: N and Δ states in the $N=0,1,2$ harmonic oscillator bands. L^P denotes angular momentum and parity, S the three-quark spin and ‘sym’=A,S,M the symmetry of the spatial wave function. Listed are all possible spin/parity combinations and assignments of experimentally observed states. Only dominant components are indicated. Assignments in the $N=2$ band are partly tentative.

N	sym	L^P	S	$N(I = 1/2)$			
2	A	1^+	$1/2$	$1/2^+$	$3/2^+$	-	-
2	M	2^+	$3/2$	$1/2^+$	$3/2^+$	$5/2^+$	$7/2^+$
2	M	2^+	$1/2$	-	$3/2^+$	$5/2^+$	-
2	M	0^+	$3/2$	-	$3/2^+$	-	-
2	M	0^+	$1/2$	$1/2^+$	$N(1710)$	-	-
2	S	2^+	$3/2$	-	-	-	-
2	S	2^+	$1/2$	-	$3/2^+$	$N(1720)$	$5/2^+$
2	S	0^+	$3/2$	-	-	-	-
2	S	0^+	$1/2$	$1/2^+$	$N(1440)$	-	-
1	M	1^-	$3/2$	$1/2^-$	$N(1650)$	$3/2^-$	$N(1700)$
1	M	1^-	$1/2$	$1/2^-$	$N(1535)$	$3/2^-$	$N(1520)$
0	S	0^+	$3/2$	-	-	-	-
0	S	0^+	$1/2$	$1/2^+$	$N(938)$	-	-

N	sym	L^P	S	$\Delta(I = 3/2)$			
2	A	1^+	$1/2$	-	-	-	-
2	M	2^+	$3/2$	-	-	-	-
2	M	2^+	$1/2$	-	$3/2^+$	$5/2^+$	-
2	M	0^+	$3/2$	-	-	-	-
2	M	0^+	$1/2$	$1/2^+$	$\Delta(1750)$	-	-
2	S	2^+	$3/2$	$1/2^+$	$\Delta(1910)$	$3/2^+$	$\Delta(1920)$
2	S	2^+	$1/2$	-	-	-	-
2	S	0^+	$3/2$	-	$3/2^+$	$\Delta(1600)$	-
2	S	0^+	$1/2$	-	-	-	-
1	M	1^-	$3/2$	-	-	-	-
1	M	1^-	$1/2$	$1/2^-$	$\Delta(1620)$	$3/2^-$	$\Delta(1700)$
0	S	0^+	$3/2$	-	$3/2^+$	$\Delta(1232)$	-
0	S	0^+	$1/2$	-	-	-	-

even with the most basic versions of the quark model, including harmonic (or linear) confinement and a spin-spin interaction, which is responsible for the octet - decuplet mass shifts. A consistent description of the ground-state electroweak properties, however, requires refined relativistic constituent quark models.

The situation for the excited states is much less clear. The assignment of some experimentally observed states with strange quarks to model configurations is only tentative and in many cases candidates are completely missing. Melde, Plessas and Sengl [46] have calculated baryon properties in relativistic constituent quark models, using one-gluon exchange and Goldstone-boson exchange for the modeling of the hyperfine interactions (see Sec. 15.7 on Dynamics). Both types of models give qualitatively comparable results, and underestimate in general experimentally observed decay widths. Nevertheless, in particular on the basis of the observed decay patterns, the authors have assigned some additional states with strangeness to the SU(3) multiplets and suggest re-assignments for a few others. Among the new assignments are states with weak experimental evidence (two or three star ratings) and partly without firm spin/parity assignments, so that further experimental efforts are necessary before final conclusions can be drawn. We have added their suggestions in Table 15.6.

In the non-strange sector there are two main problems which are illustrated in Fig. 15.4, where the experimentally observed excitation spectrum of the nucleon (N and Δ resonances) is compared to the results of a typical quark model calculation [50]. The lowest states from the $N=2$ band, the $N(1440)1/2^+$, and the $\Delta(1600)3/2^+$, appear lower than the negative parity states from the $N=1$ band (see Table 15.7) and much lower than predicted by most models. Also negative parity Δ states from the $N=3$ band ($\Delta(1900)1/2^-$, $\Delta(1940)3/2^-$, and $\Delta(1930)5/2^-$) are too low in energy. The low lying states show a clustering in groups of levels around 1700 MeV and 1900 MeV for N^* states and around 1900 MeV for Δ states which is not reflected in models.

Furthermore, many more states are predicted than observed. This has been known for a long time as the ‘missing resonance’ problem [47]. Up to an excitation energy of 2.4 GeV, about 45 N states are predicted, but only 20 are established (four- or three-star; see Note on N and Δ Resonances for the rating of the status of resonances) and 5 are tentative (two- or one-star). Even for the $N=2$ band, up to now only half of the predicted states have been observed. However, there is some recent progress. The total number of states has not much changed but the number of states with four- or three-star rating has increased from 14 to 20 compared to the 2018 PDG particle listings. Most of this progress is due to the programs concentrating on the study of meson photoproduction reactions, while the most recent partial wave analysis of elastic pion scattering and charge exchange data by Arndt and collaborators [51] found no evidence for almost half of the states listed in this review (and included in Fig. 15.4). Such analyses are of course biased against resonances which couple only weakly to the $N\pi$ channel. Quark model predictions for the couplings to other hadronic channels and to photons are given in Ref. [50]. The large experimental effort ongoing at several electron accelerators to study the baryon resonance spectrum with real and virtual photon-induced meson production reactions includes the search for as-yet-unobserved states, as well as detailed studies of the properties of the low lying states (decay patterns, electromagnetic couplings, magnetic moments, *etc.*) (see Ref. [52] for reviews). There are two major new aspects of this program. The investigation of single and double polarization observables allows, via the study of interference terms, access to small partial waves that do not leave a footprint in unpolarized cross sections. An example for the impact of such data is given by a comparison of results from different multipole analyses of pion photoproduction [53]. It shows clearly that with the inclusion of polarization observables the reaction model results start to converge. This will in the near future much improve the data basis for excited baryons in the light quark sector.

The other aspect is the study of final states with meson pairs, in particular $\pi\pi$ and $\pi\eta$ pairs, which made large progress during the last few years. This is important for higher lying states, which in the quark model may have both possible oscillations excited. Such

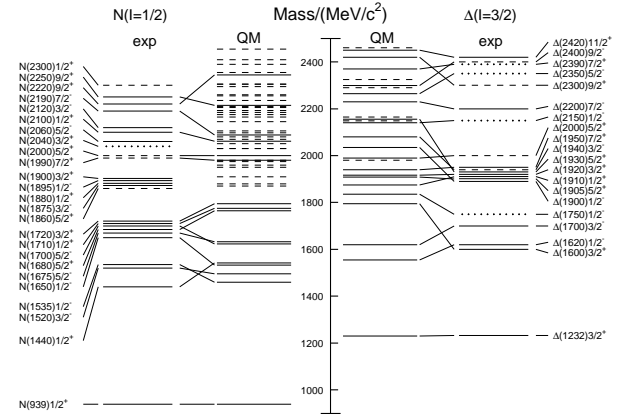


Figure 15.4: Excitation spectrum of the nucleon. Compared are the positions of the excited states identified in experiment, to those predicted by a relativized quark model calculation. Left hand side: isospin $I = 1/2$ N -states, right hand side: isospin $I = 3/2$ Δ -states. Experimental: (columns labeled ‘exp’), three- and four-star states are indicated by full lines (two-star dashed lines, one-star dotted lines). At the very left and right of the figure, the spectroscopic notation of these states is given. Quark model [50, 54]: (columns labeled ‘QM’), all states for the $N=1,2$ bands, low-lying states for the $N=3,4,5$ bands. Full lines: at least tentative assignment to observed states, dashed lines: so far no observed counterparts. Many of the assignments between predicted and observed states are highly tentative.

states can be expected to decay in sequential processes de-exciting the two oscillations step-by-step so that they couple strongly to multiple-meson final states but not to single-meson production. Detailed analyses of such data are for example given in [55, 56] and had already significant impact on partial wave analyses.

The excitation spectrum of hyperons containing s -quarks is even less well explored. Many experimental results date back to before 2000, although parameters listed in the review are in many cases updated by more modern partial wave analyses. A recent review on the quark model interpretation of the Λ and Σ states is given in Ref. [57], a new Ω^- state was reported with high significance from the Belle experiment [58]. In the near future significant progress is expected from the PANDA experiment at FAIR [59, 60].

In quark models, the number of excited states is determined by the effective degrees of freedom, while their ordering and decay properties are related to the residual quark - quark interaction. An overview of quark models for baryons is given in [61], recent discussions of baryon spectroscopy are given in [45, 62]. The effective degrees of freedom in the standard nonrelativistic quark model are three equivalent valence quarks with one-gluon exchange-motivated, flavor-independent color-magnetic interactions. The QCD aspect of gluon-gluon interactions is emphasized by the hypercentral quark model [63, 64], which includes in a natural way three-body forces between the quarks. A different class of models uses interactions which give rise to a quark - diquark clustering of the baryons: for a review see [65]. If there is a tightly bound diquark, only two degrees of freedom are available at low energies, and thus *fewer* states are predicted. Furthermore, selection rules in the decay pattern may arise from the quantum numbers of the diquark. *More* states are predicted by collective models of the baryon like the algebraic approach in [66]. In this approach, the quantum numbers of the valence quarks are distributed over a Y-shaped string-like configuration, and additional states arise *e.g.*, from vibrations of the strings. *More* states are also predicted in the framework of flux-tube models, see [67], which are motivated by lattice QCD. In addition to the quark degrees of freedom, flux-tubes responsible for the confinement of the quarks are considered as degrees of freedom. These models

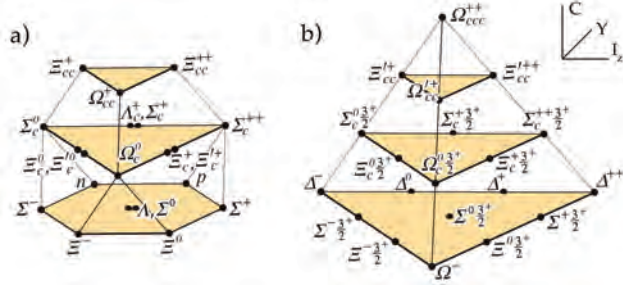


Figure 15.5: $SU(4)_f$ multiplets of ground state baryons made of $u, d, s,$ and c quarks. (a) The spin $\frac{1}{2}$ 20-plet extends the charmless $SU(3)_f$ octet to $C = 1, 2$; (b) the spin $\frac{3}{2}$ 20-plet extends the $SU(3)_f$ decuplet to $C = 1, 2, 3$.

include hybrid baryons containing explicit excitations of the gluon fields. However, since all half integral J^P quantum numbers are possible for ordinary baryons, such ‘exotics’ will be very hard to identify, and probably always mix with ordinary states. So far, the experimentally observed number of states is still far lower even than predicted by the quark–diquark models.

The influence of chiral symmetry on the excitation spectrum of the nucleon has been debated from a somewhat different perspective. Chiral symmetry, the fundamental symmetry of QCD, is strongly broken for the low lying states, resulting in large mass differences of parity partners like the $J^P=1/2^+$ $N(938)1/2^+$ ground state and the $J^P=1/2^-$ $N(1535)1/2^-$ excitation. However, at higher excitation energies there is some evidence for parity doublets and even some very tentative suggestions for full chiral multiplets of N^* and Δ resonances. An effective restoration of chiral symmetry at high excitation energies due to a decoupling from the quark condensate of the vacuum has been discussed (see Ref. [68] for recent reviews) as a possible cause. In this case, the mass generating mechanisms for low and high lying states would be essentially different. As a further consequence, the parity doublets would decouple from pions, so that experimental bias would be worse. However, parity doublets might also arise from the spin-orbital dynamics of the 3-quark system. Presently, the status of data does not allow final conclusions.

The most recent developments on the theory side are the first unquenched lattice calculations for the excitation spectrum discussed in Sec. 15.8. The results are basically consistent with the level counting of $SU(6)\otimes O(3)$ in the standard non-relativistic quark model and show no indication for quark–diquark structures or parity doubling. Consequently, there is as yet no indication from lattice that the mis-match between the excitation spectrum predicted by the standard quark model and experimental observations is due to inappropriate degrees of freedom in the quark model.

15.5.2 Charmed and bottom baryons

The naming scheme for baryons with c or b quarks follows that of the light baryons: the Λ is an isosinglet and the Σ an isotriplet with one heavy (s, c or b) quark. The Ξ is an isodoublet which contains two heavy quarks, and the Ω is an isosinglet with three heavy quarks. The number of c or b quarks is indicated by the subscripts c or b . Hyperons are baryons with at least one s quark.

For charmed baryons the addition of the c quark to the light quarks extends the flavor symmetry to $SU(4)_f$. Due to the large mass of the c quark, this symmetry is much more strongly broken than the $SU(3)_f$ of the three light quarks. Nevertheless, the $SU(4)_f$ representation is still useful for bookkeeping purposes. With the additive charm quantum number C the baryons are classified in a 3-dimensional representation with the three coordinates (I_z, Y, C) . Figure 15.5 shows the $SU(4)_f$ weight diagrams.

With four quarks the 64 possible configurations decompose into

$$4 \otimes 4 \otimes 4 = \bar{4}_A \oplus 20_S \oplus 20_{MS} \oplus 20_{MA}, \quad (15.29)$$

(for a review on $SU(N)$ symmetries see *e.g.* [69]). The subscripts

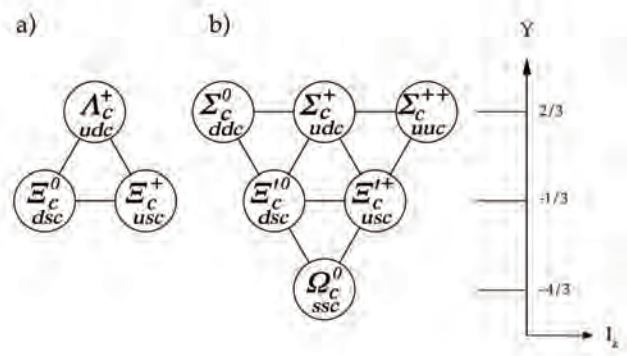


Figure 15.6: The $SU(3)_f \bar{3}$ (a) and 6 (b) ground state $J^P = 1/2^+$ representations. The structure of the 6 ground state with $J^P = 3/2^+$ is identical to the one in (b).

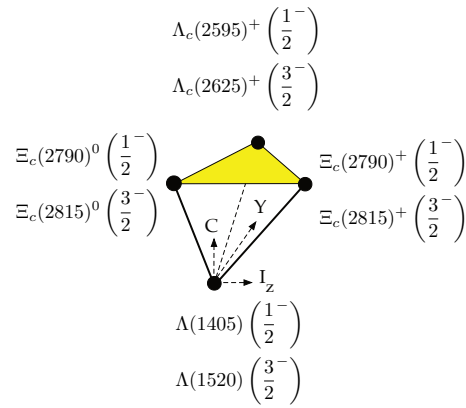


Figure 15.7: Weight diagram of the $\bar{4}$ $SU(4)_f$ multiplet with the experimentally observed negative parity baryons.

S and A refer to the symmetry and antisymmetry properties of the flavor wave functions. The flavor symmetric 20_S multiplet, associated with spin- $\frac{3}{2}$ baryons, contains the charmless $SU(3)_f$ decuplet at the bottom level. The 20_{MS} and 20_{MA} multiplets correspond to the mixed symmetric and mixed antisymmetric flavour wave functions of the spin- $\frac{1}{2}$ baryons, with the charmless octet baryons at the bottom level. There are two dsc and two usc spin- $\frac{1}{2}$ states, labeled $\Xi_c^0, \Xi_c^{\prime 0}$ and $\Xi_c^+, \Xi_c^{\prime +}$. This is because one of the qq pairs can have spin 1 (symmetric) or spin 0 (antisymmetric), giving both the total spin $j = \frac{1}{2}$ with the third quark (see also Fig. 15.6 below).

For $C = 1$ baryons the flavor decomposition of the diquark, made of $u, d,$ or s quarks, is

$$3 \otimes 3 = \bar{3}_A \oplus 6_S. \quad (15.30)$$

For ground-state baryons, the overall antisymmetry of baryon wave function (including color) requires the light diquark to be symmetric under the exchange of spin and flavor, hence both symmetric or both antisymmetric, that is spin 1 for the 6_S and spin 0 for the $\bar{3}_A$. The $\bar{3}$ then combines with the c quark to form the $J^P = 1/2^+$ states, while the 6 combines to form $J^P = 1/2^+$ or $J^P = 3/2^+$. The weight diagrams of the $\bar{3}$ and 6 ground-state representations are shown in Fig. 15.6. Within each multiplet the $C = 1$ baryons obey isospin and $SU(3)_f$ mass relations at the expected orders.

The antisymmetric quadruplet in (15.29) does not exist in the ground state but is realized for the first orbital excitations ($L = 1$). Figure 15.7 shows the weight diagram with the experimentally observed states. In the quark model the quadruplet consists of four baryons with spins coupling to $\frac{1}{2}$, leading to four $L = 1$

excitations with $J^P = \frac{1}{2}^-$ and four excitations with $\frac{3}{2}^-$. The charmed ones are the partners of the $\Lambda(1405)$ and $\Lambda(1520)$ singlets of $SU(3)_f$.

For a detailed review on charmed baryons see Ref. [62]. Quark model predictions for baryons with two heavy quarks are given in Ref. [70] and lattice results for doubly and triply charmed states are discussed in Sec. 15.8 of this *Review*.

The $C = 1$ ground state baryons have all been observed. Due to their relatively narrow widths the states are much easier to isolate than the light quark baryon resonances which require intricate partial wave analyses. The production cross sections are small, but the recent measurements at the e^+e^- B-factories, at the $p\bar{p}$ Tevatron collider, and at LHCb have boosted the field. The LHCb collaboration has published evidence for five new narrow Ω_c^0 states (*css*) [71] in proton-proton collisions. Four of these states have been confirmed by the Belle experiment in e^+e^- collisions [72]. Their quantum numbers are still unknown, but they could correspond to the $L = 1$ *ssc* orbital excitations. Constituent quark models, lattice QCD, quark-diquark models, molecular models, and pentaquark states, have been discussed to describe their structure (see e.g. [73] for references). In the meantime, also four Ω_b^- states of the *bss* type have been reported from LHCb [73]. They lie in a narrow range between 6316 - 6350 MeV, but since their intrinsic widths are on the order of just a few MeV they are well separated in the invariant mass spectra. Spectroscopy and theory in this field is rapidly evolving.

LHCb has also reported a doubly charmed Ξ_{cc}^{++} (*ccu*) baryon [74]. The quantum numbers of this state are undetermined, but its significance is already rated three stars in the current compilation. Doubly charmed baryons have a very different structure from light baryons, more resembling heavy ‘double-star’ systems with attached light ‘planets’, which opens a new window for QCD properties. The first candidate for a doubly charmed baryon Ξ_{cc}^+ (*ccd*) had been reported earlier by the SELEX experiment [75, 76]. A significance of 6.3σ was claimed for the $\Lambda_c^+ K^- \pi^+$ decay and 4.8σ for $pD^+ K^-$ but searches by other experiments have not confirmed it so far (see e.g. [77] and Refs. therein) and it is not included in the particle listings. The SELEX and LHCb masses lie in the predicted 3500 – 3700 MeV mass range (see e.g. [70]). The LHCb Ξ_{cc}^{++} state lies about 100 MeV above the SELEX one, with a mass splitting far too large for *ucc* and *dcc* isospin partners. However, it has also been discussed that due to the different production mechanisms this is not necessarily a contradiction [78].

Figure 15.8 shows the spectrum of the established singly-charmed baryons (3^* and 4^* baryons in the *Listings* with known quantum numbers). The parity of the Λ_c^+ is that of the *c* quark, defined as positive. Spin and parity have not been determined experimentally for most of the states. They follow the ordering and expectation from the quark model. Candidates for $L = 2$ orbital excitations of the Λ_c (with $J^P = \frac{3}{2}^+$ and $J^P = \frac{5}{2}^+$) have already been observed, as well as a $\frac{3}{2}^-$ state at 2940 MeV, possibly a radial $L = 1$ excitation [79].

The same $SU(4)_f$ multiplets can be constructed for the bottom baryons by replacing the *c* quark by a *b* quark. The established 3^* and 4^* bottom baryons are shown in Fig. 15.8. The quadruplet $\mathbf{4}$ contains the two negative parity candidates $\Lambda_b(5912)^0$ and $\Lambda_b(5920)^0$. It appears that the confining potential is only weakly flavour dependent. For example, the mass difference between the Ξ_b and the Λ_b is roughly the same as that between the Ξ_c and the Λ_c , the mass splitting between the spin- $\frac{1}{2}$ Ω_b and the Λ_b close to that between the spin- $\frac{1}{2}$ Ω_c and the Λ_c . The spin- $\frac{3}{2}$ states are also heavier than the spin- $\frac{1}{2}$ ones, in agreement with expectations from the spin-spin force.

The bottom hadrons can also be embedded in a larger $SU(5)_f$ group that accounts for all baryons constructed from the five quark flavors. (The existence of baryons with *t*-quarks is very unlikely due to the short lifetime of the *t*-quark.) One predicts the decomposition

$$\mathbf{5} \otimes \mathbf{5} \otimes \mathbf{5} = \overline{\mathbf{10}}_A \oplus \mathbf{40}_{MS} \oplus \mathbf{40}_{MA} \oplus \mathbf{35}_S. \quad (15.31)$$

The decuplet is not realized in the ground state. The two 40-plets have mixed symmetry ($\frac{1}{2}$ -spin) and the 35-plet is symmetric

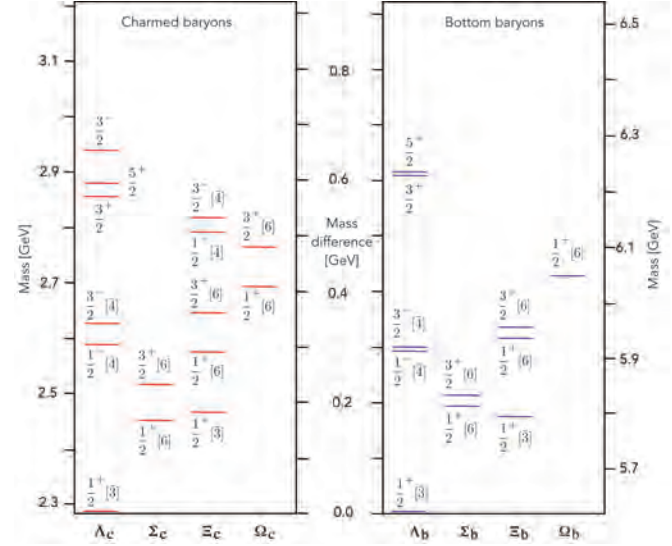


Figure 15.8: Mass spectrum of the established $C = 1$ charmed and $B = -1$ bottom baryons with known J^P . The flavor symmetry assignments are given by the square brackets. According to their isospins the $\Sigma_{c,b}$ ($\Xi_{c,b}$) consist of three (two) charged or neutral states that are nearly degenerate.

($\frac{3}{2}$ -spin). The $SU(4)_f$ spin- $\frac{1}{2}$ multiplet in Fig. 15.5 contains 20 spin- $\frac{1}{2}$ baryons and the corresponding one with bottom quarks an additional 12, giving together 32 states. Similarly there are 30 spin- $\frac{3}{2}$ baryons. One expects 75 ground state mesons from (15.31). Thus 13 ground state baryons containing both *b* and *c* quarks are predicted (8 spin- $\frac{1}{2}$ [$4\Omega + 4\Xi$] and 5 spin- $\frac{3}{2}$ [$3\Omega + 2\Xi$]).

15.6 Magnetic moments

The magnetic dipole moment of a baryon is conventionally written relative to the mass of the proton:

$$\vec{\mu}_B = g_B \mu_N \vec{\sigma}, \quad (15.32)$$

where $\mu_N = \frac{e}{2m_p}$ is the nuclear magneton (in natural units). The factor g_B is calculated by adding the quark contributions. The magnetic moment of quark *i* with charge $q_i e$ and constituent mass m_i is $\vec{\mu}_i = 2(\frac{q_i e}{2m_i})\vec{\sigma}$, hence for the three light quarks,

$$\mu_u = \frac{2}{3}\kappa_u, \quad \mu_d = -\frac{1}{3}\kappa_d, \quad \mu_s = -\frac{1}{3}\kappa_s, \quad \text{with } \kappa_i \equiv \frac{e}{2m_i}. \quad (15.33)$$

The magnetic dipole moment of a baryon is then given by

$$\mu_B = \sum_{i=1}^3 \langle B \uparrow | \mu_i \sigma_{zi} | B \uparrow \rangle, \quad (15.34)$$

where $|B \uparrow\rangle$ is the wavefunction for a baryon with its spin along the *z*-axis and $\vec{\sigma} = 2\vec{s}$. Since the quark model uses the totally symmetric $SU(6)$ wavefunctions (flavor $SU(3) \times$ spin $SU(2)$) one predicts for the proton:

$$\mu_p = \frac{4}{3}\mu_u - \frac{1}{3}\mu_d = \frac{e}{2m} \equiv \kappa, \quad (15.35)$$

assuming $m_u = m_d \simeq m$ (for the detailed derivation see e.g. Ref. [4]). For the magnetic moment of the neutron one obtains likewise

$$\mu_n = -\frac{1}{3}\mu_u + \frac{4}{3}\mu_d = -\frac{2}{3}\kappa, \quad (15.36)$$

which leads to the simple prediction $\mu_n/\mu_p = g_n/g_p = -2/3$.

The famous Frisch and Stern experiment showed for the first time that $g_p \sim 5.58 \gg 2$. Modern measurements are performed

in electromagnetic traps, see the *Listings*, while the magnetic moment of the neutron is measured with cold neutron beams. The experimental ratio $\mu_n/\mu_p = -0.6849793 \pm 0.0000003$ is impressively close to the prediction of the quark model (note that using instead the *antisymmetric* SU(6) wavefunctions would lead to $\mu_n/\mu_p = -2$ [4]). The constituent mass m of the u and d quarks can be estimated from (15.32) and (15.35): $m = 2m_p/g_p \simeq 336$ MeV.

The magnetic moment of the Λ is easy to predict: the diquark ud has isospin $i = 0$, since $i(s) = 0$ and $i(\Lambda) = 0$, and is therefore an antisymmetric isospin state. The symmetric quark model then also requires the spin to be zero, so that the magnetic moment of the Λ stems from the s quark:

$$\mu_\Lambda = \mu_s = -\frac{1}{3}\kappa_s. \quad (15.37)$$

The magnetic moment of the Λ is obtained from the Larmor precession frequency of the polarization vector in an homogeneous magnetic field. The latter is derived from the asymmetric distribution of the proton in $\Lambda \rightarrow \pi^- p$ [80]. The experimental result is listed in Table 15.8. The constituent mass of the s quark is then $m_s = -m\mu_p/3\mu_\Lambda = 509$ MeV.

Table 15.8: Quark model predictions and measured magnetic dipole moments of the ground state baryons in units of μ_N ; $\kappa \equiv \frac{e}{2m} = 2.793$ μ_N and $\kappa_s \equiv \frac{e}{2m_s} = -3\mu_\Lambda = 1.84$ μ_N . $\dagger \Sigma^0 \rightarrow \Lambda$ transition magnetic moment.

Baryon	Quark model	Experimental value
p	κ	input 2.793
n	$-\frac{2}{3}\kappa$	= -1.86 -1.913
Λ	$-\frac{1}{3}\kappa_s$	input -0.6138 \pm 0.0047
Σ^+	$\frac{8}{9}\kappa + \frac{1}{9}\kappa_s$	= 2.68 2.458 \pm 0.010
Σ^0	$\frac{2}{9}\kappa + \frac{1}{9}\kappa_s$	= 0.82
$\Sigma^{0\dagger}$	$-\frac{1}{\sqrt{3}}\kappa$	= -1.61 -1.61 \pm 0.08
Σ^-	$-\frac{4}{9}\kappa + \frac{1}{9}\kappa_s$	= -1.04 -1.160 \pm 0.025
Ξ^0	$-\frac{2}{9}\kappa - \frac{4}{9}\kappa_s$	= -1.44 -1.250 \pm 0.014
Ξ^-	$\frac{1}{9}\kappa - \frac{4}{9}\kappa_s$	= -0.51 -0.6507 \pm 0.0025
Ω^-	$-\kappa_s$	= -1.84 -2.024 \pm 0.056
Δ^{++}	2κ	= 5.58 4.52 \pm 0.67
Δ^+	κ	= 2.79 2.3 - 4.5

The magnetic moments of the other baryons (Table 15.8) are predicted from κ and κ_s . The magnetic moment of the Σ^+ is obtained by replacing the d quark in (15.35) by an s quark, and for the Σ^- the u quark by an s quark in (15.36). The magnetic moment of the Σ^+ has also been measured with the precession method using its decay into $p\pi^0$ [81], that of the $\Sigma^- \rightarrow n\pi^-$ likewise, or by detecting the X-rays emitted by cascading Σ^- captured in the Coulomb shells of target atoms. The magnetic moment is then derived from the fine-structure splitting [82].

The magnetic moments of the Ξ^0 , Ξ^- and Ω^- are obtained from the polarization of the Λ in the decays $\Lambda\pi^0$, $\Lambda\pi^-$ and ΛK^- , respectively. The SU(6) wavefunction of the (spin 3/2) Ω^- is the product of the two symmetric SU(3) flavor and SU(2) spin wavefunctions. Summing over the three s quarks one gets

$$\mu_{\Omega^-} = \sum_{i=1}^3 \langle \Omega^- \uparrow | \mu_i \sigma_{zi} | \Omega^- \uparrow \rangle = 3\mu_s = 3\mu_\Lambda. \quad (15.38)$$

The magnetic moment of the Ω^- is hard to measure, because the Ω^- is unpolarized at high energies, in contrast to the other hyperons. Polarized Ω^- hyperons have been obtained from polarized Λ and Ξ^0 impinging on a nuclear target [83].

In quark models with full isospin symmetry the magnetic moments of the Δ -resonances are simply related to the magnetic moment of the proton by $\mu_\Delta = Q_\Delta \cdot \mu_N$, ($Q_\Delta = \text{charge}$) i.e. the moment of the Δ^+ should equal the proton moment and the

moment of the Δ^{++} should be twice as large (sum of the three u -quarks). Magnetic moments of the decuplet baryons (with the exception of the Ω^-) are very difficult to measure because their lifetimes are so short that spin precession techniques cannot be used. For the Δ one can profit from an electromagnetic spin-reorientation transition inside the large width of the state. This leads to the emission of a magnetic dipole photon in reactions like $\pi^+ p \rightarrow \pi^+ p \gamma$ or $\gamma p \rightarrow \pi^0 p \gamma'$ which is related to the magnetic moment of the resonance. The first reaction has been used to study the magnetic moment of the Δ^{++} by measuring the left-right asymmetry with polarized protons [84]. The second one was used for the Δ^+ state [85,86]. Taking all experimental and systematic uncertainties into account the result spans the range from (2.3 - 4.5) μ_N , covering the quark model prediction of $\approx 2.8\mu_N$, but is not very precise.

Table 15.8 lists the current experimental values for the magnetic moments of the ground state baryons, together with the predictions from the quark model. There are significant discrepancies, but given its crudeness, the quark model performs surprisingly well.

15.7 Dynamics

Quantum chromodynamics (QCD) is well-established as the theory for the strong interactions. As such, one of the goals of QCD is to predict the spectrum of strongly-interacting particles. To date, the only first-principles calculations of spectroscopy from QCD use lattice methods. These are the subject of Sec. 15.8. These calculations are difficult and unwieldy, and many interesting questions do not have a good lattice-based method of solution. Therefore, it is natural to build models, whose ingredients are abstracted from QCD, or from the low-energy limit of QCD (such as chiral Lagrangians) or from the data itself. The words “quark model” are a shorthand for such phenomenological models. Many specific quark models exist, but most contain a similar basic set of dynamical ingredients. These include:

1. A confining interaction, which is generally spin-independent (*e.g.*, harmonic oscillator or linear confinement);
2. Different types of spin-dependent interactions:

a) commonly used is a color-magnetic flavor-independent interaction modeled after the effects of gluon exchange in QCD (see *e.g.*, Ref. [87]). For example, in the S -wave states, there is a spin-spin hyperfine interaction of the form

$$H_{HF} = -\alpha_S M \sum_{i>j} (\vec{\sigma}\lambda_a)_i (\vec{\sigma}\lambda_a)_j, \quad (15.39)$$

where M is a constant with units of energy, λ_a ($a = 1, \dots, 8$) is the set of SU(3) unitary spin matrices, defined in the review “SU(3) Isoscalar Factors and Representation Matrices,” and the sum runs over constituent quarks or antiquarks. Spin-orbit interactions, although allowed, seem to be small in general, but a tensor term is responsible for the mixing of states with the same J^P but different L, S combinations.

b) other approaches include flavor-dependent short-range quark forces from instanton effects (see *e.g.*, [88,89]). This interaction acts only on scalar, isoscalar pairs of quarks in a relative S -wave state:

$$\langle q^2; S, L, T | W | q^2; S, L, T \rangle = -4g\delta_{S,0}\delta_{L,0}\delta_{T,0}\mathcal{W} \quad (15.40)$$

where \mathcal{W} is the radial matrix element of the contact interaction.

c) a rather different and somewhat controversial approach is based on flavor-dependent spin-spin forces arising from one-boson exchange. The interaction term is of the form:

$$H_{HF} \propto \sum_{i<j} V(\vec{r}_{ij}) \lambda_i^F \cdot \lambda_j^F \vec{\sigma}_i \cdot \vec{\sigma}_j \quad (15.41)$$

where the λ_i^F are in flavor space (see *e.g.*, Ref. [90]).

3. A strange quark mass somewhat larger than the up and down quark masses, in order to split the SU(3) multiplets;
4. In the case of spin-spin interactions, a flavor-symmetric interaction for mixing $q\bar{q}$ configurations of different flavors (*e.g.*, $u\bar{u} \leftrightarrow d\bar{d} \leftrightarrow s\bar{s}$), in isoscalar channels, so as to reproduce *e.g.*, the $\eta - \eta'$ and $\omega - \phi$ mesons.

These ingredients provide the basic mechanisms that determine the hadron spectrum in the standard quark model.

15.8 Lattice Calculations of Hadronic Spectroscopy

Lattice calculations are a major source of information about QCD masses and matrix elements. The necessary theoretical background is given in Sec. 17 of this *Review*. Here we confine ourselves to some general comments and illustrations of lattice calculations for spectroscopy.

It might seem a bit out of place to have a section about lattice calculations in a review of the quark model, since to many readers, the quark model is just a model while QCD could be thought of as a construct which is something deeper than a model. But this review is, despite its title, actually an introduction to the spectroscopy and related quantities of the strong interactions. From that perspective, a presentation of lattice results is entirely appropriate.

Lattice calculations are from first principles – their input is a discretized version of the QCD Lagrangian, and the predictions of a lattice calculation are predictions of QCD, once the lattice spacing is taken to zero, the simulation volume is taken to infinity, and the quark masses are tuned to their physical values. Lattice calculations make extensive use of quark model ideas – for example, the operators used to create and annihilate hadrons are almost always based on the quark model. (This may not be clear in the lattice literature, since the final answer should not depend on the choice of operators used.)

There is only a sporadic literature connecting lattice results to the quark model (one recent example is [91]) but of course the qualitative understanding of lattice results depends as heavily on quark model ideas as does the qualitative understanding of experimental data.

In general, the cleanest lattice results come from computations of processes in which there is only one particle in the simulation volume. These quantities include masses of hadrons, simple decay constants, like pseudoscalar meson decay constants, and semileptonic form factors (such as the ones appropriate to $B \rightarrow D\ell\nu$, $K\ell\nu$, $\pi\ell\nu$). The cleanest predictions for masses are for states which have narrow decay widths and are far below any thresholds to open channels, since the effects of final state interactions are not yet under complete control on the lattice. As a simple corollary, the lightest state in a channel is easier to study than the heavier ones. “Difficult” states for the quark model (such as exotics) are also difficult for the lattice because of the lack of simple operators which couple well to them.

Good-quality modern lattice calculations will present multi-part error budgets with their predictions. A small part of the uncertainty is statistical, from sample size. Typically, the quoted statistical uncertainty includes uncertainty from a fit: it is rare that a simulation computes one global quantity which is the desired observable. Simulations which include virtual quark-antiquark pairs (also known as “dynamical quarks” or “sea quarks”) are often done at up and down quark mass values heavier than the experimental ones, and it is then necessary to extrapolate in these quark masses. Simulations can work at the physical values of the heavier quarks’ masses. They are always done at nonzero lattice spacing, and so it is necessary to extrapolate to zero lattice spacing. Some theoretical input is needed to do this. Much of the uncertainty in these extrapolations is systematic, from the choice of fitting function. Other systematics include the effect of finite simulation volume, the number of flavors of dynamical quarks actually simulated, and technical issues with how these dynamical quarks are included. The particular choice of a fiducial mass (to normalize other predictions) is not standardized; there are many possible choices, each with its own set of strengths and weaknesses, and determining it usually requires a

second lattice simulation from that used to calculate the quantity under consideration.

A systematic error of major historical interest is the “quenched approximation,” in which dynamical quarks are simply left out of the simulation. This was done because the addition of these virtual pairs presented an expensive computational problem. No generally-accepted methodology has ever allowed one to correct for quenching effects, short of redoing all calculations with dynamical quarks. Recent advances in algorithms and computer hardware have rendered it obsolete.

With these brief remarks, we turn to examples. The field of lattice QCD simulations is vast, and so it is not possible to give a comprehensive review of them in a small space. The history of lattice QCD simulations is a story of thirty years of incremental improvements in physical understanding, algorithm development, and ever faster computers, which have combined to bring the field to a present state where it is possible to carry out very high quality calculations. We present a few representative illustrations, to show the current state of the art.

15.8.1 Spectroscopy of low-lying states

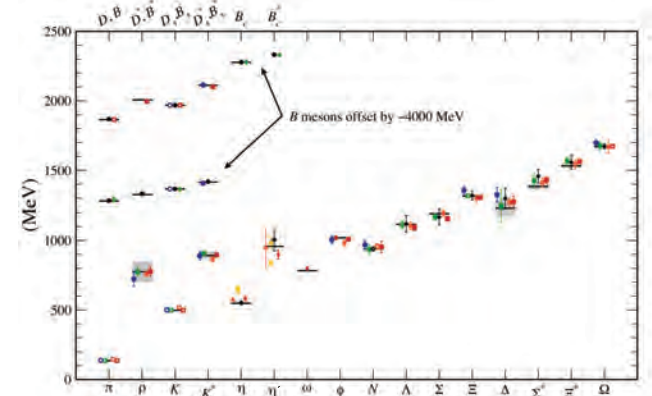


Figure 15.9: Hadron spectrum from lattice QCD. Comprehensive results for mesons and baryons are from MILC [92,93], PACS-CS [94], BMW [95], QCDSF [96], and ETM [97]. Results for η and η' are from RBC & UKQCD [17], Hadron Spectrum [98] (also the only ω mass), UKQCD [99], and Michael, Otnad, and Urbach [100]. Results for heavy-light hadrons from Fermilab-MILC [101], HPQCD [102, 103], and Mohler and Woloshyn [104]. Circles, squares, diamonds, and triangles stand for staggered, Wilson, twisted-mass Wilson, and chiral sea quarks, respectively. Asterisks represent anisotropic lattices. Open symbols denote the masses used to fix parameters. Filled symbols (and asterisks) denote results. Red, orange, yellow, green, and blue stand for increasing numbers of ensembles (*i.e.*, lattice spacing and sea quark mass) Black symbols stand for results with 2+1+1 flavors of sea quarks. Horizontal bars (gray boxes) denote experimentally measured masses (widths). b -flavored meson masses are offset by -4000 MeV.

By far, the major part of all lattice spectroscopy is concerned with that of the light hadrons, and so we illustrate results in Fig. 15.9, a comprehensive summary provided by A. Kronfeld (private communication; see also [105]).

Mesons with a valence structure of identical quark - antiquark pairs such as the eta or eta-prime, $|\eta\rangle \sim \alpha|\bar{u}u + \bar{d}d\rangle + \beta|\bar{s}s\rangle$, are at the frontier of lattice QCD calculations, because one must include the effects of “annihilation graphs” for the valence q and \bar{q} . Recently, several groups, Refs. [17, 99, 106], have reported calculations of the η and η' mesons. The numbers of [17] are typical, finding masses of 573(6) and 947(142) MeV for the η and η' . The singlet-octet mixing angle (in the conventions of Table 15.2) is $\theta_{lin} = -14.1(2.8)^\circ$.

The spectroscopy of mesons containing heavy quarks has become a truly high-precision endeavor. These simulations use Non-Relativistic QCD (NRQCD) or Heavy Quark Effective Theory

(HQET), systematic expansions of the QCD Lagrangian in powers of the heavy quark velocity, or the heavy quark mass. Terms in the Lagrangian have obvious quark analogs, but are derived directly from QCD. For example, the heavy quark potential is a derived quantity, extracted from simulations. Figs. 15.10 and 15.11 show the low lying mass spectrum for charmonium and bottomonium states from two different groups [103,107]. Most of the results are for the lightest state with a given value of quantum numbers. We return to this point below.

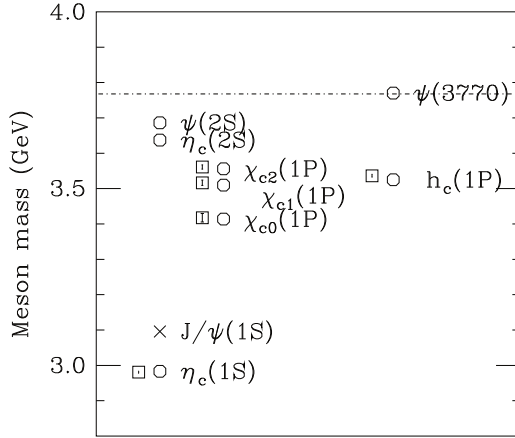


Figure 15.10: Spectroscopy of the $\bar{c}c$ spectrum, compared to lattice data from Ref. [107]. Particles whose masses are used to fix lattice parameters are shown with crosses; octagons label experimental values, and lattice results are shown as squares. The dotted line shows the threshold value for two charmed mesons.

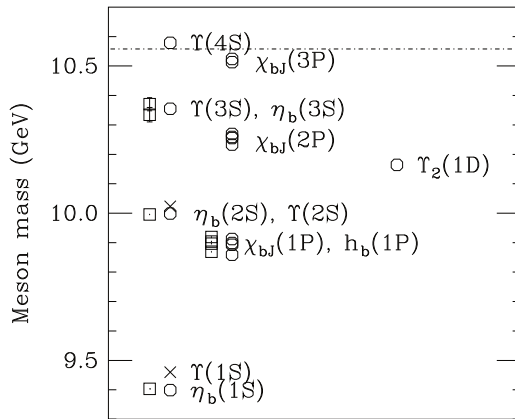


Figure 15.11: Spectroscopy of the $\bar{b}b$ system, adapted from Ref. [103]. Particles whose masses are used to fix lattice parameters are shown with crosses; octagons label experimental values, and lattice results are shown as squares. The dotted line shows the threshold value for two bottom mesons.

Fig. 15.12 shows a compilation of recent lattice results for doubly and triply charmed baryons, provided by S. Meinel [115]. The state recently announced by LHCb [74] is also shown. Note that the lattice calculations for the mass of this state were predictions, not postdictions.

15.8.2 Excited state spectroscopy

Lattice calculations of excited states are much more difficult than those for the lightest states. There are two issues:

1. The states are unstable resonances
2. There are many states with the same quantum numbers

While these two problems appear together in excited state spectroscopy, almost all lattice calculations we know of deal with them

separately (i. e. there are studies of many stable states, or studies of a single state with a single decay channel).

The first point is an issue because lattice calculations do not see decays directly; instead, they give energies of single or multiple particle states in a box of finite size. The combined mass is shifted from being the sum of the individual masses because the finite box size forces the hadrons to interact with each other. The volume-dependent mass shift yields the phase shift for the continuum scattering amplitude, which in turn can be used to extract the resonance mass and width, with some degree of modeling. So far only two-body resonances, the rho meson and a few others, have been well studied. This is an active research area. A recent review, [117], summarizes the situation, and example of a calculation of the rho meson decay width is [118]. The mass and decay width of the $f_0(500)$ have recently been computed in [119] and [120]. Ref. [121] studies the decay width of the $\Delta(1238)$.

The second point is an issue for lattice calculations since the observables which give masses have a typical functional form

$$C(t) = \sum_n A_n \exp(-E_n t). \quad (15.42)$$

E_n is the energy of the n th state and t is a parameter (the spatial distance of separation of operators) which is accessible to the lattice simulator. The contribution of excited states is exponentially suppressed at large t . The size of a given state's contribution, A_n , is related to the choice of interpolating field used to create the state. (This is where the quark model comes in.) As we move away from hadrons which can be created by the simplest quark model operators (appropriate to the lightest meson and baryon multiplets) we encounter a host of new problems: either no good interpolating fields, or too many possible interpolating fields, and many states with the same quantum numbers. Techniques for dealing with these interrelated problems vary from collaboration to collaboration, but all share common features: typically, correlation functions from many different interpolating fields are used, and the signal is extracted in what amounts to a variational calculation using the chosen operator basis. In addition to mass spectra, wave function information can be garnered from the form of the best variational wave function. Of course, the same problems which are present in the spectroscopy of the lightest hadrons (the need to extrapolate to infinite volume, physical values of the light quark masses, and zero lattice spacing) are also present. We briefly touch on three different kinds of hadrons: excited states of mesons (including hybrids), excited states of baryons, and glueballs. The quality of the data is not as good as for the ground states, and so the results continue to evolve. Shifts in the masses which occur because the state can decay are not included in the calculations.

Modern calculations use a large basis of trial states, which allow them to probe many quantum number channels simultaneously. This is vital for studying “difficult sectors” of QCD, such as the isoscalar mesons. A recent example of meson spectroscopy where this is done, by [116], is shown in Fig. 15.13. The quark masses are still heavier than their physical values, so the pion is at 392 MeV. The authors can assign a relative composition of nonstrange and strange quark content to their states, observing, for example, a nonstrange ω and a strange ϕ . Some states also have a substantial component of gluonic excitation. Note especially the three exotic channels $J^{PC} = 1^{-+}$, 0^{+-} , and 2^{+-} , with states around 2 GeV. These calculations will become more realistic as the quark masses are carried lower and resonance effects are included.

The interesting physics questions of excited baryon spectroscopy to be addressed are precisely those enumerated in the last section. An example of a recent calculation, due to Ref. [122] is shown in Fig. 15.14. Notice that the pion is not yet at its physical value. The lightest positive parity state is the nucleon, and the Roper resonance has not yet appeared as a light state.

Studies which observe a large basis of states across many volumes can probe excited state spectroscopy as resonances. These calculations are just beginning and the ones we know about are performed at unphysically heavy quark masses. Examples include the decays of an exotic $J^{PC} = 1^{-+}$ resonance [123] and the spec-

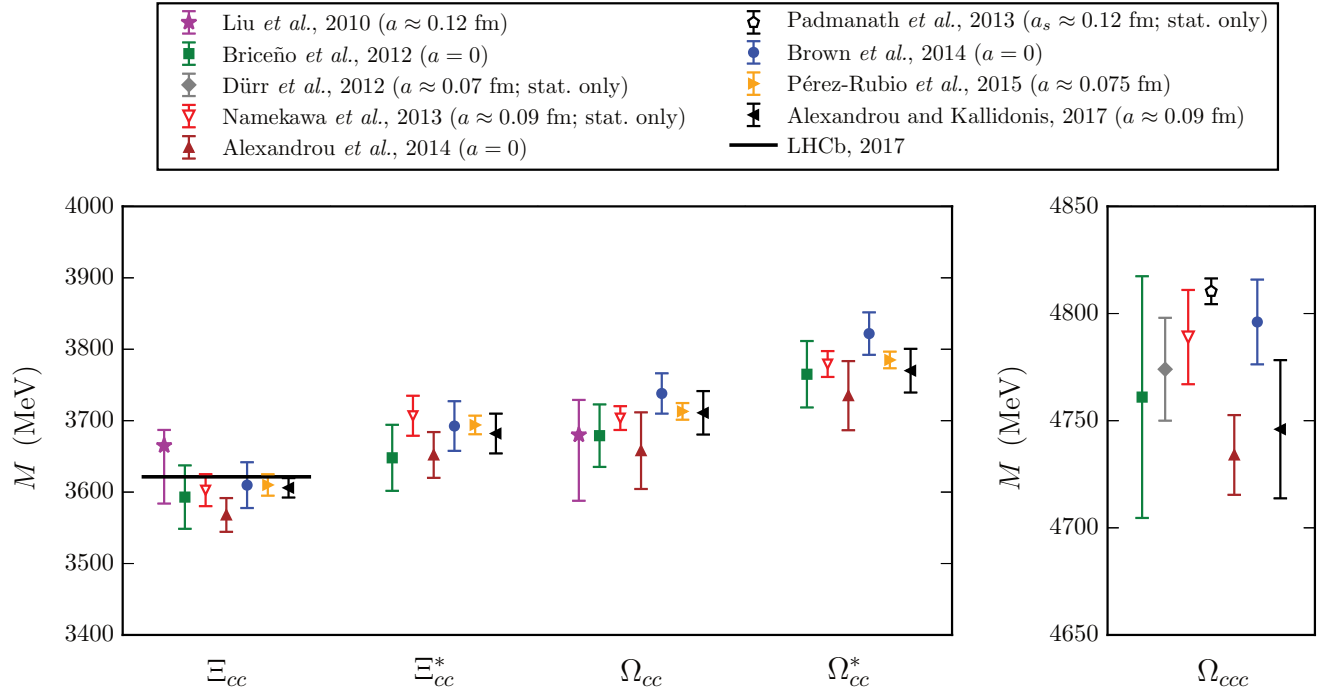


Figure 15.12: Comparison of lattice QCD results for the doubly and triply charmed baryon masses. Labels are Liu, *et al.*, [108]; Briceño, *et al.*, [109]; Namekawa, *et al.*, [110]; Padmanath, *et al.*, [111]; Alexandrou, *et al.*, [97]; Brown, *et al.*, [112]; Pérez-Rubio *et al.*, [113]; Alexandrou and Kallidonis 2017, [114]. Only calculations with dynamical light quarks are included; for the doubly charmed baryons, only calculations were performed at or extrapolated to the physical pion mass are shown. Results without estimates of systematic uncertainties are labeled “stat. only”. The lattice spacing values used in the calculations are also given; $a = 0$ indicates that the results have been extrapolated to the continuum limit. In the plot of the doubly charmed baryons, the recently announced experimental result for the Ξ_{cc}^+ mass from LHCb [74] is shown with a horizontal line.

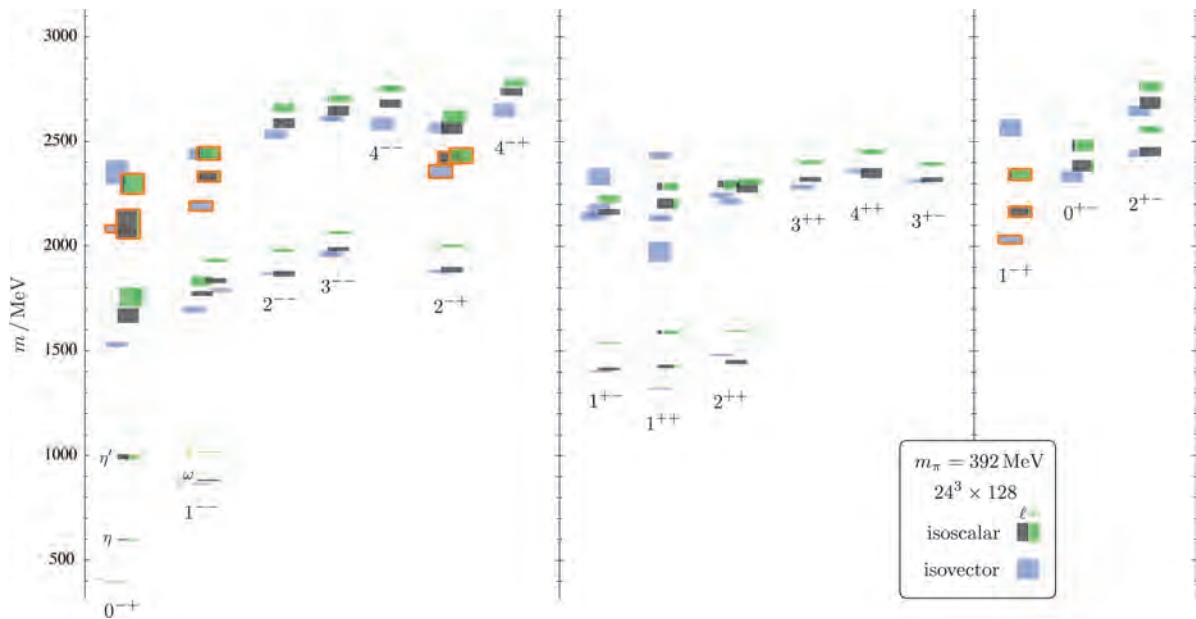


Figure 15.13: Isoscalar (green and black) and isovector (blue) spectrum from Ref. [116]. States are labeled J^{PC} . The quark mass is heavier than its physical value; $m_\pi = 392$ MeV. The vertical height of each box indicates the statistical uncertainty in the mass. Black and green indicate relative nonstrange and strange composition. Orange outlines show states with a large chromomagnetic component to their wave function, which the authors argue are hybrid states. Note the exotic states in the three rightmost columns.

trospecty of J^{--} resonances [124]. We expect to see considerable progress in this area over the next few years.

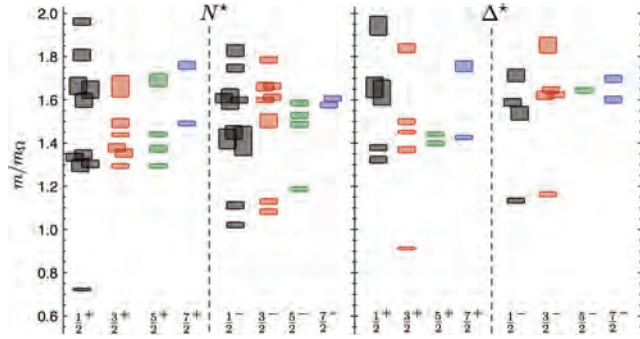


Figure 15.14: Spin-identified spectrum of nucleons and deltas, from lattices where $m_\pi = 396$ MeV, in units of the calculated Ω mass, from Ref. [122]. The colors just correspond to the different J assignments: grey for $J = 1/2$, red for $J = 3/2$, green for $J = 5/2$, blue for $J = 7/2$.

Glueballs present similar issues. In Fig. 15.3 we showed a figure from [22] presenting a lattice prediction for the glueball mass spectrum in quenched approximation. A true QCD prediction of the glueball spectrum requires dynamical light quarks, some way to deal with the mixing of glue states and quark-antiquark (and beyond) states and (because glueball operators are intrinsically noisy) high statistics. Only recently have the first useful such calculations appeared, in [125, 126]. Fig. 15.15 shows results from [125], done with dynamical u , d and s quarks at two lattice spacings, 0.123 and 0.092 fm, along with comparisons to the quenched lattice calculation of [25] and to experimental isosinglet mesons. The dynamical simulation is, of course, not the last word on this subject, but it shows that the effects of quenching seem to be small.

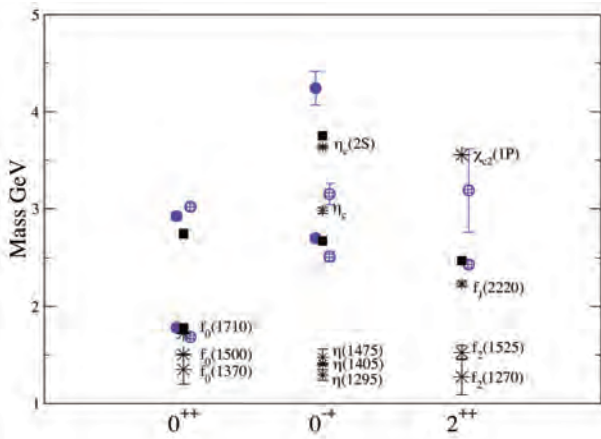


Figure 15.15: Lattice QCD predictions for glueball masses. The open and closed circles are the larger and smaller lattice spacing data of the full QCD calculation of glueball masses of Ref. [125]. Squares are the quenched data for glueball masses of Ref. [25]. The bursts labeled by particle names are experimental states with the appropriate quantum numbers.

Lattice calculations relevant to the extra states observed in the charmonium and bottomonium spectrum (Sec. 15.4) are difficult, because the states sit high in the spectrum of most channels, because of the number of nearby multiparticle states, and because it is necessary to have the technology to study heavy and light quarks together. There is a hybrid literature of studies which combines lattice calculations of the potential of static sources in a solution of a Schrödinger equation for the light quarks in a Born - Oppenheimer approximation (see [127] for context).

The system with the largest lattice literature is a bound state of two heavy quarks and two light antiquarks, for example $\bar{b}bud$. There are excellent reasons for expecting this state to be stable in the limit that the b mass goes to infinity [128] but finding the precise degree of stability at the physical b mass takes a phenomenological estimate or a lattice calculation. The $I(J^P) = 0(1^+)$ state is predicted to be stable by about 128(26) MeV [129] or 189(10) MeV [130]. (These authors put the $\bar{b}bsd$ state at 98 MeV below threshold.) These numbers are in reasonable agreement with phenomenological estimates from Refs. [128, 131].

15.8.3 Electromagnetic effects

As a final part of spectroscopy we mention electromagnetic mass splittings (such as the neutron - proton mass difference). They are interesting but difficult. These calculations are important for determining the values of the quark masses (for a discussion see Sec. 60 in this Review). Knowing that the neutron is heavier than the proton tells us that these splittings have a complicated origin. One part of the shift is because the up and down quarks have slightly different masses. The second is that the quarks have (different) charges. Phenomenologists (compare Ref. [132]) combine Coulomb forces and spin-dependent electromagnetic hyperfine interactions to model their charge effects. In order to compute hadronic mass differences on the lattice, electromagnetic interactions must be included in the simulations. This creates a host of technical issues. An important one is that electromagnetic interactions are long range, but lattice simulations are done in finite volumes. The theoretical situation is summarized in the recent Flavour Lattice Averaging Group (FLAG) review [133]. A recent calculation, Ref. [134], has presented the first results for electromagnetic mass splittings in the baryon octet, with good agreement with observation. Refs. [135–137] have performed calculations for meson splittings.

There is a small lattice literature associated with magnetic moments of baryons. The calculations are done by including a static magnetic field in the simulation and computing the energy difference between baryons in different spin states. We are aware of no calculations at physical quark masses. A recent calculation [138] used 800 and 450 MeV pions. When expressed in units of the nucleon magneton at the simulation point ($e/(2M_N(m_\pi))$) the moments are in reasonable agreement with experiment and with quark model expectations.

References

- [1] G. 't Hooft, Nucl. Phys. B **72**, 461 (1974).
- [2] G. 't Hooft, Nucl. Phys. B **75**, 461 (1974).
- [3] E. Witten, Nucl. Phys. B **160**, 57 (1979).
- [4] C. Amsler in the Quark Structure of Hadrons, Lecture Notes in Physics **949** (2018), ed. Springer.
- [5] H.-Y. Cheng, Physics Letters B **707**, 1, 116 (2012), ISSN 0370-2693, URL <https://www.sciencedirect.com/science/article/pii/S0370269311014705>.
- [6] L. Burakovsky and J. T. Goldman, Nucl. Phys. A **625**, 220 (1997), [hep-ph/9703272].
- [7] M.-C. Du and Q. Zhao, Phys. Rev. D **100**, 036005 (2019), URL <https://link.aps.org/doi/10.1103/PhysRevD.100.036005>.
- [8] H.-W. Ke and X.-Q. Li, Phys. Rev. D **99**, 036014 (2019), URL <https://link.aps.org/doi/10.1103/PhysRevD.99.036014>.
- [9] M.-L. Du *et al.*, Phys. Rev. Lett. **126**, 192001 (2021), URL <https://link.aps.org/doi/10.1103/PhysRevLett.126.192001>.
- [10] J. Schwinger, Phys. Rev. **135**, B816 (1964).
- [11] H. J. Lipkin and B.-s. Zou, Phys. Rev. D **53**, 6693 (1996).
- [12] A. Bramon, R. Escribano and M. D. Scadron, Phys. Lett. B **403**, 339 (1997), [hep-ph/9703313].
- [13] A. Aloisio *et al.* (KLOE), Phys. Lett. B **541**, 45 (2002), [hep-ex/0206010].
- [14] F. Ambrosino *et al.*, JHEP **07**, 105 (2009), [arXiv:0906.3819].

- [15] C. Amsler *et al.* (Crystal Barrel), Phys. Lett. **B294**, 451 (1992).
- [16] C. Amsler, Rev. Mod. Phys. **70**, 1293 (1998), [hep-ex/9708025].
- [17] N. H. Christ *et al.*, Phys. Rev. Lett. **105**, 241601 (2010), [arXiv:1002.2999].
- [18] T. Feldmann, Int. J. Mod. Phys. **A915**, 159 (2000).
- [19] C. Amsler and F. E. Close, Phys. Rev. **D53**, 295 (1996), [hep-ph/9507326].
- [20] R. L. Jaffe, Phys. Rev. **D15**, 267 (1977).
- [21] R. L. Jaffe, Phys. Rev. **D15**, 281 (1977).
- [22] Y. Chen *et al.*, Phys. Rev. **D73**, 014516 (2006), [hep-lat/0510074].
- [23] S.L. Olsen, Front. Phys. **10**, 121 (2015).
- [24] S. L. Olsen, T. Skwarnicki and D. Zieminska, Rev. Mod. Phys. **90**, 1, 015003 (2018), [arXiv:1708.04012].
- [25] C. J. Morningstar and M. J. Peardon, Phys. Rev. **D60**, 034509 (1999), [hep-lat/9901004].
- [26] W.-J. Lee and D. Weingarten, Phys. Rev. **D61**, 014015 (2000), [hep-lat/9910008].
- [27] G. S. Bali *et al.* (UKQCD), Phys. Lett. **B309**, 378 (1993), [hep-lat/9304012].
- [28] C. Michael, AIP Conf. Proc. **432**, 1, 657 (1998), [hep-ph/9710502].
- [29] F. E. Close and A. Kirk, Eur. Phys. J. **C21**, 531 (2001), [hep-ph/0103173].
- [30] W. Ochs, J. Phys. **G40**, 043001 (2013), [arXiv:1301.5183].
- [31] F. Br unner and A. Rebhan, Phys. Rev. Lett. **115**, 13, 131601 (2015), [arXiv:1504.05815].
- [32] C. Amsler and N. A. Tornqvist, Phys. Rept. **389**, 61 (2004).
- [33] N. Isgur and J. E. Paton, Phys. Rev. **D31**, 2910 (1985).
- [34] P. Lacock *et al.* (UKQCD), Phys. Lett. **B401**, 308 (1997), [hep-lat/9611011].
- [35] M. S. Chanowitz and S. R. Sharpe, Nucl. Phys. **B222**, 211 (1983), [Erratum: Nucl. Phys. **B228**, 588 (1983)].
- [36] T. Barnes *et al.*, Nucl. Phys. **B224**, 241 (1983).
- [37] B. Kopf *et al.* (2020), [arXiv:2008.11566].
- [38] R. Aaij *et al.* (LHCb), Phys. Rev. Lett. **115**, 072001 (2015), [arXiv:1507.03414].
- [39] R. Aaij *et al.* (LHCb), Phys. Rev. Lett. **122**, 22, 222001 (2019), [arXiv:1904.03947].
- [40] J.-J. Wu *et al.*, Phys. Rev. Lett. **105**, 232001 (2010), URL <https://link.aps.org/doi/10.1103/PhysRevLett.105.232001>.
- [41] J.-J. Wu, T.-S. H. Lee and B. S. Zou, Phys. Rev. C **85**, 044002 (2012), URL <https://link.aps.org/doi/10.1103/PhysRevC.85.044002>.
- [42] Y.-R. Liu *et al.*, Prog. Part. Nucl. Phys. **107**, 237 (2019), [arXiv:1903.11976].
- [43] F.E. Close, in *Quarks and Nuclear Forces* (Springer-Verlag, 1982), p. 56.
- [44] R.H. Dalitz and L.J. Reinders, in "Hadron Structure as Known from Electromagnetic and Strong Interactions," *Proceedings of the Hadron '77 Conference* (Veda, 1979), p. 11.
- [45] E. Klempt and J.-M. Richard, Rev. Mod. Phys. **82**, 1095 (2010), [arXiv:0901.2055].
- [46] T. Melde, W. Plessas and B. Sengl, Phys. Rev. **D77**, 114002 (2008), [arXiv:0806.1454].
- [47] N. Isgur and G. Karl, Phys. Rev. **D18**, 4187 (1978).
- [48] N. Isgur and G. Karl, Phys. Rev. **D19**, 2653 (1979), [Erratum: Phys. Rev. **D23**, 817 (1981)].
- [49] S. Capstick and W. Roberts, Prog. Part. Nucl. Phys. **45**, S241 (2000), [arXiv:nucl-th/0008028].
- [50] S. Capstick and W. Roberts, Phys. Rev. **D58**, 074011 (1998), [arXiv:nucl-th/9804070].
- [51] R. A. Arndt *et al.*, Phys. Rev. **C74**, 045205 (2006), [arXiv:nucl-th/0605082].
- [52] B. Krusche and S. Schadmand, Prog. Part. Nucl. Phys. **51**, 399 (2003), [arXiv:nucl-ex/0306023].
- [53] A. V. Anisovich *et al.*, Eur. Phys. J. **A52**, 9, 284 (2016), [arXiv:1604.05704].
- [54] S. Capstick, Phys. Rev. **D46**, 2864 (1992).
- [55] E. Gutz *et al.* (CBELSA/TAPS), Eur. Phys. J. **A50**, 74 (2014), [arXiv:1402.4125].
- [56] V. Sokhoyan *et al.* (CBELSA/TAPS), Eur. Phys. J. **A51**, 8, 95 (2015), [Erratum: Eur. Phys. J. **A51**, no.12, 187 (2015)], [arXiv:1507.02488].
- [57] E. Klempt *et al.*, Eur. Phys. J. **A56**, 261 (2020).
- [58] J. Yelton *et al.*, Phys. Rev. Lett. **121**, 052003 (2018).
- [59] G. Barruca *et al.*, Eur. Phys. J. **A57**, 154 (2021).
- [60] G. Barucca *et al.*, Eur. Phys. J. **A57**, 4, 154 (2021).
- [61] S. Capstick and W. Roberts, Prog. in Part. Nucl. Phys. **45**, 241 (2000).
- [62] V. Crede and W. Roberts, Rept. on Prog. in Phys. **76**, 076301 (2013).
- [63] M. Ferraris *et al.*, Phys. Lett. **B364**, 231 (1995).
- [64] M. M. Giannini and E. Santopinto, Chin. J. Phys. **53**, 020301 (2015), [arXiv:1501.03722].
- [65] M. Anselmino *et al.*, Rev. Mod. Phys. **65**, 1199 (1993).
- [66] R. Bijker, F. Iachello and A. Leviatan, Annals Phys. **236**, 69 (1994), [arXiv:nucl-th/9402012].
- [67] S. Capstick and P. R. Page, Phys. Rev. **C66**, 065204 (2002), [arXiv:nucl-th/0207027].
- [68] R. L. Jaffe, D. Pirjol and A. Scardicchio, Phys. Rept. **435**, 157 (2006), [hep-ph/0602010].
- [69] R. Slansky, Phys. Rept. **79**, 1 (1981).
- [70] M. Karliner and J. L. Rosner, Phys. Rev. **D90**, 9, 094007 (2014), [arXiv:1408.5877].
- [71] R. Aaij *et al.* (LHCb), Phys. Rev. Lett. **118**, 18, 182001 (2017), [arXiv:1703.04639].
- [72] Y. Yelton *et al.*, Phys. Rev. **D97**, 051102(R) (2018).
- [73] R. Aaij *et al.*, Phys. Rev. Lett. **124**, 082002 (2020).
- [74] R. Aaij *et al.* (LHCb), Phys. Rev. Lett. **119**, 11, 112001 (2017), [arXiv:1707.01621].
- [75] M. Mattson *et al.* (SELEX), Phys. Rev. Lett. **89**, 112001 (2002), [hep-ex/0208014].
- [76] A. Ocherashvili *et al.* (SELEX), Phys. Lett. **B628**, 18 (2005), [hep-ex/0406033].
- [77] R. Aaij *et al.* (LHCb), Sci. China Phys. Mech. Astron. **63**, 2, 221062 (2020), [arXiv:1909.12273].
- [78] S. G. S.J. Brodsky and S. Koshkarev, Eur. Phys. J. **C78**, 483 (2018).
- [79] R. Aaij *et al.* (LHCb), JHEP **05**, 030 (2017), [arXiv:1701.07873].
- [80] L. Schachinger *et al.*, Phys. Rev. Lett. **41**, 1348 (1978).
- [81] A. Morelos Pineda *et al.* (E761), Phys. Rev. Lett. **71**, 3417 (1993).
- [82] D. W. Hertzog *et al.*, Phys. Rev. D **37**, 1142 (1988).
- [83] N. B. Wallace *et al.*, Phys. Rev. Lett. **74**, 3732 (1995).
- [84] A. Bosshard *et al.*, Phys. Rev. D **44**, 1962 (1991).
- [85] M. Kotulla *et al.*, Phys. Rev. Lett. **27**, 272001 (2002).
- [86] S. Schumann *et al.*, Eur. Phys. J. **A43**, 269 (2010).

- [87] A. De Rujula, H. Georgi and S. L. Glashow, *Phys. Rev.* **D12**, 147 (1975).
- [88] W. H. Blask *et al.*, *Z. Phys.* **A337**, 327 (1990).
- [89] U. Loring *et al.*, *Eur. Phys. J.* **A10**, 309 (2001), [hep-ph/0103287].
- [90] L. Ya. Glozman and D. O. Riska, *Phys. Rept.* **268**, 263 (1996), [hep-ph/9505422].
- [91] T. DeGrand and E. T. Neil, *Phys. Rev. D* **101**, 3, 034504 (2020), [arXiv:1910.08561].
- [92] C. Aubin *et al.*, *Phys. Rev.* **D70**, 094505 (2004), [hep-lat/0402030].
- [93] A. Bazavov *et al.* (MILC), *Rev. Mod. Phys.* **82**, 1349 (2010), [arXiv:0903.3598].
- [94] S. Aoki *et al.* (PACS-CS), *Phys. Rev.* **D79**, 034503 (2009), [arXiv:0807.1661].
- [95] S. Durr *et al.*, *Science* **322**, 1224 (2008), [arXiv:0906.3599].
- [96] W. Bietenholz *et al.*, *Phys. Rev.* **D84**, 054509 (2011), [arXiv:1102.5300].
- [97] C. Alexandrou *et al.*, *Phys. Rev.* **D90**, 7, 074501 (2014), [arXiv:1406.4310].
- [98] J. J. Dudek *et al.*, *Phys. Rev.* **D83**, 111502 (2011), [arXiv:1102.4299].
- [99] E. B. Gregory *et al.* (UKQCD), *Phys. Rev.* **D86**, 014504 (2012), [arXiv:1112.4384].
- [100] C. Michael, K. Ottnad and C. Urbach (ETM), *Phys. Rev. Lett.* **111**, 18, 181602 (2013), [arXiv:1310.1207].
- [101] C. Bernard *et al.* (Fermilab Lattice, MILC), *Phys. Rev.* **D83**, 034503 (2011), [arXiv:1003.1937].
- [102] E. B. Gregory *et al.*, *Phys. Rev.* **D83**, 014506 (2011), [arXiv:1010.3848].
- [103] R. J. Dowdall *et al.*, *Phys. Rev.* **D86**, 094510 (2012), [arXiv:1207.5149].
- [104] D. Mohler and R. M. Woloshyn, *Phys. Rev.* **D84**, 054505 (2011), [arXiv:1103.5506].
- [105] A. S. Kronfeld, *Ann. Rev. Nucl. Part. Sci.* **62**, 265 (2012), [arXiv:1203.1204].
- [106] K. Ottnad, C. Urbach and F. Zimmermann (OTM), *Nucl. Phys.* **B896**, 470 (2015), [arXiv:1501.02645].
- [107] C. DeTar *et al.* (Fermilab Lattice, MILC), *Phys. Rev. D* **99**, 3, 034509 (2019), [arXiv:1810.09983].
- [108] L. Liu *et al.*, *Phys. Rev.* **D81**, 094505 (2010), [arXiv:0909.3294].
- [109] R. A. Briceno, H.-W. Lin and D. R. Bolton, *Phys. Rev.* **D86**, 094504 (2012), [arXiv:1207.3536].
- [110] Y. Namekawa *et al.* (PACS-CS), *Phys. Rev.* **D87**, 9, 094512 (2013), [arXiv:1301.4743].
- [111] M. Padmanath *et al.*, *Phys. Rev.* **D90**, 7, 074504 (2014), [arXiv:1307.7022].
- [112] Z. S. Brown *et al.*, *Phys. Rev.* **D90**, 9, 094507 (2014), [arXiv:1409.0497].
- [113] P. Pérez-Rubio, S. Collins and G. S. Bali, *Phys. Rev.* **D92**, 3, 034504 (2015), [arXiv:1503.08440].
- [114] C. Alexandrou and C. Kallidonis, *Phys. Rev.* **D96**, 3, 034511 (2017), [arXiv:1704.02647].
- [115] S. Meinel, private communication .
- [116] J. J. Dudek *et al.* (Hadron Spectrum), *Phys. Rev.* **D88**, 9, 094505 (2013), [arXiv:1309.2608].
- [117] R. A. Briceno, J. J. Dudek and R. D. Young, *Rev. Mod. Phys.* **90**, 2, 025001 (2018), [arXiv:1706.06223].
- [118] J. Bulava *et al.*, *Nucl. Phys.* **B910**, 842 (2016), [arXiv:1604.05593].
- [119] R. A. Briceno *et al.*, *Phys. Rev. Lett.* **118**, 2, 022002 (2017), [arXiv:1607.05900].
- [120] D. Guo *et al.*, *Phys. Rev. D* **98**, 1, 014507 (2018), [arXiv:1803.02897].
- [121] C. W. Andersen *et al.*, *Phys. Rev.* **D97**, 1, 014506 (2018), [arXiv:1710.01557].
- [122] R. G. Edwards *et al.*, *Phys. Rev.* **D84**, 074508 (2011), [arXiv:1104.5152].
- [123] A. J. Woss *et al.* (Hadron Spectrum), *Phys. Rev. D* **103**, 5, 054502 (2021), [arXiv:2009.10034].
- [124] C. T. Johnson and J. J. Dudek (Hadron Spectrum), *Phys. Rev. D* **103**, 7, 074502 (2021), [arXiv:2012.00518].
- [125] C. M. Richards *et al.* (UKQCD), *Phys. Rev.* **D82**, 034501 (2010), [arXiv:1005.2473].
- [126] E. Gregory *et al.*, *JHEP* **10**, 170 (2012), [arXiv:1208.1858].
- [127] R. F. Lebed, R. E. Mitchell and E. S. Swanson, *Prog. Part. Nucl. Phys.* **93**, 143 (2017), [arXiv:1610.04528].
- [128] E. J. Eichten and C. Quigg, *Phys. Rev. Lett.* **119**, 20, 202002 (2017), [arXiv:1707.09575].
- [129] L. Leskovec *et al.*, *Phys. Rev. D* **100**, 1, 014503 (2019), [arXiv:1904.04197].
- [130] A. Francis *et al.*, *Phys. Rev. Lett.* **118**, 14, 142001 (2017), [arXiv:1607.05214].
- [131] M. Karliner and J. L. Rosner, *Phys. Rev. Lett.* **119**, 20, 202001 (2017), [arXiv:1707.07666].
- [132] M. Karliner and J. L. Rosner (2019), [arXiv:1906.07799].
- [133] S. Aoki *et al.* (Flavour Lattice Averaging Group), *Eur. Phys. J. C* **80**, 2, 113 (2020), [arXiv:1902.08191].
- [134] S. Borsanyi *et al.*, *Science* **347**, 1452 (2015), [arXiv:1406.4088].
- [135] G. M. de Divitiis *et al.* (RM123), *Phys. Rev. D* **87**, 11, 114505 (2013), [arXiv:1303.4896].
- [136] D. Giusti *et al.*, *Phys. Rev.* **D95**, 11, 114504 (2017), [arXiv:1704.06561].
- [137] S. Basak *et al.* (MILC), *Phys. Rev. D* **99**, 3, 034503 (2019), [arXiv:1807.05556].
- [138] A. Parreno *et al.*, *Phys. Rev. D* **95**, 11, 114513 (2017), [arXiv:1609.03985].

16. Heavy-Quark and Soft-Collinear Effective Theory

Revised August 2019 by C.W. Bauer (LBNL) and M. Neubert (PRISMA, Mainz Inst. for Theor. Physics, JG U.).

16.1 Effective Field Theories

Quantum field theories provide the most precise computational tools for describing physics at the highest energies. One of their characteristic features is that they almost inevitably involve multiple length scales. When trying to determine the value of an observable, quantum field theory demands that all possible virtual states and hence all particles be included in the calculation. Since these particles have widely different masses, the final prediction is sensitive to many scales. This fact represents a formidable challenge from a practical point of view. No realistic quantum field theories can be solved exactly, so that one needs to resort to approximation schemes; these, however, are typically most straightforward when only a single scale is involved at a time.

Effective field theories (EFTs) provide a general theoretical framework to deal with the multi-scale problems of realistic quantum field theories. This framework aims at reducing such problems to a combination of separate and simpler single-scale problems; simultaneously, however, it provides an organization scheme whereby the other scales are not omitted but allowed to play their role in a separate step of the computation. The philosophy and basic principles of this approach are very generic, and correspondingly EFTs represent a widely used method in many different areas of high-energy physics, from the low-energy scales of atomic and nuclear physics to the high-energy scales of (partly yet unknown) elementary-particle physics, see [1–3] for some early references. EFTs can play a role both within analytic perturbative computations and in the context of non-perturbative numerical simulations; One of the simplest applications of EFTs to particle physics concerns the description of an underlying theory that is only probed at energy scales $E < \Lambda$. Any particle with mass $m > \Lambda$ cannot be produced as a real state and therefore only leads to short-distance virtual effects. Thus, one can construct an effective theory in which the quantum fluctuations of such heavy particles are “integrated out” from the generating functional for Green functions. This results in a simpler theory containing only those degrees of freedom that are relevant to the energy scales under consideration. In fact, the standard model of particle physics itself is widely viewed as an EFT of some yet unknown, more fundamental theory.

The development of any effective theory starts by identifying the degrees of freedom that are relevant to describe the physics at a given energy (or length) scale and constructing the Lagrangian describing the interactions among these fields. Short-distance quantum fluctuations associated with much smaller length scales are absorbed into the coefficients of the various operators in the effective theory. These coefficients are determined in a matching procedure, by requiring that the EFT reproduces the matrix elements of the full theory up to power corrections. In many cases the effective Lagrangian exhibits enhanced symmetries compared with the fundamental theory, allowing for simple and sometimes striking predictions relating different observables.

16.2 Heavy-Quark Effective Theory

Heavy-quark systems provide prime examples for applications of the EFT technology, because the hierarchy $m_Q \gg \Lambda_{\text{QCD}}$ (with $Q = b, c$) provides a natural separation of scales. Physics at the scale m_Q is of a short-distance nature and can be treated perturbatively, while for heavy-quark systems there is always also some hadronic physics governed by the confinement scale Λ_{QCD} of the strong interaction. Being able to separate the short-distance and long-distance effects associated with these two scales is crucial for any quantitative description. For instance, if the long-distance hadronic matrix elements are obtained from lattice QCD, then it is necessary to analytically compute the effects of short-wavelength modes that do not fit on the lattice. In many other instances, the long-distance physics can be encoded in a small number of hadronic parameters.

16.2.1 General idea and derivation of the effective Lagrangian

The simplest effective theory for heavy-quark systems is the heavy-quark effective theory (HQET) [4–7] (see [8, 9] for detailed discussions). It provides a simplified description of the soft interactions of a single heavy quark with light partons. This includes the interactions that bind the heavy quark with other light partons inside heavy mesons and baryons.

A softly interacting heavy quark is nearly on-shell. Its momentum may be decomposed as $p_Q = m_Q v + k$, where v is the 4-velocity of the hadron containing the heavy quark. The “residual momentum” k results from the soft interactions of the heavy quark with its environment and satisfies $v \cdot k \sim \Lambda_{\text{QCD}}$ and $k^2 \sim \Lambda_{\text{QCD}}^2$, which in the rest frame of the heavy hadron reduces to $k^\mu \sim \Lambda_{\text{QCD}}$. In the limit $m_Q \gg \Lambda_{\text{QCD}}$, the soft interactions do not change the 4-velocity of the heavy quark, which is therefore a conserved quantum number that is often used as a label on the effective heavy-quark fields. A nearly on-shell Dirac spinor has two large and two small components. We define

$$Q(x) = e^{-im_Q v \cdot x} [h_v(x) + H_v(x)], \quad (16.1)$$

where

$$h_v(x) = e^{im_Q v \cdot x} \frac{1 + \not{v}}{2} Q(x), \quad H_v(x) = e^{im_Q v \cdot x} \frac{1 - \not{v}}{2} Q(x) \quad (16.2)$$

are the large (“upper”) and small (“lower”) components of the spinor field, respectively. The extraction of the phase factor in (16.1) implies that the fields h_v and H_v carry the residual momentum k . The field H_v is $1/m_Q$ suppressed relative to h_v and describes quantum fluctuations far off the mass shell. Integrating it out using its equations of motion yields the HQET Lagrangian

$$\begin{aligned} \mathcal{L}_{\text{HQET}} = & \bar{h}_v i v \cdot D_s h_v \\ & + \frac{1}{2m_Q} \left[\bar{h}_v (iD_s)^2 h_v + C_{\text{mag}}(\mu) \frac{g}{2} \bar{h}_v \sigma_{\mu\nu} G_s^{\mu\nu} h_v \right] + \dots \end{aligned} \quad (16.3)$$

The covariant derivative $iD_s^\mu = i\partial^\mu + gA_s^\mu$ and the field strength $G_s^{\mu\nu}$ contain only the soft gluon field. Hard gluons have been integrated out, and their effects are contained in the Wilson coefficients of the operators in the effective Lagrangian. From the leading operator one derives the Feynman rules of HQET. The new operators entering at subleading order are referred to as the “kinetic energy” and “chromo-magnetic interaction”. The kinetic-energy operator corresponds to the first correction term in the Taylor expansion of the relativistic energy $E = m_Q + \vec{p}^2/2m_Q + \dots$. Lorentz invariance, which is encoded as a reparametrization invariance of the effective Lagrangian [10], ensures that its Wilson coefficient is not renormalized ($C_{\text{kin}} \equiv 1$). The coefficient C_{mag} of the chromo-magnetic operator receives corrections starting at one-loop order.

16.2.2 Spin-flavor symmetry

The leading term in the HQET Lagrangian exhibits a global spin-flavor symmetry. Its physical meaning is that, in the infinite mass limit, the properties of hadronic systems containing a single heavy quark are insensitive to the spin and flavor of the heavy quark [11, 12]. The spin symmetry results from the fact that there are no Dirac matrices in the leading term of the effective Lagrangian in (16.3), implying that the interactions of the heavy quark with soft gluons leave its spin unchanged. The flavor symmetry arises since the mass of the heavy quark does not appear at leading order. For n_Q heavy quarks moving at the same velocity, one can simply extend (16.3) by summing over n_Q identical terms for heavy-quark fields h_v^i . The result is invariant under rotations in flavor space. When combined with the spin symmetry, the symmetry group becomes promoted to $SU(2n_Q)$. These symmetries are broken by the operators at subleading power in the $1/m_Q$ expansion.

The spin-flavor symmetry leads to many interesting relations between the properties of hadrons containing a heavy quark. The most direct consequences concern the spectroscopy of such states

[13]. In the heavy-quark limit, the spin of the heavy quark and the total angular momentum j of the light degrees of freedom are separately conserved by the strong interactions. Because of heavy-quark symmetry, the dynamics is independent of the spin and mass of the heavy quark. Hadronic states can thus be classified by the quantum numbers (flavor, spin, parity, etc.) of the light degrees of freedom. The spin symmetry predicts that, for fixed $j \neq 0$, there is a doublet of degenerate states with total spin $J = j \pm \frac{1}{2}$. The flavor symmetry relates the properties of states with different heavy-quark flavor.

16.2.3 Weak decay form factors

Of particular interest are the relations between the weak decay form factors of heavy mesons, which parametrize hadronic matrix elements of currents between two mesons containing a heavy quark. These relations have been derived by Isgur and Wise [12], generalizing ideas developed by Nussinov and Wetzel [14] and Voloshin and Shifman [15]. For the purpose of this discussion, it is convenient to work with a mass-independent normalization of meson states and use velocity rather than momentum variables.

Consider the elastic scattering of a pseudoscalar meson, $P(v) \rightarrow P(v')$, induced by an external vector current coupled to the heavy quark contained in P , which acts as a color source moving with the meson's velocity v . The action of the current is to replace instantaneously the color source by one moving at velocity v' . Soft gluons need to be exchanged in order to rearrange the light degrees of freedom and build up the final state meson moving at velocity v' . This rearrangement leads to a form-factor suppression. The important observation is that, in the $m_Q \rightarrow \infty$ limit, the form factor can only depend on the Lorentz boost $\gamma = v \cdot v'$ connecting the rest frames of the initial and final-state mesons (as long as $\gamma = \mathcal{O}(1)$). In the effective theory the hadronic matrix element describing the scattering process can therefore be written as

$$\langle P(v') | \bar{h}_{v'} \gamma^\mu h_v | P(v) \rangle = \xi(v \cdot v') (v + v')^\mu, \quad (16.4)$$

with a form factor $\xi(v \cdot v')$ that is real and independent of m_Q . By flavor symmetry, the form factor remains identical when one replaces the heavy quark Q in one of the meson states by a heavy quark Q' of a different flavor, thereby turning P into another pseudoscalar meson P' . At the same time, the current becomes a flavor-changing vector current. This universal form factor is called the Isgur-Wise function [12]. For equal velocities the vector current $J^\mu = \bar{h}_v \gamma^\mu h_v$ is conserved in the effective theory, irrespective of the flavor of the heavy quarks. The corresponding conserved charges are the generators of the flavor symmetry. It follows that the Isgur-Wise function is normalized at the point of equal velocities: $\xi(1) = 1$. Since the recoil energy of the daughter meson P' in the rest frame of the parent meson P is $E_{\text{recoil}} = m_{P'} (v \cdot v' - 1)$, the point $v \cdot v' = 1$ is referred to as the zero-recoil limit. The heavy-quark spin symmetry leads to additional relations among weak decay form factors. It can be used to relate matrix elements involving vector mesons to those involving pseudoscalar mesons, which once again can be described completely in terms of the universal Isgur-Wise function.

The form factor relations imposed by heavy-quark symmetry describe the semileptonic decay processes $\bar{B} \rightarrow D \ell \bar{\nu}$ and $\bar{B} \rightarrow D^* \ell \bar{\nu}$ in the limit of infinite heavy-quark masses. They are model-independent consequences of QCD. The known normalization of the Isgur-Wise function at zero recoil can be used to obtain a model-independent measurement of the element $|V_{cb}|$ of the Cabibbo-Kobayashi-Maskawa (CKM) matrix. The semileptonic decay $\bar{B} \rightarrow D^* \ell \bar{\nu}$ is particularly well suited for this purpose [16]. Experimentally this is a very clean mode, since the reconstruction of the D^* meson mass provides a powerful rejection against background. From the theoretical point of view, it is ideal since the decay rate at zero recoil is protected by Luke's theorem against first-order power corrections in $1/m_Q$ [17]. This is described in more detail in Section 12. Corrections to the heavy-quark symmetry relations for the $\bar{B} \rightarrow D^{(*)}$ form factors near zero recoil can also be constrained using sum rules derived in the small-velocity limit [18, 19].

16.2.4 Decoupling transformation

At leading order in $1/m_Q$, the couplings of soft gluons to heavy quarks in the effective Lagrangian (16.3) can be removed by the field redefinition $h_v(x) = Y_v(x) \bar{h}_v^{(0)}(x)$, where $Y_v(x)$ is a soft Wilson line along the direction of v , extending from minus infinity to the point x . In terms of the new fields the leading-order HQET Lagrangian becomes $\mathcal{L}_{\text{HQET}} = \bar{h}_v^{(0)} i v \cdot \partial h_v^{(0)}$. It describes a free theory as far as the strong interactions of heavy quarks are concerned. However, the theory is nevertheless non-trivial in the presence of external sources. Consider, e.g., the case of a weak-interaction heavy-quark current

$$\bar{h}_{v'} \gamma^\mu (1 - \gamma_5) h_v = \bar{h}_{v'}^{(0)} \gamma^\mu (1 - \gamma_5) Y_{v'}^\dagger Y_v h_v^{(0)}, \quad (16.5)$$

where v and v' are the velocities of the heavy mesons containing the heavy quarks. Unless the two velocities are equal, corresponding to the zero-recoil limit discussed above, the object $Y_{v'}^\dagger Y_v$ is non-trivial, and hence the soft gluons do not decouple from the heavy quarks inside the current operator. One may interpret $Y_{v'}^\dagger Y_v$ as a Wilson loop with a cusp at the point x , where the two paths parallel to the different velocity vectors intersect. The presence of the cusp leads to non-trivial ultra-violet behavior (for $v \neq v'$), which is described by a cusp anomalous dimension $\Gamma_{\text{cusp}}(v \cdot v')$ that was calculated at two-loop order in [20]. It coincides with the velocity-dependent anomalous dimension of heavy-quark currents, which was introduced in the context of HQET in [21]. The interpretation of heavy quarks as Wilson lines is a useful tool, which was put forward in one of the very first papers on the subject [4]. This technology will be useful in the study of the interactions of heavy quarks with collinear degrees of freedom discussed later in this review.

16.2.5 Heavy-quark expansion for inclusive decays

The theoretical description of inclusive decays of hadrons containing a heavy quark exploits two observations [22–26]: bound-state effects related to the initial state can be calculated using the heavy-quark expansion, and the fact that the final state consists of a sum over many hadronic channels eliminates the sensitivity to the properties of individual final-state hadrons. The second feature rests on the hypothesis of quark-hadron duality, i.e. the assumption that decay rates are calculable in QCD after a smearing procedure has been applied [27]. In semileptonic decays, the integration over the lepton spectrum provides a smearing over the invariant hadronic mass of the final state (global duality). For nonleptonic decays, where the total hadronic mass is fixed, the summation over many hadronic final states provides an averaging (local duality). Since global duality is a much weaker assumption, the theoretical control of inclusive semileptonic decays is on firmer footing.

Using the optical theorem, the inclusive decay width of a hadron H_b containing a b quark can be written in the form

$$\Gamma(H_b) = \frac{1}{M_{H_b}} \text{Im} \langle H_b | i \int d^4x T \{ \mathcal{H}_{\text{eff}}(x), \mathcal{H}_{\text{eff}}(0) \} | H_b \rangle. \quad (16.6)$$

The effective weak Hamiltonian for b -quark decays consists of dimension-6 four-fermion operators and dipole operators [28]. Because of the large mass of the b quark, it follows that the separation of fields in the time-ordered product in (16.6) is small, of order $x \sim 1/m_b$. It is thus possible to construct an operator-product expansion (OPE) for the time-ordered product, in which it is represented as a series of local operators in HQET. The leading operator $\bar{h}_v h_v$ has a trivial matrix element. The next contributions arise at $\mathcal{O}(1/m_b^2)$ and give rise to two parameters $\mu_\pi^2(H_b)$ and $\mu_G^2(H_b)$, which are defined as the matrix elements of the heavy-quark kinetic energy and chromo-magnetic interaction inside the hadron H_b , respectively [29]. For the ground-state heavy mesons and baryons, one has $\mu_G^2(B) = 3(m_{B^*}^2 - m_B^2)/4 \simeq 0.36 \text{ GeV}^2$ and $\mu_G^2(\Lambda_b) = 0$. Thus, the total inclusive decay rate of a hadron H_b

can be written as [23, 24]

$$\Gamma(H_b) = \frac{G_F^2 m_b^5 |V_{cb}|^2}{192\pi^3} \left[c_1 + c_2 \frac{\mu_\pi^2(H_b)}{2m_b^2} + c_3 \frac{\mu_G^2(H_b)}{2m_b^2} + \mathcal{O}\left(\frac{1}{m_b^3}\right) + \dots \right], \quad (16.7)$$

where the prefactor arises from the loop integrations and is proportional to the fifth power of the b -quark mass. The coefficient functions c_i are calculable order by order in perturbation theory. While c_1 corresponds to the decay rate of a free heavy quark, the higher-order coefficients systematically account for bound-state effects. The coefficients of the subleading operators and of the leading operator at third order in $1/m_b$ have recently been calculated at NLO [30–34], and the heavy-quark expansion has been pushed to fifth order in $1/m_b$ [35].

From the fully inclusive width in (16.7) one can obtain the lifetime of a heavy hadron via $\tau(H_b) = 1/\Gamma(H_b)$. Due to the universality of the leading term in the heavy-quark expansion, lifetime ratios such as $\tau(B^-)/\tau(B^0)$, $\tau(\bar{B}_s^0)/\tau(B^0)$ and $\tau(A_b)/\tau(\bar{B}^0)$ are particularly sensitive to the hadronic parameters determining the power corrections in the expansion. In order to understand these ratios theoretically, it is necessary to include phase-space enhanced power corrections of order $(\Lambda_{\text{QCD}}/m_b)^3$ [36, 37] as well as short-distance perturbative effects [38] in the calculation (see [39] for a recent discussion of the status of the corresponding calculations).

A formula analogous to (16.7) can be derived for differential distributions in specific inclusive decay processes, assuming that these distributions are integrated over a sufficiently large region of phase space to ensure quark-hadron duality. Important examples are the distributions in the lepton energy and the lepton invariant mass, as well as moments of the invariant hadronic mass distribution in the semileptonic processes $\bar{B} \rightarrow X_u \ell \bar{\nu}$ and $\bar{B} \rightarrow X_c \ell \bar{\nu}$. A global fit of semileptonic decay distributions can be used to determine the CKM matrix elements $|V_{ub}|$ and $|V_{cb}|$ along with heavy-quark parameters such as the masses m_b , m_c and the hadronic parameters $\mu_\pi^2(B)$, $\mu_G^2(B)$. These determinations provide some of the most accurate values for these parameters (see e.g. [40–42]).

16.2.6 Shape functions and non-local power corrections

In certain regions of phase space, in which the hadronic final state in an inclusive heavy-hadron decay is made up of light energetic partons, the local OPE for inclusive decays must be replaced by a more complicated expansion involving hadronic matrix elements of non-local light-ray operators [43, 44]. Prominent examples are the radiative decay $\bar{B} \rightarrow X_s \gamma$ for large photon energy E_γ near $m_B/2$, and the semileptonic decay $\bar{B} \rightarrow X_u \ell \bar{\nu}$ at large lepton energy or small hadronic invariant mass. In these cases, the differential decay rates at leading order in the heavy-quark expansion can be written in the factorized form $d\Gamma = H \otimes J \otimes S$ [45], where the hard function H and the jet function J are calculable in perturbation theory. The characteristic scales for these functions are set by m_b and $(m_b \Lambda_{\text{QCD}})^{1/2}$, respectively. The soft function

$$S(\omega) = \int \frac{dt}{4\pi} e^{-i\omega t} \langle \bar{B}(v) | \bar{h}_v(tn) Y_n(tn) Y_n^\dagger(0) h_v(0) | \bar{B}(v) \rangle \quad (16.8)$$

is a non-perturbative object called the shape function [43, 44]. Here Y_n are soft Wilson lines along a light-like direction n aligned with the momentum of the hadronic final-state jet. The jet function and the shape function share a common variable $\omega \sim \Lambda_{\text{QCD}}$, and the symbol \otimes denotes a convolution in this variable.

While the hard functions are different for the decays $\bar{B} \rightarrow X_s \gamma$ and $\bar{B} \rightarrow X_u \ell \bar{\nu}$, the jet and soft functions are identical at leading order in Λ_{QCD}/m_Q . This is particularly important for the shape function, which introduces non-perturbative physics into the theoretical predictions for the decay rates in the regions of experimental interest. The fact that both processes depend on the same non-perturbative function makes it possible to use the measured shape of the $\bar{B} \rightarrow X_s \gamma$ photon spectrum to reduce the theoretical uncertainties in the determination of the CKM element $|V_{ub}|$ from semileptonic decays. In higher orders of the heavy-quark

expansion, an increasing number of subleading jet and soft functions are required to describe the decay distributions [46]. These have been analyzed in detail at order $1/m_b$ [47–49]. In the case of $\bar{B} \rightarrow X_s \gamma$ (and also in the related case of $\bar{B} \rightarrow X_s \ell \bar{\ell}$), some of these non-local effects survive in the total decay rate and give rise to irreducible hadronic uncertainties [50]. The technology for deriving the corresponding factorization theorems relies on the soft-collinear effective theory, to which we now turn.

16.3 Soft-Collinear Effective Theory

As discussed in the previous section, soft gluons that bind a heavy quark inside a heavy meson cannot change the virtuality of that heavy quark by a significant amount. The ratio Λ_{QCD}/m_Q provides the expansion parameter in HQET, which is a small parameter since $m_Q \gg \Lambda_{\text{QCD}}$. This obviously does not work when considering light quarks. However, if the energy Q of the quarks is large, the ratio Λ_{QCD}/Q provides a small parameter, which can be used to construct an effective theory. One major difference to HQET is that light energetic quarks cannot only emit soft gluons, but they can also emit collinear gluons (an energetic gluon in the same direction as the original quark), without parametrically changing their virtuality. Thus, to fully reproduce the long-distance physics of energetic quarks requires that one includes their interactions with both soft and collinear particles. The resulting effective theory is therefore called soft-collinear effective theory (SCET) [51–53] (see [54] for a review).

A single energetic particle can always be boosted to a frame where all momentum components have similar size, in which case there is no small expansion parameter. Thus, the presence of energetic particles must refer to a reference frame defined by external kinematics. SCET has a wide range of applications; some examples are the production of energetic, light states in the decay of a heavy particle in its rest frame, the production of energetic jets in collider environments, and the scattering of energetic particles off a target at rest. In this brief review we will outline the main features of this effective theory and mention a few selected applications.

16.3.1 General idea of the expansion

Consider a quark with virtuality much less than its energy Q , moving along the direction \vec{n} . It is convenient to parameterize the momentum p_n of this particle in terms of its light-cone components, defined by $(p_n^-, p_n^+, p_n^\perp) = (\vec{n} \cdot p_n, n \cdot p_n, p_n^\perp)$, where $n^\mu = (1, \vec{n})$ and $\bar{n}^\mu = (1, -\vec{n})$ are light-like vectors, and $n \cdot p_n^\perp = \bar{n} \cdot p_n^\perp = 0$. The subscript n on the momentum indicates the direction of the collinear particle. In terms of these light-cone components, the virtuality satisfies $p_n^2 = p_n^+ p_n^- + p_n^{\perp 2}$. The individual components of the momentum obey

$$(p_n^-, p_n^+, p_n^\perp) \sim Q(1, \lambda^2, \lambda), \quad (16.9)$$

where $\lambda^2 = p^2/Q^2$ is the expansion parameter of SCET. The virtuality of such an energetic particle remains parametrically unchanged if it interacts with energetic particles in the same direction n , or with soft particles with momentum scaling as

$$(p_s^-, p_s^+, p_s^\perp) \sim Q(\lambda^2, \lambda^2, \lambda^2). \quad (16.10)$$

SCET is constructed in such a way as to reproduce the long-distance dynamics arising from the interactions of collinear and soft degrees of freedom.

In the above power counting the transverse momenta of soft degrees of freedom scale as $p_s^\perp \sim Q\lambda^2$, which is much smaller than the transverse momenta $p_c^\perp \sim Q\lambda$ of collinear fields. This theory is usually called SCET_I. If the external kinematics require that the transverse momenta of both soft and collinear fields are of the same size, $p_c^\perp \sim p_s^\perp$, then the appropriate degrees of freedom have the scaling $p_c \sim Q(1, \lambda^2, \lambda)$ and $p_s \sim Q(\lambda, \lambda, \lambda)$. This theory is usually called SCET_{II} and is required, e.g., for exclusive hadronic decays such as $\bar{B} \rightarrow D\pi$, where the virtuality of both collinear and soft degrees of freedom are set by Λ_{QCD} , or for the description of transverse-momentum distributions at colliders. SCET_I power counting is assumed in the following sections, while SCET_{II} is discussed in more detail in 16.3.6.

16.3.2 Leading-order Lagrangian

The derivation of the SCET Lagrangian follows similar steps as described for HQET in Section 16.2.1. One begins by deriving the Lagrangian for a theory containing only a single collinear sector. Similar to HQET, one separates the full QCD field into two components, $q_n(x) = \psi_n(x) + \Xi_n(x)$, where (with $n \cdot \bar{n} = 2$)

$$\psi_n(x) = \frac{\not{n}\not{\bar{n}}}{4} q_n(x), \quad \Xi_n(x) = \frac{\not{\bar{n}}\not{n}}{4} q_n(x). \quad (16.11)$$

The degrees of freedom described by the field Ξ_n are far off shell and can therefore be eliminated using its equation of motion. This gives

$$\mathcal{L}_n = \bar{\psi}_n(x) \left[in \cdot D + i\mathcal{D}^\perp \frac{1}{i\bar{n} \cdot D} i\mathcal{D}^\perp \right] \frac{\not{n}}{2} \psi_n(x). \quad (16.12)$$

As a next step, one separates the large and residual momentum components by decomposing the collinear momentum into a “label” and a residual momentum, $p^\mu = P^\mu + k^\mu$ with $n \cdot P = 0$. One then performs a phase redefinition on the collinear fields, such that $\psi_n(x) = e^{iP \cdot x} \xi_n(x)$. Derivatives acting on the fields $\xi_n(x)$ now only pick out the residual momentum. Since unlike in HQET the label momentum in SCET is not conserved, one defines a label operator \mathcal{P}^μ acting as $\mathcal{P}^\mu \xi_n(x) = P^\mu \xi_n(x)$ [52], as well as a corresponding covariant label operator $i\mathcal{D}_n^\mu = \mathcal{P}^\mu + gA_n^\mu(x)$. Note that at leading order in power counting $i\mathcal{D}_n^\mu$ does not contain the soft gluon field. This leads to the final SCET Lagrangian [52,53,55,56]

$$\mathcal{L}_n = \bar{\xi}_n(x) \left[in \cdot D_n + gn \cdot A_s + i\mathcal{P}_n^\perp \frac{1}{i\bar{n} \cdot \mathcal{D}_n} i\mathcal{P}_n^\perp \right] \frac{\not{n}}{2} \xi_n(x) + \dots, \quad (16.13)$$

where we have split $in \cdot D$ into a collinear piece $in \cdot D_n = in \cdot \partial + gn \cdot A_n$ and a soft piece $gn \cdot A_s$. This latter term gives rise to the only interaction between a collinear quark and soft gluons at leading power in λ . The ellipses represent higher-order interactions between soft and collinear particles.

The Lagrangian describing collinear fields in different light-like directions is simply given by the sum of the Lagrangians for each direction n , i.e. $\mathcal{L} = \sum_n \mathcal{L}_n$. The soft gluons are the same in each individual Lagrangian. An alternative way to understand the separation between large and small momentum components is to derive the Lagrangian of SCET in position space [56]. In this case no label operators are required, and the dependence on short-distance effects is contained in non-localities at short distances. An important difference between SCET and HQET is that the SCET Lagrangian is not corrected by short distance fluctuations. The physical reason is that in the construction described above no high-momentum modes have been integrated out [56]. Such hard modes arise when different collinear sectors are coupled via some external current (e.g. in jet production at e^+e^- or hadron colliders), or when collinear particles are produced in the rest frame of a decaying heavy object (such as in B decays). Short-distance effects are then incorporated in the Wilson coefficients of the external source operators.

16.3.3 Collinear gauge invariance and Wilson lines

An important aspect of SCET is the implementation of local gauge invariance. Because the effective field operators describe modes with certain momentum scalings, the effective Lagrangian respects only residual gauge symmetries. One of them satisfies the collinear scaling

$$(\bar{n} \cdot \partial, n \cdot \partial, \partial^\perp) U_n(x) \sim Q(\lambda^2, \lambda) U_n(x), \quad (16.14)$$

and one the soft scaling

$$(\bar{n} \cdot \partial, n \cdot \partial, \partial^\perp) U_s(x) \sim Q(\lambda^2, \lambda^2, \lambda^2) U_s(x). \quad (16.15)$$

While the soft gauge transformation is common for all fields, collinear fields in different directions each transform under their own collinear gauge transformation, which means that each collinear sector, containing particles with large momenta along a certain direction, has to be separately gauge invariant under its

collinear gauge transformation. This requires the introduction of collinear Wilson lines [52]

$$W_n(x) = \text{P exp} \left[-ig \int_{-\infty}^0 ds \bar{n} \cdot A_n(s\bar{n} + x) \right], \quad (16.16)$$

which transform under collinear gauge transformations according to $W_n \rightarrow U_n W_n$. Thus, the combination $\chi_n \equiv W_n^\dagger \psi_n$ is gauge invariant. In a similar manner, one can define the gauge-invariant gluon field $B_n^\mu = g^{-1} W_n^\dagger iD_n^\mu W_n$ [57, 58]. Collinear operators in SCET are typically constructed from such collinearly gauge-invariant building blocks.

16.3.4 Derivation of factorization theorems

One of the important applications of SCET is to understand how to factorize cross sections involving energetic particles moving in different directions into simpler pieces that can either be calculated perturbatively or determined from data. Factorization theorems have been around for much longer than SCET (see [59] for a review). However, the effective theory allows for a conceptually simpler understanding of certain classes of factorization theorems [57], since most simplifications happen already at the level of the Lagrangian. The discussion in this section is valid to leading order in the power counting of the effective theory.

As discussed in the previous section, the Lagrangian of SCET does not involve any couplings between collinear particles moving in different directions. Soft gluons couple to collinear quarks only through the term $\bar{\xi}_n gn \cdot A_s (\not{n}/2) \xi_n$ in the effective Lagrangian in (16.13). This coupling is similar to the coupling of soft gluons to heavy quarks in HQET, see Section 16.2.4. It can be removed by means of the field redefinition [53]

$$\psi_n(x) = Y_n(x) \psi_n^{(0)}(x), \quad A_n^a(x) = Y_n^{ab}(x) A_n^{b(0)}(x), \quad (16.17)$$

where Y_n and Y_n^{ab} live in the fundamental and adjoint representations of $SU(3)$, respectively. This fact greatly facilitates proofs of factorization theorems in SCET. A QCD operator $O(x)$ describing the interactions of collinear partons moving in different directions can thus be written as (omitting color indices for simplicity)

$$\begin{aligned} \langle O(x) \rangle &= \\ C_O(\mu) \langle [C_{n_a}^{(0)} C_{n_b}^{(0)} C_{n_1}^{(0)} \dots C_{n_N}^{(0)}](x) [\mathcal{Y}_{n_a} \mathcal{Y}_{n_b} \mathcal{Y}_{n_1} \dots \mathcal{Y}_{n_N}](x) \rangle_\mu. \end{aligned} \quad (16.18)$$

Here $C_{n_i}^{(0)}(x)$ denotes a gauge-invariant combination of collinear fields (either quark or gluon fields) in the direction n_i . The hard matching coefficient C_O accounts for short-distance effects at the scale Q . The soft Wilson lines can either be in a color triplet or color octet representation, and are collectively denoted by \mathcal{Y}_{n_i} . Both the matrix elements and the coefficient C_O depend on the renormalization scale μ .

Having defined the operator mediating a given process, one can calculate the cross section by squaring the operator, taking the forward matrix element and integrating over the phase space of all final-state particles. The absence of interactions between collinear degrees of freedom moving along different directions or soft degrees of freedom implies that the forward matrix element can be factorized as

$$\begin{aligned} \langle \text{in} | O(x) O^\dagger(0) | \text{in} \rangle &= |C_O(\mu)|^2 \langle \text{in}_a | C_{n_a}(x) C_{n_a}^\dagger(0) | \text{in}_a \rangle_\mu \\ &\times \langle \text{in}_b | C_{n_b}(x) C_{n_b}^\dagger(0) | \text{in}_b \rangle_\mu \\ &\times \langle 0 | C_{n_1}(x) C_{n_1}^\dagger(0) | 0 \rangle_\mu \dots \langle 0 | C_{n_N}(x) C_{n_N}^\dagger(0) | 0 \rangle_\mu \\ &\times \langle 0 | [\mathcal{Y}_{n_a} \dots \mathcal{Y}_{n_N}](x) [\mathcal{Y}_{n_a} \dots \mathcal{Y}_{n_N}]^\dagger(0) | 0 \rangle_\mu. \end{aligned} \quad (16.19)$$

Thus, the matrix element can be written as a product of simpler structures, each of which can be evaluated separately.

The vacuum matrix elements of the outgoing collinear fields are determined by jet functions $J_i(\mu)$. As long as the relevant scale (for example the jet mass) is sufficiently large, these functions can

be calculated perturbatively. The matrix elements of the incoming collinear fields are non-perturbative objects $B_{p/N}(\mu)$ called beam functions for parton p in nucleon N [60]. For many applications they can be related perturbatively to the well-known parton distribution functions. Finally, the vacuum matrix element of the soft Wilson lines defines a so-called soft function $S_{ab\dots N}(\mu)$. The shared dependence on x in the above equation implies that in momentum space the various components of the factorization theorem are convoluted with one another. Deriving this convolution requires a careful treatment of the phase-space integration and the factorization of the measurement defining the cross section of interest, in particular treating the large and residual components of each momentum appropriately.

Putting all information together, the differential cross section for a proton-proton collision with N jet-like objects can schematically be written as

$$d\sigma \sim \sum_{ab} H_{ab}(\mu) [B_{a/P}(\mu) B_{b/P}(\mu)] \otimes [J_1(\mu) \dots J_N(\mu)] \otimes S_{ab\dots N}(\mu). \quad (16.20)$$

The hard function is equal to the square of the matching coefficient, $H_{ab}(\mu) = |C_O(\mu)|^2$, and the beam, jet, and soft functions and their convolution structure depend on the specific N -jet measurement. It should be mentioned that the most difficult part of traditional factorization proofs involves showing that so-called Glauber gluons do not spoil the above factorization theorem [61]. Significant progress toward the description of Glauber effects within SCET has been made in [62], where a closed form for the effective Lagrangian describing these interactions was derived. In this context, a proof of factorization requires demonstrating that this Lagrangian has no impact on a particular cross section, and such proofs have not yet been fully derived within SCET.

16.3.5 Resummation of large logarithms

SCET can be used to sum the large logarithms arising in perturbative calculations to all orders in the strong coupling constant α_s . In general, perturbation theory will generate a logarithmic dependence on any ratio of scales r in a problem. For processes that involve initial or final states with energy much in excess of their mass, there are two powers of logarithms for every power of α_s . These are referred to as Sudakov logarithms. For widely separated scales these large logarithms can spoil the convergence of fixed-order perturbation theory. One thus needs to reorganize the expansion in such a way that $\alpha_s L = \mathcal{O}(1)$ is kept fixed, with $L = \ln r$. More precisely, a proper resummation requires summing logarithms of the form $\alpha_s^n L^m$ with $m \leq (n+1)$ in the logarithm of a cross section, by writing $\ln \sigma \sim L g_0(\alpha_s L) + g_1(\alpha_s L) + \alpha_s g_2(\alpha_s L) + \dots$, with functions $g_n(x)$ that need to be determined.

The important ingredient in achieving this resummation is the fact that SCET factorizes a given cross section into simpler pieces, each of which depends on a single physical scale. The only dependence on that scale can arise through logarithms of its ratio with the renormalization scale μ . Thus, for each of the components in the factorization theorem one can choose a renormalization scale μ for which the large logarithmic terms are absent. Of course, the factorization formula requires a common renormalization scale μ in all its components, and one therefore has to use the renormalization group (RG) to evolve the various component functions from their preferred scale to the common scale μ . A novel feature of RG equations in SCET, as opposed to other EFTs, is that the anomalous dimensions entering the evolution equations of the hard, beam, jet and soft functions in a factorization formula such as (16.20) contain a single power of the logarithm of the relevant energy scale. For example, the anomalous dimension γ_H of the hard function has the form

$$\gamma_H(\mu) = c_H \Gamma_{\text{cusp}}(\alpha_s) \ln \frac{Q^2}{\mu^2} + \gamma(\alpha_s), \quad (16.21)$$

where c_H is a process-dependent coefficient and Γ_{cusp} denotes the

so-called cusp anomalous dimension [20, 63]. Collinear and soft functions have similar anomalous dimensions, which also involve a cusp and a non-cusp part. The non-cusp part γ of the anomalous dimensions is process (and observable) dependent. The presence of a logarithm in the anomalous dimension is characteristic of Sudakov problems and arises since the perturbative series contains double logarithms of scale ratios.

Solving the RG equations one can systematically resum all large logarithms of scale ratios in the factorized cross section and express the functions $g_n(\alpha_s L)$ introduced above in terms of ratios of running coupling constants. In order to compute the first two terms $L g_0(\alpha_s L) + g_1(\alpha_s L)$ in $\ln \sigma$, corresponding to the next-to-leading logarithmic (NLL) approximation, one needs two-loop expressions for the cusp anomalous dimension and β function, one-loop expressions for the non-cusp pieces in the anomalous dimensions, and tree-level matching conditions for all component functions at their characteristic scales. To calculate the next term $\alpha_s g_2(\alpha_s L)$ in the expansion, corresponding to NNLL order, one needs to go one order higher in the loop expansion, and so on.

16.3.6 Factorization and resummation in SCET_{II}

The effective theory SCET_{II} contains collinear and soft particles with momenta scaling as $(p_n^-, p_n^+, p_n^\perp) \sim Q(1, \lambda^2, \lambda)$ and $(p_s^-, p_s^+, p_s^\perp) \sim Q(\lambda, \lambda, \lambda)$. They have the same small virtuality ($p_n^2 \sim p_s^2 \sim Q^2 \lambda^2$) but differ in their rapidities. An important class of observables, for which this scaling is relevant, contains cross sections for processes in which the transverse momenta of particles are constrained by external kinematics. The prime example are the transverse-momentum distributions of electroweak gauge bosons or Higgs bosons produced at hadron colliders. The parton transverse momenta are constrained by the fact that their vector sum must be equal and opposite to the transverse momentum q_T of the boson. Standard RG evolution in the effective theory controls the logarithms arising from the fact that the virtualities of the collinear and soft modes are much smaller than the hard scale Q in the process (the boson mass). However, additional large logarithms arise since the rapidities of collinear and soft modes are parametrically different, such that $e^{|\ln c - \ln s|} \sim 1/\lambda$. These logarithms can be traced to a new source of divergences and an unusual failure of dimensional regularization. They need to be factorized in the cross section and resummed by other means.

Two equivalent approaches exist for how to deal with the additional rapidity logarithms in SCET. In the approach of [64], they are interpreted as a consequence of a ‘‘collinear anomaly’’ of the effective theory SCET_{II}, resulting from the fact that a classical rescaling symmetry of the effective Lagrangian is broken by quantum effects. The extra large logarithms can be resummed by means of simple differential equations, which typically state that to all orders in perturbation theory (and in an appropriate space) the logarithm of the cross section contains only a single extra logarithm of $\lambda \sim q_T/Q$ not contained in the hard function. Another approach to resum the rapidity logarithms uses the ‘‘rapidity renormalization group’’ [65], in which the relevant differential equations are obtained by considering a new type of scale variation in a parameter ν , which separates the phase space for collinear and soft particles along a hyperbola in the (p_-, p_+) plane. In contrast to the standard RG, there is no running coupling involved in the ν evolution, since the different contributions live at the same virtuality.

SCET_{II} also plays an important role in the study of factorization for a variety of exclusive B meson decays, such as $\bar{B} \rightarrow \pi \ell \bar{\nu}$, $\bar{B} \rightarrow K^* \gamma$ and $\bar{B} \rightarrow \pi \pi$, for which the virtualities of energetic (collinear) final-state particles are of order Λ_{QCD} , which is also the scale for the soft light degrees of freedom contained in the initial-state B meson.

16.3.7 Applications

Most of the applications of SCET are either in flavor physics, where the decay of a heavy B meson can give rise to energetic light partons, or in collider physics, where the presence of jets naturally leads to collimated sets of energetic particles. For some of these applications alternative approaches existed before the invention of SCET, but the effective theory has opened up alternative ways to understand the physics of these processes. For

many examples, however, SCET has allowed new insights and new applications. The investigation of heavy-to-light form factors has been instrumental for understanding factorization in exclusive semileptonic B decays [66]. SCET has also provided a field-theoretic basis for the QCD factorization approach to exclusive, non-leptonic decays of B mesons [67]. Using SCET methods, proofs of factorization were derived for the color-allowed decay $\bar{B}^0 \rightarrow D^+\pi^-$ [68], the color-suppressed decay $\bar{B}^0 \rightarrow D^0\pi^0$ [69], and the radiative decay $\bar{B} \rightarrow K^*\gamma$ [70]. Further examples are factorization theorems and the resummation of endpoint logarithms for quarkonia production [71], the resummation of large logarithmic terms for the thrust [72] and jet broadening [73] distributions in e^+e^- annihilation beyond NLL order, the development of new factorizable observables to veto extra jets [60, 74], all-orders factorization theorems for processes containing electroweak Sudakov logarithms [75], and the resummation of threshold (soft gluon) logarithms in momentum space for several important processes at hadron colliders [76–78]. There has also been a lot of activity describing p_T -based resummation at hadron colliders. Prominent examples are the transverse-momentum distributions of electroweak bosons [64, 65, 79]. Finally, SCET has given new insights into the jet substructure methods (see [80] for a recent review). We now describe a few of these applications in more detail.

Event-shape distributions, in particular the thrust distribution, have been measured to high accuracy at LEP [81]. They can be used for a determination of the strong coupling constant α_s . SCET has increased the theoretical accuracy in the calculations of the thrust and C -parameter distributions significantly. First, it has allowed to increase the perturbative accuracy of the thrust spectrum. The resummation of logarithms of τ , which become important for $\tau \ll 1$, has been performed to $N^3\text{LL}$ [72], two orders beyond what was previously available. Combining this resummation with the known two-loop spectrum [82, 83] gives precise perturbative predictions both at small and large values of τ . Second, the factorization of the cross section in SCET has made it possible to include non-perturbative physics through a shape function, in analogy with the B -physics case discussed in Section 16.2.6. Comparing the theoretical predictions to the measured thrust and C -parameter distributions yields a precise value of the strong coupling constant $\alpha_s(m_Z)$, which however is lower than the average value cited in Section 9 by several standard deviations [84, 85]. For more discussions on this, see Section 9.

The Higgs-boson production cross section in gluon fusion at the LHC, defined with a jet veto stating that no jet in the final state has transverse momentum above a threshold p_T^{veto} , can be factorized in the form [86, 87] (see [88] for a corresponding calculation outside the SCET framework)

$$\begin{aligned} \sigma(p_T^{\text{veto}}) = & H(m_H, \mu) \left(\frac{\nu_B}{\nu_S}\right)^{-2F_{gg}(R, p_T^{\text{veto}}, \mu)} S_{gg}(R, p_T^{\text{veto}}, \mu, \frac{\nu_S}{p_T^{\text{veto}}}) \\ & \times \int_{\tau}^1 \frac{dz}{z} B_{g/P}\left(z, R, p_T^{\text{veto}}, \mu, \frac{\nu_B}{m_H}\right) B_{g/P}\left(\frac{\tau}{z}, R, p_T^{\text{veto}}, \mu, \frac{\nu_B}{m_H}\right), \end{aligned} \quad (16.22)$$

where $\tau = m_H^2/s$, and $\mu \sim p_T^{\text{veto}}$ is a common factorization scale. The beam functions $B_{g/P}$, the soft function S_{gg} and the exponent F_{gg} all depend on the jet radius R as well as the jet clustering algorithm. The scale dependence of the hard function H is controlled by standard RG evolution in SCET. The beam functions can be factorized further into calculable collinear kernels convoluted with parton distribution functions. In addition to the renormalization scale μ , the beam and soft functions depend on two rapidity scales $\nu_B \sim m_H$ and $\nu_S \sim p_T^{\text{veto}}$, respectively. In [86] the default values $\nu_B = m_H$ and $\nu_S = p_T^{\text{veto}}$ are used for these scales, and the soft function S_{gg} is absorbed into the beam functions. In [87] the exponent F_{gg} is called $-\gamma_V^g/2$. The second factor on the right-hand side of the factorization formula (16.22), which resums large rapidity logarithms, implies that the logarithm of the jet-veto cross section contains a single large logarithm $\ln \sigma = -2F_{gg}(R, p_T^{\text{veto}}, \mu) \ln(m_H/p_T^{\text{veto}}) + \dots$ not contained in the hard function. Its coefficient can be calculated in fixed-order per-

turbation theory.

Obtaining more precise fixed-order calculations has been an important goal for many years. A major difficulty in these calculations is the proper handling of the infrared singularities that arise in both virtual and real contributions. A method based on N -jettiness (\mathcal{T}_N) slicing [89, 90] allows one to obtain the NNLO result from a much easier NLO calculation, combined with information about the singular dependence of the cross section on the \mathcal{T}_N resolution variable [74]. This has been used to compute various processes with final states containing up to one hard, colored particle [91–95]. While the NLO calculations can be performed using well established techniques, the singular dependence on \mathcal{T}_N can be calculated using SCET at NNLO. Calculations of the leading power corrections in \mathcal{T}_0/Q [96, 97] have helped to improve the numerical stability for several processes. The N -jettiness (\mathcal{T}_N) slicing method has been used prior to the fixed-order application in the combination of higher order resummation with parton showers [98, 99].

More generally, there is currently a strong effort to push the applications of SCET toward factorization and resummation at subleading power in the expansion in λ . The subleading SCET Lagrangian [56, 100] and current operators arising in B -meson decays and their anomalous dimensions [55, 56, 101–103] have been studied a long time ago. More recently, the focus has shifted to subleading operators arising in important collider processes, such as Drell-Yan or Higgs production. The general set of operators for such processes have been identified [104–106], and several of their anomalous dimensions have been calculated [106, 107]. First resummed results at subleading power have been presented for event shapes [108] and the Drell-Yan process [109].

16.4 Open issues and perspectives

HQET has successfully passed many experimental tests, and there are not many open questions that still need to be addressed. One concept that has not been derived from first principles is the notion of quark-hadron duality, which underlies the application of HQET to the description of inclusive decays of B mesons. The validity of global duality (at energies even lower than those relevant in B decays) has been tested experimentally using high-precision data on semileptonic B decays and on hadronic τ decays. However, assigning a theoretical uncertainty due to possible duality violations remains a difficult task. Another known issue is that the measured values of the CKM element $|V_{ub}|$ extracted from exclusive or inclusive decays of B mesons differ from each other by several standard deviations (see Section 76). This measurement relies on the heavy-quark limit, and the uncertainty quoted includes a theoretical estimate of the effect of power corrections arising from the finite b -quark mass. It remains an open question whether the discrepancy is due to underestimated theoretical or experimental uncertainties, or whether it may hint to the existence of new physics.

SCET, on the other hand, is still an active field of research, and new results are being obtained regularly. An important example concerns the understanding of non-global logarithms arising in hadron-collider processes with jets [110, 111]. For a long time a fully factorized form of non-global jet cross sections has not been available, despite significant progress towards this goal [112, 113]. A consistent factorization formula for non-global jet observables was developed in [114, 115]. It requires the introduction of a collinear-soft mode in the SCET Lagrangian. The first application of this formalism was to the light jet mass distribution [116], and significant steps toward an extension to NLL accuracy have been taken in [117]. It is believed that the results obtained from the factorization theorem derived in [114, 115] are equivalent to those obtained using the approaches proposed in [112, 113]. The various methods differ in the way in which they organize the all-order expansion for the appearing complicated multi-Wilson-line structures.

Another active field concerns the study of Glauber gluons in SCET [118] and their relation to the BFKL equation familiar from small- x physics [119]. A systematic account of the effects of Glauber gluons in the context of the SCET Lagrangian has been developed in [62]. The formalism has been extended to Glauber quarks in [120]. These developments set the basis for

a solid understanding of the impact of Glauber exchanges on factorization theorems. Glauber gluons also play an important role in SCET-based analysis of jet propagation in dense QCD media [121, 122], which gives rise to the jet-quenching phenomenon in heavy-ion collisions. An important open question facing some applications of SCET concerns factorized expressions containing endpoint-divergent convolution integrals.

We close this short review by mentioning a particularly nice application combining the methods of heavy-particle EFTs such as HQET and non-relativistic QCD with SCET in the context of describing the interactions of heavy dark matter (with mass $M \gg v$) with SM particles. In [123] it was realized that the interactions of heavy, weakly interacting massive particles (WIMPs) with nuclear targets can be described in a model-independent way using heavy-particle EFTs. The WIMPs are charged under $SU(2)_L$ and can interact with electroweak gauge bosons and the Higgs boson. The WIMP EFT was later extended by describing the produced, highly energetic electroweak gauge bosons in terms of soft or collinear fields in SCET [124–126]. This allows one to systematically separate all relevant mass scales, resum electroweak Sudakov logarithms and disentangle the so-called Sommerfeld enhancement from the short-distance hard annihilation process.

References

- [1] E. Witten, Nucl. Phys. **B122**, 109 (1977).
- [2] S. Weinberg, Phys. Lett. **91B**, 51 (1980).
- [3] L. J. Hall, Nucl. Phys. **B178**, 75 (1981).
- [4] E. Eichten and B. R. Hill, Phys. Lett. **B234**, 511 (1990).
- [5] H. Georgi, Phys. Lett. **B240**, 447 (1990).
- [6] B. Grinstein, Nucl. Phys. **B339**, 253 (1990).
- [7] T. Mannel, W. Roberts and Z. Ryzak, Nucl. Phys. **B368**, 204 (1992).
- [8] M. Neubert, Phys. Rept. **245**, 259 (1994), [hep-ph/9306320].
- [9] A. V. Manohar and M. B. Wise, Camb. Monogr. Part. Phys. Nucl. Phys. Cosmol. **10**, 1 (2000).
- [10] M. E. Luke and A. V. Manohar, Phys. Lett. **B286**, 348 (1992), [hep-ph/9205228].
- [11] E. V. Shuryak, Phys. Lett. **93B**, 134 (1980).
- [12] N. Isgur and M. B. Wise, Phys. Lett. **B232**, 113 (1989).
- [13] N. Isgur and M. B. Wise, Phys. Rev. Lett. **66**, 1130 (1991).
- [14] S. Nussinov and W. Wetzel, Phys. Rev. **D36**, 130 (1987).
- [15] M. A. Shifman and M. B. Voloshin, Sov. J. Nucl. Phys. **45**, 292 (1987), [Yad. Fiz.45,463(1987)].
- [16] M. Neubert, Phys. Lett. **B264**, 455 (1991).
- [17] M. E. Luke, Phys. Lett. **B252**, 447 (1990).
- [18] I. I. Y. Bigi *et al.*, Phys. Rev. **D52**, 196 (1995), [hep-ph/9405410].
- [19] N. Uraltsev, Phys. Lett. **B501**, 86 (2001), [195(2000)], [hep-ph/0011124].
- [20] G. P. Korchemsky and A. V. Radyushkin, Nucl. Phys. **B283**, 342 (1987).
- [21] A. F. Falk *et al.*, Nucl. Phys. **B343**, 1 (1990).
- [22] J. Chay, H. Georgi and B. Grinstein, Phys. Lett. **B247**, 399 (1990).
- [23] I. I. Y. Bigi, N. G. Uraltsev and A. I. Vainshtein, Phys. Lett. **B293**, 430 (1992), [Erratum: Phys. Lett. B297,477(1992)], [hep-ph/9207214].
- [24] A. V. Manohar and M. B. Wise, Phys. Rev. **D49**, 1310 (1994), [hep-ph/9308246].
- [25] T. Mannel, Nucl. Phys. **B413**, 396 (1994), [hep-ph/9308262].
- [26] A. F. Falk, M. E. Luke and M. J. Savage, Phys. Rev. **D49**, 3367 (1994), [hep-ph/9308288].
- [27] E. C. Poggio, H. R. Quinn and S. Weinberg, Phys. Rev. **D13**, 1958 (1976).
- [28] G. Buchalla, A. J. Buras and M. E. Lautenbacher, Rev. Mod. Phys. **68**, 1125 (1996), [hep-ph/9512380].
- [29] A. F. Falk and M. Neubert, Phys. Rev. **D47**, 2965 (1993), [hep-ph/9209268].
- [30] T. Becher, H. Boos and E. Lunghi, JHEP **12**, 062 (2007), [arXiv:0708.0855].
- [31] A. Alberti, P. Gambino and S. Nandi, JHEP **01**, 147 (2014), [arXiv:1311.7381].
- [32] T. Mannel, A. A. Pivovarov and D. Rosenthal, Phys. Lett. **B741**, 290 (2015), [arXiv:1405.5072].
- [33] T. Mannel, A. A. Pivovarov and D. Rosenthal, Phys. Rev. **D92**, 5, 054025 (2015), [arXiv:1506.08167].
- [34] T. Mannel and A. A. Pivovarov, Phys. Rev. **D100**, 9, 093001 (2019), [arXiv:1907.09187].
- [35] T. Mannel, S. Turczyk and N. Uraltsev, JHEP **11**, 109 (2010), [arXiv:1009.4622].
- [36] M. Neubert and C. T. Sachrajda, Nucl. Phys. **B483**, 339 (1997), [hep-ph/9603202].
- [37] M. Beneke, G. Buchalla and I. Dunietz, Phys. Rev. **D54**, 4419 (1996), [Erratum: Phys. Rev. D83,119902(2011)], [hep-ph/9605259].
- [38] M. Beneke *et al.*, Phys. Lett. **B459**, 631 (1999), [hep-ph/9808385].
- [39] M. Kirk, A. Lenz and T. Rauh, JHEP **12**, 068 (2017), [arXiv:1711.02100].
- [40] P. Gambino and C. Schwanda, Phys. Rev. **D89**, 1, 014022 (2014), [arXiv:1307.4551].
- [41] Y. Amhis *et al.* (HFLAV), Eur. Phys. J. **C77**, 12, 895 (2017), [arXiv:1612.07233].
- [42] P. Gambino, M. Jung and S. Schacht, Phys. Lett. **B795**, 386 (2019), [arXiv:1905.08209].
- [43] M. Neubert, Phys. Rev. **D49**, 3392 (1994), [hep-ph/9311325].
- [44] I. I. Y. Bigi *et al.*, Int. J. Mod. Phys. **A9**, 2467 (1994), [hep-ph/9312359].
- [45] G. P. Korchemsky and G. F. Sterman, Phys. Lett. **B340**, 96 (1994), [hep-ph/9407344].
- [46] C. W. Bauer, M. E. Luke and T. Mannel, Phys. Rev. **D68**, 094001 (2003), [hep-ph/0102089].
- [47] K. S. M. Lee and I. W. Stewart, Nucl. Phys. **B721**, 325 (2005), [hep-ph/0409045].
- [48] S. W. Bosch, M. Neubert and G. Paz, JHEP **11**, 073 (2004), [hep-ph/0409115].
- [49] M. Beneke *et al.*, JHEP **06**, 071 (2005), [hep-ph/0411395].
- [50] M. Benzke *et al.*, JHEP **08**, 099 (2010), [arXiv:1003.5012].
- [51] C. W. Bauer, S. Fleming and M. E. Luke, Phys. Rev. **D63**, 014006 (2000), [hep-ph/0005275].
- [52] C. W. Bauer and I. W. Stewart, Phys. Lett. **B516**, 134 (2001), [hep-ph/0107001].
- [53] C. W. Bauer, D. Pirjol and I. W. Stewart, Phys. Rev. **D65**, 054022 (2002), [hep-ph/0109045].
- [54] T. Becher, A. Broggio and A. Ferroglia, Lect. Notes Phys. **896**, pp.1 (2015), [arXiv:1410.1892].
- [55] J. Chay and C. Kim, Phys. Rev. **D65**, 114016 (2002), [hep-ph/0201197].
- [56] M. Beneke *et al.*, Nucl. Phys. **B643**, 431 (2002), [hep-ph/0206152].
- [57] C. W. Bauer *et al.*, Phys. Rev. **D66**, 014017 (2002), [hep-ph/0202088].
- [58] R. J. Hill and M. Neubert, Nucl. Phys. **B657**, 229 (2003), [hep-ph/0211018].
- [59] J. C. Collins, D. E. Soper and G. F. Sterman, Adv. Ser. Direct. High Energy Phys. **5**, 1 (1989), [hep-ph/0409313].

- [60] I. W. Stewart, F. J. Tackmann and W. J. Waalewijn, *Phys. Rev.* **D81**, 094035 (2010), [arXiv:0910.0467].
- [61] J. C. Collins, D. E. Soper and G. F. Sterman, *Nucl. Phys.* **B261**, 104 (1985).
- [62] I. Z. Rothstein and I. W. Stewart, *JHEP* **08**, 025 (2016), [arXiv:1601.04695].
- [63] I. A. Korchemskaya and G. P. Korchemsky, *Phys. Lett.* **B287**, 169 (1992).
- [64] T. Becher and M. Neubert, *Eur. Phys. J.* **C71**, 1665 (2011), [arXiv:1007.4005].
- [65] J.-Y. Chiu *et al.*, *JHEP* **05**, 084 (2012), [arXiv:1202.0814].
- [66] M. Beneke and T. Feldmann, *Nucl. Phys.* **B685**, 249 (2004), [hep-ph/0311335].
- [67] M. Beneke *et al.*, *Phys. Rev. Lett.* **83**, 1914 (1999), [hep-ph/9905312].
- [68] C. W. Bauer, D. Pirjol and I. W. Stewart, *Phys. Rev. Lett.* **87**, 201806 (2001), [hep-ph/0107002].
- [69] S. Mantry, D. Pirjol and I. W. Stewart, *Phys. Rev.* **D68**, 114009 (2003), [hep-ph/0306254].
- [70] T. Becher, R. J. Hill and M. Neubert, *Phys. Rev.* **D72**, 094017 (2005), [hep-ph/0503263].
- [71] S. Fleming, A. K. Leibovich and T. Mehen, *Phys. Rev.* **D68**, 094011 (2003), [hep-ph/0306139].
- [72] T. Becher and M. D. Schwartz, *JHEP* **07**, 034 (2008), [arXiv:0803.0342].
- [73] T. Becher and G. Bell, *JHEP* **11**, 126 (2012), [arXiv:1210.0580].
- [74] I. W. Stewart, F. J. Tackmann and W. J. Waalewijn, *Phys. Rev. Lett.* **105**, 092002 (2010), [arXiv:1004.2489].
- [75] J.-y. Chiu, R. Kelley and A. V. Manohar, *Phys. Rev.* **D78**, 073006 (2008), [arXiv:0806.1240].
- [76] T. Becher, M. Neubert and G. Xu, *JHEP* **07**, 030 (2008), [arXiv:0710.0680].
- [77] V. Ahrens *et al.*, *Eur. Phys. J.* **C62**, 333 (2009), [arXiv:0809.4283].
- [78] X. Liu, S. Mantry and F. Petriello, *Phys. Rev.* **D86**, 074004 (2012), [arXiv:1205.4465].
- [79] M. G. Echevarria, A. Idilbi and I. Scimemi, *JHEP* **07**, 002 (2012), [arXiv:1111.4996].
- [80] A. J. Larkoski, I. Moulton and B. Nachman (2017), [arXiv:1709.04464].
- [81] S. Kluth, *Rept. Prog. Phys.* **69**, 1771 (2006), [hep-ex/0603011].
- [82] A. Gehrmann-De Ridder *et al.*, *Phys. Rev. Lett.* **99**, 132002 (2007), [arXiv:0707.1285].
- [83] S. Weinzierl, *Phys. Rev. Lett.* **101**, 162001 (2008), [arXiv:0807.3241].
- [84] R. Abbate *et al.*, *Phys. Rev.* **D83**, 074021 (2011), [arXiv:1006.3080].
- [85] A. H. Hoang *et al.*, *Phys. Rev.* **D91**, 9, 094018 (2015), [arXiv:1501.04111].
- [86] T. Becher and M. Neubert, *JHEP* **07**, 108 (2012), [arXiv:1205.3806].
- [87] I. W. Stewart *et al.*, *Phys. Rev.* **D89**, 5, 054001 (2014), [arXiv:1307.1808].
- [88] A. Banfi *et al.*, *Phys. Rev. Lett.* **109**, 202001 (2012), [arXiv:1206.4998].
- [89] R. Boughezal, X. Liu and F. Petriello, *Phys. Rev.* **D91**, 9, 094035 (2015), [arXiv:1504.02540].
- [90] J. Gaunt *et al.*, *JHEP* **09**, 058 (2015), [arXiv:1505.04794].
- [91] R. Boughezal *et al.*, *Phys. Lett.* **B748**, 5 (2015), [arXiv:1505.03893].
- [92] R. Boughezal *et al.*, *Phys. Rev. Lett.* **116**, 15, 152001 (2016), [arXiv:1512.01291].
- [93] J. M. Campbell, R. K. Ellis and C. Williams, *JHEP* **06**, 179 (2016), [arXiv:1601.00658].
- [94] J. M. Campbell *et al.*, *JHEP* **07**, 148 (2016), [arXiv:1603.02663].
- [95] G. Heinrich *et al.*, *JHEP* **03**, 142 (2018), [arXiv:1710.06294].
- [96] I. Moulton *et al.*, *Phys. Rev.* **D95**, 7, 074023 (2017), [arXiv:1612.00450].
- [97] R. Boughezal, X. Liu and F. Petriello, *JHEP* **03**, 160 (2017), [arXiv:1612.02911].
- [98] S. Alioli *et al.*, *JHEP* **09**, 120 (2013), [arXiv:1211.7049].
- [99] S. Alioli *et al.*, *Phys. Rev.* **D92**, 9, 094020 (2015), [arXiv:1508.01475].
- [100] C. W. Bauer, D. Pirjol and I. W. Stewart, *Phys. Rev.* **D68**, 034021 (2003), [hep-ph/0303156].
- [101] D. Pirjol and I. W. Stewart, *Phys. Rev.* **D67**, 094005 (2003), [Erratum: *Phys. Rev.* **D69**, 019903(2004)], [hep-ph/0211251].
- [102] R. J. Hill *et al.*, *JHEP* **07**, 081 (2004), [hep-ph/0404217].
- [103] M. Beneke and D. Yang, *Nucl. Phys.* **B736**, 34 (2006), [hep-ph/0508250].
- [104] I. Moulton, I. W. Stewart and G. Vita, *JHEP* **07**, 067 (2017), [arXiv:1703.03408].
- [105] I. Feige *et al.*, *JHEP* **11**, 142 (2017), [arXiv:1703.03411].
- [106] M. Beneke *et al.*, *JHEP* **03**, 001 (2018), [arXiv:1712.04416].
- [107] S. Alte, M. König and M. Neubert, *JHEP* **08**, 095 (2018), [arXiv:1806.01278].
- [108] I. Moulton *et al.*, *JHEP* **08**, 013 (2018), [arXiv:1804.04665].
- [109] M. Beneke *et al.*, *JHEP* **03**, 043 (2019), [arXiv:1809.10631].
- [110] M. Dasgupta and G. P. Salam, *Phys. Lett.* **B512**, 323 (2001), [hep-ph/0104277].
- [111] R. B. Appleby and M. H. Seymour, *JHEP* **12**, 063 (2002), [hep-ph/0211426].
- [112] S. Caron-Huot, *JHEP* **03**, 036 (2018), [arXiv:1501.03754].
- [113] A. J. Larkoski, I. Moulton and D. Neill, *JHEP* **09**, 143 (2015), [arXiv:1501.04596].
- [114] T. Becher *et al.*, *Phys. Rev. Lett.* **116**, 19, 192001 (2016), [arXiv:1508.06645].
- [115] T. Becher *et al.*, *JHEP* **11**, 019 (2016), [Erratum: *JHEP* **05**, 154(2017)], [arXiv:1605.02737].
- [116] T. Becher, B. D. Pecjak and D. Y. Shao, *JHEP* **12**, 018 (2016), [arXiv:1610.01608].
- [117] M. Balsiger, T. Becher and D. Y. Shao, *JHEP* **04**, 020 (2019), [arXiv:1901.09038].
- [118] C. W. Bauer, B. O. Lange and G. Ovanesyan, *JHEP* **07**, 077 (2011), [arXiv:1010.1027].
- [119] S. Fleming, *Phys. Lett.* **B735**, 266 (2014), [arXiv:1404.5672].
- [120] I. Moulton *et al.*, *JHEP* **02**, 134 (2018), [arXiv:1709.09174].
- [121] A. Idilbi and A. Majumder, *Phys. Rev.* **D80**, 054022 (2009), [arXiv:0808.1087].
- [122] G. Ovanesyan and I. Vitev, *JHEP* **06**, 080 (2011), [arXiv:1103.1074].
- [123] R. J. Hill and M. P. Solon, *Phys. Lett.* **B707**, 539 (2012), [arXiv:1111.0016].
- [124] M. Bauer *et al.*, *JHEP* **01**, 099 (2015), [arXiv:1409.7392].
- [125] M. Baumgart, I. Z. Rothstein and V. Vaidya, *Phys. Rev. Lett.* **114**, 211301 (2015), [arXiv:1409.4415].
- [126] G. Ovanesyan, T. R. Slatyer and I. W. Stewart, *Phys. Rev. Lett.* **114**, 21, 211302 (2015), [arXiv:1409.8294].

17. Lattice Quantum Chromodynamics

Revised August 2021 by S. Hashimoto (KEK) and S.R. Sharpe (U. Washington), written September 2011 with J. Laiho (Syracuse U.)

17.1	Lattice regularization of QCD	337
17.1.1	Gauge invariance, gluon fields and the gluon action	337
17.1.2	Lattice fermions	338
17.1.3	Heavy quarks on the lattice	339
17.1.4	QED on the lattice	340
17.1.5	Basic inputs for lattice calculations	340
17.1.6	Sources of systematic error	341
17.2	Methods and status	342
17.2.1	Monte-Carlo method	342
17.2.2	Two-point functions	342
17.2.3	Three-point functions	343
17.2.4	Scattering amplitudes and resonances	343
17.2.5	Recent advances	344
17.2.6	Status of LQCD simulations	344
17.3	Physics applications	344
17.3.1	Spectrum	344
17.3.2	Decay constants and bag parameters	345
17.3.3	Form factors ($K \rightarrow \pi l\nu$, $D \rightarrow Kl\nu$, $B \rightarrow \pi l\nu$, $B \rightarrow D^{(*)} l\nu$)	345
17.3.4	Strong gauge coupling	346
17.3.5	Quark masses	346
17.3.6	Other applications	346
17.4	Outlook	347
17.5	Acknowledgments	347

Many physical processes considered in the Review of Particle Properties (RPP) involve hadrons. The properties of hadrons—which are composed of quarks and gluons—are governed primarily by Quantum Chromodynamics (QCD) (with small corrections from Quantum Electrodynamics [QED]). Theoretical calculations of these properties require non-perturbative methods, and Lattice Quantum Chromodynamics (LQCD) is a tool to carry out such calculations. It has been successfully applied to many properties of hadrons. Most important for the RPP are the calculation of electroweak decay constants and form factors, which are needed to extract Cabbibo-Kobayashi-Maskawa (CKM) matrix elements when combined with the corresponding experimental measurements. LQCD has also been used to determine other fundamental parameters of the standard model, in particular the strong gauge coupling and quark masses, as well as to predict hadronic contributions to the anomalous magnetic moment of the muon, $g_\mu - 2$.

This review describes the theoretical foundations of LQCD and sketches the methods used to calculate the quantities relevant for the RPP. It also describes the various sources of error that must be controlled in a LQCD calculation. Results for hadronic quantities are given in the corresponding dedicated reviews.

17.1 Lattice regularization of QCD

Gauge theories form the building blocks of the Standard Model. While the SU(2) and U(1) parts have weak couplings and can be studied accurately with perturbative methods, the SU(3) component—QCD—is only amenable to a perturbative treatment at high energies. The growth of the gauge coupling in the infrared—the flip-side of asymptotic freedom—requires the use of non-perturbative methods to determine the low energy properties of QCD. Lattice gauge theory, proposed by K. Wilson in 1974 [1], provides such a method, for it gives a non-perturbative definition of vector-like gauge field theories such as QCD. In lattice regularized QCD—commonly called lattice QCD or LQCD—Euclidean space-time is discretized, usually on a hypercubic lattice with lattice spacing a , with quark fields placed on sites and gauge fields on the links between sites. The lattice spacing plays the role of the ultraviolet regulator, rendering the quantum field theory finite. The continuum theory is recovered by taking the limit of vanishing lattice spacing, which can be reached by tuning the bare gauge coupling to zero according to the renormalization group.

Unlike dimensional regularization, which is commonly used in continuum QCD calculations, the definition of LQCD does not

rely on the perturbative expansion. Indeed, LQCD allows non-perturbative calculations by numerical evaluation of the path integral that defines the theory.

Practical LQCD calculations are limited by the availability of computational resources and the efficiency of algorithms. Because of this, LQCD results come with both statistical and systematic errors, the former arising from the use of Monte-Carlo integration, the latter, for example, from the use of non-zero values of a . There are also different ways in which the QCD action can be discretized, and all must give consistent results in the continuum limit, $a \rightarrow 0$. It is the purpose of this review to provide an outline of the methods of LQCD, with particular focus on applications to particle physics, and an overview of the various sources of error. This should allow the reader to better understand the LQCD results that are presented in other reviews, primarily those on “Quark Masses,” “Quark Model,” “Quantum Chromodynamics,” “CKM quark-mixing matrix,” “ V_{ud} , V_{us} , Cabibbo angle and CKM Unitarity,” “Leptonic Decays of Charged Pseudoscalar Mesons,” “ B^0 - \bar{B}^0 Mixing,” and “Semileptonic b -Hadron Decays, Determination of V_{cb} and V_{ub} .” For more extensive explanations the reader should consult the available textbooks or lecture notes, the most up-to-date of which are Refs. [2–4].

17.1.1 Gauge invariance, gluon fields and the gluon action

A key feature of the lattice formulation of QCD is that it preserves gauge invariance. This is in contrast to perturbative calculations, where gauge fixing is an essential step. The preservation of gauge invariance leads to considerable simplifications, e.g., restricting the form of operators that can mix under renormalization.

The gauge transformations of lattice quark fields are just as in the continuum: $q(x) \rightarrow V(x)q(x)$ and $\bar{q}(x) \rightarrow \bar{q}(x)V^\dagger(x)$, with $V(x)$ an arbitrary element of SU(3). The only difference is that the Euclidean space-time positions x are restricted to lie on the sites of the lattice, i.e. $x = a(n_1, n_2, n_3, n_4)$ for a hypercubic lattice, with the n_j being integers. Quark bilinears involving different lattice points can be made gauge invariant by introducing the gluon field $U_\mu(x)$. For example, for adjacent points the bilinear is $\bar{q}(x)U_\mu(x)q(x+a\hat{\mu})$, with $\hat{\mu}$ the unit vector in the μ 'th direction. (This form is used in the construction of the lattice covariant derivative.) This is illustrated in Fig. 17.1. The gluon field (or “gauge link”) is an element of the group, SU(3), in contrast to the continuum field A_μ which takes values in the Lie algebra. The bilinear is invariant if U_μ transforms as $U_\mu(x) \rightarrow V(x)U_\mu(x)V^\dagger(x+a\hat{\mu})$. The lattice gluon field is naturally associated with the link joining x and $x+a\hat{\mu}$, and corresponds in the continuum to a Wilson line connecting these two points, $P \exp(i \int_x^{x+a\hat{\mu}} dx_\mu A_\mu^{\text{cont}}(x))$ (where P indicates a path-ordered integral, and the superscript on A_μ indicates that it is a continuum field). The trace of a product of the $U_\mu(x)$ around any closed loop is easily seen to be gauge invariant and is the lattice version of a Wilson loop.

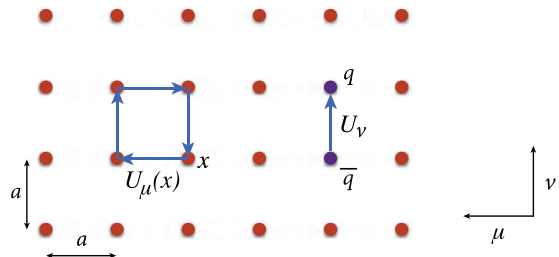


Figure 17.1: Sketch of a two-dimensional slice through the μ - ν plane of a lattice, showing gluon fields lying on links and forming either the plaquette product appearing in the gauge action or a component of the covariant derivative connecting quark and antiquark fields.

The simplest possible gauge action, usually called the Wilson gauge action, is given by the product of gauge links around elementary plaquettes:

$$S_g = \beta \sum_{x,\mu,\nu} \left[1 - \frac{1}{3} \text{ReTr}[U_\mu(x)U_\nu(x+a\hat{\mu})U_\mu^\dagger(x+a\hat{\nu})U_\nu^\dagger(x)] \right]. \quad (17.1)$$

This is illustrated in Fig. 17.1. For small a , assuming that the fields are slowly varying, one can expand the action in powers of a using $U_\mu(x) = \exp(iaA_\mu(x))$. Keeping only the leading non-vanishing term, and replacing the sum with an integral, one finds the continuum form,

$$S_g \longrightarrow \int d^4x \frac{1}{4g_{\text{lat}}^2} \text{Tr}[F_{\mu\nu}^2(x)], \quad (17.2)$$

$$(F_{\mu\nu} = \partial_\mu A_\nu - \partial_\nu A_\mu + i[A_\mu, A_\nu])$$

as long as one chooses $\beta = 6/g_{\text{lat}}^2$ for the lattice coupling. In this expression, g_{lat} is the bare gauge coupling in the lattice scheme, which can be related (by combining continuum and lattice perturbation theory) to a more conventional gauge coupling such as that in the $\overline{\text{MS}}$ scheme (see Sec. 17.3.4 below).

In practice, the lattice spacing a is non-zero, leading to discretization errors. In particular, the lattice breaks Euclidean rotational invariance (which is the Euclidean version of Lorentz invariance) down to a discrete hypercubic subgroup. One wants to reduce discretization errors as much as possible. A very useful tool for understanding and then reducing discretization errors is the Symanzik effective action: the interactions of quarks and gluons with momenta low compared to the lattice cutoff ($|p| \ll 1/a$) are described by a continuum action consisting of the standard continuum terms (e.g., the gauge action given in Eq. (17.2)) augmented by higher dimensional operators suppressed by powers of a [5]. For the Wilson lattice gauge action, the leading corrections come in at $\mathcal{O}(a^2)$. They take the form $\sum_j a^2 c_j O_6^{(j)}$, with the sum running over all dimension-six operators $O_6^{(j)}$ allowed by the lattice symmetries, and c_j unknown coefficients. Some of these operators violate Euclidean rotational invariance, and all of them lead to discretization errors of the form $a^2 \Lambda^2$ (up to $\log(a)$ corrections that will be discussed below), where Λ is a typical momentum scale for the quantity being calculated. These errors can, however, be reduced by adding corresponding operators to the lattice action and tuning their coefficients to eliminate the dimension-six operators in the effective action to a given order in perturbation theory or even non-perturbatively. This is the idea of the Symanzik improvement program [5]. In the case of the gauge action, one adds Wilson loops involving six gauge links (as opposed to the four links needed for the original plaquette action, Eq. (17.1)) to define the $\mathcal{O}(a^2)$ improved (or “Symanzik”) action [6]. In practical implementations, the improvement is either at tree-level (so that residual errors are proportional to $\alpha_s a^2$, where the coupling is evaluated at a scale $\sim 1/a$), or at one loop order (errors proportional to $\alpha_s^2 a^2$). Another popular choice is motivated by studies of renormalization group (RG) flow. It has the same terms as the $\mathcal{O}(a^2)$ improved action but with different coefficients, and is called the RG-improved or “Iwasaki” action [7].

17.1.2 Lattice fermions

Discretizing the fermion action turns out to involve subtle issues, and the range of actions being used is more extensive than for gauge fields. Recall that the continuum fermion action is $S_f = \int d^4x \bar{q}[iD_\mu \gamma_\mu + m]q$, where $D_\mu = \partial_\mu + iA_\mu$ is the gauge-covariant derivative. The simplest discretization replaces the derivative with a symmetric difference:

$$D_\mu q(x) \longrightarrow \frac{1}{2a} [U_\mu(x)q(x+a\hat{\mu}) - U_\mu(x-a\hat{\mu})^\dagger q(x-a\hat{\mu})]. \quad (17.3)$$

The factors of U_μ ensure that $D_\mu q(x)$ transforms under gauge transformations in the same way as $q(x)$, so that the discretized version of $\bar{q}(x)D_\mu \gamma_\mu q(x)$ is gauge invariant. The choice in Eq. (17.3) leads to the so-called naive fermion action. This, however, suffers from the fermion doubling problem—in d dimensions it describes 2^d equivalent fermion fields in the continuum limit. The appearance of the extra “doubler” fermions is related

to the deeper theoretical problem of formulating chirally symmetric fermions on the lattice. This is encapsulated by the Nielsen-Ninomiya theorem [8]: one cannot define lattice fermions having exact, continuum-like chiral symmetry without producing doublers. Naive lattice fermions do have chiral symmetry but at the cost of introducing 15 unwanted doublers (for $d = 4$).

There are a number of different strategies for dealing with the doubling problem, each with their own theoretical and computational advantages and disadvantages. Wilson fermions [1] add a term proportional to $a\bar{q}\Delta q$ to the fermion action (the “Wilson term”—in which Δ is a covariant lattice Laplacian). This gives a mass of $\mathcal{O}(1/a)$ to the doublers, so that they decouple in the continuum limit. The Wilson term, however, violates chiral symmetry, and also introduces discretization errors linear in a . A commonly used variant that eliminates the $\mathcal{O}(a)$ discretization error is the $\mathcal{O}(a)$ -improved Wilson (or “clover”) action [9]. In this application of Symanzik improvement, methods have been developed to remove $\mathcal{O}(a)$ terms non-perturbatively using auxiliary simulations to tune parameters [10]. Such “non-perturbative improvement” is of great practical importance as it brings the discretization error from the fermion action down to the same level as that from the gauge action.

The advantages of Wilson fermions are their theoretical simplicity and relatively low computational cost. Their main disadvantage is the lack of chiral symmetry, which makes them difficult to use in cases where mixing with wrong chirality operators can occur, particularly if this involves divergences proportional to powers of $1/a$. A related problem is the presence of potential numerical instabilities due to spurious near-zero modes of the lattice Dirac operator. There are, however, studies that successfully ameliorate these problems and increase the range of quantities for which Wilson fermions can be used (see, e.g., Refs. [11–14]).

Twisted-mass fermions [15] are a variant of Wilson fermions in which two flavors are treated together with an isospin-breaking mass term (the “twisted mass” term). The main advantage of this approach is that all errors linear in a are automatically removed (without the need for tuning of parameters) by a clever choice of twisted mass and operators [16]. A disadvantage is the presence of isospin breaking effects (such as a splitting between charged and neutral pion masses even when up and down quarks are degenerate), which, however, vanish as $a^2 \Lambda^2$ in the continuum limit. Strange and charm quarks can be added as a second pair, with a term added to split their masses [17, 18].

Staggered fermions are a reduced version of naive fermions in which there is only a single fermion Dirac component on each lattice site, with the full Dirac structure built up from neighboring sites [19]. They have the advantages of being somewhat faster to simulate than Wilson-like fermions, of preserving some chiral symmetry, and of having discretization errors of $\mathcal{O}(a^2)$. Their disadvantage is that they retain some of the doublers (3 for $d = 4$). The action thus describes four degenerate fermions in the continuum limit. These are usually called “tastes”, to distinguish them from physical flavors, and the corresponding $\text{SU}(4)$ symmetry is referred to as the “taste symmetry”. The preserved chiral symmetry in this formulation has non-singlet taste. Practical applications usually introduce one staggered fermion for each physical flavor, and remove contributions from the unwanted tastes by taking the fourth-root of the fermion determinant appearing in the path integral. The validity of this “rooting” procedure is not obvious because taste symmetry is violated for non-zero lattice spacing. Theoretical arguments, supported by numerical evidence, suggest that the procedure is valid as long as one takes the continuum limit before approaching the light quark mass region [20]. Additional issues arise for the valence quarks (those appearing in quark propagators, as described in Sec. 17.2 below), where rooting is not possible, and one must ignore the extra tastes, or account for them by including appropriate factors [21], which can be nontrivial in applications involving baryons [22].

Just as for Wilson fermions, the staggered action can be improved, so as to reduce discretization errors. The Asqtad (a -squared tadpole improved) action [23] was used until recently in many large scale simulations [24]. More recent calculations use the HISQ (highly improved staggered quark) action, introduced in

Ref. [25]. At tree-level it removes both $\mathcal{O}(a^2)$ errors and, to lowest order in the quark speed v/c , $\mathcal{O}([am]^4)$ errors. It also substantially reduces effects caused by taste-symmetry breaking. This makes it attractive not only for light quarks, but means that it is also quite accurate for heavy quarks because it suppresses $(am)^n$ errors. It is being used to directly simulate charm quarks and to approach direct simulations of bottom quarks (see, e.g., [26–28]).

There is an important class of lattice fermions, “Ginsparg-Wilson fermions,” that possess a continuum-like chiral symmetry without introducing unwanted doublers. The lattice Dirac operator D for these fermions satisfies the Ginsparg-Wilson relation $D\gamma_5 + \gamma_5 D = aD\gamma_5 D$ [29]. In the continuum, the right-hand-side vanishes, leading to chiral symmetry. On the lattice, it is non-vanishing, but with a particular form (with two factors of D) that restricts the violations of chiral symmetry in Ward-Takahashi identities to short-distance terms that do not contribute to physical matrix elements [30]. In fact, one can define a modified chiral transformation on the lattice (by including dependence on the gauge fields) such that Ginsparg-Wilson fermions have an exact chiral symmetry for on-shell quantities [31]. The net result is that such fermions essentially have the same properties under chiral transformations as do continuum fermions, including the index theorem [30]. Their leading discretization errors are of $\mathcal{O}(a^2)$.

Two types of Ginsparg-Wilson fermions are currently being used in large-scale numerical simulations. The first is Domain-wall fermions (DWF). These are defined on a five-dimensional space, in which the fifth dimension is fictitious [32]. The action is chosen so that the low-lying modes are chiral, with left- and right-handed modes localized on opposite four-dimensional surfaces. For an infinite fifth dimension, these fermions satisfy the Ginsparg-Wilson relation. In practice, the fifth dimension is kept finite, and there remains a small, controllable violation of chiral symmetry. The second type is Overlap fermions. These appeared from a completely different context and have an explicit form that exactly satisfies the Ginsparg-Wilson relation [33]. Their numerical implementation requires an approximation of the matrix sign function of a Wilson-like fermion operator, and various approaches are being used. In fact, it is possible to rewrite these approximations in terms of a five-dimensional formulation, showing that the DWF and Overlap approaches are essentially equivalent [34, 35]. Numerically, the five-dimensional approach appears to be more computationally efficient.

The various lattice fermion formulations are often combined with the technique of link smearing. Here one couples the fermions to a smoother gauge link, defined by averaging with adjacent links in a gauge invariant manner. Several closely related implementations are being used. All reduce the coupling of fermions to the short-distance fluctuations in the gauge field, leading to an improvement in the numerical stability and speed of algorithms. One cannot perform this smearing too aggressively, however, since the smearing may distort short distance physics and enhance discretization errors.

As noted above, each fermion formulation has its own advantages and disadvantages. For instance, domain-wall and overlap fermions are theoretically preferred as they have chiral symmetry without doublers, but their computational cost is greater than for other choices. If the physics application of interest and the target precision do not require near-exact chiral symmetry, there is no strong motivation to use these expensive formulations. On the other hand, there is a class of applications (including the calculation of the $\Delta I = 1/2$ amplitude for $K \rightarrow \pi\pi$ decays and the S-parameter [36]) where chiral symmetry plays an essential role and for which the use of Ginsparg-Wilson fermions is strongly favored.

17.1.3 Heavy quarks on the lattice

The fermion formulations described in the previous subsection can be used straightforwardly only for quarks whose masses are small compared to the lattice cutoff, $m_q \lesssim 1/a$. This is because there are discretization errors proportional to powers of am_q , and if $am_q \gtrsim 1$ these errors are large and uncontrolled. Present LQCD simulations typically have cutoffs in the range of $1/a = 2 - 4$ GeV (corresponding to $a \approx 0.1 - 0.05$ fm). Thus, while for the up, down and strange quarks one has $am_q \ll 1$, for bottom quarks

(with $m_b \approx 4.5$ GeV) one must use alternative approaches. Charm quarks ($m_c \approx 1.5$ GeV) are an intermediate case, allowing simulations using both direct and alternative approaches.

For the charm quark, the straightforward approach is to simultaneously reduce the lattice spacing and to improve the fermion action so as to reduce the size of errors proportional to powers of am_c . This approach has been followed successfully using the HISQ, twisted-mass and domain-wall actions [25, 26, 28, 37, 38]. It is important to note, however, that reducing a increases the computational cost because an increased number of lattice points are needed for the same physical volume. One cannot reduce the spatial size below 2–3 fm without introducing finite volume errors. Present lattices have typical sizes of $\sim 64^3 \times 128$ (with the long direction being Euclidean time), and thus allow a lattice cutoff up to $1/a \sim 4$ GeV.

This approach can, to some extent, be extended to the bottom quark, by the use of simulations with small lattice spacings [27]. This has been pursued with the HISQ action [39], using lattices of size up to $144^3 \times 288$ and lattice spacings down to $a \approx 0.03$ fm ($1/a \approx 6.6$ GeV). Extrapolation in m_b is still needed [40], however, and this makes use of the mass dependence predicted by Heavy Quark Effective Theory (HQET).

Alternative approaches for discretizing heavy quarks are motivated by effective field theories. For a bottom quark in heavy-light hadrons, one can use HQET to expand about the infinite quark-mass limit. In this limit, the bottom quark is a static color source, and one can straightforwardly write the corresponding lattice action [41]. Corrections, proportional to powers of $1/m_b$, can be introduced as operator insertions, with coefficients that can be determined non-perturbatively using existing techniques [42]. This method allows the continuum limit to be taken controlling all $1/m_b$ corrections.

Another way of introducing the $1/m_b$ corrections is to include the relevant terms in the effective action. This leads to a non-relativistic QCD (NRQCD) action, in which the heavy quark is described by a two-component spinor [43]. This approach has the advantage over HQET that it can also be used for heavy-heavy systems, such as the Upsilon states. Moreover, the bottom quark can be treated without any extrapolation in m_b . A disadvantage is that some of the parameters in this effective theory are determined perturbatively (at tree-level or at one-loop [44]), which limits the precision of the final results. Although discretization effects can be controlled with good numerical precision for a range of lattice spacings, these artifacts cannot be extrapolated away by taking the lattice spacing to zero. This is because NRQCD is a nonrelativistic effective field theory and so ceases to work when the cutoff π/a becomes much larger than the heavy-quark mass. In practice these effects are accounted for in the error budget.

This problem can be avoided if one uses HQET power counting to analyze and reduce discretization effects for heavy quarks while using conventional fermion actions [45]. For instance, one can tune the parameters of an improved Wilson quark action so that the leading HQET corrections to the static quark limit are correctly accounted for. As the lattice spacing becomes finer, the action smoothly goes over to that of a light Wilson quark action, where the continuum limit can be taken as usual. In principle, one can improve the action in the heavy quark regime up to arbitrarily high orders using HQET, but so far large-scale simulations have typically used clover improved Wilson quarks, where tuning the parameters of the action corresponds to including all corrections through next-to-leading order in HQET. Three different methods for tuning the parameters of the clover action are being used: the Fermilab [45], Tsukuba [46] and Columbia [47] approaches. An advantage of this HQET approach is that the c and b quarks can be treated on the same footing. Parameter tuning has been done perturbatively, as in NRQCD, or using non-perturbative tuning of some of the parameters [48, 49]. One can improve the effective theory including the terms beyond the next-to-leading order. The Oktay-Kronfeld action that includes dimension-six and -seven operators has been constructed [50] and used in large-scale numerical calculations [51].

Another approach is the “ratio method” introduced in Ref. [52]. Here one uses quarks with masses lying at, or slightly above, the

charm mass m_c , which can be simulated with a relativistic action, and extrapolates to m_b incorporating the behavior predicted by HQET. The particular implementation relies on the use of ratios. As an example, consider the B meson decay constant f_B . According to HQET, this scales as $1/\sqrt{m_B}$ for $m_B \gg \Lambda_{\text{QCD}}$, up to a logarithmic dependence that is calculable in perturbative QCD (but will be suppressed in the following). Here m_B is the B meson mass, which differs from m_b by $\sim \Lambda_{\text{QCD}}$. One considers the ratio $y(\lambda, m_{b'}) \equiv f_{B''} \sqrt{m_{B''}} / f_{B'} \sqrt{m_{B'}}$ for fictitious B mesons containing b quarks with unphysical masses $m_{b'}$ and $m_{b''} = \lambda m_{b'}$. HQET implies that $y(\lambda, m_{b'})$ approaches unity for large $m_{b'}$ and any fixed $\lambda > 1$. The ratios are evaluated on the lattice for the sequence of masses $m_{b'} = m_c, \lambda m_c, \lambda^2 m_c$, all well below the physical m_b , and for each the continuum limit is taken. The form of the ratio for larger values of $m_{b'}$ is obtained by fitting, incorporating the constraints implied by HQET. The result for $f_B \sqrt{m_B}$ is then obtained as a product of y 's with $f_D \sqrt{m_D}$.

17.1.4 QED on the lattice

Quarks in nature are electrically charged, and the resultant coupling to photons leads to shifts in the properties of hadrons that are generically of $\mathcal{O}(\alpha_{\text{EM}})$. Thus, for example, the proton mass is increased by ~ 1 MeV relative to that of the neutron due to its overall charge although this effect is more than compensated for by the ~ 2.5 MeV relative decrease due to the up quark being lighter than the down quark [53]. This example shows that once pure QCD, isospin-symmetric lattice calculations reach percent level accuracy, further improvement requires the inclusion of effects due to both electromagnetism and the up-down mass difference. This level of accuracy has in fact been obtained for various quantities, e.g., light hadron masses and decay constants (see Ref. [54]), and simulations including QED in addition to QCD are becoming more common.

The extension of lattice methods to include QED is straightforward, although some new subtleties arise. The essential change is that the quark must now propagate through a background field containing both gluons and photons. The gauge field U_μ that appears in the covariant derivative of Eq. (17.3) is extended from an SU(3) matrix to one living in U(3): $U_\mu \rightarrow U_\mu e^{iaq_e A_\mu^{\text{EM}}}$. Here A_μ^{EM} is the photon field, e the electromagnetic coupling, and q the charge of the quark, e.g., $q = 2/3$ for up and $-1/3$ for down and strange quarks. The lattice action for the photon that is typically used is a discretized version of the continuum action Eq. (17.2), rather than the form used for the gluons, Eq. (17.1). This “non-compact” action has the advantage that it is quadratic in A_μ^{EM} , which simplifies the QED part of the generation of configurations.

One subtlety that arises is that Gauss’ law forbids a charged particle in a box with periodic boundary conditions. This finite volume effect can be overcome by including a uniform background charge, and this can be shown to be equivalent to removing the zero-momentum mode from the photon field. This is an example of the enhanced finite-volume effects that arise in the presence of the massless photon.

Simulations including QED have progressed over the last few years, and now a full inclusion of QED has been achieved for a range of quark masses approaching the physical values [53, 55–57]. Alternative approaches have also been used: reweighting the QCD fields *a posteriori* [58, 59], and keeping only the linear term in an expansion in α_{EM} about the QCD only case [60]. In addition, some calculations have included QED effects for the valence quarks but not the sea quarks (the “electroquenched approximation”) [61–65].

The QED corrections to processes including leptons, such as the leptonic and semileptonic decays of hadrons, involve additional diagrams in which a photon propagator bridges between a hadron and a lepton. Such diagrams induce infrared divergences that cancel against soft photon radiation (Bloch-Nordsieck theorem [66]). Methods have been developed to implement this cancellation in lattice calculations, treating the soft photon analytically [67], with first results reported recently for leptonic pion and kaon decays [68, 69]. An application to semi-leptonic decays has also been discussed [70, 71].

17.1.5 Basic inputs for lattice calculations

Since LQCD is nothing but a regularization of QCD, the renormalizability of QCD implies that the number of input parameters in LQCD is the same as for continuum QCD—the strong gauge coupling $\alpha_s = g^2/(4\pi)$, the quark masses for each flavor, and the CP violating phase θ . The θ parameter is usually assumed to be zero, while the other parameters must be determined using experimental inputs.

17.1.5.1 Lattice spacing

In QCD, the gauge coupling is a function of scale. With lattice regularization, this scale is the inverse lattice spacing $1/a$, and choosing the bare gauge coupling is equivalent to fixing the lattice spacing.

In principle, a can be determined using any dimensionful quantity measured by experiments. For example, using the mass of hadron H one has $a = (am_H)^{\text{lat}}/m_H^{\text{exp}}$. One chooses quantities that can be calculated accurately on the lattice, and that are only weakly dependent on the light quark masses. The latter property minimizes errors from extrapolating or interpolating to the physical light quark masses or from mistuning of these masses.

Commonly used choices are the spin-averaged 1S-1P or 1S-2S splittings in the Upsilon system, the mass of the Ω^- baryon, and the pion decay constant f_π . Ultimately, all choices must give consistent results for a , and that this is the case provides a highly non-trivial check of both the calculational method and of QCD.

Many recent lattice calculations use intermediate length scales in place of a direct determination of the lattice spacing. These length scales, which we denote \mathcal{R} , have the advantage that they can be precisely, and relatively cheaply, computed numerically. Examples are r_0 , derived from the heavy quark potential [72], and t_0 and w_0 , determined from the gradient flow of the gauge field [73]. These scales are used in the following manner, explained here in the context of calculating a quantity Q with mass dimension d (e.g. a decay constant for which $d = 1$). In the first step, one calculates the dimensionless quantities $a^d Q$ and \mathcal{R}/a in a given lattice calculation, and forms the product $(a^d Q) \times (\mathcal{R}/a)^d = Q\mathcal{R}^d$. In a second step, one uses results available from previous dedicated lattice calculations that have determined \mathcal{R} in physical units (i.e. fm) by relating them to physical quantities as discussed above. Then one obtains $Q = (Q\mathcal{R}^d)/\mathcal{R}^d$. The results of this second step are reviewed in the latest edition of the Flavor Lattice Averaging Group (FLAG) report [74].

17.1.5.2 Light quark masses

In LQCD simulations, the up, down and strange quarks are usually referred to as the light quarks, in the sense that $m_q < \Lambda_{\text{QCD}}$. (The standard definition of Λ_{QCD} is given in the “Quantum Chromodynamics” review; in this review we are using it only to indicate the approximate non-perturbative scale of QCD.) This condition is stronger than that used above to distinguish quarks with small discretization errors, $m_q < 1/a$. Loop effects from light quarks must be included in the simulations to accurately represent QCD. At present, most simulations are done in the isospin symmetric limit $m_u = m_d \equiv m_\ell < m_s$, and are often referred to as “ $N_f = 2 + 1$ ” simulations. Increasingly, simulations also include loops of charm quarks (denoted $N_f = 2 + 1 + 1$ simulations), although the effect of charmed sea quarks on low-energy physics is generically expected to be at the sub-percent level [75–79]. Precision is now reaching the point where isospin breaking effects must be included. To do so without approximation requires simulating with nondegenerate up and down quarks (leading to $N_f = 1 + 1 + 1$ or $1 + 1 + 1 + 1$ simulations) as well as including electromagnetism (as described above). This has been done in Ref. [53]. Alternatively, one can use the perturbative approach mentioned above, expanding about the isospin symmetric theory and working to linear order in α_{EM} and $m_u - m_d$ [60, 80].

We now describe the tuning of m_ℓ , m_s and m_c to their physical values. (For brevity, we ignore isospin violation in the following discussion.) The most commonly used quantities for these tunings are, respectively, m_π , m_K and m_{η_c} . If the scale is being set by m_Ω , then one adjusts the lattice quark masses until the ratios m_π/m_Ω , m_K/m_Ω and m_{η_c}/m_Ω take their physical values. In the past, most calculations needed to extrapolate to the physical value

of m_ℓ (typically using forms based on chiral perturbation theory [ChPT]), while simulating directly at or near to the physical values of m_s and m_c . Present calculations are increasingly done with physical or near physical values of m_ℓ , requiring at most only a short extrapolation or interpolation.

17.1.5.3 Heavy quark masses

The b quark is usually treated only as a valence quark, with no loop effects included. The errors introduced by this approximation can be estimated to be $\sim \alpha_s(m_b)\Lambda_{\text{QCD}}^2/m_b^2$ and are likely to be very small. In the past, the same approximation has been made for the c quark, leading to errors $\sim \alpha_s(m_c)\Lambda_{\text{QCD}}^2/m_c^2$. (See Ref. [75] for a quantitative estimate of the effects of including the charm quark on some low energy physical quantities, and Ref. [81] for similar estimates for B -meson matrix elements.) For high precision, however, dynamical charm quarks are necessary, and some of the most recent simulations now include them.

The b quark mass can be tuned by setting heavy-heavy (\mathcal{T}) or heavy-light (B) meson masses to their experimental values. Consistency between these two determinations provides an important check that the determination of parameters in the heavy quark lattice formulations is being done correctly (see, e.g., Ref. [27,82,83]).

17.1.6 Sources of systematic error

Lattice results have statistical and systematic errors that must be quantified for any calculation in order for the result to be a useful input to phenomenology. The statistical error is due to the use of Monte Carlo importance sampling to evaluate the path integral (a method discussed below). There are, in addition, a number of systematic errors that are always present to some degree in lattice calculations, although the size of any given error depends on the particular quantity under consideration and the parameters of the ensembles being used. The most common lattice errors are reviewed below.

Although not strictly a systematic error, it is important to note that the presence of long autocorrelations in the sequence of lattice configurations generated by the Monte Carlo method can lead to underestimates of statistical errors [84]. It is known that the global topological charge of the gauge fields decorrelates very slowly with certain algorithms [84,85]. The effect of poorly sampling topological charge is expected to be most significant for the pion mass and related quantities [86–88]. This issue becomes more relevant as the precision of the final results increases.

17.1.6.1 Continuum limit

Physical results are obtained in the limit that the lattice spacing a goes to zero. The Symanzik effective theory (SET) determines the scaling of lattice artefacts with a . Most lattice calculations use improved actions with leading discretization errors of $\mathcal{O}(\alpha_s a\Lambda)$, $\mathcal{O}(a^2\Lambda^2)$, or $\mathcal{O}(\alpha_s a^2\Lambda^2)$, where Λ is a typical momentum scale in the system. Knowledge of the scaling of the leading discretization errors allows controlled extrapolation to $a = 0$ when multiple lattice spacings are available, as in current state-of-the-art calculations. Residual errors arise from the exclusion of subleading a dependence from the fits, either that due to prefactors containing powers of $\log(a)$, or from higher powers of a . The former can, in principle, be understood using the SET, and first studies of this in pure gauge QCD have been undertaken [89].

For many quantities the typical momentum scale in the system is $\sim \Lambda_{\text{QCD}} \approx 300$ MeV. Discretization errors are expected to be larger for quantities involving larger scales, for example form factors or decays involving particles with momenta larger than Λ_{QCD} .

17.1.6.2 Infinite volume limit

LQCD calculations are necessarily carried out in finite space-time boxes, leading to departures of physical quantities (masses, decay constants, etc.) from their measured, infinite volume values. These finite-volume shifts are an important systematic that must be estimated and minimized.

Typical lattices are asymmetric, with N_s points in the three spatial directions and N_t in the (Euclidean) temporal direction. The spatial and temporal sizes in physical units are thus $L_s = aN_s$ and $L_t = aN_t$, respectively. (Anisotropic lattice spacings are also sometimes used, as discussed below in Sec. 17.2.2.) Typically,

$L_t \geq 2L_s$, a longer temporal direction being used to allow excited-state contributions to correlators to decay. This means that the dominant impact of using finite volume is from the presence of a finite spatial box.

High-precision LQCD calculations are of quantities involving no more than a single strongly-interacting particle in initial and final states (with the exception of the $K \rightarrow \pi\pi$ decay amplitudes). For such quantities, once the volume exceeds about 2 fm (so that the particle is not “squeezed”), the dominant finite-volume effect comes from virtual pions wrapping around the lattice in the spatial directions. This effect is exponentially suppressed as the volume becomes large, roughly as $\sim \exp(-m_\pi L_s)$, and has been estimated using ChPT [90] or other methods [91]. The estimates suggest that finite volume shifts are sub-percent effects when $m_\pi L_s \gtrsim 4$, and most large-scale simulations use lattices satisfying this condition. This becomes challenging as one approaches the physical pion mass, for which $L_s \gtrsim 5$ fm is required.

Finite volume errors are usually determined by repeating the simulations on two or more different volumes (with other parameters fixed). If different volumes are not available, the ChPT estimate can be used, often inflated to account for the fact that the ChPT calculation is truncated at some order.

In the future, LQCD calculations involving more than a single hadron will become increasingly precise. Examples include the calculation of resonance parameters and the above-mentioned $K \rightarrow \pi\pi$ amplitudes. Finite volume effects are much larger in these cases, with power-law terms (e.g., $1/L_s^3$) in addition to exponential dependence. Indeed, as will be discussed in Sec. 17.2.4, one can use the volume dependence to indirectly extract infinite-volume quantities such as scattering lengths. Doing so, however, requires a set of lattice volumes satisfying $m_\pi L_s \gtrsim 4$ and is thus more challenging than for single-particle quantities.

17.1.6.3 Chiral extrapolation

Until recently, an important source of systematic error in LQCD calculations was the need to extrapolate in m_u and m_d (or, equivalently, in m_π). This extrapolation was usually done using functional forms based on ChPT, or with analytic functions, with the difference between different fits used as an estimate of the systematic error, which was often substantial. Increasingly, however, calculations work directly at, or very close to, the physical quark masses. This either removes entirely, or greatly reduces, the uncertainties in the extrapolation, such that this error is subdominant.

17.1.6.4 Operator matching

Many of the quantities that LQCD can precisely calculate involve hadronic matrix elements of operators from the electroweak Hamiltonian. Examples include the pion and kaon decay constants, semileptonic form factors and the kaon mixing parameter B_K (the latter defined in Eq. (17.13)). The operators in the lattice matrix elements are defined in the lattice regularization scheme. To be used in tests of the Standard Model, however, they must be matched to the continuum regularization scheme in which the corresponding Wilson coefficients have been calculated. The only case in which such matching is not needed is if the operator is a conserved or partially conserved current. Similar matching is also needed for the conversion of lattice bare quark masses to those in the continuum $\overline{\text{MS}}$ scheme.

Several methods are used to calculate the matching factors: perturbation theory (usually to one- or two-loop order), non-perturbative renormalization (NPR) using Landau-gauge quark and gluon external states [92], NPR using gauge-invariant methods based on the Schrödinger functional [93], NPR using gauge-invariant short-distance hadron correlators [94], and NPR using gauge-invariant heavy-heavy correlators [28,95]. The NPR methods replace truncation errors (which can only be approximately estimated) by statistical and systematic errors that can be determined reliably and systematically reduced.

An issue that arises in some of such calculations (e.g., for quark masses and B_K) is that, using NPR with Landau-gauge quark and gluon external states, one ends up with operators regularized in a MOM-like scheme (or a Schrödinger-functional scheme), rather than the $\overline{\text{MS}}$ scheme mostly used for calculating the Wilson coef-

ficients. To make contact with this scheme requires a purely continuum perturbative matching calculation supplemented by the operator product expansion (OPE). (The importance of power corrections is emphasized in [96].) The resultant truncation error of perturbative expansion and OPE can be minimized by pushing up the momentum scale at which the matching is done using step-scaling techniques as part of the NPR calculation [97].

It should also be noted that this final step in the conversion to the $\overline{\text{MS}}$ scheme could be avoided if continuum calculations used a MOM-like scheme or if one imposes a renormalization condition for quantities that are calculable both in the $\overline{\text{MS}}$ scheme and in LQCD, such as the hadron correlators at short distances (see, e.g., Ref. [98]).

17.2 Methods and status

Once the lattice action is chosen, it is straightforward to define the quantum theory using the path integral formulation. The Euclidean-space partition function is

$$Z = \int [dU] \prod_f [dq_f][d\bar{q}_f] e^{-S_g[U] - \sum_f \bar{q}_f (D[U] + m_f) q_f}, \quad (17.4)$$

where link variables are integrated over the SU(3) manifold, q_f and \bar{q}_f are Grassmann (anticommuting) quark and antiquark fields of flavor f , and $D[U]$ is the chosen lattice Dirac operator with m_f the quark mass in lattice units. Integrating out the quark and antiquark fields, one arrives at a form suitable for simulation:

$$Z = \int [dU] e^{-S_g[U]} \prod_f \det(D[U] + m_f). \quad (17.5)$$

The building blocks for calculations are expectation values of multi-local gauge-invariant operators, also known as “correlation functions”,

$$\begin{aligned} \langle \mathcal{O}(U, q, \bar{q}) \rangle &= \\ (1/Z) \int [dU] \prod_f [dq_f][d\bar{q}_f] \mathcal{O}(U, q, \bar{q}) e^{-S_g[U] - \sum_f \bar{q}_f (D[U] + m_f) q_f}. \end{aligned} \quad (17.6)$$

If the operators depend on the (anti-)quark fields q_f and \bar{q}_f , then integrating these fields out leads not only to the fermion determinant but also, through Wick’s theorem, to a series of quark “propagators”, $(D[U] + m_f)^{-1}$, connecting the positions of the fields.

This set-up allows one to choose, by hand, the masses of the quarks in the determinant (the sea quarks) differently from those in the propagators (valence quarks). This is called “partial quenching”, and is used by some calculations as a way of obtaining more data points from which to extrapolate both sea and valence quarks to their physical values.

17.2.1 Monte-Carlo method

Since the number of integration variables U is huge ($N_s^3 \times N_t \times 4 \times 9$), direct numerical integration is impractical and one has to use Monte-Carlo techniques. In this method, one generates a Markov chain of gauge configurations (a “configuration” being the set of U ’s on all links) distributed according to the probability measure $[dU] e^{-S_g[U]} \prod_f \det(D[U] + m_f)$. Once the configurations are generated, expectation values $\langle \mathcal{O}(U, q, \bar{q}) \rangle$ are calculated by averaging over those configurations. In this way the configurations can be used for many different calculations, and there are several large collections of ensembles of configurations (with a range of values of a , lattice sizes and quark masses) that are publicly available through the International Lattice Data Grid (ILDG). As the number of the configurations, N , is increased, the error decreases as $1/\sqrt{N}$.

The most challenging part of the generation of gauge configurations is the need to include the fermion determinant. Direct evaluation of the determinant is not feasible, as it requires $\mathcal{O}((N_s^3 \times N_t)^3)$ computations. Instead, one rewrites it in terms

of “pseudofermion” fields ϕ (auxiliary fermion fields with bosonic statistics). For example, for two degenerate quarks one has

$$\det(D[U] + m_f)^2 = \int [d\phi] e^{-\phi^\dagger (D[U] + m_f)^{-2} \phi}. \quad (17.7)$$

By treating the pseudofermions as additional integration variables in the path integral, one obtains a totally bosonic representation. The price one pays is that the pseudofermion effective action is highly non-local since it includes the inverse Dirac operator $(D[U] + m_f)^{-1}$. Thus, the large sparse matrix $(D[U] + m)$ has to be inverted every time one needs an evaluation of the effective action.

Present simulations generate gauge configurations using the Hybrid Monte Carlo (HMC) algorithm [99], or variants thereof. This algorithm combines molecular dynamics (MD) evolution in a fictitious time (which is also discretized) with a Metropolis “accept-reject” step. It makes a global update of the configuration, and is made exact by the Metropolis step. In its original form it can be used only for two degenerate flavors, but extensions (particularly the rational HMC [100]) are available for single flavors. Considerable speed-up of the algorithms has been achieved over the last two decades using a variety of techniques.

All these algorithms spend the bulk of their computational time on the repeated inversion of $(D[U] + m)$ acting on a source (which is required at every step of the MD evolution). Inversions are done using a variety of iterative algorithms, e.g., the conjugate gradient algorithm. In this class of algorithms, computational cost is proportional to the condition number of the matrix, which is the ratio of maximum and minimum eigenvalues. For $(D[U] + m)$ the smallest eigenvalue is $\approx m$, so the condition number and cost are inversely proportional to the quark mass. This is a major reason why simulations at the physical quark mass are challenging.

Recent algorithmic improvements have significantly reduced this problem. The main idea is to separate different length scales. Since the low eigenvalues of $(D[U] + m)$ are associated with long wavelength quark modes, one may project the problem onto that of a coarse-grained lattice by averaging the field within a block of sublattices and carrying out the inversion on this coarse lattice. The result is then fed back to the original lattice as an efficient *preconditioner* for the iterative solver, and the whole procedure may be nested multiple times. Variants of such methods have been implemented, specifically domain-decomposition [11,12], deflation [101–104] and multigrid [105,106]. They are increasingly used in large-scale lattice simulations.

A practical concern is the inevitable presence of correlations between configurations in the Markov chain. These are characterized by an autocorrelation length in the fictitious MD time. One aims to use configurations separated in MD time by greater than this autocorrelation length. In practice, it is difficult to measure this length accurately, see, e.g., [107], and this leads to some uncertainty in the resulting statistical errors, as well as the possibility of insufficient equilibration.

The computational cost of gauge generation grows with the lattice volume, $V_{\text{lat}} = N_s^3 N_t$, as $V_{\text{lat}}^{1+\delta}$. Here $\delta = 1/4$ for the HMC algorithm [108] and can be reduced slightly using modern variants. Such growth with V_{lat} provides a (time-dependent) limit on the largest lattice volumes that can be simulated. At present, the largest lattices being used have $N_s = 144$ and $N_t = 288$. Typically, one aims to create an ensemble of $\sim 10^3$ statistically independent configurations at each choice of parameters (a , m_q and V_{lat}). For most physical quantities of interest, this is sufficient to make the resulting statistical errors smaller than or comparable to the systematic errors.

In the past, the cost of generating gauge configurations was larger than that of performing “measurements” on those configurations. However, as the number of quantities being calculated and their complexity has increased, the balance has shifted to the point that the total cost of measurements exceeds that of generation.

17.2.2 Two-point functions

One can extract properties of stable hadrons using two-point correlation functions, $\langle O_X(x) O_Y^\dagger(0) \rangle$. Here $O_{X,Y}(x)$ are opera-

tors that have non-zero overlaps with the hadronic state of interest $|H\rangle$, *i.e.* $\langle 0|O_{X,Y}(x)|H\rangle \neq 0$. One usually Fourier transforms in the spatial directions and considers correlators as a function of Euclidean time:

$$C_{XY}(t; \mathbf{p}) = \sum_{\mathbf{x}} \langle O_X(t, \mathbf{x}) O_Y^\dagger(0) \rangle e^{-i\mathbf{p}\cdot\mathbf{x}}. \quad (17.8)$$

(Here and throughout this section all quantities are expressed in dimensionless lattice units, so that, for example, $\mathbf{p} = a\mathbf{p}_{\text{phys}}$.) By inserting a complete set of states having spatial momentum \mathbf{p} , the two-point function can be written as

$$C_{XY}(t; \mathbf{p}) = \sum_{i=0}^{\infty} \frac{1}{2E_i(\mathbf{p})} \langle 0|O_X(0)|H_i(\mathbf{p})\rangle \langle H_i(\mathbf{p})|O_Y^\dagger(0)|0\rangle e^{-E_i(\mathbf{p})t}, \quad (17.9)$$

where the energy of the i -th state $E_i(\mathbf{p})$ appears as an eigenvalue of the time evolution operator e^{-Ht} in the Euclidean time direction. The factor of $1/[2E_i(\mathbf{p})]$ is due to the relativistic normalization used for the states. For large enough t , the dominant contribution is that of the lowest energy state $|H_0(\mathbf{p})\rangle$:

$$C_{XY}(t) \xrightarrow{t \rightarrow \infty} \frac{1}{2E_0(\mathbf{p})} \langle 0|O_X(0)|H_0(\mathbf{p})\rangle \langle H_0(\mathbf{p})|O_Y^\dagger(0)|0\rangle e^{-E_0(\mathbf{p})t}. \quad (17.10)$$

One can thus obtain the energy $E_0(\mathbf{p})$, which equals the hadron mass m_H when $\vec{p} = 0$, and the product of matrix elements $\langle 0|O_X(0)|H_i(\mathbf{p})\rangle \langle H_i(\mathbf{p})|O_Y^\dagger(0)|0\rangle$.

This method can be used to determine the masses of all the stable mesons and baryons by making appropriate choices of operators. For example, if one uses the axial current, $O_X = O_Y = A_\mu = \bar{d}\gamma_\mu\gamma_5 u$, then one can determine m_{π^+} from the rate of exponential fall-off, and in addition the decay constant f_π from the coefficient of the exponential.

The expression given above for the correlator $C_{XY}(t; \mathbf{p})$ shows how, in principle, one can determine the energies of the excited hadron states having the same quantum numbers as the operators $O_{X,Y}$, by fitting the correlation function to a sum of exponentials, which is also important to precisely determine the ground-state exponential. In practice, in order to reliably identify the excited state, one often needs to use a large basis of operators and to adopt the variational approach such as that of Ref. [109]. One can also use an anisotropic lattice in which a_t , the lattice spacing in the time direction, is smaller than its spatial counterpart a_s . Using a combination of these and other technical improvements extensive excited-state spectra have been obtained [110–115].

A complication arises for states with high spins ($j \geq 4$ for bosons) because the spatial rotation group on the lattice is a discrete subgroup of the continuum group $\text{SO}(3)$. This implies that lattice operators, even when chosen to lie in irreducible representations of the lattice rotation group, have overlap with states that have a number of values of j in the continuum limit [116]. For example $j = 0$ operators can also create mesons with $j = 4$. Methods to overcome this problem in practice are available [110, 117] and have been used successfully.

17.2.3 Three-point functions

Hadronic matrix elements needed to calculate semileptonic form factors and neutral meson mixing amplitudes can be computed from three-point correlation functions. We discuss here, as a representative example, the $D \rightarrow K$ amplitude. As in the case of two-point correlation functions one constructs operators O_D and O_K having overlap, respectively, with the D and K mesons. We are interested in calculating the matrix element $\langle K|V_\mu|D\rangle$, with $V_\mu = \bar{c}\gamma_\mu s$ the vector current calculations of this contribution.

To obtain this, we use the three-point correlator

$$C_{KV_\mu D}(t_x, t_y; \mathbf{p}) = \sum_{\mathbf{x}, \mathbf{y}} \langle O_K(t_x, \mathbf{x}) V_\mu(0) O_D^\dagger(t_y, \mathbf{y}) \rangle e^{-i\mathbf{p}\cdot\mathbf{x}}, \quad (17.11)$$

and focus on the limit $t_x \rightarrow \infty$, $t_y \rightarrow -\infty$. In this example we set the D -meson at rest while the kaon carries three-momentum \mathbf{p} . Momentum conservation then implies that the weak operator

V_μ inserts three-momentum $-\mathbf{p}$. Inserting a pair of complete sets of states between each pair of operators, we find

$$C_{KV_\mu D}(t_x, t_y; \mathbf{p}) = \sum_{i,j} \frac{1}{2m_{D_i} 2E_{K_j}(\mathbf{p})} e^{-m_{D_i} t_x - E_{K_j}(\mathbf{p})|t_y|} \times \langle 0|O_K(0)|K_i(\mathbf{p})\rangle \langle K_i(\mathbf{p})|V_\mu(0)|D_j(\mathbf{0})\rangle \langle D_j(\mathbf{0})|O_D^\dagger(0)|0\rangle. \quad (17.12)$$

The matrix element $\langle K_i(\mathbf{p})|V_\mu(0)|D_j(\mathbf{0})\rangle$ can then be extracted, since all other quantities in this expression can be obtained from two-point correlation functions. Typically, one is interested in the weak matrix elements of ground states, such as the lightest pseudoscalar mesons. In the limit of large separation between the three operators in Euclidean time, the three-point correlation function yields the weak matrix element of the transition between ground states.

17.2.4 Scattering amplitudes and resonances

The methods described thus far yield matrix elements involving single, stable particles (where by stable we mean here absolutely stable to strong interaction decays). Most of the particles listed in the Review of Particle Properties are, however, unstable—they are resonances decaying into final states consisting of multiple strongly interacting particles. LQCD simulations cannot directly calculate resonance properties, but methods have been developed to do so indirectly for resonances coupled to two-particle final states in the elastic regime, starting from the seminal work of Lüscher [118].

The difficulty faced by LQCD calculations is that, to obtain resonance properties, or, more generally, scattering phase-shifts, one must calculate multiparticle scattering amplitudes in momentum space and put the external particles on their mass-shells. This requires analytically continuing from Euclidean to Minkowski momenta. Although it is straightforward in LQCD to generalize the methods described above to calculate four- and higher-point correlation functions, one necessarily obtains them at a discrete and finite set of Euclidean momenta. Analytic continuation to $p_E^2 = -m^2$ is then an ill-posed and numerically unstable problem. The same problem arises for single-particle states, but can be largely overcome by picking out the exponential fall-off of the Euclidean correlator, as described above. With a multi-particle state there is no corresponding trick, except for two particles at threshold [119], although recent ideas using smeared correlators and advanced spectral-reconstruction methods offer hope for future progress [120–123].

What LQCD can calculate are the energies of the eigenstates of the QCD Hamiltonian in a finite box. The energies of states containing two stable particles, *e.g.*, two pions, clearly depend on the interactions between the particles. It is possible to invert this dependence and, with plausible assumptions, determine the scattering phase-shifts at a discrete set of momenta from a calculation of the two-particle energy levels for a variety of spatial volumes [118]. This is a challenging calculation, but it has been carried through in several channels with quark masses approaching physical values. Channels studied include $\pi\pi$ (for $I = 2, 1$ and 0), $\bar{K}K$, $K\pi$, $\pi\omega$, $\pi\phi$, KD , DD^* and $B\pi$. For recent comprehensive reviews see [124]. Extensions to nucleon interactions are also being actively studied [125]. The formalism has been generalized to three spinless particles (both identical and nondegenerate) [126], and has been applied to three pions and kaons at maximal isospin [127]. For recent reviews, see [128].

It is also possible to extend the methodology to calculate electroweak decay amplitudes to two particles below the inelastic threshold, *e.g.*, $A(K \rightarrow \pi\pi)$ [129]. Results for both the $\Delta I = 3/2$ and $1/2$ amplitudes with physical quark masses have been obtained [130–132], the former now including a controlled continuum limit [133]. First results for the CP -violating quantity ϵ' have been obtained [131, 132].

Partial extensions of the formalism above the elastic threshold have been worked out, in particular for the case of multiple two-particle channels [134]. Another theoretical extension is to allow the calculation of form factors between a stable particle and a resonance [135], and between two resonances [136]. The former

has been used to calculate the $\gamma\pi \rightarrow \rho$ amplitude, albeit for unphysically large quark masses [137]. Finally, the formalism for using LQCD to calculate electroweak decays or transitions to three particles, e.g. $\gamma^* \rightarrow 3\pi$ and $K \rightarrow 3\pi$, has recently been worked out [138, 139].

While a systematic extension to decays with many multiparticle channels, e.g., hadronic B decays, has, however, yet to be formulated, some interesting new ideas have been recently proposed [140, 141], including a method to compute inclusive decay rates or cross sections [142, 143].

17.2.5 Recent advances

In some physics applications, one is interested in the two-point correlation function $\langle O_X(x)O_Y^\dagger(0) \rangle$ for all values of the separation x , not just its asymptotic form for large separations (which is used to determine the hadron spectrum as sketched above). A topical example is the hadronic vacuum polarization function $\Pi_{\mu\nu}(x) = \langle V_\mu(x)V_\nu(0) \rangle$ and its Fourier transform $\Pi_{\mu\nu}(q^2)$. Since the lattice is in Euclidean space-time, only space-like momenta, $q^2 = -Q^2 < 0$, are accessible. Nevertheless, this quantity is of significant interest. It is related by a dispersion relation to the cross section for $e^+e^- \rightarrow$ hadrons, and is needed for a first-principles calculation of the “hadronic vacuum polarization” contribution to the muon anomalous magnetic moment a_μ . There are a number of lattice calculations of this contribution (see, e.g., Refs. [144–160] following the pioneering work Ref. [161]; see also Ref. [162] for the summary of the status as of March 2020). Since the relevant scale is set by the muon mass m_μ , this quantity is most sensitive to the low-energy region $Q^2 \simeq m_\mu^2$ of $\Pi_{\mu\nu}(-Q^2)$, where the long-range contribution of multibody states become relevant. The lattice calculation is challenging because of this and also because the necessary precision is high (below 1%). Many systematic effects must be carefully studied and controlled in order to achieve this precision, including finite volume errors [163, 164], isospin breaking [156, 165, 166], quark-line disconnected diagrams [150, 156, 166], and QED corrections [156, 166]. Very recently, a lattice calculation has achieved the required sub-percent precision [167], a level that is comparable to the determination from the e^+e^- data. The result is, however, in tension with the data-driven approach, disagreeing with intermediate quantities by as much as 3.7σ . More calculations are anticipated to appear in the near future.

Calculations of the light-by-light scattering contribution to a_μ are also underway. These involve the calculations of four-point correlation functions with various external momenta. Ingenious methods to evaluate the contribution to a_μ have been developed by two groups and the results are in good agreement [168–175].

A summary of the theoretical studies needed to provide the hadronic quantities related to a_μ has been given by the “Muon $g - 2$ Theory Initiative” [162]. This work quotes a conservative average of all results for a_μ available before April 2019, and thus does not include the result from Ref. [167].

There are other processes for which lattice calculations can make a significant contribution to establishing a quantitative understanding. One example is the long-distance contribution to the neutral kaon mass splitting, ΔM_K . This also requires the evaluation of a four-point function, constructed from the two-point functions described above by the insertion of two electroweak Hamiltonians [176, 177]. Rare kaon decays $K \rightarrow \pi\ell^+\ell^-$ and $K \rightarrow \pi\nu\bar{\nu}$ are also important processes for which first lattice studies have appeared [178–183]. Radiative leptonic decays of pion and kaon, $\pi \rightarrow \ell\nu\gamma$ and $K \rightarrow \ell\nu\gamma$, also include two operator insertions, i.e. an electroweak Hamiltonian and an electromagnetic current, and similar techniques developed for the rare decays can be applied. First lattice results have appeared [184, 185].

17.2.6 Status of LQCD simulations

Until the 1990s, most large-scale lattice simulations were limited to the “quenched” approximation, wherein the fermion determinant is omitted from the path integral. While much of the basic methodology was developed in this era, the results obtained had uncontrolled systematic errors and were not suitable for use in placing precision constraints on the Standard Model. During the 1990s, more extensive simulations including the fermion determinant (also known as simulations with “dynam-

ical” fermions) were begun, but with unphysically heavy quark masses ($m_\ell \sim 50 - 100$ MeV), such that the extrapolation to the physical light quark masses was a source of large systematic errors [186]. During the 2000s, advances in both algorithms and computers allowed simulations to reach much smaller quark masses ($m_\ell \sim 10 - 20$ MeV) such that LQCD calculations of selected quantities with all sources of error controlled and small became available. Their results played an important role in constraints on the CKM matrix and other phenomenological analyses. In the last decade, simulations directly at the physical isospin-symmetric light quark masses have become standard, removing the need for a chiral extrapolation and thus significantly reducing the overall error. The present frontier, as noted above, is the inclusion of isospin breaking. This will be needed to push the accuracy of calculations below the percent level.

On a more qualitative level, analytic and numerical results from LQCD have demonstrated that QCD confines color and spontaneously breaks chiral symmetry. Confinement can be seen as a linearly rising potential between heavy quark and anti-quark in the absence of quark loops. Analytically, this can be shown in the strong coupling limit $g_{\text{lat}} \rightarrow \infty$ [1]. At weaker couplings there are precise numerical calculations of the potential that clearly show that this behavior persists in the continuum limit [187–189].

Chiral symmetry breaking was also demonstrated in the strong coupling limit on the lattice [19, 190], and there have been a number of numerical studies showing that this holds also in the continuum limit. The accumulation of low-lying modes of the Dirac operator, which is the analog of Cooper pair condensation in superconductors, has been observed, yielding a determination of the chiral condensate [191–197]. Many relations among physical quantities that can be derived under the assumption of broken chiral symmetry have been confirmed by a number of lattice groups [198].

17.3 Physics applications

In this section we describe the main applications of LQCD that are both computationally mature and relevant for the determination of particle properties.

A general feature to keep in mind is that, since there are many different choices for lattice actions, all of which lead to the same continuum theory, a crucial test is that results for any given quantity are consistent. In many cases, different lattice calculations are completely independent and often have very different systematic errors. Thus, final agreement, if found, is a highly non-trivial check, just as it is for different experimental measurements.

The number, variety and precision of the calculations has progressed to the point that an international collaboration, FLAG, has been formed, which aims to collect all lattice results of relevance for a variety of phenomenologically interesting quantities and provide averages of those results that pass appropriate quality criteria. The averages attempt to account for possible correlations between results (which can arise, for example, if they use common gauge configurations). The quantities considered are those we discuss in this section, with the exception of the hadron spectrum, as well as the intermediate scale-setting quantities discussed earlier. The most recent FLAG review is from 2021 [74] (see also older editions, Refs. [54, 198]). The interested reader can consult this review for very extensive discussions of the details of the calculations and of the sources of systematic errors.

We stress that the results we quote below are those obtained using the physical complement of light quarks (i.e. $N_f = 2 + 1$ or $2 + 1 + 1$ simulations).

17.3.1 Spectrum

The most basic prediction of LQCD is of the hadron spectrum. Once the input parameters are fixed as described in Sec. 17.1.5, the masses or resonance parameters of all other states can be predicted. This includes hadrons composed of light (u , d and s) quarks, as well as heavy-light and heavy-heavy hadrons. It also includes quark-model exotics (e.g., $J^{PC} = 1^{-+}$ mesons) and glueballs. Thus, in principle, LQCD calculations should be able to reproduce many of the experimental results compiled in the Review of Particle Properties. Doing so would test both that the error budgets of LQCD calculations are accurate and that QCD

indeed describes the strong interactions in the low-energy domain. The importance of the latter test can hardly be overstated.

What is the status of this fundamental test? As discussed in Sec. 1.2, LQCD calculations are most straightforward for stable, low-lying hadrons. Calculations of the properties of resonances that can decay into only two particles are more challenging, but are becoming standard in the meson sector, with the frontier being decays involving baryons. As noted above, the formalism for resonances decaying to three particles that are a mix of pions and kaons exists, but has yet to be applied to resonant channels. It is also more technically challenging to calculate masses of flavor singlet states (which can annihilate into purely gluonic intermediate states) than those of flavor non-singlets, although again algorithmic and computational advances have begun to make such calculations accessible, including first calculations that reach physical quark masses [199].

The present status for light hadrons is that fully controlled results are available for the masses of the octet light baryons, while results with less than complete control are available for the decuplet baryon resonances, the vector meson resonances and the η and η' . This is discussed in the “Quark Model” review—see, in particular, Fig. 15.9. In addition, it has been possible to calculate the isospin splitting in light mesons and baryons (due to the up-down mass difference and the incorporation of QED). There are also extensive results for heavy-light (D and B systems) and heavy-heavy (J/ψ and Υ systems). All present results, which are discussed in the “Quark Model” review, are consistent with experimental values, and several predictions have been made. We refer the reader to that review for references to the relevant work.

17.3.2 Decay constants and bag parameters

The pseudoscalar decay constants can be determined from two-point correlation functions involving the axial-vector current, as discussed in Sec. 17.2.2. The decay constant f_P of a meson P is extracted from the weak matrix element involving the axial-vector current using the definition $\langle 0|A_\mu(x)|P(\mathbf{p})\rangle = f_P p_\mu \exp(-ip \cdot x)$, where p_μ is the momentum of P and $A_\mu(x)$ is the axial-vector current. (In practice, results with the smallest errors are obtained using the pseudoscalar density $P(x)$ instead of $A_\mu(x)$.) Since they are among the simplest quantities to calculate, decay constants provide good benchmarks for lattice methods, in addition to being important inputs for flavor physics phenomenology in their own right. Results from several lattice groups for the pion and kaon decay constants now have subpercent errors. The decay constants in the charm and bottom sectors, f_D , f_{D_s} , f_B , and f_{B_s} , have also been calculated to high precision, with subpercent errors for charmed mesons, and percent-level errors for bottom mesons. Lattice results for all of these decay constants are discussed in detail in the review “Leptonic Decays of Charged Pseudoscalar Mesons.”

Another important lattice quantity is the kaon bag parameter, B_K , which is needed to turn the precise measurement of CP -violation in kaon mixing into a constraint on the Standard Model. It is defined by

$$\frac{8}{3} m_K^2 f_K^2 B_K(\mu) = \langle \bar{K}^0 | Q_{\Delta S=2}(\mu) | K^0 \rangle, \quad (17.13)$$

where m_K is the kaon mass, f_K is the kaon decay constant, $Q_{\Delta S=2} = \bar{s}\gamma_\mu(1-\gamma_5)d\bar{s}\gamma_\mu(1-\gamma_5)d$ is the four-quark operator of the effective electroweak Hamiltonian and μ is the renormalization scale. The short distance contribution to the electroweak Hamiltonian can be calculated perturbatively, but the hadronic matrix element parameterized by B_K must be computed using non-perturbative methods. In order to be of use to phenomenology, the renormalization factor of the four-quark operator must be matched to a continuum renormalization scheme, e.g., to $\overline{\text{MS}}$, as described in Sec. 17.1.6.4. Determinations with percent-level precision using different fermion actions and $N_f = 2 + 1$ light sea quarks are now available using DWF [200], staggered fermions [201], DWF valence on staggered sea quarks [202], and Wilson fermions [13]. The results are all consistent, and the present FLAG average is $\hat{B}_K = 0.7625(97)$ [74] (for original papers, see [13, 202–204]).

The bag parameters for B and B_s meson mixing are defined analogously to that for kaon mixing. The B and B_s mesons contain a valence b -quark so that calculations of these quantities must use one of the methods for heavy quarks described above. Calculations have been done using NRQCD [205, 206], the Fermilab formalism [81], and static heavy quarks [207]. All results are consistent. The FLAG averages for the quantities relevant for B_s and B mixing with $N_f = 2 + 1$, which are based on results from Refs. [81, 205, 207], are $f_{B_s} \sqrt{\hat{B}_{B_s}} = 274(8)$ MeV and $f_B \sqrt{\hat{B}_B} = 225(9)$ MeV, with their ratio (which is somewhat better determined) being $\xi = 1.206(17)$. FLAG also quotes an “average” for $N_f = 2+1+1$, which comes from a single calculation [206] and gives $f_{B_s} \sqrt{\hat{B}_{B_s}} = 256(6)$ MeV $f_B \sqrt{\hat{B}_B} = 211(6)$ MeV, and $\xi = 1.216(16)$. These are consistent with the $N_f = 2 + 1$ results at the 2σ level. Errors for quantities involving b quarks are typically larger than those for quantities involving only light quarks, although the difference has steadily decreased in recent years.

For the K , D and B systems, one can also consider the matrix elements of four-fermion operators that arise in beyond-the-standard-model (BSM) theories, which can have a different chiral structure. Knowledge of these matrix elements allows one to constrain the parameters of the BSM theories, and is complementary to direct searches at the LHC. Reliable results are now available from lattice calculations, and are reviewed by FLAG in the case of kaon mixing [74]. Complete results for D and B mixing are presented in Ref. [208, 209] and Ref. [81, 210], respectively.

The results for mixing matrix elements are used in the reviews “The CKM Quark-Mixing Matrix,” and “ $B^0 - \bar{B}^0$ Mixing.”

17.3.3 Form factors ($K \rightarrow \pi l \nu$, $D \rightarrow K l \nu$, $B \rightarrow \pi l \nu$, $B \rightarrow D^{(*)} l \nu$)

Semileptonic decay rates can be used to extract CKM matrix elements once the semileptonic form factors are known from lattice calculations. For example, the matrix element of a pseudoscalar meson P undergoing semileptonic decay to another pseudoscalar meson D is mediated by the vector current, and can be written in terms of form factors as

$$\langle D(p_D) | V_\mu | P(p_P) \rangle = f_+(q^2) (p_D + p_P - \Delta)_\mu + f_0(q^2) \Delta_\mu, \quad (17.14)$$

where $q = p_D - p_P$, $\Delta_\mu = (m_D^2 - m_P^2) q_\mu / q^2$ and V_μ is the quark vector current. The shape of the form factor is typically well determined by experiment, and the value of $f_+(q^2)$ at some reference value of q^2 is needed from the lattice in order to extract CKM matrix elements. Typically, $f_+(q^2)$ dominates the decay rate, since the contribution from $f_0(q^2)$ is suppressed when the final state lepton is light.

The form factor $f_+(0)$ for $K \rightarrow \pi l \nu$ decays is highly constrained by the Ademollo-Gatto theorem [211] and chiral symmetry. Old estimates using chiral perturbation theory combined with quark models quote sub-percent precision [212], though they suffer from some model dependence. Utilizing the constraint from the vector current conservation that $f_+(0)$ is normalized to unity in the limit of degenerate up and strange quark masses, the lattice calculation can be made very precise and has now matched the precision of the phenomenological estimates [213–220]. The present FLAG average (from $N_f = 2 + 1 + 1$ simulations) is $f_+(0) = 0.9698(17)$, based on Refs. [220].

Charm meson semileptonic decays have been calculated by different groups using methods similar to those used for charm decay constants, and results are steadily improving in precision [221–225]. For semileptonic decays involving a bottom quark, one uses HQET or NRQCD to control the discretization errors of the bottom quark. The form factors for the semileptonic decay $B \rightarrow \pi l \nu$ have been calculated in unquenched lattice QCD by a number of groups [226–231]. These B semileptonic form factors are difficult to calculate at low q^2 , *i.e.* when the mass of the B -meson must be balanced by a large pion momentum, in order to transfer a large momentum to the lepton pair. The low q^2 region has large discretization errors and very large statistical errors, while the high q^2 region is much more accessible to the lattice. For experiment, the opposite is true. To combine lattice and experimental results it has proved helpful to use the z -parameter

expansion [232]. This provides a theoretically constrained parameterization of the entire q^2 range, and allows one to obtain $|V_{ub}|$ without model dependence [233, 234].

The semileptonic decays $B \rightarrow D\ell\nu$ and $B \rightarrow D^*\ell\nu$ (and the similar decays $B_s \rightarrow D_s\ell\nu$ and $B_s \rightarrow D_s^*\ell\nu$) can be used to extract $|V_{cb}|$ once the corresponding form factors are known. The lattice calculation is most precise at zero recoil since the bulk of the systematic error cancels for appropriate ratios between $B \rightarrow D^{(*)}$ and $B \rightarrow B$ or $D^{(*)} \rightarrow D^{(*)}$ [235, 236]. The unquenched calculation of the $B \rightarrow D^{(*)}\ell\nu$ form factor at zero recoil has been performed with various formulations for the heavy quark [237–241]. Calculations at non-zero recoil have also been performed to constrain the functional form of the form factor, which can be used to extrapolate the experimental data to the zero-recoil point or to determine $|V_{cb}|$ directly at the non-zero recoil points [242]. Semileptonic decays of the Λ_b baryon can also be used to constrain $|V_{cb}|$ and $|V_{ub}|$ using lattice calculations of the relevant form factors [243, 244].

The rare decays $B \rightarrow K^{(*)}\ell^+\ell^-$ involve matrix elements similar to those needed for semileptonic decays, Eq. (17.14), except that the vector current V_μ is replaced by the operators $\bar{s}\gamma^\mu(1-\gamma_5)b$ or $\bar{s}\sigma^{\mu\nu}(1+\gamma_5)b$. Lattice calculations of the corresponding form factors involve similar techniques to those for the semileptonic form factors. The values of q^2 for which lattice calculations can be done are limited as for B semileptonic decays, and, in addition, the region of $c\bar{c}$ resonances has to be avoided. Recent lattice calculations [230, 245–247] have been used to constrain the standard model and new physics contributions.

The results discussed in this section are used in the reviews “The CKM Quark-Mixing Matrix,” “ V_{ud} , V_{us} , the Cabibbo Angle and CKM Unitarity,” and “Semileptonic b -hadron decays, determination of V_{cb} , V_{ub} .”

17.3.4 Strong gauge coupling

As explained in Sec. 17.1.5.1, for a given lattice action, the choice of bare lattice gauge coupling, g_{lat} , determines the lattice spacing a . If one then calculates a as described in Sec. 17.1.5.1, one knows the strong gauge coupling in the bare lattice scheme at the scale $1/a$, $\alpha_{\text{lat}} = g_{\text{lat}}^2/(4\pi)$. This is not, however, useful for comparing to results for α_s obtained from other inputs, such as deep inelastic scattering or jet shape variables. This is because the latter results give α_s in the $\overline{\text{MS}}$ scheme, which is commonly used in such analyses, and the conversion factor between these two schemes is known to converge extremely poorly in perturbation theory. Instead, one must use a method which directly determines α_s on the lattice in a scheme closer to $\overline{\text{MS}}$.

Several such methods have been used, all following a similar strategy. One calculates a short-distance quantity K both perturbatively (K^{PT}) and non-perturbatively (K^{NP}) on the lattice, and requires equality: $K^{\text{NP}} = K^{\text{PT}} = \sum_{i=0}^n c_i \alpha_s^i$. Solving this equation one obtains α_s at a scale related to the quantity being used. Often, α_s thus obtained is not defined in the conventional $\overline{\text{MS}}$ scheme, and one has to convert among the different schemes using perturbation theory. Unlike for the bare lattice scheme, the required conversion factors are reasonably convergent. As a final step, one uses the renormalization group to run the resulting coupling to a canonical scale (such as M_Z).

In the work of the HPQCD collaboration [248, 249], the short-distance quantities are Wilson loops of several sizes and their ratios. These quantities are perturbatively calculated through $\mathcal{O}(\alpha_s^3)$ using the V -scheme defined through the heavy quark potential. The coefficients of even higher orders are estimated using the data at various values of a . In addition, this work obtains a result for α_s by matching with α_{lat} in a tadpole-improved scheme that improves convergence.

Another choice of short-distance quantities is to use current-current correlators. Appropriate moments of these correlators are ultraviolet finite, and by matching lattice results to the *continuum* perturbative predictions, one can directly extract the $\overline{\text{MS}}$ coupling [250]. The method can be applied for light meson correlators [251–254] as well as heavy meson correlators [38, 249, 255–258]. Yet another choice of short-distance quantity is the static-quark potential, where the lattice result for the potential is compared to perturbative calculations; this method was used to compute α_s

within 2+1 flavor QCD [259–264]. There is also a determination of α_s from a comparison of lattice data for the ghost-gluon coupling with that of perturbation theory [265, 266].

With a definition of α_s given using the Schrödinger functional, one can non-perturbatively control the evolution of α_s to high-energy scales, such as 100 GeV, where the perturbative expansion converges very well. This method developed by the ALPHA collaboration [97] has been applied to 2+1-flavor QCD in [267–269].

The various lattice methods for calculating α_s have significantly different sources of systematic error. The FLAG review [74] reports an estimate $\alpha_{\overline{\text{MS}}}^{(5)}(M_Z) = 0.1184(8)$, based on Refs. [249, 254, 256, 264, 267, 269–271]. A comparison to other phenomenological determinations can be found in the “Quantum Chromodynamics” review.

17.3.5 Quark masses

Once the quark mass parameters are tuned in the lattice action, the remaining task is to convert them to those of the conventional definition. Since the quarks do not appear as asymptotic states due to confinement, the pole mass of the quark propagator is not a physical quantity. Instead, one defines the quark mass after subtracting the ultra-violet divergences in some particular way. The conventional choice is again the $\overline{\text{MS}}$ scheme at a canonical scale such as 2 or 3 GeV. Ratios such as m_c/m_s and m_b/m_c are also useful as they are free from multiplicative renormalization (in a mass-independent scheme).

As discussed in Sec. 17.1.6.4, one must convert the lattice bare quark mass to that in the $\overline{\text{MS}}$ scheme. Older calculations did so directly using perturbation theory; most recent calculations use an intermediate NPR method (e.g., RI/MOM or RI/SMOM) which is then converted to the $\overline{\text{MS}}$ scheme using perturbation theory (see, e.g., [63, 200, 272–276]).

Alternatively, one can use a definition based on the Schrödinger functional, which allows one to evolve the quark mass to a high scale non-perturbatively [277, 278]. In practice, one can reach scales as high as ~ 100 GeV, at which matching to the $\overline{\text{MS}}$ scheme can be reliably calculated in perturbation theory.

Other approaches available for heavy quarks are to match current-current correlators at short distances calculated on the lattice to those obtained in continuum perturbation theory in the $\overline{\text{MS}}$ scheme [38, 65, 249, 255–257], or to use HQET mass relations [275, 279]. This has allowed an accurate determination of m_c and m_b [95, 249, 256].

The ratio method for heavy quarks (discussed earlier) can also be used to determine m_b [280].

Results are summarized in the review of “Quark Masses.”

17.3.6 Other applications

In this review we have concentrated on applications of LQCD that are relevant to the quantities discussed in the Review of Particle Properties. We have not discussed at all several other applications that are being actively pursued by simulations. Here we list the major such applications. The reader can consult the aforementioned texts [2–4] for further details, as well as the proceedings of recent lattice conferences [281], and several recent white papers [282–288].

LQCD can be used, in principle, to simulate QCD at non-zero temperature and density, and in particular to study how confinement and chiral-symmetry breaking are lost as T and μ (the chemical potential) are increased. For example, as T is increased at $\mu = 0$, it is found that, for the physical values of the quark masses, the deconfinement and chiral-symmetry-restoration transitions are smooth crossovers, rather than phase transitions, and that they occur together. This is of relevance to heavy-ion collisions, the early Universe and neutron-star structure. In practice, finite temperature simulations are computationally tractable and relatively mature, while simulations at finite μ suffer from a “sign problem” and are at a rudimentary stage.

Another topic under active investigation is nucleon structure and inter-nucleon interactions. The simplest nucleon matrix elements are calculable with a precision that is now starting to rival that for some mesonic quantities. Of particular interest are those of the axial current (leading to g_A) and of the scalar density (with

$\langle N|\bar{s}s|N\rangle$ needed for dark matter searches), both of which are reviewed by FLAG [54, 74]. Other such matrix elements provide information on the parton distribution functions (PDFs) including their low moments. More recently, methods to directly access PDFs are being developed (see, e.g., Ref. [282] for a recent summary).

Finally, we note that there is much recent interest in studying QCD-like theories with more fermions, possibly in other representations of the gauge group (see, e.g., [284]). The main interest is to find nearly conformal theories which might be candidates for “walking technicolor” models.

17.4 Outlook

While LQCD calculations have made major strides in the last decade, and are now playing an important role in constraining the Standard Model, there are many calculations that could be done in principle but are not yet mature due to limitations in computational resources. As we move to exascale resources (10^{18} floating point operations per second), the list of mature calculations will grow. Examples that we expect to mature in the next few years are results for B meson and Λ_b baryon form factors covering the full range of q^2 ; results for excited hadrons, including quark-model exotics, at close to physical light-quark masses; results for moments of structure functions; results for the simplest nucleon matrix elements; $K \rightarrow \pi\pi$ amplitudes (allowing a prediction of ϵ'/ϵ from the Standard Model); hadronic vacuum polarization contributions to $g_\mu - 2$, the running of α_{EM} and α_s (the status of the first of which was discussed in Sec. 17.2.5); $\pi \rightarrow \gamma\gamma$ and related amplitudes; long-distance contributions to $\bar{K} \leftrightarrow K$ mixing; the light-by-light contribution to $g_\mu - 2$; and determinations of long distance contributions to rare kaon decays such as $K \rightarrow \pi\nu\bar{\nu}$. There will also be steady improvement in the precision attained for the mature quantities discussed above. As already noted, for several of these quantities, attaining the desired precision will ultimately require simulations with $m_u \neq m_d$ and the inclusion of electromagnetic effects.

17.5 Acknowledgments

We are grateful to Jack Laiho for his collaboration on previous editions of this review, and to Christine Davies, Aida El-Khadra, and Andreas Kronfeld for comments and suggestions.

References

- [1] K. G. Wilson, Phys. Rev. **D10**, 2445 (1974).
- [2] T. DeGrand & C. DeTar, “Lattice Methods for Quantum Chromodynamics,” World Scientific (2006).
- [3] C. Gattringer & C.B. Lang, “Quantum Chromodynamics on the Lattice: An Introductory Presentation,” Springer (2009).
- [4] “Modern Perspectives in Lattice QCD: quantum field theory and high performance computing” (Lecture notes of the Les Houches Summer School, Vol. 93) eds. L. Lellouch *et al.*, Oxford Univ. Press. (Aug. 2011).
- [5] W. Zimmermann, in “Lectures on Elementary Particles and Quantum Field Theory”, ed. S. Deser *et al.*, MIT Press, Cambridge, MA (1971); K. Symanzik, Nucl. Phys. **B226**, 187 (1983); K. Symanzik, Nucl. Phys. **B226**, 205 (1983).
- [6] M. Lüscher and P. Weisz, Commun. Math. Phys. **97**, 59 (1985), [Erratum: Commun. Math. Phys. **98**, 433(1985)].
- [7] Y. Iwasaki (1983), UT-HEP-118, [arXiv:1111.7054].
- [8] H. B. Nielsen and M. Ninomiya, Phys. Lett. **105B**, 219 (1981).
- [9] B. Shekholeslami and R. Wohlert, Nucl. Phys. **B259**, 572 (1985).
- [10] K. Jansen *et al.*, Phys. Lett. **B372**, 275 (1996), [hep-lat/9512009].
- [11] M. Lüscher, JHEP **05**, 052 (2003), [hep-lat/0304007].
- [12] M. Lüscher, Comput. Phys. Commun. **156**, 209 (2004), [hep-lat/0310048]; M. Lüscher, Comput. Phys. Commun. **165**, 199 (2005), [hep-lat/0409106]; M. Hasenbusch, Phys. Lett. **B519**, 177 (2001), [hep-lat/0107019]; C. Urbach *et al.*, Comput. Phys. Commun. **174**, 87 (2006), [hep-lat/0506011].
- [13] S. Dürr *et al.*, Phys. Lett. B **705**, 477 (2011), [arXiv:1106.3230].
- [14] N. Ishizuka *et al.*, Phys. Rev. **D92**, 7, 074503 (2015), [arXiv:1505.05289].
- [15] R. Frezzotti *et al.* (Alpha), JHEP **08**, 058 (2001), [hep-lat/0101001].
- [16] R. Frezzotti and G. C. Rossi, JHEP **08**, 007 (2004), [hep-lat/0306014].
- [17] R. Frezzotti and G. C. Rossi, Nucl. Phys. Proc. Suppl. **128**, 193 (2004), [hep-lat/0311008].
- [18] R. Frezzotti and G. C. Rossi, JHEP **10**, 070 (2004), [hep-lat/0407002].
- [19] L. Susskind, Phys. Rev. **D16**, 3031 (1977); N. Kawamoto and J. Smit, Nucl. Phys. B **192**, 100 (1981); H. S. Sharatchandra, H. J. Thun and P. Weisz, Nucl. Phys. B **192**, 205 (1981).
- [20] M. Golterman, PoS **CONFINEMENT8**, 014 (2008), [arXiv:0812.3110].
- [21] C. Bernard, Phys. Rev. **D73**, 114503 (2006), [hep-lat/0603011]; S. R. Sharpe, PoS **LAT2006**, 022 (2006), [hep-lat/0610094].
- [22] J. A. Bailey, Phys. Rev. D **75**, 114505 (2007), [hep-lat/0611023]; Y. Lin *et al.*, Phys. Rev. D **103**, 5, 054510 (2021), [arXiv:2010.10455].
- [23] G. P. Lepage, Phys. Rev. **D59**, 074502 (1999), [hep-lat/9809157].
- [24] A. Bazavov *et al.* (MILC), Rev. Mod. Phys. **82**, 1349 (2010), [arXiv:0903.3598].
- [25] E. Follana *et al.* (HPQCD, UKQCD), Phys. Rev. **D75**, 054502 (2007), [hep-lat/0610092].
- [26] C. T. H. Davies *et al.*, Phys. Rev. **D82**, 114504 (2010), [arXiv:1008.4018].
- [27] C. McNeile *et al.*, Phys. Rev. **D85**, 031503 (2012), [arXiv:1110.4510].
- [28] G. C. Donald *et al.*, Phys. Rev. **D86**, 094501 (2012), [arXiv:1208.2855].
- [29] P. H. Ginsparg and K. G. Wilson, Phys. Rev. **D25**, 2649 (1982).
- [30] P. Hasenfratz, V. Laliena and F. Niedermayer, Phys. Lett. **B427**, 125 (1998), [hep-lat/9801021].
- [31] M. Lüscher, Phys. Lett. **B428**, 342 (1998), [hep-lat/9802011].
- [32] D. B. Kaplan, Phys. Lett. **B288**, 342 (1992), [hep-lat/9206013]; Y. Shamir, Nucl. Phys. **B406**, 90 (1993), [hep-lat/9303005]; Y. Shamir, Nucl. Phys. **B417**, 167 (1994), [hep-lat/9310006].
- [33] H. Neuberger, Phys. Lett. **B417**, 141 (1998), [hep-lat/9707022]; H. Neuberger, Phys. Lett. **B427**, 353 (1998), [hep-lat/9801031].
- [34] A. Borici, NATO Sci. Ser. C **553**, 41 (2000), [hep-lat/9912040].
- [35] A. D. Kennedy (2006), [hep-lat/0607038].
- [36] E. Shintani *et al.* (JLQCD), Phys. Rev. Lett. **101**, 242001 (2008), [arXiv:0806.4222].
- [37] P. A. Boyle *et al.*, JHEP **12**, 008 (2017), [arXiv:1701.02644].
- [38] K. Nakayama, B. Fahy and S. Hashimoto, Phys. Rev. **D94**, 5, 054507 (2016), [arXiv:1606.01002].
- [39] A. Bazavov *et al.*, Phys. Rev. **D98**, 7, 074512 (2018), [arXiv:1712.09262].
- [40] A. Bazavov *et al.* (Fermilab Lattice, MILC, TUMQCD), Phys. Rev. **D98**, 5, 054517 (2018), [arXiv:1802.04248].
- [41] E. Eichten and B. R. Hill, Phys. Lett. **B234**, 511 (1990).
- [42] J. Heitger and R. Sommer (ALPHA), JHEP **02**, 022 (2004), [hep-lat/0310035]; B. Blossier *et al.* (ALPHA), JHEP **12**, 039 (2010), [arXiv:1006.5816].

- [43] B. A. Thacker and G. P. Lepage, Phys. Rev. **D43**, 196 (1991); G. P. Lepage *et al.*, Phys. Rev. **D46**, 4052 (1992), [hep-lat/9205007].
- [44] R. J. Dowdall *et al.* (HPQCD), Phys. Rev. **D85**, 054509 (2012), [arXiv:1110.6887].
- [45] A. X. EL-Khadra, A. S. Kronfeld and P. B. Mackenzie, Phys. Rev. **D55**, 3933 (1997), [hep-lat/9604004].
- [46] S. Aoki, Y. Kuramashi and S.-i. Tominaga, Prog. Theor. Phys. **109**, 383 (2003), [hep-lat/0107009].
- [47] N. H. Christ, M. Li and H.-W. Lin, Phys. Rev. **D76**, 074505 (2007), [hep-lat/0608006].
- [48] Y. Aoki *et al.* (RBC, UKQCD), Phys. Rev. **D86**, 116003 (2012), [arXiv:1206.2554].
- [49] N. H. Christ *et al.*, Phys. Rev. **D91**, 5, 054502 (2015), [arXiv:1404.4670].
- [50] M. B. Oktay and A. S. Kronfeld, Phys. Rev. **D78**, 014504 (2008), [arXiv:0803.0523].
- [51] J. A. Bailey *et al.*, Eur. Phys. J. **C77**, 11, 768 (2017), [arXiv:1701.00345].
- [52] B. Blossier *et al.* (ETM), JHEP **04**, 049 (2010), [arXiv:0909.3187].
- [53] S. Borsanyi *et al.*, Science **347**, 1452 (2015), [arXiv:1406.4088].
- [54] S. Aoki *et al.* (Flavour Lattice Averaging Group) (2019), [arXiv:1902.08191].
- [55] R. Horsley *et al.*, J. Phys. G **43**, 10, 10LT02 (2016), [arXiv:1508.06401].
- [56] R. Horsley *et al.* (CSSM, QCDSF, UKQCD), J. Phys. G **46**, 115004 (2019), [arXiv:1904.02304].
- [57] Z. R. Kordov *et al.* (CSSM/QCDSF/UKQCD), Phys. Rev. D **101**, 3, 034517 (2020), [arXiv:1911.02186].
- [58] S. Aoki *et al.* (HAL QCD), PTEP **2012**, 01A105 (2012), [arXiv:1206.5088].
- [59] T. Ishikawa *et al.*, Phys. Rev. Lett. **109**, 072002 (2012), [arXiv:1202.6018].
- [60] G. M. de Divitiis *et al.* (RM123), Phys. Rev. **D87**, 11, 114505 (2013), [arXiv:1303.4896].
- [61] P. Boyle *et al.*, JHEP **09**, 153 (2017), [arXiv:1706.05293].
- [62] S. Basak *et al.* (MILC), Phys. Rev. D **99**, 3, 034503 (2019), [arXiv:1807.05556].
- [63] D. Hatton *et al.* (HPQCD), Phys. Rev. D **102**, 5, 054511 (2020), [arXiv:2005.01845].
- [64] D. Hatton, C. T. H. Davies and G. P. Lepage, Phys. Rev. D **102**, 9, 094514 (2020), [arXiv:2009.07667].
- [65] D. Hatton *et al.*, Phys. Rev. D **103**, 11, 114508 (2021), [arXiv:2102.09609].
- [66] F. Bloch and A. Nordsieck, Phys. Rev. **52**, 54 (1937).
- [67] N. Carrasco *et al.*, Phys. Rev. **D91**, 7, 074506 (2015), [arXiv:1502.00257].
- [68] D. Giusti *et al.*, Phys. Rev. Lett. **120**, 7, 072001 (2018), [arXiv:1711.06537].
- [69] M. Di Carlo *et al.*, Phys. Rev. D **100**, 3, 034514 (2019), [arXiv:1904.08731].
- [70] C. T. Sachrajda *et al.*, PoS **LATTICE2019**, 162 (2019), [arXiv:1910.07342].
- [71] C.-Y. Seng *et al.*, JHEP **10**, 179 (2020), [arXiv:2009.00459].
- [72] R. Sommer, Nucl. Phys. B **411**, 839 (1994), [hep-lat/9310022].
- [73] M. Lüscher, JHEP **08**, 071 (2010), [Erratum: JHEP 03, 092 (2014)], [arXiv:1006.4518].
- [74] Y. Aoki *et al.* (2021), [arXiv:2111.09849].
- [75] M. Bruno *et al.* (ALPHA), Phys. Rev. Lett. **114**, 10, 102001 (2015), [arXiv:1410.8374].
- [76] F. Knechtli *et al.* (ALPHA), Phys. Lett. **B774**, 649 (2017), [arXiv:1706.04982].
- [77] A. Athenodorou *et al.* (ALPHA), Nucl. Phys. **B943**, 114612 (2019), [arXiv:1809.03383].
- [78] S. Cali, F. Knechtli and T. Korzec, Eur. Phys. J. **C79**, 7, 607 (2019), [arXiv:1905.12971].
- [79] S. Cali *et al.* (2021), [arXiv:2105.12278].
- [80] D. Giusti *et al.*, Phys. Rev. **D95**, 11, 114504 (2017), [arXiv:1704.06561].
- [81] A. Bazavov *et al.* (Fermilab Lattice, MILC), Phys. Rev. **D93**, 11, 113016 (2016), [arXiv:1602.03560].
- [82] R. J. Dowdall *et al.*, Phys. Rev. **D86**, 094510 (2012), [arXiv:1207.5149].
- [83] C. McNeile *et al.*, Phys. Rev. **D86**, 074503 (2012), [arXiv:1207.0994].
- [84] S. Schaefer, R. Sommer and F. Virotta (ALPHA), Nucl. Phys. **B845**, 93 (2011), [arXiv:1009.5228].
- [85] M. Lüscher, PoS **LATTICE2010**, 015 (2010), [arXiv:1009.5877].
- [86] R. Brower *et al.*, Phys. Lett. **B560**, 64 (2003), [hep-lat/0302005].
- [87] S. Aoki *et al.*, Phys. Rev. **D76**, 054508 (2007), [arXiv:0707.0396].
- [88] C. Bernard and D. Toussaint (MILC), Phys. Rev. D **97**, 7, 074502 (2018), [arXiv:1707.05430].
- [89] N. Husung, P. Marquard and R. Sommer, Eur. Phys. J. C **80**, 3, 200 (2020), [arXiv:1912.08498].
- [90] G. Colangelo, S. Dürr and C. Haefeli, Nucl. Phys. **B721**, 136 (2005), [hep-lat/0503014].
- [91] M. Lüscher, Commun. Math. Phys. **104**, 177 (1986).
- [92] G. Martinelli *et al.*, Nucl. Phys. **B445**, 81 (1995), [hep-lat/9411010].
- [93] M. Lüscher *et al.*, Nucl. Phys. **B384**, 168 (1992), [hep-lat/9207009].
- [94] G. Martinelli *et al.*, Phys. Lett. **B411**, 141 (1997), [hep-lat/9705018].
- [95] B. Colquhoun *et al.*, Phys. Rev. **D91**, 7, 074514 (2015), [arXiv:1408.5768].
- [96] D. Hatton *et al.* (HPQCD), Phys. Rev. D **100**, 11, 114513 (2019), [arXiv:1909.00756].
- [97] M. Lüscher *et al.*, Nucl. Phys. **B413**, 481 (1994), [hep-lat/9309005]; M. Della Morte *et al.* (ALPHA), Nucl. Phys. **B713**, 378 (2005), [hep-lat/0411025].
- [98] M. Tomii *et al.* (JLQCD), Phys. Rev. **D94**, 5, 054504 (2016), [arXiv:1604.08702].
- [99] S. Duane *et al.*, Phys. Lett. **B195**, 216 (1987).
- [100] M. A. Clark and A. D. Kennedy, Phys. Rev. Lett. **98**, 051601 (2007), [hep-lat/0608015].
- [101] M. Lüscher, JHEP **07**, 081 (2007), [arXiv:0706.2298].
- [102] M. Lüscher, JHEP **12**, 011 (2007), [arXiv:0710.5417].
- [103] A. Stathopoulos and K. Orginos, SIAM J. Sci. Comput. **32**, 439 (2010), [arXiv:0707.0131].
- [104] P. A. Boyle (2014), [arXiv:1402.2585].
- [105] R. Babich *et al.*, Phys. Rev. Lett. **105**, 201602 (2010), [arXiv:1005.3043].
- [106] A. Frommer *et al.*, SIAM J. Sci. Comput. **36**, A1581 (2014), [arXiv:1303.1377].
- [107] M. Bruno, S. Schaefer and R. Sommer (ALPHA), JHEP **08**, 150 (2014), [arXiv:1406.5363].
- [108] M. Creutz, Phys. Rev. **D38**, 1228 (1988); R. Gupta, G. W. Kilcup and S. R. Sharpe, Phys. Rev. **D38**, 1278 (1988).
- [109] M. Lüscher and U. Wolff, Nucl. Phys. **B339**, 222 (1990).

- [110] J. J. Dudek *et al.*, Phys. Rev. **D82**, 034508 (2010), [arXiv:1004.4930]; J. J. Dudek *et al.*, Phys. Rev. **D83**, 111502 (2011), [arXiv:1102.4299]; R. G. Edwards *et al.*, Phys. Rev. **D84**, 074508 (2011), [arXiv:1104.5152].
- [111] G. P. Engel *et al.* (BGR [Bern-Graz-Regensburg]), Phys. Rev. **D82**, 034505 (2010), [arXiv:1005.1748]; D. Mohler *et al.*, Phys. Rev. Lett. **111**, 22, 222001 (2013), [arXiv:1308.3175].
- [112] M. S. Mahbub *et al.*, Annals Phys. **342**, 270 (2014), [arXiv:1310.6803].
- [113] J. Bulava *et al.*, Nucl. Phys. **B910**, 842 (2016), [arXiv:1604.05593].
- [114] R. Brett *et al.*, Nucl. Phys. **B932**, 29 (2018), [arXiv:1802.03100].
- [115] B. Hörz and A. Hanlon, Phys. Rev. Lett. **123**, 14, 142002 (2019), [arXiv:1905.04277].
- [116] J. E. Mandula, G. Zweig and J. Govaerts, Nucl. Phys. **B228**, 91 (1983); J. E. Mandula and E. Shpiz, Nucl. Phys. **B232**, 180 (1984).
- [117] H. B. Meyer and M. J. Teper, Nucl. Phys. **B658**, 113 (2003), [hep-lat/0212026].
- [118] M. Lüscher, Commun. Math. Phys. **105**, 153 (1986); M. Lüscher, Nucl. Phys. **B364**, 237 (1991).
- [119] L. Maiani and M. Testa, Phys. Lett. **B245**, 585 (1990).
- [120] M. T. Hansen, H. B. Meyer and D. Robaina, Phys. Rev. **D96**, 9, 094513 (2017), [arXiv:1704.08993].
- [121] M. Hansen, A. Lupo and N. Tantalo, Phys. Rev. **D99**, 9, 094508 (2019), [arXiv:1903.06476].
- [122] J. Bulava and M. T. Hansen, Phys. Rev. D **100**, 3, 034521 (2019), [arXiv:1903.11735].
- [123] M. Bruno and M. T. Hansen (2020), [arXiv:2012.11488].
- [124] R. A. Briceño, J. J. Dudek and R. D. Young, Rev. Mod. Phys. **90**, 2, 025001 (2018), [arXiv:1706.06223]; N. Brambilla *et al.* (2019), [arXiv:1907.07583].
- [125] M. J. Savage, Prog. Part. Nucl. Phys. **67**, 140 (2012), [arXiv:1110.5943]; T. Inoue *et al.* (HAL QCD), Phys. Rev. **C91**, 1, 011001 (2015), [arXiv:1408.4892]; B. Hörz *et al.*, Phys. Rev. C **103**, 1, 014003 (2021), [arXiv:2009.11825].
- [126] K. Polejaeva and A. Rusetsky, Eur. Phys. J. **A48**, 67 (2012), [arXiv:1203.1241]; R. A. Briceño and Z. Davoudi, Phys. Rev. **D87**, 9, 094507 (2013), [arXiv:1212.3398]; M. T. Hansen and S. R. Sharpe, Phys. Rev. **D90**, 11, 116003 (2014), [arXiv:1408.5933]; M. T. Hansen and S. R. Sharpe, Phys. Rev. **D92**, 11, 114509 (2015), [arXiv:1504.04248]; R. Briceño, M. T. Hansen and S. R. Sharpe, Phys. Rev. **D95**, 7, 074510 (2017), [arXiv:1701.07465]; H. W. Hammer, J. Y. Pang and A. Rusetsky, JHEP **10**, 115 (2017), [arXiv:1707.02176]; R. A. Briceño, M. T. Hansen and S. R. Sharpe, Phys. Rev. **D99**, 1, 014516 (2019), [arXiv:1810.01429]; M. Mai and M. Döring, Eur. Phys. J. **A53**, 12, 240 (2017), [arXiv:1709.08222]; M. T. Hansen, F. Romero-López and S. R. Sharpe, JHEP **07**, 047 (2020), [Erratum: JHEP 02, 014 (2021)], [arXiv:2003.10974]; T. D. Blanton and S. R. Sharpe, Phys. Rev. D **103**, 5, 054503 (2021), [arXiv:2011.05520].
- [127] T. D. Blanton, F. Romero-López and S. R. Sharpe, Phys. Rev. Lett. **124**, 3, 032001 (2020), [arXiv:1909.02973]; C. Culver *et al.*, Phys. Rev. D **101**, 11, 114507 (2020), [arXiv:1911.09047]; A. Alexandru *et al.*, Phys. Rev. D **102**, 11, 114523 (2020), [arXiv:2009.12358].
- [128] M. T. Hansen and S. R. Sharpe (2019), [arXiv:1901.00483]; M. Mai, M. Döring and A. Rusetsky, Eur. Phys. J. ST **230**, 6, 1623 (2021), [arXiv:2103.00577].
- [129] L. Lellouch and M. Lüscher, Commun. Math. Phys. **219**, 31 (2001), [hep-lat/0003023].
- [130] T. Blum *et al.*, Phys. Rev. Lett. **108**, 141601 (2012), [arXiv:1111.1699]; T. Blum *et al.*, Phys. Rev. **D86**, 074513 (2012), [arXiv:1206.5142].
- [131] Z. Bai *et al.* (RBC, UKQCD), Phys. Rev. Lett. **115**, 21, 212001 (2015), [arXiv:1505.07863].
- [132] R. Abbott *et al.* (RBC, UKQCD), Phys. Rev. D **102**, 5, 054509 (2020), [arXiv:2004.09440].
- [133] T. Blum *et al.*, Phys. Rev. **D91**, 7, 074502 (2015), [arXiv:1502.00263].
- [134] V. Bernard *et al.*, JHEP **01**, 019 (2011), [arXiv:1010.6018]; M. Doring *et al.*, Eur. Phys. J. **A47**, 139 (2011), [arXiv:1107.3988]; M. T. Hansen and S. R. Sharpe, Phys. Rev. **D86**, 016007 (2012), [arXiv:1204.0826]; R. A. Briceño and Z. Davoudi, Phys. Rev. **D88**, 9, 094507 (2013), [arXiv:1204.1110].
- [135] R. Briceño, M. T. Hansen and A. Walker-Loud, Phys. Rev. **D91**, 3, 034501 (2015), [arXiv:1406.5965].
- [136] R. Briceño and M. T. Hansen, Phys. Rev. **D94**, 1, 013008 (2016), [arXiv:1509.08507].
- [137] R. Briceño *et al.*, Phys. Rev. **D93**, 11, 114508 (2016), [arXiv:1604.03530].
- [138] F. Müller and A. Rusetsky, JHEP **03**, 152 (2021), [arXiv:2012.13957].
- [139] M. T. Hansen, F. Romero-López and S. R. Sharpe, JHEP **04**, 113 (2021), [arXiv:2101.10246].
- [140] D. Agadjanov *et al.*, JHEP **06**, 043 (2016), [arXiv:1603.07205].
- [141] S. Hashimoto, PTEP **2017**, 5, 053B03 (2017), [arXiv:1703.01881].
- [142] P. Gambino and S. Hashimoto, Phys. Rev. Lett. **125**, 3, 032001 (2020), [arXiv:2005.13730].
- [143] H. Fukaya *et al.*, Phys. Rev. D **102**, 11, 114516 (2020), [arXiv:2010.01253].
- [144] X. Feng *et al.*, Phys. Rev. Lett. **107**, 081802 (2011), [arXiv:1103.4818].
- [145] P. Boyle *et al.*, Phys. Rev. **D85**, 074504 (2012), [arXiv:1107.1497].
- [146] M. Della Morte *et al.*, JHEP **03**, 055 (2012), [arXiv:1112.2894].
- [147] F. Burger *et al.* (ETM), JHEP **02**, 099 (2014), [arXiv:1308.4327].
- [148] B. Chakraborty *et al.* (HPQCD), Phys. Rev. **D89**, 11, 114501 (2014), [arXiv:1403.1778].
- [149] F. Burger *et al.*, Eur. Phys. J. C **76**, 8, 464 (2016), [arXiv:1501.05110].
- [150] B. Chakraborty *et al.*, Phys. Rev. **D93**, 7, 074509 (2016), [arXiv:1512.03270].
- [151] B. Chakraborty *et al.*, Phys. Rev. **D96**, 3, 034516 (2017), [arXiv:1601.03071].
- [152] T. Blum *et al.* (RBC/UKQCD), JHEP **04**, 063 (2016), [Erratum: JHEP05, 034(2017)], [arXiv:1602.01767].
- [153] S. Borsanyi *et al.*, Phys. Rev. **D96**, 7, 074507 (2017), [arXiv:1612.02364].
- [154] M. Della Morte *et al.*, JHEP **10**, 020 (2017), [arXiv:1705.01775].
- [155] S. Borsanyi *et al.* (Budapest-Marseille-Wuppertal), Phys. Rev. Lett. **121**, 2, 022002 (2018), [arXiv:1711.04980].
- [156] T. Blum *et al.* (RBC, UKQCD), Phys. Rev. Lett. **121**, 2, 022003 (2018), [arXiv:1801.07224].
- [157] D. Giusti, F. Sanfilippo and S. Simula, Phys. Rev. **D98**, 11, 114504 (2018), [arXiv:1808.00887].
- [158] C. T. H. Davies *et al.* (Fermilab Lattice, HPQCD, MILC), Phys. Rev. D **101**, 3, 034512 (2020), [arXiv:1902.04223].
- [159] A. Gérardin *et al.*, Phys. Rev. D **100**, 1, 014510 (2019), [arXiv:1904.03120].
- [160] C. Aubin *et al.*, Phys. Rev. D **101**, 1, 014503 (2020), [arXiv:1905.09307].

- [161] T. Blum, Phys. Rev. Lett. **91**, 052001 (2003), [hep-lat/0212018].
- [162] T. Aoyama *et al.*, Phys. Rept. **887**, 1 (2020), [arXiv:2006.04822].
- [163] T. Izubuchi *et al.* (PACS), Phys. Rev. D **98**, 5, 054505 (2018), [arXiv:1805.04250].
- [164] E. Shintani and Y. Kuramashi (PACS), Phys. Rev. D **100**, 3, 034517 (2019), [arXiv:1902.00885].
- [165] B. Chakraborty *et al.* (Fermilab Lattice, HPQCD, MILC), Phys. Rev. Lett. **120**, 15, 152001 (2018), [arXiv:1710.11212].
- [166] D. Giusti *et al.*, Phys. Rev. D **99**, 11, 114502 (2019), [arXiv:1901.10462].
- [167] S. Borsanyi *et al.*, Nature **593**, 7857, 51 (2021), [arXiv:2002.12347].
- [168] T. Blum *et al.*, Phys. Rev. Lett. **114**, 1, 012001 (2015), [arXiv:1407.2923].
- [169] T. Blum *et al.*, Phys. Rev. **D93**, 1, 014503 (2016), [arXiv:1510.07100].
- [170] J. Green *et al.*, Phys. Rev. Lett. **115**, 22, 222003 (2015), [arXiv:1507.01577].
- [171] T. Blum *et al.*, Phys. Rev. Lett. **118**, 2, 022005 (2017), [arXiv:1610.04603].
- [172] T. Blum *et al.*, Phys. Rev. **D96**, 3, 034515 (2017), [arXiv:1705.01067].
- [173] T. Blum *et al.*, “Hadronic Light-by-Light Scattering Contribution to the Muon Anomalous Magnetic Moment from Lattice QCD,” (2020), [arXiv:1911.08123].
- [174] E.-H. Chao *et al.*, Eur. Phys. J. C **80**, 9, 869 (2020), [arXiv:2006.16224].
- [175] E.-H. Chao *et al.*, Eur. Phys. J. C **81**, 7, 651 (2021), [arXiv:2104.02632].
- [176] Z. Bai *et al.*, Phys. Rev. Lett. **113**, 112003 (2014), [arXiv:1406.0916].
- [177] N. H. Christ *et al.*, Phys. Rev. D **91**, 11, 114510 (2015), [arXiv:1504.01170].
- [178] N. H. Christ *et al.* (RBC, UKQCD), Phys. Rev. **D92**, 9, 094512 (2015), [arXiv:1507.03094].
- [179] N. H. Christ *et al.* (RBC, UKQCD), Phys. Rev. **D93**, 11, 114517 (2016), [arXiv:1605.04442].
- [180] N. H. Christ *et al.*, Phys. Rev. **D94**, 11, 114516 (2016), [arXiv:1608.07585].
- [181] Z. Bai *et al.*, Phys. Rev. Lett. **118**, 25, 252001 (2017), [arXiv:1701.02858].
- [182] Z. Bai *et al.*, Phys. Rev. **D98**, 7, 074509 (2018), [arXiv:1806.11520].
- [183] N. H. Christ *et al.* (RBC, UKQCD), Phys. Rev. D **100**, 11, 114506 (2019), [arXiv:1910.10644].
- [184] C. Kane *et al.*, PoS **LATTICE2019**, 134 (2019), [arXiv:1907.00279].
- [185] A. Desiderio *et al.*, Phys. Rev. D **103**, 1, 014502 (2021), [arXiv:2006.05358].
- [186] C. Bernard *et al.*, Nucl. Phys. Proc. Suppl. **119**, 170 (2003), [hep-lat/0209086].
- [187] S. Perantonis and C. Michael, Nucl. Phys. **B347**, 854 (1990).
- [188] G. S. Bali and K. Schilling, Phys. Rev. **D46**, 2636 (1992).
- [189] S. Necco and R. Sommer, Nucl. Phys. **B622**, 328 (2002), [hep-lat/0108008].
- [190] J. M. Blairon *et al.*, Nucl. Phys. **B180**, 439 (1981).
- [191] H. Fukaya *et al.* (JLQCD), Phys. Rev. Lett. **104**, 122002 (2010), [Erratum: Phys. Rev. Lett.105,159901(2010)], [arXiv:0911.5555].
- [192] H. Fukaya *et al.* (JLQCD, TWQCD), Phys. Rev. **D83**, 074501 (2011), [arXiv:1012.4052].
- [193] L. Giusti and M. Lüscher, JHEP **03**, 013 (2009), [arXiv:0812.3638].
- [194] K. Cichy, E. Garcia-Ramos and K. Jansen, JHEP **10**, 175 (2013), [arXiv:1303.1954].
- [195] G. P. Engel *et al.*, Phys. Rev. Lett. **114**, 11, 112001 (2015), [arXiv:1406.4987].
- [196] G. P. Engel *et al.*, Phys. Rev. **D91**, 5, 054505 (2015), [arXiv:1411.6386].
- [197] G. Cossu *et al.*, PTEP **2016**, 9, 093B06 (2016), [arXiv:1607.01099].
- [198] S. Aoki *et al.*, Eur. Phys. J. **C77**, 2, 112 (2017), [arXiv:1607.00299].
- [199] G. S. Bali *et al.* (2021), [arXiv:2106.05398].
- [200] T. Blum *et al.* (RBC, UKQCD), Phys. Rev. **D93**, 7, 074505 (2016), [arXiv:1411.7017].
- [201] B. J. Choi *et al.* (SWME), Phys. Rev. **D93**, 1, 014511 (2016), [arXiv:1509.00592].
- [202] J. Laiho and R. S. Van de Water, PoS **LATTICE2011**, 293 (2011), [arXiv:1112.4861].
- [203] T. Blum *et al.* (RBC, UKQCD), Phys. Rev. D **93**, 7, 074505 (2016), [arXiv:1411.7017].
- [204] B. J. Choi *et al.* (SWME), Phys. Rev. D **93**, 1, 014511 (2016), [arXiv:1509.00592].
- [205] E. Gamiz *et al.* (HPQCD), Phys. Rev. **D80**, 014503 (2009), [arXiv:0902.1815].
- [206] R. J. Dowdall *et al.*, Phys. Rev. D **100**, 9, 094508 (2019), [arXiv:1907.01025].
- [207] Y. Aoki *et al.*, Phys. Rev. **D91**, 11, 114505 (2015), [arXiv:1406.6192].
- [208] N. Carrasco *et al.* (ETM), Phys. Rev. D **92**, 3, 034516 (2015), [arXiv:1505.06639].
- [209] A. Bazavov *et al.*, Phys. Rev. **D97**, 3, 034513 (2018), [arXiv:1706.04622].
- [210] C. T. H. Davies *et al.* (HPQCD), Phys. Rev. Lett. **124**, 8, 082001 (2020), [arXiv:1910.00970].
- [211] M. Ademollo and R. Gatto, Phys. Rev. Lett. **13**, 264 (1964).
- [212] H. Leutwyler and M. Roos, Z. Phys. **C25**, 91 (1984).
- [213] P. A. Boyle *et al.*, Phys. Rev. Lett. **100**, 141601 (2008), [arXiv:0710.5136].
- [214] V. Lubicz *et al.* (ETM), Phys. Rev. **D80**, 111502 (2009), [arXiv:0906.4728]; V. Lubicz *et al.* (ETM), PoS **LATTICE2010**, 316 (2010), [arXiv:1012.3573].
- [215] P. A. Boyle *et al.* (RBC-UKQCD), Eur. Phys. J. **C69**, 159 (2010), [arXiv:1004.0886].
- [216] A. Bazavov *et al.*, Phys. Rev. **D87**, 073012 (2013), [arXiv:1212.4993].
- [217] T. Kaneko *et al.* (JLQCD), PoS **LATTICE2012**, 111 (2012), [arXiv:1211.6180].
- [218] P. A. Boyle *et al.*, JHEP **08**, 132 (2013), [arXiv:1305.7217].
- [219] P. A. Boyle *et al.* (RBC/UKQCD), JHEP **06**, 164 (2015), [arXiv:1504.01692].
- [220] N. Carrasco *et al.*, Phys. Rev. **D93**, 11, 114512 (2016), [arXiv:1602.04113]; A. Bazavov *et al.* (Fermilab Lattice, MILC), Phys. Rev. D **99**, 11, 114509 (2019), [arXiv:1809.02827].
- [221] H. Na *et al.*, Phys. Rev. **D82**, 114506 (2010), [arXiv:1008.4562].
- [222] H. Na *et al.*, Phys. Rev. **D84**, 114505 (2011), [arXiv:1109.1501].
- [223] V. Lubicz *et al.* (ETM), Phys. Rev. **D96**, 5, 054514 (2017), [Erratum: Phys. Rev. D99, 099902(2019)], [arXiv:1706.03017].
- [224] T. Kaneko *et al.* (JLQCD), EPJ Web Conf. **175**, 13007 (2018), [arXiv:1711.11235].

- [225] B. Chakraborty *et al.* (2021), [arXiv:2104.09883].
- [226] E. Dalgic *et al.*, Phys. Rev. **D73**, 074502 (2006), [Erratum: Phys. Rev. D75,119906(2007)], [hep-lat/0601021].
- [227] J. M. Flynn *et al.*, Phys. Rev. **D91**, 7, 074510 (2015), [arXiv:1501.05373].
- [228] J. A. Bailey *et al.* (Fermilab Lattice, MILC), Phys. Rev. **D92**, 1, 014024 (2015), [arXiv:1503.07839].
- [229] B. Colquhoun *et al.*, Phys. Rev. **D93**, 3, 034502 (2016), [arXiv:1510.07446].
- [230] Z. Gelzer *et al.*, EPJ Web Conf. **175**, 13024 (2018), [arXiv:1710.09442].
- [231] B. Colquhoun, S. Hashimoto and T. Kaneko, PoS **LATTICE2018**, 274 (2018), [arXiv:1811.00227].
- [232] C. Bourrely, B. Machet and E. de Rafael, Nucl. Phys. **B189**, 157 (1981); C. G. Boyd, B. Grinstein and R. F. Lebed, Phys. Rev. Lett. **74**, 4603 (1995), [hep-ph/9412324]; T. Becher and R. J. Hill, Phys. Lett. **B633**, 61 (2006), [hep-ph/0509090]; C. Bourrely, I. Caprini and L. Lellouch, Phys. Rev. **D79**, 013008 (2009), [Erratum: Phys. Rev. D82, 099902(2010)], [arXiv:0807.2722].
- [233] M. C. Arnesen *et al.*, Phys. Rev. Lett. **95**, 071802 (2005), [hep-ph/0504209].
- [234] J. A. Bailey *et al.*, Phys. Rev. **D79**, 054507 (2009), [arXiv:0811.3640].
- [235] S. Hashimoto *et al.*, Phys. Rev. **D61**, 014502 (1999), [hep-ph/9906376].
- [236] S. Hashimoto *et al.*, Phys. Rev. **D66**, 014503 (2002), [hep-ph/0110253].
- [237] C. Bernard *et al.*, Phys. Rev. **D79**, 014506 (2009), [arXiv:0808.2519].
- [238] J. A. Bailey *et al.* (Fermilab Lattice, MILC), Phys. Rev. **D89**, 11, 114504 (2014), [arXiv:1403.0635].
- [239] J. Harrison, C. Davies and M. Wingate (HPQCD), Phys. Rev. **D97**, 5, 054502 (2018), [arXiv:1711.11013].
- [240] E. McLean *et al.*, Phys. Rev. **D99**, 11, 114512 (2019), [arXiv:1904.02046].
- [241] T. Bhattacharya *et al.* (LANL/SWME), PoS **LATTICE2018**, 283 (2018).
- [242] J. A. Bailey *et al.* (MILC), Phys. Rev. **D92**, 3, 034506 (2015), [arXiv:1503.07237]; H. Na *et al.* (HPQCD), Phys. Rev. **D92**, 5, 054510 (2015), [Erratum: Phys. Rev. D93, 19906(2016)], [arXiv:1505.03925]; T. Kaneko *et al.* (JLQCD), PoS **LATTICE2018**, 311 (2018), [arXiv:1811.00794]; E. McLean *et al.*, Phys. Rev. D **101**, 7, 074513 (2020), [arXiv:1906.00701]; J. Harrison and C. T. H. Davies (HPQCD) (2021), [arXiv:2105.11433]; A. Bazavov *et al.* (Fermilab Lattice, MILC) (2021), [arXiv:2105.14019].
- [243] W. Detmold, C. Lehner and S. Meinel, Phys. Rev. **D92**, 3, 034503 (2015), [arXiv:1503.01421].
- [244] W. Detmold and S. Meinel, Phys. Rev. **D93**, 7, 074501 (2016), [arXiv:1602.01399].
- [245] R. R. Horgan *et al.*, Phys. Rev. **D89**, 9, 094501 (2014), [arXiv:1310.3722].
- [246] J. A. Bailey *et al.*, Phys. Rev. **D93**, 2, 025026 (2016), [arXiv:1509.06235].
- [247] D. Du *et al.*, Phys. Rev. **D93**, 3, 034005 (2016), [arXiv:1510.02349].
- [248] C. T. H. Davies *et al.* (HPQCD), Phys. Rev. **D78**, 114507 (2008), [arXiv:0807.1687].
- [249] C. McNeile *et al.*, Phys. Rev. **D82**, 034512 (2010), [arXiv:1004.4285].
- [250] A. Bochkarev and P. de Forcrand, Nucl. Phys. B **477**, 489 (1996), [hep-lat/9505025].
- [251] E. Shintani *et al.*, Phys. Rev. **D82**, 7, 074505 (2010), [Erratum: Phys. Rev. D89, 099903(2014)], [arXiv:1002.0371].
- [252] R. J. Hudspith *et al.*, Mod. Phys. Lett. **A31**, 32, 1630037 (2016).
- [253] R. J. Hudspith *et al.* (2018), [arXiv:1804.10286].
- [254] S. Cali *et al.*, Phys. Rev. Lett. **125**, 242002 (2020), [arXiv:2003.05781].
- [255] I. Allison *et al.* (HPQCD), Phys. Rev. **D78**, 054513 (2008), [arXiv:0805.2999].
- [256] B. Chakraborty *et al.*, Phys. Rev. **D91**, 5, 054508 (2015), [arXiv:1408.4169].
- [257] Y. Maezawa and P. Petreczky, Phys. Rev. **D94**, 3, 034507 (2016), [arXiv:1606.08798].
- [258] P. Petreczky and J. H. Weber, Phys. Rev. D **100**, 3, 034519 (2019), [arXiv:1901.06424].
- [259] Q. Mason *et al.* (HPQCD, UKQCD), Phys. Rev. Lett. **95**, 052002 (2005), [hep-lat/0503005].
- [260] A. Bazavov *et al.*, Phys. Rev. **D86**, 114031 (2012), [arXiv:1205.6155].
- [261] A. Bazavov *et al.*, Phys. Rev. **D90**, 7, 074038 (2014), [arXiv:1407.8437].
- [262] F. Karbstein, M. Wagner and M. Weber, Phys. Rev. **D98**, 11, 114506 (2018), [arXiv:1804.10909].
- [263] H. Takaura *et al.*, JHEP **04**, 155 (2019), [arXiv:1808.01643].
- [264] A. Bazavov *et al.* (TUMQCD), Phys. Rev. D **100**, 11, 114511 (2019), [arXiv:1907.11747].
- [265] B. Blossier *et al.*, Phys. Rev. **D85**, 034503 (2012), [arXiv:1110.5829]; B. Blossier *et al.*, Phys. Rev. Lett. **108**, 262002 (2012), [arXiv:1201.5770].
- [266] S. Zafeiropoulos *et al.*, Phys. Rev. Lett. **122**, 16, 162002 (2019), [arXiv:1902.08148].
- [267] S. Aoki *et al.* (PACS-CS), JHEP **10**, 053 (2009), [arXiv:0906.3906].
- [268] P. Fritzsche *et al.*, PoS **LATTICE2014**, 291 (2014), [arXiv:1411.7648].
- [269] M. Bruno *et al.* (ALPHA), Phys. Rev. Lett. **119**, 10, 102001 (2017), [arXiv:1706.03821].
- [270] C. Ayala, X. Lobregat and A. Pineda, JHEP **09**, 016 (2020), [arXiv:2005.12301].
- [271] K. Maltman *et al.*, Phys. Rev. D **78**, 114504 (2008), [arXiv:0807.2020].
- [272] S. Dürr *et al.*, Phys. Lett. **B701**, 265 (2011), [arXiv:1011.2403].
- [273] S. Dürr *et al.*, JHEP **08**, 148 (2011), [arXiv:1011.2711].
- [274] A. T. Lytle *et al.* (HPQCD), Phys. Rev. D **98**, 1, 014513 (2018), [arXiv:1805.06225].
- [275] A. Bazavov *et al.* (Fermilab Lattice, MILC, TUMQCD), Phys. Rev. D **98**, 5, 054517 (2018), [arXiv:1802.04248].
- [276] C. Alexandrou *et al.* (2021), [arXiv:2104.13408].
- [277] S. Capitani *et al.*, Nucl. Phys. **B544**, 669 (1999), [Erratum: Nucl. Phys. B582, 762(2000)], [hep-lat/9810063].
- [278] M. Bruno *et al.* (ALPHA), PoS **LATTICE2018**, 220 (2019), [arXiv:1903.04094].
- [279] J. Komijani, JHEP **08**, 062 (2017), [arXiv:1701.00347]; N. Brambilla *et al.* (TUMQCD), Phys. Rev. D **97**, 3, 034503 (2018), [arXiv:1712.04983].
- [280] A. Bussonne *et al.* (ETM), Phys. Rev. **D93**, 11, 114505 (2016), [arXiv:1603.04306].
- [281] *Proceedings, 36th International Symposium on Lattice Field Theory*, volume PoS **LATTICE2018** (2019), URL <https://pos.sissa.it/334/>.
- [282] W. Detmold *et al.* (USQCD) (2019), [arXiv:1904.09512].
- [283] A. S. Kronfeld *et al.* (USQCD) (2019), [arXiv:1904.09931].
- [284] R. C. Brower *et al.* (USQCD) (2019), [arXiv:1904.09964].
- [285] C. Lehner *et al.* (USQCD) (2019), [arXiv:1904.09479].

[286] A. Bazavov *et al.* (USQCD) (2019), [arXiv:1904.09951].

[287] V. Cirigliano *et al.* (USQCD) (2019), [arXiv:1904.09704].

[288] B. Joó *et al.* (USQCD) (2019), [arXiv:1904.09725].

18. Structure Functions

Revised August 2021 by E.C. Aschenauer (BNL), R.S. Thorne (UCL) and R. Yoshida (ANL).

18.1 Deep inelastic scattering

High-energy lepton-nucleon scattering plays a key role in determining the partonic structure of the proton. The process $\ell N \rightarrow \ell' X$ is illustrated in Fig. 18.1. The filled circle in this figure represents the internal structure of the proton which can be expressed in terms of structure functions.

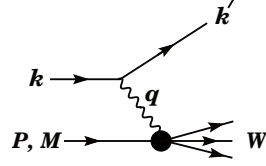


Figure 18.1: Kinematic quantities for the description of deep inelastic scattering. The quantities k and k' are the four-momenta of the incoming and outgoing leptons, P is the four-momentum of a nucleon with mass M , and W is the mass of the recoiling system X . The exchanged particle is a γ , W^\pm , or Z ; it transfers four-momentum $q = k - k'$ to the nucleon.

Invariant quantities:

$\nu = \frac{q \cdot P}{M} = E - E'$ is the lepton's energy loss in the nucleon rest frame (in earlier literature sometimes $\nu = q \cdot P$). Here, E and E' are the initial and final lepton energies in the nucleon rest frame.

$Q^2 = -q^2 = 2(E E' - \vec{k} \cdot \vec{k}') - m_\ell^2 - m_{\ell'}^2$, where m_ℓ ($m_{\ell'}$) is the initial (final) lepton mass. If $E E' \sin^2(\theta/2) \gg m_\ell^2, m_{\ell'}^2$, then

$\approx 4E E' \sin^2(\theta/2)$, where θ is the lepton's scattering angle with respect to the lepton beam direction.

$x = \frac{Q^2}{2M\nu}$ where, in the parton model, x is the fraction of the nucleon's momentum carried by the struck quark. Beyond leading order the equation remains the definition of x , but this is no longer identical to nucleon momentum fraction.

$y = \frac{q \cdot P}{k \cdot P} = \frac{\nu}{E}$ is the fraction of the lepton's energy lost in the nucleon rest frame.

$W^2 = (P + q)^2 = M^2 + 2M\nu - Q^2$ is the mass squared of the system X recoiling against the scattered lepton.

$s = (k + P)^2 = \frac{Q^2}{xy} + M^2 + m_\ell^2$ is the center-of-mass energy squared of the lepton-nucleon system.

The process in Fig. 18.1 is called deep ($Q^2 \gg M^2$) inelastic ($W^2 \gg M^2$) scattering (DIS). In what follows, the masses of the initial and scattered leptons, m_ℓ and $m_{\ell'}$, are neglected.

18.1.1 DIS cross sections

The double-differential cross section for deep inelastic scattering can be expressed in terms of kinematic variables in several ways.

$$\frac{d^2\sigma}{dx dy} = x(s - M^2) \frac{d^2\sigma}{dx dQ^2} = \frac{2\pi M\nu}{E'} \frac{d^2\sigma}{d\Omega_{N\text{rest}} dE'} \quad (18.1)$$

In lowest-order perturbation theory, the cross section for the scattering of polarized leptons on polarized nucleons can be expressed in terms of the products of leptonic and hadronic tensors associated with the coupling of the exchanged bosons at the upper and lower vertices in Fig. 18.1 (see Refs. [1–4])

$$\frac{d^2\sigma}{dx dy} = \frac{2\pi y \alpha^2}{Q^4} \sum_j \eta_j L_j^{\mu\nu} W_{\mu\nu}^j \quad (18.2)$$

For neutral-current processes, the summation is over $j = \gamma, Z$ and γZ representing photon and Z exchange and the interference

between them, whereas for charged-current interactions there is only W exchange, $j = W$. (For transverse nucleon polarization, there is a dependence on the azimuthal angle of the scattered lepton.) The lepton tensor $L_{\mu\nu}$ is associated with the coupling of the exchange boson to the leptons. For incoming leptons of charge $e = \pm 1$ and helicity $\lambda = \pm 1$,

$$\begin{aligned} L_{\mu\nu}^\gamma &= 2(k_\mu k'_\nu + k'_\mu k_\nu - (k \cdot k' - m_\ell^2)g_{\mu\nu} - i\lambda \varepsilon_{\mu\nu\alpha\beta} k^\alpha k'^\beta), \\ L_{\mu\nu}^{\gamma Z} &= (g_V^e + e\lambda g_A^e) L_{\mu\nu}^\gamma, \quad L_{\mu\nu}^Z = (g_V^e + e\lambda g_A^e)^2 L_{\mu\nu}^\gamma, \\ L_{\mu\nu}^W &= (1 + e\lambda)^2 L_{\mu\nu}^\gamma, \end{aligned} \quad (18.3)$$

where $g_V^e = -\frac{1}{2} + 2\sin^2\theta_W$, $g_A^e = -\frac{1}{2}$.

Although here the helicity basis is adopted, an alternative approach is to express the tensors in Eq. (18.3) in terms of the polarization of the lepton.

The factors η_j in Eq. (18.2) denote the ratios of the corresponding propagators and couplings to the photon propagator and coupling squared

$$\begin{aligned} \eta_\gamma &= 1; \quad \eta_{\gamma Z} = \left(\frac{G_F M_Z^2}{2\sqrt{2}\pi\alpha} \right) \left(\frac{Q^2}{Q^2 + M_Z^2} \right); \\ \eta_Z &= \eta_{\gamma Z}^2; \quad \eta_W = \frac{1}{2} \left(\frac{G_F M_W^2}{4\pi\alpha} \frac{Q^2}{Q^2 + M_W^2} \right)^2. \end{aligned} \quad (18.4)$$

The hadronic tensor, which describes the interaction of the appropriate electroweak currents with the target nucleon, is given by

$$W_{\mu\nu} = \frac{1}{4\pi} \int d^4z e^{iq \cdot z} \langle P, S | [J_\mu^\dagger(z), J_\nu(0)] | P, S \rangle, \quad (18.5)$$

where J_α is the hadronic contribution to the electromagnetic, or weak current and S denotes the nucleon-spin 4-vector, with $S^2 = -M^2$ and $S \cdot P = 0$.

18.2 Structure functions of the proton

The structure functions are defined in terms of the hadronic tensor (see Refs. [1–3])

$$\begin{aligned} W_{\mu\nu} &= \left(-g_{\mu\nu} + \frac{q_\mu q_\nu}{q^2} \right) F_1(x, Q^2) + \frac{\hat{P}_\mu \hat{P}_\nu}{P \cdot q} F_2(x, Q^2) \\ &- i\varepsilon_{\mu\nu\alpha\beta} \frac{q^\alpha P^\beta}{2P \cdot q} F_3(x, Q^2) \\ &+ i\varepsilon_{\mu\nu\alpha\beta} \frac{q^\alpha}{P \cdot q} \left[S^\beta g_1(x, Q^2) + \left(S^\beta - \frac{S \cdot q}{P \cdot q} P^\beta \right) g_2(x, Q^2) \right] \\ &+ \frac{1}{P \cdot q} \left[\frac{1}{2} (\hat{P}_\mu \hat{S}_\nu + \hat{S}_\mu \hat{P}_\nu) - \frac{S \cdot q}{P \cdot q} \hat{P}_\mu \hat{P}_\nu \right] g_3(x, Q^2) \\ &+ \frac{S \cdot q}{P \cdot q} \left[\frac{\hat{P}_\mu \hat{P}_\nu}{P \cdot q} g_4(x, Q^2) + \left(-g_{\mu\nu} + \frac{q_\mu q_\nu}{q^2} \right) g_5(x, Q^2) \right] \end{aligned} \quad (18.6)$$

where

$$\hat{P}_\mu = P_\mu - \frac{P \cdot q}{q^2} q_\mu, \quad \hat{S}_\mu = S_\mu - \frac{S \cdot q}{q^2} q_\mu \quad (18.7)$$

In [2], the definition of $W_{\mu\nu}$ with $\mu \leftrightarrow \nu$ is adopted, which changes the sign of the $\varepsilon_{\mu\nu\alpha\beta}$ terms in Eq. (18.6), although the formulae given below are unchanged. Ref. [1] tabulates the relation between the structure functions defined in Eq. (18.6) and other choices available in the literature.

The cross sections for neutral- and charged-current deep inelastic scattering on unpolarized nucleons can be written in terms of

the structure functions in the generic form

$$\begin{aligned} \frac{d^2\sigma^i}{dx dy} &= \frac{4\pi\alpha^2}{xyQ^2} \eta^i \left\{ \left(1 - y - \frac{x^2 y^2 M^2}{Q^2} \right) F_2^i \right. \\ &\quad \left. + y^2 x F_1^i \mp \left(y - \frac{y^2}{2} \right) x F_3^i \right\}, \end{aligned} \quad (18.8)$$

where $i = \text{NC, CC}$ corresponds to neutral-current ($eN \rightarrow eX$) or charged-current ($eN \rightarrow \nu X$ or $\nu N \rightarrow eX$) processes, respectively. For incoming neutrinos, $L_{\mu\nu}^W$ of Eq. (18.3) is still true, but with e, λ corresponding to the outgoing charged lepton. In the last term of Eq. (18.8), the $-$ sign is taken for an incoming e^+ or $\bar{\nu}$ and the $+$ sign for an incoming e^- or ν . The factor $\eta^{\text{NC}} = 1$ for unpolarized e^\pm beams, whereas

$$\eta^{\text{CC}} = (1 \pm \lambda)^2 \eta_W \quad (18.9)$$

with \pm for ℓ^\pm ; and where λ is the helicity of the incoming lepton and η_W is defined in Eq. (18.4); for incoming neutrinos $\eta^{\text{CC}} = 4\eta_W$. The CC structure functions, which derive exclusively from W exchange, are

$$F_1^{\text{CC}} = F_1^W, \quad F_2^{\text{CC}} = F_2^W, \quad xF_3^{\text{CC}} = xF_3^W. \quad (18.10)$$

The NC structure functions $F_2^\gamma, F_2^{\gamma Z}, F_2^Z$ are, for $e^\pm N \rightarrow e^\pm X$, given by [5],

$$F_2^{\text{NC}} = F_2^\gamma - (g_V^e \pm \lambda g_A^e) \eta_{\gamma Z} F_2^{\gamma Z} + (g_V^e{}^2 + g_A^e{}^2 \pm 2\lambda g_V^e g_A^e) \eta_Z F_2^Z \quad (18.11)$$

and similarly for F_1^{NC} , whereas

$$xF_3^{\text{NC}} = -(g_A^e \pm \lambda g_V^e) \eta_{\gamma Z} xF_3^{\gamma Z} + [2g_V^e g_A^e \pm \lambda(g_V^e{}^2 + g_A^e{}^2)] \eta_Z xF_3^Z. \quad (18.12)$$

The polarized cross-section difference

$$\Delta\sigma = \sigma(\lambda_n = -1, \lambda_\ell) - \sigma(\lambda_n = 1, \lambda_\ell), \quad (18.13)$$

where λ_ℓ, λ_n are the helicities (± 1) of the incoming lepton and nucleon, respectively, may be expressed in terms of the five structure functions $g_{1, \dots, 5}(x, Q^2)$ of Eq. (18.6). Explicitly,

$$\begin{aligned} \frac{d^2\Delta\sigma^i}{dx dy} &= \frac{8\pi\alpha^2}{xyQ^2} \eta^i \left\{ -\lambda_\ell y \left(2 - y - 2x^2 y^2 \frac{M^2}{Q^2} \right) x g_1^i \right. \\ &\quad \left. + \lambda_\ell 4x^3 y^2 \frac{M^2}{Q^2} g_2^i + 2x^2 y \frac{M^2}{Q^2} \left(1 - y - x^2 y^2 \frac{M^2}{Q^2} \right) g_3^i \right. \\ &\quad \left. - \left(1 + 2x^2 y \frac{M^2}{Q^2} \right) \left[\left(1 - y - x^2 y^2 \frac{M^2}{Q^2} \right) g_4^i + xy^2 g_5^i \right] \right\} \end{aligned} \quad (18.14)$$

with $i = \text{NC or CC}$ as before. The Eq. (18.13) corresponds to the difference of antiparallel minus parallel spins of the incoming particles for e^- or ν initiated reactions, but the difference of parallel minus antiparallel for e^+ or $\bar{\nu}$ initiated processes. For longitudinal nucleon polarization, the contributions of g_2 and g_3 are suppressed by powers of M^2/Q^2 . These structure functions give an unsuppressed contribution to the cross section for transverse polarization [1], but in this case the cross-section difference vanishes as $M/Q \rightarrow 0$.

Because the same tensor structure occurs in the spin-dependent and spin-independent parts of the hadronic tensor of Eq. (18.6) in the $M^2/Q^2 \rightarrow 0$ limit, the differential cross-section difference of Eq. (18.14) may be obtained from the differential cross section Eq. (18.8) by replacing

$$F_1 \rightarrow -g_5, \quad F_2 \rightarrow -g_4, \quad F_3 \rightarrow 2g_1, \quad (18.15)$$

and multiplying by two, since the total cross section is the average over the initial-state polarizations. In this limit, Eq. (18.8) and Eq. (18.14) may be written in the form

$$\begin{aligned} \frac{d^2\sigma^i}{dx dy} &= \frac{2\pi\alpha^2}{xyQ^2} \eta^i \left[Y_+ F_2^i \mp Y_- x F_3^i - y^2 F_L^i \right], \\ \frac{d^2\Delta\sigma^i}{dx dy} &= \frac{4\pi\alpha^2}{xyQ^2} \eta^i \left[-Y_+ g_4^i \mp Y_- 2x g_1^i + y^2 g_L^i \right], \end{aligned} \quad (18.16)$$

with $i = \text{NC or CC}$, where $Y_\pm = 1 \pm (1 - y)^2$ and

$$F_L^i = F_2^i - 2x F_1^i, \quad g_L^i = g_4^i - 2x g_5^i. \quad (18.17)$$

In the naive quark-parton model, the analogy with the Callan-Gross relations $[6]F_L^i = 0$, are the Dicus relations $[7]g_L^i = 0$. Therefore, there are only two independent polarized structure functions: g_1 (parity conserving) and g_5 (parity violating), in analogy with the unpolarized structure functions F_1 and F_3 .

18.2.1 Structure functions in the quark parton model

In the naive quark-parton model [8, 9], contributions to the structure functions F^i and g^i can be expressed in terms of the quark distribution functions $q(x, Q^2)$ of the proton, where $q = u, \bar{u}, d, \bar{d}$ etc. The quantity $q(x, Q^2)dx$ is the number of quarks (or antiquarks) of designated flavor that carry a momentum fraction between x and $x + dx$ of the proton's momentum in a frame in which the proton momentum is large. One of the most striking predictions of the quark-parton model is that the structure functions F_i, g_i scale, i.e., $F_i(x, Q^2) \rightarrow F_i(x)$ in the Bjorken limit that Q^2 and $\nu \rightarrow \infty$ with x fixed [10]. This property is related to the assumption that the transverse momentum of the partons in the infinite-momentum frame of the proton is small.

For the neutral-current processes $ep \rightarrow eX$,

$$\begin{aligned} [F_2^\gamma, F_2^{\gamma Z}, F_2^Z] &= x \sum_q [e_q^2, 2e_q g_V^q, g_V^q{}^2 + g_A^q{}^2] (q + \bar{q}), \\ [F_3^\gamma, F_3^{\gamma Z}, F_3^Z] &= \sum_q [0, 2e_q g_A^q, 2g_V^q g_A^q] (q - \bar{q}), \\ [g_1^\gamma, g_1^{\gamma Z}, g_1^Z] &= \frac{1}{2} \sum_q [e_q^2, 2e_q g_V^q, g_V^q{}^2 + g_A^q{}^2] (\Delta q + \Delta \bar{q}), \\ [g_5^\gamma, g_5^{\gamma Z}, g_5^Z] &= \sum_q [0, e_q g_A^q, g_V^q g_A^q] (\Delta \bar{q} - \Delta q), \end{aligned} \quad (18.18)$$

where $g_V^q = \pm \frac{1}{2} - 2e_q \sin^2 \theta_W$ and $g_A^q = \pm \frac{1}{2}$, with \pm according to whether q is a $u-$ or $d-$ type quark respectively. The quantity Δq is the difference $q \uparrow - q \downarrow$ of the distributions with the quark spin parallel and antiparallel to the proton spin.

For the charged-current processes $e^- p \rightarrow \nu X$ and $\bar{\nu} p \rightarrow e^+ X$, the structure functions are:

$$\begin{aligned} F_2^{W^-} &= 2x(u + \bar{d} + \bar{s} + c \dots), \\ F_3^{W^-} &= 2(u - \bar{d} - \bar{s} + c \dots), \\ g_1^{W^-} &= (\Delta u + \Delta \bar{d} + \Delta \bar{s} + \Delta c \dots), \\ g_5^{W^-} &= (-\Delta u + \Delta \bar{d} + \Delta \bar{s} - \Delta c \dots), \end{aligned} \quad (18.19)$$

where only the active flavors have been kept and where CKM mixing has been neglected. For $e^+ p \rightarrow \bar{\nu} X$ and $\nu p \rightarrow e^- X$, the structure functions F^{W^+}, g^{W^+} are obtained by the flavor interchanges $d \leftrightarrow u, s \leftrightarrow c$ in the expressions for F^{W^-}, g^{W^-} . The structure functions for scattering on a neutron are obtained from those of the proton by the interchange $u \leftrightarrow d$. For both the neutral- and charged-current processes, the quark-parton model predicts $2xF_1^i = F_2^i$ and $g_4^i = 2xg_5^i$.

Neglecting masses, the structure functions g_2 and g_3 contribute only to scattering from transversely polarized nucleons, and have no simple interpretation in terms of the quark-parton model. They arise from off-diagonal matrix elements

$\langle P, \lambda' | [J_\mu^\dagger(z), J_\nu(0)] | P, \lambda \rangle$, where the proton helicities satisfy $\lambda' \neq \lambda$. In fact, the leading-twist contributions to both g_2 and g_3 are both twist-2 and twist-3, which contribute at the same order of Q^2 . The Wandzura-Wilczek relation [11] expresses the twist-2 part of g_2 in terms of g_1 as

$$g_2^i(x) = -g_1^i(x) + \int_x^1 \frac{dy}{y} g_1^i(y). \quad (18.20)$$

However, the twist-3 component of g_2 is unknown. Similarly, there is a relation expressing the twist-2 part of g_3 in terms of g_4 . A complete set of relations, including M^2/Q^2 effects, can be found in [12].

18.2.2 Structure functions and QCD

In QCD, there are perturbative corrections to the partonic cross sections defining structure functions. Also, the radiation of hard gluons from the quarks violates the assumption that the transverse momentum of the partons is small, leading to logarithmic scaling violations, which are particularly large at small x , see Fig. 18.2. The radiation of gluons produces the evolution of the partons and structure functions. As Q^2 increases, more and more gluons are radiated, which in turn split into $q\bar{q}$ pairs. This process leads both to the softening of the initial quark momentum distributions and to the growth of the gluon density and the $q\bar{q}$ sea as x decreases.

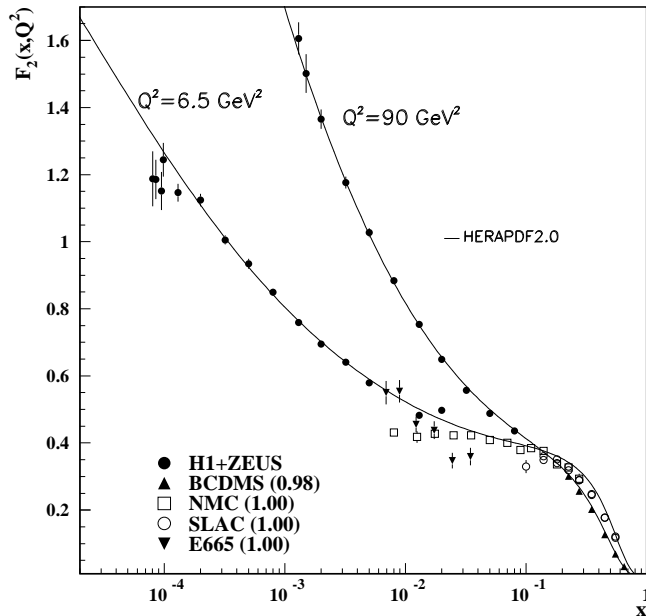


Figure 18.2: The proton structure function F_2^p given at two Q^2 values (6.5 GeV² and 90 GeV²), which exhibit scaling at the ‘pivot’ point $x \sim 0.14$. See the captions in Fig. 18.10 and Fig. 18.12 for the references of the data. The various data sets have been renormalized by the factors shown in brackets in the key to the plot, which were globally determined in a previous HERAPDF analysis [13]. The curves were obtained using the PDFs from the HERAPDF analysis [14]. In practice, data for the reduced cross section, $F_2(x, Q^2) - (y^2/Y_+)F_L(x, Q^2)$, were fitted, rather than F_2 and F_L separately. The agreement between data and theory at low Q^2 and x can be improved by a positive higher-twist correction to $F_L(x, Q^2)$ [15, 16] (see Fig. 8 of Ref. [16]), or small- x resummation [17, 18].

For $Q^2 \gg M^2$, the structure functions satisfy the factorization theorem [19],

$$F_i = \sum_a C_i^a \otimes f_a + \mathcal{O}(M^2/Q^2), \quad (18.21)$$

where \otimes denotes the convolution integral

$$C \otimes f = \int_x^1 \frac{dy}{y} C(y) f\left(\frac{x}{y}\right), \quad (18.22)$$

and where the coefficient functions C_i^a , where $a = g$ or q , are given as a power series in α_s . The scale-dependent parton distribution $f_a(x, \mu^2)$ corresponds, at a given x , to the density of parton a in the proton integrated over transverse momentum k_t up to the factorization scale μ . Typically, μ is the scale of the probe Q . For parton distributions x always refers to the nucleon momentum fraction of the parton, whereas for structure functions it retains the definition in Sec. 18.1. The parton evolution in μ is described in QCD by a DGLAP equation (see Refs. [20–23]) which has the schematic form

$$\frac{\partial f_a}{\partial \ln \mu^2} \sim \frac{\alpha_s(\mu^2)}{2\pi} \sum_b (P_{ab} \otimes f_b), \quad (18.23)$$

where the P_{ab} , which describe the parton splitting $b \rightarrow a$, are also given as a power series in α_s . Although perturbative QCD can predict, via Eq. (18.23), the evolution of the parton distribution functions from a particular scale, μ_0 , these DGLAP equations cannot predict them *a priori* at any particular μ_0 . Thus they must be measured at a starting point μ_0 before the predictions of QCD can be compared to the data at other scales, μ . In general, all observables involving a hard hadronic interaction (such as structure functions) can be expressed as a convolution of calculable, process-dependent coefficient functions and these universal parton distributions, e.g. Eq. (18.21).

Table 18.1: The main processes relevant to global PDF analyses, ordered in three groups: fixed-target experiments, HERA and the $p\bar{p}$ Tevatron / pp LHC. For each process we give an indication of their dominant partonic subprocesses, the primary partons which are probed and the approximate range of x constrained by the data. This list expands as more processes are measured and calculated with sufficient precision.

Process	Subprocess	Partons	x range
$\ell^\pm \{p, n\} \rightarrow \ell^\pm X$	$\gamma^* q \rightarrow q$	q, \bar{q}, g	$x \gtrsim 0.01$
$\ell^\pm n/p \rightarrow \ell^\pm X$	$\gamma^* d/u \rightarrow d/u$	d/u	$x \gtrsim 0.01$
$pp \rightarrow \mu^+ \mu^- X$	$u\bar{u}, d\bar{d} \rightarrow \gamma^*$	\bar{q}	$0.015 \lesssim x \lesssim 0.35$
$pn/ppp \rightarrow \mu^+ \mu^- X$	$(u\bar{d})/(u\bar{u}) \rightarrow \gamma^*$	\bar{d}/\bar{u}	$0.015 \lesssim x \lesssim 0.35$
$\nu(\bar{\nu}) N \rightarrow \mu^- (\mu^+) X$	$W^* q \rightarrow q'$	q, \bar{q}	$0.01 \lesssim x \lesssim 0.5$
$\nu N \rightarrow \mu^- \mu^+ X$	$W^* s \rightarrow c$	s	$0.01 \lesssim x \lesssim 0.2$
$\bar{\nu} N \rightarrow \mu^+ \mu^- X$	$W^* \bar{s} \rightarrow \bar{c}$	\bar{s}	$0.01 \lesssim x \lesssim 0.2$
$e^\pm p \rightarrow e^\pm X$	$\gamma^* q \rightarrow q$	q, \bar{q}, g	$10^{-4} \lesssim x \lesssim 0.1$
$e^+ p \rightarrow \bar{\nu} X$	$W^+ \{d, s\} \rightarrow \{u, c\}$	d, s	$x \gtrsim 0.01$
$e^\pm p \rightarrow e^\pm c\bar{X}, e^\pm b\bar{b}X$	$\gamma^* c \rightarrow c, \gamma^* g \rightarrow c\bar{c}$	c, b, g	$10^{-4} \lesssim x \lesssim 0.01$
$e^\pm p \rightarrow \text{jet}+X$	$\gamma^* g \rightarrow q\bar{q}$	g	$0.01 \lesssim x \lesssim 0.1$
$p\bar{p}, pp \rightarrow \text{jet}(\text{dijet})+X$	$gg, qq, qg \rightarrow 2j$	g, q	$0.00005 \lesssim x \lesssim 0.5$
$p\bar{p} \rightarrow (W^\pm \rightarrow \ell^\pm \nu) X$	$ud \rightarrow W^+, \bar{u}\bar{d} \rightarrow W^-$	$u, d, s, \bar{u}, \bar{d}, \bar{s}$	$x \gtrsim 0.05$
$pp \rightarrow (W^\pm \rightarrow \ell^\pm \nu) X$	$u\bar{d} \rightarrow W^+, d\bar{u} \rightarrow W^-$	$u, d, s, \bar{u}, \bar{d}, \bar{s}, g$	$x \gtrsim 0.001$
$p\bar{p}(pp) \rightarrow (Z \rightarrow \ell^+ \ell^-) X$	$uu, dd, \dots (u\bar{u}, \dots) \rightarrow Z$	$u, d, s, \dots (g)$	$x \gtrsim 0.001$
$pp \rightarrow W^- c, W^+ \bar{c}$	$gs \rightarrow W^- c$	s, \bar{s}	$x \sim 0.01$
$pp \rightarrow (\gamma^* \rightarrow \ell^+ \ell^-) X$	$u\bar{u}, d\bar{d}, \dots \rightarrow \gamma^*$	\bar{q}, g	$x \gtrsim 10^{-5}$
$pp \rightarrow (\gamma^* \rightarrow \ell^+ \ell^-) X$	$u\gamma, d\gamma, \dots \rightarrow \gamma^*$	γ	$x \gtrsim 10^{-2}$
$pp \rightarrow b\bar{b} X, t\bar{t} X$	$gg \rightarrow b\bar{b}, t\bar{t}$	g	$x \gtrsim 10^{-5}, 10^{-2}$
$pp \rightarrow t(\bar{t}) X,$	$bu(\bar{b}d) \rightarrow t(d\bar{t}u)$	$b, d/u$	$x \gtrsim 10^{-2}$
$pp \rightarrow \text{exclusive } J/\psi, \Upsilon$	$\gamma^*(gg) \rightarrow J/\psi, \Upsilon$	g	$x \gtrsim 10^{-5}, 10^{-4}$
$pp \rightarrow \gamma X$	$gq \rightarrow \gamma q, g\bar{q} \rightarrow \gamma \bar{q}$	g	$x \gtrsim 0.005$

It is often convenient to write the evolution equations in terms of the gluon, non-singlet (q^{NS}) and singlet (q^S) quark distributions, such that

$$q^{NS} = q_i - \bar{q}_i \quad (\text{or } q_i - q_j), \quad q^S = \sum_i (q_i + \bar{q}_i). \quad (18.24)$$

The non-singlet distributions have non-zero values of flavor quantum numbers, such as isospin and baryon number. The DGLAP evolution equations then take the form

$$\begin{aligned} \frac{\partial q^{NS}}{\partial \ln \mu^2} &= \frac{\alpha_s(\mu^2)}{2\pi} P_{qq} \otimes q^{NS}, \\ \frac{\partial}{\partial \ln \mu^2} \begin{pmatrix} q^S \\ g \end{pmatrix} &= \frac{\alpha_s(\mu^2)}{2\pi} \begin{pmatrix} P_{qq} & 2n_f P_{qg} \\ P_{gq} & P_{gg} \end{pmatrix} \otimes \begin{pmatrix} q^S \\ g \end{pmatrix}, \end{aligned} \quad (18.25)$$

where P are splitting functions that describe the probability of a given parton splitting into two others, and n_f is the number of (active) quark flavors. The leading-order Altarelli-Parisi [22] splitting functions are

$$P_{qq} = \frac{4}{3} \left[\frac{1+x^2}{(1-x)_+} \right] = \frac{4}{3} \left[\frac{1+x^2}{(1-x)_+} \right] + 2\delta(1-x), \quad (18.26)$$

$$P_{qg} = \frac{1}{2} [x^2 + (1-x)^2], \quad P_{gq} = \frac{4}{3} \left[\frac{1+(1-x)^2}{x} \right], \quad (18.27)$$

$$P_{gg} = 6 \left[\frac{1-x}{x} + x(1-x) + \frac{x}{(1-x)_+} \right] + \left[\frac{11}{2} - \frac{n_f}{3} \right] \delta(1-x), \quad (18.28)$$

where the notation $[F(x)]_+$ defines a distribution such that for any sufficiently regular test function, $f(x)$,

$$\int_0^1 dx f(x) [F(x)]_+ = \int_0^1 dx (f(x) - f(1)) F(x). \quad (18.29)$$

In general, the splitting functions can be expressed as a power series in α_s . The series contains both terms proportional to $\ln \mu^2$ and to $\ln(1/x)$ and $\ln(1-x)$. The leading-order DGLAP evolution sums up the $(\alpha_s \ln \mu^2)^n$ contributions, while at next-to-leading order (NLO) the sum over the $\alpha_s (\alpha_s \ln \mu^2)^{n-1}$ terms is included [24, 25]. The NNLO contributions to the splitting functions and the DIS coefficient functions are also all known [26–28], as are the N³LO corrections to the coefficient functions [29].

In the kinematic region of very small x , one may also sum leading terms in $\ln(1/x)$, independent of the value of $\ln \mu^2$. At leading order, LLx, this is done by the BFKL equation for the unintegrated distributions (see Refs. [32, 33]). The leading-order $(\alpha_s \ln(1/x))^n$ terms result in a power-like growth, $x^{-\omega}$ with $\omega = (12\alpha_s \ln 2)/\pi$, at asymptotic values of $\ln 1/x$. The next-to-leading $\ln 1/x$ (NLLx) contributions are also available [34, 35]. They are so large (and negative) that the results initially appeared to be perturbatively unstable. Methods, based on a combination of collinear and small- x resummations, have been developed which reorganize the perturbative series into a more stable hierarchy [36–39], and this has been used as the basis for a framework for including the corrections in phenomenological studies [40, 41]. There are some limited indications that small- x resummations become necessary for sufficient precision for $x \lesssim 10^{-3}$ at low scales [17, 18]. At sufficiently small x it is expected that evolution should also be affected by non-linear/saturation effects due to a high density of partons, i.e. the gluon density would be so high that gluon-gluon recombination effects would become significant,

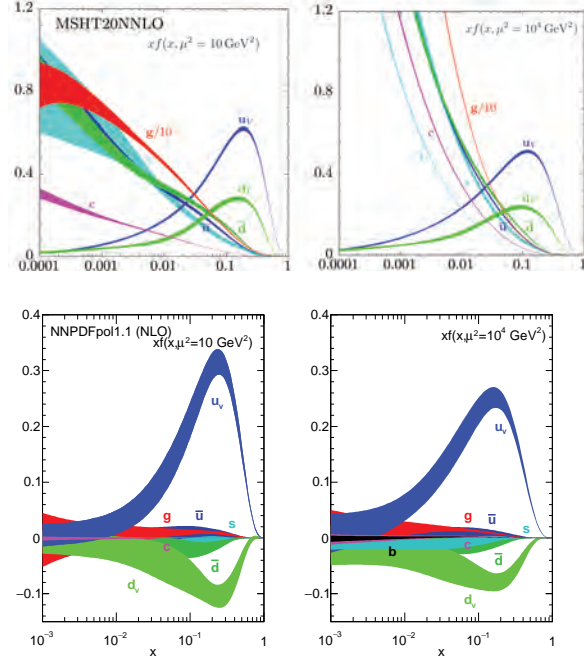


Figure 18.3: The bands are x times the unpolarized parton distributions $f(x)$ (where $f = u_v, d_v, \bar{u}, \bar{d}, s \simeq \bar{s}, c = \bar{c}, b = \bar{b}, g$) obtained in the NNLO MSHT20 global analysis [30] (top) at scales $\mu^2 = 10 \text{ GeV}^2$ (left) and $\mu^2 = 10^4 \text{ GeV}^2$ (right), with $\alpha_s(M_Z^2) = 0.118$. The polarized parton distributions $f(x)$ obtained in the NLO NNPDFpol1.1 fit [31] (bottom).

see [42–44] for reviews. However, there is not yet any very convincing indication for a non-linear regime for $Q^2 \gtrsim 2 \text{ GeV}^2$ in hadron DIS. Better evidence for saturation may be found in more exclusive final states such as dihadron correlations in proton-nucleus collisions, e.g. [45, 46].

The precision of the experimental data demands that at least NLO, and preferably NNLO, DGLAP evolution be used in comparisons between QCD theory and experiment. Beyond the leading order, it is necessary to specify, and to use consistently, both a renormalization and a factorization scheme. The renormalization scheme used almost universally is the modified minimal subtraction ($\overline{\text{MS}}$) scheme [47, 48]. The most popular choices for the factorization scheme is also $\overline{\text{MS}}$ [49]. Historically, sometimes the DIS [50] scheme was adopted, in which there are no higher-order corrections to the F_2 structure function, and this was extended to a specific definition appropriate to small x [51]. The two schemes differ in how the non-divergent pieces are assimilated in the parton distribution functions.

The discussion above relates to the Q^2 behavior of leading-twist (twist-2) contributions to the structure functions. Higher-twist terms, which involve their own non-perturbative input, exist. These die off as powers of Q ; specifically twist- n terms are damped by $1/Q^{n-2}$. Provided a cut, say $W^2 > 15 \text{ GeV}^2$ is imposed, the higher-twist terms appear to be numerically unimportant for Q^2 above a few GeV^2 , except possibly for very small x and more definitively for x close to 1 [52–54], though it is important to note that they are likely to be larger in $x F_3(x, Q^2)$ than in $F_2(x, Q^2)$ (see e.g. [55]) due to a lack of a constraining sum rule for $x F_3(x, Q^2)$.

18.3 Determination of parton distributions

The parton distribution functions (PDFs) can be determined from an analysis of data for deep inelastic lepton-nucleon scattering and for related hard-scattering processes initiated by nucleons; see Refs. [56–62] for reviews. Table 18.1 highlights some of the processes and their primary sensitivity to PDFs. LHC data are playing an increasing role [63], and new processes are continually being added to the list. Fixed-target and collider experiments have complementary kinematic reach (as is shown in Fig. 18.4),

which enables the determination of PDFs over a wide range in x and μ^2 . As more precise LHC data for W^\pm , Z , γ , jet, $b\bar{b}$ and $t\bar{t}$ production become available, tighter constraints on the PDFs are expected in a wider kinematic range. At present about half the constraint on PDFs comes from LHC data [30], but much of the constraint still comes from structure functions.

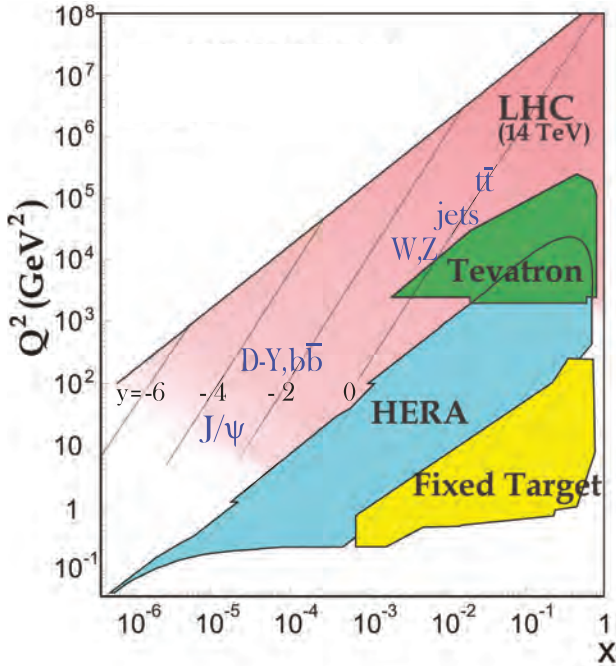


Figure 18.4: Kinematic domains in x and Q^2 probed by fixed-target and collider experiments, where here Q^2 can refer either the literal Q^2 for deep inelastic scattering, or the hard scale of the process in hadron-hadron collisions, e.g. invariant mass or transverse momentum p_T^2 . Some of the final states accessible at the LHC are indicated in the appropriate regions, where y is the rapidity. The incoming partons have $x_{1,2} = (Q/14 \text{ TeV})e^{\pm y}$ where Q is the hard scale of the process shown in blue in the figure. For example, open charm production [64] and exclusive J/ψ and Υ production [65] at high $|y|$ at the LHC may probe the gluon PDF down to $x \sim 10^{-5}$.

Recent determinations and releases of the unpolarized PDFs up to NNLO have been made by five groups: MSHT [30], NNPDF [66], CT [67], HERAPDF [14] and ABMP [68]. The CJ group produce PDFs at NLO and concentrate on the high x , low Q^2 regime, including data with lower kinematic cuts [69]. All groups start evolution at $Q_0^2 = 1-4 \text{ GeV}^2$. Most groups use input PDFs of the form $xf = x^a(\dots)(1-x)^b$ with 14-32 free parameters in total. In these cases the PDF uncertainties are made available using their best fit values, and orthogonal eigenvector sets of PDFs depending on linear combinations of the parameter variations are obtained. The uncertainty is then the quadratic sum of the uncertainties arising from each eigenvector. The NNPDF group combines a Monte Carlo representation of the probability measure in the space of PDFs with the use of neural networks. Fits are performed to a very large number of “replica” data sets obtained by allowing individual data points to fluctuate randomly by amounts determined by the size of the data uncertainties. This results in a set of replicas of unbiased PDF sets. In this case the best prediction is the average obtained using all PDF replicas and the uncertainty is the standard deviation over all replicas. It is possible to convert the eigenvectors of Hessian-based PDFs to Monte Carlo replicas [70] and *vice versa* [71].

In these analyses, the u , d and s quarks are taken to be massless, but the treatment of the heavy c and b quark masses, m_Q , differs, and has a long history, which may be traced from Refs. [72–83]. The MSHT, CT, NNPDF and HERAPDF analyses use different

variants of the General-Mass Variable-Flavour-Number Scheme (GM-VFNS). This combines fixed-order contributions to the coefficient functions (or partonic cross sections) calculated with the full m_Q dependence, with the all-order resummation of contributions via DGLAP evolution in which the heavy quarks are treated as massless after starting evolution at some transition point. Transition matrix elements are computed, following [75], which provide the boundary conditions between n_f and $n_f + 1$ PDFs. The ABMP analysis uses for structure function calculations a FFNS where only the three light (massless) quarks enter the evolution, while the heavy quarks enter the partonic cross sections with their full m_Q dependence. The GM-VFNS and FFNS approaches yield different results: in particular $\alpha_s(M_Z^2)$ and the large- x gluon PDF at large Q^2 are both significantly smaller in the FFNS. It has been argued [53, 54, 82] that the difference is due to the slow convergence of the $\ln^n(Q^2/m_Q^2)$ terms in certain regions in a FFNS. The final HERA combination of heavy flavour structure function data has been published [84], and the evolution of these measurements and their interpretation may be traced in [85].

The recent determinations of the groups fitting a variety of data and using a GM-VFNS (MSHT, NNPDF and CT) have converged, so that now a good agreement has been achieved between the resulting PDFs. Indeed, the previous round of global fit PDF sets, CT14 [86], MMHT2014 [87], and NNPDF3.0 [88], have been combined [89] using the Monte Carlo approach [70] mentioned above. The single combined set of PDFs is discussed in detail in Ref. [89]. An update for the most recent PDFs is in progress [90].

For illustration, we show in Fig. 18.3 the PDFs obtained in the NNLO MSHT analysis [30] at scales $\mu^2 = 10$ and 10^4 GeV^2 (and an equivalent plot for polarized PDFs from NNPDF [31]). The values of α_s found by MSHT [91] may be taken as representative of those resulting from the GM-VFNS analyses

$$\text{NLO} : \alpha_s(M_Z^2) = 0.1203 \pm 0.0015,$$

$$\text{NNLO} : \alpha_s(M_Z^2) = 0.1174 \pm 0.0013,$$

where the error (at 68% C.L.) corresponds to the uncertainties resulting from the data fitted (the uncertainty that might be expected from the neglect of higher orders is at least as large). A similar result is found by the NNPDF group [92], who find $\alpha_s(M_Z^2) = 0.1185 \pm 0.0012$ at NNLO and the CT group [67], who obtain $\alpha_s(M_Z^2) = 0.1164 \pm 0.0026$. The ABMP analysis [68], which uses a FFNS, finds $\alpha_s(M_Z^2) = 0.1147 \pm 0.0011$ at NNLO.

As a first step towards the inclusion of higher order electroweak corrections a recent development has been a vastly increased understanding of the photon content of the proton. Sets of PDFs with a photon contribution were considered in Refs. [93–95]. However, due to weak data constraints, the uncertainty was extremely large. Subsequently, there has been a much improved understanding of the separation into elastic and inelastic contributions [96–98]. This gives much more theoretical precision, since the elastic contribution, arising from coherent emission of a photon from the proton, can be directly related to the well-known proton electric and magnetic form factors; the model dependence of the inelastic (incoherent) contribution, related to the quark PDFs, is at the level of tens of percent. A final and decisive development directly relating the entire photon contribution to the proton structure function [99] resulted in a determination of the photon content of the proton as precise as that of the light quarks. The framework has been applied within global fits to PDFs via an iterative procedure in [100] and to provide the low-scale input photon PDF in [101, 102]. A further development is the calculation of photon-initiated collider processes directly from structure functions [103].

There are also some calculations of PDFs using lattice QCD, see [104, 105] for a recent review. There has been significant recent progress in the development of efficient algorithms for generating ensembles of gauge field configurations and in tools for extracting the required information from correlation functions. However, there remain a number of sources of systematic uncertainty; discretization effects, pion mass dependence, finite volume effects, excited state contamination and renormalization, which need to

be determined and ideally minimised. Moreover, PDFs cannot be determined directly in Euclidean lattice QCD because they depend on quantum fields at light-like separations. Traditionally the lattice has been used to determine matrix elements of twist two operators which can be related to integer moments of PDFs. Until recently these did not always agree well with determinations using global fit PDFs [104]. However, there have been recent improvements [106, 107], though uncertainties are still relatively large. An alternative approach [108] suggested the computation of the matrix elements of frame-dependent, equal-time correlators in the large momentum limit. This leads to so-called Quasi-PDFs, which in the infinite momentum frame can be related to light-cone PDFs via a matching procedure. Recent results using physical values of the light quark masses are in [109].

Comprehensive sets of PDFs are available from the LHAPDF library [110], which can be linked directly into a user's programme to provide access to recent PDFs in a standard format. This also includes many nuclear and polarized PDFs.

Nuclear PDFs: The study of the parton distributions for nucleons within nuclei, so-called nuclear parton distribution functions (nPDFs), is now reaching a level of maturity and sophistication similar to nucleon PDFs (and some nuclear target data is often included in determinations of nucleon PDFs), though they are still typically performed at NLO in perturbative QCD. The PDFs are also a function of the nucleon number of the nucleus, A . The nPDFs are obtained via fits to deep inelastic scattering data and dilepton (Drell-Yan) and pion production from proton-nucleus, and most recently also from jet and heavy flavour production data. There are a number of recent examples of NLO analyses, DSSZ [111], nCTEQ15 [112], EPPS16 [113], while NNLO analyses with a smaller selection of data types now also exist [114, 115]. The NNPDF group has recently introduced its first nuclear PDFs, with nNNPDF1.0 [116] at NNLO and based only on neutral current DIS data and nNNPDF2.0 [117] at NLO, which additionally contains charged current DIS data and vector boson production data from the LHC. A comparison of the nuclear modification factors for nCTEQ15WZ+SIH [118], EPPS16 [113] and nNNPDF2.0 [117] is shown in Fig. 18.5 where, for example, for the up quark $R_u^{Pb} = (Z_{Pb}u_{Pb} + (A_{Pb} - Z_{Pb})d_{Pb}) / (Z_{Pb}u_p + (A_{Pb} - Z_{Pb})d_p)$ i.e. it involves "physical" nuclear PDFs and is normalised such that $R_u^{Pb} = 1$ corresponds to no nuclear effects.

Much of the heavy-nucleus data included are in the form of ratios to proton or deuteron measurements. Initially most nuclear PDFs were related to a particular proton PDF via a nuclear modification factor, i.e.

$$f_i^{p/A}(x, Q^2) = R_i^A(x, Q^2) f_i^p(x, Q^2). \quad (18.30)$$

The first exception was the PDFs in [112] which parameterise the nuclear PDFs directly but are equal to proton PDFs in the limit $A = 1$, and this approach has been repeated in [115–117]. There is some variation in whether charged current neutrino DIS data is used as well as neutral current DIS data since there is no clear compatibility in the modification factors obtained [119, 120]. Recently, LHC data from vector boson production [121–124] in proton-lead collisions has been studied [125] or used directly [113, 117], and LHC jet data [126] has been included [113], giving extra constraint on the gluon within nuclei. Further information at smaller x values should soon be extracted from heavy meson production at LHCb [127], dijet production at CMS [128]. Single inclusive hadron production e.g. [129, 130], is already sometimes used. There have been PDF reweighting studies at NLO including some of these data [131–133], indicating a substantial uncertainty reduction at small x , but no fully updated nuclear PDF sets so far include them. All the PDF extractions above are based on the Hessian formulation, except for the NNPDF studies which use Monte Carlo replicas. Agreement between the different nuclear PDFs is generally good, though uncertainty is still large compared to proton PDFs. As well as improved constraints from further LHC data, nPDFs would be very significantly improved by data from a potential high-energy Electron-Ion Collider [134–136].

Double Parton Distributions Double parton scattering (DPS) occurs when two pairs of partons initiate two distinct hard scattering processes in a single collision. It becomes more prevalent at higher collider energies as the parton flux increases. Hence, it is becoming relevant at the LHC, and even more so for planning of higher energy colliders. It has a long theoretical history [137–141], and in recent years experimental studies have started. DPS is often suppressed, but this is less the case in certain kinematic regions, e.g. when the total transverse momentum of the two hard-scattering processes is small [142–145], when they have a large rapidity separation [146, 147], or when single particle production is suppressed by coupling constants, e.g. like-sign W production [148]. There have been results with some evidence for DPS found from both the Tevatron [149, 150] involving final states with multijets and photons, and at the LHC [151–153] in states with multiple vector bosons or mesons. Recent developments have been involved in putting the theoretical foundations of DPS on a much more rigorous footing and describing it in terms of well-defined double parton distributions (DPDs) which extend the concept of parton distribution functions (PDFs) to the case of two partons [142–145, 154–156]. The current knowledge of DPDs is still limited, though there are a number of attempts to impose theoretical constraints as a limit on the forms [157–159]. The DPDs can be calculated quite accurately when the transverse separation of the two partons is small, since in this limit the observed partons are produced by a splitting from a single parton. This limit is complicated by potential double counting [145], and an approach to deal with this has been devised [156]. The full splitting functions for DPS have been calculated at LO [145].

Polarized PDFs: For spin-dependent structure functions, data exists for a more restricted range of Q^2 and has lower precision, so that the scaling violations are not seen so clearly. However, spin-dependent (or polarized) parton distributions have been extracted by comparison to data using NLO global analyses which include measurements of the g_1 structure function in inclusive polarized DIS, 'flavour-tagged' semi-inclusive DIS data, open-charm production in DIS and results from polarized pp scattering at RHIC. There are recent results on DIS from JLAB [160] (for g_1^p/F_1^p), COMPASS [161, 162] and CLAS [163]. NLO analyses are given in Refs. [164–167] and more recent extractions [168, 169]. Improved parton-to-hadron fragmentation functions, needed to describe the semi-inclusive DIS (SIDIS) data, can be found in Refs. [170–173]. Only the DSSV collaboration includes in their NLO analysis to extract polarized PDFs all the world data, inclusive and semi-inclusive DIS, double spin asymmetries in jet [174], dijet [175] and inclusive π^0 -production [176], but not yet the single spin asymmetries in W^\pm, Z^0 production [177]. A determination [178], using the NNPDF methodology, concentrates just on the inclusive polarized DIS data, and finds the uncertainties on the polarized gluon PDF have been underestimated in the earlier analyses. An update to this [31], where jet and W^\pm data from pp collisions and open-charm DIS data have been included via reweighting, reduces the uncertainty and suggests a positive polarized gluon PDF. The evidence for a positive gluon polarization is strengthened by the most recent jet [179, 180] and inclusive π^0 [181] data. The DSSV group has recently implemented a Monte Carlo sampling strategy to extract helicity parton densities and their uncertainties from a reference set of longitudinally polarized scattering data [182]. Calculations of polarised PDFs on the lattice are frequently produced by the same studies as for unpolarised PDFs. These are usually in better agreement with the corresponding moments obtained from global fits, than the unpolarised PDFs, and also tend to have much more competitive uncertainties, see [104, 105] for a review and e.g. [107, 183] for more recent results.

A comparison of the polarized gluon PDFs obtained in the NLO analyses of NNPDF [31] and DSSV [182] is shown in Fig. 18.6 at scale $\mu^2 = 10 \text{ GeV}^2$. The world data of the inclusive structure function g_1 for proton and deuterium included in these analysis are shown in Fig. 18.16 and Fig. 18.17.

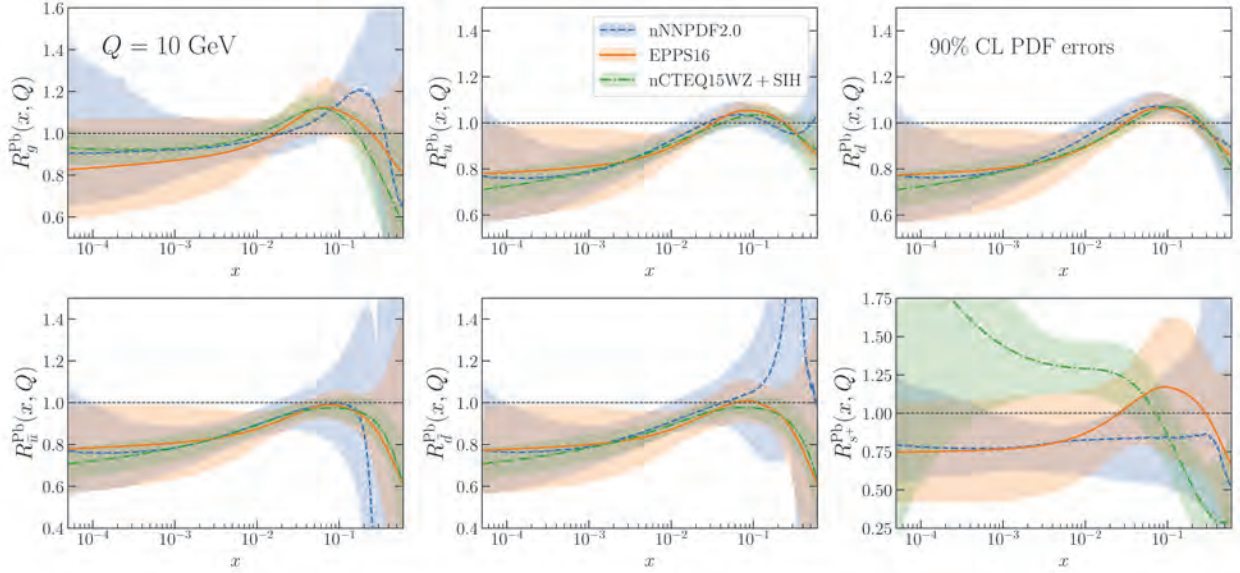


Figure 18.5: Comparison of the nNNPDF2.0, CTEQ15WZ+SIH and EPPS16 nuclear PDFs. The curves shown are ratios to the result in the limit of no nuclear corrections. Plot from NNPDF collaboration (Juan Rojo – private communication).

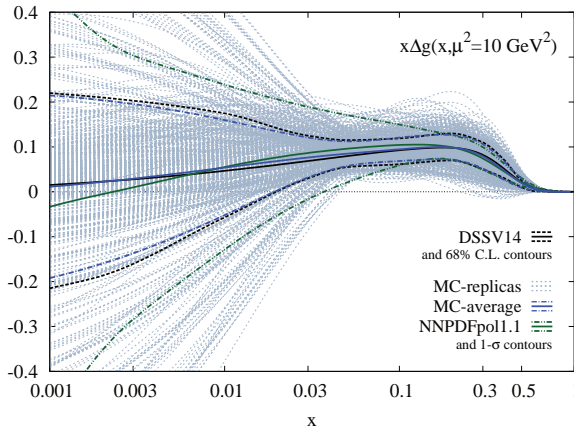


Figure 18.6: Ensemble of replicas (dotted blue lines) for the NLO gluon helicity density $\Delta g(x, Q^2)$ at $Q^2 = 10 \text{ GeV}^2$ shown along with its statistical average (solid blue line) and variance (dot-dashed blue lines). The corresponding results from the DSSV14 fit (black lines) [168] and the NNPdfpol1.1 analysis (green lines) [31] are shown for comparison. Figure taken from Ref. [182].

18.4 The hadronic structure of the photon

Besides the *direct* interactions of the photon, it is possible for it to fluctuate into a hadronic state via the process $\gamma \rightarrow q\bar{q}$. While in this state, the partonic content of the photon may be *resolved*, for example, through the process $e^+e^- \rightarrow e^+e^-\gamma^*\gamma \rightarrow e^+e^-X$, where the virtual photon emitted by the DIS lepton probes the hadronic structure of the quasi-real photon emitted by the other lepton. The perturbative LO QED contributions to this process with $\gamma \rightarrow q\bar{q}$ in conjunction with $\gamma^*q(\bar{q}) \rightarrow q(\bar{q})$, are subject to QCD corrections due to the radiation of gluons from these quarks.

Often the equivalent-photon approximation is used to express the differential cross section for deep inelastic electron–photon scattering in terms of the structure functions of the transverse quasi-real photon times a flux factor N_γ^T (for these incoming quasi-real photons of transverse polarization)

$$\frac{d^2\sigma}{dx dQ^2} = N_\gamma^T \frac{2\pi\alpha^2}{xQ^4} \left[(1 + (1-y)^2) F_2^\gamma(x, Q^2) - y^2 F_L^\gamma(x, Q^2) \right], \quad (18.31)$$

where we have used $F_2^\gamma = 2xF_T^\gamma + F_L^\gamma$ (where F_T is the transverse structure function), not to be confused with F_2^γ of Sec. 18.2. Complete formulae are given, for example, in the comprehensive review of [184].

The hadronic photon structure function, F_2^γ , evolves with increasing Q^2 from the ‘hadron-like’ behavior, calculable via the vector-meson-dominance model, to the dominating ‘point-like’ behaviour, calculable in perturbative QCD. Due to the point-like coupling, the logarithmic evolution of F_2^γ with Q^2 has a *positive* slope for all values of x , see Fig. 18.18. The ‘loss’ of quarks at large x due to gluon radiation is over-compensated by the ‘creation’ of quarks via the point-like $\gamma \rightarrow q\bar{q}$ coupling. The logarithmic evolution was first predicted in the quark–parton model ($\gamma^*\gamma \rightarrow q\bar{q}$) [185, 186], and then an improved expression was obtained using QCD corrections in the limit of large Q^2 [187]. The evolution is now known to NLO [188–190]. The NLO data analyses to determine the parton densities of the photon can be found in Refs. [191–193].

18.5 Diffractive DIS (DDIS)

Some 10% of DIS events are diffractive, $\gamma^*p \rightarrow X + p$, in which the slightly deflected proton and the cluster X of outgoing hadrons are well-separated in rapidity [194]. Besides x and Q^2 , two extra variables are needed to describe a DDIS event: the fraction x_P of the proton’s momentum transferred across the rapidity gap and t , the square of the 4-momentum transfer of the proton. The DDIS data [199, 200] are usually analysed using two levels of factorization. First, the diffractive structure function F_2^D satisfies *collinear factorization*, and can be expressed as the convolution [201]

$$F_2^D = \sum_{a=q,g} C_2^a \otimes f_{a/p}^D, \quad (18.32)$$

with the same coefficient functions as in DIS (see Eq. (18.21)), and where the diffractive parton distributions $f_{a/p}^D$ ($a = q, g$) satisfy DGLAP evolution. Second, *Regge factorization* is assumed [202],

$$f_{a/p}^D(x_P, t, z, \mu^2) = f_{IP/p}(x_P, t) f_{a/IP}(z, \mu^2), \quad (18.33)$$

where $f_{a/IP}$ are the parton densities of the Pomeron, which itself is treated like a hadron, and $z \in [x/x_P, 1]$ is the fraction of the Pomeron’s momentum carried by the parton entering the hard subprocess. The Pomeron flux factor $f_{IP/p}(x_P, t)$ is taken from Regge phenomenology. There are also secondary Reggeon contributions to Eq. (18.33). A sample of the t -integrated diffractive parton densities, obtained in this way, is shown in Fig. 18.7.

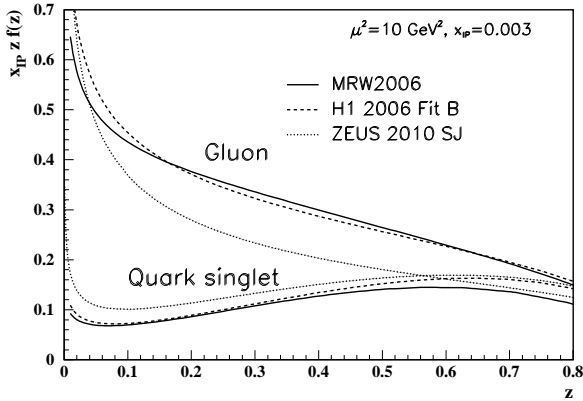


Figure 18.7: Diffractive parton distributions, $x_{IP} z f_{a/p}^D$, obtained from fitting to the ZEUS data with $Q^2 > 5 \text{ GeV}^2$ [195], H1 data with $Q^2 > 8.5 \text{ GeV}^2$ assuming Regge factorization [196], and from MRW2006 [197] using a more perturbative QCD approach [197]. Only the Pomeron contributions are shown and not the secondary Reggeon contributions, which are negligible at the value of $x_{IP} = 0.003$ chosen here. The H1 2007 Jets distribution [198] is similar to H1 2006 Fit B.

A more recent extraction of the parton densities may be found in [203].

Although collinear factorization holds as $\mu^2 \rightarrow \infty$, there are non-negligible corrections for finite μ^2 and small x_{IP} . Besides the *resolved* interactions of the Pomeron, the perturbative QCD Pomeron may also interact *directly* with the hard subprocess, giving rise to an inhomogeneous evolution equation for the diffractive parton densities analogous to the photon case. The results of the MRW analysis [197], which includes these contributions, are also shown in Fig. 18.7.

Unlike the inclusive case, the diffractive parton densities cannot be directly used to calculate diffractive hadron-hadron cross sections, since account must first be taken of “soft” rescattering effects.

18.6 Three-dimensional structure of hadrons

Generalized parton distributions (GPDs) and their complement, transverse momentum dependent distributions (TMDs) describe the three-dimensional structure of hadrons. While GPDs encode the transverse position of a parton in a nucleon, TMDs, encompassing both the parton distributions (TMD PDF) and fragmentation functions (TMD FF), encode their transverse momenta and lead to observable transverse momenta in the final state. Both TMDs and GPDs derive, via integration over the appropriate variable, from Wigner distributions [204–206] that depend on the average transverse momentum and position of partons.

18.6.1 Generalized parton distributions

The parton distributions of the proton of Sec. 18.3 are given by the diagonal matrix elements $\langle P, \lambda | \hat{O} | P, \lambda \rangle$, where P and λ are the 4-momentum and helicity of the proton, and \hat{O} is a twist-2 quark or gluon operator. However, there is new information in the so-called generalised parton distributions (GPDs) defined in terms of the off-diagonal matrix elements $\langle P', \lambda' | \hat{O} | P, \lambda \rangle$; see Refs. [207–212] for reviews. Unlike the diagonal PDFs, the GPDs cannot be regarded as parton densities, but are to be interpreted as probability amplitudes.

The physical significance of GPDs is best seen using light-cone coordinates, $z^\pm = (z^0 \pm z^3)/\sqrt{2}$, and in the light-cone gauge, $A^+ = 0$. It is conventional to define the generalised quark distri-

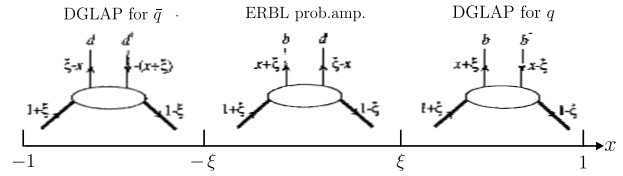


Figure 18.8: Schematic diagrams of the three distinct kinematic regions of the imaginary part of H_q . The proton and quark momentum fractions refer to \bar{P}^+ , and x covers the interval $(-1, 1)$. In the ERBL domain the GPDs are generalisations of distribution amplitudes which occur in processes such as $p\bar{p} \rightarrow J/\psi$.

butions in terms of quark operators at light-like separation

$$F_q(x, \xi, t) = \frac{1}{2} \int \frac{dz^-}{2\pi} e^{ix\bar{P}^+z^-} \langle P' | \bar{\psi}(-z/2) \gamma^+ \psi(z/2) | P \rangle \Big|_{z^+ = z^1 = z^2 = 0} = \frac{1}{2\bar{P}^+} \times \left(H_q(x, \xi, t) \bar{u}(P') \gamma^+ u(P) + E_q(x, \xi, t) \bar{u}(P') \frac{i\sigma^{+\alpha} \Delta_\alpha}{2m} u(P) \right) \quad (18.34)$$

with $\bar{P} = (P + P')/2$ and $\Delta = P' - P$, and where we have suppressed the helicity labels of the protons and spinors. We now have two extra kinematic variables:

$$t = \Delta^2, \quad \xi = -\Delta^+ / (P + P')^+. \quad (18.35)$$

We see that $-1 \leq \xi \leq 1$. Similarly, we may define GPDs \tilde{H}_q and \tilde{E}_q with an additional γ_5 between the quark operators in Eq. (18.34); and also an analogous set of gluon GPDs, H_g, E_g, \tilde{H}_g and \tilde{E}_g . After a Fourier transform with respect to the transverse components of Δ , we are able to describe the spatial distribution of partons in the impact parameter plane in terms of GPDs [213, 214].

For $P' = P$, $\lambda' = \lambda$ the matrix elements reduce to the ordinary PDFs of Sec. 18.2.1

$$H_q(x, 0, 0) = q(x), \quad H_q(-x, 0, 0) = -\bar{q}(x), \quad H_g(x, 0, 0) = xg(x), \quad (18.36)$$

$$\tilde{H}_q(x, 0, 0) = \Delta q(x), \quad \tilde{H}_q(-x, 0, 0) = \Delta \bar{q}(x), \quad \tilde{H}_g(x, 0, 0) = x\Delta g(x), \quad (18.37)$$

where $\Delta q = q \uparrow - q \downarrow$ as in Eq. (18.18). No corresponding relations exist for E, \tilde{E} as they decouple in the forward limit, $\Delta = 0$.

The functions H_g, E_g are even in x , and \tilde{H}_g, \tilde{E}_g are odd functions of x . We can introduce valence and ‘singlet’ quark distributions which are even and odd functions of x respectively. For example

$$H_q^V(x, \xi, t) \equiv H_q(x, \xi, t) + H_q(-x, \xi, t) = H_q^V(-x, \xi, t), \quad (18.38)$$

$$H_q^S(x, \xi, t) \equiv H_q(x, \xi, t) - H_q(-x, \xi, t) = -H_q^S(-x, \xi, t). \quad (18.39)$$

All the GPDs satisfy relations of the form

$$H(x, -\xi, t) = H(x, \xi, t) \quad \text{and} \quad H(x, -\xi, t)^* = H(x, \xi, t), \quad (18.40)$$

and so are real-valued functions. Moreover, the moments of GPDs, that is the x integrals of $x^n H_q$ etc., are *polynomials* in ξ of order $n + 1$. Another important property of GPDs are Ji’s sum rule [207]

$$\frac{1}{2} \int_{-1}^1 dx x (H_q(x, \xi, t) + E_q(x, \xi, t)) = J_q(t), \quad (18.41)$$

where $J_q(0)$ is the total angular momentum carried by quarks and antiquarks of flavour q , with a similar relation for gluons.

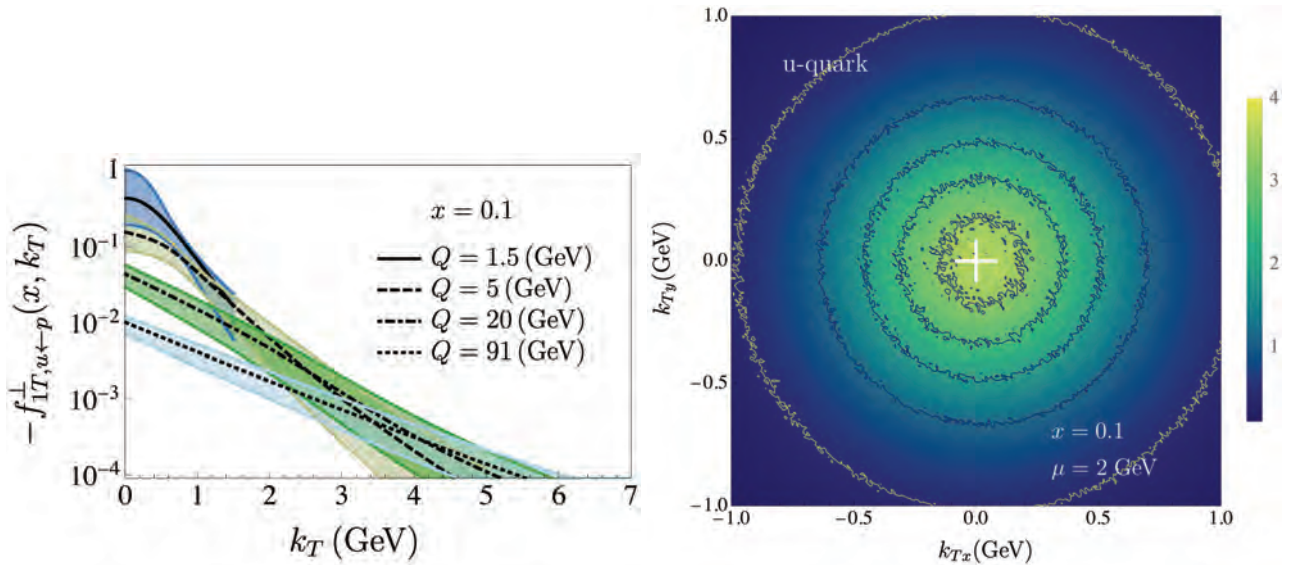


Figure 18.9: (Left) Siverts function in the momentum space for u quark [215] at $x = 0.1$ as a function of transverse momentum k_T for different values of Q . The bands are 68%CI. (Right) Momentum space density function as defined in [215] for the unpolarized u quark in a proton totally polarized in the y direction. The white cross indicates the origin with respect to which a shift of the distribution along the x -direction due to the Siverts function can be seen. The width of the patterns in the plot roughly indicates the uncertainty of the extraction.

To visualize the physical content of H_q , we Fourier expand ψ and $\bar{\psi}$ in terms of quark, antiquark creation (b, d) and annihilation (b^\dagger, d^\dagger) operators, and sketch the result in Fig. 18.8. There are two types of domain: (i) the time-like or ‘annihilation’ domain, with $|x| < |\xi|$, where the GPDs describe the wave functions of a t -channel $q\bar{q}$ (or gluon) pair and evolve according to modified ERBL equations [216,217]; (ii) the space-like or ‘scattering’ domain, with $|x| > |\xi|$, where the GPDs generalise the familiar \bar{q}, q (and gluon) PDFs and describe processes such as ‘deeply virtual Compton scattering’ ($\gamma^*p \rightarrow \gamma p$), $\gamma p \rightarrow J/\psi p$, etc., and evolve according to modified DGLAP equations. The splitting functions for the evolution of GPDs are known to NLO [218–220].

GPDs describe new aspects of proton structure and must be determined from experiment. We can parametrise them in terms of ‘double distributions’ [221,222], which reduce to diagonal PDFs as $\xi \rightarrow 0$. Alternatively, flexible $SO(3)$ -based parametrisations have been used to determine GPDs from DVCS data [223,224]; a more recent summary may be found in Ref. [225,226].

18.6.2 Transverse momentum dependent distributions

For a proton, there are eight independent transverse dependent distribution (TMD) PDFs, at leading twist, three of which correspond to the usual unpolarized, longitudinally polarized and transversely polarized quark parton distributions [227,228]. The novel TMD PDFs have physical interpretations. For example, the Siverts function [229] represents the distribution of unpolarized partons inside a transversely polarized hadron. For (pseudo)scalar particles, such as kaon and pions, there are two independent leading-twist TMD FFs, one being the ordinary unpolarized fragmentation function and the other the Collins FF [230] which is related to the probability of a polarized quark fragmenting into an unpolarized hadron.

Factorization of TMDs has been shown for semi-inclusive DIS, for the Drell-Yan process as well as for electron-positron annihilation into dihadrons [231–236]. Recently first TMD global fits have become available [237–244], although problems with consistent descriptions still remain [245,246]. The results of a recent extraction of Siverts function from a global fit to polarized Semi-Inclusive DIS, polarized pion-induced Drell-Yan and W^\pm/Z boson production data is shown in Fig. 18.9 [215].

Because TMD PDFs encode nonperturbative information about transverse momentum and polarization degrees of freedom, they are important for descriptions of multi-scale, non-inclusive collider observables, for example, production of electroweak gauge

bosons at LHC [247] and can have an effect on determination of the W boson mass [248]. The combination of TMD PDFs and FFs can give consistent global description of spin and azimuthal asymmetries and provide predictions. Some recent reviews of this rapidly developing field are given here [247,249–252].

References

- [1] J. Blumlein and N. Kochelev, Nucl. Phys. **B498**, 285 (1997), [hep-ph/9612318].
- [2] S. Forte, M. L. Mangano and G. Ridolfi, Nucl. Phys. **B602**, 585 (2001), [hep-ph/0101192].
- [3] M. Anselmino, P. Gambino and J. Kalinowski, Z. Phys. **C64**, 267 (1994), [hep-ph/9401264].
- [4] M. Anselmino, A. Efremov and E. Leader, Phys. Rept. **261**, 1 (1995), [Erratum: Phys. Rept.281,399(1997)], [hep-ph/9501369].
- [5] M. Klein and T. Riemann, Z. Phys. **C24**, 151 (1984).
- [6] C. G. Callan, Jr. and D. J. Gross, Phys. Rev. Lett. **22**, 156 (1969).
- [7] D. A. Dicus, Phys. Rev. **D5**, 1367 (1972).
- [8] J. D. Bjorken and E. A. Paschos, Phys. Rev. **185**, 1975 (1969).
- [9] R.P. Feynman, Photon Hadron Interactions (Benjamin, New York, 1972).
- [10] J. D. Bjorken, Phys. Rev. **179**, 1547 (1969).
- [11] S. Wandzura and F. Wilczek, Phys. Lett. **72B**, 195 (1977).
- [12] J. Blumlein and A. Tkabladze, Nucl. Phys. **B553**, 427 (1999), [hep-ph/9812478].
- [13] A.M. Cooper-Sarkar, private communication.
- [14] H. Abramowicz *et al.* (H1, ZEUS), Eur. Phys. J. **C75**, 12, 580 (2015), [arXiv:1506.06042].
- [15] L. A. Harland-Lang *et al.*, Eur. Phys. J. **C76**, 4, 186 (2016), [arXiv:1601.03413].
- [16] I. Abt *et al.*, Phys. Rev. **D94**, 3, 034032 (2016), [arXiv:1604.02299].
- [17] R. D. Ball *et al.*, Eur. Phys. J. **C78**, 4, 321 (2018), [arXiv:1710.05935].
- [18] H. Abdolmaleki *et al.* (xFitter Developers’ Team), Eur. Phys. J. **C78**, 8, 621 (2018), [arXiv:1802.00064].

- [19] J. C. Collins, D. E. Soper and G. F. Sterman, *Adv. Ser. Direct. High Energy Phys.* **5**, 1 (1989), [hep-ph/0409313].
- [20] V. N. Gribov and L. N. Lipatov, *Sov. J. Nucl. Phys.* **15**, 438 (1972), [*Yad. Fiz.*15,781(1972)].
- [21] L.N. Lipatov, *Sov. J. Nucl. Phys.* **20**, 95 (1975).
- [22] G. Altarelli and G. Parisi, *Nucl. Phys.* **B126**, 298 (1977).
- [23] Y. L. Dokshitzer, *Sov. Phys. JETP* **46**, 641 (1977), [*Zh. Eksp. Teor. Fiz.*73,1216(1977)].
- [24] G. Curci, W. Furmanski and R. Petronzio, *Nucl. Phys.* **B175**, 27 (1980); W. Furmanski and R. Petronzio, *Phys. Lett.* **97B**, 437 (1980).
- [25] R.K. Ellis *et al.*, *QCD and Collider Physics* (Cambridge UP, 1996).
- [26] W. L. van Neerven and E. B. Zijlstra, *Phys. Lett.* **B272**, 127 (1991); E. B. Zijlstra and W. L. van Neerven, *Phys. Lett.* **B273**, 476 (1991); E. B. Zijlstra and W. L. van Neerven, *Phys. Lett.* **B297**, 377 (1992); E. B. Zijlstra and W. L. van Neerven, *Nucl. Phys.* **B383**, 525 (1992).
- [27] S. Moch and J. A. M. Vermaseren, *Nucl. Phys.* **B573**, 853 (2000), [hep-ph/9912355].
- [28] S. Moch, J. A. M. Vermaseren and A. Vogt, *Nucl. Phys.* **B688**, 101 (2004), [hep-ph/0403192]; A. Vogt, S. Moch and J. A. M. Vermaseren, *Nucl. Phys.* **B691**, 129 (2004), [hep-ph/0404111]; S. Moch, J. A. M. Vermaseren and A. Vogt, *Phys. Lett.* **B606**, 123 (2005), [hep-ph/0411112].
- [29] J. A. M. Vermaseren, A. Vogt and S. Moch, *Nucl. Phys.* **B724**, 3 (2005), [hep-ph/0504242].
- [30] S. Bailey *et al.*, *Eur. Phys. J. C* **81**, 4, 341 (2021), [arXiv:2012.04684].
- [31] E. R. Nocera *et al.* (NNPDF), *Nucl. Phys.* **B887**, 276 (2014), [arXiv:1406.5539].
- [32] V. S. Fadin, E. A. Kuraev and L. N. Lipatov, *Phys. Lett.* **60B**, 50 (1975); E. A. Kuraev, L. N. Lipatov and V. S. Fadin, *Sov. Phys. JETP* **44**, 443 (1976), [*Zh. Eksp. Teor. Fiz.*71,840(1976)]; E. A. Kuraev, L. N. Lipatov and V. S. Fadin, *Sov. Phys. JETP* **45**, 199 (1977), [*Zh. Eksp. Teor. Fiz.*72,377(1977)].
- [33] I. I. Balitsky and L. N. Lipatov, *Sov. J. Nucl. Phys.* **28**, 822 (1978), [*Yad. Fiz.*28,1597(1978)].
- [34] V. S. Fadin and L. N. Lipatov, *Phys. Lett.* **B429**, 127 (1998), [hep-ph/9802290].
- [35] G. Camici and M. Ciafaloni, *Phys. Lett.* **B412**, 396 (1997), [Erratum: *Phys. Lett.* **B417**,390(1998)], [hep-ph/9707390]; M. Ciafaloni and G. Camici, *Phys. Lett.* **B430**, 349 (1998), [hep-ph/9803389].
- [36] M. Ciafaloni, D. Colferai and G. P. Salam, *Phys. Rev.* **D60**, 114036 (1999), [hep-ph/9905566]; M. Ciafaloni, D. Colferai and G. P. Salam, *JHEP* **07**, 054 (2000), [hep-ph/0007240].
- [37] M. Ciafaloni *et al.*, *Phys. Lett.* **B576**, 143 (2003), [hep-ph/0305254]; M. Ciafaloni *et al.*, *Phys. Rev.* **D68**, 114003 (2003), [hep-ph/0307188].
- [38] G. Altarelli, R. D. Ball and S. Forte, *Nucl. Phys.* **B742**, 1 (2006), [hep-ph/0512237]; G. Altarelli, R. D. Ball and S. Forte, *Nucl. Phys.* **B799**, 199 (2008), [arXiv:0802.0032].
- [39] C. D. White and R. S. Thorne, *Phys. Rev.* **D75**, 034005 (2007), [hep-ph/0611204].
- [40] M. Bonvini, S. Marzani and T. Peraro, *Eur. Phys. J.* **C76**, 11, 597 (2016), [arXiv:1607.02153].
- [41] M. Bonvini, S. Marzani and C. Muselli, *JHEP* **12**, 117 (2017), [arXiv:1708.07510].
- [42] Y. V. Kovchegov and E. Levin, *Quantum chromodynamics at high energy*, volume 33, Cambridge University Press (2012), ISBN 978-0-521-11257-4, 978-1-139-55768-9.
- [43] J. L. Albacete and C. Marquet, *Prog. Part. Nucl. Phys.* **76**, 1 (2014), [arXiv:1401.4866].
- [44] A. Morreale and F. Salazar, *Universe* **7**, 8, 312 (2021), [arXiv:2108.08254].
- [45] G. Giacalone and C. Marquet, *Nucl. Phys. A* **982**, 291 (2019), [arXiv:1807.06388].
- [46] X. Chu (STAR), in “28th International Workshop on Deep Inelastic Scattering and Related Subjects,” (2021), [arXiv:2110.03731].
- [47] G. 't Hooft and M. J. G. Veltman, *Nucl. Phys.* **B44**, 189 (1972).
- [48] G. 't Hooft, *Nucl. Phys.* **B61**, 455 (1973).
- [49] W. A. Bardeen *et al.*, *Phys. Rev.* **D18**, 3998 (1978).
- [50] G. Altarelli, R. K. Ellis and G. Martinelli, *Nucl. Phys.* **B143**, 521 (1978), [Erratum: *Nucl. Phys.* **B146**,544(1978)].
- [51] S. Catani, *Z. Phys. C* **70**, 263 (1996), [hep-ph/9506357].
- [52] A. D. Martin *et al.*, *Eur. Phys. J.* **C35**, 325 (2004), [hep-ph/0308087].
- [53] R. D. Ball *et al.* (NNPDF), *Phys. Lett.* **B723**, 330 (2013), [arXiv:1303.1189].
- [54] R. S. Thorne, *Eur. Phys. J.* **C74**, 7, 2958 (2014), [arXiv:1402.3536].
- [55] M. Dasgupta and B. R. Webber, *Phys. Lett.* **B382**, 273 (1996), [hep-ph/9604388].
- [56] A. De Roeck and R. S. Thorne, *Prog. Part. Nucl. Phys.* **66**, 727 (2011), [arXiv:1103.0555].
- [57] S. Forte and G. Watt, *Ann. Rev. Nucl. Part. Sci.* **63**, 291 (2013), [arXiv:1301.6754].
- [58] J. Blumlein, *Prog. Part. Nucl. Phys.* **69**, 28 (2013), [arXiv:1208.6087].
- [59] E. Perez and E. Rizvi, *Rept. Prog. Phys.* **76**, 046201 (2013), [arXiv:1208.1178].
- [60] R. D. Ball *et al.*, *JHEP* **04**, 125 (2013), [arXiv:1211.5142].
- [61] J. Gao, L. Harland-Lang and J. Rojo, *Phys. Rept.* **742**, 1 (2018), [arXiv:1709.04922].
- [62] J. J. Ethier and E. R. Nocera, *Ann. Rev. Nucl. Part. Sci.* **70**, 43 (2020), [arXiv:2001.07722].
- [63] J. Rojo *et al.*, *J. Phys.* **G42**, 103103 (2015), [arXiv:1507.00556].
- [64] V. Bertone, R. Gauld and J. Rojo, *JHEP* **01**, 217 (2019), [arXiv:1808.02034].
- [65] R. Aaij *et al.* (LHCb), *JHEP* **10**, 167 (2018), [arXiv:1806.04079].
- [66] R. D. Ball *et al.* (NNPDF), *Eur. Phys. J.* **C77**, 10, 663 (2017), [arXiv:1706.00428].
- [67] T.-J. Hou *et al.*, *Phys. Rev. D* **103**, 1, 014013 (2021), [arXiv:1912.10053].
- [68] S. Alekhin *et al.*, *Phys. Rev.* **D96**, 1, 014011 (2017), [arXiv:1701.05838].
- [69] A. Accardi *et al.*, *Phys. Rev. D* **93**, 11, 114017 (2016), [arXiv:1602.03154].
- [70] G. Watt and R. S. Thorne, *JHEP* **08**, 052 (2012), [arXiv:1205.4024].
- [71] S. Carrazza *et al.*, *Eur. Phys. J.* **C75**, 8, 369 (2015), [arXiv:1505.06736].
- [72] J. C. Collins, F. Wilczek and A. Zee, *Phys. Rev.* **D18**, 242 (1978).
- [73] E. Laenen *et al.*, *Nucl. Phys.* **B392**, 162 (1993).
- [74] M. A. G. Aivazis *et al.*, *Phys. Rev.* **D50**, 3102 (1994), [hep-ph/9312319].
- [75] M. Buza *et al.*, *Eur. Phys. J.* **C1**, 301 (1998), [hep-ph/9612398].
- [76] J. C. Collins, *Phys. Rev.* **D58**, 094002 (1998), [hep-ph/9806259].
- [77] A. Chuvakin, J. Smith and W. L. van Neerven, *Phys. Rev.* **D61**, 096004 (2000), [hep-ph/9910250].

- [78] R. S. Thorne, Phys. Rev. **D73**, 054019 (2006), [hep-ph/0601245].
- [79] R. S. Thorne and W. K. Tung, in “Proceedings, HERA and the LHC Workshop Series on the implications of HERA for LHC physics: 2006-2008,” 332–351 (2008), [2(2008)], [arXiv:0809.0714].
- [80] S. Alekhin and S. Moch, Phys. Lett. **B699**, 345 (2011), [arXiv:1011.5790].
- [81] S. Forte *et al.*, Nucl. Phys. **B834**, 116 (2010), [arXiv:1001.2312].
- [82] R. S. Thorne, Phys. Rev. **D86**, 074017 (2012), [arXiv:1201.6180].
- [83] E. G. de Oliveira *et al.*, Eur. Phys. J. **C73**, 10, 2616 (2013), [arXiv:1307.3508].
- [84] H. Abramowicz *et al.* (H1, ZEUS), Eur. Phys. J. **C78**, 6, 473 (2018), [arXiv:1804.01019].
- [85] O. Behnke, A. Geiser and M. Lisovsky, Prog. Part. Nucl. Phys. **84**, 1 (2015), [arXiv:1506.07519].
- [86] S. Dulat *et al.*, Phys. Rev. D **93**, 3, 033006 (2016), [arXiv:1506.07443].
- [87] L. A. Harland-Lang *et al.*, Eur. Phys. J. **C75**, 5, 204 (2015), [arXiv:1412.3989].
- [88] R. D. Ball *et al.* (NNPDF), JHEP **04**, 040 (2015), [arXiv:1410.8849].
- [89] J. Butterworth *et al.*, J. Phys. **G43**, 023001 (2016), [arXiv:1510.03865].
- [90] T. Cridge (PDF4LHC21 combination group), in “28th International Workshop on Deep Inelastic Scattering and Related Subjects,” (2021), [arXiv:2108.09099].
- [91] T. Cridge *et al.*, Eur. Phys. J. C **81**, 744 (2021), [arXiv:2106.10289].
- [92] R. D. Ball *et al.* (NNPDF), Eur. Phys. J. **C78**, 5, 408 (2018), [arXiv:1802.03398].
- [93] A. D. Martin *et al.*, Eur. Phys. J. **C39**, 155 (2005), [hep-ph/0411040].
- [94] R. D. Ball *et al.* (NNPDF), Nucl. Phys. **B877**, 290 (2013), [arXiv:1308.0598].
- [95] C. Schmidt *et al.*, Phys. Rev. **D93**, 11, 114015 (2016), [arXiv:1509.02905].
- [96] M. Gluck, C. Pisano and E. Reya, Phys. Lett. **B540**, 75 (2002), [hep-ph/0206126].
- [97] A. D. Martin and M. G. Ryskin, Eur. Phys. J. **C74**, 3040 (2014), [arXiv:1406.2118].
- [98] L. A. Harland-Lang, V. A. Khoze and M. G. Ryskin, Phys. Rev. **D94**, 7, 074008 (2016), [arXiv:1607.04635].
- [99] A. Manohar *et al.*, Phys. Rev. Lett. **117**, 24, 242002 (2016), [arXiv:1607.04266].
- [100] V. Bertone *et al.* (NNPDF), SciPost Phys. **5**, 1, 008 (2018), [arXiv:1712.07053].
- [101] L. A. Harland-Lang *et al.*, Eur. Phys. J. **C79**, 10, 811 (2019), [arXiv:1907.02750].
- [102] K. Xie *et al.* (CTEQ-TEA) (2021), [arXiv:2106.10299].
- [103] L. A. Harland-Lang, JHEP **03**, 128 (2020), [arXiv:1910.10178].
- [104] H.-W. Lin *et al.*, Prog. Part. Nucl. Phys. **100**, 107 (2018), [arXiv:1711.07916].
- [105] M. Constantinou *et al.*, Prog. Part. Nucl. Phys. **121**, 103908 (2021), [arXiv:2006.08636].
- [106] Y.-B. Yang *et al.*, Phys. Rev. Lett. **121**, 21, 212001 (2018), [arXiv:1808.08677].
- [107] C. Alexandrou *et al.*, Phys. Rev. D **101**, 9, 094513 (2020), [arXiv:2003.08486].
- [108] X. Ji, Phys. Rev. Lett. **110**, 262002 (2013), [arXiv:1305.1539].
- [109] C. Alexandrou *et al.*, Phys. Rev. Lett. **121**, 11, 112001 (2018), [arXiv:1803.02685].
- [110] A. Buckley *et al.*, Eur. Phys. J. **C75**, 132 (2015), [arXiv:1412.7420].
- [111] D. de Florian *et al.*, Phys. Rev. **D85**, 074028 (2012), [arXiv:1112.6324].
- [112] K. Kovarik *et al.*, Phys. Rev. **D93**, 8, 085037 (2016), [arXiv:1509.00792].
- [113] K. J. Eskola *et al.*, Eur. Phys. J. **C77**, 3, 163 (2017), [arXiv:1612.05741].
- [114] H. Khanpour and S. Atashbar Tehrani, Phys. Rev. **D93**, 1, 014026 (2016), [arXiv:1601.00939].
- [115] M. Walt, I. Helenius and W. Vogelsang, Phys. Rev. D **100**, 9, 096015 (2019), [arXiv:1908.03355].
- [116] R. Abdul Khalek, J. J. Ethier and J. Rojo (NNPDF), Eur. Phys. J. C **79**, 6, 471 (2019), [arXiv:1904.00018].
- [117] R. Abdul Khalek *et al.*, JHEP **09**, 183 (2020), [arXiv:2006.14629].
- [118] P. Duwentäster *et al.* (2021), [arXiv:2105.09873].
- [119] K. Kovarik *et al.*, Phys. Rev. Lett. **106**, 122301 (2011), [arXiv:1012.0286].
- [120] H. Paukkunen and C. A. Salgado, Phys. Rev. Lett. **110**, 21, 212301 (2013), [arXiv:1302.2001].
- [121] G. Aad *et al.* (ATLAS), Phys. Rev. **C92**, 4, 044915 (2015), [arXiv:1507.06232].
- [122] V. Khachatryan *et al.* (CMS), Phys. Lett. **B750**, 565 (2015), [arXiv:1503.05825].
- [123] V. Khachatryan *et al.* (CMS), Phys. Lett. B **759**, 36 (2016), [arXiv:1512.06461].
- [124] A. M. Sirunyan *et al.* (CMS), Phys. Lett. B **800**, 135048 (2020), [arXiv:1905.01486].
- [125] A. Kusina *et al.*, Eur. Phys. J. **C77**, 7, 488 (2017), [arXiv:1610.02925].
- [126] S. Chatrchyan *et al.* (CMS), Eur. Phys. J. **C74**, 7, 2951 (2014), [arXiv:1401.4433].
- [127] R. Aaij *et al.* (LHCb), JHEP **10**, 090 (2017), [arXiv:1707.02750].
- [128] A. M. Sirunyan *et al.* (CMS), Phys. Rev. Lett. **121**, 6, 062002 (2018), [arXiv:1805.04736].
- [129] S. Acharya *et al.* (ALICE), Eur. Phys. J. **C78**, 8, 624 (2018), [arXiv:1801.07051].
- [130] S. S. Adler *et al.* (PHENIX), Phys. Rev. Lett. **98**, 172302 (2007), [arXiv:nucl-ex/0610036].
- [131] K. J. Eskola *et al.*, JHEP **05**, 037 (2020), [arXiv:1906.02512].
- [132] K. J. Eskola, P. Paakkinen and H. Paukkunen, Eur. Phys. J. C **79**, 6, 511 (2019), [arXiv:1903.09832].
- [133] A. Kusina *et al.*, Phys. Rev. D **104**, 1, 014010 (2021), [arXiv:2012.11462].
- [134] E. C. Aschenauer *et al.*, Phys. Rev. **D96**, 11, 114005 (2017), [arXiv:1708.05654].
- [135] R. Abdul Khalek *et al.* (2021), [arXiv:2103.05419].
- [136] R. A. Khalek *et al.*, Phys. Rev. D **103**, 9, 096005 (2021), [arXiv:2102.00018].
- [137] P. V. Landshoff and J. C. Polkinghorne, Phys. Rev. D **18**, 3344 (1978).
- [138] R. Kirschner, Phys. Lett. B **84**, 266 (1979).
- [139] N. Paver and D. Treleani, Nuovo Cim. A **70**, 215 (1982).
- [140] V. P. Shelest, A. M. Snigirev and G. M. Zinovev, Phys. Lett. B **113**, 325 (1982).
- [141] M. Mekhfi, Phys. Rev. D **32**, 2371 (1985).
- [142] B. Blok *et al.*, Phys. Rev. D **83**, 071501 (2011), [arXiv:1009.2714].

- [143] M. Diehl and A. Schafer, Phys. Lett. B **698**, 389 (2011), [arXiv:1102.3081].
- [144] B. Blok *et al.*, Eur. Phys. J. C **72**, 1963 (2012), [arXiv:1106.5533].
- [145] M. Diehl, D. Ostermeier and A. Schafer, JHEP **03**, 089 (2012), [Erratum: JHEP 03, 001 (2016)], [arXiv:1111.0910].
- [146] C. H. Kom, A. Kulesza and W. J. Stirling, Phys. Rev. Lett. **107**, 082002 (2011), [arXiv:1105.4186].
- [147] C. H. Kom, A. Kulesza and W. J. Stirling, Eur. Phys. J. C **71**, 1802 (2011), [arXiv:1109.0309].
- [148] J. R. Gaunt *et al.*, Eur. Phys. J. C **69**, 53 (2010), [arXiv:1003.3953].
- [149] F. Abe *et al.* (CDF), Phys. Rev. D **56**, 3811 (1997).
- [150] V. M. Abazov *et al.* (D0), Phys. Rev. D **93**, 5, 052008 (2016), [arXiv:1512.05291].
- [151] R. Aaij *et al.* (LHCb), JHEP **06**, 047 (2017), [Erratum: JHEP 10, 068 (2017)], [arXiv:1612.07451].
- [152] M. Aaboud *et al.* (ATLAS), Phys. Lett. B **790**, 595 (2019), [arXiv:1811.11094].
- [153] A. M. Sirunyan *et al.* (CMS), Eur. Phys. J. C **80**, 1, 41 (2020), [arXiv:1909.06265].
- [154] A. V. Manohar and W. J. Waalewijn, Phys. Rev. D **85**, 114009 (2012), [arXiv:1202.3794].
- [155] B. Blok *et al.*, Eur. Phys. J. C **74**, 2926 (2014), [arXiv:1306.3763].
- [156] M. Diehl, J. R. Gaunt and K. Schönwald, JHEP **06**, 083 (2017), [arXiv:1702.06486].
- [157] J. R. Gaunt and W. J. Stirling, JHEP **03**, 005 (2010), [arXiv:0910.4347].
- [158] K. Golec-Biernat *et al.*, Phys. Lett. B **750**, 559 (2015), [arXiv:1507.08583].
- [159] M. Diehl *et al.*, Eur. Phys. J. C **80**, 5, 468 (2020), [arXiv:2001.10428].
- [160] D. Flay *et al.* (Jefferson Lab Hall A), Phys. Rev. **D94**, 5, 052003 (2016), [arXiv:1603.03612].
- [161] C. Adolph *et al.* (COMPASS), Phys. Lett. **B753**, 18 (2016), [arXiv:1503.08935].
- [162] C. Adolph *et al.* (COMPASS), Phys. Lett. **B769**, 34 (2017), [arXiv:1612.00620].
- [163] R. Fersch *et al.* (CLAS), Phys. Rev. **C96**, 6, 065208 (2017), [arXiv:1706.10289].
- [164] M. Hirai and S. Kumano (Asymmetry Analysis), Nucl. Phys. **B813**, 106 (2009), [arXiv:0808.0413].
- [165] D. de Florian *et al.*, Phys. Rev. Lett. **101**, 072001 (2008), [arXiv:0804.0422]; D. de Florian *et al.*, Phys. Rev. **D80**, 034030 (2009), [arXiv:0904.3821].
- [166] E. Leader, A. V. Sidorov and D. B. Stamenov, Phys. Rev. **D82**, 114018 (2010), [arXiv:1010.0574].
- [167] J. Blumlein and H. Bottcher, Nucl. Phys. **B841**, 205 (2010), [arXiv:1005.3113].
- [168] D. de Florian *et al.*, Phys. Rev. Lett. **113**, 1, 012001 (2014), [arXiv:1404.4293].
- [169] N. Sato *et al.* (Jefferson Lab Angular Momentum), Phys. Rev. **D93**, 7, 074005 (2016), [arXiv:1601.07782].
- [170] D. de Florian *et al.*, Phys. Rev. **D91**, 1, 014035 (2015), [arXiv:1410.6027].
- [171] D. de Florian *et al.*, Phys. Rev. **D95**, 9, 094019 (2017), [arXiv:1702.06353].
- [172] V. Bertone *et al.* (NNPDF), Eur. Phys. J. **C77**, 8, 516 (2017), [arXiv:1706.07049].
- [173] V. Bertone *et al.* (NNPDF), Eur. Phys. J. **C78**, 8, 651 (2018), [arXiv:1807.03310].
- [174] L. Adamczyk *et al.* (STAR), Phys. Rev. Lett. **115**, 9, 092002 (2015), [arXiv:1405.5134].
- [175] L. Adamczyk *et al.* (STAR), Phys. Rev. D **95**, 7, 071103 (2017), [arXiv:1610.06616].
- [176] A. Adare *et al.* (PHENIX), Phys. Rev. D **90**, 1, 012007 (2014), [arXiv:1402.6296].
- [177] J. Adam *et al.* (STAR), Phys. Rev. D **99**, 5, 051102 (2019), [arXiv:1812.04817].
- [178] R. D. Ball *et al.* (NNPDF), Nucl. Phys. **B874**, 36 (2013), [arXiv:1303.7236].
- [179] J. Adam *et al.* (STAR), Phys. Rev. D **100**, 5, 052005 (2019), [arXiv:1906.02740].
- [180] M. Abdallah *et al.* (STAR), Phys. Rev. D **103**, 9, L091103 (2021), [arXiv:2103.05571].
- [181] A. Adare *et al.* (PHENIX), Phys. Rev. D **93**, 1, 011501 (2016), [arXiv:1510.02317].
- [182] D. De Florian *et al.*, Phys. Rev. D **100**, 11, 114027 (2019), [arXiv:1902.10548].
- [183] J. Liang *et al.*, Phys. Rev. D **98**, 7, 074505 (2018), [arXiv:1806.08366].
- [184] R. Nisius, Phys. Rept. **332**, 165 (2000), [hep-ex/9912049].
- [185] T. F. Walsh and P. M. Zerwas, Phys. Lett. **44B**, 195 (1973).
- [186] R. L. Kingsley, Nucl. Phys. **B60**, 45 (1973).
- [187] E. Witten, Nucl. Phys. **B120**, 189 (1977).
- [188] W. A. Bardeen and A. J. Buras, Phys. Rev. **D20**, 166 (1979), [Erratum: Phys. Rev. D21,2041(1980)].
- [189] M. Fontannaz and E. Pilon, Phys. Rev. **D45**, 382 (1992).
- [190] M. Gluck, E. Reya and A. Vogt, Phys. Rev. **D45**, 3986 (1992).
- [191] F. Cornet, P. Jankowski and M. Krawczyk, Phys. Rev. **D70**, 093004 (2004), [hep-ph/0404063].
- [192] P. Aurenche, M. Fontannaz and J. P. Guillet, Eur. Phys. J. **C44**, 395 (2005), [hep-ph/0503259].
- [193] W. Slominski, H. Abramowicz and A. Levy, Eur. Phys. J. **C45**, 633 (2006), [hep-ph/0504003].
- [194] H. Abramowicz and A. Caldwell, Rev. Mod. Phys. **71**, 1275 (1999), [hep-ex/9903037].
- [195] S. Chekanov *et al.* (ZEUS), Nucl. Phys. **B831**, 1 (2010), [arXiv:0911.4119].
- [196] A. Aktas *et al.* (H1), Eur. Phys. J. **C48**, 715 (2006), [hep-ex/0606004].
- [197] A. D. Martin, M. G. Ryskin and G. Watt, Phys. Lett. **B644**, 131 (2007), [hep-ph/0609273].
- [198] A. Aktas *et al.* (H1), JHEP **10**, 042 (2007), [arXiv:0708.3217].
- [199] F. D. Aaron *et al.* (H1, ZEUS), Eur. Phys. J. **C72**, 2175 (2012), [arXiv:1207.4864].
- [200] F. D. Aaron *et al.* (H1), Eur. Phys. J. **C72**, 2074 (2012), [arXiv:1203.4495].
- [201] J. C. Collins, Phys. Rev. **D57**, 3051 (1998), [Erratum: Phys. Rev. D61,019902(2000)], [hep-ph/9709499].
- [202] G. Ingelman and P. E. Schlein, Phys. Lett. **152B**, 256 (1985).
- [203] M. Goharipour, H. Khanpour and V. Guzey, Eur. Phys. J. **C78**, 4, 309 (2018), [arXiv:1802.01363].
- [204] X. Ji, Phys. Rev. Lett. **91**, 062001 (2003), [hep-ph/0304037].
- [205] A. V. Belitsky, X. Ji and F. Yuan, Phys. Rev. **D69**, 074014 (2004), [hep-ph/0307383].
- [206] C. Lorce, B. Pasquini and M. Vanderhaeghen, JHEP **05**, 041 (2011), [arXiv:1102.4704].
- [207] X.-D. Ji, J. Phys. **G24**, 1181 (1998), [hep-ph/9807358].
- [208] K. Goeke, M. V. Polyakov and M. Vanderhaeghen, Prog. Part. Nucl. Phys. **47**, 401 (2001), [hep-ph/0106012].
- [209] M. Diehl, Phys. Rept. **388**, 41 (2003), [hep-ph/0307382].

- [210] A. V. Belitsky and A. V. Radyushkin, Phys. Rept. **418**, 1 (2005), [hep-ph/0504030].
- [211] S. Boffi and B. Pasquini, Riv. Nuovo Cim. **30**, 387 (2007), [arXiv:0711.2625].
- [212] K. Kumericki, S. Liuti and H. Moutarde, Eur. Phys. J. **A52**, 6, 157 (2016), [arXiv:1602.02763].
- [213] M. Burkardt, Int. J. Mod. Phys. **A18**, 173 (2003), [hep-ph/0207047].
- [214] M. Diehl, Eur. Phys. J. **C25**, 223 (2002), [Erratum: Eur. Phys. J. **C31**, 277 (2003)], [hep-ph/0205208].
- [215] M. Bury, A. Prokudin and A. Vladimirov, JHEP **05**, 151 (2021), [arXiv:2103.03270].
- [216] A. V. Efremov and A. V. Radyushkin, Phys. Lett. **94B**, 245 (1980).
- [217] G. P. Lepage and S. J. Brodsky, Phys. Rev. **D22**, 2157 (1980).
- [218] A. V. Belitsky, A. Freund and D. Mueller, Phys. Lett. **B493**, 341 (2000), [hep-ph/0008005].
- [219] A. V. Belitsky, A. Freund and D. Mueller, Nucl. Phys. **B574**, 347 (2000), [hep-ph/9912379].
- [220] V. M. Braun *et al.*, JHEP **06**, 037 (2017), [arXiv:1703.09532].
- [221] A. V. Radyushkin, Phys. Rev. **D59**, 014030 (1999), [hep-ph/9805342].
- [222] A. V. Radyushkin, Phys. Lett. **B449**, 81 (1999), [hep-ph/9810466].
- [223] K. Kumericki and D. Mueller, Nucl. Phys. **B841**, 1 (2010), [arXiv:0904.0458].
- [224] N. d'Hose, S. Niccolai and A. Rostomyan, Eur. Phys. J. **A52**, 6, 151 (2016).
- [225] M. Guidal, H. Moutarde and M. Vanderhaeghen, Rept. Prog. Phys. **76**, 066202 (2013), [arXiv:1303.6600].
- [226] M. Anselmino, M. Guidal and P. Rossi, The European Physical Journal A **52**, 6, 149 (2016), ISSN 1434-601X, URL <https://doi.org/10.1140/epja/i2016-16164-4>.
- [227] P. J. Mulders and R. D. Tangerman, Nucl. Phys. **B461**, 197 (1996), [Erratum: Nucl. Phys. **B484**, 538 (1997)], [hep-ph/9510301].
- [228] D. Boer and P. J. Mulders, Phys. Rev. **D57**, 5780 (1998), [hep-ph/9711485].
- [229] D. W. Sivers, Phys. Rev. **D41**, 83 (1990).
- [230] J. C. Collins, Nucl. Phys. **B396**, 161 (1993), [hep-ph/9208213].
- [231] X. Ji, J. Ma and F. Yuan, Phys. Rev. **D71**, 034005 (2005), [hep-ph/0404183].
- [232] J. Collins, Foundations of perturbative QCD Camb. Monogr. Part. Phys. Nucl. Phys. Cosmol. **32** (2011) 1-624 and references therein.
- [233] S. M. Aybat and T. C. Rogers, Phys. Rev. **D83**, 114042 (2011), [arXiv:1101.5057].
- [234] M. G. Echevarria, A. Idilbi and I. Scimemi, JHEP **07**, 002 (2012), [arXiv:1111.4996].
- [235] M. G. A. Buffing, A. Mukherjee and P. J. Mulders, Phys. Rev. **D88**, 054027 (2013), [arXiv:1306.5897].
- [236] T. C. Rogers and P. J. Mulders, Phys. Rev. **D81**, 094006 (2010), [arXiv:1001.2977].
- [237] A. Signori *et al.*, JHEP **11**, 194 (2013), [arXiv:1309.3507].
- [238] M. Anselmino *et al.*, JHEP **04**, 005 (2014), [arXiv:1312.6261].
- [239] U. D'Alesio *et al.*, JHEP **11**, 098 (2014), [arXiv:1407.3311].
- [240] M. G. Echevarria *et al.*, Phys. Rev. **D89**, 074013 (2014), [arXiv:1401.5078].
- [241] P. Sun *et al.*, Int. J. Mod. Phys. **A33**, 11, 1841006 (2018), [arXiv:1406.3073].
- [242] A. Bacchetta *et al.*, JHEP **06**, 081 (2017), [Erratum: JHEP **06**, 051 (2019)], [arXiv:1703.10157].
- [243] I. Scimemi and A. Vladimirov, Eur. Phys. J. **C78**, 2, 89 (2018), [arXiv:1706.01473].
- [244] V. Bertone, I. Scimemi and A. Vladimirov, JHEP **06**, 028 (2019), [arXiv:1902.08474].
- [245] J. O. Gonzalez-Hernandez *et al.*, Phys. Rev. **D98**, 11, 114005 (2018), [arXiv:1808.04396].
- [246] A. Bacchetta *et al.*, Phys. Rev. **D100**, 1, 014018 (2019), [arXiv:1901.06916].
- [247] R. Angeles-Martinez *et al.*, Acta Phys. Polon. **B46**, 12, 2501 (2015), [arXiv:1507.05267].
- [248] A. Bacchetta *et al.*, Phys. Lett. **B788**, 542 (2019), [arXiv:1807.02101].
- [249] M. Diehl, Eur. Phys. J. **A52**, 6, 149 (2016), [arXiv:1512.01328].
- [250] A. Bacchetta, Eur. Phys. J. **A52**, 6, 163 (2016).
- [251] <http://hepdata.cedar.ac.uk/pdfs>.
- [252] I. Scimemi, Adv. High Energy Phys. **2019**, 3142510 (2019), [arXiv:1901.08398].

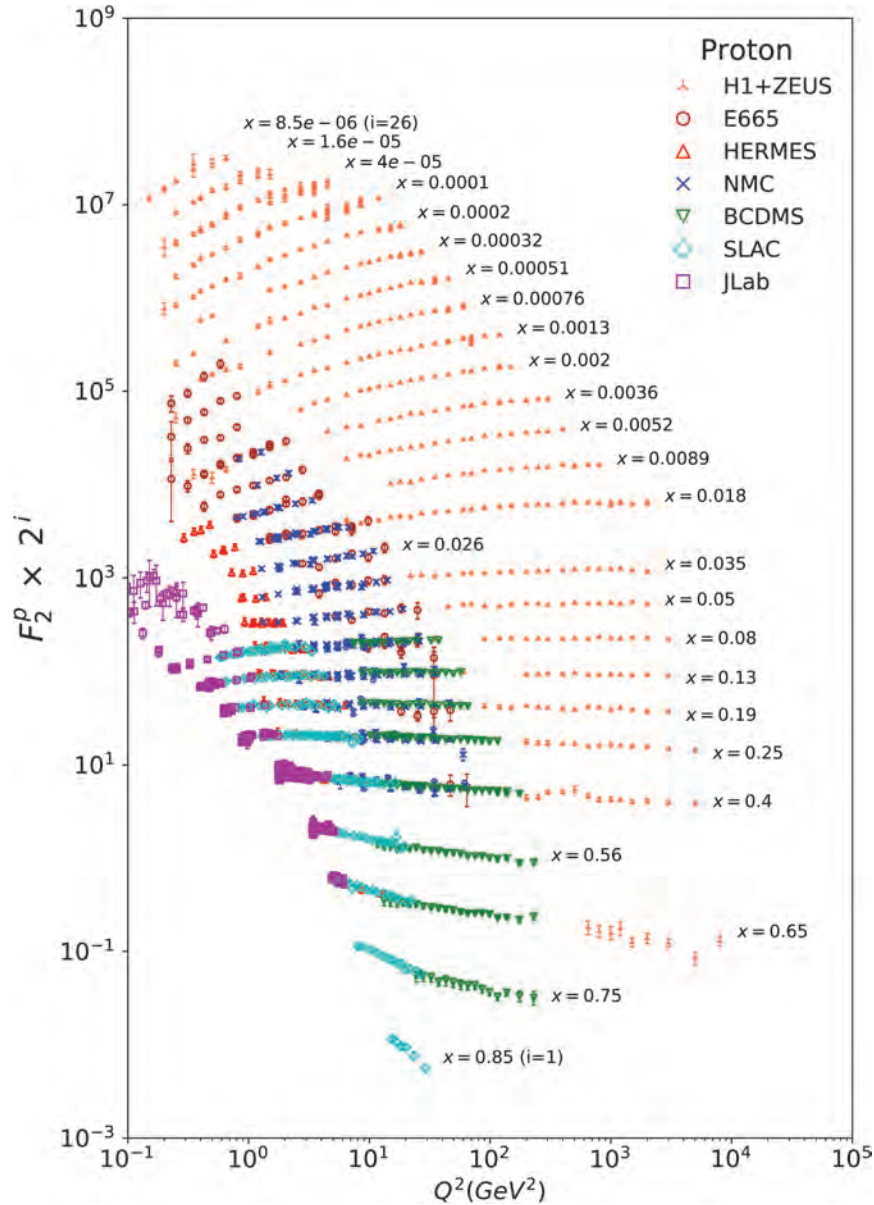


Figure 18.10: The proton structure function F_2^p measured in electromagnetic scattering of electrons and positrons on protons, and for electrons/positrons (SLAC, HERMES, JLAB) and muons (BCDMS, E665, NMC) on a fixed target. Statistical and systematic errors added in quadrature are shown. The H1+ZEUS combined values are obtained from the measured reduced cross section and converted to F_2^p with a HERAPDF NLO fit, for all measured points where the predicted ratio of F_2^p to reduced cross-section was within 10% of unity. The data are plotted as a function of Q^2 in bins of fixed x . Some points have been slightly offset in Q^2 for clarity. The H1+ZEUS combined binning in x is used in this plot; all other data are rebinned to the x values of these data. For the purpose of plotting, F_2^p has been multiplied by 2^{i_x} , where i_x is the number of the x bin, ranging from $i_x = 1$ ($x = 0.85$) to $i_x = 26$ ($x = 0.0000085$). Only data with $W^2 > 3.5 \text{ GeV}^2$ is included. Plot from CJ collaboration (Shujie Li – private communication).

References: **H1 and ZEUS**—H. Abramowicz *et al.*, *Eur. Phys. J.* **C75**, 580 (2015) (for both data and HERAPDF parameterization); **BCDMS**—A.C. Benvenuti *et al.*, *Phys. Lett.* **B223**, 485 (1989) (as given in [251]); **E665**—M.R. Adams *et al.*, *Phys. Rev.* **D54**, 3006 (1996); **NMC**—M. Arneodo *et al.*, *Nucl. Phys.* **B483**, 3 (1997); **SLAC**—L.W. Whitlow *et al.*, *Phys. Lett.* **B282**, 475 (1992); **HERMES**—A. Airapetian *et al.*, *JHEP* **1105**, 126 (2011); **JLAB**—Y. Liang *et al.*, Jefferson Lab Hall C E94-110 collaboration, nucl-ex/0410027, M.E. Christy *et al.*, Jefferson Lab Hall C E94-110 Collaboration, *Phys. Rev.* **C70**, 015206 (2004), S. Malace *et al.*, Jefferson Lab Hall C E00-116 Collaboration, *Phys. Rev.* **C80**, 035207 (2009), V. Tvasakis *et al.*, Jefferson Lab Hall C E99-118 Collaboration, *Phys. Rev.* **C81**, 055207 (2010), M. Osipenko *et al.*, Jefferson Lab Hall B CLAS6 Collaboration, *Phys. Rev.* **D67**, 092001 (2003).

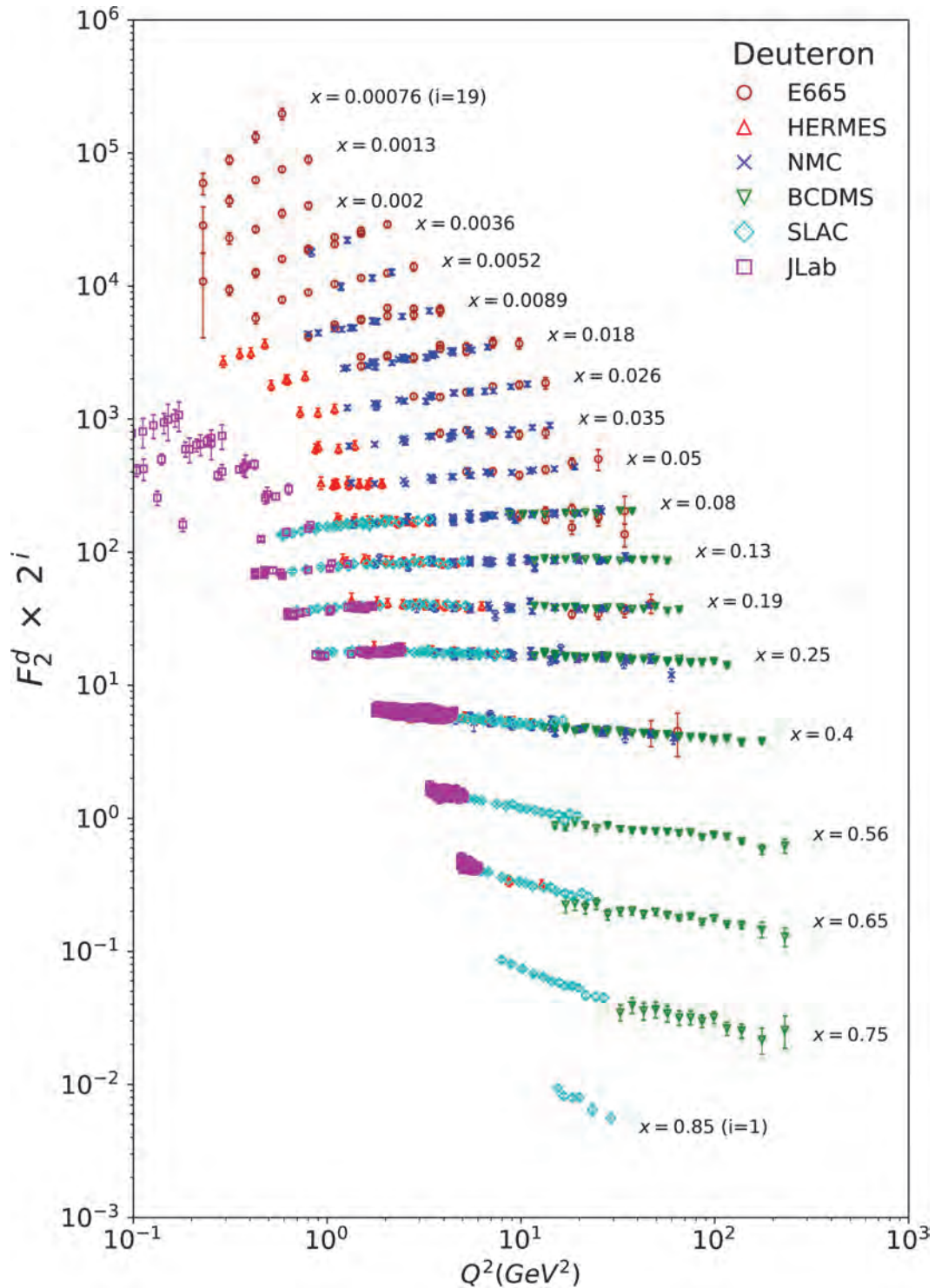


Figure 18.11: The deuteron structure function F_2^d measured in electromagnetic scattering of electrons/positrons (SLAC, HERMES, JLAB) and muons (BCDMS, E665, NMC) on a fixed target, shown as a function of Q^2 for bins of fixed x . Statistical and systematic errors added in quadrature are shown. For the purpose of plotting, F_2^d has been multiplied by 2^{i_x} , where i_x is the number of the x bin, ranging from 1 ($x = 0.85$) to 29 ($x = 0.00076$). Only data with $W^2 > 3.5 \text{ GeV}^2$ is included. Plot from CJ collaboration (Shujie Li – private communication) References: **BCDMS**—A.C. Benvenuti *et al.*, Phys. Lett. **B237**, 592 (1990). **E665**, **NMC**, **SLAC**, **HERMES**—same references as Fig. 18.10; **JLAB**—S. Malace *et al.*, Jefferson Lab Hall C E00-116 Collaboration, Phys. Rev. **C80**, 035207 (2009), V. Tvaskis *et al.*, Jefferson Lab Hall C E99-118 Collaboration, Phys. Rev. **C81**, 055207 (2010), J. Seely (MIT, LNS) *et al.*, Jefferson Lab Hall C E03-103 Collaboration, Phys. Rev. Lett. **103**, 202301 (2009), M. Osipenko *et al.*, Jefferson Lab Hall B CLAS6 Collaboration, Phys. Rev. **C73**, 045205 (2006).

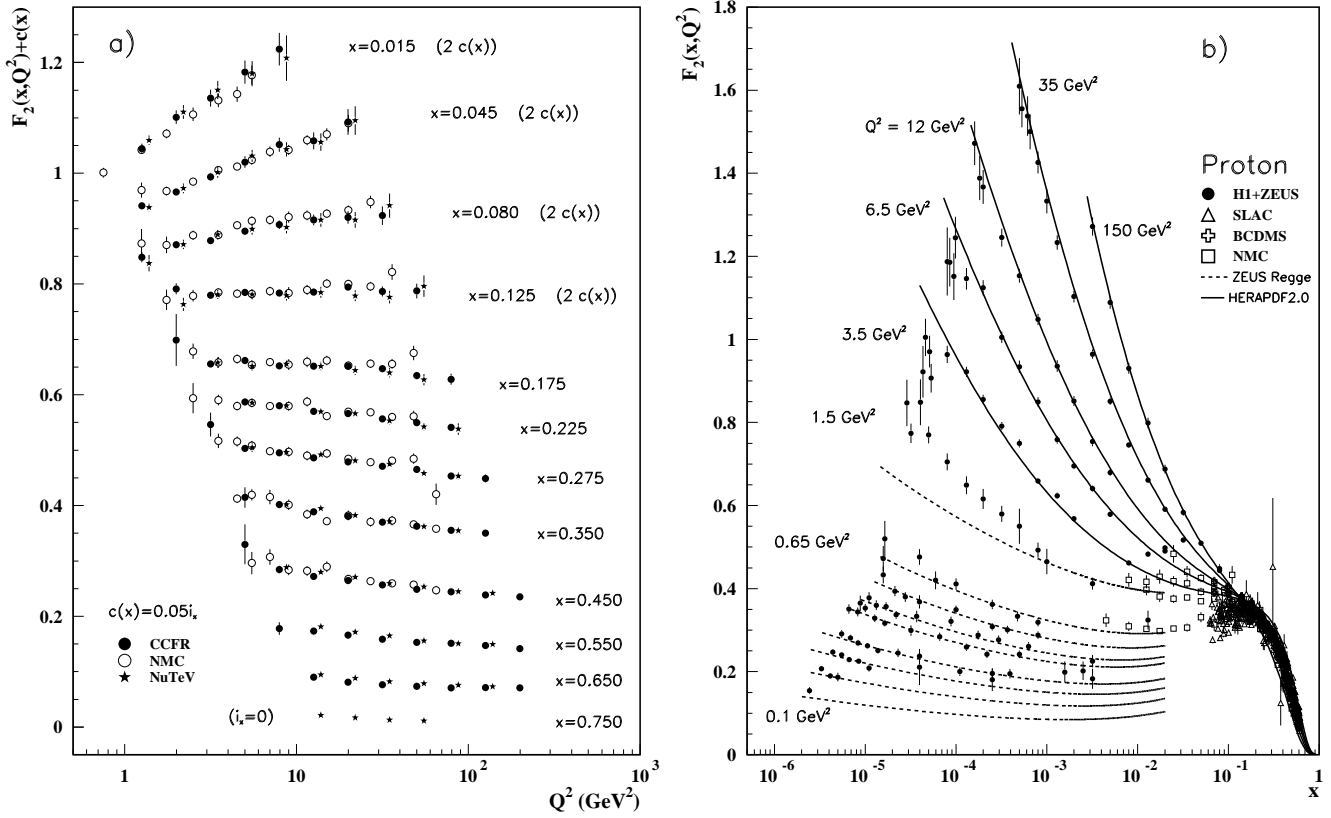


Figure 18.12: a) The deuteron structure function F_2 measured in deep inelastic scattering of muons on a fixed target (NMC) is compared to the structure function F_2 from neutrino-iron scattering (CCFR and NuTeV) using $F_2^\mu = (5/18)F_2^p - x(s + \bar{s})/6$, where heavy-target effects have been taken into account. The data are shown versus Q^2 , for bins of fixed x . The NMC data have been rebinned to CCFR and NuTeV x values. For the purpose of plotting, a constant $c(x) = 0.05i_x$ is added to F_2 , where i_x is the number of the x bin, ranging from 0 ($x = 0.75$) to 7 ($x = 0.175$). For $i_x = 8$ ($x = 0.125$) to 11 ($x = 0.015$), $2c(x)$ has been added. References: NMC—M. Arneodo *et al.*, Nucl. Phys. **B483**, 3 (1997); CCFR/NuTeV—U.K. Yang *et al.*, Phys. Rev. Lett. **86**, 2741 (2001); NuTeV—M. Tzanov *et al.*, Phys. Rev. **D74**, 012008 (2006). b) The proton structure function F_2^p mostly at small x and Q^2 , measured in electromagnetic scattering of electrons and positrons (H1, ZEUS), electrons (SLAC), and muons (BCDMS, NMC) on protons. Lines are ZEUS Regge and HERAPDF parameterizations for lower and higher Q^2 , respectively. The width of the bins can be up to 10% of the stated Q^2 . Some points have been slightly offset in x for clarity. The H1+ZEUS combined values for $Q^2 \geq 3.5$ GeV² are obtained from the measured reduced cross section and converted to F_2^p with a HERAPDF NLO fit, for all measured points where the predicted ratio of F_2^p to reduced cross-section was within 10% of unity. A turn-over is visible in the low- x points at medium Q^2 (3.5 GeV² and 6 GeV²) for the H1+ZEUS combined values. In order to obtain F_2^p from the measured reduced cross-section, F_L must be estimated; for the points shown, this estimate is obtained from HERAPDF2.0. No F_L value consistent with the HERA data can eliminate the turn-over. This may indicate that at low x and Q^2 there are contributions to the structure functions that cannot be described in standard DGLAP evolution.

References: H1 and ZEUS—F.D. Aaron *et al.*, JHEP **1001**, 109 (2010) (data for $Q^2 < 3.5$ GeV²), H. Abramowicz *et al.*, Eur. Phys. J. **C75**, 580 (2015) (data for $Q^2 \geq 3.5$ GeV² and HERAPDF parameterization); ZEUS—J. Breitweg *et al.*, Phys. Lett. **B487**, 53 (2000) (ZEUS Regge parameterization); BCDMS, NMC, SLAC—same references as Fig. 18.10.

Statistical and systematic errors added in quadrature are shown for both plots.

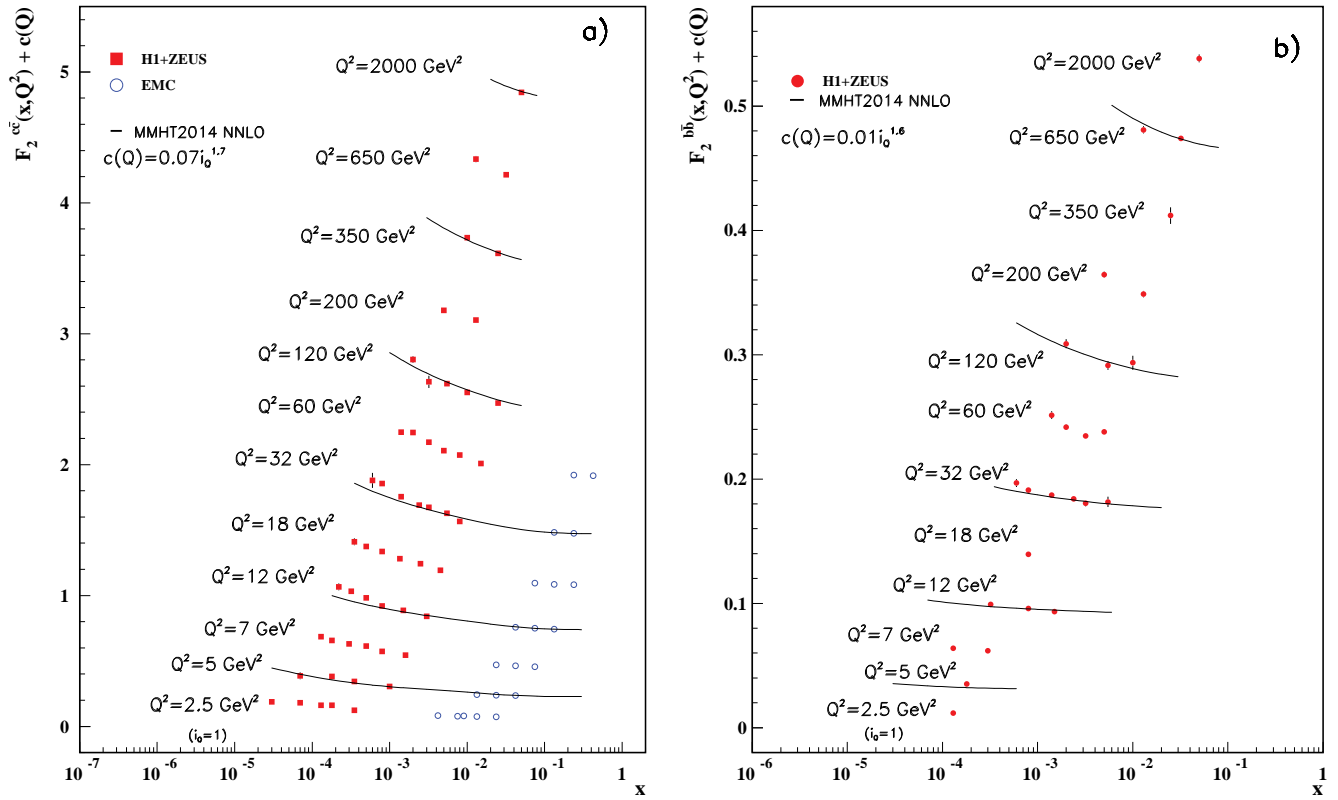


Figure 18.13: a) The charm-quark structure function $F_2^{c\bar{c}}(x)$, i.e. that part of the inclusive structure function F_2^p arising from the production of charm quarks, measured in electromagnetic scattering of positrons on protons (H1, ZEUS) (the values are obtained from the measured reduced cross section and converted to $F_2^{c\bar{c}}$ using the PDFs from the MMHT NNLO fit) and muons on iron (EMC). For the purpose of plotting, a constant $c(Q) = 0.07i_Q^{1.7}$ is added to $F_2^{c\bar{c}}$ where i_Q is the number of the Q^2 bin, ranging from 1 ($Q^2 = 2.5 \text{ GeV}^2$) to 12 ($Q^2 = 2000 \text{ GeV}^2$). References: **H1 and ZEUS run I +II combination**—H. Abramowicz *et al.*, *Eur. Phys. J.* **C78**, 473 (2018); **EMC**—J.J. Aubert *et al.*, *Nucl. Phys.* **B213**, 31 (1983).

b) The bottom-quark structure function $F_2^{b\bar{b}}(x)$. For the purpose of plotting, a constant $c(Q) = 0.01i_Q^{1.6}$ is added to $F_2^{b\bar{b}}$ where i_Q is the number of the Q^2 bin, ranging from 1 ($Q^2 = 2.5 \text{ GeV}^2$) to 12 ($Q^2 = 2000 \text{ GeV}^2$). References: **H1 and ZEUS run I combination**—H. Abramowicz *et al.*, *Eur. Phys. J.* **C78**, 473 (2018).

For both plots, statistical and systematic errors added in quadrature are shown. The data are given as a function of x in bins of Q^2 . Points may have been slightly offset in x for clarity. Some data have been rebinned to common Q^2 values. Also shown is the MMHT2014 parameterization given at several Q^2 values (L. A. Harland-Lang *et al.*, *Eur. Phys. J.* **C75**, 204 (2015)).

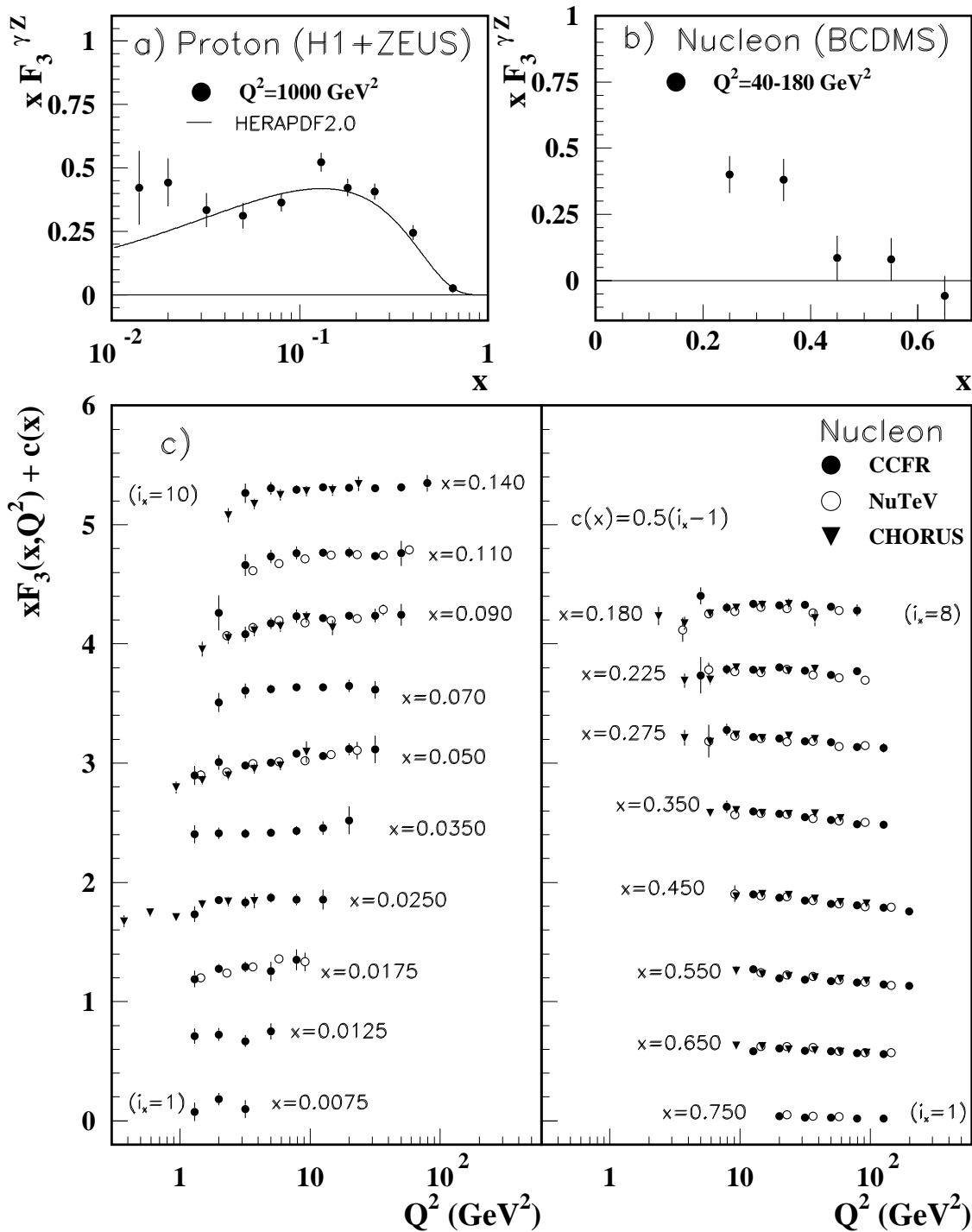


Figure 18.14: The structure function $x F_3^{\gamma Z}$ measured in electroweak scattering of **a)** electrons on protons (H1 and ZEUS) and **b)** muons on carbon (BCDMS). The line in **a)** is the HERAPDF parameterization. References: **H1 and ZEUS**—H. Abramowicz *et al.*, *Eur. Phys. J.* **C75**, 580 (2015) (for both data and HERAPDF parameterization); **BCDMS**—A. Argento *et al.*, *Phys. Lett.* **B140**, 142 (1984). **c)** The structure function $x F_3$ of the nucleon measured in ν -Fe scattering. The data are plotted as a function of Q^2 in bins of fixed x . For the purpose of plotting, a constant $c(x) = 0.5(i_x - 1)$ is added to $x F_3$, where i_x is the number of the x bin as shown in the plot. The NuTeV and CHORUS points have been shifted to the nearest corresponding x bin as given in the plot and slightly offset in Q^2 for clarity. References: **CCFR**—W.G. Seligman *et al.*, *Phys. Rev. Lett.* **79**, 1213 (1997); **NuTeV**—M. Tzanov *et al.*, *Phys. Rev.* **D74**, 012008 (2006); **CHORUS**—G. Öngüt *et al.*, *Phys. Lett.* **B632**, 65 (2006).

Statistical and systematic errors added in quadrature are shown for all plots.

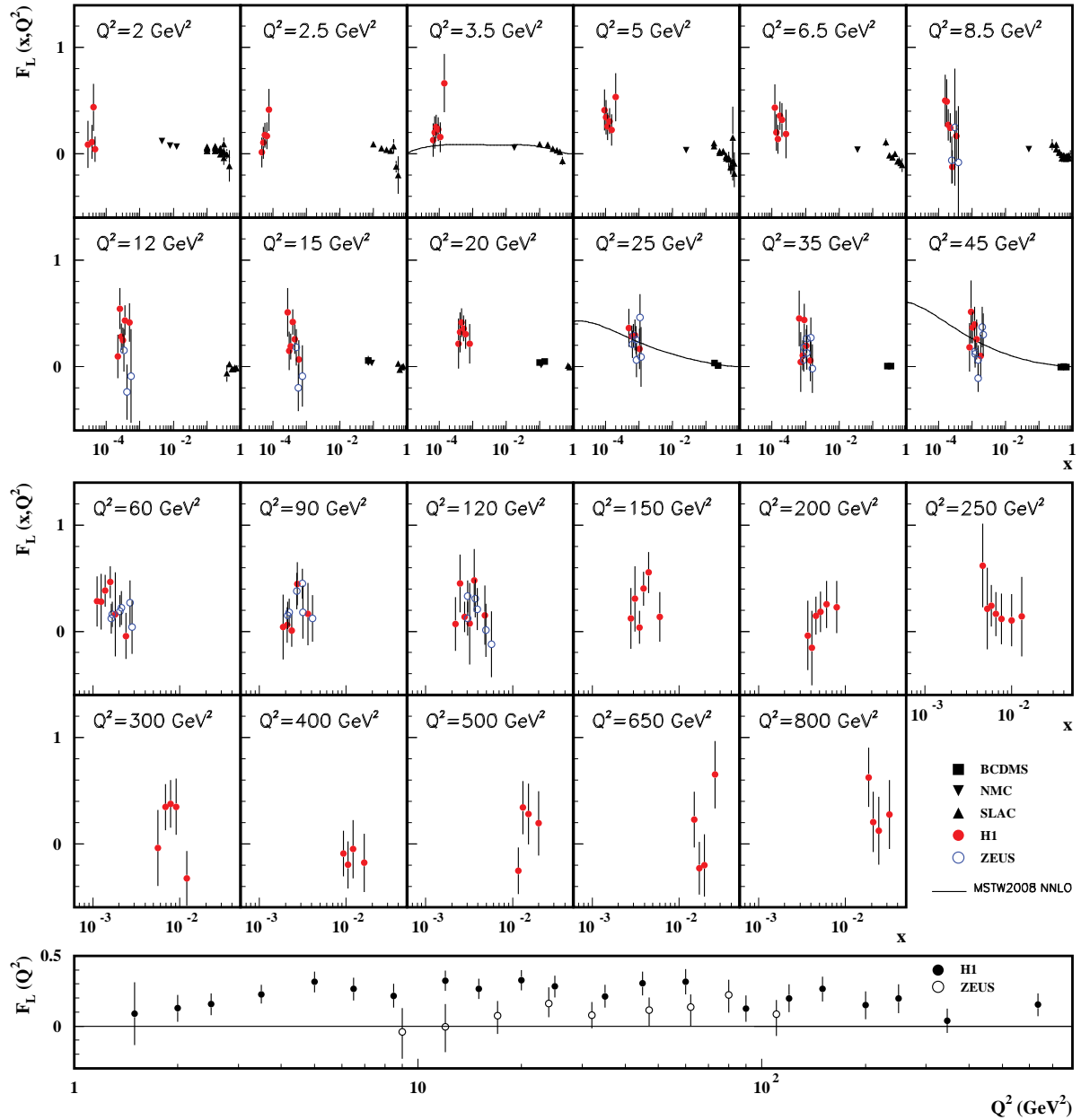


Figure 18.15: Top panels: The longitudinal structure function F_L as a function of x in bins of fixed Q^2 measured on the proton (except for the SLAC data which also contain deuterium data). BCDMS, NMC, and SLAC results are from measurements of R (the ratio of longitudinal to transverse photon absorption cross sections) which are converted to F_L by using the BDCMS parameterization of F_2 (A.C. Benvenuti *et al.*, Phys. Lett. **B223**, 485 (1989)). It is assumed that the Q^2 dependence of the fixed-target data is small within a given Q^2 bin. Some of the other data may have been rebinned to common Q^2 values. Some points have been slightly offset in x for clarity. Also shown is the MSTW2008 parameterization given at three Q^2 values (A.D. Martin *et al.*, Eur. Phys. J. **C63**, 189 (2009)). References: **H1**—V. Andreev *et al.*, Eur. Phys. J. **C74**, 2814 (2014); **ZEUS**—S. Chekanov *et al.*, Phys. Lett. **B682**, 8 (2009); H. Abramowicz *et al.*, Phys. Rev. **D90**, 072002 (2014); **BCDMS**—A. Benvenuti *et al.*, Phys. Lett. **B223**, 485 (1989); **NMC**—M. Arneodo *et al.*, Nucl. Phys. **B483**, 3 (1997); **SLAC**—L.W. Whitlow *et al.*, Phys. Lett. **B250**, 193 (1990) and numerical values from the thesis of L.W. Whitlow (SLAC-357). Bottom panel: The longitudinal structure function F_L as a function of Q^2 . Some points have been slightly offset in Q^2 for clarity. References: **H1**—V. Andreev *et al.*, Eur. Phys. J. **C74**, 2814 (2014); **ZEUS**—H. Abramowicz *et al.*, Phys. Rev. **D90**, 072002 (2014). The results shown in the bottom plot require the assumption of the validity of the QCD form for the F_2 structure function in order to extract F_L . Statistical and systematic errors added in quadrature are shown for both plots.

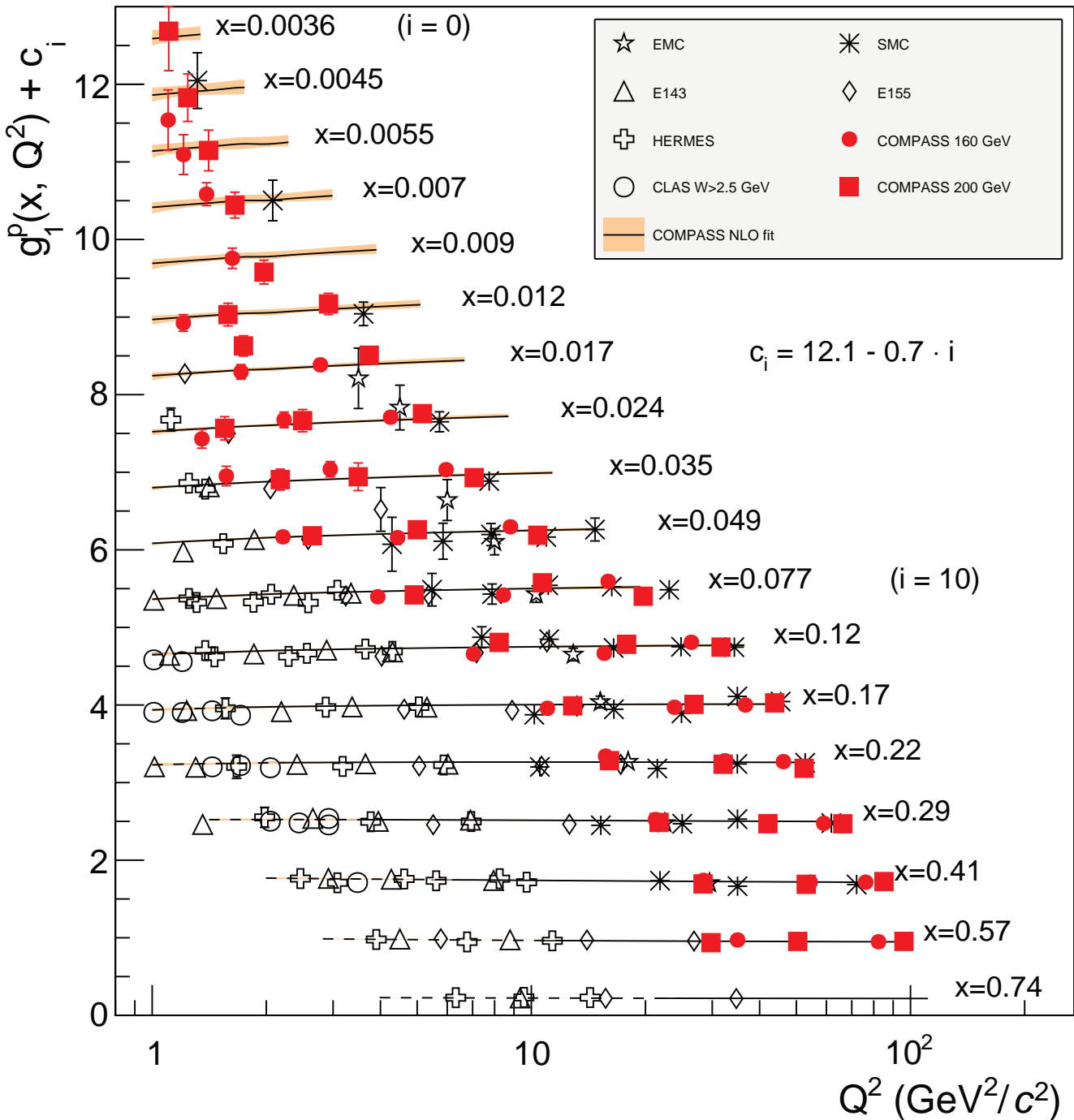


Figure 18.16: World data on the spin-dependent structure function g_1^p as a function of Q^2 for various values of x . The lines represent the Q^2 dependence for each value of x , as determined from a NLO QCD fit. The dashed ranges represent the region with $W^2 < 10$ (GeV/c²)². References: **EMC**—J. Ashman *et al.*, Phys. Lett. **B206**, 363 (1988); Nucl. Phys. **B328**, 1 (1989); **E143**—K. Abe *et al.*, Phys. Rev. **D58**, 112003 (1998); **SMC**—B. Adeva *et al.*, Phys. Rev. **D58**, 112001 (1998); **HERMES**—A. Airapetian *et al.*, Phys. Rev. **D75**, 012007 (2007); **E155**—P.L. Anthony *et al.*, Phys. Lett. **B493**, 19 (2000); **COMPASS**—M.G. Alekseev *et al.*, Phys. Lett. **B690**, 466 (2010), C. Adolph, *et al.*, Phys. Lett. **B753**, 18 (2016); **CLAS**—K.V. Dharmawardane *et al.*, Phys. Lett. **B641**, 11 (2006) (which also includes resonance region data not shown on this plot — there is also low W^2 CLAS data in Y. Prok *et al.*, Phys. Rev. **C90**, 025212 (2014) and N. Guler *et al.*, Phys. Rev. **C92**, 055201 (2015)).

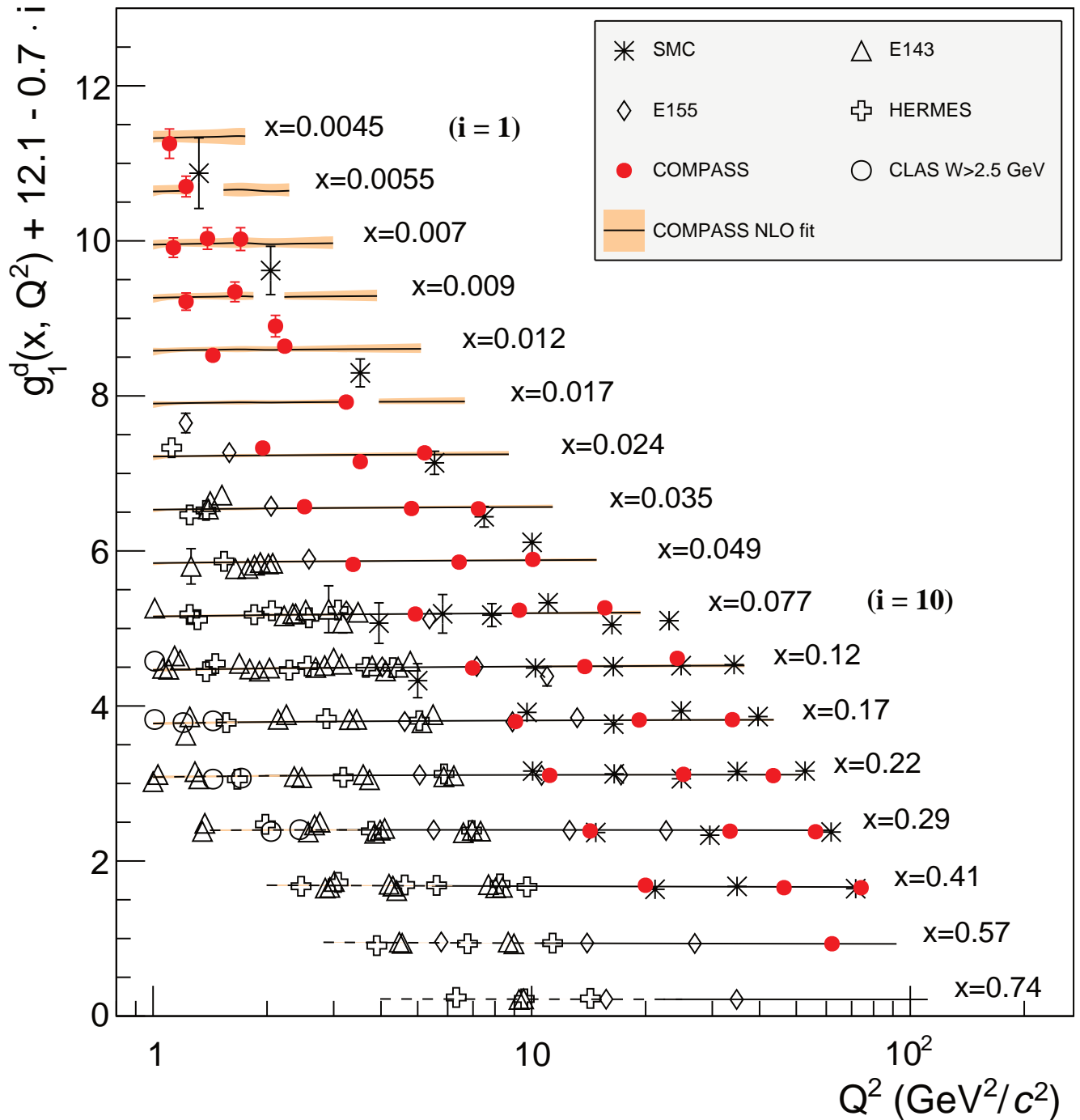


Figure 18.17: World data on the spin-dependent structure function g_1^d as a function of Q^2 for various values of x . The lines represent the Q^2 dependence for each value of x , as determined from a NLO QCD fit. The dashed ranges represent the region with $W^2 < 10$ (GeV/c^2)². **CLAS**—K.V. Dharmawardane *et al.*, Phys. Lett. **B641**, 11 (2006) **HERMES**—A. Airapetian *et al.*, Phys. Rev. **D75**, 012007 (2007); **SMC**—B. Adeva *et al.*, Phys. Rev. **D58**, 112001 (1998); **E155**—P.L. Anthony *et al.*, Phys. Lett. **B463**, 339 (1999); **E143**—K. Abe *et al.*, Phys. Rev. **D58**, 112003 (1998); **COMPASS**—C. Adolph, *et al.*, Phys. Lett. **B769**, 34 (2017);

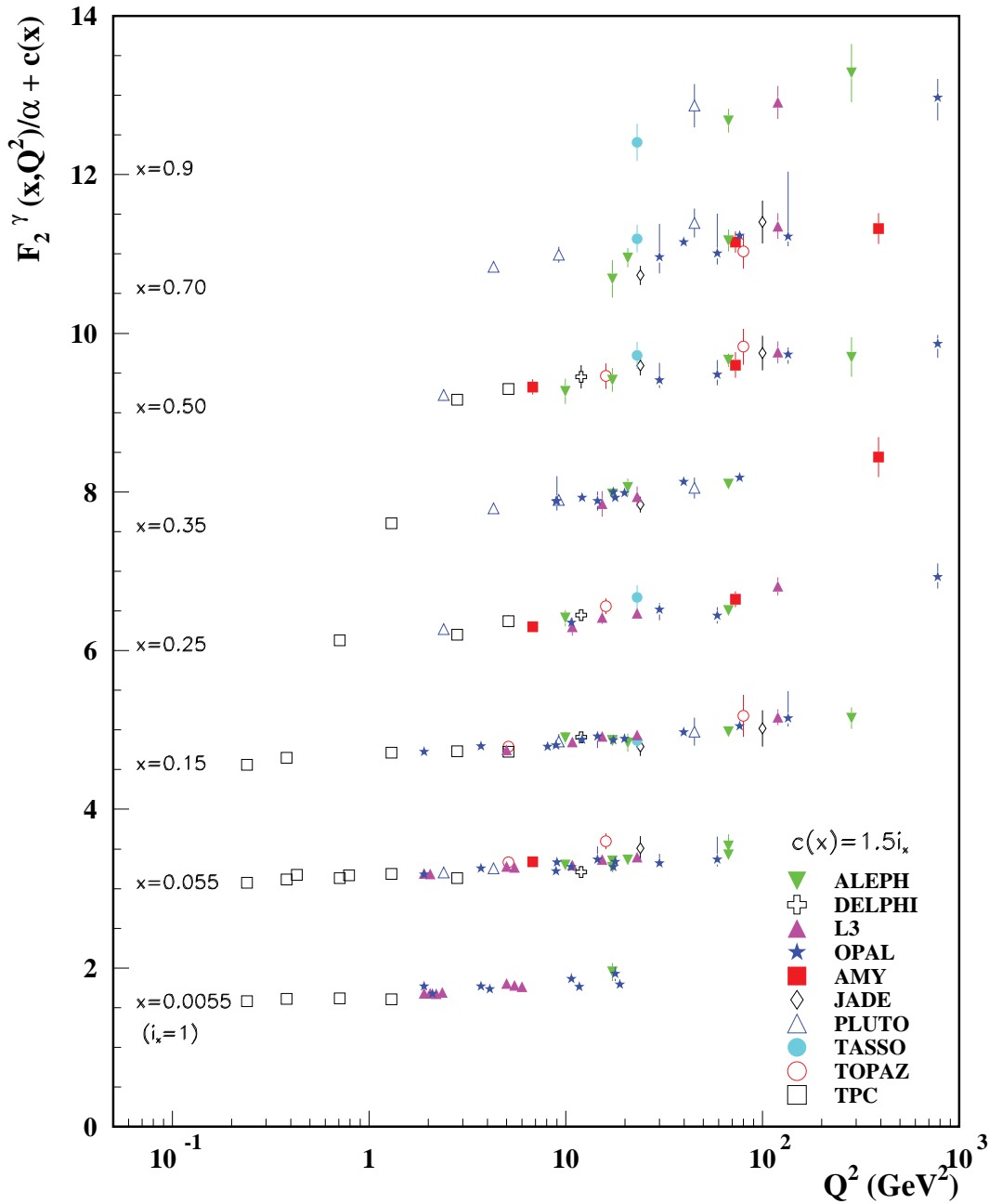


Figure 18.18: The hadronic structure function of the photon F_2^γ divided by the fine structure constant α measured in e^+e^- scattering, shown as a function of Q^2 for bins of x . Data points have been shifted to the nearest corresponding x bin as given in the plot. Some points have been offset in Q^2 for clarity. Statistical and systematic errors added in quadrature are shown. For the purpose of plotting, a constant $c(x) = 1.5i_x$ is added to F_2^γ/α where i_x is the number of the x bin, ranging from 1 ($x = 0.0055$) to 8 ($x = 0.9$). References: **ALEPH**–R. Barate *et al.*, Phys. Lett. **B458**, 152 (1999); A. Heister *et al.*, Eur. Phys. J. **C30**, 145 (2003); **DELPHI**–P. Abreu *et al.*, Z. Phys. **C69**, 223 (1995); **L3**–M. Acciarri *et al.*, Phys. Lett. **B436**, 403 (1998); M. Acciarri *et al.*, Phys. Lett. **B447**, 147 (1999); M. Acciarri *et al.*, Phys. Lett. **B483**, 373 (2000); **OPAL**–A. Ackerstaff *et al.*, Phys. Lett. **B411**, 387 (1997); A. Ackerstaff *et al.*, Z. Phys. **C74**, 33 (1997); G. Abbiendi *et al.*, Eur. Phys. J. **C18**, 15 (2000); G. Abbiendi *et al.*, Phys. Lett. **B533**, 207 (2002) (note that there is overlap of the data samples in these last two papers); **AMY**–S.K. Sahu *et al.*, Phys. Lett. **B346**, 208 (1995); T. Kojima *et al.*, Phys. Lett. **B400**, 395 (1997); **JADE**–W. Bartel *et al.*, Z. Phys. **C24**, 231 (1984); **PLUTO**–C. Berger *et al.*, Phys. Lett. **142B**, 111 (1984); C. Berger *et al.*, Nucl. Phys. **B281**, 365 (1987); **TASSO**–M. Althoff *et al.*, Z. Phys. **C31**, 527 (1986); **TOPAZ**–K. Muramatsu *et al.*, Phys. Lett. **B332**, 477 (1994); **TPC/Two Gamma**–H. Aihara *et al.*, Z. Phys. **C34**, 1 (1987).

19. Fragmentation Functions in e^+e^- , ep , and pp Collisions

Revised August 2021 by O. Biebel (Ludwig-Maximilians U.), D. de Florian (ICAS and ICIFI, UNSAM), D. Milstead (Stockholm U.) and W. Vogelsang (Tübingen U.).

19.1 Introduction to fragmentation

Quarks and gluons produced in hard-scattering reactions will ultimately give rise to the colorless hadronic bound states that may be observed in the detector. The associated hadronization process is described by fragmentation functions $D_i^h(x, \mu^2)$ ($i = q, \bar{q}, g$) which are universal functions representing, in the simplest picture, a measure of the probability density that an outgoing parton produces a hadron h . Here, x is the fraction of the parton's momentum transferred to the hadron, and μ is a 'resolution' scale known as factorization scale. The $D_i^h(x, \mu^2)$ may be viewed as the final-state analogs of the initial-state parton distribution functions (PDFs) addressed in Section 18 of this *Review*. They are also sometimes referred to as *timelike* distributions since they are primarily accessed in e^+e^- annihilation via a timelike intermediate boson. (See Refs. [1,2] for introductory reviews, and Refs. [3–5] for summaries of experimental and theoretical research in this field.)

The cleanest laboratory for the study of fragmentation functions is provided by semi-inclusive electron-positron annihilation, $e^+e^- \rightarrow \gamma/Z \rightarrow h+X$. The cross section for this reaction may be expressed in terms of 'fragmentation structure functions' $F_{T,L,A}$ that are directly related to the fragmentation functions. At center-of-mass (CM) energy $\sqrt{s} = q^2$ we have

$$\frac{1}{\sigma_0} \frac{d^2\sigma^h}{dx d\cos\theta} = \frac{3}{8}(1 + \cos^2\theta)F_T^h(x, q^2) + \frac{3}{4}\sin^2\theta F_L^h(x, q^2) + \frac{3}{4}\cos\theta F_A^h(x, q^2). \quad (19.1)$$

Here, q is the four-momentum of the intermediate photon or Z -boson, with $q^2 > 0$, and $x = 2P_h \cdot q/q^2$ with the hadron's four-momentum P_h is the fragmentation counterpart of the familiar DIS Bjorken variable. (Note that $x = 2E_h/\sqrt{s} \leq 1$ in terms of the energy E_h of the produced hadron in the CM frame of the electron positron pair.) Furthermore, in the same frame, θ is the hadron's angle relative to the electron beam direction. Eq. (19.1) is the most general form for unpolarized inclusive single-particle production via vector bosons [6]. The fragmentation structure functions F_T and F_L represent the contributions from γ/Z polarizations transverse or longitudinal with respect to the direction of motion of the hadron. The parity-violating term with the asymmetric fragmentation function F_A arises from the interference between vector and axial-vector contributions. Various normalization factors σ_0 are used in the literature, ranging from the total cross section σ_{tot} for $e^+e^- \rightarrow \text{hadrons}$, including all weak and QCD contributions, to $\sigma_0 = 4\pi\alpha^2 N_c/3s$ with $N_c = 3$, the lowest-order QED cross section for $e^+e^- \rightarrow \mu^+\mu^-$ times the number of colors N_c . LEP1 measurements of the three fragmentation structure functions are shown in Fig. 19.1.

Integration of Eq. (19.1) over all θ yields the total fragmentation structure function $F^h = F_T^h + F_L^h$:

$$\frac{1}{\sigma_0} \frac{d\sigma^h}{dx} = F^h(x, q^2) = \sum_i \int_x^1 \frac{dz}{z} C_i \left(z, \alpha_s(\mu), \frac{q^2}{\mu^2} \right) D_i^h \left(\frac{x}{z}, \mu^2 \right). \quad (19.2)$$

On the right we have written the factorized expression for the structure function in terms of a sum over convolutions of the fragmentation functions D_i^h for partons $i = u, \bar{u}, d, \bar{d}, \dots, g$ with perturbative coefficient functions C_i . Since photons and Z bosons do not distinguish between quarks and antiquarks, e^+e^- annihilation primarily constrains the combinations $D_q^h + D_{\bar{q}}^h$. Gluon fragmentation contributes only at higher order in perturbation theory or by scaling violations. Corrections to the factorized expression in Eq. (19.2) are suppressed by inverse powers of q^2 . They arise from quark and hadron mass terms and from non-perturbative effects.

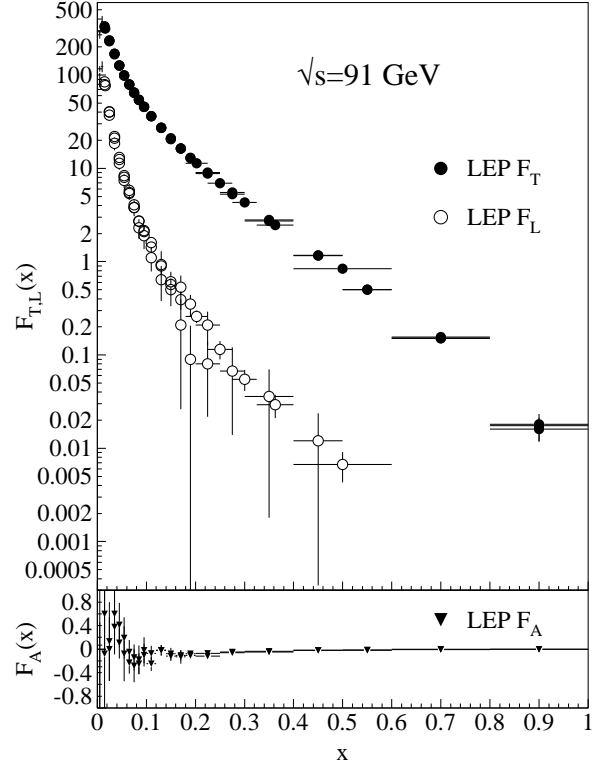


Figure 19.1: LEP1 measurements of total transverse (F_T), longitudinal (F_L), and asymmetric (F_A) fragmentation structure functions [7]. Data points with relative errors greater than 100% are omitted.

Analogous factorized expressions as in Eq. (19.2) may be written for each of the structure functions $F_{T,L,A}$ individually.

The fragmentation functions obey the momentum sum rule constraint

$$\sum_h \int_0^1 dx x D_i^h(x, \mu^2) = 1, \quad (19.3)$$

separately for each flavor i . Note that the sum rule involves a sum over all possible produced hadrons. The dependence of the functions D_i^h on the factorization scale μ^2 will be discussed in the next section.

Measurements of hadron production in deeply-inelastic lepton-proton scattering and hadron-hadron scattering are complementary to those in e^+e^- annihilation. The former process, $\ell p \rightarrow \ell' + h + X$, is known as *semi-inclusive deep-inelastic scattering (SIDIS)*. Here, in analogy with Eq. (19.2), the high virtuality of the photon in DIS also permits factorization of the cross section in terms of fragmentation functions, PDFs for the incoming proton, and perturbative hard-scattering cross sections. Likewise, factorization also occurs for $pp \rightarrow h + X$ at large transverse momentum of the produced hadron, and for $pp \rightarrow \text{jet}(h) + X$, where the hadron is part of a fully reconstructed jet. The fragmentation functions contributing to $e^+e^- \rightarrow h + X$, $\ell p \rightarrow \ell' + h + X$, and $pp \rightarrow h + X$, $pp \rightarrow \text{jet}(h) + X$ are universal in the sense that the same functions appear in the factorized expressions for the three reactions. Modern QCD analyses of fragmentation functions “globally” take into account experimental data sets for all three types of processes in order to obtain optimal sets of fragmentation functions.

Electron-positron annihilation has the advantage that there is no hadronic initial state and hence no beam remnant. This is in contrast to $\ell p \rightarrow \ell' + h + X$ or $pp \rightarrow h + X$, which are affected by hadron remnant contributions associated with the partons of the initial-state hadron(s) which are collaterally involved in the hard lepton-parton or parton-parton collision. On the other hand,

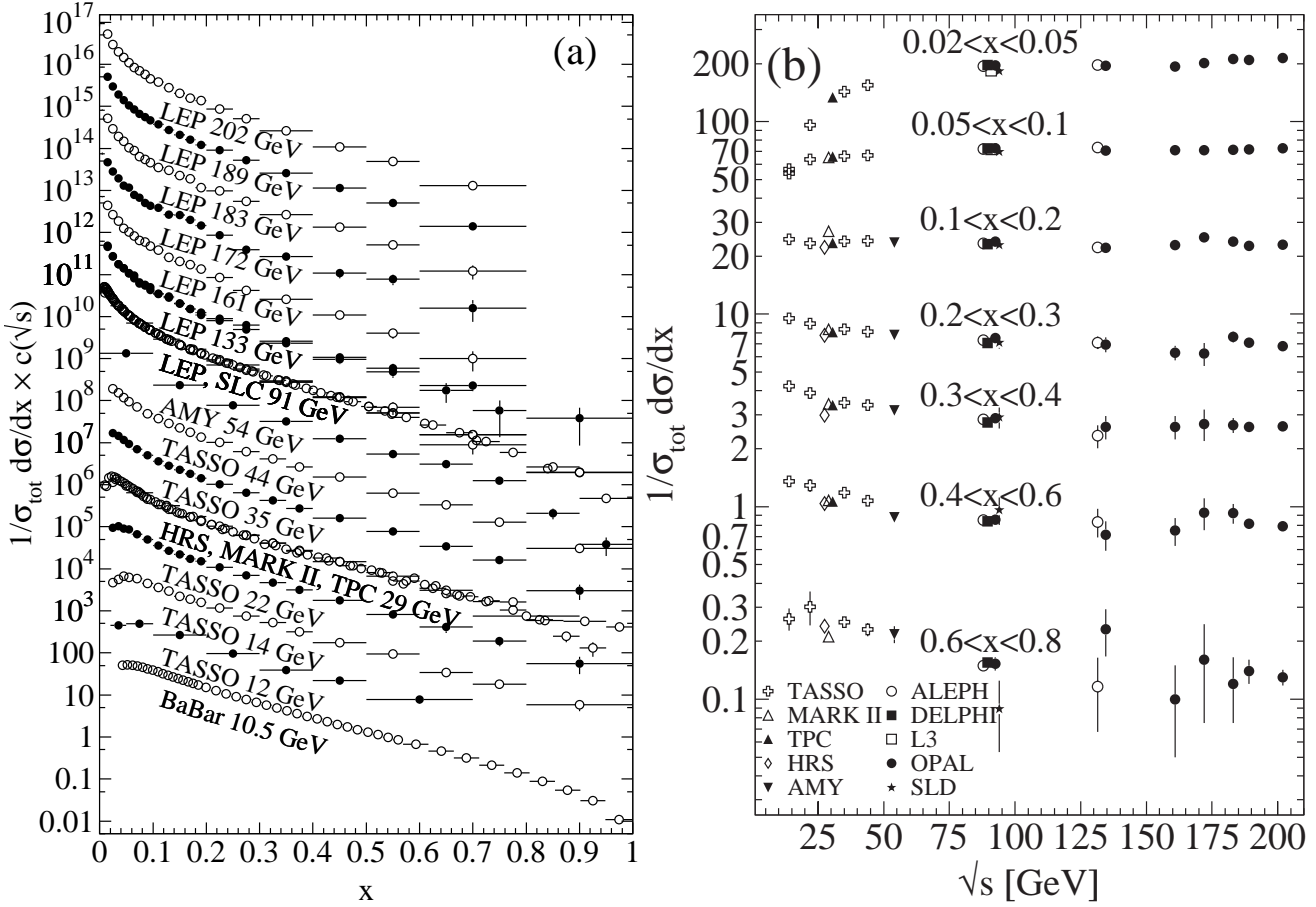


Figure 19.2: Cross section for $e^+e^- \rightarrow h + X$ for all charged hadrons [8–26], (a) for different CM energies \sqrt{s} versus x , and (b) for various ranges of x versus \sqrt{s} . For (a) the distributions have been scaled by $c(\sqrt{s}) = 10^i$ with i ranging from $i = 0$ ($\sqrt{s} = 12$ GeV) to $i = 13$ ($\sqrt{s} = 202$ GeV).

$e^+e^- \rightarrow h + X$ has little sensitivity to D_q^h and is insensitive to the charge asymmetries $D_q^h - D_{\bar{q}}^h$. These quantities are best constrained in proton-(anti-)proton and electron-proton scattering, respectively. Especially the latter provides an environment that allows the study of the influence of initial-state QCD radiation on the fragmentation process, of the partonic and spin structure of the hadron target, and of the target remnant system. (See Ref. [27] for a comprehensive review of the measurements and models of fragmentation in lepton-hadron scattering).

Moreover, unlike e^+e^- annihilation where $q^2 = s$ is fixed by the collider energy, lepton-hadron scattering has two independent scales, $Q^2 = -q^2$ and the invariant mass squared, $W^2 \approx Q^2(1-x)/x$, of the hadronic final state, which both can vary by several orders of magnitudes for a given CM energy, thus allowing the study of fragmentation in different environments by a single experiment. For example, in photoproduction the exchanged photon is quasi-real ($Q^2 \approx 0$), leading to processes akin to hadron-hadron scattering. In DIS ($Q^2 \gg 1$ GeV²), using factorization, the hadronic fragments of the struck quark can be directly compared with quark fragmentation in e^+e^- in a suitable frame. Results from lepton-hadron experiments quoted in this report primarily concern fragmentation in the DIS regime. Studies performed by lepton-hadron experiments of fragmentation with photoproduction data containing high transverse momentum jets or particles are also reported, when these are directly comparable to DIS and e^+e^- results.

Fragmentation studies in lepton-hadron collisions are usually performed in one of two frames in which the target hadron and the exchanged boson are collinear. The hadronic center-of-mass frame (HCMS) is defined as the rest system of the exchanged boson and incoming hadron, with the z^* -axis defined along the direction of the exchanged boson. The positive z^* direction de-

fines the so-called current fragmentation region. Fragmentation measurements performed in the HCMS often use the Feynman- x variable $x_F = 2p_z^*/W$, where p_z^* is the longitudinal momentum of the particle in this frame. As W is the invariant mass of the hadronic final state, x_F ranges between -1 and 1 .

The Breit system [28, 29] is related to the HCMS by a longitudinal boost such that the time component of q vanishes, i.e., $q = (0, 0, 0, -Q)$. In the parton model, the struck parton then has the longitudinal momentum $Q/2$ which becomes $-Q/2$ after the collision. As compared with the HCMS, the current fragmentation region of the Breit frame is more closely matched to the partonic scattering process, and is thus appropriate for direct comparisons of fragmentation functions in DIS with those from e^+e^- annihilation. The variable $x_p = 2p^*/Q$, where p^* is the particle's momentum in the current region of the Breit frame, is used at HERA for measurements in the Breit frame, enabling rather direct comparisons of DIS and e^+e^- results.

19.2 Scaling violations and QCD corrections

As mentioned, the coefficient functions for the fragmentation structure functions in $e^+e^- \rightarrow h + X$ are amenable to QCD perturbation theory. For each of the structure functions $F_{T,L,A}(x, q^2)$ in Eq. (19.1) (and hence for the total structure function F^h in Eq. (19.2)) the coefficient function has an expansion of the form

$$C_{a,i} \left(z, \alpha_s(\mu), \frac{q^2}{\mu^2} \right) = (1 - \delta_{aL}) \delta_{iq} \delta(1-z) + \frac{\alpha_s(\mu)}{2\pi} c_{a,i}^{(1)} \left(z, \frac{q^2}{\mu^2} \right) + \left(\frac{\alpha_s(\mu)}{2\pi} \right)^2 c_{a,i}^{(2)} \left(z, \frac{q^2}{\mu^2} \right) + \dots (19.4)$$

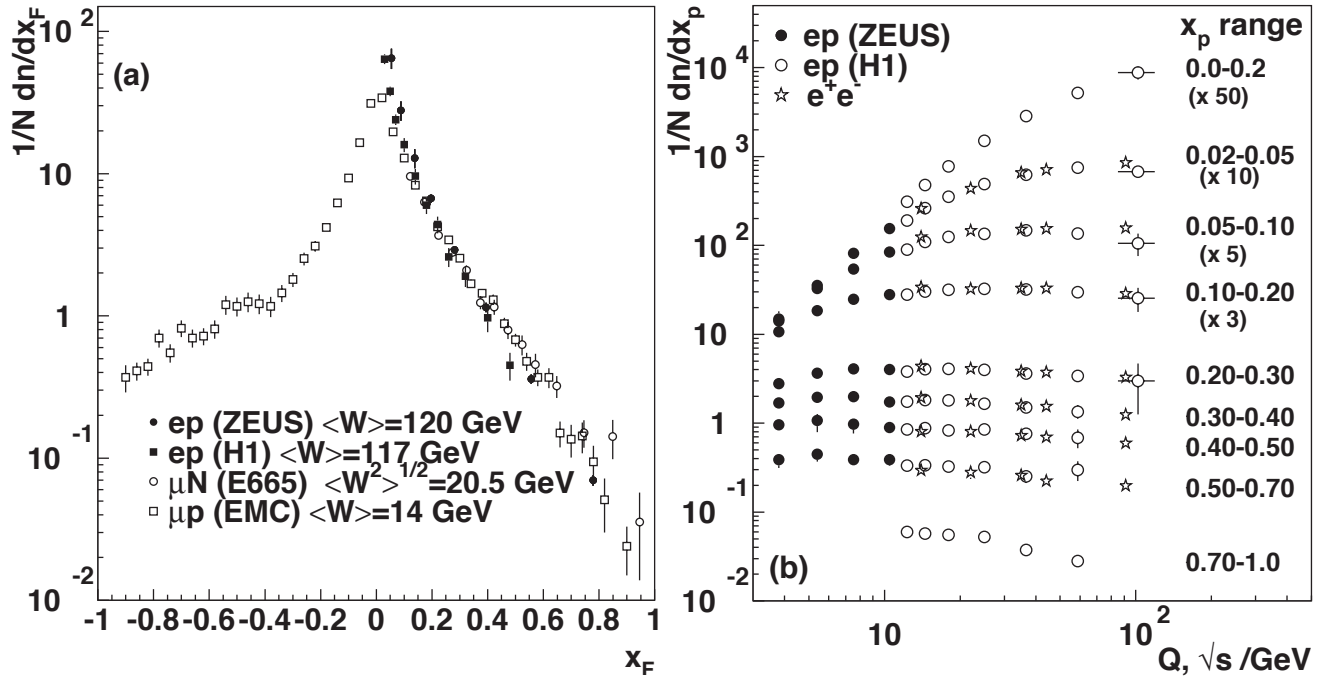


Figure 19.3: (a) The distribution $1/N \cdot dn/dx_F$ for all charged particles in DIS lepton-hadron experiments at different values of W , measured in the HCMS [30–33]. (b) Scaling violations of the fragmentation structure function for all charged particles in the current region of the Breit frame of DIS [34,35] and in e^+e^- interactions [19,36]. The data are shown as a function of \sqrt{s} for e^+e^- results, and as a function of Q for the DIS results, each within the same indicated intervals of the scaled momentum x_p . The data for the four lowest intervals of x_p are multiplied by factors 50, 10, 5, and 3, respectively for better visibility.

where $a = T, L, A$. At the zeroth order in the strong coupling α_s the coefficient functions C_g for gluons vanish, while for (anti-)quarks $C_i = g_i(s) \delta(1-z)$ (except for F_L for which the leading contribution is of order α_s , as indicated in Eq. (19.4)). Here $g_i(s)$ is the appropriate electroweak coupling. In particular, $g_i(s)$ is proportional to the squared charge of the quark i at $s \ll M_Z^2$, when weak effects can be neglected. The full electroweak prefactors $g_i(s)$ can be found in Ref. [6]. The first-order QCD corrections to the coefficient functions have been calculated in Refs. [37,38], and the second-order terms in [39–41]. Thus, the coefficient functions are known to NNLO, except for F_L . We note that beyond the leading order the coefficient functions, and hence the fragmentation functions, start to depend on the choice of factorization scheme. The standard choice in the literature is the $\overline{\text{MS}}$ scheme.

The simplest parton-model approach would predict scale-independent (‘scaling’) x -distributions for both the structure function F^h and the parton fragmentation functions D_i^h . Perturbative QCD corrections lead to logarithmic scaling violations via the evolution equations [42]

$$\frac{\partial}{\partial \ln \mu^2} D_i^h(x, \mu^2) = \sum_j \int_x^1 \frac{dz}{z} P_{ji}(z, \alpha_s(\mu^2)) D_j^h\left(\frac{x}{z}, \mu^2\right), \quad (19.5)$$

where the functions $P_{ij}(z, \alpha_s(\mu^2))$ describe the splitting process $i \rightarrow j + X$, where parton j carries the longitudinal momentum fraction z of parton i . Note that for fragmentation the relevant splitting functions are P_{ji} (rather than P_{ij} as for the PDFs) since D_j^h represents the fragmentation of the final parton. Usually the system of evolution equations is decomposed into a 2×2 flavor-singlet sector comprising the gluon and the sum of all quark and antiquark fragmentation functions, and scalar (‘non-singlet’) equations for quark-antiquark and flavor differences.

The splitting functions in Eq. (19.5) have the perturbative expansion

$$P_{ji}(z, \alpha_s) = \frac{\alpha_s}{2\pi} P_{ji}^{(0)}(z) + \left(\frac{\alpha_s}{2\pi}\right)^2 P_{ji}^{(1)}(z) + \left(\frac{\alpha_s}{2\pi}\right)^3 P_{ji}^{(2)}(z) + \dots, \quad (19.6)$$

where the leading-order (LO) functions $P^{(0)}(z)$ [42, 43] are the same as those for the initial-state parton distributions. The next-to-leading order (NLO) corrections $P^{(1)}(z)$ have been calculated in Refs. [44–48] (there are well-known misprints in the journal version of Ref. [45]). Ref. [48] also includes the spin-dependent case. The timelike functions are different from, but related to, their spacelike counterparts, see also Ref. [49]. The connections between the two sets of functions has facilitated recent calculations of the next-to-next-to-leading order (NNLO) quantities $P_{qq}^{(2)}(z)$ and $P_{gg}^{(2)}(z)$ in Eq. (19.6) [40,50]. In the same way, the corresponding off-diagonal quantities $P_{qg}^{(2)}$ and $P_{gq}^{(2)}$ were recently obtained in Ref. [51] with the help of constraints from the momentum sum rule Eq. (19.3) [50] and of the limit of $C_A = C_F = n_f$ for which QCD becomes supersymmetric. An uncertainty still remains for the $P_{qg}^{(2)}$ kernel, which however does not affect the logarithmic behavior at small and large momentum fractions. With the exception of Ref. [47], all these higher-order results refer to the standard $\overline{\text{MS}}$ scheme with a fixed number n_f of light flavors. When the threshold for the production of a heavier quark flavor is crossed in the course of the scale evolution, fragmentation functions change. The NLO treatment of these flavor thresholds in the evolution has been addressed in Ref. [52].

The phenomenological effect of scale evolution is similar in the timelike and spacelike cases: As the scale increases, one observes a scaling violation in which the x -distribution is shifted towards lower values. This can be seen from Fig. 19.2 where a set of measurements of the total fragmentation structure function in e^+e^- annihilation are shown. In particular, the figure on the right exhibits the dependence on $\sqrt{q^2} = \sqrt{s}$ at fixed values of x . QCD analyses of these data are discussed in Section 19.5 below.

The NLO coefficient functions for SIDIS, $ep \rightarrow e + h + X$, have been presented in Refs. [37, 38] Corresponding results have also been obtained for the case that a non-vanishing hadron transverse momentum is required in the HCMS frame [53,54].

Scaling violations in DIS are shown in Fig. 19.3 for both the HCMS and the Breit frames. In Fig. 1.3(a) the distribution in terms of $x_F = 2p_z^*/W$ shows a steeper slope in ep data than for the lower-energy μp data for $x_F > 0.15$, indicating the scaling

violations. At smaller values of x_F in the current jet region, the multiplicity of particles substantially increases with W , owing to the increased phase space available for the fragmentation process. The EMC data access both the current region and the region of the fragmenting target remnant system. At higher values of $|x_F|$, due to the extended nature of the remnant, the multiplicity in the target region far exceeds that in the current region. For acceptance reasons the remnant hemisphere of the HCMS is only accessible by the lower-energy fixed-target experiments.

Using hadrons from the current hemisphere in the Breit frame, measurements of fragmentation functions and the production properties of particles in ep scattering have been reported in Refs. [34, 35, 55–58]. Fig. 19.3(b) compares results from ep scattering and e^+e^- experiments; the latter results have been divided by two as they cover both event hemispheres. The agreement between the DIS and e^+e^- results is fairly good. However, processes in DIS which are not present in e^+e^- annihilation, such as boson-gluon fusion and initial-state QCD radiation, can depopulate the current region. These effects become most prominent at low values of Q and x_p . Hence, when compared with e^+e^- annihilation data at $\sqrt{s} = 5.2, 6.5$ GeV [59] not shown here, the DIS particle rates tend to lie below those observed in e^+e^- annihilation. A ZEUS study [60] finds that the direct comparability of the ep data to e^+e^- results at low scales is improved if twice the energy in the current hemisphere of the Breit frame, $2E_B^{cr}$, is used instead of $Q/2$ as the fragmentation scale. Choosing $2E_B^{cr}$ for the fragmentation scale approximates QCD radiation effects relevant at low scales, as detailed in Ref. [29].

19.3 Fragmentation functions for small particle momenta

The higher-order timelike splitting functions in Eq. (19.6) are singular at small values of x . They show a double-logarithmic enhancement, with leading terms of the form $\alpha_s^k (\ln^{2k-2} x)/x$ at the k th order of perturbation theory, corresponding to poles $\alpha_s^k (N-1)^{1-2k}$ for the Mellin moments

$$P^{(k)}(N) = \int_0^1 dx x^{N-1} P^{(k)}(x). \quad (19.7)$$

Despite large cancellations between leading and non-leading logarithms at non-asymptotic values of x , the resulting small- x rise in the timelike splitting functions dwarfs that of their spacelike counterparts for the evolution of the parton distributions in Section 18 of this *Review*, see Fig. 1 of Ref. [50]. Consequently, in fragmentation the fixed-order approximation to the evolution breaks down orders of magnitude earlier in x than in DIS.

The pattern of the known coefficients and other considerations suggest that the double-logarithmic terms sum to all-order expressions without any pole at $N = 1$, such as [61, 62]

$$P_{gg}^{LL}(N) = -\frac{1}{4} \left(N - 1 - \sqrt{(N-1)^2 \cdot 24 \alpha_s / \pi} \right) \quad (19.8)$$

for the gluon-to-gluon splitting function at leading logarithmic order. Keeping the first three terms in the resulting expansion of Eq. (19.5) around $N = 1$ and taking the Mellin inverse yields a Gaussian in the variable $\xi = \ln(1/x)$ for the small- x fragmentation functions,

$$xD(x, q^2 = s) \propto \exp \left[-\frac{1}{2\sigma^2} (\xi - \xi_p)^2 \right], \quad (19.9)$$

with the peak position and width varying with the energy as [63] (see also Ref. [2])

$$\xi_p \simeq \frac{1}{4} \ln \left(\frac{s}{\Lambda^2} \right), \quad \sigma \propto \left[\ln \left(\frac{s}{\Lambda^2} \right) \right]^{3/4}. \quad (19.10)$$

Next-to-leading logarithmic corrections to the above predictions have been calculated [64]. In the method of Ref. [65], see also Refs. [66, 67], the corrections are included in an analytical form known as the ‘modified leading logarithmic approximation’ (MLLA). Alternatively they can be used to compute higher-moment correc-

tions to the shape in Eq. (19.9) [68]. The small- x resummation of the coefficient functions for semi-inclusive e^+e^- annihilation and of the timelike spitting functions in the standard $\overline{\text{MS}}$ scheme was extended in Refs. [69–73] and has reached full next-to-next-to-leading logarithmic accuracy. Applications of these results to gluon and quark jet multiplicities have been presented in Refs. [74].

Fig. 19.4 shows the ξ distribution for charged particles produced in the current region of the Breit frame in DIS and in e^+e^- annihilation. Consistently with Eq. (19.9) (the ‘hump backed plateau’) and Eq. (19.10) the distributions have a Gaussian shape, with the peak position and area increasing with CM energy (e^+e^-) and Q^2 (DIS).

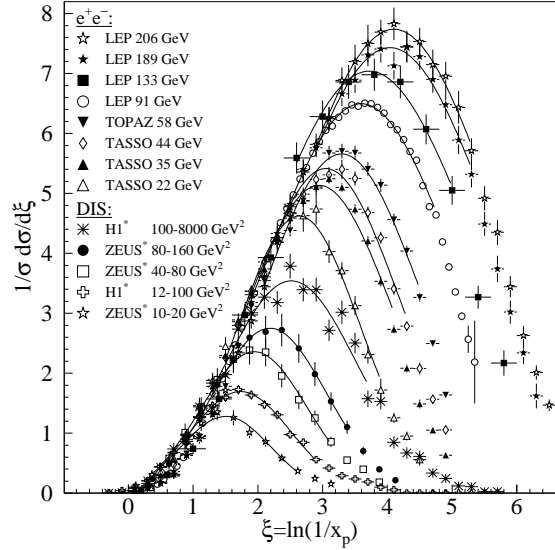


Figure 19.4: Distribution of the normalized fragmentation cross sections in $\xi = \ln(1/x_p)$ at several CM energies (e^+e^-) [10, 11, 16–19, 57, 58, 75–78] and for intervals of Q^2 (DIS). At each energy only one representative measurement is displayed. For clarity some measurements at intermediate CM energies (e^+e^-) or Q^2 ranges (DIS) are not shown. The DIS measurements (*) have been scaled by a factor of 2 for direct comparability with the e^+e^- results. Fits of simple Gaussian functions are overlaid for illustration.

The predicted energy dependence of the peak in the ξ distribution (see Eq. (19.10)) is explained by soft gluon coherence (angular ordering), *i.e.*, the destructive interference of the color wavefunction of low energy gluon radiation, which correctly predicts the suppression of hadron production at small x . Of course, a decrease at very small x is expected on purely kinematical grounds, but this would occur at particle energies proportional to their masses, *i.e.*, at $x \propto m/\sqrt{s}$ and hence $\xi \sim \frac{1}{2} \ln s$. Thus, if the suppression were purely kinematic, the peak position ξ_p would vary twice as rapidly with the energy, which is ruled out by the data in Fig. 19.5. The e^+e^- and DIS data agree well with each other, demonstrating the universality of hadronization and the MLLA prediction. Measurements of the higher moments of the ξ distribution in e^+e^- [19, 78–80] and DIS [58] have also been performed and show consistency with each other.

The average charged-particle multiplicity is another observable sensitive to fragmentation functions for small particle momenta. Perturbative predictions using both NLO [89] and MLLA [90, 91] have been obtained by solving Eq. (19.5) yielding

$$\langle n_G(Q^2) \rangle \propto \alpha_s^b(Q^2) \cdot \exp \left[\frac{c}{4\pi b_0 \sqrt{\alpha_s(Q^2)}} \cdot \left(1 + 6a_2 \frac{\alpha_s(Q^2)}{\pi} \right) \right], \quad (19.11)$$

where $b = \frac{1}{4} + \frac{10}{27} \frac{n_f}{4\pi b_0}$, $c = \sqrt{96\pi}$, with $b_0 = (33 - 2n_f)/(12\pi)$, cf. Section 9 of this *Review*, for n_f contributing quark flavors. Higher-order corrections to Eq. (19.11) are known up to next-to-next-to-next-to-leading order (N³LO), for details and references

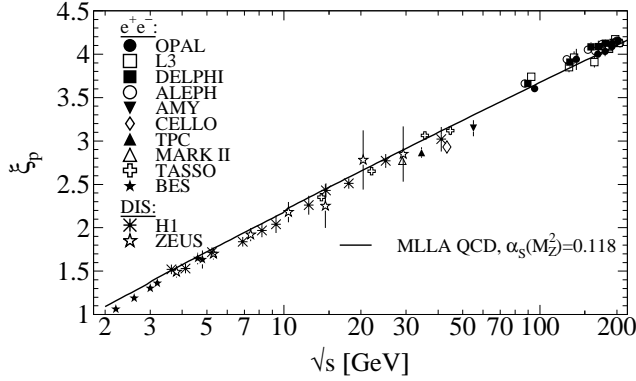


Figure 19.5: Evolution of the peak position, ξ_p , of the ξ distribution with the CM energy \sqrt{s} . The MLLA QCD prediction using $\alpha_s(s = M_Z^2) = 0.118$ is superimposed to the data of Refs. [10, 12, 15, 19, 56, 57, 76, 77, 80–88].

see [92]. The term proportional to $a_2 \approx -0.502 + 0.0421 n_f - 0.00036 n_f^2$ in Eq. (19.11) is the contribution due to NNLO corrections [93]. The quantity $\langle n_G(Q^2) \rangle$ refers to the average number of gluons, while for $\langle n_q(Q^2) \rangle$ for quarks a correction factor $1/r$ is required due to the different color factors in quark and gluon couplings, so that $\langle n_q(Q^2) \rangle = \langle n_G(Q^2) \rangle / r$. The correction factor depends only weakly on Q^2 ; higher-order corrections up to $N^3\text{LO}$ on the asymptotic value $r = C_A/C_F = 9/4$ [94] are quoted in [92].

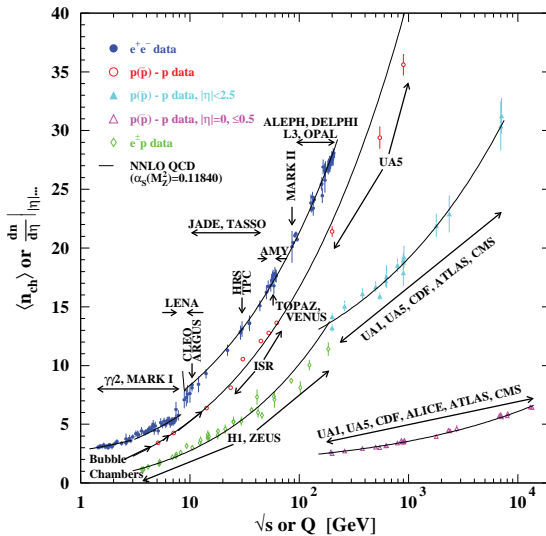


Figure 19.6: Average charged-particle multiplicity $\langle n_{\text{ch}} \rangle$ as a function of \sqrt{s} or Q for e^+e^- and $p\bar{p}$ annihilations, and pp and ep collisions. The indicated errors are statistical and systematic uncertainties added in quadrature, except when no systematic uncertainties are given. All NNLO QCD curves are from Eq. (19.11) with fitted normalization, K_{LHPD} , and offset, n_0 , using a fixed $\alpha_s(M_Z^2) = 0.1184$ [95] and for e^+e^- annihilation data $n_f = 3, 4$, or 5 depending on \sqrt{s} , else $n_f = 3$. e^+e^- : Contributions from K_S^0 and Λ decays included. Data compiled from Refs. [8, 10, 16, 16, 22, 77, 83, 96–106]; e^+p : Multiplicities have been measured in the current fragmentation region of the Breit frame. Data compiled from Refs. [35, 57, 58, 60, 107]; $p(p)\bar{p}$: Measured values above 20 GeV refer to non-single diffractive (NSD) processes. Central pseudorapidity multiplicities $(dn/d\eta)|_{\eta=0}$ refer to either $|\eta| < 2.5$ (CMS: $|\eta| < 2.4$) or $|\eta| = 0$ (UA5, CMS, ALICE: $|\eta| < 0.5$). Data compiled from Refs. [108–123].

Employing the hypothesis of ‘Local Parton-Hadron Duality’ (LPHD) [90], *i.e.*, that the color charge of partons is balanced locally in phase space and, hence, their hadronization occurs locally such that (Mellin transformed) parton and hadron inclusive

distributions directly correspond, Eq. (19.11) can be applied to describe average charged particle multiplicities obtained in e^+e^- annihilation. The equation can also be applied to $e^\pm p$ scattering if the current fragmentation region of the Breit frame is considered for measuring the average charged-particle multiplicity. Fig. 19.6 shows corresponding data and fits of Eq. (19.11) where apart from an LPHD normalization factor a constant offset has been allowed for, so that $\langle n_{\text{ch}}(Q) \rangle = K_{\text{LHPD}} \cdot \langle n_G(Q) \rangle / r + n_0$.

In hadron-hadron collisions beam remnants, *e.g.* from single-diffractive (SD) scattering where one colliding proton is negligibly deflected while hadrons related with the other colliding proton are well-separated in rapidity from the former proton, contribute to the measurement of the hadron multiplicity from a hard parton-parton scattering, making interpretation of the data more model dependent. Experimental results are usually given for inelastic processes or for non-single diffractive processes (NSD). Due to the large beam particle momenta at Tevatron and LHC, not all final state particles can be detected within the limited detector acceptance. Therefore, experiments at Tevatron and LHC quote particle multiplicities for limited ranges of pseudo-rapidity $\eta = -\ln \tan(\vartheta/2)$ or at central rapidity, *i.e.* $\eta = 0$, as shown in Fig. 19.6.

A universality of the average particle multiplicities in e^+e^- and $p(\bar{p})$ processes has been reported in Ref. [124] when considering an effective collision energy $Q_{\text{eff}} = \sqrt{s}/k$ in $p(\bar{p})$ reduced by a factor of $k \approx 3$, plus a constant offset of $n_0 \approx 2$. A more detailed review is available in Ref. [125]. According to the investigations presented in Ref. [126] the universality of the energy dependence of average particle multiplicities also applies to hadron-hadron and nucleus-nucleus collisions for both full and central rapidity multiplicities. Evidence for this universality is given by the good agreement for the energy dependence of Eq. (19.11) when fit to the $p(\bar{p})$ data as shown in Fig. 19.6.

19.4 Fragmentation models

Although the scaling violations can be calculated perturbatively, the actual form of the parton fragmentation functions is non-perturbative. Perturbative evolution gives rise to a shower of quarks and gluons (partons). Multi-parton final states from leading and higher order matrix element calculations are linked to these parton showers using factorization prescriptions, also called matching schemes, see Ref. [127] for an overview.

Phenomenological schemes are then used to model the carry-over of parton momenta and flavor to the hadrons. Implemented in Monte Carlo event generators (see Section 43 of this *Review*), these schemes have been tuned using e^+e^- data and provide good description of hadron collisions as well, thus providing evidence of the universality of fragmentation. However, e^+e^- mainly fix the quark jet fragmentation while it provides less constraints for modelling the gluon jet fragmentation.

19.5 Phenomenology of quark and gluon fragmentation functions

The fragmentation functions are solutions to the evolution equations Eq. (19.5), but need to be specified at some initial scale μ_0^2 (usually around 1 GeV^2 for light quarks and gluons, and at m_Q^2 for heavy quarks). A typical parameterization for a given light hadron is [128, 131–139]

$$D_i^h(x, \mu_0^2) = N_i x^{\alpha_i} (1-x)^{\beta_i} (1 + \gamma_i(1-x)^{\delta_i}), \quad (19.12)$$

where as indicated the normalization N_i , and the parameters α_i , β_i , γ_i and δ_i depend on the type i of the fragmenting parton. Heavy flavor fragmentation into heavy mesons is discussed in Sec. 19.8 below. The parameters of Eq. (19.12) are obtained by performing global fits to data on various hadron types for different combinations of partons and hadrons in e^+e^- , lepton-hadron and hadron-hadron collisions. We note that the choice of parameterization of the fragmentation functions at the initial scale necessarily introduces a bias since it imposes a certain form of the functions. This bias is largely avoided in neural network approaches which offer a wide flexibility of the initial functions and have recently been applied to fragmentation functions as well [130]. Sets of fragmentation functions are now available for

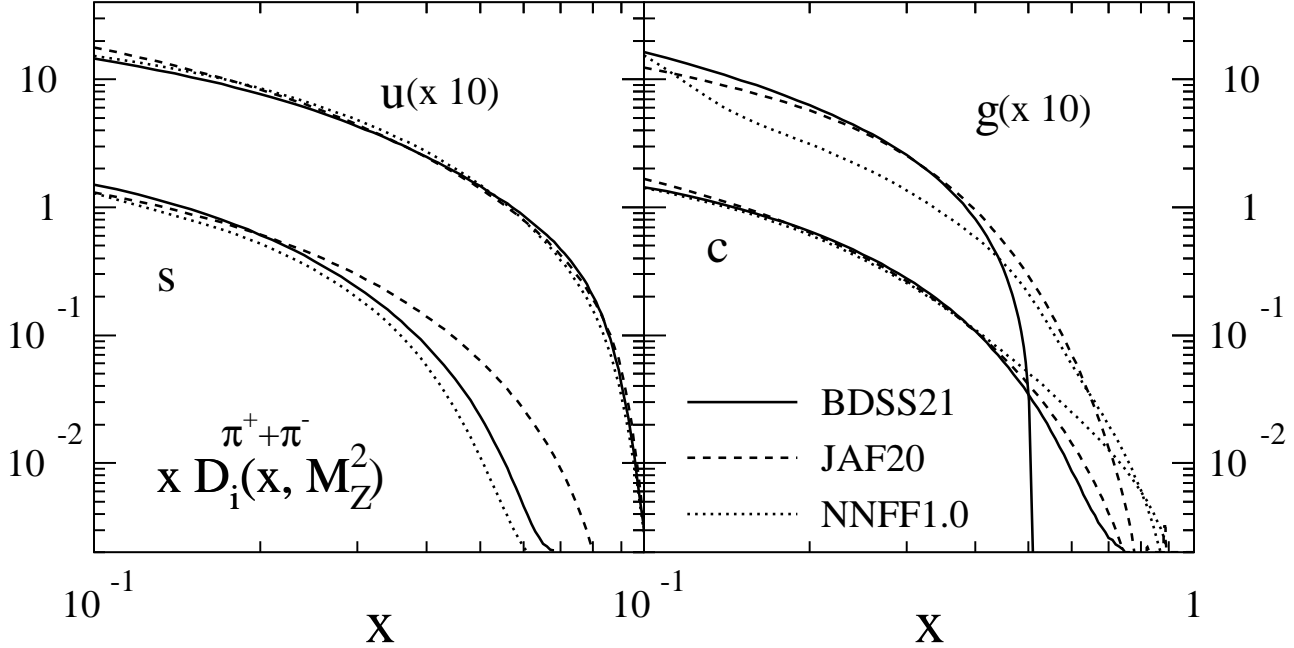


Figure 19.7: Comparison of up, strange, charm and gluon NLO fragmentation functions for $\pi^+ + \pi^-$ at the mass of the Z . The different lines correspond to the results of the analyses performed in Refs. [128–130].

pions, kaons, protons, neutrons, η mesons, Λ baryons, and charged hadrons [129, 130, 132–144]. They are all at NLO level, except for Refs. [130, 141, 144] which have been performed at NNLO level. The latter sets are restricted to the analysis of e^+e^- annihilation data. Recently, data from hadron-hadron collisions have been added in the framework of the neural network approach at NLO accuracy for charged hadrons [145]. It is noteworthy that the NNLO effects lead to an improvement in the theoretical description of the data in e^+e^- annihilation.

Data from e^+e^- annihilation present the cleanest experimental source for the measurement of fragmentation functions, but cannot be used to disentangle quark from antiquark fragmentation. Since the bulk of the e^+e^- annihilation data is obtained at the mass of the Z -boson, where the electroweak couplings are roughly the same for the different partons, it provides the most precise determination of the flavor-singlet combination of quark and antiquark fragmentation functions. Flavor-tagged results [146], distinguishing between the light quark, charm and bottom contributions are of particular value for flavor decomposition, even though those measurements cannot be unambiguously interpreted in perturbative QCD.

The most relevant source for quark-antiquark (and also flavor) separation is provided by SIDIS data. Semi-inclusive measurements are usually performed at much lower scales than for e^+e^- annihilation. The inclusion of SIDIS data in global fits allows for a wider coverage in the evolution of the fragmentation functions, resulting at the same time in a stringent test of the universality of the distributions. Charged-hadron production data in hadronic collisions also have sensitivity to (anti-)quark fragmentation functions. A recent analysis [129] performs a simultaneous extraction of parton distributions and fragmentation functions based on SIDIS data.

The gluon fragmentation function $D_g^h(x)$ can be extracted, in principle, from the longitudinal fragmentation structure function F_L in Eq. (19.2), as the coefficient functions $C_{L,i}$ for quarks and gluons are comparable at order α_s . However at NLO, *i.e.*, including the $\mathcal{O}(\alpha_s^2)$ coefficient functions $C_{L,i}^{(2)}$ [39], quark fragmentation is dominant in F_L over a large part of the kinematic range, reducing the sensitivity to D_g^h . This distribution could be determined

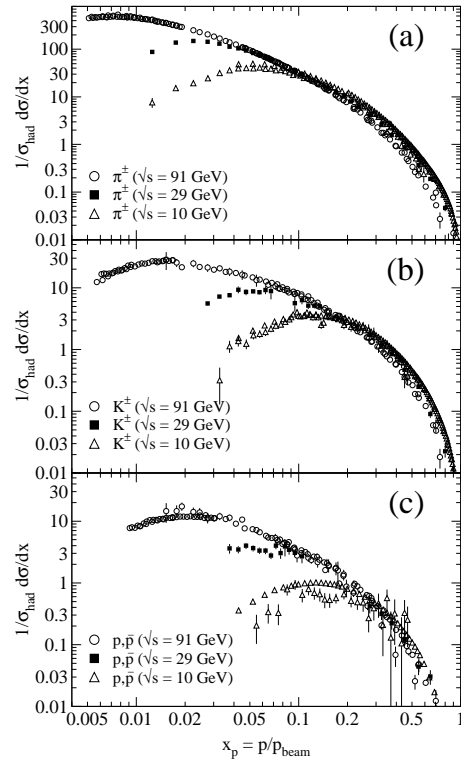


Figure 19.8: Scaled momentum spectra of (a) π^\pm , (b) K^\pm , and (c) p, \bar{p} at $\sqrt{s} = 10, 29, \text{ and } 91$ GeV [24, 26, 85, 147, 148].

also by analyzing the scale evolution of the fragmentation functions. This possibility is limited by the lack of sufficiently precise data at energy scales away from the Z -resonance and the dominance of the quark contributions at medium and large values of x . In e^+e^- annihilation, D_g^h can also be deduced from the study

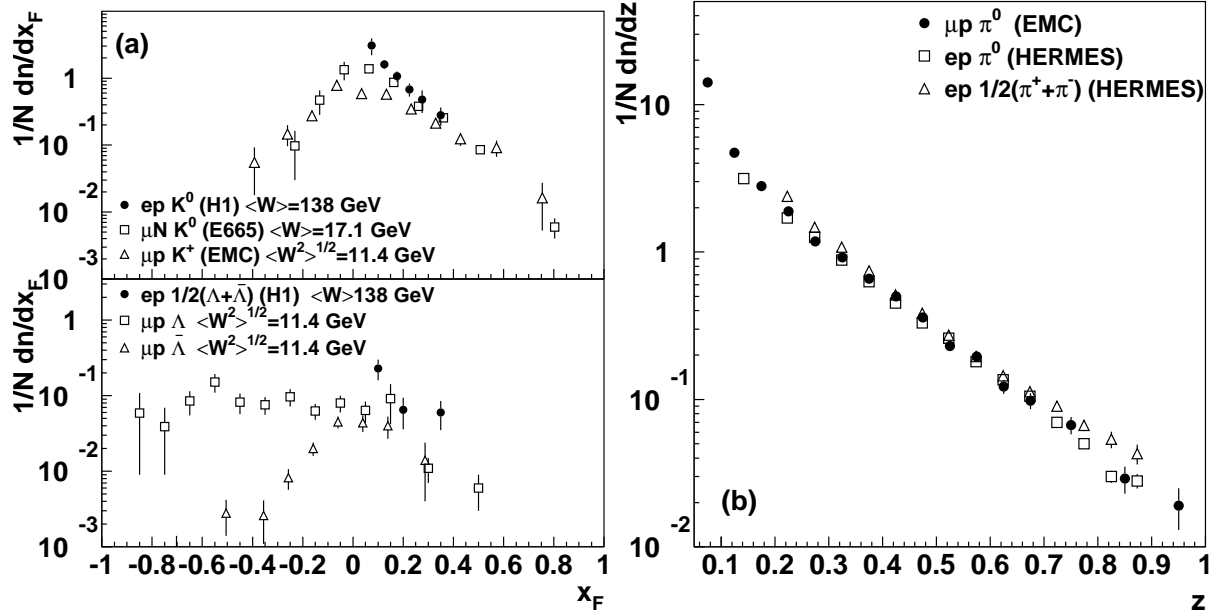


Figure 19.9: (a) $1/N \cdot dn/dx_F$ for identified strange particles in DIS at various values of W [149–151]. (b) $1/N \cdot dn/dz$ for measurements of pions in fixed-target DIS experiments [152–154].

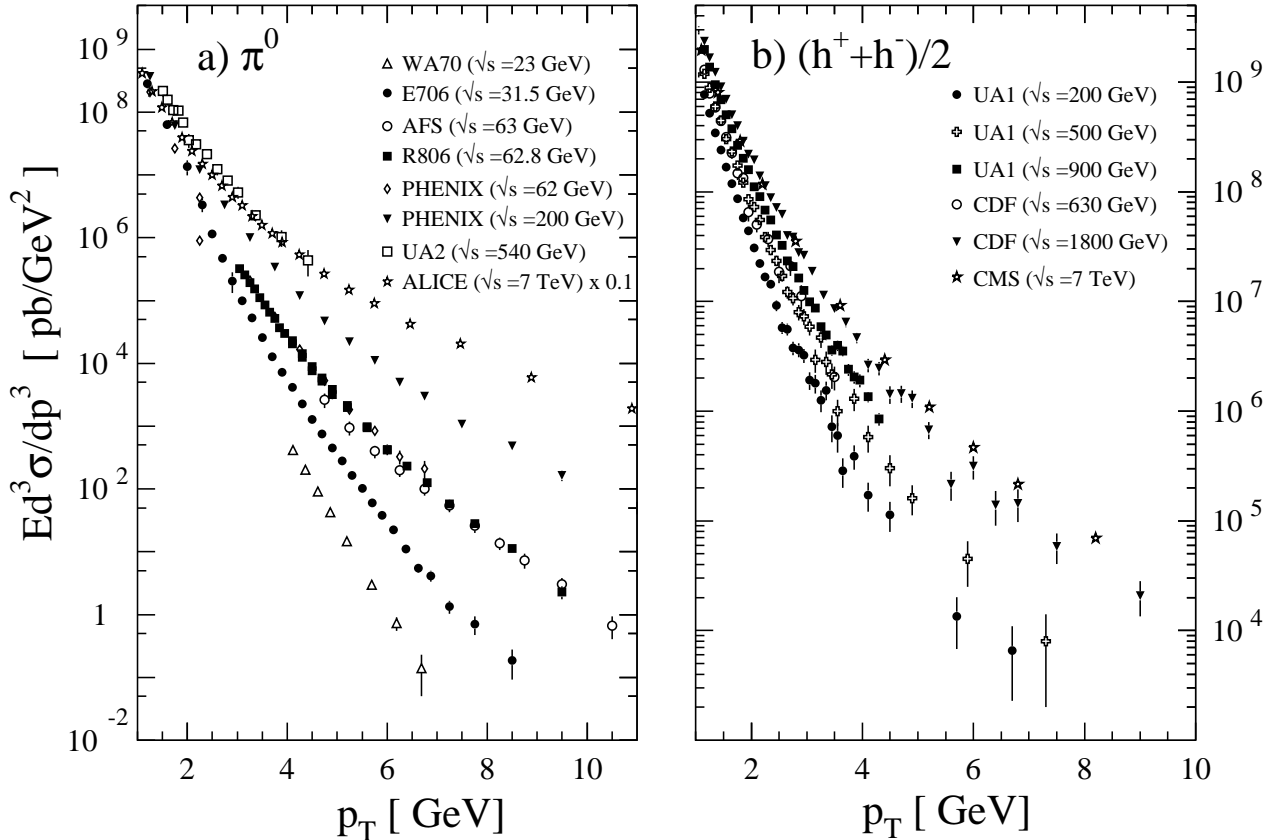


Figure 19.10: Selection of inclusive (a) π^0 and (b) charged-hadron production data from pp [118, 155–160] and $p\bar{p}$ [114, 161, 162] collisions.

of three-jet events in which the gluon jet is identified, for example, by tagging the other two jets with heavy quark decays. To leading order, the measured distributions of $x = E_{\text{had}}/E_{\text{jet}}$ for particles in gluon jets can be identified directly with the gluon fragmentation function $D_g^h(x)$.

Data for $p(\bar{p}) \rightarrow h + X$ provide much more direct constraint on D_g^h . At variance with e^+e^- annihilation and SIDIS, here gluon

fragmentation contributes already at the lowest order in the coupling constant. At large $x \gtrsim 0.5$, where information from e^+e^- is sparse, data from hadronic colliders significantly improve extractions of D_g^h [131, 132, 138, 140]. Recent LHC data has been included in the NLO analyses [128, 138, 139] of pion-fragmentation functions; see Sec.(17.7) for more details. Note that these analyses are currently the only ones that ‘globally’ incorporate avail-

Table 19.1: Classification of spin- and transverse-momentum dependent quark fragmentation functions. For simplicity we have left out the ubiquitous label for flavor i of the fragmenting quark and for hadron species h . Each of the functions carries the argument $(x, x^2 k_T^2)$ (plus dependence on a factorization scale), where $xk_T = p_T^h$ is the hadron's transverse momentum. λ and Λ are the quark's and hadron's helicities, respectively, and \vec{s}_T and \vec{S}_T are their transverse spin vectors. We have defined $[\vec{a} \times \vec{b}] \equiv a^1 b^2 - a^2 b^1$. Finally, m_h is the mass of the produced hadron.

hadron pol.	quark polarization		
	unpolarized	long. polarized	transv. polarized
unpol.	D	–	$\frac{[\vec{k}_T \times \vec{s}_T]}{m_h} H^\perp$
long. pol.	–	$\lambda \Lambda G_L$	$\frac{\vec{k}_T \cdot \vec{s}_T}{m_h} \Lambda H_L^\perp$
transv. pol.	$\frac{[\vec{k}_T \times \vec{S}_T]}{m_h} D_T^\perp$	$\frac{\vec{k}_T \cdot \vec{S}_T}{m_h} \lambda G_T^\perp$	$(\vec{s}_T \cdot \vec{S}_T) H_T + \frac{\vec{k}_T \cdot \vec{S}_T}{m_h} \frac{\vec{k}_T \cdot \vec{s}_T}{m_h} H_T^\perp$

able data from all sources, $e^+e^- \rightarrow h + X$, $ep \rightarrow e'h + X$ and $pp \rightarrow h + X$.

We note that recently a ‘hybrid’ type of high- p_T jet/hadron observable has also been considered both theoretically [163–169] and experimentally [170–177]. It is defined by an identified specific hadron found inside a fully reconstructed jet. This gives rise to a *same-side* hadron-jet momentum correlation that may be addressed using perturbative methods. One of several relevant kinematical variables (see [168] for an overview) is $z_h \equiv (\vec{p}_T^h \cdot \vec{p}_T^{\text{jet}})/(p_T^{\text{jet}})^2$, where \vec{p}_T^h and \vec{p}_T^{jet} are the transverse momenta of the hadron and the jet, respectively. The observable provides an alternative window on fragmentation functions in a more exclusive setting, enabling novel tests of the universality of fragmentation functions. Varying z_h and/or the hadron species, one can map out the fragmentation functions ‘locally’ as functions of x . This is in contrast to the single-inclusive observable $pp \rightarrow h + X$, which inevitably samples over a broad range of x . Although hadron-in-jet data are not yet routinely included in analyse of fragmentation functions, a ‘proof-of-principle’ analysis does exist [178] that shows the potential of the observable in providing constraint on fragmentation functions.

A comparison of recent NLO fits of fragmentation functions for $\pi^+ + \pi^-$ obtained by the updated version of BDSS21 [128], JAF20 [129] and NNPDF1.0 [130] is shown in Fig. 19.7. Differences among the functions for these sets are visible, especially for the gluon fragmentation function over the full range of x and for the quark functions at large momentum fractions. The differences are even larger for other species of hadrons like kaons and protons [131, 132, 136, 140]. Recent analyses [128–130, 136, 138, 139, 179, 180] estimate the uncertainties involved in the extraction of fragmentation functions.

Photonic fragmentation functions play a relevant role in the theoretical understanding of inclusive photon production in (leptonic and hadronic) high energy processes. In the spirit of the analogy between parton fragmentation functions and parton distribution functions, also photonic fragmentation functions are analogous to the photon structure function F_2^γ and to the proton's photonic parton distributions (see review on structure functions in Section 18 of this *Review*). Since photons have a pointlike coupling to quarks [181], the corresponding fragmentation functions obey inhomogeneous evolution equations and are generally decomposed into a perturbative and a non-perturbative component [135, 182, 183]. The hadronic part, sometimes approximated by the Vector Meson Dominance Model, can in principle be obtained by performing a global analysis to the available prompt photon production data [7, 12, 15, 19–21, 85, 147, 184, 185], although in practice this has not been done. We note that also the cross section for photons produced in fully reconstructed jets has been proposed [186] as a new tool for obtaining access to photon fragmentation functions, in analogy to the hadron-in-jet cross section discussed above.

19.6 Identified particles in e^+e^- and semi-inclusive DIS

There is a great wealth of measurements of e^+e^- fragmentation into identified particles. A collection of references for data on fragmentation into identified particles is provided in Table 53.1 of this *Review*. As a representative example, Figure 19.8 shows differential charged-hadron spectra as functions of the scaled hadron momentum at several CM energies.

Quantitative results of studies of scaling violations in e^+e^- fragmentation have been reported in [7, 21, 187, 188]. Scaling violations may be used to extract a value of α_s ; the values obtained are consistent with the world average (see review on QCD in Section 9 of this *Review*).

Many studies have been made of production of identified particles in lepton-hadron scattering, although fewer particle species have been measured than in e^+e^- collisions. References [149, 150, 152–154, 189–191] and [151, 192–197] are representative of the data from fixed target and ep collider experiments, respectively. QCD calculations performed at NLO provide an overall good description of the HERA data [33, 34, 58, 197–199], both for SIDIS [200] and for the hadron transverse momentum distribution [53, 201] in the kinematic regions in which the calculations are predictive. A first step towards an NNLO calculation for SIDIS has been presented in [202].

Fig. 19.9(a) compares lower-energy fixed-target and HERA data on strangeness production, showing that the HERA spectra have substantially increased multiplicities, albeit with statistical precision that is insufficient to study scaling violations. The fixed-target data show that the Λ rate substantially exceeds the $\bar{\Lambda}$ rate in the remnant region, owing to the conserved baryon number from the baryon target. Fig. 19.9(b) shows $1/N \cdot dn/dz$ for neutral and charged pion production, where z is defined as the ratio of the pion energy to that of the exchanged boson, both measured in the laboratory frame. Results are shown from the HERMES and the EMC experiments, where the HERMES data have been evolved to $\langle Q^2 \rangle = 25 \text{ GeV}^2$ at NLO QCD, in order to be comparable with the EMC data. Each of the experiments uses various kinematic cuts to ensure that the measured particles lie in the region that is expected to be associated with the struck quark. In the DIS kinematic regime accessed at these experiments, and over the range in z shown in Fig. 19.9, the z and x_F variables have similar values [30]. The precision data on identified particles can be used in the study of the quark flavor content of the proton [179, 218, 219].

Data on identified particle production can aid the investigation of the universality of jet fragmentation in e^+e^- and DIS. The strangeness suppression factor γ_s , as derived principally from tuning the Lund string model [220] within JETSET [221], is typically found to be around 0.3 in e^+e^- experiments [75], although values closer to 0.2 [222] have also been obtained. A number of measurements of so-called V^0 -particles (K^0 , Λ^0) and the relative rates of V^0 's and inclusively produced charged particles have been performed at HERA [151, 192, 223] and fixed target experiments [149].

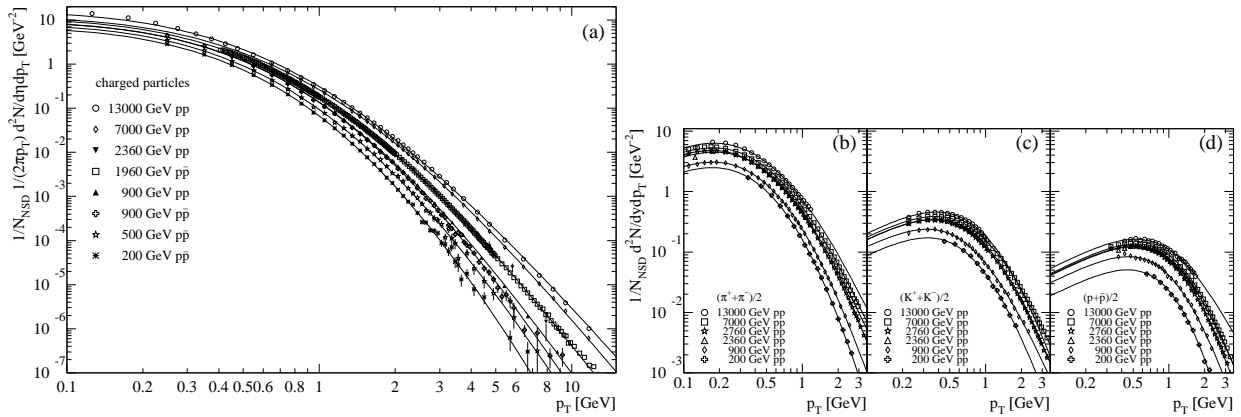


Figure 19.11: (a) Selection of inclusive charged-particle transverse momentum spectra [114, 117, 119, 121, 161, 203, 204], normalized to the non-single diffractive cross section (NSD). (b)-(d) Selection of identified charged-particle transverse momentum spectra [205–210] normalized to the NSD cross section. All spectra are scaled to the NSD cross-section using measurements of total, inelastic, elastic, single, or non-single diffractive cross sections from [211–215, 215–217]. The overall normalization uncertainty of about 3% is not shown. Superimposed are fits of the Tsallis distribution in Eq. (19.13).

These typically favour a stronger suppression ($\gamma_s \approx 0.2$) than usually obtained from e^+e^- data, although values close to 0.3 have also been obtained [224, 225].

However, when comparing the description of QCD-based models for lepton-hadron interactions and e^+e^- collisions, it is important to note that the overall description by event generators of inclusively produced hadronic final states is more accurate in e^+e^- collisions than in lepton-hadron interactions [226]. Predictions of particle rates in lepton-hadron scattering are affected by uncertainties in the modelling of the parton composition of the proton and photon, the extended target remnant, and initial and final-state QCD radiation. Furthermore, the tuning of event generators for e^+e^- collisions is typically based on a larger set of parameters and uses more observables [75] than are used when optimizing models for lepton-hadron data [227].

19.7 Fragmentation in hadron-hadron collisions

An extensive set on high-transverse momentum (p_T) single-inclusive hadron data has been collected in $h_1h_2 \rightarrow hX$ scattering processes, both at high energy colliders and fixed-target experiments [155–162, 185, 228–250]. Fig. 19.10 shows the invariant cross sections $Ed^3\sigma/dp^3$ for a compilation of neutral-pion and charged-hadron production data for energies in the range $\sqrt{s} \approx 23 - 7000$ GeV.

The differential cross section for high-transverse momentum hadron production has been computed to NLO accuracy in perturbative QCD [251]. The NLO corrections are typically large and can even double the prediction for the cross section at fixed-target energies. Nevertheless, the NLO calculations significantly under-predict the cross-section for several fixed-target energy data sets [246, 252, 253]. Different strategies have been developed to ameliorate the theoretical description at fixed-target energies. A possible phenomenological approach involves the introduction of a non-perturbative intrinsic partonic transverse momentum [160, 246, 254, 255]. Furthermore, the resummation of the dominant higher order corrections at threshold produces an enhancement of the theoretical calculation that significantly improves the description of the data [256, 257].

Data collected at high energy colliders are either included in global fit analyses or used as a test for the universality of fragmentation functions. A certain tension has been observed between data sets from RHIC and the LHC [258]. The tension can be largely resolved [128] by taking properly into account the theoretical scale dependence in the global analysis, allowing factorization and renormalization scales to vary according to the kinematics of each experiment within a conventional range.

Transverse momentum distributions can usually be fit by power laws [259]. An approach to describe the low p_T particle spectra is the Tsallis distribution [260–262], which is based on a non-extensive generalization of the Boltzmann-Gibbs statistics. The

functional form [263]

$$\frac{d^2N}{dp_T dy} = p_T \frac{dN}{dy} \frac{(n-1)(n-2)}{nT(nT + m_0(n-2))} \left[1 + \frac{m_T - m_0}{nT} \right]^{-n} \quad (19.13)$$

is frequently used to fit the transverse momentum spectra, where dN/dy is the particle's multiplicity, T and n are fit parameters of the Tsallis distribution, m_0 is either the mass of the most abundant particle, i.e. the pion for inclusive spectra, or the mass of an identified particle, and $m_T = \sqrt{p_T^2 + m_0^2}$. The parameter n is related to the non-extensive parameter $q = n/(n-1)$ of the original Tsallis formula [264], and T is connected to the temperature in the Boltzmann-Gibbs statistics. The Tsallis distribution has been very successfully fit to measured transverse momentum distributions of both inclusive charged particles and identified particle spectra for hadron-hadron collisions, see for example [265–267], for collisions of heavy nuclei, see for example [268], and also for e^+e^- collisions, see for example [269]. The energy dependence of the fitted Tsallis parameters has also been investigated in detail, see [263, 270]. Fig. 19.11 shows examples of hadron production data in pp and $p\bar{p}$ collisions compared to Tsallis distributions.

Hadron production provides a critical observable for probing the high energy-density matter produced in heavy-ion collisions. Measurements at colliders show a suppression of inclusive hadron yields at high transverse momentum for AA collisions compared to pp scattering, indicating the formation of a dense medium opaque to quark and gluons, see e.g. [271].

19.8 Heavy quark fragmentation

It was recognized very early [272] that a heavy flavored meson should retain a large fraction of the momentum of the primordial heavy quark, and therefore its fragmentation function should be much harder than that of a light hadron. In the limit of a very heavy quark, one expects the fragmentation function for a heavy quark to go into any heavy hadron to be peaked near $x = 1$.

When the heavy quark is produced at a momentum much larger than its mass, one expects important perturbative effects, enhanced by powers of the logarithm of the transverse momentum over the heavy quark mass, to intervene and modify the shape of the fragmentation function. In leading logarithmic order (*i.e.*, including all powers of $\alpha_s \log(m_Q/p_T)$), the total (*i.e.*, summed over all hadron types) perturbative fragmentation function is simply obtained by solving the leading evolution equation for fragmentation functions, Eq. (19.5), with the initial condition due to the finite mass of the heavy quark given by $D_Q(x, \mu^2)|_{\mu^2=m_Q^2} = \delta(1-x)$ and $D_i(x, \mu^2)|_{\mu^2=m_Q^2} = 0$ for $i \neq Q$ (here $D_i(x, \mu^2)$, stands for the probability to produce a heavy quark Q from parton i with a fraction x of the parton momentum).

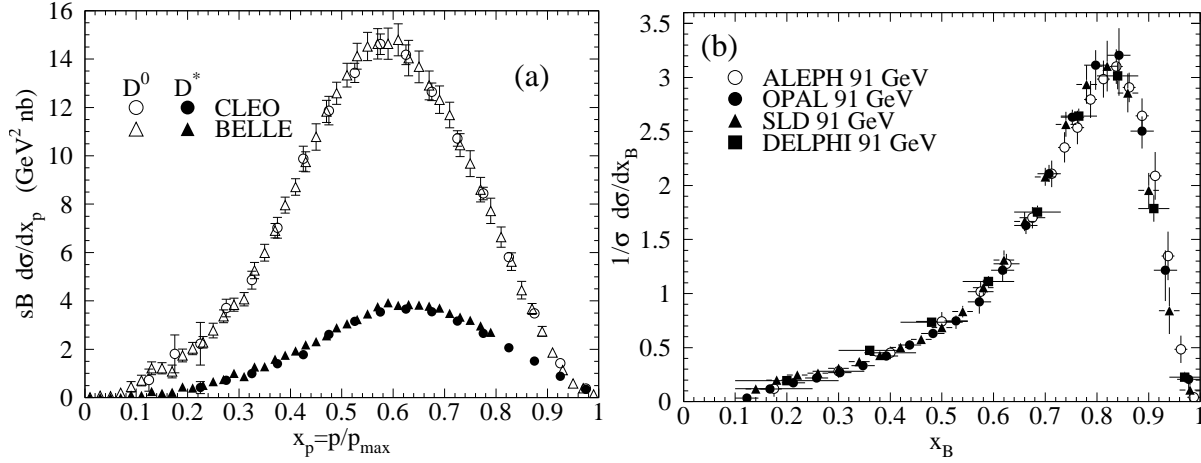


Figure 19.12: (a) Efficiency-corrected inclusive cross-section measurements for the production of D^0 and D^{*+} in e^+e^- measurements at $\sqrt{s} \approx 10.6$ GeV, excluding B decay products [273] [274]. (b) Measured e^+e^- fragmentation function of b quarks into B hadrons at $\sqrt{s} \approx 91$ GeV [275].

Several extensions of the leading logarithmic result have appeared in the literature. Next-to-leading-log (NLL) order results for the perturbative heavy quark fragmentation function have been obtained in [276]. The resummation of the dominant logarithmic contributions at large x was performed in [277] to next-to-leading-log accuracy. Fixed-order calculations of the fragmentation function at order α_s^2 in e^+e^- annihilation have appeared in [278] while the initial condition for the perturbative heavy quark fragmentation function has been extended to NNLO in [279].

Inclusion of non-perturbative effects in the calculation of the heavy-quark fragmentation function is done by convoluting the perturbative result with a phenomenological non-perturbative form. This form follows from the simple kinematical consideration that the formation of a hadron by attaching light quarks/antiquarks to the heavy quark will slightly decelerate the heavy quark. Thus, its shape will show a peak that becomes increasingly centered next to $x = 1$ the higher the quark mass. Among the most popular parameterizations we have the following:

$$\text{Peterson } et al. [280]: D_{np}(x) \propto \frac{1}{x} \left(1 - \frac{1}{x} - \frac{\epsilon}{1-x}\right)^{-2}, \quad (19.14)$$

$$\text{Kartvelishvili } et al. [281]: D_{np}(x) \propto x^\alpha(1-x), \quad (19.15)$$

$$\begin{aligned} \text{Collins \& Spiller [282]: } D_{np}(x) &\propto \left(\frac{1-x}{x} + \frac{(2-x)\epsilon_C}{1-x}\right) \times \\ &(1+x^2) \times \left(1 - \frac{1}{x} - \frac{\epsilon_C}{1-x}\right)^{-2} \end{aligned} \quad (19.16)$$

$$\text{Colangelo \& Nason [283]: } D_{np}(x) \propto (1-x)^\alpha x^\beta \quad (19.17)$$

$$\begin{aligned} \text{Bowler [284]: } D_{np}(x) &\propto x^{-(1+bm_{h,\perp}^2)} \times \\ &(1-x)^a \exp\left(-\frac{bm_{h,\perp}^2}{x}\right) \end{aligned} \quad (19.18)$$

$$\text{Braaten } et al. [285]: \text{ (see Eqs. (31), (32) in [285])} \quad (19.19)$$

where ϵ , ϵ_C , a , $bm_{h,\perp}^2$, α , and β are non-perturbative parameters that depend on the heavy hadron considered. The parameters entering the non-perturbative forms are fitted together with some model of hard radiation, which can be either a shower Monte Carlo, a leading-log or NLL calculation (which may or may not include Sudakov resummation), or a fixed order calculation. In [278], for example, the Peterson *et al.* [280] ϵ parameter for charm and bottom production is fitted from the measured distri-

butions of Refs. [286, 287] for charm, and of [288] for bottom. If the leading-logarithmic approximation (LLA) is used for the perturbative part, one finds $\epsilon_c \approx 0.05$ and $\epsilon_b \approx 0.006$; if a second order calculation is used one finds $\epsilon_c \approx 0.035$ and $\epsilon_b \approx 0.0033$; if a NLL improved fixed order $\mathcal{O}(\alpha_s^2)$ calculation is used instead of NLO $\mathcal{O}(\alpha_s)$ one finds $\epsilon_c \approx 0.022$ and $\epsilon_b \approx 0.0023$. The larger values found in the LL approximation are consistent with what is obtained in the context of parton shower models [289], as expected. The ϵ parameter for charm and bottom scales roughly with the inverse square of the heavy flavor mass. This behavior can be justified by several arguments [272, 290, 291]. It can be used to relate the non-perturbative parts of the fragmentation functions of charm and bottom quarks [278, 283, 292].

A more conventional approach [293] involves the introduction of a unique set of heavy quark fragmentation functions of non-perturbative nature that obey the usual massless evolution equations in Eq. (19.5). Finite mass terms of the form $(m_Q/p_T)^n$ are kept in the corresponding short distance coefficient function for each scattering process. Within this approach, the initial condition for the perturbative fragmentation function provides the term needed to define the correct subtraction scheme to match the massless limit for the coefficient function (see e.g. [294]). Such an implementation is in line with the variable flavor number scheme introduced for parton distributions functions, as described in Section 18 of this Review.

High statistics data for charmed-meson production near the Υ resonance (excluding decay products of B mesons) have been published [273, 274]. They include results for D and D^* , D_s (see also [295, 296]) and Λ_c . Shown in Fig. 19.12(a) are the CLEO and BELLE inclusive cross-sections times branching ratio \mathcal{B} , $sBd\sigma/dx_p$, for the production of D^0 and D^{*+} . The variable x_p approximates the light-cone momentum fraction x , but is not identical to it. The two measurements are consistent with each other.

The branching ratio \mathcal{B} represents $D^0 \rightarrow K^-\pi^+$ for the D^0 results and for the D^{*+} the product of the branching fractions for $D^{*+} \rightarrow D^0\pi^+$ and $D^0 \rightarrow K^-\pi^+$. Given the high precision of CLEO's and BELLE's data, a superposition of different parametric forms for the non-perturbative contribution is needed to obtain a good fit [52]. Older studies are reported in Refs. [287, 297, 298]. Charmed meson spectra on the Z peak have been published by OPAL and ALEPH [299, 300].

Charm quark production has also been extensively studied at HERA by the H1 and ZEUS collaborations. Measurements have been made of $D^{*\pm}$, D^\pm , and D_s^\pm mesons and the Λ_c baryon. See, for example, Refs. [301, 302].

Experimental studies of the fragmentation function for b quarks, shown in Fig. 19.12(b), have been performed at LEP and SLD [275, 288, 303]. Commonly used methods identify the B meson

through its semileptonic decay or based upon tracks emerging from the B secondary vertex. Heavy flavor contributions from gluon splitting are usually explicitly removed before fitting for the fragmentation functions. The studies in [275] fit the B spectrum using a Monte Carlo shower model supplemented with non-perturbative fragmentation functions yielding consistent results.

The experiments measure primarily the spectrum of B mesons. This defines a fragmentation function that includes the effect of the decay of higher mass excitations, like the B^* and B^{**} . In the literature (cf. details in Ref. [304]), there is sometimes ambiguity in what is defined to be the bottom fragmentation function. Instead of using what is directly measured (*i.e.*, the B meson spectrum), in some cases corrections are applied to account for B^* or B^{**} production.

Heavy-flavor production in e^+e^- collisions is the primary source of information for the role of fragmentation effects in heavy-flavor production in hadron-hadron and lepton-hadron collisions. The QCD calculations tend to underestimate the data in certain regions of phase space. Some experimental results from LHC summarized in [305] show such deviations e.g. at high transverse jet momentum and also at low di-jet separation angles, see [306] for details, and were already theoretically investigated in [307].

Both bottomed- and charmed-meson spectra have been measured at the Tevatron with unprecedented accuracy [308]. The measured spectra are in good agreement with QCD calculations (including non-perturbative fragmentation effects inferred from e^+e^- data [309]).

The HERA collaborations have produced a number of measurements of beauty production; see, for example, Refs. [301,310–313]. As for the Tevatron data, the HERA results are described well by QCD-based calculations using fragmentation models optimized with e^+e^- data.

Besides degrading the fragmentation function by gluon radiation, QCD evolution can also generate soft heavy quarks, increasing in the small x region as \sqrt{s} increases. Several theoretical studies are available on the issue of how often $b\bar{b}$ or $c\bar{c}$ pairs are produced indirectly via a gluon splitting mechanism [314–316]. Experimental results from studies on charm and bottom production via gluon splitting, given in [300,317–321], yield weighted averages of $\bar{n}_{g \rightarrow c\bar{c}} = 3.05 \pm 0.45\%$ and $\bar{n}_{g \rightarrow b\bar{b}} = 0.277 \pm 0.072\%$, respectively. The production of bottom-antibottom quark pairs via gluon splitting has also been investigated at hadron colliders, see for example [322–324].

19.9 Spin-dependent and transverse-momentum dependent fragmentation functions

The fragmentation functions we have considered so far apply to the spin-averaged case in which the polarization of the produced hadron is not observed, or the hadron has spin-0. We have also only considered ‘collinear’ fragmentation functions $D_i^h(x, \mu^2)$ which carry only one kinematical variable, the momentum fraction x . New insights into fragmentation and hadronization become available when also the dependence of fragmentation functions on the spin of the produced hadron and/or its relative transverse momentum with respect to the fragmenting parton are considered. In the latter case, one refers to the fragmentation functions as ‘transverse-momentum dependent (TMD)’ fragmentation functions.

Staying first with collinear fragmentation functions, two types of spin-dependent fragmentation functions to spin-1/2 hadrons can be considered. The helicity-dependent fragmentation function measures the transfer of longitudinal spin from the fragmenting parton to the hadron [38,325–328]. It is given by

$$\Delta D_i^h(x, \mu^2) \equiv D_{i+}^{h+}(x, \mu^2) - D_{i+}^{h-}(x, \mu^2), \quad (19.20)$$

where the superscripts \pm refer to the helicities of the parton and hadron. Λ hyperons are ideally suited for measurements of the ΔD_i^h , thanks to their self-analyzing weak decay $\Lambda \rightarrow \pi p$. Measurements of the longitudinal spin transfer to Lambda hyperons have been presented in e^+e^- (on the Z resonance), ep , and pp scattering in Refs. [329–335]. One may readily extend Eq. (19.20) to the case of transverse polarization of hadrons and quarks [336],

where the corresponding fragmentation functions are known as ‘transversity’ fragmentation functions. There are also measurements constraining these fragmentation functions [330,337,338]. A recent phenomenological analysis was presented in [339].

If the transverse-momentum (k_T) dependence of fragmentation functions is considered, there are eight types of leading-twist functions, defined by the correlations among the hadronic and partonic spin vectors and transverse-momentum vectors they represent. (For review, see [5]). We note that the eight fragmentation functions given in the table below exist separately for each quark and antiquark flavor, and a similar set may be introduced for gluons. Upon integration over the transverse momentum k_T the collinear unpolarized, helicity, and transversity fragmentation functions are reproduced.

The various fragmentation functions may be obtained from spin asymmetries and angular distributions in hadron production processes. There is a large body of precision data by now on transverse-momentum distributions in e^+e^- annihilation [340] and SIDIS [190,341] that provide constraints on the unpolarized TMD fragmentation functions D_i^h , which have been analyzed theoretically, partly also including TMD evolution effects and high orders of perturbation theory [342–349].

Besides the unpolarized functions D most of the attention in experiment and theory has been on the function H^\perp which describes the production of unpolarized (or spin-0) hadrons by transversely polarized quarks. This function is known as the ‘Collins function’ [350]. Its importance also derives from the fact that it may be used to probe the quark transversity PDF of the nucleon [351] which gives the probability of finding a transversely polarized quark with its spin aligned or anti-aligned with the spin of a transversely polarized nucleon. The transversity function is chiral-odd, and therefore not accessible through measurements of inclusive lepton-hadron scattering. The Collins effect in semi-inclusive DIS, on the other hand, provides an avenue for accessing transversity. The Collins fragmentation function is chiral-odd and T-odd, leading to a characteristic single-spin asymmetry in the azimuthal angular distribution of the produced hadron in the hadron scattering plane. A number of SIDIS [352–363] and e^+e^- experiments [364–368] have performed measurements of the Collins effect, for charged pions and kaons. These have been analyzed theoretically [369,370], leading to an extraction of the nucleon’s transversity distributions [370]. The Collins effect has also been studied in pp scattering, where one considers azimuthal transverse single-spin asymmetries for distributions of hadrons inside jets [177,371,372].

In the context of extractions of transversity PDFs also fragmentation functions for same-side pairs of hadrons with small invariant mass, *dihadrons*, have been introduced and studied [373–381]. Compared to the Collins effect, dihadron fragmentation functions have the advantage that they may be defined purely in collinear factorization. The relevant spin-dependent dihadron fragmentation function exploits a correlation between the transverse polarization of the fragmenting quark and the relative momentum of the two hadrons. In SIDIS with a transversely polarized hadron beam, the dihadron cross section then contains a specific modulation in the azimuthal orientation of the plane containing the momenta of the two hadrons. The coefficient of this modulation is a product of the spin-dependent dihadron fragmentation function and the target’s transversity PDF. The dihadron fragmentation functions may be separately extracted from measurements in e^+e^- annihilation, and the Belle experiment has presented data [382] that have been analyzed theoretically [383,384]. In lepton scattering, HERMES [385] and COMPASS [386,387] have reported data sensitive to the spin-dependent dihadron fragmentation functions, and recently the STAR experiment at RHIC has presented data in the azimuthal distribution of $\pi^+\pi^-$ pairs produced in pp scattering with one transversely polarized proton [388]. The results have been successfully used for the extraction of transversity PDFs [384,389–391].

References

- [1] G. Altarelli, Phys. Rept. **81**, 1 (1982).
- [2] R.K. Ellis *et al.*, *QCD and Collider Physics*, Cambridge

- University Press (1996).
- [3] S. Albino *et al.* (2008), [arXiv:0804.2021].
- [4] F. Arleo, *Eur. Phys. J.* **C61**, 603 (2009), [arXiv:0810.1193].
- [5] A. Metz and A. Vossen, *Prog. Part. Nucl. Phys.* **91**, 136 (2016), [arXiv:1607.02521].
- [6] P. Nason and B. R. Webber, *Nucl. Phys.* **B421**, 473 (1994), [Erratum: *Nucl. Phys.* **B480**, 755 (1996)].
- [7] D. Buskulic *et al.* (ALEPH), *Phys. Lett.* **B357**, 487 (1995), [Erratum: *Phys. Lett.* **B364**, 247 (1995)].
- [8] P. Abreu *et al.* (DELPHI), *Eur. Phys. J.* **C6**, 19 (1999).
- [9] R. Barate *et al.* (ALEPH), *Phys. Rept.* **294**, 1 (1998).
- [10] D. Buskulic *et al.* (ALEPH), *Z. Phys.* **C73**, 409 (1997).
- [11] B. Adeva *et al.* (L3), *Phys. Lett.* **B259**, 199 (1991).
- [12] Y. K. Li *et al.* (AMY), *Phys. Rev.* **D41**, 2675 (1990).
- [13] D. Bender *et al.*, *Phys. Rev.* **D31**, 1 (1985).
- [14] G. S. Abrams *et al.*, *Phys. Rev. Lett.* **64**, 1334 (1990).
- [15] A. Petersen *et al.*, *Phys. Rev.* **D37**, 1 (1988).
- [16] G. Alexander *et al.* (OPAL), *Z. Phys.* **C72**, 191 (1996).
- [17] K. Ackerstaff *et al.* (OPAL), *Z. Phys.* **C75**, 193 (1997).
- [18] G. Abbiendi *et al.* (OPAL), *Eur. Phys. J.* **C16**, 185 (2000), [hep-ex/0002012].
- [19] W. Braunschweig *et al.* (TASSO), *Z. Phys.* **C47**, 187 (1990).
- [20] K. Ackerstaff *et al.* (OPAL), *Eur. Phys. J.* **C7**, 369 (1999), [hep-ex/9807004].
- [21] P. Abreu *et al.* (DELPHI), *Phys. Lett.* **B398**, 194 (1997).
- [22] G. Abbiendi *et al.* (OPAL), *Eur. Phys. J.* **C37**, 1, 25 (2004), [hep-ex/0404026].
- [23] R. Brandelik *et al.* (TASSO), *Phys. Lett.* **114B**, 65 (1982).
- [24] K. Abe *et al.* (SLD), *Phys. Rev.* **D69**, 072003 (2004), [hep-ex/0310017].
- [25] H. Aihara *et al.* (TPC/Two Gamma), *Phys. Rev. Lett.* **61**, 1263 (1988).
- [26] M. Leitgab *et al.* (Belle), *Phys. Rev. Lett.* **111**, 062002 (2013), [arXiv:1301.6183].
- [27] W. Kittel and E.A. De Wolf, *Soft Multihadron Dynamics*, World Scientific (2005).
- [28] H.F. Jones, *Nuovo Cimento* **40A**, 1018 (1965).
- [29] K. H. Streng, T. F. Walsh and P. M. Zerwas, *Z. Phys.* **C2**, 237 (1979).
- [30] M. R. Adams *et al.* (E-665), *Phys. Lett.* **B272**, 163 (1991).
- [31] M. Arneodo *et al.* (European Muon), *Z. Phys.* **C35**, 417 (1987).
- [32] I. Abt *et al.* (H1), *Z. Phys.* **C63**, 377 (1994).
- [33] M. Derrick *et al.* (ZEUS), *Z. Phys.* **C70**, 1 (1996), [hep-ex/9511010].
- [34] J. Breitweg *et al.* (ZEUS), *Phys. Lett.* **B414**, 428 (1997), [hep-ex/9710011].
- [35] F. D. Aaron *et al.* (H1), *Phys. Lett.* **B654**, 148 (2007), [arXiv:0706.2456].
- [36] P. Abreu *et al.* (DELPHI), *Phys. Lett.* **B311**, 408 (1993).
- [37] G. Altarelli *et al.*, *Nucl. Phys.* **B160**, 301 (1979); R. Baier and K. Fey, *Z. Phys.* **C2**, 339 (1979).
- [38] D. de Florian, M. Stratmann and W. Vogelsang, *Phys. Rev.* **D57**, 5811 (1998), [hep-ph/9711387].
- [39] P. J. Rijken and W. L. van Neerven, *Phys. Lett.* **B386**, 422 (1996), [hep-ph/9604436]; P. J. Rijken and W. L. van Neerven, *Phys. Lett.* **B392**, 207 (1997), [hep-ph/9609379]; P. J. Rijken and W. L. van Neerven, *Nucl. Phys.* **B487**, 233 (1997), [hep-ph/9609377].
- [40] A. Mitov, S. Moch and A. Vogt, *Phys. Lett.* **B638**, 61 (2006), [hep-ph/0604053].
- [41] A. Mitov and S.-O. Moch, *Nucl. Phys.* **B751**, 18 (2006), [hep-ph/0604160].
- [42] V. N. Gribov and L. N. Lipatov, *Sov. J. Nucl. Phys.* **15**, 438 (1972), [*Yad. Fiz.* **15**, 781 (1972)]; V. N. Gribov and L. N. Lipatov, *Sov. J. Nucl. Phys.* **15**, 675 (1972), [*Yad. Fiz.* **15**, 1218 (1972)]; L.N. Lipatov, *Sov. J. Nucl. Phys.* **20**, 95 (1975); Yu.L. Dokshitzer, *Sov. Phys. JETP Lett.* **46**, 641 (1977); G. Altarelli and G. Parisi, *Nucl. Phys.* **B126**, 298 (1977).
- [43] H. Georgi and H. D. Politzer, *Nucl. Phys.* **B136**, 445 (1978); J. F. Owens, *Phys. Lett.* **76B**, 85 (1978); T. Uematsu, *Phys. Lett.* **79B**, 97 (1978).
- [44] G. Curci, W. Furmanski and R. Petronzio, *Nucl. Phys.* **B175**, 27 (1980).
- [45] W. Furmanski and R. Petronzio, *Phys. Lett.* **97B**, 437 (1980).
- [46] E. G. Floratos, C. Kounnas and R. Lacaze, *Nucl. Phys.* **B192**, 417 (1981).
- [47] J. Kalinowski, K. Konishi and T. R. Taylor, *Nucl. Phys.* **B181**, 221 (1981).
- [48] M. Stratmann and W. Vogelsang, *Nucl. Phys.* **B496**, 41 (1997), [hep-ph/9612250].
- [49] Yu. L. Dokshitzer, G. Marchesini and G. P. Salam, *Phys. Lett.* **B634**, 504 (2006), [hep-ph/0511302].
- [50] S. Moch and A. Vogt, *Phys. Lett.* **B659**, 290 (2008), [arXiv:0709.3899].
- [51] A. A. Almasy, S. Moch and A. Vogt, *Nucl. Phys.* **B854**, 133 (2012), [arXiv:1107.2263].
- [52] M. Cacciari, P. Nason and C. Oleari, *JHEP* **04**, 006 (2006), [hep-ph/0510032]; M. Cacciari, P. Nason and C. Oleari, *JHEP* **10**, 034 (2005), [hep-ph/0504192].
- [53] P. Aurenche *et al.*, *Eur. Phys. J.* **C34**, 277 (2004), [hep-ph/0312359]; A. Daleo, D. de Florian and R. Sassot, *Phys. Rev.* **D71**, 034013 (2005), [hep-ph/0411212]; B. A. Kniehl, G. Kramer and M. Maniatis, *Nucl. Phys.* **B711**, 345 (2005), [Erratum: *Nucl. Phys.* **B720**, 231 (2005)], [hep-ph/0411300].
- [54] B. Wang *et al.*, *Phys. Rev.* **D99**, 9, 094029 (2019), [arXiv:1903.01529].
- [55] S. Aid *et al.* (H1), *Nucl. Phys.* **B445**, 3 (1995), [hep-ex/9505003].
- [56] M. Derrick *et al.* (ZEUS), *Z. Phys.* **C67**, 93 (1995), [hep-ex/9501012].
- [57] C. Adloff *et al.* (H1), *Nucl. Phys.* **B504**, 3 (1997), [hep-ex/9707005].
- [58] J. Breitweg *et al.* (ZEUS), *Eur. Phys. J.* **C11**, 251 (1999), [hep-ex/9903056].
- [59] J. F. Patrick *et al.*, *Phys. Rev. Lett.* **49**, 1232 (1982).
- [60] S. Chekanov *et al.* (ZEUS), *JHEP* **06**, 061 (2008), [arXiv:0803.3878].
- [61] A. H. Mueller, *Phys. Lett.* **104B**, 161 (1981).
- [62] A. Bassetto *et al.*, *Nucl. Phys.* **B207**, 189 (1982).
- [63] Yu.L. Dokshitzer *et al.*, *Z. Phys.* **C15**, 324 (1982).
- [64] A. H. Mueller, *Nucl. Phys.* **B213**, 85 (1983); A. H. Mueller, *Nucl. Phys.* **B241**, 141 (1984).
- [65] Y. L. Dokshitzer, V. A. Khoze and S. I. Troian, *Int. J. Mod. Phys.* **A7**, 1875 (1992).
- [66] Yu.L. Dokshitzer *et al.*, *Basics of Perturbative QCD*, Editions Frontières (1991).
- [67] V. A. Khoze and W. Ochs, *Int. J. Mod. Phys.* **A12**, 2949 (1997), [hep-ph/9701421].
- [68] C. P. Fong and B. R. Webber, *Nucl. Phys.* **B355**, 54 (1991).
- [69] S. Albino *et al.*, *Phys. Rev. Lett.* **95**, 232002 (2005), [hep-ph/0503170].
- [70] S. Albino *et al.*, *Phys. Rev.* **D73**, 054020 (2006), [hep-ph/0510319].

- [71] S. Albino *et al.*, Nucl. Phys. **B851**, 86 (2011), [arXiv:1104.3018]; S. Albino *et al.*, Nucl. Phys. **B855**, 801 (2012), [arXiv:1108.3948].
- [72] A. Vogt, JHEP **10**, 025 (2011), [arXiv:1108.2993]; C. H. Kom, A. Vogt and K. Yeats, JHEP **10**, 033 (2012), [arXiv:1207.5631].
- [73] D. P. Anderle *et al.*, Phys. Rev. **D95**, 5, 054003 (2017), [arXiv:1611.03371].
- [74] P. Bolzoni, B. A. Kniehl and A. V. Kotikov, Phys. Rev. Lett. **109**, 242002 (2012), [arXiv:1209.5914]; P. Bolzoni, B. A. Kniehl and A. V. Kotikov, Nucl. Phys. **B875**, 18 (2013), [arXiv:1305.6017].
- [75] P. Abreu *et al.* (DELPHI), Z. Phys. **C73**, 11 (1996).
- [76] P. Abreu *et al.* (DELPHI), Z. Phys. **C73**, 229 (1997).
- [77] P. Achard *et al.* (L3), Phys. Rept. **399**, 71 (2004), [hep-ex/0406049].
- [78] R. Itoh *et al.* (TOPAZ), Phys. Lett. **B345**, 335 (1995), [hep-ex/9412015].
- [79] M. Althoff *et al.* (TASSO), Z. Phys. **C22**, 307 (1984).
- [80] M. Z. Akrawy *et al.* (OPAL), Phys. Lett. **B247**, 617 (1990).
- [81] W. Dunwoodie *et al.* (BES), Phys. Rev. **D69**, 072002 (2004), [hep-ex/0306055].
- [82] D. Buskulic *et al.* (ALEPH), Z. Phys. **C55**, 209 (1992).
- [83] A. Heister *et al.* (ALEPH), Eur. Phys. J. **C35**, 457 (2004).
- [84] P. Abreu *et al.* (DELPHI), Phys. Lett. **B275**, 231 (1992).
- [85] P. Abreu *et al.* (DELPHI), Eur. Phys. J. **C5**, 585 (1998).
- [86] P. Abreu *et al.* (DELPHI), Phys. Lett. **B459**, 397 (1999).
- [87] M. Acciarri *et al.* (L3), Phys. Lett. **B444**, 569 (1998).
- [88] TPC/TWO-GAMMA Collab.: H. Aihara *et al.*, LBL 23737.
- [89] B. R. Webber, Phys. Lett. **143B**, 501 (1984).
- [90] Y. I. Azimov *et al.*, Z. Phys. **C27**, 65 (1985).
- [91] Y. I. Azimov *et al.*, Z. Phys. **C31**, 213 (1986).
- [92] I. M. Dremin and J. W. Gary, Phys. Rept. **349**, 301 (2001), [hep-ph/0004215].
- [93] I. M. Dremin and V. A. Nechitailo, Mod. Phys. Lett. **A9**, 1471 (1994), [hep-ex/9406002].
- [94] S. J. Brodsky and J. F. Gunion, Phys. Rev. Lett. **37**, 402 (1976).
- [95] J. Beringer *et al.* (Particle Data Group), Phys. Rev. **D86**, 010001 (2012).
- [96] R. Akers *et al.* (OPAL), Z. Phys. **C68**, 203 (1995).
- [97] P. D. Acton *et al.* (OPAL), Z. Phys. **C53**, 539 (1992).
- [98] D. Buskulic *et al.* (ALEPH), Z. Phys. **C69**, 15 (1995).
- [99] P. Abreu *et al.* (DELPHI), Phys. Lett. **B372**, 172 (1996).
- [100] P. Abreu *et al.* (DELPHI), Phys. Lett. **B416**, 233 (1998).
- [101] P. Abreu *et al.* (DELPHI), Eur. Phys. J. **C18**, 203 (2000), [Erratum: Eur. Phys. J. **C25**, 493 (2002)], [hep-ex/0103031].
- [102] M. Acciarri *et al.* (L3), Phys. Lett. **B371**, 137 (1996).
- [103] M. Acciarri *et al.* (L3), Phys. Lett. **B404**, 390 (1997).
- [104] K. Nakabayashi *et al.* (TOPAZ), Phys. Lett. **B413**, 447 (1997).
- [105] K. Okabe *et al.* (VENUS), Phys. Lett. **B423**, 407 (1998).
- [106] H. Albrecht *et al.* (ARGUS), Z. Phys. **C54**, 13 (1992).
- [107] S. Chekanov *et al.* (ZEUS), Phys. Lett. **B510**, 36 (2001), [hep-ex/0104036].
- [108] J. Benecke *et al.* (Bonn-Hamburg-Munich), Nucl. Phys. **B76**, 29 (1974).
- [109] W. M. Morse *et al.*, Phys. Rev. **D15**, 66 (1977).
- [110] W. Thome *et al.* (Aachen-CERN-Heidelberg-Munich), Nucl. Phys. **B129**, 365 (1977).
- [111] A. Breakstone *et al.* (Ames-Bologna-CERN-Dortmund-Heidelberg-Warsaw), Phys. Rev. **D30**, 528 (1984).
- [112] G. J. Alner *et al.* (UA5), Phys. Rept. **154**, 247 (1987).
- [113] R. E. Ansorge *et al.* (UA5), Z. Phys. **C43**, 357 (1989).
- [114] C. Albajar *et al.* (UA1), Nucl. Phys. **B335**, 261 (1990).
- [115] F. Abe *et al.* (CDF), Phys. Rev. **D41**, 2330 (1990), [119(1989)].
- [116] K. Aamodt *et al.* (ALICE), Eur. Phys. J. **C68**, 89 (2010), [arXiv:1004.3034].
- [117] V. Khachatryan *et al.* (CMS), JHEP **02**, 041 (2010), [arXiv:1002.0621].
- [118] V. Khachatryan *et al.* (CMS), JHEP **01**, 079 (2011), [arXiv:1011.5531].
- [119] V. Khachatryan *et al.* (CMS), Phys. Rev. Lett. **105**, 022002 (2010), [arXiv:1005.3299].
- [120] G. Aad *et al.* (ATLAS), Eur. Phys. J. **C76**, 7, 403 (2016), [arXiv:1603.02439].
- [121] M. Aaboud *et al.* (ATLAS), Eur. Phys. J. **C76**, 9, 502 (2016), [arXiv:1606.01133].
- [122] J. Adam *et al.* (ALICE), Phys. Lett. **B753**, 319 (2016), [arXiv:1509.08734].
- [123] J. Adam *et al.* (ALICE), Eur. Phys. J. **C77**, 1, 33 (2017), [arXiv:1509.07541].
- [124] P. V. Chliapnikov and V. A. Uvarov, Phys. Lett. **B251**, 192 (1990).
- [125] J. F. Grosse-Oetringhaus and K. Reygers, J. Phys. **G37**, 083001 (2010), [arXiv:0912.0023].
- [126] E. K. G. Sarkisyan and A. S. Sakharov (2004), [hep-ph/0410324]; E. K. G. Sarkisyan and A. S. Sakharov, AIP Conf. Proc. **828**, 1, 35 (2006), [hep-ph/0510191]; E. K. G. Sarkisyan and A. S. Sakharov, Eur. Phys. J. **C70**, 533 (2010), [arXiv:1004.4390].
- [127] S. Hoeche *et al.*, in "HERA and the LHC: A Workshop on the implications of HERA for LHC physics: Proceedings Part A," 288–289 (2005), [hep-ph/0602031]; S. Mrenna and P. Richardson, JHEP **05**, 040 (2004), [hep-ph/0312274]; J. Alwall *et al.*, Eur. Phys. J. **C53**, 473 (2008), [arXiv:0706.2569].
- [128] I. Borsa *et al.* (2021), [arXiv:2110.14015].
- [129] E. Moffat *et al.* (Jefferson Lab Angular Momentum (JAM)), Phys. Rev. D **104**, 1, 016015 (2021), [arXiv:2101.04664].
- [130] V. Bertone *et al.* (NNPDF), Eur. Phys. J. **C77**, 8, 516 (2017), [arXiv:1706.07049].
- [131] D. de Florian, R. Sassot and M. Stratmann, Phys. Rev. **D76**, 074033 (2007), [arXiv:0707.1506].
- [132] S. Albino, B. A. Kniehl and G. Kramer, Nucl. Phys. **B803**, 42 (2008), [arXiv:0803.2768].
- [133] S. Kretzer, E. Leader and E. Christova, Eur. Phys. J. **C22**, 269 (2001), [hep-ph/0108055].
- [134] S. Kretzer, Phys. Rev. **D62**, 054001 (2000), [hep-ph/0003177].
- [135] L. Bourhis *et al.*, Eur. Phys. J. **C19**, 89 (2001), [hep-ph/0009101].
- [136] M. Hirai *et al.*, Phys. Rev. **D75**, 094009 (2007), [hep-ph/0702250].
- [137] C. A. Aidala *et al.*, Phys. Rev. **D83**, 034002 (2011), [arXiv:1009.6145].
- [138] D. de Florian *et al.*, Phys. Rev. **D91**, 1, 014035 (2015), [arXiv:1410.6027].
- [139] D. de Florian *et al.*, Phys. Rev. **D95**, 9, 094019 (2017), [arXiv:1702.06353].
- [140] D. de Florian, R. Sassot and M. Stratmann, Phys. Rev. **D75**, 114010 (2007), [hep-ph/0703242].
- [141] D. P. Anderle, F. Ringer and M. Stratmann, Phys. Rev. **D92**, 11, 114017 (2015), [arXiv:1510.05845].
- [142] E. Leader, A. V. Sidorov and D. B. Stamenov, Phys. Rev. **D93**, 7, 074026 (2016), [arXiv:1506.06381].

- [143] R. A. Khalek, V. Bertone and E. R. Nocera (2021), [arXiv:2105.08725].
- [144] H. Abdolmaleki *et al.* (xFitter) (2021), [arXiv:2105.11306].
- [145] V. Bertone *et al.* (NNPDF), Eur. Phys. J. **C78**, 8, 651 (2018), [arXiv:1807.03310].
- [146] R. Barate *et al.* (ALEPH), Eur. Phys. J. **C17**, 1 (2000); R. Akers *et al.* (OPAL), Z. Phys. **C68**, 179 (1995); G. Abbiendi *et al.* (OPAL), Eur. Phys. J. **C11**, 217 (1999), [hep-ex/9903027].
- [147] K. Abe *et al.* (SLD), Phys. Rev. **D59**, 052001 (1999), [hep-ex/9805029].
- [148] D. Buskulic *et al.* (ALEPH), Z. Phys. **C66**, 355 (1995); H. Albrecht *et al.* (ARGUS), Z. Phys. **C44**, 547 (1989); R. Akers *et al.* (OPAL), Z. Phys. **C63**, 181 (1994).
- [149] M. R. Adams *et al.* (E665), Z. Phys. **C61**, 539 (1994).
- [150] M. Arneodo *et al.* (European Muon), Z. Phys. **C34**, 283 (1987).
- [151] S. Aid *et al.* (H1), Nucl. Phys. **B480**, 3 (1996), [hep-ex/9607010].
- [152] J. J. Aubert *et al.* (European Muon), Z. Phys. **C18**, 189 (1983).
- [153] A. Airapetian *et al.* (HERMES), Eur. Phys. J. **C21**, 599 (2001), [hep-ex/0104004].
- [154] T. P. McPharlin *et al.*, Phys. Lett. **90B**, 479 (1980).
- [155] S. S. Adler *et al.* (PHENIX), Phys. Rev. Lett. **91**, 241803 (2003), [hep-ex/0304038].
- [156] B. Abelev *et al.* (ALICE), Phys. Lett. **B717**, 162 (2012), [arXiv:1205.5724].
- [157] M. Bonesini *et al.* (WA70), Z. Phys. **C38**, 371 (1988).
- [158] T. Akesson *et al.* (Axial Field Spectrometer), Sov. J. Nucl. Phys. **51**, 836 (1990), [Yad. Fiz.51,1314(1990)].
- [159] C. Kourkoumelis *et al.*, Z. Phys. **C5**, 95 (1980).
- [160] L. Apanasevich *et al.* (Fermilab E706), Phys. Rev. **D68**, 052001 (2003), [hep-ex/0204031].
- [161] F. Abe *et al.* (CDF), Phys. Rev. Lett. **61**, 1819 (1988).
- [162] M. Banner *et al.* (UA2), Phys. Lett. **115B**, 59 (1982).
- [163] M. Procura and I. W. Stewart, Phys. Rev. **D81**, 074009 (2010), [Erratum: Phys. Rev.D83,039902(2011)], [arXiv:0911.4980].
- [164] A. Jain, M. Procura and W. J. Waalewijn, JHEP **05**, 035 (2011), [arXiv:1101.4953].
- [165] M. Procura and W. J. Waalewijn, Phys. Rev. **D85**, 114041 (2012), [arXiv:1111.6605].
- [166] F. Arleo *et al.*, JHEP **04**, 147 (2014), [arXiv:1311.7356].
- [167] M. Ritzmann and W. J. Waalewijn, Phys. Rev. **D90**, 5, 054029 (2014), [arXiv:1407.3272].
- [168] T. Kaufmann, A. Mukherjee and W. Vogelsang, Phys. Rev. **D92**, 5, 054015 (2015), [arXiv:1506.01415].
- [169] Y.-T. Chien *et al.*, JHEP **05**, 125 (2016), [arXiv:1512.06851].
- [170] F. Abe *et al.* (CDF), Phys. Rev. Lett. **65**, 968 (1990).
- [171] T. A. collaboration (ATLAS) (2015).
- [172] S. Chatrchyan *et al.* (CMS), JHEP **10**, 087 (2012), [arXiv:1205.5872].
- [173] X. Lu (ALICE), Nucl. Phys. **A931**, 428 (2014), [arXiv:1407.8385].
- [174] C. Bianchin (ALICE), J. Phys. Conf. Ser. **612**, 1, 012020 (2015).
- [175] F. Krizek (ALICE), J. Phys. Conf. Ser. **668**, 1, 012018 (2016), [arXiv:1509.02024].
- [176] M. Aaboud *et al.* (ATLAS), Nucl. Phys. **A978**, 65 (2018), [arXiv:1706.02859].
- [177] L. Adamczyk *et al.* (STAR), Phys. Rev. **D97**, 3, 032004 (2018), [arXiv:1708.07080].
- [178] D. P. Anderle *et al.*, Phys. Rev. **D96**, 3, 034028 (2017), [arXiv:1706.09857].
- [179] N. Sato *et al.* (JAM) (2019), [arXiv:1905.03788].
- [180] M. Epele *et al.*, Phys. Rev. **D86**, 074028 (2012), [arXiv:1209.3240].
- [181] E. Witten, Nucl. Phys. **210**, 189 (1977).
- [182] L. Bourhis, M. Fontannaz and J. P. Guillet, Eur. Phys. J. **C2**, 529 (1998), [hep-ph/9704447].
- [183] M. Gluck, E. Reya and A. Vogt, Phys. Rev. **D48**, 116 (1993), [Erratum: Phys. Rev.D51,1427(1995)]; Erratum *ibid.* **D51**, 1427 (1995).
- [184] G. Abbiendi *et al.* (OPAL), Eur. Phys. J. **C27**, 467 (2003), [hep-ex/0209048].
- [185] G. Bocquet *et al.*, Phys. Lett. **B366**, 434 (1996).
- [186] T. Kaufmann, A. Mukherjee and W. Vogelsang, Phys. Rev. **D93**, 11, 114021 (2016), [arXiv:1604.07175].
- [187] P. Abreu *et al.* (DELPHI), Eur. Phys. J. **C13**, 573 (2000).
- [188] B. A. Kniehl, G. Kramer and B. Potter, Phys. Rev. Lett. **85**, 5288 (2000), [hep-ph/0003297].
- [189] M. Arneodo *et al.* (European Muon), Z. Phys. **C33**, 167 (1986).
- [190] A. Airapetian *et al.* (HERMES), Phys. Rev. **D87**, 074029 (2013), [arXiv:1212.5407].
- [191] C. Adolph *et al.* (COMPASS), Phys. Lett. **B764**, 1 (2017), [arXiv:1604.02695].
- [192] F. D. Aaron *et al.* (H1), Phys. Lett. **B673**, 119 (2009), [arXiv:0901.0477].
- [193] M. Derrick *et al.* (ZEUS), Z. Phys. **C68**, 29 (1995), [hep-ex/9505011].
- [194] S. Chekanov *et al.* (ZEUS), Phys. Lett. **B553**, 141 (2003), [hep-ex/0211025].
- [195] S. Chekanov *et al.* (ZEUS), Nucl. Phys. **B786**, 181 (2007), [arXiv:0705.3770].
- [196] F. D. Aaron *et al.* (H1), Eur. Phys. J. **C61**, 185 (2009), [arXiv:0810.4036].
- [197] A. Aktas *et al.* (H1), Eur. Phys. J. **C36**, 413 (2004), [hep-ex/0403056].
- [198] P. Dixon, D. Kant and G. Thompson, J. Phys. **G25**, 1453 (1999).
- [199] C. Adloff *et al.* (H1), Phys. Lett. **B462**, 440 (1999), [hep-ex/9907030].
- [200] D. Graudenz, Fortsch. Phys. **45**, 629 (1997), [hep-ph/9701334].
- [201] P. M. Nadolsky, D. R. Stump and C. P. Yuan, Phys. Rev. **D61**, 014003 (2000), [Erratum: Phys. Rev.D64,059903(2001)], [hep-ph/9906280].
- [202] D. de Florian *et al.*, Phys. Rev. **D95**, 0334027 (2017).
- [203] T. Aaltonen *et al.* (CDF), Phys. Rev. **D79**, 112005 (2009), [Erratum: Phys. Rev.D82,119903(2010)], [arXiv:0904.1098].
- [204] G. Aad *et al.* (ATLAS), New J. Phys. **13**, 053033 (2011), [arXiv:1012.5104].
- [205] B. I. Abelev *et al.* (STAR), Phys. Rev. **C75**, 064901 (2007), [arXiv:nucl-ex/0607033].
- [206] K. Aamodt *et al.* (ALICE), Eur. Phys. J. **C71**, 1655 (2011), [arXiv:1101.4110].
- [207] B. B. Abelev *et al.* (ALICE), Phys. Lett. **B736**, 196 (2014), [arXiv:1401.1250].
- [208] J. Adam *et al.* (ALICE), Eur. Phys. J. **C75**, 5, 226 (2015), [arXiv:1504.00024].
- [209] S. Chatrchyan *et al.* (CMS), Eur. Phys. J. **C72**, 2164 (2012), [arXiv:1207.4724].

- [210] A. M. Sirunyan *et al.* (CMS), Phys. Rev. **D96**, 11, 112003 (2017), [arXiv:1706.10194].
- [211] G. J. Alner *et al.* (UA5), Z. Phys. **C32**, 153 (1986).
- [212] B. Abelev *et al.* (ALICE), Eur. Phys. J. **C73**, 6, 2456 (2013), [arXiv:1208.4968].
- [213] G. Antchev *et al.* (TOTEM), EPL **101**, 2, 21004 (2013).
- [214] A. M. Sirunyan *et al.* (CMS), JHEP **07**, 161 (2018), [arXiv:1802.02613].
- [215] F. Abe *et al.* (CDF), Phys. Rev. **D50**, 5550 (1994).
- [216] F. Abe *et al.* (CDF), Phys. Rev. **D50**, 5518 (1994).
- [217] S. S. Adler *et al.* (PHENIX), Phys. Rev. **C74**, 024904 (2006), [arXiv:nucl-ex/0603010].
- [218] S. Albino *et al.*, Phys. Rev. **D75**, 034018 (2007), [hep-ph/0611029].
- [219] I. Borsa, R. Sassot and M. Stratmann, Phys. Rev. **D96**, 9, 094020 (2017), [arXiv:1708.01630].
- [220] B. Andersson *et al.*, Phys. Rept. **97**, 31 (1983).
- [221] T. Sjostrand and M. Bengtsson, Comput. Phys. Commun. **43**, 367 (1987); T. Sjostrand, Comput. Phys. Commun. **82**, 74 (1994).
- [222] P. D. Acton *et al.* (OPAL), Phys. Lett. **B305**, 407 (1993).
- [223] J. Breitweg *et al.* (ZEUS), Eur. Phys. J. **C2**, 77 (1998), [hep-ex/9711018].
- [224] D. DeProspero *et al.* (E632), Phys. Rev. **D50**, 6691 (1994).
- [225] S. Chekanov *et al.* (ZEUS), Eur. Phys. J. **C51**, 1 (2007), [hep-ex/0612023].
- [226] G. Grindhammer *et al.*, in: *Proceedings of the Workshop on Monte Carlo Generators for HERA Physics*, Hamburg, Germany, 1998/1999.
- [227] N. Brook *et al.*, in: *Proceedings of the Workshop for Future HERA Physics at HERA*, Hamburg, Germany, 1996.
- [228] D. Acosta *et al.* (CDF), Phys. Rev. **D72**, 052001 (2005), [hep-ex/0504048].
- [229] G. Arnison *et al.* (UA1), Phys. Lett. **118B**, 167 (1982).
- [230] M. Banner *et al.* (UA2), Phys. Lett. **122B**, 322 (1983).
- [231] M. Banner *et al.* (UA2, Bern-CERN-Copenhagen-Orsay-Pavia-Saclay), Z. Phys. **C27**, 329 (1985).
- [232] A. Adare *et al.* (PHENIX), Phys. Rev. **D76**, 051106 (2007), [arXiv:0704.3599].
- [233] A. Adare *et al.* (PHENIX), Phys. Rev. **D83**, 032001 (2011), [arXiv:1009.6224].
- [234] A. Adare *et al.* (PHENIX), Phys. Rev. **D86**, 092006 (2012), [arXiv:1202.4020].
- [235] A. Adare *et al.* (PHENIX), Phys. Rev. **D88**, 3, 032006 (2013), [arXiv:1209.3283].
- [236] A. Adare *et al.* (PHENIX), Phys. Rev. **D91**, 3, 032001 (2015), [arXiv:1409.1907].
- [237] A. Adare *et al.* (PHENIX), Phys. Rev. **D90**, 7, 072008 (2014), [arXiv:1406.3541].
- [238] A. Adare *et al.* (PHENIX), Phys. Rev. **D93**, 1, 011501 (2016), [arXiv:1510.02317].
- [239] I. Arsene *et al.* (BRAHMS), Phys. Rev. Lett. **98**, 252001 (2007), [hep-ex/0701041].
- [240] J. Adams *et al.* (STAR), Phys. Rev. Lett. **97**, 152302 (2006), [arXiv:nucl-ex/0602011].
- [241] J. Adams *et al.* (STAR), Phys. Lett. **B637**, 161 (2006), [arXiv:nucl-ex/0601033].
- [242] B. I. Abelev *et al.* (STAR), Phys. Rev. **D80**, 111108 (2009), [arXiv:0911.2773].
- [243] G. Agakishiev *et al.* (STAR), Phys. Rev. Lett. **108**, 072302 (2012), [arXiv:1110.0579].
- [244] L. Adamczyk *et al.* (STAR), Phys. Rev. **D89**, 1, 012001 (2014), [arXiv:1309.1800].
- [245] B. B. Abelev *et al.* (ALICE), Eur. Phys. J. **C73**, 12, 2662 (2013), [arXiv:1307.1093].
- [246] L. Apanasevich *et al.* (Fermilab E706), Phys. Rev. Lett. **81**, 2642 (1998), [hep-ex/9711017].
- [247] G. Balocchi *et al.* (UA6), Phys. Lett. **B436**, 222 (1998).
- [248] K. Aamodt *et al.* (ALICE), Eur. Phys. J. **C71**, 1594 (2011), [arXiv:1012.3257].
- [249] R. Aaij *et al.* (LHCb), Phys. Lett. **B703**, 267 (2011), [arXiv:1107.3935].
- [250] G. Aad *et al.* (ATLAS), Phys. Lett. **B758**, 67 (2016), [arXiv:1602.01633].
- [251] F. Aversa *et al.*, Nucl. Phys. **B327**, 105 (1989); D. de Florian, Phys. Rev. **D67**, 054004 (2003), [hep-ph/0210442]; B. Jager *et al.*, Phys. Rev. **D67**, 054005 (2003), [hep-ph/0211007].
- [252] U. Baur *et al.*, in "QCD and weak boson physics in Run II. Proceedings, Batavia, USA, March 4-6, June 3-4, November 4-6, 1999," 115-164 (2000), [115(2000)], [hep-ph/0005226], URL <http://lss.fnal.gov/archive/preprint/fermilab-conf-00-411-ae.shtml>.
- [253] P. Aurenche *et al.*, Eur. Phys. J. **C13**, 347 (2000), [hep-ph/9910252].
- [254] L. Apanasevich *et al.*, Phys. Rev. **D59**, 074007 (1999), [hep-ph/9808467].
- [255] U. D'Alesio and F. Murgia, Phys. Rev. **D70**, 074009 (2004), [hep-ph/0408092].
- [256] D. de Florian and W. Vogelsang, Phys. Rev. **D71**, 114004 (2005), [hep-ph/0501258].
- [257] P. Hinderer *et al.*, Phys. Rev. **D99**, 5, 054019 (2019), [arXiv:1812.00915].
- [258] D. d'Enterria *et al.*, Nucl. Phys. **B883**, 615 (2014), [arXiv:1311.1415].
- [259] G. Wilk and Z. Wlodarczyk, Eur. Phys. J. **A40**, 299 (2009), [arXiv:0810.2939].
- [260] C. Tsallis, J. Statist. Phys. **52**, 479 (1988).
- [261] C. Tsallis, Braz. J. Phys. **29**, 1 (1999).
- [262] C. Tsallis, Eur. Phys. J. **A40**, 257 (2009), [arXiv:0812.4370].
- [263] M. D. Azmi and J. Cleymans, J. Phys. **G41**, 065001 (2014), [arXiv:1401.4835].
- [264] G. Wilk and Z. Wlodarczyk, Phys. Rev. Lett. **84**, 2770 (2000), [hep-ph/9908459].
- [265] T. Bhattacharyya *et al.*, J. Phys. **G45**, 5, 055001 (2018), [arXiv:1709.07376].
- [266] S. Grigoryan, Phys. Rev. **D95**, 5, 056021 (2017), [arXiv:1702.04110].
- [267] T. Wibig, Int. J. Mod. Phys. **A29**, 1450021 (2014).
- [268] K. Saraswat, P. Shukla and V. Singh, J. Phys. Comm. **2**, 3, 035003 (2018), [arXiv:1706.04860].
- [269] K. Urmosy, G. G. Barnafoldi and T. S. Biro, Phys. Lett. **B701**, 111 (2011), [arXiv:1101.3023].
- [270] A. S. Parvan, O. V. Teryaev and J. Cleymans, Eur. Phys. J. **A53**, 5, 102 (2017), [arXiv:1607.01956].
- [271] K. Adcox *et al.* (PHENIX), Phys. Rev. Lett. **88**, 022301 (2002), [arXiv:nucl-ex/0109003]; C. Adler *et al.* (STAR), Phys. Rev. Lett. **90**, 082302 (2003), [arXiv:nucl-ex/0210033].
- [272] V. A. Khoze *et al.*, *Proceedings, Conference on High-Energy Physics, Tbilisi 1976*; J. D. Bjorken, Phys. Rev. **D17**, 171 (1978).
- [273] M. Artuso *et al.* (CLEO), Phys. Rev. **D70**, 112001 (2004), [hep-ex/0402040].
- [274] R. Seuster *et al.* (Belle), Phys. Rev. **D73**, 032002 (2006), [hep-ex/0506068].

- [275] A. Heister *et al.* (ALEPH), Phys. Lett. **B512**, 30 (2001), [hep-ex/0106051]; J. Abdallah *et al.* (DELPHI), Eur. Phys. J. **C71**, 1557 (2011), [arXiv:1102.4748]; G. Abbiendi *et al.* (OPAL), Eur. Phys. J. **C29**, 463 (2003), [hep-ex/0210031]; K. Abe *et al.* (SLD), Phys. Rev. **D65**, 092006 (2002), [Erratum: Phys. Rev. D66,079905(2002)], [hep-ex/0202031].
- [276] B. Mele and P. Nason, Phys. Lett. **B245**, 635 (1990); B. Mele and P. Nason, Nucl. Phys. **B361**, 626 (1991), [Erratum: Nucl. Phys. B921,841(2017)].
- [277] M. Cacciari and S. Catani, Nucl. Phys. **B617**, 253 (2001), [hep-ph/0107138].
- [278] P. Nason and C. Oleari, Phys. Lett. **B418**, 199 (1998), [hep-ph/9709358]; P. Nason and C. Oleari, Phys. Lett. **B447**, 327 (1999), [hep-ph/9811206]; P. Nason and C. Oleari, Nucl. Phys. **B565**, 245 (2000), [hep-ph/9903541].
- [279] K. Melnikov and A. Mitov, Phys. Rev. **D70**, 034027 (2004), [hep-ph/0404143].
- [280] C. Peterson *et al.*, Phys. Rev. **D27**, 105 (1983).
- [281] V. G. Kartvelishvili, A. K. Likhoded and V. A. Petrov, Phys. Lett. **78B**, 615 (1978).
- [282] P. D. B. Collins and T. P. Spiller, J. Phys. **G11**, 1289 (1985).
- [283] G. Colangelo and P. Nason, Phys. Lett. **B285**, 167 (1992).
- [284] M. G. Bowler, Z. Phys. **C11**, 169 (1981).
- [285] E. Braaten *et al.*, Phys. Rev. **D51**, 4819 (1995), [hep-ph/9409316].
- [286] R. Akers *et al.* (OPAL), Z. Phys. **C67**, 27 (1995).
- [287] H. Albrecht *et al.* (ARGUS), Z. Phys. **C52**, 353 (1991).
- [288] D. Buskulic *et al.* (ALEPH), Phys. Lett. **B357**, 699 (1995).
- [289] J. Chrin, Z. Phys. **C36**, 163 (1987).
- [290] R. L. Jaffe and L. Randall, Nucl. Phys. **B412**, 79 (1994), [hep-ph/9306201].
- [291] M. Cacciari and E. Gardi, Nucl. Phys. **B664**, 299 (2003), [hep-ph/0301047].
- [292] L. Randall and N. Rius, Nucl. Phys. **B441**, 167 (1995), [hep-ph/9405217].
- [293] J. C. Collins, Phys. Rev. **D58**, 094002 (1998), [hep-ph/9806259].
- [294] B. A. Kniehl *et al.*, Eur. Phys. J. **C41**, 199 (2005), [hep-ph/0502194].
- [295] S. Ahmed *et al.* (CLEO), Phys. Rev. **D62**, 112003 (2000), [hep-ex/0008015].
- [296] B. Aubert *et al.* (BaBar), Phys. Rev. **D65**, 091104 (2002), [hep-ex/0201041].
- [297] D. Bortoletto *et al.* (CLEO), Phys. Rev. **D37**, 1719 (1988), [Erratum: Phys. Rev. D39,1471(1989)].
- [298] H. Albrecht *et al.* (ARGUS), Z. Phys. **C54**, 1 (1992).
- [299] G. Alexander *et al.* (OPAL), Z. Phys. **C69**, 543 (1996).
- [300] A. Heister *et al.* (ALEPH), Phys. Lett. **B561**, 213 (2003), [hep-ex/0302003].
- [301] F. D. Aaron *et al.* (H1), Eur. Phys. J. **C65**, 89 (2010), [arXiv:0907.2643].
- [302] S. Chekanov *et al.* (ZEUS), JHEP **07**, 074 (2007), [arXiv:0704.3562]; ZEUS Collab.: H. Abramowicz *et al.*, JHEP, 1309 (2013); A. Aktas *et al.* (H1), Eur. Phys. J. **C51**, 271 (2007), [hep-ex/0701023]; F. D. Aaron *et al.* (H1), Eur. Phys. J. **C59**, 589 (2009), [arXiv:0808.1003].
- [303] B. Adeva *et al.* (L3), Phys. Lett. **B261**, 177 (1991).
- [304] O. Biebel, P. Nason and B. R. Webber (2001), [hep-ph/0109282].
- [305] H. Evans (ALICE, ATLAS, CMS, LHCb), in "Proceedings, 14th International Conference on Hadron spectroscopy (Hadron 2011): Munich, Germany, June 13-17, 2011," (2011), [arXiv:1110.5294]; E. Aguilo, in "Proceedings, 47th Rencontres de Moriond on QCD and High Energy Interactions: La Thuile, France, March 10-17, 2012," 115–120 (2012), [arXiv:1205.5678]; F. Simonetto, Journal of Physics: Conference Series **347**, 012014 (2012).
- [306] V. Khachatryan *et al.* (CMS), JHEP **03**, 136 (2011), [arXiv:1102.3194]; G. Aad *et al.* (ATLAS), Eur. Phys. J. **C71**, 1846 (2011), [arXiv:1109.6833]; S. Chatrchyan *et al.* (CMS), JHEP **04**, 084 (2012), [arXiv:1202.4617]; G. Aad *et al.* (ATLAS), Eur. Phys. J. **C73**, 2, 2301 (2013), [arXiv:1210.0441].
- [307] H. Jung *et al.*, Phys. Rev. **D85**, 034035 (2012), [arXiv:1111.1942].
- [308] D. Acosta *et al.* (CDF), Phys. Rev. Lett. **91**, 241804 (2003), [hep-ex/0307080]; D. Acosta *et al.* (CDF), Phys. Rev. **D71**, 032001 (2005), [hep-ex/0412071].
- [309] M. Cacciari and P. Nason, JHEP **09**, 006 (2003), [hep-ph/0306212]; M. Cacciari *et al.*, JHEP **07**, 033 (2004), [hep-ph/0312132]; B. A. Kniehl *et al.*, Phys. Rev. Lett. **96**, 012001 (2006), [hep-ph/0508129].
- [310] H. Abramowicz *et al.* (ZEUS), Eur. Phys. J. **C71**, 1573 (2011), [arXiv:1101.3692].
- [311] S. Chekanov *et al.* (ZEUS), Phys. Rev. **D78**, 072001 (2008), [arXiv:0805.4390].
- [312] S. Chekanov *et al.* (ZEUS), JHEP **02**, 032 (2009), [arXiv:0811.0894].
- [313] F. D. Aaron *et al.* (H1), Eur. Phys. J. **C72**, 2148 (2012), [arXiv:1206.4346].
- [314] M. L. Mangano and P. Nason, Phys. Lett. **B285**, 160 (1992).
- [315] M. H. Seymour, Nucl. Phys. **B436**, 163 (1995).
- [316] D. J. Miller and M. H. Seymour, Phys. Lett. **B435**, 213 (1998), [hep-ph/9805414].
- [317] R. Barate *et al.* (ALEPH), Phys. Lett. **B434**, 437 (1998).
- [318] P. Abreu *et al.* (DELPHI), Phys. Lett. **B405**, 202 (1997).
- [319] M. Acciarri *et al.* (L3), Phys. Lett. **B476**, 243 (2000), [hep-ex/9911016].
- [320] G. Abbiendi *et al.* (OPAL), Eur. Phys. J. **C13**, 1 (2000), [hep-ex/9908001].
- [321] K. Abe *et al.* (SLD) (1999), [hep-ex/9908028], URL <http://www-public.slac.stanford.edu/sciDoc/docMeta.aspx?slacPubNumber=SLAC-PUB-8157>.
- [322] C. Albajar *et al.* (UA1 Collaboration), Z. Phys. C **61**, 41 (1993), URL <http://cds.cern.ch/record/253028>.
- [323] R. Aaij *et al.* (LHCb), JHEP **11**, 030 (2017), [arXiv:1708.05994].
- [324] M. Aaboud *et al.* (ATLAS), Phys. Rev. **D99**, 5, 052004 (2019), [arXiv:1812.09283].
- [325] M. Burkardt and R. L. Jaffe, Phys. Rev. Lett. **70**, 2537 (1993), [hep-ph/9302232].
- [326] P. J. Mulders and R. D. Tangerman, Nucl. Phys. **B461**, 197 (1996), [Erratum: Nucl. Phys. B484,538(1997)], [hep-ph/9510301].
- [327] R. Jakob, Nucl. Phys. **A711**, 35 (2002), [hep-ph/0206271].
- [328] D. de Florian, M. Stratmann and W. Vogelsang, Phys. Rev. Lett. **81**, 530 (1998), [hep-ph/9802432].
- [329] D. Buskulic *et al.* (ALEPH), Phys. Lett. **B374**, 319 (1996).
- [330] K. Ackerstaff *et al.* (OPAL), Eur. Phys. J. **C2**, 49 (1998), [hep-ex/9708027].
- [331] G. Abbiendi *et al.* (OPAL), Phys. Lett. **B444**, 539 (1998), [hep-ex/9808006].
- [332] M. Alekseev *et al.* (COMPASS), Eur. Phys. J. **C64**, 171 (2009), [arXiv:0907.0388].
- [333] A. Airapetian *et al.* (HERMES), Phys. Rev. **D74**, 072004 (2006), [hep-ex/0607004].
- [334] G. Karyan (HERMES), Int. J. Mod. Phys. Conf. Ser. **40**, 1660067 (2016).
- [335] J. Adam *et al.* (STAR), Phys. Rev. **D98**, 11, 112009 (2018), [arXiv:1808.07634].

- [336] R. L. Jaffe, Phys. Rev. **D54**, 11, R6581 (1996), [hep-ph/9605456].
- [337] A. Airapetian *et al.* (HERMES), Phys. Rev. **D76**, 092008 (2007), [arXiv:0704.3133].
- [338] A. Moretti (COMPASS), PoS **SPIN2018**, 138 (2018), [arXiv:1901.01735].
- [339] L. Gamberg *et al.*, Phys. Lett. B **818**, 136371 (2021), [arXiv:2102.05553].
- [340] R. Seidl *et al.* (Belle), Phys. Rev. **D99**, 11, 112006 (2019), [arXiv:1902.01552].
- [341] C. Adolph *et al.* (COMPASS), Eur. Phys. J. **C73**, 8, 2531 (2013), [Erratum: Eur. Phys. J. C75, no.2, 94 (2015)], [arXiv:1305.7317].
- [342] A. Signori *et al.*, JHEP **11**, 194 (2013), [arXiv:1309.3507].
- [343] M. Anselmino *et al.*, JHEP **04**, 005 (2014), [arXiv:1312.6261].
- [344] M. G. Echevarria *et al.*, Phys. Rev. **D89**, 074013 (2014), [arXiv:1401.5078].
- [345] M. G. Echevarria, I. Scimemi and A. Vladimirov, Phys. Rev. **D93**, 1, 011502 (2016), [Erratum: Phys. Rev. D94, no.9, 099904 (2016)], [arXiv:1509.06392].
- [346] M. G. Echevarria, I. Scimemi and A. Vladimirov, JHEP **09**, 004 (2016), [arXiv:1604.07869].
- [347] A. Bacchetta *et al.*, JHEP **06**, 081 (2017), [Erratum: JHEP06,051(2019)], [arXiv:1703.10157].
- [348] M. A. Ebert, B. Mistlberger and G. Vita, JHEP **07**, 121 (2021), [arXiv:2012.07853].
- [349] M.-x. Luo *et al.*, JHEP **06**, 115 (2021), [arXiv:2012.03256].
- [350] J. C. Collins, Nucl. Phys. **B396**, 161 (1993), [hep-ph/9208213].
- [351] J. P. Ralston and D. E. Soper, Nucl. Phys. **B152**, 109 (1979).
- [352] H. Avakian *et al.* (CLAS), Phys. Rev. **D69**, 112004 (2004), [hep-ex/0301005].
- [353] A. Airapetian *et al.* (HERMES), Phys. Rev. Lett. **84**, 4047 (2000), [hep-ex/9910062].
- [354] A. Airapetian *et al.* (HERMES), Phys. Rev. **D64**, 097101 (2001), [hep-ex/0104005].
- [355] A. Airapetian *et al.* (HERMES), Phys. Rev. Lett. **94**, 012002 (2005), [hep-ex/0408013].
- [356] A. Airapetian *et al.* (HERMES), Phys. Lett. **B693**, 11 (2010), [arXiv:1006.4221].
- [357] V. Yu. Alexakhin *et al.* (COMPASS), Phys. Rev. Lett. **94**, 202002 (2005), [hep-ex/0503002].
- [358] E. S. Ageev *et al.* (COMPASS), Nucl. Phys. **B765**, 31 (2007), [hep-ex/0610068].
- [359] M. Alekseev *et al.* (COMPASS), Phys. Lett. **B673**, 127 (2009), [arXiv:0802.2160].
- [360] M. G. Alekseev *et al.* (COMPASS), Phys. Lett. **B692**, 240 (2010), [arXiv:1005.5609].
- [361] M. G. Alekseev *et al.* (COMPASS), Eur. Phys. J. **C70**, 39 (2010), [arXiv:1007.1562].
- [362] C. Adolph *et al.* (COMPASS), Phys. Lett. **B717**, 376 (2012), [arXiv:1205.5121].
- [363] C. Adolph *et al.* (COMPASS), Phys. Lett. **B744**, 250 (2015), [arXiv:1408.4405].
- [364] K. Abe *et al.* (Belle), Phys. Rev. Lett. **96**, 232002 (2006), [hep-ex/0507063].
- [365] R. Seidl *et al.* (Belle), Phys. Rev. **D78**, 032011 (2008), [Erratum: Phys. Rev. D86, 039905 (2012)], [arXiv:0805.2975].
- [366] J. P. Lees *et al.* (BaBar), Phys. Rev. **D90**, 5, 052003 (2014), [arXiv:1309.5278].
- [367] J. P. Lees *et al.* (BaBar), Phys. Rev. **D92**, 11, 111101 (2015), [arXiv:1506.05864].
- [368] M. Ablikim *et al.* (BESIII), Phys. Rev. Lett. **116**, 4, 042001 (2016), [arXiv:1507.06824].
- [369] M. Anselmino *et al.*, Phys. Rev. **D92**, 11, 114023 (2015), [arXiv:1510.05389].
- [370] Z.-B. Kang *et al.*, Phys. Rev. **D93**, 1, 014009 (2016), [arXiv:1505.05589].
- [371] F. Yuan, Phys. Rev. Lett. **100**, 032003 (2008), [arXiv:0709.3272].
- [372] Z.-B. Kang *et al.*, JHEP **11**, 068 (2017), [arXiv:1705.08443].
- [373] K. Konishi, A. Ukawa and G. Veneziano, Phys. Lett. **78B**, 243 (1978).
- [374] I. Vendramin, Nuovo Cim. **A66**, 339 (1981).
- [375] J. C. Collins, S. F. Heppelmann and G. A. Ladinsky, Nucl. Phys. **B420**, 565 (1994), [hep-ph/9305309].
- [376] R. L. Jaffe, X.-m. Jin and J. Tang, Phys. Rev. Lett. **80**, 1166 (1998), [hep-ph/9709322].
- [377] R. L. Jaffe, X.-m. Jin and J.-a. Tang, Phys. Rev. **D57**, 5920 (1998), [hep-ph/9710561].
- [378] A. Bianconi *et al.*, Phys. Rev. **D62**, 034008 (2000), [hep-ph/9907475].
- [379] M. Radici, R. Jakob and A. Bianconi, Phys. Rev. **D65**, 074031 (2002), [hep-ph/0110252].
- [380] D. de Florian and L. Vanni, Phys. Lett. **B578**, 139 (2004), [hep-ph/0310196].
- [381] A. Bacchetta and M. Radici, Phys. Rev. **D67**, 094002 (2003), [hep-ph/0212300].
- [382] A. Vossen *et al.* (Belle), Phys. Rev. Lett. **107**, 072004 (2011), [arXiv:1104.2425].
- [383] A. Courtoy *et al.*, Phys. Rev. **D85**, 114023 (2012), [arXiv:1202.0323].
- [384] M. Radici *et al.*, JHEP **05**, 123 (2015), [arXiv:1503.03495].
- [385] A. Airapetian *et al.* (HERMES), JHEP **06**, 017 (2008), [arXiv:0803.2367].
- [386] C. Adolph *et al.* (COMPASS), Phys. Lett. **B713**, 10 (2012), [arXiv:1202.6150].
- [387] C. Adolph *et al.* (COMPASS), Phys. Lett. **B736**, 124 (2014), [arXiv:1401.7873].
- [388] L. Adamczyk *et al.* (STAR), Phys. Rev. Lett. **115**, 242501 (2015), [arXiv:1504.00415].
- [389] A. Bacchetta, A. Courtoy and M. Radici, Phys. Rev. Lett. **107**, 012001 (2011), [arXiv:1104.3855].
- [390] A. Bacchetta, A. Courtoy and M. Radici, JHEP **03**, 119 (2013), [arXiv:1212.3568].
- [391] M. Radici and A. Bacchetta, Phys. Rev. Lett. **120**, 19, 192001 (2018), [arXiv:1802.05212].

20. High Energy Soft QCD and Diffraction

Written February 2020 by V.A. Khoze (Durham U.), M.G. Ryskin (Petersburg Nuclear Phys. Inst.) and M. Taševský (Prague, Inst. Phys.).

20.1 Introduction

Despite the enormous successes of Quantum Chromodynamics (QCD) (see Section 9 in [1] and [2]) there remain a number of deep questions to be answered in the domain of strong interaction physics. These concern first of all small momentum transfer processes which are generically called soft interactions.

One of the most challenging problems is the high-energy behaviour of hadronic scattering processes. At high collision energies, \sqrt{s} , soft interactions play a dominant role. Unfortunately, soft interactions cannot be described in terms of perturbative QCD. These are non-perturbative phenomena related to confinement which are generally considered in the context of the analytic S -matrix, based on *first principles*, such as analyticity, crossing symmetry and unitarity of partial waves, see e.g. [3, 4]. At high energies the most self-consistent way to perform the calculations and to describe the data is the Regge approach (see for example [5–7]), which will be considered below. As discussed in Section 20.5, this formalism could be smoothly matched with perturbative QCD calculations at larger transverse momenta. Therefore, here we will concentrate on the properties of high energy soft interactions that can be expected from the extension of the perturbative QCD domain.

The main aim of this review is to present the well-established theoretical framework, based on Regge theory and QCD, used for describing high-energy collisions. A limited number of some new experimental results, mainly from the LHC, are shown in order to demonstrate that the gross features of the data are in agreement with this approach. We are not focussing on any particular phenomenological or Monte Carlo model, which are covered in the dedicated reviews and books, see e.g. Section 43 in [1], [2, 8–14] and Chapter 2 in [15].

Typically, in multiparticle production, the secondaries¹ fill the whole available rapidity interval.² However, there exists an important class of events in which a large interval of rapidity (typically at least 4 units) is devoid of any hadronic activity. Such an interval is called a Large Rapidity Gap (LRG). The most frequent case with a LRG is elastic scattering. There are also events in which one of the incoming protons (or both) is transformed (dissociates) into a set of two or more final state particles with the mass $M \ll \sqrt{s}$ and proton quantum number. All these events have properties similar to those of the well-known from optics pattern of diffraction of a beam of light on an obstacle. By analogy, in high-energy physics, the corresponding processes are usually called diffractive. The classic example is the elastic scattering of hadrons on nuclei (see e.g. [16]), which manifests an angular distribution with a series of minima and maxima, analogous to the diffraction of light on a black disk. At LHC energies diffractive processes constitute up to 40% of the total (pp) cross section, σ_{tot} . Therefore, we will pay special attention to the description of the elastic scattering amplitude and proton diffractive dissociation. Diffraction dissociation can be considered as a quantum mechanical process caused by the fact that different components of the incoming hadron wave function have different probabilities for interaction with a target [17]. This feature allows us to probe the transverse size of the interaction region.

Note that besides being of a fundamental interest in their own right for understanding the high energy behaviour of the QCD amplitude, there are several reasons why it is important to study soft and diffractive processes. Firstly, soft interactions unavoidably give an underlying component to rare ‘hard’ events, from which we hope to extract signals for New Physics. Secondly, we should be able to estimate the probability that rapidity gaps, which oc-

cur in ‘hard’ diffractive events, survive rescattering effects, that is, survive the population of the gaps by the secondary particles from the underlying event. Thirdly, an understanding of diffractive processes is very important for evaluation of pile-up backgrounds in high-luminosity pp collisions, which have a direct impact on various experimental measurements. Pile-up corresponds to soft independent interactions in the same bunch crossing whose number rises with increasing instantaneous luminosity. And, finally, studies of diffractive processes should help in the understanding of the structure of high-energy cosmic ray cascades, which requires a very detailed knowledge of the spectra of particles carrying a large fraction x of the incoming momentum in proton-air and nucleus-air interactions, see for instance [18].

Experimentally, diffractive processes are selected using two distinct features:

1. large regions (typically at least $\Delta\eta > 4$) in the detector are devoid of hadronic activity (LRG) and/or
2. one or both incoming particles stay intact after collision and are registered by the dedicated forward detectors placed a few hundred meters from the interaction point. The momentum loss of the initial particle, $\xi = 1 - x$, is typically smaller than 0.15.

Thus, in the case of proton-proton collisions, diffractive events correspond to elastic $pp \rightarrow pp$ scattering and to $pp \rightarrow p + X$ (Single Dissociation, SD) and $pp \rightarrow X + Y$ (Double Dissociation, DD) processes, where the + sign denotes a large rapidity gap. Note that strictly speaking in high energy physics it is impossible to define (and select) rigorously purely diffractive events. We can always have some admixture of events of different origin. As a rule we call ‘diffractive’ the events with sufficiently large gap (with say $\Delta y > 4$, see above) and the vacuum quantum numbers transferred across the gap. Typically at the LHC the integrated cross sections of diffractive dissociation, σ_{SD} , σ_{DD} , are of the order of 5–10 mb depending on the gap size. Schematic diagrams of all discussed processes are shown in Fig. 20.1.

20.2 Regge pole approach

In pre-QCD times, in order to describe the behaviour of scattering amplitudes at high energy, \sqrt{s} , and small momentum-transfer squared, $-t$, Regge theory was developed and successfully applied in a wide range of energies. The Regge approach [5–7] is based on the singularities of amplitudes in the complex angular momentum, j , plane.

For instance, the measured $\pi^- p \rightarrow \pi^0 n$ amplitude behaves as

$$T_{\pi p}(s, t) \propto s^{\alpha_\rho(t)}, \quad (20.1)$$

where the process is described by the exchange of the ρ -trajectory, $j = \alpha_\rho(t) \simeq 0.5 + 0.9t$ (with $t = (p_{\pi^-} - p_{\pi^0})^2$ in GeV^2). This trajectory passes through the spin-1 ρ -meson resonance in the ‘crossed’ t -channel $\pi^- \pi^0 \rightarrow \bar{p} n$; that is, $\alpha_\rho(t = m_\rho^2) = 1$. The corresponding cross section decreases with increasing s .

On the other hand, high-energy total and elastic pp cross sections are observed to grow slowly with energy (see e.g. Section 53 in [1]) and in terms of Regge theory are dominated by the exchange of a trajectory with vacuum quantum numbers, $\sigma_{\text{tot}} \propto s^{j-1}$. The simplest possibility is to assume that the rightmost singularity in the j -plane, which drives the high-energy behaviour of the cross section, is the leading (at $t \leq 0$) Regge pole at $j = \alpha(t)$. Then the pp elastic amplitude reads

$$T_{\text{el}}(s, t) \propto s^{\alpha_{\mathbb{P}}(t)}. \quad (20.2)$$

The total cross section can then be conveniently expressed using the so called optical theorem which states that

$$s\sigma_{\text{tot}} = \text{Im}T_{\text{el}}(s, t = 0), \quad (20.3)$$

as illustrated in the upper part of Fig. 20.2, and thus

$$\sigma_{\text{tot}} \propto s^{\alpha_{\mathbb{P}}(0)-1}. \quad (20.4)$$

¹Here and in what follows, we call secondaries the new particles produced in the course of the interaction.

²For definition of particle rapidity (pseudorapidity), see Section 49.5.2 in [1]; $y = \frac{1}{2} \ln \frac{E+p_z}{E-p_z}$ ($\eta = -\ln(\tan(\theta/2))$); the correct variable is the rapidity y , however, experimentally it is simpler to use the pseudorapidity η which does not require identifying the particles, setting $m = 0$. For $p_T \gg m$, $\eta \simeq y$.

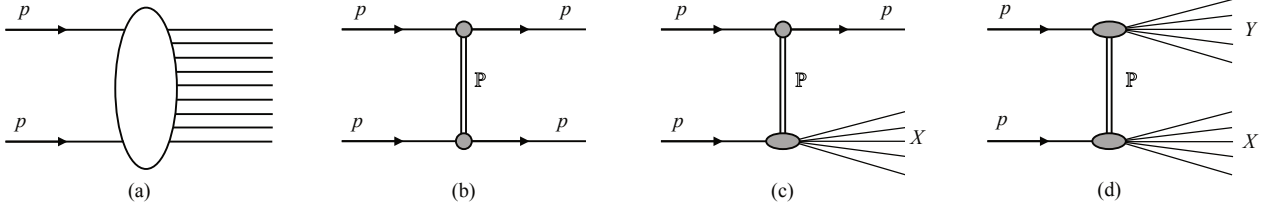


Figure 20.1: Schematic diagrams of soft pp processes. (a) non-diffractive processes, (b) elastic scattering, (c) single dissociation and (d) double dissociation. The double line corresponds to the Pomeron exchange.

$$\begin{aligned}
 \sigma_{\text{tot}} &= \sum_X \left| \text{Diagram of } p \text{ and } \bar{p} \text{ interacting via } \mathbb{P} \text{ to produce } X \right|^2 = \text{Im} \left(\text{Diagram of } p \text{ and } \bar{p} \text{ interacting via } \mathbb{P} \right) = \alpha_{\mathbb{P}}(0) \sim g_N^2 \left(\frac{s}{s_0} \right)^{\alpha_{\mathbb{P}}(0)-1} \\
 M^2 \frac{d\sigma}{dM^2} &= \left| \text{Diagram of } p \text{ and } \bar{p} \text{ interacting via } \mathbb{P} \text{ to produce } X \text{ at } t \right|^2 = \alpha_{\mathbb{P}}(t) \alpha_{\mathbb{P}}(t) = \alpha_{\mathbb{P}}(t) \alpha_{\mathbb{P}}(0) \\
 &= \underbrace{g_{3P} g_N^3 \left(\frac{M^2}{s_0} \right)^{\alpha_{\mathbb{P}}(0)-1} \left(\frac{s}{M^2} \right)^{2\alpha_{\mathbb{P}}(t)-2}}_{\text{Red bracketed term}}
 \end{aligned}$$

Figure 20.2: Illustration of the optical theorem for the total cross section and for high-mass diffractive dissociation in the absence of absorptive corrections.

The pole with the largest intercept, originally assumed to be $\alpha_{\mathbb{P}}(0) = 1$ since high-energy total cross sections were thought to have a constant asymptotic behaviour, is called the *Pomeron*³

Prior to the LHC, the energy behaviour of $pp, p\bar{p}, \pi p, Kp$ cross sections was satisfactorily reproduced by the sum of the Pomeron and secondary Reggeons (the poles at lower values of j , typically with $\alpha_{\rho}(0) \simeq 0.5$, see [22, 23] and Section 51 in [24]). However, above Tevatron energies the secondary Reggeon contributions (which all have intercepts $\alpha(0) \simeq 0.5$) are highly suppressed, which enables us to study the properties of the Pomeron only.

A popular parameterization of the elastic pp -scattering amplitude by Donnachie-Landshoff (DL) is the Regge form [25]

$$T_{\text{el}}(s, t) = \eta_P \sigma_0 F_1^2(t) s^{\alpha_{\mathbb{P}}(t)}, \quad (20.5)$$

where $\sigma_0 = 21.7$ mb [26] and η_P is the signature factor

$$\eta_P = \frac{1 + \exp(-i\pi\alpha_{\mathbb{P}}(t))}{\sin(-\pi\alpha_{\mathbb{P}}(t))}, \quad (20.6)$$

F_1 is the Dirac electromagnetic form factor of the proton and the *effective* Pomeron trajectory

$$\alpha_{\mathbb{P}}(t) = 1 + \Delta + \alpha' t \simeq 1 + 0.0808 + 0.25t, \quad (20.7)$$

with t given in GeV^2 . The intercept $\alpha_{\mathbb{P}}(0)$ just above 1 reproduces the observed slow growth of the total hadron-hadron cross sections at high energies.

However, this simple parameterization is becoming increasingly deficient at higher energies. This is because due to unitarity we have to take into account not only Regge poles, but also the cuts in the j -plane [27, 28], which correspond to the multiple exchange of Regge poles in the t -channel, see for instance [29–31]. A powerful technique to evaluate Reggeon diagrams was developed by Gribov [7, 32] (Reggeon calculus or Reggeon Field Theory (RFT)), which allows us to calculate the multi-Pomeron contributions.

20.3 Theoretical description of high-energy diffraction

Diffractive processes (see e.g. reviews [33–37]) represent a rich testing ground for the dynamics of soft interactions as well as Monte Carlo models for soft hadron-hadron physics (see for reviews e.g. [8], Section 43 in [1] and Chapter 2 in [15]).

There is no universally agreed definition of diffractive processes. Theoretically, diffraction is the effect caused by the absorption of the incoming plane-wave in some region of impact parameter, b . After a decomposition of the distorted plane-wave over the outgoing momentum, q , due to absorption we arrive at some set of plane-waves with non-zero transverse momentum, $q_t \neq 0$. Experimentally, we call diffractive the events with large rapidity gaps (LRG) in the distribution of the final state particles. However, this definition is appropriate only for the events with very large gap sizes ($\Delta\eta > 4 - 5$); otherwise gaps can also be caused by fluctuations in the hadronization process [38].

In the case of proton-proton collisions, diffraction corresponds to elastic $pp \rightarrow pp$ scattering and to the $pp \rightarrow p + X$ and $pp \rightarrow X_1 + X_2$ processes where one or both protons are allowed to dissociate into a system X with the quantum numbers of the proton. The $p \rightarrow X$ dissociation is caused by the fact that the individual components of the incoming proton wave function interact differently with the target (see Section 20.3.1).

Theoretically, high-energy diffraction may be studied from either the s -channel or the t -channel viewpoint.

20.3.1 Diffraction from the s -channel viewpoint

Unitarity plays a central role in diffractive processes. To discuss unitarity effects it is convenient to work in terms of impact parameter, b . The total cross section is closely related to the elastic scattering amplitude and the scattering into inelastic final states via the s -channel unitarity of the S -matrix (see Sections 50 and 53 in [1]), $SS^\dagger = I$, or

$$\text{disc } T \equiv T - T^\dagger = iT^\dagger T \quad (20.8)$$

³Pomeron pole was named after I. Y. Pomeranchuk. The history of the Pomeron is discussed in [19–21].

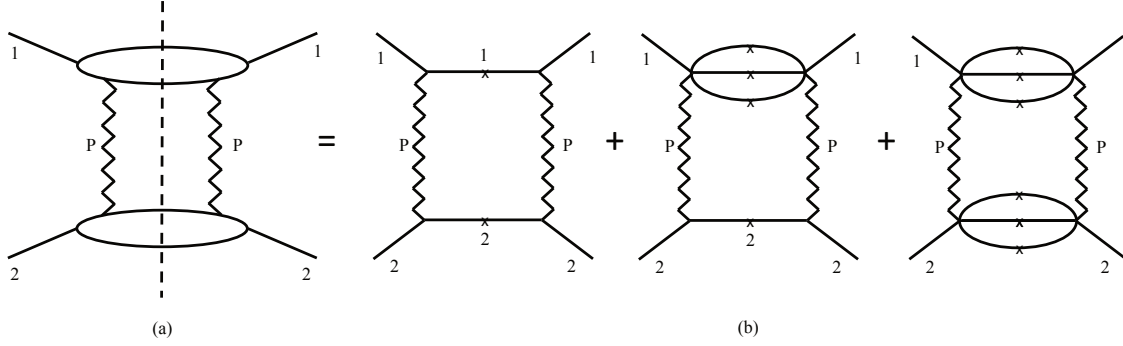


Figure 20.3: Two-Pomeron exchange in the t channel expressed as a sum over all diffractive intermediate states in the s -channel. The crosses indicate that the particles are on the mass shell.

with $S = I + iT$. If we were to focus, for example, on the unitarity for elastic and quasielastic processes, then *disc* T would simply denote a cut in s -channel between incoming and outgoing particles as visualized by crosses in Fig. 20.3.

At high energies, the s -channel unitarity relation is diagonal in the b basis such that

$$2\text{Im} T_{\text{el}}(s, b) = |T_{\text{el}}(s, b)|^2 + G_{\text{inel}}(s, b) \quad (20.9)$$

with

$$\sigma_{\text{tot}} = 2 \int d^2b \text{Im} T_{\text{el}}(s, b) \quad (20.10)$$

$$\sigma_{\text{el}} = \int d^2b |T_{\text{el}}(s, b)|^2 \quad (20.11)$$

$$\sigma_{\text{inel}} = \int d^2b [2\text{Im} T_{\text{el}}(s, b) - |T_{\text{el}}(s, b)|^2]. \quad (20.12)$$

The general solution of Eq. (20.9) is

$$T_{\text{el}}(b) = i(1 - e^{-\Omega(b)/2}) \quad (20.13)$$

and

$$G_{\text{inel}}(s, b) = 1 - e^{-\text{Re}\Omega(b)} = 1 - P_{\text{nointer}}(s, b), \quad (20.14)$$

where G_{inel} is the sum over all inelastic intermediate states and P_{nointer} is a probability to have no inelastic interactions. $G_{\text{inel}}(s, b)$ describes the b -profile of inelastic particle collisions. It satisfies the condition $0 \leq G_{\text{inel}} \leq 1$ and determines how absorptive the interaction region is at a given impact parameter (with $G_{\text{inel}} = 1$ for full absorption and $G_{\text{inel}} = 0$ for the complete dominance of elastic scattering). As seen from Eq. (20.14), $\exp(-\text{Re}\Omega(s, b))$ is the probability that no inelastic interactions occur at impact parameter b . Ω ($\text{Re}\Omega \geq 0$) is called the opacity (optical density) or eikonal. The quantity

$$S^2(b) \equiv e^{-\text{Re}\Omega(b)} = P_{\text{nointer}}(b) \quad (20.15)$$

is the so-called survival factor, which enables us to calculate the probability that the LRG survives soft rescattering.

In terms of the opacity the elastic cross section takes the form

$$\begin{aligned} \frac{d\sigma_{\text{el}}}{dt} &= \frac{1}{16\pi s^2} |T_{\text{el}}(s, t)|^2 = \frac{1}{4\pi} \left| \int d^2b e^{i\vec{q}_t \cdot \vec{b}} (1 - e^{-\Omega(b)/2}) \right|^2 \\ &= \pi \left| \int b db J_0(q_t b) (1 - e^{-\Omega(b)/2}) \right|^2, \end{aligned} \quad (20.16)$$

where $q_t = \sqrt{|t|}$ and J_0 is the zeroth-order Bessel function.

To describe the elastic scattering at one fixed energy we can always find an appropriate parameterization for the opacity $\Omega(b)$ and tune the parameters to reproduce the observed $d\sigma_{\text{el}}/dt$ cross

section. Moreover, we can fix the form of the parameterization, but choose, at each particular energy, the corresponding values of parameters; see, e.g. [39]. Alternatively, we may simply take the Fourier-Bessel transform from the experimental data [33, 40, 41]

$$\text{Im} T_{\text{el}}(b) = \int \frac{q_t dq_t}{4\pi} \sqrt{\frac{d\sigma_{\text{el}}}{dt} \frac{16\pi}{1 + \rho^2}} J_0(q_t b), \quad (20.17)$$

where the square root represents $\text{Im} T_{\text{el}}(q_t)$, with $\rho \equiv \text{Re} T_{\text{el}} / \text{Im} T_{\text{el}}$. In this way, we first determine T_{el} from the data for $d\sigma_{\text{el}}/dt$, and then calculate $\Omega(b)$ using Eq. (20.13), assuming in accordance with data that ρ is small (or $\rho(t) = \text{constant}$).

At high energies $\rho^2 \ll 1$, which is usually well justified except in the diffractive dip region (see Section 20.3.3.1 for discussion of the dip region).

The value of ρ can be derived via the dispersion relation, see [3]:

$$\begin{aligned} \frac{1}{s} \text{Re} T_{\text{el}}(s) &= \frac{1}{\pi} \int_{-\infty}^{+\infty} \frac{ds'}{s' - s} \sigma_{\text{tot}}(|s'|) \\ &= \frac{1}{\pi} \int_0^{\infty} \sigma_{\text{tot}}(s') \frac{2s ds'}{s'^2 - s^2}. \end{aligned} \quad (20.18)$$

Since we consider just the charge-parity C -even amplitude, here for negative s' we put $\sigma_{p\bar{p}} = \sigma_{pp}$. That is, for negative s' , which corresponds to the interaction with an *antiparticle*, we use the same $\sigma_{pp}(|s'|)$. The major contribution comes from $s' \simeq s$. Thus, with a good accuracy we can evaluate $\rho(t=0)$ as

$$\rho \simeq \frac{\pi}{2} \frac{\partial \ln \sigma_{\text{tot}}(s)}{\partial \ln s}. \quad (20.19)$$

20.3.2 Diffractive dissociation

The elastic cross section probes the optical density of the proton. The well known example of scattering on a black disk, with $G_{\text{inel}} = 1$ for $b < R$, gives $\sigma_{\text{el}} = \sigma_{\text{inel}} = \pi R^2$ and $\sigma_{\text{tot}} = 2\pi R^2$. In general, the absorption of the initial wave (due to inelastic channels) leads, via s -channel unitarity, to elastic scattering.

Inelastic diffraction (i.e. proton dissociation) is a consequence of the *internal structure* of hadrons. This can be conveniently described at high energies, where the lifetimes of each particular Fock component of the incoming hadron/proton wave function (the hadronic fluctuations) are large, $\tau \sim E/m^2$, and during these time intervals the corresponding Fock states can be considered as ‘frozen’. Each hadronic constituent can undergo a scattering with its own probability and thus destroys coherence of the fluctuations⁴. As a result, the outgoing superposition of states will be different from the incident particle, and will most likely contain multiparticle states, so we will have *inelastic*, as well as elastic scattering.

⁴ At high energies the configurations with different transverse separation, r , between the quarks (valence partons) can serve as an example of such Fock states. An interaction with the QCD Pomeron does not change the value of r , while the cross section $\sigma \propto \alpha_s^2 r^2$ (see Section 20.4.2 and [42–44]).

To calculate diffractive dissociation we can enlarge the set of intermediate states (p, N_a^*), from just the single elastic channel, and introduce a multichannel eikonal. However, it is more convenient to follow Good and Walker [45], and to introduce states ϕ_k diagonalising the T matrix (which e.g. in the proton case describes different $p \rightarrow N^*$, $N_a^* \rightarrow N_b^*$ transitions). Such eigenstates only undergo elastic scattering. Since there are no off-diagonal transitions,

$$\langle \phi_i | T | \phi_k \rangle = 0 \quad \text{for } i \neq k, \quad (20.20)$$

a state k cannot diffractively dissociate into a state $j \neq k$. Working in terms of the Good-Walker eigenstates ϕ_i , we have a simple one-channel eikonal for each state. We denote the orthogonal matrix which diagonalizes T by a , so that

$$T = a F a^T \quad \text{with} \quad \langle \phi_i | F | \phi_k \rangle = F_k \delta_{ik}, \quad (20.21)$$

where F_k is the probability amplitude of the hadronic process proceeding via the diffractive eigenstate ϕ_k .

Now consider the diffractive dissociation of an incoming state $|h\rangle$. We can write

$$|h\rangle = \sum_k a_{hk} |\phi_k\rangle. \quad (20.22)$$

The elastic scattering amplitude satisfies

$$\langle h | T | h \rangle = \sum_k |a_{hk}|^2 F_k = \langle F \rangle, \quad (20.23)$$

where $F_k \equiv \langle \phi_k | F | \phi_k \rangle$ and where the brackets of $\langle F \rangle$ mean that we take the average of F over the initial probability distribution of diffractive eigenstates. After the diffractive scattering described by T_{fh} , the final state $|f\rangle$ will, in general, be a different superposition of eigenstates from that of $|h\rangle$, which was shown in Eq. (20.22). Neglecting the real parts, for the cross sections at a given impact parameter b , we have

$$\begin{aligned} \frac{d\sigma_{\text{tot}}}{d^2b} &= 2 \text{Im} \langle h | T | h \rangle = 2 \sum_k |a_{hk}|^2 \text{Im} F_k = 2 \langle \text{Im} F \rangle \\ \frac{d\sigma_{\text{el}}}{d^2b} &= |\langle h | T | h \rangle|^2 = \left| \sum_k |a_{hk}|^2 F_k \right|^2 = \langle |F|^2 \rangle \\ \frac{d\sigma_{\text{el} + \text{SD}}}{d^2b} &= \sum_k |\langle \phi_k | T | h \rangle|^2 = \sum_k |a_{hk}|^2 |F_k|^2 = \langle |F|^2 \rangle. \end{aligned} \quad (20.24)$$

It follows that the cross section for the single diffractive dissociation of a proton,

$$\frac{d\sigma_{\text{SD}}}{d^2b} = \langle |F|^2 \rangle - \langle |F| \rangle^2, \quad (20.25)$$

is given by the statistical dispersion in the absorption probabilities of the diffractive eigenstates. Here the average is taken over the components k of the incoming proton which dissociates. If the averages are taken over the components of both of the incoming particles, then Eq. (20.25) is the sum of the cross sections for single and double dissociation, see Fig. 20.3.

Note that if all the components ϕ_k of the incoming proton $|h\rangle$ were absorbed equally, then the diffracted superposition would be proportional to the incident one and the probability of the inelastic diffraction would be zero. Thus if, at very high energies, the amplitudes F_k at small impact parameters are equal to the black disk limit, $F_k = i$, then diffractive production will be equal to zero in this impact parameter domain, and so will only occur in the peripheral b region where the edge of the disk becomes not completely black. Hence the impact parameter structure of diffractive dissociation and elastic scattering is drastically different in the presence of absorptive s -channel unitarity effects (see

the G_{inel} term in Eq. (20.9)). Under the assumption that amplitudes F_k at high energies cannot exceed the black disk limit, $\text{Im} F_k \leq 1$, equations 20.24 lead to the following bound

$$\frac{d\sigma_{\text{el} + \text{SD}_1 + \text{SD}_2 + \text{DD}}}{d^2b} \leq \frac{1}{2} \frac{d\sigma_{\text{tot}}}{d^2b}. \quad (20.26)$$

known as the Pumplin bound [46]⁵.

20.3.3 Diffraction from the t -channel viewpoint

The t -channel approach is based on the Regge model (see Section 20.2), where high-energy diffractive processes are mediated by the exchange of a Pomeron (\mathbb{P}). In the case of the elastic pp -scattering amplitude in the eikonal model (see Eq. (20.13)), the opacity corresponding to the exchange of one Pomeron is

$$\Omega(s, b) = \int \frac{d^2q_t}{4B^2} \Omega(s, q_t) e^{i\vec{q}_t \cdot \vec{b}} \quad (20.27)$$

with

$$\Omega(s, q_t) = \frac{1}{s} T'_{\text{el}} = -i_{\mathbb{P}}(t) g_N(t) g_N(t) \left(\frac{s}{s_0} \right)^{\text{ff}_{\mathbb{P}}(t)-1}, \quad (20.28)$$

where T'_{el} is the two-particle s -channel irreducible elastic amplitude, cf. Eq. (20.5), and $g_N(t)$ is the proton-Pomeron coupling.

If we assume an exponential t -dependence of the coupling, $g_N(t) = g_N(0) \exp(B_0 t)$, and neglect the Pomeron phase, then the opacity is

$$\Omega(s, q_t) = g_N(0) g_N(0) \left(\frac{s}{s_0} \right)^{\text{ff}_{\mathbb{P}}(0)-1} e^{Bt}, \quad (20.29)$$

with the t -slope given by

$$B = 2B_0 + \alpha'_{\mathbb{P}} \ln \left(\frac{s}{s_0} \right). \quad (20.30)$$

At high energies the opacity has a Gaussian form in the b -space:

$$\Omega(s, b) = \frac{g_N^2(0)}{4\mathbb{B}} \left(\frac{s}{s_0} \right)^{\text{ff}_{\mathbb{P}}(0)-1} e^{-b^2/4B}. \quad (20.31)$$

In terms of opacity the effective radius of interaction increases at high energies as $\sqrt{\alpha'_{\mathbb{P}} \ln(s/s_0)}$. This means that with energy increasing the differential cross section becomes steeper (the so called *shrinkage* of the diffractive peak).

If we were to take for the Pomeron the DL parametrisation [25, 26], that is to keep just the first, $T(b) = \Omega(b)/2$, term in the elastic amplitude (Eq. (20.13)) then, at LHC energies, the Gaussian would exceed the black disk limit at small b . However, the eikonal unitarization reduces the power growth of the one-Pomeron exchange cross section. Thus, in Eq. (20.31) $\Omega(s, b) \propto (s/s_0)^{\text{ff}_{\mathbb{P}}-1}$ gives an amplitude $\text{Im} T_{\text{el}}(s, b) = 1 - e^{-\Omega/2} < 1$. Hence the total cross section is limited by the size of the effective interaction area $\sigma_{\text{tot}} < 2\pi R^2$, where the interaction radius R can be estimated from Eq. (20.31) as the value of b where $\text{Re}\Omega(b)$ becomes ~ 1 .

For the parameterization of Eq. (20.31) the corresponding radius grows at very large energies as

$$b^2 = R^2 = 4B \ln \left[\frac{g_N^2(0)}{4\pi B} \left(\frac{s}{s_0} \right)^{\alpha_{\mathbb{P}}(0)-1} \right] \simeq 4\Delta \alpha'_{\mathbb{P}} \ln^2(s/s_0). \quad (20.32)$$

That is for $\Delta = 0.1$ and $\alpha'_{\mathbb{P}} = 0.25 \text{ GeV}^{-2}$ we may expect that the cross section increases as

$$\sigma_{\text{tot}} = 2\pi R^2 \simeq c \cdot \ln^2 s, \quad (20.33)$$

⁵Strictly speaking the proof of the Pumplin bound is justified only for low mass dissociation. When the masses $M_{1,2}$ become so large (say, $M_i^2 > \sqrt{s s_0}$) that the Good-Walker states $|\phi_i\rangle$, corresponding to two incoming protons overlap, we may face double counting. Therefore, the high mass dissociation will be considered in the next Section, in terms of the multi-Pomeron diagram. Here and in what follows s_0 is a constant which should be defined for a particular theoretical model or fitted from experiment.

with $c = 8\pi\Delta\alpha'_p = 0.24$ mb. This value is close to that obtained by the COMPETE parameterization ($c = 0.27$ mb [22, 24]) but much smaller than the Froissart-Lukaszuk-Martin (FLM) bound [47–49]. With $c^{\text{FLM}} = \pi/m_\pi^2 \simeq 60$ mb, see Section 20.7,

$$\sigma_{\text{tot}} \leq \frac{\pi}{m_\pi^2} \ln^2 \left(\frac{s}{s_0} \right). \quad (20.34)$$

The fact that $c = (0.24\text{--}0.27)$ mb $\ll c^{\text{FLM}} = 60$ mb demonstrates that even at the LHC we are very far from true high-energy asymptotics⁶, and the observed growth of the cross section is driven by the interactions at relatively large transverse momenta $k_t \gg m_\pi$ rather than the smallest hadron mass m_π in the denominator of Eq. (20.34).

20.3.3.1 The t -slope and dip in the elastic cross section

We first start with a relatively small one-Pomeron amplitude and consider the two-Pomeron contribution corresponding to the Ω^2 term in the expansion of the eikonal $1 - \exp(-\Omega/2)$. In this term the momentum transferred, $q_t = \sqrt{|t|}$, is divided between the two Pomerons so that each Pomeron carries about a momentum $q_t/2$. Correspondingly, the t dependence of the whole ‘two-Pomeron’ amplitude will be $\exp(2B(t/4)) = \exp(Bt/2)$ ⁷.

Since the two-Pomeron contribution has an opposite sign in comparison with the one-Pomeron exchange, their interference will result in the appearance of the first diffractive minimum which moves to smaller $|t|$ with energy increasing. Such interference effects are largely responsible for the zero in the imaginary part of the amplitude (with the minimum filled by the real part).

It is worth mentioning that the one-channel eikonal discussed so far is a rather oversimplified approximation. It provides some indications about the behaviour we may expect for the elastic cross section, but clearly it does not give the whole story. Moreover, even within the framework of the one-channel eikonal, the expectation for the elastic slope t -dependence could be masked by other effects. Firstly, there is no reason why the t -dependence of the proton-Pomeron coupling $g_N(t)$ has to be a pure exponential. Next, there exists a two-pion singularity at $t = 4m_\pi^2$ (close to the physical region) in the Pomeron trajectory which generates some curvature in the behaviour of $d\sigma_{\text{el}}/dt$ [50–52]. So there may be some compensation between the effects caused by the eikonal (arising from the interference between the different multi-Pomeron contributions), and the curvatures coming from the form of the proton-Pomeron coupling and the two-pion singularity of the Pomeron trajectory. However, an exact compensation looks quite non-trivial and a *pure* exponential behaviour of $d\sigma_{\text{el}}/dt$ looks highly unlikely.

Indeed, the measurements by the TOTEM collaboration at 8 TeV [53] and at 13 TeV [54] clearly demonstrate that the local slope of the elastic pp cross section,

$$B = d[\ln(d\sigma_{\text{el}}/dt)]/dt, \quad (20.35)$$

at $-t \lesssim 0.3$ GeV² varies with t .

20.3.3.2 High mass dissociation

Let us turn to inelastic diffractive processes that is, to single and double proton dissociations, $pp \rightarrow X+p$ and $pp \rightarrow X_1+X_2$, where the $+$ sign denotes the presence of a LRG in the distribution of final state particles. For example, for the diffractive dissociation of a proton into a system of mass M , the rapidity gap between the incoming proton and the remaining hadrons is

$$\Delta y = \ln \left(\frac{s}{M^2} \right) = \ln \left(\frac{1}{\xi} \right), \quad (20.36)$$

where $\xi = 1 - x$ and x is the initial momentum fraction (Feynman variable) carried by the outgoing proton. The masses, M , of the diffractively excited states, produced in high \sqrt{s} collisions, can be

⁶As usual, we assume $s_0 = 1$ GeV², but the qualitative conclusion does not depend on any realistic choice of s_0 .

⁷The two-Pomeron contribution has a factor of two smaller t -slope, and in terms of the impact parameter, the $\Omega^2(b)$ term is concentrated in the domain of a smaller radius. In such a simplified picture, the impact parameters corresponding to an exchange of n Pomerons will rapidly decrease with n increasing.

large. To separate dissociation from the common inelastic process, usually the condition $M^2 \ll s$ is imposed.

The simplest multi-Pomeron diagram used to describe the diffractive dissociation is the so-called triple-Pomeron graph, shown at the end of Fig. 20.2.

In the Regge pole model, the cross section for the inclusive single diffractive (SD) dissociation process [55–57] can be written in the form (see Fig. 20.2)

$$\begin{aligned} \frac{\xi d\sigma_{\text{SD}}}{dt d\xi} &= \frac{M^2 d\sigma_{\text{SD}}}{dt dM^2} \\ &= \frac{g_{3\mathbb{P}}(t) g_N(0) g_N^2(t)}{16\pi^2} \left(\frac{s}{M^2} \right)^{2\alpha_{\mathbb{P}}(t)-2} \left(\frac{M^2}{s_0} \right)^{\alpha_{\mathbb{P}}(0)-1}, \end{aligned} \quad (20.37)$$

where $g_{3\mathbb{P}}(t)$ is the triple-Pomeron coupling. The value of the coupling $g_{3\mathbb{P}}$ is usually obtained from a triple-Regge analysis of lower energy data (see e.g. [34]).

In an analogous way the cross section for double dissociation reads

$$\begin{aligned} \frac{\xi_1 \xi_2 d\sigma_{\text{DD}}}{dt d\xi_1 d\xi_2} &= \frac{M_1^2 M_2^2 d\sigma_{\text{DD}}}{dt dM_1^2 dM_2^2} \\ &= \frac{g_{3\mathbb{P}}^2(t) g_N^2(0)}{16\pi^3} \left(\frac{ss_0}{M_1^2 M_2^2} \right)^{2\alpha_{\mathbb{P}}(t)-2} \left(\frac{M_1^2 M_2^2}{s_0^2} \right)^{\alpha_{\mathbb{P}}(0)-1}, \end{aligned} \quad (20.38)$$

where t is the momentum squared transferred through the LRG. As discussed in Section 20.5, from a microscopic point of view the

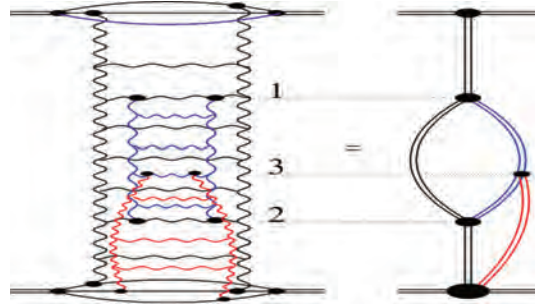


Figure 20.4: Pomeron exchange with schematic diagrams for the enhanced and semi-enhanced exchanges.

Pomeron exchange is described by a set of ladder-type diagrams (see [58–60]), which can lead to a rescattering of the intermediate partons (produced inside this ladder during the evolution), see Fig. 20.4. The left plot shows the Pomeron exchange complemented with the rescattering of partons 1 and 2 and the scattering of a parton 3 on the target. In terms of multi-Pomeron exchanges this corresponds to the diagram on the right hand side, where the Pomeron exchange is shown by the double line of a corresponding colour. The blue one is called ‘enhanced’ (its contribution is integrated over the rapidities of both upper and lower vertices, i.e. of partons 1 and 2). The loop formed by the Pomerons shown in red is called ‘semi-enhanced’ (it is integrated over the rapidity of one intermediate parton).

While the rescattering of the incoming hadron (proton) is already embedded in the eikonal formula (Eq. (20.13)), the rescattering of the intermediate partons in RFT is accounted for by the so-called enhanced diagrams⁸ with multi-Pomeron vertices, g_m^n , which couple m to n Pomerons. It is quite a challenging task to resum all the enhanced diagrams, however this was successfully performed within the framework of the QGSJET Monte Carlo [61]. An elegant approach to sum up all enhanced diagrams in the case when each extra effective Pomeron contribution is very

⁸This contribution is *enhanced* due to the large parton multiplicity.

large was proposed in [62], assuming the analyticity of the g_m^n vertices in n and m in the right half of the complex n - and m -planes. The resulting amplitude becomes a black disk.

The simplest triple-Pomeron vertex $g_2^1 = g_{3\mathbb{P}}$ produces the first multi-Pomeron graph considered above (see the end of Fig. 20.2). However, numerically the multi-Pomeron vertices are relatively small. Note also that the value of $g_{3\mathbb{P}}$, determined from the fit to experimental data (e.g. [63]), is actually an effective vertex with coupling

$$g_{\text{eff}} = g_{3\mathbb{P}} \langle S^2 \rangle, \quad (20.39)$$

which already includes the survival factor $S^2(b)$, see Eq. (20.15).

Since the opacity Ω increases with energy, at large Ω the number of multiple interactions grows as $N \propto \Omega$, leading to a smaller S^2 . An explicit analysis [64] accounting for the survival effects gives a coupling $g_{3\mathbb{P}}$ about a factor of 3 larger than g_{eff} , namely $g_{3\mathbb{P}} \simeq 0.2g_N$.

Recall that the Pomeron exchange simultaneously describes both the elastic scattering amplitude, T_{el} , and the multiparticle production cross section, G_{inel} . The discontinuity (*disc* T_{el}) of the ladder diagram corresponds to the production of secondary particles, practically homogeneously distributed over the whole available rapidity interval covered by the Pomeron, as illustrated by the right-hand diagram in Fig. 20.5.

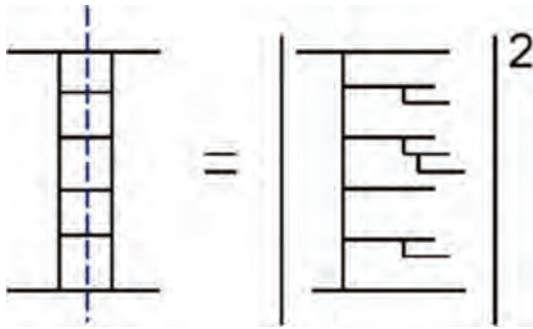


Figure 20.5: Cut Pomeron contribution to the inelastic cross section.

For the one-Pomeron case this discontinuity is called the “cut Pomeron”. Correspondingly each multi-Pomeron diagram describes a series of different processes. Cutting k Pomerons in the diagram with n Pomerons we get the inelastic interaction with the multiplicity (density of secondaries) k times larger than that, N_0 , produced by one cut Pomeron, $dN/dy = k \cdot N_0$. The remaining $n - k$ (elastic) Pomerons account for the absorptive corrections to the subprocess with k cut Pomerons. Indeed, the contribution of the diagram with n Pomerons includes also the processes with larger, $(k + i) \cdot N_0$ multiplicities (cut Pomerons), where $(i = 1, 2, \dots, n - k)$. Absorptive corrections, described by the remaining elastic Pomerons, play a role of the survival factor S^2 for the process with the fixed particle density $k \cdot N_0$. They ensure probability conservation (the sum of the probabilities of all possible different channels is equal to one) and restore unitarity. Note that the multi-Pomeron diagrams represent all possible interactions between partons from the protons and partons from the Pomerons. In the case of Monte Carlo generators, the non-enhanced multi-Pomeron contributions are included in terms of the multiple parton interaction (MPI) option, see [13,65] and Section 7.2 in [2]. However, as a rule, this option accounts mainly for the multiple interactions between the partons from the protons (incoming hadrons). The energy-momentum sharing between the various inelastic rescattering processes (including the cut and uncut Pomerons) was performed at the amplitude level within the EPOS Monte Carlo [66].

20.3.3.3 AGK cutting rules

The relation between the cross sections of subprocesses with a different number of cut Pomerons within a given diagram with n Pomerons is given by the AGK (Abramovsky-Gribov-Kancheli [67]) cutting rules. These rules include also the cut *between* the Pomerons with $k = 0$ which corresponds to the contri-

bution of the particular diagram to the elastic cross section. By applying these rules, it is possible to show the self-consistency of the approach, which was lacking in the pure Regge-pole model.

Consider a diagram where the elastic scattering amplitude is mediated by an exchange of n Pomerons. The AGK cutting rules specify the coefficients c_n^k arising when k of these Pomerons are cut. Recall that the Pomeron cut discontinuities give the corresponding inelastic contributions to σ_{tot} . The terms with $k = 0$ correspond to the diffractive cutting of the diagram (that is, the cut is between the Pomeron exchanges, and not through the Pomerons themselves), while the terms with $k = 1, 2, \dots$ describe the processes with k cut Pomerons. The coefficients $c_n^k = \sigma_n^k / |\sigma_{\text{tot}}^{(n)}|$ are ⁹

$$c_n^{k=0} = (-1)^n (2^{n-1} - 1), \quad c_n^{k \neq 0} = (-2)^{n-1} \frac{(-1)^{k-1} n!}{k!(n-k)!} \quad (20.40)$$

where $\sigma_{\text{tot}}^{(n)}$ denotes the contribution of the n -Pomeron diagram to the total cross section. Note the alternating sign of $\sigma_{\text{tot}}^{(n)}$ expressed as $(-1)^{n-1}$.

For the two-Pomeron exchange, $n = 2$, the coefficients are $+1$, -4 , or $+2$ according to whether $k = 0, 1$ or 2 Pomerons are cut, respectively. As shown in Fig. 20.6, the amplitude of the two-Pomeron exchange corresponds to a sum of three processes: i) inelastic interaction with particle density twice that caused by one Pomeron (see Fig. 20.6(c)) which enters with the coefficient ‘2’, ii) shadowing (absorptive) correction to the one-Pomeron exchange contribution, which corresponds to events with a single Pomeron density (only one Pomeron is cut), see Fig. 20.6 (b), which enters with a factor ‘-4’, and iii) diffractive elastic scattering or proton dissociation (when different components of the proton wave function correspond to different interaction cross sections), caused by the distortion of the incoming plane wave, see Fig. 20.6(a).

Note that the inclusive cross section is not affected by the multi-Pomeron contribution: $2 \times (2) + 1 \times (-4) = 0$. This is a general property of the AGK rules valid for any number of Pomerons n . Thus in order to calculate the inclusive single-particle cross section, it is sufficient to consider just the *one*-Pomeron exchange diagram.

Let us emphasize that the AGK rules provide a framework to consistently work with multi-Pomeron diagrams, that is, with the Regge cuts, accounting for their contributions to different processes (elastic scattering and diffractive dissociation, inelastic events with different densities, dN/dy , of secondaries, etc.).

Measurements of diffractive dissociation cross sections have been made in a wide range of pre-LHC energies, see e.g. [68–73]. At the LHC, cross sections of events with a LRG were measured by the ATLAS, CMS and ALICE collaborations at 7 and 8 TeV, see [74–77]. ATLAS [78] and CMS and TOTEM [79] presented first measurements of SD cross sections at 8 TeV with a tagged forward proton. While ATLAS measured inclusive SD cross section, CMS and TOTEM studied SD dijet production. Note that in [78] the measured slope $B = 7.65 \pm 0.34 \text{ GeV}^{-2}$ of the inclusive SD cross section as well as the differential distributions $\frac{\xi d\sigma_{\text{SD}}}{d\xi d\eta}$ for $0.0001 \leq \xi \leq 0.025$ are (within the experimental uncertainties) in a good agreement with the theoretical expectations [29,80]. Moreover a relatively small (in comparison with the $d\sigma_{\text{el}}/dt$) slope B indicates that the size of the triple-Pomeron vertex is much smaller than the proton size.

20.3.4 Central Diffractive processes

Processes $pp \rightarrow p + X + p$, where an object X , produced in the central rapidity region, is separated from the outgoing protons by a LRG on each side, are called Central Exclusive Production (CEP). They are described by the double Pomeron exchange (DPE) diagrams. When the mass of the central system, M_X , is large and the interaction in the M_X region can be described by

⁹In their complete form the AGK cutting rules were implemented in the QGSJET Monte Carlo [61].

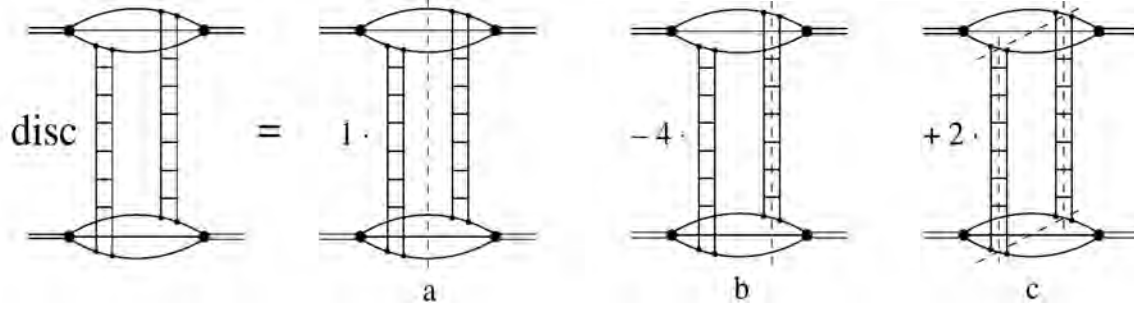


Figure 20.6: Two-Pomeron exchange diagram as a sum of different AGK cuts shown by the dashed lines.

Pomeron exchange, the corresponding cross section reads

$$\frac{\xi_1 \xi_2 d\sigma^{\text{CEP}}}{d\xi_1 dt_1 d\xi_2 dt_2} = \frac{g_N^2(t_1) g_N^2(t_2)}{(16\pi^2)^2} \left(\frac{1}{\xi_1}\right)^{2\alpha_{\mathbb{P}}(t_1)-2} \left(\frac{1}{\xi_2}\right)^{2\alpha_{\mathbb{P}}(t_2)-2} \times g_{3\mathbb{P}}^2(0) \left(\frac{M_X^2}{s_0}\right)^{\alpha_{\mathbb{P}}(0)-1}. \quad (20.41)$$

If the mass M_X is not too large or for the cases (such as exclusive Higgs boson or dijet production) where the mass M_X is comparable with the corresponding hard scale, the last factor $g_{3\mathbb{P}}^2(0)(M_X^2/s_0)^{\alpha_{\mathbb{P}}(0)-1}$ should be replaced by the corresponding ‘Pomeron-Pomeron cross section’, see for instance [81, 82].

Note that equations (20.37), (20.38) and (20.41) are written in a simplified way without accounting for absorptive corrections. That is, the cross sections in equations (20.37) (20.38) and (20.41) should be multiplied by the gap survival factor S^2 (see Eq. (20.15)).

Since the QCD Pomeron is built mainly from gluons it is natural to search for glueballs in double Pomeron exchange processes, and in particular, in CEP.

Resonance production in the Pomeron-Pomeron fusion was extensively studied at the CERN ISR at \sqrt{s} from 22 GeV to 63 GeV (see for reviews [82–84]) and, after the ISR closure in 1983, in fixed target experiments at the CERN SPS [85] and E690 at the Tevatron [86, 87]. Glueballs were actively searched for and the properties of the f_0 and f_2 production studied in detail using multiparticle spectrometers, such as the Omega facility at the CERN SPS experiments (WA76, WA91 and WA102), see for a review [85].

An important property of CEP processes, which can be expected from matching with the perturbative QCD LO (leading order) calculation, is the $J_z = 0$ dominance. Perturbatively, for the CEP of a heavy object, the leading contribution comes from a configuration with the projection of this object spin onto the beam axis $J_z = 0$ [81]. Note that the CEP cross section is suppressed at large M_X by a strong bremsstrahlung off the incoming gluons (from the Pomeron) which would violate the ‘exclusivity’. The small probability of not having such radiation is described by the Sudakov suppression factor, T_{Sud} , [88], see [81] for details.

20.3.5 Diffractive parton distributions

Selecting in Deep Inelastic Scattering (DIS) events with a LRG (see e.g. [89, 90]) or detecting the leading proton (see Section V.C. in the review [91]) we can study the parton (quark and gluon) distributions of the Pomeron¹⁰. In other words, such events can be treated as DIS on the Pomeron target with the incoming Pomeron flux given by

$$f_{\mathbb{P}}(x_{\mathbb{P}}) = \int dt \frac{g_N^2(t)}{16\pi^2} x_{\mathbb{P}}^{2(1-\alpha_{\mathbb{P}}(t))}, \quad (20.42)$$

where the proton momentum fraction transferred through the Pomeron $x_{\mathbb{P}} = \xi = M^2/s$.

These Pomeron PDFs were extracted from the HERA measurements of ep scattering with leading protons or a LRG and can be

used to describe the inclusive production of high E_T dijets or another hard process based on the collinear factorization theorem in the same way as that in non-diffractive collisions (see [91]). The inclusive measurements of these PDFs are described in [92–94], with the combined H1 and ZEUS data using tagged protons analyzed in [95]. The impact of diffractive jet measurements is addressed e.g. in [96] and the measured charm contribution is presented in [97, 98]. As far as the parton distributions are known, we can calculate the corresponding inelastic cross section of the Pomeron-proton interaction using one of the ‘general purpose’ Monte Carlo generators (see e.g. [13]), multiply it by the Pomeron flux and compare the obtained result with the Regge formula in Eq. (20.37). This approach provides another way to evaluate the triple-Pomeron vertex $g_{3\mathbb{P}}$. The corresponding analysis was performed in [99] and leads to practically the same (within the error bars) value of $g_{3\mathbb{P}} = 0.2g_N(0)$.

It is worth mentioning that in DIS at large Q^2 we are dealing with small-size objects and the rescattering effects are small. Therefore, the survival factor $S^2 \simeq 1$ and does not affect the results.

20.4 Experimental data on diffraction at high energies

20.4.1 Total and elastic cross sections

The elastic scattering of protons is a process with a special and rather simple experimental signature: the central detector is empty while the incoming protons after the collisions are detected in the dedicated forward proton detectors (FPD) placed far from the interaction point (IP). Elastic scattering data are taken in special runs in order to be able to reach different ranges of t -values and thanks to the very large value of the cross section the data can be collected with a relatively low instantaneous luminosity and hence a negligible pile-up.¹¹

These special runs usually have very few proton bunches and differ in the t range covered, which is governed roughly by the relation $t_{\text{min}} \propto d^2/\beta^*$. Here d is the distance, expressed in multiples of the beam size at the detector, from the centre of the LHC beam and β^* is defined as the distance from the IP to the point where the transverse area of the beam is twice as wide as that at the IP (see Section 31 in [1]). Note that if we work at large β^* , the incoming protons have very small angular divergence leading to small average transverse momentum, which allows us to measure very small $|t|$ values. The lowest $|t|$ values measured so far at the LHC are $4 \times 10^{-4} \text{ GeV}^2$ (ALFA) and $6 \times 10^{-4} \text{ GeV}^2$ (TOTEM) reached with the 8 TeV LHC beam configured with $\beta^* = 1 \text{ km}$ optics. The largest t values of about 4 GeV^2 were measured by TOTEM at 8 and 13 TeV with $\beta^* = 90 \text{ m}$ thanks to special triggers. Other β^* values used in special runs are 3.5 m, 11 m and 2.5 km.

There are four ways to determine the σ_{tot} value:

1. **Elastic and Inelastic.** This method does not require the optical theorem and hence no extrapolation of $d\sigma_{\text{el}}/dt$ to $t = 0$ and no ρ (defined below Eq. (20.17)) but rather the

¹¹The pile-up is formed by additional pp collisions which typically produce low- p_T particles. These may affect the signal sample and worsen various reconstruction and identification efficiencies.

¹⁰see also Section 18.5 in [1]

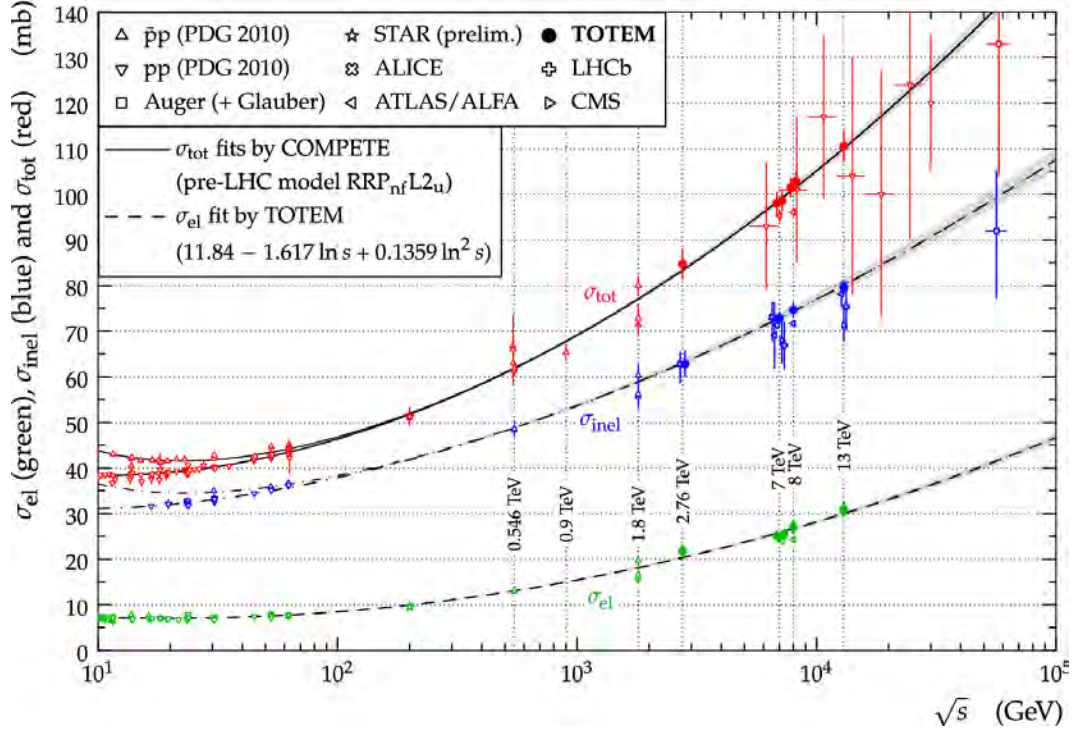


Figure 20.7: Overview of elastic (σ_{el}), inelastic (σ_{inel}) and total (σ_{tot}) cross section data for pp and $p\bar{p}$ collisions as a function of \sqrt{s} . The continuous black lines (lower for pp , upper for $p\bar{p}$) represent the best fits of the total cross section data by the COMPETE collaboration [22]. The dashed line is a fit of the elastic cross section data. The dashed-dotted lines refer to the inelastic cross section and are obtained from the difference between the continuous and dashed lines. Figure from Ref. [100].

luminosity and measuring rates N_{el} (elastic) and N_{inel} (inelastic). The total cross section is then simply:

$$\sigma_{tot} = \frac{1}{\mathcal{L}}(N_{el} + N_{inel}). \quad (20.43)$$

Of course, both N_{el} and N_{inel} should be corrected for the detector acceptance and efficiency. This is especially important for N_{inel} since the detectors never cover the whole rapidity region (i.e. the whole 4π).

- 2. Elastic only.** This approach necessitates measuring $d\sigma_{el}/dt$ and using the optical theorem with a known value of ρ . As explained in Section 20.2, the optical theorem states that $\sigma_{tot} \propto \text{Im}[T_{el}(t \rightarrow 0)]$, see Eq. (20.3). Since in practice it is not possible to measure down to $t = 0$, we need to extrapolate. To minimize the model dependence when extrapolating, it is vital to measure down to as low $|t|$ values as possible (i.e. high β^*). This method requires an independent luminosity measurement. Once the luminosity is known, $d\sigma_{el}/dt$ can be normalized and used to extract σ_{tot} using the formula:

$$\sigma_{tot}^2 = \frac{16\pi}{1 + \rho^2} \left. \frac{d\sigma_{el}}{dt} \right|_{t \rightarrow 0}. \quad (20.44)$$

- 3. Coulomb normalization.** Similarly to the previous method, this approach relies on the elastic observables only and requires a measurement of the elastic cross section at very low values of $|t|$, where it is sensitive to the theoretically well known Coulomb QED contribution $4\pi\alpha_{QED}^2/t^2$. The normalization of $d\sigma_{el}/dt$ is then determined by fitting the experimental data at very low $|t|$ using a formula including the Coulomb amplitude and its interference with the strongly interacting (the so-called nuclear) term. This method has been successfully used by UA4/2 [101] and TOTEM [102].
- 4. Luminosity-independent.** This method does not rely on the knowledge of luminosity but rather on the knowledge of N_{el} and N_{inel} and on the optical theorem: combining equations (20.43) and (20.44) with $\frac{d\sigma_{el}}{dt} = \frac{1}{\mathcal{L}} \frac{dN_{el}}{dt}$

we get

$$\sigma_{tot} = \frac{16\pi}{1 + \rho^2} \left. \frac{dN_{el}/dt}{N_{el} + N_{inel}} \right|_{t=0}, \quad (20.45)$$

where $dN_{el}/dt|_{t=0}$ corresponds to the extrapolation to $t = 0$ of the nuclear term only. By independently and simultaneously measuring N_{el} and N_{inel} , and applying the optical theorem, we can also determine the luminosity.

The TOTEM [100, 103–105] and ATLAS [106, 107] collaborations at CERN have covered an energy range from $\sqrt{s}=2.76$ TeV to 13 TeV. A compilation of high energy total pp and $p\bar{p}$ cross section measurements is shown in Fig. 20.7 (for discussion of the pre-LHC elastic scattering data see review [108]).

Despite some tension between the Tevatron CDF [109] and E811 [110] data¹² and to a lesser extent between the TOTEM [104, 105] and ATLAS [106, 107] measurements, the data clearly indicate that in the Tevatron – LHC energy interval the total cross section starts to grow *faster* than the power-law parametrization [26] describing the data below the Tevatron energy. In particular, while the DL fit [26] predicts $\sigma_{tot} = 90.7$ mb at $\sqrt{s} = 7$ TeV, the TOTEM experiment observes 98.6 ± 2.2 mb [104].

A compilation of the high-energy data on the elastic slope is shown in Fig. 20.8. It is clearly seen that in the TeV energy range the slope increases with \sqrt{s} more rapidly than the logarithmic behaviour expected in the case of one-Pomeron exchange, see Eq. (20.30). Such an acceleration of the t -slope derivative, $dB/d \ln s$, is a clear manifestation of the increasing role of the multi-Pomeron exchanges, where asymptotically the slope should rise as $\ln^2 s$, see [117]. Finally, Fig. 20.9 illustrates the energy dependence of the differential elastic pp cross section. As expected (see Section 20.3.3.1), the diffractive dip moves to smaller $|t|$ with increasing energy.

¹²The CDF 1.8 TeV point [109] is 2.8 σ higher than the corresponding E811 result [110].

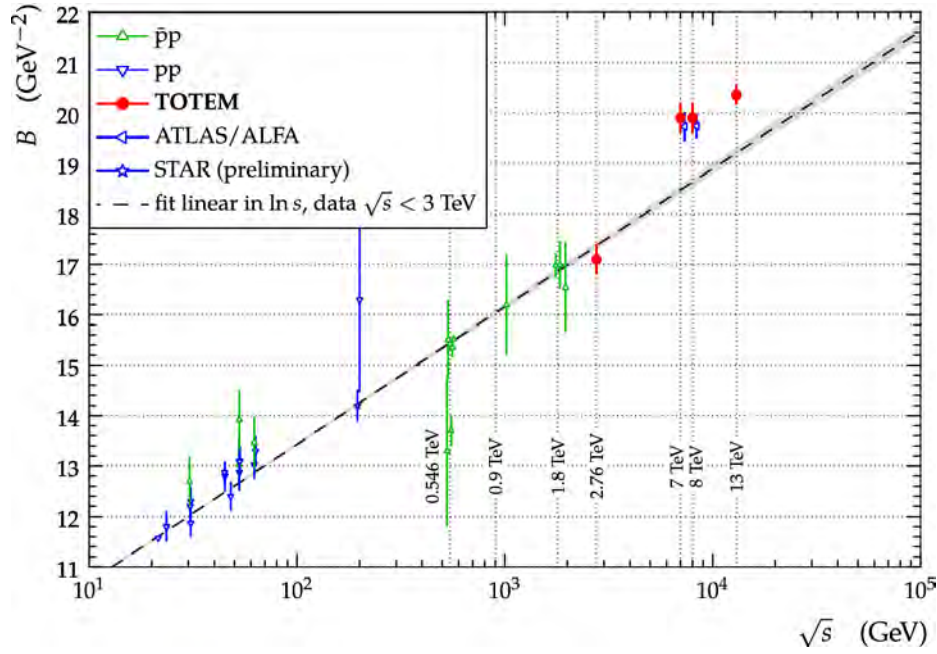


Figure 20.8: The diffractive slope B for pp and $p\bar{p}$ elastic scattering as a function of \sqrt{s} . The experimental uncertainties represent the quadratic sum of statistical and systematic uncertainties. The dashed line is a result of a linear fit to data at $\sqrt{s} < 3$ TeV. The data points come from [103–107, 111–113]. Figure from Ref. [100].

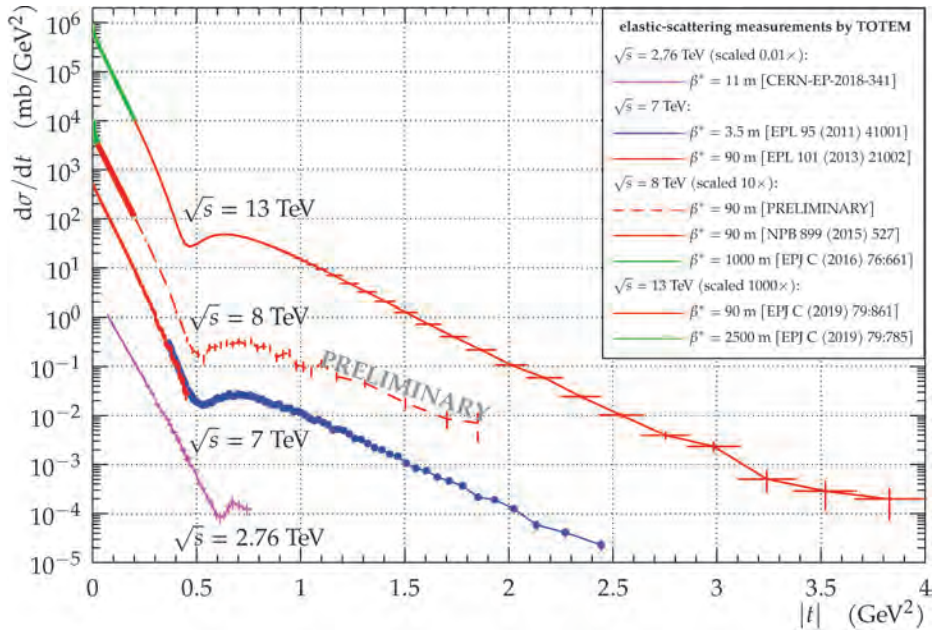


Figure 20.9: The t -dependence of the pp elastic cross section for collision energies $\sqrt{s} = 2.76$ TeV [103], 7 TeV [104, 114], 8 TeV [53, 115, 116] and 13 TeV [54, 102]. The experimental uncertainties represent the quadratic sum of statistical and systematic uncertainties. Figure from Ref. [116].

20.4.2 Diffractive vector meson production

The exclusive production of vector mesons was studied in detail at HERA (see for a review [91]). It is well described within the ‘dipole model’ (see for review and references [120]), where the incoming photon first fluctuates into a quark-antiquark, which then interacts with the target proton and, finally, with the probability given by the overlap integral between the vector meson wave function and the outgoing $q\bar{q}$ -pair, the vector meson is produced. The crucial quantity is the value of cross section, $\sigma(q\bar{q} - p)$, of elastic scattering of the $q\bar{q}$ -pair on the proton. The energy behaviour of $\sigma(q\bar{q} - p)$ is driven by the intercept, $\alpha_{\text{eff}}(0)$, of the

effective Pomeron¹³ (rightmost singularity in the j -plane), while the value of the cross section depends on the quark separation, r , in the transverse plane, $\sigma(q\bar{q} - p) \propto \alpha_s^2 \langle r^2 \rangle$ [43, 44]. Thus different processes with the same $\langle r^2 \rangle$ are driven by the same $\sigma(q\bar{q} - p)$ cross section.

In the DIS case this separation in turn is controlled by the photon virtuality, Q^2 , and the quark mass, m_q : $\langle r^2 \rangle \simeq 1/(z(1-z)Q^2 + m_q^2)$ (z is the photon momentum fraction carried by the quark). Indeed, the cross section of the ρ meson diffractive pro-

¹³Effective Pomeron means that this is not an original pole in the j -plane, but it includes the corrections (renormalizations) caused by the enhanced diagrams (see e.g. [121]).

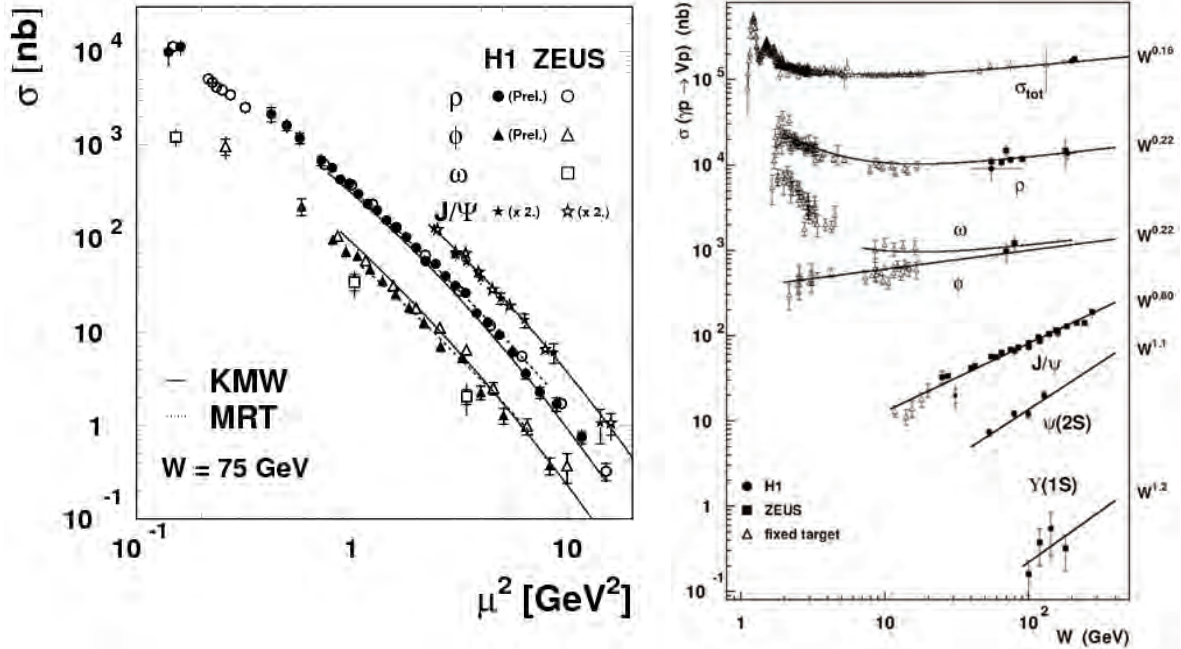


Figure 20.10: (Left) The ρ , ω , ϕ and J/ψ elastic production cross sections as a function of the scale $\mu^2 = (Q^2 + M_V^2)/4$. For readability of the figure, the J/ψ cross sections are multiplied by a factor 2. Figure from Ref. [118]. (Right) Compilation of photoproduction cross section measurements as a function of the γp centre-of-mass energy, W . The total cross section and various vector meson production cross sections are included, with the approximate power law dependences $\sigma \propto W^\delta$ indicated for each process. Figure from Ref. [119].

duction in DIS at $Q^2 = M_{J/\psi}^2$ is close (up to the difference in the quark electric charges) to that for the J/ψ photoproduction, see Fig. 20.10 (Left).

The production cross section depends non-trivially on W , the energy of the γ^*p center of mass system. It increases with W as W^n , where $n = 0.2$ for ρ, ω and ϕ (light quark)-mesons but $n = 0.8$ for J/ψ . Note that in the J/ψ case the energy dependence is close to that of the BFKL (Balitsky-Fadin-Kuraev-Lipatov) Pomeron [59, 122, 123], that is, the singularity calculated within the leading (and next-to-leading) approximation in perturbative QCD. But at lower scales the absorptive (multi-Pomeron) corrections tame the growth which leads to smaller values of n ([124–127]), see Fig. 20.10 (Right).

A similar situation reveals in the dependence of α_{eff} on Q^2 , as can be seen in Fig. 47 of [91]. At a large scale $\mu^2 = (Q^2 + M_V^2)/4$ the value of $\alpha_{\text{eff}} \simeq 1.3$ is close to the prediction for the QCD Pomeron, while for a smaller scale, the absorptive corrections described by the multi-Pomeron diagrams start to reduce the cross section, and α_{eff} decreases.

20.5 Pomeron in QCD

All features described in the previous Sections were based on *first principles*, such as analyticity (based on causality), unitarity, crossing symmetry, etc. Since QCD theory satisfies all these principles it should reveal a corresponding “Regge” behaviour. Indeed, within perturbative QCD there is a Pomeron: an even-signature singularity in the j -plane with vacuum quantum numbers. While in the old Regge theory the Regge trajectories and their couplings were phenomenological numbers fitted from experiment, perturbative QCD allows one to calculate the positions of the singularities and the corresponding couplings with $O(\alpha_s)$ and even with $O(\alpha_s^2)$ accuracy [59, 122, 123, 128–131].

In terms of Feynman diagrams, the QCD Pomeron may be viewed as a sum of multi-particle ladders built by the exchange of two t -channel (reggeized¹⁴) gluons, see the left-hand side of Fig. 20.5.

¹⁴That is, the virtual loop corrections to the one-gluon exchanges are included. These corrections are important in order to provide infrared sta-

The sum of ladder diagrams of the type of Fig. 20.5 is the simplest multiparticle structure which reproduces the power-like s^α behaviour of the Pomeron pole. In other words it corresponds to a sum of completely inelastic $2 \rightarrow n$ processes, that is, to the last term $G_{\text{inel}} = 1 - \exp(-\Omega)$ in the unitarity equation (20.9). This set of diagrams was resummed in the limit of a small QCD coupling, $\alpha_s \ll 1$, but large energy, such that $\alpha_s \ln(s/s_0) \sim O(1)$ [59]. The summation results in the rightmost singularity at $j = 1 + \omega_0 > 1$. After accounting for the next-to-leading logarithmic (NLL) corrections, the position of the singularity (Pomeron intercept) corresponds to $\omega_0 = 0.25\text{--}0.3$ depending only weakly on the scale [122, 123, 132–136], whose value is characterized by the transverse momentum, k_t , of gluons in the ladder.

It was demonstrated (see e.g. [137]) that the resummation of the $(\alpha_s \ln(1/x))^n$ terms based on the QCD Pomeron results essentially improves the description of low- x inclusive HERA data within the framework of the NNLO DGLAP evolution.

At this stage the singularity is the cut in the j -plane. However we have to account for the boundary conditions at relatively small k_t . Imposing a reasonable boundary, we arrive at a series of Regge poles in the interval from $j = 1$ to $j = 1 + \omega_0$ instead of the cut [134]. Note that the first (corresponding to the rightmost pole in the j -plane, i.e. to the pole with the largest $\text{Re } j$) eigenfunction consists of gluons with relatively small k_t , while for the next poles the k_t increases. DIS inclusive γ^*p cross sections were fitted in [135] using the QCD based approach in which Pomeron is represented by series of Regge poles obtained within the perturbative QCD BFKL approach. It was concluded that the first pole has a small coupling to the proton. It is possible that this small value of the coupling to the proton is related to the fact that the enhanced multi-Pomeron diagrams (i.e. the rescattering of intermediate partons) were neglected in the fit. The main effect of this enhanced contribution is the “renormalization” of the intercept which diminishes the effective value of ω_0 . Besides this, the enhanced diagrams provide a saturation by reducing the rise

bility of the results.

of the parton densities in the (b, k_t, y) -space (see e.g. [138, 139]).

Note that perturbative QCD allows us to understand why the values of the phenomenological multi-Pomeron vertices and the shift, ω_0 , of the intercept, are small (due to $\alpha_s \ll 1$ and some numerical factors such as N_c and π). Indeed, at the lowest α_s orders we get for the ω_0 value and the simplest multi-Pomeron vertices (see e.g. [59, 139, 140]):

$$\omega_0 \propto \frac{N_c \alpha_s}{\pi}, \quad g_{3\mathbb{P}} \propto \frac{N_c \alpha_s^2}{(N_c^2 - 1)\pi^2} \quad \text{and} \quad g_2^2 \propto \frac{N_c \alpha_s}{(N_c^2 - 1)^2}, \quad (20.46)$$

where g_2^2 is the coupling corresponding to the transition of 2 into 2 Pomerons.

20.5.1 BFKL evolution in the ‘dipole’ representation

It was shown in [141–144] that the LO BFKL Pomeron equation [59] can be written in terms of the evolution of the dipole density, $N(x_d, y_d; y)$, in rapidity y (here x_d and y_d are the transverse coordinates of two t -channel gluons which form the colour singlet dipole). Indeed, after the emission of a new gluon at point z_d , the initial colour dipole with coordinates (x_d, y_d) turns into a pair of dipoles (x_d, z_d) and (z_d, y_d) . This can be considered as a development of a ‘dipole cascade’. Moreover in this formalism it is easy to include the non-linear absorptive corrections (last term in the square brackets in Eq. (20.47)), which accounts for the rescattering of the intermediate partons (gluons) on the target proton. The corresponding contribution is described by the so-called ‘fan’ diagrams and these are the most important corrections to the linear DGLAP (Dokshitzer-Gribov-Lipatov-Altarelli-Parisi) evolution [145] in the case of DIS at not large scales but at very small momentum fraction [139].

The resulting non-linear evolution (Balitsky-Kovchegov equation [146–148]) reads

$$\begin{aligned} \frac{d}{dy} N(x_d, y_d; y) &= \frac{\alpha_s N_c}{2\pi^2} \int d^2 z_d \frac{(x_d - y_d)^2}{(x_d - z_d)^2 (y_d - z_d)^2} \\ &\times [N(x_d, z_d; y) + N(y_d, z_d; y) - N(x_d, y_d; y) \\ &\quad - N(x_d, z_d; y) N(y_d, z_d; y)]. \end{aligned} \quad (20.47)$$

For a small density N the last term in the square brackets can be neglected, and the first three terms in Eq. (20.47) reproduce the conventional BFKL equation in the coordinate representation. However, for large $N \rightarrow 1$ the right-hand side of Eq. (20.47) vanishes and we reach the saturation $N = 1$. It is worth mentioning that, as shown in [149], in terms of ‘dipole’ formalism, with the triple-Pomeron vertex generated by the ‘one dipole to two dipoles’ transition, it is possible to relate the Good-Walker approach to high mass diffraction with the triple-Pomeron diagram.

20.5.2 Distribution of secondaries: theory versus experiment

As already discussed, in terms of Feynman diagrams the cut Pomeron can be viewed as a set of ladder diagrams corresponding to a sum of completely inelastic $2 \rightarrow n$ processes, that is, to the last term $G_{\text{inel}} = 1 - \exp(-\Omega)$ in the unitarity equation (20.9). Here $n > 2$ means the production of additional $(n - 2)$ gluons which, after hadronization, form minijets.¹⁵ Therefore, in the final state driven by one Pomeron, we expect to observe gluon minijets with a flat rapidity distribution in the central (plateau) rapidity region. This would correspond to a flat pseudorapidity distribution of produced particles if they were massless. A typical pseudorapidity distribution of charged particles in inclusive events (up to $|\eta| = 7$) is shown in Fig. 20.11 (left) [150] (see also Fig. 53.1 in [1]). The central part ($|\eta| < 2.5$) was measured by CMS, while the forward region was covered by TOTEM. The dip observed at $\eta = 0$ is explained by the presence of massive particles (the Jacobian $J(p_T, m, \eta) = p_T/E \rightarrow p_T/\sqrt{p_T^2 + m^2}$ at $\eta = 0$). A photon energy spectrum is shown in Fig. 20.11 (right) [151], measured

¹⁵Minijets result from hadronization of partons emitted from the cut QCD Pomeron. Typically these are groups of hadrons with comparatively low overall $E_T \lesssim 5\text{--}10$ GeV.

by LHCf inclusively and in events with a diffraction topology, i.e. no charged particles with $p_T > 100$ MeV and $|\eta| < 2.5$ observed by ATLAS. As expected in diffractive events the energy flow decreases with E_γ more slowly than that in the inclusive case.

The energy dependence of the particle density $dN_{\text{ch}}/d\eta$ at $\eta = 0$ is shown in Fig. 20.12 (left). Neglecting absorptive corrections given by the enhanced diagrams (which mainly change (‘renormalize’) the effective Pomeron intercept $\alpha_{\text{eff}}(0) = 1 + \Delta$ [121]), we conclude that according to the AGK rules the plateau height $d\sigma/d\eta \propto s^\Delta$ is driven just by the one-Pomeron exchange with effective $\Delta \sim 0.2$ (see Section 20.3.3.3). That is, the density of secondaries observed in the inclusive process increases with increasing energy faster than the total cross section, whose growth is tamed by the multi-Pomeron diagrams. Indeed, as is seen from Fig. 20.12 (left), in the interval of collider energies $dN_{\text{ch}}/d\eta = (1/\sigma_{\text{inel}})d\sigma/d\eta \propto s^{0.115}$ (i.e. $d\sigma/d\eta \propto s^{0.215}$), while $\sigma_{\text{inel}} \propto s^{0.1}$.

Contrary to the ‘old’ Regge theory where it was *assumed* (based on the experimental data existing in the 1950s and 1960s) that all transverse momenta are limited, in QCD the k_t distributions of jets (charged particles) have a long k_t tail ($d\sigma/dk_t^2 \propto \alpha_s^2(k_t^2)/k_t^4$ at large k_t and very large energy $s \gg k_t^2$). An example of the p_T distribution of charged secondaries is shown in Fig. 20.12 (right).

Note that the mean transverse momentum of secondaries, produced via jet fragmentation, slowly increases with collision energy, see Fig. 20.13 (right). This is caused by the stronger absorption (at larger \sqrt{s}) of the gluons with a smaller k_t ($\sigma^{\text{abs}} \propto 1/k_t^2$). The growth of $\langle p_T \rangle$ with multiplicity (see Fig. 20.13 (left)) can be explained by the fact that events with larger N_{ch} correspond to a smaller impact parameter, b , where the absorption of a low k_t component is stronger and, next, larger multiplicity can be originated by the events with jets/minijets with higher p_T . Since the mean p_T of secondaries grows with \sqrt{s} , the increase with \sqrt{s} of transverse energy flow is a bit faster than that of particle density.

The model [162] based on a modification of the classic RFT allows one to trace the smooth transition from the pure perturbative, large k_t , region into the *soft* domain. A strong absorption of the low k_t partons plays a crucial role here since it produces an effective infrared cutoff, k_{sat} , and provides the possibility of extending the parton approach, used for ‘hard’ processes, to also describe high-energy soft and semihard interactions. This approach combines a description of soft physics and diffraction with jet physics in a coherent self-consistent way.

Another way is to include the soft and hard components independently [37, 66, 163, 164]. In this approach the soft part is described in terms of RFT with the phenomenological ‘soft’ Pomeron pole while the hard part is calculated in terms of the parton model for minijet production with the energy dependent cutoff $k_t > k_0(s)$. A combined description of soft and hard processes in hadronic collisions is reached within the QGSJET Monte Carlo model (e.g. [61]) in the framework of the so-called ‘semi-hard Pomeron’ approach (see e.g. [165]).

In [166] a model was constructed, which incorporated the attractive features of the two successful theoretical approaches to high energy QCD: BFKL Pomeron calculus [59, 60] and the Colour Glass Condensate/saturation [167].

20.5.2.1 Correlations

All LHC experiments routinely measure tracks with $p_T > p_{\text{min}}$, where p_{min} can vary in different studies. Typically, $p_{\text{min}} = 200$ MeV, where tracking reconstruction efficiencies are larger than 70%. In order to identify particle species, each experiment has sophisticated identification procedures usually based on the ionization energy loss, dE/dx , or other techniques, with different regions of applicability for different particle species. Thanks to usually relatively large cross sections of soft QCD processes, most of the results below come from event samples with very low or negligible pile-up.

Following the notation in [168], symmetrized inclusive particle number densities for q points at y_1, \dots, y_q (where y_i represents the 4-momentum of the i th particle), $\rho_q(y_1, \dots, y_q)$, are related to the inclusive differential cross section by

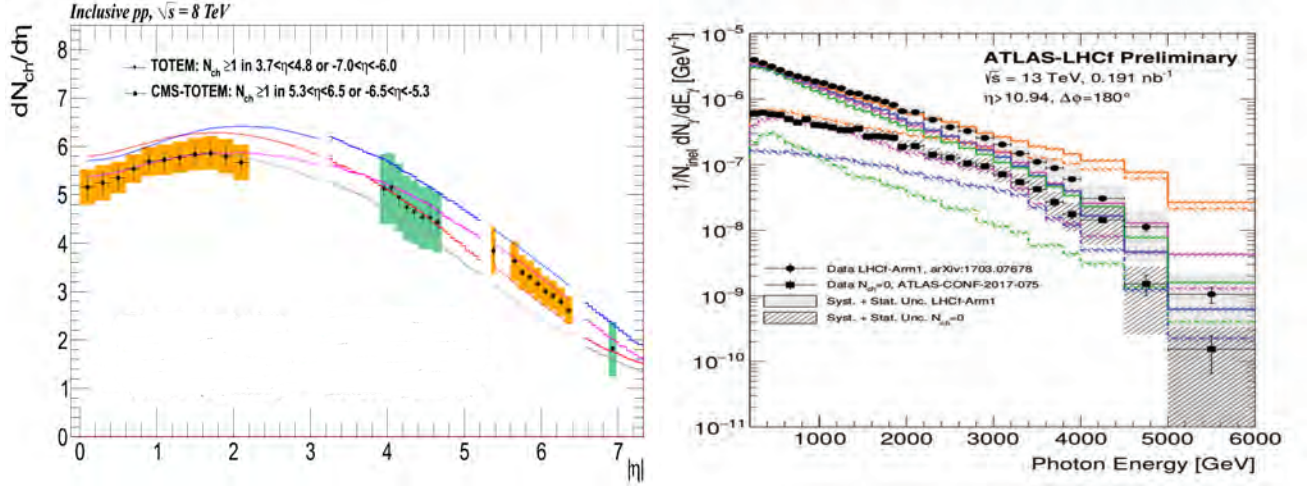


Figure 20.11: (Left) Charged-particle pseudorapidity distribution for inclusive events measured by CMS and TOTEM [150]. The error bars represent the statistical and uncorrelated systematic uncertainties between neighboring bins, while the shaded areas denote the combined statistical and full systematic uncertainties. The coloured lines indicate model predictions. (Right) Photon energy spectrum measured by LHCf at $|\eta| > 10.94$. The filled circles show the inclusive photon spectrum measured by LHCf [152] and filled squares the spectrum for $N_{ch} = 0$ events where no charged particles with $p_T > 100$ MeV and $|\eta| < 2.5$ are observed by ATLAS [153]. The coloured lines indicate model predictions. The error bars correspond to the statistical uncertainties and the shaded areas denote the combined statistical and systematic uncertainties. Figure from Ref. [151].

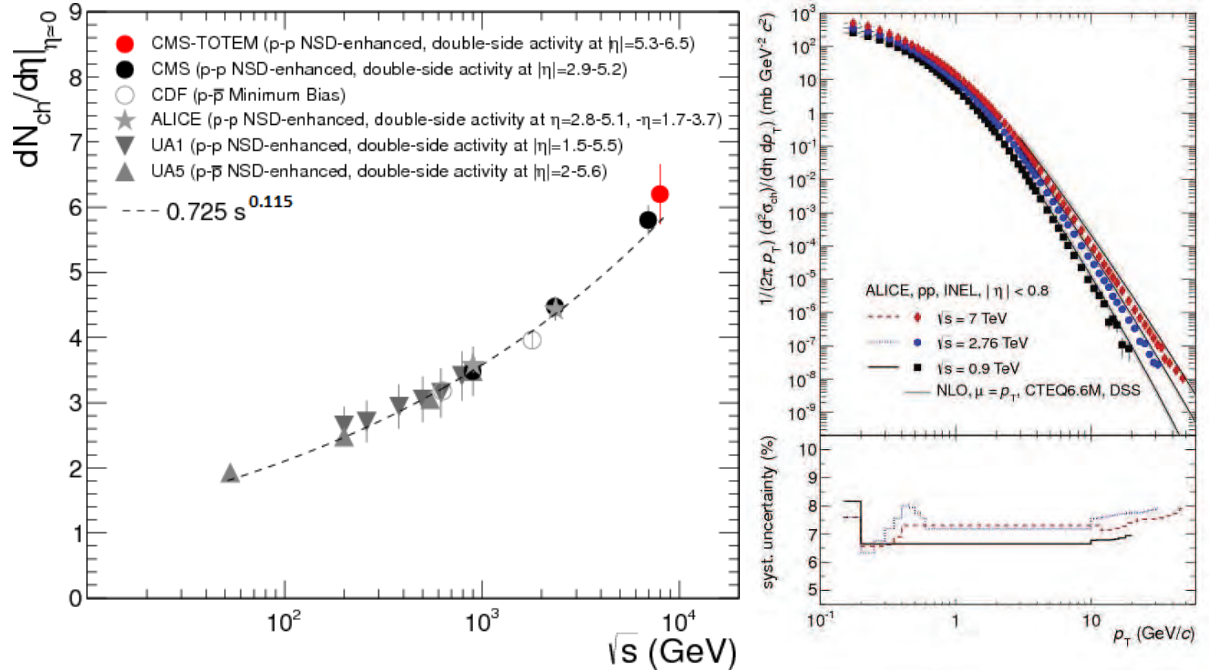


Figure 20.12: (Left) Energy dependence of the charged particle density $dN_{ch}/d\eta$ at $\eta \approx 0$ for pp and $p\bar{p}$ collisions. Shown are measurements performed with different Non-SD event selections from UA1 [154], UA5 [155], CDF [156,157], ALICE [158] and CMS [159]. The dashed line is a power-law fit to the data. Figure from Ref. [150]. (Right) Differential cross section of charged particles with $|\eta| < 0.8$ in inelastic pp collisions at $\sqrt{s} = 0.9, 2.76$ and 7 TeV as a function of p_T . Only statistical uncertainties are shown. Figure from Ref. [160].

$$\frac{1}{\sigma_{inel}} d\sigma = \rho_1(y) dy, \quad \frac{1}{\sigma_{inel}} d^2\sigma = \rho_2(y_1, y_2) dy_1 dy_2 \quad \text{etc.} \quad (20.48)$$

By integrating we get

$$\int \rho_1(y) dy = \langle n \rangle, \quad \iint \rho_2(y_1, y_2) dy_1 dy_2 = \langle n(n-1) \rangle \quad \text{etc.}, \quad (20.49)$$

where the angular brackets denote averaging over the event sample and n is the particle multiplicity.

Since the inclusive q -particle densities in general contain trivial contributions from lower-order densities, it is convenient to consider quantities C_q which vanish when one of their arguments becomes statistically independent of (uncorrelated with) the others. These quantities C_q , called correlation functions (or cumulant

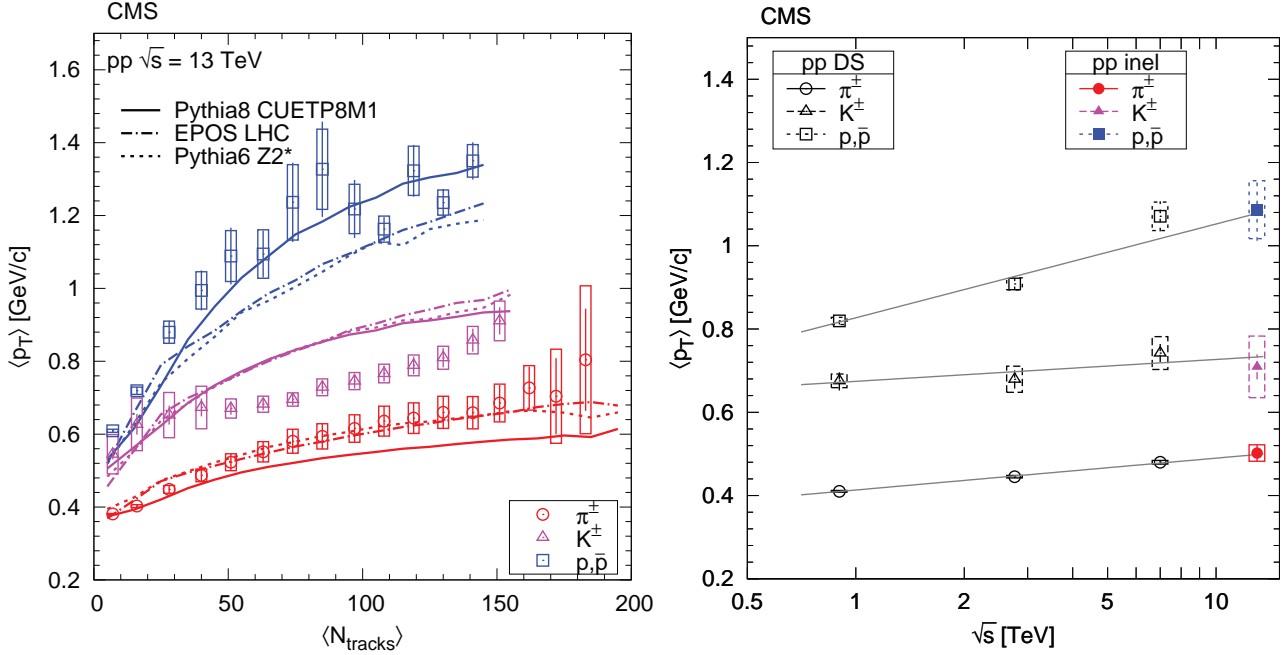


Figure 20.13: Average p_T of pions, kaons and protons in the range $|\eta| < 1.0$ as a function of (left) track multiplicity at $|\eta| < 2.4$ and (right) of center-of-mass energy where the curves show linear fits using lns. The error bars indicate the uncorrelated combined uncertainties, while the boxes show the uncorrelated systematic uncertainties. Figures from Ref. [161].

functions), are defined as:

$$\begin{aligned}
 C_2(1, 2) &= \rho_2(1, 2) - \rho_1(1)\rho_1(2), \quad C_3(1, 2, 3) \\
 &= \rho_3(1, 2, 3) - \sum_{(3)} \rho_1(1)\rho_2(2, 3) + 2\rho_1(1)\rho_1(2)\rho_1(3), \\
 C_4(1, 2, 3, 4) &= \rho_4(1, 2, 3, 4) - \sum_{(4)} \rho_1(1)\rho_3(1, 2, 3) \\
 &\quad - \sum_{(3)} \rho_2(1, 2)\rho_2(3, 4) + 2 \sum_{(6)} \rho_1(1)\rho_1(2)\rho_2(3, 4) \\
 &\quad - 6\rho_1(1)\rho_1(2)\rho_1(3)\rho_1(4).
 \end{aligned} \tag{20.50}$$

The 2D two-particle correlation function is defined as

$$C(\Delta\eta, \Delta\phi) = \frac{\rho_2(\Delta\eta, \Delta\phi)}{\rho_1(\eta_a, \phi_a)\rho_1(\eta_b, \phi_b)}. \tag{20.51}$$

The distribution $\rho_2(\Delta\eta, \Delta\phi)$ is usually interpreted as a conditional probability to observe a particle a at the phase-space point (η_a, ϕ_a) if a particle b at (η_b, ϕ_b) is observed as well, and $\Delta\eta = \eta_a - \eta_b$ and $\Delta\phi = \phi_a - \phi_b$. The distributions $\rho_1(\eta_a, \phi_a)$ and $\rho_1(\eta_b, \phi_b)$ are probabilities to observe a single particle at (η_a, ϕ_a) and (η_b, ϕ_b) , respectively. The denominator of Eq. (20.51) is constructed as a product of two single-particle distributions using an event mixing technique, where each particle in the pair comes from a different event. Experimentally, each reconstructed track is weighted by the inverse of an efficiency factor which accounts for the detector acceptance, the reconstruction and particle identification efficiencies, the contamination by secondary particles and the fraction of misreconstructed tracks.

An example of two-particle correlation functions measured in pp collisions at 7 TeV is shown in Fig. 20.14 for identical-particle pairs (right panel) and for particle-anti-particle pairs (left panel) [169].

We observe two distinct features which can be explained by short-range (in rapidity) correlations: 1) a near-side peak at $\Delta\phi \approx 0$ and 2) an away-side peak or rather a ridge at $\Delta\phi \approx \pi$. The near-side peak is considered to be caused by at least three effects:

- *fragmentation of partons scattered at a hard scale.* These relatively high p_T partons produce showers which after the

hadronization form the mini-jets which create a broad structure extending over at least one unit in $\Delta\eta$ and $\Delta\phi$.

- *resonance decays.* The decay of resonances contributes to the near-side peak at $\Delta\eta \sim 0$ and extended in $\Delta\phi$ [170–172], depending on the released kinetic energy of the given resonance. This effect is mostly visible for unlike-sign particle pairs.
- *femtoscopic correlations.* The term “femtoscopic” refers to a length scale of the order of 10^{-15} m. These correlations are present at low relative momenta of the particles in a pair (representing a very small phase-space corner, so they are practically invisible in terms of $(\Delta\eta, \Delta\phi)$) and give rise to an enhancement of the correlation function (due to Bose-Einstein quantum statistics for identical bosons) or its suppression (due to Fermi-Dirac quantum statistics for identical fermions). Besides this, at low relative momenta there are correlations caused by Coulomb and/or other final state interactions. The shape of all these effects in $(\Delta\eta, \Delta\phi)$ space depend strongly on the mass of the particle type as well as on the size of the particle-emitting system. The latter is traditionally measured in Bose-Einstein correlation (BEC) analyses and is not part of this review.

The away-side peak originates from energy-momentum conservation which manifests itself by the quark and the anti-quark going back-to-back in ϕ . In this case the rapidity width of the away-side peak is much larger than the near-side peak since in the original matrix element the quark and the antiquark can be separated by some $\Delta\eta$ interval.

As discussed in Sections 20.3.3.2 and 20.3.3.3, there may be several cut Pomerons in the same event, each giving rise to particle sets which are, in general, independent of each other (except for small Bose-Einstein correlations). This leads to long-range (in rapidity) correlations. Since the density of secondaries, dN/dy , is proportional to the number of cut Pomerons, k , the probability to observe at least one particle is proportional to $\langle k \rangle$, while the probability to observe simultaneously two particles separated by some (rather large) rapidity interval is proportional to $\langle k^2 \rangle$. Thus the long-range correlations are predicted to be $C_2 = \langle k^2 \rangle / \langle k \rangle^2 - 1 > 0$ which depends weakly on the separation $\Delta\eta$ between the two particles [173, 174]. In the case of the pure eikonal approach, neglecting the enhanced diagrams and the conservation law effects

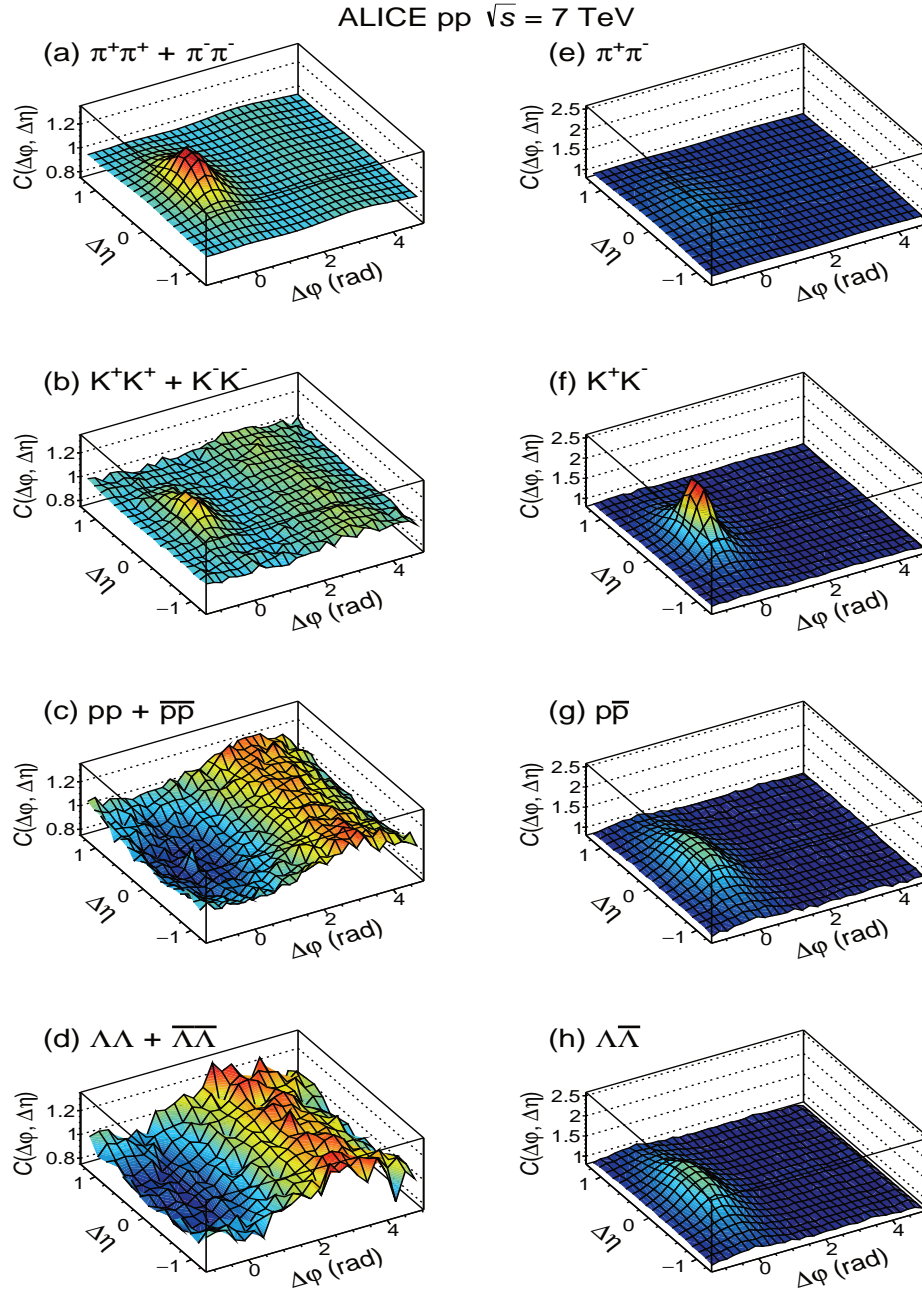


Figure 20.14: Two-particle correlation functions for identical-particle pairs: $\pi^+\pi^+ + \pi^-\pi^-$, $K^+K^+ + K^-K^-$, $pp + \bar{p}\bar{p}$, and $\Lambda\Lambda + \bar{\Lambda}\bar{\Lambda}$ (left panel) and particle–anti-particle pairs: $\pi^+\pi^-$, K^+K^- , $p\bar{p}$ and $\Lambda\bar{\Lambda}$ (right panel). Figure from Ref. [169].

in the proton fragmentation region, we expect that these long-range correlations,

$$C_2(\Delta y) = \frac{\sigma_{\text{inel}} d^2\sigma/dy_1 dy_2}{d\sigma/dy_1 d\sigma/dy_2} - 1 \sim \text{const}, \quad (20.52)$$

do not depend on the rapidity separation, $\Delta y = |y_1 - y_2|$, between the two particles. The contribution of the processes with more cut Pomerons also results in a much wider multiplicity distribution and in a larger density of soft particles coming from the ‘underlying event’.

20.5.2.2 Color reconnection

In this context, we have to mention also the so-called ‘colour reconnection’ phenomenon. This is a pure ‘soft QCD’ effect. The point is that after a number of coloured secondary partons are produced, there are different possibilities to form the colour flow between these partons and to group the partons into colourless clusters. In the process of reconnection, one rearranges the colour

flow in such a way as to minimize the size of the clusters. This is especially important when dealing with MPI contributions. The reconnection between the different cut Pomerons diminishes the final multiplicity and can change the form of the N_{ch} distributions (see e.g. Section 43.3.2 of [1] and [2, 13, 177, 178]).

20.5.2.3 Double parton scattering

The probability of MPI depends on the spatial distribution of partons in the incoming protons. The effects of MPI are suppressed if the density of partons is low and the partons from the incoming beam particles are separated from each other by a large interval in transverse coordinate space \vec{x}_t . Events in which two hard subprocesses, caused by interactions of two different parton pairs (say, $(a_1 b_1)$ and $(a_2 b_2)$), take place simultaneously, are called Double Parton Scattering (DPS). The DPS cross section is driven by the ‘double parton distributions’, $D(y_{a_1}, y_{a_2}, \dots)$, where y_{a_1} and y_{a_2} are momentum fractions carried by the partons from the proton a and the dots denote all other coordinates. As a rule,

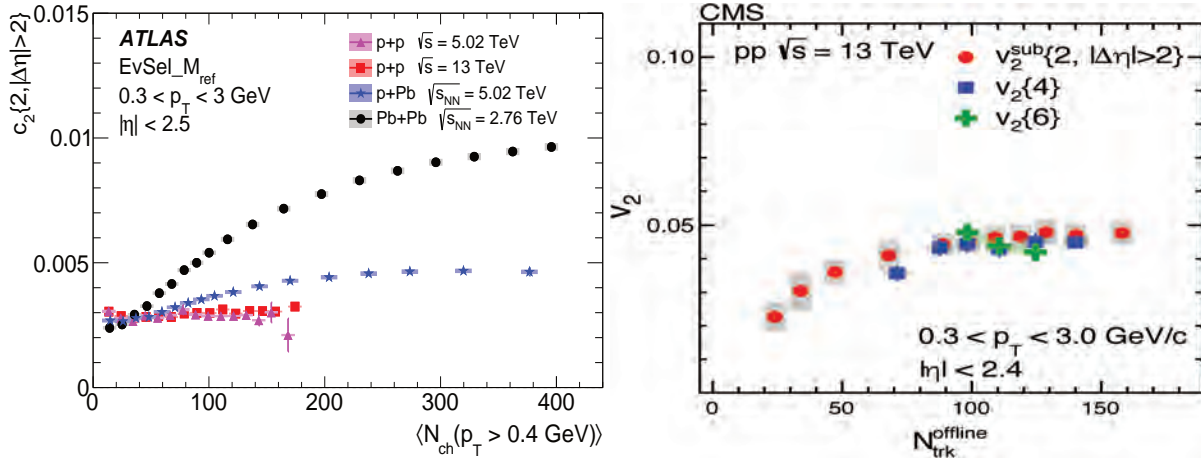


Figure 20.15: (Left) The two-particle cumulant, $c_2\{2, |\Delta\eta| > 2\}$, as a function of $\langle N_{ch}(p_T > 0.4 \text{ GeV}) \rangle$ for pp collisions at $\sqrt{s} = 5.02$ and 13 TeV , pPb collisions at $\sqrt{s_{NN}} = 5.02 \text{ TeV}$ and low-multiplicity $PbPb$ collisions at $\sqrt{s_{NN}} = 2.76 \text{ TeV}$. The data are constructed from particles with $0.3 < p_T < 3.0 \text{ GeV}$. Figure from Ref. [175]. (Right) The $v_2\{2, |\Delta\eta| > 2\}$, $v_2\{4\}$ and $v_2\{6\}$ values as a function of number of charged particles, averaged over $0.3 < p_T < 3.0 \text{ GeV}$ and $|\eta| < 2.4$, in pp collisions at $\sqrt{s} = 13 \text{ TeV}$. Figure from Ref. [176]. The error bars correspond to the statistical uncertainties, while the shaded areas denote the systematic uncertainties.

experiments study DPS processes at relatively small momentum fractions y_i . Here, correlations due to momentum conservation (like $y_{a_1} + y_{a_2} < 1$) are not so important, and with a reasonable accuracy we can assume a factorization

$$D(y_{a_1}, y_{a_2}, \dots) \propto F(y_{a_1}) \cdot F(y_{a_2}), \quad (20.53)$$

where $F(y_{a_i})$ are the single parton distributions. In such a case the DPS cross section takes the form

$$\sigma^{\text{DPS}} = c \cdot \frac{\sigma_{a_1 b_1} \sigma_{a_2 b_2}}{\sigma_{\text{eff}}}, \quad (20.54)$$

where $\sigma_{a_1 b_1}$ and $\sigma_{a_2 b_2}$ are cross sections for the two independent hard processes, while σ_{eff} characterizes the mean area occupied by the partons a_1 and b_1 ; the constant factor $c = 1/2$ if both hard processes ($a_1 b_1$) and ($a_2 b_2$) are identical, otherwise $c = 1$. Thus the DPS cross section is sensitive to the spatial separations between partons in the proton (see Section 7.2.3 in [2] and [179, 180] for more explanations and reviews).

One problem is that within this approach we assume that the partons a_1 and a_2 are produced by two independent parton showers (and similarly for the other incoming proton). On the other hand, there is a probability that from the beginning we start with the evolution of a single shower which further splits into two different branches. In this case the separation between the two partons (two shower branches) becomes very small – of the order of the inverse scale ($\sim 1/\sqrt{q^2}$) at which the splitting occurs. The exact value of this ‘splitting’ scale q^2 depends on the particular kinematics of the DPS process. So, different experiments (with different kinematical conditions) can give somewhat different values of σ_{eff} . In general, the value of σ_{eff} depends on the following features: a) on the measured process since the spatial (b_i) distributions of different incoming partons (light quarks, heavy quarks, gluons) can be different; b) on the splitting scale, $\sqrt{q^2}$, of one parton cascade into two branches. The typically high value of the splitting scale then explains the fact that the experimentally measured values of $\sigma_{\text{eff}} \sim 7\text{--}25 \text{ mb}$ (see Fig. 4 of [181]) are smaller than σ_{tot} or mostly even lower than the proton area $\pi R_p^2 \sim 22\text{--}24 \text{ mb}$ (see e.g. [182]); c) on the p_T balance, k_T , in the individual hard process (e.g. for two dijet productions $k_T = |\vec{p}_{T1} + \vec{p}_{T2}|$ where p_{T1} and p_{T2} are jet p_T ’s of the first hard process (similarly for the second hard process)). A small value of k_T indicates that there were no splittings or the splitting scale $\sqrt{q^2}$ was small and, therefore, we expect larger σ_{eff} ; d) on the contribution of single parton scatterings misidentified as DPS. For a lower scale of the hard process this contribution is larger (see [183] for more detailed discussion).

20.5.2.4 Final state interactions

The formalism of the RFT does not include ‘final state interactions’¹⁶. Therefore, besides the correlations considered in the previous Section 20.5.2.1 we have to expect the correlation caused by partons and hadrons rescattering in the final state. These effects are not crucial at lower energies, but become more important at high LHC energies, in particular in heavy-ion collisions where the particle density is large. For example, the final state interactions (FSI) lead to the formation of the collective flow of secondaries (see e.g. [185] for a review), especially in high-multiplicity events. To study the collective flow experimentally, one has to subtract correlations coming from few-particle sources such as resonance decays, mini-jets, multi-jets and BEC (so called ‘non-flow’). The non-flow can efficiently be suppressed using the sub-event method, that is by studying the azimuthal correlations between particles separated in η [186], or subtracted using the multi-particle correlation (or cumulant) techniques.

The cumulant method is based on calculating $2k$ -particle azimuthal correlations, $\text{corr}_n\{2k\}$, and cumulants $c_n\{2k\}$ (where $k = 1, 2, \dots$), for n th Fourier harmonics. The $\text{corr}_n\{2k\}$ are defined as [187, 188]:

$$\begin{aligned} \langle\langle \text{corr}_n\{2\} \rangle\rangle &= \langle\langle e^{in(\phi_1 - \phi_2)} \rangle\rangle, & \langle\langle \text{corr}_n\{4\} \rangle\rangle &= \langle\langle e^{in(\phi_1 + \phi_2 - \phi_3 - \phi_4)} \rangle\rangle, \\ \langle\langle \text{corr}_n\{6\} \rangle\rangle &= \langle\langle e^{in(\phi_1 + \phi_2 + \phi_3 - \phi_4 - \phi_5 - \phi_6)} \rangle\rangle \end{aligned}$$

and similarly for higher numbers of correlated particles. The double-brackets $\langle\langle \rangle\rangle$ denote averaging first over particles in an event and then over events within a given event class. For every event, the average is taken over all possible combinations of azimuthal angles ϕ_l ($l = 1, \dots, 2k$) of the $2k$ particles. The cumulants are then obtained from multi-particle azimuthal correlations after subtracting correlations between $2(k-1)$ particles according to the following formulae [187, 188]:

$$\begin{aligned} c_n\{2\} &= \langle\langle \text{corr}_n\{2\} \rangle\rangle, & c_n\{4\} &= \langle\langle \text{corr}_n\{4\} \rangle\rangle - 2\langle\langle \text{corr}_n\{2\} \rangle\rangle^2, \\ c_n\{6\} &= \langle\langle \text{corr}_n\{6\} \rangle\rangle - 9\langle\langle \text{corr}_n\{2\} \rangle\rangle \times \langle\langle \text{corr}_n\{4\} \rangle\rangle + 12\langle\langle \text{corr}_n\{2\} \rangle\rangle^3. \end{aligned}$$

The cumulants for higher particle multiplicities are calculated in [187, 188]. The cumulants then serve to estimate the Fourier harmonics v_n as follows [187]:

$$v_n\{2\} = \sqrt{c_n\{2\}}, \quad v_n\{4\} = \sqrt[4]{-c_n\{4\}}, \quad v_n\{6\} = \sqrt[6]{c_n\{6\}/4}.$$

¹⁶In general, final state interactions can be included into the detailed structure of the multi-Pomeron vertices. However these vertices are phenomenological objects which are not well known experimentally.

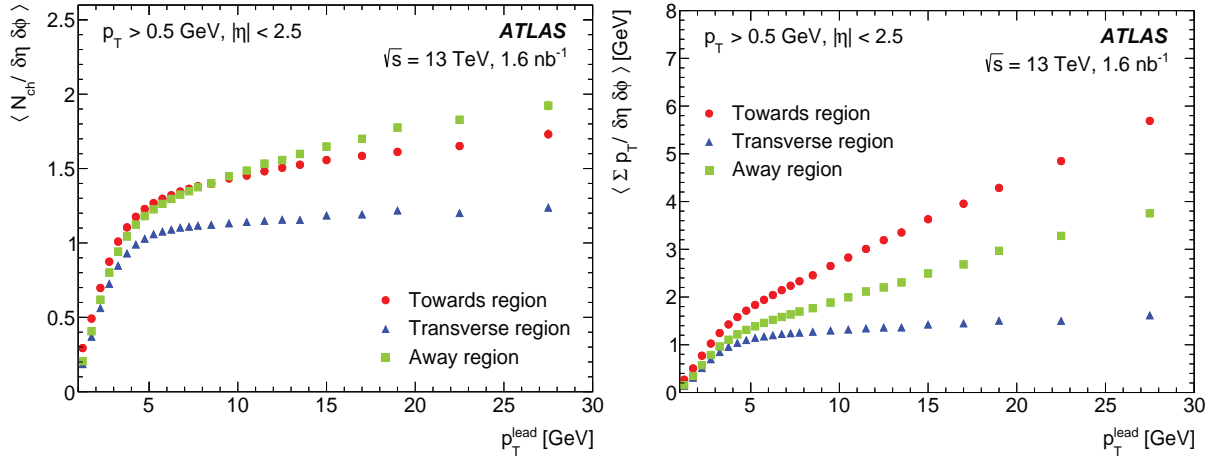


Figure 20.16: Mean charged particle density (left) and the sum of transverse momenta of secondaries (right) in events with the ‘leading’ high p_T particle as a function of p_T^{lead} in the transverse, towards and away azimuthal regions. Secondaries with $p_T > 0.5$ GeV and $|\eta| < 2.5$ are registered. The error bars (mostly hidden by the data markers) represent combined statistical and systematic uncertainties. Figures from [184].

Some of the long-range correlation ($|\Delta\eta| > 2$) results obtained on a sample of charged particles with $0.3 < p_T < 3.0$ GeV and $|\eta| < 2.4$ are summarized in Fig. 20.15. The left plot shows the cumulant c_2 measured for pp , pPb and $PbPb$ collisions [175], while the right plot shows the elliptical harmonics v_2 measured for pp collisions [176], both as functions of multiplicities of charged particles. The two-particle correlations are observed to be strongest and rising with N_{ch} for $PbPb$ collisions, and weakest and rather flat for pp collisions. The elliptical-flow harmonics for 4- and 6-particle correlations show again a rather flat multiplicity dependence (at least for large multiplicities). Within experimental uncertainties, the values of $v_2\{2\}$, $v_2\{4\}$ and $v_2\{6\}$ measured in pp collisions at 13 TeV are consistent with each other. The similarity between $v_2\{4\}$ and $v_2\{6\}$ suggests that some collective effects are occurring in pp collisions at high multiplicity and the observations are similar to those in $PbPb$ collisions, where the $v_2\{4\}$ values were measured to be close to $v_2\{6\}$ but they are both lower than $v_2\{2\}$ (not shown here).

Another example of long-range correlations is the so-called ‘ridge effect’. Here not only the ‘back-to-back’ jet correlations are registered, but also an excess of particles going in the same (in the azimuthal plane) direction as the leading (relatively high p_T) hadron. Moreover, this excess is seen at the rapidities separated from the leading hadron by a rather large interval (see e.g. [189] for a review).

It is popular to describe such FSI effects within the hydrodynamic model [190], which operates with collective (thermodynamic) variables. In terms of microscopic interactions, the collective flow can be caused by the geometry of a particular collision (the absorption is smaller for the secondaries flying in the direction orthogonal to the impact parameter vector \vec{b} [191, 192]), or by the colour reconnection at the hadronization stage [193], or accounting for the rescattering of secondaries directly, as was done, for example, in the AMPT model [194].

20.5.3 The underlying event

Except for the exclusive case, any ‘hard’ subprocess is accompanied by soft secondaries coming from initial state radiation (ISR), final state radiation (FSR) and multiple parton interaction (MPI), see Subsection 7.2.2 in [2]. These extra particles distort the signal we are looking for. In particular, they affect the isolation criteria applied to photons and charged leptons and the vertex reconstruction efficiency. In general, also the effects of colour reconnection (discussed in Section 20.5.2.2) contribute to the underlying event.

The usual procedure of estimating the amount of underlying event (UE) is to spatially divide tracks in each event according to their azimuthal angle into the Toward region (where the highest p_T jet points), the Away region (opposite to the Toward region) and to two Transverse regions. The standard observables are the

average track multiplicity per unit area and the average scalar sum of track p_T per unit area. Figure 20.16 shows the particle density and the sum of p_T for the UE in ATLAS events containing at least one charged particle with $p_T > 0.5$ GeV and $|\eta| < 2.5$ [184].

Note that by construction the largest values of $\langle p_T \rangle$ are observed in the ‘Toward’ region, while in the ‘Away’ region we observe a slightly larger density than in the Toward region. These are results of the ‘leading’ and ‘backward’ jet fragmentation. In the transverse region, mostly filled by particles from the UE, the particle density and sum of p_T per unit ($\Delta\eta, \Delta\phi$) area practically do not depend on the p_T^{lead} since these secondaries come from the other cut Pomeron(s), that is, from other ‘multiple interactions’. For low $p_T^{\text{lead}} < 2$ GeV the distributions in all three regions are close to each other. These events actually do not contain a ‘hard’ subprocess. Moreover, for a very small $p_T^{\text{lead}} \rightarrow 1$ GeV we start to select soft events with abnormally low $p_T < p_T^{\text{lead}}$ particles. Since only particles with $p_T > 0.5$ GeV are registered, the signal drops fast for $p_T^{\text{lead}} \rightarrow 1$ GeV. As a function of collision energy \sqrt{s} , the energy flow in the transverse region increases as $\sum p_T \sim s^{0.2}$ (as follows from Fig. 7 (right) in [184]) due to the larger number of MPI collisions and larger $\langle p_T \rangle$ in each collision¹⁷. As follows from this and other UE-dedicated LHC studies [195], from the comparisons of the data to the models with and without MPI, the necessity of MPI is convincingly demonstrated.

20.6 The Odderon

Apart from the even-signature singularity (Pomeron), in QCD with $N_c = 3$ there exists its counterpart, the odd-signature singularity placed at $j \simeq 1$ and formed by three t-channel reggeized gluons connected in colour space by the symmetric d^{abc} tensor of the colour $SU(3)$ group [200, 201]. This object is called the Odderon. The Odderon exchange amplitude has opposite sign for pp and $p\bar{p}$ scatterings. Its intercept is predicted to be very close to $j = 1$ [202–204], while according to perturbative estimates the coupling to the nucleon is rather small [205, 206]. The corresponding amplitude is mainly real and is about 100 times smaller than the imaginary part of the Pomeron exchange amplitude. Calculating the elastic amplitude via the eikonal formula (20.13) we have to replace the opacity $\Omega(b)$ by the sum $\Omega = \Omega_{\text{even}} + \Omega_{\text{odd}}$, where Ω_{even} is mainly real and Ω_{odd} is imaginary. Note that at $t = 0$ this QCD Odderon does not couple to mesons, and the t -slope of the Odderon amplitude is expected to be smaller than that for the Pomeron; instead of the singularity at $t = 4m_\pi^2$ in the Pomeron case, the nearest singularity in the Odderon channel is at $t = 9m_\pi^2$, see for instance [204]. Thus, in the impact parameter b space the QCD Odderon occupies an area of a smaller radius, see e.g. [207].

¹⁷Recall the stronger absorption of the low k_t partons.

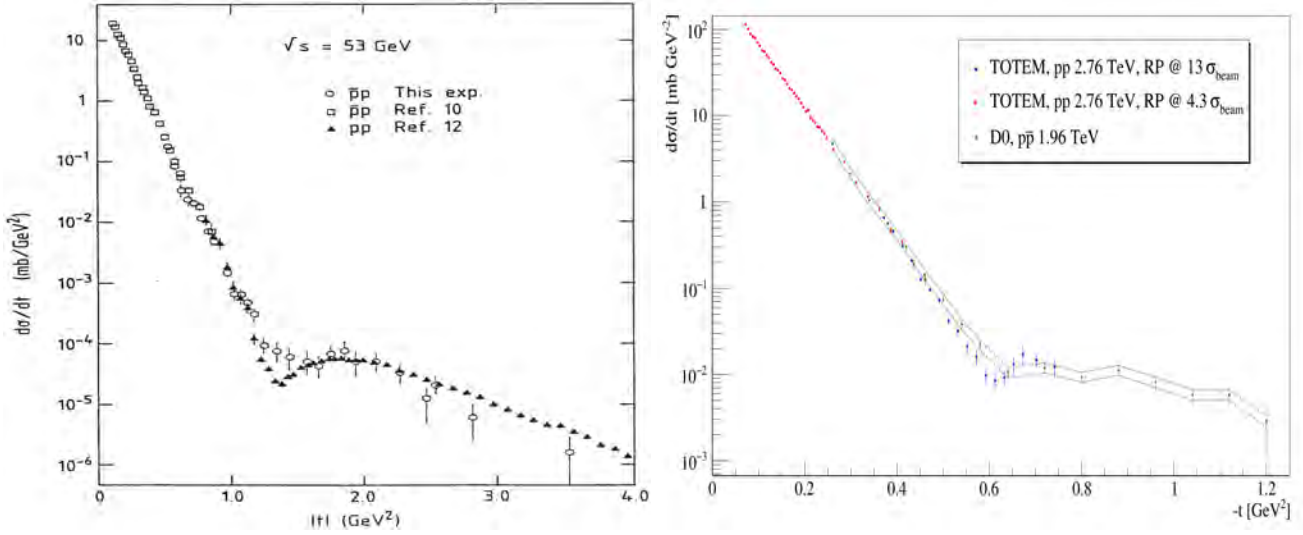


Figure 20.17: Comparison of the t -dependence of the elastic cross sections from pp and $p\bar{p}$ collisions. (Left) Data from the ISR energy of 53 GeV are shown by closed triangles [196] for pp collisions and by open circles [197] and open squares [198] for $p\bar{p}$ collisions. Only t -dependent uncertainties are shown and the systematic scale uncertainty is estimated to be $\pm 30\%$. Figure from Ref. [197]. (Right) Data from the D0 experiment at 1.96 TeV [199] are compared with data from the TOTEM experiment [103]. The green dashed line indicates the normalization uncertainty of the D0 measurement. Figure from Ref. [103].

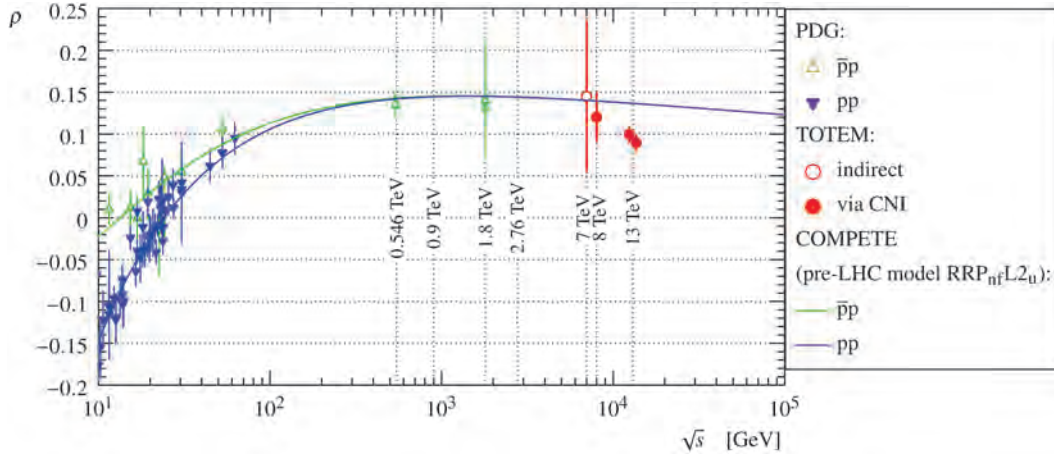


Figure 20.18: The dependence of the ρ parameter on the collision energy. The pp (blue) and $p\bar{p}$ (green) data are taken from [1]. The TOTEM measurements are marked in red. The two points at 13 TeV correspond to two fit cases, discussed in [102], using the same data. The lines represent fits to the data using the COMPETE parameterization [22]. Figure from Ref. [102].

Experimentally an indication in favour of a manifestation of the high energy C -odd amplitude was observed by comparing the elastic pp and $p\bar{p}$ cross sections in the dip region (where the contribution from the C -even amplitude has a minimum) at the CERN-ISR [197], see Fig. 20.17 (left) ¹⁸.

To get a better understanding of the Odderon effects it would be very instructive to have the $d\sigma_{el}/dt$ data for both pp and $p\bar{p}$ reactions at the same but higher energy ~ 1 TeV (ideally in the same apparatus) and, in the ideal case, to study the energy dependence.

At the moment we can only compare the pp cross section measured by TOTEM at $\sqrt{s} = 2.76$ TeV [103] with the $d\sigma/dt$ values measured by the D0 collaboration at 1.96 TeV in $p\bar{p}$ collisions [199], see Fig. 20.17 (right).

The situation looks quite intriguing, but needs further investigation. Note that in the TeV energy range the ω , ρ and ωP , ρP exchange contributions, which may be responsible for the differ-

ence between the pp and $p\bar{p}$ cross sections in the dip region at the ISR energies, are practically negligible.

Another way to search for the Odderon is to measure the real part of the elastic pp scattering amplitude via the interference with the pure QED one-photon exchange. Since the one-photon exchange amplitude contribution is sizeable only at very small $|t|$, this way we can study the Odderon at or near to $t = 0$. Indeed, the value of the ratio $\rho \equiv \text{Re}T_{el}/\text{Im}T_{el}$, obtained by TOTEM at 13 TeV ($\rho = 0.10 \pm 0.01$ [102]), turns out to be smaller than that expected for the pure even-signature amplitude, see Fig. 20.18.

Based on dispersion relations and assuming the C -even contribution only, from the known total cross sections we would rather expect $\rho \simeq 0.13$ – 0.14 . The difference could indicate that the rise of the total cross section at energies above those of the LHC slows down (see the dispersion relation, Eq. (20.19)) or this could be attributed to an Odderon contribution (see e.g. [210]). However, the Odderon exchange amplitude extracted in this analysis has opposite sign to that for the lowest- α_s -order QCD Odderon, see e.g. [205, 206, 211, 212]. Besides this, the Odderon contribution to ρ , obtained in [210], grows with \sqrt{s} (for $\sqrt{s} > 0.5$ TeV), while in QCD we expect that the Odderon contribution to ρ decreases with energy, since the QCD Odderon intercept is smaller than that of

¹⁸Note that a qualitatively similar behaviour to the $p\bar{p}$ ISR data, namely a filling in of the dip in the t -distribution, was observed by the UA4 collaboration at the CERN $S\bar{p}\bar{p}S$ collider at $\sqrt{s}=546$ and 630 GeV (see [208, 209] and in particular Fig. 2 in [209]) and by the D0 collaboration at the Tevatron at 1.96 TeV [199].

the QCD Pomeron.

It is worth mentioning also that the Odderon contribution is strongly screened by the multi-Pomeron diagrams, which facilitate the falling-off of ρ with energy increasing, see [213, 214]. On the other hand, analyzing the whole ensemble of high energy elastic pp ($p\bar{p}$) low $|t|$ data, a reasonable description can be obtained using the even-signature amplitude only, that is, without the Odderon. In particular, the RR(PL2)qc model/version of the COMPETE parameterization is consistent with the TOTEM 13 TeV data on σ_{tot} and ρ within 1σ ¹⁹. Another example is the recent analysis in [212] of the low $|t| < 0.1$ GeV² elastic data. Fitting all the low- t pp and $p\bar{p}$ data in the range of \sqrt{s} between 13 GeV and 13 TeV without Odderon, Donnachie and Landshoff [212] succeeded to describe the TOTEM cross section with less than 1σ deviation in each $d\sigma_{\text{el}}/dt$ point (see Fig. 8 of [212]). Note that in this analysis, they get a larger value of ρ close to 0.14 at 13 TeV.

It was proposed also to search for the Odderon in exclusive C -even meson ($\pi^0, \eta, f_2, \eta_c, \dots$) photoproduction (see e.g. [215, 216]). However the expected cross sections are small (e.g. for η_c) and in each channel there is a large background caused either by Pomeron-Pomeron fusion (such as CEP of the f_2 meson production in pp or pPb collisions) or due to the vector meson radiative decay (such as $\omega \rightarrow \pi^0\gamma$ for the case of pion) [217]. Up to now, no definitive Odderon signal in the C -even meson production has been observed. At the moment there exist only upper limits on the photoproduction cross sections obtained in the measurements at HERA at $\sqrt{s} \simeq 200$ GeV [218–220].

To conclude, let us emphasize that the existence of the C -odd singularity with intercept $\alpha_{\text{odd}}(0) \simeq 1$ is a firm prediction of QCD. At least in the high k_t region there is a well established C -odd three-gluon contribution to the scattering amplitude. However the expected coupling of such an Odderon singularity is numerically very small. Therefore it is quite challenging to observe its manifestation experimentally. Currently it seems to be a bit premature to draw any definite conclusion about an experimental observation of the Odderon signal.

20.7 Asymptotics

The high-energy behaviour of total hadronic cross sections has been one of the oldest problems of strong interactions over many decades, beginning from Heisenberg [221]. The most important bound obtained based on general analytical properties of scattering amplitudes is the FLM bound [47–49]. It states that the growth of the total hadronic cross section with energy does not exceed $\ln^2 s$, see Eq. (20.34).

Recall that we neglected the photon contribution as well as the whole electro-weak sector, and that the parameter in Eq. (20.34) s_0 is an *a priori* unknown scale. However, if we were to assume a reasonable hadronic scale, $s_0 \simeq 1$ GeV², we would find that Eq. (20.34) implies an unrealistically high upper bound in comparison with the cross sections observed at present collider energies. Nevertheless there is a common trend in the literature (see for instance, reviews [222, 223] and references therein) to fit phenomenologically the total cross section with $\ln^2 s$, keeping in mind the saturation of the FLM bound. Such an asymptotic behaviour is assumed also by the COMPETE collaboration [22], which achieved a comprehensive description of all soft pre-LHC data measured at $\sqrt{s} \geq 4$ GeV as well as total pp cross sections from the LHC available in the first half of 2015 (see Section 51 in [24]).

It is interesting that the Froissart-type $\ln^2 s$ asymptotics of the pp total cross section are also supported by numerical results in lattice QCD [224]. Such a behaviour is also observed in the approach [225] based on Colour Glass Condensate saturation.

Finally, it is worth mentioning that the possibility that *asymptotically* the Pomeron intercept becomes smaller than 1, $\alpha_{\mathbb{P}}(0) < 1$, and at very high energies the total cross section starts to decrease with energy, though highly unlikely, is not yet completely rejected. For instance, such a behaviour is expected in a theory with only the triple-Pomeron coupling, $g_{3\mathbb{P}}$, and which neglects the more complicated multi-Pomeron vertices g_m^n , such as the $2 \rightarrow 2$ Pomeron coupling [226, 227].

It was also argued that in the case of an increasing (with energy) cross section the only regime consistent asymptotically with both the s - and the t -channel unitarities is that of a *black disc* whose radius increases as $R = c \cdot \ln s$ [228] (i.e. $R \propto (\ln s)^\gamma$, with $\gamma = 1$ exactly).

20.8 Acknowledgements

It is a pleasure to thank Michael Albrow, Robert Cahn, Robert Ciesielski, Per Grafstrom, Frank Krauss, Paul Newman, Sergey Ostapchenko and Edward Sarkisyan-Grinbaum for discussions, suggestions and comments on this review. Special thanks to Graeme Watt who read the article through and helped to improve the presentation. MT is supported by MEYS of the Czech Republic within project LTT17018. VAK thanks the Institute of Physics of the Czech Academy of Sciences in Prague for hospitality.

References

- [1] M. Tanabashi *et al.* (Particle Data Group), Phys. Rev. **D98**, 3, 030001 (2018).
- [2] J. Campbell, J. Huston and F. Krauss, *The Black Book of Quantum Chromodynamics*, Oxford University Press (2017), ISBN 9780199652747, <https://doi.org/10.1093/oso/9780199652747.003.0004>.
- [3] R. J. Eden *et al.*, *The analytic S-matrix*, Cambridge Univ. Press, Cambridge (1966).
- [4] A. Martin, Lect. Notes Phys. **3**, 1 (1969).
- [5] P. D. B. Collins, *An Introduction to Regge Theory and High-Energy Physics*, Cambridge Monographs on Mathematical Physics, Cambridge Univ. Press, Cambridge, UK (2009), ISBN 9780521110358, URL <http://www-spires.fnal.gov/spires/find/books/www?c1=QC793.3.R4C695>.
- [6] S. Donnachie *et al.*, Camb. Monogr. Part. Phys. Nucl. Phys. Cosmol. **19**, 1 (2002).
- [7] V. N. Gribov, *The theory of complex angular momenta: Gribov lectures on theoretical physics*, Cambridge Monographs on Mathematical Physics, Cambridge University Press (2007), ISBN 9780521037037, 9780521818346, 9780511055041, URL <http://www.cambridge.org/uk/catalogue/catalogue.asp?isbn=0521307848>.
- [8] S. Ostapchenko, in “25th European Cosmic Ray Symposium (ECRS 2016) Turin, Italy, September 04-09, 2016,” (2016), [arXiv:1612.09461].
- [9] T. Sjostrand, Int. J. Mod. Phys. **A3**, 751 (1988).
- [10] B. Andersson, Camb. Monogr. Part. Phys. Nucl. Phys. Cosmol. **7**, 1 (1997).
- [11] W. Kittel and E. A. De Wolf, *Soft multihadron dynamics* (2005), ISBN 9789812562951.
- [12] I. M. Dremin and A. B. Kaidalov, Phys. Usp. **49**, 263 (2006), [Usp. Fiz. Nauk176,275(2006)].
- [13] A. Buckley *et al.*, Phys. Rept. **504**, 145 (2011), [arXiv:1101.2599].
- [14] R. Ciesielski and K. Goulianos, PoS **ICHEP2012**, 301 (2013), [arXiv:1205.1446].
- [15] K. Akiba *et al.* (LHC Forward Physics Working Group), J. Phys. **G43**, 110201 (2016), [arXiv:1611.05079].
- [16] G. D. Alkhalaf, S. L. Belostotsky and A. A. Vorobev, Phys. Rept. **42**, 89 (1978).
- [17] E. L. Feinberg and I. Y. Pomeranchuk, Doklady Akad. Nauk SSSR **93**, 439 (1953); E. L. Feinberg and I. Y. Pomeranchuk, Suppl. Nuovo Cimento **III**, serie X, 652 (1956).
- [18] R. Engel, D. Heck and T. Pierog, Ann. Rev. Nucl. Part. Sci. **61**, 467 (2011).
- [19] M. Gell-Mann, in “High-energy physics. Proceedings, 11th International Conference, ICHEP’62, Geneva, Switzerland, Jul 4-11, 1962,” 533–542 (1962).
- [20] S. Frautschi, M. Gell-Mann and F. Zachariasen, Phys. Rev. **126**, 6, 2204 (1962).

¹⁹We thank Jean-Rene Cudell for clarifying this issue.

- [21] K. G. Boreskov, A. B. Kaidalov and O. V. Kancheli, Phys. Atom. Nucl. **69**, 1765 (2006), [Yad. Fiz.69,1802(2006)].
- [22] J. R. Cudell *et al.* (COMPETE), Phys. Rev. Lett. **89**, 201801 (2002), [hep-ph/0206172].
- [23] C. Bourrely, J. Soffer and T. T. Wu, Eur. Phys. J. **C28**, 97 (2003), [hep-ph/0210264].
- [24] C. Patrignani *et al.* (Particle Data Group), Chin. Phys. **C40**, 10, 100001 (2016).
- [25] A. Donnachie and P. V. Landshoff, Nucl. Phys. **B231**, 189 (1984).
- [26] A. Donnachie and P. V. Landshoff, Phys. Lett. **B296**, 227 (1992), [hep-ph/9209205].
- [27] S. Mandelstam, Nuovo Cim. **30**, 1148 (1963).
- [28] V. N. Gribov, I. Ya. Pomeranchuk and K. A. Ter-Martirosian, Phys. Lett. **9**, 269 (1964).
- [29] V. A. Khoze, A. D. Martin and M. G. Ryskin, Int. J. Mod. Phys. **A30**, 08, 1542004 (2015), [arXiv:1402.2778].
- [30] E. Gotsman, E. Levin and U. Maor, Int. J. Mod. Phys. **A30**, 08, 1542005 (2015), [arXiv:1403.4531].
- [31] S. Ostapchenko, Phys. Rev. **D81**, 114028 (2010), [arXiv:1003.0196].
- [32] V. N. Gribov, Sov. Phys. JETP **26**, 414 (1968), [Zh. Eksp. Teor. Fiz.53,654(1967)].
- [33] U. Amaldi, M. Jacob and G. Matthiae, Ann. Rev. Nucl. Part. Sci. **26**, 385 (1976).
- [34] A. B. Kaidalov, Phys. Rept. **50**, 157 (1979).
- [35] V. Barone and E. Predazzi, *High-Energy Particle Diffraction*, volume v.565 of *Texts and Monographs in Physics*, Springer-Verlag, Berlin Heidelberg (2002), ISBN 3540421076, URL <http://www-spires.fnal.gov/spires/find/books/www?cl=QC794.6.C6B37:::2002>.
- [36] A. B. Kaidalov *et al.*, Acta Phys. Polon. **B34**, 3163 (2003), [hep-ph/0303111].
- [37] L. Frankfurt and M. Strikman, in E. M. Henley and S. D. Ellis, editors, "100 Years of Subatomic Physics," 363–423 (2013), [arXiv:1304.4308].
- [38] V. A. Khoze *et al.*, Eur. Phys. J. **C69**, 85 (2010), [arXiv:1005.4839].
- [39] D. A. Fagundes *et al.*, Phys. Rev. **D88**, 9, 094019 (2013), [arXiv:1306.0452].
- [40] R. Fiore *et al.*, Int. J. Mod. Phys. **A24**, 2551 (2009), [arXiv:0810.2902].
- [41] I. M. Dremin, Phys. Usp. **56**, 3 (2013), [Usp. Fiz. Nauk 183, 3 (2013)], [arXiv:1206.5474].
- [42] L. Frankfurt *et al.*, Phys. Rev. Lett. **101**, 202003 (2008), [arXiv:0808.0182].
- [43] G. Bertsch *et al.*, Phys. Rev. Lett. **47**, 297 (1981).
- [44] B. Z. Kopeliovich, L. I. Lapidus and A. B. Zamolodchikov, JETP Lett. **33**, 595 (1981), [Pisma Zh. Eksp. Teor. Fiz. 33, 612 (1981)].
- [45] M. L. Good and W. D. Walker, Phys. Rev. **120**, 1855 (1960).
- [46] J. Pumplin, Phys. Rev. **D8**, 2899 (1973).
- [47] M. Froissart, Phys. Rev. **123**, 1053 (1961).
- [48] A. Martin, Nuovo Cim. **A42**, 930 (1965).
- [49] L. Lukaszuk and A. Martin, Nuovo Cim. **A52**, 122 (1967).
- [50] A. A. Anselm and V. N. Gribov, Phys. Lett. **40B**, 487 (1972).
- [51] G. Cohen-Tannoudji, V. V. Ilyin and L. L. Jenkovszky, Lett. Nuovo Cim. **5S2**, 957 (1972), [Lett. Nuovo Cim.5,957(1972)].
- [52] V. A. Khoze, A. D. Martin and M. G. Ryskin, Eur. Phys. J. **C18**, 167 (2000), [hep-ph/0007359].
- [53] G. Antchev *et al.* (TOTEM), Nucl. Phys. **B899**, 527 (2015), [arXiv:1503.08111].
- [54] G. Antchev *et al.* (TOTEM), Eur. Phys. J. **C79**, 10, 861 (2019), [arXiv:1812.08283].
- [55] L. Caneschi and A. Pignotti, Phys. Rev. Lett. **22**, 1219 (1969).
- [56] O. V. Kancheli, JETP Lett. **11**, 267 (1970), [Pisma Zh. Eksp. Teor. Fiz. 11, 397 (1970)].
- [57] A. H. Mueller, Phys. Rev. **D4**, 150 (1971).
- [58] D. Amati, A. Stanghellini and S. Fubini, Nuovo Cim. **26**, 896 (1962).
- [59] V. S. Fadin, E. A. Kuraev and L. N. Lipatov, Phys. Lett. **60B**, 50 (1975); E. A. Kuraev, L. N. Lipatov and V. S. Fadin, Sov. Phys. JETP **44**, 443 (1976), [Zh. Eksp. Teor. Fiz.71,840(1976)]; E. A. Kuraev, L. N. Lipatov and V. S. Fadin, Sov. Phys. JETP **45**, 199 (1977), [Zh. Eksp. Teor. Fiz.72,377(1977)]; I. I. Balitsky and L. N. Lipatov, Sov. J. Nucl. Phys. **28**, 822 (1978), [Yad. Fiz.28,1597(1978)].
- [60] B. L. Ioffe, V. S. Fadin and L. N. Lipatov, *Quantum chromodynamics: Perturbative and nonperturbative aspects*, volume 30, Cambridge Univ. Press (2010), ISBN 9781107424753, 9780521631488, 9780511717444, URL <http://www.cambridge.org/de/knowledge/isbn/item2710695>.
- [61] S. Ostapchenko, Phys. Rev. **D83**, 014018 (2011), [arXiv:1010.1869].
- [62] J. L. Cardy, Nucl. Phys. **B75**, 413 (1974).
- [63] A. B. Kaidalov *et al.*, Phys. Lett. **45B**, 493 (1973).
- [64] E. G. S. Luna *et al.*, Eur. Phys. J. **C59**, 1 (2009), [arXiv:0807.4115].
- [65] T. Sjöstrand, Adv. Ser. Direct. High Energy Phys. **29**, 191 (2018), [arXiv:1706.02166].
- [66] K. Werner, F.-M. Liu and T. Pierog, Phys. Rev. **C74**, 044902 (2006), [hep-ph/0506232].
- [67] V. A. Abramovsky, V. N. Gribov and O. V. Kancheli, Yad. Fiz. **18**, 595 (1973), [Sov. J. Nucl. Phys. 18, 308 (1974)].
- [68] G. Alberi and G. Goggi, Phys. Rept. **74**, 1 (1981).
- [69] K. A. Goulianos, Phys. Rept. **101**, 169 (1983).
- [70] D. Bernard *et al.* (UA4), Phys. Lett. **B186**, 227 (1987).
- [71] R. E. Ansorge *et al.* (UA5), Z. Phys. **C33**, 175 (1986).
- [72] N. A. Amos *et al.* (E710), Phys. Lett. **B301**, 313 (1993).
- [73] F. Abe *et al.* (CDF), Phys. Rev. **D50**, 5535 (1994).
- [74] G. Aad *et al.* (ATLAS), Eur. Phys. J. **C72**, 1926 (2012), [arXiv:1201.2808].
- [75] V. Khachatryan *et al.* (CMS), Phys. Rev. **D92**, 1, 012003 (2015), [arXiv:1503.08689].
- [76] B. Abelev *et al.* (ALICE), Eur. Phys. J. **C73**, 6, 2456 (2013), [arXiv:1208.4968].
- [77] G. Aad *et al.* (ATLAS), Phys. Lett. **B754**, 214 (2016), [arXiv:1511.00502].
- [78] G. Aad *et al.* (ATLAS), JHEP **02**, 042 (2020), [arXiv:1911.00453].
- [79] A. M. Sirunyan *et al.* (CMS and TOTEM) (2020), [arXiv:2002.12146].
- [80] V. A. Khoze, A. D. Martin and M. G. Ryskin, Eur. Phys. J. **C73**, 2503 (2013), [arXiv:1306.2149].
- [81] V. A. Khoze, A. D. Martin and M. G. Ryskin, Eur. Phys. J. **C23**, 311 (2002), [hep-ph/0111078].
- [82] M. G. Albrow, T. D. Coughlin and J. R. Forshaw, Prog. Part. Nucl. Phys. **65**, 149 (2010), [arXiv:1006.1289].
- [83] M. Albrow, Int. J. Mod. Phys. **A29**, 1402006 (2014).
- [84] H. G. Fischer, W. Geist and M. Makariev, Int. J. Mod. Phys. **A29**, 28, 1446005 (2014).
- [85] A. Kirk, Int. J. Mod. Phys. **A29**, 28, 1446001 (2014), [arXiv:1408.1196].
- [86] M. A. Reyes *et al.* (E690), Phys. Rev. Lett. **81**, 4079 (1998).

- [87] G. Gutierrez and M. A. Reyes, *Int. J. Mod. Phys. A* **29**, 28, 1446008 (2014), [arXiv:1409.8243].
- [88] Y. L. Dokshitzer, D. Diakonov and S. I. Troian, *Phys. Rept.* **58**, 269 (1980).
- [89] M. Derrick *et al.* (ZEUS), *Phys. Lett.* **B315**, 481 (1993).
- [90] T. Ahmed *et al.* (H1), *Nucl. Phys.* **B429**, 477 (1994).
- [91] P. Newman and M. Wing, *Rev. Mod. Phys.* **86**, 3, 1037 (2014), [arXiv:1308.3368].
- [92] A. Aktas *et al.* (H1), *Eur. Phys. J.* **C48**, 715 (2006), [hep-ex/0606004].
- [93] S. Chekanov *et al.* (ZEUS), *Nucl. Phys.* **B816**, 1 (2009), [arXiv:0812.2003].
- [94] F. D. Aaron *et al.* (H1), *Eur. Phys. J.* **C72**, 2074 (2012), [arXiv:1203.4495].
- [95] F. D. Aaron *et al.* (H1, ZEUS), *Eur. Phys. J.* **C72**, 2175 (2012), [arXiv:1207.4864].
- [96] A. Aktas *et al.* (H1), *JHEP* **10**, 042 (2007), [arXiv:0708.3217].
- [97] A. Aktas *et al.* (H1), *Eur. Phys. J.* **C50**, 1 (2007), [hep-ex/0610076].
- [98] S. Chekanov *et al.* (ZEUS), *Nucl. Phys.* **B672**, 3 (2003), [hep-ex/0307068].
- [99] E. G. de Oliveira, A. D. Martin and M. G. Ryskin, *Phys. Lett.* **B695**, 162 (2011), [arXiv:1010.1366].
- [100] G. Antchev *et al.* (TOTEM), *Eur. Phys. J.* **C79**, 2, 103 (2019), [arXiv:1712.06153].
- [101] C. Augier *et al.* (UA4/2), *Phys. Lett.* **B316**, 448 (1993).
- [102] G. Antchev *et al.* (TOTEM), *Eur. Phys. J.* **C79**, 9, 785 (2019), [arXiv:1812.04732].
- [103] G. Antchev *et al.* (TOTEM), *Eur. Phys. J.* **C80**, 2, 91 (2020), [arXiv:1812.08610].
- [104] G. Antchev *et al.* (TOTEM), *EPL* **101**, 2, 21002 (2013).
- [105] G. Antchev *et al.* (TOTEM), *Phys. Rev. Lett.* **111**, 1, 012001 (2013).
- [106] G. Aad *et al.* (ATLAS), *Nucl. Phys.* **B889**, 486 (2014), [arXiv:1408.5778].
- [107] M. Aaboud *et al.* (ATLAS), *Phys. Lett.* **B761**, 158 (2016), [arXiv:1607.06605].
- [108] M. M. Block and R. N. Cahn, *Rev. Mod. Phys.* **57**, 563 (1985).
- [109] F. Abe *et al.* (CDF), *Phys. Rev.* **D50**, 5550 (1994).
- [110] C. Avila *et al.* (E811), *Phys. Lett.* **B445**, 419 (1999).
- [111] W. Guryn, “Invited talk at the Workshop on Diffraction and Low-x Physics, Reggio Calabria, Italy, August 26th–September 1st, 2018,” ; J. Adam *et al.* (STAR), *Phys. Lett. B* **808**, 135663 (2020), [arXiv:2003.12136].
- [112] K. Nakamura *et al.* (Particle Data Group), *J. Phys.* **G37**, 075021 (2010).
- [113] F. J. Nemes, *PoS DIS2017*, 059 (2018).
- [114] G. Antchev *et al.* (TOTEM), *EPL* **95**, 4, 41001 (2011), [arXiv:1110.1385].
- [115] G. Antchev *et al.* (TOTEM), *Eur. Phys. J.* **C76**, 12, 661 (2016), [arXiv:1610.00603].
- [116] J. Kaspar, “Invited talk at the meeting of the LHC Working Group on Forward Physics and Diffraction, CERN, Switzerland, December 16-17th, 2019,” .
- [117] V. A. Schegelsky and M. G. Ryskin, *Phys. Rev.* **D85**, 094024 (2012), [arXiv:1112.3243].
- [118] A. Bruni, X. Janssen and P. Marage, in “Proceedings, HERA and the LHC Workshop Series on the implications of HERA for LHC physics: 2006-2008,” 427–439 (2008), [arXiv:0812.0539].
- [119] A. Levy, in “Proceedings, 17th International Workshop on Deep-Inelastic Scattering and Related Subjects (DIS 2009): Madrid, Spain, April 26-30, 2009,” 177 (2009), [arXiv:0907.2178].
- [120] J. R. Forshaw, R. Sandapen and G. Shaw, *JHEP* **11**, 025 (2006), [hep-ph/0608161].
- [121] A. Capella *et al.*, *Nucl. Phys.* **B593**, 336 (2001), [hep-ph/0005049].
- [122] V. S. Fadin and L. N. Lipatov, *Phys. Lett.* **B429**, 127 (1998), [hep-ph/9802290].
- [123] M. Ciafaloni and G. Camici, *Phys. Lett.* **B430**, 349 (1998), [hep-ph/9803389].
- [124] F. D. Aaron *et al.* (H1), *JHEP* **05**, 032 (2010), [arXiv:0910.5831].
- [125] C. Adloff *et al.* (H1), *Eur. Phys. J.* **C13**, 371 (2000), [hep-ex/9902019].
- [126] J. Breitweg *et al.* (ZEUS), *Eur. Phys. J.* **C6**, 603 (1999), [hep-ex/9808020].
- [127] S. Chekanov *et al.* (ZEUS), *PMC Phys.* **A1**, 6 (2007), [arXiv:0708.1478].
- [128] M. Ciafaloni, *Nucl. Phys.* **B296**, 49 (1988).
- [129] S. Catani, F. Fiorani and G. Marchesini, *Phys. Lett.* **B234**, 339 (1990).
- [130] S. Catani, F. Fiorani and G. Marchesini, *Nucl. Phys.* **B336**, 18 (1990).
- [131] G. Marchesini, *Nucl. Phys.* **B445**, 49 (1995), [hep-ph/9412327].
- [132] G. P. Salam, *JHEP* **07**, 019 (1998), [hep-ph/9806482].
- [133] M. Ciafaloni and D. Colferai, *Phys. Lett.* **B452**, 372 (1999), [hep-ph/9812366].
- [134] H. Kowalski, L. N. Lipatov and D. A. Ross, *Eur. Phys. J.* **C76**, 1, 23 (2016), [arXiv:1508.05744].
- [135] H. Kowalski *et al.*, *Eur. Phys. J.* **C77**, 11, 777 (2017), [arXiv:1707.01460].
- [136] S. J. Brodsky *et al.*, *JETP Lett.* **70**, 155 (1999), [hep-ph/9901229].
- [137] R. D. Ball *et al.*, *Eur. Phys. J.* **C78**, 4, 321 (2018), [arXiv:1710.05935].
- [138] E. M. Levin and M. G. Ryskin, *Phys. Rept.* **189**, 267 (1990).
- [139] L. V. Gribov, E. M. Levin and M. G. Ryskin, *Phys. Rept.* **100**, 1 (1983).
- [140] E. M. Levin, M. G. Ryskin and A. G. Shuvaev, *Nucl. Phys.* **B387**, 589 (1992).
- [141] A. H. Mueller, *Phys. Rept.* **73**, 237 (1981).
- [142] A. H. Mueller, *Nucl. Phys.* **B415**, 373 (1994).
- [143] A. H. Mueller and B. Patel, *Nucl. Phys.* **B425**, 471 (1994), [hep-ph/9403256].
- [144] N. N. Nikolaev, B. G. Zakharov and V. R. Zoller, *JETP Lett.* **59**, 6 (1994), [hep-ph/9312268].
- [145] V. N. Gribov and L. N. Lipatov, *Sov. J. Nucl. Phys.* **15**, 438 (1972), [*Yad. Fiz.*15,781(1972)]; G. Altarelli and G. Parisi, *Nucl. Phys.* **B126**, 298 (1977); Y. L. Dokshitzer, *Sov. Phys. JETP* **46**, 641 (1977), [*Zh. Eksp. Teor. Fiz.* 73, 1216 (1977)].
- [146] I. Balitsky, *Nucl. Phys.* **B463**, 99 (1996), [hep-ph/9509348].
- [147] I. Balitsky, *Phys. Rev.* **D60**, 014020 (1999), [hep-ph/9812311].
- [148] Y. V. Kovchegov, *Phys. Rev.* **D60**, 034008 (1999), [hep-ph/9901281].
- [149] G. Gustafson, *Phys. Lett.* **B718**, 1054 (2013), [arXiv:1206.1733].
- [150] S. Chatrchyan *et al.* (CMS, TOTEM), *Eur. Phys. J.* **C74**, 10, 3053 (2014), [arXiv:1405.0722].
- [151] Q.-D. Zhou (LHCF, ATLAS), *EPJ Web Conf.* **208**, 05008 (2019).

- [152] O. Adriani *et al.* (LHCf), Phys. Lett. **B780**, 233 (2018), [arXiv:1703.07678].
- [153] M. Aaboud *et al.* (ATLAS), ATLAS-CONF-2017-075.
- [154] C. Albajar *et al.* (UA1), Nucl. Phys. **B335**, 261 (1990).
- [155] G. J. Alner *et al.* (UA5), Z. Phys. **C33**, 1 (1986).
- [156] T. Aaltonen *et al.* (CDF), Phys. Rev. **D79**, 112005 (2009), [Erratum: Phys. Rev. D82,119903(2010)], [arXiv:0904.1098].
- [157] F. Abe *et al.* (CDF), Phys. Rev. **D41**, 2330 (1990), [119(1989)].
- [158] K. Aamodt *et al.* (ALICE), Eur. Phys. J. **C68**, 89 (2010), [arXiv:1004.3034].
- [159] V. Khachatryan *et al.* (CMS), Phys. Rev. Lett. **105**, 022002 (2010), [arXiv:1005.3299].
- [160] B. B. Abelev *et al.* (ALICE), Eur. Phys. J. **C73**, 12, 2662 (2013), [arXiv:1307.1093].
- [161] A. M. Sirunyan *et al.* (CMS), Phys. Rev. **D96**, 11, 112003 (2017), [arXiv:1706.10194].
- [162] M. G. Ryskin, A. D. Martin and V. A. Khoze, Eur. Phys. J. **C71**, 1617 (2011), [arXiv:1102.2844].
- [163] X.-N. Wang, Phys. Rept. **280**, 287 (1997), [hep-ph/9605214].
- [164] S. Ostapchenko and M. Bleicher, Universe **5**, 5, 106 (2019).
- [165] F. M. Liu *et al.*, J. Phys. **G28**, 2597 (2002), [hep-ph/0109104].
- [166] E. Gotsman, E. Levin and U. Maor, Acta Phys. Polon. Supp. **8**, 777 (2015).
- [167] Y. V. Kovchegov and E. Levin, Camb. Monogr. Part. Phys. Nucl. Phys. Cosmol. **33**, 1 (2012).
- [168] E. A. De Wolf, I. M. Dremin and W. Kittel, Phys. Rept. **270**, 1 (1996), [hep-ph/9508325].
- [169] J. Adam *et al.* (ALICE), Eur. Phys. J. **C77**, 8, 569 (2017), [arXiv:1612.08975].
- [170] V. Khachatryan *et al.* (CMS), JHEP **09**, 091 (2010), [arXiv:1009.4122].
- [171] K. Eggert *et al.*, Nucl. Phys. **B86**, 201 (1975).
- [172] B. Alver *et al.* (PHOBOS), Phys. Rev. **C75**, 054913 (2007), [arXiv:0704.0966].
- [173] E. M. Levin and M. G. Ryskin, Sov. J. Nucl. Phys. **20**, 280 (1975), [Yad. Fiz.20,519(1974)].
- [174] A. Capella and A. Krzywicki, Phys. Rev. **D18**, 4120 (1978).
- [175] M. Aaboud *et al.* (ATLAS), Eur. Phys. J. **C77**, 6, 428 (2017), [arXiv:1705.04176].
- [176] V. Khachatryan *et al.* (CMS), Phys. Lett. **B765**, 193 (2017), [arXiv:1606.06198].
- [177] S. Gieseke, "Invited talk at the Workshop on Multiple Partonic Interactions at the LHC, Prague, Czech Republic, November 18th–26th, 2019," .
- [178] S. Kundu, B. Mohanty and D. Mallick (2019), [arXiv:1912.05176].
- [179] M. Diehl, D. Ostermeier and A. Schafer, JHEP **03**, 089 (2012), [Erratum: JHEP03,001(2016)], [arXiv:1111.0910].
- [180] T. Sjostrand and P. Z. Skands, JHEP **03**, 053 (2004), [hep-ph/0402078].
- [181] M. Aaboud *et al.* (ATLAS), Phys. Lett. **B790**, 595 (2019), [Phys. Lett.790,595(2019)], [arXiv:1811.11094].
- [182] M. G. Ryskin and A. M. Snigirev, Phys. Rev. **D83**, 114047 (2011), [arXiv:1103.3495].
- [183] B. Blok *et al.*, Eur. Phys. J. **C74**, 2926 (2014), [arXiv:1306.3763].
- [184] M. Aaboud *et al.* (ATLAS), JHEP **03**, 157 (2017), [arXiv:1701.05390].
- [185] R. Snellings, New J. Phys. **13**, 055008 (2011), [arXiv:1102.3010].
- [186] M. Aaboud *et al.* (ATLAS), Phys. Rev. **C97**, 2, 024904 (2018), [arXiv:1708.03559].
- [187] N. Borghini, P. M. Dinh and J.-Y. Ollitrault, Phys. Rev. **C63**, 054906 (2001), [arXiv:nucl-th/0007063].
- [188] A. Bilandzic, R. Snellings and S. Voloshin, Phys. Rev. **C83**, 044913 (2011), [arXiv:1010.0233].
- [189] W. Li, Mod. Phys. Lett. **A27**, 1230018 (2012), [arXiv:1206.0148].
- [190] B. Schenke, J. Phys. **G38**, 124009 (2011), [arXiv:1106.6012].
- [191] K. G. Boreskov, A. B. Kaidalov and O. V. Kancheli, Eur. Phys. J. **C58**, 445 (2008), [arXiv:0809.0625].
- [192] K. G. Boreskov, A. B. Kaidalov and O. V. Kancheli, Phys. Atom. Nucl. **72**, 361 (2009), [Yad. Fiz.72,390(2009)].
- [193] C. Bierlich and J. R. Christiansen, Phys. Rev. **D92**, 9, 094010 (2015), [arXiv:1507.02091].
- [194] Z.-W. Lin *et al.*, Phys. Rev. **C72**, 064901 (2005), [arXiv:nucl-th/0411110].
- [195] V. Khachatryan *et al.* (CMS), CMS-PAS-FSQ-16-008.
- [196] E. Nagy *et al.*, Nucl. Phys. **B150**, 221 (1979).
- [197] A. Breakstone *et al.*, Phys. Rev. Lett. **54**, 2180 (1985).
- [198] A. Breakstone *et al.* (AMES-BOLOGNA-CERN-DORTMUND-HEIDELBERG-WARSAW), Nucl. Phys. **B248**, 253 (1984).
- [199] V. M. Abazov *et al.* (D0), Phys. Rev. **D86**, 012009 (2012), [arXiv:1206.0687].
- [200] J. Bartels, Nucl. Phys. **B175**, 365 (1980).
- [201] J. Kwiecinski and M. Praszalowicz, Phys. Lett. **94B**, 413 (1980).
- [202] M. A. Braun (1998), [hep-ph/9805394].
- [203] J. Bartels, L. N. Lipatov and G. P. Vacca, Phys. Lett. **B477**, 178 (2000), [hep-ph/9912423].
- [204] C. Ewerz (2003), [hep-ph/0306137].
- [205] M. Fukugita and J. Kwiecinski, Phys. Lett. **83B**, 119 (1979), [625(1979)].
- [206] M. G. Ryskin, Sov. J. Nucl. Phys. **46**, 337 (1987), [Yad. Fiz.46,611(1987)].
- [207] J. Bartels, C. Contreras and G. P. Vacca, JHEP **04**, 183 (2020), [arXiv:1910.04588].
- [208] M. Bozzo *et al.* (UA4), Phys. Lett. **155B**, 197 (1985).
- [209] D. Bernard *et al.* (UA4), Phys. Lett. **B171**, 142 (1986).
- [210] E. Martynov and B. Nicolescu, Eur. Phys. J. **C79**, 6, 461 (2019), [arXiv:1808.08580].
- [211] A. Donnachie and P. V. Landshoff, Phys. Lett. **123B**, 345 (1983).
- [212] A. Donnachie and P. V. Landshoff, Phys. Lett. **B798**, 135008 (2019), [arXiv:1904.11218].
- [213] J. Finkelstein *et al.*, Phys. Lett. **B232**, 257 (1989).
- [214] V. A. Khoze, A. D. Martin and M. G. Ryskin, Phys. Lett. **B780**, 352 (2018), [arXiv:1801.07065].
- [215] W. Kilian and O. Nachtmann, Eur. Phys. J. **C5**, 317 (1998), [hep-ph/9712371].
- [216] J. Bartels *et al.*, Eur. Phys. J. **C20**, 323 (2001), [hep-ph/0102221].
- [217] L. A. Harland-Lang *et al.*, Phys. Rev. **D99**, 3, 034011 (2019), [arXiv:1811.12705].
- [218] J. Olsson (H1), in "New trends in high-energy physics: Experiment, phenomenology, theory. Proceedings, International Conference, Yalta, Crimea, Ukraine, September 22-29, 2001," 79–87 (2001), [hep-ex/0112012].
- [219] C. Adloff *et al.* (H1), Phys. Lett. **B544**, 35 (2002), [hep-ex/0206073].
- [220] T. Berndt (H1), Acta Phys. Polon. **B33**, 3499 (2002), [182(2002)].

- [221] W. Heisenberg, Z. Phys. **133**, 65 (1952).
- [222] G. Pancheri and Y. N. Srivastava, Eur. Phys. J. **C77**, 3, 150 (2017), [arXiv:1610.10038].
- [223] M. M. Block, Phys. Rept. **436**, 71 (2006), [hep-ph/0606215].
- [224] M. Giordano, E. Meggiolaro and N. Moretti, JHEP **09**, 031 (2012), [arXiv:1203.0961].
- [225] E. Ferreiro *et al.*, Nucl. Phys. **A710**, 373 (2002), [hep-ph/0206241].
- [226] P. Grassberger and K. Sundermeyer, Phys. Lett. **77B**, 220 (1978).
- [227] K. G. Boreskov, in M. Olshanetsky and A. Vainshtein, editors, “Multiple facets of quantization and supersymmetry,” 322–351 (2001), [hep-ph/0112325].
- [228] V. A. Khoze, A. D. Martin and M. G. Ryskin, Phys. Lett. **B787**, 167 (2018), [arXiv:1809.10406].

Astrophysics and Cosmology

21. Experimental tests of gravitational theory (rev.)	417
22. Big-Bang cosmology (rev.)	430
23. Inflation (rev.)	443
24. Big-Bang nucleosynthesis (rev.)	459
25. Cosmological parameters (rev.)	467
26. Neutrinos in cosmology (rev.)	476
27. Dark matter (rev.)	483
28. Dark energy (rev.)	499
29. Cosmic microwave background (rev.)	509
30. Cosmic rays (rev.)	520

21. Experimental Tests of Gravitational Theory

Revised August 2021 by T. Damour (IHES, Bures-sur-Yvette).

21.1 General Relativity

Einstein's theory of General Relativity (GR), the current “standard” theory of gravitation, describes gravity as a universal deformation of the Minkowski metric:

$$g_{\mu\nu}(x^\lambda) = \eta_{\mu\nu} + h_{\mu\nu}(x^\lambda), \text{ where } \eta_{\mu\nu} = \text{diag}(-1, +1, +1, +1). \quad (21.1)$$

GR is classically defined by two postulates, embodied in the total action defining the theory:

$$S_{\text{tot}}[g_{\mu\nu}, \psi, A_\mu, H] = c^{-1} \int d^4x (\mathcal{L}_{\text{Ein}} + \mathcal{L}_{\text{SM}}). \quad (21.2)$$

The first postulate states that the Lagrangian density describing the propagation and self-interaction of the gravitational field is

$$\mathcal{L}_{\text{Ein}}[g_{\alpha\beta}] = \frac{c^4}{16\pi G} \sqrt{g} g^{\mu\nu} R_{\mu\nu}(g_{\alpha\beta}), \quad (21.3)$$

where G denotes Newton's constant, $g = -\det(g_{\mu\nu})$, $g^{\mu\nu}$ is the matrix inverse of $g_{\mu\nu}$, and where the Ricci tensor $R_{\mu\nu} \equiv R^\alpha{}_{\mu\alpha\nu}$ is the only independent trace of the curvature tensor

$$R^\alpha{}_{\mu\beta\nu} = \partial_\beta \Gamma_{\mu\nu}^\alpha - \partial_\nu \Gamma_{\mu\beta}^\alpha + \Gamma_{\sigma\beta}^\alpha \Gamma_{\mu\nu}^\sigma - \Gamma_{\sigma\nu}^\alpha \Gamma_{\mu\beta}^\sigma, \quad (21.4)$$

$$\Gamma_{\mu\nu}^\lambda = \frac{1}{2} g^{\lambda\sigma} (\partial_\mu g_{\nu\sigma} + \partial_\nu g_{\mu\sigma} - \partial_\sigma g_{\mu\nu}). \quad (21.5)$$

The second postulate states that $g_{\mu\nu}$ (and its associated connection) couples universally, and minimally, to all the bosonic (respectively fermionic) fields of the Standard Model by replacing everywhere the Minkowski metric $\eta_{\mu\nu}$ (respectively the flat Minkowski connection). Schematically (suppressing matrix indices and labels for the various gauge fields and fermions and for the Higgs doublet),

$$\begin{aligned} \mathcal{L}_{\text{SM}}[\psi, A_\mu, H, g_{\mu\nu}] = & \\ & -\frac{1}{4} \sum \sqrt{g} g^{\mu\alpha} g^{\nu\beta} F_{\mu\nu}^a F_{\alpha\beta}^a - \sum \sqrt{g} \bar{\psi} \gamma^\mu (D_\mu + \frac{1}{4} \omega_{ij\mu} \gamma^{ij}) \psi \\ & - \frac{1}{2} \sqrt{g} g^{\mu\nu} \overline{D_\mu H} D_\nu H - \sqrt{g} V(H) - \sum \lambda \sqrt{g} \bar{\psi} H \psi. \end{aligned} \quad (21.6)$$

Here $F_{\mu\nu}^a = \partial_\mu A_\nu^a - \partial_\nu A_\mu^a + g_A f_{bc}^a A_\mu^b A_\nu^c$ and the (representation-dependent) gauge-field covariant derivative $D_\mu = \partial_\mu + g_A A_\mu^a T_a^{\text{rep}}$ are defined as in Special Relativity, while the derivative of spin- $\frac{1}{2}$ fermions also includes a coupling to the gravitational “spin-connection” $\omega_{ij\mu} = -\omega_{ji\mu}$, via its contraction with $\gamma^{ij} = \frac{1}{2}(\gamma^i \gamma^j - \gamma^j \gamma^i)$, where $i, j = 0, 1, 2, 3$ and $\gamma^i = e^\mu{}_\nu \gamma^\nu$ are usual (numerical) Dirac matrices satisfying $\gamma^i \gamma^j + \gamma^j \gamma^i = 2\eta^{ij}$. The connection components $\omega_{ij\mu}$ are defined in terms of the local orthonormal frame (vierbein) $e^i{}_\mu$ (such that $g_{\mu\nu} = \eta_{ij} e^i{}_\mu e^j{}_\nu$) used to describe the components of the various fermions ψ , and of its inverse $e_i{}^\mu$ (such that $e_i{}^\mu e^j{}_\mu = \delta_i^j$), by $\omega_{ij\mu} = \frac{1}{2} (C_{i[jk]} + C_{j[ki]} - C_{k[ij]}) e_\mu^k$ where $C_{i[jk]} = \eta_{is} C^s{}_{[jk]}$, with $C^i{}_{[jk]} \equiv (\partial_\mu e^i{}_\nu - \partial_\nu e^i{}_\mu) e_j{}^\mu e_k{}^\nu$. From the total action follow Einstein's field equations,

$$R_{\mu\nu} - \frac{1}{2} R g_{\mu\nu} = \frac{8\pi G}{c^4} T_{\mu\nu}. \quad (21.7)$$

Here $R = g^{\mu\nu} R_{\mu\nu}$ is the scalar curvature, and $T_{\mu\nu} \equiv g_{\mu\alpha} g_{\nu\beta} T^{\alpha\beta}$ where $T^{\mu\nu} = (2/\sqrt{g}) \delta \mathcal{L}_{\text{SM}} / \delta g_{\mu\nu}$ is the (symmetric) energy-momentum tensor of the Standard Model matter. The theory is invariant under arbitrary coordinate transformations: $x^\mu = f^\mu(x^\nu)$ (as well as under arbitrary local $\text{SO}(3,1)$ rotations of the vierbein, $e^i{}_\mu = \Lambda^i{}_j(x) e^j{}_\mu$). To solve the field equations Eq. (21.7), one needs to fix the coordinate gauge freedom, e.g., the “harmonic gauge” (which is the analogue of the Lorenz gauge, $\partial_\mu A^\mu = 0$, in electromagnetism) corresponds to imposing the condition $\partial_\nu (\sqrt{g} g^{\mu\nu}) = 0$.

In this *Review*, we only consider the classical limit of gravitation (i.e. classical matter and classical gravity). Quantum

gravitational effects are expected (when considered at low energy) to correct the classical action Eq. (21.2) by additional terms involving quadratic and higher powers of the curvature tensor. This suggests that the validity of classical gravity extends (at most) down to length scales of order the Planck length $L_P = \sqrt{\hbar G/c^3} \simeq 1.62 \times 10^{-33}$ cm, i.e., up to energy scales of order the Planck energy $E_P = \sqrt{\hbar c^5/G} \simeq 1.22 \times 10^{19}$ GeV. Considering quantum matter in a classical gravitational background also poses interesting challenges, notably the possibility that the zero-point fluctuations of the matter fields generate a nonvanishing vacuum energy density ρ_{vac} , corresponding to a term $-\sqrt{g} \rho_{\text{vac}}$ in \mathcal{L}_{SM} [1]. This is equivalent to adding a “cosmological constant” term $+\Lambda g_{\mu\nu}$ on the left-hand side of Einstein's equations, Eq. (21.7), with $\Lambda = 8\pi G \rho_{\text{vac}}/c^4$. Recent cosmological observations (see the following *Reviews*) suggest a positive value of Λ corresponding to $\rho_{\text{vac}} \approx (2.3 \times 10^{-3} \text{eV})^4$. Such a small value has a negligible effect on the non-cosmological tests discussed below.

21.2 Key features and predictions of GR

The definition of GR recalled above makes predictions both about the coupling of gravity to matter, and about the structure of the gravitational field beyond its previously known Newtonian aspects.

21.2.1 Equivalence Principle

First, the universal nature of the coupling between $g_{\mu\nu}$ and the Standard Model matter postulated in Eq. (21.6) entails many observable consequences that go under the generic name of “Equivalence Principle”.

A first aspect of the Equivalence Principle is that the outcome of a local non-gravitational experiment, referred to local standards, should not depend on where, when, and in which locally inertial frame, the experiment is performed. This means, for instance, that local experiments should neither feel the cosmological evolution of the Universe (constancy of the “constants”), nor exhibit preferred directions in spacetime (isotropy of space, local Lorentz invariance).

A second aspect of the Equivalence Principle is that the kinetic terms, $g^{\mu\nu} \partial_\mu \phi \partial_\nu \phi$ or $\bar{\psi} \gamma^i e_i{}^\mu \partial_\mu \psi$, of all the fields of Nature (including the gravitational field itself) are universally coupled to the same curved spacetime metric $g_{\mu\nu}(x) = \eta_{ij} e^i{}_\mu e^j{}_\nu$. This implies in particular that all massless fields should propagate with the same speed.

A third aspect of the Equivalence Principle is that two (electrically neutral) test bodies dropped at the same location and with the same velocity in an external gravitational field should fall in the same way, independently of their masses and compositions (“universality of free fall” or “Weak Equivalence Principle”). In addition, the study (using the nonlinear structure of GR) of the motion, in an external gravitational field, of bodies having a non-negligible, or even strong, self-gravity (such as planets, neutron stars, or black holes) has shown that the latter property of free-fall universality holds equally well for self-gravitating bodies (“Strong Equivalence Principle”).

A last aspect of the Equivalence Principle concerns various universality features of the gravitational redshift of clock rates. GR predicts that, when intercomparing them by means of electromagnetic signals, two (non gravity-based) clocks located along two different spacetime worldlines should exhibit a universal difference in clock rate that depends on their worldlines, but that is independent of their nature and constitution. For instance, two clocks located at two different positions in a static external Newtonian potential $U(\mathbf{x}) = \sum Gm/r$ should exhibit, when intercompared by electromagnetic signals, the difference in clock rate, $\tau_1/\tau_2 = \nu_2/\nu_1 = 1 + [U(\mathbf{x}_1) - U(\mathbf{x}_2)]/c^2 + O(1/c^4)$, (“universal gravitational redshift of clock rates”). Similarly, the comparison of atomic-transition frequencies when observing on Earth a transition that took place on a far-away galaxy should involve (at lowest order in cosmological perturbations) the universal cosmological redshift factor $1+z = a(t_{\text{reception}})/a(t_{\text{emission}})$ between the Friedmann scale factors $a(t)$ (see below).

21.2.2 Quasi-stationary, weak-field (post-Newtonian) gravity

When applied to quasi-stationary, weak-field gravitational fields, Einstein equations, Eq. (21.7), entail a spacetime structure which predicts deviations from Newtonian gravity of the first post-Newtonian (1PN) order, *i.e.*, fractionally smaller than Newtonian effects by a factor $O(v^2/c^2) \sim O(GM/(c^2r))$. The 1PN-accurate solution of Eq. (21.7) reads (in harmonic gauge)

$$\begin{aligned} g_{00} &= -1 + \frac{2}{c^2}V - \frac{2}{c^4}V^2 + O\left(\frac{1}{c^6}\right), \\ g_{0i} &= -\frac{4}{c^3}V_i + O\left(\frac{1}{c^5}\right), \\ g_{ij} &= \delta_{ij}\left[1 + \frac{2}{c^2}V\right] + O\left(\frac{1}{c^4}\right), \end{aligned} \quad (21.8)$$

where $x^0 = ct$, $i, j = 1, 2, 3$, and where the scalar, V , and vector, V_i , (retarded) potentials are defined in terms of the sources $\sigma = \frac{T^{00} + T^{ii}}{c^2}$, $\sigma_i = \frac{T^{0i}}{c}$ by

$$V = \square_{\text{ret}}^{-1}[-4\pi G\sigma]; \quad V_i = \square_{\text{ret}}^{-1}[-4\pi G\sigma_i]. \quad (21.9)$$

In GR the gravitational interaction of N moving point masses (labeled by $A = 1, \dots, N$) is described by a reduced (classical) action that admits a diagrammatic expansion:

$$S_{\text{reduced}} = S^{\text{free}} + S^{\text{tree-level}} + S^{\text{one-loop}} + \dots \quad (21.10)$$

where the free (special-relativistic) action reads

$$\begin{aligned} S^{\text{free}} &= -\sum_A \int m_A c \sqrt{-\eta_{\mu\nu} dx_A^\mu dx_A^\nu} \\ &= -\sum_A \int dt m_A c^2 \sqrt{1 - \mathbf{v}_A^2/c^2}, \end{aligned} \quad (21.11)$$

while the tree-level (one-graviton-exchange) interaction term reads

$$S^{\text{tree-level}} = -\frac{8\pi G}{c^4} \int d^4x T^{\mu\nu} \square^{-1}(T_{\mu\nu} - \frac{1}{2}T\eta_{\mu\nu}) = \int dt L^{(2)}. \quad (21.12)$$

Corresponding to the 1PN-accurate metric of Eq. (21.8), the 1PN-accurate expansion of the latter tree-level, two-body interaction Lagrangian $L^{(2)}$ reads (with $r_{AB} \equiv |\mathbf{x}_A - \mathbf{x}_B|$, $\mathbf{n}_{AB} \equiv (\mathbf{x}_A - \mathbf{x}_B)/r_{AB}$)

$$\begin{aligned} L^{(2)} &= \frac{1}{2} \sum_{A \neq B} \frac{G m_A m_B}{r_{AB}} \left[1 + \frac{3}{2c^2}(v_A^2 + v_B^2) - \frac{7}{2c^2}(\mathbf{v}_A \cdot \mathbf{v}_B) \right. \\ &\quad \left. - \frac{1}{2c^2}(\mathbf{n}_{AB} \cdot \mathbf{v}_A)(\mathbf{n}_{AB} \cdot \mathbf{v}_B) + O\left(\frac{1}{c^4}\right) \right] \end{aligned} \quad (21.13)$$

The two-body interactions, Eq. (21.13), exhibit v^2/c^2 corrections to Newton's $1/r$ potential induced by spin-2 exchange ("gravitomagnetism"). Consistency at the 1PN level, $v^2/c^2 \sim Gm/rc^2$, requires that one also considers the three-body interactions contained in the one-loop contribution $S^{\text{one-loop}}$, corresponding to terms induced by some of the three-graviton vertices and other non-linearities (terms $O(h^2)$ and $O(hT)$ in Eq. (21.15) below), *i.e.*, to the $O(V^2)$ term in Eq. (21.8):

$$L^{(3)} = -\frac{1}{2} \sum_{B \neq A \neq C} \frac{G^2 m_A m_B m_C}{r_{AB} r_{AC} c^2} + O\left(\frac{1}{c^4}\right). \quad (21.14)$$

21.2.3 Gravitational Waves in GR

The linearized approximation to Einstein's field equations, Eq. (21.7), in harmonic gauge $\partial^\nu(h_{\mu\nu} - \frac{1}{2}h\eta_{\mu\nu}) = 0$ (with $h \equiv \eta^{\mu\nu}h_{\mu\nu}$), reads

$$\square h_{\mu\nu} = -\frac{16\pi G}{c^4}(T_{\mu\nu} - \frac{1}{2}T\eta_{\mu\nu}) + O(h^2) + O(hT). \quad (21.15)$$

Outside of any source (*i.e.*, when $T_{\mu\nu} = 0$), this yields $\square h_{\mu\nu} = 0$, with $\partial^\nu(h_{\mu\nu} - \frac{1}{2}h\eta_{\mu\nu}) = 0$. The generic linearized solution (modulo the diffeomorphism freedom) of the latter vacuum Einstein equations can be written as (with $k^2 = k \cdot k = \eta_{\mu\nu}k^\mu k^\nu$, $k \cdot x = k_\mu x^\mu$)

$$h_{\mu\nu}(x) = \int d^4k \delta(k^2) \epsilon_{\mu\nu}(k) e^{ik \cdot x}, \quad (21.16)$$

where the polarization tensor $\epsilon_{\mu\nu}(k)$ must be transverse ($\epsilon_{\mu\nu}k^\nu = 0$) and traceless ($\eta^{\mu\nu}\epsilon_{\mu\nu} = 0$). In addition, $\epsilon_{\mu\nu}(k)$ can be freely submitted to the gauge freedom $\epsilon'_{\mu\nu} = \epsilon_{\mu\nu} + \xi_\mu k_\nu + \xi_\nu k_\mu$. This implies that gravitational waves (GW) propagate with the speed of light, and (like electromagnetic waves) have only two independent polarizations. In a frame where, say, $k^\mu = (ck, 0, 0, k)$, the two independent linear polarization tensors can be taken to have components only in the transverse 1-2 plane, of the following form: $\epsilon_{11}^+ = -\epsilon_{22}^+ = \epsilon^+$, with $\epsilon_{12}^+ = \epsilon_{21}^+ = 0$; or $\epsilon_{11}^\times = +\epsilon_{22}^\times = \epsilon^\times$, with $\epsilon_{12}^\times = \epsilon_{21}^\times = 0$. Under a little-group rotation of angle θ in the 1-2 plane, the two circular polarization amplitudes $\epsilon(\pm) = \epsilon^+ \mp i\epsilon^\times$ vary as $\epsilon'(\pm) = e^{\pm 2i\theta} \epsilon(\pm)$, thereby characterizing the helicity-2 nature of GWs.

When solving the inhomogeneous equation Eq. (21.15), taking into account the nonlinear contributions $O(h^2) + O(hT)$, one finds that, to lowest order, the GW amplitude emitted at large distances by a matter distribution is given by the following "quadrupole formula"

$$h_{ij}^{\text{TT}}(T, \mathbf{X}) \approx \frac{2G}{c^4} P_{ijab}^{\text{TT}}(\mathbf{N}) \frac{\dot{Q}_{ab}(T - R/c)}{R}, \quad (21.17)$$

where $Q_{ij}(t) = \int d^3x \sigma(t, \mathbf{x})(x^i x^j - \frac{1}{3}\delta_{ij} \mathbf{x}^2)$ ($a, b, i, j = 1, 2, 3$) is the quadrupole moment of the source, $R = |\mathbf{X}|$ the distance to the source, $\mathbf{N} = \mathbf{X}/R$ the unit direction from the source to the observer, and $P_{ijab}^{\text{TT}}(\mathbf{N}) = (\delta_{ia} - N_i N_a)(\delta_{jb} - N_j N_b) - \frac{1}{2}(\delta_{ij} - N_i N_j)(\delta_{ab} - N_a N_b)$ the transverse-traceless projector onto the 2-plane orthogonal to \mathbf{N} .

21.2.4 Strong gravitational fields: neutron stars and black holes

The nonlinear structure of Einstein's equations implies many predictions for strong gravitational fields that distinguish GR from Newtonian gravity. For instance, in Newtonian gravity, there is no upper limit to the dimensionless gravitational potential U/c^2 , with U satisfying Poisson's equation $\Delta U = -4\pi G\rho$, where ρ denotes the Newtonian mass density. By contrast, in GR, the dimensionless surface gravitational potential $GM/(c^2R)$ of a spherically symmetric (perfect fluid) body cannot exceed $\frac{4}{9}[2]$.

Given an equation of state $p = f(\rho)$ modeling the interior of a (cold) spherically symmetric body (say a non-rotating neutron star), Einstein equations, Eq. (21.7), with $T^{\mu\nu} = (\rho + p)u^\mu u^\nu + pg^{\mu\nu}$, and

$$g_{\mu\nu} dx^\mu dx^\nu = -e^{2\Phi(r)} c^2 dt^2 + \frac{dr^2}{1 - \frac{2GM(r)}{c^2 r}} + r^2 (d\theta^2 + \sin^2 \theta d\phi^2), \quad (21.18)$$

yield the following Tolman-Oppenheimer-Volkoff radial equations:

$$p'(r) = -\frac{G(\rho + p/c^2)(M(r) + 4\pi r^3 p/c^2)}{r^2(1 - 2GM(r)/(c^2 r))}; \quad (21.19)$$

$$M'(r) = 4\pi r^2 \rho; \quad (21.20)$$

$$\Phi'(r) = \frac{G(M(r) + 4\pi r^3 p/c^2)}{r^2(1 - 2GM(r)/(c^2 r))}. \quad (21.21)$$

In the exterior of the star ($r \geq R$), the metric takes the Schwarzschild form

$$\begin{aligned} g_{\mu\nu} dx^\mu dx^\nu &= -\left(1 - \frac{2GM}{c^2 r}\right) c^2 dt^2 + \frac{dr^2}{1 - \frac{2GM}{c^2 r}} \\ &\quad + r^2 (d\theta^2 + \sin^2 \theta d\phi^2), \end{aligned} \quad (21.22)$$

where $M \equiv M(R)$ is the total gravitational mass of the star. GR predicts, for any given $p = f(\rho)$, several (in principle) observable

features of neutron stars, such as: (i) the maximum mass of a neutron star; (ii) the relation between the radius R and the total mass M ; (iii) the dimensionless surface gravitational potential $GM/(c^2R)$ (linked to the surface redshift $\sqrt{-g_{00}} = \sqrt{1 - \frac{2GM}{c^2R}}$ measured by an observer at infinity); (iv) the moment of inertia; and (v) the Love number (tidal polarizability). The current uncertainty on the equation of state of a neutron star yields the GR-predicted approximate range for the maximum mass of non-rotating neutron stars $1.5 M_\odot \lesssim M_{\max} \lesssim 2.5 M_\odot$, and the absolute upper bound $M_{\max} < 3 M_\odot$ [3]. The surface gravitational potential of a typical neutron star is $GM/c^2 R_{\text{NS}} \simeq 0.17$, which is a factor $\sim 10^8$ higher than the surface potential of the Earth, and a mere factor 3 below the black hole limit $GM/c^2 R_{\text{BH}} = \frac{1}{2}$ to be discussed next.

The existence of a maximum mass for a neutron star led Oppenheimer and Snyder [4] to predict that the end point of stellar evolution for sufficiently heavy stars, after exhaustion of all thermonuclear sources of energy, will be what are now called “black holes.” The latter are solutions of Einstein’s equations whose past structure involves a gravitationally collapsing star, but whose presently observable structure is essentially described (for non-rotating black holes) by the vacuum Schwarzschild solution Eq. (21.22). It took many years for theoretical (and mathematical) physicists to understand that the apparent singularity of the Schwarzschild solution at $r = \frac{2GM}{c^2}$ was a coordinate singularity and that the Schwarzschild spacetime was regular at the “black hole horizon”, $R_{\text{BH}} \equiv \frac{2GM}{c^2}$. The rotating analog of the Schwarzschild spacetime is the Kerr black hole [5].

Black holes are outstanding consequences of GR which enjoy many remarkable properties, notably: (i) presence of a one-way surface (the horizon) for all waves and particles; (ii) absence of “hair” (*i.e.*, barring a possible electric charge, their structure is fully described by only two parameters, total mass, M , and total angular momentum, $J \leq GM^2/c$); (iii) existence of a spectrum of damped quasi-normal vibrational modes; and (iv) a behavior under external perturbations similar to ordinary physical objects satisfying the laws of (dissipative) thermodynamics. Moreover, though no classical waves or particles can get out of the horizon, black holes are predicted to slowly evaporate via quantum particle creation.

21.2.5 Cosmology

To complete our short tour of the main predictions of GR, let us mention that GR offers the current standard framework for describing the large-scale structure of the Cosmos, from the nearly homogeneous Big Bang (and its plausible inflationary beginning) to the current inhomogeneous Universe undergoing an accelerated expansion. The spacetime structure on large (temporal and spatial) scales is well described by a solution of Einstein’s equations of the form

$$ds^2 = -(1 + 2\Phi(t, \mathbf{x}))c^2 dt^2 + 2W_i(t, \mathbf{x})dt dx^i + a^2(t)((1 - 2\Psi(t, \mathbf{x}))\delta_{ij} + h_{ij}(t, \mathbf{x}))dx^i dx^j, \quad (21.23)$$

where, after a suitable gauge-fixing [6], $W_i(t, \mathbf{x})$ is transverse, while $h_{ij}(t, \mathbf{x})$ is transverse and traceless. The source $T^{\mu\nu}$ must involve a certain number of postulated ingredients: an inflaton field; the matter of the Standard Model; a dark matter component; and a cosmological constant contribution $T_\Lambda^{\mu\nu} = -\rho_{\text{vac}}g^{\mu\nu}$, with $\rho_{\text{vac}} \equiv c^4\Lambda/(8\pi G)$. The scale factor $a(t)$ of the Friedmann background metric $ds_0^2 = -c^2 dt^2 + a^2(t)\delta_{ij}dx^i dx^j$ satisfies the GR-predicted Friedmann equations (with vanishing spatial curvature $k = 0$),

$$H^2 \equiv \left(\frac{\dot{a}}{a}\right)^2 = \frac{8\pi G}{3}\rho_{\text{tot}}, \quad (21.24)$$

$$\frac{\ddot{a}}{a} = -\frac{4\pi G}{3}\left(\rho_{\text{tot}} + \frac{3}{c^2}p_{\text{tot}}\right), \quad (21.25)$$

while the scalar $(\Phi(t, \mathbf{x}), \Psi(t, \mathbf{x}))$, vector $(W_i(t, \mathbf{x}))$, and tensor $(h_{ij}(t, \mathbf{x}))$ inhomogeneous perturbations satisfy some GR-predicted propagation equations (coupled to matter perturbations); see [6] and the following *Reviews*. When the cosmic fluid is

well approximated by a perfect fluid, Einstein’s equations predict the following link between the scalar perturbations

$$\Phi(t, \mathbf{x}) = \Psi(t, \mathbf{x}). \quad (21.26)$$

21.3 A roadmap of parametrizations of deviations from GR, and of modified gravity

As will be discussed below, all currently performed gravitational experiments are compatible with GR. However, similarly to what is done in discussions of precision electroweak experiments, it is useful to quantify the significance of precision gravitational experiments by parameterizing possible deviations from GR. One can distinguish two main approaches to considering, and parameterizing, deviations from GR: (i) theory-agnostic phenomenological approaches; or, (ii) the study of the predictions of specific classes of alternative theories of gravity. Both types have led to useful ways of discussing tests of gravity. Both types also have their limitations. Considering them together leads to cross-fertilization.

21.3.1 Theory-agnostic phenomenological approaches to parameterizing deviations from GR

The theory-agnostic phenomenological approach is the oldest, and, arguably, the most robust one. It essentially consists in starting from specific observable predictions within the considered standard theory, and of deforming them by introducing some free parameters measuring either deviations from effects already present within the standard theory, or new effects absent from the standard theory. A classic example is the periastron advance of Mercury (and the other planets). When working within Newtonian gravity as a standard theory of gravity, the rate of periastron advance of Mercury, $\dot{\omega}$, is (when neglecting the quadrupole moment of the Sun) a calculable function of the masses and semi-major axes of the other planets of the solar system, say $\dot{\omega}^{\text{Newton}}(m_i, a_i)$. However, $\dot{\omega}$ is also a directly observable quantity, so that one can parameterize the periastron advance of Mercury by writing

$$\dot{\omega}^{\text{obs}} = \dot{\omega}^{\text{Newton}}(m_i, a_i) + \Delta\dot{\omega}. \quad (21.27)$$

Using other observable data to determine some “observed” values of the m_i ’s and a_i ’s, one can then measure the anomalous periastron precession $\Delta\dot{\omega}$ and see whether it is compatible with zero, or not. As is well-known, Leverrier used such a methodology and, in 1859, measured an anomalous periastron precession of about $\Delta\dot{\omega} \simeq 38$ arcsec/century (later re-estimated at 43 arcsec/century), which was explained in 1915 as a GR prediction. Let us discuss further examples of the use of such theory-agnostic approaches for discussing deviations from GR.

21.3.2 Parameterized post-Newtonian (PPN) formalism.

When considering the weak-field slow-motion limit appropriate to describing gravitational experiments in the solar system, it has been traditional to parameterize possible (long-range) deviations from the GR-predicted 1PN metric by introducing extra dimensionless coefficients in the various terms of the metric of Eq. (21.8). The minimal version of the parameterized post-Newtonian (PPN) formalism (essentially due to Eddington) involves only two parameters β and γ , namely

$$g_{00} = -1 + \frac{2}{c^2}V - \frac{2\beta}{c^4}V^2 + O\left(\frac{1}{c^6}\right), \quad (21.28)$$

$$g_{0i} = -\frac{2(\gamma+1)}{c^3}V_i + O\left(\frac{1}{c^5}\right), \quad (21.29)$$

$$g_{ij} = \delta_{ij}\left[1 + \frac{2\gamma}{c^2}V\right] + O\left(\frac{1}{c^4}\right), \quad (21.30)$$

with V and V_i defined by Eq. (21.9), with the same vectorial source $\sigma_i = \frac{T^{0i}}{c}$, but a modified scalar source

$$\sigma^{\text{PPN}} = \frac{1}{c^2}\left[\left(1 + (3\gamma - 2\beta - 1)\frac{V}{c^2}\right)T^{00} + \gamma T^{ii}\right]. \quad (21.31)$$

In GR, $\beta^{\text{GR}} = 1$ and $\gamma^{\text{GR}} = 1$, so that deviations from GR are parameterized by $\bar{\beta} \equiv \beta - 1$ and $\bar{\gamma} \equiv \gamma - 1$. Richer versions of the

PPN formalism (involving up to ten parameters) were developed in interaction with the study of classes of alternative theories of gravity [7, 8]. This led to parameterizing new types of contributions to the IPN metric that are absent in the GR framework.

When deriving the IPN-accurate dynamics of N point masses predicted by the PPN-modified metric, Eq. (21.28), one finds that the free Lagrangian is not modified (because we are considering here a Lorentz-invariant subclass of PPN metrics), while there are modifications of both the two-body Lagrangian, $L^{(2)}$, Eq. (21.13), and the three-body one, $L^{(3)}$, Eq. (21.14). More precisely, denoting $\eta \equiv 4\bar{\beta} - \bar{\gamma}$, the Newtonian interaction energy term in Eq. (21.13) is modified into $G_{AB}m_A m_B/r_{AB}$, with a body-dependent gravitational “constant”

$$G_{AB} = G[1 + \eta(E_A^{\text{grav}}/m_A c^2 + E_B^{\text{grav}}/m_B c^2) + O(1/c^4)], \quad (21.32)$$

where E_A^{grav} denotes the gravitational binding energy of body A . In addition, there is the additional contribution $+\bar{\gamma}(\mathbf{v}_A - \mathbf{v}_B)^2/c^2$ in the brackets on the right-hand side of $L^{(2)}$, Eq. (21.13). As for the three-body interaction term $L^{(3)}$, Eq. (21.14), it is modified by the overall factor $1 + 2\bar{\beta}$.

These results show how the introduction of the two minimal PPN deviation parameters $\bar{\beta} \equiv \beta - 1$ and $\bar{\gamma} \equiv \gamma - 1$ suffices to introduce many different observable effects. Some of them (the ones linked with $\bar{\gamma}$) concern deviations at the linearized (one-graviton-exchange) level (and affect, for instance, light deflection and time-delay effects), while the deviation parameter $\bar{\beta}$ parameterizes effects linked to the cubic vertex of Einstein’s gravity (and affects, for instance, periastron precession). Of particular interest is the fact that Eq. (21.32) shows that the combination $\eta \equiv 4\bar{\beta} - \bar{\gamma}$ parameterizes a violation of the Strong Equivalence Principle, because the gravitational interaction between self-gravitating bodies is seen to be influenced by the gravitational binding energy of each body [9]. As stated above, this effect is absent in GR (where $\eta^{\text{GR}} = 0$). This is an example where the fact of contrasting GR with some deviations from it gives physical significance to a null effect in GR (namely the universality of free fall of self-gravitating bodies).

Finally, one can extend the PPN formalism by allowing for a slow, phenomenological time variation of Newton’s constant:

$$G(t) = G_0 \left[1 + \frac{\dot{G}_0}{G_0}(t - t_0) \right]. \quad (21.33)$$

Here, one assumes that there exist units in which the masses, m_i , of elementary particles stay constant, and that G is measured in such units. A possible time variation of G then corresponds to a possible common variation of the dimensionless couplings $Gm_i^2/(\hbar c)$.

21.3.3 Parameterized post-Keplerian (PPK) formalism.

The discovery of pulsars (*i.e.*, rotating neutron stars emitting a beam of radio noise) in gravitationally bound orbits [10, 11] has given us our first experimental handle on a regime of relativistic gravity going significantly beyond the uniformly weak-field, and quasi-stationary regime of solar-system gravity. Binary pulsars allow us to probe some radiative effects, and also some strong-gravitational-field effects. In these systems, the finite speed of propagation of the gravitational interaction between the pulsar and its companion generates damping-like terms at order $(v/c)^5$ in the equations of motion [12]. These damping forces are the local counterparts of the gravitational radiation emitted at infinity by the system (“gravitational radiation reaction”). They cause the binary orbit to shrink and its orbital period P_b to decrease. The remarkable stability of pulsar clocks has allowed one to measure the corresponding very small orbital period decay $\dot{P}_b \equiv dP_b/dt \sim -(v/c)^5 \sim -10^{-12} - 10^{-14}$ in several binary systems, thereby giving us a direct experimental handle on the propagation properties of the gravitational field. In addition, the large surface gravitational potential of a neutron star allows one to probe the quasi-static strong-gravitational-field regime, as is discussed below.

It is possible to extract phenomenological (theory-independent) tests of gravity from binary pulsar data by using the parameter-

ized post-Keplerian (PPK) formalism [13]. The basis of this formalism is the fact that, after correcting for the Earth’s motion around the Sun and for the dispersion due to propagation in the interstellar plasma, the time of arrival of the N th pulse t_N can be described by a generic, parameterized “timing formula” [13, 14], whose functional form is common to the whole class of tensor-scalar gravitation theories:

$$t_N - t_0 = F[T_N(\nu_p, \dot{\nu}_p, \ddot{\nu}_p); \{p^K\}; \{p^{PK}\}]. \quad (21.34)$$

Here, T_N is the pulsar proper time corresponding to the N th turn given by $N/2\pi = \nu_p T_N + \frac{1}{2}\dot{\nu}_p T_N^2 + \frac{1}{6}\ddot{\nu}_p T_N^3$ (with $\nu_p \equiv 1/P_p$ the spin frequency of the pulsar, *etc.*), $\{p^K\} = \{P_b, T_0, e, \omega_0, x\}$ is the set of “Keplerian” parameters (notably, orbital period P_b , eccentricity e , periastron longitude ω_0 and projected semi-major axis $x = a \sin i/c$), and $\{p^{PK}\} = \{k, \gamma_{\text{timing}}, \dot{P}_b, r, s, \delta_\theta, \dot{e}, \dot{x}\}$ denotes the set of (separately measurable) “post-Keplerian” parameters. Most important among these are: the fractional periastron advance per orbit $k \equiv \dot{\omega} P_b/2\pi$; a dimensionful time-dilation parameter γ_{timing} ; the orbital period derivative \dot{P}_b ; and the “range” and “shape” parameters of the gravitational time delay caused by the companion, r and s .

Without assuming any specific theory of gravity, one can phenomenologically analyze the data from any binary pulsar by least-squares fitting the observed sequence of pulse arrival times to the timing formula of Eq. (21.34). This fit yields the “measured” values of the parameters $\{\nu_p, \dot{\nu}_p, \ddot{\nu}_p\}$, $\{p^K\}$, $\{p^{PK}\}$. Now, each specific relativistic theory of gravity predicts that, for instance, k , γ_{timing} , \dot{P}_b , r , and s (to quote parameters that have been successfully measured from some binary pulsar data) are some theory-dependent functions of the Keplerian parameters and of the (unknown) masses m_1 , m_2 of the pulsar and its companion. For instance, in GR, one finds (with $M \equiv m_1 + m_2$, $n \equiv 2\pi/P_b$),

$$\begin{aligned} k^{\text{GR}}(m_1, m_2) &= 3(1 - e^2)^{-1}(GMn/c^3)^{2/3}, \\ \gamma_{\text{timing}}^{\text{GR}}(m_1, m_2) &= en^{-1}(GMn/c^3)^{2/3}m_2(m_1 + 2m_2)/M^2, \\ \dot{P}_b^{\text{GR}}(m_1, m_2) &= -(192\pi/5)(1 - e^2)^{-7/2} \left(1 + \frac{73}{24}e^2 + \frac{37}{96}e^4 \right) \\ &\quad \times (GMn/c^3)^{5/3}m_1 m_2 / M^2, \\ r^{\text{GR}}(m_1, m_2) &= Gm_2/c^3, \\ s^{\text{GR}}(m_1, m_2) &= nx(GMn/c^3)^{-1/3}M/m_2. \end{aligned} \quad (21.35)$$

In alternative gravity theories each of the functions $k^{\text{theory}}(m_1, m_2)$, $\gamma_{\text{timing}}^{\text{theory}}(m_1, m_2)$, $\dot{P}_b^{\text{theory}}(m_1, m_2)$, *etc.*, is modified by quasi-static strong field effects (associated with the self-gravities of the pulsar and its companion), while the particular function $\dot{P}_b^{\text{theory}}(m_1, m_2)$ is further modified by radiative effects [15–18]. If one measures $N > 2$ PPK parameters from the data of a specific binary pulsar, these N measurements determine, for each given theory, N curves (defined by the N equations $k_i^{\text{theory}}(m_1, m_2) = k_i^{\text{obs}}$) in the two-dimensional mass plane (m_1, m_2) . This yields $N - 2$ tests of the specified theory, according to whether the N curves (or strips) have one point in common, as they should.

21.3.4 Parameterized-post-Friedmannian (PPF) formalisms.

We have recalled above that, in GR, the two functions, $\Phi(t, \mathbf{x})$, and $\Psi(t, \mathbf{x})$, parameterizing (in the “longitudinal gauge”) the scalar perturbations of the background Friedmann metric are related (in absence of anisotropic stresses) by Eq. (21.26). Several authors [19–28] have defined various types of parameterized-post-Friedmannian (PPF) formalisms involving (generally space and time dependent) phenomenological parameters. The simplest versions of these formalisms involve two phenomenological parameters measuring: (i) the ratio between $\Phi(t, \mathbf{x})$, and $\Psi(t, \mathbf{x})$, say (using a parametrization which parallels the usual PPN parametrization)

$$\Psi(t, \mathbf{x}) = \gamma_{\text{cosmo}}(t, \mathbf{x})\Phi(t, \mathbf{x}); \quad (21.36)$$

and (ii) the effective gravitational constant entering the Poisson equation for $\Phi(t, \mathbf{x})$, say

$$\Delta\Phi(t, \mathbf{x}) = 4\pi G_{\Phi}(t, \mathbf{x})\delta\rho(t, \mathbf{x}). \quad (21.37)$$

However, the peculiarities of cosmological observables limit the domain of applicability of such phenomenological approaches [26] (notably because the strong dependence of cosmological probes on epochs and scales obliges one to rely on specific parameterizations of the functions $\gamma_{\text{cosmo}}(t, \mathbf{x})$ and $G_{\Phi}(t, \mathbf{x})$, *e.g.*, [25, 28]). Approaches based on specific classes of modified-gravity theories allow for a more complete treatment involving, in principle, all existing cosmological observables: Big Bang nucleosynthesis, cosmic microwave background, large-scale structure, Hubble diagram, weak lensing, etc. Discussing the current cosmological tests using either such PPF formalisms, or comparisons with the predictions of modified-gravity theories, is beyond the scope of this review. See [29] for a comprehensive recent discussion. The bottom line is that all present cosmological data have been found to be compatible with GR (within the Friedmann-Lemaître-based Λ CDM model). Beyond the quantitative limits on various parameterized theoretical models [29], one should remember the striking (strong-field-type) qualitative verification of GR embodied in the fact that relativistic cosmological models give an accurate picture of the Universe over a period during which the spatial metric has been blown up by a gigantic factor, say $(1+z)^2 \sim 10^{19}$ between Big Bang nucleosynthesis and now.

21.3.5 Various phenomenological tests of GR from gravitational wave (GW) data

The observation by the US-based Laser Interferometer Gravitational-wave Observatory (LIGO), later joined by the Europe-based Virgo detector, of gravitational-wave (GW) signals [30–34], has opened up a novel testing ground for relativistic gravity. The first two observing runs of the LIGO-Virgo Collaboration (LVC) have led to the detection of GW signals from ten binary black-hole coalescences, and one binary neutron-star merger [35]. The first six months of the third observing run have led to the detection of thirty nine additional GW candidate events with a false-alarm rate smaller than two per year [36].

Several approaches have been used to either test consistency with GR, or to look for special types of possible deviations. Making accurate predictions for GW signals from coalescing black holes within GR took years of both analytical [37, 38] and numerical [39] work. Some works have started (both analytically [15, 40–44] and numerically [45–47]) to derive the corresponding predictions within some modified-gravity theories. Phenomenological approaches are very useful for parameterizing general, conceivable deviations from GR when analyzing the GW signals emitted by coalescing black holes or neutron stars.

A first phenomenological, global consistency test simply consists of measuring the noise-weighted correlation \mathcal{C} between each detected strain signal and the corresponding best-fit GR-predicted waveform. \mathcal{C}^{obs} should be equal to 1, modulo statistical (and/or systematic) errors.

Various other phenomenological tests of the structure of the GR-predicted waveforms emitted by coalescing compact binaries have been suggested. One general idea [48–50] (dubbed “parameterized post-Einsteinian formalism” in [51]) is to modify the GR-predicted Fourier-domain value $\psi(f)$ of the phase of black-hole coalescence GW signals $h(f) = A(f)e^{i\psi(f)}$ by introducing GR-deviation parameters, say

$$\psi(f) = \sum_i \left[p_i^{\text{GR,NS}}(m_1, m_2)(1 + \delta\hat{p}_i) + p_i^{\text{GR,S}}(m_1, m_2, S_1, S_2) \right] \times u_i(f). \quad (21.38)$$

Here, the $u_i(f)$ ’s define a basis of functions of the GW frequency f , and the superscript NS refers to the nonspinning contribution, while the superscript S refers to the spinning one. Such a GR-modification directly applies to the phenomenological representation [52] of $\psi(f)$, and can be generalized to any waveform model by adding the non-GR phase term $\sum_i p_i^{\text{GR,NS}}(m_1, m_2)\delta\hat{p}_i u_i(f)$ to the corresponding GR-predicted Fourier-domain phase $\psi(f)$

[53]. For instance, the leading-order (LO), quadrupolar term in the GR phase evolution during the early inspiral corresponds to $u_0(f) = f^{-5/3}$ and $p_0^{\text{GR}} = \frac{3(m_1+m_2)^2}{128m_1m_2}(\pi G(m_1+m_2)/c^3)^{-5/3}$, while the next-to-leading-order (NLO) term is a $O(v^2/c^2)$ correction $p_2^{\text{GR}}u_2(f)$ with $u_2(f) = f^{-1}$. In the phenomenological model [52] these terms (as well as the other inspiral contributions) are cut-off beyond the frequency $G(m_1+m_2)f/c^3 = 0.018$.

Each dimensionless parameter $\delta\hat{p}_i$ introduces a fractional deviation from the corresponding individual phasing GR effect having the frequency dependence $u_i(f)$, and can, in principle, be extracted by fitting the inspiral part of the observed waveform to the deformed template of Eq. (21.38). However, one must also use this deformed template for simultaneously extracting the values of m_1, m_2, S_1 , and S_2 . Together with signal-to-noise ratio (SNR) considerations, and parameter-correlation issues, this limits the applicability of such a test to introducing only one deformation parameter $\delta\hat{p}_i$ at a time. A particularly meaningful test [48] is to leave undeformed the LO and NLO terms $p_0^{\text{GR}}u_0(f) + p_2^{\text{GR}}u_2(f)$ and to vary the third coefficient p_3 parameterizing the next, “GW tail”-related $O(v^3/c^3)$ correction, with $u_3(f) = f^{-2/3}$. Another well-motivated test [51] is to introduce a new coefficient $\delta\hat{p}_{-2}$, which is absent in GR, and which parameterizes an $O((\frac{v}{c})^{-2})$ fractional correction to the LO, quadrupolar term, thereby allowing for a possible dipolar GW flux (indeed, dipolar GW radiation generally exists in theories containing scalar excitations). As p_{-2}^{GR} vanishes, $\delta\hat{p}_{-2}$ is added as an absolute deviation, scaled by the LO term p_0^{GR} .

The coalescence of two black holes, or of a black hole and a neutron star (or of two heavy-enough neutron stars) leads to the formation of a black hole that is initially formed in a perturbed state. The relaxation of the latter perturbed black hole into its stationary, equilibrium state leads to the emission of characteristic (rapidly decaying) ringing GW modes (a.k.a. quasi-normal modes) [54, 55], whose frequencies and decay times are functions of the mass (M_f) and spin ($S_f \equiv GM_f^2 a_f/c$) of the final black hole, say

$$\omega_a = (c^3/GM_f)[2\pi\hat{f}_a^{\text{QNM}}(a_f) - i/\hat{\tau}_a^{\text{QNM}}(a_f)], \quad (21.39)$$

where $a = 1, 2, \dots$ labels the various ringing modes, starting from the least-damped one. In principle, if the SNR is large enough, one can directly test for the presence of one or several of these modes in the post-merger signal, and measure both $\text{Re}(\omega_a)$ and $\text{Im}(\omega_a)$ in a theory-independent way. These phenomenological measurements then lead to null tests of GR, from which one can extract theoretical information about eventual deviations from GR [56, 57].

As recalled above, GR predicts that GWs propagate (in vacuum) at exactly the same speed as light (*i.e.*, they have the same dispersion law $g^{\mu\nu}k_\mu k_\nu = 0$ in curved spacetime). Deviations from such a universal, scale-free dispersion law can be phenomenologically parameterized in several ways. If one phenomenologically assumes that the graviton dispersion law includes a mass term, say $g^{\mu\nu}k_\mu k_\nu + m_g^2/\hbar^2 = 0$, or some more general type of frequency-dependent modification, such changes affect the phasing of the inspiral GW signal and can be directly tested [58]. When one observes *both* GWs and electromagnetic waves emitted by the same system, one can also directly test whether both types of waves propagate in the same way.

Let us now present some examples of theory-dependent discussions of experimental tests based on considering specific classes of alternative theories. The most conservative deviations from Einstein’s pure spin-2 theory are defined by adding new, bosonic, light or massless, macroscopically coupled fields.

21.3.6 Gravity tests within classes of tensor-scalar theories of gravity

The possible existence of new gravitational-strength couplings leading to deviations from Einsteinian (and Newtonian) gravity has been suggested by many natural extensions of GR, starting with the classic Kaluza-Klein idea, and continuing up to now with the study of extended supergravity theories, and of (super)string theory. In particular, a recurrent suggestion of such theories (which dates back to pioneering work by Jordan, and by

Fierz [59]) is the existence of a scalar field φ coupled both to the scalar curvature R and to the various $F_{\mu\nu}^a$ gauge-field actions. Such fields (“dilaton” or “moduli”) generically appear in string theory and are massless at the tree-level, but could acquire a self-interaction potential $V(\varphi)$ beyond the tree-level.

The exchange of such a dilaton-like field leads to several types of observational deviations from GR. For experimental limits on the gravitational inverse-square-law (down to the micrometer range) see Refs. [60–64]. If the potential $V(\varphi)$ is zero or negligible for the considered range, the coupling of φ to $F_{\mu\nu}^a$ leads to apparent violations of the weak equivalence principle, with rather specific composition-dependence [65]. Next, when neglecting the fractionally small composition-dependent effects, such a field approximately couples to the trace of the energy-momentum tensor $T = g_{\mu\nu}T^{\mu\nu}$. The most general such theory contains (after suitable field redefinitions) two arbitrary functions of the scalar field, namely the self-interaction potential $V(\varphi)$, and a matter-coupling function $a(\varphi)$:

$$\mathcal{L}_{\text{tot}}[g_{\mu\nu}, \varphi, \psi, A_\mu, H] = \frac{c^4}{16\pi G_*} \sqrt{g}(R(g_{\mu\nu}) - 2g^{\mu\nu}\partial_\mu\varphi\partial_\nu\varphi) - \sqrt{g}V(\varphi) + \mathcal{L}_{\text{SM}}[\psi, A_\mu, H, \tilde{g}_{\mu\nu}]. \quad (21.40)$$

Here G_* is a “bare” Newton constant, and the Standard Model matter is coupled not to the “Einstein” (pure spin-2) metric $g_{\mu\nu}$, but to the conformally related (“Jordan-Fierz”) metric

$$\tilde{g}_{\mu\nu} = \exp(2a(\varphi))g_{\mu\nu}. \quad (21.41)$$

The scalar field equation

$$\square_g\varphi = \frac{4\pi G}{c^4} \left(-\alpha(\varphi)T + \frac{\partial V(\varphi)}{\partial\varphi} \right), \quad (21.42)$$

features

$$\alpha(\varphi) \equiv \partial a(\varphi)/\partial\varphi, \quad (21.43)$$

as the basic (field-dependent) coupling between φ and matter [15, 66]. The best-known, special case of these theories is the one-parameter (ω) Jordan-Fierz-Brans-Dicke theory [67], with $V(\varphi) = 0$ and $a(\varphi) = \alpha_0\varphi$, leading to a field-independent coupling $\alpha(\varphi) = \alpha_0$ (with $\alpha_0^2 = 1/(2\omega + 3)$). More generally, if we consider the massless theories ($V(\varphi) = 0$) with arbitrary (non-linear) coupling function $a(\varphi)$, they modify Einstein’s predictions in the weak-field slow-motion limit appropriate to describing gravitational experiments in the solar system (1PN approximation) only through the appearance of exactly the same two “post-Einstein” dimensionless parameters $\bar{\gamma} = \gamma - 1$ and $\bar{\beta} = \beta - 1$ that entered the minimal (Eddington) PPN formalism presented above. However, we now have the following theoretical expressions relating the latter phenomenological parameters to the coupling functions entering the tensor-scalar action Eq. (21.40):

$$\bar{\gamma} = -2 \frac{\alpha_0^2}{1 + \alpha_0^2}; \quad (21.44)$$

$$\bar{\beta} = + \frac{1}{2} \frac{\beta_0\alpha_0^2}{(1 + \alpha_0^2)^2}. \quad (21.45)$$

Here $\alpha_0 \equiv \alpha(\varphi_0)$, and $\beta_0 \equiv \partial\alpha(\varphi_0)/\partial\varphi_0$, with φ_0 denoting the vacuum expectation value (VEV) of φ around the solar system. In addition, the observable value G^{obs} of the gravitational constant is found to be field-dependent and given (at a place where $\varphi = \varphi_0$) by

$$G^{\text{obs}} = G(\varphi_0) \equiv G_* \exp[2a(\varphi_0)](1 + \alpha_0^2). \quad (21.46)$$

This makes it clear that the parameter $\bar{\gamma}$ is the basic post-Einstein parameter, which measures the admixture of an additional field (here a spin-0 field) to the pure spin-2 GR. One also sees how the parameter $\bar{\beta}$ is linked to non-linear effects (here coupling terms $\beta_0(\varphi - \varphi_0)^2 T$ in the action), and how the Nordvedt parameter $\eta \equiv 4\bar{\beta} - \bar{\gamma}$ is related to the field-dependence of G^{obs} ($\eta = (\alpha_0/(1 + \alpha_0^2))\partial \ln G(\varphi_0)/\partial\varphi_0$).

The advantage of a theory-dependent approach, such as Eq. (21.40), over the phenomenological minimal PPN approach

of Eq. (21.28), is that it allows one to consistently predict the observational deviations from GR in all possible gravity regimes: the quasi-stationary weak-field regime; the wavelike weak-field regime; the strong-field regime; the cosmological regime, etc. All such observational deviations can be consistently worked out once one chooses specific forms of the coupling function $a(\varphi)$, and of $V(\varphi)$. The simple choice of a two-parameter quadratic coupling function, say $a(\varphi) = \alpha_0(\varphi - \varphi_0) + \frac{1}{2}\beta_0(\varphi - \varphi_0)^2$, has been found useful for describing many possible observable deviations from GR.

The observable consequences for binary pulsar observations of the strong-field and radiative effects linked to the coupling to φ have been explicitly worked out in Refs. [15, 43] in the case where φ is massless (see Ref. [68] for the case where φ is massive). In particular, the strong-field nature of the pulsar tests is demonstrated by the fact that some tensor-scalar theories can be as close as desired to GR in the weak-field regime of the solar-system (*i.e.*, $\bar{\gamma}$ and $\bar{\beta}$ can be as small as desired, or even exactly zero), while developing (via a “spontaneous scalarization” mechanism) differences of order unity with GR in binary pulsar experiments [17, 18].

21.3.7 Attractor and screening mechanisms in modified gravity

As will follow from the discussion of experimental data below, the comparison between the predictions of general massless tensor-scalar theories and current data shows that the basic coupling parameter α_0 must be tuned to a small value (especially when allowing for composition-dependent effects). This raises the issue of the naturalness of such small coupling parameters. It has been shown in this respect that, in many tensor-scalar theories, there is an *attractor mechanism* by which the cosmological evolution naturally drives the VEV $\varphi_0(t)$ towards a value for which the coupling parameter $\alpha_0 = \alpha(\varphi_0)$ vanishes, thereby making it natural to expect only small deviations from GR (at least for the weak-field regime) at our current cosmological epoch [69, 70].

There are other theoretical mechanisms (generally called “screening mechanisms”) that could explain why a theory of gravity whose theoretical content significantly differs from that of GR could naturally pass all the stringent, GR-compatible experimental limits that will be discussed below. In particular, when considering a self-interacting scalar field ($V(\varphi) \neq 0$), the interplay between the two terms on the right-hand side of Eq. (21.42) tends to drive the local VEV φ_0 of φ to a density-dependent value. In turn, this leads to a corresponding density-dependent effective mass $m_0(\varphi_0) = \sqrt{4\pi G\partial^2 V(\varphi_0)/\partial\varphi_0^2}$ of the φ field, and to density-dependent matter couplings [71]. Various choices of the functions $V(\varphi)$ and $a(\varphi)$ can then reduce the φ -induced deviations from GR in dense environments while still allowing for significant deviations in different (*e.g.*, cosmological) regimes [72–76].

Other screening mechanisms have been invoked, based on an environment dependence mediated by (first or second) derivatives of a scalar degree of freedom. Roughly speaking, such mechanisms involve a (possibly effective) scalar degree of freedom φ that satisfies a field equation that is more general than Eq. (21.42) in that the left-hand side, $\square_g\varphi$, is replaced by a non-linear function of φ , $\partial\varphi$ and $\partial^2\varphi$. The presence of non-linear derivative self-interactions of φ can weaken the effective coupling of φ to matter. A simple toy-model showing this weakening would be to replace Eq. (21.42) by an equation of the form

$$Z(\varphi, \partial\varphi, \partial^2\varphi)\square_g\varphi = \frac{4\pi G}{c^4} \left(-\alpha(\varphi)T + \frac{\partial V(\varphi)}{\partial\varphi} \right). \quad (21.47)$$

Such an equation is equivalent, at a first level of approximation, to replacing the gravitational constant G entering Eq. (21.42) by $G_{\text{eff}}(\varphi_0, \partial\varphi_0, \partial^2\varphi_0) \equiv G/Z_0$, where $Z_0 \equiv Z(\varphi_0, \partial\varphi_0, \partial^2\varphi_0)$. This has a screening effect if $Z_0 \gg 1$. Indeed, the replacement $G \rightarrow G_{\text{eff}}$ diminishes the strength of the interaction potential due to φ exchange by a factor of $1/Z_0$. In addition, the range of this interaction is also affected: $m_0(\varphi_0) = \sqrt{4\pi G\partial^2 V(\varphi_0)/\partial\varphi_0^2} \rightarrow m_{0\text{eff}}(\varphi_0, \partial\varphi_0, \partial^2\varphi_0) = \sqrt{4\pi G_{\text{eff}}\partial^2 V(\varphi_0)/\partial\varphi_0^2} = Z_0^{-1/2}m_0$.

Screening mechanisms based on such non-linear derivative self-interactions are often referred to as being “Vainshtein-like” because a similar mechanism was first invoked in Ref. [77] as a con-

jectural way to ensure that the extra degrees of freedom associated with a massive (rather than massless) graviton become effectively weakly coupled to matter within a large domain around gravitational sources. Here, one is considering massive deformations of the massless spin-2 metric field of GR by a very small mass, possibly of cosmological scale: $m_g \sim \hbar H_0 \sim 10^{-33}$ eV. The construction of ghost-free potential terms for a spin-2 field has turned out to be a delicate matter [78]. The phenomenology of a very-low-mass graviton is still partly uncontrolled, both because of the unknown extent to which the Vainshtein screening is really active, and because of subtle constraints linked to an eventual UV completion of the theory beyond the unusually low energy scale where it becomes strongly coupled:

$$\Lambda_{\text{strong coupling}} \sim (M_{\text{Planck}} m_0^2)^{1/3} \sim 10^{-13} \left(\frac{m_0}{\hbar H_0} \right)^{2/3} \text{ eV}. \quad (21.48)$$

The search for modified gravity theories incorporating an extra scalar degree of freedom potentially able to yield a Vainshtein-like screening led to writing down the following general class of tensor-scalar Lagrangian [79, 80]:

$$\begin{aligned} L_{\text{tot}}[g_{\mu\nu}, \varphi, \psi] = & G_2(\varphi, X) - G_3(\varphi, X) \square_g \varphi + G_4(\varphi, X) R \\ & + G_{4X}(\varphi, X) [(\square_g \varphi)^2 - \varphi^{\mu\nu} \varphi_{\mu\nu}] \\ & + G_5(\varphi, X) G^{\mu\nu} \varphi_{\mu\nu} - \frac{1}{6} G_{5X}(\varphi, X) (\square_g \varphi)^3 \\ & - 3 \square_g \varphi \varphi^{\mu\nu} + 2 \varphi_{\mu\nu} \varphi^{\mu\lambda} \varphi_{\lambda}^{\nu} + L_{\text{matter}}[g_{\mu\nu}, \psi]. \end{aligned} \quad (21.49)$$

Here $g_{\mu\nu}$ denotes the matter-coupled metric, $X \equiv -\frac{1}{2} g^{\mu\nu} \partial_\mu \varphi \partial_\nu \varphi$, $\varphi_{\mu\nu} \equiv \nabla_\mu \nabla_\nu \varphi$, $G^{\mu\nu} \equiv R^{\mu\nu} - \frac{1}{2} R g^{\mu\nu}$, and the various coefficients $G_n(\varphi, X)$ are arbitrary functions of two variables (with $G_{nX} \equiv \partial G_n / \partial X$). The field equations derived from the Lagrangian of Eq. (21.49) are only of second order in derivatives in spite of the non-linear structure of L_{tot} . This implies that the tensor-scalar theories defined by Eq. (21.49) feature three degrees of freedom, corresponding to a massless spin-2 excitation (GW) and a spin-0 excitation. Contrary to the simpler tensor-scalar theories of Eq. (21.40), it is found that the speed of propagation of GWs implied by Eq. (21.49) is generically different from the speed of light:

$$\frac{c_{\text{GW}}^2}{c^2} = \frac{G_4 - X(\dot{\varphi} G_{5X} + G_{5\varphi})}{G_4 - 2XG_{4X} - X(H\dot{\varphi} G_{5X} - G_{5\varphi})}. \quad (21.50)$$

More general modified gravity models have been proposed (see, e.g. Refs. [81, 82]). Apart from the simplest of them, most of these models have a rather artificial flavor, and do not lead to convincing alternative explanations either of dark matter or of dark energy. In addition, many of them do not lead (contrary to GR) to mathematically “well-posed” evolution problems [83–85]. This entails a serious challenge to deriving strong-field predictions for such models. It has been argued that many of these (dark-energy motivated) models should be viewed as effective field theory (EFT) approximations that need some sort of UV completion at an unusually low frequency scale [86]. In spite of these shortcomings, such models are conceptually interesting because they give examples of deviations for various predictions of GR, existing independently from each other, in various regimes. For instance, some special tensor-scalar models lead to black hole solutions modified by scalar-hair [87–89]. For other types of black holes with scalar-hair, see Ref. [90]. This shows the interest of phenomenologically testing, in a democratic and agnostic way, all conceivable deviations from GR.

Let us now turn to briefly presenting current experimental results of various phenomenological tests of the main GR predictions recalled in Section 21.2 above.

21.4 Experimental tests of the Equivalence Principle (i.e., of the matter-gravity coupling)

21.4.1 Tests of the constancy of constants

Stringent limits on a possible time variation of the basic coupling constants have been obtained by analyzing a natural fission

reactor phenomenon that took place at Oklo, Gabon, two billion years ago [91, 92]. These limits are at the 1×10^{-8} level for the fractional variation of the fine-structure constant α_{em} [92], and at the 4×10^{-9} level for the fractional variation of the ratio $m_q / \Lambda_{\text{QCD}}$ between the light quark masses and Λ_{QCD} [93]. The determination of the lifetime of Rhenium 187 from isotopic measurements of some meteorites dating back to the formation of the solar system (about 4.6 Gyr ago) yields comparably strong limits [94]. Measurements of absorption lines in astronomical spectra also give stringent limits on the variability of both α_{em} and $\mu = m_p / m_e$ at cosmological redshifts, e.g.,

$$\Delta \alpha_{\text{em}} / \alpha_{\text{em}} = (1.2 \pm 1.7_{\text{stat}} \pm 0.9_{\text{sys}}) \times 10^{-6}, \quad (21.51)$$

at redshifts $z = 1.0\text{--}2.4$ [95], and

$$|\Delta \mu / \mu| < 4 \times 10^{-7} (95\% \text{ C.L.}), \quad (21.52)$$

at a redshift $z = 0.88582$ [96]. There are also significant limits on the variation of α_{em} and $\mu = m_p / m_e$ at redshift $z \sim 10^3$ from cosmic microwave background data, e.g., $\Delta \alpha_{\text{em}} / \alpha_{\text{em}} = (3.6 \pm 3.7) \times 10^{-3}$ [97]. Direct laboratory limits (based on monitoring the frequency ratio of several different atomic clocks) on the present time variation of α_{em} , $\mu = m_p / m_e$, and $m_q / \Lambda_{\text{QCD}}$ have reached the levels [98]

$$\begin{aligned} d \ln(\alpha_{\text{em}}) / dt &= (-2.5 \pm 2.6) \times 10^{-17} \text{ yr}^{-1}, \\ d \ln(\mu) / dt &= (-1.5 \pm 3.0) \times 10^{-16} \text{ yr}^{-1}, \\ d \ln(m_q / \Lambda_{\text{QCD}}) / dt &= (7.1 \pm 4.4) \times 10^{-15} \text{ yr}^{-1}. \end{aligned} \quad (21.53)$$

There are also experimental limits on a possible dependence of coupling constants on the gravitational potential [98–100].

Experimental limits on the present time variation of the gravitational constant, Eq. (21.33), have been derived from planetary ephemerides [101], lunar laser ranging [102], and binary-pulsar data [103, 104]. The most stringent limits come from lunar-laser-ranging data [102]:

$$\frac{\dot{G}_0}{G_0} = (7.1 \pm 7.6) \times 10^{-14} \text{ yr}^{-1}. \quad (21.54)$$

21.4.2 Tests of the isotropy of space and of Local Lorentz invariance

The highest precision tests of the isotropy of space have been performed by looking for possible quadrupolar shifts of nuclear energy levels [105]. The (null) results can be interpreted as testing the fact that the various pieces in the matter Lagrangian, Eq. (21.6), are indeed coupled to the same external metric $g_{\mu\nu}$ to the 10^{-29} level.

Stringent tests of possible violations of local Lorentz invariance in gravitational interactions have been obtained both from solar-system data [8] and pulsar data [106, 107]. For astrophysical constraints on possible Planck-scale violations of Lorentz invariance, see Ref. [108].

21.4.3 Tests of the universality of free fall (weak, and strong equivalence principles)

The universality of the acceleration of free fall has been verified, for laboratory bodies, both on the ground [109, 110] (at the 10^{-13} level), and in space [111, 112] (at the 10^{-14} level):

$$\begin{aligned} (\Delta a/a)_{\text{BeTi}} &= (0.3 \pm 1.8) \times 10^{-13}; \\ (\Delta a/a)_{\text{BeAl}} &= (-0.7 \pm 1.3) \times 10^{-13}; \\ (\Delta a/a)_{\text{TiPt}} &= (-1 \pm 9(\text{stat}) \pm 9(\text{syst})) \times 10^{-15}. \end{aligned} \quad (21.55)$$

The universality of free fall has also been verified when comparing the fall of classical and quantum objects (at the 6×10^{-9} level [113]), or of two quantum objects (at the $(0.3 \pm 5.4) \times 10^{-7}$ [114], and $(1 \pm 1.4) \times 10^{-9}$, levels [115]).

The universality of free fall of self-gravitating bodies (strong equivalence principle) has been verified in both the weak-gravity, and the strong-gravity regimes. The gravitational accelerations

of the Earth and the Moon toward the Sun have been checked to agree at the 10^{-13} level [102]

$$(\Delta a/a)_{\text{EarthMoon}} = (-3 \pm 5) \times 10^{-14}. \quad (21.56)$$

The latter result constrains the Nordtvedt PPN parameter [9] $\eta \equiv 4\bar{\beta} - \bar{\gamma}$ to the 10^{-4} level:

$$\eta = (-0.2 \pm 1.1) \times 10^{-4}. \quad (21.57)$$

See below for strong-field tests of the strong equivalence principle.

Finally, the universality of the gravitational redshift of clock rates has been verified at the 10^{-4} level by comparing a hydrogen-maser clock flying on a rocket up to an altitude of about 10,000 km to a similar clock on the ground [116]. The redshift due to a height change of only 33 cm has been detected by comparing two optical clocks based on $^{27}\text{Al}^+$ ions [117]. The gravitational redshift has also been detected in the orbit of a star near the supermassive black hole at the center of our Galaxy [118, 119], and its universality has been verified at the 5% level [120].

21.5 Tests of quasi-stationary, weak-field gravity

All currently performed gravitational experiments in the solar system, including perihelion advances of planetary orbits, the bending and delay of electromagnetic signals passing near the Sun, and very accurate ranging data to the Moon obtained by laser echoes, are compatible with the post-Newtonian results of Eq. (21.15), Eq. (21.13), and Eq. (21.14). The “gravito-magnetic” interactions $\propto v_A v_B$ contained in Eq. (21.13) are involved in many of these experimental tests. They have been particularly tested in lunar-laser-ranging data [121], in the combined LAGEOS-LARES satellite data [122, 123], and in the dedicated Gravity Probe B mission [124].

To assess in a quantitative manner the results of the various solar-system tests of gravity it is convenient to express them in terms of the PPN parameters defined above. The best current limit on the post-Einstein parameter $\bar{\gamma} \equiv \gamma - 1$ is

$$\bar{\gamma} = (2.1 \pm 2.3) \times 10^{-5}, \quad (21.58)$$

as deduced from the additional Doppler shift experienced by radio-wave beams connecting the Earth to the Cassini spacecraft when they passed near the Sun [125].

The (cubic-vertex-related) post-Einstein parameter $\bar{\beta} \equiv \beta - 1$ is constrained at the 10^{-4} level both from a study of the global sensitivity of planetary ephemerides to post-Einstein parameters [101],

$$|\bar{\beta}| < 7 \times 10^{-5}, \quad (21.59)$$

and from lunar-laser-ranging data [102]

$$\bar{\beta} = (-4.5 \pm 5.6) \times 10^{-5}. \quad (21.60)$$

The periastron advance of the star S2 around the Galactic center massive black hole has been observed to agree with GR within 20% [126]. More stringent limits on $\bar{\gamma}$ (*i.e.* the coupling of φ to matter) are obtained in dilaton-like models where scalar couplings violate the Equivalence Principle [127].

21.6 Tests of strong-field gravity (neutron stars and black holes)

Experimental tests of strong-field gravity have been obtained in various physical systems, notably binary pulsars and coalescing binary black holes.

It is convenient to quantitatively express binary-pulsar tests of strong-field gravity by using the PPK formalism defined above. We recall that the measurement of N phenomenological PPK parameters leads to $N - 2$ tests of strong-field gravity. In all, *thirteen* tests of strong-field and/or radiative gravity have been obtained in the four different (double neutron-star) binary pulsar systems PSR1913+16 [10, 11, 128], PSR1534+12 [129–131], PSR J1141–6545 [132–135], and PSR J0737–3039 A,B [136–140]. These consist of $N - 2 = 5 - 2 = 3$ tests from PSR1913+16 ; $5 - 2 = 3$ tests from PSR1534+12; $4 - 2 = 2$ tests from PSR J1141–6545; and $7 - 2 = 5$ tests from PSR J0737–3039 (see,

also, Ref. [141] for additional, less accurate tests of relativistic gravity). Among these tests, four of them (those involving the measurement of the PPK parameter \dot{P}_b) probe radiative effects, and will be discussed in the following section. The four binary pulsar systems PSR1913+16, PSR1534+12, PSR J1141–6545, and PSR J0737–3039 A,B have given nine tests of quasi-static, strong-field gravity. GR passes all these tests within the measurement accuracy. Let us only highlight here some of the most accurate strong-field tests.

In the binary pulsar PSR 1534+12 [129] one has measured *five* post-Keplerian parameters: k , γ_{timing} , r , s , and (with less accuracy) \dot{P}_b [130, 131]. This yields *three* tests of relativistic gravity. Among these tests, the two involving the measurements of k , γ_{timing} , r , and s accurately probe strong field gravity, without mixing of radiative effects [130]. The most precise (10^{-3} level) of these pure strong-field tests is the one obtained by combining the measurements of k , γ_{timing} , and s ; namely, [131],

$$\left[\frac{s^{\text{obs}}}{s^{\text{GR}}[k^{\text{obs}}, \gamma_{\text{timing}}^{\text{obs}}]} \right]_{1534+12} = 1.002 \pm 0.002. \quad (21.61)$$

The discovery of the remarkable *double* binary pulsar PSR J0737–3039 A and B [136, 137] has led to the measurement of *seven* independent parameters [138–140]: five of them are the post-Keplerian parameters k , γ_{timing} , r , s , and \dot{P}_b entering the relativistic timing formula of the fast-spinning pulsar PSR J0737–3039 A; a sixth is the ratio $R = x_B/x_A$ between the projected semi-major axis of the more slowly spinning companion pulsar PSR J0737–3039 B, and that of PSR J0737–3039 A (the theoretical prediction for the ratio $R = x_B/x_A$, considered as a function of the (inertial) masses $m_1 = m_A$ and $m_2 = m_B$, is $R^{\text{theory}} = m_1/m_2 + O((v/c)^4)$ [13, 14], independently of the gravitational theory considered). Finally, the seventh parameter $\Omega_{\text{SO,B}}$ is the angular rate of (spin-orbit) precession of PSR J0737–3039 B around the total angular momentum vector [139, 140]. These seven measurements give us *five* tests of relativistic gravity [138, 142, 143], four of which are quasi-static, strong-field tests. GR passes all those tests with flying colors [143, 144]. The most accurate is at the 5×10^{-4} level:

$$\left[\frac{s^{\text{obs}}}{s^{\text{GR}}[k^{\text{obs}}, R^{\text{obs}}]} \right]_{0737-3039} = 1.0000 \pm 0.0005. \quad (21.62)$$

Binary pulsar data on other types of pulsar systems can be used to test strong-field aspects of the “strong equivalence principle,” namely the GR prediction that strong-self-gravity objects (such as neutron stars) should fall with the same acceleration as weak-self-gravity objects (such as white-dwarfs) in the (external) gravitational field created by other objects (such as the Galaxy, or another white dwarf). The first binary-pulsar tests of this property have been obtained in nearly circular binary systems (made of a neutron star and a white dwarf) falling in the field of the Galaxy, and have led to strong-field confirmations (at the 2×10^{-3} level) of the strong equivalence principle [104, 145–147]. The remarkable discovery of the pulsar PSR J0337+1715 in a hierarchical triple system [148] has allowed one to derive a much more accurate test of the strong equivalence principle because the inner binary (comprising a pulsar and a close white-dwarf companion) falls toward the outer white-dwarf companion with an acceleration that is 10^8 times larger than the Galactic acceleration. This leads to a 95% confidence level limit on a possible fractional difference in free-fall acceleration of the pulsar and its close companion of [149, 150]

$$|\Delta a/a| < 2.05 \times 10^{-6} \text{ (95\% C.L.)}. \quad (21.63)$$

.. This limit yields strong constraints on tensor-scalar gravity models.

Measurements over several years of the pulse profiles of various pulsars have detected secular changes compatible with the prediction [151] that the general relativistic spin-orbit coupling should cause a secular change in the orientation of the pulsar beam with respect to the line of sight (“geodetic precession”). Such confirmations of general-relativistic spin-orbit effects were obtained in

PSR 1913+16 [152], PSR B1534+12 [131], PSR J1141–6545 [153], PSR J0737–3039 [139, 140], and PSR J1906+0746 [154, 155]. In some cases (notably PSR 1913+16 and PSR J1906+0746) the secular change in the orientation of the pulsar beam is expected to lead to the disappearance of the beam (as seen on the Earth) on a human time scale (the second pulsar in the double system PSR J0737–3039 already disappeared in March 2008 and is expected to reappear around 2035 [140]).

Recently, the ultimate strong-field regime of black holes has started to be quantitatively probed via GW observations. The LIGO-Virgo collaboration has detected (starting in September 2015) GW signals [156], which, besides testing the radiative structure of gravity (see next section), are in excellent qualitative and quantitative agreement with the structure and dynamics of black-hole horizons in GR. Because of the mixing of strong-field effects with radiative effects during the coalescence of two black holes, and because of the lack of detailed alternative-theory predictions for this process (see, however, Refs. [45–47]), it is not easy to set quantitative limits on possible strong-field deviations from GR, independently of radiative effects. Direct tests of the existence of black-hole horizons are scarce (see, however, Sec. VIIB of [157] which reports the lack of any statistical evidence for GW echoes).

Let us also mention that the Event Horizon Telescope collaboration has obtained event-horizon-scale images of the supermassive black hole candidate in the center of the giant elliptical galaxy M87 that are “consistent with expectations for the shadow of a Kerr black hole as predicted by general relativity” [158]. For discussions of the corresponding constraints on the black hole geometry in the vicinity of the light ring see Refs. [159, 160].

21.7 Tests of radiative gravity (both in binary-pulsar data and in GW data)

Experimental confirmations of the GR predictions for the radiative structure of gravity have been obtained both in binary-pulsar data and in the observation of GW signals from coalescing compact binaries (binary black holes and binary neutron stars).

Binary-pulsar observations involving the measurement of the orbital period derivative \dot{P}_b give *direct* experimental tests of the reality of gravitational radiation, and, in particular, an experimental confirmation that the speed of propagation of gravity c_g is equal to the speed of light c (indeed, as recalled above, \dot{P}_b is a consequence of the propagation of the gravitational interaction between the two neutron stars [12]). Even in the presence of screening mechanisms within the binary system, the value of \dot{P}_b yields a measurement of the speed of propagation of GWs at the 10^{-2} level [161]. The currently most accurate binary-pulsar tests of the radiative properties of gravity come from the binary neutron-star systems PSR1913+16 and PSR J0737–3039 A,B, as well as from several neutron-star-white-dwarf systems, notably PSR J1738+0333.

After subtracting a small ($\sim 10^{-14}$ level in $\dot{P}_b^{\text{obs}} = (-2.423 \pm 0.001) \times 10^{-12}$), but significant, “Galactic” perturbing effect (linked to Galactic accelerations and to the pulsar proper motion) [162], one finds that the phenomenological test obtained by combining the measurements of the three PPK parameters ($k - \gamma_{\text{timing}} - \dot{P}_b$)₁₉₁₃₊₁₆ is passed by GR with complete success [128]:

$$\left[\frac{\dot{P}_b^{\text{obs}} - \dot{P}_b^{\text{gal}}}{\dot{P}_b^{\text{GR}}[k^{\text{obs}}, \gamma_{\text{timing}}^{\text{obs}}]} \right]_{1913+16} = 0.9983 \pm 0.0016. \quad (21.64)$$

Here $\dot{P}_b^{\text{GR}}[k^{\text{obs}}, \gamma_{\text{timing}}^{\text{obs}}]$ is the result of inserting in $\dot{P}_b^{\text{GR}}(m_1, m_2)$ the values of the masses predicted by the two equations $k^{\text{obs}} = k^{\text{GR}}(m_1, m_2)$, and $\gamma_{\text{timing}}^{\text{obs}} = \gamma_{\text{timing}}^{\text{GR}}(m_1, m_2)$. This yields experimental evidence for the reality of gravitational radiation damping forces at the $(-1.7 \pm 1.6) \times 10^{-3}$ level.

Similarly, the combined measurement in PSR J0737–3039 A,B of the three parameters k , $R \equiv x_B/x_A$, and \dot{P}_b yields another experimental test of the radiative structure of gravity at the 10^{-3} level [138–140]:

$$\left[\frac{\dot{P}_b^{\text{obs}}}{\dot{P}_b^{\text{GR}}[k^{\text{obs}}, R^{\text{obs}}]} \right]_{0737-3039} = 1.000 \pm 0.001. \quad (21.65)$$

In addition to the above tests, further very stringent tests of radiative gravity follow from the measurement of the orbital period decay \dot{P}_b of low-eccentricity pulsar-white dwarf systems. Notably, the system PSR J1738+0333 yields an intrinsic orbital decay of [163]

$$\left[\dot{P}_b^{\text{obs}} - \dot{P}_b^{\text{gal}} \right]_{1738+0333} = (-25.9 \pm 3.2) \times 10^{-15}, \quad (21.66)$$

to be compared to

$$\left[\dot{P}_b^{\text{GR}} \right]_{1738+0333} = (-27.7_{-1.9}^{+1.5}) \times 10^{-15}. \quad (21.67)$$

The fractional agreement between the (corrected) observed period decay and the GR-predicted one seems to be quantitatively less impressive than the double-neutron-star results cited above, but the crucial point is that asymmetric binary systems (such as neutron-star-white-dwarf ones) are strong emitters of dipolar gravitational radiation in tensor-scalar theories, with \dot{P}_b scaling (modulo matter-scalar couplings) like $m_1 m_2 / (m_1 + m_2)^2 (v/c)^3$, instead of the parametrically smaller GR-predicted quadrupolar radiation $\dot{P}_b \sim (v/c)^5$ [7, 15]. In view of the very small absolute value of \dot{P}_b , this makes such systems (and notably PSR J1738+0333) very sensitive probes of tensor-scalar gravity [103, 144, 163–166]. It is then useful to turn to a theory-dependent analysis of pulsar data. Such an analysis (see, e.g., [17, 130, 144, 163, 166]) leads to excluding a large portion of the parameter space of tensor-scalar gravity allowed by solar-system tests. As a result, the basic matter-scalar coupling α_0^2 is more strongly constrained, over most of the parameter space, than the best current solar-system limits of Eq. (21.58) (namely below the 10^{-5} level) [163, 166].

We now turn to the tests of radiative gravity that can be deduced from the GW data gathered from the first two observing runs of the LIGO-Virgo collaboration (LVC), and the first half of the third observing run (*i.e.* about fifty GW signals). All currently detected GW signals are consistent with GR predictions. Several phenomenological approaches were used and led to setting limits on possible deviations from GR [50, 157, 167].

A theory-agnostic quantitative assessment on possible deviations from GR is given by measuring the agreement between the full observed GW signal of coalescing binary black holes, and the GR-predicted one. The strongest such result was obtained with the first event: GW150914, which had an SNR of 24. The noise-weighted correlation between the GW150914 signal and the best-fit GR-predicted waveform was found to be $\geq 97\%$ [50, 167]. In other words, GR-violation effects that cannot be reabsorbed in a redefinition of physical parameters are limited (in a noise-weighted sense) to less than 3%.

Besides checking the agreement between the *full* observed GW signals and the corresponding best-fit full signals predicted by GR, one also tested the consistency between separate parts of the signals. A first approach [157, 167] separates: (i) the lower-frequency signal emitted during the *inspiral* phase (considered up to the innermost stable circular orbit); and (ii) the higher-frequency remaining signal emitted during the *postinspiral* phase, comprising the late-inspiral, the merger, and the ringdown. Separately fitting each of these partial signals to GR-based templates then yields separate estimates of the binary’s parameters, leading to separate estimates of the mass M_f and dimensionless spin parameter $a_f = J_f / (GM_f^2)$ of the final black hole that would be formed (in GR) by the coalescence of the two initial black holes. The consistency with GR then consists in testing whether the two estimates $(M_f, a_f)_{\text{insp}}$ and $(M_f, a_f)_{\text{postinsp}}$ are compatible with each other. They were found to be compatible for all events whose corresponding separate SNRs made such an analysis meaningful (see Figs. 3 and 4 in [157]). Quantitatively, the (population-marginalized) fractional differences

$$\begin{aligned} \frac{\Delta M_f}{\bar{M}_f} &= 2 \frac{M_f^{\text{insp}} - M_f^{\text{postinsp}}}{M_f^{\text{insp}} + M_f^{\text{postinsp}}}, \\ \frac{\Delta a_f}{\bar{a}_f} &= 2 \frac{a_f^{\text{insp}} - a_f^{\text{postinsp}}}{a_f^{\text{insp}} + a_f^{\text{postinsp}}}, \end{aligned} \quad (21.68)$$

between the two estimates were found to be consistent with zero (*i.e.* with GR) [157]

$$\begin{aligned}\frac{\Delta M_f}{M_f} &= 0.02_{-0.17}^{+0.20}, \\ \frac{\Delta a_f}{\bar{a}_f} &= -0.05_{-0.41}^{+0.36}.\end{aligned}\quad (21.69)$$

A second approach [168, 169] considers the signal of coalescing black holes in the time domain, and separates it in its *pre-merger*, and *postmerger* parts, the dividing line being the (inferred) peak of the waveform. Using various models of the postmerger signal (including either one or two black-hole ringing modes) leads to estimates of the mass and spin of the final black hole, $(M_f, a_f)_{\text{postmerger}}$. The application of this time-domain analysis to the (high SNR) first event GW150914 has shown consistency between $(M_f, a_f)_{\text{postmerger}}$, $(M_f, a_f)_{\text{premerger}}$ and $(M_f, a_f)_{\text{full signal}}$ (see Fig. 4 and Table I in [169]). This consistency confirms Hawking’s area-increase theorem with 97 % probability [169]. Applying such an analysis to the data of the second LIGO-Virgo transient catalog allows one to constrain possible deviations away from the GR-predicted frequencies and damping times of the first two quadrupolar ringing modes [157]. For instance, the population-marginalized constraint on the fractional deviation of the fundamental 220 ringing mode was found to be $\delta \hat{f}_{220} = 0.03_{-0.35}^{+0.38}$ [157] (see also Fig. 14 there). Applying the different analysis advocated in Ref. [170] allows one to derive a stronger constraint on $\delta \hat{f}_{220}$, namely $\delta \hat{f}_{220} = -0.05_{-0.05}^{+0.05}$ [171].

The parametrization of Eq. (21.38) for possible deviations in the frequency dependence of the Fourier-domain phase $\psi(f)$ of the black hole coalescence GW signal was used to measure best-fit values for each fractional deviation parameter $\delta \hat{p}_i$, considered separately (the other ones being set to zero). In all cases, the posterior distribution for each $\delta \hat{p}_i$ is consistent with the GR value, *i.e.*, $\delta \hat{p}_i^{\text{GR}} = 0$ (see Fig. 6 in [157]). The current limits on $\delta \hat{p}_i$ are (roughly) of order unity, except for the two parameters highlighted above: $\delta \hat{p}_3$ (parameterizing the $O((\frac{v}{c})^3)$ fractional correction to the LO, quadrupolar term); and $\delta \hat{p}_{-2}$ (parameterizing a possible dipolar-radiation-related $O((\frac{v}{c})^{-2})$ fractional correction to the LO, quadrupolar term). The current [157] 90%-credible interval for $\delta \hat{p}_3$ is $-0.02_{-0.10}^{+0.11}$ (when using a phenomenological model [52]), and $-0.01_{-0.10}^{+0.10}$ (when using an effective one-body model [37]). The corresponding 90%-credible intervals for a possible dipolar term $\delta \hat{p}_{-2}$ are, respectively, $(-1.0_{-4.0}^{+4.5}) \times 10^{-3}$ and $(-0.5_{-3.5}^{+3.5}) \times 10^{-3}$ [157]. For examples of the translation of these phenomenological constraints into bounds on specific gravitational theories see Refs. [172, 173].

As recalled above, GR predicts that the polarization content of GWs is pure helicity-2, *i.e.* described by the two independent components of a traceless tensor transverse to the propagation direction. A (massless) scalar excitation would add a pure-trace “breathing mode” in the plane transverse to the propagation direction. A phenomenological approach to generic metric theories of gravity would allow for up to six polarizations for a GW [174], namely two tensor, two vector and two scalar modes. The LVC tested possible polarization deviations from GR in the following way [33, 167]: they assumed that the phase evolution of the GW signal was the one predicted by GR, but they replaced the polarization structure of the signal either by a generic vector-like one, or by a generic scalar-like one. The best polarization constraints have been obtained from the GW170817 event. The latter very long (~ 100 s) and very loud ($\text{SNR} \simeq 33$) event was convincingly interpreted as coming from a binary neutron star inspiral (~ 40 Mpc away), and was associated with a subsequent γ -ray burst, followed by transient counterparts across the electromagnetic spectrum [175]. The polarization analysis of the GW170817 data has given overwhelming evidence in favor of pure tensor polarization modes in comparison to pure vector or pure scalar modes with a base-ten logarithm of the Bayes factor of $+20.81 \pm 0.08$ and $+23.09 \pm 0.08$, respectively [167]. See also Sec. VIII of [157] for an analysis that does not rely on specific waveform models.

GR also predicts that GWs are non dispersive, and propagate

at the same speed as light. One can phenomenologically modify the GR-predicted GW phase evolution by adding the putative effect of an anomalous dispersion relation of the form $E^2 = p^2 c^2 + A p^\alpha c^\alpha$. GW data have been used to set bounds on the anomalous coefficient A for various values of the exponent α . The case $\alpha = 0$ is equivalent to assuming that gravitons disperse as a massive particle [58]. Combined GW data from the second GW transient catalog lead to the following (90%-credibility) phenomenological limit on the graviton mass: $m_g \leq 1.76 \times 10^{-23} \text{eV}/c^2$ [157]. This limit is 1.8 times more stringent than the most recent Solar System bound [64].

Finally, a very constraining bound on the speed of propagation of gravity c_{GW} was derived from the observed time delay of 1.7 s between GW170817 and the associated γ -ray burst. Namely, the fractional difference between c_{GW} and $c_{\text{light}} \equiv c$ is constrained to be [176]

$$-3 \times 10^{-15} < \frac{c_{\text{GW}} - c}{c} < +7 \times 10^{-16}.\quad (21.70)$$

When comparing the latter bound to the prediction Eq. (21.50) from general second-order tensor-scalar theories, Eq. (21.49), one is led to conclude that the coupling function $G_5(\varphi, X)$ has to be ignored and that the coupling function $G_4(\varphi, X)$ has to be restricted to depend only on φ . This drastically reduces the viable tensor-scalar modified-gravity models [177–180].

21.8 Conclusions

All present experimental tests are compatible with the predictions of the current “standard” theory of gravitation, Einstein’s General Relativity. Let us recap the main tests. The universality of the coupling between matter and gravity (Equivalence Principle) has been verified at around the 10^{-14} level. Solar system experiments have tested the weak-field predictions of Einstein’s theory at the few times 10^{-5} level. The propagation properties (in the near zone) of relativistic gravity, as well as several of its static strong-field aspects, have been verified at the 10^{-3} level (or better) in several binary pulsar experiments. Interferometric detectors of gravitational radiation have given direct observational proofs of the existence, and properties, of gravitational waves (in the wave zone), and of the existence of coalescing black holes, and they have already set strong limits on possible deviations; in particular: an upper bound $|\delta \hat{p}_{-2}| \lesssim 4 \times 10^{-3}$ on a possible dipolar contribution to the GW flux; the $O(10^{-15})$ bound of Eq. (21.70) on the speed of gravity; and evidence for the tensor polarization structure of gravitational waves. In addition, laboratory experiments have set strong constraints on sub-millimeter modifications of Newtonian gravity, while many different cosmological data sets have been used to set limits on possible GR deviations on cosmological scales [29]. In spite of the uneasiness of having to assume the existence of dark matter, and the presence of an unnaturally small cosmological constant (as dark energy), General Relativity stands out as a uniquely successful description of gravity on all the scales that have been explored so far. There are no modified-gravity models which naturally pass all existing experimental tests, while either explaining away the need for dark matter or for dark energy.

References

- [1] S. Weinberg, *Rev. Mod. Phys.* **61**, 1 (1989).
- [2] H. A. Buchdahl, *Phys. Rev.* **116**, 1027 (1959).
- [3] N. Chamel *et al.*, *Int. J. Mod. Phys. E22*, 1330018 (2013), [arXiv:1307.3995].
- [4] J. R. Oppenheimer and H. Snyder, *Phys. Rev.* **56**, 455 (1939).
- [5] R. P. Kerr, *Phys. Rev. Lett.* **11**, 237 (1963).
- [6] V. F. Mukhanov, H. A. Feldman and R. H. Brandenberger, *Phys. Rept.* **215**, 203 (1992).
- [7] C. M. Will, *Theory and Experiment in Gravitational Physics*, Cambridge University Press (2018).
- [8] C. M. Will, *Living Rev. Rel.* **17**, 4 (2014), [arXiv:1403.7377].
- [9] K. Nordtvedt, *Phys. Rev.* **170**, 1186 (1968).

- [10] R. A. Hulse, *Rev. Mod. Phys.* **66**, 699 (1994).
- [11] J. H. Taylor, *Rev. Mod. Phys.* **66**, 711 (1994).
- [12] T. Damour and N. Deruelle, *Phys. Lett.* **A87**, 81 (1981); T. Damour, *C.R. Acad. Sci. Paris* **294**, 1335 (1982).
- [13] T. Damour and J. H. Taylor, *Phys. Rev.* **D45**, 1840 (1992).
- [14] T. Damour and N. Deruelle, *Ann. Inst. H. Poincaré A*, **44**, 263 (1986).
- [15] T. Damour and G. Esposito-Farese, *Class. Quant. Grav.* **9**, 2093 (1992).
- [16] C. M. Will and H. W. Zaglauer, *Astrophys. J.* **346**, 366 (1989).
- [17] T. Damour and G. Esposito-Farese, *Phys. Rev.* **D54**, 1474 (1996), [arXiv:gr-qc/9602056].
- [18] T. Damour and G. Esposito-Farese, *Phys. Rev.* **D58**, 042001 (1998), [arXiv:gr-qc/9803031].
- [19] J.-P. Uzan, *Gen. Rel. Grav.* **39**, 307 (2007), [arXiv:astro-ph/0605313].
- [20] R. Caldwell, A. Cooray and A. Melchiorri, *Phys. Rev.* **D76**, 023507 (2007), [arXiv:astro-ph/0703375].
- [21] P. Zhang *et al.*, *Phys. Rev. Lett.* **99**, 141302 (2007), [arXiv:0704.1932].
- [22] L. Amendola, M. Kunz and D. Sapone, *JCAP* **0804**, 013 (2008), [arXiv:0704.2421].
- [23] W. Hu and I. Sawicki, *Phys. Rev.* **D76**, 104043 (2007), [arXiv:0708.1190].
- [24] S. F. Daniel *et al.*, *Phys. Rev.* **D77**, 103513 (2008), [arXiv:0802.1068].
- [25] G.-B. Zhao *et al.*, *Phys. Rev.* **D79**, 083513 (2009), [arXiv:0809.3791].
- [26] J.-P. Uzan, *Gen. Rel. Grav.* **42**, 2219 (2010), [arXiv:0908.2243].
- [27] E. Bertschinger, *Phil. Trans. Roy. Soc. Lond.* **A369**, 4947 (2011), [arXiv:1111.4659].
- [28] T. Baker, P. G. Ferreira and C. Skordis, *Phys. Rev.* **D87**, 2, 024015 (2013), [arXiv:1209.2117].
- [29] M. Ishak, *Living Rev. Rel.* **22**, 1, 1 (2019), [arXiv:1806.10122].
- [30] B. P. Abbott *et al.* (LIGO Scientific, Virgo), *Phys. Rev. Lett.* **116**, 6, 061102 (2016), [arXiv:1602.03837].
- [31] B. P. Abbott *et al.* (LIGO Scientific, Virgo), *Phys. Rev. Lett.* **116**, 24, 241103 (2016), [arXiv:1606.04855].
- [32] B. P. Abbott *et al.* (LIGO Scientific, VIRGO), *Phys. Rev. Lett.* **118**, 22, 221101 (2017), [Erratum: *Phys. Rev. Lett.* **121**, no. 12, 129901 (2018)], [arXiv:1706.01812].
- [33] B. P. Abbott *et al.* (LIGO Scientific, Virgo), *Phys. Rev. Lett.* **119**, 14, 141101 (2017), [arXiv:1709.09660].
- [34] B. P. Abbott *et al.* (LIGO Scientific, Virgo), *Phys. Rev. Lett.* **119**, 16, 161101 (2017), [arXiv:1710.05832].
- [35] B. P. Abbott *et al.* (LIGO Scientific, Virgo), *Phys. Rev.* **X6**, 4, 041015 (2016), [erratum: *Phys. Rev.* **X8**, no. 3, 039903 (2018)], [arXiv:1606.04856].
- [36] R. Abbott *et al.* (LIGO Scientific, Virgo), *Phys. Rev. X* **11**, 021053 (2021), [arXiv:2010.14527].
- [37] A. Buonanno and T. Damour, *Phys. Rev.* **D62**, 064015 (2000), [arXiv:gr-qc/0001013].
- [38] L. Blanchet, *Living Rev. Rel.* **17**, 2 (2014), [arXiv:1310.1528].
- [39] F. Pretorius, *Phys. Rev. Lett.* **95**, 121101 (2005), [arXiv:gr-qc/0507014]; M. Campanelli *et al.*, *Phys. Rev. Lett.* **96**, 111101 (2006), [arXiv:gr-qc/0511048]; J. G. Baker *et al.*, *Phys. Rev. Lett.* **96**, 111102 (2006), [arXiv:gr-qc/0511103].
- [40] K. Yagi *et al.*, *Phys. Rev.* **D85**, 064022 (2012), [Erratum: *Phys. Rev.* **D93**, no. 2, 029902 (2016)], [arXiv:1110.5950].
- [41] K. Yagi, L. C. Stein and N. Yunes, *Phys. Rev.* **D93**, 2, 024010 (2016), [arXiv:1510.02152].
- [42] K. Prabhu and L. C. Stein, *Phys. Rev.* **D98**, 2, 021503 (2018), [arXiv:1805.02668].
- [43] L. Bernard, *Phys. Rev.* **D98**, 4, 044004 (2018), [arXiv:1802.10201].
- [44] F.-L. Julié and E. Berti, *Phys. Rev. D* **100**, 10, 104061 (2019), [arXiv:1909.05258].
- [45] M. Okounkova *et al.*, *Phys. Rev.* **D96**, 4, 044020 (2017), [arXiv:1705.07924].
- [46] H. Witek *et al.*, *Phys. Rev.* **D99**, 6, 064035 (2019), [arXiv:1810.05177].
- [47] M. Okounkova *et al.* (2019), [arXiv:1906.08789].
- [48] L. Blanchet and B. S. Sathyaprakash, *Phys. Rev. Lett.* **74**, 1067 (1995).
- [49] K. G. Arun *et al.*, *Phys. Rev.* **D74**, 024006 (2006), [arXiv:gr-qc/0604067].
- [50] B. P. Abbott *et al.* (LIGO Scientific, Virgo), *Phys. Rev. Lett.* **116**, 22, 221101 (2016), [Erratum: *Phys. Rev. Lett.* **121**, no. 12, 129902 (2018)], [arXiv:1602.03841].
- [51] N. Yunes and F. Pretorius, *Phys. Rev.* **D80**, 122003 (2009), [arXiv:0909.3328].
- [52] S. Khan *et al.*, *Phys. Rev.* **D93**, 4, 044007 (2016), [arXiv:1508.07253].
- [53] B. P. Abbott *et al.* (LIGO Scientific, Virgo), *Phys. Rev. Lett.* **123**, 1, 011102 (2019), [arXiv:1811.00364].
- [54] C. V. Vishveshwara, *Nature* **227**, 936 (1970).
- [55] S. L. Detweiler, *Astrophys. J.* **239**, 292 (1980).
- [56] V. Cardoso *et al.*, *Phys. Rev.* **D99**, 10, 104077 (2019), [arXiv:1901.01265].
- [57] R. McManus *et al.*, *Phys. Rev.* **D100**, 4, 044061 (2019), [arXiv:1906.05155].
- [58] C. M. Will, *Phys. Rev.* **D57**, 2061 (1998), [arXiv:gr-qc/9709011].
- [59] M. Fierz, *Helv. Phys. Acta* **29**, 128 (1956).
- [60] E. G. Adelberger, B. R. Heckel and A. E. Nelson, *Ann. Rev. Nucl. Part. Sci.* **53**, 77 (2003), [hep-ph/0307284].
- [61] D. J. Kapner *et al.*, *Phys. Rev. Lett.* **98**, 021101 (2007), [hep-ph/0611184].
- [62] A. O. Sushkov *et al.*, *Phys. Rev. Lett.* **107**, 171101 (2011), [arXiv:1108.2547].
- [63] W.-H. Tan *et al.*, *Phys. Rev. Lett.* **124**, 5, 051301 (2020).
- [64] L. Bernus *et al.*, *Phys. Rev. D* **102**, 2, 021501 (2020), [arXiv:2006.12304].
- [65] T. Damour and J. F. Donoghue, *Phys. Rev.* **D82**, 084033 (2010), [arXiv:1007.2792].
- [66] R. V. Wagoner, *Phys. Rev.* **D1**, 3209 (1970).
- [67] C. Brans and R. H. Dicke, *Phys. Rev.* **124**, 925 (1961), [142(1961)].
- [68] J. Alsing *et al.*, *Phys. Rev.* **D85**, 064041 (2012), [arXiv:1112.4903].
- [69] T. Damour and K. Nordtvedt, *Phys. Rev. Lett.* **70**, 2217 (1993).
- [70] T. Damour and A. M. Polyakov, *Nucl. Phys.* **B423**, 532 (1994), [hep-th/9401069].
- [71] K. A. Olive and M. Pospelov, *Phys. Rev.* **D77**, 043524 (2008), [arXiv:0709.3825].
- [72] J. Khoury and A. Weltman, *Phys. Rev. Lett.* **93**, 171104 (2004), [arXiv:astro-ph/0309300].
- [73] K. Hinterbichler and J. Khoury, *Phys. Rev. Lett.* **104**, 231301 (2010), [arXiv:1001.4525].
- [74] P. Brax *et al.*, *Phys. Rev.* **D82**, 063519 (2010), [arXiv:1005.3735].

- [75] A. Joyce *et al.*, Phys. Rept. **568**, 1 (2015), [arXiv:1407.0059].
- [76] C. Burrage and J. Sakstein, Living Rev. Rel. **21**, 1, 1 (2018), [arXiv:1709.09071].
- [77] A. I. Vainshtein, Phys. Lett. **39B**, 393 (1972).
- [78] C. de Rham, Living Rev. Rel. **17**, 7 (2014), [arXiv:1401.4173].
- [79] G. W. Horndeski, Int. J. Theor. Phys. **10**, 363 (1974).
- [80] C. Deffayet *et al.*, Phys. Rev. **D84**, 064039 (2011), [arXiv:1103.3260].
- [81] L. Heisenberg, Phys. Rept. **796**, 1 (2019), [arXiv:1807.01725].
- [82] T. Kobayashi, Rept. Prog. Phys. **82**, 8, 086901 (2019), [arXiv:1901.07183].
- [83] G. Papallo and H. S. Reall, Phys. Rev. **D96**, 4, 044019 (2017), [arXiv:1705.04370].
- [84] L. Bernard, L. Lehner and R. Luna, Phys. Rev. **D100**, 2, 024011 (2019), [arXiv:1904.12866].
- [85] A. D. Kovács, Phys. Rev. **D100**, 2, 024005 (2019), [arXiv:1904.00963].
- [86] C. de Rham and S. Melville, Phys. Rev. Lett. **121**, 22, 221101 (2018), [arXiv:1806.09417].
- [87] D. D. Doneva and S. S. Yazadjiev, Phys. Rev. Lett. **120**, 13, 131103 (2018), [arXiv:1711.01187].
- [88] H. O. Silva *et al.*, Phys. Rev. Lett. **120**, 13, 131104 (2018), [arXiv:1711.02080].
- [89] G. Antoniou *et al.*, Phys. Rev. D **104**, 4, 044002 (2021), [arXiv:2105.04479].
- [90] C. A. R. Herdeiro and E. Radu, Int. J. Mod. Phys. **D24**, 09, 1542014 (2015), [arXiv:1504.08209].
- [91] A.I. Shlyakhter, Nature **264**, 340 (1976).
- [92] T. Damour and F. Dyson, Nucl. Phys. **B480**, 37 (1996), [hep-ph/9606486]; C. R. Gould, E. I. Sharapov and S. K. Lamoreaux, Phys. Rev. **C74**, 024607 (2006), [arXiv:nucl-ex/0701019]; E. D. Davis and L. Hamdan, Phys. Rev. **C92**, 1, 014319 (2015), [arXiv:1503.06011]; Yu. V. Petrov *et al.*, Phys. Rev. **C74**, 064610 (2006), [hep-ph/0506186].
- [93] V. V. Flambaum and R. B. Wiringa, Phys. Rev. **C79**, 034302 (2009), [arXiv:0807.4943].
- [94] K. A. Olive *et al.*, Phys. Rev. **D69**, 027701 (2004), [arXiv:astro-ph/0309252].
- [95] M. T. Murphy, A. L. Malec and J. X. Prochaska, Mon. Not. Roy. Astron. Soc. **461**, 3, 2461 (2016), [arXiv:1606.06293].
- [96] N. Kanekar *et al.*, Mon. Not. Roy. Astron. Soc. **448**, 1, L104 (2015), [arXiv:1412.7757].
- [97] P. A. R. Ade *et al.* (Planck), Astron. Astrophys. **580**, A22 (2015), [arXiv:1406.7482].
- [98] T. Rosenband *et al.*, Science **319**, 1808 (2008); J. Guena *et al.*, Phys. Rev. Lett. **109**, 080801 (2012); R. M. Godun *et al.*, Phys. Rev. Lett. **113**, 21, 210801 (2014), [arXiv:1407.0164].
- [99] T. M. Fortier *et al.*, Phys. Rev. Lett. **98**, 070801 (2007).
- [100] R. Lange *et al.*, Phys. Rev. Lett. **126**, 1, 011102 (2021), [arXiv:2010.06620]; S. Blatt *et al.*, Phys. Rev. Lett. **100**, 140801 (2008), [arXiv:0801.1874]; T. Dent, Phys. Rev. Lett. **101**, 041102 (2008), [arXiv:0805.0318].
- [101] A. Fienga *et al.*, Cel. Mech. Dyn. Astr. **123**, Issue 2, 1 (2015).
- [102] F. Hofmann and J. Müller, Class. Quant. Grav. **35**, 3, 035015 (2018).
- [103] K. Lazaridis *et al.*, Mon. Not. R. Astron. Soc. **400**, 805 (2009), [arXiv:0908.0285].
- [104] W. W. Zhu *et al.*, Mon. Not. Roy. Astron. Soc. **482**, 3, 3249 (2019), [arXiv:1802.09206].
- [105] M. Smiciklas *et al.*, Phys. Rev. Lett. **107**, 171604 (2011), [arXiv:1106.0738].
- [106] J. F. Bell and T. Damour, Class. Quant. Grav. **13**, 3121 (1996), [arXiv:gr-qc/9606062].
- [107] L. Shao and N. Wex, Class. Quant. Grav. **29**, 215018 (2012), [arXiv:1209.4503].
- [108] S. Liberati, J. Phys. Conf. Ser. **631**, 1, 012011 (2015).
- [109] S. Schlamminger *et al.*, Phys. Rev. Lett. **100**, 041101 (2008), [arXiv:0712.0607].
- [110] T. A. Wagner *et al.*, Class. Quant. Grav. **29**, 184002 (2012), [arXiv:1207.2442].
- [111] P. Touboul *et al.*, Phys. Rev. Lett. **119**, 23, 231101 (2017), [arXiv:1712.01176].
- [112] P. Touboul *et al.* (MICROSCOPE), Class. Quant. Grav. **36**, 22, 225006 (2019), [arXiv:1909.10598].
- [113] S. Merlet *et al.*, Metrologia, **47**, L9-L11 (2010).
- [114] D. Schlippert *et al.*, Phys. Rev. Lett. **112**, 203002 (2014), [arXiv:1406.4979].
- [115] G. Rosi *et al.*, Nature Commun. **8**, 5529 (2017), [arXiv:1704.02296].
- [116] R.F.C. Vessot and M.W. Levine, Gen. Rel. Grav. **10**, 181 (1978); R. F. C. Vessot *et al.*, Phys. Rev. Lett. **45**, 2081 (1980).
- [117] C. W. Chou *et al.*, Science **329**, 1630 (2010).
- [118] R. Abuter *et al.* (GRAVITY), Astron. Astrophys. **615**, L15 (2018), [arXiv:1807.09409].
- [119] T. Do *et al.*, Science **365**, 6454, 664 (2019), [arXiv:1907.10731].
- [120] A. Amorim *et al.* (GRAVITY), Phys. Rev. Lett. **122**, 10, 101102 (2019), [arXiv:1902.04193].
- [121] J.G. Williams, S.G. Turyshev, and D.H. Boggs, Class. Quantum Grav. **29**, 184004 (2012).
- [122] I. Ciufolini and E. C. Pavlis, Nature **431**, 958 (2004).
- [123] I. Ciufolini *et al.*, Eur. Phys. J. **C76**, 3, 120 (2016), [arXiv:1603.09674].
- [124] C. W. F. Everitt *et al.*, Phys. Rev. Lett. **106**, 221101 (2011), [arXiv:1105.3456].
- [125] B. Bertotti, L. Iess and P. Tortora, Nature **425**, 374 (2003).
- [126] R. Abuter *et al.* (GRAVITY), Astron. Astrophys. **636**, L5 (2020), [arXiv:2004.07187].
- [127] J. Bergé *et al.*, Phys. Rev. Lett. **120**, 14, 141101 (2018), [arXiv:1712.00483].
- [128] J. M. Weisberg and Y. Huang, Astrophys. J. **829**, 1, 55 (2016), [arXiv:1606.02744].
- [129] A. Wolszczan, Nature **350**, 688 (1991).
- [130] J. N. Taylor, A. Wolszczan and T. Damour, Nature **355**, 132 (1993).
- [131] E. Fonseca, I. H. Stairs and S. E. Thorsett, Astrophys. J. **787**, 82 (2014), [arXiv:1402.4836].
- [132] V. M. Kaspi *et al.*, Astrophys. J. **528**, 445 (2000), [arXiv:astro-ph/9906373].
- [133] S. M. Ord, M. Bailes and W. van Straten, Astrophys. J. **574**, L75 (2002), [arXiv:astro-ph/0204421].
- [134] M. Bailes *et al.*, Astrophys. J. **595**, L49 (2003), [arXiv:astro-ph/0307468].
- [135] N. D. R. Bhat, M. Bailes and J. P. W. Verbiest, Phys. Rev. **D77**, 124017 (2008), [arXiv:0804.0956].
- [136] M. Burgay *et al.*, Nature **426**, 531 (2003), [arXiv:astro-ph/0312071].
- [137] A. G. Lyne *et al.*, Science **303**, 1153 (2004), [arXiv:astro-ph/0401086].
- [138] M. Kramer *et al.*, Science **314**, 97 (2006), [arXiv:astro-ph/0609417].

- [139] R. P. Breton *et al.*, *Science* **321**, 104 (2008), [arXiv:0807.2644].
- [140] B. Perera *et al.*, *Astrophys. J.* **721**, 1193 (2010), [arXiv:1008.1097].
- [141] R. D. Ferdman *et al.*, *Mon. Not. Roy. Astron. Soc.* **443**, 3, 2183 (2014), [arXiv:1406.5507].
- [142] M. Kramer and N. Wex, *Class. Quant. Grav.* **26**, 073001 (2009).
- [143] M. Kramer, in *Neutron Stars and Pulsars: Challenges and Opportunities after 80 Years*; M. Kramer, IAU Symp. **291**, 19 (2013), [arXiv:1211.2457].
- [144] N. Wex and M. Kramer, *Universe* **6**, 9, 156 (2020).
- [145] T. Damour and G. Schaefer, *Phys. Rev. Lett.* **66**, 2549 (1991).
- [146] M. E. Gonzalez *et al.*, *Astrophys. J.* **743**, 102 (2011), [arXiv:1109.5638].
- [147] P. C. C. Freire, M. Kramer and N. Wex, *Class. Quant. Grav.* **29**, 184007 (2012), [arXiv:1205.3751].
- [148] S. M. Ransom *et al.*, *Nature* **505**, 520 (2014), [arXiv:1401.0535].
- [149] A. M. Archibald *et al.*, *Nature* **559**, 7712, 73 (2018), [arXiv:1807.02059].
- [150] G. Voisin *et al.*, *Astron. Astrophys.* **638**, A24 (2020), [arXiv:2005.01388].
- [151] T. Damour and R. Ruffini, *C. R. Acad. Sc. Paris* **279**, série A, 971 (1974); B. M. Barker and R. F. O'Connell, *Phys. Rev.* **D12**, 329 (1975).
- [152] M. Kramer, *Astrophys. J.* **509**, 856 (1998), [arXiv:astro-ph/9808127]; J. M. Weisberg and J. H. Taylor, *Astrophys. J.* **576**, 942 (2002), [arXiv:astro-ph/0205280].
- [153] R. N. Manchester *et al.*, *Astrophys. J.* **710**, 1694 (2010), [arXiv:1001.1483].
- [154] J. van Leeuwen *et al.*, *Astrophys. J.* **798**, 2, 118 (2015), [arXiv:1411.1518].
- [155] G. Desvignes *et al.*, *Science* **365**, 6457, 1013 (2019).
- [156] B. P. Abbott *et al.* (LIGO Scientific, Virgo), *Phys. Rev.* **X9**, 3, 031040 (2019), [arXiv:1811.12907].
- [157] R. Abbott *et al.* (LIGO Scientific, Virgo), *Phys. Rev. D* **103**, 12, 122002 (2021), [arXiv:2010.14529].
- [158] K. Akiyama *et al.* (Event Horizon Telescope), *Astrophys. J.* **875**, 1, L1 (2019), [arXiv:1906.11238].
- [159] D. Psaltis *et al.* (Event Horizon Telescope), *Phys. Rev. Lett.* **125**, 14, 141104 (2020), [arXiv:2010.01055].
- [160] S. H. Völkel *et al.* (2020), [arXiv:2011.06812].
- [161] J. Beltran Jimenez, F. Piazza and H. Velten, *Phys. Rev. Lett.* **116**, 6, 061101 (2016), [arXiv:1507.05047].
- [162] T. Damour and J. H. Taylor, *Astrophys. J.* **366**, 501 (1991).
- [163] P. C. C. Freire *et al.*, *Mon. Not. Roy. Astron. Soc.* **423**, 3328 (2012), [arXiv:1205.1450].
- [164] J. Antoniadis *et al.*, *Science* **340**, 6131 (2013), [arXiv:1304.6875].
- [165] W. W. Zhu *et al.*, *Astrophys. J.* **809**, 1, 41 (2015), [arXiv:1504.00662].
- [166] L. Shao *et al.*, *Phys. Rev.* **X7**, 4, 041025 (2017), [arXiv:1704.07561].
- [167] B. P. Abbott *et al.* (LIGO Scientific, Virgo), *Phys. Rev. D* **100**, 10, 104036 (2019), [arXiv:1903.04467].
- [168] M. Isi *et al.*, *Phys. Rev. Lett.* **123**, 11, 111102 (2019), [arXiv:1905.00869].
- [169] M. Isi *et al.*, *Phys. Rev. Lett.* **127**, 1, 011103 (2021), [arXiv:2012.04486].
- [170] A. Maselli *et al.*, *Phys. Rev. D* **101**, 2, 024043 (2020), [arXiv:1910.12893].
- [171] G. Carullo, *Phys. Rev. D* **103**, 12, 124043 (2021), [arXiv:2102.05939].
- [172] S. E. Perkins *et al.*, *Phys. Rev. D* **104**, 2, 024060 (2021), [arXiv:2104.11189].
- [173] P. K. Gupta *et al.* (2021), [arXiv:2107.12111].
- [174] D. M. Eardley, D. L. Lee and A. P. Lightman, *Phys. Rev.* **D8**, 3308 (1973).
- [175] B. P. Abbott *et al.*, *Astrophys. J.* **848**, 2, L12 (2017), [arXiv:1710.05833].
- [176] B. P. Abbott *et al.* (LIGO Scientific, Virgo, Fermi-GBM, INTEGRAL), *Astrophys. J.* **848**, 2, L13 (2017), [arXiv:1710.05834].
- [177] T. Baker *et al.*, *Phys. Rev. Lett.* **119**, 25, 251301 (2017), [arXiv:1710.06394].
- [178] P. Creminelli and F. Vernizzi, *Phys. Rev. Lett.* **119**, 25, 251302 (2017), [arXiv:1710.05877].
- [179] J. Sakstein and B. Jain, *Phys. Rev. Lett.* **119**, 25, 251303 (2017), [arXiv:1710.05893].
- [180] J. M. Ezquiaga and M. Zumalacárregui, *Phys. Rev. Lett.* **119**, 25, 251304 (2017), [arXiv:1710.05901].

22. Big-Bang Cosmology

Revised August 2021 by K.A. Olive (Minnesota U.) and J.A. Peacock (Edinburgh U.).

22.1 Introduction to the standard big-bang model

The observed expansion of the Universe [1–3] is a natural (almost inevitable) result of any homogeneous and isotropic cosmological model based on general relativity. However, by itself, the Hubble expansion does not provide sufficient evidence for what we generally refer to as the Big-Bang model of cosmology. While general relativity is in principle capable of describing the cosmology of any given distribution of matter, it is extremely fortunate that our Universe appears to be homogeneous and isotropic on large scales. Together, homogeneity and isotropy allow us to extend the Copernican Principle to the Cosmological Principle, stating that all spatial positions in the Universe are essentially equivalent.

The formulation of the Big-Bang model began in the 1940s with the work of George Gamow and his collaborators, Ralph Alpher and Robert Herman. In order to account for the possibility that the abundances of the elements had a cosmological origin, they proposed that the early Universe was once very hot and dense (enough so as to allow for the nucleosynthetic processing of hydrogen), and has subsequently expanded and cooled to its present state [4, 5]. In 1948, Alpher and Herman predicted that a direct consequence of this model is the presence of a relic background radiation with a temperature of order a few K [6, 7]. Of course this radiation was observed 16 years later as the Cosmic Microwave Background (CMB) [8]. Indeed, it was the observation of this radiation that singled out the Big-Bang model as the prime candidate to describe our Universe. Subsequent work on Big-Bang nucleosynthesis further confirmed the necessity of our hot and dense past. (See Sec. 22.3.7 for a brief discussion of BBN and the review on BBN – Sec. 24 of this *Review* for a detailed discussion of BBN.) These relativistic cosmological models face severe problems with their initial conditions, to which the best modern solution is inflationary cosmology, discussed in Sec. 22.3.5 and in – Sec. 23 of this *Review*. If correct, these ideas would strictly render the term ‘Big Bang’ redundant, since it was first coined by Hoyle to represent a criticism of the lack of understanding of the initial conditions.

22.1.1 The Robertson-Walker Universe

The observed homogeneity and isotropy enable us to describe the overall geometry and evolution of the Universe in terms of two cosmological parameters accounting for the spatial curvature and the overall expansion (or contraction) of the Universe. These two quantities appear in the most general expression for a space-time metric that has a (3D) maximally symmetric subspace of a 4D space-time, known as the Robertson-Walker metric:

$$ds^2 = dt^2 - R^2(t) \left[\frac{dr^2}{1 - kr^2} + r^2 (d\theta^2 + \sin^2 \theta d\phi^2) \right]. \quad (22.1)$$

Note that we adopt $c = 1$ throughout. By rescaling the radial coordinate, we can choose the curvature constant k to take only the discrete values $+1$, -1 , or 0 corresponding to closed, open, or spatially flat geometries. In this case, it is often more convenient to re-express the metric as

$$ds^2 = dt^2 - R^2(t) \left[d\chi^2 + S_k^2(\chi) (d\theta^2 + \sin^2 \theta d\phi^2) \right], \quad (22.2)$$

where the function $S_k(\chi)$ is $(\sin \chi, \chi, \sinh \chi)$ for $k = (+1, 0, -1)$. The coordinate r [in Eq. (22.1)] and the ‘angle’ χ [in Eq. (22.2)] are both dimensionless; the dimensions are carried by the cosmological scale factor, $R(t)$, which determines proper distances in terms of the comoving coordinates. A common alternative is to define a dimensionless scale factor, $a(t) = R(t)/R_0$, where $R_0 \equiv R(t_0)$ is R at the present epoch. It is also sometimes convenient to define a dimensionless or conformal time coordinate, η , by $d\eta = dt/R(t)$. Along constant spatial sections, the proper time is defined by the time coordinate, t . Similarly, for $dt = d\theta = d\phi = 0$, the proper distance is given by $R(t)\chi$. For standard texts on cosmological models see *e.g.*, Refs. [9–16].

22.1.2 The redshift

The cosmological redshift is a direct consequence of the Hubble expansion, determined by $R(t)$. A local observer detecting light from a distant emitter sees a redshift in frequency. We can define the redshift as

$$z \equiv \frac{\nu_1 - \nu_2}{\nu_2} \simeq v_{12}, \quad (22.3)$$

where ν_1 is the frequency of the emitted light, ν_2 is the observed frequency, and v_{12} is the relative velocity between the emitter and the observer. While the definition, $z = (\nu_1 - \nu_2)/\nu_2$ is valid in general, relating the redshift to a simple relative velocity is only correct on small scales (*i.e.*, less than cosmological scales) such that the expansion velocity is non-relativistic. For light signals, we can use the metric given by Eq. (22.1) and $ds^2 = 0$ to write

$$v_{12} = \dot{R} \delta r = \frac{\dot{R}}{R} \delta t = \frac{\delta R}{R} = \frac{R_2 - R_1}{R_1}, \quad (22.4)$$

where $\delta r(\delta t)$ is the radial coordinate (temporal) separation between the emitter and observer. Noting that physical distance, D , is $R\delta r$ or δt , Eq. (22.4) gives us Hubble’s law, $v = HD$. In addition, we obtain the simple relation between the redshift and the scale factor

$$1 + z = \frac{\nu_1}{\nu_2} = \frac{R_2}{R_1}. \quad (22.5)$$

This result does not depend on the non-relativistic approximation.

22.1.3 The Friedmann equations of motion

The cosmological equations of motion are derived from Einstein’s equations

$$\mathcal{R}_{\mu\nu} - \frac{1}{2} g_{\mu\nu} \mathcal{R} = 8\pi G_N T_{\mu\nu} + \Lambda g_{\mu\nu} \quad (22.6)$$

Gliner [17] and Zeldovich [18] have pioneered the modern view, in which the Λ term is set on the rhs and interpreted as an effective energy – momentum tensor $T_{\mu\nu}$ for the vacuum of $\Lambda g_{\mu\nu}/8\pi G_N$. It is common to assume that the matter content of the Universe is a perfect fluid, for which

$$T_{\mu\nu} = -p g_{\mu\nu} + (p + \rho) u_\mu u_\nu, \quad (22.7)$$

where $g_{\mu\nu}$ is the space-time metric described by Eq. (22.1), p is the isotropic pressure, ρ is the energy density and $u = (1, 0, 0, 0)$ is the velocity vector for the isotropic fluid in co-moving coordinates. With the perfect fluid source, Einstein’s equations lead to the Friedmann equations

$$H^2 \equiv \left(\frac{\dot{R}}{R} \right)^2 = \frac{8\pi G_N \rho}{3} - \frac{k}{R^2} + \frac{\Lambda}{3}, \quad (22.8)$$

and

$$\frac{\ddot{R}}{R} = \frac{\Lambda}{3} - \frac{4\pi G_N}{3} (\rho + 3p), \quad (22.9)$$

where $H(t)$ is the Hubble parameter and Λ is the cosmological constant. The first of these is sometimes called the Friedmann equation. Energy conservation via $T^{\mu\nu}_{;\mu} = 0$, leads to a third useful equation [which can also be derived from Eq. (22.8) and Eq. (22.9)]

$$\dot{\rho} = -3H(\rho + p). \quad (22.10)$$

Eq. (22.10) can also be simply derived as a consequence of the first law of thermodynamics.

Eq. (22.8) has a simple classical mechanical analog if we neglect (for the moment) the cosmological term Λ . By interpreting $-k/R^2$ Newtonianly as a ‘total energy’, then we see that the evolution of the Universe is governed by a competition between the potential energy, $8\pi G_N \rho/3$, and the kinetic term $(\dot{R}/R)^2$. For $\Lambda = 0$, it is clear that the Universe must be expanding or contracting (except at the turning point prior to collapse in a closed Universe). The ultimate fate of the Universe is determined by the curvature constant k . For $k = +1$, the Universe will recollapse in a finite time, whereas for $k = 0, -1$, the Universe will expand indefinitely. These simple conclusions can be altered when $\Lambda \neq 0$ or more generally with some component with $(\rho + 3p) < 0$.

22.1.4 Definition of cosmological parameters

In addition to the Hubble parameter, it is useful to define several other measurable cosmological parameters. The Friedmann equation can be used to define a critical density such that $k = 0$ when $\Lambda = 0$,

$$\begin{aligned}\rho_c &\equiv \frac{3H^2}{8\pi G_N} = 1.88 \times 10^{-26} h^2 \text{ kg m}^{-3} \\ &= 1.05 \times 10^{-5} h^2 \text{ GeV cm}^{-3},\end{aligned}\quad (22.11)$$

where the scaled Hubble parameter, h , is defined by

$$\begin{aligned}H &\equiv 100 h \text{ km s}^{-1} \text{ Mpc}^{-1} \\ \Rightarrow H^{-1} &= 9.778 h^{-1} \text{ Gyr} \\ &= 2998 h^{-1} \text{ Mpc}.\end{aligned}\quad (22.12)$$

The cosmological density parameter Ω_{tot} is defined as the energy density relative to the critical density,

$$\Omega_{\text{tot}} = \rho/\rho_c. \quad (22.13)$$

Note that one can now rewrite the Friedmann equation as

$$k/R^2 = H^2(\Omega_{\text{tot}} - 1). \quad (22.14)$$

From Eq. (22.14), one can see that when $\Omega_{\text{tot}} > 1$, $k = +1$ and the Universe is closed, when $\Omega_{\text{tot}} < 1$, $k = -1$ and the Universe is open, and when $\Omega_{\text{tot}} = 1$, $k = 0$, and the Universe is spatially flat.

It is often necessary to distinguish different contributions to the density. It is therefore convenient to define present-day density parameters for pressureless matter (Ω_m) and relativistic particles (Ω_r), plus the quantity $\Omega_\Lambda = \Lambda/3H^2$. In more general models, we may wish to drop the assumption that the vacuum energy density is constant, and we therefore denote the present-day density parameter of the vacuum by Ω_v . The Friedmann equation then becomes

$$k/R_0^2 = H_0^2(\Omega_m + \Omega_r + \Omega_v - 1), \quad (22.15)$$

where the subscript 0 indicates present-day values. Thus, it is the sum of the densities in matter, relativistic particles, and vacuum that determines the overall sign of the curvature. Note that the quantity $-k/R_0^2 H_0^2$ is sometimes referred to as Ω_K . This usage is unfortunate: it encourages one to think of curvature as a contribution to the energy density of the Universe, which is not correct.

22.1.5 Standard Model solutions

Much of the history of the Universe in the standard Big-Bang model can be easily described by assuming that either matter or radiation dominates the total energy density. During inflation and again today the expansion rate for the Universe is accelerating, and domination by a cosmological constant or some other form of dark energy should be considered. In the following, we shall delineate the solutions to the Friedmann equation when a single component dominates the energy density. Each component is distinguished by an equation of state parameter $w = p/\rho$. We concentrate on solutions that expand at early times, although the Friedmann equation also permits a time-reversed contracting solution.

22.1.5.1 Solutions for a general equation of state

Let us first assume a general equation of state parameter for a single component, w , which is constant. In this case, Eq. (22.10) can be written as $\dot{\rho} = -3(1+w)\rho\dot{R}/R$ and is easily integrated to yield

$$\rho \propto R^{-3(1+w)}. \quad (22.16)$$

Note that at early times when R is small, the less singular curvature term k/R^2 in the Friedmann equation can be neglected so long as $w > -1/3$. Curvature domination occurs at rather late times (if a cosmological constant term does not dominate sooner). For $w \neq -1$, one can insert this result into the Friedmann equation Eq. (22.8), and if one neglects the curvature and cosmological constant terms, it is easy to integrate the equation to obtain,

$$R(t) \propto t^{2/[3(1+w)]}. \quad (22.17)$$

22.1.5.2 A Radiation-dominated Universe

In the early hot and dense Universe, it is appropriate to assume an equation of state corresponding to a gas of radiation (or relativistic particles) for which $w = 1/3$. In this case, Eq. (22.16) becomes $\rho \propto R^{-4}$. The ‘extra’ factor of $1/R$ is due to the cosmological redshift; not only is the number density of particles in the radiation background decreasing as R^{-3} since volume scales as R^3 , but in addition each particle’s energy is decreasing as $E \propto \nu \propto R^{-1}$. Similarly, one can substitute $w = 1/3$ into Eq. (22.17) to obtain

$$R(t) \propto t^{1/2}; \quad H = 1/2t. \quad (22.18)$$

22.1.5.3 A Matter-dominated Universe

At relatively late times, non-relativistic matter eventually dominates the energy density over radiation [see Eq. (22.3.8)]. A pressureless gas ($w = 0$) leads to the expected dependence $\rho \propto R^{-3}$ from Eq. (22.16) and, if $k = 0$, we obtain

$$R(t) \propto t^{2/3}; \quad H = 2/3t. \quad (22.19)$$

22.1.5.4 A Universe dominated by vacuum energy

If there is a dominant source of vacuum energy, V_0 , it would act as a cosmological constant with $\Lambda = 8\pi G_N V_0$ and equation of state $w = -1$. In this case, the solution to the Friedmann equation when curvature is neglected is particularly simple and leads to an exponential expansion of the Universe:

$$R(t) \propto e^{\sqrt{\Lambda/3}t}. \quad (22.20)$$

More generally we could write

$$a(t) = \sinh^{2/3}(\sqrt{3\Lambda}t/2), \quad (22.21)$$

which describes a flat Universe containing both matter and vacuum energy, with $a(t)$ being the scale factor normalized to unity when both components are equal.

A key parameter is the equation of state of the vacuum, $w \equiv p/\rho$: this need not be the $w = -1$ of Λ , and may not even be constant [19–21]. There is much interest in the more general possibility of a dynamically evolving vacuum energy, for which the name ‘dark energy’ has become commonly used. A variety of techniques exist whereby the vacuum density as a function of time may be measured, usually expressed as the value of w as a function of epoch [22, 23]. The best current measurement of the equation of state (assumed constant, but without assuming zero curvature) is $w = -1.028 \pm 0.031$ [24]. Unless stated otherwise, we will assume that the vacuum energy is a cosmological constant with $w = -1$ exactly.

The presence of vacuum energy can dramatically alter the fate of the Universe. For example, if $\Lambda < 0$, the Universe will eventually recollapse independent of the sign of k . For large values of $\Lambda > 0$ (larger than the Einstein static value needed to halt any cosmological expansion or contraction), even a closed Universe will expand forever. One way to quantify this is the deceleration parameter, q_0 , defined as

$$q_0 = - \left. \frac{R\ddot{R}}{\dot{R}^2} \right|_0 = \frac{1}{2}\Omega_m + \Omega_r + \frac{(1+3w)}{2}\Omega_v. \quad (22.22)$$

This equation shows us that $w < -1/3$ for the vacuum may lead to an accelerating expansion. To the continuing astonishment of cosmologists, such an effect has been observed; one piece of direct evidence is the supernova Hubble diagram [25–30] (see Fig. 22.1 below). Current data indicate that vacuum energy is indeed the largest contributor to the cosmological density budget, with $\Omega_v = 0.685 \pm 0.007$ and $\Omega_m = 0.315 \pm 0.007$ if $k = 0$ is assumed [24].

The existence of this constituent is without doubt the greatest puzzle raised by the current cosmological model; the final section of this review discusses some of the ways in which the vacuum-energy problem is being addressed. For more details, see the review on Dark Energy – Sec. 28.

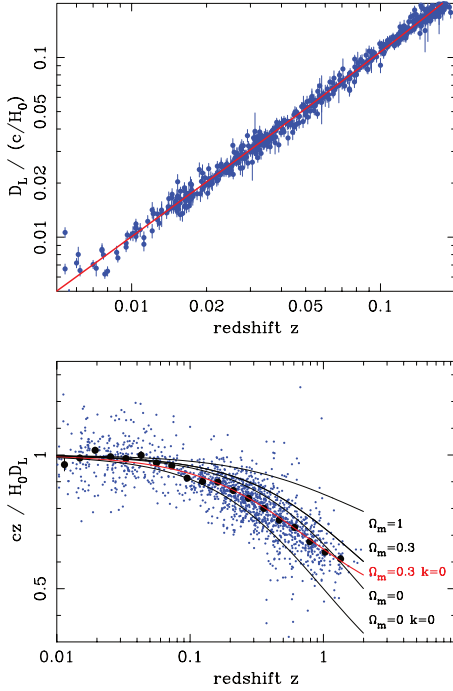


Figure 22.1: The type Ia supernova Hubble diagram, based on 1650 publicly available supernova distance estimates [28–30]. The first panel shows that for $z \ll 1$ the large-scale Hubble flow is indeed linear and uniform; the second panel shows an expanded scale, with the linear trend divided out, and with the redshift range extended to show how the Hubble law becomes nonlinear. ($\Omega_r = 0$ is assumed.) Larger points with errors show median values in redshift bins. Comparison with the prediction of Friedmann models favors a vacuum-dominated Universe.

22.2 Introduction to observational cosmology

22.2.1 Fluxes, luminosities, and distances

The key quantities for observational cosmology can be deduced quite directly from the metric.

(1) The *proper* transverse size of an object seen by us to subtend an angle $d\psi$ is its comoving size $d\psi S_k(\chi)$ times the scale factor at the time of emission:

$$dl = d\psi R_0 S_k(\chi)/(1+z). \quad (22.23)$$

(2) The apparent flux density of an object is deduced by allowing its photons to flow through a sphere of current radius $R_0 S_k(\chi)$; but photon energies and arrival rates are redshifted, and the bandwidth $d\nu$ is reduced. The observed photons at frequency ν_0 were emitted at frequency $\nu_0(1+z)$, so the flux density is the luminosity at this frequency, divided by the total area, divided by $1+z$:

$$S_\nu(\nu_0) = \frac{L_\nu([1+z]\nu_0)}{4\pi R_0^2 S_k^2(\chi)(1+z)}. \quad (22.24)$$

These relations lead to the following common definitions:

$$\begin{aligned} \text{angular-diameter distance: } D_A &= (1+z)^{-1} R_0 S_k(\chi) \\ \text{luminosity distance: } D_L &= (1+z) R_0 S_k(\chi). \end{aligned} \quad (22.25)$$

These distance-redshift relations are expressed in terms of observables by using the equation of a null radial geodesic ($R(t)d\chi = dt$) plus the Friedmann equation:

$$\begin{aligned} R_0 d\chi &= \frac{1}{H(z)} dz = \frac{1}{H_0} [(1 - \Omega_m - \Omega_v - \Omega_r)(1+z)^2 \\ &\quad + \Omega_v(1+z)^{3+3w} + \Omega_m(1+z)^3 \\ &\quad + \Omega_r(1+z)^4]^{-1/2} dz. \end{aligned} \quad (22.26)$$

The main scale for the distance here is the Hubble length, $1/H_0$. The flux density is the product of the specific intensity I_ν and the solid angle $d\Omega$ subtended by the source: $S_\nu = I_\nu d\Omega$. Combining the angular size and flux-density relations thus gives the relativistic version of surface-brightness conservation:

$$I_\nu(\nu_0) = \frac{B_\nu([1+z]\nu_0)}{(1+z)^3}, \quad (22.27)$$

where B_ν is surface brightness (luminosity emitted into unit solid angle per unit area of source). We can integrate over ν_0 to obtain the corresponding total or bolometric formula:

$$I_{\text{tot}} = \frac{B_{\text{tot}}}{(1+z)^4}. \quad (22.28)$$

This cosmology-independent form expresses Liouville's Theorem: photon phase-space density is conserved along rays.

22.2.2 Distance data and geometrical tests of cosmology

In order to confront these theoretical predictions with data, we have to bridge the divide between two extremes. Nearby objects may have their distances measured quite easily, but their radial velocities are dominated by deviations from the ideal Hubble flow, which typically have a magnitude of several hundred km s^{-1} . On the other hand, objects at redshifts $z \gtrsim 0.01$ will have observed recessional velocities that differ from their ideal values by $\lesssim 10\%$, but absolute distances are much harder to supply in this case. The traditional solution to this problem is the construction of the distance ladder: an interlocking set of methods for obtaining relative distances between various classes of object, which begins with absolute distances at the 10 to 100 pc level, and terminates with galaxies at significant redshifts. This is discussed in the article on Cosmological Parameters – Sec. 25 of this *Review*.

One of the key developments in this area has been the use of type Ia supernovae (SNe), which now allow measurement of relative distances with 5% precision. In combination with improved Cepheid data from the HST plus improved measurements of the distance to the LMC (or alternatively a direct geometrical distance to the maser galaxy NGC4258), SNe results extend the distance ladder to the point where deviations from uniform expansion are negligible, leading to the best existing Cepheid-based value for H_0 : $73.2 \pm 1.3 \text{ km s}^{-1} \text{ Mpc}^{-1}$ [31]. Better still, the analysis of high- z SNe has allowed a simple and direct test of cosmological geometry to be carried out: as shown in Fig. 22.1 and Fig. 22.2, supernova data and measurements of CMB anisotropies strongly favor a $k = 0$ model dominated by vacuum energy. It is worth noting that there is some tension (4.2σ) between the Cepheid and CMB determinations of H_0 (the latter is 67.4 ± 0.5 [24]). While it is remarkable that the two very different methods give such similar results, the formal disagreement shows that either there are unidentified systematic errors or that some new post-CDM physics is required; there is no current consensus in the community on these alternatives. We do note that a recent analysis of SNe Ia with a calibration of the tip of the red-giant branch gives a result close to that of the CMB: 69.8 ± 0.6 (stat.) ± 1.6 (sys.) $\text{km s}^{-1} \text{ Mpc}^{-1}$ [32, 33]. (See the review on Cosmological Parameters – Sec. 25 of this *Review* for a more comprehensive review of Hubble parameter determinations.)

22.2.3 Age of the Universe

The most striking conclusion of relativistic cosmology is that the Universe has not existed forever. The dynamical result for the age of the Universe may be written as

$$\begin{aligned} H_0 t_0 &= \int_0^\infty \frac{dz}{(1+z)H(z)} \\ &= \int_0^\infty \frac{dz}{(1+z)[(1+z)^2(1+\Omega_m z) - z(2+z)\Omega_v]^{1/2}}, \end{aligned} \quad (22.29)$$

where we have neglected Ω_r and chosen $w = -1$. Over the range of interest ($0.1 \lesssim \Omega_m \lesssim 1$, $|\Omega_v| \lesssim 1$), this exact answer may be approximated to a few per cent accuracy by

$$H_0 t_0 \simeq \frac{2}{3} (0.7\Omega_m + 0.3 - 0.3\Omega_v)^{-0.3}. \quad (22.30)$$

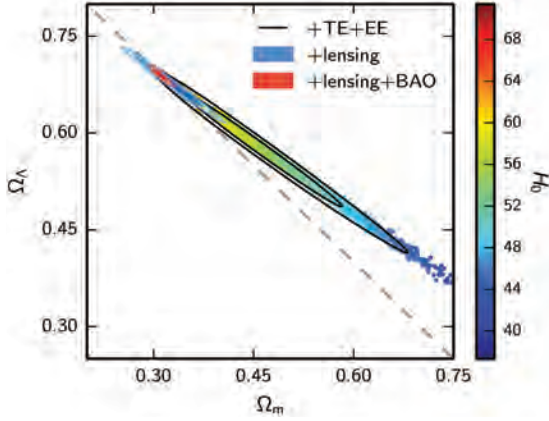


Figure 22.2: Likelihood-based probability densities over the plane Ω_Λ (i.e., Ω_ν assuming $w = -1$) vs Ω_m . The colored locus derives from *Planck* [34] and shows that the CMB alone requires a flat Universe $\Omega_\nu + \Omega_m \simeq 1$ if the Hubble constant is not too high. The SNe Ia results [35] very nearly constrain the orthogonal combination $\Omega_\nu - \Omega_m$, and the intersection of these constraints directly favors a flat model with $\Omega_m \simeq 0.3$, as does the measurement of the Baryon Acoustic Oscillation lengthscale (for which a joint constraint is shown on this plot). The CMB alone is capable of breaking the degeneracy with H_0 by using the measurements of gravitational lensing that can be made with modern high-resolution CMB data.

For the special case that $\Omega_m + \Omega_\nu = 1$, the integral in Eq. (22.29) can be expressed analytically as

$$H_0 t_0 = \frac{2}{3\sqrt{\Omega_\nu}} \ln \frac{1 + \sqrt{\Omega_\nu}}{\sqrt{1 - \Omega_\nu}} \quad (\Omega_m < 1). \quad (22.31)$$

The most accurate means of obtaining ages for astronomical objects is based on the natural clocks provided by radioactive decay. The use of these clocks is complicated by a lack of knowledge of the initial conditions of the decay. In the Solar System, chemical fractionation of different elements helps pin down a precise age for the pre-Solar nebula of 4.6 Gyr, but for stars it is necessary to attempt an a priori calculation of the relative abundances of nuclei that result from supernova explosions. In this way, a lower limit for the age of stars in the local part of the Milky Way of about 11 Gyr is obtained [36, 37].

The other major means of obtaining cosmological age estimates is based on the theory of stellar evolution. In principle, the main-sequence turnoff point in the color-magnitude diagram of a globular cluster should yield a reliable age. But these have been controversial, owing to theoretical uncertainties in the evolution model – as well as observational uncertainties in the distance, dust extinction, and metallicity of clusters. The present consensus favors ages for the oldest clusters of about 13 Gyr [38].

These methods are all consistent with the age deduced from studies of structure formation, using the microwave background and large-scale structure: $t_0 = 13.80 \pm 0.02$ Gyr [24], where the extra accuracy comes at the price of assuming the simple 6-parameter Λ CDM model to be true.

22.2.4 Horizon, isotropy, flatness problems

For photons, the radial equation of motion is just $c dt = R d\chi$. How far can a photon get in a given time? The answer is clearly

$$\Delta\chi = \int_{t_1}^{t_2} \frac{dt}{R(t)} \equiv \Delta\eta, \quad (22.32)$$

i.e., just the interval of conformal time. We can replace dt by dR/R , which the Friedmann equation says is $\propto dR/\sqrt{\rho R^2}$ at early times. Thus, this integral converges if $\rho R^2 \rightarrow \infty$ as $t_1 \rightarrow 0$, otherwise it diverges. Provided the equation of state is such that ρ changes faster than R^{-2} , light signals can only propagate a finite distance between the Big Bang and the present; there is then

said to be a particle horizon. Such a horizon therefore exists in conventional Big-Bang models, which are dominated by radiation ($\rho \propto R^{-4}$) at early times.

At late times, the integral for the horizon is largely determined by the matter-dominated phase, for which

$$D_H = R_0 \chi_H \equiv R_0 \int_0^{t(z)} \frac{dt}{R(t)} \simeq \frac{6000}{\sqrt{\Omega_m z}} h^{-1} \text{Mpc} \quad (z \gg 1). \quad (22.33)$$

The horizon at the time of formation of the microwave background ('last scattering': $z \simeq 1100$) was thus of order 100 Mpc in size, subtending an angle of about 1° . Why then are the large number of causally disconnected regions we see on the microwave sky all at the same temperature? The Universe is very nearly isotropic and homogeneous, even though the initial conditions appear not to permit such a state to be constructed.

A related problem is that the $\Omega = 1$ Universe is unstable:

$$\Omega(a) - 1 = \frac{\Omega - 1}{1 - \Omega + \Omega_\nu a^2 + \Omega_m a^{-1} + \Omega_r a^{-2}}, \quad (22.34)$$

where Ω with no subscript is the total density parameter, and $a(t) = R(t)/R_0$. This requires $\Omega(t)$ to be unity to arbitrary precision as the initial time tends to zero; a Universe of non-zero curvature today requires very finely tuned initial conditions.

22.3 The Hot Thermal Universe

22.3.1 Thermodynamics of the early Universe

As alluded to above, we expect that much of the early Universe can be described by a radiation-dominated equation of state. In addition, through much of the radiation-dominated period, thermal equilibrium is established by the rapid rate of particle interactions relative to the expansion rate of the Universe (see Sec. 22.3.3 below). In equilibrium, it is straightforward to compute the thermodynamic quantities, ρ , p , and the entropy density, s . In general, the energy density for a given particle type i can be written as

$$\rho_i = \int E_i dn_{q_i}, \quad (22.35)$$

with the density of states given by

$$dn_{q_i} = \frac{g_i}{2\pi^2} (\exp[(E_{q_i} - \mu_i)/T_i] \pm 1)^{-1} q_i^2 dq_i, \quad (22.36)$$

where g_i counts the number of degrees of freedom for particle type i , $E_{q_i}^2 = m_i^2 + q_i^2$, μ_i is the chemical potential, and the \pm corresponds to either Fermi or Bose statistics. Similarly, we can define the pressure of a perfect gas as

$$p_i = \frac{1}{3} \int \frac{q_i^2}{E_i} dn_{q_i}. \quad (22.37)$$

The number density of species i is simply

$$n_i = \int dn_{q_i}, \quad (22.38)$$

and the entropy density is

$$s_i = \frac{\rho_i + p_i - \mu_i n_i}{T_i}. \quad (22.39)$$

In the Standard Model, a chemical potential is often associated with baryon number, and since the net baryon density relative to the photon density is known to be very small (of order 10^{-9}), we can neglect any such chemical potential when computing total thermodynamic quantities.

For photons, we can compute all of the thermodynamic quantities rather easily. Taking $g_i = 2$ for the 2 photon polarization states, we have (in units where $\hbar = k_B = 1$)

$$\rho_\gamma = \frac{\pi^2}{15} T^4, \quad p_\gamma = \frac{1}{3} \rho_\gamma, \quad s_\gamma = \frac{4\rho_\gamma}{3T}, \quad n_\gamma = \frac{2\zeta(3)}{\pi^2} T^3, \quad (22.40)$$

with $2\zeta(3)/\pi^2 \simeq 0.2436$. Note that Eq. (22.10) can be converted into an equation for entropy conservation. Recognizing that $\dot{p} = s\dot{T}$, Eq. (22.10) becomes

$$d(sR^3)/dt = 0. \tag{22.41}$$

For radiation, this corresponds to the relationship between expansion and cooling, $T \propto R^{-1}$ in an adiabatically expanding Universe. Note also that both s and n_γ scale as T^3 .

22.3.2 Radiation content of the Early Universe

At the very high temperatures associated with the early Universe, massive particles are pair produced, and are part of the thermal bath. If for a given particle species i we have $T \gg m_i$, then we can neglect the mass in Eq. (22.35) to Eq. (22.39), and the thermodynamic quantities are easily computed as in Eq. (22.40). In general, we can approximate the energy density (at high temperatures) by including only those particles with $m_i \ll T$. In this case, we have

$$\rho = \left(\sum_B g_B + \frac{7}{8} \sum_F g_F \right) \frac{\pi^2}{30} T^4 \equiv \frac{\pi^2}{30} N(T) T^4, \tag{22.42}$$

where $g_{B(F)}$ is the number of degrees of freedom of each boson (fermion) and the sum runs over all boson and fermion states with $m \ll T$. The factor of $7/8$ is due to the difference between the Fermi and Bose integrals. Eq. (22.42) defines the effective number of degrees of freedom, $N(T)$, by taking into account new particle degrees of freedom as the temperature is raised. This quantity, calculated from high temperature lattice QCD, is plotted in Fig. 22.3 [39]. Near the QCD transition, there is a slight difference between the coefficient of T^4 for ρ and the coefficient of T^3 for the entropy density $s = (2\pi^2/45)N_s(T)T^3$ [40], as seen in the figure.

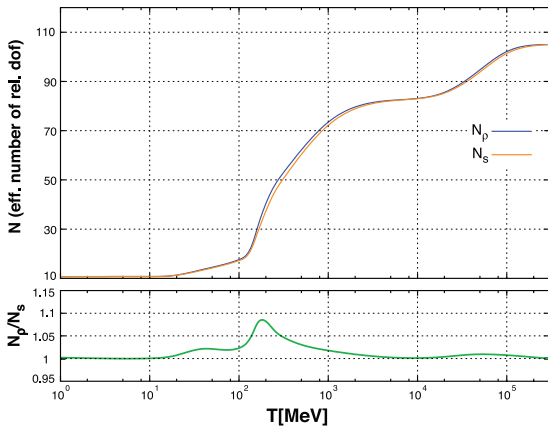


Figure 22.3: The effective numbers of relativistic degrees of freedom as a function of temperature. The sharp drop corresponds to the quark-hadron transition. The bottom panel shows the relative ratio between the number of degrees of freedom characterizing the energy density and the entropy.

The value of $N(T)$ at any given temperature depends on the particle physics model. In the standard $SU(3) \times SU(2) \times U(1)$ model, we can specify $N(T)$ up to temperatures of $O(100)$ GeV. The change in N (ignoring mass effects) can be seen in the table below.

Temperature	New Particles	$4N(T)$
$T < m_e$	γ 's + ν 's	29
$m_e < T < m_\mu$	e^\pm	43
$m_\mu < T < m_\pi$	μ^\pm	57
$m_\pi < T < T_c^\dagger$	π 's	69
$T_c < T < m_{\text{strange}}$	π 's + u, \bar{u}, d, \bar{d} + gluons	205
$m_s < T < m_{\text{charm}}$	s, \bar{s}	247
$m_c < T < m_\tau$	c, \bar{c}	289
$m_\tau < T < m_{\text{bottom}}$	τ^\pm	303
$m_b < T < m_{W,Z}$	b, \bar{b}	345
$m_{W,Z} < T < m_{\text{Higgs}}$	W^\pm, Z	381
$m_H < T < m_{\text{top}}$	H^0	385
$m_t < T$	t, \bar{t}	427

$^\dagger T_c$ corresponds to the confinement-deconfinement transition between quarks and hadrons.

At higher temperatures, $N(T)$ will be model-dependent. For example, in the minimal $SU(5)$ model, one needs to add 24 states to $N(T)$ for the charged and colored X and Y gauge bosons, another 24 from the adjoint Higgs, and another 6 scalar degrees of freedom (in addition to the 4 associated with the complex Higgs doublet already counted in the longitudinal components of W^\pm and Z , and in H) from the $\bar{5}$ of Higgs. Hence for $T > m_X$ in minimal $SU(5)$, $N(T) = 160.75$. In a supersymmetric model this would at least double.

In the radiation-dominated epoch, Eq. (22.10) can be integrated (neglecting the T -dependence of N) giving us a relationship between the age of the Universe and its temperature

$$t = \left(\frac{90}{32\pi^3 G_N N(T)} \right)^{1/2} T^{-2}. \tag{22.43}$$

Put into a more convenient form

$$t T_{\text{MeV}}^2 = 2.4 [N(T)]^{-1/2}, \tag{22.44}$$

where t is measured in seconds and T_{MeV} in units of MeV.

22.3.3 Neutrinos and equilibrium

Due to the expansion of the Universe, certain rates may be too slow to either establish or maintain equilibrium. Quantitatively, for each particle i , as a minimal condition for equilibrium, we will require that some rate Γ_i involving that type be larger than the expansion rate of the Universe, or

$$\Gamma_i > H. \tag{22.45}$$

Recalling that the age of the Universe is determined by H^{-1} , this condition is equivalent to requiring that on average, at least one interaction has occurred over the lifetime of the Universe.

A good example for a process that goes in and out of equilibrium is the weak interaction of neutrinos. On dimensional grounds, one can estimate the thermally averaged scattering cross-section:

$$\langle \sigma v \rangle \sim O(10^{-2}) T^2 / m_W^4 \tag{22.46}$$

for $T \lesssim m_W$. Recalling that the number density of leptons is $n \propto T^3$, we can compare the weak interaction rate, $\Gamma_{\text{wk}} \sim n \langle \sigma v \rangle$, with the expansion rate,

$$H = \left(\frac{8\pi G_N \rho}{3} \right)^{1/2} = \left(\frac{8\pi^3}{90} N(T) \right)^{1/2} T^2 / M_P \tag{22.47}$$

$$\simeq 1.66 N(T)^{1/2} T^2 / M_P,$$

where the Planck mass $M_P = G_N^{-1/2} = 1.22 \times 10^{19}$ GeV.

Neutrinos will be in equilibrium when $\Gamma_{\text{wk}} > H$ or

$$T > (500 m_W^4 / M_P)^{1/3} \sim 1 \text{ MeV}. \tag{22.48}$$

However, this condition assumes $T \ll m_W$; for higher temperatures, we should write $\langle \sigma v \rangle \sim O(10^{-2})/T^2$, so that $\Gamma \sim 10^{-2} T$. Thus, in the very early stages of expansion, at temperatures $T \gtrsim 10^{-2} M_P / \sqrt{N}$, equilibrium will not have been established.

Having attained a quasi-equilibrium stage, the Universe then cools further to the point where the interaction and expansion

timescales match once again. The temperature at which these rates are equal is commonly referred to as the neutrino decoupling or freeze-out temperature and is defined by $\Gamma_{\text{wk}}(T_d) = H(T_d)$. For $T < T_d$, neutrinos drop out of equilibrium. The Universe becomes transparent to neutrinos and their momenta simply redshift with the cosmic expansion. The effective neutrino temperature will simply fall with $T \sim 1/R$.

Soon after decoupling, e^\pm pairs in the thermal background begin to annihilate (when $T \lesssim m_e$). Because the neutrinos are decoupled, the energy released due to annihilation heats up the photon background relative to the neutrinos. The change in the photon temperature can be easily computed from entropy conservation. The neutrino entropy must be conserved separately from the entropy of interacting particles. A straightforward computation yields

$$T_\nu = (4/11)^{1/3} T_\gamma \simeq 1.9 \text{ K}. \quad (22.49)$$

The total entropy density is therefore given by the contribution from photons and 3 flavors of neutrinos

$$s = \frac{4}{3} \frac{\pi^2}{30} \left(2 + \frac{21}{4} (T_\nu/T_\gamma)^3 \right) T_\gamma^3 = \frac{4}{3} \frac{\pi^2}{30} \left(2 + \frac{21}{11} \right) T_\gamma^3 = 7.04 n_\gamma. \quad (22.50)$$

Similarly, the total relativistic energy density is given by

$$\rho_r = \frac{\pi^2}{30} \left[2 + \frac{21}{4} (T_\nu/T_\gamma)^4 \right] T_\gamma^4 \simeq 1.68 \rho_\gamma. \quad (22.51)$$

In practice, a small correction is needed to this, since neutrinos are not totally decoupled at e^\pm annihilation: the effective number of massless neutrino species is 3.044, rather than 3 [41].

This expression ignores neutrino rest masses, but current oscillation data require at least one neutrino eigenstate to have a mass exceeding 0.05 eV. In this minimal case, $\Omega_\nu h^2 = 6 \times 10^{-4}$, so the neutrino contribution to the matter budget would be negligibly small (which is our normal assumption). However, a nearly degenerate pattern of mass eigenstates could allow larger densities, since oscillation experiments only measure differences in m^2 values. Note that a 0.05-eV neutrino has $T_\nu = m_\nu$ at $z \simeq 296$, so the above expression for the total present relativistic density is really only an extrapolation. However, neutrinos are almost certainly relativistic at all epochs where the radiation content of the Universe is dynamically significant.

22.3.4 Field theory and phase transitions

It is very likely that the Universe has undergone one or more phase transitions during the course of its evolution [42–45]. Our current vacuum state is described by $SU(3)_c \times U(1)_{\text{em}}$, which in the Standard Model is a remnant of an unbroken $SU(3)_c \times SU(2)_L \times U(1)_Y$ gauge symmetry. Symmetry breaking occurs when a non-singlet gauge field (the Higgs field in the Standard Model) picks up a non-vanishing vacuum expectation value, determined by a scalar potential. For example, a simple (non-gauged) potential describing symmetry breaking is $V(\phi) = \frac{1}{4} \lambda \phi^4 - \frac{1}{2} \mu^2 \phi^2 + V(0)$. The resulting expectation value is simply $\langle \phi \rangle = \mu/\sqrt{\lambda}$.

In the early Universe, finite temperature radiative corrections typically add terms to the potential of the form $\phi^2 T^2$. Thus, at very high temperatures, the symmetry is restored and $\langle \phi \rangle = 0$. As the Universe cools, depending on the details of the potential, symmetry breaking will occur via a first-order phase transition in which the field tunnels through a potential barrier, or via a second-order transition in which the field evolves smoothly from one state to another (as would be the case for the above example potential).

The evolution of scalar fields can have a profound impact on the early Universe. The equation of motion for a scalar field ϕ can be derived from the energy-momentum tensor

$$T_{\mu\nu} = \partial_\mu \phi \partial_\nu \phi - \frac{1}{2} g_{\mu\nu} \partial_\rho \phi \partial^\rho \phi - g_{\mu\nu} V(\phi). \quad (22.52)$$

By associating $\rho = T_{00}$ and $p = R^{-2}(t)T_{ii}$ we have

$$\begin{aligned} \rho &= \frac{1}{2} \dot{\phi}^2 + \frac{1}{2} R^{-2}(t) (\nabla \phi)^2 + V(\phi) \\ p &= \frac{1}{2} \dot{\phi}^2 - \frac{1}{6} R^{-2}(t) (\nabla \phi)^2 - V(\phi), \end{aligned} \quad (22.53)$$

and from Eq. (22.10) we can write the equation of motion (by considering a homogeneous region, we can ignore the gradient terms)

$$\ddot{\phi} + 3H\dot{\phi} = -\partial V/\partial \phi. \quad (22.54)$$

22.3.5 Inflation

In Sec. 22.2.4, we discussed some of the problems associated with the standard Big-Bang model. However, during a phase transition, our assumptions of an adiabatically expanding Universe are generally not valid. If, for example, a phase transition occurred in the early Universe such that the field evolved slowly from the symmetric state to the global minimum, the Universe may have been dominated by the vacuum energy density associated with the potential near $\phi \simeq 0$. During this period of slow evolution, the energy density due to radiation will fall below the vacuum energy density, $\rho \ll V(0)$. When this happens, the expansion rate will be dominated by the constant $V(0)$, and we obtain the exponentially expanding solution given in Eq. (22.20). When the field evolves towards the global minimum it will begin to oscillate about the minimum, energy will be released during its decay, and a hot thermal Universe will be restored. If released fast enough, it will produce radiation at a temperature $NT_{\text{R}}^4 \lesssim V(0)$. In this reheating process, entropy has been created and the final value of RT is greater than the initial value of RT . Thus, we see that, during a phase transition, the relation $RT \sim \text{constant}$ need not hold true. This is the basis of the inflationary Universe scenario [46–48].

If, during the phase transition, the value of RT changed by a factor of $O(10^{29})$, the cosmological problems discussed above would be solved. The observed isotropy would be generated by the immense expansion; one small causal region could get blown up, and thus our entire visible Universe would have been in thermal contact some time in the past. In addition, the density parameter Ω would have been driven to 1 (with exponential precision). Density perturbations will be stretched by the expansion, $\lambda \sim R(t)$. Thus it will appear that $\lambda \gg H^{-1}$ or that the perturbations have left the horizon, where in fact the size of the causally connected region is now no longer simply H^{-1} . However, not only does inflation offer an explanation for large scale perturbations, it also offers a source for the perturbations themselves through quantum fluctuations.

Problems with early models of inflation based on either a first-order [49] or second-order [50, 51] phase transition of a Grand Unified Theory led to models invoking a completely new scalar field: the inflaton, ϕ . The potential of this field, $V(\phi)$, needs to have a very low gradient and curvature in order to match observed metric fluctuations. For a more thorough discussion of the problems of early models and a host of current models being studied see the review on inflation – Sec. 23 of this *Review*. In most current inflation models, reheated bubbles typically do not percolate, so inflation is ‘eternal’ and continues with exponential expansion in the region outside bubbles. These causally disconnected bubble Universes constitute a ‘multiverse’, where low-energy physics can vary between different bubbles. This has led to a controversial ‘anthropic’ approach to cosmology [52–54], where observer selection within the multiverse can be introduced as a means of understanding e.g. why the observed level of vacuum energy is so low (because larger values suppress growth of structure).

22.3.6 Baryogenesis

The Universe appears to be populated exclusively with matter rather than antimatter. Indeed antimatter is only detected in accelerators or in cosmic rays. However, the presence of antimatter in the latter is understood to be the result of collisions of primary particles in the interstellar medium. There is in fact strong evidence against primary forms of antimatter in the Universe. Furthermore, the density of baryons compared to the density of photons is extremely small, $\eta \sim 10^{-9}$.

The production of a net baryon asymmetry requires baryon number violating interactions, C and CP violation, and a departure from thermal equilibrium [55]. The first two of these ingredients are expected to be contained in Grand Unified Theories (GUTs) as well as in the non-perturbative sector of the Standard Model; the third can be realized in an expanding Universe where, as we have seen, interactions come in and out of equilibrium.

There are several interesting and viable mechanisms for the production of the baryon asymmetry. While we can not review any of them here in any detail, we mention some of the important scenarios. In all cases, all three ingredients listed above are incorporated. One of the first mechanisms was based on the out of equilibrium decay of a massive particle such as a superheavy GUT gauge or Higgs boson [56, 57]. A novel mechanism involving the decay of flat directions in supersymmetric models is known as the Affleck-Dine scenario [58]. There is also the possibility of generating the baryon asymmetry at the electro-weak scale using the non-perturbative interactions of sphalerons [59]. Because these interactions conserve the sum of baryon and lepton number, $B + L$, it is possible to first generate a lepton asymmetry (*e.g.*, by the out-of-equilibrium decay of a superheavy right-handed neutrino), which is converted to a baryon asymmetry at the electro-weak scale [60]. This mechanism is known as leptobaryogenesis, or simply leptogenesis.

22.3.7 Nucleosynthesis

An essential element of the standard cosmological model is Big-Bang nucleosynthesis (BBN), the theory that predicts the abundances of the light element isotopes D, ^3He , ^4He , and ^7Li . Nucleosynthesis takes place at a temperature scale of order 1 MeV. The nuclear processes lead primarily to ^4He , with a primordial mass fraction of about 25%. Lesser amounts of the other light elements are produced: about 10^{-5} of D and ^3He and about 10^{-10} of ^7Li by number relative to H. The abundances of the light elements depend almost solely on one key parameter, the baryon-to-photon ratio, η . The nucleosynthesis predictions can be compared with observational determinations of the abundances of the light elements. Consistency between theory and observations driven primarily by recent D/H measurements [61, 62] leads to a range of

$$5.8 \times 10^{-10} < \eta < 6.5 \times 10^{-10}. \quad (22.55)$$

η is related to the fraction of Ω contained in baryons:

$$\Omega_b = 3.66 \times 10^7 \eta h^{-2}, \quad (22.56)$$

or $10^{10} \eta = 274 \Omega_b h^2$. The *Planck* result [24] for $\Omega_b h^2$ of 0.0224 ± 0.0002 translates into a value of $\eta = 6.12 \pm 0.04$. This result can be used to ‘predict’ the light element abundances, which can in turn be compared with observation [63]. The resulting D/H abundance is in excellent agreement with that found in quasar absorption systems. It is in reasonable agreement with the helium abundance observed in extragalactic HII regions (once systematic uncertainties are accounted for), but is in poor agreement with the Li abundance observed in the atmospheres of halo dwarf stars [64]. See the review on BBN – Sec. 24 of this *Review* for a detailed discussion of BBN or references [65–69].

22.3.8 The transition to a matter-dominated Universe

In the Standard Model, the temperature (or redshift) at which the Universe undergoes a transition from a radiation-dominated to a matter-dominated Universe is determined by the amount of dark matter. Assuming three nearly massless neutrinos, the energy density in radiation at temperatures $T \ll 1$ MeV, is given by

$$\rho_r = \frac{\pi^2}{30} \left[2 + \frac{21}{4} \left(\frac{4}{11} \right)^{4/3} \right] T^4. \quad (22.57)$$

In the absence of non-baryonic dark matter, the matter density can be written as

$$\rho_m = m_N \eta n_\gamma, \quad (22.58)$$

where m_N is the nucleon mass. Recalling that $n_\gamma \propto T^3$ [cf. Eq. (22.40)], we can solve for the temperature or redshift at the

matter-radiation equality when $\rho_r = \rho_m$,

$$T_{\text{eq}} = 0.22 m_N \eta \quad \text{or} \quad (1 + z_{\text{eq}}) = 0.22 \eta \frac{m_N}{T_0}, \quad (22.59)$$

where T_0 is the present temperature of the microwave background. For $\eta = 6.1 \times 10^{-10}$, this corresponds to a temperature $T_{\text{eq}} \simeq 0.13$ eV or $(1 + z_{\text{eq}}) \simeq 550$. A transition this late would be problematic for structure formation (see Sec. 22.4.5).

The redshift of matter domination can be pushed back significantly if non-baryonic dark matter is present. If instead of Eq. (22.58), we write

$$\rho_m = \Omega_m \rho_c \left(\frac{T}{T_0} \right)^3, \quad (22.60)$$

we find that

$$T_{\text{eq}} = 0.9 \frac{\Omega_m \rho_c}{T_0^3} \quad \text{or} \quad (1 + z_{\text{eq}}) = 2.4 \times 10^4 \Omega_m h^2. \quad (22.61)$$

22.4 The Universe at late times

22.4.1 The CMB

One form of the infamous Olbers’ paradox says that, in Euclidean space, surface brightness is independent of distance. Every line of sight will terminate on matter that is hot enough to be ionized and so scatter photons: $T \gtrsim 10^3$ K, and the sky should therefore shine as brightly as the surface of the Sun. The reason the night sky is dark is entirely due to the expansion, which cools the radiation temperature to 2.73 K. This gives a Planck function peaking at around 1 mm to produce the CMB.

The CMB spectrum is a very accurate match to a Planck function [70]. (See the review on CMB – Sec. 29 of this *Review*.) The COBE estimate of the temperature is [71]

$$T = 2.7255 \pm 0.0006 \text{ K}. \quad (22.62)$$

The lack of any distortion of the Planck spectrum is a strong physical constraint. It is very difficult to account for in any expanding Universe other than one that passes through a hot stage. Alternative schemes for generating the radiation, such as thermalization of starlight by dust grains, inevitably generate a superposition of temperatures. What is required in addition to thermal equilibrium is that $T \propto 1/R$, so that radiation from different parts of space arrive at an observer with the same apparent temperature.

Although it is common to speak of the CMB as originating at ‘recombination’, a more accurate terminology is the era of ‘last scattering’. In practice, this takes place at $z \simeq 1100$, almost independently of the main cosmological parameters, at which time the fractional ionization is very small. This occurred when the age of the Universe was about 370,000 years. But the CMB photons themselves were not generated at this point, and were the result of thermalization at $z \sim 10^7$. (See the review on CMB – Sec. 29 of this *Review* for a full discussion of the CMB.)

22.4.2 Matter in the Universe

One of the main tasks of cosmology is to measure the density of the Universe, and how this is divided between dark matter and baryons. The baryons consist partly of stars, with $0.002 \lesssim \Omega_* \lesssim 0.003$ [72] but mainly inhabit the intergalactic medium (IGM). One powerful way in which this can be studied is via the absorption of light from distant luminous objects such as quasars. Even very small amounts of neutral hydrogen can absorb rest-frame UV photons (the Gunn-Peterson effect), and should suppress the continuum by a factor $\exp(-\tau)$, where

$$\tau \simeq 10^{4.62} h^{-1} \left[\frac{n_{\text{HI}}(z)/\text{m}^{-3}}{(1+z)\sqrt{1+\Omega_m}} \right], \quad (22.63)$$

and this expression applies while the Universe is matter dominated ($z \gtrsim 1$ in the $\Omega_m = 0.3$ $\Omega_v = 0.7$ model). At $z < 6$, the dominant effect on quasar spectra is a ‘forest’ of narrow absorption lines, which produce a mean $\tau = 1$ in the Ly α forest at about $z = 3$, and so we have $\Omega_{\text{HI}} \simeq 10^{-6.7} h^{-1}$. This is such a small number that the IGM must be very highly ionized at these redshifts, apart

from a few high-density clumps. But at $z > 6$ there is good evidence for a ‘reionization’ era at which the general IGM is not so strongly ionized [73]. As discussed below, this ionized IGM at low z is also detectable via the secondary Compton scattering of CMB photons.

The Ly α forest is of great importance in pinning down the abundance of deuterium. Because electrons in deuterium differ in reduced mass by about 1 part in 4000 compared to hydrogen, each absorption system in the Ly α forest is accompanied by an offset deuterium line. By careful selection of systems with an optimal HI column density, a measurement of the D/H ratio can be made. This has now been done with high accuracy in 10 quasars, with consistent results [61]. Combining these determinations with the theory of primordial nucleosynthesis yields a baryon density of $\Omega_b h^2 = 0.021 - 0.024$ (95% confidence) in excellent agreement with the Planck result. (See also the review on BBN – Sec. 24 of this *Review*.)

Ionized IGM can also be detected in emission when it is densely clumped, via bremsstrahlung radiation. This generates the spectacular X-ray emission from rich clusters of galaxies. Studies of this phenomenon allow us to achieve an accounting of the total baryonic material in clusters. Within the central $\simeq 1$ Mpc, the masses in stars, X-ray emitting gas, and total dark matter can be determined with reasonable accuracy (perhaps 20% rms), and this allows a minimum baryon fraction to be determined [74, 75]:

$$\frac{M_{\text{baryons}}}{M_{\text{total}}} \gtrsim 0.009 + (0.066 \pm 0.003) h^{-3/2}. \quad (22.64)$$

Because clusters are the largest collapsed structures, it is reasonable to take this as applying to the Universe as a whole. This equation implies a minimum baryon fraction of perhaps 12% (for reasonable h), which is too high for $\Omega_m = 1$ if we take $\Omega_b h^2 \simeq 0.02$ from nucleosynthesis. This is therefore one of the more robust arguments in favor of $\Omega_m \simeq 0.3$. (See the review on Cosmological Parameters – Sec. 25 of this *Review*.) This argument is also consistent with the inference on Ω_m that can be made from Fig. 22.2.

This method is much more robust than the older classical technique for weighing the Universe: ‘ $L \times M/L$ ’. The overall light density of the Universe is reasonably well determined from redshift surveys of galaxies, so that a good determination of mass M and luminosity L for a single object suffices to determine Ω_m – but only *if* the mass-to-light ratio were universal.

22.4.3 Gravitational lensing

A robust method for determining masses in cosmology is to use gravitational light deflection. Most systems can be treated as a geometrically thin gravitational lens, where the light bending is assumed to take place only at a single distance. Simple geometry then determines a mapping between the coordinates in the intrinsic source plane (S) and the observed image plane (I):

$$\alpha(D_L \theta_I) = \frac{D_S}{D_{LS}} (\theta_I - \theta_S), \quad (22.65)$$

where the angles θ_I, θ_S , and α are in general two-dimensional vectors on the sky. The distances D_{LS} etc. are given by an extension of the usual distance-redshift formula:

$$D_{LS} = \frac{R_0 S_k (\chi_S - \chi_L)}{1 + z_S}. \quad (22.66)$$

This is the angular-diameter distance for objects on the source plane as perceived by an observer on the lens.

Solutions of this equation divide into weak lensing, where the mapping between source plane and image plane is one-to-one, and strong lensing, in which multiple imaging is possible. For circularly-symmetric lenses, an on-axis source is multiply imaged into a ‘caustic’ ring, whose radius is the Einstein radius:

$$\begin{aligned} \theta_E &= \left(4GM \frac{D_{LS}}{D_L D_S} \right)^{1/2} \\ &= \left(\frac{M}{10^{11.09} M_\odot} \right)^{1/2} \left(\frac{D_L D_S / D_{LS}}{\text{Gpc}} \right)^{-1/2} \text{ arcsec}. \end{aligned} \quad (22.67)$$

The observation of ‘arcs’ (segments of near-perfect Einstein rings) in rich clusters of galaxies has thus given very accurate masses for the central parts of clusters – generally in good agreement with other indicators, such as analysis of X-ray emission from the cluster IGM [76, 77].

Gravitational lensing has also developed into a particularly promising probe of cosmological structure on 10-Mpc to 100-Mpc scales. Weak image distortions manifest themselves as an additional ellipticity of galaxy images (‘shear’), which can be observed by averaging many images together (the corresponding flux amplification is less readily detected). The result is a ‘cosmic shear’ field of order 1% ellipticity, coherent over scales of around 30 arcmin, which is directly related to the cosmic mass field. For this reason, weak lensing is seen as potentially the cleanest probe of matter fluctuations, next to the CMB. Already, impressive results have been obtained in measuring cosmological parameters, based on survey data from only $\sim 10^3$ deg 2 [78, 79]. A particular strength of lensing is its ability to measure the amplitude of mass fluctuations; this can be deduced from the amplitude of CMB fluctuations, but only with low precision on account of the poorly-known optical depth due to Compton scattering after reionization. However, the effect of weak lensing on the CMB map itself can be detected via the induced non-Gaussian signal, and this gives the CMB greater internal power [80]. The main difficulty of principle with lensing is that part of the signal is generated by small-scale density fluctuations; thus a model is required for nonlinear evolution, including astrophysical effects that separate baryons and dark matter. In this respect, the CMB is a cleaner probe of the primordial fluctuations.

22.4.4 Density fluctuations

The overall properties of the Universe are very close to being homogeneous; and yet telescopes reveal a wealth of detail on scales varying from single galaxies to large-scale structures of size exceeding 100 Mpc. The existence of these structures must be telling us something important about the initial conditions of the Big Bang, and about the physical processes that have operated subsequently. This motivates the study of the density perturbation field, defined as

$$\delta(\mathbf{x}) \equiv \frac{\rho(\mathbf{x}) - \langle \rho \rangle}{\langle \rho \rangle}. \quad (22.68)$$

A critical feature of the δ field is that it inhabits a Universe that is isotropic and homogeneous in its large-scale properties. This suggests that the statistical properties of δ should also be statistically homogeneous – *i.e.*, it is a stationary random process.

It is often convenient to describe δ as a Fourier superposition:

$$\delta(\mathbf{x}) = \sum \delta_{\mathbf{k}} e^{-i\mathbf{k} \cdot \mathbf{x}}. \quad (22.69)$$

We avoid difficulties with an infinite Universe by applying periodic boundary conditions in a cube of some large volume V . The cross-terms vanish when we compute the variance in the field, which is just a sum over modes of the power spectrum:

$$\langle \delta^2 \rangle = \sum |\delta_{\mathbf{k}}|^2 \equiv \sum P(k). \quad (22.70)$$

Note that the statistical nature of the fluctuations must be isotropic, so we write $P(k)$ rather than $P(\mathbf{k})$. The $\langle \dots \rangle$ average here is a volume average. Cosmological density fields are an example of an ergodic process, in which the average over a large volume tends to the same answer as the average over a statistical ensemble.

The statistical properties of discrete objects sampled from the density field are often described in terms of N -point correlation functions, which represent the excess probability over random for finding one particle in each of N boxes in a given configuration. For the 2-point case, the correlation function is readily shown to be identical to the autocorrelation function of the δ field: $\xi(r) = \langle \delta(x) \delta(x+r) \rangle$.

The power spectrum and correlation function are Fourier conjugates, and thus are equivalent descriptions of the density field

(similarly, k -space equivalents exist for the higher-order correlations). It is convenient to take the limit $V \rightarrow \infty$ and use k -space integrals, defining a dimensionless power spectrum, which measures the contribution to the fractional variance in density per unit logarithmic range of scale, as $\Delta^2(k) = d(\delta^2)/d \ln k = V k^3 P(k)/2\pi^2$:

$$\xi(r) = \int \Delta^2(k) \frac{\sin kr}{kr} d \ln k; \quad \Delta^2(k) = \frac{2}{\pi} k^3 \int_0^\infty \xi(r) \frac{\sin kr}{kr} r^2 dr. \quad (22.71)$$

For many years, an adequate approximation to observational data on galaxies was $\xi = (r/r_0)^{-\gamma}$, with $\gamma \simeq 1.8$ and $r_0 \simeq 5 h^{-1}$ Mpc. Modern surveys are now able to probe into the large-scale linear regime where unaltered traces of the curved post-recombination spectrum can be detected [81–83].

22.4.5 Formation of cosmological structure

The simplest model for the generation of cosmological structure is gravitational instability acting on some small initial fluctuations (for the origin of which a theory such as inflation is required). If the perturbations are adiabatic (*i.e.*, fractionally perturb number densities of photons and matter equally), the linear growth law for matter perturbations is simple:

$$\delta \propto \begin{cases} a^2(t) & (\text{radiation domination; } \Omega_r = 1); \\ a(t) & (\text{matter domination; } \Omega_m = 1). \end{cases} \quad (22.72)$$

For low-density Universes, the growth is slower:

$$d \ln \delta / d \ln a \simeq \Omega_m^\gamma(a), \quad (22.73)$$

where the parameter γ is close to 0.55 independent of the vacuum density [84, 85].

The alternative perturbation mode is isocurvature: only the equation of state changes, and the total density is initially unperturbed. These modes perturb the total entropy density, and thus induce additional large-scale CMB anisotropies [86]. Although the character of perturbations in the simplest inflationary theories are purely adiabatic, correlated adiabatic and isocurvature modes are predicted in many models; the simplest example is the curvaton, which is a scalar field that decays to yield a perturbed radiation density. If the matter content already exists at this time, the overall perturbation field will have a significant isocurvature component. Such a prediction is inconsistent with current CMB data [87], and most analyses of CMB and large-scale structure (LSS) data assume the adiabatic case to hold exactly.

Linear evolution preserves the shape of the power spectrum. However, a variety of processes mean that growth actually depends on the matter content.

1. Pressure opposes gravity effectively for wavelengths below the horizon length while the Universe is radiation dominated. The *comoving* horizon size at z_{eq} is therefore an important scale:

$$D_H(z_{\text{eq}}) = \frac{2(\sqrt{2}-1)}{(\Omega_m z_{\text{eq}})^{1/2} H_0} = \frac{16.0}{\Omega_m h^2} \text{Mpc}. \quad (22.74)$$

2. At early times, dark matter particles will undergo free streaming at the speed of light, and so erase all scales up to the horizon – a process that only ceases when the particles go nonrelativistic. For light massive neutrinos, this happens at z_{eq} ; all structure up to the horizon-scale power-spectrum break is in fact erased. Hot(cold) dark matter models are thus sometimes dubbed large(small)-scale damping models.
3. A further important scale arises where photon diffusion can erase perturbations in the matter – radiation fluid; this process is named Silk damping.

The overall effect is encapsulated in the transfer function, which gives the ratio of the late-time amplitude of a mode to its initial value (see Fig. 22.4). The overall power spectrum is thus the primordial scalar-mode power law, times the square of the transfer function:

$$P(k) \propto k^{n_s} T_k^2. \quad (22.75)$$

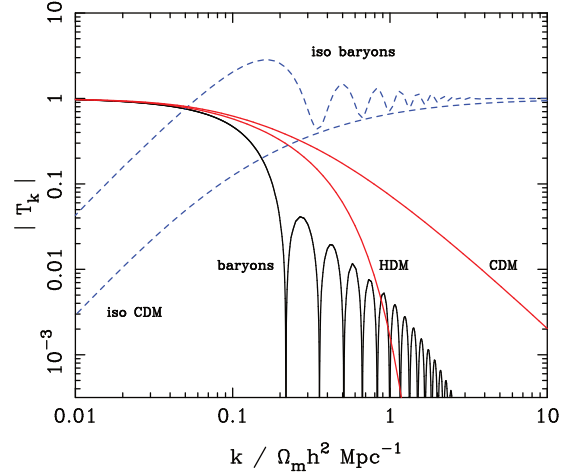


Figure 22.4: A plot of transfer functions for various models. For adiabatic models, $T_k \rightarrow 1$ at small k , whereas the opposite is true for isocurvature models. For dark-matter models, the characteristic wavenumber scales proportional to $\Omega_m h^2$. The scaling for baryonic models does not obey this exactly; the plotted cases correspond to $\Omega_m = 1$, $h = 0.5$.

The most generic power-law index is $n_s = 1$: the ‘Zeldovich’ or ‘scale-invariant’ spectrum. Inflationary models tend to predict a small ‘tilt’: $|n_s - 1| \lesssim 0.05$ [12, 13]. On the assumption that the dark matter is cold, the power spectrum then depends on 5 parameters: n_s , h , Ω_b , Ω_c ($\equiv \Omega_m - \Omega_b$), and an overall amplitude. The latter is often specified as σ_8 , the linear-theory fractional rms in density when a spherical filter of radius $8 h^{-1}$ Mpc is applied in linear theory. This scale can be probed directly via weak gravitational lensing, and also via its effect on the abundance of rich galaxy clusters. The normalization derived from samples of X-ray clusters has been given variously as [88, 89]

$$\sigma_8 = [0.746 \pm 0.012(\text{stat.}) \pm 0.022(\text{sys.})](\Omega_m/0.3)^{-0.47}; \quad (22.76)$$

$$\sigma_8 = [0.81 \pm 0.03](\Omega_m/0.3)^{-0.17}. \quad (22.77)$$

The higher figure is well consistent with *Planck*, whereas the lower is rather similar to the normalization inferred from weak lensing: $\sigma_8 \simeq [0.737^{+0.040}_{-0.036}](\Omega_m/0.3)^{-0.5}$ [78]; or $[0.759^{+0.025}_{-0.023}](\Omega_m/0.3)^{-0.5}$ [79]. These figures are both in 2.3σ tension with the *Planck* values of $(\sigma_8, \Omega_m) = (0.811 \pm 0.006, 0.315 \pm 0.007)$. If real, such a discrepancy could indicate interesting new physics; but the current evidence is not strong enough to make such a claim. However, it is worth noting that the CMB requires an almost perfect degeneracy, $\Omega_m h^3 = \text{const}$ for flat models, so that raising h as far as allowed by the CMB would require a lower density, which would reduce the tension with the amplitude of the lensing measurements.

A direct measure of mass inhomogeneity is valuable, since the galaxies inevitably are biased with respect to the mass. This means that the fractional fluctuations in galaxy number, $\delta n/n$, may differ from the mass fluctuations, $\delta \rho/\rho$. It is commonly assumed that the two fields obey some proportionality on large scales where the fluctuations are small, $\delta n/n = b \delta \rho/\rho$, but even this is not guaranteed [90].

The main shape of the transfer function is a break around the horizon scale at z_{eq} , which depends just on $\Omega_m h$ when wavenumbers are measured in observable units ($h \text{Mpc}^{-1}$). For reasonable baryon content, weak oscillations in the transfer function are also expected, and these BAOs (Baryon Acoustic Oscillations) have been clearly detected [91, 92]. As well as directly measuring the baryon fraction, the scale of the oscillations directly measures the acoustic horizon at decoupling; this can be used as an additional standard ruler for cosmological tests, and the BAO signature has become one of the most important applications of large galaxy surveys. Overall, current power-spectrum data [81–83] fa-

vor $\Omega_m h \simeq 0.20$ and a baryon fraction of about 0.15 for $n_s \simeq 1$ (see Fig. 22.5).

In principle, accurate data over a wide range of k could determine both $\Omega_m h$ and n , but in practice there is a strong degeneracy between these. In order to constrain n_s itself, it is necessary to examine data on anisotropies in the CMB.

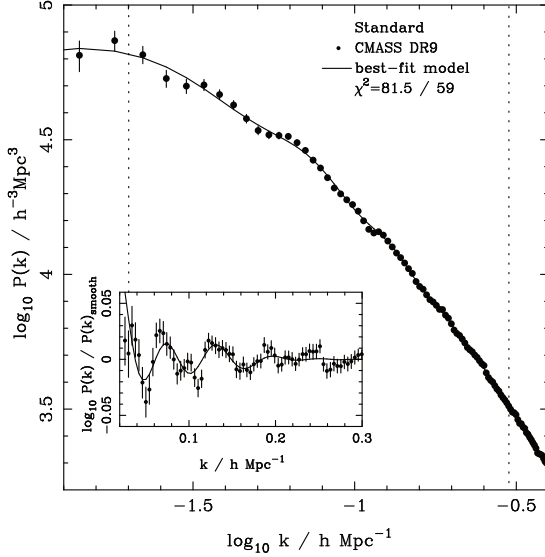


Figure 22.5: The galaxy power spectrum from the SDSS BOSS survey [83]. The solid points with error bars show the power estimate. The solid line shows a standard Λ CDM model with $\Omega_b h^2 \simeq 0.02$ and $\Omega_m h \simeq 0.2$. The inset amplifies the region where BAO features are visible. The fact that these perturb the power by $\sim 20\%$ rather than order unity is direct evidence that the matter content of the Universe is dominated by collisionless dark matter.

22.4.6 CMB anisotropies

The CMB has a clear dipole anisotropy, of magnitude 1.23×10^{-3} . This is interpreted as being due to the Earth's motion, which is equivalent to a peculiar velocity for the Milky Way of

$$v_{\text{MW}} \simeq 600 \text{ km s}^{-1} \text{ towards } (\ell, b) \simeq (270^\circ, 30^\circ). \quad (22.78)$$

A continuing challenge in cosmology is to demonstrate that this dipole is indeed kinematic, as opposed to representing a violation of large-scale isotropy. Galaxy surveys have attempted to identify the accelerating superclusters responsible for the motion [93], but there are also claims that the observed matter distribution contains an intrinsic dipole, which would be incompatible with the standard interpretation [94].

All higher-order multipole moments of the CMB are however much smaller (of order 10^{-5}), and interpreted as signatures of density fluctuations at last scattering ($\simeq 1100$). To analyze these, the sky is expanded in spherical harmonics as explained in the review on the CMB – Sec. 29 of this *Review*. The dimensionless power per $\ln k$ or ‘bandpower’ for the CMB is defined as

$$\mathcal{T}^2(\ell) = \frac{\ell(\ell+1)}{2\pi} C_\ell. \quad (22.79)$$

This function encodes information from the three distinct mechanisms that cause CMB anisotropies:

- (1) Gravitational (Sachs – Wolfe) perturbations. Photons from high-density regions at last scattering have to climb out of potential wells, and are thus redshifted.
- (2) Intrinsic (adiabatic) perturbations. In high-density regions, the coupling of matter and radiation can compress the radiation also, giving a higher temperature.
- (3) Velocity (Doppler) perturbations. The plasma has a non-zero velocity at recombination, which leads to Doppler shifts in frequency and hence shifts in brightness temperature.

Because the potential fluctuations obey Poisson's equation, $\nabla^2 \phi = 4\pi G \rho \delta$, and the velocity field satisfies the continuity equation $\nabla \cdot \mathbf{u} = -\delta$, the resulting different powers of k ensure that the Sachs-Wolfe effect dominates on large scales and adiabatic effects on small scales.

The relation between angle and comoving distance on the last-scattering sphere requires the comoving angular-diameter distance to the last-scattering sphere; because of its high redshift, this is effectively identical to the horizon size at the present epoch, D_H :

$$D_H = \frac{2}{\Omega_m H_0} \quad (\Omega_v = 0) \quad (22.80)$$

$$D_H \simeq \frac{2}{\Omega_m^{0.4} H_0} \quad (\text{flat} : \Omega_m + \Omega_v = 1).$$

These relations show how the CMB is strongly sensitive to curvature: the horizon length at last scattering is $\propto 1/\sqrt{\Omega_m}$, so that this subtends an angle that is virtually independent of Ω_m for a flat model. Observations of a peak in the CMB power spectrum at relatively large scales ($\ell \simeq 221$) are thus strongly inconsistent with zero- Λ models with low density: current CMB + BAO + lensing data require $\Omega_m + \Omega_v = 0.999 \pm 0.004$ (95%) [24]. (See *e.g.*, Fig. 22.2).

In addition to curvature, the CMB encodes information about several other key cosmological parameters. Within the compass of simple adiabatic CDM models, there are 9 of these:

$$\omega_c, \omega_b, \Omega_{\text{tot}}, h, \tau, n_s, n_t, r, Q. \quad (22.81)$$

The symbol ω denotes the physical density, Ωh^2 : the transfer function depends only on the densities of CDM (ω_c) and baryons (ω_b). Transcribing the power spectrum at last scattering into an angular power spectrum brings in the total density parameter ($\Omega_{\text{tot}} \equiv \Omega_m + \Omega_v = \Omega_c + \Omega_b + \Omega_v$) and h : there is a near-exact geometrical degeneracy [95] between these that keeps the angular-diameter distance to last scattering invariant, so that models with substantial spatial curvature and large vacuum energy cannot be ruled out without prior knowledge of the Hubble parameter. Alternatively, the CMB alone cannot measure the Hubble parameter without taking into account the line-of-sight information from CMB lensing.

A further possible degeneracy involves the tensor contribution to the CMB anisotropies. These are important at large scales (up to the horizon scales); for smaller scales, only scalar fluctuations (density perturbations) are important. Each of these components is characterized by a spectral index, n , and a ratio between the power spectra of tensors and scalars (τ). See the review on Cosmological Parameters – Sec. 25 of this *Review* for a technical definition of the r parameter. Finally, the overall amplitude of the spectrum must be specified (Q), together with the optical depth to Compton scattering owing to recent reionization (τ). Adding a large tensor contribution reduces the contrast between low ℓ and the peak at $\ell \simeq 221$ (because the tensor spectrum has no acoustic component). The previous relative height of the peak can be recovered by increasing n_s to increase the small-scale power in the scalar component; this in turn over-predicts the power at $\ell \sim 1000$, but this effect can be counteracted by raising the baryon density [96]. This approximate 3-way degeneracy is broken as we increase the range of multipoles sampled.

The reason the tensor component is introduced, and why it is so important, is that it is the only non-generic prediction of inflation. Slow-roll models of inflation involve two dimensionless parameters:

$$\epsilon \equiv \frac{M_{\text{P}}^2}{16\pi} \left(\frac{V'}{V} \right)^2, \quad \eta \equiv \frac{M_{\text{P}}^2}{8\pi} \left(\frac{V''}{V} \right), \quad (22.82)$$

where V is the inflaton potential, and dashes denote derivatives with respect to the inflation field. In terms of these, the tensor-to-scalar ratio is $r \simeq 16\epsilon$, and the spectral indices are $n_s = 1 - 6\epsilon + 2\eta$ and $n_t = -2\epsilon$. The natural expectation of inflation is that the quasi-exponential phase ends once the magnitudes of the slow-roll parameters become of order unity, so that both $n_s \neq 1$ and a significant tensor component are expected. These predictions can

be avoided in some models, but it is undeniable that observation of such features would be a great triumph for inflation. Cosmology therefore stands at a fascinating point given that the most recent CMB data reject the zero-tensor $n_s = 1$ model at more than 8σ : $n_s = 0.965 \pm 0.004$ [24]. This rejection is strong enough that it is also able to break the tensor degeneracy, so that no model with $n_s = 1$ is acceptable, whatever the value of r .

The current limit on r is < 0.036 at 95% confidence [97,98]. In conjunction with the measured value of n_s , this upper limit sits close to the prediction of a linear potential (i.e. $|\eta| \ll |\epsilon|$). Any further reduction in the limit on r will force η to be negative – i.e. a convex potential at the point where LSS scales were generated (sometimes called a ‘hilltop’), in contrast to simple early models such as $V(\phi) = m^2\phi^2$ or $\lambda\phi^4$, which are now excluded. Examples of models that are currently in excellent agreement with the Planck results are the Starobinsky model of $\mathcal{R} + \mathcal{R}^2$ gravity [99], or the Higgs-inflation model where the Higgs field is non-minimally coupled [100]. Assuming 55 e-foldings of inflation, these models predict $n_s = 0.965$ and $r = 0.0035$. Assuming that no systematic error in the CMB data can be identified, cosmology has thus passed a critical hurdle in rejecting scale-invariant fluctuations. The years ahead will be devoted to the task of searching for the tensor fluctuations – for which the main tool will be the polarization of the CMB [14].

22.4.6.1 CMB foregrounds

As the quality of CMB data improves, there is a growing interest in effects that arise along the line of sight. The CMB temperature is perturbed by dark-matter structures and by Compton scattering from ionized gas. In the former case, we have the integrated Sachs-Wolfe effect, which is sensitive to the time derivative of the gravitational potential. In the linear regime, this is damped when the Universe becomes Λ -dominated, and this is an independent way of detecting Λ [101]. The potential also causes gravitational lensing of the CMB: structures at $z \approx 1-2$ displace features on the CMB sky by about 2 arcmin over coherent degree-scale patches. Detection of these distortions allows a map to be made of overdensity projected from $z = 0$ to 1100 [80]. This is a very powerful calibration for direct studies of gravitational lensing using galaxies. Finally, Comptonization affects the CMB in two ways: the thermal Sunyaev-Zel’dovich effect measures the blurring of photon energies by hot gas, and the kinetic Sunyaev-Zel’dovich effect is sensitive to the bulk velocity of the gas. Both these effects start to dominate over the intrinsic CMB fluctuations at multipoles $\ell \gtrsim 2000$ [102].

22.4.7 Probing dark energy and the nature of gravity

The most radical element of our current cosmological model is the dark energy that accelerates the expansion. The energy density of this component is approximately $(2.2 \text{ meV})^4$ (for $w = -1$, $\Omega_v = 0.68$, $h = 0.67$), or roughly $10^{-123} M_{\text{pl}}^4$, and such an unnaturally small number is hard to understand. Various quantum effects (most simply, zero-point energy) should make contributions to the vacuum energy density. These may be truncated by new physics at high energy, but this presumably occurs at > 1 TeV scales, not meV; thus the apparent energy scale of the vacuum is at least 10^{15} times smaller than its natural value. A classic review of this situation is given by Weinberg [52], which lists extreme escape routes – especially the multiverse viewpoint, according to which low values of Λ are rare, but high values suppress the formation of structure and observers. It is certainly impressive that Weinberg used such reasoning to predict the value of Λ before any data strongly indicated a non-zero value.

But it may be that the phenomenon of dark energy is entirely illusory. The necessity for this constituent arises from using the Friedmann equation to describe the evolution of the cosmic expansion; if this equation is incorrect, it would require the replacement of Einstein’s relativistic theory of gravity with some new alternative. A frontier of current cosmological research is to distinguish these possibilities [103,104]. We also note that it has been suggested that dark energy might be an illusion even within general relativity, owing to an incorrect treatment of averaging in an inhomogeneous Universe [105,106]. Most would argue that a standard Newtonian treatment of such issues should be adequate inside the

cosmological horizon, but debate on this issue continues.

Dark Energy can differ from a classical cosmological constant in being a dynamical phenomenon [107,108], e.g., a rolling scalar field (sometimes dubbed ‘quintessence’). Empirically, this means that it is endowed with two thermodynamic properties that astronomers can try to measure: the bulk equation of state, and the sound speed. If the sound speed is close to the speed of light, the effect of this property is confined to very large scales, and mainly manifests itself in the large-angle multipoles of the CMB anisotropies [109]. The equation of state parameter governs the rate of change of the vacuum density: $d \ln \rho_v / d \ln a = -3(1+w)$, so it can be accessed via the evolving expansion rate, $H(a)$. This can be measured most cleanly by using the inbuilt natural ruler of large-scale structure: the BAO horizon scale [110]:

$$D_{\text{BAO}} \simeq 147.0 (\Omega_m h^2 / 0.1424)^{-0.253} (\Omega_b h^2 / 0.0224)^{-0.128} \text{ Mpc.} \quad (22.83)$$

Observing the equivalent acoustic scale at last scattering in the CMB yields the precise geometrical degeneracy $\Omega_m h^3 = 0.09633 \pm 0.00029$ [24].

$H(a)$ is measured by radial clustering, since $dr/dz = c/H$; clustering in the plane of the sky measures the integral of this. The expansion rate is also measured by the growth of density fluctuations, where the pressure-free growth equation for the density perturbation is $\ddot{\delta} + 2H(a)\dot{\delta} = 4\pi G\rho_0\delta$. Thus, both the scale and amplitude of density fluctuations are sensitive to $w(a)$ – but only weakly. These observables change by only typically 0.2% for a 1% change in w . Current constraints [24] place a constant w to within 5–10% of -1 , depending on the data combination chosen. A substantial improvement in this precision will require us to limit systematics in data to a few parts in 1000.

Testing whether theories of gravity require revision can also be done using data on cosmological inhomogeneities. Two separate issues arise, concerning the metric perturbation potentials Ψ and Φ , which affect respectively the time and space parts of the metric. In Einstein gravity, these potentials are both equal to the Newtonian gravitational potential, which satisfies Poisson’s equation: $\nabla^2\Phi/a^2 = 4\pi G\bar{\rho}\delta$. Empirically, modifications of gravity require us to explore a change with scale and with time of the ‘slip’ (Ψ/Φ) and the effective G on the rhs of the Poisson equation. The former aspect can only be probed via gravitational lensing, whereas the latter can be addressed on 10–100 Mpc scales via the growth of clustering. Various schemes for parameterising modified gravity exist, but a practical approach is to assume that the growth rate can be tied to the density parameter: $d \ln \delta / d \ln a = \Omega_m^\gamma(a)$ [84,85]. The parameter γ is close to 0.55 for standard relativistic gravity, but can differ by around 0.1 from this value in many non-standard models. Clearly this parameterization is incomplete, since it explicitly rejects the possibility of early dark energy ($\Omega_m(a) \rightarrow 1$ as $a \rightarrow 0$), but it is a convenient way of capturing the power of various experiments. Current data are consistent with standard Λ CDM [111], and exclude variations in slip or effective G of larger than a few times 10%.

Current planning envisages a set of satellite probes that, a decade hence, will have pursued these fundamental tests via gravitational lensing measurements over thousands of square degrees, $> 10^8$ redshifts, and photometry of > 1000 supernovae (Euclid in Europe, Roman Space Telescope in the USA) [22,23]. These experiments will measure both w and the perturbation growth rate to an accuracy of around 1%. The outcome will be either a validation of the standard relativistic vacuum-dominated Big Bang cosmology at a level of precision far beyond anything attempted to date, or the opening of entirely new directions in cosmological models. For a more complete discussion of dark energy and future probes see the review on Dark Energy – Sec. 28

References

- [1] V.M. Slipher, *Pop. Astr.* **23**, 21 (1915).
- [2] K. Lundmark, *Mon. Not. R. Astron. Soc* **84**, 747 (1924).
- [3] E. Hubble and M. L. Humason, *Astrophys. J.* **74**, 43 (1931).
- [4] G. Gamow, *Phys. Rev.* **70**, 572 (1946).
- [5] R. A. Alpher, H. Bethe and G. Gamow, *Phys. Rev.* **73**, 803 (1948).

- [6] R.A. Alpher and R.C. Herman, Phys. Rev. **74**, 1737 (1948).
- [7] R.A. Alpher and R.C. Herman, Phys. Rev. **75**, 1089 (1949).
- [8] A. A. Penzias and R. W. Wilson, Astrophys. J. **142**, 419 (1965).
- [9] P.J.E. Peebles, *Principles of Physical Cosmology*, Princeton University Press (1993).
- [10] G. Börner, *The Early Universe: Facts and Fiction*, Springer-Verlag (1988).
- [11] E.W. Kolb and M.S. Turner, *The Early Universe*, Addison-Wesley (1990).
- [12] J.A. Peacock, *Cosmological Physics*, Cambridge Univ. Press (1999).
- [13] A.R. Liddle and D. Lyth, *Cosmological Inflation and Large-Scale Structure*, Cambridge University Press (2000).
- [14] S. Dodelson, *Modern Cosmology*, Academic Press (2003).
- [15] V. Mukhanov, *Physical Foundations of Cosmology*, Cambridge University Press (2005).
- [16] S. Weinberg, *Cosmology*, Oxford Press (2008).
- [17] E.B. Gliner, Sov. Phys. JETP **22**, 378 (1966).
- [18] Ya. B. Zel'dovich, A. Krasinski and Ya. B. Zeldovich, Sov. Phys. Usp. **11**, 381 (1968), [Usp. Fiz. Nauk95,209(1968)].
- [19] P.M. Garnavich *et al.*, Astrophys. J. **507**, 74 (1998), [arXiv:astro-ph/9806396].
- [20] S. Perlmutter, M. S. Turner and M. J. White, Phys. Rev. Lett. **83**, 670 (1999), [arXiv:astro-ph/9901052].
- [21] I. Maor *et al.*, Phys. Rev. **D65**, 123003 (2002), [arXiv:astro-ph/0112526].
- [22] A. Albrecht *et al.* (2006), [arXiv:astro-ph/0609591].
- [23] J. A. Peacock *et al.* (2006), [arXiv:astro-ph/0610906].
- [24] N. Aghanim *et al.* (Planck), Astron. Astrophys. **641**, A6 (2020), [arXiv:1807.06209].
- [25] A.G. Riess *et al.*, Astrophys. J. **116**, 1009 (1998), [arXiv:astro-ph/9805201].
- [26] S. Perlmutter *et al.* (Supernova Cosmology Project), Astrophys. J. **517**, 565 (1999), [arXiv:astro-ph/9812133].
- [27] A. G. Riess, Publ. Astron. Soc. Pac. **112**, 1284 (2000), [arXiv:astro-ph/0005229].
- [28] J. L. Tonry *et al.* (Supernova Search Team), Astrophys. J. **594**, 1 (2003), [arXiv:astro-ph/0305008].
- [29] N. Suzuki *et al.*, Astrophys. J. **746**, 85 (2012), [arXiv:1105.3470].
- [30] D. M. Scolnic *et al.*, Astrophys. J. **859**, 101 (2018), [arXiv:1710.00845].
- [31] A. G. Riess *et al.*, Astrophys. J. Lett. **908**, 1, L6 (2021), [arXiv:2012.08534].
- [32] W. L. Freedman *et al.*, Astrophys. J. **882**, 34 (2019), [arXiv:1907.05922].
- [33] W. L. Freedman (2021), [arXiv:2106.15656].
- [34] Planck Collab. 2015 Results XIII, Astron. & Astrophys. **594**, A13 (2016), [arXiv:1502.10589].
- [35] P. Astier *et al.*, Astron. & Astrophys. **447**, 31 (2006), [arXiv:astro-ph/0510447].
- [36] J. A. Johnson and M. Bolte, Astrophys. J. **554**, 888 (2001), [arXiv:astro-ph/0103299].
- [37] R. Cayrel *et al.*, Nature **409**, 691 (2001), [arXiv:astro-ph/0104357].
- [38] D. A. Vandenberg *et al.*, Astrophys. J. **775**, 134 (2013), [arXiv:1308.2257].
- [39] S. Borsanyi *et al.*, Nature **539**, 7627, 69 (2016), [arXiv:1606.07494].
- [40] M. Srednicki, R. Watkins and K. A. Olive, Nucl. Phys. **B310**, 693 (1988), [247(1988)].
- [41] J. J. Bennett *et al.*, JCAP **04**, 073 (2021), [arXiv:2012.02726].
- [42] A. D. Linde, Phys. Rev. **D14**, 3345 (1976).
- [43] A. Linde, Rept. on Prog. in Phys. **42**, 389 (1979).
- [44] C.E. Vayonakis, Surv. High Energy Physics **5**, 87 (1986).
- [45] S.A. Bonometto and A. Masiero, Nuovo Cimento **9N5**, 1 (1986).
- [46] A. Linde, *Particle Physics And Inflationary Cosmology*, Harwood (1990).
- [47] K. A. Olive, Phys. Rept. **190**, 307 (1990).
- [48] D. H. Lyth and A. Riotto, Phys. Rept. **314**, 1 (1999), [hep-ph/9807278].
- [49] A. H. Guth, Phys. Rev. **D23**, 347 (1981), [Adv. Ser. Astrophys. Cosmol.3,139(1987)].
- [50] A. D. Linde, Phys. Lett. **108B**, 389 (1982), [Adv. Ser. Astrophys. Cosmol.3,149(1987)].
- [51] A. Albrecht and P. J. Steinhardt, Phys. Rev. Lett. **48**, 1220 (1982), [Adv. Ser. Astrophys. Cosmol.3,158(1987)].
- [52] S. Weinberg, Rev. Mod. Phys. **61**, 1 (1989).
- [53] L. Susskind 247–266 (2003), [hep-th/0302219].
- [54] B. Carr, *Universe or multiverse?* C.U.P. (2007).
- [55] A. D. Sakharov, Pisma Zh. Eksp. Teor. Fiz. **5**, 32 (1967), [Usp. Fiz. Nauk161,no.5,61(1991)].
- [56] S. Weinberg, Phys. Rev. Lett. **42**, 850 (1979).
- [57] D. Toussaint *et al.*, Phys. Rev. **D19**, 1036 (1979).
- [58] I. Affleck and M. Dine, Nucl. Phys. **B249**, 361 (1985).
- [59] V. A. Kuzmin, V. A. Rubakov and M. E. Shaposhnikov, Phys. Lett. **155B**, 36 (1985).
- [60] M. Fukugita and T. Yanagida, Phys. Lett. **B174**, 45 (1986).
- [61] S. Riemer-Sorensen and S. Jenssen, Universe **3**, 44 (2017), [arXiv:1502.10589].
- [62] R. J. Cooke, M. Pettini and C. C. Steidel, Astrophys. J. **855**, 2, 102 (2018), [arXiv:1710.11129].
- [63] R. H. Cyburt, B. D. Fields and K. A. Olive, Phys. Lett. **B567**, 227 (2003), [arXiv:astro-ph/0302431].
- [64] R. H. Cyburt, B. D. Fields and K. A. Olive, JCAP **0811**, 012 (2008), [arXiv:0808.2818].
- [65] K. A. Olive, G. Steigman and T. P. Walker, Phys. Rept. **333**, 389 (2000), [arXiv:astro-ph/9905320].
- [66] F. Iocco *et al.*, Phys. Rept. **472**, 1 (2009), [arXiv:0809.0631].
- [67] R. H. Cyburt *et al.*, Rev. Mod. Phys. **88**, 015004 (2016), [arXiv:1505.01076].
- [68] C. Pitrou *et al.*, Phys. Rept. **754**, 1 (2018), [arXiv:1801.08023].
- [69] B. D. Fields *et al.*, JCAP **03**, 010 (2020), [Erratum: JCAP 11, E02 (2020)], [arXiv:1912.01132].
- [70] D. J. Fixsen *et al.*, Astrophys. J. **473**, 576 (1996), [arXiv:astro-ph/9605054].
- [71] J. C. Mather *et al.*, Astrophys. J. **512**, 511 (1999), [arXiv:astro-ph/9810373].
- [72] S. Cole *et al.* (2dFGRS), Mon. Not. Roy. Astron. Soc. **326**, 255 (2001), [arXiv:astro-ph/0012429].
- [73] J. Schroeder, A. Mesinger and Z. Haiman, Mon. Not. R. Astron. Soc. **428**, 3058 (2013), [arXiv:1204.2838].
- [74] S. D. M. White *et al.*, Nature **366**, 429 (1993).
- [75] S. W. Allen, R. W. Schmidt and A. C. Fabian, Mon. Not. Roy. Astron. Soc. **334**, L11 (2002), [arXiv:astro-ph/0205007].
- [76] S. W. Allen, Mon. Not. Roy. Astron. Soc. **296**, 392 (1998), [arXiv:astro-ph/9710217].
- [77] G. P. Smith *et al.*, Mon. Not. Roy. Astron. Soc. **456**, 1, L74 (2016), [arXiv:1511.01919].

- [78] H. Hildebrandt *et al.*, *Astron. Astrophys.* **633**, A69 (2020), [arXiv:1812.06076].
- [79] A. Amon *et al.*, arXiv e-prints (2021), [arXiv:2105.13543].
- [80] Planck Collab. 2015 Results XV, *Astron. & Astrophys.* **594**, A15 (2016), [arXiv:1502.01591].
- [81] S. Cole *et al.* (2dFGRS), *Mon. Not. Roy. Astron. Soc.* **362**, 505 (2005), [arXiv:astro-ph/0501174].
- [82] W. J. Percival *et al.*, *Astrophys. J.* **657**, 645 (2007), [arXiv:astro-ph/0608636].
- [83] L. Anderson *et al.*, *Mon. Not. Roy. Astron. Soc.* **427**, 4, 3435 (2013), [arXiv:1203.6594].
- [84] E. Linder, *Phys. Rev.* **D72**, 43529 (2005), [arXiv:astro-ph/0507263].
- [85] D. Polarski and R. Gannouji, *Phys. Lett.* **B660**, 439 (2008), [arXiv:0710.1510].
- [86] G. Efstathiou and J. R. Bond, *Mon. Not. Roy. Astron. Soc.* **218**, 1, 103 (1986).
- [87] C. Gordon and A. Lewis, *Phys. Rev.* **D67**, 123513 (2003), [arXiv:astro-ph/0212248].
- [88] A. Vikhlinin *et al.*, *Astrophys. J.* **692**, 1060 (2009), [arXiv:0812.2720].
- [89] A. Mantz *et al.*, *Mon. Not. Roy. Astron. Soc.* **446**, 2205 (2015), [arXiv:1407.4516].
- [90] A. Dekel and O. Lahav, *Astrophys. J.* **520**, 24 (1999), [arXiv:astro-ph/9806193].
- [91] W. J. Percival *et al.*, *Mon. Not. Roy. Astron. Soc.* **381**, 1053 (2007), [arXiv:0705.3323].
- [92] W. J. Percival *et al.* (SDSS), *Mon. Not. Roy. Astron. Soc.* **401**, 2148 (2010), [arXiv:0907.1660].
- [93] G. Lavaux *et al.*, *Astrophys. J.* **709**, 483 (2010), [arXiv:0810.3658].
- [94] N. J. Secrest *et al.*, *Astrophys. J.* **908**, L51 (2021), [arXiv:2009.14826].
- [95] G. Efstathiou and J. R. Bond, *Mon. Not. Roy. Astron. Soc.* **304**, 75 (1999), [arXiv:astro-ph/9807103].
- [96] G. Efstathiou *et al.* (2dFGRS), *Mon. Not. Roy. Astron. Soc.* **330**, L29 (2002), [arXiv:astro-ph/0109152].
- [97] M. Tristram *et al.*, *Astron. Astrophys.* **647**, A128 (2021), [arXiv:2010.01139].
- [98] P. A. R. Ade *et al.* (BICEP/Keck), *Phys. Rev. Lett.* **127**, 15, 151301 (2021), [arXiv:2110.00483].
- [99] A. A. Starobinsky, *Phys. Lett.* **B91**, 99 (1980), [771(1980)].
- [100] F. Bezrukov and M. Shaposhnikov, *JHEP* **07**, 089 (2009), [arXiv:0904.1537].
- [101] Planck Collab. 2015 Results XXI, *Astron. & Astrophys.* **594**, A21 (2016), [arXiv:1502.01595].
- [102] Planck Collab. 2015 Results XXII, *Astron. & Astrophys.* **594**, A22 (2016), [arXiv:1502.01596].
- [103] W. Hu and I. Sawicki, *Phys. Rev.* **D76**, 4043 (2007), [arXiv:0708.1190].
- [104] B. Jain and P. Zhang, *Phys. Rev.* **D78**, 3503 (2008), [arXiv:0709.2375].
- [105] D. L. Wiltshire, *Phys. Rev. Lett.* **99**, 251101 (2007), [arXiv:0709.0732].
- [106] T. Buchert, *Gen. Rel. Grav.* **40**, 467 (2008), [arXiv:0707.2153].
- [107] I. Zlatev, L.-M. Wang and P. J. Steinhardt, *Phys. Rev. Lett.* **82**, 896 (1999), [arXiv:astro-ph/9807002].
- [108] C. Armendariz-Picon, V. Mukhanov, and P. J. Steinhardt, *Phys. Rev.* **D63**, 3510 (2001), [arXiv:astro-ph/0006373].
- [109] S. DeDeo, R.R. Caldwell, and P.J. Steinhardt, *Phys. Rev.* **D67**, 3509 (2003), [arXiv:astro-ph/0301284].
- [110] É. Aubourg *et al.*, *Phys. Rev.* **D92**, 123516 (2015), [arXiv:1411.1074].
- [111] S. F. Daniel *et al.*, *Phys. Rev.* **D81**, 123508 (2010), [arXiv:1002.1962].

23. Inflation

Revised August 2021 by J. Ellis (King's Coll. London; CERN) and D. Wands (Portsmouth U.).

23.1 Motivation and Introduction

The standard Big-Bang model of cosmology provides a successful framework in which to understand the thermal history of our Universe and the growth of cosmic structure, but it is essentially incomplete. As described in Sec. 22.2.4, Big-Bang cosmology requires very specific initial conditions. It postulates a uniform cosmological background, described by a spatially-flat, homogeneous and isotropic Robertson-Walker (RW) metric (Eq. (22.1) in “Big Bang Cosmology” review), with scale factor $R(t)$. Within this setting, it also requires an initial almost scale-invariant distribution of primordial density perturbations as seen, for example, in the cosmic microwave background (CMB) radiation (described in Chap. 29, “Cosmic Microwave Background” review), on scales far larger than the causal horizon at the time the CMB photons last scattered.

The Hubble expansion rate, $H \equiv \dot{R}/R$, in a RW cosmology is given by the Friedmann constraint equation (Eq. (22.8) in “Big Bang Cosmology” review)

$$H^2 = \frac{8\pi\rho}{3M_P^2} + \frac{\Lambda}{3} - \frac{k}{R^2}, \quad (23.1)$$

where k/R^2 is the intrinsic spatial curvature. We use natural units such that the speed of light $c = 1$ and hence we have the Planck mass $M_P = G_N^{-1/2} \simeq 10^{19}$ GeV (see “Astrophysical Constants and Parameters”). A cosmological constant, Λ , of the magnitude required to accelerate the Universe today (see Chap. 28, “Dark Energy” review) would have been completely negligible in the early Universe where the energy density $\rho \gg M_P^2 \Lambda \sim 10^{-12} (\text{eV})^4$. The standard early Universe cosmology, described in Sec. 22.1.5 in “Big Bang Cosmology” review, is thus dominated by non-relativistic matter ($p_m \ll \rho_m$) or radiation ($p_r = \rho_r/3$ for an isotropic distribution). This leads to a decelerating expansion with $\ddot{R} < 0$.

The hypothesis of inflation [1, 2] postulates a period of accelerated expansion, $\ddot{R} > 0$, in the very early Universe, preceding the standard radiation-dominated era, which offers a physical model for the origin of these initial conditions, as reviewed in [3–7]. Such a period of accelerated expansion (i) drives a curved Robertson-Walker spacetime (with spherical or hyperbolic spatial geometry) towards spatial flatness, and (ii) it also expands the causal horizon beyond the present Hubble length, so as to encompass all the scales relevant to describe the large-scale structure observed in our Universe today, via the following two mechanisms.

1. A spatially-flat Universe with vanishing spatial curvature, $k = 0$, has the dimensionless density parameter $\Omega_{tot} = 1$, where we define (Eq. (22.13) in “Big Bang Cosmology” review; see Chap. 25, “Cosmological Parameters” review for more complete definitions)

$$\Omega_{tot} \equiv \frac{8\pi\rho_{tot}}{3M_P^2 H^2}, \quad (23.2)$$

with $\rho_{tot} \equiv \rho + \Lambda M_P^2/8\pi$. If we re-write the Friedmann constraint (Eq. (23.1)) in terms of Ω_{tot} we have

$$1 - \Omega_{tot} = -\frac{k}{R^2}. \quad (23.3)$$

Observations require $|1 - \Omega_{tot,0}| < 0.005$ today [8], where the subscript 0 denotes the present-day value. Taking the time derivative of Eq. (23.3) we obtain

$$\frac{d}{dt}(1 - \Omega_{tot}) = -2\frac{\ddot{R}}{\dot{R}}(1 - \Omega_{tot}). \quad (23.4)$$

Thus in a decelerating expansion, $\dot{R} > 0$ and $\ddot{R} < 0$, any small initial deviation from spatial flatness grows, $(d/dt)|1 - \Omega_{tot}| > 0$. A small value such as $|1 - \Omega_{tot,0}| < 0.005$ today requires an even smaller value at earlier times, e.g., $|1 - \Omega_{tot}| < 10^{-5}$ at

the last scattering of the CMB, which appears unlikely, unless for some reason space is exactly flat. However, an extended period of accelerated expansion in the very early Universe, with $\dot{R} > 0$ and $\ddot{R} > 0$ and hence $(d/dt)|1 - \Omega_{tot}| < 0$, can drive Ω_{tot} sufficiently close to unity, so that $|1 - \Omega_{tot,0}|$ remains unobservable small today, even after the radiation- and matter-dominated eras, for a wide range of initial values of Ω_{tot} .

2. The comoving distance (the present-day proper distance) traversed by light between cosmic time t_1 and t_2 in an expanding Universe can be written, (see Eq. (22.32) in “Big Bang Cosmology” review), as

$$D_0(t_1, t_2) = R_0 \int_{t_1}^{t_2} \frac{dt}{R(t)} = R_0 \int_{\ln R_1}^{\ln R_2} \frac{d(\ln R)}{\dot{R}}. \quad (23.5)$$

In standard decelerated (radiation- or matter-dominated) cosmology the integrand, $1/\dot{R}$, decreases towards the past, and there is a finite comoving distance traversed by light (a particle horizon) since the Big Bang ($R_1 \rightarrow 0$). For example, the comoving size of the particle horizon at the CMB last-scattering surface ($R_2 = R_{lss}$) corresponds to $D_0 \sim 100$ Mpc, or approximately 1° on the CMB sky today (see Sec. 22.2.4 in “Big Bang Cosmology” review). However, during a period of inflation, $1/\dot{R}$ increases towards the past, and hence the integral (Eq. (23.5)) diverges as $R_1 \rightarrow 0$, allowing an arbitrarily large causal horizon, dependent only upon the duration of the accelerated expansion. Assuming that the Universe inflates with a finite Hubble rate H_* at $t_1 = t_*$, ending with $H_{end} < H_*$ at $t_2 = t_{end}$, we have

$$D_0(t_*, t_{end}) > \left(\frac{R_0}{R_{end}}\right) H_*^{-1} (e^{N_*} - 1), \quad (23.6)$$

where $N_* \equiv \ln(R_{end}/R_*)$ describes the duration of inflation, measured in terms of the logarithmic expansion (or “e-folds”) from $t_1 = t_*$ up to the end of inflation at $t_2 = t_{end}$, and R_0/R_{end} is the subsequent expansion from the end of inflation to the present day. If inflation occurs above the TeV scale, the comoving Hubble scale at the end of inflation, $(R_0/R_{end})H_{end}^{-1}$, is less than one astronomical unit ($\sim 10^{11}$ m), and a causally-connected patch can encompass our entire observable Universe today, which has a size $D_0 > 30$ Gpc, if there were more than 40 e-folds of inflation ($N_* > 40$). If inflation occurs at the GUT scale (10^{15} GeV) then we require more than 60 e-folds.

Producing an accelerated expansion in general relativity requires an energy-momentum tensor with negative pressure, $p < -\rho/3$ (see Eq. (22.9) in “Big Bang Cosmology” review and Chap. 28, “Dark Energy” review), quite different from the hot dense plasma of relativistic particles in the hot Big Bang. However a positive vacuum energy $V > 0$ does exert a negative pressure, $p_V = -\rho_V$. The work done by the cosmological expansion must be negative in this case so that the local vacuum energy density remains constant in an expanding Universe, $\dot{\rho}_V = -3H(\rho_V + p_V) = 0$. Therefore, a false vacuum state can drive an exponential expansion, corresponding to a de Sitter spacetime with a constant Hubble rate $H^2 = 8\pi\rho_V/3M_P^2$ on spatially-flat hypersurfaces.

A constant vacuum energy V , equivalent to a cosmological constant Λ in the Friedmann equation Eq. (23.1), cannot provide a complete description of inflation in the early Universe, since inflation must necessarily have come to an end in order for the standard Big-Bang cosmology to follow. A phase transition to the present true vacuum is required to release the false vacuum energy into the energetic plasma of the hot Big Bang and produce the large total entropy of our observed Universe today. Thus, we must necessarily study dynamical models of inflation, where the time-invariance of the false vacuum state is broken by a time-dependent field. A first-order phase transition would produce a very inhomogeneous Universe [9] unless a time-dependent scalar field leads to a rapidly changing percolation rate [10–12]. However,

a second-order phase transition [13, 14], controlled by a slowly-rolling scalar field, can lead to a smooth classical exit from the vacuum-dominated phase.

As a spectacular bonus, quantum fluctuations in that scalar field could provide a source of almost scale-invariant density fluctuations [15, 16], as detected in the CMB (see Chap. 29), which are thought to be the origin of the structures seen in the Universe today.

Accelerated expansion and primordial perturbations can also be produced in some modified gravity theories (e.g., [1, 17]), which introduce additional non-minimally coupled degrees of freedom. Such inflation models can often be conveniently studied by transforming variables to an ‘Einstein frame’ in which Einstein’s equations apply with minimally coupled scalar fields [18–20].

In the following we will review scalar field cosmology in general relativity and the spectra of primordial fluctuations produced during inflation, before studying selected inflation models.

23.2 Scalar Field Cosmology

The energy-momentum tensor for a canonical scalar field ϕ with self-interaction potential $V(\phi)$ is given in Eq. (22.52) in “Big Bang Cosmology” review. In a homogeneous background this corresponds to a perfect fluid with density

$$\rho = \frac{1}{2}\dot{\phi}^2 + V(\phi), \tag{23.7}$$

and isotropic pressure

$$p = \frac{1}{2}\dot{\phi}^2 - V(\phi), \tag{23.8}$$

while the 4-velocity is proportional to the gradient of the field, $u^\mu \propto \nabla^\mu \phi$.

A field with vanishing potential energy acts like a stiff fluid with $p = \rho = \dot{\phi}^2/2$, whereas if the time-dependence vanishes we have $p = -\rho = -V$ and the scalar field is uniform in time and space. Thus a classical, potential-dominated scalar-field cosmology, with $p \simeq -\rho$, can naturally drive a quasi-de Sitter expansion; the slow time-evolution of the energy density weakly breaks the exact $O(1, 3)$ symmetry of four-dimensional de Sitter spacetime down to a Robertson-Walker (RW) spacetime, where the scalar field plays the role of the cosmic time coordinate.

In a scalar-field RW cosmology the Friedmann constraint equation (Eq. (23.1)) reduces to

$$H^2 = \frac{8\pi}{3M_P^2} \left(\frac{1}{2}\dot{\phi}^2 + V \right) - \frac{k}{R^2}, \tag{23.9}$$

while energy conservation (Eq. (22.10) in “Big Bang Cosmology” review) for a homogeneous scalar field reduces to the Klein-Gordon equation of motion (Eq. (22.54) in “Big Bang Cosmology” review)

$$\ddot{\phi} = -3H\dot{\phi} - V'(\phi). \tag{23.10}$$

The evolution of the scalar field is thus driven by the potential gradient $V' = dV/d\phi$, subject to damping by the Hubble expansion $3H\dot{\phi}$.

If we define the Hubble slow-roll parameter

$$\epsilon_H \equiv -\frac{\dot{H}}{H^2}, \tag{23.11}$$

then we see that inflation ($\dot{R} > 0$ and hence $\dot{H} > -H^2$) requires $\epsilon_H < 1$. In this case the spatial curvature decreases relative to the scalar field energy density as the Universe expands. Hence, in the following we drop the spatial curvature and consider a spatially-flat RW cosmology, assuming that inflation has lasted sufficiently long that our observable Universe is very close to spatially flatness. However, we note that bubble nucleation, leading to a first-order phase transition during inflation, can lead to homogeneous hypersurfaces with a hyperbolic (‘open’) geometry, effectively resetting the spatial curvature inside the bubble [21]. This is the basis of so-called open inflation models [22–24], where inflation inside the bubble has a finite duration, leaving a finite negative spatial curvature.

In a scalar field-dominated cosmology (Eq. (23.11)) gives

$$\epsilon_H = \frac{3\dot{\phi}^2}{2V + \dot{\phi}^2}, \tag{23.12}$$

in which case we see that inflation requires a potential-dominated expansion, $\dot{\phi}^2 < V$.

23.2.1 Slow-Roll Inflation

It is commonly assumed that the field acceleration term, $\ddot{\phi}$, in (Eq. (23.10)) can be neglected, in which case one can give an approximate solution for the inflationary attractor [25]. This slow-roll approximation reduces the second-order Klein-Gordon equation (Eq. (23.10)) to a first-order system, which is over-damped, with the potential gradient being approximately balanced against to the Hubble damping:

$$3H\dot{\phi} \simeq -V', \tag{23.13}$$

and at the same time that the Hubble expansion (Eq. (23.9)) is dominated by the potential energy

$$H^2 \simeq \frac{8\pi}{3M_P^2} V(\phi), \tag{23.14}$$

corresponding to $\epsilon_H \ll 1$.

A necessary condition for the validity of the slow-roll approximation is that the potential slow-roll parameters

$$\epsilon \equiv \frac{M_P^2}{16\pi} \left(\frac{V'}{V} \right)^2, \quad \eta \equiv \frac{M_P^2}{8\pi} \left(\frac{V''}{V} \right), \tag{23.15}$$

are small, i.e., $\epsilon \ll 1$ and $|\eta| \ll 1$, requiring the potential to be correspondingly flat. If we identify V'' with the effective mass of the field, we see that the slow-roll approximation requires that the mass of the scalar field must be small compared with the Hubble scale. We note that the Hubble slow-roll parameter (Eq. (23.11)) coincides with the potential slow-roll parameter, $\epsilon_H \simeq \epsilon$, to leading order in the slow-roll approximation.

The slow-roll approximation allows one to determine the Hubble expansion rate as a function of the scalar field value, and vice versa. In particular, we can express, in terms of the scalar field value during inflation, the total logarithmic expansion, or number of “e-folds”:

$$\begin{aligned} N_* &\equiv \ln \left(\frac{R_{end}}{R_*} \right) \\ &= \int_{t_*}^{t_{end}} H dt \simeq - \int_{\phi_*}^{\phi_{end}} \sqrt{\frac{4\pi}{\epsilon}} \frac{d\phi}{M_P} \text{ for } V' > 0. \end{aligned} \tag{23.16}$$

Given that the slow-roll parameters are approximately constant during slow-roll inflation, $d\epsilon/dN \simeq 2\epsilon(\eta - 2\epsilon) = \mathcal{O}(\epsilon^2)$, we have

$$N_* \simeq \frac{4}{\sqrt{\epsilon}} \frac{\Delta\phi}{M_P}. \tag{23.17}$$

Since we require $N > 40$ to solve the flatness, horizon and entropy problems of the standard Big Bang cosmology, we require either very slow roll, $\epsilon < 0.01$, or a large change in the value of the scalar field relative to the Planck scale, $\Delta\phi > M_P$.

23.2.2 Reheating

Slow-roll inflation can lead to an exponentially large Universe, close to spatial flatness and homogeneity, but the energy density is locked in the potential energy of the scalar field, and needs to be converted to particles and thermalised to recover a hot Big Bang cosmology at the end of inflation [26, 27]. This process is usually referred to as reheating, although there was not necessarily any preceding thermal era. Reheating can occur when the scalar field evolves towards the minimum of its potential, converting the potential energy first to kinetic energy. This can occur either through the breakdown of the slow-roll condition in single-field models, or due to an instability triggered by the inflaton reaching

a critical value, in multi-field models known as hybrid inflation models [28].

Close to a simple minimum, the scalar field potential can be described by a quadratic function, $V = m^2\phi^2/2$, where m is the mass of the field. We can obtain slow-roll inflation in such a potential at large field values, $\phi \gg M_P$. However, for $\phi \ll M_P$ the field approaches an oscillatory solution:

$$\phi(t) \simeq \frac{M_P}{\sqrt{3\pi}} \frac{\sin(mt)}{mt}. \quad (23.18)$$

For $|\phi| < M_P$ the Hubble rate drops below the inflaton mass, $H < m$, and the field oscillates many times over a Hubble time. Averaging over several oscillations, $\Delta t \gg m^{-1}$, we find $\langle \dot{\phi}^2/2 \rangle_{\Delta t} \simeq \langle m^2\phi^2/2 \rangle_{\Delta t}$ and hence

$$\langle \rho \rangle_{\Delta t} \simeq \frac{M_P^2}{6\pi t^2}, \quad \langle p \rangle_{\Delta t} \simeq 0. \quad (23.19)$$

This coherent oscillating field corresponds to a condensate of non-relativistic massive inflaton particles, driving a matter-dominated era at the end of inflation, with scale factor $R \propto t^{2/3}$.

The inflaton condensate can lose energy through perturbative decays due to terms in the interaction Lagrangian, such as

$$\mathcal{L}_{int} \subset -\lambda_i \sigma \phi \chi_i^2 - \lambda_j \phi \bar{\psi}_j \psi_j \quad (23.20)$$

that couple the inflation to scalar fields χ_i or fermions ψ_j , where σ has dimensions of mass and the λ_i are dimensionless couplings. When the mass of the inflaton is much larger than the decay products, the decay rate is given by [29]

$$\Gamma_i = \frac{\lambda_i^2 \sigma^2}{8\pi m}, \quad \Gamma_j = \frac{\lambda_j^2 m}{8\pi}. \quad (23.21)$$

These decay products must in turn thermalise with Standard Model particles before we recover conventional hot Big Bang cosmology. An upper limit on the reheating temperature after inflation is given by [27]

$$T_{rh} = 0.2 \left(\frac{100}{g_*} \right)^{1/4} \sqrt{M_P \Gamma_{tot}}, \quad (23.22)$$

where g_* is the effective number of degrees of freedom and Γ_{tot} is the total decay rate for the inflaton, which is required to be less than m for perturbative decay.

The baryon asymmetry of the Universe must be generated after the main release of entropy during inflation, which is an important constraint on possible models. Also, the fact that the inflaton mass is much larger than the mass scale of the Standard Model opens up the possibility that it may decay into massive stable or metastable particles that could be connected with dark matter, constraining possible models. For example, in the context of supergravity models the reheat temperature is constrained by the requirement that gravitinos are not overproduced, potentially destroying the successes of Big Bang nucleosynthesis. For a range of gravitino masses one must require $T_{rh} < 10^9$ GeV [30, 31].

The process of inflaton decay and reheating can be significantly altered by interactions leading to space-time dependences in the effective masses of the fields. In particular, parametric resonance can lead to explosive, non-perturbative decay of the inflaton in some cases, a process often referred to as preheating [26, 32]. For example, an interaction term of the form

$$\mathcal{L}_{int} \subset -\lambda^2 \phi^2 \chi^2, \quad (23.23)$$

leads to a time-dependent effective mass for the χ field as the inflaton ϕ oscillates. This can lead to non-adiabatic particle production if the bare mass of the χ field is small for large couplings or for rapid changes of the inflaton field. The process of preheating is highly model-dependent, but it highlights the possible role of non-thermal particle production after and even during inflation.

23.3 Primordial Perturbations from Inflation

Although inflation was originally discussed as a solution to the problem of initial conditions required for homogeneous and isotropic hot Big Bang cosmology, it was soon realised that inflation also offered a mechanism to generate the inhomogeneous initial conditions required for the formation of large-scale structure [15–17, 33].

23.3.1 Metric Perturbations

In a homogeneous classical inflationary cosmology driven by a scalar field, the inflaton field is uniform on constant-time hypersurfaces, $\phi = \phi_0(t)$. However, quantum fluctuations inevitably break the spatial symmetry leading to an inhomogeneous field:

$$\phi(t, x^i) = \phi_0(t) + \delta\phi(t, x^i). \quad (23.24)$$

At the same time, one should consider inhomogeneous perturbations of the RW spacetime metric (see, e.g., [34–36]):

$$ds^2 = (1 + 2A)dt^2 - 2RB_i dt dx^i - R^2 [(1 + 2C)\delta_{ij} + \partial_i \partial_j E + h_{ij}] dx^i dx^j, \quad (23.25)$$

where A , B , E and C are scalar perturbations while h_{ij} represents transverse and tracefree, tensor metric perturbations. Vector metric perturbations can be eliminated using Einstein constraint equations in a scalar field cosmology.

The tensor perturbations remain invariant under a temporal gauge transformation $t \rightarrow t + \delta t(t, x^i)$, but both the scalar field and the scalar metric perturbations transform. For example, we have

$$\delta\phi \rightarrow \delta\phi - \dot{\phi}_0 \delta t, \quad C \rightarrow C - H \delta t. \quad (23.26)$$

However, there are gauge invariant combinations, such as [37]

$$Q = \delta\phi - \frac{\dot{\phi}_0}{H} C, \quad (23.27)$$

which describes the scalar field perturbations on spatially-flat ($C = 0$) hypersurfaces. This is simply related to the curvature perturbation on uniform-field ($\delta\phi = 0$) hypersurfaces:

$$\mathcal{R} = C - \frac{H}{\dot{\phi}_0} \delta\phi = -\frac{H}{\dot{\phi}_0} Q, \quad (23.28)$$

which coincides in slow-roll inflation, $\rho \simeq \rho(\phi)$, with the curvature perturbation on uniform-density hypersurfaces [16]

$$\zeta = C - \frac{H}{\dot{\rho}_0} \delta\rho. \quad (23.29)$$

Thus scalar field and scalar metric perturbations are coupled by the evolution of the inflaton field.

23.3.2 Gravitational waves from inflation

The tensor metric perturbation, h_{ij} in Eq. (23.25), is gauge-invariant and decoupled from the scalar perturbations at first order. This represents the free excitations of the spacetime, i.e., gravitational waves, which are the simplest metric perturbations to study at linear order.

Each tensor mode, with wavevector \vec{k} , has two linearly-independent transverse and trace-free polarization states:

$$h_{ij}(\vec{k}) = h_{\vec{k}} q_{ij} + \bar{h}_{\vec{k}} \bar{q}_{ij}. \quad (23.30)$$

The linearised Einstein equations then yield the same evolution equation for the amplitude as that for a massless field in RW spacetime:

$$\ddot{h}_{\vec{k}} + 3H\dot{h}_{\vec{k}} + \frac{k^2}{R^2} h_{\vec{k}} = 0, \quad (23.31)$$

(and similarly for $\bar{h}_{\vec{k}}$). This can be re-written in terms of the conformal time, $\eta = \int dt/R$, and the conformally rescaled field:

$$u_{\vec{k}} = \frac{M_P R h_{\vec{k}}}{\sqrt{32\pi}}. \quad (23.32)$$

This conformal field then obeys the wave equation for a canonical scalar field in Minkowski spacetime with a time-dependent mass:

$$u_{\vec{k}}'' + \left(k^2 - \frac{R''}{R}\right) u_{\vec{k}} = 0. \quad (23.33)$$

During slow-roll

$$\frac{R''}{R} \simeq (2 - \epsilon)R^2 H^2. \quad (23.34)$$

This makes it possible to quantise the linearised metric fluctuations, $u_{\vec{k}} \rightarrow \hat{u}_{\vec{k}}$, on sub-Hubble scales, $k^2/R^2 \gg H^2$, where the background expansion can be neglected.

Crucially, in an inflationary expansion, where $\dot{R} > 0$, the comoving Hubble length $H^{-1}/R = 1/\dot{R}$ decreases with time. Thus, all modes start inside the Hubble horizon and it is possible to take the initial field fluctuations to be in a vacuum state at early times or on small scales:

$$\langle u_{\vec{k}_1} u_{\vec{k}_2} \rangle = \frac{i}{2} (2\pi)^3 \delta^{(3)}(\vec{k}_1 + \vec{k}_2). \quad (23.35)$$

In terms of the amplitude of the tensor metric perturbations, this corresponds to

$$\langle h_{\vec{k}_1} h_{\vec{k}_2} \rangle = \frac{1}{2} \frac{\mathcal{P}_t(k_1)}{4\pi k_1^3} (2\pi)^3 \delta^{(3)}(\vec{k}_1 + \vec{k}_2), \quad (23.36)$$

where the factor 1/2 appears due to the two polarization states that contribute to the total tensor power spectrum:

$$\mathcal{P}_t(k) = \frac{64\pi}{M_P^2} \left(\frac{k}{2\pi R}\right)^2. \quad (23.37)$$

On super-Hubble scales, $k^2/R^2 \ll H^2$, we have the growing mode solution to Eq. (23.33), $u_{\vec{k}} \propto R$, corresponding to $h_{\vec{k}} \rightarrow$ constant, i.e., tensor modes are frozen-in on super-Hubble scales, both during and after inflation. Thus, connecting the initial vacuum fluctuations on sub-Hubble scales to the late-time power spectrum for tensor modes at Hubble exit during inflation, $k = R_* H_*$, we obtain

$$\mathcal{P}_t(k) \simeq \frac{64\pi}{M_P^2} \left(\frac{H_*}{2\pi}\right)^2. \quad (23.38)$$

In the de Sitter limit, $\epsilon \rightarrow 0$, the Hubble rate becomes time-independent and the tensor spectrum on super-Hubble scales becomes scale-invariant [39]. However slow-roll evolution leads to weak time dependence of H_* and thus a scale-dependent spectrum on large scales, with a spectral tilt

$$n_t \equiv \frac{d \ln \mathcal{P}_T}{d \ln k} \simeq -2\epsilon_*. \quad (23.39)$$

23.3.3 Density Perturbations from single-field inflation

The inflaton field fluctuations on spatially-flat hypersurfaces are coupled to scalar metric perturbations at first order, but these can be eliminated using the Einstein constraint equations to yield an evolution equation

$$\ddot{Q}_{\vec{k}} + 3H\dot{Q}_{\vec{k}} + \left[\frac{k^2}{R^2} + V'' - \frac{8\pi}{M_P^2 R^3} \frac{d}{dt} \left(\frac{R^3 \dot{\phi}^2}{H}\right)\right] Q_{\vec{k}} = 0. \quad (23.40)$$

Terms proportional to M_P^{-2} represent the effect on the field fluctuations of gravity at first order. As can be seen, this vanishes in the limit of a constant background field, and hence is suppressed in the slow-roll limit, but it is of the same order as the effective mass, $V'' = 3\eta H^2$, so must be included if we wish to model deviations from exact de Sitter symmetry.

This wave equation can also be written in the canonical form for a free field in Minkowski spacetime if we define [37]

$$v_{\vec{k}} \equiv RQ_{\vec{k}}, \quad (23.41)$$

to yield

$$v_{\vec{k}}'' + \left(k^2 - \frac{z''}{z}\right) v_{\vec{k}} = 0, \quad (23.42)$$

where we define

$$z \equiv \frac{R\dot{\phi}}{H}, \quad \frac{z''}{z} \simeq (2 + 5\epsilon - 3\eta)R^2 H^2, \quad (23.43)$$

where the last approximate equality holds to leading order in the slow-roll approximation.

As previously done for gravitational waves, we quantise the linearised field fluctuations $v_{\vec{k}} \rightarrow \hat{v}_{\vec{k}}$ on sub-Hubble scales, $k^2/R^2 \gg H^2$, where the background expansion can be neglected. Thus, we impose

$$\langle v_{\vec{k}_1} v_{\vec{k}_2}' \rangle = \frac{i}{2} \delta^{(3)}(\vec{k}_1 + \vec{k}_2). \quad (23.44)$$

In terms of the field perturbations, this corresponds to

$$\langle Q_{\vec{k}_1} Q_{\vec{k}_2} \rangle = \frac{\mathcal{P}_Q(k_1)}{4\pi k_1^3} (2\pi)^3 \delta^{(3)}(\vec{k}_1 + \vec{k}_2), \quad (23.45)$$

where the power spectrum for vacuum field fluctuations on sub-Hubble scales, $k^2/R^2 \gg H^2$, is simply

$$\mathcal{P}_Q(k) = \left(\frac{k}{2\pi R}\right)^2, \quad (23.46)$$

yielding the classic result for the vacuum fluctuations for a massless field in de Sitter at Hubble exit, $k = R_* H_*$:

$$\mathcal{P}_Q(k) \simeq \left(\frac{H}{2\pi}\right)_*^2. \quad (23.47)$$

In practice there are slow-roll corrections due to the small but finite mass (η) and field evolution (ϵ) [40].

Slow-roll corrections to the field fluctuations are small on sub-Hubble scales, but can become significant as the field and its perturbations evolve over time on super-Hubble scales. Thus, it is helpful to work instead with the curvature perturbation, ζ defined in equation (Eq. (23.29)), which remains constant on super-Hubble scales for adiabatic density perturbations both during and after inflation [16,41]. Thus we have an expression for the primordial curvature perturbation on super-Hubble scales produced by single-field inflation:

$$\mathcal{P}_\zeta(k) = \left[\left(\frac{H}{\dot{\phi}}\right)^2 \mathcal{P}_Q(k) \right]_* \simeq \frac{4\pi}{M_P^2} \left[\frac{1}{\epsilon} \left(\frac{H}{2\pi}\right)^2 \right]_*. \quad (23.48)$$

Comparing this with the primordial gravitational wave power spectrum (Eq. (23.38)) we obtain the tensor-to-scalar ratio for single-field slow-roll inflation

$$r \equiv \frac{\mathcal{P}_t}{\mathcal{P}_\zeta} \simeq 16\epsilon_*. \quad (23.49)$$

Note that the scalar amplitude is boosted by a factor $1/\epsilon_*$ during slow-roll inflation, because small scalar field fluctuations can lead to relatively large curvature perturbations on hypersurfaces defined with respect to the density if the potential energy is only weakly dependent on the scalar field, as in slow-roll. Indeed, the de Sitter limit is singular, since the potential energy becomes independent of the scalar field at first order, $\epsilon \rightarrow 0$, and the curvature perturbation on uniform-density hypersurfaces becomes ill-defined.

We note that in single-field inflation the tensor-to-scalar ratio and the tensor tilt (Eq. (23.39)) at the same scale are both determined by the first slow-roll parameter at Hubble exit, ϵ_* , giving rise to an important consistency test for single-field inflation:

$$n_t = -\frac{r}{8}. \quad (23.50)$$

This may be hard to verify if r is small, making any tensor tilt n_t difficult to measure. On the other hand, it does offer a way to rule out single-field slow-roll inflation if either r or n_t is large.

Given the relatively large scalar power spectrum, it has proved easier to measure the scalar tilt, conventionally defined as $n_s - 1$.

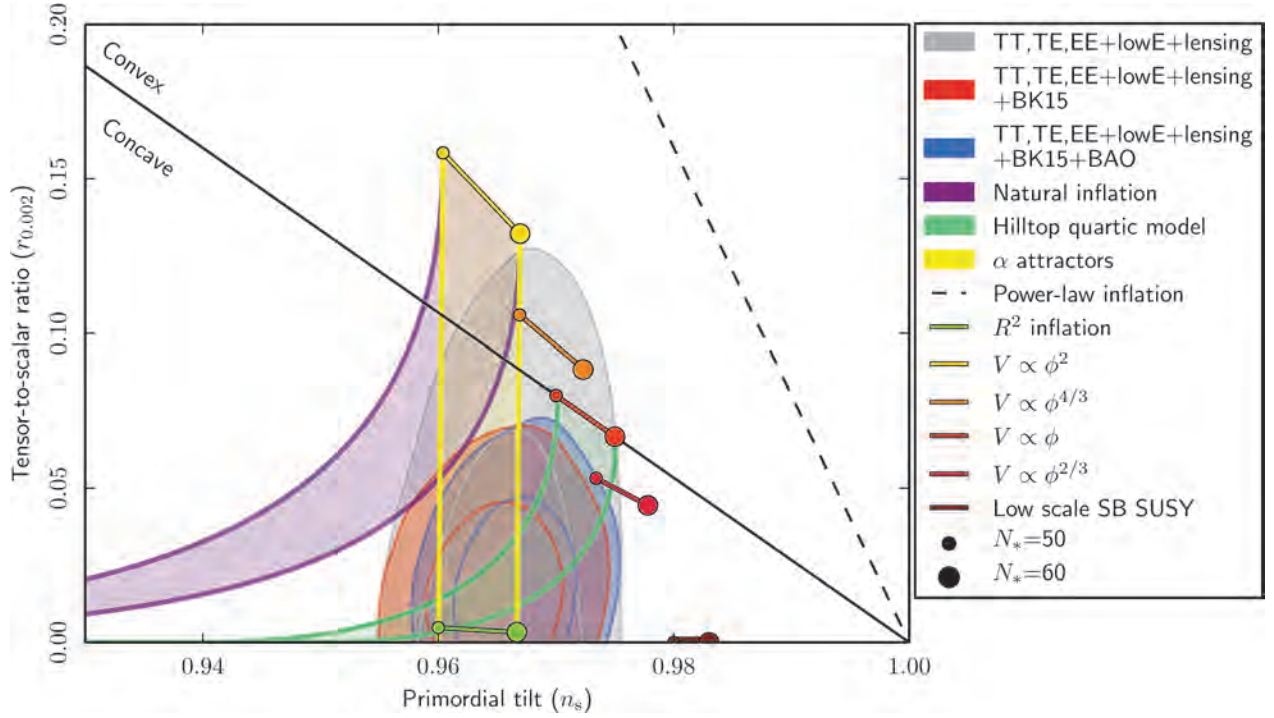


Figure 23.1: The marginalized joint 68 and 95% CL regions for the tilt in the scalar perturbation spectrum, n_s , and the relative magnitude of the tensor perturbations, r , obtained from the *Planck* 2018 and lensing data alone, and their combinations with BICEP2/Keck Array (BK15) and (optionally) BAO data, confronted with the predictions of some of the inflationary models discussed in this review. This figure is taken from [38].

Slow-roll corrections lead to slow time-dependence of both H_* and ϵ_* , giving a weak scale-dependence of the scalar power spectrum:

$$n_s - 1 \equiv \frac{d \ln \mathcal{P}_\zeta}{d \ln k} \simeq -6\epsilon_* + 2\eta_*, \quad (23.51)$$

and a running of this tilt at second-order in slow-roll:

$$\frac{dn_s}{d \ln k} \simeq -8\epsilon_*(3\epsilon_* - 2\eta_*) - 2\xi_*^2, \quad (23.52)$$

where the running introduces a new slow-roll parameter at second-order:

$$\xi^2 = \frac{M_P^4}{64\pi^2} \frac{V'V'''}{V^2}. \quad (23.53)$$

23.3.4 Observational Bounds

The observed scale-dependence of the power spectrum makes it necessary to specify the comoving scale, k , at which quantities are constrained and hence the Hubble-exit time, $k = a_* H_*$, when the corresponding theoretical quantities are calculated during inflation. This is usually expressed in terms of the number of e-folds from the end of inflation [42]:

$$N_*(k) \simeq 67 - \ln \left(\frac{k}{a_0 H_0} \right) + \frac{1}{4} \ln \left(\frac{V_*^2}{M_P^4 \rho_{end}} \right) + \frac{1}{12} \ln \left(\frac{\rho_{rh}}{\rho_{end}} \right) - \frac{1}{12} \ln(g_*), \quad (23.54)$$

where H_0^{-1}/a_0 is the present comoving Hubble length. Different models of reheating and and thus different reheat temperatures and densities, ρ_{rh} in Eq. (23.54), lead to a range of possible values for N_* corresponding to a fixed physical scale, and hence we have a range of observational predictions for a given inflation model, as seen in Fig. 23.1.

The *Planck* 2018 temperature and polarization data (see Chap. 29, “Cosmic Microwave Background” review) are consistent with a smooth featureless power spectrum over a range of comoving

wavenumbers, $0.008 h^{-1} \text{ Mpc}^{-1} \leq k \leq 0.1 h \text{ Mpc}^{-1}$. In the absence of running, the data measure the spectral index to be [38]

$$n_s = 0.9649 \pm 0.0042, \quad (23.55)$$

corresponding to a deviation from scale-invariance exceeding the 7σ level. If running of the spectral tilt is included in the model, this is constrained to be [38]

$$\frac{dn_s}{d \ln k} = -0.0045 \pm 0.0067 \quad (23.56)$$

at the 95% CL, assuming no running of the running. The most recent analysis [43] of the BICEP, Keck Array and *Planck* data places an upper bound on the tensor-to-scalar ratio

$$r < 0.036, \quad (23.57)$$

at the 95% CL.

These observational bounds can be converted into bounds on the slow-roll parameters and hence the potential during slow-roll inflation. Setting higher-order slow-roll parameters (beyond second-order in horizon-flow parameters [44]) to zero, the *Planck* collaboration obtain the following 95% CL bounds when lensing and BK15 data are included [38]

$$\epsilon < 0.0044, \quad (23.58)$$

$$\eta = -0.015 \pm 0.006, \quad (23.59)$$

$$\xi^2 = 0.0029_{-0.0069}^{+0.0073}, \quad (23.60)$$

which can be used to constrain models, as discussed in the next Section.

Fig. 23.1, which is taken from [38], compares observational CMB constraints on the tilt, n_s , in the spectrum of scalar perturbations and the ratio, r , between the magnitudes of tensor and scalar perturbations. Important rôles are played by data from the *Planck* satellite and on lensing, the BICEP2/Keck Array (BK15) and measurements of baryon acoustic oscillations (BAO). The reader is referred to [38] for technical details. These experimental constraints are compared with the predictions of some

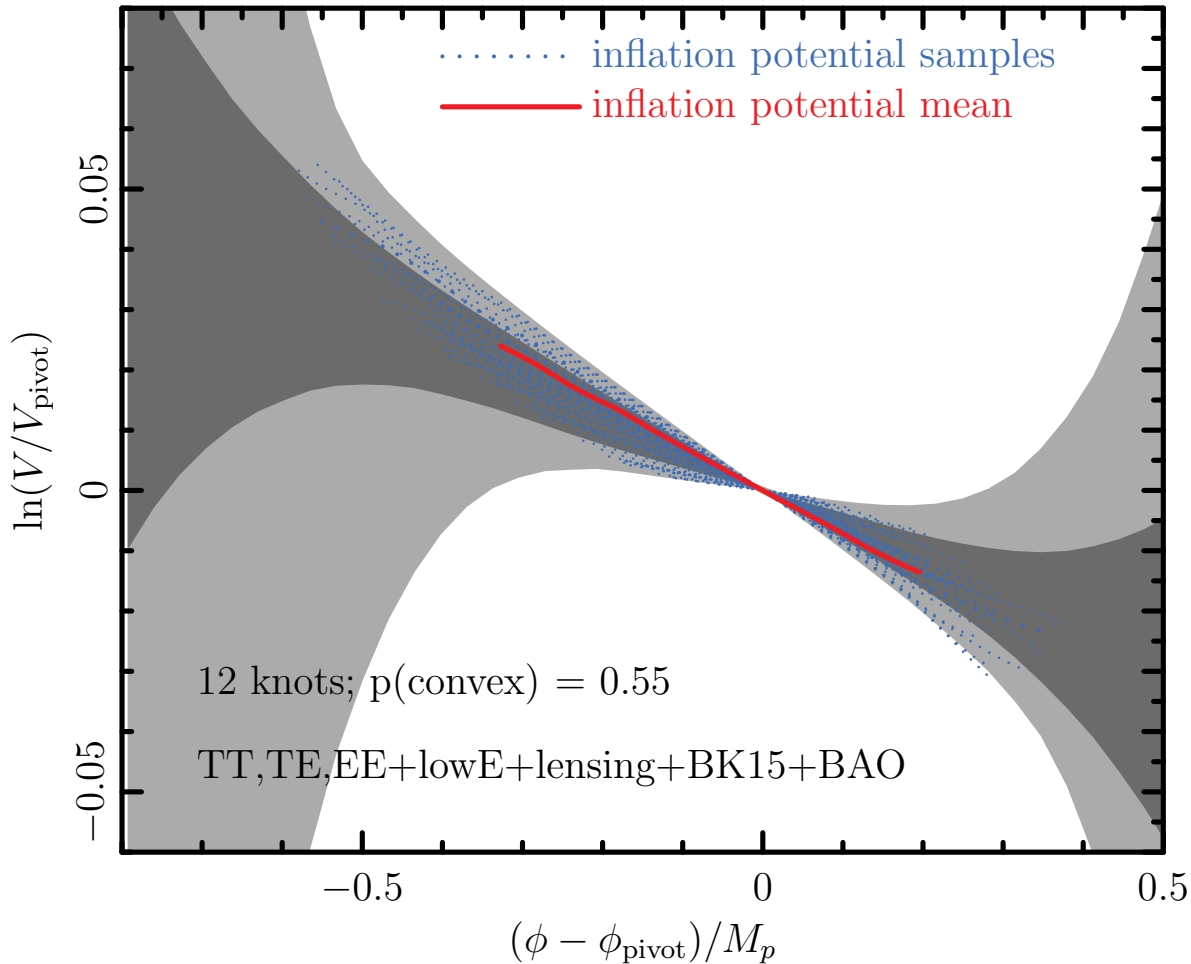


Figure 23.2: The result of reconstructing a single-field inflaton potential using a cubic-spline power-spectrum mode expansion and the the full *Planck*, lensing, BK15 and BAO data set. This figure is taken from [38].

of the inflationary models discussed in this review. Generally speaking, models with a concave potential are favored over those with a convex potential, and models with power-law inflation are now excluded, as opposed to models with de Sitter-like (quasi-)exponential expansion.

There is no significant evidence for local features within the range of inflaton field values probed by the data [38]. However, the data may be used to reconstruct partially the effective inflationary potential over a range of inflaton field values, assuming that it is suitably smooth. The result of one such exercise by the *Planck* collaboration [38] in the framework of a generic single-field inflaton potential is shown in Fig. 23.2. This reconstruction assumes a cubic-spline power-spectrum mode expansion and employs the full *Planck*, lensing, BK15 and BAO data set. The reader is again referred to [38] for technical details. We see that the effective inflaton potential is relatively well reconstructed over field values ϕ within ± 0.5 of the chosen pivot value, but the potential is only very weakly constrained for larger values of $|\phi - \phi_{pivot}|$, providing wide scope for inflationary model-builders.

23.4 Models

23.4.1 Pioneering Models

The paradigm of the inflationary Universe was proposed in [2], where it was pointed out that an early period of (near-)exponential expansion, in addition to resolving the horizon and flatness problems of conventional Big-Bang cosmology as discussed above (the possibility of a de Sitter phase in the early history of the Universe was also proposed in the non-minimal gravity model of [1], with the motivation of avoiding an initial singularity), would also dilute the prior abundance of any unseen heavy, (meta-)stable particles, as exemplified by monopoles

in grand unified theories (GUTs; see Chap. 93, “Grand Unified Theories” review). The original proposal was that this inflationary expansion took place while the Universe was in a metastable state (a similar suggestion was made in [45, 46], where in [45] it was also pointed out that such a mechanism could address the horizon problem) and was terminated by a first-order transition due to tunnelling through a potential barrier. However, it was recognized already in [2] that this ‘old inflation’ scenario would need modification if the transition to the post-inflationary Universe were to be completed smoothly without generating unacceptable inhomogeneities.

This ‘graceful exit’ problem was addressed in the ‘new inflation’ model of [13] (see also [14] and footnote [39] of [2]), which studied models based on an $SU(5)$ GUT with an effective potential of the Coleman-Weinberg type (i.e., dominated by radiative corrections), in which inflation could occur during the roll-down from the local maximum of the potential towards a global minimum. However, it was realized that the Universe would evolve to a different minimum from the Standard Model [47], and it was also recognized that density fluctuations would necessarily be too large [15], since they were related to the GUT coupling strength.

These early models of inflation assumed initial conditions enforced by thermal equilibrium in the early Universe. However, this assumption was questionable: indeed, it was not made in the model of [1], in which a higher-order gravitational curvature term was assumed to arise from quantum corrections, and the assumption of initial thermal equilibrium was jettisoned in the ‘chaotic’ inflationary model of [48]. These are the inspirations for much recent inflationary model building, so we now discuss them in more detail, before reviewing contemporary models.

In this section we will work in natural units where we set the reduced Planck mass to unity, i.e., $8\pi/M_P^2 = 1$. All masses are thus relative to the reduced Planck scale.

23.4.2 R^2 Inflation

The first-order Einstein-Hilbert action, $(1/2) \int d^4x \sqrt{-g} R$, where R is the Ricci scalar curvature, is the minimal possible theory consistent with general coordinate invariance. However, it is possible that there might be non-minimal corrections to this action, and the unique second-order possibility is

$$S = \frac{1}{2} \int d^4x \sqrt{-g} \left(R + \frac{R^2}{6M^2} \right). \quad (23.61)$$

It was pointed out in [1] that an R^2 term could be generated by quantum effects, and that (Eq. (23.61)) could lead to de Sitter-like expansion of the Universe. Scalar density perturbations in this model were calculated in [17]. Because the initial phase was (almost) de Sitter, these perturbations were (approximately) scale-invariant, with magnitude $\propto M$. It was pointed out in [17] that requiring the scalar density perturbations to lie in the range 10^{-3} to 10^{-5} , consistent with upper limits at that time, would require $M \sim 10^{-3}$ to 10^{-5} in Planck units, and it was further suggested that these perturbations could lead to the observed large-scale structure of the Universe, including the formation of galaxies.

Although the action (Eq. (23.61)) does not contain an explicit scalar field, [17] reduced the calculation of density perturbations to that of fluctuations in the scalar curvature R , which could be identified (up to a factor) with a scalar field of mass M . The formal equivalence of R^2 gravity (Eq. (23.61)) to a theory of gravity with a massive scalar ϕ had been shown in [18], see also [19]. The effective scalar potential for what we would nowadays call the ‘inflaton’ [49] takes the form

$$S = \frac{1}{2} \int d^4x \sqrt{-g} \left[R + (\partial_\mu \phi)^2 - \frac{3}{2} M^2 (1 - e^{-\sqrt{2/3} \phi})^2 \right] \quad (23.62)$$

when the action is written in the Einstein frame, and the potential is shown as the solid black line in Fig. 23.3. Using (Eq. (23.48)), one finds that the amplitude of the scalar density perturbations in this model is given by

$$\Delta_{\mathcal{R}} = \frac{3M^2}{8\pi^2} \sinh^4 \left(\frac{\phi}{\sqrt{6}} \right), \quad (23.63)$$

The measured magnitude of the density fluctuations in the CMB requires $M \simeq 1.3 \times 10^{-5}$ in Planck units (assuming $N_* \simeq 55$), so one of the open questions in this model is why M is so small. Obtaining $N_* \simeq 55$ also requires an initial value of $\phi \simeq 5.5$, i.e., a super-Planckian initial condition, and another issue for this and many other models is how the form of the effective potential is protected and remains valid at such large field values. Using Eq. (23.51) one finds that $n_s \simeq 0.965$ for $N_* \simeq 55$ and using (Eq. (23.49)) one finds that $r \simeq 0.0035$. These predictions are consistent with the present data from *Planck* and other experiments, as seen in Fig. 23.1.

23.4.3 Chaotic Models with Power-Law Potentials

As has already been mentioned, a key innovation in inflationary model-building was the suggestion to abandon the questionable assumption of a thermal initial state, and consider ‘chaotic’ initial conditions with very general forms of potential [48]. (Indeed, the R^2 model discussed above can be regarded as a prototype of this approach.) The chaotic approach was first proposed in the context of a simple power-law potential of the form $\mu^{4-\alpha} \phi^\alpha$, and the specific example of $\lambda \phi^4$ was studied in [48]. Such models make the following predictions for the slow-roll parameters ϵ and η :

$$\epsilon = \frac{1}{2} \left(\frac{\alpha}{\phi} \right)^2, \quad \eta = \frac{\alpha(\alpha-1)}{\phi^2}, \quad (23.64)$$

leading to the predictions

$$r \approx \frac{4\alpha}{N_*}, \quad n_s - 1 \approx -\frac{\alpha+2}{2N_*}, \quad (23.65)$$

which are shown in Fig. 23.1 for some illustrative values of α . We note that the prediction of the original ϕ^4 model lies out of the frame, with values of r that are too large and values of n_s that are too small. The ϕ^3 model has similar problems, and would in any case require modification in order to have a well-defined minimum. The simplest possibility is ϕ^2 , but this is now also disfavored by the data, at the 95% CL if only the *Planck* data are considered, and more strongly if other data are included, as seen in Fig. 23.1. (For non-minimal models of quadratic inflation that avoid this problem, see, e.g., [51].)

Indeed, as can be seen in Fig. 23.1, all single-field models with a convex potential (i.e., one curving upwards) are disfavored compared to models with a concave potential.

23.4.4 Hilltop Models

This preference for a concave potential motivates interest in ‘hilltop’ models [52], whose starting-point is a potential of the form

$$V(\phi) = \Lambda^4 \left[1 - \left(\frac{\phi}{\mu} \right)^p + \dots \right], \quad (23.66)$$

where the \dots represent extra terms that yield a positive semi-definite potential. To first order in the slow-roll parameters, when $x \equiv \phi/\mu$ is small, one has

$$n_s \simeq 1 - p(p-1)\mu^{-2} \frac{x^{p-2}}{(1-x^p)} - \frac{3}{8}r, \quad r \simeq 8p^2\mu^{-2} \frac{x^{2p-2}}{(1-x^p)^2}. \quad (23.67)$$

As seen in Fig. 23.1, a hilltop model with $p = 4$ can be compatible with the *Planck* and other measurements, if $\mu \gg M_P$.

23.4.5 D-Brane Inflation

Many scenarios for inflation involving extra dimensions have been proposed, e.g., the possibility that observable physics resides on a three-dimensional brane, and that there is an inflationary potential that depends on the distance between our brane and an antibrane, with a potential of the form [53]

$$V(\phi) = \Lambda^4 \left[1 - \left(\frac{\mu}{\phi} \right)^p + \dots \right]. \quad (23.68)$$

In this scenario the effective potential vanishes in the limit $\phi \rightarrow \infty$, corresponding to complete separation between our brane and the antibrane. The predictions for n_s and r in this model can be obtained from (Eq. 23.67) by exchanging $p \leftrightarrow -p$, and are also consistent with the *Planck* and other data.

23.4.6 Natural Inflation

Also seen in Fig. 23.1 are the predictions of ‘natural inflation’ [54], in which one postulates a non-perturbative shift symmetry that suppresses quantum corrections, so that a hierarchically small scale of inflation, $H \ll M_P$, is technically natural. In the simplest models, there is a periodic potential of the form

$$V(\phi) = \Lambda^4 \left[1 + \cos \left(\frac{\phi}{f} \right) \right], \quad (23.69)$$

where f is a dimensional parameter reminiscent of an axion decay constant (see the next subsection) [55], which must have a value $> M_P$. Natural inflation can yield predictions similar to quadratic inflation (which are no longer favored, as already discussed), but can also yield an effective convex potential. Thus, it may lead to values of r that are acceptably small, but for values of n_s that are in tension with the data, as seen in Fig. 23.1.

23.4.7 Axion Monodromy Models

The effective potentials in stringy models [56,57] motivated by axion monodromy may be of the form

$$V(\phi) = \mu^{4-\alpha} \phi^\alpha + \Lambda^4 e^{-C \left(\frac{\phi}{\phi_0} \right)^{p_\Lambda}} \cos \left[\gamma + \frac{\phi}{f} \left(\frac{\phi}{\phi_0} \right)^{p_f+1} \right], \quad (23.70)$$

where μ, Λ, f and ϕ_0 are parameters with the dimension of mass, and C, p, p_Λ, p_f and γ are dimensionless constants, generalizing the potential ([54]) in the simplest models of natural inflation. The oscillations in (Eq. 23.70) are associated with the axion field, and powers $p_\Lambda, p_f \neq 0$ may arise from ϕ -dependent evolutions of

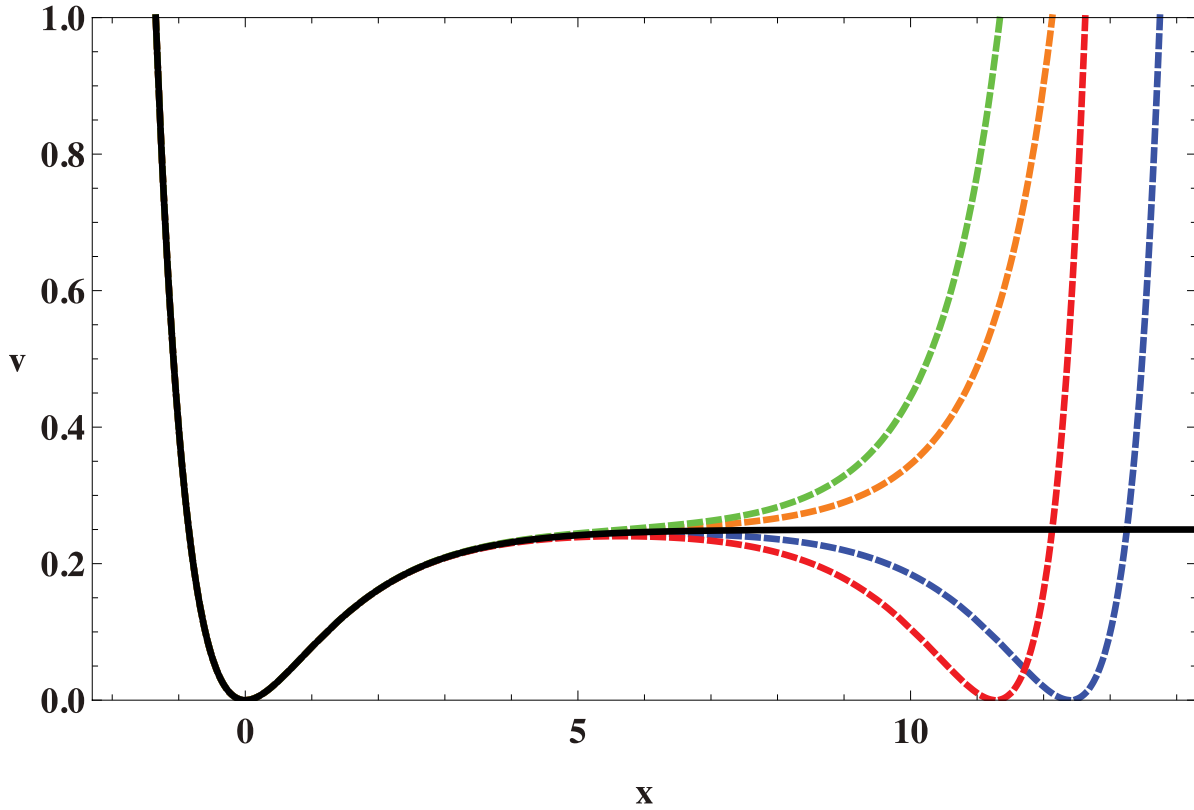


Figure 23.3: The inflationary potential V in the R^2 model (solid black line) compared with its form in various no-scale models discussed in detail in [50] (dashed coloured lines).

string moduli. Since the exponential prefactor in (Eq. 23.70) is due to non-perturbative effects that may be strongly suppressed, the oscillations may be unobservable small. Specific string models having ϕ^α with $\alpha = 4/3, 1$ or $2/3$ have been constructed in [56,57], providing some motivation for the low-power models mentioned above.

As seen in Fig. 23.1, the simple axion monodromy models with the power $\alpha = 4/3$ or 1 are no longer compatible with the current CMB data at the 95% CL, while $\alpha = 2/3$ is only marginally compatible at 95% CL. The *Planck* Collaboration has also searched for characteristic effects associated with the second term in (Eq. (23.70)), such as a possible drift in the modulation amplitude (setting $p_A = C = 0$), and a possible drifting frequency generated by $p_f \neq 0$, without finding any compelling evidence [38].

23.4.8 Higgs Inflation

Since the energy scale during inflation is commonly expected to lie between the Planck and TeV scales, it may serve as a useful bridge with contacts both to string theory or some other quantum theory of gravity, on the one side, and particle physics on the other side. However, as the above discussion shows, much of the activity in building models of inflation has been largely independent of specific connections with these subjects, though some examples of string-motivated models of inflation were mentioned above.

The most economical scenario for inflation might be to use as inflaton the only established scalar field, namely the Higgs field (see Chap.11, “Status of Higgs boson physics” review). A specific model assuming a non-minimal coupling of the Higgs field h to gravity was constructed in [58]. Its starting-point is the action

$$S = \int d^4x \sqrt{-g} \left[\frac{M^2 + \xi h^2}{2} R + \frac{1}{2} \partial_\mu h \partial^\mu h - \frac{\lambda}{4} (h^2 - v^2)^2 \right], \quad (23.71)$$

where v is the Higgs vacuum expectation value. The model requires $\xi \gg 1$, in which case it can be rewritten in the Einstein

frame as

$$S = \int d^4x \sqrt{-g} \left[\frac{1}{2} R + \frac{1}{2} \partial_\mu \chi \partial^\mu \chi - U(\chi) \right], \quad (23.72)$$

where the effective potential for the canonically-normalized inflaton field χ has the form

$$U(\chi) = \frac{\lambda}{4\xi^2} \left[1 + \exp\left(-\frac{2\chi}{\sqrt{6}M_P}\right) \right]^{-2}, \quad (23.73)$$

which is similar to the effective potential of the R^2 model at large field values. As such, the model inflates successfully if $\xi \simeq 5 \times 10^4 m_h/(\sqrt{2}v)$, with predictions for n_s and r that are indistinguishable from the predictions of the R^2 model shown in Fig. 23.1.

This model is very appealing, but must confront several issues. One is to understand the value of ξ , and another is the possibility of unitarity violation. However, a more fundamental issue is whether the effective quartic Higgs coupling is positive at the scale of the Higgs field during inflation. Extrapolations of the effective potential in the Standard Model using the measured values of the masses of the Higgs boson and the top quark indicate that probably $\lambda < 0$ at this scale [59], though there are still significant uncertainties associated with the appropriate input value of the top mass and the extrapolation to high renormalization scales.

23.4.9 Supersymmetric Models of Inflation

Supersymmetry [60] is widely considered to be a well-motivated possible extension of the Standard Model that might become apparent at the TeV scale. It is therefore natural to consider supersymmetric models of inflation. These were originally proposed because of the problems of the new inflationary theory [13,14] based on the one-loop (Coleman-Weinberg) potential for breaking SU(5). Several of these problems are related to the magnitude of the effective potential parameters: in any model of inflation based on an elementary scalar field, some parameter in the effective potential must be small in natural units, e.g., the quartic

coupling λ in a chaotic model with a quartic potential, or the mass parameter μ in a model of chaotic quadratic inflation. These parameters are renormalized multiplicatively in a supersymmetric theory, so that the quantum corrections to small values would be

under control. Hence, it was suggested that inflation cries out for supersymmetry [61], though non-supersymmetric resolutions of the problems of Coleman-Weinberg inflation are also possible: see, e.g., Ref. [62].

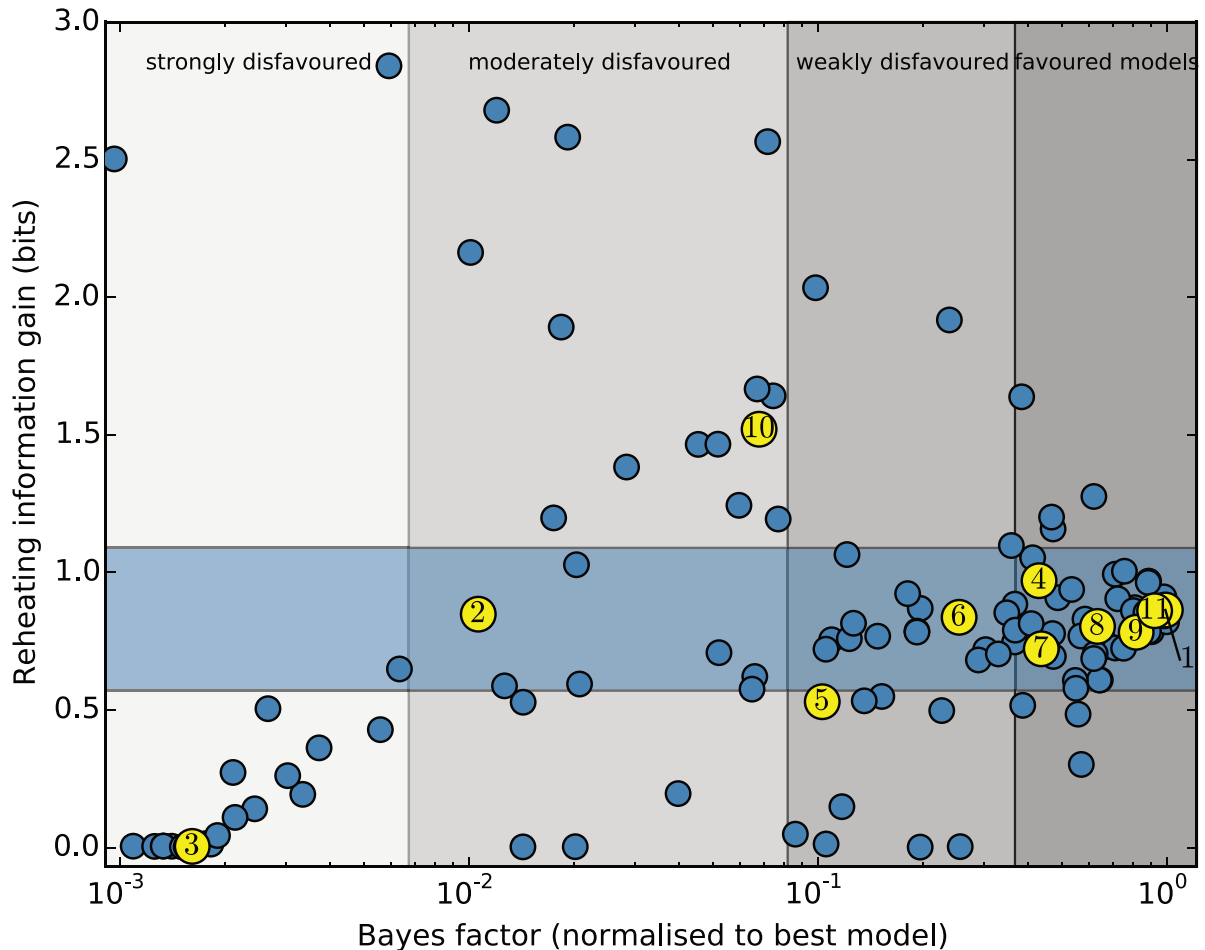


Figure 23.4: The Bayes factors calculated in [63] for a large sample of inflationary models using *Planck* 2015 data [64]. Those highlighted in yellow are featured in this review, according to the numbers listed in the text.

In the Standard Model there is only one scalar field that could be a candidate for the inflaton, namely the Higgs field discussed above, but even the minimal supersymmetric extension of the Standard Model (MSSM) contains many scalar fields. However, none of these is a promising candidate for the inflaton. The minimal extension of the MSSM that may contain a suitable candidate is the supersymmetric version of the minimal seesaw model of neutrino masses, which contains the three supersymmetric partners of the heavy singlet (right-handed) neutrinos. One of these singlet sneutrinos $\tilde{\nu}$ could be the inflaton [65]: it would have a quadratic potential, the mass coefficient required would be $\sim 10^{13}$ GeV, very much in the expected ballpark for singlet (right-handed) neutrino masses, and sneutrino inflaton decays also could give rise to the cosmological baryon asymmetry via leptogenesis. However, as seen in Fig. 23.1 and already discussed, a purely quadratic inflationary potential is no longer favored by the data. This difficulty could in principle be resolved in models with multiple sneutrinos [66], or by postulating a trilinear sneutrino coupling and hence a superpotential of Wess-Zumino type [67], which can yield successful inflation with predictions intermediate between those of natural inflation and hilltop inflation in Fig. 23.1.

Finally, we note that it is also possible to obtain inflation via supersymmetry breaking, as in the model [68] whose predictions are illustrated in Fig. 23.1.

23.4.10 Supergravity Models

Any model of early-Universe cosmology, and specifically inflation, must necessarily incorporate gravity. In the context of supersymmetry this requires an embedding in some supergravity theory [69, 70]. An $\mathcal{N} = 1$ supergravity theory is specified by three functions: a Hermitian function of the matter scalar fields ϕ^i , called the Kähler potential K , that describes its geometry, a holomorphic function of the superfields, called the superpotential W , which describes their interactions, and another holomorphic function $f_{\alpha\beta}$, which describes their couplings to gauge fields V_α [71].

The simplest possibility is that the Kähler metric is flat:

$$K = \phi^i \phi_i^* , \quad (23.74)$$

where the sum is over all scalar fields in the theory, and the simplest inflationary model in minimal supergravity had the superpotential [72]

$$W = m^2(1 - \phi)^2 , \quad (23.75)$$

Where ϕ is the inflaton. However, this model predicts a tilted scalar perturbation spectrum, $n_s = 0.933$, which is now in serious disagreement with the data from *Planck* and other experiments shown in Fig. 23.1.

Moreover, there is a general problem that arises in any supergravity theory coupled to matter, namely that, since its ef-

fective scalar potential contains a factor of e^K , scalars typically receive squared masses $\propto H^2 \sim V$, where H is the Hubble parameter [73], an issue called the ‘ η problem’. The theory given by (Eq. (23.75)) avoids this η problem, but a generic supergravity inflationary model encounters this problem of a large inflaton mass. Moreover, there are additional challenges for supergravity inflation associated with the spontaneous breaking of local supersymmetry [74–76].

Various approaches to the η problem in supergravity have been proposed, including the possibility of a shift symmetry [77], and one possibility that has attracted renewed attention recently is no-scale supergravity [78, 79]. This is a form of supergravity with a Kähler potential that can be written in the form [80]

$$K = -3 \ln \left(T + T^* - \frac{\sum_i |\phi^i|^2}{3} \right), \quad (23.76)$$

which has the special property that it naturally has a flat potential, at the classical level and before specifying a non-trivial superpotential. As such, no-scale supergravity is well-suited for constructing models of inflation. Adding to its attraction is the feature that compactifications of string theory to supersymmetric four-dimensional models yield effective supergravity theories of the no-scale type [81]. There are many examples of superpotentials that yield effective inflationary potentials for either the T field (which is akin to a modulus field in some string compactification) or a ϕ field (generically representing matter) that are of the same form as the effective potential of the R^2 model (Eq. (23.62)) when the magnitude of the inflaton field $\gg 1$ in Planck units, as required to obtain sufficiently many e-folds of inflation, N_* [82, 83]. This framework also offers the possibility of using a suitable superpotential to construct models with effective potentials that are similar, but not identical, to the R^2 model, as shown by the dashed coloured lines in Fig. 23.3.

23.4.11 Other Exponential Potential Models

This framework also offers the possibility [82] of constructing models in which the asymptotic constant value of the potential at large inflaton field values is approached via a different exponentially-suppressed term:

$$V(\phi) = A \left[1 - \delta e^{-B\phi} + \mathcal{O}(e^{-2B\phi}) \right], \quad (23.77)$$

where the magnitude of the scalar density perturbations fixes A , but δ and B are regarded as free parameters. In the case of R^2 inflation $\delta = 2$ and $B = \sqrt{2/3}$. In a model such as (Eq. (23.77)), one finds at leading order in the small quantity $e^{-B\phi}$ that

$$\begin{aligned} n_s &= 1 - 2B^2 \delta e^{-B\phi}, \\ r &= 8B^2 \delta^2 e^{-2B\phi}, \\ N_* &= \frac{1}{B^2 \delta} e^{+B\phi}. \end{aligned} \quad (23.78)$$

yielding the relations

$$n_s = 1 - \frac{2}{N_*}, r = \frac{8}{B^2 N_*^2}. \quad (23.79)$$

This model leads to the class of predictions labeled by ‘ α attractors’ [84] in Fig. 23.1. There are generalizations of the simplest no-scale model (Eq. (23.76)) with prefactors before the $\ln(\dots)$ that are 1 or 2, leading to larger values of $B = \sqrt{2}$ or 1, respectively, and hence smaller values of r than in the R^2 model.

23.5 Model Comparison

Given a particular inflationary model, one can obtain constraints on the model parameters, informed by the likelihood, corresponding to the probability of the data given a particular choice of parameters (see Sec. 40, “Statistics” review). In the light of the detailed constraints on the statistical distribution of primordial perturbations now inferred from high-precision observations of the cosmic microwave background, it is also possible to make quantitative comparison of the statistical evidence for or against different inflationary models. This can be done either

by comparing the logarithm of the maximum likelihood that can be obtained for the data using each model, i.e., the minimum χ^2 (with some correction for the number of free parameters in each model), or by a Bayesian model comparison [85] (see also Sec. 40.3.3 in “Statistics” review).

In such a Bayesian model comparison one computes [7] the evidence, $\mathcal{E}(\mathcal{D}|\mathcal{M}_A)$ for a model, \mathcal{M}_A , given the data \mathcal{D} . This corresponds to the likelihood, $\mathcal{L}(\theta_{Aj}) = p(\mathcal{D}|\theta_{Aj}, \mathcal{M}_A)$, integrated over the assumed prior distribution, $\pi(\theta_{Aj}|\mathcal{M}_A)$, for all the model parameters θ_{Aj} :

$$\mathcal{E}(\mathcal{D}|\mathcal{M}_A) = \int \mathcal{L}(\theta_{Aj}) \pi(\theta_{Aj}|\mathcal{M}_A) d\theta_{Aj}. \quad (23.80)$$

The posterior probability of the model given the data follows from Bayes’ theorem

$$p(\mathcal{M}_A|\mathcal{D}) = \frac{\mathcal{E}(\mathcal{D}|\mathcal{M}_A) \pi(\mathcal{M}_A)}{p(\mathcal{D})}, \quad (23.81)$$

where the prior probability of the model is given by $\pi(\mathcal{M}_A)$. Assuming that all models are equally likely a priori, $\pi(\mathcal{M}_A) = \pi(\mathcal{M}_B)$, the relative probability of model A relative to a reference model, in the light of the data, is thus given by the Bayes factor

$$B_{A,ref} = \frac{\mathcal{E}(\mathcal{D}|\mathcal{M}_A)}{\mathcal{E}(\mathcal{D}|\mathcal{M}_{ref})}. \quad (23.82)$$

Computation of the multi-dimensional integral (Eq. (23.80)) is a challenging numerical task. Even using an efficient sampling algorithm requires hundreds of thousands of likelihood computations for each model, though slow-roll approximations can be used to calculate rapidly the primordial power spectrum using the APSIC numerical library [7] for a large number of single-field, slow-roll inflation models.

The change in χ^2 for selected slow-roll models relative to the Starobinsky R^2 inflationary model, used as a reference, is given in Table 23.1 (taken from [38]). All the other inflation models require a substantial amplitude of tensor modes, and so have an increased χ^2 with respect to the Starobinsky and other models with a scalar tilt but small tensor modes. Table 23.1 also shows the Bayesian evidence for ($\ln B_{A,ref} > 0$) or against ($\ln B_{A,ref} < 0$) a selection of inflation models using the *Planck* analysis priors [38]. The Starobinsky R^2 inflationary model may be chosen as a reference [38] that provides a good fit to current data. Higgs inflation [58] is indistinguishable using current data, making the model comparison “inconclusive” on the Jeffrey’s scale ($|\ln B_{A,ref}| < 1$). (Recall, though, that this model is disfavored by the measured values of the Higgs and top quark masses [59].) We note that although α -attractor models can provide a good fit to the data, they are disfavored relative to the Starobinsky model due to their larger prior volume. There is now strong evidence ($|\ln B_{A,ref}| > 5$) against large-field models such as chaotic inflation with a quadratic or a quartic potential. Indeed, over 30% of the slow-roll inflation models considered in Ref. [7] are strongly disfavored by the *Planck* data.

Table 23.1: Observational evidence for and against selected inflation models: $\Delta\chi^2$ and the Bayes factors are calculated relative to the Starobinsky R^2 inflationary model, which is treated as a reference. Results from *Planck* 2018 analysis [38].

Model	$\Delta\chi^2$	$\ln B_{A,ref}$
R^2 inflation	0	0
Power-law potential $\phi^{2/3}$	+4.0	-4.6
Power-law potential ϕ^2	+21.6	< -10
Power-law potential ϕ^4	+75.3	< -10
Natural inflation	+9.9	-6.6
Hilltop quartic model	-0.3	-1.4

The Bayes factors for a wide selection of slow-roll inflationary models are displayed in Fig. 23.4, which is adapted from Fig. 3

in [63], where more complete descriptions of the models and the calculations of the Bayes factors using *Planck* 2015 data [64] are given. Models discussed in this review are highlighted in yellow, and numbered as follows: (1) R^2 inflation (Sec. 23.4.2) and models with similar predictions, such as Higgs inflation (Sec. 23.4.8) and no-scale supergravity inflation (Sec. 23.4.10); chaotic inflation models (2) with a ϕ^2 potential; (3) with a ϕ^4 potential; (4) with a $\phi^{2/3}$ potential, and (5) with a ϕ^p potential marginalising over $p \in [0.2, 6]$ (Sec. 23.4.3); hilltop inflation models (6) with $p = 2$; (7) with $p = 4$ and (8) marginalising over p (Sec. 23.4.4); (9) brane inflation (Sec. 23.4.5); (10) natural inflation (Sec. 23.4.6); (11) exponential potential models such as α -attractors (Sec. 23.4.11). As seen in Fig. 23.4 and discussed in the next Section, constraints on reheating are starting to provide additional information about models of inflation.

23.6 Constraints on Reheating

One connection between inflation and particle physics is provided by inflaton decay, whose products are expected to have thermalized subsequently. As seen in (Eq. (23.54)), the number of e-folds required during inflation depends on details of this reheating process, including the matter density upon reheating, denoted by ρ_{th} , which depends in turn on the inflaton decay rate Γ_ϕ . We see in Fig. 23.1 that, within any specific inflationary model, both n_s and particularly r are sensitive to the value of N_* . In particular, the one- σ uncertainty in the experimental measurement of n_s is comparable to the variation in many model predictions for $N_* \in [50, 60]$. This implies that the data start to constrain scenarios for inflaton decay in many models. For example, it is clear from Fig. 23.1 that $N_* = 60$ would be preferred over $N_* = 50$ in a chaotic inflationary model with a quadratic potential.

As a specific example, let us consider R^2 models and related models such as Higgs and no-scale inflation models that predict small values of r [86]. As seen in Fig. 23.1, within these models the combination of *Planck*, BICEP2/Keck Array and BAO data would require a limited range of n_s , corresponding to a limited range of N_* , as seen by comparing the left and right vertical axes in Fig. 23.5:

$$N_* \gtrsim 52 \quad (68\% \text{ CL}), \quad N_* \gtrsim 44 \quad (95\% \text{ CL}). \quad (23.83)$$

Within any specific model for inflaton decay, these bounds can be translated into constraints on the effective decay coupling. For example, if one postulates a two-body inflaton decay coupling y , the bounds (Eq. (23.83)) can be translated into bounds on y . This is illustrated in Fig. 23.5, where any value of N_* (on the left vertical axis), projected onto the diagonal line representing the correlation predicted in R^2 -like models, corresponds to a specific value of the inflaton decay rate Γ_ϕ/m (lower horizontal axis) and hence y (upper horizontal axis):

$$y \gtrsim 10^{-5} \quad (68\% \text{ CL}), \quad y \gtrsim 10^{-15} \quad (95\% \text{ CL}). \quad (23.84)$$

These bounds are not very constraining – although the 68% CL lower bound on y is already comparable with the electron Yukawa coupling – but can be expected to improve significantly in the coming years and thereby provide significant information on the connections between inflation and particle physics.

23.7 Beyond Single-Field Slow-Roll Inflation

There are numerous possible scenarios beyond the simplest single-field models of slow-roll inflation. These include theories in which non-canonical fields are considered, such as k-inflation [87] or DBI inflation [88], and multiple-field models, such as the curvaton scenario [89]. As well as altering the single-field predictions for the primordial curvature power spectrum (Eq. (23.48)) and the tensor-scalar ratio (Eq. (23.49)), they may introduce new quantities that vanish in single-field slow-roll models, such as isocurvature matter perturbations, corresponding to entropy fluctuations in the photon-to-matter ratio, at first order:

$$S_m = \frac{\delta n_m}{n_m} - \frac{\delta n_\gamma}{n_\gamma} = \frac{\delta \rho_m}{\rho_m} - \frac{3}{4} \frac{\delta \rho_\gamma}{\rho_\gamma}. \quad (23.85)$$

Another possibility is non-Gaussianity in the distribution of the primordial curvature perturbation (see Chap. 29, “Cosmic Mi-

crowave Background” review), encoded in higher-order correlators such as the primordial bispectrum [90]

$$\langle \zeta(\mathbf{k})\zeta(\mathbf{k}')\zeta(\mathbf{k}'') \rangle \equiv (2\pi)^3 \delta(\mathbf{k} + \mathbf{k}' + \mathbf{k}'') B_\zeta(k, k', k''), \quad (23.86)$$

which is often expressed in terms of a dimensionless non-linearity parameter

$$f_{NL} \propto B_\zeta(k, k', k'') / P_\zeta(k) P_\zeta(k').$$

The three-point function (Eq. (23.86)) can be thought of as defined on a triangle whose sides are $\mathbf{k}, \mathbf{k}', \mathbf{k}''$, of which only two are independent, since they sum to zero. Further assuming statistical isotropy ensures that the bispectrum depends only on the magnitudes of the three vectors, k, k' and k'' . The search for f_{NL} and other non-Gaussian effects was a prime objective of the *Planck* data analysis [91, 92].

23.7.1 Effective Field Theory of Inflation

Since slow-roll inflation is a phase of accelerated expansion with an almost constant Hubble parameter, one may think of inflation in terms of an effective theory where the de Sitter spacetime symmetry is spontaneously broken down to RW symmetry by the time-evolution of the Hubble rate, $\dot{H} \neq 0$. There is then a Goldstone boson, π , associated with the spontaneous breaking of time-translation invariance, which can be used to study model-independent properties of inflation. The Goldstone boson describes a spacetime-dependent shift of the time coordinate, corresponding to an adiabatic perturbation of the matter fields:

$$\delta\phi_i(t, \vec{x}) = \phi_i(t + \pi(t, \vec{x})) - \phi_i(t). \quad (23.87)$$

Thus adiabatic field fluctuations can be absorbed into the spatial metric perturbation, \mathcal{R} in Eq. (23.28) at first order, in the comoving gauge:

$$\mathcal{R} = -H\pi, \quad (23.88)$$

where we define π on spatially-flat hypersurfaces. In terms of inflaton field fluctuations, we can identify $\pi \equiv \delta\phi/\dot{\phi}$, but in principle this analysis is not restricted to inflation driven by scalar fields.

The low-energy effective action for π can be obtained by writing down the most general Lorentz-invariant action and expanding in terms of π . The second-order effective action for the free-field wave modes, π_k , to leading order in slow roll is then

$$S_\pi^{(2)} = - \int d^4x \sqrt{-g} \frac{M_P^2 \dot{H}}{c_s^2} \left[\dot{\pi}_k^2 - \frac{c_s^2}{R^2} (\nabla\pi)^2 \right], \quad (23.89)$$

where ϵ_H is the Hubble slow-roll parameter (Eq. (23.11)). We identify c_s^2 with an effective sound speed, generalising canonical slow-roll inflation, which is recovered in the limit $c_s^2 \rightarrow 1$.

The scalar power spectrum on super-Hubble scales (Eq. (23.48)) is enhanced for a reduced sound speed, leading to a reduced tensor-scalar ratio (Eq. (23.49))

$$\mathcal{P}_\zeta(k) \simeq \frac{4\pi}{M_P^2} \frac{1}{c_s^2 \epsilon} \left(\frac{H}{2\pi} \right)_*^2, \quad r \simeq 16(c_s^2 \epsilon)_*. \quad (23.90)$$

At third perturbative order and to lowest order in derivatives, one obtains [94]

$$S_\pi^{(3)} = \int d^4x \sqrt{-g} \frac{M_P^2 (1 - c_s^2) \dot{H}}{c_s^2} \left[\frac{\dot{\pi} (\nabla\pi)^2}{R^2} - \left(1 + \frac{2}{3} \frac{\tilde{c}_3}{c_s^2} \right) \dot{\pi}^3 \right]. \quad (23.91)$$

Note that this expression vanishes for canonical fields with $c_s^2 = 1$. For $c_s^2 \neq 1$ the cubic action is determined by the sound speed and an additional parameter \tilde{c}_3 . Both terms in the cubic action give rise to primordial bispectra that are well approximated by equilateral bispectra. However, the shapes are not identical, so one can find a linear combination for which the equilateral bispectra of each term cancel, giving rise to a distinctive orthogonal-type bispectrum [94].

Analysis based on *Planck* 2018 temperature and polarization data has placed bounds on several bispectrum shapes including

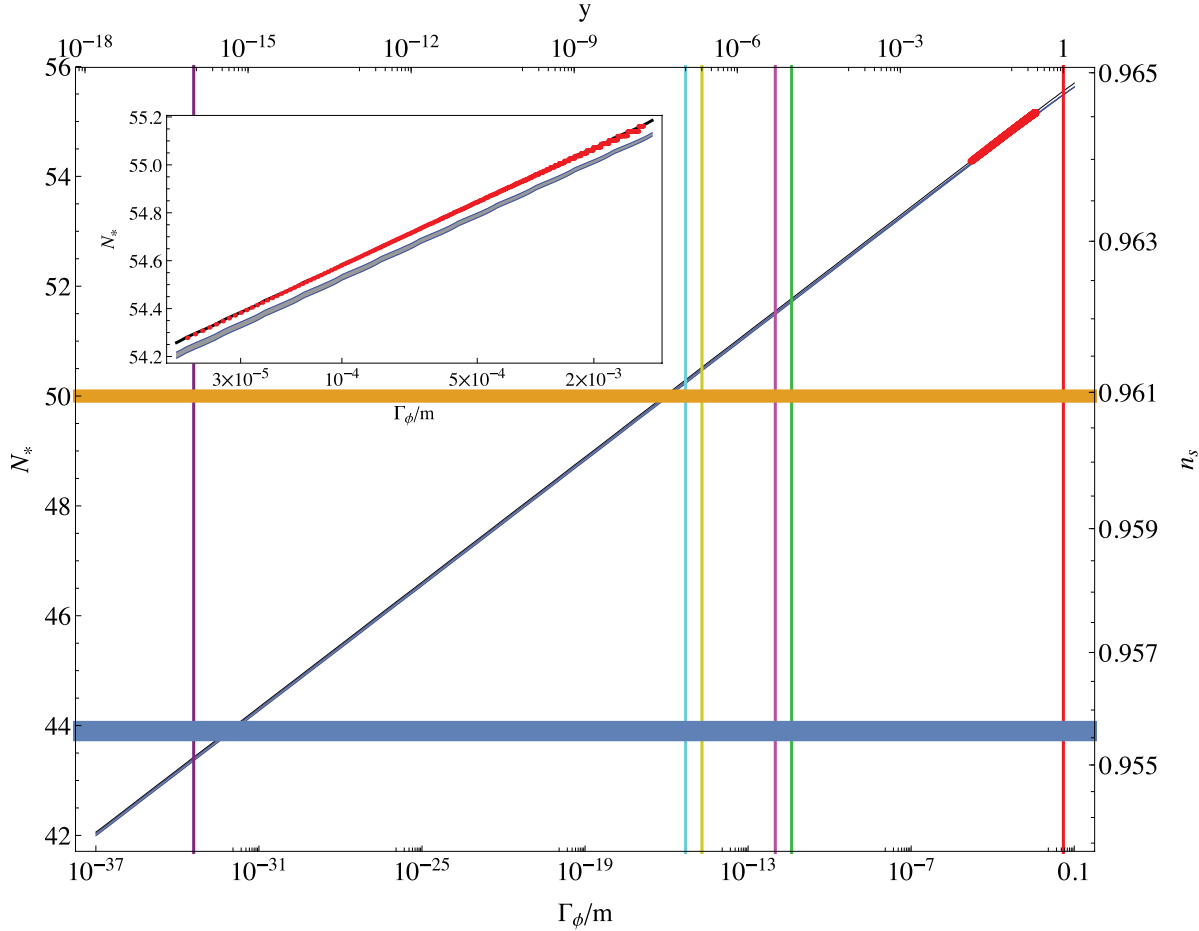


Figure 23.5: The values of N_* (left axis) and n_s (right axis) in R^2 inflation and related models for a wide range of decay rates, Γ_ϕ/m , (bottom axis) and corresponding two-body couplings, y (top axis). The diagonal red line segment shows full numerical results over a restricted range of Γ_ϕ/m (which are shown in more detail in the insert), while the diagonal blue strip represents an analytical approximation described in [86]. The difference between these results is indistinguishable in the main plot, but is visible in the insert. The horizontal yellow and blue lines show the 68 and 95% CL lower limits from the *Planck* 2015 data [64], and the vertical coloured lines correspond to specific models of inflaton decay. Figure taken from [93].

equilateral and orthogonal shapes [92]:

$$f_{NL}^{equil} = -26 \pm 47, \quad f_{NL}^{orthog} = -38 \pm 24 \quad (68\% \text{ CL}). \quad (23.92)$$

For the simplest case of a constant sound speed, and marginalising over \tilde{c}_3 , this provides a bound on the inflaton sound speed [92]

$$c_s \geq 0.021 \quad (95\% \text{ CL}). \quad (23.93)$$

For a specific model such as DBI inflation [88], corresponding to $\tilde{c}_3 = 3(1 - c_s^2)/2$, one obtains a tighter bound [92]:

$$c_s^{DBI} \geq 0.086 \quad (95\% \text{ CL}). \quad (23.94)$$

The *Planck* team have analysed a wide range of non-Gaussian templates from different inflation models, including tests for deviations from an initial Bunch-Davies vacuum state, direction-dependent non-Gaussianity, and feature models with oscillatory bispectra [92]. No individual feature or resonance is above the three- σ significance level after accounting for the look-elsewhere effect. These results are consistent with the simplest canonical, slow-roll inflation models, but do not rule out most alternative models; rather, bounds on primordial non-Gaussianity place important constraints on the parameter space for non-canonical models.

23.7.2 Multi-Field Fluctuations

There is a very large literature on two- and multi-field models of inflation, most of which lies beyond the scope of this review [95,96]. However, two important general topics merit being

mentioned here, namely residual isocurvature perturbations and the possibility of non-Gaussian effects in the primordial perturbations.

One might expect that other scalar fields besides the inflaton might have non-negligible values that evolve and fluctuate in parallel with the inflaton, without necessarily making the dominant contribution to the energy density during the inflationary epoch. However, the energy density in such a field might persist beyond the end of inflation before decaying, at which point it might come to dominate (or at least make a non-negligible contribution to) the total energy density. In such a case, its perturbations could end up generating the density perturbations detected in the CMB. This could occur due to a late-decaying scalar field [89] or a field fluctuation that modulates the end of inflation [97] or the inflaton decay [98].

23.7.2.1 Isocurvature Perturbations

Primordial perturbations arising in single-field slow-roll inflation are necessarily adiabatic, i.e., they affect the overall density without changing the ratios of different contributions, such as the photon-matter ratio, $\delta(n_\gamma/n_m)/(n_\gamma/n_m)$. This is because inflaton perturbations represent a local shift of the time, as described in section Sec. 23.7.1:

$$\pi = \frac{\delta n_\gamma}{\dot{n}_\gamma} = \frac{\delta n_m}{\dot{n}_m}. \quad (23.95)$$

However, any light scalar field (i.e., one with effective mass less than the Hubble scale) acquires a spectrum of nearly scale-

invariant perturbations during inflation. Fluctuations orthogonal to the inflaton in field space are decoupled from the inflaton at Hubble-exit, but can affect the subsequent evolution of the density perturbation. In particular, they can give rise to local variations in the equation of state (non-adiabatic pressure perturbations) that can alter the primordial curvature perturbation ζ on super-Hubble scales. Since these fluctuations are statistically independent of the inflaton perturbations at leading order in slow-roll [96], non-adiabatic field fluctuations can only increase the scalar power spectrum with respect to adiabatic perturbations at Hubble exit, while leaving the tensor modes unaffected at first perturbative order. Thus, the single-field result for the tensor-scalar ratio (Eq. (23.49)) becomes an inequality [99]

$$r \leq 16\epsilon_* . \quad (23.96)$$

Hence, an observational upper bound on the tensor-scalar ratio does not bound the slow-roll parameter ϵ in multi-field models.

If all the scalar fields present during inflation eventually decay completely into fully thermalized radiation, these field fluctuations are converted fully into adiabatic perturbations in the primordial plasma [100]. On the other hand, non-adiabatic field fluctuations can also leave behind primordial isocurvature perturbations (Eq. (23.85)) after inflation. In multi-field inflation models it is thus possible for non-adiabatic field fluctuations to generate both curvature and isocurvature perturbations leading to correlated primordial perturbations [101].

The amplitudes of any primordial isocurvature perturbations (Eq. (23.85)) are strongly constrained by the current CMB data, especially on large angular scales. Using temperature and low- ℓ polarization data yields the following bound on the amplitude of cold dark matter isocurvature perturbations at scale $k = 0.002h^{-1}\text{Mpc}^{-1}$ (marginalising over the correlation angle and in the absence of primordial tensor perturbations) [38]:

$$\frac{\mathcal{P}_{S_m}}{\mathcal{P}_\zeta + \mathcal{P}_{S_m}} < 0.025 \text{ (95\% CL)} . \quad (23.97)$$

For fully (anti-)correlated isocurvature perturbations, corresponding to a single isocurvature field providing a source for both the curvature and residual isocurvature perturbations, the bounds become significantly tighter [38]:

$$\frac{\mathcal{P}_{S_m}}{\mathcal{P}_\zeta + \mathcal{P}_{S_m}} < 0.0002 \text{ (95\% CL), correlated} , \quad (23.98)$$

$$\frac{\mathcal{P}_{S_m}}{\mathcal{P}_\zeta + \mathcal{P}_{S_m}} < 0.003 \text{ (95\% CL), anti-correlated} \quad (23.99)$$

23.7.2.2 Local-Type Non-Gaussianity

Since non-adiabatic field fluctuations in multi-field inflation may lead to the evolution of the primordial curvature perturbation at all orders, it becomes possible to generate significant non-Gaussianity in the primordial curvature perturbation. Non-linear evolution on super-Hubble scales leads to local-type non-Gaussianity, where the local integrated expansion is a non-linear function of the local field values during inflation, $N(\phi_i)$. While the field fluctuations at Hubble exit, $\delta\phi_{i*}$, are Gaussian in the slow-roll limit, the curvature perturbation, $\zeta = \delta N$, becomes a non-Gaussian distribution [102]:

$$\zeta = \sum_i \frac{\partial N}{\partial \phi_i} \delta\phi_i + \frac{1}{2} \sum_{i,j} \frac{\partial^2 N}{\partial \phi_i \partial \phi_j} \delta\phi_i \delta\phi_j + \dots \quad (23.100)$$

with non-vanishing bispectrum in the squeezed limit ($k_1 \approx k_2 \gg k_3$):

$$B_\zeta(k_1, k_2, k_3) \approx \frac{12}{5} f_{NL}^{local} \frac{\mathcal{P}_\zeta(k_1)}{4\pi k_1^3} \frac{\mathcal{P}_\zeta(k_3)}{4\pi k_3^3} , \quad (23.101)$$

where

$$\frac{6}{5} f_{NL}^{local} = \frac{\sum_{i,j} \frac{\partial^2 N}{\partial \phi_i \partial \phi_j}}{\left(\sum_i \frac{\partial N}{\partial \phi_i}\right)^2} . \quad (23.102)$$

Both equilateral and orthogonal bispectra, discussed above in the context of generalised single field inflation, vanish in the squeezed limit, enabling the three types of non-Gaussianity to be distinguished by observations, in principle.

Non-Gaussianity during multi-field inflation is highly model dependent, though f_{NL}^{local} can often be smaller than unity in multi-field slow-roll inflation [103]. Scenarios where a second light field plays a role during or after inflation can make distinctive predictions for f_{NL}^{local} , such as $f_{NL}^{local} = -5/4$ in some curvaton scenarios [102, 104] or $f_{NL}^{local} = 5$ in simple modulated reheating scenarios [98, 105]. By contrast the constancy of ζ on super-Hubble scales in single-field slow-roll inflation leads to a very small non-Gaussianity [106, 107], and in the squeezed limit we have the simple result $f_{NL}^{local} = 5(1 - n_S)/12$ [108, 109].

A combined analysis of the *Planck* 2018 temperature and polarization data [92] yields the following range for f_{NL}^{local} defined in (Eq. (23.102)):

$$f_{NL}^{local} = -1 \pm 5 \text{ (68\% CL)} . \quad (23.103)$$

This sensitivity is sufficient to rule out parameter regimes giving rise to relatively large non-Gaussianity, but insufficient to probe $f_{NL}^{local} = \mathcal{O}(\epsilon)$, as expected in single-field models, or the range $f_{NL}^{local} = \mathcal{O}(1)$ found in the simplest two-field models.

Local-type primordial non-Gaussianity can also give rise to a striking scale-dependent bias in the distribution of collapsed dark matter halos and thus the galaxy distribution [110, 111]. Bounds from high-redshift galaxy surveys are not currently competitive with the best CMB constraints. The most recent analysis [112] based on the clustering of quasars in the final data release (DR16) of the extended Baryon acoustic Oscillation Spectroscopic Survey (eBOSS) yields

$$f_{NL}^{local} = -12 \pm 21 \text{ (68\% CL)} . \quad (23.104)$$

23.8 Initial Conditions and Fine-tuning

This review is based on the assumption that the inflationary paradigm is valid. However, it remains the object of many criticisms (see, e.g., [113]), many of them related to the perceived unnaturalness of the required initial conditions.

Most work on inflation is done in the context of RW cosmology, which assumes a high degree of symmetry, or small inhomogeneous perturbations (usually first order) about an RW cosmology. The isotropic RW space-time is an attractor for many homogeneous but anisotropic cosmologies in the presence of a false vacuum energy density [114], or a scalar field with suitable self-interaction potential energy [115, 116]. However it is much harder to establish the range of highly inhomogeneous initial conditions that yield a successful RW Universe, with only limited studies initially (see, e.g., [117, 118]). A related open question is the general nature of the pre-inflationary state of the inflaton and other fields that could have provided initial conditions suitable for inflation [113]. They would need to have satisfied non-trivial homogeneity and isotropy conditions, and one may ask how these could have arisen, whether these are plausible, and whether there may be some observable signature of the pre-inflationary state. These and other criticisms of inflation were addressed in [119], which presented studies of the sensitivity of inflation to the initial conditions. Complementing the studies reported in [119], there have been numerical relativity investigations of highly inhomogeneous initial conditions [120–122]. The general conclusion is that inflation is rather robust with respect to inhomogeneities in the initial conditions in both the scalar field profile and the extrinsic curvature, including large tensor perturbations.

To quantify the fine-tuning of initial conditions requires a measure in the space of possible cosmologies [123], however it has been argued that some of the measures historically used to frame this problem are formally invalid [124]. It is sometimes also objected that inflationary models predict the existence of a multiverse, and potentially a loss of predictive power [125], if it undergoes the process termed eternal inflation [126–128]. However, whether this is actually a bug or a feature remains a topic of debate [129, 130]. The existence of the multiverse is a purely philosophical problem, unless it has observable consequences, e.g., in the CMB.

One might expect signatures of any pre-inflationary state to appear at large angular scales, i.e., low multipoles ℓ . Indeed, various anomalies have been noted in the large-scale CMB anisotropies, as also discussed in Chap. 29, the ‘‘Cosmic Microwave Background’’ review, including a possible suppression of the quadrupole and other very large-scale anisotropies, an apparent feature in the range $\ell \approx 20$ to 30, and a possible hemispheric asymmetry. However, none of these are highly significant statistically, in view of the limitations due to cosmic variance [64]. They cannot yet be regarded as signatures of initial conditions, the multiverse or some pre-inflationary dynamics, such as might emerge from string theory.

A different kind of initial condition problem, called the trans-Planckian problem [131], is that the perturbations now seen in the CMB would have had wavelengths shorter than the Planck length at the onset of inflation. However, under quite general and conservative assumptions the usual inflationary predictions would be quite robust [132], with the possibility of $\mathcal{O}((H/m_P)^n)$ corrections that might have interesting signatures in the CMB [133].

When inflation was first proposed [1] [2] there was no evidence for the existence of scalar fields or the accelerated expansion of the Universe. The situation has changed dramatically in recent years with the observational evidence that the cosmic expansion is currently accelerating and with the discovery of a scalar particle, namely the Higgs boson (see Chap. 11, ‘‘Status of Higgs boson physics’’ review). Combined with the lack of any widely accepted alternative model for the origin of cosmic structure, these discoveries have lent support to the idea of a primordial accelerated expansion driven by a scalar field, i.e., cosmological inflation. In parallel, successive CMB experiments have been consistent with generic predictions of inflationary models, although without yet providing irrefutable evidence. It was concluded in [119] that the inflationary paradigm is not currently in trouble. However, we note that inflation via a formally elementary scalar inflaton should probably only be regarded as an effective field theory valid at energy densities hierarchically smaller than the Planck scale. It should eventually be embedded in a suitable ultraviolet completion, on which inflationary dynamics may be our clearest window.

23.9 Future Probes of Inflation

Prospective future CMB experiments, both ground- and space-based are reviewed in the separate PDG ‘‘Cosmic Microwave Background’’ review, Chap. 29. The main emphasis in CMB experiments in the coming years will be on ground-based experiments providing improved measurements of B -mode polarization and greater sensitivity to the tensor-to-scalar ratio r , and more precise measurements at higher ℓ that will constrain n_s better. As is apparent from Fig. 23.1 and the discussion of models such as R^2 inflation, there is a strong incentive to reach a $5\text{-}\sigma$ sensitivity to $r \sim 3$ to 4×10^{-3} . This could be achieved with a moderately-sized space mission with large sky coverage [134], improvements in de-lensing and foreground measurements. The discussion in Sec. 23.3 (see also Fig. 23.5), also brought out the importance of reducing the uncertainty in n_s , as a way to constrain post-inflationary reheating and the connection to particle physics. CMB temperature anisotropies probe primordial density perturbations down to comoving scales of order 50 Mpc, beyond which scale secondary sources of anisotropy dominate. CMB spectral distortions could potentially constrain the amplitude and shape of primordial density perturbations on comoving scales from Mpc to kpc due to distortions caused by the Silk damping of pressure waves in the radiation dominated era, before the last scattering of the CMB photons but after the plasma can be fully thermalised [135].

Improved sensitivity to non-Gaussianities is also a priority. In addition to CMB measurements, future large-scale structure surveys will also have roles to play as probes into models of inflation, for which there are excellent prospects. High-redshift galaxy surveys are sensitive to local-type non-Gaussianity due to the scale-dependent bias induced on large scales. Upcoming surveys such as DESI may reach $\Delta f_{NL} \sim 4$ [136] comparable with the *Planck* sensitivity. In the future, radio surveys such as SKA will measure large-scale structure out to redshift $z \sim 3$ [137], initially through mapping the intensity of the neutral hydrogen 21-cm line, and eventually through radio galaxy surveys which will probe local-

type non-Gaussianity to $f_{NL} \sim 1$.

Galaxy clustering using DESI and *Euclid* satellite data could also constrain the running of the scalar tilt to a precision of $\Delta\alpha_s \approx 0.0028$, a factor of 2 improvement on *Planck* constraints, or a precision of 0.0016 using LSST data [136].

As an example of a proposed future satellite mission, *SPHEREx* [138] will use measurements of the galaxy power spectrum to target a measurement of the running of the scalar spectral index with a sensitivity $\Delta\alpha_s \sim 10^{-3}$ and local-type primordial non-Gaussianity, $\Delta f_{NL} \sim 1$. Including information from the galaxy bispectrum one might reduce the measurement error on non-Gaussianity to $\Delta f_{NL} \sim 0.2$, making it possible to distinguish between single-field slow-roll models and alternatives such as the curvaton scenario for the origin of structure, which generate $f_{NL} \sim 1$.

Acknowledgements

The authors are grateful to Vincent Vennin for his careful reading of this manuscript and preparing Fig. 23.4 for this review. The work of J.E. was supported in part by the UK STFC via the research grant ST/L000258/1 and in part by the Estonian Research Council via a Mobilitas Pluss grant. The work of D.W. was supported in part by the UK STFC research grant ST/S000550/1.

References

- [1] A. A. Starobinsky, Phys. Lett. **B91**, 99 (1980), [Adv. Ser. Astrophys. Cosmol.3,130(1987)].
- [2] A. H. Guth, Phys. Rev. **D23**, 347 (1981), [Adv. Ser. Astrophys. Cosmol.3,139(1987)].
- [3] K. A. Olive, Phys. Rept. **190**, 307 (1990).
- [4] D. H. Lyth and A. Riotto, Phys. Rept. **314**, 1 (1999), [hep-ph/9807278].
- [5] A.R. Liddle and D.H. Lyth, *Cosmological inflation and large-scale structure* (Cambridge University Press, 2000).
- [6] D. Baumann, in ‘‘Physics of the large and the small, TASI 09, proceedings of the Theoretical Advanced Study Institute in Elementary Particle Physics, Boulder, Colorado, USA, 1-26 June 2009,’’ 523–686 (2011), [arXiv:0907.5424].
- [7] J. Martin, C. Ringeval and V. Vennin, Phys. Dark Univ. **5-6**, 75 (2014), [arXiv:1303.3787]; J. Martin *et al.*, JCAP **1403**, 039 (2014), [arXiv:1312.3529]; J. Martin, Astrophys. Space Sci. Proc. **45**, 41 (2016), [arXiv:1502.05733].
- [8] P. A. R. Ade *et al.* (Planck), Astron. Astrophys. **594**, A13 (2016), [arXiv:1502.01589].
- [9] A. H. Guth and E. J. Weinberg, Nucl. Phys. **B212**, 321 (1983).
- [10] D. La and P. J. Steinhardt, Phys. Rev. Lett. **62**, 376 (1989), [Erratum: Phys. Rev. Lett.62,1066(1989)].
- [11] A. D. Linde, Phys. Lett. **B249**, 18 (1990).
- [12] F. C. Adams and K. Freese, Phys. Rev. **D43**, 353 (1991), [hep-ph/0504135].
- [13] A. D. Linde, Phys. Lett. **108B**, 389 (1982), [Adv. Ser. Astrophys. Cosmol.3,149(1987)].
- [14] A. Albrecht and P. J. Steinhardt, Phys. Rev. Lett. **48**, 1220 (1982), [Adv. Ser. Astrophys. Cosmol.3,158(1987)].
- [15] W. H. Press, Phys. Scripta **21**, 702 (1980); S. W. Hawking, Phys. Lett. **115B**, 295 (1982); A. A. Starobinsky, Phys. Lett. **117B**, 175 (1982); A. H. Guth and S. Y. Pi, Phys. Rev. Lett. **49**, 1110 (1982).
- [16] J. M. Bardeen, P. J. Steinhardt and M. S. Turner, Phys. Rev. **D28**, 679 (1983).
- [17] V. F. Mukhanov and G. V. Chibisov, JETP Lett. **33**, 532 (1981), [Pisma Zh. Eksp. Teor. Fiz.33,549(1981)].
- [18] K. S. Stelle, Gen. Rel. Grav. **9**, 353 (1978).
- [19] B. Whitt, Phys. Lett. **145B**, 176 (1984).
- [20] D. Wands, Class. Quant. Grav. **11**, 269 (1994), [arXiv:gr-qc/9307034].
- [21] S. R. Coleman and F. De Luccia, Phys. Rev. **D21**, 3305 (1980).

- [22] M. Sasaki *et al.*, Phys. Lett. **B317**, 510 (1993).
- [23] M. Bucher, A. S. Goldhaber and N. Turok, Phys. Rev. **D52**, 3314 (1995), [hep-ph/9411206].
- [24] A. D. Linde and A. Mezhlumian, Phys. Rev. **D52**, 6789 (1995), [arXiv:astro-ph/9506017].
- [25] A. R. Liddle, P. Parsons and J. D. Barrow, Phys. Rev. **D50**, 7222 (1994), [arXiv:astro-ph/9408015].
- [26] L. Kofman, A. D. Linde and A. A. Starobinsky, Phys. Rev. **D56**, 3258 (1997), [hep-ph/9704452].
- [27] B. A. Bassett, S. Tsujikawa and D. Wands, Rev. Mod. Phys. **78**, 537 (2006), [arXiv:astro-ph/0507632].
- [28] A. D. Linde, Phys. Rev. **D49**, 748 (1994), [arXiv:astro-ph/9307002].
- [29] A. D. Dolgov and A. D. Linde, Phys. Lett. **116B**, 329 (1982).
- [30] J. R. Ellis *et al.*, Nucl. Phys. **B238**, 453 (1984), [,223(1983)].
- [31] M. Kawasaki and T. Moroi, Prog. Theor. Phys. **93**, 879 (1995), [hep-ph/9403364].
- [32] J. H. Traschen and R. H. Brandenberger, Phys. Rev. **D42**, 2491 (1990).
- [33] G. V. Chibisov and V. F. Mukhanov, Mon. Not. Roy. Astron. Soc. **200**, 535 (1982).
- [34] H. Kodama and M. Sasaki, Prog. Theor. Phys. Suppl. **78**, 1 (1984).
- [35] V.F. Mukhanov, H.A. Feldman and R.H. Brandenberger, Phys. Rept. **215**, 203 (1992).
- [36] K. A. Malik and D. Wands, Phys. Rept. **475**, 1 (2009), [arXiv:0809.4944].
- [37] V. F. Mukhanov, Sov. Phys. JETP **67**, 1297 (1988), [Zh. Eksp. Teor. Fiz.94N7,1(1988)].
- [38] Y. Akrami *et al.* (Planck), Astron. Astrophys. **641**, A10 (2020), [arXiv:1807.06211].
- [39] A. A. Starobinsky, JETP Lett. **30**, 682 (1979), [,767(1979)].
- [40] E. D. Stewart and D. H. Lyth, Phys. Lett. **B302**, 171 (1993), [arXiv:gr-qc/9302019].
- [41] D. Wands *et al.*, Phys. Rev. **D62**, 043527 (2000), [arXiv:astro-ph/0003278].
- [42] A. R. Liddle and S. M. Leach, Phys. Rev. **D68**, 103503 (2003), [arXiv:astro-ph/0305263].
- [43] P. A. R. Ade *et al.* (BICEP/Keck), Phys. Rev. Lett. **127**, 15, 151301 (2021), [arXiv:2110.00483].
- [44] S.M. Leach, A.R. Liddle, J. Martin, and D.J. Schwarz, Phys. Rev. **D66**, 23515 (2002).
- [45] D. Kazanas, Astrophys. J. **241**, L59 (1980).
- [46] K. Sato, Mon. Not. Roy. Astron. Soc. **195**, 467 (1981).
- [47] A. Billore and K. Tamvakis, Nucl. Phys. **B200**, 329 (1982); J. D. Breit, S. Gupta and A. Zaks, Phys. Rev. Lett. **51**, 1007 (1983).
- [48] A. D. Linde, Phys. Lett. **129B**, 177 (1983).
- [49] D. V. Nanopoulos, K. A. Olive and M. Srednicki, Phys. Lett. **127B**, 30 (1983).
- [50] J. Ellis, D. V. Nanopoulos and K. A. Olive, Phys. Rev. Lett. **111**, 111301 (2013), [Erratum: Phys. Rev. Lett.111,no.12,129902(2013)], [arXiv:1305.1247].
- [51] T. S. Koivisto and F. R. Urban, JCAP **1503**, 03, 003 (2015), [arXiv:1407.3445].
- [52] L. Boubekeur and D. H. Lyth, JCAP **0507**, 010 (2005), [hep-ph/0502047].
- [53] G. R. Dvali, Q. Shafi and S. Solganik, in “4th European Meeting From the Planck Scale to the Electroweak Scale (Planck 2001) La Londe les Maures, Toulon, France, May 11-16, 2001,” (2001), [hep-th/0105203]; J. Garcia-Bellido, R. Rabadan and F. Zamora, JHEP **01**, 036 (2002), [hep-th/0112147]; S. Kachru *et al.*, JCAP **0310**, 013 (2003), [hep-th/0308055].
- [54] F. C. Adams *et al.*, Phys. Rev. **D47**, 426 (1993), [hep-ph/9207245].
- [55] E. Pajer and M. Peloso, Class. Quant. Grav. **30**, 214002 (2013), [arXiv:1305.3557].
- [56] E. Silverstein and A. Westphal, Phys. Rev. **D78**, 106003 (2008), [arXiv:0803.3085].
- [57] L. McAllister, E. Silverstein and A. Westphal, Phys. Rev. **D82**, 046003 (2010), [arXiv:0808.0706].
- [58] F. L. Bezrukov and M. Shaposhnikov, Phys. Lett. **B659**, 703 (2008), [arXiv:0710.3755].
- [59] D. Buttazzo *et al.*, JHEP **12**, 089 (2013), [arXiv:1307.3536].
- [60] H. P. Nilles, Phys. Rept. **110**, 1 (1984); H. E. Haber and G. L. Kane, Phys. Rept. **117**, 75 (1985).
- [61] J.R. Ellis *et al.*, Phys. Lett. **118B**, 335 (1982).
- [62] N. Okada and Q. Shafi (2013), [arXiv:1311.0921].
- [63] J. Martin, C. Ringeval and V. Vennin, Phys. Rev. **D93**, 10, 103532 (2016), [arXiv:1603.02606].
- [64] P. A. R. Ade *et al.* (Planck), Astron. Astrophys. **594**, A20 (2016), [arXiv:1502.02114].
- [65] H. Murayama *et al.*, Phys. Rev. Lett. **70**, 1912 (1993).
- [66] J. Ellis, M. Fairbairn and M. Sueiro, JCAP **1402**, 044 (2014), [arXiv:1312.1353].
- [67] D. Croon, J. Ellis and N. E. Mavromatos, Phys. Lett. **B724**, 165 (2013), [arXiv:1303.6253].
- [68] G. R. Dvali, Q. Shafi and R. K. Schaefer, Phys. Rev. Lett. **73**, 1886 (1994), [hep-ph/9406319].
- [69] D. V. Nanopoulos *et al.*, Phys. Lett. **123B**, 41 (1983).
- [70] A. B. Goncharov and A. D. Linde, Phys. Lett. **139B**, 27 (1984).
- [71] E. Cremmer *et al.*, Nucl. Phys. **B212**, 413 (1983), [,413(1982)].
- [72] R. Holman, P. Ramond and G. G. Ross, Phys. Lett. **137B**, 343 (1984).
- [73] E. J. Copeland *et al.*, Phys. Rev. **D49**, 6410 (1994), [arXiv:astro-ph/9401011]; E. D. Stewart, Phys. Rev. **D51**, 6847 (1995), [hep-ph/9405389].
- [74] G. D. Coughlan *et al.*, Phys. Lett. **131B**, 59 (1983); A. S. Goncharov, A. D. Linde and M. I. Vysotsky, Phys. Lett. **147B**, 279 (1984); T. Banks, D. B. Kaplan and A. E. Nelson, Phys. Rev. **D49**, 779 (1994), [hep-ph/9308292]; B. de Carlos *et al.*, Phys. Lett. **B318**, 447 (1993), [hep-ph/9308325]; M. Kawasaki, T. Moroi and T. Yanagida, Phys. Lett. **B370**, 52 (1996), [hep-ph/9509399].
- [75] J. R. Ellis, D. V. Nanopoulos and M. Quiros, Phys. Lett. **B174**, 176 (1986).
- [76] T. Moroi, M. Yamaguchi and T. Yanagida, Phys. Lett. **B342**, 105 (1995), [hep-ph/9409367].
- [77] M. Kawasaki, M. Yamaguchi and T. Yanagida, Phys. Rev. Lett. **85**, 3572 (2000), [hep-ph/0004243]; K. Nakayama, F. Takahashi and T. T. Yanagida, JCAP **1308**, 038 (2013), [arXiv:1305.5099].
- [78] E. Cremmer *et al.*, Phys. Lett. **133B**, 61 (1983).
- [79] A. S. Goncharov and A. D. Linde, Class. Quant. Grav. **1**, L75 (1984); C. Kounnas and M. Quiros, Phys. Lett. **151B**, 189 (1985).
- [80] J. R. Ellis, C. Kounnas and D. V. Nanopoulos, Nucl. Phys. **B247**, 373 (1984).
- [81] E. Witten, Phys. Lett. **155B**, 151 (1985).
- [82] J. Ellis, D. V. Nanopoulos and K. A. Olive, JCAP **1310**, 009 (2013), [arXiv:1307.3537].
- [83] J. Ellis *et al.*, Class. Quant. Grav. **33**, 9, 094001 (2016), [arXiv:1507.02308].
- [84] R. Kallosh, A. Linde and D. Roest, JHEP **11**, 198 (2013), [arXiv:1311.0472].

- [85] A. R. Liddle, *Mon. Not. Roy. Astron. Soc.* **377**, L74 (2007), [arXiv:astro-ph/0701113].
- [86] C. T. Byrnes and E. R. M. Tarrant, *JCAP* **1507**, 007 (2015), [arXiv:1502.07339].
- [87] C. Armendariz-Picon, T. Damour and V. F. Mukhanov, *Phys. Lett.* **B458**, 209 (1999), [hep-th/9904075].
- [88] M. Alishahiha, E. Silverstein and D. Tong, *Phys. Rev.* **D70**, 123505 (2004), [hep-th/0404084].
- [89] K. Enqvist and M. S. Sloth, *Nucl. Phys.* **B626**, 395 (2002), [hep-ph/0109214]; D. H. Lyth and D. Wands, *Phys. Lett.* **B524**, 5 (2002), [hep-ph/0110002]; T. Moroi and T. Takahashi, *Phys. Lett.* **B522**, 215 (2001), [Erratum: *Phys. Lett.* **B539**, 303(2002)], [hep-ph/0110096].
- [90] N. Bartolo *et al.*, *Phys. Rept.* **402**, 103 (2004), [arXiv:astro-ph/0406398].
- [91] P. A. R. Ade *et al.* (Planck), *Astron. Astrophys.* **594**, A17 (2016), [arXiv:1502.01592].
- [92] Y. Akrami *et al.* (Planck), *Astron. Astrophys.* **641**, A9 (2020), [arXiv:1905.05697].
- [93] J. Ellis *et al.*, *JCAP* **1507**, 07, 050 (2015), [arXiv:1505.06986].
- [94] L. Senatore, K. M. Smith and M. Zaldarriaga, *JCAP* **1001**, 028 (2010), [arXiv:0905.3746].
- [95] C. Gordon *et al.*, *Phys. Rev.* **D63**, 023506 (2001), [arXiv:astro-ph/0009131]; R. Easther *et al.*, *Phys. Rev. Lett.* **112**, 161302 (2014), [arXiv:1312.4035]; J. Ellis *et al.*, *JCAP* **1501**, 010 (2015), [arXiv:1409.8197]; S. Renaux-Petel and K. Turzynski, *JCAP* **1506**, 06, 010 (2015), [arXiv:1405.6195].
- [96] C. T. Byrnes and D. Wands, *Phys. Rev.* **D74**, 043529 (2006), [arXiv:astro-ph/0605679].
- [97] D. H. Lyth, *JCAP* **0511**, 006 (2005), [arXiv:astro-ph/0510443].
- [98] G. Dvali, A. Gruzinov and M. Zaldarriaga, *Phys. Rev.* **D69**, 023505 (2004), [arXiv:astro-ph/0303591].
- [99] D. Wands *et al.*, *Phys. Rev.* **D66**, 043520 (2002), [arXiv:astro-ph/0205253].
- [100] S. Weinberg, *Phys. Rev.* **D67**, 123504 (2003), [arXiv:astro-ph/0302326].
- [101] D. Langlois, *Phys. Rev.* **D59**, 123512 (1999), [arXiv:astro-ph/9906080].
- [102] D. H. Lyth and Y. Rodriguez, *Phys. Rev. Lett.* **95**, 121302 (2005), [arXiv:astro-ph/0504045].
- [103] F. Vernizzi and D. Wands, *JCAP* **0605**, 019 (2006), [arXiv:astro-ph/0603799].
- [104] M. Sasaki, J. Valiviita and D. Wands, *Phys. Rev.* **D74**, 103003 (2006), [arXiv:astro-ph/0607627].
- [105] G. Dvali, A. Gruzinov and M. Zaldarriaga, *Phys. Rev.* **D69**, 083505 (2004), [arXiv:astro-ph/0305548].
- [106] D. S. Salopek and J. R. Bond, *Phys. Rev.* **D43**, 1005 (1991).
- [107] A. Gangui *et al.*, *Astrophys. J.* **430**, 447 (1994), [arXiv:astro-ph/9312033].
- [108] J. M. Maldacena, *JHEP* **05**, 013 (2003), [arXiv:astro-ph/0210603].
- [109] V. Acquaviva *et al.*, *Nucl. Phys.* **B667**, 119 (2003), [arXiv:astro-ph/0209156].
- [110] N. Dalal *et al.*, *Phys. Rev.* **D77**, 123514 (2008), [arXiv:0710.4560].
- [111] S. Matarrese and L. Verde, *Astrophys. J.* **677**, L77 (2008), [arXiv:0801.4826].
- [112] E.-M. Mueller *et al.* (2021), [arXiv:2106.13725].
- [113] A. Ijjas, P. J. Steinhardt and A. Loeb, *Phys. Lett.* **B723**, 261 (2013), [arXiv:1304.2785].
- [114] R. M. Wald, *Phys. Rev.* **D28**, 2118 (1983).
- [115] M. Heusler, *Phys. Lett.* **B253**, 33 (1991).
- [116] Y. Kitada and K.-i. Maeda, *Phys. Rev.* **D45**, 1416 (1992).
- [117] D. S. Goldwirth and T. Piran, *Phys. Rept.* **214**, 223 (1992).
- [118] T. Vachaspati and M. Trodden, *Phys. Rev.* **D61**, 023502 (1999), [arXiv:gr-qc/9811037].
- [119] D. Chowdhury *et al.*, *Phys. Rev. D* **100**, 8, 083537 (2019), [arXiv:1902.03951].
- [120] W. E. East *et al.*, *JCAP* **1609**, 09, 010 (2016), [arXiv:1511.05143].
- [121] K. Clough *et al.*, *JCAP* **1709**, 09, 025 (2017), [arXiv:1608.04408].
- [122] K. Clough, R. Flauger and E. A. Lim, *JCAP* **1805**, 05, 065 (2018), [arXiv:1712.07352].
- [123] G. W. Gibbons, S. W. Hawking and J. M. Stewart, *Nucl. Phys.* **B281**, 736 (1987).
- [124] J. S. Schiffrin and R. M. Wald, *Phys. Rev.* **D86**, 023521 (2012), [arXiv:1202.1818].
- [125] A. Ijjas, P. J. Steinhardt and A. Loeb, *Phys. Lett.* **B736**, 142 (2014), [arXiv:1402.6980].
- [126] A. Vilenkin, *Phys. Rev.* **D27**, 2848 (1983).
- [127] A. D. Linde, *Phys. Lett.* **B175**, 395 (1986).
- [128] A. S. Goncharov, A. D. Linde and V. F. Mukhanov, *Int. J. Mod. Phys.* **A2**, 561 (1987).
- [129] A. H. Guth, D. I. Kaiser and Y. Nomura, *Phys. Lett.* **B733**, 112 (2014), [arXiv:1312.7619].
- [130] A. Linde, in “Proceedings, 100th Les Houches Summer School: Post-Planck Cosmology: Les Houches, France, July 8 - August 2, 2013,” 231–316 (2015), [arXiv:1402.0526].
- [131] J. Martin and R. H. Brandenberger, *Phys. Rev.* **D63**, 123501 (2001), [hep-th/0005209].
- [132] R. H. Brandenberger and J. Martin, *Mod. Phys. Lett.* **A16**, 999 (2001), [arXiv:astro-ph/0005432].
- [133] J. Martin and R. H. Brandenberger, in “Recent developments in theoretical and experimental general relativity, gravitation and relativistic field theories. Proceedings, 9th Marcel Grossmann Meeting, MG’9, Rome, Italy, July 2-8, 2000. Pts. A-C,” 2001–2002 (2000), [arXiv:astro-ph/0012031].
- [134] A. Kogut *et al.*, *JCAP* **1107**, 025 (2011), [arXiv:1105.2044].
- [135] J. Chluba, J. Hamann and S. P. Patil, *Int. J. Mod. Phys.* **D24**, 10, 1530023 (2015), [arXiv:1505.01834].
- [136] A. Font-Ribera *et al.*, *JCAP* **1405**, 023 (2014), [arXiv:1308.4164].
- [137] R. Maartens *et al.* (SKA Cosmology SWG), *PoS AASKA14*, 016 (2015), [arXiv:1501.04076].
- [138] O. Doré *et al.* (2014), [arXiv:1412.4872].

24. Big Bang Nucleosynthesis

Revised August 2021 by B.D. Fields (Astronomy, Illinois U.; Physics, Illinois U.), P. Molaro (INAF-OATS Trieste; IFPU) and S. Sarkar (Rudolf Peierls, Oxford U.).

24.1 Abstract

Big-Bang nucleosynthesis (BBN) offers the deepest reliable probe of the early Universe, being based on well-understood Standard Model physics [1]. Predictions of the abundances of the light elements, D, ^3He , ^4He , and ^7Li , synthesized at the end of the *first three minutes*, are in good overall agreement with the primordial abundances inferred from observational data, thus validating the standard hot Big-Bang cosmology (see [2–5] for reviews). This is particularly impressive given that these abundances span nine orders of magnitude – from $^4\text{He}/\text{H} \sim 0.08$ down to $^7\text{Li}/\text{H} \sim 10^{-10}$ (ratios by number). Thus BBN provides powerful constraints on possible deviations from the standard cosmology, and on new physics beyond the Standard Model [6–9].

24.2 Theory

The synthesis of the light elements is sensitive to physical conditions in the early radiation-dominated era at a temperature $T \sim 1$ MeV, corresponding to an age $t \sim 1$ s. At higher temperatures, weak interactions were in thermal equilibrium, thus fixing the ratio of the neutron and proton number densities to be $n/p = e^{-Q/T}$, where $Q = 1.293$ MeV is the neutron-proton mass difference. As the temperature dropped, the neutron-proton inter-conversion rate per nucleon, $\Gamma_{n \leftrightarrow p} \sim G_{\text{F}}^2 T^5$, fell faster than the Hubble expansion rate, $H \sim \sqrt{g_* G_{\text{N}}} T^2$, where g_* counts the number of relativistic particle species determining the energy density in radiation (see ‘Big Bang Cosmology’ — Sec. 22 of this *Review*). This resulted in departure from chemical equilibrium (freeze-out) at $T_{\text{fr}} \sim (g_* G_{\text{N}}/G_{\text{F}}^4)^{1/6} \simeq 1$ MeV. The neutron fraction at this time, $n/p = e^{-Q/T_{\text{fr}}} \simeq 1/6$, is thus sensitive to every known physical interaction, since Q is determined by both strong and electromagnetic interactions while T_{fr} depends on the weak as well as gravitational interactions. Moreover, the sensitivity to the Hubble expansion rate affords a probe of, *e.g.*, the number of relativistic neutrino species [10]. After freeze-out, the neutrons were free to β -decay, so the neutron fraction dropped to $n/p \simeq 1/7$ by the time nuclear reactions began. A simplified analytic model of freeze-out yields the n/p ratio to an accuracy of $\sim 1\%$ [11, 12].

The rates of these reactions depend on the density of baryons (strictly speaking, nucleons), which is usually expressed normalized to the relic blackbody photon density as $\eta \equiv n_{\text{b}}/n_{\gamma}$. As we shall see, all the light-element abundances can be explained with $\eta_{10} \equiv \eta \times 10^{10}$ in the range 6.143 ± 0.190 . With n_{γ} fixed by the present CMB temperature 2.7255 K (see ‘Cosmic Microwave Background’ — Sec. 29 of this *Review*), this can be stated as the allowed range for the baryon mass density today, $\rho_{\text{b}} = (4.2 \pm 0.1) \times 10^{-31}$ g cm $^{-3}$, or as the baryonic fraction of the critical density, $\Omega_{\text{b}} = \rho_{\text{b}}/\rho_{\text{crit}} \simeq \eta_{10} h^{-2}/274 = (0.02244 \pm 0.00069) h^{-2}$, where $h \equiv H_0/100$ km s $^{-1}$ Mpc $^{-1}$ is the present Hubble parameter (see ‘The Cosmological Parameters’ — Sec. 25 of this *Review*).

The nucleosynthesis chain begins with the formation of deuterium in the process $p(n, \gamma)\text{D}$. However, photo-dissociation by the high number density of photons delays production of deuterium (and other complex nuclei) until well after T drops below the binding energy of deuterium, $\Delta_{\text{D}} = 2.23$ MeV. The quantity $\eta^{-1} e^{-\Delta_{\text{D}}/T}$, *i.e.*, the number of photons per baryon above the deuterium photo-dissociation threshold, falls below unity at $T \simeq 0.1$ MeV; nuclei can then begin to form without being immediately photo-dissociated again. Only 2-body reactions, such as $\text{D}(p, \gamma)^3\text{He}$ and $^3\text{He}(\text{D}, p)^4\text{He}$ are important because the density by this time has become rather low – comparable to that of air!

Nearly all neutrons end up bound in the most stable light element ^4He . Heavier nuclei do not form in any significant quantity both because of the absence of stable nuclei with mass number 5 or 8 (which impedes nucleosynthesis via $n^4\text{He}$, $p^4\text{He}$ or $^4\text{He}^4\text{He}$ reactions), and the large Coulomb barriers for reactions such as $^3\text{He}(^4\text{He}, \gamma)^7\text{Li}$ and $^3\text{He}(^4\text{He}, \gamma)^7\text{Be}$. Hence the primordial mass fraction of ^4He , $Y_{\text{p}} \equiv \rho(^4\text{He})/\rho_{\text{b}}$, can be estimated by the simple

counting argument

$$Y_{\text{p}} = \frac{2(n/p)}{1 + n/p} \simeq 0.25 \quad (24.1)$$

where strictly speaking this gives the baryon fraction in ^4He , which is what we will quote throughout. This differs slightly from the mass fraction due to small binding energy corrections.

There is little sensitivity here to the actual nuclear reaction rates for the production of ^4He . Nuclear rates are, however, critically important in determining the other ‘left-over’ abundances: D and ^3He at the level of a few times 10^{-5} by number relative to H, and $^7\text{Li}/\text{H}$ at the level of about 10^{-10} (when η_{10} is in the range 1–10). These values can be understood in terms of approximate analytic arguments [12, 13].

The elemental abundances shown in Fig. 24.1 as a function of η_{10} were calculated using an updated version [14] of the Wagoner code [1]; other versions [15–17] too are publicly available. The ^4He curve includes small corrections due to radiative processes at zero and finite temperatures [18], non-equilibrium neutrino heating during e^{\pm} annihilation [19], and finite nucleon mass effects [20]; the range primarily reflects the 2σ uncertainty in the neutron lifetime. The spread in the curves for D, ^3He , and ^7Li corresponds to the 2σ uncertainties in nuclear cross sections, as estimated by Monte Carlo methods [21–24]. The input nuclear data have been carefully reassessed [2, 14, 21–31], leading to improved precision for the abundance predictions. In particular, the uncertainty in $^7\text{Li}/\text{H}$ at interesting values of η has been reduced recently by a factor ~ 2 , a consequence of a similar reduction in the error budget [32] for the dominant mass-7 production channel $^3\text{He}(^4\text{He}, \gamma)^7\text{Be}$. Polynomial fits to the predicted abundances and the error correlation matrix have been given in refs. [23, 33]. The boxes in Fig 24.1 show the observationally inferred primordial abundances with their associated uncertainties, as discussed below.

The nuclear reaction cross sections important for BBN have all been measured at the relevant energies. Recently however there have been substantial advances in the precision of light element observations (*e.g.*, D/H) and in the determination of cosmological parameters (*e.g.*, from *Planck*). This motivates corresponding improvement in BBN predictions and thus in the key reaction cross sections. Recent measurements of $\text{D}(p, \gamma)^3\text{He}$ by the LUNA collaboration have significantly improved the precision of D/H predictions [34]. Even so, the nuclear uncertainties still leave D/H prediction errors larger than those of the observations [14, 30, 31]. The $\text{D}(\text{D}, n)^3\text{He}$ and $\text{D}(\text{D}, p)^3\text{He}$ reactions now not only dominate the uncertainty budget, but they can give significantly different D/H predictions depending on whether one uses just the empirical determination of the cross sections, or also uses theory to guide the functional form. Clearly, more experimental data is needed.

An additional experimental parameter important in determining the light element abundances is the neutron lifetime, τ_n , which normalizes (the inverse of) $\Gamma_{n \leftrightarrow p}$. Its value has been revised downwards to $\tau_n = 879.4 \pm 0.6$ s (see *N Baryons Listing*).

24.3 Observations: the Light Element Abundances

BBN theory predicts the universal abundances of D, ^3He , ^4He , and ^7Li which are essentially fixed by $t \sim 180$ s. However, abundances are *derived* at much later epochs, after stellar nucleosynthesis commenced. Stars produce heavy elements such as C, N, O, and Fe (“metals”), while the ejected remains of stellar processing alters the light element abundances from their primordial values. Thus, one seeks astrophysical sites with low metal abundances to measure light element abundances that are closer to primordial.

BBN is the only significant source of deuterium which is entirely destroyed when it is cycled into stars [35]. Thus, any detection provides a lower limit to primordial D/H, and an upper limit on η_{10} . The best proxy to the primordial value of D is its measure in distant and chemically unprocessed matter, where stellar processing (astration) is minimal [35]. This has become possible with the advent of large telescopes, but after nearly three decades of observational efforts we have only 16 determinations listed in Table

24.1 [36–49].

High-resolution spectra reveal the presence of D in high-redshift, low-metallicity quasar absorption systems via its isotopically shifted Lyman- α absorption features, though, unfortunately, these are often obscured or contaminated by the hydrogen features of the Lyman- α forest.

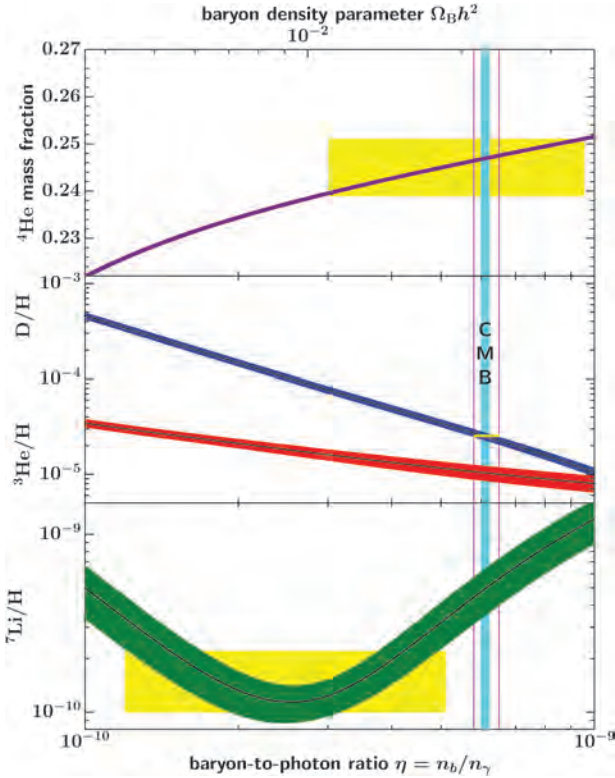


Figure 24.1: The primordial abundances of ${}^4\text{He}$, D, ${}^3\text{He}$, and ${}^7\text{Li}$ as predicted by the standard model of Big-Bang nucleosynthesis — the bands show the 95% CL range [50]. Boxes indicate the observed light element abundances. The narrow vertical band indicates the CMB measure of the cosmic baryon density, while the wider band indicates the BBN D+ ${}^4\text{He}$ concordance range (both at 95% CL).

A few DLA systems show D lines resolved up to the higher members of the Lyman series. Recent determinations [40, 42] and re-analyses [41, 49, 51] provide strikingly improved precision over earlier work. The weighted mean of the 11 most precise measurements in Table 24.1 is (with 1% precision):

$$D/H|_p \times 10^6 = (25.47 \pm 0.25). \quad (24.2)$$

Considering all the 16 extant determinations, the weighted mean is $D/H|_p \times 10^6 = (25.36 \pm 0.26)$, while different selections provide $D/H|_p \times 10^6 = (25.27 \pm 0.30)$ [51] or $D/H|_p \times 10^6 = (25.45 \pm 0.25)$ [52], all consistent with each other. Metallicities of the absorbers are $(0.001 - 0.03) \times \text{Solar}$, i.e. at a level where no significant astration is expected [37, 53]. D/H shows no correlation with metallicity, redshift, or the neutral hydrogen column density $N(\text{HI})$ ($= \int_{\text{los}} n_{\text{HI}} ds$) integrated over the line-of-sight through the absorber. In the Galaxy D/H measurements are anti-correlated with metal abundances, which suggests that interstellar D partly resides in dust particles [54]. However, in the absorbers where deuterium is measured, the dust content is quite small as implied by Solar proportions of the abundances of refractory and non refractory elements. This is consistent with the measured D/H being truly representative of the primordial value.

The primordial ${}^4\text{He}$ abundance is best determined through recombination emission lines of He and H in the most metal-poor extragalactic HII (ionized) regions, *viz.* blue compact galaxies, generally found at low redshift. There is now a large body of

data on ${}^4\text{He}$ and CNO in these galaxies, with over 1000 such systems in the Sloan Digital Sky Survey alone [59]. These data confirm that the stellar contribution to the helium abundance is positively correlated with metal production, so extrapolation to zero metallicity gives the primordial ${}^4\text{He}$ abundance Y_p . However, HII regions are complex systems and several physical parameters enter in the He/H determination, notably the electron density and temperature, as well as reddening. Thus, systematic effects dominate the uncertainties in the abundance determination [60, 61]. A major step forward has been the inclusion of the He $\lambda 10830$ infrared emission line which shows a strong dependence on the electron density and is thus useful to break the degeneracy with the temperature, allowing for a more robust helium abundance determination. In recent works the underlying ${}^4\text{He}$ stellar absorption, and/or the newly derived values of the HeI-recombination and H-excitation-collisional coefficients are addressed and the ${}^4\text{He}$ abundances have increased significantly. Some recent results are reported in Table 24.2.

There is a reassuring convergence towards the value of $Y_p = 0.245$ between detailed analyses of specific extragalactic HII regions with other (statistically more significant) analyses of many systems. Thus our recommended ${}^4\text{He}$ abundance is:

$$Y_p = 0.245 \pm 0.003. \quad (24.3)$$

The central value is close to the mean/weighted average of the values in Table 24.2, however we caution that combining these partially overlapping data sets is not straightforward. The uncertainty reflects the combined statistical and systematic errors, with the latter, estimated to be ± 0.002 [67], being dominant.

The best suited objects for the determination of primordial ${}^7\text{Li}$ are metal-poor stars in the Galactic halo, which have metallicities going down to 10^{-6} of the Solar value [68]. Observations have long shown [69–72] that ${}^7\text{Li}$ does not vary significantly in halo dwarfs with metallicities $\lesssim 1/30$ of Solar — the *Spite plateau* [69, 73]. Recent observations show a puzzling drop in the Li/H abundance in metal-poor stars with $[\text{Fe}/\text{H}] < -3.0$ [74–76]. This becomes particularly acute at the very low metallicity end where only one star out of the seven dwarfs with metallicities $[\text{Fe}/\text{H}] \lesssim -4.5$ shows a ${}^7\text{Li}$ abundance close to the Spite Plateau, while in the others where it ought to be present it is either lower or totally absent [68, 77]. The reason for the increase in scatter at low metallicity is unknown and prevents derivation of the primordial ${}^7\text{Li}$ value by extrapolation to zero metallicity [75, 76].

To estimate the primordial ${}^7\text{Li}$ value we consider only stars with metallicity in the range $-2.8 < [\text{Fe}/\text{H}] < -1.5$ [76], where no scatter in excess of the observational errors is observed. This yields:

$$\text{Li}/\text{H}|_p = (1.6 \pm 0.3) \times 10^{-10}. \quad (24.4)$$

Strictly speaking the suggested primordial ${}^7\text{Li}$ abundance should be considered a *lower bound* rather than a measure. In fact, ${}^7\text{Li}$ in Pop II stars may have been partially destroyed due to mixing of the outer layers with the hotter interior [78]. Such processes can be constrained by the absence of significant scatter in ${}^7\text{Li}$ versus T_{eff} [71], but ${}^7\text{Li}$ depletion by a factor as large as ~ 1.8 may have occurred [71, 79]. Stellar determination of Li abundances typically sum over both ${}^6\text{Li}$ and ${}^7\text{Li}$ isotopes. However, high-precision measurements indicate ${}^6\text{Li}/{}^7\text{Li} \leq 0.05$, thus confirming that ${}^7\text{Li}$ is dominant [80].

The primordial abundance of ${}^3\text{He}$ has the poorest observational determination of all of the light nuclides. The only data available come from the Solar system and from solar-metallicity HII regions in the Galaxy [81]. Therefore, inferring the primordial ${}^3\text{He}$ abundance is problematic, compounded by the fact that stellar nucleosynthesis models for ${}^3\text{He}$ are in conflict with observations. Consequently, we consider it inappropriate to use ${}^3\text{He}$ (and also D+ ${}^3\text{He}$) as a cosmological probe.

Table 24.1: D/H measurements. For systems with multiple measurements we used the most recent one which is generally more precise.

QSO	z_{em}	z_{abs}	$\log N(\text{HI})$	[X/H]	(D/H) $\times 10^6$	Ref
QSO 2206–199	2.56	2.076	20.436 \pm 0.008	-2.04	16.5 \pm 3.5	[55]
QSO 0347–3819	3.22	3.025	20.63 \pm 0.09	-1.25	22.4 \pm 6.7	[56]
SDSS J1134+5742	3.52	3.411	17.95 \pm 0.05	<-4.2	20.4 \pm 6.1	[44]
QSO CTQ 247	3.02	2.621	20.45 \pm 0.10	-1.99	28.0 \pm 8.0	[46]
SDSS 1337+3152	3.17	3.168	20.41 \pm 0.15	-2.68	12.0 \pm 5.0	[57]
SDSS J1419+0829	3.03	3.049	20.392 \pm 0.003	-1.92	25.1 \pm 0.5	[39]
HS 0105+1619	2.65	2.536	19.40 \pm 0.01	-1.77	25.8 \pm 1.5	[39]
QSO B0913+0715	2.78	2.618	20.312 \pm 0.008	-2.40	25.3 \pm 1.0	[39]
SDSS J1358+0349	2.89	2.853	20.524 \pm 0.006	-2.33	26.2 \pm 0.7	[40]
SDSS J1358+6522	3.17	3.067	20.50 \pm 0.01	-2.33	25.8 \pm 1.0	[39]
SDSS J1558–0031	2.82	2.702	20.75 \pm 0.03	-1.55	24.0 \pm 1.4	[39]
PKS 1937–1009	3.78	3.256	18.09 \pm 0.03	-1.87	24.5 \pm 2.8	[58]
QSO J1444+2919	2.66	2.437	19.983 \pm 0.010	-2.04	19.7 \pm 3.3	[42]
PKS 1937–1009	3.78	3.572	17.925 \pm 0.006	-2.26	26.2 \pm 0.5	[49]
QSO 1009+2956	2.63	2.504	17.362 \pm 0.005	-2.50	24.8 \pm 4.1	[52]
QSO 1243+307	2.55	2.525	19.761 \pm 0.026	-2.77	23.9 \pm 1.0	[51]
Weighted mean of all 16					25.38 \pm 0.25	
Weighted mean of the most recent 11					25.47 \pm 0.25	

Table 24.2: Recent primordial ^4He measurements in extragalactic HII regions.

$Y_{\text{p}}(^4\text{He})$	$\pm 1\sigma_{\text{stat}}$	$\pm 1\sigma_{\text{sys}}$	$\pm 1\sigma_{\text{tot}}$	# systems	Ref
0.2453	0.0034			16	[62]
0.2451	0.0019	0.0018	0.0026	1	[63]
0.243	0.005			16	[64]
0.2462	0.0022			120	[65]
0.2436	0.0040			54	[66]
0.2448	0.0027	0.0018	0.0033	7	[67]

24.4 Concordance, Dark Matter, and the CMB

We now use the observed light element abundances to test the theory. We first consider standard BBN, which is based on Standard Model physics alone, so $N_{\nu} = 3$ and the only free parameter is the baryon-to-photon ratio η . (The implications of BBN for physics beyond the Standard Model will be considered below). Thus, any abundance measurement determines η , and additional measurements overconstrain the theory and thereby provide a consistency check.

While the η ranges spanned by the boxes in Fig 24.1 do not all overlap, they are all within a factor ~ 2 of each other. In particular, the lithium abundance corresponds to η values that are inconsistent with that of the (now very precise) D/H abundance as well as the less-constraining ^4He abundance. This discrepancy marks the *lithium problem*. The problem could simply reflect difficulty in determining the primordial lithium abundance, or could hint at a more fundamental omission in the theory. The possibility that lithium reveals new physics is addressed in detail in the next section. If however we exclude the lithium constraint because its inferred abundance suffers from systematic uncertainties, then D/H and ^4He are in agreement. The concordant η range is essentially determined by D/H, and yields [50]

$$\eta_{10} = 6.143 \pm 0.190 \quad (24.5)$$

where the errors are 1σ . Despite the lithium problem, the overall concordance remains remarkable: using only well-established microphysics we can extrapolate back to $t \sim 1$ s to predict light element abundances spanning nine orders of magnitude, in approximate agreement with observation. This is a major success for the standard cosmology, and inspires confidence in extrapolation back to such early times.

This concordance provides a measure of the baryon content:

$$\Omega_{\text{b}}h^2 = 0.02244 \pm 0.00069 \quad (24.6)$$

where again errors are 1σ , a result that plays a key role in our

understanding of the matter budget of the Universe. First of all $\Omega_{\text{b}} \ll 1$, *i.e.*, baryons cannot close the Universe [82]. Furthermore, the cosmic density of (optically) luminous matter is $\Omega_{\text{lum}} \simeq 0.0024h^{-1}$ [83], so that $\Omega_{\text{b}} \gg \Omega_{\text{lum}}$: most baryons are optically dark, probably in the form of a diffuse intergalactic medium [84]. Finally, given that $\Omega_{\text{m}} \sim 0.3$ (see the ‘Dark Matter’ and ‘Cosmological Parameters’ reviews), we infer that most matter in the Universe is not only dark, but also takes some non-baryonic (more precisely, non-nucleonic) form.

The BBN prediction for the cosmic baryon density can be tested through precision measurements of CMB temperature fluctuations (see the ‘Cosmic Microwave Background’ review). One can determine η from the amplitudes of the acoustic peaks in the CMB angular power spectrum [85], making it possible to compare two measures of η using very different physics, at two widely separated epochs. In the standard cosmology, there is no change in η between BBN and CMB decoupling, thus, a comparison of η_{BBN} and η_{CMB} is a key test. Agreement would endorse the standard picture, while disagreement could point to new physics during/-between the BBN and CMB epochs.

The analysis described in the Cosmic Microwave Background review (Sec.29), based on *Planck* TT, TE, EE + lowE data and lensing, yields $\Omega_{\text{b}}h^2 = 0.02237 \pm 0.00015$ [86], which corresponds to $\eta_{10} = 6.12 \pm 0.04$ [87]. This result depends weakly on the primordial helium abundance, and the fiducial *Planck* analysis uses BBN theory to fix $Y_{\text{p}}(\eta)$. Without BBN theory, the *Planck* TT, TE, EE + lowE data plus lensing give $\Omega_{\text{b}}h^2 = 0.02230 \pm 0.00021$, corresponding to $\eta_{10} = 6.104 \pm 0.058$. As shown in Fig. 24.1, this CMB estimate of the baryon density (narrow vertical band) is consistent with the BBN range, *i.e.*, in good agreement with the value inferred from high-redshift D/H measurements and local ^4He determinations; together these observations span diverse environments from redshifts $z \sim 1000$ to the present. Combining the CMB and BBN sharpens the baryon measures to $\eta_{10} = 6.129 \pm 0.039$ and $\Omega_{\text{b}}h^2 = 0.02239 \pm 0.00014$.

The ${}^4\text{He}$ abundance is proportional to the n/p ratio when the weak-interaction rate falls behind the Hubble expansion rate at $T_{\text{fr}} \sim 1$ MeV. The presence of additional neutrino flavors (or of any other relativistic species) at this time increases g_* , hence the expansion rate, leading to a larger value of T_{fr} , n/p , and therefore Y_{p} [10, 88]. In the Standard Model at $T = 1$ MeV, $g_* = 5.5 + \frac{7}{4}N_\nu$, where N_ν is the *effective* number of (nearly) massless neutrino flavors. The helium curves in 24.1 were computed taking $N_\nu = 3$; small corrections for non-equilibrium neutrino heating [19] are included in the thermal evolution and lead to an effective $N_\nu = 3.044$ compared to assuming instantaneous neutrino freezeout (see ‘Big Bang Cosmology’ — Sec. 22 of this *Review*). The computed ${}^4\text{He}$ abundance scales as $\Delta Y_{\text{p}} \simeq 0.013 \Delta N_\nu$ [11]. Clearly the central value for N_ν from BBN will depend on η , which is independently determined (with weaker sensitivity to N_ν) by the adopted D or ${}^7\text{Li}$ abundance. For example, if the best value for the observed primordial ${}^4\text{He}$ abundance is 0.249, then, for $\eta_{10} \sim 6$, the central value for N_ν is very close to 3. A maximum likelihood analysis on η and N_ν based on ${}^4\text{He}$ and D abundances nearly identical to those above finds the (correlated) 95% CL ranges to be $\eta_{10} = 6.090 \pm 0.055$ and $N_\nu = 2.843 \pm 0.154$ [50, 89]. Identical results are obtained using a simpler method to extract such bounds based on χ^2 statistics, given a set of input abundances [90].

The CMB damping tail is sensitive to the primordial ${}^4\text{He}$ abundance independently of both BBN and local ${}^4\text{He}$ measurements [91]. The *Planck* analysis using TT, TE, EE+lowE and lensing but not the BBN $Y_{\text{p}}(\eta)$ relation gives a ${}^4\text{He}$ mass fraction $0.239^{+0.024}_{-0.025}$, and nucleon fraction $Y_{\text{p}} = 0.240^{+0.24}_{-0.25}$, both at 95% CL [86]. This is consistent with the HII region helium abundance determination. Moreover, this value is consistent with the Standard ($N_\nu = 3$) BBN prediction for Y_{p} with the *Planck*-determined baryon density. This concordance represents a successful CMB-only test of BBN.

The precision determination of the baryon density using the CMB motivates using this as an input to BBN calculations. Within the context of the Standard Model, BBN then becomes a zero-parameter theory, and the light element abundances are completely determined to within the uncertainties in η_{CMB} and the BBN theoretical errors. Comparison with the observed abundances then can be used to test the astrophysics of post-BBN light element evolution [92]. Alternatively, one can consider possible physics beyond the Standard Model (*e.g.*, which might change the expansion rate during BBN) and then use all of the abundances to test such models; this is discussed in 23.6 below.

24.5 The Lithium Problem

As Fig. 24.1 shows, stellar Li/H measurements are inconsistent with the D/H (and CMB), given the error budgets we have quoted. Recent updates in nuclear cross sections and stellar abundance systematics *increase* the discrepancy to over 5σ , depending on the stellar abundance analysis adopted [25]. For instance, the value of $\text{Li}/\text{H}|_{\text{p}} = (4.72 \pm 0.7) \times 10^{-10}$ [50] is a factor 3.1 higher than in eq.24.4 which is a 4.4σ discrepancy.

Stars that have been accreted by the Milky Way about 10 Gyrs ago from the Gaia-Enceladus-Sausage galaxy have the same abundances as those in the Milky Way, showing that the Li problem is universal [93, 94]. The question then becomes pressing as to whether this mismatch comes from systematic errors in the observed abundances, and/or uncertainties in stellar astrophysics or nuclear inputs, or whether there might be new physics at work [9]. Nuclear inputs (cross sections) for BBN reactions are constrained by extensive laboratory measurements; to increase ${}^7\text{Be}$ destruction requires enhancement of otherwise subdominant processes that can be attained by missed resonances in a few reactions such as ${}^7\text{Be}(d,p)2\alpha$ if the compound nuclear state properties are particularly favorable [29, 95–97]. However, experimental searches have now closed off these possibilities [98–100], making a *nuclear fix* increasingly unlikely.

Another means to solve the lithium problem is by *in situ* destruction over the long lifetimes of the host halo stars. Stellar depletion mechanisms include diffusion, rotationally induced mixing, or pre-main-sequence depletion. These effects certainly oc-

cur, but to reduce lithium to the required levels generally requires some *ad hoc* mechanism and fine tuning of the initial stellar parameters [79, 101–103]. General features of diffusive models are a dispersion in the Li abundances and a pronounced downturn in the Li abundances at the hot end of the Li plateau. Some extra turbulence needs to be invoked to limit diffusion in the hotter stars and to restore uniform Li abundance along the Spite plateau [103]. Li abundances for over 100 000 field stars have been obtained in the GALAH (Galactic Archeology with HERMES) survey. Warm stars with $[\text{Fe}/\text{H}]$ in between -1.0 and -0.5 form an elevated plateau consistent with the BBN prediction and it has been suggested that this could have been also true for the more metal poor stars which have evolved further [104]. Li destruction in the pre-Main sequence phase has been also proposed [102].

Observations of interstellar lithium in low-metallicity systems probe lithium abundances not subject to stellar depletion. Measurements of interstellar Li/H in the Small Magellanic Cloud lie near the primordial level, but also are consistent with Milky Way stellar abundances at that metallicity ($\sim 1/4$ solar) [105]. Additional such measurements in more metal-poor systems would be of great interest.

As nuclear and astrophysical solutions to the lithium problem become increasingly constrained, the possibility of new physics arises. Nucleosynthesis models in which the baryon-to-photon ratio is inhomogeneous can alter abundances for a given η_{BBN} , but will overproduce ${}^7\text{Li}$ [106]. Entropy generation by some non-standard process could have decreased η between the BBN era and CMB decoupling, however the lack of spectral distortions in the CMB rules out any significant energy injection up to a redshift $z \sim 10^7$ [107]. The most intriguing resolution of the lithium problem thus involves new physics during BBN [7–9]

We summarize the general features of such solutions here, and later consider examples in the context of specific particle physics models. Many proposed solutions introduce perturbations to light-element formation during BBN; while all element abundances may suffer perturbations, the interplay of ${}^7\text{Li}$ and D is often the most important *i.e.* observations of D often provide the strongest constraints on the allowed perturbations to ${}^7\text{Li}$. In this connection it is important to note that the new, very precise determination of D/H will significantly constrain the ability of such models to ameliorate or solve the lithium problem.

A well studied class of models invokes the injection of suprathermal hadronic or electromagnetic particles due to decays of dark matter particles. The effects are complex and depend on the nature of the decaying particles and their branchings and spectra. However, the models that most successfully solve the lithium problem generally feature non-thermal nucleons, which dissociate all light elements. Dissociation of even a small fraction of ${}^4\text{He}$ introduces a large abundance of free neutrons, which quickly thermalize. The thermal neutrons drive the ${}^7\text{Be}(n,p){}^7\text{Li}$ conversion of ${}^7\text{Be}$. The resulting ${}^7\text{Li}$ has a lower Coulomb barrier relative to ${}^7\text{Be}$ and is readily destroyed via ${}^7\text{Li}(p,\alpha){}^4\text{He}$ [108, 109]. But ${}^4\text{He}$ dissociation also produces D directly as well as via nonthermal neutron $n(p,\gamma)d$ reactions. This introduces a tension between Li/H reduction and D/H enhancement that becomes increasingly restrictive with the increasing precision of deuterium observations. Indeed, this now forces particle injection scenarios to make very small ${}^7\text{Li}$ perturbations — far short of the level needed. An exception is a recent model wherein MeV-scale decays by construction avoid ${}^4\text{He}$ dissociation and associated D/H overproduction, instead *borrowing* neutrons by dissociating only deuterons [110].

Another important class of models retains the standard cosmic particle content, but changes their interactions via time variations in the fundamental constants [111–117]. Here too, the details are model-dependent, but scenarios that solve or alleviate the lithium problem often feature perturbations to the deuteron binding energy. A weaker D binding leads to the D bottleneck being overcome later, so that element formation commences at a lower temperature and lower density. This leads in turn to slower nuclear rates that freeze out earlier. The net result is a *higher* final D/H, due to less efficient processing into ${}^4\text{He}$, but also *lower* Li, due to suppressed production via ${}^3\text{He}(\alpha,\gamma){}^7\text{Be}$.

The *cosmological lithium problem* remains an unresolved issue

in BBN. Nevertheless, the remarkable concordance between the CMB and the D (as well as ^4He) abundance, is a non-trivial success, and provides important constraints on the early Universe.

24.6 Beyond the Standard Model

Given the simple physics underlying BBN, it is remarkable that it still provides the most effective test for the cosmological viability of ideas concerning physics beyond the Standard Model. Although baryogenesis and inflation must have occurred at higher temperatures in the early Universe, we do not as yet have ‘standard models’ for these, so BBN still marks the boundary between the established and the speculative in Big Bang cosmology. It might appear possible to push the boundary back to the quark-hadron transition at $T \sim \Lambda_{\text{QCD}}$, or electroweak symmetry breaking at $T \sim 1/\sqrt{G_{\text{F}}}$; however, so far no observable relics of these epochs have been identified, either theoretically or observationally. Thus, although the Standard Model provides a precise description of physics up to the Fermi scale, cosmology cannot be traced in detail before the BBN era.

The CMB power spectrum in the damping tail is independently sensitive to N_ν (e.g. [118]). The CMB value N_ν^{CMB} probes the cosmic radiation content at (re)combination, so a discrepancy would imply new physics or astrophysics. Indeed, observations by the South Pole Telescope implied $N_\nu^{\text{CMB}} = 3.85 \pm 0.62$ [119], prompting discussion of *dark radiation* such as sterile neutrinos [120]. However, *Planck* 2018 results give $N_\nu^{\text{CMB}} = 2.92^{+0.36}_{+0.37}$, 95% CL, when using Planck TT, TE, EE+lowE, a result quite consistent with 3 Standard Model neutrinos [86] (and adjusting for the CMB’s measurement of $N_{\text{eff}} = 3.044$ due to neutrino heading effects [121–123]).

Just as one can use the measured helium abundance to place limits on g_* [88, 112, 124–126], any changes in the strong, weak, electromagnetic, or gravitational coupling constants, arising e.g., from the dynamics of new dimensions, can be similarly constrained [127], as can any speed-up of the expansion rate in, e.g., scalar-tensor theories of gravity [128].

The limits on N_ν can be translated into limits on other types of particles or particle masses that would affect the expansion rate of the Universe during nucleosynthesis. For example, consider *sterile* neutrinos with only right-handed interactions of strength $G_{\text{R}} < G_{\text{F}}$. Such particles would decouple at higher temperature than (left-handed) neutrinos, so their number density ($\propto T^3$) relative to neutrinos would be reduced by any subsequent entropy release, e.g., due to annihilations of massive particles that become non-relativistic between the two decoupling temperatures. Thus, (relativistic) particles with less than full strength weak interactions contribute less to the energy density than particles that remain in equilibrium up to the time of nucleosynthesis [129]. If we impose $N_\nu < 4$ as an illustrative constraint, then the three right-handed neutrinos must have a temperature $3(T_{\nu_{\text{R}}}/T_{\nu_{\text{L}}})^4 < 1$. Since the temperature of the decoupled ν_{R} is determined by entropy conservation (see ‘Big Bang Cosmology’ — Sec. 22 of this *Review*), $T_{\nu_{\text{R}}}/T_{\nu_{\text{L}}} = [(43/4)/g_*(T_{\text{d}})]^{1/3} < 0.76$, where T_{d} is the decoupling temperature of the ν_{R} . This requires $g_*(T_{\text{d}}) > 24$, so decoupling must have occurred at $T_{\text{d}} > 140$ MeV. The decoupling temperature is related to G_{R} through $(G_{\text{R}}/G_{\text{F}})^2 \sim (T_{\text{d}}/3 \text{ MeV})^{-3}$, where 3 MeV is the decoupling temperature for ν_{L} s. This yields a limit $G_{\text{R}} \lesssim 10^{-2} G_{\text{F}}$. The above argument sets lower limits on the masses of new Z' gauge bosons to which right-handed neutrinos would be coupled in models of superstrings [130], or extended technicolour [131]. Similarly a Dirac magnetic moment for neutrinos, which would allow the right-handed states to be produced through scattering and thus increase g_* , can be significantly constrained [132], as can any new interactions for neutrinos that have a similar effect [133–135]. Right-handed states can be populated directly by helicity-flip scattering if the neutrino mass is large enough, and this property has been used to infer a bound of $m_{\nu_\tau} \lesssim 1$ MeV (taking $N_\nu < 4$) [136]. If there is mixing between active and sterile neutrinos then the effect on BBN is more complicated [137, 138].

BBN limits on the cosmic expansion rate constrain supersymmetric scenarios in which the neutralino or gravitino are very light, so that they contribute to g_* [139]. A gravitino in the mass range $\sim 10^{-4} - 10$ eV will affect the expansion rate of the Universe sim-

ilarly to a light neutralino (which is however now probably ruled out by collider data, especially the decays of the Higgs-like boson). The net contribution to N_ν then ranges between 0.74 and 1.69, depending on the gravitino and slepton masses [140].

The limit on the expansion rate during BBN can also be translated into bounds on the mass/lifetime of non-relativistic particles that decay during BBN. This results in an even faster speed-up rate, and typically also changes the entropy [141–143]. If the decays include Standard Model particles, the resulting electromagnetic [144] [92, 130, 145] and/or hadronic [146, 147] cascades can strongly perturb the light elements, which leads to even stronger constraints. Such arguments have been applied to rule out an MeV mass for ν_τ , which decays during nucleosynthesis [148].

Decaying-particle arguments have proved very effective in probing supersymmetry. Light-element abundances generally are complementary to accelerator data in constraining SUSY parameter space, with BBN reaching to values kinematically inaccessible to the LHC. Much recent interest has focused on the case in which the next-to-lightest supersymmetric particle is metastable and decays during or after BBN. The constraints on unstable particles discussed above imply stringent bounds on the allowed abundance of such particles [108]; if the metastable particle is charged (e.g., the stau), then it is possible for it to form atom-like electromagnetic bound states with nuclei, and the resulting impact on light elements can be quite complex [8, 95, 149]. Moreover, SUSY decays can destroy ^7Li and/or produce ^6Li , leading to a possible supersymmetric solution to the lithium problems noted above [150] (see [7] for a review).

These arguments impose powerful constraints on supersymmetric inflationary cosmology [92, 130, 145–147], particularly thermal leptogenesis [151]. These limits can be evaded only if the gravitino is massive enough to decay before BBN, i.e., $m_{3/2} \gtrsim 50$ TeV [152] (which would be unnatural), or if it is in fact the lightest supersymmetric particle and thus stable [130, 145, 153, 154]. Similar constraints apply to moduli – very weakly coupled fields in string theory that obtain an electroweak-scale mass from supersymmetry breaking [155].

Finally, we mention that BBN places powerful constraints on the possibility that there are new large dimensions in nature, perhaps enabling the scale of quantum gravity to be as low as the electroweak scale [156]. Thus, Standard Model fields may be localized on a *brane*, while gravity alone propagates in the *bulk*. It has been further noted that the new dimensions may be non-compact, even infinite [157], and the cosmology of such models has attracted considerable attention. The expansion rate in the early Universe can be significantly modified, so BBN is able to set interesting constraints on such possibilities [158, 159].

References

- [1] R. V. Wagoner, W. A. Fowler and F. Hoyle, *Astrophys. J.* **148**, 3 (1967).
- [2] D. N. Schramm and M. S. Turner, *Rev. Mod. Phys.* **70**, 303 (1998), [arXiv:astro-ph/9706069].
- [3] G. Steigman, *Ann. Rev. Nucl. Part. Sci.* **57**, 463 (2007), [arXiv:0712.1100].
- [4] F. Iocco *et al.*, *Phys. Rept.* **472**, 1 (2009), [arXiv:0809.0631].
- [5] R. H. Cyburt *et al.*, *Rev. Mod. Phys.* **88**, 015004 (2016), [arXiv:1505.01076].
- [6] S. Sarkar, *Rept. on Prog. in Phys.* **59**, 1493 (1996).
- [7] K. Jedamzik and M. Pospelov, *New J. Phys.* **11**, 105028 (2009), [arXiv:0906.2087].
- [8] M. Pospelov and J. Pradler, *Ann. Rev. Nucl. Part. Sci.* **60**, 539 (2010), [arXiv:1011.1054].
- [9] B. D. Fields, *Ann. Rev. Nucl. Part. Sci.* **61**, 47 (2011), [arXiv:1203.3551].
- [10] P.J.E. Peebles, *Phys. Rev. Lett.* **16**, 411 (1966).
- [11] J. Bernstein, L. S. Brown and G. Feinberg, *Rev. Mod. Phys.* **61**, 25 (1989).
- [12] S. Mukhanov, *Int. J. Theor. Phys.* **143**, 669 (2004).
- [13] R. Esmailzadeh, G. D. Starkman and S. Dimopoulos, *Astrophys. J.* **378**, 504 (1991).

- [14] T.-H. Yeh, K. A. Olive and B. D. Fields, *JCAP* **03**, 046 (2021), [arXiv:2011.13874].
- [15] L. Kawano, Technical report (1992), URL <https://ui.adsabs.harvard.edu/abs/1992STIN...9225163K>.
- [16] A. Arbey *et al.*, *Comput. Phys. Commun.* **248**, 106982 (2020), [arXiv:1806.11095].
- [17] R. Consiglio *et al.*, *Computer Physics Communications* **233**, 237 (2018), [arXiv:1712.04378].
- [18] S. Esposito *et al.*, *Nucl. Phys.* **B568**, 421 (2000), [arXiv:astro-ph/9906232].
- [19] S. Dodelson and M. S. Turner, *Phys. Rev.* **D46**, 3372 (1992).
- [20] D. Seckel (1993), [hep-ph/9305311].
- [21] R. H. Cyburt, B. D. Fields and K. A. Olive, *New Astron.* **6**, 215 (2001), [arXiv:astro-ph/0102179].
- [22] M. S. Smith, L. H. Kawano and R. A. Malaney, *Astrophys. J. Suppl.* **85**, 219 (1993).
- [23] G. Fiorentini *et al.*, *Phys. Rev.* **D58**, 063506 (1998), [arXiv:astro-ph/9803177].
- [24] A. Coc *et al.*, *Astrophys. J.* **744**, 158 (2012), [arXiv:1107.1117].
- [25] R. H. Cyburt, B. D. Fields and K. A. Olive, *JCAP* **0811**, 012 (2008), [arXiv:0808.2818].
- [26] K. M. Nollett and S. Burles, *Phys. Rev.* **D61**, 123505 (2000), [arXiv:astro-ph/0001440].
- [27] R. H. Cyburt, *Phys. Rev.* **D70**, 023505 (2004), [arXiv:astro-ph/0401091].
- [28] P. D. Serpico *et al.*, *JCAP* **0412**, 010 (2004), [arXiv:astro-ph/0408076].
- [29] R. N. Boyd *et al.*, *Phys. Rev.* **D82**, 105005 (2010), [arXiv:1008.0848].
- [30] C. Pitrou *et al.*, *Mon. Not. Roy. Astron. Soc.* **502**, 2, 2474 (2021), [arXiv:2011.11320].
- [31] O. Pisanti *et al.*, *JCAP* **04**, 020 (2021), [arXiv:2011.11537].
- [32] R.H. Cyburt and B. Davids, *Phys. Rev.* **C78**, 012 (2008).
- [33] S. Burles, K. M. Nollett and M. S. Turner, *Astrophys. J.* **552**, L1 (2001), [arXiv:astro-ph/0010171].
- [34] V. Mossa *et al.*, *Nature* **587**, 7833, 210 (2020).
- [35] R. I. Epstein, J. M. Lattimer and D. N. Schramm, *Nature* **263**, 198 (1976).
- [36] S. D'Odorico *et al.*, *Astron. & Astrophys.* **368**, L21 (2001).
- [37] D. Romano *et al.*, *Mon. Not. Roy. Astron. Soc.* **369**, 295 (2006), [arXiv:astro-ph/0603190].
- [38] M. Pettini and D. V. Bowen, *Astrophys. J.* **560**, 41 (2001), [arXiv:astro-ph/0104474].
- [39] R. Cooke *et al.*, *Astrophys. J.* **781**, 1, 31 (2014), [arXiv:1308.3240].
- [40] R. J. Cooke *et al.*, *Astrophys. J.* **830**, 2, 148 (2016), [arXiv:1607.03900].
- [41] E.O. Zavarygin *et al.*, arXiv:1706.09512(2017).
- [42] S. A. Balashev *et al.*, *Mon. Not. Roy. Astron. Soc.* **458**, 2, 2188 (2016), [arXiv:1511.01797].
- [43] S. A. Levshakov *et al.*, *Astrophys. J.* **565**, 696 (2002), [arXiv:astro-ph/0105529].
- [44] M. Fumagalli, J. M. O'Meara and J. X. Prochaska, *Science* **334**, 1245 (2011), [arXiv:1111.2334].
- [45] R. Srianand *et al.*, *Mon. Not. Roy. Astron. Soc.* **405**, 1888 (2010), [arXiv:1002.4620].
- [46] P. Noterdaeme *et al.*, *Astron. Astrophys.* **542**, L33 (2012), [arXiv:1205.3777].
- [47] M. Pettini and R. Cooke, *Mon. Not. Roy. Astron. Soc.* **425**, 2477 (2012), [arXiv:1205.3785].
- [48] S. Riemer-Sørensen *et al.*, *Mon. Not. Roy. Astron. Soc.* **447**, 2925 (2015), [arXiv:1412.4043].
- [49] S. Riemer-Sørensen *et al.*, *Mon. Not. Roy. Astron. Soc.* **468**, 3, 3239 (2017), [arXiv:1703.06656].
- [50] B. D. Fields *et al.*, *JCAP* **2020**, 3, 010 (2020), [arXiv:1912.01132].
- [51] R. J. Cooke, M. Pettini and C. C. Steidel, *Astrophys. J.* **855**, 2, 102 (2018), [arXiv:1710.11129].
- [52] E. O. Zavarygin *et al.*, *Mon. Not. Roy. Astron. Soc.* **477**, 4, 5536 (2018), [arXiv:1706.09512].
- [53] F. van de Voort *et al.*, *Mon. Not. Roy. Astron. Soc.* **477**, 1, 80 (2018), [arXiv:1704.08254].
- [54] J. L. Linsky *et al.*, *Astrophys. J.* **647**, 1106 (2006), [arXiv:astro-ph/0608308].
- [55] M. Pettini and D. V. Bowen, *Astrophys. J.* **560**, 1, 41 (2001), [arXiv:astro-ph/0104474].
- [56] S. D'Odorico, M. Dessauges-Zavadsky and P. Molaro, *Astron. Astrophys.* **368**, L21 (2001), [arXiv:astro-ph/0102162].
- [57] R. Srianand *et al.*, *Mon. Not. Roy. Astron. Soc.* **405**, 3, 1888 (2010), [arXiv:1002.4620].
- [58] S. Riemer-Sørensen *et al.*, *Mon. Not. Roy. Astron. Soc.* **447**, 3, 2925 (2015), [arXiv:1412.4043].
- [59] Y. I. Izotov, T. X. Thuan and N. G. Guseva, *Mon. Not. Roy. Astron. Soc.* **445**, 1, 778 (2014), [arXiv:1408.6953].
- [60] Y. I. Izotov *et al.*, *Astrophys. J.* **527**, 757 (1999), [arXiv:astro-ph/9907228].
- [61] K. A. Olive and E. D. Skillman, *Astrophys. J.* **617**, 29 (2004), [arXiv:astro-ph/0405588].
- [62] E. Aver *et al.*, *JCAP* **2021**, 3, 027 (2021), [arXiv:2010.04180].
- [63] M. Valerdi *et al.*, *Astrophys. J.* **876**, 2, 98 (2019), [arXiv:1904.01594].
- [64] V. Fernández *et al.*, *Mon. Not. Roy. Astron. Soc.* **487**, 3, 3221 (2019), [arXiv:1905.09215].
- [65] O. A. Kurichin *et al.*, *Mon. Not. Roy. Astron. Soc.* **502**, 2, 3045 (2021), [arXiv:2101.09127].
- [66] T. Hsyu *et al.*, *Astrophys. J.* **896**, 1, 77 (2020), [arXiv:2005.12290].
- [67] M. Valerdi, A. Peimbert and M. Peimbert, *Mon. Not. Roy. Astr. Soc.* **505**, 3, 3624 (2021), [arXiv:2105.12260].
- [68] D. S. Aguado *et al.*, *Astrophys. J. Lett.* **874**, 2, L21 (2019), [arXiv:1904.04892].
- [69] M. Spite and F. Spite, *Nature* **297**, 483 (1982).
- [70] E. Vangioni-Flam *et al.*, *New Astron.* **4**, 245 (1999), [arXiv:astro-ph/9811327].
- [71] S. G. Ryan *et al.*, *Astrophys. J.* **530**, L57 (2000), [arXiv:astro-ph/9905211].
- [72] P. Bonifacio and P. Molaro, *Mon. Not. Roy. Astron. Soc.* **285**, 847 (1997), [arXiv:astro-ph/9611043].
- [73] R. Rebolo, P. Molaro and J. E. Beckman, *Astron. Astrophys.* **192**, 192 (1988).
- [74] P. Bonifacio *et al.*, *Astron. & Astrophys.* **462**, 851 (2007).
- [75] W. Aoki *et al.*, *Astrophys. J.* **698**, 1803 (2009), [arXiv:0904.1448].
- [76] L. Sbordone *et al.*, *Astron. & Astrophys.* **522**, A26 (2010).
- [77] P. Bonifacio *et al.*, *Astron. Astrophys.* **612**, A65 (2018), [arXiv:1801.03935].
- [78] M.H. Pinsonneault *et al.*, *Astrophys. J.* **574**, 389 (2002).
- [79] A. J. Korn *et al.*, *Nature* **442**, 657 (2006), [arXiv:astro-ph/0608201].
- [80] R. Cayrel *et al.*, *Astron. & Astrophys.* **473**, L37 (2007).
- [81] D. S. Balser and T. M. Bania, *Astrophys. J.* **156**, 6, 280 (2018), [arXiv:1810.09422].
- [82] H. Reeves *et al.*, *Astrophys. J.* **179**, 909 (1973).

- [83] M. Fukugita and P. J. E. Peebles, *Astrophys. J.* **616**, 643 (2004), [arXiv:astro-ph/0406095].
- [84] R. Cen and J. P. Ostriker, *Astrophys. J.* **514**, 1 (1999), [arXiv:astro-ph/9806281].
- [85] G. Jungman *et al.*, *Phys. Rev.* **D54**, 1332 (1996), [arXiv:astro-ph/9512139].
- [86] Planck Collaboration *et al.*, arXiv e-prints arXiv:1807.06209 (2018), [arXiv:1807.06209].
- [87] P.A.R. Ade *et al.*, *Astron. & Astrophys.* **594**, A13 (2016).
- [88] G. Steigman, D. N. Schramm and J. E. Gunn, *Phys. Lett.* **B66**, 202 (1977), [159(1977)].
- [89] B. D. Fields *et al.*, *JCAP* **2020**, 11, E02 (2020).
- [90] E. Lisi, S. Sarkar and F. L. Villante, *Phys. Rev.* **D59**, 123520 (1999), [hep-ph/9901404].
- [91] R. Trotta and S. H. Hansen, *Phys. Rev.* **D69**, 023509 (2004), [arXiv:astro-ph/0306588].
- [92] R. H. Cyburt, B. D. Fields and K. A. Olive, *Phys. Lett.* **B567**, 227 (2003), [arXiv:astro-ph/0302431].
- [93] P. Molaro, G. Cescutti and X. Fu, *Mon. Not. Roy. Astron. Soc.* **496**, 3, 2902 (2020), [arXiv:2006.00787].
- [94] J. D. Simpson *et al.*, *Mon. Not. Roy. Astron. Soc.* (2021).
- [95] R. H. Cyburt *et al.*, *JCAP* **1305**, 014 (2013), [arXiv:1303.0574].
- [96] N. Chakraborty, B. D. Fields and K. A. Olive, *Phys. Rev.* **D83**, 063006 (2011), [arXiv:1011.0722].
- [97] C. Broggin *et al.*, *JCAP* **1206**, 030 (2012), [arXiv:1202.5232].
- [98] P. D. O'Malley *et al.*, *Phys. Rev.* **C84**, 042801 (2011).
- [99] F. Hammache *et al.*, *Phys. Rev.* **C88**, 6, 062802 (2013), [arXiv:1312.0894].
- [100] M. W. Paris *et al.*, *Nucl. Data Sheets* **120**, 184 (2014), [arXiv:1304.3153].
- [101] P. Molaro *et al.*, *Memorie della Soc. Astronomica Italiana Supp.* **22**, 233 (2012).
- [102] X. Fu *et al.*, *Mon. Not. R. Astron. Soc.* **452**, 325 (2015).
- [103] O. Richard, G. Michaud and J. Richer, *Astrophys. J.* **619**, 538 (2005), [arXiv:astro-ph/0409672].
- [104] X. Gao *et al.*, *Mon. Not. Roy. Astron. Soc.* **497**, 1, L30 (2020), [arXiv:2006.05173].
- [105] J. C. Howk *et al.*, *Nature* **489**, 7414, 121 (2012), [arXiv:1207.3081].
- [106] K. Jedamzik and J. B. Rehm, *Phys. Rev.* **D64**, 023510 (2001), [arXiv:astro-ph/0101292].
- [107] D. J. Fixsen *et al.*, *Astrophys. J.* **473**, 576 (1996), [arXiv:astro-ph/9605054].
- [108] M. Kawasaki, K. Kohri and T. Moroi, *Phys. Rev.* **D71**, 083502 (2005), [arXiv:astro-ph/0408426].
- [109] K. Jedamzik, *Phys. Rev.* **D70**, 063524 (2004), [arXiv:astro-ph/0402344].
- [110] A. Goudelis, M. Pospelov and J. Pradler, *Phys. Rev. Lett.* **116**, 21, 211303 (2016), [arXiv:1510.08858].
- [111] J. D. Barrow, *Phys. Rev.* **D35**, 1805 (1987).
- [112] B. A. Campbell and K. A. Olive, *Phys. Lett.* **B345**, 429 (1995), [hep-ph/9411272].
- [113] L. Bergstrom, S. Iguri and H. Rubinstein, *Phys. Rev.* **D60**, 045005 (1999), [arXiv:astro-ph/9902157].
- [114] V. V. Flambaum and E. V. Shuryak, *Phys. Rev.* **D65**, 103503 (2002), [hep-ph/0201303].
- [115] A. Coc *et al.*, *Phys. Rev.* **D76**, 023511 (2007), [arXiv:astro-ph/0610733].
- [116] J. C. Berengut *et al.*, *Phys. Rev.* **D87**, 8, 085018 (2013), [arXiv:1301.1738].
- [117] C. J. A. P. Martins, *Astron. Astrophys.* **646**, A47 (2021), [arXiv:2012.10505].
- [118] Z. Hou *et al.*, *Phys. Rev.* **D87**, 083008 (2013), [arXiv:1104.2333].
- [119] R. Keisler *et al.*, *Astrophys. J.* **743**, 28 (2011), [arXiv:1105.3182].
- [120] J. Hamann *et al.*, *Phys. Rev. Lett.* **105**, 181301 (2010), [arXiv:1006.5276].
- [121] K. Akita and M. Yamaguchi, *JCAP* **2020**, 8, 012 (2020), [arXiv:2005.07047].
- [122] J. Froustey, C. Pitrou and M. C. Volpe, *JCAP* **2020**, 12, 015 (2020), [arXiv:2008.01074].
- [123] J. J. Bennett *et al.*, *JCAP* **04**, 073 (2021), [arXiv:2012.02726].
- [124] F. S. Accetta, L. M. Krauss and P. Romanelli, *Phys. Lett.* **B248**, 146 (1990).
- [125] K. M. Nollett and R. E. Lopez, *Phys. Rev.* **D66**, 063507 (2002), [arXiv:astro-ph/0204325].
- [126] C. Bambi, M. Giannotti and F. L. Villante, *Phys. Rev.* **D71**, 123524 (2005), [arXiv:astro-ph/0503502].
- [127] E. W. Kolb, M. J. Perry and T. P. Walker, *Phys. Rev.* **D33**, 869 (1986).
- [128] A. Coc *et al.*, *Phys. Rev.* **D73**, 083525 (2006), [arXiv:astro-ph/0601299].
- [129] K. A. Olive, D. N. Schramm and G. Steigman, *Nucl. Phys.* **B180**, 497 (1981).
- [130] J. R. Ellis *et al.*, *Phys. Lett.* **167B**, 457 (1986).
- [131] L. M. Krauss, J. Terning and T. Appelquist, *Phys. Rev. Lett.* **71**, 823 (1993), [hep-ph/9305265].
- [132] J. A. Morgan, *Phys. Lett.* **102B**, 247 (1981).
- [133] E. W. Kolb, M. S. Turner and T. P. Walker, *Phys. Rev.* **D34**, 2197 (1986).
- [134] J. A. Grifols and E. Masso, *Mod. Phys. Lett.* **A2**, 205 (1987).
- [135] K. S. Babu, R. N. Mohapatra and I. Z. Rothstein, *Phys. Rev. Lett.* **67**, 545 (1991).
- [136] A. D. Dolgov, S. H. Hansen and D. V. Semikoz, *Nucl. Phys.* **B524**, 621 (1998), [hep-ph/9712284].
- [137] K. Enqvist, K. Kainulainen and M. J. Thomson, *Nucl. Phys.* **B373**, 498 (1992).
- [138] A. D. Dolgov, *Phys. Rept.* **370**, 333 (2002), [hep-ph/0202122].
- [139] J. A. Grifols, R. N. Mohapatra and A. Riotto, *Phys. Lett.* **B400**, 124 (1997), [hep-ph/9612253].
- [140] H. K. Dreiner *et al.*, *Phys. Rev.* **D85**, 065027 (2012), [arXiv:1111.5715].
- [141] K. Sato and M. Kobayashi, *Prog. Theor. Phys.* **58**, 1775 (1977).
- [142] D. A. Dicus *et al.*, *Phys. Rev.* **D17**, 1529 (1978).
- [143] R. J. Scherrer and M. S. Turner, *Astrophys. J.* **331**, 19 (1988), [Astrophys. J.331,33(1988)].
- [144] D. Lindley, *Mon. Not. R. Astron. Soc.* **188**, 15 (1979).
- [145] J. R. Ellis *et al.*, *Nucl. Phys.* **B373**, 399 (1992).
- [146] M. H. Reno and D. Seckel, *Phys. Rev.* **D37**, 3441 (1988).
- [147] S. Dimopoulos *et al.*, *Nucl. Phys.* **B311**, 699 (1989).
- [148] S. Sarkar and A. M. Cooper-Sarkar, *Phys. Lett.* **148B**, 347 (1984).
- [149] M. Kawasaki, K. Kohri and T. Moroi, *Phys. Lett.* **B649**, 436 (2007), [hep-ph/0703122].
- [150] K. Jedamzik *et al.*, *JCAP* **0607**, 007 (2006), [hep-ph/0512044].
- [151] S. Davidson *et al.*, *Phys. Rev.* **466**, 105 (2008).
- [152] S. Weinberg, *Phys. Rev. Lett.* **48**, 1303 (1982).

- [153] R. H. Cyburt *et al.*, Phys. Rev. **D67**, 103521 (2003), [arXiv:astro-ph/0211258].
- [154] M. Bolz, A. Brandenburg and W. Buchmuller, Nucl. Phys. **B606**, 518 (2001), [Erratum: Nucl. Phys.B790,336(2008)], [hep-ph/0012052].
- [155] G. D. Coughlan *et al.*, Physics Letters B **131**, 1-3, 59 (1983).
- [156] N. Arkani-Hamed, S. Dimopoulos and G. R. Dvali, Phys. Rev. **D59**, 086004 (1999), [hep-ph/9807344].
- [157] L. Randall and R. Sundrum, Phys. Rev. Lett. **83**, 3370 (1999), [hep-ph/9905221].
- [158] J. M. Cline, C. Grojean and G. Servant, Phys. Rev. Lett. **83**, 4245 (1999), [hep-ph/9906523].
- [159] P. Binetruy *et al.*, Phys. Lett. **B477**, 285 (2000), [hep-th/9910219].

25. Cosmological Parameters

Revised September 2021 by O. Lahav (UCL) and A.R. Liddle (ULisboa).

25.1 Parametrizing the Universe

Rapid advances in observational cosmology have led to the establishment of a precision cosmological model, with many of the key cosmological parameters determined to one or two significant figure accuracy. Particularly prominent are measurements of cosmic microwave background (CMB) anisotropies, with the highest precision observations being those of the *Planck* Satellite [1, 2] which supersede the landmark *WMAP* results [3, 4]. However the most accurate model of the Universe requires consideration of a range of observations, with complementary probes providing consistency checks, lifting parameter degeneracies, and enabling the strongest constraints to be placed.

The term ‘cosmological parameters’ now has a wide scope, and may include the parameterization of some functions as well as simple numbers describing properties of the Universe. The original usage referred to the parameters describing the global dynamics of the Universe, such as its expansion rate and curvature. Now we wish to know how the matter budget of the Universe is built up from its constituents: baryons, photons, neutrinos, dark matter, and dark energy. We also need to describe the nature of perturbations in the Universe, through global statistical descriptors such as the matter and radiation power spectra. There may be additional parameters describing the physical state of the Universe, such as the ionization fraction as a function of time during the era since recombination. Typical comparisons of cosmological models with observational data now feature between five and ten parameters.

25.1.1 The global description of the Universe

Ordinarily, the Universe is taken to be a perturbed Robertson–Walker space-time, with dynamics governed by Einstein’s equations. This is described in detail in the Big-Bang Cosmology chapter in this volume. Using the density parameters Ω_i for the various matter species and Ω_Λ for the cosmological constant, the Friedmann equation can be written

$$\sum_i \Omega_i + \Omega_\Lambda - 1 = \frac{k}{R^2 H^2}, \quad (25.1)$$

where the sum is over all the different species of material in the Universe. This equation applies at any epoch, but later in this article we will use the symbols Ω_i and Ω_Λ to refer specifically to the present-epoch values.

The complete present-epoch state of the homogeneous Universe can be described by giving the current-epoch values of all the density parameters and the Hubble constant h (the present-day Hubble parameter being written $H_0 = 100h \text{ km s}^{-1} \text{ Mpc}^{-1}$). A typical collection would be baryons Ω_b , photons Ω_γ , neutrinos Ω_ν , and cold dark matter Ω_c (given charge neutrality, the electron density is guaranteed to be too small to be worth considering separately and is effectively included with the baryons). The spatial curvature can then be determined from the other parameters using Eq. (25.1). The total present matter density $\Omega_m = \Omega_c + \Omega_b$ may be used in place of the cold dark matter density Ω_c .

These parameters also allow us to track the history of the Universe, at least back until an epoch where interactions allow interchanges between the densities of the different species; this is believed to have last happened at neutrino decoupling, shortly before Big-Bang Nucleosynthesis (BBN). To probe further back into the Universe’s history requires assumptions about particle interactions, and perhaps about the nature of physical laws themselves.

The standard neutrino sector has three flavors. For neutrinos of mass in the range $5 \times 10^{-4} \text{ eV}$ to 1 MeV, the density parameter in neutrinos is predicted to be

$$\Omega_\nu h^2 = \frac{\sum m_\nu}{93.14 \text{ eV}}, \quad (25.2)$$

where the sum is over all families with mass in that range (higher masses need a more sophisticated calculation). We use units with $c = 1$ throughout. Results on atmospheric and Solar neutrino oscillations [5] imply non-zero mass-squared differences between the

three neutrino flavors. These oscillation experiments cannot tell us the absolute neutrino masses, but within the normal assumption of a mass hierarchy suggest a lower limit of approximately 0.06 eV for the sum of the neutrino masses (see the Neutrino chapter).

Even a mass this small has a potentially observable effect on the formation of structure, as neutrino free-streaming damps the growth of perturbations. Analyses commonly now either assume a neutrino mass sum fixed at this lower limit, or allow the neutrino mass sum to be a variable parameter. To date there is no decisive evidence of any effects from either neutrino masses or an otherwise non-standard neutrino sector, and observations impose quite stringent limits; see the Neutrinos in Cosmology chapter. However, we note that the inclusion of the neutrino mass sum as a free parameter can affect the derived values of other cosmological parameters.

25.1.2 Inflation and perturbations

A complete model of the Universe must include a description of deviations from homogeneity, at least statistically. Indeed, the most powerful probes of the parameters described above come from the evolution of perturbations, so their study is naturally intertwined with the determination of cosmological parameters.

There are many different notations used to describe the perturbations, both in terms of the quantity used to and the definition of the statistical measure. We use the dimensionless power spectrum Δ^2 as defined in the Big Bang Cosmology section (also denoted \mathcal{P} in some of the literature). If the perturbations obey Gaussian statistics, the power spectrum provides a complete description of their properties.

From a theoretical perspective, a useful quantity to describe the perturbations is the curvature perturbation \mathcal{R} , which measures the spatial curvature of a comoving slicing of the space-time. A simple case is the Harrison–Zeldovich spectrum, which corresponds to a constant $\Delta_{\mathcal{R}}^2$. More generally, one can approximate the spectrum by a power law, writing

$$\Delta_{\mathcal{R}}^2(k) = \Delta_{\mathcal{R}}^2(k_*) \left[\frac{k}{k_*} \right]^{n_s - 1}, \quad (25.3)$$

where n_s is known as the spectral index, always defined so that $n_s = 1$ for the Harrison–Zeldovich spectrum, and k_* is an arbitrarily chosen scale. The initial spectrum, defined at some early epoch of the Universe’s history, is usually taken to have a simple form such as this power law, and we will see that observations require n_s close to one. Subsequent evolution will modify the spectrum from its initial form.

The simplest mechanism for generating the observed perturbations is the inflationary cosmology, which posits a period of accelerated expansion in the Universe’s early stages [6, 7]. It is a useful working hypothesis that this is the sole mechanism for generating perturbations, and it may further be assumed to be the simplest class of inflationary model, where the dynamics are equivalent to that of a single scalar field ϕ with canonical kinetic energy slowly rolling on a potential $V(\phi)$. One may seek to verify that this simple picture can match observations and to determine the properties of $V(\phi)$ from the observational data. Alternatively, more complicated models, perhaps motivated by contemporary fundamental physics ideas, may be tested on a model-by-model basis (see more in the Inflation chapter in this volume).

Inflation generates perturbations through the amplification of quantum fluctuations, which are stretched to astrophysical scales by the rapid expansion. The simplest models generate two types, density perturbations that come from fluctuations in the scalar field and its corresponding scalar metric perturbation, and gravitational waves that are tensor metric fluctuations. The former experience gravitational instability and lead to structure formation, while the latter can influence the CMB anisotropies. Defining slow-roll parameters (with primes indicating derivatives with respect to the scalar field, and $m_{\text{Pl}} \equiv \sqrt{\hbar c/G}$ the Planck mass) as

$$\epsilon = \frac{m_{\text{Pl}}^2}{16\pi} \left(\frac{V'}{V} \right)^2, \quad \eta = \frac{m_{\text{Pl}}^2}{8\pi} \frac{V''}{V}, \quad (25.4)$$

which should satisfy $\epsilon, |\eta| \ll 1$, the spectra can be computed using the slow-roll approximation as

$$\Delta_{\mathcal{R}}^2(k) \simeq \frac{8}{3m_{\text{Pl}}^4} \frac{V}{\epsilon} \Big|_{k=aH}, \quad \Delta_{\mathcal{T}}^2(k) \simeq \frac{128}{3m_{\text{Pl}}^4} V \Big|_{k=aH}. \quad (25.5)$$

In each case, the expressions on the right-hand side are to be evaluated when the scale k is equal to the Hubble radius during inflation. The symbol ‘ \simeq ’ here indicates use of the slow-roll approximation, which is expected to be accurate to a few percent or better.

From these expressions, we can compute the spectral indices [8]:

$$n_s \simeq 1 - 6\epsilon + 2\eta \quad ; \quad n_t \simeq -2\epsilon. \quad (25.6)$$

Another useful quantity is the ratio of the two spectra, defined by

$$r \equiv \frac{\Delta_{\mathcal{T}}^2(k_*)}{\Delta_{\mathcal{R}}^2(k_*)}. \quad (25.7)$$

We have

$$r \simeq 16\epsilon \simeq -8n_t, \quad (25.8)$$

which is known as the consistency equation.

One could consider corrections to the power-law approximation, which we discuss later. However, for now we make the working assumption that the spectra can be approximated by such power laws. The consistency equation shows that r and n_t are not independent parameters, and so the simplest inflation models give initial conditions described by three parameters, usually taken as $\Delta_{\mathcal{R}}^2$, n_s , and r , all to be evaluated at some scale k_* , usually the ‘statistical center’ of the range explored by the data. Alternatively, one could use the parametrization V , ϵ , and η , all evaluated at a point on the putative inflationary potential.

After the perturbations are created in the early Universe, they undergo a complex evolution up until the time they are observed in the present Universe. When the perturbations are small, this can be accurately followed using a linear theory numerical code such as **CAMB** or **CLASS** [9]. This works right up to the present for the CMB, but for density perturbations on small scales non-linear evolution is important and can be addressed by a variety of semi-analytical and numerical techniques. However the analysis is made, the outcome of the evolution is in principle determined by the cosmological model and by the parameters describing the initial perturbations, and hence can be used to determine them.

Of particular interest are CMB anisotropies. Both the total intensity and two independent polarization modes are predicted to have anisotropies. These can be described by the radiation angular power spectra C_ℓ as defined in the CMB article in this volume, and again provide a complete description if the density perturbations are Gaussian.

25.1.3 The standard cosmological model

We now have most of the ingredients in place to describe the cosmological model. Beyond those of the previous subsections, we need a measure of the ionization state of the Universe. The Universe is known to be highly ionized at redshifts below 5 or so (otherwise radiation from distant quasars would be heavily absorbed in the ultra-violet), and the ionized electrons can scatter microwave photons, altering the pattern of observed anisotropies. The most convenient parameter to describe this is the optical depth to scattering τ (*i.e.*, the probability that a given photon scatters once); in the approximation of instantaneous and complete reionization, this could equivalently be described by the redshift of reionization z_1 .

As described in Sec. 25.4, models based on these parameters are able to give a good fit to the complete set of high-quality data available at present, and indeed some simplification is possible. Observations are consistent with spatial flatness, and the inflation models so far described automatically generate negligible spatial curvature, so we can set $k = 0$; the density parameters then must sum to unity, and so one of them can be eliminated. The neutrino energy density is often not taken as an independent parameter; provided that the neutrino sector has the standard interactions, the neutrino energy density, while relativistic, can be

related to the photon density using thermal physics arguments, and a minimal assumption takes the neutrino mass sum to be that of the lowest mass solution to the neutrino oscillation constraints, namely 0.06 eV. In addition, there is no observational evidence for the existence of tensor perturbations (with the upper limits now starting to become constraining on models), and so r could be set to zero. This leaves seven parameters, which is the smallest set that can usefully be compared to the present cosmological data. This model is referred to by various names, including Λ CDM, the concordance cosmology, and the standard cosmological model.

Of these parameters, only Ω_γ is accurately measured directly. The radiation density is dominated by the energy in the CMB, and the COBE satellite FIRAS experiment determined its temperature to be $T = 2.7255 \pm 0.0006$ K [10],¹ corresponding to $\Omega_\gamma = 2.47 \times 10^{-5} h^{-2}$. It typically can be taken as fixed when fitting other data. Hence the minimum number of cosmological parameters varied in fits to data is six, though as described below there may additionally be many ‘nuisance’ parameters necessary to describe astrophysical processes influencing the data.

In addition to this minimal set, there is a range of other parameters that might prove important in future as the data-sets further improve, but for which there is so far no direct evidence, allowing them to be set to specific values for now. We discuss various speculative options in the next section. For completeness at this point, we mention one other interesting quantity, the helium fraction, which is a non-zero parameter that can affect the CMB anisotropies at a subtle level. It is usually fixed in microwave anisotropy studies, but the data are approaching a level where allowing its variation may become mandatory.

In conventional parameter estimation, a set of parameters is chosen by hand and the aim is to constrain their values. The higher-level inference problem of model selection instead compares different choices of parameter sets, as is necessary to assess whether observations are pointing towards inclusion of new physical effects. Bayesian inference offers an attractive framework for cosmological model selection, setting a tension between model predictiveness and ability to fit the data [11], and its use is becoming widespread.

25.1.4 Derived parameters

The parameter list of the previous subsection is sufficient to give a complete description of cosmological models that agree with observational data. However, it is not a unique parameterization, and one could instead use parameters derived from that basic set. Parameters that can be obtained from the set given above include the age of the Universe, the present horizon distance, the present neutrino background temperature, the epoch of matter–radiation equality, the epochs of recombination and decoupling, the epoch of transition to an accelerating Universe, the baryon-to-photon ratio, and the baryon-to-dark-matter density ratio. In addition, the physical densities of the matter components, $\Omega_i h^2$, are often more useful than the density parameters. The density perturbation amplitude can be specified in many different ways other than the large-scale primordial amplitude, for instance, in terms of its effect on the CMB, or by specifying a short-scale quantity, a common choice being the present linear-theory mass dispersion on a radius of $8 h^{-1}$ Mpc, known as σ_8 .

Different types of observation are sensitive to different subsets of the full cosmological parameter set, and some are more naturally interpreted in terms of some of the derived parameters of this subsection than on the original base parameter set. In particular, most types of observation feature degeneracies whereby they are unable to separate the effects of simultaneously varying specific combinations of several of the base parameters.

25.2 Extensions to the standard model

At present, there is no positive evidence in favor of extensions of the standard model. These are becoming increasingly constrained

¹All quoted uncertainties in this article are $1\sigma/68\%$ confidence and all upper limits are 95% confidence. Cosmological parameters sometimes have significantly non-Gaussian uncertainties. Throughout we have rounded central values, and especially uncertainties, from original sources, in cases where they appear to be given to excessive precision.

by the data, though there always remains the possibility of trace effects at a level below present observational capability.

25.2.1 More general perturbations

The standard cosmology assumes adiabatic, Gaussian perturbations. Adiabaticity means that all types of material in the Universe share a common perturbation, so that if the space-time is foliated by constant-density hypersurfaces, then all fluids and fields are homogeneous on those slices, with the perturbations completely described by the variation of the spatial curvature of the slices. Gaussianity means that the initial perturbations obey Gaussian statistics, with the amplitudes of waves of different wavenumbers being randomly drawn from a Gaussian distribution of width given by the power spectrum. Note that gravitational instability generates non-Gaussianity; in this context, Gaussianity refers to a property of the initial perturbations, before they evolve.

The simplest inflation models, based on one dynamical field, predict adiabatic perturbations and a level of non-Gaussianity that is too small to be detected by any experiment so far conceived. For present data, the primordial spectra are usually assumed to be power laws.

25.2.1.1 Non-power-law spectra

For typical inflation models, it is an approximation to take the spectra as power laws, albeit usually a good one. As data quality improves, one might expect this approximation to come under pressure, requiring a more accurate description of the initial spectra, particularly for the density perturbations. In general, one can expand $\ln \Delta_{\mathcal{R}}^2$ as

$$\ln \Delta_{\mathcal{R}}^2(k) = \ln \Delta_{\mathcal{R}}^2(k_*) + (n_{s,*} - 1) \ln \frac{k}{k_*} + \frac{1}{2} \left. \frac{dn_s}{d \ln k} \right|_* \ln^2 \frac{k}{k_*} + \dots, \quad (25.9)$$

where the coefficients are all evaluated at some scale k_* . The term $dn_s/d \ln k|_*$ is often called the running of the spectral index [12]. Once non-power-law spectra are allowed, it is necessary to specify the scale k_* at which the spectral index is defined.

25.2.1.2 Isocurvature perturbations

An isocurvature perturbation is one that leaves the total density unperturbed, while perturbing the relative amounts of different materials. If the Universe contains N fluids, there is one growing adiabatic mode and $N-1$ growing isocurvature modes (for reviews see Ref. [7] and Ref. [13]). These can be excited, for example, in inflationary models where there are two or more fields that acquire dynamically-important perturbations. If one field decays to form normal matter, while the second survives to become the dark matter, this will generate a cold dark matter isocurvature perturbation.

In general, there are also correlations between the different modes, and so the full set of perturbations is described by a matrix giving the spectra and their correlations. Constraining such a general construct is challenging, though constraints on individual modes are beginning to become meaningful, with no evidence that any other than the adiabatic mode must be non-zero.

25.2.1.3 Seeded perturbations

An alternative to laying down perturbations at very early epochs is that they are seeded throughout cosmic history, for instance by topological defects such as cosmic strings. It has long been excluded that these are the sole original of structure, but they could contribute part of the perturbation signal, current limits being just a few percent [14]. In particular, cosmic defects formed in a phase transition ending inflation is a plausible scenario for such a contribution.

25.2.1.4 Non-Gaussianity

Multi-field inflation models can also generate primordial non-Gaussianity (reviewed, *e.g.*, in Ref. [7]). The extra fields can either be in the same sector of the underlying theory as the inflaton, or completely separate, an interesting example of the latter being the curvaton model [15]. Current upper limits on non-Gaussianity are becoming stringent, but there remains strong motivation to push down those limits and perhaps reveal trace non-Gaussianity in

the data. If non-Gaussianity is observed, its nature may favor an inflationary origin, or a different one such as topological defects.

25.2.2 Dark matter properties

Dark matter properties are discussed in the Dark Matter chapter in this volume. The simplest assumption concerning the dark matter is that it has no significant interactions with other matter, and that its particles have a negligible velocity as far as structure formation is concerned. Such dark matter is described as ‘cold,’ and candidates include the lightest supersymmetric particle, the axion, and primordial black holes. As far as astrophysicists are concerned, a complete specification of the relevant cold dark matter properties is given by the density parameter Ω_c , though those seeking to detect it directly need also to know its interaction properties.

Cold dark matter is the standard assumption and gives an excellent fit to observations, except possibly on the shortest scales where there remains some controversy concerning the structure of dwarf galaxies and possible substructure in galaxy halos. It has long been excluded for all the dark matter to have a large velocity dispersion, so-called ‘hot’ dark matter, as it does not permit galaxies to form; for thermal relics the mass must be above about 1 keV to satisfy this constraint, though relics produced non-thermally, such as the axion, need not obey this limit. However, in future further parameters might need to be introduced to describe dark matter properties relevant to astrophysical observations. Suggestions that have been made include a modest velocity dispersion (warm dark matter) and dark matter self-interactions. There remains the possibility that the dark matter is comprised of two separate components, *e.g.*, a cold one and a hot one, an example being if massive neutrinos have a non-negligible effect.

25.2.3 Relativistic species

The number of relativistic species in the young Universe (omitting photons) is denoted N_{eff} . In the standard cosmological model only the three neutrino species contribute, and its baseline value is assumed fixed at 3.044 (the small shift from 3 is because of a slight predicted deviation from a thermal distribution [16]). However other species could contribute, for example an extra neutrino, possibly of sterile type, or massless Goldstone bosons or other scalars. It is hence interesting to study the effect of allowing this parameter to vary, and indeed although 3.044 is consistent with the data, most analyses currently suggest a somewhat higher value (*e.g.*, Ref. [17]).

25.2.4 Dark energy and modified gravity

While the standard cosmological model given above features a cosmological constant, in order to explain observations indicating that the Universe is presently accelerating, further possibilities exist under the general headings of ‘dark energy’ and ‘modified gravity’. These topics are described in detail in the Dark Energy chapter in this volume. This article focuses on the case of the cosmological constant, since this simple model is a good match to existing data. We note that more general treatments of dark energy/modified gravity will lead to weaker constraints on other parameters.

25.2.5 Complex ionization history

The full ionization history of the Universe is given by the ionization fraction as a function of redshift z . The simplest scenario takes the ionization to have the small residual value left after recombination up to some redshift z_1 , at which point the Universe instantaneously reionizes completely. Then there is a one-to-one correspondence between τ and z_1 (that relation, however, also depending on other cosmological parameters). An accurate treatment of this process will track separate histories for hydrogen and helium. While currently rapid ionization appears to be a good approximation, as data improve a more complex ionization history may need to be considered.

25.2.6 Varying ‘constants’

Variation of the fundamental constants of Nature over cosmological times is another possible enhancement of the standard cosmology. There is a long history of study of variation of the gravitational constant G_N , and more recently attention has been

drawn to the possibility of small fractional variations in the fine-structure constant. There is presently no observational evidence for the former, which is tightly constrained by a variety of measurements. Evidence for the latter has been claimed from studies of spectral line shifts in quasar spectra at redshift $z \simeq 2$ [18], but this is presently controversial and in need of further observational study.

25.2.7 Cosmic topology

The usual hypothesis is that the Universe has the simplest topology consistent with its geometry, for example that a flat Universe extends forever. Observations cannot tell us whether that is true, but they can test the possibility of a non-trivial topology on scales up to roughly the present Hubble scale. Extra parameters would be needed to specify both the type and scale of the topology; for example, a cuboidal topology would need specification of the three principal axis lengths and orientation. At present, there is no evidence for non-trivial cosmic topology [19].

25.3 Cosmological Probes

The goal of the observational cosmologist is to utilize astronomical information to derive cosmological parameters. The transformation from the observables to the parameters usually involves many assumptions about the nature of the data, as well as of the dark sector. Below we outline the physical processes involved in each of the major probes, and the main recent results. The first two subsections concern probes of the homogeneous Universe, while the remainder consider constraints from perturbations.

In addition to statistical uncertainties we note three sources of systematic uncertainties that will apply to the cosmological parameters of interest: (i) due to the assumptions on the cosmological model and its priors (*i.e.*, the number of assumed cosmological parameters and their allowed range); (ii) due to the uncertainty in the astrophysics of the objects (*e.g.*, light-curve fitting for supernovae or the mass–temperature relation of galaxy clusters); and (iii) due to instrumental and observational limitations (*e.g.*, the effect of ‘seeing’ on weak gravitational lensing measurements, or beam shape on CMB anisotropy measurements).

These systematics, the last two of which appear as ‘nuisance parameters’, pose a challenging problem to the statistical analysis. We attempt a statistical fit to the whole Universe with 6 to 12 parameters, but we might need to include hundreds of nuisance parameters, some of them highly correlated with the cosmological parameters of interest (for example time-dependent galaxy biasing could mimic the growth of mass fluctuations). Fortunately, there is some astrophysical prior knowledge on these effects, and a small number of physically-motivated free parameters would ideally be preferred in the cosmological parameter analysis.

25.3.1 Measures of the Hubble constant

In 1929, Edwin Hubble discovered the law of expansion of the Universe by measuring distances to nearby galaxies. The slope of the relation between the distance and recession velocity is defined to be the present-epoch Hubble constant, H_0 . Astronomers argued for decades about the systematic uncertainties in various methods and derived values over the wide range $40 \text{ km s}^{-1} \text{ Mpc}^{-1} \lesssim H_0 \lesssim 100 \text{ km s}^{-1} \text{ Mpc}^{-1}$.

One of the most reliable results on the Hubble constant came from the Hubble Space Telescope (HST) Key Project [20]. This study used the empirical period–luminosity relation for Cepheid variable stars, and calibrated a number of secondary distance indicators: Type Ia Supernovae (SNe Ia), the Tully–Fisher relation, surface-brightness fluctuations, and Type II Supernovae. This approach has been further extended. Based on HST photometry of 75 Milky Way Cepheids and Gaia EDR3 parallaxes, the SH0ES team derived $H_0 = 73.2 \pm 1.3 \text{ km s}^{-1} \text{ Mpc}^{-1}$ [21].

Three other methods have been used recently. One is a calibration of the tip of the red-giant branch applied to Type Ia supernovae, the Carnegie–Chicago Hubble Programme (CCHP) finding $H_0 = 69.8 \pm 0.6$ (stat.) ± 1.6 (sys.) $\text{km s}^{-1} \text{ Mpc}^{-1}$ [22]. The second uses the method of time delay in gravitationally-lensed quasars; Birrer et al. [23] find $H_0 = 67.4^{+4.1}_{-3.2} \text{ km s}^{-1} \text{ Mpc}^{-1}$ from a sample of 40 lenses (which includes as a subset the six systems previously used by the HOLiCOW collaboration [24] who

obtained a higher value). A third method that came to fruition recently is based on gravitational waves; the ‘bright standard siren’ method applied to the binary neutron star GW170817 yields $H_0 = 70^{+12}_{-8} \text{ km s}^{-1} \text{ Mpc}^{-1}$ [25]. Adding two ‘dark standard siren’ systems shifts this to $H_0 = 72^{+12}_{-8} \text{ km s}^{-1} \text{ Mpc}^{-1}$ [26], still dominated by the single bright siren system. When many more gravitational-wave events have been acquired, the future uncertainties on H_0 from standard sirens will get smaller.

The determination of H_0 by the *Planck* Collaboration [2] gives a lower value than most of the above methods, $H_0 = 67.4 \pm 0.5 \text{ km s}^{-1} \text{ Mpc}^{-1}$. As they discuss, there is strong degeneracy of H_0 with other parameters, particularly Ω_m and the neutrino mass. It is worth noting that using the ‘inverse distance ladder’ method gives a result $H_0 = 67.8 \pm 1.3 \text{ km s}^{-1} \text{ Mpc}^{-1}$ [27], close to the *Planck* result. The inverse distance ladder relies on absolute-distance measurements from baryon acoustic oscillations (BAOs) to calibrate the intrinsic magnitude of the SNe Ia (rather than nearby Cepheids and parallax). This measurement was derived from 207 spectroscopically-confirmed Type Ia supernovae from the Dark Energy Survey (DES), an additional 122 low-redshift SNe Ia, and measurements of BAOs. A combination of DES Year 3 (Y3) clustering and weak lensing with BAO and BBN (assuming Λ CDM) gives $H_0 = 67.6 \pm 0.9 \text{ km s}^{-1} \text{ Mpc}^{-1}$ [28]. The completed Extended Baryon Oscillation Spectroscopic Survey (eBOSS) [29] inverse distance ladder result, within an assumed extended cosmological model, is $H_0 = 68.2 \pm 0.8 \text{ km s}^{-1} \text{ Mpc}^{-1}$, also close to the *Planck* value.

The tension between the H_0 values from *Planck* and the traditional cosmic distance ladder methods, with the SH0ES result deviating from *Planck* by 4.2σ , is under intense investigation for potential systematic effects. There is possibly a trend for higher H_0 derived from the nearby Universe and a lower H_0 from the early Universe, which has led some researchers to propose a time-variation of the dark energy component or other exotic scenarios. Ongoing studies are addressing the question of whether the Hubble tension is due to systematics in at least one of the probes, or a signature of new physics.

Figure 25.1 shows a selection of recent H_0 values, summarizing the current status of the Hubble constant tension. We note that while the tension remains highly significant, its severity has somewhat lessened compared to our assessment in the previous edition of this article two years ago.

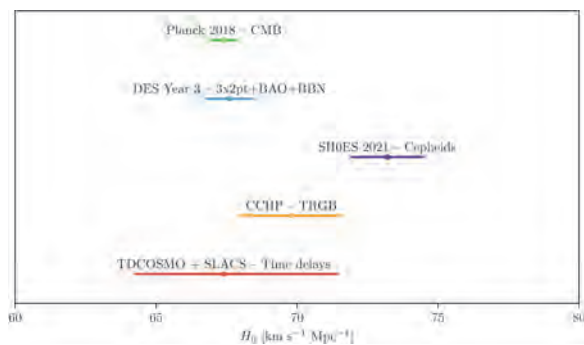


Figure 25.1: A selection of recent H_0 measurements from the various projects as described in the text. The standard-siren determinations are omitted as they are too wide for the plot. Figure courtesy of Pablo Lemos.

25.3.2 Supernovae as cosmological probes

Empirically, the peak luminosity of SNe Ia can be used as an efficient distance indicator (*e.g.*, Ref. [30]), thus allowing cosmology to be constrained via the distance–redshift relation. The favorite theoretical explanation for SNe Ia is the thermonuclear disruption of carbon–oxygen white dwarfs. Although not perfect ‘standard candles’, it has been demonstrated that by correcting for a relation between the light-curve shape, color, and luminosity at max-

imum brightness, the dispersion of the measured luminosities can be greatly reduced. There are several possible systematic effects that may affect the accuracy of the use of SNe Ia as distance indicators, *e.g.*, evolution with redshift and interstellar extinction in the host galaxy and in the Milky Way.

Two major studies, the Supernova Cosmology Project and the High- z Supernova Search Team, found evidence for an accelerating Universe [31], interpreted as due to a cosmological constant or a dark energy component. When combined with the CMB data (which indicate near flatness, *i.e.*, $\Omega_m + \Omega_\Lambda \simeq 1$), the best-fit values were $\Omega_m \simeq 0.3$ and $\Omega_\Lambda \simeq 0.7$. Most results in the literature are consistent with the $w = -1$ cosmological constant case. The most-used sample currently is the Pantheon compilation [32]. This sample of 1048 spectroscopically-confirmed SNe Ia gives $\Omega_m = 0.298 \pm 0.022$ (stat+sym) for an assumed flat Λ CDM model. In combination with the CMB, for a flat w CDM model these data give $w = -1.03 \pm 0.04$ and $\Omega_m = 0.307 \pm 0.012$. For comparison, an analysis of a sample of 207 spectroscopically-confirmed DES SNe Ia combined with 122 low-redshift SNe [33] yielded $\Omega_m = 0.331 \pm 0.038$ for an assumed flat Λ CDM model. Future experiments will refine constraints on the cosmic equation of state $w(z)$.

25.3.3 Cosmic microwave background

The physics of the CMB is described in detail in the CMB chapter in this volume. Before recombination, the baryons and photons are tightly coupled, and the perturbations oscillate in the potential wells generated primarily by the dark matter perturbations. After decoupling, the baryons are free to collapse into those potential wells. The CMB carries a record of conditions at the time of last scattering, often called primary anisotropies. In addition, it is affected by various processes as it propagates towards us, including the effect of a time-varying gravitational potential (the integrated Sachs-Wolfe effect), gravitational lensing, and scattering from ionized gas at low redshift.

The primary anisotropies, the integrated Sachs-Wolfe effect, and the scattering from a homogeneous distribution of ionized gas, can all be calculated using linear perturbation theory. Available codes include CAMB and CLASS [9], the former widely used embedded within the analysis package CosmoMC [34] and in higher-level analysis packages such as CosmoSIS [35] and CosmoLike [36]. Gravitational lensing is also calculated in these codes. Secondary effects, such as inhomogeneities in the reionization process, and scattering from gravitationally-collapsed gas (the Sunyaev-Zeldovich or SZ effect), require more complicated, and more uncertain, calculations.

The upshot is that the detailed pattern of anisotropies depends on all of the cosmological parameters. In a typical cosmology, the anisotropy power spectrum [usually plotted as $\ell(\ell + 1)C_\ell$] features a flat plateau at large angular scales (small ℓ), followed by a series of oscillatory features at higher angular scales, the first and most prominent being at around one degree ($\ell \simeq 200$). These features, known as acoustic peaks, represent the oscillations of the photon-baryon fluid around the time of decoupling. Some features can be closely related to specific parameters—for instance, the location in multipole space of the set of peaks probes the spatial geometry, while the relative heights of the peaks probe the baryon density—but many other parameters combine to determine the overall shape.

The 2018 data release from the *Planck* satellite [1] gives the most powerful results to date on the spectrum of CMB temperature anisotropies, with a precision determination of the temperature power spectrum to beyond $\ell = 2000$. The Atacama Cosmology Telescope (ACT) and South Pole Telescope (SPT) experiments extend these results to higher angular resolution, though without full-sky coverage. *Planck* and the polarization-sensitive versions of ACT and SPT give the state of the art in measuring the spectrum of E -polarization anisotropies and the correlation spectrum between temperature and polarization. These are consistent with models based on the parameters we have described, and provide accurate determinations of many of those parameters [2]. Primordial B -mode polarization has not been detected (although the gravitational lensing effect on B modes has been measured).

The data provide an exquisite measurement of the location of the set of acoustic peaks, determining the angular-diameter distance of the last-scattering surface. In combination with other data this strongly constrains the spatial geometry, in a manner consistent with spatial flatness and excluding significantly-curved Universes. CMB data give a precision measurement of the age of the Universe. The CMB also gives a baryon density consistent with, and at higher precision than, that coming from BBN. It affirms the need for both dark matter and dark energy. It shows no evidence for dynamics of the dark energy, being consistent with a pure cosmological constant ($w = -1$). The density perturbations are consistent with a power-law primordial spectrum, and there is no indication yet of tensor perturbations. The current best-fit for the reionization optical depth from CMB data, $\tau = 0.054$, is in line with models of how early structure formation induces reionization.

Planck has also made the first all-sky map of the CMB lensing field, which probes the entire matter distribution in the Universe and adds some additional constraining power to the CMB-only data-sets. These measurements are compatible with the expected effect in the standard cosmology.

25.3.4 Galaxy clustering

The power spectrum of density perturbations is affected by the nature of the dark matter. Within the Λ CDM model, the power spectrum shape depends primarily on the primordial power spectrum and on the combination $\Omega_m h$, which determines the horizon scale at matter-radiation equality, with a subdominant dependence on the baryon density. The matter distribution is most easily probed by observing the galaxy distribution, but this must be done with care since the galaxies do not perfectly trace the dark matter distribution. Rather, they are a ‘biased’ tracer of the dark matter [37]. The need to allow for such bias is emphasized by the observation that different types of galaxies show bias with respect to each other. In particular, scale-dependent and stochastic biasing may introduce a systematic effect on the determination of cosmological parameters from redshift surveys [38]. Prior knowledge from simulations of galaxy formation or from gravitational lensing data could help to quantify biasing. Furthermore, the observed 3D galaxy distribution is in redshift space, *i.e.*, the observed redshift is the sum of the Hubble expansion and the line-of-sight peculiar velocity, leading to linear and non-linear dynamical effects that also depend on the cosmological parameters. On the largest length scales, the galaxies are expected to trace the location of the dark matter, except for a constant multiplier b to the power spectrum, known as the linear bias parameter. On scales smaller than 20 Mpc or so, the clustering pattern is ‘squashed’ in the radial direction due to coherent infall, which depends approximately on the parameter $\beta \equiv \Omega_m^{0.6}/b$ (on these shorter scales, more complicated forms of biasing are not excluded by the data). On scales of a few Mpc, there is an effect of elongation along the line of sight (colloquially known as the ‘finger of God’ effect) that depends on the galaxy velocity dispersion.

25.3.4.1 Baryon acoustic oscillations

The power spectra of the 2-degree Field (2dF) Galaxy Redshift Survey and the Sloan Digital Sky Survey (SDSS) are well fit by a Λ CDM model and both surveys showed first evidence for baryon acoustic oscillations (BAOs) [39, 40]. When eBOSS is combined with *Planck*, Pantheon Type Ia Supernovae and other probes the result is $w_p = -1.020 \pm 0.032$ at the pivot redshift $z_p = 0.29$ [29]. Similar results for w were obtained *e.g.* by the WiggleZ survey [41].

25.3.4.2 Redshift distortion

There is continuing interest in the ‘redshift distortion’ effect. This distortion depends on cosmological parameters [42] via the perturbation growth rate in linear theory $f(z) = d \ln \delta / d \ln a \simeq \Omega_m^\gamma(z)$, where $\gamma \simeq 0.55$ for the Λ CDM model and may be different for modified gravity models. By measuring $f(z)$ it is feasible to constrain γ and rule out certain modified gravity models [43, 44]. We note the degeneracy of the redshift-distortion pattern and the geometric distortion (the so-called Alcock-Paczynski effect [45]), *e.g.*, as illustrated by the WiggleZ survey [46] and eBOSS [29].

25.3.4.3 Limits on neutrino mass from galaxy surveys and other probes

Large-scale structure data place constraints on Ω_ν due to the neutrino free-streaming effect [47]. Presently there is no clear detection, and upper limits on neutrino mass are commonly estimated by comparing the observed galaxy power spectrum with a four-component model of baryons, cold dark matter, a cosmological constant, and massive neutrinos. Such analyses also assume that the primordial power spectrum is adiabatic, scale-invariant, and Gaussian. Potential systematic effects include biasing of the galaxy distribution and non-linearities of the power spectrum. An upper limit can also be derived from CMB anisotropies alone, while combination with additional cosmological data-sets can improve the results.

The most recent results on neutrino mass upper limits and other neutrino properties are summarized in the Neutrinos in Cosmology chapter in this volume. The latest cosmological data constrain the sum of neutrino masses to be below 0.2 eV or even 0.1 eV depending on the assumed priors and systematics (e.g. Refs. [2, 29].) Since the lower limit on this sum from oscillation experiments (assuming normal hierarchy) is 0.06 eV it is expected that future cosmological surveys will soon detect effects from the neutrino mass. Also, current cosmological datasets are in good agreement with the standard value for the effective number of neutrino species $N_{\text{eff}} = 3.044$.

25.3.5 Clustering in the inter-galactic medium

It is commonly assumed, based on hydrodynamic simulations, that the neutral hydrogen in the inter-galactic medium (IGM) can be related to the underlying mass distribution. It is then possible to estimate the matter power spectrum from the absorption observed in quasar spectra, the so-called Lyman- α forest. The usual procedure is to measure the power spectrum of the transmitted flux, and then to infer the mass power spectrum. Photoionization heating by the ultraviolet background radiation and adiabatic cooling by the expansion of the Universe combine to give a simple power-law relation between the gas temperature and the baryon density. It also follows that there is a power-law relation between the optical depth τ and ρ_b . Therefore, the observed flux $F = \exp(-\tau)$ is strongly correlated with ρ_b , which itself traces the mass density. The matter and flux power spectra can be related by a biasing function that is calibrated from simulations. There are two variants of Lyman-alpha analyses: 1-dimensional power spectra from individual lines-of-sight that probe small (\sim Mpc) scales, and 3-dimensional Lyman-alpha BAO analyses that measure large-scale correlations (over \sim 100 Mpc scales) using neighbouring quasar lines-of-sight.

The latest BOSS and eBOSS datasets have provided measurements of the BAO scale both in the Lyman- α absorption and in its cross correlation with quasars at an effective redshift $z = 2.3$ [29, 48]. The results agree within $1.5\text{-}\sigma$ with the *Planck* CMB flat- Λ estimation for BAO scale. Such measurements will improve with the Dark Energy Spectroscopic Instrument (DESI) and other future spectroscopic surveys. The Lyman- α flux power spectrum has also been used to constrain the nature of dark matter, for example limiting the amount of warm dark matter [49].

25.3.6 Weak gravitational lensing

Images of background galaxies are distorted by the gravitational effect of mass variations along the line of sight. Deep gravitational potential wells, such as galaxy clusters, generate ‘strong lensing’ leading to arcs, arclets, and multiple images, while more moderate perturbations give rise to ‘weak lensing’. Weak lensing is now widely used to measure the mass power spectrum in selected regions of the sky (see Ref. [50] for reviews). Since the signal is weak, the image of deformed galaxy shapes (the ‘shear map’) must be analyzed statistically to measure the power spectrum, higher moments, and cosmological parameters. There are various systematic effects in the interpretation of weak lensing, e.g., due to atmospheric distortions during observations, the redshift distribution of the background galaxies (usually depending on the accuracy of photometric redshifts), the intrinsic correlation

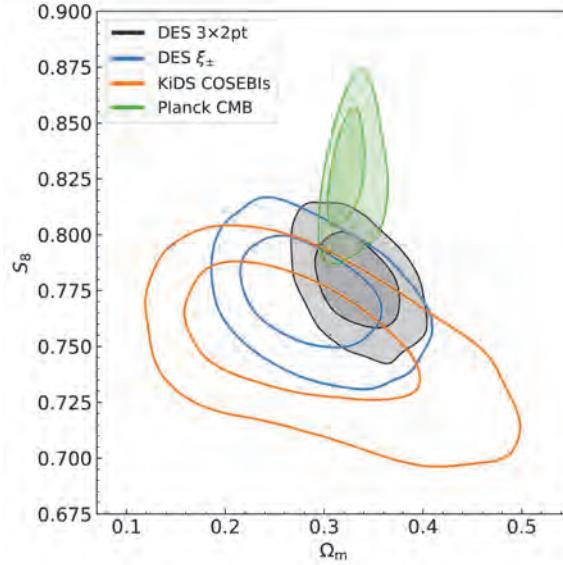


Figure 25.2: Marginalized posterior contours (inner 68% confidence level, outer 95% confidence level) in the Ω_m – S_8 plane. The plot shows a subset of the cases shown in Figure 19 of Ref. [28]: KiDS weak lensing alone, DES Y3 weak lensing alone, DES Y3 combined weak lensing and galaxy clustering (3x2pt), and Planck CMB. Figure courtesy of Michael Troxel and the DES collaboration.

of galaxy shapes, and non-linear modeling uncertainties.

Weak-lensing measurements from the Kilo-Degree Survey (KiDS) [51], the Subaru Hyper-Suprime-Cam (HSC) [52], and DES Y3 [53] have constrained the clumpiness parameter $S_8 \equiv \sigma_8(\Omega_m/0.3)^{0.5}$. Each of these surveys has yielded S_8 lower by about 2σ than S_8 derived from *Planck*. This tension is not yet resolved. Figure 25.2 shows the Ω_m – S_8 constraints derived from of KiDS (weak lensing) and DES Y3 (weak lensing with and without galaxy clustering) versus the CMB constraint from *Planck*. Results from weak lensing from DES, combined with other probes, are described in the next section.

25.3.7 Other probes

Other probes that have been used to constrain cosmological parameters, but that are not presently competitive in terms of accuracy, are the integrated Sachs-Wolfe effect [54,55], the number density or composition of galaxy clusters [56], and galaxy peculiar velocities which probe the mass fluctuations in the local Universe [57].

25.4 Bringing probes together

Although it contains two ingredients—dark matter and dark energy—which have not yet been verified by laboratory experiments, the Λ CDM model is almost universally accepted by cosmologists as the best description of the present data. The approximate values of some of the key parameters are $\Omega_b \simeq 0.05$, $\Omega_c \simeq 0.25$, $\Omega_\Lambda \simeq 0.70$, and a Hubble constant $h \simeq 0.70$. The spatial geometry is very close to flat (and usually assumed to be precisely flat), and the initial perturbations Gaussian, adiabatic, and nearly scale-invariant.

The most powerful data source is the CMB, which on its own supports all these main tenets. Values for some parameters, as given in Ref. [2], are reproduced in Table 25.1. These particular results presume a flat Universe. The constraints are somewhat strengthened by adding additional data-sets, BAO being shown in the Table as an example, though most of the constraining power resides in the CMB data. Similar constraints at lower precision were previously obtained by the *WMAP* collaboration.

If the assumption of spatial flatness is lifted, it turns out that the primary CMB on its own constrains the spatial curvature fairly weakly, due to a parameter degeneracy in the angular-diameter distance. However, inclusion of other data readily re-

Table 25.1: Parameter constraints reproduced from Ref. [2] (Table 2, column 5), with some additional rounding. Both columns assume the Λ CDM cosmology with a power-law initial spectrum, no tensors, spatial flatness, a cosmological constant as dark energy, and the sum of neutrino masses fixed to 0.06 eV. Above the line are the six parameter combinations actually fit to the data (θ_{MC} is a measure of the sound horizon at last scattering); those below the line are derived from these. The first column uses *Planck* primary CMB data plus the *Planck* measurement of CMB lensing. This column gives our present recommended values. The second column adds in data from a compilation of BAO measurements described in Ref. [2]. The perturbation amplitude $\Delta_{\mathcal{R}}^2$ (denoted A_s in the original paper) is specified at the scale 0.05 Mpc^{-1} . Uncertainties are shown at 68% confidence.

	<i>Planck</i> TT,TE,EE+lowE+lensing	+BAO
$\Omega_b h^2$	0.02237 ± 0.00015	0.02242 ± 0.00014
$\Omega_c h^2$	0.1200 ± 0.0012	0.1193 ± 0.0009
$100 \theta_{\text{MC}}$	1.0409 ± 0.0003	1.0410 ± 0.0003
n_s	0.965 ± 0.004	0.966 ± 0.004
τ	0.054 ± 0.007	0.056 ± 0.007
$\ln(10^{10} \Delta_{\mathcal{R}}^2)$	3.044 ± 0.014	3.047 ± 0.014
h	0.674 ± 0.005	0.677 ± 0.004
σ_8	0.811 ± 0.006	0.810 ± 0.006
Ω_m	0.315 ± 0.007	0.311 ± 0.006
Ω_Λ	0.685 ± 0.007	0.689 ± 0.006

moves this degeneracy. Simply adding the *Planck* lensing measurement, and with the assumption that the dark energy is a cosmological constant, yields a 68% confidence constraint on $\Omega_{\text{tot}} \equiv \sum \Omega_i + \Omega_\Lambda = 1.011 \pm 0.006$ and further adding BAO makes it 0.9993 ± 0.0019 [2]. Results of this type are normally taken as justifying the restriction to flat cosmologies.

One derived parameter that is very robust is the age of the Universe, since there is a useful coincidence that for a flat Universe the position of the first peak is strongly correlated with the age. The CMB data give 13.797 ± 0.023 Gyr (assuming flatness). This is in good agreement with the ages of the oldest globular clusters and with radioactive dating.

The baryon density Ω_b is now measured with high accuracy from CMB data alone, and is consistent with and more precise than the determination from BBN. The value quoted in the Big-Bang Nucleosynthesis chapter in this volume is $\Omega_b h^2 = 0.0224 \pm 0.0007$.

While Ω_Λ is measured to be non-zero with very high confidence, there is no evidence of evolution of the dark energy density. As described in the Dark Energy chapter in this volume a combination of CMB, SN, and BAO measurements, assuming a flat Universe, found $w = -1.03 \pm 0.03$ [29], consistent with the cosmological constant case $w = -1$. Allowing more complicated forms of dark energy weakens the limits.

The data provide strong support for the main predictions of the simplest inflation models: spatial flatness and adiabatic, Gaussian, nearly scale-invariant density perturbations. But it is disappointing that there is no sign of primordial gravitational waves; combining *Planck* and *WMAP* with BICEP2/Keck Array BK18 data (plus BAO data to help constrain n_s) gives a 95% confidence upper limit of $r < 0.036$ at the scale 0.05 Mpc^{-1} [58]. The density perturbation spectral index is clearly required to be less than one by current data, though the strength of that conclusion can weaken if additional parameters are included in the model fits.

Tests have been made for various types of non-Gaussianity, a particular example being a parameter f_{NL} that measures a quadratic contribution to the perturbations. Various non-Gaussian shapes are possible (see Ref. [59] for details), and current

constraints on the popular ‘local’, ‘equilateral’, and ‘orthogonal’ types (combining CMB temperature and polarization data) are $f_{\text{NL}}^{\text{local}} = -1 \pm 5$, $f_{\text{NL}}^{\text{equil}} = -26 \pm 47$, and $f_{\text{NL}}^{\text{ortho}} = -38 \pm 24$ respectively (these look weak, but prominent non-Gaussianity requires the product $f_{\text{NL}} \Delta_{\mathcal{R}}$ to be large, and $\Delta_{\mathcal{R}}$ is of order 10^{-5}). Clearly none of these give any indication of primordial non-Gaussianity.

While the above results come from the CMB alone, other probes are becoming competitive (especially when considering more complex cosmological models), and so combination of data from different sources is of growing importance. We note that it has become fashionable to combine probes at the level of power-spectrum data vectors, taking into account nuisance parameters in each type of measurement. Discussions on ‘tension’ in resulting cosmological parameters depend on the statistical approaches used. Commonly the cosmology community works within the Bayesian framework, and assesses agreement amongst data sets with respect to a model via Bayesian Evidence, essentially the denominator in Bayes’s theorem.

As an example of results, combining DES Y3 (position–position clustering, galaxy–galaxy lensing, and weak lensing shear) with *Planck*, BAO and RSD measurements from eBOSS, and type Ia supernovae from the Pantheon dataset compilation has shown the datasets to be mutually compatible and yields very tight constraints on cosmological parameters: $S_8 \equiv \sigma_8(\Omega_m/0.3)^{0.5} = 0.812 \pm 0.008$, and $\Omega_m = 0.306_{-0.005}^{+0.004}$ in Λ CDM, and $w = -1.03 \pm 0.03$ in w CDM [28] matching the constraint in Ref. [29]. The combined measurement of the Hubble constant within Λ CDM gives $H_0 = 68.0_{-0.3}^{+0.4} \text{ km s}^{-1} \text{ Mpc}^{-1}$, still leaving substantial tension with the SH0ES measurement described earlier. Future analyses and the next generation of surveys will test for deviations from Λ CDM, for example epoch-dependent $w(z)$ and modifications to General Relativity.

25.5 Outlook for the future

The concordance model is now well-established, and there seems little room left for any dramatic revision of this paradigm. A measure of the strength of that statement is how difficult it has proven to formulate convincing alternatives.

Should there indeed be no major revision of the current paradigm, we can expect future developments to take one of two directions. Either the existing parameter set will continue to prove sufficient to explain the data, with the parameters subject to ever-tightening constraints, or it will become necessary to deploy new parameters. The latter outcome would be very much the more interesting, offering a route towards understanding new physical processes relevant to the cosmological evolution. There are many possibilities on offer for striking discoveries, for example:

- the cosmological effects of a neutrino mass may be unambiguously detected, shedding light on fundamental neutrino properties;
- detection of primordial non-Gaussianities would indicate that non-linear processes influence the perturbation generation mechanism;
- detection of variation in the dark-energy density (*i.e.*, $w \neq -1$) would provide much-needed experimental input into its nature.

These provide more than enough motivation for continued efforts to test the cosmological model and improve its accuracy. Over the coming years, there are a wide range of new observations that will bring further precision to cosmological studies. Indeed, there are far too many for us to be able to mention them all here, and so we will just highlight a few areas.

The CMB observations will improve in several directions. A current frontier is the study of polarization, for which power spectrum measurements have now been made by several experiments. Detection of primordial B -mode anisotropies is the next major goal and a variety of projects are targeting this, though theory gives little guidance as to the likely signal level. Future CMB projects that are approved include *LiteBIRD* and the Simons Observatory.

An impressive array of cosmology surveys are already operational, under construction, or proposed, including the ground-

based Hyper Suprime Camera (HSC) and Rubin-LSST imaging surveys, spectroscopic surveys such as DESI and space missions *Euclid* and the Roman Wide-Field Infrared Survey (WFIRST).

An exciting area for the future is radio surveys of the redshifted 21-cm line of hydrogen. Because of the intrinsic narrowness of this line, by tuning the bandpass the emission from narrow redshift slices of the Universe will be measured to extremely high redshift, probing the details of the reionization process at redshifts up to perhaps 20, as well as measuring large-scale features such as the BAOs. LOFAR and CHIME are the first instruments able to do this and have begun operations. In the longer term, the Square Kilometre Array (SKA) will take these studies to a precision level.

The development of the first precision cosmological model is a major achievement. However, it is important not to lose sight of the motivation for developing such a model, which is to understand the underlying physical processes at work governing the Universe's evolution. From that perspective, progress has been much less dramatic. For instance, there are many proposals for the nature of the dark matter, but no consensus as to which is correct. The nature of the dark energy remains a mystery. Even the baryon density, now measured to an accuracy of a percent, lacks an underlying theory able to predict it within orders of magnitude. Precision cosmology may have arrived, but at present many key questions remain to motivate and challenge the cosmology community.

References

- [1] Planck Collab. 2018 Results I, *Astron. Astrophys.* **641**, A1 (2020), [arXiv:1807.06205].
- [2] Planck Collab. 2018 Results VI, *Astron. Astrophys.* **641**, A6 (2020), [arXiv:1807.06209].
- [3] C. L. Bennett *et al.* (WMAP), *Astrophys. J. Suppl.* **208**, 20 (2013), [arXiv:1212.5225].
- [4] G. Hinshaw *et al.* (WMAP), *Astrophys. J. Suppl.* **208**, 19 (2013), [arXiv:1212.5226].
- [5] S. Fukuda *et al.* (Super-Kamiokande), *Phys. Rev. Lett.* **85**, 3999 (2000), [hep-ex/0009001]; Q. R. Ahmad *et al.* (SNO), *Phys. Rev. Lett.* **87**, 071301 (2001), [arXiv:nucl-ex/0106015].
- [6] E.W. Kolb and M.S. Turner, *The Early Universe*, Addison-Wesley (Redwood City, 1990).
- [7] D.H. Lyth and A.R. Liddle, *The Primordial Density Perturbation*, Cambridge University Press (2009).
- [8] A. R. Liddle and D. H. Lyth, *Phys. Lett.* **B291**, 391 (1992), [arXiv:astro-ph/9208007].
- [9] A. Lewis, A. Challinor and A. Lasenby, *Astrophys. J.* **538**, 473 (2000), [arXiv:astro-ph/9911177]; D. Blas, J. Lesgourgues and T. Tram, *JCAP* **1107**, 034 (2011), [arXiv:1104.2933].
- [10] D. J. Fixsen, *Astrophys. J.* **707**, 916 (2009), [arXiv:0911.1955].
- [11] M. Hobson *et al.* (eds). *Bayesian Methods in Cosmology*, Cambridge University Press (2009).
- [12] A. Kosowsky and M. S. Turner, *Phys. Rev.* **D52**, R1739 (1995), [arXiv:astro-ph/9504071].
- [13] K. A. Malik and D. Wands, *Phys. Rept.* **475**, 1 (2009), [arXiv:0809.4944].
- [14] Planck Collab. 2013 Results XXV, *Astron. Astrophys.* **571**, A25 (2014), [arXiv:1303.5085].
- [15] D. H. Lyth and D. Wands, *Phys. Lett.* **B524**, 5 (2002), [hep-ph/0110002]; K. Enqvist and M. S. Sloth, *Nucl. Phys.* **B626**, 395 (2002), [hep-ph/0109214]; T. Moroi and T. Takahashi, *Phys. Lett.* **B522**, 215 (2001), [Erratum: *Phys. Lett.* **B539**, 303(2002)], [hep-ph/0110096].
- [16] J. J. Bennett *et al.*, *JCAP* **04**, 073 (2021), [arXiv:2012.02726].
- [17] S. Riemer-Sorensen, D. Parkinson and T. M. Davis, *Publ. Astron. Soc. Austral.* **30**, e029 (2013), [arXiv:1301.7102].
- [18] J. K. Webb *et al.*, *Phys. Rev. Lett.* **107**, 191101 (2011), [arXiv:1008.3907]; J. A. King *et al.*, *Mon. Not. Roy. Astron. Soc.* **422**, 3370 (2012), [arXiv:1202.4758]; P. Molaro *et al.*, *Astron. & Astrophys.* **555**, 68 (2013).
- [19] Planck Collab. 2015 Results XVIII, *Astron. Astrophys.* **594**, A18 (2016), [arXiv:1502.01593].
- [20] W. L. Freedman *et al.* (HST), *Astrophys. J.* **553**, 47 (2001), [arXiv:astro-ph/0012376].
- [21] A. G. Riess *et al.*, *Astrophys. J. Lett.* **908**, 1, L6 (2021), [arXiv:2012.08534].
- [22] W. L. Freedman (2021), [arXiv:2106.15656].
- [23] S. Birrer *et al.*, *Astron. Astrophys.* **643**, A165 (2020), [arXiv:2007.02941].
- [24] K. C. Wong *et al.* (2019), [arXiv:1907.04869].
- [25] B. P. Abbott *et al.* (LIGO Scientific, Virgo, 1M2H, Dark Energy Camera GW-E, DES, DLT40, Las Cumbres Observatory, VINROUGE, MASTER), *Nature* **551**, 7678, 85 (2017), [arXiv:1710.05835].
- [26] A. Palmese *et al.* (DES), *Astrophys. J. Lett.* **900**, 2, L33 (2020), [arXiv:2006.14961].
- [27] E. Macaulay *et al.* (DES), *Mon. Not. Roy. Astron. Soc.* **486**, 2, 2184 (2019), [arXiv:1811.02376].
- [28] T. M. C. Abbott *et al.* (DES) (2021), [arXiv:2105.13549].
- [29] S. Alam *et al.* (eBOSS), *Phys. Rev. D* **103**, 8, 083533 (2021), [arXiv:2007.08991].
- [30] B. Leibundgut, *Ann. Rev. Astron. Astrophys.* **39**, 67 (2001).
- [31] A. G. Riess *et al.* (Supernova Search Team), *Astron. J.* **116**, 1009 (1998), [arXiv:astro-ph/9805201]; P. M. Garnavich *et al.* (Supernova Search Team), *Astrophys. J.* **509**, 74 (1998), [arXiv:astro-ph/9806396]; S. Perlmutter *et al.* (Supernova Cosmology Project), *Astrophys. J.* **517**, 565 (1999), [arXiv:astro-ph/9812133].
- [32] D. M. Scolnic *et al.*, *Astrophys. J.* **859**, 2, 101 (2018), [arXiv:1710.00845].
- [33] T. M. C. Abbott *et al.* (DES), *Astrophys. J.* **872**, 2, L30 (2019), [arXiv:1811.02374].
- [34] A. Lewis and S. Bridle, *Phys. Rev.* **D66**, 103511 (2002), [arXiv:astro-ph/0205436].
- [35] J. Zuntz *et al.*, *Astron. Comput.* **12**, 45 (2015), [arXiv:1409.3409].
- [36] E. Krause and T. Eifler, *Mon. Not. Roy. Astron. Soc.* **470**, 2, 2100 (2017), [arXiv:1601.05779].
- [37] N. Kaiser, *Astrophys. J.* **284**, L9 (1984).
- [38] A. Dekel and O. Lahav, *Astrophys. J.* **520**, 24 (1999), [arXiv:astro-ph/9806193].
- [39] D. J. Eisenstein *et al.* (SDSS), *Astrophys. J.* **633**, 560 (2005), [arXiv:astro-ph/0501171].
- [40] S. Cole *et al.* (2dFGRS), *Mon. Not. Roy. Astron. Soc.* **362**, 505 (2005), [arXiv:astro-ph/0501174].
- [41] D. Parkinson *et al.*, *Phys. Rev.* **D86**, 103518 (2012), [arXiv:1210.2130].
- [42] N. Kaiser, *Mon. Not. Roy. Astron. Soc.* **227**, 1 (1987).
- [43] L. Guzzo *et al.*, *Nature* **451**, 541 (2008), [arXiv:0802.1944].
- [44] A. Nusser and M. Davis, *Astrophys. J.* **736**, 93 (2011), [arXiv:1101.1650].
- [45] C. Alcock and B. Paczynski, *Nature* **281**, 358 (1979).
- [46] C. Blake *et al.*, *Mon. Not. Roy. Astron. Soc.* **425**, 405 (2012), [arXiv:1204.3674].
- [47] J. Lesgourgues and S. Pastor, *Phys. Rept.* **429**, 307 (2006), [arXiv:astro-ph/0603494].
- [48] H. du Mas des Bourboux *et al.*, *Astrophys. J.* **901**, 2, 153 (2020), [arXiv:2007.08995].
- [49] M. Viel *et al.*, *Phys. Rev.* **D88**, 043502 (2013), [arXiv:1306.2314].
- [50] A. Refregier, *Ann. Rev. Astron. Astrophys.* **41**, 645 (2003), [arXiv:astro-ph/0307212]; R. Massey *et al.*, *Nature* **445**, 286 (2007), [arXiv:astro-ph/0701594]; H. Hoekstra and B. Jain, *Ann. Rev. Nucl. Part. Sci.* **58**, 99 (2008), [arXiv:0805.0139].

- [51] M. Asgari *et al.* (KiDS), *Astron. Astrophys.* **645**, A104 (2021), [arXiv:2007.15633].
- [52] C. Hikage *et al.* (HSC), *Publ. Astron. Soc. Jap.* **71**, 2, 43 (2019), [arXiv:1809.09148].
- [53] L. F. Secco *et al.* (DES) (2021), [arXiv:2105.13544].
- [54] R. G. Crittenden and N. Turok, *Phys. Rev. Lett.* **75**, 2642 (1995), [arXiv:astro-ph/9505120].
- [55] Planck Collab. 2015 Results XXI, *Astron. Astrophys.* **594**, A21 (2016), [arXiv:1502.01595].
- [56] Planck Collab. 2015 Results XXIV, *Astron. Astrophys.* **594**, A24 (2016), [arXiv:1502.01597].
- [57] A. Dekel, *Ann. Rev. Astron. Astrophys.* **32**, 371 (1994), [arXiv:astro-ph/9401022].
- [58] P. A. R. Ade *et al.* (BICEP/Keck), *Phys. Rev. Lett.* **127**, 15, 151301 (2021), [arXiv:2110.00483].
- [59] Planck Collab. 2018 Results IX, *Astron. Astrophys.* **641**, A9 (2020), [arXiv:1905.05697].

26. Neutrinos in Cosmology

Revised August 2021 by J. Lesgourgues (TTK, RWTH) and L. Verde (ICC, U. of Barcelona; ICREA, Barcelona).

26.1 Standard neutrino cosmology

Neutrinos leave detectable imprints on cosmological observations that can then be used to constrain neutrino properties. This is a great example of the remarkable interconnection and interplay between nuclear physics, particle physics, astrophysics and cosmology (for general reviews see *e.g.*, [1–4]). Present cosmological data are already providing constraints on neutrino properties not only complementary but also competitive with terrestrial experiments; for instance, upper bounds on the total neutrino mass have shrunk by a factor of about 20 in the past 19 years. Forthcoming cosmological data may soon provide key information, not obtainable in other ways like *e.g.*, a measurement of the absolute neutrino mass scale.

A relic neutrino background pervading the Universe (the Cosmic Neutrino background, $C\nu B$) is a generic prediction of the standard hot Big Bang model (see Big Bang Nucleosynthesis – Chap. 24 of this *Review*). While it has not yet been detected directly, it has been indirectly confirmed by the accurate agreement of predictions and observations of: *a*) the primordial abundance of light elements (see Big Bang Nucleosynthesis – Chap. 24 of this *Review*; *b*) the power spectrum of Cosmic Microwave Background (CMB) anisotropies (see Cosmic Microwave Background – Chap. 29 of this *Review*); and *c*) the large scale clustering of cosmological structures. Within the hot Big Bang model such good agreement would fail dramatically without a $C\nu B$ with properties matching closely those predicted by the standard neutrino decoupling process (*i.e.*, involving only weak interactions).

We will illustrate below that cosmology is sensitive to the following neutrino properties: their density, related to the number of active (*i.e.*, left-handed, see Neutrino Mass, Mixing, and Oscillations – Chap. 14 of this *Review*) neutrino species, and their masses. At first order, cosmology is sensitive to the total neutrino mass, but is blind to the mixing angles and CP violation phase as discussed in Neutrino Mass, Mixing, and Oscillations (Chap. 14 of this *Review*). This makes cosmological constraints nicely complementary to measurements from terrestrial neutrino experiments.

The minimal cosmological model, Λ CDM, currently providing a good fit to most cosmological data sets (with the exception of some data in tension, discussed in The Cosmological Parameters Chap. 25 of this *Review*), assumes that the only massless or light (subkeV) relic particles since the Big Bang Nucleosynthesis (BBN) epoch are photons and active neutrinos. Extended models with light sterile neutrinos, light thermal axions or other light relics – sometimes referred to as “dark radiation” – would produce effects similar to, and potentially degenerate with, those of active neutrinos. Thus neutrino bounds are often discussed together with limits on such scenarios. In case of anomalies in cosmological data, it might not be obvious to discriminate between interpretation in terms of active neutrinos with non-standard decoupling, additional production mechanisms, non-standard interactions, etc., or in terms of some additional light particles. Such extensions have been recently explored as a possible way to resolve the H_0 tension between late and early Universe determinations [5–8], but are not widely favoured [9–11].

Hence neutrino density and mass bounds can be derived under the assumption of no additional massless or light relic particles, and the neutrino density measured in that way provides a test of standard (*i.e.*, involving only weak interactions) neutrino decoupling.

In that model, the three active neutrino types thermalize in the early Universe, with a negligible leptonic asymmetry. Then they can be viewed as three propagating mass eigenstates sharing the same temperature and identical Fermi-Dirac distributions, thus with no visible effects of flavour oscillations. Neutrinos decouple gradually from the thermal plasma at temperatures $T \sim 2$ MeV. In the instantaneous neutrino decoupling limit, *i.e.*, assuming that neutrinos were fully decoupled at the time when electron-positrons annihilate and release entropy in the thermal bath, the neutrino-to-photon density ratio between the time of electron-positron an-

ihilation and the non-relativistic transition of neutrinos would be given by

$$\frac{\rho_\nu}{\rho_\gamma} = \frac{7}{8} N_{\text{eff}} \left(\frac{4}{11} \right)^{4/3}, \quad (26.1)$$

with $N_{\text{eff}} = 3$, and the last factor comes from the fourth power of the temperature ratio $T_\nu/T_\gamma = (4/11)^{1/3}$ (see Big Bang Cosmology – Chap. 22 in this *Review*). In the above formula, N_{eff} is called the effective number of neutrino species because it can be viewed as a convenient parametrisation of the relativistic energy density of the Universe beyond that of photons, in units of one neutrino in the instantaneous decoupling limit. Precise simulations of neutrino decoupling and electron-positron annihilation, taking into account flavor oscillations, provide precise predictions for the actual phase-space distribution of relic neutrinos [12–15]. These distributions differ from the instantaneous decoupling approximation through a combination of a small shift in the photon temperature and small non-thermal distortions, all at the percent level. The final result for the density ratio ρ_ν/ρ_γ in the relativistic regime can always be expressed as in Eq. (26.1), but with a different value of N_{eff} . The most recent analyses, that includes the effect of neutrino oscillations with the present values of the mixing parameters, an improved calculation of the collision terms and the most recent results on plasma thermodynamics QED corrections, gives $N_{\text{eff}} = 3.044$ [16, 17]. The precise number density ratio n_ν/n_γ can also be derived from such studies, and is important for computing the ratio $\Omega_\nu h^2 / \sum_i m_i$ (ratio of the physical density of neutrinos in units of the critical density to the sum of neutrino masses) in the non-relativistic regime.

The neutrino temperature today, $T_\nu^0 \simeq 1.7 \times 10^{-4}$ eV $\simeq 1.9$ K, is smaller than at least two of the neutrino masses, since the two squared-mass differences are $|\Delta m_{31}^2|^{1/2} > |\Delta m_{21}^2|^{1/2} > T_\nu^0$ (see Neutrino mass, Mixing, and oscillations – Chap. 14 of this *Review*). Thus at least two neutrino mass eigenstates are non-relativistic today and behave as a small “hot” fraction of the total dark matter (they cannot be all the dark matter, as explained in Chap. 27 in this *Review*). This fraction of hot dark matter can be probed by cosmological experiments, for two related reasons, as we now describe.

First, neutrinos are the only known particles behaving as radiation at early times (during the CMB acoustic oscillations) and dark matter at late times (during structure formation), which has consequences on the background evolution. Neutrinos become non-relativistic when their mass is equal to their average momentum, given for any Fermi-Dirac-distributed particle by $\langle p \rangle = 3.15 T$. Thus the redshift of the non-relativistic transition is given by $z_i^{\text{nr}} = m_i / (3.15 T_\nu^0) - 1 = m_i / [0.53 \text{ meV}] - 1$ for each eigenstate of mass m_i , giving for instance $z_i^{\text{nr}} = 110$ for $m_i = 60$ meV, corresponding to a time deep inside the matter-dominated regime. Second, until the non-relativistic transition, neutrinos travel at the speed of light, and later on they move at a typical velocity $\langle v_i/c \rangle = 3.15 T_\nu(z) / m_i = 0.53(1+z) \text{ meV} / m_i$, which is several orders of magnitude larger than that of the dominant cold (or even of possibly warm) dark matter component(s). This brings their characteristic diffusion scale, called the “free-streaming length”, to cosmological relevant values, with consequences on gravitational clustering and the growth of structure.

Once neutrinos are non-relativistic, their energy density is given by $\rho_\nu \simeq \sum m_i n_i$. Since the number densities n_i are equal to each other (up to negligible corrections coming from flavour effects in the decoupling phase), the total mass ($\sum m_\nu$) = $m_1 + m_2 + m_3$ can be factorized out. It is possible that the lightest neutrino is still relativistic today, in which case this relation is slightly incorrect, but given that the total density is always strongly dominated by that of non-relativistic neutrinos, the error made is completely negligible. Using the expression for n_i/n_γ obtained from precise neutrino decoupling studies, and knowing n_γ from the measurement of the CMB temperature, one can compute ρ_ν^0 , the total neutrino density today, in units of the critical density ρ_{crit}^0 [15]:

$$\Omega_\nu = \frac{\rho_\nu^0}{\rho_{\text{crit}}^0} = \frac{\sum m_\nu}{93.14 h^2 \text{ eV}}, \quad (26.2)$$

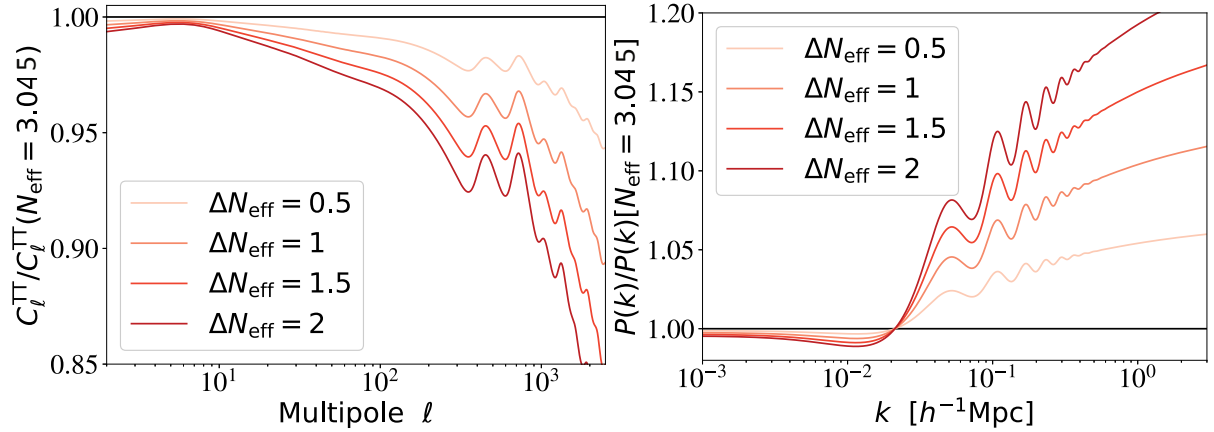


Figure 26.1: Ratio of the CMB C_ℓ^{TT} (left, including lensing effects) and matter power spectrum $P(k)$ (right, computed for each model in units of $(h^{-1}\text{Mpc})^3$) for different values of $\Delta N_{\text{eff}} \equiv N_{\text{eff}} - 3.044$ over those of a reference model with $\Delta N_{\text{eff}} = 0$. In order to minimize and better characterise the effect of N_{eff} on the CMB, the parameters that are kept fixed are $\{z_{\text{eq}}, z_\Lambda, \omega_b, \tau\}$ and the primordial spectrum parameters. Fixing $\{z_{\text{eq}}, z_\Lambda\}$ is equivalent to fixing the fractional density of total radiation, of total matter and of cosmological constant $\{\Omega_r, \Omega_m, \Omega_\Lambda\}$ while increasing the Hubble parameter as a function of N_{eff} . The statistical errors on the C_ℓ are $\sim 1\%$ for a band power of $\Delta\ell = 30$ at $\ell \sim 1000$. The error on $P(k)$ is estimated to be of the order of 5%.

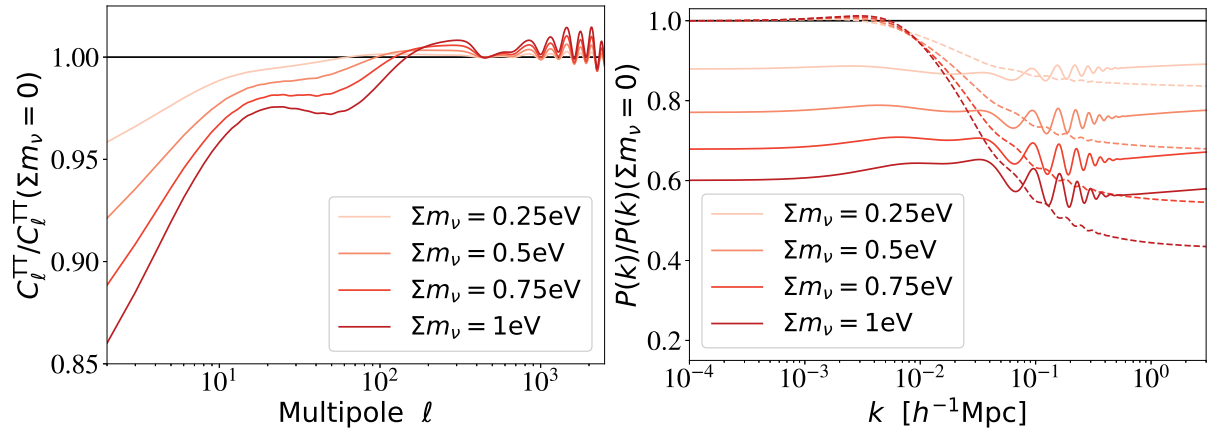


Figure 26.2: Ratio of the CMB C_ℓ^{TT} and matter power spectrum $P(k)$ (computed for each model in units of $(h^{-1}\text{Mpc})^3$) for different values of $\sum m_\nu$ over those of a reference model with massless neutrinos. In order to minimize and better characterise the effect of $\sum m_\nu$ on the CMB, the parameters that are kept fixed are ω_b, ω_c, τ , the angular scale of the sound horizon θ_s and the primordial spectrum parameters (solid lines). This implies that we are increasing the Hubble parameter h as a function of $\sum m_\nu$. For the matter power spectrum, in order to single out the effect of neutrino free-streaming on $P(k)$, the dashed lines show the spectrum ratio when $\{\omega_m, \omega_b, \Omega_\Lambda\}$ are kept fixed. For comparison, the error on $P(k)$ is of the order of 5% with current observations, and the fractional C_ℓ errors are of the order of $1/\sqrt{\ell}$ at low ℓ .

and the total neutrino average number density today: $n_\nu^0 = 339.5 \text{ cm}^{-3}$. Here h is the Hubble constant in units of $100 \text{ km s}^{-1} \text{ Mpc}^{-1}$.

26.2 Effects of neutrino properties on cosmological observables

As long as they are relativistic, *i.e.*, until some time deep inside the matter-dominated regime for neutrinos with a mass $m_i \ll 3.15 T_\nu^{\text{eq}} \sim 1.5 \text{ eV}$ (see Big Bang Cosmology, Chap. 22 in this *Review*), neutrinos enhance the density of radiation: this effect is parameterised by N_{eff} and can be discussed separately from the effect of the mass that will be described later in this section. Increasing N_{eff} impacts the observable spectra of CMB anisotropies and matter fluctuations through background and perturbation effects.

26.2.1 Effect of N_{eff} on the CMB

The background effects depend on what is kept fixed when increasing N_{eff} . If the densities of other species are kept fixed, a higher N_{eff} implies a smaller redshift of radiation-to-matter equality, with very strong effects on the CMB spectrum: when the amount of expansion between radiation-to-matter equality and

photon decoupling is larger, the CMB peaks are suppressed. This effect is not truly characteristic of the neutrino density, since it can be produced by varying several other parameters. Hence, to characterise the effect of N_{eff} , it is more useful and illuminating to enhance the density of total radiation, of total matter and of Λ by exactly the same amount, in order to keep the redshift of radiation-to-matter equality z_{eq} and matter-to- Λ equality z_Λ fixed [18–20]. The primordial spectrum parameters, the baryon density $\omega_b \equiv \Omega_b h^2$ and the optical depth to reionization τ can be kept fixed at the same time, since we can simply vary N_{eff} together with the Hubble parameter h with fixed $\{\omega_b, \Omega_c, \Omega_\Lambda\}$. The impact of such a transformation is shown in Fig. 26.1 for the CMB temperature spectrum C_ℓ^{TT} (defined in Chap. 29 in this *Review*) and for the matter power spectrum $P(k)$ (defined in Chap. 22 in this *Review*) for several representative values of N_{eff} . These effects are within the reach of cosmological observations given current error bars, as discussed in Section 26.3.1 (for instance, with the *Planck* satellite data, the statistical error on the C_ℓ 's is of the order of one per cent for a band power of $\Delta\ell = 30$ at $\ell \sim 1000$).

With this transformation, the main background effect of N_{eff}

is an increase in the diffusion scale (or Silk damping scale, see Cosmic Microwave Background – Chap. 29 in this *Review*) at the time of decoupling, responsible for the decrease in C_l^{TT} at high l , plus smaller effects coming from a slight increase in the redshift of photon decoupling [18–20]. At the level of perturbations, a higher N_{eff} implies that photons feel gravitational forces from a denser neutrino component; this tends to decrease the acoustic peaks (because neutrinos are distributed in a smoother way than photons) and to shift them to larger scales / smaller multipoles (because photon perturbations traveling at the speed of sound in the photon-baryon fluid feel some dragging effect from neutrino perturbations travelling at the speed of light) [18, 20, 21]. The effect of increasing N_{eff} on the polarization spectrum features are the same as on the temperature spectrum: an increased Silk damping, and a shift in the acoustic peak amplitude and location - the latter effect is even more clear in the polarization spectrum, in which the location of acoustic peaks does not get further influenced by a Doppler effect like for temperature. The combination of these effects is truly characteristic of the radiation density parameter N_{eff} and cannot be mimicked by other parameters; thus N_{eff} can be accurately measured from the CMB alone. However, there are correlations between N_{eff} and other parameters. In particular, we have seen (Fig. 26.1) that in order to minimise the effect of N_{eff} on the CMB spectrum, one should vary h at the same time, hence there is a correlation between N_{eff} and h , which implies that independent measurements reducing the error bar on h also reduce that on N_{eff} . Note that this correlation is not equivalent to a perfect degeneracy, so both parameters can anyway be constrained with CMB data alone.

26.2.2 Effect of N_{eff} on the matter spectrum

We have discussed the effect of increasing N_{eff} while keeping z_{eq} and ω_b fixed, because the latter two quantities are very accurately constrained by CMB data. This implies that ω_c increases with N_{eff} , and that the ratio $\omega_b/\omega_c = \Omega_b/\Omega_c$ decreases. However, the ratio of baryonic-to-dark matter has a strong impact on the shape of the matter power spectrum, because until the time of decoupling of the baryons from the photons, CDM experiences gravitational collapse, while baryons are kept smoothly distributed by photon pressure and affected by acoustic oscillations. The decrease of Ω_b/Ω_c following from the increase of N_{eff} gives more weight to the most clustered of the two components, namely the dark matter one, and produces an enhancement of the small-scale matter power spectrum and a damping of the amplitude of baryon acoustic oscillations (BAOs), clearly visible in Fig. 26.1 (right plot). The scale of BAOs is also slightly shifted by the same neutrino dragging effect as for CMB peaks [24].

The increase in the small-scale matter power spectrum is also responsible for a last effect on the CMB spectra: the CMB last scattering surface is slightly more affected by weak lensing from large-scale structures. This tends to smooth the maxima, the minima, and the damping scale of the CMB spectra [25].

26.2.3 Effect of neutrino masses on the CMB

Neutrino eigenstates with a mass $m_i \ll 0.6$ eV become non-relativistic after photon decoupling. They contribute to the non-relativistic matter budget today, but not at the time of equality or recombination. If we increase the neutrino mass while keeping fixed the density of baryons and dark matter (ω_b and ω_c), the early cosmological evolution remains fixed and independent of the neutrino mass, until the time of the non-relativistic transition. Thus one might expect that the CMB temperature and polarization power spectra are left invariant. This is not true for four reasons.

First, the neutrino density enhances the total non-relativistic density at late times, $\omega_m = \omega_b + \omega_c + \omega_\nu$, where $\omega_\nu \equiv \Omega_\nu h^2$ is given as a function of the total mass $\sum m_\nu$ by Eq. (26.2). The late background evolution impacts the CMB spectrum through the relation between scales on the last scattering surface and angles on the sky, and through the late ISW effect (see Cosmic Microwave Background – Chap. 29 of this *Review*). These two effects depend respectively on the angular diameter distance to recombination, $d_A(z_{\text{rec}})$, and on the redshift of matter-to- Λ equality. Increasing $\sum m_\nu$ tends to modify these two quantities. By playing with h

and Ω_Λ , it is possible to keep one of them fixed, but not both at the same time. Since the CMB measures the angular scale of acoustic oscillations with exquisite precision, and is only loosely sensitive to the late ISW effect due to cosmic variance, we choose in Fig. 26.2 to play with the Hubble parameter in order to maintain a fixed scale $d_A(z_{\text{rec}})$. With such a choice, an increase in neutrino mass comes together with a decrease in the late ISW effect explaining the depletion of the CMB spectrum for $l \leq 20$. The fact that both $\sum m_\nu$ and h enter the expression of $d_A(z_{\text{rec}})$ implies that measurements of the neutrino mass from CMB data are strongly correlated with h . Second, the non-relativistic transition of neutrinos affects the total pressure-to-density ratio of the Universe, and causes a small variation of the metric fluctuations. If this transition takes place not too long after photon decoupling, this variation is observable through the early ISW effect [20, 26, 27]. It is responsible for the dip seen in Fig. 26.2 for $20 \leq l \leq 200$. Third, when the neutrino mass is higher, the CMB spectrum is less affected by the weak lensing effect induced by the large-scale structure at small redshift. This is due to a decrease in the matter power spectrum described in the next paragraphs. This reduced lensing effect is responsible for most of the oscillatory patterns visible in Fig. 26.2 (left plot) for $l \geq 200$. Fourth, the neutrinos with the smallest momenta start to be non-relativistic earlier than the average ones. The photon perturbations feel this through their gravitational coupling with neutrinos. This leads to a small enhancement of C_l^{TT} for $l \geq 500$, hardly visible on Fig. 26.2 because it is balanced by the lensing effect.

26.2.4 Effect of neutrino masses on the matter spectrum

The physical effect of neutrinos on the matter power spectrum is related to their velocity dispersion. Neutrinos free-stream over large distances without falling into small potential wells. The free-streaming scale is roughly defined as the distance travel by neutrinos over a Hubble time scale $t_H = (a/\dot{a})$, and approximates the scale below which neutrinos remain very smooth. On larger scales, they cluster in the same way as cold dark matter. The power spectrum of total matter fluctuations, related to the squared fluctuation δ_m^2 with $\delta_m \equiv \delta_b + \delta_c + \delta_\nu$, gets a negligible contribution from the neutrino component on small scales, and is reduced by a factor $(1 - 2f_\nu)$, where $f_\nu = \omega_\nu/\omega_m$. Additionally, on scales below the free-streaming scale, the growth of ordinary cold dark matter and baryon fluctuations is modified by the fact that neutrinos contribute to the background density, but not to the density fluctuations. This changes the balance between the gravitational forces responsible for clustering, and the Hubble friction term slowing it down. Thus the growth rate of CDM and baryon fluctuations is reduced [28]. This results today in an additional suppression of the small-scale linear matter power spectrum by approximately $(1 - 6f_\nu)$. These two effects sum up to a factor $(1 - 8f_\nu)$ [29] (more precise approximations can be found in [2, 20]). The non-linear spectrum is even more suppressed on mildly non-linear scales [3, 30–34].

This effect is often illustrated by plots of the matter power spectrum ratio with fixed parameters $\{\omega_m, \omega_b, \Omega_\Lambda\}$ and varying f_ν , *i.e.*, with the CDM density adjusted to get a fixed total dark matter density [2, 20, 29] (see Fig. 26.2, right plot, dashed lines). This transformation does not leave the redshift of equality z_{eq} invariant, and has very large effects on the CMB spectra. If one follows the logic of minimizing CMB variations and fixing z_{eq} like in the previous paragraphs, the increase in $\sum m_\nu$ must take place together with an increase of h , which tends to suppress the large-scale power spectrum, by approximately the same amount as the neutrino free-streaming effect [35]. In that case, the impact of neutrino masses on the matter power spectrum appears as an overall amplitude suppression, which can be seen in Fig. 26.2 (right plot, solid lines). The oscillations on intermediate wavenumbers come from a small shift in the BAO scale [35]. This global effect is not degenerate with a variation of the primordial spectrum amplitude A_s , because it only affects the matter power spectrum, and not the CMB spectra. However, the amplitude of the CMB temperature and polarization spectrum is given by the combination $A_s e^{-2\tau}$. Hence a measurement of τ is necessary in order to fix A_s from CMB data, and avoid a parameter degeneracy between $\sum m_\nu$ and A_s [35–37].

Table 26.1: Summary of N_{eff} constraints.

	Model	95%CL	Ref.
CMB alone			
P118[TT,TE,EE+lowE]	$\Lambda\text{CDM}+N_{\text{eff}}$	$2.92^{+0.36}_{-0.37}$	[22]
CMB + background evolution + LSS			
P118[TT,TE,EE+lowE+lensing] + BAO	$\Lambda\text{CDM}+N_{\text{eff}}$	$2.99^{+0.34}_{-0.33}$	[22]
” + BAO + R21	$\Lambda\text{CDM}+N_{\text{eff}}$	3.34 ± 0.14 (68%CL)	[11]
”	+5-params.	2.85 ± 0.23 (68%CL)	[23]

A few of the neutrino mass effects described above –free-streaming scale, early ISW– depend on individual masses m_i , but most of them depend only on the total mass through f_ν –suppression of the matter power spectrum, CMB lensing, shift in angular diameter distance–. Because the latter effects are easier to measure, cosmology is primarily sensitive to the total mass $\sum m_\nu$ [38, 39]. The possibility that future data sets might be able to measure individual masses or the mass hierarchy, despite systematic errors and parameter degeneracies, has recently become a subject of investigation [40, 41].

26.3 Cosmological Constraints on neutrino properties

In this review we focus on cosmological constraints on the abundance and mass of ordinary active neutrinos. Several stringent but model-dependent constraints on non-standard neutrinos (*e.g.*, sterile neutrinos, active neutrinos with interactions beyond the weak force, unstable neutrinos with invisible decay, etc.) can also be found in the literature.

26.3.1 Neutrino abundance

Table 26.1 shows a list of constraints on N_{eff} obtained with several combination of data sets. ‘P118’ denotes the *Planck* 2018 data, composed of a high- ℓ temperature+polarization likelihood (TT,TE,EE), low- ℓ polarization (low E) and CMB lensing spectrum likelihood (lensing) based on lensing extraction from quadratic estimators [22]. ‘BAO’ refers to measurements of the BAO scale (and hence of the angular diameter distance) from various recent data sets, described in detail in the references given in the table. ‘R21’ refers to the distance ladder local measurement of the Hubble scale from cepheids and supernovae [42].

Within the framework of a 7-parameter cosmological model ($\Lambda\text{CDM}+N_{\text{eff}}$), the constraint on N_{eff} from the *Planck* 2018 data release [TT,TE,EE+lowE] is $N_{\text{eff}} = 2.92^{+0.36}_{-0.37}$ (95%CL). This number is perfectly compatible with the prediction of the standard neutrino decoupling model, $N_{\text{eff}} = 3.044$, and can be viewed as a proof of self-consistency of the cosmological model.

The bounds can be tightened by adding information on the low-redshift background expansion from BAOs, or local H_0 measurements. Finally, one can also add information on large scale structure (LSS), *i.e.*, on the growth rate and clustering amplitude of matter as a function of scale. However, LSS data are not very constraining for the N_{eff} parameter, and the only LSS data included in Table 26.1 is the measurement of the CMB lensing spectrum. All combinations of *Planck* 2018 data with BAO or CMB lensing constraints return measurements consistent with the standard expectation.

The situation is different with the inclusion of the low-redshift measurement of H_0 by R21 [42], known to be in tension with *Planck* in the ΛCDM framework. As explained in Section 26.2, the positive correlation between N_{eff} and h means that inclusion of the H_0 measurement pushes N_{eff} to higher values, $N_{\text{eff}} = 3.34 \pm 0.14$ (68%CL, P118[TT,TE,EE+lowE+lensing] + BAO + R21) [11], compatible with the standard expectation at the $\sim 2.1\sigma$ level. However, the N_{eff} extension to the ΛCDM model does not reduce the tension significantly enough to be an appealing solution. It remains to be seen whether the $> 4.2\sigma$ tension between CMB data and direct measurements of H_0 results from systematics, or from a departure from the ΛCDM model [11, 46–49].

The error bars on N_{eff} degrade mildly when the data are analysed in the context of more extended cosmological scenarios. Adding only the total neutrino mass as an 8th free parameter

has a negligible impact on the bounds.

The authors of Ref. [23] take a more extreme point of view and fit a 12-parameter model to P118[TT,TE,EE+lowE+lensing] data; they obtain $N_{\text{eff}} = 2.95 \pm 0.24$ (68% CL), showing that it is very difficult with current cosmological data to accommodate shifts of more than 0.5 from the standard N_{eff} value, and to obtain good fits with, for instance, a fourth (sterile) thermalized neutrino. This is interesting since the anomalies in some oscillation data could be interpreted as evidence for at least one sterile neutrino with a large mixing angle, which would need to be thermalised unless non-standard interactions come into play [5]. In other words cosmology disfavors the explanation of the oscillation anomalies in terms of extra neutrinos if they are thermalized.

26.3.2 Are they really neutrinos, as expected?

While a value of N_{eff} significantly different from zero (at more than 15σ) and consistent with the expected number 3.044 yields a powerful indirect confirmation of the $C\nu B$, departures from standard N_{eff} could be caused by any ingredient affecting the early-time expansion rate of the Universe. Extra relativistic particles (either decoupled, self-interacting, or interacting with a dark sector), a background of gravitational waves, an oscillating scalar field with quartic potential, departures from Einstein gravity, or large extra dimensions are some of the possibilities for such ingredients. In principle one could even assume that the cosmic neutrino background never existed or has decayed (like in the “neutrinoless Universe” model of [50]) while another dark radiation component is responsible for N_{eff} . At least, cosmological data allow to narrow the range of possible interpretations of $N_{\text{eff}} \simeq 3$ to the presence of decoupled relativistic relics like standard neutrinos. Indeed, free-streaming particles leave specific signatures in the CMB and LSS spectra, because their density and pressure perturbations, bulk velocities and anisotropic stress also source the metric perturbations. These signatures can be tested in several ways.

A first approach consists of introducing a self-interaction term in the neutrino equations [6, 7]. Ref. [8] finds that current CMB and BAO data are compatible with no self-interactions. The upper limit to the effective coupling constant G_{eff} for a Fermi-like four-fermions interaction at 95% confidence is $\log_{10}(G_{\text{eff}}\text{MeV}^2) < -0.8$ for P115+BAO. Note however that neutrino self-interactions as strong as $\log_{10}(G_{\text{eff}}\text{MeV}^2) \simeq -1.4$ could reconcile CMB temperature and BAO data with the direct H_0 measurement of Ref [42], but such interactions seem to be hardly compatible with BBN, laboratory constraints [10] and CMB polarization [9, 11].

A second approach consists of introducing two phenomenological parameters, c_{eff} and c_{vis} (see *e.g.*, [51–53]): c_{eff}^2 generalizes the linear relation between isotropic pressure perturbations and density perturbations, while c_{vis}^2 modifies the neutrino anisotropic stress equation. While relativistic free-streaming species have $(c_{\text{eff}}^2, c_{\text{vis}}^2) = (1/3, 1/3)$, a perfect relativistic fluid would have $(c_{\text{eff}}^2, c_{\text{vis}}^2) = (1/3, 0)$. Other values do not necessarily refer to a concrete model, but make it possible to interpolate between these limits. *Planck* data strongly suggests $(c_{\text{eff}}^2, c_{\text{vis}}^2) = (1/3, 1/3)$ [54, 55].

Finally, Ref. [21] (resp. [24]) shows that current data are precise enough to detect the “neutrino drag” effect mentioned in Sec. 26.2 through the measurement of the CMB peak (resp. BAO) scale. These findings show that current cosmological data are able to detect not just the average density of some relativistic relics, but also their anisotropies.

Table 26.2: Summary of $\sum m_\nu$ constraints.

	Model	95% CL (eV)	Ref.
CMB alone			
P18[TT+lowE]	Λ CDM+ $\sum m_\nu$	< 0.54	[22]
P18[TT,TE,EE+lowE]	Λ CDM+ $\sum m_\nu$	< 0.26	[22]
CMB + probes of background evolution			
P18[TT+lowE] + BAO	Λ CDM+ $\sum m_\nu$	< 0.13	[43]
P18[TT,TE,EE+lowE]+BAO	Λ CDM+ $\sum m_\nu$ +5 params.	< 0.515	[23]
CMB + LSS			
P18[TT+lowE+lensing]	Λ CDM+ $\sum m_\nu$	< 0.44	[22]
P18[TT,TE,EE+lowE+lensing]	Λ CDM+ $\sum m_\nu$	< 0.24	[22]
CMB + probes of background evolution + LSS			
P18[TT,TE,EE+lowE] + BAO + RSD	Λ CDM+ $\sum m_\nu$	< 0.10	[43]
P18[TT+lowE+lensing] + BAO + Lyman- α	Λ CDM+ $\sum m_\nu$	< 0.087	[44]
P18[TT,TE,EE+lowE] + BAO + RSD + Pantheon + DES	Λ CDM+ $\sum m_\nu$	< 0.13	[45]

26.3.3 Neutrino masses

Table 26.2 shows a list of constraints on $\sum m_\nu$ obtained with several combinations of data sets. The acronyms ‘‘P18’’ and ‘‘BAO’’ have been described in the previous subsection, while ‘‘Pantheon’’ refers to the supernovae Type Ia compilation of [56], ‘‘RSD’’ to Redshift Space Distorsions in the eBOSS galaxy survey [43], and ‘‘Lyman- α ’’ to the one-dimensional flux power spectrum of eBOSS quasars [44].

Given that most determinations of N_{eff} are compatible with the standard prediction, $N_{\text{eff}} = 3.044$, it is reasonable to adopt this value as a theoretical prior and to investigate neutrino mass constraints in the context of a minimal 7-parameter model, Λ CDM+ $\sum m_\nu$. Under this assumption, the most robust constraints come from *Planck* 2018 temperature and polarization data alone: $\sum m_\nu < 0.26$ eV (95%CL) [22]. Among the four effects of neutrino masses on the CMB spectra described before, current bounds are dominated by the first and the third effects (modified late background evolution, and distortions of the temperature and polarization spectra through weak lensing).

Adding measurements of the BAO scale is crucial, since the determination of the angular diameter distance at small redshift allows us to break parameter degeneracies, for instance between $\sum m_\nu$ and h . The combination of P18[TT,TE,EE+lowE] with the most recent BAO measurements, including the eBOSS Data Release 16 (DR16), gives $\sum m_\nu < 0.13$ eV (95%CL) [43]. Supernovae data are less constraining than BAO data for the neutrino mass determination.

Because the parameter correlation between $\sum m_\nu$ and H_0 is negative, the inclusion of distance ladder data provides stronger bounds on neutrinos masses, down to $\sum m_\nu < 0.097$ eV (95% CL) when including P18[TT,TE,EE+lowE]+R18 [22], where R18 refers to the 2018 estimate of the Hubble rate by [57]. However, such bounds are subject to caution, since they come from a combination of discrepant data sets (at the $> 3\sigma$ level).

It is interesting to add LSS data sets, sensitive to the small-scale suppression of the matter power spectrum due to neutrino free-streaming. Some conservative LSS information comes from the eBOSS survey, which infers the growth rate of structures from Redshift Space Distorsions (RSD) and tightens the bound down to $\sum m_\nu < 0.10$ eV (95%CL) [43]. This already challenges the inverted hierarchy mass scheme, which predicts $\sum m_\nu \geq 0.11$ eV. The inclusion of CMB lensing data from *Planck* 18 improves the CMB-only bound, but hardly affects the latest joint CMB+BAO+RSD bounds [58]. The most recent Ly α forest data from eBOSS combined with P18[TT,TE,EE+lowE+lensing] and BAO data provides the strongest bound to date, $\sum m_\nu < 0.087$ eV (95% CL). It should however be noticed that the full DES 3-year data prefer a lower σ_8 value than the *Planck* best fit, relaxing the bound to $\sum m_\nu < 0.13$ eV (95%CL, P18[TT,TE,EE+lowE+lensing]+BAO+RSD+Pantheon+DES) [45].

Upper bounds on neutrino masses become weaker when the data are analysed in the context of extended cosmological models, but only by a small amount. Floating N_{eff} instead of fixing it to 3.044 has no significant impact on the neutrino mass bounds reported

in the previous paragraphs. Even in the extreme case considered by Ref. [23], with 12 free cosmological parameters, one can see in Table 26.2 that the bound from *Planck* 2018 (without lensing) + BAO increases from 0.13 eV to 0.52 eV (95% CL) only. This shows that current cosmological data are precise enough to disentangle the effect of several extended cosmological parameters, and that neutrino mass bounds are becoming increasingly robust.

26.4 Future prospects and outlook

The cosmic neutrino background has been detected indirectly at very high statistical significance. Direct detection experiments are now being planned, *e.g.*, at the Princeton Tritium Observatory for Light, Early Universe, Massive-neutrino Yield (PTOLEMY) [59]. The detection prospects crucially depend on the exact value of neutrino masses and on the enhancement of their density at the location of the Earth through gravitational clustering in the Milky Way and its sub-halos – an effect however expected to be small [60–62].

Over the past few years the upper limit on the sum of neutrino masses has become increasingly stringent, first indicating that the mass ordering is hierarchical and recently putting the inverted hierarchy under pressure and favouring the normal hierarchy (although quantitative estimates of how disfavoured the inverted hierarchy is vary depending on assumptions, see *e.g.* [63–65]) which has consequences for planning future double beta decay experiments.

Neutrino mass and density bounds are expected to keep improving significantly over the next years, thanks to new LSS experiments like DESI [66], Euclid [67], LSST [68], SPHEREx [69] and SKA [70], in combinations with new CMB experiments like Simons Observatory [71], CMB-S4 [72] or LiteBird [73]. If the Λ CDM model is confirmed, and if neutrinos have standard properties, the total neutrino mass should be detected at the level of at least 3–4 σ even at the minimum level allowed by oscillations. This is the conclusion reached by several independent studies, using different dataset combinations (see *e.g.*, [37, 74–79]). One should note that at the minimum level allowed by oscillations $\sum m_\nu \sim 0.06$, neutrinos constitute $\sim 0.5\%$ of the Universe matter density, and their effects on the matter power spectrum is only at the 5% level, implying that exquisite control of systematic errors will be crucial to achieve the required accuracy. At this level, the information coming from the power spectrum shape is more powerful than that coming from geometrical measurements (*e.g.*, BAO). But exploiting the shape information requires improved understanding of the non-linear regime, and of galaxy bias for galaxy surveys. The fact that different surveys and different data set combinations have enough statistical power to reach this level, offers a much needed redundancy and the possibility to perform consistency checks which in turns helps immensely with the control of systematic errors and in making the measurement robust. Using the entire Universe as a particle detector, the on-going and future observational efforts hold the exciting prospect to provide a measurement of the sum of neutrino masses and possibly indication of their mass hierarchy.

References

- [1] A. D. Dolgov, Phys. Rept. **370**, 333 (2002), [hep-ph/0202122].
- [2] J. Lesgourgues and S. Pastor, Phys. Rept. **429**, 307 (2006), [arXiv:astro-ph/0603494].
- [3] S. Hannestad, Prog. Part. Nucl. Phys. **65**, 185 (2010), [arXiv:1007.0658].
- [4] J. Lesgourgues *et al.*, *Neutrino Cosmology*, Cambridge University Press (2013), ISBN 978-1-108-70501-1, 978-1-139-60341-6.
- [5] M. Archidiacono *et al.*, JCAP **1608**, 08, 067 (2016), [arXiv:1606.07673].
- [6] L. Lancaster *et al.*, JCAP **1707**, 07, 033 (2017), [arXiv:1704.06657].
- [7] I. M. Oldengott *et al.*, JCAP **1711**, 11, 027 (2017), [arXiv:1706.02123].
- [8] M. Park *et al.*, Phys. Rev. D **100**, 6, 063524 (2019), [arXiv:1904.02625].
- [9] C. D. Kreisch, F.-Y. Cyr-Racine and O. Doré, Phys. Rev. D **101**, 12, 123505 (2020), [arXiv:1902.00534].
- [10] N. Blinov *et al.*, Phys. Rev. Lett. **123**, 19, 191102 (2019), [arXiv:1905.02727].
- [11] N. Schöneberg *et al.* (2021), [arXiv:2107.10291].
- [12] J. Birrell, C.-T. Yang and J. Rafelski, Nucl. Phys. **B890**, 481 (2014), [arXiv:1406.1759].
- [13] G. Mangano *et al.*, Nucl. Phys. **B729**, 221 (2005), [hep-ph/0506164].
- [14] E. Grohs *et al.*, Phys. Rev. **D93**, 8, 083522 (2016), [arXiv:1512.02205].
- [15] P. F. de Salas and S. Pastor, JCAP **1607**, 07, 051 (2016), [arXiv:1606.06986].
- [16] J. Froustey, C. Pitrou and M. C. Volpe, JCAP **12**, 015 (2020), [arXiv:2008.01074].
- [17] J. J. Bennett *et al.*, JCAP **04**, 073 (2021), [arXiv:2012.02726].
- [18] S. Bashinsky and U. Seljak, Phys. Rev. **D69**, 083002 (2004), [arXiv:astro-ph/0310198].
- [19] Z. Hou *et al.*, Phys. Rev. **D87**, 083008 (2013), [arXiv:1104.2333].
- [20] J. Lesgourgues *et al.*, *Neutrino cosmology* (Cambridge University Press, 2013).
- [21] B. Follin *et al.*, Phys. Rev. Lett. **115**, 9, 091301 (2015), [arXiv:1503.07863].
- [22] N. Aghanim *et al.* (Planck) (2018), [arXiv:1807.06209].
- [23] E. Di Valentino, A. Melchiorri and J. Silk, JCAP **01**, 013 (2020), [arXiv:1908.01391].
- [24] D. Baumann *et al.*, Nature Phys. **15**, 465 (2019), [arXiv:1803.10741].
- [25] A. Lewis and A. Challinor, Phys. Rept. **429**, 1 (2006), [arXiv:astro-ph/0601594].
- [26] J. Lesgourgues and S. Pastor, Adv. High Energy Phys. **2012**, 608515 (2012), [arXiv:1212.6154].
- [27] Z. Hou *et al.*, Astrophys. J. **782**, 74 (2014), [arXiv:1212.6267].
- [28] J. R. Bond, G. Efstathiou and J. Silk, Phys. Rev. Lett. **45**, 1980 (1980), [61(1980)].
- [29] W. Hu, D. J. Eisenstein and M. Tegmark, Phys. Rev. Lett. **80**, 5255 (1998), [arXiv:astro-ph/9712057].
- [30] S. Bird, M. Viel and M. G. Haehnelt, Mon. Not. Roy. Astron. Soc. **420**, 2551 (2012), [arXiv:1109.4416].
- [31] C. Wagner, L. Verde and R. Jimenez, Astrophys. J. **752**, L31 (2012), [arXiv:1203.5342].
- [32] C. J. Todero Peixoto, V. de Souza and P. L. Biermann, JCAP **1507**, 07, 042 (2015), [arXiv:1502.00305].
- [33] J. Brandbyge and S. Hannestad, JCAP **1710**, 10, 015 (2017), [arXiv:1706.00025].
- [34] J. Adamek, R. Durrer and M. Kunz, JCAP **1711**, 11, 004 (2017), [arXiv:1707.06938].
- [35] M. Archidiacono *et al.*, JCAP **1702**, 02, 052 (2017), [arXiv:1610.09852].
- [36] A. Liu *et al.*, Phys. Rev. **D93**, 4, 043013 (2016), [arXiv:1509.08463].
- [37] R. Allison *et al.*, Phys. Rev. **D92**, 12, 123535 (2015), [arXiv:1509.07471].
- [38] J. Lesgourgues, S. Pastor and L. Perotto, Phys. Rev. **D70**, 045016 (2004), [hep-ph/0403296].
- [39] A. Slosar, Phys. Rev. **D73**, 123501 (2006), [arXiv:astro-ph/0602133].
- [40] R. Jimenez *et al.*, JCAP **1005**, 035 (2010), [arXiv:1003.5918].
- [41] R. Jimenez, C. P. Garay and L. Verde, Phys. Dark Univ. **15**, 31 (2017), [arXiv:1602.08430].
- [42] A. G. Riess *et al.*, Astrophys. J. Lett. **908**, 1, L6 (2021), [arXiv:2012.08534].
- [43] S. Alam *et al.* (eBOSS), Phys. Rev. D **103**, 8, 083533 (2021), [arXiv:2007.08991].
- [44] N. Palanque-Delabrouille *et al.*, JCAP **04**, 038 (2020), [arXiv:1911.09073].
- [45] T. M. C. Abbott *et al.* (DES) (2021), [arXiv:2105.13549].
- [46] J. L. Bernal, L. Verde and A. G. Riess, JCAP **1610**, 10, 019 (2016), [arXiv:1607.05617].
- [47] L. Verde, T. Treu and A. G. Riess, Nature Astron. **3**, 891 (2019), [arXiv:1907.10625].
- [48] J. L. Bernal *et al.*, Phys. Rev. D **103**, 10, 103533 (2021), [arXiv:2102.05066].
- [49] E. Di Valentino *et al.*, Class. Quant. Grav. **38**, 15, 153001 (2021), [arXiv:2103.01183].
- [50] J. F. Beacom, N. F. Bell and S. Dodelson, Phys. Rev. Lett. **93**, 121302 (2004), [arXiv:astro-ph/0404585].
- [51] W. Hu, Astrophys. J. **506**, 485 (1998), [arXiv:astro-ph/9801234].
- [52] W. Hu *et al.*, Phys. Rev. **D59**, 023512 (1999), [arXiv:astro-ph/9806362].
- [53] M. Gerbino, E. Di Valentino and N. Said, Phys. Rev. **D88**, 6, 063538 (2013), [arXiv:1304.7400].
- [54] B. Audren *et al.*, JCAP **1503**, 036 (2015), [arXiv:1412.5948].
- [55] P. A. R. Ade *et al.* (Planck), Astron. Astrophys. **594**, A13 (2016), [arXiv:1502.01589].
- [56] D. M. Scolnic *et al.*, Astrophys. J. **859**, 2, 101 (2018), [arXiv:1710.00845].
- [57] A. G. Riess *et al.*, Astrophys. J. **855**, 2, 136 (2018), [arXiv:1801.01120].
- [58] E. Di Valentino, S. Gariazzo and O. Mena (2021), [arXiv:2106.15267].
- [59] S. Betts *et al.*, in “Proceedings, 2013 Community Summer Study on the Future of U.S. Particle Physics: Snowmass on the Mississippi (CSS2013): Minneapolis, MN, USA, July 29-August 6, 2013,” (2013), [arXiv:1307.4738], URL <http://www.slac.stanford.edu/econf/C1307292/docs/submittedArxivFiles/1307.4738.pdf>.
- [60] A. Ringwald and Y. Y. Y. Wong, JCAP **0412**, 005 (2004), [hep-ph/0408241].
- [61] F. Villaescusa-Navarro *et al.*, JCAP **1303**, 019 (2013), [arXiv:1212.4855].
- [62] P. F. de Salas *et al.*, JCAP **1709**, 09, 034 (2017), [arXiv:1706.09850].
- [63] F. Simpson *et al.*, JCAP **1706**, 06, 029 (2017), [arXiv:1703.03425].

- [64] S. Hannestad and T. Schwetz, *JCAP* **1611**, 11, 035 (2016), [arXiv:1606.04691].
- [65] S. Roy Choudhury and S. Hannestad (2019), [arXiv:1907.12598].
- [66] A. Aghamousa *et al.* (DESI) (2016), [arXiv:1611.00036].
- [67] R. Laureijs *et al.* (EUCLID) (2011), [arXiv:1110.3193].
- [68] Paul A. Abell *et al.*, LSST Science and LSST Project Collaborations, <http://lss.fnal.gov/archive/test-tm/2000/fermilab-tm-2495-a.pdf> (2009) arXiv:0912.0201.
- [69] J. Bock and SPHEREx Science Team, in “American Astronomical Society Meeting Abstracts #231,” volume 231 of *American Astronomical Society Meeting Abstracts*, 354.21 (2018).
- [70] <http://www.skatelescope.org>.
- [71] P. Ade *et al.* (Simons Observatory), *JCAP* **02**, 056 (2019), [arXiv:1808.07445].
- [72] K. N. Abazajian *et al.* (CMB-S4) (2016), [arXiv:1610.02743].
- [73] M. Hazumi *et al.*, *J. Low Temp. Phys.* **194**, 5-6, 443 (2019).
- [74] C. Carbone *et al.*, *JCAP* **1103**, 030 (2011), [arXiv:1012.2868].
- [75] J. Hamann, S. Hannestad and Y. Y. Y. Wong, *JCAP* **1211**, 052 (2012), [arXiv:1209.1043].
- [76] B. Audren *et al.*, *JCAP* **1301**, 026 (2013), [arXiv:1210.2194].
- [77] R. Pearson and O. Zahn, *Phys. Rev.* **D89**, 4, 043516 (2014), [arXiv:1311.0905].
- [78] F. Villaescusa-Navarro, P. Bull and M. Viel, *Astrophys. J.* **814**, 2, 146 (2015), [arXiv:1507.05102].
- [79] T. Brinckmann *et al.*, *JCAP* **1901**, 059 (2019), [arXiv:1808.05955].

27. Dark Matter

Revised August 2021 by L. Baudis (Zurich U.) and S. Profumo (UC Santa Cruz).

27.1 The case for dark matter

Modern cosmological models invariably include an electromagnetically close-to-neutral, non-baryonic matter species with negligible velocity from the standpoint of structure formation, generically referred to as “cold dark matter” (CDM; see The Big-Bang Cosmology—Sec. 22 of this *Review*). For the benchmark Λ CDM cosmology adopted in the Cosmological Parameters—Sec. 25 of this *Review*, the DM accounts for 26.4% of the critical density in the universe, or 84.4% of the total matter density. The nature of only a small fraction, between at least 0.5% (given neutrino oscillations) and at most 1.6% (from combined cosmological constraints), of the non-baryonic matter content of the universe is known: the three Standard Model neutrinos (see the Neutrino Masses, Mixing, and Oscillations—Sec. 14 of this *Review*). The fundamental makeup of the large majority of the DM is, as of yet, unknown.

Assuming the validity of General Relativity, DM is observed to be ubiquitous in gravitationally collapsed structures of size ranging from the smallest known galaxies [1] to galaxies of size comparable to the Milky Way [2], to groups and clusters of galaxies [3]. The mass-to-light ratio is observed to saturate at the largest collapsed scales to a value indicative, and close to, what inferred from other cosmological observations for the universe as a whole [4]. In such collapsed structures, the existence of DM is inferred directly using tracers of mass enclosed within a certain radius such as stellar velocity dispersion, rotation curves in axisymmetric systems, the virial theorem, gravitational lensing, and measures of the amount of non-dark, i.e. baryonic, mass such as stellar number counts and tracers of gas density such as X-ray emission [5]. The global DM abundance as determined from cosmological probes is discussed in Sec. 22.

The picture of structure formation in modern cosmology heavily relies on, and can be considered an independent and exceptionally strong motivation for, DM. Baryonic density fluctuations at CMB decoupling are observed to be at most on the order of $\delta\rho_b/\rho_b|_{\text{rec}} \approx 10^{-5}$; since density perturbations grow linearly with the scale factor in the linear regime, absent any other matter fluid, one would predict that

$$\delta\rho_b/\rho_b|_{\text{today}} \approx \frac{\delta\rho_b/\rho_b|_{\text{rec}}}{a_{\text{rec}}} \approx 10^{-2}, \quad (27.1)$$

at odds with the observed highly non-linear structures in the universe, $\delta\rho_b/\rho_b|_{\text{obs}} \gg 1$. The presence of a dominant non-relativistic (“cold”) pressure-less matter component decoupled from the thermal bath well before recombination allows instead for the prediction of a matter power spectrum in remarkable agreement with observations [6].

Assuming deviations of gravitational interactions on large scales from general relativity or from its Newtonian limit, certain effects, attributed in the standard scenario to DM, can be explained by modified gravity [7]. Usually such theories mimic the effects otherwise attributed to DM on a limited range of scales, but fail globally, and especially at the largest scales. Key issues that at present appear highly problematic in the framework of theories of modified gravity without DM include (i) predicting the correct spectrum of density perturbations, (ii) predicting the observed anisotropy power spectrum of the CMB, and (iii) explaining weak lensing and X-ray observations of merging clusters such as 1E 0657-558 (the “Bullet” cluster) [8]. The inferred relative speed of gravitational and electromagnetic radiation in GW170817 additionally excludes a significant swath of modified theories of gravity where the two speeds (of gravitational and electromagnetic waves) differ [9].

27.2 Properties of dark matter candidates

Electric charge: The “darkness” of DM can be quantified based on constraints from the CMB and large-scale structure: if the DM is charged, or “milli-charged” (for instance via a kinetic mixing with a dark photon field, producing an effective

suppressed coupling to the visible photon field), it might impact the baryon-photon plasma during recombination; in turn, DM density fluctuations can be suppressed by radiation pressure and photon diffusion, additionally altering the baryon acoustic peak structure. [10] finds that the most stringent constraints stem from the requirement that the DM be completely decoupled from the baryon-photon plasma at recombination, yielding a maximal “milli-electric” charge, in units of the electron charge, of $3.5 \times 10^{-7} (m_{\text{DM}}/1 \text{ GeV})^{0.58}$ for $m_{\text{DM}} > 1 \text{ GeV}$, and of $4.0 \times 10^{-7} (m_{\text{DM}}/1 \text{ GeV})^{0.35}$ for $m_{\text{DM}} < 1 \text{ GeV}$. Limits also exist from structure formation on how optically dark and dissipationless the DM should be.

Self-interactions: Observations of merging clusters [8] and of the ellipticity of certain galaxies as inferred from X-rays [11] constrain the level of DM-DM self interactions. The figure of merit is the ratio of the DM-DM cross section and the DM mass [12] (see Ref. [13] for a review), $\sigma_{\text{DM-DM}}/m_{\text{DM}} < 0.47 \text{ cm}^2/\text{g} \approx 0.84 \text{ barn}/\text{GeV}$ at 95% C.L.. Assuming a velocity dependence in $\sigma_{\text{DM-DM}}$, “self-interacting DM” has been advocated as a possible solution to certain possible small-scale structure issues in the standard non-collisional ($\sigma_{\text{DM-DM}} \approx 0$) setup [13, 14] (see Sec. 27.4).

Mass: Lower Limits: Model-independent lower limits for very small DM masses are due to quantum effects: for fermionic DM particles, the phase-space density $f(\vec{x}, \vec{p})$ is bounded from above due to Pauli’s exclusion principle, $f < gh^{-3}$, with g the number of internal degrees of freedom and h Planck’s constant; observations of the velocity dispersion (or, equivalently, measures of the enclosed mass) and physical density in dwarf galaxies, lead to a lower limit on fermionic DM masses, sometimes known as the Tremaine-Gunn limit [15]. Using the Fornax dwarf, Ref. [16] finds $m_F > 70 \text{ eV}$. More stringent limits can be drawn from Lyman- α observations, although such limits depend on the thermal history of the DM. In the case of bosonic DM, the Compton wavelength of an ultra-light species might erase small-scale structure, in conflict with CMB and large-scale structure [17], Lyman- α observations [18, 19], and measurements of high-redshift galaxy luminosity functions and the Milky Way satellite luminosity function [20–22]: these observations indicate that $m_B \gtrsim 10^{-22} \text{ eV}$.

Mass: Upper Limits: General upper limits exist on the mass of the DM constituent from the stability against tidal disruption of structures immersed in DM halos, such as galactic disks and globular clusters, and of individual small galaxies. The most stringent limits can be derived using wide halo binaries [23] and the stability of the star cluster within Eridanus II [24]. Such limits constrain an individual, point-like DM constituent, assuming it makes up 100% of the DM, to be lighter than around $5 M_{\odot}$. (Notice that the mass limits discussed here do not assume any specific production mechanism, and do not depend on the observed cosmological DM density).

Stability: The DM lifetime must be long compared to cosmological timescales [25].

27.3 Genesis of dark matter

The generation of DM in the early universe can proceed via thermal or non-thermal production, or both, or it may result from a particle-antiparticle asymmetry.

Freeze-out: The process of chemical decoupling from the high-temperature, high-density thermal bath (freeze-out) as a paradigm for particle production in the early universe is both a predictive and a successful one. The possibility that just like light elements, neutrinos, and CMB photons, particle DM also originated from a thermal decoupling process has thus garnered significant attention.

A particle species *chemically* decouples when the rate Γ for the species’ number-changing processes drops below the Hubble rate H . Rough estimates for the abundance of relics can be obtained by (i) calculating the freeze-out (i.e. “decoupling”) temperature $T_{\text{f.o.}}$, corresponding to $H(T_{\text{f.o.}}) \sim \Gamma(T_{\text{f.o.}})$, (ii) equating the comoving number density at freeze-out and today, eventually (iii) obtaining the physical density of relic particles today. This procedure assumes that entropy is conserved between $T_{\text{f.o.}}$ and today, an assumption that could well be violated, especially for

heavy relics that decouple early, for instance by entropy injection episodes [26]. Notice also that the freeze-out calculation strongly depends on the assumed background cosmology, and changes e.g. if the early universe is not radiation-dominated around DM decoupling.

The calculation of the freeze-out relic abundance hinges on a Boltzmann equation relating the Liouville operator to the collision operator acting on the phase space density. Under a variety of simplifying assumptions including homogeneity and isotropy, it is possible to reduce the relevant equation for the number density n of a single species pair-annihilating with particles in the thermal bath via 2-to-2 processes to

$$\frac{dn}{dt} - 3Hn = -\langle\sigma v\rangle (n^2 - n_{\text{eq}}^2), \quad (27.2)$$

where $\langle\sigma v\rangle$ is the thermally-averaged pair-annihilation cross section times relative velocity (see Ref. [27]), and n_{eq} is the equilibrium number density. Relics for which the freeze-out temperature is much larger than the particle mass (and thus that freeze-out as ultra-relativistic) are called *hot* relics; if the opposite is true, the relic is instead considered *cold*.

A straightforward calculation shows that to leading order the frozen-out density of *hot* relics is *linearly proportional to the relic particle mass*. The comoving number density $Y = n/s$, where s is the entropy density, for a hot relic is approximately given by its equilibrium value,

$$Y_{\text{f.o.}} \simeq Y_{\text{eq}} \simeq 0.278 \frac{g_{\text{eff}}}{g_{*s}}, \quad (27.3)$$

where g_{eff} is the relic's effective number of degrees of freedom, and g_{*s} is the number of entropic relativistic degrees of freedom, both calculated at $T_{\text{f.o.}}$. The resulting relic abundance, assuming an iso-entropic expansion, is

$$\Omega_{\text{hot}} h^2 = \frac{m Y_{\text{f.o.}} s_0 h^2}{\rho_c} \simeq \frac{m}{93 \text{ eV}}, \quad (27.4)$$

with s_0 the entropy density today, and with the latter equality holding for the case of SM neutrinos, with a freeze-out temperature around 1 MeV (which enters in the final relic abundance through the degrees of freedom dependence on the right-hand-side of Eq. (27.3)).

For *cold* relics, the leading-order dependence of the relic abundance on the DM particle properties is an *inverse proportionality relation to the pair-annihilation cross section*,

$$\Omega_{\text{cold}} h^2 \simeq 0.1 \left(\frac{x_{\text{f.o.}}}{20} \right) \left(\frac{10^{-8} \text{ GeV}^{-2}}{\sigma_{DM+DM \leftrightarrow \text{anything}}} \right), \quad (27.5)$$

where $x \equiv m_{\text{DM}}/T$. In turn, the freeze-out temperature is approximately given by the solution to the equation

$$\sqrt{x} \cdot e^{-x} = \left(m_{\text{DM}} \cdot M_P \cdot \sigma_{DM+DM \leftrightarrow \text{anything}} \right)^{-1}, \quad (27.6)$$

where $M_P \simeq 2.435 \times 10^{18}$ GeV is the reduced Planck mass. As a result, $T_{\text{f.o.}} \simeq m_{\text{DM}}/x_{\text{f.o.}}$, with $x_{\text{f.o.}}$ a number between 10 and 50, depending on the cross section, with only a logarithmic dependence on the DM mass. Since for electroweak-scale cross sections and masses $\sigma_{DM+DM} \simeq 10^{-8} \text{ GeV}^{-2}$, “weakly-interacting massive particles”, or WIMPs have gained exceptional popularity. Notice that Eq. (27.5) bears, however, no connection to the weak scale [28], despite the relation being known as “WIMP miracle”.

Numerous scenarios exist, including notably supersymmetry [29,30] and models with universal extra dimensions [31,32] where the relic abundance of the DM is controlled by processes involving a slightly heavier, unstable, co-annihilating species [33]. In this case the calculation of the abundance of the stable species proceeds similarly to what outlined above, with an effective pair-annihilation cross section that captures the effects of co-annihilation replacing the pair-annihilation cross section [30].

Freeze-in: Collisional processes can lead to the production of out-of-equilibrium particles that progressively accumulate over cosmic time, a process sometimes called *freeze-in*. The abundance

of the frozen-in particles produced at a given redshift depends on the product of the production rate times the Hubble time at that redshift. Freeze-in generally implies that the lightest observable-sector particles decay to the DM with relatively long lifetimes, giving peculiar signals at colliders (see e.g. [34]). Gravitinos are an example of DM candidates possibly produced via a freeze-in type scenario, albeit the portal coupling is in that case via a higher dimensional, Planck-suppressed operator [35].

Cannibalization and other dark-sector number-changing processes: Thermal processes can drive the abundance of the DM beyond simple 2-to-2 number-changing interactions. For instance, DM can “cannibalize” [36,37] itself if $n \rightarrow 2$ processes exist. In this case, a critical aspect is whether or not the DM sector is in thermal contact with the Standard Model thermal bath. If it is, $n \rightarrow 2$ processes can drive the relic abundance, e.g. in the Strongly Interacting Massive Particles (SIMP) scenario [38]. Models exist where the *kinetic decoupling* (i.e. the decoupling from the *thermal equilibrium velocity distribution*) of the two sectors drives the abundance of the DM (elastically decoupling relics, or ELDERS [39]). When the two sectors are not in thermal contact, $n \rightarrow 2$ processes heat the DM sector dramatically, rapidly affecting the temperature ratio between the visible and dark sectors [36,38]. If the relevant cross sections are large enough, and the DM mass light enough, significant effects can arise in structure formation [36].

Non-thermal production: DM production can proceed via processes out of thermal equilibrium (“non-thermal” production). These include DM production via the decay of a “mother” particle [40,41] (or of topological defects [42], moduli [43] etc.) to the DM, or production via gravitational effects.

Asymmetric DM: An enticing alternative possibility for DM production is that of *asymmetric* DM [44,45]: the relic DM abundance arises from an asymmetry between anti-DM and DM. This asymmetry may or may not be related to the baryon-antibaryon asymmetry. If it is, then depending on the model and its thermal history, a relation exists between the mass of the DM and the proton mass. A variety of proposals have been put forward where alternately baryogenesis is explained from a DM sector asymmetry, or vice-versa (see e.g. Ref. [46] for a review).

Primordial Black Holes production: A qualitatively stand-alone class of DM candidates, primordial black holes (PBHs), arises from entirely different mechanisms from what reviewed above. PBHs are thought to originate from gravitational collapse of large density fluctuations in the early universe [47,48]. The over-densities could be produced in a variety of ways, such as topological defects like cosmic strings, necklaces or domain walls, curvature fluctuations from a period of ultra-slow-roll, a sound speed “resonance”, an early phase of matter domination, or sub-horizon phenomena including a phase transition and pre-heating. Albeit the calculation depends on the details of gravitational collapse, the formation time is connected to the PBH mass via $M = \gamma M_{\text{PBH}} \simeq 2 \times 10^5 \gamma \left(\frac{t}{1 \text{ s}} \right) M_{\odot}$, with $\gamma \simeq (1/\sqrt{3})^3$ during radiation domination [49].

27.4 Density and velocity distribution of dark matter

27.4.1 Local density and velocity distribution

The density and distribution of DM in the Milky Way encipher relevant dynamical information about our Galaxy, and are particularly important for direct and indirect detection experiments. The *local density* (ρ_0) is an average over a volume of a few hundred parsecs in the Solar neighbourhood.

To determine the local density from observations, two classes of methods are used [50]. So-called *local measures* rely on the vertical motion of tracer stars in the vicinity of the Sun, while *global measures* extrapolate ρ_0 from the measured rotation curve, with additional assumptions about the Galactic halo shape. Conversely, by comparing the extrapolated local density with the one obtained from local measures, one can constrain the local shape of the Milky Way halo. A major source of uncertainty on ρ_0 is the contribution of baryons (stars, gas, stellar remnants) to the local dynamical mass. For instance, the motion of tracer stars used in local measures is dictated by the total potential generated by

baryons and DM, and a robust baryonic census must be available to infer the additional contribution from DM. Recent determinations from global methods lie in the range $(0.2 - 0.6) \text{ GeV/cm}^3$, while new studies of the local DM density from *Gaia* satellite data yield $(0.3 - 1.5) \text{ GeV/cm}^3$, depending on the type of stars used in the study.

Other observational quantities that enter in the phase space distribution of DM, and provide constraints on mass models of the Milky Way are the local circular speed v_c and the escape velocity v_{esc} . The local circular speed is measured by various methods, roughly divided into measurements of the Sun's velocity with respect to an object assumed to be at rest with respect to the Galactic centre or direct measurements of the local radial force. These methods yield values of $v_c = (218 - 246) \text{ km/s}$. A recent estimate of the escape velocity, defined as the speed above which objects are not gravitationally bound to our galaxy, is $v_{esc} = 533^{+54}_{-41} \text{ km/s}$ [51].

The local velocity distribution of DM particles can not be measured directly at present, and is mostly derived from simulations. In general, experiments use the simplest, so-called *Standard Halo Model (SHM)* for their data analysis. It assumes an isotropic, isothermal sphere of DM particles with a density profile of $\rho(r) \propto r^{-2}$, for which the velocity distribution is Maxwellian, with a velocity dispersion $\sigma_v = v_c/\sqrt{2}$. This distribution, which formally extends to infinity, is truncated at v_{esc} [52]. Earlier high resolution, dark-matter-only simulations found velocity distributions that markedly deviated from a Maxwell-Boltzmann distribution and in addition revealed components above the dominant smooth distribution, including narrow spikes due to tidal streams. Recent hydrodynamical simulations of Milky Way-like galaxies including baryons, which have a non-negligible effect on the DM distribution in the Solar neighbourhood, find velocity distributions that are indeed close to Maxwellian, arguing that the SHM is a good approximation.

Ultimately the goal is to determine the velocity distribution from observations (for example by studying the motion of stars that share the same kinematics as the DM), and the *Gaia* satellite data offers a unique opportunity to study the various stellar populations. Recently it was revealed that the local stellar halo has two components: a quasi-spherical, weakly rotating structure with metal-poor stars, and a flattened, radially anisotropic structure of metal-rich stars, which arose due to accretion of a large $(10^{11} - 10^{12} M_\odot)$ dwarf galaxy around $(8-10) \times 10^9 \text{ y}$ ago [53]. The expectation is that the local DM halo shows a similar bimodal structure, and first velocity distributions of the two components - using the stellar populations as tracers - were inferred in [54]. In Ref. [55], an updated halo model is introduced: it includes the anisotropic structure seen in the *Gaia* data and provides an analytic expression for the velocity distribution. The value of the local DM density is updated to $(0.55 \pm 0.17) \text{ GeV/cm}^3$, where the 30% error accounts for the systematics. The circular rotation and the escape speeds are updated to $v_c = (233 \pm 3) \text{ km/s}$ and $v_{esc} = 528^{+24}_{-25} \text{ km/s}$.

27.4.2 Small-scale challenges

The ΛCDM framework is tremendously successful at explaining the observed large-scale structures of the Universe (corresponding to distances $\geq 1 \text{ Mpc}$, the typical inter-galactic distance), as well as the main properties of galaxies that form within DM haloes, see the comprehensive review in Ref. [56]. The observed large-scale structure is consistent with point-like, cold DM particles that interact purely via the gravitational force. But in the past decades, observations at scales below $\sim 1 \text{ Mpc}$, where structure formation becomes strongly nonlinear, turned out more problematic to be described within the ΛCDM model. The main *small-scale challenges* are known as: the missing satellites problem, the cusp-core problem and the too-big-to-fail problem. Initially these issues, which are not all independent of one another, arose by comparing theoretical predictions from dark-matter-only simulations to observation. While their most likely solutions are in dissipative, baryonic physics (such gas cooling, star formation, supernovae feedback), see the recent review in Ref. [57], the small-scale problems could in addition call for a modification or an extension of the ΛCDM paradigm. Most importantly, the ever increasing amount

of data on the satellites of the MW and M31 are used to constrain alternative DM models.

The missing satellites problem: High-resolution cosmological simulations of DM haloes the size of the MW predict hundreds or thousands of subhaloes with masses that are in principle large enough to allow for galaxy formation ($> 10^7 M_\odot$). Yet less than ~ 100 satellite galaxies with masses down to $\sim 300 M_\odot$ are known to orbit our galaxy within 300 kpc. Galaxies in the field show a similar under-abundance. One solution could be that galaxy formation becomes increasingly inefficient as the halo mass drops, and thus the smallest DM haloes have naturally failed to form galaxies.

The cusp-core problem: The mass density profiles of DM haloes in ΛCDM simulations rise steeply at small radii, $\rho(r) \propto r^{-\gamma}$, with $\gamma \simeq 0.8 - 1.4$. This is in contrast to the observed density profiles of many low-mass galaxies (albeit not all), the rotation curves of which are best fit with constant-density cores, $\gamma \simeq 0 - 0.5$. A related issue is that simulations predict more DM than measured in the central regions of galaxies (also known as the central density problem). A likely solution is that baryonic feedback modifies the structure of DM haloes. Hydrodynamic simulations which include the effects of baryons on galaxy formation have shown that baryonic feedback (e.g., supernova-driven blowouts) can erase the central cusps and produce core-like density profiles.

The too-big-to-fail problem: This problem is related to the fact that the local Universe contains fewer galaxies with large central densities ($\simeq 10^{10} M_\odot$) compared to ΛCDM predictions. DM haloes of such masses are thought to be too massive to have failed to form stars (hence the name of the problem), especially if lower-mass subhaloes are capable of doing so. The bright MW satellites are generally associated with subhaloes (e.g., from the Aquarius and Via Lactea II ΛCDM simulations), however not with the most massive ones. A similar issue is present in Andromeda and in field galaxies outside the Local Group.

The solutions that were briefly mentioned above do not require modifications to the ΛCDM framework. Other solutions involve either modifications of linear theory predictions (via the nature of the DM particle, e.g., Warm DM - WDM) or modifications of nonlinear predictions (via DM models that involve a self-interaction of DM particles - SIDM). WDM models postulate particles with masses at the keV-scale, and the observed number of dark-matter-dominated satellites is used to set a lower limit on the number of subhaloes in the MW and thus a lower limit on the particle's mass [57]. Current constraints are in the range $m_{WDM} > (1.6 - 2.3) \text{ keV}$. Cosmological simulations with SIDM find that $\sigma/m_{SIDM} \simeq (0.5-10) \text{ cm}^2/\text{g}$ can alleviate the cusp-core and too-big-to-fail problems, giving rise to DM cores in dwarf galaxies with sizes of $(0.3-1.5) \text{ kpc}$ [13]. Galaxy clusters provide important constraints, and their large central DM densities prefer models with $\sigma/m_{DM} \lesssim 0.1 \text{ cm}^2/\text{g}$ [58]. Thus, if SIDM is to solve the small-scale CDM problems and obey the constraints observed on the scales of clusters, σ must depend on the velocity of the particle: it must increase as the rms speed of the particle decreases from the scale of clusters ($v \sim 10^3 \text{ km/s}$) to the scale of dwarf galaxies ($v \sim 10 \text{ km/s}$).

27.5 Dark matter models

Particle DM model building is deeply intertwined with the question of the nature of physics beyond the Standard Model (BSM) of particle physics¹. Directions in this area have followed a few strategies, including, but not limited to

(1) pursuing DM candidates embedded in frameworks that include solutions to other open issues in particle physics, for example WIMPs in connection with electroweak-scale new physics that addresses the hierarchy problem, such as supersymmetry (see the Supersymmetry reviews Sec. 88 and 88); axions in connection with frameworks that address the strong *CP* problem (see Axions and Other Similar Particles—Sec. 90); sterile neutrinos in connection with the problem of neutrino masses and mixing (see

¹Notice that this includes the case of PBHs, as successful formation of the correct number density of PBHs involves new ingredients beyond standard cosmology and particle physics

the Neutrino Masses, Mixing, and Oscillations—Sec. 14); or (2) *ad hoc*, or *bottom-up* models built with the intent of addressing or explaining a putative experimental (e.g. particle physical anomalies) or observational (e.g. astronomical) signal.

WIMPs: The WIMP paradigm has been a preferred framework chiefly because it often arises in beyond the Standard Model scenarios that address the hierarchy problem whilst also providing a simple mechanism to explain the observed relic abundance via the “WIMP miracle” described above. Perhaps the most notable example of a framework containing a paradigmatic WIMP is the minimal supersymmetric extension to the Standard Model, if the lightest supersymmetric particle is a neutralino (the mass eigenstate resulting from the mixing of the supersymmetric partners to the Higgses and to the SU(2) and hypercharge gauge bosons, and, possibly, of additional singlet scalars); purely SU(2) sneutrinos have long been ruled out by direct detection, but with suitable mixing with “inert” (gauge-singlet) sneutrinos they can also play the role of WIMP candidates. For more details see the the Supersymmetry—Sec. 88 and 89 in this *Review*. Other non-supersymmetric WIMP models include models with a Higgs or Z (or Z') portal, universal extra dimensions [32], and other models with extra (warped or flat) dimensions, little Higgs theories, technicolor and composite Higgs theories, among others (see e.g. the review in [59]).

Axions and axion-like particles: Axions are an especially compelling example of a broad category of DM candidates encompassing very light scalar or pseudoscalar fields. The QCD axion provides a solution to the strong CP problem, and is at present a viable DM candidate (see Sec. 90 for details on motivations, production mechanisms, and detection prospects for the QCD axion). Ultra-light, bosonic DM generally implies the imprint of quantum effects on macroscopic scales (hence the name of *wave* or *fuzzy* DM). Specifically, some of the small-scale issues mentioned in sec. 27.4 can be addressed if the de Broglie wavelength of the DM, of mass m_a and velocity v_a ,

$$\frac{\lambda}{2\pi} = \frac{\hbar}{m_a v_a} \simeq 1.9 \text{ kpc} \left(\frac{10^{-22} \text{ eV}}{m_a} \right) \left(\frac{10 \text{ km/s}}{v_a} \right) \quad (27.7)$$

is comparable to the size of the smallest observed gravitationally collapsed structures, roughly, for a self-gravitating system of mass M , a scale $r \simeq GM/v^2$. The typical expectation is the formation of a soliton-like core in the DM density profile of size λ , thus inversely proportional to the DM mass, with an upper limit on the central density of around

$$\rho_s \lesssim 7 M_\odot/\text{pc}^3 \left(\frac{m_a}{10^{-22} \text{ eV}} \right)^6 \left(\frac{M}{10^9 M_\odot} \right) \quad (27.8)$$

for a halo of virial mass M . Additionally, wave DM predicts that halos lighter than around $10^7 (m_a/10^{-22} \text{ eV})^{-3/2} M_\odot$ should not exist [60], and that the number of halos in the local universe with a mass at or less $10^9 (m_a/10^{-22} \text{ eV})^{-4/3} M_\odot$ [61] be significantly depleted, addressing in part the too big to fail and missing satellite problems (see Sec. 27.4 above). Light bosonic DM is necessarily produced non-thermally [62], and the connection with the visible sector need not, but might, exist.

Dark photons: Light *vector* bosons such as a “dark photon” V with a mass below $m_V < 2m_e$, can be cosmologically stable (depending upon its kinetic mixing coupling with the visible photon) and be a viable DM candidate. Light dark photons can be produced in the early universe through scattering or annihilation via processes such as $\gamma e^\pm \rightarrow V e^\pm$ or $e^+ e^- \rightarrow V \gamma$, or via resonant photon-dark photon conversion, or from a condensate seeded by inflationary perturbations [63], or from a misalignment mechanism similar to the one commonly invoked for axion production; constraints on the parameter space stem from a combination of direct detection experiments, where the dark photon is absorbed and leads to a large ionization signal, from stellar cooling constraints from the Sun, horizontal branch stars, and red giants, and from CMB and the diffuse radiation from the $V \rightarrow 3\gamma$ decay mode. More broadly, light dark (pseudo-)scalars and vectors can be best constrained with experiments that rely on their wave-like behaviour and/or on their possible “portal” with the

visible sector. A broad assortment of experiments is sensitive to the range of masses between 10^{-22} eV and 10^{-2} eV . Among these experimental efforts, the lowest masses are probed by torsion balance experiments [64, 65], atom interferometry [66], comagnetometers [67, 68], and even gravitational wave detectors [69]; at increasing masses, if the light bosons couple electromagnetically, they can generate effective currents which are detectable with different apparatus depending on the relevant, mass-dependent target frequency. The experimental portfolio includes the broadband axion search ABRACADABRA [70, 71], the LC resonator DM Radio [72], lumped-element LC resonators [73], and cavity resonators such as HAYSTAC [74] and ADMX [75].

Sterile Neutrinos: Sterile (gauge-singlet) neutrinos, assumed to share a Dirac mass term with ordinary, SU(2) $_L$ -active neutrinos, have long been considered viable DM candidates [76]. The mostly-sterile mass eigenstate participates in SU(2) $_L$ interactions via a mixing parameter $\theta \ll 1$ that controls much of the particle’s phenomenology. In particular, the sterile neutrino possesses an inverse-lifetime on the order of $\tau^{-1} \sim G_F^2 m_\nu^5 \theta^2$, forcing the mixing to not exceed

$$\theta < 3.3 \times 10^{-4} \left(\frac{10 \text{ keV}}{m_\nu} \right)^5 \quad (27.9)$$

in order for the lifetime to exceed the age of the universe. While the main decay channel is to three active neutrinos, observationally the radiative decay mode to one neutrino plus a photon is much more relevant, giving rise to a quasi-monochromatic photon line at half the sterile neutrino mass. A recent tentative signal at 3.5 keV was reported from stacked observations of clusters of galaxies, individual clusters [77, 78], and the Galactic center [79] with both the XMM and Chandra X-ray observatories. The signal however was not detected in a large sample of galaxies and groups of galaxies [80] and dwarf galaxies [81], and especially Draco [82], shedding strong doubts on its sterile neutrino decay origin. Future observations with increased energy resolution might conclusively pinpoint the origin of the 3.5 keV emission [83].

Models with rich dark sectors: The absence of any conclusive signals from DM as a particle thus far motivates the hypothesis that the DM be charged under some new “hidden” dark-sector force, an idea that dates back many decades [84], including in the guise of “mirror DM” (more recently in the context of “neutral naturalness”). Top-down motivation for hidden-sector DM comes from string theory [85], although TeV-scale BSM framework such as supersymmetry and composite Higgs models can also naturally accommodate hidden sectors [86]. Although no coupling of the visible sector to the hidden sector need exist in principle, there are a few reasons to expect it [87]. The mass scale for hidden-sector DM is broader than, but overlapping with, that for WIMPs (this latter being limited to roughly between a few GeV and a few TeV). In particular, while some motivation exists for electroweak-scale hidden sectors, light, sub-GeV hidden sectors have a strong theoretical underpinning, and offer novel detection avenues and opportunities. The phenomenology of hidden-sector DM depends primarily on the nature of the force and its force carrier. The most-widely considered cases are (pseudo-)scalar and (axial-)vector mediators. Among the structures for the mediators’ coupling to the visible sector, renormalizable “portals” include the $H^\dagger H$ operator, through Lagrangian terms of the type $(\mu\phi + \lambda\phi^2)H^\dagger H$, coupling to the hypercharge field strength $B^{\mu\nu}$ via kinetic mixing, $e' B_{\mu\nu} F'^{\mu\nu}$, and the “neutrino” portal, $y_n L H N$, where L is the lepton doublet of any generation, N is a right-handed neutrino, H is the SM Higgs doublet, and y_n the Yukawa coupling. Other possibilities are for instance a vector mediator directly coupled to SM fermions charged under its corresponding symmetry [88], or a Z' associated to U(1) $_{B-L}$. Additional possibilities, arising for instance from vector couplings to anomalous global symmetries of the SM like baryon or lepton number, also exist [87]. The accelerator program necessary to probe hidden-sector DM often involves small-scale colliders and fixed-target experiments, with experiments utilizing missing energy and momentum offering the best sensitivity. Beam-dump experiments can test large ranges of DM-mediator couplings as long as mediators decay or scatter inside the detector (see e.g. the recent review [89]). Such exper-

iments can also probe dark sectors with light vectors coupled to visible matter besides gauge kinetic mixing: an instance are neutrino trident scattering used to place bounds on e.g. $L_\mu - L_\tau$ Z' gauge bosons. Being virtually unconstrained, the phenomenology of dark sectors can be arbitrarily rich, with possibilities ranging from dark non-Abelian gauge interactions creating non-trivial self-interacting and/or particle number-changing dynamics, to models of “dynamical” DM, with multi-component, unstable DM candidates and a time-variable effective total DM abundance and equation of state [90].

27.6 Laboratory detection of dark matter

Laboratory searches for DM particles can be roughly classified in direct detection experiments, axion searches (see Axions and Other Similar Particles—Sec. 90), and searches at accelerators and colliders.

27.6.1 Searches at Accelerators and Colliders

Various searches for dark matter have been carried out by the CMS and ATLAS collaborations at the LHC in pp collisions [91–95]. In general, these assume that dark matter particles escape the detector without interacting leading to significant amounts of missing energy and momentum.

Searches for DM with the LHC and other colliders have targeted DM models that interact with the SM via Higgs or Z boson exchange, effective field theories with heavy mediators, UV-complete models such as supersymmetry, models with long-lived particles, and models with rich dark sectors. The experimental program correspondingly includes searches for invisible-particle production mediated by a SM boson, generic searches for invisible particles produced via new particle mediators, and specific searches for complete models.

There are a variety of types of signals for DM, as noted by Ref. [91]:

- (a) the imbalance in the transverse momentum in an event due to the presence of DM particles, produced together with one Standard Model particle,
- (b) a bump in the di-jet or di-lepton invariant mass distributions, or
- (c) an excess of events in the di-jet angular distribution, produced by a dark matter mediator. No signal for DM has been observed in the LHC experiments so far. Instead, limits are set on masses, couplings, and cross-sections. The latter can be compared, generally in a model-dependent way, with direct detection experiments.

Searches strategies are designed to optimize signal-to-noise by selecting search-specific cuts: a model-independent instance is initial-state electromagnetic or strong-interaction radiation plus missing transverse energy. Collider searches for DM inform, and are informed, by DM searches through direct or indirect detection (see below), and, if possible, by the inferred thermal relic DM abundance. The collider searches alone cannot prove that a discovery is of dark matter.

In the latter category, searches for DM with the LHC and other colliders have targeted DM models that interact with the SM via Higgs or Z boson exchange, effective field theories with heavy mediators, UV-complete models such as supersymmetry, models with long-lived particles, and models with rich dark sectors. The experimental program correspondingly includes searches for invisible-particle production mediated by a SM boson, generic searches for invisible particles produced via new particle mediators, and specific searches for complete models. Searches strategies are designed to optimize signal-to-noise by selecting specific search-specific cuts: a model-independent instance is initial-state electromagnetic or strong-interaction radiation plus missing transverse energy.

New fixed-target experiments are increasingly probing lighter, sub-GeV dark sectors; thermal, or quasi-thermal relics (such as asymmetric, SIMP, ELDER DM models) provide sharp, largely model-independent experimental targets in the case of direct annihilation to Standard Model particles; even “secluded” annihilation to dark-sector particles can be probed with fixed-target experiments, albeit with some model-dependent caveats. Accelerator searches provide unique ways to test light DM models in

that they present a lower dependence on the DM particle nature, that could e.g. drive suppressed velocity-dependent direct detection cross sections, and on kinematic thresholds that can similarly suppress rates with other search strategies; additionally, accelerator searches offer opportunities to explore dark sectors in greater detail than other search strategies [87].

Experimental approaches to explore scenarios with a light DM χ and mediator A' include (i) searches for missing mass in exclusive reactions such as $e^+e^- \rightarrow \gamma(A'\chi\bar{\chi})$ or $e^-p \rightarrow e^-p(A'\chi\bar{\chi})$, (ii) missing momentum/energy, e.g. in fixed-target reactions such as $eZ \rightarrow eZ(A'\chi\bar{\chi})$, (iii) electron and proton beam dump, where the DM particle is detected from scattering in a downstream detector after being produced in the beam dump, (iv) direct dark photon searches, when the mediator cannot decay to the dark matter, $m_{A'} < 2m_\chi$. Current facilities actively probing the methods listed above include APEX and HPS and JLab, MiniBooNE at Fermilab, NA64 at CERN, and TREK at J-PARC. Future experiments that will eventually contribute to covering the mentioned thermal targets include Belle-II at KEK, MAGIX at MESA, PADME at LNF, SHIP at CERN, VEPP3 at BINP, BDX at JLab, COHERENT at ORNL, DarkLight at JLab, LDMX at SLAC or JLab, MMAPS at Cornell, SBN at Fermilab, and SeaQuest [87].

27.6.2 Direct detection formalism

Direct detection experiments mostly aim to observe elastic or inelastic scatters of Galactic DM particles with atomic nuclei, or with electrons in the detector material. Predicted event rates assume a certain mass and scattering cross section, as well as a set of astrophysical parameters: the local density ρ_0 , the velocity distribution $f(\vec{v})$, and the escape velocity v_{esc} (see Sec. 27.4).

Interactions with atomic nuclei: For DM scattering off nuclei, the differential scattering rate R as a function of nuclear recoil energy E_R is

$$\frac{dR(E_R, t)}{dE_R} = N_T \frac{\rho_0}{m_{\text{DM}}} \int_{v > v_{\min}} v f(\vec{v} + \vec{v}_E(t)) \frac{d\sigma(E_R, v)}{dE_R} d^3v, \quad (27.10)$$

where N_T is the number of target nuclei, m_{DM} is the mass of the DM particles, $v = |\vec{v}|$ is the speed of the particle in the experiment’s rest frame, $f(\vec{v} + \vec{v}_E(t))$ is the velocity distribution in the Earth’s frame, v_{\min} is the minimum speed of the DM particles that can cause a recoil energy E_R and σ is the scattering cross section on the nucleus [29, 114]. For elastic scattering, the minimum velocity is $v_{\min} = (m_N E_R / 2m_r^2)^{1/2}$, with m_N being the mass of the nucleus, and $m_r = (m_N m_{\text{DM}}) / (m_N + m_{\text{DM}})$ the reduced mass of the nucleus-DM system. In case of inelastic scattering, the minimum speed becomes $v_{\min} = (m_N E_R / 2m_r^2)^{1/2} + E^* / (2m_N E_R)^{1/2}$, with the nuclear excitation energy E^* , for part of the kinetic energy of the incoming particle will be spent on exciting the nucleus. The prompt de-excitation energy, if observed in addition to the nuclear recoil energy, will boost the region-of-interest to higher energies [115].

If one assumes the standard, leading order spin-independent (SI) and spin-dependent (SD) interactions, which couple to the charge/mass and spin of the nucleus, respectively, the differential cross section is proportional to the inverse squared speed of the DM particle, $d\sigma/dE_R \propto v^{-2}$, and the dependence on the velocity distribution can be expressed as:

$$g(v_{\min}, t) = \int_{v > v_{\min}} \frac{f(\vec{v} + \vec{v}_E(t))}{v} d^3v. \quad (27.11)$$

This functions allows for the comparison of various experimental results independently of the underlying velocity distribution [116], for a given DM mass. The time-integrated differential cross section is the sum of the SI and SD contributions:

$$\frac{d\sigma(E_R, v)}{dE_R} = \frac{m_N}{2m_r^2 v^2} \left(\sigma_0^{SI} F_{SI}^2(E_R) + \sigma_0^{SD} F_{SD}^2(E_R) \right), \quad (27.12)$$

where $F^2(E_R)$ are the nuclear form factors and σ_0 the cross sections in the limit of zero momentum transfer. Since the in-

Table 27.1: Best constraints from direct detection experiments on the SI (at high >5 GeV and low < 5 GeV masses) and SD DM-nucleon couplings.

Experiment	Target	Fiducial mass [kg]	Cross section [cm ²]	DM mass [GeV]	Ref.
Spin independent high mass (>5 GeV)					
XENON1T	Xe	1042	4.1×10^{-47}	30	[96]
PandaX-II	Xe	364	2.2×10^{-46}	30	[97]
LUX	Xe	118	1.1×10^{-46}	50	[98]
SuperCDMS	Ge	12	1.0×10^{-44}	46	[99]
DarkSide-50	Ar	46	1.14×10^{-44}	100	[100]
DEAP-3600	Ar	2000	3.9×10^{-45}	100	[101]
Spin independent low mass (<5 GeV)					
LUX (Migdal)	Xe	118	6.9×10^{-38}	2	[102]
XENON1T (Migdal)	Xe	1042	3×10^{-40}	2	[103]
XENON1T (ionisation only)	Xe	1042	3.6×10^{-41}	3	[104]
DarkSide-50 (ionisation only)	Ar	20	1×10^{-41}	2	[105]
SuperCDMS (CDMSlite)	Ge	0.6	2×10^{-40}	2	[106]
CRESST	CaWO ₄ - O	0.024	1×10^{-39}	2	[107]
NEWS-G	Ne	0.3	1×10^{-38}	2	[108]
DAMIC	Si	0.3	1×10^{-41}	7	[109]
Spin dependent proton					
PICO60	C ₃ F ₈ - F	49	3.2×10^{-41}	25	[110]
Spin dependent neutron					
XENON1T	Xe	1042	6.3×10^{-42}	30	[111]
PandaX-II	Xe	364	1.6×10^{-41}	40	[112]
LUX	Xe	118	1.6×10^{-41}	35	[113]

coming particle velocity is $v/c \sim 10^{-3}$, the nuclear recoil energy is at most tens of keV (much smaller than typical nuclear binding energies per nucleon), and the momentum transfer $q = (2m_N E_R)^{1/2} \sim \mathcal{O}(10-100 \text{ MeV})$. This implies that $1/q$ can be of the same order as nuclear radii $R \sim A^{1/3} \text{ fm}$, and that nuclei are not point-like from the perspective of a DM particle. The cross sections will thus involve nuclear form factors. These were calculated in [117] and [118] for the SI and SD case, respectively, for specific target nuclei, while the cross sections are often expressed in terms of single-nucleon cross sections and effective couplings of the DM particle to protons and neutrons. In the SI case, all the nucleons in the nucleus contribute coherently to the cross section (under the assumption of iso-spin independence in the DM couplings). Dominant sources of uncertainty are the nucleon sigma terms, especially for Higgs-dominated interactions, where the couplings are proportional to the quark masses. An overview is presented in Ref. [119]. For SD scattering, the nuclear spin contents due to the protons and neutrons must be considered.

The interactions of DM particles with nuclei can be treated in a non-relativistic effective field theory (NR-EFT) approach, which considers more general DM scenarios based on the lowest-order, four-field operators that describe the couplings to nucleons. These operators, which correspond to different types of interactions between the DM and quark fields, can be momentum- and velocity-dependent, and might be leading when momentum-independent interactions are suppressed, or even vanish in the limit of zero momentum [120, 121]. In Ref. [121, 122] all 15 operators (arising from 20 possible bilinear combinations between the DM and nucleon fields) which obey Galilean-invariance, T -symmetry and are Hermitian are written out up to quadratic order in q , and the nuclear response functions evaluated in shell-model calculations for DM targets made of F, Na, Ge, I and Xe isotopes. The connection to particle physics within the context of *simplified DM models* is made in Ref. [123, 124], where the simplified models assume a single DM particle with one mediator which couples it to quarks. More recently the DM-nucleus scattering was also analysed in the framework of chiral effective field theory (Ch-EFT), a low-energy effective theory of QCD, which allows for a consistent derivation of the nuclear responses beyond the leading-order expressions [125, 126]. Ch-EFT preserves the QCD symmetries, and predicts DM couplings to two nucleons (e.g., when the hypothetical particle couples to a virtual pion exchanged between the nucleons). It also provides a power counting that suggests a hier-

archy of the various NR-EFT operators, which is however approximate given that the couplings between the DM and the Standard Model fields are not known. The generalized SI structure factors for spin-1/2 and spin-0 DM particles and various isotopes of F, Si, Ar, Ge and Xe employed in direct detection experiments are provided in Ref. [126].

Scattering off bound electrons and absorption: For DM particle masses below the GeV-scale, most searches for DM-nucleus scattering rapidly lose sensitivity, due to energy thresholds around a few 100 eV - few keV. As an example, a light DM particle with a mass of 100 MeV and $v \propto 10^{-3}c$ will induce a nuclear recoil energy of about 0.5 eV in a target made of argon. Another strategy is to search for DM scattering off bound electrons, allowing for all of the kinetic energy (50 eV in the above case) to be transferred to the material [127]. The leading possibilities are ionisation, excitation, and molecular dissociation processes, which typically require energies of (1-10) eV, and thus allow to probe scattering of DM particles with masses down to the $\mathcal{O}(\text{MeV})$ range.

For a bound electron with binding energy E_B DM particle masses of $m_{\text{DM}} \geq 250 \text{ keV} \times E_B/1 \text{ eV}$ can in principle be probed. The signal depends on the material, and can consist of one or more electrons (in semiconductors, noble liquids, graphene), one or more photons (in scintillators) or phonons (in superconductors and superfluids) and quasiparticles (in superconductors). As an example, the differential event rate for ionization in atoms is given by

$$\frac{dR_{\text{ion}}}{d \ln E_R} = N_T \frac{\rho_0}{m_{\text{DM}}} \frac{d\langle \sigma_{\text{ion}} v \rangle}{d \ln E_R}, \quad (27.13)$$

where E_R is the recoil energy transferred to the electron, $\langle \sigma_{\text{ion}} v \rangle$ is the thermally averaged ionization cross section and N_T is the number of target atoms per unit mass. The cross section is related to the non relativistic DM-electron elastic scattering cross section (σ_e):

$$\begin{aligned} \frac{dR_{\text{ion}}}{d \ln E_R} &= \frac{6.2}{A} \left(\frac{\rho_0}{0.4 \text{ GeV cm}^{-3}} \right) \left(\frac{\sigma_e}{10^{-40} \text{ cm}^2} \right) \left(\frac{10 \text{ MeV}}{m_{\text{DM}}} \right) \\ &\times \frac{d\langle \sigma_{\text{ion}} v \rangle / d \ln E_R}{10^{-3} \sigma_e} \frac{\text{events}}{\text{kg d}} \end{aligned} \quad (27.14)$$

Predicted differential rates in various materials (He, Ar, Ge, Xe) and for different particle masses are shown in [127], together

with cross section sensitivities as a function of mass and expected background rates from neutrinos.

Two classes of DM candidates, axion-like-particles (ALPs) and dark (or hidden) photons (see Sec. 27.5), can be absorbed in a target material by interactions with bound electrons via the axioelectric effect, which is analogous to the photoelectric effect: a boson is absorbed by a bound electron, which is then ejected from the atom [63,128,129]. The dark photon arises in extensions of the SM by a new massive or massless $U(1)'$ field, coupled to the SM $U(1)_Y$ via a kinetic mixing term κ , see Sec. 27.5. The absorption cross section of a massive, NR particle m_V with coupling $e' = e\kappa$ to electrons is (in natural units, and for energies $E_V \ll m_e$)

$$\sigma_{abs} = \frac{\alpha'}{\alpha} \left(\frac{E_V}{2m_e} \right)^2 \sigma_{pe}, \quad (27.15)$$

where σ_{pe} is the photoelectric cross section, and an analogue to the electromagnetic fine structure constant α is introduced, $\alpha' = (e\kappa)^2/4\pi$. The rate per atom is

$$R \simeq \frac{\rho_0}{m_V} \times \kappa^2 \sigma_{pe}. \quad (27.16)$$

Since the kinetic energy of the dark photon is negligible compared to its rest energy, a mono-energetic peak at its mass is expected in the spectrum of a direct detection experiment. Dark photons with a thermally generated abundance are excluded by direct detection experiments [63], however non-thermal mechanisms (e.g., via perturbations during inflation) could create the relic abundance, see Section 27.3.

Similarly to axions, ALPs arise in the spontaneous breaking of a global symmetry, and are phenomenologically described by a mass m_a and a decay constant f_a . Unlike for QCD axions, however, there is no strict relation between m_a and f_a . The coupling strength to electrons with mass m_e is parameterised by $g_{ae} = 2m_e/f_a$, and the absorption cross section of a particle with incoming velocity v_a is related to the cross section for the photoelectric effect as

$$\sigma_{abs} v_a \simeq \frac{3E_a^2}{4\pi\alpha f_a^2} \sigma_{pe} = \frac{3g_{ae}^2}{4\pi\alpha} \left(\frac{E_a}{2m_e} \right)^2 \sigma_{pe}. \quad (27.17)$$

As in the case of the dark photon, the signature is a mono-energetic peak at the mass of the particle, broadened by the energy resolution of the detector. Constraints on the couplings of ALPs and dark photons to electrons from direct detection experiments in m_a and m_V mass ranges from $\sim (1-10^4)$ eV were derived in Ref. [130,131], and compared to indirect limits from anomalous energy losses in the Sun, in red-giant and horizontal-branch stars. For a detailed discussion of axion and ALP searches, we refer to the *Axion* review.

27.6.3 Current and future direct detection technologies

Direct detection experiments aim to observe the small (keV-scale and below) and rare (fewer than ~ 1 event/(kg y)) signals which are induced by DM particle scatters in a detector, mostly in the form of ionisation, scintillation or lattice vibrations. A majority of experiments detects more than one signal, which allows to distinguish between scattering off of electrons (electronic recoils, ER) and off of atomic nuclei (nuclear recoils, NR). A 3D position resolution is required to define central detector regions (or fiducial volumes) with low background rates from surrounding materials, and the distinction between single- versus multiple-scatters rejects a significant fraction of backgrounds, given that DM will scatter at most once. We refer to [132,133] for recent reviews of the field.

Specific signatures: For NRs, the shape of the differential recoil spectrum is exponentially falling with recoil energy, and depends on the mass of the particle and on the nuclear mass. Unless $m_{DM} \gg m_N$, m_{DM} can in principle be determined from the measured recoil spectrum, where multiple targets will provide tighter constraints [134]. The Earth's motion through the MW induces a seasonal variation of the total event rate and a forward-backward asymmetry in a directional signal [135,136]. The annual modulation is due to the Earth's motion in the Galactic rest frame, which is a superposition of the Earth's rotation around the Sun

and the Sun's rotation around the Galactic center. Since the Earth's orbital speed is much smaller than the Sun's speed, the expected amplitude of the modulation is $\simeq 5\%$. In the SHM, the period is one year, and the phase is 150 d (June 2), when both speeds add up maximally. This expectation is modified for different DM distributions, e.g. in the case of sub-structures such as clumps and streams [137,138] and a DM disc [139]. In addition, the modulation changes phase at a specific recoil energy (known as crossing-energy) [140], which depends on the DM and nuclear mass, allowing to in principle determine m_{DM} if low energy thresholds can be achieved. A powerful signature is provided by the ability to detect the axis and direction of the recoiling nucleus. Since the DM flux in the laboratory frame is peaked in the direction of motion of the Sun towards the constellation Cygnus, the recoil spectrum is peaked in the opposite direction. The observation of such a dipole feature would provide a 'smoking-gun' evidence for DM, where the forward-backward rates can differ by a factor of ~ 10 , depending on the energy threshold. Ref. [141] provides a recent review of the theoretical framework and of the discovery reach of directional detectors.

Backgrounds, including neutrinos: Early direct detection experiments employing low-background Ge spectrometers featured background levels around 2 events/(kg d keV), while the latest generation of liquid Xe experiments reduced this noise by four orders of magnitude, to 2×10^{-4} events/(kg d keV). Nonetheless, the measured energy spectra are still dominated by interactions due to the radioactivity of detector components, followed by cosmic muons and their secondaries such as fast neutrons. The cosmic and environmental radiation are suppressed by going deep underground and surrounding the experiments with appropriate shielding structures (mainly large water Cherenkov detectors for the current and next-generation detectors). Activation of materials via cosmic-ray interactions produce long-lived radio-nuclides (e.g., ^{39}Ar , ^{60}Co , ^{68}Ge , ^{32}Si , etc), while long-lived, human-made isotopes (^{85}Kr , ^{137}Cs , etc) can mix with detector materials or generate surface backgrounds. For details, we refer to *Section 36.6* of this *Review*.

The final backgrounds will be due to the irreducible neutrino flux from the Sun, the atmosphere and the diffuse supernovae background [142]. Solar pp-neutrinos will dominate the electronic recoil background due to elastic neutrino-electron scatters, at a level of $\sim (10-25)$ events/(t y) below energies of ~ 100 keV, while coherent elastic neutrino-nucleus scatters ($\text{CE}\nu\text{NS}$) from ^8B solar neutrinos will induce up to $\sim 10^3$ events/(t y) for high-A targets, at nuclear recoil energies below $\sim \text{few}$ keV. Nuclear recoils from atmospheric neutrinos and the diffuse supernovae neutrino background will yield event rates in the range $(1-5)$ events/(100 t y), depending on the detector material. In general, ^8B and atmospheric neutrinos will impact light (≤ 6 GeV) and heavy (100 GeV and above) DM searches for cross sections on nucleons below $\sim 10^{-45}$ cm² and $\sim 10^{-49}$ cm², respectively. The precise cross sections where neutrinos constitute a dominant background depend however on the uncertainties on the flux of each neutrino source, and on the astrophysical parameters that enter in the DM signal models [143]. For very low energy thresholds to nuclear recoils, e.g. 10-30 eV in Ge and Si detectors, $\text{CE}\nu\text{NS}$ due to the ^7Be neutrino flux become relevant for exposures of ~ 50 kg y [144]. For DM searches with electron recoils via DM-electron scattering and dark photon or ALP absorption, solar neutrinos will also limit the sensitivity to DM masses in the range $\sim (1-10^3)$ MeV and $\sim (1-10^3)$ eV, respectively, for large exposures ~ 1 t y, as shown in Ref. [145].

Solid-state cryogenic detectors: Current experiments using the bolometric technique (see *Section 36.5* of this *Review*), together with either charge or light readout, are SuperCDMS (Si, Ge) at Soudan, EDELWEISS (Ge) at the Laboratoire Souterrain de Modane (LSM) and CRESST (CaWO₄) at the Laboratori Nazionali del Gran Sasso (LNGS). These experiments are optimised for low-mass DM searches, and can probe masses down to ~ 0.2 GeV. CDMSlite also operates detectors at higher bias voltages to amplify the phonon signals produced by drifting charges and thus have access to light DM around 1.5 GeV. The goal of their future phases is to probe the low-mass region down to cross

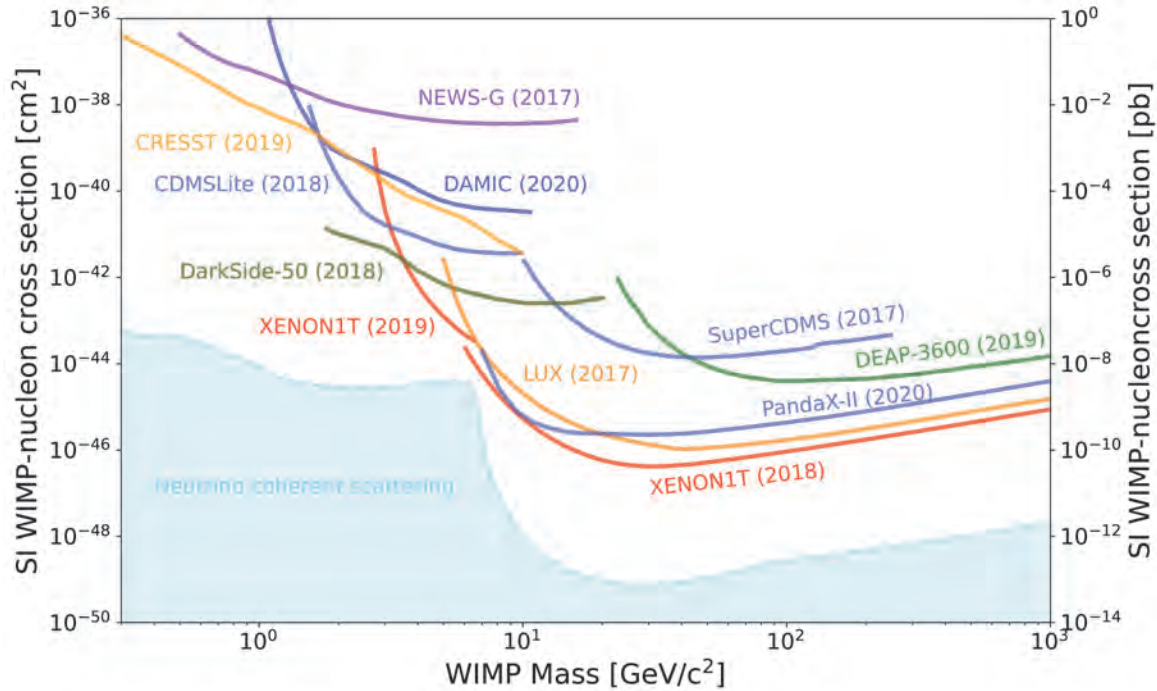


Figure 27.1: Upper limits on the SI DM-nucleon cross section as a function of DM mass.

sections of 10^{-43} – 10^{-44} cm^2 . Much smaller, gram-scale versions of cryogenic detectors can have single-charge resolution and thus probe low-mass DM via inelastic electron recoils. A SuperCDMS single-charge sensitive Si detector placed upper limits on DM interacting with electrons for masses between (0.5 – 10^4) MeV, as well as on dark photon kinetic mixing for dark photon masses in the range (1.5 – 40) eV. With Ge crystals operated at Soudan, SuperCDMS constrained dark photons and ALPs in the mass range 40 eV to 500 keV.

Germanium ionisation detectors operated at 77 K can reach sub-keV energy thresholds and low backgrounds, but lack the ability to distinguish electronic from nuclear recoils. The CDEX-10 experiment, located at the China Jinping Underground Laboratory (CJPL), uses p-type, point-contact Ge detectors operated in liquid nitrogen, and probes DM masses down to 3 GeV. It also reported constraints on the kinetic mixing of dark photons in the mass range 0.1–4.0 keV. The neutrinoless double beta experiments Majorana Demonstrator and GERDA have obtained constraints on the couplings of ALPs and dark photons to electrons, with masses between (6–100) keV and (60–1000) keV, respectively.

Noble liquids: Liquid argon (LAr) and liquid xenon (LXe) are employed as DM targets, while R&D on liquid helium and neon is ongoing. We refer to Ref. [146] for a review of the liquid noble gas detector technology in low-energy physics, as well to Section 36.4 of this Review. At present the best constraints on DM-nucleus interactions come from experiments using xenon: the LUX experiment which was operated at SURFi, PandaX-II at CJPL and XENON1T at LNGS. These experiments probe particle masses down to ~ 6 GeV (when using both light and charge signals) and the SI DM-nucleon cross section down to 4.1×10^{-47} cm^2 (at 30 GeV). LAr experiments use the powerful pulse shape discrimination (PSD) that allows for distinguishing between ER and NR events, at the expense of higher energy thresholds than in LXe. The DarkSide-50 TPC at LNGS sets a minimum upper limit on the SI, DM-nucleon cross section of 1.09×10^{-44} cm^2 at 126 GeV, while the single-phase experiment DEAP-3600 at SNOLAB constrains the SI cross section to values below 3.9×10^{-45} cm^2 at 100 GeV.

In noble liquids, sub-GeV DM particles can be searched for by observing inelastic, ER processes following a low-energy nuclear recoil: excitation and ionisation of the recoiling atom (the hypothetical Migdal effect) and a bremsstrahlung photon [147].

As an example, LUX and XENON1T constrained DM particle masses between (0.3 – 5) GeV via bremsstrahlung photons and Migdal electrons. Even lower masses are accessible when using the amplified, charge signal only, at the expense of giving up discrimination between ERs and NRs. XENON1T probed particle masses down to 60 MeV, while DarkSide-50 published constraints on WIMP masses as low as 1.8 GeV. DM masses at the MeV-scale can also be probed by exploiting the scattering off electrons. The XENON1T experiment presented a light DM search with ionisation signals, with a background level of < 1 event/(t d keV) above 0.4 keV. LXe TPCs also search for solar axions, Galactic ALPs and dark photons. PandaX-II and LUX set upper limits on the axion-electron coupling of 3.5×10^{-12} in the mass range (10^{-5} – 1) eV for solar axions, and probe couplings around 4×10^{-13} in the mass range (1 – 10) keV for Galactic ALPs [148, 149]. XENON1T observed an excess of events over known backgrounds at energies below 7 keV, which can be explained by solar axions (3.4σ) or bosonic dark matter with a mass around 2.3 keV (3.0σ), where the former is in strong tension with stellar constraints [150].

The next generation of liquefied noble gas detectors are in construction (DarkSide-20k), commissioning (LZ), operation (PandaX-4T and XENONnT) or at the design and R&D stage (ARGO, DARWIN). These will increase the sensitivity to various DM candidates by 1–2 orders of magnitude, with the ultimate goal of exploring the experimentally accessible parameter space, until the backgrounds from neutrinos will start dominating the event rates.

Room temperature scintillators: Several large DM experiments using high-purity NaI(Tl) crystals are acquiring data in various underground laboratories. Of these, DAMA/LIBRA at LNGS has the highest mass, 250 kg, and the largest exposure: 1.33 ty with an energy threshold of 1 keV and 2.46 ty with an energy threshold of 2 keV. It is the only experiment in the field that reported an annually modulated event rate with a statistical significance of 12.9σ C.L. (20 annual cycles), with a modulation amplitude around 0.02 events/(kg d keV) in the energy region (1–4) keV. These findings were interpreted as due to DM interactions via nuclear or electronic recoils. The ANAIS experiment at Canfranc operates 112.5 kg of NaI(Tl) scintillators with an energy threshold of 1 keV and a background rate of 3.6 events/(kg d keV) in the (1–6) keV region. A blind analysis of 3y of data, for an exposure of 314 kgy is consistent with an absence of mod-

ulation at 3.3σ . The COSINE-100 experiment, located at the Yangyang Underground Laboratory, operates 106 kg of NaI(Tl) crystals in a liquid scintillator, with an energy threshold of 2 keV and a background rate of 3.6 events/(kg d keV). Results from a 97.7 kg y exposure in the (2-6) keV energy range are consistent, at 68.3% C.L., with both the null hypothesis and DAMA/LIBRA's best fit value in the same energy range. A larger exposure and a reduced energy threshold are required to test DAMA/LIBRA for 3σ coverage. The SABRE experiment plans to operate a total of 50 kg of NaI(Tl) crystals, focussing on reaching a background level of 0.1 events/(kg d keV), an order of magnitude below DAMA/LIBRA. Twin detectors will be installed at LNGS and at the Stawell Underground Physics Laboratory in the Southern hemisphere. While a DM-induced signal is expected to have the same phase in both hemispheres, seasonal or site-related effects would show different amplitudes and phases in the twin detectors. The COSINUS R&D project aims to develop a cryogenic scintillating bolometer with undoped NaI crystals with phonon and light readout, the ratio of which allows for particle discrimination. The hope is that it will shed light on the type of interactions responsible for the modulated signal.

Room temperature ionisation detectors: Silicon charged-coupled devices (CCDs) are employed for low-mass DM searches, as well as for hidden photon searches in the eV-mass range. Ionisation events induced in bulk silicon of high-resistivity, fully depleted CCDs are observed with charge resolutions around $1-2e^-$ and extremely low leakage currents, at the level of few $e^- \text{ mm}^{-2} \text{ d}^{-1}$. The position of an energy deposit is reconstructed in 3 dimensions and the particle type (electron, neutron, muon, α -particles, etc) is reconstructed based on the recorded track pattern.

The DAMIC experiment at SNOLAB yielded new constraints on DM-electron scattering, and on the hidden-photon kinetic mixing parameter in the mass range (1-30) eV with an exposure of 7.6 kg d and on low-mass WIMPs with an exposure of 11 kg d. The SENSEI projects employ the skipper technology to achieve single-electron sensitivity. A run with a 2 g detector in the MINOS cavern at Fermilab yielded world-leading constraints on DM-electron scattering for a large range of sub-GeV dark matter masses. The skipper technology will also be employed in the next stage of the DAMIC programme, DAMIC-M at LSM, which plans for a kg-size mass. The goal is to achieve thresholds of 2-3 electrons and to probe the DM-nucleon cross section down to $\text{few} \times 10^{-43} \text{ cm}^2$ around 2-3 GeV and the DM-electron cross section down to $2 \times 10^{-41} \text{ cm}^2$ at 10 MeV mass.

The NEWS-G collaboration operates spherical proportional counters filled with a noble gas. Advantages of this technology are the low intrinsic electronic noise and a high amplification gain, allowing for low energy thresholds down to single-electron detection, and the possibility to use different light targets (He, Ne, etc). A 60 cm diameter chamber operated at LSM with a gas mixture of Ne + CH₄ (0.7%) at 3.1 bar, excluded SI, WIMP-nucleon cross sections above $4.4 \times 10^{-37} \text{ cm}^2$ at 0.5 GeV after an exposure of 9.6 kg d with an energy threshold ~ 100 eV. The next iteration, a 140 cm sphere detector made of very low radioactivity copper (few $\mu\text{Bq/kg}$ of ²³⁸U and ²³²Th) is under construction at SNOLAB.

Superheated liquid detectors: Investigation of the spin-dependent interaction channel calls for target nuclei with uneven total angular momentum. A particularly favourable candidate is ¹⁹F, the spin of which is carried mostly by the unpaired proton, yielding a cross section which is almost a factor of ten higher than of other employed nuclei with spin (e.g., ²³Na, ⁷³Ge, ¹²⁷I, ¹²⁹Xe, ¹³¹Xe). Fluorine is part of the target of experiments using superheated liquids, such as the ones operated by the PICO and MOSCAB collaborations. A search in the PICO-60 C₃F₆ bubble chamber at SNOLAB with an exposure of 1404 kg d and an energy threshold of 2.45 keV, yielded the most stringent constraint on the DM-proton SD cross section at $3.2 \times 10^{-41} \text{ cm}^2$ for a 25 GeV particle mass. In construction is a ton-scale detector (PICO-500) to be deployed in the cube area hall of SNOLAB. MOSCAB successfully built and tested a geyser-concept bubble chamber, the operation of which is based on a continuous process

of evaporation and condensation, with the detector recovering its superheated state automatically after each event. After first results in a surface laboratory, the detector was moved underground to LNGS for science data taking.

Directional detectors: Detectors capable of measuring the direction of the recoiling nucleus would unequivocally confirm the Galactic origin of a signal and could probe the region below the neutrino floor [151, 152]. Because nuclear recoils have a range which is about 10 times smaller than the one of Compton recoils of the same energy, gaseous detectors have an excellent intrinsic background rejection if they can measure the range of events precisely. Several directional detectors are presently in operation, where a 1 m³ detector has a typical mass of a few 100 g and can measure the sense of an incoming nuclear recoil above a few tens of keV. Cygnus is a proto-collaboration which coordinates the R&D efforts for gas based TPCs with 1 keV threshold.

A new technique is based on fine-grained nuclear emulsions (solid-state detectors with silver halide crystals uniformly dispersed in a gelatine film, where each crystal works as a sensor for charged particles), as proposed by the NEWSdm collaboration. These act as target and nanometric tracking device, and the expected NR tracks are sub- μm in size. Due to the small crystal size and larger number density, a superior spatial resolution compared to gaseous detectors is obtained. Simulations show that to reach the neutrino floor, exposures of 10 t y and 100 t y are required if a 30 nm and 50 nm threshold for detecting the track length is reached. This requires further R&D, since current emulsions allow for 100 nm tracking and target masses are around 1 kg, with 10 kg y exposures planned. A proposed approach for the directional detection of sub-GeV DM is to use two-dimensional materials such as monolayer graphene [153], from which the DM particle can eject electrons. Their energy and direction, correlated with the direction of the incoming DM, can be measured for instance with the proposed PTOLEMY experiment.

New techniques: To probe light (sub-GeV) DM particles, either via scatters off electrons or via couplings to phonons, new techniques beyond the ones discussed above are proposed. The DM particle mass that can be accessed in DM-electron scattering in noble liquids and semiconductors is limited by the minimum ionisation/excitation energy and the size of the band gap, respectively (at the $\sim\text{eV}$ -scale). To reach lower energy thresholds, materials with smaller band gaps for electron excitations ($\sim\text{meV}$), such as superconductors and superfluids, as well as Dirac materials were recently proposed [154]. These would in principle allow for the detection of keV-scale DM. Other ideas to detect keV-MeV scale DM are to observe NRs in superfluid He, via collective excitation modes in the fluid [155], or based on the breaking of chemical bonds between atoms [156].

Even lighter DM, with masses in the meV-eV range, could be detected via absorption on a conduction electron in a superconductor, followed by the emission of an athermal phonon [157]. Another proposed target for light DM are polar materials (for example GaAs, sapphire), which are especially sensitive for scattering through an ultralight dark photon, via excitation of single optical phonons [158]. If an anisotropic crystal such as sapphire is employed, a daily modulation interaction rate could be established [159]. A new class of detectors for bosonic DM, based on resonant absorption onto a gas of small polyatomic molecules, is proposed in [160]. The DM would effectively act as a laser that resonantly excites transitions in molecules when its mass closely matches the transition energy. While DM with SI couplings can efficiently excite phonons, it has been shown in [161] that if DM couples to the electron spin, magnon excitations (quanta of collective spin wave excitations) in materials with magnetic dipole order may also offer a promising detection avenue. Yet another approach for sub-GeV DM is to employ superconducting nanowires as both target and sensor, and first bounds on DM-electron interactions were already placed from a 4.3 ng tungsten-silicide prototype with a 0.8 eV energy threshold [162].

The detection of light DM via collective excitations in condensed matter systems and other methods is a rapidly evolving field, and a growing area of research at the interface of DM physics, condensed matter and materials science. We refer to Ref. [87, 163]

for discussions of some of these new directions and models. Critical challenges are to detect these very small energy depositions, and to reliably assess the background noise.

Table 27.1 summarises the most stringent constraints on the DM-nucleon SI and SD cross sections, and Figure 27.1 shows the best constraints for SI couplings in the cross section versus DM mass parameter space, above masses of 0.3 GeV.

27.7 Astrophysical detection of dark matter

DM as a microscopic constituent can have measurable, macroscopic effects on astrophysical systems. Indirect DM detection refers to the search for the annihilation or decay debris from DM particles, resulting in detectable species, including especially gamma rays, neutrinos, and antimatter particles. The production rate of such particles depends on (i) the annihilation (or decay) rate (ii) the density of pairs (respectively, of individual particles) in the region of interest, and (iii) the number of final-state particles produced in one annihilation (decay) event. In formulae, the rate for production of a final state particle f per unit volume from DM annihilation can be cast as

$$\Gamma_f^A = c \frac{\rho_{\text{DM}}^2}{m_{\text{DM}}^2} \langle \sigma v \rangle N_f^A, \quad (27.18)$$

where $\langle \sigma v \rangle$ indicates the thermally-averaged cross section for DM annihilation times relative velocity [27], calculated at the appropriate temperature, ρ_{DM} is the physical density of DM, and N_f^A is the number of final state particles f produced in one individual annihilation event. The constant c depends on whether the DM is its own antiparticle, in which case $c = 1/2$, or if there is a mixture of DM particles and antiparticles (in case there is no asymmetry, $c = 1/4$). The analog for decay is

$$\Gamma_f^D = \frac{\rho_{\text{DM}}}{m_{\text{DM}}} \frac{1}{\tau_{\text{DM}}} N_f^D, \quad (27.19)$$

with the same conventions for the symbols, and where τ_{DM} is the DM's lifetime.

Gamma Rays: DM annihilation to virtually any final state produces gamma rays: emission processes include the dominant two-photon decay mode of neutral pions resulting from the hadronization of strongly-interacting final states; final state radiation; and internal bremsstrahlung, the latter two including, possibly, the emission of massive gauge or Higgs bosons subsequently producing photons via their decay products. Similarly, neutrinos are produced from charged pion decay and from radiative processes. The flux of gamma rays and neutrinos is calculated integrating the rate Γ_f per steradian (simply meaning, for isotropic emission, $\Gamma_f/(4\pi)$) along the line of sight within the appropriate angular region (the *differential flux* is obtained in the same way by simply replacing N_f with the differential flux at production, at the appropriate redshift in the case of cosmologically distant sources),

$$\phi_f = \int_{\Delta\Omega} d\Omega \int_{\text{l.o.s.}} dl \frac{\Gamma_f}{4\pi}. \quad (27.20)$$

It is customary to factor out, in the expression for the rate, a *particle physics* factor, depending upon the DM particle mass and its annihilation or decay rate, and an *astrophysical* factor, which only depends on the observational target. The latter is sometimes denoted with $J_{\Delta\Omega}(\psi)$ with ψ indicating the direction of the line of sight. Although different conventions are in use, a common choice is to define

$$J_{\Delta\Omega}(\psi) = \int_{\Delta\Omega} \int_{\text{l.o.s.}(\psi)} \rho_{\text{DM}}^2(l, \Omega) dl d\Omega. \quad (27.21)$$

For a target with uniform density ρ and radius r at a distance $d \gg r$, such that the target is entirely within the solid angle $\Delta\Omega$,

$$J \simeq \frac{4\pi r^3 \rho_{\text{DM}}^2}{3d^2}. \quad (27.22)$$

Searches for gamma-ray emission from DM annihilation have focused on targets chosen based on a variety of considerations,

primarily intended to maximize signal to noise. Nearby dwarf spheroidal galaxies contain very small amounts of gas, and do not host any significant astrophysical background at gamma-ray or X-ray frequencies, and are thus an optimal target choice for DM searches. An accurate determination of the DM density profile in these objects results in somewhat large systematics when deriving constraints from the non-observation of emission from DM; future optical surveys will help pinpoint with greater accuracy stellar kinematics and thus reduce such uncertainty; a second target is the inner region of the Milky Way: while nearby and potentially hosting a large density of DM, the Galactic center region is however very bright at almost any wavelength, making the extraction of a signal highly problematic; nearby clusters of galaxies are also known to host significant astrophysical emission, but are potentially ideally suited to constrain DM decay. Finally, putative nearby DM clumps are also a possible source of a bright DM signal (albeit from an unknown direction), as is the annihilation of DM in all halos at all redshifts.

DM annihilation and decay can lead to striking spectral features. Since the process happens typically at very low particle velocities, if the DM pair-annihilates e.g. to two photons or two neutrinos, the final-state particles will be nearly monoenergetic, with an energy close to the DM particle mass and a width proportional to the DM velocity in units of c (if a $\gamma\gamma$ line is present electroweak symmetry also implies a $Z\gamma$ line, if kinematically allowed). No astrophysical processes are known to produce lines at gamma-ray or neutrino energies in the GeV and above (with, perhaps, the possible exception of cold pulsar winds [164]) making this channel virtually background-free. At lower energy, lines are expected from radiative decay modes of candidates such as sterile neutrinos (see Sec. 27.5). DM annihilation or decay can lead to additional spectral features besides lines. These include (one or more) “boxes” [165], produced by boosted final states decaying to monochromatic photons (such as e.g. neutral pions), or combinations thereof. Processes occurring at higher redshift can distort these spectral features by smearing them to lower energies. Neglecting gamma-ray attenuation, the flux of gamma rays from all redshift can be cast as

$$\frac{dN_\gamma}{dE_\gamma}(E_\gamma) = \frac{c}{8\pi} \int \frac{\langle \sigma v \rangle \rho_{\text{DM}}(z) dz}{H(z)(1+z)^3 m_{\text{DM}}^2} \left(\frac{dN_\gamma}{dE'} \right)_{E'=E_\gamma(1+z)}. \quad (27.23)$$

While the calculation of the differential spectrum of gamma rays from a given final state f , dN_γ^f/dE_γ , is carried out using numerical tools, such as PYTHIA [166] that reproduce hadronization and particle decay for masses well above a few GeV, in the sub-GeV range gamma-ray production follows primarily from meson decay and radiative processes well outside the range of applicability of the Altarelli-Parisi splitting function. The MeV gamma-ray range will soon be probed with forthcoming satellites [167]. Recently a code that provides the expected gamma-ray spectrum for sub-GeV DM, **Hazma**, has become available [168].

Observations with the Fermi Large Area Telescope (LAT) and with ground-based facilities such as HESS, VERITAS, MAGIC, and HAWC have provided an unprecedented picture of the gamma-ray sky ideally suited to look for a signal from DM annihilation or decay for DM particles from a few GeV mass up to several TeV. The LAT has provided some of the most stringent constraints to-date on DM pair-annihilation for a variety of annihilation final states, chiefly from stacked observations of nearby satellite dwarf spheroidal galaxies [169]. Excesses of gamma rays over the expected diffuse and point-source background have been claimed, most importantly from the direction of the inner Galaxy, where a signal from DM annihilation might be especially bright [170, 171]. The nature of this excess is quite controversial: while the morphology and spectrum fall within what expected for a standard WIMP with a mass of a few tens of GeV [172], unresolved point sources, including especially an (expected) population of millisecond pulsars (MSPs) have been advocated as a possible plausible counterpart [173]. Statistical methods to discriminate between DM and MSPs have been utilized [174, 175], but recent studies indicate that such results might not be conclusive [176]. Large uncertainties in the Galactic diffuse background emission model are addition-

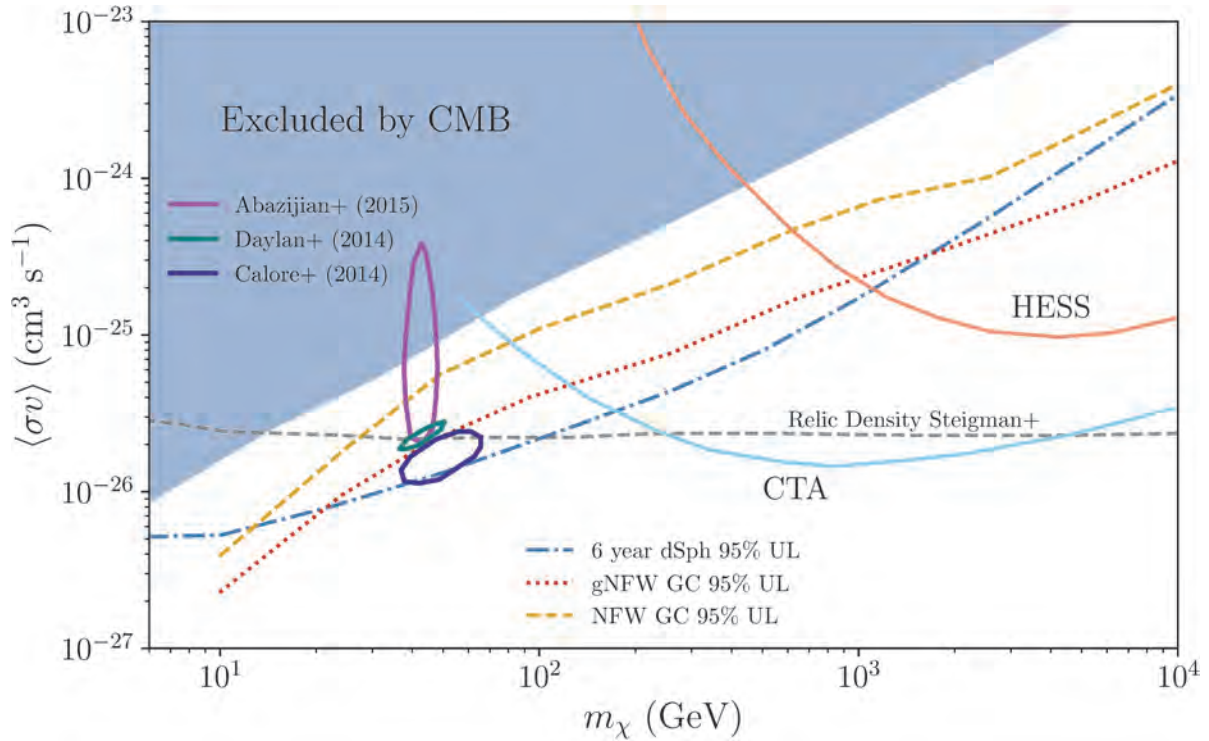


Figure 27.2: Upper limits and projected sensitivity from CTA on the pair-annihilation rate versus the DM mass from gamma-ray and CMB observations (figure courtesy of Logan Morrison).

ally known to exist, and possible plague the morphological and spectral information [177, 178]. Other notable potential gamma-ray excesses include a diffuse emission from the Andromeda galaxy (M31) [179–181], possibly in excess of what expected from cosmic-ray models [182]; and a diffuse emission at 511 keV energy in the inner Galaxy from Integral-SPI observations [183]; such emission has known astrophysical counterparts [184], as well as several proposed DM explanations (e.g. [185]).

While DM annihilation and decay typically occurs at low velocities, the possibility of “boosted” DM has also been considered [186]. In this case, the DM particle might dominantly pair-annihilate to a lighter dark species, which does interact with Standard Model particle, and could be detected with neutrino telescopes or direct detection experiments. Future facilities that promise to widen the reach of gamma-ray searches for DM include especially the Cherenkov Telescope Array (CTA), see fig. 27.2.

Neutrinos: DM can be captured in celestial bodies in significant amounts, depending on the DM scattering cross section off of nucleons, the DM mass, and the DM flux incident on the celestial body of interest. For DM masses at or around the GeV scale, evaporation from the celestial body plays an important role [187]. If enough DM accumulates, DM annihilation inside the celestial body can then lead to the production of Standard Model particles. Such particles can heat up the body, if they lose most of their energy before escaping. Utilizing models for heat production in planets, or stellar interior models in the case of stars, constraints can be put on DM particle properties. Of note are constraints from anomalous warming of cold planets such as Uranus [188], alterations to the stellar structure or the Sun’s seismic activity [189], and anomalous Earth heat flow [190]. Alternately, DM annihilation in celestial bodies can result in the production of particles that can escape the body. Within the Standard Model, the only such instance is annihilation to neutrinos, but, similarly to the boosted DM case the DM can annihilate to a (stable or unstable) dark-sector particles, whose decay or interactions can be detected on Earth [191, 192]. For direct annihilation to neutrinos, given the lower limit on the DM mass from evaporation, the typical neutrino energies usually exceed the energy of neutrinos from the Sun, the best target for this type of searches, making this a virtually

background-free DM search. Significant neutrino fluxes can only be achieved, however, if near-equilibration is reached between the capture and annihilation rates. In turn, this requires large-enough DM-nucleon scattering cross sections, to-date very close to the limits from direct detection (see sec. 27.6). Only spin-dependent cross section, and capture in the Sun usually provide large-enough neutrino fluxes. IceCube and ANTARES searches for an anomalous flux of high-energy neutrinos from the Sun yielded null results, which can be interpreted as constraints on spin-dependent nucleon-DM interactions under the assumption of equilibration and of specific annihilation final states [193, 194]. Lower-threshold detectors, including DeepCore [195] and PINGU [196], can produce interesting limits on lower-mass DM candidates above the evaporation threshold.

Cosmic-ray Antimatter: Stable charged particles produced by decays of products of, or directly from DM annihilation or decay, populate the cosmic radiation and are a prime target for indirect DM searches. To maximize signal to noise, searches focus on relatively rare particle species, such as positrons, antiprotons, and antinuclei. While in certain models the production of particles and antiparticles is not symmetric [197], generally DM annihilation or decay produces as many particles as antiparticles in the final state. Charged particles produced by DM propagate and lose energy prior to reaching detectors. The transport of charged particles is customarily carried out in the context of diffusion models such as the Galactic “leaky box” setup, see e.g. [198]. While progress in constraining the uncertain propagation and energy-loss processes has been steady with improved data from new detectors such as PAMELA [199] and AMS-02 [200], the calculation of the particle flux at Earth from that at production suffers from significant uncertainties [198].

An excess of high-energy positrons over the standard secondary production from inelastic cosmic-ray interactions has been firmly established by several experiments, most recently and with the highest statistics by AMS-02 [201]. The excess has been ascribed to DM annihilation, although strong constraints from the non-observation of corresponding anomalies in other channels, such as antiprotons and gamma rays, and the peculiar spectral shape, force DM models to be quite convoluted (see e.g. [202]). Alter-

nately, excess *primary* positrons can be produced in the magnetosphere of nearby pulsars [203, 204]. This latter explanation was questioned in [205] in connection with the detection of a TeV halo around two candidate pulsars, leading to the determination of a highly suppressed diffusion coefficient within the pulsar nebula; with such low diffusion coefficient, positrons from the pulsars would not contribute significantly to the flux at Earth; Ref. [206], however, showed that likely the diffusion coefficient is not constant, and that if it increases outside the nebula, as expected from other cosmic-ray measurements, pulsars can still be considered as the counterpart to the positron excess. Other explanations for the excess, albeit somewhat controversial, and increasingly constrained by data, also exist [207, 208].

The antiproton spectrum in the cosmic radiation as measured by AMS-02 [200] also exhibits features that might be considered as excess flux between 10 and 20 GeV, and energies above 100 GeV [209], which have been interpreted as possible signal of DM annihilation; more realistically, however, systematic uncertainties in the antiproton production cross section, in cosmic-ray transport, reacceleration at high energy and, at low energy, solar modulation make it extremely difficult to assess the robustness of the excesses [210, 211].

Antinuclei such as anti-deuterium and anti-helium could also form as a result of DM annihilation or decay. While baryon number conservation forces the typical kinetic energy of antinuclei produced in inelastic cosmic-ray processes to large values, antinuclei arising from hadronization of DM-initiated jets have low energy, offering optimal signal-to-noise when a low-energy cut on the antinucleus kinetic energy is used [212–216]. Specific detector designs have been developed to single out low-energy cosmic-ray antinuclei (e.g. $E < 0.25$ GeV/nucleon in the case of the General Antiparticle Spectrometer, or GAPS [217]). The detection of even a single antinucleus would have considerable importance as a possible sign of new physics [218].

Multi-wavelength studies: Electrons and positrons from DM lose energy quite efficiently, radiating at a variety of wavelengths. This *secondary* radiative emission presents spectral and morphological features that might provide an important additional indirect detection channel. The most efficient energy loss mechanisms for high-energy electrons and positrons are inverse Compton (IC) up-scattering of background photons, and synchrotron radiation in the presence of magnetic fields. Depending on the DM mass, the emitted light from synchrotron peaks at MHz-GHz frequencies, while the IC emission at X-ray to gamma-ray frequencies, depending on the energy of the background radiation, typically ranging from CMB photons up to starlight photons [219–221]. The calculation of the secondary emission from DM entails both solving the transport of the electrons and positrons from DM, and for the radiative emission; codes exist that perform these calculations for certain astrophysical environments [222–224], with diffusion playing an increasingly critical role in smaller and smaller structures such as dwarf galaxies [220]. It has been demonstrated that for large magnetic fields and for certain final states, the synchrotron emission is more constraining than the gamma-ray emission [225].

Stellar Physics: Microscopic properties of the DM can meaningfully alter, and thus be constrained by, several astrophysical environments, from planets and stars, up to the universe as a whole. DM particles light enough to be produced in collisional processes inside stars, with typically temperatures in the keV, or supernovae, with energy scales in the MeV, lead to an additional energy-loss mechanism, if capable of escaping the system. If this is the case, the increased needed energy output would also result in an increased neutrino flux, leading to constraints on the masses and couplings of the DM, see e.g. [226] for a comprehensive review. DM annihilation can even have fueled early stages of stellar evolution, perhaps with measurable consequences [227]. DM capture in neutron stars could lead to the collapse of the star into black holes; the existence of neutron stars in DM-rich environments can thus be used to constrain the mass and interaction cross section of DM with nucleons [228] and even relatively light, but stable, primordial black holes [229].

Cosmology: Energy injection from DM processes in the early

universe, as well as the contribution of DM to the effective relativistic degrees of freedom, are severely constrained from data on Big Bang Nucleosynthesis (see Sec. 24 in this *Review*) and on the energy and anisotropy power spectrum of the CMB (see Sec. 29). Codes exist that perform the calculation of the constraints on particle DM models [168, 230].

PBH Detection: Macroscopic DM candidates can gravitationally perturb structure and compromise the stability of, for instance, globular clusters such as Eridanus II [24], and/or disrupt wide binaries [231]. This constrains the maximal mass of a macroscopic DM candidate to not much more than $5 M_{\odot}$ [231] (see also [24]). In the specific case of primordial black holes, strong constraints also stem from the acceleration of charged particles around and after recombination, with significant effects on the CMB [232], albeit a lively debate exists over the accretion efficiency around such objects at high redshift [233, 234]. Whether or not PBH in the solar-mass range can be 100% of the DM is therefore disputed at present. Other effects produced by macroscopic, massive DM candidates are the microlensing of stars [235, 236] and quasars [237], femtolensing of gamma-ray bursts [238], and neutron star capture [229]. It is important to note that recently constraints from both microlensing and femtolensing have been corrected after the realization of important finite-size source and wave effects [236, 239, 240], leaving a substantial window, at PBH masses $10^{17} \lesssim M_{\text{BH}}/g \lesssim 10^{21}$ where PBH can be 100% of the DM. Light black holes, $M_{\text{BH}} \lesssim 10^{17}$ g, are also constrained by the non-detection of products of evaporation [241]; future MeV gamma-ray detectors are slated to significantly improve such constraints and to enable the direct detection of Hawking radiation [242]. If evaporation shuts down at or near the Planck scale, Planck-scale relic PBH are generally expected to carry electric charge and to be detectable with direct detection and neutrino experiments, or with paleo-detectors [243].

References

- [1] J. D. Simon, arXiv e-prints arXiv:1901.05465 (2019), [arXiv:1901.05465].
- [2] P. Salucci, *Astron. Astrophys. Rev.* **27**, 1, 2 (2019), [arXiv:1811.08843].
- [3] S. W. Allen, A. E. Evrard and A. B. Mantz, *Ann. Rev. Astron. Astrophys.* **49**, 409 (2011), [arXiv:1103.4829].
- [4] N. A. Bahcall *et al.*, *ApJ* **541**, 1 (2000).
- [5] S. D. M. White, G. Efstathiou and C. S. Frenk, *Mon. Not. Roy. Astron. Soc.* **262**, 1023 (1993).
- [6] A. J. S. Hamilton and M. Tegmark, *Mon. Not. Roy. Astron. Soc.* **330**, 506 (2002), [arXiv:astro-ph/0008392].
- [7] B. Famaey and S. McGaugh, *Living Rev. Rel.* **15**, 10 (2012), [arXiv:1112.3960].
- [8] S. W. Randall *et al.*, *Astrophys. J.* **679**, 1173 (2008), [arXiv:0704.0261].
- [9] R. H. Sanders, *Int. J. Mod. Phys. D* **27**, 14, 14 (2018), [arXiv:1805.06804].
- [10] S. D. McDermott, H.-B. Yu and K. M. Zurek, *Phys. Rev. D* **83**, 063509 (2011), [arXiv:1011.2907].
- [11] D. A. Buote *et al.*, *Astrophys. J.* **577**, 183 (2002), [arXiv:astro-ph/0205469].
- [12] D. Harvey *et al.*, *Science* **347**, 1462 (2015), [arXiv:1503.07675].
- [13] S. Tulin and H.-B. Yu, *Phys. Rept.* **730**, 1 (2018), [arXiv:1705.02358].
- [14] D. N. Spergel and P. J. Steinhardt, *Phys. Rev. Lett.* **84**, 3760 (2000), [arXiv:astro-ph/9909386].
- [15] S. Tremaine and J. E. Gunn, *Phys. Rev. Lett.* **42**, 407 (1979), [66(1979)].
- [16] L. Randall, J. Scholtz and J. Unwin, *Mon. Not. Roy. Astron. Soc.* **467**, 2, 1515 (2017), [arXiv:1611.04590].
- [17] R. Hlozek *et al.*, *Phys. Rev. D* **91**, 10, 103512 (2015), [arXiv:1410.2896].

- [18] E. Armengaud *et al.*, *Mon. Not. Roy. Astron. Soc.* **471**, 4, 4606 (2017), [arXiv:1703.09126].
- [19] M. Nori *et al.*, *Mon. Not. Roy. Astron. Soc.* **482**, 3, 3227 (2019), [arXiv:1809.09619].
- [20] B. Bozek *et al.*, *Mon. Not. Roy. Astron. Soc.* **450**, 1, 209 (2015), [arXiv:1409.3544].
- [21] H.-Y. Schive *et al.*, *Astrophys. J.* **818**, 1, 89 (2016), [arXiv:1508.04621].
- [22] E. O. Nadler *et al.*, *Astrophys. J.* **878**, 2, L32 (2019), [*Astrophys. J. Lett.* 878,32(2019)], [arXiv:1904.10000].
- [23] M. A. Monroy-Rodríguez and C. Allen, *ApJ* **790**, 2, 159 (2014), [arXiv:1406.5169].
- [24] T. D. Brandt, *Astrophys. J.* **824**, 2, L31 (2016), [arXiv:1605.03665].
- [25] B. Audren *et al.*, *JCAP* **1412**, 12, 028 (2014), [arXiv:1407.2418].
- [26] M. Dutra *et al.*, *JCAP* **1803**, 037 (2018), [arXiv:1801.05447].
- [27] P. Gondolo and G. Gelmini, *Nucl. Phys.* **B360**, 145 (1991).
- [28] J. L. Feng and J. Kumar, *Phys. Rev. Lett.* **101**, 231301 (2008), [arXiv:0803.4196].
- [29] G. Jungman, M. Kamionkowski and K. Griest, *Phys. Rept.* **267**, 195 (1996), [hep-ph/9506380].
- [30] J. Edsjo *et al.*, *JCAP* **0304**, 001 (2003), [hep-ph/0301106].
- [31] G. Servant and T. M. P. Tait, *Nucl. Phys.* **B650**, 391 (2003), [hep-ph/0206071].
- [32] D. Hooper and S. Profumo, *Phys. Rept.* **453**, 29 (2007), [hep-ph/0701197].
- [33] K. Griest and D. Seckel, *Phys. Rev.* **D43**, 3191 (1991).
- [34] R. T. Co *et al.*, *JCAP* **1512**, 12, 024 (2015), [arXiv:1506.07532].
- [35] V. S. Rychkov and A. Strumia, *Phys. Rev.* **D75**, 075011 (2007), [hep-ph/0701104].
- [36] E. D. Carlson, M. E. Machacek and L. J. Hall, *Astrophys. J.* **398**, 43 (1992).
- [37] D. Pappadopulo, J. T. Ruderman and G. Trevisan, *Phys. Rev.* **D94**, 3, 035005 (2016), [arXiv:1602.04219].
- [38] Y. Hochberg *et al.*, *Phys. Rev. Lett.* **113**, 171301 (2014), [arXiv:1402.5143].
- [39] E. Kufflik *et al.*, *Phys. Rev. Lett.* **116**, 22, 221302 (2016), [arXiv:1512.04545].
- [40] W. B. Lin *et al.*, *Phys. Rev. Lett.* **86**, 954 (2001), [arXiv:astro-ph/0009003].
- [41] G. B. Gelmini and P. Gondolo, *Phys. Rev.* **D74**, 023510 (2006), [hep-ph/0602230].
- [42] M. Hindmarsh, R. Kirk and S. M. West, *JCAP* **1403**, 037 (2014), [arXiv:1311.1637].
- [43] T. Moroi and L. Randall, *Nucl. Phys.* **B570**, 455 (2000), [hep-ph/9906527].
- [44] P. Hut and K. A. Olive, *Phys. Lett.* **87B**, 144 (1979).
- [45] S. Nussinov, *Phys. Lett.* **165B**, 55 (1985).
- [46] K. M. Zurek, *Phys. Rept.* **537**, 91 (2014), [arXiv:1308.0338].
- [47] Y. B. Zel'dovich and I. D. Novikov, *Soviet Ast.* **10**, 602 (1967).
- [48] S. Hawking, *Mon. Not. Roy. Astron. Soc.* **152**, 75 (1971).
- [49] B. J. Carr, *ApJ* **201**, 1 (1975).
- [50] J. I. Read, *J. Phys.* **G41**, 063101 (2014), [arXiv:1404.1938].
- [51] T. Piffel *et al.*, *Astron. Astrophys.* **562**, A91 (2014), [arXiv:1309.4293].
- [52] A. M. Green, *J. Phys.* **G44**, 8, 084001 (2017), [arXiv:1703.10102].
- [53] A. Helmi *et al.*, *Nature* **7729**, 985 (2018).
- [54] L. Necib, M. Lisanti and V. Belokurov (2018), [arXiv:1807.02519].
- [55] N. W. Evans, C. A. J. O'Hare and C. McCabe, *Phys. Rev.* **D99**, 2, 023012 (2019), [arXiv:1810.11468].
- [56] J. S. Bullock and M. Boylan-Kolchin, *Ann. Rev. Astron. Astrophys.* **55**, 343 (2017), [arXiv:1707.04256].
- [57] J. Zavala and C. S. Frenk (2019), [arXiv:1907.11775].
- [58] K. E. Andrade *et al.* (2019), [arXiv:1901.00507].
- [59] G. Servant, in "Particle dark matter," 164–189 (2010).
- [60] L. Hui *et al.*, *Phys. Rev.* **D95**, 4, 043541 (2017), [arXiv:1610.08297].
- [61] A. Fattahi *et al.* (2016), [arXiv:1607.06479].
- [62] D. J. E. Marsh, *Phys. Rept.* **643**, 1 (2016), [arXiv:1510.07633].
- [63] H. An *et al.*, *Phys. Lett.* **B747**, 331 (2015), [arXiv:1412.8378].
- [64] P. W. Graham and S. Rajendran, *Phys. Rev.* **D88**, 035023 (2013), [arXiv:1306.6088].
- [65] P. W. Graham *et al.*, *Phys. Rev.* **D93**, 7, 075029 (2016), [arXiv:1512.06165].
- [66] A. Arvanitaki *et al.*, *Phys. Rev.* **D97**, 7, 075020 (2018), [arXiv:1606.04541].
- [67] P. W. Graham *et al.*, *Phys. Rev.* **D97**, 5, 055006 (2018), [arXiv:1709.07852].
- [68] I. M. Bloch *et al.* (2019), [arXiv:1907.03767].
- [69] A. Pierce, K. Riles and Y. Zhao, *Phys. Rev. Lett.* **121**, 6, 061102 (2018), [arXiv:1801.10161].
- [70] Y. Kahn, B. R. Safdi and J. Thaler, *Phys. Rev. Lett.* **117**, 14, 141801 (2016), [arXiv:1602.01086].
- [71] R. Henning *et al.* (ABRACADABRA), in "Proceedings, 13th Patras Workshop on Axions, WIMPs and WISPs, (PATRAS 2017): Thessaloniki, Greece, 15 May 2017 - 19, 2017," 28–31 (2018).
- [72] S. Chaudhuri *et al.*, *Phys. Rev.* **D92**, 7, 075012 (2015), [arXiv:1411.7382].
- [73] P. Sikivie, N. Sullivan and D. B. Tanner, *Phys. Rev. Lett.* **112**, 13, 131301 (2014), [arXiv:1310.8545].
- [74] B. M. Brubaker *et al.*, *Phys. Rev.* **D96**, 12, 123008 (2017), [arXiv:1706.08388].
- [75] G. Rybka (ADMX), *Phys. Dark Univ.* **4**, 14 (2014).
- [76] S. Dodelson and L. M. Widrow, *Phys. Rev. Lett.* **72**, 17 (1994), [hep-ph/9303287].
- [77] E. Bulbul *et al.*, *Astrophys. J.* **789**, 13 (2014), [arXiv:1402.2301].
- [78] A. Boyarsky *et al.*, *Phys. Rev. Lett.* **113**, 251301 (2014), [arXiv:1402.4119].
- [79] T. E. Jeltema and S. Profumo, *Mon. Not. Roy. Astron. Soc.* **450**, 2, 2143 (2015), [arXiv:1408.1699].
- [80] M. E. Anderson, E. Churazov and J. N. Bregman, *Mon. Not. Roy. Astron. Soc.* **452**, 4, 3905 (2015), [arXiv:1408.4115].
- [81] D. Malyshev, A. Neronov and D. Eckert, *Phys. Rev.* **D90**, 103506 (2014), [arXiv:1408.3531].
- [82] T. E. Jeltema and S. Profumo, *Mon. Not. Roy. Astron. Soc.* **458**, 4, 3592 (2016), [arXiv:1512.01239].
- [83] F. A. Aharonian *et al.* (Hitomi), *Astrophys. J.* **837**, 1, L15 (2017), [arXiv:1607.07420].
- [84] I. Yu. Kobzarev, L. B. Okun and I. Ya. Pomeranchuk, *Sov. J. Nucl. Phys.* **3**, 6, 837 (1966), [*Yad. Fiz.* 3,1154(1966)].
- [85] M. J. Strassler and K. M. Zurek, *Phys. Lett.* **B651**, 374 (2007), [hep-ph/0604261].
- [86] M. J. Strassler (2006), [hep-ph/0607160].
- [87] M. Battaglieri *et al.*, in "U.S. Cosmic Visions: New Ideas in Dark Matter," (2017), [arXiv:1707.04591].

- [88] Y. Kahn *et al.*, JHEP **05**, 002 (2017), [arXiv:1609.09072].
- [89] J. Alexander *et al.* (2016), [arXiv:1608.08632], URL <http://lss.fnal.gov/archive/2016/conf/fermilab-conf-16-421.pdf>.
- [90] K. R. Dienes and B. Thomas, Phys. Rev. **D85**, 083523 (2012), [arXiv:1106.4546].
- [91] N. Trevisani (ATLAS, CMS), Universe **4**, 11, 131 (2018).
- [92] E. Tolley (ATLAS), PoS **ICHEP2018**, 171 (2019).
- [93] W. C. Kalderon (ATLAS), PoS **DIS2018**, 085 (2018).
- [94] D. Vannerom (CMS), PoS **DIS2019**, 111 (2019).
- [95] G. Gómez-Ceballos (CMS), PoS **EDSU2018**, 014 (2018).
- [96] E. Aprile *et al.* (XENON), Phys. Rev. Lett. **121**, 11, 111302 (2018), [arXiv:1805.12562].
- [97] Q. Wang *et al.* (PandaX-II), Chin. Phys. C **44**, 12, 125001 (2020), [arXiv:2007.15469].
- [98] D. S. Akerib *et al.* (LUX), Phys. Rev. Lett. **118**, 2, 021303 (2017), [arXiv:1608.07648].
- [99] R. Agnese *et al.* (SuperCDMS), Phys. Rev. Lett. **120**, 6, 061802 (2018), [arXiv:1708.08869].
- [100] P. Agnes *et al.* (DarkSide), Phys. Rev. **D98**, 10, 102006 (2018), [arXiv:1802.07198].
- [101] R. Ajaj *et al.* (DEAP), Phys. Rev. **D100**, 022004 (2019), [arXiv:1902.04048].
- [102] D. S. Akerib *et al.* (LUX), Phys. Rev. Lett. **122**, 13, 131301 (2019), [arXiv:1811.11241].
- [103] E. Aprile *et al.* (XENON) (2019), [arXiv:1907.12771].
- [104] E. Aprile *et al.* (2019), [arXiv:1907.11485].
- [105] P. Agnes *et al.* (DarkSide), Phys. Rev. Lett. **121**, 8, 081307 (2018), [arXiv:1802.06994].
- [106] R. Agnese *et al.* (SuperCDMS), Phys. Rev. **D99**, 6, 062001 (2019), [arXiv:1808.09098].
- [107] A. H. Abdelhameed *et al.* (CRESST) (2019), [arXiv:1904.00498].
- [108] Q. Arnaud *et al.* (NEWS-G), Astropart. Phys. **97**, 54 (2018), [arXiv:1706.04934].
- [109] A. Aguilar-Arevalo *et al.* (DAMIC), Phys. Rev. Lett. **125**, 241803 (2020), [arXiv:2007.15622].
- [110] C. Amole *et al.* (PICO), Phys. Rev. **D100**, 2, 022001 (2019), [arXiv:1902.04031].
- [111] E. Aprile *et al.* (XENON), Phys. Rev. Lett. **122**, 14, 141301 (2019), [arXiv:1902.03234].
- [112] J. Xia *et al.* (PandaX-II), Phys. Lett. **B792**, 193 (2019), [arXiv:1807.01936].
- [113] D. S. Akerib *et al.* (LUX), Phys. Rev. Lett. **118**, 25, 251302 (2017), [arXiv:1705.03380].
- [114] J. D. Lewin and P. F. Smith, Astropart. Phys. **6**, 87 (1996).
- [115] J. R. Ellis, R. A. Flores and J. D. Lewin, Phys. Lett. **B212**, 375 (1988).
- [116] P. J. Fox, J. Liu and N. Weiner, Phys. Rev. **D83**, 103514 (2011), [arXiv:1011.1915].
- [117] L. Vietze *et al.*, Phys. Rev. **D91**, 4, 043520 (2015), [arXiv:1412.6091].
- [118] P. Klos *et al.*, Phys. Rev. **D88**, 8, 083516 (2013), [Erratum: Phys. Rev. **D89**, no. 2, 029901 (2014)], [arXiv:1304.7684].
- [119] J. Ellis, N. Nagata and K. A. Olive, Eur. Phys. J. **C78**, 7, 569 (2018), [arXiv:1805.09795].
- [120] J. Fan, M. Reece and L.-T. Wang, JCAP **1011**, 042 (2010), [arXiv:1008.1591].
- [121] A. L. Fitzpatrick *et al.*, JCAP **1302**, 004 (2013), [arXiv:1203.3542].
- [122] N. Anand, A. L. Fitzpatrick and W. C. Haxton, Phys. Rev. **C89**, 6, 065501 (2014), [arXiv:1308.6288].
- [123] M. I. Gresham and K. M. Zurek, Phys. Rev. **D89**, 12, 123521 (2014), [arXiv:1401.3739].
- [124] J. B. Dent *et al.*, Phys. Rev. **D92**, 6, 063515 (2015), [arXiv:1505.03117].
- [125] D. Gazda, R. Catena and C. Forssén, Phys. Rev. **D95**, 10, 103011 (2017), [arXiv:1612.09165].
- [126] M. Hoferichter *et al.*, Phys. Rev. **D99**, 5, 055031 (2019), [arXiv:1812.05617].
- [127] R. Essig, J. Mardon and T. Volansky, Phys. Rev. **D85**, 076007 (2012), [arXiv:1108.5383].
- [128] F. T. Avignone, III *et al.*, Phys. Rev. **D35**, 2752 (1987).
- [129] M. Pospelov, A. Ritz and M. B. Voloshin, Phys. Rev. **D78**, 115012 (2008), [arXiv:0807.3279].
- [130] I. M. Bloch *et al.*, JHEP **06**, 087 (2017), [arXiv:1608.02123].
- [131] Y. Hochberg, T. Lin and K. M. Zurek, Phys. Rev. **D95**, 2, 023013 (2017), [arXiv:1608.01994].
- [132] M. Schumann (2019), [arXiv:1903.03026].
- [133] J. Billard *et al.* (2021), [arXiv:2104.07634].
- [134] M. Pato *et al.*, Phys. Rev. **D83**, 083505 (2011), [arXiv:1012.3458].
- [135] A. K. Drukier, K. Freese and D. N. Spergel, Phys. Rev. **D33**, 3495 (1986).
- [136] D. N. Spergel, Phys. Rev. **D37**, 1353 (1988).
- [137] D. Stiff, L. M. Widrow and J. Frieman, Phys. Rev. **D64**, 083516 (2001), [arXiv:astro-ph/0106048].
- [138] K. Freese *et al.*, Phys. Rev. Lett. **92**, 111301 (2004), [arXiv:astro-ph/0310334].
- [139] T. Bruch *et al.*, Astrophys. J. **696**, 920 (2009), [arXiv:0804.2896].
- [140] M. J. Lewis and K. Freese, Phys. Rev. **D70**, 043501 (2004), [arXiv:astro-ph/0307190].
- [141] F. Mayet *et al.*, Phys. Rept. **627**, 1 (2016), [arXiv:1602.03781].
- [142] L. E. Strigari, New J. Phys. **11**, 105011 (2009), [arXiv:0903.3630].
- [143] C. A. J. O'Hare, Phys. Rev. **D94**, 6, 063527 (2016), [arXiv:1604.03858].
- [144] L. E. Strigari, Phys. Rev. **D93**, 10, 103534 (2016), [arXiv:1604.00729].
- [145] R. Essig, M. Sholapurkar and T.-T. Yu, Phys. Rev. **D97**, 9, 095029 (2018), [arXiv:1801.10159].
- [146] V. Chepel and H. Araujo, JINST **8**, R04001 (2013), [arXiv:1207.2292].
- [147] M. J. Dolan, F. Kahlhoefer and C. McCabe, Phys. Rev. Lett. **121**, 10, 101801 (2018), [arXiv:1711.09906].
- [148] C. Fu *et al.* (PandaX), Phys. Rev. Lett. **119**, 18, 181806 (2017), [arXiv:1707.07921].
- [149] D. S. Akerib *et al.* (LUX), Phys. Rev. Lett. **118**, 26, 261301 (2017), [arXiv:1704.02297].
- [150] E. Aprile *et al.* (XENON), Phys. Rev. D **102**, 7, 072004 (2020), [arXiv:2006.09721].
- [151] P. Grothaus, M. Fairbairn and J. Monroe, Phys. Rev. **D90**, 5, 055018 (2014), [arXiv:1406.5047].
- [152] C. A. J. O'Hare *et al.*, Phys. Rev. **D92**, 6, 063518 (2015), [arXiv:1505.08061].
- [153] Y. Hochberg *et al.*, Phys. Lett. **B772**, 239 (2017), [arXiv:1606.08849].
- [154] Y. Hochberg *et al.*, Phys. Rev. **D97**, 1, 015004 (2018), [arXiv:1708.08929].
- [155] S. Knapen, T. Lin and K. M. Zurek, Phys. Rev. **D95**, 5, 056019 (2017), [arXiv:1611.06228].
- [156] R. Essig *et al.*, Phys. Rev. **D95**, 5, 056011 (2017), [arXiv:1608.02940].

- [157] Y. Hochberg, T. Lin and K. M. Zurek, *Phys. Rev.* **D94**, 1, 015019 (2016), [arXiv:1604.06800].
- [158] S. Knapen *et al.*, *Phys. Lett.* **B785**, 386 (2018), [arXiv:1712.06598].
- [159] S. Griffin *et al.*, *Phys. Rev.* **D98**, 11, 115034 (2018), [arXiv:1807.10291].
- [160] A. Arvanitaki, S. Dimopoulos and K. Van Tilburg, *Phys. Rev.* **X8**, 4, 041001 (2018), [arXiv:1709.05354].
- [161] T. Trickle, Z. Zhang and K. M. Zurek (2019), [arXiv:1905.13744].
- [162] Y. Hochberg *et al.*, *Phys. Rev. Lett.* **123**, 15, 151802 (2019), [arXiv:1903.05101].
- [163] T. Lin, *PoS* **333**, 009 (2019), [arXiv:1904.07915].
- [164] F. Aharonian, D. Khangulyan and D. Malyshev, *Astron. Astrophys.* **547**, A114 (2012), [arXiv:1207.0458].
- [165] K. K. Boddy *et al.*, *Phys. Rev.* **D94**, 9, 095027 (2016), [arXiv:1606.07440].
- [166] T. Sjöstrand (2019), [arXiv:1907.09874].
- [167] M. Tavani *et al.* (e-ASTROGAM), *JHEAp* **19**, 1 (2018), [arXiv:1711.01265].
- [168] A. Coogan, L. Morrison and S. Profumo (2019), [arXiv:1907.11846].
- [169] M. Ackermann *et al.* (Fermi-LAT), *Phys. Rev. Lett.* **115**, 23, 231301 (2015), [arXiv:1503.02641].
- [170] D. Hooper and L. Goodenough, *Phys. Lett.* **B697**, 412 (2011), [arXiv:1010.2752].
- [171] M. Ackermann *et al.* (Fermi-LAT), *Astrophys. J.* **840**, 1, 43 (2017), [arXiv:1704.03910].
- [172] F. Calore, I. Cholis and C. Weniger, *JCAP* **1503**, 038 (2015), [arXiv:1409.0042].
- [173] K. N. Abazajian and M. Kaplinghat, *Phys. Rev.* **D86**, 083511 (2012), [Erratum: *Phys. Rev.* **D87**, 129902 (2013)], [arXiv:1207.6047].
- [174] S. K. Lee, M. Lisanti and B. R. Safdi, *JCAP* **1505**, 05, 056 (2015), [arXiv:1412.6099].
- [175] T. Daylan *et al.*, *Phys. Dark Univ.* **12**, 1 (2016), [arXiv:1402.6703].
- [176] R. K. Leane and T. R. Slatyer (2019), [arXiv:1904.08430].
- [177] E. Carlson, T. Linden and S. Profumo, *Phys. Rev. Lett.* **117**, 11, 111101 (2016), [arXiv:1510.04698].
- [178] M. Ajello *et al.* (Fermi-LAT), *Astrophys. J.* **819**, 1, 44 (2016), [arXiv:1511.02938].
- [179] M. Ackermann *et al.* (Fermi-LAT), *Astrophys. J.* **836**, 2, 208 (2017), [arXiv:1702.08602].
- [180] A. McDaniel, T. Jeltema and S. Profumo, *Phys. Rev.* **D97**, 10, 103021 (2018), [arXiv:1802.05258].
- [181] C. Karwin *et al.* (2019), [arXiv:1903.10533].
- [182] A. McDaniel, T. Jeltema and S. Profumo, *Phys. Rev.* **D100**, 2, 023014 (2019), [arXiv:1903.06833].
- [183] R. L. Kinzer *et al.*, *Astrophys. J.* **559**, 282 (2001).
- [184] R. M. Bandyopadhyay *et al.*, *Mon. Not. Roy. Astron. Soc.* **392**, 1115 (2009), [arXiv:0810.3674].
- [185] D. P. Finkbeiner and N. Weiner, *Phys. Rev.* **D76**, 083519 (2007), [arXiv:astro-ph/0702587].
- [186] K. Agashe *et al.*, *JCAP* **1410**, 10, 062 (2014), [arXiv:1405.7370].
- [187] T. Damour and L. M. Krauss, *Phys. Rev. Lett.* **81**, 5726 (1998), [arXiv:astro-ph/9806165].
- [188] S. L. Adler, *Phys. Lett.* **B671**, 203 (2009), [arXiv:0808.2823].
- [189] J. Casanellas and I. Lopes, *Astrophys. J.* **765**, L21 (2013), [arXiv:1212.2985].
- [190] G. D. Mack, J. F. Beacom and G. Bertone, *Phys. Rev.* **D76**, 043523 (2007), [arXiv:0705.4298].
- [191] J. Smolinsky and P. Tanedo, *Phys. Rev.* **D95**, 7, 075015 (2017), [Erratum: *Phys. Rev.* **D96**, no.9, 099902 (2017)], [arXiv:1701.03168].
- [192] C. Niblaeus, A. Beniwal and J. Edsjo (2019), [arXiv:1903.11363].
- [193] M. G. Aartsen *et al.* (IceCube), *JCAP* **1604**, 04, 022 (2016), [arXiv:1601.00653].
- [194] S. Adrian-Martinez *et al.* (ANTARES), *Phys. Lett.* **B759**, 69 (2016), [arXiv:1603.02228].
- [195] C. R. Das *et al.*, *Phys. Lett.* **B725**, 297 (2013), [arXiv:1110.5095].
- [196] M. G. Aartsen *et al.* (IceCube), *J. Phys.* **G44**, 5, 054006 (2017), [arXiv:1607.02671].
- [197] Y. Zhao and K. M. Zurek, *JHEP* **07**, 017 (2014), [arXiv:1401.7664].
- [198] A. W. Strong, I. V. Moskalenko and V. S. Ptuskin, *Ann. Rev. Nucl. Part. Sci.* **57**, 285 (2007), [arXiv:astro-ph/0701517].
- [199] O. Adriani *et al.* (PAMELA), *Phys. Rev. Lett.* **111**, 081102 (2013), [arXiv:1308.0133].
- [200] M. Aguilar *et al.* (AMS), *Phys. Rev. Lett.* **117**, 9, 091103 (2016).
- [201] M. Aguilar *et al.* (AMS), *Phys. Rev. Lett.* **110**, 141102 (2013).
- [202] S. Profumo, F. Queiroz and C. Siqueira (2019), [arXiv:1903.07638].
- [203] D. Hooper, P. Blasi and P. D. Serpico, *JCAP* **0901**, 025 (2009), [arXiv:0810.1527].
- [204] S. Profumo, *Central Eur. J. Phys.* **10**, 1 (2011), [arXiv:0812.4457].
- [205] A. U. Abeysekara *et al.* (HAWC), *Science* **358**, 6365, 911 (2017), [arXiv:1711.06223].
- [206] S. Profumo *et al.*, *Phys. Rev.* **D97**, 12, 123008 (2018), [arXiv:1803.09731].
- [207] R. Cowsik, B. Burch and T. Madziwa-Nussinov, *Astrophys. J.* **786**, 124 (2014), [arXiv:1305.1242].
- [208] K. Blum, B. Katz and E. Waxman, *Phys. Rev. Lett.* **111**, 21, 211101 (2013), [arXiv:1305.1324].
- [209] M.-Y. Cui *et al.*, *Phys. Rev. Lett.* **118**, 19, 191101 (2017), [arXiv:1610.03840].
- [210] A. Reinert and M. W. Winkler, *JCAP* **1801**, 01, 055 (2018), [arXiv:1712.00002].
- [211] M. W. Winkler, *JCAP* **1702**, 02, 048 (2017), [arXiv:1701.04866].
- [212] F. Donato, N. Fornengo and P. Salati, *Phys. Rev.* **D62**, 043003 (2000), [hep-ph/9904481].
- [213] K. Mori *et al.*, *Astrophys. J.* **566**, 604 (2002), [arXiv:astro-ph/0109463].
- [214] H. Baer and S. Profumo, *JCAP* **0512**, 008 (2005), [arXiv:astro-ph/0510722].
- [215] E. Carlson *et al.*, *Phys. Rev.* **D89**, 7, 076005 (2014), [arXiv:1401.2461].
- [216] M. Cirelli *et al.*, *JHEP* **08**, 009 (2014), [arXiv:1401.4017].
- [217] R. Bird *et al.*, in "36th International Cosmic Ray Conference (ICRC 2019) Madison, Wisconsin, USA, July 24-August 1, 2019," (2019), [arXiv:1908.03154].
- [218] A. Coogan and S. Profumo, *Phys. Rev.* **D96**, 8, 083020 (2017), [arXiv:1705.09664].
- [219] S. Colafrancesco, S. Profumo and P. Ullio, *Astron. Astrophys.* **455**, 21 (2006), [arXiv:astro-ph/0507575].
- [220] S. Colafrancesco, S. Profumo and P. Ullio, *Phys. Rev.* **D75**, 023513 (2007), [arXiv:astro-ph/0607073].
- [221] S. Profumo and P. Ullio (2010), [arXiv:1001.4086].

- [222] T. E. Jeltema and S. Profumo, *JCAP* **0811**, 003 (2008), [arXiv:0808.2641].
- [223] M. Cirelli *et al.*, *JCAP* **1103**, 051 (2011), [Erratum: *JCAP*1210,E01(2012)], [arXiv:1012.4515].
- [224] A. McDaniell *et al.*, *JCAP* **1709**, 09, 027 (2017), [arXiv:1705.09384].
- [225] E. Storm *et al.*, *Astrophys. J.* **768**, 106 (2013), [arXiv:1210.0872].
- [226] G. G. Raffelt, *Stars as laboratories for fundamental physics* (1996), ISBN 9780226702728, URL <http://wwwth.mpp.mpg.de/members/raffelt/mypapers/199613.pdf>.
- [227] D. Spolyar, K. Freese and P. Gondolo, *Phys. Rev. Lett.* **100**, 051101 (2008), [arXiv:0705.0521].
- [228] S. Dimopoulos, J. Preskill and F. Wilczek, *Phys. Lett.* **119B**, 320 (1982).
- [229] P. Pani and A. Loeb, *JCAP* **1406**, 026 (2014), [arXiv:1401.3025].
- [230] H. Liu, G. W. Ridgway and T. R. Slatyer (2019), [arXiv:1904.09296].
- [231] M. A. Monroy-Rodríguez and C. Allen, *Astrophys. J.* **790**, 2, 159 (2014), [arXiv:1406.5169].
- [232] M. Ricotti, J. P. Ostriker and K. J. Mack, *Astrophys. J.* **680**, 829 (2008), [arXiv:0709.0524].
- [233] S. Bird *et al.*, *Phys. Rev. Lett.* **116**, 20, 201301 (2016), [arXiv:1603.00464].
- [234] V. Poulin *et al.*, *Phys. Rev.* **D96**, 8, 083524 (2017), [arXiv:1707.04206].
- [235] P. Tisserand *et al.* (EROS-2), *Astron. Astrophys.* **469**, 387 (2007), [arXiv:astro-ph/0607207].
- [236] H. Niikura *et al.*, *Nat. Astron.* **3**, 6, 524 (2019), [arXiv:1701.02151].
- [237] E. Mediavilla *et al.*, *Astrophys. J.* **706**, 1451 (2009), [arXiv:0910.3645].
- [238] A. Barnacka, J. F. Glicenstein and R. Moderski, *Phys. Rev.* **D86**, 043001 (2012), [arXiv:1204.2056].
- [239] A. Katz *et al.*, *JCAP* **1812**, 005 (2018), [arXiv:1807.11495].
- [240] N. Smyth *et al.* (2019), [arXiv:1910.01285].
- [241] B. J. Carr *et al.*, *Phys. Rev.* **D81**, 104019 (2010), [arXiv:0912.5297].
- [242] A. Coogan, L. Morrison and S. Profumo, *Phys. Rev. Lett.* **126**, 17, 171101 (2021), [arXiv:2010.04797].
- [243] B. V. Lehmann *et al.*, *JCAP* **10**, 046 (2019), [arXiv:1906.06348].

28. Dark Energy

Revised August 2021 by D.H. Weinberg (Ohio State U.) and M. White (UC Berkeley; LBNL).

28.1 Repulsive Gravity and Cosmic Acceleration

In the first modern cosmological model, Einstein [1] modified his field equation of General Relativity (GR), introducing a “cosmological term” that enabled a solution with time-independent, spatially homogeneous matter density ρ_m and constant positive space curvature. Although Einstein did not frame it this way, one can view the “cosmological constant” Λ as representing a constant energy density of the vacuum [2], whose repulsive gravitational effect balances the attractive gravity of matter and thereby allows a static solution. After the development of dynamic cosmological models [3,4] and the discovery of cosmic expansion [5], the cosmological term appeared unnecessary, and Einstein and de Sitter [6] advocated adopting an expanding, homogeneous and isotropic, spatially flat, matter-dominated Universe as the default cosmology until observations dictated otherwise. Such a model has matter density equal to the critical density, $\Omega_m \equiv \rho_m/\rho_c = 1$, and negligible contribution from other energy components [7].

By the mid-1990s, the Einstein-de Sitter model was showing numerous cracks, under the combined onslaught of data from the cosmic microwave background (CMB), large-scale galaxy clustering, and direct estimates of the matter density, the expansion rate (H_0), and the age of the Universe. As noted in a number of papers from this time, introducing a cosmological constant offered a potential resolution of many of these tensions, yielding the most empirically successful version of the inflationary cold dark matter scenario. In the late 1990s, supernova surveys by two independent teams provided direct evidence for accelerating cosmic expansion [8,9], establishing the cosmological constant model (with $\Omega_m \simeq 0.3$, $\Omega_\Lambda \simeq 0.7$) as the preferred alternative to the $\Omega_m = 1$ scenario. Shortly thereafter, CMB evidence for a spatially flat Universe [10,11], and thus for $\Omega_{\text{tot}} \simeq 1$, cemented the case for cosmic acceleration by firmly eliminating the free-expansion alternative with $\Omega_m \ll 1$ and $\Omega_\Lambda = 0$. Today, the accelerating Universe is well established by multiple lines of independent evidence from a tight web of precise cosmological measurements.

As discussed in the Big Bang Cosmology article of this *Review* (Sec. 22), the scale factor $R(t)$ of a homogeneous and isotropic Universe governed by GR grows at an accelerating rate if the pressure $p < -\frac{1}{3}\rho$ (in $c = 1$ units). A cosmological constant has $\rho_\Lambda = \text{constant}$ and pressure $p_\Lambda = -\rho_\Lambda$ (see Eq. 22.10), so it will drive acceleration if it dominates the total energy density. However, acceleration could arise from a more general form of “dark energy” that has negative pressure, typically specified in terms of the equation-of-state-parameter $w = p/\rho$ ($= -1$ for a cosmological constant). Furthermore, the conclusion that acceleration requires a new energy component beyond matter and radiation relies on the assumption that GR is the correct description of gravity on cosmological scales. The title of this article follows the common but inexact usage of “dark energy” as a catch-all term for the origin of cosmic acceleration, regardless of whether it arises from a new form of energy or a modification of GR. Our account here draws on the much longer review of cosmic acceleration by Ref. [12], which provides background explanation and extensive literature references for the discussion in Secs. 28.2 and 28.3.

Below we will use the abbreviation Λ CDM to refer to a model with cold dark matter, a cosmological constant, inflationary initial conditions, standard radiation and neutrino content, and a flat Universe with $\Omega_{\text{tot}} = 1$ (though we will sometimes describe this model as “flat Λ CDM” to emphasize this last restriction). We will use w CDM to denote a model with the same assumptions but a free, constant value of w . Models with the prefix “o” (*e.g.*, o w CDM) allow non-zero space curvature.

28.2 Theories of Cosmic Acceleration

28.2.1 Dark Energy or Modified Gravity?

A cosmological constant is the mathematically simplest, and perhaps the physically simplest, theoretical explanation for the accelerating Universe. The problem is explaining its unnaturally small magnitude, as discussed in Sec. 22.4.7 of this *Review*. An alternative (which still requires finding a way to make the cos-

mological constant zero or at least negligibly small) is that the accelerating cosmic expansion is driven by a new form of energy such as a scalar field [13] with potential $V(\phi)$. The energy density and pressure of the field $\phi(\mathbf{x})$ take the same forms as for inflationary scalar fields, given in Eq. (22.52) of the Big Bang Cosmology article. In the limit that $\frac{1}{2}\dot{\phi}^2 \ll |V(\phi)|$, the scalar field acts like a cosmological constant, with $p_\phi \simeq -\rho_\phi$. In this scenario, today’s cosmic acceleration is closely akin to the epoch of inflation, but with radically different energy and timescale.

More generally, the value of $w = p_\phi/\rho_\phi$ in scalar field models evolves with time in a way that depends on $V(\phi)$ and on the initial conditions $(\phi_i, \dot{\phi}_i)$; some forms of $V(\phi)$ have attractor solutions in which the late-time behavior is insensitive to initial values. Many forms of time evolution are possible, including ones where w is approximately constant and broad classes where w “freezes” towards or “thaws” away from $w = -1$, with the transition occurring when the field comes to dominate the total energy budget. If ρ_ϕ is even approximately constant, then it becomes dynamically insignificant at high redshift, because the matter density scales as $\rho_m \propto (1+z)^3$. “Early dark energy” models are ones in which ρ_ϕ is a small but not negligible fraction (*e.g.*, a few percent) of the total energy throughout the matter- and radiation-dominated eras, tracking the dominant component before itself coming to dominate at low redshift.

Instead of introducing a new energy component, one can attempt to modify gravity in a way that leads to accelerated expansion [14]. One option is to replace the Ricci scalar \mathcal{R} with a function $\mathcal{R} + f(\mathcal{R})$ in the gravitational action [15]. Other changes can be more radical, such as introducing extra dimensions and allowing gravitons to “leak” off the brane that represents the observable Universe (the “DGP” model [16]). The DGP example has inspired a more general class of “galileon” and massive gravity models. Constructing viable modified gravity models is challenging, in part because it is easy to introduce theoretical inconsistencies (such as “ghost” fields with negative kinetic energy), but above all because GR is a theory with many high-precision empirical successes on solar system scales [17]. Modified gravity models typically invoke screening mechanisms that force model predictions to approach those of GR in regions of high density or strong gravitational potential. Screening offers potentially distinctive signatures, as the strength of gravity (*i.e.*, the effective value of G_N) can vary by order unity in environments with different gravitational potentials.

More generally, one can search for signatures of modified gravity by comparing the history of cosmic structure growth to the history of cosmic expansion. Within GR, these two are linked by a consistency relation, as described below (Eq. (28.2)). Modifying gravity can change the predicted rate of structure growth, and it can make the growth rate dependent on scale or environment. In some circumstances, modifying gravity alters the combinations of potentials responsible for gravitational lensing and the dynamics of non-relativistic tracers (such as galaxies or stars) in different ways (see Sec. 22.4.7 in this *Review*), leading to order unity mismatches between the masses of objects inferred from lensing and those inferred from dynamics in unscreened environments.

At present there are no fully realized and empirically viable modified gravity theories that explain the observed level of cosmic acceleration. The constraints on $f(\mathcal{R})$ models now force them so close to GR that they cannot produce acceleration without introducing a separate dark energy component [18]. The DGP model is empirically ruled out by several tests, including the expansion history, the integrated Sachs-Wolfe effect, and redshift-space distortion measurements of the structure growth rate [19]. The near-simultaneous arrival of gravitational waves and electromagnetic signals from the neutron star merger event GW170817, which shows that gravitational waves travel at almost exactly the speed of light, is a further strong constraint on modified gravity theories [20]. The elimination of models should be considered an important success of the program to empirically test theories of cosmic acceleration. However, it is worth recalling that there was no fully realized gravitational explanation for the precession of Mercury’s orbit prior to the completion of GR in 1915, and the fact that no complete and viable modified gravity theory exists

today does not mean that one will not arise in the future. In the meantime, we can continue empirical investigations that can tighten restrictions on such theories or perhaps point towards the gravitational sector as the origin of accelerating expansion.

28.2.2 Expansion History and Growth of Structure

The main line of empirical attack on dark energy is to measure the history of cosmic expansion and the history of matter clustering with the greatest achievable precision over a wide range of redshift. Within GR, the expansion rate $H(z)$ is governed by the Friedmann equation (see the articles on Big Bang Cosmology and Cosmological Parameters—Secs. 22 and 25 in this *Review*). For dark energy with an equation of state $w(z)$, the cosmological constant contribution to the expansion, Ω_Λ , is replaced by a redshift-dependent contribution. The evolution of the dark energy density follows from Eq. (22.10),

$$\begin{aligned} \Omega_{\text{de}} \frac{\rho_{\text{de}}(z)}{\rho_{\text{de}}(z=0)} &= \Omega_{\text{de}} \exp \left[3 \int_0^z [1 + w(z')] \frac{dz'}{1+z'} \right] \\ &= \Omega_{\text{de}} (1+z)^{3(1+w)}, \end{aligned} \quad (28.1)$$

where the second equality holds for constant w . If Ω_m , Ω_r , and the present value of Ω_{tot} are known, then measuring $H(z)$ pins down $w(z)$. (Note that Ω_{de} is the same quantity denoted Ω_v in Sec. 22, but we have adopted the ‘de’ subscript to avoid implying that dark energy is necessarily a vacuum effect.)

While some observations can probe $H(z)$ directly, others measure the distance-redshift relation. The basic relations between angular diameter distance or luminosity distance and $H(z)$ are given in Ch. 22—and these are generally unaltered in time-dependent dark energy or modified gravity models. For convenience, in later sections, we will sometimes refer to the comoving angular distance, $D_{A,c}(z) = (1+z)D_A(z)$.

In GR-based linear perturbation theory, the density contrast $\delta(\mathbf{x}, t) \equiv \rho(\mathbf{x}, t)/\bar{\rho}(t) - 1$ of pressureless matter grows in proportion to the linear growth function $G(t)$ (not to be confused with the gravitational constant G_N), which follows the differential equation

$$\ddot{G} + 2H(z)\dot{G} - \frac{3}{2}\Omega_m H_0^2 (1+z)^3 G = 0. \quad (28.2)$$

To a good approximation, the logarithmic derivative of $G(z)$ is

$$f(z) \equiv -\frac{d \ln G}{d \ln(1+z)} \simeq \left[\Omega_m (1+z)^3 \frac{H_0^2}{H^2(z)} \right]^\gamma, \quad (28.3)$$

where $\gamma \simeq 0.55$ for relevant values of cosmological parameters [21]. In an $\Omega_m = 1$ Universe, $G(z) \propto (1+z)^{-1}$, but growth slows when Ω_m drops significantly below unity. One can integrate Eq. (28.3) to get an approximate integral relation between $G(z)$ and $H(z)$, but the full (numerical) solution to Eq. (28.2) should be used for precision calculations. Even in the non-linear regime, the amplitude of clustering is determined mainly by $G(z)$, so observations of non-linear structure can be used to infer the linear $G(z)$, provided one has good theoretical modeling to relate the two.

In modified gravity models the growth rate of gravitational clustering may differ from the GR prediction. A general strategy to test modified gravity, therefore, is to measure both the expansion history and the growth history to see whether they yield consistent results for $H(z)$ or $w(z)$.

28.2.3 Parameters

Constraining a general history of $w(z)$ is nearly impossible, because the dark energy density, which affects $H(z)$, is given by an integral over $w(z)$, and distances and the growth factor involve a further integration over functions of $H(z)$. Oscillations in $w(z)$ over a range $\Delta z/(1+z) \ll 1$ are therefore extremely difficult to constrain. It has become conventional to phrase constraints or projected constraints on $w(z)$ in terms of a linear evolution model,

$$w(a) = w_0 + w_a(1-a) = w_p + w_a(a_p - a), \quad (28.4)$$

where $a \equiv (1+z)^{-1}$, w_0 is the value of w at $z = 0$, and w_p is the value of w at a ‘pivot’ redshift $z_p \equiv a_p^{-1} - 1$, where it

is best constrained by a given set of experiments. For typical data combinations, $z_p \simeq 0.5$. This simple parameterization can provide a good approximation to the predictions of many physically motivated models for observables measured with percent-level precision. A widely used ‘Figure of Merit’ (FoM) for dark energy experiments [22] is the projected combination of errors $[\sigma(w_p)\sigma(w_a)]^{-1}$. Ambitious future experiments with 0.1–0.3% precision on observables can constrain richer descriptions of $w(z)$, which can be characterized by principal components.

There has been less convergence on a standard parameterization for describing modified gravity theories. Deviations from the GR-predicted growth rate can be described by a deviation $\Delta\gamma$ in the index of Eq. (28.3), together with an overall multiplicative offset relative to the $G(z)$ expected from extrapolating the CMB-measured fluctuation amplitude to low redshift. However, these two parameters may not accurately capture the growth predictions of all physically interesting models. Another important parameter to constrain is the ratio of the gravitational potentials governing space curvature and the acceleration of non-relativistic test particles. The possible phenomenology of modified gravity models is rich [23], which enables many consistency tests but complicates the task of constructing parameterized descriptions.

The more general set of cosmological parameters is discussed elsewhere in this *Review* (Sec. 25), but here we highlight a few that are particularly important to the dark energy discussion.

- The dimensionless Hubble parameter $h \equiv H_0/100 \text{ km s}^{-1} \text{ Mpc}^{-1}$ determines the present day value of the critical density and the overall scaling of distances inferred from redshifts.
- Ω_m and Ω_{tot} affect the expansion history and the distance-redshift relation.
- The sound horizon $r_s = \int_0^{t_{\text{rec}}} c_s(t) dt/a(t)$, the comoving distance that pressure waves can propagate between $t = 0$ and recombination, determines the physical scale of the acoustic peaks in the CMB and the baryon acoustic oscillation (BAO) feature in low-redshift matter clustering [24].
- The amplitude of matter fluctuations, conventionally represented by the quantity $\sigma_8(z)$, scales the overall amplitude of growth measures such as weak lensing or redshift-space distortions (discussed in the next section).

Specifically, $\sigma_8(z)$ refers to the rms fluctuation of the matter overdensity $\rho/\bar{\rho}$ in spheres of radius $8 h^{-1} \text{ Mpc}$, computed from the linear theory matter power spectrum at redshift z , and σ_8 on its own refers to the value at $z = 0$ (just like our convention for Ω_m).

While discussions of dark energy are frequently phrased in terms of values and errors on quantities like w_p , w_a , $\Delta\gamma$, and Ω_{tot} , parameter precision is the means to an end, not an end in itself. The underlying goal of empirical studies of cosmic acceleration is to address two physically profound questions:

1. Does acceleration arise from a breakdown of GR on cosmological scales or from a new energy component that exerts repulsive gravity within GR?
2. If acceleration is caused by a new energy component, is its energy density constant in space and time, as expected for a fundamental vacuum energy, or does it show variations that indicate a dynamical field?

Substantial progress towards answering these questions, in particular any definitive rejection of the cosmological constant ‘null hypothesis,’ would be a major breakthrough in cosmology and fundamental physics.

28.3 Observational Probes

We briefly summarize the observational probes that play the greatest role in current constraints on dark energy. Further discussion can be found in other articles of this *Review*, in particular Secs. 25 (Cosmological Parameters) and 29 (The Cosmic Microwave Background), and in Ref. [12], which provides extensive references to background literature. Recent observational results from these methods are discussed in Sec. 28.4.

28.3.1 Methods, Sensitivity, Systematics

Cosmic Microwave Background Anisotropies: Although CMB anisotropies provide limited information about dark energy on their own, CMB constraints on the geometry, matter content, and radiation content of the Universe play a critical role in dark energy studies when combined with low-redshift probes. In particular, CMB data supply measurements of $\theta_s = r_s/D_{A,c}(z_{\text{rec}})$, the angular size of the sound horizon at recombination, from the angular location of the acoustic peaks, measurements of $\Omega_m h^2$ and $\Omega_b h^2$ from the heights of the peaks, and normalization of the amplitude of matter fluctuations at z_{rec} from the amplitude of the CMB fluctuations themselves. *Planck* data yield a 0.18% determination of r_s , which scales as $(\Omega_m h^2)^{-0.25}$ for cosmologies with standard matter and radiation content. The uncertainty in the matter fluctuation amplitude at the epoch of recombination is 0.5%. Secondary anisotropies, including the integrated Sachs-Wolfe effect, the Sunyaev-Zel'dovich (SZ, [25]) effect, and weak lensing of primary anisotropies, provide additional information about dark energy by constraining low-redshift structure growth.

Type Ia Supernovae (SN): Type Ia supernovae, produced by the thermonuclear explosions of white dwarfs, exhibit 10–15% scatter in peak luminosity after correction for light curve duration (the time to rise and fall) and color (which is a diagnostic of dust extinction). Since the peak luminosity is not known *a priori*, supernova surveys constrain ratios of luminosity distances at different redshifts. If one is comparing a high-redshift sample to a local calibrator sample measured with much higher precision (and distances inferred from Hubble's law), then one essentially measures the luminosity distance in $h^{-1}\text{Mpc}$, constraining the combination $hD_L(z)$. With distance uncertainties of 5–8% per well observed supernova, a sample of around 100 SNe is sufficient to achieve sub-percent statistical precision. The 1–2% systematic uncertainties in current samples are dominated by uncertainties associated with photometric calibration and dust extinction corrections plus the observed dependence of luminosity on host galaxy properties. Another potential systematic is redshift evolution of the supernova population itself, which can be tested by analyzing subsamples grouped by spectral properties or host galaxy properties to confirm that they yield consistent results.

Baryon Acoustic Oscillations (BAO):

Pressure waves that propagate in the pre-recombination photon-baryon fluid imprint a characteristic scale in the clustering of matter and galaxies, which appears in the galaxy correlation function as a localized peak at the sound horizon scale r_s , or in the power spectrum as a series of oscillations. Since observed galaxy coordinates consist of angles and redshifts, measuring this “standard ruler” scale in a galaxy redshift survey determines the angular diameter distance $D_A(z)$ and the expansion rate $H(z)$, which convert coordinate separations to comoving distances. Errors on the two quantities are correlated, and in existing galaxy surveys the best determined combination is approximately $D_V(z) = [czD_{A,c}^2(z)/H(z)]^{1/3}$. As an approximate rule of thumb, a survey that fully samples structures at redshift z over a comoving volume V , and is therefore limited by cosmic variance rather than shot noise, measures $D_{A,c}(z)$ with a fractional error of $0.005(V/10\text{Gpc}^3)^{-1/2}$ and $H(z)$ with a fractional error 1.6–1.8 times higher. The most precise BAO measurements to date come from large galaxy redshift surveys probing $z < 0.8$, and these will be extended to higher redshifts by future projects. At redshifts $z > 2$, BAO can also be measured in the Lyman- α forest of intergalactic hydrogen absorption towards background quasars, where the fluctuating absorption pattern provides tens or hundreds of samples of the density field along each quasar sightline. For Lyman- α forest BAO, the best measured parameter combination is more heavily weighted towards $H(z)$ because of strong redshift-space distortions that enhance clustering in the line-of-sight direction. Radio intensity mapping, which maps large-scale structure in redshifted 21-cm hydrogen emission without resolving individual galaxies, offers a potentially promising route to measuring BAO over large volumes at relatively low cost, but the technique is still under development. Photometric redshifts in optical imaging surveys can be used to measure BAO in the angular direction, though the typical distance precision is a fac-

tor of 3–4 lower compared to a well sampled spectroscopic survey of the same area, and angular BAO measurements do not directly constrain $H(z)$. BAO distance measurements complement SN distance measurements by providing absolute rather than relative distances (with precise calibration of r_s from the CMB) and by having greater achievable precision at high redshift thanks to the increasing comoving volume available. Theoretical modeling suggests that BAO measurements from even the largest feasible redshift surveys will be limited by statistical rather than systematic uncertainties.

Weak Gravitational Lensing: Gravitational light bending by a clustered distribution of matter shears the shapes of higher redshift background galaxies in a spatially coherent manner, producing a correlated pattern of apparent ellipticities. By studying the weak lensing signal for source galaxies binned by photometric redshift (estimated from broad-band colors), one can probe the history of structure growth. “Cosmic shear” weak lensing uses the correlation of source ellipticities to deduce the clustering of intervening matter. “Galaxy-galaxy lensing” (GGL) uses the correlation between a shear map and a foreground galaxy sample to measure the average mass profile around the foreground galaxies, which can be combined with galaxy clustering to constrain total matter clustering. For a specified expansion history, the predicted signals scale approximately as $\sigma_8 \Omega_m^\alpha$, with $\alpha \simeq 0.3\text{--}0.5$. The predicted signals also depend on the distance-redshift relation, so weak lensing becomes more powerful in concert with SN or BAO measurements that can pin this relation down independently. The most challenging systematics are shape measurement biases, biases in the distribution of photometric redshifts, and intrinsic alignments of galaxy orientations that could contaminate the lensing-induced signal. Weak lensing of CMB anisotropies is an increasingly powerful tool, in part because it circumvents many of these observational and astrophysical systematics. Predicting the large-scale weak lensing signal is straightforward in principle, but the number of independent modes on large scales is small, and the inferences are therefore dominated by sample variance. Exploiting small-scale measurements, for tighter constraints, requires modeling the effects of complex physical processes such as star formation and feedback on the matter power spectrum. Strong gravitational lensing can also provide constraints on dark energy, either through time delay measurements that probe the absolute distance scale, or through measurements of multiple-redshift lenses that constrain distance ratios. The primary uncertainty for strong lensing constraints is modeling the mass distribution of the lens systems.

Clusters of Galaxies: Like weak lensing, the abundance of massive dark-matter halos probes structure growth by constraining $\sigma_8 \Omega_m^\alpha$, where $\alpha \simeq 0.3\text{--}0.5$. These halos can be identified as dense concentrations of galaxies or through the signatures of hot ($10^7\text{--}10^8\text{K}$) gas in X-ray emission or SZ distortion of the CMB. The critical challenge in cluster cosmology is calibrating the relation $P(M_{\text{halo}}|O)$ between the halo mass as predicted from theory and the observable O used for cluster identification. Measuring the stacked weak lensing signal from clusters has emerged as a promising approach to achieve percent-level accuracy in calibration of the mean relation, which is required for clusters to remain competitive with other growth probes. This method requires accurate modeling of completeness and contamination of cluster catalogs, projection effects on cluster selection and weak lensing measurements, and possible baryonic physics effects on the mass distribution within clusters.

Redshift-Space Distortions (RSD) and the Alcock-Paczynski (AP) Effect: Redshift-space distortions of galaxy clustering, induced by peculiar motions, probe structure growth by constraining the parameter combination $f(z)\sigma_8(z)$, where $f(z)$ is the growth rate defined by Eq. (28.3). Uncertainties in theoretical modeling of non-linear gravitational evolution and the non-linear bias between the galaxy and matter distributions currently limit application of the method to large scales (comoving separations $r \gtrsim 10h^{-1}\text{Mpc}$ or wavenumbers $k \lesssim 0.2h\text{Mpc}^{-1}$). A second source of anisotropy arises if one adopts the wrong cosmological metric to convert angles and redshifts into comoving separations, a phenomenon known as the Alcock-Paczynski effect [27]. Demanding isotropy

Table 28.1: A selection of major dark-energy experiments, based on Ref. [26]. Abbreviations in the “Data” column refer to optical (Opt) or near-infrared (NIR) imaging (I) or spectroscopy (S). For spectroscopic experiments, the “Spec- z ” column lists the primary redshift range for galaxies (gals), quasars (QSOs), or the Lyman- α forest (Ly α F). Abbreviations in the “Methods” column are weak lensing (WL), clusters (CL), supernovae (SN), baryon acoustic oscillations (BAO), and redshift-space distortions (RSD).

Project	Dates	Area/deg ²	Data	Spec- z Range	Methods
BOSS	2008–2014	10,000	Opt-S	0.3–0.7 (gals) 2–3.5 (Ly α F)	BAO/RSD
KiDS	2011–2019	1350	Opt-I	—	WL/CL
DES	2013–2019	5000	Opt-I	—	WL/CL SN/BAO
eBOSS	2014–2018	7500	Opt-S	0.6–2.0 (gal/QSO) 2–3.5 (Ly α F)	BAO/RSD
SuMIRE	2014–2024	1500	Opt-I	—	WL/CL
HETDEX	2017–2023	450	Opt/NIR-S	0.8–2.4 (gals)	BAO/RSD
DESI	2021–2026	14,000	Opt-S	1.9 < z < 3.5 (gals) 0–1.7 (gals) 2–3.5 (Ly α F)	BAO/RSD
VRO/LSST	2022–2032	20,000	Opt-I	—	WL/CL SN/BAO
<i>Euclid</i>	2022–2028	15,000	Opt-I	—	WL/CL
			NIR-S	0.7–2.2 (gals)	BAO/RSD
<i>Roman</i>	2026–2031	2200	NIR-I	—	WL/CL/SN
			NIR-S	1.0–3.0 (gals)	BAO/RSD

of clustering at redshift z constrains the parameter combination $H(z)D_A(z)$. The main challenge for the AP method is correcting for the anisotropy induced by peculiar velocity RSD.

Low Redshift Measurement of H_0 : The value of H_0 sets the current value of the critical density $\rho_c = 3H_0^2/8\pi G_N$, and combination with CMB measurements provides a long lever arm for constraining the evolution of dark energy. The challenge in conventional H_0 measurements is establishing distances to galaxies that are “in the Hubble flow,” *i.e.*, far enough away that their peculiar velocities are small compared to the expansion velocity $v = H_0 d$. This can be done by building a ladder of distance indicators tied to stellar parallax on its lowest rung, or by using gravitational-lens time delays or geometrical measurements of maser data to circumvent this ladder.

28.3.2 Dark Energy Experiments

Most observational applications of these methods now take place in the context of large cosmological surveys, for which constraining dark energy and modified gravity theories is a central objective. Table 28.1 lists a selection of recent, ongoing, and planned dark-energy experiments, taken originally from the Snowmass 2013 Dark Energy Facilities review [26], which focused on projects in which the U.S. has either a leading role or significant participation. References and links to further information about these projects can be found in Ref. [26]. We have adjusted some of the dates in this Table relative to those in Ref. [26] and added the European-led KiloDegree Survey (KiDS). Dates in the Table correspond to the duration of survey observations, and the final cosmological results frequently require 1–3 years of analysis and modeling beyond the end of data taking.

Beginning our discussion with imaging surveys, the Dark Energy Survey (DES) has observed 1/8 of the sky to a depth roughly 2 magnitudes deeper than the Sloan Digital Sky Survey (SDSS), enabling weak lensing measurements with much greater statistical precision, cluster measurements calibrated by weak lensing, and angular BAO measurements based on photometric redshifts. With repeated imaging of selected fields, DES has identified thousands of Type Ia SNe, which together with spectroscopic follow-up data enable significant improvements on the current state-of-the-art for supernova (SN) cosmology. Cosmological results from weak lensing and galaxy clustering analyses of the 3-year (Y3) DES data set are presented in Ref. [28] and discussed further below, while the first cosmological results from the DES supernova survey are presented in Ref. [29]. KiDS and the Subaru Hyper-Suprime Camera (HSC) collaboration are carrying out op-

tical imaging surveys similar to the DES weak lensing survey, smaller in area but with greater depth and sharper image quality. Weak lensing cosmology results from 1000 deg² of KiDS imaging are reported by Refs. [30,31] and from the first year of HSC imaging by Refs. [32,33], all discussed further below. The HSC survey is one component of the Subaru Measurement of Images and Redshifts (SuMIRE) project. Beginning in the early 2020s, the Legacy Survey of Space and Time (LSST) of the Vera Rubin Observatory (VRO) will scan the southern sky to SDSS-like depth every four nights. LSST imaging co-added over its decade-long primary survey will reach extraordinary depth, enabling weak lensing, cluster, and photometric BAO studies from billions of galaxies. Additionally, LSST time-domain monitoring will identify and measure light curves for thousands of Type Ia SNe per year.

Turning to spectroscopic surveys, the Baryon Oscillation Spectroscopic Survey (BOSS) and its successor eBOSS used fiber-fed optical spectrographs to map the redshift-space distributions of millions of galaxies and quasars. These 3-dimensional maps enable BAO and RSD measurements, and Lyman- α forest spectra of high-redshift quasars extend these measurements to redshifts $z > 2$. As discussed below, the eBOSS Collaboration has now published BAO and RSD analyses from the final data sets of the BOSS and eBOSS programs. The Hobby-Eberly Telescope Dark Energy Experiment (HETDEX) uses integral field spectrographs to detect Lyman- α emission-line galaxies at $z \simeq 1.9$ –3.5, probing a small sky area but a substantial comoving volume. The Dark Energy Spectroscopic Instrument (DESI) follows a strategy similar to BOSS/eBOSS but on a much grander scale, using a larger telescope (4-m vs. 2.5-m) and a much higher fiber multiplex (5000 vs. 1000) to survey an order-of-magnitude more galaxies. After commissioning and survey validation observations, DESI began full operations in May 2021, and it has already measured more galaxy redshifts than BOSS and eBOSS combined. A new Prime Focus Spectrograph (PFS) for the Subaru telescope will enable the spectroscopic component of SuMIRE, with the large telescope aperture and wavelength sensitivity that extends to the near-infrared (NIR) allowing it to probe a higher redshift galaxy population than DESI, over a smaller area of sky.

Compared to ground-based observations, space observations afford higher angular resolution and a far lower NIR sky background. The *Euclid* mission and the *Nancy Grace Roman Space Telescope* (formerly *WFIRST*) will exploit these advantages, conducting large area imaging surveys for weak lensing and cluster studies and slitless spectroscopic surveys of emission-line galaxies for BAO and RSD studies. *Roman* will also incorporate an imag-

ing and spectrophotometric supernova (SN) survey, extending to redshift $z \simeq 1.7$. Survey details are likely to evolve prior to launch, but in the current designs one can roughly characterize the difference between the *Euclid* and *Roman* dark-energy experiments as “wide vs. deep,” with planned survey areas of 15,000 deg² and 2200 deg², respectively. For weak lensing shape measurements, *Euclid* will use a single wide optical filter, while *Roman* will use three NIR filters. The *Euclid* galaxy redshift survey will cover a large volume at relatively low space density, while the *Roman* survey will provide denser sampling of structure in a smaller volume. There are numerous synergies among the LSST, *Euclid*, and *Roman* dark energy programs, as discussed in Ref. [34].

28.4 Current Constraints on Expansion, Growth, and Dark Energy

The last decade has seen dramatic progress in measurements of the cosmic expansion history and structure growth, leading to much tighter constraints on the parameters of dark energy models. CMB data from the *WMAP* and *Planck* satellites and from higher resolution ground-based experiments have provided an exquisitely detailed picture of structure at the recombination epoch and the first CMB-based measures of low-redshift structure through lensing and SZ cluster counts. Cosmological supernova samples have increased in size from tens to many hundreds, with continuous coverage from $z = 0$ to $z \simeq 1.4$, alongside major improvements in data quality, analysis methods, and detailed understanding of local populations. BAO measurements have advanced from the first detections to 1–2% precision at multiple redshifts, with increasingly sophisticated methods for testing systematics, fitting models, and evaluating statistical errors. Advances in X-ray, SZ, and weak-lensing observations of large samples of galaxy clusters allow a multi-faceted approach to mass calibration, improving statistical precision but also revealing sources of astrophysical uncertainty. Cluster constraints have been joined, and for the present superseded, by the first precise matter-clustering constraints from cosmic-shear weak lensing and galaxy-galaxy lensing, and by redshift-space distortion measurements that probe different aspects of structure growth at (presently) lower precision. The precision of low-redshift H_0 measurements has sharpened from the roughly 10% error of the *HST* Key Project [35] to 2–3% in recent analyses.

As an illustration of current measurements of the cosmic expansion history, Fig. 28.1 compares distance-redshift measurements from SN and BAO data to the predictions for a flat Universe with a cosmological constant. SN cosmology relies on compilation analyses that try to bring data from different surveys probing distinct redshift ranges to a common scale. Here we use the “joint light curve analysis” (JLA) sample of Ref. [37], who carried out a careful intercalibration of the 3-year Supernova Legacy Survey (SNLS3, [39]) and the full SDSS-II Supernova Survey [3] data in combination with several local supernova samples and high-redshift supernovae from *HST*. Results from the Union2.1 sample [40], which partly overlaps JLA but has different analysis procedures, would be similar. Other state-of-the-art supernova data sets include the Pan-STARRS1 sample incorporated in the PANTHEON compilation [41] and the sample of spectroscopically confirmed supernovae from DES [29]. For illustration purposes, we have binned the JLA data in redshift and plotted the diagonal elements of the covariance matrix as error bars, and we have converted the SN luminosity distances to an equivalent comoving angular diameter distance. Because the peak luminosity of a fiducial SN Ia is an unknown free parameter, the SN distance measurements could all be shifted up and down by a constant multiplicative factor; cosmological information resides in the relative distances as a function of redshift. The normalization used here corresponds to a Hubble parameter $h = 0.674$.

For the BAO data points in Fig. 28.1 we have used the compilation in Table 3 (the “BAO-only” row) from the summary cosmology paper by the eBOSS collaboration [38], where one can find references for the original data sources. The individual BAO measurements come (in order of increasing redshift) from the SDSS-II main galaxy sample and from luminous red galaxies, emission line galaxies, and quasars mapped by BOSS and eBOSS. The two high-

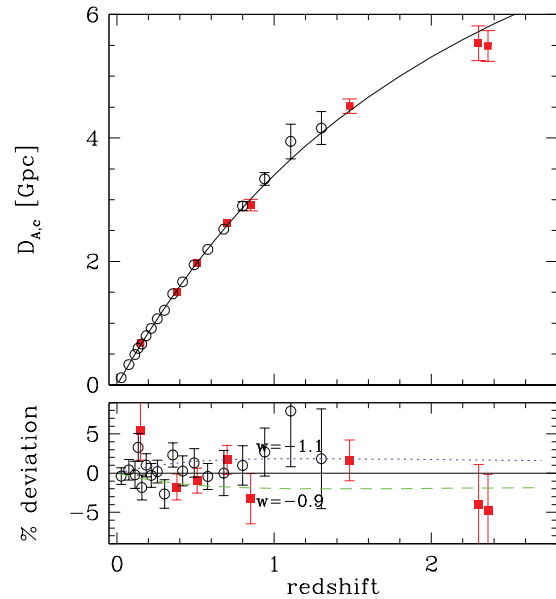


Figure 28.1: Distance-redshift relation measured from Type Ia SN and BAO compared to the predictions (black curve) of a flat Λ CDM model with $\Omega_m = 0.315$ and $h = 0.674$, the best-fit parameters inferred from *Planck* CMB data [36]. Circles show binned luminosity distances from the JLA SN sample [37], multiplied by $(1+z)^{-1}$ to convert to comoving angular diameter distance. Red squares show BAO distance measurements from the SDSS-II, BOSS, and eBOSS surveys as compiled in Ref. [38]. The lower panel plots residuals from the Λ CDM prediction, with dashed and dotted curves that show the effect of changing w by ± 0.1 while all other parameters are held fixed. Note that the SN data points can be shifted up or down by a constant factor to account for freedom in the peak luminosity, while the BAO points are calibrated to 0.2% precision by the sound horizon scale computed from *Planck* data. The errors on the BAO data points are approximately independent, but not entirely so. In the upper panel, error bars are plotted only at $z > 0.7$ to avoid visual confusion. The two Lyman- α forest data points are slightly offset from their effective redshift of $z = 2.33$ for clarity.

est redshift points, both with an effective $z \approx 2.3$, come from the auto-correlation of the Lyman- α forest in high-redshift ($z > 2$) quasars from BOSS and eBOSS and from the cross-correlation of the Lyman- α forest with the quasars themselves. The BAO measurements are converted to absolute distances using the sound horizon scale $r_s = 147.09$ Mpc from *Planck* 2018 CMB data, whose 0.18% uncertainty is small compared to the current BAO measurement errors. For the $z = 0.15$ and $z = 1.5$ data points we have converted values of D_V to $D_{A,c}$, while for other redshifts we use the $D_{A,c}$ determinations measured directly by the transverse BAO. The galaxy and Lyman- α forest analyses also measure $H(z)$ at the same redshifts, providing further leverage on expansion history that is not captured in Fig. 28.1.

The plotted cosmological model has $\Omega_m = 0.315$ and $h = 0.674$, the best-fit values from *Planck* (TT+TE+EE+lowE+lensing) assuming $w = -1$ and $\Omega_{tot} = 1$ [36]. The SN, BAO, and CMB data sets, probing a wide range of redshifts with radically different techniques, are for the most part mutually consistent with the predictions of a flat Λ CDM cosmology. This consistency has held steady or improved as the measurements themselves have improved over the past decade. Dotted and dashed curves in the lower panel of Fig. 28.1 show the effect of changing w by ± 0.1 with all other parameters held fixed, which leads to significantly worse agreement with the data. However, such a single-parameter comparison does not capture the impact of parameter degeneracies or the ability of complementary data sets to break them, and if one instead forced a match to CMB data by changing h and Ω_m when changing w then the predicted BAO distances would diverge at

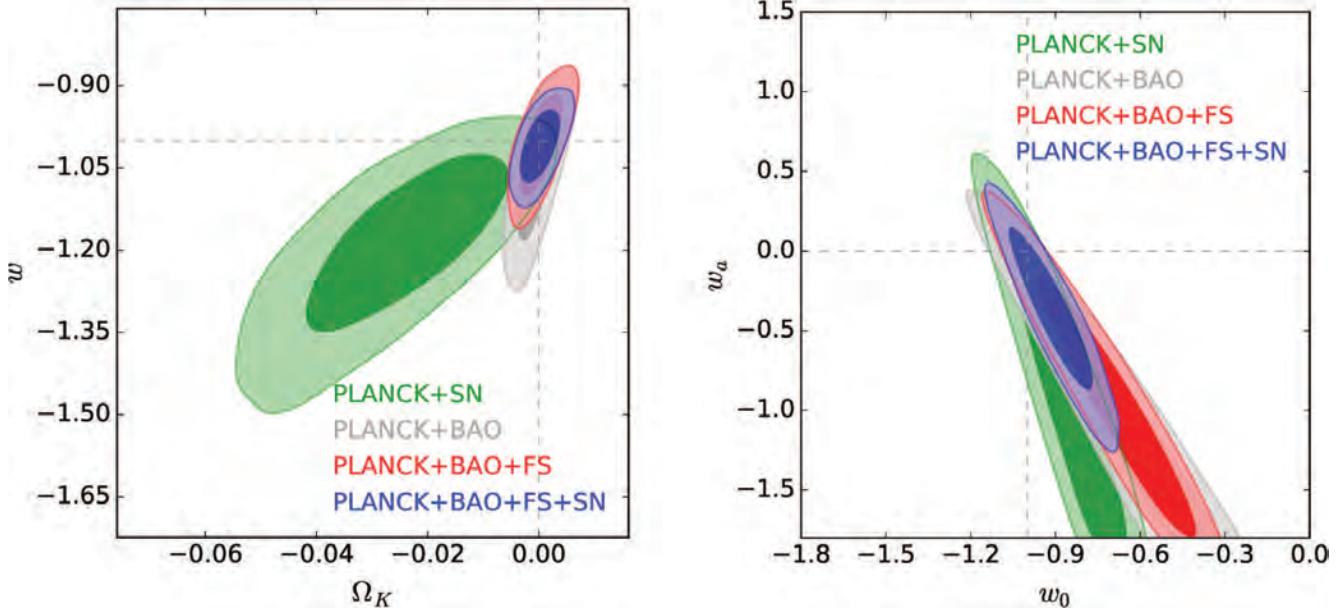


Figure 28.2: Constraints on dark energy model parameters from combinations of CMB, BAO, galaxy clustering, and supernova (SN) data, taken from Ref. [42]. The left panel shows 68% and 95% confidence contours in the $owCDM$ model, with constant equation-of-state parameter w and non-zero space curvature $\Omega_K \equiv 1 - \Omega_{\text{tot}}$. Green and gray contours show the combination of *Planck* CMB data with SN or BAO data, respectively. Red contours combine CMB, BAO, and the full shape (FS) of redshift-space galaxy clustering. Blue contours add SN data to this combination. The right panel shows confidence contours for the same data combinations in the w_0w_aCDM model, which assumes a flat Universe and an evolving equation of state with $w(a) = w_0 + w_a(1 - a)$.

$z = 0$ rather than converging there. Other good representations of recent observational constraints on the cosmic expansion history include Fig. 11 of Ref. [41] for SNIa and Fig. 2 of Ref. [38] for BAO.

Fig. 28.2, taken from Ref. [42], presents constraints on models that allow a free but constant value of w with non-zero space curvature ($owCDM$, left panel) or the evolving equation of state of Eq. (28.4) in a flat Universe (w_0w_aCDM , right panel). Green contours show constraints from the combination of *Planck* 2015 CMB data and the JLA supernova sample. Gray contours show the combination of *Planck* with BAO measurements from BOSS, 6dFGS [43], and SDSS-II [44]. Red contours adopt a more aggressive analysis of the BOSS galaxy data that uses the full shape (FS) of the redshift-space power spectrum and correlation function, modeled via perturbation theory, in addition to the measurement of the BAO scale itself. The full shape analysis improves the constraining power of the data, primarily because measurement of the Alcock-Paczynski effect on sub-BAO scales helps to break the degeneracy between $D_{A,c}(z)$ and $H(z)$. Blue contours show constraints from the full combination of CMB, BAO+FS, and SN data. Supernovae provide fine-grained relative distance measurements with good bin-by-bin precision at $z < 0.7$ (see Fig. 28.1), which is complementary to BAO for constraining redshift evolution of w . In both classes of model, the flat Λ CDM parameters ($w = w_0 = -1$, $\Omega_K = w_a = 0$) lie within the 68% confidence contour. Many recent papers feature constraint diagrams analogous to Fig. 28.2, and the constraints within this parameter space have tightened moderately with new data while remaining consistent with flat Λ CDM.

The precision on dark energy parameters depends, of course, on both the data being considered and the flexibility of the model being assumed. For $wCDM$, Ref. [38] find $w = -1.026 \pm 0.033$ using *Planck* CMB data, BAO measurements from SDSS-II and BOSS/eBOSS, and SN measurements from the Pantheon compilation. With the addition of eBOSS RSD data and DES $3 \times 2pt$ measurements, they constrain a more flexible model (ow_0w_aCDM) that allows non-zero curvature and an evolving equation-of-state (Eq. 28.4), finding

$$w_p = -1.020 \pm 0.032 \quad (28.5)$$

at a pivot redshift $z_p = 0.29$, a tight constraint on curvature

$$1 - \Omega_{\text{tot}} = -0.0023 \pm 0.0022 \quad (28.6)$$

but only a loose constraint on the evolution parameter

$$w_a = -0.48^{+0.36}_{-0.30}. \quad (28.7)$$

Obtaining a tight constraint on w_p in such a flexible cosmological model requires measurements that have complementary sensitivity to its multiple free parameters, and the precision of Eq. (28.5) is a testament to the remarkable improvements in cosmological measurements over the past decade.

A flat Λ CDM model fit to *Planck* CMB data alone predicts $H_0 = 67.4 \pm 0.5 \text{ km s}^{-1} \text{ Mpc}^{-1}$ (see Chapter 29 of this *Review*). This prediction and its error bar are sensitive to the assumptions of constant dark energy and a flat Universe. However, by adding BAO and supernova data one can construct an “inverse distance ladder” to measure H_0 precisely, even with a general dark energy model and free curvature [45]. Ref. [38] applies this approach to obtain $H_0 = 68.2 \pm 0.81 \text{ km s}^{-1} \text{ Mpc}^{-1}$. As discussed in Sec. 25.3.1 of this *Review*, some recent measurements from low-redshift data yield higher values of H_0 . Fig. 28.3 compares the CMB-anchored H_0 estimates cited above to distance-ladder estimates that use Cepheid [46] or tip-of-the-red-giant-branch (TRGB) [47] stars to calibrate Type Ia supernova luminosities, and to an entirely independent estimate that uses gravitational-lens time delays [48]. The Cepheid estimate is discrepant with the CMB-anchored estimates at a statistically significant level (Ref. [46] quotes 4.2σ relative to *Planck* Λ CDM), while the TRGB calibration yields an intermediate result that is consistent with either the “high” or “low” values of H_0 . Strong lensing inferences of H_0 depend on the mass profiles of the lensing galaxies and halos. The two strong lensing values in Fig. 28.3, both from Ref. [48], use the same lensing time delay data but either a loose prior or an independent dynamical constraint on these profiles. Earlier strong lensing analyses made stronger assumptions about mass profiles and inferred smaller H_0 uncertainties [49].

The tension in H_0 could reflect some combination of statistical flukes and systematic errors in one or more of the data sets employed in these analyses. However, if the resolution lies in new physics rather than measurement errors, then this is probably

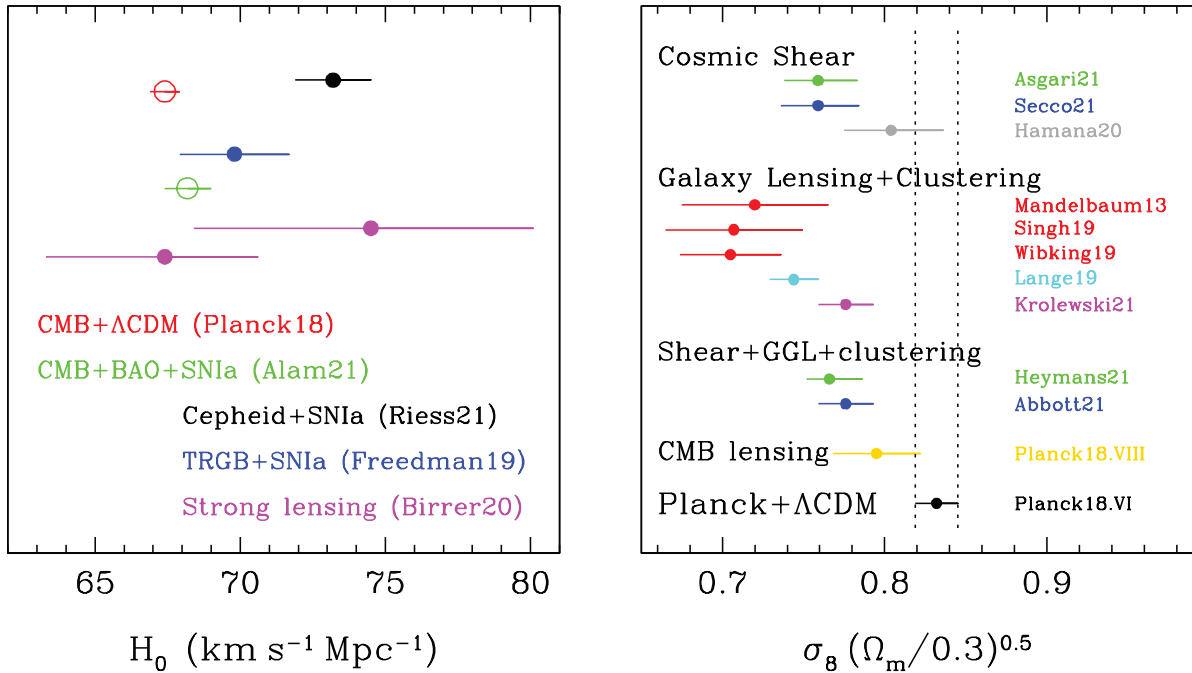


Figure 28.3: Tensions between low-redshift cosmological measurements and the predictions of a CMB-normalized Λ CDM model. All error bars are 1σ ; see text for observational references. (Left) Open circles show values of H_0 for flat Λ CDM with *Planck* parameters (red) or a general dark energy model constrained by a combination of CMB, BAO, and supernova data (green). Filled circles show distance-ladder estimates based on Cepheid (black) or TRGB (blue) calibration of SNIa luminosities, or an independent estimate using gravitational-lens time delays with two alternative constraints on lens mass profiles (magenta). (Right) Matter clustering characterized by the parameter combination $\sigma_8(\Omega_m/0.3)^{0.5}$, as predicted by a *Planck*-normalized Λ CDM model (vertical dotted lines, black hexagon) and estimated from weak gravitational lensing using: cosmic shear from KiDS-1000 (green), DES Y3 (blue) or HSC Y1 (gray), galaxy clustering and galaxy-galaxy lensing of SDSS galaxies (red, cyan) or galaxy clustering and CMB lensing of WISE galaxies (magenta), and the “ $3 \times 2pt$ ” analyses of KiDS-1000 (green) and DES Y3 (blue). Points of the same color are based on the same weak-lensing data. The “CMB lensing” point (gold) shows the value of σ_8 for $\Omega_m = 0.3$ inferred from *Planck* CMB lensing, a measurement that is independent of the “Planck+ Λ CDM” prediction and weighted to somewhat higher redshift than the other weak-lensing points.

physics that operates in the *pre-recombination* Universe, rescaling the BAO standard ruler in a way that shifts the Λ CDM and inverse-distance-ladder values upward. Models with extra relativistic degrees of freedom or dark energy that is dynamically significant in the early Universe can achieve this effect by increasing the early expansion rate, but they are tightly constrained by the damping tail of CMB anisotropies and by the shape of the galaxy power spectrum. A finely tuned model in which early dark energy decays rapidly after recombination can mitigate the tension between CMB data and local H_0 measurements [50], though it still prefers H_0 values below those of Ref. [46]. Numerous theory papers have examined possible physical solutions to the H_0 tension, all of which involve significant modifications to the Λ CDM scenario.

The amplitude of CMB anisotropies is proportional to the amplitude of density fluctuations present at recombination, and by assuming GR and a specified dark energy model one can extrapolate the growth of structure forward to the present day to predict σ_8 . Probes of low-redshift structure yield constraints in the (σ_8, Ω_m) plane, which can be summarized in terms of the parameter combination $S_8 \equiv \sigma_8(\Omega_m/0.3)^{0.5}$. As discussed in earlier editions of this *Review*, many but not all weak-lensing and cluster studies to date yield S_8 values lower than those predicted for *Planck*-normalized Λ CDM. The right panel of Fig. 28.3 illustrates the current state-of-play, comparing a selection of recently published S_8 estimates to the *Planck*+ Λ CDM prediction of $S_8 = 0.832 \pm 0.013$.

The first three points show recent cosmic-shear weak-lensing estimates from KiDS [30], DES [51], and HSC [33]. The next four points use galaxy-galaxy lensing in combination with galaxy clustering. Ref. [52] used weak-lensing data from SDSS imaging and the SDSS main galaxy redshift catalog, restricting the analysis to scales well described by perturbation theory. Refs. [53]

and [54] used the same weak-lensing data but the BOSS LOWZ galaxy sample, and they employed two quite different approaches to model the clustering and lensing signals into the strongly non-linear regime ($r \approx 1 h^{-1} \text{Mpc}$) so that they could fully exploit the constraining power of the data. Ref. [55] found a strong discrepancy on these non-linear scales between the predictions of a *Planck*-normalized Λ CDM model and the galaxy-galaxy lensing of BOSS CMASS galaxies, measured from 250 deg^2 of deep imaging from the Canada-France-Hawaii Telescope. Ref. [56], plotted in Fig. 28.3, revisited these data with a more general modeling approach and showed that the discrepancy persists over a range of redshift and galaxy stellar mass. The last point in this group, from Ref. [57], uses the clustering of galaxies in the WISE satellite’s all-sky infrared survey and the cross-correlation of these galaxies with *Planck* CMB-lensing, with galaxy redshifts estimated from photometry.

The third set of points in this panel shows S_8 estimates that combine cosmic shear with galaxy-galaxy lensing and galaxy clustering (a.k.a. “ 3×2 ” analyses because they combine three 2-point correlations), restricted to fairly large scales in the perturbative regime. These points come from analyses of the KiDS-1000 data set [31] and the DES Y3 data set [28]. The “CMB lensing” point shows the matter-clustering amplitude inferred from *Planck* CMB lensing; we have evaluated Eq. (38) of Ref. [58] at $\Omega_m = 0.3$ and adopted the same fractional error. Although the background being lensed is the CMB, this is still a measurement of low-redshift clustering, albeit with an effective redshift that is higher than that of the other weak lensing analyses. For multipoles $l > 100$ roughly half of the expected signal comes from structure at $z < 2$ and nearly all from $z < 10$ [59].

The HSC cosmic shear and *Planck* CMB lensing measurements are both consistent with the *Planck*+ Λ CDM prediction at $\sim 1\sigma$, and most but not all of the remaining points are individually

consistent at $\sim 2\sigma$. However, it is clear that the low redshift data prefer a value of S_8 below the predicted value. As a simple (but arguably appropriate) characterization of these measurements, we have averaged together estimates from the same weak lensing experiment (*i.e.*, points of the same color), then averaged the values from the seven experiments to obtain the mean estimate $S_8 = 0.766 \pm 0.012$, where the quoted uncertainty is simply the dispersion of the seven estimates divided by $\sqrt{N-1} = \sqrt{6}$. The $\sim 8\%$ discrepancy with the predicted $S_8 = 0.832 \pm 0.013$ is thus statistically significant if we assume that the errors (both statistical and systematic) of each measurement are independent. Using a much more sophisticated approach to data combination, but before the availability of the DES Y3 results, Ref. [60] found a slightly higher central value and slightly tighter error bar, $S_8 = 0.7769 \pm 0.0095$. However, common systematics might affect multiple weak lensing measurements, and any downward revision of the *Planck*+ Λ CDM central value would weaken the tension.

In the two years since the last edition of this *Review*, the precision and systematics tests of the weak lensing measurements have improved significantly. The evidence for a discrepancy between the predicted and inferred values of S_8 has not become obviously stronger or obviously weaker as a result of these improvements. It remains possible that the tension seen in Fig. 28.3 represents a true deviation between the clustering growth extrapolated forward from the early Universe and the clustering of matter at late times. Because the expansion history is well constrained by BAO and SN data, it is difficult to change low-redshift matter clustering by simply changing the equation of state of dark energy. Instead, a deviation between predicted and observed clustering might point towards modified gravity, decaying dark matter, or coupling between dark matter and dark energy.

Final results from KiDS, DES, and HSC may clarify this situation over the next two years. Cluster weak lensing from the same surveys can achieve S_8 constraints with comparable statistical power, though systematic biases associated with cluster selection have thus far been a limiting factor. CMB lensing constraints will improve with higher angular resolution data from the South Pole Telescope and the Atacama Cosmology Telescope and their successors. The DESI survey will soon allow the first RSD-based measurements of structure growth at the 1–2% level, providing an entirely distinct route to probe the clustering tension hinted at by weak lensing data.

28.5 Summary and Outlook

Figure 28.2 focuses on model parameter constraints, but to describe the observational situation it is more useful to characterize the precision, redshift range, and systematic uncertainties of the basic expansion and growth measurements. At present, supernova surveys constrain distance ratios at the 1–2% level in redshift bins of width $\Delta z = 0.1$ out to $z \approx 0.8$, with larger but still interesting error bars out to $z \approx 1.3$. Estimated systematic uncertainties are comparable to statistical uncertainties and include effects of photometric calibration, dust reddening, host-galaxy correlations, and possible evolution of the SN population. BAO surveys have measured the angular diameter distance $D_{A,c}(z)$ and the expansion rate $H(z)$ over the range $0 < z < 2.5$, calibrated to absolute units using the CMB-based value of the sound horizon r_s . For $D_{A,c}(z)$, the final analyses of BOSS/eBOSS achieve precision of 1.6–1.8% in three overlapping redshift bins from luminous galaxies at $z = 0.2 - 1.0$, 2.6% from quasars at $z \approx 1.5$, and 2.9% from the Lyman- α forest at $z \approx 2.3$. For $H(z)$, the precision at the same redshifts is 2.6–3.0%, 4.1%, and 2.1%, respectively. SDSS, DES, KiDS, and HSC have used combinations of weak lensing and galaxy clustering to measure the parameter combination $S_8 = \sigma_8(\Omega_m/0.3)^{0.5}$ with estimated precision of 2–4%, and the cross-correlation of WISE galaxies with *Planck* CMB lensing achieves similar precision. These estimates account for identified systematic uncertainties, but the measurements and modeling are challenging, and it is possible that the systematics are underestimated. Our simple average of these measurements, treating them as independent and using their dispersion as an empirical estimate of uncertainty, yields an error on the mean of 1.5%. The statistical power of these weak lensing surveys is concentrated at $z \approx 0.2 - 0.8$, and they provide useful constraints at lower preci-

sion on redshift evolution over this range and on individual values of Ω_m and σ_8 . RSD measurements constrain the similar parameter combination $f(z)\sigma_8(z)$, but they do not yet have precision competitive with that of weak lensing measurements. Distance-ladder estimates of H_0 now span a small range, using overlapping data but distinct treatments of key steps; individual studies quote uncertainties of 2–3%, with similar statistical and systematic contributions.

Planck data and higher resolution ground-based experiments now measure CMB anisotropies with exquisite precision; for example, CMB measurements now constrain the physical size of the BAO sound horizon to 0.2% and the angular scale of the sound horizon to 0.01%. A flat Λ CDM model with standard radiation and neutrino content can fit the CMB data and the BAO and SN distance measurements to within their estimated uncertainties. The value of H_0 implied by this model disagrees with recent Cepheid+SN Ia distance-ladder measurements of H_0 at a $\sim 4\sigma$ level. This disagreement persists in models that allow non-zero curvature and low redshift evolution of $w(z)$, provided one assumes standard pre-recombination physics to compute the sound horizon r_s . The discrepancy could reflect underestimated systematic uncertainties in the Cepheid-based H_0 estimate, or it could be a sign of new physics in the early Universe that rescales r_s . Over the next few years, improved parallax data from *HST* and *Gaia*, discovery of new SNIa in nearby galaxies, and observing programs on the *James Webb Space Telescope (JWST)* should allow further improvements and systematics checks in the Cepheid distance ladder. It will be equally important to bring the TRGB calibration method to a comparable level of precision and systematics control, and to understand any differences between the Cepheid and TRGB distance scales. Strong lensing time delays and gravitational wave standard sirens may provide useful independent tests if their systematic uncertainties can be sufficiently well controlled. Improving measurements of the CMB damping tail from ground-based experiments will provide increasingly strong constraints on resolutions of the H_0 -tension that invoke novel pre-recombination physics.

Extrapolating forward from the CMB anisotropies measured by *Planck* implies a low redshift value of S_8 that is higher than recent direct estimates from weak gravitational lensing and galaxy clustering. Comparing the *Planck* central value to the simple average of recent experiments discussed in §28.4 implies a difference of 8.6%: $S_8 = 0.832 \pm 0.013$ vs. $S_8 = 0.766 \pm 0.012$. This disagreement could reflect a common systematic that biases several of the weak lensing analyses in the same direction, and it would be weakened if the *Planck* S_8 value were high because of an unlucky statistical fluctuation or a residual systematic. If real, this discrepancy could point towards modified gravity, decaying dark matter, or coupling between dark matter and dark energy.

Analyses of the final (6-year) DES data could plausibly achieve a factor of two or more improvement on current uncertainties, along with more stringent internal cross-checks, from a combination of deeper imaging, improved weak lensing calibration, and modeling that exploits measurements in the non-linear clustering regime. The final KiDS and HSC data sets will be smaller than DES, but still large enough to achieve competitive precision with independent observations and analyses. Higher signal-to-noise CMB lensing maps cross-correlated with galaxies will provide independent tests that avoid some of the systematic uncertainties of optical weak lensing. Collectively these efforts could achieve an unambiguous determination of the amplitude of low redshift matter clustering at the 1–2% level.

The DESI galaxy redshift survey will soon exceed the size of the existing SDSS and BOSS/eBOSS surveys, ultimately by a factor of ~ 10 . DESI will enable high precision BAO measurements of expansion history at $z \approx 0.7-1.4$ and, for the first time, percent-level measurements of structure growth through RSD. Cross-correlation of DESI galaxies with cosmic shear or CMB lensing maps will achieve high precision while sidestepping many of the systematics that affect pure imaging surveys. Precise BAO and RSD measurements at higher redshifts will come from DESI Lyman- α forest maps and the HETDEX and Subaru PFS galaxy surveys. The BAO measurements will complement increasingly

precise measurements of the relative distance scale at $z < 1$ from the DES photometric supernova sample and from improved local supernova samples ($z < 0.1$) that provide a low-redshift anchor. Large galaxy samples will also enable more powerful applications of the Alcock-Paczynski effect and parameter measurements based on voids or higher order clustering statistics.

The next five years will see another major leap in observational capabilities with the advent of LSST, *Euclid*, and *Roman*. LSST will be the ultimate ground-based optical weak-lensing experiment, measuring several billion galaxy shapes over 20,000 deg² of the southern hemisphere sky, and it will detect and monitor many thousands of SNe per year. *Euclid* and *Roman* also have weak lensing as a primary science goal, taking advantage of the high angular resolution and extremely stable image quality achievable from space. Both missions plan large spectroscopic galaxy surveys, which will provide better sampling at high redshifts than DESI or PFS because of the lower infrared sky background above the atmosphere. *Roman* is also designed to carry out what should be the ultimate supernova cosmology experiment, with deep, high resolution, near-IR observations and the stable calibration achievable with a space platform. The 2020s will also see dramatic advances in CMB lensing from the Simons Observatory and, potentially, CMB-S4 and/or a space-based probe; cross-correlation with galaxy surveys allows precise tomographic measurements of clustering as a function of redshift.

If the anomalies suggested in Fig. 28.3 are real, then the experiments of the 2020s will map out their redshift, scale, and environment dependence in great detail, providing detailed empirical constraints on dynamical dark energy or modified gravity models. If these tensions dissipate with improved measurements, then the experiments of the 2020s will achieve much more stringent tests of the Λ CDM paradigm, with the potential to reveal deviations that are still within the statistical uncertainties of current data. The critical clue to the origin of cosmic acceleration could also come from a surprising direction, such as laboratory, solar-system, or gravitational wave tests that challenge GR, time variation of fundamental “constants,” or anomalous behavior of gravity in some astronomical environments. Experimental advances along these multiple axes could confirm today’s relatively simple, but frustratingly incomplete, “standard model” of cosmology, or they could force yet another radical revision in our understanding of energy, or gravity, or the spacetime structure of the Universe.

References

- [1] A. Einstein, *Sitzungsber. Preuss. Akad. Wiss. Berlin (Math. Phys.)*, 142 (1917).
- [2] Ya. B. Zel’dovich, A. Krasinski and Ya. B. Zel’dovich, *Sov. Phys. Usp.* **11**, 381 (1968), [*Gen. Rel. Grav.*40,1557(2008); *Usp. Fiz. Nauk*95,209(1968)].
- [3] A. Friedman, *Z. Phys.* **10**, 377 (1922), [*Gen. Rel. Grav.*31,1991(1999)].
- [4] G. Lemaître, *Annales de la Societe Scietifique de Bruxelles* **47**, 49 (1927).
- [5] E. Hubble, *Proc. Nat. Acad. Sci.* **15**, 168 (1929).
- [6] A. Einstein and W. de Sitter, *Proc. Nat. Acad. Sci.* **18**, 213 (1932).
- [7] For background and definitions, see Big-Bang Cosmology – Sec. 22 of this *Review*.
- [8] A. G. Riess *et al.* (Supernova Search Team), *Astron. J.* **116**, 1009 (1998), [arXiv:astro-ph/9805201].
- [9] S. Perlmutter *et al.* (Supernova Cosmology Project), *Astrophys. J.* **517**, 565 (1999), [arXiv:astro-ph/9812133].
- [10] P. de Bernardis *et al.* (Boomerang), *Nature* **404**, 955 (2000), [arXiv:astro-ph/0004404].
- [11] S. Hanany *et al.*, *Astrophys. J.* **545**, L5 (2000), [arXiv:astro-ph/0005123].
- [12] D. H. Weinberg *et al.*, *Phys. Rept.* **530**, 87 (2013), [arXiv:1201.2434].
- [13] C. Wetterich, *Nucl. Phys.* **B302**, 668 (1988), [arXiv:1711.03844].
- [14] A. Joyce *et al.*, *Phys. Rept.* **568**, 1 (2015), [arXiv:1407.0059].
- [15] S. M. Carroll *et al.*, *Phys. Rev.* **D70**, 043528 (2004), [arXiv:astro-ph/0306438].
- [16] G. R. Dvali, G. Gabadadze and M. Porrati, *Phys. Lett.* **B485**, 208 (2000), [hep-th/0005016].
- [17] C.M. Will, *Living Reviews in Relativity*, **9**, 3 (2006). See also the chapter on Experimental Tests of Gravitational Theory – in this *Review*.
- [18] J. Wang, L. Hui and J. Khoury, *Phys. Rev. Lett.* **109**, 241301 (2012), [arXiv:1208.4612].
- [19] M. Fairbairn and A. Goobar, *Phys. Lett.* **B642**, 432 (2006), [arXiv:astro-ph/0511029]; Y.-S. Song, I. Sawicki and W. Hu, *Phys. Rev.* **D75**, 064003 (2007), [arXiv:astro-ph/0606286]; C. Blake *et al.*, *Mon. Not. Roy. Astron. Soc.* **415**, 2876 (2011), [arXiv:1104.2948].
- [20] T. Baker *et al.*, *Phys. Rev. Lett.* **119**, 25, 251301 (2017), [arXiv:1710.06394].
- [21] E. V. Linder, *Phys. Rev.* **D72**, 043529 (2005), [arXiv:astro-ph/0507263].
- [22] This is essentially the FoM proposed in the Dark Energy Task Force (DETF) report, A. Albrecht *et al.*, *astro-ph/0609591*, though they based their FoM on the area of the 95 in the $w_0 - w_a$ plane.
- [23] T. Baker *et al.*, *Rev. Mod. Phys.* **93**, 1, 015003 (2021), [arXiv:1908.03430].
- [24] For high accuracy, the impact of acoustic oscillations must be computed with a full Boltzmann code, but the simple integral for r_s captures the essential physics and the scaling with cosmological parameters.
- [25] R. A. Sunyaev and Ya. B. Zel’dovich, *Astrophys. Space Sci.* **7**, 3 (1970).
- [26] D. Weinberg *et al.* (2013), [arXiv:1309.5380].
- [27] C. Alcock and B. Paczynski, *Nature* **281**, 358 (1979).
- [28] T. M. C. Abbott *et al.* (DES) (2021), [arXiv:2105.13549].
- [29] T. M. C. Abbott *et al.* (DES), *Astrophys. J.* **872**, 2, L30 (2019), [arXiv:1811.02374].
- [30] M. Asgari *et al.* (KiDS), *Astron. Astrophys.* **645**, A104 (2021), [arXiv:2007.15633].
- [31] C. Heymans *et al.*, *Astron. Astrophys.* **646**, A140 (2021), [arXiv:2007.15632].
- [32] C. Hikage *et al.* (HSC), *Publ. Astron. Soc. Jap.* **71**, 2, Publications of the Astronomical Society of Japan, Volume 71, Issue 2, April 2019, 43, <https://doi.org/10.1093/pasj/psz010> (2019), [arXiv:1809.09148].
- [33] T. Hamana *et al.*, *Publ. Astron. Soc. Jap.* **72**, 1, Publications of the Astronomical Society of Japan, Volume 72, Issue 1, February 2020, 16, <https://doi.org/10.1093/pasj/psz138> (2020), [arXiv:1906.06041].
- [34] B. Jain *et al.* (2015), [arXiv:1501.07897].
- [35] W. L. Freedman *et al.* (HST), *Astrophys. J.* **553**, 47 (2001), [arXiv:astro-ph/0012376].
- [36] N. Aghanim *et al.* (Planck) (2018), [arXiv:1807.06209].
- [37] M. Betoule *et al.*, *Astron. & Astrophys.* **568**, 22 (2014).
- [38] S. Alam *et al.* (eBOSS), *Phys. Rev. D* **103**, 8, 083533 (2021), [arXiv:2007.08991].
- [39] M. Sullivan *et al.* (SNLS), *Astrophys. J.* **737**, 102 (2011), [arXiv:1104.1444].
- [40] N. Suzuki *et al.* (Supernova Cosmology Project), *Astrophys. J.* **746**, 85 (2012), [arXiv:1105.3470].
- [41] D. M. Scolnic *et al.*, *Astrophys. J.* **859**, 2, 101 (2018), [arXiv:1710.00845].
- [42] S. Alam *et al.* (BOSS), *Mon. Not. Roy. Astron. Soc.* **470**, 3, 2617 (2017), [arXiv:1607.03155].
- [43] F. Beutler *et al.*, *Mon. Not. Roy. Astron. Soc.* **416**, 3017 (2011), [arXiv:1106.3366].

- [44] A. J. Ross *et al.*, Mon. Not. Roy. Astron. Soc. **449**, 1, 835 (2015), [arXiv:1409.3242].
- [45] E. Aubourg *et al.*, Phys. Rev. **D92**, 12, 123516 (2015), [arXiv:1411.1074].
- [46] A. G. Riess *et al.*, Astrophys. J. Lett. **908**, 1, L6 (2021), [arXiv:2012.08534].
- [47] W.L. Friedman, Astron. J. **882** (2019) 34.
- [48] S. Birrer *et al.*, Astron. Astrophys. **643**, A165 (2020), [arXiv:2007.02941].
- [49] K. C. Wong *et al.* (2019), [arXiv:1907.04869].
- [50] V. Poulin *et al.*, Phys. Rev. Lett. **122**, 22, 221301 (2019), [arXiv:1811.04083].
- [51] L. F. Secco *et al.* (DES) (2021), [arXiv:2105.13544].
- [52] R. Mandelbaum *et al.*, Mon. Not. Roy. Astron. Soc. **432**, 1544 (2013), [arXiv:1207.1120].
- [53] S. Singh *et al.*, Mon. Not. Roy. Astron. Soc. **491**, 1, 51 (2020), [arXiv:1811.06499].
- [54] B. D. Wibking *et al.*, Mon. Not. Roy. Astron. Soc. **492**, 2, 2872 (2020), [arXiv:1907.06293].
- [55] A. Leauthaud *et al.*, Mon. Not. Roy. Astron. Soc. **467**, 3, 3024 (2017), [arXiv:1611.08606].
- [56] J. U. Lange *et al.*, Mon. Not. Roy. Astron. Soc. **488**, 4, 5771 (2019), [arXiv:1906.08680].
- [57] A. Krolewski, S. Ferraro and M. White (2021), [arXiv:2105.03421].
- [58] N. Aghanim *et al.* (Planck) (2018), [arXiv:1807.06210].
- [59] A. Lewis and A. Challinor, Phys. Rept. **429**, 1 (2006), [arXiv:astro-ph/0601594].
- [60] C. García-García *et al.* (2021), [arXiv:2105.12108].

29. Cosmic Microwave Background

Revised August 2021 by D. Scott (U. of British Columbia) and G.F. Smoot (HKUST; UC Berkeley; LBNL; DIPC; Paris U.).

29.1 Introduction

The energy content in electromagnetic radiation from beyond our Galaxy is dominated by the cosmic microwave background (CMB), discovered in 1965 [1]. The spectrum of the CMB is well described by a blackbody function with $T = 2.7255$ K. This spectral form is a main supporting pillar of the hot Big Bang model for the Universe. The lack of any observed deviations from a blackbody spectrum constrains physical processes over cosmic history at redshifts $z \lesssim 10^7$ (see earlier versions of this review).

Currently the key CMB observable is the angular variation in temperature (or intensity) correlations, and to a growing extent polarization [2]. Since the first detection of these anisotropies by the Cosmic Background Explorer (*COBE*) satellite in 1992 [3], there has been intense activity to map the sky at increasing levels of sensitivity and angular resolution by ground-based and balloon-borne measurements. These were joined in 2003 by the first results from NASA's Wilkinson Microwave Anisotropy Probe (*WMAP*) [4], which were improved upon by analyses of data added every 2 years, culminating in the 9-year results [5]. In 2013 we had the first results [6] from the third generation CMB satellite, ESA's *Planck* mission [7], which were enhanced by results from the 2015 *Planck* data release [8, 9], and then the final 2018 *Planck* data release [10, 11]. Additionally, CMB anisotropies have been extended to smaller angular scales by ground-based experiments, particularly the Atacama Cosmology Telescope (ACT) [12] and the South Pole Telescope (SPT) [13]. Together these observations have led to a stunning confirmation of the 'Standard Model of Cosmology.' In combination with other astrophysical data, the CMB anisotropy measurements place quite precise constraints on a number of cosmological parameters, and have launched us into an era of precision cosmology. With the CMB now having been studied for more than half a century, the program to map temperature anisotropies is effectively wrapping up, and attention is increasingly focussing on polarization measurements as the future arena in which to test fundamental physics.

29.2 CMB Spectrum

It is well-known that the spectrum of the microwave background is very precisely that of blackbody radiation, whose temperature evolves with redshift as $T(z) = T_0(1+z)$ in an expanding Universe. As a direct test of its cosmological origin, this relationship has been tested by measuring the strengths of emission and absorption lines in high-redshift systems [14].

Measurements of the spectrum are consistent with a blackbody distribution over more than three decades in frequency (there is a claim by ARCADE [15] of a possible unexpected extragalactic emission signal at low frequency, but the interpretation is debated [16]). All viable cosmological models predict a very nearly Planckian spectrum to within the current observational limits. Because of this, measurements of deviations from a blackbody spectrum have received little attention in recent years, with only a few exceptions. However, that situation will eventually change, since proposed experiments [17] have the potential to dramatically improve the constraints on energy release in the early Universe. It now seems feasible to probe spectral distortion mechanisms that are *required* in the standard picture, such as those arising from the damping and dissipation of relatively small-scale primordial perturbations, or the average effect of inverse Compton scattering. A more ambitious goal would be to reach the precision needed to detect the residual lines from the cosmological recombination of hydrogen and helium and hence test whether conditions at $z \gtrsim 1000$ accurately follow those in the standard picture [18].

29.3 Description of CMB Anisotropies

Observations show that the CMB contains temperature anisotropies at the 10^{-5} level and polarization anisotropies at the 10^{-6} (and lower) level, over a wide range of angular scales. These anisotropies are usually expressed using a spherical harmonic expansion

of the CMB sky:

$$T(\theta, \phi) = \sum_{\ell m} a_{\ell m} Y_{\ell m}(\theta, \phi) \quad (29.1)$$

(with the linear polarization pattern written in a similar way using the so-called spin-2 spherical harmonics). Increasing angular resolution requires that the expansion goes to higher multipoles. Because there are only very weak phase correlations seen in the CMB sky and since we notice no preferred direction, the vast majority of the cosmological information is contained in the temperature 2-point function, *i.e.*, the variance as a function only of angular separation. Equivalently, the anisotropy power per unit $\ln \ell$ is $\ell \sum_m |a_{\ell m}|^2 / 4\pi$.

29.3.1 The Monopole

The CMB has a mean temperature of $T_\gamma = 2.7255 \pm 0.0006$ K (1σ) [19], which can be considered as the monopole component of CMB maps, a_{00} . Since all mapping experiments involve difference measurements, they are insensitive to this average level; monopole measurements can only be made with absolute temperature devices, such as the FIRAS instrument on the *COBE* satellite [20]. The measured kT_γ is equivalent to 0.234 meV or $4.60 \times 10^{-10} m_e c^2$. A blackbody of the measured temperature has a number density $n_\gamma = (2\zeta(3)/\pi^2) T_\gamma^3 \simeq 411 \text{ cm}^{-3}$, energy density $\rho_\gamma = (\pi^2/15) T_\gamma^4 \simeq 4.64 \times 10^{-34} \text{ g cm}^{-3} \simeq 0.260 \text{ eV cm}^{-3}$, and a fraction of the critical density $\Omega_\gamma \simeq 5.38 \times 10^{-5}$.

29.3.2 The Dipole

The largest anisotropy is in the $\ell = 1$ (dipole) first spherical harmonic, with amplitude 3.3621 ± 0.0010 mK [10]. The dipole is interpreted to be the result of the Doppler boosting of the monopole caused by the Solar System motion relative to the nearly isotropic blackbody field, as broadly confirmed by measurements of the radial velocities of local galaxies (*e.g.*, Ref. [21]); the intrinsic part of the signal is expected to be 2 orders of magnitude smaller (and fundamentally difficult to distinguish). The motion of an observer with velocity $\beta \equiv v/c$ relative to an isotropic Planckian radiation field of temperature T_0 produces a Lorentz-boosted temperature pattern

$$T(\theta) = T_0(1 - \beta^2)^{1/2} / (1 - \beta \cos \theta) \\ \simeq T_0 \left[1 + \beta \cos \theta + (\beta^2/2) \cos 2\theta + \mathcal{O}(\beta^3) \right]. \quad (29.2)$$

At every point in the sky, one observes a blackbody spectrum, with temperature $T(\theta)$. The spectrum of the dipole has been confirmed to be the differential of a blackbody spectrum [22]. At higher order there are additional effects arising from aberration and from modulation of the anisotropy pattern, which have also been observed [23].

The implied velocity for the Solar System barycenter is $v = 369.82 \pm 0.11 \text{ km s}^{-1}$, assuming a value $T_0 = T_\gamma$, towards $(l, b) = (264.021^\circ \pm 0.011^\circ, 48.253^\circ \pm 0.005^\circ)$ [10]. Such a Solar System motion implies a velocity for the Galaxy and the Local Group of galaxies relative to the CMB. The derived value is $v_{\text{LG}} = 620 \pm 15 \text{ km s}^{-1}$ towards $(l, b) = (271.9^\circ \pm 2.0^\circ, 29.6^\circ \pm 1.4^\circ)$ [10], where most of the error comes from uncertainty in the velocity of the Solar System relative to the Local Group.

The dipole is a frame-dependent quantity, and one can thus determine the 'CMB frame' (in some sense this is a special frame) as that in which the CMB dipole would be zero. Any velocity of the receiver relative to the Earth and the Earth around the Sun is removed for the purposes of CMB anisotropy studies, while our velocity relative to the Local Group of galaxies and the Local Group's motion relative to the CMB frame are normally removed for cosmological studies. The dipole is now routinely used as a primary calibrator for mapping experiments, either via the time-varying orbital motion of the Earth, or through the cosmological dipole measured by satellite experiments.

29.3.3 Higher-Order Multipoles

The variations in the CMB temperature maps at higher multipoles ($\ell \geq 2$) are interpreted as being mostly the result of per-

turbations in the density of the early Universe, manifesting themselves at the epoch of the last scattering of the CMB photons. In the hot Big Bang picture, the expansion of the Universe cools the plasma so that by a redshift $z \simeq 1100$ (with little dependence on the details of the model), the hydrogen and helium nuclei can bind electrons into neutral atoms, a process usually referred to as ‘recombination’ [24]. Before this epoch, the CMB photons were tightly coupled to the baryons, while afterwards they could freely stream towards us. By measuring the $a_{\ell m}$ s we are thus learning directly about physical conditions in the early Universe.

A statistically-isotropic sky means that all m s are equivalent, *i.e.*, there is no preferred axis, so that the temperature correlation function between two positions on the sky depends only on angular separation and not orientation. Together with the assumption of Gaussian statistics (*i.e.*, no correlations between the modes), the 2-point function of the temperature field (or equivalently the power spectrum in ℓ) then fully characterizes the anisotropies. The power summed over all m s at each ℓ is $(2\ell+1)C_\ell/(4\pi)$, where $C_\ell \equiv \langle |a_{\ell m}|^2 \rangle$. Thus, averages of $a_{\ell m}$ s over m can be used as estimators of the C_ℓ s to constrain their expectation values, which are the quantities predicted by a theoretical model. For an idealized full-sky observation, the variance of each measured C_ℓ (*i.e.*, the variance of the variance) is $[2/(2\ell+1)]C_\ell^2$. This sampling uncertainty (known as ‘cosmic variance’) comes about because each C_ℓ is χ^2 distributed with $(2\ell+1)$ degrees of freedom for our observable volume of the Universe. For fractional sky coverage, f_{sky} , this variance is increased by $1/f_{\text{sky}}$ and the modes become partially correlated.

It is important to understand that theories predict the expectation value of the power spectrum, whereas our sky is a single realization. Hence, the cosmic variance is an unavoidable source of uncertainty when constraining models; it dominates the scatter at lower ℓ s, while the effects of instrumental noise and resolution dominate at higher ℓ s [25].

Theoretical models generally predict that the $a_{\ell m}$ modes are Gaussian random fields to high precision, matching the empirical tests, *e.g.*, standard slow-roll inflation’s non-Gaussian contribution is expected to be at least an order of magnitude below current observational limits [26]. Although non-Gaussianity of various forms is possible in early Universe models, tests show that Gaussianity is an extremely good simplifying approximation [27]. The only current indications of any non-Gaussianity or statistical anisotropy are some relatively weak signatures at large scales, seen in both *WMAP* [28] and *Planck* data [29], but not of high enough significance to reject the simplifying assumption. Nevertheless, models that deviate from the inflationary slow-roll conditions can have measurable non-Gaussian signatures. So while the current observational limits make the power spectrum the dominant probe of cosmology, it is worth noting that higher-order correlations are becoming a tool for constraining otherwise viable theories.

29.3.4 Angular Resolution and Binning

There is no one-to-one conversion between multipole ℓ and the angle subtended by a particular spatial scale projected onto the sky. However, crudely speaking, a single spherical harmonic $Y_{\ell m}$ corresponds to angular variations of $\theta \sim \pi/\ell$. CMB maps contain anisotropy information from the size of the map (or in practice some fraction of that size) down to the beam-size of the instrument, σ (the standard deviation of the beam, in radians). One can think of the effect of a Gaussian beam as rolling off the power spectrum with the function $e^{-\ell(\ell+1)\sigma^2}$.

For less than full sky coverage, the ℓ modes become correlated. Hence, experimental results are usually quoted as a series of ‘band powers,’ defined as estimators of $\ell(\ell+1)C_\ell/2\pi$ over different ranges of ℓ . Because of the strong foreground signals in the Galactic plane, even ‘all-sky’ surveys, such as *WMAP* and *Planck*, involve a cut sky. The amount of binning required to obtain uncorrelated estimates of power also depends on the map size.

29.4 Cosmological Parameters

The current ‘Standard Model’ of cosmology contains around 10 free parameters, only six of which are required to have non-null values (see The Cosmological Parameters—Sec. 25 of this *Review*).

The basic framework is the Friedmann-Robertson-Walker (FRW) metric (*i.e.*, a Universe that is approximately homogeneous and isotropic on large scales), with density perturbations laid down at early times and evolving into today’s structures (see Big-Bang cosmology—Sec. 22 of this *Review*). The most general possible set of density variations is a linear combination of an adiabatic density perturbation and some isocurvature perturbations. Adiabatic means that there is no change to the entropy per particle for each species, *i.e.*, $\delta\rho/\rho$ for matter is $(3/4)\delta\rho/\rho$ for radiation. Isocurvature means that the set of individual density perturbations adds to zero, for example, matter perturbations compensate radiation perturbations so that the total energy density remains unperturbed, *i.e.*, $\delta\rho$ for matter is $-\delta\rho$ for radiation. These different modes give rise to distinct (temporal) phases during growth, with those of the adiabatic scenario being fully consistent with the data. Models that generate mainly isocurvature type perturbations (such as most topological defect scenarios) are not viable. However, an admixture of the adiabatic mode with up to 1.7% isocurvature contribution (depending on details of the mode) is still allowed [30].

29.4.1 Initial Condition Parameters

Within the adiabatic family of models, there is, in principle, a free function describing the variation of comoving curvature perturbations, $\mathcal{R}(\mathbf{x}, t)$. The great virtue of \mathcal{R} is that, on large scales, it is constant in time on super-horizon scales for a purely adiabatic perturbation. There are physical reasons to anticipate that the variance of these perturbations will be described well by a power law in scale, *i.e.*, in Fourier space $\langle |\mathcal{R}|_k^2 \rangle \propto k^{n_s-4}$, where k is wavenumber and n_s is the spectral index as usually defined. So-called ‘scale-invariant’ initial conditions (meaning gravitational potential fluctuations that are independent of k) correspond to $n_s = 1$. In inflationary models [31] (see Inflation—Sec. 23 of this *Review*), perturbations are generated by quantum fluctuations, which are set by the energy scale of inflation, together with the slope and higher derivatives of the inflationary potential. One generally expects that the Taylor series expansion of $\ln \mathcal{R}_k(\ln k)$ has terms of steadily decreasing size. For the simplest models, there are thus two parameters describing the initial conditions for density perturbations, namely the amplitude and slope of the power spectrum. These can be explicitly defined, for example, through

$$\mathcal{P}_{\mathcal{R}}^2 \equiv k^3 \langle |\mathcal{R}|_k^2 \rangle / 2\pi^2 \simeq A_s (k/k_0)^{n_s-1}, \quad (29.3)$$

with $A_s \equiv \mathcal{P}_{\mathcal{R}}^2(k_0)$ and $k_0 = 0.05 \text{ Mpc}^{-1}$, say. There are other equally valid definitions of the amplitude parameter (see also Secs. 22, 23, and 25 of this *Review*), and we caution that the relationships between some of them can be cosmology-dependent. In slow-roll inflationary models, this normalization is proportional to the combination $V^3/(V')^2$, for the inflationary potential $V(\phi)$. The slope n_s also involves V'' , and so the combination of A_s and n_s can constrain potentials.

Inflation generates tensor (gravitational wave) modes, as well as scalar (density perturbation) modes. This fact introduces another parameter, measuring the amplitude of a possible tensor component, or equivalently the ratio of the tensor to scalar contributions. The tensor amplitude is $A_t \propto V$, and thus one expects a larger gravitational wave contribution in models where inflation happens at higher energies. The tensor power spectrum also has a slope, often denoted n_t , but since this seems unlikely to be measured in the near future (and there is also a consistency relation with tensor amplitude), it is sufficient for now to focus only on the amplitude of the gravitational wave component. It is most common to define the tensor contribution through r , the ratio of tensor to scalar perturbation spectra at some fixed value of k (*e.g.*, $k = 0.002 \text{ Mpc}^{-1}$ or $k = 0.05 \text{ Mpc}^{-1}$, although it was historically defined in terms of the ratio of contributions at $\ell = 2$). Different inflationary potentials will lead to different predictions, *e.g.*, for 50 e-folds, $\lambda\phi^4$ inflation gives $r = 0.32$ and $m^2\phi^2$ inflation gives $r = 0.16$ (both now strongly disfavored by the data), while other models can have arbitrarily small values of r . In any case, whatever the specific definition, and whether they come from inflation or something else, the ‘initial conditions’ give rise to a minimum of three parameters, A_s , n_s , and r .

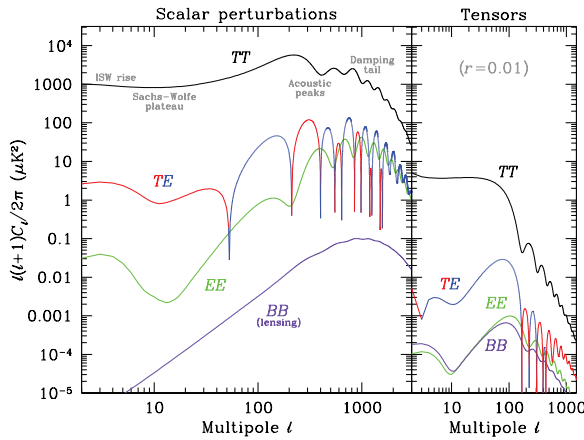


Figure 29.1: Theoretical CMB anisotropy power spectra, using the best-fitting Λ CDM model from *Planck*, calculated using CAMB. The panel on the left shows the theoretical expectation for scalar perturbations, while the panel on the right is for tensor perturbations, with an amplitude set to $r = 0.01$ for illustration. Note that the horizontal axis is logarithmic here. For the well-measured scalar TT spectrum, the regions, each covering roughly a decade in ℓ , are labeled as in the text: the ISW rise; Sachs-Wolfe plateau; acoustic peaks; and damping tail. The TE cross-correlation power spectrum changes sign, indicated here by plotting the absolute value, but switching color for the negative parts.

29.4.2 Background Cosmology Parameters

The FRW cosmology requires an expansion parameter (the Hubble constant, H_0 , often represented through $H_0 = 100 h \text{ km s}^{-1} \text{ Mpc}^{-1}$) and several parameters to describe the matter and energy content of the Universe. These are usually given in terms of the critical density, *i.e.*, for species ‘x,’ $\Omega_x \equiv \rho_x / \rho_{\text{crit}}$, where $\rho_{\text{crit}} \equiv 3H_0^2 / 8\pi G$. Since physical densities $\rho_x \propto \Omega_x h^2 \equiv \omega_x$ are what govern the physics of the CMB anisotropies, it is these ω s that are best constrained by CMB data. In particular, CMB observations constrain $\Omega_b h^2$ for baryons and $\Omega_c h^2$ for cold dark matter (with $\rho_m = \rho_c + \rho_b$ for the sum).

The contribution of a cosmological constant Λ (or other form of dark energy, see Dark Energy—Sec. 28) is usually included, together with a parameter that quantifies the curvature, $\Omega_K \equiv 1 - \Omega_{\text{tot}}$, where $\Omega_{\text{tot}} = \Omega_m + \Omega_\Lambda$. The radiation content, while in principle a free parameter, is precisely enough determined by the measurement of T_γ that it can be considered fixed, and makes a $< 10^{-4}$ contribution to Ω_{tot} today.

Astrophysical processes at relatively low redshift can also affect the C_ℓ s, with a particularly significant effect coming through reionization. The Universe became reionized at some redshift z_i , long after recombination, affecting the CMB through the integrated Thomson scattering optical depth:

$$\tau = \int_0^{z_i} \sigma_T n_e(z) \frac{dt}{dz} dz, \quad (29.4)$$

where σ_T is the Thomson cross-section, $n_e(z)$ is the number density of free electrons (which depends on astrophysics), and dt/dz is fixed by the background cosmology. In principle, τ can be determined from the small-scale matter power spectrum, together with the physics of structure formation and radiative feedback processes; however, this is a sufficiently intractable calculation that in practice τ needs to be considered as a free parameter.

Thus, we have eight basic cosmological parameters, namely A_s , n_s , r , h , $\Omega_b h^2$, $\Omega_c h^2$, Ω_{tot} , and τ . One can add additional parameters to this list, particularly when using the CMB in combination with other data sets. The next most relevant ones might be: $\Omega_\nu h^2$, the massive neutrino contribution; w ($\equiv p/\rho$), the equation of state parameter for the dark energy; and $dn_s/d \ln k$, measuring deviations from a constant spectral index. To these 11 one could of course add further parameters describing additional physics, such as details of the reionization process, features in the ini-

tial power spectrum, a sub-dominant contribution of isocurvature modes, *etc.*

As well as these underlying parameters, there are other (dependent) quantities that can be obtained from them. Such derived parameters include the actual Ω s of the various components (*e.g.*, Ω_m), the variance of density perturbations at particular scales (*e.g.*, σ_8), the angular scale of the sound horizon (θ_*), the age of the Universe today (t_0), the age of the Universe at recombination, reionization, *etc.* (see The Cosmological Parameters—Sec. 25).

29.5 Physics of Anisotropies

The cosmological parameters affect the anisotropies through the well understood physics of the evolution of linear perturbations within a background FRW cosmology. There are very effective, fast, and publicly-available software codes for computing the CMB temperature, polarization, and matter power spectra, *e.g.*, CMBFAST [32], CAMB [33], and CLASS [34]. These have been tested over a wide range of cosmologies and are considered to be accurate to much better than the 1% level [35], so that numerical errors are less than 10% of the parameter uncertainties for *Planck* [6].

For pedagogical purposes, it is easiest to focus on the temperature anisotropies, before moving to the polarization power spectra. A description of the physics underlying the C_ℓ^{TT} s can be separated into four main regions (the first two combined below), as shown in the top left part of Fig. 29.1.

29.5.1 The ISW Rise, $\ell \lesssim 10$, and Sachs-Wolfe Plateau, $10 \lesssim \ell \lesssim 100$

The horizon scale (or more precisely, the angle subtended by the Hubble radius) at last scattering corresponds to $\ell \simeq 100$. Anisotropies at larger scales have not evolved significantly, and hence directly reflect the ‘initial conditions.’ Temperature variations are $\delta T/T = -(1/5)\mathcal{R}(\mathbf{x}_{\text{LSS}}) \simeq (1/3)\delta\phi/c^2$, where $\delta\phi$ is the perturbation to the gravitational potential, evaluated on the last-scattering surface (LSS). This is a result of the combination of gravitational redshift and intrinsic temperature fluctuations, and is usually referred to as the Sachs-Wolfe effect [36].

Assuming that a nearly scale-invariant spectrum of curvature (and corresponding density) perturbations was laid down at early times (*i.e.*, $n_s \simeq 1$, meaning equal power per decade in k), then $\ell(\ell+1)C_\ell \simeq \text{constant}$ at low ℓ s. This effect is hard to see unless the multipole axis is plotted logarithmically (as in Fig. 29.1, and part of Fig. 29.2).

Time variation of the potentials (*i.e.*, time-dependent metric perturbations) at late times leads to an upturn in the C_ℓ s in the lowest several multipoles; any deviation from a total equation of state $w = 0$ has such an effect. So the dominance of the dark energy at low redshift (see Dark Energy—Sec. 28) makes the lowest ℓ s rise above the plateau. This is usually called the integrated Sachs-Wolfe effect (or ISW rise), since it comes from the line integral of $\dot{\phi}$; it has been confirmed through correlations between the large-angle anisotropies and large-scale structure [37]. Specific models can also give additional contributions at low ℓ (*e.g.*, perturbations in the dark-energy component itself [38]), but typically these are buried in the cosmic variance.

In principle, the mechanism that produces primordial perturbations could generate scalar, vector, and tensor modes. However, the vector (vorticity) modes decay with the expansion of the Universe. The tensors (transverse trace-free perturbations to the metric) generate temperature anisotropies through the integrated effect of the locally-anisotropic expansion of space. Since the tensor modes also redshift away after they enter the horizon, they contribute only to angular scales above about 1° (see Fig. 29.1). Hence, some fraction of the low- ℓ signal could be due to a gravitational wave contribution, although small amounts of tensors are essentially impossible to discriminate from other effects that might raise the level of the plateau. Nevertheless, the tensors *can* be distinguished using polarization information (see Sec. 29.7).

29.5.2 The Acoustic Peaks, $100 \lesssim \ell \lesssim 1000$

On sub-degree scales, the rich structure in the anisotropy spectrum is the consequence of gravity-driven acoustic oscillations oc-

curing before the atoms in the Universe became neutral [39]. Perturbations inside the horizon at last scattering have been able to evolve causally and produce anisotropy at the last-scattering epoch, which reflects this evolution. The frozen-in phases of these sound waves imprint a dependence on the cosmological parameters, which gives CMB anisotropies their great constraining power.

The underlying physics can be understood as follows. Before the Universe became neutral, the proton-electron plasma was tightly coupled to the photons, and these components behaved as a single ‘photon-baryon fluid.’ Perturbations in the gravitational potential, dominated by the dark-matter component, were steadily evolving. They drove oscillations in the photon-baryon fluid, with photon pressure providing most of the restoring force and baryons giving some additional inertia. The perturbations were quite small in amplitude, $\mathcal{O}(10^{-5})$, and so evolved linearly. That means each Fourier mode developed independently, and hence can be described as a driven harmonic oscillator, with frequency determined by the sound speed in the fluid. Thus, the fluid density underwent oscillations, giving time variations in temperature. These combine with a velocity effect, which is $\pi/2$ out of phase and has its amplitude reduced by the sound speed.

After the Universe recombined, the radiation decoupled from the baryons and could travel freely towards us. At that point, the (temporal) phases of the oscillations were frozen-in, and became projected on the sky as a harmonic series of peaks and troughs in power. The main peak is the mode that went through 1/4 of a period, reaching maximal compression. The even peaks are maximal *under*-densities, which are generally of smaller amplitude because the rebound has to fight against the baryon inertia. The troughs, which do not extend to zero power, are partially filled by the Doppler effect because they are at the velocity maxima.

The physical length scale associated with the peaks is the sound horizon at last scattering, which can be straightforwardly calculated. This length is projected onto the sky, leading to an angular scale that depends on the geometry of space, as well as the distance to last scattering. Hence, the angular position of the peaks is a sensitive probe of a particular combination of cosmological parameters. In fact, the angular scale, θ_* , is the most precisely measured observable, and hence is usually treated as an element of the cosmological parameter set.

One additional effect arises from reionization at redshift z_i . A fraction of photons (τ) will be isotropically scattered at $z < z_i$, partially erasing the anisotropies at angular scales smaller than those subtended by the Hubble radius at z_i . This corresponds typically to ℓ s above about 10, depending on the specific reionization model. The acoustic peaks are therefore reduced by a factor $e^{-2\tau}$ relative to the plateau.

These peaks were a clear theoretical prediction going back to about 1970 [40]. One can think of them as a snapshot of stochastic standing waves. Since the physics governing them is simple and their structure rich, one can see how they encode extractable information about the cosmological parameters. Their empirical existence started to become clear around 1994 [41], and the emergence, over the following decade, of a coherent series of acoustic peaks and troughs is a triumph of modern cosmology. This picture has received further confirmation with the detection in the power spectrum of galaxies (at redshifts $z \lesssim 1$) of the imprint of these same acoustic oscillations in the baryon component [42], as well as through detection of the expected oscillations in CMB polarization power spectra (see Sec. 29.7).

29.5.3 The Damping Tail, $\ell \gtrsim 1000$

The recombination process is not instantaneous, which imparts a thickness to the LSS. This leads to a damping of the anisotropies at the highest ℓ s, corresponding to scales smaller than that subtended by this thickness. One can also think of the photon-baryon fluid as having imperfect coupling, so that there is diffusion between the two components, and hence the amplitudes of the oscillations decrease with time. These effects lead to a damping of the C_{ℓ} s, sometimes called ‘Silk damping’ [43], which cuts off the anisotropies at multipoles above about 2000. So, although in principle it is possible to measure to ever smaller scales, this becomes increasingly difficult in practice.

29.5.4 Gravitational Lensing Effects

An extra effect at high ℓ s comes from gravitational lensing, caused by structures at low redshift along the line of sight to the LSS. The C_{ℓ} s are convolved with a smoothing function in a calculable way, partially flattening the peaks and troughs, generating a power-law tail at the highest multipoles, and complicating the polarization signal [44]. The expected effects of lensing on the CMB have been definitively detected through the 4-point function, which correlates temperature gradients and small-scale anisotropies (enabling a map of the lensing potential to be constructed [45]), as well as through the smoothing effect on the shape of the C_{ℓ} s. Lensing is important because it gives an independent estimate of A_s , breaking the parameter combination $A_s e^{-2\tau}$ that is largely degenerate in the temperature anisotropy power spectra. Lensing is an example of a ‘secondary effect,’ *i.e.*, the processing of anisotropies due to relatively nearby structures (see Sec. 29.8.2). Galaxies and clusters of galaxies give several such effects; all are expected to be of low amplitude, but are increasingly important at the highest ℓ s. Such effects carry additional cosmological information (about evolving gravitational potentials in the low-redshift Universe) and are receiving more attention as experiments push to higher sensitivity and angular resolution. The lensing power spectrum can potentially constrain dark-energy evolution, while future measurements at high ℓ are a particularly sensitive probe of the sum of the neutrino masses [46].

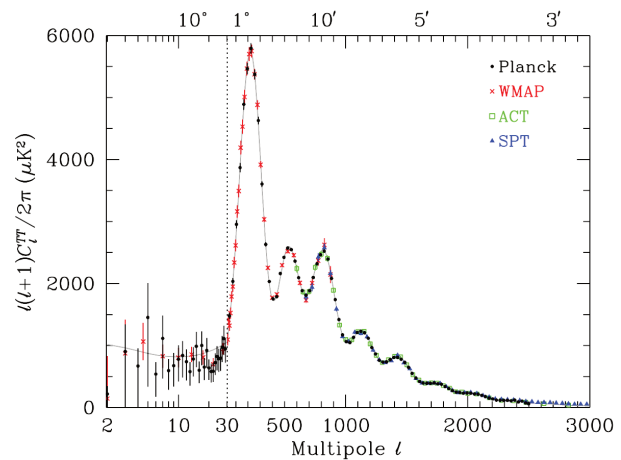


Figure 29.2: CMB temperature anisotropy band-power estimates from the *Planck*, *WMAP*, ACT, and SPT experiments. Note that the widths of the multipole bands vary between experiments and have not been plotted. This figure represents only a selection of the most recent available experimental results, and some points with large error bars have been omitted. At the higher multipoles these band-powers involve subtraction of particular foreground models, and so proper analysis requires simultaneous fitting of CMB and foregrounds over multiple frequencies. The horizontal axis here is logarithmic for the lowest multipoles, to show the Sachs-Wolfe plateau, and linear for the other multipoles. The acoustic peaks and damping region are very clearly observed, with no need for a theoretical line to guide the eye; however, the curve plotted is the best-fit *Planck* Λ CDM model.

29.6 Current Temperature Anisotropy Data

There has been a steady improvement in the quality of CMB data that has led to the development of the present-day cosmological model. The most robust constraints currently available come from *Planck* satellite [47, 48] data (together with constraints from non-CMB cosmological data sets), although smaller-scale results from the ACT [49] and SPT [50] experiments are beginning to add useful constraining power. We plot power spectrum estimates from these experiments in Fig. 29.2, along with *WMAP* data [5] to show the consistency (see previous versions of this review for data from earlier experiments). Comparisons among data sets show consistency, both in maps and in derived power spectra (up

to systematic uncertainties in the overall calibration for some experiments). This makes it clear that systematic effects are largely under control.

The band-powers shown in Fig. 29.2 are in very good agreement with a ‘ Λ CDM’ model. As described earlier, several (at least seven) of the peaks and troughs are quite apparent. For details of how these estimates were arrived at, the strength of correlations between band-powers, and other information required to properly interpret them, the original papers should be consulted.

29.7 CMB Polarization

Thomson scattering of an anisotropic radiation field also generates linear polarization and the CMB is predicted to be polarized, at the level of roughly 5% of the temperature anisotropies [51]. Polarization is a spin-2 field on the sky, and the algebra of the modes in multipole space is strongly analogous to spin-orbit coupling in quantum mechanics [52]. The linear polarization pattern can be decomposed in a number of ways, with two quantities required for each pixel in a map, often given as the Q and U Stokes parameters. However, the most intuitive and physical decomposition is a geometrical one, splitting the polarization pattern into a part that comes from a divergence (often referred to as the ‘ E mode’) and a part with a curl (called the ‘ B mode’) [53]. More explicitly, the modes are defined in terms of second derivatives of the polarization amplitude, with the Hessian for the E modes having principal axes in the same sense as the polarization, while the B -mode pattern can be thought of as a 45° rotation of the E -mode pattern. Globally one sees that the E modes have $(-1)^\ell$ parity (like the spherical harmonics), while the B modes have $(-1)^{\ell+1}$ parity.

The existence of this linear polarization allows for six different cross-power spectra to be determined from data that measure the full temperature and polarization anisotropy information. Parity considerations make two of these zero, and we are left with four potential observables, C_ℓ^{TT} , C_ℓ^{TE} , C_ℓ^{EE} , and C_ℓ^{BB} (see Fig. 29.1). Because scalar perturbations have no handedness, the B -mode power spectrum can only be sourced by vectors or tensors. Moreover, since inflationary scalar perturbations give only E modes, while tensors generate roughly equal amounts of E and B , then the determination of a non-zero B -mode signal is a way to measure the gravitational-wave contribution (and thus potentially derive the energy scale of inflation). However, since the signal is expected to be rather weak, one must first eliminate the foreground contributions and other systematic effects down to very low levels. In addition, CMB lensing creates B modes from E modes, further complicating the extraction of a tensor signal.

Like with temperature, the polarization C_ℓ s exhibit a series of acoustic peaks generated by the oscillating photon-baryon fluid. The main ‘ EE ’ power spectrum has peaks that are out of phase with those in the ‘ TT ’ spectrum because the polarization anisotropies are sourced by the fluid velocity. The ‘ TE ’ part of the polarization and temperature patterns comes from correlations between density and velocity perturbations on the last-scattering surface, which can be both positive and negative, and is of larger amplitude than the EE signal. There is no polarization Sachs-Wolfe effect, and hence no large-angle plateau. However, scattering during a recent period of reionization can create a polarization ‘bump’ at large angular scales.

Because the polarization anisotropies have only a small fraction of the amplitude of the temperature anisotropies, they took longer to detect. The first measurement of a polarization signal came in 2002 from the DASI experiment [54], which provided a convincing detection, confirming the general paradigm, but of low enough significance that it lent no real constraint to models. Despite dramatic progress since then, it is still the case that polarization data mainly support the basic paradigm, while reducing error bars on parameters by only around 20%. However, there are exceptions to this, specifically in the reionization optical depth, and the potential to constrain primordial gravitational waves. Moreover the situation is expected to change dramatically as more of the available polarization modes are measured.

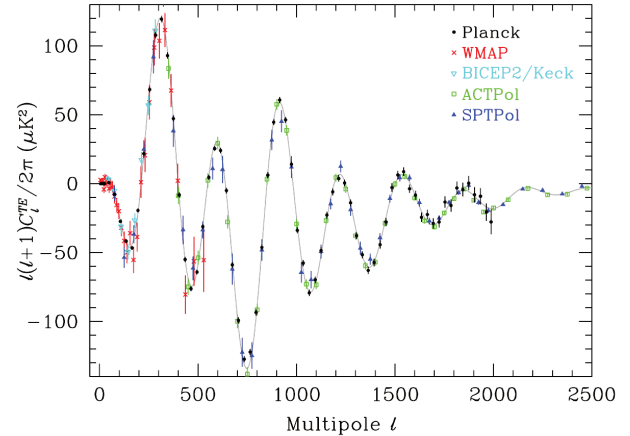


Figure 29.3: Cross-power spectrum band-powers of the temperature anisotropies and E -mode polarization signal from *Planck* (the low multipole data have been binned here), as well as *WMAP*, *BICEP2/Keck*, *ACTPol*, and *SPTPol*. The curve is the best fit to the *Planck* temperature, polarization, and lensing band-powers. Note that each data point is an average over a band of multipoles, and hence to compare in detail with a model one has to integrate the theoretical curve through the band.

29.7.1 T - E Power Spectrum

Since the T and E skies are correlated, one has to measure the TE power spectrum, as well as TT and EE , in order to extract all the cosmological information. This TE signal has now been mapped out extremely accurately by *Planck* [48], and these band-powers are shown in Fig. 29.3, along with those from *WMAP* [55] and *BICEP2/Keck* [56], with *ACTPol* [57] and *SPTPol* [58] extending to smaller angular scales. The anti-correlation at $\ell \simeq 150$ and the peak at $\ell \simeq 300$ were the first features to become distinct, but now a whole series of oscillations is clearly seen in this power spectrum (including at least six peaks and troughs [10]). The measured shape of the cross-correlation power spectrum provides supporting evidence for the general cosmological picture, as well as directly constraining the thickness of the last-scattering surface. Since the polarization anisotropies are generated in this scattering surface, the existence of correlations at angles above about a degree demonstrates that there were super-Hubble fluctuations at the recombination epoch. The sign of this correlation also confirms the adiabatic paradigm.

The overall picture of the source of CMB polarization and its oscillations has also been confirmed through tests that average the maps around both temperature hot spots and cold spots [59]. One sees precisely the expected patterns of radial and tangential polarization configurations, as well as the phase shift between polarization and temperature. This leaves no doubt that the oscillation picture is the correct one and that the polarization is coming from Thomson scattering at $z \simeq 1100$.

29.7.2 E - E Power Spectrum

Experimental band-powers for C_ℓ^{EE} from *Planck*, *WMAP*, *BICEP2/Keck* Array [56], *ACTPol* [57], and *SPTPol* [58] are shown in Fig. 29.4. Without the benefit of correlating with the temperature anisotropies (*i.e.*, measuring C_ℓ^{TE}), the polarization anisotropies are very weak and challenging to measure. Nevertheless, the oscillatory pattern is now well established and the data closely match the TT -derived theoretical prediction. In Fig. 29.4 one can clearly see the ‘shoulder’ expected at $\ell \simeq 140$, the first main peak at $\ell \simeq 400$ (corresponding to the first trough in C_ℓ^{TT}), and the series of oscillations that is out of phase with those of the temperature anisotropy power spectrum (including four or five peaks and troughs [10]).

Perhaps the most unique result from the polarization measurements is at the largest angular scales ($\ell < 10$) in C_ℓ^{TE} and C_ℓ^{EE} , where there is evidence for an excess signal (not visible in

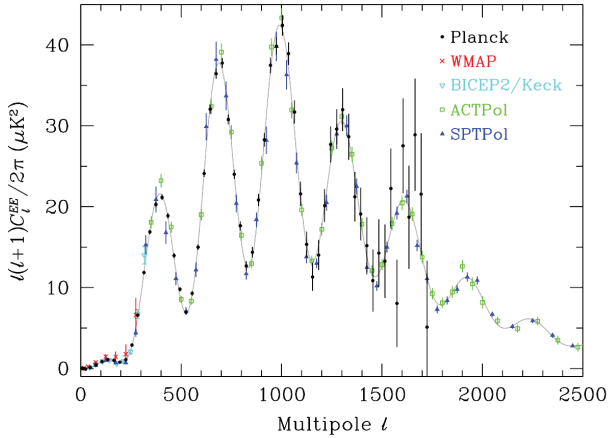


Figure 29.4: Power spectrum of E -mode polarization from *Planck*, together with *WMAP*, BICEP2/Keck, ACTPol, and SPTPol. Note that some band-powers with larger uncertainties have been omitted and that the unbinned *Planck* low- ℓ data have been binned here. Also plotted is the best-fit theoretical model from *Planck* temperature, polarization, and lensing data.

Fig. 29.4) compared to that expected from the temperature power spectrum alone. This is precisely the signal anticipated from an early period of reionization, arising from Doppler shifts during the partial scattering at $z < z_i$. The amplitude of the signal indicates that the first stars, presumably the source of the ionizing radiation, formed around $z \simeq 8$ (although the uncertainty is still quite large). Since this corresponds to a scattering optical depth $\tau \simeq 0.06$, then roughly 6% of CMB photons were re-scattered at the reionization epoch, with the other 94% last scattering at $z \simeq 1100$. However, estimates of the amplitude of this reionization excess have come down since the first measurements by *WMAP* (indicating that this is an extremely difficult measurement to make) and the latest *Planck* results have reduced the value further [11, 60].

29.7.3 B - B Power Spectrum

The expected amplitude of C_{ℓ}^{BB} is very small, and so measurements of this polarization curl-mode are extremely challenging. The first indication of the existence of the BB signal came from the detection of the expected conversion of E modes to B modes by gravitational lensing, through a correlation technique using the lensing potential and polarization measurements from SPT [61]. However, the real promise of B modes lies in the detection of primordial gravitational waves at larger scales. This tensor signature could be seen either in the ‘recombination bump’ at around $\ell = 100$ (caused by an ISW effect as gravitational waves redshift away at the last-scattering epoch) or the ‘reionization bump’ at $\ell \lesssim 10$ (from additional scattering at low redshifts).

Results from the BICEP2 experiment [62] in 2014 suggested a detection of the primordial B -mode signature around the recombination peak. BICEP2 mapped a small part of the CMB sky with the best sensitivity level reached at that time (below 100 nK), but at a single frequency. Higher frequency data from *Planck* indicated that much of the BICEP2 signal was due to dust within our Galaxy, and a combined analysis by the BICEP2, Keck Array, and *Planck* teams [63] indicated that the data are consistent with no primordial B modes. The current constraint from *Planck* data alone is $r < 0.069$ (95% at $k = 0.05 \text{ Mpc}^{-1}$ [11, 60]) using all CMB power spectra, and this limit is reduced to $r < 0.044$ with the inclusion of BICEP2/Keck Array data [60, 64]. The most constraining limit is $r < 0.036$ from a combination of BICEP2, Keck Array, and BICEP3 data, using *WMAP* and *Planck* maps to help remove foregrounds [65].

Several experiments are continuing to push down the sensitivity of B -mode measurements, motivated by the enormous importance of a future detection of this telltale signature of inflation (or other

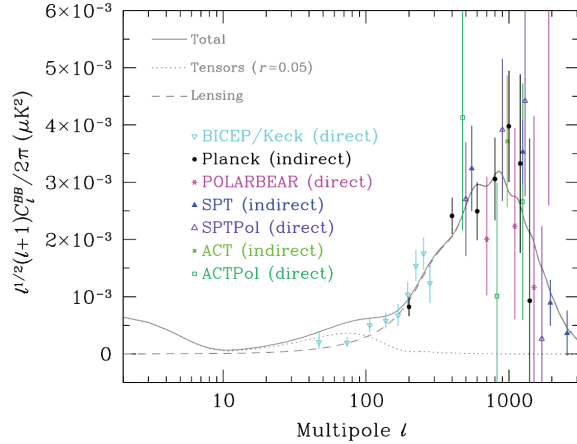


Figure 29.5: Power spectrum of B -mode polarization, including results from the BICEP2/BICEP3/Keck Array combined analysis, *Planck*, POLARBEAR, SPT, and ACT. Note that some of the measurements are direct estimates of B modes on the sky, while others are only sensitive to the lensing signal and come from combining E -mode and lensing potential measurements. Several earlier experiments reported upper limits, which are all off the top of this plot. A logarithmic horizontal axis is adopted here and the y -axis has been divided by a factor of $\sqrt{\ell}$ in order to show all three theoretically expected contributions: the low- ℓ reionization bump; the $\ell \simeq 100$ recombination peak; and the high- ℓ lensing signature. The dotted line is for a tensor (primordial gravitational wave) fraction $r = 0.05$, simply as an example, with all other cosmological parameters set at the best *Planck*-derived values, for which model the expected lensing B modes have also been shown with a dashed line.

physics at the highest energies). A compilation of experimental results for C_{ℓ}^{BB} is shown in Fig. 29.5, coming from a combination of direct estimates of the B modes (BICEP2/BICEP3/Keck Array [65], POLARBEAR [66], SPTPol [67], and ACTPol [57]) and indirect determinations of the lensing B modes based on estimating the effect of measured lensing on measured E modes (*Planck* [68], SPT [61], and ACT [69]). Additional band-power estimates are expected from these and other experiments in the near future, with the Simons Observatory [70], the so-called ‘Stage 4’ CMB project [71] and the *LiteBIRD* satellite [72], holding great promise for pushing down to the $r \sim 0.001$ level.

29.7.4 ϕ - ϕ Power Spectrum

One further CMB observable that can be measured is the gravitational lensing deflection, leading to the construction of a map of the lensing potential. The latest *Planck* results [73] give a map that is detected at the 40σ level using a minimum-variance procedure from the 4-point function of temperature and polarization data. From this, estimates can be constructed of $C_{\ell}^{\phi\phi}$, the lensing-potential power spectrum, which is found to be consistent with predictions from the best-fit temperature and polarization model.

We can think of each sky pixel as possessing three independent quantities that can be measured, namely T , E , and ϕ (and potentially B , if that becomes detectable). Determining the constraining power comes down to counting $Y_{\ell m}$ modes [74], as well as appreciating that some modes help to break particular parameter degeneracies. We have only scratched the surface of CMB lensing so far, and it is expected that future small-scale experiments will be able to extract more of the cosmological information. Further constraints can also be derived on the lower- z Universe by cross-correlating CMB lensing with other cosmological tracers of large-scale structure. Additionally, small-scale lensing, combined with E -mode measurements, can be used to ‘delens’ CMB B -mode data, which will be important for pushing down into the $r \lesssim 0.01$ regime [75].

29.8 Complications

There are a number of issues that complicate the interpretation of CMB anisotropy data (and are considered to be *signal* by many astrophysicists), some of which we sketch out below.

29.8.1 Foregrounds

The microwave sky contains significant emission from our Galaxy and from extragalactic sources [76]. Fortunately, the frequency dependence of these various sources is in general substantially different from that of the CMB anisotropy signals. The combination of Galactic synchrotron, bremsstrahlung, and dust emission reaches a minimum at a frequency of roughly 100 GHz (or wavelength of about 3 mm). As one moves to greater angular resolution, the minimum moves to slightly higher frequencies, but becomes more sensitive to unresolved (point-like) sources.

At frequencies around 100 GHz, and for portions of the sky away from the Galactic plane, the foregrounds are typically 1 to 10% of the CMB anisotropies. By making observations at multiple frequencies, it is relatively straightforward to separate the various components and determine the CMB signal to the few per cent level. For greater sensitivity, it is necessary to use the spatial information and statistical properties of the foregrounds to separate them from the CMB. Furthermore, at higher ℓ s it is essential to carefully model extragalactic foregrounds, particularly the clustering of infrared-emitting galaxies, which dominate the measured power spectrum as we move into the damping tail.

The foregrounds for CMB polarization follow a similar pattern to those for temperature, but are intrinsically brighter relative to CMB anisotropies. *WMAP* showed that the polarized foregrounds dominate at large angular scales, and that they must be well characterized in order to be discriminated [77]. *Planck* has shown that it is possible to characterize the foreground polarization signals, with synchrotron dominating at low frequencies and dust at high frequencies [78]. On smaller scales there are no strongly-polarized foregrounds, and hence it is in principle easier to measure foreground-free modes at high multipoles in polarization than in temperature. Although foreground contamination will no doubt become more complicated as we push down in sensitivity, making analysis more difficult, for the time being, foreground contamination is not a fundamental limit for CMB experiments.

29.8.2 Secondary Anisotropies

With increasingly precise measurements of the primary anisotropies, there is growing theoretical and observational interest in ‘secondary anisotropies,’ pushing experiments to higher angular resolution and sensitivity. These secondary effects arise from the processing of the CMB due to ionization history and the evolution of structure, including gravitational lensing (which was already discussed) and patchy reionization effects [79]. Additional information can thus be extracted about the Universe at $z \ll 1000$. This tends to be most effectively done through correlating CMB maps with other cosmological probes of structure. Secondary signals are also typically non-Gaussian, unlike the primary CMB anisotropies.

A secondary signal of great current interest is the Sunyaev-Zeldovich (SZ) effect [80], which is Compton scattering ($\gamma e \rightarrow \gamma' e'$) of the CMB photons by hot electrons in intergalactic plasma. This creates spectral distortions by transferring energy from the electrons to the photons. It is particularly important for clusters of galaxies, through which one observes a partially Comptonized spectrum, resulting in a decrement at radio wavelengths and an increment in the submillimeter.

The imprint on the CMB sky is of the form $\Delta T/T = y f(x)$, with the y parameter being the integral of Thomson optical depth times $kT_e/m_e c^2$ through the cluster, and $f(x)$ describing the frequency dependence. This is simply $x \coth(x/2) - 4$ for a non-relativistic gas (the electron temperature in a cluster is typically a few keV), where the dimensionless frequency $x \equiv h\nu/kT_\gamma$. As well as this ‘thermal’ SZ effect, there is also a smaller ‘kinetic’ effect due to the bulk motion of the cluster gas, giving $\Delta T/T \sim \tau(v/c)$, with either sign, but having the same spectrum as the primary CMB anisotropies.

A significant advantage in finding galaxy clusters via the SZ

effect is that the signal is largely independent of redshift, so in principle clusters can be found to arbitrarily large distances. The SZ effect can be used to find and study individual clusters, and to obtain estimates of the Hubble constant. There is also the potential to constrain cosmological parameters, such as the clustering amplitude σ_8 and the equation of state of the dark energy, through counts of detected clusters as a function of redshift. The promise of the method has been realized through detections of clusters purely through the SZ effect by SPT [81], ACT [82], and *Planck* [83]. Results from *Planck* clusters [84] suggest a somewhat lower value of σ_8 than inferred from CMB anisotropies, but there are still systematic uncertainties that might encompass the difference, and a more recent analysis of SPT-detected clusters shows better agreement [85]. Further analysis of scaling relations among cluster properties should enable more robust cosmological constraints to be placed in future, so that we can understand whether this ‘tension’ might be a sign of new physics.

29.8.3 Higher-order Statistics

Although most of the CMB anisotropy information is contained in the power spectra, there will also be weak signals present in higher-order statistics. These can measure any primordial non-Gaussianity in the perturbations, as well as non-linear growth of the fluctuations on small scales and other secondary effects (plus residual foreground contamination of course). There are an infinite variety of ways in which the CMB could be non-Gaussian [26]; however, there is a generic form to consider for the initial conditions, where a quadratic contribution to the curvature perturbations is parameterized through a dimensionless number f_{NL} . This weakly non-linear component can be constrained in several ways, the most popular being through measurements of the bispectrum (or 3-point function).

The constraints depend on the shape of the triangles in harmonic space, and it has become common to distinguish the ‘local’ or ‘squeezed’ configuration (in which one side is much smaller than the other two) from the ‘equilateral’ configuration. Other configurations are also relevant for specific theories, such as ‘orthogonal’ non-Gaussianity, which has positive correlations for $k_1 \simeq 2k_2 \simeq 2k_3$, and negative correlations for the equilateral configuration. The latest results from the *Planck* team [86] are $f_{\text{NL}}^{\text{local}} = 1 \pm 5$, $f_{\text{NL}}^{\text{equil}} = -26 \pm 47$, and $f_{\text{NL}}^{\text{ortho}} = -38 \pm 24$.

These results are consistent with zero, but are at a level that is now interesting for model predictions. The amplitude of f_{NL} expected is small, so that a detection of $f_{\text{NL}} \gg 1$ would rule out all single-field, slow-roll inflationary models. It is still possible to improve upon these *Planck* results, and it certainly seems feasible that a measurement of primordial non-Gaussianity may yet be within reach. Non-primordial detections of non-Gaussianity from expected signatures have already been made. For example, the bispectrum and trispectrum contain evidence of gravitational lensing, the ISW effect, and Doppler boosting. For now the primordial signal is elusive, but should it be detected, then detailed measurements of non-Gaussianity will become a unique probe of inflationary-era physics. Because of that, much effort continues to be devoted to honing predictions and measurement techniques, with the expectation that we will need to go beyond the CMB (e.g., 3D galaxy surveys) to dramatically improve the constraints.

29.8.4 Anomalies

Several features seen in the *Planck* data [29,59,87] confirm those found earlier with *WMAP* [28], showing mild deviations from a simple description of the sky; these are often referred to as ‘anomalies.’ One such feature is the lack of power in the multipole range $\ell \simeq 20\text{--}30$ [11,48]. Other examples involve the breaking of statistical anisotropy, caused by alignment of the lowest multipoles, as well as a somewhat excessive cold spot and a power asymmetry between hemispheres. No such feature is significant at more than the roughly 3σ level, and the importance of ‘*a posteriori*’ statistics here has been emphasized by many authors. Since these effects are at large angular scales, where cosmic variance dominates, the results will not increase in significance with more data, although there is the potential for more sensitive polarization measurements to provide independent tests.

29.9 Constraints on Cosmological Parameters

The most striking outcome of the last couple of decades of experimental results is that the standard cosmological paradigm continues to be in very good shape. A large amount of high-precision data on the power spectrum is adequately fit with fewer than 10 free parameters (and only six need non-trivial values). The framework is that of FRW models, which have nearly flat geometry, containing dark matter and dark energy, and with adiabatic perturbations having close to scale-invariant initial conditions.

Within this basic picture, the values of the cosmological parameters can be constrained. Of course, more stringent bounds can be placed on models that cover a restricted parameter space, *e.g.*, assuming that $\Omega_{\text{tot}} = 1$ or $r = 0$. More generally, the constraints depend upon the adopted prior probability distributions, even if they are implicit, for example by restricting the parameter freedom or their ranges (particularly where likelihoods peak near the boundaries), or by using different choices of other data in combination with the CMB. As the data become even more precise, these considerations will be less important, but for now we caution that restrictions on model space and choice of non-CMB data sets and priors need to be kept in mind when adopting specific parameter values and uncertainties.

There are some combinations of parameters that fit the CMB anisotropies almost equivalently. For example, there is a nearly exact geometric degeneracy, where any combination of Ω_{m} and Ω_{Λ} that provides the same angular-diameter distance to last scattering will give nearly identical C_{ℓ} s. There are also other less exact degeneracies among the parameters. Such degeneracies can be broken when using the CMB results in combination with other cosmological data sets. Particularly useful are complementary constraints from baryon acoustic oscillations, galaxy clustering, the abundance of galaxy clusters, weak gravitational lensing measurements, and Type Ia supernova distances. For an overview of some of these other cosmological constraints, see The Cosmological Parameters—Sec. 25 of this *Review*.

Within the context of a 6-parameter family of models (which fixes $\Omega_{\text{tot}} = 1$, $dn_{\text{s}}/d\ln k = 0$, $r = 0$, and $w = -1$) the *Planck* results for TT , together with TE , EE , and CMB lensing, yield [11]: $\ln(10^{10} A_{\text{s}}) = 3.044 \pm 0.014$; $n_{\text{s}} = 0.965 \pm 0.004$; $\Omega_{\text{b}} h^2 = 0.02237 \pm 0.00015$; $\Omega_{\text{c}} h^2 = 0.1200 \pm 0.0012$; $100\theta_{*} = 1.04092 \pm 0.00031$; and $\tau = 0.054 \pm 0.007$. Other parameters can be derived from this basic set, including $h = 0.674 \pm 0.005$, $\Omega_{\Lambda} = 0.685 \pm 0.007$ ($= 1 - \Omega_{\text{m}}$) and $\sigma_8 = 0.811 \pm 0.006$. Somewhat different (although consistent) values are obtained using other data combinations, such as including BAO, supernova, H_0 , or weak-lensing constraints (see Sec. 25 of this *Review*). However, the results quoted above are currently the best available from CMB data alone.

The standard cosmological model still fits the data well, with the error bars on the parameters continuing to shrink. Improved measurement of higher acoustic peaks has dramatically reduced the uncertainty in the θ_{*} parameter, which is now detected at $> 3000\sigma$. The evidence for $n_{\text{s}} < 1$ is now at the 8σ level from *Planck* data alone. The value of the reionization optical depth has decreased compared with earlier estimates; it is convincingly detected, but still not at very high significance.

Constraints can also be placed on parameters beyond the basic six, particularly when including other astrophysical data sets. Relaxing the flatness assumption, the constraint on Ω_{tot} is 1.011 ± 0.006 . Note that for h , the CMB data alone provide only a very weak constraint if spatial flatness is not assumed. However, with the addition of other data (particularly powerful in this context being a compilation of BAO measurements; see Sec. 25 of this *Review*), the constraints on the Hubble constant and curvature improve considerably, leading to $\Omega_{\text{tot}} = 0.9993 \pm 0.0019$ [11].

For $\Omega_{\text{b}} h^2$ the CMB-derived value is generally consistent with completely independent constraints from Big Bang nucleosynthesis (see Sec. 24 of this *Review*). Related are constraints on additional neutrino-like relativistic degrees of freedom, which lead to $N_{\text{eff}} = 2.99 \pm 0.17$ (including BAO), *i.e.*, no evidence for extra neutrino species.

The best published limit on the tensor-to-scalar ratio is $r <$

0.036 (measured at $k = 0.05 \text{ Mpc}^{-1}$) from BICEP/Keck Array [65]. The detailed limit will depend on how the slope n_{t} is restricted and whether $dn_{\text{s}}/d\ln k \neq 0$ is allowed. The joint constraints on n_{s} and r allow specific inflationary models to be tested [30,88]. Looking at the (n_{s}, r) plane, this means that $m^2 \phi^2$ (mass-term quadratic) inflation is disfavored by the data, as well as $\lambda \phi^4$ (self-coupled) inflation.

The addition of the dark-energy equation of state w adds the partial degeneracy of being able to fit a ridge in (w, h) space, extending to low values of both parameters. This degeneracy is broken when the CMB is used in combination with other data sets, *e.g.*, adding a compilation of BAO and supernova data gives $w = -1.028 \pm 0.031$. Constraints can also be placed on more general dark energy and modified-gravity models [89]. However, when extending the search space, one needs to be careful not to over-interpret some tensions between data sets as evidence for new physics.

For the reionization optical depth, a reanalysis of *Planck* data in 2016 resulted in a reduction in the value of τ , with the tightest result giving $\tau = 0.055 \pm 0.009$, and the newest analysis gives similar numbers. This corresponds to $z_1 = 7.8\text{--}8.8$ (depending on the functional form of the reionization history), with an uncertainty of ± 0.9 [90]. This redshift is only slightly higher than that suggested from studies of absorption lines in high- z quasar spectra [91] and Ly α -emitting galaxies [92], perhaps hinting that the process of reionization was not as complex as previously suspected. The important constraint provided by CMB polarization, in combination with astrophysical measurements, thus allows us to investigate how the first stars formed and brought about the end of the cosmic dark ages.

29.10 Particle Physics Constraints

CMB data place limits on parameters that are directly relevant for particle physics models. For example, there is a limit on the sum of the masses of the neutrinos, $\Sigma m_{\nu} < 0.12 \text{ eV}$ (95%) [11] coming from *Planck* together with BAO measurements (although limits are weaker when considering both N_{eff} and Σm_{ν} as free parameters). This assumes the usual number density of fermions, which decoupled when they were relativistic. The limit is tantalizingly only a factor of a few higher than the minimum value coming from neutrino mixing experiments (see Neutrino Mixings—Secs. 14 and 26). As well as being an indirect probe of the neutrino background, *Planck* data also require that the neutrino background has perturbations, *i.e.*, that it possesses a sound speed $c_{\text{s}}^2 \simeq 1/3$, as expected [9].

The current suite of data suggests that $n_{\text{s}} < 1$, with a best-fitting value about 0.035 below unity. This is already quite constraining for inflationary models, particularly along with r limits. There is no current evidence for running of the spectral index, with $dn_{\text{s}}/d\ln k = -0.004 \pm 0.007$ from *Planck* alone [11] (with a similar value when BAO data are included), although this is less of a constraint on models. Similarly, primordial non-Gaussianity is being probed to interesting levels, although tests of simple inflationary models will only come with significant reductions in uncertainty.

The large-angle anomalies, such as the hemispheric modulation of power and the dip in power at $\ell \simeq 20\text{--}30$, have the potential to be hints of new physics. Such effects might be expected in a Universe that has a large-scale power cut-off, or anisotropy in the initial power spectrum, or is topologically non-trivial. However, cosmic variance and *a posteriori* statistics limit the significance of these anomalies, absent the existence of a model that naturally yields some of these features (and ideally also predicting other phenomena that can be tested).

Constraints on ‘cosmic birefringence’ (*i.e.*, rotation of the plane of CMB polarization that generates non-zero TB and EB power) can be used to place limits on theories involving parity violation, Lorentz violation, or axion-photon mixing [93].

It is possible to place limits on additional areas of physics [94], for example annihilating dark matter [9,9], primordial magnetic fields [95], and time variation of the fine-structure constant [96], as well as the neutrino chemical potential, a contribution of warm dark matter, topological defects, or physics beyond general relativity. Further particle physics constraints will follow as the

smaller-scale and polarization measurements continue to improve.

The CMB anisotropy measurements precisely pin down physics at the time of last-scattering, and so any change of physics can be constrained if it affects the relevant energies or timescales. Future, higher sensitivity measurements of the CMB frequency spectrum will push the constraints back to cover energy injection at much earlier times (~ 1 year). Comparison of CMB and BBN observables extend these constraints to timescales of order seconds, and energies in the MeV range. And to the extent that inflation provides an effective description of the generation of perturbations, the inflationary observables may constrain physics at GUT-type energy scales.

More generally, careful measurement of the CMB power spectra and non-Gaussianity can in principle put constraints on physics at the highest energies, including ideas of string theory, extra dimensions, colliding branes, *etc.* At the moment any calculation of predictions appears to be far from definitive. However, there is a great deal of activity on implications of string theory for the early Universe, and hence a chance that there might be observational implications for specific scenarios.

29.11 Fundamental Lessons

More important than the precise values of parameters is what we have learned about the general features that describe our observable Universe. Beyond the basic hot Big Bang picture, the CMB has taught us that:

- the (observable) Universe is very close to isotropic;
- the Universe recombined at $z \sim 1000$ and started to become ionized again at $z \sim 10$;
- the geometry of the Universe is close to flat;
- both dark matter and dark energy are required;
- gravitational instability is sufficient to grow all of the observed large structures in the Universe;
- topological defects were not important for structure formation;
- there were ‘synchronized’ super-Hubble modes generated in the early Universe;
- the initial perturbations were predominantly adiabatic in nature;
- the primordial perturbation spectrum has a slightly red tilt;
- the perturbations had close to Gaussian (*i.e.*, maximally random) initial conditions.

These features form the basis of the cosmological standard model, Λ CDM, for which it is tempting to make an analogy with the Standard Model of particle physics (see earlier Sections of this *Review*). The cosmological model is much further from any underlying ‘fundamental theory,’ which might ultimately provide the values of the parameters from first principles. Nevertheless, any genuinely complete ‘theory of everything’ must include an explanation for the values of these cosmological parameters in addition to the parameters of the Standard Model of particle physics.

29.12 Future Directions

Given the significant progress in measuring the CMB sky, which has been instrumental in tying down the cosmological model, what can we anticipate for the future? There will be a steady improvement in the precision and confidence with which we can determine the appropriate cosmological parameters. Ground-based experiments operating at smaller angular scales will continue to place tighter constraints on the damping tail, lensing, and cross-correlations. New polarization experiments at small scales will probe further into the damping tail, without the limitation of extragalactic foregrounds. And polarization experiments at large angular scales will push down the limits on primordial B modes.

Planck, the third generation CMB satellite mission, was launched in May 2009, and produced a large number of papers, including a set of cosmological studies based on the first two full surveys of the sky (accompanied by a public release of data products) in 2013, a further series coming from analysis of the full mission data release in 2015 (eight surveys for the Low Frequency Instrument and five surveys for the High Frequency Instrument),

and a third series derived from a final analysis of the 2018 data release, including full constraints from polarization data. *Planck* data currently dominate constraints on models (but that situation will change soon).

A set of cosmological parameters is now known to percent-level accuracy, and that may seem sufficient for many people. However, we should certainly demand more of measurements that describe *the entire observable Universe!* Hence a lot of activity in the coming years will continue to focus on determining those parameters with increasing precision. This necessarily includes testing for consistency among different predictions of the cosmological Standard Model, and searching for signals that might require additional physics.

A second area of focus will be the smaller-scale anisotropies and ‘secondary effects.’ There is a great deal of information about structure formation at $z \ll 1000$ encoded in the CMB sky. This may involve higher-order statistics and cross-correlations with other large-scale structure tracers, as well as spectral signatures, with many experiments targeting the galaxy cluster SZ effect. The current status of CMB lensing is similar (in terms of total signal-to-noise) to the quality of the first CMB anisotropy measurements by *COBE*, and thus we can expect that experimental probes of lensing will improve dramatically in the coming years. All of these investigations can provide constraints on the dark-energy equation of state, for example, which is a major area of focus for several future cosmological surveys at optical wavelengths. CMB lensing also promises to yield a measurement of the sum of the neutrino masses.

A third direction is increasingly sensitive searches for specific signatures of physics at the highest energies. The most promising of these may be the primordial gravitational wave signals in C_{ℓ}^{BB} , which could be a probe of the $\sim 10^{16}$ GeV energy range. There are several ground- and balloon-based experiments underway that are designed to search for the polarization B modes. Additionally, non-Gaussianity holds the promise of constraining models beyond single-field slow-roll inflation.

Anisotropies in the CMB have proven to be the premier probe of cosmology and the early Universe. Theoretically the CMB involves well-understood physics in the linear regime, and is under very good calculational control. A substantial and improving set of observational data now exists. Systematics appear to be under control and are not currently a limiting factor. And so for the next several years we can expect an increasing amount of cosmological information to be gleaned from CMB anisotropies, with the prospect also of some genuine surprises.

References

- [1] A. A. Penzias and R. W. Wilson, *Astrophys. J.* **142**, 419 (1965); R. H. Dicke *et al.*, *Astrophys. J.* **142**, 414 (1965).
- [2] M. White, D. Scott and J. Silk, *Ann. Rev. Astron. Astrophys.* **32**, 319 (1994); W. Hu and S. Dodelson, *Ann. Rev. Astron. Astrophys.* **40**, 171 (2002), [arXiv:astro-ph/0110414]; A. Challinor and H. Peiris, in M. Novello and S. Perez, editors, “American Institute of Physics Conference Series,” volume 1132, 86–140 (2009), [arXiv:0903.5158].
- [3] G. F. Smoot *et al.*, *Astrophys. J. Lett.* **396**, L1 (1992).
- [4] C. L. Bennett *et al.*, *Astrophys. J. Supp.* **148**, 1 (2003), [arXiv:astro-ph/0302207].
- [5] G. Hinshaw *et al.*, *Astrophys. J. Supp.* **208**, 19 (2013).
- [6] Planck Collab. 2013 Results XVI, *Astron. Astrophys.* **571**, A16 (2014).
- [7] J. A. Tauber *et al.*, *Astron. Astrophys.* **520**, A1 (2010); Planck Collab. 2013 Results I, *Astron. Astrophys.* **571**, A1 (2014), [arXiv:1303.5062].
- [8] Planck Collab. 2015 Results I, *Astron. Astrophys.* **594**, A1 (2016), [arXiv:1502.01582].
- [9] Planck Collab. 2015 Results XIII, *Astron. Astrophys.* **594**, A13 (2016), [arXiv:1502.01589].
- [10] Planck Collab. 2018 Results I, *Astron. Astrophys.* **641**, A1 (2020), [arXiv:1807.06205].

- [11] Planck Collab. 2018 Results VI, *Astron. Astrophys.* **641**, A6 (2020), [arXiv:1807.06209].
- [12] D. S. Swetz *et al.*, *Astrophys. J. Supp.* **194**, 41 (2011), [arXiv:1007.0290].
- [13] J. E. Carlstrom *et al.*, *Proc. Astron. Soc. Pacific* **123**, 568 (2011), [arXiv:0907.4445].
- [14] P. Noterdaeme *et al.*, *Astron. Astrophys.* **526**, L7 (2011), [arXiv:1012.3164]; S. Muller *et al.*, *Astron. Astrophys.* **551**, A109 (2013), [arXiv:1212.5456].
- [15] D. J. Fixsen *et al.*, *Astrophys. J.* **734**, 5 (2011), [arXiv:0901.0555].
- [16] J. Singal *et al.*, *Proc. Astron. Soc. Pacific* **130**, 985, 036001 (2018), [arXiv:1711.09979].
- [17] A. Kogut *et al.*, *J. Cosmology Astropart. Phys.* **2011**, 7, 025 (2011), [arXiv:1105.2044]; P. André *et al.*, *J. Cosmology Astropart. Phys.* **2014**, 2, 006 (2014), [arXiv:1310.1554]; J. Delabrouille *et al.*, *Experimental Astronomy*, in press (2021), [arXiv:1909.01591].
- [18] V. Desjacques *et al.*, *Mon. Not. R. Astron. Soc.* **451**, 4460 (2015), [arXiv:1503.05589].
- [19] D. J. Fixsen, *Astrophys. J.* **707**, 916 (2009), [arXiv:0911.1955].
- [20] J. C. Mather *et al.*, *Astrophys. J.* **512**, 511 (1999), [arXiv:astro-ph/9810373].
- [21] Y. Hoffman, H. M. Courtois and R. B. Tully, *Mon. Not. R. Astron. Soc.* **449**, 4494 (2015), [arXiv:1503.05422].
- [22] D. J. Fixsen *et al.*, *Astrophys. J.* **420**, 445 (1994).
- [23] Planck Collab. 2013 Results XXVII, *Astron. Astrophys.* **571**, A27 (2014), [arXiv:1303.5087].
- [24] S. Seager, D. D. Sasselov and D. Scott, *Astrophys. J. Supp.* **128**, 407 (2000), [arXiv:astro-ph/9912182].
- [25] L. Knox, *Phys. Rev.* **D52**, 4307 (1995), [arXiv:astro-ph/9504054].
- [26] N. Bartolo *et al.*, *Phys. Rep.* **402**, 103 (2004), [arXiv:astro-ph/0406398].
- [27] Planck Collab. 2013 Results XXIV, *Astron. Astrophys.* **571**, A24 (2014), [arXiv:1303.5084].
- [28] C. L. Bennett *et al.*, *Astrophys. J. Supp.* **192**, 17 (2011), [arXiv:1001.4758].
- [29] Planck Collab. 2013 Results XXIII, *Astron. Astrophys.* **571**, A23 (2014), [arXiv:1303.5083].
- [30] Planck Collab. 2018 Results X, *Astron. Astrophys.* **641**, A10 (2020), [arXiv:1807.06211].
- [31] A. R. Liddle and D. H. Lyth, *Cosmological Inflation and Large-Scale Structure*, Cambridge University Press, Cambridge (2000).
- [32] U. Seljak and M. Zaldarriaga, *Astrophys. J.* **469**, 437 (1996), [arXiv:astro-ph/9603033].
- [33] A. Lewis, A. Challinor and A. Lasenby, *Astrophys. J.* **538**, 473 (2000), [arXiv:astro-ph/9911177].
- [34] D. Blas, J. Lesgourgues and T. Tram, *J. Cosmology Astropart. Phys.* **7**, 034 (2011), [arXiv:1104.2933].
- [35] U. Seljak *et al.*, *Phys. Rev.* **D68**, 083507 (2003), [arXiv:astro-ph/0306052].
- [36] R. K. Sachs and A. M. Wolfe, *Astrophys. J.* **147**, 73 (1967).
- [37] R. G. Crittenden and N. Turok, *Phys. Rev. Lett.* **76**, 575 (1996), [arXiv:astro-ph/9510072]; Planck Collab. 2015 Results XXI, *Astron. Astrophys.* **594**, A21 (2016), [arXiv:1502.01595].
- [38] W. Hu *et al.*, *Phys. Rev.* **D59**, 2, 023512 (1998), [arXiv:astro-ph/9806362].
- [39] W. Hu, N. Sugiyama and J. Silk, *Nature* **386**, 37 (1997), [arXiv:astro-ph/9604166].
- [40] P. J. E. Peebles and J. T. Yu, *Astrophys. J.* **162**, 815 (1970); Sunyaev, R. A. and Zeldovich, Ya. B., *Astron. Astrophys. Supp.* **7**, 3 (1970).
- [41] D. Scott, J. Silk and M. White, *Science* **268**, 829 (1995), [arXiv:astro-ph/9505015].
- [42] D. J. Eisenstein, *New Astron. Rev.* **49**, 360 (2005).
- [43] J. Silk, *Astrophys. J.* **151**, 459 (1968).
- [44] M. Zaldarriaga and U. Seljak, *Phys. Rev.* **D58**, 023003 (1998), [arXiv:astro-ph/9803150].
- [45] Planck Collab. 2013 Result XVII, *Astron. Astrophys.* **571**, A17 (2014), [arXiv:1303.5077].
- [46] M. Kaplinghat, L. Knox and Y.-S. Song, *Phys. Rev. Lett.* **91**, 24, 241301 (2003), [arXiv:astro-ph/0303344].
- [47] Planck Collab. 2013 Results XV, *Astron. Astrophys.* **571**, A15 (2014), [arXiv:1303.5075].
- [48] Planck Collab. 2018 Results V, *Astron. Astrophys.* **641**, A5 (2020), [arXiv:1907.12875].
- [49] S. Das *et al.*, *J. Cosmology Astropart. Phys.* **4**, 014 (2014), [arXiv:1301.1037].
- [50] K. T. Story *et al.*, *Astrophys. J.* **779**, 86 (2013), [arXiv:1210.7231].
- [51] W. Hu and M. White, *New Astron.* **2**, 323 (1997), [arXiv:astro-ph/9706147].
- [52] W. Hu and M. J. White, *Phys. Rev.* **D56**, 596 (1997), [arXiv:astro-ph/9702170].
- [53] M. Zaldarriaga and U. Seljak, *Phys. Rev.* **D55**, 1830 (1997), [arXiv:astro-ph/9609170]; M. Kamionkowski, A. Kosowsky and A. Stebbins, *Phys. Rev.* **D55**, 7368 (1997), [arXiv:astro-ph/9611125].
- [54] J. M. Kovac *et al.*, *Nature* **420**, 772 (2002), [arXiv:astro-ph/0209478].
- [55] D. Larson *et al.*, *Astrophys. J. Supp.* **192**, 16 (2011), [arXiv:1001.4635].
- [56] Keck Array and BICEP2 Collabs. V, *Astrophys. J.* **811**, 126 (2015), [arXiv:1502.00643].
- [57] S. K. Choi *et al.*, *J. Cosmology Astropart. Phys.* **2020**, 12, 045 (2020), [arXiv:2007.07289].
- [58] A. T. Crites *et al.*, *Astrophys. J.* **805**, 36 (2015), [arXiv:1411.1042].
- [59] Planck Collab. 2018 Results VII, *Astron. Astrophys.* **641**, A7 (2020), [arXiv:1906.02552].
- [60] M. Tristram *et al.*, *Astron. Astrophys.* **647**, A128 (2021), [arXiv:2010.01139].
- [61] D. Hanson *et al.*, *Phys. Rev. Lett.* **111**, 14, 141301 (2013), [arXiv:1307.5830].
- [62] BICEP2 Collab., *Phys. Rev. Lett.* **112**, 24, 241101 (2014), [arXiv:1403.3985].
- [63] BICEP2/Keck and Planck Collabs., *Phys. Rev. Lett.* **114**, 10, 101301 (2015), [arXiv:1502.00612].
- [64] BICEP2 and Keck Array Collab., *Phys. Rev. Lett.* **121**, 22, 221301 (2018), [arXiv:1810.05216].
- [65] BICEP/Keck Collab., *Phys. Rev. Lett.* **127**, 151301 (2021), [arXiv:2110.00483].
- [66] POLARBEAR Collab., *Astrophys. J.* **848**, 121 (2017), [arXiv:1705.02907].
- [67] R. Keisler *et al.*, *Astrophys. J.* **807**, 151 (2015), [arXiv:1503.02315].
- [68] Planck Collab. 2015 Results XV, *Astron. Astrophys.* **594**, A15 (2016), [arXiv:1502.01591].
- [69] A. van Engelen *et al.*, *Astrophys. J.* **808**, 7 (2015), [arXiv:1412.0626].
- [70] P. Ade *et al.* (Simons Observatory Collab.), *J. Cosmology Astropart. Phys.* **2019**, 2, 056 (2019), [arXiv:1808.07445].

- [71] K. N. Abazajian *et al.*, ArXiv e-prints (2016), [arXiv:1610.02743].
- [72] M. Hazumi *et al.*, in “S.P.I.E. Conf. Ser.”, volume 11443, 114432F (2020), [arXiv:2101.12449].
- [73] Planck Collab. 2018 Results VIII, *Astron. Astrophys.* **641**, A8 (2020), [arXiv:1807.06210].
- [74] D. Scott *et al.*, *J. Cosmology Astropart. Phys.* **2016**, 6, 046 (2016), [arXiv:1603.03550].
- [75] L. Knox and Y.-S. Song, *Phys. Rev. Lett.* **89**, 1, 011303 (2002), [arXiv:astro-ph/0202286]; M. Kesden, A. Cooray and M. Kamionkowski, *Phys. Rev. Lett.* **89**, 011304 (2002), [arXiv:astro-ph/0202434]; C. M. Hirata and U. Seljak, *Phys. Rev. D* **68**, 8, 083002 (2003), [arXiv:astro-ph/0306354].
- [76] Planck Collab. 2013 Results XII, *Astron. Astrophys.* **571**, A12 (2014), [arXiv:1303.5072]; Planck Collab. 2015 Results X, *Astron. Astrophys.* **594**, A10 (2016), [arXiv:1502.01588]; Planck Collab. 2018 Results IV, *Astron. Astrophys.* **641**, A4 (2020), [arXiv:1807.06208].
- [77] B. Gold *et al.*, *Astrophys. J. Supp.* **192**, 15 (2011), [arXiv:1001.4555].
- [78] Planck Collab. Interm. Results XXX, *Astron. Astrophys.* **586**, A133 (2016), [arXiv:1409.5738].
- [79] M. Millea *et al.*, *Astrophys. J.* **746**, 4 (2012), [arXiv:1102.5195].
- [80] Sunyaev, R. A. and Zeldovich, Ya. B., *Ann. Rev. Astron. Astrophys.* **18**, 537 (1980).
- [81] R. Williamson *et al.*, *Astrophys. J.* **738**, 139 (2011), [arXiv:1101.1290].
- [82] M. Hilton *et al.*, *Astrophys. J. Supp.* **253**, 1, 3 (2021), [arXiv:2009.11043].
- [83] Planck Collab. Early Results VIII, *Astron. Astrophys.* **536**, A8 (2011), [arXiv:1101.2024].
- [84] Planck Collab. 2013 Results XX, *Astron. Astrophys.* **571**, A20 (2014), [arXiv:1303.5080].
- [85] T. de Haan *et al.*, *Astrophys. J.* **832**, 95 (2016), [arXiv:1603.06522].
- [86] Planck Collab. 2018 Results IX, *Astron. Astrophys.* **641**, A9 (2020), [arXiv:1905.05697].
- [87] Planck Collab. 2015 Results XVI, *Astron. Astrophys.* **594**, A16 (2016), [arXiv:1506.07135].
- [88] Planck Collab. 2013 Results XXII, *Astron. Astrophys.* **571**, A22 (2014), [arXiv:1303.5082]; Planck Collab. 2015 Results XX, *Astron. Astrophys.* **594**, A20 (2016), [arXiv:1502.02114].
- [89] Planck Collab. 2015 Results XIV, *Astron. Astrophys.* **594**, A14 (2016), [arXiv:1502.01590].
- [90] Planck Collab. Interm. Results XLVI, *Astron. Astrophys.* **596**, A107 (2016), [arXiv:1605.02985].
- [91] X. Fan, C. L. Carilli and B. Keating, *Ann. Rev. Astron. Astrophys.* **44**, 415 (2006), [arXiv:astro-ph/0602375].
- [92] C. A. Mason *et al.*, *Astrophys. J.* **856**, 1, 2 (2018), [arXiv:1709.05356].
- [93] Planck Collab. Interm. Results XLIX, *Astron. Astrophys.* **596**, A110 (2016), [arXiv:1605.08633].
- [94] M. Kamionkowski and A. Kosowsky, *Ann. Rev. Nucl. Part. Sci.* **49**, 77 (1999), [arXiv:astro-ph/9904108].
- [95] Planck Collab. 2015 Results XIX, *Astron. Astrophys.* **594**, A19 (2016), [arXiv:1502.01594].
- [96] Planck Collab. Interm. Results XXIV, *Astron. Astrophys.* **580**, A22 (2015), [arXiv:1406.7482].

30. Cosmic Rays

Revised October 2021 by J.J. Beatty (Ohio State U.), J. Matthews (Louisiana State U.) and S.P. Wakely (Chicago U.; Chicago U., Kavli Inst.).

Cosmic rays are a population of energetic elementary particles and nuclei with a steeply falling, nearly power-law spectrum extending from a few MeV to tens of J per particle. Primary cosmic rays can be measured directly by experiments in space or on balloons at energies where there is sufficient flux (§30.1). Atmospheric interactions of primary cosmic rays produce fluxes of secondary elementary particles which can be detected in the atmosphere (§30.2), at the Earth's surface (§30.3), and underground (§30.4). At high energies, air showers of particles generated by a single primary can be detected (§30.5). These showers can be reconstructed to determine the energy, direction, and composition of the incident particle. Gamma-ray photons are observed both as diffuse fluxes and as steady-state and transient emission from sources (§30.6). Energetic neutrinos are closely linked to high energy protons and nuclei, both through production at astrophysical sites of particle acceleration and by production during propagation of extremely high energy particles (§30.7).

30.1 Primary Spectra from Direct Measurements

The cosmic radiation incident at the top of the terrestrial atmosphere includes all stable charged particles and nuclei with lifetimes of order 10^6 years or longer. When discussing the astrophysical origin of cosmic rays, “primary” cosmic rays are those particles accelerated at astrophysical sources and “secondaries” are those particles produced in interaction of the primaries with interstellar gas¹. Thus electrons, protons and helium, as well as carbon, oxygen, iron, and other nuclei synthesized in stars, are primaries. Nuclei such as lithium, beryllium, and boron (which are not abundant end-products of stellar nucleosynthesis) are secondaries. Antiprotons and positrons are also in large part secondary. Whether a small fraction of these particles may be primary is a question of current interest.

There are four different ways to describe the spectra of the components of the cosmic radiation: (1) By particles per unit rigidity. Propagation (and probably also acceleration) through cosmic magnetic fields depends on the gyroradius or *magnetic rigidity*, R , which is the gyroradius multiplied by the magnetic field strength:

$$R = \frac{pc}{Ze} = r_L B \quad (30.1)$$

(2) By particles per energy-per-nucleon. Fragmentation of nuclei propagating through the interstellar gas depends on the energy per nucleon, since that quantity is approximately conserved when a nucleus breaks up on interaction with the gas. (3) By nucleons per energy-per-nucleon. Production of secondary cosmic rays in the atmosphere depends on the intensity of nucleons per energy-per-nucleon, approximately independently of whether the incident nucleons are free protons or bound in nuclei. (4) By particles per energy-per-nucleus. Air shower experiments that use the atmosphere as a calorimeter generally measure a quantity that is related to total energy per particle.

The units of differential intensity I are $[\text{m}^{-2} \text{s}^{-1} \text{sr}^{-1} \mathcal{E}^{-1}]$, where \mathcal{E} represents the units of one of the four variables listed above.

Apart from particles associated with solar flares², the cosmic radiation comes from outside the solar system. The incoming charged particles are “modulated” by the solar wind, the expanding magnetized plasma generated by the Sun, which decelerates and partially excludes the lower energy Galactic cosmic rays from the inner solar system. There is a significant anti-correlation between solar activity (which has an alternating eleven-year cycle) and the intensity of the cosmic rays with rigidities below about 10 GV. In addition, the lower-energy cosmic rays are affected by

¹‘Primary’ and ‘secondary’ are used in a different but analogous sense when discussing cosmic ray interactions in the atmosphere.

²Energetic particles accelerated by the Sun and at other sites within the heliosphere and at its boundary are outside the scope of this review.

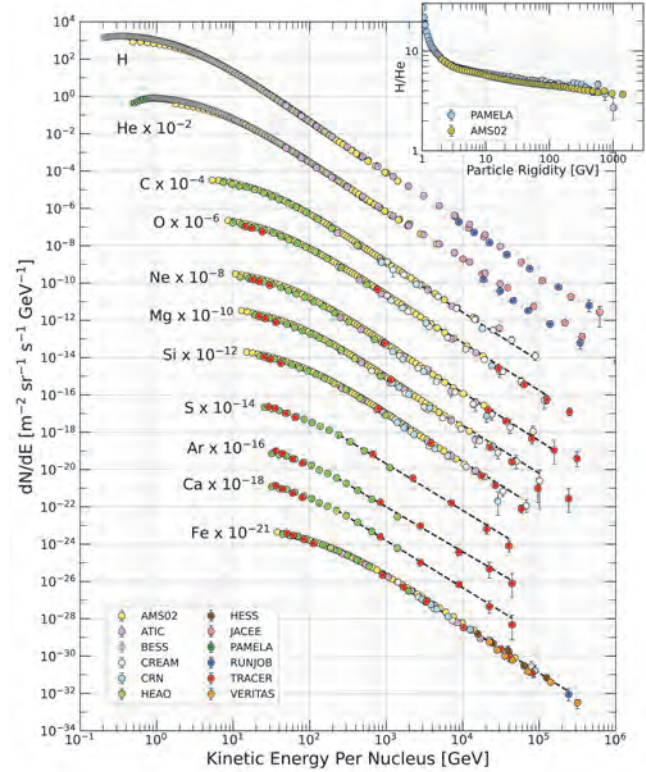


Figure 30.1: Fluxes of nuclei of the primary cosmic radiation in particles per energy-per-nucleus are plotted vs energy-per-nucleus using data from Refs. [1–15]. The inset shows the H/He ratio as a function of rigidity [1, 3].

the geomagnetic field, which they must penetrate to reach the top of the atmosphere. Thus the intensity of any component of the cosmic radiation in the GeV range depends both on the location and time.

The intensity of primary nucleons in the energy range from several GeV to somewhat beyond 100 TeV is given approximately by

$$I_N(E) \approx 1.8 \times 10^4 (E/1 \text{ GeV})^{-\alpha} \frac{\text{nucleons}}{\text{m}^2 \text{ s sr GeV}}, \quad (30.2)$$

where E is the energy-per-nucleon (including rest mass energy), α ($\equiv \gamma + 1$) ≈ 2.7 is the differential spectral index of the cosmic-ray flux, and γ is the integral spectral index. About 74% of the primary nucleons are free protons and about 70% of the rest are nucleons bound in helium nuclei. The fractions of the primary nuclei are nearly constant over this energy range. Fractions of both primary and secondary incident nuclei are listed in Table 30.1. Figure 30.1 shows the major nuclear components for kinetic energies greater than 0.22 GeV/nucleus. Figure 30.2 shows the relative abundances of low-energy (0.2 GeV/nucleon) cosmic rays compared to the present-day solar system. Secondary cosmic rays contribute to increased abundances of rare elements and a reduced even-odd effect. A useful compendium of experimental data for cosmic-ray nuclei and electrons is described in [16].

The composition and energy spectra of nuclei are typically interpreted in the context of propagation models, in which the sources of the primary cosmic radiation are located within the Galaxy [23]. The ratio of secondary to primary nuclei is observed to decrease with increasing energy, a fact often interpreted to mean that the lifetime of cosmic rays in the Galaxy decreases with energy. Measurements of radioactive “clock” isotopes in the low energy cosmic radiation are consistent with a lifetime in the Galaxy of about 15 Myr [24].

Cosmic rays are nearly isotropic at most energies due to diffu-

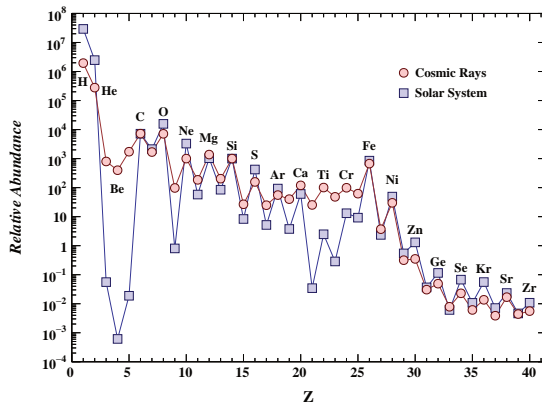


Figure 30.2: Cosmic ray elemental abundances compared to abundances in present-day solar system material. Abundances are normalised to $\text{Si}=10^3$. Cosmic ray abundances are from AMS-02 (H,He) [3, 17], ACE/CRIS (Li-Ni) [18, 19], and TIGER/Super-TIGER (Cu-Zr) [20, 21]. Solar system abundances are from Table 6 of Ref. [22].

sive propagation in the Galactic magnetic field. Several collaborations [25–29] have observed anisotropy on various angular scales at the level of about 10^{-3} for cosmic rays with energy of a few TeV, possibly due the direction of local Galactic magnetic fields, motion of the solar system in the Galaxy, and to the distribution of sources [30].

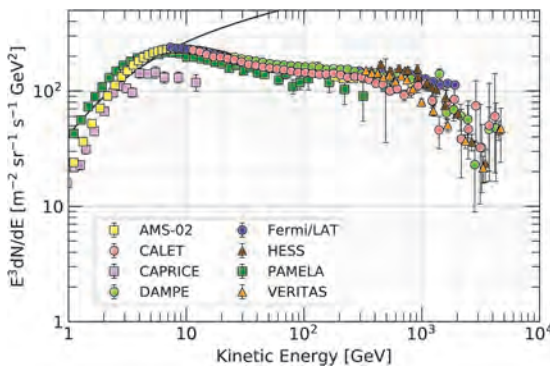


Figure 30.3: Differential spectrum of electrons plus positrons (except PAMELA data, which are electrons only) multiplied by E^3 [31–39]. The line shows the proton spectrum [40] multiplied by 0.01.

The spectrum of electrons and positrons incident at the top of the atmosphere is generally expected to steepen by one power of E

Table 30.1: Relative abundances F of cosmic-ray nuclei at 10.6 GeV/nucleon normalized to oxygen ($\equiv 1$) [9]. The oxygen flux at kinetic energy of 10.6 GeV/nucleon is $3.29 \times 10^{-2} (\text{m}^2 \text{ s sr GeV/nucleon})^{-1}$. Abundances of hydrogen and helium are from Refs. [2–4]. Note that one can not use these values to extend the cosmic-ray flux to high energy because the power law indices for each element may differ slightly.

Z	Element	F	Z	Element	F
1	H	550	13–14	Al-Si	0.19
2	He	34	15–16	P-S	0.03
3–5	Li-B	0.40	17–18	Cl-Ar	0.01
6–8	C-O	2.20	19–20	K-Ca	0.02
9–10	F-Ne	0.30	21–25	Sc-Mn	0.05
11–12	Na-Mg	0.22	26–28	Fe-Ni	0.12

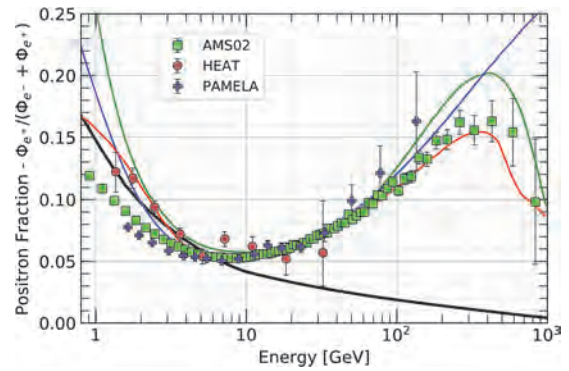


Figure 30.4: The positron fraction (ratio of the flux of e^+ to the total flux of e^+ and e^-) [33, 41–43]. The heavy black line is a model of pure secondary production [44] and the three thin lines show three representative attempts to model the positron excess with different phenomena: green: dark matter decay [45]; blue: propagation physics [46]; red: production in pulsars [47]. The ratio below 10 GeV is dependent on the intensity and polarity of the solar magnetic field.

above an energy of 5 GeV because of radiative energy loss effects in the Galaxy. Most modern measurements of the combined electron+positron spectrum at high energy, which includes data from spectrometers, calorimeters, and ground-based air Cherenkov telescopes, reveal a relatively smooth spectrum to approximately 1 TeV, where evidence of a cutoff has been reported [35, 37, 39].

The PAMELA [41, 42] and AMS-02 [48, 49] satellite experiments measured the positron to electron ratio to increase above 10 GeV instead of the expected decrease [44] at higher energy, confirming earlier hints seen by the HEAT balloon-borne experiment [43]. The structure in the electron spectrum, as well as the increase in the positron fraction, may be related to contributions from individual nearby sources (supernova remnants or pulsars) emerging above a background suppressed at high energy by synchrotron losses [50]. Other explanations have invoked propagation effects [46] or dark matter decay/annihilation processes (see, e.g., [45]). The significant disagreement in the ratio below ~ 10 GeV is attributable to differences in charge-sign dependent solar modulation effects present near Earth at the times of measurement.

The ratio of antiprotons to protons is $\sim 2 \times 10^{-4}$ [51] at around 10–20 GeV, and there is clear evidence [52] for the kinematic suppression at lower energy that is the signature of secondary antiprotons. The \bar{p}/p ratio also shows a strong dependence on the phase and polarity of the solar cycle [53] in the opposite sense to that of the positron fraction. There is at this time no evidence for a significant primary component of antiprotons. No antihelium or antideuteron has been found in the cosmic radiation. The best measured upper limit on the ratio antihelium/helium is currently approximately 1×10^{-7} [54]. The upper limit on the flux of antideuterons around 1 GeV/nucleon is approximately $2 \times 10^{-4} (\text{m}^2 \text{ s sr GeV/nucleon})^{-1}$ [55].

A useful method for calculating the effect of solar modulation including time, charge-sign, and rigidity-dependent effects is given in Ref. [56].

30.2 Cosmic Rays in the Atmosphere

Figure 30.5 shows the vertical fluxes of the major cosmic-ray components in the atmosphere in the energy region where the particles are most numerous (except for electrons, which are most numerous near their critical energy, which is about 81 MeV in air). Except for protons and electrons near the top of the atmosphere, all particles are produced in interactions of the primary³ cosmic rays in the air. Muons and neutrinos are products of the decay chain of charged mesons, while electrons and photons originate in

³When discussing cosmic rays in the atmosphere, ‘primary’ is used to denote the original particle and ‘secondary’ to denote the particles produced in interactions.

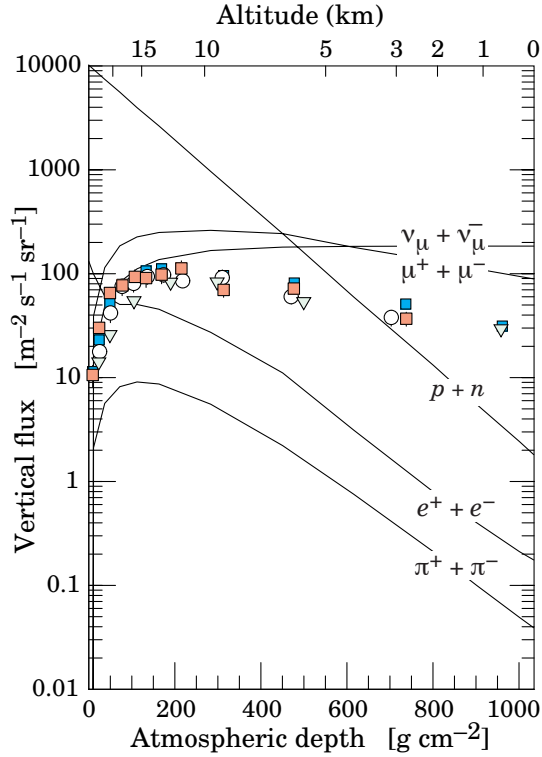


Figure 30.5: Vertical fluxes of cosmic rays in the atmosphere with $E > 1$ GeV estimated from the nucleon flux of Eq. (30.2). The experimental points show measurements of negative muons with $E_\mu > 1$ GeV [57–62].

decays of neutral mesons.

Most measurements are made at ground level or near the top of the atmosphere, but there are also measurements of muons and electrons from airplanes and balloons. Fig. 30.5 shows measurements of negative muons [57–62]. Since μ^+ (μ^-) are produced in association with ν_μ ($\bar{\nu}_\mu$), the measurement of muons near the maximum of the intensity curve for the parent pions serves to calibrate the atmospheric ν_μ ($\bar{\nu}_\mu$) beam [63]. Because muons typically lose almost 2 GeV in passing through the atmosphere, the comparison near the production altitude is important for the sub-GeV range of ν_μ ($\bar{\nu}_\mu$) energies.

The flux of cosmic rays through the atmosphere is described by a set of coupled cascade equations with boundary conditions at the top of the atmosphere to match the primary spectrum. Numerical or Monte Carlo calculations are needed to account accurately for decay and energy-loss processes, and for the energy-dependences of the cross sections and of the primary spectral index γ . Approximate analytic solutions are, however, useful in limited regions of energy [64, 65]. For example, the vertical intensity of charged pions with energy $E_\pi \ll \epsilon_\pi = 115$ GeV is

$$I_\pi(E_\pi, X) \approx \frac{Z_{N\pi}}{\lambda_N} I_N(E_\pi, 0) e^{-X/\Lambda} \frac{X E_\pi}{\epsilon_\pi} \quad (30.3)$$

where Λ is the characteristic length for exponential attenuation of the parent nucleon flux in the atmosphere. This expression has a maximum at $X = \Lambda \approx 121 \pm 4$ g cm $^{-2}$ [66], which corresponds to an altitude of 15 kilometers. The quantity $Z_{N\pi}$ is the spectrum-weighted moment that characterizes the inclusive distribution of charged pions in interactions of a spectrum of nucleons with nuclei of the atmosphere. The intensity of low-energy pions is much less than that of nucleons because $Z_{N\pi} \approx 0.079$ is small and because most pions with energy much less than the critical energy ϵ_π decay rather than interact.

30.3 Cosmic rays at the surface

30.3.1 Muons

Muons are the most numerous charged particles at sea level (see Fig. 30.5). Most muons are produced high in the atmosphere (typically 15 km) and lose about 2 GeV to ionization before reaching the ground. Their energy and angular distribution reflect a convolution of the production spectrum, energy loss in the atmosphere, and decay. For example, 2.4 GeV muons have a decay length of 15 km, which is reduced to 8.7 km by energy loss. The mean energy of muons at the ground is ≈ 4 GeV. The energy spectrum is almost flat below 1 GeV, steepens gradually to reflect the primary spectrum in the 10–100 GeV range, and steepens further at higher energies because pions with $E_\pi > \epsilon_\pi$ tend to interact in the atmosphere before they decay. Asymptotically ($E_\mu \gg 1$ TeV), the energy spectrum of atmospheric muons is one power steeper than the primary spectrum. The integral intensity of vertical muons above 1 GeV/c at sea level is ≈ 70 m $^{-2}$ s $^{-1}$ sr $^{-1}$ [67, 68], with recent measurements [62, 69, 70] favoring a lower normalization by 10–15%. Experimentalists are familiar with this number in the form $I \approx 1$ cm $^{-2}$ min $^{-1}$ for horizontal detectors. The overall angular distribution of muons at the ground as a function of zenith angle θ is $\propto \cos^2 \theta$, which is characteristic of muons with $E_\mu \sim 3$ GeV. At lower energy the angular distribution becomes increasingly steep, while at higher energy it flattens, approaching a sec θ distribution for $E_\mu \gg \epsilon_\pi$ and $\theta < 70^\circ$.

Figure 30.6 shows the muon energy spectrum at sea level for two angles. At large angles low energy muons decay before reaching the surface and high energy pions decay before they interact, thus the average muon energy increases. An approximate extrapolation formula valid when muon decay is negligible ($E_\mu > 100/\cos \theta$ GeV) and the curvature of the Earth can be neglected ($\theta < 70^\circ$) is

$$\frac{dN_\mu}{dE_\mu d\Omega} \approx \frac{0.14 E_\mu^{-2.7}}{\text{cm}^2 \text{ s sr GeV}} \times \left\{ \frac{1}{1 + \frac{1.1 E_\mu \cos \theta}{115 \text{ GeV}}} + \frac{0.054}{1 + \frac{1.1 E_\mu \cos \theta}{850 \text{ GeV}}} \right\} \quad (30.4)$$

where the two terms give the contribution of pions and charged kaons. Eq. (30.4) neglects a small contribution from charm and heavier flavors which is negligible except at very high energy [75].

The muon charge ratio reflects the excess of π^+ over π^- and K^+ over K^- in the forward fragmentation region of proton initiated interactions together with the fact that there are more free and bound protons than free and bound neutrons in the primary spectrum. The increase with energy of μ^+/μ^- shown in Fig. 30.7 reflects the increasing importance of kaons in the TeV range [76] and indicates a significant contribution of associated production by cosmic-ray protons ($p \rightarrow \Lambda + K^+$). The same process is even more important for atmospheric neutrinos at high energy.

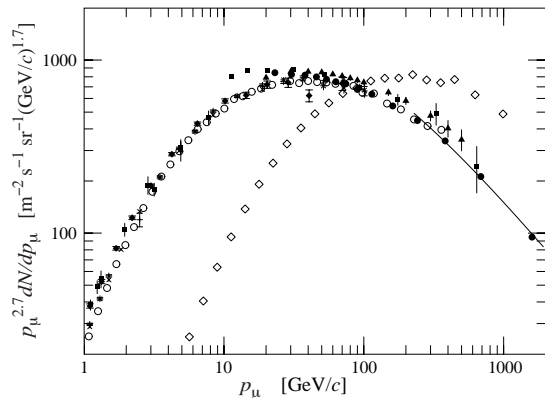


Figure 30.6: Spectrum of muons at $\theta = 0^\circ$ (\blacklozenge [67], \blacksquare [71], \blacktriangledown [72], \blacktriangle [73], \times , $+$ [69], \circ [62], and \bullet [70] and $\theta = 75^\circ$ \diamond [74]). The line plots the result from Eq. (30.4) for vertical showers.

30.3.2 Electromagnetic component

At the ground, this component consists of electrons, positrons, and photons primarily from cascades initiated by decay of neutral and charged mesons. Muon decay is the dominant source of low-energy electrons at sea level. Decay of neutral pions is more important at high altitude or when the energy threshold is high. Knock-on electrons also make a small contribution at low energy [77]. The integral vertical intensity of electrons plus positrons is very approximately 30, 6, and $0.2 \text{ m}^{-2}\text{s}^{-1}\text{sr}^{-1}$ above 10, 100, and 1000 MeV respectively [68, 78], but the exact numbers depend sensitively on altitude, and the angular dependence is complex because of the different altitude dependence of the different sources of electrons [77, 79]. The ratio of photons to electrons plus positrons is approximately 1.3 above 1 GeV and 1.7 below the critical energy [79].

30.3.3 Nucleons

Nucleons above $1 \text{ GeV}/c$ at ground level are degraded remnants of the primary cosmic radiation. The intensity is approximately $I_N(E, 0) \times \exp(-X/\cos\theta\Lambda)$ for $\theta < 70^\circ$. At sea level, about 1/3 of the nucleons in the vertical direction are neutrons (up from $\approx 10\%$ at the top of the atmosphere as the n/p ratio approaches equilibrium). The integral intensity of vertical protons above $1 \text{ GeV}/c$ at sea level is $\approx 0.9 \text{ m}^{-2}\text{s}^{-1}\text{sr}^{-1}$ [68, 80].

30.4 Cosmic Rays Underground

Only muons and neutrinos penetrate to significant depths underground. The muons produce tertiary fluxes of photons, electrons, and hadrons.

30.4.1 Muons

As discussed in Section 34.6 of this *Review*, muons lose energy by ionization and by radiative processes: bremsstrahlung, direct production of e^+e^- pairs, and photonuclear interactions. The total muon energy loss may be expressed as a function of the

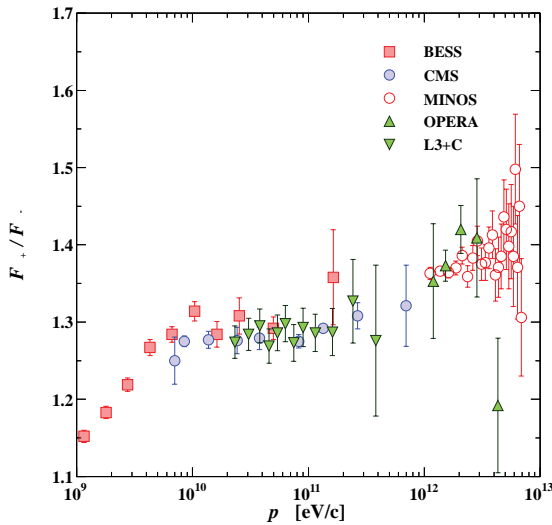


Figure 30.7: Muon charge ratio as a function of the muon momentum from Refs. [62, 70, 76, 81, 82].

Table 30.2: Average muon range R and energy loss parameters calculated for standard rock. Range is given in km-water-equivalent, or 10^5 g cm^{-2} .

E_μ GeV	R km.w.e.	a $\frac{\text{MeV cm}^2}{\text{g}}$	b_{brems}	b_{pair} 10^{-6}	b_{nucl} $\text{g}^{-1} \text{cm}^2$	$\sum b_i$	$\sum b_{\text{ice}}$
10	0.05	2.17	0.70	0.70	0.50	1.90	1.66
10^2	0.41	2.44	1.10	1.53	0.41	3.04	2.51
10^3	2.45	2.68	1.44	2.07	0.41	3.92	3.17
10^4	6.09	2.93	1.62	2.27	0.46	4.35	3.78

amount of matter traversed as

$$-\frac{dE_\mu}{dX} = a + bE_\mu \quad (30.5)$$

where a is the ionization loss and b is the fractional energy loss by the three radiation processes. Both are slowly varying functions of energy. The quantity $\epsilon \equiv a/b$ ($\approx 500 \text{ GeV}$ in standard rock) defines a critical energy below which continuous ionization loss is more important than radiative losses. Table 30.2 shows a and b values for standard rock, and b for ice, as a function of muon energy. The second column of Table 30.2 shows the muon range in standard rock ($A = 22$, $Z = 11$, $\rho = 2.65 \text{ g cm}^{-3}$). These parameters are quite sensitive to the chemical composition of the rock, which must be evaluated for each location.

The intensity of muons underground can be estimated from the muon intensity in the atmosphere and their rate of energy loss. To the extent that the mild energy dependence of a and b can be neglected, Eq. (30.5) can be integrated to provide the following relation between the energy $E_{\mu,0}$ of a muon at production in the atmosphere and its average energy E_μ after traversing a thickness X of rock (or ice or water):

$$E_{\mu,0} = (E_\mu + \epsilon)e^{bX} - \epsilon. \quad (30.6)$$

Especially at high energy, however, fluctuations are important and an accurate calculation requires a simulation that accounts for stochastic energy-loss processes [83].

There are two depth regimes for which Eq. (30.6) can be simplified. For $X \ll b^{-1} \approx 2.5 \text{ km water equivalent}$, $E_{\mu,0} \approx E_\mu(X) + aX$, while for $X \gg b^{-1}$ $E_{\mu,0} \approx (\epsilon + E_\mu(X)) \exp(bX)$. Thus at shallow depths the differential muon energy spectrum is approximately constant for $E_\mu < aX$ and steepens to reflect the surface muon spectrum for $E_\mu > aX$, whereas for $X > 2.5 \text{ km-water-equivalent (km.w.e.)}$ the differential spectrum underground is again constant for small muon energies but steepens to reflect the surface muon spectrum for $E_\mu > \epsilon \approx 0.5 \text{ TeV}$. In the deep regime the shape is independent of depth although the intensity decreases exponentially with depth. In general the muon spectrum at slant depth X is

$$\frac{dN_\mu(X)}{dE_\mu} = \frac{dN_\mu}{dE_{\mu,0}} \frac{dE_{\mu,0}}{dE_\mu} = \frac{dN_\mu}{dE_{\mu,0}} e^{bX} \quad (30.7)$$

where $E_{\mu,0}$ is the solution of Eq. (30.6) in the approximation neglecting fluctuations.

Fig. 30.8 shows the vertical muon intensity versus depth. In constructing this “depth-intensity curve,” each group has taken account of the angular distribution of the muons in the atmosphere, the map of the overburden at each detector, and the properties of the local medium in connecting measurements at various slant depths and zenith angles to the vertical intensity. Use of data from a range of angles allows a fixed detector to cover a wide range of depths. The flat portion of the curve is due to muons produced locally by charged-current interactions of ν_μ . The inset shows the vertical intensity curve for water and ice [90–93]. It is not as steep as the one for rock because of the lower muon energy loss in water.

30.4.2 Atmospheric Neutrinos

Because neutrinos have small interaction cross sections, measurements of atmospheric neutrinos require a deep detector to avoid backgrounds. There are two types of measurements: contained (or semi-contained) events, in which the vertex is determined to originate inside the detector, and neutrino-induced muons. The latter are muons that enter the detector from zenith angles so large (*e.g.*, nearly horizontal or upward) that they cannot be muons produced in the atmosphere. In neither case is the neutrino flux measured directly. What is measured is a convolution of the neutrino flux and cross section with the properties of the detector (which includes the surrounding medium in the case of entering muons). This section focuses on neutrinos below about 1 TeV. For discussion of atmospheric neutrinos in the TeV–PeV region including a prompt component produced by charmed meson decays, see Ref. [64].

Table 30.3: Measured fluxes ($10^{-9} \text{ m}^{-2} \text{ s}^{-1} \text{ sr}^{-1}$) of neutrino-induced muons as a function of the effective minimum muon energy E_μ .

$E_\mu >$	1 GeV	1 GeV	1 GeV	2 GeV	3 GeV	3 GeV
Ref.	CWI [95]	Baksan [96]	MACRO [97,98]	IMB [99,100]	Kam [101]	SuperK [102]
F_μ	2.17 ± 0.21	2.77 ± 0.17	2.29 ± 0.15	2.26 ± 0.11	1.94 ± 0.12	1.74 ± 0.07

Contained and semi-contained events reflect neutrinos in the sub-GeV to multi-GeV region where the product of increasing cross section and decreasing flux is maximum. In the GeV region the neutrino flux and its angular distribution depend on the geomagnetic location of the detector and, to a lesser extent, on the phase of the solar cycle. Naively, we expect $\nu_\mu/\nu_e = 2$ from counting neutrinos of the two flavors coming from the chain of pion and muon decays. Contrary to expectation, however, the numbers of the two classes of events are similar rather than different by a factor of two. This is now understood to be a consequence of neutrino flavor oscillations [103]. (See the article on neutrino properties in this *Review*.)

Two well-understood properties of atmospheric cosmic rays provide a standard for comparison of the measurements of atmospheric neutrinos to expectation. These are the “sec θ effect” and the “east-west effect” due to the Earth’s magnetic field [104]. The former refers originally to the enhancement of the flux of > 10 GeV muons (and neutrinos) at large zenith angles because the parent pions propagate more in the low density upper atmosphere where decay is enhanced relative to interaction. For neutrinos from muon decay, the enhancement near the horizontal becomes important for $E_\nu > 1$ GeV and arises mainly from the increased pathlength through the atmosphere for muon decay in flight. Fig. 14.4 from Ref. [105] shows a comparison between measurement and expectation for the zenith angle dependence of multi-GeV electron-like (mostly ν_e) and muon-like (mostly ν_μ) events separately. The ν_e show an enhancement near the horizon-

tal and approximate equality for nearly upward ($\cos \theta \approx -1$) and nearly downward ($\cos \theta \approx 1$) events. There is, however, a very significant deficit of upward ($\cos \theta < 0$) ν_μ events, which have long pathlengths comparable to the radius of the Earth. This feature is the principal signature for atmospheric neutrino oscillations [103].

Muons that enter the detector from outside after production in charged-current interactions of neutrinos naturally reflect a higher energy portion of the neutrino spectrum than contained events because the muon range increases with energy as well as the cross section. The relevant energy range is $\sim 10 < E_\nu < 1000$ GeV, depending somewhat on angle. Neutrinos in this energy range show a sec θ effect similar to muons (see Eq. (30.4)). This causes the flux of horizontal neutrino-induced muons to be approximately a factor two higher than the vertically upward flux. The upper and lower edges of the horizontal shaded region in Fig. 30.8 correspond to horizontal and vertical intensities of neutrino-induced muons. Table 30.3 gives the measured fluxes of upward-moving neutrino-induced muons averaged over the lower hemisphere. Generally the definition of minimum muon energy depends on where it passes through the detector. The tabulated effective minimum energy estimates the average over various accepted trajectories.

30.5 Air Showers

So far we have discussed inclusive or uncorrelated fluxes of various components of the cosmic radiation. An air shower is caused by a single cosmic ray with energy high enough for the cascade that it creates in the atmosphere to be detectable at the ground. The shower has a hadronic core, which acts as a collimated source of electromagnetic sub-showers, generated mostly from $\pi^0 \rightarrow \gamma\gamma$ decays. The resulting electrons and positrons are the most numerous charged particles in the shower, and are accompanied by about ten times as many photons with a mean energy of ~ 10 MeV. The number of muons, produced by decays of charged mesons, is an order of magnitude lower. Air showers spread over a large area on the ground, and arrays of detectors operated for long times are important for studying cosmic rays with primary energy $E_0 > 100$ TeV, where the low flux makes measurements with small detectors in balloons and satellites impractical.

Greisen [120] gives the following approximate analytic expressions for the numbers and lateral distributions of particles in showers at ground level. The total number of muons N_μ with energies above 1 GeV is

$$N_\mu(> 1\text{GeV}) \approx 0.95 \times 10^5 \left(N_e/10^6 \right)^{3/4}, \quad (30.8)$$

where N_e is the total number of charged particles in the shower (not just e^\pm). The number of muons per square meter, ρ_μ , as a function of the lateral distance r (in meters) from the center of the shower is

$$\rho_\mu = \frac{1.25 N_\mu}{2\pi \Gamma(1.25)} \left(\frac{1}{320} \right)^{1.25} r^{-0.75} \left(1 + \frac{r}{320} \right)^{-2.5}, \quad (30.9)$$

where Γ is the gamma function. The number density of charged particles is

$$\rho_e = C_1(s, d, C_2) x^{(s-2)} (1+x)^{(s-4.5)} (1+C_2 x^d). \quad (30.10)$$

Here s , d , and C_2 are parameters in terms of which the overall normalization constant $C_1(s, d, C_2)$ is given by

$$C_1(s, d, C_2) = \frac{N_e}{2\pi r_1^2} [B(s, 4.5 - 2s) C_2 B(s + d, 4.5 - d - 2s)]^{-1}, \quad (30.11)$$

where $B(m, n)$ is the beta function. The values of the parameters depend on shower size (N_e), depth in the atmosphere, identity of the primary nucleus, etc. For showers with $N_e \approx 10^6$ at sea level,

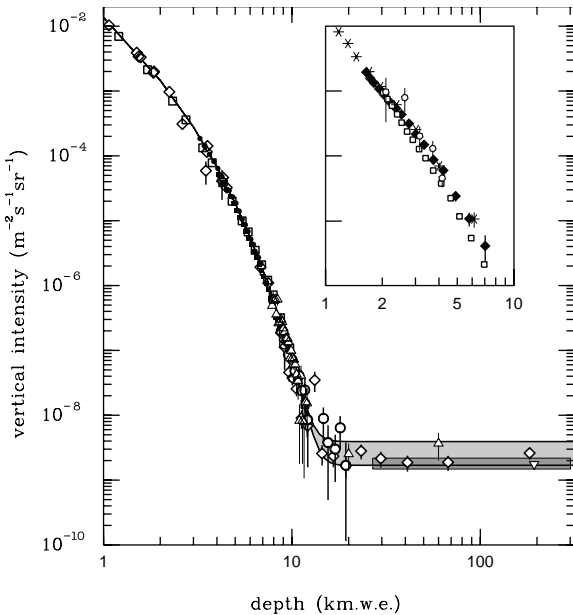


Figure 30.8: Vertical muon intensity vs depth (1 km.w.e. = 10^5 g cm^{-2} of standard rock). The experimental data are from: \diamond : the compilations of Crouch [84], \square : Baksan [85], \circ : LVD [86], \bullet : MACRO [87], \blacksquare : Frejus [88], and \triangle : SNO [89]. The shaded area at large depths represents neutrino-induced muons of energy above 2 GeV. The upper line is for horizontal neutrino-induced muons, the lower one for vertically upward muons. Darker shading shows the muon flux measured by the SuperKamiokande experiment. The inset shows the vertical intensity curve for water and ice published in Refs. [90–93]. Additional data extending to slant depths of 13 km are available in [94].

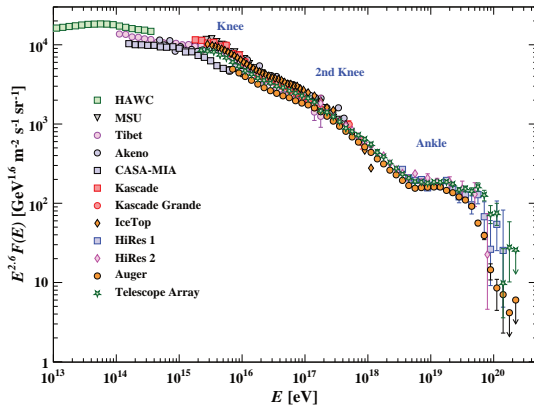


Figure 30.9: The all-particle spectrum as a function of E (energy-per-nucleus) from air shower measurements [106–119]

Greisen uses $s = 1.25$, $d = 1$, and $C_2 = 0.088$. For showers with average $N_e \approx 6 \times 10^7$ at the Akeno array [109], $d = 1.3$, $C_2 = 0.2$ and s is fitted for each shower with typical values between 0.95 and 1.15. Finally, x is r/r_1 , where r_1 is the Molière radius, which depends on the density of the atmosphere and hence on the altitude at which showers are detected. At sea level $r_1 \approx 78$ m, and it increases with altitude as the air density decreases. (See the section on electromagnetic cascades in the article on the passage of particles through matter in this *Review*).

The lateral spread of a shower is determined largely by Coulomb scattering of the many low-energy electrons and is characterized by the Molière radius, which depends on density and thus on temperature and pressure. The lateral spread of the muons (ρ_μ) is larger and depends on the transverse momenta of the muons at production as well as multiple scattering.

There are large fluctuations in development from shower to shower, even for showers initiated by primaries of the same energy and mass—especially for small showers, which are usually well past maximum development when observed at the ground. Thus the shower size N_e and primary energy E_0 are only related in an average sense, and even this relation depends on depth in the atmosphere. One estimate of the relation is [109]

$$E_0 \sim 3.9 \times 10^6 \text{ GeV} (N_e/10^6)^{0.9} \quad (30.12)$$

for vertical showers with $10^{14} < E < 10^{17}$ eV at 920 g cm^{-2} (965 m above sea level). As E_0 increases, the shower maximum (on average) moves down into the atmosphere and the relation between N_e and E_0 changes. Moreover, because of fluctuations, N_e as a function of E_0 is not correctly obtained by inverting Eq. (30.12). At the maximum of shower development, there are approximately 0.66 particles per GeV of primary energy.

The muon and electron lateral distributions used in reconstructing experimental data must be adapted taking into consideration the altitude of the observations and the characteristics of the detectors used. Useful examples include the Akeno [109] and Volcano Ranch [121] arrays. Compilations of useful lateral distribution functions and discussion of their applications are given in Refs. [122, 123].

Cosmic ray shower development is sensitive to hadronic physics in the forward region above energies that can be probed at accelerators. Specialized simulation codes such as CORSIKA [124] include both the relevant physics and methods for efficiently dealing with the large number of particles in high energy air showers. Hadronic interaction models used to interpret air shower measurements now incorporate data from the LHC, reducing the extrapolation required. However, differences between the simulated and observed properties of showers remain. Most notably, the observed muon content of showers near 10^{19} eV exceeds that given by models by 30–60% [125].

There are three common types of air shower detectors: shower arrays that measure a ground parameter related to shower size N_e and muon number N_μ as well as the lateral distribution on

the ground, optical Cherenkov and radio detectors that detect forward-beamed emission by the charged particles of the shower, and ‘fluorescence’ detectors that measure nitrogen scintillation excited by the charged particles in the shower. The fluorescence light is emitted isotropically so the showers can be observed from the side. Detection of radiofrequency emission from showers via geomagnetic and Askaryan mechanisms has been successfully employed in recent experiments [126]. Detailed simulations and cross-calibrations between different types of detectors are necessary to establish the primary energy spectrum from air-shower experiments.

Figure 30.9 shows the “all-particle” spectrum. The differential energy spectrum has been multiplied by $E^{2.6}$ in order to display the features of the steep spectrum that are otherwise difficult to discern. The steepening that occurs between 10^{15} and 10^{16} eV is known as the *knee* of the spectrum. Another steepening occurs around 10^{17} eV, known as the *second knee*. The feature around $10^{18.5}$ eV is called the *ankle* of the spectrum.

Cosmic ray experiments have systematic differences in their energy scales. For ground-based air-shower arrays, these are dependent on an assumed composition and on the hadronic interaction model used when interpreting the data. Systematic errors in energy scale are simplest when plotting $\frac{dN}{d \ln E} = E \frac{dN}{dE}$. When the spectrum is multiplied by a different power of energy, systematic errors in energy scale result in an apparent shift in the normalization of the spectrum; for example, when the spectrum is multiplied by $E^{2.6}$ a systematic shift of 10% in the energy scale results in a 16% change in the normalization of the plotted flux. See Ref. [64], §2.5.2 for further discussion of this issue.

In the energy range above 10^{17} eV, the fluorescence technique [127] is particularly useful because it can establish the primary energy in a nearly model-independent way by observing most of the longitudinal development of each shower, from which E_0 is obtained by integrating the energy deposition in the atmosphere. The result, however, depends strongly on the light absorption in the atmosphere and the calculation of the aperture of the detector.

Assuming the cosmic-ray spectrum below 10^{18} eV is of Galactic origin, the knee could indicate that most cosmic accelerators in the Galaxy have reached their maximum energy for acceleration of protons. Some types of expanding supernova remnants, for example, are estimated not to be able to accelerate protons above energies in the range of 10^{15} eV. Further observations of the PeV gamma-ray sources recently detected by LHAASO [128] may provide insight into the types of objects that act as Galactic sources near the knee and energies to which they can accelerate cosmic rays. Effects of propagation and confinement in the Galaxy [129] also need to be considered. A discussion of models of the knee may be found in Ref. [130].

The second knee may have a similar origin to the knee, but corresponding to steepening of the spectrum of heavy nuclei, particularly iron. The Cascade-Grande experiment has reported observation of a second steepening of the spectrum near 8×10^{16} eV, with evidence that this structure is accompanied by a transition to electron-poor showers resulting from heavy primaries [112]. Cascade Grande has also reported that the spectrum of light nuclei is steeper than the all-particle spectrum below the second knee and flattens in the vicinity of the second knee [131]. IceCube has performed a composition analysis using coincident surface (IceTop) and in-ice data, and finds that the mean logarithmic mass increases between 5×10^{15} eV and 10^{17} eV [132]. Together, these data are suggestive that the knee and second knee may result from a *Peters cycle*, with a steepening of the spectrum of each primary element taking place at the same rigidity but different energy per particle [133].

The Auger Observatory and Telescope Array (TA) have studied composition using the depth of shower maximum X_{max} , a quantity that correlates strongly with $\ln E/A$ and with the interaction cross section of the primary particle. The Auger Collaboration [134], using a post-LHC hadronic interaction model, reports a light composition below 2×10^{18} eV and becoming heavier above that energy, with the mean mass intermediate between protons and iron at 3×10^{19} eV. The TA Collaboration [135], using a different post-LHC model, has interpreted their data as implying a

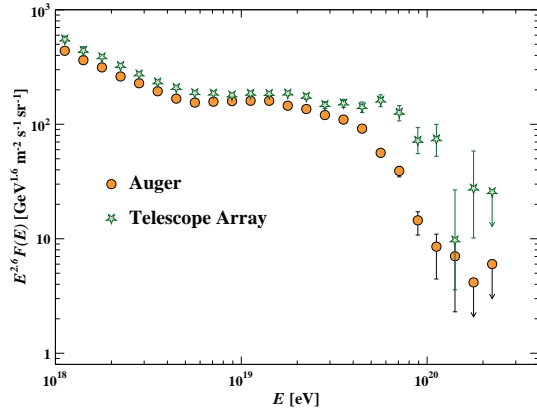


Figure 30.10: Expanded view of the highest energy portion of the cosmic-ray spectrum from data of the Pierre Auger Observatory [115–117, 139] and the Telescope Array [118, 119]. The small difference in the normalization of the spectra corresponds to a difference in energy scale of 9%.

light primary composition (mainly p and He) of ultrahigh-energy cosmic-rays (UHECR) from 1.3×10^{18} to 4×10^{19} eV. The Auger and TA Collaborations have also conducted a thorough joint analysis [136] and state that, at the current level of statistics and understanding of systematics, both data sets are compatible with being drawn from the same parent distribution, and that the TA data is compatible both with a light composition below 10^{19} eV and with the mixed composition above 10^{19} eV as reported by the Auger Collaboration.

Possible contributions to the origin of the ankle include a higher energy population of particles overtaking a lower energy population, for example an extragalactic flux beginning to dominate over the Galactic flux (e.g. Ref. [127]). Another proposed mechanism is that the dip structure in the region of the ankle is due to $p\gamma \rightarrow e^+ + e^-$ energy losses of extragalactic protons on the 2.7 K cosmic microwave radiation (CMB) [137]. The latter mechanism requires that the composition in this energy range is predominantly protons. A study of the correlation between the depth of shower maximum and the surface detector signal in hybrid showers by the Auger Collaboration favors a mixed composition at the ankle, disfavoring the dip model [138].

The propagation of the highest energy cosmic rays over extragalactic distances is predicted to result in a rapid steepening of the spectrum (called the GZK feature) around 5×10^{19} eV, resulting from the onset of inelastic interactions of UHE cosmic rays with the cosmic microwave background [140, 141]. Photo-dissociation of heavy nuclei in the mixed composition model [142] would have a similar effect. The HiRes detector, Auger Observatory, and the Telescope Array have all detected evidence of a suppression consistent with the GZK effect [114–116, 118, 143], with a steepened spectrum extending beyond 10^{20} eV. The differential energy spectra measured by the TA and Auger collaborations agree within systematic errors except at the very highest energies (Fig. 30.10). Both collaborations have also reported evidence for a steepening of the spectrum around $10^{19.2}$ eV, dubbed the ‘instep’ [115, 144].

Cosmic rays above 5×10^{19} eV are predominantly from nearby sources (< 100 Mpc). Differences between the Auger Observatory and Telescope Array spectra above this energy may reflect differences in the spectra between the northern and southern hemispheres. The Auger Collaboration has reported the observation of a dipole of amplitude $6.6_{-0.8}^{+1.2}\%$ for cosmic rays with energies above 8×10^{18} eV. The direction of the dipole indicates an extragalactic origin for these particles [145–147]. There are also hints of structure at smaller angular scales. TA has reported a ‘hot spot’ in the Northern Hemisphere at energies above 5.7×10^{19} eV of radius $\sim 20^\circ$ with a chance probability of this excess with respect to an isotropic distribution of 3.7×10^{-4} [148]. The Auger Collaboration has also reported an excess of events above 3.7×10^{19} eV in a region near the radio-loud active galaxy Centaurus A with

a post-trial significance of 3.9σ , and a correlation of the distribution of ultrahigh energy events with several catalogs of nearby astrophysical objects, with starburst galaxies giving the highest significance at 4.5σ [149]. TA has also observed a similar correlation of cosmic arrival directions above 4.9×10^{19} eV with starburst galaxies with a significance of 4.3σ [148].

30.6 Gamma Rays

There is a well-studied flux of cosmic gamma rays (gamma rays defined here as having energy greater than 1 MeV) present at the top of the atmosphere. This flux has been measured with multiple space and ground-based instruments [Cite PDG 36.2.2] across a broad range of energies.

Contributions to the flux include steady and transient emissions from numerous Galactic and extragalactic sources, as well as diffuse components originating from both inside and outside the Galaxy. The source-associated contributions include photons from a range of objects and phenomena such as supernova remnants, pulsars, active galactic nuclei, GRBs, and more. These contributions have been well documented in reviews (e.g., [150]) and in catalogs in the MeV [151, 152] GeV [153] and TeV [154] energy ranges. LHAASO has recently observed photon spectra from several sources extending to ~ 1 PeV and beyond [128, 155].

The majority of photons detected at higher energies are characterized as diffuse emission unassociated with discrete sources. The Large Area Telescope (LAT) of the Fermi Gamma-Ray Space Telescope has examined this radiation in detail for energies above 50 MeV [156]. The dominant component comes from the plane of the Galaxy (i.e., $|b| \lesssim 10$ deg) and is referred to as the Galactic diffuse emission. It can be attributed largely to interactions of high energy cosmic hadrons and electrons with interstellar matter and photon fields, leading to emission from π^0 decay, inverse Compton scattering and bremsstrahlung [153, 157]. Ground-based all-sky gamma detectors have extended these measurements to TeV energies and beyond in certain regions of the Galactic Plane [158–160].

In addition to the Galactic flux, there is a lower-intensity component to the diffuse emission that appears to be isotropic across the sky. This is thought to be extragalactic in origin and is often referred to as the isotropic gamma-ray background (IGRB). The IGRB has been measured by the LAT above 100 MeV and has an energy spectrum that can be described by a power-law with index -2.3 and an exponential cutoff at approximately 280 GeV, with a total intensity of $(7.2 \pm 0.6) \times 10^{-6} \text{cm}^{-2} \text{s}^{-1} \text{sr}^{-1}$ [161]. Above energies of tens of TeV most emission is likely of local origin, due to Mpc and shorter attenuation lengths for interactions with cosmic microwave and infrared photons fields - this is referred to as the gamma-ray horizon [162, 163].

30.7 High-Energy Astrophysical Neutrinos

Neutrinos are expected to be produced in hadronic interactions in a variety of astrophysical objects. IceCube has reported a population of astrophysical neutrino events extending from tens of TeV to beyond ten PeV [164, 173, 174]. Multimessenger observations of the flaring blazar TXS 0506+056 have identified this object as a high-energy neutrino source [175, 176].

There is also expected to be a neutrino flux produced in cosmic ray GZK interactions. Measuring this *cosmogenic*⁴ neutrino flux above 10^{18} eV would help resolve the UHECR uncertainties mentioned above. One half of the energy that UHECR protons lose in photoproduction interactions that cause the GZK effects ends up in neutrinos [177]. Heavier nuclei produce lower energy neutrinos due to the lower energy of their constituent nucleons. The magnitude of the cosmogenic neutrino flux depends strongly on the cosmic-ray spectrum at acceleration, the cosmic-ray composition, the cosmological evolution of the cosmic-ray sources, and the energy of the Galactic-extragalactic transition.

The expected rate of cosmogenic neutrinos is lower than current limits obtained by IceCube [164], the Auger Observatory [167], RICE [166, 178], and ANITA [168], which are shown in Fig. 30.11 together with a models for cosmogenic neutrino production [171, 172] and the Waxman-Bahcall benchmark flux of

⁴Here we use cosmogenic to denote neutrinos produced by photoproduction during propagation, and astrophysical to denote neutrinos produced by other mechanisms or close to sources.

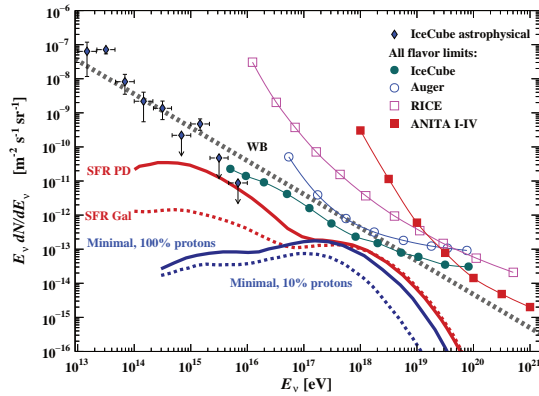


Figure 30.11: The best-fit IceCube *astrophysical* all-flavor neutrino flux [164]. Also shown are differential limits on the flux of *cosmogenic* neutrinos set by four experiments [165–168]. The IceCube limit on cosmogenic neutrinos accounts for a nuisance background of astrophysical neutrinos. The curves show the Waxman-Bahcall benchmark flux (solid grey) [169,170], cosmogenic models with cosmic ray sources with maximum proton energy of $10^{20.5}$ eV evolving with the star-formation rate in proton dip (solid red) and Galactic composition (dashed red) scenarios [171], and ‘minimal’ cosmogenic models with protons constituting 100% (solid blue) and 10% (dashed red) of the cosmic rays [172].

neutrinos produced in cosmic ray sources [169, 170]. At production, the dominant component of neutrinos comes from π^\pm decays and has flavor content $\nu_e:\nu_\mu:\nu_\tau = 1:2:0$. After oscillations, the arriving cosmogenic neutrinos are expected to be a 1:1:1 mixture of flavors. The sensitivity of each experiment depends on neutrino flavor, and all limits are expressed as three-flavor limits assuming a 1:1:1 mixture.

References

- [1] O. Adriani *et al.* (PAMELA), *Science* **332**, 69 (2011).
- [2] M. Aguilar *et al.* (AMS), *Phys. Rev. Lett.* **114**, 171103 (2015).
- [3] M. Aguilar *et al.* (AMS), *Phys. Rev. Lett.* **115**, 21, 211101 (2015).
- [4] K. Abe *et al.*, *Astrophys. J.* **822**, 2, 65 (2016).
- [5] M. J. Christ *et al.*, *Astrophys. J.* **502**, 278 (1998).
- [6] A.D. Panov *et al.* (ATIC Collab.), *Bull. Russian Acad. of Science, Physics*, **73**, 564 (2009).
- [7] V. A. Derbina *et al.* (RUNJOB), *Astrophys. J.* **628**, L41 (2005).
- [8] H. S. Ahn *et al.*, *Astrophys. J.* **707**, 593 (2009).
- [9] J.J. Engelmann *et al.* (HEAO3-C2 Collab.), *Astron. & Astrophys.* **233**, 96 (1990).
- [10] D. Müller *et al.* (CRN Collab.), *Astrophys. J.* **374**, 356 (1991).
- [11] M. Ave *et al.*, *Astrophys. J.* **678**, 262 (2008).
- [12] F. Aharonian *et al.* (H.E.S.S.), *Phys. Rev.* **D75**, 042004 (2007).
- [13] A. Archer *et al.* (VERITAS), *Phys. Rev.* **D98**, 2, 022009 (2018).
- [14] M. Aguilar *et al.*, *Phys. Rev. Lett.* **124**, 21, 211102 (2020).
- [15] M. Aguilar *et al.*, *Phys. Rev. Lett.* **126**, 4, 041104 (2021).
- [16] D. Maurin *et al.*, *Astron. & Astrophys.* **569**, A32 (2014).
- [17] M. Aguilar *et al.* (AMS), *Phys. Rev. Lett.* **119**, 25, 251101 (2017).
- [18] K. Lave *et al.*, *Astrophys. J.* **770**, 117 (2013).
- [19] G. DeNolfo *et al.*, *Adv. Space Res.* **38**, 1558 (2006).
- [20] R. Murphy *et al.*, *Astrophys. J.* **831**, 148 (2016).
- [21] B. Rauch *et al.*, *Astrophys. J.* **697**, 2083 (2009).
- [22] K. Lodders, H. Palme and H.P.Gail, *Landolt-Börnstein, New Series*, volume VI/4b, chapter 4.4, 560, Springer-Verlag (2009).
- [23] A. W. Strong, I. V. Moskalenko and V. S. Ptuskin, *Ann. Rev. Nucl. Part. Sci.* **57**, 285 (2007).
- [24] R.A. Mewaldt *et al.*, *Space Science Reviews* 99,27(2001).
- [25] A. A. Abdo *et al.*, *Astrophys. J.* **698**, 2121 (2009).
- [26] A. U. Abeysekara *et al.* (HAWC, IceCube), *Astrophys. J.* **871**, 1, 96 (2019).
- [27] M. Amenomori *et al.*, *Astrophys. J.* **711**, 119 (2010).
- [28] M. G. Aartsen *et al.*, *Astrophys. J.* **826**, 2, 220 (2016), [arXiv:1603.01227].
- [29] M. Amenomori *et al.*, *Astrophys. J.* **836**, 2, 153 (2017), [arXiv:1701.07144].
- [30] M. Ahlers and P. Mertsch, *Progr. Part. and Nucl. Phys.* **94**, 184 (2017), [arXiv:1612.01873].
- [31] O. Adriani *et al.* (PAMELA), *Phys. Rev. Lett.* **106**, 201101 (2011).
- [32] M. Boezio *et al.*, *Astrophys. J.* **532**, 653 (2000).
- [33] M. Aguilar *et al.* (AMS), *Phys. Rev. Lett.* **122**, 10, 101101 (2019).
- [34] S. Abdollahi *et al.* (Fermi-LAT), *Phys. Rev.* **D95**, 8, 082007 (2017).
- [35] G. Ambrosi *et al.* (DAMPE), *Nature* **552**, 63 (2017).
- [36] O. Adriani *et al.* (CALET), *Phys. Rev. Lett.* **122**, 18, 181102 (2019).
- [37] F. Aharonian *et al.* (H.E.S.S.), *Phys. Rev. Lett.* **101**, 261104 (2008).
- [38] F. Aharonian *et al.* (H.E.S.S.), *Astron. Astrophys.* **508**, 561 (2009).
- [39] A. Archer *et al.* (VERITAS), *Phys. Rev.* **D98**, 6, 062004 (2018).
- [40] Y. Shikaze *et al.*, *Astropart. Phys.* **28**, 154 (2007).
- [41] O. Adriani *et al.* (PAMELA), *Nature* **458**, 607 (2009).
- [42] O. Adriani *et al.*, *Phys. Rev. Lett.* **102**, 051101 (2009).
- [43] J.J. Beatty *et al.*, *Phys. Rev. Lett.* **93**, 24112 (2004).
- [44] I. V. Moskalenko and A. W. Strong, *Astrophys. J.* **493**, 694 (1998).
- [45] A. Ibarra, D. Tran and C. Weniger, *Int. J. Mod. Phys.* **A28**, 1330040 (2013).
- [46] D. Gaggero *et al.*, *Phys. Rev. Lett.* **111**, 021102 (2013).
- [47] P.-F. Yin *et al.*, *Phys. Rev.* **D88**, 2, 023001 (2013).
- [48] M. Aguilar *et al.* (AMS), *Phys. Rev. Lett.* **110**, 141102 (2013).
- [49] L. Accardo *et al.* (AMS), *Phys. Rev. Lett.* **113**, 121101 (2014).
- [50] J. Nishimura *et al.*, *Adv. Space Research* **19**, 767 (1997).
- [51] A. S. Beach *et al.*, *Phys. Rev. Lett.* **87**, 271101 (2001).
- [52] A. Yamamoto *et al.*, *Adv. Space Research* **42**, 443(2008).
- [53] Y. Asaoka *et al.*, *Phys. Rev. Lett.* **88**, 51101 (2002).
- [54] K. Abe *et al.*, *Phys. Rev. Lett.* **108**, 131301 (2012).
- [55] H. Fuke *et al.*, *Phys. Rev. Lett.* **95**, 081101 (2005).
- [56] I. Cholis, D. Hooper and T. Linden, *Phys. Rev.* **D93**, 4, 043016 (2016).
- [57] R. Bellotti *et al.*, *Phys. Rev.* **D53**, 35 (1996).
- [58] R. Bellotti *et al.* (WiZard/MASS2), *Phys. Rev.* **D60**, 052002 (1999).
- [59] M. Boezio *et al.* (WiZard/CAPRICE), *Phys. Rev.* **D62**, 032007 (2000).
- [60] M. Boezio *et al.*, *Phys. Rev.* **D67**, 072003 (2003).
- [61] S. Coutu *et al.*, *Phys. Rev.* **D62**, 032001 (2000).

- [62] S. Haino *et al.*, Phys. Lett. **B594**, 35 (2004).
- [63] T. Sanuki *et al.*, Phys. Rev. **D75**, 043005 (2007).
- [64] T.K. Gaisser, R. Engel, and E. Resconi, *Cosmic Rays and Particle Physics (second edition)*, Cambridge University Press (2016).
- [65] P. Lipari, Astropart. Phys. **1**, 195 (1993).
- [66] E. Mocchiutti *et al.*, in *Proc. 28th Int. Cosmic Ray Conf.*, Tsukuba, 1627 (2003). [<http://adsabs.harvard.edu/abs/2003ICRC...3.1627M>].
- [67] M. P. De Pascale *et al.*, J. Geophys. Res. **98**, A3, 3501 (1993).
- [68] P.K.F. Grieder, *Cosmic Rays at Earth*, Elsevier Science (2001).
- [69] J. Kremer *et al.*, Phys. Rev. Lett. **83**, 4241 (1999).
- [70] P. Achard *et al.* (L3), Phys. Lett. **B598**, 15 (2004).
- [71] O. C. Allkofer, K. Carstensen and D. W. Dau, Phys. Lett. **36B**, 425 (1971).
- [72] B. C. Rastin, J. Phys. **G10**, 1609 (1984).
- [73] C. A. Ayre *et al.*, J. Phys. **G1**, 584 (1975).
- [74] H. Jokisch *et al.*, Phys. Rev. **D19**, 1368 (1979).
- [75] C. G. S. Costa, Astropart. Phys. **16**, 193 (2001).
- [76] P. Adamson *et al.* (MINOS), Phys. Rev. **D76**, 052003 (2007).
- [77] S. Hayakawa, *Cosmic Ray Physics*, Wiley, Interscience, New York (1969).
- [78] R.R. Daniel and S.A. Stephens, Revs. Geophysics & Space Sci. **12**, 233 (1974).
- [79] K.P. Beuermann and G. Wibberenz, Can. J. Phys. **46**, S1034 (1968).
- [80] I. S. Diggory *et al.*, J. Phys. **A7**, 741 (1974).
- [81] V. Khachatryan *et al.* (CMS), Phys. Lett. **B692**, 83 (2010).
- [82] N. Agafonova *et al.* (OPERA), Eur. Phys. J. **C67**, 25 (2010).
- [83] P. Lipari and T. Stanev, Phys. Rev. **D44**, 3543 (1991).
- [84] M. Crouch, in *Proc. 20th Int. Cosmic Ray Conf.*, Moscow, **6**, 165 (1987) [<http://adsabs.harvard.edu/abs/1987ICRC...6..165C>].
- [85] Yu.M. Andreev, V.I. Gurentzov, and I.M. Kogai, in *Proc. 20th Int. Cosmic Ray Conf.*, Moscow, **6**, 200 (1987), [<http://adsabs.harvard.edu/abs/1987ICRC...6..200A>].
- [86] M. Aglietta *et al.* (LVD), Astropart. Phys. **3**, 311 (1995).
- [87] M. Ambrosio *et al.* (MACRO), Phys. Rev. **D52**, 3793 (1995).
- [88] C. Berger *et al.* (FREJUS), Phys. Rev. **D40**, 2163 (1989).
- [89] C. Waltham *et al.*, in *Proc. 27th Int. Cosmic Ray Conf.*, Hamburg, 991 (2001), [<http://adsabs.harvard.edu/abs/2001ICRC...3..991W>].
- [90] I. A. Belolaptikov *et al.* (BAIKAL), Astropart. Phys. **7**, 263 (1997).
- [91] J. Babson *et al.* (DUMAND), Phys. Rev. **D42**, 3613 (1990).
- [92] P. Desiati *et al.*, in *Proc. 28th Int. Cosmic Ray Conf.*, Tsukuba, 1373 (2003) [<http://adsabs.harvard.edu/abs/2003ICRC...3.1373D>].
- [93] T. Pradier (ANTARES), in “Proceedings, 43rd Rencontres de Moriond on Electroweak Interactions and Unified Theories: La Thuile, Italy, March 1-8, 2008,” 423–430 (2008).
- [94] S. Aiello *et al.* (NEMO), Astropart. Phys. **66**, 1 (2015).
- [95] F. Reines *et al.*, Phys. Rev. Lett. **15**, 429 (1965).
- [96] M.M. Boliev *et al.*, in *Proc. 3rd Int. Workshop on Neutrino Telescopes* (ed. Milla Baldo Ceolin), 235 (1991).
- [97] M. Ambrosio *et al.* (MACRO), Phys. Lett. **B434**, 451 (1998).
- [98] F. Ronga (MACRO), in “Proceedings, 26th International Cosmic Ray Conference (ICRC), August 17-25, 1999, Salt Lake City: Invited, Rapporteur, and Highlight Papers,” volume 2, 172 (1999), URL http://krusty.physics.utah.edu/~icrc1999/root/vol2/h4_1_07.pdf.
- [99] R. Becker-Szendy *et al.*, Phys. Rev. Lett. **69**, 1010 (1992).
- [100] *Proc. 25th Int. Conf. High-Energy Physics*, Singapore (eds. K.K. Phua and Y. Yamaguchi, World Scientific), 662 1991.
- [101] S. Hatakeyama *et al.* (Kamiokande), Phys. Rev. Lett. **81**, 2016 (1998).
- [102] Y. Fukuda *et al.* (Super-Kamiokande), Phys. Rev. Lett. **82**, 2644 (1999).
- [103] Y. Fukuda *et al.* (Super-Kamiokande), Phys. Rev. Lett. **81**, 1562 (1998).
- [104] T. Futagami *et al.* (Super-Kamiokande), Phys. Rev. Lett. **82**, 5194 (1999).
- [105] Y. Ashie *et al.* (Super-Kamiokande), Phys. Rev. **D71**, 112005 (2005).
- [106] R. Alfaro *et al.* (HAWC), Phys. Rev. **D96**, 12, 122001 (2017).
- [107] Yu. A. Fomin *et al.*, *Proc. 22nd Int. Cosmic Ray Conf.*, Dublin, **2**, 85 (1991) [<http://adsabs.harvard.edu/abs/1991ICRC...2...85F>].
- [108] M. Amenomori *et al.*, Astrophys. J. **268**, 1165 (2008).
- [109] M. Nagano *et al.*, J. Phys. **G10**, 1295 (1984).
- [110] M. A. K. Glasmacher *et al.*, Astropart. Phys. **10**, 291 (1999).
- [111] T. Antoni *et al.* (KASCADE), Astropart. Phys. **24**, 1 (2005).
- [112] W. D. Apel *et al.* (KASCADE Grande), Phys. Rev. Lett. **107**, 171104 (2011).
- [113] K. Andeen, M. Plum *et al.*, (IceCube Collab.), *Proceedings of Science* (ICRC2019), 172 (2019).
- [114] R. U. Abbasi *et al.* (HiRes), Phys. Rev. Lett. **100**, 101101 (2008).
- [115] A. Aab *et al.* (Pierre Auger), Phys. Rev. Lett. **125**, 12, 121106 (2020), [arXiv:2008.06488].
- [116] A. Aab *et al.* (Pierre Auger), Phys. Rev. D **102**, 6, 062005 (2020), [arXiv:2008.06486].
- [117] P. Abreu *et al.*, Eur. Phys. J. C **81** (2021).
- [118] D. Ivanov *et al.*, (Telescope Array Collab.), *Proceedings of Science* (ICRC2019), 298 (2019).
- [119] R. U. Abbasi *et al.* (Telescope Array), Astrophys. J. **865**, 1, 74 (2018), [arXiv:1803.01288].
- [120] K. Greisen, Ann. Rev. Nucl. Sci. **10**, 63 (1960).
- [121] J. Linsley, *Proc. 15th. Internat. Cosmic Ray Conf. (Plovdiv)*, **12**, 56-65, 89-96. (Available from ADS).
- [122] M. Nagano and A. Watson, Rev. Mod. Phys. **72**, 689 (2000).
- [123] A. Haungs *et al.*, Rep. Prog. Phys. (2003).
- [124] <https://www.iap.kit.edu/corsika/>.
- [125] A. Aab *et al.* (Pierre Auger), Phys. Rev. Lett. **117**, 19, 192001 (2016).
- [126] T. Huege, Phys. Rept. **620**, 1 (2016).
- [127] D. J. Bird *et al.* (HiRes), Astrophys. J. **424**, 491 (1994).
- [128] Z. Cao *et al.*, Nature **594**, 7861, 33 (2021).
- [129] V.S. Ptuskin *et al.*, Astron. & Astrophys. **268**, 726 (1993).
- [130] J. R. Hoerandel, Astropart. Phys. **21**, 241 (2004).
- [131] W. D. Apel *et al.*, Phys. Rev. **D87**, 081101 (2013), [arXiv:1304.7114].
- [132] M. G. Aartsen *et al.* (IceCube) (2019), [arXiv:1906.04317].
- [133] B. Peters, Nuovo Cimento **XXII**, 800 (1961).
- [134] J. Bellido *et al.* (Auger Collab.), Proceedings of Science (ICRC2017), 506 (2017).

- [135] D. Ikeda *et al.* (TA Collab.), *Proceedings of Science*(ICRC2017), 515 (2017).
- [136] V. de Souza *et al.* (TA and Auger Collabs.), *Proceedings of Science*(ICRC2017), 522 (2017).
- [137] V. Berezhinsky, A. Z. Gazizov and S. I. Grigorieva, *Phys. Rev.* **D74**, 043005 (2006).
- [138] A. Aab *et al.* (Pierre Auger), *Phys. Lett. B* **762**, 288 (2016), [arXiv:1609.08567].
- [139] V. Novotny *et al.*, (Auger Collab.), *Proceedings of Science* (ICRC2021), 324 (2021).
- [140] K. Greisen, *Phys. Rev. Lett.* **16**, 748 (1966).
- [141] G. T. Zatsepin and V. A. Kuzmin, *JETP Lett.* **4**, 78 (1966), [Pisma Zh. Eksp. Teor. Fiz.4,114(1966)].
- [142] D. Allard *et al.*, *Astron. & Astrophys.* **443**, L29 (2005).
- [143] R. U. Abbasi *et al.* (HiRes), *Astropart. Phys.* **32**, 53 (2009).
- [144] D. Ivanov *et al.*, *Proceedings of Science* (ICRC2021), 341(2021).
- [145] A. Aab *et al.*, *Science* **357**, 1266 (2017).
- [146] A. Aab *et al.*, *Astrophys. J.* **868**, 1 (2018).
- [147] E. Roulet *et al.*, (Auger Collab.), *Proceedings of Science* (ICRC2019), 408 (2019).
- [148] T. Fujii *et al.*, (Telescope Array Collab.), *Proceedings of Science* (ICRC2021), 392 (2021).
- [149] L. Caccianiga *et al.*, (Auger Collab.), *Proceedings of Science* (ICRC2019), 206 (2019).
- [150] A. De Angelis and M. Mollinari, *European Physical Journal Plus* **133**, 8, 324 (2018), [arXiv:1805.05642].
- [151] V. Schönfelder *et al.*, *Astron. Astrophys. Suppl.* **143**, 145 (2000), [arXiv:astro-ph/0002366].
- [152] I. S. D. Centre, “Integral general reference catalog,” <https://www.isdc.unige.ch/integral/science/catalogue>.
- [153] S. Abdollahi *et al.*, *Astrophys. J. Suppl.* **247**, 1, 33 (2020), [arXiv:1902.10045].
- [154] S. Wakely and D. Horan, “Tevcat,” <http://tevcat.uchicago.edu>.
- [155] Z. Cao *et al.*, *Science* **373**, 6553, 425 (2021).
- [156] M. Ackermann *et al.*, *Astrophys. J.* **750**, 1, 3 (2012), [arXiv:1202.4039].
- [157] F. Acero *et al.*, *Astrophys. J. Suppl.* **223**, 2, 26 (2016), [arXiv:1602.07246].
- [158] R. Atkins *et al.*, *Phys. Rev. Lett.* **95**, 25, 251103 (2005), [arXiv:astro-ph/0502303].
- [159] B. Bartoli *et al.*, *Astrophys. J.* **806**, 1, 20 (2015), [arXiv:1507.06758].
- [160] M. Amenomori *et al.*, *Phys. Rev. Lett.* **126**, 14, 141101 (2021), [arXiv:2104.05181].
- [161] M. Ackermann *et al.*, *Astrophys. J.* **799**, 1, 86 (2015), [arXiv:1410.3696].
- [162] T. M. Kneiske, K. Mannheim and D. H. Hartmann, in S. Ritz, N. Gehrels and C. R. Shrader, editors, “Gamma 2001: Gamma-Ray Astrophysics,” volume 587 of *American Institute of Physics Conference Series*, 358–362 (2001).
- [163] S. P. Wakely, in S. R. Magill and R. Yoshida, editors, “Calorimetry in High Energy Physics: XII,” volume 867 of *American Institute of Physics Conference Series*, 139–147 (2006).
- [164] M. G. Aartsen *et al.* (IceCube), *Astrophys. J.* **809**, 1, 98 (2015).
- [165] M. G. Aartsen *et al.* (IceCube), *Phys. Rev.* **D98**, 6, 062003 (2018).
- [166] I. Kravchenko *et al.*, *Phys. Rev.* **D85**, 062004 (2012).
- [167] F. Pedriera *et al.*, (Auger Collab.), *Proceedings of Science* (ICRC2019), 172 (2019).
- [168] C. Deaconu *et al.*, (ANITA Collab.), *Proceedings of Science* (ICRC2019), 867 (2019).
- [169] E. Waxman and J. N. Bahcall, *Phys. Rev.* **D59**, 023002 (1999).
- [170] E. Waxman, *The Origin of IceCube’s Neutrinos: Cosmic Ray Accelerators Embedded in Star Forming Calorimeters* (2017), [arXiv:1511.00815].
- [171] K. Kotera, D. Allard and A. V. Olinto, *JCAP* **1010**, 013 (2010).
- [172] M. Ahlers and F. Halzen, *Phys. Rev.* **D86**, 083010 (2012).
- [173] M. G. Aartsen *et al.* (IceCube), *Science* **342**, 1242856 (2013).
- [174] M. G. Aartsen *et al.* (IceCube), *Phys. Rev. Lett.* **113**, 101101 (2014).
- [175] M. G. Aartsen *et al.* (IceCube, Fermi-LAT, MAGIC, AGILE, ASAS-SN, HAWC, H.E.S.S., INTEGRAL, Kanata, Kiso, Kapteyn, Liverpool Telescope, Subaru, Swift NuSTAR, VERITAS, VLA/17B-403), *Science* **361**, eaat1378 (2018).
- [176] M. G. Aartsen *et al.* (IceCube), *Science* **361**, 6398, 147 (2018).
- [177] V. S. Berezhinsky and G. T. Zatsepin, *Phys. Lett.* **28B**, 423 (1969).
- [178] I. Kravchenko *et al.*, *Phys. Rev.* **D73**, 082002 (2006).

Experimental Methods and Colliders

31. Accelerator physics of colliders (rev.)	533
32. High-energy collider parameters (rev.)	543
33. Neutrino beam lines at high-energy proton synchrotrons (rev.)	548
34. Passage of particles through matter (rev.)	549
35. Particle detectors at accelerators (rev.)	565
36. Particle detectors for non-accelerator phys. (rev.)	618
37. Radioactivity and radiation protection (rev.)	646
38. Commonly used radioactive sources (rev.)	652

31. Accelerator Physics of Colliders

Revised August 2021 by V. Shiltsev (FNAL) and F. Zimmermann (CERN).

This article provides background for the High-Energy Collider Parameter Tables that follow and some additional information; see in-depth review and a comprehensive list of references in [1]; citations below are limited to widely used textbooks and open access seminal papers and reviews.

31.1 Energy and Luminosity

Collisions of two beams of particles accelerated to high energies $E_{1,2}$ provide access to center-of-mass energies (c.m.e.) $E_{\text{c.m.e.}} \approx 2\sqrt{E_1 E_2}$, assuming a typically small or zero crossing angle. Most of the 31 colliders that have ever reached the operational stage (seven are operational now) used equal masses and energies of colliding particles, with c.m.e. equal to twice the beam energy $E_{\text{c.m.e.}} = 2E_b$. Other machines collide beams of unequal energies, such as electron-proton or electron-ion colliders, or asymmetric B -factories, that produce new short-lived particles, whose decays are more easily detected and analyzed with a Lorentz boost.

In an accelerator, charged particles gain energy from an electric field, which usually varies in time at a high frequency ranging from 100s of kHz to 10s of GHz. With proper phasing to the RF field over distance l , the energy gain of a particle with charge Ze is proportional to the average accelerating gradient G , i.e. $\Delta E_b = ZeGl$. In principle, the highest beam accelerating gradients achieved to date in operational machines or beam test facilities ($G \approx 100$ MV/m in 12 GHz normal-conducting RF cavities and 31.5 MV/m in 1.3 GHz superconducting ones) allow accessing high energies over reasonably long linear accelerators (linacs), but cost considerations often call for minimization of RF acceleration via repeated use of the same RF system which, in that case, would boost the energy in small portions $\Delta E_b = ZeV_{\text{RF}}$ per turn every time a particle passes through the total cavity voltage V_{RF} . Such an arrangement can be realized either in the form of storage-ring circular colliders or also through novel schemes based on, e.g., recirculating linear accelerators (RLAs) with or without energy recovery. Circular colliders are by far the most common; here, the momentum and energy of ultra-relativistic particles are determined by the bending radius inside the dipole magnets, ρ , and by the average magnetic field B of these magnets:

$$p = ZeB\rho \quad \text{or} \quad E_b [\text{GeV}] = 0.3Z(B\rho) [\text{Tm}]. \quad (31.1)$$

Such *synchrotron condition* assures approximately constant radius of the beam orbit during acceleration. Transverse focusing by quadrupole magnets is needed to keep particles inside the rather limited space provided by the accelerator beam pipe passing through the magnet apertures. The maximum field of normal-conducting (NC) magnets is about 2 T, due to the saturation of ferromagnetic materials, and, while this is sufficient for lower energy colliders, such as most e^+e^- storage rings, it is not adequate for frontier-energy hadron (or muon) beams, because of the implied need for excessively long accelerator tunnels and prohibitively high total magnet power consumption. The development of superconducting (SC) magnets that employ high electric current carrying Nb-Ti wires cooled by liquid helium below 5 K, opened up the way towards higher fields and to hadron colliders at record energies [2]. For example, the 14 TeV c.m.e. LHC at CERN, uses double-bore SC magnets with a maximum field of 8.3 T at a temperature of 1.9 K, in a tunnel of $C = 26.7$ km circumference (dipole-magnet bending radius $\rho = 2800$ m). The double-bore design allows acceleration of the same particle type in opposite directions and also the operation with different particle species (e.g., protons and heavy ions) in the two apertures, while a single bore magnet implies the use of particles and antiparticles for the collider application. As the production of anti-particles is energy consuming and therefore limited, this concept opens the door to high-performance hadron colliders.

The exploration of rare nuclear and high energy particle physics phenomena requires not only an appropriately high energy, but also a sufficiently large number of detectable reactions. The number of events of interest N_{exp} is given by the product of the cross section of the reaction under study, σ_{exp} , and the time integral

over the instantaneous *luminosity*, \mathcal{L} :

$$N_{\text{exp}} = \sigma_{\text{exp}} \cdot \int \mathcal{L}(t) dt. \quad (31.2)$$

In the Tables, luminosity is stated in the units of $\text{cm}^{-2}\text{s}^{-1}$. The integral on the right is referred to as integrated luminosity \mathcal{L}_{int} , and, reflecting the smallness of typical particle-interaction cross-sections is often reported in units of inverse femto- or attobarn, e.g., $1 \text{ ab}^{-1} = 10^{42} \text{ cm}^2$. Colliders usually employ bunched beams of particles with approximately Gaussian distributions, and for two bunches containing N_1 and N_2 particles colliding head-on with frequency f_{coll} , a basic expression for the luminosity is

$$\mathcal{L} = f_{\text{coll}} \frac{N_1 N_2}{4\pi\sigma_x^* \sigma_y^*} \mathcal{F} \quad (31.3)$$

where σ_x^* and σ_y^* characterize the rms transverse beam sizes in the horizontal and vertical directions at the interaction point, and \mathcal{F} is a factor of order 1, that takes into account inefficient geometric overlapping of the beams due to a crossing angle and finite bunch length, and dynamic effects, such as the mutual focusing of the two beam during the collision (see below). Having n_b bunches per beam increases the frequency of collisions $f_{\text{coll}} = n_b f_0$ where f_0 is either the revolution frequency of a circular collider or the repetition rate of a linear one. To achieve a high luminosity, one, therefore, has to maximize the population and number of bunches, either producing these narrowly or focusing them tightly, and colliding them at high frequencies at dedicated locations, where products of their reactions can be registered by particle detectors.

Subsequent sections in this report briefly expand on the beam dynamics behind collider design, comment on the realization of collider performance in a selection of today's facilities, and end with some remarks on future possibilities.

31.2 Beam Dynamics

Given the enormous and highly concentrated power carried by modern high energy particle beams, the main concern of beam dynamics in colliders is stability of motion of i) individual particles in accelerators, ii) single high-intensity beams of many particles moving together, and iii) colliding beams [3–5].

31.2.1 Single Particle Dynamics

While a reference particle at the nominal energy proceeds along the design trajectory (reference orbit) mostly determined by transverse magnetic dipole fields, other particles in the bunch are kept close by through the focusing effect of quadrupole fields. Assume that the reference particle carries a right-handed Cartesian coordinate system, with the co-moving z -coordinate pointed in the direction of motion along the reference trajectory, $z = s - vt$ (with v the reference particle velocity, and t time). The independent variable is the distance s of the reference particle along this trajectory, rather than time t , and for simplicity this reference path is taken to be planar. The transverse coordinates are x (horizontal) and y (vertical), where $\{x, z\}$ defines the plane of the reference trajectory.

Several time scales are involved, and this is reflected in the approximations used in formulating the equations of motion. All of today's high-energy colliders are alternating gradient synchrotrons or, respectively, storage rings and the shortest time scale is set by so-called *betatron oscillations*. The linearized equations of motion of a particle displaced from the reference trajectory are:

$$x'' + K_x(s)x = 0, \quad y'' + K_y(s)y = 0, \quad z' = -x/\rho(s), \quad (31.4)$$

with $K_x \equiv \frac{Ze}{p} \frac{\partial B_y}{\partial x} + \frac{1}{\rho^2}$ and $K_y \equiv -\frac{Ze}{p} \frac{\partial B_y}{\partial x}$

where $\rho = p/ZeB_y$ is the radius of curvature due to the field on the reference orbit. The prime denotes d/ds and the Maxwell equation in vacuum $\nabla \times \mathbf{B} = \mathbf{0}$ helps to eliminate $B_x(s)$ using the relation $\partial B_x/\partial y = \partial B_y/\partial x$. In this linear approximation, the vertical magnetic field $B_y(s)$ in the (x, z) -plane contains only

dipole and quadrupole terms, which are treated as static in time, but s -dependent.

The solutions of the Hill's equations (31.4) for x and y with a restoring force periodic in s are those of quasi-harmonic oscillators:

$$x(s) = \sqrt{2J_x\beta_x} \cos \psi_x, \quad x'(s) = -\sqrt{\frac{2J_x}{\beta_x}} [\alpha_x \cos \psi_x + \sin \psi_x], \quad (31.5)$$

where the *action* J_x is a constant of integration, $\alpha_x = \alpha_x(s) \equiv -(1/2)d\beta_x(s)/ds$, and the envelope of oscillations is modulated by the *beta-function* $\beta_x(s)$. A solution of the same form describes the motion in y . The betatron oscillation phase advances according to $d\psi_x/ds = 1/\beta_x$; that is, $2\pi\beta_x$ also plays the role of a local wavelength of oscillations along the orbit. An extremely important parameter for circular machines is the *tune*, Q_x , which is the number of such oscillations per turn about the closed path:

$$Q_x = \frac{1}{2\pi} \oint d\psi_x = \frac{1}{2\pi} \oint \frac{ds}{\beta_x(s)}. \quad (31.6)$$

While the integer part of the tune $[Q_{x,y}]$ generally characterizes the extent of the focusing lattice, it is the fractional part of the tune $\{Q_{x,y}\}$ that needs to be well defined and controlled by the machine operators in order to stay away from potentially detrimental resonances, which may occur under conditions of $kQ_x + lQ_y = m$, where k, l , and m are integers. For example, for the LHC a combination of horizontal and vertical tunes — also called the *working point* — equal to $(Q_x, Q_y) = (64.31, 59.32)$ has been selected, such that resonances up to the order of $|k| + |l| = 10$ or 12 are avoided. These resonances are driven by high order multipole components of the fields in the magnets, or by self-fields of the beam, or by the electromagnetic fields of the opposite bunch. Normally, the nonlinear components are very weak compared to linear ones, nevertheless, when the nonlinear resonance condition is encountered, the amplitudes of particle oscillations could grow over the beam lifetime, resulting in the escape of the particles to the machine aperture, in the increase of the average beam size, or in both; either of these is highly undesirable phenomena. Careful analysis of nonlinear beam dynamics is instrumental in determining and optimizing the *dynamic aperture*, which is defined as the maximum amplitude of a bounded particle motion.

Neglecting for now all nonlinear effects and usually small $x - y$ coupling, and considering only the linear dynamics, the beta-function is well defined and satisfies the following equation:

$$2\beta_x\beta_x'' - \beta_x'^2 + 4\beta_x^2 K_x = 4. \quad (31.7)$$

In a region free of magnetic fields, such as in the neighborhood of a collider interaction point (IP), usually occupied by particle detectors, a symmetric solution of Eq. (31.7) is a parabola:

$$\beta_x(s) = \beta_x^* + \frac{s^2}{\beta_x^*}, \quad (31.8)$$

where, in this case, s denotes the longitudinal distance from the IP. The location of the beam waist usually coincides with the IP and corresponds to the minimum value of the beta-function β_x^* ; the asterisk is used to indicate IP parameters.

Note that individual quadrupole magnet focuses particles in one plane and defocuses in another, see Eq.(31.4), and a standard way to provide focusing in both planes is to employ an alternating gradient periodic focusing lattice, consisting of a sequence of equally-spaced quadrupoles with a magnetic field gradient equal in magnitude, but alternating in sign ("focusing quadrupole - drift space - defocusing quadrupole - drift space" — known as a *FODO cell*), Eq. (31.7) has stable periodic solutions $\beta_x(s), \beta_y(s)$ in both planes provided that the focal length of the quadrupoles is longer than half the focusing-lens spacing L , i.e., $f = p/(eB_2l) > L/2$ (where l is the length of a quadrupole magnet, here assumed to be short $l \ll L$, and $B_2 \equiv |\partial B_y/\partial x|$ the quadrupoles' field gradient). In that case, the beta-functions have maxima at the focusing quadrupoles and minima at the defocusing ones, equal to, for example, $\beta_{\max, \min} = (2 \pm \sqrt{2})L$ in the case of $f = L/\sqrt{2}$, which

corresponds to a betatron phase advance $\Delta\psi_{x,y} = 90^\circ$ per FODO cell.

Expressing the invariant J_x in terms of x, x' yields

$$J_x = \frac{1}{2} (\gamma_x x^2 + 2\alpha_x x x' + \beta_x x'^2) = \frac{x^2 + (\alpha_x x + \beta_x x')^2}{2\beta_x} \quad (31.9)$$

with $\gamma_x = \gamma_x(s) \equiv (1 + \alpha_x^2(s))/\beta_x(s)$. In a periodic system, these *Courant-Snyder parameters* [6] or *Twiss parameters* $\alpha(s), \beta(s), \gamma(s)$ are usually defined by the focusing lattice; in a single pass system such as a linac, the parameters may be selected to match the $x-x'$ distribution of the input beam. For a given position s in the ring, the transverse particle motion in $\{x, x' \equiv dx/ds\}$ phase space describes an ellipse, the area of which is $2\pi J_x$, where the horizontal action J_x is a constant of motion and independent of s . If the interior of that ellipse is populated by an ensemble of non-interacting and non-radiating particles, that area, given the name *emittance*, is constant over the trajectory as well and would only change with energy. In a typical case of the particle's energy change rate being much slower than betatron motion, and considering a Hamiltonian system (i.e., a hadron collider or a linear collider, either without significant synchrotron radiation), the adiabatic invariant $\int p_x dx$ is conserved, and given that for small angles $p_x = x' \cdot \beta\gamma mc^2$, it is common practice to consider an energy-independent *normalized emittance* that is equal to the product of the emittance and relativistic factor $\beta\gamma/\pi$ and denoted by ε_n . For a beam with a Gaussian distribution in $\{x, x'\}$, average action value $\langle J_x \rangle$ and standard deviations σ_x , and $\sigma_{x'}$, the definition of the normalized rms emittance is

$$\varepsilon_{nx} \equiv \beta\gamma \langle J_x \rangle = \beta\gamma \frac{\sigma_x^2(s)}{\beta_x(s)} = \beta\gamma \frac{\sigma_{x'}^2(s)}{\gamma_x(s)}, \quad (31.10)$$

with a corresponding expression for the other transverse direction, y . The angular brackets denote an average over the beam distribution. For 1D Gaussian beam, 95% of the particles are contained within $\{x, x'\}$ phase space area of $6\pi\varepsilon_n/(\beta\gamma)$. Normalized beam emittances are conserved over the acceleration cycle in linear, static focusing lattices $K_{x,y}(s)$, and consequently, one would expect the same ε_n at the hadron (or linear) collider top energy as the one coming from the very initial low energy particle source. Unfortunately, that is rarely the case as many time-varying or nonlinear phenomena come into play. In an e^-/e^+ storage ring, the normalized emittance is not preserved during acceleration, but at each energy the beam's equilibrium emittance is determined by the effect of synchrotron radiation as a balance between radiation damping and quantum excitation [7]. In such a ring, for a given accelerator optics, the normalized equilibrium emittance increases with the third power of the beam energy [8].

As for the description of a particle's longitudinal motion, one takes the fractional momentum deviation $\Delta p/p$ from that of the reference particle as the variable conjugate to z . The factors $K_{x,y}$ and ρ in Hill's equations (31.4) are dependent on momentum p , leading to a number of effects: first, the trajectory of off-momentum particles deviates by $\Delta x(s) = D_x(s)(\Delta p/p)$, where the *dispersion function* $D_x(s)$ is determined by the magnetic lattice and is usually positive, periodic, and of the order of $\sim \rho/Q_x^2$. Second, the radius of curvature and orbit path-length C vary with the momentum and, to first order, are characterized by the momentum compaction factor α_c ,

$$\alpha_c \equiv \frac{\Delta C/C}{\Delta p/p} = \frac{1}{C} \oint \frac{D_x(s)}{\rho(s)} ds, \quad (31.11)$$

which typically is of order $1/Q_x^2$. Energy deviations also result in changes of machine focusing lattice properties and variations of the particle tunes, characterized by the *chromaticity* $Q'_{x,y} \equiv \Delta Q_{x,y}/(\Delta p/p)$. The natural chromaticity due to momentum dependence of the quadrupole focusing is negative and large $\sim -Q_{x,y}$. Corresponding chromatic tune variations can, therefore, become unacceptably large even for relatively small energy deviations $(\Delta p/p) \sim (0.1 - 1) \cdot 10^{-3}$. To assure transverse particle stability, usually, the chromaticity is partially or fully com-

compensated by additional sextupole magnets placed at locations of non-zero dispersion.

Radiofrequency electric fields in s direction provide a longitudinal focusing effect, allowing a stable increase of particle energy. The frequency f_s of such longitudinal *synchrotron oscillations* is (expressed in units of revolution frequency f_0 , to become the synchrotron tune Q_s)

$$Q_s \equiv \frac{f_s}{f_0} = \sqrt{\frac{(\alpha_c - 1/\gamma^2)hZeV_{\text{RF}} \sin(\phi_s)}{2\pi\beta cp}}, \quad (31.12)$$

where $h = f_{\text{RF}}/f_0$ denotes the RF harmonic number, V_{RF} the RF voltage, and $\phi_s = \cos^{-1}(\Delta E/Z_eV_{\text{RF}})$ the synchronous phase, with ΔE the average energy loss per turn (e.g. due to synchrotron radiation and impedance). The synchrotron tune Q_s determines the amplitude of longitudinal oscillations for a particle with an initial momentum offset, e.g., the rms bunch length σ_z relates to the rms momentum spread $\delta p/p$ as:

$$\sigma_z = \frac{c(\alpha_c - 1/\gamma^2)}{2\pi Q_s f_0} \left(\frac{\delta p}{p} \right). \quad (31.13)$$

Similarly to the case of transverse oscillations, the area of the longitudinal phase space $\{\Delta E, \Delta t\}$, or $\{\gamma\beta\delta p/p = (1/\beta)\Delta\gamma, z = \beta c\Delta t\}$, encircled by a moving particle is an adiabatic invariant, and the corresponding normalized *longitudinal emittance* $\varepsilon_{n,L} = \beta\gamma mc\sigma_z(\delta p/p)$ is a generally conserved quantity in hadron accelerators and also in linear accelerators. In the case of lepton storage rings, synchrotron radiation determines the equilibrium relative momentum spread, which grows linearly with beam energy [7, 8], and the corresponding bunch length follows from Eq. (31.13). In hadron synchrotrons, the longitudinal emittance sometimes is intentionally blown up during acceleration, so as to preserve longitudinal beam stability.

Longitudinal oscillations are the slowest of all the periodic processes which take place in the accelerators. For example, in the LHC, the frequency of synchrotron oscillations at the top energy of 7 TeV is about $f_s = 23$ Hz, the revolution frequency is $f_0 = 11.3$ kHz, the frequency of betatron oscillations is about $Q_{x,y}f_{\text{rev}} \simeq 700$ kHz and the RF frequency is $f_{\text{RF}} = 400.8$ MHz ($h = 35640$). It should be noted that longitudinal motion is practically absent in linacs. In the absence of bending dipoles, dispersion $D_x(s)$ is zero and so are the momentum compaction factor α_c and the synchrotron tune Q_s . As a result, ultrarelativistic particles in a linac barely change their relative positions during acceleration despite significant energy spread.

Highest-energy circular colliders face a serious impediment in the form of synchrotron radiation (SR) that causes an energy loss per turn of

$$\Delta E_{\text{SR}} = \frac{1}{3\varepsilon_0} \frac{Z^2 e^2 \beta^3 \gamma^4}{\rho}, \quad (31.14)$$

here, ε_0 is the permittivity of vacuum. For electrons and positrons it is equal to $\Delta E_{\text{SR}} = 88.5$ [keV/turn] $E_b^4[\text{GeV}]/\rho[\text{m}]$ and requires correspondingly high total RF voltage per turn to replenish the loss. Above a few hundred GeV, the SR energy loss becomes comparable to beam energy $\Delta E_{\text{SR}} \sim E_b$, which makes circular e^+e^- colliders impractical for c.m.e. above ~ 500 GeV.

Dynamics of the particle spin and sophisticated methods to maintain beam polarization along the acceleration chain, from the polarized sources to collisions, dedicated spin matching procedures to enable self polarization in e^+/e^- storage rings and the *resonant depolarization* method of ultra-precise c.m.e. calibration are described in [9].

31.2.2 High Intensity Beams

Ultimate collider luminosity calls for high beam currents $I_b = Ze f_0 n_b N$. Three related major difficulties include growing RF demands to compensate the synchrotron-radiation power loss $P = I_b \Delta E_{\text{SR}}$ in e^+/e^- beams, the advent of so-called *coherent* or (*collective*) *beam instabilities*, and growing demands for minimization of radiation due to inevitable particle losses. Many types of single- and multi-bunch instabilities are caused by beam interactions with electromagnetic fields induced by the beam itself due

to the *impedance* of the vacuum chambers and RF cavities [4], or caused by unstable clouds of secondary particles, like electrons or ions, which are formed around the circulating beams [10]. These instabilities can develop as quickly as within tens to thousands of turns and need to be controlled. Mechanisms that are routinely employed to avoid coherent instabilities include the use of nonlinear magnets to generate sufficient spread of the tunes and therefore, provide *Landau damping*, fast beam-based transverse and longitudinal feedback systems, and electron/ion clearing (either by weak magnetic or electric fields or by modulation of the primary beam current profile rendering secondaries unstable, or by reducing the yield of secondary electrons via either a special coating or extensive *beam scrubbing* of the vacuum chamber walls).

High current beam operation is sensitive to even minuscule fractional intensity losses caused by particles' scattering at a large angle or with a large energy loss, sufficient for either the particle amplitudes $\sqrt{2J_{x,y}\beta_{x,y}(s)}$, or their dispersive position deviations $\Delta x = D_x(s)(\delta p/p)$ to exceed the available transverse aperture, usually set by collimators (otherwise, by the vacuum chamber and magnet apertures). This can be due to residual vacuum molecules near the beam orbit or Compton scattering off thermal photons, due to Coulomb scattering off other particles within the same bunch (*Touschek effect*), or due to collisions with opposite beam particles and fields, such as inelastic interaction of protons, Bhabha scattering $e^+e^- \rightarrow e^+e^-$, or radiative Bhabha scattering $e^+e^- \rightarrow e^+e^-\gamma$ (see corresponding chapters in [11]).

Particles can also get lost on the aperture as a result of much slower mechanisms of diffusion caused either by the above processes with smaller scattering amplitudes, but stochastically repeated many times, such as intensity-dependent multiple Coulomb *intra-beam scattering* [12], by external noises such as ground motion or magnetic field fluctuations, or via chaotic mechanisms like Arnold diffusion, modulational diffusion, or resonance streaming in nonlinear fields, enhanced by minor tune modulations. Diffusion leads to a slow evolution of the beam distribution function and appearance of highly unwanted large-amplitude tails and beam emittance growth. The only way to counteract it is to arrange *beam cooling* (damping of particle oscillations). The cooling requires a reaction force opposite to particle momentum arranged such that, on average, the corresponding dissipative particle energy loss is compensated for by external power [13, 14].

In the case of electron or positron storage rings, such cooling occurs naturally due to synchrotron radiation and provides an automatic route to achieve small equilibrium emittances through a balance between radiation damping and excitation of oscillations by random radiation of individual photons. Fast radiation damping allows *top-up injection* of new particles without removing existing ones, a useful method to maximize the integrated luminosity of circular e^+e^- colliders. Synchrotron radiation damping will also be an important cooling mechanism for future energy-frontier hadron colliders, like the proposed FCC-hh and SppC (see below).

Four other methods of beam cooling have been developed and successfully employed to attain low emittances, namely *electron cooling* and *stochastic cooling* of heavy particles (ions and antiprotons), *laser cooling* of ion beams, and the *ionization cooling* of muons.

To avoid damage or excessive irradiation of accelerator components so that these remain accessible for maintenance in the tunnel, sophisticated collimation systems are utilized. These systems usually employ a series of targets or primary collimators which scatter the halo particles, and numerous absorbers (sometimes as many as a hundred, which intercept particles in dedicated locations) [15, Ch.9.7]. In the highest energy modern and future colliders, extreme total beam energies $n_b N E_b$ ranging from MJs to GJs and impacting energy surface densities reaching many GJ/mm² pose one of the biggest challenges for high efficiency and robust particle collimation.

31.2.3 High Luminosity Collisions

Eq. (31.3) for luminosity can be recast in terms of normalized transverse emittances Eq. (31.10) and the beta-functions β^* at

the IP as:

$$\mathcal{L} = f_0 \gamma m_b \frac{N^2}{4\pi \sqrt{\varepsilon_{nx} \beta_x^* \varepsilon_{ny} \beta_y^*}} \mathcal{F}. \quad (31.15)$$

Here, equal bunch populations N are assumed in two Gaussian beams with the same emittances. Naturally, to achieve a high luminosity, one has to maximize the total beam populations $n_b N$ within the lowest possible emittances, and collide the beams at high frequency at locations where the focusing beam optics provides the lowest possible values of the amplitude functions β^* , the so-called *low-beta insertion*. The latter requires sophisticated systems of strong focusing elements, sometimes occupying quite a significant fraction of the collider's total length. The lowest $\beta_{x,y}^*$ is determined by the maximum field gradients and apertures in the interaction region (IR) magnets and the effectiveness of compensation of chromatic and nonlinear aberrations.

The typical geometric reduction factor is $\mathcal{F} \approx 1$, and it rarely drops below 0.5 for the majority of colliders, unless this is specifically required by physics processes under study. The reduction due to the *hourglass effect* is caused by the increase in transverse beam sizes as one proceeds away from the IP, where $\beta(s)$ grows parabolically, as in Eq. (31.8). For long round bunches the effect scales as $\mathcal{F} \approx \sqrt{\pi} A \exp(A^2) \operatorname{erfc}(A)$, where $A = \beta^*/\sigma_z$. Nonzero beam crossing angles θ_c in the horizontal plane and long bunches (rms bunch length σ_z) will reduce the luminosity, too, by a factor $\mathcal{F} \approx 1/(1 + \Phi^2)^{1/2}$, where the parameter $\Phi = \sigma_z \tan(\theta_c/2)/\sigma_x^*$ is known as the *Piwiński angle*.

One of the most common limits to producing high luminosity arises from electric and magnetic forces of the opposite bunch at the IPs, characterized by a dimensionless *beam-beam parameter*:

$$\xi_{x,y} = \frac{r_0 N \beta_{x,y}^*}{2\pi \gamma \sigma_{x,y}^* (\sigma_x^* + \sigma_y^*)}, \quad (31.16)$$

where $r_0 = Z^2 e^2 / (4\pi \varepsilon_0 m c^2)$ is the classical radius of the colliding particle (with charge Ze and mass m). From Eqs. (31.3) or (31.15) and (31.16), one can note that the path to higher luminosity via higher beam intensity and smaller beam sizes almost automatically calls for a higher beam-beam parameter as $\mathcal{L} \propto \xi$. Cited in the Tables, the beam-beam parameter is roughly equal to the betatron tune shift experienced by small-amplitude particles – positive in the case of opposite charge beams, like e^+e^- , and negative for same charge beams as in pp collisions. Beam-beam forces can lead to coherent effects, such as unstable beam oscillations or blow-up of one beam's size while the other beam remains small or even shrinks (*flip-flop effect*). The tune spread arising from ξ and the nonlinear nature of beam-beam interactions results in strong diffusion along high-order transverse resonances $kQ_x + lQ_y = m$ and, ultimately, in beam size growth and beam losses. Operational experience indicates that the aforementioned effects are tolerable below certain *beam-beam limit* of $\xi_{x,y} \approx 0.003 - 0.012$ in hadron colliders [16], and – due to strong synchrotron radiation damping – an order of magnitude higher one in e^+e^- colliders, with maximum $\xi_{x,y} \approx 0.03 - 0.12$ [17, 18]. The accessible beam-beam parameter range can also be restricted by coherent beam-beam instabilities. These various limits translate into a maximum allowed single bunch intensity N and call for an increase of the number of bunches n_b to achieve higher luminosities.

In linear colliders, where each bunch collides only once, with typically much smaller beam size and experiencing much stronger forces, the strength of the collision is measured by the ratio of the rms bunch length σ_z to the beam-beam focal length. This ratio, called *disruption parameter* D_y , is related to ξ_y via $D_y = 4\pi \sigma_z \xi_y / \beta_y^*$. Significant disruption leads to effectively smaller beam size and a resulting luminosity enhancement; it also makes the collision more sensitive to small offsets, resulting in a *kink instability*. Additional beam-beam effects arising in the collisions at linear colliders are the emission of *beamstrahlung* (synchrotron radiation in the field of the opposing beam), along with e^+e^- pair creation, and depolarization by various mechanisms.

Beamstrahlung is relevant for both linear colliders, where it may significantly degrade the luminosity spectrum, and for future

highest-energy circular colliders, where it may limit the beam lifetime, and also increases the energy spread and bunch length of the stored beam. For both types of colliders, the beamstrahlung is mitigated by making the colliding beams as flat as possible at the interaction point ($\sigma_x^* \gg \sigma_y^*$). The photon energy spectrum of the beamstrahlung is characterized by the parameter $\Upsilon = (2/3)\hbar\omega_c/E_b$ [19], with $\hbar\omega_c$ denoting the critical photon energy. The spectrum strongly deviates from the classical synchrotron radiation spectrum for Υ approaching or exceeding 1.

For hadron colliders, two fundamental luminosity limits are the beam lifetime, determined by burn-off in the collisions due to inelastic pp interaction $dN/dt = -\mathcal{L}\sigma_{in}$, and the radiation from the collision debris, which may induce “quenches” (transitions to the normal-conducting state) of the superconducting final quadrupole magnets, and, in the long term, affect the equipment lifetime. Another limit on the achievable integrated luminosity in circular colliders is set by the minimum or average turnaround time (the time between the beam abort at the end of a physics fill and the start of the next physics collisions). Achieving practical filling times with many bunches in the collider requires either fast cycling injector machines and/or the top-up injection operation. The latter makes the average luminosity of circular electron-positron colliders approximately equal to the peak luminosity.

31.3 Recent High Energy Colliders

In this and the following section, elaboration is made on various issues associated with some of the recently operating colliders, particularly factors which impact integrated luminosity. Only general references are provided, where further information can be obtained. A more complete list of recent colliders and their parameters can be found in the High-Energy Collider Parameters tables.

31.3.1 Tevatron

The first superconducting synchrotron in history, the Tevatron [20] was converted into a proton-antiproton collider in 1985. Its 4.4 T dipole magnets employed Nb-Ti superconducting cable operating at 4.5 K, requiring what was then the world's largest cryogenic system. With \sqrt{s} up to 1.96 TeV it was the highest energy collider for 25 years and delivered more than 12 fb^{-1} of the integrated luminosity to each $p\bar{p}$ detector experiments (CDF and D0) before being shut off in 2011. The route to high integrated luminosity in the Tevatron was governed by the antiproton production rate, the turn-around time to produce another store, and the resulting optimization of store time [21]. The antiproton production complex consisted of three 8 GeV \bar{p} accelerators (the Accumulator, Debuncher, and Recycler – the latter was the first high energy accelerator built with permanent magnets), and employed 25 independent stochastic cooling systems and one pioneering high-energy electron cooling set-up to accumulate up to a record high value of $25 \cdot 10^{10} \bar{p}$ per hour. Despite severe parasitic long-range interactions of the two beams, each consisting of 36 bunches placed on helical orbits by two dozen $\pm 150 \text{ kV}$ high-voltage (HV) separators, a total beam-beam tune shift parameter of $n_{IP}\xi \approx 0.025-0.03$ was achieved, a record for hadron beams, with $n_{IP} = 2$ primary collision points. Other notable advances in the accelerator science and technology included advanced longitudinal beam manipulation techniques of *slip-stacking* and *momentum mining* and the first operational use of *electron lenses* for beam collimation and for compensation of long-range beam-beam effects [22]. The Tevatron ultimately achieved luminosities a factor of 430 higher than the original design specification.

31.3.2 HERA

The first lepton-proton collider, the 6.4 km long Hadron-Elektron-Ring-Anlage (HERA) at DESY in Germany [23], operated between 1992 and 2007 and delivered nearly 1 fb^{-1} of integrated luminosity at \sqrt{s} of about 320 GeV to the electron-proton collider experiments H1 and ZEUS [24, Ch.10.5]. It was the first facility to employ both applications of superconductivity: 5 T magnets in the 920 GeV proton ring and SRF accelerating structures to provide about 12 MW of RF power to compensate for synchrotron radiation losses of 30 GeV lepton beams (positrons or electrons, in a conventional-magnet ring). With proper orbit and

optics control, the HERA lepton beam would naturally become transversely polarized to about 60% (within about 40 minutes) thanks to the *Sokolov-Ternov effect*. Special magnets called *spin rotators* were implemented on either side of the collider IPs to produce 30–45% longitudinal polarization at the experiments.

31.3.3 LEP

Installed in a tunnel of 26.7 km circumference, LEP [25] was the largest circular e^+e^- collider built so far. LEP was operated from 1989 to 2000 with beam energies ranging from 45.6 to 104.5 GeV. The synchrotron radiation loss per turn reached some 3% of beam energy and it was the total available RF voltage and power, respectively, that determined LEP maximum energy and luminosity of $10^{32} \text{ cm}^{-2}\text{s}^{-1}$. At a beam energy of 98 GeV, LEP operated with a beam-beam parameter $\xi \approx 0.083$, i.e., the total beam-beam tune shift for four interaction points was $n_{\text{IP}}|\xi| \approx 0.33$. In the last year of operation, 288 SRF cavities were powered by 36 klystrons with an average power of 0.6 MW each and provided $V_{\text{RF}} = 3.63 \text{ GV}$. Up to about 60 GeV, LEP used resonant depolarization to measure the beam energy with 0.001% accuracy.

31.3.4 SLC

Based on an existing 3-km long 2.85 GHz warm RF linac, the SLC [26] was the first and only linear collider. It was operated from 1987 to 1998 with a constant beam energy of 45.6 GeV, up to about 80% electron-beam polarization, quasi-flat beams, a final-focus optics with local chromatic correction based on four interleaved sextupoles and $\beta_y^* \approx 1 \text{ mm}$. In its last year, SLC achieved a peak luminosity of about $3 \times 10^{30} \text{ cm}^{-2}\text{s}^{-1}$, roughly half of the design value. The SLC had a high-efficiency positron source providing $5 \times 10^{12} e^+$ per s for 120 Hz injection into the linac. It also employed the *BNS damping* to suppress the single-bunch beam break up instability, and also demonstrated an about 2-fold increase of luminosity from *disruption enhancement* due to the mutual focusing of the colliding electron and positron bunches at the interaction point.

31.4 Presently Operating Colliders

31.4.1 LHC

With a beam energy of 6.5 TeV (to be raised, first, to 6.8 TeV and, then, to the design value of 7 TeV, through consolidation and magnet training), the superconducting Large Hadron Collider [27] presently is the world's highest energy collider. In the latest runs, peak luminosities of up to $2.1 \times 10^{34} \text{ cm}^{-2}\text{s}^{-1}$ have been achieved - more than twice the design value (the current status is best checked at the Web site [28]). To meet its luminosity goals, the LHC operates with a high beam current of approximately 0.5 A, leading to stored energies of about 330 MJ per beam. Controlled energy deposition and component protection are given a high priority and a sophisticated highly efficient system of more than 100 beam collimators is employed [29]. At the energy of 6.5 or 7 TeV per particle, synchrotron radiation poses a challenge, as the cryogenic system must remove roughly 7 kW due to synchrotron radiation, intercepted with a specially designed *beamscreen* inside the vacuum chamber, at a temperature of about 5–20 K, to be compared with a temperature of 1.9 K for the magnet cold bore. The elevated temperature allows for a more energy-efficient removal of beam-induced heat. The beamscreen also provides an effective cryo-pump for the vacuum system. When synchrotron-radiation photons hit the beamscreen, they can generate photoelectrons. These photoelectrons, and also any other electrons generated in the vacuum system, e.g. by residual-gas ionization, are accelerated in the electric field of the beam and may multiply via secondary-electron emission, with consequent electron cloud development. To mitigate this issue, the beamscreen is regularly subjected to beam-induced surface conditioning (*scrubbing*), thereby lowering the secondary emission yield. The two proton beams of 2556 bunches spaced by 25 ns are contained in separate pipes throughout most of the circumference and are brought together into a single 130 m long beam pipe at the interaction points. To avoid approximately 30 head-on collisions a small crossing angle of about 0.3 mrad is employed, which reduces the luminosity by about 15%. Still, the bunches moving in one direction experience multiple long-range encounters with the counter-rotating bunches and

the resulting perturbations of the particle motion substantially contribute to the beam lifetime reduction. The dominant source of approximately 8 hour characteristic luminosity decay time is proton burn-off due to inelastic pp interaction with $\sigma_{\text{in}} \approx 81 \text{ mbarn}$, corresponding to *pile-up* of up to 50 (number of events per individual bunch crossing). In special physics runs with a few bunches and large β^* , the LHC achieved a head-on beam-beam tune shift of $n_{\text{IP}}|\xi| \approx 0.02$ with $n_{\text{IP}} = 2$ [30], about twice as high as in regular operation.

The Tables also show the LHC luminosity performance in Pb-Pb collisions, which for the ATLAS and CMS experiments well exceeded the design value, while for the ALICE experiment, the luminosity is *levelled* near the Pb-Pb design value of $10^{27} \text{ cm}^{-2}\text{s}^{-1}$. The LHC can also provide Pb-p collisions as it did in 2013 and 2016, and other ion-ion or ion-proton collisions, at different energies.

In the coming years, an ambitious upgrade program, HL-LHC [31], with the accompanying LHC Injectors Upgrade [32], has as its target an order-of-magnitude increase in integrated luminosity through doubling the proton beam current, the utilization of new larger aperture Nb₃Sn superconducting final quadrupoles to allow squeezing the β^* to as low as 10 cm, superconducting compact *crab cavities* and luminosity leveling also for ATLAS and CMS as its key ingredients.

31.4.2 Electron-Positron Rings

Asymmetric energies of the two beams allow for the enhancement of *B*-physics research and for interesting interaction region designs. SuperKEKB operates with 7 GeV electron and 4 GeV positron beams since 2018 and is aiming for luminosities of $8 \times 10^{35} \text{ cm}^{-2}\text{s}^{-1}$ [33]. By summer 2021, a world record luminosity in excess of $3 \times 10^{34} \text{ cm}^{-2}\text{s}^{-1}$ has been reached, still at rather low beam currents. Vertical beam-beam tune shifts of $\xi_y \approx 0.5$ for the 4 GeV positron beam, and $\xi_y \approx 0.03$ for the 7 GeV electron beam have been achieved. These values are still about a factor of two lower than at the previous KEKB. Since 2020 SuperKEKB operates with a virtual *crab-waist* collision scheme, first developed for the FCC-ee design [34]. The original crab-waist scheme, based on additional sextupole magnets, was earlier implemented at DAΦNE [35]. The general crab-waist concept combines a large Piwinski angle Φ , and an extremely low β_y^* ($\ll \sigma_z$) with the cancellation of the transverse betatron resonances which occur under conditions of $kQ_x + lQ_y = n$, where k, l, n are integers. The latter is achieved by means of existing or additional electromagnetic sextupoles with special betatron phase advances to the collision point [36]. The crab-waist collision scheme has become a design choice for all proposed future e^+e^- circular colliders.

Beside SuperKEKB and DAΦNE, three other e^+e^- ring colliders currently in operation are VEPP-2000 with \sqrt{s} up to 2.0 GeV, BEPC-II with \sqrt{s} up to 4.6 GeV and VEPP-4M with maximum c.m.e. of 12 GeV [1].

31.4.3 RHIC

The Relativistic Heavy Ion Collider [37] employs 3.45 T Nb-Ti superconducting magnets, and collides combinations of fully-stripped ions such as H-H ($p-p$), p -Al, p -Au, d -Au, h -Au, Cu-Cu, Cu-Au, Zr-Zr, Ru-Ru, Au-Au, and U-U over a wide energy range. The high charge per particle (+79 for gold, for instance) makes intra-beam scattering of particles within the bunch a special concern, even for seemingly moderate bunch intensities. In 2012, 3-D stochastic cooling was successfully implemented in RHIC [38] and is now routinely used. With stochastic cooling, steady increases in the bunch intensity, and numerous other upgrades, RHIC now operates at 44 times the Au-Au design average luminosity. Unique among high energy colliders, RHIC heavy ions beams cross the *transition energy* $\gamma_{\text{rmt}} = 1/\sqrt{\alpha_c}$ during acceleration - see Eqs.(31.11, 31.12) - a point where the derivative with respect to momentum of the revolution period is zero. This period of time is kept as short as allowed by the magnet ramp rate and must be dealt with carefully.

RHIC is also unique in its ability to accelerate and collide polarized proton beams. As proton beam polarization must be maintained from its low-energy source, successful acceleration through the myriad of depolarizing resonance conditions in high energy

circular accelerators has taken years to accomplish [39]. An energy of 255 GeV per proton with 60% final polarization per beam has been realized. As part of a scheme to compensate the head-on beam-beam effect, electron lenses operated routinely during the record high beam-beam parameter polarized proton operation at 100 GeV energy in 2015 [40].

31.5 Future High Energy Colliders and Prospects

Modern nuclear physics and high energy particle physics face critical questions which require next-generation high-energy and high-intensity experiments using hadron-hadron, lepton-lepton, and lepton-proton colliding-beam facilities. Understanding the structure of the proton and neutron directly from the dynamics of their quarks and gluons governed by the quantum chromodynamics calls for new ion-ion and electron-ion colliders. Two types of colliders are generally aspired by the HEP community [41]: i) Higgs factories with a c.m.e. of 240–250 GeV in e^+e^- collisions for precision studies of the Higgs boson ($m_H = 125$ GeV) and exploration of the Higgs sector in greater detail, including measurements of Higgs couplings to fermions and vector bosons, self-coupling, rare decays, mass and width, that can also deliver other electroweak precision physics, e.g. on the Z -pole (91 GeV c.m.e.), at the W -pair threshold (about 160 GeV), and when run as a top quark factory (365–380 GeV); and ii) colliders to explore the energy frontier for potential discoveries through direct searches with c.m.e. levels significantly beyond those of the LHC in pp , $\mu\mu$ and e^+e^- interactions. In addition, precision physics at future high-luminosity factories operating at the τ -charm energy also provides sensitivity to new physics at multi-TeV energies and beyond. A comprehensive review of the future colliders' projects, ideas, and R&D activities can be found in Ref. [1]. Below we only briefly summarize leading collider proposals for construction over the next several decades which rely mostly on currently available technologies, such as normal-conducting (NC) or SC RF and/or NC or SC magnets, some of them requiring reasonable scope and duration mission-oriented development programs, as well as advanced schemes based on plasma acceleration and other innovative ideas. Tentative parameters of some of the colliders discussed, or mentioned, in this section are summarized in Table 31.1 and Table 31.2.

31.5.1 Ion-Ion and Electron-Ion Colliders

NICA (Nuclotron-based Ion Collider fAcility) is a new accelerator complex under construction at the Joint Institute for Nuclear Research (JINR, Dubna, Russia) to study properties of hot and dense baryonic matter, strong interactions between quarks and gluons, and spin physics [42]. NICA will provide a variety of beam species, ranging from protons and polarized deuterons to massive gold ions. The 500 m circumference SC magnet based collider is designed for average luminosity in heavy ion and light ion interactions at $\sqrt{s_{NN}}=4\text{--}11$ GeV of $1 \times 10^{27} \text{ cm}^{-2} \text{ s}^{-1}$ for a variety of nuclei up to $^{197}\text{Au}^{79+}$, and for polarized proton and deuteron collisions at $\sqrt{s}=12\text{--}27$ GeV with $\mathcal{L}=(1\text{--}10) \times 10^{31} \text{ cm}^{-2} \text{ s}^{-1}$. NICA major accelerator challenges include strong intrabeam scattering and space-charge effects which will be mitigated by extensive use of electron and stochastic cooling systems.

The recently announced Electron-Ion Collider (EIC) for nuclear physics research will be built at Brookhaven National Laboratory in the US and arrange collisions between an the reconfigured RHIC with a 41–275 GeV proton beam and a 5–18 GeV electron beam stored in a new ring (eRHIC) [43]. The EIC physics requirements [44], include highly polarized ($P_{e,n} \sim 70\%$) electron and nucleon beams (as the precision of measurements of interest scales as $\mathcal{L}P_e^2P_n^2$), a spectrum of ion beams from deuterons to the heaviest nuclei (U or Pb), variable c.m.e. values from $\sqrt{s}=20$ GeV to 140 GeV, high luminosities of up to $10^{33\text{--}34} \text{ cm}^{-2} \text{ s}^{-1}$, as well as possibilities of having more than one interaction region. Main accelerator design challenges on the path to the required energy, luminosity, and polarization, include the development of SRF crab-cavities and advanced SC magnets for interaction region focusing, energy-recovery linac (ERL) based electron cooling of hadron beams, essential to attain luminosities two orders of magnitude beyond the predecessor HERA ep collider, and high

intensity polarized particle sources, augmented by the development of special magnets and operational techniques to preserve the polarization through the acceleration process to the collisions, including swap-out injection.

31.5.2 Higgs/Electroweak Factories

Higgs factory proposals generally aim at improving the precision of coupling measurements of Higgs boson, top quark, W and Z by an order of magnitude or more compared with previous studies. Two proposals for ~ 100 km circumference circular e^+e^- colliders have recently gained momentum: the Future Circular Collider (FCC-ee) at CERN [34] and the Circular Electron-Positron Collider (CEPC) in China [45]. Design philosophy of these machines assumes use of the maximum RF power available to compensate $O(100$ MW) synchrotron radiation losses $P_{SR} = 2I \cdot \Delta E_{SR}$ and operation at the beam-beam limit ξ_y that yields peak luminosity:

$$\mathcal{L} = \frac{3}{16\pi r_0^2 (m_e c^2)} \frac{P_{SR} \xi_y \rho}{\beta_y^* \gamma^3}, \quad (31.17)$$

that scales approximately as $1/E_b^{3.5}$ for practical limits on P , ξ_y and β_y^* . The short beam lifetime at the high target luminosity, due to radiative Bhabha scattering, requires these machines to be constructed with a full-energy injector ring installed in the same tunnel to *top off* the electron and positron currents in the collider rings operating at constant energy. Beamstrahlung introduces an additional beam lifetime limitation depending on momentum acceptance (so that achieving sufficient off-momentum dynamic aperture becomes one of the design challenges), as well as some bunch lengthening.

These ambitious, large-scale projects based on well-established technologies are not extendable to TeV or multi-TeV energies, but they offer several important advantages that include the potential for much higher luminosities and, thus, higher precision, the ability to operate multiple experiments simultaneously, and their 100 km circular tunnels that could later house $O(100$ TeV) hadron colliders.

For more than four decades, efforts have been devoted to developing high-gradient RF technology linear e^+e^- colliders in order to overcome the synchrotron radiation limitations of circular e^+e^- machines. The International Linear Collider (ILC), with a c.m.e. of 250 GeV in e^+e^- collisions, has been under consideration for more than two decades and could potentially be upgraded to $\sqrt{s}=500$ GeV and further to 1 TeV. CERN's Compact Linear Collider (CLIC) design, developed since the mid-1980s, also includes possible upgrades, from an initial 380 GeV c.m.e. to ultimately 3 TeV, which would enable searches for new particles of significantly higher masses.

The primary challenge confronting a high energy, high luminosity single pass collider design is the beam power requirement, so that measures must be taken to keep the demand within bounds as illustrated in a transformed Eq.(31.15):

$$\mathcal{L} = \frac{1}{8\pi\alpha r_0} \frac{P_{\text{wall}}}{\sqrt{s}} \frac{\eta}{\sigma_y^*} N_\gamma H_D. \quad (31.18)$$

Here, P_{wall} is the total wall-plug power of the collider, to be converted into beam power $P_b = 2f_0 N E_b$ with efficiency η , $N_\gamma \approx 2\alpha r_0 N / \sigma_x^*$ is the number of beamstrahlung photons emitted per e^\pm (α denotes the fine-structure constant), and the last factor H_D , typically between 1 and 2, represents the enhancement of luminosity due to the *pinch effect*, the additional focusing occurring during the collision of oppositely charged bunches. The management of P_{wall} leads to an upward push on the bunch population N with an attendant rise in the energy radiated due to the electromagnetic field of one bunch acting on the particles of the other (beamstrahlung). Keeping a significant fraction of the luminosity close to the nominal energy represents a design goal, which is met if N_γ does not exceed a value of about 1. A consequence is the use of flat beams, where N_γ is managed by the beam width, and luminosity adjusted by the beam height, thus the explicit appearance of the vertical beam size σ_y^* .

The ILC [46, 47] is based on 1.3 GHz superconducting accelerating structures with 31.5 MV/m average gradient, up to 8 nm

Table 31.1: Tentative parameters of selected future e^+e^- high-energy colliders. Parameters associated with different beam energy scenarios are comma-separated; H and V indicate horizontal and vertical directions.

	FCC-ee	CEPC	ILC	CLIC
Species	e^+e^-	e^+e^-	e^+e^-	e^+e^-
Beam energy E_b (GeV)	46, 120, 183	46, 120	125, 250	190, 1500
Circumference or length (km)	97.75	100	20.5, 31	11, 50
Interaction regions	2	2	1	1
Est. integrated luminosity per experiment ($\text{ab}^{-1}/\text{year}$)	26, 0.9, 0.17	4, 0.4	0.2, 0.3	0.1, 0.6
Peak lumi. \mathcal{L} ($10^{34}\text{cm}^{-2}\text{s}^{-1}$)	230, 8.5, 1.55	32, 3	1.4, 1.8	1.5, 6
Rep.rate (Hz, f_{rev} for rings)	3067	3000	5	50
Polarization (%)	$\geq 10, 0, 0$	5–10, 0	80/30 (e^-/e^+)	80/0 (e^-/e^+)
Time between collisions (μs)	0.02, 0.99, 3.4	0.025, 0.68	0.55	0.0005
Energy spread (rms, 10^{-3})	1.3, 1.65, 2.0	0.8, 1.3	e^- : 1.9, 1.2 e^+ : 1.5, 0.7	3.5
Bunch length σ_z (rms, mm)	12.1, 5.3, 2.5	8.5, 4.4	0.3	0.07, 0.044
IP beam size σ^* (rms, μm)	H: 6.4, 14, 38 V: 0.03, 0.04, 0.07	H: 6.0, 21 V: 0.04, 0.06	H: 0.52, 0.47 V: 0.008, 0.006	H: 0.15, 0.04 V: 0.003, 0.001
Emittance, ε_n (rms, μm)	H: 24, 148, 520 V: 0.09, 0.3, 1.0	H: 16, 284 V: 0.14, 0.6	H: 5, 10 V: 0.035, 0.035	H: 0.95, 0.66 V: 0.03, 0.02
β^* at interaction point (cm)	H: 15, 30, 100 V: 0.08, 0.1, 0.16	H: 20, 36 V: 0.1, 0.15	H: 1.3, 1.1 V: 0.041, 0.048	H: 0.8, 0.69 V: 0.01, 0.0068
Full crossing angle θ_c (mrad)	30	33	14	20
Crossing scheme	crab waist	crab waist	crab crossing	crab crossing
Piwinski angle $\Phi = \sigma_z \theta_c / (2\sigma_x^*)$	28.5, 5.8, 1.0	23.8, 3.5	0	0
Beam-beam param. ξ_y (10^{-3})	133, 118, 126	79, 109	n/a	n/a
Disruption parameter D_y	0.9, 1.3, 1.1	0.4, 1.1	35, 25	13, 8
Average Upsilon Υ (10^{-2})	0.02, 0.05, 0.08	0.01, 0.04	3, 6	17, 500
RF frequency f_{RF} (MHz)	400, 400, 800	650	1300	11994
Particles per bunch N (10^{10})	17, 18, 23	8, 15	2	0.52, 0.37
Bunches per beam n_b	16640, 328, 48	12000, 242	1312 (pulse)	352, 312 (trains at 50 Hz)
Average beam current I_b (mA)	1390, 29, 5.4	461, 17.4	0.021	0.014, 0.009
Injection energy (GeV)	on E_b (top off)	on E_b (top off)	5.0 (linac)	9.0 (linac)
RF gradient G (MV/m)	1.3, 9.8, 19.8	3.6, 19.7	31.5	72, 100
Total SR power loss (MW)	100	33, 60	n/a	n/a
Total beam power (MW)	n/a	n/a	5.3, 10.5	5.6, 28
Key technology	—	—	high grad. SC RF	two-beam accel.

vertical beam size at the IP, and luminosity comparable to the LHC. Progress toward higher field gradients and Q values continues to be made, with nitrogen-doping techniques being a recent example [48]. CLIC is based on a novel two-beam acceleration scheme [49]. Here, NC copper high-gradient 12 GHz accelerating structures are powered by a high-current 1.9 GeV drive beam to efficiently enable accelerating gradients of up to 100 MV/m (though optimal $G=70$ MV/m for the first CLIC stage at $\sqrt{s}=380$ GeV, and for this stage an alternative RF power drive option with 12 GHz klystrons powering is also being considered). To reach their design luminosities, both CLIC and ILC require unprecedented rates of positron production about 40 times the world record set by the SLC positron source, and very tight control of imperfections, such as $O(10\ \mu\text{m})$ accuracy of pre-alignment of the main linac and beam delivery system components at the level, suppression of fast vibrations of the quadrupoles due to ground motion to $O(1\ \text{nm})$ level at frequencies above 1 Hz, advanced beam-based trajectory tuning, and mitigation of the effect of wakefields [50].

There are a number of alternative ideas proposed for studies of the Higgs/Electroweak physics, such as high-energy, high-luminosity e^+e^- collider in a 100 km tunnel using ERLs to accelerate particles to collision energy in 4 to 6 passes and return up to 81% of the energy back into the SRF cavities on deceleration turns, thus, lowering the required facility power several-fold [51]; similar power recovery in one pass can greatly improve efficiency of linear colliders [52–54]; an arrangement of $\gamma\gamma$ collision through near-IP conversion of high energy electron beams into intense photon beams by backward Compton scattering off a high-power laser [55] or off an FEL photon pulse [56]; $\mu\mu$ Higgs factory with unprecedented 0.004% energy resolution [57], and a high-energy lepton-hadron collider bringing into collision a 60-GeV electron

beam from an ERL with the 7 TeV protons circulating in the LHC (LHeC) [58]. At lower energies, Super Tau-Charm Factory proposals aim at the production and precise study of charmonium states and of the tau lepton [59].

31.5.3 Energy Frontier Circular Colliders

Several hadron and lepton colliders have been proposed to extend the energy reach beyond the LHC. As noted above, ambitious plans have been proposed to upgrade the FCC and CEPC to hadron colliders – FCC-hh at CERN and Super Proton Proton Collider (SPPC) in China, respectively – by means of next- or next-next generation SC magnets installed in the arc sections of the 100 km rings, so as to enable \sqrt{s} of the order 100 TeV or above [60, 61]. Comparable discovery reach is expected for a circular 10–14 TeV muon collider [62], significantly beyond that of practical e^+e^- linear colliders.

The maximum beam energy Eq.(31.1) is directly proportional to the magnetic field and to the ring circumference, hence, the hadron colliders rely on the development of the technology of 16T Nb₃Sn dipole magnets (FCC-hh) [63] or 12 T iron-based superconducting magnets (SPPC) [64]. Though higher fields are possible with high-temperature superconductors (HTS), more cost-effective might be hybrid magnet designs incorporating Nb-Ti, Nb₃Sn, and an inner layer of HTS and providing fields of about 20 T. Another important technology is the cryogenic beam vacuum system, which has to cope with unusually high levels of synchrotron radiation (up to 5 MW in total, for FCC-hh) in a cold environment. The beam-screen intercepting the radiation inside the cold bore of the magnets should operate at 50 K — significantly higher temperature than in the LHC.

Design luminosities of these hadron colliders $O(10^{35}\ \text{cm}^{-2}\text{s}^{-1})$

Table 31.2: Tentative parameters of selected future high-energy hadronic colliders. Parameters associated with different particle species for NICA and EIC, and different beam-energy scenarios for a muon collider, are comma-separated. Quantities are, where appropriate, r.m.s.; unless noted otherwise, energies refer to beam energy; H and V indicate horizontal and vertical directions. Parameters of HL-LHC can be found in the High-Energy Collider Parameters review tables.

	NICA	EIC	FFC-hh	SPPC	$\mu\mu$ collider
Species	ion-ion, pp	ep , e -ion	pp	pp	$\mu^+\mu^-$
Beam energy E_b (TeV)	10^{-3} ·(4.5/u, 13)	0.01(e),0.275(p)	50	37.5	0.063, 5
Circumference C (km)	0.503	3.834	97.75	100	0.3, 10
Interaction regions	2	1(2)	4	2	1, 2
Est. integr. luminosity per exp. ($\text{ab}^{-1}/\text{year}$)	$10^{-8,-3}$ (ii , pp)	0.1	0.2–1.0	0.4	0.001, 2.0
Peak luminosity \mathcal{L} ($10^{34}\text{cm}^{-2}\text{s}^{-1}$)	$10^{-7,-2}$ (ii , pp)	1.05	5–30	10	0.008, 20
Rep.rate (Hz, f_{rev} for rings)	$5.9\cdot 10^5$	$7.8\cdot 10^4$	3067	3000	15, 5
Time between collisions (μs)	0.077	0.009	0.025	0.025	1, 33
Energy spread (rms, 10^{-3})	1.6 (Au)	0.6 (e), 0.7 (p)	0.1	0.2	0.04, 1
Bunch length σ_z (rms, mm)	600	7 (e), 60 (p)	80	75.5	63, 1.5
IP beam size σ^* (H/V rms, μm)	360	95/8.5	6.7–3.5 (init.)	6.8 (init.)	75, 0.9
Emittance ε_n (H/V rms, mm mrad)	1.1	11.3/1.0 (e), 9.2/1.6 (p)	2.2 (init.)	2.4 (init.)	200, 25
Beta function at IP β^* (H/V cm)	60	45/5.6 (e), 80/7.2 (p)	110–30	75	1.7, 0.15
Beam-beam param. ξ (10^{-3} H/V)	25	72/100 (e),12 (p)	5–15	7.5	22, 78
RF frequency f_{RF} (MHz)	13/39	591	400	400/200	805/1300
Particles per bunch N (10^{10})	0.23	17.2(e), 6.9(p)	10	15	400, 180
Bunches per beam n_b	22	1160	10400	10080	1
Average beam current I_b (mA)	480	2500(e),1000 (p)	500	730	640, 9 (peak)
Injection energy (GeV)	1–3.8	on E_b (e), 25 (p)	3300	2100	on E_b
Peak magnetic field B (T)	1.8	0.248 (e), 3.80 (p)	16	12	10
Polarization (%)	0(i), >50(p)	> 70(e), >70(p)	0	0	0
SR power loss/beam (MW)	10^{-6}	10(e), < 10^{-6} (p)	2.4	1.1	10^{-3} , 0.16
Key technology	electron and stoch. cooling	strong hadron cooling	16 T Nb ₃ Sn magnets	HTS magnets	muon prod. & cooling

will result in a pile-up of events per crossing $O(500)$ (from up to 50 in LHC) and fast intensity drop due to burn-off. Significant radiation damping of beam emittances will naturally level luminosity evolution, though the total beam-beam tune shift $n_{\text{IP}}\xi \sim (0.01 - 0.03)$ might need a special control as it will increase during the store [65].

Future hadron colliders are characterized by record high stored beam energy – 8.4 GJ in FCC-hh – rendering machine protection a paramount concern. A very challenging multi-stage collimation system is needed to avoid local beam loss spikes near cold magnets, which would induce magnet quenches. The primary and secondary collimators of the LHC are based on carbon-carbon composite material. For the future hadron colliders, ever stronger materials are being developed and examined, which also feature higher conductivity and, hence, lower impedance. More advanced options include the use of short bent crystals as primary collimators [66] and the deployment of hollow electron-beam lenses as non-destructible collimators [67].

It is noteworthy that machines like FCC-hh or SPPC can additionally be used for ion-ion/ion-proton collisions; their high-energy proton beams can also be collided with high-intensity $O(60)$ GeV electrons from an ERL resulting in c.m.e. of 3.5 TeV.

The lifetime of the muon, $\gamma\tau_0$ where $\tau_0=2.2\mu\text{s}$, is sufficient to allow fast acceleration to high energy before most, or all, of the muons decay, and storage for some $300B$ turns in a ring with an average bending magnets field of B (in units of Tesla). The muon to electron mass ratio of 210 implies removal of the synchrotron radiation barrier and possibility of a muon collider facility scale to a level compatible with on-site placement at existing accelerator laboratories. High-energy muon colliders, as presently conceived, are predicted to be more compact, more power-efficient and significantly less expensive than the equivalent energy-frontier hadron or e^+e^- machines [68], and a neutrino factory could potentially be realized in the course of their construction [69]. The Higgs

production cross-section in the s -channel is enhanced by a factor of $(m_\mu/m_e)^2$ compared to that in e^+e^- collisions.

The average luminosity of a muon collider,

$$\langle \mathcal{L} \rangle = f_0 \gamma^2 \frac{c\tau_0}{2C} \frac{n_b N^2}{4\pi\varepsilon_n \beta^*} \mathcal{F} = B P_b \frac{N r_0}{4\pi\varepsilon_n \beta^*} \gamma \left(\frac{c\tau_0 \mathcal{F}}{8\pi e} \right), \quad (31.19)$$

scales with B , the total beam power P_b , and the beam brightness – the third factor above is nothing but the muon beam-beam tune shift Eq. (31.16). There is an obvious incentive to have all the particles in just one bunch per beam. The beta-function at the two IPs $\beta^* \approx \sigma_z$ scales as $1/\gamma$ within certain range of energies, giving overall scaling $\langle \mathcal{L} \rangle \propto \gamma^2$ with other limiting parameters fixed. The main challenges to luminosity achievement with decaying particles are related to production and fast cooling and acceleration of $O(10^{12})$ muons per bunch without emittance degradation. A multi-TeV c.m.e. high luminosity $O(10^{34}\text{cm}^{-2}\text{s}^{-1})$ muon collider would consist of [70]: (i) a high power proton driver (e.g., 8 GeV 2–4 MW H^- SRF linac), (ii) pre-target accumulation and compressor rings, in which high intensity 1–3 ns long proton bunches are formed, (iii) a liquid-mercury or other high-power target for converting the proton beam into a tertiary muon beam with energy of about 200 MeV, (iv) a multi-stage ionization cooling section that reduces transverse and longitudinal emittances by several orders of magnitude and creates a low emittance beam, similarly to that recently demonstrated [71], (v) a multistage acceleration system, possibly employing either rapid cycling synchrotrons or RLAs to accelerate muons in a modest number of turns up to the final energy using superconducting RF technology, and, finally, (vi) a 3–14 km diameter collider ring, where counter-propagating muon beams are stored and collide over the roughly 3000 turns corresponding to the muon lifetime.

The intense neutrino flux originating from the multi-TeV muon beams decaying in the collider poses another challenge — the need

to minimize the environmental impact. The collider complex is usually located underground and when the produced neutrinos emerge at the surface, a small fraction interacts with the rock (and other material) and produces ionizing radiation dose scaling as γ^3 . The impact of this neutrino-induced radiation can be mitigated, for example, by continually adjusting the orbits of the beams to spread them out on a wider area, by deeper collider tunnels or with a further reduced emittance of the muon beam so that the required luminosity could be obtained using a substantially smaller number of muons.

31.5.4 Plasma Acceleration and Other Advanced Concepts

Since about the mid-1950s, it has been understood that collective plasma-based accelerators promise extremely large accelerating gradients, approximately three orders of magnitude greater than ~ 100 MV/m obtained in conventional breakdown limited RF structures [72]. Ionized plasmas can sustain electron plasma density waves with electric fields in excess of $E_0 = cm_e\omega_p/\epsilon$ or

$$E_0 \approx 96 \text{ [V/m]} \sqrt{n_0[\text{cm}^{-3}]}, \quad (31.20)$$

where n_0 denotes the ambient electron number density and $\omega_p = \sqrt{e^2 n_0 / (m_e \epsilon_0)}$ is the electron plasma frequency [73].

Such gradients can be effectively excited by either powerful external pulses of laser light or by electron bunches if they are shorter than the plasma wavelength $\lambda_p = c/\omega_p \approx 1 \text{ mm} \times \sqrt{10^{15} \text{ cm}^{-3}/n_0}$, or by longer beams of protons if their charge density is modulated with the period of λ_p . In the past decade, we have seen impressive progress in the plasma wakefield acceleration of high-quality beams. Laser-driven electron energy gain of about 8 GeV over 20 cm of plasma with density $3 \times 10^{17} \text{ cm}^{-3}$ has been demonstrated at the BELLA facility at the Lawrence Berkeley National Laboratory (LBNL) [74]. Short electron bunches were used to boost the energy of externally injected electron bunches by 9 GeV over 1.3 m of $\sim 10^{17} \text{ cm}^{-3}$ plasma at the FACET facility in SLAC [75]. The AWAKE experiment at CERN used self-modulating long 450 GeV proton bunches to accelerate electrons to 2 GeV over 10 m of 10^{15} cm^{-3} plasma [76].

Whether plasma acceleration will find application in an HEP facility is not yet clear, given the necessity of staging and phase-locking acceleration in multiple plasma chambers. Another critical issue is the power efficiency η for a collider based on plasma acceleration, whose luminosity would still be described by Eq.(31.18). In addition, many novel ideas and approaches have been proposed to extend the energy reach of future particle colliders, reduce their cost, and improve their luminosity or energy efficiency. Those include: i) *cold normal-conducting RF* based TeV-class linear e^+e^- collider operating copper accelerating cavities at liquid nitrogen temperature and promising significantly lower linac cost and power per GeV than in the ILC (SRF cavities at 2 K) and CLIC (room temperature RF structures) [77]; ii) *dielectric wakefield accelerators* in which resonant dielectric accelerating structures are fed by ultra-short RF pulses of wakefields driven by either collinear or preceding high charge electron bunches and withstand 270 MV/m operational accelerating gradients [78]; iii) *dielectric laser accelerators* – micron-size dielectric accelerating structures driven by a laser and supporting $O(1 \text{ GV/m})$ accelerating fields [79]; iv) compact *linear muon crystal colliders* with ultimate energies $O(1\text{--}10 \text{ PeV})$ [80] based on 1–10 TeV/m wakefield acceleration of muons (instead of electrons or hadrons) channeling between the planes in crystals or inside carbon nanotubes (CNT) with charge carrier density $\sim 10^{20\text{--}22} \text{ cm}^{-3}$ [81]; v) the *Gamma Factory* concept [82], where frequent bursts of gamma rays are generated by repeatedly colliding a partially stripped heavy-ion beam circulating in the LHC, or in a future higher-energy hadron storage ring like the FCC-hh, with a conventional laser pulse, profiting from two Lorentz boosts. Active R&D programs are presently underway worldwide to determine the suitability of novel technologies for use in future high-energy colliders.

References

- [1] V. Shiltsev and F. Zimmermann, *Reviews of Modern Physics* **93**, 1, 015006 (2021).
- [2] A. Tollestrup and E. Todesco, in “Reviews Of Accelerator Science And Technology: Volume 1,” 185–210, World Scientific (2008).
- [3] D. A. Edwards and M. J. Syphers, *An introduction to the physics of high energy accelerators*, John Wiley & Sons, New York, NY (2008).
- [4] A. W. Chao, *Physics of collective beam instabilities in high energy accelerators*, Wiley, New York, NY (1993), URL <https://cds.cern.ch/record/246480>.
- [5] S.-Y. Lee, *Accelerator physics*, World Scientific, Singapore (2018).
- [6] E. D. Courant and H. S. Snyder, *Annals of physics* **3**, 1, 1 (1958).
- [7] H. Wiedemann, *Particle accelerator physics*, Springer Nature (2015), URL <https://library.oapen.org/handle/20.500.12657/23641>.
- [8] M. Sands, *Conf. Proc. C* **6906161**, 257 (1969).
- [9] S.-Y. Lee, *Spin dynamics and snakes in synchrotrons*, World Scientific Publishing Company (1997).
- [10] F. Zimmermann, *Physical Review Special Topics-Accelerators and Beams* **7**, 12, 124801 (2004).
- [11] A. W. Chao *et al.*, editors, *Handbook of accelerator physics and engineering*, World Scientific, Hackensack, USA (2013), ISBN 9789814415842, URL <http://www.worldscientific.com/worldscibooks/10.1142/8543>.
- [12] A. Piwinski, J. D. Bjorken and S. K. Mtingwa, *Physical Review Accelerators and Beams* **21**, 11, 114801 (2018).
- [13] V. Parkhomchuk and A. Skrinsky, *Reviews of Accelerator Science and Technology* **1**, 01, 237 (2008).
- [14] M. Minty and F. Zimmermann, *Measurement and control of charged particle beams*, Springer Nature (2003), URL <https://library.oapen.org/handle/20.500.12657/23642>.
- [15] S. Myers, *Particle Physics Reference Library: Volume 3: Accelerators and Colliders*, volume 3, Springer Nature (2020), URL <https://library.oapen.org/handle/20.500.12657/39571>.
- [16] V. Shiltsev *et al.*, *Physical Review Special Topics-Accelerators and Beams* **8**, 10, 101001 (2005).
- [17] J. T. Seeman, *Observations of the beam-beam interaction*, Springer (1986).
- [18] R. Assmann, M. Lamont and S. Myers, *Nucl. Phys. B Proc. Suppl.* **109**, 17 (2002).
- [19] K. Yokoya and P. Chen, *Lect. Notes Phys.* **400**, 415 (1992).
- [20] H. T. Edwards, *Annual Review of Nuclear and Particle Science* **35**, 1, 605 (1985).
- [21] V. Lebedev and V. Shiltsev, *Accelerator physics at the Tevatron collider*, Springer (2014).
- [22] S. D. Holmes and V. D. Shiltsev, *Annual Review of Nuclear and Particle Science* **63**, 435 (2013).
- [23] G. Voss and B. Wiik, *Annual Review of Nuclear and Particle Science* **44**, 1, 413 (1994).
- [24] S. Myers and H. Schopper, *Landolt Börnstein* **21** (2013).
- [25] D. Brandt *et al.*, *Reports on Progress in Physics* **63**, 6, 939 (2000).
- [26] N. Phinney, *eConf* **C00082**, MO102 (2000), [arXiv:physics/0010008].
- [27] L. Evans, *Annual Review of Nuclear and Particle Science* **61**, 435 (2011).
- [28] CERN, “The Large Hadron Collider web site: <http://lhc.web.cern.ch/lhc/>,”.
- [29] G. Valentino *et al.*, *Physical Review Special Topics-Accelerators and Beams* **15**, 5, 051002 (2012).
- [30] J. Wenninger (2019), URL <https://cds.cern.ch/record/2668326>.

- [31] G. Apollinari *et al.*, Technical Report CERN Yellow Report: Monograph 2017-007-M (2017).
- [32] H. Damerou *et al.*, *LHC Injectors Upgrade, Technical Design Report* (2014), URL <https://cds.cern.ch/record/1976692>.
- [33] Y. Ohnishi *et al.*, *Progress of Theoretical and Experimental Physics* **2013(3)**, 3 (2013).
- [34] M. Benedikt *et al.*, *The European Physical Journal Special Topics* **228**, 2, 261 (2019).
- [35] M. Zobov *et al.*, *Physical Review Letters* **104**, 17, 174801 (2010).
- [36] P. Raimondi, D. N. Shatilov and M. Zobov (2007), [arXiv:physics/0702033].
- [37] M. Harrison, S. Peggs and T. Roser, *Annual Review of Nuclear and Particle Science* **52**, 1, 425 (2002).
- [38] M. Blaskiewicz, J. M. Brennan and K. Mernick, *Phys. Rev. Lett.* **105**, 094801 (2010).
- [39] M. Bai *et al.*, *Physical Review Letters* **96**, 17, 174801 (2006).
- [40] W. Fischer *et al.*, *Phys. Rev. Lett.* **115**, 26, 264801 (2015).
- [41] 2020 Update of the European Strategy for Particle Physics by the European Strategy Group, <https://home.cern/sites/home.web.cern.ch/files/2020-06/2020UpdateEuropeanStrategy.pdf> (2020), accessed: June 20, 2020.
- [42] V. Kekelidze *et al.*, *The European Physical Journal A* **52**, 8, 211 (2016).
- [43] E. Beebe-Wang (ed.) *et al.*, Technical Report BNL Formal Report BNL-211943-2019-FORE, Brookhaven (2019).
- [44] A. Accardi *et al.*, *The European Physical Journal A* **52**, 9, 268 (2016).
- [45] CEPC Study Group (2018), [arXiv:1809.00285].
- [46] C. Adolphsen *et al.*, Technical Report arXiv:1306.6328. CERN-ATS-2013-037. IHEP-AC-ILC-2013-001. ILC-REPORT-2013-040. INFN-13-04-LNF. JINR-E9-2013-35. JLAB-R-2013-01. LLNL-TR-635539. comments: See also <http://www.linearcollider.org/ILC/TDR>. The full list of signatories is inside the Report, URL <http://cds.cern.ch/record/1601969>.
- [47] L. Evans and S. Michizono (Linear Collider) (2017), [arXiv:1711.00568].
- [48] A. Grassellino *et al.*, *Supercond. Sci. Technol.* **26**, 102001 (2013), [arXiv:1306.0288].
- [49] T. K. Charles *et al.* (CLICdp, CLIC), CERN Yellow Rep. Monogr. **1802**, 1 (2018), [arXiv:1812.06018].
- [50] T. O. Raubenheimer, *Physical Review Special Topics-Accelerators and Beams* **3**, 12, 121002 (2000).
- [51] V. N. Litvinenko, T. Roser and M. Chamizo-Llatas, *Physics Letters B* **804**, 135394 (2020), ISSN 0370-2693, URL <http://www.sciencedirect.com/science/article/pii/S0370269320301982>.
- [52] M. Tigner, *Il Nuovo Cimento* (1955-1965) **37**, 3, 1228 (1965).
- [53] U. Amaldi, *Physics Letters B* **61**, 3, 313 (1976).
- [54] V. I. Telnov, *JINST* **16**, 12, P12025 (2021), [arXiv:2105.11015].
- [55] V. Telnov, *Journal of Instrumentation* **9**, 09, C09020 (2014).
- [56] The ERL Study Group — Angal-Kalinin, Deepa and others, A Contribution to the European Strategy for Particle Physics (2021).
- [57] Y. Alexahin, E. Gianfelice-Wendt and V. Kapin, *Journal of Instrumentation* **13**, 11, P11002 (2018).
- [58] P. Agostini *et al.*, “The Large Hadron-Electron Collider at the HL-LHC,” (2020), [arXiv:2007.14491].
- [59] P. Piminov, *Physics of Particles and Nuclei Letters* **15**, 7, 732 (2018).
- [60] M. Benedikt *et al.*, *The European Physical Journal Special Topics* **228**, 4, 755 (2019), ISSN 1951-6401, URL <https://doi.org/10.1140/epjst/e2019-900087-0>.
- [61] CEPC Study Group (2018), [arXiv:1809.00285].
- [62] H. Al Ali *et al.* (2021), [arXiv:2103.14043].
- [63] D. Schoerling and A. V. Zlobin, *Nb3Sn Accelerator Magnets: Designs, Technologies and Performance*, Springer Nature (2019).
- [64] E. Kong *et al.*, *International Journal of Modern Physics A* **34**, 13n14, 1940003 (2019).
- [65] M. Benedikt, D. Schulte and F. Zimmermann, *Phys. Rev. ST Accel. Beams* **18**, 101002 (2015).
- [66] W. Scandale and A. Taratin, *Physics Reports* **815**, 1 (2019).
- [67] V. Shiltsev, *Journal of Instrumentation* **16**, 03, P03039 (2021).
- [68] K. R. Long *et al.*, *Nature Physics* **17**, 3, 289 (2021).
- [69] S. Geer, *Annual Review of Nuclear and Particle Science* **59**, 347 (2009).
- [70] C. Ankenbrandt *et al.*, *Physical Review Special Topics-Accelerators and Beams* **2**, 8, 081001 (1999).
- [71] M. Bogomilov *et al.*, *Nature* **578**, 53 (2020).
- [72] V. Veksler, *The Soviet Journal of Atomic Energy* **2**, 5, 525 (1957).
- [73] T. Tajima and J. M. Dawson, *Physical Review Letters* **43**, 4, 267 (1979).
- [74] A. Gonsalves *et al.*, *Physical Review Letters* **122**, 8, 084801 (2019).
- [75] M. Litos *et al.*, *Plasma Physics and Controlled Fusion* **58**, 3, 034017 (2016).
- [76] E. Adli *et al.*, *Nature* **561**, 7723, 363 (2018).
- [77] K. L. Bane *et al.* (2018), [arXiv:1807.10195].
- [78] C. Jing, *Reviews of Accelerator Science and Technology* **9**, 127 (2016).
- [79] E. Peralta *et al.*, *Nature* **503**, 7474, 91 (2013).
- [80] V. D. Shiltsev, *Physics-Uspekhi* **55**, 10, 965 (2012).
- [81] T. Tajima and M. Cavenago, *Physical Review Letters* **59**, 13, 1440 (1987).
- [82] M. W. Krasny (2015), [arXiv:1511.07794].

32. High-Energy Collider Parameters

High-Energy Collider Parameters: e^+e^- Colliders (I)

Table 32.1: Updated in March 2022 with numbers received from representatives of the colliders (contact E. Pianori, LBNL). The table shows the parameter values achieved. Quantities are, where appropriate, r.m.s.; unless noted otherwise, energies refer to beam energy; H and V indicate horizontal and vertical directions; s.c. stands for superconducting. Parameters for the defunct SPEAR, DORIS, PETRA, PEP, TRISTAN, and VEPP-2M colliders may be found in our 1996 edition (Phys. Rev. **D54**, 1 July 1996, Part I).

	VEPP-2000 (Novosibirsk)	VEPP-4M (Novosibirsk)	BEPC (China)	BEPC-II (China)	DAΦNE (Frascati)
Physics start date	2010	1994	1989	2008	1999
Physics end date	—	—	2005	—	—
Maximum beam energy (GeV)	1.0	6	2.5	1.89 (2.474 max)	0.510
Delivered integrated luminosity per exp. (fb^{-1})	0.25	0.05	0.11	34.5	≈ 4.7 in 2001-2007 ≈ 2.7 w/crab-waist ≈ 6.8 since Nov 2014
Luminosity ($10^{30} \text{ cm}^{-2}\text{s}^{-1}$)	50	20	12.6 at 1.843 GeV 5 at 1.55 GeV	1000	453
Time between collisions (μs)	0.04	0.6	0.8	0.008	0.0027
Full crossing angle (μ rad)	0	0	0	2.2×10^4	5×10^4
Energy spread (units 10^{-3})	0.71	1	0.58 at 2.2 GeV	0.52	0.40
Bunch length (cm)	4	5	≈ 5	≈ 1.2	low current: 1 at 15mA: 2
Beam radius (10^{-6} m)	125 (round)	H:1000 V:30	H:890 V:37	H:347 V:4.5	H:260 V:4.8
Free space at interaction point (m)	± 0.5	± 2	± 2.15	± 0.63	± 0.295
Luminosity lifetime (hr)	continuous	2	7–12	1.5	0.2
Turn-around time (min)	continuous	18	32	4 (topping up)	2 (topping up)
Injection energy (GeV)	0.2–1.0	1.8	1.55	1.89	on energy
Transverse emittance (10^{-9} m)	H:150 V:150	H:200 V:20	H:660 V:28	H:121 V:1.56	H:260 V:2.6
β^* , amplitude function at interaction point (m)	H:0.05 - 0.11 V:0.05 - 0.11	H:0.75 V:0.05	H:1.2 V:0.05	H:1.0 V:0.0129	H:0.26 V:0.009
Beam-beam tune shift per crossing (units 10^{-4})	H:850 V:850	500	350	383	440/894 (crab-waist run/test)
RF frequency (MHz)	172	180	199.53	499.8	368.667
Particles per bunch (units 10^{10})	8	15	20 at 2 GeV 11 at 1.55 GeV	3.8	e^- : 3.2 e^+ : 2.1
Bunches per ring per species	1	2	1	119	100 to 110 (120 buckets)
Average beam current per species (mA)	160	80	40 at 2 GeV 22 at 1.55 GeV	851	e^- : 1250 e^+ : 800
Circumference or length (km)	0.024	0.366	0.2404	0.23753	0.098
Interaction regions	2	1	2	1	1
Magnetic length of dipole (m)	1.1	2	1.6	outer ring: 1.6 inner ring: 1.41	outer ring: 1.2 inner ring: 1
Length of standard cell (m)	12	7.2	6.6	outer ring: 6.6 inner ring: 6.2	n/a
Phase advance per cell (deg)	H:745 V:385	65	≈ 60	60–90 non-standard cells	—
Dipoles in ring	8	78	40 + 4 weak	84 + 8 weak	8
Quadrupoles in ring	24 + 4 s.c.	150	68	134+2 s.c.	48
Peak magnetic field (T)	2.4	0.6	0.903 at 2.8 GeV	outer ring: 0.677 inner ring: 0.766	1.2

High-Energy Collider Parameters: e^+e^- Colliders (II)

Table 32.2: Updated in March 2020 with numbers received from representatives of the colliders (contact E. Pianori, LBNL). The table shows the parameter values achieved. Quantities are, where appropriate, r.m.s.; unless noted otherwise, energies refer to beam energy; H and V indicate horizontal and vertical directions; s.c. stands for superconducting. ILC and CLIC parameters are documented in the Accelerator physics of colliders review.

	CESR (Cornell)	CESR-C (Cornell)	LEP (CERN)	SLC (SLAC)
Physics start date	1979	2002	1989	1989
Physics end date	2002	2008	2000	1998
Maximum beam energy (GeV)	6	6	100 - 104.6	50
Delivered integrated luminosity per experiment (fb^{-1})	41.5	2.0	0.221 at Z peak 0.501 at 65 - 100 GeV 0.275 at >100 GeV	0.022
Luminosity ($10^{30} \text{ cm}^{-2}\text{s}^{-1}$)	1280 at 5.3 GeV	76 at 2.08 GeV	24 at Z peak 100 at > 90 GeV	2.5
Time between collisions (μs)	0.014 to 0.22	0.014 to 0.22	22	8300
Full crossing angle (μ rad)	± 2000	± 3300	0	0
Energy spread (units 10^{-3})	0.6 at 5.3 GeV	0.82 at 2.08 GeV	0.7→1.5	1.2
Bunch length (cm)	1.8	1.2	1.0	0.1
Beam radius (μm)	H:460 V:4	H:340 V:6.5	H:200→300 V:2.5→8	H:1.5 V:0.5
Free space at interaction point (m)	± 2.2 (± 0.6 to REC quads)	± 2.2 (± 0.3 to PM quads)	± 3.5	± 2.8
Luminosity lifetime (hr)	2-3	2-3	20 at Z peak 10 at > 90 GeV	—
Turn-around time (min)	5 (topping up)	1.5 (topping up)	50	120 Hz (pulsed)
Injection energy (GeV)	1.8-6	1.5-6	22	45.64
Transverse emittance (10^{-9} m)	210 1	120 3.5	H:20-45 V:0.25→1	H:0.5 V:0.05
β^* , amplitude function at interaction point (m)	1.0 0.018	0.94 0.012	1.5 0.05	0.0025 0.0015
Beam-beam tune shift per crossing (10^{-4}) or disruption	250 620	e^- : 420 (H), 280 (V) e^+ : 410 (H), 270 (V)	830	0.75 (H) 2.0 (V)
RF frequency (MHz)	500	500	352.2	2856
Particles per bunch (units 10^{10})	1.15	4.7	45 in collision 60 in single beam	4.0
Bunches per ring per species	9 trains of 5 bunches	8 trains of 3 bunches	4 trains of 1 or 2	1
Average beam current per species (mA)	340	72	4 at Z peak 4→6 at > 90 GeV	0.0008
Beam polarization (%)	—	—	55 at 45 GeV 5 at 61 GeV	e^- : 80
Circumference or length (km)	0.768	0.768	26.66	1.45 +1.47
Interaction regions	1	1	4	1
Magnetic length of dipole (m)	1.6-6.6	1.6-6.6	11.66/pair	2.5
Length of standard cell (m)	16	16	79	5.2
Phase advance per cell (deg)	45-90 (no standard cell)	45-90 (no standard cell)	102/90	108
Dipoles in ring	86	84	3280 + 24 inj. + 64 weak	460+440
Quadrupoles in ring	101 + 4 s.c.	101 + 4 s.c.	520 + 288 + 8 s.c.	—
Peak magnetic field (T)	0.3 / 0.8 at 8 GeV	0.3 / 0.8 at 8 GeV, 2.1 wigglers at 1.9 GeV	0.135	0.597

High-Energy Collider Parameters: e^+e^- Colliders (III)

Table 32.3: Updated in March 2022 with numbers received from representatives of the colliders (contact E. Pianori, LBNL). The table shows the parameter values achieved. Design parameters for SuperKEKEB may be found in our 2018 edition (Phys. Rev. **D98**, 030001 (2018)) Quantities are, where appropriate, r.m.s.; unless noted otherwise, energies refer to beam energy; H and V indicate horizontal and vertical directions; s.c. stands for superconducting.

	KEKB (KEK)	PEP-II (SLAC)	SuperKEKB (KEK)
Physics start date	1999	1999	2018
Physics end date	2010	2008	—
Maximum beam energy (GeV)	e^- : 8.33 (8.0 nominal) e^+ : 3.64 (3.5 nominal)	e^- : 7–12 (9.0 nominal) e^+ : 2.5–4 (3.1 nominal)	e^- : 7 e^+ : 4
Delivered integrated luminosity per exp. (fb^{-1})	1040	557	307
Luminosity ($10^{30} \text{ cm}^{-2}\text{s}^{-1}$)	21083	12069 (design: 3000)	3.81×10^4
Time between collisions (μs)	0.00590 or 0.00786	0.0042	0.0065
Full crossing angle (μ rad)	$\pm 11000^*$	0	± 41500
Energy spread (units 10^{-3})	0.7	e^-/e^+ : 0.61/0.77	e^-/e^+ : 0.64/0.81
Bunch length (cm)	0.65	e^-/e^+ : 1.1/1.0	e^-/e^+ : 0.6/0.6
Beam radius (μm)	H: 124 (e^-), 117 (e^+) V: 1.9	157 4.7	e^- : 16.6 (H), 0.24 (V) e^+ : 17.9 (H), 0.24 (V)
Free space at interaction point (m)	+0.75/−0.58 (+300/−500) mrad cone	± 0.2 , ± 300 mrad cone	e^- : +1.20/−1.28, e^+ : +0.78/−0.73 (+300/−500) mrad cone
Luminosity lifetime (hr)	continuous	continuous	continuous
Turn-around time (min)	continuous	continuous	continuous
Injection energy (GeV)	e^-/e^+ : 8.0/3.5 (nominal)	e^-/e^+ : 9.0/3.1 (nominal)	e^-/e^+ : 7/4
Transverse emittance (10^{-9} m)	e^- : 24 (57^\dagger) (H), 0.61 (V) e^+ : 18 (55^\dagger) (H), 0.56 (V)	e^- : 48 (H), 1.8 (V) e^+ : 24 (H), 1.8 (V)	e^- : 4.6 (H), 0.058 (V) e^+ : 4.0 (H), 0.058 (V)
β^* , amplitude function at interaction point (m)	e^- : 1.2 (0.27^\dagger) (H), 0.0059 (V) e^+ : 1.2 (0.23^\dagger) (H), 0.0059 (V)	e^- : 0.50 (H), 0.012 (V) e^+ : 0.50 (H), 0.012 (V)	e^- : 0.060 (H), 1×10^{-3} (V) e^+ : 0.080 (H), 1×10^{-3} (V)
Beam-beam tune shift per crossing (units 10^{-4})	e^- : 1020 (H), 900 (V) e^+ : 1270 (H), 1290 (V)	e^- : 703 (H), 498 (V) e^+ : 510 (H), 727 (V)	e^- : 15 (H), 315 (V) e^+ : 27 (H), 433 (V)
RF frequency (MHz)	508.887	476	508.887
Particles per bunch (units 10^{10})	e^-/e^+ : 4.7/6.4	e^-/e^+ : 5.2/8.0	e^-/e^+ : 2.76/3.52
Bunches per ring per species	1585	1732	1476
Average beam current per species (mA)	e^-/e^+ : 1188/1637	e^-/e^+ : 1960/3026	e^-/e^+ : 640/819
Beam polarization (%)	—	—	—
Circumference or length (km)	3.016	2.2	3.016
Interaction regions	1	1	1
Magnetic length of dipole (m)	e^-/e^+ : 5.86/0.915	e^-/e^+ : 5.4/0.45	e^-/e^+ : 5.9/4.0
Length of standard cell (m)	e^-/e^+ : 75.7/76.1	15.2	e^-/e^+ : 75.7/76.1
Phase advance per cell (deg)	450	e^-/e^+ : 60/90	450
Dipoles in ring	e^-/e^+ : 116/112	e^-/e^+ : 192/192	e^-/e^+ : 116/112
Quadrupoles in ring	e^-/e^+ : 452/452	e^-/e^+ : 290/326	e^-/e^+ : 466/460
Peak magnetic field (T)	e^-/e^+ : 0.25/0.72	e^-/e^+ : 0.18/0.75	e^-/e^+ : 0.22/0.19

*KEKB was operated with crab crossing from 2007 to 2010.

† With dynamic beam-beam effect.

High-Energy Collider Parameters: ep , $\bar{p}p$, pp Colliders

Table 32.4: Updated in March 2022 with numbers received from representatives of the colliders (contact E. Pianori, LBNL). The table shows the parameter values achieved. Parameters for the defunct $Spp\bar{p}S$ collider may be found in our 2002 edition (Phys. Rev. D66, 010001 (2002)). Quantities are, where appropriate, r.m.s.; unless noted otherwise, energies refer to beam energy; H and V indicate horizontal and vertical directions; s.c. stands for superconducting.

	HERA (DESY)	TEVATRON* (Fermilab)	RHIC Brookhaven	LHC (CERN)		
Physics start date	1992	1987	2001	2009	2015	2029 (HL-LHC)
Physics end date	2007	2011	—	—		
Particles collided	ep	$p\bar{p}$	pp (polarized)	pp		
Maximum beam energy (TeV)	e : 0.030 p : 0.92	0.980	0.255 55% polarization	4.0	6.5	7.0
Max. delivered integrated luminosity per exp. (fb^{-1})	0.8	12	0.38 at 100 GeV 1.3 at 250/255 GeV	23.3 at 4.0 TeV 6.1 at 3.5 TeV	160	250/y
Luminosity ($10^{30} \text{ cm}^{-2} \text{ s}^{-1}$)	75	431	245 (pk) 160 (avg)	7.7×10^3	2.1×10^4	5.0×10^4 (leveled)
Time between collisions (ns)	96	396	107	49.90	24.95	24.95
Full crossing angle (μ rad)	0	0	0	290	$320 \rightarrow 260^\dagger$	500
Energy spread (units 10^{-3})	e : 0.91 p : 0.2	0.14	0.15	0.1445	0.105	0.129
Bunch length (cm)	e : 0.83 p : 8.5	p : 50 \bar{p} : 45	60	9.4	8	9
Beam radius (10^{-6} m)	e : 110 (H), 30 (V) p : 111 (H), 30 (V)	p : 28 \bar{p} : 16	85	18.8	8.5^\ddagger	7^\ddagger
Free space at interaction point (m)	± 2	± 6.5	16	38	38	38
Initial luminosity decay time, $-L/(dL/dt)$ (hr)	10	6 (avg)	7.5	≈ 6	≈ 8	≈ 7.5 (leveled)
Turn-around time (min)	e : 75, p : 135	90	25	180	150	145
Injection energy (TeV)	e : 0.012 p : 0.040	0.15	0.023	0.450	0.450	0.450
Transverse emittance (10^{-9} m)	e : 20 (H), 3.5 (V) p : 5 (H), 5 (V)	p : 3 \bar{p} : 1	11	0.59	0.29	0.33
β^* , ampl. function at interaction point (m)	e : 0.6 (H), 0.26 (V) p : 2.45 (H), 0.18 (V)	0.28	0.65	0.6	$0.3 \rightarrow 0.25^\S$	$0.6 \rightarrow 0.15^\S$
Beam-beam tune shift per crossing (units 10^{-4})	e : 190 (H), 450 (V) p : 12 (H), 9 (V)	p : 120 \bar{p} : 120	73	72	45	86
RF frequency (MHz)	e : 499.7 p : 208.2/52.05	53	accel: 9 store: 28	400.8	400.8	400.8
Particles per bunch (units 10^{10})	e : 3 p : 7	p : 26 \bar{p} : 9	18.5	16	11	22
Bunches per ring per species	e : 189 p : 180	36	111	1380	2556 2544 (i.r. 1/5 ¶)	2760 2748 (i.r. 1/5 ¶)
Average beam current per species (mA)	e : 40 p : 90	p : 70 \bar{p} : 24	257	400	510	1100
Circumference (km)	6.336	6.28	3.834	26.659		
Interaction regions	2 colliding beams 1 fixed target (e beam)	2 high \mathcal{L}	6 total, 2 high \mathcal{L}	4 total, 2 high \mathcal{L}		
Magnetic length of dipole (m)	e : 9.185; p : 8.82	6.12	9.45	14.3		
Length of standard cell (m)	e : 23.5 p : 47	59.5	29.7	106.90		
Phase advance per cell (deg)	e : 60 p : 90	67.8	84	90		
Dipoles in ring	e : 396 p : 416	774	192 per ring + 12 common	1232 main dipoles		
Quadrupoles in ring	e : 580 p : 280	216	246 per ring	482 2-in-1 24 1-in-1		
Magnet types	e : C-shaped p : s.c., col., warm iron	s.c., $\cos\theta$ warm iron	s.c., $\cos\theta$ cold iron	s.c., 2-in-1 cold iron		
Peak magnetic field (T)	e : 0.274; p : 5	4.4	3.5	8.3 $^\parallel$		

*Other TEVATRON parameters: \bar{p} source accum. rate: $25 \times 10^{10} \text{ hr}^{-1}$; max. no. of \bar{p} stored: 3.4×10^{12} (Accumulator), 6.1×10^{12} (Recycler).

† Variable crossing angle decreasing during the fill with the reduction in bunch population

‡ Minimum beam radius during levelling

§ β^* levelling

¶ Number of bunches colliding at the interaction regions (i.r.) 1 (ATLAS) and 5 (CMS).

$^\parallel$ Value for design beam energy of 7 TeV.

High-Energy Collider Parameters: Heavy Ion Colliders

Table 32.5: Updated in March 2022 with numbers received from representatives of the collider (contact E. Pianori, LBNL) The table shows the parameter values achieved. For the LHC, only maximum values for the ATLAS and CMS experiments are provided (ALICE and LHCb have different requirements for energy and luminosity). Design values for a high-luminosity upgrade are also given. Quantities are, where appropriate, r.m.s.; unless noted otherwise, energies refer to beam energy; s.c. stands for superconducting. pk and avg denote peak and average values.

	RHIC (Brookhaven)			LHC (CERN)			
	2000	2012 / 2018 / 2018 / 2012 / 2004 2021 / 2014 / 2002 / 2015 / 2015		2010	2012	2017	≥ 2022 (high lum.)*
Physics start date	2000			2010	2012	2017	≥ 2022 (high lum.)*
Physics end date		—			—		
Particles collided	Au Au	U U / Zr Zr / Ru Ru / Cu Au / Cu Cu O O / h Au / d Au / p Au / p Al		Pb Pb	p Pb	Xe Xe	Pb Pb
Max. beam energy (TeV/n)	0.1	0.1		2.51	p:6.5 Pb:2.56	2.72	2.76
$\sqrt{s_{NN}}$ (TeV)	0.2	0.2		5.02	8.16	5.44	5.5
Max. delivered int. nucleon-pair lumin. per exp. (pb^{-1})	2639 (at 100 GeV/n)	21 / 36 / 36.9 / 167 / 60 8.2 / 43 / 169 / 124 / 63 (all at 100 GeV/n)		77.8	194	0.05	$\approx 121/y$
Luminosity ($10^{27} \text{ cm}^{-2} \text{ s}^{-1}$)	pk: 15.5 avg: 8.7	pk: 0.4 / 4.8 / 3.8 / 12 / 21 450 / 170 / 850 / 880 / 7600 avg: 0.6 / 2.2 / 2.1 / 10 / 8 230 / 100 / 500 / 450 / 3800		6.1	900	0.4	6.4 (leveled)
Time between collisions (ns)	107	107 / 107 / 107 / 107 / 321 107 / 107 / 107 / 107 / 107		74.9 / 149.7	99.8 / 149.7	≈ 5500	49.9
Full crossing angle (μ rad)	0	0		320	280	300	340
Energy spread (units 10^{-3})	0.75	0.75		0.11	0.11	0.11	0.11
Bunch length (cm)	30	30		8.0	p / Pb: 9 / 11.5	11	7.9
Beam radius (10^{-6} m)	114^\dagger	123^\ddagger / 87^\ddagger / 88^\ddagger / 163^\ddagger / 145^\ddagger 100^\ddagger / 136^\ddagger / 124^\ddagger / 147^\ddagger / 128^\ddagger		21	19	12	17
Free space at inter. point (m)	16	16		38	38	38	38
Initial luminosity decay time, $-L/(dL/dt)$ (hr)	1	-0.35^\S / ∞^\S / ∞^\S / ∞^\ddagger / 1.8 ∞ / 0.6 / ∞^\ddagger / 0.5 / 0.25		3.3	≈ 2	≈ 6	∞
Turn-around time (min)	30	60^\P / 40^\P / 40^\P / 160^\P / 90^\P 45^\P / 45^\P / 90^\P / 60^\P / 50^\P		≈ 180	150	180	≈ 200
Injection energy (TeV/n)	0.011	0.011		0.177	p / Pb: 0.45 / 0.177	0.188	0.177
Transverse emittance (10^{-9} m)	19^\ddagger	22^\ddagger / 10.7^\ddagger / 11.2^\ddagger / 38^\ddagger / 23^\ddagger 12^\ddagger / 19^\ddagger / 22^\ddagger / 26^\ddagger / 21^\ddagger		0.85	0.29	0.3	0.5
β^* , ampl. function at interaction point (m)	0.7	0.7 / 0.7 / 0.7 / 0.7 / 0.9 0.7 / 1.0 / 0.7 / 0.8 / 0.8		0.5	0.5	0.4	0.5
Beam-beam tune shift per crossing (units 10^{-4})	39^\ddagger	6^\ddagger / 18^\ddagger / 21^\ddagger / 14^\ddagger , 14^\ddagger / 30^\ddagger / 34^\ddagger 42^\ddagger , 22^\ddagger / 40^\ddagger , 27^\ddagger / 53^\ddagger , 41^\ddagger / 80^\ddagger , 59^\ddagger		15	15	≈ 10	4.3
RF frequency (MHz)		accel: 28, store: 197		400.8	400.8	400.8	400.8
Particles per bunch (units 10^{10})	0.20	0.03 / 0.1 / 0.1 / 0.4, 0.13 / 0.45 / 0.85 4.5, 0.13 / 13, 0.20 / 22.5, 0.16 / 24, 1.1		0.022 (r.m.s.)	p:2.6 Pb:0.022	0.027	0.018
Bunches per ring per species	111	111 / 111 / 111 / 111 / 37 106 / 111 / 111 / 111 / 111		733	p:540 Pb:684	16	1240
Average beam current per species (mA)	224	38 / 56 / 61 / 160,138 / 60 / 95 125,143 / 181,213 / 313,176 / 334,199		23.8	p:16 Pb:15	0.54	33
Circumference (km)		3.834			26.659		
Interaction regions		6 total, 2 high \mathcal{L}			4 total, 3 high \mathcal{L}		
Magnetic length of dipole (m)		9.45			14.3		
Length of standard cell (m)		29.7			106.90		
Phase advance per cell (deg)	93	84 / 84 / 84 / 84 / 84 / 84 93 / 84(d), 93 / 84(p), 93 / 84(p), 93			90		
Dipoles in ring		192 per ring, + 12 common			1232, main dipoles		
Quadrupoles in ring		246 per ring			482 2-in-1, 24 1-in-1		
Magnet Type		s.c. $\cos \theta$, cold iron			s.c., 2 in 1, cold iron		
Peak magnetic field (T)		3.5			8.3		

* High luminosity upgrade expected ≥ 2022 ; will extend throughout HL-LHC running. Very preliminary, conservative estimates.

† Initial value, increases (decreases) without (with) cooling

‡ Negative or infinite decay time is effect of cooling.

§ luminosity leveled to flat after set to target value, with cooling

¶ measured minimum, not theoretical

33. Neutrino Beam Lines at High-Energy Proton Synchrotrons

Revised August 2021 with numbers verified by representatives of the synchrotrons (contact C.-J. Lin, LBNL). For existing (future) neutrino beam lines the latest achieved (design) values are given.

The main source of neutrinos at proton synchrotrons is from the decay of pions and kaons produced by protons striking a nuclear target. There are different schemes to focus the secondary particles to enhance neutrino flux and/or tune the neutrino energy profile. In wide-band beams (WBB), the neutrino parent mesons are focused over a wide momentum range to obtain maximum neutrino intensity. In narrow-band beams (NBB), the secondary particles are first momentum-selected to produce a monochromatic parent beam. Another approach to generate a narrow-band neutrino spectrum is to select neutrinos that are emitted off-axis relative to the momentum of the parent mesons. For a comprehensive review of the topic, including other historical neutrino beam lines, see the article by S. E. Kopp, "Accelerator-based neutrino beams," Phys. Rept. **439**, 101 (2007).

	PS (CERN)				SPS (CERN)				PS (KEK)	Main Ring (JPARC)
Date	1963	1969	1972	1983	1977	1977	1995	2006	1999	2021
Proton Kinetic Energy (GeV)	20.6	20.6	26	19	350	350	450	400	12	30 (50)
Protons per Cycle (10^{12})	0.7	0.6	5	5	10	10	36	48	6	270 (330)
Cycle Time (s)	3	2.3	-	-	-	-	14.4	6	2.2	2.48 (2.1)
Beam Power (kW)	0.8	0.9	-	-	-	-	180	510	5	515 (750)
Target	-	-	-	-	-	-	Be	Graphite	Al	Graphite
Target Length (cm)	-	-	-	-	-	-	290	130	66	91
Secondary Focussing	1-horn WBB	3-horn WBB	2-horn WBB	bare target	dichromatic NBB	2-horn WBB	2-horn WBB	2-horn WBB	2-horn WBB	3-horn off-axis
Decay Pipe Length (m)	-	-	-	-	-	-	110	1090	200	96
$\langle E_\nu \rangle$ (GeV)	1.5	1.5	1.5	1	50,150 [†]	20	24.3	17	1.3	0.6
Experiments	HLBC, Spark Ch.	HLBC, Spark Ch.	GGM, Aachen-Padova	CDHS, CHARM	CDHS, CHARM, BEBC	GGM, CDHS, CHARM, BEBC	NOMAD, CHORUS	OPERA, ICARUS	K2K	T2K

	Main Ring (Fermilab)					Booster (Fermilab)	Main Injector (Fermilab)			
Date	1974	1979	1976	1991	1998	2002, (2022)	2005	2017	2021	(2026)
Proton Kinetic Energy (GeV)	300	400	350	800	800	8	120	120	120	(60 – 120)
Protons per Cycle (10^{12})	10	10	13	10	12	4.5	37	54	55 (65)	(75)
Cycle Time (s)	-	-	-	60	60	0.2	2	1.333	1.2	(1.2)
Beam Power (kW)	-	-	-	20	25	29	350	720	840 (1000)	(1200)
Target	-	-	-	-	BeO	Be	Graphite	Graphite	Graphite	(Graphite)
Target Length (cm)	-	-	-	-	31	71	95	120	120	(150-220)
Secondary Focussing	dichromatic NBB	2-horn WBB	1-horn WBB	quad trip.	SSQT WBB	1-horn WBB	2-horn WBB	2-horn off-axis	2-horn off-axis	(3-horn WBB)
Decay Pipe Length (m)	400	400	400	400	400	50	675	675	675	(220)
$\langle E_\nu \rangle$ (GeV)	50,180 [†]	25	100	90,260	70,180	1	3-20 [‡]	2	2	(2.5)
Experiments	CITF, HPWF, 15' BC	15' BC	HPWF 15' BC	15' BC, CCFRR	NuTeV	MiniBooNE, SciBooNE, MicroBooNE, (SBND, ICARUS)	MINOS, MINERνA	NOνA, MINERνA, MINOS+	NOνA	LBNF/ DUNE

[†]Pion and kaon peaks in the momentum-selected channel.

[‡]Tunable WBB energy spectrum.

34. Passage of Particles Through Matter

Revised August 2021 by D.E. Groom (LBNL) and S.R. Klein (NSD LBNL; UC Berkeley).

34.1	Notation	549
34.2	Electronic energy loss by heavy particles	549
34.2.1	Moments and cross sections	549
34.2.2	Maximum energy transfer to an electron in a single collision	550
34.2.3	Stopping power at intermediate energies	550
34.2.4	Mean excitation energy	550
34.2.5	Density effect	550
34.2.6	Energy loss at low energies	551
34.2.7	Energetic knock-on electrons (δ rays)	553
34.2.8	Restricted energy loss rates for relativistic ionizing particles	553
34.2.9	Fluctuations in energy loss	553
34.2.10	Energy loss in mixtures and compounds	554
34.2.11	Ionization yields	554
34.3	Multiple scattering through small angles	554
34.4	Photon and electron interactions in matter	555
34.4.1	Collision energy losses by e^\pm	555
34.4.2	Radiation length	556
34.4.3	Bremsstrahlung energy loss by e^\pm	556
34.4.4	Critical energy	556
34.4.5	Energy loss by photons	557
34.4.6	Bremsstrahlung and pair production at very high energies	558
34.4.7	Photonuclear and electronuclear interactions at still higher energies	559
34.5	Electromagnetic cascades	559
34.6	Muon energy loss at high energy	560
34.7	Cherenkov and transition radiation	561
34.7.1	Optical Cherenkov radiation	561
34.7.2	Coherent radio Cherenkov radiation	562
34.7.3	Transition radiation	562

This review covers the interactions of photons and electrically charged particles in matter, concentrating on energies of interest for high-energy physics and astrophysics and processes of interest for particle detectors (ionization, Cherenkov radiation, transition radiation). Much of the focus is on particles heavier than electrons (π^\pm , p , etc.). Although the charge number z of the projectile is included in the equations, only $z = 1$ is discussed in detail. Muon radiative losses are discussed, as are photon/electron interactions at high to ultrahigh energies. Neutrons are not discussed.

34.1 Notation

The notation and important numerical values are shown in Table 34.1.

34.2 Electronic energy loss by heavy particles

34.2.1 Moments and cross sections

The electronic interactions of fast charged particles with speed $v = \beta c$ occur in *single collisions with energy losses* W [1], leading to ionization, atomic, or collective excitation. Most frequently the energy losses are small (for 90% of all collisions the energy losses are less than 100 eV). In thin absorbers few collisions will take place and the total energy loss will show a large variance [1]; also see Sec. 34.2.9 below. For particles with charge ze more massive than electrons (“heavy” particles), scattering from free electrons is adequately described by the Rutherford differential cross section [2, 3].

$$\frac{d\sigma_R(W; \beta)}{dW} = \frac{2\pi r_e^2 m_e c^2 z^2}{\beta^2} \frac{(1 - \beta^2 W/W_{\max})}{W^2}, \quad (34.1)$$

where W_{\max} , the maximum energy transfer possible in a single collision, is discussed below. It differs from the classical cross section by the factor $(1 - \beta^2 W/W_{\max})$, which arises when the spin of the target electrons is taken into account.

Table 34.1: Summary of variables used in this section. The kinematic variables β and γ have their usual relativistic meanings.

Symb.	Definition	Value or (usual) units
$m_e c^2$	electron mass $\times c^2$	0.510 998 950 00(15) MeV
r_e	classical electron radius $e^2/4\pi\epsilon_0 m_e c^2$	2.817 940 3227(19) fm
α	fine structure constant $e^2/4\pi\epsilon_0 \hbar c$	1/137.035 999 139(31)
N_A	Avogadro’s number	6.022 140 857(74) $\times 10^{23}$ mol $^{-1}$
ρ	density	g cm $^{-3}$
x	mass per unit area	g cm $^{-2}$
M	incident particle mass	MeV/ c^2
E	incident part. energy $\gamma M c^2$	MeV
T	kinetic energy, $(\gamma - 1) M c^2$	MeV
W	energy transfer to an electron in a single collision	MeV
W_{\max}	Maximum possible energy transfer to an electron in a single collision	MeV
k	bremsstrahlung photon energy	MeV
z	charge number of incident particle	
Z	atomic number of absorber	
A	atomic mass of absorber	g mol $^{-1}$
K	$4\pi N_A r_e^2 m_e c^2$ (Coefficient for dE/dx)	0.307 075 MeV mol $^{-1}$ cm 2
I	mean excitation energy	eV (<i>Nota bene!</i>)
$\delta(\beta\gamma)$	density effect correction to ionization energy loss	
$\hbar\omega_p$	plasma energy $\sqrt{4\pi N_e r_e^3 m_e c^2}/\alpha$	$\sqrt{\rho \langle Z/A \rangle} \times 28.816$ eV $\hookrightarrow \rho$ in g cm $^{-3}$
N_e	electron density	(units of r_e) $^{-3}$
w_j	weight fraction of the j th element in a compound or mixt.	
n_j	\times number of j th kind of atoms in a compound or mixture	
X_0	radiation length	g cm $^{-2}$
E_c	critical energy for electrons	MeV
$E_{\mu c}$	critical energy for muons	GeV
E_s	scale energy $\sqrt{4\pi/\alpha} m_e c^2$	21.2052 MeV
R_M	Molière radius	g cm $^{-2}$

Bethe’s original theory applied only to energies above which atomic effects are not important. The free-electron cross section (Eq. (34.1)) was used to extend the cross section to W_{\max} . This free-electron approximation is not valid if W is not large compared to electron binding energies. For this energy regime Bethe [4, 5] used “Born Theorie” to obtain the differential cross section

$$\frac{d\sigma_B(W; \beta)}{dW} = \frac{d\sigma_R(W; \beta)}{dW} B(W). \quad (34.2)$$

Electronic binding is accounted for by the correction factor $B(W)$. Examples of $B(W)$ and $d\sigma_B/dW$ can be seen in Figs. 5 and 6 of Ref. [1]. For a given material, the correction results in introducing an *effective ionization energy* I “which is a geometric average of the excitation energies of the medium weighed by the corresponding oscillator strength.” [6]. The nontrivial task of finding these values is discussed in Sec. 34.2.4.

At high energies the stopping power is further modified by polarization of the medium, and this “density effect,” discussed in Sec. 34.2.5, must also be included.

The mean number of collisions with energy loss between W and $W + dW$ occurring in a distance δx is $N_e \delta x (d\sigma/dW) dW$, where $d\sigma(W; \beta)/dW$, where the cross section is the Rutherford formula if free electrons can be assumed and the Bethe form where binding energy is important. It is convenient to define the moments

$$M_j(\beta) = N_e \delta x \int W^j \frac{d\sigma(W; \beta)}{dW} dW, \quad (34.3)$$

so that M_0 is the mean number of collisions in δx , M_1 is the mean energy loss in δx , $(M_2 - M_1)^2$ is the variance, *etc.* The number of collisions is Poisson-distributed with mean M_0 . N_e is either measured in electrons/g ($N_e = N_A Z/A$) or electrons/cm³ ($N_e = N_A \rho Z/A$). The former is used throughout this chapter, since quantities of interest (dE/dx , X_0 , *etc.*) vary smoothly with composition when there is no density dependence.

34.2.2 Maximum energy transfer to an electron in a single collision

For a point-like particle with mass $M \gg m_e$,

$$W_{\max} = \frac{2m_e c^2 \beta^2 \gamma^2}{1 + 2\gamma m_e/M + (m_e/M)^2}. \quad (34.4)$$

In older references [2, 9] the “low-energy” approximation $W_{\max} = 2m_e c^2 \beta^2 \gamma^2$, valid for $2\gamma m_e \ll M$, is often implicit. For a pion in copper, the error thus introduced into dE/dx is greater than 6% at 100 GeV. For $2\gamma m_e \gg M$, $W_{\max} = M c^2 \beta^2 \gamma$.

At energies of order 100 GeV, the maximum 4-momentum transfer to the electron can exceed 1 GeV/c, where hadronic structure effects modify the cross sections. This problem has been investigated by J.D. Jackson [10], who concluded that for incident hadrons (but not for large nuclei) corrections to dE/dx are negligible below energies where radiative effects dominate. While the cross section for rare hard collisions is modified, the average stopping power, dominated by many softer collisions, is almost unchanged.

34.2.3 Stopping power at intermediate energies

The mean rate of energy loss by moderately relativistic charged heavy particles is well described by the “Bethe equation” [2, 4, 5, 9],

$$\left\langle -\frac{dE}{dx} \right\rangle = K z^2 \frac{Z}{A} \frac{1}{\beta^2} \left[\frac{1}{2} \ln \frac{2m_e c^2 \beta^2 \gamma^2 W_{\max}}{I^2} - \beta^2 - \frac{\delta(\beta\gamma)}{2} \right]. \quad (34.5)$$

Eq. (34.5) is valid in the region $0.1 \lesssim \beta\gamma \lesssim 1000$ with an accuracy of a few percent. At $\beta\gamma \sim 0.1$ the projectile speed is comparable to atomic electron “speed,” and at $\beta\gamma \sim 1000$ radiative effects begin to be important (Sec. 34.6). Both limits are Z dependent. A minor dependence on M at high energies is introduced through W_{\max} , but for all practical purposes the stopping power in a given material is a function of β alone. Small corrections are discussed in Sec. 34.2.6.^{1,2}

This is the *mass stopping power*; with the symbol definitions and values given in Table 34.1, the units are MeV g⁻¹cm². As can be seen from Fig. 34.2, dE/dx defined in this way is about the same for most materials, decreasing slowly with Z . The *linear stopping power*, in MeV/cm, is $\rho dE/dx$, where ρ is the density in g/cm³.

The stopping power at first falls as $1/\beta^\alpha$ where $\alpha \approx 1.7$ – 1.5 , decreasing with increasing Z , and reaches a broad minimum at $\beta\gamma = 3.8$ – 3.0 as Z rises from 6 to 82. It then inexorably rises as the argument of the logarithmic term increases. Two independent mechanisms contribute. Two thirds of the rise is produced by the explicit $\beta^2 \gamma^2$ dependence through the relativistic flattening and extension of the particle’s electric field. Rather than producing ionization at greater and greater distances, the field polarizes the medium, cancelling the increase in the logarithmic term at high energies. This is taken into account by the density-effect correction $\delta(\beta\gamma)$. The other third is introduced by the $\beta^2 \gamma$ dependence of W_{\max} , the maximum possible energy transfer to a recoil electron. “Hard collision” events increasingly extend the tail of the energy loss distribution, increasing the mean but with little effect on the position of the maximum, the most probable energy loss.

Few concepts in high-energy physics are as misused as dE/dx , since the mean is weighted by rare events with large single-collision energy losses. Even with samples of hundreds of events

¹For incident spin 1/2 particles, $(W_{\max}/E)^2/4$ is included in the square brackets. Although this correction is within the uncertainties in the total stopping power, its inclusion avoids a systematic bias.

²In this section, “ dE/dx ” will be understood to mean the mass stopping power “ $(-dE/dx)$.”

in a typical detector, the mean energy loss cannot be obtained dependably. Far better and more easily measured is the most probable energy loss, discussed in Sec. 34.2.9. The most probable energy loss in a typical detector is considerably smaller than the mean given by the Bethe equation. It does not continue to rise with the mean stopping power, but approaches a “Fermi plateau.”

In analysing TPC data (Sec. 35.6.5), the same end is often accomplished by using a restricted energy loss, the mean of 50%–70% of the samples with the smallest signals as the estimator.

Although it must be used with cautions and caveats, dE/dx as described in Eq. (34.5) still forms the basis of much of our understanding of energy loss by charged particles. Extensive tables are available [6, 7] and pdg.lbl.gov/current/AtomicNuclearProperties/.

For heavy projectiles, like ions, additional terms are required to account for higher-order photon coupling to the target, and to account for the finite target radius. These can change dE/dx by a factor of two or more for the heaviest nuclei in certain kinematic regimes [11].

The function as computed for muons on copper is shown as the “Bethe” region of Fig. 34.1. Mean energy loss behavior below this region is discussed in Sec. 34.2.6, and the radiative effects at high energy are discussed in Sec. 34.6. Only in the Bethe region is it a function of β alone; the mass dependence is more complicated elsewhere. The stopping power in several other materials is shown in Fig. 34.2. Except in hydrogen, particles with the same speed have similar rates of energy loss in different materials, although there is a slow decrease in the rate of energy loss with increasing Z . The qualitative behavior difference at high energies between a gas (He in the figure) and the other materials shown in the figure is due to the density-effect correction, $\delta(\beta\gamma)$, discussed in Sec. 34.2.5. The stopping power functions are characterized by broad minima whose position drops from $\beta\gamma = 3.5$ to 3.0 as Z goes from 7 to 100. The values of minimum ionization as a function of atomic number are shown in Fig. 34.3.

In practical cases, most relativistic particles (*e.g.*, cosmic-ray muons) have mean energy loss rates close to the minimum; they are “minimum-ionizing particles,” or mip’s.

Eq. (34.5) may be integrated to find the total (or partial) “continuous slowing-down approximation” (CSDA) range R for a particle which loses energy only through ionization and atomic excitation. Since dE/dx depends only on β , R/M is a function of E/M or pc/M . In practice, range is a useful concept only for low-energy hadrons ($R \lesssim \lambda_I$, where λ_I is the nuclear interaction length), and for muons below a few hundred GeV (above which radiative effects dominate). Fig. 34.4 shows R/M as a function of $\beta\gamma$ ($= p/Mc$) for a variety of materials.

The mass scaling of dE/dx and range is valid for the electronic losses described by the Bethe equation, but not for radiative losses.

34.2.4 Mean excitation energy

“The determination of the mean excitation energy is the principal non-trivial task in the evaluation of the Bethe stopping-power formula” [15]. Recommended values have varied substantially with time. Estimates based on experimental stopping-power measurements for protons, deuterons, and alpha particles and on oscillator-strength distributions and dielectric-response functions were given in ICRU 49 [6]. See also ICRU 37 [12]. These values, shown in Fig. 34.5, have since been widely used. Machine-readable versions can also be found [16].

34.2.5 Density effect

As the particle energy increases, its electric field flattens and extends, so that the distant-collision contribution to the logarithmic term in Eq. (34.5) increases as $\beta^2 \gamma^2$. However, real media become polarized, limiting the field extension and effectively truncating this part of the logarithmic rise [2, 3, 6, 17, 18]. At very high energies,

$$\delta(\beta\gamma)/2 \rightarrow \ln(\hbar\omega_p/I) + \ln \beta\gamma - 1/2, \quad (34.6)$$

where $\delta(\beta\gamma)/2$ is the density effect correction introduced in Eq. (34.5) and $\hbar\omega_p$ is the plasma energy defined in Table 34.1. A comparison with Eq. (34.5) shows that dE/dx then grows as

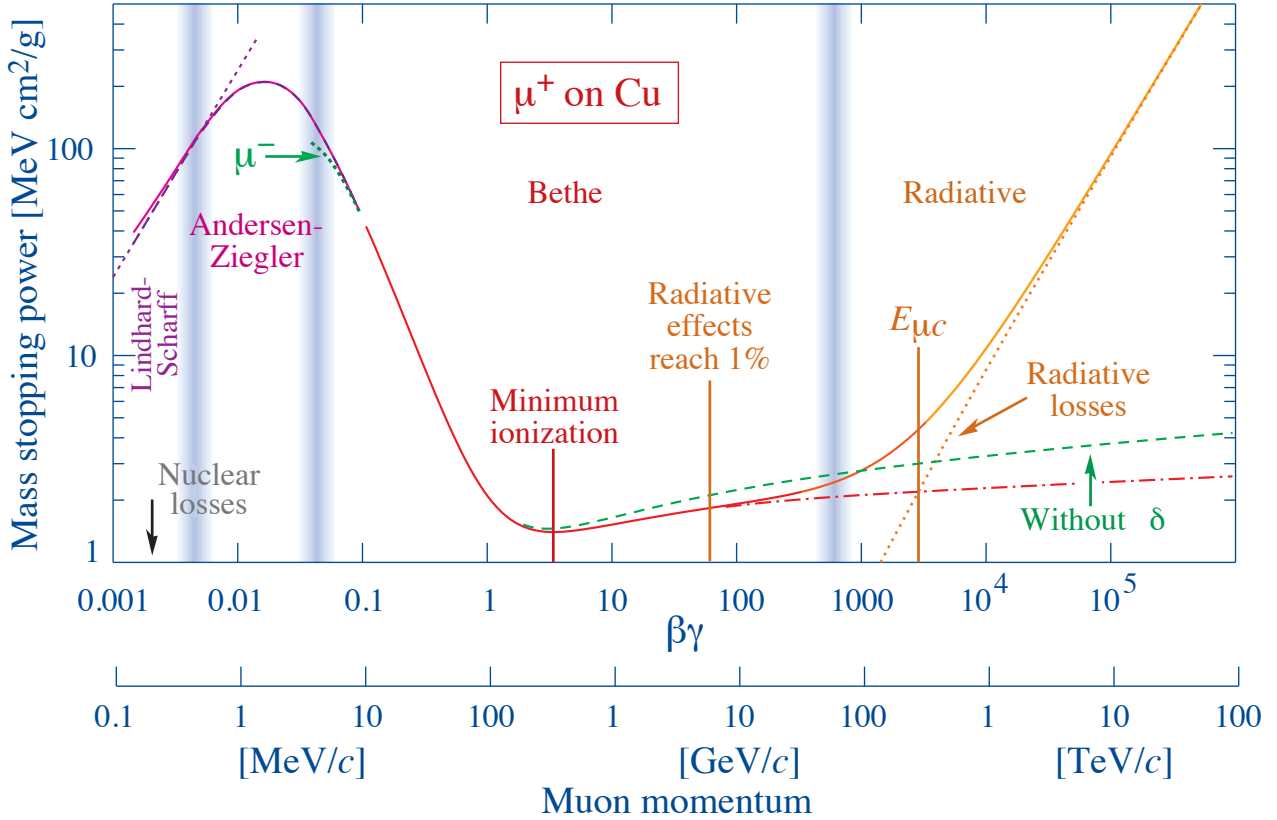


Figure 34.1: Mass stopping power (dE/dx) for positive muons in copper as a function of $\beta\gamma = p/Mc$ over nine orders of magnitude in momentum (12 orders of magnitude in kinetic energy). Solid curves indicate the total stopping power. Data below the break at $\beta\gamma \approx 0.1$ are taken from ICRU 49 [6] assuming only β dependence, and data at higher energies are from [7]. Vertical bands indicate boundaries between different approximations discussed in the text. The short dotted lines labeled “ μ^- ” illustrate the “Barkas effect,” the dependence of stopping power on projectile charge at very low energies [8]. dE/dx in the radiative region is not simply a function of β .

In T_{\max} rather than $\ln \beta^2 \gamma^2 T_{\max}$, and that the mean excitation energy I is replaced by the plasma energy $\hbar\omega_p$. An example of the ionization stopping power as calculated with and without the density effect correction is shown in Fig. 34.1. Since the plasma frequency scales as the square root of the electron density, the correction is much larger for a liquid or solid than for a gas, as is illustrated in Fig. 34.2.

The density effect correction is usually computed using Sternheimer’s parameterization [17]:

$$\delta(\beta\gamma) = \begin{cases} 2(\ln 10)x - \bar{C} & \text{if } x \geq x_1; \\ 2(\ln 10)x - \bar{C} + a(x_1 - x)^k & \text{if } x_0 \leq x < x_1; \\ 0 & \text{if } x < x_0 \text{ (nonconductors);} \\ \delta_0 10^{2(x-x_0)} & \text{if } x < x_0 \text{ (conductors)} \end{cases} \quad (34.7)$$

Here $x = \log_{10} \beta\gamma = \log_{10}(p/Mc)$. \bar{C} (the negative of the C used in Ref. [17]) is obtained by equating the high-energy case of Eq. (34.7) with the limit given in Eq. (34.6). The other parameters are adjusted to give a best fit to the results of detailed calculations for momenta below $Mc \exp(x_1)$. For nonconductors the correction is 0 below $\beta\gamma = 10^{x_0}$, corresponding to 100–200 MeV for pions and 1–2 GeV for protons. For conductors it decreases rapidly below this point. Parameters for the elements and nearly 200 compounds and mixtures of interest are published in a variety of places, notably in Ref. [18]. A recipe for finding the coefficients for nontabulated materials is given by Sternheimer and Peierls [19] and is summarized in Ref. [7].

The remaining relativistic rise comes from the $\beta^2\gamma$ growth of W_{\max} , which in turn is due to (rare) large energy transfers to a few electrons. When these events are excluded, the energy deposit in an absorbing layer approaches a constant value, the Fermi plateau (see Sec. 34.2.8 below). At even higher energies (*e.g.*, > 332 GeV

for muons in iron, and at a considerably higher energy for protons in iron), radiative effects are more important than ionization losses. These are especially relevant for high-energy muons, as discussed in Sec. 34.6.

34.2.6 Energy loss at low energies

The theory of energy loss by ionization and excitation as given by Bethe is based on a first-order Born approximation. It assumes free electrons, and should be valid when the projectile’s speed is large compared to that of the atomic electrons. This presents a problem at low energies, where W_{\max} is less than the K shell binding energy. However, Mott showed that the Born approximation can be applied at energies much smaller than atomic binding energies [20]; the incident particle can be treated by classical mechanics since its wavelength is shorter than atomic dimensions. The Born method is actually better justified when its speed is not large compared to the K electron speed [5].

Higher-order corrections must still be made to extend the Bethe equation (Eq. (34.5)) to low energies. An improved approximation for the terms in the square brackets of Eq. (34.5) at low energies is obtained with

$$L(\beta) = L_a(\beta) - \frac{C(\beta)}{Z} + zL_1(\beta) + z^2L_2(\beta). \quad (34.8)$$

Here L_a is the square-bracketed terms of Eq. (34.5), C/Z is the sum of shell corrections and zL_1 and z^2L_2 are Barkas and Bloch correction terms [6, 21]. With these corrections, the Bethe treatment is accurate to about 1% down to $\beta \approx 0.05$, or about 1 MeV for protons (0.13 MeV for muons). Values of L_a , C/Z , L_1 , and L_2 in the range $T = 0.3$ –30 MeV for a proton traversing aluminum can be found in Table I of Ref. [21].

Shell correction $-C/Z$. As the speed of the projectile decreases, the contribution to the stopping power from K shell electrons de-

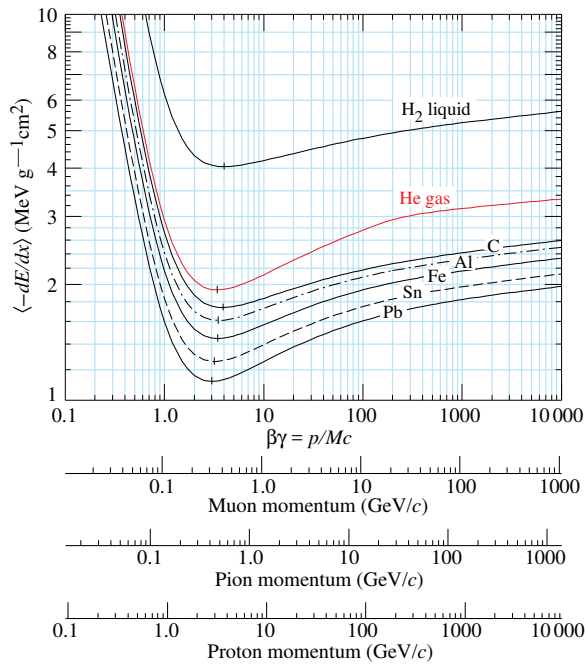


Figure 34.2: Mean energy loss rate in liquid (bubble chamber) hydrogen, gaseous helium, carbon, aluminum, iron, tin, and lead. Radiative effects, relevant for muons and pions, are not included. These become significant for muons in iron for $\beta\gamma \gtrsim 1000$, and at lower momenta for muons in higher- Z absorbers. See Fig. 34.23.

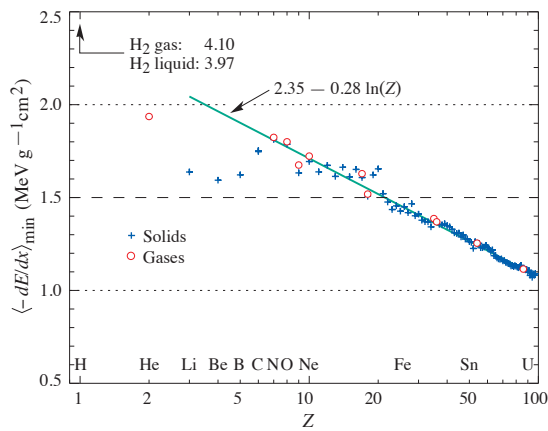


Figure 34.3: Mass stopping power at minimum ionization for the chemical elements. The straight line is fitted for $Z > 6$. A simple functional dependence on Z is not to be expected, since dE/dx also depends on other variables.

creases, and at even lower velocities contributions from L and higher shells further reduce it. The correction $(C_K + C_L + \dots)/Z$ is should be included in the square brackets of Eq. (34.5). It is calculated and tabulated (for a few common materials) in a number of places; Refs. [6, 12, 21] are especially useful. As an example, the shell correction for a 30 MeV proton traversing aluminum is 0.6%, increasing to 9.9% as the proton's energy decreases to 0.3 MeV.

Barkas correction zL_1 . Qualitatively, one might imagine an atom's electron cloud slightly recoiling at the approach of a negative projectile and being attracted toward an approaching positive projectile. Hence the stopping power for negative particles should be slightly smaller than the stopping power for positive particles. In a 1956 paper, Barkas *et al.* noted that negative pions possibly had a longer range than positive pions [8]. The effect has been measured for a number of negative/positive particle pairs, and more recently in detailed studies with antiprotons at the CERN LEAR facility [22]. Since no complete theory exists, an empirical

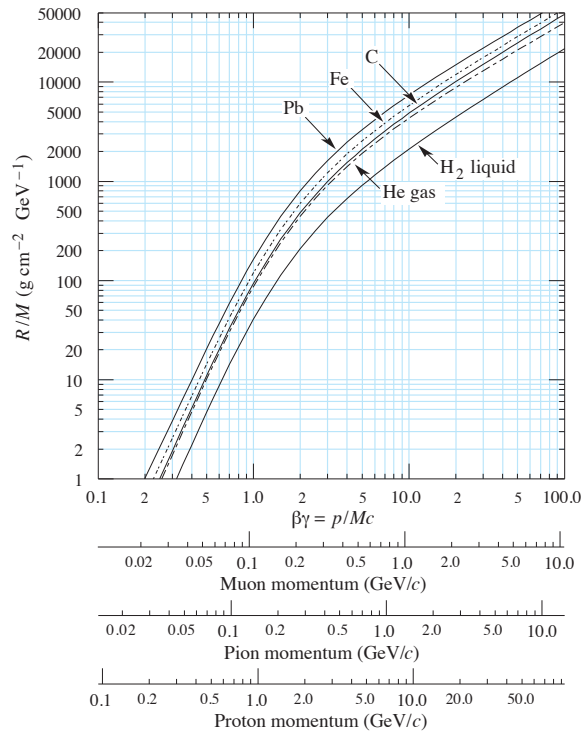


Figure 34.4: Range of heavy charged particles in liquid (bubble chamber) hydrogen, helium gas, carbon, iron, and lead. For example: For a K^+ whose momentum is 700 MeV/ c , $\beta\gamma = 1.42$. For lead we read $R/M \approx 396$, and so the range is 195 g cm $^{-2}$ (17 cm).

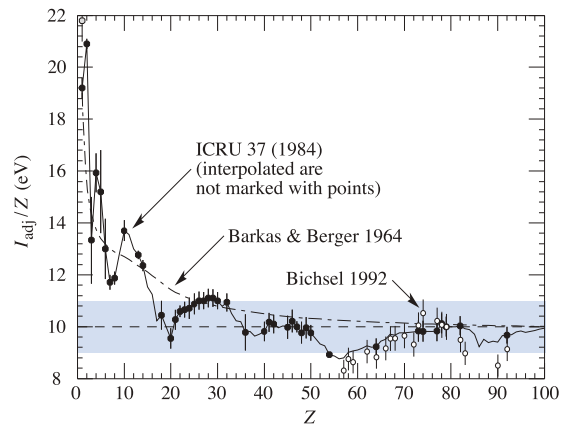


Figure 34.5: Mean excitation energies (divided by Z) as adopted by the ICRU [12]. Those based on experimental measurements are shown by symbols with error flags; the interpolated values are simply joined. The grey point is for liquid H $_2$; the black point at 19.2 eV is for H $_2$ gas. The open circles show more recent determinations by Bichsel [13]. The dash-dotted curve is from the approximate formula of Barkas [14] used in early editions of this Review.

approach is necessary. A 1972 harmonic-oscillator model by Ashley *et al.* [23] is often used; it has two parameters determined by experimental data. For protons in aluminum, L_1/L_a is less than 0.1% at 30 MeV, but increases to 17% as T decreases to 0.3 MeV. This correction is indicated in Fig. 34.1.

Bloch correction z^2L_2 . Bloch's extension of Bethe's theory introduced a low-energy correction that takes account of perturbations of the atomic wave functions. The form obtained by Lindhard and Sørensen [11] is used *e.g.* in Refs. [6, 21]. For protons in aluminum, $-L_2/L_1$ is less than 0.3% at 3.0 MeV, but rises to 7%

when the energy has fallen to 0.3 MeV.

For the interval $0.01 < \beta < 0.05$ there is no satisfactory theory. For protons, one usually relies on the phenomenological fitting formulae developed by Andersen and Ziegler [6, 24]. As tabulated in ICRU 49 [6], the nuclear plus electronic proton stopping power in copper is $113 \text{ MeV cm}^2 \text{ g}^{-1}$ at $T = 10 \text{ keV}$ ($\beta\gamma = 0.005$), rises to a maximum of $210 \text{ MeV cm}^2 \text{ g}^{-1}$ at $T \approx 120 \text{ keV}$ ($\beta\gamma = 0.016$), then falls to $118 \text{ MeV cm}^2 \text{ g}^{-1}$ at $T = 1 \text{ MeV}$ ($\beta\gamma = 0.046$). Above 0.5–1.0 MeV the corrected Bethe theory is adequate.

For particles moving more slowly than $\approx 0.01c$ (more or less the speed of the outer atomic electrons), Lindhard has been quite successful in describing electronic stopping power, which is proportional to β [25]. Finally, we note that at even lower energies, e.g., for protons of less than several hundred eV, non-ionizing nuclear recoil energy loss dominates the total energy loss [6, 25, 26].

34.2.7 Energetic knock-on electrons (δ rays)

The distribution of secondary electrons with kinetic energies $T \gg I$ is [2]

$$\frac{d^2 N}{dT dx} = \frac{1}{2} K z^2 \frac{Z}{A} \frac{1}{\beta^2} \frac{F(T)}{T^2} \quad (34.9)$$

for $I \ll T \leq W_{\max}$, where W_{\max} is given by Eq. (34.4). Here β is the speed of the primary particle. The factor F is spin-dependent, but is about unity for $T \ll W_{\max}$. For spin-0 particles $F(T) = (1 - \beta^2 T/W_{\max})$; forms for spins 1/2 and 1 are also given by Rossi [2] (Sec. 2.3, Eqs. 7 and 8). Additional formulae are given in [27]. Equation Eq. (34.9) is inaccurate for T close to I [28].

δ rays of even modest energy are rare. For a $\beta \approx 1$ particle, for example, on average only one collision with $T_e > 10 \text{ keV}$ will occur along a path length of 90 cm of argon gas [1].

A δ ray with kinetic energy T_e and corresponding momentum p_e is produced at an angle θ given by

$$\cos \theta = (T_e/p_e)(p_{\max}/W_{\max}), \quad (34.10)$$

where p_{\max} is the momentum of an electron with the maximum possible energy transfer W_{\max} .

34.2.8 Restricted energy loss rates for relativistic ionizing particles

Further insight can be obtained by examining the mean energy deposit by an ionizing particle when energy transfers are restricted to $T \leq W_{\text{cut}} \leq W_{\max}$. The restricted energy loss rate is

$$-\frac{dE}{dx} \Big|_{T < W_{\text{cut}}} = K z^2 \frac{Z}{A} \frac{1}{\beta^2} \left[\frac{1}{2} \ln \frac{2m_e c^2 \beta^2 \gamma^2 W_{\text{cut}}}{I^2} - \frac{\beta^2}{2} \left(1 + \frac{W_{\text{cut}}}{W_{\max}} \right) - \frac{\delta}{2} \right]. \quad (34.11)$$

This form approaches the normal Bethe function (Eq. (34.5)) as $W_{\text{cut}} \rightarrow W_{\max}$. It can be verified that the difference between Eq. (34.5) and Eq. (34.11) is equal to $\int_{W_{\text{cut}}}^{W_{\max}} T(d^2 N/dT dx) dT$, where $d^2 N/dT dx$ is given by Eq. (34.9).

Since W_{cut} replaces W_{\max} in the argument of the logarithmic term of Eq. (34.5), the $\beta\gamma$ term producing the relativistic rise in the close-collision part of dE/dx is replaced by a constant, and $|dE/dx|_{T < W_{\text{cut}}}$ approaches the constant ‘‘Fermi plateau.’’ (The density effect correction δ eliminates the explicit $\beta\gamma$ dependence produced by the distant-collision contribution.) This behavior is illustrated in Fig. 34.6, where restricted loss rates for two examples of W_{cut} are shown in comparison with the full Bethe dE/dx and the Landau-Vavilov most probable energy loss (to be discussed in Sec. 34.2.9 below).

‘‘Restricted energy loss’’ is cut at the total mean energy, not the single-collision energy above W_{cut} . It is of limited use. The most probable energy loss, discussed in the next Section, is far more useful in situations where single-particle energy loss is observed.

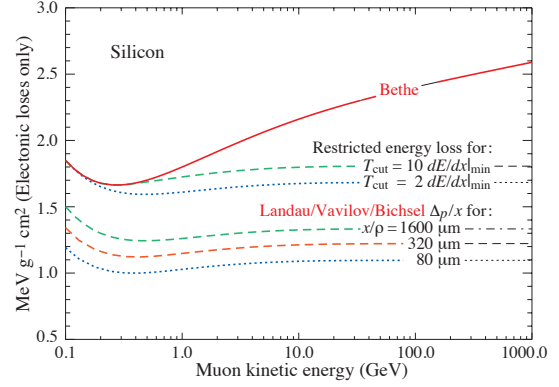


Figure 34.6: Bethe dE/dx , two examples of restricted energy loss, and the Landau most probable energy per unit thickness in silicon. The change of Δ_p/x with thickness x illustrates its $a \ln x + b$ dependence. Minimum ionization $(dE/dx)_{\min}$ is $1.664 \text{ MeV g}^{-1} \text{ cm}^2$. Radiative losses are excluded. The incident particles are muons.

34.2.9 Fluctuations in energy loss

For detectors of moderate thickness x (e.g. scintillators or LAr cells),³ the energy loss probability distribution $f(\Delta; \beta\gamma, x)$ is adequately described by the highly-skewed Landau (or Landau-Vavilov) distribution [29, 30].

The most probable energy loss is [31]⁴

$$\Delta_p = \xi \left[\ln \frac{2mc^2 \beta^2 \gamma^2}{I} + \ln \frac{\xi}{I} + j - \beta^2 - \delta(\beta\gamma) \right], \quad (34.12)$$

where $\xi = (K/2) \langle Z/A \rangle z^2 (x/\beta^2) \text{ MeV}$ for a detector with a thickness x in g cm^{-2} , and $j = 0.200$ [31].⁵ While dE/dx is independent of thickness, Δ_p/x scales as $a \ln x + b$. The density correction $\delta(\beta\gamma)$ was not included in Landau’s or Vavilov’s work, but it was later included by Bichsel [31]. The high-energy behavior of $\delta(\beta\gamma)$ (Eq. (34.6)) is such that

$$\Delta_p \xrightarrow{\beta\gamma \gtrsim 100} \xi \left[\ln \frac{2mc^2 \xi}{(h\omega_p)^2} + j \right]. \quad (34.13)$$

Thus the Landau-Vavilov most probable energy loss, like the restricted energy loss, reaches a Fermi plateau. The Bethe dE/dx and Landau-Vavilov-Bichsel Δ_p/x in silicon are shown as a function of muon energy in Fig. 34.6. The energy deposit in the $1600 \mu\text{m}$ case is roughly the same as in a 3 mm thick plastic scintillator.

The distribution function for the energy deposit by a 10 GeV muon going through a detector of about this thickness is shown in Fig. 34.7. In this case the most probable energy loss is 62% of the mean $(M_1(\langle \Delta \rangle)/M_1(\infty))$. Folding in experimental resolution displaces the peak of the distribution, usually toward a higher value. 90% of the collisions $(M_1(\langle \Delta \rangle)/M_1(\infty))$ contribute to energy deposits below the mean. It is the very rare high-energy-transfer collisions, extending to W_{\max} at several GeV, that drives the mean into the tail of the distribution. The large weight of these rare events makes the mean of an experimental distribution consisting of a few hundred events subject to large fluctuations and sensitive to cuts. *The mean of the energy loss given by the Bethe equation, Eq. (34.5), is thus ill-defined experimentally and*

³‘‘Moderate thickness’’ means $G \lesssim 0.05\text{--}0.1$, where G is given by Rossi Ref. [2], Eq. 2.7(10). It is Vavilov’s κ [29]. G is proportional to the absorber’s thickness, and as such parameterizes the constants describing the Landau distribution. These are fairly insensitive to thickness for $G \lesssim 0.1$, the case for most detectors.

⁴Practical calculations can be expedited by using the tables of δ and β from the text versions of the muon energy loss tables to be found at pdg.lbl.gov/current/AtomicNuclearProperties.

⁵Rossi [2], Talman [32], and others give somewhat different values for j . The most probable loss is not sensitive to its value.

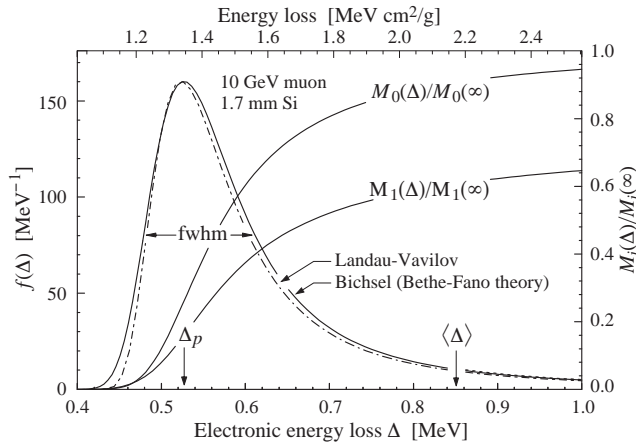


Figure 34.7: Electronic energy deposit distribution for a 10 GeV muon traversing 1.7 mm of silicon, the stopping power equivalent of about 0.3 cm of PVT-based scintillator [1, 13, 33]. The Landau-Vavilov function (dot-dashed) uses a Rutherford cross section without atomic binding corrections but with a kinetic energy transfer limit of W_{\max} . The solid curve was calculated using Bethe-Fano theory. $M_0(\Delta)$ and $M_1(\Delta)$ are the cumulative 0th moment (mean number of collisions) and 1st moment (mean energy loss) in crossing the silicon. (See Sec. 34.2.1). The fwhm of the Landau-Vavilov function is about 4ξ for detectors of moderate thickness. Δ_p is the most probable energy loss, and $\langle\Delta\rangle$ divided by the thickness is the Bethe dE/dx .

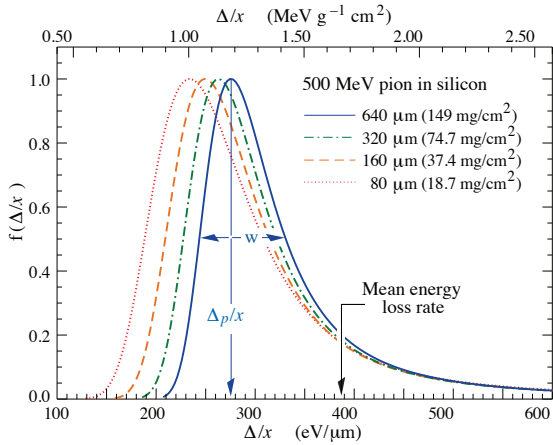


Figure 34.8: Straggling functions in silicon for 500 MeV pions, normalized to unity at the most probable value Δ_p/x . The width w is the full width at half maximum.

is not useful for describing energy loss by single particles.⁶ It rises as $\ln\gamma$ because W_{\max} increases as γ at high energies. The most probable energy loss should be used.

A practical example: For muons traversing 0.25 inches (0.64 cm) of PVT (polyvinyltoluene) based plastic scintillator, the ratio of the most probable E loss rate to the mean loss rate via the Bethe equation is [0.69, 0.57, 0.49, 0.42, 0.38] for $T_\mu = [0.01, 0.1, 1, 10, 100]$ GeV. Radiative losses add less than 0.5% to the total mean energy deposit at 10 GeV, but add 7% at 100 GeV. The most probable E loss rate rises slightly beyond the minimum ionization energy, then is essentially constant.

The Landau distribution fails to describe energy loss in thin absorbers such as gas TPC cells [1] and Si detectors [31], as can be seen *e.g.* in Fig. 1 of Ref. [1] for an argon-filled TPC cell. Also see Talman [32]. While Δ_p/x may be calculated adequately with Eq. (34.12), the distributions are significantly wider than the

⁶It does find application in dosimetry, where only bulk deposit is relevant.

Landau width $w = 4\xi$ Ref. [31], Fig. 15. Examples for 500 MeV pions incident on thin silicon detectors are shown in Fig. 34.8. For very thick absorbers the distribution is less skewed but never approaches a Gaussian.

The most probable energy loss, scaled to the mean loss at minimum ionization, is shown in Fig. 34.9 for several silicon detector thicknesses.

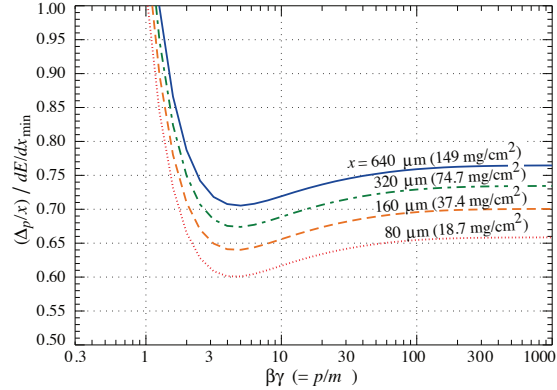


Figure 34.9: Most probable energy loss in silicon, scaled to the mean loss of a minimum ionizing particle, 388 eV/μm (1.66 MeV $g^{-1}cm^2$).

34.2.10 Energy loss in mixtures and compounds

A mixture or compound can be thought of as made up of thin layers of pure elements in the right proportion (Bragg additivity). In this case,

$$\left\langle \frac{dE}{dx} \right\rangle = \sum w_j \left\langle \frac{dE}{dx} \right\rangle_j, \quad (34.14)$$

where $dE/dx|_j$ is the mean rate of energy loss (in MeV $g\ cm^{-2}$) in the j th element. Eq. (34.5) can be inserted into Eq. (34.14) to find expressions for $\langle Z/A \rangle$, $\langle I \rangle$, and $\langle \delta \rangle$; for example, $\langle Z/A \rangle = \sum w_j Z_j/A_j = \sum n_j Z_j / \sum n_j A_j$. However, $\langle I \rangle$ as defined this way is an underestimate, because in a compound electrons are more tightly bound than in the free elements, and $\langle \delta \rangle$ as calculated this way has little relevance, because it is the electron density that matters. If possible, one uses the tables given in Refs. [18, 34], or the recipes given in [19] (repeated in Ref. [7]), that include effective excitation energies and interpolation coefficients for calculating the density effect correction for the chemical elements and nearly 200 mixtures and compounds. Otherwise, use the recipe for δ given in Refs. [7, 19], and calculate $\langle I \rangle$ following the discussion in Ref. [15]. (Note the “13%” rule!)

34.2.11 Ionization yields

The Bethe equation describes energy loss via excitation and ionization. Many gaseous detectors (proportional counters or TPCs) or liquid ionization detectors count the number of electrons or positive ions from ionization, rather than the ionization energy. As a further complication, the electron liberated in the initial ionization often has enough energy to ionize other atoms or molecules; this process can happen several times. The number of electron-ion pairs per unit length is typically three or more times the original number. Ion or electron counting is a proxy for a direct dE/dx measurement. Calibrations link the number of observed ions to the traversing particle’s dE/dx .

The details depend on the gases (or liquids) and the particular detector involved. A useful discussion of the physics is provided in Sec.35.6 of this Review.

34.3 Multiple scattering through small angles

A charged particle traversing a medium is deflected by many small-angle scatters. Most of this deflection is due to Coulomb scattering from nuclei as described by the Rutherford cross section. (However, for hadronic projectiles, the strong interactions also contribute to multiple scattering.) For many small-angle scatters the net scattering and displacement distributions are Gaussian via the central limit theorem. Less frequent “hard” scatters

produce non-Gaussian tails. These Coulomb scattering distributions are well-represented by the theory of Molière [35]. Accessible discussions are given by Rossi [2] and Jackson [3], and exhaustive reviews have been published by Scott [36] and Motz *et al.* [37]. Experimental measurements have been published by Bichsel [38] (low energy protons) and by Shen *et al.* [39] (relativistic pions, kaons, and protons).⁷

If we define

$$\theta_0 = \theta_{\text{plane}}^{\text{rms}} = \frac{1}{\sqrt{2}} \theta_{\text{space}}^{\text{rms}}, \quad (34.15)$$

then it is sufficient for many applications to use a Gaussian approximation for the central 98% of the projected angular distribution, with an rms width given by Lynch & Dahl [40]:

$$\begin{aligned} \theta_0 &= \frac{13.6 \text{ MeV}}{\beta c p} z \sqrt{\frac{x}{X_0}} \left[1 + 0.088 \log_{10} \left(\frac{x z^2}{X_0 \beta^2} \right) \right] \\ &= \frac{13.6 \text{ MeV}}{\beta c p} z \sqrt{\frac{x}{X_0}} \left[1 + 0.038 \ln \left(\frac{x z^2}{X_0 \beta^2} \right) \right] \end{aligned} \quad (34.16)$$

Here p , βc , and z are the momentum, speed, and charge number of the incident particle, and x/X_0 is the thickness of the scattering medium in radiation lengths (defined below). This takes into account the p and z dependence quite well at small Z , but for large Z and small x the β -dependence is not well represented. Further improvements are discussed in Ref. [40].

Eq. (34.16) describes scattering from a single material, while the usual problem involves the multiple scattering of a particle traversing many different layers and mixtures. Since it is from a fit to a Molière distribution, it is incorrect to add the individual θ_0 contributions in quadrature; the result is systematically too small. It is much more accurate to apply Eq. (34.16) once, after finding x and X_0 for the combined scatterer.

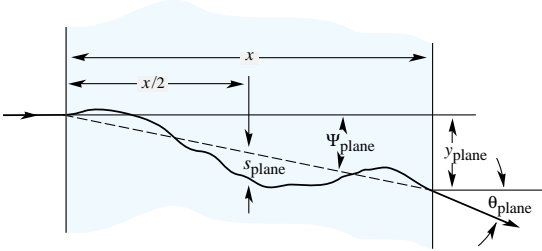


Figure 34.10: Quantities used to describe multiple Coulomb scattering. The particle is incident in the plane of the figure.

The nonprojected (space) and projected (plane) angular distributions are given approximately by [35]

$$\frac{1}{2\pi \theta_0^2} \exp \left(-\frac{\theta_{\text{space}}^2}{2\theta_0^2} \right) d\Omega, \quad (34.17)$$

$$\frac{1}{\sqrt{2\pi} \theta_0} \exp \left(-\frac{\theta_{\text{plane}}^2}{2\theta_0^2} \right) d\theta_{\text{plane}}, \quad (34.18)$$

where θ is the deflection angle. In this approximation, $\theta_{\text{space}}^2 \approx (\theta_{\text{plane},x}^2 + \theta_{\text{plane},y}^2)$, where the x and y axes are orthogonal to the direction of motion, and $d\Omega \approx d\theta_{\text{plane},x} d\theta_{\text{plane},y}$. Deflections into $\theta_{\text{plane},x}$ and $\theta_{\text{plane},y}$ are independent and identically distributed. Fig. 34.10 shows these and other quantities sometimes used to describe multiple Coulomb scattering. They are

$$\psi_{\text{plane}}^{\text{rms}} = \frac{1}{\sqrt{3}} \theta_{\text{plane}}^{\text{rms}} = \frac{1}{\sqrt{3}} \theta_0, \quad (34.19)$$

$$y_{\text{plane}}^{\text{rms}} = \frac{1}{\sqrt{3}} x \theta_{\text{plane}}^{\text{rms}} = \frac{1}{\sqrt{3}} x \theta_0, \quad (34.20)$$

⁷Shen *et al.*'s measurements show that Bethe's simpler methods of including atomic electron effects agrees better with experiment than does Scott's treatment.

$$s_{\text{plane}}^{\text{rms}} = \frac{1}{4\sqrt{3}} x \theta_{\text{plane}}^{\text{rms}} = \frac{1}{4\sqrt{3}} x \theta_0. \quad (34.21)$$

All the quantitative estimates in this section apply only in the limit of small $\theta_{\text{plane}}^{\text{rms}}$ and in the absence of large-angle scatters. The random variables s , ψ , y , and θ in a given plane are correlated. Obviously, $y \approx x\psi$. In addition, y and θ have the correlation coefficient $\rho_{y\theta} = \sqrt{3}/2 \approx 0.87$. For Monte Carlo generation of a joint $(y_{\text{plane}}, \theta_{\text{plane}})$ distribution, or for other calculations, it may be most convenient to work with independent Gaussian random variables (z_1, z_2) with mean zero and variance one, and then set

$$y_{\text{plane}} = z_1 x \theta_0 (1 - \rho_{y\theta}^2)^{1/2} / \sqrt{3} + z_2 \rho_{y\theta} x \theta_0 / \sqrt{3} \quad (34.22a)$$

$$= z_1 x \theta_0 / \sqrt{12} + z_2 x \theta_0 / 2; \quad (34.22b)$$

$$\theta_{\text{plane}} = z_2 \theta_0. \quad (34.22c)$$

Note that the second term for y_{plane} equals $x \theta_{\text{plane}}/2$ and represents the displacement that would have occurred had the deflection θ_{plane} all occurred at the single point $x/2$.

For heavy ions the multiple Coulomb scattering has been measured and compared with various theoretical distributions [41].

34.4 Photon and electron interactions in matter

At low energies electrons and positrons primarily lose energy by ionization, although other processes (Møller scattering, Bhabha scattering, e^+ annihilation) contribute, as shown in Fig. 34.11. While ionization loss rates rise logarithmically with energy, bremsstrahlung losses rise nearly linearly (fractional loss is nearly independent of energy), and dominates above the critical energy (Sec. 34.4.4 below), a few tens of MeV in most materials.

34.4.1 Collision energy losses by e^\pm

Stopping power differs somewhat for electrons and positrons, and both differ from stopping power for heavy particles because of the kinematics, spin, charge, and the identity of the incident electron with the electrons that it ionizes. Complete discussions and tables can be found in Refs. [12, 15, 34].

For electrons, large energy transfers to atomic electrons (taken as free) are described by the Møller cross section. From Eq. (34.4), the maximum energy transfer in a single collision should be the entire kinetic energy, $W_{\text{max}} = m_e c^2 (\gamma - 1)$, but because the particles are identical, the maximum is half this, $W_{\text{max}}/2$. (The results are the same if the transferred energy is ϵ or if the transferred energy is $W_{\text{max}} - \epsilon$. The stopping power is by convention calculated for the faster of the two emerging electrons.) The first moment of the Møller cross section [27] (divided by dx) is the stopping power:

$$\begin{aligned} \left\langle -\frac{dE}{dx} \right\rangle &= \frac{1}{2} K \frac{Z}{A} \frac{1}{\beta^2} \left[\ln \frac{m_e c^2 \beta^2 \gamma^2 \{m_e c^2 (\gamma - 1)/2\}}{I^2} + (1 - \beta^2) \right. \\ &\quad \left. - \frac{2\gamma - 1}{\gamma^2} \ln 2 + \frac{1}{8} \left(\frac{\gamma - 1}{\gamma} \right)^2 - \delta \right] \end{aligned} \quad (34.23)$$

The logarithmic term can be compared with the logarithmic term in the Bethe equation (Eq. (34.2)) by substituting $W_{\text{max}} = m_e c^2 (\gamma - 1)/2$. Electron-positron scattering is described by the fairly complicated Bhabha cross section [27]. There is no identical particle problem, so $W_{\text{max}} = m_e c^2 (\gamma - 1)$. The first moment of the Bhabha equation yields

$$\begin{aligned} \left\langle -\frac{dE}{dx} \right\rangle &= \frac{1}{2} K \frac{Z}{A} \frac{1}{\beta^2} \left[\ln \frac{m_e c^2 \beta^2 \gamma^2 \{m_e c^2 (\gamma - 1)\}}{2I^2} + 2 \ln 2 \right. \\ &\quad \left. - \frac{\beta^2}{12} \left(23 + \frac{14}{\gamma + 1} + \frac{10}{(\gamma + 1)^2} + \frac{4}{(\gamma + 1)^3} \right) - \delta \right]. \end{aligned} \quad (34.24)$$

Following ICRU 37 [12], the density effect correction δ has been added to Uehling's equations [27] in both cases.

For heavy particles, shell corrections were developed assuming that the projectile is equivalent to a perturbing potential whose center moves with constant speed. This assumption has no sound

theoretical basis for electrons. The authors of ICRU 37 [12] estimated the possible error in omitting it by assuming the correction was twice as great as for a proton of the same speed. At $T = 10$ keV, the error was estimated to be $\approx 2\%$ for water, $\approx 9\%$ for Cu, and $\approx 21\%$ for Au.

As shown in Fig. 34.11, stopping powers for e^- , e^+ , and heavy particles are not dramatically different. In silicon, the minimum value for electrons is 1.50 MeV cm²/g (at $\gamma = 3.3$); for positrons, 1.46 MeV cm²/g (at $\gamma = 3.7$), and for muons, 1.66 MeV cm²/g (at $\gamma = 3.58$).

34.4.2 Radiation length

High-energy electrons predominantly lose energy in matter by bremsstrahlung, and high-energy photons by e^+e^- pair production. The characteristic amount of matter traversed for these related interactions is called the radiation length X_0 , usually measured in g cm⁻². It is the mean distance over which a high-energy electron loses all but $1/e$ of its energy by bremsstrahlung. It is also the appropriate scale length for describing high-energy electromagnetic cascades. X_0 has been calculated and tabulated by Y.S. Tsai [42]:

$$\frac{1}{X_0} = 4\alpha r_e^2 \frac{N_A}{A} \left\{ Z^2 [L_{\text{rad}} - f(Z)] + Z L'_{\text{rad}} \right\}. \quad (34.25)$$

For $A = 1$ g mol⁻¹, $4\alpha r_e^2 N_A/A = (716.408 \text{ g cm}^{-2})^{-1}$. L_{rad} and L'_{rad} are given in Table 34.2. The function $f(Z)$ is an infinite sum, but for elements up to uranium can be represented to 4-place accuracy by

$$f(Z) = a^2 \left[(1 + a^2)^{-1} + 0.20206 - 0.0369 a^2 + 0.0083 a^4 - 0.002 a^6 \right], \quad (34.26)$$

where $a = \alpha Z$ [43].

Table 34.2: Tsai's L_{rad} and L'_{rad} , for use in calculating the radiation length in an element using Eq. (34.25).

Element	Z	L_{rad}	L'_{rad}
H	1	5.31	6.144
He	2	4.79	5.621
Li	3	4.74	5.805
Be	4	4.71	5.924
Others	> 4	$\ln(184.15 Z^{-1/3})$	$\ln(1194 Z^{-2/3})$

The radiation length in a mixture or compound may be approximated by

$$1/X_0 = \sum w_j/X_j, \quad (34.27)$$

where w_j and X_j are the fraction by weight and the radiation length for the j th element.

34.4.3 Bremsstrahlung energy loss by e^\pm

At very high energies and except at the high-energy tip of the bremsstrahlung spectrum, the cross section can be approximated in the "complete screening case" as [42]

$$d\sigma/dk = (1/k)4\alpha r_e^2 \left\{ \left(\frac{4}{3} - \frac{4}{3}y + y^2 \right) [Z^2(L_{\text{rad}} - f(Z)) + Z L'_{\text{rad}}] + \frac{1}{9}(1-y)(Z^2 + Z) \right\}, \quad (34.28)$$

where $y = k/E$ is the fraction of the electron's energy transferred to the radiated photon. At small y (the "infrared limit") the term on the second line ranges from 1.7% (low Z) to 2.5% (high Z) of the total. If it is ignored and the first line simplified with the definition of X_0 given in Eq. (34.25), we have

$$\frac{d\sigma}{dk} = \frac{A}{X_0 N_A k} \left(\frac{4}{3} - \frac{4}{3}y + y^2 \right). \quad (34.29)$$

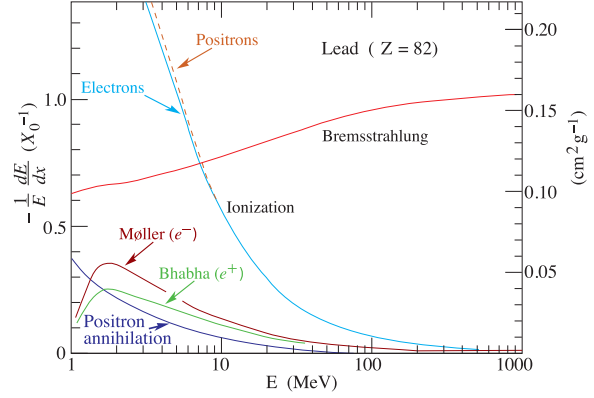


Figure 34.11: Fractional energy loss per radiation length in lead as a function of electron or positron energy. Electron (positron) scattering is considered as ionization when the energy loss per collision is below 0.255 MeV, and as Møller (Bhabha) scattering when it is above. Adapted from Fig. 3.2 from Messel and Crawford, *Electron-Photon Shower Distribution Function Tables for Lead, Copper, and Air Absorbers*, Pergamon Press, 1970. Messel and Crawford use $X_0(\text{Pb}) = 5.82$ g/cm², but we have modified the figures to reflect the value given in the Table of Atomic and Nuclear Properties of Materials ($X_0(\text{Pb}) = 6.37$ g/cm²).

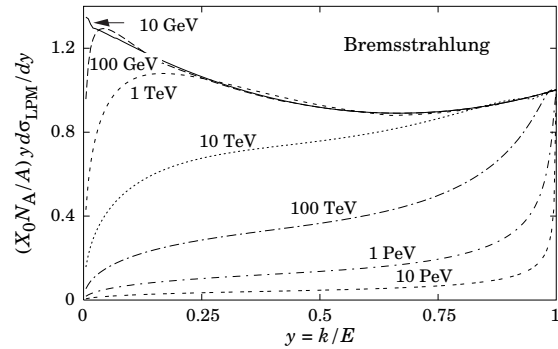


Figure 34.12: The normalized bremsstrahlung cross section $k d\sigma_{\text{LPM}}/dk$ in lead versus the fractional photon energy $y = k/E$. The vertical axis has units of photons per radiation length.

This cross section (times k) is shown by the top curve in Fig. 34.12.

This formula is accurate except near $y = 1$, where screening may become incomplete, and near $y = 0$, where the infrared divergence is removed by the interference of bremsstrahlung amplitudes from nearby scattering centers (the LPM effect) [44, 45] and dielectric suppression [46, 47]. These and other suppression effects in bulk media are discussed in Sec. 34.4.6.

With decreasing energy ($E \lesssim 10$ GeV) the high- y cross section drops and the curves become rounded as $y \rightarrow 1$. Curves of this familiar shape can be seen in Rossi [2] (Figs. 2.11.2,3); see also the review by Koch & Motz [48].

Except at these extremes, and still in the complete-screening approximation, the number of photons with energies between k_{min} and k_{max} emitted by an electron travelling a distance $d \ll X_0$ is

$$N_\gamma = \frac{d}{X_0} \left[\frac{4}{3} \ln \left(\frac{k_{\text{max}}}{k_{\text{min}}} \right) - \frac{4(k_{\text{max}} - k_{\text{min}})}{3E} + \frac{k_{\text{max}}^2 - k_{\text{min}}^2}{2E^2} \right]. \quad (34.30)$$

34.4.4 Critical energy

An electron loses energy by bremsstrahlung at a rate nearly proportional to its energy, while the ionization loss rate varies only logarithmically with the electron energy. The *critical energy* E_c is sometimes defined as the energy at which the two loss rates are equal [49]. Among alternate definitions is that of Rossi [2], who defines the critical energy as the energy at which the ion-

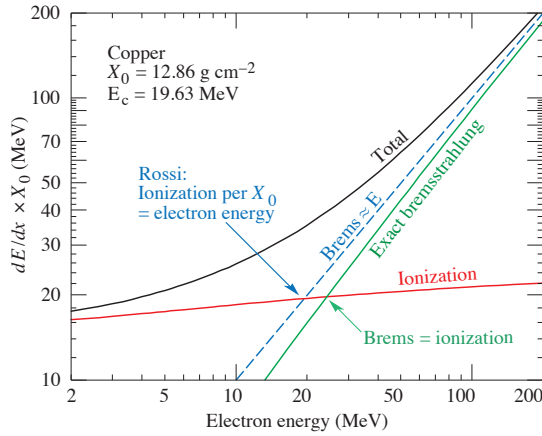


Figure 34.13: Two definitions of the critical energy E_c .

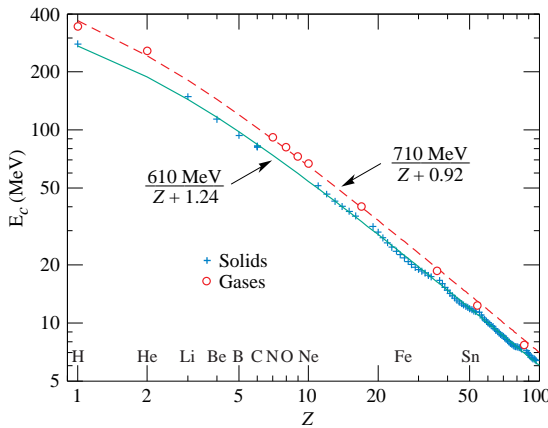


Figure 34.14: Electron critical energy for the chemical elements, using Rossi’s definition [2]. The fits shown are for solids and liquids (solid line) and gases (dashed line). The rms deviation is 2.2% for the solids and 4.0% for the gases.

ization loss per radiation length is equal to the electron energy. Equivalently, it is the same as the first definition with the approximation $|dE/dx|_{\text{brems}} \approx E/X_0$. This form has been found to describe transverse electromagnetic shower development more accurately (see below). These definitions are illustrated in the case of copper in Fig. 34.13.

The accuracy of approximate forms for E_c has been limited by the failure to distinguish between gases and solid or liquids, where there is a substantial difference in ionization at the relevant energy because of the density effect. We distinguish these two cases in Fig. 34.14. Fits were also made with functions of the form $a/(Z + b)^\alpha$, but α was found to be essentially unity. Since E_c also depends on A , I , and other factors, such forms are at best approximate.

Values of E_c for both electrons and positrons in more than 300 materials at pdg.lbl.gov/current/AtomicNuclearProperties.

34.4.5 Energy loss by photons

Contributions to the photon cross section in a light element (carbon) and a heavy element (lead) are shown in Fig. 34.15. At low energies it is seen that the photoelectric effect dominates, although Compton scattering, Rayleigh scattering, and photonuclear absorption also contribute. The photoelectric cross section is characterized by discontinuities (absorption edges) as thresholds for photoionization of various atomic levels are reached. Photon attenuation lengths for a variety of elements are shown in Fig. 34.16, and data for $30 \text{ eV} < k < 100 \text{ GeV}$ for all elements are available from the web pages given in the caption. Here k is the photon energy.

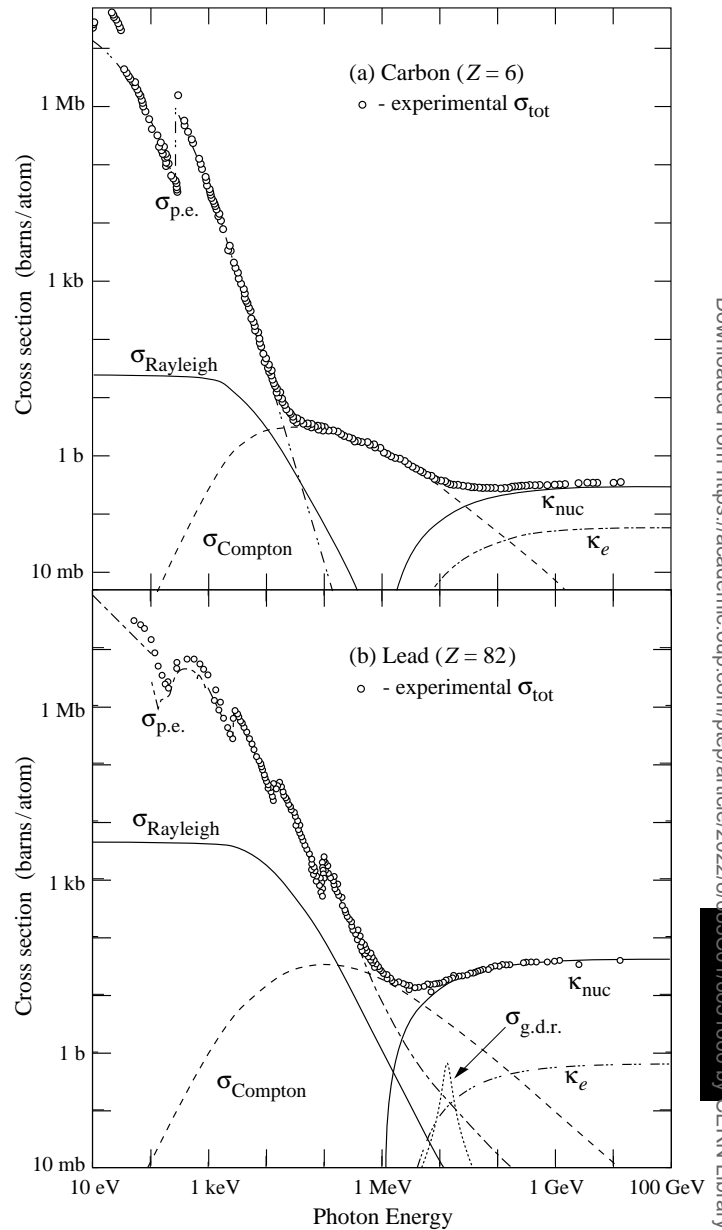


Figure 34.15: Photon total cross sections as a function of energy in carbon and lead, showing the contributions of different processes [50]:

- $\sigma_{\text{p.e.}}$ = Atomic photoelectric effect (electron ejection, photon absorption)
- σ_{Rayleigh} = Rayleigh (coherent) scattering—atom neither ionized nor excited
- σ_{Compton} = Incoherent scattering (Compton scattering off an electron)
- κ_{nuc} = Pair production, nuclear field
- κ_e = Pair production, electron field
- $\sigma_{\text{g.d.r.}}$ = Photonuclear interactions, most notably the Giant Dipole Resonance [51]. In these interactions, the target nucleus is usually broken up.

Original figures through the courtesy of John H. Hubbell (NIST).

The increasing domination of pair production as the energy increases is shown in Fig. 34.17. Using approximations similar to those used to obtain Eq. (34.29), Tsai’s formula for the differential cross section [42] reduces to

$$\frac{d\sigma}{dx} = \frac{A}{X_0 N_A} \left[1 - \frac{4}{3}x(1-x) \right] \quad (34.31)$$

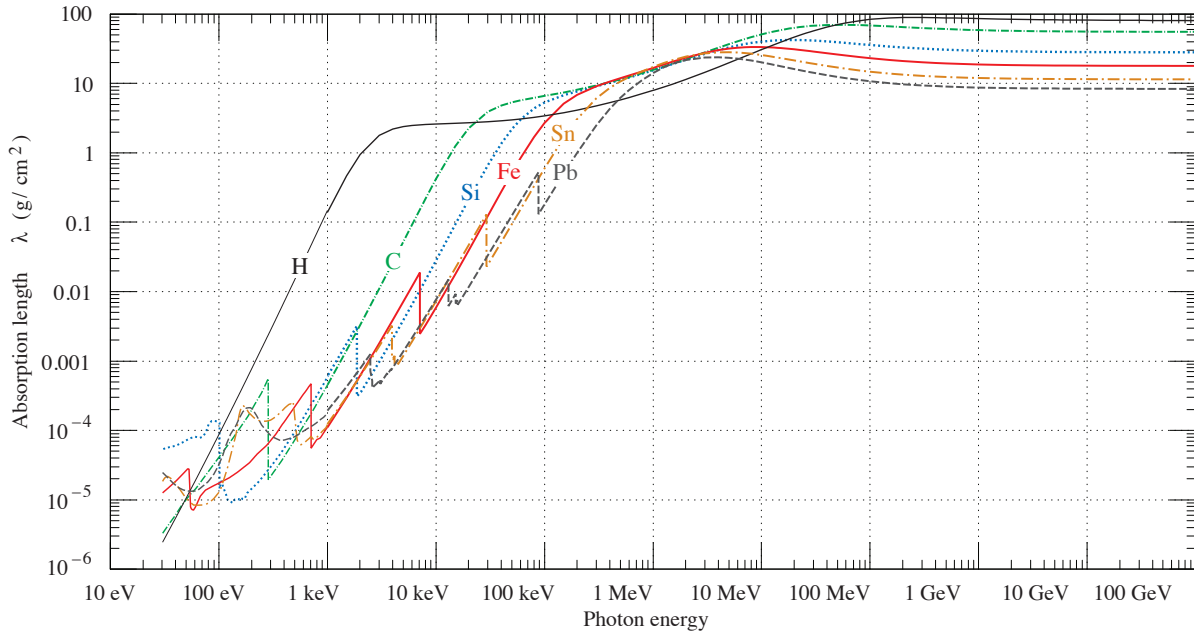


Figure 34.16: The photon mass attenuation length (or mean free path) $\lambda = 1/(\mu/\rho)$ for various elemental absorbers as a function of photon energy. The mass attenuation coefficient is μ/ρ , where ρ is the density. The intensity I remaining after traversal of thickness t (in mass/unit area) is given by $I = I_0 \exp(-t/\lambda)$. The accuracy is a few percent. For a chemical compound or mixture, $1/\lambda_{\text{eff}} \approx \sum_{\text{elements}} w_Z/\lambda_Z$, where w_Z is the proportion by weight of the element with atomic number Z . The processes responsible for attenuation are given in Fig. 34.11. Since coherent processes are included, not all these processes result in energy deposition. The data for $30 \text{ eV} < E < 1 \text{ keV}$ are from Ref. [52], those for $1 \text{ keV} < E < 100 \text{ GeV}$ from Ref. [53].

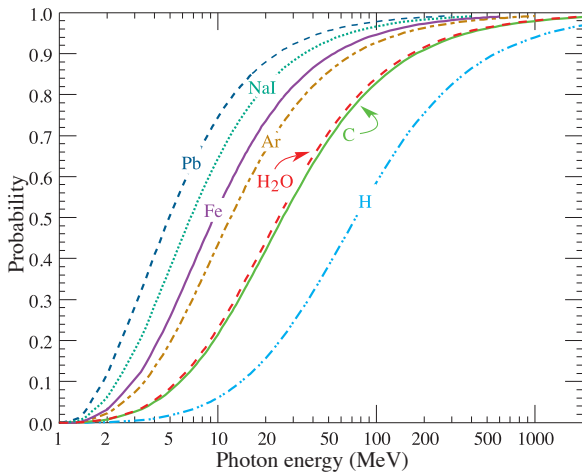


Figure 34.17: Probability P that a photon interaction will result in conversion to an e^+e^- pair. Except for a few-percent contribution from photonuclear absorption around 10 or 20 MeV, essentially all other interactions in this energy range result in Compton scattering off an atomic electron. For a photon attenuation length λ (Fig. 34.16), the probability that a given photon will produce an electron pair (without first Compton scattering) in thickness t of absorber is $P[1 - \exp(-t/\lambda)]$.

in the complete-screening limit valid at high energies. Here $x = E/k$ is the fractional energy transfer to the pair-produced electron (or positron), and k is the incident photon energy. The cross section is very closely related to that for bremsstrahlung, since the Feynman diagrams are variants of one another. The cross section is of necessity symmetric between x and $1 - x$, as can be seen by the solid curve in Fig. 34.18. See the review by Motz, Olsen, & Koch for a more detailed treatment [54]. Eq. (34.31) may be integrated to find the high-energy limit for the total e^+e^-

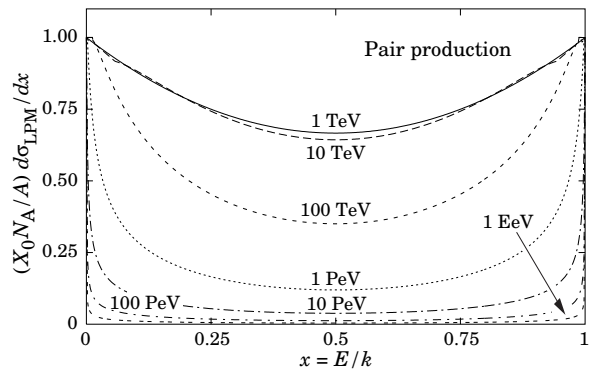


Figure 34.18: The normalized pair production cross section $d\sigma_{LPM}/dx$, versus fractional electron energy $x = E/k$.

pair-production cross section:

$$\sigma = \frac{7}{9}(A/X_0N_A). \tag{34.32}$$

Equation Eq. (34.32) is accurate to within a few percent down to energies as low as 1 GeV, particularly for high- Z materials.

34.4.6 Bremsstrahlung and pair production at very high energies

At ultrahigh energies, Eqns. 34.28–34.32 will fail because of quantum mechanical interference between amplitudes from different scattering centers. Since the longitudinal momentum transfer to a given center is small ($\propto k/E(E - k)$, in the case of bremsstrahlung), the interaction is spread over a comparatively long distance called the formation length ($\propto E(E - k)/k$) via the uncertainty principle. In alternate language, the formation length is the distance over which the highly relativistic electron and the photon “split apart.” The interference is usually destructive. Calculations of the “Landau-Pomeranchuk-Migdal” (LPM) effect may be made semi-classically based on the average multiple scattering, or more rigorously using a quantum transport approach [44, 45].

In amorphous media, bremsstrahlung is suppressed if the photon energy k is less than $E^2/(E + E_{LPM})$ [45], where⁸

$$E_{LPM} = (m_e c^2)^2 \alpha \frac{X_0}{4\pi\hbar c \rho} = (7.7 \text{ TeV/cm}) \times \frac{X_0}{\rho}. \quad (34.33)$$

Since physical distances are involved, X_0/ρ , in cm, appears. The energy-weighted bremsstrahlung spectrum for lead, $k d\sigma_{LPM}/dk$, is shown in Fig. 34.12. With appropriate scaling by X_0/ρ , other materials behave similarly.

For photons, pair production is reduced for $E(k - E) > k E_{LPM}$. The pair-production cross sections for different photon energies are shown in Fig. 34.18.

If $k \ll E$, several additional mechanisms can also produce suppression. When the formation length is long, even weak factors can perturb the interaction. For example, the emitted photon can coherently forward scatter off of the electrons in the media. Because of this, for $k < \omega_p E/m_e \sim 10^{-4}$, bremsstrahlung is suppressed by a factor $(km_e/\omega_p E)^2$ [47]. Magnetic fields can also suppress bremsstrahlung.

In crystalline media, the situation is more complicated, with coherent enhancement or suppression possible. The cross section depends on the electron and photon energies and the angles between the particle direction and the crystalline axes [56].

34.4.7 Photonuclear and electronuclear interactions at still higher energies

At still higher photon and electron energies, where the bremsstrahlung and pair production cross-sections are heavily suppressed by the LPM effect, photonuclear and electronuclear interactions predominate over electromagnetic interactions.

At photon energies above about 10^{20} eV, for example, photons usually interact hadronically. The exact cross-over energy depends on the model used for the photonuclear interactions. These processes are illustrated in Fig. 34.19. At still higher energies ($\gtrsim 10^{23}$ eV), photonuclear interactions can become coherent, with the photon interaction spread over multiple nuclei. Essentially, the photon coherently converts to a ρ^0 , in a process that is somewhat similar to kaon regeneration [57].

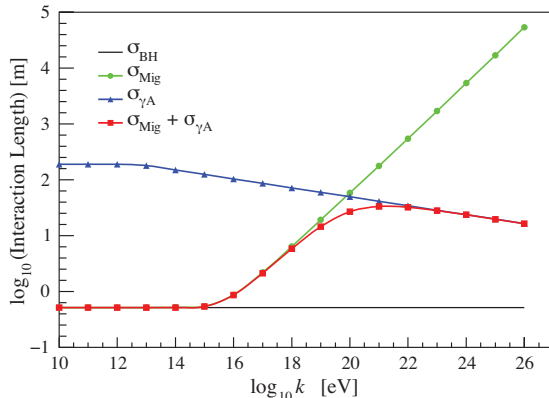


Figure 34.19: Interaction length for a photon in ice as a function of photon energy for the Bethe-Heitler (BH), LPM (Mig) and photonuclear (γA) cross sections [57]. The Bethe-Heitler interaction length is $9X_0/7$, and X_0 is 0.393 m in ice.

Similar processes occur for electrons. As electron energies increase and the LPM effect suppresses bremsstrahlung, electronuclear interactions become more important. At energies above 10^{21} eV, these electronuclear interactions dominate electron energy loss [57].

34.5 Electromagnetic cascades

When a high-energy electron or photon is incident on a thick absorber, it initiates an electromagnetic cascade as pair production

⁸This definition differs from that of Ref. [55] by a factor of two. E_{LPM} scales as the 4th power of the mass of the incident particle, so that $E_{LPM} = (1.4 \times 10^{10} \text{ TeV/cm}) \times X_0/\rho$ for a muon.

and bremsstrahlung generate more electrons and photons with lower energy. The longitudinal development is governed by the high-energy part of the cascade, and therefore scales as the radiation length in the material. Electron energies eventually fall below the critical energy, and then dissipate their energy by ionization and excitation rather than by the generation of more shower particles. In describing shower behavior, it is therefore convenient to introduce the scale variables

$$t = x/X_0, \quad y = E/E_c, \quad (34.34)$$

so that distance is measured in units of radiation length and energy in units of critical energy.

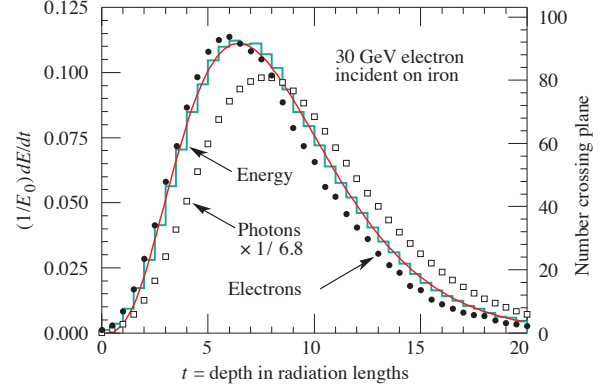


Figure 34.20: An EGS4 simulation of a 30 GeV electron-induced cascade in iron. The histogram shows fractional energy deposition per radiation length, and the curve is a gamma-function fit to the distribution. Circles indicate the number of electrons with total energy greater than 1.5 MeV crossing planes at $X_0/2$ intervals (scale on right) and the squares the number of photons with $E \geq 1.5$ MeV crossing the planes (scaled down to have same area as the electron distribution).

Longitudinal profiles from an EGS4 [58] simulation of a 30 GeV electron-induced cascade in iron are shown in Fig. 34.20. The number of particles crossing a plane (very close to Rossi's Π function [2]) is sensitive to the cutoff energy, here chosen as a total energy of 1.5 MeV for both electrons and photons. The electron number falls off more quickly than energy deposition. This is because, with increasing depth, a larger fraction of the cascade energy is carried by photons. Exactly what a calorimeter measures depends on the device, but it is not likely to be exactly any of the profiles shown. In gas counters it may be very close to the electron number, but in glass Cherenkov detectors and other devices with “thick” sensitive regions it is closer to the energy deposition (total track length). In such detectors the signal is proportional to the “detectable” track length T_d , which is in general less than the total track length T . Practical devices are sensitive to electrons with energy above some detection threshold E_d , and $T_d = T F(E_d/E_c)$. An analytic form for $F(E_d/E_c)$ obtained by Rossi [2] is given by Fabjan in Ref. [59]; see also Amaldi [60].

The mean longitudinal profile of the energy deposition in an electromagnetic cascade is reasonably well described by a gamma distribution [61]:

$$\frac{dE}{dt} = E_0 b \frac{(bt)^{a-1} e^{-bt}}{\Gamma(a)} \quad (34.35)$$

The maximum t_{\max} occurs at $(a - 1)/b$. We have made fits to shower profiles in elements ranging from carbon to uranium, at energies from 1 GeV to 100 GeV. The energy deposition profiles are well described by Eq. (34.35) with

$$t_{\max} = (a - 1)/b = 1.0 \times (\ln y + C_j), \quad j = e, \gamma, \quad (34.36)$$

where $C_e = -0.5$ for electron-induced cascades and $C_\gamma = +0.5$ for photon-induced cascades. To use Eq. (34.35), one finds $(a - 1)/b$ from Eq. (34.36) and Eq. (34.34), then finds a either by assuming

$b \approx 0.5$ or by finding a more accurate value from Fig. 34.21. The results are very similar for the electron number profiles, but there is some dependence on the atomic number of the medium. A similar form for the electron number maximum was obtained by Rossi in the context of his “Approximation B,” [2] (see Fabjan’s review in Ref. [59]), but with $C_e = -1.0$ and $C_\gamma = -0.5$; we regard this as superseded by the EGS4 result.

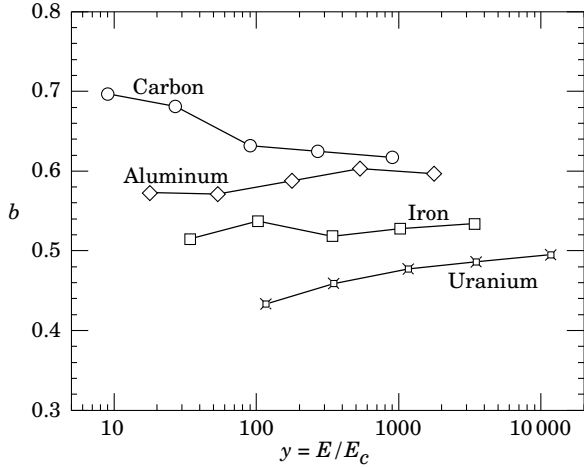


Figure 34.21: Fitted values of the scale factor b for energy deposition profiles obtained with EGS4 for a variety of elements for incident electrons with $1 \leq E_0 \leq 100$ GeV. Values obtained for incident photons are essentially the same.

The “shower length” $X_s = X_0/b$ is less conveniently parameterized, since b depends upon both Z and incident energy, as shown in Fig. 34.21. As a corollary of this Z dependence, the number of electrons crossing a plane near shower maximum is underestimated using Rossi’s approximation for carbon and seriously overestimated for uranium. Essentially the same b values are obtained for incident electrons and photons. For many purposes it is sufficient to take $b \approx 0.5$.

The length of showers initiated by ultra-high energy photons and electrons is somewhat greater than at lower energies since the first or first few interaction lengths are increased via the mechanisms discussed above.

The gamma function distribution is very flat near the origin, while the EGS4 cascade (or a real cascade) increases more rapidly. As a result Eq. (34.35) fails badly for about the first two radiation lengths; it was necessary to exclude this region in making fits.

Because fluctuations are important, Eq. (34.35) should be used only in applications where average behavior is adequate. Grindhammer *et al.* have developed fast simulation algorithms in which the variance and correlation of a and b are obtained by fitting Eq. (34.35) to individually simulated cascades, then generating profiles for cascades using a and b chosen from the correlated distributions [62].

The transverse development of electromagnetic showers in different materials scales fairly accurately with the *Molière radius* R_M , given by [63, 64]

$$R_M = X_0 E_s/E_c, \quad (34.37)$$

where $E_s \approx 21$ MeV (Table 34.1), and the Rossi definition of E_c is used.

In a material containing a weight fraction w_j of the element with critical energy E_{cj} and radiation length X_j , the Molière radius is given by

$$\frac{1}{R_M} = \frac{1}{E_s} \sum \frac{w_j E_{cj}}{X_j}. \quad (34.38)$$

Measurements of the lateral distribution in electromagnetic cascades are shown in Refs. [63, 64]. On the average, only 10% of the energy lies outside the cylinder with radius R_M . About 99% is contained inside of $3.5R_M$, but at this radius and beyond composition effects become important and the scaling with R_M fails.

The distributions are characterized by a narrow core, and broaden as the shower develops. They are often represented as the sum of two Gaussians.

At high enough energies, the LPM effect (Sec. 34.4.6) reduces the cross sections for bremsstrahlung and pair production, and hence can cause significant elongation of electromagnetic cascades [45].

34.6 Muon energy loss at high energy

At sufficiently high energies, radiative processes become more important than ionization for all charged particles. For muons and pions in materials such as iron, this “critical energy” occurs at several hundred GeV. (There is no simple scaling with particle mass, but for protons the “critical energy” is much, much higher.) Radiative effects dominate the energy loss of energetic muons found in cosmic rays or produced at the newest accelerators. These processes are characterized by small cross sections, hard spectra, large energy fluctuations, and the associated generation of electromagnetic and (in the case of photonuclear interactions) hadronic showers [65–73]. As a consequence, at these energies the treatment of energy loss as a uniform and continuous process is for many purposes inadequate.

It is convenient to write the average rate of muon energy loss as [74]

$$\langle -dE/dx \rangle = a(E) + b(E)E. \quad (34.39)$$

Here $a(E)$ is the ionization energy loss given by Eq. (34.5), and $b(E)$ is the sum of e^+e^- pair production, bremsstrahlung, and photonuclear contributions. To the approximation that these slowly-varying functions are constant, the mean range x_0 of a muon with initial energy E_0 is given by

$$x_0 \approx (1/b) \ln(1 + E_0/E_{\mu c}), \quad (34.40)$$

where $E_{\mu c} = a/b$.

Fig. 34.22 shows contributions to $b(E)$ for iron. Since $a(E) \approx 0.002$ GeV g⁻¹ cm², $b(E)E$ dominates the energy loss above several hundred GeV, where $b(E)$ is nearly constant. The rates of energy loss for muons in hydrogen, uranium, and iron are shown in Fig. 34.23 [7].

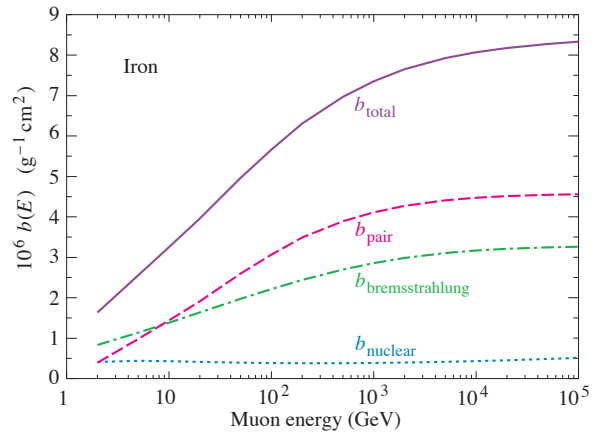


Figure 34.22: Contributions to the fractional energy loss by muons in iron due to e^+e^- pair production, bremsstrahlung, and photonuclear interactions, as obtained from Groom *et al.* [7] except for post-Born corrections to the cross section for direct pair production from atomic electrons.

The “muon critical energy” $E_{\mu c}$ can be defined more exactly as the energy at which radiative and ionization losses are equal, and can be found by solving $E_{\mu c} = a(E_{\mu c})/b(E_{\mu c})$. This definition corresponds to the solid-line intersection in Fig. 34.13, and is different from the Rossi definition we used for electrons. It serves the same function: below $E_{\mu c}$ ionization losses dominate, and above $E_{\mu c}$ radiative effects dominate. The dependence of $E_{\mu c}$ on atomic number Z is shown in Fig. 34.24.

The radiative cross sections are expressed as functions of the fractional energy loss ν . The bremsstrahlung cross section goes

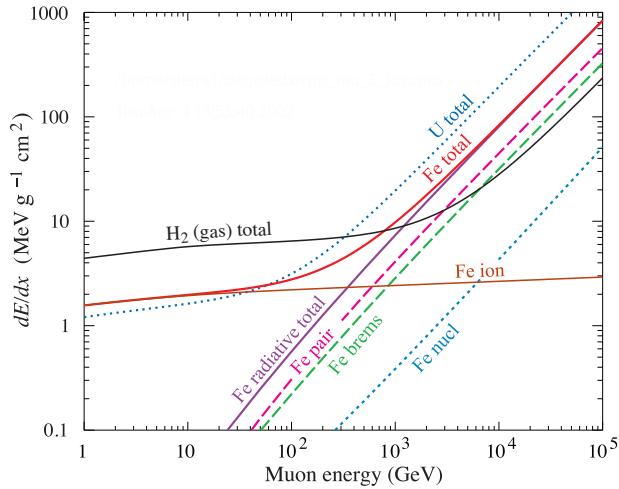


Figure 34.23: The average energy loss of a muon in hydrogen, iron, and uranium as a function of muon energy. Contributions to dE/dx in iron from ionization and pair production, bremsstrahlung and photonuclear interactions are also shown.

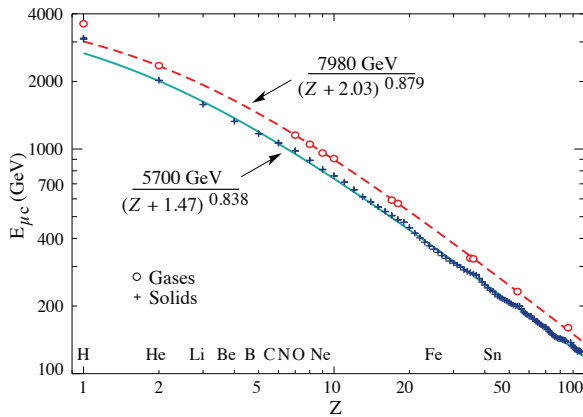


Figure 34.24: Muon critical energy for the chemical elements, defined as the energy at which radiative and ionization energy loss rates are equal [7]. The equality comes at a higher energy for gases than for solids or liquids with the same atomic number because of a smaller density effect reduction of the ionization losses. The fits shown in the figure exclude hydrogen. Alkali metals fall 3–4% above the fitted function, while most other solids are within 2% of the function. Among the gases the worst fit is for radon (2.7% high).

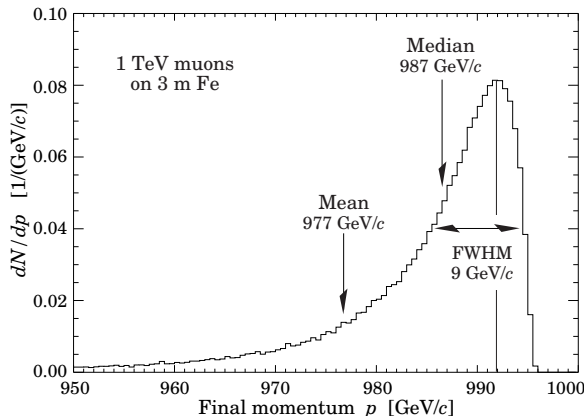


Figure 34.25: The momentum distribution of 1 TeV/c muons after traversing 3 m of iron as calculated by S.I. Striganov [7].

roughly as $1/\nu$ over most of the range, while for the pair production case the distribution goes as ν^{-3} to ν^{-2} [75]. “Hard” losses are therefore more probable in bremsstrahlung, and in fact energy losses due to pair production may very nearly be treated as continuous. The simulated momentum distribution of an incident 1 TeV/c muon beam after it crosses 3 m of iron is shown in Fig. 34.25 [7]. The most probable loss is 8 GeV, or 3.4 MeV $g^{-1}cm^2$. The full width at half maximum is 9 GeV/c, or 0.9%. The radiative tail is almost entirely due to bremsstrahlung, although most of the events in which more than 10% of the incident energy lost experienced relatively hard photonuclear interactions. The latter can exceed detector resolution [76], necessitating the reconstruction of lost energy. Tables in Ref. [7] list the stopping power as 9.82 MeV $g^{-1}cm^2$ for a 1 TeV muon, so that the mean loss should be 23 GeV (≈ 23 GeV/c), for a final momentum of 977 GeV/c, far below the peak. This agrees with the indicated mean calculated from the simulation. Electromagnetic and hadronic cascades in detector materials can obscure muon tracks in detector planes and reduce tracking efficiency [77].

34.7 Cherenkov and transition radiation [3, 78, 79]

A charged particle radiates if its speed is greater than the local phase speed of light (Cherenkov radiation) or if it crosses suddenly from one medium to another with different optical properties (transition radiation). Neither process is important for energy loss, but both are used in high-energy and cosmic-ray physics detectors.

34.7.1 Optical Cherenkov radiation

The angle θ_c of Cherenkov radiation, relative to the particle’s direction, for a particle with speed βc in a medium with index of refraction n is

$$\begin{aligned} \cos \theta_c &= (1/n\beta) \\ \text{or } \tan \theta_c &= \sqrt{\beta^2 n^2 - 1} \\ &\approx \sqrt{2(1 - 1/n\beta)} \quad \text{for small } \theta_c, \text{ e.g. in gases. (34.41)} \end{aligned}$$

The threshold speed β_t is $1/n$, and $\gamma_t = 1/(1 - \beta_t^2)^{1/2}$. Therefore, $\beta_t \gamma_t = 1/(2\delta + \delta^2)^{1/2}$, where $\delta = n - 1$. Values of δ for various commonly used gases are given as a function of pressure and wavelength in Ref. [80]. See its Table 6.1 for values at atmospheric pressure. Data for other commonly used materials are given in Ref. [81].

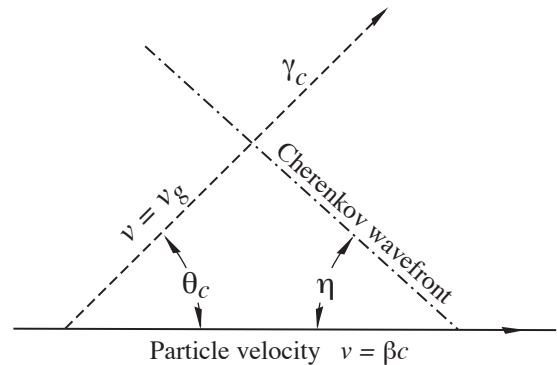


Figure 34.26: Cherenkov light emission and wavefront angles. In a dispersive medium, $\theta_c + \eta \neq 90^\circ$.

Practical Cherenkov radiator materials are dispersive. Let ω be the photon’s frequency, and let $k = 2\pi/\lambda$ be its wavenumber. The photons propagate at the group speed $v_g = d\omega/dk = c/[n(\omega) + \omega(dn/d\omega)]$. In a non-dispersive medium, this simplifies to $v_g = c/n$.

In his classical paper, Tamm [82] showed that for dispersive media the radiation is concentrated in a thin conical shell whose

vertex is at the moving charge, and whose opening half-angle η is

$$\cot \eta = \left[\frac{d}{d\omega} (\omega \tan \theta_c) \right]_{\omega_0} = \left[\tan \theta_c + \beta^2 \omega n(\omega) \frac{dn}{d\omega} \cot \theta_c \right]_{\omega_0}, \quad (34.42)$$

where ω_0 is the central value of the small frequency range under consideration. (See Fig. 34.26.) This cone has a opening half-angle η , and, unless the medium is non-dispersive ($dn/d\omega = 0$), $\theta_c + \eta \neq 90^\circ$. The Cherenkov wavefront ‘sideslips’ along with the particle [83]. This effect has timing implications for ring imaging Cherenkov counters [84], but it is probably unimportant for most applications.

The number of photons produced per unit path length of a particle with charge ze and per unit energy interval of the photons is

$$\frac{d^2 N}{dE dx} = \frac{\alpha z^2}{hc} \sin^2 \theta_c = \frac{\alpha^2 z^2}{r_e m_e c^2} \left(1 - \frac{1}{\beta^2 n^2(E)} \right) \approx 370 \sin^2 \theta_c(E) \text{ eV}^{-1} \text{ cm}^{-1} \quad (z = 1), \quad (34.43)$$

or, equivalently,

$$\frac{d^2 N}{dx d\lambda} = \frac{2\pi\alpha z^2}{\lambda^2} \left(1 - \frac{1}{\beta^2 n^2(\lambda)} \right). \quad (34.44)$$

The index of refraction n is a function of photon energy $E = \hbar\omega$, as is the sensitivity of the transducer used to detect the light. For practical use, Eq. (34.43) must be multiplied by the the transducer response function and integrated over the region for which $\beta n(\omega) > 1$. Further details are given in the discussion of Cherenkov detectors in the Particle Detectors section (Sec. 35.5 of this Review).

When two particles are close together (lateral separation $\lesssim 1$ wavelength), the electromagnetic fields from the particles may add coherently, affecting the Cherenkov radiation. Because of their opposite charges, the radiation from an e^+e^- pair at close separation is suppressed compared to two independent leptons [85].

34.7.2 Coherent radio Cherenkov radiation

Coherent Cherenkov radiation is produced by many charged particles with a non-zero net charge moving through matter on an approximately common “wavefront”—for example, the electrons and positrons in a high-energy electromagnetic cascade. The signals can be visible for energies above 10^{16} eV; see Sec. 36.3.3 for more details. The phenomenon is called the Askaryan effect [86]. Near the end of a shower, when typical particle energies are below E_c (but still relativistic), a charge imbalance develops. Photons can Compton-scatter atomic electrons, and positrons can annihilate with atomic electrons to contribute even more photons which can in turn Compton scatter. These processes result in a roughly 20% excess of electrons over positrons in a shower. The net negative charge leads to coherent radio Cherenkov emission. The radiation includes a component from the decelerating charges (as in bremsstrahlung). Because the emission is coherent, the electric field strength is proportional to the shower energy, and the signal power increases as its square. The electric field strength also increases linearly with frequency, up to a maximum frequency determined by the lateral spread of the shower. This cutoff occurs at about 1 GHz in ice, and scales inversely with the Moliere radius. At low frequencies, the radiation is roughly isotropic, but, as the frequency rises toward the cutoff frequency, the radiation becomes increasingly peaked around the Cherenkov angle. The radiation is linearly polarized in the plane containing the shower axis and the photon direction. A measurement of the signal polarization can be used to help determine the shower direction. The characteristics of this radiation have been nicely demonstrated in a series of experiments at SLAC [87]. A detailed discussion of the radiation can be found in Ref. [88].

34.7.3 Transition radiation

The energy radiated when a particle with charge ze crosses the boundary between vacuum and a medium with plasma frequency ω_p is

$$I = \alpha z^2 \gamma \hbar \omega_p / 3, \quad (34.45)$$

where

$$\hbar \omega_p = \sqrt{4\pi N_e r_e^3} m_e c^2 / \alpha = \sqrt{\rho \text{ (in g/cm}^3\text{)} \langle Z/A \rangle} \times 28.81 \text{ eV}. \quad (34.46)$$

For styrene and similar materials, $\hbar \omega_p \approx 20$ eV; for air it is 0.7 eV.

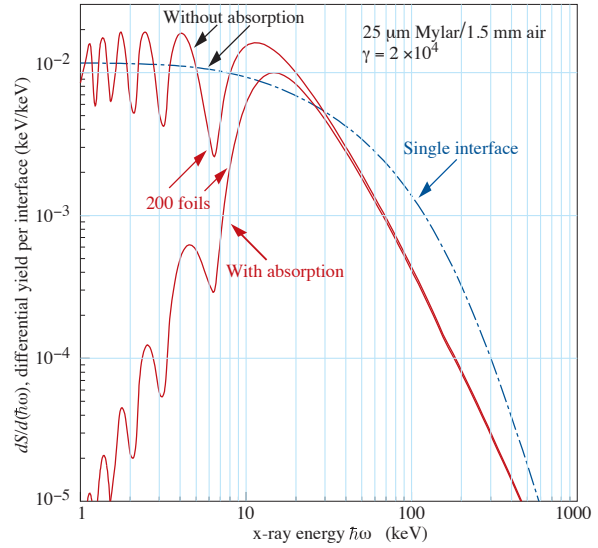


Figure 34.27: X-ray photon energy spectra for a radiator consisting of 200 25 μm thick foils of Mylar with 1.5 mm spacing in air (solid lines) and for a single surface (dashed line). Curves are shown with and without absorption. Adapted from Ref. [89].

The number spectrum $dN_\gamma/d(\hbar\omega)$ diverges logarithmically at low energies and decreases rapidly for $\hbar\omega/\gamma\hbar\omega_p > 1$. About half the energy is emitted in the range $0.1 \leq \hbar\omega/\gamma\hbar\omega_p \leq 1$. Inevitable absorption in a practical detector removes the divergence. For a particle with $\gamma = 10^3$, the radiated photons are in the soft x-ray range 2 to 40 keV. The γ dependence of the emitted energy thus comes from the hardening of the spectrum rather than from an increased quantum yield.

The number of photons with energy $\hbar\omega > \hbar\omega_0$ is given by the answer to problem 13.15 in Ref. [3],

$$N_\gamma(\hbar\omega > \hbar\omega_0) = \frac{\alpha z^2}{\pi} \left[\left(\ln \frac{\gamma \hbar \omega_p}{\hbar \omega_0} - 1 \right)^2 + \frac{\pi^2}{12} \right], \quad (34.47)$$

within corrections of order $(\hbar\omega_0/\gamma\hbar\omega_p)^2$. The number of photons above a fixed energy $\hbar\omega_0 \ll \gamma\hbar\omega_p$ thus grows as $(\ln \gamma)^2$, but the number above a fixed fraction of $\gamma\hbar\omega_p$ (as in the example above) is constant. For example, for $\hbar\omega > \gamma\hbar\omega_p/10$, $N_\gamma = 2.519 \alpha z^2 / \pi = 0.59\% \times z^2$.

The particle stays “in phase” with the x ray over a distance called the formation length, $d(\omega) = (2c/\omega)(1/\gamma^2 + \omega_p^2/\omega^2)^{-1}$. Most of the radiation is produced in this distance. Here θ is the x-ray emission angle, characteristically $1/\gamma$. For $\theta = 1/\gamma$ the formation length has a maximum at $d(\gamma\omega_p/\sqrt{2}) = \gamma c/\sqrt{2}\omega_p$. In practical situations it is tens of μm .

Since the useful x-ray yield from a single interface is low, in practical detectors it is enhanced by using a stack of N foil radiators—foils L thick, where L is typically several formation lengths—separated by gas-filled gaps. The amplitudes at successive interfaces interfere to cause oscillations about the single-interface spectrum. At increasing frequencies above the position of the last interference maximum ($L/d(\omega) = \pi/2$), the formation zones, which have opposite phase, overlap more and more and the

spectrum saturates, $dI/d\omega$ approaching zero as $L/d(\omega) \rightarrow 0$. This is illustrated in Fig. 34.27 for a realistic detector configuration.

For regular spacing of the layers fairly complicated analytic solutions for the intensity have been obtained [89,90]. Although one might expect the intensity of coherent radiation from the stack of foils to be proportional to N^2 , the angular dependence of the formation length conspires to make the intensity $\propto N$.

References

- [1] H. Bichsel, Nucl. Instrum. Meth. **A562**, 154 (2006).
- [2] B. Rossi, *High Energy Particles*, Prentice-Hall, Inc., Englewood Cliffs, NJ, 1952.
- [3] J.D. Jackson, *Classical Electrodynamics*, 3rd edition, (John Wiley and Sons, New York, 1998).
- [4] H.A. Bethe, *Zur Theorie des Durchgangs schneller Korpuskularstrahlen durch Materie*, H. Bethe, Ann. Phys. **5**, 325 (1930).
- [5] M. S. Livingston and H. A. Bethe, Rev. Mod. Phys. **9**, 245 (1937).
- [6] "Stopping Powers and Ranges for Protons and Alpha Particles," ICRU Report No. 49 (1993); Tables and graphs are available at physics.nist.gov/PhysRefData/Star/Text/PSTAR.html and physics.nist.gov/PhysRefData/Star/Text/ASTAR.html.
- [7] D.E. Groom, N.V. Mokhov, and S.I. Striganov, "Muon stopping-power and range tables: 10 MeV–100 TeV," Atomic Data and Nuclear Data Tables **78**, 183–356 (2001). Since submission of this paper it has become likely that post-Born corrections to the direct pair production cross section should be made. Code used to make Figs. 34.22–34.24 included these corrections [D.Yu. Ivanov *et al.*, Phys. Lett. **B442**, 453 (1998)]. The effect is negligible except at high Z . (It is less than 1% for iron.); The introductory text of the paper can be found at pdg.lbl.gov/current/AtomicNuclearProperties/adndt.pdf

Extensive printable and machine-readable tables for muons are given at pdg.lbl.gov/current/AtomicNuclearProperties/.
- [8] W. H. Barkas, W. Birnbaum and F. M. Smith, Phys. Rev. **101**, 778 (1956).
- [9] U. Fano, Ann. Rev. Nucl. Part. Sci. **13**, 1 (1963).
- [10] J. D. Jackson, Phys. Rev. **D59**, 017301 (1999).
- [11] J. Lindhard and A. H. Sørensen, Phys. Rev. **A53**, 2443 (1996).
- [12] "Stopping Powers for Electrons and Positrons," ICRU Report No. 37 (1984); Tables and graphs are available at physics.nist.gov/PhysRefData/Star/Text/ESTAR.html.
- [13] H. Bichsel, Phys. Rev. **A46**, 5761 (1992).
- [14] W.H. Barkas and M.J. Berger, *Tables of Energy Losses and Ranges of Heavy Charged Particles*, NASA-SP-3013 (1964).
- [15] S.M. Seltzer and M.J. Berger, Int. J. of Applied Rad. **33**, 1189 (1982).
- [16] physics.nist.gov/PhysRefData/XrayMassCoef/tab1.html.
- [17] R. M. Sternheimer, Phys. Rev. **88**, 851 (1952).
- [18] R. M. Sternheimer, M. J. Berger and S. M. Seltzer, Atom. Data Nucl. Data Tabl. **30**, 261 (1984); Minor errors are corrected in Ref. 5. Chemical composition for the tabulated materials is given in Ref. 10.
- [19] R. M. Sternheimer and R. F. Peierls, Phys. Rev. **B3**, 3681 (1971).
- [20] N. F. Mott, Proceedings of the Cambridge Philosophical Society **27**, 553 (1931).
- [21] H. Bichsel, Phys. Rev. **A65**, 5, 052709 (2002).
- [22] S. P. Møller *et al.*, Phys. Rev. **A56**, 4, 2930 (1997).
- [23] J. C. Ashley, R. H. Ritchie and W. Brandt, Phys. Rev. B **5**, 2393 (1972).
- [24] H.H. Andersen and J.F. Ziegler, *Hydrogen: Stopping Powers and Ranges in All Elements*. Vol. 3 of *The Stopping and Ranges of Ions in Matter* (Pergamon Press 1977).
- [25] J. Lindhard, Kgl. Danske Videnskab. Selskab, Mat.-Fys. Medd. **28**, No. 8 (1954); J. Lindhard, M. Scharff, and H.E. Schiøtt, Kgl. Danske Videnskab. Selskab, Mat.-Fys. Medd. **33**, No. 14 (1963).
- [26] J.F. Ziegler, J.F. Biersac, and U. Littmark, *The Stopping and Range of Ions in Solids*, Pergamon Press 1985.
- [27] E.A. Uehling, Ann. Rev. Nucl. Sci. **4**, 315 (1954) (For heavy particles with unit charge, but e^\pm cross sections and stopping powers are also given).
- [28] N.F. Mott and H.S.W. Massey, *The Theory of Atomic Collisions*, Oxford Press, London, 1965.
- [29] P. V. Vavilov, Sov. Phys. JETP **5**, 749 (1957), [Zh. Eksp. Teor. Fiz.32,920(1957)].
- [30] L.D. Landau, J. Exp. Phys. (USSR) **8**, 201 (1944).
- [31] H. Bichsel, Rev. Mod. Phys. **60**, 663 (1988).
- [32] R. Talman, Nucl. Instrum. Meth. **159**, 189 (1979).
- [33] H. Bichsel, Ch. 87 in the Atomic, Molecular and Optical Physics Handbook, G.W.F. Drake, editor (Am. Inst. Phys. Press, Woodbury NY, 1996).
- [34] S.M. Seltzer and M.J. Berger, Int. J. of Applied Rad. **35**, 665 (1984). This paper corrects and extends the results of Ref. [15].
- [35] H. A. Bethe, Phys. Rev. **89**, 1256 (1953).
- [36] W. T. Scott, Rev. Mod. Phys. **35**, 231 (1963).
- [37] J. W. Motz, H. Olsen and H. W. Koch, Rev. Mod. Phys. **36**, 881 (1964).
- [38] H. Bichsel, Phys. Rev. **112**, 182 (1958).
- [39] G. Shen *et al.*, Phys. Rev. **D20**, 1584 (1979).
- [40] G. R. Lynch and O. I. Dahl, Nucl. Instrum. Meth. **B58**, 6 (1991).
- [41] M. Wong *et al.*, Med. Phys. **17**, 163 (1990).
- [42] Y.-S. Tsai, Rev. Mod. Phys. **46**, 815 (1974), [Erratum: Rev. Mod. Phys.49,521(1977)].
- [43] H. Davies, H. A. Bethe and L. C. Maximon, Phys. Rev. **93**, 788 (1954).
- [44] L. D. Landau and I. Pomeranchuk, Dokl. Akad. Nauk Ser. Fiz. **92**, 535 (1953); **92**, 735 (1953). These papers are available in English in L. Landau, *The Collected Papers of L.D. Landau*, Pergamon Press, 1965; A. B. Migdal, Phys. Rev. **103**, 1811 (1956).
- [45] S. Klein, Rev. Mod. Phys. **71**, 1501 (1999).
- [46] M.L. Ter-Mikaelian, SSSR **94**, 1033 (1954); M.L. Ter-Mikaelian, *High Energy Electromagnetic Processes in Condensed Media* (John Wiley and Sons, New York, 1972).
- [47] P. L. Anthony *et al.*, Phys. Rev. Lett. **76**, 3550 (1996).
- [48] H. W. Koch and J. W. Motz, Rev. Mod. Phys. **31**, 920 (1959).
- [49] M.J. Berger and S.M. Seltzer, "Tables of Energy Losses and Ranges of Electrons and Positrons," National Aeronautics and Space Administration Report NASA-SP-3012 (Washington DC 1964).
- [50] Curves for these and other elements, compounds, and mixtures may be obtained from nist.gov/pml/xcom-photon-cross-sections-database. The photon total cross section is approximately flat for at least two decades beyond the energy range shown.
- [51] B. L. Berman and S. C. Fultz, Rev. Mod. Phys. **47**, 713 (1975).
- [52] www.cxro.lbl.gov/optical_constants/pert_form.html.
- [53] physics.nist.gov/PhysRefData/XrayMassCoef/tab3.html.
- [54] J. W. Motz, H. A. Olsen and H. W. Koch, Rev. Mod. Phys. **41**, 581 (1969).

- [55] P. L. Anthony *et al.*, Phys. Rev. Lett. **75**, 1949 (1995).
- [56] U. I. Uggerhøj, Rev. Mod. Phys. **77**, 1131 (2005).
- [57] L. Gerhardt and S. R. Klein, Phys. Rev. **D82**, 074017 (2010).
- [58] W.R. Nelson, H. Hirayama, and D.W.O. Rogers, “The EGS4 Code System,” SLAC-265, Stanford Linear Accelerator Center (Dec. 1985).
- [59] *Experimental Techniques in High Energy Physics*, ed. T. Ferbel (Addison-Wesley, Menlo Park CA 1987).
- [60] U. Amaldi, Phys. Scripta **23**, 409 (1981).
- [61] E. Longo and I. Sestili, Nucl. Instrum. Meth. **128**, 283 (1975), [Erratum: Nucl. Instrum. Meth.135,587(1976)].
- [62] G. Grindhammer *et al.*, in *Proceedings of the 1988 Summer Study on High Energy Physics in the 1990’s*, Snowmass, CO, June 27 – July 15, 1990, edited by F.J. Gilman and S. Jensen, (World Scientific, Teaneck, NJ, 1989) p. 151.
- [63] W. R. Nelson *et al.*, Phys. Rev. **149**, 201 (1966).
- [64] G. Bathow *et al.*, Nucl. Phys. **B20**, 592 (1970).
- [65] H. Bethe and W. Heitler, Proc. Roy. Soc. Lond. **A146**, 83 (1934); H.A. Bethe, *Proc. Cambridge Phil. Soc.* **30**, 542 (1934).
- [66] A.A. Petrukhin and V.V. Shestakov, Can. J. Phys. **46**, S377 (1968).
- [67] V.M. Galitskii and S.R. Kel’ner, Sov. Phys. JETP **25**, 948 (1967).
- [68] S.R. Kel’ner and Yu.D. Kotov, Sov. J. Nucl. Phys. **7**, 237 (1968).
- [69] R.P. Kokoulin and A.A. Petrukhin, in *Proceedings of the International Conference on Cosmic Rays*, Hobart, Australia, August 16–25, 1971, Vol. **4**, p. 2436 .
- [70] A. I. Nikishov, Sov. J. Nucl. Phys. **27**, 677 (1978), [Yad. Fiz.27,1281(1978)].
- [71] Yu. M. Andreev, L. B. Bezrukov and E. V. Bugaev, Phys. Atom. Nucl. **57**, 2066 (1994), [Yad. Fiz.57,2146(1994)].
- [72] L. B. Bezrukov and E. V. Bugaev, Yad. Fiz. **33**, 1195 (1981), [Sov. J. Nucl. Phys.33,635(1981)].
- [73] N.V. Mokhov and C.C. James, The MARS Code System User’s Guide, Fermilab-FN-1058-APC (2018), mars.fnal.gov/; N. Mokhov *et al.*, Prog. Nucl. Sci. Tech. **4**, 496 (2014).
- [74] P. H. Barrett *et al.*, Rev. Mod. Phys. **24**, 3, 133 (1952).
- [75] A. Van Ginneken, Nucl. Instrum. Meth. **A251**, 21 (1986).
- [76] U. Becker *et al.*, Nucl. Instrum. Meth. **A253**, 15 (1986).
- [77] J.J. Eastman and S.C. Loken, in *Proceedings of the Workshop on Experiments, Detectors, and Experimental Areas for the Supercollider*, Berkeley, CA, July 7–17, 1987, edited by R. Donaldson and M.G.D. Gilchriese (World Scientific, Singapore, 1988), p. 542.
- [78] *Methods of Experimental Physics*, L.C.L. Yuan and C.-S. Wu, editors, Academic Press, 1961, Vol. 5A, p. 163.
- [79] W.W.M. Allison and P.R.S. Wright, “The Physics of Charged Particle Identification: dE/dx , Cherenkov Radiation, and Transition Radiation,” p. 371 in *Experimental Techniques in High Energy Physics*, T. Ferbel, editor, (Addison-Wesley 1987).
- [80] E.R. Hayes, R.A. Schluter, and A. Tamosaitis, “Index and Dispersion of Some Cherenkov Counter Gases,” ANL-6916 (1964).
- [81] T. Ypsilantis, in “Proceedings of the Symposium on Particle Identification at High Luminosity Hadron Colliders, Apr 5-7, 1989 Batavia, Ill.”, 0661–676 (1989).
- [82] I. Tamm, J. Phys. U.S.S.R., **1**, 439 (1939).
- [83] H. Motz and L.I. Schiff, Am. J. Phys. **21**, 258 (1953).
- [84] B. N. Ratcliff, Nucl. Instrum. Meth. **A502**, 211 (2003).
- [85] S. K. Mandal, S. R. Klein and J. D. Jackson, Phys. Rev. **D72**, 093003 (2005).
- [86] G. A. Askar’yan, Sov. Phys. JETP **14**, 2, 441 (1962), [Zh. Eksp. Teor. Fiz.41,616(1961)].
- [87] P. W. Gorham *et al.*, Phys. Rev. **D72**, 023002 (2005).
- [88] E. Zas, F. Halzen and T. Stanev, Phys. Rev. **D45**, 362 (1992).
- [89] M. L. Cherry *et al.*, Phys. Rev. **D10**, 3594 (1974); M. L. Cherry, Phys. Rev. **D17**, 2245 (1978).
- [90] B. Dolgoshein, Nucl. Instrum. Meth. **A326**, 434 (1993).

35. Particle Detectors at Accelerators

Revised 2021. See the various sections for authors.

35.1	Introduction	565
35.2	Photon detectors	565
35.2.1	Vacuum photodetectors	566
35.2.2	Gaseous photon detectors	567
35.2.3	Solid-state photon detectors	567
35.2.4	Superconducting photon detectors	568
35.3	Organic scintillators	568
35.3.1	Scintillation mechanism	568
35.3.2	Plastic scintillator practicalities	569
35.3.3	Liquid scintillator practicalities	569
35.4	Inorganic scintillators	570
35.5	Cherenkov detectors	572
35.6	Gaseous detectors	574
35.6.1	Energy loss and charge transport in gases	574
35.6.2	Multi-Wire Proportional and Drift Chambers	577
35.6.3	High Rate Effects	578
35.6.4	Micro-Pattern Gas Detectors	578
35.6.5	Time-projection chambers	581
35.6.6	Transition radiation detectors (TRD's)	582
35.6.7	Resistive-plate chambers	584
35.7	LAr Time Projection Chamber	586
35.7.1	Introduction	586
35.7.2	A Mass of ultra-pure Liquid Argon	587
35.7.3	Charge and Light Signals	587
35.7.4	LAr TPC topologies	588
35.7.5	Prospect - written October 2021	589
35.7.6	Acknowledgement	589
35.8	Semiconductor detectors	589
35.8.1	Signal generation	590
35.8.2	Typical detectors	591
35.8.3	Radiation Damage	592
35.9	Low-noise detector readout	593
35.9.1	Principal noise origins	594
35.9.2	Equivalent noise analysis	594
35.9.3	Timing measurements	596
35.9.4	Digital signal processing	596
35.9.5	What to use when?	596
35.10	Calorimeters	597
35.10.1	Introduction	597
35.10.2	Electromagnetic calorimeters	599
35.10.3	Hadronic calorimeters	600
35.10.4	Free electron drift velocities in liquid ionization chambers	604
35.11	Accelerator-based neutrino detectors	605
35.11.1	Introduction	605
35.11.2	Signals and Backgrounds	605
35.11.3	Instances of Neutrino Detector Technology	606
35.11.4	Outlook	608
35.12	Superconducting magnets for collider detectors	609
35.12.1	Solenoid Magnets	609
35.12.2	Properties of collider detector magnets	609
35.12.3	Toroidal magnets	609
35.13	Measurement of particle momenta in a uniform magnetic field	610

35.1 Introduction

This review summarizes the detector technologies employed at accelerator particle physics experiments. Several of these detectors are also used in a non-accelerator context and examples of such applications will be provided. The detector techniques which are specific to non-accelerator particle physics experiments are the subject of Chap. 36. More detailed discussions of detectors and their underlying physics can be found in books by Kolanoski & Wermes [1], Ferbel [2], Kleinknecht [3], Knoll [4], Green [5], Leroy & Rancoita [6], and Grupen [7].

In Table 35.1 are given typical resolutions and deadtimes of common charged particle detectors. The quoted numbers are usually based on typical devices, and should be regarded only as rough approximations for new designs. The spatial resolution refers to

the intrinsic detector resolution, i.e. without multiple scattering. We note that analog detector readout can provide better spatial resolution than digital readout by measuring and averaging the deposited charge in neighboring channels. Quoted ranges attempt to be representative of both possibilities. The time resolution is defined by how accurately the time at which a particle crossed the detector can be determined. The deadtime is the minimum separation in time between two resolved hits on the same channel. Typical performance of calorimetry and particle identification are provided in the relevant sections below.

Table 35.1: Typical resolutions and deadtimes of common charged particle detectors. Revised November 2021.

Detector Type	Intrinsic Spatial Resolution (rms)	Time Resolution	Dead Time
Resistive plate chamber	50 μ m	50–1000 ps*	10 ns [†]
Liquid argon TPC	0.5–1 mm [‡]	0.01–1 μ s [§]	— [¶]
Scintillation tracker	\sim 100 μ m	100 ps/n	10 ns
Bubble chamber	10–150 μ m	1 ms	50 ms**
Wire chambers (proportional & drift chambers)	50–100 μ m	5–10 ns ^{††}	2–200 ns ^{‡‡}
Micro-pattern gas detect.	30–40 μ m	5–10 ns ^{††}	2–200 ns ^{‡‡}
Silicon strips/pixels	\lesssim 10 μ m ^{§§}	few ns ^{¶¶} ^{‡‡}	\lesssim 50 ns ^{‡‡}

*LHC: \sim 2mm gap, \sim 1ns. HL-LHC: \sim 1mm gap, \sim 350ps. Timing RPC: \sim 50ps

[†]Limited by amplifier and discriminator bandwidth, usually around 100MHz

[‡]Detector geometry dependent

[§]Using the scintillation signal

[¶]No deadtime for medium

^{||} n = index of refraction.

**Multiple pulsing time.

^{††}For fast particles

^{‡‡}Depending/limited by the amplifying electronics [8]

^{§§}Depending on electrode pitch, best values around 2–4 μ m have been achieved

^{¶¶}Resolutions < 100 ps are reached in dedicated pixel developments

35.2 Photon detectors

Revised August 2021 by P. Križan (Ljubljana U; Jozef Stefan Inst.).

Most detectors in high-energy, nuclear, and astrophysics rely on the detection of photons in or near the visible range, 100 nm \lesssim $\lambda \lesssim$ 1000 nm, or 1 eV $\lesssim E \lesssim$ 10 eV. This range covers scintillation and Cherenkov radiation as well as the light detected in many astronomical observations.

Generally, photodetection involves generating a detectable electrical signal proportional to the (usually very small) number of incident photons. The process involves three distinct steps:

1. generation of a primary photoelectron or electron-hole (e - h) pair by an incident photon by the photoelectric or photoconductive effect,
2. multiplication of the photoelectron or electron-hole pair signal to detectable levels, usually by one or more multiplicative bombardment steps and/or an avalanche process, and,
3. detection of charges induced by secondary electrons.

The important characteristics of a photodetector include the following:

1. quantum efficiency (QE or ϵ_Q): the average number of primary photoelectrons generated per incident photon ($0 \leq \epsilon_Q \leq 1$; in silicon more than one e - h pair per incident photon can be generated for $\lambda \lesssim 165$ nm),
2. collection efficiency (CE or ϵ_C): the overall acceptance factor other than the generation of photoelectrons ($0 \leq \epsilon_C \leq 1$),
3. gain (G): the number of electrons collected for each photoelectron generated,

4. dark current or dark noise: the electrical signal when there is no incident photon,
5. precision of measuring the intensity I of the incoming light: electronic noise (ENC or N_e) and statistical fluctuations in the amplification process compound the Poisson distribution of n_γ photons from a given source:

$$\frac{\sigma(I)}{\langle I \rangle} = \sqrt{\frac{f_N}{n_\gamma \epsilon_Q \epsilon_C} + \left(\frac{N_e}{G n_\gamma \epsilon_Q \epsilon_C} \right)^2}, \quad (35.1)$$

where f_N , or the excess noise factor (ENF), is the contribution to the intensity distribution variance due to multiplication statistics [9],

6. dynamic range, linearity and saturation: relation between the number of incident photons and the sensor output in the pulsed mode,
7. time dependence of the response: this includes the transit time, which is the time between the arrival of the photon and the electrical pulse, and the transit time spread, and
8. rate capability: maximal rate of light pulses at which detection is still possible.

The QE is a strong function of the photon wavelength (λ), and is usually quoted at maximum, together with a range of λ where the QE is comparable to its maximum. Spatial uniformity and linearity with respect to the number of photons are highly desirable in a photodetector response.

Optimization of these factors involves many trade-offs and varies widely between applications. For example, while a large gain is desirable, attempts to increase the gain for a given device also increases the ENF and after-pulsing ("echos" of the main pulse). In solid-state devices, a higher QE often requires a compromise in the timing properties. In other types, coverage of large areas by focusing photoelectrons increases the transit time spread.

Other important considerations also are highly application-specific. These include the photon flux and wavelength range, the total area to be covered, and the efficiency required, the volume available to accommodate the detectors, characteristics of the environment such as chemical composition, temperature, magnetic field, ambient background, as well as ambient radiation of different types, mode of operation (continuous or triggered), bias (high-voltage) requirements, power consumption, calibration needs, aging, cost, and so on. Several technologies employing different phenomena for the three steps described above, and many variants within each, offer a wide range of solutions to choose from. The salient features of the main technologies and the common variants are described below. Some key characteristics are summarized in Table 35.2.

35.2.1 Vacuum photodetectors

Vacuum photodetectors can be broadly subdivided into three types: photomultiplier tubes, microchannel plate photomultiplier tubes, and hybrid photodetectors.

35.2.1.1 Photomultiplier tubes

A versatile class of photon detectors, vacuum photomultiplier tube (PMT) has been employed by a vast majority of all particle physics experiments to date [9]. Both "transmission-" and "reflection-type" PMTs are widely used. In the former, the photocathode material is deposited on the inside of a transparent window through which the photons enter, while in the latter, the photocathode material rests on a separate surface that the incident photons strike. The cathode material has a low work function, chosen for the wavelength band of interest. When a photon hits the cathode and liberates an electron (the photoelectric effect), the latter is accelerated and guided by electric fields to impinge on a secondary-emission electrode, or dynode, which then emits several (~ 5) secondary electrons. The multiplication process is repeated typically about 10 times in series to generate a sufficient number of electrons, which are collected at the anode for delivery to the external circuit. The total gain of a PMT depends on the applied high voltage V as $G = AV^k$, where $k \approx 0.7-0.8$ (depending on the dynode material), n is the number of dynodes in the

chain, and A a constant (which also depends on n). Typically, G is in the range of 10^5-10^7 ; time resolution is $O(1ns)$ but can be as good as ≈ 100 ps for certain PMT types.

A large variety of PMTs covers a wide span of wavelength ranges from infrared (IR) to extreme ultraviolet (XUV) [10]. They are categorized by the window materials, photocathode materials, dynode structures, and anode configurations. Common window materials are borosilicate glass for IR to near-UV, fused quartz and sapphire (Al_2O_3) for UV, and MgF_2 or LiF for XUV. The choice of photocathode materials include a variety of mostly Cs- and/or Sb-based compounds such as CsI, CsTe, bi-alkali (SbRbCs, SbKCs), multi-alkali (SbNaKCs), GaAs(Cs), GaAsP(Cs), etc. Sensitive wavelengths and peak quantum efficiencies for these materials are summarized in Table-35.3. Typical dynode structures used in PMTs are circular cage, line focusing, box-and-grid, venetian blind, and fine mesh.

Multianode PMTs (MaPMTs) of up to 5×5 cm² in size are based on the parallel (side-by-side) arrangement of several dynode channels and anodes in the same tube, requiring advanced micro-machining and processing techniques. Fast PMTs with very large windows—measuring up to 508 mm across—have been developed for detection of Cherenkov radiation in neutrino experiments such as Super-Kamiokande and KamLAND among many others. Specially prepared low-radioactivity glass is used to make these PMTs, and they are also able to withstand the high pressure of the surrounding liquid.

PMTs are vulnerable to magnetic fields—sometimes even the geomagnetic field causes large orientation-dependent gain changes. A high-permeability metal shield is often necessary. However, proximity-focused PMTs, e.g. the fine-mesh types, can be used even in a high magnetic field (≥ 1 T) if the direction of electric field of the tube is close to the direction of the external magnetic field. CMS uses custom-made vacuum phototriodes (VPT) mounted on the back face of projective lead tungstate crystals to detect scintillation light in the endcap sections of its electromagnetic calorimeters, which are inside a 3.8 T superconducting solenoid. A VPT employs a single dynode (thus, $G \approx 10$) placed close to the photocathode, and a mesh anode plane between the two, to help it cope with the strong magnetic field, which is not too unfavorably oriented with respect to the photodetector axis in the endcaps (within 25°), but where the radiation level is too high for Avalanche Photodiodes (APDs) like those used in the barrel section.

35.2.1.2 Microchannel plate photomultiplier tubes

A typical microchannel plate photomultiplier tube (MCP-PMT) consists of two or more ~ 1 mm thick glass plates with densely packed $O(10 \mu m)$ -diameter cylindrical holes, or "microchannels", sitting between the transmission-type photocathode and anode planes, separated by $O(1$ mm) gaps. Instead of discrete dynodes, the inner surface of each cylindrical hole with a length-to-diameter ratio of 40-100 serves as a continuous dynode for the entire cascade of multiplicative bombardments initiated by a photoelectron. Gain fluctuations are reduced by operating each of the MCPs in the saturation mode. MCPs are stacked in a "chevron" configuration that alternates their bias angle; this reduces ion and photon feed-back effects and optimizes the overall amplification gain.

MCP-PMTs are thin, offer good spatial resolution, have excellent time resolution (~ 20 ps), and can tolerate magnetic fields up to 0.1 T and axial fields up to 1–2 T. The technology has significantly evolved over the past 10 years [11]. A main breakthrough was the introduction of the atomic layer deposition (ALD) coatings on the MCP surfaces to increase the lifetime (>20 C/cm² of charge accumulated on the anode) and gain. The Large Area Picosecond Photo-Detector (LAPPD) project [12] is an important attempt to produce at a reasonable cost large (20 by 20 cm²) sensors with a transit time spread of 50-70 ps.

35.2.1.3 Hybrid photon detectors

Hybrid photon detectors (HPD) combine the sensitivity of a vacuum PMT with the excellent spatial and energy resolutions of a silicon sensor [13]. A single photoelectron ejected from the photocathode is accelerated through a large potential difference of

Table 35.2: Representative characteristics of some photodetectors commonly used in particle physics.

Type	λ (nm)	$\epsilon_Q \epsilon_C$	Gain	Risetime (ns)	Single photon time resol. (ps)	Area (mm ²)	1-p.e noise (Hz)	HV (V)
PMT *	115–1700	0.15–0.25	10^5 – 10^7	0.7–10	~ 200	10^2 – 10^5	10 – 10^4	500–3000
MCP-PMT*	115–650	0.01–0.10	10^3 – 10^7	0.15–0.3	~ 20	10^2 – 10^4	0.1–200	500–3500
HPD*	115–850	0.1–0.3	10^3 – 10^4	$O(1)$	~ 1000	10^2 – 10^5	10 – 10^3	$\sim 2 \times 10^4$
HAPD*	115–850	0.1–0.3	10^4 – 10^5	$O(1)$	~ 30	10^2 – 10^5	10 – 10^3	$\sim 1 \times 10^4$
GPD*	115–500	0.15–0.3	10^3 – 10^6	$O(0.1)$	~ 100	$O(10)$	10 – 10^3	300–2000
APD	300–1700	~ 0.7	10 – 10^8	$O(1)$	- †	10 – 10^3	1 – 10^3	400–1400
SiPM	125–1000	0.15–0.4	10^5 – 10^6	~ 1	~ 50	1–10	$O(10^5)$	30–60

*These devices often come in multi-anode configurations. In such cases, area and noise are to be considered on a “per readout-channel” basis.

†No single photon detection possible.

~ 20 kV before it impinges on the silicon sensor/anode. The gain nearly equals the maximum number of e - h pairs that could be created from the entire kinetic energy of the accelerated electron: $G \approx eV/w$, where e is the electronic charge, V is the applied potential difference, and $w \approx 3.7$ eV is the mean energy required to create an e - h pair in Si at room temperature. Since the gain is achieved in a single step, one can expect to have the excellent resolution of a simple Poisson statistic with large mean, but in fact it is even better, thanks to the Fano effect discussed in Sec. 35.8.

Low-noise electronics must be used to read out HPDs if one intends to take advantage of the low fluctuations in gain, *e.g.* when counting small numbers of photons. HPDs can have the same $\epsilon_Q \epsilon_C$ and window geometries as PMTs and can be segmented down to ~ 50 μm . However, they require rather high biases and will not function in a magnetic field. The exception is proximity-focused devices (\Rightarrow no (de)magnification) in an axial field. With time resolutions of ~ 10 ps and superior rate capability, proximity-focused HPDs can be an alternative to MCP-PMTs. Applications of HPDs include the CMS hadronic calorimeter and the RICH detector in LHCb. Large-size HPDs with sophisticated focusing may be suitable for future water Cherenkov experiments.

Hybrid APDs (HAPDs) add an avalanche multiplication step following the electron bombardment to boost the gain by a factor of ~ 50 . This affords a higher gain and/or a lower bias voltage, but also increases the detector capacitance and fluctuations in multiplication. The forward RICH detector of Belle II uses a 144-channel device of this type [14].

Table 35.3: Properties of photocathode and window materials commonly used in vacuum photodetectors. [10]

Photocathode material	λ (nm)	Window material	Peak ϵ_Q (λ/nm)
CsI	115–200	MgF ₂	0.13 (130)
CsTe	115–320	MgF ₂	0.17 (200)
Bi-alkali	300–650	Borosilicate	0.27 (390)
	160–650	Synthetic Silica	0.27 (390)
"Ultra Bi-alkali"	300–650	Borosilicate	0.43 (350)
	160–650	Synthetic Silica	0.43 (350)
Multi-alkali	300–850	Borosilicate	0.20 (375)
	160–850	Synthetic Silica	0.25 (380)
GaAsP(Cs)	280–720	Borosilicate	0.40 (480–530)

35.2.2 Gaseous photon detectors

In a gaseous photon detector (GPD) a photoelectron in a suitable gas mixture initiates an avalanche in a high-field region, producing a large number of secondary impact-ionization electrons. In principle the charge multiplication and collection processes are identical to those employed in gaseous tracking detectors such as multiwire proportional chambers (MWPC), micromesh gaseous detectors (Micromegas), or gas electron multipliers (GEM). These are discussed in Sec. 35.6.4.

The devices can be divided into two types depending on the

photosensitive material. One type uses solid photocathode materials much in the same way as PMTs. Since it is resistant to gas mixtures typically used in tracking chambers, CsI is a common choice. In the other type, photoionization occurs on suitable molecules vaporized and mixed in the drift volume. Most gases have photoionization work functions in excess of 10 eV, which would limit their sensitivity to wavelengths far too short. However, vapors of tetrakis dimethyl-amine ethylene (TMAE) or triethyl-amine (TEA), which have smaller work functions (5.3 eV for TMAE and 7.5 eV for TEA), are suited for XUV photon detection [15]. Since devices like GEMs offer sub-mm spatial resolution, GPDs are often used as position-sensitive photon detectors. They can be made into flat panels to cover large areas ($O(1 \text{ m}^2)$), can operate in high magnetic fields, and are relatively inexpensive. Many of the ring imaging Cherenkov (RICH) detectors have used GPDs for the detection of Cherenkov light [16–19]. Special care must be taken to suppress the ion-feedback and photon-feedback processes in GPDs. It is also important to maintain high purity of the gas as minute traces of O₂ or H₂O can significantly degrade the detection efficiency.

35.2.3 Solid-state photon detectors

In a phase of rapid development, solid-state photodetectors are competing with vacuum- or gas-based devices for many existing applications and making way for a multitude of new ones. Compared to traditional vacuum- and gaseous photodetectors, solid-state devices are more compact, lightweight, rugged, tolerant to magnetic fields, and often cheaper. They also allow fine pixelization, are easy to integrate into large systems, and can operate at low electric potentials, while matching or exceeding most performance criteria.

Silicon photodiodes (PD) are widely used in high-energy physics as particle detectors and in a large number of applications as photon detectors. The structure is discussed in some detail in Sec. 35.8. In its simplest form, the PD is a reverse-biased p - n junction. Photons with energies above the indirect bandgap energy (wavelengths shorter than about 1050 nm, depending on the temperature) can create e - h pairs (the photoconductive effect), which are collected on the p and n sides, respectively. Often, as in the PDs used for crystal scintillator readout in CLEO, L3, Belle, BaBar, and GLAST, intrinsic silicon is doped to create a p - i - n structure. The reverse bias increases the thickness of the depleted region; in the case of these particular detectors, to full depletion at a depth of about 100 μm . Increasing the depletion depth decreases the capacitance (and hence electronic noise) and extends the red response. Quantum efficiency can exceed 90%, but falls toward the red because of the decrease of the light absorption probability in silicon; the absorption length reaches 100 μm at 985 nm. However, since $G = 1$, electronic signal amplification is necessary. Optimal low-noise amplifiers are slow, but, even so, noise limits the minimum detectable signal in room-temperature devices to several hundred photons.

In APDs, an exponential cascade of impact ionizations initiated by the original photogenerated e - h pair under a large reverse-bias voltage leads to an avalanche multiplication [20–23], and eventually to breakdown in Geiger-mode APDs. As a result, de-

tectable electrical response can be obtained from low-intensity optical signals down to single photons. Excellent junction uniformity is critical, and a guard ring is generally used as a protection against edge breakdown. Well-designed APDs, such as those used in CMS crystal-based electromagnetic calorimeter, have achieved $\epsilon_Q \epsilon_C \approx 0.7$ with sub-ns response time. The sensitive wavelength window and gain depend on the semiconductor used. The gain is typically 10–200 in linear and up to 10^8 in Geiger mode of operation. Stability and close monitoring of the operating temperature are important for linear-mode operation, and substantial cooling is often necessary.

One of the most promising recent developments in the field is SiPMs ("Silicon Photomultiplier"), a device consisting of large arrays ($O(10^3)$) of tiny APDs packed over a small area ($O(1 \text{ mm}^2)$) and operated in a limited Geiger mode [24–26]. Although each cell only offers a binary output, linearity with respect to the number of photons is achieved by summing the cell outputs. The sum of all cells is proportional to the number of photons received so long as the probability of an individual cell receiving multiple photons during a single time gate is negligible. SiPMs are being adopted as the preferred solution for various purposes including medical imaging, e.g. positron emission tomography (PET). These compact, rugged, and economical devices allow auto-calibration through decent separation of photoelectron peaks and offer gains of $O(10^6)$ at a moderate bias voltage ($\sim 30 \text{ V}$). However, the single-photoelectron noise of a SiPM, being the logical "or" of $O(10^3)$ Geiger APDs, is rather large: $O(10\text{--}100 \text{ kHz/mm}^2)$ at room temperature. Intensive R&D in recent years [27] led to a substantial reduction in dark count rates and in correlated noise levels, resulting in coverage of larger areas and in a wider range of applications. One way to further improve the signal-to-noise ratio in SiPMs is by using dedicated light collectors, either as quartz Winston cone like arrays [28] or suitably designed meta-materials [29]. In this way, photons propagate from a larger entry window to a considerably smaller semiconductor sensor, resulting in an improved signal photon to dark-count ratio. Intense R&D is expected to improve radiation hardness of these sensors. The fabrication of the sensors and the front-end electronics combined in the same process with the goal of making SiPMs extremely easy to use has already been successful (digital SiPMs) [30], and remains a topic of intense R&D.

More solid-state light sensors have either been developed or are potentially interesting for use in HEP experiments. The Run 2 DØ detector used 86000 Visible-light photon counters (VLPC) to read the optical signal from its scintillating-fiber tracker and scintillator-strip preshower detectors. These light sensors utilize the formation of an impurity band only 50 meV below the conduction band in As-doped Si to generate strong ($G \approx 5 \times 10^4$) yet sharp response to single photons with $\epsilon_Q \approx 0.9$ [31–33]. Only a very small bias ($\sim 7 \text{ V}$) is needed, but high sensitivity to infrared photons requires cooling below 10 K. Another interesting light sensor that has not yet found its use in HEP instrumentation are quantum dots, realized by nanometer-sized semiconductor 'particles' embedded in a semiconductor bulk.

35.2.4 Superconducting photon detectors

In this rapidly developing technology field, three most established technologies are the superconducting nano-wire single photon detector (SNSPD), the transition edge sensor (TES), and the microwave kinetic inductance detector (MKID). An SNSPD consists of a thin (4 nm) and narrow (100–250 nm) superconducting nanostrip that is current-biased just below its critical current. Absorption of a photon generates a resistive domain in the superconducting nanostrip, which leads to a transient voltage signal that can be detected. SNSPDs offer a unique combination of speed, both in terms of count rate ($\sim \text{GHz}$) and low timing jitter ($< 3 \text{ ps}$ [34]), large range of wavelength sensitivity from VUV (120 nm) to mid-IR ($10 \mu\text{m}$), high detection efficiencies (approaching 100% for UV to near-IR), and low dark count rates ($\sim 5\text{--}10 \text{ Hz}$), making them appealing for a wide variety of demanding applications.

Examples of present use in particle physics are small nanowire detectors for dark matter and dark photons. Work is in progress that could make these sensors relevant to HEP applications by

increasing the area (using 300 mm wafers and larger) and pixel size, coupling via windows to cryogenic stages, and readout of arrays (superconducting electronics for data processing). While the performance of these sensors is impressive, an application in large accelerator-based detectors would require an extensive R&D program because of the severe cryogenic requirements.

35.3 Organic scintillators

Written August 2021 by S. C. Eno (U. Maryland) and Matthieu Hamel (Paris-Saclay U. CEA, LIST).

Organic scintillators produce light when transversed by a charged particle. They can be broadly categorized into four types: single crystal, liquid, plastic, and a recently emerged glass [35]. The most useful scintillators produce photons with wavelengths between 370–750 nm (blue to red), typically peaking at 425 nm [36] via a series of processes that are initialized when charged particles interact with the material via both excitation and ionization/recombination (see Sec. 34.2 of this *Review*). Typical photon yields are about 1 photon per 100 eV of energy deposit [37], although the collected and transduced signal can be much lower. Methods to guide the light towards the photon-electron converter, such as diffusive paint, reflectors, photonic crystals, or light guides, may be required to optimize light yield.

Organic scintillators have found use in a wide variety of detectors [38]. Plastics are mostly used in collider detectors, and liquids in neutrino experiments. Ease of fabrication into desired shapes and low cost has made plastic scintillator ideal for large detectors. In the form of scintillating fiber, it has found widespread use in tracking and calorimetry. Demand for large volume detectors (e.g. neutrino detectors: MiniBooNE, NOvA) has led to increased use of liquid scintillator, which can be very low cost.

35.3.1 Scintillation mechanism

Plastic and liquid scintillators are based on an aromatic "matrix" such as benzene. The p electrons form both "pi" and "sigma" bonds between the atoms; the pi bonds are responsible for scintillation. Scintillation is produced via standard photophysical interactions, shown schematically in Fig. 35.1. While there have been claims of delayed light production on long time scales (labeled "phosphorescence" in the figure), this is still a subject of active debate in the community. As aromatic molecules scintillate in the ultraviolet (UV), useful scintillators have one or several fluorophores dissolved into the matrix as dopants. Common fluorophores include 2,5-diphenyloxazole, *p*-terphenyl, 9,10-diphenylanthracene (9,10-DPA), 1,4-bis(2-methylstyryl)benzene (bis-MSB) and 1,4-bis(5-phenyl-2-oxazolyl)benzene (POPOP). Each molecule has its own role: the matrix (whether liquid or plastic) is where most of the radiation/matter interaction occurs. After radiation interaction, ions may recombine giving birth to excited molecules (excitons). Excitons in the matrix are transferred to a "primary fluorophore", whose concentration is typically 1–3 weight % in commercial plastic and liquid scintillators. This concentration is large enough to ensure exciton transfer is primarily via the Förster mechanism, a resonant dipole-dipole interaction which decreases at sixth the power of the distance between molecules. The concentration, however, can be up to the solubility limit. Transfer via the Förster mechanism increases both speed and light output of the organic scintillator. To reduce reabsorption of the emitted light by the matrix or the primary fluorophore, and the resulting shortened attenuation length, a "secondary fluorophore" is also used to shift the light to longer wavelengths. Transfer from the primary to the secondary is generally radiative. Typical secondary concentrations in plastic and liquids are 0.01–0.2 weight %. The chain of emission and absorption from the matrix to the subsequent fluorophores is shown in Fig. 35.2. Scintillators with two fluorophores typically have absorption lengths of several meters. The longest attenuation lengths require a third fluorophore: when the matrix is transparent up to 1 cm, adding a primary fluorophore increases the light transmission up to $\approx 10 \text{ cm}$, whereas the ternary cocktail is transparent up to 2 m and longer [39].

For most scintillators, decay times are in the ns range; rise times are much faster. Sub-ns timing resolutions have been achieved [40].

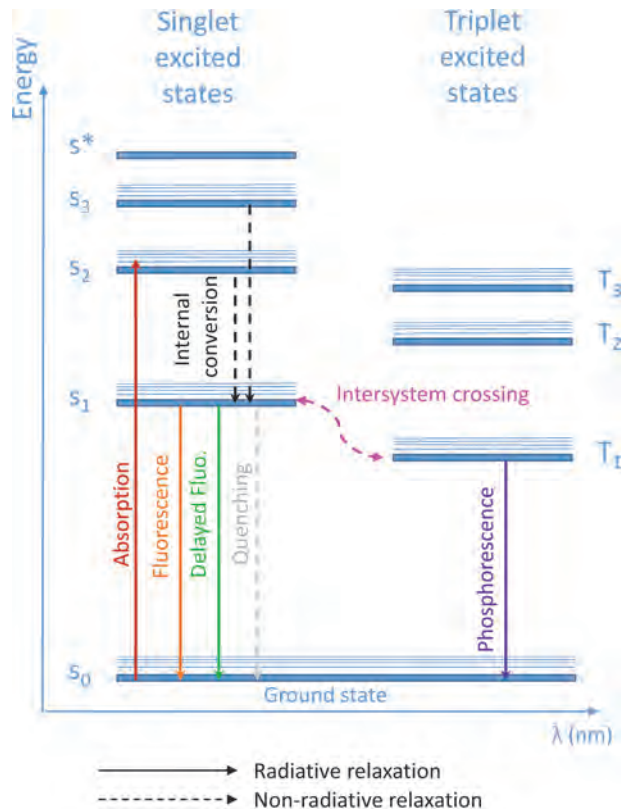


Figure 35.1: Schematic of scintillation mechanism. Schematic of typical excitation and de-excitation of matrix modules.

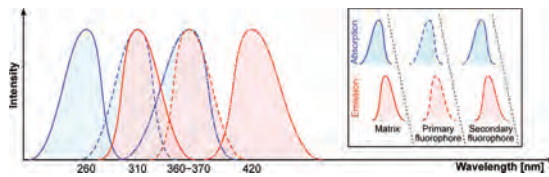


Figure 35.2: Schematic of scintillation mechanism. Typical emission and absorption spectra for the matrix, the primary, and the secondary fluorophore

Organic scintillators do not respond linearly to the ionization density. Very dense ionization tracks, with large dE/dx , emit less light than expected compared to minimum-ionizing particles. A widely used semi-empirical model by Birks posits that recombination and quenching effects between the excited molecules reduce the light yield [41]. These effects are more pronounced the greater the density of the excited molecules. Birks' formula is

$$\frac{d\mathcal{L}}{dx} = \mathcal{L}_0 \frac{dE/dx}{1 + kB dE/dx}, \quad (35.2)$$

where \mathcal{L} is the luminescence, \mathcal{L}_0 is the luminescence at low specific ionization density, and the product kB is known as Birks' constant, which must be determined for each scintillator by measurement. The value of kB for polystyrene is 0.126 mm/MeV, which is large enough to play an important role in compensation in scintillator-based calorimetry. The high hydrogen content of plastic, which enhances the neutron interaction cross section, as well as its large mass stopping power, also contributes to calorimetry compensation. In the case of large dE/dx values (e.g. with alpha particles), ion recombination may lead to the creation of triplet excited states instead of singlet excited states. If two triplet states are close enough (typically in the order of 10\AA), then triplet-triplet annihilation may occur following the Dexter process [42], leading to delayed fluorescence. This phenomenon is useful for α/β or neutron/ γ discrimination.

Extensive research searching for new efficient molecules that can act as matrix, primary, or secondary fluorophores, is ongoing [43]. Other chemical modifications can affect the scintillator emission wavelength and decay time, or be used e.g. as stabilizers or to enhance thermal neutron sensitivity. Other parameters that can be modified are the density and the effective atomic number.

35.3.2 Plastic scintillator practicalities

Most commercial plastic scintillators use either polystyrene (PS) or poly(vinyltoluene) (PVT) as matrix. A variety of manufacturing techniques [43] are used in the production of plastic scintillator. Cast plastic has the highest light yield, while extruded scintillator is less expensive and allows creation of the scintillator and coating with a diffusive reflector in a single process. 3D printing of plastic scintillator is being actively pursued [44]. Plastic scintillator is also used to produce scintillating, wavelength-shifting, and clear fibers. These fibers can be useful to guide light to photodetectors, and as the active element in the type of calorimeter pioneered by the RD52/DREAM collaboration [45]. They have even been used in the construction of trackers [46, 47].

Plastic scintillators are reliable, robust, and convenient. However, exposure to solvent vapors, high temperatures, mechanical flexing, irradiation, or rough handling will cause degradation. The surface is a particularly fragile region and can "craze" – develop microcracks which degrade transmission of light by total internal reflection. Crazing is particularly likely where oils, solvents, or fingerprints have contacted the surface or when mechanical stresses are present. The light yield is influenced by several environmental factors: it decreases with the partial pressure of oxygen [48] and increases with increasing magnetic field. Water vapour can also diffuse into plastic and cause clouding.

Plastics are susceptible to radiation damage [49]. At high enough dose, the visible color of the plastic can change to yellow or (at high enough dose) even brown. During irradiation, broken molecular bonds ("radicals") absorb light, generally strongly in the UV, with tails to longer wavelengths. Because of this, shifting the light to longer wavelengths reduces the decrease in light output and in attenuation length due to radiation effects. Radicals produce mostly temporary damage that "anneals" when the irradiation ends, as the bonds can reform. Radicals can also polymerize via cross linking, and this leads to a permanent reduction in light yield [50]. In an inert atmosphere at room temperature, the bond reformation timescale is on the order of a month. Oxygen, which diffuses into the plastic during radiation to a depth that scales as the inverse square root of dose rate, can quickly bind to the radicals, reducing but not eliminating temporary damage at the price of a small increased permanent damage [51–53]. After irradiation, oxygen, if present, will diffuse through the entire sample, leading to oxide formation and speeding the annealing process. The decrease in light output due to permanent damage depends on the dose rate. Lower dose rates show large light losses for the same dose. The ratio of the light output to the unirradiated light output can roughly be parameterized as an exponential. For dose rates typical of current collider detectors at the Large Hadron Collider (from a few 10^{-3} to 10 Gy/hr), an exponential dose constant of tens of kGy is observed.

35.3.3 Liquid scintillator practicalities

Liquid scintillators have been used in large scale neutrino experiments 36.3.1.1 due to their low cost. They can hermetically fill any vessel shape. Liquid scintillators are also, due to the mobility of the molecules, much less susceptible to radiation damage.

Care must be taken to avoid dissolved water, solvents such as isopropyl alcohol, and oxygen, which reduce light yield. As they can dissolve many materials (e.g. plastics, adhesives, paints...) care must be taken in their handling. Flammability concerns limit their use in practical experiments in intense radiation fields.

35.4 Inorganic scintillators

Revised August 2021 by C.L. Woody (BNL) and R.-Y. Zhu (HEP California Inst. of Technology).

Inorganic crystals form a class of scintillating materials with much higher densities than organic plastic scintillators (typically $\sim 4\text{--}8\text{ g/cm}^3$) with a variety of different properties for use as scintillation detectors. Due to their high density and high effective atomic number, they can be used in applications where high stopping power or a high conversion efficiency for electrons or photons is required. These include total absorption electromagnetic calorimeters (see Sec. 35.10.2), which consist of a totally active absorber (as opposed to a sampling calorimeter), as well as serving as gamma ray detectors over a wide range of energies. Many of these crystals also have very high light output, and can therefore provide excellent energy resolution down to very low energies (\sim few hundred keV).

Some crystals are intrinsic scintillators in which the luminescence is produced by a part of the crystal lattice itself. However, other crystals require the addition of a dopant, typically fluorescent ions such as thallium (Tl) or cerium (Ce) which is responsible for producing the scintillation light. However, in both cases, the scintillation mechanism is the same. Energy is deposited in the crystal by ionization, either directly by charged particles, or by the conversion of photons into electrons or positrons which subsequently produce ionization. This energy is transferred to the luminescent centers which then radiate scintillation photons. The light yield L in terms of the number of scintillation photons produced per MeV of energy deposit in the crystal can be expressed as [54]

$$L = 10^6 S \cdot Q / (\beta \cdot E_g), \quad (35.3)$$

where $\beta \cdot E_g$ is the energy required to create an e-h pair expressed as a multiple of the band gap energy E_g (eV), S is the efficiency of energy transfer to the luminescent center and Q is the quantum efficiency of the luminescent center. The values of β , S and Q are crystal dependent and are the main factors in determining the intrinsic light yield of the scintillator. The decay time of the scintillator is mainly dominated by the decay time of the luminescent center.

Table-35.4 lists the basic properties of some commonly used inorganic crystals. NaI(Tl) is one of the most common and widely used scintillators, with an emission that is well matched to a bi-alkali photomultiplier tube, but it is highly hygroscopic and difficult to work with, and has a rather low density. CsI(Tl) and CsI(Na) have high light yield, low cost, and are mechanically robust (high plasticity and resistance to cracking). However, they need careful surface treatment and are slightly and highly hygroscopic respectively. Pure CsI has identical mechanical properties as CsI(Tl), but a faster emission at shorter wavelength and a much lower light output.

Undoped BaF₂ has a fast component with a less than 0.6 ns decay time, and is the fastest known scintillator. However, it also has a slow component with a much longer decay time (~ 630 ns). Bismuth germanate (Bi₄Ge₃O₁₂ or BGO) has a high density, and consequently a short radiation length X_0 and Molière radius R_M . Similar to CsI(Tl), BGO's emission is well-matched to the spectral sensitivity of photodiodes, and it is easy to handle and not hygroscopic. Lead tungstate (PbWO₄ or PWO) has a very high density, with a very short X_0 and R_M , but its intrinsic light yield is rather low.

Cerium doped lutetium oxyorthosilicate (Lu₂SiO₅:Ce, or LSO:Ce) [55] and cerium doped lutetium-yttrium oxyorthosilicate (Lu_{2(1-x)}Y_{2x}SiO₅, LYSO:Ce) [56] are dense crystal scintillators which have a high light yield and a fast decay time. Only the properties of LSO:Ce are listed in Table-35.4 since the properties of LYSO:Ce are similar to that of LSO:Ce except a slightly lower density than LSO:Ce depending on the yttrium fraction (typically 5 to 10%) in LYSO:Ce. This material is also featured with excellent radiation hardness [57, 58], so is expected to be used where extraordinary radiation hardness is required.

Also listed in Table-35.4 are other fluoride crystals such as PbF₂ as a Cherenkov material and CeF₃, which have been shown to provide excellent energy resolution in calorimeter applications.

Table-35.4 also includes cerium doped lanthanum tri-halides, such as LaBr₃ [59] and CeBr₃ [60], which are brighter and faster than LSO:Ce, but they are highly hygroscopic and have a lower density. The FWHM energy resolution measured for these materials coupled to a PMT with bi-alkali photocathode for 0.662 MeV γ -rays from a ¹³⁷Cs source is about 3%, and has recently been improved to 2% by co-doping with cerium and strontium [61], which is the best among all inorganic crystal scintillators. For this reason, LaBr₃ and CeBr₃ are expected to be used in applications where a good energy resolution for low energy photons are required, such as homeland security.

Beside the crystals listed in Table-35.4, a number of new crystals are being developed that may have potential applications in high energy or nuclear physics. Of particular interest is the family of yttrium and lutetium perovskites and garnet, which include YAP (YAlO₃:Ce), LuAP (LuAlO₃:Ce), YAG (Y₃Al₅O₁₂:Ce) and LuAG (Lu₃Al₅O₁₂:Ce) and their mixed compositions. These have been shown to be linear over a large energy range [62], and have the potential for providing good intrinsic energy resolution.

Aiming at the best jet-mass resolution inorganic scintillators are being investigated for HEP calorimeters with dual readout for both Cherenkov and scintillation light to be used at future linear lepton colliders. These materials may be used for an electromagnetic calorimeter [63] or a homogeneous hadronic calorimetry (HHCAL) detector concept, including both electromagnetic and hadronic parts [64, 65]. Because of the unprecedented volume (70 to 100 m³) foreseen for the HHCAL detector concept the materials must be (1) dense (to minimize the leakage) and (2) cost-effective. It should also be UV transparent (for effective collection of the Cherenkov light) and allow for a clear discrimination between the Cherenkov and scintillation light. The preferred scintillation light is thus at a longer wavelength, and not necessarily bright or fast. Dense crystals, scintillating glasses and ceramics offer a very attractive implementation for this detector concept [66].

The fast scintillation light provides timing information about electromagnetic interactions and showers, which may be used to mitigate pile-up effects and/or for particle identification since the time development of electromagnetic and hadronic showers, as well as minimum ionizing particles, are different. The timing information is primarily determined by the scintillator rise time and decay time, and the number of photons produced. For fast timing, it is important to have a large number of photons emitted in the initial part of the scintillation pulse, e.g. in the first ns, since one is often measuring the arrival time of the particle in the crystal using the leading edge of the light pulse. A good example of this is BaF₂, which has $\sim 10\%$ of its light in its fast component with a decay time of less than 0.6 ns. Recent investigation shows that doping with yttrium in BaF₂ reduces its slow component significantly, while keeping its ultrafast scintillation component unchanged [67, 68]. The light propagation can spread out the arrival time of the scintillation photons at the photodetector due to time dispersion [69]. The time response of the photodetector also plays a major role in achieving good time resolution with fast scintillating crystals.

Table-35.4 gives the light output of other crystals relative to NaI(Tl) and their dependence to the temperature variations measured for 1.5 X_0 cube crystal samples with a Tyvek paper wrapping and a full end face coupled to a photodetector [70]. The quantum efficiency of the photodetector is taken out to facilitate a direct comparison of crystal's light output. However, the useful signal produced by a scintillator is usually quoted in terms of the number of photoelectrons per MeV produced by a given photodetector. The relationship between the light yield (LY) in number of photons/MeV produced ($N_{\text{photons/MeV}}$) and the light output in number of photoelectrons/MeV detected involves the factors for the light collection efficiency (LC) and the quantum efficiency (QE) of the photodetector:

$$N_{\text{p.e./MeV}} = LY \cdot LC \cdot QE. \quad (35.4)$$

LC depends on the size and shape of the crystal, and includes effects such as the transmission of scintillation light within the crystal (i.e., the bulk attenuation length of the material), scattering from within the crystal, reflections and scattering from the

Table 35.4: Properties of several inorganic crystals. Most of the notation is defined in Sec. 6 of this Review.

Parameter:	ρ	MP	X_0^*	R_M^*	dE/dx^*	λ_I^*	τ_{decay}	λ_{max}	n^\dagger	Relative output [‡]	Hygro-scopic?	$d(\text{LY})/dT$ [§]
Units:	g/cm^3	$^\circ\text{C}$	cm	cm	MeV/cm	cm	ns	nm				$\%/^\circ\text{C}^\S$
NaI(Tl)	3.67	651	2.59	4.13	4.8	42.9	245	410	1.85	100	yes	-0.2
BGO	7.13	1050	1.12	2.23	9.0	22.8	300	480	2.15	21	no	-0.9
BaF ₂	4.89	1280	2.03	3.10	6.5	30.7	650 ^s	300 ^s	1.50	36 ^s	no	-1.9 ^s
							<0.6 ^f	220 ^f		4.1 ^f		0.1 ^f
CsI(Tl)	4.51	621	1.86	3.57	5.6	39.3	1220	550	1.79	165	slight	0.4
CsI(Na)	4.51	621	1.86	3.57	5.6	39.3	690	420	1.84	88	yes	0.4
CsI(pure)	4.51	621	1.86	3.57	5.6	39.3	30 ^s	310	1.95	3.6 ^s	slight	-1.4
							6 ^f			1.1 ^f		
PbWO ₄	8.30	1123	0.89	2.00	10.1	20.7	30 ^s	425 ^s	2.20	0.3 ^s	no	-2.5
							10 ^f	420 ^f		0.077 ^f		
LSO(Ce)	7.40	2050	1.14	2.07	9.6	20.9	40	402	1.82	85	no	-0.2
PbF ₂	7.77	824	0.93	2.21	9.4	21.0	-	-	-	Cherenkov	no	-
CeF ₃	6.16	1460	1.70	2.41	8.42	23.2	30	340	1.62	7.3	no	0
LaBr ₃ (Ce)	5.29	783	1.88	2.85	6.90	30.4	20	356	1.9	180	yes	0.2
CeBr ₃	5.23	722	1.96	2.97	6.65	31.5	17	371	1.9	165	yes	-0.1

* Numerical values calculated using formulae in this review.

[†] Refractive index at the wavelength of the emission maximum.

[‡] Relative light output measured for samples of 1.5 X_0 cube with a Tyvek paper wrapping and a full end face coupled to a photodetector. The quantum efficiencies of the photodetector are taken out.

[§] Variation of light yield with temperature evaluated at the room temperature.

^f = fast component, ^s = slow component

crystal surfaces, and re-bouncing back into the crystal by wrapping materials. These factors can vary considerably depending on the sample, but can be in the range of ~ 10 –60%. The internal light transmission depends on the intrinsic properties of the material, e.g. the density and type of the scattering centers and defects that can produce internal absorption within the crystal, and can be highly affected by factors such as radiation damage, as discussed below.

The quantum efficiency depends on the type of photodetector used to detect the scintillation light, which is typically ~ 15 –30% for photomultiplier tubes and $\sim 70\%$ for silicon photodetectors for visible wavelengths. The quantum efficiency of the detector is usually highly wavelength dependent and should be matched to the particular crystal of interest to give the highest quantum yield at the wavelength corresponding to the peak of the scintillation emission. Fig. 35.3 shows the quantum efficiencies of two photodetectors, a Hamamatsu R2059 PMT with bi-alkali cathode and a Hamamatsu S8664 avalanche photodiode (APD) as a function of wavelength. Also shown in the figure are emission spectra of three crystal scintillators, BGO, LSO:Ce/LYSO:Ce and CsI(Tl), and the numerical values of the emission weighted quantum efficiency. The area under each emission spectrum is proportional to crystal's light yield, as shown in Table-35.4, where the quantum efficiencies of the photodetector has been taken out. Results with different photodetectors can be significantly different. For example, the response of CsI(Tl) relative to NaI(Tl) with a standard photomultiplier tube with a bi-alkali photo-cathode, e.g. Hamamatsu R2059, would be 45 rather than 165 because of the photomultiplier's low quantum efficiency at longer wavelengths. For scintillators which emit in the UV, a detector with a quartz window should be used.

For very low energy applications (typically below 1 MeV), non-proportionality of the scintillation light yield may be important. It has been known for a long time that the conversion factor between the energy deposited in a crystal scintillator and the number of photons produced is not constant. It is also known that the energy resolution measured by all crystal scintillators for low energy γ -rays is significantly worse than the contribution from photo-electron statistics alone, indicating an intrinsic contribution from the scintillator itself. Precision measurement using low energy electron beam shows that this non-proportionality is crystal dependent [71]. Recent study on this issue also shows that this effect is also sample dependent even for the same crystal [72]. Further work is therefore needed to fully understand this subject.

One important issue related to the application of a crystal scin-

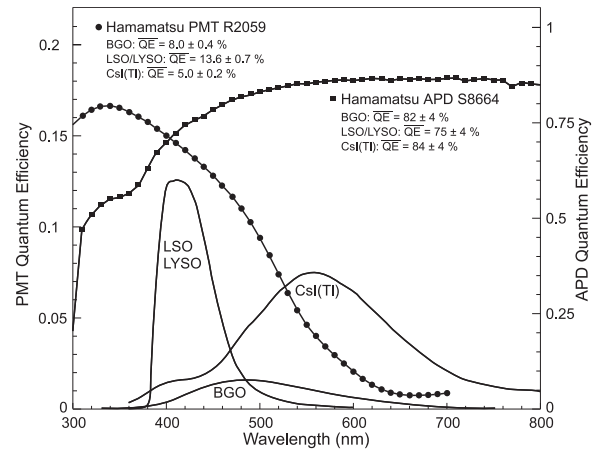


Figure 35.3: The quantum efficiencies of two photodetectors, a Hamamatsu R2059 PMT with bi-alkali cathode and a Hamamatsu S8664 avalanche photodiode (APD), are shown as a function of wavelength. Also shown in the figure are emission spectra of three crystal scintillators, BGO, LSO and CsI(Tl), and the numerical values of the emission weighted quantum efficiencies. The area under each emission spectrum is proportional to crystal's light yield.

tillator is its radiation hardness. Stability of its light output, or the ability to track and monitor the variation of its light output in a radiation environment, is required for high resolution and precision calibration [73]. All known crystal scintillators suffer from ionization dose induced radiation damage [74], where a common damage phenomenon is the appearance of radiation induced absorption caused by the formation of color centers originated from the impurities or point defects in the crystal. This radiation induced absorption reduces the light attenuation length in the crystal, and hence its light output. For crystals with high defect density, a severe reduction of light attenuation length may cause a distortion of the light response uniformity, leading to a degradation of the energy resolution. Additional radiation damage effects may include a reduced intrinsic scintillation light yield (damage to the luminescent centers) and an increased phosphorescence (afterglow). For crystals to be used in a high precision calorimeter in a radiation environment, its scintillation mechanism must not

be damaged and its light attenuation length in the expected radiation environment must be long enough so that its light response uniformity, and thus its energy resolution, does not change.

While radiation damage induced by ionization dose is well understood [75], investigation is on-going to understand radiation damage caused by hadrons, including both charged hadrons [76] and neutrons [77]. Two additional fundamental processes may cause defects by hadrons: displacement damage and nuclear breakup. While charged hadrons can produce all three types of damage (and it's often difficult to separate them), neutrons can produce only the last two, and electrons and photons only produce ionization damage. Studies on hadron induced radiation damage to lead tungstate [78] show a proton-specific damage component caused by fragments from fission induced in lead and tungsten by particles in the hadronic shower. The fragments cause a severe, local damage to the crystalline lattice due to their extremely high energy loss over a short distance [78]. Recent investigation also sees evidence of neutron-specific damage in various crystals [77].

Most of the crystals listed in Table-35.4 have been used in high energy or nuclear physics experiments when the ultimate energy resolution for electrons and photons is desired. Examples are the Crystal Ball NaI(Tl) calorimeter at SPEAR, the L3 BGO calorimeter at LEP, the CLEO CsI(Tl) calorimeter at CESR, the KTeV CsI calorimeter at the Tevatron, and the BaBar, BELLE and BES III CsI(Tl) calorimeters at PEP-II, KEK and BEPC II, respectively. Because of their high density and relative low cost, PWO calorimeters are used by CMS and ALICE at LHC, by CLAS and PrimEx at CEBAF and by PANDA at GSI. Similarly, PbF₂ calorimeters are used by the A4 experiment at MAINZ and by the g-2 experiment at Fermilab. A CsI calorimeter is being built for the Mu2e experiment at Fermilab. An LYSO:Ce calorimeter is being built for the COMET experiment at J-PARC, and an LYSO:Ce crystal-based precision timing layer is being built for the CMS experiment at the HL-LHC.

35.5 Cherenkov detectors

Revised July 2021 by J. Schwiening (GSI Darmstadt).

Although devices using Cherenkov radiation are often thought of as only particle identification (PID) detectors, in practice they are used over a much broader range of applications including; (1) fast particle counters; (2) hadronic PID; (3) electromagnetic calorimeters (EMC); and (4) tracking detectors performing complete event reconstruction. Examples of applications from each category include; (1) the BaBar luminosity detector [79] and the Quartic fast timing counter for the ATLAS Forward Proton Detector, designed to measure small angle scatters at the LHC [80]; (2) the hadronic PID detectors at the B factory detectors—DIRC in BaBar [81], and the modern Imaging Aerogel and TOP counters at Belle II [82]; (3) the CMS Hadron Forward calorimeter based on Cherenkov light emitted in quartz fibers embedded in a steel absorber [83]; and (4) large water Cherenkov counters such as Super-Kamiokande [84].

Cherenkov counters contain two main elements; (1) a radiator through which the charged particle passes, and (2) a photodetector. As Cherenkov radiation is a weak source of photons, light collection and detection must be as efficient as possible. The refractive index n and the particle's path length through the radiator L appear in the Cherenkov relations allowing the tuning of these quantities for particular applications. One or more of the properties of Cherenkov radiation discussed in the Passages of Particles through Matter section (Sec. 34 of this *Review*) are utilized in Cherenkov detectors: the prompt emission of a light pulse; the existence of a velocity threshold for radiation; and the dependence of the Cherenkov cone half-angle θ_c and the number of emitted photons on the velocity of the particle v_p and the refractive index n of the medium. The Cherenkov angle can be calculated as

$$\cos \theta_c = \frac{1}{n(E)\beta}, \quad (35.5)$$

where $\beta = v_p/c$ with c being the speed of light, and E the photon energy. The number of photoelectrons ($N_{p.e.}$) detected in a given

device with radiator of length L is

$$N_{p.e.} = L \frac{\alpha^2 z^2}{r_e m_e c^2} \int \epsilon(E) \sin^2 \theta_c(E) dE, \quad (35.6)$$

where $\epsilon(E)$ is the efficiency for collecting the Cherenkov light and transducing it into photoelectrons, and $\alpha^2/(r_e m_e c^2) = 370 \text{ cm}^{-1} \text{ eV}^{-1}$. The quantities ϵ and θ_c are functions of the photon energy. As the typical energy dependent variation of the index of refraction is modest, a quantity called the *Cherenkov detector quality factor* N_0 can be defined as

$$N_0 = \frac{\alpha^2 z^2}{r_e m_e c^2} \int \epsilon dE, \quad (35.7)$$

so that, taking the charge number $z = 1$ (the usual case in high-energy physics),

$$N_{p.e.} \approx L N_0 \langle \sin^2 \theta_c \rangle. \quad (35.8)$$

This definition of the quality factor N_0 is not universal, nor, indeed, very useful for those common situations where ϵ factorizes as $\epsilon = \epsilon_{\text{coll}} \epsilon_{\text{det}}$ with the geometrical photon collection efficiency (ϵ_{coll}) varying substantially for different tracks while the photon detector efficiency (ϵ_{det}) remains nearly track independent. In this case, it can be useful to explicitly remove (ϵ_{coll}) from the definition of N_0 . A typical value of N_0 for a photomultiplier (PMT) detection system working in the visible and near UV, and collecting most of the Cherenkov light, is about 100 cm^{-1} . Practical counters, utilizing a variety of different photodetectors, have values ranging between about 30 and 180 cm^{-1} . Radiators can be chosen from a variety of transparent materials (Sec. 34 of this *Review* and Table 6). In addition to refractive index, the choice requires consideration of factors such as material density, radiation length and radiation hardness, transmission bandwidth, absorption length, chromatic dispersion, optical workability (for solids), availability, and cost. When the momenta of particles to be identified is high, the refractive index must be set close to one, so that the photon yield per unit length is low and a long particle path in the radiator is required. Recently, the gap in refractive index that has traditionally existed between gases and liquid or solid materials has been partially closed with transparent *silica aerogels* with indices that range between about 1.007 and 1.13.

Cherenkov counters may be classified as either *imaging* or *threshold* types, depending on whether they do or do not make use of Cherenkov angle (θ_c) information. Imaging counters may be used to track particles as well as identify them. The recent development of very fast photodetectors such as micro-channel plate PMTs (MCP-PMT) (see 35.2 of this *Review*) also potentially allows very fast Cherenkov based time of flight (TOF) detectors of either class [85]. The track timing resolution of imaging detectors can be extremely good as it scales approximately as $\frac{1}{\sqrt{N_{p.e.}}}$.

Threshold Cherenkov detectors [86], in their simplest form, make a yes/no decision based

on whether the particle is above or below the Cherenkov threshold velocity $\beta_t = 1/n$. A straightforward enhancement of such detectors uses the number of observed photoelectrons (or a calibrated pulse height) to discriminate between species or to set probabilities for each particle species [87]. This strategy can increase the momentum range of particle separation by a modest amount (to a momentum some 20% above the threshold momentum of the heavier particle in a typical case).

Careful designs give $\langle \epsilon_{\text{coll}} \rangle \gtrsim 90\%$. For a photomultiplier with a typical bi-alkali cathode, $\int \epsilon_{\text{det}} dE \approx 0.27 \text{ eV}$, so that

$$N_{p.e.}/L \approx 90 \text{ cm}^{-1} \langle \sin^2 \theta_c \rangle \quad (i.e., N_0 = 90 \text{ cm}^{-1}). \quad (35.9)$$

Suppose, for example, that n is chosen so that the threshold for species a is p_t ; that is, at this momentum species a has velocity $\beta_a = 1/n$. A second, lighter, species b with the same momentum has velocity β_b , so $\cos \theta_c = \beta_a/\beta_b$, and

$$N_{p.e.}/L \approx 90 \text{ cm}^{-1} \frac{m_a^2 - m_b^2}{p_t^2 + m_a^2}. \quad (35.10)$$

For K/π separation at $p = p_t = 1(5)$ GeV/ c , $N_{p.e.}/L \approx 16(0.8)$ cm $^{-1}$ for π 's and (by design) 0 for K 's.

For limited path lengths $N_{p.e.}$ will usually be small. The overall efficiency of the device is controlled by Poisson fluctuations, which can be especially critical for separation of species where one particle type is dominant. Moreover, the effective number of photoelectrons is often less than the average number calculated above due to additional equivalent noise from the photodetector (see the discussion of the excess noise factor in 35.2 of this *Review*). It is common to design for at least 10 photoelectrons for the high velocity particle in order to obtain a robust counter. As rejection of the particle that is below threshold depends on *not* seeing a signal, electronic and other background noise, especially overlapping tracks, can be important. Physics sources of light production for the below threshold particle, such as decay to an above threshold particle, scintillation light, or the production of delta rays in the radiator, often limit the separation attainable, and need to be carefully considered. Well designed, modern multi-channel counters, such as the ACC at Belle [88], can attain adequate particle separation performance over a substantial momentum range.

Imaging counters make the most powerful use of the information available by measuring the ring-correlated angles of emission of the individual Cherenkov photons. They typically provide positive ID information both for the “wanted” and the “unwanted” particles, thus reducing mis-identification substantially. Since low-energy photon detectors can measure only the position (and, perhaps, a precise detection time) of the individual Cherenkov photons (not the angles directly), the photons must be “imaged” onto a detector so that their angles can be derived [89]. Typically the optics map the Cherenkov cone onto (a portion of) a distorted “circle” at the photodetector. Though the imaging process is directly analogous to familiar imaging techniques used in telescopes and other optical instruments, there is a somewhat bewildering variety of methods used in a wide variety of counter types with different names. Some of the imaging methods used include (1) focusing by a lens or mirror; (2) proximity focusing (i.e., focusing by limiting the emission region of the radiation); and (3) focusing through an aperture (a pinhole). In addition, the prompt Cherenkov emission coupled with the speed of some modern photon detectors allows the use of (4) time imaging, a method which is little used in conventional imaging technology, and may allow some separation with particle TOF. Finally, (5) correlated tracking (and event reconstruction) can be performed in large water counters by combining the individual space position and time of each photon together with the constraint that Cherenkov photons are emitted from each track at the same polar angle (Sec. 36.3.1 of this *Review*).

In a simple model of an imaging PID counter, the fractional error on the particle velocity (δ_β) is given by

$$\delta_\beta = \frac{\sigma_\beta}{\beta} = \tan \theta_c \sigma(\theta_c), \quad (35.11)$$

where

$$\sigma(\theta_c) = \frac{\langle \sigma(\theta_i) \rangle}{\sqrt{N_{p.e.}}} \oplus C, \quad (35.12)$$

and $\langle \sigma(\theta_i) \rangle$ is the average single photoelectron resolution, as defined by the optics, detector resolution and the intrinsic chromaticity spread of the radiator index of refraction averaged over the photon detection bandwidth. C combines a number of other contributions to resolution including, (1) correlated terms such as tracking, alignment, and multiple scattering, (2) hit ambiguities, (3) background hits from random sources, and (4) hits coming from other tracks. The actual separation performance is also limited by physics effects such as decays in flight and particle interactions in the material of the detector. In many practical cases, the performance is limited by these effects.

For a $\beta \approx 1$ particle of momentum (p) well above threshold entering a radiator with index of refraction (n), the number of σ separation (N_σ) between particles of mass m_1 and m_2 is approximately

$$N_\sigma \approx \frac{|m_1^2 - m_2^2|}{2p^2 \sigma(\theta_c) \sqrt{n^2 - 1}}. \quad (35.13)$$

In practical counters, the angular resolution term $\sigma(\theta_c)$ varies between about 0.1 and 5 mrad depending on the size, radiator, and photodetector type of the particular counter. The range of momenta over which a particular counter can separate particle species extends from the point at which the number of photons emitted becomes sufficient for the counter to operate efficiently as a threshold device ($\sim 20\%$ above the threshold for the lighter species) to the value in the imaging region given by the equation above. For example, for $\sigma(\theta_c) = 2$ mrad, a fused silica radiator ($n = 1.474$), or a fluorocarbon gas radiator (C_5F_{12} , $n = 1.0017$), would separate π/K 's from the threshold region starting around $0.15(3)$ GeV/ c through the imaging region up to about $4.2(18)$ GeV/ c at better than 3σ .

Many different imaging counters have been built during the last several decades [85]. Among the earliest examples of this class of counters are the very limited acceptance

Differential Cherenkov detectors, designed for particle selection in high momentum beam lines. These devices use optical focusing and/or geometrical masking to select particles having velocities in a specified region. With careful design, a velocity resolution of $\sigma_\beta/\beta \approx 10^{-4}$ – 10^{-5} can be obtained [86].

Practical multi-track *Ring-Imaging Cherenkov detectors* (generally called RICH counters) are a more recent development. RICH counters are sometimes further classified by ‘generations’ that differ based on historical timing, performance, design, and photodetection techniques. Prototypical examples of first generation RICH counters are those used in the DELPHI and SLD detectors at the LEP and SLC Z factory e^+e^- colliders [85]. They have both liquid (C_6F_{14} , $n = 1.276$) and gas (C_5F_{12} , $n = 1.0017$) radiators, the former being proximity imaged with the latter using mirrors. The phototransducers are a TPC/wire-chamber combination. They are made sensitive to photons by doping the TPC gas (usually, ethane/methane) with $\sim 0.05\%$ TMAE (tetrakis(dimethylamino)ethylene). Great attention to detail is required, (1) to avoid absorbing the UV photons to which TMAE is sensitive, (2) to avoid absorbing the single photoelectrons as they drift in the long TPC, and (3) to keep the chemically active TMAE vapor from interacting with materials in the system. In spite of their unforgiving operational characteristics, these counters attained good $e/\pi/K/p$ separation over wide momentum ranges (from about 0.25 to 20 GeV/ c) during several years of operation at LEP and SLC. Related but smaller acceptance devices include the OMEGA RICH at the CERN SPS, and the RICH in the balloon-borne CAPRICE detector [85].

Later generation counters [85] generally operate at much higher rates, with more detection channels, than the first generation detectors just described. They also utilize faster, more forgiving photon detectors, covering different photon detection bandwidths. Radiator choices have broadened to include materials such as lithium fluoride, fused silica, and aerogel. Vacuum-based photodetection systems (*e.g.*, single or multi anode PMTs, MCP-PMTs, or hybrid photodiodes (HPD)) have become increasingly common (see 35.2 of this *Review*). They handle high rates, and can be used with a wide choice of radiators. Examples include (1) the SELEX RICH at Fermilab, which mirror focuses the Cherenkov photons from a neon radiator onto a camera array made of ~ 2000 PMTs to separate hadrons over a wide momentum range (to well above 200 GeV/ c for heavy hadrons); (2) the NA62 RICH at CERN, which uses a 17 m long tank filled with neon gas as radiator and spherical mirrors to focus the photons on two arrays of 2000 PMTs to separate pions from muons for momenta between 15 and 35 GeV/ c ; (3) the CBM RICH under construction at FAIR where the Cherenkov photons, produced in about 30 m 3 of CO $_2$ radiator gas, are mirror-focused on arrays of multi-anode PMTs (MaPMTs) with a total of about 55,000 pixels, to identify electrons with momenta up to 10 GeV/ c ; and (4) the LHCb detector now running at the LHC. It uses two separate counters. One volume contains C $_4$ F $_{10}$ (originally in combination with aerogel, which was removed in 2015) while the second volume contains CF $_4$. Photons are mirror-focused onto detector arrays of HPDs to cover a π/K separation momentum range between 1 and 150 GeV/ c . Further upgrades, including the replacement of the

HPDs by MaPMTs and improved readout electronics, are necessary to deal with increases in luminosity.

Other fast detection systems that use solid cesium iodide (CsI) photocathodes or triethylamine (TEA) doping in proportional chambers are useful with certain radiator types and geometries. Examples include (1) the CLEO-III RICH at CESR that uses a LiF radiator with TEA doped proportional chambers; (2) the ALICE detector at the LHC that uses proximity focused liquid (C_6F_{14} radiators and solid CsI photocathodes (similar photodetectors have been used for several years by the HADES and COMPASS detectors), and the hadron blind detector (HBD) in the PHENIX detector at RHIC that couples a low index CF_4 radiator to a photodetector based on electron multiplier (GEM) chambers with reflective CsI photocathodes [85].

Recent technological advances in the production of aerogel with improved transparency in the UV range and finely tuned refractive indices enable several new RICH designs. The innovative hybrid geometry of the CLAS12 RICH, with complex photon paths that feature multiple passes through the aerogel tiles, is only possible due to the improved scattering length of the aerogel. It minimizes the material inside of the detector acceptance as well as the cost of the photon sensor array. Beam tests have demonstrated that the counter will be able to provide clean π/K separation up to 8 GeV/c. The forward endcap Aerogel RICH (ARICH) for the Belle II upgrade at KEKB, designed to provide clean π/K separation for momenta up to 3.5 GeV/c, is an example of the so-called focusing aerogel approach [90]. The radiator is a dual-layer aerogel, with a thickness of 20 mm for each layer and increasing refractive indices of $n = 1.045$ and $n = 1.055$ along the particle path. The Cherenkov ring images from the two layers overlap on the array of Hybrid Avalanche Photo Detectors (HAPDs), which provide efficient single photon detection in the 1.5 T magnetic field.

A DIRC (Detection [of] Internally Reflected Cherenkov [light]) is a distinctive, compact RICH subtype first used in the BaBar detector [81]. A DIRC “inverts” the usual RICH principle for use of light from the radiator by collecting and imaging the total internally reflected light rather than the transmitted light. It utilizes the optical material of the radiator in two ways, simultaneously: as a Cherenkov radiator and as a light pipe. The magnitudes of the photon angles are preserved during transport by the flat, rectangular cross section radiators, allowing the photons to be efficiently transported to a detector outside the path of the particle where they may be imaged in up to three independent dimensions (the usual two in space and, due to the long photon paths lengths, one in time). Because the index of refraction in the radiator is large ($n \sim 1.47$ for fused silica), the momentum range with good π/K separation goes up to 4–5 GeV/c. It is plausible, but difficult, to extend it up to about 10 GeV/c with an improved design.

The BaBar experiment at the asymmetric PEP-II e^+e^- collider studied CP violation in $\Upsilon(4S)$ decays. Excellent pion/kaon separation for particle momenta up to 4 GeV/c was required. The BaBar DIRC used 4.9 m long, rectangular bars made from synthetic fused silica as radiator and light guide. The photons were imaged via a “pin-hole” through an expansion region filled with 6 000 liters of purified water onto an array of 10 752 densely packed photomultiplier tubes placed at a distance of about 1.2 m from the bar end. During more than 8 years of operation, the BaBar DIRC achieved π/K separation of 2.5 standard deviations or more up to 4 GeV/c momentum. For a pion identification rate around 85% the DIRC provided a kaon misidentification rate well below 1% up to 3 GeV/c.

The next generation of DIRC detectors [91] takes advantage of the new, very fast, pixelated photodetectors becoming available, such as MaPMTs and MCP-PMTs. They typically utilize either time imaging or lens/mirror-focused optics, or both, leading not only to a precision measurement of the Cherenkov angle, but in some cases, to a precise measurement of the particle time of flight, and/or to correction of the chromatic dispersion in the radiator. Examples [85] include (1) the Belle II Time of Propagation (TOP) counter that emphasizes precision timing for both Cherenkov imaging and TOF to perform π/K separation of at

least 3 standard deviations up to 4 GeV/c; (2) the DIRC upgrade of the GlueX experiment at Jefferson Lab that places four decommissioned BaBar DIRC modules, coupled to upgraded optics and readout, perpendicular to the beamline, the first application of a DIRC in a detector endcap; (3) the PANDA Barrel DIRC at FAIR, to be installed in 2025, that will be the first DIRC counter to use lens focusing and is expected to provide more than 3 standard deviations π/K separation up to 3.5 GeV/c; and (4) the TORCH proposal being developed for an LHCb upgrade in 2027 which uses DIRC imaging for individual photons with fast photon detectors to provide particle separation via particle TOF with a precision of 10–15 ps per track over a flight path length of 9.5m.

35.6 Gaseous detectors

35.6.1 Energy loss and charge transport in gases

Revised November 2021 by F. Sauli (CERN) and M. Titov (IRFU, CEA, Université Paris-Saclay).

Gas-filled detectors use the localized ionization produced by charged particles, generally after charge multiplication. The statistics of ionization processes, having asymmetries in the ionization trails, affect the coordinate determination deduced from the measurement of drift time, or of the center of gravity of the collected charge. For thin gas layers, the width of the energy loss distribution can be larger than its average, requiring multi-sampling devices or truncated mean analysis to achieve good particle identification. In the truncated mean method for calculating $\langle dE/dx \rangle$, the ionization measurements along the track length are broken into many samples and then a fixed fraction of high-side (and sometimes also low-side) values are rejected [92].

Table 35.5: Properties of noble and molecular gases at normal temperature and pressure (NTP: 20° C, one atm). E_X , E_I : first excitation, ionization energy; W_I : average energy for creation of ion pair; $dE/dx|_{\min}$, N_P , N_T : differential energy loss, primary and total number of electron-ion pairs per cm, for unit charge minimum ionizing particles. Values often differ, depending on the source, and those in the table should be taken only as approximate.

Gas	Density, mg cm ⁻³	E_X eV	E_I eV	W_I eV	$dE/dx _{\min}$ keV cm ⁻¹	N_P cm ⁻¹	N_T cm ⁻¹
H ₂	0.084	10.8	13.6	37	0.34	5.2	9.2
He	0.179	19.8	24.6	41.3	0.32	3.5	8
Ne	0.839	16.7	21.6	37	1.45	13	40
Ar	1.66	11.6	15.7	26	2.53	25	97
Xe	5.495	8.4	12.1	22	6.87	41	312
CH ₄	0.667	8.8	12.6	30	1.61	28	54
C ₂ H ₆	1.26	8.2	11.5	26	2.91	48	112
iC ₄ H ₁₀	2.49	6.5	10.6	26	5.67	90	220
CO ₂	1.84	7.0	13.8	34	3.35	35	100
CF ₄	3.78	10.0	16.0	35–52	6.38	52–63	120

The energy loss of charged particles and photons in matter is discussed in Sec. 34. Every ionization process is a quantum mechanical transition initiated by the Coulomb field of the particle and the field created by neighbouring polarizable atoms; the average energy losses are described by the Bethe-Bloch formula with Sternheimer’s density effect corrections. The fluctuations caused by Rutherford scattering on quasi-free electrons follow a Landau distribution and the influence of atomic shells is described by the photoabsorption ionization (PAI) model, which allows simulation of each energy transfer [93], with relaxation cascades and simulation of delta-electrons [94]. Table 35.5 provides values of relevant parameters in some commonly used gases at NTP for unit-charge minimum-ionizing particles (MIPs) [95] [96]. When an ionizing particle passes through the gas it creates electron-ion pairs; often the ejected electrons have sufficient energy to further ionize the medium. The number of pairs is known as cluster-size distribution, because the secondary electrons are created in the immedi-

ate vicinity of the primary encounter and, together with the primary electrons, form clusters of one, several, or sometimes many, electron-ion pairs. As shown in Table 35.5, the total number of pairs (N_T) is a few times larger than the number of primaries (N_P). For different conditions and for mixtures, and neglecting energy transfer processes (*e.g.* Penning effect), one can scale the density, N_P , and N_T with temperature and pressure assuming a perfect gas law.

The probability for a released electron to have an energy E or larger follows an approximate $1/E^2$ dependence (Rutherford law), shown in Fig. 35.4 for Ar at NTP (dotted line, left scale). More detailed estimates taking into account the electronic structure of the medium are shown in the figure, for three values of the particle velocity factor $\beta\gamma$ [97]. The dot-dashed line provides, on the right scale, the practical range of electrons (including scattering) of energy E . As an example, about 0.6% of released electrons have 1 keV or more energy, substantially increasing the total ionization loss. The practical range of 1 keV electrons in argon (dot-dashed line, right scale) is 70 μm and this can contribute to the error in the coordinate determination.

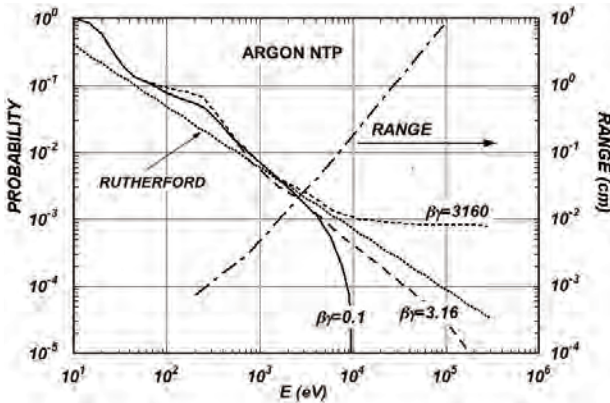


Figure 35.4: Probability of single collisions in which released electrons have an energy E or larger (left scale) and practical range of electrons in Ar at NTP (dot-dashed curve, right scale) [97].

Garfield⁺⁺ [98], together with HEED [94], Degrad [99], Magboltz [100, 101], SRIM, ANSYS, COMSOL, and neBEM [102] software packages represent the core simulation tools for microscopic modelling of gaseous detector response. The number of electron-ion pairs per primary ionization, or cluster size depends little on the medium; it can be computed with the programs mentioned above or experimentally measured. For example, there is about 1% probability for primary clusters to contain ten or more electron-ion pairs in argon [103].

Once released in the gas, and under the influence of an applied electric field, electrons and ions drift in opposite directions and diffuse towards the electrodes. The electron-molecule collision cross sections are determined by the details of atomic and molecular structure and depends strongly on the electron energy and therefore on the electric field \mathbf{E} for most gases. High values of the total electron scattering cross section reduce the electron diffusion and increase the drift velocity; a large inelasticity implies that high fields are required to raise the electron energy. For noble gases, the inelastic cross section is zero until the electrons reach the first excitation and ionization energies $\mathcal{O}(10 \text{ eV})$; on the contrary, for molecular gases, like CH_4 , inelastic channels, involving rotational and vibrational levels, open up at energies above $\sim 0.1 \text{ eV}$. Large drift velocities are achieved by adding polyatomic gases (usually hydrocarbons C_xH_y , CO_2 , CF_4) having large inelastic component at moderate energies of a few eV; this results in the electron “cooling” into the energy range of the Ramsauer-Townsend minimum (at $\sim 0.5 \text{ eV}$) of the elastic (“momentum-transfer”) cross-section in Ar [96]. Under these circumstances, it is not surprising that the addition of very small quantities of one gas to another can dramatically modify the average electron energy and alter the dependence of the drift velocity (v_d) on \mathbf{E}/P and temperature; this has a particularly strong effect for noble gases, as illustrated in Fig. 35.5

for Ar. Carbon tetrafluoride (CF_4) has the largest drift velocity and the lowest electron diffusion among known gases due to the sizeable Ramsauer-Townsend dip in the elastic cross-section which coincides with a very large vibrational modes. Another principal role of the polyatomic gas is to absorb the ultraviolet photons emitted by the excited noble gas atoms. Addition of molecular gases (hydrocarbons or CO_2 are widely used in the proportional counters as a quencher) to noble gas allows to dissipate a good fraction of energy through rotational and vibrational radiationless transitions without the creation of photons or ions. On the contrary, CF_4 has a small quenching cross-section of excited Ar states and light emission in CF_4 (from the far UV to the visible light) is a complex process, involving the creation of CF_3^+ excited states [104].

Extensive collections of experimental data [105] and theoretical calculations based on transport theory permit evaluation of drift and diffusion properties in pure gases and their mixtures; modern compilations of the electron-molecule cross sections are available at the open-access website LXCAT [106]. Fig. 35.5 and Fig. 35.6 show drift velocity and transverse diffusion for some commonly used gases at NTP, computed with the Magboltz program [100, 101]. For different conditions, the horizontal axis must be scaled inversely with the gas density. Standard deviations for longitudinal (σ_L) and transverse diffusion (σ_T) are given for one cm of drift, and scale with the the square root of the drift distance.

In a simple approximation, gas kinetic theory provides the drift velocity v_d as a function of the mean collision time τ and the electric field \mathbf{E} : $v_d = eE\tau/m_e$ (Townsend’s expression). In the presence of an external magnetic field, the Lorentz force acting on electrons between collisions deflects the drifting electrons and modifies the drift properties. The electron trajectories, velocities and diffusion parameters can be computed with Magboltz. The friction force model provides an approximate expression for the vector drift velocity \mathbf{v} as a function of electric and magnetic field vectors \mathbf{E} and \mathbf{B} , of the Larmor frequency $\omega = eB/m_e$, and of the mean collision time τ (more precise calculation is available in Magboltz, which computes drift velocity by tracing electrons at the microscopic level through numerous collisions with gas molecules):

$$\mathbf{v} = \frac{e}{m_e} \frac{\tau}{1 + \omega^2\tau^2} \left(\mathbf{E} + \frac{\omega\tau}{B} (\mathbf{E} \times \mathbf{B}) + \frac{\omega^2\tau^2}{B^2} (\mathbf{E} \cdot \mathbf{B})\mathbf{B} \right) \quad (35.14)$$

To a good approximation, and for moderate fields, one can assume that the energy of the electrons is not affected by B , and use for τ the values deduced from the drift velocity at $B = 0$ (the Townsend expression). For \mathbf{E} perpendicular to \mathbf{B} , the drift angle relative to the electric field vector is $\tan\theta_B = \omega\tau$ and $v = (E/B)(\omega\tau/\sqrt{1 + \omega^2\tau^2})$. For parallel electric and magnetic fields, drift velocity and longitudinal diffusion are not affected, while the transverse diffusion can be strongly reduced: $\sigma_T(B) = \sigma_T(B = 0)/\sqrt{1 + \omega^2\tau^2}$. As an example, the dotted line in Fig. 35.6 represents σ_T for the classic Ar/ CH_4 (90:10) mixture at 4 T. Large values of $\omega\tau \sim 20$ at 5 T are consistent with the measurement of diffusion coefficient in Ar/ CF_4 / iC_4H_{10} (95:3:2). This reduction is exploited to substantially improve spatial resolution in the Drift (Sec. 35.6.2) and Time Projection Chambers (Sec. 35.6.5).

In some mixtures containing molecules with electronic affinity, electrons can be captured to form negative ions. Capture cross sections vary considerably with an energy and, hence, the electric field; as a consequence, the three-body electron attachment coefficients may differ significantly for the same additive in different mixtures. As an example, at moderate fields (up to 1 kV/cm) the addition of 0.1% of oxygen to an Ar/ CO_2 mixture results in an electron capture probability about twenty times larger than in Ar/ CH_4 . Among common molecules, the largest electron affinities are found for the halogenides, O_2 and H_2O . The attachment probability in O_2 or H_2O is large at low fields and electron energies close to thermal, but decreases at increasing fields. On the contrary, CF_4 is not electronegative at low and moderate fields, but has a large electron capture cross section at fields above $\sim 8 \text{ kV/cm}$, before reaching the avalanche field strengths. Depending on the mixture and detector geometry, some signal reduction and energy resolution loss is expected in this gas.

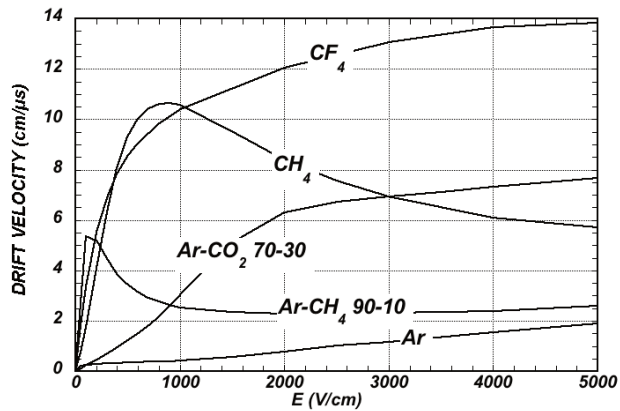


Figure 35.5: Computed electron drift velocity as a function of electric field in several gases at NTP and $B = 0$ [100, 101].

If the electric field is increased sufficiently, electrons gain enough energy between collisions to excite and ionize molecules. Above a gas-dependent threshold, the mean free path for ionization, λ_i , decreases exponentially with the field; its inverse, $\alpha = 1/\lambda_i$, is named the first Townsend coefficient. In wire chambers, most of the increase of avalanche particle density occurs very close to the anode wires, and a simple electrostatic consideration shows that the largest fraction of the detected signal is due to the motion of positive ions receding from the wires. The electron component, although very fast, contributes very little to the signal. This determines the characteristic shape of the detected signals in the proportional mode: a fast rise followed by a gradual increase. The slow component, the so-called “ion tail” that limits the time resolution of the detector, is usually removed by differentiation of the signal. In uniform fields, N_0 initial electrons multiply over a length x forming an electron avalanche of size $N = N_0 e^{\alpha x}$; N/N_0 is the gain of the detector. Fig. 35.7 shows examples of Townsend coefficients for several gas mixtures, computed with Magboltz [100, 101].

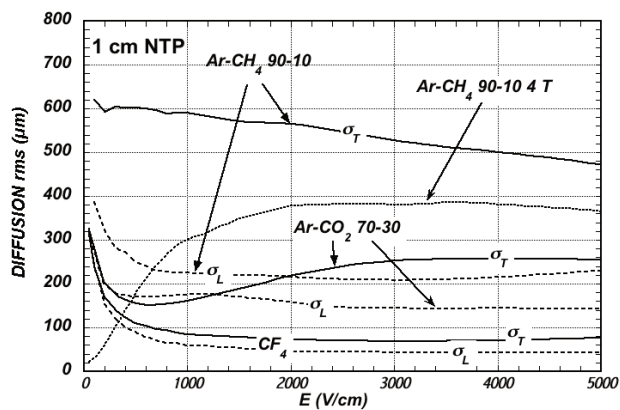


Figure 35.6: Electron longitudinal diffusion (σ_L) (dashed lines) and transverse diffusion (σ_T) (full lines) for 1 cm of drift at NTP and $B = 0$. The dotted line shows σ_T for the P10 mixture at 4 T [100, 101].

Additional ionizing energy transfer mechanisms due to the excited noble gas atoms, called collisional Penning energy transfers, occur when the excitation energy of a noble gas is higher than the ionization potential of an admixture gas. The energy transfer rate, probability that an excited atom ionizes a quenching agent, is a priori not known for a mixture but can be extracted from the fits of the experimental gas gain data [107] using the Magboltz simulations [100, 101]. In the gain calculations, the Penning adjusted Townsend coefficient is defined in terms of the total production frequencies of the noble gas excitations and direct ionizations of the mixture. Systematic gas gain measurements for varying mix-

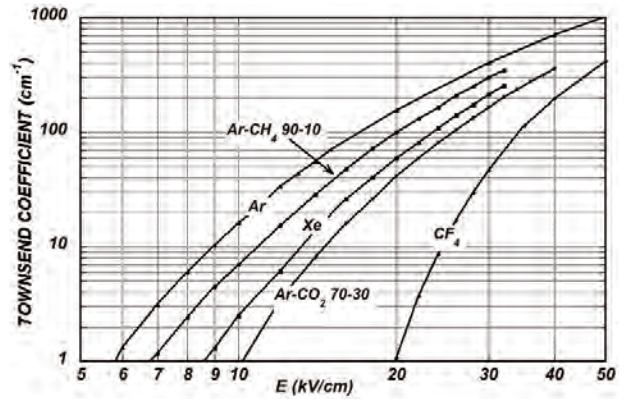


Figure 35.7: Computed first Townsend coefficient α as a function of electric field in several gases at NTP [100, 101].

ing ratios and pressures are critical for determining the efficiency of the different mechanisms involved in the transfers. Collisional energy transfer mostly scales linearly with the gas pressure and the fraction of quenching gas in the mixture, while ionization by photons emitted from excitations is independent of the medium [108]. In addition, collisional Penning transfers of some higher excited states can occur before they decay at atmospheric pressure and are not restricted to metastable states of the excited noble gas. For example, the impact of the Penning effect on gas gain is roughly a factor 10 in Ar-CO₂ mixtures and exceeding a factor of 100 in Ar-C₂H₂ mixtures [108].

Positive ions released by the primary ionization or produced in the avalanches drift and diffuse under the influence of the electric field. Negative ions may also be produced by electron attachment to gas molecules. The drift velocity of ions in the fields encountered in gaseous detectors (up to few kV/cm) is typically about three orders of magnitude smaller than for electrons. The ion mobility μ , the ratio of drift velocity to electric field, is constant for a given ion type up to very high fields. Values of ions mobility at NTP are given in Table 35.6 [109]. For different temperatures and pressures, the mobility can be scaled inversely with the density assuming an ideal gas law. Both the longitudinal and transverse diffusion of ions are proportional to the square root of the drift time, with a coefficient that depends on temperature but not on the ion mass. It has been historically assumed that, due to a very effective charge transfer mechanism, only ions with the lowest ionization potential survive after a short path in the mixture. However, recent experimental data suggests that the signal ions, in e.g. CO₂-quenched mixtures of Ar and Ne are CO₂⁺·(CO₂)_n cluster ions, and not CO₂⁺ or noble gas ions [110]. Since the cluster ions are slower than the initial ions, the signals induced by ion motion are altered. The effect can be present in constant-field detectors and TPCs (see Sec. 35.6.5), and might affect devices such as Micromegas (see Sec. 35.6.4) and drift tubes. A negative-ion TPC can be used to expand the reach of directional dark matters searches [111].

Table 35.6: Mobility of ions in gases and mixtures at NTP [109].

Gas	Mobility μ (cm ² V ⁻¹ s ⁻¹)
He	10.4
Ne	4.7
Ar	1.54
Ar/CH ₄	1.87
Ar/CO ₂	1.72
CH ₄	2.26
CO ₂	1.09

35.6.2 Multi-Wire Proportional and Drift Chambers

Revised November 2021 by F. Sauli (CERN) and M. Titov (IRFU, CEA, Université Paris-Saclay).

Single-wire counters that detect the ionization produced in a gas by a charged particle, followed by charge multiplication and collection around a thin (typically 20 – 50 μm diameter) wire, have been used for decades. Good energy resolution is obtained in the proportional amplification mode, while very large saturated pulses can be detected in the streamer and Geiger modes [112].

Modern fully electronic devices, multiwire proportional chambers (MWPCs) [113, 114] introduced in the late 1960's, detect, localize and measure energy deposit by charged particles over large areas. A mesh of parallel anode wires at a suitable potential, inserted between two cathodes, acts almost as a set of independent proportional counters (see Fig. 35.8a). Electrons released in the gas volume drift towards the anodes and produce avalanches in the increasing field. Analytic expressions for the electric field can be found in many textbooks. The fields close to the wires $E(r)$, in the drift region E_D , and the capacitance C per unit length of anode wire are approximately given by

$$E(r) = \frac{CV_0}{2\pi\epsilon_0} \frac{1}{r} \quad E_D = \frac{CV_0}{2\epsilon_0 s} \quad C = \frac{2\pi\epsilon_0}{\pi(\ell/s) - \ln(2\pi a/s)}, \quad (35.15)$$

where r is the distance from the center of the anode, s the wire spacing, ℓ and V_0 the distance and potential difference between anode and cathode, and a the anode wire radius.

Because of electrostatic forces, anode wires are in equilibrium only for a perfect geometry. Small deviations result in forces displacing the wires alternatively below and above the symmetry plane, sometimes with catastrophic results [115]. These displacement forces are countered by the mechanical tension of the wire, up to a maximum unsupported stable length, L_M [116], above which the wire displaces:

$$L_M = \frac{s}{CV_0} \sqrt{4\pi\epsilon_0 T_M} \quad (35.16)$$

The maximum tension T_M depends on the wire diameter and modulus of elasticity. Table 35.7 gives approximate values for tungsten and the corresponding maximum stable wire length under reasonable assumptions for the operating voltage ($V_0 = 5$ kV) [117]. Internal supports and spacers can be used in the construction of longer detectors to overcome limits on the wire length imposed by Eq. (35.16).

Table 35.7: Maximum tension T_M and stable unsupported length L_M for tungsten wires with spacing s , operated at $V_0 = 5$ kV. No safety factor is included.

Wire diameter (μm)	T_M (newton)	s (mm)	L_M (cm)
10	0.16	1	25
20	0.65	2	85

Traditionally, several simplifying assumptions are made in such analytical calculations: electrostatic force acting on the wire does not change during wire movements, or varies linearly with the displacement, the wire shape is parabolic; only one wire moves at a time. Therefore, for complicated electrode geometries the approximations listed above are not applicable. The advantage of numerical integrations using Garfield⁺⁺ program is to simulate the collective movement of all wires, which are difficult analytically, and to consider all forces acting on a wire: forces between anode wire and other electrodes (wires, cathode) and a gravitational force [118].

Detection of charge on the wires over a predefined threshold provides the transverse coordinate to the wire with an accuracy comparable to that of the wire spacing. The coordinate along each wire can be obtained by measuring the ratio of collected charge at the two ends of resistive wires. The cathode planes can be fabricated in the form of group of wires or isolated strips, which are often patterned in orthogonal directions. Making use of

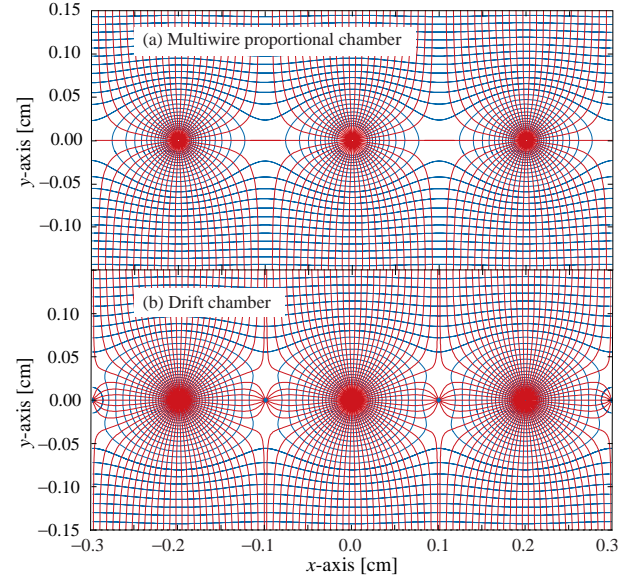


Figure 35.8: Electric field lines and equipotentials in (a) a multiwire proportional chamber and (b) a drift chamber.

the charge profile induced by avalanches on segmented cathodes, the so-called electronic center-of-gravity (COG) method allows localization of tracks to sub-mm accuracy. Due to the statistics of energy loss and asymmetric ionization clusters, the position accuracy is ~ 50 μm rms for fast particles perpendicular to the wire plane, but degrades to ~ 250 μm at 30° to the normal [119].

Drift chambers, developed in the early '70's, can be used to estimate the space coordinate perpendicular to the wires by exploiting the arrival time of electrons at the anodes if the time of interaction is known [120]. The distance between anode wires (e.g. Au-plated W) is usually several cm, allowing coverage of large areas at reduced cost. In the original design, a thicker wire (the field wire, often from Cu-Be or Al) at the proper voltage, placed between the anode wires, removes the low-field region at the midpoint between anodes and improves charge collection (Fig. 35.8b). In some drift chamber designs, and with the help of suitable voltages applied to field-shaping electrodes, the electric field structure is adjusted to improve the linearity of space-to-drift-time relation, resulting in better spatial resolution [121].

Drift chambers can reach a longitudinal spatial resolution from timing measurement of order 100 μm (rms) or better for minimum ionizing particles, depending on the geometry and operating conditions. However, a degradation of resolution is observed [122] due to primary ionization statistics for tracks close to the anode wires, caused by the spread in arrival time of the nearest ionization clusters. The effect can be reduced by operating the detector at higher pressures. Sampling the drift time on rows of anodes led to the concept of multiple arrays such as the multi-drift module [123] and the JET chamber [124]. A measurement of drift time, together with the recording of charge sharing from the two ends of the anode wires provides the coordinates of segments of tracks. An ultimate drift chamber design is the Time Projection Chamber (TPC) concept [125], which provides 3D precision tracking with low material budget and enables particle identification through differential energy loss dE/dx measurement or cluster counting dN_{cl}/dx techniques. In all cases, a good knowledge of electron drift velocity and diffusion properties is required. This has to be combined with the knowledge of the electric fields in the structures [101]. Accumulation of ions in the gas volume may induce gain reduction and field distortions, especially for long drift distances in TPC (see Sec. 35.6.5). An important major innovation is related to the replacement of MWPC with Micro-Pattern Gaseous Detectors (MPGD) (see Sec. 35.6.4) for the TPC endplate readout, which offers many advantages: reduced track-angle, and negligible $E \times B$ track distortion effects, narrower pad

response function (PRF), and intrinsic suppression of Ion Back Flow (IBF). For an overview of detectors exploiting the drift time for coordinate measurement see Refs. [116,126].

Multiwire and drift chambers have been operated with a variety of gas fillings and operating modes, depending on experimental requirements. The so-called “Magic Gas,” a mixture of argon, isobutane and Freon [114], permits very high and saturated gains ($\sim 10^6$). This gas mixture was used in early wire chambers, but was found to be susceptible to severe aging processes. DAFNE’s KLOE Drift Chamber and the recent version of it developed for the MEG2 experiment [127] are the precursors of the next generation of ultralight central trackers for future colliders. Since the main contribution in terms of radiation length is related to tungsten wires, high transparency can be achieved thanks to the development of new wire materials (e.g. carbon monofilaments) and novel approaches for the wiring and assembly procedures. Drift chambers have been operated with a light helium/hydrocarbon mixtures, which are not reliable for long-term, high-rate operation [128]. Dedicated R&D is necessary to find an alternative hydrocarbon-free mixture adapted to the desired performance at future colliders.

Although very powerful in terms of performance, multi-wire structures have reliability problems when used in harsh or hard-to-access environments, since a single broken wire can disable the entire detector. Introduced in the 1980s, straw and drift tube systems make use of large arrays of proportional counters encased in individual enclosures, each acting as an independent wire counter [129]. Techniques for low-cost mass production of these detectors have been developed for large experiments, such as the Transition Radiation Tracker and the Drift Tubes arrays for CERN’s LHC experiments [130]. The state-of-the-art NA62 straw tracker utilizes new construction techniques of ultrasonic welding to close the straw and to keep them straight and withstand the vacuum pressure without breaking [131]. Future efforts for straw detectors, e.g. COMET Phase-II at JPARC or Mu2e-II at Fermilab, will focus on ultra-thin wall development, long and thin wire handling, precise mechanics and innovative designs.

35.6.3 High Rate Effects

Revised November 2021 by F. Sauli (CERN) and M. Titov (IRFU, CEA, Université Paris-Saclay).

The production of positive ions in the avalanches and their slow drift before neutralization result in a rate-dependent accumulation of positive charge in the detector. This may result in significant field distortion, gain reduction and degradation of spatial resolution. As shown in Fig. 35.9 [132], the proportional gain drops above a charge production rate around 10^9 electrons per second and mm of wire, independently of the avalanche size. For a proportional gain of 10^4 and 100 electrons per track, this corresponds to a particle flux of $10^3 \text{ s}^{-1} \text{ mm}^{-1}$ (1 kHz/mm² for 1 mm wire spacing). For the description of rate effects in MPGD, see Sec. 35.6.4.

Although almost any gas can be used to operate wire chambers, CF_4 -based mixtures have been preferred due to their properties. Their main advantage for the use in large volume detectors are high drift velocity, low diffusion, non-flammability and low sensitivity to neutrons; also they do not form polymers in avalanches.

However, the problem of greenhouse gases, such as CF_4 , could become a fundamental limitation for their future applications in gaseous detectors; due to the EU regulations their prices might go up and future availability is unknown. Performance studies of several eco-friendly mixtures have been initiated, together with a better understanding of their long-term ageing effects [133] (see also Sec. 35.6.4).

Ageing phenomena (formation of polymer deposits on the electrodes) constitute one of the most complex and serious potential problems which could limit or severely impair the use of gaseous detectors in unprecedented harsh radiation environments and lead to operational instabilities [134] [128]. The process has been extensively investigated, often with conflicting results. Several causes have been identified, including organic pollutants and silicone oils. Addition of small amounts of water in many (but not all) cases has been shown to extend the lifetime of the detectors.

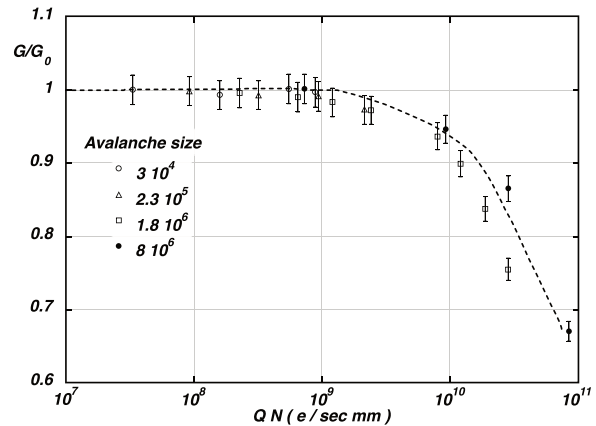


Figure 35.9: Charge rate dependence of normalized gas gain G/G_0 (relative to zero counting rate) in proportional thin-wire detectors [132]. Q is the total charge in single avalanche; N is the particle rate per wire length.

Addition of fluorinated gases (e.g., CF_4) or oxygen may result in an etching action that can overcome polymer formation, or even eliminate already existing deposits. However, the issue of long-term survival of gas detectors with these gases is controversial. Under optimum operating conditions, a total collected charge of a few coulombs per cm of wire can usually be reached before noticeable degradation occurs. This corresponds, for one mm spacing and at a gain of 10^4 , to a total particle flux of $\sim 10^{14}$ MIPs/cm².

35.6.4 Micro-Pattern Gas Detectors

Revised November 2021 by F. Sauli (CERN) and M. Titov (IRFU, CEA, Université Paris-Saclay).

Despite various improvements, position-sensitive detectors based on wire structures are limited by basic diffusion processes and space charge effects to localization accuracies of 50–100 μm [135]. Industrial advances in microelectronics and photolithographic technology on flexible and standard PCB substrates has favored the invention, in the last years of the 20th century, of novel Micro-Pattern Gaseous Detectors (MPGD) [136–138]. Since the very beginning, the goal was the development of novel devices with high rate capability (up to 10^6 Hz/mm²) and excellent spatial resolution (down to 30 μm), single photo-electron time resolution in the ns-range, large sensitive area and dynamic range, superior radiation hardness and low-cost for large area coverage. Nowadays, a broad family of MPGD technologies are being developed and optimized for numerous applications, such as [139,140]: Micro-Strip Gas Chamber (MSGC), Gas Electron Multiplier (GEM), Micro-Mesh Gaseous Structure (Micromegas), Thick GEMs (THGEM), also referred to in the literature as Large Electron Multipliers (LEM), Resistive Plate WELL (RPWELL), GEM-derived architecture (μ -RWELL), Micro-Pixel Gas Chamber (μ -PIC), and an integrated readout of gaseous detectors (Gridpix) using solid-state pixel chips (e.g. Medipix or Timepix).

The MSGC concept, invented in 1988, was the first of the micro-structure gas chambers [136]. It consists of a set of tiny parallel metal strips laid on a thin resistive support, alternatively connected as anodes and cathodes and resembles a multi-anode proportional counter. Through an accurate and simple photolithography process, the anode strips can be made very narrow ($\sim 10 \mu\text{m}$) with a typical pitch (distance between strips) of $\sim 100 \mu\text{m}$. When appropriate potentials are applied to the electrodes, electrons released in the drift volume move toward the strips and multiply in the high-field region. Owing to the small anode-to-cathode distance, the fast removal of positive ions by nearby cathode strips reduces space charge build-up, and improves significantly the rate capability, compared to wire counter. Despite their promising performance, experience with MSGCs has raised serious concerns about their long-term behavior. There are several major processes, particularly at high rates, leading to the MSGC operational instabilities: substrate charging-up and time-dependent distur-

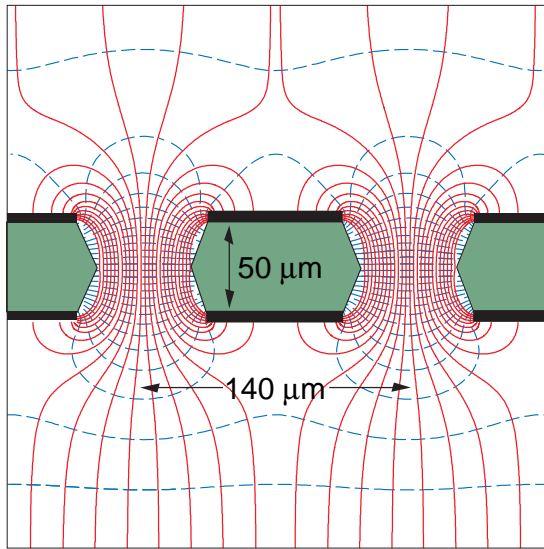


Figure 35.10: Schematic view and typical dimensions of the hole structure in the GEM amplification cell. Electric field lines (solid) and equipotentials (dashed) are shown. Electron trajectories do not strictly follow the field lines as drifting electrons scatter isotropically with gas molecules and diffuse transversally.

tions of the electric field, surface deposition of polymers (“aging”) during sustained irradiation, and destructive micro-discharges under exposure to heavily ionizing particles [141]. The physical parameters used to manufacture and operate these detectors (substrate material, metal of strips, type and purity of the gas mixture) appeared to play dominant roles in determining the medium- and long-term stability. The problems encountered inspired the development of novel structures, using modern photolithographic processes: GEM, Micromegas and others, having increased reliability and radiation hardness.

A GEM detector consists of a thin-foil copper-insulator-copper sandwich chemically perforated to obtain a high density of holes in which avalanches occur [137, 142]. The hole diameter is typically between $25\ \mu\text{m}$ and $150\ \mu\text{m}$, while the corresponding distance between holes varies between $50\ \mu\text{m}$ and $200\ \mu\text{m}$. The central insulator is usually (in the original design) a polyimide foil, with a thickness of $50\ \mu\text{m}$. Application of a potential difference between the two metal sides of the GEM generates the electric fields indicated in Fig. 35.10. Each hole acts as an independent proportional counter. Electrons released by the primary ionization particle in the upper conversion region (above the GEM foil) drift into the holes, where charge multiplication occurs in the high electric field ($50\text{--}70\ \text{kV/cm}$), and are transferred into the gap below the GEM. Systematic measurements with cascaded multi-GEM structures confirm that the gains and charge transfer processes are predictable from electrostatic considerations and avalanche development models; an overall gas gain well above 10^4 can be reached in the presence of highly ionizing particles, while strongly reducing the risk of discharges [143]. Other important parameters such as attachment, diffusion depend on the gas mixture composition and E/P . The majority of the charges created in the avalanche process follow the field lines and are collected by the metallic electrodes; owing however to diffusion, some may deposit on the dielectric surfaces, modifying the field and affecting gain and transparency of the structures [144]. This effect is known as “charging-up” effect; its time constant and amplitude depend largely on the shape of the holes.

The micro-mesh gaseous structure (Micromegas) is a thin parallel-plate avalanche counter, as shown in Fig. 35.11 [138]. It consists of a drift region and a narrow multiplication gap ($25\text{--}150\ \mu\text{m}$) between a thin metal grid (micromesh) and the read-out electrode (strips or pads of conductor printed on an insulator board). Electrons from the primary ionization drift through the mesh into the narrow multiplication gap, where they are ampli-

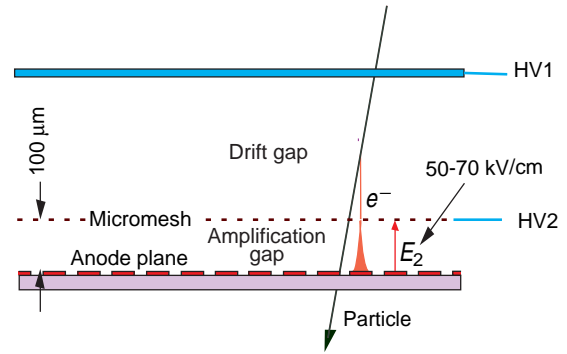


Figure 35.11: Schematic drawing of the Micromegas detector.

fied. The electric field is mostly homogeneous in both the drift (electric field $\sim 1\ \text{kV/cm}$) and amplification ($50\text{--}70\ \text{kV/cm}$) regions and exhibits a funnel-like shape close to the openings of the micromesh: field lines are compressed into a small diameter of the order of a few microns, depending on the electric field ratio between the two gaps. In the narrow multiplication region, small variations of the amplification gap are approximately compensated by an inverse variation of the Townsend coefficient from the electric field, resulting in a more uniform gain. The transverse size of the electron avalanche due to diffusion is of the order of $10\text{--}15\ \mu\text{m}$, depending on the gas mixture, the electric field, and the gap width, giving rise to excellent spatial resolution ($12\ \mu\text{m}$ for MIPs) [145]. Most positive ions are quickly removed by the micromesh; this prevents space-charge accumulation and induces very fast signals ($\sim 100\ \text{ns}$ length) due to electrons with a (fast) tail due to ions. Efforts have been also focused on producing Micromegas detector using innovative manufacturing techniques - the “Bulk” and “MicroBulk” technologies [146].

The absence of space-charge effects in GEMs at the highest rates reached so far, thanks to its fine-pitch structure of a few hundred microns, improves the maximum rate capability by more than two orders of magnitude compared to MWPC (see Fig. 35.12) [147] [148]. Even larger rate capability has been reported for Micromegas [149].

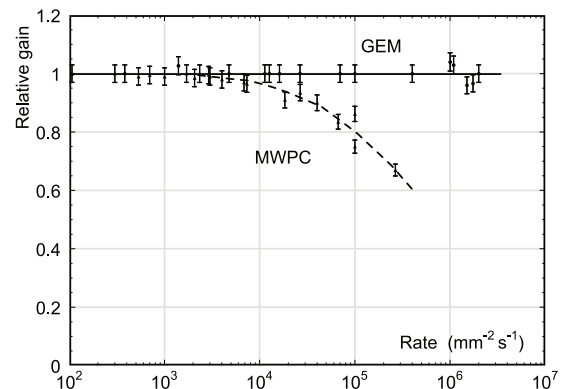


Figure 35.12: Normalized gas gain as a function of particle rate for MWPC [147] and GEM [148].

The fine granularity and high-rate capability of GEM and Micromegas can be fully exploited by using high-density pixel read-out with a size corresponding to the intrinsic width of the detected avalanche charge. An elegant solution is the use of a CMOS pixel ASIC, assembled directly below the GEM or Micromegas amplification structure. Modern wafer post-processing technology allows an integration of a small-scale micromesh grid directly on top of a Timepix chip, thus forming an integrated MPGD readout, called GridPix concept (see Fig. 35.13) [150]. With this arrangement, avalanche electrons are collected on the metalized input pads, exposed to the gas and signals are induced at the input gate of a charge-sensitive preamplifier. Every pixel is then directly con-

nected to the amplification and digitization circuits, integrated in the underlying CMOS layers. A thin insulating layer, e.g. a few μm of silicon nitride, is usually deposited on top of CMOS ASIC to protect against destructive discharges across the $\mathcal{O}(50 \mu\text{m})$ amplification gap. The GridPix concept provides the high granularity needed to resolve individual electron clusters (separated by an average distance of a few hundred microns) and to determine energy loss by the cluster counting technique, rather than by the charge measurement, with a precision of better than 3%. Despite the enormous challenges, real breakthrough was the development of the TPC readout endplate with a 160 GridPix ASICs, each 2 cm^2 , corresponding to 10.5 million pixels, demonstrating for the first time the feasibility of large-area MPGD with CMOS pixel readout [151]. New structures, where a GEM foil is facing the Medipix chip, forming the GEMpix detector, are in use for medical applications [152] as well as for monitoring the radioactive waste [153].

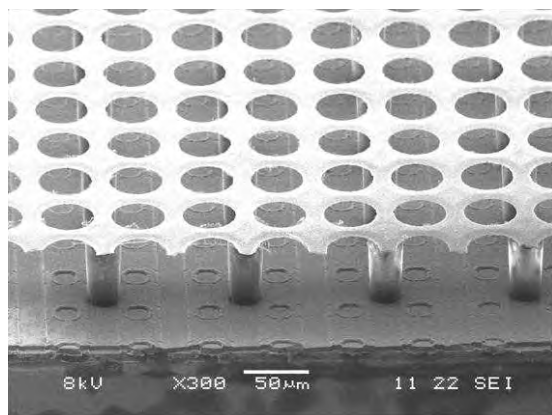


Figure 35.13: Photo of the Micromegas ('GridPix') detector. The grid holes can be accurately aligned with readout pixels of Timepix CMOS chip. The insulating pillars are centered between the grid holes, thus avoiding dead regions.

Gaseous detectors represent the most cost-effective solution to cover very large areas with photosensitive elements. MPGD-based gaseous photomultipliers, conceived with the aim to overcome the limitations of MWPCs, with semi-transparent or reflective photocathodes (PC), allow to minimize PC aging due to the ion and photon feedback and to avoid secondary effects causing electrical instability. For RICH applications requiring large-area coverage and moderate spatial resolution, coarser macro-patterned structures (e.g. THGEM with typical thickness of 0.4–1 mm and hole spacing of 0.7–1.2 mm) offer an interesting cheaper solution [154]. These are derived from the GEM design, scaling up ~ 10 -fold geometrical parameters, and can be mass-produced with standard PCB technology and mechanical drilling of large number of holes: some millions per square meter. Systematic studies to find the optimal electrostatic configuration revealed that the presence of a rim, a circular region around the holes where metal is etched away, plays a major role in THGEM performance. A small or zero rim allows to achieve better gain stability in time and under irradiation, while large rims permit to attain larger maximum gain and to reduce discharges, at the cost of significant charging up of the insulating surface, which modify the electric field. Therefore, in spite of the enhanced gain performance, the use of large rim THGEMs must be avoided to guarantee stable detector performance [155]. MPGDs are now in operation for single photon detection in the COMPASS RICH where a hybrid architecture formed by two THGEM layers (one covered by CsI-PC) and a Micromegas, acting as a third amplification stage, has been adopted.

Lately, closed geometry THGEM-based structures (RPWELL) [156], in common with some MPGDs invented at the end of the last century – C.A.T. and WELL, with resistive anodes have been developed, combining THGEM and RPC properties. This concept consists of a single-faced THGEM, copper-clad on its top

side only, mounted directly on top of a resistive film deposited on a thin insulating sheet. Compared to THGEM with an induction gap, higher gains could be achieved in RPWELL for lower applied voltage across the THGEM electrode, due to the larger electric field within the closed holes. Another promising GEM-derived architecture is that of the μ -RWELL [157], with its \sim seven-fold smaller pitch with respect to the RPWELL. Two different layouts for resistive stage have been studied: the simplest one is based on a single-resistive Diamond-Like Carbon (DLC) layer, and grounding by edges (2D charge evacuation for low-rates $\mathcal{O}(\text{kHz}/\text{cm}^2)$) and a more sophisticated scheme using double-resistive layer with a through-vias between them and the grounding done by means of the readout electrodes (3D charge evacuation for high-rate $\mathcal{O}(\text{MHz}/\text{cm}^2)$ applications) [158]. The μ -PIC structure is an industrially produced PCB including anode strips on one side and orthogonal cathode strips on the other one. A regular pattern of uncoated regions is present along the cathode strips; an electric conductor buried in the thin PCB substrate transfers the anode voltage to a "dot" at the center of each of the uncoated cathode zones. Electron avalanches occur under the high-electric field around the point-like anodes; the electric field near cathode edges is weaker than in MSGCs, resulting in a lower discharge probability. A resistive coating of the cathode strips (e.g. using DLC layers) ensures tolerance to occasional discharges [159].

A big step in the direction of large-size applications has been obtained both with conceptual consolidation and industrial and cost-effective manufacturing of MPGDs by developing new fabrication techniques: resistive Micromegas (to suppress destructive sparks in hadron environments) [160] and single-mask and self-stretching GEM techniques (to enable production of large-size foils and significantly reduce detector assembly time) [161]. Scaling up of MPGDs to very large single unit detectors of $\mathcal{O}(\text{m}^2)$, has facilitated their use in the High Luminosity LHC upgrades: Micromegas will instrument an area of $\mathcal{O}(1000 \text{ m}^2)$ in the New Small Wheel of the ATLAS Muon endcaps, while GEMs will be used in the CMS Muon system and for the ALICE TPC readout. Exploiting the Micromegas, GEM, and μ -RWELL ability to measure both position and arrival time of the charge released in the drift gap, a novel μ -TPC concept has been developed; it permits achieving nearly constant spatial resolution over a wide range of particle incident angles and allows 3D track reconstruction with a single MPGD layer [162]. Although normally used as planar detectors, GEM, Micromegas, and μ -RWELL can be bent to form cylindrically curved ultra-light inner tracking systems, without support and cooling structures [163].

The consolidation of the better-established technologies has been accompanied with flourishing of novel ones, often specific to well-defined applications. Modern technologies have been also derived from Micromegas and GEM concepts, hybrid approaches combining different elements in a single device, gaseous with non-gaseous detectors, as is the case for optical read-out. MPGD hybridization, a strategy aiming to strengthen the detector performance, remains a valid asset for addressing future experimental challenges such as high granularity and picosecond-precision timing (e.g. PICOSEC-Micromegas concept [164]). A clear direction for future developments is that of resistive materials and related detector architectures. Their usage improves detector stability, making possible a higher gain in a single multiplication layer. Recent DLC resistive layers studies are the key ingredients for increasing the rate capability of MPGDs [165]. Future developments call for novel materials as well as for new fabrication techniques. Contributions to the detector concepts are required in several domains: resistive materials, solid-state photon and neutron converters, innovative nanotechnology components. Material studies can contribute to requirements related to low out-gassing, radiation hardness, radio-purity, converter robustness, and eco-friendly gases. The development of the next generation of MPGDs can largely profit from emerging technologies as those related to MicroElectroMechanical Systems (MEMS), sputtering, novel photoconverters, 3D printing of amplifying structures and cooling circuits, etc. Nowadays, many intensive MPGD R&D activities and their diversified applications are pursued within the world-wide CERN-RD51 collaboration [166].

35.6.5 Time-projection chambers

Revised July 2021 by C. Lippmann (GSI Darmstadt).

The Time Projection Chamber (TPC) concept was invented by David Nygren in the 1970's [167]. It consists of a cylindrical or square field cage that is filled with a gaseous (or liquid) detection medium. Charged particles produce tracks of ionization electrons that drift in a uniform electric field towards a position-sensitive amplification stage which provides a 2D projection of the particle trajectories. The third coordinate can be calculated from the arrival times of the drifted electrons. The start for this drift time measurement is usually derived from an external detector, e.g. a fast interaction trigger detector.

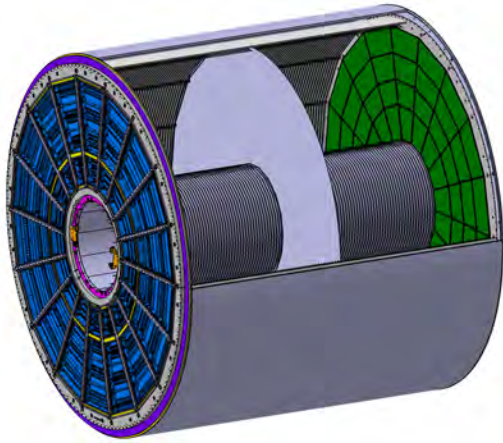


Figure 35.14: Schematic view of the ALICE TPC [168, 169]. The drift volume with 5 m diameter is divided into two halves, each providing 2.5 m drift length. The amplification stage has recently been upgraded from wire planes to GEMs.

This section focuses on the gas-filled TPCs that are often used in particle or nuclear physics experiments at accelerators on account of their low material budget. For neutrino physics (Sec. 35.11) or for detecting rare events (Sec. 36.4), on the contrary, usually high density and large active mass are required, and a liquid detection medium is favored.

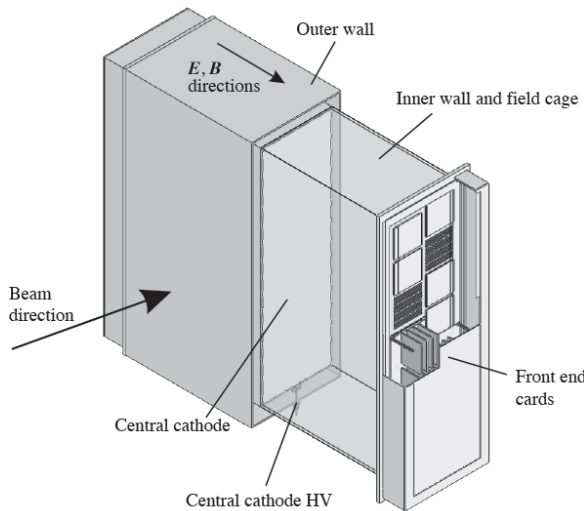


Figure 35.15: One of the 3 TPC modules for the near detector of the T2K experiment [170]. The size is $2 \times 2 \times 0.8 \text{ m}^3$. Micromegas devices are used for gas amplification and readout.

The TPC enables full 3D measurements of charged particle

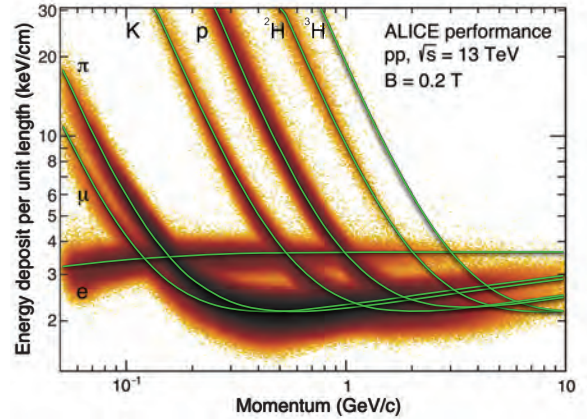


Figure 35.16: Energy deposit versus momentum measured in the ALICE TPC.

tracks, which gives it a distinct advantage over other tracking detector designs which record information only in two-dimensional detector planes and have less overall segmentation. The track points recorded in a TPC are basically adjacent, which facilitates the track finding enormously. This advantage is often exploited for pattern recognition in events with large numbers of particles, e.g. heavy-ion collisions. Two examples of modern large-volume gaseous TPCs are shown in (Figure 35.14) and (Figure 35.15).

Identification of the charged particles crossing the TPC is possible by simultaneously measuring their momentum and specific energy deposit through ionisation (dE/dx). The momentum, as well as the charge sign, are calculated from a helix fit to the particle trajectory in the presence of a magnetic field (typically parallel to the drift field). For this application, precise spatial measurements in the plane transverse to the magnetic field are most important. The specific energy deposit is estimated from many charge measurements along the particle trajectory (e.g. one measurement per anode wire or per row of readout pads). As the charge collected per readout segment depends on the track angle and on the ambient conditions, the measured values are corrected for the effective length of the track segments and for variations of the gas temperature and pressure. The most probable value of the corrected signal amplitudes for a given track provides the best estimator for the specific energy deposit (see Sec. 34.2.3); it is usually approximated by the truncated mean, i.e. the average of the 50%–70% smallest values. The resulting particle identification performance is illustrated in (Figure 35.16), for the ALICE TPC.

The dependence of the achievable energy resolution on the number of measurements N , on the thickness of the sampling layers t , and on the gas pressure P can be estimated using an empirical formula [171]:

$$\sigma_{dE/dx} = 0.41 N^{-0.43} (tP)^{-0.32}. \quad (35.17)$$

Typical values at nominal pressure are $\sigma_{dE/dx} = 4.5$ to 7.5% , with $t = 0.4$ to 1.5 cm and $N = 40$ up to more than 300. The record, with an unprecedented energy resolution of 3%, is held by the PEP-4/9 TPC [172], due to the high gas pressure of 8.5 bar.

The greatest challenges for a large TPC are due to the length of the drift of up to a few meters. In particular, it can make the device sensitive to small distortions in the electric field. Such distortions can arise from a number of sources, e.g. imperfections in the field cage construction or the presence of ions in the drift volume. The electron drift in a TPC in the presence of a magnetic field is defined by Eq. (35.14). The $E \times B$ term of Eq. (35.14) vanishes for perfectly aligned electric and magnetic fields, which can be difficult to achieve in practice. Furthermore, the electron drift depends on the $\omega\tau$ factor, which is defined by the gas mixture and the magnetic field strength. The electrons will tend to follow the magnetic field lines for $\omega\tau > 1$, or the electric field lines for $\omega\tau < 1$. The former mode of operation makes the TPC less

sensitive to non-uniformities of the electric field, which is usually desirable.

The drift of the ionization electrons is superposed with a random diffusion motion which degrades their position information. The ultimate resolution of a single position measurement is limited to around

$$\sigma_x = \frac{\sigma_D \sqrt{L}}{\sqrt{n}}, \quad (35.18)$$

where σ_D is the transverse diffusion coefficient for 1 cm drift, L is the drift length in cm and n is the effective number of electrons collected. Without a magnetic field, $\sigma_{D,B=0} \sqrt{L}$ is typically a few mm after a drift of $L = 100$ cm. However, in a strong magnetic field parallel to the drift field, a large value of $\omega\tau$ can significantly reduce diffusion:

$$\frac{\sigma_{D,B>0}}{\sigma_{D,B=0}} = \frac{1}{\sqrt{1 + \omega^2 \tau^2}}. \quad (35.19)$$

This factor can reach values of up to 10. In practice, the final resolution limit due to diffusion typically lies around $\sigma_x = 100 \mu\text{m}$.

The drift and diffusion of electrons depend strongly on the gas mixture. The optimal gas mixture varies according to the environment in which the TPC will operate. In all cases, the oxygen concentration must be kept very low (few ten parts per million in a large TPC) in order to avoid electron loss through attachment.

Ideally, the drift velocity should depend only weakly on the electric field at the nominal operating condition. The classic Ar/CH₄ (90:10) mixture, known as P10, has a drift velocity maximum of 5 cm/ μs at an electric field of only 125 V/cm (Figure 35.5). In this regime, the electron arrival time is not affected by small variations in the ambient conditions. Moreover, low electric fields simplify the design and operation of the field cage. The mixture has a large transverse diffusion at $B = 0$, but this can be reduced significantly in a strong magnetic field due to the relatively large value of $\omega\tau$.

For some applications organic gases like CH₄ are not desirable since they may cause aging. An alternative is to replace CH₄ with CO₂. An Ar/CO₂ (90:10) mixture has a low transverse diffusion at all magnetic field strengths, but does not provide a saturated drift velocity for the typical electric fields used in TPCs (up to a few 100 V/cm). As a consequence, it is quite sensitive to the ambient conditions. Freon admixtures like CF₄ can be an attractive option for a TPC as well, since the resulting gas mixtures provide high drift velocities at low electric fields. However, the use of CF₄ always needs to be thoroughly validated for compatibility with all materials of the detector and the gas system.

Historically, the amplification stages used in gaseous TPCs have been planes of anode wires operated in proportional mode. The performance is limited by effects related to the feature size (wire spacing) of a few mm. Since near the wires the electric and magnetic fields are not parallel, the incoming ionisation electrons are displaced in the direction of the wires (“wire $E \times B$ effect”), which degrades the resolution. The smaller feature sizes of Micro-Pattern Gas Detectors (MPGDs) like GEMs and Micromegas lead to many advantages as compared to wire planes (see Sec. 35.6.4). In particular, $E \times B$ effects in the amplification stage are much smaller. Moreover, the signal induction process in MPGDs leads to a very narrow pad response, allowing for a much finer segmentation, which improves the separation for two very close tracks. Combinations of MPGDs with silicon sensors have resulted in the highest granularity readout systems so far (see Sec. 35.6.4). These devices make it possible to count the number of ionization clusters along the length of a track, which can, in principle, improve the particle identification capability. However, the big challenge for such a system is the huge number of readout channels for a TPC of a typical size.

The accumulation of the positive ions created by the ionization from the particle tracks can lead to time-dependent distortions of the drift field. Due to their low drift velocity, ions from many events may coexist in the drift volume. To reduce the effect of such a build-up of space charge, Argon can be replaced by Neon as the main component of the gas mixture. Neon features a lower

number of ionisation electrons per unit of track length (see 35.5) and a higher ion mobility (see 35.6).

Of greater concern are the ions produced in the gas amplification stage. In order to prevent them from entering the drift volume, large TPCs built until now have a gating grid. The gating grid can be switched to transparent mode (usually in the presence of an interaction trigger) to allow the ionization electrons to pass into the amplification region. After all electrons have reached the amplification region, it is usually closed such that it is rendered opaque to electrons and ions. However, a gating grid implies a principal rate limitation to a few kHz. Different groups are therefore working towards the goal of continuous readout, for applications where a triggered operation would lead to unacceptable data loss (e.g. ALICE [169], sPHENIX [173]). The employed readout schemes are based on MPGDs, as these can be optimised in order to drastically reduce the ion back-flow at the same effective gain as MWPCs. Extensive work has been carried out during the 2010’s to design such readout structures. In ALICE and sPHENIX ion back-flow values below 1 % are achieved with a thorough adjustment of the various fields in a quadruple GEM system. Similar levels of ion back-flow can be reached with Micromegas detectors [174]. For triggered operation, on the other hand, a combination of a MPGD and a gating structure may be an attractive solution.

35.6.6 Transition radiation detectors (TRD’s)

Revised July 2021 by P. Nevski (BNL) and A. Romaniouk (Insbbruck U.; MEPHI Moscow).

Transition radiation (TR) x-rays are produced when a highly relativistic particle ($\gamma \gtrsim 10^3$) crosses a refractive index interface, as discussed in Sec. 34.7. Since the TR yield is about a few % per boundary crossing, radiation from multiple surface crossings (e.g., a stack of foils) is used in practical detectors. The x-rays, ranging from a few keV to a few dozen keV or more, are emitted in a forward direction at small angles (within few mrad) to the particle trajectory. The TR intensity for a single boundary crossing always increases with γ , but, for multiple boundary crossings, interference leads to saturation above a Lorentz factor $\gamma_{\text{sat}} = 0.6 \omega_1 \sqrt{\ell_1 \ell_2} / c$ [175], where ω_1 is the radiator material plasma frequency, ℓ_1 is its thickness, and ℓ_2 the spacing between material elements. The probability density function of TR is a fairly complex function of γ , radiator parameters, photon energy (ω) and its emission angle (θ). For well defined radiator parameters a measured two-dimensional distribution of photon energy vs its reconstructed emission angle is in very good agreement with the theory predictions [176].

Integration over the angle yields the TR spectrum, which typically features many maxima (see Sec. 34.7). Most of the TR energy is emitted near the last maximum of the spectra determined by radiator material parameters at $\omega_{\text{max}} = \ell_1 \omega_1^2 / 2\pi c$. The effective TR photon emission starts at about $\gamma_{\text{thr}} = \ell_1 \omega_1 / c$. By varying radiator parameters one may optimize the particle separation for a given range of the γ -factor. The angular distribution of TR photons has a few maxima and extends up to $\theta_{\text{max}} = (1/\gamma^2 + \omega_2^2/\omega^2)^{1/2}$ [177]. For a single foil the largest part of the TR energy is emitted around the most probable angle $\theta = (1/\gamma^2 + \omega_2^2/\omega^2)^{1/2}$, where ω_2 is the plasma frequency of the gas surrounding the radiator material elements. However, in case of multiple interfaces, interference effects may significantly change this angle and more realistic expression for the angle which corresponds to the last interference maximum of the energy spectra is $\theta \approx \sqrt{1.4\pi^2/\gamma_{\text{sat}}^2 - 1/\gamma^2}$ [176]. The higher is the gamma-factor, the larger is the angle of the first interference maximum. It reaches almost its asymptotic limit at $\gamma = \gamma_{\text{sat}}$. This effect is illustrated in Fig. 35.17 [176] which shows two-dimensional distribution of the TR photon energy versus the reconstructed production angle obtained in 20 GeV electron beam with the radiator containing a stack of foils of 15.5 μm thickness spaced by 210 μm (the left plot) using a Si-pixel detector. TR produced by 20 GeV electrons is emitted mostly around $\theta \sim 0.9$ mrad. All features of this distribution are well reproduced with MC simulations (the right plot).

The simplified numerical expressions can be used for practical

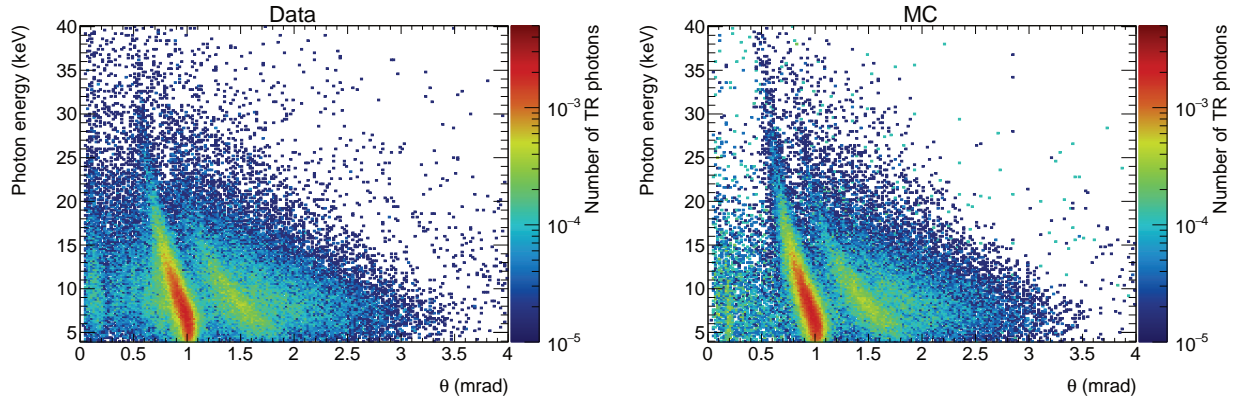


Figure 35.17: Two dimensional distributions of photon energy versus reconstructed production angle obtained with the polypropylene radiator with 20 GeV/c electron beam. Data - the left plot, MC - the right plot. Z-axis is a number of photons per particle [176]

estimation of the main TR production parameters [176]: $\theta \sim 1.2/\omega_1\sqrt{l_1l_2}$, $\gamma_{thr} \sim 3 \times 10^3 \omega_1 l_1$, $\gamma_{sat} \sim 3 \times 10^3 \omega_1 \sqrt{l_1l_2}$ and $\omega_{max} = 0.65 l_1 \omega_1^2$, where θ in mrad, ω_1 in eV, ω_{max} in keV and l_1 and l_2 in mm.

In the simplest concept, a detector module might consist of a low- Z TR radiator followed by a high- Z active layer made of proportional counters filled with a Xe-rich gas mixture. The atomic number considerations follow from the dominant photoelectric absorption cross section per atom going roughly as Z^n/ω^3 , where n varies between 4 and 5 over the region of interest.¹ To minimize self-absorption, materials such as polypropylene, Mylar, carbon, and (rarely) lithium in the form of foils, fibers or foams are used as radiators. The TR signal in the active regions is in most cases superimposed upon the particle ionization losses, which are proportional to Z . In most of the detectors used in particle physics the radiator parameters are chosen to provide $\gamma_{sat} \approx 3000$. Those detectors normally work as threshold devices, ensuring the best electron/pion separation in the momentum range $1 \text{ GeV}/c \lesssim p \lesssim 150 \text{ GeV}/c$.

One can distinguish two design concepts—“thick” and “thin” detectors. In “thick” detectors the radiator, optimized for a fixed total radiation length at maximum TR yield and maximum TR absorption in the detector, consists of few hundred foils (for instance 300 20 μm thick polypropylene foils). Most of the TR photons are absorbed in the radiator itself. To maximise the number of TR photons reaching the detector, part of the radiator far from the active layers is often made of thicker foils, which shifts the x-ray spectrum to higher energies. The detector thickness, about 2-4 cm for Xe-filled gas chambers, is optimized to absorb most of the incoming x-ray spectrum. A classical detector is composed of several similar modules which respond nearly independently. Such detectors were used in the UA2, NA34 and other experiments [178], are being used in the ALICE experiment [179, 180] and are built for the CBM experiment [181]. In another TRD concept a fine granular radiator/detector structure exploits the soft part of the TR spectrum more efficiently. This can be achieved, for instance, by distributing small-diameter straw-tube detectors uniformly or in thin layers throughout the radiator material. This approach allows to realise a TRD as an integral part of a tracking detector providing many points of measurements on the particle track. Even with a relatively thin radiator stack, radiation below 4 keV is mostly lost in the radiators themselves. However, for photon energies above this value, the absorption is reduced and the radiation can be registered by several consecutive detector layers, thus creating a strong TR build-up effect. Descriptions of detectors using this approach in both accelerator and space experiments can be found in [179, 182–185]. For example, in the ATLAS TR tracker (TRT), charged particles on average cross about 35 straw tube layers embedded in the radiator material [182]. The effec-

tive thickness of the Xe gas per straw is about 2.5 mm and the average number of foils per straw is about 40 with an effective foil thickness of about 18 μm . In this approach straw walls also act as radiator and make some contribution to the TR spectrum.

Although the values mentioned above are typical for most of the plastic radiators used with Xe-based detectors, they vary significantly depending on the detector requirements. Careful simulations are usually needed to build a detector optimized for a particular application. For TRD simulations the codes are based on well understood TR emission formulas (see for instance [177] for regular radiators and [186] for irregular radiators). They are realised as the stand-alone simulation programs [176, 187, 188] or GEANT4 based ones [189] and give both a good agreement of the TR energy spectra and of the angular distributions with data [176, 190, 191].

The discrimination between electrons and pions can be based on the charge deposition measured in each detection module, on the number of clusters – energy depositions observed above an optimal threshold (usually it is 5–7 keV), or on more sophisticated methods such as analyzing the pulse shape as a function of time. The total energy measurement technique is more suitable for thick gas volumes, which absorb most of the TR radiation and where the ionization loss fluctuations are relatively small. The cluster-counting method works better for detectors with thin gas layers, where the fluctuations of the ionization losses are bigger. Cluster-counting replaces the Landau-Vavilov distribution of background ionization energy losses with the Poisson statistics of δ -electrons, responsible for the distribution tails. The latter distribution is narrower than the Landau-Vavilov distribution. In practice, most of the experiments use a likelihood method, which exploits detailed knowledge of the detector response for different particles and gives the best separation. The more parameters are considered, the better achievable separation power. The neural network method is the most powerful tool. When it used by the ALICE TRD (ALICE point in Fig. 35.18) it lead to an increase of the rejection power by another factor of 2–3 with respect to the likelihood method [179].

The major factor in the performance of any TRD is its overall length. This is illustrated in Fig. 35.18, which shows, for a variety of detectors, the pion efficiency at a fixed electron efficiency of 90% as a function of the overall detector length. As TRD performance depends on particle energy, the experimental data in this figure covering a range of particle energies from 1 GeV to 40 GeV, are rescaled to an energy of 10 GeV when possible. Phenomenologically, the rejection power against pions increases as $5 \cdot 10^{L/38}$, where the range of validity is $L \approx 20$ –100 cm. Apart from the beam energy variations, the observed scattering of the points in the plot reflects how effectively the detector space is used and how well the exact response to different particles is taken into account in the analysis. For instance, the ATLAS TRT was built as a compromise between TR and tracking requirements; that is why the test-beam prototype result (lower point) is better than the real End-Cap TRT performance at the LHC shown in Fig. 35.18

¹ Photon absorption coefficients for the elements (via a NIST link), and $dE/dx|_{\min}$ and plasma energies for many materials are given in <https://pdg.lbl.gov/current/AtomicNuclearProperties>.

for different regions in the detector (in agreement with MC).

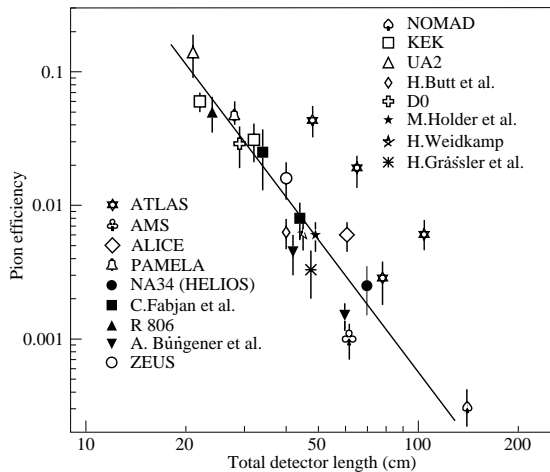


Figure 35.18: Pion efficiency measured (or predicted) for different TRDs as a function of the detector length for a fixed electron efficiency of 90%. The plot is based on the table given in [178]. Results from more recent detectors are added from [179, 183–185, 192].

In most cases, recent TRDs combine particle identification with charged-track measurement in the same detector [179, 181, 184]. This is particularly important for collider experiments, where the available space for the inner detector is very limited. For a modest increase of the radiation length due to the radiator ($\sim 4\% X_0$), a significant enhancement of the electron identification was obtained in the case of the ATLAS TRT. Here, the combination of the two detector functions provides a powerful tool for electron identification even at very high particle densities.

In addition to the enhancement of the electron identification during offline data analysis, TRD signatures are often used in the trigger algorithms at collider experiments. The ALICE experiment [180] is a good example for the use of the TRD in a First Level Trigger. In the ATLAS experiment, the TRT information is used in the High Level Trigger (HLT) algorithms. At increasing luminosities, the electron trigger output rate becomes so high, that a significant increase of the calorimeter energy threshold is required to keep it at an acceptable level. This may affect the trigger efficiency of very important physics channels (e.g. $W \rightarrow e\nu$ inclusive decay). Even a very soft TR cut at the HLT level, which preserves high electron efficiency (98%), allows to suppress a significant part of fake triggers and enhance the purity for physics events with electrons in a final state. The TRT also plays a crucial role in the studies where an electron suppression is required (e.g. hadronic mode of τ -decays). TR information is a completely independent tool for electron identification and allows to study systematic uncertainties of other electron reconstruction methods.

Electron identification is not the only TRD application. Some TRDs for particle astrophysics are designed to directly measure the Lorentz factor of high-energy nuclei by using the quadratic dependence of the TR yield on nuclear charge; see, for instance, in [193]. The radiator configuration (ℓ_1, ℓ_2) is tuned to extend the TR yield rise up to $\gamma \approx 10^5$ using the more energetic part of the TR spectrum (up to 100 keV). High density radiator materials (such as Al) are the best for this purpose. Direct absorption of the TR-photons of these energies with thin detectors becomes problematic and TR detection methods based on Compton scattering have been proposed, see in [194].

The high granularity of the semiconductor pixel or microstrip detectors provides spatial separation of the TR photons and dE/dx losses at relatively modest distances between radiator and detector. These detectors may be the basis for novel devices which combine precise tracking and PID properties [176, 188, 195]. Use of the TR production angle in addition to its energy can help to improve PID properties of the TRD. The presence of a magnetic field could enhance the separation between TR photons and

dE/dx losses [196]. New detector techniques for TRDs are also under consideration. GasPixel detectors allow to reconstruct a track segment with a space point accuracy of $< 30 \mu\text{m}$ and exploit all details of the particle tracks to highlight individual TR clusters in the gas, see in [197]. Thin films of heavy scintillators might be a very attractive option for non-gas based TRD [198].

35.6.7 Resistive-plate chambers

Revised August 2021 by G. Aielli (Rome U. Tor Vergata).

The resistive-plate chamber (RPC) is a gaseous detector working at atmospheric pressure developed by R. Santonico and R. Cardarelli in the early 1980's [199]. A precursor of the RPC is the Pestov spark chamber [200] [201] having a metallic plate cathode and a thick glass plate anode, designed to work at 12 bars to obtain an outstanding 0.1 ns time resolution. Although the original purpose of RPCs was to provide a competitive alternative to large scintillator counters, the RPC's potential for timing tracker systems was quickly recognized given its high detection efficiency ($>95\%$), excellent temporal and spatial resolutions and ease of constructing large-format single frame detectors. The RPC, as sketched in Fig. 35.19, is a large planar capacitor with two parallel high bulk resistivity electrode plates ($10^9\text{--}10^{13} \Omega\text{-cm}$) separated by a set of insulating spacers. The spacers define a gap in the range from a few millimeters down to 0.1 mm with a precision of a few μm . The gap is filled with a suitable atmospheric-pressure gas mixture which serves as a target for ionizing radiation. The gas gap thickness practically determines the time resolution of the RPC, on the other side the limit for reaching full detection efficiency at atmospheric pressure is typically 1 mm (also influenced by the gas molecular weight). Since the primary ionization for sub-millimeter gas gaps is limited, multiple gaps can be combined to effectively obtain a very high detection efficiency [202]. The electrodes are most commonly made of high pressure phenolic-melaminic laminate (HPL), commonly referred to as "bakelite",

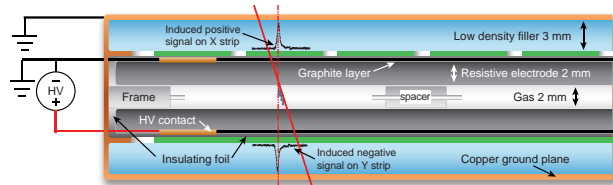


Figure 35.19: Schematic cross section of a generic single gap RPC.

or glass. A uniform electric field of several kV/mm, is established on the gas gap, sufficient to promptly multiply the primary ionization. This is realized through a moderately conductive coating ($\sim 10^5 \Omega/\square$) placed on the external faces of the electrodes. The conductivity sufficiently low to be transparent to the fast avalanche signal transients, and high enough to suppress field gradients. Due to the high electrode resistivity in RPCs, the time constant of the equivalent RC circuit ($\tau = \rho\epsilon_r$ being ρ the electrode resistivity and ϵ_r its dielectric constant) is much longer than discharge processes. Therefore only the locally-stored electrostatic energy contributes to the discharge, preventing the formation of sparks and leaving the rest of the detector field unaffected. The gas-facing surface of HPL electrodes are commonly coated with a few μm -thick layer of polymerized linseed oil [203] with the function of smoothing the electrode surface, improving the electric field uniformity. It also has the function of protecting the electrode from the being eventually etched by free radicals generated in the discharge e.g. in presence of fluorocarbons. It is generally assumed that the linseed oil layer has a resistivity comparable to the electrode's one, due to the absence of the Malter effect. In the early stage of the avalanche multiplication, the uniform electric field of RPCs exponentially amplifies each primary ionization cluster in function of its distance from the location of the primary ionization. Therefore RPC signals spectrum would be broad and exponentially distributed (unlike gaseous detectors where ionization and amplification occur in separate regions) having the most probable amplitude close the zero. For increasingly

larger avalanches, the space-charge progressively saturates the avalanche growth from exponential to linear, producing a peaked signal spectrum, essential to efficiently separate the signal from the noise [204]. For gains exceeding the Meek limit, the avalanche undergoes a transition to "streamer", connecting the electrodes with a plasma filament which exhausts all the locally-available energy [205], generating an almost fixed amplitude signal. This prevents any further evolution of the discharge. The streamer mode was the first ever used by RPCs, until the introduction of very electronegative gases and more sensitive front end electronics, permitted to detect the precursor avalanche independently on the streamer [206,207] Any of this operating regimes can be used in RPC detectors, depending on the applications.

As with other gaseous detectors, the gas mixture is optimized for each specific application. In general it needs to contain a UV photons quencher to limit the occurrence of photon feedback from the avalanches to the cathode, suppressing the spurious counts, and one or more electronegative components, to extend the avalanche growth, free from streamers, to as high as possible electric fields [208]. The role of the electronegative molecule is to capture slow electrons preventing their recombination with emission of photons, known to be the mediators for the transition to streamer. As a reference, the mixture for stable avalanche operation in ATLAS and CMS is $C_2H_2F_4/i-C_4H_10/SF_6=94.5\%/5\%/0.3\%$.

The avalanche induces a fast electron signal on a set of metallic readout electrodes (e.g. pads or strips) commonly placed externally and insulated from the resistive electrodes. The signal is isotropically distributed with respect to the field direction and present with equal but opposite amplitude on both electrodes. This feature allows to place readout electrodes on both RPC sides with equivalent performance. The induced charge density can be ideally calculated for a simplified RPC model [209] [210] as: $\sigma(x) = A/\cosh[(r)/\delta]$ where A is a normalization constant, r is the distance from the center of the avalanche axis and $\delta = (g + 2d)/\pi$ depends on the gap and electrode width (g and d , respectively). Depending on the specific RPC layout and geometry, the interplay between graphite and pick-up electrodes typically broadens, by means of a diffusion-like process, such distribution [210] [211]. This effect mostly preserves the impact position information, which can be obtained using the charge centroid method, with the drawback of increasing the signal space occupancy. Sensitivity to the high-frequency spectrum of electron avalanche signals over large RPC areas, requires a correspondingly adequate Faraday cage and readout design. At the same time, to preserve the excellent timing features of the RPC signal, the front end electronics should have a short rise time (ideally \ll than the signal rise time) and low noise, although these requirements could be in competition [212].

35.6.7.1 RPC types and applications

RPCs are generally classified in two categories depending on the gas gap structure: single gap RPCs (described above) and multiple gap RPCs [202] (typically referred as mRPCs or timing RPCs). While they are both based on the same principle they have different construction techniques, performance and limitations, making them suitable for different applications. Due to its simplicity and robustness, the single gap RPC is ideal for covering very large surfaces. Typical detector systems can have sensitive surface areas up to $\sim 10^4$ m², with single module areas of a few m², and a space-time resolution down to ~ 0.4 ns \times 100 μ m [213] [214].

Representative examples are the muon systems of ATLAS [215] and CMS [216] or ground and underground based cosmic rays [217] and neutrino arrays [218]. Interesting to note that CMS implements a bi-gap structure, i.e. the pickup signal is sandwiched by 2 single gas gaps, both contributing to the signal induction, improving efficiency and time resolution with respect to the single gas gap. Relevant new trends for single gap RPC applications are represented by new Dark Matter search experiments such as CODEX-B [219] and ANUBIS [220], in both cases exploiting RPCs to enclose and instrument large detection volumes with a good space-time tracker. Single gap RPCs have also recently demonstrated good candidates for application in tracking calorimetry [221].

The mRPC [222], as sketched in Fig. 35.20, segments the sensitive target by means of a stack of floating glass electrodes separated by a monofilament (i.e. fishing line), sandwiched between two external electrodes providing the high-voltage bias. The electrically-floating glass electrodes assume a potential determined by the avalanche processes occurring between them. An extensive description can be found in [223]. It has been observed that higher time resolution is inversely correlated to the gas gap size so this configuration allows for smaller gas thicknesses while maintaining a sufficient total gas thickness. This tends to separate primary clusters avalanches in different gas gaps, treating them independently, and determines a shorter avalanche growth time, increasing time resolution by one order of magnitude with respect to the classic RPCs [224]. The mechanical fragility of sub-mm-gap structures makes this technique less suitable for very large detector areas. Moreover the only material nowadays practically suitable for building such structures is soda-lime glass with resistivity above 10^{12} Ω -cm, limiting the rate capability to about 500 Hz/cm² [225].

mRPCs have been largely used in Time Of Flight systems such as ALICE [226], HADES [227], FOPI [228] and BESSIII [229], and in applications such as timing PET [230]. In perspective mRPC will be used for upgraded and new nuclear physics experiments such as CBM@FAIR [231] and SoLID [232].

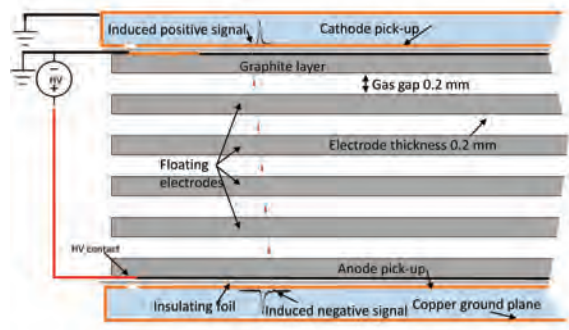


Figure 35.20: Schematic cross section of a generic multi gap RPC.

35.6.7.2 Time and space resolution

Space-time uncertainties in RPCs are determined by the statistical fluctuations of the primary and secondary ionization, the avalanche multiplication rate which is function of the electric field, and on the Signal/Noise ratio of the front-end electronics. The intrinsic signal latency is commonly in a few ns range (avalanche growth time to produce a detectable signal), making the RPC suitable for applications where a low latency is essential.

The gas gap size is a crucial feature for the RPC timing performance: producing the same total charge (for a detectable signal) in a smaller gas gap implies the necessity of increasing the Townsend coefficient by increasing the electric field, reducing at the same time the total signal duration and the related time fluctuations; moreover the chance of having multiple clusters in the same gas gap reduces with the gaps size, suppressing the charge collection fluctuations [233], which can be relevant for gas gap size ≈ 500 μ m. Typical timing performances range from around 1 ns with a 2 mm gas gap, down to 20 ps for a stack of several 0.1 mm gaps [234].

The intrinsic position sensitivity of an RPC is in the range of tens of μ m depending on the avalanche footprint fluctuations, influenced also by the gap size. In typical RPC applications the pickup electrodes pitch L (~ 1 cm) is much broader than the intrinsic resolution, and being readout via a discriminator, the spatial resolution is limited in the range of $L/\sqrt{12}$. A much better result is obtained by using a finer electrodes granularity and measuring the charge in each strip collecting the avalanche charge, so to reconstruct the charge centroid. It has been demonstrated recently, through charge centroid techniques, that the RPC avalanche space-time localization is better than ~ 50 ps \times 40 μ m [235] [236].

35.6.7.3 Rate capability and ageing

RPC rate capability is limited by the voltage drop on resistive electrodes, $\Delta V = V_a - V_{\text{gas}} = I \cdot R$ [237]. Here V_a is the applied voltage, V_{gas} is the effective voltage on the gas, $R = \rho \cdot d/S$ is the total electrode resistance, ρ being the resistivity and d/S the sample thickness and surface respectively, and I is the working current. Assuming uniform irradiation we can express $I = \phi \cdot S \cdot \langle Q \rangle$ where ϕ is the particle fluence and $\langle Q \rangle$ is average charge per avalanche. So we obtain a state equation for the RPC rate capability:

$$\Delta V/\phi = \rho \cdot d \cdot \langle Q \rangle$$

A large I not only limits the rate capability but also affects the long term performance of the detector since the working current, associated to discharges, depletes the conductive properties of HPL electrodes [238]. In presence of fluorocarbons and water, discharges generate hydrofluoric acid (HF) which damages internal detector surfaces, especially if made of glass, known to be not resistant to HF [239]. The practical way to suppress HF formation in glass RPCs is preventing water vapor contamination. Conversely, HPL electrodes, coated with linseed oil, are relatively resistant to HF, but the presence water can not be avoided since it mediates the HPL conduction. In this case the HF damage is mitigated by removing it with a forced flow of gas through the gas gap. Operating in the streamer regime puts low requirements on the front end electronics sensitivity, but generally limits the counting rate capability to ~ 100 Hz/cm². Higher-rate operation can be achieved by reducing gas gain in favor of electronic amplification, operating the detector in avalanche mode. Increasing concentrations of electronegative gases, such as C₂H₂F₄ and SF₆ [208], shifts the streamer transition to higher gains. The avalanche signal has a higher dynamic range, a drawback which puts a further stress on the performance request on the front-end electronics. With these techniques, stable performance at high rates (e.g. 10 kHz/cm²) has been achieved for large area single gap RPCs [212]. Two complementary strategies rely either on the natural redundancy and higher signal yield of multiple micro gap structures [240] or on electrodes made with lower resistivity materials [241]. Lowering the electrode resistivity in presence of high uniform field, finds a limit in the increasing probability of larger discharge events and overall noise. In this case, to safely lower the electrode resistivity, a safety margin would be given by operating with a lower electric field, and a correspondingly lower average charge per count.

35.6.7.4 A new detector: the Resistive Cylindrical Counter

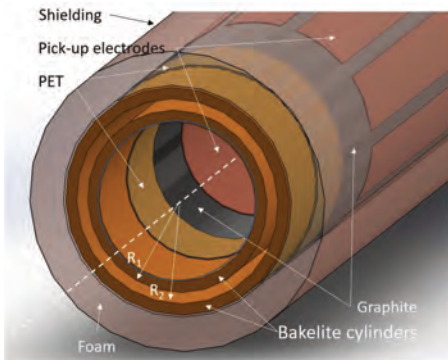


Figure 35.21: Schematic drawing of an RCC.

The RCC, illustrated in fig. 35.20, has been recently proposed as an evolution of the RPC [242] and is essentially an RPC warped to a cylindrical shape. The idea is to combine the advantages of parallel plate geometry and high pressure drift tubes in a single detector. The electric field $E(r)$, which is uniform in RPCs, here depends instead on the distance from the axis r , according to $E(r) = -\frac{V}{r \ln(R_1/R_2)}$. By choosing appropriate values for R_1 , R_2 , V and its polarization (the innermost cylinder is the cathode), it is possible to virtually segment the cylindrical gap in an innermost sensitive layer, where the field is sufficiently high to start the avalanche multiplication, and an outermost layer where the

drift happens, increasing the induced signal with lower or no multiplication at all. This effect is called geometrical quenching and limits the avalanche growth without the necessity of electronegative gases. Moreover a geometrically quenched avalanche would have a much better prompt to total charge ratio, lowering the total operative current, hence increasing the rate capability. The cylindrical structure has a further major advantage with respect to the planar one, it can be easily pressurized overcoming the RPC limitation of working at atmospheric pressure only. Pressurization on one side increases the gaseous target density, thus increasing the efficiency of narrow gaps, on the other, it could largely improve RPC time resolution since the Townsend coefficient $\alpha = A p \cdot \exp(-Bp/E)$ (where p is the pressure, E the electric field and A, B are constants), as we learn from the RPC precursor, the Pestov spark chamber [201]. RCC concept can be exploited to reach \sim ps resolution and counting rates sufficient for many FCC applications. On the other side, being insensitive to the environmental pressure, potentially extends its range to space and under water applications.

35.7 LAr Time Projection Chamber

Written August 2021 by F. Pietropaolo (CERN; INFN, Padua) and S. Pordes (FNAL).

35.7.1 Introduction

Liquid argon is an attractive material for particle detection. Energy deposition in the argon produces scintillation light and ionization electrons; in the presence of a moderate electric field, a significant fraction of the electrons escape recombination, making them available for detection as a charge signal. Typical values for a minimum ionizing particle are $\sim 40,000$ photons/MeV at zero field (lower at finite fields) and $\sim 30,000$ electrons/MeV at a field of 500 V/cm. That the liquid has a relative density of 1.4 and that the free electrons can be drifted many meters with minimal dispersion makes it particularly attractive for use in massive time-projection chambers (TPC) to study rare processes, as realized in [243] and [244]. Since that time, the liquid argon TPC (LAr TPC) has been developed into a detector that combines mm³ resolution with particle identification, calorimetry, and 100% live time. Detectors with masses up to 600 tons have been built and operated and detectors of 10's of kilotons are being planned.

The operation of a liquid argon time projection chamber requires

1. a cryostat and cryogenic system to maintain a mass of ultrapure liquid argon clean, cold and calm,
2. an electric field that permeates the volume of liquid argon and allows electrons liberated by deposition of energy in the argon to escape recombination, and drifts them to the charge sensors,
3. an array of charge sensors and associated electronics to amplify and digitize the charge signals,
4. sensors to detect the scintillation light, and associated electronics,
5. a data-acquisition system to read out and record the data,
6. software to reconstruct and interpret the data.

Surveys of previous, present and proposed detectors are described in the literature - see references [245] and [246] and detailed descriptions of detectors which have operated in experiments are given in descriptions [247–253].

This article provides a description of some of the challenges in achieving items 1 to 4 and of some of the solutions presently adopted. Topics 5 and 6 are not discussed. They are crucial to the successful exploitation of the LAr TPC technology and the subject of intense activity; interested readers may note the references. [254–256]. References are also given for a number of ancillary devices - cameras that can operate in the liquid argon [253], monitors to provide a rapid measurement of the purity of the argon [257, 258], ionization lasers to measure distortions of the drift field due to space charge or electrical problems [259] - that have been developed to improve performance. A list of experiments with their masses is also given in 35.14.

35.7.2 A Mass of ultra-pure Liquid Argon

Argon is abundant in the atmosphere (0.93% by volume, 1.3% by mass) as a result of the decay of ^{40}K in the earth's surface. The stable isotopes of argon are ^{40}Ar (99.6%), ^{36}Ar (0.33%) and ^{38}Ar (0.06%). Argon in the atmosphere is exposed to cosmic rays, forming the unstable isotope ^{39}Ar (lifetime 388 yr, β^- , endpoint 565 keV) at the level of 1 Bq/kg [260, 261]. Liquid argon is commercially available as a by-product in the distillation of air to produce nitrogen and oxygen. Some properties of argon are given in table 35.8; for many more see [262].

Table 35.8: Some physical properties of liquid argon from [263].

Property	Unit	Value
Boiling Point (<i>BP</i>) at 1013 hPa	K	87.3
Density (ρ) at 1013 hPa	kg m^{-3}	1395
$d(BP)/dP$	K hPa^{-1}	9×10^{-3}
$d\rho/dT$	$\text{kg m}^{-3} \text{K}^{-1}$	-6.2
Latent Heat of Evaporation	kJ kg^{-1}	161
Freezing Point (1013 hPa)	K	83.8

Critical to any LAr TPC are the cryostat and the cryogenic and purification system to maintain the argon liquid, ultra-clean and calm. Evacuatable double-walled vacuum cryostats are practical for detectors with a mass of O(100) t. Larger evacuatable cryostats would not be feasible and given the demonstration that ultra-clean argon can be achieved without initial evacuation [258], current and proposed mid-size and larger detectors sit in foam-insulated non-evacuatable cryostats based on a technology used in liquefied natural gas transport [253]. A convenient feature of these cryostats is that their components (inner walls, insulation, outer structures) are modular and of a size suited to assembly underground.

The absence of electronegative contaminants from the liquid argon is crucial to ensure the ionization electrons drift from their point of production to the charge sensors without being captured and their drift motion becoming too slow to detect. The major potential contaminants are environmental oxygen, nitrogen and water. Oxygen and water capture electrons; the scintillation light is affected by all three but at much higher levels of contamination. The loss of the charge signal depends on the product of the concentration of contaminant, the cross section for electron capture, and the time taken to reach the sensors. This combination leads to the quality of the argon being described in terms of 'electron lifetime', τ . To set a scale, the electron capture time in liquid argon with a concentration of oxygen of 1 ppb (part per billion by volume - all concentrations here are by volume) is $\sim 300 \mu\text{s}$ [264, 265], largely independent of electric field in our range of interest. For detectors with electron drift times in the milliseconds, the oxygen level must be well below 0.1 ppb to avoid losing most of the signal. The capture time for water has not been measured directly; the one indirect measurement in the literature [266] suggests water is more potent than oxygen. Nitrogen does not affect the free electron lifetime at levels up to many ppm but it does affect light production [267] and transmission [268] at the few ppm level. Oxygen at the ppm level affects light production [269]; its effect in TPCs is usually ignored given the requirements for electron drift.

The atmosphere is removed from the cryostat volume either by evacuation or a controlled purging with argon [270]; purging achieves ppm levels of oxygen and nitrogen gas which on dilution in the liquid present a negligible (ppb) level compared to the levels in the commercially provided argon. With the cryostat ready for cooldown and filling, a purification system is required to purify the commercial argon delivered from its typical ppm oxygen and water levels to the level required for TPC operation. Commercial argon is available with acceptable levels of nitrogen ($< 2\text{ppm}$) and typically no further reduction of the nitrogen level is provided. Molecular sieve and activated copper on alumina [271] are commonly used to remove water and oxygen, respectively. This purification is performed in the liquid phase and the discovery that purification with standard materials is effective at cryogenic temperatures [272] allowed for an enormous gain in throughput compared to purification in the gas phase. The purification system delivers essentially pure argon - which then mixes with any

contaminants from outgassing or leaks that escaped the stringent leak-check. To avoid the build-up of contaminants, many small systems recirculate the boil-off gas through purifying filters, while all large systems circulate the liquid and boil-off gas continuously through the purification system. Schematics of experiment cryogenics systems are shown in [248, 250, 253]. While reconstructed tracks eventually determine the argon quality, so-called 'purity monitors', double-gridded ionization chambers, are often installed to give rapid feedback on the purity of the liquid [253].

35.7.3 Charge and Light Signals

Figure 35.22 (left) shows how the electron and scintillation yields for a minimum ionizing particle (m.i.p.) change with electric field. The free electron yield from the passage of a charged particle can be calculated from 'W_{el}' = 23.6 eV [273], the energy deposit that generates one ion-electron pair, the dE/dx of the particle, and 'R' the (unfortunately labeled) fraction of electrons that escape recombination - see figure 35.22 (left). Measurements of electron yield have been made at various electric fields and at different ionization densities [274–278] and show good consistency. Of the models proposed to predict recombination [279, 280], none is fully successful; the so-called 'box model' [281] which considers the situation of mobile electrons and stationary ions makes more realistic assumptions than previous models and its form is commonly used. The data from [277] which are some of the most comprehensive are described by the form $R = \frac{0.8}{(1+0.049(dE/dx)/\rho\mathcal{E})}$ where dE/dx is in $\text{MeV g}^{-1} \text{cm}^2$ and \mathcal{E} in kV/cm . At a drift field of 500 V/cm, R for a minimum ionizing particle is $\sim 70\%$. A comprehensive summary and analysis of charge yield is given in [282].

The movement of the free electron charge towards the charge sensors is characterized by the drift velocity, the charge loss due to impurities, and the diffusion. The drift velocity depends on the strength of the electric field and slightly on the argon temperature (see table 35.9); a measurement of drift velocity vs electric field from [283] with a fit from [284] is shown in 35.22 (right). At an electric field of 500 V/cm, the drift velocity is $\sim 1.55 \text{ m/ms}$ at 89 K. The charge loss depends on the purity of the liquid. For a drift of duration, t , the fraction of charge that survives to the sense electrodes is $e^{-t/\tau}$ where τ is the electron lifetime. Values of τ exceeding tens of ms have been achieved [285–287]. Diffusion broadens the charge distribution as it travels to the sensor. The diffusion coefficient, D, defines the contribution to the spatial distribution of the charge at the sensor from diffusion after a drift of time, t , via $\sigma_D^2 = 2Dt$. Several measurements of the longitudinal diffusion component, D_L , have been made with a typical value around $0.4 \text{ mm}^2/\text{ms}$ [276, 288–290]. For a 3 ms drift, this gives a contribution of $(0.4 \cdot 6)^{1/2} \text{ mm}$, $\sim 1.5 \text{ mm}$, to the spread of the charge.

The scintillation light comes from the decay of excited argon dimers, Ar_2^* , (excimers) produced through direct excitation and through recombination of ionized argon ions and electrons [303]. The contribution of the latter process is reduced in the presence of an electric field as shown in figure 35.22, (left). The excimer is produced either in a singlet ('allowed' decay) or in a triplet spin state ('forbidden' (spin-flip) decay), with lifetimes of $\sim 6 \text{ ns}$ and $\sim 1.5 \mu\text{s}$ respectively. The states are almost degenerate and photons are emitted, somewhat inconveniently [304], in the VUV with a spectrum peaked at 128 nm with a $\pm 8 \text{ nm}$ (FWHM) spread [295]. The relative populations of the two states depends on the ionization density; typically 1:3 (singlet:triplet) for minimum ionizing and 3:1 for highly ionizing nuclear fragments [299]. As described in Section 36.4.1, this effect is exploited in argon-based WIMP dark matter searches to distinguish electromagnetic background from the nuclear recoil candidate signal. The long lifetime of the triplet state makes it sensitive to quenching impurities such as nitrogen or oxygen to which the excitation energy of the dimer can be transferred without the subsequent emission of a visible photon [267, 269].

The propagation of the scintillation is affected by two processes: absorption and Rayleigh scattering. While the large Stokes shift [305] makes pure LAr transparent to its own scintillation light, methane at the few ppb level [306] and nitrogen at the few ppm [268] level lead to light absorption. Rayleigh scattering

Table 35.9: Some Detector Relevant Properties of liquid argon.

Property	Unit	Value
Stopping Power (m.i.p.)	MeV g ⁻¹ cm ²	1.51
Radiation Length	g cm ⁻²	19.6
Nuclear Interaction / Collision Length	g cm ⁻²	120 / 76
W _{el} , Energy to form one electron-ion pair	eV	23.6 (±0.3) [273, 291]
Ion mobility	cm ² V ⁻¹ s ⁻¹	1.6 × 10 ⁻³ [292]
Temperature dependence of drift velocity	% K ⁻¹	-1.7 [284]
Longitudinal diffusion coefficient, D _L	mm ² ms ⁻¹	0.4 (see text)
W _{ph} , Energy to produce one scint. photon (m.i.p.)	eV	25 [293, 294]
Scintillation photon wavelength (vacuum)	nm	128 ± 8 (FWHM) [295]
Scintillation light inverse velocity	ns m ⁻¹	7.46 (±0.08) [296]
Rayleigh scattering length (predicted)	m	0.9 (±0.2) [296–298]
Scintillation Decay times fast/slow	ns	6 (±1)/1500 (±100) [267, 299, 300]
Dielectric strength	kV cm ⁻¹	>40 [301, 302]

increases the effective travel distance of photons between their production point and their detection and for detectors where the distance between origin and detection covers a range of many meters, the short Rayleigh scattering length for argon scintillation has a serious effect on the uniformity of detection. In this situation, the long lifetime of the triplet state can be exploited by the use of dopants to which the argon dimers can transfer their excitation energy with subsequent photon emission. Xenon, where almost complete transfer of the long-lived state energy is achieved at a concentration of 10's of ppm (mass), is a leading candidate. [307, 308].

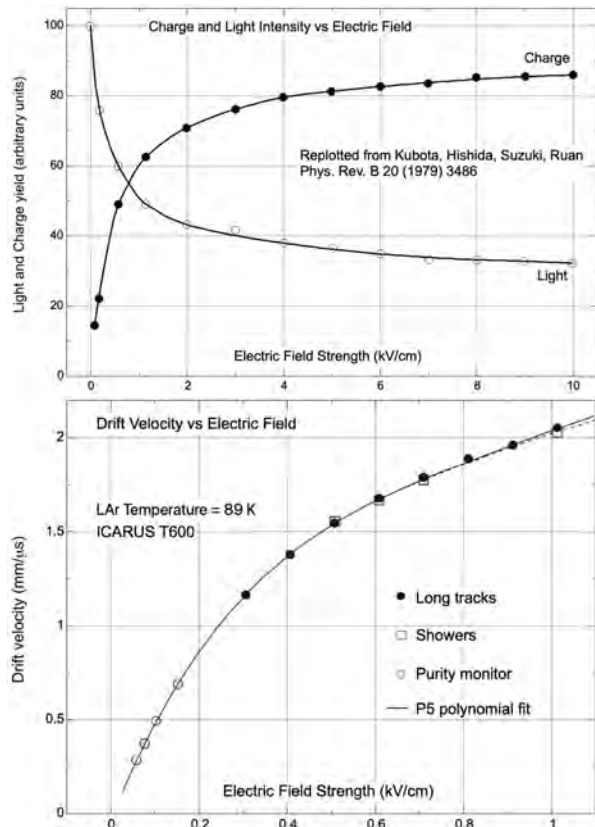


Figure 35.22: (top) the form of the light yield and the charge yield vs electric field redrawn from [303]; (bottom) electron drift velocity vs electric field redrawn from [283].

35.7.4 LAr TPC topologies

There are two basic LAr TPC formats: the single-phase design where all the detector elements are in the liquid, and the dual-

phase design which drifts the electrons upwards and extracts them from the liquid into a thin layer of argon gas above the liquid to allow amplification of the signal [309]. (Charge amplification in the liquid is difficult to achieve given that there is no equivalent to the Ramsauer minimum that occurs in the gas phase [310, 311].) The dual-phase format is popular in dark matter searches where electroluminescence produced by the extracted electrons in the argon gas is exploited (see Chapter 36.4); scaling up detectors with charge gain ([312, 313] to kilotons for neutrino experiments has not yet proved successful. In single-phase detectors, the drift direction can be either horizontal or vertical. Currently operating detectors come in a range of sizes but the basic form of a cathode and field cage generating a field which drives the ionization electrons to planes of charge sensors at ground potential is universal. A standard criterion is to make the TPC drift as long as considered possible to maximize the detector mass for a given channel count; this can result in a single drift volume; two drift volumes with a common cathode, or multiple drift volumes with multiple common cathodes. An exception is the DUNE near detector TPC; it is segmented into many small TPCs to help resolve the large interaction rate [314].

The drift field is produced by a planar cathode at -HV, a graded field-cage surrounding the active volume, and the sensing electrodes at a potential near ground which form the anode. The field cage is designed to produce a uniform electric field throughout the drift region although for detectors at surface, the slow-moving positive ions generated by the flux of cosmic rays distort the field, particularly for TPCs with long drift [282, 287, 315–317]. Particular challenges in the drift field system are the feed-through [248, 318] that brings the voltage from the HV supply outside the cryostat to the cathode (the cathode can sit at (-ve) voltages up to 300 kV), avoiding damage to the electronics from a potential cathode discharge [253], and ensuring the integrity of the field-cage resistor chain [319]. Avoiding discharge and current draw in a medium chosen because it allows electron flow is possibly the hardest challenge in the technology.

To date, the sensor arrangement for large detectors has used vertical planes of wires as sense electrodes and a horizontal electric field. A schematic is shown in figure 35.23.

The sense planes are perpendicular to the drift direction and arranged in a stack with the wires in each plane oriented at a different angle. (While the schematic shows three planes, in principle only two are needed.) The wire-pitch, p , is a few mm and the plane spacing is similar. As indicated in figure 35.23, the planes are biased such that all field lines from the drift region pass through the intermediate planes and terminate on the final plane as shown in 35.23. (The condition for transparency across one plane is derived in [320].) The drift electrons follow the field lines, inducing bi-polar current pulses on the first two planes, and terminate on the last one, the collection plane, producing a unipolar signal [321].

The raw signal rise and fall times are a few μ s as determined by the electron drift velocity and the plane spacing, and any geometric effects from the track angles. The signals from each wire

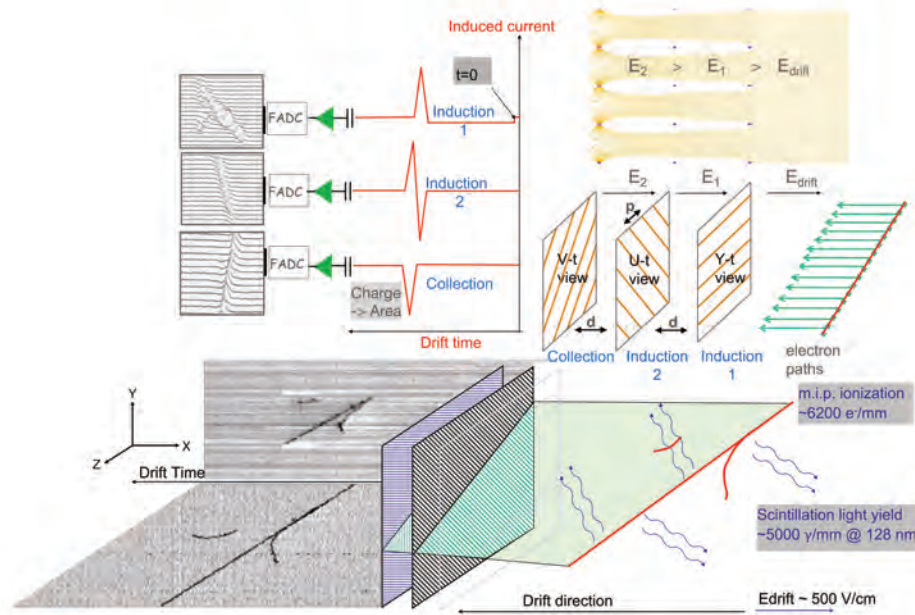


Figure 35.23: Schematic of an event in the ICARUS 3 t LAr TPC; *Top (from right to left):* field lines from drift region to collection wires, electron flow & arrangement of wire-planes, signal shapes on the wires, and wave-forms from the continuous readout and digitization; *Bottom:* the passage of a muon. The gray scale on the track indicates the ionization density.

are recorded as wave-forms spanning the maximum drift time at typically 2 or 2.5 MHz sampling rate. The intersection of wires on different planes which record signals at the same time, and the drift time converted to a distance knowing the drift velocity give the position of the charge source.

The design of large (> kiloton) detectors faces an intrinsic electrical challenge in that long (> few m) cables from the sense electrodes to the first-stage amplifier will introduce an unacceptable amount of noise through their capacitance, and attempts to avoid such cables leads to impractical constraints on the charge sensor geometry; both of these are emphasized in [321]. To address this problem, CMOS based ASIC amplifiers that operate in the cold and can be placed next to the charge sensor (wire or strip or pixel) have been developed, their design rules and robustness validated, and successfully deployed [322,323]. The subsequent problem that individual feed-throughs for each signal in a detector with hundreds of thousands of channels complicate the cryostat structure and raise the specter of leaks has been resolved by the development of flash-ADC and signal multiplexers [324] that also operate in the liquid. These implementations have resulted in equivalent noise charge levels of a few hundred electrons [287, 325] to be compared with a charge yield for a m.i.p. of 30,000 e/MeV. With such low noise, energy depositions well below 1 MeV are quite accessible.

Large LAr detectors usually contain a system to detect the primary scintillation light. These provide an event time for drift time measurement [326], a trigger [327,328], calorimetry that can be independent of and complementary to the charge [287], and event position information [254]. Given the VUV nature of the scintillation, a wavelength shifter is typically used to move the light into the visible [304]. Photo-multiplier tubes that operate in liquid argon were developed under the ICARUS program [329], while some recent systems are based on Silicon Photo-Multipliers. This latter approach separates the light collection from the light-to-electrical signal transducer, and many designs for the first task are being pursued [253, 330, 331].

35.7.5 Prospect - written October 2021

The successful operation [332] of the ICARUS T600 TPC served as clear demonstration of the feasibility of the liquid argon TPC technology on a massive scale. Since this milestone, the liquid argon TPC community has expanded and the technology has continued to evolve. Notable developments include in-liquid elec-

tronics, the adoption of Silicon Photo-Multipliers and new light collection technologies, the use of dopants in the argon to improve the light performance, improved techniques for wavelength shifting, the adoption of a cryostat technology which permits detector masses of tens of kilotons and, in a major change to the standard single-phase topology, the implementation of pixelated readout to replace projective geometry in busy environments [333]. Technical R&D is continuing; as examples, the vertical-drift single-phase design for the second DUNE far-detector that uses strips on perforated printed circuit boards as charge sensors [334], a dual-phase TPC readout [335] using fast cameras to read out the scintillation light produced in the gas region in place of a charge readout; a light detection system powered and readout using optical fiber allowing the readout to operate at any potential and therefore anywhere in the TPC (including on the cathode), and plans to replace the classic HV feed-through and filter with continuous semi-conductive cable. An abundance of data from recent experiments is encouraging insights into the liquid argon medium as in [282,336] and revealing new phenomena. For a taste, see [337]. The ground is fertile, busy, and full of opportunity.

35.7.6 Acknowledgement

We thank Drs Thorsten Lux and Stefania Bordini for their enormous and invaluable help.

35.8 Semiconductor detectors

Revised August 2021 by N. Wermes (Bonn U.).

Semiconductor detectors provide outstanding detection opportunities in terms of position, energy and also time resolution, often in combination. In accelerator experiments they are most widely used as position sensing devices or as photodetectors (Sec. 35.2), for example in calorimeters (Sec. 35.10) or in imaging Cherenkov detectors (Sec. 35.5). Comparing in particular with gaseous detectors, main features are high density and low ionization threshold, providing in high resistivity substrates comparatively large signals without intrinsic amplification. Silicon detectors with active layers only 100–300 μm thick provide adequately large and fast signals (of order nanoseconds). Challenges are the purity of a semiconductor material, characterized by its mobility-lifetime product and its radiation resistance. Modern semiconductor detectors are strongly connected with integrated circuit technology allowing on one hand for the formation of high-density micron-scale electrodes

on large wafers (6–8 in \approx 15–20 cm diameter sensor wafers) and for amplification and readout circuits connected to them on the other (a typical CMOS wafer reticle is 26×33 mm²).

Some important material properties of common semiconductors used as detectors are summarized in Tab. 35.10. While for particle tracking the excellent position resolution is the main (but not the only) interest, high stopping power and high energy resolution are key parameters in X-ray, gamma-ray, and β spectroscopy, *e.g.*, in neutrinoless double beta decay searches. Due to its small bandgap germanium excels in energy resolution, but needs to be operated at very low temperatures to reduce thermally generated reverse bias current. GaAs, CdTe and CdZnTe (CZT, with the bandgap depending on the Cd to Zn ratio) also feature high atomic numbers and hence much higher stopping power which is important especially for X-ray absorption. Diamond, fabricated by chemical vapor deposition (CVD) and strictly speaking classifying as an insulator, features low Z and large radiation length X_0 . It is used for particle detection especially in environments with high particle flux thanks to its radiation hardness (Sec. 35.8.3), especially regarding its low leakage current.

Materials R&D for radiation sensors extends to other bulk semiconductors as well, as for example ZnS, SiC or InP, and also to new material structures. Examples are semiconductor Quantum Dots – realized by nanometer-sized semiconductor ‘particles’ embedded in a semiconductor bulk, or Graphene, which – as a zero bandgap 2D material – features extraordinarily high conductivity (electrical and thermal). A bandgap can be introduced by structuring, doping, and other means, hence rendering transistor and sensor realizations possible. The interested reader is referred to reference [338] or [339], for example.

Operating without intrinsic amplification, semiconductor detectors crucially depend on low-noise electronics (see Sec. 35.9), so the detection sensitivity is determined largely by signal charge and input capacitance. Reviews of semiconductor detectors and electronics can be found for example in Refs. [1, 8, 340, 341]

35.8.1 Signal generation

35.8.1.1 Creation of charges

Semiconductor detectors are solid state ionization chambers. Absorbed energy forms electron-hole (e - h) pairs, *i.e.*, negative and positive charge carriers, which induce a signal current on electrodes when moving under an applied electric field (see Sec. 35.8.1.2). In order for the signal charge carriers to (freely) drift in the electric field and to become detectable, semiconductors must feature small intrinsic charge carrier densities (as *e.g.* in GaAs, CZT or diamond) or they must be depleted by reverse bias junction configurations (as for Si or Ge). In addition, they should feature low intrinsic density of defects which can act as trapping or generation/recombination centers (see Sec. 35.8.3).

The minimum energy required to form an e - h pair is the bandgap energy (1.12 eV in Si, 0.66 eV in Ge). However, impinging radiation or particles also release energy into lattice vibrations (phonons). In an “indirect” semiconductor like Si the valance band maximum is not at the same position in k -space (crystal-momentum space) as the conduction-band minimum and additional momentum transfer is required for a band transition to occur. For few-eV photons this momentum kick must come from lattice phonons which are Bose-Einstein distributed and hence cause a steep rise of photon absorption probability between 1.12 eV and about 3.4 eV, which is the “direct” energy gap without k -transfer. For much larger energy deposits the mean energy w_i required to produce an e - h pair assumes a constant value of 3.65 eV at room temperature; for other semiconductors consult Tab. 35.10.

For minimum-ionizing particles, the most probable charge deposition in a 300 μ m thick silicon detector is about 3.7 fC (\sim 23 000 electrons). In tracking detectors a particle’s energy loss and scattering in the detector material should be minimal (large X_0), whereas for energy spectroscopy, *e.g.* of X-ray photons, the stopping power should be maximized by choosing high- Z semiconductors. A smaller bandgap produces a larger signal and improves energy resolution, but also (exponentially) increases thermally excited carrier generation, following the Fermi-Dirac distribution law. In order to cope with excessive leakage currents at room temperature, Ge diodes are typically operated at liquid nitrogen

temperature (77 K). In pure Si at 300 K the carrier concentration is $n \approx 10^{10}$ cm⁻³ (Tab. 35.10), corresponding to a resistivity in the order of $\rho \approx (e\mu n)^{-1} \approx 400$ k Ω cm. In reality, crystal imperfections and minute impurity concentrations limit Si carrier concentrations to about 10^{11} cm⁻³ at 300 K ($\rho \approx 40$ k Ω cm). In practice, wafer resistivities up to 20 k Ω cm are available, with mass production ranging from 1 to 10 k Ω cm.

Since both electronic and lattice excitations are involved in digesting absorbed energy (in a correlated way), the variance in the number of charge carriers $N = E/w_i$ produced by fixed absorbed energy E (for example by an X-ray photon) follows binomial statistics and is, due to the energy constraint, reduced by the Fano factor F (about 0.1 in Si and Ge) relative to Poisson statistics. Thus, $\sigma_N = \sqrt{FN}$ and the energy resolution is $\sigma_E/E = \sqrt{Fw_i/E}$. However, the measured signal fluctuations are usually dominated by electronic noise or energy-loss fluctuations deposited in the detector. The electronic noise contributions depend on the detector leakage current and the electrode capacitance as well as on pulse shaping (shaping time) in the signal processing electronics (see Sec. 35.9).

Electric field strength and shape inside the semiconductor bulk are important for efficient signal charge collection, governed by the applied external voltage as well as by space charges. The latter naturally exists in junction detectors (see Sec. 35.8.2.1) leading (for constant space charge) to a linear decrease of the field strength from the junction boundary into the space charge region. Space charge can also occur from ionized lattice defects, either naturally existent as for example in GaAs or created by irradiation in any semiconductor material. This can lead to low field regions as well as to changes in the field’s shape (deviating from linear), both of which usually deteriorate the charge collection properties of a detector.

For X-ray detection a major effort is to find high- Z materials with a bandgap that is sufficiently large to allow for room-temperature operation while still providing good energy resolution. Compound semiconductors, *e.g.* CZT, can allow this, but typically suffer from charge collection problems, characterized by the product $\mu\tau$ of mobility and carrier lifetime. In Si and Ge $\mu\tau$ is orders of magnitude larger than in compound semiconductors (see Tab. 35.10) for both electrons and holes. Since for holes $\mu\tau$ is typically much smaller than for electrons, detector configurations where the electron contribution to the charge signal near the readout electrode dominates—*e.g.*, strip or pixel structures with electron collection—can provide better performance (see also next section).

35.8.1.2 Signal Formation

The signal and its pulse shape depend on the instantaneous carrier velocity $\vec{v}(\vec{x}) = \mu\vec{E}(\vec{x})$ and the electrode geometry, which determine the distribution of induced current according to the Shockley-Ramo theorem

$$i_S(t) = Ne \vec{E}_w(\vec{x}) \vec{v}(\vec{x}(t)), \quad (35.20)$$

where Ne represents a drifting charge cloud of N elementary charges, $\vec{E}_w(\vec{x})$ is the “weighting field”, which accounts for the coupling of the charge to a specific electrode, and \vec{v} is the drift velocity. Note that the mobility is in general field dependent, $\mu = \mu(E)$, with $v \approx \text{const}$ at high fields (velocity saturation, in Si approaching 10^7 cm/s at $E > 10^4$ V/cm). Both, electron and hole movements contribute to an electrode’s signal. Hence, if the carrier mobility is very different for electrons and holes, like *e.g.* in CdTe where $\mu_h \ll \mu_e$, a photon signal, for example, becomes absorption-point dependent. Integration of the induced current signal on an electrode yields the “collected charge”. For a simple parallel-plate geometry with two electrodes the weighting field is constant, whereas for structured electrode geometries, like for example strips or pixels, E_w is position dependent which for small electrodes (compared to the sensor dimensions) strongly enhances the contribution of the movement close to the electrode (“small-pixel effect”). More details and practical accounts on the Shockley-Ramo theorem and its usage can be found in [1, 8] and references therein.

During the movement the charge cloud spreads due to diffusion

widecaptionscale=1,tabularstretch=1.2]

Table 35.10: Properties of some detector-relevant semiconductors; temperature-dependent quantities given at 300 K (from [1] and references therein).

Property	Si	Ge	GaAs	CdTe (CZT)	Diamond
atomic number (Z)	14	32	31/33	48/(30)/52	6
density ρ (g/cm ³)	2.328	5.327	5.32	5.85	3.51
semiconductor type	indirect	indirect	direct	direct	indirect
bandgap E_G (eV)	1.12	0.66	1.424	1.44(1.44–2.2)	5.5
intr. carrier density (cm ⁻³)	1.01×10^{10}	2.4×10^{13}	2.1×10^6	10^7	≈ 0
radiation length X_0 (cm)	9.36	2.30	2.29	1.52	12.15
average energy w_i for (e/h) creation (eV)	3.65	2.96	4.35	4.43	13.1
mobility (cm ² /Vs)					
electrons μ_n	1450	3900	8500	1050	$\approx 1800^*$
holes μ_h	500	1800	400	90	$\approx 2300^*$
lifetime					
electrons τ_e	$>100 \mu\text{s}$	$\sim \text{ms}$	1–10 ns	0.1–2 μs	$\approx 100 \text{ ns}$
holes τ_h	$>100 \mu\text{s}$	$\sim \text{ms}$	20 ns	0.1–1 μs	$\approx 50 \text{ ns}$

* Approximate averages. Values quoted in the literature for the mobility in diamond vary strongly.

(typically 5 μm for 300 μm thickness) such that more than one electrode might collect charge (“charge sharing”), an effect that usually improves position resolution. Charge collection time decreases with increasing bias voltage (*i.e.* field strength), and can be reduced further by operating the detector with “overbias”, *i.e.*, a bias voltage exceeding the value required to fully deplete the device. Note that in partial depletion the electric field goes to zero at the end of the depletion zone, whereas overbias adds a constant electric field component. At an average field of $E = 10^4 \text{ V/cm}$, the onset of velocity saturation, the collection times for Si are about 15 ps/ μm for electrons and 30 ps/ μm for holes. In typical fully-depleted detectors, 200–300 μm thick, electrons are collected within about 5–10 ns, and holes within about 15–25 ns.

Position resolution is ultimately limited by transverse diffusion and by the emission of δ electrons. Performance also depends on optimal usage of charge sharing between neighboring electrodes and on noise. Resolutions of 2–4 μm (rms) have been obtained. In magnetic fields, Lorentz drift deflects the electron and hole trajectories increasing the spatial spreading. Total spreading and hence charge sharing between electrodes can be tuned (increased or decreased) by tilting the detector relative to the incoming (average) particle direction.

35.8.2 Typical detectors

35.8.2.1 Junction detectors

A p - n junction operated in reverse bias forms a sensitive region depleted of mobile charges and sets up an electric field that sweeps charge liberated by radiation to the electrodes. Detectors typically use an asymmetric structure, for example a highly doped p electrode and a lightly doped n region – or vice versa, so that the depletion region extends predominantly into the lightly doped bulk volume.

In a planar Si (or Ge) device the thickness of the depleted region is

$$d = \sqrt{2\epsilon(V + V_{bi})/Ne} = \sqrt{2\rho\mu\epsilon(V + V_{bi})} \quad (35.21)$$

$$\approx \frac{0.5}{\mu\text{m}} \times \sqrt{\frac{\rho V}{\Omega \text{ cm} \cdot \text{V}}} \quad \text{for } n\text{-type Si}$$

$$\approx \frac{0.3}{\mu\text{m}} \times \sqrt{\frac{\rho V}{\Omega \text{ cm} \cdot \text{V}}} \quad \text{for } p\text{-type Si}$$

with (values for Si)

V = external bias voltage

V_{bi} = “built-in” voltage ($\approx 0.5 \text{ V}$ for typically used resistivities)

N = doping concentration

e = elementary charge

ϵ = dielectric constant = $11.9 \epsilon_0 \approx 1 \text{ pF/cm}$

ρ = resistivity (typically 1–10 $\text{k}\Omega \text{ cm}$)

μ = charge carrier mobility ($\sim 1450 \text{ cm}^2/\text{Vs}$ (electrons), $\sim 500 \text{ cm}^2/\text{Vs}$ (holes) [342])

The conductive p and n regions together with the depleted volume form a capacitor with capacitance per unit area

$$C = \frac{\epsilon}{d} \approx \frac{1 \text{ pF/cm}}{d} \quad \text{in Si.} \quad (35.22)$$

In strip and pixel detectors (see next section) the capacitance is dominated by the fringing capacitance to neighboring electrodes as the electrode pitch is usually much smaller than the sensor thickness. For example, the strip-to-strip Si fringing capacitance is about 1–1.5 pF per cm of strip length at a strip pitch of 25–50 μm .

Large volume ($\sim 10^2 - 10^3 \text{ cm}^3$) germanium detectors are commonly configured cylindrical, for example, a cylindrical n -type crystal with 5–10 cm diameter and 10 cm length with an inner 5–10 mm diameter n^+ electrode and an outer p^+ layer forming the diode junction. Germanium can be grown with fairly low impurity levels, $10^9 - 10^{10} \text{ cm}^{-3}$ (HPGe, high-purity germanium), so these large volumes can be depleted with several kilovolts.

Diamond, featuring free charge carrier densities close to zero, needs no depletion and is operated as a parallel plate capacitor with insulator dielectrics. Still, substantial bias voltage is required to overcome charge trapping.

35.8.2.2 Detectors with structured electrodes

In HEP experiments semiconductor detectors usually aim at good position resolution achieved with electrodes patterned in “strips” or “pixels” with typical dimension scales (electrode pitch) of 50–100 μm , or in “pads” ($\text{mm}^2\text{-cm}^2$) if coarser granularity is affordable for the benefit of fewer channels.

Electrodes are usually placed “planar”, *i.e.*, at the surface of the sensing Si bulk, or can sometimes be shaped as columns or trenches running normal to the surface and hence parallel to the average direction of impinging particles, which increases radiation tolerance due to the shorter drift distances [343] (see also Sec. 35.8.3).

Various readout structures have been developed for pixels, *e.g.*, CCDs, DEPFETs as well as hybrid or monolithic pixels that either split or rather merge the sensing and readout IC functionality, as is illustrated in Fig. 35.24. Hybrid pixel devices utilize separate sensors and readout ICs connected by two-dimensional arrays of solder or indium bumps (for more details see *e.g.* [340, 344]). Monolithic pixel detectors combine sensing and readout in one chip with proper shielding of either function by exploiting multiwell IC technology.

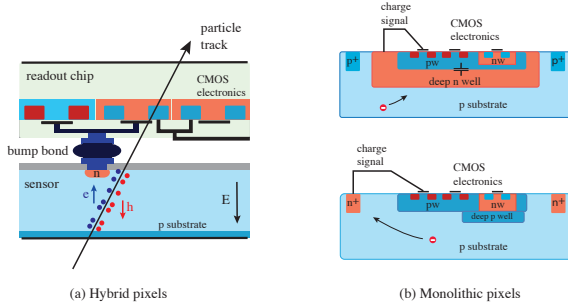


Figure 35.24: Pixel detectors: (a) hybrid pixels (one cell); (b) monolithic pixels (one cell): (top) DMAPS with large collection electrode, (bottom) DMAPS with small collection electrode.

The hybrid approach excels in optimally utilizing chip and sensor technologies (see *e.g.* [345]); its disadvantage is complex and cost intensive assembly. Monolithic pixels, on the contrary, combine sensing and readout functionalities. Realized as MAPS (monolithic active pixel sensors) standard CMOS wafers are used with a Si epitaxial layer usually as the sensitive part, where charge collection is largely governed by slow and non-directional charge diffusion. Depleted MAPS (DMAPS) exploit non-standard high resistivity wafers (typically >1 k Ω cm) and high bias voltage (up to ~ 300 V) resulting in charge collection by directed drift motion. Charge collecting electrodes are deep wells (n-wells in Fig. 35.24(b)), either formed as large structures to fully contain the CMOS circuitry (top) or as small nodes, set aside the electronics (bottom), with obvious pros and cons resulting from shorter average drift distance (large electrode) versus much smaller capacitance (small electrode). The former benefits radiation tolerance, whereas the latter allows for smaller pixels and benefits from small sensor capacitance in noise and timing performance. However, in both approaches radiation tolerance levels to the order of 10^{15} n_{eq}/cm^2 (fluence) and 1 MGy (ion. dose) have been demonstrated.

A high spatial resolution, but less radiation-tolerant variant of the monolithic approach are SOI (silicon on insulator) pixels (see *e.g.* [346]), where a high-resistivity supporting wafer, employed for particle sensing, connects through an embedded insulator (a buried oxide layer, BOX) to the CMOS circuitry. The BOX separates the sensing volume from the electronics layer and provides shielding.

DEPFET pixels (see *e.g.* [347]) contain one transistor in every cell which—apart from a normal (external) gate electrode—is controlled by an “internal gate” (a local n -implant) about $1\ \mu\text{m}$ underneath the surface. By appropriately biasing from two diode structures on either side of the bulk together with the internal gate, a local potential minimum for electrons is created underneath the transistor channel which gathers the released ionization electrons, thus modulating the transistor’s channel current by about $0.5\ \text{nA}$ per collected electron. Very thin sensors and $O(\mu\text{m})$ spatial resolutions have been achieved.

35.8.2.3 Timing with silicon detectors

Essential for precision timing (< 100 ps) are steep signal rise and low noise (see Eq. (35.37) in Section 35.9). Thin detectors with high E-fields and short amplifier rise times are necessary to achieve the required small collection times and fast amplification. Columnar electrodes (normal to the surface) with small diameter and small pitch are a suitable choice by design but they require non-standard fabrication processes. Planar electrode geometries that include an implanted low-gain ($g = 10\text{--}50$) amplification structure on either top or bottom electrode side to maximize the slew rate (dS/dt , with S = “signal”, *e.g.* an induced current or a voltage), are employed in so-called LGADs (low gain avalanche diodes, Fig. 35.25). Electrons created from ionizing traversing particles are accelerated in a high field towards an amplification layer near the top electrode, where they create a multitude of e - h pairs. They induce a very fast and large signal rise, mainly governed by the holes’ movement away from the amplification layer. Sufficiently

low amplification gain minimizes excess noise contributions and avoids creation of hole-induced avalanches moving in opposite direction to electron avalanches.

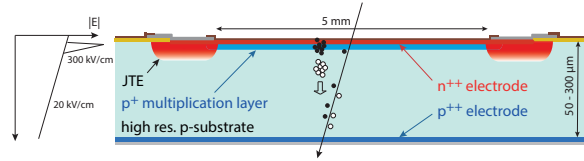


Figure 35.25: LGAD amplification structure for precision timing. Amplification occurs inside the structure boundaries in a highly doped p - n junction near the surface (JTE = Junction Termination Extension, deep n-well).

The achievable time resolution has several contributions:

$$\sigma_t^2 = \left(\frac{\sigma_S^{thr}}{dS/dt} \right)^2 + \left(\frac{\sigma_n}{dS/dt} \right)^2 + \sigma_{arrival}^2 + \sigma_{dist}^2 + \sigma_{TDC}^2. \quad (35.23)$$

The first term represents “time walk” coming from Landau fluctuations, defined as originating from number and energy transfer fluctuations in the energy loss process (see *e.g.* [1]) with σ_S^{thr} being the signal height variations at discriminator threshold. This term can be kept minimal, *e.g.*, by employing constant fraction discrimination or by applying corrections using amplitude information. The second term is noise jitter, which can also be expressed as t_r/SNR with t_r = rise time, SNR = signal-to-noise ratio. Both first terms are made small by large signal slew rates. An irreducible contribution comes from fluctuations in non-uniform depositions of charge along the particle path (including fluctuations in the amplification process) which causes an intrinsic jitter in the arrival time (third term)². The thinner the detector the less disturbing is this effect. The fourth contribution is signal distortion due to non-uniform weighting field regions and variations in (non-saturated) drift velocities. The final term denotes time fluctuations due to uncertainties in the digitization, which can, however, be made negligible with GHz TDCs. Timing precisions of order 30 ps have been reached. More elaborate discussions on timing in silicon detectors can be found *e.g.* in [348]; more details on LGADs are given in [349].

35.8.3 Radiation Damage

High channel density and response times in the nanosecond range renders micro-patterned semiconductor detectors particularly suited for high particle rates. This is usually accompanied by high radiation causing damage of sensors and front-end electronics. Radiation damage occurs through two basic mechanisms:

1. *Bulk damage* due to displacement of atoms from their lattice sites resulting in defect energy levels inside the band gap. This leads to increased leakage current, carrier trapping, and build-up of space charge that changes the required operating voltage. Displacement damage results from non-ionizing energy loss (NIEL) and the energy imparted to the recoil atoms can initiate a chain of subsequent displacements including “damage clusters”. Hence, it is critical to consider both, particle type and energy. Conventionally, for silicon the received NIEL is normalized to the damage level caused by 1 MeV neutrons and specified in units of neutron-equivalent fluence Φ_{eq} with units n_{eq}/cm^2 .
2. *Surface damage* due to charge build-up in surface layers and formation of interface traps at *e.g.* Si-SiO₂ boundaries. These cause thin charge carrier layers at the silicon surface, leading to increased surface leakage currents in sensors or circuits affecting electrode isolation or transistor characteristics, respectively. The effects of charge build-up are strongly dependent on the device structure and on fabrication details. The damage is dominantly due to ionizing energy loss (IEL)

²In LGAD literature these fluctuations are sometimes also referred to as “Landau fluctuations”.

and hence proportional to the absorbed total ionization dose (TID) measured in Gy (or rad), independent of particle type.

The increase in reverse bias generation current due to bulk damage is $\Delta I_L = \alpha \Phi_{eq} V$, where V is the volume under an electrode and $\alpha \simeq 4 \times 10^{-17}$ A/cm, a universal constant when normalized to temperature (conventionally 20°C), and given after annealing for 80 min at 60°C. Note that for devices with intrinsic amplification, generation current is amplified accordingly. The reverse bias leakage current depends strongly on temperature

$$I_L(T) \propto T^2 \exp\left(-\frac{E_a}{2kT}\right), \quad (35.24)$$

where $E_a \approx 1.2$ eV (activation energy), so rather modest cooling can reduce the current substantially (~ 6 -fold reduction in cooling from room temperature to 0°C).

For bulk damage in silicon the *NIEL hypothesis* is a good first order description of the observed damage (especially regarding I_L). It states that all lattice radiation damage in silicon linearly scales with NIEL and can be traced back to the abundance of primary defects (point defects and clusters), irrespective of their initial distribution over energy and space, that is, regardless of topology and origin of the damage. Under the NIEL hypothesis, the observed differences in damage caused by neutrons, protons, pions and electrons are hence usually scaled to each other.

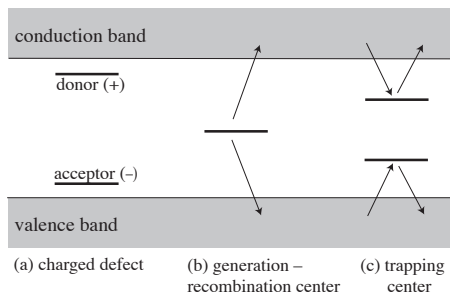


Figure 35.26: Characteristic locations of energy levels caused by bulk radiation damage and their main effects on device operation.

Three main bulk displacement damage effects are sketched in Figure 35.26: (a) defects acting as charged donors/acceptors, (b) deep defects (near the middle of the bandgap) causing increased leakage current, and (c) carrier trapping centers. Damage effects are not constant with time; for example, the negative space charge first anneals reaching a stable damage minimum (beneficial annealing) and then electrically active defects (negative space charge) build up on the time scale of months (reverse annealing).

Acceptor- (typically dominant) or donor-like states, when ionized, build up space charge, which in turn requires an increase in the applied voltage to sweep signal charge through the detector thickness. For n -type silicon, acceptor buildup with fluence initially leads to a decrease in the required bias voltage until (effective) positive and negative space charges balance; only little bias voltage is required for operation (point of effective space charge inversion, also called “type” inversion). At larger fluences the negative space charge dominates, and the required operating voltage increases proportional to the increasing effective space charge density N_{eff} , also called effective doping concentration. Today, p -type silicon is the preferred choice for sensors operating in high radiation environments for reasons of cost-effectiveness in production and high radiation hardness due to electron collection in high electric- and high weighting-field regions at segmented n^+ electrodes. Dopant removal, *e.g.*, through phosphorous or boron reactions with crystal defects, also plays an important role in more complex sensor structures like for example DMAPS or LGADs. Various techniques have been applied to neutralize “active” damage sites, for example by oxygen or carbon enrichment for n -type/ p -type substrates with different successes (for more details see *e.g.* [350, 351]).

Deep level defects (Fig. 35.26(b)) typically are the origin of leakage current increase, whereas trapping centers (Fig. 35.26(c))

dominate carrier lifetime and signal loss at high fluences beyond 10^{15} $n_{\text{eq}}/\text{cm}^2$. The safe limit on operating voltage ultimately limits the detector lifetime. Strip and pixel detectors specifically designed for high voltages have been extensively operated at bias voltages of 500–600 V.

Strip and pixel detectors have remained functional in large detectors even at particle fluences beyond 10^{15} $n_{\text{eq}}/\text{cm}^2$ where charge loss due to recombination and trapping becomes significant. The high SNR obtainable with low capacitance pixel structures extends detector lifetime. The higher mobility of electrons makes them less sensitive to carrier lifetime than holes, so detector configurations that emphasize the electron contribution to the charge signal are advantageous, *e.g.*, n^+ strips or pixels on a p - or n -substrate. The occupancy of the defect charge states is strongly temperature dependent; competing processes can increase or decrease space charge and the required operating voltage. It is critical to choose the operating temperature judiciously (-30°C to 0°C in typical collider detectors) and to limit warm-up periods during maintenance. Detailed discussions of the current understanding of radiation effects can be found in [350, 351].

Tolerance against surface damage, especially in SiO_2 layers and in trenches of CMOS transistor structures, largely depends on the feature size of a technology and on appropriately designed circuitry. Deep submicron technology nodes of 130 nm and 65 nm sustain total ionization doses of up to 5 MGy (500 Mrad), corresponding to fluences of up to 5×10^{15} cm^{-2} of minimum ionizing pions or protons.

35.9 Low-noise detector readout

Revised November 2021 by N. Wermes (Bonn U.), revised November 2013 by H. Spieler (LBNL).

Many detectors rely critically on low-noise readout electronics, for best energy resolution or to allow low thresholds for high detection efficiencies. A typical detector front-end is shown in Fig. 35.27.

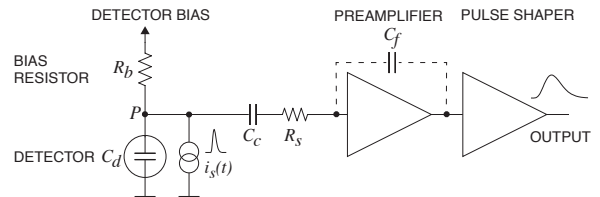


Figure 35.27: Typical detector front-end. The dashed circuit part is a charge-sensitive amplifier (CSA) realization.

In a model relevant for most readout applications, the detector, represented by a capacitance C_d , delivers a delta-function-shaped current signal, represented by a current source in parallel. Bias voltage is applied through resistor R_b and the signal is (often) coupled to the amplifier through a blocking capacitor C_c . The series resistance R_s represents the sum of all resistances present in the input signal path, *e.g.*, the electrode resistance, any input protection networks, and parasitic resistances in the input transistor. The amplification stage contains the preamplifier providing gain and a pulse shaper (characterized by a shaping time τ), which tailors the overall frequency response to optimize the signal-to-noise ratio (SNR) while limiting the duration of the signal pulse to accommodate the signal pulse rate. For a given input signal, purely random noise leads to a gaussianly smeared signal distribution behind the shaper. Even if not explicitly stated, all amplifiers provide some form of pulse shaping due to their limited frequency response.

It is useful to distinguish between noise inherent to a detector’s signal amplification and processing circuitry (per channel) on the one hand, depending on the detector specifics and the experimental environment (*e.g.* the data rate), and — on the other hand — external noise sources introduced *e.g.* by systems external to a specific readout circuit often resulting in “common-mode” noise, *i.e.* common to all channels. External noise can be introduced for

example from power supplies, digital signal switching, RF pick-up, or can come from effects due to “common grounding” allowing noise to couple to the current loop connecting the detector to the preamplifier. These noise sources differ from setup to setup and must be dealt with – and should at best be eliminated – individually. In the following, therefore, only the noise inherent to typical detector signal processing is discussed.

35.9.1 Principal noise origins

As principal noise origins in circuit elements we mainly distinguish “thermal noise” resulting from velocity fluctuations of charge carriers (Brownian motion), as well as “shot noise” and “ $1/f$ noise”, both resulting from charge carrier number fluctuations. Shot noise is due to emission statistics of electrons crossing a barrier, $1/f$ noise is often – especially in MOSFETs – due to charge trapping–detrapping processes leading to a spectral behavior as $1/f^\alpha$ with $\alpha = 0.5 \dots 2$. Further noise nomenclature, like for example RTS (random telegraph signal) noise, also called “burst noise” or “popcorn noise”, is in its origin like $1/f$ noise usually related to trapping/detrapping processes. The popping-up nature of individual RTS bursts eventually leads to the $1/f$ noise spectral density when noise of several traps with (very) different trapping times are superimposed. RTS noise is omitted in the following for simplicity reasons.

35.9.2 Equivalent noise analysis

The equivalent circuit for noise analysis (Fig. 35.28) shows contributions of the mentioned noise sources at several circuit points. Originating from fluctuations, noise is expressed as the variance $\langle i^2 \rangle$ or $\langle v^2 \rangle$ of a noise current or voltage distribution. Shot noise, such as that produced in a semiconductor detector by leakage current fluctuations, is represented by a current noise generator in parallel with the detector and the amplifier input. The statistical fluctuations in a charge measurement will scale with the square root of the total number of recorded charges, so this noise contribution increases with the measurement (shaping) time. Thermal noise in resistors produces a white noise, *i.e.* a noise power density independent of frequency. Hence limiting the bandwidth by a shaper, *i.e.*, increasing the shaping time, will decrease the noise at the expense of slowing down the detector response. Usually, resistors shunting the input act as noise current sources and resistors in series with the amplifier input act as noise voltage sources, so that they are often referred to as “parallel” and “series” noise. Thermal fluctuations in the bias resistor result in fluctuations of the voltage at point P in Fig. 35.27 and its noise current source $\langle i_b^2 \rangle$ has the same effect as the shot noise current $\langle i_d^2 \rangle$ from the detector. Conversely, the series resistor R_s acts as a voltage noise generator $\langle v_s^2 \rangle$ for the amplifier input.

Shot noise and thermal noise have a “white” frequency distribution, *i.e.*, the (power) spectral densities (f = frequency) $d\langle i^2 \rangle/df$ and $d\langle v^2 \rangle/df$ are constant with magnitudes

$$\begin{aligned} d\langle i_d^2 \rangle &= 2eI_d df, \\ d\langle i_b^2 \rangle &= \frac{4kT}{R_b} df, \\ d\langle v_s^2 \rangle &= 4kTR_s df, \end{aligned} \quad (35.25)$$

where e is the elementary charge, I_d the detector leakage current, and k, T Boltzmann constant and temperature. Hence, in a 1 k Ω resistor at room temperature, for example, one finds a current-independent thermal noise of $\sqrt{d\langle i^2 \rangle/df} = 4 \text{ pA}/\sqrt{\text{Hz}}$ or $\sqrt{d\langle v^2 \rangle/df} = 4 \text{ nV}/\sqrt{\text{Hz}}$, respectively. For $1/f$ noise, by contrast, the spectral power density is proportional to $1/f^\alpha$ ($\alpha = 0.5\text{--}2$) with a device specific proportionality constant. In what follows, we will assume $\alpha = 1$ for simplicity reasons, noting though that more complex models exist.

An important noise source is the preamplifier input stage, very often dominated by the first amplification transistor. In what follows we assume a MOSFET at this point, as the large majority of amplification circuits is based on MOS transistors. Noise sources in bipolar amplification is shortly mentioned at the end of this section. A MOS transistor’s channel features thermal noise with “resistance” $1/g_m$, where $g_m = \partial I/\partial V$ is the transconductance. Correction factor(s) for parametrization depend on the transistor

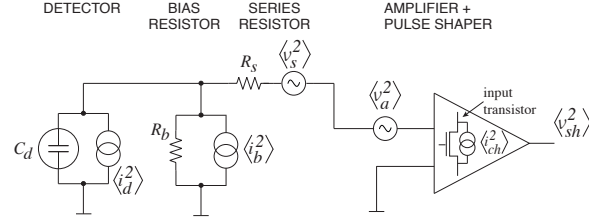


Figure 35.28: Equivalent circuit for noise analysis.

operation point. Conventionally, a factor γ is applied varying between 0.5 and 1 when temperature dependence is implicit, but is commonly taken as $\gamma \approx 2/3$ for operation in strong inversion and 0.5 in weak inversion.

In addition, especially in MOSFETs, there is $1/f$ noise originating from trapping/detrapping processes of charge carriers at the channel’s Si–SiO₂ interface. The channel’s current noise is equivalent to a voltage noise at the transistor input (the gate) via

$$\langle i_{ch}^2 \rangle = \langle (g_m v_a)^2 \rangle \quad (35.26)$$

leading to respective noise power spectral densities of

$$\frac{d\langle v_a^2 \rangle}{df} = 4kT\gamma \frac{1}{g_m} + K_f \frac{1}{C'_{ox} WL} \frac{1}{f}, \quad (35.27)$$

where the individual (uncorrelated) noise contributions add in quadrature. The “ $1/f$ noise constant” K_f has magnitude in the order of $10^{-24} - 10^{-26} \text{ J}$ depending on the device type and the technology³. C'_{ox} is the oxide capacitance per unit area, and W, L are width and length of the gate.

Particle and radiation detectors typically convert the deposited energy into charge (usually e-ion or e-h pairs) which can be measured by integrating the current induced on an electrode by the drifting charge pairs (see *e.g.* Sec. 35.8) employing a “charge-sensitive (pre)amplifier” (CSA), realized by feeding back the preamp’s output to the input through capacitor C_f (dashed circuit part of Fig. 35.27). The feedback capacitance must be discharged for the next pulse to appear, for example by a resistor, a (constant) current source or a switch. Noise contributions from such components can usually be kept small in comparison.

For a CSA the noise output voltage after the preamplifier (v_{pa}^2) relates to the input (current or voltage) noise sources via the transimpedance $1/\omega C_f$ as

$$\langle v_{pa}^2 \rangle = \langle i_{in}^2 \rangle \left(\frac{1}{\omega C_f} \right)^2 \quad \text{or} \quad \langle v_{pa}^2 \rangle = \langle v_{in}^2 \rangle \left(\frac{\omega C_D}{\omega C_f} \right)^2 \quad (35.28)$$

with $\omega = 2\pi f$. The capacitance C_D includes the detector capacitance C_d plus all capacitances shunting the input. Considering only the (usually) dominant noise sources, being the detector shot noise as well as the transistor channel noise, and neglecting the resistor parallel and serial noise sources of (35.25) by choosing R_b large and keeping R_s small, one obtains

$$\frac{d\langle v_{pa}^2 \rangle}{d\omega} = \sum_{k=-2}^0 c_k \omega^k \quad (35.29)$$

with

$$c_{-2} = \frac{e}{\pi} I_d \frac{1}{C_f^2}, \quad c_{-1} = K_f \frac{1}{C'_{ox} WL} \frac{C_D^2}{C_f^2}, \quad c_0 = \frac{2\gamma}{\pi} kT \frac{1}{g_m} \frac{C_D^2}{C_f^2}, \quad (35.30)$$

which correspond to the discussed main noise components, c_{-2} : shot noise, c_{-1} : $1/f$ noise, c_0 : thermal noise, respectively.

The filtering effect of the shaper limits the bandwidth of the system and is generally described by a transfer function $H(\omega)$ for

³Other $1/f$ noise parametrizations also exist with correspondingly different numerical values for K_f .

$\langle v_{pa}^2 \rangle$ integrated over the full bandwidth

$$\langle v_{sh}^2 \rangle = \int_0^\infty \frac{d\langle v_{pa}^2 \rangle}{d\omega} |H(\omega)|^2 d\omega \quad (35.31)$$

with $\langle v_{sh}^2 \rangle$ being the shaper output voltage noise. $H(\omega)$ depends on the filter circuit, *i.e.* the shape of the pulse formed by the shaper, and is characterized by a characteristic time τ , the shaping time, which can, for example, be the peaking time of a semi-gaussian pulse or the sampling interval in a correlated double-sampler (see *e.g.* [8]). The peaking time is an important quantity for readout systems since for peaking times large compared to the duration of the input signal the amplitude at peaking time corresponds to the total input charge.

For a simple time-invariant CR–RC filter, consisting of a high-pass followed by a low-pass filter with equal time constants, the transfer function is

$$|H(\omega)|^2 = A^2 \left(\frac{\omega\tau}{1 + \omega^2\tau^2} \right)^2 \quad (35.32)$$

and (35.29) becomes

$$\langle v_{sh}^2 \rangle = \frac{\pi}{4} A^2 \left(c_{-2}\tau + \frac{2}{\pi}c_{-1} + c_0\frac{1}{\tau} \right) \quad (35.33)$$

with A being an overall gain factor.

The system noise for a charge measurement is conveniently expressed as an equivalent noise charge (ENC) referring the noise to the equivalent signal of one electron at the input:

$$\text{ENC}^2 = \frac{\langle v_{sh}^2 \rangle}{v_{\text{signal}}^2 (1e^-)}. \quad (35.34)$$

While being dimensionless by definition, ENC is commonly expressed as an equivalent number of electrons (e^-) at the input or alternatively as equivalent Coulombs (C) when multiplying by the elementary charge or as equivalent deposited energy (eV), where $1e^-$ equivalent charge corresponds to 3.65 eV of equivalent deposited energy in Si.

A charge of one electron at the input yields a voltage signal (peak) behind the shaper of $v_{\text{signal}} = \frac{A}{2.71} \frac{e}{C_f}$. Hence with (35.34) and (35.33) one obtains:

$$\begin{aligned} \text{ENC}^2 (e^-) &= \frac{(2.71)^2}{4e^2} \left(eI_d\tau + 2C_D^2 K_f \frac{1}{C'_{ox}WL} + \gamma \frac{2kT}{g_m} \frac{C_D^2}{\tau} \right) \\ &= a_{\text{shot}}\tau + a_{1/f}C_D^2 + a_{\text{therm}}\frac{C_D^2}{\tau}, \end{aligned} \quad (35.35)$$

where 2.71 is Euler's number resulting from the amplitude peak value behind the (CR–RC) shaper (for $t = \tau$), while e is the elementary charge and (e^-) explicitly denotes equivalent number of electrons.

Equation (35.35) accentuates the main noise dependencies of the system. The contribution from parallel current shot noise (*i.e.* detector leakage) increases with shaping time, *i.e.* with pulse duration, whereas thermal noise (here serial voltage noise at the gate, originating from transistor channel noise) decreases with increasing shaping time, *i.e.* with reduced bandwidth. Noise with a $1/f$ spectrum depends only on the ratio of upper to lower cutoff frequencies (low pass to high pass time constants) and is hence independent of τ for a given shaper topology. Furthermore, the contribution of serial noise voltage ($1/f$ and thermal noise) to ENC increases with input (detector) capacitance C_D . Pulse shapers can be designed to optimize the noise performance of a system or to mitigate operation variations with time (*e.g.* due to radiation damage) deteriorating the performance, at the expense of loss of simplicity. For example, a shaper with one high-pass filter followed by four cascaded low-pass filters, increases the pulse symmetry and tends to decrease the current noise, but increases the voltage noise contributions for the circuit of Fig. 35.28, if the same peaking time is assured by adjusting the individual time constants

of the filter stages. If instead the low-pass filters cause the peaking time of the pulse to increase, the opposite can be true. More details about shaping filters can be found *e.g.* in [8, 352–354].

Figure 35.29 shows a typical example of eq. (35.35) displaying ENC as a function of shaping time τ for a system. At short shaping times, thermal noise dominates, whereas for longer shaping times the shot noise contribution takes over. The total noise has a minimum at a shaping time where shot and thermal noise contributions are equal. The minimum is flattened by the presence of $1/f$ noise. Increasing the detector capacitance increases the thermal and $1/f$ contributions and shifts the noise minimum to larger shaping times. One can hence exploit the shaping time dependence of the total noise to determine the individual noise contributions of a system.

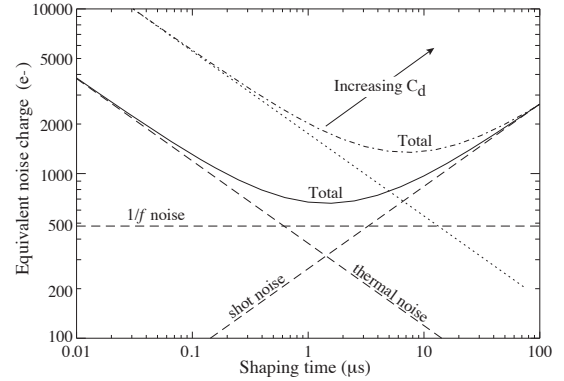


Figure 35.29: Equivalent noise charge *vs* shaping time. Changing the detector capacitance C_D affects thermal and $1/f$ noise contributions and moves the noise minimum as indicated by the dotted and dash-dotted lines. The $1/f$ noise contribution is small for the chosen parameters ($C_D = 20$ pF, $I_d = 10$ nA, $g_m = 1$ mS) in this example.

For quick estimates (35.35) is cast into a useful equation for a typical CSA-shaper system [1]:

$$\begin{aligned} \text{ENC}^2 (e^-) &= 11 \frac{I_d}{\text{nA}} \frac{\tau}{\text{ns}} + 740 \frac{1}{WL/(\mu\text{m}^2)} \frac{C_D^2}{(100\text{fF})^2} \\ &+ 4000 \frac{1}{g_m/\text{mS}} \frac{C_D^2/(100\text{fF})^2}{\tau/\text{ns}}, \end{aligned} \quad (35.36)$$

where $\gamma = 2/3$, $K_f = 33 \times 10^{-25}$ J, and $C'_{ox} = 6$ fF/ μm^2 has been used, the latter being typical for CMOS technologies as employed for example for the detector readout chips of the LHC experiments and their upgrades. Generally, noise performance is improved by reducing the detector capacitance and leakage current, judiciously selecting all resistances in the input circuit, and by choosing the optimum shaping time constant. Another noise contribution to consider is the fact that noise can cross-couple from the neighboring front-ends in detectors with structured electrodes through the inter-electrode capacitance.

As mentioned, the noise parameters of the amplifier depend primarily on the input device (input transistor(s)). In field-effect transistors, the input noise current contribution of the transistor itself is very small. Hence, if the experiment's time structure permits, reducing the detector leakage current and increasing the bias resistance will allow long shaping times with correspondingly lower noise. For amplifiers employing bipolar transistors, shot noise sources originate from both, base-emitter and collector-base, junctions and from the series resistance at the base which is especially important for small structures optimized for radiation hardness. For the shot-noise contribution, the input base current I_B sets a lower bound on the noise current, such that these devices are best at short shaping times.

35.9.2.0.1 Examples Using (35.36) one finds for a typical pixel detector (before heavy irradiation) with $C_D = 200$ fF, $I_d =$

1 nA, $\tau = 50$ ns, $W = 20$ μm , $L = 0.5$ μm , $g_m = 0.5$ mS:

$$\text{ENC}^2 \approx (24 e^-)^2 \Big|_{\text{shot}} + (17 e^-)^2 \Big|_{1/f} + (25 e^-)^2 \Big|_{\text{therm}} \approx (40 e^-)^2.$$

For a typical silicon microstrip detector after radiation damage (fluence $\gtrsim 10^{14}$ $\text{n}_{\text{eq}}/\text{cm}^2$, assuming no degradation of the front-end electronics due to radiation) one obtains for $C_D = 20$ pF, $I_d = 1$ μA , $\tau = 50$ ns, $W = 2000$ μm , $L = 0.4$ μm , $g_m = 5$ mS:

$$\text{ENC}^2 \approx (750 e^-)^2 \Big|_{\text{shot}} + (200 e^-)^2 \Big|_{1/f} + (800 e^-)^2 \Big|_{\text{therm}} \approx (1100 e^-)^2.$$

Apart from the larger leakage current, the larger capacitance of strips compared to pixels leads to a much worse noise performance which can only be partially compensated by allowing more power in the amplification transistor, *i.e.*, by increasing g_m .

A liquid argon calorimeter cell is a suitable example of a detector with a large electrode capacitance with typical parameters (similar to the ATLAS central electromagnetic calorimeter, see Sec. 35.10). Using $C_D = 1.5$ nF, $I_d = < 2$ μA , $\tau = 50$ ns, $W = 3000$ μm , $L = 0.25$ μm , $g_m = 100$ mS, one obtains:

$$\begin{aligned} \text{ENC}^2 &\approx (1000 e^-)^2 \Big|_{\text{shot}} + (15000 e^-)^2 \Big|_{1/f} + (13500 e^-)^2 \Big|_{\text{therm}} \\ &\approx (20200 e^-)^2. \end{aligned}$$

Here only a small (negligible) parallel shot noise (leakage current) contribution is assumed, which is typical for liquid argon calorimeters.

Practical noise levels range from $\sim 1e^-$ for CCD's at long shaping times to $\sim 10^4 e^-$ in high-capacitance liquid argon calorimeters. Gaseous micropattern detectors like GEMs or MicroMegas (see Sec. 35.6.4) typically feature noise levels between $1000 e^-$ and $1500 e^-$, depending on the ability to correct for common-mode noise. Silicon strip detectors typically operate at levels of $\sim 10^3 e^-$, whereas pixel detectors with fast readout typically have noise levels below about 100 electrons.

35.9.3 Timing measurements

In timing measurements, the slope-to-noise ratio must be optimized, rather than the signal-to-noise ratio alone, so the rise time t_r of the pulse is important. The "jitter" σ_t of the timing distribution is

$$\sigma_t = \frac{\sigma_n}{(dS/dt)_{\text{trig}}} \approx \frac{t_r}{\text{SNR}}, \quad (35.37)$$

where σ_n is the rms noise, SNR the signal-to-noise ratio and the "slew rate" dS/dt , *i.e.* the derivative of the signal, is evaluated at the trigger level. The rise-time of a CSA again depends on the detector and feedback capacitances and on the amplifier transconductance

$$t_r \propto \frac{C_D}{C_f \cdot g_m}. \quad (35.38)$$

To increase dS/dt without incurring excessive noise, the amplifier bandwidth should match the rise-time of the detector signal. The 10% to 90% rise time of an amplifier with bandwidth f_U is $0.35/f_U$. For example, an oscilloscope with 350 MHz bandwidth has a 1 ns rise time. For cascaded amplifiers the individual rise times add in quadrature to first order.

As increasing SNR also improves the time resolution, minimizing the total input capacitance is extremely important for timing measurements (see also Sec. 35.8). At high signal-to-noise ratios, the time jitter can be much smaller than the rise time. The time-mark distribution of pulses may shift with the signal level ("time walk"), but this can be corrected by various means, either in hardware or in software.

For applications aiming at extreme time resolution a charge sensitive (integrating) amplification is not optimal. Transimpedance or voltage amplifiers converting current/voltage to voltage are preferred. Also, when aiming for picosecond timing using voltage amplifiers, *e.g.*, with LGAD detectors having C_D of $\mathcal{O}(\text{pF})$ (see Sec. 35.8), not only the preamplifier rise time t_r but also the signal pulse duration t_d at the preamplifier input is important, *i.e.*, the preamplifier must react draining the charge from C_D before

the input voltage $v_{in} = Q_S/C_D$ ($Q_S =$ signal charge) reaches its peak. Both times must reasonably match, $t_r \approx t_d$, resulting in a time jitter of [355]

$$\sigma_t^2 \approx \frac{C_D^2}{Q_S^2} \frac{d\langle v_n^2 \rangle}{df} t_d, \quad (35.39)$$

where $d\langle v_n^2 \rangle/df$ is the voltage noise spectral density.

35.9.4 Digital signal processing

The filtering principles apply to both analog and digital signal processing. In digital signal processing the pulse shaper shown in Fig. 35.27 is replaced by an analog to digital converter (ADC) followed by a digital processor that determines the pulse shape. Digital signal processing allows great flexibility in implementing filtering functions. The software can be changed readily to adapt to a wide variety of operating conditions and it is possible to implement filters that are impractical or even impossible using analog circuitry. However, this comes at the expense of increased circuit complexity and increased demands on the ADC compared to analog shaping.

If the sampling rate of the ADC is too low, high frequency components will be transferred to lower frequencies ("aliasing"). The sampling rate of the ADC must be high enough to capture the maximum frequency component of the input signal. Apart from missing information on the fast components of the pulse, under-sampling introduces spurious artifacts. If the frequency range of the input signal is much larger than the sampling rate, the noise at the higher frequencies will be transferred to lower frequencies and will increase the noise level in the frequency range of pulses formed in the subsequent digital shaper. The Nyquist criterion states that the sampling frequency must be at least twice the maximum relevant input frequency. This requires that the bandwidth of the circuitry preceding the ADC must be limited. The most reliable technique is to insert a low-pass filter.

The digitization process also introduces inherent noise, since the voltage range ΔV corresponding to a minimum bit step introduces quasi-random fluctuations relative to the exact amplitude

$$\sigma_n = \frac{\Delta V}{\sqrt{12}}. \quad (35.40)$$

When the Nyquist condition is fulfilled the noise bandwidth Δf_n is spread nearly uniformly and extends to 1/2 the sampling frequency f_S , so the spectral noise density is

$$\frac{\sigma_n}{\sqrt{\Delta f_n}} = \frac{\Delta V}{\sqrt{12}} \cdot \frac{1}{\sqrt{f_S/2}} = \frac{\Delta V}{\sqrt{6f_S}}. \quad (35.41)$$

Sampling at a higher frequency spreads the total noise over a larger frequency range, so oversampling can be used to increase the effective resolution. In practice, this quantization noise is increased by the ADC's differential non-linearity. Furthermore, the equivalent input noise of ADCs is often rather high, so the overall gain of the stages preceding the ADC must be sufficiently large for the preamplifier to override the ADC input noise.

35.9.5 What to use when?

When implemented properly, digital signal processing provides significant advantages in systems where the shape of detector signal pulses changes greatly, for example in large semiconductor detectors for gamma rays or in gaseous detectors (*e.g.* TPCs) where the duration of the current pulse varies with drift time, which can range over orders of magnitude. Analog signal processing is best or most efficient in systems that require fast time response, but the high power requirements of high-speed ADCs are prohibitive. Systems that are not sensitive to pulse shape can use fixed shaping time constants and rather simple filters (like CR-RC), which can be either continuous or sampled. In high density systems that require small circuit area and low power (*e.g.*, in strip and pixel detectors), analog filtering often yields the required response and tends to be most efficient.

As stressed already in the introduction, it is important to consider that additional noise is often introduced externally. Recognizing additional noise sources and minimizing cross-coupling

to the detector current loop is often essential to obtain the best overall noise performance. Understanding basic physics and its practical effects is important in forming a broad view of the detector system and recognizing potential problems (*e.g.* modified data), rather than merely following standard recipes.

More comprehensive treatments of low noise detector readout and signal processing can be found, for example, in [8, 352, 354] and in [1, 344].

35.10 Calorimeters

35.10.1 Introduction

Revised August 2021 by F. Sefkow (DESY, Hamburg) and F. Simon (Werner-Heisenberg-Inst.).

A calorimeter measures the energy and direction of particles by absorption in the detector material and registration of the energy deposited in an (ideally) contained electromagnetic (EM) or hadronic shower. Calorimeters are central components of modern high energy physics experiments, due to their ability to measure not only the energy of charged particles (with the exception of muons), but also of photons and neutral hadrons, thus enabling the reconstruction of π^0 and η decays and of exclusive final states involving long-lived neutral kaons, or neutrons. They are indispensable for the measurement of particle jets and for the reconstruction of total event properties, which, via the measurement of missing energy (or missing transverse energy in hadron colliders), enable the detection of the presence of "invisible" particles such as neutrinos and hypothetical particles such as dark-matter candidates. Calorimeters are also important for the identification of particle species, using information on the longitudinal and transverse shape of the energy deposition to separate electrons, photons, hadrons and muons. While the performance of calorimeters is typically assessed by the quality of their energy measurements, position resolution, both for EM and hadronic showers, is also highly relevant, for example for the reconstruction of effective jet masses. The capability to measure high-level observables that serve to classify events, such as particle and jet energies, missing energy and isolated leptons, makes calorimeters central components of the trigger systems in high-energy physics experiments.

In collider experiments, the importance of calorimeters tends to increase with increasing collision energies since the relative energy resolution improves with increasing particle energy while the depth required for full containment of the showers shows only logarithmic growth with energy. This is in contrast to the precision of track-based measurements, which is decreasing with increasing momentum. With recent advances in timing capabilities calorimeters are also contributing to the rejection of pile-up from multiple interactions within the same bunch crossings at colliders.

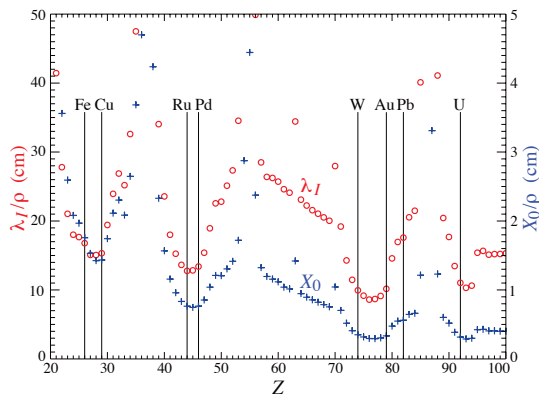


Figure 35.30: Nuclear interaction length λ_I/ρ (circles) and radiation length X_0/ρ (+s) in cm for the chemical elements with $Z > 20$ and $\lambda_I < 50$ cm.

The characteristic length scale for EM showers is the radiation length X_0 , which ranges from 1.8 cm (13.8 g cm^{-2}) in iron to 3.2 mm (6.0 g cm^{-2}) in uranium for materials used to generate

showers in calorimeters.⁴ Similarly, the characteristic nuclear interaction length λ_I varies from 16.8 cm (132.1 g cm^{-2}) (Fe) to 11.0 cm (209 g cm^{-2}) (U).⁵ There is a premium on small λ_I/ρ and X_0/ρ (both with units of length). These quantities are shown for elements with $Z > 20$ in Fig. 35.30. The minima for both X_0 and λ_I correspond to elements between W and Au. Some of these elements are very difficult to work with (*e.g.* W) or expensive (*e.g.* Au), so, depending on the application (size of the required calorimeter) other materials, such as Fe, Cu, Pb, and different alloys like brass and CuW are often chosen. For EM calorimeters high Z is preferred; here Pb is a popular choice, while W provides even higher density and is generally affordable due to the limited volume of EM systems.

Most existing calorimeters are subdivided into a front EM section (ECAL) and a hadronic part (HCAL) behind; electrons and photons are measured in the ECAL, while hadrons and jets are measured in the combined ECAL and HCAL system. The detailed design depends on energy range and performance requirements as well as on size and cost constraints for the entire system. EM calorimeters tend to be 15–30 X_0 deep, while hadronic calorimeters are usually optimised for cost and performance at 5–8 λ_I . The depth of the ECAL typically corresponds to approximately 1 λ_I , with the exact value depending on the material. This means that approximately 70% of all hadronic showers will already begin in the electromagnetic calorimeter, making its response to a hadronic cascade highly relevant for the overall performance of the system. The choice of the calorimeter technology for the ECAL is thus a result of simultaneous optimisation for EM and hadronic performance of the overall system.

Sampling calorimeters consist of a high-density, normally metallic absorber sandwiched (or threaded) with an active material which generates a signal in response to shower particles. The active medium may be a scintillator, a noble liquid, a gas, silicon, or a Cherenkov radiator. These active media all have a relatively low Z , a significantly lower density, and larger X_0 and λ_I values than typical absorber materials. The average radiation and interaction lengths in the full detector are thus larger than those of the absorber alone.

There are also *homogeneous calorimeters*, in which the entire volume contributes to the signal. Homogeneous calorimeters may be built with inorganic heavy scintillating crystals or non-scintillating Cherenkov radiators such as lead glass and lead fluoride. Nuclear interaction lengths in inorganic crystals range from 17.8 cm (LuAlO_3) to 42.2 cm (NaI). Materials with low X_0 used in large systems are for example BGO with $\lambda_I = 22.3$ cm and $X_0 = 1.12$ cm, and PbWO_4 (20.3 cm and 0.89 cm). Properties of these and other commonly used inorganic crystal scintillators can be found in Table 35.4. Cryogenic noble liquids, where scintillation light and/or ionization can be detected, are also suitable materials for homogeneous detectors.

Homogeneous calorimeters at colliders are usually only used for the EM section. For the use of homogeneous calorimeters for hadron energy measurement, the large differences in the response to EM and hadronic parts of the shower are a significant challenge, as is the three-dimensional segmentation. This is still requiring substantial R&D, including the search for affordable materials. In non-accelerator physics experiments or at neutrino beams, homogeneous calorimeters, where the sensitive medium can be water or ice, scintillator, a noble liquid or the atmosphere itself, are used to detect both EM and hadronic showers.

Comprehensive tables of particle-physics calorimeters are given as Appendix C in Ref. [356].

35.10.1.1 Energy Resolution and System Performance

The energy resolution of calorimeters is a complex observable, due to the variety of contributing processes with different energy dependencies, and response functions often not perfectly Gaussian. Nevertheless, a simplified picture is useful in practice, and in particular for EM calorimeters also numerically accurate. For hadronic calorimeters additional complications must be taken into

⁴ $X_0 = 120 \text{ g cm}^{-2} Z^{-2/3}$ to better than 5% for $Z > 23$.

⁵ $\lambda_I = 37.8 \text{ g cm}^{-2} A^{0.312}$ to within 0.8% for $Z > 15$.

See <https://pdg.lbl.gov/current/AtomicNuclearProperties> for actual values.

account. In such a simplified picture, due to the stochastic nature of shower evolution, the intrinsic calorimeter energy resolution, σ , is proportional to \sqrt{E} , as the number of charged particles, or the total ionising track length in a shower are on average proportional to the incident particle energy E . The relative resolution σ/E therefore improves with A/\sqrt{E} , where A denotes the so-called *stochastic term*. The readout system of the active medium will contribute noise to the resolution, $\sigma_N = B$, which in general is not energy-dependent. Effects that are proportional to the total deposited energy result in a *constant term*, $\sigma_C = C \cdot E$. Different sources contribute to this term, depending on the type of calorimeter. For both EM and hadronic calorimeters, imperfections of the detector, inhomogeneities such as density variations or those introduced by the detector mechanics, instabilities in time, imperfections of the readout or incorrect calibration of channels contribute. Shower leakage, which depends on particle energy, also contributes to the resolution with approximately linear dependence on energy. In non-compensating hadronic calorimeters, fluctuations of the EM fraction f_{em} from shower to shower, together with the energy dependence of the average f_{em} value, can lead to a significant constant term that often dominates over the instrumental effects. Adding up all contributions in quadrature yields the standard parameterisation of the relative energy resolution of a calorimeter:

$$\frac{\sigma}{E} = \frac{A}{\sqrt{E}} \oplus \frac{B}{E} \oplus C. \quad (35.42)$$

In particular the effects specific to hadronic showers give rise to non-Gaussian distributions of the energy response. Therefore care must be used in performance comparisons, as different parameterisations of the line shape and different definitions of the resolution are in use. In some cases, a linear rather than a quadratic addition of the stochastic and constant term may provide a better description of the energy resolution as a function of energy. It should be noted that the individual terms then lose the simplified interpretation discussed above, and care has to be taken when comparing performance based on fits to the energy dependence of the resolution.

Typically, primarily the stochastic term — which is determined by the calorimeter design in terms of material and geometry — is considered in order to describe the overall properties of a calorimeter. For the calorimeters of the multi-purpose experiments at the LHC, the stochastic terms are 3 – 10% for electromagnetic and 50 – 80% for hadronic calorimeters. In practice, the energy resolution of a calorimeter at high energies is limited by the constant term C , which in the EM case mainly reflects the precision and stability of the mechanical construction, electronic readout system and calibration. Typical constant terms are a few per-mil for EM and a few percent for hadronic calorimeters. For concrete examples and references see Tables 35.11 and 35.13.

For sampling calorimeters, the stochastic term depends on the *sampling fraction* f_{samp} , i.e. the ratio of energies deposited in the active and passive material. Also the *sampling frequency* enters, which is determined by the number N of different sampling elements present in the region in which the shower develops. The stochastic term A scales approximately with $1/\sqrt{f_{\text{samp}}}$, and for given f_{samp} and total depth, with $1/\sqrt{N}$.

While the energy resolution for single hadrons (most commonly pions) is often used as the key performance criterion for a hadronic calorimeter, it has to be noted that this value is only of limited relevance in high-energy physics experiments. In most experiments, the calorimetric measurement of hadrons is based on the combined system consisting of ECAL and HCAL. Moreover, for the physics capabilities of a detector at a high-energy particle collider, also the combined calorimetric resolution for single hadrons is not a sufficient criterion to fully characterise hadronic performance, but rather the jet energy resolution, the resolution for missing (transverse) energy, and the capability to cope with high background and pile-up levels. These quantities cannot be measured directly with prototypes in beam tests, and strongly depend on overall system aspects and reconstruction tools. However, the performance in these observables can be reliably inferred from system simulations once the simulated response to single particles and

the simulated topology of showers has been validated in detail by beam tests.

Besides energy resolution, response linearity is an important factor in the design of calorimeters. While a non-linear response for single particles can be corrected for if appropriate calibration measurements exist, such corrections deteriorate the energy resolution, in particular in the case of superposition of several showers, as it often occurs in jets. Sources for non-linearities can be intrinsic to the design, for example due to saturation effects in the active medium with increasing energy density, due to leakage, or connected to shower physics as discussed in section 35.10.3.

The energy resolution for hadrons is intrinsically limited by large event-to-event fluctuations of the shower evolution and of "invisible" components not contributing to the detector signal. It remains the limiting factor for single particles and for the high-level performance for jets and total event properties. This has motivated intense research in the past decades. One direction aims at improving the hadronic resolution by extracting additional signals to disentangle the shower composition, e.g. with so-called dual read-out methods, and is explained in the hadron calorimeter section 35.10.3. Another, so-called "particle flow" approach described below optimises the combination of measurements of individual particles in different detector components. Ideally, both methods can be combined.

35.10.1.2 Role of Simulations

Simulations have become indispensable for the design of detectors and the development of reconstruction algorithms. Since event-to-event fluctuations drive calorimeter performance, Monte Carlo techniques that accurately model the evolution of particle cascades in material are required. By far the most common computer code in use today is the *GEANT4* toolkit [357, 358], which provides a step-based simulation of the passage of particles through matter. Thanks to the relative simplicity of EM cascades, simulations of EM showers are typically highly accurate. The modelling of hadronic showers is more complex, and suffers from larger uncertainties. Significant improvement has been achieved in this area, moving from simpler parameterised models to physics-driven interaction models. From early on, detailed codes and data describing nuclear break-up and neutron transport like *CALOR* [359] or *FLUKA* [360, 361] contributed crucially to the understanding of hadron calorimetry. The simulations reproduce the general features of the substructure of hadronic showers, characterised by dense shower activity and sparser ionising track segments, and their accuracy is adequate for most purposes of quantitative design optimisations. Details of the implementation of physics models in *GEANT4* are discussed in [362].

35.10.1.3 Particle flow approach

In a typical collider experiment, the EM and hadronic calorimeter system surrounds a charged-particle tracking volume devised for momentum measurement in a magnetic field. Matching tracks to calorimetric energy deposits provides corrections for the magnetic deflection of the charged particles, necessary for the reconstruction of invariant masses in multi-jet final states, or of the total momentum imbalance. Furthermore, for charged particles the track-based measurements are far more precise for particles in jets with energies of up to several hundred GeV, so using these instead of calorimeter energies may optimise the jet energy resolution. This so-called "particle flow" approach aims at reconstructing each particle individually, using a combination of the best measurements from the detector.

About 60% of the energy in a typical jet is carried by charged particles, predominantly hadrons, 30% by photons and only 10% by long-lived neutral hadrons (K_L^0 and n), for which hadronic calorimetry is unavoidable. Assuming, as motivated by detector designs proposed for a future Higgs factory, 15%/√ E (GeV) for photons and 55%/√ E (GeV) for hadrons, then, in the ideal case, where each particle is resolved, a jet energy resolution of 19%/√ E (GeV) could be obtained. Here the dominant part (18%/√ E (GeV)) is still due to the calorimeter resolution for the neutral hadrons.

The particle flow method places high demands on the imaging

capabilities of the calorimeters, and on the pattern recognition performance of the reconstruction algorithms. Only energy deposits not associated with charged particles and not identified as photons, will be interpreted as neutral hadrons. In practice, this cannot always be done unambiguously, and mis-assignments give rise to an additional measurement uncertainty, which is called *confusion*. For simulated detectors at proposed future Higgs factories jet energy resolutions of 3–4% have been demonstrated, significantly larger than in the ideal case, but sufficient for the required efficient separation of W and Z hadronic final states.

Particle flow-like techniques were first applied in the ALEPH detector [363], which achieved a jet energy resolution of $60\%/\sqrt{E}$, or 6.2 GeV for hadronic Z decays. More recently, particle flow techniques are successfully used in the CMS experiment [364], for example improving the missing energy resolution by one third over a wide range.

The Pandora particle flow algorithm (PFA) [365] is the most developed and best performing today in the context of future lepton colliders. The algorithms make use of topological information, including the sub-structure of showers, as well as the compatibility of calorimetric and track-based measurements. In this way the purely calorimetric performance for the jet is either retained or improved. In the framework of studies for CLIC [366], it was shown that the required jet energy resolution of 3.5% can be achieved with the PF technique for jet energies up to 1500 GeV.

For the use of energy-momentum matching in the assignment of energy depositions, and for energy flow treatment of dense jets, particle flow calorimeters with their emphasis on imaging must still feature a good energy resolution. Furthermore, the neutral hadron energy uncertainty is the dominant contribution to the jet resolution for low energy jets, where particles are well separated, while at higher energies the confusion effects take over.

High granularity in all three space dimensions comparable to or smaller than the length scales of particle showers given by X_0 and ρ_M for both ECAL and HCAL brings additional advantages; for example it offers ideal conditions for the application of software compensation methods, which improves the intrinsic resolution and also reduces "confusion" [367]. A particular strength is the possibility to use topological information such as the reconstructed starting point of the shower for the estimation of leakage. Moreover, the combination of fine-grained topological reconstruction and cuts on cluster-wise timing with a precision of few tens of pico-seconds allows for powerful pile-up rejection. This extends the application range of particle flow methods towards collider environments with less benign background conditions, like multi-TeV e^+e^- collisions, and it is an asset on its own for high-intensity hadron colliders, even if particle flow methods are difficult to apply.

The performance of highly granular calorimeters depends, among others, on the particle separation and pattern recognition capabilities and on the single particle energy and timing resolution. They are thus not only optimised for energy measurement, but also for multi-dimensional shower reconstruction and particle separation in space and time.

35.10.2 Electromagnetic calorimeters

Revised October 2021 by C.L. Woody (BNL) and R.-Y. Zhu (HEP California Inst. of Technology).

The development of electromagnetic showers is discussed in the section on "Passage of Particles Through Matter" (Sec. 34 of this *Review*). Formulae are given which approximately describe average showers, but since the physics of electromagnetic showers is well understood, a detailed and reliable Monte Carlo simulation is possible. EGS4 [368] and GEANT [357] have emerged as the standards.

Electromagnetic calorimeters are devices that are designed to measure the total energy of electrons and photons by total absorption. They come in two general categories: homogeneous and sampling. In a homogeneous calorimeter, all of the particle's energy is deposited in the active detector volume and is used to produce a measurable signal (either scintillation light, Cherenkov light or charge). Homogeneous electromagnetic calorimeters are typically constructed using high density, high Z inorganic scintil-

lating crystals such as BaF₂, BGO, CsI, CsI(Tl), LYSO, NaI(Tl) and PWO, non-scintillating Cherenkov radiators such as lead glass and lead fluoride (PbF₂), or ionizing noble liquids such as liquid argon, liquid krypton or liquid xenon. The properties of some commonly used inorganic crystal scintillators can be found in Table 35.4. Total absorption homogeneous calorimeters such as those built with heavy crystal scintillators provide the best energy resolution for measuring electromagnetic showers and are generally used when the best possible performance is required, particularly at lower energies. Attention, however, needs to be paid to radiation damage in inorganic scintillators when exposed to the typical environment of high luminosity proton colliders, as discussed below and in Section 35.4.

A sampling calorimeter consists of an active medium which generates a signal and a passive medium which functions as an absorber. In this case, most of the particle's energy is deposited in the absorber and only a fraction of the energy is detected in the active medium. The ratio of energy in the sampling medium to the total energy in calorimeter is called the sampling fraction. The active medium may be a scintillator, an ionizing noble liquid, a semiconductor, or a gas ionization detector. The absorber is typically a heavy metal with a high Z such as lead, tungsten, iron, copper, or depleted uranium. The active material is interspersed with the passive absorber in a variety of ways, e.g. by using alternating plates of active material and absorber or embedding the active material, such as scintillating fibers, into the absorber. The main difficulty in this approach is extracting the signal from the active material. One possibility is a simple stack of alternating absorber and active material, which, however, usually leads to gaps for services and hence non-uniformities. This can be improved by using a so-called "spaghetti" design, where scintillating fibers are brought to the front or back of the detector and read out. This can also be done with either wavelength shifting plates or fibers, such as in a so-called "shashlik" design where wavelength shifting fibers run through the stack of alternating scintillator and absorber plates and are read out at one end, or embedding wavelength shifting fibers in the scintillating plates which are then brought out to the edges or back of the detector and read out. For ionization detectors, there is also an "accordion" design which avoids all gaps for services and where the absorber plates are folded into an accordion shape along with interspersed electrodes to collect the ionization charge [369]. While these readout schemes are generally more complicated than those for homogeneous calorimeters, the sampling calorimeter design allows the construction of large calorimeters at much lower cost than homogeneous calorimeters.

The energy resolution σ_E/E of a calorimeter can be parameterized as $a/\sqrt{E} \oplus b \oplus c/E$, where \oplus represents addition in quadrature and E and σ_E are in GeV. The stochastic term a represents statistics-related fluctuations such as intrinsic shower fluctuations, photoelectron statistics, dead material at the front of the calorimeter, and sampling fluctuations for minimum ionizing particles. For a fixed number of radiation lengths, the stochastic term a for a sampling calorimeter is expected to be proportional to $\sqrt{t/f}$, where t is plate thickness and f is sampling fraction [370–372]. The stochastic term a is typically of the order of a few percent for a homogeneous calorimeter, and is generally in the range of 8 to 20% for sampling calorimeters, depending on the sampling fraction.

The main contributions to the systematic, or constant, term b are detector non-uniformity and calibration uncertainties. In the case of hadronic cascades discussed below, non-compensation also contributes deviations from \sqrt{E} scaling. Another important contribution to the energy resolution of calorimeters that are used in high radiation environments such as high luminosity colliders is radiation damage of the active medium. Radiation damage can induce optical absorption in scintillating materials which reduces the measured light output and produces non-uniformities in light collection. This can be mitigated by developing radiation-hard active media [373], by reducing the signal path length [374] and by frequent *in situ* calibration and monitoring [73,372]. With effort, the constant term b can be reduced to below one percent. The term c is due mainly to electronic noise summed over the readout

Table 35.11: Resolution of typical electromagnetic calorimeters. E is in GeV.

Technology (Experiment)	Depth	Energy resolution	Date
NaI(Tl) (Crystal Ball)	$20X_0$	$2.7\%/E^{1/4}$	1983
$\text{Bi}_4\text{Ge}_3\text{O}_{12}$ (BGO) (L3)	$22X_0$	$2\%/\sqrt{E} \oplus 0.7\%$	1993
CsI (KTeV)	$27X_0$	$2\%/\sqrt{E} \oplus 0.45\%$	1996
CsI(Tl) (BaBar)	$16\text{--}18X_0$	$2.3\%/E^{1/4} \oplus 1.4\%$	1999
CsI(Tl) (BELLE)	$16X_0$	1.7% for $E_\gamma > 3.5$ GeV	1998
CsI(Tl) (BES III)	$15X_0$	2.5% for $E_\gamma = 1$ GeV	2010
PbWO_4 (PWO) (CMS)	$25X_0$	$3\%/\sqrt{E} \oplus 0.5\% \oplus 0.2/E$	1997
PbWO_4 (PWO) (ALICE)	$19X_0$	$3.6\%/\sqrt{E} \oplus 1.2\%$	2008
Lead glass (OPAL)	$20.5X_0$	$5\%/\sqrt{E}$	1990
Liquid Kr (NA48)	$27X_0$	$3.2\%/\sqrt{E} \oplus 0.42\% \oplus 0.09/E$	1998
Scintillator/depleted U (ZEUS)	$20\text{--}30X_0$	$18\%/\sqrt{E}$	1988
Scintillator/Pb (CDF)	$18X_0$	$13.5\%/\sqrt{E}$	1988
Scintillator fiber/Pb spaghetti (KLOE)	$15X_0$	$5.7\%/\sqrt{E} \oplus 0.6\%$	1995
Liquid Ar/Pb (NA31)	$27X_0$	$7.5\%/\sqrt{E} \oplus 0.5\% \oplus 0.1/E$	1988
Liquid Ar/Pb (SLD)	$21X_0$	$8\%/\sqrt{E}$	1993
Liquid Ar/Pb (H1)	$20\text{--}30X_0$	$12\%/\sqrt{E} \oplus 1\%$	1998
Liquid Ar/depl. U (DØ)	$20.5X_0$	$16\%/\sqrt{E} \oplus 0.3\% \oplus 0.3/E$	1993
Liquid Ar/Pb accordion (ATLAS)	$25X_0$	$10\%/\sqrt{E} \oplus 0.4\% \oplus 0.3/E$	1996

channels required to measure the shower energy (typically a few Molière radii).

The position resolution depends on the effective Molière radius and the transverse granularity of the calorimeter. Like the energy resolution, it can be factored as $a/\sqrt{E} \oplus b$, where a is the stochastic term, typically of the order of a few mm to 20 mm, and b can be as small as a fraction of mm for a dense calorimeter with fine granularity. Fine granularity also helps particle flow analysis discussed in the hadron calorimeters section below.

Electromagnetic calorimeters may also provide angular measurements for electrons and photons. This is particularly important for photon-related physics to identify the correct primary vertex, since photons are not detected by the tracking system of the overall experiment. The typical photon angular resolution is about $45 \text{ mrad}/\sqrt{E}$, which can be achieved by implementing longitudinal segmentation [369] for a sampling calorimeter or by adding a preshower detector [375] for a homogeneous calorimeter without longitudinal segmentation.

There have been many electromagnetic calorimeters built and used in particle physics experiments for a variety of applications. Table 35.11 provides a short list of the major ones used in some of the larger experiments. Also listed are calorimeter depths in radiation lengths (X_0) and the achieved energy resolution. Whenever possible, the performance of the calorimeters *in situ* is quoted, which is usually in good agreement with prototype test beam results as well as EGS or GEANT simulations, provided that all systematic effects are properly included. Details about detector design and performance can be found in Appendix C of reference [372] and Proceedings of the International Conference series on Calorimetry in High Energy Physics.

35.10.3 Hadronic calorimeters

Revised August 2021 by F. Sefkow (DESY, Hamburg) and F. Simon (Werner-Heisenberg-Inst.).

Hadronic calorimetry [356, 376, 377] is considerably more complex than electromagnetic (EM) calorimetry due to the wider range and different nature of physical processes contributing to shower development and energy deposition, which in turn are characterised by different length and time scales. Hadronic showers are initiated by inelastic strong interactions of highly-energetic charged and neutral hadrons with atomic nuclei. These interactions result in the production of secondary particles, which drive the development of the shower. Among these are energetic hadrons, as well as lower-energy nucleons, photons and nuclear fragments. Energy transferred to nuclear break-up, excitation or

recoil does not, in general, produce a signal, but remains *invisible*, and event-to-event fluctuations of this invisible energy deposit ultimately limit the resolution of hadronic calorimeters (HCALs).

The length scale of the interaction of relativistic hadrons is given by the nuclear interaction length λ_I . As discussed in Section 35.10.1, λ_I is a factor 10 to 30 larger than X_0 for common materials used in the construction of calorimeters. HCALs thus require a significantly larger geometrical depth for full containment than electromagnetic calorimeters (ECALs), albeit not by the factor suggested by the ratio of λ_I/X_0 due to the different nature of the showers. A key role is played by the production of π^0 s and their subsequent decay into two photons. These result in the formation of electromagnetic sub-showers which evolve on the scale given by the radiation length X_0 , and thus require sufficiently fine sampling of the shower activity to capture also this electromagnetic component. The two different length scales occurring in hadronic showers, and the large fluctuations of hadronic, electromagnetic and invisible activity, result in significant event-to-event variations of the energy response and of the shower topology. This topology is characterized by a lumpy structure, with compact regions of high local energy density originating from electromagnetic sub-showers, and sparser hadronic activity with minimum-ionizing hadrons.

Figure 35.31 (left) shows the distribution of the longitudinal position of the first inelastic interaction measured for pion-induced hadronic showers with the highly-granular scintillator-steel HCAL of the CALICE collaboration [378]. The figure illustrates the exponential distribution, with a slope consistent with the pion interaction length expected from the geometry and material composition of the calorimeter. This distribution is well reproduced by simulations using GEANT4 [357, 362]. Figure 35.31 (right) shows the mean longitudinal shower profile, given by the mean energy deposition in each calorimeter layer, both relative to the front face of the calorimeter (dots, without corrections for dead cells) and relative to the measured shower starting point given by the first inelastic interaction (filled histogram). The latter is much more compact than the former, which is a convolution of the latter with the distribution of shower starting point shown in the left panel of the figure. This shows that the detector depth required for adequate shower containment is significantly influenced by the fluctuations of the position of the first hadronic interaction. Detection of this position allows for an estimate of leakage from a finite calorimeter volume, and it enables stringent tests of shower evolution models. In the past years, motivated by precision needs at the next generation of e^+e^- colliders, the CALICE

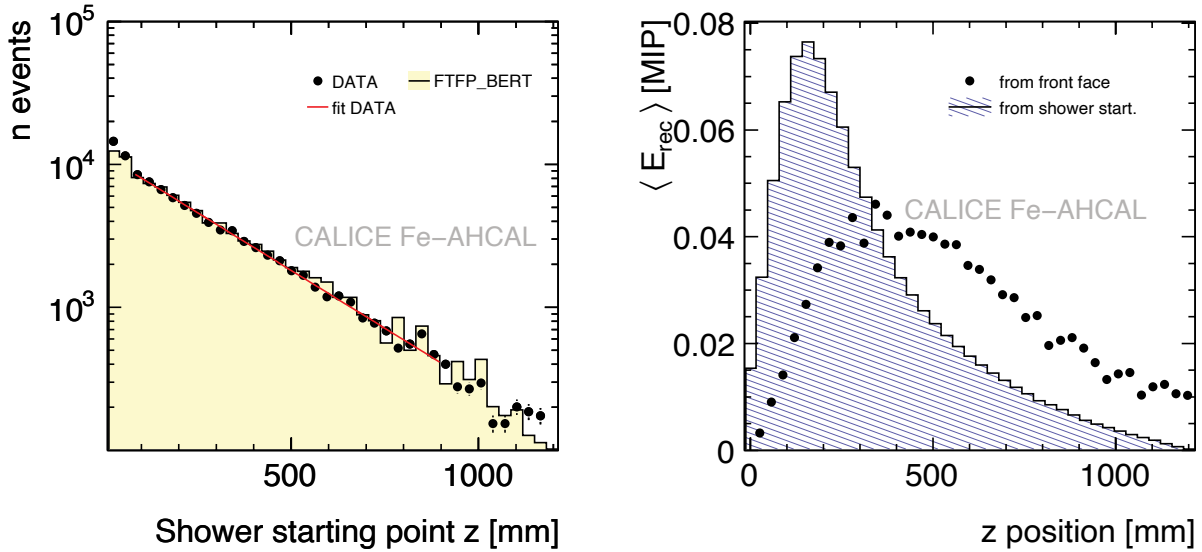


Figure 35.31: Longitudinal profile of hadronic showers induced by 45 GeV negative pions measured in the CALICE highly-granular steel-scintillator sampling calorimeter [378]. Left: Reconstructed position of the first inelastic interaction, compared to simulations (GEANT4 9.4p03, FTFP_BERT), and an exponential fit yielding a slope consistent with the expected pion interaction length. Right: Longitudinal shower profile measured from the front face of the calorimeter (dots, without corrections for dead cells) and relative to the position of the shower start given by the first inelastic interaction (filled histogram). The visible energy is given in units of the most probable energy loss of a minimum-ionizing particle (MIP). The integrals of the distributions are normalized to unity.

collaboration has constructed a number of prototypes with high 3-dimensional spatial granularity and recorded large sets of data at test beams, allowing for studies of shower evolution processes in unprecedented detail. The refined simulations support the trend to proceed from research focused on understanding the global intrinsic properties of showers, e.g. for the purpose of compensation, towards the study of detailed information, in space, time, and energy deposition type, through many and multiple readout channels.

In an inelastic hadronic collision a significant fraction f_{em} of the energy is removed from further hadronic interaction by the production of secondary π^0/η 's, whose decay photons generate high-energy electromagnetic showers. Charged secondaries (π^\pm, p, \dots) deposit energy via ionization and excitation, but also interact with nuclei, producing evaporation neutrons, spallation protons and neutrons, and heavier spallation fragments. The charged collision products produce detectable ionization, as do the showering γ -rays from the prompt de-excitation of highly excited nuclei. The recoiling nuclei generate little or no detectable signal, as mentioned previously. The neutrons lose kinetic energy in elastic collisions which generate ionization signals via recoiling protons, thermalize on a time scale of several μs , and are finally captured, with the production of more γ -rays—usually outside the acceptance gate of the electronics. Between endothermic spallation losses, nuclear recoils, and late neutron capture, a significant fraction of the hadronic energy (20%–40%, depending on the absorber and energy of the incident particle) is used to overcome nuclear binding energies and is therefore lost or “invisible.”

In a hadron-nucleus collision a large fraction of the incident energy is carried by a “leading particle” with the same quark content as the incident hadron. If the projectile is a charged pion, the leading particle is usually a pion, which can be neutral and hence contributes to the EM sector. This is not true for incident protons. The result is an increased mean hadronic fraction for incident protons.

The complexity of hadronic showers also has a significant impact on the energy measurement. In contrast to EM showers, hadronic cascade processes are characterised by the production of relatively few high-energy particles. The number multiplicity of these particles produced in hadronic interactions increases only logarithmically with energy. The lost energy and f_{em} are

highly variable from event to event, and on average increase with increasing energy [379]. Electromagnetic sub-showers typically result in a higher response than the hadronic parts of the cascade, where undetectable energy loss due to nuclear dissociation, the long time scales and the material dependence of neutron signals, as well as other effects reduce the measured signal. This difference in response is often expressed by the $\langle h/e \rangle$ ratio, a calorimeter-dependent quantity which is smaller than unity for many, but not all, HCALs. The increase of the electromagnetic fraction with energy thus introduces a non-linear contribution to the response. Combined with the significant event-by-event fluctuations between electromagnetic and hadronic fractions of the showers and between different hadronic processes the non-equality of h and e deteriorates the energy resolution of HCALs. Different strategies to address this exist, as discussed further below.

Most large HCALs are parts of complex 4π detectors at colliding beam facilities. To date, all these HCALs are sampling calorimeters. This choice is imposed by the physics of hadronic showers, both by the required depth for containment which favours high-density materials with short λ_I , and by the differences in response to electromagnetic and hadronic parts of the cascade, which are particularly severe for homogeneous calorimeters. Common absorber materials are Fe, Cu, Pb, and U, with W also used occasionally. A large variety of different active materials are used, depending on application and optimisation, from plastic scintillators (plates, tiles, bars, fibers), crystals and Cherenkov media, silicon, liquid argon (LAR), to gaseous detectors. The energy loss of particles in the active medium is either detected directly by collecting charge, or via scintillation or Cherenkov light observed with conventional photomultipliers (PMTs), photodiodes or silicon photomultipliers (SiPMs). The choice of both active and passive materials is driven by different, sometimes conflicting, constraints, including performance requirements, space and other mechanical boundary conditions, radiation tolerance, and cost considerations.

A wide range of different geometries of absorbers and sensors is used, with design choices depending on the chosen priorities of addressing these constraints, also considering the need to bring the signals to the outside of the detector while achieving a hermetic coverage and other constraints. In this context it is important to note that a classic sandwich structure with absorber plates and

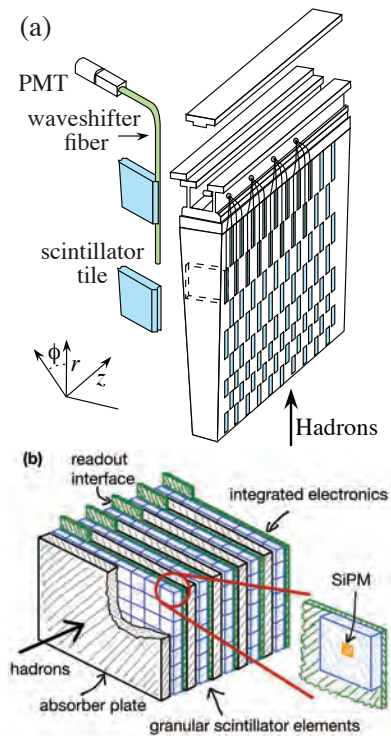


Figure 35.32: Two examples of geometrical structures of scintillator-based HCALS. (a) A wedge of the ATLAS central tile calorimeter consisting of scintillator tiles in iron, read out via wavelength-shifting fibers and PMTs [380]. The coordinate system is that of the ATLAS calorimeter within the experiment, with the z axis along the beam direction, r pointing radially outward, and ϕ being the azimuthal angle. (b) An illustration of the “SiPM-on-tile” structure used in the CALICE analogue HCAL prototype, and in the CMS High-Granularity Calorimeter (HG-CAL), highly granular calorimeters with steel absorbers and small scintillator tiles directly read out via SiPMs with embedded electronics [377, 381, 385].

active elements approximately perpendicular to the particle incidence is not required, and arbitrary orientations are viable for good calorimetric measurements, as long as channelling, meaning the extended passage of primary particles through low-density active regions, is excluded. Figure 35.32 shows two examples of plastic scintillator-based calorimeters to illustrate differences in design between coarsely-segmented and highly-granular calorimeters. The ATLAS tile calorimeter [380] uses scintillator tiles coupled to wavelength-shifting fibers which collect the light from the tiles and guide them to PMTs outside of the active region of the calorimeter. The calorimeter is segmented in ϕ (azimuthal angle) and η (pseudorapidity, defined as $\eta = -\ln \tan(\theta/2)$, where θ is the angle relative to the beam axis), with coarse longitudinal segmentation. The technological prototype of the CALICE analogue HCAL, a highly granular SiPM-on-tile calorimeter is based on scintillator tiles directly coupled to SiPMs, which, together with the front-end electronics, are embedded inside of the active volume of the calorimeter. The CMS HGCAL [381] uses the same concept in part of the detector, and in addition embeds elements for digital data concentration and power distribution in the active volume. Other detector solutions include scintillating fibres threading an absorber [382], liquid-argon-filled tubes [383] and the “accordion” LAr detector [384]. The latter has zig-zag absorber plates to minimize channelling effects; the calorimeter is hermetic (no cracks), and plates are oriented so that cascades cross the same plate repeatedly.

In particular, but not exclusively, the combination of heavy absorber materials (Pb, U) with plastic scintillators allows the construction of HCALS that have a near-equal response to electromagnetic and hadronic parts of the cascade, so-called compensat-

ing calorimeters [386]. In this first study, it was recognized that nuclear fission can amplify the hadronic signal when using uranium absorbers. However, the key drivers of compensation are the reduction of the electromagnetic response with high-Z absorbers and an increased sensitivity to neutrons, which are strongly correlated to otherwise invisible energy loss due to nuclear dissociation, with a homogeneous active medium [387–391]. Since the electromagnetic cross section increases, and the critical energy decreases with Z , and since most of the energy of an electromagnetic shower is deposited by low-energy, short-range electrons, a disproportionate fraction of the total electromagnetic energy is deposited in the absorber in the high- Z case. Hydrogenous active media, such as organic scintillators, have a high sensitivity to spallation neutrons via elastic $n-p$ scattering. The number of produced neutrons is highly correlated with the invisible energy of the hadronic cascade. Increasing the sensitivity to these particles can thus boost the visible hadronic signal. Achieving compensation requires carefully-chosen sampling fractions and frequencies, with the response to the hadronic parts of the shower also sensitive to the integration time of the electronics due to the time structure of the neutron component of the signal.

Since Cherenkov light, for example in quartz plates or fibers, or in crystals, is produced only by relativistic particles in the cascade and thus predominantly by the electromagnetic component of the shower, such media are less common in hadronic than in ECALS. Notable exceptions are applications that require high radiation tolerance, and dual-readout calorimeters which specifically exploit this feature, as discussed below.

Silicon offers high compactness, high granularity, high radiation tolerance, long-term stability and fast charge collection, and is thus an interesting active material for sampling calorimeters. A thorough overview of the development and of the features of this technology can be found in a recent review paper [392]. The first silicon-based calorimeter in a collider experiment was a HCAL, the H1 PLUG calorimeter [393] covering the very forward region of the H1 experiment at HERA. The SICAPO collaboration has demonstrated the conceptual possibility of constructing compensating HCALS using silicon sensors [394]. Silicon is currently the technology of choice for several ECALS for future Higgs factories [395–397]. It is also being used extensively in the CMS HGCAL [381] in both electromagnetic and hadronic sections, complemented by scintillator tiles with on-tile SiPM readout where the radiation levels allow.

More generally, high-granularity calorimeters play an increasingly important role, in particular motivated by the use of particle-flow algorithms for global event reconstruction (see Section 35.10.1). The associated technologies for both electromagnetic and HCALS have been pioneered by the CALICE collaboration, which has built and tested an increasingly sophisticated series of “imaging” calorimeters with a highly granular readout [398]. In the area of HCALS, this includes the scintillator-based analog HCAL [399] with the latest SiPM-on-tile technological prototype with fully-integrated electronics having approximately 22,000 channels [385], as well as digital [400] and semidigital [401] calorimeters using gas detectors, such as RPCs (Sec. 35.6.7) and micropattern gas detectors (Sec. 35.6.4), with channel counts of up to 500,000. The large numbers of channels of high-granularity calorimeters presents a significant integration challenge for full detector systems, and requires the full integration of the front-end electronics inside of the active volume of the detector, as well as very compact data concentration and interface units. The first such detector in construction for a collider experiment is the CMS HGCAL [381]. The total silicon area of this detector amounts to about 600 m², and about 240,000 SiPMs are foreseen. The calibration of such calorimeters requires the monitoring of a large number of cells, which is achieved in-situ using reconstructed track segments within hadronic showers [381, 402] or externally identified muons. For this method, the capability to detect the most probable energy loss of a minimum-ionizing particle in a single cell is essential. This is required over the full lifetime of the detector, also after the active elements have received significant radiation damage, resulting in increased noise and reduced charge or signal collection efficiency. Due to the large number of cells contribut-

ing to the measurement of one shower, the requirements on the precision of the calibration of individual cells is relaxed relative to the global energy calibration of the calorimeter.

The energy resolution of HCALs is severely affected by fluctuations between different components of the cascade, exacerbated by differences in response to purely hadronic and to electromagnetic sub-showers. In many detectors, fluctuations in the electromagnetic energy fraction, f_{em} , and the related, consequential variations in nuclear energy dissociation losses, represent the biggest single contribution to the hadron energy resolution. One strategy to address this problem is the construction of intrinsically-compensating calorimeters, which imposes stringent constraints on materials and geometries as discussed above. Compensating calorimeters are not used in current large collider experiments, and are at the moment not considered for future collider detectors. Two different strategies are presently followed to improve the energy resolution in non-compensating calorimeters: Offline weighting or software compensation in longitudinally-segmented or in highly-granular calorimeters; and dual-readout calorimetry.

Software compensation techniques exploit the fact that electromagnetic sub-showers typically have a higher spatial density than the purely hadronic parts of the cascade. Amplitude (or energy-density) dependent weights are applied in the reconstruction to reduce the effects of shower-to-shower fluctuations. These techniques were pioneered by the CDHS collaboration for a longitudinally segmented steel-plastic scintillator calorimeter [403], where an improvement of the energy resolution of 10% (at 10 GeV) to 30% (at 140 GeV) for charged pion showers was achieved. Similar techniques were successfully applied in the H1 [404] liquid argon calorimeter system resulting in a stochastic term of $51\%/\sqrt{E}$, and in the ATLAS [405] endcap calorimeters, also based on liquid argon, with an energy resolution of $84\%/\sqrt{E}$. Inspired by these approaches, a software compensation technique using the detailed spatial information provided by highly-granular calorimeters of the CALICE collaboration has been developed, achieving up to 25% improvement of the energy resolution compared to the resolution without software compensation, resulting in a stochastic term of $45\%/\sqrt{E}$ [406] in a scintillator tile calorimeter with steel absorbers. This technique has also been successfully transferred to particle-flow reconstruction [407], resulting in an improvement of the jet-energy resolution in simulated events by 8% - 15%, depending on jet energy. Highly-granular calorimeters with software compensation and particle-flow reconstruction are currently studied as the baseline configuration for several Higgs-factory detectors.

The *dual-readout method*, originally proposed by Mockett in 1983 [408], measures f_{em} event by event in parallel to the total deposited energy. It uses the fact that most of the relativistic particles in the shower originate from the electromagnetic part, and that only those produce Cherenkov light, while the signal of the hadronic part is mostly due to non-relativistic protons. In practice either two different active media, e.g. scintillator and quartz, are used to register scintillation and Cherenkov light, respectively, or the optical signals from the two processes occurring in heavy crystals are disentangled, using their different spectral, directional or timing properties.

The Cherenkov and scintillation signals, normalised to the response for electrons, are given by

$$C = [f_{em} + (h/e)_C(1 - f_{em})]E, \quad (35.43)$$

$$S = [f_{em} + (h/e)_S(1 - f_{em})]E, \quad (35.44)$$

respectively, which can be solved for the fraction f_{em} and the energy

$$E = (\xi S - C)/(\xi - 1), \quad (35.45)$$

where $\xi = [1 - (h/e)_C]/[1 - (h/e)_S]$ and $(h/e)_{C,S}$ denote the average ratios of hadronic to electromagnetic response in the Cherenkov and scintillator parts, respectively. This is illustrated in Figure 35.33, which shows their correlation for a set of simulated negative pion events [409] using FLUKA [361].

It was noted that the method demands a steep slope ξ , which implies that the scintillator read-out should be as compensating

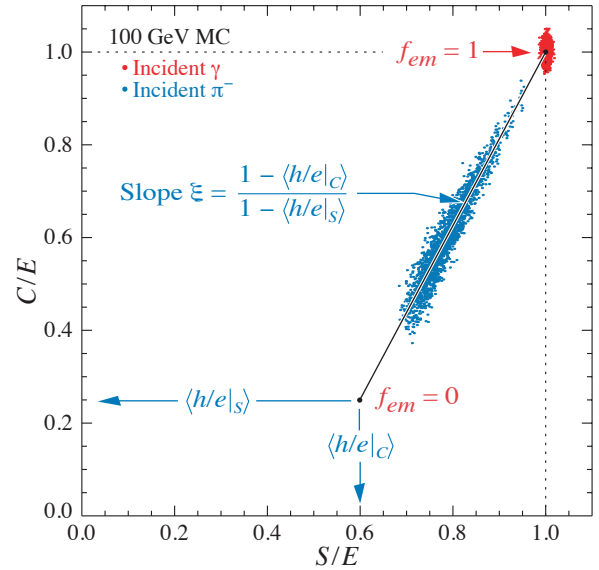


Figure 35.33: Scatter plot of Monte Carlo C/E (Cherenkov) vs S/E (scintillator) signals for individual events in a dual-readout calorimeter for 100 GeV negative pions and photons. Hadronic events are shown in blue, and scatter about the indicated event locus. Electromagnetic events cluster about $(C/E, S/E) = (1,1)$. In this case worse resolution (fewer p.e.'s) was assumed for the Cherenkov events, leading to the “elliptical” distribution.

as possible, which however reduces the room for improvement by adding Cherenkov information.

The method was tested by the DREAM/RD52 collaboration [410, 411], using a 1 ton copper matrix with embedded quartz and scintillating fibers. The value of ξ was about 3 in this detector. With this detector, a resolution of $70\%/\sqrt{E(\text{GeV})}$ was obtained for single hadrons [412]. Due to the small size of the module, this includes contributions from transverse leakage which prevent the full exploitation of key features of dual readout, and thus underestimates the potential of the method.

The separate Cherenkov read-out evidently provides excellent pion-electron separation for particle identification. In another RD52 prototype, each fiber is read out individually by SiPMs, giving also a superior transverse granularity. A fiber-based calorimeter with full solid-angle coverage requires a pointing geometry due to the limited or missing longitudinal segmentation. The resulting challenges for a mechanical design are studied in the framework of the IDEA detector concept [413].

Table 35.12 shows selected examples of the energy resolution of HCALs for single charged pions achieved in beam tests. The examples are selected to illustrate the performance achieved with different designs ranging from intrinsic compensation to software compensation and dual readout, with a focus on results by R&D projects. It should be noted that the exact values of the different resolution terms depend on the functional form used in the fit, here the addition in quadrature is used for the cases where more than just the stochastic term is quoted. The results shown in the table illustrate that (close to) compensating calorimeters with optimized sampling fraction and frequency, such as HELIOS (U-plastic scintillator) and SPACAL (Pb-plastic scintillator), achieve a very good energy resolution. The comparison with Bernardi *et al.*, which has the same Pb/scintillator ratio by volume as SPACAL, but coarser sampling in a sandwich structure, illustrates the importance of the geometrical details. Beyond the examples shown in the table, liquid argon has also been explored as an active medium, for example in the context of the SLD detector with different absorber options [418]. Due to the reduced sensitivity to neutrons in the shower, not the same resolution as for plastic-scintillator-based systems is achieved. This technology has also been used in the D0 experiment, as discussed below. The dual-readout method has the potential to reach or surpass this

Table 35.12: Energy resolution of selected hadron calorimeters for single charged hadrons obtained in beam tests.

Calorimeter	Passive	Active	Resolution	Ref.
Bernardi <i>et al.</i>	Pb	Scintillator layers	$44.2\%/\sqrt{E}$ §	[414]
CALICE AHCAL	Fe	Scintillator tiles	$44.3\%/\sqrt{E} \oplus 1.8\%$ †	[406]
CALICE W-AHCAL	W	Scintillator tiles	$57.9\%/\sqrt{E} \oplus 4.6\% \oplus 0.065/E$ §	[415]
CDHS	Fe	Scintillator layers	$58\%/\sqrt{E}$ ‡	[403]
DREAM/RD52	Pb	Scint.+ Quartz fibers	$70\%/\sqrt{E}$ *	[412]
HELIOS	U	Scintillator layers	$34\%/\sqrt{E}$ §	[416]
SPACAL	Pb	Scintillating fibers	$33.3\%/\sqrt{E} \oplus 2.2\%$ §	[417]

§ Bernardi *et al.*, CALICE W-AHCAL, HELIOS, SPACAL: (near-)compensating calorimeters.
† CALICE AHCAL: Local software compensation exploiting the high granularity of the calorimeter.
‡ CDHS: Offline weighting using longitudinal information.
* DREAM/RD52: Due to the relatively small transverse size of the detector lateral leakage was significant, deteriorating the energy resolution with respect to the full potential of the dual readout method.

performance, but would require a prototype sufficiently large for full longitudinal and transverse shower containment for an experimental demonstration. The two CALICE calorimeters shown, which use the same active elements (5 mm thick scintillator tiles) but different absorbers (21.4 mm Fe vs 10 mm W + 4 mm Fe) per layer, illustrate the impact of the absorber choice on energy resolution and reconstruction possibilities. While the tungsten-based W-AHCAL setup is very close to compensating, the steel-based AHCAL achieves a better energy resolution when software compensation is applied, profiting from the finer sampling of the electromagnetic parts of the cascade and the correction for shower-to-shower fluctuations of the electromagnetic fraction in the reconstruction. In the case of tungsten, software compensation does not significantly improve the energy resolution, as expected. The comparison of the CALICE AHCAL performance with the one of CDHS illustrates the benefits of higher granularity for software compensation techniques, but it should be noted that the absorber thickness of the latter is 25 mm, with the same scintillator thickness as in the case of CALICE.

As explained in the introduction, in most high-energy physics experiments, the HCAL follows after an ECAL, making the response of the latter to hadronic cascades highly relevant for the overall performance of the combined ECAL HCAL system. For scenarios where the electromagnetic and the HCAL have very different $\langle h/e \rangle$, as is typically the case for crystal-based ECALS, the fluctuations of the fraction of the hadronic shower contained within the ECAL result in a significant deterioration of the energy resolution for hadrons. A deterioration of the hadronic performance also results from larger amounts of not-instrumented material, e.g. supports and services, between electromagnetic and hadronic sections. In particle-flow calorimeters, a large value of the λ_I/X_0 ratio of the absorber material, like in tungsten, maximises the longitudinal separation of electromagnetic and hadronic showers. This is reflected in the design of particle-flow-based detector concepts for future Higgs Factories.

Table 35.13 summarizes the single hadron energy resolution obtained from test beams of the combined ECAL and HCAL systems of the large multi-purpose experiments at HERA, the Tevatron and at the LHC. These systems are examples of different optimization strategies. D0 and ZEUS are near-compensating systems with the same technology in ECAL and HCAL emphasizing hadronic performance. ATLAS and H1 use sampling ECALS with good electromagnetic resolution and weighting techniques exploiting longitudinal and transverse shower information for hadronic energy reconstruction. CMS, with a crystal ECAL and a scintillator-brass HCAL, prioritizes electromagnetic performance, with very different $\langle h/e \rangle$ in the electromagnetic and hadronic system. Of the detectors shown in the table, CMS has the best electromagnetic resolution by a comfortable margin, but consequently the weakest hadronic resolution. The best hadronic performance is achieved with the compensating calorimeter of ZEUS, which however has a weaker electromagnetic performance than the other calorimeter systems shown here. It should be noted that an excellent single-hadron resolution in general does not fully

propagate into the jet-energy performance. Inactive material in front of the calorimeter can significantly worsen the energy resolution for jets, with an impact in particular on lower-energy particles. For example, the core of the invariant mass distribution of hadronically-decaying Z^0 bosons measured in ZEUS, which had a superconducting coil in front of the calorimeter, is well described by a Gaussian with a σ of 6 GeV [425], approximately 40% wider than would be expected for a jet-energy resolution that is identical to the single-hadron performance.

35.10.4 Free electron drift velocities in liquid ionization chambers

Revised August 2009 by W. Walkowiak (Siegen U.).

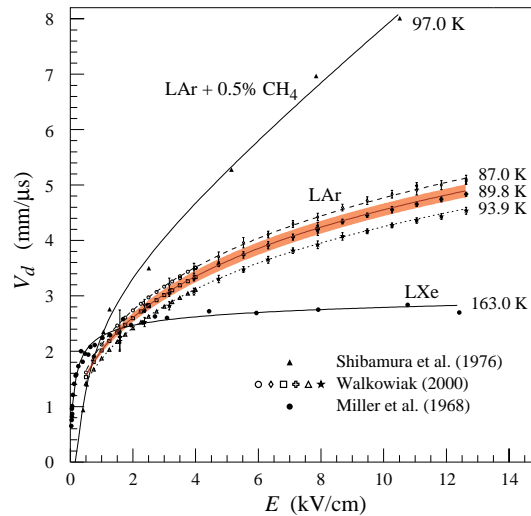


Figure 35.34: Drift velocity of free electrons as a function of electric field strength for LAr [284], LAr + 0.5% CH₄ [426] and LXe [427]. The average temperatures of the liquids are indicated. Results of a fit to an empirical function [428] are superimposed. In case of LAr at 91 K the error band for the global fit [284] including statistical and systematic errors as well as correlations of the data points is given. Only statistical errors are shown for the individual LAr data points.

Drift velocities of free electrons in LAr [284] are given as a function of electric field strength for different temperatures of the medium in Fig. 35.34. The drift velocities in LAr have been measured using a double-gridded drift chamber with electrons produced by a laser pulse on a gold-plated cathode. The average temperature gradient of the drift velocity of the free electrons in LAr is described [284] by

$$\frac{\Delta v_d}{\Delta T v_d} = (-1.72 \pm 0.08) \%/\text{K}. \quad (35.46)$$

Table 35.13: Energy resolution of selected combined electromagnetic and hadronic calorimeter systems in past and present high-energy collider experiments for single hadrons. The results are taken from beam tests of prototypes with the electromagnetic calorimeter upstream of the hadronic calorimeter.

Experiment	technology (ECAL, HCAL)	Combined hadronic resolution	Reference
H1	Pb/LAr, Steel / LAr	$46\%/\sqrt{E} \oplus 2.6\% \oplus 0.73/E$	[419]
ZEUS	depleted U / plastic scintillator	$35\%/\sqrt{E}$	[420]
CDF	Pb/plastic scint., Steel/plastic scint.	$68\%/\sqrt{E} \oplus 4.1\%$	[421]
D0	depleted U / LAr	$44.6\%/\sqrt{E} \oplus 3.9\%$	[422]
ATLAS	Pb/LAr, Steel/plastic scintillator	$52\%/\sqrt{E} \oplus 3.0\% \oplus 1.6/E$	[423]
CMS	PbWO ₄ , brass/plastic scintillator	$84.7\%/\sqrt{E} \oplus 7.4\%$	[424]

Previous measurements [426, 427, 429, 430] range from 13% higher [427] to 18% lower [429] than these measurements. They used different techniques and show drift velocities for free electrons which cannot be explained by the temperature dependence mentioned above.

Drift velocities of free electrons in LXe [426] as a function of electric field strength are also displayed in Fig. 35.34. The drift velocity saturates for $|E| > 3$ kV/cm, and decreases with increasing temperature for LXe as well as measured e.g. by [431].

The addition of small concentrations of other molecules like N₂, H₂ and CH₄ in solution to the liquid typically increases the drift velocities of free electrons above the saturation value [426, 429], see example for CH₄ admixture to LAr in Fig. 35.34. Therefore, actual drift velocities are critically dependent on even small additions or contaminations.

35.11 Accelerator-based neutrino detectors

Written by M.O. Wascko (Imperial Coll. London). Minor revision in October 2021 by F. Pietropaolo (CERN; INFN, Padua) and S.H. Pordes (FNAL).

35.11.1 Introduction

Accelerator-based neutrino experiments span many orders of magnitude in neutrino energy, from a few MeV to hundreds of GeV. This wide range of neutrino energy is driven by the many physics applications of accelerator-based neutrino beams. Foremost among them is neutrino oscillation, which varies as the ratio L/E_ν , where L is the neutrino baseline (distance traveled), and E_ν is the neutrino energy. But accelerator-based neutrino beams have also been used to study the nature of the weak interaction, to probe nucleon form factors and structure functions, and to study nuclear structure.

The first accelerator-based neutrino experiment used neutrinos from the decays of high energy pions in flight to show that the neutrinos emitted from pion decay are different from the neutrinos emitted by beta decay [432]. The field of accelerator-based neutrino experiments would likely not have expanded beyond this without Simon van der Meer's invention of the magnetic focusing horn [433], which significantly increased the flux of neutrinos aimed toward the detector. In this mini-review, we focus on experiments employing decay-in-flight beams—pions, kaons, charmed mesons, and taus—producing fluxes of neutrinos and antineutrinos from ~ 10 MeV to ~ 100 GeV.

Neutrino interactions with matter proceed only through the weak interaction, making the cross section extremely small and requiring high fluxes of neutrinos and large detector masses in order to achieve satisfactory event rates. Therefore, neutrino detector design is a balancing act taking into account sufficient numbers of nuclear targets (often achieved with inactive detector materials), adequate sampling/segmentation to ensure accurate reconstruction of the tracks and showers produced by neutrino-interaction secondary particles, and practical readout systems to allow timely analysis of data.

35.11.2 Signals and Backgrounds

The neutrino interaction processes available increase with increasing neutrino energy as interaction thresholds are crossed; in general neutrino-interaction cross sections grow with energy; for a detailed discussion of neutrino interactions see [434]. The multiplicity of secondary particles from each interaction process grows in complexity with neutrino energy, while the forward-boost due to increasing E_ν compresses the occupied phase space in the lab frame, impacting detector designs. Because decay-in-flight beams produce neutrinos at well-defined times, leading to very small duty factors, the predominant backgrounds usually stem from unwanted beam-induced neutrino interactions, i.e. neutrinos interacting via other processes than the one being studied. A noteworthy exception is time projection chambers, wherein the long drift times can admit substantially more cosmic backgrounds than most other detection methods. Cosmic backgrounds are more rare at higher energies because the secondary particles produced by neutrino interactions yield detector signals that resemble cosmic backgrounds less and less.

Below, we describe a few of the dominant neutrino interaction processes, with a focus on the final state particle content and topologies.

35.11.2.1 Charged-Current Quasi-Elastic Scattering and Pion Production

Below ~ 2 GeV neutrino energy, the dominant neutrino-nucleus interaction process is quasi-elastic (QE) scattering. In the charged current (CC) mode, the CCQE base neutrino reaction is $\nu_\ell n \rightarrow \ell^- p$, where $\ell = e, \mu, \tau$, and similarly for antineutrinos, $\bar{\nu}_\ell p \rightarrow \ell^+ n$. The final state particles are a charged lepton, and perhaps a recoiling nucleon if it is given enough energy to escape the nucleus. Detectors designed to observe this process should have good single-particle track resolution for muon neutrino interactions, but should have good μ/e separation for electron neutrino interactions. Because the interaction cross section falls sharply with Q^2 , the lepton typically carries away more of the neutrino's kinetic energy than the recoiling nucleon. The fraction of backward-scattered leptons is large, however, so detectors with 4π coverage are desirable. The dominant backgrounds in this channel tend to come from single pion production events in which the pion is not detected.

Near 1 GeV, the quasi-elastic cross section is eclipsed by pion production processes. A typical single pion production (CC1 π) reaction is $\nu_\ell n \rightarrow \ell^- \pi^+ n$, but many more final state particle combinations are possible. Single pion production proceeds through the coherent channel and many incoherent processes, dominated by resonance production. With increasing neutrino energy, higher-order resonances can be excited, leading to multiple pions in the final state. Separating these processes from quasi-elastic scattering, and indeed from each other, requires tagging, and ideally reconstructing, the pions. Since these processes can produce neutral pions, electromagnetic (EM) shower reconstruction is more important here than it is for the quasi-elastic channel. The predominant backgrounds for pion production change with increasing neutrino energy. Detection of pion processes is also complicated because near threshold the quasi-elastic channel creates pion backgrounds through final state interactions of the recoiling nucleon, and at higher energies backgrounds come from

migration of multiple pion events in which one or more pions is not detected.

35.11.2.2 Deep Inelastic Scattering

Beyond a few GeV, the neutrino has enough energy to probe the nucleon at the parton scale, leading to deep inelastic scattering (DIS). In the charged-current channel, the DIS neutrino reaction is $\nu_\ell N \rightarrow \ell^- X$, where N is a nucleon and X encompasses the entire recoiling hadronic system. The final state particle reconstruction revolves around accurate reconstruction of the lepton momentum and containment and reconstruction of the hadronic shower energy. Because of the high neutrino energies involved, DIS events are very forward boosted, and can have extremely long particle tracks. For this reason, detectors measuring DIS interactions must be large to contain the hadronic showers in the detector volume.

35.11.2.3 Neutral Currents

Neutrino interactions proceeding through the neutral current (NC) channel are identified by the lack of a charged lepton in the final state. For example, the NC elastic reaction is $\nu_\ell N \rightarrow \nu_\ell N$, and the NC DIS reaction is $\nu_\ell N \rightarrow \nu_\ell X$. NC interactions are suppressed relative to CC interactions by a factor involving the weak mixing angle; the primary backgrounds for NC interactions come from CC interactions in which the charged lepton is misidentified.

35.11.3 Instances of Neutrino Detector Technology

Below we describe many of the actual detectors that have been built and operated for use in accelerator-based neutrino beams.

35.11.3.1 Spark Chambers

In the first accelerator-based neutrino beam experiment, Lederman, Schwartz, and Steinberger [432] used an internally-triggered spark chamber detector, filled with 10 tons of Al planes and surrounded by external scintillator veto planes, to distinguish muon tracks from electron showers, and hence muon neutrinos from electron neutrinos. The inactive Al planes served as the neutrino interaction target and as radiators for EM shower development. The detector successfully showed the presence of muon tracks from neutrino interactions. It was also sensitive to the hadronic showers induced by NC interactions, which were unknown at the time. In 1963, CERN also built and ran a large (20 ton) Al plane spark chamber in a wideband beam based on the PS accelerator [435]. More than a decade later, the Aachen-Padova [436] experiment at CERN employed a 40 ton Al spark chamber in the PS-WBB.

35.11.3.2 Bubble Chambers

Several large bubble chamber detectors were employed as accelerator neutrino detectors in the 1970s and 80s, performing many of the first studies of the properties of the weak interaction. Bubble chambers provide exquisite granularity in the reconstruction of secondary particles, allowing very accurate separation of interaction processes. However, the extremely slow and labor-intensive acquisition and analysis of the data from photographic film led to them being phased out in favor of electronically read out detectors.

The Gargamelle [437] detector at CERN used Freon and propane gas targets to make the first observation of neutrino-induced NC interactions and more. The BEBC [438] detector at CERN was a bubble chamber that was alternately filled with liquid hydrogen, deuterium, and a neon-hydrogen mixture; BEBC was also outfitted with a track-sensitive detector to improve event tagging, and sometimes used with a small emulsion chamber. The SKAT [439] Freon bubble chamber was exposed to wideband neutrino and antineutrino beams at the Serpukhov laboratory in the former Soviet Union. A series of American bubble chambers in the 1970's and 1980's made measurements on free nucleons that are still crucial inputs for neutrino-nucleus scattering predictions. The 12-foot bubble chamber at ANL [440] in the USA used both deuterium and hydrogen targets, as did the 7-foot bubble chamber at BNL [441]. Fermilab's 15 foot bubble chamber [442] used deuterium and neon targets.

35.11.3.3 Iron Tracking Calorimeters

Because of the forward boost of high energy interactions, long detectors made of magnetized iron interspersed with active de-

tector layers have been very successfully employed. The long magnetized detectors allow measurements of the momentum of penetrating muons. The iron planes also act as shower-inducing layers, allowing separation of EM and hadronic showers; the large number of iron planes provide enough mass for high statistics and/or shower containment. Magnetized iron spectrometers have been used for studies of the weak interaction, measurements of structure functions, and searches for neutrino oscillation. Non-magnetized iron detectors have also been successfully employed as neutrino monitors for oscillation experiments and also for neutrino-nucleus interaction studies.

The Caltech-Fermilab counter (CITF) [440] combined a 92 ton iron-scintillator target-calorimeter detector with a downstream toroidal magnet to perform early studies of weak interactions—including observations of neutral currents. The CDHS [443] detector used layers of magnetized iron modules interspersed with wire drift chambers, with a fiducial mass of 1250 t, to detect neutrinos in the range 10–200 GeV. Within each iron module, 5 cm (or 15 cm) iron plates were interspersed with scintillation counters. The MINOS [444] detectors, a near detector of 980 t at FNAL and a far detector of 5500 t in the Soudan Underground Laboratory (SUL), were functionally identical magnetized iron calorimeters, comprised of iron plates interleaved with layers of 4 cm wide plastic scintillator strips in alternating orientations. The T2K [445] on-axis detector, INGRID, consists of 16 non-magnetized iron scintillator sandwich detectors, each with nine 6.5 cm iron plane (7.1 t total) interspersed between layers of 5 cm wide plastic scintillator strips readout out by multi-pixel photon counters (MPPCs) coupled to WLS fibers. Fourteen of the IN-GRID modules are arranged in a cross-hair configuration centered on the neutrino beam axis.

35.11.3.4 Cherenkov Detectors

Open volume water Cherenkov detectors were originally built to search for proton decay. Large volumes of ultra-pure water were lined with photomultipliers to collect Cherenkov light emitted by the passage of relativistic charged particles. See Sec. 36.3.1 for a detailed discussion of deep liquid detectors for rare processes. The Cherenkov light, which has significant production in the visible range, appears on the walls of the detectors in distinctive ring patterns, and topological characteristics of the rings are employed to separate muon-induced rings from electron-induced with very high accuracy. As neutrino detectors, Cherenkov detectors optimize the design balance since the entire neutrino target is also active detector medium.

When used to detect \sim GeV neutrinos, the detector medium acts as a natural filter for final state particles below the Cherenkov threshold; this feature has been exploited successfully by the K2K, MiniBooNE (using mineral oil instead of water), and T2K neutrino oscillation experiments. This makes event reconstruction simple and robust since electrons and muons have very different signatures, but does require making assumptions when inferring neutrino energy since not all final state particles are observed. At higher energies Cherenkov detectors become less accurate because the overlapping rings from many final state particles become increasingly difficult to resolve.

The second-generation Cherenkov detector in Japan, Super-Kamiokande [84] (Super-K), comprises 22.5 kt of water viewed by 50 cm photomultiplier tubes with 40% photocathode coverage; it is surrounded by an outer detector region viewed by 20 cm photomultipliers. Super-K is the far detector for K2K and T2K, and is described in greater detail elsewhere in this review. The K2K experiment also employed a 1 kt water Cherenkov detector in the suite of near detectors [446], with 40% photocathode coverage. The MiniBooNE detector at FNAL was a 0.8 kt [447] mineral oil Cherenkov detector, with 20 cm photomultipliers giving 10% photocathode coverage, surrounded by a veto detector also with 20 cm photomultipliers.

Table 35.14: Properties of detectors for accelerator-based neutrino beams. Revised in October 2021 by F. Pietropaolo (CERN; INFN, Padua) and S.H. Pordes (FNAL).

Name	Type	Target	Total Mass (fiducial) [t]	$\langle E_\nu \rangle$ [GeV]	Location	Dates
Lederman et al.	Spark	Al	10	[0.2-3]	BNL	1962
CERN-spark.	Spark	Al	20	1.5	CERN	1963
Serpukhov	Spark	Al	20	[3-30]	IHEP	1974-82
Aachen-Padova	Spark	Al	40(20)	1.4	CERN	1976-77
Gargamelle	Bubble	Freon	12	[1-10]	CERN	1970-79
BEBC	Bubble	H,D,Ne-H	2-42	[50-150] & 20	CERN	1977-84
SKAT	Bubble	Freon	8	7	IHEP	1976-1987
ANL-12ft	Bubble	H,D	1-2	0.5	ANL	1970
BNL-7ft	Bubble	HD	0.4-0.9	1.3,3	BNL	1976-82
Fermilab-15ft	Bubble	D, Ne	1,20	[50-180] & [25-100]	FNAL	1973-92
CITF	Iron	Fe	92	[50-180]	FNAL	1974-83
CDHS	Iron	Fe	1250(520)	10-200	CERN	1976-84
MINOS	Iron	Fe	980(23.7), 5.5k (4.2k)	3	FNAL, SUL	2005-2012
MINOS+	Iron	Fe	980, 5.5k	4-10	FNAL, SUL	2013-2016
INGRID	Iron	Fe	160	0.6-3	J-PARC	2010-
Super-Kamiokande	Cherenkov	H ₂ O	50k (22.5k)	0.6	Kamioka	1996-
HyperK	Cherenkov	H ₂ O	260k(190k)	0.6	Kamioka	2027-
K2K-1kt	Cherenkov	H ₂ O	25	0.8	KEK	1998-2004
MiniBooNE	Cherenkov	CH ₂	818(440)	0.5	FNAL	2002-19
HWPF	Scintillation	CH ₂ , Fe	160	[50-180]	FNAL	1974-78
LSND	Scintillation	CH ₂	167	0.003-0.06	LANL	1993-1998
NOvA	Scintillation	CH ₂	300, 14k	2	FNAL,Ash River	2014-
SciBar	Scintillation	CH	15(9.5)	0.6	KEK	2003-2004
SciBooNE,	Scintillation	CH	15(9.5)	0.8	FNAL	2007-08
ICARUS	LArTPC	Ar	760(476)	17	LNGS	2006-12
ICARUS	LArTPC	Ar	760(476)	0.8	FNAL	2020-
Argoneut	LArTPC	Ar	0.025	3	FNAL	2009-10
MicroBooNE	LArTPC	Ar	170(85)	0.8	FNAL	2014-
DUNE	LArTPC	Ar	70(40)	3	FNAL	2026-
FNAL-E-531	Emulsion	Ag, Br	0.009	22	FNAL	1984
CHORUS	Emulsion	Ag, Br	0.8	27	CERN	1994-97
DONuT	Emulsion	Fe	0.26	53	FNAL	1997
OPERA	Emulsion	Pb	1.25k	17	LNGS	2008-12
NINJA	Emulsion	Fe	0.002(0.001)	0.6	J-PARC	2015-
CHARM	Hybrid	CaCO ₃	(27),156(122)	20	CERN	1978-84
CHARM-II	Hybrid	glass	692	20	CERN	1984-91
BNL-E-734	Hybrid	CH ₂	172	1.3	BNL	1981-86
BNL-E-776	Hybrid	concrete	240	1.4	BNL	1986
NOMAD	Hybrid	CH	2.9(2.7)	27	CERN	1995-98
CCFR	Hybrid	Fe	690	[30-260]	FNAL	1985-88
NuTeV	Hybrid	Fe	690	[70-180]	FNAL	1996-97
MINERvA	Hybrid	CH,H ₂ O,Fe,Pb,C,He	8	3.8	FNAL	2010-19
T2K-ND280	Hybrid	CH,H ₂ O	2	0.6	J-PARC	2010-

35.11.3.5 Scintillation Detectors

Liquid and solid scintillator detectors also employ fully (or nearly fully) active detector media. Typically organic scintillators, which emit into the ultraviolet range, are dissolved in mineral oil or plastic and read out by photomultipliers coupled to wavelength shifters (WLS). Open volume scintillation detectors lined with photomultipliers are conceptually similar to Cherenkov detectors, although energy reconstruction is calorimetric in nature as opposed to kinematic (see also Sec. 36.3.1). For higher energies and higher particle multiplicities, it becomes beneficial to use segmented detectors to help distinguish particle tracks and showers from each other.

The HWPF collaboration [448] employed a 2 t liquid scintillator total-absorption hadron calorimeter followed by a magnetic spectrometer to observe neutral current events in the early days of Fermilab. The LSND [449] detector at LANL was a 130 t open volume liquid scintillator detector employed to detect relatively low energy (<300 MeV) neutrinos. The NOvA [450] detectors use segmented volumes of liquid scintillator in which the scintillation light is collected by WLS fibers in the segments that are coupled to avalanche photodiodes (APDs) at the ends of the volumes. The

NOvA far detector, located in Ash River, MN, is comprised of 896 layers of 15.6 m long extruded PVC scintillator cells for a total mass of 14 kt; the NOvA near detector is comprised of 214 layers of 4.1 m scintillator volumes for a total mass of 300 t. Both are placed in the NuMI beamline at 0.8° off-axis. The SciBar (Scintillation Bar) detector was originally built for K2K at KEK in Japan and then re-used for SciBooNE [451] at FNAL. SciBar used plastic scintillator strips with 1.5 cm×2.5 cm rectangular cross section, read out by multianode photomultipliers (MAPMTs) coupled to WLS fibers, arranged in alternating horizontal and vertical layers. Both SciBooNE and K2K employed an EM calorimeter downstream of SciBar and a muon range detector (MRD) downstream of that.

35.11.3.6 Liquid Argon Time Projection Chambers

Liquid argon time projection chambers (LAr-TPCs) were conceived in the 1970s as a way to achieve a fully active detector with sub-centimeter track reconstruction [452]. A massive volume of purified liquid argon is put under a strong electric field (hundreds of V/cm), so that the liberated electrons from the paths of ionizing particles can be drifted to the edge of the volume and read out, directly by collecting charge from wire planes or non-destructively

through charge induction in the wire planes. Dual-phase readout methods have also been developed, in which the charge is drifted vertically and then passed through an amplification region inside a gas volume above the liquid volume; the bottom of the liquid volume is equipped with a PMT array for detecting scintillation photons from the liquid argon. The first large scale LAr-TPC was the ICARUS T-600 module [453], comprising 760 t of liquid argon with a charge drift length of 1.5 m read out by wires with 3 mm pitch, which operated in LNGS, both standalone and also exposed to the CNGS high energy neutrino beam. The ICARUS detector has been transported to Fermilab and is being installed in an on-axis position in the Booster Neutrino Beamline, where it will also be exposed to off-axis neutrinos from the NuMI beamline. The ArgoNeUT [454] detector at FNAL, with fiducial mass 25 kg of argon read out with 4 mm pitch wires, was exposed to the NuMI neutrino and antineutrino beams. The MicroBooNE [455] detector at FNAL comprises 170 t (85t active) of liquid Ar, read out with 3 mm wire pitch, which began collecting data in the Booster Neutrino Beam Oct 2015. A LAr-TPC has also been chosen as the multi-kton detector design for the future DUNE neutrino oscillation experiment, from FNAL to Sanford Underground Research Facility .

35.11.3.7 Emulsion Detectors

Photographic film emulsions have been employed in particle physics experiments since the 1940s [456]. Thanks to advances in scanning technology and automation [457], they have been successfully employed as neutrino detectors. Emulsions are used for experiments observing CC tau neutrino interactions, where the short lifetime of the tau, $\tau_\tau = 2.90 \times 10^{-13}$ s, leading to the short mean path length, $c \times \tau = 87 \mu\text{m}$, requires extremely precise track resolution. They are employed in hybrid detectors in which the emulsion bricks are embedded inside fine-grained tracker detectors. In the data analysis, the tracker data are used to select events with characteristics typical of a tau decay in the final state, such as missing energy and unbalanced transverse momentum. The reconstructed tracks are projected back into an emulsion brick and used as the search seed for a neutrino interaction vertex.

E531 [458] at Fermilab tested many of the emulsion-tracker hybrid techniques employed by later neutrino experiments, in a detector with approximately 9 kg of emulsion target. The CHORUS [457] experiment at CERN used 1,600 kg of emulsion, in a hybrid detector with a fiber tracker, high resolution calorimeter, and muon spectrometer, to search for $\nu_\mu \rightarrow \nu_\tau$ oscillation. The DONuT [459] experiment at FNAL used a hybrid detector, with 260 kg of emulsion bricks interspersed with fiber trackers, followed by a magnetic spectrometer, and calorimeter, to make the first direct observation of tau neutrino CC interactions. The OPERA [460] [462] experiment used an automated hybrid emulsion detector, with 1,25x0 t of emulsion, to make the first direct observation of the appearance of ν_τ in a ν_μ beam. Recently, the NINJA collaboration has developed an emulsion cloud chamber detector to observe neutrinos in the J-PARC neutrino beam [463].

35.11.3.8 Hybrid Detectors

In the previous neutrino detector examples, one can point to a specific detection technology or configuration that defines a category of detectors. In this section we look at detectors that combine multiple elements or techniques, without one facet being specifically dominant or crucial; we call these detectors hybrids.

The CHARM detector [464] at CERN was built to study neutral-current interactions and search for muon neutrino oscillation. It was a fine-grained ionization calorimeter tracker with approximately 150 t of marble as neutrino target, surrounded by a magnetized iron muon system for tagging high angle muons, and followed downstream by a muon spectrometer. The CHARM II detector [465] at CERN comprised a target calorimeter followed by a downstream muon spectrometer. Each target calorimeter module consists of a 4.8 cm thick glass plate followed by a layer of plastic streamer tubes, with spacing 1 cm, instrumented with 2 cm wide pickup strips. Every fifth module is followed by a 3 cm thick scintillator layer. The total mass of the target calorimeter was 692 t.

The Brookhaven E-734 [466] detector was a tracking calorimeter made up of 172 t liquid scintillator modules interspersed with proportional drift tubes, followed by a dense EM calorimeter and a muon spectrometer downstream of that. The detector was exposed to a wideband horn-focused beam with peak neutrino energy near 1 GeV. The Brookhaven E-776 [467] experiment comprised a finely segmented EM calorimeter, with 2.54 cm concrete absorbers interspersed with planes of drift tubes and acrylic scintillation counters, with total mass 240 t, followed by a muon spectrometer.

The FNAL Lab-E neutrino detector was used by the CCFR [468] and NuTeV [469] collaborations to perform a series of experiments in the Fermilab high energy neutrino beam ($50 \text{ GeV} < E_\nu < 300 \text{ GeV}$). The detector was comprised of six iron target calorimeter modules, with 690 t total target mass, followed by three muon spectrometer modules, followed by two drift chambers. Each iron target calorimeter module comprised 5.2 cm thick steel plates interspersed with liquid scintillation counters and drift chambers.

The NOMAD [470] detector at CERN consisted of central tracker detector inside a 0.4 T dipole magnet (the magnet was originally used by the UA1 experiment at CERN) followed by a hadronic calorimeter and muon detectors downstream of the magnet. The main neutrino target is 3 t of drift chambers followed downstream by transition radiation detectors which are followed by an EM calorimeter. NOMAD was exposed to the same wideband neutrino beam as was CHORUS.

MINERvA [471] is a hybrid detector based around a central plastic scintillator tracker: 8.3 t of plastic scintillator strips with triangular cross section read out by MAPMTs coupled to WLS fibers. The scintillator tracker is surrounded by electromagnetic and hadronic calorimetry, which is achieved by interleaving thin lead (steel) layers between the scintillator layers for the ECAL (HCAL). MINERvA is situated upstream of the MINOS near detector which acts as a muon spectrometer. Upstream of the scintillator tracker is a nuclear target region containing inactive layers of C (graphite), Pb, Fe (steel), and O (water). MINERvA's physics goals span a wide range of neutrino-nucleus interaction studies, from form factors to nuclear effects.

T2K [445] in Japan employs two near detectors at 280 m from the neutrino beam target, one centered on the axis of the horn-focused J-PARC neutrino beam and one placed 2.5° off-axis. The on-axis detector, INGRID, is described above. The 2.5° off-axis detector, ND280, employs the UA1 magnet (at 0.2 T) previously used by NOMAD. Inside the magnet volume are three separate detector systems: the trackers, the Pi0 Detector (P0D), and several ECAL modules. The tracker detectors comprise two fine-grained scintillator detectors (FGDs), read out by MPPCs coupled to WLS fibers, interleaved between three gas TPCs read out by micro-megas planes. The downstream FGD contains inactive water layers in addition to the scintillators. Upstream of the tracker is the P0D, a sampling tracker calorimeter with active detector materials comprising plastic scintillator read out by MPPCs and WLS fibers, and inactive sheets of brass radiators and refillable water modules. Surrounding the tracker and P0D, but still inside the magnet, are lead-scintillator EM sampling calorimeters.

35.11.4 Outlook

Detectors for accelerator-based neutrino beams have been in use, and constantly evolving, for six decades now. The rich program of neutrino oscillation physics and attendant need for newer and better neutrino-nucleus scattering measurements means that more neutrino detectors with broader capabilities will be needed in the coming decades.

One of the most intriguing prospects is a large volume, high pressure gas time projection chamber (HPTPC). With the prospect of megawatt power accelerator-based neutrino beams, it is entirely feasible to collect high statistics data sets with a gas target. The low momentum thresholds for particle detection, and excellent momentum resolution and particle identification capabilities, of an HPTPC would open a new window into the physics of neutrino-nucleus scattering. Moreover, the ability to change the gas mixtures in the HPTPC would allow measurements in the same detector on multiple nuclear targets, which would, in

turn, allow unprecedentedly accurate constraints and tuning of neutrino-nucleus interaction models.

35.12 Superconducting magnets for collider detectors

Revised August 2019 by Y. Makida (KEK).

35.12.1 Solenoid Magnets

In all cases SI unit are assumed, so that the magnetic field, B , is in Tesla, the stored energy, E , is in joules, the dimensions are in meters, and vacuum permeability of $\mu_0 = 4\pi \times 10^{-7}$.

The magnetic field (B) in an simple solenoid with a flux return iron yoke, in which the magnetic field is lower than magnetic saturation of < 2 T, is given by

$$B = \frac{\mu_0 n I}{L} \quad (35.47)$$

where n is the number of turns, I is the current and L is the coil length.

In an air-core solenoid case, the central field is given by

$$B(0, 0) = \mu_0 n I \frac{1}{\sqrt{L^2 + 4R^2}}, \quad (35.48)$$

where R is the coil radius.

In most cases, momentum analysis is made by measuring the circular trajectory of the passing particles according to $p = mv = qrB$, where p is the momentum, m the mass, q the charge, r the bending radius. The sagitta, s , of the trajectory is given by

$$s = q B \ell^2 / 8p, \quad (35.49)$$

where ℓ is the path length in the magnetic field. In a practical momentum measurement in colliding beam detectors, it is more effective to increase the magnetic volume than the field strength, since

$$dp/p \propto p/B \ell^2, \quad (35.50)$$

where ℓ corresponds to the solenoid coil radius R . The energy stored in the magnetic field of any magnet is calculated by integrating B^2 over all space:

$$E = \frac{1}{2\mu_0} \int B^2 dV \quad (35.51)$$

If the coil thin and inside an iron return yoke, (which is the case if it is to superconducting coil), then

$$E \approx (B^2/2\mu_0)\pi R^2 L. \quad (35.52)$$

For a detector in which the calorimetry is outside the aperture of the solenoid, the coil must be transparent in terms of radiation and absorption lengths. This usually means that the superconducting solenoid and its cryostat is of minimum real thickness and is made of a material with long radiation length. There are two major contributors to the thickness of a thin solenoid:

1. The conductor consisting of the current-carrying superconducting material (usually Nb-Ti/Cu) and the quench protecting stabilizer (usually aluminum) are wound on the inside of a structural support cylinder (usually aluminum alloy). The coil thickness scales as $B^2 R$, so the thickness in radiation lengths (X_0) is

$$t_{\text{coil}}/X_0 = (R/\sigma_h X_0)(B^2/2\mu_0), \quad (35.53)$$

where t_{coil} is the physical thickness of the coil, X_0 the average radiation length of the coil/stabilizer material, and σ_h is the hoop stress in the coil [472]. $B^2/2\mu_0$ is the magnetic pressure. In large detector solenoids, the aluminum stabilizer and support cylinders dominate the thickness; the superconductor (Nb-Ti/Cu) contributes a smaller fraction. The main coil and support cylinder components typically contribute about 2/3 of the total thickness in radiation lengths.

2. Another contribution to the material comes from the outer cylindrical shell of the vacuum vessel. Since this shell is susceptible to buckling collapse, its thickness is determined by the diameter, length and the modulus of the material of which it is fabricated. The outer vacuum shell represents about 1/3 of the total thickness in radiation length.

35.12.2 Properties of collider detector magnets

The physical dimensions, central field stored energy and thickness in radiation lengths normal to the beam line of the superconducting solenoids associated with the major collider are given in Table 35.15 [473]. Fig. 35.35 shows thickness in radiation lengths as a function of $B^2 R$ in various collider detector solenoids.

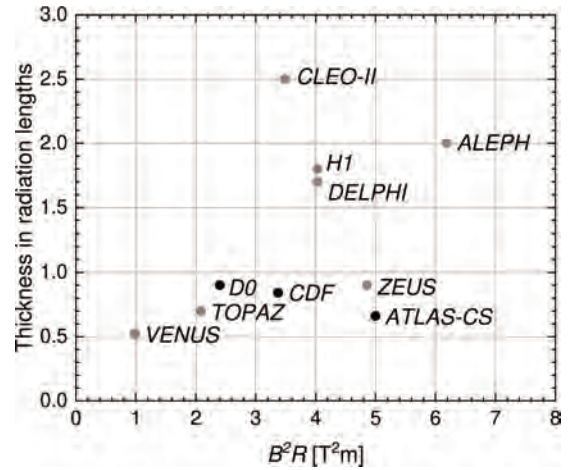


Figure 35.35: Magnet wall thickness in radiation length as a function of $B^2 R$ for various detector solenoids. Gray entries are for magnets no longer in use.

The ratio of stored energy to cold mass (E/M) is a useful performance measure. It can also be expressed as the ratio of the stress, σ_h , to twice the equivalent density, ρ , in the coil [472]:

$$\frac{E}{M} = \frac{E}{\rho 2\pi t_{\text{coil}} RL} \approx \frac{\sigma_h}{2\rho} \quad (35.54)$$

The E/M ratio in the coil is approximately equivalent to H ,^{||} the enthalpy of the coil, and it determines the average coil temperature rise after energy absorption in a quench:

$$E/M = H(T_2) - H(T_1) \approx H(T_2) \quad (35.55)$$

where T_2 is the average coil temperature after the full energy absorption in a quench, and T_1 is the initial temperature. E/M ratios of 5, 10, and 20 kJ/kg correspond to ~ 65 , ~ 80 , and ~ 100 K, respectively. The E/M ratios of various detector magnets are shown in Fig. 35.36 as a function of total stored energy. One would like the cold mass to be as small as possible to minimize the thickness, but temperature rise during a quench must also be minimized. An E/M ratio as large as 12 kJ/kg is designed into the CMS solenoid, with the possibility that about half of the stored energy can go to an external dump resistor. Thus the coil temperature can be kept below 80 K if the energy extraction system works well. The limit is set by the maximum temperature that the coil design can tolerate during a quench. This maximum local temperature should be < 130 K (50 K + 80 K), so that thermal expansion effects, which are remarkable beyond 80 K, in the coil are manageable less than 50 K.

35.12.3 Toroidal magnets

Toroidal coils uniquely provide a closed magnetic field without the necessity of an iron flux-return yoke. Because no field exists at the collision point and along the beam line, there is, in

^{||}The enthalpy, or heat content, is called H in the thermodynamics literature. It is not to be confused with the magnetic field intensity B/μ .

Table 35.15: Progress of superconducting magnets for particle physics detectors.

Experiment	Laboratory	B [T]	Radius [m]	Length [m]	Energy [MJ]	X/X_0	E/M [kJ/kg]
TOPAZ*	KEK	1.2	1.45	5.4	20	0.70	4.3
CDF*	Tsukuba/Fermi	1.5	1.5	5.07	30	0.84	5.4
VENUS*	KEK	0.75	1.75	5.64	12	0.52	2.8
AMY*	KEK	3	1.29	3	40	†	
CLEO-II*	Cornell	1.5	1.55	3.8	25	2.5	3.7
ALEPH*	Saclay/CERN	1.5	2.75	7.0	130	2.0	5.5
DELPHI*	RAL/CERN	1.2	2.8	7.4	109	1.7	4.2
ZEUS*	INFN/DESY	1.8	1.5	2.85	11	0.9	5.5
H1*	RAL/DESY	1.2	2.8	5.75	120	1.8	4.8
BaBar*	INFN/SLAC	1.5	1.5	3.46	27	†	3.6
D0*	Fermi	2.0	0.6	2.73	5.6	0.9	3.7
BELLE*	KEK	1.5	1.8	4	42	†	5.3
BES-III	IHEP	1.0	1.475	3.5	9.5	†	2.6
ATLAS-CS	ATLAS/CERN	2.0	1.25	5.3	38	0.66	7.0
ATLAS-BT	ATLAS/CERN	1	4.7–9.75	26	1080	(Toroid)†	
ATLAS-ET	ATLAS/CERN	1	0.825–5.35	5	2 × 250	(Toroid)†	
CMS	CMS/CERN	4	6	12.5	2600	†	12
SiD**	ILC	5	2.9	5.6	1560	†	12
ILD**	ILC	4	3.8	7.5	2300	†	13
SiD**	CLIC	5	2.8	6.2	2300	†	14
ILD**	CLIC	4	3.8	7.9	2300	†	13
FCC**		6	6	23	54000	†	12

* No longer in service
 ** Conceptual design in future
 † EM calorimeter is inside solenoid, so small X/X_0 is not a goal

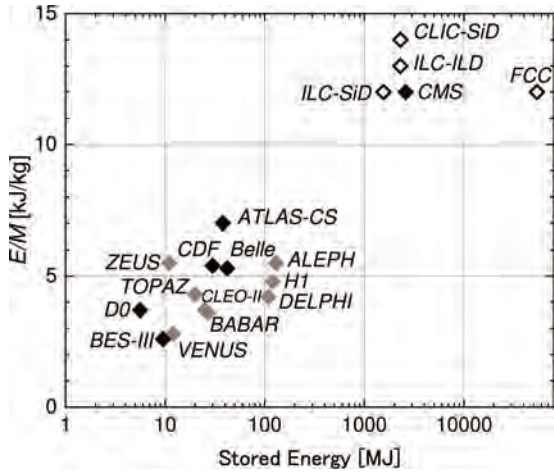


Figure 35.36: Ratio of stored energy to cold mass for major detector solenoids. Gray indicates magnets no longer in operation.

principle, no effect on the beam. On the other hand, the field profile generally has $1/r$ dependence. The particle momentum may be determined by measurements of the deflection angle combined with the sagitta. The deflection (bending) power BL is

$$BL \approx \int_{R_i}^{R_0} \frac{B_i R_i dR}{R \sin \theta} = \frac{B_i R_i}{\sin \theta} \ln(R_0/R_i), \quad (35.56)$$

where R_i is the inner coil radius, R_0 is the outer coil radius, and θ is the angle between the particle trajectory and the beam line axis. The momentum resolution given by the deflection may be expressed as

$$\frac{\Delta p}{p} \propto \frac{p}{BL} \approx \frac{p \sin \theta}{B_i R_i \ln(R_0/R_i)}. \quad (35.57)$$

The momentum resolution is better in the forward/backward (smaller θ) direction. The geometry has been found to be optimal when $R_0/R_i \approx 3-4$. In practical designs, the coil is divided into 6–12 lumped coils in order to have reasonable acceptance and

accessibility. This causes the coil design to be much more complex. The mechanical structure needs to sustain the decentering force between adjacent coils, and the peak field in the coil is 3–5 times higher than the useful magnetic field for the momentum analysis [474].

35.13 Measurement of particle momenta in a uniform magnetic field

The trajectory of a particle with momentum p (in GeV/c) and charge ze in a constant magnetic field \vec{B} is a helix, with radius of curvature R and pitch angle λ . The radius of curvature and momentum component perpendicular to \vec{B} are related by

$$p \cos \lambda = 0.3 z B R, \quad (35.58)$$

where B is in tesla and R is in meters.

The distribution of measurements of the curvature $k \equiv 1/R$ is approximately Gaussian. The curvature error for a large number of uniformly spaced measurements on the trajectory of a charged particle in a uniform magnetic field can be approximated by

$$(\delta k)^2 = (\delta k_{\text{res}})^2 + (\delta k_{\text{ms}})^2, \quad (35.59)$$

where δk = curvature error
 δk_{res} = curvature error due to finite measurement resolution

δk_{ms} = curvature error due to multiple scattering.

If many (≥ 10) uniformly spaced position measurements are made along a trajectory in a uniform medium,

$$\delta k_{\text{res}} = \frac{\epsilon}{L'^2} \sqrt{\frac{720}{N+4}}, \quad (35.60)$$

where N = number of points measured along track
 L' = the projected length of the track onto the bending plane
 ϵ = measurement error for each point, perpendicular to the trajectory.

If a vertex constraint is applied at the origin of the track, the coefficient under the radical becomes 320.

For arbitrary spacing of coordinates s_i measured along the projected trajectory and with variable measurement errors ϵ_i the curvature error δk_{res} is calculated from:

$$(\delta k_{\text{res}})^2 = \frac{4}{w} \frac{V_{ss}}{V_{ss} V_{s^2 s^2} - (V_{ss^2})^2}, \quad (35.61)$$

where V are covariances defined as $V_{s^m s^n} = \langle s^m s^n \rangle - s^m \langle s^n \rangle$ with $\langle s^m \rangle = w^{-1} \sum (s_i^m / \epsilon_i^2)$ and $w = \sum \epsilon_i^{-2}$.

The contribution due to multiple Coulomb scattering is approximately

$$\delta k_{\text{ms}} \approx \frac{(0.016)(\text{GeV}/c)z}{Lp\beta \cos^2 \lambda} \sqrt{\frac{L}{X_0}}, \quad (35.62)$$

- where p = momentum (GeV/c)
 z = charge of incident particle in units of e
 L = the total track length
 X_0 = radiation length of the scattering medium (in units of length; the X_0 defined elsewhere must be multiplied by density)
 β = the kinematic variable v/c .

More accurate approximations for multiple scattering may be found in the section on Passage of Particles Through Matter (Sec. 34 of this *Review*). The contribution to the curvature error is given approximately by $\delta k_{\text{ms}} \approx 8s_{\text{plane}}^{\text{rms}}/L^2$, where $s_{\text{plane}}^{\text{rms}}$ is defined there.

References

- [1] H. Kolanoski and N. Wermes, *Particle Detectors - Fundamentals and Applications*, Oxford University Press (2020), ISBN 978-0-19-885836-2.
- [2] T. Ferbel, *Experimental techniques in high energy physics; 1st ed.*, Frontiers in physics, Addison-Wesley, Menlo Park, CA (1987), URL <https://cds.cern.ch/record/110951>.
- [3] K. Kleinknecht, *Detectors for particle radiation* (1998), ISBN 978-0-521-64854-7.
- [4] G. Knoll, *Radiation Detection and Measurement (4th ed.)*, John Wiley, Hoboken, NJ (2010), ISBN 978-0-470-13148-0.
- [5] D. Green, *The physics of particle detectors*, Cambridge University Press, Cambridge, UK (2000), ISBN 9780521675680.
- [6] C. Leroy and P.-G. Rancoita, *Principles of radiation interaction in matter and detection*, World Scientific, Singapore (2011), ISBN 978-981-238-909-1.
- [7] C. Grupen and B. Schwartz, *Particle detectors*, Cambridge University Press, Cambridge, UK (2008), ISBN 9780521187954.
- [8] H. Spieler, *Semiconductor Detector Systems*, Oxford University Press, Oxford (2005), ISBN 978-0-19-852784-8.
- [9] K. Arisaka, Nucl. Instrum. Meth. **A442**, 80 (2000).
- [10] N. Matsunaga (ed.), *Photomultiplier Tubes: Basics and Applications*, 4th edition, Hamamatsu Photonics K.K., Hamamatsu (2017), https://www.hamamatsu.com/resources/pdf/etd/PMT_handbook_v4E.pdf.
- [11] M. Böhm *et al.*, JINST **15**, 11, C11015 (2020).
- [12] M. J. Minot *et al.*, Nuovo Cim. C **43**, 1, 11 (2020).
- [13] A. Braem *et al.*, Nucl. Instrum. Meth. **A518**, 574 (2004).
- [14] S. Korpar *et al.*, Nucl. Instrum. Meth. A **766**, 145 (2014).
- [15] R. Arnold *et al.*, Nucl. Instrum. Meth. **A314**, 465 (1992).
- [16] P. Mangeot *et al.*, Nucl. Instrum. Methods **A216**, 79 (1983).
- [17] R. Apsimon *et al.*, IEEE Trans. **NS33**, 112 (1986).
- [18] R. Arnold *et al.*, Nucl. Instrum. Meth. **A270**, 255 (1988).
- [19] D. Aston *et al.*, Nucl. Instrum. Meth. **A283**, 582 (1989).
- [20] R. Haitz *et al.*, J. Appl. Phys. **36**, 3123 (1965).
- [21] R. McIntyre, IEEE Trans. Electron Devices **13**, 164 (1966).
- [22] H. Dautet *et al.*, Applied Optics, **32**, 3894 (1993).
- [23] Perkin-Elmer Optoelectronics, *Avalanche Photodiodes: A User's Guide*, (2003).
- [24] P. Buzhan *et al.*, Nucl. Instrum. Meth. **A504**, 48 (2003).
- [25] Z. Sadygov *et al.*, Nucl. Instrum. Methods **A504**, 301 (2003).
- [26] V. Golovin and V. Savelev, Nucl. Instrum. Meth. **A518**, 560 (2004).
- [27] F. Simon, Nuclear Instruments and Methods in Physics Research Section A: Accelerators, Spectrometers, Detectors and Associated Equipment **926**, 85–100 (2019), ISSN 0168-9002, URL <http://dx.doi.org/10.1016/j.nima.2018.11.042>.
- [28] S. Korpar *et al.*, Nucl. Instrum. Meth. **A766**, 107 (2014).
- [29] R. H. Pots *et al.*, Nucl. Instrum. Meth. **A940**, 254 (2019).
- [30] D. R. Schaart *et al.*, Nuclear Instruments and Methods in Physics Research Section A: Accelerators, Spectrometers, Detectors and Associated Equipment **809**, 31 (2016).
- [31] M. Petrov, M. Stapelbroek, and W. Kleinhans, Appl. Phys. Lett. **51**, 406 (1987).
- [32] M. Atac and M. Petrov, IEEE Trans. **NS36**, 163 (1989).
- [33] M. Atac *et al.*, Nucl. Instrum. Meth. **A314**, 56 (1992).
- [34] B. Korzh *et al.*, Nature Photonics **14**, 250 (2020).
- [35] J. S. Carlson *et al.*, J. Am. Chem. Soc. **139**, 28, 9621 (2017).
- [36] J.B. Birks, *The Theory and Practice of Scintillation Counting*, Pergamon, London (1964).
- [37] D. Clark, Nucl. Instrum. Meth. **117**, 1, 295 (1974).
- [38] Y. Kharzheev, Ann. Rev. Nucl. Part. **4**, 1 (2017).
- [39] S. Moser *et al.*, Rad. Phys. and Chem. **41**, 1, 31 (1993), ISSN 0969-806X.
- [40] M. Moszyński and B. Bengtson, Nucl. Instrum. Methods **158**, 1 (1979).
- [41] J. B. Birks, Proc. Phys. Soc. **A64**, 874 (1951).
- [42] D. Dexter, J. Chem. Phys. **21**, 836 (1953).
- [43] M. Hamel, *Plastic scintillators: chemistry and applications*, Springer (2021), ISBN 978-3-030-73487-9.
- [44] J. Son, D. Lee and et al., J. Korean Phys. Soc **73**, 887 (2018).
- [45] S. Lee, M. Livan and R. Wigmans, Rev. Mod. Phys. **90**, 025002 (2018).
- [46] R. C. Ruchti, Ann. Rev. Nucl. Part. **46**, 281 (1996).
- [47] C. Joram, G. Haefeli and B. Leverington, JINST **10**, 08, C08005 (2015).
- [48] D. Horstmann and U. Holm, Radiat. Phys. Chem. **41**, 1, 395 (1993), ISSN 0969-806X.
- [49] Y. Kharzheev, Phys. Part. Nucl. **50**, 1, 42 (2019).
- [50] C. Zorn, in F. Sauli, editor, "Instrumentation in high-energy physics, Advanced Series on Directions in High Energy Physics," volume 9, 218, World Scientific (1992).
- [51] CMS Collaboration, J. Instrum. **15**, 06, P06009 (2020).
- [52] K. Gillen and R. Clough, Polymer **38**, 1929 (1992).
- [53] T. Seguchi *et al.*, Radiat. Phys. Chem. **17**, 195 (1981), ISSN 0146-5724.
- [54] S.E. Derenzo, W.-S. Choong and W.W. Moses, Phys. Med. Biol. **59**, 3261 (2014).
- [55] C. Melcher and J. Schweitzer, Nucl. Instrum. Methods **A314**, 212 (1992).
- [56] D.W. Cooke *et al.*, J. Appl. Phys. **88**, 7360 (2000).
- [57] J.M. Chen *et al.*, IEEE Trans. **NS54**, 718 (2007).
- [58] J.M. Chen *et al.*, IEEE Trans. **NS54**, 1319 (2007).
- [59] E.V.D. van Loef *et al.*, Nucl. Instrum. Methods **A486**, 254 (2002).
- [60] W. Drozdowski *et al.*, IEEE Trans. **NS55**, 1391 (2008).
- [61] M.S. Alekhin *et al.*, Appl. Phys. Lett. **102**, 161915 (2013).
- [62] C. Kuntner *et al.* (Crystal Clear), Nucl. Instrum. Meth. **A493**, 131 (2002).
- [63] N. Akchurin *et al.*, Nucl. Instrum. Meth. **A595**, 359 (2008).
- [64] H. Wenzel, Journal of Physics: Conference Series **404**, 012049 (2012).
- [65] A. Benaglia *et al.*, IEEE Transactions on Nuclear Science **63**, 2, 574 (2016).

- [66] R.H. Mao, L.Y. Zhang and R.Y. Zhu, IEEE Trans. **NS59**, 2229 (2012).
- [67] R. Y. Zhu, TIPP 2017, SPPHY 213, 70 (2018).
- [68] C. Hu *et al.*, IEEE Transactions on Nuclear Science **66**, 7, 1854 (2019).
- [69] W.W. Moses, W.-S. Choong and S.E. Derenzo, Acta Physica Polonica **B7**, 725 (2014).
- [70] R.H. Mao, L.Y. Zhang and R.Y. Zhu, IEEE Trans. **NS55**, 2425 (2008).
- [71] B.D. Rooney and J.D. Valentine, IEEE Trans. **NS44**, 509 (1997).
- [72] W.W. Moses *et al.*, IEEE Trans. **NS55**, 1049 (2008).
- [73] G. Gratta, H. Newman and R. Y. Zhu, Ann. Rev. Nucl. Part. Sci. **44**, 453 (1994).
- [74] R.-Y. Zhu, in "Handbook of Particle Detection and Imaging," 1–25, Springer International Publishing (2020).
- [75] F. Yang *et al.*, IEEE Trans. **NS63**, 612 (2016).
- [76] F. Yang *et al.*, IEEE Trans. **NS64**, 665 (2017).
- [77] C. Hu *et al.*, IEEE Transactions on Nuclear Science **67**, 6, 1086 (2020).
- [78] G. Dissertori *et al.*, Nucl. Instrum. Methods **745**, 1 (2014), and references therein.
- [79] S. Ecklund, C. Field and G. Mazaheri, Nucl. Instr. and Meth. Res. Sect. **A463**, 68 (2001).
- [80] M. G. Albrow *et al.*, JINST **7**, P10027 (2012), [arXiv:1207.7248].
- [81] B. Aubert *et al.* (BaBar), Nucl. Instr. and Meth. Res. Sect. **A479**, 1 (2002), [hep-ex/0105044].
- [82] E. Torassa (Belle-II PID Group), Nucl. Instr. and Meth. Res. Sect. **A824**, 152 (2016).
- [83] G. Bayatian *et al.* (CMS), Eur. Phys. J. **C53**, 139 (2008).
- [84] Y. Fukuda *et al.* (Super-Kamiokande), Nucl. Instrum. Meth. **A501**, 418 (2003).
- [85] Proceedings of the International Workshops on Ring Imaging Cherenkov Detectors, Nucl. Instr. and Meth. Res. Sect. **A343**, 1 (1993); Nucl. Instr. and Meth. Res. Sect. **A371**, 1 (1996); Nucl. Instr. and Meth. Res. Sect. **A433**, 1 (1999); Nucl. Instr. and Meth. Res. Sect. **A502**, 1 (2003); Nucl. Instr. and Meth. Res. Sect. **A553**, 1 (2005); Nucl. Instr. and Meth. Res. Sect. **A595**, 1 (2008); Nucl. Instr. and Meth. Res. Sect. **A639**, 1 (2011); Nucl. Instr. and Meth. Res. Sect. **A766**, 1 (2014); Nucl. Instr. and Meth. Res. Sect. **A876**, 1 (2017); Nucl. Instr. and Meth. Res. Sect. **A 952**, 1 (2019).
- [86] J. Litt and R. Meunier, Ann. Rev. Nucl. Part. Sci. **23**, 1 (1973).
- [87] D. Bartlett *et al.*, Nucl. Instr. and Meth. Res. Sect. **A260**, 55 (1987).
- [88] A. Abashian *et al.*, Nucl. Instr. and Meth. Res. Sect. **A479**, 117 (2002).
- [89] B. N. Ratcliff, Nucl. Instr. and Meth. Res. Sect. **A502**, 211 (2003).
- [90] T. Iijima *et al.*, Nucl. Instr. and Meth. Res. Sect. **A548**, 383 (2005), [arXiv:physics/0504220].
- [91] B. Ratcliff and J. Va'vra, Nucl. Instrum. Meth. **A**, 163442 (2020).
- [92] W. Blum, W. Riegler, and L. Rolandi, *Particle Detection with Drift Chambers*, Springer-Verlag, Berlin (2008).
- [93] R. M. Sternheimer and R. F. Peierls, Phys. Rev. B **3**, 3681 (1971); L. Landau, J. Phys. (USSR) **8**, 201 (1944); W. W. M. Allison and J. H. Cobb, Ann. Rev. Nucl. Part. Sci. **30**, 253 (1980).
- [94] I. Smirnov, Nucl. Instrum. Meth. **A554**, 474 (2005); I. Smirnov, HEED - High Energy Electro Dynamics, <http://ismirnov.web.cern.ch/ismirnov/heed>.
- [95] L.G. Christophorou, *Atomic and Molecular Radiation Physics*, John Wiley & Sons, Hoboken (1971); J. Berkowitz, *Atomic and Molecular Photoabsorption*, Academic Press, Cambridge (2015).
- [96] F. Sauli, *Gaseous Radiation Detectors: Fundamentals and Applications*, Cambridge University Press (2014).
- [97] H. Bichsel, Nucl. Instrum. Meth. **A562**, 154 (2006).
- [98] R. Veenhof, Garfield - Simulation of Gaseous Detectors, <http://garfield.web.cern.ch/garfield/>.
- [99] Degrad - cluster size distribution and primary cluster distribution in gas mixtures for minimum ionising particles and X-rays, <http://magboltz.web.cern.ch/magboltz/>.
- [100] S. F. Biagi, Nucl. Instrum. Meth. **A421**, 1-2, 234 (1999).
- [101] S. Biagi, R. Veenhof, Magboltz - Boltzmann transport equations for electrons in gas mixtures under the influence of electric and magnetic fields, <http://magboltz.web.cern.ch/magboltz/>.
- [102] S. Mukhopadhyay and N. Majumdar, in "17th DAE-BRNS High Energy Physics Symposium," (2007), [arXiv:physics/0703009].
- [103] H. Fischle, J. Heintze and B. Schmidt, Nucl. Instrum. Meth. **A301**, 202 (1991).
- [104] M. M. F. R. Fraga *et al.*, Nucl. Instrum. Meth. A **504**, 88 (2003).
- [105] A. Peisert and F. Sauli, "Drift and diffusion of electrons in gases: A compilation (with an introduction to the use of computing program)," CERN-84-08, CERN-YELLOW-84-08 (1984).
- [106] <https://fr.lxcat.net/instructions/categories.php>.
- [107] O. Şahin, T. Z. Kowalski and R. Veenhof, Nucl. Instrum. Meth. A **768**, 104 (2014).
- [108] O. Şahin *et al.*, JINST **5**, 05, P05002 (2010); O. Şahin, JINST **16**, 03, P03026 (2021).
- [109] E. McDaniel and E. Mason, *The Mobility and Diffusion of Ions in Gases*, John Wiley & Sons, Hoboken (1973); G. Schultz, G. Charpak and F. Sauli, Rev. Phys. Appl. **12**, 1, 67 (1977).
- [110] Y. Kalkan *et al.*, JINST **10**, 07, P07004 (2015).
- [111] T. Ikeda *et al.*, JINST **15**, 07, P07015 (2020), [arXiv:2004.09706].
- [112] G.F. Knoll, *Radiation Detection and Measurement*, 3rd edition, John Wiley & Sons, New York (1999).
- [113] G. Charpak *et al.*, Nucl. Instrum. Methods **A62**, 262 (1968).
- [114] G. Charpak and F. Sauli, Ann. Rev. Nucl. Sci. **34**, 285 (1984).
- [115] G. Charpak *et al.*, Nucl. Instrum. Methods **A97**, 377 (1971).
- [116] W. Blum, W. Riegler, and L. Rolandi, *Particle Detection with Drift Chambers*, Springer-Verlag, Berlin (2008).
- [117] T. Ferbel (ed.), *Experimental Techniques in High Energy Physics*, Addison-Wesley, Menlo Park, CA (1987), see "Principles of Operation of Multiwire Proportional and Drift Chambers".
- [118] R. Veenhof, Nucl. Instrum. Meth. A **419**, 726 (1998).
- [119] G. Charpak *et al.*, Nucl. Instrum. Methods **A167**, 455 (1979).
- [120] A.H. Walenta *et al.*, Nucl. Instrum. Methods **A92**, 373 (1971).
- [121] A. Breskin *et al.*, Nucl. Instrum. Methods **A124**, 189 (1975).
- [122] A. Breskin *et al.*, Nucl. Instrum. Methods **A156**, 147 (1978).
- [123] R. Bouclier *et al.*, Nucl. Instrum. Meth. **A265**, 78 (1988), [556(1987)].

- [124] H. Drumm *et al.*, Nucl. Instrum. Methods **A176**, 333 (1980).
- [125] D.R. Nygren and J.N. Marx, Phys. Today **31N10**, 46 (1978).
- [126] C. Grupen, *Particle Detectors*, Cambridge Monographs on Particle Physics, Nuclear Physics and Cosmology, Cambridge University Press (2008).
- [127] G. F. Tassielli *et al.*, JINST **15**, 09, C09051 (2020), [arXiv:2006.02378].
- [128] M. Titov, ICFA Instrum. Bull. **26**, 002 (2004), [arXiv:physics/0403055]; M. Titov *et al.*, ICFA Instrum. Bull. **24**, 22 (2002), [hep-ex/0204005].
- [129] P. S. Baringer *et al.*, Nucl. Instrum. Meth. **A254**, 542 (1987).
- [130] J. Virdee, Phys. Reports **403**, 401 (2004).
- [131] A. Sergi, Phys. Procedia **37**, 530 (2012).
- [132] A. H. Walenta, Phys. Scripta **23**, 354 (1981).
- [133] <https://indico.cern.ch/event/1022051/>.
- [134] J. A. Kadyk, Nucl. Instrum. Meth. A **300**, 436 (1991); J. Va'vra, ICFA Instrum. Bull. **24**, 1 (2002).
- [135] M. Aleksa *et al.*, Nucl. Instrum. Meth. **A446**, 435 (2000).
- [136] A. Oed, Nucl. Instrum. Meth. **A263**, 351 (1988).
- [137] F. Sauli, Nucl. Instrum. Meth. **A386**, 531 (1997).
- [138] Y. Giomataris *et al.*, Nucl. Instrum. Meth. **A376**, 29 (1996).
- [139] Input to the European Particle Physics Strategy no. 87 (2019), S. Dalla Torre, E. Oliveri, L. Ropelewski, M. Titov, Development of the Micro-Pattern Gaseous Detector Technologies: an overview of the CERN-RD51 Collaboration, <https://indico.cern.ch/event/765096/contributions/3295721>.
- [140] F. Sauli, *Micro-pattern gaseous detectors principles of operation and applications*, World Scientific, Singapore (2020).
- [141] R. Bouclier *et al.*, Nucl. Instrum. Meth. A **381**, 289 (1996); Y. Bagaturia *et al.*, Nucl. Instrum. Meth. A **490**, 223 (2002).
- [142] A. Bressan *et al.*, Nucl. Instrum. Meth. **A425**, 262 (1999).
- [143] S. Bachmann *et al.*, Nucl. Instrum. Meth. **A479**, 294 (2002); A. Bressan *et al.*, Nucl. Instrum. Meth. **A424**, 321 (1999).
- [144] M. Alfonsi *et al.*, Nucl. Instrum. Meth. A **671**, 6 (2012).
- [145] J. Derre *et al.*, Nucl. Instrum. Meth. A **459**, 523 (2001).
- [146] I. Giomataris *et al.*, Nucl. Instrum. Meth. A **560**, 405 (2006); S. Andriamonje *et al.*, JINST **5**, P02001 (2010).
- [147] A. Breskin *et al.*, Nucl. Instrum. Meth. **124**, 189 (1975).
- [148] J. Benlloch *et al.*, IEEE Trans. Nucl. Sci. **45**, 234 (1998).
- [149] Y. Giomataris, Nucl. Instrum. Meth. **A419**, 239 (1998).
- [150] M. Chefdeville *et al.*, Nucl. Instrum. Meth. A **556**, 490 (2006).
- [151] M. Lupberger *et al.*, IEEE Trans. Nucl. Sci. **64**, 5, 1159 (2017).
- [152] J. Leidner, F. Murtas and M. Silari, Applied Sciences **11**, 1 (2021).
- [153] A. Curioni *et al.*, Nucl. Instrum. Meth. A **849**, 60 (2017).
- [154] R. Chechik *et al.*, Nucl. Instrum. Meth. A **535**, 303 (2004); M. Alexeev *et al.*, JINST **8**, C12005 (2013).
- [155] S. Dalla Torre, Nucl. Instrum. Meth. A **639**, 111 (2011).
- [156] L. Molari *et al.*, JINST **12**, 10, P10017 (2017), [arXiv:1707.00125].
- [157] G. Bencivenni *et al.*, JINST **10**, 02, P02008 (2015), [arXiv:1411.2466].
- [158] G. Bencivenni *et al.*, JINST **15**, 09, C09034 (2020).
- [159] F. Yamane *et al.*, Nucl. Instrum. Meth. A **951**, 162938 (2020), [arXiv:1901.03836].
- [160] T. Alexopoulos *et al.*, Nucl. Instrum. Meth. A **640**, 110 (2011).
- [161] D. Abbaneo *et al.*, Nucl. Instrum. Meth. A **718**, 383 (2013).
- [162] T. Alexopoulos *et al.*, Nucl. Instrum. Meth. A **617**, 161 (2010); L. Lavezzi *et al.*, in "2017 IEEE Nuclear Science Symposium and Medical Imaging Conference," (2017), [arXiv:1803.07266].
- [163] A. Balla *et al.*, Nucl. Instrum. Meth. A **732**, 221 (2013).
- [164] J. Bortfeldt *et al.*, Nucl. Instrum. Meth. A **903**, 317 (2018), [arXiv:1712.05256].
- [165] RD51 DLC Workshop Report, RD51-NOTE-2021-002 (2021).
- [166] RD51 Collaboration: <https://rd51-public.web.cern.ch/>; S. Dalla Torre *et al.* (2018), [arXiv:1806.09955].
- [167] D.R. Nygren and J.N. Marx, Phys. Today **31N10**, 46 (1978).
- [168] J. Alme *et al.*, Nucl. Instrum. Meth. **A622**, 316 (2010), [arXiv:1001.1950].
- [169] J. Adolfsson *et al.*, Journal of Instrumentation **16**, 03, P03022 (2021), URL <https://doi.org/10.1088/1748-0221/16/03/p03022>.
- [170] N. Abgrall *et al.* (T2K ND280 TPC), Nucl. Instrum. Meth. A **637**, 25 (2011), [arXiv:1012.0865].
- [171] A. H. Walenta *et al.*, Nucl. Instrum. Meth. **161**, 45 (1979).
- [172] H. Aihara *et al.*, IEEE Trans. **NS30**, 63 (1983).
- [173] K. Dehmelt (sPHENIX), PoS **MPGD2017**, 044 (2019).
- [174] P. Colas, I. Giomataris and V. Lepeltier, Nucl. Instrum. Meth. **A535**, 226 (2004).
- [175] X. Artru, G. B. Yodh and G. Mennessier, Phys. Rev. **D12**, 1289 (1975).
- [176] J. Alozy *et al.*, Nucl. Instrum. Meth. **A961**, 163681 (2020).
- [177] M. L. Cherry *et al.*, Phys. Rev. **D10**, 3594 (1974).
- [178] B. Dolgoshein, Nucl. Instrum. Meth. **A326**, 434 (1993).
- [179] A. Andronic and J. P. Wessels, Nucl. Instrum. Meth. **A666**, 130 (2012).
- [180] S. Acharya *et al.* (ALICE), Nucl. Instrum. Meth. **A881**, 88 (2018), [arXiv:1709.02743].
- [181] M. Petris *et al.*, Nucl. Instrum. Meth. **A714**, 17 (2013).
- [182] T. Akesson *et al.* (ATLAS TRT), Nucl. Instrum. Meth. **A522**, 131 (2004).
- [183] M. Ambriola *et al.*, Nucl. Instrum. Meth. **A522**, 77 (2004).
- [184] J. Adelman (ATLAS), Nucl. Instrum. Meth. **A706**, 33 (2013).
- [185] T. Kirm (AMS 02 TRD), Nucl. Instrum. Meth. **A706**, 43 (2013).
- [186] G. M. Garibian, L. A. Gevorgian and C. Yang, Nucl. Instrum. Meth. **125**, 133 (1975).
- [187] P. Nevski, Nucl. Instrum. Meth. **A522**, 116 (2004).
- [188] J. Alozy *et al.*, Nucl. Instrum. Meth. **A927**, 1 (2019), [arXiv:1901.11265].
- [189] V. M. Grishin and S. S. Sadilov, Nucl. Instrum. Meth. **A522**, 122 (2004).
- [190] B. Beischer *et al.*, Nucl. Instrum. Meth. **A583**, 485 (2007).
- [191] A. A. Savchenko *et al.*, JINST **15**, 06, C06024 (2020).
- [192] T. Akesson *et al.* (ATLAS TRT), Nucl. Instrum. Meth. **A412**, 200 (1998).
- [193] M. Ave *et al.*, Nucl. Instrum. Meth. **A654**, 140 (2011).
- [194] M. L. Cherry, Nucl. Instrum. Meth. **A706**, 39 (2013).
- [195] J. Alozy *et al.*, J. Phys. Conf. Ser. **1690**, 1, 012041 (2020).
- [196] M. Brigida *et al.*, Nucl. Instrum. Meth. **A706**, 69 (2013).
- [197] F. Hartjes *et al.*, Nucl. Instrum. Meth. **A706**, 59 (2013).
- [198] V. V. Berdnikov *et al.*, Nucl. Instrum. Meth. **A706**, 65 (2013).

- [199] R. Santonico and R. Cardarelli, Nucl. Instrum. Meth. **187**, 377 (1981).
- [200] V. Parkhomchuck, Y. Pestov and N. Petrovykh, Nuclear Instruments and Methods **93**, 2, 269 (1971).
- [201] G. V. Fedotov, Y. N. Pestov and K. N. Putilin, in "International Conference on Instrumentation for Colliding Beam Physics," 127–131 (1982).
- [202] E. Cerron Zeballos *et al.*, Nucl. Instrum. Meth. **A374**, 132 (1996).
- [203] J. Juita *et al.*, Fire Science Reviews **1** (2012).
- [204] G. Aielli *et al.*, Nucl. Instrum. Meth. **A508**, 6 (2003).
- [205] R. Cardarelli, R. Santonico and V. Makeev, Nucl. Instrum. Meth. **A382**, 470 (1996).
- [206] R. Cardarelli, A. Di Ciaccio and R. Santonico, Nucl. Instrum. Meth. **A333**, 399 (1993).
- [207] R. Cardarelli, Sci Acta **8**, 159 (1993).
- [208] P. Camarri *et al.*, Nucl. Instrum. Meth. **A414**, 317 (1998).
- [209] L. Pontecorvo, ATLAS Muon Internal note **20** (1993).
- [210] W. Riegler, JINST **11**, 11, P11002 (2016).
- [211] R. Santonico, Nucl. Instrum. Meth. **A456**, 1 (2000).
- [212] R. Cardarelli *et al.*, JINST **8**, P01003 (2013).
- [213] G. Aielli *et al.*, JINST **9**, 09, C09030 (2014).
- [214] R. Santonico, JINST **9**, 11, C11007 (2014).
- [215] G. Aad *et al.* (ATLAS), JINST **3**, S08003 (2008).
- [216] S. Chatrchyan *et al.* (CMS), JINST **3**, S08004 (2008).
- [217] G. Aielli *et al.*, Nucl. Instrum. Meth. A **562**, 92 (2006).
- [218] A. Bertolin *et al.*, Nucl. Instrum. Meth. A **602**, 631 (2009).
- [219] Aielli, Giulio *et al.*, Eur. Phys. J. C **80**, 12, 1177 (2020).
- [220] M. Bauer *et al.*, "Anubis: Proposal to search for long-lived neutral particles in cern service shafts," (2019), [arXiv:1909.13022].
- [221] M. Bedjidian *et al.*, JINST **6**, P02001 (2011), [arXiv:1011.5969].
- [222] P. Fonte, A. Smirnitsky and M. C. S. Williams (ALICE), Nucl. Instrum. Meth. **A443**, 201 (2000).
- [223] M. Abbrescia, V. Peskov and P. Fonte, *Resistive Gaseous Detectors: Designs, Performance, and Perspectives*, Wiley (2018), ISBN 9783527340767.
- [224] W. Riegler and C. Lippmann, Nucl. Instrum. Meth. **A508**, 14 (2003).
- [225] P. Fonte (AIDA2020), "Validation of new resistive materials for RPCs," .
- [226] A. Akindinov *et al.*, Eur. Phys. J. Plus **128**, 44 (2013).
- [227] D. Belver *et al.*, Nucl. Instrum. Meth. A **602**, 687 (2009).
- [228] A. Schuttauf (FOPI), Nucl. Instrum. Meth. A **533**, 65 (2004).
- [229] M. Ablikim *et al.*, Nucl. Instrum. Meth. A **614**, 3, 345 (2010), ISSN 0168-9002.
- [230] A. Blanco *et al.*, IEEE Symposium Conference Record Nuclear Science 2004. **4**, 2356 (2004).
- [231] I. Deppner and N. Herrmann, JINST **15**, 10, C10030 (2020).
- [232] J. P. Chen *et al.*, "A white paper on solid (solenoidal large intensity device)," (2014), [arXiv:1409.7741].
- [233] M. Benoit *et al.*, Journal of Instrumentation **11** (2015).
- [234] S. An *et al.*, Nucl. Instrum. Meth. **A594**, 39 (2008).
- [235] A. Blanco *et al.*, JINST **7**, P11012 (2012).
- [236] C. Jacobaeus *et al.*, Nucl. Instrum. Meth. **A513**, 244 (2003), [arXiv:physics/0210006].
- [237] G. Aielli *et al.*, Nucl. Instrum. Meth. **A456**, 82 (2000).
- [238] G. Aielli *et al.*, Nucl. Instrum. Meth. **533**, 1, 86 (2004), ISSN 0168-9002, proceedings of the Seventh International Workshop on Resistive Plate Chambers and Related Detectors.
- [239] H. Sakai *et al.*, Nucl. Instrum. Meth. **A484**, 153 (2002).
- [240] R. Santonico, JINST **8**, P04023 (2013).
- [241] L. Lopes *et al.*, Nucl. Instrum. Meth. **A533**, 69 (2004).
- [242] R. Cardarelli, JINST **16**, 05, C05004 (2021).
- [243] C. Rubbia, "The liquid-argon time projection chamber: a new concept for neutrino detectors: CERN-EP-INT-77-8," (1977), URL <https://cds.cern.ch/record/117852>.
- [244] H. H. Chen and J. F. Lathrop, Nucl. Instrum. Meth. **150**, 585 (1978).
- [245] A. Marchionni, Ann. Rev. Nucl. Part. Sci. **63**, 269 (2013), [arXiv:1307.6918].
- [246] K. Majumdar and K. Mavrokoridis, Appl. Sciences **11**, 6, 2455 (2021), [arXiv:2103.06395].
- [247] F. Arneodo *et al.* (The ICARUS-Milano Collaboration), Phys. Rev. D **74**, 112001 (2006).
- [248] S. Amerio *et al.* (ICARUS), Nucl. Instrum. Meth. A **527**, 329 (2004).
- [249] C. Anderson *et al.* (ArgoNeuT), JINST **7**, P10019 (2012), [arXiv:1205.6747].
- [250] R. Acciarri *et al.* (MicroBooNE), JINST **12**, 02, P02017 (2017), [arXiv:1612.05824].
- [251] R. Acciarri *et al.* (LArIAT), JINST **15**, 04, P04026 (2020), [arXiv:1911.10379].
- [252] C. E. Taylor *et al.* (CAPTAIN), Nucl. Instrum. Meth. A **1001**, 165131 (2021), [arXiv:2008.11422].
- [253] A. A. Abud *et al.* (DUNE (protoDUNE-SP)) (2021), [arXiv:2108.01902].
- [254] P. Abratenko *et al.* (MicroBooNE), JINST **16**, 06, P06043 (2021), [arXiv:2011.01375].
- [255] M. Wang *et al.* (2020), [arXiv:2009.04509].
- [256] B. Abi *et al.* (DUNE), Phys. Rev. D **102**, 9, 092003 (2020), [arXiv:2006.15052].
- [257] G. Carugno *et al.* (ICARUS), Nucl. Instrum. Meth. A **292**, 580 (1990).
- [258] M. Adamowski *et al.*, JINST **9**, P07005 (2014), [arXiv:1403.7236].
- [259] C. Adams *et al.* (MicroBooNE), JINST **15**, 07, P07010 (2020), [arXiv:1910.01430].
- [260] H. Loosli, Earth and Planetary Science Letters **63**, 1, 51 (1983), ISSN 0012-821X.
- [261] P. Benetti *et al.* (WARP), Nucl. Instrum. Meth. A **574**, 83 (2007), [arXiv:astro-ph/0603131].
- [262] "Summary of Liquid Argon Properties," Accessed August 2021, URL <https://lar.bnl.gov/properties/>.
- [263] E. W. Lemmon *et al.*, "NIST Standard Reference Database 23: Reference Fluid Thermodynamic and Transport Properties-REFPROP, Version 10.0, National Institute of Standards and Technology," (2018), URL <https://www.nist.gov/srd/refprop>.
- [264] G. Bakale, U. Sowada and W. F. Schmidt, The Journal of Physical Chemistry **80**, 23, 2556 (1976).
- [265] A. Bettini *et al.* (ICARUS), Nucl. Instrum. Meth. A **305**, 177 (1991).
- [266] R. Andrews *et al.*, Nucl. Instrum. Meth. A **608**, 251 (2009).
- [267] R. Acciarri *et al.* (WArP), JINST **5**, P06003 (2010), [arXiv:0804.1217].
- [268] B. J. P. Jones *et al.*, JINST **8**, P07011 (2013), [Erratum: JINST **8**, E09001 (2013)], [arXiv:1306.4605].
- [269] R. Acciarri *et al.* (WArP), JINST **5**, P05003 (2010), [arXiv:0804.1222].

- [270] W. Jaskierny *et al.* (Fermilab-TM-2384-E), Technical Report (2006), URL <https://lss.fnal.gov/archive/test-tm/2000/fermilab-tm-2384-e.pdf>.
- [271] Sigma-Aldrich 4A, BASF Copper Getter CU-0226S.
- [272] P. Cennini *et al.*, Nucl. Instrum. Meth. A **333**, 567 (1993).
- [273] M. Miyajima *et al.*, Phys. Rev. A **9**, 1438 (1974).
- [274] R. T. Scalettar *et al.*, Phys. Rev. A **25**, 2419 (1982).
- [275] E. Aprile *et al.*, Nucl. Instrum. Meth. A **261**, 519 (1987).
- [276] P. Cennini *et al.* (ICARUS), Nucl. Instrum. Meth. A **345**, 230 (1994).
- [277] S. Amoruso *et al.* (ICARUS), Nucl. Instrum. Meth. A **523**, 275 (2004).
- [278] R. Acciarri *et al.* (ArgoNeuT), JINST **8**, P08005 (2013), [arXiv:1306.1712].
- [279] G. Jaffe, Annalen der Physik **42**, 12, 303 (1913).
- [280] L. Onsager, Phys. Rev. **54**, 554 (1938).
- [281] J. Thomas and D. A. Imel, Phys. Rev. A **36**, 614 (1987).
- [282] T. Yang, Instruments **5**, 1, 2 (2020), [arXiv:2012.01319].
- [283] S. Amoruso *et al.* (ICARUS), Nucl. Instrum. Meth. A **516**, 68 (2004).
- [284] W. Walkowiak, Nucl. Instrum. Meth. A **449**, 288 (2000).
- [285] M. Antonello *et al.* (ICARUS), JINST **9**, 12, P12006 (2014), [arXiv:1409.5592].
- [286] V. Meddage (MicroBooNE), in “Meeting of the APS Division of Particles and Fields,” (2017), [arXiv:1710.00396].
- [287] B. Abi *et al.* (DUNE), JINST **15**, 12, P12004 (2020), [arXiv:2007.06722].
- [288] Y. Li *et al.*, Nucl. Instrum. Meth. A **816**, 160 (2016), [arXiv:1508.07059].
- [289] P. Agnes *et al.* (DarkSide), Nucl. Instrum. Meth. A **904**, 23 (2018), [arXiv:1802.01427].
- [290] P. Abratenko *et al.* (MicroBooNE), JINST **16**, 09, P09025 (2021), [arXiv:2104.06551].
- [291] M. Miyajima *et al.*, Phys. Rev. A **10**, 1452 (1974).
- [292] N. Gee *et al.*, Journal of Applied Physics **57**, 4, 1097 (1985).
- [293] T. Doke *et al.*, Nucl. Instrum. Meth. A **269**, 291 (1988).
- [294] T. Doke, K. Masuda and E. Shibamura, Nucl. Instrum. Meth. A **291**, 617 (1990).
- [295] T. Heindl *et al.*, EPL **91**, 6, 62002 (2010), [arXiv:1511.07718].
- [296] M. Babicz *et al.*, JINST **15**, 09, P09009 (2020), [arXiv:2002.09346].
- [297] G. M. Seidel, R. E. Lanou and W. Yao, Nucl. Instrum. Meth. A **489**, 189 (2002), [hep-ex/0111054].
- [298] E. Grace and J. A. Nikkel, Nucl. Instrum. Meth. A **867**, 204 (2017), [arXiv:1502.04213].
- [299] A. Hitachi *et al.*, Phys. Rev. B **27**, 5279 (1983).
- [300] P. Adhikari *et al.* (DEAP), Eur. Phys. J. C **80**, 4, 303 (2020), [arXiv:2001.09855].
- [301] B. Abi *et al.* (DUNE), JINST **15**, 08, T08010 (2020), [arXiv:2002.03010].
- [302] M. Auger *et al.*, JINST **11**, 03, P03017 (2016), [arXiv:1512.05968].
- [303] S. Kubota *et al.*, Phys. Rev. B **20**, 8, 3486 (1979).
- [304] M. Kuźniak and A. M. Szalc, Instruments **5**, 1, 4 (2020), [arXiv:2012.15626].
- [305] F. Spiegelmann and J.-P. Malrieu, Chemical Physics Letters **57**, 2, 214 (1978), ISSN 0009-2614.
- [306] B. Jones *et al.*, JINST **8**, P12015 (2013), [arXiv:1308.3658].
- [307] A. Buzulutskov, EPL **117**, 3, 39002 (2017), [arXiv:1702.03612].
- [308] J. Soto-Oton (DUNE), in “International Conference on Technology and Instrumentation in Particle Physics,” (2021), [arXiv:2109.05858].
- [309] B. A. Dolgoshein, V. N. Lebedenko and B. U. Rodionov, JETP Letters (1970), URL http://jetpletters.ru/ps/1724/article_26181.pdf.
- [310] J. Lekner, Phys. Rev. **158**, 130 (1967).
- [311] E. Shibamura *et al.*, Phys. Rev. A **20**, 6, 2547 (1979).
- [312] A. Badertscher *et al.*, JINST **8**, P04012 (2013), [arXiv:1301.4817].
- [313] B. Aimard *et al.* (WA105), JINST **16**, 08, P08063 (2021), [arXiv:2104.08227].
- [314] A. Abed Abud *et al.* (DUNE) (2021), [arXiv:2103.13910].
- [315] P. Abratenko *et al.* (MicroBooNE), JINST **15**, 12, P12037 (2020), [arXiv:2008.09765].
- [316] M. Antonello *et al.* (ICARUS), JINST **15**, 07, P07001 (2020), [arXiv:2001.08934].
- [317] S. Palestini, Instruments **5**, 1, 9 (2021), [arXiv:2102.06082].
- [318] C. Cantini *et al.*, JINST **12**, 03, P03021 (2017), [arXiv:1611.02085].
- [319] J. Asaadi *et al.*, JINST **9**, P09002 (2014), [arXiv:1406.5216].
- [320] O. Bunemann, T. E. Cranshaw and J. A. Harvey, Canadian Journal of Research **27a**, 5, 191 (1949).
- [321] V. Radeka *et al.*, J. Phys. Conf. Ser. **308**, 012021 (2011).
- [322] H. Chen *et al.*, Phys. Procedia **37**, 1287 (2012).
- [323] S. Li *et al.*, IEEE Transactions on Nuclear Science **60**, 6, 4737 (2013).
- [324] H. Chen *et al.*, Nucl. Instrum. Meth. A **936**, 271 (2019).
- [325] R. Acciarri *et al.* (MicroBooNE), JINST **12**, 08, P08003 (2017), [arXiv:1705.07341].
- [326] P. Cennini *et al.* (ICARUS), Nucl. Instrum. Meth. A **432**, 240 (1999).
- [327] D. Caratelli (MicroBooNE), JINST **15**, 03, C03023 (2020).
- [328] B. Ali-Mohammadzadeh *et al.* (ICARUS), JINST **15**, 10, T10007 (2020), [arXiv:2006.05261].
- [329] A. Ankowski *et al.* (ICARUS), Nucl. Instrum. Meth. A **556**, 146 (2006).
- [330] N. Anfimov *et al.*, JINST **15**, 07, C07022 (2020).
- [331] E. Segreto *et al.*, JINST **15**, 05, C05045 (2020).
- [332] C. Rubbia *et al.* (ICARUS), JINST **6**, P07011 (2011), [arXiv:1106.0975].
- [333] D. A. Dwyer *et al.*, JINST **13**, 10, P10007 (2018), [arXiv:1808.02969].
- [334] B. Baibussinov *et al.* (ICARUS), JINST **13**, 03, T03001 (2018), [arXiv:1711.06781].
- [335] A. Lowe *et al.*, Instruments **4**, 4, 35 (2020), [arXiv:2011.02292].
- [336] E. Segreto, Phys. Rev. D **103**, 4, 043001 (2021), [arXiv:2012.06527].
- [337] “Lidine 2021,” Accessed October 2021, URL <https://indico.physics.ucsd.edu/event/1/book-of-abstracts.pdf>.
- [338] A. Rogalski, Adv. Opt. Photon. **11**, 2, 314 (2019).
- [339] V. Saraswat, R. Jacobberger and M. Arnold, ACS Nano **15**:3, 3674–3708 (2021).
- [340] F. Hartmann, *Evolution of Silicon Sensor Technology in Particle Physics*, volume 275 of *Springer Tracts in Modern Physics*, Springer (2017), ISBN 978-3-319-64434-9, 978-3-319-64436-3.
- [341] G. Lutz and R. Klanner, *Particle Physics Reference Library (Vol. 2, Ch. 5., Solid State Detectors)*, Springer Nature (2020), ISBN 978-3-030-35317-9, 978-3-030-35318-6.
- [342] Landolt-Börnstein, Springer (Berlin), 2002, https://doi.org/10.1007/10832182_456 and https://doi.org/10.1007/10832182_458.

- [343] C. Da Via *et al.*, Nucl. Instrum. Meth. **587**, 243 (2008).
- [344] L. Rossi *et al.*, *Pixel Detectors – From Fundamentals to Applications*, Springer, Berlin (2006), ISBN 978-3-540-28332-4, 978-3-540-28333-1.
- [345] M. Garcia-Sciveres and N. Wermes, Rept. Prog. Phys. **81**, 6, 066101 (2018), [arXiv:1705.10150].
- [346] Y. Arai *et al.*, Nucl. Instrum. Meth. A **623**, 186 (2010).
- [347] H.-G. Moser *et al.*, PoS **VERTEX2007**, 022 (2007).
- [348] W. Riegler and G. Aglieri Rinella, JINST **12**, 11, P11017 (2017), [arXiv:1706.04883].
- [349] H. F. W. Sadrozinski, A. Seiden and N. Cartiglia, Rept. Prog. Phys. **81**, 2, 026101 (2018), [arXiv:1704.08666].
- [350] G. Kramberger, *Particle Physics Reference Library (Vol. 2, Ch. 21., Solid State Detectors for High Radiation Environments)*, Springer Nature (2020), ISBN 978-3-030-35317-9, 978-3-030-35318-6.
- [351] M. Moll, IEEE Trans. Nucl. Sci. **65**, 8, 1561 (2018).
- [352] W. Blum, L. Rolandi and W. Riegler, *Particle detection with drift chambers*, Particle Acceleration and Detection, Springer (2008), ISBN 978-3-540-76683-4, 978-3-540-76684-1.
- [353] F. S. Goulding, Nucl. Instrum. Meth. **100**, 493 (1972).
- [354] V. Radeka, Ann. Rev. Nucl. Part. Sci. **38**, 217 (1988).
- [355] C. Agapopoulou *et al.*, JINST **15**, 07, P07007 (2020).
- [356] R. Wigmans, *Calorimetry*, International Series of Monographs on Physics, Oxford University Press (2017).
- [357] S. Agostinelli *et al.* (GEANT4), Nucl. Instrum. Meth. A **506**, 250 (2003).
- [358] J. Allison *et al.*, IEEE Trans. Nucl. Sci. **53**, 270 (2006).
- [359] T. Gabriel and L. Charlton (1997).
- [360] T. T. Böhlen *et al.*, Nucl. Data Sheets **120**, 211 (2014).
- [361] A. Ferrari *et al.* (2005).
- [362] J. Allison *et al.*, Nucl. Instrum. Meth. A **835**, 186 (2016).
- [363] D. Buskulic *et al.* (ALEPH), Nucl. Instrum. Meth. A **360**, 481 (1995).
- [364] A. M. Sirunyan *et al.* (CMS), JINST **12**, 10, P10003 (2017), [arXiv:1706.04965].
- [365] M. A. Thomson, Nucl. Instrum. Meth. A **611**, 25 (2009), [arXiv:0907.3577].
- [366] L. Linssen *et al.* (2012), [arXiv:1202.5940].
- [367] H. L. Tran *et al.*, Eur. Phys. J. C **77**, 10, 698 (2017), [arXiv:1705.10363].
- [368] W.R. Nelson, H. Hirayama, and D.W.O. Rogers, SLAC-265 (1985).
- [369] ATLAS Collab., CERN/LHCC 96-41 (1996).
- [370] D. Hitlin *et al.*, Nucl. Instrum. Meth. **137**, 225 (1976).
- [371] W. J. Willis and V. Radeka, Nucl. Instrum. Meth. **120**, 221 (1974).
- [372] R. Wigmans, *Calorimetry: Energy Measurement in Particle Physics*, Inter. Series of Monographs on Phys. **107**, Second Edition, Oxford Scholarship Online (2017).
- [373] R. Y. Zhu, Nucl. Instrum. Meth. A **413**, 297 (1998).
- [374] R.Y. Zhu, Journal of Physics: Conference Series **587**, 012055 (2015).
- [375] CMS Collab., CERN/LHCC 97-33 (1997).
- [376] C. Leroy and P. Rancoita, Rept. Prog. Phys. **63**, 505 (2000).
- [377] F. Sefkow and F. Simon, *Calorimeters*, in Fleck I., Titov M., Grupen C., Buvat I. (eds) Handbook of Particle Detection and Imaging, Springer (2021), ISBN 978-3-319-47999-6.
- [378] C. Adloff *et al.* (CALICE), JINST **8**, 07005 (2013).
- [379] T. A. Gabriel *et al.*, Nucl. Instrum. Meth. A **338**, 336 (1994).
- [380] F. Ariztizabal *et al.* (RD-34), Nucl. Instrum. Meth. A **349**, 384 (1994).
- [381] CMS, CERN-LHCC-2017-023, CMS-TDR-019 (2017).
- [382] N. Akchurin *et al.*, Nucl. Instrum. Meth. A **399**, 202 (1997).
- [383] A. Artamonov *et al.*, JINST **3**, P02010 (2008).
- [384] B. Aubert *et al.*, Nucl. Instrum. Meth. A **321**, 467 (1992).
- [385] F. Sefkow and F. Simon (CALICE), J. Phys. Conf. Ser. **1162**, 1, 012012 (2019), [arXiv:1808.09281].
- [386] C. W. Fabjan *et al.*, Nucl. Instrum. Meth. **141**, 61 (1977).
- [387] J. Brau *et al.*, Nucl. Instrum. Meth. A **238**, 489 (1985).
- [388] H. Brückmann and H. Kowalski, ZEUS Int. Note 86/026 DESY, Hamburg (1986).
- [389] R. Wigmans, Nucl. Instrum. Meth. A **259**, 389 (1987).
- [390] R. Wigmans, Nucl. Instrum. Meth. A **265**, 273 (1988).
- [391] J. E. Brau and T. A. Gabriel, Nucl. Instrum. Meth. A **275**, 190 (1989).
- [392] J. C. Brient, R. Rusack and F. Sefkow, Ann. Rev. Nucl. Part. Sci. **68**, 271 (2018).
- [393] E. Fretwurst *et al.* (1989), URL <http://cds.cern.ch/record/368113>.
- [394] E. Borchi *et al.* (SICAPO), Nucl. Instrum. Meth. A **279**, 57 (1989).
- [395] H. Abramowicz *et al.* (2013), [arXiv:1306.6329].
- [396] N. Alipour Tehrani *et al.* (CLICdp) (2017), CLICdp-Note-2017-001.
- [397] N. Bacchetta *et al.* (2019), [arXiv:1911.12230].
- [398] <https://twiki.cern.ch/twiki/bin/view/CALICE/CaliceDetectors>.
- [399] C. Adloff *et al.* (CALICE), JINST **5**, P05004 (2010), [arXiv:1003.2662].
- [400] M. Chefdeville *et al.* (CALICE), Nucl. Instrum. Meth. A **939**, 89 (2019), [arXiv:1901.08818].
- [401] G. Baulieu *et al.*, JINST **10**, 10, P10039 (2015), [arXiv:1506.05316].
- [402] C. Adloff *et al.* (CALICE), JINST **8**, P09001 (2013), [arXiv:1305.7027].
- [403] H. Abramowicz *et al.*, Nucl. Instrum. Meth. **180**, 429 (1981).
- [404] B. Andrieu *et al.* (H1 Calorimeter Group), Nucl. Instrum. Meth. A **336**, 499 (1993).
- [405] C. Cojocararu *et al.* (ATLAS Liquid Argon EMEC/HEC), Nucl. Instrum. Meth. A **531**, 481 (2004), [arXiv:physics/0407009].
- [406] C. Adloff *et al.* (CALICE), J. Instr. **7**, 09, P09017 (2012).
- [407] H. L. Tran *et al.*, The European Physical Journal C **77**, 10, 698 (2017).
- [408] P. Mockett, SLAC-267, 335 (1983).
- [409] D. E. Groom, Nucl. Instrum. Meth. A **572**, 633 (2007), erratum: Nucl. Instrum. Meth. A **593**, 628 (2008).
- [410] R. Wigmans, *Proc. 7th Inter. Conf. on Calorimetry in High Energy Physics*, 182 World Scientific, River Edge, NJ, (1998);
- [411] S. Lee, M. Livan and R. Wigmans, Rev. Mod. Phys. **90**, 2, 025002 (2018).
- [412] S. Lee *et al.*, Nucl. Instrum. Meth. A **866**, 76 (2017), [arXiv:1703.09120].
- [413] M. Antonello *et al.*, JINST **15**, 06, C06015 (2020).
- [414] E. Bernardi *et al.*, Nucl. Instrum. Meth. A **262**, 229 (1987).
- [415] M. Chefdeville *et al.* (CALICE), JINST **10**, 12, P12006 (2015), [arXiv:1509.00617].
- [416] T. Akesson *et al.*, Nucl. Instrum. Meth. A **262**, 243 (1987).
- [417] D. Acosta *et al.*, Nucl. Instrum. Meth. A **308**, 481 (1991).
- [418] R. Dubois *et al.*, IEEE Trans. Nucl. Sci. **33**, 194 (1986).
- [419] B. Andrieu *et al.* (H1 Calorimeter Group), Nucl. Instrum. Meth. A **336**, 460 (1993).

- [420] A. Bernstein *et al.* (ZEUS Barrel Calorimeter Group), Nucl. Instrum. Meth. A **336**, 23 (1993).
- [421] J.-b. Liu (CDF), in “7th International Conference on Calorimetry in High-Energy Physics (ICCHEP 97),” 237–240 (1997).
- [422] S. Abachi *et al.* (D0), Nucl. Instrum. Meth. A **324**, 53 (1993).
- [423] G. Aad *et al.* (ATLAS), JINST **3**, S08003 (2008).
- [424] S. Abdullin *et al.* (USCMS, ECAL/HCAL), Eur. Phys. J. C **60**, 359 (2009), [Erratum: Eur.Phys.J.C 61, 353–356 (2009)].
- [425] H. Abramowicz *et al.* (ZEUS), Phys. Lett. B **718**, 915 (2013), [arXiv:1210.5511].
- [426] E. Shibamura *et al.*, Nucl. Instrum. Methods **A316**, 184 (1975).
- [427] L. S. Miller, S. Howe and W. E. Spear, Phys. Rev. **166**, 871 (1968).
- [428] A.M. Kalinin *et al.*, ATLAS-LARG-NO-058 (1996).
- [429] K. Yoshino, U. Sowada and W. F. Schmidt, Phys. Rev. **A14**, 438 (1976).
- [430] A.O. Allen *et al.*, NSRDS-NBS-58 (1976).
- [431] P. Benetti *et al.*, Nucl. Instrum. Methods **A32**, 361 (1993).
- [432] G. Danby *et al.*, Phys. Rev. Lett. **9**, 36 (1962).
- [433] S. van der Meer (1961).
- [434] J. A. Formaggio and G. P. Zeller, Rev. Mod. Phys. **84**, 1307 (2012), [arXiv:1305.7513].
- [435] H. Faissner, “CERN Spark Chamber Neutrino Experiment”, INSPIRE-1377455.
- [436] H. Faissner *et al.*, Phys. Lett. **68B**, 377 (1977).
- [437] F. J. Hasert *et al.* (Gargamelle Neutrino), Nucl. Phys. **B73**, 1 (1974).
- [438] N. Armenise *et al.* (BEBC TST Neutrino), Phys. Lett. **81B**, 385 (1979).
- [439] A.E. Asratien *et al.*, Phys. Lett. **79**, 497 (1978).
- [440] S. J. Barish *et al.*, Phys. Rev. **D16**, 3103 (1977).
- [441] N. J. Baker *et al.*, Phys. Rev. **D23**, 2499 (1981).
- [442] J. W. Chapman *et al.*, Phys. Rev. **D14**, 5 (1976).
- [443] M. Holder *et al.*, Nucl. Instrum. Meth. **148**, 235 (1978).
- [444] I. Ambats *et al.* (MINOS) (1998).
- [445] K. Abe *et al.* (T2K), Nucl. Instrum. Meth. **A659**, 106 (2011), [arXiv:1106.1238].
- [446] M. H. Ahn *et al.* (K2K), Phys. Rev. **D74**, 072003 (2006), [hep-ex/0606032].
- [447] A. A. Aguilar-Arevalo *et al.* (MiniBooNE), Nucl. Instrum. Meth. **A599**, 28 (2009), [arXiv:0806.4201].
- [448] A. C. Benvenuti *et al.*, Nucl. Instrum. Meth. **125**, 447 (1975).
- [449] C. Athanassopoulos *et al.* (LSND), Nucl. Instrum. Meth. **A388**, 149 (1997), [arXiv:nucl-ex/9605002].
- [450] D. S. Ayres *et al.* (NOvA) (2007).
- [451] K. Hiraide *et al.* (SciBooNE), Phys. Rev. **D78**, 112004 (2008), [arXiv:0811.0369].
- [452] C. Rubbia, CERN-EP-INT-77-08 (1977).
- [453] S. Amerio *et al.* (ICARUS), Nucl. Instrum. Meth. **A527**, 329 (2004).
- [454] C. Anderson *et al.*, JINST **7**, 10020 (2012).
- [455] H. Chen *et al.*, FERMILAB-PROPOSAL-0974 (2007).
- [456] D. H. Perkins, Nature **159**, 126 (1947).
- [457] S. Aoki *et al.*, Nucl. Instrum. Meth. **A447**, 361 (2000).
- [458] N. Uhida *et al.*, Nucl. Instrum. Methods **224**, 50 (1984).
- [459] K. Kodama *et al.*, Nucl. Instrum. Meth. **B93**, 340 (1994).
- [460] T. Adam *et al.*, Nucl. Instrum. Meth. **A577**, 523 (2007), [arXiv:physics/0701153].
- [461] D. Di Ferdinando (OPERA), Radiat. Meas. **44**, 840 (2009), [arXiv:0812.0451].
- [462] R. Acquafredda *et al.* (OPERA), New J. Phys. **8**, 303 (2006), [hep-ex/0611023].
- [463] T. Fukuda *et al.*, PTEP **2017**, no. 6, 063C02 (2017).
- [464] A. N. Diddens *et al.* (CERN-Hamburg-Amsterdam-Rome-Moscow), Nucl. Instrum. Meth. **178**, 27 (1980).
- [465] D. Geiregat *et al.* (CHARM-II), Nucl. Instrum. Meth. **A325**, 92 (1993).
- [466] L. A. Ahrens *et al.*, Nucl. Instrum. Meth. **A254**, 515 (1987).
- [467] G. Gidal, LBL-91 Suppl., Rev. (1985).
- [468] W. K. Sakumoto *et al.*, Nucl. Instrum. Meth. **A294**, 179 (1990).
- [469] D. A. Harris *et al.* (NuTeV), Nucl. Instrum. Meth. **A447**, 377 (2000), [hep-ex/9908056].
- [470] J. Altegoer *et al.* (NOMAD), Nucl. Instrum. Meth. **A404**, 96 (1998).
- [471] L. Aliaga *et al.* (MINERvA), Nucl. Instrum. Meth. **A743**, 130 (2014), [arXiv:1305.5199].
- [472] A. Yamamoto, Nucl. Instrum. Meth. **A453**, 445 (2000).
- [473] A. Yamamoto and Y. Makida, Nucl. Instrum. Meth. **A494**, 255 (2002).
- [474] T. M. Taylor, Phys. Scripta **23**, 459 (1981).
- [475] R. L. Gluckstern, Nucl. Instrum. Meth. **24**, 381 (1963).
- [476] V. Karimaki, Nucl. Instrum. Meth. **A410**, 284 (1998).

36. Particle Detectors for Non-Accelerator Physics

Revised 2021. See the various sections for authors.

36.1	Introduction	618
36.2	High-energy cosmic-ray hadron and gamma-ray detectors	618
36.2.1	Atmospheric fluorescence detectors	618
36.2.2	Atmospheric Cherenkov telescopes for high-energy gamma ray astronomy	620
36.3	Large neutrino detectors	621
36.3.1	Deep liquid detectors for rare processes	621
36.3.2	Neutrino telescopes	623
36.3.3	Radio emission from (ultra-)high energy particle showers	627
36.4	Large time-projection chambers for rare event detection	630
36.4.1	Dark matter and other low energy signals	631
36.4.2	$0\nu\beta\beta$ Decay	632
36.5	Sub-kelvin detectors	633
36.5.1	Motivation for Sub-kelvin Detectors	633
36.5.2	Detector Types	633
36.5.3	Experimental Applications	636
36.6	Low-radioactivity background techniques	638
36.6.1	Introduction	638
36.6.2	Radio-purity assay	638
36.6.3	Radon and its progeny	639
36.6.4	Surface backgrounds	639
36.6.5	Mitigation of backgrounds and active background discrimination	640

36.1 Introduction

Non-accelerator experiments have become increasingly important in particle physics and astrophysics. From them comes the evidence of physics beyond the SM, with the discovery of neutrino oscillations and adiabatic flavor conversion. Explored energies range from the MeV scale to above the EeV, some 24 orders of magnitude. The physics and the design of the detectors vary as a consequence. Some experiments look at astrophysical high-energy phenomena using the atmosphere as a detector in the fluorescence and Cherenkov observatories or the polar ice and the ocean water in neutrino telescopes. Experiments on extremely rare events, such as neutrino-less double beta decay, solar neutrinos and dark matter induced scattering, need dedicated fully equipped deep underground laboratories, existing in different countries. Critical is the research to push back the ultra-low radioactive background frontier, with dedicated facilities in these laboratories. Detectors range from hyper-pure liquid scintillators, both organic and not, to thermalized and ballistic phonon detectors at the sub-Kelvin temperature, to dual phase noble fluid TPCs, etc. Space-based detectors also use some unique instrumentation, but these are beyond the present scope of this review. Gravitational wave detectors are not included as well.

36.2 High-energy cosmic-ray hadron and gamma-ray detectors

36.2.1 Atmospheric fluorescence detectors

Revised March 2022 by L.R. Wiencke (Colorado School of Mines).

Cosmic-ray fluorescence detectors (FDs) use the atmosphere as a giant calorimeter to measure isotropic scintillation light that traces the development profiles of extensive air showers. An extensive air shower (EAS) is produced by the interactions of ultra high-energy ($E > 10^{17}$ eV) subatomic particles in the stratosphere and upper troposphere. The amount of scintillation light generated by an EAS is proportional to the energy deposited in the atmosphere and nearly independent of the primary species. With energies extending beyond 10^{20} eV these are the highest energy subatomic particles known to exist. In addition to particle arrival directions, energy spectra and primary composition, the astroparticle science investigated with FDs also includes multi-messenger studies, searches for high energy photons, neutrinos,

monopoles and deeply penetrating forms of dark matter. The Pierre Auger Observatory FD also measures UV scintillation that traces the development of ring-shaped atmospheric transient luminous events, called Elves, in the ionosphere that are initiated by strong lightning [1].

Previous experiments with FDs included the pioneering Fly's Eye [2,3], and the High Resolution Fly's Eye (HiRes and HiRes prototype) [4]. A history of the fluorescence technique includes earlier studies in the 1950's and 1960's [5]. The current generation of experiments include the Telescope Array (TA) [6] in the northern hemisphere, and the much larger Pierre Auger Observatory (Auger) [7] in the southern hemisphere. Both are hybrid observatories. Their FD telescopes overlook sparse arrays of particle detectors on the ground. Select parameters are listed in Table 36.1. TA and Auger have each one FD site populated with additional telescopes that view up to 60° in elevation to measure lower EASs using a combination of scintillation and direct Cherenkov light. As part of a fourfold coverage upgrade of TA (TAx4), 12 HiRes refurbished telescopes have been installed at the north and south-east sites of TA. A set of prototype FD telescopes, dubbed FAST [8], have observed EASs at the TA site using design that features wide field of view PMTs, fast timing and economical optics for a next-generation ground-based observatory.

The fluorescence light is emitted primarily between 290 and 430 nm (Figure 36.1) with major lines at 337, 357, and 391 nm, when relativistic charged particles, primarily electrons and positrons, excite nitrogen molecules in air, resulting in transitions of the 1P and 2P systems. Reviews and references for the pioneering and recent laboratory measurements of fluorescence yield, $Y(\lambda, P, T, u)$, including dependence on wavelength (λ), temperature (T), pressure (p), and humidity (u) may be found in Refs. [9–11]. The results of various laboratory experiments have been combined (Figure 36.2) to obtain an absolute average and uncertainty for $Y(337 \text{ nm}, 800 \text{ hPa}, 293 \text{ K}, \text{ dry air})$ of $7.04 \pm 0.24 \text{ ph/MeV}$ after corrections for different electron beam energies and other factors. The units of ph/MeV correspond to the number of fluorescence photons produced per MeV of energy deposited in the atmosphere by the electromagnetic component of an EAS.

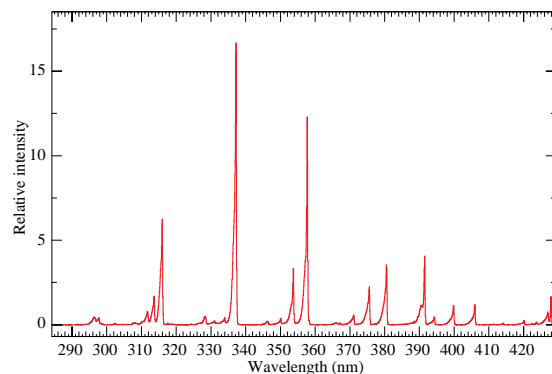


Figure 36.1: Measured fluorescence spectrum excited by 3 MeV electrons in dry air at 800 hPa and 293 K. Airfly experiment. Figure from Ref [12].

An FD element (telescope) consists of a non-tracking spherical mirror of less than astronomical quality, a “camera” of photomultiplier tubes (PMTs) near the focal plane, and a flash ADC readout system with a pulse and track-finding trigger scheme [7, 14]. The major experiments listed in Table 36.1 all use conventional PMTs (for example, Hamamatsu R9508 or Photonis XP3062) with grounded cathodes and AC coupled readout. Segmented mirrors have been fabricated from slumped or slumped/polished glass with an anodized aluminum coating or fabricated using shaped aluminum that was then chemically anodized with AlMgSiO_5 . A broadband UV filter (custom fabricated, BG-3, or Schott MUG-6) reduces background light such as starlight, airglow, man-made light pollution, and airplane strobe-lights.

Table 36.1: Parameters of major fluorescence detectors. Note 1: Year when all FD sites were operational. Note 2: At TA 1 of the 3 FD sites features 24 telescopes from the HiRes experiment. Note 3: A-C for one telescope where A is the full area and C the area obscured by the camera and support structures. Thus A-C is the effective light collecting area. For the modified Schmidt design at Auger, the area of the entrance pupil, A, is listed because the pupil is smaller than the mirror and thus defines the entrance aperture. For the other experiments, the area of the mirror, A, is listed

Observatory	Fly's Eye	HiRes	Telescope Array	Pierre Auger
Location	Dugway UT US	Dugway UT US	Delta UT US	Malargüe AR
Start-End	1981-1992	1996-2006	2008-present	2005-present
Sites (note 1)	2 (1986)	2 (1999)	3 (2008)	4 (2008)
Separation	3.3 km	12.6 km	31-40 km	39-62 km
Telescopes/site	67,18	21,42	12+8,12,14+10+4	6, 6, 6, 6+3
Pixel FOV	5.5°	1°	1°	1.5°
Telescope FOV	≈18° × ≈18°	16° × 13.5°	18° × 15° (note 2)	30° × 28.1°
Azi × Elv				
Light collection area (note 3)	1.95 m ² - 0.25 m ²	3.72 m ² - 0.5 m ²	6.8 m ² - 0.85 m ² (for 2 sites)	3.80 m ² - 0.80 m ² (modified schmidt)
Energy Scale	≤40%	≈20%	≈20%	14%
Uncertainty				

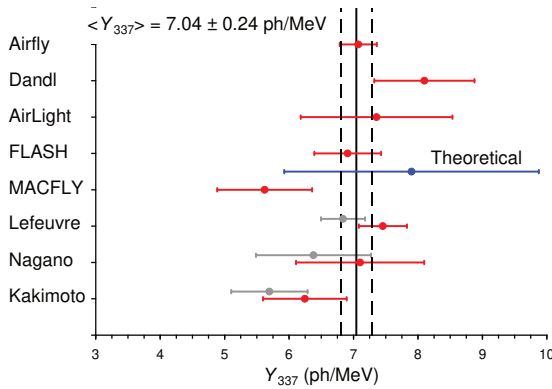


Figure 36.2: Fluorescence yield values and associated uncertainties at 337 nm (Y_{337}) in dry air at 800 hPa and 293 K. The methodology and corrections that were applied to obtain the average and the uncertainty are discussed extensively in this reference. The vertical axis denotes different laboratory experiments that measured FY. The gray bars show three of the original measurements to illustrate the scale of the corrections applied. Figure from Ref [13].

At 10^{20} eV, where the flux drops below 1 EAS/km²century, the aperture for an eye of adjacent FD telescopes that span the horizon can reach 10^4 km² sr. FD operation requires (nearly) moonless nights and clear atmospheric conditions, which typically imposes a duty cycle of about 10%. Arrangements of LEDs, calibrated diffuse sources [15], pulsed UV lasers [16], LIDARs¹ and IR detectors that are sensitive to clouds are used for photometric calibration, atmospheric calibration [17], and determination of exposure [18]. For purposes of optical transmission, the atmosphere is treated as having a dominant molecular component and a secondary aerosol component. The latter is well described [19] by molecular scattering theory and models derived from radiosonde measurements. The aerosol component can include dust, haze and pollution and the aerosol optical depth profile must be measured on site in the UV during FD data taking.

The EAS generates a track consistent with a light source moving at $v = c$ across the FOV. The number of photons (N_γ) as a function of atmospheric depth (X) can be expressed as [10]

$$\frac{dN_\gamma}{dX} = \frac{dE_{\text{dep}}^{\text{tot}}}{dX} \int Y(\lambda, P, T, u) \cdot \tau_{\text{atm}}(\lambda, X) \cdot \varepsilon_{\text{FD}}(\lambda) d\lambda, \quad (36.1)$$

where $\tau_{\text{atm}}(\lambda, X)$ is the atmospheric transmission, including

¹LIDAR stands for "Light Detection and Ranging" and refers here to systems that measure atmospheric properties from the light scattered backwards from laser pulses directed into the sky.

wavelength (λ) dependence, and $\varepsilon_{\text{FD}}(\lambda)$ is the FD efficiency. $\varepsilon_{\text{FD}}(\lambda)$ includes geometric factors and collection efficiency of the optics, quantum efficiency of the PMTs, and other throughput factors. The typical systematic uncertainties, τ_{atm} (10%) and ε_{FD} (photometric calibration 10%), currently dominate the systematic uncertainty the absolute EAS energy scale. FD energy resolution, defined as event-to-event statistical uncertainty, is typically less than 10% for final data samples used for science analysis.

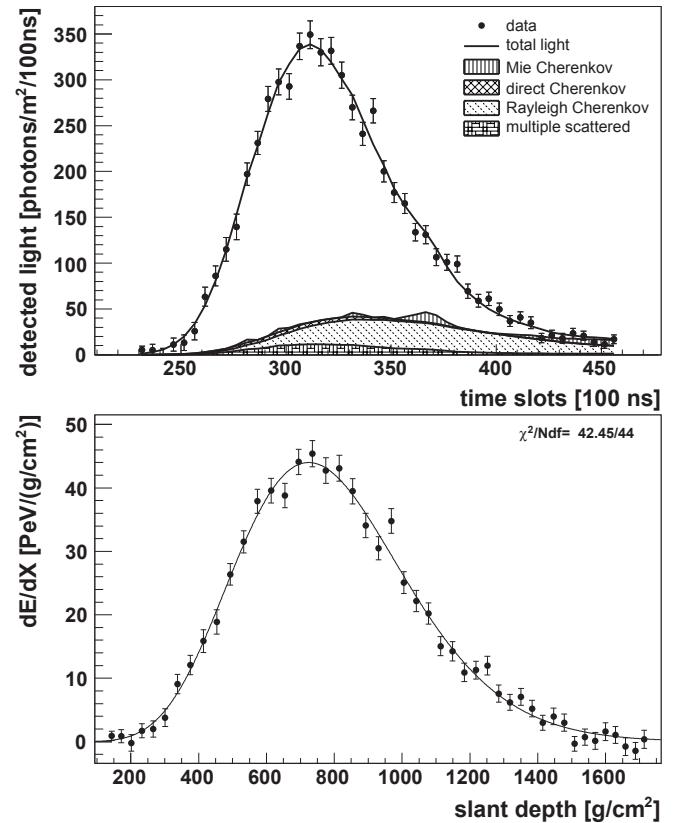


Figure 36.3: Example light profile (left) of one EAS recorded by the Pierre Auger FD and the corresponding profile (right) of energy deposited in the atmosphere vs atmospheric slant depth. The light profiles include the estimated components of Cherenkov light that have been scattered out of the forward beam by the molecular and aerosol (Mie) components of the atmosphere. The reconstructed energy of this EAS was $3.0 \pm 0.2 \times 10^{19}$ eV. Figure from Ref [20].

Analysis methods to reconstruct the EAS profile and deconvolve

the contributions of re-scattered scintillation light, and direct and scattered Cherenkov light are described in [2] and more recently in [21]. The EAS energy is typically obtained by integrating over the Gaisser-Hillas function [22]

$$E_{\text{cal}} = \int_0^{\infty} [w_{\text{max}} \left(\frac{X - X_0}{X_{\text{max}} - X_0} \right)^{(X_{\text{max}} - X_0)/\lambda} e^{(X_{\text{max}} - X)/\lambda}] dX, \quad (36.2)$$

where E_{cal} is the energy of electromagnetic energy component of the EAS and X_{max} is the atmospheric slant depth at which the shower reaches its maximum energy deposit rate. This maximum dE/dX is denoted as w_{max} . X_0 and λ are two shape parameters. The energy of the primary cosmic ray is obtained by correcting E_{cal} upward by about 10% to account for the invisible energy carried by particles that do not interact in the atmosphere. Auger recently reported a data-driven method to estimate the invisible energy from the muon number at ground level and X_{max} to reduce systematic uncertainties [23]. Energy resolution, $\Delta E/E$, of 15–20% is achievable, provided the geometric fit of the EAS axis is constrained, typically by multi-eye stereo projection or hybrid observations, and the profile fit of EAS development along the track is constrained by the observed rise and fall about X_{max} . An example of a recorded EAS light profile and its corresponding dE/dX development profile are shown in Fig. 36.3. The EAS generates a track consistent with a light source moving at $v = c$ across the FOV. The number of photons (N_γ) as a function of atmospheric depth (X) can be expressed as [10]

An FD that would look down on the earth's atmosphere from space orbit to view a much larger area than ground based instruments is an active area of R&D. Prototypes that have been built and flown in orbit include the pioneering TUS instrument [24], [25] operated 2016–2018 onboard the Lomonosov satellite. The JEM-EUSO collaboration has flown prototype FD telescopes on two stratospheric balloon flights [26] and [27] with a third in preparation. The Mini-EUSO [28] FD is recording terrestrial UV emission by looking down through a 25 cm diameter UV window from inside the International Space Station. The Probe of Extreme Multimessenger Astrophysics (POEMMA) project has completed a detailed conceptual design study for a twin-satellite mission [29] that would observe UHECRs and PeV scale cosmogenic tau neutrinos.

36.2.2 Atmospheric Cherenkov telescopes for high-energy gamma ray astronomy

Revised August 2019 by J. Holder (Delaware U.; Delaware U., Bartol Inst.).

A wide variety of astrophysical objects are now known to produce high-energy γ -ray photons. Leptonic or hadronic particles, accelerated to relativistic energies in the source, produce γ -rays typically through inverse Compton boosting of ambient photons or through the decay of neutral pions produced in hadronic interactions. At energies below ~ 30 GeV, γ -ray emission can be efficiently detected using satellite or balloon-borne instrumentation, with an effective area approximately equal to the size of the detector (typically $< 1 \text{ m}^2$). At higher energies, a technique with much larger effective collection area is desirable to measure astrophysical γ -ray fluxes, which decrease rapidly with increasing energy. Atmospheric Cherenkov detectors achieve effective collection areas of $> 10^5 \text{ m}^2$ by employing the Earth's atmosphere as an intrinsic part of the detection technique.

As described in Chapter 30, a hadronic cosmic ray or high energy γ -ray incident on the Earth's atmosphere triggers a particle cascade, or air shower. Relativistic charged particles in the cascade generate Cherenkov radiation, which is emitted along the shower direction, resulting in a light pool on the ground with a radius of $\sim 130 \text{ m}$. Cherenkov light is produced throughout the cascade development, with the maximum emission occurring when the number of particles in the cascade is largest, at an altitude of $\sim 10 \text{ km}$ for primary energies of 100 GeV–1 TeV. Following absorption and scattering in the atmosphere, the Cherenkov light at ground level peaks at a wavelength, $\lambda \approx 300\text{--}350 \text{ nm}$. The photon density is typically ~ 100 photons/ m^2 for a 1 TeV primary, arriv-

ing in a brief flash of a few nanoseconds duration. This Cherenkov pulse can be detected from any point within the light pool radius by using large reflecting surfaces to focus the Cherenkov light on to fast photon detectors (Fig. 36.4).

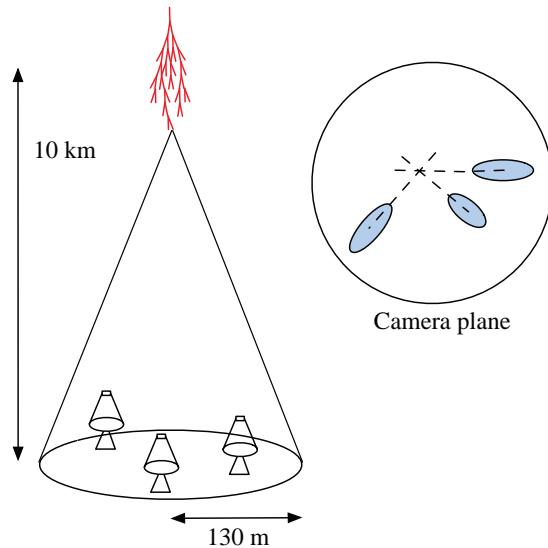


Figure 36.4: A schematic illustration of an imaging atmospheric Cherenkov telescope array. The primary particle initiates an air shower, resulting in a cone of Cherenkov radiation. Telescopes within the Cherenkov light pool record elliptical images; the intersection of the long axes of these images indicates the arrival direction of the primary, and hence the location of a γ -ray source in the sky

Modern atmospheric Cherenkov telescopes, such as those built and operated by the VERITAS [30], H.E.S.S. [31] and MAGIC [32] collaborations, consist of large ($> 100 \text{ m}^2$) segmented mirrors on steerable altitude-azimuth mounts. A camera made from an array of photosensors is placed at the focus of each mirror and used to record a Cherenkov image of each air shower. In these imaging atmospheric Cherenkov telescopes, single-anode photomultiplier tubes (PMTs) have traditionally been used (2048, in the case of H.E.S.S. II), but silicon devices now feature in more modern designs. The telescope cameras typically cover a field-of-view of $3\text{--}10^\circ$ in diameter. Images are recorded at kHz rates, the vast majority of which are due to showers with hadronic cosmic-ray primaries. The shape and orientation of the Cherenkov images are used to discriminate γ -ray photon events from this cosmic-ray background, and to reconstruct the photon energy and arrival direction. γ -ray images result from purely electromagnetic cascades and appear as narrow, elongated ellipses in the camera plane. The long axis of the ellipse corresponds to the vertical extension of the air shower, and points back towards the source position in the field-of-view. If multiple telescopes are used to view the same shower (“stereoscopy”), the source position is simply the intersection point of the various image axes. Cosmic-ray primaries produce secondaries with large transverse momenta, which initiate sub-showers. Their images are consequently wider and less regular than those with γ -ray primaries and, since the original charged particle has been deflected by Galactic magnetic fields before reaching the Earth, the images have no preferred orientation.

The measurable differences in Cherenkov image orientation and morphology provide the background discrimination which makes ground-based γ -ray astronomy possible. For point-like sources, such as distant active galactic nuclei, modern instruments can reject over 99.999% of the triggered cosmic-ray events, while retaining up to 50% of the γ -ray population. In the case of spatially extended sources, such as Galactic supernova remnants, the background rejection is less efficient, but the technique can be used to produce γ -ray maps of the emission from the source. The angular resolution depends upon the number of telescopes which view the

image and the energy of the primary γ -ray, but is typically less than 0.1° per event (68% containment radius) at energies above a few hundred GeV.

The total Cherenkov yield from the air shower is proportional to the energy of the primary particle. The image intensity, combined with the reconstructed distance of the shower core from each telescope, can therefore be used to estimate the primary energy. The energy resolution of this technique, also energy-dependent, is typically 15–20% at energies above a few hundred GeV. Energy spectra of γ -ray sources can be measured over a wide range, depending upon the instrument characteristics, source properties (flux, spectral slope, elevation angle, *etc.*), and exposure time. The effective energy range is typically from 30 GeV to 100 TeV and peak sensitivity lies in the range from 100 GeV to a few TeV.

The first astrophysical source to be convincingly detected using the imaging atmospheric Cherenkov technique was the Crab Nebula [33], with an integral flux of 2.1×10^{-11} photons $\text{cm}^{-2} \text{s}^{-1}$ above 1 TeV [34]. Modern imaging atmospheric Cherenkov telescopes have sensitivity sufficient to detect sources with less than 1% of the Crab Nebula flux in a few tens of hours. The TeV source catalog now consists of over 200 sources (see e.g. Ref. [35]). A large fraction of these were detected by scanning the Galactic plane from the southern hemisphere with the H.E.S.S. telescope array [36]. Recent reviews of the field include [37] and [38], and a historical overview can be found in [39].

Major upgrades of the existing telescope arrays have recently been completed, including the addition of a 28 m diameter central telescope to H.E.S.S. (H.E.S.S. II). Development is also underway for the next generation instrument, the Cherenkov Telescope Array (CTA), which will consist of a northern and a southern hemisphere observatory, with a combined total of more than 100 telescopes [40]. Telescopes of three different sizes are planned, spread over an area of $> 1 \text{ km}^2$, providing wider energy coverage, improved angular and energy resolutions, and an order of magnitude improvement in sensitivity relative to existing imaging atmospheric Cherenkov telescopes. Baseline telescope designs are similar to existing devices, but exploit technological developments such as dual mirror optics and silicon photo-detectors.

36.3 Large neutrino detectors

36.3.1 Deep liquid detectors for rare processes

Revised August 2021 by K. Scholberg (Duke U.) and C.W. Walter (Duke U.).

Deep, large detectors for rare processes tend to be multipurpose with physics reach that includes not only solar, reactor, supernova and atmospheric neutrinos, but also searches for baryon number violation and lepton number violation, searches for exotic particles and beyond-the-standard-model physics, and neutrino and cosmic-ray astrophysics in different energy regimes. The detectors may also serve as targets for long-baseline neutrino beams for neutrino oscillation physics studies. In general, detector design considerations can be divided into high- and low-energy regimes, for which background and event reconstruction issues differ. The high-energy regime, from about 100 MeV to a few hundred GeV, is relevant for proton decay searches, atmospheric neutrinos and high-energy astrophysical neutrinos. The low-energy regime (a few tens of MeV or less) is relevant for supernova, solar, reactor and geological neutrinos.

Large water Cherenkov and scintillator detectors (see Table 36.2) usually consist of a volume of transparent liquid viewed by photomultiplier tubes (PMTs) (see Sec 35.2); the liquid serves as active target. PMT hit charges and times are recorded and digitized, and triggering is usually based on coincidence of PMT hits within a time window comparable to the detector's light-crossing time. Because photosensors lining an inner surface represent a driving cost that scales as surface area, very large volumes can be used for comparatively reasonable cost. Some detectors are segmented into subvolumes individually viewed by PMTs, and may include other detector elements (*e.g.*, tracking detectors). Devices to increase light collection, *e.g.*, reflectors or waveshifter plates, may be employed. A common configuration is to have at least one concentric outer layer of liquid material separated from the

inner part of the detector to serve as shielding against ambient background. If optically separated and instrumented with PMTs, an outer layer may also serve as an active veto against entering cosmic rays and other background events. The PMTs for large detectors typically range in size from 20 cm to 51 cm diameter, and typical quantum efficiencies are in the 20–25% range for scintillation and water-Cherenkov photons. PMTs with higher quantum efficiencies, 35% or higher, have recently become available. The active liquid volume requires purification and there may be continuous recirculation of liquid. For large homogeneous detectors, the event interaction vertex is determined using relative timing of PMT hits, and energy deposition is determined from the number of recorded photoelectrons. A “fiducial volume” is usually defined within the full detector volume, some distance away from the PMT array. Inside the fiducial volume, enough PMTs are illuminated per event that reconstruction is considered reliable, and furthermore, entering background from the enclosing walls is suppressed by a buffer of self-shielding. PMT and detector optical parameters are calibrated using laser, LED, or other light sources. Quality of event reconstruction typically depends on photoelectron yield, pixelization and timing.

Because in most cases one is searching for rare events, large detectors are usually sited underground to reduce cosmic-ray-related background (see Chapter 30). The minimum depth required varies according to the physics goals [41].

36.3.1.1 Liquid scintillator detectors

Past and current large underground detectors based on hydrocarbon scintillators include LVD, MACRO, Baksan, Borexino, KamLAND and SNO+; JUNO is a future detector. Experiments at nuclear reactors include CHOOZ, Double CHOOZ, Daya Bay, and RENO. Organic liquid scintillators (see Section 35.3) for large detectors are chosen for high light yield and attenuation length, good stability, compatibility with other detector materials, high flash point, low toxicity, appropriate density for mechanical stability, and low cost. They may be doped with waveshifters and stabilizing agents. Popular choices are pseudocumene (1,2,4-trimethylbenzene) with a few g/L of the PPO (2,5-diphenyloxazole) fluor, and linear alkylbenzene (LAB), with light yield $\sim 10^4$ photons/MeV. In a typical detector configuration there will be active or passive regions of undoped scintillator, non-scintillating mineral oil or water surrounding the inner neutrino target volume. A thin vessel or balloon made of nylon, acrylic or other material transparent to scintillation light may contain the inner target; if the scintillator is buoyant with respect to its buffer, ropes may hold the balloon in place. For phototube surface coverages in the 20–40% range, yields in the few hundreds of photoelectrons per MeV of energy deposition can be obtained. Typical energy resolution is about $5 - 7\% / \sqrt{E(\text{MeV})}$ [42, 43], and typical position reconstruction resolution is a few tens of cm at $\sim 1 \text{ MeV}$, scaling as $\sim N^{-1/2}$, where N is the number of photoelectrons detected.

Shallow detectors for reactor neutrino oscillation experiments require excellent muon veto capabilities. For $\bar{\nu}_e$ detection via inverse beta decay on free protons, $\bar{\nu}_e + p \rightarrow n + e^+$, the neutron is captured by a proton on a $\sim 180 \mu\text{s}$ timescale, resulting in a 2.2 MeV γ ray, observable by Compton scattering and which can be used as a tag in coincidence with the positron signal. The positron annihilation γ rays may also contribute. Inverse beta decay tagging may be improved by addition of Gd at $\sim 0.1\%$ by mass, which for natural isotope abundance has a $\sim 49,000$ barn cross-section for neutron capture (in contrast to the 0.3 barn cross-section for capture on free protons). Gd capture takes $\sim 30 \mu\text{s}$, and is followed by a cascade of γ rays adding up to about 8 MeV. Gadolinium doping of scintillator requires specialized formulation to ensure adequate attenuation length and stability.

Scintillation detectors have an advantage over water Cherenkov detectors in the lack of Cherenkov threshold and the high light yield. However, scintillation light emission is nearly isotropic, and therefore directional capabilities are relatively weak. Liquid scintillator is especially suitable for detection of low-energy events. Radioactive backgrounds are a serious issue, and include long-lived cosmogenics such as ^{14}C . To go below a few MeV, very

Table 36.2: Properties of large detectors for rare processes. If total target mass is divided into large submodules, the number of subdetectors is indicated in parentheses. Projects with first data expected in 2023 or later are indicated in italics.

Detector	Mass, kton (modules)	PMTs (diameter, cm)	ξ	p.e./MeV	Dates
Baksan	0.33, scint (3150)	1/module (15)	segmented	40	1980–
MACRO	0.56, scint (476)	2-4/module (20)	segmented	18	1989–2000
LVD	1, scint. (840)	3/module (15)	segmented	15	1992–
KamLAND	0.41*, scint	1325(43)+554(51) [†]	34%	460	2002–
Borexino	0.1*, scint	2212 (20)	30%	500	2007–
SNO+	0.78, scint [‡]	9394 (20)	47%	400–600	2021–
CHOOZ	0.005, scint (Gd)	192 (20)	15%	130	1997–1998
Double Chooz	0.017, scint (Gd)(2)	534/module (20)	13%	180	2011–2017
Daya Bay	0.160, scint (Gd)(8)	192/module (20)	5.6% [§]	100	2011–2020
RENO	0.032, scint (Gd)(2)	342/module (25)	12.6%	100	2011–
<i>JUNO</i>	20.0*, scint	17613 (51)/25600 (8)	77.9%	1200	2023 (exp.)
IMB-1	3.3*, H ₂ O	2048 (12.5)	1%	0.25	1982–1985
IMB-2	3.3*, H ₂ O	2048 (20)	4.5%	1.1	1987–1990
Kam I	0.88/0.78*, H ₂ O	1000/948 (51)	20%	3.4	1983–1985
Kam II	1.04*, H ₂ O	948 (51)	20%	3.4	1986–1990
Kam III	1.04*, H ₂ O	948 (51)	20% [¶]	4.3	1990–1995
SK I	22.5*, H ₂ O	11146 (51)	40%	6	1996–2001
SK II	22.5*, H ₂ O	5182 (51)	19%	3	2002–2005
SK III-V	22.5*, H ₂ O	11129 (51)	40%	6	2006–2020
SK-Gd	22.5*, H ₂ O (Gd)	11129 (51)	40%	6	2020–
<i>Hyper-K</i>	187*, H ₂ O	>20000 (51)**	>20%	>6	2027 (exp.)
SNO	1, D ₂ O/1.7, H ₂ O	9438 (20)	31% ^{††}	9	1999–2006
<i>DUNE</i>	40*, Ar (4)	TBD ^{‡‡}	TBD ^{‡‡}	TBD ^{‡‡}	2029 (exp.)

*Indicates typical fiducial mass used for data analysis; this may vary by physics topic.

[†]Measurements made before 2003 only considered data from the 43 cm PMTs.

[‡]SNO+ ran with water fill from May 2017 to July 2019.

[§]The effective Daya Bay coverage is 12% with top and bottom reflectors.

[¶]The effective Kamiokande III coverage was 25% with light collectors.

^{||}A second staged module is being investigated.

**Additional photosensor modules and PMTs are planned.

^{††}The effective SNO coverage was 54% with light collectors.

^{‡‡}Photodetector technology and coverage varies according to TPC type and is not yet fully determined.

careful selection of materials and purification of the scintillator is required (see Section 36.6). Fiducialization and tagging can reduce background. One can also dissolve neutrinoless double beta decay ($0\nu\beta\beta$) isotopes in scintillator. This has been realized by KamLAND-Zen, which deployed a 1.5 m-radius balloon containing enriched Xe dissolved in scintillator inside KamLAND, and ¹³⁰Te is planned for SNO+.

36.3.1.2 Water Cherenkov detectors

Very large imaging water detectors reconstruct ten-meter-scale Cherenkov rings produced by charged particles (see Section 35.5). The first such large detectors were IMB and Kamiokande. The only currently existing instance of this class of detector, with fiducial mass of 22.5 kton and total mass of 50 kton, is Super-Kamiokande (Super-K, SK). Hyper-Kamiokande (Hyper-K) plans at least one, and possibly two, detectors with 187-kton fiducial mass. For volumes of this scale, absorption and scattering of Cherenkov light are non-negligible, and a wavelength-dependent factor $\exp(-d/L(\lambda))$ (where d is the distance from emission to the sensor and $L(\lambda)$ is the attenuation length of the medium) must be included in the integral of Eq. (35.6) for the photoelectron yield. Attenuation lengths on the order of 100 meters have been achieved.

Cherenkov detectors are excellent electromagnetic calorimeters, and the number of Cherenkov photons produced by an e/γ is nearly proportional to its kinetic energy. For massive particles, the number of photons produced is also related to the energy, but not linearly. For any type of particle, the *visible energy* E_{vis} is defined as the energy of an electron which would produce the same number of Cherenkov photons. The number of collected photoelectrons depends on the scattering and attenuation in the water along with the photo-cathode coverage, quantum efficiency and the optical parameters of any external light collection systems or protective material surrounding them. Event-by-event correc-

tions are made for geometry and attenuation. For a typical case, in water $N_{\text{p.e.}} \sim 15 \xi E_{\text{vis}}(\text{MeV})$, where ξ is the effective fractional photosensor coverage. Cherenkov photoelectron yield per MeV of energy is relatively small compared to that for scintillator, e.g., ~ 6 p.e./MeV for Super-K with a PMT surface coverage of $\sim 40\%$. In spite of light yield and Cherenkov threshold issues, the intrinsic directionality of Cherenkov light allows individual particle tracks to be reconstructed. Vertex and direction fits are performed using PMT hit charges and times, requiring that the hit pattern be consistent with a Cherenkov ring.

High-energy (~ 100 MeV or more) neutrinos from the atmosphere or beams interact with nucleons; for the nucleons bound inside the ¹⁶O nucleus, nuclear effects must be considered both at the interaction and as the particles leave the nucleus. Various event topologies, with final-state particles contained, exiting, or entering the detector, can be distinguished by their timing and fit patterns, and by presence or absence of light in a veto. At high energies, multi-photoelectron hits are likely and the charge collected by each PMT (rather than the number of PMTs firing) must be used; the energy resolution in this case is approximately $2\%/\sqrt{\xi E_{\text{vis}}(\text{GeV})}$. The absolute energy scale in this regime can be known to $\sim 2\text{--}3\%$ using cosmic-ray muon energy deposition, Michel electrons and π^0 from atmospheric neutrino interactions. Typical vertex resolutions for GeV energies are a few tens of cm [44]. Angular resolution for determination of the direction of a charged particle track is a few degrees. For a neutrino interaction, because some final-state particles are usually below Cherenkov threshold, knowledge of direction of the incoming neutrino direction itself is generally worse than that of the lepton direction, and dependent on neutrino energy.

Multiple particles in an interaction (so long as they are above Cherenkov threshold) may be reconstructed, allowing for the exclusive reconstruction of final states. In searches for proton decay,

multiple particles can be kinematically reconstructed to form a decaying nucleon. High-quality particle identification is also possible: γ rays and electrons shower, and electrons scatter, which results in fuzzy rings, whereas muons, pions and protons make sharp rings. These patterns can be quantitatively separated with high reliability using maximum likelihood methods [45]. Sources of background for high energy interactions include misidentified cosmic muons and anomalous light patterns when the PMTs sometimes “flash” and emit photons themselves. The latter class of events can be removed using its distinctive PMT signal patterns, which may be repeated. More information about high energy event selection and reconstruction may be found in reference [46].

In spite of the fairly low light yield, large water Cherenkov detectors may be employed for reconstructing low-energy events, down to *e.g.* $\sim 4\text{--}5$ MeV for Super-K [47]. Low-energy neutrino interactions of solar neutrinos in water are predominantly elastic scattering off atomic electrons; single electron events are then reconstructed. At solar neutrino energies, the visible energy resolution ($\sim 30\%/\sqrt{\xi E_{\text{vis}}(\text{MeV})}$) is about 20% worse than photoelectron counting statistics would imply. Using an electron LINAC and/or nuclear sources, approximately 0.5% determination of the absolute energy scale has been achieved at solar neutrino energies. Angular resolution is limited by multiple scattering in this energy regime ($25\text{--}30^\circ$). At these energies, radioactive backgrounds become a dominant issue. These backgrounds include radon in the water itself or emanated from detector materials, and γ rays from the rock and detector materials. In the few to tens of MeV range, radioactive products of cosmic-ray-muon-induced spallation are troublesome, and are removed by proximity in time and space to preceding muons, at some cost in dead time. Gadolinium doping using 0.2% $\text{Gd}_2(\text{SO}_4)_3$ has now been initiated for Super-K to improve selection of low-energy $\bar{\nu}_e$ and other events with accompanying neutrons [48].

The Sudbury Neutrino Observatory (SNO) detector [49] is the only instance of a large heavy water detector. In addition to an outer 1.7 kton of light water, SNO contained 1 kton of D_2O , giving it unique sensitivity to neutrino neutral current ($\nu_x + d \rightarrow \nu_x + p + n$), and charged current ($\nu_e + d \rightarrow p + p + e^-$) deuteron breakup reactions. The neutrons were detected in three ways: via capture on deuterons, via capture on dissolved ^{35}Cl , and via specialized ^3He counters.

36.3.1.3 Noble liquid detectors

Noble liquids scintillate and can be used as the active medium for particle detection. Detectors employing argon and xenon are also used as time-projection chambers (TPCs), either as dual-phase low-energy recoil detectors, or as track-imaging detectors. Noble-liquid detectors with low energy (few to few tens of keV) capability for detecting electronic and nuclear recoils are employed for dark matter and other rare event searches and are described in Sec. 36.4. These detectors can also be employed for some of the same physics (baryon number violation, astrophysical neutrino transient searches, etc.) as for the other large detectors described here, especially as they approach tens of ton scale and higher (*e.g.*, DARWIN, DarkSide-20, ARGO). Track-imaging time-projection chambers, which are described in detail Section 36.4, have a dynamic range reaching down to the few to few tens of MeV scale, enabling sensitivity to *e.g.*, solar and supernova burst neutrinos. Surface LArTPCs have significant cosmic backgrounds, but may still have sensitivity to astrophysical transients such as supernova burst neutrinos. DUNE will be sufficiently deep to have sensitivity to steady-state low-energy neutrino sources such as solar neutrinos.

36.3.2 Neutrino telescopes

Revised November 2021 by U.F. Katz (Erlangen U.) and C. Spiering (DESY, Zeuthen).

The primary goal of neutrino telescopes (NTs) is the detection of astrophysical neutrinos, in particular those which are expected to accompany the production of high-energy cosmic rays in astrophysical accelerators. NTs in addition address a variety of other fundamental physics issues like the indirect search for dark matter, studies of neutrino oscillations, searches for exotic particles

like magnetic monopoles or study of cosmic rays and their interactions [50–52]. Electromagnetic radio frequency detectors for high energy neutrinos are discussed in “Radio emission from (ultra-) high energy particle showers” section 36.3.3.

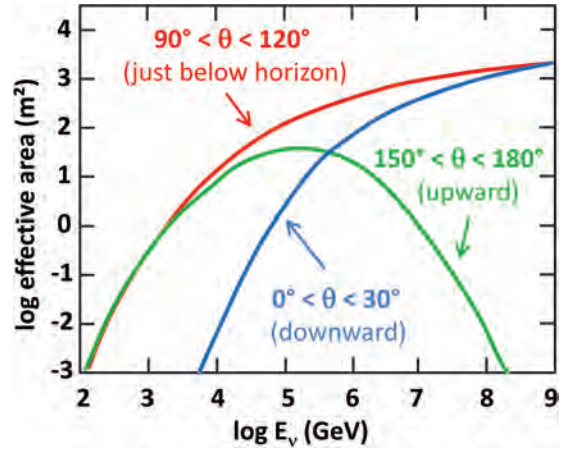


Figure 36.5: Average over the effective ν_μ and $\bar{\nu}_\mu$ areas for IceCube as an example of a cubic-kilometre NT, as a function of neutrino energy for three intervals of the zenith angle θ . The values shown here correspond to a specific event selection for point source searches.

NTs are large-volume arrays of “optical modules” (OMs) installed in open transparent media like water or ice, at depths that completely block the daylight. The OMs are sensitive to individual photons of the Cherenkov light induced by charged secondary particles produced in reactions of high-energy neutrinos in or around the instrumented volume. The time of photon-induced signals (“hits”) is registered with a precision of a few nanoseconds. The neutrino energy, E_ν , and direction can be reconstructed from the hit pattern recorded. NTs typically target an energy range $E_\nu \gtrsim 100$ GeV; sensitivity to lower energies is achieved in dedicated setups with denser instrumentation.

In detecting cosmic neutrinos, three sources of backgrounds have to be considered: (i) *atmospheric neutrinos* from cosmic-ray interactions in the atmosphere, which can be separated from cosmic neutrinos on a statistical basis, or, for down-going neutrinos, by vetoing accompanying muons; (ii) down-going punch-through *atmospheric muons* from cosmic-ray interactions, which are suppressed by several orders of magnitude with respect to the ground level due to the large detector depths and can be further reduced by selecting upward-going or high-energy neutrinos or by self-veto methods; (iii) random backgrounds due to photomultiplier (PMT) dark counts, ^{40}K decays (mainly in sea water) or bioluminescence (only water). Note that atmospheric neutrinos and muons allow for investigating neutrino oscillations and cosmic ray anisotropies, respectively.

In the last decade, it has become obvious that a precise measurement of the energy-zenith-distribution of atmospheric neutrinos in the energy range from a few to about 100 GeV may allow for determining the neutrino mass hierarchy by exploiting matter-induced oscillation effects in the Earth [53, 54].

Neutrinos can interact with target nucleons N through charged current ($\bar{\nu}_\ell N \rightarrow \ell^\mp X$, CC) or neutral current ($\bar{\nu}_\ell N \rightarrow \bar{\nu}_\ell X$, NC) processes. A CC reaction of a $\bar{\nu}_\mu$ produces a muon track and a hadronic particle cascade, whereas all NC reactions and CC reactions of $\bar{\nu}_e$ produce particle cascades only. CC interactions of $\bar{\nu}_\tau$ can have either signature, depending on the τ decay mode. Of particular interest is the so-called double-bang signature, where the τ decays sufficiently far away from the primary interaction to create a second, distinguishable cascade (typically at PeV energies and above). In most astrophysical models, neutrinos are expected to be produced through the $\pi/K \rightarrow \mu \rightarrow e$ decay chain, *i.e.*, with a flavour ratio $\nu_e : \nu_\mu : \nu_\tau \approx 1 : 2 : 0$. For sources outside the solar system, neutrino oscillations turn this ratio to $\nu_e : \nu_\mu : \nu_\tau \approx 1 : 1 : 1$ upon arrival on Earth.

The total neutrino-nucleon cross section is about 10^{-34} cm² at $E_\nu = 20$ TeV and rises roughly linearly with E_ν below this energy and as $E_\nu^{0.3-0.5}$ above, flattening out towards high energies. The CC:NC cross-section ratio is about 2:1. At energies above several TeV, neutrino absorption in the Earth becomes noticeable; for vertically upward-moving neutrinos (zenith angle $\theta = 180^\circ$), the survival probability is 74 (27, < 2)% for 10 (100, 1000) TeV. The energy transferred to the final-state lepton varies between 0 and 100% of E_ν , with a mean of 50% (65%) for neutrinos (antineutrinos) at 10 GeV and 75% for both neutrinos and antineutrinos at 10 PeV.

The final-state lepton follows the initial (anti)neutrino direction with an average mismatch angle of about $\langle\phi_{\nu\ell}\rangle \approx 1^\circ/(E_\nu/\text{TeV})^{0.55}$, with a steeper decrease beyond 10 TeV, reaching 0.005° at 1 PeV [55]. These values indicate the intrinsic kinematic limit to the angular resolution of NTs. For CC $\bar{\nu}_\mu$ reactions at energies above about 10 TeV, the angular resolution is dominated by the muon reconstruction accuracy of a few times 0.1° at most. For muon energies $E_\mu \gtrsim 1$ TeV, the increasing light emission due to radiative processes allows for reconstructing E_μ from the measured Cherenkov light intensity with an accuracy of $\sigma(\log E_\mu) \approx 0.3$; at lower energies, E_μ can be estimated from the length of the muon track if it is contained in the detector. These properties make CC $\bar{\nu}_\mu$ reactions the prime channel for the identification of individual astrophysical neutrino sources.

Hadronic and electromagnetic particle cascades at the relevant energies are 5–20 m long, *i.e.*, short compared to typical OM spacings. The total amount of Cherenkov light provides a direct measurement of the cascade energy with an accuracy of about 20% at energies above 10 TeV and 10% beyond 100 TeV for events contained in the instrumented volume. Except for double-bang events, the neutrino flavour and reaction mechanism can, however, be determined on a statistical basis at best, and neutrinos from NC reactions or τ decays may carry away significant “invisible” energy. Above 100 TeV, the average directional reconstruction accuracy of cascades is better than 10 (2) degrees in polar ice (sea water), the difference being due to the inhomogeneity of the ice and stronger light scattering in ice. These features, together with the small background of atmospheric $\bar{\nu}_e$ and $\bar{\nu}_\tau$ events, makes the cascade channel particularly interesting for searches for a diffuse, high-energy excess of extraterrestrial over atmospheric neutrinos. Cascade events can also be used to complement the muon channel in searches for point sources or transient signals, albeit with inferior angular accuracy compared to muon tracks.

The detection efficiency of a NT is quantified by its effective area, *e.g.*, the fictitious area for which the full incoming neutrino flux would be recorded (see Figure 36.5). The increase with E_ν is due to the rise of neutrino cross section and muon range, while neutrino absorption in the Earth causes the decrease at large θ for large E_ν . Identification of downward-going neutrinos requires strong cuts against atmospheric muons, hence the cut-off towards low E_ν at low θ . Due to the small cross section, the effective area is many orders of magnitude smaller than the geometrical dimension of the detector; a $\bar{\nu}_\mu$ with 1 TeV can, *e.g.*, be detected with a probability of the order 10^{-6} if the NT is on its path.

Due to the long muon range, CC interactions of up-going $\bar{\nu}_\mu$ can be detected from far outside the instrumented volume. This method also works for horizontal neutrinos up to about 10° above the horizon (depth dependent), where the background from atmospheric muons become prohibitive. Alternatively, one can select events that start inside the instrumented volume and thus remove incoming muons that generate early hits in the outer layers of the detector. Such a veto-based event selection is sensitive to neutrinos of all flavours from all directions, albeit with a reduced efficiency since a part of the instrumented volume is sacrificed for the veto. Such a muon veto, or vetoing events with a coincident signal in the surface array, also rejects down-going atmospheric neutrinos that are accompanied by muons from the same air shower and thus reduces the atmospheric-neutrino background. Actually, the breakthrough in detecting high-energy cosmic neutrinos was first achieved with this technique.

Note that the fields of view of NTs at the South Pole and in the

Northern hemisphere are complementary for each reaction channel and neutrino energy.

36.3.2.1 The Projects

Table 36.3 lists past, present and future neutrino telescope projects and their main parameters.

36.3.2.2 Properties of media

The efficiency and quality of event reconstruction depend strongly on the optical properties (absorption and scattering length, intrinsic optical activity) of the medium in the spectral range of alkali photocathodes (300–550 nm). Large absorption lengths result in a better light collection, large scattering lengths in superior angular resolution. Deep-sea sites typically have effective scattering lengths of > 100 m and, at their peak transparency around 450 nm, absorption lengths of 50–65 m. The absorption length for Lake Baikal is 22–24 m. The properties of South Polar ice vary strongly with depth; at the peak transparency wavelength (400 nm), the scattering length is between 5 and 75 m and the absorption length between 15 and 250 m, with the best values in the depth region 2200–2450 m and the worst ones in the layer 1950–2100 m.

Noise rates measured by PMTs with a diameter of 25 cm in deep polar ice are about 0.5 kHz per PMT and almost entirely due to radioactivity in the OM components. The corresponding rates in sea water are typically 60 kHz, mostly due to ^{40}K decays. Bioluminescence activity can locally cause rates on the MHz scale for seconds; the frequency and intensity of such “bursts” depends strongly on the sea current, the season, the geographic location, and the geometry of the detector elements. Experience from ANTARES shows that these backgrounds are manageable without a major loss of efficiency or experimental resolution.

36.3.2.3 Technical realisation

Optical modules (OMs) and PMTs: An OM is a pressure-tight glass sphere housing one or several PMTs with a time resolution in the nanosecond range, and in most cases also electronics for control, HV generation, operation of calibration LEDs, time synchronisation and signal digitisation.

Hybrid PMTs with 37 cm diameter have been used for NT-200, conventional hemispheric PMTs with 20 cm diameter for AMANDA and with 25 cm diameter for ANTARES, IceCube and Baikal-GVD. A novel concept has been chosen for KM3NeT. Each OM (43 cm) is equipped with 31 PMTs (7.5 cm), plus control, calibration and digitisation electronics. Advantages are that (i) the overall photocathode area exceeds that of a 25 cm PMT by more than a factor of 3; (ii) the individual readout of the PMTs results in a very good separation between one- and two-photoelectron signals which is essential for online data filtering and random background suppression; (iii) the hit pattern on an OM provides directional information; (iv) no mu-metal shielding against the Earth magnetic field is required. Figure 36.6 shows the OM designs of IceCube and KM3NeT.

Readout and data filtering: In current NTs the PMT data are digitised in situ: for ANTARES and Baikal-GVD in special electronics containers close to the OMs, for IceCube and KM3NeT inside the OMs. For IceCube, data are transmitted via electrical cables of up to 3.3 km length, depending on the location of the strings and the depth of the OMs; for ANTARES, KM3NeT and Baikal-GVD optical fibre connections have been chosen (several 10 km for the first two and 4 km for GVD).

The full digitised waveforms of the IceCube OMs are transmitted to the surface for pulses appearing in local coincidences on a string; for other pulses, only time and charge information is provided. For ANTARES (time and charge) and KM3NeT (time and time over threshold), all PMT signals above an adjustable threshold are sent to shore.

The raw data are subsequently processed on online computer farms, where multiplicity- and topology-driven filter algorithms are applied to select event candidates. The filter output data rate is about 10 GByte/day for ANTARES and of the order 1 TByte/day for IceCube (100 GByte/day transferred via satellite) and KM3NeT.

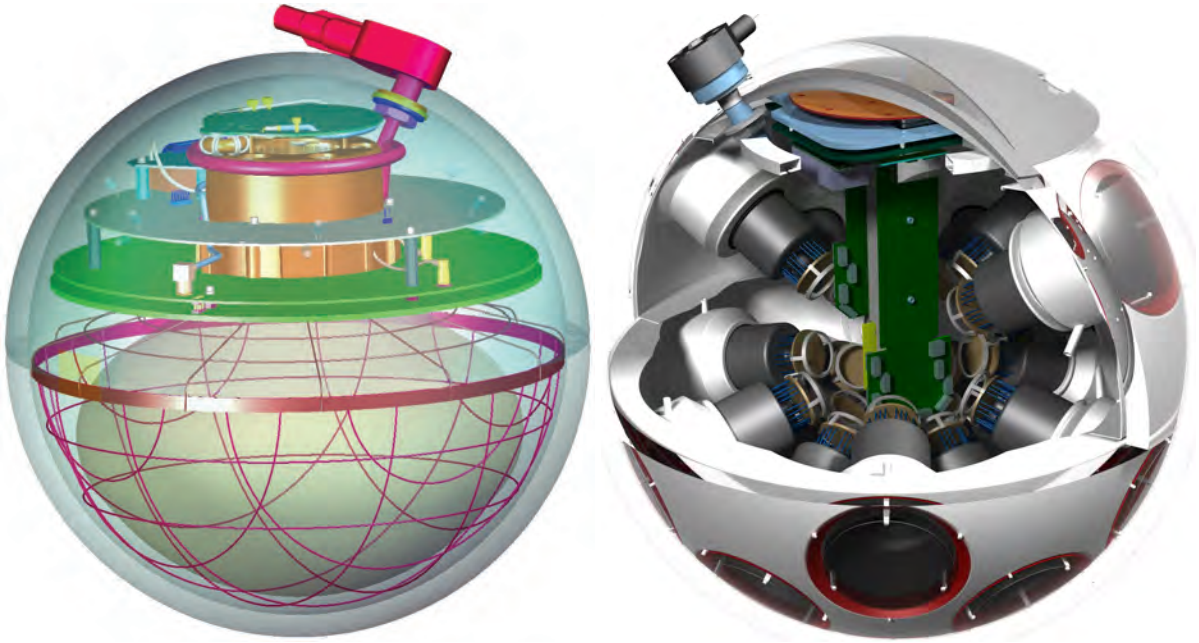


Figure 36.6: Schematic views of the digital OMs of IceCube (left) and KM3NeT (right).

Table 36.3: Past, present and future NT projects and their main parameters. The milestone years give the times of project start, of first data taking with partial configurations, of detector completion, and of project termination. Projects with first data expected past 2022 are indicated in italics. The size refers to the largest instrumented volume reached during the project development. See [52] for references to the different projects where unspecified.

Experiment	Milestones	Location	Size (km ³)	Remarks
DUMAND	1978/--/1995	Pacific Ocean		Terminated due to technical/funding problems
NT-200	1980/1993/1998/2015	Lake Baikal	10 ⁻⁴	First proof of principle
GVD [56]	2012/2015/--	Lake Baikal	0.5–1.5	High-energy ν astronomy first 8 clusters installed
NESTOR	1991/--/--	Med. Sea		2004 data taking with prototype
NEMO	1998/--/--	Med. Sea		R&D project, prototype tests
AMANDA	1990/1996/2000/2009	South Pole	0.015	First deep-ice NT
ANTARES	1997/2006/2008/--	Med. Sea	0.010	First deep-sea NT
IceCube [57]	2001/2005/2010/--	South Pole	1.0	First km ³ -sized detector
<i>IceCube-Gen2</i> [58, 59]	2014/--/--	South Pole	5–10	Planned extension of IceCube covering low and high energies, a surface array and radio detection
KM3NeT/ARCA [54]	2013/2021/--	Med. Sea	ca. 1	High-energy configuration for neutrino astronomy. Under construction, data taking with 8 strings
KM3NeT/ORCA [54]	2014/2020/--	Med. Sea	0.007	Low-energy configuration for neutrino mass hierarchy. Under construction, data taking with 10 strings
<i>KM3NeT Phase 3</i>	2013/--/--	Med. Sea	ca. 3	6 ARCA blocks + ORCA
<i>P-ONE</i> [60]	2018/--/--	Pacific Ocean	$\mathcal{O}(1)$	Possible future NT, R&D phase

Calibration: For efficient event recognition and reconstruction, the OM timing must be synchronised at the few-nanosecond level and the OM positions and orientations must be known to a few 10 cm and a few degrees, respectively. Time calibration is achieved by sending time synchronisation signals to the OM electronics and also by light calibration signals emitted in situ at known times by LED or laser flashers (ANTARES, KM3NeT). Precise position calibration is achieved by measuring the travel time of light calibration signals sent from OM to OM (IceCube) or acoustic

signals sent from transducers at the sea floor to receivers on the detector strings (ANTARES, KM3NeT, Baikal-GVD). Absolute pointing and angular resolution can be determined by measuring the “shadow of the moon” (*i.e.*, the directional depletion of muons generated in cosmic-ray interactions). IceCube and ANTARES have both shown that they have angular resolution below 1°, confirming MC calculations which indicate a precision of $\approx 0.5^\circ$ for energies above 10 TeV. For KM3NeT, simulations indicate that sub-degree precision in the absolute pointing can be

reached within a few weeks of operation.

Detector configurations: IceCube [57] (see Figure 36.7) consists of 5160 Digital OMs (DOMs) installed on 86 strings at depths of 1450 to 2450 m in the Antarctic ice; except for the DeepCore region, string distances are 125 m and vertical distances between OMs 17 m. 324 further DOMs are installed in IceTop, an array of detector stations on the ice surface above the strings. DeepCore is a high-density sub-array at large depths (*i.e.*, in the best ice layer) at the centre of IceCube.

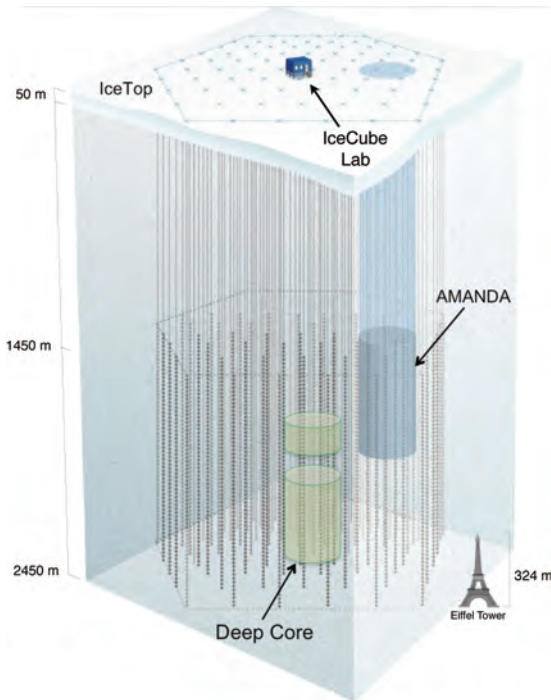


Figure 36.7: Schematic view of the IceCube neutrino observatory comprising the deep-ice detector including its nested dense part DeepCore, and the surface air shower array IceTop. The IceCube Lab houses data acquisition electronics and the computer farm for online processing. Operation of AMANDA was terminated in 2009.

The NT200 detector in Lake Baikal at a depth of 1100 m consisted of 8 strings attached to an umbrella-like frame, with 12 pairs of OMs per string. The diameter of the instrumented volume was 42 m, its height 70 m. Meanwhile (2021), the Baikal collaboration has installed the first eight clusters of a future cubic-kilometre array, GVD [56]. A first phase, covering a volume of about 0.7 km^3 , will consist of 14 clusters, each with 288 OMs at 8 strings; its completion is scheduled for 2024. A next stage could cover up to 1.5 km^3 .

ANTARES (see [52] and references therein) comprises 12 strings with lateral distances of 60–70 m, each carrying 25 triplets of OMs at vertical distances of 14.5 m. The OMs are located at depths of 2.1–2.4 km, starting 100 m above the sea floor. An additional string holds devices for calibration and environmental monitoring. A system to investigate the feasibility of acoustic neutrino detection has also been implemented.

KM3NeT will consist of building blocks of 115 strings each, with 18 OMs per string. Operation of prototypes and the first strings deployed have successfully verified the KM3NeT technology [61]. In the upcoming phase 2.0 of its staged implementation, KM3NeT aims at two building blocks for neutrino astronomy, with vertical distances between OMs of 36 m and a lateral distance between adjacent strings of 90 m (ARCA, for *Astroparticle Research with Cosmics in the Abyss*) and at one block for the measurement of the neutrino mass hierarchy, with vertical distances between OMs of 9 m and a lateral distance between adjacent strings of about 20 m (ORCA, for *Oscillation Research with Cosmics in the Abyss*) [54]. The installation of ARCA near Capo Passero, East of Sicily (depth

3440 m) and of ORCA near Toulon (depth 2450 m) is ongoing and as of now (August 2021) for each of both six strings have been deployed and are continuously operated. Completion of the full ARCA (ORCA) arrays is planned for 2026 (2025). The possibility of directing a neutrino beam from the Protvino accelerator to ORCA (P2O) is also under study [62].

P-ONE (*Pacific Ocean Neutrino Experiment*) [60] is a new initiative in an early R&D phase, envisaging a large NT in the Pacific Ocean off the Canadian coast. It is intended to use an existing deep-sea cable infrastructure and to optimise the sensitivity for horizontal neutrinos with energies of about 100 TeV and beyond.

36.3.2.4 Results

Atmospheric neutrino fluxes have been precisely measured with AMANDA ($\bar{\nu}_\mu$), with IceCube and ANTARES ($\bar{\nu}_\mu$, $\bar{\nu}_e$) and have recently also been detected with KM3NeT ($\bar{\nu}_\mu$); the results are in agreement with predicted spectra.

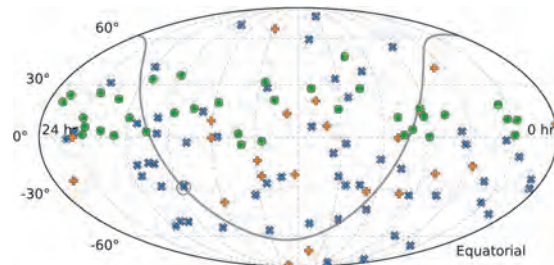


Figure 36.8: Arrival directions of IceCube candidate events for cosmic neutrinos in equatorial coordinates. The plot contains 82 HESE events, with shower-like events marked as blue \times and muon tracks as orange $+$, and in addition 36 through-going muons tracks with an energy deposit exceeding 200 TeV (green circles). Approximately 40% of the events are expected to originate from atmospheric backgrounds. The grey curve denotes the Galactic Plane and the grey circle the Galactic Centre (from [63]).

In 2013, an excess of track and cascade events between 30 TeV and 1 PeV above background expectations was reported by IceCube; this analysis used the data taken in 2010 and 2011 and for the first time employed containment conditions and an atmospheric muon veto for suppression of down-going atmospheric neutrinos (High-Energy Starting Event analysis, HESE). The observed excess reached a significance of 5.7σ in a subsequent analysis of 3 years of data [64] and increased in significance since then. The excess is therefore interpreted to be due to an astrophysical neutrino flux. A consistent observation has also been made by ANTARES [65], albeit with much lower significance. The skymap of HESE and high-energy through-going muon events (see Figure 36.8) does not indicate statistically significant event clusters, nor deviations from an isotropic cosmic neutrino flux. Meanwhile the energy range of IceCube analyses has been extended down to about 10 TeV and the high-energy excess confirmed; also, events with through-going muons showed a corresponding excess of cosmic origin. In [66], the various analyses have been combined. Assuming the cosmic neutrino flux to be isotropic, flavour-symmetric and ν - $\bar{\nu}$ -symmetric at Earth, the all-flavour spectrum is well described by a power law with normalisation $6.7^{+1.1}_{-1.2} \times 10^{-18} \text{ GeV}^{-1} \text{ s}^{-1} \text{ sr}^{-1} \text{ cm}^{-2}$ at 100 TeV and a spectral index -2.50 ± 0.09 for energies between 25 TeV and 2.8 PeV. A spectral index of -2 , an often quoted benchmark value, is disfavoured with a significance of 3.8σ .

Multi-messenger observations triggered by a high-energy IceCube neutrino event in 2017 (see Figure 36.9 for an event display), together with a neutrino excess from the same celestial direction in the 2014/15 archival IceCube data, yielded evidence for a first neutrino signal related to a known astronomical object, the blazar² TXS 0506+056 [67, 68]. Multi-messenger investigations in conjunction with gravitational waves, ultra-high-energy cosmic rays or gamma-ray observations have not revealed further,

²An Active Galactic Nucleus with a relativistic jet outflow pointing to the observer.

similarly significant neutrino signals to date. Also, no further astrophysical neutrino sources were found in a recent combined IceCube/ANTARES search for steady sources [69].

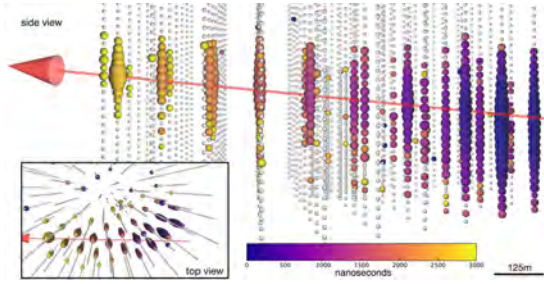


Figure 36.9: Display of the event IceCube-170922A, consistent with a neutrino from the blasar TXS 0506+056. The deposited energy is 24 TeV, the most probable neutrino energy is 290 TeV. The colour code indicates the signal timing (blue: early; yellow: late), the size of the coloured circles is a logarithmic measure of the light intensity registered per DOM. The arrow indicates the reconstructed neutrino direction, corresponding to a zenith angle of $5.7_{-0.3}^{+0.5}$ degrees below horizon. Figure from [67].

IceCube has reported an energy-dependent anisotropy of cosmic-ray induced muons, a measurement of the neutrino-nucleon cross section using neutrino absorption in Earth, and the observation of a cascade event consistent with the process $\bar{\nu}_e + e^- \rightarrow W^- \rightarrow \text{hadrons}$ (Glashow resonance).

No indications for neutrino fluxes from dark matter annihilations or for other exotic phenomena have been found.

At lower energies, down to 10 GeV, IceCube/DeepCore, ANTARES and meanwhile also KM3NeT have identified clear signals of oscillations of atmospheric neutrinos. The closely spaced OMs of DeepCore allow for selecting a very pure sample of low-energy $\bar{\nu}_\mu$ (6–56 GeV) that produce upward moving muons inside the detector. The neutrino energy is determined from the energy of the hadronic shower at the vertex and the muon range. Fits to the energy/zenith-dependent deficit of muon neutrinos provide constraints on the oscillation parameters $\sin^2 \theta_{23}$ and Δm_{23}^2 . The analysis of the same dependence for cascade-like events provides a $\sim 3\sigma$ evidence for ν_τ appearance – an important measurement to test the unitarity of the PMNS matrix [70].

See [71–73] for summaries of status, recent results and future plans of IceCube, ANTARES, KM3NeT, and GVD.

36.3.2.5 Plans beyond 2021

Within the future IceCube-Gen2 project, it is planned to extend the sensitivity of IceCube towards both higher and lower energies. To increase the detector sensitivity at high energies, a large-volume extension is envisaged, combined with a radio array for highest-energy neutrinos and a surface array providing also a powerful veto against atmospheric events [58, 59]. A substantially denser instrumentation of a sub-volume of DeepCore will be achieved with 7 closely spaced strings to be deployed in 2024/25 (the IceCube Upgrade), aiming to cover a low-energy program, to better calibrate the existing IceCube detector and the archival data, and to test new technologies. More information on the future extensions of GVD and KM3NeT and on P-ONE are given above, in Table 36.3 and in [54, 72].

36.3.3 Radio emission from (ultra-)high energy particle showers

Revised October 2021 by S.R. Klein (NSD LBNL; UC Berkeley) and A. Nelles (DESY, Zeuthen; Erlangen U.).

Coherent radio-frequency (RF) electromagnetic radiation is an attractive signature to search for particle cascades produced by interactions of high-energy particles. RF signatures have been used to study both cosmic-ray air showers and to search for neutrino-induced showers. This article will discuss the radio signal generation, the relevant energy regime and the application in detectors. Air showers are discussed in more detail in two recent reviews [74, 75]. At lower energies, incoherent optical Cherenkov

radiation is frequently used, as discussed in "Neutrino telescopes" section 36.3.2. This article uses the general definitions and properties of neutrino telescopes as described in 36.3.2.

36.3.3.1 Signal generation and its characteristics

As discussed in the "Passage of Particles Through Matter" review Sec. 34 the electromagnetic component of a high energy shower gives rise to radio emission. For the signal generation itself the type of primary particle is irrelevant. However, the signal medium is important. It must be non-conducting (and non-absorptive at RF frequencies). The different shower length scales (radiation length, X_0) between air and the solid materials used for neutrino searches leads to surprisingly large differences in shower development. Due to the interaction with the medium the shower contains more electrons than positrons, which results in a net charge excess and leads to coherent Cherenkov emission, also known as Askaryan effect [76–78]. In air, during propagation through the geomagnetic field, the relative motion of electrons and positrons is affected, which leads to a varying transverse current, usually referred to as the geomagnetic effect [74]. Both effects may be described more generally as being due to radiation from a time-varying net charge [79]. Their relative importance is governed by the density of the medium, as the electric field scales as the net charge excess, and a lower density allows the geomagnetic effect to gain importance. Thus, in solid materials the emission from the Askaryan effect dominates, but it is a $< 20\%$ correction in air showers.

Coherent radiation is possible at wavelengths longer than the instantaneous thickness of the shower along an observer's line of sight. Since air showers have a larger extent than showers in solid media, their coherent radiation appears at lower frequencies.

High-frequency radiation is concentrated around the Cherenkov angle θ_C . Viewed directly on the Cherenkov cone, the electric field strength, ϵ_{Ch} at a frequency f from an electromagnetic shower from a ν_e with energy E_ν in ice may be roughly parameterized as [80, 81]

$$\epsilon_{Ch} (\text{V/mMHz}) = 2.53 \times 10^{-7} \frac{E_\nu}{1 \text{TeV}} \frac{f}{f_c} \left[\frac{1}{1 + (f/f_c)^{1.44}} \right]. \quad (36.3)$$

The electric field strength increases linearly with frequency, up to a cut-off frequency f_c , which is set by the transverse size of the shower [82, 83]. The maximum wavelength c/f_c is roughly the Moliere radius divided by $\cos(\theta_C)$ where θ_C is the Cherenkov angle. The cutoff frequencies depend on the density (which affects the Moliere radius). They are about 1 GHz in ice, about 3 GHz in the lunar regolith, and below 100 MHz in air.

Near f_c , radiation is narrowly concentrated around θ_C [82, 83]. At lower frequencies, the limited length of the emitting region leads to a broadening in emission angle around the Cherenkov cone. Away from θ_C , the electric field from Eq. (36.3) is reduced by [80],

$$\frac{\epsilon}{\epsilon_{Ch}} = \exp \left(-\frac{1}{2} \frac{(\theta - \theta_C)^2}{(2.2^\circ \times [1 \text{GHz}/f])^2} \right). \quad (36.4)$$

The angular distribution of the signal around θ_C can be parameterized by a Gaussian peak modulated by a $\sin \theta$. In both ice and the lunar regolith, θ_C is about 56° , in air only 1° . Close to θ_C , the 1 GHz maximum frequency in ice/regolith leads to a generated pulse width of ≈ 1 nsec.

These equations are appropriate for ice. More general parameterizations can be found in [81, 84].

More accurate calculations of the predicted radio signal, in particular air showers are not easily parameterized, but require detailed Monte Carlo simulations. For air showers, these are built on microscopic air shower simulations, calculate the emission from all individual particles in the shower development and add them for different observer positions [74]. For neutrinos, most approaches calculate (directly or from a parameterization) the Askaryan signal from a shower profile. The signal is then propagated through the medium and into an antenna model [81].

At energies above 10^{16} eV in ice, the Landau-Pomeranchuk-Migdal effect lengthens electromagnetic showers, by reducing the

cross-sections for bremsstrahlung and pair production [85]. The lengthening of the shower leads to a narrowing of the radio emission around the Cherenkov cone, and a reduction in high-frequency emission away from the cone [81]. At higher energies, this leads to two separate components of the Askaryan radiation from a neutrino interaction: an un-altered component from the hadronic portion of the shower and an angularly narrowed component from the LPM-lengthened electromagnetic shower. The width of the narrowed component scales as $E_\nu^{1/3}$. If these two components can be observed separately, they could, in principle, be combined to determine the inelasticity of the neutrino interaction [86], allowing for improved measurements of low- x parton distributions and searches for beyond-standard-model interactions.

Similarly, energetic outgoing μ^\pm and τ^\pm from neutrino interactions will dominantly lose energy via stochastic pair production and photonuclear interactions. These secondary particles will produce electromagnetic showers that can be detected by radio detectors, if they are above threshold energy. This will enable multiple detections of the same particle track and thus present interesting reconstruction opportunities [87].

At still higher energies, above 10^{20} eV, the LPM effect strengthens, and the electromagnetic shower splits into multiple subshowers with significant separation. When these separations become large enough, the subshowers will effectively become independent radiators, with the total emission showing substantial event-by-event variation, depending on the division into subshowers [85]. Because of this, many experiments that study higher energy (well above 10^{20} eV) neutrinos focus on the hadronic shower from the struck nucleus. This contains an average of only about 20% of the energy, but with fewer large fluctuations.

36.3.3.2 Energy regime of radio detectors

The electric field amplitude is linearly proportional to the shower energy. Since the signal is a radio wave, the field amplitude decreases as $1/R$, plus potential absorption in the intervening medium, while the energy fluence decreases as $1/R^2$, again, plus potential absorption. The detection threshold depends on the distance to the antenna and the bandwidth and noise characteristics of the antenna and detector. For an antenna located in the detection medium, at a distance of 1 km the typical threshold is around 10^{17} eV. For stand-off (remote sensing) detectors, the threshold rises roughly linearly with the distance. These thresholds can be reduced by using directional antennas and/or combining the signals from multiple antennas using beam-forming techniques.

RF detectors are used to search for energetic neutrinos from three types of sources: astrophysical objects (*i.e.* extending measurements of the neutrino energy spectrum observed at TeV to PeV energies upward in energy), cosmogenic neutrinos associated with cosmic-ray-cosmic microwave background radiation (CMBR) interactions, and neutrinos from beyond-standard-model physics. These types are very roughly associated with energies below 10^{18} eV, the energy range 10^{18} to 10^{20} eV, and above 10^{20} eV.

Cosmogenic neutrinos are produced when ultra-high energy (UHE) protons with energy $E > 5 \times 10^{19}$ eV interact with photons from the CMBR, infrared light from old stars, and other extragalactic background light. These protons are excited to a Δ^+ resonance which may decay via $\Delta^+ \rightarrow n\pi^+$, leading to neutrinos with energies above 10^{18} eV [88, 89]. The cosmogenic neutrino signal depends heavily on the fraction of UHE cosmic-rays that are protons. For a 100% proton composition (disfavored by most data [90]), observing a cosmogenic neutrino signal of at least a few events per year requires a solid or liquid detector with an active volume of about 100 km^3 .

To reach the effective volumes necessary to observe the expected low fluxes of UHE neutrinos, common, naturally occurring, non-conducting solid (or potentially liquid) media, with a long absorption length for radio waves are needed. Optical Cherenkov and acoustical detectors are limited by short (< 100 m) attenuation lengths [91] so would require a prohibitively expensive number of sensors. The radio detection technique has been used to detect air showers, targeting neutrinos as well as cosmic rays, and to search for neutrino showers in ice, salt domes and the lunar regolith.

36.3.3.3 Reconstruction of particle energy and direction and background suppression

Since radio detectors view the interaction from afar, the reconstruction techniques differ from optical neutrino telescopes.

Radio detection is a calorimetric measurement, thus provides good energy estimates of the shower energy. The energy fluence (integrated pulse power) of the signal scales quadratically with shower energy. It also depends on the distance to the shower, through potential attenuation losses and the usual $1/R$ loss in electric field amplitude. The arrival times in antennas and a spherical wave approximation can be used to determine the interaction vertex, although some uncertainty due to the viewing angle with respect to the Cherenkov angle may remain, if not corrected for by using the frequency information. If the radio signal travels through media where the index of refraction varies (like the firm of glacial ice), then ray-tracing techniques may be required to follow the signal back to the interaction point. For buried antennas, the bending of the signal trajectories due to the index of refraction creates an opportunity. For some geometries, there may be two paths to the detector: a 'direct' path, with minor bending, and a second where the signal is bent beyond horizontal, bouncing off the surface before reaching the antenna. By measuring the time difference between the two paths, the distance to the interaction vertex may be determined; this greatly simplifies the energy determination [92, 93]. For most neutrino interactions (except for ν_e charged-current interactions), the shower energy is less than the neutrino energy. The uncertainty on the interaction inelasticity is a major contributor to the uncertainty in the neutrino energy, along with uncertainties on the distance between the antenna(s) and the interaction vertex [94].

Reconstruction of the neutrino arrival direction depends on several aspects of the signal. First, the direction from the antenna to the interaction site must be determined. This can be done by using the relative timing from separated antennas, or using beam-forming techniques with multi-element arrays. For air showers, the signal arrival direction is (almost) equal to the particle arrival direction, with corrections being obtainable by fitting a hyperbolic wavefront [74, 75].

For showers in solid/liquid media, the arrival direction with respect to the interaction point - antenna vector is determined from two additional angles. The frequency spectrum can be used to determine the angle between signal arrival direction and Cherenkov cone according to Eq. (36.4) [95]. The second angle can be determined from the polarization of the signal. The radio signal is produced with a linear polarization in the plane containing both the particle direction and the radio wave direction. These two angles can be combined to determine the direction, subject to a (usually) four-fold ambiguity, due to uncertainty as to whether the antenna is inside or outside the Cherenkov cone, and because the particle direction can be flipped 180° without affecting the observed signal. Often, some of these solutions can be rejected because they correspond to long path lengths through the Moon or the Earth, where the neutrino would be absorbed.

Spectral information is crucial for the reconstruction and background rejection. However, large bandwidth antennas typically disperse (*i.e.* broaden) the pulses. As long as the dispersion can be compensated for and backgrounds controlled, a large bandwidth detector is the most sensitive.

All radio experiments must contend with background. Common sources are anthropogenic noise, antenna/preamp noise, charge generated by blowing snow, lightning, and, at low frequencies, radiation from the Milky Way. While narrowband noise impacts triggering and contaminates signal quality, impulsive backgrounds could mimic a signal. One of the major issues for radio-detection experiments is anthropogenic noise. Most anthropogenic noise has distinctive characteristics (such as being narrow-band, and coming from near the horizon) which makes it relatively easy to reject during data analysis, via narrow-band filters and other techniques [74]. However, these factors complicate triggering and reduce data purity. This is even an issue in Antarctica, where communication radios and passing satellites can mimic showers, at least at the trigger level. The need to limit anthropogenic noise has led most experimental groups to select remote locations for

their detectors. Still, experiments have used approaches to reduce trigger-level noise, and/or to reject background at the analysis level. For example, for multi-element arrays, the threshold drops as the square root of number of antennas, since the signal adds in-phase while the backgrounds add with random phases [96].

Most dedicated air shower experiments have used radio antennas in combination with at least one other detector technology, such as scintillation counters, if the site quality is not sufficient and/or computing power on autonomous stations is limited. One exception is ARIANNA, which is located in an uninhabited part of Antarctica, enabling them to efficiently self-trigger on air showers [97].

Lunar experiments (discussed below) use different techniques to reduce the anthropogenic background. Some experiments use multiple antennas, separated by at least hundreds of meters; by requiring a coincidence within a small time window, anthropogenic noise can be rejected. With good enough timing, beam-forming techniques can be used to further reduce the background. An alternative approach is to use beam forming with multiple feed antennas viewing a single reflector, to ensure that the signal points back to the moon.

Due to the similarity in the radio emission of air showers and neutrino showers, the more abundant cosmic rays can act as background to neutrino searches. In-ice detectors need to suppress in-air emission that is refracted into the ice, emission that is created from developing air showers continuing in the ice, as well as from stochastic energy-losses of atmospheric muons. Lunar experiments may face challenges in separating neutrino interactions from cosmic ray interactions.

36.3.3.4 Recent experiments

Figure 36.10 shows some current limits from neutrino searches, including from prototype arrays. Except for LOFAR, which is fully operational, projected limits from future experiments are not shown in the figure.

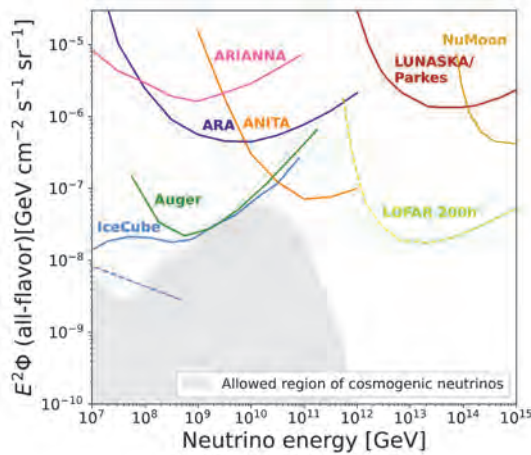


Figure 36.10: Representative 3-flavor (summed, assuming equal fluxes of each flavor) differential (over one decade in energy) limits from different experiments and prototype experiments. Shown are limits from the IceCube ultra-high energy ν search [98], the Auger search for earth-skimming ν_τ [99], the LUNASKA/Parkes [100] and NuMoon lunar searches [101], the ANITA balloon experiment [102], ARA [103] and ARIANNA prototypes [104], along with projections for the LOFAR array [105]. The dashed blue line is the extrapolation of the IceCube through-going ν_μ flux measured at lower energies (few 10s of TeV to 10 PeV), with spectral index $\alpha = -2.28$ [106]. Because of the long extrapolation, this should only be treated as a rough reference. The ARA and ARIANNA limits are from prototype arrays, and indicate the energy range that might be covered, with far higher sensitivity by larger arrays. The shaded area is the allowed region for cosmogenic neutrinos, from a recent global analysis that included the measured cosmic-ray spectrum and composition [107].

i. Ice

The most common dense medium transparent to radio waves is ice. Natural ice is an attractive medium for neutrino detection with radio attenuation lengths from over 300 m to 1 km [108]. The attenuation length varies with frequency and ice temperature, with higher attenuation in warmer ice. Although glacial ice is mostly uniform, the top ≈ 100 m of ice, the 'firn,' exhibits a gradual transition from packed snow at the surface (typically $\rho = 0.35$ g/cm³) to solid ice ($\rho = 0.92$ g/cm³) below [109]. The thickness of the firn varies with location; it is thicker in central Antarctica than in the coastal ice sheets or in Greenland. The varying density has several implications.

The index of refraction depends linearly on the density, so radio waves curve downward in the firn. This bending reduces the effective volume of surface or aerial antennas. A surface antenna cannot see near-surface interactions at large horizontal distances. There are also indications that the increase in firn density is non-monotonic [110, 111]. This leads to non-monotonic changes in index of refraction which may create waveguides that trap a small fraction of the radio energy and propagate it horizontally.

In one type of experiment, antennas mounted on high-altitude balloons observe the ice from above. Radio signals from in-ice neutrino interactions propagate to the surface, traverse the ice-air interface, and then travel to the balloon. The surface roughness of the ice can affect signals as they transition from the ice to the atmosphere. The best known example, ANITA, has made four flights around Antarctica, floating at an altitude around 35 km [112]. Its 32/40/48 (depending on the flight) dual-polarization horn antennas scanned the surrounding ice, out to the horizon (650 km away). Because of the small angle of incidence, ANITA could use polarization information to separate signals from background; ν signals should be vertically polarized, while most background from cosmic-ray air showers should be horizontally polarized.

As with all radio-detection experiments, ANITA had to contend with anthropogenic backgrounds. The ANITA collaboration uses their multiple antennas as a phased array to achieve good pointing accuracy, with a resolution of 0.2-0.4° in elevation, and 0.5-1.1° in azimuth. They rejected all events that pointed toward known or suspected areas of human activity. ANITA has set the most stringent flux limits yet on neutrinos with energies above 10²⁰ eV [102]. The ANITA experiment has also reported several anomalous events, matching cosmic ray signals, but with unexpected polarization signature, which the collaboration has indicated might be from Earth-skimming ν_τ [113, 114]. However, this interpretation is controversial.

Because of the significant source-detector separation, ANITA is most sensitive at energies above 10¹⁹ eV. A lower energy threshold requires a smaller antenna-target separation.

Other ice based experiments use antennas located within the active volume, allowing them to reach thresholds around 10¹⁷ eV, or lower with phased array antennas. This approach was pioneered by the RICE experiment [115] which buried 18 half-wave dipole antennas in holes drilled for AMANDA at the South Pole, at depths from 100 to 300 m. The hardware was sensitive from 200 MHz to 1 GHz. Each antenna fed an in-situ preamplifier which transmitted the signals to surface digitizing electronics.

More recently, two groups have deployed prototype arrays which have explored different detector concepts. The Askaryan Radio Array (ARA) deployed surface and buried antennas at the South Pole [116], while the Antarctic Ross Iceshelf Antenna Neutrino Array (ARIANNA) installed surface antennas on the Ross Ice Shelf [104], about 110 km north of McMurdo station. ARIANNA offered the possibility of detecting downward-going ν , from the radio waves reflected off the ice-sea water interface on the bottom of the Ross Ice Shelf, while ARA took advantage of the colder, deeper ice at the South Pole, with its longer radio attenuation length. ARA buried antennas up to 200 m deep to be able to observe a larger portion of ice, due to the refraction of the signal in the firn. In contrast, ARIANNA deployed antennas just below the surface, allowing them to use high-gain, but large log periodic dipole antennas. Recently, phased-array trigger techniques have been demonstrated that can reduce the energy threshold by a

factor of several [96, 117].

Both experiments use stations which operate independently, spaced far enough to maximize sensitivity, but where only a small fraction of neutrino events will be visible in multiple stations. Each station includes multiple antennas, which will be sensitive to both horizontal and vertical polarization. The expected angular resolution is a few degrees [95].

In 2021, the Radio Neutrino Observatory Greenland (RNO-G) started deploying stations at Summit Station. RNO-G is planned to consist of 35 stations, which employ ARIANNA-style surface antennas, an ARA-style phased array and deep antennas, and draw heavily on ANITA's electronics heritage [118].

ii. The Moon

Because of its large size and non-conducting regolith, and the availability of large radio-telescopes, the Moon is an attractive target [119]. Conventional radio-telescopes are quite well suited to lunar neutrino searches, with natural beam widths not too dissimilar from the size of the Moon. Still, there are experimental challenges. The attenuation length is typically estimated to be $9m/f(\text{GHz})$ [120], so only near-surface interactions can be studied. The composition of the lunar regolith is not well known, and there are significant uncertainties due to this uncertainty. One big limitation of lunar experiments is that the 385,000 km target-antenna separation leads to energy thresholds above 10^{20} eV.

The effective volume probed by experiments depends on the geometry, which itself depends on the frequency range used. At high frequencies f , the electric field strength is high, leading to a lower energy threshold, but the sensitive volume is limited because the Cherenkov cone only points toward the Earth for a narrow range of geometries. Lower frequency radiation is more isotropic, so the effective volume is larger, but, because the electric field is weaker, the energy threshold is higher. The $1/f$ dependence of the attenuation length in the lunar regolith further increases the effective volume at low frequencies. The frequency range affects the energy dependence of the sensitivity. As can be seen in Fig. 36.10, a low-frequency experiment like NuMoon (which covered 115-180 MHz) has good sensitivity, but only above about 10^{14} GeV, while Lunaska/Parkes, which observed in the range 1200-1500 MHz, has a higher flux limit, but is sensitive above about $10^{12.5}$ GeV.

Current limits and projected sensitivities are sensitive to many details. A recent review [121] compared different radio-detection experiments using a common framework, and found some significant shifts in sensitivities due to, e.g. different assumptions about lunar composition and inelasticities.

With modern technology, it is increasingly viable to search over very broad frequency ranges [122]. One technical challenge is due to dispersion (frequency dependent time delays) in the ionosphere. Dispersion can be largely removed with a de-dispersion filter, using either analog circuitry or post-collection digital processing.

iii. Air

Radio detection in air is sensitive to all particles inducing air showers. Radio-detection can be used to determine the energy of cosmic rays, as done by e.g. the Auger and Tunka-Rex experiments [123, 124]. Radio signals can also be used to infer the altitude for shower-maximum, where the shower contains the most particles, as done by e.g. the LOFAR and Tunka-Rex collaborations [124, 125]. This altitude is sensitive to the cosmic-ray composition. Reconstructing the particle arrival direction is much easier in air since the Cherenkov angle, and thus the radio wavefront, aligns with the axis to 1° . Radio-detection is also useful for energy cross-calibrations between different experiments and may be able to provide an independent energy scale calibration for air shower arrays [126].

One variation on the radio-detection approach is to look for radio emission from Earth-skimming ν_τ . Although ν_τ are much less commonly produced than ν_μ and ν_e , over astrophysical distances, oscillations lead to a $\nu_e : \nu_\mu : \nu_\tau$ ratio near $1 : 1 : 1$, for almost all non-exotic acceleration and propagation mechanisms [127].

If the ν_τ traverse the Earth and interact while traveling upward, near the surface, the resulting τ^\pm may exit the Earth before decaying. 83% of the time, the decay produces a hadronic or electromagnetic shower in the atmosphere [128]. Experiments have searched for these upgoing showers, and for the resulting optical Cherenkov and coherent RF radiation. The threshold energy dependence for these searches depends on several factors, notably including the average τ^\pm decay length, which increases linearly with energy; the Pierre Auger observatory sets stringent limits on the neutrino flux at energies above 10^{17} eV [99].

36.3.3.5 Future experiments

Looking ahead, RNO-G [118] will continue deployment until 2024 and reach the largest yearly sensitivity of any radio array thus far. Further out, the proposed IceCube Gen2 expansion includes a substantial radio array component [59], which will be sensitive to both neutrinos from the ice and air showers from cosmic rays. PUEO, a successor of ANITA has been funded and is scheduled for its first flight in 2024 [129].

In the near future, several large radio detector arrays should reach significantly lower energies for lunar neutrino detection. The LOFAR array is taking data with 36 detector clusters spread over Northern Europe [105]. In the longer term, the Square Kilometer Array (SKA) with its 1 km^2 effective area will push thresholds down to near 10^{20} eV [122]. The SKA will also study air showers.

A number of dedicated prototype ν_τ radio-detection experiments exist. The GRAND Collaboration recently proposed to deploy a 10,000 antenna array, eventually growing to 200,000 antennas spread over $200,000 \text{ km}^2$. Its stations are simple autonomous units that sample the 30-100 MHz range using antennas optimized for near-horizontal signals [130]. The first phase GRAND-proto 300 is scheduled for deployment in 2021. The Pierre Auger Collaboration is currently upgrading their surface array to include radio antennas at all water Cherenkov detectors. This array will improve the sensitivity of the instrument to horizontal showers, both for composition sensitivity for cosmic rays and for the detection of Earth skimming neutrinos [131].

36.4 Large time-projection chambers for rare event detection

Revised October 2019 by T. Shutt (SLAC).

Rare event searches require detectors that combine large target masses and low levels of radioactivity, and that are located deep underground to eliminate cosmic-ray related backgrounds. Past and present efforts include searches for the scattering of particle dark matter, neutrinoless double beta decay, and the measurement of solar neutrinos, while next generation experiments will also probe coherent scattering of solar, atmospheric and diffuse supernova background neutrinos. Large time projection chambers (TPCs) [132], adapted from particle collider experiments, have emerged as a leading technology for these efforts. Events are measured in a central region confined by a field cage and usually filled with a liquid noble element target. Ionization electrons are drifted (in the z direction) to an anode region by use of electrode grids and field shaping rings, where their magnitude and $x - y$ location is measured. In rare event searches (with no external trigger available) scintillation generated at the initial event site is also measured, and the time difference between this prompt signal and the later-arriving charge signal gives the event location in z for a known electron drift speed. Thus, 3D imaging is achieved in a monolithic central volume. The relatively slow readout due to the drift of charges ($\sim 1/2 \text{ ms/m}$ at 1 kV/cm) [133] is not a major pile-up concern in low background experiments. Noble elements have relatively high light yields (comparable to or exceeding the best inorganic scintillators), and the charge signal can be amplified by multiplication or electroluminescence. Radioactive backgrounds are distinguished by event imaging, the separate measurements of charge and light, and scintillation pulse shape. For recent reviews of noble element detectors, see [134-137].

Methods for achieving very low radioactive backgrounds are discussed in general in section 35.6. The basic architecture of large TPCs is very favorable for this application because gas or liquid targets can be relatively easily purified, while the gener-

ally more radioactive readout and support materials are confined to the periphery. The 3D imaging of the TPC then allows self shielding in the target material, which is quite powerful when the target is large compared to mean scattering lengths of order ~ 10 cm for \sim MeV neutrons and gammas from radioactivity. Most recent experiments have immersed the TPCs in hermetic water shields to eliminate external radioactive backgrounds, and several are also using an active scintillator inner layer to further veto backgrounds from detector materials. While other target fluids are possible, almost all recent efforts have used Xe and Ar. In LHe and LNe the mobility of electrons is $\sim 10^3$ times lower than in the heavier noble elements due to the formation "bubbles" around electrons. [138, 139] It is worth noting that scintillation and electron drift are possible in a number of organic fluids, possibly providing a route to economical large detectors, but with much reduced performance compared to noble elements.

In noble element targets, all non-noble impurities are readily removed (e.g., by chemical reaction in a commercial getter) so that only radioactive noble isotopes are a significant background concern. Xe, Ne and He have no long lived radioactive isotopes (apart from the ^{136}Xe , discussed below, and the very long-lived ^{124}Xe [140]). Kr has ~ 0.3 MBq/kg of the beta emitter ^{85}Kr created by nuclear fuel reprocessing [141], making it unusable as a target, while the ~ 1 Bq/kg level of the beta emitter ^{39}Ar [142] is a nuisance for Ar-based experiments. Both of these can be backgrounds in other target materials, as can Rn emanating from detector components. Relatively low background materials are available for most of the structures surrounding the central target, with the exception of radioactive glasses and ceramics usually present in PMTs, feedthroughs and electrical components. Very low background PMTs with synthetic quartz windows, available over the last 15 years (see, e.g., [143]), have been a key enabling technology for dark matter searches. Radio-clean SiPMs and related Si-based photon detectors are increasingly being used in cases where their dark rates (which are significantly higher than PMTs) can be tolerated.

An important technical challenge in liquid detectors is achieving the high voltages needed for electron drift and measurement. In general, quench gases which stabilize charge gain and speed electron transport in wire chambers cannot be used, since these absorb and/or quench scintillation light and can trap electrons. It is also important to suppress low-level emission of electrons and associated photons which can otherwise swamp low energy signals. Drift of electrons over meter scales with minimal loss from attachment on trace levels of dissolved impurities (e.g., O_2) has so far required continuous circulating purification.

36.4.1 Dark matter and other low energy signals

A major goal of low background experiments is detection of WIMP (Weakly Interacting Massive Particle) dark matter through scattering on nuclei in a terrestrial detector (for a recent review, see [144]). Energy transfers are generally small, a few tens of keV at most. Liquid noble TPCs distinguish single nuclear recoils (NR) from dark matter from the dominant background of electron recoils (ER) from gamma rays and beta decays by rejecting multiple scatters, and, as described below, based on both the ratio of charge to light and the scintillation pulse shape. Neutrons are a NR background, but are present at much lower rates than gammas and betas, and also undergo significant multiple scattering. To detect small charge signals, a dual phase technique is used wherein electrons from interactions in the liquid target are drifted to the liquid surface and extracted with high field (~ 5 kV/cm) into the gas phase where they create an amplified electroluminescence signal which is usually measured by an array of PMTs located just above the liquid. (While both charge multiplication and electroluminescence are possible in liquid, they require very high fields created by very small electron structures and thus have not seen widespread adoption. For recent progress see [145]) This technique readily measures single electrons with \sim cm $x - y$ resolution.

The measurement of the initial scintillation signal, by contrast, suffers from loss upon reflection from the TPC walls, and inefficiency in the readout, and usually limits the energy threshold. In LXe, the ~ 178 nm wavelength is just long enough to be trans-

mitted through high purity synthetic quartz PMTs windows, and, remarkably, PTFE immersed in LXe has $\sim 97\%$ reflectivity. [146] The ~ 128 nm scintillation light of LAr requires waveshifting (usually using TPB) both for reflectivity (usually on PTFE) and for efficient measurement. With both liquids, a second sensor array at the bottom of the TPC is used to maximize light collection, and total photon efficiencies have been in the 10-15% range. Typical raw yields for ER are several tens of electrons and photons per keV, and, in LXe, a NR threshold of ~ 5 keV has been achieved [147].

The microscopic processes leading to signals in liquid nobles are complex. Energy deposited by an event generates pairs of free electron and ions, and also atoms in their lowest excited state. The latter rapidly form excimers which de-excite by emitting light. Excimers arise in both triplet and singlet states which have the same energy but different decay times. In an event track, some fraction of electrons recombine with ions, while the rest escape and are measured. Each recombined ion creates an additional excimer, and hence another photon. Finally, some part of the energy is lost as heat - a small fraction for ER but a dominant and energy dependent fraction for NR. The branching into these various modes depends on drift field, energy, and particle type, requiring extensive calibrations. These have largely been carried out for LXe (see, e.g., [148]), and have been incorporated into the NEST Monte Carlo framework. [149]

This complexity also gives rise to discrimination between ER and NR: for the same visible energy, the slower NR create short, denser tracks and generate a higher fraction of initial excitons, leading to a smaller ratio of measured charge to light. NR also generate a higher ratio of short-lived singlet state to long-lived triplet states than ER, so that the scintillation signal itself gives pulse shape discrimination (PSD). Charge/light discrimination has been well mapped in LXe, and, remarkably, is very high ($>99.9\%$) below ~ 10 keV for NR. [147] It has only recently been measured in LAr [150], and has not yet played an important role in LAr based experiments. Qualitatively, PSD is similar in LXe and LAr - strong at high energy and weak at low energy. However it is well mapped only in LAr where it is very high above ~ 50 keV, achieving values above $\sim 10^8$. [151]

This extremely powerful PSD in LAr is sufficient to overcome the ER background from ^{39}Ar , which is roughly 10^7 times higher than the fundamental low energy ER background from p-p solar neutrinos. In a multi-ton detector the event rate from ^{39}Ar poses a significant pile-up challenge, and the DarkSide collaboration is pursuing ^{39}Ar reduction through two methods. One, for which a factor 1400 reduction in ~ 50 kg Ar has been demonstrated, is extracting "aged" Ar from underground (cosmic ray shielded) gas deposits in which the 269 yr half-life ^{39}Ar has decayed. [152] The other method is removal by distillation. The need for ^{39}Ar depleted Ar negates the much lower raw material cost of Ar compared to Xe. Kr must also be removed from both Xe and Ar experiments (and Ar must be from Xe experiments), comparatively easy tasks compared to isotopic separation. This is done through distillation or a chromatographic technique. In current LXe experiments the remaining dominant ER backgrounds is the beta decay of a daughter of ^{222}Rn in the active LXe, where the Rn has emanated from detector materials or external plumbing. Rn will be even more important as experiments scale up in size, but can in principle be reduced by better materials screening and online Rn separation, again by either distillation or chromatography. Neutrons are in general some six orders of magnitude less abundant than gamma rays and betas in U and Th decay chains, but they naturally scatter in the WIMP energy range, and their single scatters cannot be discriminated against. Self shielding is less powerful for neutrons than gamma rays, so that they are an increasingly important background at the current ton scale and future larger experiments, both in Ar and Xe. Active outer shielding layers which tag and veto neutrons are being included in most next generation experiments.

The WIMP sensitivity is a combination of backgrounds, discrimination, and WIMP scattering rates. The scattering rates are model dependent, but are in general dominated by spin-independent coherent scattering on the full nucleus. This has an

A^2 dependence, favoring high mass targets. The energy spectrum is close to a falling exponential, so that the lowest possible energy threshold maximizes sensitivity. Experiments using LXe TPCs have had the leading sensitivity for standard WIMP dark matter for well over a decade, for all but the lowest WIMP masses. The ton-scale XENON1T [153] achieved a WIMP-nucleon sensitivity of $4.1 \times 10^{-47} \text{ cm}^2$ at 30 GeV mass, closely followed by PANDAX-II [154] and LUX [155]. The next generation ~ 7 tonne experiments LZ [156] and XENONnT [157], and ~ 4 tonne PandaX-4T [158] are currently in late stages of construction. The DarkSide program is carrying out WIMP searches with LAr TPCs. The 50 kg DarkSide-50 achieved a sensitivity $\gtrsim 40$ times poorer than XENON1T. A 50 ton scale-up, DarkSide-20 is being pursued which features SIPMs instead of PMTs. [159]. (The best current limit using LAr is not from a TPC, but instead the scintillation-only DEAP-3600 experiment. [151])

LZ and XENONnT project sensitivity to WIMPs about a decade above the “floor” of coherent scattering of astrophysical neutrinos, which, absent a directional measurement (see below), are essentially indistinguishable from WIMPs. DARWIN, a proposed a 50 ton LXe TPC would approach the practical limit set by this floor for WIMP masses above ~ 5 GeV [160], while ARGO a ~ 200 ton LAr detector would achieve similar sensitivity for WIMPs masses well above ~ 50 GeV. [159]

There has been recent interest in models featuring low mass dark matter. These give rise to low energy recoils, and also strongly favor low mass target nuclei (despite the A^2 rate penalty). This has led to renewed focus on events below the scintillation threshold, where the charge signal alone achieves very low threshold due to the gain of the electroluminescence readout. This preserves $x - y$ spatial information, but only very weak depth information based on electron diffusion. Thus it is subject to the high backgrounds at the top and bottom of the active region, and decays of Rn daughters on grids. While the first such results came from XENON10, a recent result in LAr from DarkSide-50 extends to much lower dark matter mass because of the lower mass of Ar. To maximize the sensitivity of such searches in the future, studies have begun to understand and minimize the sources of electron backgrounds from both radioactivity and spurious sources such as field emission from grids. There is also an effort to develop a superfluid He TPC [161] read out with superconducting sensors (similar to the proposed HERON solar neutrino experiment). The rich set of signals in this case - scintillation, retons, and ionization - potentially offer significant background rejection.

Measurement of NR recoil track direction would provide proof of the galactic origin of a dark matter signal since the prevailing WIMP direction varies on a daily basis as the earth spins. This cannot be achieved for the sub-micron tracks in any existing solid or liquid technology, but the mm-scale tracks in a low pressure gas (typically, $P \sim 50$ Torr) could be imaged with sufficiently dense instrumentation. Directionality can be established with $O(10^2)$ events by measuring just the track direction, while, with finer resolution that distinguishes the diffuse (dense) tail and dense (diffuse) head of NR (ER) tracks, only $O(10)$ events are required. Such imaging requires a high energy threshold, decreasing WIMP sensitivity, but also powerfully rejecting less dense ER background tracks.

A variety of TPC configurations are being pursued to accomplish this, most with a CF_4 target. The longest established effort, DRIFT, avoids diffusion washing out tracks for electron drift distances greater than ~ 20 cm by attaching electrons to CS_2 , which drifts with vastly reduced diffusion. Other efforts drift electrons directly and use a variety of techniques for their measurement: DMTPC (electroluminescence + CCDs), MIMAC (MicroMegas), NEWAGE (GEMs), and D^3 (Si pixels). A related suggestion is that the amount of recombination in a high pressure Xe gas with an electron-cooling additive could be sensitive to the angle between the track and electric field [162], eliminating the need for track imaging. Directional measurements appear to be the only possibility to push beyond the floor of coherent neutrino scatters [163], though at the cost of enormous target mass and channel count.

36.4.2 $0\nu\beta\beta$ Decay

Another major class of rare event search is neutrinoless double beta decay ($0\nu\beta\beta$). A limited set of nuclei are unstable against simultaneous beta decay of two neutrons. Fortuitously, this includes the Xe isotope ^{136}Xe (Q-value 2458 keV), which can be used as the active material in a detector, and which, as an inert gas, can also be more readily enriched from its natural 8.9% abundance than any other $\beta\beta$ isotope. Observation of the lepton-number violating neutrinoless version of this decay would establish that neutrinos are Majorana particles and provide a direct measure of neutrino mass. For a recent review, see [137, 164]. The signal in $0\nu\beta\beta$ decay is distinctive: the full Q-value energy of the nuclear decay appears as equal energy back-to-back recoil electrons. A large TPC is advantageous for observing this low rate decay for all the reasons described above. The first detector to observe the standard model process two neutrino double beta decay was a gaseous TPC which imaged the two electrons tracks from ^{82}Se embedded in a foil. [165] Modern TPCs use Xe as the detector medium.

The dominant background is gamma rays originating outside the active volume. Most of these undergo multiple Compton-scatters which are efficiently recognized and rejected through sub-cm position resolution, though the few percent of gammas at this energy that photoabsorb are not. Self shielding of gamma rays in the double beta decay energy window is less powerful than in the low energy dark matter window, since in the former case there is some small probability of penetrating to some depth followed by the modestly small probability of photo-absorption. The latter case consists of three small probability processes: penetration to some depth, a very low-energy scatter, and the gamma exiting without a second interaction. Because of this and the fact that background and the signal are both electron recoils (i.e., NR/ER discrimination is of no value), the requirements on radioactivity in all the surrounding materials of a $\beta\beta$ TPC are much more stringent than an otherwise similar dark matter detector, unless other background rejection tools are available. However $\beta\beta$ searches are insensitive to low energy backgrounds (e.g., ^{85}Kr and ^{39}Ar) important for dark matter.

Very good energy resolution is crucial to avoid background from $2\nu\beta\beta$ decays and gammas including the prominent 2615 keV line from ^{208}Tl in the Th chain. Here a combined charge and light measurement largely eliminates the otherwise dominant fluctuations in recombination which lead to anti-correlated fluctuations in charge and light. Because of the high energy of the $\beta\beta$ signal, charge can be read out directly, and the scintillation measurement is easily tolerant of the dark rates of SiPMs. These goals have led $\beta\beta$ detectors to have somewhat different optimization than dark matter detectors, although the next generation large Xe dark matter experiments (LZ, XENONnT, DARWIN) have significant $\beta\beta$ reach.

The recently completed EXO-200 experiment used a single-phase LXe TPC with roughly 110 active kg of Xe enriched to 80.7% ^{136}Xe to achieve one of the best $\beta\beta$ search limits [166]. The energy resolution obtained is (FWHM) of 2.71% (at 2458 keV), and lower values in LXe appear possible. A multi-ton successor experiment, nEXO, has been proposed which would fully cover the inverted neutrino mass hierarchy. [167] EXO-200 featured LAAPDs for light readout, and direct charge readout, while nEXO will use SiPMs.

A related but different approach is to use high pressure gaseous Xe TPC. [168] The lower density requires a large apparatus for given target mass, but has two significant advantages. The larger track size allows the two-electron topology of $0\nu\beta\beta$ events to be distinguished from single electrons from photoabsorption of background gammas. In addition, the low recombination fraction in the gas phase suppresses recombination fluctuations, allowing higher energy resolution. Recent progress with a 5 kg prototype by the NEXT collaboration has demonstrated the topology based discrimination, and, notably, 1% (FWHM) energy resolution. A ~ 100 kg detector is now under construction, and ton-scale designs being studied. Finally, a long-standing idea that would provide definitive identification of a $0\nu\beta\beta$ signal is to extract and tag the ionized Ba daughter via atomic physics techniques [169], either

in gas or liquid and gas phases. Significant recent progress by both the EXO and NEXT collaborations has now achieved the key milestone of demonstrating single Ba ion sensitivity in test setups. [170–172]

36.5 Sub-kelvin detectors

Written October 2021 by O. Cremonesi (INFN, Milano-Bicocca), L. Hsu (FNAL) and G. Signorelli (INFN, Pisa).

36.5.1 Motivation for Sub-kelvin Detectors

Detectors operating below 1 K are referred to as low-temperature detectors (LTDs). The advantage of using LTDs over conventional detectors resides in their better energy resolutions, lower noise, and improved energy thresholds, which can all be achieved with a versatile choice in materials. In certain applications, these advantages outweigh the potential drawbacks of cooling and reading out a detector payload at sub-kelvin temperatures, and thus enable exploration of new frontiers in fundamental physics, astrophysics and cosmology. Among the endeavors enabled by LTDs are direct searches for dark matter over a wide mass range, precision experiments to measure the electron neutrino mass, searches for neutrinoless double-beta decay, and X-ray observation of the Universe. Large arrays of LTDs are also employed to measure the properties of the cosmic microwave background (CMB) spectrum whose parameters are determined by fundamental physics. These include dark matter and dark energy densities, the sum of neutrino masses and the number of light relativistic species, as well as probing the physics of inflation at energy scales of $\sim 10^{16}$ GeV. This article presents a brief overview of LTDs, their features, and several applications. More detailed treatment of this subject is available in the literature [173–176].

The advantages of LTDs are enabled by the detection of very low energy excitations (e.g. phonons and quasiparticles). In a typical interaction, energy from an incident particle is dissipated through excitation of secondary particles such as electrons, ions, holes, photons, phonons etc. These particles will in turn produce their own secondaries. Thus there is a cascade down in energy until the original energy deposit is converted entirely into heat and the detector reaches thermal equilibrium. Prior to the equilibrium phase, the energy at any given moment is partitioned among multiple excitation modes. Conventional particle detectors work by sensing the higher energy excitation modes, such as ionization and scintillation, which require an average minimum energy of few eV to 10's of eV to produce. For such detectors, a large fraction of the deposited energy remains undetected in the form of heat. Furthermore, the measurements are subject to the fluctuations inherent in the partition of energy across different excitation modes. Secondaries that don't eventually escape the detector, will de-excite or recombine to dissipate their energy in the form of phonons and quasiparticles, which are characterized by energies in the range of meV down to μ eV. These can be detected by LTDs at various stages of their final degradation towards thermal equilibrium. Thus LTDs allow for energy resolutions and operational thresholds much lower than detectors that only sense scintillation and ionization. Furthermore, LTDs provide a precise energy measurement owing to the relatively large number of excitation quanta that can be detected. In fact, LTDs designed to measure thermal phonons achieve the highest possible energy resolutions with optimal noise performance.

At thermal equilibrium, energy E deposited in an LTD causes a temperature rise $\Delta T = E/C$ where C is the heat capacity. Thermal equilibrium is characterized by the condition where the average heat flowing to an LTD equals the average heat flowing from the LTD (into a proper heat sink or bath). In this state, the ideal intrinsic energy resolution is determined by the statistical fluctuations in the phonon system. Fluctuations in the total number of phonons in the LTD absorber have variance C/k_B , which yields a minimum resolution of $\Delta E^2 = k_B T^2 C$ to the device energy resolution, where k_B is Boltzmann's constant. Thus, the smaller the heat capacity, the more sensitive the response of the calorimeter and the better the energy resolution. The most relevant feature of this result is that the latter is independent of the energy deposition. The heat capacity itself is the product of the detector volume (V) and the specific heat (c_p). Optimization

of LTD response can be achieved by using small detector volumes and materials with low specific heat. Noise contributions from additional sources will increase the variance and are generally parameterized as a multiplicative factor ($\xi \gtrsim 1$) to the variance expression above.

Similarly, the power P from incident particles or radiation can be measured through a temperature rise given by $\Delta T = P/G$, where G is the thermal conductance to a weakly linked bath held at constant temperature. Power fluctuations are limited by G and have a spectral density of $S_P = NE P^2 = 4k_B T^2 G$, where $NE P$ is the noise equivalent power, defined as the power in a 1 Hz bandwidth that gives a response signal with an equal amplitude to the noise. Hence lower conductance yields better sensitivities. To minimize thermal conductance in precise power measurements, weak thermal links can be realized by using thin membranes or by decoupling the electron and phonon systems. However, a compromise must be made. While lower G yields better noise metrics, conversely, larger G is needed to dissipate all incident power (which can be large in the case of CMB detectors) or to have a faster detector response (the characteristic response time being $\tau = C/G$).

LTDs that measure power are sometimes referred to as *bolometers* in literature, as opposed to *calorimeters* that measure energy, generating some confusion. In principle, there is no clear distinction between a calorimeter and a bolometer. The operation mode is generally determined by the ratio of the characteristic time constant and the average time between the arrival of incident particles or quanta [177]. Yet another convention is to refer to *non-equilibrium* LTDs as those detectors that measure incident energy or power by counting excitations that have energy $\gg k_B T$. In such detectors, energy resolution is determined by the statistical fluctuations of the energy partition, similar to conventional ionization detectors but with a much lower average excitation energy and hence a larger number of excitation quanta.

Table 36.4: Low temperature dependence on temperature (T) for specific heat, based on different material classes. In the table below Θ_D is the Debye temperature and T_C is the transition temperature of the superconductor.

Heat Capacity	Material
$\left(\frac{T}{\Theta_D}\right)^3$	Dielectric and diamagnetic
T	Conductor
$\exp\left(-\frac{2T_C}{T}\right)$	Superconductor
$\left(\frac{\mu_B B}{k_B T}\right)^2 \operatorname{sech}^2\left(\frac{\mu_B B}{k_B T}\right)$	Paramagnet (in magnetic field \mathbf{B})

A variety of possible detector materials and sensor technologies makes LTDs very versatile and highly customizable. Dielectric, superconducting and paramagnetic materials are often used owing to the fact that at very low temperatures, the specific heat decreases strongly as a function of T (see table 36.4). Superconductors offer additional advantages: the abrupt change in resistance when a material transitions from its normal to superconducting state enables highly sensitive measures of temperature changes. Additionally, the existence of a small (less than a meV) but distinct energy gap that is required to break a Cooper pair, provides a means to measure energy deposits by counting the resulting quasiparticles (QP). QP relaxation processes are typically faster than thermal processes making these detectors suitable for high-rate photo-counting. In summary, both the sensitivity and energy resolution of an LTD benefit greatly from low temperature operation.

36.5.2 Detector Types

A generalized LTD calorimeter consists of an absorber in thermal contact with a phonon or quasiparticle sensor, and a thermal link to a heat bath at a constant temperature (see figure

36.11). The absorber provides the mass necessary for the interaction of the particle and a fast and complete thermalization of the deposited energy. The sensor accomplishes the task of translating the particle interaction into measurable parameters. It is generally sensitive to equilibrium phonons (e.g. thermistors and MMCs) and thus provides a precise measurement of the temperature. However, non-equilibrium (e.g. STJ's) and mixed (e.g. TES) phonon sensors have been devised and implemented in many applications as well. The goal of the thermal link is to cool the absorber down to its equilibrium temperature after the absorption of a particle. In monolithic detectors the thermometer and absorber are identical, while in composite detectors the thermometer is attached to a separate absorber. This basic design applies to single-event particle detection as well as for continuous radiation measurement devices. In the case of the latter, a suitable absorber whose mass is irrelevant, e.g. an antenna at the end of a waveguide, collects the incident power and dissipates it onto a resistive (e.g. Au) film, which is put in contact with a sensor capable of detecting tiny temperature changes (e.g. semiconductor thermistors, transition-edge sensors, and kinetic inductance detectors, to name a few).

Superconducting Tunnel Junctions (STJs) and Kinetic Inductance Detectors (KIDs) are examples of non-equilibrium detectors. STJs exploit Josephson tunnelling of particles and QPs between two superconductors. The superconductors act as radiation absorbers, and are separated by a thin insulating layer. When such a junction is DC biased at a voltage just below the gap voltage, the excess quasiparticles generated by the incoming radiation are detected as a tunneling-current proportional to the incoming energy. Statistical fluctuations in the tunnelling process limit the energy resolution which is given by:

$$\sigma_E = \sqrt{\varepsilon(F + G)E_0}, \quad (36.5)$$

where $\varepsilon \sim \Delta$, the band-gap, while $F \sim 0.2$ and $G > 1$ are the Fano factor and tunnelling fluctuation respectively. STJs have been proven to be excellent single photon and UV-VIS spectroscopic detectors with near theoretical energy resolutions, high detection efficiencies and excellent time resolution. In astrophysics they are used as mixers to detect radiation in the 100 GHz to 1 THz range by exploiting the non-linear behaviour of its current versus voltage characteristic curve. STJs share similar design elements to charge qubits, which are being used for the development of quantum computers. Such qubits have also recently been used in dark matter searches as single photon detectors to evade the standard quantum limit in measurement noise [178]. Despite their extremely good energy resolutions, STJs cannot be scaled-up to produce sensors with large observing volumes due to readout complexity and the difficulty in uniformly suppressing the superconducting Josephson current, which is superimposed on the QP current.

KIDs exploit the variation of the kinetic energy T stored in a superconductor by Cooper pairs whose inertia acts as an effective inductance, given by:

$$T = \frac{1}{2}nm^*v^2 = \frac{1}{2}LI^2 \quad (36.6)$$

where n is the number density of Cooper pairs, $m^* = 2m_e$ is the Cooper pair mass and $I = 2nev$ is the Cooper pair current. $L = m_e/2ne$ is defined as Kinetic Inductance and is inversely proportional to the number of Cooper pairs [179]. When a KID is placed in series with a superconducting capacitor, the resonance frequency of the circuit will be temporarily shifted by incident radiation, which converts Cooper pairs to QPs, thus changing the effective inductance. The presence and amount of radiation is observed as a change in amplitude or phase of a tuned sinusoidal signal that is sent through the circuit. In practice the change in L is small, and very high Q microwave resonance circuits are needed to sense this variation (hence the name MKIDs, for Microwave-KIDs). Furthermore, only areas of the film where large currents are flowing will be sensitive to pair breaking, thus making the response of a distributed KID position dependent. To overcome this issue, QP trapping (by coupling two superconductors with different band-gaps) is used for absorbing optical photons and X-rays.

To detect lower frequencies (e.g. in the 100-1000 GHz range for CMB) a lumped element resonator (LEKID), with little current variation across the device, is used. The device itself, based on a series LC circuit inductively coupled to a microstrip feed line, can act as the absorber as well as the sensing element in a detector system. Macroscopic devices (few mm^2) can be fabricated by shaping the inductor in the form of a meander coupled to an inter-digitated capacitor [180]. The theoretical noise limit of these devices is governed by generation-recombination noise and takes the form:

$$NEP_{QP} = 2\Delta \sqrt{\frac{n_{QP}}{\tau_{QP}}}, \quad (36.7)$$

where n_{QP} and τ_{QP} are the QP number and lifetime respectively. KIDs are easy to fabricate, very sensitive, broad band and easily multiplexable: they can be coupled with a single microstrip that simultaneously reads 1000s of detectors resonating at different frequencies. They provide therefore a promising solution for deploying large arrays of detectors with applications to high-energy physics, astronomy or CMB measurements, although there are still some challenges, especially at frequencies below 100 GHz, related to their worse noise performance when compared to other LTDs, and to the choice of materials with a sufficiently small energy-gap.

Semiconductor thermistors are resistive elements characterised by a strong dependence of the resistance on the temperature. Usually, they consist of small crystals of germanium or silicon with a dopant concentration slightly below the metal-to-insulator transition. However, they can also be realized in the form of amorphous films such as NbSi. At low temperatures, their resistivity (ρ) is governed by variable range hopping (VRH) conduction and is described by the expression $\rho(T) = \rho_0 \exp((T_0/T)^\gamma)$, where T_0 and ρ_0 are parameters controlled by the doping level, while γ depends on the compensation level K (ratio of acceptor to donor concentrations). For low values of K it is well approximated by $1/4$ while it converges to $1/2$ as K increases.

Semiconductor thermistors are high impedance devices (1–100 $\text{M}\Omega$) whose performance is usually parameterized in terms of the logarithmic sensitivity $\alpha = d \log R / d \log T$, typically in the range of 1–10. Silicon thermistors are fabricated using a multiple ion implantation process in high purity silicon wafers to produce a thin and uniformly doped box-like volume. The best germanium thermistors are fabricated starting from bulk, high-purity germanium crystals doped by means of neutron irradiation in the core of a nuclear reactor, referred to as nuclear transmutation doping (NTD). Individual sensors are then produced by dicing the irradiated samples and finishing them by hand. The great advantage of NTDs is the highly uniform doping level over large volumes which results in a better signal to noise ratio with respect to other doping techniques. The doping level depends on the isotopic composition of the starting material and the irradiation time.

The weak coupling to the heat sink can be provided by the electrical leads used for the read-out. However, nowadays microelectronic planar technologies and silicon micromachining are more commonly preferred, and sensors are suspended on thin silicon nitride membranes or thin silicon beams. Thermistors are read-out in an approximately constant current biasing configuration obtained by inserting large load resistors in the bias circuit, which allows for direct conversion of the thermal signal (ΔT) into a voltage signal (ΔV).

Semiconductor thermistors are very practical to use with some drawbacks. One of these is related to their high impedance which requires a JFET front-end placed as close as possible to the device in order to minimize the signal integration on parasitic electrical capacitances. This can represent a technical challenge, because JFETs must be maintained at significantly higher temperatures ($\gtrsim 100$ K). Furthermore, deviations from the exponential behaviour of the conductivity have been observed at low temperatures. They are usually described in terms of a finite thermal coupling between electrons and phonons which results in an intrinsic limit to the signal rise times, which is of the order of hundreds of milliseconds at temperatures below 100 mK. Nevertheless, semiconductor thermistors are an established and robust technology, and arrays of detectors based on these devices have been widely

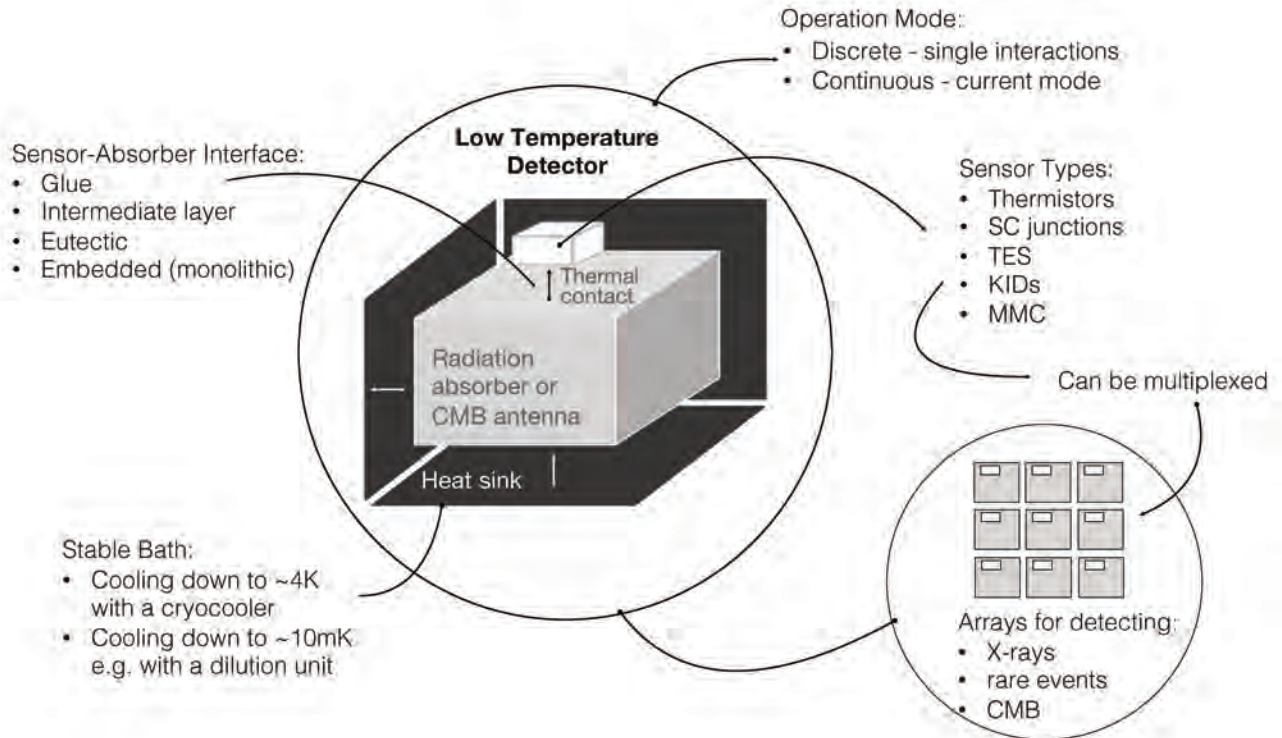


Figure 36.11: A generalized LTD consists of an absorber, a sensor and a thermal link to a stable-temperature bath. Biasing schemes and readout is described in detail in the text for individual sensor types.

used for neutrinoless double beta decay searches, neutrino mass measurements and X-ray spectroscopy. Energy resolutions lower than 5 eV have been achieved with Sn or HgTe absorbers.

Superconducting Transition Edge Sensors (TESs) exploit the sharp transition between superconducting and normal conducting phases, yielding a high sensitivity to temperature variations. Temperature perturbations, and hence resistance changes, are sensed as modulations in the current through the TES. TESs are operated in a constant voltage biasing configuration where Joule heating, arising from the current flowing in the TES, decreases with a rise in resistance, which then brings the TES back to its nominal operating temperature. This electrothermal feedback (EFT) is achieved by providing a TES with a voltage bias whose power, $P_J = V_{\text{bias}}^2/R(T)$, heats the TES to its nominal operation point, the superconducting transition temperature. Operation in ETF mode improves linearity, speeds up response (to faster than $\tau = C/G$), and in some cases it provides tolerance for T_C (critical temperature) variation between multiple TESs in a large array. The low impedance in this configuration makes them well-suited for readout by SQUID (Superconducting QUantum Interference Device) based amplifiers. Logarithmic sensitivities $\alpha = d \log R/d \log T$ of the order of several hundreds can be achieved. By using different superconductors, or superconductor-metal pairs patterned in suitable shapes, a wide range of resistances, transition temperatures and time constants are obtainable to meet the requirements of the desired application [181].

Nano-TESs are fabricated by lithographic techniques in the form of long (few μm) and narrow (nm) wires that exhibit extremely small NEPs due to their reduced C and G , enabling single-photon sensing. Superconducting Nanowire Single-Photon Detectors (SNSPDs) are similarly patterned superconductors or superconducting bilayers maintained at a temperature well below their T_C . When a DC current just below the critical current is driven through the nanowire, the absorption of a single photon causes the formation of a hot spot that drives the superconductor to a normal conducting state, resulting in a very fast (tens of pi-

coseconds) current pulse through a shunt resistor. For this reason, nano-TESs and SNSPDs are used as single photon detectors for light dark matter and axion searches in applications where large detecting mass is not critical [182].

Magnetic Metallic Calorimeters (MMC) exploit paramagnetic sensors exposed to a weak magnetic field with a weak thermal link to a heat bath. A temperature rise causes a change in the sensor magnetization, which is sensed by a SQUID magnetometer. A common material is an Au:Er mixture, with the addition of a few hundred ppm of enriched ^{166}Er , which is needed to reduce the unwanted contribution of nuclear magnetic moments of other Er isotopes. The read-out is non-dissipative and avoids the noise sources common to the dissipative devices. The use of a metallic host ensures relatively fast time response, since the typical spin-electron relaxation times are of the order of 0.1 microseconds at ~ 50 mK [183]. For an optimized MMC, the energy resolution is given by $\Delta_E = \sqrt{2k_B T^2 C (\tau_0/\tau_1)^{1/4}}$, where τ_0 (order of microsecond) and τ_1 (order of millisecond) denote the signal rising and decay times respectively [173]. In order to obtain a fast and efficient energy thermalization, MMC are typically fabricated from gold. The intrinsically large heat capacity of the paramagnet does not spoil the temperature sensitivity and allows the use of relatively large gold absorbers without degrading the device performance. Furthermore, thermal isolation from the heat sink is not generally an issue. Owing to the simple concept of these devices, MMC can be precisely customized and fabricated by employing standard microtechnology. Planar MMC arrays characterized by an excellent energy resolution, large dynamic range and good linearity have been successfully used for the detection of soft X-rays.

Performance and technological constraints limit the maximum size of LTDs. To improve overall experimental sensitivities, a large number of sensors must be deployed, typically at temperatures of a few tens of mK, where cooling power is limited to a few μW . To reduce the readout complexity and the heat load at the colder stages, multiplexing (MUX) techniques are often employed. Multiplexing consists of reading multiple detectors out

through a limited number of lines that traverse room temperature to cryogenic temperatures [184]. In frequency-domain multiplexing (FDM), a tuned superconducting LC circuit is placed in series with each sensor, and a frequency comb of AC biases (usually in the MHz range) is sent to a group of sensors in parallel. A synchronous demodulation of the amplified current signal allows the recovery of the resistance variation of each detector. Microwave-multiplexing (μ MUX) represents a variation of this concept, based on the usage of rf-SQUIDS, where the frequency comb is in the GHz range. Alternatively, the signal from a single detector can be recovered by readout of one detector at a time (time-domain multiplexing, TDM). KIDs have been gaining popularity owing to the fact that they naturally form resonant circuits, hence multiplexing in the frequency domain is readily achieved by adjusting their capacitance.

36.5.3 Experimental Applications

LTDs are sensitive over a wide range of energy, from centimetre wavelength (\sim meV) through the visible spectrum (\sim eV) up to the X-ray domain (\sim keV) and beyond. Several broad categories of LTD applications towards measurements of fundamental physics are described in more detail in the text below and summarized in tables 36.5 and 36.6.

Bolometric detectors are favored as microwave detectors owing to their nearly constant response over frequency, playing an important role in far-infrared astronomy and in the survey of the cosmic background radiation. The high-frequency instrument of the Planck satellite (HFI) used spiderweb bolometers read by NTD-Ge thermistors, but current experiments use mainly TESs or, more recently, KIDs. Depending on the objective of the experiment, antenna coupling or absorber coupling is used. In the former case, the bolometer detects one polarization and one (or a few) modes of the radiation, while absorber-coupled bolometers do not distinguish between polarizations. In order to avoid the absorption or emission from Earth's atmosphere, many (CMB) instruments are operated by observatories located at high altitude, dry places (such as the Atacama desert or Antarctica), balloon-borne platforms, or from space. In Table 36.5, we list a subset of the ongoing or planned CMB experiments (see Section 29 of this Review for the details on present challenges). In the Atacama desert in Chile, CLASS is taking data, POLARBEAR is being upgraded to Simons Array and ACTPol is being upgraded to AdvancedACT-Pol, the next big step being the deployment of the Simons Observatory. At the South Pole, SPTPol has been upgraded to SPT-3G, while BICEP3 and BICEP array will constitute the South Pole Observatory. The most powerful upgrade in terms of both size and sensitivity will be CMB-S4, a consortium of telescopes both at the Pole and in Chile. In the Canary islands, QUIJOTE and GroundBIRD are operating and LSPE/STRIP is in preparation. QUBIC will soon start operations in Argentina and AliCPT is in preparation in Tibet. Regarding balloon projects, SPIDER and EBEX were already launched while LSPE/SWIPE and PIPER will be in the near future. Finally from space, after the success of Planck, LiteBIRD has been selected by the Japan Aerospace Exploration Agency (JAXA) as the next strategic large mission to be launched in the 2020s.

The incoming radiation couples directly to the antenna probes (as in BICEP/Keck) or through micro-machined horn waveguides (AdvancedACT-Pol, CLASS) or lenslets (Simons Array, SPT-3G), depending on the frequency range. All of these experiments have focal planes with hundreds to hundreds of thousands of sensors. To optimize focal plane occupancy, multi-mode or multi-chroic, dual polarization sensitive detectors are used. In the former case, the sensitivity is enhanced by collecting power from a larger number of modes at the expense of angular resolution. In the latter, one single mode of the radiation is focused on a broad band antenna, and on-chip polarization separation and band-pass filters split the signal in different frequency bands directing the power to different absorbers and sensors.

Experimental design is driven by a trade-off between the sensitivity and the complexity of the production processes and readout. On the one front, single-sensor NEP at the level of 10^{-21} W/ $\sqrt{\text{Hz}}$ has been achieved in laboratories and research centers. Meanwhile, efforts are in place for the industrialization of the fabrica-

tion processes, which is essential for scaling up production for the large number of detectors needed for future experiments.

Massive cryogenic calorimeters have been proposed since the 1980's as particle detectors for the search of rare processes (e.g. dark matter, neutrinoless double beta decay) [185]. Almost simultaneously, the use of arrays of small mass calorimeters was suggested for X-ray astrophysics [186] and precision measurements of the neutrino mass [187, 188]. Although essential to understanding the nature of neutrinos, neutrinoless double beta decay (NDBD) has eluded discovery (or definitive exclusion) for over 50 years. Calorimetric techniques provide the best sensitivities to NDBD. However, before the advent of low temperature calorimeters (LTC), only a few isotopes (^{48}Ca , ^{136}Xe and ^{76}Ge) could be utilized for NDBD studies with the calorimetric approach. This limitation was removed by the advancement of LTC's, and in particular by CUORE, which takes advantage of the naturally high abundance of ^{130}Te in TeO_2 crystals. Additionally, the operation of CUORE at LNGS [189] has demonstrated that the technical challenges of operating ton-sized LTD detectors in a deep, underground location are surmountable. Currently, the most promising future approach is based on the hybrid approach of scintillating LTCs, which unfortunately cannot be used for ^{130}Te . Now, new projects are being proposed based on different scintillating compounds. In particular ^{100}Mo is the choice of CUPID [190] (NTD thermistors glued to $\text{Li}_2^{100}\text{MoO}_4$ crystals), which will use the same infrastructure of CUORE and follows from the successful operation of several demonstrators (CUPID-0 [191] and CUPID-Mo [192]), and AMORE (MMC sensors on $\text{Ca}^{100}\text{MoO}_4$ or $\text{Li}_2^{100}\text{MoO}_4$ crystals) [193]. With an energy resolution comparable to germanium diodes and a mass of the order of a ton, these experiments aim to probe the inverted hierarchy of neutrino masses. The slow response of these detectors is still a dominant limitation because pile-up may prove to be a serious background. Extremely pure materials, careful assembly procedures, and deep underground laboratories are therefore necessary.

In the 1980's, the calorimetric technique was recognized as a feasible approach to make a direct measurement of the neutrino mass from the end-point of a beta spectrum. Thus, LTCs were proposed as a possible alternative to the standard spectrometric measurements [194]. Calorimetric measurements offer a number of advantages: i) a weak dependence on the final excited states, ii) no source effects (e.g. self-absorption), and iii) lack of back-scattering from the detector. Therefore LTCs provide a faithful reconstruction of the beta spectral shape over a broad energy range below the end-point. However, the difficulty in resolving a small fraction of the spectrum near the end-point is a serious limitation that strongly constrains the source strength and the statistics that need to be accumulated. Such an inconvenience can be mitigated by selecting beta emitters with a small Q value, owing to the fact that the fraction of counts in an interval, δ close to Q, scales as $(\delta/Q)^3$. However, this is generally at the cost of choosing decays with more complex nuclear transitions. In addition, LTCs may be affected by specific systematics (e.g. solid state effects). Ultimately it is recognized that spectrometers and calorimeters have complicated but different systematic effects. It is therefore critical to develop complementary experiments exploiting both techniques.

LTCs were initially proposed as perfect calorimeters to measure the energy spectrum of a low Q beta emitter embedded in an absorber. However, the requirements of excellent energy resolution and a low rate (to avoid pileup) requires a very large number, $O(10^4 - 10^6)$, of small mass devices (micro-calorimeters). Early experiments used ^{187}Re , which is a long-lived beta emitter that is naturally abundant in rhenium samples and is characterised by a very low Q value (2.4709 keV [199]). A large number of ^{187}Re based experiments have been developed over the years (MANU [200], MIBETA [201], MARE [202]). Nowadays a different approach is preferred and is based on the measurement of the atomic radiation following electron capture, typically in ^{163}Ho which is also characterized by a very low Q (2.837 keV [203]). Different experiments have been proposed to face the challenge: ECHO in Germany [195] (using MMC sensors), HOLMES in Italy [196] and NUMECS [197] in the US (using TESs). The very large number

Table 36.5: Some selected experiments using LTDs to measure the CMB. These experiments constrain the physics of inflation and the absolute mass, hierarchy, and number of neutrino species. The experiment location determines the part of the sky that is observed. The size of the aperture determines the angular resolution. The table also indicates the type of sensor used, the number of sensors, the frequency range, and the number of frequency bands. Data for planned upgrades or future experiments are provided in parentheses.

Sub-K CMB Experiment	Location	Aperture	Sensor type	# Sensors (planned)	Frequency (planned)	Bands (planned)
Ground-based						
Atacama Cosmology Telescope (2007–)	Chile	6 m	TES	5,614	30–230 GHz	5
BICEP/Keck (2006–)	South Pole	26/68 cm	TES	2,500	95–270 GHz	6
CLASS (2015–)	Chile	60 cm	TES	3,488	40–220 GHz	4
GroundBIRD (2021–)	Canary Island	30 cm	MKID	322	145–220 GHz	2
POLARBEAR / Simons Array (2012–)	Chile	3.5 m	TES	1,274 (22,764)	150 GHz (90–280 GHz)	1 (4)
South Pole Telescope (2007–)	South Pole	10 m	TES	16,260	90–220 GHz	3
Simons Observatory (2022–)	Chile	6 m/0.5 m	TES	(60,000)	(27–280 GHz)	(6)
CMB-S4 (2024–)	Chile + South Pole	21 telescopes	TES	(500,000)	(20–280 GHz)	(11)
Balloon						
EBEX (2013–)	McMurdo	1.5 m	TES	~1,000	150–410 GHz	3
PIPER (2016–)	New Mexico	2 m	TES	5,120	200–600 GHz	4
SPIDER (2014–)	McMurdo	30 cm	TES	1,959	90–280 GHz	3
LSPE (2022–)	Longyearbyen	60 cm	TES	(326)	(140–270 GHz)	(3)
Satellite						
Planck HFI (2003–2013)	L2	1.5 m	NTD	52	100–857 GHz	9
LiteBIRD (2028–)	L2	20–40 cm	TES	(4,508)	(34–448 GHz)	(15)

Table 36.6: Selected experiments using low temperature calorimeters. The table shows currently or soon-to-be operating experiments that will search for dark matter or neutrino properties. The dates refer to the start of the program.

Sub-K Experiment	Location	Detection mode	Absorber (Total mass)	Sensor type	# Sensor # Crystal
WIMPs					
CRESST III (2016)	LNGS Italy	Athermal phonon and scint.	CaWO ₄ /Al ₂ O ₃	TES	10
EDELWEISS † (_SubGeV)	LSM Modane France	Thermal phonon and ion.	Ge	NTD Ge	-
SuperCDMS (2023)	SNOLAB Canada	Athermal phonon and ion.	Ge/Si	TES	24
Neutrino mass					
ECHO [195] (2012)	Heidelberg Germany	Thermal phonon	Au: ¹⁶³ Ho (0.2 μg)	MMC	16
HOLMES [196] (2015)	Milan Italy	Thermal phonon	implanted ¹⁶³ Ho (18 μg)	TES	1000
NUMECS† [197] (2015)	LANL USA	Thermal phonon	implanted ¹⁶³ Ho	TES	4096
0νββ decay					
CUORE [189, 198] (2015)	LNGS Italy	Thermal phonon	^{nat} TeO ₂ (741 kg)	NTD Ge	988
CUPID [190] (2015)	LNGS Italy	Phonon and scint.	Li ¹⁰⁰ MoO ₄ (450 kg)	NTD Ge	1596
AMoRe-I [193] (2018)	Y2L South Korea	Phonon and scint.	Ca ¹⁰⁰ MoO ₄ /Li ²¹⁰⁰ MoO ₄ (6 kg)	MMC	13/5

†No payload size quoted for experiments that are primarily in R&D phase.

of microcalorimeters needed to obtain sensitivities comparable to spectrometric measurements is a serious challenge, both for the readout and the thermal heat load. An alternative readout based on the use of KIDs, for their multiplexing capability, has been proposed and is presently under development.

Traditional searches for WIMP-like dark matter aim to measure the scatter of a massive dark matter particle off of a target nucleus. Similar to detectors employed for neutrinoless double beta decay, these searches benefit from large-mass absorbers for

the target because the dark matter interaction rate scales directly with the number of nuclei in the target and hence its mass. Among the most successful experiments to date, are those that combine the detection of phonons with another channel such as ionization energy (EDELWEISS and SuperCDMS) or scintillation light (CRESST). This simultaneous, dual measurement takes advantage of the fact that the energy deposited in the absorber is partitioned into these channels differently depending on whether the initial particle interaction produces electron or nuclear recoils (or

both). This particle identification allows for the rejection of background from natural sources of radiation, which most commonly manifest themselves as electron recoils in the detector.

In recent years, multi-ton liquid noble detectors have outclassed LTD-based technologies in searches for heavy (>10 GeV/ c^2) dark matter owing to their ability to more easily and cheaply scale to large target masses. However, the lower thresholds achieved by LTDs continue to make them the technology of choice for low-mass dark matter searches. New advances have enabled these detectors to reach much lower energy thresholds than previously obtained, albeit sometimes at the cost of being able to detect energy in more than one channel as described above. For example, the use of an electric field to generate Neganov-Trofimov-Luke [204, 205] phonons in proportion to the applied voltage, has enabled the detection of single electron hole pairs in Si detectors with thresholds as low as a few eV (SuperCDMS HVeV). This and similar advances in Ge LTDs (EDELWEISS_SubGeV) have enabled sensitive searches for dark photons and dark matter that scatters off electrons [206, 207]. Next generation experiments such as SPICE/HERALD aim to further optimize the intrinsic energy resolution of TES detectors, coupled with a strategic choice of target materials (superfluid He and polar crystals) to enable sensitivities to dark matter with masses below an MeV/ c^2 [208]. Current state-of-the-art axion searches use SQUID based quantum amplifiers such as Josephson Parametric Amplifiers along with resonant cavities operating below 100 mK to look for a signal above fluctuations in the thermal noise [209]. Future axion experiments are also working to close the sensitivity gap between particle and wave-like dark matter with the help of LTDs. Broad-band axion searches in the THz range are being proposed, which will make use of TES, SNSPDs or KIDs for single photon detection [210]. Finally, LTD-based dark matter detectors are also actively employed to study coherent neutrino scattering, owing to the fact that the hypothesized signal from dark matter-nucleus scattering is nearly identical to that from neutrino-nucleus scattering, with both inducing nuclear recoils in a similar energy range [211, 212].

36.6 Low-radioactivity background techniques

Revised October 2021 by Al. Ianni (INFN, LNGS) and S. Schönert (Munich Tech. U.).

36.6.1 Introduction

The study of rare phenomena in fundamental physics, such as proton decay, neutrinoless double beta decay, dark matter, and MeV-scale neutrino interactions, requires extremely low levels of background radiation. Experiments searching for these rare events record electron recoils or nuclear recoils in the energy scale from a few eV to several MeV. The detector technologies used are multiple from organic and cryogenic liquid scintillators, to bolometers, solid state calorimeters, gaseous detectors, and crystal scintillators. As far as the background contamination is concerned at some extent the application defines the requirements, although the common denominator is that an extreme reduction of all background sources is essential. Leading experiments in rare events search have achieved trace contaminations that generate background events in the region of interest (ROI) as low as order of 50 pBq/kg. As a first and crucial step, a dedicated radio-purity assay of the detector set-up components has to be carried out. Over the last fifty years, special screening and cleaning techniques have been developed to measure and mitigate ultra-low levels of background. In order to characterize the background sources we refer to Heusser [213] and identify the following five main categories:

- environmental radioactivity in the location where the detector is installed;
- radioimpurities in the detector and shielding;
- radon and its progenies;
- cosmic rays and induced radioactivity;
- neutrons from natural fission, (α, n) reactions, and from cosmic-ray muons interactions.

The energy range affected by these background sources is mainly <10 MeV. All materials contain traces of long-lived primordial ra-

dioimpurities, such as ^{238}U , ^{232}Th , ^{235}U ($^{238}\text{U}/^{235}\text{U} \sim 138$), and ^{40}K ($^{40}\text{K}/K^{\text{nat}} \sim 1.17 \times 10^{-4}$). We recall that 1 ppt of ^{238}U and ^{232}Th corresponds to 12.36 and 4.06 $\mu\text{Bq/kg}$, respectively; 1 ppb of K^{nat} corresponds to 30.25 $\mu\text{Bq/kg}$. In the Earth's crust the abundance of uranium and thorium is of the order of 1 – 10 ppm which corresponds to about 10 – 100 Bq/kg. Taking into account these contamination levels and the low background requirements, a fundamental background reduction and mitigation is essential to carry out rare phenomena research.

Besides primordial radionuclides other radioactive elements are produced through interactions with matter of secondary cosmic ray particles. Among these so-called cosmogenic radionuclides we recall, in particular, ^3H , ^{14}C , ^7Be , ^{39}Ar , ^{42}Ar , and, in copper, steel and iron often used as shielding materials, $^{57,60}\text{Co}$.

A third category of background source in our environment consists of anthropogenic radionuclides. These are artificially produced mainly through nuclear reactions in nuclear power plants, nuclear fuel reprocessing plants, and nuclear weapons testing. Anthropogenic background elements of concern for rare phenomena are ^{85}Kr , ^{137}Cs , ^{241}Am , ^{60}Co , and ^{90}Sr . The concentration of ^{85}Kr ($T_{1/2}=10.76$ y, $Q_{\beta}=687$ keV) in air has been slowly increasing since World War Two with a present activity of order 1 Bq/ m^3 . As a consequence ^{85}Kr is a crucial background in experiments making use of nitrogen, xenon, and argon from air.

Once detectors components radioactive backgrounds have been assayed and reduced by a careful selection campaign, which can last several years, a further step to push the background level beyond the screening possibilities is needed to reach the required sensitivity. For this purpose special active vetos, purification methods, and offline analyses have been developed. A meticulous background understanding and mitigation is crucial to explain any possible signal excess which may be detected. Background mitigation techniques are based on:

- use of radio-pure materials that absorb ionizing radiation;
- identify radio-pure material for detector construction;
- perform advanced surface and sub-surface cleaning treatment;
- reduce muon flux with underground detector deployment and using active vetos;
- exploit advanced detection and tagging techniques to discriminate signal from background.

In the following we describe radio-assay and background mitigation techniques developed and exploited in the framework of rare phenomena searches in deep underground laboratories.

36.6.2 Radio-purity assay

The radio-purity assay of detector components is a basic prerequisite to be carried out in low counting experiments. Several techniques are exploited for radio-purity assay. They are complementary to characterise the radio-purity of materials for shielding or core detector components. Next generation experiments radioassay campaign requires a considerable effort and organization for several years [214–216].

Gamma spectroscopy (GS) via high purity germanium (HPGe) detectors is a powerful and crucial technique [213]. It is nondestructive and thanks to the energy resolution allows to distinguish various radionuclides elements. Radiation from ^{238}U and ^{232}Th comes with all decay products in the radioactive chains. However, if secular equilibrium is broken, this crucial information can be addressed by separating different gamma-ray lines characterizing elements in the decay chains. In the ^{238}U chain one can have three sub-chains out of equilibrium. The first sub-chain can be assessed through ^{234}Th direct progeny of ^{238}U . The second sub-chain, which originates from ^{226}Ra , can be probed by ^{214}Pb and ^{214}Bi . A third sub-chain, which starts from ^{210}Pb , cannot be efficiently probed by GS, yet is of crucial importance and alternative methods must be used. In the ^{232}Th chain again one can probe two sub-chains which can be out of secular equilibrium: the first one through ^{228}Ac from ^{228}Ra ; the second from ^{228}Th can be measured through ^{212}Pb , ^{212}Bi and ^{208}Tl . The technology for HPGe operated in deep underground counting facilities [217, 218] or in shallow laboratories with an efficient active

veto shielding [219] has been boosted to sensitivities of the order of 10–100 $\mu\text{Bq/kg}$ by carefully selecting detector components, electronics and sample handling systems. The HPGe screening method requires order of ≥ 100 g of material, and weeks of acquisition to produce a reliable measurement.

A second crucial technique is based on inductively coupled plasma mass spectrometry (ICP-MS) [220]. This technique can probe primordial parents activity at the level of 1 $\mu\text{Bq/kg}$. It is a destructive method and often needs special sample preparation on a small quantity of material. The ICP-MS does not measure the radioactive decay of isotopes but determines their concentration. At present, it is the most sensitive and rapid screening technique which allows to select materials at sub-ppt level of impurities. The drawback is that ICP-MS cannot assess whether the uranium and thorium chains are out of equilibrium and to reach ultra-high sensitivities one needs to carefully prepare and handle the samples in a cleanroom environment. ICP-MS screening must be coupled with other methods to properly assess the radio-purity of materials in the context of rare events searches. The Glow Discharge Mass Spectroscopy (GDMS) is a trace element analysis technique somehow alternative to ICP-MS. An advantage of GDMS is the possibility to determine the bulk composition of the sample, assuming homogeneity. Sensitivities of the order of 10 ppt can be achieved.

A third screening technique is based on neutron activation analysis (NAA) [221]. A sample exposed to a neutrons flux can be activated to form radioactive isotopes which can be detected using HPGe detectors or ICP-MS. Considering the difficulties to irradiate samples, this method is not often used. NAA can probe sensitivities at the level of 0.01 $\mu\text{Bq/kg}$. This method is not destructive and the irradiated sample can be used if the activated products are not long-lived.

In case out of secular equilibrium conditions are measured for uranium and thorium from GS screening, a rigorous assessment cannot avoid radon emanation measurements. This matter is discussed in Section 36.6.3.

Complementarity between radio-purity assay techniques is a crucial parameter to design detectors for rare phenomena searches. As it has been pointed out above, requirements can be more stringent than the best sensitivity which can be obtained with the current radioassay techniques. In these cases, a number of prototype detectors have been built and operated to prove the feasibility to reach ultra-low backgrounds.

36.6.3 Radon and its progeny

Radon is considered to be rare in nature because most of its isotopes are short-lived. However, ^{222}Rn ($T_{1/2}=3.82$ d) is of particular concern in our context. ^{222}Rn is produced by ^{226}Ra and is a radioactive noble gas which can move within active detector components. ^{222}Rn daughters are heavy metals which can deposit on surfaces. If diffusive ^{222}Rn is supported by ^{226}Ra this can deposit on surfaces the long-lived ^{210}Pb , which is a major concern for low counting experiments. In addition, due to ~ 100 keV nuclear recoil energies from alpha decays in the ^{226}Ra sub-chain, eventually ^{210}Pb can be implanted into a sub-surface layer of a material exposed to radon. This sub-surface contamination can remain even after surface cleaning. Surface contamination of ^{210}Pb is a serious background for direct dark matter experiments through alpha decay of ^{210}Po , which can generate neutrons by (α ,n) reactions. Low energy beta/gamma emissions from ^{210}Pb are also a concern. Therefore, radon-free cleanrooms are essential for the assembly of the detector components. Effective radon abatement systems are available for this purpose.

In assembling and commissioning rare events experiments, special care must be dedicated to the estimate of radon emanation of the materials and continuous radon monitoring. For this purpose different methods for radon assay have been developed and exploited since the beginning of solar neutrino observations. ^{222}Rn atoms are collected inside an exhalation chamber for several half-lives before adsorption and counting. Detection limits of the order of 100 μBq (about 50 ^{222}Rn atoms) can be obtained with ~ 50 l stainless steel electro-polished chambers [222]. This limit can be pushed down to 30 μBq for 1-liter scale chamber. Emanation of large vessels (cryostats, storage tanks, purification columns)

can be determined by collecting exhaled radon into transportable charcoal traps [223]. The same method can be used for liquid samples. In this case instead of evacuating the exhalation chamber into a charcoal trap, He is flushed through a sparger tube for about 10 times the volume of the liquid used. Sensitivities of the order of 10 $\mu\text{Bq/kg}$ have been reached.

Nitrogen or synthetic air is often used in rare events experiments for purging, stripping, and assembling the experimental apparatus. These gases might contain radon. In gases ^{222}Rn can also be detected using electrostatic collection of ^{218}Po and ^{214}Po [224, 225]. Sensitivities of the order of mBq/m^3 can be obtained. In Borexino three grades of nitrogen purity were used: regular purity, high purity, and low argon and krypton purity. The regular purity is obtained from boil-off gas and has radon, measured with the method reported above, at the level of $< 100\mu\text{Bq/m}^3$. For stripping the purified liquid scintillator a higher purity is needed. To remove radon from regular purity nitrogen a dedicated absorber plant has been built. This system can reduce radon by a factor of 100. Finally, we mention that not only radon is found in nitrogen. For specific applications the long-lived ^{39}Ar and ^{85}Kr in nitrogen are an important source of background.

36.6.4 Surface backgrounds

Surface contamination of long-lived ^{222}Rn daughters can be challenging in low-counting experiments. Considering required sensitivities of the next generation experiments, this source of background has to be properly quantified and mitigated. Therefore, exposure to ^{222}Rn should be monitored and limited to reduce build-up of ^{210}Pb on surfaces. In addition, ^{222}Rn exposure could also produce sub-surface contamination as discussed in Section 36.6.3. For one cannot avoid radon contamination in many circumstances during production of detector components, it is crucial to quantify the effectiveness of cleaning aiming at removing surface contamination of ^{210}Pb , ^{210}Bi , and ^{210}Po . A simple cleaning procedure, which implies degreasing, wiping, and rinsing the material surfaces is not effective in removing these surface contaminants. Studies of cleaning procedures have been carried out exposing stainless steel, copper and other materials to a strong radon source. Etching and electropolishing with subsequential passivation and rinsing have been investigated in great details. Several recipes for etching and electropolishing have been proposed [226]. Electropolishing has been shown to be very effective in reducing ^{210}Pb , ^{210}Bi , and ^{210}Po from both copper and stainless steel by a factor greater than 100. Etching, which is easier to perform than electropolishing, followed by passivation and rinsing with deionized water is effective in reducing ^{210}Pb and ^{210}Bi by a factor between 50 and 100. However, it is less effective for ^{210}Po , which in copper is very poorly reduced. Removing ^{210}Po from surfaces is crucial, therefore, naturally ^{210}Po contaminated copper and stainless steel surfaces have been deeply investigated with a high sensitivity (1mBq/m^2) alpha spectrometer [227]. After multi-etching steps (≥ 3), followed by a passivation, a reduction of order 100 has been obtained. On the contrary, static etching (single step) is poorly effective. Electropolishing, or multi-etching are recommended in case copper is in direct contact with the active core of the detector and ultra-high radio-purity is essential or when copper electroforming cannot be used. Electroplating of a thin layer of high radio-pure copper onto the surface of less radio-pure copper has also been investigate to mitigate surface background [227]. This technique is shown to be near-perfect in reducing surface activity of ^{210}Po when electroformed copper is used [227].

Besides copper and steel other materials often used, such as polyethylene and teflon, have been investigated to understand how to reduce radon plate-out contaminations [228].

As far as surface contamination is concerned particulate fallout in cleanrooms environment could be of concern. In general, chemical composition of dust reflects local composition of soil and dust. This is not necessarily true in cleanroom spaces, where the composition of dust depends on ongoing activities and handled materials [229]. The rate of fallout is an important information in the framework of rare events experiments, where assembling is performed in cleanrooms. The ^{210}Pb contamination, inferred from stable lead measured by ICP-MS, due to dust fallout has been

investigated [229]. This contamination has a different origin with respect to ^{210}Pb from radon progeny implantation. Ultimately, one can conclude that radon exposure is more crucial than dust fallout. Therefore, the best practice for rare events experiments to face surface background contamination is to perform cleaning and assembling in a radon-free cleanroom environment.

36.6.5 Mitigation of backgrounds and active background discrimination

In this Section we discuss a selection of different background mitigation techniques used in experiments to search for rare events in deep underground laboratories. This includes both the avoidance or reduction of specific radioactive contamination, as well as active background suppression techniques based on specific event features and topologies.

- *Mitigation of ^{222}Rn daughters deposition.* In dark matter direct search radiogenic (α, n) reactions due to radioactive decays are of great concern. The emitted neutron can mimic a nuclear recoil induced by a dark matter particle interaction. In the DarkSide-50 and LUX-ZEPLIN (LZ) experiments to mitigate this background, cleaning of parts and assembling of the dual-phase Time Projection Chamber have been carried out in a radon-free cleanroom with ^{222}Rn activity of the order of $\lesssim 50 \text{ mBq/m}^3$.
- *Underground argon.* Liquid argon is an excellent scintillator to search for dark matter interactions due to the high electron-recoils rejection power through pulse shape discrimination. Events from $\beta-\gamma$ background can be rejected at the level of 10^7 or better with respect to nuclear-recoils. Moreover, liquid argon is used as an active shield in GERDA and the upcoming LEGEND experiment searching for neutrinoless double beta decay. However, a major drawback for dark matter search is due to the fact that atmospheric argon contains about 1 Bq/kg of cosmogenic ^{39}Ar ($T_{1/2}=269 \text{ y}$, $Q_{\beta}=565 \text{ keV}$) [230]. For neutrinoless double beta decay search with GERDA and LEGEND, ^{42}Ar ($T_{1/2}=32.9 \text{ y}$, $Q_{\beta}=599 \text{ keV}$) with its short lived progeny ^{42}K ($T_{1/2}=12 \text{ h}$, $Q_{\beta}=3525 \text{ keV}$) is a major source of background. This limits significantly the dark matter and neutrinoless double beta decay sensitivity search. Therefore, a source of argon with reduced ^{39}Ar and ^{42}Ar is crucial. Centrifugation or differential thermal diffusion are established methods to separate $^{39/42}\text{Ar}$ and ^{40}Ar . However, this is an expensive method for a large fiducial mass. Argon from underground natural gas reservoirs is shown to contain low ^{39}Ar [231], and it is expected that ^{42}Ar is similar or even better reduced. Therefore, the use of underground argon mitigates the $^{39/42}\text{Ar}$ backgrounds. DarkSide-50, with a mass of 150 kg of underground argon, has shown that this source of argon contains ^{39}Ar at a level reduced by a factor of $(1.4 \pm 0.3) \times 10^3$ with respect to atmospheric argon.
- *Electro-formed copper.* High radio-purity copper is often used as shielding and as core detectors components. The radioimpurities in the copper can be a dominant source of external background. Copper electro-forming is a technique used to reduce this background component in rare events experiments. Copper electro-forming is a well known process to obtain ultra-high radio-purity copper. This technique has been used in the framework of the Majorana Demonstrator experiment to search for neutrinoless double beta decay and in ANAIS to search for dark matter annual modulation. Subppm levels in uranium and thorium have been achieved with electro-formed copper.
- *Background suppression using topological event information.* In addition to rigorous selection of high-purity target and shielding materials from external radiation, additional active suppression techniques must usually be employed in low background experiments to achieve the appropriate experimental sensitivities. While signal and background events may be indistinguishable if only their energy deposition is measured, their event features may differ significantly in time and space. Liquid scintillators use the characteristic photon

emission time distributions to distinguish between electron- and alpha-like signals [232] and nuclear recoils [233], respectively. High-purity germanium detectors use the time evolution of the induced charges to separate point-like signal candidates for neutrinoless double-beta decay events from background signals induced, for example, by gamma interactions with multiple interactions within a crystal, or from β or α events on the n+ or p+ electrodes [234]. The operation of bare high-purity germanium detectors in an instrumented liquid argon shield enabled the GERDA experiment to identify backgrounds with signal-like event topology within the HPGe detectors, but with random energy deposition in the surrounding liquid argon. These synergistic background suppression techniques enabled for a first time ever a quasi background-free search for neutrinoless double beta decays with GERDA.

The NEXT experiment for neutrinoless double beta decay in ^{136}Xe exploits differences in the spatial ionization patterns of double beta decay and single electron events to reject the background [235]. The former is characterized by two Bragg peaks at opposite ends of the tracks, the latter on the contrary displays only one peak. The combination of topology information and good energy resolution offer a powerful tool for background rejection.

In addition, the 3D location of detected events in a multivariate fit, which accounts for spacial surface and bulk distributions of signal and background together with other properties, such as pulse shape and topological features, is a powerful tool for background mitigation.

- *Signal detection in rare events searches.* In direct dark matter experiments electron recoil events have to be mitigated with respect to nuclear recoil events. In semiconductor bolometers, operating at a few tens of mK under a bias electric field and used as calorimeters, drifting charges produce a large phonon signal proportional to the ionization, which allows to discriminate electron recoils by the combination of charge and phonon signals [236]. In scintillating bolometers the phonon and light signals are used for the same purpose [237]. Cryogenic scintillators, such as xenon and argon, in time projection chambers offer a strong electron recoils background mitigation through the detection of a primary scintillation signal in liquid and a secondary signal in gas from the drift and extraction of ionization electrons. This background mitigation technique is also being used for neutrinoless double beta decay with ^{136}Xe . The accurate fiducialization and good rejection of multiple-scattering events allow dark matter optimized experiments to attempt a search for this very rare phenomenon.
- *Neutron tagging in dark matter searches.* Present and next generation experiments need large neutron tagging detectors. In DarkSide-50 a dedicated active veto has been developed to both suppress and measure *in situ* the rate of neutron-induced background events [238]. The detector consists of a boron-loaded liquid scintillator, which serves both as shielding against γ -rays and as a tag for neutrons. Neutrons are thermalised and captured on ^{10}B . Experimental data has shown a neutron rejection power greater than 99.1% with 5% concentration of TMB in 30 tonnes pseudocumene-based liquid scintillator. The LZ direct dark matter detector with a central TPC of 7 tonnes of liquid xenon makes use of an outer Gd-loaded liquid scintillator neutron tagging veto, which works similarly to the DarkSide-50 veto, replacing boron with gadolinium. The 22 tonnes liquid scintillator is based on linear alkyl benzene (LAB) as solvent. This detector has been designed to operate with a neutron tagging efficiency greater than 95%. The nuclear-recoil background is reduced by a factor of 10. The XENONnT detector makes use of a cylindrical stainless steel tank filled with Gd-loaded water, which surrounds the cryostat with a TPC of 5.9 tonnes of active liquid xenon. The Gd concentration in water is 0.2% in mass. Neutrons leaving the TPC volume will be moderated and captured by the Gd with a probability of 91%. The gamma-rays emitted after the capture are detected from

Cherenkov photons, providing a neutron tagging.

- *Mitigation of cosmogenic background.* In recent years the required sensitivity to search for dark matter and neutrinoless double beta decay asks for a strong reduction of cosmogenic background. We have emphasized that muons can produce neutrons that can enter the active volume of the detector from the surrounding rock or from external detector components. The yield of these so-called *cosmogenic neutrons* depend on the muon energies and the material properties of the medium the muon passes through. In addition, muons can produce by spallation radioisotopes inside the detector active volume. Cosmogenic backgrounds are a function of depth and experimental design, and can limit the sensitivity to search for rare events. Most of these radioisotopes are short-lived and their effect can be easily removed by an active veto based on the time correlation with a crossing muon. However, a number of cosmogenic radioisotopes are long-lived and they require an important consideration. Mitigation of these cosmogenic backgrounds produced in-situ deep underground are a major challenge for upcoming and future experiments. Optimizing the detector design and analysis strategies at a given depth equals an effective muon flux reduction. In particular, we mention two discrimination techniques for muon-induced isotopes: 1) ^{11}C tagging by a three-fold coincidence between the crossing muon, the capture of the ejected neutron from ^{12}C , and the ^{11}C decay [239]; 2) similar delayed coincidence tagging can be exploited to mitigate the background due to ^{77}Ge and its metastable state ^{77m}Ge , which have been identified as dominant cosmogenic background in the search for neutrinoless double beta decay of ^{76}Ge .
- *Purification.* A number of high efficiency specific purification methods have been developed for different detectors in order to remove long-lived radio-isotopes, ^{39}Ar , ^{85}Kr , and ^{210}Pb progeny. For organic liquid scintillators, distillation and water extraction have been shown to be very effective to reach radiopurity levels of the order of $10^{-5}\mu\text{Bq/kg}$ or better in uranium and thorium, and $10^{-3}\mu\text{Bq/kg}$ in ^{210}Pb [240]. Distillation has been used to reduce ^{85}Kr in xenon by a factor of 10^3 [241]. Cryogenic distillation will be used to reduce the isotopic abundance of ^{39}Ar in argon extracted from underground with a 350 m column in the ARIA project [242]. For semiconductors [243] and scintillating crystals [244] zone-refining has been exploited to remove impurities at the cost of a small fraction of material kept after the purification.
- *Direct isotope tagging.* In neutrinoless double beta decay in order to explore half-lives greater than 10^{28} y one needs an almost background-free detector. A robust method to reject backgrounds from radioactive decays would be the identification of the daughter atom of the double beta decaying nucleus: for example, for ^{136}Xe , the $^{136}\text{Ba}^{2+}$. Important step forwards to establish a valid and promising method for this tagging have been recently made [245, 246].

References

- [1] A. Aab *et al.* (Pierre Auger), *Earth and Space Science* **7**, 4, e2019EA000582 (2020), URL <https://agupubs.onlinelibrary.wiley.com/doi/abs/10.1029/2019EA000582>.
- [2] R. M. Baltrusaitis *et al.*, *Nucl. Instrum. Meth.* **A240**, 410 (1985).
- [3] D. J. Bird *et al.* (HiRes), *Astrophys. J.* **424**, 491 (1994).
- [4] T. Abu-Zayyad *et al.*, *Nucl. Instrum. Meth.* **A450**, 253 (2000).
- [5] A. Watson **210**, 00001 (2019), [arXiv:1901.06676].
- [6] H. Tokuno *et al.*, *Nucl. Instrum. Meth.* **A676**, 54 (2012), [arXiv:1201.0002].
- [7] J. Abraham *et al.* (Pierre Auger), *Nucl. Instrum. Meth.* **A620**, 227 (2010), [arXiv:0907.4282].
- [8] M. M. Malacari *et al.* (FAST), *Astroparticle Physics* **119**, 102430 (2020), ISSN 0927-6505, URL <https://www.sciencedirect.com/science/article/pii/S0927650520300037>.
- [9] F. Arqueros, J. R. Hoerandel and B. Keilhauer, *Nucl. Instrum. Meth.* **A597**, 23 (2008), [arXiv:0807.3844].
- [10] F. Arqueros, J. R. Hoerandel and B. Keilhauer, *Nucl. Instrum. Meth.* **A597**, 1 (2008), [arXiv:0807.3760].
- [11] J. Rosado, F. Blanco and F. Arqueros, *Astropart. Phys.* **34**, 164 (2010), [arXiv:1004.3971].
- [12] M. Ave *et al.* (AIRFLY), *Astropart. Phys.* **28**, 41 (2007), [arXiv:astro-ph/0703132].
- [13] J. Rosado, F. Blanco and F. Arqueros, *Astropart. Phys.* **55**, 51 (2014), [arXiv:1401.4310].
- [14] J. H. Boyer *et al.*, *Nucl. Instrum. Meth.* **A482**, 457 (2002).
- [15] J. T. Brack *et al.*, *Astropart. Phys.* **20**, 653 (2004).
- [16] B. Fick *et al.*, *JINST* **1**, 11, P11003 (2006).
- [17] J. Abraham *et al.* (Pierre Auger), *Astropart. Phys.* **33**, 108 (2010), [arXiv:1002.0366].
- [18] P. Abreu *et al.* (Pierre Auger), *Astropart. Phys.* **34**, 368 (2011), [arXiv:1010.6162].
- [19] R. Thalman *et al.* *Journal of Quantitative Spectroscopy and Radiative Transfer*, **147**, 171 (2014), Erratum-ibid. **189**, 281 (2017).
- [20] J. Abraham *et al.* [Pierre Auger Collab.], *Nucl. Instrum. Methods* **A789**, 172 (2015).
- [21] M. Unger *et al.*, *Nucl. Instrum. Meth.* **A588**, 433 (2008), [arXiv:0801.4309].
- [22] T.K. Gaisser and A.M. Hillas, *Proc. 15th Int. Cosmic Ray Conf. Bulgarska Akademiia na Naukite, Conf. Papers* **8**, 353 (1978), (archived at <http://adsabs.harvard.edu/abs/1977ICRC....8..353G>).
- [23] A. e. a. T. P. A. C. Aab (The Pierre Auger Collaboration), *Phys. Rev. D* **100**, 082003 (2019), URL <https://link.aps.org/doi/10.1103/PhysRevD.100.082003>.
- [24] P. A. Klimov *et al.*, *Space Sci. Rev.* **212**, 3-4, 1687 (2017), [arXiv:1706.04976].
- [25] B. A. e. a. Khrenov, *Cosmic Research* **58**, 5, 317 (2020).
- [26] G. Abdellaoui *et al.* (JEM-EUSO), *Journal of Instrumentation* **13**, 5 (2018), ISSN 17480221.
- [27] J. e. a. Adams, *Experimental Astronomy* (2021).
- [28] F. Capel *et al.*, *Advances in Space Research* **62**, 2954 (2018).
- [29] A. O. *et al.*, *Journal of Cosmology and Astroparticle Physics* **2021**, 06, 007 (2021), URL <https://doi.org/10.1088/1475-7516/2021/06/007>.
- [30] J. Holder *et al.*, *AIP Conf. Proc.* **1085**, 657 (2009), [arXiv:0810.0474].
- [31] F. Aharonian *et al.* (H.E.S.S.), *Astron. Astrophys.* **457**, 899 (2006), [arXiv:astro-ph/0607333].
- [32] J. Albert *et al.* (MAGIC), *Astrophys. J.* **674**, 1037 (2008), [arXiv:0705.3244].
- [33] T. C. Weekes *et al.*, *Astrophys. J.* **342**, 379 (1989).
- [34] A. M. Hillas *et al.*, *Astrophys. J.* **503**, 744 (1998).
- [35] <http://tevcat.uchicago.edu/>.
- [36] F. Aharonian *et al.* (H.E.S.S.), *Astrophys. J.* **636**, 777 (2006), [arXiv:astro-ph/0510397].
- [37] M. de Naurois and D. Mazin, *Comptes Rendus Physique* **16**, 610 (2015), [arXiv:1511.00463].
- [38] N. Park, *PoS ICRC2017*, arXiv:1808.10495 (2018), [arXiv:1808.10495].
- [39] A. M. Hillas, *Astropart. Phys.* **43**, 19 (2013).
- [40] B. S. Acharya *et al.* (CTA Consortium), *Astropart. Phys.* **43**, 3 (2013).
- [41] A. Bernstein *et al.*, *Report on the Depth Requirements for a Massive Detector at Homestake* (2009), [arXiv:0907.4183].
- [42] K. Eguchi *et al.* (KamLAND), *Phys. Rev. Lett.* **90**, 021802 (2003), [hep-ex/0212021].

- [43] G. Alimonti *et al.* (Borexino), Nucl. Instrum. Meth. A **600**, 568 (2009), [arXiv:0806.2400].
- [44] Y. Ashie *et al.* (Super-Kamiokande), Phys. Rev. **D71**, 112005 (2005), [hep-ex/0501064].
- [45] S. Kasuga *et al.*, Phys. Lett. **B374**, 238 (1996).
- [46] M. Shiozawa (Super-Kamiokande), Nucl. Instrum. Meth. **A433**, 240 (1999).
- [47] K. Abe *et al.* (Super-Kamiokande), Phys. Rev. **D83**, 052010 (2011), [arXiv:1010.0118].
- [48] J. F. Beacom and M. R. Vagins, Phys. Rev. Lett. **93**, 171101 (2004), [hep-ph/0309300].
- [49] J. Boger *et al.* (SNO), Nucl. Instrum. Meth. **A449**, 172 (2000), [arXiv:nucl-ex/9910016].
- [50] T. K. Gaisser, F. Halzen and T. Stanev, Phys. Rept. **258**, 173 (1995), [Erratum: Phys. Rept.271,355(1996)], [hep-ph/9410384].
- [51] J.G. Learned and K. Mannheim, Ann. Rev. Nucl. and Part. Sci. **50**, 679 (2000).
- [52] U. F. Katz and C. Spiering, Prog. Part. Nucl. Phys. **67**, 651 (2012), [arXiv:1111.0507].
- [53] M. G. Aartsen *et al.* (IceCube), J. Phys. **G44**, 5, 054006 (2017), [arXiv:1607.02671].
- [54] S. Adrián-Martínez *et al.* (KM3NeT), J. Phys. **G43**, 8, 084001 (2016), [arXiv:1601.07459].
- [55] A. Gazizov and M. P. Kowalski, Comput. Phys. Commun. **172**, 203 (2005), [arXiv:astro-ph/0406439].
- [56] A. D. Avrorin *et al.*, Phys. Part. Nucl. **46**, 2, 211 (2015).
- [57] M. G. Aartsen *et al.* (IceCube), JINST **12**, 03, P03012 (2017), [arXiv:1612.05093].
- [58] M. G. Aartsen *et al.* (IceCube) (2014), [arXiv:1412.5106].
- [59] M. G. Aartsen *et al.* (IceCube-Gen2), J. Phys. G **48**, 6, 060501 (2021), [arXiv:2008.04323].
- [60] M. Agostini *et al.* (P-ONE), Nature Astron. **4**, 10, 913 (2020), [arXiv:2005.09493].
- [61] S. Adrián-Martínez *et al.* (KM3NeT), Eur. Phys. J. **C74**, 9, 3056 (2014), [arXiv:1405.0839].
- [62] A. V. Akindinov *et al.*, Eur. Phys. J. **C79**, 9, 758 (2019), [arXiv:1902.06083].
- [63] C. Kopper (for the IceCube Collab.), contribution to ICRC2017.
- [64] M. G. Aartsen *et al.* (IceCube), Phys. Rev. Lett. **113**, 101101 (2014), [arXiv:1405.5303].
- [65] A. Albert *et al.* (ANTARES), Astrophys. J. **853**, 1, L7 (2018), [arXiv:1711.07212].
- [66] M. G. Aartsen *et al.* (IceCube), Astrophys. J. **809**, 1, 98 (2015), [arXiv:1507.03991].
- [67] M. G. Aartsen *et al.* (IceCube, Fermi-LAT, MAGIC, AGILE, ASAS-SN, HAWC, H.E.S.S., INTEGRAL, Kanata, Kiso, Kapteyn, Liverpool Telescope, Subaru, Swift NuSTAR, VERITAS, VLA/17B-403), Science **361**, 6398, eaat1378 (2018), [arXiv:1807.08816].
- [68] M. G. Aartsen *et al.* (IceCube), Science **361**, 6398, 147 (2018), [arXiv:1807.08794].
- [69] A. Albert *et al.* (ANTARES, IceCube), Astrophys. J. **892**, 92 (2020), [arXiv:2001.04412].
- [70] M. G. Aartsen *et al.* (IceCube), Phys. Rev. **D99**, 3, 032007 (2019), [arXiv:1901.05366].
- [71] M. Kowalski (for the IceCube and IceCube-Gen2 Collabs.), contribution to ICRC2021.
- [72] P. Coyle, contribution to ICRC2021.
- [73] G. Dzhilkibaev (for the Baikal Collab.), contribution to ICRC2021.
- [74] T. Huege, Phys. Rept. **620**, 1 (2016), [arXiv:1601.07426].
- [75] F. G. Schroder, Prog. Part. Nucl. Phys. **93**, 1 (2017), [arXiv:1607.08781].
- [76] G. A. Askar'yan, Sov. Phys. JETP **14**, 2, 441 (1962), [Zh. Eksp. Teor. Fiz.41,616(1961)].
- [77] G.A. Askaryan, Sov. Phys. JETP **21**, 658 (1965).
- [78] E. Zas, F. Halzen and T. Stanev, Phys. Rev. D **45**, 362 (1992).
- [79] C. W. James *et al.*, Phys. Rev. **E84**, 056602 (2011), [arXiv:1007.4146].
- [80] J. Alvarez-Muniz, R. A. Vazquez and E. Zas, Phys. Rev. **D62**, 063001 (2000), [arXiv:astro-ph/0003315].
- [81] C. Glaser *et al.*, Eur. Phys. J. C **80**, 77 (2020), [arXiv:1906.01670].
- [82] D. Saltzberg *et al.*, Phys. Rev. Lett. **86**, 2802 (2001), [hep-ex/0011001].
- [83] O. Scholten *et al.*, J. Phys. Conf. Ser. **81**, 012004 (2007).
- [84] J. Alvarez-Muñiz *et al.*, Phys. Rev. D **74**, 023007 (2006), URL <https://link.aps.org/doi/10.1103/PhysRevD.74.023007>.
- [85] L. Gerhardt and S. R. Klein, Phys. Rev. **D82**, 074017 (2010), [arXiv:1007.0039].
- [86] J. Alvarez-Muniz, R. A. Vazquez and E. Zas, Phys. Rev. **D61**, 023001 (2000), [arXiv:astro-ph/9901278].
- [87] D. García-Fernández, A. Nelles and C. Glaser, Phys. Rev. D **102**, 8, 083011 (2020), [arXiv:2003.13442].
- [88] K. Greisen, Phys. Rev. Lett. **16**, 748 (1966).
- [89] G. T. Zatsepin and V. A. Kuzmin, JETP Lett. **4**, 78 (1966), [Pisma Zh. Eksp. Teor. Fiz.4,114(1966)].
- [90] V. de Souza (Pierre Auger, Telescope Array), PoS **ICRC2017**, 522 (2018).
- [91] R. Abbasi *et al.* (IceCube), Astropart. Phys. **34**, 382 (2011), [arXiv:1004.1694].
- [92] P. Allison *et al.* (ARA), Astropart. Phys. **108**, 63 (2019), [arXiv:1712.03301].
- [93] A. Anker *et al.* (ARIANNA), JCAP **1911**, 030 (2019), [arXiv:1909.02677].
- [94] J. A. Aguilar *et al.* (RNO-G) (2021), [arXiv:2107.02604].
- [95] I. Plaisier *et al.* (RNO-G), PoS **395**, 1026 (2021).
- [96] A. G. Viereg, K. Bechtol and A. Romero-Wolf, JCAP **1602**, 02, 005 (2016), [arXiv:1504.08006].
- [97] S. W. Barwick *et al.* (ARIANNA), Astropart. Phys. **90**, 50 (2017), [arXiv:1612.04473].
- [98] M. G. Aartsen *et al.* (IceCube), Phys. Rev. **D98**, 6, 062003 (2018), [arXiv:1807.01820].
- [99] A. Aab *et al.* (Pierre Auger), JCAP **1910**, 10, 022 (2019), [arXiv:1906.07422].
- [100] J. D. Bray *et al.*, Phys. Rev. **D91**, 6, 063002 (2015), [arXiv:1502.03313].
- [101] O. Scholten *et al.*, Phys. Rev. Lett. **103**, 191301 (2009), [arXiv:0910.4745].
- [102] P. W. Gorham *et al.* (ANITA), Phys. Rev. **D99**, 12, 122001 (2019), [arXiv:1902.04005].
- [103] P. Allison *et al.* (ARA), Phys. Rev. D **102**, 4, 043021 (2020), [arXiv:1912.00987].
- [104] A. Anker *et al.* (ARIANNA), JCAP **03**, 053 (2020), [arXiv:1909.00840].
- [105] T. Winchen *et al.*, J. Phys. Conf. Ser. **1181**, 1, 012077 (2019), [arXiv:1903.08472].
- [106] J. Stettner (IceCube), PoS **ICRC2019**, 1017 (2019), [arXiv:1908.09551].
- [107] A. van Vliet, R. Alves Batista and J. R. Hörandel, Phys. Rev. D **100**, 2, 021302 (2019), [arXiv:1901.01899].
- [108] S. Barwick *et al.*, Journal of Glaciology **51**, 173, 231–238 (2005).

- [109] J.A. Dowdeswell and S. Evans, Rept. on Prog. in Phys. **67**, 1821 (2004).
- [110] S. W. Barwick *et al.*, JCAP **1807**, 07, 055 (2018), [arXiv:1804.10430].
- [111] C. Deaconu *et al.*, Phys. Rev. **D98**, 4, 043010 (2018), [arXiv:1805.12576].
- [112] P. W. Gorham *et al.* (ANITA), Phys. Rev. Lett. **103**, 051103 (2009), [arXiv:0812.2715].
- [113] P. W. Gorham *et al.* (ANITA), Phys. Rev. Lett. **121**, 16, 161102 (2018), [arXiv:1803.05088].
- [114] P. W. Gorham *et al.* (ANITA), Phys. Rev. Lett. **126**, 7, 071103 (2021), [arXiv:2008.05690].
- [115] I. Kravchenko *et al.* (RICE), Phys. Rev. **D73**, 082002 (2006), [arXiv:astro-ph/0601148].
- [116] P. Allison *et al.* (ARA), Phys. Rev. **D93**, 8, 082003 (2016), [arXiv:1507.08991].
- [117] J. Avva *et al.*, Nucl. Instrum. Meth. **A869**, 46 (2017), [arXiv:1605.03525].
- [118] J. A. Aguilar *et al.* (RNO-G), JINST **16**, 03, P03025 (2021), [arXiv:2010.12279].
- [119] R.D. Dagkesamanskii and I.M. Zheleznykh, Sov. Phys. JETP Lett. **50**, 233 (1989).
- [120] G. R. Olhoeft and D. W. Strangway, Earth and Planetary Science Letters **24**, 3, 394 (1975).
- [121] J. D. Bray, Astropart. Phys. **77**, 1 (2016), [arXiv:1601.02980].
- [122] C. W. James *et al.*, EPJ Web Conf. **135**, 04001 (2017), [arXiv:1704.05336].
- [123] A. Aab *et al.* (Pierre Auger), Phys. Rev. Lett. **116**, 24, 241101 (2016), [arXiv:1605.02564].
- [124] P. A. Bezyazeev *et al.* (Tunka-Rex), Phys. Rev. **D97**, 12, 122004 (2018), [arXiv:1803.06862].
- [125] S. Buitink *et al.* (LOFAR), Phys. Rev. **D90**, 8, 082003 (2014), [arXiv:1408.7001].
- [126] K. Mulrey *et al.* (LOFAR), JCAP **11**, 017 (2020), [arXiv:2005.13441].
- [127] J. G. Learned and S. Pakvasa, Astropart. Phys. **3**, 267 (1995), [hep-ph/9405296].
- [128] J. L. Feng *et al.*, Phys. Rev. Lett. **88**, 161102 (2002), [hep-ph/0105067].
- [129] A. G. Viereg (PUEO), PoS **ICRC2021**, 1029 (2021).
- [130] J. Álvarez Muñoz *et al.* (GRAND), Sci. China Phys. Mech. Astron. **63**, 1, 219501 (2020), [arXiv:1810.09994].
- [131] P. Abreu *et al.* (Pierre Auger), PoS **ICRC2021**, 262 (2021).
- [132] D. R. Nygren, in "Proceedings, 1975 PEP Summer Study, Berkeley, July 28-August 20, 1975," 126–133 (1975).
- [133] L. S. Miller, S. Howe and W. E. Spear, Phys. Rev. **166**, 871 (1968), URL <https://link.aps.org/doi/10.1103/PhysRev.166.871>.
- [134] E. Aprile and T. Doke, Rev. Mod. Phys. **82**, 2053 (2010), [arXiv:0910.4956].
- [135] V. Chepel and H. Araujo, JINST **8**, R04001 (2013), [arXiv:1207.2292].
- [136] D. Gonzalez-Diaz, F. Monrabal and S. Murphy, Nucl. Instrum. Meth. **A878**, 200 (2018), [arXiv:1710.01018].
- [137] J. J. Gomez-Cadenas, F. Monrabal Capilla and P. Ferrario, Front.in Phys. **7**, 51 (2019), [arXiv:1903.02435].
- [138] H. J. Maris, Journal of the Physical Society of Japan **77**, 11, 111008 (2008), URL <https://doi.org/10.1143/JPSJ.77.111008>.
- [139] L. Bruschi, G. Mazzi and M. Santini, Phys. Rev. Lett. **28**, 1504 (1972), URL <https://link.aps.org/doi/10.1103/PhysRevLett.28.1504>.
- [140] E. Aprile *et al.*, Nature **568**, 7753, 532 (2019), URL <https://doi.org/10.1038/s41586-019-1124-4>.
- [141] K. Winger *et al.*, Journal of Environmental Radioactivity **80**, 2, 183 (2005), ISSN 0265-931X, URL <http://www.sciencedirect.com/science/article/pii/S0265931X04002887>.
- [142] H. Loosli, Earth and Planetary Science Letters **63**, 1, 51 (1983), ISSN 0012-821X, URL <http://www.sciencedirect.com/science/article/pii/0012821X83900213>.
- [143] E. Aprile *et al.* (XENON), Eur. Phys. J. **C75**, 11, 546 (2015), [arXiv:1503.07698].
- [144] M. Schumann, J. Phys. **G46**, 10, 103003 (2019), [arXiv:1903.03026].
- [145] E. Aprile *et al.*, JINST **9**, 11, P11012 (2014), [arXiv:1408.6206].
- [146] F. Neves *et al.*, JINST **12**, 01, P01017 (2017), [arXiv:1612.07965].
- [147] D. S. Akerib *et al.* (LUX Collaboration), Phys. Rev. D **97**, 102008 (2018), URL <https://link.aps.org/doi/10.1103/PhysRevD.97.102008>.
- [148] D. S. Akerib *et al.* (LUX), Phys. Rev. **D95**, 1, 012008 (2017), [arXiv:1610.02076].
- [149] M. Szydagis *et al.*, Journal of Instrumentation **6**, 10, P10002 (2011), URL <https://doi.org/10.1088/2F1748-0221%2F6%2F10%2Fp10002>.
- [150] M. Kimura *et al.*, Phys. Rev. **D100**, 3, 032002 (2019), [arXiv:1902.01501].
- [151] R. Ajaj *et al.* (DEAP), Phys. Rev. **D100**, 2, 022004 (2019), [arXiv:1902.04048].
- [152] P. Agnes *et al.* (DarkSide), Phys. Rev. **D93**, 8, 081101 (2016), [Addendum: Phys. Rev.D95,no.6,069901(2017)], [arXiv:1510.00702].
- [153] E. Aprile *et al.* (XENON), Phys. Rev. Lett. **119**, 18, 181301 (2017), [arXiv:1705.06655].
- [154] X. Cui *et al.* (PandaX-II), Phys. Rev. Lett. **119**, 18, 181302 (2017), [arXiv:1708.06917].
- [155] D. S. Akerib *et al.*, Phys. Rev. Lett. **118**, 25, 251302 (2017).
- [156] D. S. Akerib *et al.* (LUX-ZEPLIN) (2018), [arXiv:1802.06039].
- [157] E. Aprile *et al.* (XENON), JCAP **1604**, 04, 027 (2016), [arXiv:1512.07501].
- [158] H. Zhang *et al.* (PandaX), Sci. China Phys. Mech. Astron. **62**, 3, 31011 (2019), [arXiv:1806.02229].
- [159] C. E. Aalseth *et al.*, Eur. Phys. J. Plus **133**, 131 (2018), [arXiv:1707.08145].
- [160] J. Aalbers *et al.*, Journal of Cosmology and Astroparticle Physics **2016**, 11, 017 (2016), URL <https://doi.org/10.1088/2F1475-7516%2F2016%2F11%2F017>.
- [161] W. Guo and D. N. McKinsey, Phys. Rev. **D87**, 11, 115001 (2013), [arXiv:1302.0534].
- [162] D. R. Nygren, J. Phys. Conf. Ser. **460**, 012006 (2013).
- [163] C. A. J. O'Hare *et al.*, Phys. Rev. **D92**, 6, 063518 (2015), [arXiv:1505.08061].
- [164] S. M. Bilenky and C. Giunti, Mod. Phys. Lett. **A27**, 1230015 (2012), [arXiv:1203.5250].
- [165] S. R. Elliott, A. A. Hahn and M. K. Moe, Phys. Rev. Lett. **59**, 2020 (1987), URL <http://link.aps.org/doi/10.1103/PhysRevLett.59.2020>.
- [166] G. Anton *et al.* (EXO-200), Phys. Rev. Lett. **123**, 16, 161802 (2019), [arXiv:1906.02723].
- [167] S. A. Kharusi *et al.* (nEXO) (2018), [arXiv:1805.11142].
- [168] D. Nygren, Nucl. Instrum. Meth. **A603**, 337 (2009).
- [169] M. K. Moe, Phys. Rev. **C44**, 931 (1991), [1019(1991)].
- [170] A. D. McDonald *et al.*, Phys. Rev. Lett. **120**, 13, 132504 (2018), [arXiv:1711.04782].

- [171] C. Chambers *et al.* (nEXO), *Nature* **569**, 7755, 203 (2019), [arXiv:1806.10694].
- [172] P. Thapa *et al.* (2019), [arXiv:1904.05901].
- [173] C. Enss, editor, *Cryogenic particle detection*, volume 99 of *Topics in applied physics*, Springer, Berlin, Germany (2005).
- [174] K. Pretzl, *Cryogenic Detectors* (2020).
- [175] *Proc. of the Low Temperature Detectors for Neutrinos and Dark Matter*, Low Temperature Detectors for Neutrinos and Dark Matter (start 1987).
- [176] G. H. Rieke, *Detection of Light*, Cambridge University Press, 3rd edition (2021).
- [177] H. Kraus, *Superconductor Science and Technology* **9**, 10, 827 (1996), URL <https://doi.org/10.1088/0953-2048/9/10/001>.
- [178] A. V. Dixit *et al.*, *Phys. Rev. Lett.* **126**, 14, 141302 (2021), [arXiv:2008.12231].
- [179] J. Zmuidzinas, *Annual Review of Condensed Matter Physics* **3**, 1, 169 (2012), URL <https://doi.org/10.1146/annurev-conmatphys-020911-125022>.
- [180] S. Doyle *et al.*, *Journal of Low Temperature Physics* **151**, 1, 530 (2008), URL <https://doi.org/10.1007/s10909-007-9685-2>.
- [181] K. Irwin and G. Hilton, *Transition-Edge Sensors*, 63–150, Springer Berlin Heidelberg, Berlin, Heidelberg (2005), ISBN 978-3-540-31478-3, URL https://doi.org/10.1007/10933596_3.
- [182] F. Paolucci and F. Giazotto, *Instruments* **5**, 2 (2021), ISSN 2410-390X, URL <https://www.mdpi.com/2410-390X/5/2/14>.
- [183] S. B. Bandler *et al.*, *J. Low Temp. Phys.* **93**, 709 (1993).
- [184] D. Prele, *Journal of Instrumentation* **10**, 08, C08015 (2015), URL <https://doi.org/10.1088/1748-0221/10/08/c08015>.
- [185] E. Fiorini and T. Niinikoski, *Nucl. Instrum. Meth. A* **224**, 83 (1984).
- [186] S. H. Moseley, J. C. Mather and D. McCammon, “Thermal detectors as x-ray spectrometers,” (1984).
- [187] V. Barger and D. Cline (1985), telemark, 1984.
- [188] A. Blasi *et al.* (1985), I.N.F.N./BE-85/2, internal report.
- [189] D. Q. Adams *et al.* (CUORE) (2021), [arXiv:2104.06906].
- [190] W. R. Armstrong *et al.* (CUPID) (2019), [arXiv:1907.09376].
- [191] O. Azzolini *et al.* (CUPID), *Phys. Rev. Lett.* **123**, 3, 032501 (2019), [arXiv:1906.05001].
- [192] E. Armengaud *et al.* (CUPID), *Phys. Rev. Lett.* **126**, 18, 181802 (2021), [arXiv:2011.13243].
- [193] V. Alenkov *et al.*, *Eur. Phys. J. C* **79**, 9, 791 (2019), [arXiv:1903.09483].
- [194] D. Mccammon *et al.* (1984).
- [195] L. Gastaldo *et al.*, *Eur. Phys. J. ST* **226**, 8, 1623 (2017).
- [196] B. Alpert *et al.*, *Eur. Phys. J. C* **75**, 3, 112 (2015), [arXiv:1412.5060].
- [197] M. P. Croce *et al.*, *J. Low Temp. Phys.* **184**, 3-4, 958 (2016), [arXiv:1510.03874].
- [198] R. Ardito *et al.* (2005), [hep-ex/0501010].
- [199] P. Filianin *et al.*, *Phys. Rev. Lett.* **127**, 7, 072502 (2021), [arXiv:2108.07039].
- [200] D. Pergolesi *et al.*, *Nucl. Instrum. Meth. A* **559**, 349 (2006).
- [201] M. Sisti *et al.*, *Nuclear Instruments and Methods in Physics Research Section A: Accelerators, Spectrometers, Detectors and Associated Equipment* **520**, 1, 125 (2004), ISSN 0168-9002, proceedings of the 10th International Workshop on Low Temperature Detectors, URL <https://www.sciencedirect.com/science/article/pii/S0168900203031814>.
- [202] E. Ferri *et al.*, *Phys. Procedia* **61**, 227 (2015).
- [203] C. Velte, *Measurement of a high energy resolution and high-statistics 163Ho electron capture spectrum for theECHO experiment.*, Ph.D. thesis, U. Heidelberg (main) (2020).
- [204] P. Luke *et al.*, *Nucl. Instrum. Meth. A* **289**, 406 (1990).
- [205] B. Neganov *et al.*, *J Low Temp Phys* **93**, 417–422 (1993), URL <https://doi.org/10.1007/BF00693454>.
- [206] I. Alkhatib *et al.* (SuperCDMS), *Phys. Rev. Lett.* **127**, 8, 081802 (2021), [arXiv:2011.09183].
- [207] Q. Arnaud *et al.* (EDELWEISS), *Phys. Rev. Lett.* **125**, 14, 141301 (2020), [arXiv:2003.01046].
- [208] *Snowmass2021-Letter of Interest The TESSERACT Dark Matter Project* (2020).
- [209] T. Braine *et al.* (ADMX), *Phys. Rev. Lett.* **124**, 10, 101303 (2020), [arXiv:1910.08638].
- [210] *Snowmass2021-Letter of Interest Opening the Terahertz Axion Window* (2020).
- [211] C. Bellenghi *et al.*, *Eur. Phys. J. C* **79**, 9, 727 (2019), [arXiv:1905.10611].
- [212] I. Colantoni *et al.*, *J. Low Temp. Phys.* **199**, 3-4, 593 (2020).
- [213] G. Heusser, *Ann. Rev. Nucl. Part. Sci.* **45**, 543 (1995).
- [214] D. S. Akerib *et al.*, *The European Physical Journal C* **80**, 11 (2020), URL <https://doi.org/10.1140/2Fepjc/2Fs10052-020-8420-x>.
- [215] D. S. Leonard *et al.*, *Nucl. Instrum. Meth. A* **871**, 169 (2017), [arXiv:1703.10799].
- [216] N. Abgrall *et al.* (Majorana), *Nucl. Instrum. Meth. A* **823**, 83 (2016), [arXiv:1603.08483].
- [217] M. Laubenstein, *International Journal of Modern Physics A* **32**, 30, 1743002 (2017), URL <https://doi.org/10.1142/S0217751x17430023>.
- [218] P. Scovell *et al.*, *Astroparticle Physics* **97**, 160 (2018), URL <https://doi.org/10.1016/j.astropartphys.2017.11.006>.
- [219] G. Heusser *et al.*, *The European Physical Journal C* **75**, 11 (2015), URL <https://doi.org/10.1140/2Fepjc/2Fs10052-015-3704-2>.
- [220] N. Jakubowski, *Analytical and Bioanalytical Chemistry* **392**, 5, 775 (2008), URL <https://doi.org/10.1007/2Fs00216-008-2374-4>.
- [221] M. Clemenza, *J. Radioanal. Nucl. Chem.* **318**, 3, 1765 (2018).
- [222] G. Heusser *et al.*, *Applied Radiation and Isotopes* **52**, 3, 691 (2000), URL <https://doi.org/10.1016/2Fs0969-8043%2899%2900231-6>.
- [223] M. Wojcik, G. Zuzel and H. Simgen, *International Journal of Modern Physics A* **32**, 30, 1743004 (2017), URL <https://doi.org/10.1142/2Fs0217751x17430047>.
- [224] Y. Takeuchi *et al.*, *Nuclear Instruments and Methods in Physics Research Section A: Accelerators, Spectrometers, Detectors and Associated Equipment* **421**, 1-2, 334 (1999), URL <https://doi.org/10.1016/2Fs0168-9002%2898%2901204-2>.
- [225] J. Kiko, *Nuclear Instruments and Methods in Physics Research Section A: Accelerators, Spectrometers, Detectors and Associated Equipment* **460**, 2-3, 272 (2001), URL <https://doi.org/10.1016/2Fs0168-9002%2800%2901082-2>.
- [226] E. Hoppe *et al.*, *Nuclear Instruments and Methods in Physics Research Section A: Accelerators, Spectrometers, Detectors and Associated Equipment* **579**, 1, 486 (2007), URL <https://doi.org/10.1016/2Fj.nima.2007.04.101>.
- [227] R. Bunker *et al.*, *Nuclear Instruments and Methods in Physics Research Section A: Accelerators, Spectrometers, Detectors and Associated Equipment* **967**, 163870 (2020), URL <https://doi.org/10.1016/j.nima.2020.163870>.

- [228] S. Bruenner *et al.*, The European Physical Journal C **81**, 4 (2021), URL <https://doi.org/10.1140/epjc/s10052-021-09047-2>.
- [229] M. L. di Vacri *et al.*, Nucl. Instrum. Meth. A **994**, 165051 (2021), [arXiv:2006.12746].
- [230] H. Loosli, Earth and Planetary Science Letters **63**, 1, 51 (1983), URL <https://doi.org/10.1016%2F0012-821x%2883%2990021-3>.
- [231] D. Acosta-Kane *et al.*, Nuclear Instruments and Methods in Physics Research Section A: Accelerators, Spectrometers, Detectors and Associated Equipment **587**, 1, 46 (2008), URL <https://doi.org/10.1016%2Fj.nima.2007.12.032>.
- [232] G. Ranucci, in “IEEE Symposium Conference Record Nuclear Science 2004.”, volume 2, 804–809 Vol. 2 (2004).
- [233] P. Adhikari *et al.*, The European Physical Journal C **80**, 4 (2020), URL <https://doi.org/10.1140%2Fepjc%2Fs10052-020-7789-x>.
- [234] D. Budjáš *et al.*, Journal of Instrumentation **4**, 10, P10007 (2009), URL <https://doi.org/10.1088/1748-0221/4/10/p10007>.
- [235] A. Simón *et al.* (NEXT), JHEP **21**, 146 (2020), [arXiv:2102.11931].
- [236] R. Agnese *et al.* (SuperCDMS Collaboration), Phys. Rev. Lett. **120**, 061802 (2018), URL <https://link.aps.org/doi/10.1103/PhysRevLett.120.061802>.
- [237] W. Westphal *et al.*, Nucl. Instrum. Meth. A **559**, 372 (2006).
- [238] S. Westerdale, E. Shields and F. Calaprice, Astroparticle Physics **79**, 10 (2016), URL <https://doi.org/10.1016%2Fj.astropartphys.2016.01.005>.
- [239] H. Back *et al.* (Borexino Collaboration), Phys. Rev. C **74**, 045805 (2006), URL <https://link.aps.org/doi/10.1103/PhysRevC.74.045805>.
- [240] J. Benziger *et al.*, Nuclear Instruments and Methods in Physics Research Section A: Accelerators, Spectrometers, Detectors and Associated Equipment **587**, 2-3, 277 (2008), URL <https://doi.org/10.1016/j.nima.2007.12.043>.
- [241] K. Abe *et al.*, Nucl. Instrum. Meth. A **716**, 78 (2013), [arXiv:1301.2815].
- [242] P. Agnes *et al.*, The European Physical Journal C **81**, 4 (2021), URL <https://doi.org/10.1140/epjc/s10052-021-09121-9>.
- [243] K.-P. Gradwohl *et al.*, Journal of Instrumentation **15**, 12, P12010 (2020), URL <https://doi.org/10.1088/1748-0221/15/12/p12010>.
- [244] B. Suerfu, F. Calaprice and M. Souza, Physical Review Applied **16**, 1 (2021), URL <https://doi.org/10.1103/physrevapplied.16.014060>.
- [245] I. Rivilla *et al.*, Nature **583**, 7814, 48 (2020), URL <https://doi.org/10.1038/s41586-020-2431-5>.
- [246] A. McDonald *et al.*, Physical Review Letters **120**, 13 (2018), URL <https://doi.org/10.1103/physrevlett.120.132504>.

37. Radioactivity and Radiation Protection

Revised August 2021 by S. Roesler (CERN) and M. Silari (CERN).

37.1 Definitions [1–3]

It would be desirable if legal protection limits could be expressed in directly measurable *physical quantities*. However, this does not allow quantifying biological effects of the exposure of the human body and its detriment to ionizing radiation.

For this reason, dose limits are expressed in terms of so-called *protection quantities* which, although calculable, are not measurable. Protection quantities are used to quantify the extent of exposure of the human body to ionizing radiation from both whole and partial body external irradiation and from intakes of radionuclides.

In order to demonstrate compliance with dose limits, so-called *operational quantities* are typically used, which aim at providing conservative estimates of protection quantities. Often radiation protection detectors used for individual and area monitoring are calibrated in terms of operational quantities and, thus, these quantities become “measurable”.

37.1.1 Physical quantities

• **Fluence, Φ** (unit: $1/\text{m}^2$): The fluence is the quotient of the sum of the particle track lengths dl in the volume dV

$$\Phi = dl/dV .$$

It can also be expressed in terms of number of particles dN incident upon a small sphere of cross-sectional area da

$$\Phi = dN/da .$$

• **Absorbed dose, D** (unit: gray, $1 \text{ Gy}=1 \text{ J/kg}=100 \text{ rad}$): The absorbed dose is the energy imparted by ionizing radiation in a volume element of a specified material divided by the mass of this volume element.

• **Kerma, K** (unit: gray): Kerma is the sum of the initial kinetic energies of all charged particles set in motion by indirectly ionizing radiation in a volume element of the specified material divided by the mass of this volume element.

• **Linear energy transfer, L or LET** (unit: J/m , often given in $\text{keV}/\mu\text{m}$, $1 \text{ keV}/\mu\text{m} \approx 1.602 \times 10^{-10} \text{ J/m}$): The linear energy transfer is the mean energy, dE , lost by a charged particle owing to collisions with electrons in traversing a distance dl in matter. *Low-LET radiation*: X rays and gamma rays (accompanied by charged particles due to interactions with the surrounding medium) or light charged particles such as electrons that produce sparse ionizing events far apart at a molecular scale ($L < 10 \text{ keV}/\mu\text{m}$). *High-LET radiation*: neutrons and heavy charged particles that produce ionizing events densely spaced at a molecular scale ($L > 10 \text{ keV}/\mu\text{m}$). While the above LET definition refers to electronic stopping power only, at low energy nuclear stopping power could be a significant fraction of the total stopping power.

• **Activity, A** (unit: Becquerel, $1 \text{ Bq}=1/\text{s}=27 \text{ pCi}$): Activity is the expectation value of the number of nuclear decays occurring in a given quantity of material per unit time.

37.1.2 Protection quantities

• **Organ absorbed dose, D_T** (unit: gray): The mean absorbed dose in an organ or tissue T of mass m_T is defined as

$$D_T = \frac{1}{m_T} \int_{m_T} D dm .$$

• **Equivalent dose, H_T** (unit: sievert, $1 \text{ Sv}=1 \text{ J/kg}=100 \text{ rem}$):

The equivalent dose H_T in an organ or tissue T is equal to the sum of the absorbed doses $D_{T,R}$ in the organ or tissue caused by different radiation types R weighted with so-called radiation weighting factors w_R :

$$H_T = \sum_R w_R \times D_{T,R} .$$

It expresses long-term risks (primarily cancer and leukemia) from low-level chronic exposure. The values for w_R recommended by ICRP [2] are given in Table 37.1.

Table 37.1: Radiation weighting factors, w_R .

Radiation type	w_R
Photons, electrons and muons	1
Neutrons, $E_n < 1 \text{ MeV}$	$2.5 + 18.2 \times \exp[-(\ln E_n)^2/6]$
$1 \text{ MeV} \leq E_n \leq 50 \text{ MeV}$	$5.0 + 17.0 \times \exp[-(\ln(2E_n))^2/6]$
$E_n > 50 \text{ MeV}$	$2.5 + 3.25 \times \exp[-(\ln(0.04E_n))^2/6]$
Protons and charged pions	2
Alpha particles, fission fragments, heavy ions	20

• **Effective dose, E** (unit: sievert): The sum of the equivalent doses, weighted by the tissue weighting factors w_T ($\sum_T w_T = 1$) of several organs and tissues T of the body that are considered to be most sensitive [2], is called “effective dose”:

$$E = \sum_T w_T \times H_T . \quad (37.1)$$

37.1.3 Operational quantities

• **Dose equivalent, H** (unit: sievert): The dose equivalent at a point in tissue is given by:

$$H = D \times Q \quad (37.2)$$

where D is the absorbed dose and Q is the quality factor at that point. The quality factor at a point in tissue, is given by:

$$Q = \frac{1}{D} \int_{L=0}^{\infty} Q(L) D_L dL$$

where D_L is the distribution of D in unrestricted linear energy transfer L at the point of interest, and $Q(L)$ is the quality factor as a function of L . The integration is to be performed over D_L , due to all charged particles, excluding their secondary electrons.

• **Ambient dose equivalent, $H^*(10)$** (unit: sievert): The dose equivalent at a point in a radiation field that would be produced by the corresponding expanded and aligned field in a 30 cm diameter sphere of unit density tissue (so-called ICRU sphere/tissue with a mass composition of 76.2% oxygen, 11.1% carbon, 10.1% hydrogen and 2.6% nitrogen) at a depth of 10 mm on the radius vector opposing the direction of the aligned field. Ambient dose equivalent is the operational quantity for *area monitoring*.

• **Personal dose equivalent, $H_p(d)$** (unit: sievert): The dose equivalent in ICRU tissue at an appropriate depth, d , below a specified point on the human body. The specified point is normally taken to be where the individual dosimeter is worn. For the assessment of effective dose, $H_p(10)$ with a depth $d = 10 \text{ mm}$ is chosen, and for the assessment of the dose to the skin and to the hands and feet the personal dose equivalent, $H_p(0.07)$, with a depth $d = 0.07 \text{ mm}$, is used. Personal dose equivalent is the operational quantity for *individual monitoring*.

37.1.4 Dose conversion coefficients

Dose conversion coefficients allow direct calculation of protection or operational quantities from particle fluence and are functions of particle type, energy and irradiation configuration. The most common coefficients are those for effective dose and ambient dose equivalent. The former are based on simulations in which the dose to organs of anthropomorphic phantoms is calculated for approximate actual conditions of exposure, such as irradiation of the front of the body (antero-posterior irradiation) or isotropic irradiation.

Conversion coefficients from fluence to effective dose are given for anterior-posterior irradiation and various particle types in Fig. 37.1 [4]. For example, the effective dose from an anterior-posterior irradiation in a field of 1-MeV neutrons with a fluence of 1 neutron per cm^2 is about 290 pSv. In Monte Carlo simulations such coefficients allow multiplication with fluence at scoring

time such that effective dose to a human body at the considered location is directly obtained.

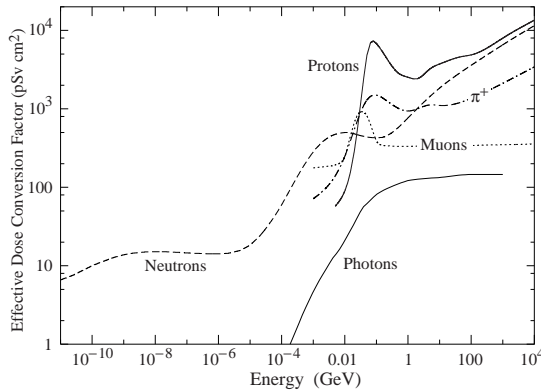


Figure 37.1: Fluence to effective dose conversion coefficients for anterior-posterior irradiation and various particle types [4].

37.2 Radiation levels [5]

• Natural background radiation:

On a worldwide average, the annual whole-body dose equivalent due to all sources of natural background radiation ranges from 1.0 to 13 mSv (0.1–1.3 rem) with an annual average of 2.4 mSv [6]. In certain areas values up to 50 mSv (5 rem) have been measured. A large fraction (typically more than 50%) originates from inhaled natural radioactivity, mostly radon and radon daughters [7]. The latter can vary by more than one order of magnitude: it is 0.1–0.2 mSv in open areas, 2 mSv on average in a house and more than 20 mSv in poorly ventilated mines.

• **Cosmic ray background radiation:** At sea level, the whole-body dose equivalent due to cosmic ray background radiation is dominated by muons; at higher altitudes also nucleons contribute. Dose equivalent rates range from less than 0.1 $\mu\text{Sv/h}$ at sea level to a few $\mu\text{Sv/h}$ at aircraft altitudes. Details on cosmic ray fluence levels are given in the Cosmic Rays section (Sec. 30 of this Review).

37.3 Health effects of ionizing radiation

Radiation can cause two types of health effects, deterministic and stochastic:

• **Deterministic effects** are tissue reactions which cause injury to a population of cells if a given threshold of absorbed dose is exceeded. The severity of the reaction increases with dose. The quantity in use for tissue reactions is the absorbed dose, D . When particles other than photons and electrons (low- LET radiation) are involved, a Relative Biological Effectiveness (RBE)-weighted dose may be used. The RBE of a given radiation is the reciprocal of the ratio of the absorbed dose of that radiation to the absorbed dose of a reference radiation (usually X rays) required to produce the same degree of biological effect. It is a complex quantity that depends on many factors such as cell type, dose rate, fractionation, etc.

• **Stochastic effects** are malignant diseases and heritable effects for which the probability of an effect occurring, but not its severity, is a function of dose without threshold.

• **Lethal dose:** The whole-body dose from penetrating ionizing radiation resulting in 50% mortality in 30 days (assuming no medical treatment) is 2.5–4.5 Gy (250–450 rad)¹, as measured internally on the body longitudinal center line. The surface dose varies due to variable body attenuation and may be a strong function of energy.

• Cancer induction:

The cancer induction probability is about 5% per Sv on average for the entire population [3].

• **Recommended effective dose limits:** The International Commission on Radiological Protection (ICRP) recommends a

limit for radiation workers of 20 mSv effective dose per year averaged over 5 years, with the provision that the dose should not exceed 50 mSv in any single year [3]. The limit in the EU-countries and Switzerland is 20 mSv per year, in the U.S. it is 50 mSv per year (5 rem per year). Many physics laboratories in the U.S. and elsewhere set lower limits. The effective dose limit for the general public is typically 1 mSv per year.

37.4 Prompt neutrons at accelerators

Neutrons dominate the radiation environment outside thick shielding (*e.g.*, > 1 m of concrete) for high energy (> a few hundred MeV) electron and hadron accelerators. In addition, for accelerators with energies above about 10 GeV, muons contribute significantly at small angles with regard to the beam, even behind several meters of shielding. Another special case are synchrotron light sources where particular care has to be taken to shield the very intense low-energy photons extracted from the electron synchrotron into the experimental areas. Due to its importance at high energy accelerators this section focuses on prompt neutrons.

37.4.1 Electron accelerators

At electron accelerators, neutrons are generated via photonuclear reactions from bremsstrahlung photons. Neutron production takes place above a threshold value which varies from 10 to 19 MeV for light nuclei (with important exceptions, such as 2.23 MeV for deuterium and 1.67 MeV for beryllium) and from 4 to 6 MeV for heavy nuclei. It is commonly described by different mechanisms depending on the photon energy: the giant dipole resonance interactions (from threshold up to about 30 MeV, often the dominant process), the quasi-deuteron effect (between 30 MeV and a few hundred MeV), the delta resonance mechanism (between 200 MeV and a few GeV) and the vector meson dominance model at higher energies.

The giant dipole resonance reaction consists in a collective excitation of the nucleus, in which neutrons and protons oscillate in the direction of the photon electric field. The oscillation is damped by friction in a few cycles, with the photon energy being transferred to the nucleus in a process similar to evaporation. Nucleons emitted in the dipolar interaction have an anisotropic angular distribution, with a maximum at 90° , while those leaving the nucleus as a result of evaporation are emitted isotropically with a Maxwellian energy distribution described as [8]:

$$\frac{dN}{dE_n} = \frac{E_n}{T^2} e^{-E_n/T}, \quad (37.3)$$

where T is a nuclear ‘temperature’ (in units of MeV) characteristic of the particular target nucleus and its excitation energy. For heavy nuclei the ‘temperature’ generally lies in the range of $T = 0.5$ – 1.0 MeV. Neutron yields from semi-infinite targets per kW of electron beam power are plotted in Fig. 37.2 as a function of the electron beam energy [8].

While for thick targets neutron production is mainly due to photonuclear interactions, for thin targets (thickness of fractions of the radiation length) electronuclear interactions are the dominating process.

Typical neutron energy spectra outside of concrete (80 cm thick, 2.35 g/cm³) and iron (40 cm thick) shields are shown in Fig. 37.3. In order to compare these spectra to those caused by proton beams (see below) the spectra are scaled by a factor of 100, which roughly corresponds to the difference in the high energy hadronic cross sections for photons and hadrons (*e.g.*, the fine structure constant). The shape of these spectra are generally characterized by a low-energy peak at around 1 MeV (evaporation neutrons) and a high-energy shoulder at around 70–80 MeV. In case of concrete shielding, the spectrum also shows a pronounced peak at thermal neutron energies.

37.4.2 Proton accelerators

At proton accelerators, neutron yields emitted per incident proton by different target materials are roughly independent of proton energy between 20 MeV and 1 GeV, and are given by the ratio C : Al : Cu-Fe : Sn : Ta-Pb = 0.3 : 0.6 : 1.0 : 1.5 : 1.7 [12]. Above about 1 GeV, the neutron yield is proportional to E^m , where $0.80 \leq m \leq 0.85$ [13].

¹ RBE -weighted when necessary

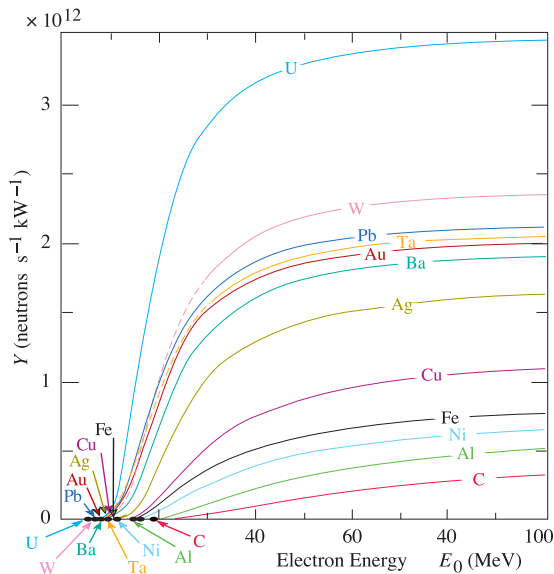


Figure 37.2: Neutron yields from semi-infinite targets per kW of electron beam power, as a function of the electron beam energy, disregarding target self-shielding [8].

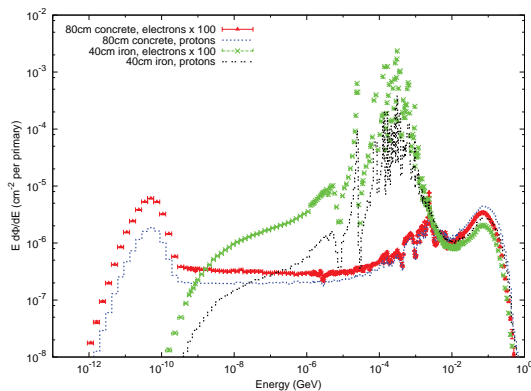


Figure 37.3: Neutron energy spectra calculated with the FLUKA code [9–11] from 25 GeV proton and electron beams on a thick copper target. Spectra are evaluated at 90° to the beam direction behind 80 cm of concrete or 40 cm of iron. All spectra are normalized per beam particle. For better visualization, spectra for electron beam are multiplied by a factor of 100.

Typical neutron energy spectra outside of concrete and iron shielding are shown in Fig. 37.3. Here, the radiation fields are caused by a 25 GeV proton beam interacting with a thick copper target. The comparison of these spectra with those for an electron beam of the same energy reflects the difference in the hadronic cross sections between photons and hadrons above a few 100 MeV. Differences are increasing towards lower energies because of different interaction mechanisms. Furthermore, the slight shift in energy above about 100 MeV follows from the fact that the energies of the interacting photons are lower than 25 GeV. Apart from this the shapes of the two spectra are similar.

The neutron-attenuation length is shown in Fig. 37.4 for concrete and mono-energetic broad-beam conditions. It reaches an asymptotic value of about 117 g/cm^2 above 200 MeV. As the cascade through thick shielding is carried by particles with energies between about 100 MeV and 300 MeV (in this energy range non-elastic cross sections are at minimum and are dominated by quasi-elastic processes leading to low attenuation) this value is equal to the equilibrium attenuation length for particles emitted at 90° in concrete.

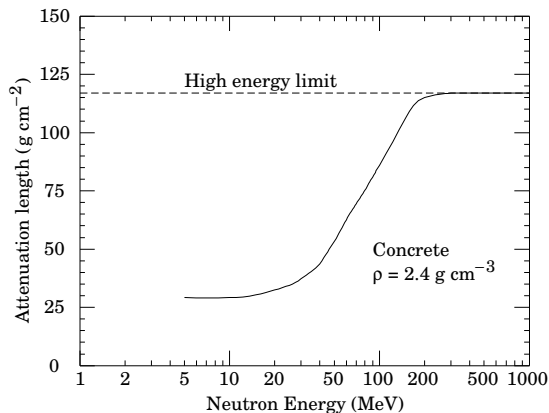


Figure 37.4: The variation of the attenuation length for mono-energetic neutrons in concrete as a function of neutron energy [12].

37.5 Photon sources

The dose equivalent rate in tissue (in mSv/h) from a gamma point source emitting one photon of energy E (in MeV) per second at a distance of 1 m is $4.6 \times 10^{-9} \mu_{en}/\rho E$, where μ_{en}/ρ is the mass energy absorption coefficient. The latter has a value of $0.029 \pm 0.004 \text{ cm}^2/\text{g}$ for photons in tissue over an energy range between 60 keV and 2 MeV (see Ref. [14] for tabulated values).

Similarly, the dose equivalent rate in tissue (in mSv/h) at the surface of a semi-infinite slab of uniformly activated material containing 1 Bq/g of a gamma emitter of energy E (in MeV) is $2.9 \times 10^{-4} R_\mu E$, where R_μ is the ratio of the mass energy absorption coefficients of the photons in tissue and in the material.

37.6 Accelerator-induced radioactivity

Typical medium- and long-lived activation products in metallic components of accelerators are ^{22}Na , ^{46}Sc , ^{48}V , ^{51}Cr , ^{54}Mn , ^{55}Fe , ^{59}Fe , ^{56}Co , ^{57}Co , ^{58}Co , ^{60}Co , ^{63}Ni and ^{65}Zn . Gamma-emitting nuclides dominate doses from external irradiation at longer decay times (more than one day) while at short decay times β^+ emitters are also important (through photons produced by β^+ annihilation). Due to their short range, β^- emitters are relevant, for example, only for dose to the skin and eyes or for doses due to inhalation or ingestion. Fig. 37.5 and Fig. 37.6 illustrate the contributions of gamma and β^+ emitters to the total dose rate at 12.4 cm distance to a copper sample [15]. The sample was activated by the stray radiation field created by a 120 GeV mixed hadron beam dumped in a copper target during about 8 hours at intensities between $10^7 - 10^8$ hadrons per second. Here, the contributions by individual nuclides were calculated analytically assuming exponential decay of the nuclide inventory present at 20 minute cooling time. The total dose rate, however, also includes decay chains and as such also contributions from daughter nuclides.

Typically, dose rates at a certain decay time are mainly determined by radionuclides having a half-life of the order of the decay time. Extended irradiation periods might be an exception to this general rule as in this case the activity of long-lived nuclides can build up sufficiently so that it dominates that one of short-lived even at short cooling times.

Activation in concrete is dominated by ^{24}Na (short decay time) and ^{22}Na (long decay time). Both nuclides can be produced either by low-energy neutron reactions on the sodium-component in the concrete or by spallation reactions on silicon, calcium and other constituents such as aluminum. At long decay times nuclides of radiological interest in activated concrete can also be ^{60}Co , ^{152}Eu , ^{154}Eu and ^{134}Cs , all of which produced by (n,γ) -reactions with traces of natural cobalt, europium and cesium. Thus, such trace elements might be important even if their content in concrete is only a few parts per million or less by weight.

The explicit simulation of radionuclide production with general-purpose Monte Carlo codes has become the most commonly applied method to calculate induced radioactivity and its radiologi-

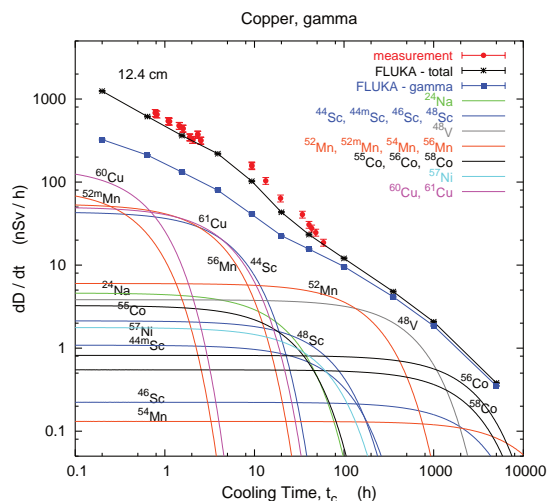


Figure 37.5: Contribution of individual gamma-emitting nuclides to the total dose rate at 12.4 cm distance to an activated copper sample [15].

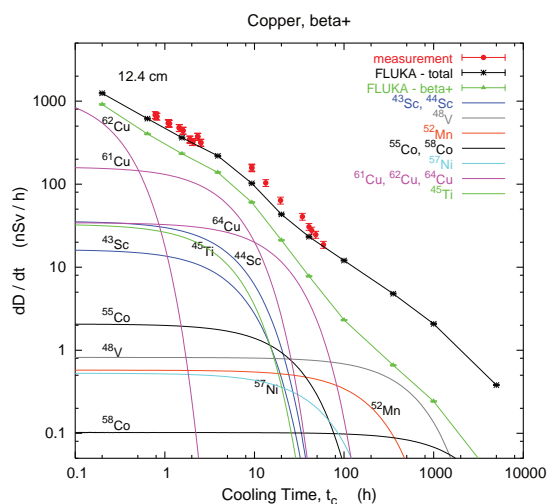


Figure 37.6: Contribution of individual positron-emitting nuclides to the total dose rate at 12.4 cm distance to an activated copper sample [15].

cal consequences [15] (see also Sec. 37.8). They are complemented by analytical codes based on folding particle fluence spectra with nuclide production cross sections. ActiWiz [16, 17] is an example of such a code targeting the domain of radiological characterization and material optimization. It allows for calculating nuclide inventories by convolution of fluence spectra with nuclide production data for 85 chemical elements and arbitrary compounds from threshold to an energy of 100 TeV.

37.7 Radiation protection instrumentation

The capacity to distinguish and measure the high-LET (mostly neutrons) and the low-LET components (photons, electrons, muons) of the radiation field at workplaces is of primary importance to evaluate the exposure of personnel. At proton accelerators the prompt dose equivalent outside a shield is mainly due to neutrons, with some contribution from photons and, to a minor extent, charged particles. At high-energy electron accelerators the dominant stray radiation during operation consists also of neutrons, because the shielding is normally thick enough to absorb most of the bremsstrahlung photons. Most of the personnel exposure at accelerator facilities is often received during maintenance

interventions, and is due to gamma/beta radiation coming from residual radioactivity in accelerator components.

Radiation detectors used both for radiation surveys and area monitoring are normally calibrated in ambient dose equivalent $H^*(10)$.

37.7.1 Neutron detectors

• **Rem counters:** A rem counter [18] is a portable detector consisting of a thermal neutron counter embedded in a polyethylene moderator, with a response function that approximately follows the curve of the conversion coefficients from neutron fluence to $H^*(10)$ over a wide energy range. Conventional rem counters provide a response to neutrons up to approximately 10–15 MeV, extended-range units are heavier as they include a converter consisting of a material with high mass number to correctly measure $H^*(10)$ up to several hundred MeV [19].

• **Bonner Sphere Spectrometer (BSS):** A BSS [20] consists of a thermal neutron detector at the centre of moderating spheres of different diameters made of polyethylene (PE) or a combination of PE and a high-A material to enhance its response to high energy neutrons (similar to rem counters). Each sphere has a different response function versus neutron energy, and the neutron energy, at which the sensitivity peaks, increases with sphere diameter. The energy resolution of the system is rather low but satisfactory for radiation protection purposes. The neutron spectrum is obtained by unfolding the experimental counts of the BSS with its response matrix by a computer code that is often based on an iterative algorithm such as GRAVEL [21] and MAXED [22]. BSS exist in active (using ^3He or BF_3 proportional counters or ^6LiI scintillators) and passive versions (using CR-39 track detectors or LiF), for use *e.g.* in strongly pulsed fields. With ^3He counters the discrimination with respect to gamma rays and noise is excellent.

• **Bubble detectors:** A bubble detector [23] is a dosimeter based on a super-heated emulsion (super-heated droplets suspended in a gel) contained in a vial and acting as a continuously sensitive, miniature bubble chamber. The total number of bubbles evolved from the radiation-induced nucleation of drops gives an integrated measure of the total neutron exposure. Various techniques exist to record and count the bubbles, *e.g.*, visual inspection, automated reading with video cameras or acoustic counting. Bubble detectors are insensitive to low-LET radiation. Super-heated emulsions are used as personal, area and environmental dosimeters, as well as neutron spectrometers.

• **Track etched detectors (TEDs)** [24] are based on the preferential dissolution of suitable, mostly insulator, materials along the damage trails of charged particles of sufficiently high-energy deposition density. The detectors are effectively not sensitive to radiation which deposits the energy through the interactions of particles with low LET. These dosimeters are generally able to determine neutron ambient dose equivalent down to around 100 μSv . They are used both as personal dosimeters and for area monitoring, *e.g.*, in BSS.

37.7.2 Photon detectors [25]

• **Geiger Müller (GM) counters:** GM counters are low cost devices simple to operate. They work in pulse mode and since they only count radiation-induced events, any spectrometric information is lost. In general they are calibrated in terms of air kerma, for instance in a ^{60}Co field. The response of GM counters to photons is constant within 15% for energies up to 2 MeV and shows considerable energy dependence above.

• **Ionization chambers:** Ionization chambers are gas-filled detectors used both as hand-held instruments (*e.g.*, for radiation surveys) and environmental monitors. They are normally operated in current mode although pulse-mode operation is also possible. They possess a relatively flat response to a wide range of X- and gamma ray energies (typically from 10 keV to several MeV), can measure radiation over a wide intensity range and are capable of discriminating between the beta and gamma components of a radiation field (by use of, *e.g.*, a beta window). Pressurized ion chambers (filled, *e.g.*, with Ar or H gas to several tens of bars) are used for environmental and stray radiation monitoring applications. They have good sensitivity to neutrons and charged hadrons in addition to low LET radiation (gammas and muons),

with the response function to the former being strongly non-linear with energy.

• **Proportional counters:** Proportional counters are another type of gas-filled detector, operated in pulse mode. They are normally of cylindrical geometry, with a thin central wire (the anode) on the axis of a hollow tube (the cathode). The initial electron charge created by the interaction of the radiation with the gas is amplified by the multiplication process (Townsend avalanche) produced by the strong electric field in a narrow volume around the anode. The generated pulses are still proportional to the original number of ion pairs but are much larger than in an ionization chamber, yielding a much improved signal-to-noise ratio. Proportional counters are also used for neutron detection: the rem counter and BSS discussed in the previous sections typically employ ^3He or BF_3 filled tubes with a large sensitivity to thermal neutrons.

• **Scintillators:** Scintillation-based detectors are used in radiation protection as hand-held probes and in fixed installations, *e.g.*, portal monitors. A scintillation detector or counter is obtained coupling a scintillator to an electronic light sensor such as a photomultiplier tube (PMT), a photodiode or a silicon photomultiplier (SiPM). There is a wide range of scintillating materials, inorganic (such as CsI and BGO), organic or plastic; they find application in both photon dosimetry and spectrometry.

37.7.3 Operation in pulsed radiation fields

There are many practical situations with particle accelerators used for scientific, industrial and medical applications where the time structure of the stray radiation limits the use of active monitors or requires specifically designed electronics. Pulsed neutron and gamma fields may be present because of beam losses at, *e.g.*, targets, collimators and beam dumps. The time duration of a single burst can range from a few ns to about 1 ms with a typical repetition rate in the range 0.1–100 Hz. Conventional detectors generally suffer from dead time effects and have strong limitations in the measurements of pulsed fields. Severe under response has been observed, *e.g.*, in commercial rem counters, with tremendous underestimation of the ambient dose equivalent, $H^*(10)$, up to three orders of magnitude [26]. The common techniques used to correct the response of radiation detectors which include dead-time corrections operate properly in a steady-state radiation field, whereas it is much more difficult to cope with dead time losses in a pulsed radiation field of unknown time structure and burst dose. Generally speaking the monitoring instrumentation must be chosen on the basis of the knowledge of the radiation field. Detectors with specifically designed electronics must be employed in pulsed field conditions in place of conventional rem counters for neutrons, such as the LUPIN detector [27]. If real-time monitoring is not required, passive detectors or dosimeters such as TEDs mentioned in Sec. 37.7.1 or LiF mentioned in Sec. 37.7.5 can be employed, as they are insensitive to the time structure of the radiation.

37.7.4 Operation in presence of magnetic fields

There may be circumstances in which a radiation survey needs to be performed in the presence of a magnetic field. This may be the case for example for measurements on activated detector components in the underground experimental areas of CERN LHC experiments without switching off the intense magnetic field of the detectors; or measurements of the residual radioactivity of permanent magnets sometimes used in particle accelerators. In hospitals, one of most advanced diagnostic modalities is PET-MRI, in which PET imaging uses radioactive substances (radio-pharmaceuticals) in proximity of the strong magnetic field of the MRI scanner. Most of the commercial survey meters do not operate correctly or do not function at all in the presence of even comparatively weak magnetic fields below 0.3 T, and often already at 0.1 T. This is either because of the presence of components in their electronics sensitive to magnetic field (*e.g.* inductive elements), ferromagnetic materials in general (such as shells, screws and frames), battery drain/heating or LCD screen failure. An instrument called B-RAD has recently been developed [28] that overcomes the above limitations and is now commercially available. It is a hand-held instrument for gamma dose rate and gamma spectrometry measurements, consisting of a central unit

(housing a microcontroller, magnetic field insensitive electronic circuitry, the battery and two displays) and a probe connected through a cable, certified to operate up to 3 T fields. The probe uses a $\text{LaBr}_3(\text{Ce})$ crystal coupled to an array of silicon photomultipliers. The excellent scintillation properties and the high photon resolution of the scintillator (3.3% FWHM at 662 keV) make the device capable of operating in the energy range from 30 keV to 2 MeV photons with a very fast response.

37.7.5 Personal dosimeters

Personal dosimeters, calibrated in $H_p(10)$, are worn by persons exposed to ionizing radiation for professional reasons to record the dose received. They are typically passive detectors, either film, track etched detectors, $^6\text{Li}/^7\text{Li}$ -based dosimeters (*e.g.* LiF), optically stimulated luminescence (OSL) or radiophotoluminescence detectors (RPL) but semi-active dosimeters using miniaturized ion-chambers also exist, like the Direct Ion Storage (DIS) dosimeters in use at CERN.

Electronic personal dosimeters are small active units for on-line monitoring of individual exposure, designed to be worn on the body. They can give an alarm on both the integral dose received or dose rate once a pre-set threshold is exceeded.

37.8 Monte Carlo codes for radiation protection studies

The use of general-purpose particle interaction and transport Monte Carlo codes is often the most accurate and efficient choice for assessing radiation protection quantities at accelerators. Due to the vast spread of such codes to all areas of particle physics and the associated extensive benchmarking with experimental data, the modeling has reached an unprecedented accuracy. Furthermore, most codes allow the user to simulate all aspects of a high energy particle cascade in one and the same run: from the first interaction of a TeV nucleus over the transport and re-interactions (hadronic and electromagnetic) of the produced secondaries, to detailed nuclear fragmentation, the calculation of radioactive decays and even of the electromagnetic shower caused by the radiation from such decays. A brief account of the codes most widely used for radiation protection studies at high energy accelerators is given in the following.

• **FLUKA [9–11]:** FLUKA is a general-purpose particle interaction and transport code. It comprises all features needed for radiation protection, such as detailed hadronic and nuclear interaction models up to 10 PeV, full coupling between hadronic and electromagnetic processes and numerous variance reduction options. The latter include weight windows, region importance biasing, and leading particle, interaction, and decay length biasing (among others). The capabilities of FLUKA are unique for studies of induced radioactivity, especially with regard to nuclide production, decay, and transport of residual radiation. In particular, particle cascades by prompt and residual radiation are simulated in parallel based on the microscopic models for nuclide production and a solution of the Bateman equations for activity build-up and decay.

• **GEANT4 [29–31]:** GEANT4 is an object-oriented toolkit consisting of a kernel that provides the framework for particle transport, including tracking, geometry description, material specifications, management of events and interfaces to external graphics systems. The kernel also provides interfaces to physics processes. It allows the user to freely select the physics models that best serve the particular application needs. Implementations of interaction models exist over an extended range of energies, from optical photons and thermal neutrons to high-energy interactions required for the simulation of accelerator and cosmic ray experiments. To facilitate the use of variance reduction techniques, general-purpose biasing methods such as importance biasing, weight windows, and a weight cut-off method have been introduced directly into the toolkit. Other variance reduction methods, such as leading particle biasing for hadronic processes, come with the respective physics packages.

• **MARS15 [32,33]:** The MARS15 code system is a set of Monte Carlo programs for the simulation of hadronic and electromagnetic cascades. It covers a wide energy range: 1 keV to 100 TeV for muons, charged hadrons, heavy ions and electromagnetic showers;

and 0.00215 eV to 100 TeV for neutrons. Hadron-nucleus interactions as well as practically all other strong, weak and electromagnetic interactions in the entire energy range can be simulated either inclusively or exclusively. MARS15 uses ENDFB-VII nuclear data to handle interactions of neutrons with energies below 14 MeV. Several variance reduction techniques, such as weight windows, particle splitting, and Russian roulette, are available. A tagging module allows tagging the origin of a given signal for source term or sensitivity analyses. The geometry module allows either a basic solid body representation option or a ROOT-based powerful engine. Further features of MARS15 include a MAD-MARS merge for a convenient creation of accelerator models and multi-turn tracking and cascade simulation in accelerator and beamline lattices.

• **MCNP6 [34, 35]:** MCNP6 is the latest version of the Monte Carlo N-Particle transport (MCNP) family of neutron interaction and transport codes and, therefore, features one of the most comprehensive and detailed descriptions of the related physical processes. It transports 37 different particle types, including ions and electromagnetic particles. The neutron interaction and transport modules use standard evaluated data libraries mixed with physics models where such libraries are not available. The transport is continuous in energy. MCNP6 contains one of the most powerful implementations of variance reduction techniques. Spherical mesh weight windows can be created by a generator in order to focus the simulation time on certain spatial regions of interest. In addition, a more generalized phase space biasing is also possible through energy- and time-dependent weight windows. Other biasing options include pulse-height tallies with variance reduction and criticality source convergence acceleration.

• **PHITS [36, 37]:** The Particle and Heavy-Ion Transport code System PHITS was among the first general-purpose codes to simulate the transport and interactions of heavy ions in a wide energy range, from 10 MeV/nucleon to 100 GeV/nucleon. It is based on the high-energy hadron transport code NMTC/JAM that was extended to heavy ions. The transport of low-energy neutrons employs cross sections from evaluated nuclear data libraries such as ENDF and JENDL below 20 MeV. Electromagnetic interactions are simulated based on the ITS code in the energy range between 1 keV and 100 MeV for electrons and positrons and between 1 keV and 100 GeV for photons. Several variance reduction techniques, including weight windows and region importance biasing, are available.

References

- [1] International Commission on Radiation Units and Measurements, *Fundamental Quantities and Units for Ionizing Radiation*, ICRU Report 60 (1998).
- [2] ICRP, 2010. *Conversion Coefficients for Radiological Protection Quantities for External Radiation Exposures*, ICRP Publication 116, Annals of the ICRP 40(2-5).
- [3] ICRP Publication 103, *The 2007 Recommendations of the International Commission on Radiological Protection*, Annals of the ICRP, Elsevier (2007).
- [4] M. Pelliccioni, *Radiation Protection Dosimetry* **88**, 279 (2000).
- [5] E. Pochin, *Nuclear Radiation: Risks and Benefits*, Clarendon Press, Oxford, 1983.
- [6] United Nations, *Report of the United Nations Scientific Committee on the Effect of Atomic Radiation*, General Assembly, Official Records A/63/46 (2008).
- [7] G. Cinelli *et al.*, *European Atlas of Natural Radiation*, G. Cinelli, M. De Cort, and T. Tollefsen, editor(s), Publications Office of the European Union, Luxembourg, 2019, ISBN 978-92-76-08259-0, JRC116795.
- [8] W. P. Swanson, *Radiological Safety Aspects of the Operation of Electron Linear Accelerators*, IAEA Technical Reports Series No. 188 (1979) (1979).
- [9] A. Ferrari, *et al.*, FLUKA: A Multi-particle Transport Code, CERN-2005-010 (2005), SLAC-R-773, INFN-TC-05-11, <http://www.fluka.org>, <http://fluka.cern>.
- [10] T. T. Böhlen *et al.*, *Nucl. Data Sheets* **120**, 211 (2014).
- [11] G. Battistoni *et al.*, *Annals of Nuclear Energy* **82**, 10 (2015).
- [12] R.H. Thomas and G.R. Stevenson, *Radiological Safety Aspects of the Operation of Proton Accelerators*, SSC-N-354 (1986), IAEA Technical Report Series No. 283 (1988).
- [13] T. Gabriel *et al.*, *Nucl. Instrum. Meth. A* **338**, 336 (1994).
- [14] <http://physics.nist.gov/PhysRefData/XrayMassCoef/cover.html>.
- [15] S. Roesler, *et al.*, “Simulation of Remanent Dose Rates and Benchmark Measurements at the CERN-EU High Energy Reference Field Facility,” in *Proceedings of the Sixth International Meeting on Nuclear Applications of Accelerator Technology*, San Diego, CA, 1-5 June 2003, 655–662 (2003).
- [16] C. Theis and H. Vincke, “The use of ActiWiz in operational radiation protection,” in *Proceedings of the Twelfth Meeting of Task-Force on Shielding Aspects of Accelerators, Targets and Irradiation Facilities of Accelerator Technology, SATIF12* FNAL, 28-30 April 2014, Nuclear Science Report NEA/NSC/R 3, (2015).
- [17] C. Theis and H. Vincke, “ActiWiz3 an overview of the concepts, architecture and new features,” CERN Technical Note CERN-RP-2016-117-REPORTS-TN (2016), <http://actiwiz.web.cern.ch>.
- [18] I.O. Andersson and J. Braun, “A neutron rem counter with uniform sensitivity from 0.025 eV to 10 MeV” in *Proceedings of the IAEA Symposium on Neutron dosimetry*, IAEA, Vienna, Vol. II, 87–95, (1963).
- [19] C. Birattari, *et al.*, *Radiation Protection Dosimetry* **76**, 135 (1998).
- [20] R.L. Bramblett, R.I. Ewing and T.W. Bonner, *Nucl. Instrum. Methods* **9**, 1 (1960).
- [21] M. Matzke, PTB, Braunschweig PTBN-19, (1994).
- [22] M. Reginatto and P. Goldhagen, *Health Physics* **77**, 579 (1999).
- [23] F. d’Errico, *Nucl. Instrum. Methods* **B184**, 229 (2001).
- [24] K. Becker, Dosimetric applications of track etching, in *Topics in Radiation Dosimetry* Ed. F.H. Attix, Academic Press, London, 79–143, (1972).
- [25] G.F. Knoll, *Radiation detection and measurements*, Wiley (2010).
- [26] M. Caresana *et al.*, *Nucl. Instrum. Meth. A* **737**, 203 (2014).
- [27] M. Caresana, *et al.*, A new version of the LUPIN detector: Improvements and latest experimental verification, *Review of Scientific Instruments* **85**, 065102 (2014).
- [28] D. Celeste, A. Curioni, A. Fazzi, M. Silari and V. Varoli, B-RAD: a radiation survey meter for operation in intense magnetic fields *Journal of Instrumentation* **14**, T05007 (2019).
- [29] S. Agostinelli *et al.* (GEANT4), *Nucl. Instrum. Meth. A* **506**, 250 (2003).
- [30] J. Allison *et al.*, *IEEE Trans. Nucl. Sci.* **53**, 270 (2006).
- [31] J. Allison *et al.*, *Nucl. Instrum. Meth. A* **835**, 186 (2016), <http://geant4.cern.ch>.
- [32] N.V. Mokhov and C.C. James, The MARS Code System User’s Guide, Fermilab-FN-1058-APC (2018), <https://mars.fnal.gov>.
- [33] N. Mokhov *et al.*, *Prog. Nucl. Sci. Tech.* **4**, 496 (2014), [arXiv:1409.0033].
- [34] J.T. Goorley, *et al.*, *Nuclear Technology* **180**, 298 (2012).
- [35] C.J. Werner (editor), MCNP Users Manual - Code Version 6.2, Los Alamos National Laboratory report, LA-UR-17-29981 (2017), <https://mcnp.lanl.gov>.
- [36] T. Sato, *et al.*, *Journal of Nuclear Science and Technology* **55**, 684 (2018).
- [37] T. Sato, *et al.*, PHITS Particle and Heavy Ion Transport code System, Version 3.10 (2019), <https://phits.jaea.go.jp>.

38. Commonly Used Radioactive Sources

Revised April 2021 by D.E. Groom (LBNL).

Table 38.1: Radioactive sources

Nuclide	Half-life	Type of Decay	Particle		Photon	
			Energy (MeV)	Emission prob.	Energy (MeV)	Emission prob.
²² ₁₁ Na	2.603 y	β^+ , EC	0.546	90%	0.511 1.275	Annih. 100%
⁵¹ ₂₄ Cr	27.70 d	EC			0.320 V K x rays	10% 100%
Neutrino calibration source						
⁵⁴ ₂₅ Mn	0.855 y	EC			0.835 Cr K x rays	100% 26%
⁵⁵ ₂₆ Fe	2.747 y	EC			Mn K x rays: 0.00590 0.00649	24.4% 2.86%
⁵⁷ ₂₇ Co	271.8 d	EC			0.014 0.122 0.136 Fe K x rays	9% 86% 11% 58%
⁶⁰ ₂₇ Co	5.271 y	β^-	0.317	99.9%	1.173 1.333	99.9% 99.9%
⁶⁸ ₃₂ Ge	271.0 d	EC			Ga K x rays	42%
\rightarrow ⁶⁸ ₃₁ Ga	67.8 m	β^+ , EC	1.899	90%	0.511 1.077	Annih. 3%
⁹⁰ ₃₈ Sr	28.8 y	β^-	0.546	100%		
\rightarrow ⁹⁰ ₃₉ Y	2.67 d	β^-	2.279	100%		
¹⁰⁶ ₄₄ Ru	371.5 d	β^-	0.039	100%		
\rightarrow ¹⁰⁶ ₄₅ Rh	30.1 s	β^-	3.546	79%	0.512 0.622	21% 10%
¹⁰⁹ ₄₈ Cd	1.265 y	EC	0.063 e^- 0.084 e^-	42% 44%	0.088 Ag K x rays	3.7% 100%
¹¹³ ₅₀ Sn	115.1 d	EC	0.364 e^- 0.388 e^-	28% 6%	0.392 In K x rays	65% 97
¹³⁷ ₅₅ Cs	30.0 y	β^-	0.514 1.176	94% 6%	0.662	85%
¹³³ ₅₆ Ba	10.55 y	EC	0.045 e^- 0.075 e^-	50% 6%	0.081 0.356 Cs K x rays	33% 62% 121%
¹⁵² ₆₃ Eu	13.537 y	EC β^-		72.1% 27.9%	Many γ 's 0.1218–1.408 MeV	
²⁰⁷ ₈₃ Pb	32.9 y	EC	0.481 e^- 0.975 e^- 1.047 e^-	2% 7% 2%	0.569 1.063 1.770 Pb K x rays	98% 75% 7% 78%
²²⁸ ₉₀ Th	1.912 y	6 α : 3 β^- :	5.341 – 8.785 0.334 – 2.246		0.239 0.583 2.614	44% 31% 36%
$\left(\begin{array}{cccccc} \rightarrow \text{}^{224}\text{Ra} & \rightarrow \text{}^{220}\text{Rn} & \rightarrow \text{}^{216}\text{Po} & \rightarrow \text{}^{212}\text{Pb} & \rightarrow \text{}^{212}\text{Bi} & \rightarrow \text{}^{212}\text{Po} \\ \text{}^{224}\text{Ra} & \text{}^{220}\text{Rn} & \text{}^{216}\text{Po} & \text{}^{212}\text{Pb} & \text{}^{212}\text{Bi} & \text{}^{212}\text{Po} \\ 361 \text{ d} & 55.8 \text{ s} & 0.148 \text{ s} & 10.64 \text{ h} & 60.54 \text{ m} & 300 \text{ ns} \end{array} \right)$						
²⁴¹ ₉₅ Am	432.6 y	α	5.443 5.486	13% 84%	0.060 Np L x rays	36% 38%
²⁴¹ ₉₅ Am/Be	432.6 y	neutrons ($E = 4$ MeV) and γ 's (4.43 MeV from ⁹ Be(α , n))				
²⁴⁴ ₉₆ Cm	18.11 y	α	5.763 5.805	24% 76%	Pu L x rays	$\sim 9\%$
²⁵² ₉₈ Cf	2.645 y	α (97%)	6.076 6.118	15% 82%		
Fission (3.1%): Average 7.8 γ 's/fission; $\langle E_\gamma \rangle = 0.88$ MeV ≈ 4 neutrons/fission; $\langle E_n \rangle = 2.14$ MeV						

“Emission probability” is the probability per decay of a given emission; because of cascades these may total more than 100%. Only principal emissions are listed. EC means electron capture, and e^- means monoenergetic internal conversion (Auger) electron. The intensity of 0.511 MeV e^+e^- annihilation photons depends upon the number of stopped positrons. Endpoint β^\pm energies are listed. In some cases when energies are closely spaced, the γ -ray values are approximate weighted averages. Radiation from short-lived daughter isotopes is included where relevant.

Isotopic data may be found at https://physics.nist.gov/cgi-bin/Compositions/stand_alone.pl.

Neutron sources: See *e.g.* J. Liu *et al.*, “Neutron Calibration Sources in the Daya Bay Experiment” [1]. ⁵¹Cr calibration of neutrino detectors is discussed in *e.g.* J.N. Abdurashitov *et al.*, “Measurement of the response of a gallium metal solar neutrino experiment to neutrinos from a ⁵¹Cr source” [2]. The use of ⁷⁵Se and other isotopes has also been proposed.

References

- [1] J. Liu *et al.*, Nucl. Instrum. Meth. A **797**, 260 (2015), [arXiv:1504.07911].
- [2] J. N. Abdurashitov *et al.* (SAGE), Phys. Rev. C **59**, 2246 (1999), [hep-ph/9803418].

Mathematical Tools or Statistics, Monte Carlo, Group Theory

39. Probability (rev.)	655
40. Statistics (rev.)	660
41. Machine Learning (new)	676
42. Monte Carlo techniques (rev.)	713
43. Monte Carlo event generators (rev.)	717
44. Monte Carlo neutrino event generators (rev.)	729
45. Monte Carlo particle numbering scheme (rev.)	733
46. Clebsch-Gordan coefficients, spherical harmonics, and d functions	737
47. SU(3) isoscalar factors and representation matrices	738
48. SU(n) multiplets and Young diagrams	739

39. Probability

Revised August 2021 by G. Cowan (RHUL).

39.1 General

Further discussion of probability can be found, *e.g.*, in Refs. [1–8].

An abstract definition of probability can be given by considering a set S , called the sample space, and possible subsets A, B, \dots , the interpretation of which is left open. The probability P is a real-valued function defined by the following axioms due to Kolmogorov [9]:

1. For every subset A in S , $P(A) \geq 0$;
2. For disjoint subsets (*i.e.*, $A \cap B = \emptyset$), $P(A \cup B) = P(A) + P(B)$;
3. $P(S) = 1$.

In addition, one defines the conditional probability $P(A|B)$ (read as P of A given B) as

$$P(A|B) = \frac{P(A \cap B)}{P(B)}. \tag{39.1}$$

From this definition and using the fact that $A \cap B$ and $B \cap A$ are the same, one obtains *Bayes' theorem*,

$$P(A|B) = \frac{P(B|A)P(A)}{P(B)}. \tag{39.2}$$

From the three axioms of probability and the definition of conditional probability, one obtains the *law of total probability*,

$$P(B) = \sum_i P(B|A_i)P(A_i), \tag{39.3}$$

for any subset B and for disjoint A_i with $\cup_i A_i = S$. This can be combined with Bayes' theorem (Eq. (39.2)) to give

$$P(A|B) = \frac{P(B|A)P(A)}{\sum_i P(B|A_i)P(A_i)}, \tag{39.4}$$

where the subset A could, for example, be one of the A_i .

The most commonly used interpretation of the elements of the sample space are outcomes of a repeatable experiment. The probability $P(A)$ is assigned a value equal to the limiting frequency of occurrence of A . This interpretation forms the basis of *frequentist statistics*.

The elements of the sample space might also be interpreted as *hypotheses*, *i.e.*, statements that are either true or false, such as ‘The mass of the W boson lies between 80.3 and 80.5 GeV.’ Upon repetition of a measurement, however, such statements are either always true or always false, *i.e.*, the corresponding probabilities in the frequentist interpretation are either 0 or 1. Using *subjective probability*, however, $P(A)$ is interpreted as the degree of belief that the hypothesis A is true. Subjective probability is used in *Bayesian* (as opposed to frequentist) statistics. Bayes' theorem can be written

$$P(\text{theory}|\text{data}) \propto P(\text{data}|\text{theory})P(\text{theory}), \tag{39.5}$$

where ‘theory’ represents some hypothesis and ‘data’ is the outcome of the experiment. Here $P(\text{theory})$ is the *prior* probability for the theory, which reflects the experimenter’s degree of belief before carrying out the measurement, and $P(\text{data}|\text{theory})$ is the probability to have gotten the data actually obtained, given the theory, which is also called the *likelihood*.

Bayesian statistics provides no fundamental rule for obtaining the prior probability, which may depend on previous measurements, theoretical prejudices, *etc.* Once this has been specified, however, Eq. (39.5) tells how the probability for the theory must be modified in the light of the new data to give the *posterior* probability, $P(\text{theory}|\text{data})$. As Eq. (39.5) is stated as a proportionality, the probability must be normalized by summing (or integrating) over all possible hypotheses.

39.2 Random variables

A *random variable* is a numerical characteristic assigned to an element of the sample space. In the frequency interpretation of probability, it corresponds to an outcome of a repeatable experiment. Let x be a possible outcome of an observation. If x can take on any value from a continuous range, we write $f(x; \theta)dx$ as the probability that the measurement’s outcome lies between x and $x + dx$. The function $f(x; \theta)$ is called the *probability density function* (p.d.f.), which may depend on one or more parameters θ . If x can take on only discrete values (*e.g.*, the non-negative integers), then we use $f(x; \theta)$ to denote the probability to find the value x . In the following the term p.d.f. is often taken to cover both the continuous and discrete cases, although technically the term density should only be used in the continuous case.

The p.d.f. is always normalized to unity. Both x and θ may have multiple components and are then often written as vectors. If θ is unknown, we may wish to estimate its value from a given set of measurements of x ; this is a central topic of *statistics* (see Sec. 40).

The *cumulative distribution function* $F(a)$ is the probability that $x \leq a$:

$$F(a) = \int_{-\infty}^a f(x) dx. \tag{39.6}$$

Here and below, if x is discrete-valued, the integral is replaced by a sum. The endpoint a is expressly included in the integral or sum. Then $0 \leq F(x) \leq 1$, $F(x)$ is nondecreasing, and $P(a < x \leq b) = F(b) - F(a)$. If x is discrete, $F(x)$ is flat except at allowed values of x , where it has discontinuous jumps equal to $f(x)$.

Any function of random variables is itself a random variable, with (in general) a different p.d.f. The *expectation value* of any function $u(x)$ is

$$E[u(x)] = \int_{-\infty}^{\infty} u(x) f(x) dx, \tag{39.7}$$

assuming the integral is finite. The expectation value is linear, *i.e.*, for any two functions u and v of x and constants c_1 and c_2 , $E[c_1 u + c_2 v] = c_1 E[u] + c_2 E[v]$.

The n^{th} moment of a random variable x is

$$\alpha_n \equiv E[x^n] = \int_{-\infty}^{\infty} x^n f(x) dx, \tag{39.8a}$$

and the n^{th} central moment of x (or moment about the mean, α_1) is

$$m_n \equiv E[(x - \alpha_1)^n] = \int_{-\infty}^{\infty} (x - \alpha_1)^n f(x) dx. \tag{39.8b}$$

The most commonly used moments are the mean μ and variance σ^2 :

$$\mu \equiv \alpha_1, \tag{39.9a}$$

$$\sigma^2 \equiv V[x] \equiv m_2 = \alpha_2 - \mu^2. \tag{39.9b}$$

The mean is the location of the ‘center of mass’ of the p.d.f., and the variance is a measure of the square of its width. Note that $V[cx + k] = c^2 V[x]$. It is often convenient to use the *standard deviation* of x , σ , defined as the square root of the variance.

Any odd moment about the mean is a measure of the skewness of the p.d.f. The simplest of these is the dimensionless coefficient of skewness $\gamma_1 = m_3/\sigma^3$.

The fourth central moment m_4 provides a convenient measure of the tails of a distribution. For the Gaussian distribution (see Sec. 39.4), one has $m_4 = 3\sigma^4$. The *kurtosis* is defined as $\gamma_2 = m_4/\sigma^4 - 3$, *i.e.*, it is zero for a Gaussian, positive for a *leptokurtic* distribution with longer tails, and negative for a *platykurtic* distribution with tails that die off more quickly than those of a Gaussian.

The *quantile* x_α is the value of the random variable x at which the cumulative distribution is equal to α . That is, the quantile

is the inverse of the cumulative distribution function, *i.e.*, $x_\alpha = F^{-1}(\alpha)$. An important special case is the *median*, x_{med} , defined by $F(x_{\text{med}}) = 1/2$, *i.e.*, half the probability lies above and half lies below x_{med} . (More rigorously, x_{med} is a median if $P(x \geq x_{\text{med}}) \geq 1/2$ and $P(x \leq x_{\text{med}}) \geq 1/2$. If only one value exists, it is called ‘*the median*.’)

Under a monotonic change of variable $x \rightarrow y(x)$, the quantiles of a distribution (and hence also the median) obey $y_\alpha = y(x_\alpha)$. In general the expectation value and *mode* (most probable value) of a distribution do not, however, transform in this way.

Let x and y be two random variables with a *joint* p.d.f. $f(x, y)$. The *marginal* p.d.f. of x (the distribution of x with y unobserved) is

$$f_1(x) = \int_{-\infty}^{\infty} f(x, y) dy, \tag{39.10}$$

and similarly for the marginal p.d.f. $f_2(y)$. The *conditional* p.d.f. of y given fixed x (with $f_1(x) \neq 0$) is defined by $f_3(y|x) = f(x, y)/f_1(x)$, and similarly $f_4(x|y) = f(x, y)/f_2(y)$. From these, we immediately obtain Bayes’ theorem (see Eqs. (39.2) and (39.4)),

$$f_4(x|y) = \frac{f_3(y|x)f_1(x)}{f_2(y)} = \frac{f_3(y|x)f_1(x)}{\int f_3(y|x')f_1(x') dx'}. \tag{39.11}$$

The mean of x is

$$\mu_x = \int_{-\infty}^{\infty} \int_{-\infty}^{\infty} x f(x, y) dx dy = \int_{-\infty}^{\infty} x f_1(x) dx, \tag{39.12}$$

and similarly for y . The *covariance* of x and y is

$$\text{cov}[x, y] = E[(x - \mu_x)(y - \mu_y)] = E[xy] - \mu_x \mu_y. \tag{39.13}$$

A dimensionless measure of the covariance of x and y is given by the *correlation coefficient*,

$$\rho_{xy} = \text{cov}[x, y]/\sigma_x \sigma_y, \tag{39.14}$$

where σ_x and σ_y are the standard deviations of x and y . It can be shown that $-1 \leq \rho_{xy} \leq 1$.

Two random variables x and y are *independent* if and only if

$$f(x, y) = f_1(x)f_2(y). \tag{39.15}$$

If x and y are independent, then $\rho_{xy} = 0$; the converse is not necessarily true. If x and y are independent, $E[u(x)v(y)] = E[u(x)]E[v(y)]$, and $V[x+y] = V[x] + V[y]$; otherwise, $V[x+y] = V[x] + V[y] + 2\text{cov}[x, y]$, and $E[uv]$ does not necessarily factorize.

Consider a set of n continuous random variables $\mathbf{x} = (x_1, \dots, x_n)$ with joint p.d.f. $f(\mathbf{x})$, and a set of n new variables $\mathbf{y} = (y_1, \dots, y_n)$, related to \mathbf{x} by means of a function $\mathbf{y}(\mathbf{x})$ that is one-to-one, *i.e.*, the inverse $\mathbf{x}(\mathbf{y})$ exists. The joint p.d.f. for \mathbf{y} is given by

$$g(\mathbf{y}) = f(\mathbf{x}(\mathbf{y}))|J|, \tag{39.16}$$

where $|J|$ is the absolute value of the determinant of the square matrix $J_{ij} = \partial x_i / \partial y_j$ (the Jacobian determinant). If the transformation from \mathbf{x} to \mathbf{y} is not one-to-one, the \mathbf{x} -space must be broken into regions where the function $\mathbf{y}(\mathbf{x})$ can be inverted, and the contributions to $g(\mathbf{y})$ from each region summed.

Given a set of functions $\mathbf{y} = (y_1, \dots, y_m)$ with $m < n$, one can construct $n - m$ additional independent functions, apply the procedure above, then integrate the resulting $g(\mathbf{y})$ over the unwanted y_i to find the marginal distribution of those of interest.

For a one-to-one transformation of discrete random variables, the probability is obtained by simple substitution; no Jacobian is necessary because in this case f is a probability rather than a probability density. If the transformation is not one-to-one, then one must sum the probabilities for all values of the original variable that contribute to a given value of the transformed variable. If f depends on a set of parameters $\boldsymbol{\theta}$, a change to a different parameter set $\boldsymbol{\eta}(\boldsymbol{\theta})$ is made by simple substitution; no Jacobian is used.

39.2.1 Propagation of errors

Consider n random variables $\mathbf{x} = (x_1, \dots, x_n)$ and m functions $\mathbf{y}(\mathbf{x}) = (y_1(\mathbf{x}), \dots, y_m(\mathbf{x}))$. Suppose here that the mean values $\boldsymbol{\mu} = (\mu_1, \dots, \mu_n) = E[\mathbf{x}]$ are known, although in practice they will only be estimated, and suppose we also know or have estimated the covariance matrix $V_{ij} = \text{cov}[x_i, x_j]$. The goal of *error propagation* is to determine the covariance matrix for the functions, $U_{ij} = \text{cov}[y_i, y_j]$. In particular, the diagonal elements $U_{ii} = V[y_i]$ give the variances. The new covariance matrix can be found by expanding the functions $\mathbf{y}(\mathbf{x})$ about the means $\boldsymbol{\mu}$ to first order in a Taylor series. Using this one finds

$$U_{ij} \approx \sum_{k,l} \left. \frac{\partial y_i}{\partial x_k} \frac{\partial y_j}{\partial x_l} \right|_{\boldsymbol{\mu}} V_{kl}. \tag{39.17}$$

This can be written in matrix notation as $U \approx AVA^T$ where the matrix of derivatives A is

$$A_{ij} = \left. \frac{\partial y_i}{\partial x_j} \right|_{\boldsymbol{\mu}}, \tag{39.18}$$

and A^T is its transpose. The approximation is exact if $\mathbf{y}(\mathbf{x})$ is linear. If this is not the case, the approximation can break down if, for example, $\mathbf{y}(\mathbf{x})$ is significantly nonlinear close to $\boldsymbol{\mu}$ in a region of a size comparable to the standard deviations of \mathbf{x} .

39.3 Characteristic functions

The characteristic function $\phi(u)$ associated with the p.d.f. $f(x)$ is essentially its Fourier transform, or the expectation value of e^{iux} :

$$\phi(u) = E[e^{iux}] = \int_{-\infty}^{\infty} e^{iux} f(x) dx. \tag{39.19}$$

Once $\phi(u)$ is specified, the p.d.f. $f(x)$ is uniquely determined and vice versa; knowing one is equivalent to the other. Characteristic functions are useful in deriving a number of important results about moments and sums of random variables.

It follows from Eqs. (39.8) and (39.19) that the n^{th} moment of a random variable x that follows $f(x)$ is given by

$$i^{-n} \left. \frac{d^n \phi}{du^n} \right|_{u=0} = \int_{-\infty}^{\infty} x^n f(x) dx = \alpha_n. \tag{39.20}$$

Thus it is often easy to calculate all the moments of a distribution defined by $\phi(u)$, even when $f(x)$ cannot be written down explicitly.

If the p.d.f.s $f_1(x)$ and $f_2(y)$ for independent random variables x and y have characteristic functions $\phi_1(u)$ and $\phi_2(u)$, then the characteristic function of the weighted sum $ax + by$ is $\phi_1(au)\phi_2(bu)$. The rules of addition for several important distributions (*e.g.*, that the sum of two Gaussian distributed variables also follows a Gaussian distribution) easily follow from this observation.

Let the (partial) characteristic function corresponding to the conditional p.d.f. $f_2(x|z)$ be $\phi_2(u|z)$, and the p.d.f. of z be $f_1(z)$. The characteristic function after integration over the conditional value is

$$\phi(u) = \int \phi_2(u|z)f_1(z) dz. \tag{39.21}$$

Suppose we can write ϕ_2 in the form

$$\phi_2(u|z) = A(u)e^{ig(u)z}. \tag{39.22}$$

Then

$$\phi(u) = A(u)\phi_1(g(u)). \tag{39.23}$$

The cumulants (semi-invariants) κ_n of a distribution with characteristic function $\phi(u)$ are defined by the relation

$$\phi(u) = \exp \left[\sum_{n=1}^{\infty} \frac{\kappa_n}{n!} (iu)^n \right] = \exp \left(i\kappa_1 u - \frac{1}{2} \kappa_2 u^2 + \dots \right). \tag{39.24}$$

The values κ_n are related to the moments α_n and m_n . The first few relations are

$$\begin{aligned} \kappa_1 &= \alpha_1 \quad (= \mu, \text{ the mean}) \\ \kappa_2 &= m_2 = \alpha_2 - \alpha_1^2 \quad (= \sigma^2, \text{ the variance}) \\ \kappa_3 &= m_3 = \alpha_3 - 3\alpha_1\alpha_2 + 2\alpha_1^3. \end{aligned} \tag{39.25}$$

39.4 Commonly used probability distributions

Table 39.1 gives a number of common probability density functions and corresponding characteristic functions, means, and variances. Further information may be found in Refs. [1–8] [10], and [11], which has particularly detailed tables. Monte Carlo techniques for generating each of them may be found in our Sec. 42.4 and in Ref. [10]. We comment below on all except the trivial uniform distribution.

39.4.1 Binomial and multinomial distributions

A random process with exactly two possible outcomes which occur with fixed probabilities is called a *Bernoulli* process. If the probability of obtaining a certain outcome (a “success”) in an individual trial is p , then the probability of obtaining exactly r successes ($r = 0, 1, 2, \dots, N$) in N independent trials, without regard to the order of the successes and failures, is given by the binomial distribution $f(r; N, p)$ in Table 39.1. If r and s are binomially distributed with parameters (N_r, p) and (N_s, p) , then $t = r + s$ follows a binomial distribution with parameters $(N_r + N_s, p)$. If there are m possible outcomes for each trial having probabilities p_1, p_2, \dots, p_m , then the joint probability to find r_1, r_2, \dots, r_m of each outcome after a total of N independent trials is given by the multinomial distribution as shown in Table 39.1. We can regard outcome i as “success” and all the rest as “failure”, so individually, any of the r_i follow a binomial distribution for N trials and a success probability p_i .

39.4.2 Poisson distribution

The Poisson distribution $f(n; \nu)$ gives the probability of finding exactly n events in a given interval of x (e.g., space or time) when the events occur independently of one another and of x at an average rate of ν per the given interval. The variance σ^2 equals ν . It is the limiting case $p \rightarrow 0, N \rightarrow \infty, Np = \nu$ of the binomial distribution. The Poisson distribution approaches the Gaussian distribution for large ν .

For example, a large number of radioactive nuclei of a given type will result in a certain number of decays in a fixed time interval. If this interval is small compared to the mean lifetime, then the probability for a given nucleus to decay is small, and thus the number of decays in the time interval is well modeled as a Poisson variable.

39.4.3 Normal or Gaussian distribution

The normal (or Gaussian) probability density function $f(x; \mu, \sigma^2)$ given in Table 39.1 has mean $E[x] = \mu$ and variance $V[x] = \sigma^2$. Comparison of the characteristic function $\phi(u)$ given in Table 39.1 with Eq. (39.24) shows that all cumulants κ_n beyond κ_2 vanish; this is a unique property of the Gaussian distribution. Some other properties are:

$$\begin{aligned} P(x \text{ in range } \mu \pm \sigma) &= 0.6827, \\ P(x \text{ in range } \mu \pm 0.6745\sigma) &= 0.5, \\ E[|x - \mu|] &= \sqrt{2/\pi}\sigma = 0.7979\sigma, \\ \text{half-width at half maximum} &= \sqrt{2 \ln 2}\sigma = 1.177\sigma. \end{aligned}$$

For a Gaussian with $\mu = 0$ and $\sigma^2 = 1$ (the *standard normal*) the cumulative distribution, often written $\Phi(x)$, is related to the error function erf by

$$F(x; 0, 1) \equiv \Phi(x) = \frac{1}{2} [1 + \text{erf}(x/\sqrt{2})]. \tag{39.26}$$

The error function and standard Gaussian are tabulated in many references (e.g., Ref. [11, 12]) and are available in software packages such as ROOT [13]. For a mean μ and variance σ^2 , replace x by $(x - \mu)/\sigma$. The probability of x in a given range can be calculated with Eq. (40.71).

For x and y independent and normally distributed, $z = ax + by$ follows a normal p.d.f. $f(z; a\mu_x + b\mu_y, a^2\sigma_x^2 + b^2\sigma_y^2)$; that is, the weighted means and variances add.

The Gaussian derives its importance in large part from the *central limit theorem*:

If independent random variables x_1, \dots, x_n are distributed according to any p.d.f. with finite mean and variance, then the sum $y = \sum_{i=1}^n x_i$ will have a p.d.f. that approaches a Gaussian for large n . If the p.d.f.s of the x_i are not identical, the theorem still holds under somewhat more restrictive conditions. The mean and variance are given by the sums of corresponding terms from the individual x_i . Therefore, the sum of a large number of fluctuations x_i will be distributed as a Gaussian, even if the x_i themselves are not.

For a set of n Gaussian random variables \mathbf{x} with means $\boldsymbol{\mu}$ and covariances $V_{ij} = \text{cov}[x_i, x_j]$, the p.d.f. for the one-dimensional Gaussian is generalized to

$$f(\mathbf{x}; \boldsymbol{\mu}, V) = \frac{1}{(2\pi)^{n/2} \sqrt{|V|}} \exp \left[-\frac{1}{2} (\mathbf{x} - \boldsymbol{\mu})^T V^{-1} (\mathbf{x} - \boldsymbol{\mu}) \right], \tag{39.27}$$

where the determinant $|V|$ must be greater than 0. For diagonal V (independent variables), $f(\mathbf{x}; \boldsymbol{\mu}, V)$ is the product of the p.d.f.s of n Gaussian distributions.

For $n = 2$, $f(\mathbf{x}; \boldsymbol{\mu}, V)$ is

$$\begin{aligned} f(x_1, x_2; \mu_1, \mu_2, \sigma_1, \sigma_2, \rho) &= \frac{1}{2\pi\sigma_1\sigma_2\sqrt{1-\rho^2}} \\ &\times \exp \left\{ \frac{-1}{2(1-\rho^2)} \left[\frac{(x_1 - \mu_1)^2}{\sigma_1^2} - \frac{2\rho(x_1 - \mu_1)(x_2 - \mu_2)}{\sigma_1\sigma_2} \right. \right. \\ &\quad \left. \left. + \frac{(x_2 - \mu_2)^2}{\sigma_2^2} \right] \right\}. \end{aligned} \tag{39.28}$$

The characteristic function for the multivariate Gaussian is

$$\phi(\mathbf{u}; \boldsymbol{\mu}, V) = \exp \left[i\boldsymbol{\mu} \cdot \mathbf{u} - \frac{1}{2} \mathbf{u}^T V \mathbf{u} \right]. \tag{39.29}$$

If the components of \mathbf{x} are independent, then Eq. (39.29) is the product of the characteristic functions of n Gaussians.

For an n -dimensional Gaussian distribution for \mathbf{x} with mean $\boldsymbol{\mu}$ and covariance matrix V , the marginal distribution for any single x_i is a one-dimensional Gaussian with mean μ_i and variance V_{ii} . The equation $(\mathbf{x} - \mathbf{a})^T V^{-1} (\mathbf{x} - \mathbf{a}) = C$, where C is any positive number, defines an n -dimensional ellipse centered about \mathbf{a} . If \mathbf{a} is equal to the mean $\boldsymbol{\mu}$, then C is a random variable obeying the χ^2 distribution for n degrees of freedom, which is discussed in the following section. The probability that \mathbf{x} lies outside the ellipsoid for a given value of C is given by $1 - F_{\chi^2}(C; n)$, where F_{χ^2} is the cumulative χ^2 distribution. This may be read from Fig. 40.1. For example, the “ s -standard-deviation ellipsoid” occurs at $C = s^2$. For the two-variable case ($n = 2$), the point \mathbf{x} lies outside the one-standard-deviation ellipsoid with 61% probability. The use of these ellipsoids as indicators of probable error is described in Sec. 40.4.2.2; the validity of those indicators assumes that $\boldsymbol{\mu}$ and V are correct.

39.4.4 Log-normal distribution

If a random variable y follows a Gaussian distribution with mean μ and variance σ^2 , then $x = e^y$ follows a log-normal distribution, as given in Table 39.1. As a consequence of the central limit theorem described in Sec. 39.4.3, the distribution of the product of a large number of positive random variables approaches a log-normal. It is bounded below by zero and is thus well suited for modeling quantities that are intrinsically non-negative such as an efficiency. One can implement a log-normal model for a random variable x by defining $y = \ln x$ so that y follows a Gaussian distribution.

39.4.5 χ^2 distribution

If x_1, \dots, x_n are independent Gaussian random variables, the sum $z = \sum_{i=1}^n (x_i - \mu_i)^2 / \sigma_i^2$ follows the χ^2 p.d.f. with n degrees

Table 39.1: Some common probability density functions, with corresponding characteristic functions and means and variances. In the Table, $\Gamma(k)$ is the gamma function, equal to $(k - 1)!$ when k is an integer; ${}_1F_1$ is the confluent hypergeometric function of the 1st kind [11].

Distribution	Probability density function f (variable; parameters)	Characteristic function $\phi(u)$	Mean	Variance
Uniform	$f(x; a, b) = \begin{cases} 1/(b - a) & a \leq x \leq b \\ 0 & \text{otherwise} \end{cases}$	$\frac{e^{ibu} - e^{iau}}{(b-a)iu}$	$\frac{a+b}{2}$	$\frac{(b-a)^2}{12}$
Binomial	$f(r; N, p) = \frac{N!}{r!(N-r)!} p^r q^{N-r}$ $r = 0, 1, 2, \dots, N; \quad 0 \leq p \leq 1; \quad q = 1 - p$	$(q + pe^{iu})^N$	Np	Npq
Multinomial	$f(r_1, \dots, r_m; N, p_1, \dots, p_m) = \frac{N!}{r_1! \dots r_m!} p_1^{r_1} \dots p_m^{r_m}$	$(\sum_{k=1}^m p_k e^{iu_k})^N$	$E[r_i] = Np_i$	$\text{cov}[r_i, r_j] = Np_i(\delta_{ij} - p_j)$
Poisson	$f(n; \nu) = \frac{\nu^n e^{-\nu}}{n!}; \quad n = 0, 1, 2, \dots; \quad \nu > 0$	$\exp[\nu(e^{iu} - 1)]$	ν	ν
Normal (Gaussian)	$f(x; \mu, \sigma^2) = \frac{1}{\sigma\sqrt{2\pi}} \exp(-(x - \mu)^2/2\sigma^2)$	$\exp(i\mu u - \frac{1}{2}\sigma^2 u^2)$	μ	σ^2
Multivariate Gaussian	$f(\mathbf{x}; \boldsymbol{\mu}, \mathbf{V}) = \frac{1}{(2\pi)^{n/2} \sqrt{ \mathbf{V} }} \times \exp[-\frac{1}{2}(\mathbf{x} - \boldsymbol{\mu})^T \mathbf{V}^{-1}(\mathbf{x} - \boldsymbol{\mu})]$ $-\infty < x_j < \infty; \quad -\infty < \mu_j < \infty; \quad \mathbf{V} > 0$	$\exp[i\boldsymbol{\mu} \cdot \mathbf{u} - \frac{1}{2}\mathbf{u}^T \mathbf{V} \mathbf{u}]$	\mathbf{u}	V_{jk}
Log-normal	$f(x; \mu, \sigma^2) = \frac{1}{\sigma\sqrt{2\pi}} \frac{1}{x} \exp(-(\ln x - \mu)^2/2\sigma^2)$ $0 < x < \infty; \quad -\infty < \mu < \infty; \quad \sigma > 0$	—	$\exp(\mu + \sigma^2/2)$	$\exp(2\mu + \sigma^2) \times [\exp(\sigma^2) - 1]$
χ^2	$f(z; n) = \frac{z^{n/2-1} e^{-z/2}}{2^{n/2} \Gamma(n/2)}; \quad z \geq 0$	$(1 - 2iu)^{-n/2}$	n	$2n$
Student's t	$f(t; n) = \frac{1}{\sqrt{n\pi}} \frac{\Gamma[(n+1)/2]}{\Gamma(n/2)} \left(1 + \frac{t^2}{n}\right)^{-(n+1)/2}$ $-\infty < t < \infty; \quad n \text{ not required to be integer}$	—	0 for $n > 1$	$n/(n - 2)$ for $n > 2$
Gamma	$f(x; \lambda, k) = \frac{x^{k-1} \lambda^k e^{-\lambda x}}{\Gamma(k)}; \quad 0 \leq x < \infty; \quad k \text{ not required to be integer}$	$(1 - iu/\lambda)^{-k}$	k/λ	k/λ^2
Beta	$f(x; \alpha, \beta) = \frac{\Gamma(\alpha+\beta)}{\Gamma(\alpha)\Gamma(\beta)} x^{\alpha-1} (1-x)^{\beta-1}$ $0 \leq x \leq 1$	${}_1F_1(\alpha; \alpha + \beta; iu)$	$\frac{\alpha}{\alpha+\beta}$	$\frac{\alpha\beta}{(\alpha+\beta)^2(\alpha+\beta+1)}$

of freedom, which we denote by $\chi^2(n)$. More generally, for n correlated Gaussian variables as components of a vector \mathbf{X} with covariance matrix V , $z = \mathbf{X}^T V^{-1} \mathbf{X}$ follows $\chi^2(n)$ as in the previous section. For a set of z_i , each of which follows $\chi^2(n_i)$, $\sum z_i$ follows $\chi^2(\sum n_i)$. For large n , the χ^2 p.d.f. approaches a Gaussian with a mean and variance given by $\mu = n$ and $\sigma^2 = 2n$, respectively (here the formulae for μ and σ^2 are valid for all n).

The χ^2 p.d.f. is often used in evaluating the level of compatibility between observed data and a hypothesis for the p.d.f. that the data might follow. This is discussed further in Sec. 40.3.2 on significance tests.

39.4.6 Student's t distribution

Suppose that y and x_1, \dots, x_n are independent and Gaussian distributed with mean 0 and variance 1. We then define

$$z = \sum_{i=1}^n x_i^2 \quad \text{and} \quad t = \frac{y}{\sqrt{z/n}}. \tag{39.30}$$

The variable z thus follows a $\chi^2(n)$ distribution. Then t is distributed according to Student's t distribution with n degrees of freedom, $f(t; n)$, given in Table 39.1.

If defined through gamma functions as in Table 39.1, the parameter n is not required to be an integer. As $n \rightarrow \infty$, the distribution approaches a Gaussian, and for $n = 1$ it is a *Cauchy* or *Breit-Wigner* distribution.

As an example, consider the *sample mean* $\bar{x} = \sum x_i/n$ and the *sample variance* $s^2 = \sum (x_i - \bar{x})^2/(n-1)$ for normally distributed x_i with unknown mean μ and variance σ^2 . The sample mean has a Gaussian distribution with a variance σ^2/n , so the variable $(\bar{x} - \mu)/\sqrt{\sigma^2/n}$ is normal with mean 0 and variance 1. The quantity $(n-1)s^2/\sigma^2$ is independent of this and follows $\chi^2(n-1)$.

The ratio

$$t = \frac{(\bar{x} - \mu)/\sqrt{\sigma^2/n}}{\sqrt{(n-1)s^2/\sigma^2}} = \frac{\bar{x} - \mu}{\sqrt{s^2/n}} \tag{39.31}$$

is distributed as $f(t; n - 1)$. The unknown variance σ^2 cancels, and t can be used to test the hypothesis that the true mean is some particular value μ .

39.4.7 Gamma distribution

For a process that generates events as a function of x (e.g., space or time) according to a Poisson distribution, the distance in x from an arbitrary starting point (which may be some particular event) to the k^{th} event follows a *gamma* distribution, $f(x; \lambda, k)$. The Poisson parameter μ is λ per unit x . The special case $k = 1$ (i.e., $f(x; \lambda, 1) = \lambda e^{-\lambda x}$) is called the *exponential* distribution. A sum of k' exponential random variables x_i is distributed as $f(\sum x_i; \lambda, k')$.

The parameter k is not required to be an integer. For $\lambda = 1/2$ and $k = n/2$, the gamma distribution reduces to the $\chi^2(n)$ distribution.

39.4.8 Beta distribution

The beta distribution describes a continuous random variable x in the interval $[0, 1]$. By scaling and translation one can easily generalize it to have arbitrary endpoints. In Bayesian inference about the parameter p of a binomial process, if the prior p.d.f. is a beta distribution $f(p; \alpha, \beta)$ then the observation of r successes out of N trials gives a posterior beta distribution $f(p; r + \alpha, N - r + \beta)$ (Bayesian methods are discussed further in Sec. 40). The uniform distribution is a beta distribution with $\alpha = \beta = 1$.

References

[1] H. Cramér, *Mathematical Methods of Statistics*, (Princeton Univ. Press, New Jersey, 1958).

- [2] A. Stuart and J.K. Ord, *Kendall's Advanced Theory of Statistics*, Vol. 1 *Distribution Theory* 6th Ed., (Halsted Press, New York, 1994), and earlier editions by Kendall and Stuart.
- [3] F.E. James, *Statistical Methods in Experimental Physics*, 2nd Ed., (World Scientific, Singapore, 2006).
- [4] L. Lyons, *Statistics for Nuclear and Particle Physicists*, (Cambridge University Press, New York, 1986).
- [5] B.R. Roe, *Probability and Statistics in Experimental Physics*, 2nd Ed., (Springer, New York, 2001).
- [6] R.J. Barlow, *Statistics: A Guide to the Use of Statistical Methods in the Physical Sciences*, (John Wiley, New York, 1989).
- [7] S. Brandt, *Data Analysis*, 3rd Ed., (Springer, New York, 1999).
- [8] G. Cowan, *Statistical Data Analysis*, (Oxford University Press, Oxford, 1998).
- [9] A.N. Kolmogorov, *Grundbegriffe der Wahrscheinlichkeitsrechnung*, (Springer, Berlin, 1933); *Foundations of the Theory of Probability*, 2nd Ed., (Chelsea, New York 1956).
- [10] Ch. Walck, *Hand-book on Statistical Distributions for Experimentalists*, University of Stockholm Internal Report SUF-PFY/96-01, available from www.physto.se-walck.
- [11] M. Abramowitz and I. Stegun, eds., *Handbook of Mathematical Functions*, (Dover, New York, 1972).
- [12] F.W.J. Olver *et al.*, eds., *NIST Handbook of Mathematical Functions*, (Cambridge University Press, 2010); A companion Digital Library of Mathematical Functions is available at dlmf.nist.gov.
- [13] R. Brun and F. Rademakers, *Nucl. Instrum. Meth.* **A389**, 81 (1997); See also root.cern.ch.

40. Statistics

Revised August 2021 by G. Cowan (RHUL).

This chapter gives an overview of statistical methods used in high-energy physics. In statistics, we are interested in using a given sample of data to make inferences about a probabilistic model, *e.g.*, to assess the model's validity or to determine the values of its parameters. There are two main approaches to statistical inference, which we may call frequentist and Bayesian.

In frequentist statistics, probability is interpreted as the limiting frequency of the outcome of a repeatable experiment. The most important tools in this framework are parameter estimation, covered in Section 40.2, statistical tests, discussed in Section 40.3, and confidence intervals, which are constructed so as to cover the true value of a parameter with a specified probability, as described in Section 40.4.2. Note that in frequentist statistics one does not define a probability for a hypothesis or for the value of a parameter.

In Bayesian statistics, the subjective interpretation of probability is used to quantify one's *degree of belief* in a hypothesis. This allows one to define a probability density function (p.d.f.) for a parameter, which reflects one's knowledge about where its true value lies.

Bayesian methods provide a natural means to include additional information, which in general may be subjective; in fact they *require* prior probabilities for the hypotheses (or parameters) in question, *i.e.*, the degree of belief about the parameters' values, before carrying out the measurement. Using Bayes' theorem (Eq. (39.4)), the prior degree of belief is updated by the data from the experiment. Bayesian methods for interval estimation are discussed in Sections 40.4.1 and 40.4.2.4.

For many inference problems, the frequentist and Bayesian approaches give similar numerical values, even though they answer different questions and are based on fundamentally different interpretations of probability. In some important cases, however, the two approaches may yield very different results. For a discussion of Bayesian vs. non-Bayesian methods, see references written by a statistician [1], by a physicist [2], or the detailed comparison in Ref. [3].

40.1 Fundamental concepts

Consider an experiment whose outcome is characterized by one or more data values, which we can write as a vector \mathbf{x} . A *hypothesis* H is a statement about the probability for the data, often written $P(\mathbf{x}|H)$. (We will usually use a capital letter for a probability and lower case for a probability density. Often the term p.d.f. is used loosely to refer to either a probability or a probability density.) This could, for example, define completely the p.d.f. for the data (a *simple* hypothesis), or it could specify only the functional form of the p.d.f., with the values of one or more parameters not determined (a *composite* hypothesis).

If the probability $P(\mathbf{x}|H)$ for data \mathbf{x} is regarded as a function of the hypothesis H , then it is called the *likelihood* of H , usually written $L(H)$. Often the hypothesis is characterized by one or more parameters θ , in which case $L(\theta) = P(\mathbf{x}|\theta)$ is called the likelihood function.

In some cases one can obtain at least approximate frequentist results using the likelihood evaluated only with the data obtained, for example, when determining confidence regions with Eq. (40.74). In general, however, the frequentist approach requires a full specification of the probability model $P(\mathbf{x}|H)$ both as a function of the data \mathbf{x} and hypothesis H .

In the Bayesian approach, inference is based on the posterior probability for H given the data \mathbf{x} , which represents one's degree of belief that H is true given the data. This is obtained from Bayes' theorem (39.4), which can be written

$$P(H|\mathbf{x}) = \frac{P(\mathbf{x}|H)\pi(H)}{\int P(\mathbf{x}|H')\pi(H') dH'}. \quad (40.1)$$

Here $P(\mathbf{x}|H)$ is the likelihood for H , which depends only on the data actually obtained. The quantity $\pi(H)$ is the prior probability for H , which represents one's degree of belief for H before carrying out the measurement. The integral in the denominator (or sum, for discrete hypotheses) serves as a normalization factor. If H

is characterized by a continuous parameter θ then the posterior probability is a p.d.f. $p(\theta|\mathbf{x})$. Note that the likelihood function itself is not a p.d.f. for θ .

40.2 Parameter estimation

Here we review *point estimation* of parameters, first with an overview of the frequentist approach and its two most important methods, maximum likelihood and least squares, treated in Sections 40.2.2 and 40.2.3. The Bayesian approach is outlined in Sec. 40.2.6.

An *estimator* $\hat{\theta}$ (written with a hat) is a function of the data used to estimate the value of the parameter θ . Sometimes the word 'estimate' is used to denote the value of the estimator when evaluated with given data. There is no fundamental rule dictating how an estimator must be constructed. One tries, therefore, to choose that estimator which has the best properties. The most important of these are (a) *consistency*, (b) *bias*, (c) *efficiency*, and (d) *robustness*.

(a) An estimator is said to be *consistent* if the estimate $\hat{\theta}$ converges in probability (see Ref. [3]) to the true value θ as the amount of data increases. This property is so important that it is possessed by all commonly used estimators.

(b) The *bias*, $b = E[\hat{\theta}] - \theta$, is the difference between the expectation value of the estimator and the true value of the parameter. The expectation value is taken over a hypothetical set of similar experiments in which $\hat{\theta}$ is constructed in the same way. When $b = 0$, the estimator is said to be unbiased. The bias depends on the chosen metric, *i.e.*, if $\hat{\theta}$ is an unbiased estimator of θ , then $\hat{\theta}^2$ is not in general an unbiased estimator for θ^2 .

(c) *Efficiency* is the ratio of the minimum possible variance for any estimator of θ to the variance $V[\hat{\theta}]$ of the estimator $\hat{\theta}$. For the case of a single parameter, under rather general conditions the minimum variance is given by the Rao-Cramér-Fréchet bound,

$$\sigma_{\min}^2 = \left(1 + \frac{\partial b}{\partial \theta}\right)^2 / I(\theta), \quad (40.2)$$

where

$$I(\theta) = E \left[\left(\frac{\partial \ln L}{\partial \theta} \right)^2 \right] = -E \left[\frac{\partial^2 \ln L}{\partial \theta^2} \right] \quad (40.3)$$

is the *Fisher information*, L is the likelihood, and the operator $E[\]$ in (40.3) is the expectation value with respect to the data. For the final equality to hold, the range of allowed data values must not depend on θ .

The *mean-squared error*,

$$\text{MSE} = E[(\hat{\theta} - \theta)^2] = V[\hat{\theta}] + b^2, \quad (40.4)$$

is a measure of an estimator's quality which combines bias and variance.

(d) *Robustness* is the property of being insensitive to departures from assumptions about the p.d.f., *e.g.*, owing to uncertainties in the distribution's tails.

It is not in general possible to optimize simultaneously for all the measures of estimator quality described above. For some common estimators, the properties above are known exactly. More generally, it is possible to evaluate them by Monte Carlo simulation. Note that they will in general depend on the unknown θ .

40.2.1 Estimators for mean, variance, and median

Suppose we have a set of n independent measurements, x_1, \dots, x_n , each assumed to follow a p.d.f. with unknown mean μ and unknown variance σ^2 (the measurements do not necessarily have to follow a Gaussian distribution). Then

$$\hat{\mu} = \frac{1}{n} \sum_{i=1}^n x_i \quad (40.5)$$

$$\hat{\sigma}^2 = \frac{1}{n-1} \sum_{i=1}^n (x_i - \hat{\mu})^2 \quad (40.6)$$

are unbiased estimators of μ and σ^2 . The variance of $\hat{\mu}$ is σ^2/n and the variance of $\hat{\sigma}^2$ is

$$V\left[\hat{\sigma}^2\right] = \frac{1}{n} \left(m_4 - \frac{n-3}{n-1} \sigma^4 \right), \quad (40.7)$$

where m_4 is the 4th central moment of x (see Eq. (39.8)). For Gaussian distributed x_i , this becomes $2\sigma^4/(n-1)$ for any $n \geq 2$, and for large n the standard deviation of $\hat{\sigma}$ is $\sigma/\sqrt{2n}$. For any n and Gaussian x_i , $\hat{\mu}$ is an efficient estimator for μ , and the estimators $\hat{\mu}$ and $\hat{\sigma}^2$ are uncorrelated. Otherwise the arithmetic mean (40.5) is not necessarily the most efficient estimator; this is discussed further in Sec. 8.7 of Ref. [4].

If σ^2 is known, it does not improve the estimate $\hat{\mu}$, as can be seen from Eq. (40.5); however, if μ is known, one can substitute it for $\hat{\mu}$ in Eq. (40.6) and replace $n-1$ by n to obtain an estimator of σ^2 still with zero bias but smaller variance. If the x_i have different, known variances σ_i^2 , then the weighted average

$$\hat{\mu} = \frac{1}{w} \sum_{i=1}^n w_i x_i, \quad (40.8)$$

where $w_i = 1/\sigma_i^2$ and $w = \sum_i w_i$, is an unbiased estimator for μ with a smaller variance than an unweighted average. The standard deviation of $\hat{\mu}$ is $1/\sqrt{w}$.

As an estimator for the median x_{med} , one can use the value \hat{x}_{med} such that half the x_i are below and half above (the sample median). If there are an even number of observations and the sample median lies between two observed values, the estimator is set by convention to their arithmetic average. If the p.d.f. of x has the form $f(x-\mu)$ and μ is both mean and median, then for large n the variance of the sample median approaches $1/[4nf^2(0)]$, provided $f(0) > 0$. Although estimating the median can often be more difficult computationally than the mean, the resulting estimator is generally more robust, as it is insensitive to the exact shape of the tails of a distribution.

40.2.2 The method of maximum likelihood

Suppose we have a set of measured quantities \mathbf{x} and the likelihood $L(\boldsymbol{\theta}) = P(\mathbf{x}|\boldsymbol{\theta})$ for a set of parameters $\boldsymbol{\theta} = (\theta_1, \dots, \theta_M)$. The *maximum likelihood* (ML) estimators for $\boldsymbol{\theta}$ are defined as the values that give the maximum of L . Because of the properties of the logarithm, it is usually easier to work with $\ln L$, and since both are maximized for the same parameter values $\boldsymbol{\theta}$, the ML estimators can be found by solving the *likelihood equations*,

$$\frac{\partial \ln L}{\partial \theta_i} = 0, \quad i = 1, \dots, M. \quad (40.9)$$

Often the solution must be found numerically. Maximum likelihood estimators are important because they are asymptotically (*i.e.*, for large data samples) unbiased, efficient and have a Gaussian sampling distribution under quite general conditions, and the method has a wide range of applicability.

In general the likelihood function is obtained from the probability of the data under assumption of the parameters. An important special case is when the data consist of *i.i.d.* (independent and identically distributed) values. Here one has a set of n statistically independent quantities $\mathbf{x} = (x_1, \dots, x_n)$, where each component follows the same p.d.f. $f(x; \boldsymbol{\theta})$. In this case the joint p.d.f. of the data sample factorizes and the likelihood function is

$$L(\boldsymbol{\theta}) = \prod_{i=1}^n f(x_i; \boldsymbol{\theta}). \quad (40.10)$$

In this case the number n of observations (usually individual “events” in particle physics) is regarded as fixed. If, however, the probability to observe n events itself depends on the parameters $\boldsymbol{\theta}$, then this dependence should be included in the likelihood. For example, if n follows a Poisson distribution with mean μ and the independent x values all follow $f(x; \boldsymbol{\theta})$, then the likelihood becomes

$$L(\boldsymbol{\theta}) = \frac{\mu^n}{n!} e^{-\mu} \prod_{i=1}^n f(x_i; \boldsymbol{\theta}). \quad (40.11)$$

Equation (40.11) is often called the *extended likelihood* (see, *e.g.*, Refs. [5–7]). If μ is given as a function of $\boldsymbol{\theta}$, then including the probability for n given $\boldsymbol{\theta}$ in the likelihood provides additional information about the parameters. This therefore leads to a reduction in their statistical uncertainties and in general changes their estimated values.

In evaluating the likelihood function, it is important that any normalization factors in the p.d.f. that involve $\boldsymbol{\theta}$ be included. However, we will only be interested in the maximum of L and in ratios of L at different values of the parameters; hence any multiplicative factors that do not involve the parameters that we want to estimate may be dropped, including factors that depend on the data but not on $\boldsymbol{\theta}$.

Under a one-to-one change of parameters from $\boldsymbol{\theta}$ to $\boldsymbol{\eta}$, the ML estimators $\hat{\boldsymbol{\theta}}$ transform to $\boldsymbol{\eta}(\hat{\boldsymbol{\theta}})$. That is, the ML solution is invariant under change of parameter. However, other properties of ML estimators, in particular the bias, are not invariant under change of parameter.

The inverse V^{-1} of the covariance matrix $V_{ij} = \text{cov}[\hat{\theta}_i, \hat{\theta}_j]$ for a set of ML estimators can be estimated by using

$$(\hat{V}^{-1})_{ij} = - \left. \frac{\partial^2 \ln L}{\partial \theta_i \partial \theta_j} \right|_{\hat{\boldsymbol{\theta}}}. \quad (40.12)$$

Equation (40.12) holds for a sufficiently large data sample (or for a small sample only in special cases, *e.g.*, where the means of Gaussian distributed data are linear functions of the parameters); otherwise it can result in a misestimation of the variances. Under the conditions where the equation is valid, L has a Gaussian form and $\ln L$ is (hyper)parabolic. In this case, s times the standard deviations σ_i of the estimators for the parameters can be obtained from the hypersurface defined by the $\boldsymbol{\theta}$ such that

$$\ln L(\boldsymbol{\theta}) = \ln L_{\text{max}} - s^2/2, \quad (40.13)$$

where $\ln L_{\text{max}}$ is the value of $\ln L$ at the solution point (compare with Eq. (40.74)). The minimum and maximum values of θ_i on the hypersurface then give an approximate s -standard deviation confidence interval for θ_i (see Section 40.4.2.2).

40.2.2.1 ML with binned data

If the total number of data values x_i , ($i = 1, \dots, n_{\text{tot}}$), is small, the unbinned maximum likelihood method, *i.e.*, use of Equation (40.10) (or (40.11) for extended ML), is preferred since binning can only result in a loss of information, and hence larger statistical errors for the parameter estimates. If the sample is large, it can be convenient to bin the values in a histogram with N bins, so that one obtains a vector of data $\mathbf{n} = (n_1, \dots, n_N)$ with expectation values $\boldsymbol{\mu} = E[\mathbf{n}]$ and probabilities $f(\mathbf{n}; \boldsymbol{\mu})$. Suppose the mean values $\boldsymbol{\mu}$ can be determined as a function of a set of parameters $\boldsymbol{\theta}$. Then one may maximize the likelihood function based on the contents of the bins.

As mentioned in Sec. 40.2.2, the total number of events $n_{\text{tot}} = \sum_i n_i$ can be regarded either as fixed or as a random variable. If it is fixed, the histogram follows a multinomial distribution,

$$f_M(\mathbf{n}; \boldsymbol{\theta}) = \frac{n_{\text{tot}}!}{n_1! \dots n_N!} p_1^{n_1} \dots p_N^{n_N}, \quad (40.14)$$

where we assume the probabilities p_i are given functions of the parameters $\boldsymbol{\theta}$. The distribution can be written equivalently in terms of the expected number of events in each bin, $\mu_i = n_{\text{tot}} p_i$. If the n_i are regarded as independent and Poisson distributed, then the data are instead described by a product of Poisson probabilities,

$$f_P(\mathbf{n}; \boldsymbol{\theta}) = \prod_{i=1}^N \frac{\mu_i^{n_i}}{n_i!} e^{-\mu_i}, \quad (40.15)$$

where the mean values μ_i are given functions of $\boldsymbol{\theta}$. The total number of events n_{tot} thus follows a Poisson distribution with mean $\mu_{\text{tot}} = \sum_i \mu_i$.

When using maximum likelihood with binned data, one can find the ML estimators and at the same time obtain a statistic

usable for a test of goodness-of-fit (see Sec. 40.3.2). Maximizing the likelihood $L(\theta) = f_{M/P}(\mathbf{n}; \theta)$ is equivalent to maximizing the likelihood ratio $\lambda(\theta) = f_{M/P}(\mathbf{n}; \theta) / f(\mathbf{n}; \hat{\mu})$, where in the denominator $f(\mathbf{n}; \mu)$ is a model with an adjustable parameter for each bin, $\mu = (\mu_1, \dots, \mu_N)$, and the corresponding estimators are $\hat{\mu} = (n_1, \dots, n_N)$ (called the “saturated model”). Equivalently one often minimizes the quantity $-2 \ln \lambda(\theta)$. For independent Poisson distributed n_i this is [8]

$$-2 \ln \lambda(\theta) = 2 \sum_{i=1}^N \left[\mu_i(\theta) - n_i + n_i \ln \frac{n_i}{\mu_i(\theta)} \right], \quad (40.16)$$

where for bins with $n_i = 0$, the last term in (40.16) is zero. The expression (40.16) without the terms $\mu_i - n_i$ also gives $-2 \ln \lambda(\theta)$ for multinomially distributed n_i , *i.e.*, when the total number of entries is regarded as fixed. In the limit of zero bin width, minimizing (40.16) is equivalent to maximizing the unbinned extended likelihood function (40.11); in the corresponding multinomial case without the $\mu_i - n_i$ terms one obtains Eq. (40.10).

A smaller value of $-2 \ln \lambda(\hat{\theta})$ corresponds to better agreement between the data and the hypothesized form of $\mu(\theta)$. The value of $-2 \ln \lambda(\hat{\theta})$ can thus be translated into a *p*-value as a measure of goodness-of-fit, as described in Sec. 40.3.2. Assuming the model is correct, then according to Wilks’ theorem [9], for sufficiently large μ_i and provided certain regularity conditions are met, the minimum of $-2 \ln \lambda$ as defined by Eq. (40.16) follows a χ^2 distribution (see, *e.g.*, Ref. [8]). If there are N bins and M fitted parameters, then the number of degrees of freedom for the χ^2 distribution is $N - M$ if the data are treated as Poisson-distributed, and $N - M - 1$ if the n_i are multinomially distributed.

Suppose the n_i are Poisson-distributed and the overall normalization $\mu_{\text{tot}} = \sum_i \mu_i$ is taken as an adjustable parameter, so that $\mu_i = \mu_{\text{tot}} p_i(\theta)$, where the probability to be in the *i*th bin, $p_i(\theta)$, does not depend on μ_{tot} . Then by minimizing Eq. (40.16), one obtains that the area under the fitted function is equal to the sum of the histogram contents, *i.e.*, $\sum_i \hat{\mu}_i = \sum_i n_i$. This is a property not possessed by the estimators from the method of least squares (see, *e.g.*, Sec. 40.2.3 and Ref. [7]).

40.2.2.2 *Frequentist treatment of nuisance parameters*

Suppose we want to determine the values of parameters θ using a set of measurements \mathbf{x} described by a probability model $P(\mathbf{x}|\theta)$. In general the model is not perfect, which is to say it cannot provide an accurate description of the data even at the most optimal point of its parameter space. As a result, the estimated parameters can have a systematic bias.

One can improve the model by including in it additional parameters. That is, $P(\mathbf{x}|\theta)$ is replaced by a more general model $P(\mathbf{x}|\theta, \nu)$, which depends on parameters of interest θ and *nuisance parameters* ν . The additional parameters are not of intrinsic interest but must be included for the model to be sufficiently accurate for some point in the enlarged parameter space.

Although including additional parameters may eliminate or at least reduce the effect of systematic uncertainties, their presence will result in increased statistical uncertainties for the parameters of interest. This occurs because the estimators for the nuisance parameters and those of interest will in general be correlated, which results in an enlargement of the contour defined by Eq. (40.13).

To reduce the impact of the nuisance parameters one often tries to constrain their values by means of control or calibration measurements, say, having data \mathbf{y} . For example, some components of \mathbf{y} could represent estimates of the nuisance parameters, often from separate experiments. Suppose the measurements \mathbf{y} are statistically independent from \mathbf{x} and are described by a model $P(\mathbf{y}|\nu)$. The joint model for both \mathbf{x} and \mathbf{y} is in this case therefore the product of the probabilities for \mathbf{x} and \mathbf{y} , and thus the likelihood function for the full set of parameters is

$$L(\theta, \nu) = P(\mathbf{x}|\theta, \nu) P(\mathbf{y}|\nu). \quad (40.17)$$

Note that in this case if one wants to simulate the experiment by means of Monte Carlo, both the primary and control mea-

surements, \mathbf{x} and \mathbf{y} , must be generated for each repetition under assumption of fixed values for the parameters θ and ν .

Using all of the parameters (θ, ν) in Eq. (40.13) to find the statistical errors in the parameters of interest θ is equivalent to using the *profile likelihood*, which depends only on θ . It is defined as

$$L_p(\theta) = L(\theta, \hat{\nu}(\theta)), \quad (40.18)$$

where the double-hat notation indicates the profiled values of the parameters ν , defined as the values that maximize L for the specified θ . The profile likelihood is discussed further in Section 40.3.2.1 in connection with hypothesis tests.

40.2.3 *The method of least squares*

The *method of least squares* (LS) coincides with the method of maximum likelihood in the following special case. Consider a set of N independent measurements y_i at known points x_i . The measurement y_i is assumed to be Gaussian distributed with mean $\mu(x_i; \theta)$ and known variance σ_i^2 . The goal is to construct estimators for the unknown parameters θ . The log-likelihood function contains the sum of squares

$$\chi^2(\theta) = -2 \ln L(\theta) + \text{constant} = \sum_{i=1}^N \frac{(y_i - \mu(x_i; \theta))^2}{\sigma_i^2}. \quad (40.19)$$

The parameter values that maximize L are the same as those which minimize χ^2 .

The minimum of the chi-square function in Equation (40.19) defines the least-squares estimators $\hat{\theta}$ for the more general case where the y_i are not Gaussian distributed as long as they are independent. If they are not independent but rather have a covariance matrix $V_{ij} = \text{cov}[y_i, y_j]$, then the LS estimators are determined by the minimum of

$$\chi^2(\theta) = (\mathbf{y} - \mu(\theta))^T V^{-1} (\mathbf{y} - \mu(\theta)), \quad (40.20)$$

where $\mathbf{y} = (y_1, \dots, y_N)$ is the (column) vector of measurements, $\mu(\theta)$ is the corresponding vector of predicted values, and the superscript T denotes the transpose. If the y_i are not Gaussian distributed, then the LS and ML estimators will not in general coincide.

Often one further restricts the problem to the case where $\mu(x_i; \theta)$ is a linear function of the parameters, *i.e.*,

$$\mu(x_i; \theta) = \sum_{j=1}^m \theta_j h_j(x_i). \quad (40.21)$$

Here the $h_j(x)$ are m linearly independent functions, *e.g.*, $1, x, x^2, \dots, x^{m-1}$ or Legendre polynomials. We require $m < N$ and at least m of the x_i must be distinct.

Minimizing χ^2 in this case with m parameters reduces to solving a system of m linear equations. Defining $H_{ij} = h_j(x_i)$ and minimizing χ^2 by setting its derivatives with respect to the θ_i equal to zero gives the LS estimators,

$$\hat{\theta} = (H^T V^{-1} H)^{-1} H^T V^{-1} \mathbf{y} \equiv D \mathbf{y}. \quad (40.22)$$

The covariance matrix for the estimators $U_{ij} = \text{cov}[\hat{\theta}_i, \hat{\theta}_j]$ is given by

$$U = D V D^T = (H^T V^{-1} H)^{-1}, \quad (40.23)$$

or equivalently, its inverse U^{-1} can be found from

$$(U^{-1})_{ij} = \frac{1}{2} \frac{\partial^2 \chi^2}{\partial \theta_i \partial \theta_j} \Big|_{\theta=\hat{\theta}} = \sum_{k,l=1}^m h_i(x_k) (V^{-1})_{kl} h_j(x_l). \quad (40.24)$$

The LS estimators can also be found from the expression

$$\hat{\theta} = U \mathbf{g}, \quad (40.25)$$

where the vector \mathbf{g} is defined by

$$\mathbf{g}_i = \sum_{j,k=1}^m y_j h_i(x_k) (V^{-1})_{jk}. \quad (40.26)$$

For the case of uncorrelated y_i , for example, one can use (40.25) with

$$(U^{-1})_{ij} = \sum_{k=1}^N \frac{h_i(x_k)h_j(x_k)}{\sigma_k^2}, \quad (40.27)$$

$$g_i = \sum_{k=1}^N \frac{y_k h_i(x_k)}{\sigma_k^2}. \quad (40.28)$$

Expanding $\chi^2(\boldsymbol{\theta})$ about $\hat{\boldsymbol{\theta}}$, one finds that the contour in parameter space defined by

$$\chi^2(\boldsymbol{\theta}) = \chi^2(\hat{\boldsymbol{\theta}}) + 1 = \chi_{\min}^2 + 1 \quad (40.29)$$

has tangent planes located at plus-or-minus-one standard deviation $\sigma_{\hat{\boldsymbol{\theta}}}$ from the LS estimates $\hat{\boldsymbol{\theta}}$ (the relation is approximate if the fit function $\mu(x; \boldsymbol{\theta})$ is nonlinear in the parameters).

In constructing the quantity $\chi^2(\boldsymbol{\theta})$ one requires the variances or, in the case of correlated measurements, the covariance matrix. Often these quantities are not known *a priori* and must be estimated from the data. In this case the least-squares and maximum-likelihood methods are no longer exactly equivalent even for Gaussian distributed measurements. An important example is where the measured value y_i represents the event count in a histogram bin. If, for example, y_i represents a Poisson variable, for which the variance is equal to the mean, then one can either estimate the variance from the predicted value, $\mu(x_i; \boldsymbol{\theta})$, or from the observed number itself, y_i . In the first option, the variances become functions of the parameters, and as a result the estimators may need to be found numerically. The second option can be undefined if y_i is zero, and for small y_i , the variance will be poorly estimated. In either case, one should constrain the normalization of the fitted curve to the correct value, *i.e.*, one should determine the area under the fitted curve directly from the number of entries in the histogram (see Ref. [7], Section 7.4). As noted in Sec. 40.2.2.1, this issue is avoided when using the method of extended maximum likelihood with binned data by minimizing Eq. (40.16). In that case if the expected number of events μ_{tot} does not depend on the other fitted parameters $\boldsymbol{\theta}$, then its extended ML estimator is equal to the observed total number of events.

As the minimum value of the χ^2 represents the level of agreement between the measurements and the fitted function, it can be used for assessing the goodness-of-fit; this is discussed further in Section 40.3.2.

40.2.4 Parameter estimation with constraints

In some applications one is interested in using a set of measured quantities $\mathbf{y} = (y_1, \dots, y_N)$ to estimate a set of parameters $\boldsymbol{\theta} = (\theta_1, \dots, \theta_M)$ subject to a number of constraints. For example, one may have measured coordinates from two tracks, and one wishes to estimate their momentum vectors subject to the constraint that the tracks have a common vertex. The parameters can also include momenta of undetected particles such as neutrinos, as long as the constraints from conservation of energy and momentum and from known masses of particles involved in the reaction chain provide enough information for these quantities to be inferred.

A set of K constraints can be given in the form of equations

$$c_k(\boldsymbol{\theta}) = 0, \quad k = 1, \dots, K. \quad (40.30)$$

In some problems it may be possible to define a new set of parameters $\boldsymbol{\eta} = (\eta_1, \dots, \eta_L)$ with $L = M - K$ such that every point in $\boldsymbol{\eta}$ -space automatically satisfies the constraints. If this is possible then the problem reduces to one of estimating $\boldsymbol{\eta}$ with, *e.g.*, maximum likelihood or least squares and then transforming the estimators back into $\boldsymbol{\theta}$ -space.

In many cases it may be difficult or impossible to find an appropriate transformation $\boldsymbol{\eta}(\boldsymbol{\theta})$. Suppose that the parameters are determined through minimizing an objective function such as $\chi^2(\boldsymbol{\theta})$ in the method of least squares. Here one may enforce the con-

straints by finding the stationary points of the *Lagrange function*

$$\mathcal{L}(\boldsymbol{\theta}, \boldsymbol{\lambda}, \mathbf{y}) = \chi^2(\boldsymbol{\theta}, \mathbf{y}) + \sum_{k=1}^K \lambda_k c_k(\boldsymbol{\theta}) \quad (40.31)$$

with respect to both the parameters $\boldsymbol{\theta}$ and a set of *Lagrange multipliers* $\boldsymbol{\lambda} = (\lambda_1, \dots, \lambda_K)$. Combining the parameters and Lagrange multipliers into an $(M + K)$ -component vector $\boldsymbol{\gamma} = (\theta_1, \dots, \theta_M, \lambda_1, \dots, \lambda_K)$, the solutions for $\boldsymbol{\gamma}$, *i.e.*, the estimators $\hat{\boldsymbol{\gamma}}$, are found (*e.g.*, numerically) from the system of equations

$$F_i(\boldsymbol{\gamma}, \mathbf{y}) \equiv \frac{\partial \mathcal{L}}{\partial \gamma_i} = 0, \quad i = 1, \dots, M + K. \quad (40.32)$$

To obtain the covariance matrix of the estimated parameters one can find solutions $\hat{\boldsymbol{\gamma}}$ corresponding to the expectation values of the data $\langle \mathbf{y} \rangle$ and expand $F_i(\hat{\boldsymbol{\gamma}}, \mathbf{y})$ to first order about these values. This gives (see, *e.g.*, Sec. 11.6 of Ref. [7]) linearized approximations for the estimators, $\hat{\boldsymbol{\gamma}}(\mathbf{y}) \approx \tilde{\boldsymbol{\gamma}} + C(\mathbf{y} - \langle \mathbf{y} \rangle)$, where the matrix $C = -A^{-1}B$, and A and B are given by

$$A_{ij} = \left[\frac{\partial F_i}{\partial \gamma_j} \right]_{\tilde{\boldsymbol{\gamma}}, \langle \mathbf{y} \rangle} \quad \text{and} \quad B_{ij} = \left[\frac{\partial F_i}{\partial y_j} \right]_{\tilde{\boldsymbol{\gamma}}, \langle \mathbf{y} \rangle}. \quad (40.33)$$

In practice the values $\langle \mathbf{y} \rangle$ and corresponding solutions $\tilde{\boldsymbol{\gamma}}$ are estimated using the data from the actual measurement. Using this approximation for $\hat{\boldsymbol{\gamma}}(\mathbf{y})$, one can find the covariance matrix $U_{ij} = \text{cov}[\hat{\gamma}_i, \hat{\gamma}_j]$ of the estimators for the γ_i in terms of that of the data $V_{ij} = \text{cov}[y_i, y_j]$ using error propagation (cf. Eqs. (39.17) and (39.18)),

$$U = CVC^T. \quad (40.34)$$

The upper-left $M \times M$ block of the matrix U gives the covariance matrix for the estimated parameters $\text{cov}[\hat{\theta}_i, \hat{\theta}_j]$. One can show for linear constraints that $\text{cov}[\hat{\theta}_i, \hat{\theta}_j]$ is also given by the upper-left $M \times M$ block of $2A^{-1}$. If the parameters are estimated using the method of least squares, then the number of degrees of freedom for the distribution of the minimized χ^2 is increased by the number of constraints, *i.e.*, it becomes $N - M + K$. Further details can be found in, *e.g.*, Ch. 8 of Ref. [4] and Ch. 7 of Ref. [10].

40.2.5 Unfolding

An important class of parameter estimation problem involves measurement of the differential distribution of a kinematic variable in the form of a histogram with N bins. The data thus consist of the vector of measured data values $\mathbf{n} = (n_1, \dots, n_N)$, with expectation values $\nu_i = E[n_i]$. The n_i are usually independent and often modeled as Poisson distributed, from which it follows that the maximum-likelihood estimators are $\hat{\nu}_i = n_i$ for all i .

Because of the limited acceptance and resolution of the experiment, however, the measured values of the kinematic variable in question differ in general from their true values, and as a consequence the form of the data histogram is distorted relative to what would be obtained with perfect resolution. The desired parameters are not, therefore, the ν_i but rather one wants to estimate the expected number of entries in a given bin that would be found with a perfect detector. We call this the “true histogram” and denote it with $\boldsymbol{\mu} = (\mu_1, \dots, \mu_M)$, where the number of bins M is not required to equal that of the observed histogram. The μ_i are related to the expected numbers of events in the observed histogram by

$$\nu_i = \sum_{j=1}^M R_{ij} \mu_j + \beta_i, \quad (40.35)$$

where β_i here represents the expected number of events in bin i due to background processes and the $N \times M$ *response matrix* R_{ij} gives the probability for an event to be observed in bin i of $\boldsymbol{\nu}$ given that the true value of the variable was in bin j of $\boldsymbol{\mu}$. For purposes of this discussion let us suppose that the response matrix and expected background values are known. There are two main approaches to this type of problem, which we can call *unfolding* and *folding*.

In unfolding, one treats the true histogram μ as the parameters of interest. The result is thus given by estimators $\hat{\mu}$ and the corresponding covariance matrix $U_{ij} = \text{cov}[\hat{\mu}_i, \hat{\mu}_j]$. Provided the response matrix can be inverted, the maximum-likelihood solution is easily found as $\hat{\mu} = R^{-1}(\mathbf{n} - \beta)$. If the response matrix allows for significant migration of events between bins, then the variances of these estimators can be very large, sometimes to the point where the $\hat{\mu}$ bear essentially no resemblance to the true μ . In such cases the estimators can be found by maximizing a linear combination of the log-likelihood and a regularization function that imposes some degree of smoothness on the unfolded distribution. In achieving a reduction in variance one inevitably introduces some bias into the estimators.

In the approach of folding, by contrast, to test a given model prediction for the true histogram μ it is first “folded” with the response matrix and corrected for expected background to give the corresponding ν according to Eq. (40.35), and these are compared to the corresponding \mathbf{n} using, e.g., a likelihood ratio as shown in Sec. 40.2.2.1. In this way, one avoids any bias due to regularization.

To account for systematic uncertainties, the response matrix and background values may not be expressed as constants but rather as functions of nuisance parameters θ . These may be constrained by auxiliary measurements \mathbf{u} with pdf $p(\mathbf{u}|\theta)$ so that the full likelihood becomes (as in Eq. (40.17) but with different notation)

$$L(\mu, \theta) = P(\mathbf{n}|\nu(\mu, \theta))p(\mathbf{u}|\theta). \quad (40.36)$$

Here the mean values $\nu = R(\theta)\mu + \beta(\theta)$ now depend on both the true histogram parameters μ as well as the nuisance parameters θ . Thus to record enough information for a future analysis using folding one must provide all of the ingredients used above: the primary data \mathbf{n} , the auxiliary measurements \mathbf{u} , and also the response matrix $R(\theta)$ and expected backgrounds $\beta(\theta)$ as functions of the nuisance parameters. If unfolding is used, then future model tests or comparisons with other experiments can be carried out directly using the estimators $\hat{\mu}$ and their covariance matrix.

If several distributions are unfolded, then to combine these in a test of a given model one should know how estimators for bins of different distributions are correlated, as can arise, e.g., through common systematic effects. If only the unfolded distributions and their separate covariance matrices are reported, however, then information on such correlations is not retained. In folding, one can include information on correlated systematic effects if the ingredients (R and β) are known in terms of nuisance parameters that are common to different distributions.

In unfolding, the estimators for μ can be constructed either by maximizing the log-likelihood using Eq. (40.36) or in the case where regularization is required one can maximize $\varphi(\mu, \theta) = \ln L(\mu, \theta) + \tau S(\mu)$, where the *regularization function* $S(\mu)$ reflects the smoothness of the true histogram and serves to reduce the variances of the estimators. Possible functions are based on the mean squared second derivative (a commonly used type of Tikhonov regularization) or the entropy of the true histogram. The parameter τ fixes the relative weighting of the log-likelihood and the regularization function and thus determines the balance between the bias and variance of the resulting estimators. Further discussion of the unfolding problem including methods for choosing the regularization function and parameter, as well as techniques that employ other types of regularization such as the iterative Bayes (Richardson-Lucy) method, can be found in Refs. [7, 10–12] and references therein.

40.2.6 The Bayesian approach

In the frequentist methods discussed above, probability is associated only with data, not with the value of a parameter. This is no longer the case in Bayesian statistics, however, which we introduce in this section. For general introductions to Bayesian statistics see, e.g., Refs. [13–16].

Suppose the outcome of an experiment is characterized by a vector of data \mathbf{x} , whose probability distribution depends on an unknown parameter (or parameters) θ that we wish to determine. In Bayesian statistics, all knowledge about θ is summarized by

the posterior p.d.f. $p(\theta|\mathbf{x})$, whose integral over any given region gives the degree of belief for θ to take on values in that region, given the data \mathbf{x} . It is obtained by using Bayes’ theorem,

$$p(\theta|\mathbf{x}) = \frac{P(\mathbf{x}|\theta)\pi(\theta)}{\int P(\mathbf{x}|\theta')\pi(\theta') d\theta'}, \quad (40.37)$$

where $P(\mathbf{x}|\theta)$ is the likelihood function, i.e., the joint p.d.f. for the data viewed as a function of θ , evaluated with the data actually obtained in the experiment, and $\pi(\theta)$ is the prior p.d.f. for θ . Note that the denominator in Eq. (40.37) serves to normalize the posterior p.d.f. to unity.

As it can be difficult to report the full posterior p.d.f. $p(\theta|\mathbf{x})$, one would usually summarize it with statistics such as the mean (or median) value, and covariance matrix. In addition one may construct intervals with a given probability content, as is discussed in Sec. 40.4.1 on Bayesian interval estimation.

40.2.6.1 Priors

Bayesian statistics supplies no unique rule for determining the prior $\pi(\theta)$; this reflects the analyst’s subjective degree of belief (or state of knowledge) about θ before the measurement was carried out. For the result to be of value to the broader community, whose members may not share these beliefs, it is important to carry out a *sensitivity analysis*, that is, to show how the result changes under a reasonable variation of the prior probabilities.

One might like to construct $\pi(\theta)$ to represent complete ignorance about the parameters by setting it equal to a constant. A problem here is that if the prior p.d.f. is flat in θ , then it is not flat for a nonlinear function of θ , and so a different parametrization of the problem would lead in general to a non-equivalent posterior p.d.f.

For the special case of a constant prior, one can see from Bayes’ theorem (40.37) that the posterior is proportional to the likelihood, and therefore the mode (peak position) of the posterior is equal to the ML estimator. The posterior mode, however, will change in general upon a transformation of parameter. One may use as the Bayesian estimator a summary statistic other than the mode, such as the median, which is invariant under parameter transformation. But this will not in general coincide with the ML estimator.

The difficult and subjective nature of encoding personal knowledge into priors has led to what is called *objective Bayesian statistics*, where prior probabilities are based not on an actual degree of belief but rather derived from formal rules. These give, for example, priors which are invariant under a transformation of parameters, or ones which result in a maximum gain in information for a given set of measurements. For an extensive review see, e.g., Ref. [17].

Objective priors do not in general reflect degree of belief, but they could in some cases be taken as possible, although perhaps extreme, subjective priors. The posterior probabilities as well therefore do not necessarily reflect a degree of belief. However one may regard investigating a variety of objective priors to be an important part of the sensitivity analysis. Furthermore, use of objective priors with Bayes’ theorem can be viewed as a recipe for producing estimators or intervals which have desirable frequentist properties.

An important procedure for deriving objective priors is due to Jeffreys. According to *Jeffreys’ rule* one takes the prior as

$$\pi(\theta) \propto \sqrt{\det(I(\theta))}, \quad (40.38)$$

where

$$I_{ij}(\theta) = -E \left[\frac{\partial^2 \ln P(\mathbf{x}|\theta)}{\partial \theta_i \partial \theta_j} \right] \quad (40.39)$$

is the *Fisher information matrix*. One can show that the Jeffreys prior leads to inference that is invariant under a transformation of parameters. One should note that the Jeffreys prior does not in general correspond to one’s degree of belief about the value of a parameter. As examples, the Jeffreys prior for the mean μ of a Gaussian distribution is a constant, and for the mean of a Poisson distribution one finds $\pi(\mu) \propto 1/\sqrt{\mu}$.

Neither the constant nor $1/\sqrt{\mu}$ priors can be normalized to unit area and are therefore said to be *improper*. This can be allowed because the prior always appears multiplied by the likelihood function, and if the likelihood falls to zero sufficiently quickly then one may have a normalizable posterior density.

An important type of objective prior is the reference prior due to Bernardo and Berger [18]. To find the reference prior for a given problem one considers the Kullback-Leibler divergence $D_n[\pi, p]$ of the posterior $p(\theta|\mathbf{x})$ relative to a prior $\pi(\theta)$, obtained from a set of i.i.d. data $\mathbf{x} = (x_1, \dots, x_n)$:

$$D_n[\pi, p] = \int p(\theta|\mathbf{x}) \ln \frac{p(\theta|\mathbf{x})}{\pi(\theta)} d\theta. \quad (40.40)$$

This is effectively a measure of the gain in information provided by the data. The reference prior is chosen so that the expectation value of this information gain is maximized for the limiting case of $n \rightarrow \infty$, where the expectation is computed with respect to the marginal distribution of the data,

$$p(\mathbf{x}) = \int p(\mathbf{x}|\theta)\pi(\theta) d\theta. \quad (40.41)$$

For a single, continuous parameter the reference prior is usually identical to the Jeffreys prior. In the multiparameter case an iterative algorithm exists, which requires sorting the parameters by order of inferential importance. Often the result does not depend on this order, but when it does, this can be part of a sensitivity analysis. Further discussion and applications to particle physics problems can be found in Ref. [19].

40.2.6.2 Bayesian treatment of nuisance parameters

As discussed in Sec. 40.2.2, a model may depend on parameters of interest θ as well as on nuisance parameters ν , which must be included for an accurate description of the data. Knowledge about the values of ν may be supplied by control measurements, theoretical insights, physical constraints, etc. Suppose, for example, one has data \mathbf{y} from a control measurement which is characterized by a probability $P(\mathbf{y}|\nu)$. Suppose further that before carrying out the control measurement one's state of knowledge about ν is described by an initial prior $\pi_0(\nu)$, which in practice is often taken to be a constant or in any case very broad. By using Bayes' theorem (40.1) one obtains the updated prior $\pi(\nu)$ (*i.e.*, now $\pi(\nu) = \pi(\nu|\mathbf{y})$, the probability for ν given \mathbf{y}),

$$\pi(\nu|\mathbf{y}) \propto P(\mathbf{y}|\nu)\pi_0(\nu). \quad (40.42)$$

In the absence of a model for $P(\mathbf{y}|\nu)$ one may make some reasonable but *ad hoc* choices in order to approximate $\pi(\nu)$. For a single nuisance parameter ν , for example, one might characterize the uncertainty by a p.d.f. $\pi(\nu)$ centered about its nominal value with a certain standard deviation σ_ν . Often a Gaussian p.d.f. provides a reasonable model for one's degree of belief about a nuisance parameter; in other cases, more complicated shapes may be appropriate. If, for example, the parameter represents a non-negative quantity then a log-normal or gamma p.d.f. can be a more natural choice than a Gaussian truncated at zero. Note also that truncation of the prior of a nuisance parameter ν at zero will in general make $\pi(\nu)$ nonzero at $\nu = 0$, which can lead to an unnormalizable posterior for a parameter of interest that appears multiplied by ν .

The likelihood function, prior, and posterior p.d.f.s all depend on both θ and ν , and are related by Bayes' theorem, as usual. Note that the likelihood here only refers to the primary measurement \mathbf{x} . Once any control measurements \mathbf{y} are used to find the updated prior $\pi(\nu)$ for the nuisance parameters, this information is fully encapsulated in $\pi(\nu)$ and the control measurements do not appear further.

One can obtain the posterior p.d.f. for θ alone by integrating over the nuisance parameters, *i.e.*,

$$p(\theta|\mathbf{x}) = \int p(\theta, \nu|\mathbf{x}) d\nu. \quad (40.43)$$

Such integrals can often not be carried out in closed form, and if the number of nuisance parameters is large, then they can be difficult to compute with standard Monte Carlo methods. *Markov Chain Monte Carlo* (MCMC) techniques are often used for computing integrals of this type (see Sec. 42.6).

40.3 Statistical tests

In addition to estimating parameters, one often wants to assess the validity of certain statements concerning the data's underlying distribution. Frequentist *hypothesis tests*, described in Sec. 40.3.1, provide a rule for accepting or rejecting hypotheses depending on the outcome of a measurement. In *significance tests*, covered in Sec. 40.3.2, one gives the probability to obtain a level of incompatibility with a certain hypothesis that is greater than or equal to the level observed with the actual data. In the Bayesian approach, the corresponding procedure is based fundamentally on the posterior probabilities of the competing hypotheses. In Sec. 40.3.3 we describe a related construct called the Bayes factor, which can be used to quantify the degree to which the data prefer one or another hypothesis.

40.3.1 Hypothesis tests

A frequentist *test* of a hypothesis (often called the null hypothesis, H_0) is a rule that states for which data values \mathbf{x} the hypothesis is rejected. A region of \mathbf{x} -space called the critical region, w , is specified such that there is no more than a given probability under H_0 , α , called the *size* or *significance level* of the test, to find $\mathbf{x} \in w$. If the data are discrete, it may not be possible to find a critical region with exact probability content α , and thus we require $P(\mathbf{x} \in w|H_0) \leq \alpha$. If the data are observed in the critical region, H_0 is rejected.

The data \mathbf{x} used to construct a test could be, for example, a set of values that characterizes an individual event. In this case the test corresponds to classification as, *e.g.*, signal or background. Alternatively the data could represent a set of values from a collection of events. Often one is interested in knowing whether all of the events are of a certain type (background), or whether the sample contains at least some events of a new type (signal). Here the background-only hypothesis plays the role of H_0 , and in the alternative H_1 both signal and background are present. Rejecting H_0 is, from the standpoint of frequentist statistics, the required step to establish discovery of the signal process.

The critical region is not unique. Its choice should take into account the probabilities for the data predicted by some alternative hypothesis (or set of alternatives) H_1 . Rejecting H_0 if it is true is called a *type-I error*, and occurs by construction with probability no greater than α . Not rejecting H_0 if an alternative H_1 is true is called a *type-II error*, and for a given test this will have a certain probability $\beta = P(\mathbf{x} \notin w|H_1)$. The quantity $1 - \beta$ is called the *power* of the test of H_0 with respect to the alternative H_1 . A strategy for defining the critical region can therefore be to maximize the power with respect to some alternative (or alternatives) given a fixed size α .

To maximize the power of a test of H_0 with respect to the alternative H_1 , the *Neyman-Pearson lemma* states that the critical region w should be chosen such that for all data values \mathbf{x} inside w , the likelihood ratio

$$\lambda(\mathbf{x}) = \frac{f(\mathbf{x}|H_1)}{f(\mathbf{x}|H_0)} \quad (40.44)$$

is greater than or equal to a given constant c_α , and everywhere outside the critical region one has $\lambda(\mathbf{x}) < c_\alpha$, where the value of c_α is determined by the size of the test α . Here H_0 and H_1 must be simple hypotheses, *i.e.*, they should not contain undetermined parameters.

It is convenient to define the test using a scalar function of the data \mathbf{x} called a *test statistic*, $t(\mathbf{x})$, such that the boundary of the critical region is given by a surface of constant $t(\mathbf{x})$. The Neyman-Pearson lemma is equivalent to the statement that the likelihood ratio (40.44) represents the optimal test statistic. It can be difficult in practice, however, to determine $\lambda(\mathbf{x})$, since this requires knowledge of the joint p.d.f.s $f(\mathbf{x}|H_0)$ and $f(\mathbf{x}|H_1)$. Often one does not have explicit formulae for these, but rather

Monte Carlo models that allow one to generate instances of \mathbf{x} that follow the p.d.f.s.

In the case where the likelihood ratio (40.44) cannot be used explicitly, there exist a variety of other multivariate methods for constructing a test statistic that may approach its performance. These are based on machine-learning algorithms that use samples of *training data* corresponding to the hypotheses in question, often generated from Monte Carlo models. Further information on Machine Learning can be found in Sec. 41 of this Review.

The multivariate algorithms designed to classify events into signal and background types also form the basis of tests of the hypothesis that a sample of events consists of background only. Such a test can be constructed using the distributions of the test statistic $t(\mathbf{x})$ for event classification obtained from a multivariate algorithm such as a Neural Network output. The distributions $p(t|s)$ and $p(t|b)$ for signal and background events, respectively, are used to construct the likelihood ratio of the signal-plus-background hypothesis relative to that of background only. To the extent that the test statistic $t(\mathbf{x})$ approximates the likelihood ratio (or a monotonic function thereof) for individual events given by (40.44), the resulting test of the background-only hypothesis for the event sample will have maximum power with respect to the signal-plus-background alternative (see Ref. [20]).

40.3.2 Tests of significance (goodness-of-fit)

Often one wants to quantify the level of agreement between the data and a hypothesis without explicit reference to alternative hypotheses. This can be done by defining a statistic t whose value reflects in some way the level of agreement between the data and the hypothesis. The analyst must decide what values of the statistic correspond to better or worse levels of agreement with the hypothesis in question; the choice will in general depend on the relevant alternative hypotheses.

The hypothesis in question, H_0 , will determine the p.d.f. $f(t|H_0)$ for the statistic. The significance of a discrepancy between the data and what one expects under the assumption of H_0 is quantified by giving the p -value, defined as the probability to find t in the region of equal or lesser compatibility with H_0 than the level of compatibility observed with the actual data. For example, if t is defined such that large values correspond to poor agreement with the hypothesis, then the p -value would be

$$p = \int_{t_{\text{obs}}}^{\infty} f(t|H_0) dt, \quad (40.45)$$

where t_{obs} is the value of the statistic obtained in the actual experiment.

The p -value is a function of the data, and is therefore itself a random variable. If the hypothesis used to compute the p -value is true, then for continuous data p will be uniformly distributed between zero and one. Note that the p -value is not the probability for the hypothesis; in frequentist statistics, this is not defined.

The p -value should not be confused with the size (significance level) of a test, or the confidence level of a confidence interval (Section 40.4), both of which are pre-specified constants. We may formulate a hypothesis test, however, by defining the critical region to correspond to the data outcomes that give the lowest p -values, so that finding $p \leq \alpha$ implies that the data outcome was in the critical region. When constructing a p -value, one generally chooses the region of data space deemed to have lower compatibility with the model being tested as one having higher compatibility with a given alternative, such that the corresponding test will have a high power with respect to this alternative. For data generated according to the alternative, the distribution of the p -value of H_0 will be concentrated at low values.

When searching for a new phenomenon, one tries to reject the hypothesis H_0 that the data are consistent with known (e.g., Standard Model) processes. If the p -value of H_0 is sufficiently low, then one is willing to accept that some alternative hypothesis is true. Often one converts the p -value into an effective significance Z , defined as an equivalent number of standard deviations of a Gaussian distributed random variable. In a search for an intrinsically positive signal, i.e., where only upward fluctuations of the

estimated rate appear signal like, this is defined as

$$Z = \Phi^{-1}(1 - p). \quad (40.46)$$

Here Φ is the cumulative distribution of the standard Gaussian, and Φ^{-1} is its inverse (quantile) function. In this way, a p -value of 1/2 gives $Z = 0$, i.e., having an estimated signal rate of zero corresponds to zero significance. If either positive or negative data fluctuations would indicate evidence of the signal, then one defines

$$Z = \Phi^{-1}(1 - p/2). \quad (40.47)$$

In this case an estimated signal rate of zero gives $p = 1$ and $Z = 0$.

Often in particle physics the level of significance where an effect is said to qualify as a discovery is $Z = 5$, i.e., a 5σ effect, corresponding to a p -value of 2.87×10^{-7} . One's actual degree of belief that a new process is present, however, will depend in general on other factors as well, such as the plausibility of the new signal hypothesis and the degree to which it can describe the data, one's confidence in the model that led to the observed p -value, and possible corrections for multiple observations out of which one focuses on the smallest p -value obtained (the "look-elsewhere effect", discussed in Section 40.3.2.2).

40.3.2.1 Treatment of nuisance parameters for frequentist tests

Suppose one wants to test hypothetical values of parameters θ , but the model also contains nuisance parameters ν . To find a p -value for θ we can construct a test statistic q_θ such that larger values constitute increasing incompatibility between the data and the hypothesis. Then for an observed value of the statistic $q_{\theta, \text{obs}}$, the p -value of θ is

$$p_\theta(\nu) = \int_{q_{\theta, \text{obs}}}^{\infty} f(q_\theta|\theta, \nu) dq_\theta, \quad (40.48)$$

which depends in general on the nuisance parameters ν . In the strict frequentist approach, θ is rejected only if the p -value is less than α for all possible values of the nuisance parameters.

The difficulty described above is effectively solved if we can define the test statistic q_θ in such a way that its distribution $f(q_\theta|\theta)$ is independent of the nuisance parameters. Although exact independence is only found in special cases, it can be achieved approximately by use of the *profile likelihood ratio*. This is given by the profile likelihood from Eq.(40.18) divided by the value of the likelihood at its maximum, i.e., when evaluated with the ML estimators $\hat{\theta}$ and $\hat{\nu}$:

$$\lambda_p(\theta) = \frac{L(\theta, \hat{\nu}(\theta))}{L(\hat{\theta}, \hat{\nu})}. \quad (40.49)$$

Wilks' theorem [9] states that, providing certain general conditions are satisfied, the distribution of $-2 \ln \lambda_p(\theta)$, under assumption of θ , approaches a χ^2 distribution in the limit where the data sample is very large, independent of the values of the nuisance parameters ν . Here the number of degrees of freedom is equal to the number of components of θ . More details on use of the profile likelihood are given in Refs. [21, 22] and in contributions to the PHYSTAT conferences [23]; explicit formulae for special cases can be found in Ref. [24]. Further discussion on how to incorporate systematic uncertainties into p -values can be found in Ref. [25].

Even with use of the profile likelihood ratio, for a finite data sample the p -value of hypothesized parameters θ will retain in general some dependence on the nuisance parameters ν . Ideally one would find the the maximum of $p_\theta(\nu)$ from Eq. (40.48) explicitly, but that is often impractical. An approximate and computationally feasible technique is to use $p_\theta(\hat{\nu}(\theta))$, where $\hat{\nu}(\theta)$ are the profiled values of the nuisance parameters as defined in Section 40.2.2.2. The resulting p -value is correct if the true values of the nuisance parameters are equal to the profiled values used; otherwise it could be either too high or too low. This is discussed further in Section 40.4.2 on confidence intervals.

One may also treat model uncertainties in a Bayesian manner but then use the resulting model in a frequentist test. Suppose the uncertainty in a set of nuisance parameters ν is characterized

by a Bayesian prior p.d.f. $\pi(\boldsymbol{\nu})$. This can be used to construct the marginal (also called the prior predictive) model for the data \boldsymbol{x} and parameters of interest $\boldsymbol{\theta}$,

$$P_m(\boldsymbol{x}|\boldsymbol{\theta}) = \int P(\boldsymbol{x}|\boldsymbol{\theta}, \boldsymbol{\nu})\pi(\boldsymbol{\nu}) d\boldsymbol{\nu}. \quad (40.50)$$

The marginal model does not represent the probability of data that would be generated if one were really to repeat the experiment, as in that case one would assume that the nuisance parameters do not vary. Rather, the marginal model represents a situation in which every repetition of the experiment is carried out with new values of $\boldsymbol{\nu}$, randomly sampled from $\pi(\boldsymbol{\nu})$. It is in effect an average of models each with a given $\boldsymbol{\nu}$, where the average is carried out with respect to the prior p.d.f. $\pi(\boldsymbol{\nu})$.

The marginal model for the data \boldsymbol{x} can be used to determine the distribution of a test statistic Q , which can be written

$$P_m(Q|\boldsymbol{\theta}) = \int P(Q|\boldsymbol{\theta}, \boldsymbol{\nu})\pi(\boldsymbol{\nu}) d\boldsymbol{\nu}. \quad (40.51)$$

In a search for a new signal process, the test statistic can be based on the ratio of likelihoods corresponding to the experiments where signal and background events are both present, L_{s+b} , to that of background only, L_b . Often the likelihoods are evaluated with the profiled values of the nuisance parameters, which may give improved performance. It is important to note, however, that it is through use of the marginal model for the distribution of Q that the uncertainties related to the nuisance parameters are incorporated into the result of the test. Different choices for the test statistic itself only result in variations of the power of the test with respect to different alternatives.

40.3.2.2 The look-elsewhere effect

The “look-elsewhere effect” relates to multiple measurements used to test a single hypothesis. The classic example is when one searches in a distribution for a peak whose position is not predicted in advance. Here the no-peak hypothesis is tested using data in a given range of the distribution. In the frequentist approach the correct p -value of the no-peak hypothesis is the probability, assuming background only, to find a signal as significant as the one found or more so anywhere in the search region. This can be substantially higher than the probability to find a peak of equal or greater significance in the particular place where it appeared. There is in general some ambiguity as to what constitutes the relevant search region or even the broader set of relevant measurements. Although the desired p -value is well defined once the search region has been fixed, an exact treatment can require extensive computation.

The “brute-force” solution to this problem by Monte Carlo involves generating data under the background-only hypothesis and for each data set, fitting a peak of unknown position and recording a measure of its significance. To establish a discovery one often requires a p -value smaller than 2.87×10^{-7} , corresponding to a 5σ or larger effect. Determining this with Monte Carlo thus requires generating and fitting a very large number of experiments, perhaps several times 10^7 . In contrast, if the position of the peak is fixed, then the fit to the distribution is much easier, and furthermore one can in many cases use formulae valid for sufficiently large samples that bypass completely the need for Monte Carlo (see, e.g., [24]). However, this fixed-position or “local” p -value would not be correct in general, as it assumes the position of the peak was known in advance.

A method that allows one to modify the local p -value computed under assumption of a fixed position to obtain an approximation to the correct “global” value using a relatively simple calculation is described in Ref. [26]. Suppose a test statistic q_0 , defined so that larger values indicate increasing disagreement with the data, is observed to have a value u . Furthermore suppose the model contains a nuisance parameter such as the peak position that is only defined under the signal model (there is no peak in the background-only model). An approximation for the global p -value is found to be

$$p_{\text{global}} \approx p_{\text{local}} + \langle N_u \rangle, \quad (40.52)$$

where $\langle N_u \rangle$, which is much smaller than one in cases of interest, is the mean number of “upcrossings” (as defined in [26]) of the statistic q_0 above the level u in the range of the nuisance parameter considered (e.g., the mass range).

The value of $\langle N_u \rangle$ can be estimated from the number of upcrossings $\langle N_{u_0} \rangle$ above some much lower value, u_0 , by using a relation due to Davis [27],

$$\langle N_u \rangle \approx \langle N_{u_0} \rangle e^{-(u-u_0)/2}. \quad (40.53)$$

By choosing u_0 sufficiently low, the value of $\langle N_u \rangle$ can be estimated by simulating only a very small number of experiments, or even from the observed data, rather than of the order 10^7 needed if one is dealing with a 5σ effect.

40.3.2.3 Goodness-of-fit with the method of least squares

When estimating parameters using the method of least squares, one obtains the minimum value of the quantity χ^2 (40.19). This statistic can be used to test the *goodness-of-fit*, i.e., the test provides a measure of the significance of a discrepancy between the data and the hypothesized functional form used in the fit. It may also happen that no parameters are estimated from the data, but that one simply wants to compare a histogram, e.g., a vector of Poisson distributed numbers $\boldsymbol{n} = (n_1, \dots, n_N)$, with a hypothesis for their expectation values $\mu_i = E[n_i]$. As the distribution is Poisson with variances $\sigma_i^2 = \mu_i$, the χ^2 (40.19) becomes *Pearson's χ^2 statistic*,

$$\chi^2 = \sum_{i=1}^N \frac{(n_i - \mu_i)^2}{\mu_i}. \quad (40.54)$$

If the hypothesis $\boldsymbol{\mu} = (\mu_1, \dots, \mu_N)$ is correct, and if the expected values μ_i in (40.54) are sufficiently large (or equivalently, if the measurements n_i can be treated as following a Gaussian distribution), then the χ^2 statistic will follow the χ^2 p.d.f. with the number of degrees of freedom equal to the number of measurements N minus the number of fitted parameters.

Alternatively, one may fit parameters and evaluate goodness-of-fit by minimizing $-2 \ln \lambda$ from Eq. (40.16). One finds that the distribution of this statistic approaches the asymptotic limit faster than does Pearson's χ^2 . Therefore if one uses the asymptotic χ^2 p.d.f. as the statistic's approximate sampling distribution to compute a p -value, one obtains in general a more accurate result from $-2 \ln \lambda$ than from Pearson's χ^2 (see Ref. [8] and references therein).

Assuming the goodness-of-fit statistic follows a χ^2 p.d.f., the p -value for the hypothesis is then

$$p = \int_{\chi^2}^{\infty} f(z; n_d) dz, \quad (40.55)$$

where $f(z; n_d)$ is the χ^2 p.d.f. and n_d is the appropriate number of degrees of freedom. Values are shown in Fig. 40.1 or obtained, e.g., from the ROOT function `TMath::Prob`. If the asymptotic conditions for using the χ^2 p.d.f. do not hold, the statistic can still be defined as before, but its p.d.f. must be determined by other means in order to obtain the p -value, e.g., using a Monte Carlo calculation.

Since the mean of the χ^2 distribution is equal to n_d , one expects in a “reasonable” experiment to obtain $\chi^2 \approx n_d$. Hence the quantity χ^2/n_d is sometimes reported. Since the p.d.f. of χ^2/n_d depends on n_d , however, one must report n_d as well if one wishes to determine the p -value. The p -values obtained for different values of χ^2/n_d are shown in Fig. 40.2.

If the minimized χ^2 value indicates a low level of agreement between data and hypothesis, one may be tempted to expect a high degree of uncertainty for any fitted parameters. Poor goodness-of-fit, however, does not mean that one will have large statistical errors for parameter estimates. If, for example, the error bars (or covariance matrix) used in constructing the χ^2 are underestimated, then this will lead to underestimated statistical errors for the fitted parameters and an increased value of the minimized χ^2 . The standard deviations of estimators that one finds from, say, Eq. (40.13) reflect how widely the estimates would be distributed

if one were to repeat the measurement many times, assuming that the hypothesis and measurement errors used in the χ^2 are also correct. They do not include the systematic error which may result from an incorrect hypothesis or incorrectly estimated measurement errors in the χ^2 .

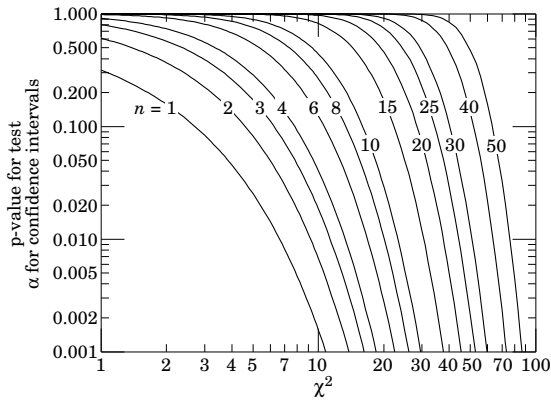


Figure 40.1: One minus the χ^2 cumulative distribution, $1 - F(\chi^2; n)$, for n degrees of freedom. This gives the p -value for the χ^2 goodness-of-fit test as well as one minus the coverage probability for confidence regions (see Sec. 40.4.2.2).

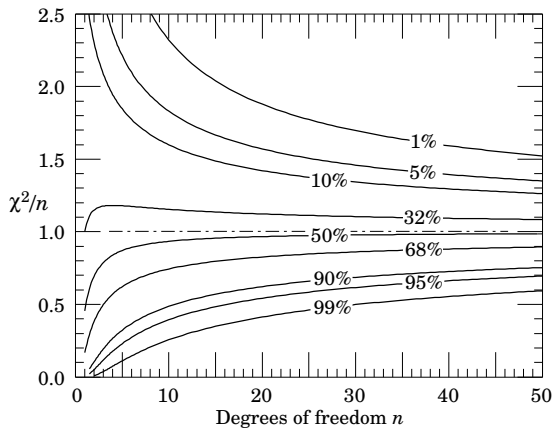


Figure 40.2: The ‘reduced’ χ^2 , equal to χ^2/n , for n degrees of freedom. The curves show as a function of n the χ^2/n that corresponds to a given p -value.

40.3.3 Bayes factors

In Bayesian statistics, all of one’s knowledge about a model is contained in its posterior probability, which one obtains using Bayes’ theorem (Eq. (40.37)). Thus one could reject a hypothesis H if its posterior probability $P(H|\mathbf{x})$ is sufficiently small. The difficulty here is that $P(H|\mathbf{x})$ is proportional to the prior probability $P(H)$, and there will not be a consensus about the prior probabilities for the existence of new phenomena. Nevertheless one can construct a quantity called the Bayes factor (described below), which can be used to quantify the degree to which the data prefer one hypothesis over another, and is independent of their prior probabilities.

Consider two models (hypotheses), H_i and H_j , described by vectors of parameters θ_i and θ_j , respectively. Some of the components will be common to both models and others may be distinct. The full prior probability for each model can be written in the form

$$\pi(H_i, \theta_i) = P(H_i)\pi(\theta_i|H_i). \quad (40.56)$$

Here $P(H_i)$ is the overall prior probability for H_i , and $\pi(\theta_i|H_i)$ is the normalized p.d.f. of its parameters. For each model, the

posterior probability is found using Bayes’ theorem,

$$P(H_i|\mathbf{x}) = \frac{\int P(\mathbf{x}|\theta_i, H_i)P(H_i)\pi(\theta_i|H_i) d\theta_i}{P(\mathbf{x})}, \quad (40.57)$$

where the integration is carried out over the internal parameters θ_i of the model. The ratio of posterior probabilities for the models is therefore

$$\frac{P(H_i|\mathbf{x})}{P(H_j|\mathbf{x})} = \frac{\int P(\mathbf{x}|\theta_i, H_i)\pi(\theta_i|H_i) d\theta_i}{\int P(\mathbf{x}|\theta_j, H_j)\pi(\theta_j|H_j) d\theta_j} \frac{P(H_i)}{P(H_j)}. \quad (40.58)$$

The *Bayes factor* is defined as

$$B_{ij} = \frac{\int P(\mathbf{x}|\theta_i, H_i)\pi(\theta_i|H_i) d\theta_i}{\int P(\mathbf{x}|\theta_j, H_j)\pi(\theta_j|H_j) d\theta_j}. \quad (40.59)$$

This gives what the ratio of posterior probabilities for models i and j would be if the overall prior probabilities for the two models were equal. If the models have no nuisance parameters, *i.e.*, no internal parameters described by priors, then the Bayes factor is simply the likelihood ratio. The Bayes factor therefore shows by how much the probability ratio of model i to model j changes in the light of the data, and thus can be viewed as a numerical measure of evidence supplied by the data in favor of one hypothesis over the other.

Although the Bayes factor is by construction independent of the overall prior probabilities $P(H_i)$ and $P(H_j)$, it does require priors for all internal parameters of a model, *i.e.*, one needs the functions $\pi(\theta_i|H_i)$ and $\pi(\theta_j|H_j)$. In a Bayesian analysis where one is only interested in the posterior p.d.f. of a parameter, it may be acceptable to take an unnormalizable function for the prior (an improper prior) as long as the product of likelihood and prior can be normalized. Improper priors are, however, only defined up to an arbitrary multiplicative constant, and so the Bayes factor would depend on this constant. Furthermore, although the range of a constant normalized prior is unimportant for parameter determination (provided it is wider than the likelihood), this is not so for the Bayes factor when such a prior is used for only one of the hypotheses. So to compute a Bayes factor, all internal parameters must be described by normalized priors that represent meaningful probabilities over the entire range where they are defined.

An exception to this rule may be considered when the identical parameter appears in the models for both numerator and denominator of the Bayes factor. In this case one can argue that the arbitrary constants would cancel. One must exercise some caution, however, as parameters with the same name and physical meaning may still play different roles in the two models.

Both integrals in Equation (40.59) are of the form

$$m = \int P(\mathbf{x}|\theta)\pi(\theta) d\theta, \quad (40.60)$$

which is similar to the marginal likelihood seen previously in Eq. (40.50) (in some fields this quantity is called the *evidence*). Computing marginal likelihoods can be difficult; in many cases it can be done with the nested sampling algorithm [28] as implemented, *e.g.*, in the program *MultiNest* [29]. A review of Bayes factors can be found in Ref. [30].

40.4 Intervals and limits

When the goal of an experiment is to determine a parameter θ , the result is usually expressed by quoting, in addition to the point estimate, some sort of interval which reflects the statistical precision of the measurement. In the simplest case, this can be given by the parameter’s estimated value $\hat{\theta}$ plus or minus an estimate of the standard deviation of $\hat{\theta}$, $\hat{\sigma}_{\hat{\theta}}$. If, however, the p.d.f. of the estimator is not Gaussian or if there are physical boundaries on the possible values of the parameter, then one usually quotes instead an interval according to one of the procedures described below.

In reporting an interval or limit, the experimenter may wish to

- communicate as objectively as possible the result of the experiment;
- provide an interval that is constructed to cover on average the true value of the parameter with a specified probability;
- provide the information needed by the consumer of the result to draw conclusions about the parameter or to make a particular decision;
- draw conclusions about the parameter that incorporate stated prior beliefs.

With a sufficiently large data sample, the point estimate and standard deviation (or for the multiparameter case, the parameter estimates and covariance matrix) satisfy essentially all of these goals. For small data samples, no single method for quoting an interval will achieve all of them.

In addition to the goals listed above, the choice of method may be influenced by practical considerations such as ease of producing an interval from the results of several measurements. Of course the experimenter is not restricted to quoting a single interval or limit; one may choose, for example, first to communicate the result with a confidence interval having certain frequentist properties, and then in addition to draw conclusions about a parameter using a judiciously chosen subjective Bayesian prior. It is recommended, however, that there be a clear separation between these two aspects of reporting a result. In the remainder of this section, we assess the extent to which various types of intervals achieve the goals stated here.

40.4.1 Bayesian intervals

As described in Sec. 40.2.6, a Bayesian posterior probability may be used to determine regions that will have a given probability of containing the true value of a parameter. In the single parameter case, for example, an interval (called a Bayesian or credible interval) $[\theta_{\text{lo}}, \theta_{\text{up}}]$ can be determined which contains a given fraction $1 - \alpha$ of the posterior probability, *i.e.*,

$$1 - \alpha = \int_{\theta_{\text{lo}}}^{\theta_{\text{up}}} p(\theta|\mathbf{x}) d\theta. \quad (40.61)$$

Sometimes an upper or lower limit is desired, *i.e.*, θ_{lo} or θ_{up} can be set to a physical boundary or to plus or minus infinity. In other cases, one might be interested in the set of θ values for which $p(\theta|\mathbf{x})$ is higher than for any θ not belonging to the set, which may constitute a single interval or a set of disjoint regions; these are called highest posterior density (HPD) intervals. Note that HPD intervals are not invariant under a nonlinear transformation of the parameter.

If a parameter is constrained to be non-negative, then the prior p.d.f. can simply be set to zero for negative values. An important example is the case of a Poisson variable n , which counts signal events with unknown mean s , as well as background with mean b , assumed known. For the signal mean s , one often uses the prior

$$\pi(s) = \begin{cases} 0 & s < 0 \\ 1 & s \geq 0 \end{cases}. \quad (40.62)$$

This prior may be regarded as providing an interval whose frequentist properties can be studied, rather than as representing a degree of belief. For example, to obtain an upper limit on s , one may proceed as follows. The likelihood for s is given by the Poisson distribution for n with mean $s + b$,

$$P(n|s) = \frac{(s+b)^n}{n!} e^{-(s+b)}, \quad (40.63)$$

along with the prior (40.62) in (40.37) gives the posterior density for s . An upper limit s_{up} at confidence level (or here, rather, *credibility* level) $1 - \alpha$ can be obtained by requiring

$$1 - \alpha = \int_{-\infty}^{s_{\text{up}}} p(s|n) ds = \frac{\int_{-\infty}^{s_{\text{up}}} P(n|s) \pi(s) ds}{\int_{-\infty}^{\infty} P(n|s) \pi(s) ds}, \quad (40.64)$$

where the lower limit of integration is effectively zero because of the cut-off in $\pi(s)$. By relating the integrals in Eq. (40.64) to

incomplete gamma functions, the solution for the upper limit is found to be

$$s_{\text{up}} = \frac{1}{2} F_{\chi^2}^{-1}[p, 2(n+1)] - b, \quad (40.65)$$

where $F_{\chi^2}^{-1}$ is the quantile of the χ^2 distribution (inverse of the cumulative distribution). Here the quantity p is

$$p = 1 - \alpha (1 - F_{\chi^2}[2b, 2(n+1)]), \quad (40.66)$$

where F_{χ^2} is the cumulative χ^2 distribution. For both F_{χ^2} and $F_{\chi^2}^{-1}$ above, the argument $2(n+1)$ gives the number of degrees of freedom. For the special case of $b = 0$, the limit reduces to

$$s_{\text{up}} = \frac{1}{2} F_{\chi^2}^{-1}(1 - \alpha; 2(n+1)). \quad (40.67)$$

It happens that for the case of $b = 0$, the upper limit from Eq. (40.67) coincides numerically with the frequentist upper limit discussed in Section 40.4.2.3. Values for $1 - \alpha = 0.9$ and 0.95 are given by the values μ_{up} in Table 40.3. The frequentist properties of confidence intervals for the Poisson mean found in this way are discussed in Refs. [2] and [31].

As in any Bayesian analysis, it is important to show how the result changes under assumption of different prior probabilities. For example, one could consider the Jeffreys prior as described in Sec. 40.2.6. For this problem one finds the Jeffreys prior $\pi(s) \propto 1/\sqrt{s+b}$ for $s \geq 0$ and zero otherwise. As with the constant prior, one would not regard this as representing one's prior beliefs about s , both because it is improper and also as it depends on b . Rather it is used with Bayes' theorem to produce an interval whose frequentist properties can be studied.

If the model contains nuisance parameters then these are eliminated by marginalizing, as in Eq. (40.43), to obtain the p.d.f. for the parameters of interest. For example, if the parameter b in the Poisson counting problem above were to be characterized by a prior p.d.f. $\pi(b)$, then one would first use Bayes' theorem to find $p(s, b|n)$. This is then marginalized to find $p(s|n) = \int p(s, b|n) \pi(b) db$, from which one may determine an interval for s . One may not be certain whether to extend a model by including more nuisance parameters. In this case, a Bayes factor may be used to determine to what extent the data prefer a model with additional parameters, as described in Section 40.3.3.

40.4.2 Frequentist confidence intervals

The unqualified phrase "confidence intervals" refers to frequentist intervals obtained with a procedure due to Neyman [32], described below. The boundary of the interval (or in the multiparameter case, region) is given by a specific function of the data, which would fluctuate if one were to repeat the experiment many times. The *coverage probability* refers to the fraction of intervals in such an ensemble that contain the true parameter value. Confidence intervals are constructed so as to have a coverage probability greater than or equal to a given *confidence level*, regardless of the true parameter's value. It is important to note that in the frequentist approach, such a probability is not meaningful for a fixed interval. In this section we discuss several techniques for producing intervals that have, at least approximately, this property of coverage.

40.4.2.1 The Neyman construction for confidence intervals

Consider a p.d.f. $f(x; \theta)$ where x represents the outcome of the experiment and θ is the unknown parameter for which we want to construct a confidence interval. The variable x could (and often does) represent an estimator for θ . Using $f(x; \theta)$, we can find using a pre-defined rule and probability $1 - \alpha$ for every value of θ , a set of values $x_1(\theta, \alpha)$ and $x_2(\theta, \alpha)$ such that

$$P(x_1 < x < x_2; \theta) = \int_{x_1}^{x_2} f(x; \theta) dx \geq 1 - \alpha. \quad (40.68)$$

If x is discrete, the integral is replaced by the corresponding sum. In that case there may not exist a range of x values whose summed probability is exactly equal to a given value of $1 - \alpha$, and one requires by convention $P(x_1 < x < x_2; \theta) \geq 1 - \alpha$.

This is illustrated for continuous x in Fig. 40.3: a horizontal line segment $[x_1(\theta, \alpha), x_2(\theta, \alpha)]$ is drawn for representative values of θ . The union of such intervals for all values of θ , designated in the figure as $D(\alpha)$, is known as a *confidence belt*. Typically the curves $x_1(\theta, \alpha)$ and $x_2(\theta, \alpha)$ are monotonic functions of θ , which we assume for this discussion.

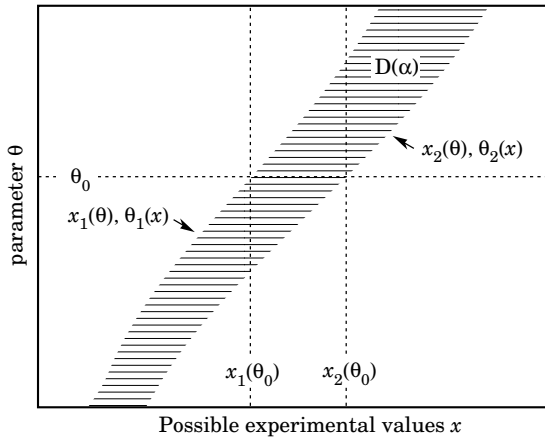


Figure 40.3: Construction of the confidence belt (see text).

Upon performing an experiment to measure x and obtaining a value x_0 , one draws a vertical line through x_0 . The confidence interval for θ is the set of all values of θ for which the corresponding line segment $[x_1(\theta, \alpha), x_2(\theta, \alpha)]$ is intercepted by this vertical line. Such confidence intervals are said to have a *confidence level* (CL) equal to $1 - \alpha$.

Now suppose that the true value of θ is θ_0 , indicated in the figure. We see from the figure that θ_0 lies between $\theta_1(x)$ and $\theta_2(x)$ if and only if x lies between $x_1(\theta_0)$ and $x_2(\theta_0)$. The two events thus have the same probability, and since this is true for any value θ_0 , we can drop the subscript 0 and obtain

$$1 - \alpha = P(x_1(\theta) < x < x_2(\theta)) = P(\theta_2(x) < \theta < \theta_1(x)). \quad (40.69)$$

In this probability statement, $\theta_1(x)$ and $\theta_2(x)$, *i.e.*, the endpoints of the interval, are the random variables and θ is an unknown constant. If the experiment were to be repeated a large number of times, the interval $[\theta_1, \theta_2]$ would vary, covering the fixed value θ in a fraction $1 - \alpha$ of the experiments.

The condition of coverage in Eq. (40.68) does not determine x_1 and x_2 uniquely, and additional criteria are needed. One possibility is to choose *central intervals* such that the probabilities to find x below x_1 and above x_2 are each $\alpha/2$. In other cases, one may want to report only an upper or lower limit, in which case one of $P(x \leq x_1)$ or $P(x \geq x_2)$ can be set to α and the other to zero. Another principle based on *likelihood ratio ordering* for determining which values of x should be included in the confidence belt is discussed below.

When the observed random variable x is continuous, the coverage probability obtained with the Neyman construction is $1 - \alpha$, regardless of the true value of the parameter. Because of the requirement $P(x_1 < x < x_2) \geq 1 - \alpha$ when x is discrete, one obtains in that case confidence intervals that include the true parameter with a probability greater than or equal to $1 - \alpha$.

An equivalent method of constructing confidence intervals is to consider a test (see Sec. 40.3) of the hypothesis that the parameter's true value is θ (assume one constructs a test for all physical values of θ). One then excludes all values of θ where the hypothesis would be rejected in a test of size α or less. The remaining values constitute the confidence interval at confidence level $1 - \alpha$. If the critical region of the test is characterized by having a p -value $p_\theta \leq \alpha$, then the endpoints of the confidence interval are found in practice by solving $p_\theta = \alpha$ for θ .

In the procedure outlined above, one is still free to choose the test to be used; this corresponds to the freedom in the Neyman construction as to which values of the data are included in the

confidence belt. One possibility is to use a test statistic based on the *likelihood ratio*,

$$\lambda(\theta) = \frac{f(x; \theta)}{f(x; \hat{\theta})}, \quad (40.70)$$

where $\hat{\theta}$ is the value of the parameter which, out of all allowed values, maximizes $f(x; \theta)$. The confidence belt is taken to contain the values of x that give the greatest values of $\lambda(\theta)$. This results in the intervals described in Ref. [33] by Feldman and Cousins.

If the model contains nuisance parameters ν , then these can be incorporated into the test (or the p -values) used to determine the limit by profiling as discussed in Section 40.3.2.1. As mentioned there, the strict frequentist approach is to regard the parameter of interest θ as excluded only if it is rejected for all possible values of ν . The resulting interval for θ will then cover the true value with a probability greater than or equal to the nominal confidence level for all points in ν -space.

If the p -value is based on the profiled values of the nuisance parameters, *i.e.*, with $\nu = \hat{\nu}(\theta)$ used in Eq. (40.48), then the resulting interval for the parameter of interest will have the correct coverage if the true values of ν are equal to the profiled values. Otherwise the coverage probability may be too high or too low. This procedure has been called *profile construction* in particle physics [34] (see also [25]).

40.4.2.2 Gaussian distributed measurements

An important example of constructing a confidence interval is when the data consists of a single random variable x that follows a Gaussian distribution; this is often the case when x represents an estimator for a parameter and one has a sufficiently large data sample. If there is more than one parameter being estimated, the multivariate Gaussian is used. For the univariate case with known σ , the probability that the measured value x will fall within $\pm\delta$ of the true value μ is

$$\begin{aligned} 1 - \alpha &= \frac{1}{\sqrt{2\pi}\sigma} \int_{\mu-\delta}^{\mu+\delta} e^{-(x-\mu)^2/2\sigma^2} dx \\ &= \text{erf}\left(\frac{\delta}{\sqrt{2}\sigma}\right) = 2\Phi\left(\frac{\delta}{\sigma}\right) - 1, \end{aligned} \quad (40.71)$$

where erf is the Gaussian error function, which is rewritten in the final equality using Φ , the Gaussian cumulative distribution. Fig. 40.4 shows a $\delta = 1.64\sigma$ confidence interval unshaded. The choice $\delta = \sigma$ gives an interval called the *standard error* which has $1 - \alpha = 68.27\%$ if σ is known. Values of α for other frequently used choices of δ are given in Table 40.1.

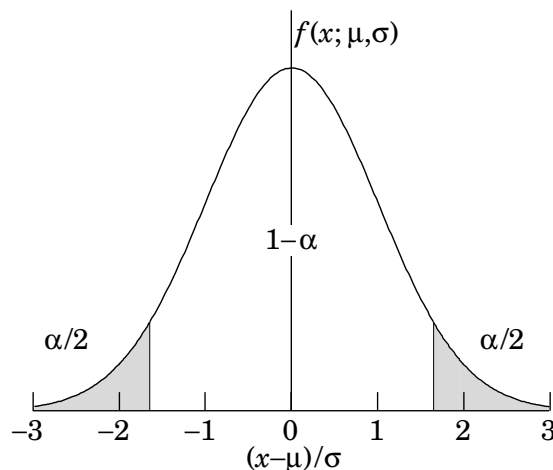


Figure 40.4: Illustration of a symmetric 90% confidence interval (unshaded) for a Gaussian-distributed measurement of a single quantity. Integrated probabilities, defined by $\alpha = 0.1$, are as shown.

Table 40.1: Area of the tails α outside $\pm\delta$ from the mean of a Gaussian distribution.

α	δ	α	δ
0.3173	1σ	0.2	1.28σ
4.55×10^{-2}	2σ	0.1	1.64σ
2.7×10^{-3}	3σ	0.05	1.96σ
6.3×10^{-5}	4σ	0.01	2.58σ
5.7×10^{-7}	5σ	0.001	3.29σ
2.0×10^{-9}	6σ	10^{-4}	3.89σ

We can set a one-sided (upper or lower) limit by excluding above $x + \delta$ (or below $x - \delta$). The values of α for such limits are half the values in Table 40.1.

The relation (40.71) can be re-expressed using the cumulative distribution function for the χ^2 distribution as

$$\alpha = 1 - F(\chi^2; n), \quad (40.72)$$

for $\chi^2 = (\delta/\sigma)^2$ and $n = 1$ degree of freedom. This can be seen as the $n = 1$ curve in Fig. 40.1 or obtained by using, e.g., the ROOT function `TMath::Prob`. For multivariate measurements of, say, M parameter estimates $\hat{\theta} = (\hat{\theta}_1, \dots, \hat{\theta}_M)$, construction of the confidence region requires the full covariance matrix $V_{ij} = \text{cov}[\hat{\theta}_i, \hat{\theta}_j]$, which can be estimated as described in Sections 40.2.2 and 40.2.3. Under fairly general conditions with the methods of maximum-likelihood or least-squares in the large sample limit, the estimators will be distributed according to a multivariate Gaussian centered about the true (unknown) values θ , and furthermore, the likelihood function itself will take on a Gaussian shape.

The standard error ellipse for the pair (θ_i, θ_j) is shown in Fig. 40.5, corresponding to a contour $\chi^2 = \chi_{\min}^2 + 1$ or $\ln L = \ln L_{\max} - 1/2$. The ellipse is centered about the estimated values $\hat{\theta}$, and the tangents to the ellipse give the standard deviations of the estimators, σ_i and σ_j . The angle of the major axis of the ellipse is given by

$$\tan 2\phi = \frac{2\rho_{ij}\sigma_i\sigma_j}{\sigma_j^2 - \sigma_i^2}, \quad (40.73)$$

where $\rho_{ij} = \text{cov}[\hat{\theta}_i, \hat{\theta}_j]/\sigma_i\sigma_j$ is the correlation coefficient.

The correlation coefficient can be visualized as the fraction of the distance σ_i from the ellipse's horizontal center-line at which the ellipse becomes tangent to vertical, *i.e.*, at the distance $\rho_{ij}\sigma_i$ below the center-line as shown. As ρ_{ij} goes to $+1$ or -1 , the ellipse thins to a diagonal line.

It could happen that one of the parameters, say, θ_j , is known from previous measurements to a precision much better than σ_j , so that the current measurement contributes almost nothing to the knowledge of θ_j . However, the current measurement of θ_i and its dependence on θ_j may still be important. In this case, instead of quoting both parameter estimates and their correlation, one sometimes reports the value of θ_i , which minimizes χ^2 at a fixed value of θ_j , such as the PDG best value. This θ_i value lies along the dotted line between the points where the ellipse becomes tangent to vertical, and has statistical error σ_{inner} as shown on the figure, where $\sigma_{\text{inner}} = (1 - \rho_{ij}^2)^{1/2}\sigma_i$. Instead of the correlation ρ_{ij} , one reports the dependency $d\hat{\theta}_i/d\theta_j$, which is the slope of the dotted line. This slope is related to the correlation coefficient by $d\hat{\theta}_i/d\theta_j = \rho_{ij} \times \frac{\sigma_i}{\sigma_j}$.

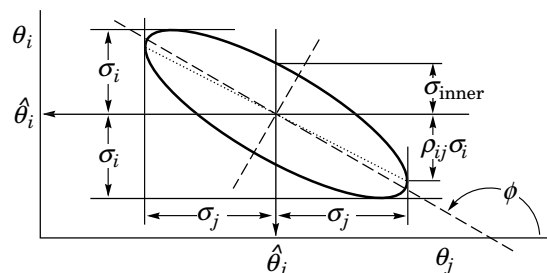
As in the single-variable case, because of the symmetry of the Gaussian function between θ and $\hat{\theta}$, one finds that contours of constant $\ln L$ or χ^2 cover the true values with a certain, fixed probability. That is, the confidence region is determined by

$$\ln L(\theta) \geq \ln L_{\max} - \Delta \ln L, \quad (40.74)$$

or where a χ^2 has been defined for use with the method of least-squares,

$$\chi^2(\theta) \leq \chi_{\min}^2 + \Delta\chi^2. \quad (40.75)$$

Values of $\Delta\chi^2$ or $2\Delta \ln L$ are given in Table 40.2 for several values of the coverage probability $1 - \alpha$ and number of fitted parameters

**Figure 40.5:** Standard error ellipse for the estimators $\hat{\theta}_i$ and $\hat{\theta}_j$. In the case shown the correlation is negative.

M . For Gaussian distributed data, these are related by $\Delta\chi^2 = 2\Delta \ln L = F_{\chi_M^2}^{-1}(1 - \alpha)$, where $F_{\chi_M^2}^{-1}$ is the chi-square quantile (inverse of the cumulative distribution) for M degrees of freedom.

Table 40.2: Values of $\Delta\chi^2$ or $2\Delta \ln L$ corresponding to a coverage probability $1 - \alpha$ in the large data sample limit, for joint estimation of M parameters.

$(1 - \alpha)$ (%)	$M = 1$	$M = 2$	$M = 3$
68.27	1.00	2.30	3.53
90.	2.71	4.61	6.25
95.	3.84	5.99	7.82
95.45	4.00	6.18	8.03
99.	6.63	9.21	11.34
99.73	9.00	11.83	14.16

For non-Gaussian data samples, the probability for the regions determined by Equations (40.74) or (40.75) to cover the true value of θ becomes independent of θ only in the large-sample limit. So for a finite data sample these are not exact confidence regions according to our previous definition. Nevertheless, they can still have a coverage probability only weakly dependent on the true parameter, and approximately as given in Table 40.2. In any case, the coverage probability of the intervals or regions obtained according to this procedure can in principle be determined as a function of the true parameter(s), for example, using a Monte Carlo calculation.

One of the practical advantages of intervals that can be constructed from the log-likelihood function or χ^2 is that it is relatively simple to produce the interval for the combination of several experiments. If N independent measurements result in log-likelihood functions $\ln L_i(\theta)$, then the combined log-likelihood function is simply the sum,

$$\ln L(\theta) = \sum_{i=1}^N \ln L_i(\theta). \quad (40.76)$$

This can then be used to determine an approximate confidence interval or region with Eq. (40.74), just as with a single experiment.

40.4.2.3 Poisson or binomial data

Another important class of measurements consists of counting a certain number of events, n . In this section, we will assume these are all events of the desired type, *i.e.*, there is no background. If n represents the number of events produced in a reaction with cross section σ , say, in a fixed integrated luminosity \mathcal{L} , then it follows a Poisson distribution with mean $\mu = \sigma\mathcal{L}$. If, on the other hand, one has selected a larger sample of N events and found n of them to have a particular property, then n follows a binomial distribution where the parameter p gives the probability for the event to possess the property in question. This is appropriate, *e.g.*, for estimates of branching ratios or selection efficiencies based on a given total number of events.

For the case of Poisson distributed n , limits on the mean value μ can be found from the Neyman procedure as discussed in Sec-

tion 40.4.2.1 with n used directly as the statistic x . The upper and lower limits are found to be

$$\mu_{\text{lo}} = \frac{1}{2} F_{\chi^2}^{-1}(\alpha_{\text{lo}}; 2n), \quad (40.77a)$$

$$\mu_{\text{up}} = \frac{1}{2} F_{\chi^2}^{-1}(1 - \alpha_{\text{up}}; 2(n+1)), \quad (40.77b)$$

where confidence levels of $1 - \alpha_{\text{lo}}$ and $1 - \alpha_{\text{up}}$ refer separately to the corresponding intervals $\mu \geq \mu_{\text{lo}}$ and $\mu \leq \mu_{\text{up}}$, and $F_{\chi^2}^{-1}$ is the quantile of the χ^2 distribution (inverse of the cumulative distribution). For central confidence intervals at confidence level $1 - \alpha$, set $\alpha_{\text{lo}} = \alpha_{\text{up}} = \alpha/2$.

Table 40.3: Lower and upper (one-sided) limits for the mean μ of a Poisson variable given n observed events in the absence of background, for confidence levels of 90% and 95%.

n	$1 - \alpha = 90\%$		$1 - \alpha = 95\%$	
	μ_{lo}	μ_{up}	μ_{lo}	μ_{up}
0	–	2.30	–	3.00
1	0.105	3.89	0.051	4.74
2	0.532	5.32	0.355	6.30
3	1.10	6.68	0.818	7.75
4	1.74	7.99	1.37	9.15
5	2.43	9.27	1.97	10.51
6	3.15	10.53	2.61	11.84
7	3.89	11.77	3.29	13.15
8	4.66	12.99	3.98	14.43
9	5.43	14.21	4.70	15.71
10	6.22	15.41	5.43	16.96

It happens that the upper limit from Eq. (40.77b) coincides numerically with the Bayesian upper limit for a Poisson parameter, using a uniform prior p.d.f. for μ . Values for confidence levels of 90% and 95% are shown in Table 40.3. For the case of binomially distributed n successes out of N trials with probability of success p , the upper and lower limits on p are found to be

$$p_{\text{lo}} = \frac{n F_F^{-1}[\alpha_{\text{lo}}; 2n, 2(N-n+1)]}{N-n+1 + n F_F^{-1}[\alpha_{\text{lo}}; 2n, 2(N-n+1)]}, \quad (40.78a)$$

$$p_{\text{up}} = \frac{(n+1) F_F^{-1}[1 - \alpha_{\text{up}}; 2(n+1), 2(N-n)]}{(N-n) + (n+1) F_F^{-1}[1 - \alpha_{\text{up}}; 2(n+1), 2(N-n)]}. \quad (40.78b)$$

Here F_F^{-1} is the quantile of the F distribution (also called the Fisher-Snedecor distribution; see Ref. [4]).

40.4.2.4 Parameter exclusion in cases of low sensitivity

An important example of a statistical test arises in the search for a new signal process. Suppose the parameter μ is defined such that it is proportional to the signal cross section. A statistical test may be carried out for hypothesized values of μ , which may be done by computing a p -value, p_{μ} , for all μ . Those values not rejected in a test of size α , *i.e.*, for which one does not find $p_{\mu} \leq \alpha$, constitute a confidence interval with confidence level $1 - \alpha$.

In general one will find that for some regions in the parameter space of the signal model, the predictions for data are almost indistinguishable from those of the background-only model. This corresponds to the case where μ is very small, as would occur, *e.g.*, in a search for a new particle with a mass so high that its production rate in a given experiment is negligible. That is, one has essentially no experimental sensitivity to such a model.

One would prefer that if the sensitivity to a model (or a point in a model's parameter space) is very low, then it should not be excluded. Even if the outcomes predicted with or without signal are identical, however, the probability to reject the signal model will equal α , the type-I error rate. As one often takes α to be 5%, this would mean that in a large number of searches covering a broad range of a signal model's parameter space, there would inevitably be excluded regions in which the experimental

sensitivity is very small, and thus one may question whether it is justified to regard such parameter values as disfavored.

Exclusion of models to which one has little or no sensitivity occurs, for example, if the data fluctuate very low relative to the expectation of the background-only hypothesis. In this case the resulting upper limit on μ may be anomalously low. As a means of controlling this effect one often determines the mean or median limit under assumption of the background-only hypothesis, as discussed in Sec. 40.5.

One way to mitigate the problem of excluding models to which one is not sensitive is the CL_s method, where the measure used to test a parameter is increased for decreasing sensitivity [35,36]. The procedure is based on a statistic called CL_s , which is defined as

$$\text{CL}_s = \frac{p_{\mu}}{1 - p_b}, \quad (40.79)$$

where p_b is the p -value of the background-only hypothesis. In the usual formulation of the method, both p_{μ} and p_b are defined using a single test statistic, and the definition of CL_s above assumes this statistic is continuous; more details can be found in Refs. [35,36].

A point in a model's parameter space is regarded as excluded if one finds $\text{CL}_s \leq \alpha$. As the denominator in Eq. (40.79) is always less than or equal to unity, the exclusion criterion based on CL_s is more stringent than the usual requirement $p_{\mu} \leq \alpha$. In this sense the CL_s procedure is conservative, and the coverage probability of the corresponding intervals will exceed the nominal confidence level $1 - \alpha$. If the experimental sensitivity to a given value of μ is very low, then one finds that as p_{μ} decreases, so does the denominator $1 - p_b$, and thus the condition $\text{CL}_s \leq \alpha$ is effectively prevented from being satisfied. In this way the exclusion of parameters in the case of low sensitivity is suppressed.

The CL_s procedure has the attractive feature that the resulting intervals coincide with those obtained from the Bayesian method in two important cases: the mean value of a Poisson or Gaussian distributed measurement with a constant prior. The CL_s intervals overcover for all values of the parameter μ , however, by an amount that depends on μ .

The problem of excluding parameter values to which one has little sensitivity is particularly acute when one wants to set a one-sided limit, *e.g.*, an upper limit on a cross section. Here one tests a value of a rate parameter μ against the alternative of a lower rate, and therefore the critical region of the test is taken to correspond to data outcomes with a low event yield. If the number of events found in the search region fluctuates low enough, however, it can happen that all physically meaningful signal parameter values, including those to which one has very little sensitivity, are rejected by the test.

Another solution to this problem, therefore, is to replace the one-sided test by one based on the likelihood ratio, where the critical region is not restricted to low rates. This is the approach followed in the Feldman-Cousins procedure described in Section 40.4.2.1. The critical region for the test of a given value of μ contains data values characteristic of both higher and lower rates. As a result, for a given observed rate one can in general obtain a two-sided interval. If, however, the parameter estimate $\hat{\mu}$ is sufficiently close to the lower limit of zero, then only high values of μ are rejected, and the lower edge of the confidence interval is at zero. Note, however, that the coverage property of $1 - \alpha$ pertains to the entire interval, not to the probability for the upper edge μ_{up} to be greater than the true value μ . For parameter estimates increasingly far away from the boundary, *i.e.*, for increasing signal significance, the point $\mu = 0$ is excluded and the interval has nonzero upper and lower edges.

An additional difficulty arises when a parameter estimate is not significantly far away from the boundary, in which case it is natural to report a one-sided confidence interval (often an upper limit). It is straightforward to force the Neyman prescription to produce only an upper limit by setting $x_2 = \infty$ in Eq. (40.68). Then x_1 is uniquely determined and the upper limit can be obtained. If, however, the data come out such that the parameter estimate is not so close to the boundary, one might wish to report a central confidence interval (*i.e.*, an interval based on a two-sided test with equal upper and lower tail areas). As pointed out by Feldman and

Cousins [33], if the decision to report an upper limit or two-sided interval is made by looking at the data (“flip-flopping”), then in general there will be parameter values for which the resulting intervals have a coverage probability less than $1 - \alpha$. With the confidence intervals suggested in [33], the prescription determines whether the interval is one- or two-sided in a way which preserves the coverage probability (and are thus said to be *unified*).

The intervals according to this method for the mean of Poisson variable in the absence of background are given in Table 40.4. (Note that α in Ref. [33] is defined following Neyman [32] as the coverage probability; this is opposite the modern convention used here in which the coverage probability is $1 - \alpha$.) The values of $1 - \alpha$ given here refer to the coverage of the true parameter by the whole interval $[\mu_1, \mu_2]$. In Table 40.3 for the one-sided upper limit, however, $1 - \alpha$ refers to the probability to have $\mu_{\text{up}} \geq \mu$ (or $\mu_{\text{lo}} \leq \mu$ for lower limits).

Table 40.4: Unified confidence intervals $[\mu_1, \mu_2]$ for a the mean of a Poisson variable given n observed events in the absence of background, for confidence levels of 90% and 95%.

n	$1 - \alpha = 90\%$		$1 - \alpha = 95\%$	
	μ_1	μ_2	μ_1	μ_2
0	0.00	2.44	0.00	3.09
1	0.11	4.36	0.05	5.14
2	0.53	5.91	0.36	6.72
3	1.10	7.42	0.82	8.25
4	1.47	8.60	1.37	9.76
5	1.84	9.99	1.84	11.26
6	2.21	11.47	2.21	12.75
7	3.56	12.53	2.58	13.81
8	3.96	13.99	2.94	15.29
9	4.36	15.30	4.36	16.77
10	5.50	16.50	4.75	17.82

A potential difficulty with unified intervals arises if, for example, one constructs such an interval for a Poisson parameter s of some yet to be discovered signal process with, say, $1 - \alpha = 0.9$. If the true signal parameter is zero, or in any case much less than the expected background, one will usually obtain a one-sided upper limit on s . In a certain fraction of the experiments, however, a two-sided interval for s will result. Since, however, one typically chooses $1 - \alpha$ to be only 0.9 or 0.95 when setting limits, the value $s = 0$ may be found below the lower edge of the interval before the existence of the effect is well established. It must then be communicated carefully that in excluding $s = 0$ at, say, 90% or 95% confidence level from the interval, one is not necessarily claiming to have discovered the effect, for which one would usually require a higher level of significance (e.g., 5σ).

Another possibility is to construct a Bayesian interval as described in Section 40.4.1. The presence of the boundary can be incorporated simply by setting the prior density to zero in the unphysical region. More specifically, the prior may be chosen using formal rules such as the reference prior or Jeffreys prior mentioned in Sec. 40.2.6.

In particle physics a widely used prior for the mean μ of a Poisson distributed measurement has been the uniform distribution for $\mu \geq 0$. This prior does not follow from any fundamental rule nor can it be regarded as reflecting a reasonable degree of belief, since the prior probability for μ to lie between any two finite values is zero. The procedure above can be more appropriately regarded as a way for obtaining intervals with frequentist properties that can be investigated. The resulting upper limits have a coverage probability that depends on the true value of the Poisson parameter, and is nowhere smaller than the stated probability content. Lower limits and two-sided intervals for the Poisson mean based on uniform priors undercover, however, for some values of the parameter, although to an extent that in practical cases may not be too severe [2, 31].

In any case, it is important to always report sufficient information so that the result can be combined with other measurements.

Often this means giving an unbiased estimator and its standard deviation, even if the estimated value is in the unphysical region.

It can also be useful with a frequentist interval to calculate its subjective probability content using the posterior p.d.f. based on one or several reasonable guesses for the prior p.d.f. If it turns out to be significantly less than the stated confidence level, this warns that it would be particularly misleading to draw conclusions about the parameter’s value from the interval alone.

40.5 Experimental sensitivity

In this section we describe methods for characterizing the sensitivity of a search for a new physics signal. As discussed in Sec. 40.3, an experimental analysis can often be formulated as a test of hypothetical model parameters. Therefore we may quantify the sensitivity by giving the results that we expect from such a test under specific assumptions about the signal process.

Here to be concrete we will consider a parameter μ proportional to the rate of a signal process, although the concepts described in this section may be easily generalized to other parameters. One may wish to establish discovery of the signal process by testing and rejecting the hypothesis that $\mu = 0$, and in addition one often wants to test nonzero values of μ to construct a confidence interval (e.g., limits) as described in Sec. 40.4. In the frequentist framework, the result of each tested value of μ is the p -value p_μ or equivalently the significance $Z_\mu = \Phi^{-1}(1 - p_\mu)$, where as usual Φ is the standard Gaussian cumulative distribution and its inverse Φ^{-1} is the standard Gaussian quantile.

Prior to carrying out the experiment, one generally wants to quantify what significance Z_μ is expected under given assumptions for the presence or absence of the signal process. Specifically, for the significance of a test of $\mu = 0$ (the discovery significance) one usually quotes the Z_0 one would expect if the signal is present at a given nominal rate, which we can define in general to correspond to $\mu = 1$. For limits, one often gives the expected limit under assumption of the background-only ($\mu = 0$) model. These quantities are used to optimize the analysis and to quantify the experimental sensitivity, that is, to characterize how likely it is to make a discovery if the signal is present, and to say what values of μ one may be able to exclude if the signal is in fact absent.

First we clarify the notion of *expected significance*. Because the significance Z_μ is a function of the data, it is itself a random quantity characterized by a certain sampling distribution. This distribution depends on the assumed value of μ , which is not necessarily the same as the hypothesized value of μ being tested. We may therefore consider the distribution $f(Z_\mu|\mu')$, i.e., the distribution of Z_μ that would be obtained by considering data samples generated under assumption of μ' . In a similar way one can talk about the sampling distribution of an upper limit for μ , $f(\mu_{\text{up}}|\mu')$.

One can identify the expected significance or limit with either the mean or median of these distributions, but the median may be preferred since it is invariant under monotonic transformations. For example, the monotonic relation between p -value and significance, $p = 1 - \Phi(Z)$, then gives $\text{med}[p_\mu|\mu'] = 1 - \Phi(\text{med}[Z_\mu|\mu'])$, whereas the corresponding relation does not hold in general for the mean.

In some cases one may be able to write down approximate formulae for the distributions of Z_μ and for limits, but more generally they must be determined from Monte Carlo calculations. In many cases of interest, the significance Z_μ and the limits on μ will have approximate Gaussian distributions.

As an example, consider a Poisson counting experiment, where the result consists of an observed number n of events, modeled as a Poisson distributed variable with a mean of $\mu s + b$. Here s and b , the expected numbers of events from signal and background processes, are taken to be known. If we are interested in discovering the signal process we test and try to reject the hypothesis $\mu = 0$. To characterize the experimental sensitivity, we want to give the discovery significance expected under the assumption of $\mu = 1$.

In the limit where its mean value is large, the Poisson variable n can be approximated as an almost continuous Gaussian variable with mean $\mu s + b$ and standard deviation $\sigma = \sqrt{\mu s + b}$. In the usual case where a physical signal model corresponds to $\mu > 0$,

the p -value of $\mu = 0$ is the probability to find n greater than or equal to the value observed,

$$p_0 = \Phi\left(\frac{n-b}{\sqrt{b}}\right), \quad (40.80)$$

and the corresponding significance is $Z_0 = \Phi^{-1}(1-p_0) = (n-b)/\sqrt{b}$. The median (here equal to the mean) of n assuming $\mu = 1$ is $s+b$, and therefore the median discovery significance is

$$\text{med}[Z_0|\mu=1] = \frac{s}{\sqrt{b}}. \quad (40.81)$$

The figure of merit “ s/\sqrt{b} ” has been widely used in particle physics as a measure of expected discovery significance. A better approximation for the Poisson counting experiment, however, may be obtained by testing $\mu = 0$ using the likelihood ratio (40.49) $\lambda(0) = L(0)/L(\hat{\mu})$, where

$$L(\mu) = \frac{(\mu s + b)^n}{n!} e^{-(\mu s + b)} \quad (40.82)$$

is the likelihood function, and $\hat{\mu} = (n-b)/s$ is the ML estimator. In this example there are no nuisance parameters, as s and b are taken to be known. For the case where the relevant signal models correspond to positive μ , one may test the $\mu = 0$ hypothesis with the statistic $q_0 = -2\ln\lambda(0)$ when $\hat{\mu} > 0$, *i.e.*, an excess is observed, and $q_0 = 0$ otherwise. One can show (see, *e.g.*, [24]) that in the large-sample limit, the discovery significance is then $Z_0 = \sqrt{q_0}$, for which one finds

$$Z_0 = \sqrt{2\left(n \ln \frac{n}{b} + b - n\right)} \quad (40.83)$$

for $n > b$ and $Z_0 = 0$ otherwise. To approximate the expected discovery significance assuming $\mu = 1$, one may simply replace n with the expected value $E[n|\mu=1] = s+b$ (the so-called “Asimov data set”), giving

$$\text{med}[Z_0|\mu=1] = \sqrt{2\left((s+b) \ln\left(1 + \frac{s}{b}\right) - s\right)}. \quad (40.84)$$

This has been shown in Ref. [24] to provide a good approximation to the median discovery significance for values of s of several and for b well below unity. The right-hand side of Eq. (40.84) reduces to s/\sqrt{b} in the limit $s \ll b$.

Beyond the simple Poisson counting experiment, in general one may test values of a parameter μ with more complicated functions of the measured data to obtain a p -value p_μ , and from this one can quote the equivalent significance Z_μ or find, *e.g.*, an upper limit μ_{up} . In this case as well one may quantify the experimental sensitivity by giving the significance Z_μ expected if the data are generated with a different value of the parameter μ' . In some problems, finding the sampling distribution of the significance or limits may be possible using large-sample formulae as described, *e.g.*, in Ref. [24]. In other cases a Monte Carlo study may be needed. Using whatever method of calculation is most appropriate, one usually quotes the expected (mean or, preferably, median) significance or limit as the primary measures of experimental sensitivity.

Even if the true signal is present at its nominal rate, the actual discovery significance Z_0 obtained from the real data is subject to statistical fluctuations and will not in general be equal to its expected value. In an analogous way, the observed limit will differ from the expected limit even if the signal is absent. Upon observing such a difference one would like to know how large this is compared to expected statistical fluctuations. Therefore, in addition to the observed significance and limits it is useful to communicate not only their expected values but also a measure of the width of their distributions.

As the distributions of significance and limits are often well approximated by a Gaussian, one may indicate the intervals corresponding to plus-or-minus one and/or two standard deviations. If the distributions are significantly non-Gaussian, one may use

instead the quantiles that give the same probability content, *i.e.*, [0.1587, 0.8413] for $\pm 1\sigma$, [0.02275, 0.97725] for $\pm 2\sigma$. An upper limit found significantly below the background-only expectation may indicate a strong downward fluctuation of the data, or perhaps as well an incorrect estimate of the background rate.

The procedures described above pertain to frequentist hypothesis tests and limits. Bayesian limits, just like those found from a frequentist procedure, are functions of the data and one may therefore find, usually with approximations or Monte Carlo studies, their sampling distribution and corresponding mean (or, preferably, median) and standard deviation.

When trying to establish discovery of a signal process, the Bayesian approach may employ a Bayes factor as described in Sec. 40.3.3. In the case of the Poisson counting experiment with the likelihood from Eq. (40.82), the log of the Bayes factor that compares $\mu = 1$ to $\mu = 0$ is $\ln B_{10} = \ln(L(1)/L(0)) = n \ln(1+s/b) - s$. That is, the expectation value, assuming $\mu = 1$, of $\ln B_{10}$ for this problem is

$$E[\ln B_{10}|\mu=1] = (s+b) \ln\left(1 + \frac{s}{b}\right) - s. \quad (40.85)$$

Comparing this to Eq. (40.84), one finds $\text{med}[Z_0|1] = \sqrt{2E[\ln B_{10}|1]}$. Thus for this particular problem the frequentist median discovery significance can be related to the corresponding Bayes factor in a simple way.

In some analyses, the goal may not be to establish discovery of a signal process but rather to measure, as accurately as possible, the signal rate. If we consider again the Poisson counting experiment described by the likelihood function of Eq. (40.82), the ML estimator $\hat{\mu} = (n-b)/s$ has a variance, assuming $\mu = 1$, of

$$V[\hat{\mu}] = V\left[\frac{n-b}{s}\right] = \frac{1}{s^2} V[n] = \frac{s+b}{s^2}, \quad (40.86)$$

so that the standard deviation of $\hat{\mu}$ is $\sigma_{\hat{\mu}} = \sqrt{s+b}/s$. One may therefore use $s/\sqrt{s+b}$ as a figure of merit to be maximized in order to obtain the best measurement accuracy of a rate parameter. The quantity $s/\sqrt{s+b}$ is also the expected significance with which one rejects s assuming the signal is absent, and thus can be used to optimize the expected upper limit on s .

References

- [1] B. Efron, *Am. Stat.* **40**, 11 (1986).
- [2] R. D. Cousins, *Am. J. Phys.* **63**, 398 (1995).
- [3] A. Stuart, J.K. Ord, and S. Arnold, *Kendall's Advanced Theory of Statistics*, Vol. 2A: *Classical Inference and the Linear Model*, 6th ed., Oxford Univ. Press (1999), and earlier editions by Kendall and Stuart. The likelihood-ratio ordering principle is described at the beginning of Ch. 23. Chapter 26 compares different schools of statistical inference.
- [4] F. James, *Statistical methods in experimental physics* (2006), ISBN 9789812567956.
- [5] L. Lyons, *Statistics for Nuclear and Particle Physicists* (1986), ISBN 9780521379342, URL <http://www.cambridge.org/uk/catalogue/catalogue.asp?isbn=0521255406>.
- [6] R. J. Barlow, *Nucl. Instrum. Meth.* **A297**, 496 (1990).
- [7] G. Cowan, *Statistical data analysis* (1998), ISBN 9780198501565.
- [8] S. Baker and R. D. Cousins, *Nucl. Instrum. Meth.* **221**, 437 (1984).
- [9] S. S. Wilks, *Annals Math. Statist.* **9**, 1, 60 (1938).
- [10] O. Behnke *et al.*, editors, *Data analysis in high energy physics*, Wiley-VCH, Weinheim, Germany (2013), ISBN 9783527410583, 9783527653447, 9783527653430, URL <http://www.wiley-vch.de/publish/dt/books/ISBN3-527-41058-9>.
- [11] S. Schmitt, *EPJ Web of Conferences* **137**, 11008 (2017), ISSN 2100-014X, URL <http://dx.doi.org/10.1051/epjconf/201713711008>.

- [12] L. Brenner *et al.*, Int. J. Mod. Phys. A **35**, 24, 2050145 (2020), [arXiv:1910.14654].
- [13] A. O'Hagan and J.J. Forster, *Bayesian Inference*, (2nd edition, volume 2B of *Kendall's Advanced Theory of Statistics*, Arnold, London, 2004).
- [14] D. Sivia and J. Skilling, *Data Analysis: A Bayesian Tutorial*, (Oxford University Press, 2006).
- [15] P.C. Gregory, *Bayesian Logical Data Analysis for the Physical Sciences*, (Cambridge University Press, 2005).
- [16] J.M. Bernardo and A.F.M. Smith, *Bayesian Theory*, (Wiley, 2000).
- [17] Robert E. Kass and Larry Wasserman, J. Am. Stat. Assoc. **91**, 1343 (1996).
- [18] J.M. Bernardo, J. R. Statist. Soc. **B41**, 113 (1979); J.M. Bernardo and J.O. Berger, J. Am. Stat. Assoc. **84**, 200 (1989). See also J.M. Bernardo, *Reference Analysis*, in *Handbook of Statistics*, 25 (D.K. Dey and C.R. Rao, eds.), 17-90, Elsevier (2005) and references therein.
- [19] L. Demortier, S. Jain and H. B. Prosper, Phys. Rev. **D82**, 034002 (2010), [arXiv:1002.1111].
- [20] K. Cranmer, J. Pavez and G. Louppe (2015), [arXiv:1506.02169].
- [21] N. Reid, *Likelihood Inference in the Presence of Nuisance Parameters*, *Proceedings of PHYSTAT2003*, L. Lyons, R. Mount, and R. Reitmeyer, eds., eConf C030908, Stanford, 2003.
- [22] W. A. Rolke, A. M. Lopez and J. Conrad, Nucl. Instrum. Meth. **A551**, 493 (2005), [arXiv:physics/0403059].
- [23] Links to the *Proceedings of the PHYSTAT* conference series (Durham 2002, Stanford 2003, Oxford 2005, and Geneva 2007, 2011) can be found at phystat.org.
- [24] G. Cowan *et al.*, Eur. Phys. J. **C71**, 1554 (2011), [Erratum: Eur. Phys. J. **C73**, 2501 (2013)], [arXiv:1007.1727].
- [25] L. Demortier, *P-Values and Nuisance Parameters*, *Proceedings of PHYSTAT 2007*, CERN-2008-001, p. 23.
- [26] E. Gross and O. Vitells, Eur. Phys. J. **C70**, 525 (2010), [arXiv:1005.1891].
- [27] R. B. Davies, Biometrika **74**, 33 (1987).
- [28] J. Skilling, *Nested Sampling*, *AIP Conference Proceedings*, **735**, 395-405 (2004).
- [29] F. Feroz, M. P. Hobson and M. Bridges, Mon. Not. Roy. Astron. Soc. **398**, 1601 (2009), [arXiv:0809.3437].
- [30] R. E. Kass and A. E. Raftery, J. Am. Statist. Assoc. **90**, 430, 773 (1995).
- [31] B. P. Roe and M. B. Woodroffe, Phys. Rev. **D63**, 013009 (2001), [hep-ex/0007048].
- [32] J. Neyman, Phil. Trans. Roy. Soc. Lond. **A236**, 767, 333 (1937); Reprinted in *A Selection of Early Statistical Papers on J. Neyman*, (University of California Press, Berkeley, 1967).
- [33] G. J. Feldman and R. D. Cousins, Phys. Rev. **D57**, 3873 (1998), [arXiv:physics/9711021]; This paper does not specify what to do if the ordering principle gives equal rank to some values of x . Eq. 21.6 of Ref. [3] gives the rule: all such points are included in the acceptance region (the domain $D(\alpha)$). Some authors have assumed the contrary, and shown that one can then obtain null intervals.
- [34] K. Cranmer, in "Statistical Problems in Particle Physics, Astrophysics and Cosmology (PHYSTAT 05): Proceedings, Oxford, UK, September 12-15, 2005," 112-123 (2005), [arXiv:physics/0511028], URL http://www.physics.ox.ac.uk/phystat05/proceedings/files//Cranmer_LHCStatisticalChallenges.ps.
- [35] A. L. Read, in "Workshop on confidence limits, CERN, Geneva, Switzerland, 17-18 Jan 2000: Proceedings," 81-101 (2000), URL <http://weblib.cern.ch/abstract?CERN-OPEN-2000-205>.
- [36] T. Junk, Nucl. Instrum. Meth. **A434**, 435 (1999), [hep-ex/9902006].

41. Machine Learning

Written November 2021 by K. Cranmer (NYU), U. Seljak (UC Berkeley; LBNL) and K. Terao (SLAC; Stanford U.).

41.1	Introduction	676	41.5.3.13	Transformer and multi-head attention	696
41.1.1	A gentle introduction with a representative example	677	41.5.3.14	Graph networks and geometric deep learning	696
41.2	Fundamental concepts	677	41.5.4	Deep generative models	697
41.2.1	Loss, risk, empirical risk	677	41.5.4.1	Variational auto-encoders	698
41.2.2	Generalization	678	41.5.4.2	Generative adversarial networks	698
41.3	Common tasks and their associated loss functions	678	41.5.4.3	Normalizing flows, autoregressive models, and score based models	699
41.3.1	Supervised learning	678	41.6	Learning algorithms	700
41.3.1.1	Regression	678	41.6.1	Gradient-based optimization	700
41.3.1.2	A note on regularization	679	41.6.2	Stochastic gradient descent	700
41.3.1.3	Classification	679	41.6.3	Optimization algorithms	700
41.3.2	Unsupervised learning	680	41.6.4	Automatic differentiation and back propagation	700
41.3.2.1	Density estimation	680	41.6.5	The vanishing and exploding gradient problems	701
41.3.2.2	Representation learning, compression, and auto-encoders	681	41.6.6	Early stopping	701
41.3.2.3	Clustering	681	41.6.7	Initialization of model parameters	701
41.3.3	Optimal control, reinforcement learning, and active learning	682	41.6.8	Input normalization	701
	Reinforcement learning	682	41.6.9	Batch normalization	701
	Multi-arm bandits	682	41.6.10	Transfer learning: pre-training and fine-tuning	702
	Bayesian optimization	682	41.6.11	Zero, one, and a few shot learning	702
	Connection to experimental design	683	41.7	Incorporating uncertainty	702
	Active learning	683	41.7.1	Propagation of errors	703
41.3.4	Anomaly detection and out-of-distribution detection	683	41.7.2	Domain adaptation	703
41.3.5	Simulation-based inference	684	41.7.3	Parameterized models	704
41.3.5.1	Differentiable simulations	684	41.7.4	Data augmentation	704
41.3.5.2	Unfolding as an inverse problem	684	41.7.5	Aleatoric and epistemic uncertainty	704
41.4	Data representations, inductive bias, and example applications	685	41.7.6	Model averaging and Bayesian machine learning	705
41.5	Flavors of ML models	686	41.7.7	Connection to probabilistic machine learning	705
41.5.1	Support vector machines and kernel machines	686	41.8	Infrastructure for deployment in experiments	706
	Maximum-margin classifiers	686			
	Soft margins and slack variables	686			
	The dual problem	686			
	The kernel trick	686			
	Support vector regression	687			
	Kernel ridge regression	687			
	Gaussian Process Regression (kriging)	687			
41.5.2	Decision trees	687			
	Tree-based models	687			
	Ensemble methods	688			
	Bagging	688			
	Random forests	688			
	AdaBoost	689			
	Gradient boosting	689			
41.5.3	Neural networks	689			
41.5.3.1	Feed-forward multi-layer perceptron	689			
41.5.3.2	Activation functions	689			
41.5.3.3	Softmax	690			
41.5.3.4	The rise of deep learning	690			
41.5.3.5	Convolutional neural networks	690			
41.5.3.6	Pooling	690			
41.5.3.7	CNN architectures for image analysis	691			
	Region Convolutional Neural Network	691			
	U-Net	691			
41.5.3.8	Residual networks and skip connections	692			
41.5.3.9	Recurrent neural networks	692			
41.5.3.10	LSTM and GRU	694			
41.5.3.11	Attention	694			
41.5.3.12	Scaled dot-product attention	695			

41.1 Introduction

This chapter gives an overview of the core concepts of machine learning that are relevant to particle physics with some examples of applications to the energy, intensity, cosmic, and accelerator frontiers. Machine learning (ML) is an enormous field that has grown substantially in the last decade, propelled largely by the emergence of so-called deep learning (DL) [1, 2]. ML has a long history in particle physics going back to the late 1980s and early 1990s, see Refs. [3–5] for recent reviews.

Physicists are exploring and contributing to machine learning at an unprecedented rate, which poses a challenge for those that wish to have an up-to-date view of the field. This motivated an effort to create *A Living Review of Machine Learning for Particle and Nuclear Physics* [6], which can be downloaded here: <https://github.com/iml-wg/HEPML-LivingReview>. As of the time of this writing, the Living Review includes over 500 references organized hierarchically by topic. While we make references to some of these papers, this chapter focuses on the methodology and does not attempt to give a comprehensive review of the applications.

Despite the connotations of machine learning and artificial intelligence as a mysterious and radical departure from traditional approaches, we stress that machine learning has a mathematical formulation that is closely tied to statistics, the calculus of variations, approximation theory, and optimal control theory.

The topic can be organized along a few axes, which we use to organize this section. First, there are different learning paradigms, for example supervised learning, unsupervised learning, and reinforcement learning. We focus on the first two in this review, since reinforcement learning is less commonly used in particle physics. Within these paradigms there are various tasks; for example, classification and regression – which have been the primary use of ML in particle physics – are examples of supervised learning. In addition to the learning paradigm and tasks, there are various types of machine learning models that generically process some input and produce some output. The types of models vary based on what it is they are modelling (*e.g.* so-called discriminative vs. generative

models), as well as the way that they are implemented (e.g. neural networks, decision trees, and kernel machines). Next, there are the issues around training or learning within the context of a given task and model class, which connects to optimization and regularization. We will briefly discuss the various considerations that emerge in the application of machine learning methods to physics, such as the treatment of systematic uncertainty, the interpretability of the models, the incorporation of symmetry, etc..

41.1.1 A gentle introduction with a representative example

We will use a specific, familiar example to introduce the various ingredients in context before factorizing and abstracting them. Consider the task of *classifying energy deposits* in a particle detector as electrons or protons. For this example, let the detector data consist of energy deposits in d sensors so that the data can be represented as *feature vector* $x \in \mathbb{R}^d$. Different components of x may have different units (e.g. units of energy, momentum, position etc.). Due to the complex interactions of particles in the detector, we do not have an explicit probability model for the high-dimensional data for the electron and proton scenarios, but we do have a simulator that allows us to generate Monte Carlo samples for each. This allows us to assemble a *training dataset* $\{x_i, y_i\}_{i=1, \dots, n}$, where y is used as a *label* to identify how the example was generated (e.g. $y = 0$ for electrons and $y = 1$ for protons). We would like to find a function $f : x \rightarrow y$ that is able to accurately *predict* the label on new data. Because we have feature-label pairs, this is considered a *supervised learning* problem. We can use a *neural network* to provide a flexible family of functions $f_\phi : \mathbb{R}^d \rightarrow \mathbb{R}$, where ϕ denotes the internal parameters of the neural network (i.e. the weights and biases that we will discuss in Sec.41.5.3). The goal of the *training procedure* is to find the value of the parameters ϕ that provide the ‘best’ predictions, but since no model is perfect, we must be explicit about the trade-offs. This is made concrete through a *loss function* $\mathcal{L}(f_\phi(x), y)$. For this example, instead of the obvious zero-one loss (which is 0 if $f_\phi(x)$ equals y and 1 if they are not), we choose to use the squared-loss $\mathcal{L}_{\text{sq}}(f_\phi(x), y) = (y - f_\phi(x))^2$ (which may seem *ad hoc* now, but will be motivated in Sec. 41.3.1.3). We can evaluate the average of the loss on the training set of size n , which is referred to as the *empirical risk* $\mathcal{R}_{\text{emp}}(f_\phi) = \sum_{i=1}^n \mathcal{L}(f_\phi(x), y)/n$. *Training* refers to numerically minimizing the empirical risk (often referred to as the *training loss* through some abuse of terminology). We can numerically optimize the model through *gradient descent*, which iteratively adjusts the parameters of the network according to $\phi^{t+1} = \phi^t - \lambda \nabla_{\phi} \mathcal{R}_{\text{emp}}(f_\phi)$, where λ is referred to as the *learning rate*. Once the optimization is complete and we obtain the solution $\hat{\phi}$, it is natural to assess the quality of the trained model $f_{\hat{\phi}}$ on an independent *testing dataset*. The empirical risk evaluated on the testing set is often larger than on the training set, and large differences indicate *overfitting*, which indicates that the model does not generalize well to the unseen data. The ability to accurately predict on unseen data is referred to as *generalization* and the empirical risk on the test data provides a measure of the *generalization error*. In order to reduce the *generalization error* one might explore different model choices (e.g. neural network architectures), additional regularization terms in the loss function, different learning rates, optimization algorithms, or early stopping criterion in the optimization. Once trained, the model can be applied to data. In order to produce a binary electron vs. proton decision from the continuous output of the neural network, we must threshold (i.e. classify as proton if $f_{\hat{\phi}}(x) > k$). The choice of the threshold k is often referred to as a working point and it sets the tradeoff between electron and proton efficiency, fake-rates, purity, etc. These familiar concepts in particle physics are usually referred to in different terms in machine learning and a *receiver operating characteristic curve*, or ROC curve, is used to summarize the tradeoff between true positive rate (TPR) and false positive rate (FPR). Importantly, the characterization of the efficiency / rejection (or equivalently the ROC curve) requires labeled data. In a particle physics context, it is recognized that the simulation is not perfect and the mismodelling is associated to the presence of systematic uncertainty. In machine learning, the discrepancy between the distribution of the training dataset

and the distribution of the data that the model will be applied to in practice is referred to as *domain shift* or *distribution shift*. While mismodelling in the training dataset might lead to a less-than-optimal classifier in practice, the real source of systematic uncertainty comes from mismatch between the data used to characterize the performance of the classifier and the unlabeled data that the classifier is applied to. This motivates the use of data-driven methods to calibrate the resulting model.

This example provides a vertical slice through the various aspects of supervised machine learning in particle physics. Now we factorize and abstract the various ingredients in order to provide a more general treatment with a broader scope.

41.2 Fundamental concepts

41.2.1 Loss, risk, empirical risk

The term *learning* in machine learning generally refers to optimization of some objective, which can be thought of as maximizing utility or minimizing *risk*. The risk brings together three main ingredients. The first is the *model family* \mathcal{F} (where $f \in \mathcal{F}$ is the quantity that we vary during optimization), the second is the *loss function* \mathcal{L} , and the third is a data distribution $p(u)$. The *risk* for a model $f \in \mathcal{F}$ is defined as its expected loss

$$\mathcal{R}[f] := \mathbb{E}_{p(u)}[\mathcal{L}(u, f(u))] \equiv \int \mathcal{L}(u, f(u)) p(u) du, \quad (41.1)$$

where $\mathbb{E}_p[\cdot]$ refers to the expectation with respect to the distribution p . In the context of supervised learning, the distribution $p(u)$ describes a joint distribution over the features x and the labels y (i.e. $p(u) = p(x, y)$), the model only depends on the features $f(u) = f(x)$, and the loss function takes on the special form $\mathcal{L}(u, f(u)) = \mathcal{L}(y, f(x))$. In the context of unsupervised learning there are no labels, and $u = x$. Written this way, the risk is a functional, and the idealized goal for machine learning is to solve the optimization problem

$$f^* = \arg \min_{f \in \mathcal{F}} \mathcal{R}[f], \quad (41.2)$$

where \mathcal{F} would include all possible functions.

One of the defining characteristics of machine learning in practice is that one does not know the data distribution $p(u)$, but does have access to samples from that distribution, i.e. $\{u_i\}_{i=1, \dots, n}$ with $u_i \stackrel{i.i.d.}{\sim} p(u)$. This leads to the corresponding *empirical risk*

$$\mathcal{R}_{\text{emp}}[f] := \mathbb{E}_{\hat{p}(u)}[\mathcal{L}(u, f(u))] \equiv \frac{1}{n} \sum_{i=1}^n \mathcal{L}(u_i, f(u_i)), \quad (41.3)$$

where $\hat{p}(u) = \frac{1}{n} \sum_{i=1}^n \delta(u - u_i)$ is referred to as the empirical distribution of the dataset $\{u_i\}_{i=1, \dots, n}$. The *empirical risk minimization* principle is a core idea in statistical learning theory [7], which approximates f^* with its empirical analogue

$$\hat{f} = \arg \min_{f \in \hat{\mathcal{F}}} \mathcal{R}_{\text{emp}}[f], \quad (41.4)$$

where $\hat{\mathcal{F}}$ are all possible functions parametrized by the model parameters ϕ . In an idealized infinite parameter limit machine learning functions, such as neural networks, are universal approximators, such that they cover all functions and $\mathcal{F} = \hat{\mathcal{F}}$. For finite size networks this may or may not be a valid assumption. Expressivity of the network characterizes this universality property and is a function of the network architecture and its parameters such as width and depth of neural network layers. If the expressivity is too small it leads to underfitting. However, an equally important consideration is the risk of overfitting if we optimize equation 41.4 for too long.

While the loss function may quantify some well-motivated notion of (negative) utility, it is also common to design loss functions so that f^* has some desired property. While in practice one does not know the data distribution $p(u)$, it is constructive to imagine that one does and analyze Eq. 41.2 with the calculus of variations. In Secs. 41.3 we will consider several such loss functions where one can show that the corresponding f^* has the desired property even

if the form of the loss is not obvious from the point of view of utility. Furthermore, there are often multiple loss functions that can lead to the same f^* . Then one can think of machine learning as applied calculus of variations where one solves Eq. 41.4 with a sufficiently flexible model, powerful optimization algorithms, and practical considerations to break the degeneracy between different loss functions that lead to the same f^* .

41.2.2 Generalization

With a sufficiently flexible model, it is possible to fit the training dataset very well, though the model might not *generalize* well to unseen data due to overfitting. More concretely, for a non-negative loss function one might have $\mathcal{R}_{\text{emp}}[\hat{f}] \rightarrow 0$, while the true risk might be large ($\mathcal{R}[\hat{f}] \gg 0$). The gap between the $\mathcal{R}[\hat{f}] - \mathcal{R}_{\text{emp}}[\hat{f}]$ is typically referred to as the *excess risk*¹. While it is generally not possible to evaluate $\mathcal{R}[\hat{f}]$ exactly because we do not know $p(u)$, we can use an independent testing dataset (also called validation dataset) to obtain an unbiased estimate of it. This *cross-validation* method motivates the test – train split of the data.

Intuitively, a model with many parameters has more flexibility and is more prone to overfitting. A common and intuitive heuristic is that one should not fit a model with more parameters than there are data points. However, a more careful treatment reveals that this heuristic can be both pessimistic and optimistic. For example, the single-parameter model $f_\phi(x) = \text{sign}(\sin(\phi x))$ can perfectly classify any assignment of labels on data (x_i, y_i) with $x \in \mathbb{R}$ and $y \in \{-1, 1\}$ and generalize poorly. Conversely, sometimes highly over-parameterized models (that have large subspaces of their parameters where $\mathcal{R}_{\text{emp}}[\hat{f}_\phi] \rightarrow 0$) might generalize well [8,9]. Often this is achieved through *regularization*, both explicit and implicit (section 41.3.1.2).

Structural risk minimization is a modification to the empirical risk minimization principle that was introduced by Vapnik and Chervonenkis to account for the potential for overfitting [7]. However, the bounds are based on a worst-case type analysis and are often very weak. Recall that while one cannot calculate the true risk, one can obtain an unbiased estimate of it with a held-out, independent testing sample. Thus one can empirically compare the generalization error of two models and find that one generalizes better than the other even if the bounds might suggest the opposite. One of the major conceptual shifts that happened with the rise of deep learning was to more fully appreciate that these bounds and structural risk minimization were not a good learning principle in practice and that more theoretical work is needed to close the gap between formal bounds and empirical estimates of generalization error.

41.3 Common tasks and their associated loss functions

We now move to common tasks encountered in machine learning and their associated loss functions.

41.3.1 Supervised learning

Supervised learning generally refers to the class of problems where the training dataset are presented as input-output pairs $\{x_i, y_i\}_{i=1, \dots, n}$, where $x_i \in \mathcal{X}$ are the input features and $y_i \in \mathcal{Y}$ are the corresponding target labels. Furthermore, it is typically assumed that $(x_i, y_i) \stackrel{i.i.d.}{\sim} p(x, y)$, though $p(x, y)$ is usually not known explicitly. Finally, the loss function in supervised learning takes on the special form $\mathcal{L}(y, f(x))$. The resulting trained model is then used to predict the labels for dataset where labels are not available.

In what follows we will make use of the equalities $p(x, y) = p(x|y)p(y) = p(y|x)p(x)$ and Bayes theorem, which is discussed in Sec. 39.1. We will also use the notation $x \sim p(x)$ to indicate that the random variable x is being drawn, sampled, or generated from the distribution $p(x)$.

¹Similarly, the gap between the true risk of the learned model and the true risk of the optimal model (i.e. $\mathcal{R}[\hat{f}] - \mathcal{R}[f^*]$) is referred to as the *regret*. This quantity is mainly of interest for theoretical analysis of machine learning algorithms, and not of practical concern since usually neither term is tractable.

41.3.1.1 Regression

The goal of regression is to predict a label $y \in \mathcal{Y}$ given an input feature vector $x \in \mathcal{X}$. Typically, the label is a real-valued scalar, but \mathcal{X} can be \mathbb{R}^d or some more structured target (e.g. an image, sequence, graph, quantile, or distribution). When \mathcal{Y} is discrete, the task is usually referred to as classification; however, the two are closely related and *logistic regression* is an example where the model predicts a continuous probability associated to the possible label values. In elementary statistical language, the target label y is often called a dependent variable, while the feature x is called the independent variable. In classical statistics, one often assumes a model for the data such as

$$y_i = f_\phi(x_i) + e_i, \quad (41.5)$$

where e_i is an additive error term that is often assumed to be independent of x and often assumed to be normally distributed. This leads to classic approaches like least-squares (see Sec. 40.2.3), and when the model f_ϕ is linear in ϕ (not in x !) one has linear regression that has a closed-form solution. However, we can relax these assumptions and consider the general case of an arbitrary joint distribution $p(x, y)$, which can be written as $p(y|x)p(x)$ without loss of generality. Consider the *squared error* as a loss function, which leads to the mean-squared error (MSE) for the empirical risk:

$$\mathcal{L}_{\text{MSE}}(y, f(x)) = (y - f(x))^2. \quad (41.6)$$

One might expect that the squared error would only be appropriate in the case that the conditional distribution $p(y|x)$ is normally distributed, but one can use the calculus of variations to show that in general

$$f_{\text{MSE}}^*(x) = \mathbb{E}_{p(y|x)}[y], \quad (41.7)$$

that is the optimal regressor for the MSE is the conditional expectation of y given x .

One issue with the squared-error as a loss function is that it is sensitive to outliers. Alternatively, one can use the absolute error $|y - f(x)|$ as a loss function². However, the discontinuous derivative of the absolute (L1) error leads to challenges in optimization. As a result there are various other loss functions, such as the Huber loss, that aim to be both robust and more amenable to optimization that we do not discuss here.

Note that these this framing of regression yields a function $f(x)$ that only provides a point estimate for y . An alternative approach to regression is to model the full conditional distribution $p(y|x)$. One such example is Gaussian Process regression, which is discussed in Sec. 41.5.1. In that probabilistic approach, one can still obtain a point estimator, such as the conditional expectation or the maximum a posteriori (MAP) estimator

$$f^*(x) = \arg \max_y p(y|x), \quad (41.8)$$

and one can also derive uncertainty estimates on the predicted value y . In this setting, the prior distribution on the model family is closely related to the concept of regularization, which we touch on in Sec. in Sec. 41.3.1.2 and in Sec. 41.5.1.

When one directly models $p(y|x)$, or goes further to model the joint distribution $p(x, y) = p(y|x)p(x)$, then one can use maximum likelihood for the loss function. In that approach, the problem is really one of density estimation, which is a type of unsupervised learning that we discuss in Sec. 41.3.2.1. These two approaches are a classic examples of two different approaches to modelling. Regression with $f_{\text{MSE}}^*(x)$ is the prototypical example of *discriminative* modelling, while modelling the joint distribution is a prototypical example of *generative* modelling. Generally, discriminative approaches with supervised learning out perform generative approaches when there is sufficient data, but generative approaches can be beneficial in data-starved settings [10].

²The absolute error and squared error are often denoted as L1 and L2 errors, respectively, in reference to the corresponding norms.

41.3.1.2 A note on regularization

The trained model \hat{f} , or equivalently, the parameters of the trained model $\hat{\phi}$ can be thought of as point estimates of f^* , and there is a correspondence to the issues of bias and variance discussed in Sec. 40.2 on parameter estimation. Generically, there is a bias–variance tradeoff, and when the number of parameters is large and the number of data points is not much larger, introducing a small bias can often lead to a significant reduction in variance. This motivates the explicit addition of a *regularization* term to the loss function, which will introduce some bias $f_{\text{reg}}^* \neq f^*$. A common form for regularization is to penalize by the L2 norm of the parameters (*i.e.* $\|\phi\|^2$), which is referred to as *Tikhonov regularization*. This appears in the form of penalized maximum likelihood, and it is also commonly used in unfolding [11]. One can also interpret the regularization term as an explicit prior on the parameters, and the resulting model as the Bayesian maximum a posteriori (MAP) estimator. When paired with linear regression this is known as *ridge regression*, and when paired with kernel machines (see Sec. 41.5.1) this gives rise to kernel ridge regression or Gaussian process regression.

Another form of regularization is to restrict the model class $\hat{\mathcal{F}}$. For example, a neural network and a sequence of narrow step functions (delta functions) can both be shown to be universal approximators in infinite parameter size limit, but on real world examples the former generalizes much better than the latter. Within the class of neural network models, convolutional neural networks are a subset of generic feedforward neural networks that enforce translational symmetry (see Sec. 41.5.3.5 for more discussion). Similarly, one might restrict to Lipschitz continuous functions. These types of choices are often encoded in the architecture of a neural network and are broadly referred to as *inductive bias* in the model.

In addition to explicit regularization terms in the loss function or through restrictions to the model class, it is also possible to regularize implicitly. One implicit regularization is through early stopping [11, 12], where we monitor the loss on training dataset and the loss on test dataset. While the training dataset loss continues to decrease with more gradient descent cycles, the test loss may not, and early stopping stops the training when test loss flattens out or begins to increase. Another powerful form of regularization used in deep learning models is known as *dropout* [13], which randomly removes some parts of the model during training and can be thought of as implementing a type of model averaging [14]. What is more surprising is that in the case of highly over-parameterized models where there is a large degenerate parameter space that achieves zero loss, $\Phi_0 = \{\phi | \mathcal{R}_{\text{emp}}[f_\phi] = 0\}$, that the dynamics of the optimization algorithm that is used will break the degeneracy and favor some particular $\hat{\phi} \in \Phi_0$ as if an additional regularization term was secretly included. Despite zero loss and over-parametrization, the corresponding generalization error may be small, a phenomenon called *benign overfitting* [15]. Importantly, the dynamics of different optimization algorithms will have different implicit regularization effects, and thus favor different parameter points in Φ_0 that will have different generalization error [16]. Understanding this interaction is a topic of contemporary research in machine learning [17].

41.3.1.3 Classification

The goal of classification is to predict one of a finite number of class labels $y \in \mathcal{Y}$ given an input feature vector $x \in \mathbb{X}$. It is similar to regression in this way, but the focus is on discrete target space \mathcal{Y} . An important special case is when the label can only take on one of two values (*e.g.* “signal” or “background”), which is referred to as binary classification and is equivalent to simple hypothesis testing in statistics. It is common for a classifier to be the composition of a model $g: \mathcal{X} \rightarrow \mathbb{R}^{|\mathcal{Y}|}$ that predicts continuous probabilities for each class (*i.e.* $g(x) \approx p(y|x)$) followed by an operation that then chooses the discrete label $y \in \mathcal{Y}$, such as a fixed threshold or $f(x) = \arg \max g(x) \approx \arg \max_y p(y|x)$. This is the case for both classical methods like logistic regression and modern, deep learning approaches to classification; therefore, we will use the term probabilistic classifier for $g(x)$ or just classifier

when it is clear in context.

An intuitive loss function for classification is the zero-one loss, which simply counts the number of mis-classifications:

$$\mathcal{L}_{0/1}(y, f(x)) = \begin{cases} 0, & \text{if } f(x) = y \\ 1, & \text{otherwise.} \end{cases} \quad (41.9)$$

The zero-one loss can also be written as $\mathcal{L}_{0/1}(y, f(x)) = \mathbf{1}(y \neq f(x))$, where $\mathbf{1}(\cdot)$ is the indicator function. The zero-one loss is non-differentiable, so it does not pair well with gradient-based optimization.

For binary classification, one can use $y = \{0, 1\}$ as numerical values for the class labels and the mean-squared error $\mathcal{L}_{\text{MSE}}(y, f(x))$ in Eq. 41.6 for the loss function. The resulting model will approximate f_{MSE}^* , the conditional expectation of Eq. 41.7 takes on the form

$$\begin{aligned} f_{\text{MSE}}^*(x) &= \mathbb{E}_{p(y|x)}[y] \rightarrow p(y=1|x) \\ &= \frac{p(x|y=1)p(y=1)}{p(x|y=0)p(y=0) + p(x|y=1)p(y=1)}. \end{aligned} \quad (41.10)$$

That is the MSE loss for binary classification leads to the Bayesian posterior probability that the label $y = 1$ given the feature vector x .

Equation 41.10 highlights an important general feature of supervised learning relevant for particle physics, which is that the joint distribution $p(x, y)$ of the training dataset implies a prior distribution $p(y)$ on the labels or classes. This prior distribution need not reflect a degree of belief or the frequency in real data, it represents the frequency in the training dataset. However, it is important to keep in mind that when applying the resulting model to a different dataset with the same conditional distribution (data likelihood) $p(x|y)$ for the features and a different prior $p'(y)$ for the labels that the probabilistic interpretation of the result will not be properly calibrated. A common choice for binary classification is to use a balanced training dataset with $p(y=0) = p(y=1) = \frac{1}{2}$, while in many cases the true $p'(y=1)$ in the experimental data might be very small (*i.e.* low signal-to-background), unknown, or zero (*i.e.* a hypothetical particle that does not exist).

If $p'(y)$ and $p(y)$ are known then the Bayes theorem can be used to re-calibrate the posterior $p(y|x)$ from one prior to another. One example of such re-calibration is the correspondence of binary classification to simple hypothesis tests in frequentist statistics discussed in Sec. 40.3.1 of the Statistics chapter. In that setting, the Neyman-Pearson lemma states that the optimal classifier is given by the likelihood-ratio. Adapting to the notation of this chapter, we have

$$f_{\text{N.P.}}^*(x) = \frac{p(x|y=1)}{p(x|y=0)}, \quad (41.11)$$

which does not depend on the prior probabilities $p'(y=0)$ or $p'(y=1)$ as in Eq. 41.10, or, equivalently, assumes equal priors $p'(y=0) = p'(y=1)$. From Bayes theorem, we have the identity $p(y=1|x)/p(y=0|x) = [p(x|y=1)p(y=1)]/[p(x|y=0)p(y=0)]$, which can be used to show that the two functions are related by a one-to-one, monotonic transformation

$$f_{\text{N.P.}}^*(x) = \frac{p(y=0)}{p(y=1)} \frac{f_{\text{MSE}}^*(x)}{1 - f_{\text{MSE}}^*(x)}, \quad (41.12)$$

which is referred to as the *likelihood-ratio trick*, which plays an important role in simulation-based inference (see Sec. 41.3.5). Importantly, the monotonic transformation does not impact the tradeoff of type-I and type-II error (or, equivalently, the FPR and TPR), therefore the ROC curve for $f_{\text{N.P.}}^*(x)$ and $f_{\text{MSE}}^*(x)$ are identical and do not depend on the prior probabilities $p(y)$. This property has been leveraged in the context of *weakly supervised* approaches [18] and enables one to train a classifier on data without access to labels as long as one has two datasets with different ratios $p(y=1)/p(y=0)$ and the same conditional distribution $p(x|y)$ of the features given the labels.

A generalization of the binary loss function for classification of Eq. 41.10, which applies to multiple classes, is the *cross-entropy* loss

$$\mathcal{L}_{\text{xe}}(y, f(x)) = - \sum_{c \in \mathcal{Y}} \mathbf{1}(y = c) \log(f_c(x)), \quad (41.13)$$

where $f : \mathcal{X} \rightarrow \mathbb{R}^{|\mathcal{Y}|}$ and the indicator function picks out the term in the sum for the corresponding class label y . This loss can be derived from maximizing the posterior of Eq. 41.57 using a discrete set of class labels y , which identifies $f_c(x) = \tilde{f}(y = c|x) = p(y = c|x)$ and thus enforces the constraint $\sum_c f_c(x) = 1$ and $f_c(x) \geq 0$ (for all $x \in \mathcal{X}$, e.g. by using the *softmax* function). The notation is aligned with the interpretation of $\tilde{f}(y|x)$ as a conditional distribution, i.e. an approximation to the true posterior $p(y|x)$. The risk associated to the cross entropy loss function is

$$\begin{aligned} \mathcal{R}_{\text{xe}}[f] &= \mathbb{E}_{p(x,y)} \left[- \sum_{c \in \mathcal{Y}} \mathbf{1}(y = c) \log f_c(x) \right] \\ &= - \sum_{c \in \mathcal{Y}} p(y = c) \mathbb{E}_{p(x|y)} [\log \tilde{f}(y = c|x)]. \end{aligned} \quad (41.14)$$

This is equivalent to $\mathcal{R}_{\text{xe}}[f] = \mathbb{E}_{p(x)} [H[p(y|x), \tilde{f}(y|x)]]$, where $H[p, f] = \mathbb{E}_p[-\log f]$ is the cross-entropy between the two distributions. One can use a Lagrange multiplier λ to enforce the normalization constraint (e.g. equation 41.10) and the calculus of variations to show that

$$f_{\text{x.e.,c}}^*(x) = \lambda p(x, y = c) = \lambda p(y = c|x)p(x) = p(y = c|x). \quad (41.15)$$

This approach is closely related to the loss functions that are used for density estimation, the forward Kullback–Leibler (KL) divergence, and the maximum likelihood estimation. Minimizing cross entropy $H[p, f_\phi]$ with respect to ϕ is equivalent to minimizing the forward KL divergence

$$KL(p||f_\phi) := \mathbb{E}_p[\log p(x)] - \log f_\phi = H[p, f_\phi] - H[p], \quad (41.16)$$

where $H[p] := \int p(x) \log p(x) dx$ is the entropy and independent of f_ϕ . The KL divergence $KL(p||f) \geq 0$, and equal if and only if $p = f$.

One can also consider the reverse KL divergence $KL[f_\phi||p]$, which is also minimized by $f_\phi = p$; however, this requires one to be able to generate samples $x_i \sim f_\phi(x)$ and be able to evaluate the probability density $p(x_i)$. Often this is not the case for real world data, but this approach is useful in the context of variational inference, where $f_\phi(x)$ is an approximation to the posterior of x , and $p(x)$ is the likelihood times the prior, which can be evaluated on samples x_i drawn from f_ϕ . Because likelihood times prior is not normalized this KL divergence optimizes the lower bound to the normalization (Evidence Lower Bound Objective or ELBO).

The forward KL is also closely related to the variational free energy principle in statistical mechanics where $H[f_\phi]$ represents the entropy of the variational distribution, $p(x) \propto \exp(-E(x)/kT)$ is the Boltzman factor for the state x with energy $E(x)$, and $H[f_\phi, p] = \mathbb{E}_{f_\phi}[E(x)]$ represents the expected energy for the variational distribution. As is well known to physicists, minimizing the free energy involves a balance between minimizing the energy and maximizing the entropy.

In some cases it is possible to augment the training dataset with an unbiased, stochastic estimate of $p(y = c|x)$ that we denote $s_c(x, z)$. For example, when the simulation involves latent variables z (i.e. Monte Carlo truth quantities), then the simulation encodes $p(x, z|y)$, the joint distribution over the observed features x and the latent variables z conditioned on the class y . In many cases the simulation evolves through a Markov process (e.g. the detector response only depends on the momenta of the incoming particles z , not the details of the hard scattering y). In that case, it is often possible to calculate $s_c(x, z) = p(y = c|x, z)$ for each training sample [19]. Using the identity, $\mathbb{E}_{p(z|x)} [p(y|x, z)] = p(y|x)$, we see that $s_c(x, z)$ is an unbiased estimator of $p(y = c|x)$.

In this case, one can use $s_c(x, z)$ in place of the indicator function in Eq. 41.13 to construct an improved (lower-variance) loss function that reproduces the same cross-entropy risk function^{3,4}

$$\begin{aligned} \mathcal{R}'_{\text{xe}}[f] &= \mathbb{E}_{p(x,y,z)} \left[- \sum_{c \in \mathcal{Y}} s_c(x, z) \log f_c(x) \right] \\ &= - \sum_{c \in \mathcal{Y}} \mathbb{E}_{p(x)} [p(y = c|x) \log f_c(x)], \end{aligned} \quad (41.17)$$

which yields the same optimal classifier $f_{\text{x.e.,c}}^*(x) = p(y = c|x)$ [20, 21].

We note that unlike in the binary classification case, the multi-class classifier is sensitive to the priors $p(y)$ used in training. This leads to complications as often the class proportions are unknown. For example, one might be interested in classifying a signal when multiple backgrounds are present and the relative proportion of those different background components is uncertain. Ideally one would like the class proportions for the background components used in training to match those in the data, which presents an additional training challenge if those proportions are heavily unbalanced.

41.3.2 Unsupervised learning

Unsupervised learning generally refers to the class of problems that use unlabeled training dataset $\{x_i\}_{i=1,\dots,n}$, where $x_i \in \mathcal{X}$ are the input features. Furthermore, it is typically assumed that $(x_i) \stackrel{i.i.d.}{\sim} p(x)$, though $p(x)$ is usually not known explicitly. Finally, the loss function in supervised learning takes on the special form $\mathcal{L}(x, f(x))$.

A related concept is that of self-supervised learning, which also aims to distill useful features in the data without requiring supervision labels for every sample in the input data. Self-supervised methods can make use of large unsupervised datasets and build meaningful representations by performing data augmentation, and learning the latent space mapping that is insensitive to it. For example, in the case of galaxy images one may augment the data by performing image rotations, adding noise, size scaling, adding point spread function smoothing etc., all of which are realistic transformations expected in a real galaxy image survey [22]. Self-supervised learning then learns the latent space representation where all of these augmentations of the same training sample result in the same latent space position. This training is augmented with contrastive learning, which ensures that different training samples do not all collapse to the same latent space position. When this latent space representation is used for downstream tasks such as classification it outperforms other forms of supervised learning [23].

41.3.2.1 Density estimation

The goal of density estimation is to estimate a distribution $p(x)$ based on samples $\{x_i\}_{i=1,\dots,n}$ with $x_i \stackrel{i.i.d.}{\sim} p(x)$. Conceptually, this is the same goal as when fitting a parameterized distribution $f(x; \theta)$ to data using the method of maximum likelihood as described in Sec. 40.2.2 of the chapter on statistics. In practice, the difference in the machine learning context has to do with the flexibility of the model and the dimensionality of the data. A highly-flexible model, which can effectively approximate any distribution, is referred to as a non-parametric model (though, ironically, usually this means the model has many parameters). In contrast, typical maximum likelihood fits in particle physics are based on restricted families of distributions with relatively few parameters and the data is typically one- or two-dimensional, though occasionally five- or six-dimensional.

Maximizing the likelihood function in Eq. 40.10 $\mathcal{L}(\theta) =$

³A similar approach can also be used for the squared-error, see Ref. [20].

⁴The right hand side of Eqs. 41.14 and 41.17 are written in a different form, but are equivalent.

$\prod_{i=1}^n f(x_i; \theta)$ is equivalent to minimizing the empirical risk:

$$\mathcal{R}_{\text{emp,xe}}[f_\phi] = -\frac{1}{n} \sum_{i=1}^n \log f_\phi(x), \quad (41.18)$$

where we adopt the notion used in this chapter. The loss is simply $\mathcal{L}(x, f_\phi(x)) = -\log f_\phi(x)$, and the corresponding risk is

$$\mathcal{R}_{\text{xe}}[f_\phi] = \mathbb{E}_{p(x)}[-\log f_\phi(x)], \quad (41.19)$$

which is the cross entropy $H[p, f_\phi]$. For density estimation, the model is usually constructed to enforce $\int f_\phi(x) dx = 1$ and $f_\phi(x) \geq 0$ so that it can be interpreted as a distribution. With this constraint, one can show that $f_{\text{xe}}^*(x) = p(x)$.

The concepts of generalization and overfitting are particularly acute in unsupervised learning, where the likelihood maximization of equation 41.18, combined with universal approximator assumption, must converge onto $\hat{p}(x) = \frac{1}{n} \sum_{i=1}^n \delta(x - x_i)$, the empirical distribution of the dataset $\{x_i\}_{i=1, \dots, n}$. This distribution has the highest likelihood on the training dataset and the lowest likelihood on the test data where it gives $\hat{p}(x) = 0$. as long as the test dataset are not identical to the training dataset. So the empirical distribution of the training dataset has the worst possible generalization property, yet it is the solution we converge to for sufficiently expressive architectures in the absence of any regularization. In contrast, in supervised learning we often observe the phenomenon of benign overfitting, where even zero loss can generalize well.

In addition to approaches to density estimation that involve learning in the sense of minimizing a loss or risk function, we note that there are also classical density estimation techniques such as histogramming and kernel density estimation [24–26].

41.3.2.2 Representation learning, compression, and auto-encoders

A recurring topic in machine learning and statistics is how to represent the data. Much of classical statistics involves constructing a low-dimensional summary statistic that extracts the relevant information from the data for a particular task (a sufficient statistic in language of classical statistics). There is a spectrum of representations with trade-offs. At one end of this spectrum is lossless compression that allows you to encode the data into a smaller, intermediate representation that carries all the information since it can be decoded back into the original data. At the other end of the spectrum is something like the likelihood-ratio, which is a single scalar that carries the relevant information needed for hypothesis testing for a single hypothesis, but it discards all the other information that might be needed for other tasks (such as testing other hypotheses). An intermediate point in this spectrum is the process of feature engineering, which refers to the creation of new features \mathcal{X}' from the original features \mathcal{X} in hopes that the down-stream task will be easier with the new features. For example, instead of working directly with the energy and momentum of particles, one might compute invariant masses, angles between particles, etc. This type of feature engineering generally improved performance for shallow neural networks, decision trees, etc.; however, with the rise of deep learning this is often no longer necessary and often limits performance compared to working with the original features. One can think of the intermediate layers of a neural network between the input and the output a representation of the data that is good for the task at hand, and by training all the layers of the network simultaneously (or “end-to-end”) one can see the intermediate layers as a learned representations. For a review see Ref. [27].

An example of a linear dimensionality reduction representation and data compression is principal component analysis (PCA) of data $x \in \mathbb{R}^d$ at fixed latent space dimensionality k ($k < d$), which finds the orthogonal linear transformation, O ,

$$O : \mathbb{R}^k \rightarrow \mathbb{R}^d, z \mapsto Oz, OO^T = I_d \quad (41.20)$$

that maximizes the data variance in the latent space. Maximizing the variance of the transformed data is equivalent to minimizing

the average reconstruction error (the residual variance in data space),

$$\mathcal{L}_{a.e.}(x, f(x)) = \|x - f(x)\|^2. \quad (41.21)$$

A PCA can thus be interpreted as a linear, orthogonal model that is trained to minimize the L_2 -distance between the input data and the reconstructed data given the fixed dimensionality k . In practice, the PCA problem can be solved analytically without the use of optimization algorithms or the loss function: the principal components are given by the eigenvectors of the data covariance matrix.

A suitable latent space dimensionality, k , is chosen by ordering the eigenvalues, λ_i , of the data covariance in descending order, and keeping only the first few eigenvectors that correspond to the largest eigenvalues. The cut is often made at dimensionalities that capture around 90% of the data variance. For many data sets this results in $k \ll d$. The average reconstruction error that originates from the discarded eigenvalues is $\sigma_{\text{recon}}^2 = \sum_{i=k+1}^d \lambda_i$.

Another common type of representation learning and nonlinear dimensionality reduction is based on the *auto-encoder* $f = g \circ e : \mathcal{X} \rightarrow \mathcal{X}$, where $e : \mathcal{X} \rightarrow \mathcal{Z}$ is referred to as the *encoder* and $g : \mathcal{Z} \rightarrow \mathcal{X}$ is referred to as the *generator* or *decoder*. Typically the dimensionality of \mathcal{Z} is much less than \mathcal{X} , and $z = e(x)$ can be thought of as a compressed representation of the input. The intermediate space \mathcal{Z} is sometimes referred to as the *bottleneck* or the *latent space* of the auto-encoder. If the bottleneck is sufficiently large and the encoder and decoder are sufficiently flexible, then the function f could just be the identity (*i.e.* lossless compression). However, if the encoder and decoder are not sufficiently flexible or the dimensionality of the latent space is not large enough there will be some reconstruction error. Therefore the reconstruction error of Eq. 41.21 serves as a natural loss function of an auto-encoder.

Once trained, the encoder $e(x)$ can be used independently of the decoder to provide a generic low-dimensional representation of the data. The flexibility of this approach is attractive; however, there are no guarantees that this representation will be optimal for the other task. Indeed, the transition from pre-trained auto-encoders to end-to-end learning is one of the important trends that characterized the onset of the deep learning era.

While achieving zero reconstruction error may seem good as it would imply lossless compression, it often performs poorly in practice. First, the encoder may be overfit to the training dataset and not generalize well to held out data. Secondly, it may not be robust to domain shift (see Sec. 41.7.2). One approach to address these issues is the *denoising auto-encoder*, which uses a form of regularization that corrupts the input with noise $x' \sim q(x'|x)$ while still targeting reconstruction of the uncorrupted input x .

$$\mathcal{L}_{d.a.e.}(x, f(x)) = \|x - f(x')\|^2 \quad \text{with} \quad x' \sim q(x'|x), \quad (41.22)$$

where $q(x'|x)$ is some probability distribution such as a multivariate normal.

41.3.2.3 Clustering

The goal of clustering is to group the data $\{x_i\}_{i=1, \dots, n}$ into k groups, or *clusters*, usually with $k \ll n$. Intuitively, if two data points belong to the same cluster, then they should be similar in some sense. Conversely, if two data points are very different, then they should be assigned to different clusters. The notion of similarity usually is based on some heuristic, and there are a variety of algorithmic and probabilistic clustering algorithms. In some cases k is specified, while in others it is determined by the clustering algorithm. There is also a distinction between flat clustering that directly partitions the data into k clusters and hierarchical clustering where clusters are nested hierarchically as the name suggests. In many cases clustering uses some notion of distance $d(x_i, x_j)$, which may be the L_p norm $\|x_i - x_j\|_p$.

One of the most common clustering algorithms is known as *k*-means, where k is specified by the user and results in sets $S = \{S_1, \dots, S_k\}$ that minimize the variance of each cluster. Thus,

the objective is

$$\begin{aligned} \arg \min_{\mathbf{S}} \sum_{i=1}^k \sum_{\mathbf{x} \in S_i} \|\mathbf{x} - \boldsymbol{\mu}_i\|^2 &= \arg \min_{\mathbf{S}} \sum_{i=1}^k |S_i| \text{Var } S_i \\ &= \arg \min_{\mathbf{S}} \sum_{i=1}^k \frac{1}{2|S_i|} \sum_{\mathbf{x}, \mathbf{y} \in S_i} \|\mathbf{x} - \mathbf{y}\|^2 \end{aligned} \quad (41.23)$$

where $\boldsymbol{\mu}_i$ is the mean of points in S_i .

While k -means and many other clustering algorithms are defined in terms of an optimization problem, the optimization objective is often not representative of the actual notions of performance in a given context. As a result, there are a number of quantities used for the evaluation and assessment of the resulting clustering. These include Davies–Bouldin index, Dunn index, Rand index, Jaccard index, purity, F-measure, Hopkins statistic, *etc.* [28].

41.3.3 Optimal control, reinforcement learning, and active learning

Many problems in science and engineering can be cast as a control problem, which comprises a cost functional that is a function of state and some control variables that specify some underlying dynamical system. This is relevant for the control of accelerators where the dynamical system is physical. This formalism can also be used to describe the design of experiments, planning of an observational survey, and other decision making processes relevant to the scientific method. There is a tremendous amount of literature on the subject, and it is closely connected to planning, dynamic programming, and reinforcement learning. Optimal control can be seen as an extension of the calculus of variations, and thus generalizes the framing of learning presented in Sec. 41.2.

Optimal control theory deals with finding a control for a dynamical system over a period of time such that the objective function is optimized. The underlying system can be discrete or continuous and may be deterministic or stochastic. The commonalities and differences between optimal control and reinforcement learning can be best understood through the formalism of a Markov decision process (MDP), which is a discrete-time stochastic control process. We follow common notation, such as that found in Wikipedia.

A Markov decision process comprises four components often organized as a 4-tuple (S, A, P_a, R_a) , where: S is a set of states called the state space, A is a set of actions called the action space, $P_a(s, s') = \Pr(s_{t+1} = s' \mid s_t = s, a_t = a)$ is the probability that action a in state s at time t will lead to state s' at time $t + 1$, $R_a(s, s')$ is the immediate reward (or expected immediate reward) received after transitioning from state s to state s' , due to action a .

The policy function π is a mapping from state space to action space that can be either deterministic or probabilistic. For examples, the policy that drives a computer chess playing system, decides which move to make given the current state of the board. Similarly, policies dictate which experiment should be built next, which field of the sky should be observed, or how to adjust the operational parameters of an accelerator. The dynamics of the resulting system are then fixed by combining the policy with the underlying MDP. The evolution of the resulting dynamical system behaves like a Markov chain since the action chosen in state s is completely determined by $\pi(s)$ and $\Pr(s_{t+1} = s' \mid s_t = s, a_t = a)$ implies the Markov transition matrix $\Pr(s_{t+1} = s' \mid s_t = s)$.

The objective optimal control is to choose a policy π that will maximize a cumulative function of the instantaneous rewards R_a . A common choice is the expected discounted sum:

$$\mathbb{E} \left[\sum_{t=0}^{\infty} \gamma^t R_{a_t}(s_t, s_{t+1}) \right], \quad (41.24)$$

where $a_t \sim \pi(s_t)$ are the actions given by the policy, the expectation computed with respect to the distribution $s_{t+1} \sim P_{a_t}(s_t, s_{t+1})$, and γ is the discount factor satisfying

$0 \leq \gamma \leq 1$. The discount factor is usually close to 1 and sometimes reparameterized as $\gamma = 1/(1+r)$, where r is called the discount rate. A lower discount factor motivates the decision maker to favor taking actions early, rather than postpone them indefinitely.

A policy that maximizes the objective function is called an optimal policy and denoted π^* , though the optimal policy need not be unique. Importantly, the Markov property implies that the optimal policy is only a function of the current state. Dynamic programming can be used to find the optimal policy for MDPs with finite state and action spaces. For instance, in value iteration (a.k.a. backward induction) can be used to solve the “Bellman equation” [29]. For continuous-time systems, the optimal policy is defined by the Hamilton–Jacobi–Bellman equation [30].

In many settings, it is assumed that the state s is fully known when action is to be taken and there are no latent variables. When this assumption is not true, the problem is called a partially observable MDP. These problems are generally more difficult and the dynamic programming algorithms do not directly apply [31].

Reinforcement learning The main difference between the classical dynamic programming methods and reinforcement learning (RL) algorithms is that the latter do not assume knowledge of an exact mathematical model of the MDP and they target large MDPs where exact methods become infeasible. For example, RL was used in the context of jet physics to search for the most likely jet clustering when the number of constituents was too large for the exact dynamic programming algorithm to be used [32]. In addition, RL can be used when the probabilities or rewards are unknown. Instead, the transition probabilities are often accessed indirectly through interaction with a real or simulated environment. For example, in Q-learning one uses experience to estimate the array $Q(s, a)$ defined as

$$Q(s, a) = \sum_{s'} P_a(s, s') (R_a(s, s') + \gamma V(s')). \quad (41.25)$$

While this function is also unknown, it can be estimated during learning based on (s, a) pairs together with the outcome s' .

Numerous variations to RL exist, which include so-called model-based and model-free approaches (referring to models of the instantaneous rewards and the state transitions) and on-policy and off-policy (which describes how the actions taken during learning are related to the current policy). See Ref. [33] for an introduction and Ref. [34] for a recent review.

Multi-arm bandits Multi-arm bandit problems are a classic reinforcement learning problem where one tries to maximize the expected gain by allocating a limited set of resources to various alternatives. The name is a reference to a gambler with a fixed amount of money that must choose between multiple slot machines (or “one-armed” bandits) when the payoff for the individual machines is unknown. A hallmark of multi-arm bandit problems is that they involve a trade-off between exploration (playing machines to estimate their payoff) and exploitation (playing machines with the highest estimated payoff). Multi-armed bandits are used to manage large projects, organizations, and scheduling problems. The theory has a long history going back to Robbins in 1952 that used it to study the sequential design of experiments [35] and Gittins who derived an optimal policy under some conditions [36].

Bayesian optimization A closely related set of techniques involve optimizing some expensive black box function $f(x)$. For instance, the function may be computationally expensive to evaluate or low-latency, *e.g.* it may involve manually re-configuring a system. This is particularly relevant for analysis optimization in particle physics where evaluating $f(x)$ involves processing large numbers of simulated collisions. Another common use case involves optimizing the hyperparameters of a learning algorithm.

Without any assumptions about the function $f(x)$ this is hopeless; however, if one assumes something about the functions (*e.g.*

some notion of smoothness) then one can leverage function evaluations $\{f(x_t)\}_{t=1,\dots,T}$ to say something about what value the function might take on at other values of x . This is usually cast in Bayesian terms, and Gaussian processes (Section 41.5.1) are often used to model the distribution over $f(x)$. The optimization techniques that use this framing are generically referred to as Bayesian Optimization [37].

Optimization in this context is usually characterized by an *exploration-exploitation* trade-off, similar to what is found in multi-arm bandits. Here, exploration refers to function evaluations that characterize the function in regions that haven't been evaluated, while exploitation refers to evaluations near what is predicted to be its maximum. This setting is similar to reinforcement learning in that it involves sequential decisions (*i.e.* where to evaluate the function next), but usually the target function $f(x)$ is assumed to be static. In that sense, the state referred to in the language of an MDP is the state of knowledge about the function after sequential evaluations $\{f(x_t)\}_{t=1,\dots,T}$. The reward at time t is not the value of the function $f(x_t)$, but some quantity that characterizes what was learned about the function's maximum. In this literature, one often refers to the *acquisition function*, which plays a similar role as the expected value of the reward in RL. Common acquisition functions include the probability of improvement, the expected improvement, and an upper-confidence bound [38].

Connection to experimental design In the context of physics experiments we often want to build the next generation experiment which can reach certain target precision on parameters of interest that the experiment can measure. To achieve this precision we may deploy the concept of *experimental design*, where we the objective is to optimize some objective that quantifies the expected performance of an experiment. Moreover, we would like to achieve this within some constraints such as a minimal cost. Such problems are often solved using the Fisher matrix optimization, where Fisher matrix can be viewed as the expectation of the inverse covariance matrix. We can define

$$t(x|\theta_0) := \nabla_{\theta} \log p(x|\theta)|_{\theta_0}, \quad (41.26)$$

where $t(x|\theta_0)$ is referred to by statisticians as the score [20]. The score plays an important role in the classical statistics as it is a sufficient statistic when $p(x|\theta)$ is in the exponential family, and through the Rao-Cramér-Fréchet bound on the variance of an estimator for θ , and is used to define the Fisher information matrix $I_{ij}(\theta) := \mathbb{E}_{p(x|\theta)}[t_i(x|\theta)t_j(x|\theta)]$. The Fisher information, in turn is an important object in experimental design. In particle physics, the score is closely related to the concept of optimal observables. The corresponding diagonal element of the inverse of the Fisher matrix thus provides expected uncertainty estimation of a given parameter, and is a lower bound to the error of an unbiased estimator (Cramér-Rao bound). In experimental design we vary the experiment parameters within the constraints such as the total cost to minimize this uncertainty. This framework has been widely used in cosmology, where Fisher analysis is the foundation of any experiment proposal.

Active learning Active learning is closely related to Bayesian optimization, described above. In Bayesian optimization one estimates the function $f(x)$ from some set of evaluations $\{y_t = f(x_t)\}_{t=1,\dots,T}$; however, the goal is to find the maximum $x^* = \arg \max_x f(x)$. In active learning, the goal is not to find the maximum of $f(x)$, but to approximate the function as one does in supervised learning. The main difference compared to vanilla supervised learning is that the labeled training dataset isn't provided a priori in a passive way, but the learning algorithm actively decides where to generate $(x_t, y_t = f(x_t))$ pairs. The function $f(x)$ is sometimes referred to as an *oracle*. Active learning is particularly attractive when obtaining labelled data is a costly process.

More broadly, a challenge of many machine learning applications is obtaining labeled data, which can be a costly process. If a system could learn from small amounts of data, and choose by itself what data it would like the user to label via an external process called oracle, it would make machine learning more

powerful. Such frameworks are also called Experiment Design or Active Learning. In Active Learning, a model is trained on a small amount of data (the initial training dataset), and an acquisition function (often based on the model's uncertainty) decides on which data points to ask for a label. The acquisition function selects one or more points from a pool of unlabelled data points, with the pool points lying outside of the training dataset. Once we label the selected data points, these are added to the training dataset, and a new model is trained on the updated training dataset. This process is then repeated, with the training dataset increasing in size over time. The advantage of such systems is that they often result in dramatic reductions in the amount of labelling required to train an ML system (and therefore cost and time).

41.3.4 Anomaly detection and out-of-distribution detection

Unsupervised anomaly detection techniques detect anomalies in an unlabeled test data set under the assumption that the majority of the in-distribution data are normal under some measure, while out-of-distribution (OOD) data are not. In the context of auto-encoders a popular technique is to use the reconstruction error of Eq. 41.21 to identify an outlier as one with a large reconstruction error [39, 40]. One issue with this method is that for higher dimensional latent space and flexible neural network architectures the encoder-decoder map become identity for any input data, $f(x) = x$, regardless of whether input x is from the in-distribution training dataset or from the out-of-distribution data. The choice of auto-encoder latent space dimensionality is thus an important hyperparameter that must be tuned.

Another set of anomaly detection techniques construct a model representing normal behavior from a given In Distribution training dataset, and then test the likelihood of a test instance to be generated by the utilized model. For instance, one can use density estimation methods such as normalizing flows (section 41.5.4.3) to learn the density (likelihood) of the In Distribution training dataset $p(x)$, and apply it to the test data. The expectation is that out-of-distribution data will have a lower density (likelihood) under the in-distribution density model. This expectation is however not always met in high dimensions and the method suffers because likelihood based training is sensitive to the smallest variance directions [41]: for example, a zero variance pixels leads to an infinite $p(x)$, and noise must be added to regularize it. But low variance directions may contain little or no information on the global structure of the image, so there is a mismatch between the training objective and outlier detection objective. A related issue is that of typicality: an in-distribution likelihood will typically be lower than the maximum value. For a Gaussian likelihood the typical set is on average be $n/2$ in log likelihood below the peak value, where n is the dimensionality of the data. So an out-of-distribution dataset that is closer to the peak would be preferred in terms of likelihood even though its distribution does not match the in-distribution data. If this happens by chance on low variance directions which dominate the likelihood, normalizing flows can assign higher likelihoods to out-of-distribution data than to in-distribution training dataset [42]. A number of techniques have been proposed to circumvent these limitations, such as likelihood regret [43], likelihood-ratio [41], likelihood in auto-encoder latent space [44], and Wasserstein distance training of the likelihood $p(x)$ [45]. These methods can achieve better anomaly detection performance than the auto-encoder reconstruction error [44, 46].

Supervised anomaly detection techniques require a data set that has been labeled as in-distribution and out-of-distribution and involves training a classifier (the key difference to many other statistical classification problems is the inherent unbalanced nature of outlier detection). These methods assume some form for what out-of-distribution data may look like, and their success relies on whether the assumed form is a realistic representation of actual out-of-distribution data. When this assumption is valid these methods can be more powerful than unsupervised methods, but the reverse is also true. A hybrid between the two approaches is to train a classifier without labels [47]. All these approaches are largely complementary to each other [48]. An example of different anomaly detection methods applied to HEP is LHC Olympics

2020 and Dark Machines challenges [49, 50].

41.3.5 Simulation-based inference

The goal of simulation-based inference (related to, but distinct from, likelihood-free inference) is to extend the statistical procedures described in the Chapter on Statistics (e.g. parameter estimation, hypothesis tests, confidence intervals, and Bayesian posterior distributions) to the situation where one does not know the explicit likelihood $p(x|\theta)$, the probability of the data given the parameters θ , but has access to a simulator that defines the likelihood $p(x|\theta)$ implicitly [51, 52]. In a typical setup we would like to solve the so called inverse problem of getting the posterior of the parameters given the data, $p(\theta|x)$, but we cannot use Bayes theorem directly because we do not have explicit $p(x|\theta)$.

In particle physics, the simulators usually use Monte Carlo event generators (see Sec. 43) to sample unobserved latent variables z , such as the z_p phase space of the hard scattering (see Sec. 49.4), z_s associated to showering and hadronization, and z_d associated to the interaction of particles with the detector (see Sec. 34). As such, the full simulation chain can be expressed symbolically as

$$\begin{aligned}
 p(x|\theta) &= \int dz_p p(x, z|\theta) \\
 &= \int dz_d \int dz_s \int dz_p p(x|z_d)p(z_d|z_s)p(z_s|z_p)p(z_p|\theta),
 \end{aligned}
 \tag{41.27}$$

where θ are the Lagrangian parameters that dictate the hard scattering. Evaluating the likelihood is intractable as it would require evaluating the integral above for each event.

While the likelihood is intractable, simulators provide the ability to generate synthetic data $x_i \stackrel{i.i.d.}{\sim} p(x|\theta)$ for any value of the parameters θ . One can use a suitable proposal distribution $\tilde{p}(\theta)$, sample $\theta_i \stackrel{i.i.d.}{\sim} \tilde{p}(\theta)$, generate synthetic data $x_i \sim p(x|\theta_i)$, and then assemble a training dataset $\{x_i, \theta_i\}_{i=1, \dots, n}$ that can be used to train various machine learning models.

There is thus a close analogy between Simulation-based Inference and data driven machine learning tasks discussed so far, replacing θ with y . One difference is that in simulation-based inference we can always generate new samples by running additional simulations, while we typically view training dataset in machine learning as fixed. This property of Simulation-based Inference enables Active Learning, where the additional simulations are chosen such as to minimize the error on the desired statistical inference task. Another difference is that we often have access to the joint likelihood $p(x, z|\theta)$, where z are unobserved latent variables⁵.

Typically in particle physics, one uses histograms or kernel density estimation to model the distribution of observables (low-dimensional summary statistics such as the invariant mass) of simulated data [53]. Alternatively, one can use an explicit parametric family (such as a falling exponential, a Gaussian distribution, etc.) to model $\hat{f}(x|\theta) \approx p(x|\theta)$. That model is then used as a surrogate for the unknown density implicitly defined by the simulator. A related approach is known as Approximate Bayesian Computation (ABC), which approximates the likelihood through an acceptance probability that synthetic data is sufficiently close to the observed data [54, 55]. In practice, these techniques are limited to low-dimensional representations of the data. Thus the potential of recent machine learning approaches to simulation-based inference is to extend this approach to higher-dimensional data, while maintaining the already well-established statistical procedures.

For instance, one can use normalizing flows (see Sec. 41.5.4.3) and the loss functions for density estimation (see Sec. 41.3.2.1) to learn a surrogate model for the likelihood $\hat{f}(x|\theta) \approx p(x|\theta)$ [56]. Similarly, one can use conditional density estimation to learn a surrogate model for the posterior $\hat{f}(\theta|x) \approx p(\theta|x)$, which may involve including the prior-to-proposal ratio $\tilde{p}(\theta)/p(\theta)$ [57]. In addition to the unsupervised learning

⁵For this reason we prefer to use simulation-based inference instead of likelihood-free inference: joint likelihood $p(x, z|\theta)$ is often available, it is the marginal integral over latent space z that is assumed to be intractable.

techniques, one can also use supervised learning to learn the likelihood-ratio $r(x|\theta_0, \theta_1) = p(x|\theta_0)/p(x|\theta_1)$ by leveraging the likelihood-ratio trick of Eq. 41.12 [20, 58].

In some cases one can also augment the training dataset to include the joint likelihood-ratio

$$r(x_i, z_i|\theta_0, \theta_1) := p(x_i, z_i|\theta_0)/p(x_i, z_i|\theta_1), \tag{41.28}$$

which can be used to reduce the variance for the squared-error loss or the improved cross-entropy estimator of Eq. 41.17 [20, 21]. While the marginal likelihood $p(x|\theta)$ is intractable due to the high-dimensional integral over the latent space, the joint likelihood is often tractable since no integration is necessary. In addition, one can often augment the training dataset with the joint score

$$t(x_i, z_i|\theta_0) := \nabla_{\theta} \log p(x_i, z_i|\theta)|_{\theta_0}. \tag{41.29}$$

Regressing on the joint score with the squared loss function $\mathcal{L}(t(x, z|\theta_0), f(x)) = (t(x, z|\theta_0) - f(x))^2$ corresponds to risk functional

$$\mathcal{R}_{\text{score}}[f] := \mathbb{E}_{p(x, z|\theta_0)}[(\nabla_{\theta} \log p(x_i, z_i|\theta)|_{\theta_0} - f(x))^2]. \tag{41.30}$$

One can show with the calculus of variations that the risk is minimized by the score of equation 41.26.

41.3.5.1 Differentiable simulations

One of the approaches to make inference feasible in high dimensional latent space is to make simulations differentiable with respect to all of its parameters, global variables θ and latent variables z . Latent variable models are known in Machine Learning as generative models and are discussed below, but latent variable models are also common in scientific applications. As an example, in cosmology one can view the initial conditions of the large scale structure or cosmic microwave background as Gaussian distributed latent variables.

While differentiable simulations have traditionally not been developed for scientific applications, the success of Machine Learning, where backpropagation algorithm combined with gradient descent optimization (see Sec. 41.6.1) is the basis of its recent advances, has inspired a new look at this. One recent example is FlowPM cosmological N-body simulation, which takes advantage of Mesh-Tensorflow to achieve a GPU-accelerated, distributed, and differentiable simulation [59].

One broad class of inference problems where gradients make the problem simpler are the so called inverse problems. As a simple example let's assume the data x are observed with some Gaussian noise with known variance σ^2 , equal for all data points. The likelihood of the data can be written as

$$\log p(x|z, \theta) = -\frac{N}{2} \log[2\pi\sigma^2] - \frac{\|x - g(z, \theta)\|^2}{2\sigma^2}. \tag{41.31}$$

Here $g(z, \theta)$ is the forward model (generator or decoder), i.e. the simulation output in the absence of noise. The joint distribution is $p(x, z|\theta) = p(x|z, \theta)p(z|\theta)$, where $p(z|\theta)$ is the prior of latent space variables, assumed to be known, with a known gradient with respect to θ and z . In this case the gradients $\nabla_{\theta} \log p(x, z|\theta)$ and $\nabla_z \log p(x, z|\theta)$ are available when the simulation forward model gradients $\nabla_{\theta} g(z, \theta)$ and $\nabla_z g(z, \theta)$ are available.

Availability of simulation gradients in turn enables gradient based optimization or sampling. In sampling approach one can use Monte Carlo Markov Chains to obtain the posterior samples of latent space z and parameter space θ [60]. In optimization approach one can find the best-fit point \hat{z} , which is the MAP estimate of the latent space variables z given x and fixed θ [61]. Another optimization approach is Variational Inference, which attempts to model the posterior probability distribution using optimization. This is discussed further in Section 41.5.4.

41.3.5.2 Unfolding as an inverse problem

While much of the work on simulation-based inference described above is aimed at inferring the parameters θ of the simulator, there is also work that aims to infer the latent variables z . Here it is useful to think of the parameters θ as parameters of a theory, such as masses, coupling constants, or Lagrangian parameters, while z

might describe the kinematics of a collision before the detector response.

Inferring the distribution $p(z|\{x_1, \dots, x_n\})$ from a dataset of multiple observations is commonly referred to as unfolding in particle physics, and deconvolution in other contexts. Unfolding is a classic inverse problem, and the collection of ideas being used for machine-learning based simulation-based inference are also being applied in this setting. Examples of recent work exploring these approaches are Refs. [62–73]. In addition, there has been work to infer the posterior distribution for an individual event $p(z|x_i)$ using probabilistic programming techniques [74–76].

41.4 Data representations, inductive bias, and example applications

In Sec. 41.3 we describe the input data as living in an abstract space $x_i \in \mathcal{X}$. In this section, we briefly describe some of the common types of structured data that are encountered in physics and refer to the corresponding model classes that have been developed to work with them. We will describe the model classes in more detail in the following section.

The most basic and common type of data structure is when $\mathcal{X} = \mathbb{R}^d$. This is often referred to as *tabular data* since the entire data set $\{x_i\}_{i=1, \dots, n}$ can be thought of as a table with n rows and d columns. It is common to think of an individual entry x_i as a vector in d -dimensional Euclidean space, where the coordinates correspond to the columns of this table. In some cases individual components of x_i might be integers or take on only discrete values, in which case describing the space of the data as real-valued is a slight abuse of notation and representation. For many years this was the dominant type of data in high energy physics as it is a natural input type for shallow neural networks, multi-layer perceptrons, support vector machines, and tree-based methods found in popular tools such as TMVA [77].

For categorical data, one typically uses a numerical representation such as *integer encoding* where different categories are mapped to integers with a corresponding dictionary. Another common representation of categorical data is based on the so-called *one-hot encoding* (aka ‘one-of-K’ or ‘dummy’), in which case the category is mapped to a k -dimensional binary vector where k is the number of categories and each component of this vector corresponds to a particular category. In the one-hot encoding, only one of the components is non-zero. Finally, there are approaches in one learns an *embedding* that maps discrete categories into \mathbb{R}^d ; an example of this is Word2Vec [78]. Interestingly, such embeddings can preserve various types of semantics; for instance, the vector `walking-walk` is similar to the vectors `swimming-swam` as are the vectors connecting countries and their capital cities. This allows for a loose sense of algebra on the word embeddings such as `walking-swimming+swam = walk`. Similar types of embeddings have also been used in a number of scientific use-cases including biological sequences (e.g. DNA, RNA, and Proteins) for bioinformatics applications [79].

Particle physics data often is represented with an extension of the simple tabular data structure where the number of columns is not fixed. For instance, if the rows correspond to data for individual collisions, the number of electrons (and positrons) reconstructed in the event is variable. Thus the number of columns needed to represent the energy, momentum, and charge of these particles is also variable. A common solution to this problem is to fix a maximum number of particles and then *truncate* and *zero-pad* to fit the data into a fixed tabular representation, though this is not the natural representation of the data and it leads to a loss of information.

Sequential data is also commonly encountered in physics (e.g. in time series). Here an individual entry $x_i = (x_i^1, \dots, x_i^t, \dots, x_i^{T_i})$ where t is index for the ordered sequence, T_i is the length of the sequence (which might be variable), and the data associated to each ‘time’ $x_i^t \in \mathbb{R}^d$. This is similar to the previous example where the energy, momentum, and charge of the t -th electron in the i -th event would be x_i^t and the electrons might be sorted according to their energy or transverse momentum. Sequential data is also encountered in natural language processing, where x_i^t correspond to individual words in a sentence. Recurrent neural networks (see

Sec. 41.5.3.9) are particularly well suited to sequential data. Examples applications from the Living Review include [80–85].

Image-like data is one of the most dominant forms of data in industrial applications of deep learning, is very relevant for astronomy and cosmology, and also appears in particle physics in various forms. Image-like data typically involves d -dimensional features associated to a regular grid or lattice that does not vary across the individual instances x_i . The canonical example is a standard image from a camera with $W \times H$ pixels where the p -th pixel has data $x_i^p \in \mathbb{R}^3$ corresponding to the three *channels* in the RGB color model. It is important to recognize that the data corresponding to the 2-dimensional image is not 2-dimensional; instead, it is $(W \times H \times c)$ -dimensional, where c is the number of channels. In astronomy, an image may be grey scale ($c = 1$) or there may be more *channels* ($c > 3$) corresponding to different color filters. In other applications, the grid or lattice might be 3- or 4-dimensional. For example, the data associated to a regularly segmented calorimeter can be thought of as a 3-dimensional image and the data associated to a lattice simulation of a classical or quantum system can be thought of as a 4-dimensional image. Convolutional neural networks, described in Sec. 41.5.3.5, are particularly well suited to image-like data. Example applications from the Living Review include [81, 86–108].

It is also possible that the the data (or features) associated to one ‘pixel’ or lattice site may itself be structured. For example, the single read-out plane of a Liquid Argon time projection chamber (LArTPC) may involve a 1-dimensional or 2-dimensional grid, but the data associated to each ‘pixel’ is itself a sequence or waveform. Example applications in Neutrino Physics from the Living Review include [109–139]. Similarly, in lattice quantum chromodynamics, the data associate to a particular site (or link) would be group valued (e.g. $x_i^p \in SU(3)$ as in Refs. [140, 141]).

Both sequential and image-like data have a notion of temporal or spatial structure. While it is possible to unroll an image into a $(W \times H \times c)$ -dimensional vector, that would erase the spatial structure and obfuscate the fact that nearby pixels are highly correlated. Similarly, one could permute the time index for sequential data, but that would destroy the temporal structure of the data. The complementary point of view is that the model class should also be aware of the structure of the data. Recurrent neural networks and convolutional neural networks are good examples of what is called *inductive bias* as the models do incorporate something about the structure of the data that they are expected to be used with. In some cases this can be formalized in terms of symmetry. For example, if we train model to classify images of cats and dogs, we would like it’s prediction to be invariant to where in the image the cat is. This type of translational invariance can be enforced in the design of the model class.

While permuting the elements of a sequence destroys the temporal structure of a time series, attaching a temporal index t to a set of objects with features x_i^t can also be problematic. If the data corresponding to x_i really are a set $\{x_i^1, \dots, x_i^{T_i}\}$ (e.g. a point cloud), then we would like the output of the model to be *permutation invariance*. A standard sequential or convolutional model will not generally be permutation invariant, but recently models such as Deep Sets, various types of graph neural networks, and transformers can be made to enforce permutation symmetry. Example applications from the Living Review include [100, 142–152].

The temporal and spatial structure of sequences and image like data can also be generalized. For instance, a 1-dimensional sequence can be generalized to a tree structured data like one finds in the hierarchical clustering of jets or as in a directed-acyclic graph (DAG). Generalizations of recurrent neural networks have been constructed that can operate over these more complex data structures [153, 154]. More generally, one can consider graph-structured data composed of nodes and edges or multi-graphs that group together three nodes into faces or k nodes into k -edges. Graph neural networks are a class of models that work with this type of data. The emerging subfield of geometric deep learning aims to unify the notation, terminology, and theory that connect these considerations of the structure of the data and the corresponding model architecture. Example applications in the Living Review include [121, 128, 131, 132, 134, 155–181].

If the data are expected to have a symmetry associated to them but one is working with a model class that does not enforce this symmetry, then *data augmentation* is a common procedure used to improve generalization performance. Here one starts with an initial dataset $\{x_i\}_{i=1,\dots,n}$ and produces an augmented dataset $\{x'_i\}_{i'=1,\dots,n'}$ through some data augmentation strategy. For example, one might apply a random rotation $R_{i'}$ to an image to produce $x'_i = R_{i'}(x_i)$ if one assumes rotational invariance in the underlying problem.

In some cases some of the individual features (components) of x are functions of other features. For instance, one may include components of a four-vector (E, p_x, p_y, p_z) as well as redundant information such as transverse momentum, azimuthal angles, rapidity, etc. In this case, the data is restricted to a lower-dimensional surface embedded in \mathcal{X} . Even if the features aren't redundant, statistically the data are often effectively restricted to a small subspace of statistically likely samples and those that are exceedingly unlikely. For instance, the space of natural images is a small and highly structured subspace of all possible images, which are dominated by what we would perceive visually as noise. The term *data manifold* is used to describe this restricted subspace where the data are to be found, even though it does not necessarily satisfy the formal requirements of a manifold in the mathematical sense.

These considerations on the structure of the data not only apply not to the input data $x_i \in \mathcal{X}$, but also to the output data $y_i \in \mathcal{Y}$. For instance, one might want a sequence-to-sequence model as in machine translation of written text [182] or to learn a function that takes sets as input and produces graphs as output as in the Set2Graph mode [183]. One might also want the input and output of the model to be different in representations of an underlying symmetry group and for the model to enforce group-equivariance [140, 141]. The development of the necessary modelling components to enable practitioners to compose and train these types of models is a significant development for the field of physics.

41.5 Flavors of ML models

41.5.1 Support vector machines and kernel machines

Support Vector Machines (SVM) are a class of supervised learning models used for classification and regression. The learning algorithm involves a convex optimization problem that has a unique solution and can be solved with quadratic programming techniques. In this sense, they are robust and easier to characterize than neural networks that involve non-convex optimization. While their history goes back to Vapnik and Chervonenkis in the 1960s, they gained popularity after Bernhard Boser, Isabelle Guyon and Vladimir Vapnik suggested a way to create nonlinear classifiers by applying the kernel trick in 1992 [184]. Originally they were developed for binary classification and only supported the restricted case where the training dataset can be separated without errors, but in 1995 Cortes and Vapnik extended the technique to non-separable training dataset [185]. A variant targeting regression, known as support vector regression (SVR), was developed in 1997 [186]. The theory around support vector machines was well developed, and they dominated machine learning research for roughly a decade before the rise of deep learning (see Sec. 41.5.3.4).

Maximum-margin classifiers Linear support vector machines are used for binary classification, where $\mathcal{X} = \mathbb{R}^d$ and the target labels are conventionally defined as $\mathcal{Y} = \{-1, 1\}$. The classification is simply based on which side of a hyperplane the data lie. Any hyperplane can be written as the set of points x satisfying $w^T x - b = 0$, where $w, b \in \mathbb{R}^d$ are the parameters of the model. The vector w is normal to the hyperplane, but not necessarily normalized. The quantity $\frac{b}{\|w\|}$ quantifies the offset of the hyperplane from the origin along the normal vector w .

If the training dataset is linearly separable, then there is a region bounded by two parallel hyperplanes, called the *margin*, that separate the two classes of data. The maximum margin classifier is uniquely defined by making the distance between these two hyperplanes as large as possible. The boundaries of the margin

can be defined by $w^T x_i - b = \pm 1$, and the width of the margin is given by $\frac{2}{\|w\|}$. Figure 41.1 illustrates this for $x \in \mathbb{R}^2$.

Since the width of the margin is maximized when $\|w\|$ is minimized, we can state the goal of the (hard) maximum-margin classifier in the linear separable case as the following constrained optimization problem: Minimize $\|w\|^2$ subject to the constraint $y_i(w^T x_i - b) \geq 1$ for $i = 1, \dots, n$. The w and b that solve this problem uniquely determine the resulting classifier, $\hat{y}(x) = \text{sgn}(w^T x - b)$.

This geometric description makes it clear that the maximum-margin hyperplane is completely determined by those x_i that lie nearest to it: the eponymous *support vectors*.

Soft margins and slack variables Often the data will not be linearly separable and thus the hard-margin optimization problem described above has no solution. Such a non-separable case can be accommodated with the use of so-called *slack variables*. One slack variable $\xi_i > 0$ is introduced for each data point. As shown in Figure 41.1 (right), if a data point x_i is outside the margin and correctly classified as in the separable case, then $\xi_i = 0$. If it is within the margin but still correctly classified, then $0 < \xi_i < 1$. If it is misclassified, then $\xi_i > 1$. The new constrained optimization problem is to minimize

$$\sum_i \xi_i + \lambda \|w\|^2 \quad (41.32)$$

subject to the constraints $y_i(w^T x_i - b) \geq 1 - \xi_i$ and $\xi_i > 0$ for $i = 1, \dots, n$. Effectively, this corresponds to minimizing $\sum_i \max(0, 1 - y_i(w^T x_i - b)) + \lambda \|w\|^2$, where the first term is called the *hinge loss*.

The dual problem In the language of convex optimization, linear programming, and quadratic programming the optimization problems stated above for the hard and soft maximum-margin classifiers define the *primal* objective to be minimized. There is a *Lagrange dual* problem where the solution corresponds to maximization with $\min_{\phi} L(\phi) = \sup_{\alpha > 0} \tilde{L}(\phi, \alpha)$, where α are Lagrange multipliers. While it is not apparent in the primal formulation of the constrained optimization problems, the solution to the dual problem takes on the form

$$\hat{y}(x) = \text{sgn}\left(\sum_i y_i \alpha_i x_i^T x - b\right), \quad (41.33)$$

where the $\alpha_i > 0$ for the support vectors and otherwise zero. This reformulation is plausible since the orientation of the maximum-margin hyperplanes defined by w is completely specified by the support vectors. The crucial observation for the kernel trick described below is that the final model is defined in terms of coefficients and the inner product $\langle x_i, x \rangle_{\mathcal{X}} = x_i^T x$.

The kernel trick One approach to obtain non-linear decision boundaries is to introduce a non-linear mapping $\varphi: \mathcal{X} \rightarrow \mathcal{V}$ that embeds the data in some higher-dimensional space \mathcal{V} . One can then use the linear SVM described above in the space \mathcal{V} . This is not unlike the many neural network models where the first layers use a non-linear activation function while the last layer is linear.

The *kernel trick* avoids the explicit mapping φ that is needed to get linear learning algorithms to learn a nonlinear function or decision boundary. This is possible because the solution to the dual problem in Eq. 41.33 is represented in terms of inner products $\langle \varphi(x_i), \varphi(x) \rangle_{\mathcal{V}} = \varphi(x_i)^T \varphi(x)$ corresponding to the candidate point x and the support vectors x_i . Thus all that is needed is a way to evaluate the inner products. A *kernel* or a kernel function $k: \mathcal{X} \times \mathcal{X} \rightarrow \mathbb{R}$ is a function that can be expressed as an inner product in another space \mathcal{V} via $k(x, x') = \langle \varphi(x), \varphi(x') \rangle_{\mathcal{V}}$. Critically, one does not need to ever evaluate the map $\varphi(x')$, which is implicitly defined by the kernel. In some cases the kernel is straight forward to evaluate, even though the target space \mathcal{V} is implicitly defined by the kernel would be infinite dimensional.

The choice of the kernel is roughly the analog of the architecture of a neural network. It dictates the types of non-linearities the

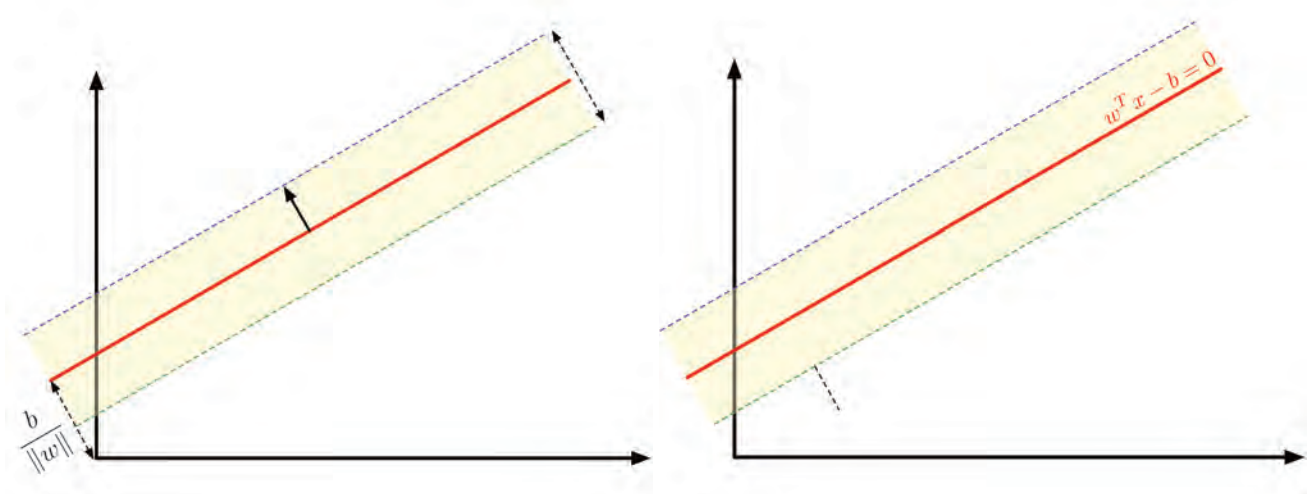


Figure 41.1: Illustration of a maximum margin classifier for a linear support vector machine in the separable case (left) and with the soft-margin and slack variables ξ (right).

SVM can implement in the input space. It also provides an opportunity to encode prior knowledge from physics such as symmetries, length scales, *etc.* There are also connections between very wide neural networks with random weights and biases and the kernel of a Gaussian process [187–189], which, when applied to deep networks, lead to the concept of neural tangent kernel [190]. While it is beyond the scope of this chapter, the interested reader may also be curious to understand the connections as formalized in the language of Reproducing kernel Hilbert spaces (RKHS) [191].

Support vector regression There are a few flavors of SVR. In Vapnik’s ϵ -SVR formulation is similar to the picture for classification, but the boundary hyperplane serves as the prediction and the width of the margin for which there is no penalty is ϵ . Again, one can introduce a non-linear map $\phi(x)$ explicitly or implicitly via the corresponding kernel $k(x, x')$. One can view the predictive model as $\hat{y}(x) = w^T \phi(x) - b$ and the goal of the optimization problem is to minimize

$$\|w\|^2 + C \sum_i (\xi_i + \xi_i^*) \quad (41.34)$$

where ξ_i and ξ_i^* are slack variables associated to the model over or under-estimating $y_i \in \mathbb{R}$. The constrained optimization is subject to $w^T x_i - b - y_i \leq \epsilon + \xi_i$, $y_i - w^T x_i + b \leq \epsilon + \xi_i^*$, $\xi_i, \xi_i^* \geq 0$ for $i = 1 \dots, n$. The solution to the dual problem leads to a kernelized representation of the solution

$$\hat{y}(x) = \sum_i (\alpha_i^* - \alpha_i) K(x, x_i) - b, \quad (41.35)$$

where the α_i, α_i^* are the parameters of the dual problem. In libraries like `libsvm` the output of the algorithm is just $\alpha_i^* - \alpha_i$ for $i = 1 \dots, n$.

Kernel ridge regression Kernel Ridge Regression (KRR) uses the same model as in SVR; however, it uses a different loss function. KRR uses the squared error loss while support vector regression uses the ϵ -insensitive loss function (*i.e.* no penalty is incurred if the prediction is within ϵ). Both are combined with l2 regularization (the $\|w\|^2$ term). While SVR leads to a sparse solution that only depends on the support vectors, it can be slow to solve the constrained convex optimization problem. In contrast, KRR can be done in closed-form and is typically faster to train for medium-sized datasets. The consequence is that the learned model is non-sparse and thus slower than SVR to evaluate at prediction-time.

Gaussian Process Regression (kriging) Another variation on kernel-based regression is Gaussian process regression (GPR), also referred to as *kriging*. Again the model is based on the kernel trick. While KRR aims to minimize the mean-squared error loss $(y_i - \hat{y}(x_i))^2$ along with an l2 regularization term proportional to $\|w\|^2$, GPR elevates these terms to a probabilistic interpretation where the first is proportional to a log-likelihood for Gaussian $N(y_i | \hat{y}(x_i), \sigma)$ likelihood and the second corresponds to the log of a Gaussian prior on w_i . This is related to the discussion on Tikhonov regularization found in Sec. 41.3.1.2. GPR goes further and uses a mean function $m(x)$ and kernel $k(x, x')$ to define a probabilistic model for $y(x)$ and $y(x')$ that includes correlations. For any finite number of points $\{x_j\}_{j=1, \dots, m}$, the Gaussian process defines the joint distribution for the values that $f(x_i)$ might take. Typically, one specifies the prior mean $m(x)$ and prior covariance function $k(x, x')$ and then conditions on the training dataset $\{x_i, y_i\}_{i=1, \dots, n}$. The posterior can then be evaluated for an independent set of points $\{x_j\}_{j=1, \dots, m}$. The posterior mean is typically used as the prediction equivalent to SVR and KRR, but GPR also gives a meaningful notion of uncertainty in the predictions, and can be viewed as a realization of kernel Bayesian regression [192].

One advantage of GPR is that one can work with a family of kernel functions parameterized by some hyperparameters η . One can then optimize the hyperparameters via gradient-ascent on the marginal likelihood function. In contrast, hyperparameter tuning in SVR and KRR typically requires a grid search or some other black-box optimization procedure evaluated on held out data or some form of cross-validation.

Rasmussen and Williams provides an excellent review of Gaussian processes [193]. Numerically, Gaussian Process libraries are confronted with computing the log determinant of the covariance kernel, which naively scales like $\mathcal{O}(n^3)$ in computational complexity. However, recently there have been a number of numerical advances that make these methods fast and scalable to large datasets [194, 195]. While Gaussian Processes are used more widely in cosmology, they are not widely used in particle physics or astro-particle physics. Recent works explore the design of physics-inspired kernels and use Gaussian Processes to model the intensity for a Poisson point process like those found in experimental particle physics and γ -ray and X-ray astronomy [196–198]. Gaussian Processes are also extensively used in Bayesian Optimization (Section 41.3.3).

41.5.2 Decision trees

Tree-based models Classification and Regression Trees (CART) typically partition the input space into J disjoint regions $\mathcal{X} = \mathcal{X}^1 \cup \dots \cup \mathcal{X}^J$ through a sequence of $J - 1$ binary splits based

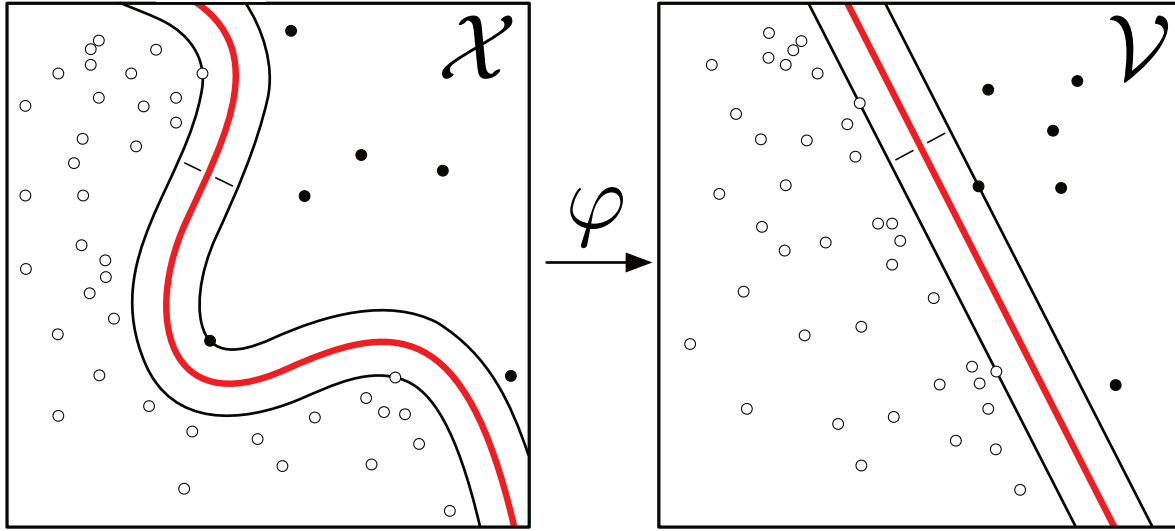


Figure 41.2: Figure depicting the nonlinear SVM decision boundary in \mathcal{X} (left) and the corresponding linear maximum margin classifier in \mathcal{Y} (right). Figure adapted from Kernel_Macine.svg Wikimedia Commons (CC BY-SA 4.0) by Cranmer.

on an individual components of $x \in \mathcal{X}$ (e.g. $x_4 < 0.7$) [199]. The model is piecewise constant and assigns the value $b_j \in \mathcal{Y}$ to the j -th terminal region \mathcal{X}^j . The model can be written

$$\hat{y}(x) = f_\phi(x) = \sum_j b_j \mathbf{1}(x \in \mathcal{X}^j). \quad (41.36)$$

The parameters ϕ of the model comprise the components index and thresholds for the successive splittings and the coefficients b_j .

Tree learning refers to the algorithm used to choosing the tree structure and determining the predictions at leaf nodes. Optimization of the tree structure involves a difficult discrete optimization since the change in the loss with respect to the tree structure is non-differentiable and it is intractable to explore the combinatorially large space of possible trees with brute force. Therefore, the discrete optimization component of tree learning typically involves some approximate algorithm based on heuristics. In contrast, optimization of the b_j for a given tree structure can exploit gradient-based optimization algorithms.

Common approaches to building the decision tree start with a root node and grow with splits based on individual attributes (components of x). These are referred to as top-down induction strategies. There are various impurity heuristics used for choosing the best attribute to split on such as the Gini index, cross-entropy and mis-classification error. Generally they aim to find a split that will refine the the terminal nodes such that they have higher purity than the parent node.

Because most tree learning algorithms consider splits aligned with individual feature components, there are some failure modes for tree-based models. However, tree-based models work well with tabular data that is composed of a mix of continuous and discrete features. Tools such as XGBoost [200] are widely used in data science competitions such as Kaggle and the boosted decision trees (BDTs) implemented in StatPatternRecognition [201] and TMVA [77] have been one of the most used techniques in particle physics [3].

Individual trees are often referred to as weak-learners and they can be combined in various ways described below. Regularization is also an important consideration with tree-based models as one can always learn a tree that assigns exactly one training dataset point per terminal node and memorize the training dataset exactly. One approach to this is called *pre-pruning*, which simply terminates the growing of the trees if the number of training samples reaching the terminal node drops below some threshold, the purity of a terminal nodes is below some threshold, or if the improvement in purity due to a proposed split is not above a

threshold. Another regularization approach is called *post-pruning*, which uses a validation data set that is disjoint from the training dataset to probe generalization performance. In this approach, after initially growing a tree with the training dataset, one considers a sequences of pruned trees where splits are removed based on some heuristic. One finds the tree in this sequence of pruned trees that minimizes the generalization error on the validation set. Alternatively, in tools such as XGBoost there is an explicit regularization term included in the loss function (see Eq. 41.43).

Ensemble methods The idea of ensemble methods is to combine multiple models into a more performant one by exploiting the bias-variance tradeoff [202]. This is most commonly achieved through averaging (e.g. bagging and random forests), which primarily reduces variance, or boosting (e.g. AdaBoost and gradient boosting), which primarily reduces bias. Here bias refers to the difference between the Bayes optimal model and the average model produced by the learning procedure with different training sets and variance quantifies how much the learned model varies from one training set to another.

The motivation of boosting is to combine the outputs of many “weak” models to produce a more expressive model. Compared to averaging techniques like bagging and random forests, the model is built sequentially on modified versions of the data and the final predictions are combined through a weighted sum

$$\hat{y}(x) = \sum_{t=1}^T \beta_t \hat{y}_t(x), \quad (41.37)$$

where β_t expand the parameters of the model ϕ .

Bagging The idea behind bagging (bootstrap aggregating) is to create T bootstrap training datasets B_1, \dots, B_T drawn from the training dataset $\{x_i, y_i\}_{i=1, \dots, n}$, then learn a model \hat{y}_t for each, and finally construct an average model $\hat{y}(x) = (1/T) \sum_t \hat{y}_t(x)$. If one had T independent training datasets each of size n , then the bias of the average model would be the same as the original model, but the variance would be reduced by a factor of T . By using bootstrap resampling, the bias may increase but the reduction in variance often dominates, which leads to improved performance.

Random forests Random forests refers to a type of “perturb and combine algorithm” that combines bagging and random attribute subset selection. Again one builds trees $\hat{y}_t(x)$ from bootstrap training datasets B_t , but instead of choosing the best split

among all attributes, one select the best split among a random subset of k attributes. If k includes all attributes, then it is equivalent to bagging.

AdaBoost In AdaBoost (adaptive boost) the sequence of trees $\hat{y}_1, \dots, \hat{y}_T$ are trained with reweighted versions of the original training dataset such that the weight of individual training sample is based on the prediction error in the previous iteration [203]. This requires working with a loss function that and learning procedure for the individual iterations that is amenable to weighted training dataset $\{x_i, y_i, w_i\}_{i=1, \dots, n}$. Incorporating the weights w_i is straight forward when the risk is expressed as an expectation, since the empirical risk of Eq. 41.3 is just replaced with the weighted average. Similarly, the heuristic for many of the tree-based learning algorithms (e.g. the Gini index) also have natural generalizations with weighted events.

In the context of classification, the weighted error of the model $\hat{y}_t(x)$ is

$$\text{err}_t = \frac{\sum_i w_i^{(t)} \mathbf{1}[y_i \neq \hat{y}_t(x_i)]}{\sum_i w_i^{(t)}}. \quad (41.38)$$

Based on this weighted error, the coefficient β_t of the component $\hat{y}_t(x)$ in Eq. 41.37 is given by

$$\beta_t = \log \left(\frac{1 - \text{err}_t}{\text{err}_t} \right). \quad (41.39)$$

Then for the next iteration the weights of the misclassified events are updated as $w^{(t+1)} = w^{(t)} \exp(\beta_t)$ and then renormalized so that the sum of all weights is 1. This reweighted dataset is then used to train the next model $\hat{y}_{t+1}(x)$ and the entire procedure is initialized with uniform weights $w_i^{t=0} = 1/n$.

There is an analogous procedure for regression with the squared loss function based on the residuals $r_i = y_i - \hat{y}_t(x_i)$ (see for example Ref. [77] for details).

Gradient boosting One of the most powerful forms of tree based models, which is implemented in the tool **XGBoost** is referred to as *gradient boosting* [204]. In this setup, the model is purely additive as in the case of random forests, so the model is Eq. 41.37 with all $\beta_t = 1$. Note this is without loss of generality since the β_t can be absorbed into the b_j of Eq. 41.36. As with AdaBoost, the model is built sequentially through the sequence $\hat{y}_1, \dots, \hat{y}_T$.

At each iteration, a new term f_t will be added to the sum in Eq. 41.37. For a given decision tree defined by splits on attributes, one can approximate the objective function (the loss function \mathcal{L} plus a regularization term Ω) as a function of b_j in a second order Taylor series:

$$\begin{aligned} \text{obj}^{(t)} = \sum_{i=1}^n [\mathcal{L}(y_i, \hat{y}_i^{(t-1)}) + g_i f_t(x_i) + \frac{1}{2} h_i f_t^2(x_i)] + \Omega(f_t) + \\ + \text{constant}, \end{aligned} \quad (41.40)$$

where

$$g_i = \partial_{\hat{y}_i^{(t-1)}} \mathcal{L}(y_i, \hat{y}_i^{(t-1)}) \quad (41.41)$$

and

$$h_i = \partial_{\hat{y}_i^{(t-1)}}^2 \mathcal{L}(y_i, \hat{y}_i^{(t-1)}) \quad (41.42)$$

In **XGBoost**, the regularization term is taken to be

$$\Omega(f) = \gamma J + \frac{1}{2} \lambda \sum_{j=1}^J b_j^2, \quad (41.43)$$

where J is the number of terminal nodes in the tree. With the second-order approximation of the objective, one can directly solve for the optimal b_j for the next tree and the corresponding value of the optimized objective function. The improvement in the objective function can then be used as a heuristic for choosing the best split. Specifically, define $G_j = \sum_{i \in I_j} g_i$ and

$H_j = \sum_{i \in I_j} h_i$, where I_j is the set of indices of data points assigned to the j -th leaf. The heuristic used in **XGBoost** for splitting a node is

$$\text{Gain} = \frac{1}{2} \left[\frac{G_L^2}{H_L + \lambda} + \frac{G_R^2}{H_R + \lambda} - \frac{(G_L + G_R)^2}{H_L + H_R + \lambda} \right] - \gamma. \quad (41.44)$$

This formula can be interpreted as the score on the new left leaf plus the score on the new right leaf minus the score on the original leaf minus a regularization penalty on the additional leaf. If the gain from splitting a leaf is smaller than γ , then the total Gain is negative and the split will not be added, which can be seen as implementing a form of pruning.

41.5.3 Neural networks

In this section we focus on the different types of components used in modern neural network architectures. Gradient-based optimization techniques are most commonly used for training neural networks, and they are described in Sec. 41.6.1. Similarly, other important aspects to effectively training neural network models such as parameter initialization, early stopping, etc. are discussed in Sec. 41.6.

The vanishing and exploding gradient problem is a common challenge for gradient-based optimization of neural networks and is described in Sec. 41.6.5. That problem is referred to repeatedly in this section because it has motivated the development of numerous architectural components described below.

41.5.3.1 Feed-forward multi-layer perceptron

One of the core components in neural networks is the fully-connected, feedforward network or *multi-layer perceptron* (MLP), which is composed of L layers: $f = f^{(L)} \circ \dots \circ f^{(1)}$. The l^{th} layer defines a function that maps a d_{l-1} -dimensional input vector, called *features*, to an d_l -dimensional output $f^{(l)} : \mathbb{R}^{d_{l-1}} \rightarrow \mathbb{R}^{d_l}$. A unit responsible for producing an individual output in d_l -dimensional output is called a *neuron* or a *filter* interchangeably. For $l < L$, the functions f_l are called hidden layers, and the number of neurons (d_l) is referred to as the width of the hidden layers. The layers in an MLP take on the form:

$$f^{(l)}(u) = \sigma^{(l)}(W^{(l)}u + b^{(l)}), \quad (41.45)$$

where $W^{(l)} \in \mathbb{R}^{d_l \times d_{l-1}}$ is called the *weight matrix*, the components of the vector $b^{(l)} \in \mathbb{R}^{d_l}$ are referred to as the *biases*, $u \in \mathbb{R}^{d_{l-1}}$ is the input from the previous layer, $W^{(l)}u$ denotes a matrix-vector product, and $\sigma^{(l)}$ is a non-linear *activation function* that is usually applied element-wise. The parameters of the network comprise the full collection of weights and biases, $\phi = (W^{(1)}, \dots, W^{(L)}, b^{(1)}, \dots, b^{(L)})$.

41.5.3.2 Activation functions

The activation functions σ in neural networks are nonlinear functions and key to the expressiveness of the resulting family of functions. Two traditionally used functions are *logistic* and *hyperbolic tangent* functions. These functions are bounded to be $(0, 1)$ and $(-1, 1)$ respectively, and are symmetric about the input value of zero. On the other hand, away from the zero input value, a gradient of both functions quickly vanishes and this poses a challenge in using gradient-based optimization method (see Sec. 41.6.1). This can be avoided, to some extent, by normalizing the input values and carefully initializing the values of $W^{(l)}$ and $b^{(l)}$. These are discussed in Sec. 41.6.7, 41.6.8 and 41.6.9. Yet, it becomes difficult to maintain a null input value for a *deep* neural network, a model with many layers. Instead, a popular choice for a deep neural network is *Rectified Linear Unit* (ReLU):

$$\sigma(x) = \begin{cases} x & \text{if } x > 0 \\ 0 & \text{otherwise} \end{cases} \quad (41.46)$$

which computational cost is small and provides the gradient does not vanish for $x \in (0, +\infty)$ [205,206]. An alternative to preserve a non-zero gradient in negative input values are called *Leaky ReLU* and modifies the output to $0.01x$ for $x \in (-\infty, 0)$ [207]. Another variant, called *Parametric ReLU* (PReLU), turns the coefficient

0.01 into a variable that is optimized as a part of the model during optimization [208].

The choice of activation functions depends on the model architecture and applications. As described, while the use of ReLU types are a typical choice for a deep neural network, a logistic function is a popular choice at the final layer for classification tasks. Recently, in the area of neural scene representation, sinusoidal activation functions have been found to be surprisingly effective [209].

41.5.3.3 Softmax

A softmax function is often used to normalize elements of a discrete vector u , or to interpret the output as a probability over a set of n discrete categories. Given a real-valued input vector $u \in \mathbb{R}^n$, the softmax function computes the output vector $v \in \mathbb{R}^n$ the i -th component is given by:

$$v_i = \frac{\exp(u_i)}{\sum_{j=1}^n \exp(u_j)}. \quad (41.47)$$

The result has the property that $v_i \in (0, 1)$ and $\sum v_i = 1$. The components of the input vector u are often referred to as *logits* in reference to their connection to the logistic function used in logistic regression. The softmax function is commonly used as the last layer in multi-class classifier. The softmax is also used in the context of attention (see Sec. 41.5.3.11).

41.5.3.4 The rise of deep learning

There are a number of universal approximation theorems in the theory of neural networks. One of the first was that even with one hidden layer ($L = 2$), an MLP can approximate any continuous function if the non-linear activation function σ not a polynomial and the width d_1 is large enough [210]. However, it is often more efficient (in terms of the number of parameters) to increase the *depth* of the network L [211].

Training a deep network (*i.e.* $L > 2$) that generalizes well can be more difficult, requiring large training datasets, many gradient updates, and suitable regularization. The introduction of large labeled training sets, advances in computing (*e.g.* graphic processing units or GPUs which enabled orders of magnitude acceleration in parallel computation including matrix multiplies [212]), development of ReLU, research progress in initialization and optimization algorithms for model parameters, and regularization techniques like *dropout* [13] all played an important role in the rise of *deep learning* [2, 213]. Though the name deep learning was originally a reference to the depth L of such networks, modern deep learning is characterized more by the composition of various types of modules that are trained through gradient-based optimization. Below we introduce some other common network architectures.

41.5.3.5 Convolutional neural networks

Convolutional Neural Networks (CNNs) are widely used for image-like data. They implement the convolution of the input image u and a *filter* W (also referred to as a kernel). The parameters of the filter are learnable and the convolution involves traversing over input and calculating the inner product of the filter W with the part of the input in the *receptive field*, which has the same spatial shape as the filter and is centered at the target pixel. At each location – indexed by i and j below – there is a pixel that may have a vector of features associated with it. In the context of CNNs, these components of these features – indexed by c and c' below – are often referred to as *channels* in reference to the red, green, and blue color channels in a traditional image. The convolution operation is often denoted with a $*$, and the result can be expressed as

$$v_c(j) = (W * u_c)(j) = \sum_{c'} \sum_i W_{c,c'}(i) u_{c'}(“j - i”), \quad (41.48)$$

where “ $j - i$ ” is shorthand for the pixel index corresponding to the translation from pixel j to i . By repeating the operation over all pixels, the result of a kernel convolution is also an image as

illustrated in Figure 41.3. Note that the the number of channels in the output v does not need to be the same as in the input, and the collection of filters $W_{c,c'}$ is often referred to as a filter bank. The entire image for a fixed channel index is often referred to as a *feature map*.

A key feature of the CNN architecture is that it is *equivariant* to translations, meaning that if the input image is shifted (*e.g.* $u(i) \rightarrow u'(i) = u(i - k)$), then the output is also shifted by the same amount (*e.g.* $v(j) \rightarrow v'(j) = v(j - k)$). This equivariance property is a natural consequence of using convolutions. A fully connected MLP would not generally have this symmetry; however, it is enlightening to imagine transferring the computation performed by a CNN to the weights and biases of a fully connected MLP, which would result in duplicating the weights of the filters multiple times. In this view, the CNN can be interpreted as a fully connected MLP with *shared weights*, which would maintain the equivariance property. This view is helpful for gaining intuition about the inductive bias of models and makes clear that a CNN is a subset of the fully connected MLPs that satisfy the translation equivariance property.

The discussion above makes it clear that CNNs will have fewer parameters than the corresponding fully connected MLP, which can alleviate the optimization challenge. In addition, the convolutional structure allows for data to be reused effectively as patterns in one part of an image in the training dataset effectively contribute to learning that pattern anywhere in the image. Larger kernel sizes allow for the filters to learn more complicated patterns, but at the expense of having more parameters and needing more data to train (the extreme case being a kernel size that is the size of the entire image, which would be equivalent to a fully connected MLP). In practice, kernel sizes of 3 are popular, 5 is sometimes used, and larger kernels are rarely used.

A kernel convolution involves three hyperparameters, the size of kernel (typically an odd number so that the filter has an unambiguous center), *stride*, and *padding*. The stride is the number of pixels between each target pixel (*i.e.* the center of the filter). The stride size of 1 implies the target pixels are adjacent, and a stride of 2 implies skipping 1 pixel in between (along each spatial axis). Padding is an operation to expand the input image by a specified number of pixels (*i.e.* “padding size”) for when the target pixel is near the edge and the filter would extend beyond the input image. In Figure 41.3, the input image is 4×4 pixels, the kernel is of size 3, and no (zero) padding is applied. The result is a smaller image. Alternatively, With the padding of size 1, the output would retain the 4×4 shape of the input image.

A kernel size of 1 is also frequently used and is referred to as a 1×1 *convolution*. While it cannot capture a geometrical features, it can perform linear operations on the input features, including increasing or decreasing the number of features. When combined with a non-linearity and stacked repeatedly this can be seen as a small MLP attached to an individual pixel, and for this reason the 1×1 convolution is sometimes referred to as a *network-in-network* [214]. This is often used to extract more powerful features to be used by the latter layers, and also to compress features when the next layers may be computationally demanding such as a block of many convolution layers with a large kernel size [215, 216].

One may wonder how CNNs identify features with a spatial size larger than a typical kernel size. One mechanism for this is by stacking multiple convolutional layers – *e.g.* the composition of two 3×3 kernels will lead to an effective 4×4 kernel. In addition, a typical CNN architecture uses pooling (described below), which effectively down-samples the image so that it can be processed at different resolutions. The effective receptive field in the input image may be much larger than the kernel size in this case. An alternative approach is to use an *inception module* which is designed to extract features simultaneously using kernels of different size [215].

41.5.3.6 Pooling

Pooling plays an important role in convolutional neural networks both practically and in terms of their mathematical properties. A pooling operation is a type of aggregation or down-sampling that takes many pixels as input and produce one pixel for output. Typically, the pooling operation is applied indepen-

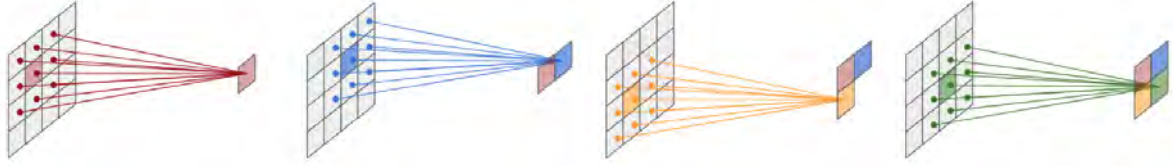


Figure 41.3: A pictorial description of a kernel convolution over four input pixels. It takes a product of the weight matrix (kernel) and the local input matrix centered at a target pixel. The operation is repeated over the input image using the same kernel. The size of the output image depends on the size of the kernel, stride, and padding. In this figure, the kernel size of 3, stride of 1, and padding of 0 is used.

dently for each channel or feature component. The most popular pooling operations are *max* and *average* pooling. Max-pooling picks the highest activation pixel value within the specified receptive field, while the average pooling computes the average pixel value in the receptive field. The idea of pooling generalizes to other architectures, including graph neural networks where the receptive field includes the neighbors of a particular node in the graph (see Sec. 41.5.3.14). The pooling operation gives rise to robustness of the model to small, local deformations in the input, a property called *geometric stability* [217–219]. This type of local deformation is important and distinct from the equivariance to rigid translations provided by the convolutional structure. Repeated pooling operations that eventually lead to a single feature vector with no spatial index is what gives rise to the invariance of common CNN architectures to translations (*i.e.* an image with a dog will be labeled ‘dog’ even independent of where the dog is in the image).

On the practical side, it is also beneficial to reduce the dimensionality of the input to a smaller hidden state representation. This can be done either a convolution operation with the stride size larger than 1, or employing a *pooling*.

A typical CNN for extracting a 1-dimensional array of features is designed with repeating blocks of convolution layers and pooling operations [220]. Figure 41.4 shows an example evolution of a data tensor through the succession of a convolution and pooling operations in order to extract a 1-dimensional array of features, which then can be fed into a block of MLP for an image classification (or a regression) task. This type of an architecture is referred to as an *encoder* or *feature extractor*.

The reduction in the spatial size of an image is performed *slowly*, typically by a factor of 2, which is the minimum possible reduction factor. After the reduction of the spatial extent, the number of channels is typically increased (also by a factor of 2 in most cases), converging one set of feature maps into a larger number of down-sampled feature maps. There may be more than one convolution layer within each spatial resolution (*i.e.* in between pooling operations). Following these design principles, CNN encoders typically become *deep*, consisting of dozens or sometimes hundreds of convolution layers, and face challenges of vanishing gradients problem (see Sec. 41.6.5). A standard practice to mitigate this issue is explicitly *normalize* the input tensor input at each convolution layer using algorithms like *Batch Normalization*. This will be discussed in Sec. 41.6.9.

41.5.3.7 CNN architectures for image analysis

There are three major categories of computer vision tasks where CNNs are often used:

- *Image classification or regression* requires a prediction of single value for the whole image (*i.e.* a category or target value)
- *Object detection* produces a list location information for arbitrary number of objects in the input image
- *Semantic segmentation* outputs an image of the same spatial dimension as the input, in which every pixel is segmented by a predicted value for a target task (classification or regression).

As discussed previously, a CNN feature extractor followed by MLP is often used for image classification and regression tasks in wide range of applications including particle physics. Many successful

CNN architectures for object detection and semantic segmentation applications share key designs which we briefly discuss below.

Region Convolutional Neural Network (R-CNN) is one of the most successful design for object detection [221]. R-CNN is explored in HEP experiments where the number and location of signal (e.g. neutrino interactions) are not known a priori in large image data such as neutrino detectors [3, 116, 222].

R-CNN consists of multiple CNNs. The first is a feature extractor which produces a spatially compressed feature tensor. The second CNN applies 1×1 convolution to predict two information: an *object score* which indicates whether there is an object in this (spatially compressed) pixel or not, and prediction of the location and size of a rectangular, axis-aligned bounding box that contains the object (if exists). This second CNN is called *Region Proposal Network (RPN)*, and the bounding box is called *Region of Interest (ROI)*. The the size of a bounding box is not directly solved by a regression. Instead, the model requires a set of pre-defined *anchor* boxes, which sizes and aspect ratios are hyperparameters, and predict the object score, location, and size (as a multiplicative factor to the defined anchor box) for each anchor box. This allows RPN to detect multiple objects with different aspect ratios even if they are within the same receptive field in the original input image. For each ROI with an object score above threshold (hyperparameter), the third CNN operates in the corresponding sub-field of an already-compressed tensor (*i.e.* by the first CNN) to perform a classification for an object inside the ROI.

This approach can produce multiple ROIs for the same object with a high overlap. Those predictions are reduced using Non-Maximum Suppression (NMS) algorithm. Given a list of bounding boxes with confidence scores, NMS takes the box with the highest score, and computes the Intersection-over-Union (IoU) of this box and all the rest of boxes. Boxes with the IoU higher than a threshold (hyperparameter) are eliminated as they are likely to represent the same object. Then NMS repeats the same operation for the box with the second highest score among the remaining boxes. This is repeated till the list is exhausted.

U-Net is one of the of most successful models used for semantic segmentation [223]. As the output of U-Net is also an image, it gives some interpretability compared to models for an image-level classification or regression tasks. The model is used widely in HEP experiments in both 2D and 3D image data [112, 113, 118, 125, 127].

The architecture of U-Net consists of a CNN encoder and *decoder*. A decoder consists of convolution and *convolution-transpose* layer (also called strided transpose-convolution, or rarely deconvolution). The operation of a convolution transpose can be seen an opposite of a convolution: for every pixel in an input image, its value is multiplied to the kernel and copied to the output. 3×3 kernel in transpose-convolution layer fills 3×3 pixels in the output tensor. The concept of padding and the stride are also applied to the output tensor. For instance, the stride 2 transpose-convolution fills 3×3 fields centered at every other pixel (*i.e.* stride 2) for every input pixel. The spatial size of an output tensor is therefore determined by the spatial size of an input tensor, stride, and padding. In the decoder of U-Net, convolution-transpose layers are used to up-sample spatially compressed feature tensors back to the original image resolution. The

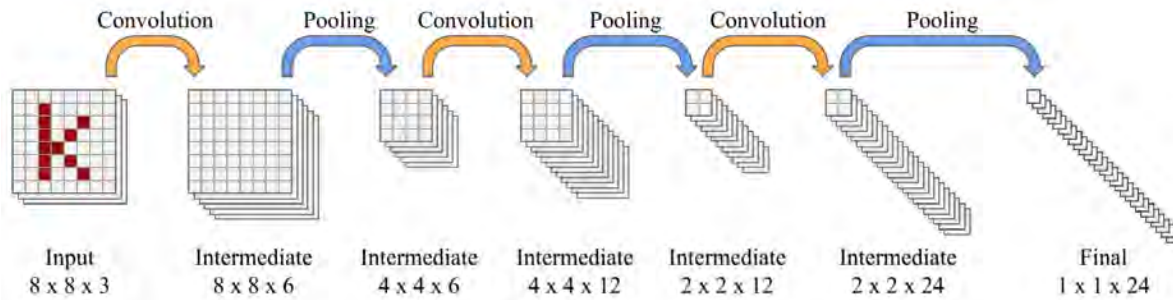


Figure 41.4: An example CNN architecture to extract a 1-dimensional array of features from an image via succession of convolution layers and pooling operations. The (square) kernel, stride, and padding size of a convolution operation are 3, 1, and 1 in respective order. The pooling operation uses a square kernel size of 2. The number of filters at the first convolution layer is 6, and is increased by a factor of 2 at subsequent convolution layers.

stride size of a convolution-transpose layer is almost always 2 in order to *slowly* transform the spatial size, and standard convolution layers (with stride 1) are placed in-between up-sampling operations. Because the output of the decoder has the same size as the input image, features for every pixel can be used for either a classification or a regression task at the pixel-level.

The idea behind encoder-decoder architecture is to extract features in the encoder, and the decoder interpolates those features back to the original spatial resolution. The down-sampling operation (e.g. max-pooling) in the encoder is, however, a lossy process where spatial information is permanently lost. This prevents a simple encoder-decoder architecture to perform a semantic segmentation task at the level of precision required for science research and industrial use. Interesting observation made by the U-Net authors is a symmetry in the encoder-decoder architecture in which there are tensors of corresponding (i.e. the same) spatial size between two parts of the model. This observation inspired them to concatenate the intermediate tensors in the encoder block to the intermediate tensors of the corresponding size in the decoder block before convolution layers are applied in the decoder, which dramatically improved the performance of semantic segmentation. This is a type of a *skip connection* discussed below.

41.5.3.8 Residual networks and skip connections

The representation power of a neural network increases as more hidden layers are added, but gradient-based optimization of deep models can be notoriously difficult due to vanishing gradients (see Sec. 41.6.5). One of powerful techniques to address this challenge is a *residual network* (ResNet), which is a modular architecture design that can be applied to neural network models [216]. Suppose a $f^*(x)$ as the target transformation to be learned by a few stacked layers where x is the input to the first layer. The authors of ResNet hypothesized that it may be easier for a model to learn a residual transformation $\hat{f}(x) := f^*(x) - x$, thus the objective to learn is $\hat{f}(x) + x$ where $\hat{f}(x)$ denotes the output of stacked layers. This form assumes $\hat{f}(x)$ and x share the same tensor dimension and size. If they differ in the feature dimension, equivalently the count of channels in an image tensor, one could use 1×1 convolutions to transform and match the dimension. The design is modular as it can be applied per a stack of convolution layers (e.g. U-ResNet introduced for LArTPC detectors uses ResNet modules within a U-Net architecture [112, 113]) widely in the present applications.

The authors of ResNet successfully demonstrated an improved performance of some models at the depth exceeding 1000 layers where the non-residual counter part could not improve the accuracy beyond a few dozens of layers. This remarkable success was due to the *skip connections* in ResNet, namely the element-wise addition of the input to the output at each block of convolution layers as shown in Figure 41.5. Without the presence of the skip connections, the gradients from the loss function is forced to go through all convolution layers (i.e. the reverse direction of orange arrows in Figure 41.5), which results in the gradient being altered at every convolution layer. The layers closer to the input receive

altered gradients by the continuously updated weights of deeper layers, making conversion difficult and slow. The skip connections provides the path for the gradient to flow directly to the preceding layers. As a result, the gradient can flow more directly to preceding layers and allows simultaneous optimization across layers. It is possible, however, that some convolution layers in ResNet may learn an identity mapping, thus contributing no effect to solving a given task despite consuming computing power.

Another type of skip connections is a concatenation of feature maps, in which case the input and the output of a block of convolution layers do not necessarily have to have the same number of features. This is shown to be very powerful in number of popular model architectures including U-Net [223] and DenseNet [224]. In this case, the input features are re-used: the next block of hidden layers can learn an optimal way to combine the input and the output of the preceding block (i.e. it could learn a simple addition operation, which makes it identical to ResNet). In DenseNet, input to a convolution layer is concatenated with the output of all preceding convolution layers of the same spatial dimension, thus $x_l = f_l([x_1, x_2, \dots, x_{l-1}])$ where x_l is the output of l -th layer f_l and $[x_1, \dots, x_{l-1}]$ denotes a concatenation of the inputs. In U-Net, tensors from the encoder block are concatenated with the tensors in the decoder block where they have the same size in spatial dimensions. This was critical for achieving a high spatial resolution for *semantic segmentation*, a class of tasks in Computer Vision to classify every pixel in an image among the predefined set of types (semantics), because the geometrical features at each spatial resolution is otherwise lost via pooling operation in the encoder block [223].

41.5.3.9 Recurrent neural networks

Recurrent Neural Networks (RNNs) [225] are a family of neural networks designed for sequential data (e.g. time series). Consider sequential data where x_t represents each step in a sequence with $t \in [1, n]$. A typical RNN takes the following form:

$$h_t = g_h(h_{t-1}, x_t, \theta) \quad (41.49)$$

where h_t and θ denote the *hidden state* of the system and parameters of g_h , the RNN model. The term *recurrent* refers the nature of the model operating on the previous state of the system (and hence the whole history). RNNs operate on three types of tasks:

- *One-to-many* takes a single input and generates a sequence (e.g. generates a sequence data, such as a sentence or waveform, given a category).
- *Many-to-one* takes a sequence and generates an output (e.g. sequence-labeling).
- *Many-to-many* takes a sequence and generates a sequence where the length of input and output sequence may be same (e.g. classification of individual element in a sequence) or different (e.g. sequence to sequence mapping).

Figure 41.6 shows an example for a many-to-many task, where $\{x_t\}_{t=1:n}$, $\{y_t\}_{t=1:n}$, and $\{h_t\}_{t=0:n}$ denote the inputs, outputs,

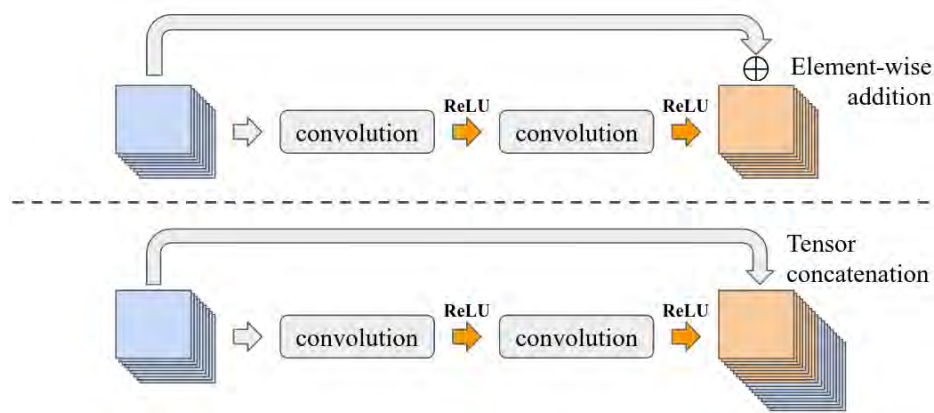


Figure 41.5: Two types of skip connections: the top is from ResNet where the input is element-wise added to the output tensor of a block of convolution layers while the bottom shows a concatenation of the input to the output tensor as employed in other models including U-Net and DenseNet.

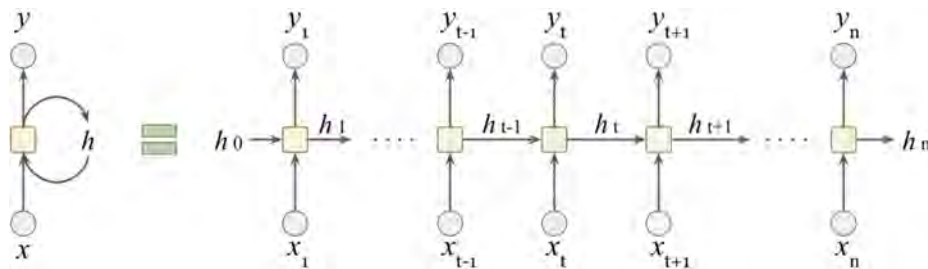


Figure 41.6: Pictorial description of a RNN (on the left) which takes an input and produces an output at every step with a hidden-to-hidden connection. The right diagram is unrolled over discrete steps. The yellow box represents a cell: a set of operations unique to each architecture.

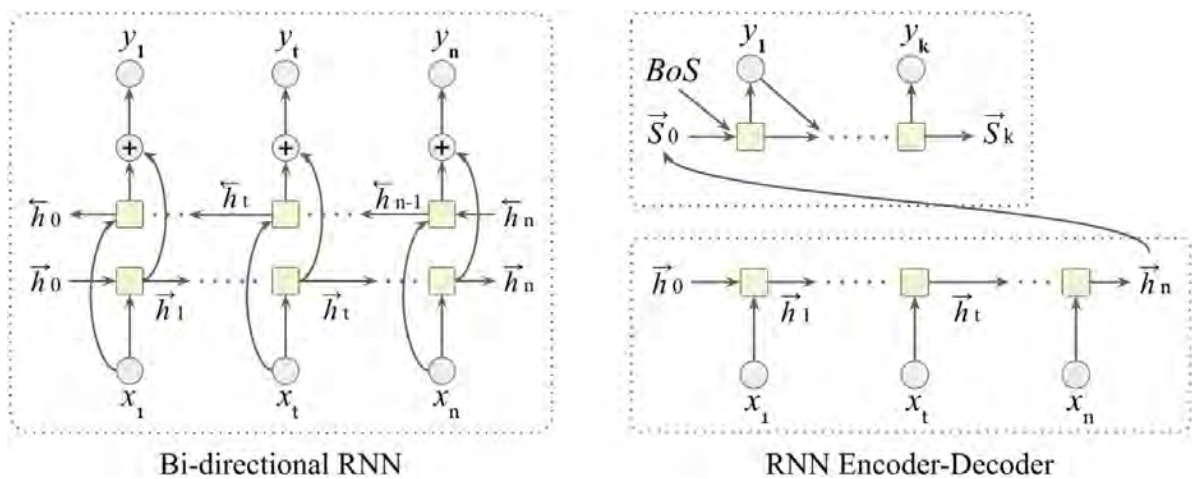


Figure 41.7: Bi-directional RNN (left) provides contexts in the preceding and subsequent parts of the input sequence. RNN encoder-decoder (right) can generate an output with a different sequence length from an input. Each cell in the decoder may take a previously generated element, starting from a special marker that signals the beginning of the sequence (BoS) and ending when the end of sequence is generated.

and hidden states respectively. A set of operations at each time step is called a *cell*. A simple RNN cell may look like:

$$\begin{aligned} h_t &= g_h(Wx_t + Vh_{t-1} + b) \\ y_t &= g_o(Uh_t) \end{aligned} \quad (41.50)$$

where $W \in \mathbb{R}^{d_h \times d_i}$, $V \in \mathbb{R}^{d_h \times d_h}$, $U \in \mathbb{R}^{d_o \times d_h}$ are matrices g_h and g_o represent functions. d_i , d_h , and d_o are the dimension of input, hidden state, and output. $b \in \mathbb{R}^{d_h}$ is a bias term. An example application is sequence-labeling where the goal is for y_t to classify each input x_t in the sequence. In that case, one might use $g_h = \tanh$ and $g_o = \text{softmax}$ and use a loss function that averages classification accuracy over the sequence.

Variations in RNN architectures result from the design of cells (described below) and flow of information across the cells. For instance, a bi-directional RNN (Figure 41.7 left) employs two sets of RNNs, one processing the sequence in the forward direction and the other in the backward direction, and the hidden states from both directions are then combined to capture the context from both parts of the sequence. An RNN encoder-decoder (Figure 41.7 right) use one RNN to generate a context vector that encodes the whole input sequence, and use a separate RNN to generate

another sequence from the encoded context. This can be used for machine translation.

41.5.3.10 LSTM and GRU

An RNN applies the same functions g_h and g_o in Eq. 41.50 repeatedly for each element of the sequence. This repeated component is similar to the shared weights for a convolutional filter in a CNN.

A hyperbolic tangent (\tanh) is traditionally a popular choice for g_h as it regulates the magnitude of the hidden states and prevents it from diverging. Yet, this simple model is challenging to train for a long sequence of data [226, 227]. This is partially due to the fact that \tanh contributes to the vanishing gradient problem and because repeated multiplication of the same weight matrices (i.e. V and W in Eq. 41.50) can lead to gradients that can either explode or vanish (see Sec. 41.6.5). Additionally, the way the signal accumulates means that changes early in the sequence have different impact from changes late in the sequence.

Long Short-Term Memory (LSTM) [228] is a model designed to address the issue of vanishing gradient for RNNs. In this model, a *context* is introduced as a way to enable the model to hold long-term memory while the hidden states remain to hold short-term memory. The context c_t and hidden state h_t at step t are computed as follows:

$$\begin{aligned} c_t &= f_t \odot c_{t-1} + i_t \odot \tilde{c}_t \\ h_t &= o_t \odot c_t \end{aligned} \quad \text{where} \quad \begin{aligned} f_t &= \sigma(W^f x_t + V^f h_{t-1} + b^f) \\ i_t &= \sigma(W^i x_t + V^i h_{t-1} + b^i) \\ o_t &= \sigma(W^o x_t + V^o h_{t-1} + b^o) \\ \tilde{c}_t &= \tanh(W^c x_t + V^c h_{t-1} + b^c) \end{aligned} \quad (41.51)$$

where σ and \odot denote logistic function and an element-wise (i.e. Hadamard) product and f_t , i_t , and o_t are referred to as *gates*. Each gate outputs a value between 0 and 1, and is associated with unique weights, W and V , and a bias b . One can see c_t is a combination of the previous context vector c_{t-1} and a new context vector \tilde{c}_t . The *forget gate* f_t controls which and how much of the past context should be kept or forgotten. The *input gate* i_t controls how much of the present context \tilde{c}_t should propagate to the current state c_t . The output gate o_t controls which and how much of the context vector should represent the present hidden state h_t . From Figure 41.8, one can see that the context vector c_t

evolves with a gated addition operation. As such, it can be seen as an uninterrupted path for gradients to flow. This is similar to a residual connection (see ResNet in Sec. 41.5.3.8), which enabled training of CNNs with thousands of layers.

Another gated model to solve a vanishing gradient problem is the *Gated Recurrent Unit* (GRU) [182]. The GRU is similar to the LSTM with a few simplifications: the GRU merges the context vector and the hidden states and combines three gates into two. As a result, it requires less computational resources while retaining a similar level of performance for long sequences. The GRU operations are defined as follows:

$$\begin{aligned} r_t &= \sigma(W^r x_t + V^r h_{t-1} + b^r) \\ z_t &= \sigma(W^z x_t + V^z h_{t-1} + b^z) \\ \tilde{h}_t &= \tanh(W^h x_t + V^h (r_t \odot h_{t-1}) + b^h) \end{aligned} \quad \text{where} \quad (41.52)$$

where r_t and z_t are referred to as *reset* and *update* gate. As one can see in Figure 41.6, the reset gate in GRU performs the same task as the forget gate in LSTM by removing or reducing the elements of its memory (i.e. the hidden state). The update gate z_t determines the relative proportion of the previous hidden state h_{t-1} and the new context \tilde{h}_t to be mixed in producing the new hidden state.

In addition to sequential data, the LSTM and GRU units can be used for data that has a tree-like structure. In this setting, the networks are often referred to as recursive neural networks or TreeRNN and they have found applications in natural language processing and jet physics [153, 154, 229–231].

41.5.3.11 Attention

Many tasks encountered in machine learning can be divided into subtasks. For example, classifying each pixel of an image or element of a sequence, predicting a target for each node in a graph, etc.. For each subtask the model may need to draw upon information from the entire input, but some parts of the input will be more relevant than others. At some point, the model will

need to form a representation for the input as context for the subtask at hand. A fixed length vector c as a global context for this subtask is possible, but this approach scales poorly as the size of the input and number of subtasks grow. Either the size of the global context must grow or it will not have the capacity to represent all the relevant information, which would lead to a degradation in performance.

The idea behind *attention* is intuitive: one still forms a representation for the entire input, but different parts of the input are weighted differently according to the task at hand. By making the weights a learnable component, the network can learn to attend to the relevant parts of the input. A softmax function is a natural way to represent attention as it assigns a positive value to each component of the input and sums to one. Then for the i -th task, one can simply form a task-specific context c_i by computing the weighted average of the hidden state representations h_j for each component of the input. Let α_{ij} be the weights assigned to the j -th input for the i -th task, such that $\sum_j \alpha_{ij} = 1$. We can satisfy this naturally if for each i the α_{ij} are computed from the logits β_{ij} using a softmax function that normalizes by summing over j .

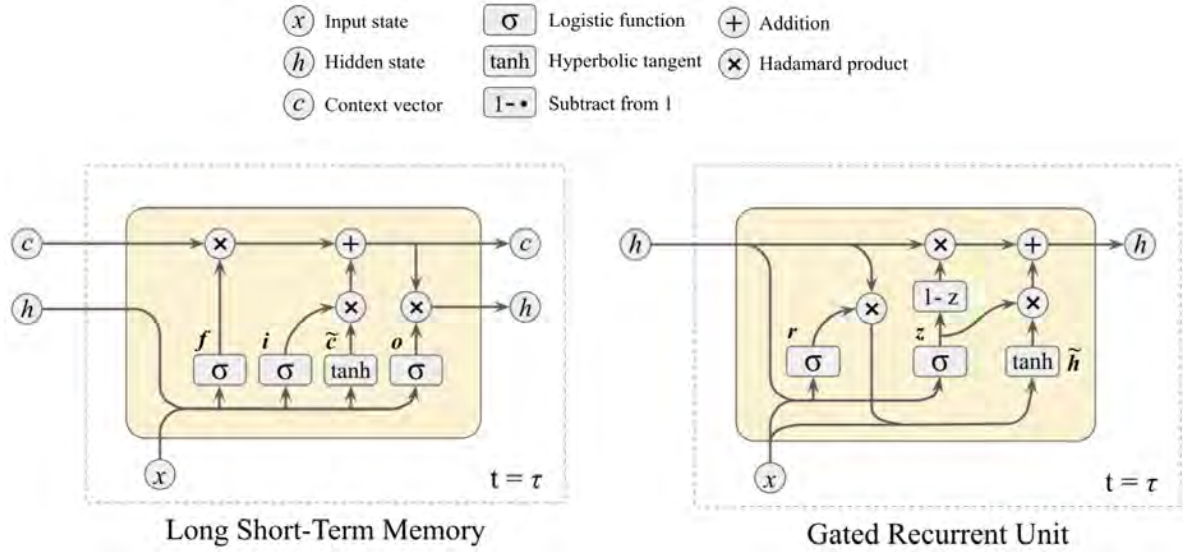


Figure 41.8: LSTM (left) and GRU (right) are both gated neural network designed to address a vanishing gradient problem for RNNs.

Putting these ingredients together, we have the *additive attention mechanism*

$$c_i = \sum_{j=1}^n \alpha_{ij} h_j \quad \text{where} \quad \alpha_{ij} = \text{softmax}(\beta_{ij}) \text{ over } j. \tag{41.53}$$

As in the case of a multi-class classifier, the logits β_{ij} can be computed from a network component with learnable parameters. For instance, in the case of a cell of an RNN encoder-decoder network (see Fig. 41.7) that is decoding element i with an incoming input state s_{i-1} , the logits for the attention mechanism could be computed as follows

$$\beta_{ij} = U \tanh(W s_{i-1} + \tilde{W} h_j + b_i), \tag{41.54}$$

where U, W, \tilde{W} are the weights and b is the bias term of the model. Fig. 41.9 from Ref. [232] illustrates the full attention mechanism. The idea was implemented by a model called *RNNSearch* which made a breakthrough in machine translation by combining a bi-directional RNN with an additive attention mechanism [233].

We end this section by noting that the softmax α_{ij} can be used to visualize the influence of the j -th input element on the i -th output element, which improves interpretability of the model. An example of this from Ref. [232] is shown in Fig. 41.10.

41.5.3.12 Scaled dot-product attention

Shortly after the introduction of RNNSearch, the attention mechanism has been recognized as a powerful tool. One such variant is *scaled dot-product attention*, which is most widely recognized as the foundation of the *Transformer* architecture [234], which is described in more detail below.

In additive attention (Eq. 41.53) the hidden representations h_j were combined through a weighted average based on the coefficients α_{ij} , resulting in a task-specific context vector c_i . In the literature around scaled dot-product attention, multi-head attention, and transformers, the hidden states that will be combined are referred to as *values*, and they are often arranged in a matrix labeled $V \in \mathbb{R}^{m \times d_v}$, where the m rows of the matrix correspond to individual hidden state vectors of length d_v . The α_{ij} can also be represented as a $n \times m$ matrix α resulting from applying the softmax function to the $n \times m$ matrix β , normalized independently for each row. With this notation, Eq. 41.53 could be rewritten as $c = \text{softmax}(\beta)V$, where the softmax is normalized per row.

In scaled dot-product attention, the basic structure will be different, but instead of using a non-linear network component to compute the logits β as in Eq. 41.54, the logits will be computed

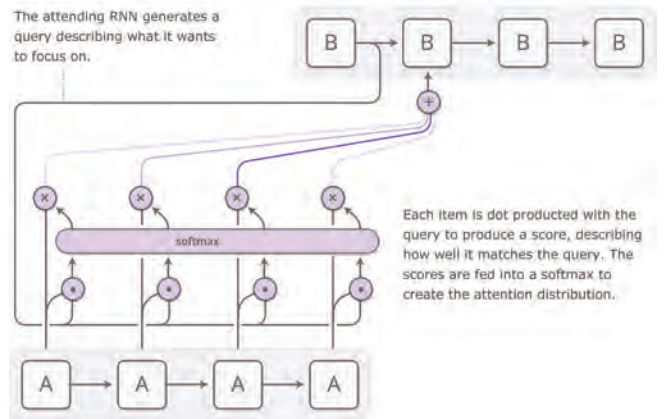


Figure 41.9: An illustration of the attention mechanism From Olah and Carter, “Attention and Augmented Recurrent Neural Networks”. Lower boxes labeled A represent input elements in the sequence and upper boxes labeled B indicate output elements. The left-most line originating from the first B corresponds to the state s_{i-1} in the text.

by forming a dot product between an incoming *query* and a *key*. The set of n query vectors can be arranged into the matrix $Q \in \mathbb{R}^{n \times d}$ and the set of d key vectors can be arranged into the matrix (transpose) $K^T \in \mathbb{R}^{d \times m}$. When the dot product between a particular query vector $q_i \in \mathbb{R}^d$ and key vector $k_j \in \mathbb{R}^d$ is large, then the resulting logit β_{ij} and attention weight α_{ij} will be large. One can interpret the keys as trying to detect certain types of queries and routing the attention to the relevant value. Typically, the dot-product is scaled by a factor of $1/\sqrt{d}$. The resulting task-dependent context is $c_i = \text{softmax}_j(q_i \cdot k_j / \sqrt{d})v_j$, where softmax_j indicates that normalizing sum runs over the index j . A common, though sometimes confusing, notation is simply

$$c = \text{Attention}(Q, K, V) = \text{softmax} \left(\frac{QK^T}{\sqrt{d}} \right) V, \tag{41.55}$$

where c is a $n \times d_v$ matrix organizing the n context vectors of length d_v that are tailored summaries of the input vector for each of the n tasks.

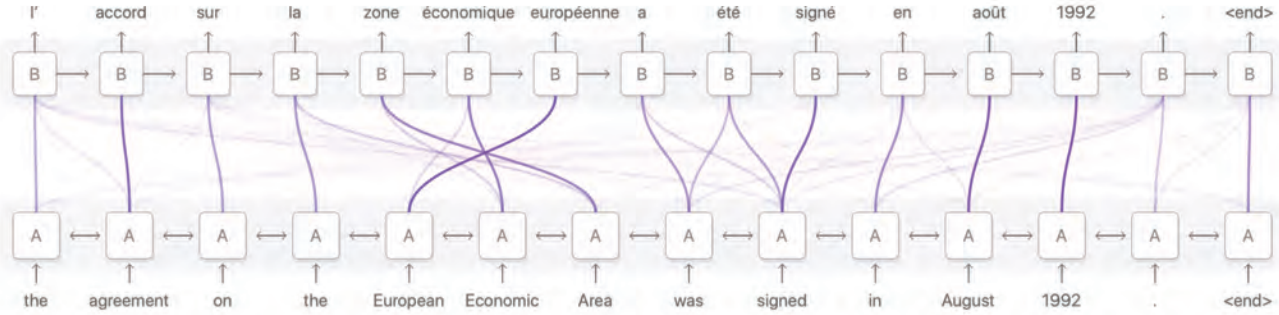


Figure 41.10: Visualization of the attention weights in a sequence-to-sequence problem taken from Olah & Carter, "Attention and Augmented Recurrent Neural Networks". The thickness of the lines is proportional to the attention weights α_{ij} .

41.5.3.13 Transformer and multi-head attention

The Transformer architecture is a powerful encoder-decoder model based on the scaled-dot product attention mechanism. It was originally designed for sequential data like RNNSearch, and subsequently used in other areas of research including computer vision. One advantage of scaled-dot product attention compared to the approach used in RNNSearch (Eq. 41.54) is that computing the logits β_{ij} (and thus the attention weights) does not involve any sequential processing. This allows the models to better leverage parallelism of the hardware to train much more expressive models than before. In place of the gated unites of an RNN that are key to avoiding the vanishing gradient problem, the Transformer architecture employs a residual connections at every attention module (i.e. the input tensor is added to the output as in Fig 41.5).

The second major ingredient in the Transformer architecture is the multi-head attention mechanism. A multi-head attention module executes multiple scaled dot-product attention in parallel. The query Q , key K , and value V matrices in each scaled dot-product attention module is obtained by applying a linear transformation (with learnable weights) to the common Q , K , and V input matrices. Each of them can be considered as a different (albeit rotated) perspective to derive attention.

For a sequence-to-sequence mapping task, the output of encoder is used to derive key K and value V matrices for the multi-head attention module in the decoder. The decoder is then responsible for mapping between the key-value features derived from the input (the encoder) and the queries from the decoder (which is still executed sequentially) in order to produce the final decoded output.

Finally, we note that the Transformer architecture does not just employ an attention mechanism in the decoder. By employing attention in the encoder as well the model has more capacity to "interpret" the input – a concept referred to as self-attention.

Models such as these have made breakthroughs in many areas of scientific and industrial research [235].

41.5.3.14 Graph networks and geometric deep learning

Graphs are a powerful data structure for representing structure data. A graph consists of nodes as elements and edges between them. Graphs are sufficiently flexible to describe many types of structured data including images and sequences. Graph-based neural networks can also be seen as a generalization of many common types of machine learning models such as recurrent networks, convolutional neural networks, etc. [219]. The term geometric deep learning refers to this recent formulation that focuses largely on the symmetries of the data.

An earlier attempt to organize the variations on different flavors of graph-based neural networks can be found in Ref. [236]. In their formalism a Graph Network may be represented as $G(\mathbf{u}, V, E)$ where \mathbf{u} represents an array of global features, $V = \{\mathbf{v}_i\}_{i=1:N^v}$ represents a set of N^v nodes with \mathbf{v}_i as features for the i -th node (e.g. such as RGB channels if a node represents a pixel in image data), and $E = \{(\mathbf{e}_k, r_k, s_k)\}_{k=1:N^e}$ represents a set of N^e edges with \mathbf{e}_k as features for the k -th edge. An edge may be (bi-)directional where r_k and s_k denotes the destination and origin nodes respectively. The features of a graph may evolve with three update functions ϕ and and three aggregate functions ρ :

$$\begin{aligned}
 \mathbf{e}'_k &= \phi^e(\mathbf{e}_k, \mathbf{v}_{r_k}, \mathbf{v}_{s_k}, \mathbf{u}) & \mathbf{e}'_i &= \rho^{e \rightarrow v}(E'_i) & \text{where } E'_i &= \{(\mathbf{e}'_k, r_k, s_k)\}_{r_k=i, k=1:N^e} \\
 \mathbf{v}'_i &= \phi^v(\bar{\mathbf{e}}_i, \mathbf{v}_i, \mathbf{u}) & \bar{\mathbf{e}}' &= \rho^{e \rightarrow u}(E') & \text{where } E' &= \cup_i E'_i = \{(\mathbf{e}'_k, r_k, s_k)\}_{k=1:N^e} \\
 \mathbf{u}' &= \phi^u(\bar{\mathbf{e}}', \bar{\mathbf{v}}', \mathbf{u}) & \bar{\mathbf{v}}' &= \rho^{v \rightarrow u}(V') & \text{where } V' &= \{\mathbf{v}'_i\}_{i=1:N^v}
 \end{aligned}
 \tag{41.56}$$

where \mathbf{e}' , \mathbf{v}' , and \mathbf{u}' denote the updated node, edge, and graph features. In Graph Networks, three types of information are updated in the following order. The first step is ϕ^e to update every edge. The second step updates every node: for i -th node, compute $\rho^{e \rightarrow v}$ to aggregate updated attributes from the edges with $r_k = i$ then compute ϕ^v to update the node attributes. The third step updates the graph attributes through ϕ^u which takes the original state \mathbf{u} , aggregated node and edge attributes by $\rho^{v \rightarrow u}$ and $\rho^{e \rightarrow u}$ respectively.

Graph Neural Networks [237] (GNNs) are the class of neural networks that work on graph-structured data. A direct analog in Computer Vision and physics is the point cloud data type, which is an unordered set of points. Operations on point cloud need to be permutation invariant (e.g. \min , \max , $+$, \cdot), and analysis of 3-dimensional physical object represented by point cloud need to be rotation and translation invariant as in the case for an image. PointNet [238, 239], a GNN that performs an object classification

on point cloud of 3-dimensional positions, treats each point as a node, applies MLPs as ϕ^v to update node features, and global max-pooling operation as $\rho^{v \rightarrow u}$. There is no explicit edge definition in PointNet (though the model applies affine transformation to all points using Spatial Transformer Network [240], which could be considered as a separate graph operation, to introduce rotation and translation invariance and to capture topological features). Deep Sets [241] follows the same manner except ϕ^v takes the global entities \mathbf{u} . This is same for PointNet when performing point cloud segmentation: ϕ^v takes a step of simply concatenating \mathbf{u} to node entities to combine a local and global features. Dynamic Graph CNN [242] is a variant that (re)define edges dynamically using attention mechanism: $\rho^{e \rightarrow v}$ aggregates k neighbor nodes where the inter-node distance is defined as a Cartesian distance in the feature space. ϕ^v remains a MLP and, while edges are defined, there is no associated entity. A similar technique is used in Non-Local Neural Network [243] to efficiently propagate local

feature information to points that may be far in the 3D cartesian coordinate. Message Passing Neural Network [244] (MPNN) explicitly defines a feature vector as edge entities. In MPNN, $\rho^{e \rightarrow v}$ performs element-wise sum of features and feed into ϕ^e , explicitly passing features across nodes as the name suggests. While these are representative models that are frequently used in particle physics applications [117, 121, 132, 142, 156, 183, 245, 246], it is only a tiny fraction of GNN models developed over the past decade.

Graph-based models are particularly interesting for science applications because they often offer a natural way to organize the entities in the data and encode how those components should interact each other. This particular type of inductive bias is referred to as *relational inductive bias* in Ref. [237]. The structure of the graph is both an opportunity and a responsibility as one needs to define the graph structure including the edges to define the mode. A naive approach may be defining a fully-connected graph. However, for applications on hundreds of thousands of nodes (e.g. high resolution 3D point cloud), this may require a prohibitive amount of memory and computation. On the other hand, if the graph is too sparse, it may negatively impact the performance. One may need to compare the model performance among differently constructed graphs and balance against computational burden. Ideally the graph would be based on some knowledge of the interactions, but in the absence of such knowledge, popular graph construction methods include fully-connected, k -Nearest Neighbors, a Delaunay graph, and Minimum Spanning Tree.

Classification and regression tasks for graphs can be formulated such that the prediction is made for the entire graph or its individual nodes or edges. Graph-level prediction is like classifying an entire image, while node-level prediction is like semantic segmentation where individual pixels are classified. For clustering of points, GNNs can approximate a transformation function for nodes into the latent space where an optimal clustering of points can be performed. Alternatively, one can formulate clustering as an edge classification task. A comprehensive review on particle physics applications have been made available recently [247].

41.5.4 Deep generative models

Deep generative models are powerful machine learning models that can learn complex, high-dimensional distributions and generate samples from them. Because of their inherently probabilistic formulation, generative models are rapidly becoming an indispensable tool for scientific data analysis in a range of domains. Generative models can be contrasted against discriminative models that are primarily used for supervised learning tasks. Roughly, discriminative models are used for prediction and $f(x)$ provides a point estimate of the target y , and they are more closely connected to function approximation. In contrast, generative models describe the data distribution $p(x)$ (or the joint data distribution $p(x, y)$ in a supervised setting). An enlightening discussion of these two approaches can be found in Ref. [10].

There are a number of different types of deep generative models that have various pros and cons as they do not all have the same capabilities. We will focus on Variational Auto-Encoders (VAEs) [248, 249], Generative Adversarial Networks (GANs) [250, 251], and Normalizing Flows (NFs) [252–256], though there other approaches have been explored in this quickly developing area of research. Consider these three distinct types of functionality:

- **generation:** ability to sample or “generate” a data point $x_i \sim p(x)$.
- **likelihood for generated data:** ability to evaluate the probability density (likelihood) $p(x_i)$ for a data point x_i sampled from the model $x_i \sim p(x)$.
- **likelihood for arbitrary data:** ability to evaluate the probability density $p(x_i)$ for an arbitrary data point $x_i \in \mathcal{X}$.

Each of the models above can be used for generation; however, only normalizing flows provide all three capabilities. For reasons that we will describe below, GANs and VAEs do not provide a tractable likelihood function, and they are sometimes referred to as *implicit models*. This establishes a connection to simulation-based inference where most scientific simulators are also implicit

models with an intractable likelihood. Because normalizing flows have a tractable likelihood, they can be trained via maximum likelihood (Eq. 41.18) as described in Sec. 41.3.2.1. GANs and VAEs, on the other hand, need to employ some other loss function to be trained. In the case of VAEs, training is based on the ELBO used in variational inference (see Sec. 41.3.1.3 and the discussion around the reverse KL divergence below Eq. 41.16). While GANs are also implicit models they data they can generate is typically restricted to a lower-dimensional manifold $\mathcal{M} \subset \mathcal{X}$, meaning that almost all real training dataset doesn’t “live on” the subspace of possibilities that the model can produce. In this case, the likelihood is for almost all data is zero, and so even ELBO-based training will not work. The breakthrough idea introduced in Ref. [250] was to use adversarial training where a classifier would be used to quantify how different the data generated from the model is from the data from the target distribution.

VAEs, GANs, and normalizing flows introduce a mapping $g(z, \theta)$ from a base random variable z to the space of the data \mathcal{X} . The map $g(z, \theta)$ is typically implemented with a neural network. The random variable z is sampled from some known base distribution $p(z)$ that is both easy to sample and has a density that is easy to evaluate. Typically, the base distribution is a multivariate normal.

In the literature on GANs and normalizing flows, this base random variable is often referred to as a latent variable and $p(z)$ is often referred to as a prior distribution, but this may cause confusion as the relationship between z and the observed x is deterministic. Typically, one would reserve the term latent variable for situations where one must marginalize (integrate) over z to obtain the marginal likelihood as in $p(x) = \int p(x, z) dz$. In this integral would involve a delta function imposing the deterministic relationship $x = g(z, \theta)$. A more natural interpretation of the relationship between x and z is through the change of variables formula, which is the essence of normalizing flows.

In the case of VAEs, the one additionally adds some normally-distributed (Gaussian) random noise ϵ to the output so that $x = g(z, \theta) + \epsilon$. In this case, x and z are not deterministically related and z is a legitimate latent variable in the model and $p(z)$ can be interpreted as the prior on that latent variable. In this case, the model can populate the full space of the data. Unfortunately, the marginal likelihood $p(x) = \int p(x, z) dz$ involves an intractable integral, thus maximum likelihood training is infeasible. However, the likelihood term $p(x|z)$ is tractable (*i.e.* the Gaussian noise), so training with the ELBO is possible.

Note that the dimensionality of z need not be the same as that of x . If $z \in \mathbb{R}^q$ and $\mathcal{X} = \mathbb{R}^d$ with $q < d$, then all points $g(z, \theta)$ will lie on a d -dimensional surface in \mathbb{R}^d . In the case of a VAE, the Gaussian noise ϵ means that the generated data x will be distributed in a thin region around the surface defined by $g(z, \theta)$. The presence of a bottleneck (*i.e.* $q < d$) leads to advantages and disadvantages. The disadvantages for GANs is that the likelihood assigned to almost all real world data (*i.e.* data not generated by the model) will be zero, so training is more difficult and many tasks in probabilistic inference won’t be applicable. However, often real world data is also effectively described by a low-dimensional subspace in the full space of the data – random images look like noise, while natural images are in some sense special. For this reason, images produced by GANs for instance often have better visual quality than those produced by other techniques. This points to the ambiguity encountered in quantifying how close two distributions are, and also motivates the use of distance measures such as the Earth Movers distance or Wasserstein distance [257, 258]. Conversely, the lack of a bottleneck (*i.e.* $q = d$) leads to very large models and scalability issues when the data is high dimensional.

Recent work has also focused on combining ideas from VAEs, GANs, and normalizing flows so that the generative model does involve a bottleneck but can still provide tractable likelihoods for density estimation restricted to that manifold [44, 46, 252, 259, 260]. Some of these models can also be used in the context of anomaly detection and out of distribution detection by identifying data that is off the manifold.

The parametrization of the mapping (the architecture of the neural network) should match the structure of the data and be

expressive enough. For problems with explicit symmetries it is beneficial to include them into the architecture of the network explicitly, which restricts the allowed space of the models and matches their inductive bias (implicit regularization inherently built into the choice of architecture of the network) to the data. Different architectures have been proposed [255, 261–263], and to achieve the best performance on a new dataset one needs extensive hyperparameter explorations [264].

41.5.4.1 Variational auto-encoders

The auto-encoder was described in Sec. 41.3.2.2 as model for compression and representation learning. The model is $f = g \circ e : \mathcal{X} \rightarrow \mathcal{X}$, where $e : \mathcal{X} \rightarrow \mathcal{Z}$ is referred to as the *encoder* and $g : \mathcal{Z} \rightarrow \mathcal{X}$ is referred to as the *generator* or *decoder*. The standard auto-encoder is not a probabilistic model, but additional probabilistic structure can be added.

One approach is VAE mentioned above [248, 249]. By equipping the latent space with a prior distribution $p(z)$, the decoder of the auto-encoder $g(z, \theta)$ implies a distribution on a manifold in the output space \mathcal{X} . VAEs additionally add some normally-distributed (Gaussian) random noise ϵ to the output so that $x = g(z, \theta) + \epsilon$. This implies that $p_\theta(x|z)$ is a tractable quantity, and it is interpreted as the likelihood in this context.

In a VAE one also elevates the encoder to have a probabilistic form. Instead of encoding $z = e(x)$ in a deterministic way, one seeks a distribution over z given x . A natural target for the probabilistic encoder would be to probabilistically invert the decoder. This inverse problem is solved by the posterior distribution $p(z|x)$ via Bayes theorem

$$p(z|x) = \frac{p(x|z)p(z)}{p(x)}. \quad (41.57)$$

While the likelihood and the prior may both be tractable, the normalizing constant $p(x) = \int p(x, z) dz$ involves an intractable integral (the same intractable integral that makes maximum likelihood training of the VAE infeasible).

One approach to Bayesian inference in these settings is variational inference (VI). In VI one approximates the posterior with some parametric family $q_\phi(z|x)$ in a parametric form, and then uses optimization to optimize the ELBO with respect to its parameters ϕ .

$$\begin{aligned} \text{ELBO} &= \mathbb{E}_{q(z)} \log p(x|z) - D_{KL}[q(z)||p(z)] \\ &\leq \log \mathbb{E}_{q(z)} \left[\frac{p(x, z)}{q(z)} \right] = \log p(x), \end{aligned} \quad (41.58)$$

where we used Jensen's inequality for concave functions (\log) and the reverse Kullback-Leibler (KL) divergence term is

$$D_{KL}[q(z)||p(z)] = \mathbb{E}_{q(z)} [\log q(z) - \log p(z)] \geq 0. \quad (41.59)$$

In a VAE, the variational model for the posterior $q_\phi(z|x)$ is often assumed to be an uncorrelated Gaussian (this is often called mean field approximation) defined by the mean μ and variance Σ . Instead of optimizing the mean and variance independently for each x , VAEs use neural networks to predict the mean $\mu_\phi(x)$ and the variance $\Sigma_\phi(x)$. This is called *amortized inference*, since after an up-front training cost the approximate posterior $q_\phi(z|x)$ can be evaluated efficiently with a single forward pass of the neural network. Note the standard auto-encoder is recovered if one only used the mean $\mu_\phi(x)$ for the encoder and did not add noise ϵ to the decoder.

Both the probabilistic encoder $q_\phi(z|x)$ and the probabilistic decoder $p_\theta(x|z)$ are trained jointly by optimizing the ELBO. Unlike the standard auto-encoder, which only minimizes the reconstruction error, ELBO optimization of Eq. 41.58 has a trade-off between minimizing the reconstruction error in the first term (averaged over the approximate posterior $q(z)$), which encourages high quality reconstructions, and minimizing the KL divergence term, which forces the posterior $q(z)$ to be as close to the chosen prior $p(z)$, and thus controls the sample quality by matching the aggregate posterior with a chosen prior distribution [265]. This term regularizes the VAE latent space, such that every sample drawn

from the prior $p(z)$ correspond to a valid sample. Successful VAE training requires to find a delicate balance between the two contributing terms to the ELBO. Whether the VAE training process succeeds in striking this balance depends on a number of factors, including the network architectures, the chosen prior and the class of allowed posterior distributions. Once trained, the VAE can be used as a generative model by sampling from the prior $z_i \sim p(z)$ and then decoding according to $p_\theta(x|z) = g(z, \theta) + \epsilon$.

VAEs allow for expressive architectures, enjoy the benefits of regularization through data compression and have a firm theoretical foundation. Compared to GANs [250], VAEs are of particular interest to the scientific community as they provide a lower bound to the marginal likelihood (albeit potentially with a large gap) and a posterior distribution for the latent variables.

It is also interesting to consider a special case of the auto-encoder and VAE where the encoder and decoder are restricted to be linear transformations, which is effectively PCA. In PCA the (linear) decoder can be written $g(z) = Oz$, where O is a matrix. As in the case of the auto-encoder, PCA is not a probabilistic model, but probabilistic structure can be added. Probabilistic PCA [266] assumes that the latent variables follow a Gaussian distribution with mean zero and covariance Λ , where Λ is a diagonal matrix with the rank-ordered eigenvalues λ_i along its diagonal. The true distribution of the PCA components may be non-Gaussian, but a Gaussian is the maximum entropy approximation given their first two moments. Note that in Probabilistic PCA these moments are measured on training dataset (when finding the principal components).

One can generalize Probabilistic PCA to use non-linear encoder and decoder as in an auto-encoder. A Gaussian prior is a poor ansatz for the latent space distribution of data proceed by an auto-encoder. Instead one can learn the density of the training samples in latent space using a normalizing flow. This model was introduced in \mathcal{M} -flows [46] and in Probabilistic Auto-Encoder (PAE) [44], which achieves similar performance to a VAE in terms of sample quality without explicit ELBO optimization. In all these cases the dimensionality of the latent space is a hyperparameter to be chosen or optimized by the user. Unlike a standard VAE, these models do not add noise to the decoded output, thus the data is strictly restricted to the manifold defined by the decoder $g(z, \theta)$. However, unlike a GAN there is a well defined way to take an arbitrary data point x , project it onto the manifold, and calculate the density of the data point projected onto the manifold. Thus these models can also be used in the context of anomaly detection and out of distribution detection by identifying data that is off the manifold.

41.5.4.2 Generative adversarial networks

GANs [250] also typically choose a low dimensional latent space z with a known prior distribution $p(z)$, typically a normal (Gaussian) distribution with zero mean and unit variance. GANs do not add noise to the output $g(z, \theta)$, so the likelihood $p(x|z)$ (and marginal likelihood $p(x)$) for almost all of the data space is 0, which precludes training by maximum likelihood and the ELBO. Instead of training on ELBO, GANs train on a dissimilarity measure defined implicitly by a discriminator $D(x)$ (also referred to as the critic). Calculating the dissimilarity often involves its own learning problem (*i.e.* adversarial training of the discriminator).

The training is usually framed as a mini-max game

$$\begin{aligned} \min_g \max_D \mathcal{L}_{\text{GAN}} &= \\ \min_g \max_D \{ \mathbb{E}_{x \sim p(x)} \log D(x) + \mathbb{E}_{z \sim p(z)} \log [1 - D(g(z))] \}. \end{aligned} \quad (41.60)$$

The goal of the discriminator is to distinguish between true and generated data, hence we want to maximize this loss with respect to D , assigning 1 to true data and 0 to generated data. The goal of generator is to fool the discriminator such that it cannot distinguish between true and generated data, hence we want to minimize this loss with respect to g at fixed D . This can be viewed as a game theoretical setup in a zero sum game between generator and discriminator.

Instead of this game theory interpretation we can view the internal objective $\max_D \mathcal{L}_{\text{GAN}}$ as an implicit loss function that mea-

sures the dissimilarity between the target and generated distributions. The loss of Eq. 41.60 corresponds to the Jensen-Shannon (JS) divergence, which is a symmetrized form of KL divergence. However, JS divergence is hard to directly work with, and the adversarial training could bring many problems such as vanishing gradient, mode collapse (tendency of generator to cluster the samples around the training samples, with holes between them) and non-convergence [257, 258]. One of the core issues is that the distribution generated by the GAN is restricted to a manifold and the KL divergence isn't well defined in this case (because p is not absolutely continuous with respect to q). To address these issues Wasserstein GANs train on

$$\min_g \max_D \mathcal{L}_{WGAN} = \min_g \max_D \{\mathbb{E}_{x \sim p(x)} D(x) - \mathbb{E}_{z \sim p(z)} D(g(z))\}. \quad (41.61)$$

Here again the goal of discriminator is to make the loss as large as possible between the true data and the generated data, while the goal of generator is to make it as small as possible, so that the discriminator cannot distinguish between the two. There is no requirement for $D(x)$ to be between 0 and 1, which helps with the above mentioned problems of JS divergence. Instead, this is replaced with a requirement that $D(x)$ is 1-Lipschitz, i.e. the absolute value of the norm of the gradient of the discriminator output with respect to the input has to be less or equal to 1.

Eq. 41.61 can be interpreted as the dual form of the 1-Wasserstein distance between the true and generated distribution [267]. Wasserstein distances are a measure of dissimilarity between two distributions used in the context of Optimal Transport, mathematical theory of how to optimally transport one distribution to another. Since the transport distance increases with the separation between the two distributions when they are non-overlapping, there is no gradient collapse that plagues other measures. In its primal form p-Wasserstein distance, $p \in [1, \infty)$, between two probability distributions p_1 and p_2 , is defined as $W_p(p_1, p_2) = \inf_{\gamma \in \Pi(p_1, p_2)} \left(\mathbb{E}_{(x,y) \sim \gamma} [|x - y|^p] \right)^{\frac{1}{p}}$, where $\Pi(p_1, p_2)$ is the set of all possible joint distributions $\gamma(x, y)$ with marginalized distributions p_1 and p_2 . In 1D the Wasserstein distance has a closed form solution via Cumulative Distribution Functions (CDFs), but this evaluation is intractable in high dimensions.

In the dual form of 1-Wasserstein distance, one instead maximizes Eq. 41.61 over all possible functions $D(x)$ that are 1-Lipschitz. One way to implement this is through weight clipping of the parameters of discriminator network, but a simpler solution is to add a gradient norm penalty term explicitly to the loss function [268].

Because of the discriminative nature of the dissimilarity measure defined in data space, GANs often generate more realistic samples than VAE or normalizing flows in high dimensions such as natural images. However, GANs do not provide an encoder from data to latent space, do not provide a tractable likelihood $p(x)$.

41.5.4.3 Normalizing flows, autoregressive models, and score based models

Normalizing Flows (NF) provide a powerful framework for density estimation and sampling [252–256, 269]. These models map the data x to latent variables z through a sequence of invertible transformations $f = f_1 \circ f_2 \circ \dots \circ f_n$, such that $z = f(x)$ or $x = g(z) = f^{-1}(x)$. As in the VAE and GAN, z is modelled as a random number with a simple base distribution $p_Z(z)$, which is typically chosen to be a standard normal (Gaussian) distribution. The probability density of the model be evaluated using the change of variables formula:

$$p_X(x) = p_Z(f(x)) \left| \det \left(\frac{\partial f(x)}{\partial x} \right) \right| = p_Z(f(x)) \prod_{l=1}^n \left| \det \left(\frac{\partial f_l(x)}{\partial x} \right) \right|, \quad (41.62)$$

where we have added subscripts to $p_X(x)$ and $p_Z(z)$ for clarity. The Jacobian determinant $\det \left(\frac{\partial f_l(x)}{\partial x} \right)$ must be efficient to compute for density estimation to be practical, and the transformation f_l should be easy to invert for sampling. In contrast to VAE and

GANs, standard normalizing flows preserve the dimensionality of the data space as they are invertible (though there are normalizing flows that are defined on lower dimensional manifolds embedded in the data space [44, 46, 252, 259, 260]). As such, they do not have the problems of GANs and VAEs they can be trained via maximum likelihood (Eq. 41.18) as described in Sec. 41.3.2.1.

There are several popular architectures of NFs. A method used by NICE, RealNVP and Glow [253–255] is to split the space into two disjoint sets z_1 and z_2 , and then use an identity forward map $z \rightarrow x$ for x_1 , $x_1 = z_1$, and an affine transformation for x_2 of the form

$$x_2 = \exp(s(z_1)) \odot z_2 + m(z_1), \quad (41.63)$$

where \odot is elementwise product and $m(z_1)$, $s(z_1)$ are neural networks. The Jacobian of this map is lower triangular, and its determinant is simply the product of elements along the diagonal, which is tractable, as is the inverse of the transformation. At the next layer one then performs a different split of dimensions into z_1 and z_2 . The affine transformation can be further generalized to a nonlinear form using rational splines [270].

One can interpret the sequence of invertible transformations $f_1 \circ f_2 \circ \dots \circ f_n$ as n discrete time steps in a continuous flow. In particular, one can think of a continuous-time flow described by an ordinary differential equation (ODE) and then interpret the discrete time steps as the result of a numerical integration of that ODE. This is the approach taken by the Pfjord algorithm [271] and other variants.

A different approach creating a deep generative model with a tractable likelihood is to model $p(x)$ autoregressively as

$$p(x) = \prod_{i=1}^n p(x_i | x_1, x_2, \dots, x_{i-1}). \quad (41.64)$$

This form describes each new dimension conditionally on all previous dimensions. It can model a general likelihood $p(x)$ as a sequence of conditional 1d distributions, whose conditional dependence on the parameters x_1, x_2, \dots, x_{i-1} can be modeled with neural networks. If x is a time series this form imposes a causal structure where x_i depends on all previous times x_j , $j < i$. WaveNet [272] and PixelCNN [273] are two well known examples. Sampling from an autoregressive model is sequential, and can be slow in high dimensions. Inverse autoregressive flow reverses this process and makes sampling fast, but the likelihood evaluation is slow. Some normalizing flows have autoregressive coupling layers, such as Masked Autoregressive Flow (MAF) [269].

All of the methods above use maximum likelihood training of likelihood $p(x)$ against network parameters, so the training is to minimize KL divergence between the data distribution and a Gaussian in latent space. This can be overly sensitive to small variance directions that dominate the likelihood, without being sensitive to the global structure of the data. An alternative is to use Optimal Transport Wasserstein distance between the density of the generated samples and the data, which can be evaluated either in data space or in latent space. As Wasserstein distance is difficult to evaluate in high dimensions, one can instead use slices, 1d projections of the data along different directions in high dimensional space, to build the flow [45]. Along each slice direction one obtains the 1d marginal distribution that can be mapped to a Normal distribution using a cumulative distribution function method. In 1d the Jacobian and the inverse transformation are tractable. The projection directions are chosen to maximize the sliced 1d Wasserstein distance between the data and the distribution generated by the samples, or between the inverse flow from the data to the latent space and the target distribution (typically chosen as the Normal distribution). Because this training is less sensitive to small variance directions than maximum likelihood training it achieves better results on anomaly detection tasks [45].

One can reduce the architectural restrictions imposed by normalizing flows or autoregressive models by modeling the “score” $\nabla_x \log p(x)$ instead of $p(x)$. Note this usage of the term “score” is non-standard and goes back to Ref. [274]; the standard use of the term score is theta of Eq. 41.26. Score-based training avoids the normalization requirement. Score based models learn gradients of log probability density functions on a large number of

noise-perturbed data distributions, and then generate samples by Langevin-type sampling. The resulting generative models, called score-based generative models [275] or diffusion probabilistic models [276], have several advantages over existing model families. They achieve GAN-level sample quality without adversarial training, and enable exact log-likelihood computation through their connection to continuous-time flows, which can be represented as a probability flow ordinary differential equation [276]. The main advantage is that the distribution $p(x)$ can be specified solely by its gradient, which can subsequently be sampled from using Langevin dynamics. This is similar to the gradient based Monte Carlo Markov Chain methods (such as Langevin or Hamiltonian Monte Carlo) that sample from Bayesian posteriors without directly estimating the normalizing constant. This in turn enables more flexible model architectures than what can be used in normalizing flows or autoregressive models.

We end by noting that normalizing flows, autoregressive models, and other deep generative models that provide a tractable likelihood are incredibly powerful tools for simulation-based inference. They can provide surrogate models trained from large simulated datasets when the simulators have intractable likelihood functions, which is usually the case. As described in Sec. 41.3.5, one would like to work with models that can provide conditional density estimation in order to model either the likelihood $p(x|\theta)$ or the posterior $p(\theta|x)$ [56, 57]. These techniques are being actively explored and applied to a number of scientific problems.

41.6 Learning algorithms

41.6.1 Gradient-based optimization

Given a parameterized model $f(x, \theta)$ and a loss function $\mathcal{L}(x, \theta)$, where x and θ denotes data and model parameters, one way to optimize θ is to first apply an appropriate initialization, $\theta_{t=0}$ (e.g. Sec. 41.6.7 for neural networks), and perform an iterative update:

$$\theta_t = \theta_{t-1} - \lambda \nabla_{\theta} \mathcal{L}(x, \theta), \quad (41.65)$$

where λ is a small, real valued hyperparameter called *learning rate*. To see how this works, define $\delta\theta \equiv \theta_t - \theta_{t-1}$ and consider $\delta(\nabla_{\theta} \mathcal{L}(x, \theta))$:

$$\delta(\nabla_{\theta} \mathcal{L}(x, \theta)) \approx \delta\theta \cdot \nabla_{\theta} \mathcal{L}(x, \theta) = -\lambda |\nabla_{\theta} \mathcal{L}(x, \theta)|^2 \quad (41.66)$$

which would monotonically decrease the loss function, and locally move the parameter values in the desired direction of loss function minimization. This algorithm is called *Gradient Descent*. We note that λ needs to be sufficiently small for the approximation to hold. When λ is too large, this can be a cause of a gradient explosion discussed in Sec. 41.6.7.

41.6.2 Stochastic gradient descent

Stochastic Gradient Descent (SGD) follows GD but replaces the exact gradient term $\nabla_{\theta} \mathcal{L}(x, \theta)$ with a stochastic approximation, where we subsample the data in the loss function using N samples, where $N < n$,

$$\nabla_{\theta} \mathbb{E}_{\hat{p}(x)} \mathcal{L} \approx \frac{1}{N} \sum_i^N \nabla_{\theta} \mathcal{L}_i, \quad (41.67)$$

where \mathcal{L}_i is the loss function for data sample i . It should be noted that N needs to be randomly and independently sampled for the approximation to hold. Implementation of SGD follows three steps: take new samples of size N , approximate the gradient, then update the parameters θ .

In the case of optimizing the loss using a static database (*i.e.* one cannot take new N samples for every update), *mini-batch learning* is often employed. This replaces the first step with a randomly sampled *batch* of data, which is a subset of all the samples in the database. In this case, however, since a batch of data used for each parameter update is not entirely independent, a model may overfit. In practice, a part of the whole dataset is reserved as a *validation* sample, and the model performance is carefully monitored during the optimization process to avoid overfitting via an early stopping criterion (see Sec. 41.6.6 and Fig. 41.11).

SGD with slowly decreasing learning rate can be shown to converge to a local minimum almost surely under mild conditions,

and to a global minimum for unimodal loss functions. SGD may also prevent getting stuck in shallow local minima of the loss function, thereby reaching a better local minimum for multi-modal loss functions. The noise in SGD with a constant learning rate can be viewed as a form of Langevin dynamics, which under proper conditions on the learning rate and mini-batch size converges to the stationary posterior distribution of the weights [277]. Thus SGD at a constant learning rate can be viewed as a sampler bouncing around and exploring the posterior surface for better solutions, descending onto the best found solution as the learning rate is decreased, a process related to temperature annealing in global optimization.

Another advantage of SGD is simply the computational cost: rather than evaluating the loss over all the data samples at each update, we use a small subset of data instead at each update. Furthermore, mini-batching can take advantage of vectorization libraries and GPU architectures. Large batch training requires specialized methods of training, such as Layer-wise Adaptive Rate Scaling (LARS).

41.6.3 Optimization algorithms

GD and SGD are the basic building blocks for more advanced optimization algorithms. One can improve the convergence rate of gradient based optimization by considering the learning rate λ to depend on individual θ_i . Second order algorithms such as Newton's method take into account second order derivatives (Hessian) to find the minimum, and give an exact solution in a single update when the loss is quadratic around the peak. However, this requires a matrix inversion of the Hessian, which is exceedingly expensive in ML applications, where the number of network parameters is very large. As a consequence, second order optimization is rarely used in ML.

There are several improvements to the basic SGD even in the absence of Hessian information. Momentum based optimization takes a physics perspective of a viscous fluid in an external potential, where one updates current velocity with the potential gradient (force), followed by an update in position based on velocity. This approach therefore uses previous gradients in addition to the current one to compute a running average of the gradient, with a forgetting factor that controls how far back the averaging goes. This helps move faster towards the minimum in ravines, where gradient descent is usually inefficient due to the high condition number of the Hessian.

One way to make the learning rate dependent on θ_i is to consider the gradient norm squared $(\nabla_{\theta_i} \mathcal{L})^2$. RMSprop learns its running average and then reduces the learning rate in directions with a large average gradient norm squared, thereby reducing the oscillations along that direction. ADAM (Adaptive Moment Estimation) combines the momentum and gradient norm ideas, computing running averages of both the gradient and the gradient norm squared, each with its own forgetting factor [278].

41.6.4 Automatic differentiation and back propagation

In practice, $f(x, \theta)$ might take a complex form and may include a large set of parameters. The term $\nabla_{\theta} \mathcal{L} = \nabla_{\theta} \mathcal{L}(f(x, \theta))$ requires computing partial derivatives with respect to individual parameter θ_i . If f is a composite model (*i.e.* $f = f_n(f_{n-1}(\dots, \theta_{n-1}), \theta_n)$), and if all of $f_{i:1,n}$ are differentiable, a chain rule can be applied:

$$\nabla_{\theta_i} \mathcal{L} = \frac{\partial \mathcal{L}(f(x, \theta))}{\partial \theta_i} = \frac{\partial \mathcal{L}}{\partial x_n} \cdot \frac{\partial x_n}{\partial x_{n-1}} \dots \frac{\partial x_i}{\partial \theta_i} \quad (41.68)$$

where x_n denotes the output of n -th composite function f_n . In order to compute $\nabla_{\theta_i} \mathcal{L}$ for f_i , it needs computation of a gradient at all preceding (or subsequent if seen in the forward context) functions. As the gradients accumulate across differentiable functions in the reverse order of the model composition, this technique is called *back propagation* [225]. An example of f that satisfies conditions to apply back propagation is a neural network, which consists of repeating blocks of a (differentiable) activation function and an affine transformation.

When the model $f(x, \theta)$ is implemented as a computer program in practice, *automatic differentiation* (AD), also called *algorithmic differentiation*, is used to compute the derivatives. AD ex-

exploits the fact that any computer program consists of a sequence of elementary arithmetic operations (i.e. addition, subtraction, multiplication, division) and functions (e.g. log, exp, sin, cos) and apply chain rules to compute the target derivative. AD has advantages over traditional approaches including symbolic and numerical differentiation. The symbolic differentiation faces a serious difficulty of converting a program into a single expression, and the numerical differentiation suffers from round-off errors. Finally, both methods scale poorly in speed of computation for calculating partial derivatives with a large number of inputs. AD delivers much faster speed and does not suffer from increasing errors for calculating higher derivatives.

There are two modes of AD: the *forward* and *backward* mode. Consider a composite function $f(x, \theta) = f_n(f_{n-1}(\dots f_1(x, \theta_1) \dots), \theta_{n-1}), \theta_n$. The forward mode applies the chain rule in the same order of the forward evaluation of f by computing $\partial f_1/\partial x$ first, then $\partial f_2/\partial f_1$, and continue to $\partial f_n/\partial f_{n-1}$. The backward mode traverses the reverse direction: starting from the last (outer-most) function $\partial f_n/\partial f_{n-1}$, next $\partial f_{n-1}/\partial f_{n-2}$, and continue to $\partial f_1/\partial x$. Therefore, the back propagation of gradients can be implemented using the backward AD, in which the target variable to be differentiated is fixed and the derivative is computed with respect to each sub-expression recursively as shown in Eq. 41.68. The forward mode is simpler to implement as the order of gradient calculation follows the order of composite functions to be executed. The reverse mode typically requires less amount of computation than the forward mode, but more memory is required to store intermediate function output values to calculate derivatives efficiently. Another consideration is the mapping of dimensionality $f: \mathbb{R}^k \rightarrow \mathbb{R}^\ell$ as it concerns the number of variables to sweep from each end. The forward mode is efficient when $k \ll \ell$ while the reverse mode takes an advantage if $\ell \ll k$. For instance, in the case of an image classification where $(k, \ell) = (\text{pixel count}, 1)$, the reverse AD is more efficient.

41.6.5 The vanishing and exploding gradient problems

Gradient based optimization crucially depends on the size of gradient with respect to each model parameter. If the magnitude of gradient is too large with respect to the distance to an optimal parameter value, it may repeatedly overshoot the target and cause an oscillation preventing convergence. If the gradient is too small, it may take an impractically long time to converge. As shown in Eq. 41.68, the gradient of i -th function f_i is a product of gradients from the subsequent functions. If those gradients are too large or too small, the magnitude can either increase or decrease exponentially in the number of layers. These are called *exploding* and *vanishing* gradient problem respectively.

Modern deep neural networks consist with many composite functions (i.e. layers) and are particularly prone to this effect. Let us consider a simple RNN. From Eq. 41.50, we can write the back-propagating gradient:

$$\frac{\partial h_t}{\partial h_{t-1}} = \text{diagonal}(f'(Wx_t + Vh_{t-1} + b1))W \quad (41.69)$$

where f' denotes the derivative of an activation function. The gradient of the contribution to the loss \mathcal{L}_i from the i -th element in the sequence with respect to the j -th hidden state h_j is therefore:

$$\frac{\partial \mathcal{L}_i}{\partial h_j} = \frac{\partial \mathcal{L}_i}{\partial h_i} V^{i-j} \prod_{j < t \leq i} \text{diagonal}(f'(Wx_t + Vh_{t-1} + b1)) \quad (41.70)$$

where we can see that V contributes multiplicatively with $i - j$ powers when $i - j > 1$. This example is explored in depth for recurrent models [226, 227] but is common for all types of deep neural networks.

In practice, one may explicitly inspect the magnitude of gradients propagating across layers to ensure an effective optimization. One way to mitigate an exploding gradient is to set the maximum gradient value δ_{\max} as a model hyperparameter and *clip* any larger gradients δ where it appears in the back propagation:

$$\delta = \frac{\delta_{\max}}{\|\delta\|} \text{diff}[\|\delta\| > \delta_{\max}]. \quad (41.71)$$

This is called *gradient clipping* [227].

Alternatively, there are many architecture designs that are motivated by the vanishing and exploding gradient problem or which aim to help propagate gradients across many layers. These considerations drove the design of gated models like the LSTM and GRU for sequential data and also motivated the ReLU non-linearity. Other example architectural designs or components motivated by these considerations include identity mapping and skip connections used in ResNet, U-Net, and DenseNet, which allow gradients to flow across many layers.

Other factors contributing to vanishing and exploding gradient include initialization of model parameters and normalization of input data. These factors contribute in keeping the magnitude of activation, which also concerns the magnitude of gradient, within a reasonable range. A recommended practice for a gradient-based optimization of a neural network is to maintain the input values centered around zero and a similar level of covariance across the inputs (and the outputs that are the inputs to the next layer) [279]. These factors are discussed in the following.

41.6.6 Early stopping

Early stopping is a form of regularization used to avoid overfitting when an iterative method, such as gradient descent, is used as a learning algorithm. Imagine a plot of the training loss and test loss as a function of iterations (*i.e.* parameter updates). As learning proceeds, the training loss will generally decrease. However, the test loss will often decrease initially and then start to increase, which is the classic sign of overfitting as shown in Fig. 41.11. The basic idea of early stopping is simply to stop training before overfitting takes place. In some approaches to early stopping theoretical analysis of the learning problem provides a prescription for when to stop the training [280]; however, the most straight forward approaches use a held-out validation dataset to monitor the generalization performance [281].

41.6.7 Initialization of model parameters

An improper initialization can slow down the optimization process or even result in a loss of convergence. While $b^{(l)}$ is typically initialized to zero, $W^{(l)}$ values need to be stochastic to avoid identical updates during optimization. One way is to sample $W^{(l)}$ from a zero-centered Gaussian distribution with a small variance (e.g. 0.01) [282]. However, this method does not guarantee the same variance in the input to each layer, which depends on the size of the input layer, and makes it difficult to train a deep neural network [220]. The *Xavier* initialization takes this into account and sets the variance of a Gaussian distribution to be $\sigma^2 = 1/d^{(l-1)}$ assuming a symmetric activation function around zero, such as a logistic function or hyperbolic tangent [283]. The *He* initialization uses the variance $\sigma^2 = 0.5/d^{(l-1)}$, and is a simple extension of Xavier initialization for leaky, parametric, and standard ReLU activation [208].

41.6.8 Input normalization

Input data to a neural network is often pre-processed for the same goals discussed previously: values are shift to have the mean of zero and scaled to keep a similar covariance across features. Furthermore, a data may be transformed using techniques including PCA and whitening (sphering) to keep input features independent and uncorrelated from each other [279].

41.6.9 Batch normalization

Even with careful normalization of the input data and initialization of model parameters, the mean and covariance of the data representations in hidden layers will evolve during training and may pose challenges for learning for downstream layers. This is called an *internal covariate shift* [284] and may cause negative effects to an optimization process. Accordingly, techniques to explicitly normalize features in between hidden layers are often employed for a deep neural network. One of them is *Batch Normalization*, which shifts and scales the input to a hidden layer:

$$\tilde{u}^{(l)} = \gamma \frac{u^{(l)} - \mu_B}{\sqrt{\sigma_B^2 + \epsilon}} + \beta \quad (41.72)$$

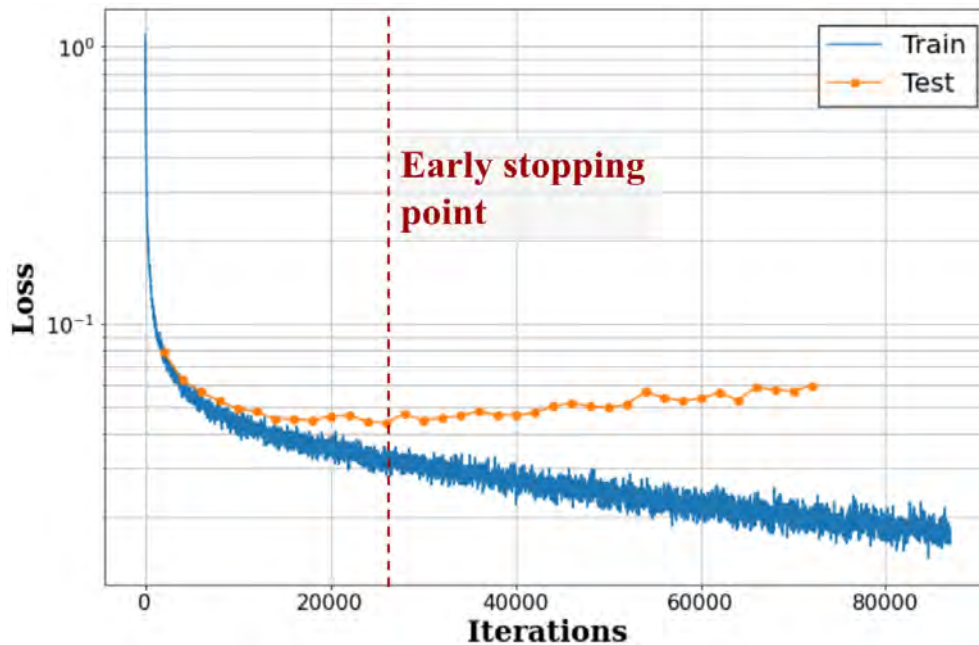


Figure 41.11: An example instance of overfitting. The training loss (vertical axis) shown in blue decreasing over iterations (horizontal axis) while the loss values evaluated on test samples shown in orange start to increase at around 26,000 iterations as indicated by the vertical line.

where $u^{(l)}$ and $\tilde{u}^{(l)}$ refer to the raw and normalized input to the l -th layer, μ_B and σ_B represent the mean and mean-squared-error of $u^{(l)}$ calculated using a *batch* of input data used to update the network parameters. γ and β are part of model parameters that are updated during the optimization. After optimization is complete, these parameters are fixed for model evaluation during production. ϵ is a small, fixed constant value to ensure numerical stability. While it is popular (especially in Computer Vision), a downside of BN is its dependency on the batch size. In situations where the batch size is limited to be a small number (e.g. memory limitation for a large data or a model), the performance using BN could degrade since β and γ values may not be generalized for the dataset during training.

There are several variants to batch normalization with considerations on how to group a subset of values in u^l . For instance, an image naturally has three groupings: a set of pixels across spatial axis, features within one pixel (i.e. image *channels*), alongside with a grouping across multiple images (i.e. *batch*). Different groupings have been studied and found and some are found effective to particular type of applications: Layer Normalization groups values along the channel and spatial dimensions [285], Instance Normalization groups along the spatial dimension but not along the batch nor channel [286], and Group Normalization is similar to Layer Normalization but forms multiple sub-groups of channels [287]. These variants does not apply normalization across samples within a batch, and thus agnostic to the batch size.

41.6.10 Transfer learning: pre-training and fine-tuning

Transfer learning is a technique to improve performance and accelerate optimization process by reusing a pre-trained machine learning model for a new task. Two tasks and data sets for each task may be different: the idea is that fundamental features may be reusable across different data and tasks. Transfer learning typically takes two steps: the first is to alter the model or data if necessary, then train (*fine-tuning*) the model. The first step is required, for example, when solving a different task that requires a different architecture (e.g. regression v.s. classification), or when input data format requires a change (e.g. original model trained on three channel image, such as RGB images, while new data has a single channel). Transfer learning has been widely practiced in the field of Computer Vision where large, labeled data sets

are available [288–291]: a CNN trained for classifying images of an animal can be largely reused for object detection, or even for analyzing image data in science (e.g. particle trajectories recorded by an imaging detector). It is a critical aspect for the development of generic AI as well as interdisciplinary sharing of models across research fields.

For sequential models, transfer learning had been challenging before the appearance of Transformer. While Transformer was initially introduced for machine translation, Generative Pre-trained Transformer (GPT-1) showed that the model can be generalized to multiple NLP tasks by achieving the state-of-the-art in several seemingly different tasks including a sentence classification, semantic similarity, question answering and commonsense reasoning [292].

41.6.11 Zero, one, and a few shot learning

Fine-tuning (and thus transfer learning) may not be necessary if model is well generalized: humans can picture an imaginary animal in mind just from descriptions, or perform a task that he or she has never done before. One-shot learning is an extreme case of transfer learning where only one example is presented at the fine-tuning stage [293]. A similar variant is called a few-shot learning (fine-tuning using a few examples). This is possible only if the model has already learned the solution during the pre-training and the example is used to map the solution to the task. Zero-shot [294–296] learning is even more extreme where the model is given a new task without any example. This is only possible if the task is already learned during the pre-training in an implicit or unsupervised manner since zero-shot training implies that the model was never trained for the task.

41.7 Incorporating uncertainty

A fundamental aspect of data analysis is the quantification of uncertainty. This broad topic includes the traditional distinction between statistical and systematic uncertainty, procedures for propagation of errors, and the incorporation of uncertainty in to the statistical models (e.g. with nuisance parameters) that are used in Bayesian or frequentist statistical procedures (see Sec. 40). Accounting for systematic uncertainty can be seen as a requirement, but ideally systematic uncertainties are also taken into account in the design of the analysis so as to mitigate their effect. The introduction of machine learning into the analysis pipeline

requires revisiting the techniques used for uncertainty quantification and exposes many fundamental issues that have nothing to do with the use of machine learning per se. See Ref. [297] for a recent review on this topic.

In machine learning research and industrial settings, the mismatch between the data distribution $p_{\text{train}}(x, y)$ used for training and the data distribution $p_{\text{prod}}(x, y)$ that the model will be applied to in production is referred to as *covariate shift* or *domain shift*. For example, one might train a classifier to identify cats and dogs with images from a well lit studio and then apply the classifier on images taken in doors with poor lighting conditions and a scratched lens. Not surprisingly, the mis-classification rate of the classifier will be different between the two settings.

Physicists are keenly aware that the simulations that we use to describe the data are not perfect, and this mismodelling corresponds to a large fraction of the of systematic uncertainties accounted for in published works. Since simulated data is often used to train machine learning models (*i.e.* $p_{\text{train}}(x, y)$), it is important to understand and account for how this mismodelling will influence results when applied to real data (*i.e.* $p_{\text{prod}}(x, y)$).

One of the primary approaches to incorporating this type uncertainty is to introduce nuisance parameters ν corresponding to the uncertain inputs to the simulation and to parameterize various types of perturbations (*e.g.* corrections to efficiencies, energy scales, *etc.*) in hopes that the resulting family of distributions $p(x|y, \nu)$ is flexible enough to encompass the true data distribution for class y . In this approach one does not have just two “domains” for the data (*i.e.* p_{train} and p_{prod}), but a continuous family of domains parameterized by the nuisance parameters ν .

With this framing in mind, there are several approaches to incorporating uncertainty into an analysis that includes ML-based components:

- **propagation of errors:** one works with a model $f(x)$ and simply characterizes how uncertainty in the data distribution propagate through the function to the down-stream task irrespective of how it was trained.
- **domain adaptation:** one incorporates knowledge of the distribution for domains (or the parameterized family of distributions $p(x|y, \nu)$) into the training procedure so that the performance of $f(x)$ for the down-stream task is robust or insensitive to the uncertainty in ν .
- **parameterized models:** instead of learning a single function of the data $f(x)$, one learns a family of functions $f(x; \nu)$ that is explicitly parameterized in terms of nuisance parameters and then accounts for the dependence on the nuisance parameters in the down-stream task.
- **data augmentation:** one trains a model $f(x)$ in the usual way using training dataset from multiple domains by sampling from some distribution over ν .

In this setting it is best to consider the trained model $f(x)$ or $f(x; \nu)$ to be a fixed function and decouple the variability associated to training or the choice of architecture. The fact that one could have chosen a different architecture or learning algorithm should be treated in the same way as other choices that are made in the data analysis pipeline. While it is reasonable to want downstream inference and decisions to be robust to these choices, they are of a different nature than the uncertainty in the modelling of the data distribution. We return to this point in Sections 41.7.5 and 41.7.6.

41.7.1 Propagation of errors

In this Section we consider the common scenario in which one has used some machine learning technique to train a model $f(x)$ for classification or regression and wants to assess the sensitivity of the output of $f(x)$ to uncertainty in the input x . We regard the function $f(x)$ as fixed and we are not concerned with how the model was trained.

Propagating uncertainty through a ML-based model $f(x)$ is not fundamentally different than for any other function, and one can use the standard propagation of errors formula of Sec. 39.2.1. As always, it is important to recognize the limitations of the propagation of errors formula, which is accurate when the uncertainty

on x is Gaussian and the function $f(x)$ is approximately linear within the region set by the uncertainty on x .

Similarly, classifiers are often used for particle identification or event selection. In that case, one is primarily interested in the efficiency ϵ to satisfy a cut on the classifier output. The efficiency depends on the distribution $p(x|y)$ through the equation $\epsilon_y = P(f(x) > f_{\text{cut}}|y) = \int H(f(x) - f_{\text{cut}})p(x|y)dx$, where H is the Heaviside step function and y is an index or label for the category of data that is being considered (*e.g.* signal or background, electron or jet, *etc.*). Thus, the question in this context is what is the uncertainty on the efficiency ϵ_y due to uncertainty in the distribution $p(x|y)$. In practice, the quantification of the uncertainty in the efficiency ϵ_y is usually based on either a calibration measurement on real data or estimated with simulated data. These procedures typically treat the classifier as a black-box, and thus nothing precludes using those procedures on a ML-based classifier. An early example of this approach for b-tagging can be found in Ref. [298].

In the case where simulation is used to estimate the efficiency ϵ_y and its uncertainty, one usually varies nuisance parameters ν associated to the simulation. One then uses simulated samples to approximate $\epsilon_y(\nu) = P(f(x) > f_{\text{cut}}|y, \nu) = \int H(f(x) - f_{\text{cut}})p(x|y, \nu)dx$. Again, the procedure for incorporating uncertainty isn’t fundamentally different if the classifier $f(x)$ is based on machine learning or a hand-crafted observable.

41.7.2 Domain adaptation

While estimating the uncertainty for a ML-based model is not fundamentally different than any other hand-crafted observable used for regression or classification, the worry of many physicists is that by working with a high-dimensional set of features x that one is more susceptible to mismodelling of subtle correlations. This is a valid concern, and it should be appreciated that a great deal of prior knowledge and physical insight goes into the construction of hand-crafted observables so that they will be robust to the most uncertain aspects of data. However, much of this craft is based on heuristics that are difficult to systematize. Furthermore, one can only validate that such an observable is robust if one can explicitly evaluate the performance for a perturbed distribution. Thus in the settings where one can validate the robustness to a perturbed scenario ν_0 , one must have access to $p(x|y, \nu_0)$.

One approach to formalize this type of robustness is to consider the dependence on the distribution of the output of the model $f(x)$ to the nuisance parameters. In statistics, if the distribution of f is independent of the nuisance parameters, then f is referred to as a *pivotal quantity*. This is a property that we can incorporate directly into the training procedure to target a particular notion of robustness. The authors of Ref. [299] introduced an adversarial approach (similar to what is used in the generative adversarial network of Sec. 41.5.4.2) to penalize a model during training if the distribution of the output varies with the nuisance parameters. To construct the training dataset $\{x_i, y_i, \nu_i\}_{i=1, \dots, n}$, one must sample y and ν according to some proposal distribution (similar to a prior, but only used for the creation of training dataset, not necessarily for statistical inference), corresponding to a joint distribution $p(x, y, \nu)$. Instead of minimizing the target loss \mathcal{L}_f (*e.g.* cross-entropy, squared-error, *etc.*) with respect to the parameters ϕ_f that parameterize the model f , one trains with a minimax strategy that also includes an adversary q with parameters ϕ_r . The trained model is characterized by the saddle point

$$\hat{\phi}_f, \hat{\phi}_r = \arg \min_{\phi_f} \arg \max_{\phi_r} E_\lambda(\phi_f, \phi_r), \quad (41.73)$$

where the value function E_λ includes the target loss as well as a regularization term associated to the adversary

$$E_\lambda(\phi_f, \phi_r) = \mathcal{L}_f(\phi_f) - \lambda \mathcal{L}_r(\phi_f, \phi_r). \quad (41.74)$$

The constant λ is a hyperparameter, since generially there is a tradeoff between the two terms and only in special cases can the model that minimizes \mathcal{L}_f also be a pivotal quantity. The regularization term

$$\mathcal{L}_r(\phi_f, \phi_r) = \mathbb{E}_{p(x, y, \nu)}[-\log q_{\phi_r}(\nu|f_{\phi_f}(x))] \quad (41.75)$$

is an example of conditional density estimation (see Sec. 41.3.2.1), where the model $q_{\phi_r}(\nu|f)$ is trying to predict the distribution of the nuisance parameter ν given the output of the model $f(x)$. This term is maximized when f is independent of ν . Earlier work had also used an adversarial technique for domain adaptation, but was limited to just two domains [300–302], while here ν parameterizes a continuous family of distributions and can have multiple components corresponding to different sources of uncertainty. Furthermore, the previous work aimed to make the distribution for a high-dimensional, intermediate representation of the data be invariant to the domain shift as opposed to just the final output $f(x)$.

One way of interpreting Eq. 41.73 is that the goal is to minimize a regularized loss function $\tilde{\mathcal{L}}(\phi_f) = \arg \max_{\phi_r} E_{\lambda}(\phi_f, \phi_r)$, where the optimization with respect to ϕ_r is not exposed. This motivates another approach in which the regularization is not achieved through a learned adversary, but by a measure of discrepancy between distributions that can be computed directly from samples. In particular, the authors of Ref. [303] proposed the use of *distance correlation* to avoid what can be a challenging min-max optimization problem.

In either case, the optimization of the hyperparameter λ is based on the downstream task. For example, in Ref. [299] considered the case where f was a signal vs. background binary classifier where the nuisance parameter ν was associated to uncertainty in the background model. The hyperparameter λ was then optimized to maximize the approximate median significance (AMS). Similarly, the authors of Refs. [304] and [303] considered new physics searches in the context of boosted jet tagging, where the hyperparameter controls the sculpting of the side-bands used for background estimation.

While these strategies modify the training procedure so that the sensitivity to the nuisance parameters is reduced, it does not typically eliminate it. As a result, one still needs to propagate the uncertainty in the data distribution through the learned model as described in the preceding section.

Note, this adversarial technique has also been employed in other settings where one would like to decorrelate the output of the classifier with an observed quantity so that it can be used for background estimation [304]. Widely used alternative approaches to decorrelation include uboost [305] and DDT [306]. Other examples of the domain adaptation and decorrelation use cases from the Living Review include [299, 303–318].

41.7.3 Parameterized models

An alternative to learning a model $f(x)$ that is pivotal — *i.e.* whose distribution is independent of the nuisance parameter ν — is to learn a family of models $f(x; \nu)$ that is parameterized in terms of the nuisance parameters. In general, there is a tradeoff between the two terms of Eq. 41.74 for a single model $f(x)$. In a parameterized model, $f(x; \nu)$ optimizes the performance of the model for every value of ν . Parameterized classifiers were first advocated in Ref. [58] in the context of simulation-based inference (see Sec. 41.7.7) and in Ref. [319] for new physics searches. It has also been applied to simulation-based inference for effective field theory parameters in Ref. [19] and Ref. [320] provides additional pedagogical examples.

The training of a parameterized model is similar to the standard procedure. For example, if one originally wanted to minimize the squared loss function $\mathcal{L}(y, f(x)) = (y - f(x))^2$ with training dataset $\{x_i, y_i\}_{i=1, \dots, n}$, then the corresponding training procedure for the parameterized model would be as follows. One would need to construct a training set $\{x_i, y_i, \nu_i\}_{i=1, \dots, n}$ as described in the preceding section, construct a parameterized model $f(x; \nu)$ that takes as input the original feature vector x as well as the nuisance parameters ν , and then train using the same loss $\mathcal{L}(y, f(x; \nu)) = (y - f(x; \nu))^2$.

One complication of the parameterized approach is that it is no longer possible to evaluate the model on a dataset $\{x_i\}$ and pass on only $\{f_i\}$ for downstream analysis tasks since $f(x_i; \nu)$ still depends on ν . Instead, one delay evaluating the model to some downstream stage when the dependence on ν would accounted for. For example, in the context of a likelihood based analysis where one is testing a hypothesis where the nuisance param-

eters take on a particular value ν_{test} , then one will consider the data distribution $p(x|\nu_{\text{test}})$, and at that point one would evaluate the model at the corresponding nuisance parameter value, *i.e.* $f(x; \nu_{\text{test}})$. Explicit examples are given in Refs. [19, 58, 297, 320]. While this may seem complicated, it actually corresponds to what is done in a typical likelihood-based fit when the statistical model has nuisance parameters; *i.e.* the likelihood-ratio corresponds to the model $f(x; \nu)$ as in Eq. 41.12.

41.7.4 Data augmentation

An intuitive approach to building in robustness to systematic effects that can lead to domain shift, is simply to augment the training dataset so that it includes examples corresponding to several values of the nuisance parameter or systematic variations. As before one can construct a dataset $\{x_i, y_i, \nu_i\}_{i=1, \dots, n}$, but instead of leveraging the information about ν_i , one simply discards this information. This corresponds to sampling from the marginal distribution $x_i, y_i \sim p(x, y) = \int d\nu p(x, y|\nu)p(\nu)$, and is often referred to as *smearing*. One can then use this smeared dataset for supervised learning in the traditional way. While it is possible that this approach will lead to improved robustness to systematic variations (*i.e.* generalization for ν other than the nominal value) than if systematic uncertainty weren't considered at all, this intuitive approach has several shortcomings. The approach does not yield a pivotal quantity as in the adversarial approach, so propagation of uncertainty through the network is still required. Moreover, there is no direct way to control the trade-off between independence from the nuisance parameter and the original target loss as in the adversarial approach. Finally, it can lead to significant performance loss compared to what is possible with the parameterized approach. These trade-offs were studied in Refs. [319, 320] with both pedagogical and physically-motivated examples.

41.7.5 Aleatoric and epistemic uncertainty

In the machine learning and risk assessment literature, uncertainty is often characterized in terms of *aleatoric* and *epistemic* uncertainty [321–324]. Familiarity with these terms is useful, but the distinction between the two can be ambiguous, the terms are not always consistently used, and they do not clearly map onto the concepts used in physics.

For example, Ref. [323], states that “roughly speaking, aleatoric (aka statistical) uncertainty refers to the notion of randomness, that is, the variability in the outcome of an experiment which is due to inherently random effects”, while “epistemic (aka systematic) uncertainty refers to uncertainty caused by a lack of knowledge (about the best model)”. This seems clear enough, but in that same reference (and in Ref. [325]) the aleatoric uncertainty is considered irreducible, while the epistemic uncertainty could be reduced with additional information. This may seem backwards for many physicists since often in particle physics, we think of how uncertainties scale as we collect more data but keep the experimental design fixed. In that case, the statistical uncertainty will be reduced with time while the systematic uncertainty will remain constant⁶. There is no paradox here, it is simply a different point of view. The emphasis of the risk assessment community is not on collecting more data with the same experimental design, but collecting different types of data that will inform the models themselves. Clearly even for physicists, data from new experiments or calibration measurements could also reduce our systematic uncertainties. While there are exceptions in the literature, the bulk of it associates aleatoric uncertainty with the randomness of classical probability (*i.e.* the statistical uncertainty associated to repeating the same experiment many times) and epistemic uncertainty with our state of knowledge.

Perhaps a more important distinction between the perspective of physicists and machine learning researchers has to do with the use of the term “model” and what exactly is uncertain. In physics, the systematic and epistemic uncertainty is typically associated to our understanding of the underlying physics and “the model” usually refers to the physics model, detector model encapsulated

⁶Further complicating the relationship between the terms is that many experimental uncertainties that are characterized as systematic are actually statistical in nature as auxiliary measurements and control regions are used to constrain the corresponding nuisance parameters.

in a simulation. In contrast, for machine learning research, “the model” usually refers to the trained model $\hat{f} \in \mathcal{F}$ used as described in Section 41.2.1 (or the class of functions \mathcal{F} itself). This makes sense if we recall that in the bulk of machine learning research, one has little insight into the process that generated the data (*e.g.* images of cats and dogs, natural language, *etc.*). In that sense, the epistemic uncertainty in machine learning is usually associated to uncertainty in the model parameters ϕ after training, which would be reduced if one could collect more training dataset (see Ref. [324] for this point of view).

In the literature on Uncertainty Quantification (UQ), which is more closely connected to physics given the role of computer simulations, the terminology is more fine grained and less ambiguous. That community uses the terms parameter uncertainty (*i.e.* nuisance parameters), structural uncertainty (*i.e.* misspecification), algorithmic uncertainty (*i.e.* numerical uncertainty), experimental uncertainty (*i.e.* uncertainty from experimental resolution and statistical fluctuations), and interpolation uncertainty (*i.e.* uncertainty due to interpolating between different parameter values due to lack of computational resources).

41.7.6 Model averaging and Bayesian machine learning

The core of Bayesian machine learning is the model averaging view. Here one often takes a more ambitious view of learning than described in Sec. 41.2.1, which is framed mainly as function approximation. While in Sec. 41.2.1, the goal is to find a function that minimizes the risk, in Bayesian machine learning one explicitly builds a probability model $q_\phi(x, y)$ for the training dataset $\mathcal{D} = \{x_i, y_i\}_{i=1, \dots, n}$. It is the same change in perspective that one has when one views the squared error loss function $\mathcal{L}_{MSE} = (y - f_\phi(x))^2$ as the log-likelihood for a probability model $y \sim N(f(x), \sigma)$. In addition, one assumes some prior on the model parameters $p(\phi)$, which is often a Gaussian distribution, and is analogous to Tikhonov regularization (see Sec. 41.3.1.2). With this view in mind, a single trained model $\hat{f} = f_{\hat{\phi}}$ is the MAP point estimate and the more complete Bayesian solution is the entire posterior distribution over the model parameters $p(\phi|\mathcal{D})$. With this view, it is clear how increasing the number of training examples n will lead to a reduction in uncertainty on ϕ . However, this notion of epistemic uncertainty has little to do with the notion of systematic uncertainty as the term is used by particle physicists.

Bayesian methods can be applied to non-probabilistic regression problems, in which case they can provide uncertainty quantification. Consider the case of regression in traditional (non-Bayesian) machine learning. The trained model $f_{\hat{\phi}}(x)$ is used to predict the target label y . For a fixed x , the model does not provide any notion of uncertainty on the prediction. One could propagate uncertainty on x through $f(x)$, but that is also not the desired quantity to characterize the intrinsic spread $p(y|x)$ in the data, which may exist even if x has negligible uncertainty. In contrast, Gaussian process regression (a Bayesian method) does provide a natural way to communicate the uncertainty on the prediction, which is possible because one first had to specify a prior on the mean and covariance of the Gaussian process.

In the context of Bayesian deep learning and Bayesian Neural Networks, one would place a prior on the weights and biases of the neural network $p(\phi)$ and then use one of the many emerging techniques to calculate the approximate posterior $p(\phi|\mathcal{D})$. However, we should recognize that we have little-to-no insight into the parameters of a deep neural network, so the prior on ϕ is hardly well-justified. Furthermore, just as in all Bayesian approaches, the prior is not invariant to reparametrizing the model: $\phi \rightarrow \eta(\phi)$. While it is difficult to justify the choice of the prior on the parameters (and, thus, the resulting posterior), the resulting model may perform well empirically. In such high-dimensional parameter spaces, the bias-variance tradeoff can be dramatic.

Bayesian model averaging (BMA) performs Bayesian average over the posterior $p(\phi|\mathcal{D})$. This can be applied to any quantity f_ϕ , such as a regression or classification prediction y . Suppose we can draw from the posterior $\phi \sim p(\phi|\mathcal{D})$. For each draw we can evaluate the predicted regression variable $y = f_\phi(x) + \epsilon$, where ϵ is some noise to account for uncertainty in the predictions. We

can denote this process as a draw from $p(y|x, \phi)$, $y \sim p(y|x, \phi) = N(f_\phi(x), \sigma_\epsilon^2)$, where σ_ϵ^2 is the noise variance. The BMA then performs

$$p(y|x, \mathcal{D}) = \int d\phi p(\phi|\mathcal{D}) p(y|x, \phi). \quad (41.76)$$

In practice $p(y|x, \phi)$ is evaluated by drawing samples of y and ϕ , so the posterior is defined implicitly by the samples. For example, the mean prediction is obtained by averaging $f_\phi(x)$ over the samples of ϕ , and the covariance matrix is similarly evaluated by averaging the second moments over the samples of ϕ .

Ref. [326] provides a different perspective on BMA analyzed in what are referred to as the \mathcal{M} -open and \mathcal{M} -closed settings [326]. The \mathcal{M} -closed setting refers to the situation where the true data generating process is in the space of models, even if it is unknown to us. In contrast, the \mathcal{M} -open setting refers to when the true data generating process is not in model space (*i.e.* the model is mis-specified). Interestingly, in the \mathcal{M} -open case one can potentially do better than any one model in the model class by considering an average over the models, since averaging can create a new model that is not in the model class. BMA provides one such averaging, but other averages, which are not weighted by $p(\phi|\mathcal{D})$, can be a better choice. When the weights of each model are optimized against appropriate loss the resulting procedure is called stacking, which has been shown to be superior to BMA in the \mathcal{M} -open setting [326]. Ref. [327] performed experiments indicating that in some cases model averaging can also improve predictive uncertainty estimates under domain shifts.

Neural network model averaging beyond BMA comes in several different flavors. Two successful model averaging procedures are Monte Carlo dropout [328], which uses dropout ensembling, and deep ensembles [329], which use random initialization ensembling. These methods may not only be superior to BMA, they are also often significantly faster than BMA. Whether these model averages are an approximation to BMA, or an alternative to it, remains a debated topic, and both views have been advocated. BMA itself can be accelerated using approximate methods, such as stochastic Variational Inference with reparametrization trick [330].

41.7.7 Connection to probabilistic machine learning

We end this Section by reinforcing the connection between uncertainty quantification in traditional machine learning and the more probabilistic approaches to machine learning exemplified by simulation-based inference (see Sec 41.3.5) and deep generative models (see Sec. 41.5.4). In the standard approach to supervised learning (*e.g.* classification and regression) the model $f(x)$ provides a point estimate for y . Estimating an uncertainty on y goes a step further, but the complete picture would be to model the posterior distribution $p(y|x)$. Gaussian processes (see Sec. 41.5.1) are an example, but the form of the models is limited to Gaussian posteriors. In Sec 41.3.5 we discussed approaches to model $p(y|x)$ using conditional density estimation [51, 56, 57]. If we extend this task to include a family of distributions parameterized by some nuisance parameters ν , then the task is to model $p(y|x, \nu)$, which is structurally similar.

In the context of classification, the output is already probabilistic, and the interpretation of the resulting classifier is $\hat{f}_{MSE}(x) \approx p(y = 1|x)$ (see Eq. 41.10). Incorporating the dependence on the nuisance parameter, then connects to the likelihood-ratio trick (see Eq. 41.12), approaches to simulation-based inference that involve learning the likelihood-ratio, and the parameterized approaches described in Sec. 41.7.3.

If one pairs the training procedure for classification, regression, or density estimation used in the approaches above with model averaging techniques such as BMA, then it would be possible to incorporate both uncertainty associated to finite training dataset and the uncertainty associated to systematic uncertainties. However, as described in Sec. 41.7.5 and Sec. 41.7.1, it is not clear that in physics applications it is desirable to account for the variability associated to training when the more common practice is to regard the trained model $\hat{f}(x)$ as fixed.

While these probabilistic approaches to machine learning are attractive conceptually, it is known in the machine learning community that classifiers often are poorly calibrated and often overly

confident in their predictions. This is a problem even if one regards the trained model $\hat{f}(x)$ as fixed. Various approaches, including model averaging, are being pursued to improve the calibration of trained models, but the problem is unlikely to be eliminated entirely. Miscalibration can be verified by evaluating the true positive and false positive rates on held out data. This is common practice in experimental particle physics, where the output of a binary classifier is rarely taken at face value. Instead, the true and false positive rates are estimated with simulated data or control samples as described in Sec. 41.7.1. Furthermore, the true and false positives can be characterized as a function of the nuisance parameters. These procedures can be used to help calibrate parameterized models based on the likelihood-ratio trick (see Refs. [58, 320]). Unfortunately, calibration in the context of density estimation is more challenging. This connects to topics and challenges in anomaly detection (see Sec. 41.3.4).

41.8 Infrastructure for deployment in experiments

The software and computing needs of training a machine learning model are different than those encountered when it deployed for use. In machine learning jargon, the two stages are often referred to as *training* and *inference*, where inference might refer to making a prediction for y given x in a classification or regression problem. Sometimes this transition also involves using different programming languages for implementing the trained model from the ones used for training them. Modern machine learning frameworks support various serialization formats to exchange trained models. For instance, ONNX provides an open source format for many types of models and is widely supported and can be found in many frameworks, tools, and hardware. This is important when integrating a trained model into the large software frameworks used by the large experiments.

While hardware acceleration with GPUs is important for efficiently training modern machine learning techniques, there are also advantages of hardware acceleration at inference time. This may include GPUs or Field Programmable Gate Arrays (FPGAs), and the Living Review includes many example works focusing on efficient inference for a given hardware architecture [81, 108, 331–340]. For applications where latency is a key concern (eg triggering at collider experiments), various accelerators have been investigated [167, 171, 341–355]. In addition, some solutions for deployment of ML models involve deployment in the cloud [356, 357].

References

- [1] Y. Lecun, Y. Bengio and G. Hinton, *Nature* **521**, 7553, 436 (2015), ISSN 14764687.
- [2] J. Schmidhuber, *Neural Networks* **61**, 85 (2015).
- [3] A. Radovic *et al.*, *Nature* **560**, 7716, 41 (2018).
- [4] D. Guest, K. Cranmer and D. Whiteson, *Ann. Rev. Nucl. Part. Sci.* **68**, 161 (2018), [arXiv:1806.11484].
- [5] G. Carleo *et al.*, *Rev. Mod. Phys.* **91**, 4, 045002 (2019), [arXiv:1903.10563].
- [6] M. Feickert and B. Nachman (2021), [arXiv:2102.02770].
- [7] V. Vapnik, *The nature of statistical learning theory*, Springer science & business media (2013).
- [8] C. Zhang *et al.*, *Communications of the ACM* **64**, 3, 107 (2021).
- [9] P. Nakkiran *et al.*, arXiv preprint arXiv:1912.02292 (2019).
- [10] A. Y. Ng and M. I. Jordan, in T. G. Dietterich, S. Becker and Z. Ghahramani, editors, “Advances in Neural Information Processing Systems 14 [Neural Information Processing Systems: Natural and Synthetic, NIPS 2001, December 3–8, 2001, Vancouver, British Columbia, Canada],” 841–848, MIT Press (2001), URL <https://proceedings.neurips.cc/paper/2001/hash/7b7a53e239400a13bd6be6c91c4f6c4e-Abstract.html>.
- [11] M. Kuusela and V. M. Panaretos, *Ann. Appl. Stat.* **9**, 1671 (2015), [arXiv:1505.04768].
- [12] L. Rosasco, A. Tacchetti and S. Villa, *CoRR abs/1405.0042* (2014), URL <http://arxiv.org/abs/1405.0042>.
- [13] G. E. Hinton *et al.*, *CoRR abs/1207.0580* (2012), [arXiv:1207.0580], URL <http://arxiv.org/abs/1207.0580>.
- [14] P. Baldi and P. J. Sadowski, *Advances in neural information processing systems* **26**, 2814 (2013).
- [15] M. Belkin, S. Ma and S. Mandal, in J. G. Dy and A. Krause, editors, “Proceedings of the 35th International Conference on Machine Learning, ICML 2018, Stockholm, Sweden, July 10–15, 2018,” volume 80 of *Proceedings of Machine Learning Research*, 540–548, PMLR (2018), URL <http://proceedings.mlr.press/v80/belkin18a.html>.
- [16] S. Gunasekar *et al.*, in J. Dy and A. Krause, editors, “Proceedings of the 35th International Conference on Machine Learning,” volume 80 of *Proceedings of Machine Learning Research*, 1832–1841, PMLR (2018), URL <http://proceedings.mlr.press/v80/gunasekar18a.html>.
- [17] L. Zdeborová, *Nature Physics* **16**, 6, 602 (2020).
- [18] E. M. Metodiev, B. Nachman and J. Thaler, *JHEP* **10**, 174 (2017), [arXiv:1708.02949].
- [19] J. Brehmer *et al.*, *Phys. Rev.* **D98**, 5, 052004 (2018), [arXiv:1805.00020].
- [20] J. Brehmer *et al.*, *Proc. Nat. Acad. Sci.* 201915980 (2020), [arXiv:1805.12244].
- [21] M. Stoye *et al.* (2018), [arXiv:1808.00973].
- [22] M. A. Hayat *et al.*, *ApJ Letters* **911**, 2, L33 (2021).
- [23] T. Chen *et al.*, in “Proceedings of the 37th International Conference on Machine Learning, ICML 2020, 13–18 July 2020, Virtual Event,” volume 119 of *Proceedings of Machine Learning Research*, 1597–1607, PMLR (2020), URL <http://proceedings.mlr.press/v119/chen20j.html>.
- [24] E. Parzen, *The annals of mathematical statistics* **33**, 3, 1065 (1962).
- [25] R. A. Davis, K.-S. Lii and D. N. Politis, in “Selected Works of Murray Rosenblatt,” 95–100, Springer (2011).
- [26] K. S. Cranmer, *Comput. Phys. Commun.* **136**, 198 (2001), [hep-ex/0011057].
- [27] Y. Bengio, A. Courville and P. Vincent, *IEEE transactions on pattern analysis and machine intelligence* **35**, 8, 1798 (2013).
- [28] https://en.wikipedia.org/wiki/Cluster_analysis.
- [29] R. E. Bellman, *Dynamic Programming*, Princeton University Press, USA (1957), ISBN 069107951X.
- [30] D. E. Kirk, *Optimal control theory: an introduction*, Courier Corporation (2004).
- [31] K. J. Åström, *Journal of Mathematical Analysis and Applications* **10**, 174 (1965).
- [32] J. Brehmer *et al.*, in “34th Conference on Neural Information Processing Systems,” (2020), [arXiv:2011.08191].
- [33] R. S. Sutton and A. G. Barto, Cambridge, MA **22447** (1998).
- [34] K. Arulkumaran *et al.*, *IEEE Signal Processing Magazine* **34**, 6, 26 (2017).
- [35] H. Robbins, *Bulletin of the American Mathematical Society* **58**, 5, 527 (1952).
- [36] J. C. Gittins, *Journal of the Royal Statistical Society: Series B (Methodological)* **41**, 2, 148 (1979).
- [37] J. Mockus, *Bayesian approach to global optimization: theory and applications*, volume 37, Springer Science & Business Media (2012).
- [38] E. Brochu, V. M. Cora and N. De Freitas, arXiv preprint arXiv:1012.2599 (2010).

- [39] M. Farina, Y. Nakai and D. Shih, *Physical Review D* **101**, 7 (2020), ISSN 2470-0029, URL <http://dx.doi.org/10.1103/PhysRevD.101.075021>.
- [40] T. Heimel *et al.*, *SciPost Physics* **6**, 3 (2019), ISSN 2542-4653, URL <http://dx.doi.org/10.21468/SciPostPhys.6.3.030>.
- [41] J. Ren *et al.*, in H. M. Wallach *et al.*, editors, “Advances in Neural Information Processing Systems 32: Annual Conference on Neural Information Processing Systems 2019, NeurIPS 2019, December 8-14, 2019, Vancouver, BC, Canada,” 14680–14691 (2019).
- [42] E. T. Nalisnick *et al.*, in “7th International Conference on Learning Representations, ICLR 2019, New Orleans, LA, USA, May 6-9, 2019,” OpenReview.net (2019), URL <https://openreview.net/forum?id=H1xwNhCcYm>.
- [43] Z. Xiao, Q. Yan and Y. Amit, arXiv preprint arXiv:2003.02977 (2020).
- [44] V. Böhm and U. Seljak, arXiv preprint arXiv:2006.05479 (2020).
- [45] B. Dai and U. Seljak, in M. Meila and T. Zhang, editors, “Proceedings of the 38th International Conference on Machine Learning, ICML 2021, 18-24 July 2021, Virtual Event,” volume 139 of *Proceedings of Machine Learning Research*, 2352–2364, PMLR (2021), URL <http://proceedings.mlr.press/v139/dai21a.html>.
- [46] J. Brehmer and K. Cranmer (2020), [arXiv:2003.13913].
- [47] E. M. Metodiev, B. Nachman and J. Thaler, *Journal of High Energy Physics* **2017**, 10 (2017), ISSN 1029-8479, URL [http://dx.doi.org/10.1007/JHEP10\(2017\)174](http://dx.doi.org/10.1007/JHEP10(2017)174).
- [48] J. H. Collins *et al.*, *The European Physical Journal C* **81**, 7 (2021), ISSN 1434-6052, URL <http://dx.doi.org/10.1140/epjc/s10052-021-09389-x>.
- [49] G. Kasieczka *et al.* (2021), [arXiv:2101.08320].
- [50] T. Aarrestad *et al.* (2021), [arXiv:2105.14027].
- [51] K. Cranmer, J. Brehmer and G. Louppe, *Proc. Nat. Acad. Sci.* **117**, 48, 30055 (2020), [arXiv:1911.01429].
- [52] J. Brehmer and K. Cranmer, *Artificial Intelligence for Particle Physics*, chapter Simulation-based inference methods for particle physics, World Scientific Publishing Co (2021).
- [53] P. J. Diggle and R. J. Gratton, in “Journal of the Royal Statistical Society: Series B (Methodological),” volume 46, 193–212 (1984), ISSN 0035-9246.
- [54] D. B. Rubin, *The Annals of Statistics* **12**, 4, 1151 (1984), ISSN 0090-5364, URL <https://doi.org/10.1214/aos/1176346785>.
- [55] M. A. Beaumont, W. Zhang and D. J. Balding, *Genetics* **162**, 4, 2025 (2002), ISSN 00166731.
- [56] K. Cranmer and G. Louppe, *J. Brief Ideas* (2016), 10.5281/zenodo.198541.
- [57] G. Papamakarios and I. Murray, in “Advances in Neural Information Processing Systems,” 1036–1044 (2016), ISSN 10495258, [arXiv:1605.06376].
- [58] K. Cranmer, J. Pavez and G. Louppe, arXiv:1506.02169 (2015), [arXiv:1506.02169], URL <http://arxiv.org/abs/1506.02169>.
- [59] C. Modi, F. Lanusse and U. Seljak, “Flowpm: Distributed tensorflow implementation of the fastpm cosmological n-body solver,” (2020), [arXiv:2010.11847].
- [60] J. Jasche and B. D. Wandelt, *Mon. Not. Roy. Astron. Soc.* **432**, 894 (2013), [arXiv:1203.3639].
- [61] U. Seljak *et al.*, *JCAP* **12**, 009 (2017), [arXiv:1706.06645].
- [62] A. Andreassen *et al.*, *Phys. Rev. Lett.* **124**, 18, 182001 (2020), [arXiv:1911.09107].
- [63] K. Datta, D. Kar and D. Roy (2018), [arXiv:1806.00433].
- [64] M. Bellagente *et al.* (2019), [arXiv:1912.00477].
- [65] N. D. Gaganashvili (2010), [arXiv:1004.2006].
- [66] A. Glazov (2017), [arXiv:1712.01814].
- [67] M. Bellagente *et al.* (2020), [arXiv:2006.06685].
- [68] M. Vandegar *et al.*, in A. Banerjee and K. Fukumizu, editors, “Proceedings of The 24th International Conference on Artificial Intelligence and Statistics,” volume 130 of *Proceedings of Machine Learning Research*, 2107–2115, PMLR (2021), [arXiv:2011.05836], URL <https://proceedings.mlr.press/v130/vandegar21a.html>.
- [69] P. Baroň (2021), [arXiv:2104.03036].
- [70] A. Andreassen *et al.* (2021), [arXiv:2105.04448].
- [71] P. Komiske, W. P. McCormack and B. Nachman (2021), [arXiv:2105.09923].
- [72] V. Andreev *et al.* (H1) (2021), [arXiv:2108.12376].
- [73] M. Arratia *et al.* (2021), [arXiv:2109.13243].
- [74] T. A. Le, A. G. Baydin and F. Wood, in “Proceedings of the 20th International Conference on Artificial Intelligence and Statistics, AISTATS 2017,” volume 54 of *Proceedings of Machine Learning Research*, 1338–1348, PMLR, Fort Lauderdale, FL, USA (2017), [arXiv:1610.09900].
- [75] A. G. Baydin *et al.* (2018), [arXiv:1807.07706].
- [76] A. G. Baydin *et al.*, International Conference for High Performance Computing, Networking, Storage and Analysis, SC arXiv:1907.03382 (2019), ISSN 21674337, [arXiv:1907.03382].
- [77] A. Hocker *et al.*, PoS **ACAT**, 040 (2007), [arXiv:physics/0703039].
- [78] T. Mikolov *et al.*, arXiv preprint arXiv:1301.3781 (2013).
- [79] E. Asgari and M. R. Mofrad, *PloS one* **10**, 11, e0141287 (2015).
- [80] D. Guest *et al.*, *Phys. Rev.* **D94**, 11, 112002 (2016), [arXiv:1607.08633].
- [81] T. Q. Nguyen *et al.*, *Comput. Softw. Big Sci.* **3**, 1, 12 (2019), [arXiv:1807.00083].
- [82] E. Bols *et al.* (2020), [arXiv:2008.10519].
- [83] K. Goto *et al.*, “Development of a Vertex Finding Algorithm using Recurrent Neural Network,” (2021), [arXiv:2101.11906].
- [84] R. T. de Lima (2021), [arXiv:2102.06128].
- [85] Technical Report ATL-PHYS-PUB-2017-003, CERN, Geneva (2017), URL <http://cdsweb.cern.ch/record/2255226>.
- [86] J. Pumplin, *Phys. Rev. D* **44**, 2025 (1991).
- [87] J. Cogan *et al.*, *JHEP* **02**, 118 (2015), [arXiv:1407.5675].
- [88] L. G. Almeida *et al.*, *JHEP* **07**, 086 (2015), [arXiv:1501.05968].
- [89] L. de Oliveira *et al.*, *JHEP* **07**, 069 (2016), [arXiv:1511.05190].
- [90] Technical Report ATL-PHYS-PUB-2017-017, CERN, Geneva (2017), URL <http://cds.cern.ch/record/2275641>.
- [91] J. Lin *et al.*, *JHEP* **10**, 101 (2018), [arXiv:1807.10768].
- [92] P. T. Komiske *et al.*, *Phys. Rev.* **D98**, 1, 011502 (2018), [arXiv:1801.10158].
- [93] J. Barnard *et al.*, *Phys. Rev.* **D95**, 1, 014018 (2017), [arXiv:1609.00607].
- [94] P. T. Komiske, E. M. Metodiev and M. D. Schwartz, *JHEP* **01**, 110 (2017), [arXiv:1612.01551].
- [95] G. Kasieczka *et al.*, *JHEP* **05**, 006 (2017), [arXiv:1701.08784].
- [96] S. Macaluso and D. Shih, *JHEP* **10**, 121 (2018), [arXiv:1803.00107].
- [97] J. Li, T. Li and F.-Z. Xu (2020), [arXiv:2008.13529].
- [98] J. Li and H. Sun (2020), [arXiv:2009.00170].
- [99] J. S. H. Lee *et al.*, *J. Korean Phys. Soc.* **74**, 3, 219 (2019), [arXiv:2012.02531].

- [100] J. Collado *et al.*, “Learning to Isolate Muons,” (2021), [arXiv:2102.02278].
- [101] Y.-L. Du, D. Pablos and K. Tywoniuk (2020), [arXiv:2012.07797].
- [102] J. Filipek *et al.* (2021), [arXiv:2105.04582].
- [103] Technical Report ATL-PHYS-PUB-2019-028, CERN, Geneva (2019), URL <http://cds.cern.ch/record/2684070>.
- [104] M. Andrews *et al.* (2018), [arXiv:1807.11916].
- [105] Y.-L. Chung, S.-C. Hsu and B. Nachman (2020), [arXiv:2009.05930].
- [106] Y.-L. Du *et al.*, Eur. Phys. J. C **80**, 6, 516 (2020), [arXiv:1910.11530].
- [107] M. Andrews *et al.* (2021), [arXiv:2104.14659].
- [108] A. A. Pol *et al.* (2021), [arXiv:2105.05785].
- [109] A. Aurisano *et al.*, JINST **11**, 09, P09001 (2016), [arXiv:1604.01444].
- [110] R. Acciarri *et al.* (MicroBooNE), JINST **12**, 03, P03011 (2017), [arXiv:1611.05531].
- [111] L. Hertel *et al.* (2017), URL https://dl4physicalsciences.github.io/files/nips_dlps_2017_7.pdf.
- [112] C. Adams *et al.* (MicroBooNE), Phys. Rev. **D99**, 9, 092001 (2019), [arXiv:1808.07269].
- [113] L. Dominé and K. Terao (DeepLearnPhysics), Phys. Rev. D **102**, 1, 012005 (2020), [arXiv:1903.05663].
- [114] S. Aiello *et al.* (KM3NeT) (2020), [arXiv:2004.08254].
- [115] C. Adams, K. Terao and T. Wongjirad (2020), [arXiv:2006.01993].
- [116] L. Dominé *et al.* (DeepLearnPhysics), Phys. Rev. D **104**, 3, 032004 (2021), [arXiv:2006.14745].
- [117] F. Drielsma *et al.* (DeepLearnPhysics), Phys. Rev. D **104**, 7, 072004 (2021), [arXiv:2007.01335].
- [118] D. H. Koh *et al.* (DeepLearnPhysics) (2020), [arXiv:2007.03083].
- [119] H. Yu *et al.*, JINST **16**, 01, P01036 (2021), [arXiv:2007.12743].
- [120] F. Psihas *et al.* (2020), [arXiv:2008.01242].
- [121] S. Alonso-Monsalve *et al.*, Phys. Rev. D **103**, 3, 032005 (2021), [arXiv:2009.00688].
- [122] P. Abratenko *et al.* (MicroBooNE) (2020), [arXiv:2010.08653].
- [123] B. Clerbaux *et al.* (2020), [arXiv:2011.08847].
- [124] J. Liu *et al.* (2020), [arXiv:2012.06181].
- [125] P. Abratenko *et al.* (MicroBooNE) (2020), [arXiv:2012.08513].
- [126] S. Y.-C. Chen *et al.* (2020), [arXiv:2012.12177].
- [127] R. Acciarri *et al.* (SBND) (2020), [arXiv:2012.01301].
- [128] Z. Qian *et al.* (2021), [arXiv:2101.04839].
- [129] R. Abbasi *et al.* (IceCube), “A Convolutional Neural Network based Cascade Reconstruction for the IceCube Neutrino Observatory,” (2021), [arXiv:2101.11589].
- [130] F. Drielsma *et al.*, in “34th Conference on Neural Information Processing Systems,” (2021), [arXiv:2102.01033].
- [131] M. Rossi and S. Vallecorsa, in “25th International Conference on Computing in High-Energy and Nuclear Physics,” (2021), [arXiv:2103.01596].
- [132] J. Hewes *et al.* (2021), [arXiv:2103.06233].
- [133] R. Acciarri *et al.* (ArgoNeuT) (2021), [arXiv:2103.06391].
- [134] V. Belavin, E. Trofimova and A. Ustyuzhanin (2021), [arXiv:2104.02040].
- [135] D. Maksimović, M. Nieslony and M. Wurm (2021), [arXiv:2104.13426].
- [136] A. Gavrikov and F. Ratnikov, in “25th International Conference on Computing in High-Energy and Nuclear Physics,” (2021), [arXiv:2106.02907].
- [137] J. García-Méndez *et al.* (2021), [arXiv:2107.13654].
- [138] K. Carloni *et al.* (2021), [arXiv:2110.10766].
- [139] P. Abratenko *et al.* (MicroBooNE) (2021), [arXiv:2110.11874].
- [140] D. Boyda *et al.*, Phys. Rev. D **103**, 7, 074504 (2021), [arXiv:2008.05456].
- [141] G. Kanwar *et al.*, Phys. Rev. Lett. **125**, 12, 121601 (2020), [arXiv:2003.06413].
- [142] P. T. Komiske, E. M. Metodiev and J. Thaler, JHEP **01**, 121 (2019), [arXiv:1810.05165].
- [143] H. Qu and L. Gouskos, Phys. Rev. D **101**, 5, 056019 (2020), [arXiv:1902.08570].
- [144] V. Mikuni and F. Canelli, Eur. Phys. J. Plus **135**, 6, 463 (2020), [arXiv:2001.05311].
- [145] J. Shlomi *et al.* (2020), [arXiv:2008.02831].
- [146] M. J. Dolan and A. Ore (2020), [arXiv:2012.00964].
- [147] M. J. Fenton *et al.* (2020), [arXiv:2010.09206].
- [148] J. S. H. Lee *et al.* (2020), [arXiv:2012.03542].
- [149] V. Mikuni and F. Canelli (2021), [arXiv:2102.05073].
- [150] A. Shmakov *et al.* (2021), [arXiv:2106.03898].
- [151] C. Shimmin (2021), [arXiv:2107.02908].
- [152] Technical Report ATL-PHYS-PUB-2020-014, CERN, Geneva (2020), URL <https://cds.cern.ch/record/2718948>.
- [153] G. Louppe *et al.*, Journal of High Energy Physics **2019**, 1, 57 (2019), ISSN 10298479, [arXiv:1702.00748].
- [154] T. Cheng (2017), [arXiv:1711.02633].
- [155] I. Henrion *et al.* (2017), URL https://dl4physicalsciences.github.io/files/nips_dlps_2017_29.pdf.
- [156] X. Ju *et al.*, 33rd Annual Conference on Neural Information Processing Systems (2020), [arXiv:2003.11603].
- [157] M. Abdughani *et al.*, JHEP **08**, 055 (2019), [arXiv:1807.09088].
- [158] J. Arjona Martínez *et al.*, Eur. Phys. J. Plus **134**, 7, 333 (2019), [arXiv:1810.07988].
- [159] J. Ren, L. Wu and J. M. Yang, Phys. Lett. B **802**, 135198 (2020), [arXiv:1901.05627].
- [160] E. A. Moreno *et al.*, Eur. Phys. J. C **80**, 1, 58 (2020), [arXiv:1908.05318].
- [161] S. R. Qasim *et al.*, Eur. Phys. J. C **79**, 7, 608 (2019), [arXiv:1902.07987].
- [162] A. Chakraborty, S. H. Lim and M. M. Nojiri, JHEP **19**, 135 (2020), [arXiv:1904.02092].
- [163] A. Chakraborty *et al.* (2020), [arXiv:2003.11787].
- [164] M. Abdughani *et al.* (2020), [arXiv:2005.11086].
- [165] E. Bernreuther *et al.* (2020), [arXiv:2006.08639].
- [166] J. Shlomi, P. Battaglia and J.-R. Vlimant, Machine Learning: Science and Technology **2**, 2, 021001 (2021), ISSN 2632-2153, URL <http://dx.doi.org/10.1088/2632-2153/abbf9a>.
- [167] Y. Iiyama *et al.*, Front. Big Data **3**, 598927 (2020), [arXiv:2008.03601].
- [168] X. Ju and B. Nachman, Phys. Rev. D **102**, 075014 (2020), [arXiv:2008.06064].
- [169] N. Choma *et al.* (2020), [arXiv:2007.00149].
- [170] Jun Guo and Jimmian Li and Tianjun Li (2020), [arXiv:2010.05464].
- [171] A. Heintz *et al.*, 34th Conference on Neural Information Processing Systems (2020), [arXiv:2012.01563].

- [172] Y. Verma and S. Jena (2020), [arXiv:2012.08515].
- [173] F. A. Dreyer and H. Qu (2020), [arXiv:2012.08526].
- [174] J. Pata *et al.* (2021), [arXiv:2101.08578].
- [175] C. Biscarat *et al.*, in “25th International Conference on Computing in High-Energy and Nuclear Physics,” (2021), [arXiv:2103.00916].
- [176] S. Thais and G. DeZoort (2021), [arXiv:2103.06509].
- [177] G. Dezoort *et al.* (2021), [arXiv:2103.16701].
- [178] Y. Verma and S. Jena (2021), [arXiv:2103.14906].
- [179] A. Hariri, D. Dyachkova and S. Gleyzer (2021), [arXiv:2104.01725].
- [180] O. Atkinson *et al.* (2021), [arXiv:2105.07988].
- [181] P. Konar, V. S. Ngairangbam and M. Spannowsky (2021), [arXiv:2109.14636].
- [182] K. Cho *et al.*, in “Conference on Empirical Methods in Natural Language Processing (EMNLP 2014),” (2014).
- [183] H. Serviansky *et al.*, in H. Larochelle *et al.*, editors, “Advances in Neural Information Processing Systems,” volume 33, 22080–22091, Curran Associates, Inc. (2020), URL <https://proceedings.neurips.cc/paper/2020/file/fb4ab556bc42d6f0ee0f9e24ec4d1af0-Paper.pdf>.
- [184] B. E. Boser, I. M. Guyon and V. N. Vapnik, in “Proceedings of the fifth annual workshop on Computational learning theory,” 144–152 (1992).
- [185] C. Cortes and V. Vapnik, *Machine learning* **20**, 3, 273 (1995).
- [186] H. Drucker *et al.*, *Advances in neural information processing systems* **9**, 155 (1997).
- [187] R. M. Neal, University of Toronto (1994).
- [188] C. K. Williams, *Advances in neural information processing systems* 295–301 (1997).
- [189] J. Lee *et al.*, in “6th International Conference on Learning Representations, ICLR 2018, Vancouver, BC, Canada, April 30 - May 3, 2018, Conference Track Proceedings,” OpenReview.net (2018), URL <https://openreview.net/forum?id=B1EA-M-OZ>.
- [190] A. Jacot, C. Hongler and F. Gabriel, in S. Bengio *et al.*, editors, “Advances in Neural Information Processing Systems 31: Annual Conference on Neural Information Processing Systems 2018, NeurIPS 2018, December 3-8, 2018, Montréal, Canada,” 8580–8589 (2018), URL <https://proceedings.neurips.cc/paper/2018/hash/5a4be1fa34e62bb8a6ec6b91d2462f5a-Abstract.html>.
- [191] T. Hofmann, B. Schölkopf and A. J. Smola, *The Annals of Statistics* 1171–1220 (2008).
- [192] C. M. Bishop, *Pattern recognition and machine learning*, springer (2006).
- [193] C. K. Williams and C. E. Rasmussen, *Gaussian processes for machine learning*, volume 2, MIT press Cambridge, MA (2006).
- [194] S. Ambikasaran *et al.*, *IEEE transactions on pattern analysis and machine intelligence* **38**, 2, 252 (2015).
- [195] J. R. Gardner *et al.*, arXiv preprint arXiv:1809.11165 (2018).
- [196] M. Frate *et al.* (2017), [arXiv:1709.05681].
- [197] S. Mishra-Sharma and K. Cranmer, in “34th Conference on Neural Information Processing Systems,” (2020), [arXiv:2010.10450].
- [198] J. W. Foster *et al.*, *Phys. Rev. Lett.* **127**, 5, 051101 (2021), [arXiv:2102.02207].
- [199] L. Breiman *et al.* (1984).
- [200] “Xgboost,” <https://xgboost.readthedocs.io/>.
- [201] I. Narsky (2005), [arXiv:physics/0507143].
- [202] G. Louppe, arXiv preprint arXiv:1407.7502 (2014).
- [203] Y. Freund and R. E. Schapire, *Journal of computer and system sciences* **55**, 1, 119 (1997).
- [204] J. H. Friedman, *Annals of statistics* 1189–1232 (2001).
- [205] K. Fukushima, *Biological Cybernetics* **36**, 193 (1980).
- [206] V. Nair and G. E. Hinton, in “ICML,” (2010).
- [207] A. L. Maas, A. Y. Hannun and A. Y. Ng, in “in ICML Workshop on Deep Learning for Audio, Speech and Language Processing,” (2013).
- [208] K. He *et al.*, *IEEE International Conference on Computer Vision (ICCV 2015)* **1502** (2015).
- [209] V. Sitzmann *et al.*, in “Proc. NeurIPS,” (2020).
- [210] G. Cybenko, *Mathematics of control, signals and systems* **2**, 4, 303 (1989).
- [211] O. Delalleau and Y. Bengio, in J. Shawe-Taylor *et al.*, editors, “Advances in Neural Information Processing Systems,” volume 24, Curran Associates, Inc. (2011), URL <https://proceedings.neurips.cc/paper/2011/file/8e6b42f1644ecb1327dc03ab345e618b-Paper.pdf>.
- [212] R. Raina, A. Madhavan and A. Y. Ng, in “Proceedings of the 26th Annual International Conference on Machine Learning,” ICML ’09, 873–880, Association for Computing Machinery, New York, NY, USA (2009), ISBN 9781605585161, URL <https://doi.org/10.1145/1553374.1553486>.
- [213] Y. LeCun, “Deep Learning est mort. Vive Differentiable Programming!” <https://www.facebook.com/yann.lecun/posts/10155003011462143> (2018), <https://www.facebook.com/yann.lecun/posts/10155003011462143>, <https://tecburst.io/deep-learning-est-mort-vive-differentiable-programming-5060d3c55074>.
- [214] M. Lin, Q. Chen and S. Yan, arXiv preprint arXiv:1312.4400 (2013).
- [215] C. Szegedy *et al.*, in “2015 IEEE Conference on Computer Vision and Pattern Recognition (CVPR),” 1–9 (2015).
- [216] K. He *et al.*, in “2016 IEEE Conference on Computer Vision and Pattern Recognition (CVPR),” 770–778 (2016).
- [217] N. Cohen and A. Shashua, *CoRR* **abs/1605.06743** (2016), URL <http://arxiv.org/abs/1605.06743>.
- [218] A. Bietti, L. Venturi and J. Bruna, arXiv preprint arXiv:2106.07148 (2021).
- [219] M. M. Bronstein *et al.*, arXiv preprint arXiv:2104.13478 (2021).
- [220] K. Simonyan and A. Zisserman, *CoRR* **abs/1409.1556** (2015).
- [221] S. Ren *et al.*, in C. Cortes *et al.*, editors, “Advances in Neural Information Processing Systems,” volume 28, Curran Associates, Inc. (2015), URL <https://proceedings.neurips.cc/paper/2015/file/14bfa6bb14875e45bba028a21ed38046-Paper.pdf>.
- [222] M. collaboration, *Journal of Instrumentation* **12**, 03, P03011 (2017), URL <https://doi.org/10.1088/1748-0221/12/03/p03011>.
- [223] O. Ronneberger, P. Fischer and T. Brox, in N. Navab *et al.*, editors, “Medical Image Computing and Computer-Assisted Intervention – MICCAI 2015,” 234–241, Springer International Publishing, Cham (2015), ISBN 978-3-319-24574-4.
- [224] G. Huang *et al.*, in “2017 IEEE Conference on Computer Vision and Pattern Recognition (CVPR),” 2261–2269 (2017).
- [225] D. Rumelhart, G. Hinton and R. Williams.
- [226] Y. Bengio, P. Simard and P. Frasconi, *Neural Networks, IEEE Transactions on* **5**, 2, 157 (1994).
- [227] R. Pascanu, T. Mikolov and Y. Bengio, in S. Dasgupta and D. McAllester, editors, “Proceedings of the 30th International Conference on Machine Learning,” volume 28 of *Proceedings of Machine Learning Research*, 1310–1318, PMLR, Atlanta, Georgia, USA (2013), URL <https://proceedings.mlr.press/v28/pascanu13.html>.

- [228] S. Hochreiter and J. Schmidhuber, *Neural Computation* **9**, 8, 1735 (1997).
- [229] R. Socher *et al.*, in “ICML,” (2011).
- [230] R. Socher *et al.*, in “Proceedings of the 2011 conference on empirical methods in natural language processing,” 151–161 (2011).
- [231] X. Chen *et al.*, in “Proceedings of the 2015 conference on empirical methods in natural language processing,” 793–798 (2015).
- [232] C. Olah and S. Carter, *Distill* (2016), URL <http://distill.pub/2016/augmented-rnns>.
- [233] D. Bahdanau, K. Cho and Y. Bengio (2015), 3rd International Conference on Learning Representations, ICLR 2015 ; Conference date: 07-05-2015 Through 09-05-2015.
- [234] A. Vaswani *et al.*, in I. Guyon *et al.*, editors, “Advances in Neural Information Processing Systems,” volume 30, Curran Associates, Inc. (2017), URL <https://proceedings.neurips.cc/paper/2017/file/3f5ee243547dee91fbd053c1c4a845aa-Paper.pdf>.
- [235] R. Bommasani *et al.*, arXiv preprint arXiv:2108.07258 (2021).
- [236] P. Battaglia *et al.*, arXiv (2018), URL <https://arxiv.org/pdf/1806.01261.pdf>.
- [237] M. Gori, G. Monfardini and F. Scarselli, in “Proceedings. 2005 IEEE International Joint Conference on Neural Networks, 2005.”, volume 2, 729–734 vol. 2 (2005).
- [238] C. R. Qi *et al.*, in “Proceedings of the IEEE Conference on Computer Vision and Pattern Recognition (CVPR),” (2017).
- [239] C. Qi *et al.*, in “NIPS,” (2017).
- [240] M. Jaderberg *et al.*, in C. Cortes *et al.*, editors, “Advances in Neural Information Processing Systems,” volume 28, Curran Associates, Inc. (2015), URL <https://proceedings.neurips.cc/paper/2015/file/33ceb07bf4eeb3da587e268d663aba1a-Paper.pdf>.
- [241] M. Zaheer *et al.*, in I. Guyon *et al.*, editors, “Advances in Neural Information Processing Systems,” volume 30, Curran Associates, Inc. (2017), URL <https://proceedings.neurips.cc/paper/2017/file/f22e4747da1aa27e363d86d40ff442fe-Paper.pdf>.
- [242] Y. Wang *et al.*, *ACM Transactions on Graphics* **38** (2018).
- [243] X. Wang *et al.*, in “2018 IEEE/CVF Conference on Computer Vision and Pattern Recognition (CVPR),” 7794–7803, IEEE Computer Society, Los Alamitos, CA, USA (2018), URL <https://doi.ieeecomputersociety.org/10.1109/CVPR.2018.00813>.
- [244] J. Gilmer *et al.*, in D. Precup and Y. W. Teh, editors, “Proceedings of the 34th International Conference on Machine Learning,” volume 70 of *Proceedings of Machine Learning Research*, 1263–1272, PMLR (2017), URL <https://proceedings.mlr.press/v70/gilmer17a.html>.
- [245] N. Choma *et al.* (IceCube) (2018), [arXiv:1809.06166].
- [246] S. R. Qasim *et al.*, *The European Physical Journal C* **79**, 7 (2019), ISSN 1434-6052, URL <http://dx.doi.org/10.1140/epjc/s10052-019-7113-9>.
- [247] J. Shlomi, P. Battaglia and J.-R. Vlimant, *Machine Learning: Science and Technology* **2**, 2, 021001 (2021), URL <https://doi.org/10.1088/2632-2153/abbf9a>.
- [248] D. P. Kingma and M. Welling, arXiv preprint arXiv:1312.6114 (2013).
- [249] D. J. Rezende, S. Mohamed and D. Wierstra, in “Proceedings of the 31th International Conference on Machine Learning, ICML 2014, Beijing, China, 21-26 June 2014,” volume 32 of *JMLR Workshop and Conference Proceedings*, 1278–1286, JMLR.org (2014), URL <http://proceedings.mlr.press/v32/rezende14.html>.
- [250] I. J. Goodfellow *et al.*, in Z. Ghahramani *et al.*, editors, “Advances in Neural Information Processing Systems 27: Annual Conference on Neural Information Processing Systems 2014, December 8-13 2014, Montreal, Quebec, Canada,” 2672–2680 (2014), URL <http://papers.nips.cc/paper/5423-generative-adversarial-nets>.
- [251] A. Radford, L. Metz and S. Chintala, in Y. Bengio and Y. LeCun, editors, “4th International Conference on Learning Representations, ICLR 2016, San Juan, Puerto Rico, May 2-4, 2016, Conference Track Proceedings,” (2016), URL <http://arxiv.org/abs/1511.06434>.
- [252] D. Rezende and S. Mohamed, *Proceedings of the 32nd International Conference on Machine Learning* **37**, 1530 (2015), URL <http://proceedings.mlr.press/v37/rezende15.html>.
- [253] L. Dinh, D. Krueger and Y. Bengio, 3rd International Conference on Learning Representations, ICLR 2015 - Workshop Track Proceedings (2015), [arXiv:1410.8516].
- [254] L. Dinh, J. Sohl-Dickstein and S. Bengio, in “5th International Conference on Learning Representations, ICLR 2017, Toulon, France, April 24-26, 2017, Conference Track Proceedings,” OpenReview.net (2017), URL <https://openreview.net/forum?id=HkpbnH91x>.
- [255] D. P. Kingma and P. Dhariwal, in S. Bengio *et al.*, editors, “Advances in Neural Information Processing Systems 31: Annual Conference on Neural Information Processing Systems 2018, NeurIPS 2018, December 3-8, 2018, Montréal, Canada,” 10236–10245 (2018).
- [256] I. Kobyzev, S. Prince and M. Brubaker, *IEEE Transactions on Pattern Analysis and Machine Intelligence* (2020).
- [257] M. Arjovsky and L. Bottou, in “5th International Conference on Learning Representations, ICLR 2017, Toulon, France, April 24-26, 2017, Conference Track Proceedings,” OpenReview.net (2017), URL https://openreview.net/forum?id=Hk4_qw5xe.
- [258] M. Wiatrak and S. V. Albrecht, arXiv preprint arXiv:1910.00927 (2019).
- [259] D. J. Rezende *et al.*, in “International Conference on Machine Learning,” 8083–8092, PMLR (2020).
- [260] M. C. Gemici, D. Rezende and S. Mohamed, arXiv preprint arXiv:1611.02304 (2016).
- [261] A. van den Oord, O. Vinyals and K. Kavukcuoglu, in I. Guyon *et al.*, editors, “Advances in Neural Information Processing Systems 30: Annual Conference on Neural Information Processing Systems 2017, December 4-9, 2017, Long Beach, CA, USA,” 6306–6315 (2017).
- [262] T. Karras *et al.*, in “6th International Conference on Learning Representations, ICLR 2018, Vancouver, BC, Canada, April 30 - May 3, 2018, Conference Track Proceedings,” OpenReview.net (2018), URL <https://openreview.net/forum?id=Hk99zCeAb>.
- [263] T. Karras, S. Laine and T. Aila, in “IEEE Conference on Computer Vision and Pattern Recognition, CVPR 2019, Long Beach, CA, USA, June 16-20, 2019,” 4401–4410, Computer Vision Foundation / IEEE (2019), URL http://openaccess.thecvf.com/content_CVPR_2019/html/Karras_A_Style-Based_Generator_Architecture_for_Generative_Adversarial_Networks_CVPR_2019_paper.html.
- [264] M. Lucic *et al.*, in S. Bengio *et al.*, editors, “Advances in Neural Information Processing Systems 31: Annual Conference on Neural Information Processing Systems 2018, NeurIPS 2018, December 3-8, 2018, Montréal, Canada,” 698–707 (2018).
- [265] A. A. Alemi *et al.*, in J. G. Dy and A. Krause, editors, “Proceedings of the 35th International Conference on Machine Learning, ICML 2018, Stockholm, Sweden, July 10-15, 2018,” volume 80 of *Proceedings of Machine Learning Research*, 159–168, PMLR (2018), URL <http://proceedings.mlr.press/v80/alemi18a.html>.

- [266] M. E. Tipping and C. M. Bishop, *Journal of the Royal Statistical Society: Series B (Statistical Methodology)* **61**, 3, 611 (1999), URL <https://rss.onlinelibrary.wiley.com/doi/abs/10.1111/1467-9868.00196>.
- [267] M. Arjovsky, S. Chintala and L. Bottou, arXiv preprint arXiv:1701.07875 (2017).
- [268] L. Mescheder, S. Nowozin and A. Geiger, in I. Guyon *et al.*, editors, “Advances in Neural Information Processing Systems,” volume 30, Curran Associates, Inc. (2017), URL <https://proceedings.neurips.cc/paper/2017/file/4588e674d3f0faf985047d4c3f13ed0d-Paper.pdf>.
- [269] G. Papamakarios, I. Murray and T. Pavlakou, in “Advances in Neural Information Processing Systems,” 2335–2344 (2017).
- [270] C. Durkan *et al.*, in H. M. Wallach *et al.*, editors, “Advances in Neural Information Processing Systems 32: Annual Conference on Neural Information Processing Systems 2019, NeurIPS 2019, December 8–14, 2019, Vancouver, BC, Canada,” 7509–7520 (2019).
- [271] W. Grathwohl *et al.*, in “7th International Conference on Learning Representations, ICLR 2019, New Orleans, LA, USA, May 6–9, 2019,” OpenReview.net (2019), URL <https://openreview.net/forum?id=rJxgknCck7>.
- [272] A. van den Oord *et al.*, arXiv:1609.03499 (2016), [arXiv:1609.03499], URL <http://arxiv.org/abs/1609.03499>.
- [273] A. van den Oord *et al.*, in D. D. Lee *et al.*, editors, “Advances in Neural Information Processing Systems 29: Annual Conference on Neural Information Processing Systems 2016, December 5–10, 2016, Barcelona, Spain,” 4790–4798 (2016), URL <https://proceedings.neurips.cc/paper/2016/hash/b1301141feffabac455e1f90a7de2054-Abstract.html>.
- [274] A. Hyvärinen and P. Dayan, *Journal of Machine Learning Research* **6**, 4 (2005).
- [275] Y. Song and S. Ermon, in Wallach *et al.* [358], 11895–11907, URL <https://proceedings.neurips.cc/paper/2019/hash/3001ef257407d5a371a96dcd947c7d93-Abstract.html>.
- [276] Y. Song *et al.*, CoRR **abs/2011.13456** (2020), [arXiv:2011.13456], URL <https://arxiv.org/abs/2011.13456>.
- [277] S. Mandt, M. D. Hoffman and D. M. Blei, *J. Mach. Learn. Res.* **18**, 134:1 (2017), URL <http://jmlr.org/papers/v18/17-214.html>.
- [278] D. P. Kingma and J. Ba, arXiv e-prints arXiv:1412.6980 (2014), [arXiv:1412.6980].
- [279] Y. LeCun *et al.*, *Efficient backprop*, 9–48, *Lecture Notes in Computer Science (including subseries Lecture Notes in Artificial Intelligence and Lecture Notes in Bioinformatics)*, Springer Verlag (2012), ISBN 9783642352881, copyright: Copyright 2021 Elsevier B.V., All rights reserved.
- [280] Y. Yao, L. Rosasco and A. Caponnetto, *Constructive Approximation* **26**, 2, 289 (2007).
- [281] L. Prechelt, in “Neural Networks: Tricks of the trade,” 55–69, Springer (1998).
- [282] A. Krizhevsky, I. Sutskever and G. Hinton, *Neural Information Processing Systems* **25** (2012).
- [283] X. Glorot and Y. Bengio, in Y. W. Teh and M. Titterton, editors, “Proceedings of the Thirteenth International Conference on Artificial Intelligence and Statistics,” volume 9 of *Proceedings of Machine Learning Research*, 249–256, PMLR, Chia Laguna Resort, Sardinia, Italy (2010), URL <http://proceedings.mlr.press/v9/glorot10a.html>.
- [284] S. Ioffe and C. Szegedy, CoRR **abs/1502.03167** (2015), [arXiv:1502.03167], URL <http://arxiv.org/abs/1502.03167>.
- [285] J. L. Ba, J. R. Kiros and G. E. Hinton, “Layer normalization,” (2016), [arXiv:1607.06450].
- [286] D. Ulyanov, A. Vedaldi and V. Lempitsky, “Instance normalization: The missing ingredient for fast stylization,” (2017), [arXiv:1607.08022].
- [287] Y. Wu and K. He, “Group normalization,” (2018), [arXiv:1803.08494].
- [288] T.-Y. Lin *et al.*, in D. Fleet *et al.*, editors, “Computer Vision – ECCV 2014,” 740–755, Springer International Publishing, Cham (2014), ISBN 978-3-319-10602-1.
- [289] O. Russakovsky *et al.*, *International Journal of Computer Vision (IJCV)* **115**, 3, 211 (2015).
- [290] M. Cordts *et al.*, in “Proc. of the IEEE Conference on Computer Vision and Pattern Recognition (CVPR),” (2016).
- [291] L. Yi *et al.*, SIGGRAPH Asia (2016).
- [292] A. Radford *et al.* (2018), URL https://s3-us-west-2.amazonaws.com/openai-assets/research-covers/language-unsupervised/language_understanding_paper.pdf.
- [293] L. Fei-Fei, R. Fergus and P. Perona, *IEEE Transactions on Pattern Analysis and Machine Intelligence* **28**, 4, 594 (2006).
- [294] H. Larochelle, D. Erhan and Y. Bengio, in “Proceedings of the 23rd National Conference on Artificial Intelligence - Volume 2,” AAAI’08, 646–651, AAAI Press (2008), ISBN 9781577353683.
- [295] M. Palatucci *et al.*, in Y. Bengio *et al.*, editors, “Advances in Neural Information Processing Systems,” volume 22, Curran Associates, Inc. (2009), URL <https://proceedings.neurips.cc/paper/2009/file/1543843a4723ed2ab08e18053ae6dc5b-Paper.pdf>.
- [296] R. Socher *et al.*, in “Proceedings of the 26th International Conference on Neural Information Processing Systems - Volume 1,” NIPS’13, 935–943, Curran Associates Inc., Red Hook, NY, USA (2013).
- [297] T. Dorigo and P. De Castro Manzano (2020), [arXiv:2007.09121].
- [298] R. Barate *et al.* (ALEPH), *Phys. Lett. B* **412**, 173 (1997).
- [299] G. Louppe, M. Kagan and K. Cranmer, in I. Guyon *et al.*, editors, “Advances in Neural Information Processing Systems,” volume 30, Curran Associates, Inc. (2017), [arXiv:1611.01046], URL <https://papers.nips.cc/paper/2017/hash/48ab2f9b45957ab574cf005eb8a76760-Abstract.html>.
- [300] H. Edwards and A. Storkey, arXiv preprint arXiv:1511.05897 (2015).
- [301] Y. Ganin and V. Lempitsky, in “International conference on machine learning,” 1180–1189, PMLR (2015).
- [302] H. Ajakan *et al.*, ArXiv e-prints (2014), [arXiv:1412.4446].
- [303] G. Kasieczka and D. Shih, *Phys. Rev. Lett.* **125**, 12, 122001 (2020), [arXiv:2001.05310].
- [304] C. Shimmin *et al.*, *Phys. Rev.* **D96**, 7, 074034 (2017), [arXiv:1703.03507].
- [305] J. Stevens and M. Williams, *JINST* **8**, P12013 (2013), [arXiv:1305.7248].
- [306] J. Dolen *et al.*, *JHEP* **05**, 156 (2016), [arXiv:1603.00027].
- [307] I. Moutl, B. Nachman and D. Neill, *JHEP* **05**, 002 (2018), [arXiv:1710.06859].
- [308] L. Bradshaw *et al.* (2019), [arXiv:1908.08959].
- [309] ATL-PHYS-PUB-2018-014 (2018), URL <http://cds.cern.ch/record/2630973>.
- [310] L.-G. Xia, *Nucl. Instrum. Meth.* **A930**, 15 (2019), [arXiv:1810.08387].
- [311] C. Englert *et al.*, *Eur. Phys. J.* **C79**, 1, 4 (2019), [arXiv:1807.08763].
- [312] S. Wunsch *et al.* (2019), [arXiv:1907.11674].
- [313] A. Rogozhnikov *et al.*, *JINST* **10**, 03, T03002 (2015), [arXiv:1410.4140].

- [314] C. Collaboration, *Machine Learning: Science and Technology* (2020).
- [315] J. M. Clavijo, P. Glaysher and J. M. Katzy (2020), [arXiv:2005.00568].
- [316] G. Kasieczka *et al.* (2020), [arXiv:2007.14400].
- [317] O. Kitouni *et al.* (2020), [arXiv:2010.09745].
- [318] A. Ghosh and B. Nachman (2021), [arXiv:2109.08159].
- [319] P. Baldi *et al.*, *Eur. Phys. J.* **C76**, 5, 235 (2016), [arXiv:1601.07913].
- [320] A. Ghosh, B. Nachman and D. Whiteson (2021), [arXiv:2105.08742].
- [321] W. L. Oberkampf *et al.*, *Reliability Engineering & System Safety* **85**, 1, 11 (2004), ISSN 0951-8320, alternative Representations of Epistemic Uncertainty, URL <https://www.sciencedirect.com/science/article/pii/S0951832004000493>.
- [322] A. O'Hagan and J. E. Oakley, *Reliability Engineering & System Safety* **85**, 1, 239 (2004), ISSN 0951-8320, alternative Representations of Epistemic Uncertainty, URL <https://www.sciencedirect.com/science/article/pii/S0951832004000638>.
- [323] E. Hüllermeier and W. Waegeman, *CoRR* **abs/1910.09457** (2019), URL <http://arxiv.org/abs/1910.09457>.
- [324] A. Kendall and Y. Gal, in I. Guyon *et al.*, editors, "Advances in Neural Information Processing Systems," volume 30, Curran Associates, Inc. (2017), URL <https://proceedings.neurips.cc/paper/2017/file/2650d6089a6d640c5e85b2b88265dc2b-Paper.pdf>.
- [325] A. D. Kiureghian and O. Ditlevsen, *Structural Safety* **31**, 2, 105 (2009), ISSN 0167-4730, risk Acceptance and Risk Communication, URL <https://www.sciencedirect.com/science/article/pii/S0167473008000556>.
- [326] Y. Yao *et al.*, *Bayesian Analysis* **13**, 3 (2018), ISSN 1936-0975, URL <http://dx.doi.org/10.1214/17-BA1091>.
- [327] J. Snoek *et al.*, in Wallach *et al.* [358], 13969–13980, URL <https://proceedings.neurips.cc/paper/2019/hash/8558cb408c1d76621371888657d2eb1d-Abstract.html>.
- [328] Y. Gal and Z. Ghahramani, in M. Balcan and K. Q. Weinberger, editors, "Proceedings of the 33rd International Conference on Machine Learning, ICML 2016, New York City, NY, USA, June 19-24, 2016," volume 48 of *JMLR Workshop and Conference Proceedings*, 1050–1059, JMLR.org (2016), URL <http://proceedings.mlr.press/v48/gal16.html>.
- [329] B. Lakshminarayanan, A. Pritzel and C. Blundell, in I. Guyon *et al.*, editors, "Advances in Neural Information Processing Systems 30: Annual Conference on Neural Information Processing Systems 2017, December 4-9, 2017, Long Beach, CA, USA," 6402–6413 (2017), URL <https://proceedings.neurips.cc/paper/2017/hash/9ef2ed4b7fd2c810847ffa5fa85bce38-Abstract.html>.
- [330] D. P. Kingma, T. Salimans and M. Welling, *CoRR* **abs/1506.02557** (2015), URL <http://arxiv.org/abs/1506.02557>.
- [331] G. C. Strong (2020), [arXiv:2002.01427].
- [332] V. V. Gligorov and M. Williams, *JINST* **8**, P02013 (2013), [arXiv:1210.6861].
- [333] D. W. III *et al.* (2017), URL https://dl4physicalsciences.github.io/files/nips_dlps_2017_3.pdf.
- [334] D. Bourgeois, C. Fitzpatrick and S. Stahl (2018), [arXiv:1808.00711].
- [335] J. Alimena, Y. Iiyama and J. Kieseler (2020), [arXiv:2004.10744].
- [336] C. Balázs *et al.* (DarkMachines High Dimensional Sampling Group) (2021), [arXiv:2101.04525].
- [337] F. Rehm *et al.* (2021), [arXiv:2103.10142].
- [338] C. Mahesh *et al.*, in "34th Conference on Neural Information Processing Systems," (2021), [arXiv:2104.06622].
- [339] S. Amrouche *et al.* (2021), [arXiv:2105.01160].
- [340] P. Goncharov *et al.*, in "24th International Scientific Conference of Young Scientists and Specialists," (2021), [arXiv:2109.08982].
- [341] J. Duarte *et al.*, *JINST* **13**, 07, P07027 (2018), [arXiv:1804.06913].
- [342] J. Ngadiuba *et al.*, *Mach. Learn.: Sci. Tech.* **2**, 1, 015001 (2020), [arXiv:2003.06308].
- [343] S. Summers *et al.*, *JINST* **15**, 05, P05026 (2020), [arXiv:2002.02534].
- [344] J. Krupa *et al.* (2020), [arXiv:2007.10359].
- [345] L. R. M. Mohan *et al.* (2020), [arXiv:2008.09210].
- [346] S. Carrazza, J. M. Cruz-Martinez and M. Rossi (2020), [arXiv:2009.06635].
- [347] D. S. Rankin *et al.*, 2020 IEEE/ACM International Workshop on Heterogeneous High-performance Reconfigurable Computing (H2RC) 38 (2020), [arXiv:2010.08556].
- [348] M. Rossi, S. Carrazza and J. M. Cruz-Martinez (2020), [arXiv:2012.08221].
- [349] T. Aarrestad *et al.* (2021), [arXiv:2101.05108].
- [350] B. Hawks *et al.* (2021), [arXiv:2102.11289].
- [351] T. Teixeira, L. Andrade and J. M. de Seixas (2021), [arXiv:2103.12467].
- [352] T. M. Hong *et al.* (2021), [arXiv:2104.03408].
- [353] G. Di Guglielmo *et al.* (2021), [arXiv:2105.01683].
- [354] M. Migliorini *et al.* (2021), [arXiv:2105.04428].
- [355] E. Govorkova *et al.* (2021), [arXiv:2108.03986].
- [356] V. Kuznetsov, L. Giommi and D. Bonacorsi (2020), [arXiv:2007.14781].
- [357] O. Sunneborn Gudnadottir *et al.*, *EPJ Web Conf.* **251**, 02054 (2021), [arXiv:2109.00264].
- [358] H. M. Wallach *et al.*, editors, *Advances in Neural Information Processing Systems 32: Annual Conference on Neural Information Processing Systems 2019, NeurIPS 2019, December 8-14, 2019, Vancouver, BC, Canada* (2019), URL <https://proceedings.neurips.cc/paper/2019>.

42. Monte Carlo Techniques

Revised September 2021 by G. Cowan (RHUL).

Monte Carlo techniques are often the only practical way to evaluate difficult integrals or to sample random variables governed by complicated probability density functions. Here we describe an assortment of methods for sampling some commonly occurring probability density functions.

42.1 Sampling the uniform distribution

Most Monte Carlo sampling or integration techniques assume a “random number generator,” which generates uniform statistically independent values on the half open interval $[0, 1)$; for reviews see, *e.g.*, Refs. [1, 2].

Uniform random number generators are available in software libraries such as CLHEP [3], and ROOT [4]. For example, in addition to a basic congruential generator `TRandom` (see below), ROOT provides three more sophisticated routines: `TRandom1` implements the RANLUX generator [5] based on the method by Lüscher, and allows the user to select different quality levels, trading off quality with speed; `TRandom2` is based on the maximally equidistributed combined Tausworthe generator by L’Ecuyer [6]; the `TRandom3` generator implements the Mersenne twister algorithm of Matsumoto and Nishimura [7]. All of the algorithms produce a periodic sequence of numbers, and to obtain effectively random values, one must not use more than a small subset of a single period. The Mersenne twister algorithm has an extremely long period of $2^{19937} - 1$. A recent review of high-quality random number generators can be found in Ref. [8].

The performance of the generators can be investigated with tests such as DIEHARD [9] or TestU01 [10]. Many commonly available congruential generators fail these tests and often have sequences (typically with periods less than 2^{32}), which can be easily exhausted on modern computers. A short period is a problem for the `TRandom` generator in ROOT, which, however, has the advantage that its state is stored in a single 32-bit word. The generators `TRandom1`, `TRandom2`, or `TRandom3` have much longer periods, with `TRandom3` being recommended by the ROOT authors as providing the best combination of speed and good random properties. For further information see, *e.g.*, Ref. [11].

42.2 Inverse transform method

If the desired probability density function is $f(x)$ on the range $-\infty < x < \infty$, its cumulative distribution function (expressing the probability that $x \leq a$) is given by Eq. (39.6). If a is chosen with probability density $f(a)$, then the integrated probability up to point a , $F(a)$, is itself a random variable which will occur with uniform probability density on $[0, 1)$. Suppose u is generated according to a uniformly distributed in $(0, 1)$. If x can take on any value, and ignoring the endpoints, we can then find a unique x chosen from the p.d.f. $f(x)$ for a given u if we set

$$u = F(x) , \tag{42.1}$$

provided we can find an inverse of F , defined by

$$x = F^{-1}(u) . \tag{42.2}$$

This method is shown in Fig. 42.1a. It is most convenient when one can calculate by hand the inverse function of the indefinite integral of f . This is the case for some common functions $f(x)$ such as $\exp(x)$, $(1 - x)^n$, and $1/(1 + x^2)$ (Cauchy or Breit-Wigner), although it does not necessarily produce the fastest generator. Standard libraries contain software to implement this method numerically, working from functions or histograms in one or more dimensions, *e.g.*, the UNU.RAN package [12], available in ROOT. For a discrete distribution, $F(x)$ will have a discontinuous jump of size $f(x_k)$ at each allowed $x_k, k = 1, 2, \dots$. Choose u from a uniform distribution on $(0, 1)$ as before. Find x_k such that

$$F(x_{k-1}) < u \leq F(x_k) \equiv \text{Prob}(x \leq x_k) = \sum_{i=1}^k f(x_i) ; \tag{42.3}$$

then x_k is the value we seek (note: $F(x_0) \equiv 0$). This algorithm is illustrated in Fig. 42.1b.

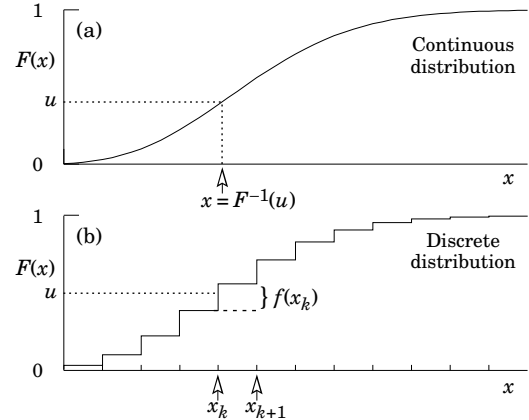


Figure 42.1: Use of a random number u chosen from a uniform distribution $(0,1)$ to find a random number x from a distribution with cumulative distribution function $F(x)$.

42.3 Acceptance-rejection method (Von Neumann)

Very commonly an analytic form for $F(x)$ is unknown or too complex to work with, so that obtaining an inverse as in Eq. (42.2) is impractical. We suppose that for any given value of x , the probability density function $f(x)$ can be computed, and further that enough is known about $f(x)$ that we can enclose it entirely inside a shape which is C times an easily generated distribution $h(x)$, as illustrated in Fig. 42.2. That is, $Ch(x) \geq f(x)$ must hold for all x . Frequently $h(x)$ is uniform or is a normalized

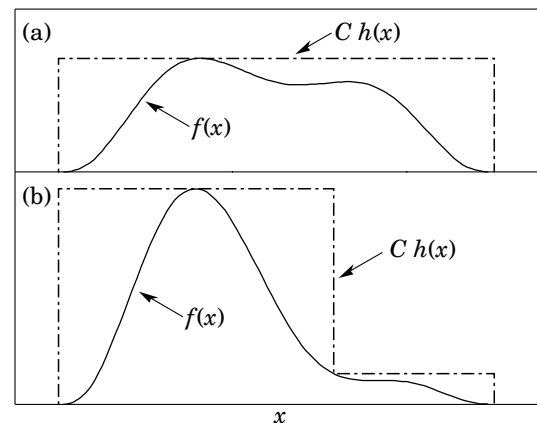


Figure 42.2: Illustration of the acceptance-rejection method. Random points are chosen inside the upper bounding figure, and rejected if the ordinate exceeds $f(x)$. The lower figure illustrates a method to increase the efficiency (see text).

sum of uniform distributions. Note that both $f(x)$ and $h(x)$ must be normalized to unit area, and therefore, the proportionality constant $C > 1$. To generate $f(x)$, first generate a candidate x according to $h(x)$. Calculate $f(x)$ and the height of the envelope $Ch(x)$; generate u and test if $uCh(x) \leq f(x)$. If so, accept x ; if not reject x and try again. If we regard x and $uCh(x)$ as the abscissa and ordinate of a point in a two-dimensional plot, these points will populate the entire area $Ch(x)$ in a smooth manner; then we accept those which fall under $f(x)$. The efficiency is the ratio of areas, which must equal $1/C$; therefore we must keep C as close as possible to 1.0. Therefore, we try to choose $Ch(x)$ to be as close to $f(x)$ as convenience dictates, as in the lower part of Fig. 42.2.

42.4 Algorithms

Algorithms for generating random numbers belonging to many different distributions are given for example by Press [13], Ahrens and Dieter [14], Rubinstein [15], Devroye [16], Walck [17] and Gentle [18]. For many distributions, alternative algorithms exist, varying in complexity, speed, and accuracy. For time-critical applications, these algorithms may be coded in-line to remove the significant overhead often encountered in making function calls.

In the examples given below, we use the notation for the variables and parameters given in Table 39.1. Variables named “ u ” are assumed to be independent and uniform on $[0,1]$. Denominators must be verified to be non-zero where relevant.

42.4.1 Exponential decay

This is a common application of the inverse transform method, and uses the fact that if u is uniformly distributed in $[0,1]$, then $(1-u)$ is as well. Consider an exponential p.d.f. $f(t) = (1/\tau)\exp(-t/\tau)$ that is truncated so as to lie between two values, a and b , and renormalized to unit area. To generate decay times t according to this p.d.f., first let $\alpha = \exp(-a/\tau)$ and $\beta = \exp(-b/\tau)$; then generate u and let

$$t = -\tau \ln(\beta + u(\alpha - \beta)). \tag{42.4}$$

For $(a,b) = (0, \infty)$, we have simply $t = -\tau \ln u$. (See also Sec. 42.4.6.)

42.4.2 Isotropic direction in 3D

Isotropy means the density is proportional to solid angle, the differential element of which is $d\Omega = d(\cos\theta)d\phi$. Hence $\cos\theta$ is uniform $(2u_1 - 1)$ and ϕ is uniform $(2\pi u_2)$. For alternative generation of $\sin\phi$ and $\cos\phi$, see the next subsection.

42.4.3 Sine and cosine of random angle in 2D

Generate u_1 and u_2 . Then $v_1 = 2u_1 - 1$ is uniform on $(-1,1)$, and $v_2 = u_2$ is uniform on $(0,1)$. Calculate $r^2 = v_1^2 + v_2^2$. If $r^2 > 1$, start over. Otherwise, the sine (S) and cosine (C) of a random angle (i.e., uniformly distributed between zero and 2π) are given by

$$S = 2v_1v_2/r^2 \quad \text{and} \quad C = (v_1^2 - v_2^2)/r^2. \tag{42.5}$$

42.4.4 Gaussian distribution

If u_1 and u_2 are uniform on $(0,1)$, then

$$z_1 = \sin(2\pi u_1)\sqrt{-2 \ln u_2} \quad \text{and} \quad z_2 = \cos(2\pi u_1)\sqrt{-2 \ln u_2} \tag{42.6}$$

are independent and Gaussian distributed with mean 0 and $\sigma = 1$.

There are many variants of this basic algorithm, which may be faster. For example, construct $v_1 = 2u_1 - 1$ and $v_2 = 2u_2 - 1$, which are uniform on $(-1,1)$. Calculate $r^2 = v_1^2 + v_2^2$, and if $r^2 > 1$ start over. If $r^2 < 1$, it is uniform on $(0,1)$. Then

$$z_1 = v_1\sqrt{\frac{-2 \ln r^2}{r^2}} \quad \text{and} \quad z_2 = v_2\sqrt{\frac{-2 \ln r^2}{r^2}} \tag{42.7}$$

are independent numbers chosen from a normal distribution with mean 0 and variance 1. $z'_i = \mu + \sigma z_i$ distributes with mean μ and variance σ^2 .

For a multivariate Gaussian with an $n \times n$ covariance matrix V , one can start by generating n independent Gaussian variables, $\{\eta_j\}$, with mean 0 and variance 1 as above. Then the new set $\{x_i\}$ is obtained as $x_i = \mu_i + \sum_j L_{ij}\eta_j$, where μ_i is the mean of x_i , and L_{ij} are the components of L , the unique lower triangular matrix that fulfils $V = LL^T$. The matrix L can be easily computed by the following recursive relation (Cholesky’s method):

$$L_{jj} = \left(V_{jj} - \sum_{k=1}^{j-1} L_{jk}^2 \right)^{1/2}, \tag{42.8a}$$

$$L_{ij} = \frac{V_{ij} - \sum_{k=1}^{j-1} L_{ik}L_{jk}}{L_{jj}}, \quad j = 1, \dots, n; \quad i = j + 1, \dots, n, \tag{42.8b}$$

where $V_{ij} = \rho_{ij}\sigma_i\sigma_j$ are the components of V . For $n = 2$ one has

$$L = \begin{pmatrix} \sigma_1 & 0 \\ \rho\sigma_2 & \sqrt{1 - \rho^2}\sigma_2 \end{pmatrix}, \tag{42.9}$$

and therefore the correlated Gaussian variables are generated as $x_1 = \mu_1 + \sigma_1\eta_1$, $x_2 = \mu_2 + \rho\sigma_2\eta_1 + \sqrt{1 - \rho^2}\sigma_2\eta_2$.

42.4.5 $\chi^2(n)$ distribution

To generate a variable following the χ^2 distribution for n degrees of freedom, use the Gamma distribution with $k = n/2$ and $\lambda = 1/2$ using the method of Sec. 42.4.6.

42.4.6 Gamma distribution

All of the following algorithms are given for $\lambda = 1$. For $\lambda \neq 1$, divide the resulting random number x by λ .

- If $k = 1$ (the exponential distribution), accept $x = -\ln u$. (See also Sec. 42.4.1.)
- If $0 < k < 1$, initialize with $v_1 = (e+k)/e$ (with $e = 2.71828\dots$ being the natural log base). Generate u_1, u_2 . Define $v_2 = v_1u_1$.

Case 1: $v_2 \leq 1$. Define $x = v_2^{1/k}$. If $u_2 \leq e^{-x}$, accept x and stop, else restart by generating new u_1, u_2 .

Case 2: $v_2 > 1$. Define $x = -\ln([v_1 - v_2]/k)$. If $u_2 \leq x^{k-1}$, accept x and stop, else restart by generating new u_1, u_2 . Note that, for $k < 1$, the probability density has a pole at $x = 0$, so that return values of zero due to underflow must be accepted or otherwise dealt with.

- Otherwise, if $k > 1$, initialize with $c = 3k - 0.75$. Generate u_1 and compute $v_1 = u_1(1 - u_1)$ and $v_2 = (u_1 - 0.5)\sqrt{c/v_1}$. If $x = k + v_2 - 1 \leq 0$, go back and generate new u_1 ; otherwise generate u_2 and compute $v_3 = 64v_1^3u_2^2$. If $v_3 \leq 1 - 2v_2^2/x$ or if $\ln v_3 \leq 2\{[k - 1] \ln[x/(k - 1)] - v_2\}$, accept x and stop; otherwise go back and generate new u_1 .

42.4.7 Binomial distribution

Begin with $k = 0$ and generate u uniform in $[0,1]$. Compute $P_k = (1 - p)^n$ and store P_k into B . If $u \leq B$ accept $r_k = k$ and stop. Otherwise, increment k by one; compute the next P_k as $P_k \cdot (p/(1 - p)) \cdot (n - k)/(k + 1)$; add this to B . Again, if $u \leq B$, accept $r_k = k$ and stop, otherwise iterate until a value is accepted. If $p > 1/2$, it will be more efficient to generate r from $f(r; n, q)$, i.e., with p and q interchanged, and then set $r_k = n - r$.

42.4.8 Poisson distribution

Iterate until a successful choice is made: Begin with $k = 1$ and set $A = 1$ to start. Generate u . Replace A with uA ; if now $A < \exp(-\mu)$, where μ is the Poisson parameter, accept $n_k = k - 1$ and stop. Otherwise increment k by 1, generate a new u and repeat, always starting with the value of A left from the previous try.

Note that the Poisson generator used in ROOT’s `TRandom` classes before version 5.12 (including the derived classes `TRandom1`, `TRandom2`, `TRandom3`) uses a Gaussian approximation when μ exceeds a given threshold. This may be satisfactory (and much faster) for some applications. To do this, generate z from a Gaussian with zero mean and unit standard deviation; then use $x = \max(0, [\mu + z\sqrt{\mu} + 0.5])$ where $[\]$ signifies the greatest integer \leq the expression. The routines from Numerical Recipes [13] and CLHEP’s routine `RandPoisson` do not make this approximation (see, e.g., Ref. [11]).

42.4.9 Student’s t distribution

Generate u_1 and u_2 uniform in $(0,1)$; then $t = \sin(2\pi u_1)[n(u_2^{-2/n} - 1)]^{1/2}$ follows the Student’s t distribution for $n > 0$ degrees of freedom (n not necessarily an integer).

Alternatively, generate x from a Gaussian with mean 0 and $\sigma^2 = 1$ according to the method of 42.4.4. Next generate y ,

an independent gamma random variate, according to 42.4.6 with $\lambda = 1/2$ and $k = n/2$. Then $z = x/\sqrt{y/n}$ is distributed as a t with n degrees of freedom.

For the special case $n = 1$, the Breit-Wigner distribution, generate u_1 and u_2 ; set $v_1 = 2u_1 - 1$ and $v_2 = 2u_2 - 1$. If $v_1^2 + v_2^2 \leq 1$ accept $z = v_1/v_2$ as a Breit-Wigner distribution with unit area, center at 0.0, and FWHM 2.0. Otherwise start over. For center M_0 and FWHM Γ , use $W = z\Gamma/2 + M_0$.

42.4.10 Beta distribution

The choice of an appropriate algorithm for generation of beta distributed random numbers depends on the values of the parameters α and β . For, e.g., $\alpha = 1$, one can use the transformation method to find $x = 1 - u^{1/\beta}$, and similarly if $\beta = 1$ one has $x = u^{1/\alpha}$. For more general cases see, e.g., Refs. [17, 18] and references therein.

42.5 Importance sampling and weighted Monte Carlo

Often the goal of a Monte Carlo calculation is to determine an expectation value of a function $h(x)$, where x is a (single or vector) random variable that follows a pdf $f(x)$,

$$E_f[h(x)] = \int h(x)f(x) dx \equiv \mu . \tag{42.10}$$

A Monte-Carlo estimator $\hat{\mu}_{MC}$ for μ is the average of N values of $h(x)$ where x is sampled (generated) from $f(x)$, i.e., $\hat{\mu}_{MC} = \frac{1}{N} \sum_{i=1}^N h(x_i)$. This has a variance

$$V[\hat{\mu}_{MC}] = \frac{1}{N} V_f[h(x)] = \frac{1}{N} (E_f[h^2(x)] - \mu^2) . \tag{42.11}$$

By using the method of *importance sampling*, one can achieve a reduction in this variance and thus a more accurate determination of the expectation value for a given number of random values generated. The key idea is to rewrite the expectation value in Eq. (42.10) as

$$\mu = \int h(x)f(x) dx = \int \frac{h(x)f(x)}{g(x)} g(x) dx = E_g \left[\frac{h(x)f(x)}{g(x)} \right] , \tag{42.12}$$

where $g(x)$ is any other pdf of x with the same support as $f(x)$ (i.e., nonzero for the same region of x). Thus the desired quantity μ is the expectation value with respect to g of $h(x)f(x)/g(x)$. It can be estimated by generating N values of x sampled from g and computing

$$\hat{\mu}_{IS} = \frac{1}{N} \sum_{i=1}^N \frac{h(x_i)f(x_i)}{g(x_i)} . \tag{42.13}$$

The variance of $\hat{\mu}_{IS}$ is given by

$$V[\hat{\mu}_{IS}] = \frac{1}{N} V_g \left[\frac{h(x)f(x)}{g(x)} \right] = \frac{1}{N} \left(E_g \left[\frac{h^2(x)f^2(x)}{g^2(x)} \right] - \mu^2 \right) , \tag{42.14}$$

By choosing $g(x)$ such that $h(x)f(x)/g(x)$ is as constant as possible, the variance of $\hat{\mu}_{IS}$ can be substantially reduced. One can show (see, e.g., Refs. [19, 20]) that the variance is minimized when $g(x) \propto |h(x)|f(x)$.

An alternative importance sampling estimator can be constructed by replacing the number of generated values N in Eq. (42.13) by the sum $\sum_{i=1}^N f(x_i)/g(x_i)$. This can give an even smaller variance at the price of a small bias. It can be of further advantage in problems where the pdf $f(x)$ is known only up to a normalization constant, which then cancels (see Refs. [19, 20]).

A closely related application of importance sampling is the use of weighted Monte Carlo to compute the probability $P_f(x \in A)$ for x to be in a specified region A :

$$P_f(x \in A) = \int_A f(x) dx . \tag{42.15}$$

It may be, however, that one does not have an MC model capable of generating $x \sim f(x)$, but rather one can generate x according to a different density $g(x)$. The probability $P_f(x \in A)$ can be written

$$P_f(x \in A) = \frac{\int_A \frac{f(x)}{g(x)} g(x) dx}{\int_A g(x) dx} \int_A g(x) dx = E_g[w(x)|x \in A] P_g(x \in A) , \tag{42.16}$$

where $w(x) = f(x)/g(x)$ is the *weight function* and $P_g(x \in A) = \int_A g(x) dx$ is the probability to find $x \in A$ assuming $x \sim g(x)$. That is, $P_f(x \in A)$ is the conditional expectation value of $w(x)$ with respect to $g(x)$ given $x \in A$ multiplied by the probability to find $x \in A$ under assumption of $g(x)$.

Suppose N values of x are generated according to $g(x)$ and m of them are found in the region A . Then the probability to be in A for $x \sim g(x)$ can be estimated by m/N , and the expectation value above can be obtained from the average of the weights in A . Therefore the desired probability $P_f(x \in A)$ can be estimated using

$$\hat{P}_f(x \in A) = \frac{1}{m} \sum_{i=1}^m w_i \times \frac{m}{N} = \frac{1}{N} \sum_{i=1}^m w_i , \tag{42.17}$$

where $w_i = w(x_i)$ and the sum includes only the m values of x found in A . That is, when generating the x values according to $g(x)$ instead of $f(x)$, the number of events m found in A is replaced by the corresponding sum of weights. The variance of $\hat{P}_f(x \in A)$ can be found from

$$\widehat{V}[\hat{P}_f(x \in A)] = \frac{1}{N^2} \sum_{i=1}^m w_i^2 . \tag{42.18}$$

By choosing $g(x)$ so that a larger fraction of x values are sampled in the ‘‘important’’ region A , one can reduce the variance of the estimated probability for a given total number of generated values.

42.6 Markov Chain Monte Carlo

In applications involving generation of random numbers following a multivariate distribution with a high number of dimensions, the transformation method may not be possible and the acceptance-rejection technique may have too low of an efficiency to be practical. If it is not required to have independent random values, but only that they follow a certain distribution, then Markov Chain Monte Carlo (MCMC) methods can be used. In depth treatments of MCMC can be found, e.g., in the texts by Robert and Casella [19], Liu [20], and the review by Neal [21]. HEP-oriented software for MCMC is available from the Bayesian Analysis Toolkit (BAT) [22, 23].

MCMC is particularly useful in connection with Bayesian statistics, where a p.d.f. $p(\theta)$ for an n -dimensional vector of parameters $\theta = (\theta_1, \dots, \theta_n)$ is obtained, and one needs the marginal distribution of a subset of the components. Here one samples θ from $p(\theta)$ and simply records the marginal distribution for the components of interest.

A simple and broadly applicable MCMC method is the Metropolis-Hastings algorithm, which allows one to generate multidimensional points θ distributed according to a target p.d.f. that is proportional to a given function $p(\theta)$. It is not necessary to have

$p(\theta)$ normalized to unit area, which is useful in Bayesian statistics, as posterior probability densities are often determined only up to an unknown normalization constant.

To generate points that follow $p(\theta)$, one first needs a proposal p.d.f. $q(\theta; \theta_0)$, which can be (almost) any p.d.f. from which independent random values θ can be generated, and which contains as a parameter another point in the same space θ_0 . For example, a multivariate Gaussian centered about θ_0 can be used. Beginning at an arbitrary starting point θ_0 , the Hastings algorithm iterates the following steps:

1. Generate a value θ using the proposal density $q(\theta; \theta_0)$;
2. Form the Hastings test ratio, $\alpha = \min \left[1, \frac{p(\theta)q(\theta_0; \theta)}{p(\theta_0)q(\theta; \theta_0)} \right]$;
3. Generate a value u uniformly distributed in $[0, 1]$;
4. If $u \leq \alpha$, take $\theta_1 = \theta$. Otherwise, repeat the old point, *i.e.*, $\theta_1 = \theta_0$.
5. Set $\theta_0 = \theta_1$ and return to step 1.

If one takes the proposal density to be symmetric in θ and θ_0 , then this is the *Metropolis-Hastings* algorithm, and the test ratio becomes $\alpha = \min[1, p(\theta)/p(\theta_0)]$. That is, if the proposed θ is at a value of probability higher than θ_0 , the step is taken. If the proposed step is rejected, the old point is repeated.

Methods for assessing and optimizing the performance of the algorithm are discussed in, *e.g.*, Refs. [19–21]. One can, for example, examine the autocorrelation as a function of the lag k , *i.e.*, the correlation of a sampled point with that k steps removed. This should decrease as quickly as possible for increasing k .

Generally one chooses the proposal density so as to optimize some quality measure such as the autocorrelation. For certain problems it has been shown that one achieves optimal performance when the acceptance fraction, that is, the fraction of points with $u \leq \alpha$, is around 40%. This can be adjusted by varying the width of the proposal density. For example, one can use the proposal p.d.f. a multivariate Gaussian with the same covariance matrix as that of the target p.d.f., but scaled by a constant.

References

- [1] F. James, *Comput. Phys. Commun.* **60**, 329 (1990).
- [2] P. L'Ecuyer, *Proc. 1997 Winter Simulation Conference*, IEEE Press, Dec. 1997, 127–134.
- [3] L. Lonnblad, *Comput. Phys. Commun.* **84**, 307 (1994).
- [4] R. Brun and F. Rademakers, *Nucl. Instrum. Meth.* **A389**, 81 (1997); See also root.cern.ch.
- [5] F. James, *Comput. Phys. Commun.* **79**, 111 (1994), [Erratum: *Comput. Phys. Commun.* **97**, 357 (1996)]; M. Luscher, *Comput. Phys. Commun.* **79**, 100 (1994), [[hep-lat/9309020](https://arxiv.org/abs/hep-lat/9309020)].
- [6] P. L'Ecuyer, *Mathematics of Computation*, **65**, 213 (1996) and **65**, 225 (1999).
- [7] M. Matsumoto and T. Nishimura, *ACM Transactions on Modeling and Computer Simulation*, Vol. 8, No. 1, January 1998, 3–30.
- [8] F. James and L. Moneta, *Comput. Softw. Big Sci.* **4**, 2, 12 p (2019), 4 figures, [[arXiv:1903.01247](https://arxiv.org/abs/1903.01247)], URL <http://cds.cern.ch/record/2678858>.
- [9] Much of DIEHARD is described in: G. Marsaglia, *A Current View of Random Number Generators*, keynote address, *Computer Science and Statistics: 16th Symposium on the Interface*, Elsevier (1985).
- [10] P. L'Ecuyer and R. Simard, *ACM Transactions on Mathematical Software* **33**, 4, Article 1, December 2007.
- [11] J. Heinrich, CDF Note CDF/MEMO/STATISTICS/PUBLIC/8032, 2006.
- [12] UNU.RAN is described at statmath.wu.ac.at/software/unuran; See also W. Hörmann, J. Leydold, and G. Derflinger, *Automatic Nonuniform Random Variate Generation*, (Springer, New York, 2004).
- [13] W.H. Press *et al.*, *Numerical Recipes*, 3rd edition, (Cambridge University Press, New York, 2007).
- [14] J.H. Ahrens and U. Dieter, *Computing* **12**, 223 (1974).
- [15] R.Y. Rubinstein, *Simulation and the Monte Carlo Method*, (John Wiley and Sons, Inc., New York, 1981).
- [16] L. Devroye, *Non-Uniform Random Variate Generation*, (Springer-Verlag, New York, 1986); Available online at luc.devroye.org/rnbookindex.html.
- [17] C. Walck, *Handbook on Statistical Distributions for Experimentalists*, University of Stockholm Report SUF-PFY/96-01, available from www.fysik.su.se/~walck.
- [18] J.E. Gentle, *Random Number Generation and Monte Carlo Methods*, 2nd ed., (Springer, New York, 2003).
- [19] C.P. Robert and G. Casella, *Monte Carlo Statistical Methods*, 2nd ed., (Springer, New York, 2004).
- [20] J.S. Liu, *Monte Carlo Strategies in Scientific Computing*, (Springer, New York, 2001).
- [21] R.M. Neal, *Probabilistic Inference Using Markov Chain Monte Carlo Methods*, Technical Report CRG-TR-93-1, Dept. of Computer Science, University of Toronto, available from www.cs.toronto.edu/~radford/res-mcmc.html.
- [22] A. Caldwell, D. Kollar, K. Kröninger, *Comput. Phys. Commun.* **180** (2009) pages 2197–2209.
- [23] Schulz, O., Beaujean, F., Caldwell, A. et al., *SN Computer Science* **2**, 210 (2021).

43. Monte Carlo Event Generators

Revised July 2021 by P. Nason (INFN, Milano-Bicocca; Milano-Bicocca U.) and P. Skands (Monash U.).

General-purpose Monte Carlo (GPMC) generators like HERWIG [1–3], PYTHIA [4,5], and SHERPA [6], provide detailed simulations of high-energy collisions. They play an essential role in QCD modeling (in particular for aspects beyond fixed-order perturbative QCD) and in data analysis and the planning of new experiments, where they are used together with detector simulation to estimate signals and backgrounds in high-energy processes. They are built from several components, that describe the physics starting from very short distance scales, up to the typical scale of hadron formation and decay. Since QCD is weakly interacting at short distances (below a femtometer), the components of the GPMC dealing with short-distance physics are based upon perturbation theory. At larger distances, all soft hadronic phenomena, like hadronization and the formation of the underlying event in hadron collisions, cannot be computed from first principles at present, and one must rely upon QCD-inspired models.

The purpose of this review is to illustrate the main components of these generators. It is divided into four sections. The first one deals with short-distance, perturbative phenomena. The basic concepts leading to the simulations of the dominant QCD processes are illustrated here. In the second section, the nonperturbative transition from partons to hadrons (“hadronization”) is treated. The two most popular hadronization models, the string and cluster models, are illustrated. The basics of the implementation of decay chains of unstable “primary” hadrons into stable “secondaries” is also illustrated here. In the third section, models for soft hadron physics are discussed. These include models for the underlying event and for low- p_{\perp} (“minimum-bias”) interactions. Issues of collective effects, such as Bose-Einstein and color-reconnection effects, are also discussed here. The fourth section briefly introduces the challenges of MC uncertainty estimates and tuning.

We use natural units throughout, such that $c = 1$ and $\hbar = 1$, with energies, momenta and masses measured in GeV, and times and distances measured in GeV^{-1} .

43.1 Short-distance physics in GPMC generators

The short-distance components of a GPMC generator deal with the computation of the primary process at hand, with decays of short-lived particles, and with the generation of QCD and QED radiation. QCD radiation is computable in perturbation theory as long as the time scales involved are well below $1/\Lambda$, where Λ is a typical hadronic scale of few hundred MeV. Because of the presence of logarithmic enhancements due to both collinear and soft emissions, this description involves an indefinite number of final-state particles that are emitted at time scales below $1/\Lambda$. In e^+e^- annihilation into hadrons, for example, the time scale of the primary process is of the order of the inverse of the annihilation energy Q . Collinear and soft emissions take place at all time scales between $1/Q$ and $1/\Lambda$. Technically, the computation of the dominant collinear and soft radiation is carried out by the so called shower algorithms. Historically, “Parton Shower” algorithms were first developed for resummation of collinear singularities. We will briefly describe this approach in this section. We stress, however, that many modern generators adopt approaches that focus initially upon soft singularities, leading to “Dipole Showers”, discussed in Sec. 43.1.3.

Collinear singularities arise when the angle between two emitted light partons becomes small. For example, in a process in which a quark and a gluon are emitted, if the angle θ among them is very small (and is smaller than the angles among all other pairs of light partons in the process) the squared amplitude factorizes as follows

$$|M_{qg}|^2 d\Phi_{qg} \approx |M_q|^2 d\Phi_q \frac{\alpha_s}{2\pi} P_{q,gg}(z) dz \frac{d\phi}{2\pi} \frac{d\theta^2}{\theta^2} \quad (43.1)$$

where M_{qg} , $d\Phi_{qg}$ are the amplitude and phase space when both the gluon and the quark are emitted; M_q , $d\Phi_q$ are the amplitude and phase space when only the quark is emitted; $z = E_q/(E_q + E_g)$

is the fraction of energy carried by the quark; ϕ is the azimuth of the splitting plane, and $P_{q,gg}(z) = C_F(1+z^2)/(1-z)$ is the Altarelli-Parisi splitting kernel for gluon emission from a quark line, with color factor $C_F = 4/3$. The factorized form of Eq. (43.1) is due to the fact that for small angle the process is dominated by a single amplitude in which the splitting quark is almost on shell and hence propagates for long distances. We define the energy scale corresponding to the inverse of this distance as the *hardness* of the splitting process, so that larger hardness corresponds to shorter distance. We can define the hardness t as the product $E^2\theta^2$, or as the virtuality of the splitting parton p^2 , or as a measure of the relative transverse momentum in the splitting such as the k_t of an emitted parton relative to its parent, defined by

$$\begin{aligned} p^2 &= 2E^2z(1-z)(1-\cos\theta) \approx z(1-z)E^2\theta^2, \\ k_t^2 &= z^2(1-z)^2E^2\theta^2. \end{aligned} \quad (43.2)$$

If the region of small values of z and $1-z$ was not important, these definitions would be equivalent. In QCD we also have soft divergences, arising when soft gluons are emitted. In Eq. (43.1) they appear as $z \rightarrow 1$, because of the $1/(1-z)$ singularity of $P_{q,gg}(z)$. Thus, we expect that the choice of the appropriate ordering variable will be relevant when dealing with soft divergences (see Sec. 43.3). The $d\theta^2/\theta^2$ factor in Eq. (43.1) can be equivalently written in terms of the hardness dt/t . After integration, it gives rise to a logarithmic factor $\log(Q^2/\Lambda^2)$. We can have many subsequent splittings, that we can describe by applying Eq. (43.1) recursively, as long as the splittings are strongly ordered in decreasing hardness. This means that, from a typical final-state configuration, by clustering together final-state parton pairs with the smallest hardness recursively, we can reconstruct a branching tree, that may be viewed as the splitting history of the event. We stress that all hardness values between the hardness of the primary process and the cutoff scale Λ are equally involved here. The collinear approximation is applied recursively to splitting processes that have much smaller hardness with respect to all previous ones.

By integrating over the phase space, a process with n collinear splittings will be of order $(\alpha_s(Q^2)\log(Q^2/\Lambda^2))^n$ with respect to the primary process. Since $\alpha_s(Q^2) \propto 1/\log(Q^2/\Lambda^2)$ [7], these corrections are not small. The so-called KLN theorem [8,9] guarantees that large logarithmic enhancements arising from final-state collinear splitting cancel against the virtual corrections in inclusive cross sections, order by order in perturbation theory. Furthermore, the factorization theorem guarantees that initial-state collinear singularities can be factorized into the parton density functions (PDFs) [7]. Therefore, the cross section for the basic process remains accurate up to corrections of higher orders in $\alpha_s(Q)$, provided it is interpreted as an inclusive cross section, rather than as a bare partonic cross section. For example, the leading order (LO) cross section for $e^+e^- \rightarrow q\bar{q}$ is a good LO estimate of the e^+e^- cross section for the production of a pair of quarks accompanied by an arbitrary number of collinear and soft gluons, but is not a good estimate of the cross section for the production of a $q\bar{q}$ pair with no extra radiation. In summary, perturbation theory at fixed order can yield increasingly accurate predictions for inclusive observables, but cannot be used to describe the indefinite sequence of collinear and soft radiations that accompany the hard partons.

Parton-Shower algorithms are used to compute the cross section for generic hard processes including all dominant collinear radiation. These algorithms begin with the generation of the kinematics of the basic process, performed with a probability proportional to its LO partonic cross section. This is interpreted physically as the inclusive cross section for the basic process, followed by an arbitrary sequence of shower splittings. The algorithm then assigns a probability to each splitting sequence, so that the initial LO cross section is partitioned into the cross sections for a multitude of final states of arbitrary multiplicity, with their sum equal to the cross section of the primary process. This property of the GPMCs reflects the KLN cancellation mentioned earlier, and it is often called “unitarity of the shower process”, a name that reminds us that the KLN cancellation itself is a consequence

of unitarity. The fact that a quantum mechanical process can be described in terms of composition of probabilities, rather than amplitudes, follows from the collinear approximation. In fact, because of strong ordering, a radiated parton cannot be collinear to more than one parton in the amplitude, and this suppresses interference effects.

We now illustrate the basic parton-shower algorithm, as first introduced in Ref. [10]. (For more pedagogical introductions see Ref. [11] and references therein.) For simplicity, we consider the example of e^+e^- annihilation into $q\bar{q}$ pairs, where we only have to deal with final state radiation (FSR). We consider all final states that can be built by dressing the q and \bar{q} partons with an indefinite number of splitting processes. By recursively clustering together final state parton pairs with the smallest relative hardness, from each final state configuration we can construct two trees rooted at the q and \bar{q} partons. The momenta of all intermediate lines of the tree diagrams are then uniquely determined from the final-state momenta. Hardnesses in the trees are ordered. One assigns to each splitting vertex the hardness t , the energy fractions z and $1-z$ of the two generated partons, and the azimuth ϕ of the splitting process with respect to the momentum of the incoming parton. For definiteness, we assume that z and ϕ are defined in the center-of-mass (CM) frame of the e^+e^- collision. The differential cross section for a given final state is given by the product of the differential cross section for the initial $e^+e^- \rightarrow q\bar{q}$ process, multiplied by a factor

$$\Delta_i(t_m, t_n) \frac{\alpha_s(t)}{2\pi} P_{i,jk}(z) \frac{dt_m}{t_m} dz \frac{d\phi}{2\pi} \quad (43.3)$$

for each intermediate line arising from the n^{th} and ending in the m^{th} splitting vertex. $\Delta_i(t_m, t_n)$ is the so-called Sudakov form factor

$$\Delta_i(t_m, t_n) = \exp \left[- \int_{t_m}^{t_n} \frac{dq^2}{q^2} \frac{\alpha_s(q^2)}{2\pi} \sum_{jk} P_{i,jk}(z) dz \frac{d\phi}{2\pi} \right]. \quad (43.4)$$

The suffixes i and jk represent the parton species of the incoming and final partons, respectively, and $P_{i,jk}(z)$ are the Altarelli-Parisi [12] splitting kernels. Notice that the endpoints on the z integration depend upon the definition of hardness. For example, in case of virtuality or transverse momentum ordering, the z integration is automatically cut-off near the extremes, see eq. (1.2). When this is not the case (as, for example, for angular ordering) an explicit cut-off on z must be introduced, corresponding to the requirement that an emission must have some minimum energy to be distinguishable from no emission. For lines originating at the primary vertex, the scale t_n is replaced by the typical scale of the primary process and for lines ending without any further splitting the scale t_m is replaced by t_0 , an infrared cutoff defined by the shower hadronization scale (at which the charges are screened by hadronization) or, for an unstable particle, its width (a source cannot emit radiation with a period exceeding its lifetime).

Eq. (43.3) can be obtained by iterating formula Eq. (43.1) recursively, with two important corrections: a) the strong coupling is evaluated at a scale corresponding to the hardness of the splitting process; b) the presence of the Sudakov form factor. Both these modifications arise from the inclusion of all collinear-dominant virtual corrections.

Notice that the Sudakov form factor for a small hardness interval $\Delta_i(t, t + \delta t)$ is equal to one minus the integrated emission probability of Eq. (43.3), i.e. it can be interpreted as the probability of no emission in the interval $t, t + \delta t$. From this, it immediately follows that $\Delta_i(t_m, t_n)$ can be interpreted as the no-emission probability in the full t_m, t_n interval. This interpretation allows to formulate the shower process as a probabilistic algorithm. We first notice that $0 < \Delta_i(t_m, t_n) \leq 1$, where the upper extreme is reached for $t_m = t_n$, and the lower extreme is approached for $t_m = t_0$. Starting from each of the partons in the primary process (e.g., $e^+e^- \rightarrow q\bar{q}$), event generation then proceeds recursively as follows. Given a parton exiting a vertex with hardness t_n , (taken to be of order the annihilation scale Q^2 for the first branching) one seeks a solution of the equation $r = \Delta_i(t_m, t_n)$, with $r \in [0, 1]$

a uniform random number, and solves it for the hardness of the next branching t_m . If $t_m \leq t_0$, no splitting is generated and the line is interpreted as a final parton. If $t_m > t_0$, a branching is generated at the scale t_m . Its z value and the final parton species jk are generated with a probability proportional to $P_{i,jk}(z)$. The azimuth is generated uniformly, neglecting angular correlations (see Sec. 43.1.1). This procedure is started with each of the primary process partons, and is applied recursively to all generated partons. It may generate an arbitrary number of partons, and it stops when no final-state partons undergo further splitting.

The four-momenta of the final-state partons are reconstructed from the momenta of the initial ones, and from the whole sequence of splitting variables, subject to overall momentum conservation. Different algorithms employ different strategies to treat recoil effects due to momentum conservation, which may be applied either locally for each splitting, or globally for the entire set of partons (a procedure called *momentum reshuffling*.) This has a subleading effect with respect to the collinear approximation.

We emphasize that the shower cross sections described above can be derived from perturbative QCD by keeping only the collinear-dominant real and virtual contributions to the cross section. As such it is unpredictable for large-angle radiation. It is thus unsafe to rely upon Parton Shower Monte Carlo alone to compute backgrounds to new physics signals that are characterized by several widely separated jets.

A Shower Monte Carlo builds its final state as if it developed from an iterative process, often with each intermediate stage made available to the user. It should be remarked that the meaning of these intermediate stages is only relevant within the approximation adopted by the generator, and could also differ in different implementations.

43.1.1 Angular correlations

In gluon-splitting processes ($g \rightarrow q\bar{q}$, $g \rightarrow gg$) in the collinear approximation, the distribution of the split pair is not uniform in azimuth, and the Altarelli-Parisi splitting functions are recovered only after azimuthal averaging. This dependence is due to the interference of positive and negative helicity states for the gluon that undergoes splitting. Spin correlations propagate through the splitting process, and determine acausal correlations of the EPR kind [13]. A method to partially account for these effects was introduced in Ref. [14], in which the azimuthal correlation between two successive splittings is computed by averaging over polarizations. This can then be applied at each branching step. Acausal correlations are argued to be small, and are discarded with this method, that is still used in PYTHIA [4]. A method that fully includes spin correlation effects was later proposed [15], and has been implemented in HERWIG [3, 16].

43.1.2 Initial-state radiation

Initial-state radiation (ISR) arises because incoming particles may undergo collinear radiation before entering the hard-scattering process. In doing so, they acquire a non-vanishing transverse momentum, and their virtuality becomes negative (spacelike). It turns out to be convenient to develop the ISR shower starting with the highest hardness (i.e. with the hard process) and ending with the smallest (i.e. with the incoming parton in the hadron). Unlike the case of FSR, however, hardness ordering is opposite to time ordering in the ISR case. A corresponding backwards-evolution algorithm was formulated by Sjöstrand [17], and was basically adopted in all shower models. It can be illustrated by considering a primary interaction initiated by a quark where no collinear emission of hardness $\geq t$ have taken place, and the same process where the quark also emits a collinear gluon of hardness t . The respective cross sections are proportional to

$$|M_q(x)|^2 dx f_q(x, t), \quad \text{and} \quad |M_q(x)|^2 dx \frac{\alpha_s(t)}{2\pi} f_q(x/z, t) P_{q,qg}(z) dz \frac{d\mathbf{CE}}{2\pi} \frac{dt}{t}. \quad (43.5)$$

Here f_q is the quark PDF in the incoming hadron, x is the fraction of momentum of the incoming quark that enters the basic process, while x/z is the fraction of momentum of the incoming quark *before* it emits the collinear gluon. The elementary *emission probability* is the ratio of the second over the first expression

in Eq. (43.5). In analogy with the final state radiation case, this ratio will appear in the exponent of the Sudakov form factor, that (after the inclusion of all splitting subprocesses) is given by

$$\Delta_i^{\text{ISR}}(t, t') = \exp \left[- \int_{t'}^t \frac{dt''}{t''} \frac{\alpha_S(t'')}{2\pi} \int_x^1 \frac{dz}{z} \sum_{jk} P_{j,ik}(z) \frac{f_j(t'', x/z)}{f_i(t'', x)} \right]. \quad (43.6)$$

Notice that there are two uses of the PDFs: they are used to compute the cross section for the basic hard process, and they control ISR via backward evolution. Since the evolution is generated with leading-logarithmic accuracy, it is acceptable to use two different PDF sets for these two tasks, provided they agree at the LO level.

In the context of GPMC evolution, each ISR emission generates a finite amount of transverse momentum. Details on how the recoils generated by these transverse “kicks” are distributed among other partons in the event, in particular the ones involved in the hard process, constitute one of the main areas of difference between existing algorithms, see Ref. [11]. An additional $\mathcal{O}(1 \text{ GeV})$ of “primordial k_T ” is typically added, to represent the sum of unresolved and/or non-perturbative motion below the shower cutoff scale.

43.1.3 Soft emissions and QCD coherence

Soft singularities arise in QCD due to the real or virtual emission of soft gluons. For example, the cross section for the emission of a soft gluon in e^+e^- annihilation into hadrons is given by

$$\begin{aligned} d\sigma_{q\bar{q}g} &\approx d\sigma_{q\bar{q}} \frac{4}{3} (4\pi\alpha_S) \left[\frac{2 p_q \cdot p_{\bar{q}}}{p_q \cdot l p_{\bar{q}} \cdot l} \right] \frac{d^3l}{2l^0(2\pi)^3} \\ &= d\sigma_{q\bar{q}} \frac{\alpha_S}{2\pi} \frac{4}{3} \frac{d^0\phi}{l^0} \frac{d\phi}{2\pi} \frac{d\cos\theta}{1-\cos^2\theta}, \end{aligned} \quad (43.7)$$

where p_q , $p_{\bar{q}}$ and l are the quark, antiquark and gluon momentum, and θ and ϕ are the polar and azimuthal angle of the gluon momentum with respect to the quark direction. Since the gluon is soft, we may assume that p_q and $p_{\bar{q}}$ are unaffected by the gluon emission. The soft singularity is manifest in the $d^0\phi/l^0$ factor. Notice that also collinear singularities are present at the same time when $\theta \rightarrow 0$ and $\theta \rightarrow \pi$, corresponding to the gluon becoming collinear to either the quark or the antiquark. It is easy to check that in the collinear limits Eq. (43.7) becomes equivalent to Eq. (43.1) with $P_{q,qq}(z) = (4/3)2/(1-z)$, i.e. the limiting form of $P_{q,qq}(z)$ when z approaches 1. Thus, soft singularities coexist with collinear ones, so that two potentially large logarithms can arise simultaneously due to gluon emission.

Unlike the case of collinear emission, soft emission is not tied to a single emitting particle. The amplitude for the emission of a soft gluon from an external (incoming or outgoing) line with momentum p is proportional to $p \cdot \epsilon/p \cdot l$. When squaring the amplitude, products like the one appearing in the square bracket of Eq. (43.1) arise for all pairs of external particles, with the product of a single emission amplitude with itself appearing only if $p^2 > 0$, i.e. for massive colored particles. Thus, interference plays here a crucial role. This is unlike the case of collinear singularities, where because of strong ordering a radiated parton cannot be collinear to more than one other parton.

It was shown in a set of publications (see Ref. [18]) that, within the conventional parton-shower formalism based on collinear factorization, the region of collinear and soft emissions can be correctly described by using the angle of the emissions as the ordering variable, rather than the virtuality, and by setting the argument of α_S at the splitting vertex equal to the relative parton transverse momentum after the splitting. Physically, the ordering in angle approximates the coherent interference arising from large-angle soft emission from a bunch of collinear partons. Without this effect, the particle multiplicity would grow too rapidly with energy, in conflict with e^+e^- data. For this reason, angular ordering is used as the default evolution variable in all versions of HERWIG (see Ref. [19]). To partially account for soft interference effects,

an angular veto is imposed on the virtuality-ordered evolution in PYTHIA 6 [20].

A radical alternative formulation of QCD cascades first proposed in Ref. [21] focuses upon soft emission, rather than collinear emission, as the basic splitting mechanism. It then becomes natural to consider a branching process where it is a parton pair (i.e. a dipole) rather than a single parton, that emits a soft parton. Adding a suitable correction for non-soft, collinear partons, one can simultaneously achieve the correct logarithmic structure for both the collinear and soft emissions in the so called leading color approximation, i.e. when terms suppressed by a power of the number of colors are neglected. The ARIADNE [22] and VINCIA [23] programs are based on this approach. Dipole-type showers [24] are also used by default in SHERPA [25] and exist as an option in HERWIG [26]. An alternative dipole-based model is available in PYTHIA and SHERPA via the DIRE [27] plugin. The p_\perp -ordered showers in PYTHIA 6 and 8 represent a hybrid, combining collinear splitting kernels with dipole kinematics [28].

43.1.4 Resummation

Shower Monte Carlo generators perform resummation of all-order collinear- and/or soft-enhanced perturbative contributions, and it is thus natural to compare them to QCD resummation calculations [7]. The latter start from the definition of specific infrared-safe observables, that develop towers of large logarithms in certain regions of phase space, typically organized as

$$A(\alpha_S) \exp[Lg_0(\alpha_S L) + g_1(\alpha_S L) + g_2(\alpha_S L) + \dots] \quad (43.8)$$

where L is the large logarithm, α_S is the strong coupling constant evaluated at some hard scale, and the functions A and g_i have an all-order expansion in their arguments. We talk about N^{LL} accuracy if all g_i functions for $i \leq n$ have been computed correctly in the resummation formula. In particular we talk about LL accuracy if the function g_0 is given correctly, NLL accuracy if g_2 is correct, and so on.

In general, a dedicated resummation calculation must be performed for each new observable. The predictions of shower MCs, on the other hand, are cast in terms of complete sets of final-state momenta, on which one can evaluate any observable; i.e., the shower algorithm itself is normally independent of the specific observable(s) under study. Because of this, it is not easy to qualifying the accuracy of a shower MC using the same criteria adopted in resummation calculation. In spite of this fact, shower MCs perform generally quite well in the description of observables that require resummation. This is related to their inclusion of several universal but formally subleading aspects. There is no guarantee, however, that the shower MC should perform to a certain level of accuracy for all distributions that require resummation. Thus, a more systematic treatment of subleading effects is quite desirable.

Several studies have appeared in the literature, aiming at either improving the current shower algorithms or formulate totally new ones, in such a way that the theoretical accuracy can be discussed in more precise terms [29–34]. In particular, in refs [29–31] (the PanScales collaboration), it was shown that criteria for defining the accuracy of Shower Generators can indeed be given on a quite general ground. They identified two such criteria: the first one regards the multi-parton real matrix-elements generated by the shower algorithm, that are required to be accurate in the region of phase space that are relevant for N^{LL} accuracy. The second one regards the implementation of the virtual corrections, and it requires that for a large class of shape variables the shower MC must agree with the resummed calculation at the N^{LL} level. The PanScale collaboration has also constructed shower algorithms that, at least in the leading color approximation, are NLL accurate according to these criteria.

43.1.5 Massive quarks

Quark masses act as a cut-off on collinear singularities. If the mass of a quark is below, or of the order of Λ , its effect in the shower is small. For larger quark masses, like in c , b , or t production, it is the mass, rather than the typical hadronic scale, that cuts off collinear radiation. For a quark with energy E and mass m_Q , the divergent behavior $d\theta/\theta$ of the collinear splitting process

is regulated for $\theta \leq \theta_0 = m_Q/E$. We thus expect less collinear activity for heavy quarks than for light ones, which in turn is the reason why heavy quarks carry a larger fraction of the momentum acquired in the hard production process.

This feature can be implemented with different levels of sophistication. Using the fact that soft emission exhibits a zero at zero emission angle, older parton shower algorithms simply limited the shower emission to be not smaller than the angle θ_0 . More modern approaches are used in both PYTHIA, where mass effects are included using a kind of matrix-element correction method [35], and in HERWIG++ and SHERPA, where a generalization of the Altarelli-Parisi splitting kernel is used for massive quarks [36].

43.1.6 Color information

In event generators, quarks and antiquarks are represented by color lines, with arrows indicating the direction of color flow. In the limit of infinitely many colors (called the leading color approximation), each such line can be associated with a unique label; the probability for two quarks (or antiquarks) to have the same color (anticolor) vanishes. Moreover, in the same limit gluons can be represented by a pair of color lines with opposite arrows, as can be realized e.g. from the SU(3) group relation $8 = 3 \otimes \bar{3} \ominus 1$. The rules for color propagation are:



During the shower development, partons are connected by color lines. We can have a quark directly connected by a color line to an antiquark, or via an arbitrary number of intermediate gluons, as shown in Fig. 43.1. It is also possible for a set of gluons to be connected cyclically in color, as e.g. in the decay $\Upsilon \rightarrow ggg$. The

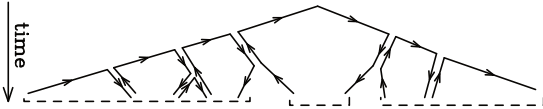


Figure 43.1: Color development of a shower in e^+e^- annihilation. Color-neutral clusters of partons are indicated by the dashed under-brackets.

color information is used in angular-ordered showers, where the angle of color-connected partons (i.e. partons connected by the same color line) determines the initial angle for the shower development, and in dipole showers, where dipoles are always color-connected partons. It is also used in hadronization models, where the initial strings or clusters used for hadronization are formed by color-neutral clusters of partons.

43.1.7 Electromagnetic (and weak) corrections

The physics of photon emission from charged particles, and of photon splittings to pairs of charged fermions, can also be treated with a shower MC algorithm. High-energy electrons and quarks, for example, are accompanied by bremsstrahlung photons. Also here, similarly to the QCD case, electromagnetic corrections are of order $\alpha_{em} \ln(Q/m)$, where m is the mass of the radiating particle, or even of order $\alpha_{em} \ln(Q/m) \ln(E_\gamma/E)$ for soft γ emissions, so that, especially for the case of electrons, their inclusion in the simulation process is mandatory. This is done in most GPMCs (for a comparative study see [37]), which typically agree in collinear (DGLAP) limits but differ in whether and how soft (multipole) QED interference effects are handled. The specialized generator PHOTOS [38] is sometimes used as an afterburner for an improved treatment of QED radiation in non-hadronic resonance decays.

For photon emissions off leptons, the shower can be continued down to virtualities arbitrarily close to the lepton mass shell (unlike the case in QCD). In practice, an infrared cutoff is still required for the shower algorithm to terminate. Therefore, there is always an energy cut-off for emitted photons that depends upon the implementations [37]. In the case of electrons, this energy is typically of the order of its mass. Electromagnetic radiation below this scale is not enhanced by collinear singularities, and is thus bound to be soft, so that the electron momentum is not affected by it.

For photons emitted from quarks, we have instead the obvious

limitation that the photon wavelength cannot exceed the typical hadronic size. Longer-wavelength photons are in fact emitted by hadrons, rather than quarks. This last effect is in practice never modeled by existing shower MC implementations. Thus, electromagnetic radiation from quarks is cut off at a typical hadronic scale. Finally, hadron (and τ) decays involving charged particles can produce additional soft bremsstrahlung. This is implemented in a general way in HERWIG++/HERWIG 7 [39] and SHERPA [40].

At energies significantly above the electroweak (EW) scale, showers involving emissions (and splittings) of weak gauge and Higgs bosons can also be relevant, with recent implementations based on collinear limits ranging from weak-boson emissions from fermions in PYTHIA 8 [41], to triple-boson couplings in HERWIG 7 [42], to the full set of EW branching processes in VINCIA [43].

43.1.8 Beyond-the-Standard-Model Physics

The inclusion of processes for physics beyond the Standard Model (BSM) in event generators is to some extent only a matter of implementing the relevant hard processes and (chains of) decays, with the level of difficulty depending on the complexity of the model and the degree of automation [44, 45]. Notable exceptions are long-lived colored particles [46], particles in exotic color representations, and particles showering under new gauge symmetries, with a growing set of implementations documented in the individual GPMC manuals. Further complications that may be relevant are finite-width effects (discussed in Sec. 43.1.9) and the assumed threshold behavior.

In addition to code-specific implementations [11], there are a few commonly adopted standards that are useful for transferring information and events between codes. Currently, the most important of these is the Les Houches Event File (LHEF) standard [47], normally used to transfer parton-level events from a hard-process generator to a shower generator. Another important standard is the Supersymmetry Les Houches Accord (SLHA) format [48], originally used to transfer information on supersymmetric particle spectra and couplings, but by now extended to apply also to more general BSM frameworks and incorporated within the LHEF standard [49].

43.1.9 Decay Chains and Particle Widths

In most BSM processes and some SM ones, an important aspect of the event simulation is how decays of short-lived particles, such as top quarks, EW and Higgs bosons, and new BSM resonances, are handled. We here briefly summarize the spectrum of possibilities, but emphasize that there is no universal standard. Users are advised to check whether the treatment of a given code is adequate for the physics study at hand.

The appearance of an unstable resonance as a physical particle at an intermediate stage of the event generation implies that its production and decay processes are treated as being factorized. This is valid up to corrections of order Γ/m_0 , with Γ the width and m_0 the pole mass. States whose widths are a substantial fraction of their mass should instead be treated as intrinsically off-shell internal propagator lines.

For states treated as physical particles, two aspects are relevant: the mass distribution of the decaying particle itself and the distributions of its decay products. For the former, matrix-element generators often use a simple δ function at m_0 . The next level up, typically used in GPMCs, is to use a Breit-Wigner distribution, which formally resums higher-order virtual corrections to the mass distribution. Note, however, that this still only generates an improved picture for *moderate* fluctuations away from m_0 . Similarly to above, particles that are significantly off-shell (in units of Γ) should not be treated as resonant, but rather as internal off-shell propagator lines. In most GPMCs, further refinements are included, for instance by letting Γ be a function of m (“running widths”) and by limiting the magnitude of the allowed fluctuations away from m_0 . We finally point out that NLO+PS generators have appeared that can deal with resonances including off-shell effects, non-resonance contributions and interference of radiation generated in resonance decay and production, see [50] and references therein. A new “interleaved” shower treatment also allows for interference between production and decay in the Vincia model [43].

For the distributions of the decay products, the simplest treatment is again to assign them their respective m_0 values, with a uniform phase-space distribution. A more sophisticated treatment distributes the decay products according to the differential decay matrix elements, capturing at least the internal dynamics and helicity structure of the decay process, including EPR-like correlations. Further refinements include polarizations of the external states [51] and assigning the decay products their own Breit-Wigner distributions, the latter of which opens the possibility to include also intrinsically off-shell decay channels, like $H \rightarrow WW^*$.

GPMC manuals often give instructions on how to include new decay modes, at varying levels of sophistications ranging from simple uniform phase-space sampling (which the user can reweight a posteriori) and step-function thresholds, to fully matrix-element weighted decay implementations including potential off-shell / threshold effects.

During subsequent showering of the decay products, most parton-shower models will preserve the total invariant mass of the decayed resonance, so as not to skew the original resonance shape. In the context of passing externally generated LHEF files [47] to a GPMC for showering, note that this is only possible if the intermediate resonances are present (with status code 2) in the LHEF event record [52].

43.1.10 Matching and Merging with Fixed-Order Matrix Elements

Shower algorithms are based upon a combination of the collinear (small-angle) and soft (small-energy) approximations and are thus normally inaccurate for hard, wide-angle emissions (i.e., additional well-resolved jets). They also contain only the leading singular pieces of next-to-leading order (NLO) and higher corrections to the basic process.

Traditional GPMCs, like HERWIG and PYTHIA, have included for a long time the so called Matrix Element Corrections (MEC), first formulated in Ref. [53] with later developments summarized in Ref. [11]. They are typically available for $2 \rightarrow 1$ or $1 \rightarrow 2$ processes, like DIS, vector boson and Higgs production and decays, and top decays. The MEC corrects the emission of the hardest jet at large angles, so that it becomes exact at LO. A generalization of the method to multiple emissions was formulated in [54].

Aside from MECs implemented directly in the GPMCs, the improvements on the parton-shower description of hard collisions have been made in two main directions: the so called Matrix Elements and Parton Shower matching (ME+PS from now on), and the matching of NLO calculations and Parton Showers (NLO+PS). We now discuss each of these, and then briefly summarize techniques becoming available for combining them.

The ME+PS method allows one to use tree-level matrix elements for hard, large-angle emissions. It was first formulated in the so-called CKKW paper [55], and several variants have appeared, including the CKKW-L, MLM, pseudoshower and MESS methods, see Refs. [11, 56, 57] and references therein. So called “Truncated Showers” are required [58] to maintain color coherence when interfacing to angular-ordered parton showers, and care must be taken to use consistent α_s choices for the real (ME-driven) and virtual (PS-driven) corrections [59].

In the ME+PS method one typically starts by generating LO matrix elements for the production of the basic process plus a certain number $\leq n$ of other partons. A minimum separation is imposed on the produced partons, requiring, for example, that the relative transverse momentum in any pair of partons is above a given cut Q_{cut} . One then reweights these amplitudes in such a way that, in the strongly ordered region, the virtual effects that are included in the shower algorithm (i.e. running couplings and Sudakov form factors) are also accounted for. At this stage, before parton showers are added, the generated configurations are tree-level accurate at large angle, and at small angle they match the results of the shower algorithm, except that there are no emissions below the scale Q_{cut} , and no final states with more than n partons. These kinematic configurations are thus fed into a GPMC, that must generate all splittings with relative transverse momentum below the scale Q_{cut} , for initial events with less than n partons, or below the scale of the smallest pair transverse momentum, for

events with n partons. The matching parameter Q_{cut} must be chosen to be large enough for fixed-order perturbation theory to hold, but small enough so that the shower is accurate for emissions below it. Notice that the accuracy achieved with MEC is equivalent to that of ME+PS with $n = 1$, where MEC has the advantage of not having a matching parameter Q_{cut} .

The popularity of the ME+PS method is due to the fact that processes with many jets often appear as backgrounds to new-physics searches. These jets are typically required to be well separated, and to have large transverse momenta. These kinematic configurations are exactly those for which pure shower algorithms are unreliable, hence it is mandatory to describe them using at least LO matrix elements.

Several ME+PS implementations use existing LO generators, like ALPGEN [60], MADGRAPH [61], and others summarized in Ref. [56], for the calculation of the matrix elements, and feed the partonic events to a GPMC like PYTHIA or HERWIG using the Les Houches Interface for User Processes (LHI/LHEF) [47, 52]. SHERPA and HERWIG 7 also include their own matrix-element generators.

The NLO+PS methods promote the accuracy of the generation of the basic process from LO to NLO in QCD. They must thus include the radiation of one extra parton with tree-level accuracy, since this radiation constitutes a NLO correction to the basic process. They must also include NLO virtual corrections. They can be viewed as an extension of the MEC methods with the inclusion of NLO virtual corrections. They are however more general, since they are applicable to processes of arbitrary complexity. Two of these methods are now widely used: MC@NLO [62] and POWHEG [58, 63], with several alternative methods now also being pursued, see Ref. [11] and references therein.

NLO+PS generators produce NLO accurate distributions for inclusive quantities, and generate the hardest jet with tree-level accuracy. It should be recalled, though, that in $2 \rightarrow 1$ processes like Z/W production, GPMCs including MEC and weighted by a constant K factor may perform nearly as well, and, if suitably tuned, may even yield a better description of data. In this context, note also that the optimal tuning of an NLO+PS generator may well be different from that of the pure PS.

Several NLO+PS processes are implemented in the MC@NLO program [62], together with the AMCNLO development [64], and in the POWHEG-BOX framework [63]. HERWIG 7 supports its own variants of POWHEG and MC@NLO for several processes. SHERPA instead implements a variant of the MC@NLO method.

For applications that require an accurate description of more than one hard, large-angle jet associated with the primary process, ME+PS schemes are still superior to NLO+PS ones. Ideally, one would like to improve NLO generators in such a way that also the production of associated jets achieves NLO accuracy. The FFX [65], UNLOPS [66], MiNLO [67] and MEPS@NLO [68] methods address this problem. The solution of this problem is also a prerequisite for the construction of NNLO+PS generators, i.e. generators that, besides being NLO accurate for the production of an associated jet, are also NNLO accurate for fully inclusive observables. Three different approaches have appeared in the literature for dealing with this problem: the UN²NLOPS, based upon UNLOPS method [69]; methods extending the MiNLO approach by reweighting [70] and by the so called MiNNLO_{PS} technique [71]; and the GENEVA method [72]. Several processes have been implemented with the MiNLO related and GENEVA methods, mostly for the production of color singlet systems, with the exception of the recent MiNNLO_{PS} implementation of $t\bar{t}$ production (see refs. [73, 74] for an extensive list of references).

43.2 Hadronization Models

In the context of GPMCs, *hadronization* denotes the process by which a set of colored partons (*after* showering) is transformed into a set of “primary hadrons”, which may then subsequently decay further (to “secondary hadrons”). This non-perturbative transition takes place at the *hadronization scale* Q_{had} , which by construction is equal to the infrared cutoff of the parton shower. In the absence of a first-principles solution to the relevant dynamics, GPMCs use QCD-inspired phenomenological models to describe this transition.

An important result in “quenched” lattice QCD (see Chap. 17

of PDG book) is that the potential energy between two partons with opposite color charges grows linearly with their separation, at distances greater than about a femtometer. This is known as “linear confinement”, and it forms the starting point for the *string model of hadronization*, discussed below in Sec. 43.2.1. Alternatively, a property of perturbative QCD called “preconfinement” is the basis of the *cluster model of hadronization*, discussed in Sec. 43.2.2.

A key difference between MC hadronization models and the fragmentation-function (FF) formalism used to describe inclusive hadron spectra in perturbative QCD (see Chap. 9 and Chap. 19 of PDG book) is that FFs can be defined at an arbitrary perturbative scale Q while MC hadronization models are intrinsically defined at the scale Q_{had} . Direct comparisons are therefore only meaningful if the perturbative evolution between Q and Q_{had} is taken into account. FFs are calculable in pQCD, given a non-perturbative initial condition obtained by fits to hadron spectra. In the MC context, one can prove that the correct QCD evolution of the FFs arises from the shower formalism, with the hadronization model providing an explicit parameterization of the non-perturbative component. However, the MC modeling of shower and hadronization includes much more information on the final state since it is fully exclusive (i.e., it addresses all particles in the final state explicitly), while FFs only describe inclusive spectra. This exclusivity also enables MC models to make use of the color-flow information coming from the perturbative shower evolution (see Sec. 43.1.6) to determine between which partons confining potentials should arise. E.g., in the string picture, the nonperturbative limit of a QCD dipole is a string piece [75].

Given an exact hadronization model, its dependence on the scale Q_{had} should in principle be compensated by the corresponding scale dependence of the shower algorithm, which stops generating branchings at the scale Q_{had} . However, due to their complicated and fully exclusive nature, it is generally not possible to enforce this compensation automatically in MC models. One must therefore be aware that the nonperturbative model parameters must be “retuned” by hand if the infrared cutoff is modified. Any other changes to the perturbative part of the calculation, such as matching to further (fixed-order or resummed) coefficients, may also necessitate a retuning. Tuning is discussed briefly in Sec. 43.4.

Finally, it should be emphasized that the so-called “parton level” that can be obtained by switching off hadronization in a GPMC, is not a universal concept, since each model defines Q_{had} differently (e.g. via a cutoff in p_{\perp} , invariant mass, etc., with different tunes using different values for the cutoff). Comparisons to distributions at this level may therefore be used to provide an idea of the overall impact of hadronization corrections within a given model, but should be avoided in the context of physical observables.

43.2.1 The String Model

Starting from early concepts [76], several hadronization models based on strings have been proposed [11]. Of these, the most widely used today is the so-called Lund model [77, 78], implemented in PYTHIA [4, 5]. We concentrate on that particular model here, though many of the overall concepts would be shared by any string-inspired method.

Consider a quark and an antiquark that have a large relative momentum and which are in an overall color-singlet state, such as the $q\bar{q}$ pair produced at the end of the shower in the center of Fig. 43.1). As the charges move apart, linear confinement implies that a potential $V(r) = \kappa r$ is reached for large distances r . (At short distances, there is a Coulomb term $\propto 1/r$ as well, but this is neglected in the Lund string.) This potential describes a string with tension $\kappa \sim 1 \text{ GeV/fm} \sim 0.2 \text{ GeV}^2$. The physical picture is that of a color flux tube being stretched between the q and the \bar{q} . As the string grows, the nonperturbative creation of quark-antiquark pairs can break the string, via the process illustrated in Fig. 43.2. If either of the resulting string pieces after the break still has a large invariant mass, new breaks will then continue to occur until every piece has a mass of order a typical hadron. In nature, quantum mechanics ensures that these masses are (Breit-Wigner-distributed around) those of the physical hadron states in QCD, while in an algorithmic implementation, this is less trivial

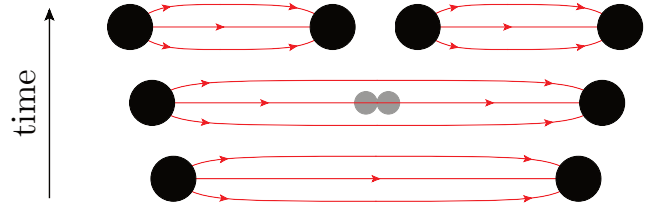


Figure 43.2: Illustration of string breaking by quark pair-creation in the string field.

to impose. Within the Lund model, the constraint that each final string piece must have a mass consistent with that of physical hadron is addressed by first noting that each breakup vertex is spacelike separated from all others (the string cannot break again in the forward lightcone of a point where it has already broken); since the breakups are therefore causally disconnected, they do not have to be considered in any particular order. The Lund model exploits this to perform the fragmentation in an outwards-in manner [78], splitting off one physical hadron at a time from either the left or right endpoint (chosen randomly in each step).

The first hadron to be generated (starting either from the left or right) is thus the “outermost” one (sometimes called the “first-rank” hadron), formed by combining the original hadronizing endpoint quark (or antiquark) q_0 with an antiquark (or quark) \bar{q}_1 produced by the first breakup. The new leftover quark (or antiquark) q_1 becomes the string endpoint for the next iteration, in a Markov chain which continues, alternating randomly between the left and right ends of the string, until finally a small last bit of string is decayed directly to two hadrons, with no energy left over.

Not only does this allow for the hadron that is split off in each step to be assigned a physical mass, the fact that the fragmentation spectrum should be independent of whether one performs the fragmentation from left to right or vice versa places a strong constraint on the form of the nonperturbative *fragmentation function*, $f(z)$, which governs the probability for the hadron produced in a given step to take a fraction $z \in [0, 1]$ of the remaining energy. Thus, in the Lund model, causality dictates that the fragmentation function should be of the form,

$$f(z) \propto \frac{1}{z} (1-z)^a \exp\left(-\frac{b(m_h^2 + p_{\Gamma} h^2)}{z}\right). \quad (43.9)$$

This is known as the Lund symmetric fragmentation function (normalized to unit integral). The dimensionless parameter a dampens the hard tail of the fragmentation function, towards $z \rightarrow 1$, and may in principle be flavor-dependent, while b , with dimension GeV^{-2} , is a universal constant related to the string tension [78] which determines the behavior in the soft limit, $z \rightarrow 0$. Note that the dependence on the hadron mass, m_h , in $f(z)$ implies that heavier hadrons have higher $\langle z \rangle$. We return to the transverse momentum $p_{\Gamma} h$ below.

The model is Lorentz invariant, so considerations involving boosted string systems are straightforward, involving the usual Lorentz effects.

As a by-product, the probability distribution in invariant time τ of $q\bar{q}$ breakup vertices, or equivalently $\Gamma = (\kappa\tau)^2$, is also obtained, with $dP/d\Gamma \propto \Gamma^a \exp(-b\Gamma)$ implying an area law for the color flux, and the average breakup time lying along a hyperbola of constant invariant time $\tau_0 \sim 10^{-23} \text{ s}$ [78].

For massive endpoints (e.g. c and b quarks), which do not move along straight lightcone sections, the exponential suppression with string area leads to modifications of the form $f(z) \rightarrow f(z)/z^{b m_Q^2}$, with m_Q the mass of the heavy quark [79]. Although different forms, such as the Peterson formula [80], can also be used to describe inclusive heavy-meson spectra (see Sec 19.8 of PDG book), such choices are not strictly consistent with causality in the string framework.

43.2.1.1 Strings with Gluons

In the string model, energetic gluons lead to transverse “kinks” on strings, illustrated in Fig. 43.3. The order of these kinks follows from the color ordering produced by the parton shower, cf. the $\bar{q}gggq$ and $\bar{q}gq$ systems on the left and right part of Fig. 43.1. (Modifications to this order, by possible color reconnection/rearrangement effects, are discussed in Sec. 43.3.2.) Thus gluons

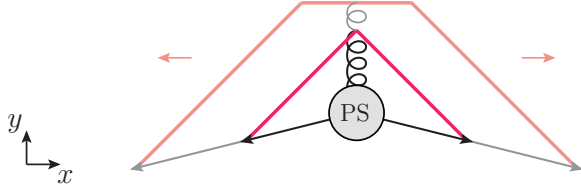


Figure 43.3: Schematic illustration of an $e^+e^- \rightarrow qq\bar{q}$ configuration emerging from the parton shower (PS). Snapshots of string positions are shown at two different times (full and shaded lines respectively). The gluon forms a transverse kink which grows in the y direction until all the gluon’s kinetic energy has been used up.

effectively build up a transverse structure in the originally one-dimensional object, with infinitely soft ones smoothly absorbed into the string. Note: cyclic topologies made entirely of gluons (closed strings) are also possible, e.g. in decays such as $H \rightarrow gg$ or $\Upsilon \rightarrow ggg$. The space-time evolution is more involved when kinks are taken into account [78], but no additional free parameters need to be introduced. The main difference between quark and gluon hadronization stems from the fact that gluons are connected to two string pieces (one on either side), while quarks are only connected to a single string piece. Hence, the relative rate of energy loss per unit invariant time — and consequently also the rate of hadron production — is larger by a factor of 2 for gluons (analogously to the ratio of gluon to quark color charges $C_A/C_F = 2.25$).

43.2.1.2 Transverse Momentum and Flavors

For each breakup vertex, quantum mechanical tunneling is assumed to control the masses and p_T kicks (transverse to the string axis, in a frame in which the string itself has no transverse motion) that can be produced, leading to a Gaussian suppression

$$\text{Prob}(m_q^2, p_T q^2) \propto \exp\left(\frac{-\pi m_q^2}{\kappa}\right) \exp\left(\frac{-\pi p_T q^2}{\kappa}\right), \quad (43.10)$$

where m_q is the mass of the produced quark flavor and p_T is the nonperturbative transverse momentum imparted to it by the breakup process, with a universal average value of $\langle p_T q^2 \rangle = \kappa/\pi \sim (250 \text{ MeV})^2$. The antiquark has the same mass and opposite p_T .

In an MC model with a fixed shower cutoff t_0 , the effective amount of p_T in string breaks may be larger than the purely nonperturbative κ/π above, to account for effects of additional (unresolved) radiation below t_0 .

From the mass term in Eq. (43.10), one concludes that charm and bottom quarks are too heavy to be produced in string breaks, while strange quarks will be suppressed relative to up and down ones. Lacking unambiguous and precise mass definitions for light quarks, however, the effective amount of strangeness suppression is normally extracted from experimental data, using observables such as K/π , K^*/ρ , and ϕ/K^* ratios.

Baryon production can also be incorporated, at various levels of sophistication. The simplest option is to allow string breaks to produce pairs of *diquarks*, loosely bound states of two quarks in an overall $\bar{3}$ representation. Again, the relative rate of such pairs is extracted from data, e.g. using p/π or Λ/K ratios. Since the perturbative shower splittings do not produce diquarks, the optimal value for this parameter is mildly correlated with the amount of $g \rightarrow q\bar{q}$ splittings in the shower. More sophisticated

options, including the so-called “popcorn” mechanism, are discussed in Ref. [78]. Finally, the PYTHIA framework also allows for baryon string junctions [81]. These represent epsilon tensors in color space (analogously to how color dipoles represent Kronecker deltas), and are used, e.g., to model the fragmentation of baryon beam remnants. They can also be created (in pairs of junctions and antijunctions) in some color-reconnection scenarios [82], making the effective baryon-to-meson ratios in such models dependent on the amount and type of color reconnections that occur in each event.

The next step of the algorithm is the assignment of the produced quarks within hadron multiplets. Using a nonrelativistic classification of spin states, the hadronizing q may combine with the \bar{q}' from a newly created breakup to produce a hadron of a given spin S and angular momentum L . The lowest-lying pseudoscalar and vector meson multiplets, and spin-1/2 and -3/2 baryons, are assumed to dominate in a string framework¹, but individual rates are not predicted by the model, and hence the ratios of spin-1 to spin-0 mesons and diquarks are free parameters (modulo a factor 3 from spin counting) which must be constrained by data. In that context, it is often advisable to begin with the heaviest states, since so-called feed-down from the decays of higher-lying hadron states complicates the extraction for lighter particles, see Sec. 43.2.3.

43.2.2 The Cluster Model

The cluster hadronization model is based on *preconfinement*, i.e., on the observation [83,84] that the color structure of a perturbative QCD shower evolution at any scale Q_0 is such that color-singlet subsystems of partons (labeled “clusters”) occur with a universal invariant mass distribution which is power suppressed at large masses. For any starting scale $Q \gg Q_0 \gg \Lambda_{\text{QCD}}$, only the number of such clusters depends on Q , while the shape of their mass distribution only depends on Q_0 and on Λ_{QCD} .

Following early models based on this universality [10,85], the cluster model developed by Webber [86] has for many years been a hallmark of the HERWIG generators, with an alternative implementation [87] now available in the SHERPA generator. The key idea, in addition to preconfinement, is to force “by hand” all gluons to split into quark-antiquark pairs at the end of the parton shower. Compared with the string description, this effectively amounts to viewing gluons as “seeds” for string breaks, rather than as kinks in a continuous object. After the splittings, a new set of low-mass color-singlet clusters is obtained, formed only by quark-antiquark pairs. These can be decayed to on-shell hadrons in a simple manner, with the relative yields of different hadron species mainly governed by their masses and the size of the phase space.

The algorithm starts by generating the forced $g \rightarrow q\bar{q}$ breakups, and by assigning flavors and momenta to the produced quark pairs. For a typical shower cutoff corresponding to a gluon virtuality of $Q_{\text{had}} \sim 1 \text{ GeV}$, the p_T generated by the splittings can be neglected. The constituent light-quark masses, $m_{u,d} \sim 300 \text{ MeV}$ and $m_s \sim 450 \text{ MeV}$, imply a suppression (typically even an absence) of strangeness production. In principle, the model also allows for diquarks to be produced at this stage, but due to the larger constituent masses this would only become relevant for shower cutoffs larger than 1 GeV.

If a cluster formed in this way has an invariant mass above some cutoff value, typically 3–4 GeV, it is forced to undergo sequential $1 \rightarrow 2$ cluster breakups, along an axis defined by the constituent partons of the original cluster, until all sub-cluster masses fall below the cutoff value. Due to the preservation of the original axis in these breakups, this treatment has some resemblance to the string-like picture, though the nonperturbative p_\perp kicks generated in this way are generally larger, up to half the allowed cluster mass.

Next, on the low-mass side of the spectrum, some clusters are allowed to decay directly to a single hadron, with nearby clusters absorbing any excess momentum. This improves the description of the high- z part of the spectrum — where the hadron carries almost

¹In PYTHIA, the four $L = 1$ meson multiplets (scalar, tensor, and 2 pseudovectors) are also available but are disabled by default, since many states (and their decays) are poorly known.

all the momentum of its parent jet — at the cost of introducing one additional parameter, controlling the probability for single-hadron cluster decay.

Having obtained a final distribution of small-mass clusters, now with a strict cutoff at 3–4 GeV and with the component destined to decay to single hadrons already removed, the remaining clusters are interpreted as a smoothed-out spectrum of excited mesons, each of which decays isotropically to two hadrons, with relative probabilities proportional to the available phase space for each possible two-hadron combination that is consistent with the cluster’s internal flavors, including spin degeneracy. It is important that all the light members (containing only uds) of each hadron multiplet be included, as the absence of members can lead to unphysical isospin or SU(3) flavor violation. Typically, the lightest pseudoscalar, vector, scalar, even and odd charge conjugation pseudovector, and tensor multiplets of light mesons are included. In addition, some excited vector multiplets of light mesons may be available. For baryons, usually only the lightest flavor-octet, -decuplet and -singlet baryons are present, although both the HERWIG++ and SHERPA implementations now include some heavier baryon multiplets as well.

Differently from the string model, the mechanism of phase-space suppression employed here leads to a natural enhancement of the lighter pseudoscalars, and no parameters beyond the spectrum of hadron masses need to be introduced at this point. The phase space also limits the transverse momenta of the produced hadrons relative to the jet axis.

Note that, since the masses and decays of excited heavy-flavor hadrons in particular are not well known, there is some freedom in the model to adjust these, which in turn will affect their relative phase-space populations.

43.2.3 Hadron and τ Decays

Of the so-called primary hadrons, originating directly from string breaks and/or cluster decays (see above), many are unstable and so decay further, until a set of particles is obtained that can be considered stable on time scales relevant to the given measurement. (A typical hadron-collider definition of a “stable particle” $c\tau \geq 10$ mm includes weakly-decaying strange hadrons K , Λ , Σ^\pm , Ξ^\pm , Ξ , Ω .) The decay modeling can therefore have a significant impact on final particle yields and spectra, especially for the lowest-lying hadronic states, which receive the largest relative contributions from decays (feed-down). This interplay also implies that hadronization parameters may need to be retuned if significant changes to the decay treatment are made.

Particle summary tables, such as those given elsewhere in this *Review*, represent a condensed summary of the available experimental measurements and hence may be incomplete and/or exhibit inconsistencies within the experimental precision. In an MC decay package, on the other hand, all information must be quantified and consistent, with all branching ratios summing to unity. When adapting particle summary information for use in a decay package, a number of choices must therefore be made. The amount of ambiguity increases as more excited hadron multiplets are added to the simulation, about which less and less is known from experiment, with each GPMC making its own choices.

A related choice is how to distribute the decay products differentially in phase space, in particular which matrix elements to use. Historically, MC generators contained matrix elements only for selected (generator-specific) classes of hadron and τ decays, coupled with a Breit-Wigner smearing of the masses, truncated at the edges of the physical decay phase space (the treatment of decay thresholds can be important for certain modes [11]). A more sophisticated treatment can then be obtained by reweighting the generated events using the obtained particle four-momenta and/or by using specialized external packages such as EVTGEN [88] for hadron decays and TAUOLA [89] for τ decays.

More recently, HERWIG++ and SHERPA include helicity-dependence in τ decays [6, 90], with a more limited treatment available in PYTHIA 8 [5]. The HERWIG++ and SHERPA generators have also included significantly improved internal simulations of hadron decays, which include spin correlations between those decays for which matrix elements are used. Photon-bremsstrahlung effects are discussed in Sec. 43.1.7.

HERWIG++ and PYTHIA include the probability for B mesons to oscillate into \bar{B} ones before decay. SHERPA and EVTGEN also include CP -violating effects and, for common decay modes of the neutral meson and its antiparticle, the interference between the direct decay and oscillation followed by decay.

We end on a note of warning on double counting. This may occur if a particle can decay via an intermediate on-shell resonance. An example is $a_1 \rightarrow \pi\pi\pi$ which may proceed via $a_1 \rightarrow \rho\pi$, $\rho \rightarrow \pi\pi$. If these decay channels of the a_1 are both included, each with their full partial width, a double counting of the on-shell $a_1 \rightarrow \rho\pi$ contribution would result. Such cases are normally dealt with consistently in the default MC generator packages, so this warning is mostly for users that wish to edit decay tables on their own.

43.3 Models for Soft Hadron-Hadron Physics

43.3.1 Underlying Event

In the GPMC context, “underlying event” (UE) denotes any additional activity *beyond* the basic process and its associated ISR and FSR activity. The UE is thus only defined in the context of events selected with a “hard” (i.e., high- p_\perp) trigger which defines the basic process at hand. The dominant contribution to the UE is believed to come from additional color exchanges between the colliding hadronic states. These multiple exchanges can be modeled either as additional perturbative (mainly t -channel gluon) exchanges, called multiple parton-parton interactions (MPI), or nonperturbatively using so-called cut pomerons (roughly equivalent to exchange of gluons with $p_\perp \rightarrow 0$). The experimental observation that events with a hard trigger are accompanied by a higher-than-average level of associated activity is called the “jet pedestal” effect.

The most clearly identifiable consequence of MPI is arguably the possibility of observing several hard parton-parton interactions in one and the same hadron-hadron event. Typically, these are QCD $2 \rightarrow 2$ interactions, which produce additional back-to-back jet pairs, with each pair having a small value of $\text{sum}(\vec{p}_\perp)$. The fraction of MPI that give rise to additional reconstructible jets is, however, small. Soft interactions, that exchange color and a small amount of momentum without giving rise to observable jets, are much more plentiful, and can give significant corrections to the color flow and total scattered energy of the event. This affects the final-state activity in a more global way, increasing hadron-multiplicity and summed E_T distributions, and contributing to the break-up of the beam remnants in the forward direction.

The first detailed Monte Carlo model for perturbative MPI was proposed in Ref. [91], and with some variation this still forms the basis for most modern implementations. Some useful additional references can be found in Ref. [11]. The first crucial observation is that the t -channel propagators appearing in perturbative QCD $2 \rightarrow 2$ scattering almost go on shell at low p_T , causing the differential cross sections to behave roughly as

$$d\sigma_{2 \rightarrow 2} \propto \frac{dt}{t^2} \sim \frac{dp_T^2}{p_T^4}. \quad (43.11)$$

This cross section represents the inclusive scattering of partons against partons in perturbative QCD, summed over all partons. Thus, if a single hadron-hadron scattering contains *two* parton-parton interactions, that event will contribute twice to the parton-parton cross section $\sigma_{2 \rightarrow 2}$ but only once to the hadron-hadron one σ_{tot} , and so on. In the limit that all the parton-parton interactions are independent and equivalent, one has

$$\sigma_{2 \rightarrow 2} = \langle n \rangle \sigma_{\text{tot}}, \quad (43.12)$$

with $\langle n \rangle$ the average number of parton-parton interactions, typically defined with some minimal $p_T > p_{\perp, \text{min}}$ to render the parton-parton cross section finite. The probability for n parton-parton scatterings then follows a Poisson distribution,

$$\mathcal{P}_n = \langle n \rangle^n \frac{\exp(-\langle n \rangle)}{n!}. \quad (43.13)$$

This simple argument expresses unitarity; instead of the total hadron-hadron interaction cross section diverging as the parton-parton $p_T \rightarrow 0$ (which would violate unitarity), we have restated

the problem so that it is now the number of *parton-parton interactions per hadron-hadron collision* that diverges, with the total hadron-hadron cross section remaining finite. At LHC energies, the parton-parton scattering cross sections computed using the LO QCD cross section folded with modern PDFs become larger than the total pp one for $p_{\perp\min}$ values of order 4–5 GeV (see e.g. [92, 93]). One therefore expects the average number of perturbative MPI to exceed unity at around that scale.

Two ingredients remain to fully regulate the remaining divergence. Firstly, the interactions cannot use up more momentum than is available in the parent hadron. This suppresses the large- n tail of the estimate above. In PYTHIA-based models, the MPI are ordered in p_T , and the parton densities for each successive interaction are explicitly constructed so that the sum of x fractions can never be greater than unity. In the HERWIG models, the Poisson estimate of $\langle n \rangle$ above is used as an initial guess, but the generation of actual MPI is stopped once the energy-momentum conservation limit is reached. Both of these approaches generate momentum (conservation) correlations among the MPI.

The second ingredient invoked to suppress the number of interactions, at low p_T and x , is color screening; if the wavelength $\sim 1/p_T$ of an exchanged colored parton becomes larger than a typical color-anticolor separation distance, it will only see an *average* color charge that vanishes in the limit $p_T \rightarrow 0$. This provides an infrared cutoff for MPI similar to that provided by the hadronization scale for parton showers. A first estimate of the color-screening cutoff would be the proton size, $p_{\perp\min} \approx \hbar/r_p \approx 0.3 \text{ GeV} \approx \Lambda_{\text{QCD}}$, but empirically this appears to be far too low. In current models, one replaces the proton radius r_p in the above formula by a “typical color screening distance,” i.e., an average size of a region within which the net compensation of a given color charge occurs. This number is not known from first principles [94] and is perceived of simply as an effective cutoff parameter. The simplest choice is to introduce a step function $\Theta(p_T - p_{\perp\min})$. Alternatively, one may note that the jet cross section is divergent like $\alpha_S^2(p_T^2)/p_T^4$, cf. Eq. (43.11), and that therefore a factor

$$\frac{\alpha_S^2(p_T^2 + p_{T0}^2)}{\alpha_S^2(p_T^2)} \frac{p_T^4}{(p_T^2 + p_{T0}^2)^2} \quad (43.14)$$

would smoothly regulate the divergences, now with p_{T0} as the free parameter. Regardless of whether it is imposed as a smooth (PYTHIA and SHERPA) or steep (HERWIG++) function, this is effectively the main “tuning” parameter in such models.

Note that the numerical value obtained for the cross section depends upon the PDF set used, and therefore the optimal value to use for the cutoff will also depend on this choice. Note also that the cutoff does not have to be energy-independent. Higher energies imply that parton densities can be probed at smaller x values, where the number of partons rapidly increases. Partons then become closer packed and the color screening distance d decreases. The uncertainty on the energy and/or x scaling of the cutoff is a major concern when extrapolating between different collider energies [95].

We now turn to the origin of the observational fact that hard jets appear to sit on top of a higher “pedestal” of underlying activity than events with no hard jets. This is interpreted as a consequence of impact-parameter-dependence: in peripheral collisions, only a small fraction of events contain any high- p_T activity, whereas central collisions are more likely to contain at least one hard scattering; a high- p_T triggered sample will therefore be biased towards small impact parameters, b . The ability of a model to describe both the UE in events with a hard trigger as well as the activity in inclusive “minimum-bias” (MB) samples (see below) therefore depends upon its modeling of the b -dependence, and correspondingly the impact-parameter shape constitutes another main tuning parameter.

For each impact parameter b , the number of interactions $\tilde{n}(b)$ can still be assumed to be distributed according to Eq. (43.13), again modulo momentum conservation, but now with the mean value of the Poisson distribution depending on impact parameter, $\langle \tilde{n}(b) \rangle$. This causes the final n -distribution (integrated over b) to be wider than a Poissonian.

Finally, there are two perturbative modeling aspects which go beyond the introduction of MPI themselves: 1) parton showers off the MPI, and 2) perturbative parton-rescattering effects. Without showers, MPI models would generate very sharp peaks for back-to-back MPI jets, caused by unshowered partons passed directly to the hadronization model. However, with the exception of the oldest PYTHIA6 model, all GPMC models do include such showers [11], and hence should exhibit more realistic (i.e., broader and more decorrelated) MPI jets. On the initial-state side, the main questions are whether and how correlated multi-parton densities are taken into account and, as discussed previously, how the showers are regulated at low p_T and/or low x . Although none of the MC models currently impose a rigorous correlated multi-parton evolution, all of them include some elementary aspects. The most significant for parton-level results is arguably momentum conservation, which is enforced explicitly in all the models. The so-called “interleaved” models [28] attempt to go a step further, generating an explicitly correlated multi-parton evolution in which flavor sum rules are imposed to conserve, e.g. the total numbers of valence and sea quarks [81].

Perturbative rescattering in the final state can occur if partons are allowed to undergo several distinct interactions, with showering activity possibly taking place in-between. This has so far not been studied extensively, but a first exploratory model is available [96]. In the initial state, parton rescattering/recombination effects have so far not been included in any of the GPMC models.

43.3.2 Bose-Einstein and Color-Reconnection Effects

In the context of e^+e^- collisions, Bose-Einstein (BE) correlations have mostly been discussed as a source of uncertainty on high-precision W mass determinations at LEP [97]. In hadron-hadron (and nucleus-nucleus) collisions, however, BE correlations are used extensively to study the space-time structure of hadronizing matter (“femtoscopy”).

In MC models of hadronization, each string break or particle/cluster decay is normally factorized from all other ones. This reduces the number of variables that must be considered in each step, but also makes it intrinsically difficult to introduce correlations among particles from different breaks/decays. In GPMCs, a few semi-classical models are available within the PYTHIA 6 and 8 generators [98], in which the BE effect is mimicked by an attractive interaction between pairs of identical particles in the final state, with no higher correlations included. Variants of this model differ mainly by the assumed shape of the correlation function and how overall momentum conservation is handled.

As discussed in Sec. 43.2, leading-color (“planar”) color flows are used to set up the hadronizing systems (clusters or strings) at the hadronization stage. If the systems do not overlap significantly in space and time, subleading-color ambiguities and/or nonperturbative reconnections are expected to be small. However, if the density of displaced color charges is sufficiently high that several systems can overlap significantly, full-color and/or reconnection effects should become progressively larger.

In the specific context of MPI, a crucial question is how color is neutralized *between* different MPI systems, including the remnants. The large rapidity differences involved imply large invariant masses (though normally low p_T), and hence large amounts of (soft) particle production. Indeed, in the context of soft-inclusive physics, it is these “inter-system” strings/clusters that furnish the dominant particle-production mechanism, and hence their modeling is an essential part of the soft-physics description, affecting topics such as MB/UE multiplicity and p_T distributions, rapidity gaps, and precision mass measurements. Reviews of color-reconnection effects can be found in [11, 82].

43.3.3 Minimum-Bias Events and Diffraction

The term “minimum bias” (MB) originates from the experimental requirement of a minimal number of tracks (or hits) in a given instrumented region. In order to make MC predictions for such observables, all possible contributions to the relevant phase-space region must be accounted for. There are essentially four types of physics processes, which together make up the total hadron-

hadron (hh) cross section: 1) elastic scattering²: $hh \rightarrow hh$, 2) single diffractive dissociation: $hh \rightarrow h + \text{gap} + X$, with X denoting anything that is not the original beam particle, and “gap” denoting a rapidity region devoid of observed activity; 3) double diffractive dissociation: $hh \rightarrow X + \text{gap} + X$, and 4) inelastic non-diffractive scattering: everything else. A fifth class may also be defined, called central diffraction ($hh \rightarrow h + \text{gap} + X + \text{gap} + h$). Note that different terminologies exist [99]: in experimental settings, diffraction is typically defined by an observable gap, of some minimal size in rapidity, while in the MC context, each diffractive physics process produces a whole spectrum of gaps, with small ones suppressed but not excluded.

The inelastic non-diffractive part of the cross section is typically modeled either by smoothly regulating and extending the perturbative QCD scattering cross sections all the way to zero p_{\perp} [91] (PYTHIA and SHERPA), or by regulating the QCD cross sections with a sharp cutoff [100] and adding a separate class of nonperturbative scatterings below that scale [101] (HERWIG). See also Sec. 43.3.1. In all cases, the most important ingredients are: 1) the IR regularization of the perturbative scattering cross sections, including their PDF dependence, 2) the assumed matter distribution of the colliding hadrons, possibly including multi-parton correlations [81] and/or x dependence [102], and 3) additional soft-QCD effects such as color reconnections, discussed in Sec. 43.3.2.

Currently, there are essentially three methods for simulating diffraction in the main MC models: 1) in PYTHIA 6, one picks a diffractive mass according to parameterized cross sections $\propto dM^2/M^2$ [103]. This mass is represented as a string, which is hadronized as described in Sec. 43.2.1, though differences in the effective scale of the hadronization may necessitate a (re)tuning of the hadronization parameters for diffraction; 2) in PYTHIA 8, the high-mass tail beyond $M \sim 10$ GeV is augmented by a partonic description in terms of pomeron PDFs [104], allowing diffractive jet production including showers and underlying event [105]; 3) the PHOJET and DPMJET programs also include central diffraction and rely directly on a formulation in terms of pomerons (color-singlet multi-gluon states) [106–108]. Cut pomerons correspond to exchanges of soft gluons while uncut ones give elastic and diffractive topologies as well as virtual corrections that help preserve unitarity. So-called “hard pomerons” provide a transition to the perturbative regime. Hadronization is still handled using the Lund string model, so there is some overlap with the above models at the hadronization stage. In addition, a pomeron-based package exists for HERWIG [109], and an effort is underway to construct an MC implementation of the “KMR” model [94] within the SHERPA generator. Color reconnections (Sec. 43.3.2) may also play a role in creating rapidity gaps and the underlying event (Sec. 43.3.1) in filling them.

43.4 Uncertainties and Tuning

The accuracy that can be achieved by a GPMC model depends on the sophistication of the theory models it incorporates, on the available constraints on its free parameters, and on the nature of the observable(s) under study. Using existing data (or more accurate theory calculations) to constrain the model parameters is referred to as generator tuning. Although tuned models do tend to yield improved results also for observables that they have not been tuned to, the question of evaluating the remaining uncertainties reliably is still far from solved. It is worth noting, however, that all of the GPMCs now provide options for automatic evaluation of perturbative shower uncertainties (e.g., via renormalization-scale variations), in the form of vectors of alternative event weights [110–112]. One must be aware that these variations are not necessarily exhaustive and significant weight fluctuations can be a problem for processes with large shower phase spaces. Nonperturbative uncertainties must normally still be evaluated by varying salient model parameters by hand. A general method called eigentunes [113] is also available, based on global fits to data.

Typically, the overall event properties are determined by only a few, very important parameters, such as the value of α_s , for

perturbative corrections, and the shape of the fragmentation functions, for nonperturbative ones. More parameters may then be introduced to describe successively more detailed aspects (e.g., the rates and decays of individual hadron species), but these should have progressively less impact on the overall modeling. One may therefore take a factorized approach, first constraining the perturbative parameters and thereafter the nonperturbative ones, in order of decreasing significance to the overall modeling. Furthermore, by identifying which measurements are most sensitive to each parameter, this ordering can be reflected in the way that data is selected and applied to constrain the models. Thus, measurements sensitive to global event properties would typically be applied first, to constrain the most inclusive parameters, and so on for progressively more exclusive aspects.

At LO \times LL, perturbation theory is doing well if it agrees with an IR safe measurement within $\sim 10\%$. It would therefore not make much sense to tune a GPMC beyond roughly 5% (it might even be dangerous, due to overfitting). The advent of NLO Monte Carlos may reduce this number slightly, but only for quantities for which one expects NLO precision. For quantities governed by nonperturbative physics, uncertainties are larger. For some quantities, e.g. ones for which the underlying modeling is known to be poor, an order-of-magnitude agreement or worse may have to be accepted. Note further that the unitarity of shower and hadronization models implies that the Born-level cross-section normalization is not tunable, hence in tuning contexts one tends to focus on the shapes of distributions rather than their normalizations.

In the context of LO \times LL GPMC tuning, subleading aspects of coupling-constant and PDF choices are relevant. In particular, one should be aware that the choice of QCD Λ parameter $\Lambda_{\text{MC}} = 1.569\Lambda_{\overline{\text{MS}}}$ (for 5 active flavors) improves the predictions of coherent shower algorithms at the NLL level for a class of relevant observables [114], and hence this scheme is often considered the baseline for shower tuning. The question of LO vs. NLO PDFs is more involved [11], but it should be emphasized that the gluon PDF at (very) low x is important for determining the level of the underlying event in MPI models (Sec. 43.3.1), and hence the MB/UE tuning (and energy scaling [95]) is linked to the choice of PDF in such models. Further issues and an example of a specific recipe that could be followed in a realistic set-up can be found in Ref. [92]. A useful online resource can be found at the mc-plots.cern.ch website [115], based on the RIVET tool [116].

Recent years have seen the emergence of automated tools to reduce the amount of both computer and manpower required for tuning [113]. Automating the human expert input is more difficult. In the tools currently on the market, this is addressed by a combination of input solicited from the GPMC authors (e.g., which parameters and ranges to consider, which observables constitute a complete set, etc) and a set of weights determining the relative priority given to each bin in each distribution. The final result is therefore still subjective but at least reproducible. When backed by careful demonstrations of sensitivities, correlations, and uncertainties, the quality of the resulting tunes is by now competitive. The field is still burgeoning, with future sophistications to be expected.

References

- [1] G. Corcella *et al.*, JHEP **01**, 010 (2001), [hep-ph/0011363].
- [2] M. Bahr *et al.*, Eur. Phys. J. C **58**, 639 (2008), [arXiv:0803.0883].
- [3] J. Bellm *et al.*, Eur. Phys. J. C **76**, 4, 196 (2016), [arXiv:1512.01178].
- [4] T. Sjostrand, S. Mrenna and P. Z. Skands, JHEP **05**, 026 (2006), [hep-ph/0603175].
- [5] T. Sjöstrand *et al.*, Comput. Phys. Commun. **191**, 159 (2015), [arXiv:1410.3012].
- [6] T. Gleisberg *et al.*, JHEP **02**, 007 (2009), [arXiv:0811.4622].
- [7] QCD summary, PDG.
- [8] T. Kinoshita, J. Math. Phys. **3**, 650 (1962).
- [9] T. Lee and M. Nauenberg, Phys. Rev. **133**, B1549 (1964).
- [10] G. C. Fox and S. Wolfram, Nucl. Phys. B **168**, 285 (1980).

²The QED elastic cross section diverges and is normally a non-default option.

- [11] A. Buckley *et al.*, Phys. Rept. **504**, 145 (2011), [arXiv:1101.2599].
- [12] G. Altarelli and G. Parisi, Nucl. Phys. B **126**, 298 (1977).
- [13] A. Einstein, B. Podolsky and N. Rosen, Phys. Rev. **47**, 777 (1935).
- [14] B. Webber, Phys. Lett. B **193**, 91 (1987).
- [15] J. C. Collins, Nucl. Phys. B **304**, 794 (1988).
- [16] I. Knowles, Comput. Phys. Commun. **58**, 271 (1990).
- [17] T. Sjostrand, Phys. Lett. B **157**, 321 (1985).
- [18] G. Marchesini and B. Webber, Nucl. Phys. B **310**, 461 (1988).
- [19] S. Gieseke, P. Stephens and B. Webber, JHEP **12**, 045 (2003), [hep-ph/0310083].
- [20] M. Bengtsson and T. Sjostrand, Nucl. Phys. B **289**, 810 (1987).
- [21] G. Gustafson and U. Pettersson, Nucl. Phys. B **306**, 746 (1988).
- [22] L. Lonnblad, Comput. Phys. Commun. **71**, 15 (1992).
- [23] W. T. Giele, D. A. Kosower and P. Z. Skands, Phys. Rev. D **78**, 014026 (2008), [arXiv:0707.3652].
- [24] Z. Nagy and D. E. Soper, JHEP **10**, 024 (2005), [hep-ph/0503053].
- [25] S. Schumann and F. Krauss, JHEP **03**, 038 (2008), [arXiv:0709.1027].
- [26] S. Platzer and S. Gieseke, Eur. Phys. J. C **72**, 2187 (2012), [arXiv:1109.6256].
- [27] S. Höche and S. Prestel, Eur. Phys. J. C **75**, 9, 461 (2015), [arXiv:1506.05057].
- [28] T. Sjostrand and P. Z. Skands, Eur. Phys. J. C **39**, 129 (2005), [hep-ph/0408302].
- [29] M. Dasgupta *et al.*, JHEP **09**, 033 (2018), [Erratum: JHEP **03**, 083 (2020)], [arXiv:1805.09327].
- [30] M. Dasgupta *et al.*, Phys. Rev. Lett. **125**, 5, 052002 (2020), [arXiv:2002.11114].
- [31] A. Karlberg *et al.*, Eur. Phys. J. C **81**, 8, 681 (2021), [arXiv:2103.16526].
- [32] J. R. Forshaw, J. Holguin and S. Plätzer, JHEP **09**, 014 (2020), [arXiv:2003.06400].
- [33] J. R. Forshaw, J. Holguin and S. Plätzer, JHEP **08**, 145 (2019), [arXiv:1905.08686].
- [34] Z. Nagy and D. E. Soper, Phys. Rev. D **99**, 5, 054009 (2019), [arXiv:1902.02105].
- [35] E. Norrbin and T. Sjostrand, Nucl. Phys. B **603**, 297 (2001), [hep-ph/0010012].
- [36] S. Catani *et al.*, Nucl. Phys. B **627**, 189 (2002), [hep-ph/0201036].
- [37] J. Cembranos *et al.*, JHEP **09**, 077 (2013), [arXiv:1305.2124].
- [38] N. Davidson, T. Przedzinski and Z. Was, Comput. Phys. Commun. **199**, 86 (2016), [arXiv:1011.0937].
- [39] K. Hamilton and P. Richardson, JHEP **07**, 010 (2006), [hep-ph/0603034].
- [40] M. Schonherr and F. Krauss, JHEP **12**, 018 (2008), [arXiv:0810.5071].
- [41] J. R. Christiansen and T. Sjöstrand, JHEP **04**, 115 (2014), [arXiv:1401.5238].
- [42] M. R. Masouminia and P. Richardson (2021), [arXiv:2108.10817].
- [43] H. Brooks, P. Skands and R. Verheyen (2021), [arXiv:2108.10786].
- [44] A. Semenov, Comput. Phys. Commun. **180**, 431 (2009), [arXiv:0805.0555].
- [45] N. D. Christensen and C. Duhr, Comput. Phys. Commun. **180**, 1614 (2009), [arXiv:0806.4194].
- [46] M. Fairbairn *et al.*, Phys. Rept. **438**, 1 (2007), [hep-ph/0611040].
- [47] J. Alwall *et al.*, Comput. Phys. Commun. **176**, 300 (2007), [hep-ph/0609017].
- [48] P. Z. Skands *et al.*, JHEP **07**, 036 (2004), [hep-ph/0311123].
- [49] J. Alwall *et al.* (2007), [arXiv:0712.3311].
- [50] T. Ježo *et al.*, Eur. Phys. J. C **76**, 12, 691 (2016), [arXiv:1607.04538].
- [51] P. Richardson, JHEP **11**, 029 (2001), [hep-ph/0110108].
- [52] E. Boos *et al.*, in “2nd Les Houches Workshop on Physics at TeV Colliders,” (2001), [hep-ph/0109068].
- [53] M. Bengtsson and T. Sjostrand, Phys. Lett. B **185**, 435 (1987).
- [54] W. Giele, D. Kosower and P. Skands, Phys. Rev. D **84**, 054003 (2011), [arXiv:1102.2126].
- [55] S. Catani *et al.*, JHEP **11**, 063 (2001), [hep-ph/0109231].
- [56] J. Alwall *et al.*, Eur. Phys. J. C **53**, 473 (2008), [arXiv:0706.2569].
- [57] H. Brooks and C. T. Preuss, Comput. Phys. Commun. **264**, 107985 (2021), [arXiv:2008.09468].
- [58] P. Nason, JHEP **11**, 040 (2004), [hep-ph/0409146].
- [59] B. Cooper *et al.*, Eur. Phys. J. C **72**, 2078 (2012), [arXiv:1109.5295].
- [60] M. L. Mangano *et al.*, JHEP **07**, 001 (2003), [hep-ph/0206293].
- [61] J. Alwall *et al.*, JHEP **06**, 128 (2011), [arXiv:1106.0522].
- [62] S. Frixione and B. R. Webber, JHEP **06**, 029 (2002), [hep-ph/0204244].
- [63] S. Alioli *et al.*, JHEP **06**, 043 (2010), [arXiv:1002.2581].
- [64] J. Alwall *et al.*, JHEP **07**, 079 (2014), [arXiv:1405.0301].
- [65] R. Frederix and S. Frixione, JHEP **12**, 061 (2012), [arXiv:1209.6215].
- [66] L. Lönnblad and S. Prestel, JHEP **03**, 166 (2013), [arXiv:1211.7278].
- [67] K. Hamilton, P. Nason and G. Zanderighi, JHEP **10**, 155 (2012), [arXiv:1206.3572].
- [68] S. Hoeche *et al.*, JHEP **04**, 027 (2013), [arXiv:1207.5030].
- [69] S. Höche, Y. Li and S. Prestel, Phys. Rev. D **91**, 7, 074015 (2015), [arXiv:1405.3607].
- [70] K. Hamilton *et al.*, JHEP **05**, 082 (2013), [arXiv:1212.4504].
- [71] P. F. Monni *et al.*, JHEP **05**, 143 (2020), [arXiv:1908.06987].
- [72] S. Alioli *et al.*, JHEP **06**, 089 (2014), [arXiv:1311.0286].
- [73] J. Mazzitelli *et al.*, Phys. Rev. Lett. **127**, 6, 062001 (2021), [arXiv:2012.14267].
- [74] S. Alioli *et al.*, Phys. Lett. B **818**, 136380 (2021), [arXiv:21103.01214].
- [75] G. Gustafson 193–198 (1986).
- [76] X. Artru and G. Mennessier, Nucl. Phys. B **70**, 93 (1974).
- [77] B. Andersson *et al.*, Phys. Rept. **97**, 31 (1983).
- [78] B. Andersson, *The Lund model*, volume 7, Cambridge University Press (2005), ISBN 978-0-521-01734-3, 978-0-521-42094-5, 978-0-511-88149-7.
- [79] M. Bowler, Z. Phys. C **11**, 169 (1981).
- [80] C. Peterson *et al.*, Phys. Rev. D **27**, 105 (1983).
- [81] T. Sjostrand and P. Z. Skands, JHEP **03**, 053 (2004), [hep-ph/0402078].
- [82] J. R. Christiansen and P. Z. Skands, JHEP **08**, 003 (2015), [arXiv:1505.01681].
- [83] D. Amati and G. Veneziano, Phys. Lett. B **83**, 87 (1979).

- [84] A. Bassetto, M. Ciafaloni and G. Marchesini, *Phys. Lett. B* **83**, 207 (1979).
- [85] R. D. Field and S. Wolfram, *Nucl. Phys. B* **213**, 65 (1983).
- [86] B. Webber, *Nucl. Phys. B* **238**, 492 (1984).
- [87] J.-C. Winter, F. Krauss and G. Soff, *Eur. Phys. J. C* **36**, 381 (2004), [arXiv:1404.5630].
- [88] D. Lange, *Nucl. Instrum. Meth. A* **462**, 152 (2001).
- [89] S. Jadach *et al.*, *Comput. Phys. Commun.* **76**, 361 (1993).
- [90] D. Grellscheid and P. Richardson (2007), [arXiv:0710.1951].
- [91] T. Sjostrand and M. van Zijl, *Phys. Rev. D* **36**, 2019 (1987).
- [92] P. Skands, S. Carrazza and J. Rojo, *Eur. Phys. J. C* **74**, 8, 3024 (2014), [arXiv:1404.5630].
- [93] M. Bahr, J. M. Butterworth and M. H. Seymour, *JHEP* **01**, 065 (2009), [arXiv:0806.2949].
- [94] M. Ryskin, A. Martin and V. Khoze, *Eur. Phys. J. C* **71**, 1617 (2011), [arXiv:1102.2844].
- [95] H. Schulz and P. Skands, *Eur. Phys. J. C* **71**, 1644 (2011), [arXiv:1103.3649].
- [96] R. Casalbuoni *et al.*, *JHEP* **01**, 035 (2009), [arXiv:0812.1982].
- [97] (2005), [hep-ex/0511027].
- [98] L. Lonnblad and T. Sjostrand, *Eur. Phys. J. C* **2**, 165 (1998), [hep-ph/9711460].
- [99] V. Khoze *et al.*, *Eur. Phys. J. C* **69**, 85 (2010), [arXiv:1005.4839].
- [100] J. Butterworth, J. R. Forshaw and M. Seymour, *Z. Phys. C* **72**, 637 (1996), [hep-ph/9601371].
- [101] M. Bahr *et al.*, in “1st International Workshop on Multiple Partonic Interactions at the LHC,” 239–248 (2009), [arXiv:0905.4671].
- [102] R. Corke and T. Sjostrand, *JHEP* **05**, 009 (2011), [arXiv:1101.5953].
- [103] G. A. Schuler and T. Sjostrand, *Phys. Rev. D* **49**, 2257 (1994).
- [104] G. Ingelman and P. Schlein, *Phys. Lett. B* **152**, 256 (1985).
- [105] S. Navin (2010), [arXiv:1005.3894].
- [106] P. Aurenche *et al.*, *Comput. Phys. Commun.* **83**, 107 (1994), [hep-ph/9402351].
- [107] F. W. Bopp, R. Engel and J. Ranft, in “LAFEX International School on High-Energy Physics (LISHEP 98) Session A: Particle Physics for High School Teachers - Session B: Advanced School in HEP - Session C: Workshop on Diffractive Physics,” 729–741 (1998), [hep-ph/9803437].
- [108] S. Roesler, R. Engel and J. Ranft, in “International Conference on Advanced Monte Carlo for Radiation Physics, Particle Transport Simulation and Applications (MC 2000),” 1033–1038 (2000), [hep-ph/0012252].
- [109] B. E. Cox and J. R. Forshaw, *Comput. Phys. Commun.* **144**, 104 (2002), [hep-ph/0010303].
- [110] J. Bellm *et al.*, *Phys. Rev. D* **94**, 3, 034028 (2016), [arXiv:1605.08256].
- [111] S. Mrenna and P. Skands, *Phys. Rev. D* **94**, 7, 074005 (2016), [arXiv:1605.08352].
- [112] E. Bothmann, M. Schönherr and S. Schumann, *Eur. Phys. J. C* **76**, 11, 590 (2016), [arXiv:1606.08753].
- [113] A. Buckley *et al.*, *Eur. Phys. J. C* **65**, 331 (2010), [arXiv:0907.2973].
- [114] S. Catani, B. Webber and G. Marchesini, *Nucl. Phys. B* **349**, 635 (1991).
- [115] A. Karneyeu *et al.*, *Eur. Phys. J. C* **74**, 2714 (2014), [arXiv:1306.3436].
- [116] A. Buckley *et al.*, *Comput. Phys. Commun.* **184**, 2803 (2013), [arXiv:1003.0694].

44. Monte Carlo Neutrino Generators

Revised September 2021 by H. Gallagher (Tufts U.) and Y. Hayato (Kamioka Observatory, ICRR, UTokyo; Kavli IPMU (WPI), UTokyo).

Monte Carlo neutrino generators are programs or libraries which simulate neutrino interactions with electrons, nucleons and nuclei. In this capacity their usual task is to take an input neutrino and nucleus and produce a set of 4-vectors for particles emerging from the interaction, which are then input to full detector simulations. Since these generators have to simulate not only the initial interaction of neutrinos with target particles, but re-interactions of the generated particles in the nucleus, they contain a wide range of elementary particle and nuclear physics. Viewed more broadly, they are the access point for neutrino experimentalists to the theory inputs needed for analysis. Examples include cross section libraries for event rate calculations and parameter uncertainties and reweighting tools for systematic error evaluation.

Neutrino experiments typically operate in neutrino beams that are neither completely pure nor mono-energetic. Generators are a crucial component in the convolution of beam flux, neutrino interaction physics, and detector response that is necessary to make predictions about observable quantities. Generated events are used to define experimental analyses, like event selection criteria, for efficiency determination and background subtraction. Similarly they are used to relate reconstructed quantities back to true quantities. In these various capacities they are used from the detector design stage through the extraction of physics measurements from reconstructed observable. Monte Carlo neutrino generators play unique and important roles in the experimental study of neutrino interactions and oscillations.

There are several neutrino event generators available, such as ANIS [1], GENIE [2, 3], GiBUU [4, 5], MARLEY [6], NEGN [7], NEUT [8], NUANCE [9], the FLUKA routines NUNDIS/-NUNRES [10, 11], and NuWro [12], as well as tools to facilitate cross-generator comparisons, such as NUISANCE [13]. Historically, experiments would develop their own generators. This was often because they were focused on a particular measurement, energy range, or target, and wanted to ensure that the best physics was included for them. These ‘home-grown’ generators were often tuned primarily or exclusively to the neutrino data most similar to the data that the experiment would be collecting. A major advance in the field was the introduction of conference series devoted to the topic of neutrino interaction physics, NuINT (<https://indico.cern.ch/event/703880/>) and NuFACT (<https://indico.cern.ch/event/855372/>) in particular. Event generator comparisons have been a regular staple of the NuINT conference series from its inception, and a great deal of information on this topic can be found in the Proceedings of these meetings. These meetings have facilitated experiment-theory discussions leading to the first generator developed by a theory group (NuWro) [12], the extension of established nuclear interaction codes (FLUKA and GiBUU) to include neutrino-nuclear processes [4, 5, 10, 11], and inclusion of theorists in existing generator development teams.

These activities have led to more careful scrutiny of the crucial hadron and nuclear theory inputs to these generators, which is evaluated in particular through comparisons to electron-scattering data. At this point in time all simulation codes face challenges in describing the full extent of the lepton scattering data, and the tension between incorporating the best available theory versus obtaining the best agreement with the data plays out in a variety of ways within the field. For the field to make progress, inclusion of state of the art theory needs to be coupled to global analyses that correctly incorporate correlations between measurements. Given the rapid pace of new data and the complexity of analyses, this is a significant challenge for the field in the coming years.

There are many neutrino experiments which use various sources of neutrinos, from reactors, accelerators, the atmosphere, and astrophysical sources, thereby covering a range of energies from MeV to TeV. Much of the emphasis has been on the few-GeV region in the generators, as this is the relevant energy range for short- and long-baseline neutrino oscillation experiments. These gen-

erators use the impulse approximation, which treats the nucleus as a collection of independent nucleons and the primary interaction occurs between the probe and a single nucleon, for most of the initial interaction, and subsequently simulates the interactions of secondary particles in the nucleus in semi-classical ways. Semi-classical hadron transport approaches are commonly used as they are able to simulate a variety of nuclei in a single model, fully describe complex multi-particle final states, and for practical considerations as these approaches are fast. However, there are several challenges facing these simulations coming mainly from the complexity of the nuclear physics, and the need to avoid double counting in combining perturbative and non-perturbative models for the neutrino-nucleon scattering processes. The overall validity of this impulse approximation-based scheme, and in particular the importance of scattering channels that involve more than one nucleon, is a crucial question that is the topic of much current work. While generators share many common ingredients, differences in implementation, parameter values, and approaches to avoid double counting can yield dramatically different predictions [14]. In the following sections, interaction models and their implementations, including final-state interactions of hadrons produced in the nuclei, are described.

In order to assure their validity, neutrino event generators are tuned and validated against a wide variety of data. This means that the quality of the outputs from generators is limited by the quality of experimental data. The existing neutrino-nucleon and neutrino-nucleus scattering data sets are not restrictive enough to eliminate many approaches. On the other hand, there are various precise data sets, which use photon, charged lepton, and hadron probes. These data sets are extensively used to validate the generators. The results from these external data tuning exercises are important for experiments as they quantify the uncertainty on model parameters, needed by experiments in the evaluation of generator-related systematic errors. Electron scattering data plays an important role in determining the vector contribution to the form-factors and structure functions, as well as in evaluating specific aspects of the nuclear model [15, 16]. Hadron scattering data is used in validating the nuclear model, in particular of interactions between hadrons produced in the primary interaction and the residual target nucleus (final state interactions). As mentioned, tuning of neutrino-nucleon scattering and hadronization models relies heavily on the previous generation of high energy neutrino scattering and hydrogen and deuterium bubble chamber experiments. More recent data from the K2K, MiniBooNE, NOMAD, SciBooNE, MINOS, T2K, ArgoNEUT, MINERvA, NOvA, MicroBooNE, ICARUS, SBND and Ninja experiments has been, or will be, used for this purpose, although caution is advisable due to possible biases that mis-modeled nuclear effects might introduce. In practice, there are often choices to be made about which models to include in an overall simulation, and which data sets to use for tuning. The process of developing a comprehensive tune in GENIE is discussed in Ref. [3].

However, all the recent experiments use nuclear targets and it is challenging to disentangle the neutrino-nucleon interaction from the effects of the nuclear environment. For example, it is difficult to separate charged current quasi-elastic scattering from the multi-nucleon quasi-elastic like scattering or single pion production, in which a pion is absorbed in the nucleus. Sometimes, there are tensions between the data sets from different experiments. Data on multi-pion and meson production are limited, but are anticipated to be measured in the near future experiments. Next generation experiments are expected to provide better detection capabilities with higher statistics and these data will help in evaluating and validating the models implemented in the generators.

44.1 Neutrino-Nucleon Scattering

Event generators typically begin with free-nucleon cross sections which are then embedded into a nuclear physics model. The most important processes are quasi-elastic (elastic for neutral current (NC)) scattering, resonance production, and non-resonant inelastic scattering, which make comparable contributions for few-GeV interactions. The neutrino cross sections in this energy range can be seen in Figure 52.1 of this *Review*.

44.1.1 Quasi-Elastic Scattering

The cross section for the neutrino nucleon charged current quasi-elastic scattering is described in terms of the leptonic and hadronic weak currents, where dominant contributions to the hadronic current come from the vector (V) and axial-vector (A) form factors. Contributions from the pseudo-scalar form factor (P) are typically small for muon and electron neutrinos and are related to the axial form factor (A) assuming partially conserved axial currents (PCAC). Owing to isospin symmetry, the vector form factors are related to those measured by precise electron scattering experiments [17]. Therefore, most of the generators use parametrizations of these form factors taken directly from the data. For the axial form factor there is no such precise experiment, and most of the generators use a dipole form [18]. Generally, the value of axial form factor at $q^2 = 0$ (q is the four-momentum transfer) is extracted from the polarized nucleon beta decay experiment. However, the selection of the axial vector mass parameter depends on each generator, with values typically around 1.00 GeV/c². Recently, there are several attempts to use the other functions for the axial form factors [19, 20] and some generators have already implemented these form factors [8, 21].

44.1.2 Inelastic Production

Most generators use the prescriptions of Rein-Sehgal [22] to simulate neutrino-induced single pion production, or updated versions that incorporate lepton mass terms and pion pole contributions [23, 24]. To obtain the cross section for a particular channel, they calculate the amplitude for the production of each resonance multiplied by the probability for the decay of that resonance into that particular channel. Implementation differences include the number of resonances included, whether the amplitudes are added coherently or incoherently, the invariant mass range over which the model is used, how non-resonant backgrounds are included, inclusion of lepton mass terms, and the model parameter values (in particular the axial mass). In this model it is also possible to calculate the cross-sections of single photon, and η production by changing the decay probability of the resonances, which are included in some of the programs. However, it is known that discrepancies exist between the recent pion electro/photo-production data and the results from the simulation data with the same framework, i.e. vector part of this model. There are several attempts to overcome this issue [25] and some of the generators started using more appropriate form factors. Recently, there are approaches that improve the theoretical description of non-resonant contributions in the resonance region, [26–28], and which account for interference between resonant and non-resonant amplitudes. This work is expected to be implemented in the generators soon. GiBUU and NuWro generators do not use the Rein-Sehgal model, and instead rely directly on electro-production data for the vector contribution and fit bubble chamber data to determine the remaining parameters for the axial contribution [29–32]. The dynamical coupled-channel model, which has been developed to simulate various electro- and photo-meson productions, was extended to simulate the neutrino single pion production [33]. In this approach pion-nucleon scattering is used to fix the form of the axial current at $q^2 = 0$. This model is also being implemented and expected to be available in some of the generators in future.

44.1.3 Deep and Shallow Inelastic Scattering

For this process the fundamental target shifts from the nucleon to its quark constituents. Therefore, the generators construct the nucleon structure functions F_2 and xF_3 from parton distributions for high Q^2 (the DIS regime: $W \gtrsim 2$ GeV/c² and $Q^2 \gtrsim 1$ GeV²) to calculate the direction and momentum of the lepton. The first challenge is in extending this picture to the lower values of Q^2 and W that dominate the available phase space for few-GeV interactions (the so-called ‘shallow inelastic scattering’, or SIS regime). GRV98LO parton distribution functions [34] with the corrections proposed in [35, 36] are widely used, while others [10] implement their own modifications to the parton distributions at low Q^2 . Both DIS and SIS generate hadrons but their production depends on each generator’s implementation of a hadronization model as described in the next section. There are various difficulties not only in the actual hadronization but the relation with the single

meson production. It is necessary to avoid double counting between the resonance and SIS/DIS models, and all generators are different in this regard. The scheme chosen can have a significant impact on the results of simulations at a few-GeV neutrino energies. For simulating ultra-high energy interactions currently being studied with neutrino telescopes, fully partonic descriptions, which utilize beyond-leading-order pQCD calculations [37, 38] are the norm [39].

44.2 Hadronization Models

For hadrons produced via baryonic resonances, the underlying model amplitudes and resonance branching fractions can be used to fully characterize the hadronic system. For shallow- and deep-inelastic scattering, a hadronization model is required. Most generators use PYTHIA [40] for this purpose, although some with modified parameters. In addition some implement their own models to handle invariant masses that are too low for PYTHIA, typically somewhere around 2.0 GeV/c². Such models rely heavily on measurements of neutrino hadro-production in high-resolution devices, such as bubble chambers and the CHORUS [41] and NOMAD experiments [42], to construct empirical parametrizations that reproduce the key features of the data [43, 44]. The basic ingredients are the empirical observations that average charged particle multiplicities increase logarithmically with the invariant mass of the hadronic system, and that the distribution of charged particle multiplicities about this average are described by a single function (an observation known as KNO scaling [45]). The multiplicity of the neutral particles are usually obtained by scaling the charged particle multiplicity. Simple parametrizations to more accurately reproduce differences observed in the forward/backward hemispheres of hadronic systems are included in GENIE, NEUT, and NuWro.

44.3 Nuclear Physics

The nuclear physics relevant to neutrino-nucleus scattering at few-GeV energies is complicated, involving Fermi motion, nuclear binding, Pauli blocking, in-medium modifications of form factors and hadronization, intranuclear rescattering of hadrons, and many-body scattering mechanisms including long- and short-range nucleon-nucleon correlations.

44.3.1 Treatment of nuclear effects

In order to obtain the cross-section off nucleons in the nucleus, it is necessary to take into account various in-medium effects. Most of the models used for neutrino-nuclear scattering kinematics were developed in the context of few-GeV inclusive electron scattering, by experiments going back nearly 50 years. The basic models employed in event generators rely on impulse approximation schemes, the most simple of which is the Relativistic Fermi Gas Model. The most common implementations have been the Smith-Moniz [46] and Bodek-Ritchie [47] models. However, the results from neutrino-nucleus scattering experiments in 2000 and afterwards, beginning with K2K, MiniBooNE have shown large discrepancies from the naive expectation from the models. Most striking differences are a suppression of forward going muons (low Q^2), a high Q^2 enhancement in the event rate, and an overall larger than expected number of observed events. In order to reproduce the data, the quasi-elastic axial mass was used as the effective parameter and increased by roughly 20% from the nominal values obtained by an earlier generation of bubble chamber experiments using hydrogen or deuterium [18]. This inconsistency between nucleon and nucleus targets suggests that the simple nuclear model is not appropriate in describing the data. Moreover, these simple Fermi-Gas models are not expected to describe the kinematical distributions of final state nucleons. Therefore, several generators have to implement better models, such as local Fermi-Gas model or more sophisticated models. Within the electron scattering community, the analogous calculations have for decades relied on spectral functions, which incorporate information about nucleon momenta and binding energies in the impulse approximation scheme [15]. Therefore, most of the generators have implemented the realistic spectral functions in their latest releases.

Actually, the discrepancies in small q^2 could not be solved alone

by just introducing the local Fermi-gas model nor spectral function models. This implies that the additional medium correction effects are needed to be taken into account. One of the implemented solutions is the local Fermi-Gas model with medium correction calculated using the random phase approximation, which is known to give large suppression in small q^2 [48,49]. Although, the fundamental parts of the models are same, actual implementations are quite different between the generators. Especially, the constructions of the final state hadron kinematics are quite different. Especially for the quasi-elastic scattering case, treatment of the nucleon masses in the nucleus, the binding and the separation energies are sometimes quite different [50]. Recently, Super-Scaling model with relativistic mean field theory effects (SuSAv2) [51, 52] is implemented in some of the generators. Indications of the suppression in small q^2 in the single pion productions were also observed in K2K and MiniBooNE and it is clearly observed at the MINER ν A and NO ν A experiments. However, the models to explain the suppression have not been implemented, other than the phenomenological ones. Also, q^2 dependence of the cross-section is largely model and parameter dependent. Further studies of newly implemented single pion models may give new insights. The cause of the discrepancy of small q^2 seems to be identified but the issue of the observed interaction rates are not solved. This implies that there must be some interaction channels which are missing and not considered in the generators.

These led to a revisit of the role played by excitation of multiple particle-hole states in the nucleus, and the experimental study of these scattering channels is an area of intense experimental interest [53]. The contribution of these scattering processes is an extremely active area of theoretical research as well, with significant implications for generators and analyses [54]. Several approaches, ranging from strictly phenomenological descriptions to full theoretical calculations, have recently been incorporated into generators [55–57]. One example of a phenomenological approach utilizes an Effective Spectral Function [58] and a Transverse Enhancement Model [59], which together encapsulate information derived from electron scattering experiments at relevant kinematics. The microscopic model of Nieves and collaborators is now available in GENIE and NEUT [60,61]. SuSAv2 model [52] also has capability to simulate this multi-nucleon quasi-elastic like interaction and is also implemented in GENIE.

One of the challenges in incorporating full theoretical models of these processes is that they are typically slow, so generators have developed new approaches whereby much of the computation is done offline, and the generators simply read in the hadronic tensor components. This allows for a full prediction of the lepton kinematics, however the ability to simulate the hadronic component of these multinucleon states then relies on separate models. The other challenge is that the theoretical models are not designed to describe exclusive final states. These approaches, while making simulations computationally tractable, neglect correlations between the lepton and hadron kinematics. Also, there are limitations of the model itself to describe some of the kinematic regions. However, the generators need to simulate final all the state particles and thus, several assumptions are made by authors of the generators from time to time.

Also, it is known from photo and electro-nuclear scattering that the Delta width is affected by Pauli blocking and collisional broadening. These effects are included in some, but not all generators.

The remnant nucleus after the scattering is usually in an excited state. Therefore, the remnant may emit gamma-rays, additional nucleons or an alpha particle during the de-excitation process. This de-excitation gamma-ray is used in searching for proton decay in water Cherenkov detectors. Some generators have implemented this process. NEUT implemented the de-excitation process but only for Oxygen. Recently, GENIE has de-excitation processes for various nuclei.

When scattering from a nucleus, coherent scattering of various kinds is possible. Most simulations incorporate, at least, coherent neutral and charged single pion production. While the interaction rate for these interactions is typically around a percent of the total yield, the unique kinematic features of these events can make them potential backgrounds for oscillation searches. Imple-

mented in Monte Carlo are several PCAC-based methods [62,63]. Microscopic models, valid at lower neutrino energies [64–67], have also been implemented in several generators. One commonly used model by Rein and Sehgal [62] predicts a cross section for charged-current coherent pion production that is much larger than what is observed by K2K, MINER ν A and T2K. However, the cross-section is sensitive to the pion cross-section used in the model as parameters and improved models with lepton mass correction [63] give better agreement with the recent data. This improved model is implemented in most of the generators. In addition to coherent pion production, some generators can simulate coherent single photon production [68] and coherent elastic neutrino-nucleus scattering.

44.3.2 Hadron Production in Nuclei

Neutrino pion production is one of the dominant neutrino scattering mechanisms in the few-GeV region and the pions produced in the nucleus have quite large interaction cross sections. Therefore, pion intranuclear scattering can have sizable effects on the results of simulations at these energies. Also, recent neutrino oscillation experiments use the observed information of protons and pions more extensively, in addition to the charged leptons. Therefore, most generators implement this physics through an intranuclear cascade simulation. In generators which utilize cascade models, a hadron, which has been formed in the nucleus, is moved step by step until it interacts with a nucleon or escapes from the nucleus. The probabilities of each interaction in nucleus are usually given as the mean free paths and used to determine whether the hadron has interacted or not. If the hadron is found to have interacted, appropriate final states are selected. Usually, absorption, elastic, charge exchange, and inelastic scatterings including particle productions are simulated as intranuclear interactions. The determination method of the kinematics for the final state particles heavily depends on the generators but most of them use experimentally validated models to simulate hadron interactions in nucleus. No two intranuclear cascade simulations implemented in neutrino event generators are the same [69]. In all cases hadrons propagate from an interaction vertex chosen based on the density distribution of the target nucleus. In determining the generated position of the hadrons in nucleus, the concept of the formation length is sometimes employed. Based on this idea, the hadronization process is not instantaneous and it takes some time before generating the hadrons [12]. The basis for formation times are measurements at relatively high energy and Q^2 , and most generators that employ the concept do not apply them to resonance interactions.

GiBUU does not employ an intranuclear cascade simulation, instead, it utilizes a semi-classical transport model in coupled channels that describes the space-time evolution of a many body system in the presence of potentials and a collision term [4]. This approach assures consistency between nuclear effects in the initial state, such as Fermi motion, Pauli blocking, hadron self-energies [70], and modified cross sections, and the final state, such as particle re-interactions, since the two are derived from the same model. This model has been previously used to describe a wide variety of nuclear interaction data. Similarly, the hadronic simulation of the NUNDIS/NUNRES programs are handled by the well-established FLUKA hadronic simulation package [10]. Recently, GENIE included the interface to the external hadronic simulation package INCL++ [71].

References

- [1] A. Gazizov and M. P. Kowalski, *Comput. Phys. Commun.* **172**, 203 (2005), [arXiv:astro-ph/0406439].
- [2] C. Andreopoulos *et al.*, *Nucl. Instrum. Meth.* **A614**, 87 (2010), [arXiv:0905.2517].
- [3] J. Tena-Vidal *et al.* (GENIE) (2021), [arXiv:2104.09179].
- [4] O. Buss *et al.*, *Phys. Rept.* **512**, 1 (2012), [arXiv:1106.1344].
- [5] K. Gallmeister, U. Mosel and J. Weil, *Phys. Rev.* **C94**, 3, 035502 (2016), [arXiv:1605.09391].
- [6] S. Gardiner, C. Grant, E. Panic, and R. Svoboda, <http://www.marleygen.org>.
- [7] D. Autiero, *Nucl. Phys. Proc. Suppl.* **139**, 253 (2005).

- [8] Y. Hayato and L. Pickering, *Eur. Phys. J. Spec. Top.* (2021), [arXiv:2106.15809].
- [9] D. Casper, *Nucl. Phys. Proc. Suppl.* **112**, 161 (2002), [hep-ph/0208030].
- [10] G. Battistoni *et al.*, *Acta Phys. Polon.* **B40**, 2491 (2009).
- [11] T. T. Böhlen *et al.*, *Nucl. Data Sheets* **120**, 211 (2014).
- [12] T. Golan, C. Juszczak and J. T. Sobczyk, *Phys. Rev.* **C86**, 015505 (2012), [arXiv:1202.4197].
- [13] P. Stowell *et al.*, *JINST* **12**, 01, P01016 (2017), [arXiv:1612.07393].
- [14] M. Betancourt *et al.*, *Phys. Rept.* **773-774**, 1 (2018), [arXiv:1805.07378].
- [15] O. Benhar, D. Day and I. Sick, *Rev. Mod. Phys.* **80**, 189 (2008), [arXiv:nucl-ex/0603029].
- [16] B. Schmookler *et al.* (CLAS), *Nature* **566**, 7744, 354 (2019), [arXiv:2004.12065].
- [17] A. Bodek *et al.*, *Eur. Phys. J.* **C53**, 349 (2008), [arXiv:0708.1946].
- [18] H. Gallagher, G. Garvey and G. P. Zeller, *Ann. Rev. Nucl. Part. Sci.* **61**, 355 (2011).
- [19] E. Tomasi-Gustafsson, G. I. Gakh and C. Adamuscin, *Phys. Rev.* **C73**, 045204 (2006), [arXiv:nucl-th/0512039].
- [20] B. Bhattacharya, R. J. Hill and G. Paz, *Phys. Rev.* **D84**, 073006 (2011), [arXiv:1108.0423].
- [21] A. S. Meyer *et al.*, *Phys. Rev.* **D93**, 11, 113015 (2016), [arXiv:1603.03048].
- [22] D. Rein and L. M. Sehgal, *Annals Phys.* **133**, 79 (1981).
- [23] K. S. Kuzmin, V. V. Lyubushkin and V. A. Naumov, *Mod. Phys. Lett. A* **19**, 2815 (2004), [hep-ph/0312107].
- [24] C. Berger and L. M. Sehgal, *Phys. Rev. D* **76**, 113004 (2007), [arXiv:0709.4378].
- [25] K. M. Graczyk and J. T. Sobczyk, *Phys. Rev.* **D77**, 053001 (2008), [Erratum: *Phys. Rev. D* **79**, 079903 (2009)], [arXiv:0707.3561].
- [26] M. Kabirnezhad, *Phys. Rev.* **D97**, 1, 013002 (2018), [arXiv:1711.02403].
- [27] M. Kabirnezhad, *Phys. Rev. D* **102**, 5, 053009 (2020), [arXiv:2006.13765].
- [28] E. Hernandez, J. Nieves and M. Valverde, *Phys. Rev. D* **76**, 033005 (2007), [hep-ph/0701149].
- [29] O. Lalakulich and E. A. Paschos, *Phys. Rev.* **D71**, 074003 (2005), [hep-ph/0501109].
- [30] J. A. Nowak, *Phys. Scripta* **T127**, 70 (2006), [hep-ph/0607081].
- [31] T. Leitner *et al.*, *Phys. Rev. C* **79**, 034601 (2009), [arXiv:0812.0587].
- [32] L. Alvarez-Ruso, S. K. Singh and M. J. Vicente Vacas, *Phys. Rev.* **C57**, 2693 (1998), [arXiv:nucl-th/9712058].
- [33] S. X. Nakamura, H. Kamano and T. Sato, *Phys. Rev.* **D92**, 7, 074024 (2015), [arXiv:1506.03403].
- [34] M. Glück, E. Reya and A. Vogt, *Eur. Phys. J.* **C5**, 461 (1998), [hep-ph/9806404].
- [35] A. Bodek and U. K. Yang, *J. Phys.* **G29**, 1899 (2003), [hep-ex/0210024].
- [36] A. Bodek, U. K. Yang and Y. Xu (2021), [arXiv:2108.09240].
- [37] A. Cooper-Sarkar, P. Mertsch and S. Sarkar, *JHEP* **08**, 042 (2011), [arXiv:1106.3723].
- [38] V. Bertone, R. Gauld and J. Rojo, *JHEP* **01**, 217 (2019), [arXiv:1808.02034].
- [39] A. Garcia and A. Heijboer (KM3NeT), *PoS ICRC2019*, 895 (2020), [arXiv:1908.10077].
- [40] T. Sjostrand, S. Mrenna and P. Z. Skands, *JHEP* **05**, 026 (2006), [hep-ph/0603175].
- [41] A. Kayis-Topaksu *et al.* (CHORUS), *Eur. Phys. J.* **C51**, 775 (2007), [arXiv:0707.1586].
- [42] J. Altegoer *et al.* (NOMAD), *Phys. Lett.* **B445**, 439 (1999).
- [43] T. Yang *et al.*, *Eur. Phys. J.* **C63**, 1 (2009), [arXiv:0904.4043].
- [44] J. A. Nowak and J. T. Sobczyk, *Acta Phys. Polon.* **B37**, 2371 (2006), [hep-ph/0608108].
- [45] Z. Koba, H. B. Nielsen and P. Olesen, *Nucl. Phys.* **B40**, 317 (1972).
- [46] R. A. Smith and E. J. Moniz, *Nucl. Phys.* **B43**, 605 (1972), [Erratum: *Nucl. Phys.* **B101**, 547 (1975)].
- [47] A. Bodek and J. L. Ritchie, *Phys. Rev.* **D24**, 1400 (1981).
- [48] M. C. Martinez *et al.*, *Phys. Rev. C* **73**, 024607 (2006), [arXiv:nucl-th/0505008].
- [49] J. Nieves, J. E. Amaro and M. Valverde, *Phys. Rev. C* **70**, 055503 (2004), [Erratum: *Phys. Rev. C* **72**, 019902 (2005)], [arXiv:nucl-th/0408005].
- [50] A. Bodek and T. Cai, *Eur. Phys. J. C* **79**, 4, 293 (2019), [arXiv:1801.07975].
- [51] J. A. Caballero *et al.*, *Phys. Lett.* **B653**, 366 (2007), [arXiv:0705.1429].
- [52] R. González-Jiménez *et al.*, *Phys. Rev. C* **90**, 3, 035501 (2014), [arXiv:1407.8346].
- [53] X. G. Lu *et al.* (MINERvA) (2021), [arXiv:2107.02064].
- [54] L. Alvarez-Ruso *et al.*, *Prog. Part. Nucl. Phys.* **100**, 1 (2018), [arXiv:1706.03621].
- [55] T. Katori, *AIP Conf. Proc.* **1663**, 1, 030001 (2015), [arXiv:1304.6014].
- [56] M. Alam *et al.* (2015), [arXiv:1512.06882].
- [57] C. Wilkinson *et al.*, *Phys. Rev.* **D93**, 7, 072010 (2016), [arXiv:1601.05592].
- [58] A. Bodek, M. E. Christy and B. Coopersmith, *Eur. Phys. J.* **C74**, 10, 3091 (2014), [arXiv:1405.0583].
- [59] A. Bodek, H. S. Budd and M. E. Christy, *Eur. Phys. J.* **C71**, 1726 (2011), [arXiv:1106.0340].
- [60] J. Nieves, I. Ruiz Simo and M. J. Vicente Vacas, *Phys. Rev.* **C83**, 045501 (2011), [arXiv:1102.2777].
- [61] R. Gran *et al.*, *Phys. Rev.* **D88**, 11, 113007 (2013), [arXiv:1307.8105].
- [62] D. Rein and L. M. Sehgal, *Nucl. Phys.* **B223**, 29 (1983).
- [63] C. Berger and L. M. Sehgal, *Phys. Rev.* **D79**, 053003 (2009), [arXiv:0812.2653].
- [64] L. Alvarez-Ruso *et al.*, *Phys. Rev.* **C75**, 055501 (2007), [Erratum: *Phys. Rev. C* **80**, 019906 (2009)], [arXiv:nucl-th/0701098].
- [65] L. Alvarez-Ruso, L. S. Geng and M. J. Vicente Vacas, *Phys. Rev.* **C76**, 068501 (2007), [Erratum: *Phys. Rev. C* **80**, 029904 (2009)], [arXiv:0707.2172].
- [66] J. E. Amaro *et al.*, *Phys. Rev. D* **79**, 013002 (2009), [arXiv:0811.1421].
- [67] S. X. Nakamura *et al.*, *Phys. Rev. C* **81**, 035502 (2010), [arXiv:0910.1057].
- [68] E. Wang, L. Alvarez-Ruso and J. Nieves, *Phys. Rev. C* **89**, 1, 015503 (2014), [arXiv:1311.2151].
- [69] S. Dytman *et al.*, *Phys. Rev. D* **104**, 5, 053006 (2021), [arXiv:2103.07535].
- [70] S. K. Singh, M. J. Vicente-Vacas and E. Oset, *Phys. Lett. B* **416**, 23 (1998), [Erratum: *Phys. Lett. B* **423**, 428 (1998)].
- [71] A. Boudard *et al.*, *Phys. Rev. C* **87**, 014606 (2013), URL <https://link.aps.org/doi/10.1103/PhysRevC.87.014606>.

45. Monte Carlo Particle Numbering Scheme

Revised August 2021 by F. Krauss (Durham U.), S. Navas (Granada U.), P. Richardson (Durham U.) and T. Sjöstrand (Lund U.).

The Monte Carlo particle numbering scheme presented here is intended to facilitate interfacing between matrix-element generators, event generators, detector simulators, and analysis packages used in particle physics, and is widely accepted as the “industry standard”. The numbering scheme was introduced in 1988 [1], and has since been revised and expanded in the light of new information on hadronic resonances, and expanded to encompass as yet undiscovered and hypothetical particles.

The general form is a 7-digit number:

$$\pm n \ n_r \ n_L \ n_{q_1} \ n_{q_2} \ n_{q_3} \ n_J .$$

This encodes information about the particle’s spin, flavor content, and internal quantum numbers. A 9-digit extension is used specifically for tetra- and penta-quark states, and a distinct 10-digit scheme is used for encoding (hyper)nuclear states. The details are as follows:

1. Particles are given positive numbers, antiparticles negative numbers. The PDG convention for mesons is used, so that K^+ and B^+ are particles.
2. Quarks and leptons are numbered consecutively starting from 1 and 11 respectively; to do this they are first ordered by family and within families by weak isospin.
3. In composite quark systems (diquarks, mesons, and baryons) $n_{q_{1-3}}$ are quark numbers used to specify the quark content, while the rightmost digit $n_J = 2J + 1$ gives the system’s spin (except for the K_S^0 and K_L^0). The scheme does not cover particles of spin $J > 4$.
4. Diquarks have 4-digit numbers with $n_{q_1} \geq n_{q_2}$ and $n_{q_3} = 0$.
5. The numbering of mesons is guided by the nonrelativistic (L - S decoupled) quark model, as listed in Tables 15.2, 15.3, and 15.4.
 - (a) The numbers specifying the meson’s quark content conform to the convention $n_{q_1} = 0$ and $n_{q_2} \geq n_{q_3}$. The special case K_L^0 is the sole exception to this rule.
 - (b) The quark numbers of flavorless, light (u, d, s) mesons are: 11 for the member of the isotriplet (π^0, ρ^0, \dots), 22 for the lighter isosinglet (η, ω, \dots), and 33 for the heavier isosinglet (η', ϕ, \dots). Since isosinglet mesons are often large mixtures of $u\bar{u} + d\bar{d}$ and $s\bar{s}$ states, 22 and 33 are assigned by mass and do not necessarily specify the dominant quark composition.
 - (c) The special numbers 310 and 130 are given to the K_S^0 and K_L^0 respectively.
 - (d) The fifth digit n_L is reserved to distinguish mesons of the same total (J) but different spin (S) and orbital (L) angular momentum quantum numbers. For $J > 0$ the numbers are: $(L, S) = (J - 1, 1)$ $n_L = 0$, $(J, 0)$ $n_L = 1$, $(J, 1)$ $n_L = 2$ and $(J + 1, 1)$ $n_L = 3$. For the exceptional case $J = 0$ the numbers are $(0, 0)$ $n_L = 0$ and $(1, 1)$ $n_L = 1$ (*i.e.* $n_L = L$). See Table 45.1.
 - (e) If a set of physical mesons correspond to a (non-negligible) mixture of basis states, differing in their internal quantum numbers, then the lightest physical state gets the smallest basis state number. For example the $K_1(1270)$ is numbered 10313 ($1^1P_1 K_{1B}$) and the $K_1(1400)$ is numbered 20313 ($1^3P_1 K_{1A}$).
 - (f) The sixth digit n_r is used to label mesons radially excited above the ground state.
 - (g) Numbers have been assigned for complete $n_r = 0$ S - and P -wave multiplets, even where states remain to be identified.
 - (h) In some instances assignments within the $q\bar{q}$ meson model are only tentative; here best guess assignments are made.

Table 45.1: Meson numbering logic. Here qq stands for $n_{q_2} n_{q_3}$.

J	$L = J - 1, S = 1$			$L = J, S = 0$			$L = J, S = 1$			$L = J + 1, S = 1$		
	code	J^{PC}	L	code	J^{PC}	L	code	J^{PC}	L	code	J^{PC}	L
0	—	—	—	00qq1	0 ⁻⁺	0	—	—	—	10qq1	0 ⁺⁺	1
1	00qq3	1 ⁻⁻	0	10qq3	1 ⁺⁻	1	20qq3	1 ⁺⁺	1	30qq3	1 ⁻⁻	2
2	00qq5	2 ⁺⁺	1	10qq5	2 ⁻⁺	2	20qq5	2 ⁻⁻	2	30qq5	2 ⁺⁺	3
3	00qq7	3 ⁻	2	10qq7	3 ⁺⁻	3	20qq7	3 ⁺⁺	3	30qq7	3 ⁻	4
4	00qq9	4 ⁺⁺	3	10qq9	4 ⁻⁺	4	20qq9	4 ⁻⁻	4	30qq9	4 ⁺⁺	5

- (i) Many states appearing in the Meson Listings are not yet assigned within the $q\bar{q}$ model. Here $n_{q_{2-3}}$ and n_J are assigned according to the state’s likely flavors and spin; all such unassigned light isoscalar states are given the flavor code 22. Within these groups $n_L = 0, 1, 2, \dots$ is used to distinguish states of increasing mass. These states are flagged using $n = 9$. It is to be expected that these numbers will evolve as the nature of the states are elucidated. Codes are assigned to all mesons which are listed in the one-page table at the end of the Meson Summary Table as long as they have a preferred or established spin. Additional heavy meson states expected from heavy quark spectroscopy are also assigned codes.
6. The numbering of baryons is again guided by the nonrelativistic quark model, see Table 15.6. This numbering scheme is illustrated through a few examples in Table 45.2.
 - (a) The numbers specifying a baryon’s quark content are such that in general $n_{q_1} \geq n_{q_2} \geq n_{q_3}$.
 - (b) Two states exist for $J = 1/2$ baryons containing 3 different types of quarks. In the lighter baryon ($\Lambda, \Xi, \Omega, \dots$) the light quarks are in an antisymmetric ($J = 0$) state while for the heavier baryon ($\Sigma^0, \Xi', \Omega', \dots$) they are in a symmetric ($J = 1$) state. In this situation n_{q_2} and n_{q_3} are reversed for the lighter state, so that the smaller number corresponds to the lighter baryon.
 - (c) For excited baryons a scheme is adopted, where the n_r label is used to denote the excitation bands in the harmonic oscillator model, see Sec. 15.5. Using the notation employed there, n_r is given by the N -index of the D_N band identifier.
 - (d) Further degeneracies of excited hadron multiplets with the same excitation number n_r and spin J are lifted by labelling such multiplets with the n_L index according to their mass, as given by its N or Δ -equivalent.
 - (e) In such excited multiplets extra singlets may occur, the $\Lambda(1520)$ being a prominent example. In such cases the ordering is reversed such that the heaviest quark label is pushed to the last position: $n_{q_3} > n_{q_1} > n_{q_2}$.
7. The gluon, when considered as a gauge boson, has official number 21. In codes for glueballs, however, 9 is used to allow a notation in close analogy with that of hadrons.
8. The pomeron and odderon trajectories and a generic reggeon trajectory of states in QCD are assigned codes 990, 9990, and 110 respectively, where the final 0 indicates the indeterminate nature of the spin, and the other digits reflect the expected “valence” flavor content. We do not attempt a complete classification of all reggeon trajectories, since there is currently no need to distinguish a specific such trajectory from its lowest-lying member.
9. Two-digit numbers in the range 21–30 are provided for the Standard Model gauge and Higgs bosons.
10. Codes 81–100 are reserved for generator-specific pseudoparticles and concepts. Codes 901–930, 1901–1930, 2901–2930, and 3901–3930 are for additional components of Standard Model parton distribution functions, where the latter three ranges are intended to distinguish left/ right/ longitudinal components. Codes 998 and 999 are reserved for GEANT tracking purposes.

Table 45.2: Some examples of octet (top) and decuplet (bottom) members for the numbering scheme for excited baryons. Here qqq stands for $n_{q_1}n_{q_2}n_{q_3}$. See the text for the definition of the notation. The numbers in parenthesis correspond to the mass of the baryons. The states marked as (?) are not experimentally confirmed.

J^P	(D, L_N^P)	$n_r n_L n_{q_1} n_{q_2} n_{q_3} n_J$	N	Λ_8	Σ	Ξ	Λ_1
Octet							
1/2 ⁺	(56, 0 ₀ ⁺)	00qqq2	(939)	(1116)	(1193)	(1318)	—
1/2 ⁺	(56, 0 ₂ ⁺)	20qqq2	(1440)	(1600)	(1660)	(1690)	—
1/2 ⁺	(70, 0 ₂ ⁺)	21qqq2	(1710)	(1810)	(1880)	(?)	(?)
1/2 ⁻	(70, 1 ₁ ⁻)	10qqq2	(1535)	(1670)	(1620)	(1750)	(1405)
Decuplet							
J^P	(D, L_N^P)	$n_r n_L n_{q_1} n_{q_2} n_{q_3} n_J$	Δ	Σ	Ξ	Ω	
3/2 ⁺	(56, 0 ₀ ⁺)	00qqq4	(1232)	(1385)	(1530)	(1672)	
3/2 ⁺	(56, 0 ₂ ⁺)	20qqq4	(1600)	(1690)	(?)	(?)	
1/2 ⁻	(70, 1 ₁ ⁻)	11qqq2	(1620)	(1750)	(?)	(?)	
3/2 ⁻	(70, 1 ₁ ⁻)	12qqq4	(1700)	(?)	(?)	(?)	

11. The search for physics beyond the Standard Model is an active area, so these codes are also standardized as far as possible.

- (a) A standard fourth generation of fermions is included by analogy with the first three.
- (b) The graviton and the boson content of a two-Higgs-doublet scenario and of additional $SU(2) \times U(1)$ groups are found in the range 31–40.
- (c) “One-of-a-kind” exotic particles are assigned numbers in the range 41–80. The subrange 61–80 can be used for new heavier fermions in generic models, where partners to the SM fermions would have codes offset by 60. If required, however, other assignments could be made.
- (d) Fundamental supersymmetric particles are identified by adding a nonzero n to the particle number. The superpartner of a boson or a left-handed fermion has $n = 1$ while the superpartner of a right-handed fermion has $n = 2$. When mixing occurs, such as between the winos and charged Higgsinos to give charginos, or between left and right sfermions, the lighter physical state is given the smaller basis state number.
- (e) Technicolor states have $n = 3$, with technifermions treated like ordinary fermions. States which are ordinary color singlets have $n_r = 0$. Color octets have $n_r = 1$. If a state has non-trivial quantum numbers under the topcolor groups $SU(3)_1 \times SU(3)_2$, the quantum numbers are specified by $tech, ij$, where i and j are 1 or 2. n_L is then $2i + j$. The coloron, V_8 , is a heavy gluon color octet and thus is 3100021.
- (f) Excited (composite) quarks and leptons are identified by setting $n = 4$ and $n_r = 0$.
- (g) Within several scenarios of new physics, it is possible to have colored particles sufficiently long-lived for color-singlet hadronic states to form around them. In the context of supersymmetric scenarios, these states are called R -hadrons, since they carry odd R -parity. R -hadron codes, defined here, should be viewed as templates for corresponding codes also in other scenarios, for any long-lived particle that is either an unflavored color octet or a flavored color triplet. The R -hadron code is obtained by combining the SUSY particle code with a code for the light degrees of freedom, with as many intermediate zeros removed from the former as required to make place for the latter at the end. (To exemplify, a sparticle $n00000n_{\bar{q}}$ combined with quarks q_1 and q_2 obtains code $n00n_{\bar{q}}n_{q_1}n_{q_2}n_J$.) Specifically, the new-particle spin decouples in the limit of large masses, so that the final n_J digit is defined by the spin state of the light-quark system alone. An appropriate number of n_q digits is used to define the ordinary-quark content. As usual, 9 rather than 21 is used to denote a gluon/gluino in composite states. The sign of the hadron agrees with that of the constituent new particle (a color triplet) where

there is a distinct new antiparticle, and else is defined as for normal hadrons. Particle names are R with the flavor content as lower index.

- (h) A black hole in models with extra dimensions has code 5000040. Kaluza-Klein excitations in models with extra dimensions have $n = 5$ or $n = 6$, to distinguish excitations of left- or right-handed fermions or, in case of mixing, the lighter or heavier state (cf. 11d). The nonzero n_r digit gives the radial excitation number, in scenarios where the level spacing allow these to be distinguished. Should the model also contain supersymmetry, excited SUSY states would be denoted by an $n_r > 0$, with $n = 1$ or 2 as usual. Should some colored states be long-lived enough that hadrons would form around them, the coding strategy of 11g applies, with the initial two nn_r digits preserved in the combined code.
 - (i) Magnetic monopoles and dyons are assumed to have one unit of Dirac monopole charge and a variable integer number $n_{q_1}n_{q_2}n_{q_3}$ units of electric charge. Codes $411n_{q_1}n_{q_2}n_{q_3}0$ are then used when the magnetic and electrical charge sign agree and $412n_{q_1}n_{q_2}n_{q_3}0$ when they disagree, with the overall sign of the particle set by the magnetic charge. For now no spin information is provided.
 - (j) The nature of Dark Matter (DM) is not known, and therefore a definitive classification is too early. Candidates within specific scenarios are classified therein, such as 1000022 for the lightest neutralino. Generic fundamental states can be given temporary codes in the range 51–60, with 51, 52 and 53 reserved for spin 0, 1/2 and 1 ones (this could also be an axion state). Generic mediators of s-channel DM pair creation of annihilation can be given codes 54 and 55 for spin 0 or 1 ones. Separate antiparticles, with negative codes, may or may not exist. More elaborate new scenarios should be constructed with $n = 5$ and $n_r = 9$.
 - (k) Hidden Valley particles have $n = 4$ and $n_r = 9$, and trailing numbers in agreement with their nearest-analog standard particles, as far as possible. Thus 4900021 is the gauge boson g_v of a confining gauge field, 490000 n_{q_v} and 490001 n_{ℓ_v} fundamental constituents charged or not under this, 4900022 is the γ_v of a non-confining field, and 4900 $n_{q_v1}n_{q_v2}n_J$ a Hidden Valley meson.
12. Occasionally program authors add their own states. To avoid confusion, these should be flagged by setting $nn_r = 99$.
 13. Concerning the non-99 numbers, it may be noted that only quarks, excited quarks, squarks, and diquarks have $n_{q_3} = 0$; only diquarks, baryons, and the odderon have $n_{q_1} \neq 0$; and only mesons, the reggeon, and the pomeron have $n_{q_1} = 0$ and $n_{q_2} \neq 0$. Concerning mesons (not antimesons), if n_{q_1} is odd then it labels a quark and an antiquark if even.
 14. The 9-digit tetra-quark codes are $\pm 1n_r n_L n_{q_1} n_{q_2} 0 n_{q_3} n_{q_4} n_J$. For the particle $q_1 q_2$ is a diquark and $\bar{q}_3 \bar{q}_4$ an antiquark,

sorted such that $n_{q_1} \geq n_{q_2}, n_{q_3} \geq n_{q_4}, n_{q_1} \geq n_{q_3}$, and $n_{q_2} \geq n_{q_4}$ if $n_{q_1} = n_{q_3}$. For the antiparticle, given with a negative sign, $\bar{q}_1\bar{q}_2$ is an antiquark and q_3q_4 a diquark, with the same sorting except that either $n_{q_1} > n_{q_3}$ or $n_{q_2} > n_{q_4}$ (so that flavour-diagonal states are particles). The n_r, n_L , and n_J numbers have the same meaning as for ordinary hadrons.

15. The 9-digit penta-quark codes are $\pm 1n_r n_L n_{q_1} n_{q_2} n_{q_3} n_{q_4} n_{q_5} n_J$, sorted such that $n_{q_1} \geq n_{q_2} \geq n_{q_3} \geq n_{q_4}$. In the particle the first four are quarks and the fifth an antiquark while the opposite holds in the antiparticle, which is given with a negative sign. The n_r, n_L , and n_J numbers have the same meaning as for ordinary hadrons.

16. Nuclear codes are given as 10-digit numbers $\pm 10LZZZAAAI$. For a (hyper)nucleus consisting of n_p protons, n_n neutrons and n_A Λ 's, $A = n_p + n_n + n_A$ gives the total baryon number, $Z = n_p$ the total charge and $L = n_A$ the total number of strange quarks. I gives the isomer level, with $I = 0$ corresponding to the ground state and $I > 0$ to excitations, see [2], where states denoted m, n, p, q translate to $I = 1-4$. As examples, the deuteron is 1000010020 and ^{235}U is 1000922350. To avoid ambiguities, nuclear codes should not be applied to a single hadron, like p, n or Λ^0 , where quark-contents-based codes already exist.

QUARKS		DIQUARKS		LIGHT I = 1 MESONS		LIGHT I = 0 MESONS (u \bar{u} , d \bar{d} , s \bar{s} admixtures)		STRANGE MESONS	
d	1	(dd) ₁	1103	π^0	111	η	221	K_L^0	130
u	2	(ud) ₀	2101	π^+	211	$\eta'(958)$	331	K_S^0	310
s	3	(ud) ₁	2103	$a_0(980)^0$	9000111	$f_0(500)$	9000221	K^0	311
c	4	(uu) ₁	2203	$a_0(980)^+$	9000211	$f_0(980)$	9010221	K^+	321
b	5	(sd) ₀	3101	$\pi(1300)^0$	100111	$\eta(1295)$	100221	$K^*(700)^0$	9000311
t	6	(sd) ₁	3103	$\pi(1300)^+$	100211	$\eta(1405)$	9020221	$K^*(700)^+$	9000321
b'	7	(su) ₀	3201	$a_0(1450)^0$	10111	$\eta(1475)$	100331	$K^*(1430)^0$	10311
t'	8	(su) ₁	3203	$a_0(1450)^+$	10211	$f_0(1370)$	10221	$K^*(1430)^+$	10321
LEPTONS		(ss) ₁	3303	$\pi(1800)^0$	9010111	$f_0(1405)$	9020221	$K(1460)^0$	100311
e ⁻	11	(cd) ₀	4101	$\pi(1800)^+$	9010211	$\eta(1760)$	9040221	$K(1460)^+$	100321
ν_e	12	(cd) ₁	4103	$\rho(1800)^0$	113	$f_0(1500)$	9030221	$K(1830)^0$	9010311
μ^-	13	(cu) ₀	4201	$\rho(1800)^+$	213	$f_0(1710)$	10331	$K(1830)^+$	9010321
ν_μ	14	(cu) ₁	4203	$b_1(1235)^0$	10113	$\eta(1760)$	9040221	$K^*(1950)^0$	9020311
τ^-	15	(cs) ₀	4301	$b_1(1235)^+$	10213	$f_0(2020)$	9050221	$K^*(1950)^+$	9020321
ν_τ	16	(cs) ₁	4303	$\rho(770)^0$	113	$f_0(2100)$	9060221	$K^*(892)^0$	313
τ^+	17	(cc) ₁	4403	$\rho(770)^+$	213	$f_0(2200)$	9070221	$K^*(892)^+$	323
$\nu_{\tau'}$	18	(bd) ₀	5101	$b_1(1235)^0$	10113	$\eta(2225)$	9080221	$K_1(1270)^0$	10313
GAUGE AND HIGGS BOSONS		(bd) ₁	5103	$a_1(1260)^0$	20113	$\omega(782)$	223	$K_1(1270)^+$	10323
g	(9) 21	(bu) ₀	5201	$a_1(1260)^+$	20213	$\phi(1020)$	333	$K_1(1400)^0$	20313
γ	22	(bu) ₁	5203	$\pi_1(1400)^0$	9000113	$h_1(1170)$	10223	$K_1(1400)^+$	20323
Z^0	23	(bs) ₀	5301	$\pi_1(1400)^+$	9000213	$f_1(1285)$	20223	$K^*(1410)^0$	100313
W^+	24	(bs) ₁	5303	$\rho(1450)^0$	100113	$h_1(1380)$	10333	$K^*(1410)^+$	100323
h^0/H_1^0	25	(bc) ₀	5401	$\rho(1450)^+$	100213	$f_1(1420)$	20333	$K_1(1650)^0$	9000313
Z'/Z_2^0	32	(bc) ₁	5403	$\pi_1(1600)^0$	9010113	$\omega(1420)$	100223	$K_1(1650)^+$	9000323
Z''/Z_3^0	33	(bb) ₁	5503	$\pi_1(1600)^+$	9010213	$f_1(1510)$	9000223	$K^*(1680)^0$	30313
W'/W_2^+	34			$a_1(1640)^0$	9020113	$h_1(1595)$	9010223	$K^*(1680)^+$	30323
H^0/H_2^0	35			$a_1(1640)^+$	9020213	$\omega(1650)$	30223	$K_2^*(1430)^0$	315
A^0/H_3^0	36			$\rho(1700)^0$	30113	$\phi(1680)$	100333	$K_2^*(1430)^+$	325
H^+	37			$\rho(1700)^+$	30213	$f_2(1270)$	225	$K_2(1580)^0$	9000315
H^{++}	38			$\rho(1900)^0$	9030113	$f_2(1430)$	9000225	$K_2(1580)^+$	9000325
a^0/H_4^0	40			$\rho(1900)^+$	9030213	$f_2'(1525)$	335	$K_2(1770)^0$	10315
SPECIAL PARTICLES				$\rho(2150)^0$	9040113	$f_2(1565)$	9010225	$K_2(1770)^+$	10325
G (graviton)	39			$\rho(2150)^+$	9040213	$f_2(1640)$	9020225	$K_2(1820)^0$	20315
R^0	41			$\pi_2(1670)^0$	10115	$\eta_2(1645)$	10225	$K_2(1820)^+$	20325
LQ^c	42			$\pi_2(1670)^+$	10215	$f_2(1810)$	9030225	$K_2^*(1980)^0$	9010315
DM ($S=0$)	51			$\nu_e L$	1000011	$\eta_2(1870)$	10335	$K_2^*(1980)^+$	9010325
DM ($S=1/2$)	52			$\nu_\mu L$	1000012	$f_2(1910)$	9040225	$K_2(2250)^0$	9020315
DM ($S=1$)	53			$\nu_\tau L$	1000013	$f_2(1950)$	9050225	$K_2(2250)^+$	9020325
reggeon	110			μL	1000013	$f_2(2010)$	9060225	$K_3^*(1780)^0$	317
pomeron	990			τ_1^-	1000015 ^a	$f_2(2150)$	9070225	$K_3^*(1780)^+$	327
odderon	9990			τ_1^+	1000015 ^a	$f_2(2300)$	9080225	$K_3(2320)^0$	9010317
				τ_2^-	1000016	$f_2(2340)$	9090225	$K_3(2320)^+$	9010327
				τ_2^+	1000016	$\omega_3(1670)$	227	$K_4^*(2045)^0$	319
				\tilde{d}_L	2000001	$\phi_3(1850)$	337	$K_4^*(2045)^+$	329
				\tilde{u}_L	2000002	$f_4(2050)$	229	$K_4(2500)^0$	9000319
				\tilde{u}_R	2000002	$f_J(2220)$	9000229	$K_4(2500)^+$	9000329
				\tilde{s}_R	2000003	$f_4(2300)$	9010229		
				\tilde{c}_R	2000004				
				\tilde{b}_2	2000005 ^a				
				\tilde{t}_2	2000006 ^a				
				\tilde{e}_R	2000011				
				$\tilde{\mu}_R$	2000013				
				$\tilde{\tau}_2$	2000015 ^a				
				\tilde{g}	1000021				
				$\tilde{\chi}_1^0$	1000022 ^b				
				$\tilde{\chi}_2^0$	1000023 ^b				
				$\tilde{\chi}_3^0$	1000025 ^b				
				$\tilde{\chi}_4^0$	1000035 ^b				
				$\tilde{\chi}_2^+$	1000037 ^b				
				\tilde{G}	1000039				

for MC internal use
81-100, 901-930,
998-999, 1901-1930,
2901-2930, and
3901-3930

CHARMED MESONS						CHARMED BARYONS		BOTTOM BARYONS	
D^+	411	B_c^{*+}	10541	$\Upsilon(11020)$	9010553	Λ_c^+	4122	Λ_b^0	5122
D^0	421	B_c^{*+}	543	$\chi_{b2}(1P)$	555	Σ_c^{*+}	4222	Σ_b^-	5112
$D_0^*(2400)^+$	10411	$B_{c1}(L)^+$	10543	$\eta_{b2}(1D)$	10555	Σ_c^+	4212	Σ_b^0	5212
$D_0^*(2400)^0$	10421	$B_{c1}(H)^+$	20543	$\Upsilon_2(1D)$	20555	Σ_c^0	4112	Σ_b^+	5222
$D^*(2010)^+$	413	B_{c2}^{*+}	545	$\chi_{b2}(2P)$	100555	Σ_c^{*0}	4224	Σ_b^{*-}	5114
$D^*(2007)^0$	423	<hr/> $c\bar{c}$ MESONS <hr/>		$\eta_{b2}(2D)$	110555	Σ_c^{*+}	4214	Σ_b^{*0}	5214
$D_1(2430)^+$	10413	$\eta_c(1S)$	441	$\Upsilon_2(2D)$	120555	Σ_c^0	4114	Σ_b^{*+}	5224
$D_1(2420)^0$	10423	$\chi_{c0}(1P)$	10441	$\chi_{b2}(3P)$	200555	Ξ_c^+	4232	Ξ_b^-	5132
$D_1(H)^+$	20413	$\eta_c(2S)$	100441	$\Upsilon_3(1D)$	557	Ξ_c^0	4132	Ξ_b^0	5232
$D_1(2430)^0$	20423	$J/\psi(1S)$	443	$\Upsilon_3(2D)$	100557	Ξ_c^{*+}	4322	Ξ_b^+	5312
$D_2^*(2460)^+$	415	$h_c(1P)$	10443	<hr/> LIGHT BARYONS <hr/>		Ξ_c^{*0}	4312	Ξ_b^0	5322
$D_2^*(2460)^0$	425	$\chi_{c1}(1P)$	20443	p	2212	Ξ_c^+	4324	Ξ_b^+	5314
D_s^+	431	$\psi(2S)$	100443	n	2112	Ξ_c^{*0}	4314	Ξ_b^{*0}	5324
$D_{s0}^*(2317)^+$	10431	$\psi(3770)$	30443	Δ^{++}	2224	Ω_c^0	4332	Ω_b^-	5332
D_s^{*+}	433	$\psi(4040)$	9000443	Δ^+	2214	Ω_c^{*0}	4334	Ω_b^{*-}	5334
$D_{s1}(2536)^+$	10433	$\psi(4160)$	9010443	Δ^0	2114	Ξ_{cc}^+	4412	Ξ_b^0	5142
$D_{s1}(2460)^+$	20433	$\psi(4415)$	9020443	Δ^-	1114	Ξ_{cc}^{*+}	4414	Ξ_b^{bc}	5242
$D_{s2}^*(2573)^+$	435	$\chi_{c2}(1P)$	445	<hr/> STRANGE BARYONS <hr/>		Ξ_{cc}^{*0}	4424	Ξ_b^+	5412
		$\chi_{c2}(3930)$	100445	Λ	3122	Ξ_{cc}^+	4432	Ξ_b^{bc}	5422
<hr/> BOTTOM MESONS <hr/>		<hr/> $b\bar{b}$ MESONS <hr/>		Σ^+	3222	Ω_{cc}^+	4434	Ξ_b^{*0}	5414
B^0	511	$\eta_b(1S)$	551	Σ^0	3212	Ω_{cc}^{*+}	4444	Ξ_b^+	5424
B^+	521	$\chi_{b0}(1P)$	10551	Σ^-	3112	Ω_{cc}^{*0}	4444	Ω_b^{bc}	5342
B_s^{*0}	10511	$\eta_b(2S)$	100551	Σ^{*+}	3224 ^c	Ω_b^{*0}	5434	Ω_b^{*0}	5434
B_s^{*+}	10521	$\chi_{b0}(2P)$	110551	Σ^{*0}	3214 ^c	Ω_b^{bc}	5444	Ω_b^{bc}	5444
B_s^{*0}	513	$\eta_b(3S)$	200551	Σ^{*-}	3114 ^c	Ξ_{bb}^+	5512	Ξ_{bb}^+	5512
B^{*+}	523	$\chi_{b0}(3P)$	210551	Ξ^0	3322	Ξ_{bb}^0	5522	Ξ_{bb}^0	5522
$B_1(L)^0$	10513	$\Upsilon(1S)$	553	Ξ^-	3312	Ξ_{bb}^{*0}	5524	Ξ_{bb}^{*0}	5524
$B_1(L)^+$	10523	$h_b(1P)$	10553	Ξ^{*0}	3324 ^c	Ω_{bb}^+	5532	Ω_{bb}^+	5532
$B_1(H)^0$	20513	$\chi_{b1}(1P)$	20553	Ξ^{*-}	3314 ^c	Ω_{bb}^{*+}	5542	Ω_{bb}^{*+}	5542
$B_1(H)^+$	20523	$\Upsilon_1(1D)$	30553	Ω^-	3334	Ω_{bb}^{*0}	5544	Ω_{bb}^{*0}	5544
B_2^{*0}	515	$\Upsilon(2S)$	100553			Ω_{bbb}	5554	Ω_{bbb}	5554
B_2^{*+}	525	$h_b(2P)$	110553			<hr/> PENTAQUARKS <hr/>			
B_s^0	531	$\chi_{b1}(2P)$	120553			Θ^+	100221132 [*]		
B_{s0}^{*0}	10531	$\Upsilon_1(2D)$	130553			Φ^{--}	100331122 [*]		
B_{s0}^{*+}	533	$\Upsilon(3S)$	200553						
$B_{s1}(L)^0$	10533	$h_b(3P)$	210553						
$B_{s1}(H)^0$	20533	$\chi_{b1}(3P)$	220553						
B_{s2}^{*0}	535	$\Upsilon(4S)$	300553						
B_c^+	541	$\Upsilon(10860)$	9000553						

Footnotes to the tables:

*) Numbers or names in bold face are new or have changed since the 2020 *Review*.

a) Particularity in the third generation, the left and right sfermion states may mix, as shown.

The lighter mixed state is given the smaller number.

b) The physical $\tilde{\chi}$ states are admixtures of the pure $\tilde{\gamma}$, \tilde{Z}^0 , \tilde{W}^+ ,

\tilde{H}_1^0 , \tilde{H}_2^0 , and \tilde{H}^+ states.

c) Σ^{*+} and Ξ^{*-} are alternate names for $\Sigma(1385)$ and $\Xi(1530)$.

References

[1] G. P. Yost *et al.* (Particle Data Group), Phys. Lett. **B204**, 1 (1988).
 [2] G. Audi *et al.*, Nucl. Phys. **A729**, 3 (2003).

46. Clebsch-Gordan Coefficients, Spherical Harmonics, and d Functions

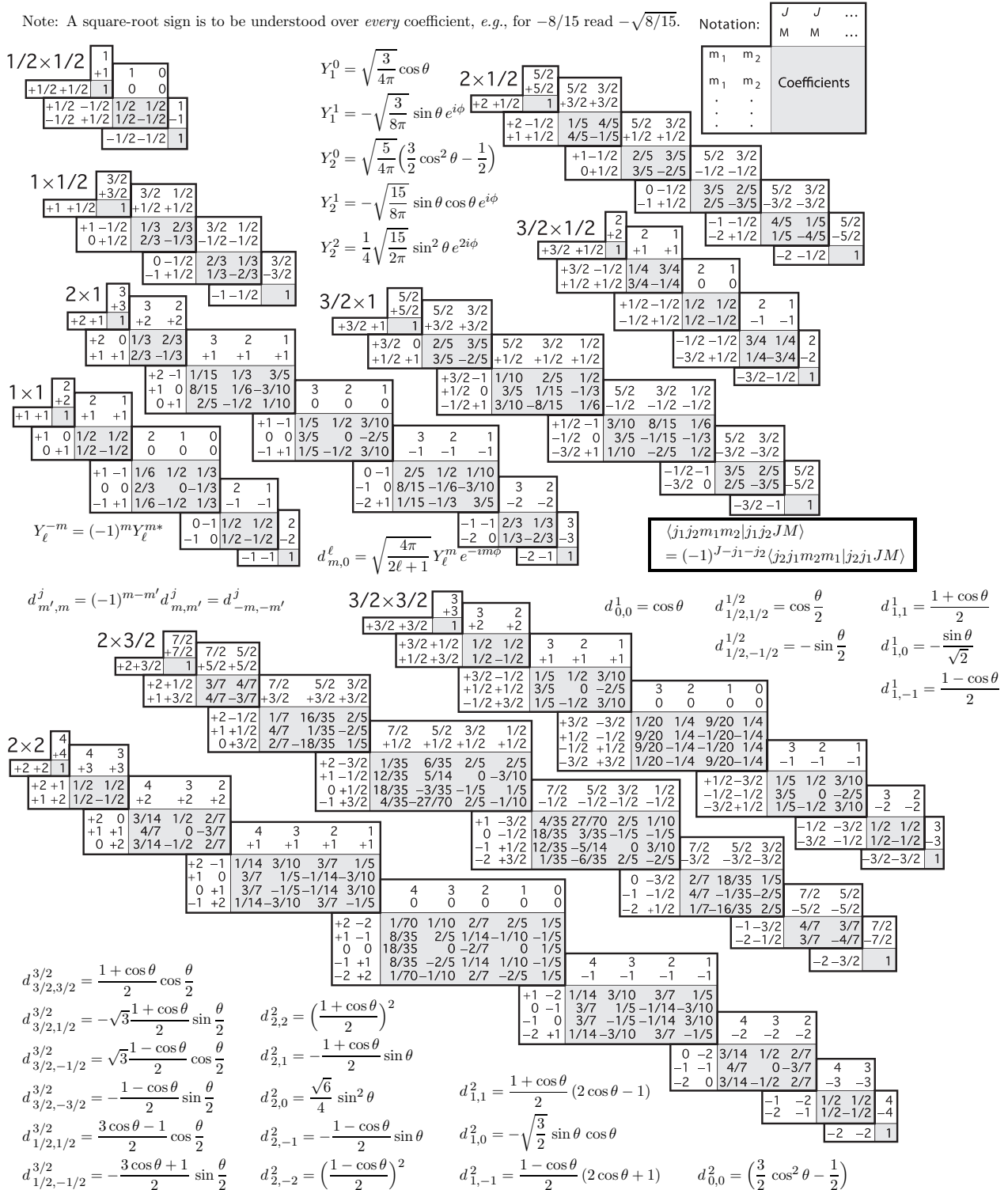


Figure 46.1: The sign convention is that of Wigner (*Group Theory*, Academic Press, New York, 1959), also used by Condon and Shortley (*The Theory of Atomic Spectra*, Cambridge Univ. Press, New York, 1953), Rose (*Elementary Theory of Angular Momentum*, Wiley, New York, 1957), and Cohen (*Tables of the Clebsch-Gordan Coefficients*, North American Rockwell Science Center, Thousand Oaks, Calif., 1974).

47. SU(3) Isoscalar Factors and Representation Matrices

Revised August 2019 by R. Kelly (LBNL).

The most commonly used SU(3) isoscalar factors, corresponding to the singlet, octet, and decuplet content of $8 \otimes 8$ and $10 \otimes 8$, are shown at the right. The notation uses particle names to identify the coefficients, so that the pattern of relative couplings may be seen at a glance. We illustrate the use of the coefficients below. See J.J de Swart, Rev. Mod. Phys. **35**, 916 (1963) for detailed explanations and phase conventions.

A $\sqrt{}$ is to be understood over every integer in the matrices; the exponent 1/2 on each matrix is a reminder of this. For example, the $\Xi \rightarrow \Omega K$ element of the $10 \rightarrow 10 \otimes 8$ matrix is $-\sqrt{6}/\sqrt{24} = -1/2$.

Intramultiplet relative decay strengths may be read directly from the matrices. For example, in decuplet \rightarrow octet + octet decays, the ratio of $\Omega^* \rightarrow \Xi K$ and $\Delta \rightarrow N \pi$ partial widths is, from the $10 \rightarrow 8 \times 8$ matrix,

$$\frac{\Gamma(\Omega^* \rightarrow \Xi K)}{\Gamma(\Delta \rightarrow N \pi)} = \frac{12}{6} \times (\text{phase space factors}). \quad (47.1)$$

Including isospin Clebsch-Gordan coefficients, we obtain, e.g.,

$$\frac{\Gamma(\Omega^{*-} \rightarrow \Xi^0 K^-)}{\Gamma(\Delta^+ \rightarrow p \pi^0)} = \frac{1/2}{2/3} \times \frac{12}{6} \times p.s.f. = \frac{3}{2} \times p.s.f. \quad (47.2)$$

Partial widths for $8 \rightarrow 8 \otimes 8$ involve a linear superposition of 8_1 (symmetric) and 8_2 (antisymmetric) couplings. For example,

$$\Gamma(\Xi^* \rightarrow \Xi \pi) \sim \left(-\sqrt{\frac{9}{20}} g_1 + \sqrt{\frac{3}{12}} g_2 \right)^2. \quad (47.3)$$

The relations between g_1 and g_2 (with de Swart's normalization) and the standard D and F couplings that appear in the interaction Lagrangian,

$$\mathcal{L} = -\sqrt{2} D \text{Tr}(\{\bar{B}, B\}M) + \sqrt{2} F \text{Tr}([\bar{B}, B]M), \quad (47.4)$$

where $[\bar{B}, B] \equiv \bar{B}B - B\bar{B}$ and $\{\bar{B}, B\} \equiv \bar{B}B + B\bar{B}$, are

$$D = \frac{\sqrt{30}}{40} g_1, \quad F = \frac{\sqrt{6}}{24} g_2. \quad (47.5)$$

Thus, for example,

$$\Gamma(\Xi^* \rightarrow \Xi \pi) \sim (F - D)^2 \sim (1 - 2\alpha)^2, \quad (47.6)$$

where $\alpha \equiv F/(D + F)$. (This definition of α is de Swart's. The alternative $D/(D + F)$, due to Gell-Mann, is also used.)

The generators of SU(3) transformations, λ_a ($a = 1, 8$), are 3×3 matrices that obey the following commutation and anticommutation relationships:

$$[\lambda_a, \lambda_b] \equiv \lambda_a \lambda_b - \lambda_b \lambda_a = 2i f_{abc} \lambda_c \quad (47.7)$$

$$\{\lambda_a, \lambda_b\} \equiv \lambda_a \lambda_b + \lambda_b \lambda_a = \frac{4}{3} \delta_{ab} I + 2d_{abc} \lambda_c, \quad (47.8)$$

where I is the 3×3 identity matrix, and δ_{ab} is the Kronecker delta symbol. The f_{abc} are odd under the permutation of any pair of indices, while the d_{abc} are even. The nonzero values are:

$1 \rightarrow 8 \otimes 8$

$$(A) \rightarrow (N\bar{K} \ \Sigma\pi \ \Lambda\eta \ \Xi K) = \frac{1}{\sqrt{8}} \begin{pmatrix} 2 & 3 & -1 & -2 \end{pmatrix}^{1/2}$$

$8_1 \rightarrow 8 \otimes 8$

$$\begin{pmatrix} N \\ \Sigma \\ \Lambda \\ \Xi \end{pmatrix} \rightarrow \begin{pmatrix} N\pi & N\eta & \Sigma K & \Lambda K \\ N\bar{K} & \Sigma\pi & \Lambda\pi & \Sigma\eta & \Xi K \\ N\bar{K} & \Sigma\pi & \Lambda\eta & \Xi K \\ \Sigma\bar{K} & \Lambda\bar{K} & \Xi\pi & \Xi\eta \end{pmatrix} = \frac{1}{\sqrt{20}} \begin{pmatrix} 9 & -1 & -9 & -1 \\ -6 & 0 & 4 & 4 \\ 2 & -12 & -4 & -2 \\ 9 & -1 & -9 & -1 \end{pmatrix}^{1/2}$$

$8_2 \rightarrow 8 \otimes 8$

$$\begin{pmatrix} N \\ \Sigma \\ \Lambda \\ \Xi \end{pmatrix} \rightarrow \begin{pmatrix} N\pi & N\eta & \Sigma K & \Lambda K \\ N\bar{K} & \Sigma\pi & \Lambda\pi & \Sigma\eta & \Xi K \\ N\bar{K} & \Sigma\pi & \Lambda\eta & \Xi K \\ \Sigma\bar{K} & \Lambda\bar{K} & \Xi\pi & \Xi\eta \end{pmatrix} = \frac{1}{\sqrt{12}} \begin{pmatrix} 3 & 3 & 3 & -3 \\ 2 & 8 & 0 & 0 \\ 6 & 0 & 0 & 6 \\ 3 & 3 & 3 & -3 \end{pmatrix}^{1/2}$$

$10 \rightarrow 8 \otimes 8$

$$\begin{pmatrix} \Delta \\ \Sigma \\ \Xi \\ \Omega \end{pmatrix} \rightarrow \begin{pmatrix} N\pi & \Sigma K \\ N\bar{K} & \Sigma\pi & \Lambda\pi & \Sigma\eta & \Xi K \\ \Sigma\bar{K} & \Lambda\bar{K} & \Xi\pi & \Xi\eta \\ \Xi\bar{K} \end{pmatrix} = \frac{1}{\sqrt{12}} \begin{pmatrix} -6 & 6 \\ -2 & 2 & -3 & 3 & 2 \\ 3 & -3 & 3 & 3 \\ 12 \end{pmatrix}^{1/2}$$

$8 \rightarrow 10 \otimes 8$

$$\begin{pmatrix} N \\ \Sigma \\ \Lambda \\ \Xi \end{pmatrix} \rightarrow \begin{pmatrix} \Delta\pi & \Sigma K \\ \Delta\bar{K} & \Sigma\pi & \Sigma\eta & \Xi K \\ \Sigma\pi & \Xi K \\ \Sigma\bar{K} & \Xi\pi & \Xi\eta & \Omega K \end{pmatrix} = \frac{1}{\sqrt{15}} \begin{pmatrix} -12 & 3 \\ 8 & -2 & -3 & 2 \\ -9 & 6 \\ 3 & -3 & -3 & 6 \end{pmatrix}^{1/2}$$

$10 \rightarrow 10 \otimes 8$

$$\begin{pmatrix} \Delta \\ \Sigma \\ \Xi \\ \Omega \end{pmatrix} \rightarrow \begin{pmatrix} \Delta\pi & \Delta\eta & \Sigma K \\ \Delta\bar{K} & \Sigma\pi & \Sigma\eta & \Xi K \\ \Sigma\bar{K} & \Xi\pi & \Xi\eta & \Omega K \\ \Xi\bar{K} & \Omega\eta \end{pmatrix} = \frac{1}{\sqrt{24}} \begin{pmatrix} 8 & 15 & 3 & -6 \\ 8 & 8 & 0 & -8 \\ 12 & 3 & -3 & -6 \\ 12 & 12 & -12 \end{pmatrix}^{1/2}$$

abc	f_{abc}	abc	d_{abc}	abc	d_{abc}
123	1	118	$1/\sqrt{3}$	355	1/2
147	1/2	146	1/2	366	-1/2
156	-1/2	157	1/2	377	-1/2
246	1/2	228	$1/\sqrt{3}$	448	$-1/(2\sqrt{3})$
257	1/2	247	-1/2	558	$-1/(2\sqrt{3})$
345	1/2	256	1/2	668	$-1/(2\sqrt{3})$
367	-1/2	338	$1/\sqrt{3}$	778	$-1/(2\sqrt{3})$
458	$\sqrt{3}/2$	344	1/2	888	$-1/\sqrt{3}$
678	$\sqrt{3}/2$				

The λ_a 's are

$$\lambda_1 = \begin{pmatrix} 0 & 1 & 0 \\ 1 & 0 & 0 \\ 0 & 0 & 0 \end{pmatrix} \quad \lambda_2 = \begin{pmatrix} 0 & -i & 0 \\ i & 0 & 0 \\ 0 & 0 & 0 \end{pmatrix} \quad \lambda_3 = \begin{pmatrix} 1 & 0 & 0 \\ 0 & -1 & 0 \\ 0 & 0 & 0 \end{pmatrix}$$

$$\lambda_4 = \begin{pmatrix} 0 & 0 & 1 \\ 0 & 0 & 0 \\ 1 & 0 & 0 \end{pmatrix} \quad \lambda_5 = \begin{pmatrix} 0 & 0 & -i \\ 0 & 0 & 0 \\ i & 0 & 0 \end{pmatrix} \quad \lambda_6 = \begin{pmatrix} 0 & 0 & 0 \\ 0 & 0 & 1 \\ 0 & 1 & 0 \end{pmatrix}$$

$$\lambda_7 = \begin{pmatrix} 0 & 0 & 0 \\ 0 & 0 & -i \\ 0 & i & 0 \end{pmatrix} \quad \lambda_8 = \frac{1}{\sqrt{3}} \begin{pmatrix} 1 & 0 & 0 \\ 0 & 1 & 0 \\ 0 & 0 & -2 \end{pmatrix}$$

Equation (47.7) defines the Lie algebra of SU(3). A general d -dimensional representation is given by a set of $d \times d$ matrices satisfying Eq. (47.7) with the f_{abc} given above. Equation (47.8) is specific to the defining 3-dimensional representation.

48. SU(n) Multiplets and Young Diagrams

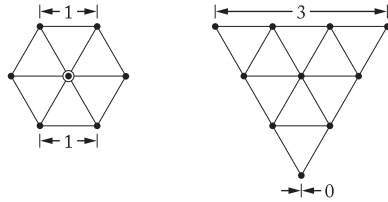
Revised August 2019 by C.G. Wohl (LBNL).

This note tells (1) how SU(n) particle multiplets are identified or labeled, (2) how to find the number of particles in a multiplet from its label, (3) how to draw the Young diagram for a multiplet, and (4) how to use Young diagrams to determine the overall multiplet structure of a composite system, such as a 3-quark or a meson-baryon system.

In much of the literature, the word “representation” is used where we use “multiplet,” and “tableau” is used where we use “diagram.”

48.1 Multiplet labels

An SU(n) multiplet is uniquely identified by a string of (n-1) nonnegative integers: (α, β, γ, ...). Any such set of integers specifies a multiplet. For an SU(2) multiplet such as an isospin multiplet, the single integer α is the number of steps from one end of the multiplet to the other (i.e., it is one fewer than the number of particles in the multiplet). In SU(3), the two integers α and β are the numbers of steps across the top and bottom levels of the multiplet diagram. Thus the labels for the SU(3) octet and decuplet



are (1,1) and (3,0). For larger n, the interpretation of the integers in terms of the geometry of the multiplets, which exist in an (n-1)-dimensional space, is not so readily apparent.

The label for the SU(n) singlet is (0, 0, ..., 0). In a flavor SU(n), the n quarks together form a (1, 0, ..., 0) multiplet, and the n antiquarks belong to a (0, ..., 0, 1) multiplet. These two multiplets are conjugate to one another, which means their labels are related by (α, β, ...) ↔ (... , β, α).

48.2 Number of particles

The number of particles in a multiplet, N = N(α, β, ...), is given as follows (note the pattern of the equations). In SU(2), N = N(α) is

$$N = \frac{(\alpha + 1)}{1} . \tag{48.1}$$

In SU(3), N = N(α, β) is

$$N = \frac{(\alpha + 1)}{1} . \frac{(\beta + 1)}{1} . \frac{(\alpha + \beta + 2)}{2} . \tag{48.2}$$

In SU(4), N = N(α, β, γ) is

$$N = \frac{(\alpha+1)}{1} . \frac{(\beta+1)}{1} . \frac{(\gamma+1)}{1} . \frac{(\alpha+\beta+2)}{2} . \frac{(\beta+\gamma+2)}{2} . \frac{(\alpha+\beta+\gamma+3)}{3} . \tag{48.3}$$

Note that in Eq. (48.3) there is no factor with (α + γ + 2): only a consecutive sequence of the label integers appears in any factor. One more example should make the pattern clear for any SU(n). In SU(5), N = N(α, β, γ, δ) is

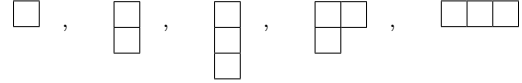
$$N = \frac{(\alpha+1)}{1} . \frac{(\beta+1)}{1} . \frac{(\gamma+1)}{1} . \frac{(\delta+1)}{1} . \frac{(\alpha+\beta+2)}{2} . \frac{(\beta+\gamma+2)}{2} . \frac{(\gamma+\delta+2)}{2} . \frac{(\alpha+\beta+\gamma+3)}{3} . \frac{(\beta+\gamma+\delta+3)}{3} . \frac{(\alpha+\beta+\gamma+\delta+4)}{4} . \tag{48.4}$$

From the symmetry of these equations, it is clear that multiplets that are conjugate to one another have the same number of particles, but so can other multiplets. For example, the SU(4) multi-

plets (3,0,0) and (1,1,0) each have 20 particles. Try the equations and see.

48.3 Young diagrams

A Young diagram consists of an array of boxes (or some other symbol) arranged in one or more left-justified rows, with each row being at least as long as the row beneath. The correspondence between a diagram and a multiplet label is: The top row juts out α boxes to the right past the end of the second row, the second row juts out β boxes to the right past the end of the third row, etc. A diagram in SU(n) has at most n rows. There can be any number of “completed” columns of n boxes buttressing the left of a diagram; these don’t affect the label. Thus in SU(3) the diagrams



represent the multiplets (1,0), (0,1), (0,0), (1,1), and (3,0). In any SU(n), the quark multiplet is represented by a single box, the antiquark multiplet by a column of (n-1) boxes, and a singlet by a completed column of n boxes.

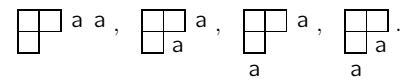
48.4 Coupling multiplets together

The following recipe tells how to find the multiplets that occur in coupling two multiplets together. To couple together more than two multiplets, first couple two, then couple a third with each of the multiplets obtained from the first two, etc.

First a definition: A sequence of the letters a, b, c, ... is admissible if at any point in the sequence at least as many a’s have occurred as b’s, at least as many b’s have occurred as c’s, etc. Thus abcd and aabcb are admissible sequences and abb and acb are not. Now the recipe:

(a) Draw the Young diagrams for the two multiplets, but in one of the diagrams replace the boxes in the first row with a’s, the boxes in the second row with b’s, etc. Thus, to couple two SU(3) octets (such as the π-meson octet and the baryon octet), we start with and . The unlettered diagram forms the upper left-hand corner of all the enlarged diagrams constructed below.

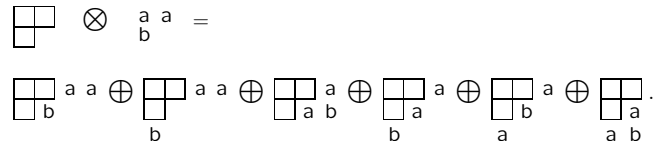
(b) Add the a’s from the lettered diagram to the right-hand ends of the rows of the unlettered diagram to form all possible legitimate Young diagrams that have no more than one a per column. In general, there will be several distinct diagrams, and all the a’s appear in each diagram. At this stage, for the coupling of the two SU(3) octets, we have:



(c) Use the b’s to further enlarge the diagrams already obtained, subject to the same rules. Then throw away any diagram in which the full sequence of letters formed by reading right to left in the first row, then the second row, etc., is not admissible.

(d) Proceed as in (c) with the c’s (if any), etc.

The final result of the coupling of the two SU(3) octets is:



Here only the diagrams with admissible sequences of a’s and b’s and with fewer than four rows (since n = 3) have been kept. In terms of multiplet labels, the above may be written

$$(1, 1) \otimes (1, 1) = (2, 2) \oplus (3, 0) \oplus (0, 3) \oplus (1, 1) \oplus (1, 1) \oplus (0, 0) .$$

In terms of numbers of particles, it may be written

$$8 \otimes 8 = 27 \oplus 10 \oplus \overline{10} \oplus 8 \oplus 8 \oplus 1 .$$

The product of the numbers on the left here is equal to the sum on the right, a useful check. (See also Sec. 15 on the Quark Model.)

Kinematics, Cross-Section Formulae, and Plots

49. Kinematics (rev.)	743
50. Resonances (rev.)	747
51. Cross-section formulae for specific processes (rev.)	756
52. Neutrino cross section measurements (rev.)	765
53. Plots of cross sections and related quantities (rev.)	770

49. Kinematics

Reviewed August 2021 by D. Miller (Glasgow), D.R. Tovey (Sheffield), written January 2000 by J.D. Jackson (LBNL).

Throughout this section units are used in which $\hbar = c = 1$. The following conversions are useful: $\hbar c = 197.3 \text{ MeV fm}$, $(\hbar c)^2 = 0.3894 \text{ (GeV)}^2 \text{ mb}$.

49.1 Lorentz transformations

The energy E and 3-momentum \mathbf{p} of a particle of mass m form a 4-vector $p = (E, \mathbf{p})$ whose square $p^2 \equiv E^2 - |\mathbf{p}|^2 = m^2$. The velocity of the particle is $\boldsymbol{\beta} = \mathbf{p}/E$. The energy and momentum (E^*, \mathbf{p}^*) viewed from a frame moving with velocity $\boldsymbol{\beta}_f$ are given by

$$\begin{pmatrix} E^* \\ \mathbf{p}_{\parallel}^* \end{pmatrix} = \begin{pmatrix} \gamma_f & -\gamma_f \boldsymbol{\beta}_f \\ -\gamma_f \boldsymbol{\beta}_f & \gamma_f \end{pmatrix} \begin{pmatrix} E \\ p_{\parallel} \end{pmatrix}, \quad p_T^* = p_T, \quad (49.1)$$

where $\gamma_f = (1 - \beta_f^2)^{-1/2}$ and p_T (p_{\parallel}) are the components of \mathbf{p} perpendicular (parallel) to $\boldsymbol{\beta}_f$. Other 4-vectors, such as the space-time coordinates of events, of course transform in the same way. The scalar product of two 4-momenta $p_1 \cdot p_2 = E_1 E_2 - \mathbf{p}_1 \cdot \mathbf{p}_2$ is invariant (frame independent).

49.2 Center-of-mass energy and momentum

In the collision of two particles of masses m_1 and m_2 the total center-of-mass energy can be expressed in the Lorentz-invariant form

$$\begin{aligned} E_{\text{cm}} &= [(E_1 + E_2)^2 - (\mathbf{p}_1 + \mathbf{p}_2)^2]^{1/2}, \\ &= [m_1^2 + m_2^2 + 2E_1 E_2 (1 - \beta_1 \beta_2 \cos \theta)]^{1/2}, \end{aligned} \quad (49.2)$$

where θ is the angle between the particles. In the frame where one particle (of mass m_2) is at rest (lab frame),

$$E_{\text{cm}} = (m_1^2 + m_2^2 + 2E_{1 \text{ lab}} m_2)^{1/2}. \quad (49.3)$$

The velocity of the center-of-mass in the lab frame is

$$\boldsymbol{\beta}_{\text{cm}} = \mathbf{p}_{\text{lab}} / (E_{1 \text{ lab}} + m_2), \quad (49.4)$$

where $\mathbf{p}_{\text{lab}} \equiv \mathbf{p}_{1 \text{ lab}}$ and

$$\gamma_{\text{cm}} = (E_{1 \text{ lab}} + m_2) / E_{\text{cm}}. \quad (49.5)$$

The c.m. momenta of particles 1 and 2 are of magnitude

$$p_{\text{cm}} = p_{\text{lab}} \frac{m_2}{E_{\text{cm}}}. \quad (49.6)$$

For example, if a 0.80 GeV/c kaon beam is incident on a proton target, the center of mass energy is 1.699 GeV and the center of mass momentum of either particle is 0.442 GeV/c. It is also useful to note that

$$E_{\text{cm}} dE_{\text{cm}} = m_2 dE_{1 \text{ lab}} = m_2 \beta_{1 \text{ lab}} dp_{1 \text{ lab}}. \quad (49.7)$$

49.3 Lorentz-invariant amplitudes

The matrix elements for a scattering or decay process are written in terms of an invariant amplitude $-i\mathcal{M}$. As an example, the S -matrix for $2 \rightarrow 2$ scattering is related to \mathcal{M} by

$$\langle p'_1 p'_2 | S - 1 | p_1 p_2 \rangle = i(2\pi)^4 \delta^4(p_1 + p_2 - p'_1 - p'_2) \mathcal{M}(p_1, p_2; p'_1, p'_2). \quad (49.8)$$

The state normalization is such that

$$\langle p' | p \rangle = (2\pi)^3 2E_p \delta^3(\mathbf{p}' - \mathbf{p}), \quad (49.9)$$

with $E_p = \sqrt{\mathbf{p}^2 + m^2}$.

For a $2 \rightarrow 2$ scattering process producing unstable particles $1'$ and $2'$ decaying via $1' \rightarrow 3'4'$ and $2' \rightarrow 5'6'$ the matrix element for the complete process can be written in the narrow width

approximation as:

$$\begin{aligned} \mathcal{M}(12 \rightarrow 3'4'5'6') &= \\ &= \sum_{h_{1'}, h_{2'}} \frac{\mathcal{M}(12 \rightarrow 1'2') \mathcal{M}(1' \rightarrow 3'4') \mathcal{M}(2' \rightarrow 5'6')}{(m_{3'4'}^2 - m_{1'}^2 + im_{1'}\Gamma_{1'})(m_{5'6'}^2 - m_{2'}^2 + im_{2'}\Gamma_{2'})}. \end{aligned} \quad (49.10)$$

Here, m_{ij} is the invariant mass of particles i and j , m_k and Γ_k are the mass and total width of particle k , and the sum runs over the helicities of the intermediate particles. This enables the cross section for such a process to be written as the product of the cross section for the initial $2 \rightarrow 2$ scattering process with the branching ratios (relative partial decay rates) of the subsequent decays. A more sophisticated treatment, beyond the narrow width approximation, can be found in the review on "Resonances".

49.4 Particle decays

The partial decay rate of a particle of mass M into n bodies in its rest frame is given in terms of the Lorentz-invariant matrix element \mathcal{M} by

$$d\Gamma = \frac{(2\pi)^4}{2M} |\mathcal{M}|^2 d\Phi_n(P; p_1, \dots, p_n), \quad (49.11)$$

where $d\Phi_n$ is an element of n -body phase space given by

$$d\Phi_n(P; p_1, \dots, p_n) = \delta^4(P - \sum_{i=1}^n p_i) \prod_{i=1}^n \frac{d^3 p_i}{(2\pi)^3 2E_i}. \quad (49.12)$$

This phase space is reduced by combinatoric factors whenever there are identical particles in the final state. The phase space can be generated recursively, viz.

$$\begin{aligned} d\Phi_n(P; p_1, \dots, p_n) &= d\Phi_j(q; p_1, \dots, p_j) \\ &\times d\Phi_{n-j+1}(P; q, p_{j+1}, \dots, p_n) (2\pi)^3 dq^2, \end{aligned} \quad (49.13)$$

where $q^2 = (\sum_{i=1}^j E_i)^2 - |\sum_{i=1}^j \mathbf{p}_i|^2$. This form is particularly useful in the case where a particle decays into another particle that subsequently decays.

49.4.1 Survival probability

If a particle of mass M has mean proper lifetime $\tau (= 1/\Gamma)$ and has momentum (E, \mathbf{p}) , then the probability that it lives for a time t_0 or greater before decaying is given by

$$P(t_0) = e^{-t_0 \Gamma/\gamma} = e^{-Mt_0 \Gamma/E}, \quad (49.14)$$

and the probability that it travels a distance x_0 or greater is

$$P(x_0) = e^{-Mx_0 \Gamma/|\mathbf{p}|}. \quad (49.15)$$

49.4.2 Two-body decays

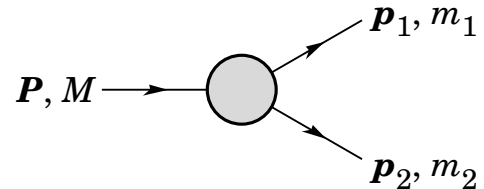


Figure 49.1: Definitions of variables for two-body decays.

In the rest frame of a particle of mass M , decaying into 2 particles labeled 1 and 2,

$$E_1 = \frac{M^2 - m_2^2 + m_1^2}{2M}, \quad (49.16)$$

$$|\mathbf{p}_1| = |\mathbf{p}_2| = \frac{1}{2M} \sqrt{\lambda(M^2, m_1^2, m_2^2)}, \quad (49.17)$$

and

$$d\Gamma = \frac{1}{32\pi^2} |\mathcal{M}|^2 \frac{|\mathbf{p}_1|}{M^2} d\Omega, \quad (49.18)$$

where $\lambda(\alpha, \beta, \gamma) = \alpha^2 + \beta^2 + \gamma^2 - 2\alpha\beta - 2\alpha\gamma - 2\beta\gamma$ is the Källén function and $d\Omega = d\phi_1 d(\cos\theta_1)$ is the solid angle of particle 1. The invariant mass M can be determined from the energies and momenta using Eq. (49.2) with $M = E_{\text{cm}}$.

49.4.3 Three-body decays

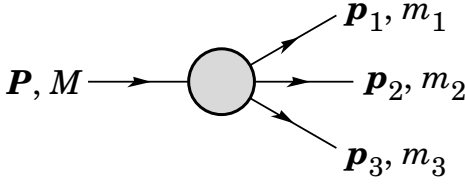


Figure 49.2: Definitions of variables for three-body decays.

Defining $p_{ij} = p_i + p_j$ and $m_{ij}^2 = p_{ij}^2$, then $m_{12}^2 + m_{23}^2 + m_{13}^2 = M^2 + m_1^2 + m_2^2 + m_3^2$ and $m_{12}^2 = (P - p_3)^2 = M^2 + m_3^2 - 2ME_3$, where E_3 is the energy of particle 3 in the rest frame of M . In that frame, the momenta of the three decay particles lie in a plane. The relative orientation of these three momenta is fixed if their energies are known. The momenta can therefore be specified in space by giving three Euler angles (α, β, γ) that specify the orientation of the final system relative to the initial particle. The direction of any one of the particles relative to the frame in which the initial particle is described can be specified in space by two angles (α, β) while a third angle, γ , can be set as the azimuthal angle of a second particle around the first [1]. Then

$$d\Gamma = \frac{1}{(2\pi)^5} \frac{1}{16M} |\mathcal{M}|^2 dE_1 dE_3 d\alpha d(\cos\beta) d\gamma. \quad (49.19)$$

Alternatively

$$d\Gamma = \frac{1}{(2\pi)^5} \frac{1}{16M^2} |\mathcal{M}|^2 |\mathbf{p}_1^*| |\mathbf{p}_3| dm_{12} d\Omega_1^* d\Omega_3, \quad (49.20)$$

where $(|\mathbf{p}_1^*|, \Omega_1^*)$ is the momentum of particle 1 in the rest frame of 1 and 2, and Ω_3 is the angle of particle 3 in the rest frame of the decaying particle. $|\mathbf{p}_1^*|$ and $|\mathbf{p}_3|$ are given by

$$|\mathbf{p}_1^*| = \frac{1}{2m_{12}} \sqrt{\lambda(m_{12}^2, m_1^2, m_2^2)}, \quad (49.21a)$$

and

$$|\mathbf{p}_3| = \frac{1}{2M} \sqrt{\lambda(M^2, m_{12}^2, m_3^2)}. \quad (49.21b)$$

[Compare with Eq. (49.17).]

If the decaying particle is a scalar, or we average over its spin states, then integration over the angles in Eq. (49.19) gives

$$\begin{aligned} d\Gamma &= \frac{1}{(2\pi)^3} \frac{1}{8M} |\overline{\mathcal{M}}|^2 dE_1 dE_3 \\ &= \frac{1}{(2\pi)^3} \frac{1}{32M^3} |\overline{\mathcal{M}}|^2 dm_{12}^2 dm_{23}^2. \end{aligned} \quad (49.22)$$

This is the standard form for the Dalitz plot.

49.4.3.1 Dalitz plot

For a given value of m_{12}^2 , the range of m_{23}^2 is determined by its values when \mathbf{p}_2 is parallel or antiparallel to \mathbf{p}_3 :

$$(m_{23}^2)_{\text{max}} = (E_2^* + E_3^*)^2 - \left(\sqrt{E_2^{*2} - m_2^2} - \sqrt{E_3^{*2} - m_3^2} \right)^2, \quad (49.23a)$$

$$(m_{23}^2)_{\text{min}} = (E_2^* + E_3^*)^2 - \left(\sqrt{E_2^{*2} - m_2^2} + \sqrt{E_3^{*2} - m_3^2} \right)^2. \quad (49.23b)$$

Here $E_2^* = (m_{12}^2 - m_1^2 + m_2^2)/2m_{12}$ and $E_3^* = (M^2 - m_{12}^2 - m_3^2)/2m_{12}$ are the energies of particles 2 and 3 in the m_{12} rest frame. The scatter plot in m_{12}^2 and m_{23}^2 is called a Dalitz plot.

If $|\overline{\mathcal{M}}|^2$ is constant, the allowed region of the plot will be uniformly populated with events [see Eq. (49.22)]. A nonuniformity in the plot gives immediate information on $|\overline{\mathcal{M}}|^2$. For example, in the case of $D \rightarrow K\pi\pi$, bands appear when $m_{(K\pi)} = m_{K^*(892)}$, reflecting the appearance of the decay chain $D \rightarrow K^*(892)\pi \rightarrow K\pi\pi$.

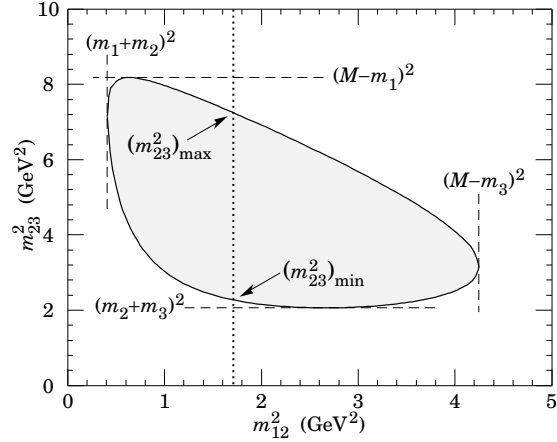


Figure 49.3: Dalitz plot for a three-body final state. In this example, the state is $\pi^+ K^0 p$ at 3 GeV. Four-momentum conservation restricts events to the shaded region.

49.4.4 Kinematic limits

49.4.4.1 Three-body decays

In a three-body decay (Fig. 49.2) the maximum of $|\mathbf{p}_3|$, [given by Eq. (49.21)], is achieved when $m_{12} = m_1 + m_2$, *i.e.*, particles 1 and 2 have the same vector velocity in the rest frame of the decaying particle. If, in addition, $m_3 > m_1, m_2$, then $|\mathbf{p}_3|_{\text{max}} > |\mathbf{p}_1|_{\text{max}}, |\mathbf{p}_2|_{\text{max}}$. The distribution of m_{12} values possesses an end-point or maximum value at $m_{12} = M - m_3$. This can be used to constrain the mass difference of a parent particle and one invisible decay product.

49.4.4.2 Sequential two-body decays

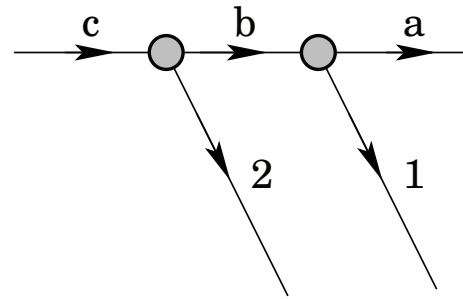


Figure 49.4: Particles participating in sequential two-body decay chain. Particles labeled 1 and 2 are visible while the particle terminating the chain (a) is invisible.

When a heavy particle initiates a sequential chain of two-body decays terminating in an invisible particle, constraints on the masses of the states participating in the chain can be obtained from end-points and thresholds in invariant mass distributions of the aggregated decay products. For the two-step decay chain depicted in Fig. 49.4 the invariant mass distribution of the two visible particles possesses an end-point given by:

$$(m_{12}^{\text{max}})^2 = \frac{(m_c^2 - m_b^2)(m_b^2 - m_a^2)}{m_b^2}, \quad (49.24)$$

provided particles 1 and 2 are massless. If visible particle 1 has

non-zero mass m_1 then Eq. (49.24) is replaced by

$$(m_{12}^{\max})^2 = m_1^2 + \frac{(m_c^2 - m_b^2)}{2m_b^2} \times \left(m_1^2 + m_b^2 - m_a^2 + \sqrt{(-m_1^2 + m_b^2 - m_a^2)^2 - 4m_1^2 m_a^2} \right) \quad (49.25)$$

See Refs. [2] and [3] for other cases.

49.4.5 Multibody decays

The above results may be generalized to final states containing any number of particles by combining some of the particles into “effective particles” and treating the final states as 2 or 3 “effective particle” states. Thus, if $p_{ijk\dots} = p_i + p_j + p_k + \dots$, then

$$m_{ijk\dots} = \sqrt{p_{ijk\dots}^2}, \quad (49.26)$$

and $m_{ijk\dots}$ may be used in place of *e.g.*, m_{12} in the relations in Sec. 49.4.3 or Sec. 49.4.4 above.

49.5 Cross sections

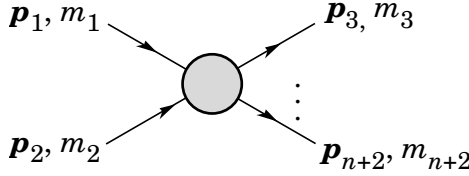


Figure 49.5: Definitions of variables for production of an n -body final state.

The differential cross section is given by

$$d\sigma = \frac{(2\pi)^4 |\mathcal{M}|^2}{4\sqrt{(p_1 \cdot p_2)^2 - m_1^2 m_2^2}} \times d\Phi_n(p_1 + p_2; p_3, \dots, p_{n+2}). \quad (49.27)$$

[See Eq. (49.12).] In the rest frame of m_2 (lab),

$$\sqrt{(p_1 \cdot p_2)^2 - m_1^2 m_2^2} = m_2 p_{1\text{lab}}; \quad (49.28a)$$

while in the center-of-mass frame

$$\sqrt{(p_1 \cdot p_2)^2 - m_1^2 m_2^2} = p_{1\text{cm}} \sqrt{s}. \quad (49.28b)$$

49.5.1 Two-body reactions

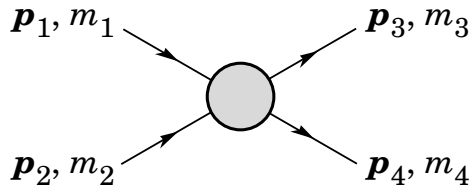


Figure 49.6: Definitions of variables for a two-body final state.

Two particles of momenta p_1 and p_2 and masses m_1 and m_2 scatter to particles of momenta p_3 and p_4 and masses m_3 and m_4 ; the Lorentz-invariant Mandelstam variables are defined by

$$s = (p_1 + p_2)^2 = (p_3 + p_4)^2 = m_1^2 + 2E_1 E_2 - 2\mathbf{p}_1 \cdot \mathbf{p}_2 + m_2^2, \quad (49.29)$$

$$t = (p_1 - p_3)^2 = (p_2 - p_4)^2 = m_1^2 - 2E_1 E_3 + 2\mathbf{p}_1 \cdot \mathbf{p}_3 + m_3^2, \quad (49.30)$$

$$u = (p_1 - p_4)^2 = (p_2 - p_3)^2 = m_1^2 - 2E_1 E_4 + 2\mathbf{p}_1 \cdot \mathbf{p}_4 + m_4^2, \quad (49.31)$$

and they satisfy

$$s + t + u = m_1^2 + m_2^2 + m_3^2 + m_4^2. \quad (49.32)$$

The two-body cross section may be written as

$$\frac{d\sigma}{dt} = \frac{1}{64\pi s} \frac{1}{|\mathbf{p}_{1\text{cm}}|^2} |\mathcal{M}|^2. \quad (49.33)$$

In the center-of-mass frame

$$t = (E_{1\text{cm}} - E_{3\text{cm}})^2 - (p_{1\text{cm}} - p_{3\text{cm}})^2 - 4p_{1\text{cm}} p_{3\text{cm}} \sin^2(\theta_{\text{cm}}/2) = t_0 - 4p_{1\text{cm}} p_{3\text{cm}} \sin^2(\theta_{\text{cm}}/2), \quad (49.34)$$

where θ_{cm} is the angle between particle 1 and 3. The limiting values t_0 ($\theta_{\text{cm}} = 0$) and t_1 ($\theta_{\text{cm}} = \pi$) for $2 \rightarrow 2$ scattering are

$$t_0(t_1) = \left[\frac{m_1^2 - m_3^2 - m_2^2 + m_4^2}{2\sqrt{s}} \right]^2 - (p_{1\text{cm}} \mp p_{3\text{cm}})^2. \quad (49.35)$$

In the literature the notation t_{\min} (t_{\max}) for t_0 (t_1) is sometimes used, which should be discouraged since $t_0 > t_1$. The center-of-mass energies and momenta of the incoming particles are

$$E_{1\text{cm}} = \frac{s + m_1^2 - m_2^2}{2\sqrt{s}}, \quad E_{2\text{cm}} = \frac{s + m_2^2 - m_1^2}{2\sqrt{s}}, \quad (49.36)$$

For $E_{3\text{cm}}$ and $E_{4\text{cm}}$, change m_1 to m_3 and m_2 to m_4 . Then

$$p_{i\text{cm}} = \sqrt{E_{i\text{cm}}^2 - m_i^2} \text{ and } p_{1\text{cm}} = \frac{p_{1\text{lab}} m_2}{\sqrt{s}}. \quad (49.37)$$

Here the subscript lab refers to the frame where particle 2 is at rest. [For other relations see Eqs. (49.2)–(49.4).]

49.5.2 Inclusive reactions

Choose some direction (usually the beam direction) for the z -axis; then the energy and momentum of a particle can be written as

$$E = m_T \cosh y, \quad p_x, p_y, p_z = m_T \sinh y, \quad (49.38)$$

where m_T , conventionally called the ‘transverse mass’, is given by

$$m_T^2 = m^2 + p_x^2 + p_y^2. \quad (49.39)$$

and the rapidity y is defined by

$$y = \frac{1}{2} \ln \left(\frac{E + p_z}{E - p_z} \right) = \ln \left(\frac{E + p_z}{m_T} \right) = \tanh^{-1} \left(\frac{p_z}{E} \right). \quad (49.40)$$

Note that the definition of the transverse mass in Eq. (49.39) differs from that used by experimentalists at hadron colliders (see Sec. 49.6.1 below). Under a boost in the z -direction to a frame with velocity β , $y \rightarrow y - \tanh^{-1} \beta$. Hence, the shape of the rapidity distribution dN/dy is invariant, as are differences in rapidity. The invariant cross section may also be rewritten

$$E \frac{d^3\sigma}{d^3p} = \frac{d^3\sigma}{d\phi dy p_T dp_T} \Rightarrow \frac{d^2\sigma}{\pi dy d(p_T^2)}. \quad (49.41)$$

The second form is obtained using the identity $dy/dp_z = 1/E$, and the third form represents the average over ϕ .

Feynman’s x variable is given by

$$x = \frac{p_z}{p_{z\text{max}}} \approx \frac{E + p_z}{(E + p_z)_{\text{max}}} \quad (p_T \ll |p_z|). \quad (49.42)$$

In the c.m. frame,

$$x \approx \frac{2p_{z\text{cm}}}{\sqrt{s}} = \frac{2m_T \sinh y_{\text{cm}}}{\sqrt{s}} \quad (49.43)$$

and

$$= (y_{\text{cm}})_{\text{max}} = \ln(\sqrt{s}/m). \quad (49.44)$$

The invariant mass M of the two-particle system described in Sec. 49.4.2 can be written in terms of these variables as

$$M^2 = m_1^2 + m_2^2 + 2[E_T(1)E_T(2) \cosh \Delta y - \mathbf{p}_T(1) \cdot \mathbf{p}_T(2)], \quad (49.45)$$

where

$$E_T(i) = \sqrt{|\mathbf{p}_T(i)|^2 + m_i^2}, \quad (49.46)$$

and $\mathbf{p}_T(i)$ denotes the transverse momentum vector of particle i .

For $p \gg m$, the rapidity [Eq. (49.40)] may be expanded to obtain

$$y = \frac{1}{2} \ln \frac{\cos^2(\theta/2) + m^2/4p^2 + \dots}{\sin^2(\theta/2) + m^2/4p^2 + \dots} \\ \approx -\ln \tan(\theta/2) \equiv \eta \quad (49.47)$$

where $\cos \theta = p_z/p$. The pseudorapidity η defined by the second line is approximately equal to the rapidity y for $p \gg m$ and $\theta \gg 1/\gamma$, and in any case can be measured when the mass and momentum of the particle are unknown. From the definition one can obtain the identities

$$\sinh \eta = \cot \theta, \quad \cosh \eta = 1/\sin \theta, \quad \tanh \eta = \cos \theta. \quad (49.48)$$

49.6 Transverse variables

At hadron colliders, a significant and unknown proportion of the energy of the incoming hadrons in each event escapes down the beam-pipe. Consequently, if invisible particles are created in the final state, their net momentum can only be constrained in the plane transverse to the beam direction. Defining the z -axis as the beam direction, this net momentum is equal to the missing transverse energy vector

$$\mathbf{E}_T^{\text{miss}} = -\sum_i \mathbf{p}_T(i), \quad (49.49)$$

where the sum runs over the transverse momenta of all visible final state particles.

49.6.1 Single production with semi-invisible final state

Consider a single heavy particle of mass M produced in association with visible particles which decays as in Fig. 49.1 to two particles, of which one (labeled particle 1) is invisible. The mass of the parent particle can be constrained with the quantity M_T

defined by

$$M_T^2 \equiv [E_T(1) + E_T(2)]^2 - [\mathbf{p}_T(1) + \mathbf{p}_T(2)]^2 \\ = m_1^2 + m_2^2 + 2[E_T(1)E_T(2) - \mathbf{p}_T(1) \cdot \mathbf{p}_T(2)], \quad (49.50)$$

where

$$\mathbf{p}_T(1) = \mathbf{E}_T^{\text{miss}}. \quad (49.51)$$

This quantity is called the ‘transverse mass’ by hadron collider experimentalists but it should be noted that it is quite different from that used in the description of inclusive reactions [Eq. (49.39)]. The distribution of event M_T values possesses an end-point at $M_T^{\text{max}} = M$. If $m_1 = m_2 = 0$ then

$$M_T^2 = 2|\mathbf{p}_T(1)||\mathbf{p}_T(2)|(1 - \cos \phi_{12}), \quad (49.52)$$

where ϕ_{ij} is defined as the angle between particles i and j in the transverse plane.

49.6.2 Pair production with semi-invisible final states

Consider two identical heavy particles of mass M produced such that their combined center-of-mass is at rest in the transverse plane (Fig. 49.7). Each particle decays to a final state consisting of an invisible particle of fixed mass m_1 together with an additional visible particle. M and m_1 can be constrained with the variables M_{T2} and M_{CT} which are defined in Refs. [4] and [5].

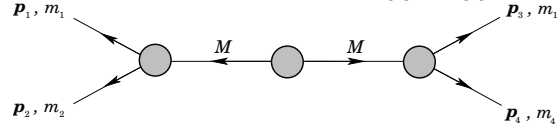


Figure 49.7: Definitions of variables for pair production of semi-invisible final states. Particles 1 and 3 are invisible while particles 2 and 4 are visible.

References

- [1] J.D. Jackson in *High Energy Physics, Les Houches 1965 Summer School*, GORDON AND BREACH Science Publishers (1965), p. 348.
- [2] I. Hinchliffe *et al.*, Phys. Rev. **D55**, 5520 (1997), [hep-ph/9610544].
- [3] B. C. Allanach *et al.*, JHEP **09**, 004 (2000), [hep-ph/0007009].
- [4] C. G. Lester and D. J. Summers, Phys. Lett. **B463**, 99 (1999), [hep-ph/9906349].
- [5] D. R. Tovey, JHEP **04**, 034 (2008), [arXiv:0802.2879].

50. Resonances

Revised August 2021 by D.M. Asner (BNL) and C. Hanhart (Jülich).

50.1 General Considerations

Perturbative methods can be applied to systems of quarks and gluons only for large momentum transfers (see review on ‘Quantum Chromodynamics’) and, under certain conditions, to some properties of systems that contain heavy quarks or very large momentum scales (see review on ‘Heavy-quark and soft-collinear effective theory’). Dealing with Quantum Chromodynamics (QCD) in the low momentum transfer region is a very complicated, non-perturbative problem. Accordingly, most hadrons are resonances, which means that they appear as poles of the S -matrix in the complex plane on unphysical sheets. These resonances can show up either in so-called formation experiments,

$$A + B \rightarrow \mathbf{R} \rightarrow C_1 + \dots + C_n,$$

where they become visible in an energy scan (for example, the R -function measured in e^+e^- annihilations — *cf.* the corresponding plots in the review on ‘Plots of Cross Sections and Related Quantities’), or together with a spectator particle S in production experiments of the kind

$$\begin{aligned} A + B \rightarrow \mathbf{R} + S &\rightarrow [C_1 + \dots + C_n] + S, \\ Z \rightarrow \mathbf{R} + S &\rightarrow [C_1 + \dots + C_n] + S, \end{aligned}$$

where the first reaction corresponds to an associated production, the second is a decay (see ‘Review of Multibody Charm Analyses’). In the latter case, the resonance properties are commonly extracted from a Dalitz-plot analysis (see review on ‘Kinematics’) or projections thereof.

Resonance phenomena are very rich: while typical hadronic widths are of the order of 100 MeV (*e.g.*, for the meson resonances $\rho(770)$ or $\psi(4040)$ or the baryon resonance $\Delta(1232)$) corresponding to a lifetime of 10^{-23} s, the widths can also be as small as a few MeV (*e.g.* of $\phi(1020)$ or J/ψ) or as large as several hundred MeV (*e.g.* of the meson resonances $f_0(500)$ or $D_1(2430)$ or the baryon resonance $N(2190)$).

Typically, a resonance appears as a peak in the total cross section. If the structure is narrow and if there are no relevant thresholds or other resonances nearby, the resonance properties may be extracted employing a Breit–Wigner parameterization, if necessary improved by using an energy-dependent width (*cf.* Sec. 50.3.1 of this review). However, in general, unitarity and analyticity call for the use of more refined tools. When there are overlapping resonances with the same quantum numbers, the resonance terms should not simply be added but combined in a non-trivial way either in a K -matrix approach (*cf.* Sec. 50.3.2 of this review) or using other advanced methods (*cf.* Sec. 50.3.6 of this review). Additional constraints from the S -matrix allow one to build more reliable amplitudes and, in turn, to reduce the systematic uncertainties of the resonance parameters: pole locations and residues. In addition, for broad resonances there is no direct relation between pole location and the total width/lifetime — then, the pole residues need to be used in order to quantify the decay properties.

For simplicity, throughout this review the formulas are given for resonances in a system of distinguishable, scalar particles. The additional complications that appear in the presence of spins can be controlled in the helicity framework developed by Jacob and Wick [1], or in a non-covariant [2] or covariant [3] tensor-operator formalisms. Within these approaches, sequential (cascade) decays are commonly treated as a coherent sum of two-body interactions. Most of the expressions below are given for two-body kinematics.

50.1.1 Properties of the S -matrix

The unitary operator that connects asymptotic *in* and *out* states is called the S -matrix. The scattering amplitude is defined as the interacting part of the S matrix. For a two-particles scattering process, it reads:

$$\begin{aligned} i(2\pi)^4 \delta^4(p_1 + p_2 - p'_1 - p'_2) \mathcal{M}(p_1, p_2; p'_1, p'_2)_{ba} = \\ = \text{out} \langle p'_1 p'_2, b | S - 1 | p_1 p_2, a \rangle_{\text{in}} \end{aligned} \quad (50.1)$$

where $|p_1 p_2, a\rangle$ and $|p'_1 p'_2, b\rangle$ are asymptotic states of two non-interacting particles with momentum p_1, p_2 and p'_1, p'_2 . The channel labels a and b are multi-indices specifying all additional properties of the channel. In general, \mathcal{M} is a matrix in channel space. For a single-particle state, we employ the relativistic normalization,

$$\langle p' | p \rangle = (2\pi)^3 2E_p \delta^3(\vec{p}' - \vec{p}), \quad (50.2)$$

with $E_p = \sqrt{\vec{p}^2 + m^2}$. The Mandelstam variables $s = (p_1 + p_2)^2$, $t = (p_1 - p'_1)^2$, and $u = (p_1 - p'_2)^2$ are the invariant variables describing the scattering. With these definitions the process in Eq. (50.1) is referred to as the s -channel scattering, where the total energy of the interacting system is given by \sqrt{s} , while the variable t is related to the scattering angle, *i.e.* the angle between the momenta of the particles 1 and 1' in the center-of-momentum frame. The variable u is not independent of s and t , but the relation

$$s + t + u = m_1^2 + m_2^2 + m_{1'}^2 + m_{2'}^2,$$

holds, where the m_i denote the masses of the incoming and outgoing particles, $i \in 1, 1', 2, 2'$. Therefore, the reaction amplitude is a function of two variables, $\mathcal{M}(s, t)$. The function $\mathcal{M}(s, t)$ is a multi-valued function due to the complex branch points in the Mandelstam variables. Branch points appear whenever there is a channel opening. Each two-particle threshold introduces a square-root singularity and the number of Riemann sheets doubles. For resonances coupled to multi-particle states with odd number of particles the threshold branch point is logarithmic [4]. The branch points appear in the complex plane of an unphysical sheet when there is a resonance in a subsystem of the final-state particles [4]. The cuts related to the openings of the crossed channels are located on the left-hand side of the complex plane, and, therefore, are referred to as the left-hand cuts. Triangle topologies can induce logarithmic branch points on the unphysical sheets often called triangle singularities (TS) [4–6].

Poles of reaction amplitude refer either to bound states or to resonances. The former poles are located on the physical sheet, the latter are located on unphysical sheets. Naturally, those located on the unphysical sheet closest to the physical one, often called the second sheet, have usually the largest impact on observables. Moreover, as follows from analyticity, if there is a pole at some complex value of s , there must be another pole at its complex conjugate value, s^* . For a single-channel case this is illustrated in Fig. 50.1: the pole with a negative imaginary part is closer to the physical axis and thus influences the observables in the vicinity of the resonance region more strongly. However, at the threshold both poles are equally distant and accordingly equally important. Any of these singularities can lead to some structure in the observables (see also Ref. [7]). If certain kinematical constraints are met, especially the TS can mimic resonance signals, as claimed in Refs. [8–13] or cause significant changes of resonance signals [14]. In addition to not all bumps being resonances, not every resonance generates a bump in all observables. For instance, there is no clear trace of the $N(1440)1/2^+$, the so called Roper resonance, in the πN observables or phase shifts, although careful analyses reveal a pole [15].

In case of two relevant channels we are faced with four Riemann sheets. Then, the sheet that is the closest to the physical axis changes, as the energy increases. This can be seen from the illustration in Fig. 50.2: for energies higher than the first, but lower than the second threshold, the sheet that connects smoothly to the upper half plane of the physical sheet (11) is sheet (21). However, for energies above the second threshold this role is taken over by sheet (22). Accordingly, a pole on sheet (21), but above the second threshold, will show up in data only as a cusp exactly at the second threshold. Sheet (12), on the other hand, is remote for all energies.

The analyticity principle of the S -matrix forbids any singularities on the first Riemann sheet except poles and branch points on the real axis. Unitarity constrains the imaginary part of the amplitude on the real axis as further discussed in the following

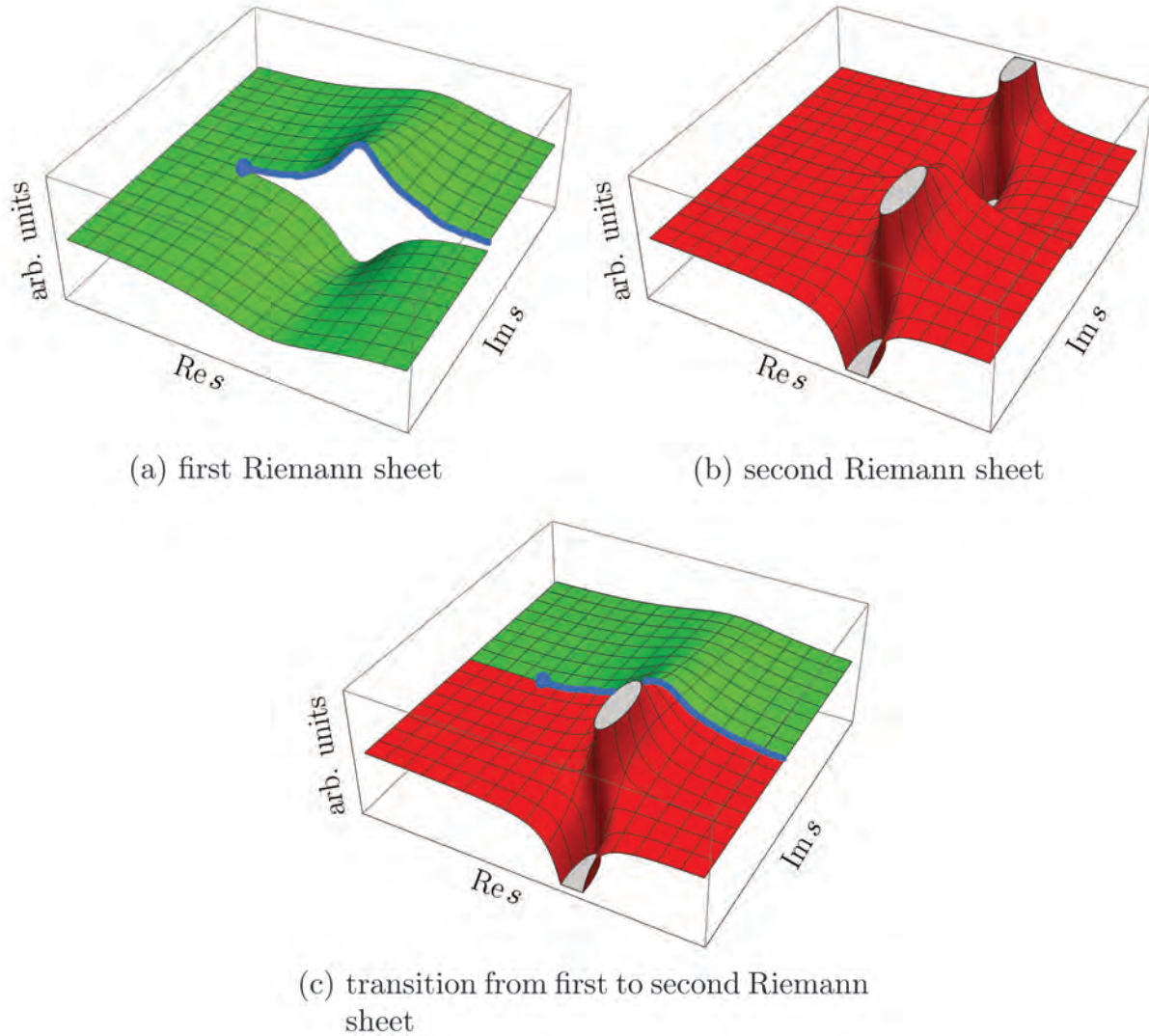


Figure 50.1: Imaginary part of a typical single-channel scattering amplitude with an isolated resonance. The blue line shows the physical range of the Mandelstam variable s : it is real and starts from the threshold shown by the blue dot. Plot (a) shows the imaginary part of the amplitude in the complex s -plane that corresponds to the first or physical sheet (green surface), plot (b) shows the related unphysical or the second sheet (red surface) which contains the resonance poles, and plot (c) shows the analytic continuation of the same amplitude from the upper half plane of the physical sheet to the lower half plane of the unphysical sheet. The two sheets are connected smoothly along the real axis above the threshold.

section. Further constraints come, *e.g.*, from crossing symmetry and duality [16]. Approaches based on analyticity and crossing symmetry, implemented via dispersion theory, like the Roy equations [17] or variants thereof, were developed and applied to $\pi\pi \rightarrow \pi\pi$ scattering [18–20], πK scattering [21], $\gamma\gamma \rightarrow \pi\pi$ [22] as well as pion-nucleon scattering [23, 24].

50.1.2 Consequences from unitarity

In what follows, scattering amplitudes, \mathcal{M} , and production amplitudes, \mathcal{A} , will be distinguished, since unitarity puts different constraints on these. For the scattering amplitude, all considered channels are supposed to be of comparable importance, while for the production amplitudes we require that the initial state is only weakly coupled and, therefore, the probability of the time-reversed reaction is negligibly small compared to the other coupled channels. Most of the strong-interaction processes are then described by the scattering amplitude, *e.g.* $\pi^+\pi^- \rightarrow K\bar{K}$, or $D^0\bar{D}^0 \rightarrow D^0\bar{D}^0$. Examples for production processes are $e^+e^- \rightarrow \pi^+\pi^-$, $\tau \rightarrow K^-\pi^0\nu$, $B^0 \rightarrow J/\psi\pi^+\pi^-$.

Unitarity of the S matrix, $S^\dagger S = 1$, which is equivalent to

the conservation of probability, translates to a constraint for the imaginary part of the reaction amplitude. The amplitude is real below the first threshold. Above the threshold, the discontinuity across the cut related to the threshold branch point, obeys the relation [25]:

$$\mathcal{M}_{ba} - \mathcal{M}_{ab}^* = i(2\pi)^4 \sum_c \int d\Phi_c \mathcal{M}_{cb}^* \mathcal{M}_{ca}, \quad (50.3)$$

where Φ_c is the invariant phase space for channel c . The sum includes only open channels, *i.e.* those for which the production threshold is below the energy of the scattered system. Complementary, the channels with the threshold higher than the energy of the system are called closed. Using time-reversal symmetry, and $\text{Disc } \mathcal{M}(s, t) = 2i \text{Im}(\mathcal{M}(s + i\epsilon, t))$ for the s -channel, the optical theorem follows:

$$\text{Im } \mathcal{M}_{aa}(s, 0) = 2q_a \sqrt{s} \sigma_{\text{tot}}(a \rightarrow \text{anything}). \quad (50.4)$$

Here, q_a is the momentum of particles in their center-of-

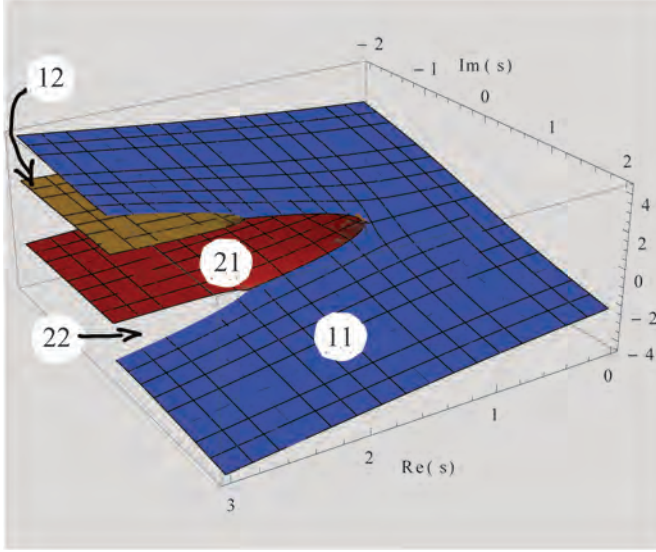


Figure 50.2: Cut structure of the S -matrix in the presence of two-channels. The four sheets are labelled as (ij) with $i = 1, 2$ and $j = 1, 2$ referring to the doubling of the sheets at the first and the second thresholds, respectively.

momentum frame,

$$q_a = \frac{\lambda^{1/2}(s, m_{1,a}^2, m_{2,a}^2)}{2\sqrt{s}}, \quad (50.5)$$

where $\lambda(x, y, z) = x^2 + y^2 + z^2 - 2xy - 2yz - 2zx$ is the Källén function, $m_{1,a}$ and $m_{2,b}$ are the masses of the two particles in the channel a , cf. Eq. (17) of the review on “Kinematics”. The value $t = 0$ in Eq. (50.4) corresponds to forward scattering.

The unitarity relation for a production amplitude for a channel a is given by

$$\mathcal{A}_a - \mathcal{A}_a^* = i(2\pi)^4 \sum_c \int d\Phi_c \mathcal{M}_{ca}^* \mathcal{A}_c. \quad (50.6)$$

Note that production amplitude written as a linear combination of the scattering amplitudes satisfies Eq. (50.6) due to Eq. (50.3). This solution is often practical, especially, when the scattering matrix is well known, as for example for $\pi\pi$ system below 1.1 GeV [26, 27]. However, it should be understood that this kind of treatment is only approximate, since it imports the analytic structure of the scattering amplitude including its left-hand cuts to the production amplitude which in general has a different cut structure. A more sophisticated application of the two-body-unitarity constraints from Eq. (50.6) is the Khuri-Treiman framework often employed to study three-body decays [28]. The standard procedure here is to derive the equations for the production amplitude for small values of the mass of the decaying particle in the scattering domain and relate it to the decay kinematics by an analytic continuation in the decay mass. The method was successfully applied to various decays of light mesons, $\eta \rightarrow 3\pi$ in Refs. [29–34], $\phi/\omega \rightarrow 3\pi$ in Ref. [35, 36], $\eta' \rightarrow \eta\pi\pi$ in Ref. [37], as well as to the charm-mesons decays $D^+ \rightarrow K^0/\pi^0/\pi^+$ [38, 39].

50.1.3 Partial-wave decomposition

It is often convenient to expand the scattering amplitude in partial waves. Since resonances have a well-defined spin, they appear only in a specific partial wave of the reaction amplitude. For scalar particles the expansion reads:

$$\mathcal{M}_{ba}(s, t) = \sum_{j=0}^{\infty} (2j+1) \mathcal{M}_{ba}^j(s) P_j(\cos(\theta)), \quad (50.7)$$

where j denotes the total angular momentum and the $P_j(\cos(\theta))$ denotes the Legendre polynomials. In the presence of spins an

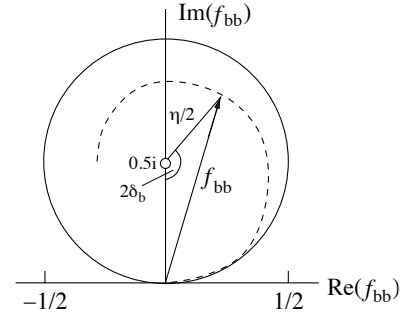


Figure 50.3: Argand plot showing a diagonal element of a partial-wave amplitude, a_{bb} , as a function of energy. The amplitude leaves the unitary circle (solid line) as soon as inelasticity sets in, $\eta < 1$ (dashed line).

expansion more complicated than Eq. (50.7) is necessary. In the absence of spins the parameter j coincides with the orbital angular momentum of the particle pairs in the initial and the final state. To simplify notations we will drop the label j for the single-argument function $\mathcal{M}_{ba}(s)$. The unitarity constraint for $\mathcal{M}_{ba}(s)$ reads,

$$\text{Im } \mathcal{M}_{ba}(s) = \sum_c \mathcal{M}_{cb}(s)^* \rho_c(s) \mathcal{M}_{ca}(s) \quad (50.8)$$

with $\rho_c(s)$ being a factor that is related to the two-body phase space in Eq. (12) of the review on “Kinematics”,

$$\rho_c(s) = \frac{(2\pi)^4}{2} \int d\Phi_2 = \frac{1}{16\pi} \frac{2|\vec{q}_c|}{\sqrt{s}}, \quad (50.9)$$

with the momentum q_c being defined in Eq. (50.5). Note that in case of the two particles being identical the inclusion of symmetry factors becomes necessary. The partial-wave amplitude $f_{ba}(s)$ is introduced via

$$f_{ba}(s) = \sqrt{\rho_b} \mathcal{M}_{ba}(s) \sqrt{\rho_a}. \quad (50.10)$$

From the unitarity condition Eq. (50.8) it follows that $\text{Im } f_{ba}^{-1} = -\delta_{ba}$. Moreover, $\mathbb{I} + 2if$ is a unitary matrix. Hence, the diagonal elements of f can be parameterized as,

$$f_{bb} = (\eta_b \exp(2i\delta_b) - 1)/2i, \quad (50.11)$$

where δ_b denotes the phase shift for the scattering from channel b to channel b , η_b is elasticity parameter — also called inelasticity. One has $0 \leq \eta_b \leq 1$, where $\eta_b = 1$ is referred to as a purely elastic scattering. The evolution of the partial-wave amplitude f_{bb} with energy can be displayed as a trajectory in the Argand plot, as shown in Fig. 50.3. In case of a two-channel problem, $\eta_b = \eta_a = \eta$, and the off-diagonal element is $f_{ba} = \sqrt{1 - \eta^2/2} \exp(i(\delta_b + \delta_a))$. The unitarity condition Eq. (50.11) sets the limit to the squared amplitude f_{bb} :

$$|f_{bb}|^2 = \frac{1}{4}(\eta_b^2 - 2\eta_b \cos(2\delta_b) + 1) \leq \frac{1}{4}(\eta_b + 1)^2, \quad (50.12)$$

where the maximum value is achieved for $\delta_b = \pi/2$. For the partial-wave-projected scattering amplitude the unitarity bound reads:

$$|\mathcal{M}_{bb}| \leq \frac{1}{2\rho_b}(\eta_b + 1) \leq \frac{8\pi}{q_b} \sqrt{s}, \quad (50.13)$$

where the second inequality comes from $\eta_b \leq 1$. For energies much larger than the masses of the scattering particles. One finds that the upper bound for $|\mathcal{M}_{bb}|$ tends to 16π for large s .

The partial-wave-projected production amplitude $\mathcal{A}(s)$ (the label j is dropped for consistency) is also constrained by unitarity. From Eq. (50.6) it follows:

$$\text{Im } \mathcal{A}_a = \sum_b \mathcal{M}_{ba}^* \rho_b \mathcal{A}_b, \quad (50.14)$$

where the sum runs over all open channels. For elastic processes, the sum collapses to the channel a . In this case, the phase of \mathcal{A}_a must agree with the phase of \mathcal{M}_{aa} since the left-hand side of Eq. (50.14) is a real number. The statement is known as the Watson theorem [40].

50.2 Properties of resonances

The main characteristics of a resonance is its pole position in the complex s -plane, s_R . The pole mass M_R and pole width Γ_R are introduced via the pole parameters

$$\sqrt{s_R} = M_R - i\Gamma_R/2. \quad (50.15)$$

Note that the standard Breit–Wigner parameters M_{BW} and Γ_{BW} , also introduced below, in general, deviate from the pole parameters, *e.g.*, due to finite width effects and the influence of thresholds. It should be stressed, however, that the pole location s_R as well as the pole residues to be introduced below, are the only resonance properties that are model- and parametrisation independent.

In addition to the pole position, a resonance is characterized by its couplings to the various channels called residues. The Baryon Particle Listings give the elastic pole residues and normalized transition residues. However, different conventions are used in the two sectors, which are shortly outlined here.

In the close vicinity of the resonance pole the scattering matrix \mathcal{M} can be written as

$$\lim_{s \rightarrow s_R} (s - s_R)\mathcal{M}_{ba} = -\mathcal{R}_{ba}. \quad (50.16)$$

The residues are calculated via an integration along a closed contour around the pole using

$$\mathcal{R}_{ba} = -\frac{1}{2\pi i} \oint ds \mathcal{M}_{ba}. \quad (50.17)$$

The factorization of the residue $(\mathcal{R}_{ba})^2 = \mathcal{R}_{aa} \times \mathcal{R}_{bb}$ allows one to introduce pole couplings according to

$$\tilde{g}_a = \mathcal{R}_{ba} / \sqrt{\mathcal{R}_{bb}}. \quad (50.18)$$

The pole couplings characterize the transition strength of a given resonance to some channel a independently of how the particular resonance was produced. For a two-particle decays in the S -wave, one may define a partial width and a branching fraction for a resonance via

$$\Gamma_{R \rightarrow a} = \frac{|\tilde{g}_a|^2}{M_R} \rho_a(M_R^2) \quad \text{and} \quad \text{Br}_a = \Gamma_{R \rightarrow a} / \Gamma_R, \quad (50.19)$$

where M_R and Γ_R were introduced in Eq. (50.15). This expression was used to define a two-photon width for the broad

$f_0(500)$ [41, 42] as well as in the corresponding section of the Meson Particle Listings. Analogously, one should use residues to quantify the coupling of resonances to certain production channels [43]. For an application of this formalism to the coupling of the $K_0^*(1430)$ resonance to a leptonic current see Ref. [44]. Equation (50.19) defines a partial-decay width independent of the reaction used to extract the parameters. For a narrow resonances it maps smoothly onto the other common definition of the branching fraction, discussed in Eq. (50.20) more closely related to observables. For broad, overlapping resonances, however, it should be understood that Eq. (50.19) serves the purpose to convert the residues to quantities that allow for a more direct comparison of resonance transitions to different channels. In case of resonances with significant couplings to channels that are still closed at the resonance mass, Eq. (50.19) cannot be used since the phase-space factor yields zero.

In the baryon sector, it is common to define the residue of the pole of the f_{ba} amplitude defined in Eq. (50.10) in variable \sqrt{s} instead of s . Accordingly, in the baryon listings the elastic pole residue, which refers to $\pi N \rightarrow \pi N$ scattering, is related to the residues introduced above via

$$r_{\pi N, \pi N} = \frac{\rho_{\pi N}(s_R)}{\sqrt{4s_R}} \mathcal{R}_{\pi N, \pi N}, \quad (50.20)$$

where s_R is the position of the pole. For evaluation of the phase-space factor for the complex argument, analytic continuation is required.

In the literature there are alternative definitions of a branching fraction, which are more close to what is observed in experiment than what follows from Eq. (50.19). Usually those are defined from the probability of the decay of a resonance to a certain channel as provided by the corresponding amplitude on the real axis, where the measurements are performed. It should be understood that in order to isolate an individual resonance in an amplitude defined on the real axis in general some model dependence is unavoidable (*e.g.* this is possible if the amplitude is provided by a sum of Breit–Wigner functions, however, since such a sum violates unitarity the parametrisation comes with an intrinsic theoretical uncertainty difficult to quantify). Having that said one may define the partial width of a resonance alternatively via

$$\Gamma_{R \rightarrow a} = \frac{(2\pi)^4}{2M_R} \int |\mathcal{A}_a|^2 d\Phi_a, \quad (50.21)$$

where \mathcal{A}_a is the decay amplitude of the resonance into channel a , which for multi-body final states may even contain resonances in a subchannel. For the two-body decay of a narrow, isolated resonance, \mathcal{A}_a is to a good approximation just \tilde{g}_a and we get back to Eq. (50.19). If the mass of the decaying resonance lies below the threshold of the final state, an integration over the resonance line-shape needs to be employed in addition. For example, for some generic three-body decay with two of the final-state particles going through a resonance one commonly defines (avoiding complications from spins or centrifugal barrier factors), for simplicity written in terms of Breit–Wigner functions (see next section)

$$\begin{aligned} \text{Br}_{R \rightarrow cR'} \text{Br}_{R' \rightarrow ab} &= (2\pi)^3 \int_{m_{\min R}^2}^{\infty} dm^2 \left| \frac{g_{R \rightarrow R'c}}{M_{BW R}^2 - m^2 - iM_{BW R} \Gamma_R(m^2)} \right|^2 \\ &\times (2\pi)^3 \int_{m_{\min R'}^2}^{(m-m_c)^2} dm_{ab}^2 \left| \frac{g_{R' \rightarrow ab}}{M_{BW R'}^2 - m_{ab}^2 - iM_{BW R'} \Gamma_{R'}(m_{ab}^2)} \right|^2 \int d\Phi_{ab} \int d\Phi_{R'(m_{ab}^2)c}, \end{aligned} \quad (50.22)$$

where $\Gamma_{R'(\prime)}(m^2)$ denotes the energy dependent width of resonance R (R') (details are given in the next section), $d\Phi_{R'(m_{ab}^2)c}$ denotes the two-body phase space for resonance R' , at a fixed mass m_{ab} , and particle c for a total energy m , and $d\Phi_{ab}$ the two-body phase space for particles a and b for a total energy m_{ab} , respectively. Furthermore, $m_{\min R'(\prime)}^2$ denotes the threshold of the lightest channel resonance R (R') couples to. For example, employing the parameters of the decay of $N^*(1520)$ to ρN one ob-

serves that the equation given above only allows the tail of the ρ -meson to contribute to the partial width of the $N^*(1520)$. If in a certain experiment the kinematics do not allow for a scan of the complete line shape of the mother particle, the appropriate procedure to determine the partial width in the approximation outlined above is to determine the effective resonance parameters from a fit to data and to then evaluate Eq. (50.22) in the limits given there. As stressed above, Eq. (50.22) is correct only,

if the use of Breit–Wigner functions is indeed justified for the mother and the daughter particles, which is often not the case. Then, to compare with experiment, the amplitudes need to be parametrised in a more sophisticated way and branching ratios can model independently only be defined via the residues.

In studies of decays where resonance R is very narrow, the first integral in Eq. (50.22) is obsolete and m in the boundaries of the second integral gets fixed to the mass of the mother particle. For recent use of such formulas for B -decays see, e.g., Refs. [45–48]. They were applied to study the three-pion system in Ref. [49].

50.3 Common parameterizations

In general, there is no universal, model-independent recipe to build scattering amplitudes. However, a few approaches presented in this section are practical to extract resonance properties in experimental analyses. The systematic theory uncertainties need to be assessed from a range of model variations that are permitted by general S -matrix principles and that provide a sufficient quality of description of the available data.

50.3.1 The Breit–Wigner parametrization

The relativistic Breit–Wigner parametrization provides a propagator for a single, isolated resonance,

$$\mathcal{A}(s) = \frac{N_a(s)}{M_{\text{BW}}^2 - s - iM_{\text{BW}}\Gamma(s)} \quad (50.23)$$

where M_{BW} is the Breit–Wigner mass, and $\Gamma_{\text{BW}} = \Gamma(M_{\text{BW}}^2)$ is the Breit–Wigner width. The function $\Gamma(s)$ is determined by the channels that the resonance can decay to. The numerator function $N_a(s)$ is specific to the production process. It includes kinematic factors and couplings related to the production process and the decay. Breit–Wigner functions with a s -independent width are justified only, if there is no relevant threshold in the vicinity of the resonance.

To give a concrete example, we consider a resonance observed in the channel a , that is also coupled to a set of channels labeled by index $b = 1, 2, \dots$, with the orbital angular momentum l_b . Couplings to the channels are denoted, g_b .

$$N_a(s) = \alpha g_a n_a(s) \quad (50.24)$$

$$\Gamma(s) = \frac{1}{M_{\text{BW}}} \sum_b g_b^2 \rho_b(s) n_b^2(s) \quad (50.25)$$

where the factor $n_a(s)$ includes the kinematic threshold factor q^{l_a} , and the barrier factor $F_{l_a}(q_a/q_0)$ that regularize the high-energy behaviour:

$$n_a = (q_a/q_0)^{l_a} F_{l_a}(q_a/q_0), \quad (50.26)$$

with l_a being the orbital angular momentum in channel a , $q_a(s)$ is defined in Eq. (50.5), and q_0 denotes some conveniently chosen momentum scale. The factor $(q_a)^l$ guarantees the correct threshold behavior. The rapid growth of this factor for angular momenta $l > 0$ is commonly compensated at higher energies by a phenomenological form factor, here denoted by $F_{l_a}(q_a, q_0)$. Often, the Blatt-Weisskopf form factors, $F_j(q/q_0)$, are used [50–52]:

$$F_0^2(z) = 1, \quad (50.27)$$

$$F_1^2(z) = 1/(1+z^2),$$

$$F_2^2(z) = 1/(9+3z^2+z^4),$$

with the scale parameter $R = 1/q_0$ in the range from 1 GeV^{-1} to 5 GeV^{-1} . Instead of using coupling constant in Eq. (50.25), one can define the energy-dependent partial width:

$$\Gamma_b(s) = \Gamma_{\text{BW},b} \frac{\rho_b(s)}{\rho_b(M_{\text{BW}}^2)} \left(\frac{q_b}{q_{\text{B}}} \right)^{2l_b} \frac{F_{l_b}^2(q_b, q_0)}{F_{l_b}^2(q_{\text{B}}, q_0)}. \quad (50.28)$$

Here q_{B} are the values of the break-up momentum evaluated at $s = M_{\text{BW}}^2$. The substitution is possible only for those channels where the threshold of the decay channel is located below the nominal resonance mass, otherwise, Eq. (50.25) should be used.

The Breit–Wigner parametrization provides an effective description of resonance phenomena. However, the parameters agree with the pole parameters only if the resonance is narrow, isolated (no nearby resonances in the same partial wave) and the background is smooth. Otherwise, the Breit–Wigner parameters deviate from the pole parameters and are reaction-dependent. If there is more than one resonance in one partial wave that significantly couples to the same channel, it is in general incorrect to use a sum of Breit–Wigner functions, for this usually leads to a violation of unitarity constraints, and hence, a non-quantifiable bias to resonance properties which are inferred from the reaction amplitude. In case of overlapping resonances in the same partial wave more refined methods should be used, like the K -matrix approach described in the next section.

50.3.2 K -matrix approach and Flatté parameterizations

The K -matrix method is a general construction for coupled-channel scattering amplitudes \mathcal{M}_{ba} that guarantees two-particle unitarity, but does not allow for the inclusion of left-hand cuts [53]. The amplitude reads,

$$n_b \mathcal{M}_{ba}^{-1} n_a = \mathcal{K}_{ba}^{-1} - i\delta_{ba} \rho_a n_a^2, \quad (50.29)$$

where \mathcal{K}_{ba} is a real function, a subject to modeling. The factor n_a , defined in Eq. (50.26), becomes important for waves with non-zero angular momentum. As there is no unique rigorous recipe to build \mathcal{K} , various parameterizations thereof have to be studied, in order to get access to the theoretical systematic uncertainty. One possible choice for the K -matrix is

$$\mathcal{K}_{ba}(s) = \sum_R \frac{g_b^R g_a^R}{m_R^2 - s} + \sum_{i=0}^{N_{\text{b.g.}}} b_{ba}^{(i)} s^i, \quad (50.30)$$

where m_R is referred to as the bare mass of the resonance R (not to be confused with the physical mass), the g_a^R are the bare couplings of the resonance R to the channel a (not to be confused with the residues). The $b_{ba}^{(i)}$ are matrices parameterizing the non-pole parts of the K -matrix. As long as all parameters appearing in Eq. (50.30) are real the amplitude is unitary. From the ansatz given above the scattering amplitude \mathcal{M} can be calculated directly using the matrix form,

$$\mathcal{M} = n[1 - \mathcal{K} i \rho n^2]^{-1} \mathcal{K} n, \quad (50.31)$$

where the diagonal matrix in the channel space $n = \text{diag}(n_a, n_b, \dots)$. As an alternative to Eq. (50.30), the same functional form as on the right side of Eq. (50.30) can be used to parameterize the inverse K -matrix, called by authors of Ref. [54] the M -matrix. Many other alternative expressions in the K -matrix framework are used for amplitude studies in lattice-QCD calculations [55–57].

Evaluation of the K -matrix amplitude for the multichannel problem requires an analytic continuation already on the real axis. For a given closed channel c , the factor $q_c(s)$ that enters ρ_c and n_c has to be calculated below the corresponding threshold, *i.e.* in the unphysical region of the particular channel c . This is done using analytic continuation as described *e.g.* in Refs. [27, 58]:

$$q_c = i\sqrt{-q_c^2} \quad \text{for } q_c^2 < 0. \quad (50.32)$$

The resulting line shape above and below the threshold of channel c is called the Flatté parameterization [58]. The continuation given above stays on the physical sheet. To reach the unphysical sheet the negative square root needs to be chosen. If the coupling of a resonance to the channel opening nearby is very strong, the Flatté parameterization shows a scaling invariance and does not allow for an extraction of individual partial decay widths, but only of ratios [59]. The position of the resonance poles can be determined by a study of the zeros of the analytic function $\det[1 - \mathcal{K} i \rho n^2]$. Due to the ρ factor, this determinant has a complicated multisheet structure, however, the closest unphysical sheet is always the one which is determined by the heaviest threshold below the studied point in s (*cf.* Fig. 50.2).

50.3.3 Scattering-length approximation

A scattering length, a , is defined as the first term in an expansion of the scattering phase shift introduced in Eq. (50.11). For S -waves one finds,

$$q \cot \delta = 1/a + O(q^2), \quad (50.33)$$

where q is the break-up momentum of the scattering system. The sign convention used in Eq. (50.33) is the one commonly employed in particle physics. In this convention a positive scattering length indicates attraction; if, however, the attraction is strong enough to generate a bound state, the scattering length changes sign and turns negative. A negative scattering length also occurs for repulsive interactions. Note that in nuclear physics the leading term in the expansion of Eq. (50.33) is usually defined as $-1/a$ such that *e.g.* a bound state would be related to a positive scattering length. Employing Eq. (50.33) the scattering amplitude reads

$$\mathcal{M}(s) = \frac{8\pi\sqrt{s}}{1/a - iq(s)}. \quad (50.34)$$

The scattering length is proportional to the value of the amplitude at threshold. A scattering length approximation is applicable only in a very limited energy range, however, might well be appropriate to analyse the recently discovered narrow near-threshold states [60,61] from this point of view, *e.g.*, in Refs. [62–64]. Moreover, it is possible to introduce the effect of a weakly coupled lower channel. To see this one might start from

$$\mathcal{K} = \begin{pmatrix} \gamma & \beta \\ \beta & 0 \end{pmatrix}, \quad (50.35)$$

with β, γ being real numbers. It leads to

$$\mathcal{M}_{\text{el.}}(s) = \frac{1}{1/(\gamma + i\beta^2\rho_{\text{inel.}}(s)) - i\rho(s)}, \quad (50.36)$$

with $\rho_{\text{inel.}}(s)$ being the phase-space factor of the inelastic channel. The scattering length for the amplitude in Eq. (50.36) obtains an imaginary part due to the coupling to the lower channel,

$$a = \frac{1}{8\pi\sqrt{s_{\text{thr}}}} (\gamma + i\beta^2\rho_{\text{inel.}}(s_{\text{thr}})). \quad (50.37)$$

If the function $\beta^2\rho_{\text{inel.}}(s)$ does not vary significantly in the energy range studied, the scattering-length approximation with a complex value is justified. For large values of a the amplitude of Eq. (50.36) develops a near-threshold pole located on the physical or unphysical sheet for negative or positive values of γ , respectively. While easy to use, it is important to stress, however, that the approximation in Eq. (50.35) is a specific choice of the dynamic function that produces a single pole near the physical region pointing at a hadronic molecule nature of the state studied [64–67]. Virtual states are discussed in this context in Ref. [68]. For practical analyses, various modifications of the parameterization have to be tested.

50.3.4 Two methods to build the production amplitude

When the unitary scattering amplitude is fixed, it can be used to build the production amplitude in a way that it is consistent with unitarity [52,69].

1. The Q -vector approach is discussed in Ref. [52,54,70]. It reads,

$$A_a(s) = \sum_c \mathcal{M}_{ac}(s) Q_c(s) / n_c, \quad Q_c(s) = \sum_i Q_c^{(i)} s^i. \quad (50.38)$$

The unitarity condition of Eq. (50.14) is satisfied when $Q_c(s)$ is a real function and in particular does not have singularities above the lowest threshold for all channels c . Besides these conditions $Q_c(s)$ is arbitrary. Note that in the Q -vector approach the left hand cuts of the scattering matrix $\mathcal{M}_{ac}(s)$ get imported to the production amplitude which might generate a wrong analytic structure. If this problem is relevant needs to be investigated on a case-by-case basis. In a study of

$\gamma\gamma \rightarrow \pi\pi$, *cf.* Ref. [41,42] a low-order polynomial is claimed to be sufficient to parametrize the energy dependence of the function $Q_c(s)$. The Q -vector method is convenient, if the full matrix \mathcal{M} is known, *cf.* Ref. [54].

2. The P -vector is a parameterization that exploits the K -matrix of the scattering amplitude [53,69]. It contains two components: the background term B_c that is coupled to the K -matrix via an intermediate loop represented by the $i\rho$ factor, and the “direct” resonance production term with couplings α_c^R :

$$A_a(s) = n_a \sum_c \left[1 - \mathcal{K} i\rho n^2 \right]_{ac}^{-1} P_c, \quad (50.39)$$

$$P_c = \sum_R \frac{\alpha_c^R g_c^R}{m_R^2 - s} + B_c.$$

Again, unitarity requires the parameters B_c and α_c^R to be real. Here, the masses m_R and the couplings g_c^R need to agree with those in \mathcal{K} in Eq. (50.30).

An important difference between the methods is to be noticed [69]. When the two-particle scattering amplitude goes to zero, the production amplitude in the Q -vector method vanishes for finite values of Q_c , while it stays finite in the P -vector approach. An version of the P -vector approach that exploits the analytic properties of production amplitudes [69,71,72] is widely used, *e.g.* in the dispersive Khuri-Treiman framework [28,73] for the construction of three-body-decay amplitudes.

50.3.5 Further improvements: Chew-Mandelstam function

The K -matrix described above usually allows one to get a proper fit of physical amplitudes and it is easy to deal with, however, it also has an important deficit: it violates constraints from analyticity — *e.g.*, ρ_a , given by Eq. (50.9), is ill-defined at $s = 0$, and for unequal masses it develops an unphysical cut (see left panel of Fig. 50.4). A method to improve the analytic properties was suggested in Refs. [74–78]. It replaces the phase-space factor $i\rho_a(s)$ in Eq. (50.29) by the analytic function $\Sigma_a(s)$ that produces the identical imaginary part on the right-hand cut. This function is called the Chew-Mandelstam function and for S -waves it reads [72,76]:

$$\Sigma_a(s) = \frac{1}{16\pi^2} \left[\frac{2q_a}{\sqrt{s}} \log \frac{m_1^2 + m_2^2 - s + 2\sqrt{s}q_a}{2m_1m_2} - (m_1^2 - m_2^2) \left(\frac{1}{s} - \frac{1}{(m_1 + m_2)^2} \right) \log \frac{m_1}{m_2} \right], \quad (50.40)$$

where m_1 and m_2 are masses of the final-state particles in channel a , $s_{\text{thra}} = (m_1 + m_2)^2$. The function along the real axis is plotted in the right panel of Fig. 50.4. For channels with $j > 0$, the threshold behavior has to be incorporated properly. This can be done, *e.g.*, by computing the dispersion integral

$$\Sigma_a(s + i0) = \frac{s - s_{\text{thra}}}{\pi} \int_{s_{\text{thra}}}^{\infty} \frac{\rho_a(s') n_a^2(s')}{(s' - s_{\text{thra}})(s' - s - i0)} ds'. \quad (50.41)$$

A further discussion of the calculation of the Chew-Mandelstam function can be found in Refs. [79,80].

If there is only a single resonance in a given channel, it is possible to feed the imaginary part of the Breit-Wigner function, Eq. (50.23) with an energy-dependent width, directly into a dispersion integral to get a resonance propagator with the correct analytic structure [81,82].

50.3.6 Two-potential decomposition

Another advanced technique to construct the scattering amplitude which is widely used in the literature [83–87] is based on the two-potential formalism [88]. The method is usually formulated for the full unprojected amplitude $\mathcal{M}_{ba}(s, t)$, however, in order to simplify the discussion we present the equations in the partial-wave-projected form.

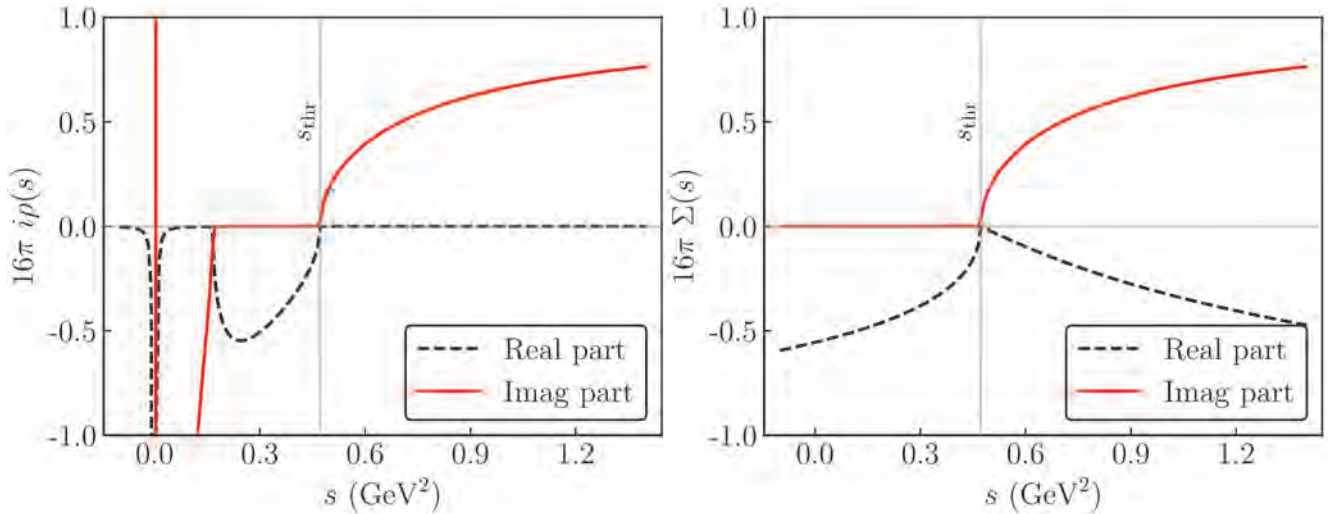


Figure 50.4: Comparison of the $i\rho$ function (left plot) to the Chew-Mandelstam function from Eq. (50.40) (right plot), evaluated for the case of S -wave $\eta\pi$ scattering. The values of s are taken slightly above the real axis, $s + i0$. The solid red line shows the imaginary part that is the same for both functions above threshold. The dashed black line presents the real part. One finds indications of the unphysical left-hand singularities of the function $i\rho$ on the left plot, while the Chew-Mandelstam function is analytic below the two-particle threshold.

The scattering amplitude \mathcal{M} is decomposed into a pole part and a non-pole part, often called background (b.g.)

$$\mathcal{M}(s) = \mathcal{M}^{\text{b.g.}}(s) + \mathcal{M}^{\text{pole}}(s). \quad (50.42)$$

The splitting given in Eq. (50.42) is not unique and model-dependent (see, *e.g.*, the discussions in Refs. [89,90]). The background scattering matrix is assumed to be unitary by itself. One option is to parameterize it, *e.g.* at low energies directly in terms of phase shifts and inelasticities — see, *e.g.*, Refs. [44,87,91]. In this case the vertex functions $\Omega(s)_{ab}$ introduced below can be written in terms of an Omnes matrix [91], which reduces to the well-known Omnes function in the single-channel case [71]. Alternatively, it can be computed based on some potential, $V^{\text{b.g.}}$, fed into a proper scattering equation.

The complete amplitude \mathcal{M} of Eq. (50.42) is unitary, if the pole part is chosen as

$$\mathcal{M}^{\text{pole}}(s) = \Omega(s) [1 - V^{\text{R}}(s)\Sigma^u(s)]^{-1} V^{\text{R}}(s) \Omega^T(s). \quad (50.43)$$

where the resonance potential reads in channel space

$$V_{ab}^{\text{R}}(s) = \sum_R \frac{g_a^{\text{R}} g_b^{\text{R}}}{M_R^2 - s}, \quad (50.44)$$

Σ_{ab}^u denotes the self-energy matrix, and g_a^{R} and M_R denote the bare coupling of the resonance R to channel a and its bare mass, respectively. A relation analogous to Eq. (50.6) holds for the normalized vertex functions, however, with the final state interaction provided by $\mathcal{M}^{\text{b.g.}}$

$$\text{Disc } \Omega_{ab}(s) = 2i \sum_c \mathcal{M}_{ca}^{\text{b.g.*}}(s) \rho_c(s) \Omega_{cb}(s). \quad (50.45)$$

The discontinuity of the self-energy matrix $\Sigma^u(s)$ is

$$\text{Disc } \Sigma_{ab}^u(s) = 2i \sum_c \Omega_{ca}^*(s) \rho_c(s) \Omega_{cb}(s). \quad (50.46)$$

The real part of Σ^u can be calculated from Eq. (50.46) via a properly subtracted dispersion integral. If $\mathcal{M}^{\text{b.g.}}$ is unitary, the use of Eq. (50.43) leads to a unitary full amplitude, *cf.* Eq. (50.42). However, the pole term alone is unitary only for a vanishing background amplitude. In this situation the amplitude just described reduces to the analytically improved K -matrix of Sec. 50.3.5. While the omission of non-pole terms is a bad approximation

for, *e.g.*, scalar-isoscalar $\pi\pi$ interactions at low energies [92], it typically works well for higher partial waves.

The algebra of the two potential splitting presented in Eq. (50.42) is found to be very practical in various other cases, beyond the pole-background separation. It was employed in Refs. [87,91] to treat the pion vector and scalar form factor, respectively, over a sizable energy range including inelasticities. A similar decomposition applied to the $3 \rightarrow 3$ scattering problem provided a way to isolate the non-separable one-particle exchange singularity from the short-range resonance interaction [93].

Acknowledgement

We are very grateful to Mikhail Mikhasenko, who gave vital input to improve this review and to Ulf-G. Meißner for valuable comments on the manuscript.

References

- [1] M. Jacob and G. C. Wick, *Annals Phys.* **7**, 404 (1959), [*Annals Phys.*281,774(2000)].
- [2] C. Zemach, *Phys. Rev.* **140B**, 97, 109 (1965).
- [3] A. V. Anisovich *et al.*, *J. Phys.* **G28**, 15 (2002), [*hep-ph/0105330*].
- [4] V. N. Gribov, Y. L. Dokshitzer and J. Nyiri, *Strong Interactions of Hadrons at High Energies – Gribov Lectures on Theoretical Physics*, Cambridge University Press, Cambridge (2009).
- [5] L. Landau, *Nucl. Phys.* **13**, 181 (1959).
- [6] R. Cutkosky, *J. Math. Phys.* **1**, 429 (1960).
- [7] A rapid change in an amplitude is not an unambiguous signal of a singularity of the S -matrix [94], however, for realistic interactions this connection holds.
- [8] S. Coleman and R. E. Norton, *Nuovo Cim.* **38**, 438 (1965).
- [9] C. Schmid, *Phys. Rev.* **154**, 5, 1363 (1967).
- [10] I. J. R. Aitchison and C. Kacser, *Il Nuovo Cimento A* (1965-1970) **40**, 2, 576 (1965), ISSN 1826-9869, URL <https://doi.org/10.1007/BF02721045>.
- [11] M. Mikhasenko, B. Ketzer and A. Sarantsev, *Phys. Rev.* **D91**, 9, 094015 (2015), [*arXiv:1501.07023*].
- [12] M. Bayar *et al.*, *Phys. Rev.* **D94**, 7, 074039 (2016), [*arXiv:1609.04133*].
- [13] F. Aceti, L. R. Dai and E. Oset, *Phys. Rev.* **D94**, 9, 096015 (2016), [*arXiv:1606.06893*].

- [14] J.-J. Wu *et al.*, Phys. Rev. Lett. **108**, 081803 (2012), [arXiv:1108.3772].
- [15] L. D. Roper, Phys. Rev. Lett. **12**, 340 (1964).
- [16] M. Fukugita and K. Igi, Phys. Rept. **31**, 237 (1977).
- [17] S. M. Roy, Phys. Lett. **36B**, 353 (1971).
- [18] B. Ananthanarayan *et al.*, Phys. Rept. **353**, 207 (2001), [hep-ph/0005297].
- [19] G. Colangelo, J. Gasser and H. Leutwyler, Nucl. Phys. **B603**, 125 (2001), [hep-ph/0103088].
- [20] R. Garcia-Martin *et al.*, Phys. Rev. **D83**, 074004 (2011), [arXiv:1102.2183].
- [21] P. Buettiker, S. Descotes-Genon and B. Moussallam, Eur. Phys. J. **C33**, 409 (2004), [hep-ph/0310283].
- [22] M. Hoferichter, D. R. Phillips and C. Schat, Eur. Phys. J. **C71**, 1743 (2011), [arXiv:1106.4147].
- [23] G. E. Hite and F. Steiner, Nuovo Cim. A **18**, 237 (1973).
- [24] M. Hoferichter *et al.*, Phys. Rept. **625**, 1 (2016), [arXiv:1510.06039].
- [25] M. P. Peskin and D. V. Schroeder, *An Introduction to Quantum Field Theory*, Westview Press, 1995.
- [26] R. Garcia-Martin *et al.*, Phys. Rev. D **83**, 074004 (2011), [arXiv:1102.2183].
- [27] V. V. Anisovich and A. V. Sarantsev, Eur. Phys. J. **A16**, 229 (2003), [hep-ph/0204328].
- [28] N. N. Khuri and S. B. Treiman, Phys. Rev. **119**, 1115 (1960).
- [29] J. Kambor, C. Wiesendanger and D. Wyler, Nucl. Phys. B **465**, 215 (1996), [hep-ph/9509374].
- [30] A. V. Anisovich and H. Leutwyler, Phys. Lett. B **375**, 335 (1996), [hep-ph/9601237].
- [31] P. Guo *et al.*, Phys. Lett. **B771**, 497 (2017), [arXiv:1608.01447].
- [32] M. Albaladejo and B. Moussallam, Eur. Phys. J. **C77**, 8, 508 (2017), [arXiv:1702.04931].
- [33] G. Colangelo *et al.*, Eur. Phys. J. **C78**, 11, 947 (2018), [arXiv:1807.11937].
- [34] K. Kampf *et al.*, Phys. Rev. D **101**, 7, 074043 (2020), [arXiv:1911.11762].
- [35] F. Niecknig, B. Kubis and S. P. Schneider, Eur. Phys. J. **C72**, 2014 (2012), [arXiv:1203.2501].
- [36] I. V. Danilkin *et al.*, Phys. Rev. **D91**, 9, 094029 (2015), [arXiv:1409.7708].
- [37] T. Isken *et al.*, Eur. Phys. J. **C77**, 7, 489 (2017), [arXiv:1705.04339].
- [38] F. Niecknig and B. Kubis, JHEP **10**, 142 (2015), [arXiv:1509.03188].
- [39] F. Niecknig and B. Kubis, Phys. Lett. **B780**, 471 (2018), [arXiv:1708.00446].
- [40] K. M. Watson, Phys. Rev. **95**, 228 (1954).
- [41] D. Morgan and M. R. Pennington, Z. Phys. **C37**, 431 (1988), [Erratum: Z. Phys. C39,590(1988)].
- [42] D. Morgan and M. R. Pennington, Z. Phys. **C48**, 623 (1990).
- [43] B. Moussallam, Eur. Phys. J. C **71**, 1814 (2011), [arXiv:1110.6074].
- [44] L. Von Detten *et al.*, Eur. Phys. J. C **81**, 5, 420 (2021), [arXiv:2103.01966].
- [45] R. Aaij *et al.* (LHCb), Phys. Rev. D **94**, 7, 072001 (2016), [arXiv:1608.01289].
- [46] R. Aaij *et al.* (LHCb), Phys. Rev. D **92**, 1, 012012 (2015), [arXiv:1505.01505].
- [47] R. Aaij *et al.* (LHCb), Phys. Rev. D **91**, 9, 092002 (2015), [Erratum: Phys.Rev.D 93, 119901 (2016)], [arXiv:1503.02995].
- [48] R. Aaij *et al.* (LHCb), Phys. Rev. D **102**, 112003 (2020), [arXiv:2009.00026].
- [49] M. Aghasyan *et al.* (COMPASS), Phys. Rev. D **98**, 9, 092003 (2018), [arXiv:1802.05913].
- [50] J. M. Blatt and V. F. Weisskopf, *Theoretical nuclear physics*, Springer, New York (1952), ISBN 9780471080190.
- [51] F. Von Hippel and C. Quigg, Phys. Rev. **D5**, 624 (1972).
- [52] S. U. Chung *et al.*, Annalen Phys. **4**, 404 (1995).
- [53] I. J. R. Aitchison, Nucl. Phys. **A189**, 417 (1972).
- [54] K. L. Au, D. Morgan and M. R. Pennington, Phys. Rev. **D35**, 1633 (1987).
- [55] J. J. Dudek, R. G. Edwards and D. J. Wilson (Hadron Spectrum), Phys. Rev. **D93**, 9, 094506 (2016), [arXiv:1602.05122].
- [56] R. A. Briceno *et al.*, Phys. Rev. **D97**, 5, 054513 (2018), [arXiv:1708.06667].
- [57] A. J. Woss *et al.* (2019), [arXiv:1904.04136].
- [58] S. M. Flatte, Phys. Lett. **63B**, 224 (1976).
- [59] V. Baru *et al.*, Eur. Phys. J. **A23**, 523 (2005), [arXiv:nucl-th/0410099].
- [60] S. K. Choi *et al.* (Belle), Phys. Rev. Lett. **91**, 262001 (2003), [hep-ex/0309032].
- [61] R. Aaij *et al.* (LHCb), Phys. Rev. Lett. **122**, 22, 222001 (2019), [arXiv:1904.03947].
- [62] E. Braaten and J. Stapleton, Phys. Rev. **D81**, 014019 (2010), [arXiv:0907.3167].
- [63] V. Baru *et al.*, Eur. Phys. J. **A44**, 93 (2010), [arXiv:1001.0369].
- [64] C. Fernández-Ramírez *et al.* (JPAC), Phys. Rev. Lett. **123**, 9, 092001 (2019), [arXiv:1904.10021].
- [65] D. Morgan, Nucl. Phys. **A543**, 632 (1992).
- [66] V. Baru *et al.*, Phys. Lett. **B586**, 53 (2004), [hep-ph/0308129].
- [67] F.-K. Guo *et al.*, Rev. Mod. Phys. **90**, 1, 015004 (2018), [arXiv:1705.00141].
- [68] I. Matuschek *et al.*, Eur. Phys. J. A **57**, 3, 101 (2021), [arXiv:2007.05329].
- [69] I. J. R. Aitchison (2015), [arXiv:1507.02697].
- [70] R. N. Cahn and P. V. Landshoff, Nucl. Phys. **B266**, 451 (1986).
- [71] R. Omnes, Nuovo Cim. **8**, 316 (1958).
- [72] J. L. Basdevant and E. L. Berger, Phys. Rev. **D16**, 657 (1977).
- [73] I. J. R. Aitchison and R. Pasquier, Phys. Rev. **152**, 4, 1274 (1966).
- [74] G. J. Gounaris and J. J. Sakurai, Phys. Rev. Lett. **21**, 244 (1968).
- [75] M. R. Pennington *et al.*, Eur. Phys. J. **C56**, 1 (2008), [arXiv:0803.3389].
- [76] J. A. Oller and E. Oset, Phys. Rev. **D60**, 074023 (1999), [hep-ph/9809337].
- [77] N. N. Achasov and A. V. Kiselev, Phys. Rev. **D83**, 054008 (2011), [arXiv:1011.4446].
- [78] A. V. Anisovich *et al.*, Phys. Rev. **D84**, 076001 (2011).
- [79] J. H. Reid and N. N. Trofimenkoff, J. Math. Phys. **25**, 3540 (1984).
- [80] J. A. Oller and U. G. Meissner, Phys. Lett. B **500**, 263 (2001), [hep-ph/0011146].
- [81] E. L. Lomon and S. Pacetti, Phys. Rev. **D85**, 113004 (2012), [Erratum: Phys. Rev. D86,039901(2012)], [arXiv:1201.6126].
- [82] B. Moussallam, Eur. Phys. J. **C73**, 2539 (2013), [arXiv:1305.3143].
- [83] I. R. Afnan and B. Blankleider, Phys. Rev. **C22**, 1638 (1980).
- [84] A. D. Lahiff and I. R. Afnan, Phys. Rev. **C60**, 024608 (1999), [arXiv:nucl-th/9903058].

- [85] A. Matsuyama, T. Sato and T. S. H. Lee, Phys. Rept. **439**, 193 (2007), [arXiv:nucl-th/0608051].
- [86] D. Ronchen *et al.*, Eur. Phys. J. **A49**, 44 (2013), [arXiv:1211.6998].
- [87] C. Hanhart, Phys. Lett. **B715**, 170 (2012), [arXiv:1203.6839].
- [88] K. Nakano, Phys. Rev. **C26**, 1123 (1982).
- [89] D. Djukanovic, J. Gegelia and S. Scherer, Phys. Rev. **D76**, 037501 (2007), [arXiv:0707.2030].
- [90] M. Doring *et al.*, Phys. Lett. **B681**, 26 (2009), [arXiv:0903.1781].
- [91] S. Ropertz, C. Hanhart and B. Kubis, Eur. Phys. J. **C78**, 12, 1000 (2018), [arXiv:1809.06867].
- [92] J. Gasser and U. G. Meissner, Nucl. Phys. **B357**, 90 (1991).
- [93] M. Mikhasenko *et al.*, JHEP **08**, 080 (2019), [arXiv:1904.11894].
- [94] G. Calucci, L. Fonda and G. C. Ghirardi, Phys. Rev. **166**, 1719 (1968).

51. Cross-Section Formulae for Specific Processes

Revised August 2019 by H. Baer (Oklahoma U.) and R.N. Cahn (LBNL).

PART I: STANDARD MODEL PROCESSES

Setting aside leptonproduction (for which, see Sec. 16 of this *Review*), the cross sections of primary interest are those with light incident particles, e^+e^- , $\gamma\gamma$, $q\bar{q}$, gq , gg , etc., where g and q represent gluons and light quarks. The produced particles include both light particles and heavy ones - t , W , Z , and the Higgs boson H . We provide the production cross sections calculated within the Standard Model for several such processes.

51.1 Resonance Formation

Resonant cross sections are generally described by the Breit-Wigner formula (Sec. 50.3 of this *Review*).

$$\sigma(E) = \frac{2J+1}{(2S_1+1)(2S_2+1)} \frac{4\pi}{k^2} \left[\frac{\Gamma^2/4}{(E-E_0)^2 + \Gamma^2/4} \right] B_{in} B_{out}, \quad (51.1)$$

where E is the c.m. energy, J is the spin of the resonance, and the number of polarization states of the two incident particles are $2S_1+1$ and $2S_2+1$. The c.m. momentum in the initial state is k , E_0 is the c.m. energy at the resonance, and Γ is the full width at half maximum height of the resonance. The branching fraction for the resonance into the initial-state channel is B_{in} and into the final-state channel is B_{out} . For a narrow resonance, the factor in square brackets may be replaced by $\pi\Gamma\delta(E-E_0)/2$.

51.2 Production of light particles

The production of point-like, spin-1/2 fermions in e^+e^- annihilation through a virtual photon, $e^+e^- \rightarrow \gamma^* \rightarrow f\bar{f}$, at c.m. energy squared s is given by

$$\frac{d\sigma}{d\Omega} = N_c \frac{\alpha^2}{4s} \beta [1 + \cos^2\theta + (1-\beta^2)\sin^2\theta] Q_f^2, \quad (51.2)$$

where β is v/c for the produced fermions in the c.m., θ is the c.m. scattering angle, and Q_f is the charge of the fermion. The factor N_c is 1 for charged leptons and 3 for quarks. In the ultrarelativistic limit, $\beta \rightarrow 1$,

$$\sigma = N_c Q_f^2 \frac{4\pi\alpha^2}{3s} = N_c Q_f^2 \frac{86.8 \text{ nb}}{s(\text{GeV}^2)}. \quad (51.3)$$

The cross section for the annihilation of a $q\bar{q}$ pair into a distinct pair $q'\bar{q}'$ through a gluon is completely analogous up to color factors, with the replacement $\alpha \rightarrow \alpha_s$. Treating all quarks as massless, averaging over the colors of the initial quarks and defining $t = -s \sin^2(\theta/2)$, $u = -s \cos^2(\theta/2)$, one finds [1]

$$\frac{d\sigma}{d\Omega}(q\bar{q} \rightarrow q'\bar{q}') = \frac{\alpha_s^2}{9s} \frac{t^2 + u^2}{s^2}. \quad (51.4)$$

Crossing symmetry gives

$$\frac{d\sigma}{d\Omega}(qq' \rightarrow qq') = \frac{\alpha_s^2}{9s} \frac{s^2 + u^2}{t^2}. \quad (51.5)$$

If the quarks q and q' are identical, we have

$$\frac{d\sigma}{d\Omega}(q\bar{q} \rightarrow q\bar{q}) = \frac{\alpha_s^2}{9s} \left[\frac{t^2 + u^2}{s^2} + \frac{s^2 + u^2}{t^2} - \frac{2u^2}{3st} \right], \quad (51.6)$$

and by crossing

$$\frac{d\sigma}{d\Omega}(qq \rightarrow qq) = \frac{\alpha_s^2}{9s} \left[\frac{t^2 + s^2}{u^2} + \frac{s^2 + u^2}{t^2} - \frac{2s^2}{3ut} \right]. \quad (51.7)$$

Annihilation of e^+e^- into $\gamma\gamma$ has the cross section

$$\frac{d\sigma}{d\Omega}(e^+e^- \rightarrow \gamma\gamma) = \frac{\alpha^2}{2s} \frac{u^2 + t^2}{tu}. \quad (51.8)$$

The related QCD process also has a triple-gluon coupling. The cross section is

$$\frac{d\sigma}{d\Omega}(q\bar{q} \rightarrow gg) = \frac{8\alpha_s^2}{27s} (t^2 + u^2) \left(\frac{1}{tu} - \frac{9}{4s^2} \right). \quad (51.9)$$

The crossed reactions are

$$\frac{d\sigma}{d\Omega}(qg \rightarrow qg) = \frac{\alpha_s^2}{9s} (s^2 + u^2) \left(-\frac{1}{su} + \frac{9}{4t^2} \right) \quad (51.10)$$

and

$$\frac{d\sigma}{d\Omega}(gg \rightarrow q\bar{q}) = \frac{\alpha_s^2}{24s} (t^2 + u^2) \left(\frac{1}{tu} - \frac{9}{4s^2} \right). \quad (51.11)$$

Finally,

$$\frac{d\sigma}{d\Omega}(gg \rightarrow gg) = \frac{9\alpha_s^2}{8s} \left(3 - \frac{ut}{s^2} - \frac{su}{t^2} - \frac{st}{u^2} \right). \quad (51.12)$$

Lepton-quark scattering is analogous (neglecting Z exchange)

$$\frac{d\sigma}{d\Omega}(eq \rightarrow eq) = \frac{\alpha^2}{2s} e_q^2 \frac{s^2 + u^2}{t^2}. \quad (51.13)$$

where e_q is the charge of the quark. For neutrino scattering with the four-Fermi interaction

$$\frac{d\sigma}{d\Omega}(\nu d \rightarrow \ell^- u) = \frac{G_F^2 s}{4\pi^2}, \quad (51.14)$$

where the Cabibbo angle suppression is ignored. Similarly

$$\frac{d\sigma}{d\Omega}(\nu\bar{u} \rightarrow \ell^- \bar{d}) = \frac{G_F^2 s}{4\pi^2} \frac{(1 + \cos\theta)^2}{4}. \quad (51.15)$$

To obtain the formulae for deep inelastic scattering (presented in more detail in Section 18) we consider quarks of type i carrying a fraction $x = Q^2/(2M\nu)$ of the nucleon's energy, where $\nu = E - E'$ is the energy lost by the lepton in the nucleon rest frame. With $y = \nu/E$ we have the correspondences

$$1 + \cos\theta \rightarrow 2(1-y),$$

$$d\Omega_{cm} \rightarrow 4\pi f_i(x) dx dy, \quad (51.16)$$

where the latter incorporates the quark distribution, $f_i(x)$. In this way we find

$$\begin{aligned} \frac{d\sigma}{dx dy}(eN \rightarrow eX) &= \frac{4\pi\alpha^2 x s}{Q^4} \frac{1}{2} [1 + (1-y)^2] \\ &\times \left[\frac{4}{9}(u(x) + \bar{u}(x) + \dots) + \frac{1}{9}(d(x) + \bar{d}(x) + \dots) \right] \end{aligned} \quad (51.17)$$

where now $s = 2ME$ is the cm energy squared for the electron-nucleon collision, and we have suppressed contributions from higher mass quarks.

Similarly,

$$\frac{d\sigma}{dx dy}(\nu N \rightarrow \ell^- X) = \frac{G_F^2 x s}{\pi} [(d(x) + \dots) + (1-y)^2(\bar{u}(x) + \dots)] \quad (51.18)$$

and

$$\frac{d\sigma}{dx dy}(\bar{\nu} N \rightarrow \ell^+ X) = \frac{G_F^2 x s}{\pi} [(\bar{d}(x) + \dots) + (1-y)^2(u(x) + \dots)]. \quad (51.19)$$

Quasi-elastic neutrino scattering ($\nu\mu n \rightarrow \mu^- p$, $\bar{\nu}\mu p \rightarrow \mu^+ n$) is directly related to the crossed reaction, neutron decay. The formula for the differential cross section is presented, for example, in N.J. Baker *et al.*, Phys. Rev. **D23**, 2499 (1981).

51.3 Hadroproduction of heavy quarks

For hadroproduction of heavy quarks $Q = c, b, t$, it is important to include mass effects in the formulae. For $q\bar{q} \rightarrow Q\bar{Q}$, one has

$$\frac{d\sigma}{d\Omega}(q\bar{q} \rightarrow Q\bar{Q}) = \frac{\alpha_s^2}{9s^3} \sqrt{1 - \frac{4m_Q^2}{s}} \times \left[(m_Q^2 - t)^2 + (m_Q^2 - u)^2 + 2m_Q^2 s \right], \quad (51.20)$$

while for $gg \rightarrow Q\bar{Q}$ one has

$$\begin{aligned} \frac{d\sigma}{d\Omega}(gg \rightarrow Q\bar{Q}) = & \frac{\alpha_s^2}{32s} \sqrt{1 - \frac{4m_Q^2}{s}} \left[\frac{6}{s^2} (m_Q^2 - t)(m_Q^2 - u) - \right. \\ & \left. - \frac{m_Q^2 (s - 4m_Q^2)}{3(m_Q^2 - t)(m_Q^2 - u)} + \frac{4}{3} \frac{(m_Q^2 - t)(m_Q^2 - u) - 2m_Q^2 (m_Q^2 + t)}{(m_Q^2 - t)^2} \right. \\ & \left. + \frac{4}{3} \frac{(m_Q^2 - t)(m_Q^2 - u) - 2m_Q^2 (m_Q^2 + u)}{(m_Q^2 - u)^2} - 3 \frac{(m_Q^2 - t)(m_Q^2 - u) + m_Q^2 (u - t)}{s(m_Q^2 - t)} \right. \\ & \left. - 3 \frac{(m_Q^2 - t)(m_Q^2 - u) + m_Q^2 (t - u)}{s(m_Q^2 - u)} \right]. \quad (51.21) \end{aligned}$$

51.4 Production of Weak Gauge Bosons

51.4.1 W and Z resonant production

Resonant production of a single W or Z is governed by the partial widths

$$\Gamma(W \rightarrow \ell_i \bar{\nu}_i) = \frac{\sqrt{2} G_F m_W^3}{12\pi} \quad (51.22)$$

$$\Gamma(W \rightarrow q_i \bar{q}_j) = 3 \frac{\sqrt{2} G_F |V_{ij}|^2 m_W^3}{12\pi} \quad (51.23)$$

$$\begin{aligned} \Gamma(Z \rightarrow f\bar{f}) = & N_c \frac{\sqrt{2} G_F m_Z^3}{6\pi} \\ & \times \left[(T_3 - Q_f \sin^2 \theta_W)^2 + (Q_f \sin^2 \theta_W)^2 \right]. \quad (51.24) \end{aligned}$$

The weak mixing angle is θ_W . The CKM matrix elements are indicated by V_{ij} and N_c is 3 for $q\bar{q}$ final states and 1 for leptonic final states.

The full differential cross section for $f_i \bar{f}_j \rightarrow (W, Z) \rightarrow f_i' \bar{f}_j'$ is given by

$$\begin{aligned} \frac{d\sigma}{d\Omega} = & \frac{N_c^f}{N_c^{i'}} \cdot \frac{1}{256\pi^2 s} \cdot \frac{s^2}{(s - M^2)^2 + s\Gamma^2} \\ & \times \left[(L^2 + R^2)(L'^2 + R'^2)(1 + \cos^2 \theta) \right. \\ & \left. + (L^2 - R^2)(L'^2 - R'^2)2 \cos \theta \right] \quad (51.25) \end{aligned}$$

where M is the mass of the W or Z . The couplings for the W are $L = (8G_F m_W^2 / \sqrt{2})^{1/2} V_{ij} / \sqrt{2}$; $R = 0$ where V_{ij} is the corresponding CKM matrix element, with an analogous expression for L' and R' . For Z , the couplings are $L = (8G_F m_Z^2 / \sqrt{2})^{1/2} (T_3 - \sin^2 \theta_W Q)$; $R = -(8G_F m_Z^2 / \sqrt{2})^{1/2} \sin^2 \theta_W Q$, where T_3 is the weak isospin of the initial left-handed fermion and Q is the initial fermion's electric charge. The expressions for L' and R' are analogous. The color factors $N_c^{i'f}$ are 3 for initial or final quarks and 1 for initial or final leptons.

51.4.2 Production of pairs of weak gauge bosons

The cross section for $f\bar{f} \rightarrow W^+W^-$ is given in term of the couplings of the left-handed and right-handed fermion f , $\ell = 2(T_3 - Qx_W)$, $r = -2Qx_W$, where T_3 is the third component of weak isospin for the left-handed f , Q is its electric charge (in units of the proton charge), and $x_W = \sin^2 \theta_W$:

$$\begin{aligned} \frac{d\sigma}{dt} = & \frac{2\pi\alpha^2}{N_c s^2} \left\{ \left[\left(Q + \frac{\ell + r}{4x_W} \frac{s}{s - m_Z^2} \right)^2 \right. \right. \\ & \left. \left. + \left(\frac{\ell - r}{4x_W} \frac{s}{s - m_Z^2} \right)^2 \right] A(s, t, u) \right. \\ & \left. + \frac{1}{2x_W} \left(Q + \frac{\ell}{2x_W} \frac{s}{s - m_Z^2} \right) \right. \\ & \left. (\Theta(-Q)I(s, t, u) - \Theta(Q)I(s, u, t)) \right. \\ & \left. + \frac{1}{8x_W^2} (\Theta(-Q)E(s, t, u) + \Theta(Q)E(s, u, t)) \right\}, \quad (51.26) \end{aligned}$$

where $\Theta(x)$ is 1 for $x > 0$ and 0 for $x < 0$, and where

$$\begin{aligned} A(s, t, u) = & \left(\frac{tu}{m_W^4} - 1 \right) \left(\frac{1}{4} - \frac{m_W^2}{s} + 3 \frac{m_W^4}{s^2} \right) + \frac{s}{m_W^2} - 4, \\ I(s, t, u) = & \left(\frac{tu}{m_W^4} - 1 \right) \left(\frac{1}{4} - \frac{m_W^2}{2s} - \frac{m_W^4}{st} \right) + \frac{s}{m_W^2} - 2 + 2 \frac{m_W^2}{t}, \\ E(s, t, u) = & \left(\frac{tu}{m_W^4} - 1 \right) \left(\frac{1}{4} + \frac{m_W^4}{t^2} \right) + \frac{s}{m_W^2}, \quad (51.27) \end{aligned}$$

and s, t, u are the usual Mandelstam variables with $s = (p_f + p_{\bar{f}})^2$, $t = (p_f - p_{W^-})^2$, $u = (p_f - p_{W^+})^2$. The factor N_c is 3 for quarks and 1 for leptons.

The analogous cross-section for $q_i \bar{q}_j \rightarrow W^\pm Z^0$ is

$$\begin{aligned} \frac{d\sigma}{dt} = & \frac{\pi\alpha^2 |V_{ij}|^2}{6s^2 x_W^2} \left\{ \left(\frac{1}{s - m_W^2} \right)^2 \left[\left(\frac{9 - 8x_W}{4} \right) (ut - m_W^2 m_Z^2) \right. \right. \\ & \left. \left. + (8x_W - 6) s (m_W^2 + m_Z^2) \right] \right. \\ & \left. + \left[\frac{ut - m_W^2 m_Z^2 - s(m_W^2 + m_Z^2)}{s - m_W^2} \right] \left[\frac{\ell_j}{t} - \frac{\ell_i}{u} \right] \right. \\ & \left. + \frac{ut - m_W^2 m_Z^2}{4(1 - x_W)} \left[\frac{\ell_j^2}{t^2} + \frac{\ell_i^2}{u^2} \right] + \frac{s(m_W^2 + m_Z^2)}{2(1 - x_W)} \frac{\ell_i \ell_j}{tu} \right\}, \quad (51.28) \end{aligned}$$

where ℓ_i and ℓ_j are the couplings of the left-handed q_i and q_j as defined above. The CKM matrix element between q_i and q_j is V_{ij} .

The cross section for $q_i \bar{q}_j \rightarrow Z^0 Z^0$ is

$$\frac{d\sigma}{dt} = \frac{\pi\alpha^2}{96} \frac{\ell_i^4 + r_i^4}{x_W^2 (1 - x_W^2)^2 s^2} \left[\frac{t}{u} + \frac{u}{t} + \frac{4m_Z^2 s}{tu} - m_Z^4 \left(\frac{1}{t^2} + \frac{1}{u^2} \right) \right]. \quad (51.29)$$

51.5 Production of Higgs Bosons

51.5.1 Resonant Production

The Higgs boson of the Standard Model can be produced resonantly in the collisions of quarks, leptons, W or Z bosons, gluons, or photons. The production cross section is thus controlled by the partial width of the Higgs boson into the entrance channel and its total width. The branching fractions for the Standard Model Higgs boson are shown in Fig. 1 of the ‘‘Searches for Higgs bosons’’

review in the Particle Listings section, as a function of the Higgs boson mass. The partial widths are given by the relations

$$\Gamma(H \rightarrow f\bar{f}) = \frac{G_F m_H^2 N_c}{4\pi\sqrt{2}} \left(1 - 4m_f^2/m_H^2\right)^{3/2}, \quad (51.30)$$

$$\Gamma(H \rightarrow W^+W^-) = \frac{G_F m_H^3 \beta_W}{32\pi\sqrt{2}} (4 - 4a_W + 3a_W^2), \quad (51.31)$$

$$\Gamma(H \rightarrow ZZ) = \frac{G_F m_H^3 \beta_Z}{64\pi\sqrt{2}} (4 - 4a_Z + 3a_Z^2), \quad (51.32)$$

where N_c is 3 for quarks and 1 for leptons and where $a_W = 1 - \beta_W^2 = 4m_W^2/m_H^2$ and $a_Z = 1 - \beta_Z^2 = 4m_Z^2/m_H^2$. The decay to two gluons proceeds through quark loops, with the t quark dominating [2]. Explicitly,

$$\Gamma(H \rightarrow gg) = \frac{\alpha_s^2 G_F m_H^3}{36\pi^3 \sqrt{2}} \left| \sum_q I(m_q^2/m_H^2) \right|^2, \quad (51.33)$$

where $I(z)$ is complex for $z < 1/4$. For $z < 2 \times 10^{-3}$, $|I(z)|$ is small so the light quarks contribute negligibly. For $m_H < 2m_t$, $z > 1/4$ and

$$I(z) = 3 \left[2z + 2z(1-4z) \left(\sin^{-1} \frac{1}{2\sqrt{z}} \right)^2 \right], \quad (51.34)$$

which has the limit $I(z) \rightarrow 1$ as $z \rightarrow \infty$.

51.5.2 Higgs Boson Production in W^* and Z^* decay

The Standard Model Higgs boson can be produced in the decay of a virtual W or Z (“Higgstrahlung”) [3, 4]: In particular, if k is the c.m. momentum of the Higgs boson,

$$\sigma(q_i \bar{q}_j \rightarrow WH) = \frac{\pi \alpha^2 |V_{ij}|^2}{36 \sin^4 \theta_W} \frac{2k}{\sqrt{s}} \frac{k^2 + 3m_W^2}{(s - m_W^2)^2} \quad (51.35)$$

$$\sigma(f\bar{f} \rightarrow ZH) = \frac{2\pi \alpha^2 (\ell_f^2 + r_f^2)}{48 N_c \sin^4 \theta_W \cos^4 \theta_W} \frac{2k}{\sqrt{s}} \frac{k^2 + 3m_Z^2}{(s - m_Z^2)^2}, \quad (51.36)$$

where ℓ and r are defined as above.

51.5.3 W and Z Fusion

Just as high-energy electrons can be regarded as sources of virtual photon beams, at very high energies they are sources of virtual W and Z beams. For Higgs boson production, it is the longitudinal components of the W s and Z s that are important [5]. The distribution of longitudinal W s carrying a fraction y of the electron’s energy is [6]

$$f(y) = \frac{g^2}{16\pi^2} \frac{1-y}{y}, \quad (51.37)$$

where $g = e/\sin \theta_W$. In the limit $s \gg m_H \gg m_W$, the partial decay rate is $\Gamma(H \rightarrow W_L W_L) = (g^2/64\pi)(m_H^3/m_W^2)$ and in the equivalent W approximation [7]

$$\begin{aligned} \sigma(e^+e^- \rightarrow \bar{\nu}_e \nu_e H) &= \frac{1}{16m_W^2} \left(\frac{\alpha}{\sin^2 \theta_W} \right)^3 \\ &\times \left[\left(1 + \frac{m_H^2}{s} \right) \log \frac{s}{m_H^2} - 2 + 2 \frac{m_H^2}{s} \right]. \end{aligned} \quad (51.38)$$

There are significant corrections to this relation when m_H is not large compared to m_W [8]. For $m_H = 150$ GeV, the estimate is too high by 51% for $\sqrt{s} = 1000$ GeV, 32% too high at $\sqrt{s} = 2000$ GeV, and 22% too high at $\sqrt{s} = 4000$ GeV. Fusion of ZZ to make a Higgs boson can be treated similarly. Identical formulae apply for Higgs production in the collisions of quarks whose charges permit

the emission of a W^+ and a W^- , except that QCD corrections and CKM matrix elements are required. Even in the absence of QCD corrections, the fine-structure constant ought to be evaluated at the scale of the collision, say m_W . All quarks contribute to the ZZ fusion process.

51.6 Inclusive hadronic reactions

One-particle inclusive cross sections $E d^3\sigma/d^3p$ for the production of a particle of momentum p are conveniently expressed in terms of rapidity y (see above) and the momentum p_T transverse to the beam direction (in the c.m.):

$$E \frac{d^3\sigma}{d^3p} = \frac{d^3\sigma}{d\phi dy p_T dp_T}. \quad (51.39)$$

In appropriate circumstances, the cross section may be decomposed as a partonic cross section multiplied by the probabilities of finding partons of the prescribed momenta:

$$\sigma_{\text{hadronic}} = \sum_{ij} \int dx_1 dx_2 f_i(x_1) f_j(x_2) d\hat{\sigma}_{\text{partonic}}, \quad (51.40)$$

The probability that a parton of type i carries a fraction of the incident particle’s that lies between x_1 and $x_1 + dx_1$ is $f_i(x_1)dx_1$ and similarly for partons in the other incident particle. The partonic collision is specified by its c.m. energy squared $\hat{s} = x_1 x_2 s$ and the momentum transfer squared \hat{t} . The final hadronic state is more conveniently specified by the rapidities y_1, y_2 of the two jets resulting from the collision and the transverse momentum p_T . The connection between the differentials is

$$dx_1 dx_2 d\hat{t} = dy_1 dy_2 \frac{\hat{s}}{s} dp_T^2, \quad (51.41)$$

so that

$$\begin{aligned} \frac{d^3\sigma}{dy_1 dy_2 dp_T^2} &= \\ &\frac{\hat{s}}{s} \left[f_i(x_1) f_j(x_2) \frac{d\hat{\sigma}}{d\hat{t}}(\hat{s}, \hat{t}, \hat{u}) + f_i(x_2) f_j(x_1) \frac{d\hat{\sigma}}{d\hat{t}}(\hat{s}, \hat{u}, \hat{t}) \right], \end{aligned} \quad (51.42)$$

where we have taken into account the possibility that the incident parton types might arise from either incident particle. The second term should be dropped if the types are identical: $i = j$.

51.7 Two-photon processes

In the Weizsäcker-Williams picture, a high-energy electron beam is accompanied by a spectrum of virtual photons of energies ω and invariant-mass squared $q^2 = -Q^2$, for which the photon number density is

$$dn = \frac{\alpha}{\pi} \left[1 - \frac{\omega}{E} + \frac{\omega^2}{E^2} - \frac{m_e^2 \omega^2}{Q^2 E^2} \right] \frac{d\omega}{\omega} \frac{dQ^2}{Q^2}, \quad (51.43)$$

where E is the energy of the electron beam. The cross section for $e^+e^- \rightarrow e^+e^-X$ is then [9]

$$d\sigma_{e^+e^- \rightarrow e^+e^-X}(s) = dn_1 dn_2 d\sigma_{\gamma\gamma \rightarrow X}(W^2), \quad (51.44)$$

where $W^2 = m_X^2$. Integrating from the lower limit $Q^2 = m_e^2 \frac{\omega_i^2}{E_i(E_i - \omega_i)}$ to a maximum Q^2 gives

$$\begin{aligned} \sigma_{e^+e^- \rightarrow e^+e^-X}(s) &= \frac{\alpha^2}{\pi^2} \int_{z_{th}}^1 \frac{dz}{z} \\ &\times \left[\left(\ln \frac{Q_{max}^2}{zm_e^2} - 1 \right)^2 f(z) + \frac{1}{3} (\ln z)^3 \right] \sigma_{\gamma\gamma \rightarrow X}(zs), \end{aligned} \quad (51.45)$$

where

$$f(z) = \left(1 + \frac{1}{2}z \right)^2 \ln(1/z) - \frac{1}{2}(1-z)(3+z). \quad (51.46)$$

The appropriate value of Q_{max}^2 depends on the properties of the produced system X . For production of hadronic systems, $Q_{max}^2 \approx m_\rho^2$, while for lepton-pair production, $Q^2 \approx W^2$. For production of a resonance with spin $J \neq 1$, we have

$$\begin{aligned} \sigma_{e^+e^- \rightarrow e^+e^-R}(s) &= (2J+1) \frac{8\alpha^2 \Gamma_{R \rightarrow \gamma\gamma}}{m_R^3} \\ &\times \left[f(m_R^2/s) \left(\ln \frac{m_V^2 s}{m_e^2 m_R^2} - 1 \right)^2 - \frac{1}{3} \left(\ln \frac{s}{M_R^2} \right)^3 \right], \end{aligned} \quad (51.47)$$

where m_V is the mass that enters into the form factor for the $\gamma\gamma \rightarrow R$ transition, typically m_ρ .

PART II: PROCESSES BEYOND THE STANDARD MODEL

51.8 Production of supersymmetric particles

In supersymmetric (SUSY) theories (see Supersymmetric Particle Searches in this *Review*), every boson has a fermionic superpartner, and every fermion has a bosonic superpartner. The minimal supersymmetric Standard Model (MSSM) is a direct supersymmetrization of the Standard Model (SM), although a second Higgs doublet is needed to avoid triangle anomalies [10]. Under *soft* SUSY breaking, superpartner masses are lifted above the SM particle masses. In weak scale SUSY, the superpartners are invoked to stabilize the weak scale under radiative corrections, so the superpartners are expected to have masses of order the TeV scale.

51.8.1 Gluino and squark production

The superpartners of gluons are the color octet, spin- $\frac{1}{2}$ gluinos (\tilde{g}), while each helicity component of quark flavor has a spin-0 squark partner, e.g. \tilde{q}_L and \tilde{q}_R . Third generation left- and right- squarks are expected to have large mixing, resulting in mass eigenstates \tilde{q}_1 and \tilde{q}_2 , with $m_{\tilde{q}_1} < m_{\tilde{q}_2}$ (here, q denotes any of the SM flavors of quarks and \tilde{q}_i the corresponding flavor and type ($i = L, R$ or $1, 2$) of squark). Gluino pair production ($\tilde{g}\tilde{g}$) takes place via either glue-gluon or quark-antiquark annihilation [11].

The subprocess cross sections are usually presented as differential distributions in the Mandelstam variables s , t and u . Note that for a $2 \rightarrow 2$ scattering subprocess $ab \rightarrow cd$, the Mandelstam variable $s = (p_a + p_b)^2 = (p_c + p_d)^2$, where p_a is the 4-momentum of particle a , and so forth. The variable $t = (p_c - p_a)^2$, where c and a are taken conventionally to be the most similar particles in the subprocess. The variable u would then be equal to $(p_d - p_a)^2$. Note that since s , t and u are squares of 4-vectors, they are invariants in any inertial reference frame.

Gluino pair production at hadron colliders is described by:

$$\begin{aligned} \frac{d\sigma}{dt}(gg \rightarrow \tilde{g}\tilde{g}) &= \frac{9\pi\alpha_s^2}{4s^2} \left\{ \frac{2(m_{\tilde{g}}^2 - t)(m_{\tilde{g}}^2 - u)}{s^2} \right. \\ &+ \frac{(m_{\tilde{g}}^2 - t)(m_{\tilde{g}}^2 - u) - 2m_{\tilde{g}}^2(m_{\tilde{g}}^2 + t)}{(m_{\tilde{g}}^2 - t)^2} \\ &+ \frac{(m_{\tilde{g}}^2 - t)(m_{\tilde{g}}^2 - u) - 2m_{\tilde{g}}^2(m_{\tilde{g}}^2 + u)}{(m_{\tilde{g}}^2 - u)^2} + \frac{m_{\tilde{g}}^2(s - 4m_{\tilde{g}}^2)}{(m_{\tilde{g}}^2 - t)(m_{\tilde{g}}^2 - u)} \\ &- \frac{(m_{\tilde{g}}^2 - t)(m_{\tilde{g}}^2 - u) + m_{\tilde{g}}^2(u - t)}{s(m_{\tilde{g}}^2 - t)} \\ &\left. - \frac{(m_{\tilde{g}}^2 - t)(m_{\tilde{g}}^2 - u) + m_{\tilde{g}}^2(t - u)}{s(m_{\tilde{g}}^2 - u)} \right\}, \end{aligned} \quad (51.48)$$

where α_s is the strong fine structure constant. Also,

$$\begin{aligned} \frac{d\sigma}{dt}(q\bar{q} \rightarrow \tilde{g}\tilde{g}) &= \frac{8\pi\alpha_s^2}{9s^2} \left\{ \frac{4}{3} \left(\frac{m_{\tilde{g}}^2 - t}{m_{\tilde{q}}^2 - t} \right)^2 + \frac{4}{3} \left(\frac{m_{\tilde{g}}^2 - u}{m_{\tilde{q}}^2 - u} \right)^2 \right. \\ &+ \frac{3}{s^2} [(m_{\tilde{g}}^2 - t)^2 + (m_{\tilde{g}}^2 - u)^2 + 2m_{\tilde{g}}^2 s] \\ &- 3 \frac{[(m_{\tilde{g}}^2 - t)^2 + m_{\tilde{g}}^2 s]}{s(m_{\tilde{q}}^2 - t)} \\ &\left. - 3 \frac{[(m_{\tilde{g}}^2 - u)^2 + m_{\tilde{g}}^2 s]}{s(m_{\tilde{q}}^2 - u)} + \frac{1}{3} \frac{m_{\tilde{g}}^2 s}{(m_{\tilde{q}}^2 - t)(m_{\tilde{q}}^2 - u)} \right\}. \end{aligned} \quad (51.49)$$

Gluinos can also be produced in association with squarks: $\tilde{g}\tilde{q}_i$ production, where \tilde{q}_i represents any of the various types (left, right- or mixed) and flavors of squarks. The subprocess cross section is independent of whether the squark is the right-, left- or mixed type:

$$\begin{aligned} \frac{d\sigma}{dt}(gq \rightarrow \tilde{g}\tilde{q}_i) &= \frac{\pi\alpha_s^2}{24s^2} \frac{[\frac{16}{3}(s^2 + (m_{\tilde{q}_i}^2 - u)^2) + \frac{4}{3}s(m_{\tilde{q}_i}^2 - u)]}{s(m_{\tilde{g}}^2 - t)(m_{\tilde{q}_i}^2 - u)^2} \\ &\times \left((m_{\tilde{g}}^2 - u)^2 + (m_{\tilde{q}_i}^2 - m_{\tilde{g}}^2)^2 + \frac{2sm_{\tilde{g}}^2(m_{\tilde{q}_i}^2 - m_{\tilde{g}}^2)}{(m_{\tilde{g}}^2 - t)} \right). \end{aligned} \quad (51.50)$$

There are many different subprocesses for production of squark pairs. Since left- and right- squarks generally have different masses and different decay patterns, we present the differential cross section for each subprocess of \tilde{q}_i ($i = L, R$ or $1, 2$) separately. (In early literature, the following formulae were often combined into a single equation which didn't differentiate the various squark types.) The result for $gg \rightarrow \tilde{q}_i\tilde{q}_i$ is:

$$\begin{aligned} \frac{d\sigma}{dt}(gg \rightarrow \tilde{q}_i\tilde{q}_i) &= \frac{\pi\alpha_s^2}{4s^2} \left\{ \frac{1}{3} \left(\frac{m_{\tilde{q}}^2 + t}{m_{\tilde{q}}^2 - t} \right)^2 + \frac{1}{3} \left(\frac{m_{\tilde{q}}^2 + u}{m_{\tilde{q}}^2 - u} \right)^2 \right. \\ &+ \frac{3}{32s^2} (8s(4m_{\tilde{q}}^2 - s) + 4(u - t)^2) + \frac{7}{12} \\ &- \frac{1}{48} \frac{(4m_{\tilde{q}}^2 - s)^2}{(m_{\tilde{q}}^2 - t)(m_{\tilde{q}}^2 - u)} \\ &+ \frac{3}{32} \frac{[(t - u)(4m_{\tilde{q}}^2 + 4t - s) - 2(m_{\tilde{q}}^2 - u)(6m_{\tilde{q}}^2 + 2t - s)]}{s(m_{\tilde{q}}^2 - t)} \\ &+ \frac{3}{32} \frac{[(u - t)(4m_{\tilde{q}}^2 + 4u - s) - 2(m_{\tilde{q}}^2 - t)(6m_{\tilde{q}}^2 + 2u - s)]}{s(m_{\tilde{q}}^2 - u)} \\ &\left. + \frac{7}{96} \frac{[4m_{\tilde{q}}^2 + 4t - s]}{m_{\tilde{q}}^2 - t} + \frac{7}{96} \frac{[4m_{\tilde{q}}^2 + 4u - s]}{m_{\tilde{q}}^2 - u} \right\}, \end{aligned} \quad (51.51)$$

which has an obvious $u \leftrightarrow t$ symmetry.

For $q\bar{q} \rightarrow \tilde{q}_i\tilde{q}_i$ with the same initial and final state flavors, we have

$$\begin{aligned} \frac{d\sigma}{dt}(q\bar{q} \rightarrow \tilde{q}_i\tilde{q}_i) &= \frac{2\pi\alpha_s^2}{9s^2} \left\{ \frac{1}{(t - m_{\tilde{q}}^2)^2} + \frac{2}{s^2} - \frac{2/3}{s(t - m_{\tilde{q}}^2)} \right\} \\ &\times [-st - (t - m_{\tilde{q}_i}^2)^2], \end{aligned} \quad (51.52)$$

while if initial and final state flavors are different ($q\bar{q} \rightarrow \tilde{q}_i\tilde{q}'_i$) we

instead have

$$\frac{d\sigma}{dt}(q\bar{q} \rightarrow \tilde{q}'_i \bar{\tilde{q}}'_i) = \frac{4\pi\alpha_s^2}{9s^4} \left[-st - (t - m_{\tilde{q}'_i}^2)^2 \right]. \quad (51.53)$$

If the two initial state quarks are of different flavors, then we have

$$\frac{d\sigma}{dt}(q\bar{q}' \rightarrow \tilde{q}_i \bar{\tilde{q}}'_i) = \frac{2\pi\alpha_s^2}{9s^2} \frac{-st - (t - m_{\tilde{q}_i}^2)^2}{(t - m_{\tilde{q}}^2)^2}. \quad (51.54)$$

If the initial quarks are of different flavor and final state squarks are of different type ($i \neq j$) then

$$\frac{d\sigma}{dt}(q\bar{q}' \rightarrow \tilde{q}_i \bar{\tilde{q}}'_j) = \frac{2\pi\alpha_s^2}{9s^2} \frac{m_{\tilde{q}}^2 s}{(t - m_{\tilde{q}}^2)^2}. \quad (51.55)$$

For same-flavor initial state quarks, but final state unlike-type squarks, we also have

$$\frac{d\sigma}{dt}(q\bar{q} \rightarrow \tilde{q}_i \bar{\tilde{q}}'_j) = \frac{2\pi\alpha_s^2}{9s^2} \frac{m_{\tilde{q}}^2 s}{(t - m_{\tilde{q}}^2)^2}. \quad (51.56)$$

There also exist cross sections for quark-quark annihilation to squark pairs. For same flavor quark-quark annihilation to same flavor/same type final state squarks,

$$\begin{aligned} \frac{d\sigma}{dt}(qq \rightarrow \tilde{q}_i \tilde{q}_i) &= \\ &= \frac{\pi\alpha_s^2}{9s^2} m_{\tilde{q}}^2 s \left\{ \frac{1}{(t - m_{\tilde{q}}^2)^2} + \frac{1}{(u - m_{\tilde{q}}^2)^2} - \frac{2/3}{(t - m_{\tilde{q}}^2)(u - m_{\tilde{q}}^2)} \right\}, \end{aligned} \quad (51.57)$$

while if the final type squarks are different ($i \neq j$), we have

$$\begin{aligned} \frac{d\sigma}{dt}(qq \rightarrow \tilde{q}_i \tilde{q}_j) &= \\ &= \frac{2\pi\alpha_s^2}{9s^2} \times \left\{ \frac{[-st - (t - m_{\tilde{q}_i}^2)(t - m_{\tilde{q}_j}^2)]}{(t - m_{\tilde{q}}^2)} + \frac{[-su - (u - m_{\tilde{q}_i}^2)(u - m_{\tilde{q}_j}^2)]}{(u - m_{\tilde{q}}^2)} \right\}. \end{aligned} \quad (51.58)$$

If initial/final state flavors are different, but final state squark types are the same, then

$$\frac{d\sigma}{dt}(qq' \rightarrow \tilde{q}_i \tilde{q}'_i) = \frac{2\pi\alpha_s^2}{9s^2} \frac{m_{\tilde{q}}^2 s}{(t - m_{\tilde{q}}^2)^2}. \quad (51.59)$$

If initial quark flavors are different and final squark types are different, then

$$\frac{d\sigma}{dt}(qq' \rightarrow \tilde{q}_i \tilde{q}'_j) = \frac{2\pi\alpha_s^2}{9s^2} \frac{-st - (t - m_{\tilde{q}_i}^2)(t - m_{\tilde{q}_j}^2)}{(t - m_{\tilde{q}}^2)^2}. \quad (51.60)$$

51.8.2 Gluino and squark associated production

In the MSSM, the charged spin- $\frac{1}{2}$ winos and higgsinos mix to make chargino states $\chi_{1,2}^{\pm}$, with $m_{\chi_{1,2}^{\pm}} < m_{\chi_{2,3}^{\pm}}$. The spin- $\frac{1}{2}$ neutral bino, wino and higgsino fields mix to give four neutralino mass eigenstates $\chi_{1,2,3,4}^0$ ordered according to mass. We sometimes denote the charginos and neutralinos collectively as -inos for notational simplicity

For gluino and squark production in association with charginos and neutralinos [12], the quark-squark-neutralino couplings¹ are defined by the interaction Lagrangian terms

$$\mathcal{L}_{\tilde{f}f\tilde{\chi}_i^0} = \left[iA_{\tilde{\chi}_i^0}^f \tilde{f}_L^{\dagger} \tilde{\chi}_i^0 P_L f + iB_{\tilde{\chi}_i^0}^f \tilde{f}_R^{\dagger} \tilde{\chi}_i^0 P_R f + \text{h.c.} \right]$$

¹The couplings $A_{\tilde{\chi}_i^0}^f$ and $B_{\tilde{\chi}_i^0}^f$ are given explicitly in Ref. [13] in Eq. (8.87). Also, the couplings $A_{\tilde{\chi}_i^{\pm}}^d$ and $A_{\tilde{\chi}_i^{\pm}}^u$ are given in Eq. (8.93). The couplings X_i^j and Y_i^j are given by Eq. (8.103), while the x_i and y_i couplings are given in Eq. (8.100). Finally, the couplings W_{ij} are given in Eq. (8.101).

, where $A_{\tilde{\chi}_i^0}^f$ and $B_{\tilde{\chi}_i^0}^f$ are coupling constants involving gauge couplings, neutralino mixing elements and in the case of third generation fermions, Yukawa couplings. Their form depends on the conventions used for setting up the MSSM Lagrangian, and can be found in various reviews [14] and textbooks [13, 15]. P_L and P_R are the usual left- and right- spinor projection operators and f denotes any of the SM fermions u, d, e, ν_e, \dots . The fermion-sfermion- chargino couplings have the form $\mathcal{L} = \left[iA_{\tilde{\chi}_i^{\pm}}^d \tilde{u}_L^{\dagger} \tilde{\chi}_i^{\pm} P_L d + iA_{\tilde{\chi}_i^{\pm}}^u \tilde{d}_L^{\dagger} \tilde{\chi}_i^{\pm} P_L u + \text{h.c.} \right]$ for u and d quarks, where the $A_{\tilde{\chi}_i^{\pm}}^d$ and $A_{\tilde{\chi}_i^{\pm}}^u$ couplings are again convention-dependent, and can be found in textbooks. The superscript c denotes ‘‘charge conjugate spinor’’, defined by $\psi^c \equiv C\bar{\psi}^T$.

The subprocess cross sections for chargino-squark associated production occur via squark exchange and are given by

$$\frac{d\sigma}{dt}(\tilde{u}g \rightarrow \tilde{\chi}_i^{\pm} \tilde{d}_L) = \frac{\alpha_s}{24s^2} |A_{\tilde{\chi}_i^{\pm}}^u|^2 \psi(m_{\tilde{d}_L}, m_{\tilde{\chi}_i^{\pm}}, t), \quad (51.61)$$

$$\frac{d\sigma}{dt}(dg \rightarrow \tilde{\chi}_i^{\pm} \tilde{u}_L) = \frac{\alpha_s}{24s^2} |A_{\tilde{\chi}_i^{\pm}}^d|^2 \psi(m_{\tilde{u}_L}, m_{\tilde{\chi}_i^{\pm}}, t), \quad (51.62)$$

while neutralino-squark production is given by

$$\frac{d\sigma}{dt}(qg \rightarrow \tilde{\chi}_i^0 \tilde{q}) = \frac{\alpha_s}{24s^2} \left(|A_{\tilde{\chi}_i^0}^q|^2 + |B_{\tilde{\chi}_i^0}^q|^2 \right) \psi(m_{\tilde{q}}, m_{\tilde{\chi}_i^0}, t), \quad (51.63)$$

where

$$\begin{aligned} \psi(m_1, m_2, t) &= \frac{s + t - m_1^2}{2s} - \frac{m_1^2(m_2^2 - t)}{(m_1^2 - t)^2} \\ &+ \frac{t(m_2^2 - m_1^2) + m_2^2(s - m_2^2 + m_1^2)}{s(m_1^2 - t)}. \end{aligned} \quad (51.64)$$

Here, the variable t is given by the square of ‘‘squark-minus-quark’’ four-momentum. The neutralino-gluino associated production cross section also occurs via squark exchange and is given by

$$\begin{aligned} \frac{d\sigma}{dt}(q\bar{q} \rightarrow \tilde{\chi}_i^0 \tilde{g}) &= \frac{\alpha_s}{18s^2} \left(|A_{\tilde{\chi}_i^0}^q|^2 + |B_{\tilde{\chi}_i^0}^q|^2 \right) \left[\frac{(m_{\tilde{\chi}_i^0}^2 - t)(m_{\tilde{g}}^2 - t)}{(m_{\tilde{q}}^2 - t)^2} \right. \\ &+ \left. \frac{(m_{\tilde{\chi}_i^0}^2 - u)(m_{\tilde{g}}^2 - u)}{(m_{\tilde{q}}^2 - u)^2} - \frac{2\eta_i \eta_{\tilde{g}} m_{\tilde{g}} m_{\tilde{\chi}_i^0} s}{(m_{\tilde{q}}^2 - t)(m_{\tilde{q}}^2 - u)} \right], \end{aligned} \quad (51.65)$$

where η_i is the sign of the neutralino mass eigenvalue and $\eta_{\tilde{g}}$ is the sign of the gluino mass eigenvalue. We also have chargino-gluino associated production:

$$\begin{aligned} \frac{d\sigma}{dt}(\tilde{u}d \rightarrow \tilde{\chi}_i^{\pm} \tilde{g}) &= \frac{\alpha_s}{18s^2} \left[|A_{\tilde{\chi}_i^{\pm}}^u|^2 \frac{(m_{\tilde{\chi}_i^{\pm}}^2 - t)(m_{\tilde{g}}^2 - t)}{(m_{\tilde{d}_L}^2 - t)^2} \right. \\ &+ |A_{\tilde{\chi}_i^{\pm}}^d|^2 \frac{(m_{\tilde{\chi}_i^{\pm}}^2 - u)(m_{\tilde{g}}^2 - u)}{(m_{\tilde{u}_L}^2 - u)^2} + \left. \frac{2\eta_{\tilde{g}} \text{Re}(A_{\tilde{\chi}_i^{\pm}}^u - A_{\tilde{\chi}_i^{\pm}}^d) m_{\tilde{g}} m_{\tilde{\chi}_i^{\pm}} s}{(m_{\tilde{d}_L}^2 - t)(m_{\tilde{u}_L}^2 - u)} \right], \end{aligned} \quad (51.66)$$

where $\hat{t} = (\tilde{g} - d)^2$ and in the third term one must take the real part of the in general complex coupling constant product.

51.8.3 Slepton and sneutrino production

The subprocess cross section for $\tilde{\ell}_L \tilde{\nu}_{\ell L}$ production ($\ell = e$ or μ) occurs via s -channel W exchange and is given by

$$\frac{d\sigma}{dt}(d\tilde{u} \rightarrow \tilde{\ell}_L \tilde{\nu}_{\ell L}) = \frac{g^4 |D_W(s)|^2}{192\pi s^2} \left(tu - m_{\tilde{\ell}_L}^2 m_{\tilde{\nu}_{\ell L}}^2 \right), \quad (51.67)$$

where $D_W(s) = 1/(s - M_W^2 + iM_W\Gamma_W)$ is the W -boson propagator denominator. The production of $\tilde{\tau}_1 \tilde{\nu}_{\tau}$ is given as above, but

replacing $m_{\tilde{\ell}_L} \rightarrow m_{\tilde{\tau}_1}$, $m_{\tilde{\nu}_{\ell_L}} \rightarrow m_{\tilde{\nu}_\tau}$ and multiplying by an overall factor of $\cos^2 \theta_\tau$ (where θ_τ is the tau-slepton mixing angle). Similar substitutions hold for $\tilde{\tau}_2 \tilde{\nu}_\tau$ production, except the overall factor is $\sin^2 \theta_\tau$.

Table 51.1: The constants α_f and β_f that appear in the SM neutral current Lagrangian. Here $t \equiv \tan \theta_W$ and $c \equiv \cot \theta_W$.

f	q_f	α_f	β_f
ℓ	-1	$\frac{1}{4}(3t - c)$	$\frac{1}{4}(t + c)$
ν_ℓ	0	$\frac{1}{4}(t + c)$	$-\frac{1}{4}(t + c)$
u	$\frac{2}{3}$	$-\frac{5}{12}t + \frac{1}{4}c$	$-\frac{1}{4}(t + c)$
d	$-\frac{1}{3}$	$\frac{1}{12}t - \frac{1}{4}c$	$\frac{1}{4}(t + c)$

The subprocess cross section for $\tilde{\ell}_L \tilde{\bar{\ell}}_L$ production occurs via s -channel γ and Z exchange, and depends on the neutral current interaction, with fermion couplings to γ and Z^0 given by $\mathcal{L}_{\text{neutral}} = -e q_f \bar{f} \gamma^\mu f A_\mu + e f \gamma^\mu (\alpha_f + \beta_f \gamma_5) f Z_\mu$ (with values of q_f , α_f , and β_f given in Table-51.1).

The subprocess cross section is given by

$$\frac{d\sigma}{dt}(q\bar{q} \rightarrow \tilde{\ell}_L \tilde{\bar{\ell}}_L) = \frac{e^4}{24\pi s^2} \left(tu - m_{\tilde{\ell}_L}^4 \right) \times \left\{ \frac{q_\ell^2 q_q^2}{s^2} + (\alpha_\ell - \beta_\ell)^2 (\alpha_q^2 + \beta_q^2) |D_Z(s)|^2 + \frac{2q_\ell q_q \alpha_q (\alpha_\ell - \beta_\ell) (s - M_Z^2)}{s} |D_Z(s)|^2 \right\}, \quad (51.68)$$

where $D_Z(s) = 1/(s - M_Z^2 + iM_Z \Gamma_Z)$. The cross section for sneutrino production is given by the same formula, but with α_ℓ , β_ℓ , q_ℓ and $m_{\tilde{\ell}_L}$ replaced by α_ν , β_ν , 0 and $m_{\tilde{\nu}_L}$, respectively. The cross section for $\tilde{\tau}_1 \tilde{\bar{\tau}}_1$ production is obtained by replacing $m_{\tilde{\ell}_L} \rightarrow m_{\tilde{\tau}_1}$ and $\beta_\ell \rightarrow \beta_\ell \cos 2\theta_\tau$. The cross section for $\tilde{\ell}_R \tilde{\bar{\ell}}_R$ production is given by substituting $\alpha_\ell - \beta_\ell \rightarrow \alpha_\ell + \beta_\ell$ and $m_{\tilde{\ell}_L} \rightarrow m_{\tilde{\ell}_R}$ in the equation above. The cross section for $\tilde{\tau}_2 \tilde{\bar{\tau}}_2$ production is obtained from the formula for $\tilde{\ell}_R \tilde{\bar{\ell}}_R$ production by replacing $m_{\tilde{\ell}_R} \rightarrow m_{\tilde{\tau}_2}$ and $\beta_\ell \rightarrow \beta_\ell \cos 2\theta_\tau$.

Finally, the cross section for $\tilde{\tau}_1 \tilde{\bar{\tau}}_2$ production occurs only via Z exchange, and is given by

$$\frac{d\sigma}{dt}(q\bar{q} \rightarrow \tilde{\tau}_1 \tilde{\bar{\tau}}_2) = \frac{d\sigma}{dt}(q\bar{q} \rightarrow \tilde{\tau}_1 \tilde{\bar{\tau}}_2) = \frac{e^4}{24\pi s^2} (\alpha_q^2 + \beta_q^2) \beta_\ell^2 \sin^2 2\theta_\tau |D_Z(s)|^2 (ut - m_{\tilde{\tau}_1}^2 m_{\tilde{\tau}_2}^2). \quad (51.69)$$

51.8.4 Chargino and neutralino pair production

51.8.4.1 $\tilde{\chi}_i^- \tilde{\chi}_j^0$ production

The subprocess cross section for $d\bar{u} \rightarrow \tilde{\chi}_i^- \tilde{\chi}_j^0$ depends on Lagrangian couplings

$$\mathcal{L}_{W\bar{u}d} = -\frac{g}{\sqrt{2}} \bar{u} \gamma_\mu P_L d W^{+\mu} + \text{h.c.}$$

$$\mathcal{L}_{W\tilde{\chi}_i^- \tilde{\chi}_j^0} = -g(-i)^{\theta_j} \bar{\tilde{\chi}}_i^- [X_i^j + Y_i^j \gamma_5] \gamma_\mu \tilde{\chi}_j^0 W^{-\mu} + \text{h.c.}$$

$$\mathcal{L}_{q\bar{q}\tilde{\chi}_i^-} = iA_{\tilde{\chi}_i^-}^d \bar{u}_L^\dagger \tilde{\chi}_i^- P_L d + iA_{\tilde{\chi}_i^-}^u \bar{d}_L^\dagger \tilde{\chi}_i^- P_L u + \text{h.c.}$$

and

$$\mathcal{L}_{q\bar{q}\tilde{\chi}_j^0} = iA_{\tilde{\chi}_j^0}^q \bar{q}_L^\dagger \tilde{\chi}_j^0 P_L q + \text{h.c.}$$

Contributing diagrams include W exchange and also \tilde{d}_L and \tilde{u}_L squark exchange. The X_i^j and Y_i^j couplings are new, and again convention-dependent: the cross section formulae works if

the interaction Lagrangian is written in the above form, so that the couplings can be suitably extracted. The term $\theta_j = 0$ (1) if $m_{\tilde{\chi}_j^0} > 0$ (< 0); it comes about because the neutralino field must be re-defined by a $-i\gamma_5$ transformation if its mass eigenvalue is negative [13]. The subprocess cross section is given in terms of dot products of four momenta, where particle labels are used to denote their four-momenta; note that all mass terms in the cross section formulae are positive definite, so that the signs of mass eigenstates have been absorbed into the Lagrangian couplings, as for instance in Ref. [13]. We then have

$$\frac{d\sigma}{dt}(d\bar{u} \rightarrow \tilde{\chi}_i^- \tilde{\chi}_j^0) = \frac{1}{192\pi s^2}$$

$$\left[T_W + T_{\tilde{d}_L} + T_{\tilde{u}_L} + T_{W\tilde{d}_L} + T_{W\tilde{u}_L} + T_{\tilde{d}_L\tilde{u}_L} \right] \quad (51.70)$$

where

$$T_W = 8g^4 |D_W(s)|^2 \left\{ [X_i^{j2} + Y_i^{j2}] (\tilde{\chi}_j^0 \cdot d\tilde{\chi}_i^- \cdot \bar{u} + \tilde{\chi}_j^0 \cdot \bar{u}\tilde{\chi}_i^- \cdot d) + 2(X_i^j Y_i^j) (\tilde{\chi}_j^0 \cdot d\tilde{\chi}_i^- \cdot \bar{u} - \tilde{\chi}_j^0 \cdot \bar{u}\tilde{\chi}_i^- \cdot d) + [X_i^{j2} - Y_i^{j2}] m_{\tilde{\chi}_i^-} m_{\tilde{\chi}_j^0} d \cdot \bar{u} \right\}, \quad (51.71)$$

$$T_{\tilde{d}_L} = \frac{4|A_{\tilde{\chi}_i^-}^u|^2 |A_{\tilde{\chi}_j^0}^d|^2}{[(\tilde{\chi}_i^- - \bar{u})^2 - m_{\tilde{d}_L}^2]^2} d \cdot \tilde{\chi}_j^0 \tilde{\chi}_i^- \cdot \bar{u}, \quad (51.72)$$

$$T_{\tilde{u}_L} = \frac{4|A_{\tilde{\chi}_i^-}^d|^2 |A_{\tilde{\chi}_j^0}^u|^2}{[(\tilde{\chi}_j^0 - \bar{u})^2 - m_{\tilde{u}_L}^2]^2} \bar{u} \cdot \tilde{\chi}_j^0 \tilde{\chi}_i^- \cdot d \quad (51.73)$$

$$T_{W\tilde{d}_L} = \frac{-\sqrt{2}g^2 \text{Re}[A_{\tilde{\chi}_j^0}^{d*} A_{\tilde{\chi}_i^-}^u (-i)^{\theta_j}](s - M_W^2) |D_W(s)|^2}{(\tilde{\chi}_i^- - \bar{u})^2 - m_{\tilde{d}_L}^2} \times \left\{ 8(X_i^j + Y_i^j) \tilde{\chi}_j^0 \cdot d\bar{u} \cdot \tilde{\chi}_i^- + 4(X_i^j - Y_i^j) m_{\tilde{\chi}_i^-} m_{\tilde{\chi}_j^0} d \cdot \bar{u} \right\} \quad (51.74)$$

$$T_{W\tilde{u}_L} = \frac{\sqrt{2}g^2 \text{Re}[A_{\tilde{\chi}_i^-}^{d*} A_{\tilde{\chi}_j^0}^u (-i)^{\theta_j}](s - M_W^2) |D_W(s)|^2}{(\tilde{\chi}_j^0 - \bar{u})^2 - m_{\tilde{u}_L}^2} \times \left\{ 8(X_i^j - Y_i^j) \tilde{\chi}_j^0 \cdot \bar{u}d \cdot \tilde{\chi}_i^- + 4(X_i^j + Y_i^j) m_{\tilde{\chi}_i^-} m_{\tilde{\chi}_j^0} d \cdot \bar{u} \right\} \quad (51.75)$$

and

$$T_{\tilde{d}_L\tilde{u}_L} = -\frac{4\text{Re}[A_{\tilde{\chi}_j^0}^d A_{\tilde{\chi}_i^-}^{u*} A_{\tilde{\chi}_i^-}^{d*} A_{\tilde{\chi}_j^0}^u] m_{\tilde{\chi}_i^-} m_{\tilde{\chi}_j^0} d \cdot \bar{u}}{[(\tilde{\chi}_i^- - \bar{u})^2 - m_{\tilde{d}_L}^2][(\tilde{\chi}_j^0 - \bar{u})^2 - m_{\tilde{u}_L}^2]}. \quad (51.76)$$

51.8.4.2 Chargino pair production

The subprocess cross section for $d\bar{d} \rightarrow \tilde{\chi}_i^- \tilde{\chi}_i^+$ ($i = 1, 2$) depends on Lagrangian couplings $\mathcal{L} = e\tilde{\chi}_i^- \gamma_\mu \tilde{\chi}_i^+ A^\mu - e \cot \theta_W \tilde{\chi}_i^- \gamma_\mu (x_i - y_i \gamma_5) \tilde{\chi}_i^+ Z^\mu$ and also $\mathcal{L} \ni iA_{\tilde{\chi}_i^-}^d \bar{u}_L^\dagger \tilde{\chi}_i^- P_L d + iA_{\tilde{\chi}_i^-}^u \bar{d}_L^\dagger \tilde{\chi}_i^- P_L u + \text{h.c.}$

Contributing diagrams include s -channel γ , Z^0 exchange and t -channel \tilde{u}_L exchange [16, 17]. The couplings x_i and y_i are again new and as usual convention-dependent.

The subprocess cross section is given by

$$\frac{d\sigma}{dt}(d\bar{d} \rightarrow \tilde{\chi}_i^- \tilde{\chi}_i^+) = \frac{1}{192\pi s^2} [T_\gamma + T_Z + T_{\tilde{u}_L} + T_{\gamma Z} + T_{\gamma\tilde{u}_L} + T_{Z\tilde{u}_L}] \quad (51.77)$$

where

$$T_\gamma = \frac{32e^4 q_d^2}{s^2} \left[d \cdot \tilde{\chi}_i^+ \bar{d} \cdot \tilde{\chi}_i^- + d \cdot \tilde{\chi}_i^- \bar{d} \cdot \tilde{\chi}_i^+ + m_{\tilde{\chi}_i^-}^2 d \cdot \bar{d} \right] \quad (51.78)$$

$$T_Z = 32e^4 \cot^2 \theta_W |D_Z(s)|^2 \left\{ (\alpha_d^2 + \beta_d^2)(x_i^2 + y_i^2) \left[d \cdot \tilde{\chi}_i^+ \bar{d} \cdot \tilde{\chi}_i^- + d \cdot \tilde{\chi}_i^- \bar{d} \cdot \tilde{\chi}_i^+ + m_{\tilde{\chi}_i^-}^2 d \cdot \bar{d} \right] \mp 4\alpha_d \beta_d x_i y_i \left[d \cdot \tilde{\chi}_i^+ \bar{d} \cdot \tilde{\chi}_i^- - d \cdot \tilde{\chi}_i^- \bar{d} \cdot \tilde{\chi}_i^+ \right] - 2y_i^2 (\alpha_d^2 + \beta_d^2) m_{\tilde{\chi}_i^-}^2 d \cdot \bar{d} \right\}, \quad (51.79)$$

$$T_{\tilde{u}_L} = \frac{4|A_{\tilde{\chi}_i^-}^d|^4}{[(d - \tilde{\chi}_i^-)^2 - m_{\tilde{u}_L}^2]^2} d \cdot \tilde{\chi}_i^- \bar{d} \cdot \tilde{\chi}_i^+ \quad (51.80)$$

$$T_{\gamma Z} = \frac{64e^4 \cot \theta_W q_d (s - M_Z^2) |D_Z(s)|^2}{s} \times$$

$$\left\{ \alpha_d x_i \left(d \cdot \tilde{\chi}_i^+ \bar{d} \cdot \tilde{\chi}_i^- + d \cdot \tilde{\chi}_i^- \bar{d} \cdot \tilde{\chi}_i^+ + m_{\tilde{\chi}_i^-}^2 d \cdot \bar{d} \right) \pm \beta_d y_i \left(d \cdot \tilde{\chi}_i^- \bar{d} \cdot \tilde{\chi}_i^+ - d \cdot \tilde{\chi}_i^+ \bar{d} \cdot \tilde{\chi}_i^- \right) \right\} \quad (51.81)$$

$$T_{\gamma \tilde{u}_L} = \mp \frac{8e^2 q_d}{s} \frac{|A_{\tilde{\chi}_i^-}^d|^2}{[(d - \tilde{\chi}_i^-)^2 - m_{\tilde{u}_L}^2]} \left\{ 2\bar{d} \cdot \tilde{\chi}_i^+ d \cdot \tilde{\chi}_i^- + m_{\tilde{\chi}_i^-}^2 d \cdot \bar{d} \right\} \quad (51.82)$$

and

$$T_{Z\tilde{u}_L} = \mp 8e^2 \cot \theta_W |D_Z(s)|^2 \frac{|A_{\tilde{\chi}_i^-}^d|^2 (s - M_Z^2)}{[(d - \tilde{\chi}_i^-)^2 - m_{\tilde{u}_L}^2]} (\alpha_d - \beta_d) \times \left\{ 2(x_i \mp y_i) d \cdot \tilde{\chi}_i^- \bar{d} \cdot \tilde{\chi}_i^+ + m_{\tilde{\chi}_i^-}^2 (x_i \pm y_i) d \cdot \bar{d} \right\} \quad (51.83)$$

using the upper of the sign choices.

The cross section for $u\bar{u} \rightarrow \tilde{\chi}_i^+ \tilde{\chi}_i^-$ can be obtained from the above by replacing $\alpha_d \rightarrow \alpha_u$, $\beta_d \rightarrow \beta_u$, $q_d \rightarrow q_u$, $\tilde{u}_L \rightarrow \tilde{d}_L$, $A_{\tilde{\chi}_i^-}^d \rightarrow A_{\tilde{\chi}_i^-}^u$, $d \rightarrow \bar{u}$, $\bar{d} \rightarrow u$ and adopting the lower of the sign choices everywhere.

The cross section for $q\bar{q} \rightarrow \tilde{\chi}_1^- \tilde{\chi}_2^+$, $\tilde{\chi}_1^+ \tilde{\chi}_2^-$ can occur via Z and \tilde{q}_L exchange. It is usually much smaller than $\tilde{\chi}_{1,2}^- \tilde{\chi}_{1,2}^+$ production, so the cross section will not be presented here. It can be found in Appendix A of Ref. [13].

51.8.4.3 Neutralino pair production

Neutralino pair production via $q\bar{q}$ fusion takes place via s -channel Z exchange plus t - and u -channel left- and right- squark exchange (5 diagrams) [17, 18]. The Lagrangian couplings (see previous footnote*) needed include terms given above plus terms of the form $\mathcal{L} = W_{ij} \tilde{\chi}_i^0 \gamma_\mu (\gamma_5)^{\theta_i + \theta_j + 1} \tilde{\chi}_j^0 Z^\mu$. The couplings W_{ij} depend only on the *higgsino* components of the neutralinos i and j . The subprocess cross section is given by:

$$\frac{d\sigma}{dt}(q\bar{q} \rightarrow \tilde{\chi}_i^0 \tilde{\chi}_j^0) = \frac{1}{192\pi s^2} [T_Z + T_{\tilde{q}_L} + T_{\tilde{q}_R} + T_{Z\tilde{q}_L} + T_{Z\tilde{q}_R}] \quad (51.84)$$

where

$$T_Z = 128e^2 |W_{ij}|^2 (\alpha_q^2 + \beta_q^2) |D_Z(s)|^2 \left[q \cdot \tilde{\chi}_i^0 \bar{q} \cdot \tilde{\chi}_j^0 + q \cdot \tilde{\chi}_j^0 \bar{q} \cdot \tilde{\chi}_i^0 - \eta_i \eta_j m_{\tilde{\chi}_i^0} m_{\tilde{\chi}_j^0} q \cdot \bar{q} \right], \quad (51.85)$$

$$T_{\tilde{q}_L} = 4|A_{\tilde{\chi}_i^0}^q|^2 |A_{\tilde{\chi}_j^0}^q|^2 \left\{ \frac{q \cdot \tilde{\chi}_i^0 \bar{q} \cdot \tilde{\chi}_j^0}{[(\tilde{\chi}_i^0 - q)^2 - m_{\tilde{q}_L}^2]^2} + \frac{q \cdot \tilde{\chi}_j^0 \bar{q} \cdot \tilde{\chi}_i^0}{[(\tilde{\chi}_j^0 - q)^2 - m_{\tilde{q}_L}^2]^2} - \eta_i \eta_j \frac{m_{\tilde{\chi}_i^0} m_{\tilde{\chi}_j^0} q \cdot \bar{q}}{[(\tilde{\chi}_i^0 - q)^2 - m_{\tilde{q}_L}^2][(\tilde{\chi}_j^0 - q)^2 - m_{\tilde{q}_L}^2]} \right\} \quad (51.86)$$

$$T_{\tilde{q}_R} = 4|B_{\tilde{\chi}_i^0}^q|^2 |B_{\tilde{\chi}_j^0}^q|^2 \left\{ \frac{q \cdot \tilde{\chi}_i^0 \bar{q} \cdot \tilde{\chi}_j^0}{[(\tilde{\chi}_i^0 - q)^2 - m_{\tilde{q}_R}^2]^2} + \frac{q \cdot \tilde{\chi}_j^0 \bar{q} \cdot \tilde{\chi}_i^0}{[(\tilde{\chi}_j^0 - q)^2 - m_{\tilde{q}_R}^2]^2} - \eta_i \eta_j \frac{m_{\tilde{\chi}_i^0} m_{\tilde{\chi}_j^0} q \cdot \bar{q}}{[(\tilde{\chi}_i^0 - q)^2 - m_{\tilde{q}_R}^2][(\tilde{\chi}_j^0 - q)^2 - m_{\tilde{q}_R}^2]} \right\} \quad (51.87)$$

$$T_{Z\tilde{q}_L} = 16e(\alpha_q - \beta_q)(s - M_Z^2) |D_Z(s)|^2$$

$$\left\{ \frac{\text{Re}(W_{ij} A_{\tilde{\chi}_i^0}^{q*} A_{\tilde{\chi}_j^0}^q)}{[(\tilde{\chi}_i^0 - q)^2 - m_{\tilde{q}_L}^2]} \left[2q \cdot \tilde{\chi}_i^0 \bar{q} \cdot \tilde{\chi}_j^0 - \eta_i \eta_j m_{\tilde{\chi}_i^0} m_{\tilde{\chi}_j^0} q \cdot \bar{q} \right] + \eta_i \eta_j \frac{\text{Re}(W_{ij} A_{\tilde{\chi}_i^0}^q A_{\tilde{\chi}_j^0}^{q*})}{[(\tilde{\chi}_j^0 - q)^2 - m_{\tilde{q}_L}^2]} \left[2q \cdot \tilde{\chi}_j^0 \bar{q} \cdot \tilde{\chi}_i^0 - \eta_i \eta_j m_{\tilde{\chi}_i^0} m_{\tilde{\chi}_j^0} q \cdot \bar{q} \right] \right\} \quad (51.88)$$

$$T_{Z\tilde{q}_R} = 16e(\alpha_q + \beta_q)(s - M_Z^2) |D_Z(s)|^2$$

$$\left\{ \frac{\text{Re}(W_{ij} B_{\tilde{\chi}_i^0}^{q*} B_{\tilde{\chi}_j^0}^q)}{[(\tilde{\chi}_i^0 - q)^2 - m_{\tilde{q}_R}^2]} \left[2q \cdot \tilde{\chi}_i^0 \bar{q} \cdot \tilde{\chi}_j^0 - \eta_i \eta_j m_{\tilde{\chi}_i^0} m_{\tilde{\chi}_j^0} q \cdot \bar{q} \right] + \frac{\text{Re}(W_{ij} B_{\tilde{\chi}_i^0}^q B_{\tilde{\chi}_j^0}^{q*})}{[(\tilde{\chi}_j^0 - q)^2 - m_{\tilde{q}_R}^2]} \left[2q \cdot \tilde{\chi}_j^0 \bar{q} \cdot \tilde{\chi}_i^0 - \eta_i \eta_j m_{\tilde{\chi}_i^0} m_{\tilde{\chi}_j^0} q \cdot \bar{q} \right] \right\}. \quad (51.89)$$

As before, $\eta_i = \pm 1$ corresponding to whether the neutralino mass eigenvalue is positive or negative. When $i = j$ in the above formula, one must remember to integrate over just 2π steradians of solid angle to avoid double counting in the total cross section.

51.9 Universal extra dimensions

In the Universal Extra Dimension (UED) model of Ref. [19] (see Ref. [20] for a review of models with extra spacetime dimensions), the Standard Model is embedded in a five dimensional theory, where the fifth dimension is compactified on an S_1/Z_2 orbifold. Each SM chirality state is then the zero mode of an infinite tower of Kaluza-Klein excitations labeled by $n = 0 - \infty$. A KK parity is usually assumed to hold, where each state is assigned KK-parity $P = (-1)^n$. If the compactification scale is around a TeV, then the $n = 1$ (or even higher) KK modes may be accessible to collider searches.

Of interest for hadron colliders are the production of massive $n \geq 1$ quark or gluon pairs. These production cross sections have been calculated in Ref. [21, 22]. We list here results for the $n = 1$ case only with $M_1 = 1/R$ (R is the compactification radius) and s , t and u are the usual Mandelstam variables; more general formulae can be found in Ref. [22]. The superscript * stands for any KK excited state, while \bullet stands for left chirality states and \circ stands for right chirality states.

$$\frac{d\sigma}{dt} = \frac{1}{16\pi s^2} T \quad (51.90)$$

where

$$T(q\bar{q} \rightarrow g^* g^*) = \frac{2g_s^4}{27} \left[M_1^2 \left(-\frac{4s^3}{t'^2 u'^2} + \frac{57s}{t' u'} - \frac{108}{s} \right) + \frac{20s^2}{t' u'} - 93 + \frac{108t' u'}{s^2} \right] \quad (51.91)$$

and

$$T(gg \rightarrow g^* g^*) = \frac{9g_s^4}{27} \left[3M_1^4 \frac{s^2 + t'^2 + u'^2}{t'^2 u'^2} - 3M_1^2 \frac{s^2 + t'^2 + u'^2}{s t' u'} + 1 + \frac{(s^2 + t'^2 + u'^2)^3}{4s^2 t'^2 u'^2} - \frac{t' u'}{s^2} \right] \quad (51.92)$$

where $t' = t - M_1^2$ and $u' = u - M_1^2$.

Also,

$$T(q\bar{q} \rightarrow q_1^* \bar{q}_1^*) = \frac{4g_s^4}{9} \left[\frac{2M_1^2}{s} + \frac{t'^2 + u'^2}{s^2} \right],$$

$$T(q\bar{q} \rightarrow q_1^* \bar{q}_1^*) = \frac{g_s^4}{9} \left[2M_1^2 \left(\frac{4}{s} + \frac{s}{t'^2} - \frac{1}{t'} \right) + \frac{23}{6} + \frac{2s^2}{t'^2} + \frac{8s}{3t'} + \frac{6t'}{s} + \frac{8t'^2}{s^2} \right], \quad (51.96)$$

$$T(qq \rightarrow q_1^* \bar{q}_1^*) = \frac{g_s^4}{27} \left[M_1^2 \left(6 \frac{t'}{u'^2} + 6 \frac{u'}{t'^2} - \frac{s}{t'u'} \right) + 2 \left(3 \frac{t'^2}{u'^2} + 3 \frac{u'^2}{t'^2} + 4 \frac{s^2}{t'u'} - 5 \right) \right],$$

$$T(gg \rightarrow q_1^* \bar{q}_1^*) = g_s^4 \left[M_1^4 \frac{-4}{t'u'} \left(\frac{s^2}{6t'u'} - \frac{3}{8} \right) + M_1^2 \frac{4}{s} \left(\frac{s^2}{6t'u'} - \frac{3}{8} \right) + \frac{s^2}{6t'u'} - \frac{17}{24} + \frac{3t'u'}{4s^2} \right],$$

$$T(gq \rightarrow g^* \bar{q}_1^*) = \frac{-g_s^4}{3} \left[\frac{5s^2}{12t'^2} + \frac{s^3}{t'^2 u'} + \frac{11su'}{6t'^2} + \frac{5u'^2}{12t'^2} + \frac{u'^3}{st'^2} \right],$$

$$T(q\bar{q}' \rightarrow q_1^* \bar{q}_1'^*) = \frac{g_s^4}{18} \left[4M_1^4 \frac{s}{t'^2} + 5 + 4 \frac{s^2}{t'^2} + 8 \frac{s}{t'} \right],$$

$$T(qq' \rightarrow q_1^* \bar{q}_1'^*) = \frac{2g_s^4}{9} \left[-M_1^2 \frac{s}{t'^2} + \frac{1}{4} + \frac{s^2}{t'^2} \right],$$

$$T(qq \rightarrow q_1^* \bar{q}_1^{\circ}) =$$

$$\frac{g_s^4}{9} \left[M_1^2 \left(\frac{2s^3}{t'^2 u'^2} - \frac{4s}{t'u'} \right) + 2 \frac{s^4}{t'^2 u'^2} - 8 \frac{s^2}{t'u'} + 5 \right],$$

$$T(q\bar{q}' \rightarrow q_1^* \bar{q}_1'^{\circ}) = \frac{g_s^4}{9} \left[2M_1^2 \left(\frac{1}{t'} + \frac{u'}{t'^2} \right) + \frac{5}{2} + \frac{4u'}{t'} + \frac{2u'^2}{t'^2} \right],$$

and

$$T(qq' \rightarrow q_1^* \bar{q}_1'^{\circ}) = \frac{g_s^4}{9} \left[-2M_1^2 \left(\frac{1}{t'} + \frac{u'}{t'^2} \right) + \frac{1}{2} + \frac{2u'^2}{t'^2} \right].$$

51.10 Large extra dimensions

In the ADD theory [23] with large extra dimensions (LED), the SM particles are confined to a 3-brane, while gravity propagates in the bulk. It is assumed that the n extra dimensions are compactified on an n -dimensional torus of volume $(2\pi r)^n$, so that the fundamental $4+n$ dimensional Planck scale M_* is related to the usual 4-dimensional Planck scale M_{Pl} by $M_{Pl}^2 = M_*^{n+2} (2\pi r)^n$. If $M_* \sim 1$ TeV, then the $M_W - M_{Pl}$ hierarchy problem is just due to gravity propagating in the large extra dimensions.

In these theories, the KK-excited graviton states $G_{\mu\nu}^n$ for $n = 1 - \infty$ can be produced at collider experiments. The graviton couplings to matter are suppressed by $1/M_{Pl}$, so that graviton emission cross sections $d\sigma/dt \sim 1/M_{Pl}^2$. However, the mass splittings between the excited graviton states can be tiny, so the graviton eigenstates are usually approximated by a continuum distribution. A summation (integration) over all allowed graviton emissions ends up cancelling the $1/M_{Pl}^2$ factor, so that observable cross section rates can be attained. Some fundamental production formulae for a KK graviton (denoted G) of mass m at hadron colliders include the subprocesses

$$\frac{d\sigma_m}{dt}(f\bar{f} \rightarrow \gamma G) = \frac{\alpha Q_f^2}{16N_f s M_{Pl}^2} F_1\left(\frac{t}{s}, \frac{m^2}{s}\right), \quad (51.93)$$

where Q_f is the charge of fermion f and N_f is the number of QCD colors of f . Also,

$$\frac{d\sigma_m}{dt}(q\bar{q} \rightarrow gG) = \frac{\alpha_s}{36 s M_{Pl}^2} F_1\left(\frac{t}{s}, \frac{m^2}{s}\right), \quad (51.94)$$

$$\frac{d\sigma_m}{dt}(gg \rightarrow qG) = \frac{\alpha_s}{96 s M_{Pl}^2} F_2\left(\frac{t}{s}, \frac{m^2}{s}\right), \quad (51.95)$$

$$\frac{d\sigma_m}{dt}(gg \rightarrow gG) = \frac{3\alpha_s}{16 s M_{Pl}^2} F_3\left(\frac{t}{s}, \frac{m^2}{s}\right), \quad (51.96)$$

where

$$F_1(x, y) = \frac{1}{x(y-1-x)} \left[-4x(1+x)(1+2x+2x^2) + y(1+6x+18x^2+16x^3) - 6y^2x(1+2x) + y^3(1+4x) \right] \quad (51.97)$$

$$F_2(x, y) = -(y-1-x)F_1\left(\frac{x}{y-1-x}, \frac{y}{y-1-x}\right) \quad (51.98)$$

and

$$F_3(x, y) = \frac{1}{x(y-1-x)} \left[1+2x+3x^2+2x^3+x^4 - 2y(1+x^3) + 3y^2(1+x^2) - 2y^3(1+x) + y^4 \right]. \quad (51.99)$$

These formulae must then be multiplied by the graviton density of states formula

$dN = S_{n-1} \frac{M_{Pl}^2}{M_*^{n+2}} m^{n-1} dm$ to gain the cross section

$$\frac{d^2\sigma}{dt dm} = S_{n-1} \frac{M_{Pl}^2}{M_*^{n+2}} m^{n-1} \frac{d\sigma_m}{dt} \quad (51.100)$$

where $S_n = \frac{(2\pi)^{n/2}}{\Gamma(n/2)}$ is the surface area of an n -dimensional sphere of unit radius.

Virtual graviton processes can also be searched for at colliders. For instance, in Ref. [24] the cross section for Drell-Yan production of lepton pairs via gluon fusion was calculated, where it is found that, in the center-of-mass system

$$\frac{d\sigma}{dz}(gg \rightarrow \ell^+ \ell^-) = \frac{\lambda^2 s^3}{64\pi M_*^8} (1-z^2)(1+z^2) \quad (51.101)$$

where $z = \cos\theta$ and λ is a model-dependent coupling constant ~ 1 . Formulae for Drell-Yan production via $q\bar{q}$ fusion can also be found in Refs. [24, 25].

51.11 Warped extra dimensions

In the Randall-Sundrum model [26] of warped extra dimensions, the arena for physics is a 5-d anti-deSitter (AdS_5) spacetime, for which a non-factorizable metric exists with a metric warp factor $e^{-2\sigma(\phi)}$. It is assumed that two opposite tension 3-branes exist within AdS_5 at the two ends of an S_1/Z_2 orbifold parameterized by co-ordinate ϕ which runs from $0 - \pi$. The 4-D solution of the Einstein equations yields $\sigma(\phi) = kr_c|\phi|$, where r_c is the compactification radius of the extra dimension and $k \sim M_{Pl}$. The 4-D effective action allows one to identify $\bar{M}_{Pl}^2 = \frac{M^3}{k} (1 - e^{-2kr_c\pi})$, where M is the 5-D Planck scale. Physical particles on the TeV scale (SM) brane have mass $m = e^{-kr_c\pi} m_0$, where m_0 is a fundamental mass of order the Planck scale. Thus, the weak scale-Planck scale hierarchy occurs due to the existence of the exponential warp factor if $kr_c \sim 12$.

In the simplest versions of the RS model, the TeV-scale brane contains only SM particles plus a tower of KK gravitons. The RS gravitons have mass $m_n = kx_n e^{-kr_c\pi}$, where the x_i are roots of Bessel functions $J_1(x_n) = 0$, with $x_1 \simeq 3.83$, $x_2 \simeq 7.02$ etc. While the RS zero-mode graviton couplings suppressed by $1/\bar{M}_{Pl}$ and are thus inconsequential for collider searches, the $n = 1$ and higher modes have couplings suppressed instead by $\Lambda_\pi = e^{-kr_c\pi} \bar{M}_{Pl} \sim TeV$. The $n = 1$ RS graviton should have width $\Gamma_1 = \rho m_1 x_1^2 (k/\bar{M}_{Pl})^2$, where ρ is a constant depending on how many decay modes are open. The formulae for dilepton production via virtual RS graviton exchange can be gained from the above formulae for the ADD scenario via the replacement [27]

$$\frac{\lambda}{M_*^4} \rightarrow \frac{i^2}{8\Lambda_\pi^2} \sum_{n=1}^{\infty} \frac{1}{s - m_n^2 + im_n \Gamma_n}. \quad (51.102)$$

References

- [1] J. F. Owens, E. Reya and M. Gluck, Phys. Rev. **D18**, 1501 (1978).
- [2] F. Wilczek, Phys. Rev. Lett. **39**, 1304 (1977).
- [3] B. L. Ioffe and V. A. Khoze, Sov. J. Part. Nucl. **9**, 50 (1978), [Fiz. Elem. Chast. Atom. Yadra9,118(1978)].
- [4] J. R. Ellis, M. K. Gaillard and D. V. Nanopoulos, Nucl. Phys. **B106**, 292 (1976).
- [5] R. N. Cahn and S. Dawson, Phys. Lett. **136B**, 196 (1984), [Erratum: Phys. Lett.138B,464(1984)].
- [6] S. Dawson, Nucl. Phys. **B249**, 42 (1985).
- [7] M. S. Chanowitz and M. K. Gaillard, Phys. Lett. **142B**, 85 (1984).
- [8] R. N. Cahn, Nucl. Phys. **B255**, 341 (1985), [Erratum: Nucl. Phys.B262,744(1985)].
- [9] V. M. Budnev *et al.*, Phys. Rept. **15**, 181 (1975), see for an exhaustive treatment.
- [10] See *e.g.* H.Haber, *Supersymmetry, Part I (Theory), this Review*.
- [11] P. R. Harrison and C. H. Llewellyn Smith, Nucl. Phys. **B213**, 223 (1983), [Erratum: Nucl. Phys.B223,542(1983)]; S. Dawson, E. Eichten and C. Quigg, Phys. Rev. **D31**, 1581 (1985); V. D. Barger *et al.*, Phys. Rev. **D31**, 528 (1985); H. Baer and X. Tata, Phys. Lett. **160B**, 159 (1985).
- [12] H. Baer, D. D. Karatas and X. Tata, Phys. Rev. **D42**, 2259 (1990).
- [13] Weak Scale Supersymmetry: From Superfields to Scattering Events, H. Baer and X. Tata (Cambridge University Press) 2006.
- [14] H. E. Haber and G. L. Kane, Phys. Rept. **117**, 75 (1985).
- [15] Theory and Phenomenology of Sparticles, M. Drees, R. Godbole, and P. Roy (World Scientific) 2005.
- [16] A. Bartl, H. Fraas and W. Majerotto, Z. Phys. **C30**, 441 (1986).
- [17] H. Baer *et al.*, Int. J. Mod. Phys. **A4**, 4111 (1989).
- [18] A. Bartl, H. Fraas and W. Majerotto, Nucl. Phys. **B278**, 1 (1986).
- [19] T. Appelquist, H.-C. Cheng and B. A. Dobrescu, Phys. Rev. **D64**, 035002 (2001), [hep-ph/0012100].
- [20] For a review of models with extra spacetime dimensions, see G. Giudice and J. Wells, *Extra Dimensions, this Review*.
- [21] J. M. Smillie and B. R. Webber, JHEP **10**, 069 (2005), [hep-ph/0507170].
- [22] C. Macesanu, C. D. McMullen and S. Nandi, Phys. Rev. **D66**, 015009 (2002), [hep-ph/0201300].
- [23] N. Arkani-Hamed, S. Dimopoulos and G. R. Dvali, Phys. Lett. **B429**, 263 (1998), [hep-ph/9803315]; N. Arkani-Hamed, S. Dimopoulos and G. R. Dvali, Phys. Rev. **D59**, 086004 (1999), [hep-ph/9807344].
- [24] J. L. Hewett, Phys. Rev. Lett. **82**, 4765 (1999), [hep-ph/9811356].
- [25] G. F. Giudice, R. Rattazzi and J. D. Wells, Nucl. Phys. **B544**, 3 (1999), [hep-ph/9811291]; E. A. Mirabelli, M. Perelstein and M. E. Peskin, Phys. Rev. Lett. **82**, 2236 (1999), [hep-ph/9811337]; T. Han, J. D. Lykken and R.-J. Zhang, Phys. Rev. **D59**, 105006 (1999), [hep-ph/9811350].
- [26] L. Randall and R. Sundrum, Phys. Rev. Lett. **83**, 3370 (1999), [hep-ph/9905221].
- [27] H. Davoudiasl, J. L. Hewett and T. G. Rizzo, Phys. Rev. Lett. **84**, 2080 (2000), [hep-ph/9909255].

52. Neutrino Cross Section Measurements

Revised August 2021 by G.P. Zeller (FNAL).

Neutrino cross sections are an essential ingredient in all neutrino experiments. Interest in neutrino scattering has increased due to the need for such information in the interpretation of neutrino oscillation data [1] and given that uncertainties in neutrino-nucleus scattering remain a dominant source of systematic uncertainty in many neutrino oscillation measurements, for example [2]. Historically, neutrino scattering results on both charged current (CC) and neutral current (NC) channels have been collected over many decades using a variety of targets, analysis techniques, and detector technologies. With the advent of intense neutrino sources constructed for neutrino oscillation investigations, experiments are now remeasuring such interaction cross sections with a renewed appreciation for nuclear effects¹ and the need for more precise neutrino flux estimations. This work summarizes accelerator-based neutrino cross section measurements performed in the $\sim 0.1 - 300$ GeV range with an emphasis on inclusive, quasi-elastic (pionless), and pion production processes, areas where we have the most experimental input at present (Table 52.1). For a more comprehensive discussion of neutrino cross sections, including neutrino-electron elastic scattering and lower energy neutrino measurements, the reader is directed to a review of this subject [3]. Here, we survey existing experimental data on neutrino interactions and do not attempt to provide a census of the associated theoretical calculations [4], which are both critical and plentiful. Companion electron-nucleus scattering data are additionally playing an increased role in neutrino event generator development through such efforts as the $e4\nu$ collaboration.

Table 52.1: List of beam properties, nuclear targets, and run durations for modern accelerator-based neutrino experiments studying neutrino scattering.

Experiment	beam	$\langle E_\nu \rangle, \langle E_{\bar{\nu}} \rangle$ GeV	neutrino target(s)	run period
ArgoNeuT	$\nu, \bar{\nu}$	4.3, 3.6	Ar	2009 – 2010
ICARUS (at CNGS)	ν	20.0	Ar	2010 – 2012
ICARUS (at FNAL)	ν	0.8	Ar	2021 –
K2K	ν	1.3	CH, H ₂ O	2003 – 2004
MicroBooNE	ν	0.8	Ar	2015 – 2020
MINERvA	$\nu, \bar{\nu}$	3.5 (LE), 5.5 (ME)	He, C, CH, H ₂ O, Fe, Pb	2009 – 2019
MiniBooNE	$\nu, \bar{\nu}$	0.8, 0.7	CH ₂	2002 – 2019
MINOS	$\nu, \bar{\nu}$	3.5, 6.1	Fe	2004 – 2016
NOMAD	$\nu, \bar{\nu}$	23.4, 19.7	C-based	1995 – 1998
NOvA	$\nu, \bar{\nu}$	2.0, 2.0	CH ₂	2010 –
SciBooNE	$\nu, \bar{\nu}$	0.8, 0.7	CH	2007 – 2008
T2K	$\nu, \bar{\nu}$	0.6, 0.6	CH, H ₂ O, Fe	2010 –

52.1 Inclusive Scattering

Over the years, many experiments have measured the total inclusive charged current cross section for neutrino ($\nu_\mu N \rightarrow \mu^- X$) and antineutrino ($\bar{\nu}_\mu N \rightarrow \mu^+ X$) scattering covering a broad range of neutrino energies. As can be seen in Fig. 52.1, the inclusive cross section approaches a linear dependence on neutrino energy. This behavior is expected for point-like scattering of neutrinos from quarks, an assumption which breaks down at lower energies. Modern measurements of such inclusive scattering cross sections and their target nuclei are summarized in Table 52.2.

To provide a more complete picture, single and double differential cross sections for such inclusive scattering processes have also been reported. These include measurements on iron from NuTeV [5] and on a variety of nuclear targets from ArgoNeuT [6,7], MicroBooNE [8], MINERvA [9–11], NINJA [12], and T2K [13,14]. More recently, MINERvA has provided measurements in terms of longitudinal and transverse muon momenta [10,11], MicroBooNE has measured the first double differential cross sections in argon [8],

and T2K has provided the first measurement of the antineutrino inclusive cross section at low energy [15] (Fig. 52.1).

At high energy, the inclusive cross section is dominated by deep inelastic scattering (DIS). Several neutrino experiments have measured DIS cross sections for specific targets and final states, for example, MINERvA has measured ratios of muon neutrino inclusive and DIS cross sections on a variety of nuclear targets including lead, iron, and carbon [16,17]. The reader is referred to a recent review of measurements in the shallow and deep inelastic scattering regions [18]. Other experiments have measured opposite-sign dimuon production, the most recent being from CHORUS [19], NOMAD [20], and NuTeV [21].

The aforementioned measurements have all been performed using beams of muon neutrinos and antineutrinos. For the first time, measurements of inclusive electron neutrino cross sections have also been reported, most recently by MicroBooNE [22] and T2K [23–25].

Table 52.2: Published measurements of neutrino and antineutrino CC inclusive cross sections from modern accelerator-based neutrino experiments.

experiment	measurement	target
ArgoNeuT	ν_μ [6, 7], $\bar{\nu}_\mu$ [7]	Ar
MicroBooNE	ν_μ [8, 26], ν_e [22]	Ar
MINERvA	ν_μ [9–11, 16, 17, 27], $\bar{\nu}_\mu$ [27], $\bar{\nu}_\mu/\nu_\mu$ [28]	CH, C/CH, Fe/CH, Pb/CH
MINOS	ν_μ [29], $\bar{\nu}_\mu$ [29]	Fe
NINJA	ν_μ [12], $\bar{\nu}_\mu$ [12]	H ₂ O
NOMAD	ν_μ [30]	C
SciBooNE	ν_μ [31]	CH
T2K	ν_μ [13, 14, 32–34], ν_e [23–25], $\bar{\nu}_\mu/\nu_\mu$ [15]	CH, H ₂ O, Fe

At lower neutrino energies, the inclusive cross section is an additionally complex combination of quasi-elastic scattering and pion production processes, two areas we discuss next.

52.2 Quasi-elastic scattering

Quasi-elastic (QE) scattering is the dominant neutrino interaction for neutrino energies less than ~ 1 GeV and represents a large fraction of the signal samples in many neutrino oscillation experiments, which is why this process has received considerable attention in recent years. Historically, neutrino (antineutrino) quasi-elastic scattering refers to the process, $\nu_\mu n \rightarrow \mu^- p$ ($\bar{\nu}_\mu p \rightarrow \mu^+ n$), where a charged lepton and single nucleon are ejected in the elastic interaction of a neutrino (or antineutrino) with a nucleon in the target material. This is the final state one would strictly observe, for example, in scattering off of a *free* nucleon target. There were many early measurements of neutrino QE scattering that span back to the 1970's [3]. In many of these initial measurements, bubble chamber experiments employed light targets (hydrogen or deuterium) and required both the detection of the final state muon and single nucleon²; thus the final state was clear and elastic kinematic conditions could be verified. The situation is more complicated, of course, for heavier nuclear targets used in modern neutrino experiments. In this case, nuclear effects can impact the size and shape of the cross section as well as the final state composition, kinematics, and topology. Due to intranuclear hadron rescattering and the effects of correlations between target nucleons, additional particles may be ejected in the final state; hence, a QE interaction on a nuclear target does not necessarily imply the ejection of a lepton and a *single* nucleon. One therefore needs to take care in defining what one means by neutrino QE scattering when scattering off targets heavier than hydrogen or deuterium. Because of this, modern experiments tend to instead report cross sections for processes involving pionless (e.g., nucleon-only) final states, often referred to as CC 0π or QE-like reactions in recent literature. Such measurements are

¹Nuclear effects refer to kinematic and final state effects which impact neutrino scattering off nuclei. Such effects can be significant and are particularly relevant given that modern neutrino experiments make use of nuclear targets to increase their event yields.

²In the case of deuterium, many experiments additionally observed the spectator proton.

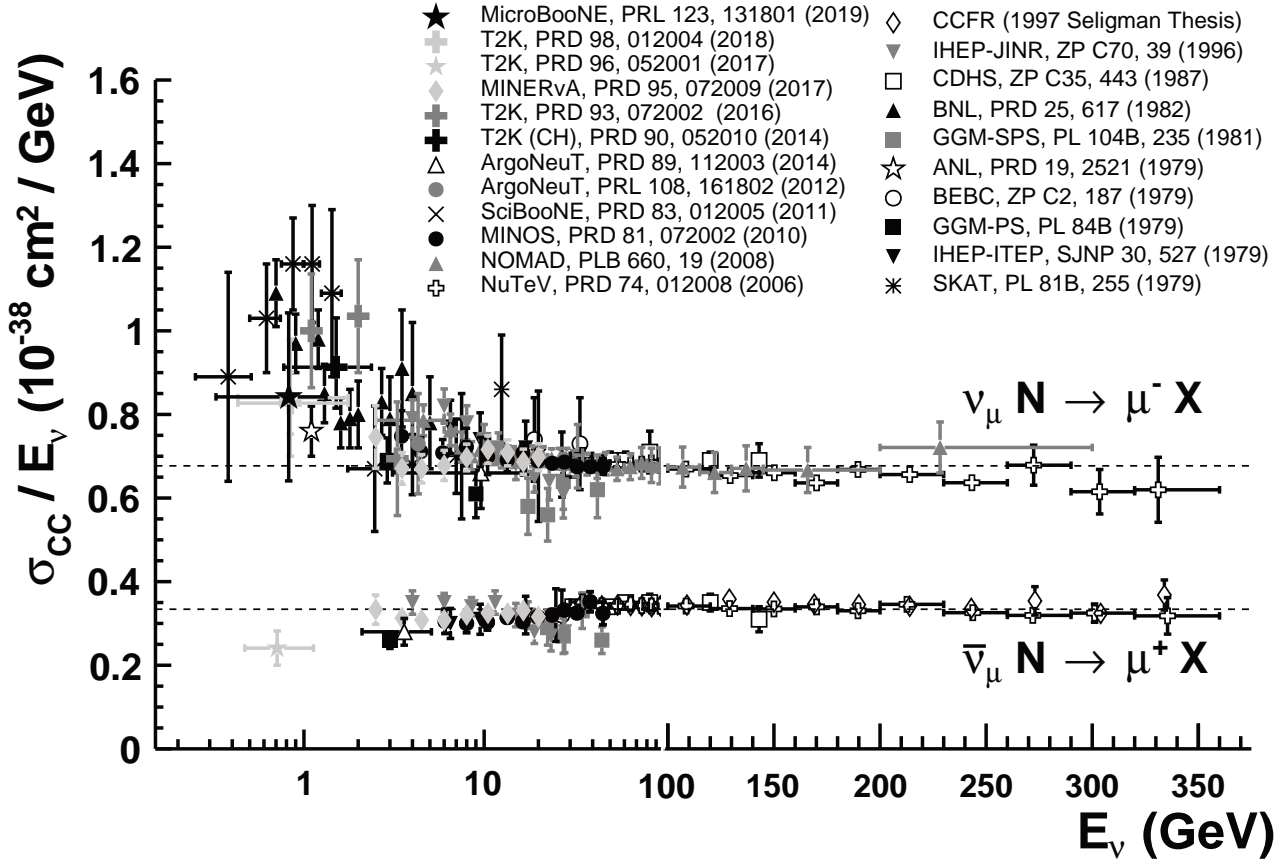


Figure 52.1: Measurements of per nucleon ν_μ and $\bar{\nu}_\mu$ CC inclusive scattering cross sections divided by neutrino energy as a function of neutrino energy. Note the transition between logarithmic and linear scales occurring at 100 GeV. Neutrino cross sections are typically twice as large as their corresponding antineutrino counterparts, although this difference can be larger at lower energies. NC cross sections (not shown) are generally smaller compared to their CC counterpart.

summarized in Table 52.3. Many modern experiments have also recently opted to report nucleon-only cross sections as a function of observed final state particle kinematics [35–48]. Such measurements can be more difficult to directly compare between experiments but have the advantage of being much less model-dependent and provide more stringent tests of the theory than historical cross sections as a function of derived quantities such as neutrino energy (E_ν) or 4-momentum transfer (Q^2). More recent work has been done to develop a means to directly compare experimental measurements produced in these less model-dependent forms [49].

The topic of neutrino QE scattering began drawing considerable attention following the first double differential cross section measurements of this process that revealed a significantly larger cross section than originally anticipated, predominantly in the backwards muon scattering region [40, 41]. Such an enhancement was observed many years prior in transverse electron-nucleus scattering [68] and was attributed to the presence of correlations between nucleons in the target nucleus. As a result, the impact of such nuclear effects on neutrino QE scattering has recently become the subject of intense experimental and theoretical scrutiny with implications on event rates, nucleon emission, neutrino energy reconstruction, and neutrino versus antineutrino cross sections. The reader is referred to reviews of the situation in [4, 69, 70]. To help drive further progress in understanding the underlying nuclear contributions, pionless (e.g., nucleon-only) cross sections have been reported for the first time in the form of double-differential distributions by MiniBooNE [40, 41], MINERvA [35–37, 55], and T2K [42–46]. Such double-differential cross sections in terms of final state particle kinematics reduce the model-dependence of the reported data, provide the most robust measurements available, and allow a more rigorous two-dimensional test of the underlying

nuclear theory. MINERvA and T2K have been especially prolific in recent years in probing this interaction process (Table 52.3). Neutrino experiments have also launched dedicated studies of the hadronic side of these interactions, including ArgoNeuT [50, 71], MicroBooNE [47, 48], MINERvA [54], and T2K [67]. MINERvA has been the first modern experiment to measure neutron emission in antineutrino interactions [72]. T2K has probed ratios of oxygen to carbon [45] and asymmetries between neutrino and antineutrino scattering [46] to glean more information on the nature of the underlying nuclear effects. In addition, the exploration of transverse kinematic variables and momentum imbalances in pionless neutrino scattering is allowing better constraints on the various nuclear contributions to the cross section. Such scrutiny includes recent evaluations from MINERvA [35, 36, 38, 39] and T2K [67]. With the MiniBooNE results having first revealed these additional complexities in neutrino-nucleus QE scattering, measurements from multiple neutrino experiments, on multiple targets, and using a variety of kinematic information have been crucial in gaining a better handle on the underlying nuclear physics impacting neutrino-nucleus interactions. What we once thought was “simple” QE scattering is in fact not so simple.

In addition to such charged current investigations, measurements of the neutral current counterpart of this channel have also been performed. The most recent NC elastic scattering cross section measurements include those from BNL E734 [73], MiniBooNE [59, 60], Super-K [63], and T2K [66]. A number of measurements of the Cabibbo-suppressed antineutrino QE hyperon production cross section have additionally been reported [74, 75], although not in recent years.

Table 52.3: Published modern measurements of neutrino CC and NC scattering cross sections with nucleon-only final states.

experiment	measurement	target
ArgoNeuT	2p [50]	Ar
K2K	M_A [51]	H ₂ O
MicroBooNE	$\frac{d\sigma}{dp_\mu} \frac{d\sigma}{dp_p} \frac{d\sigma}{d\cos\theta_\mu} \frac{d\sigma}{d\cos\theta_p}$ [47, 48]	Ar
MINERvA	$\frac{d^2\sigma}{dp_T dp_{ }}$ [35–37], $\frac{d\sigma}{d\delta p_{Tx}} \frac{d\sigma}{d\delta p_{Ty}}$ [38], $\frac{d\sigma}{dp_n} \frac{d\sigma}{d\delta\alpha_T}$ [39]	CH, Fe, Pb
	$\frac{d\sigma}{dQ^2}$ [52, 53], 1p [54], $\frac{d^2\sigma}{dE_{avail} dq_3}$ [55], $\frac{d\sigma}{dQ^2}$ [56], ν_e [57]	
MiniBooNE	$\frac{d^2\sigma}{dT_\mu d\theta_\mu}$ [40, 41], M_A [58], NC [59, 60]	CH ₂
MINOS	M_A [61]	Fe
NOMAD	M_A , $\sigma(E_\nu)$ [62]	C
Super-K	NC [63]	H ₂ O
T2K	$\frac{d^2\sigma}{dT_\mu d\theta_\mu}$ [42–46], $\sigma(E_\nu)$ [64], M_A [65], NC [66], $\frac{d\sigma}{d\delta p_T} \frac{d\sigma}{d\delta\alpha_T}$ [67], O/C [45]	CH, H ₂ O

52.3 Pion Production

In addition to such elastic scattering processes, neutrinos can also inelastically scatter producing a nucleon excited state (Δ , N^*). Such baryonic resonances quickly decay, most often to a nucleon and single-pion final state. Historically, experiments have measured various exclusive final states associated with these reactions, the majority of which have been on hydrogen and deuterium targets [3]. There have been several recent re-analyses of this data to better understand the consistency between data sets [76], nucleon form factors [77], and non-resonant contributions [78]. Also, modern measurements of neutrino-induced pion production have since been performed on a variety of nuclear targets (Table 52.4).

Table 52.4: Summary of modern measurements of NC and CC scattering cross sections involving a single pion or multiple pions in the final state.

experiment	π^\pm	π^0	target
ArgoNeuT	CC [79, 80]	NC [81]	Ar
K2K	CC [82, 83]	CC [84], NC [85]	CH, H ₂ O
MicroBooNE	–	CC [86]	Ar
MINERvA	CC [87–92]	CC [88, 93–95], NC [96]	CH
MiniBooNE	CC [97, 98]	CC [99], NC [100, 101]	CH ₂
MINOS	–	NC [102]	Fe
NOMAD	–	NC [103]	C
NOvA	–	NC [104]	C
SciBooNE	CC [105]	NC [106, 107]	CH
T2K	CC [108–111]	–	CH, H ₂ O

In addition to resonance production processes, neutrinos can also coherently scatter off of the entire nucleus and produce a distinctly forward-scattered single pion final state. Both CC ($\nu_\mu A \rightarrow \mu^- A \pi^+$, $\bar{\nu}_\mu A \rightarrow \mu^+ A \pi^-$) and NC ($\nu_\mu A \rightarrow \nu_\mu A \pi^0$, $\bar{\nu}_\mu A \rightarrow \bar{\nu}_\mu A \pi^0$) processes are possible in this case. Even though the level of coherent pion production is small compared to their resonant counterpart, observations exist across a broad energy range and on multiple nuclear targets [112]. More recently, several modern neutrino experiments have either measured or set limits on coherent pion production cross sections including ArgoNeuT [79], K2K [83], MINERvA [89, 91], MiniBooNE [101], MINOS [102], NOMAD [103], NOvA [104], SciBooNE [105, 107], and T2K [83].

As with inclusive and quasi-elastic scattering, a new appreciation for the significance of nuclear effects has also surfaced in pion production physics, again due to the use of heavy nuclear targets in modern neutrino experiments. Many experiments have been careful to report cross sections for various detected final states, thereby not correcting for large and uncertain nuclear effects (e.g., pion rescattering, charge exchange, and absorption) which can introduce significant sources of uncertainty and model dependence. Providing the most comprehensive survey of neutrino single-pion production to date, MiniBooNE has published a total of 16 single- and double-differential cross sections for both the final state muon (in the case of CC scattering) and pions in these interactions; thus, providing the first measurements of such final state kinematic distributions [97–100]. At similar neutrino energies, T2K

has provided new data [108] including the first measurement of the Adler angles in neutrino-nucleus scattering [110] and the first exploration of transverse kinematic imbalances in pion production processes [111]. MINERvA has produced a similar accompaniment of measurements at higher neutrino energies [88, 90, 92, 94]. Importantly, MINERvA has been working towards an improved nuclear model [95] and one that can potentially describe all of the pion reaction channels simultaneously, an issue that many experiments have struggled with up until now [88]. ArgoNeuT [80, 81] and MicroBooNE [86] have since been adding new information on single pion production in argon. Regardless of the interaction channel or target material, differential cross section measurements in terms of observed final state particle kinematics are preferred for their reduced model dependence and for the additional kinematic information they provide. Such a new direction has been the focus of modern measurements as opposed to the reporting of more model-dependent, historical cross sections as a function of E_ν or Q^2 . Together with similar results for other interaction channels, a better understanding and modeling of nuclear effects will be possible moving forward. MINERvA [113] has already taken a large step in this direction by explicitly tuning the physics in existing neutrino event generators to best fit the experimental data on pion production.

It should be noted that baryonic resonances can also decay to multi-pion, other mesonic (K , η , ρ , etc.), and even photon final states. Experimental results for these channels are typically sparse or non-existent [3]; however, photon production processes can comprise an important background for $\nu_\mu \rightarrow \nu_e$ appearance searches in some detectors and thus have become the focus of recent experimental investigations, most notably in NOMAD [114] and T2K [115, 116]. There have also been several recent measurements of kaon final states produced in neutrino NC and CC scattering in MINERvA [117–119] that are providing needed background constraints for certain nucleon decay searches.

52.4 Outlook

Neutrino experiments continue to produce critical neutrino scattering measurements on nuclei as they accumulate increased statistics and pursue new ways of reporting their measurements. Analysis of a broad energy range of data from MINERvA is providing some of the most detailed analysis of nuclear effects in neutrino interactions by examining multiple nuclei in a single experiment. Data from ArgoNeuT and MicroBooNE (and soon also ICARUS and SBND) are probing deeper into complex neutrino final states using the superior capabilities of liquid argon time projection chambers, while the T2K and NOvA near detectors continue to collect high statistics samples in intense neutrino beams. Together with dedicated discussions between experiments on how best to report neutrino cross section measurements [120] and with accompanying work being advanced by theorists to further improve nuclear model calculations [4], we are starting to significantly advance our understanding of neutrino-nucleus scattering.

52.5 Acknowledgments

The author thanks Anne Schukraft (Fermilab) for help in preparing the plots and content of this review.

References

- [1] O. Benhar *et al.*, Phys. Rept. **700**, 1 (2017), [arXiv:1501.06448].
- [2] M. A. Acero *et al.* (NOvA, R. Group), Eur. Phys. J. C **80**, 12, 1119 (2020), [arXiv:2006.08727].
- [3] J. A. Formaggio and G. P. Zeller, Rev. Mod. Phys. **84**, 1307 (2012), [arXiv:1305.7513].
- [4] L. Alvarez-Ruso *et al.*, Prog. Part. Nucl. Phys. **100**, 1 (2018), [arXiv:1706.03621].
- [5] M. Tzanov *et al.* (NuTeV), Phys. Rev. **D74**, 012008 (2006), [hep-ex/0509010].
- [6] C. Anderson *et al.* (ArgoNeuT), Phys. Rev. Lett. **108**, 161802 (2012), [arXiv:1111.0103].
- [7] R. Acciarri *et al.* (ArgoNeuT), Phys. Rev. **D89**, 11, 112003 (2014), [arXiv:1404.4809].
- [8] P. Abratenko *et al.* (MicroBooNE), Phys. Rev. Lett. **123**, 13, 131801 (2019), [arXiv:1905.09694].
- [9] P. A. Rodrigues *et al.* (MINERvA), Phys. Rev. Lett. **116**, 071802 (2016), [Addendum: Phys. Rev. Lett. **121**, no. 20, 209902 (2018)], [arXiv:1511.05944].
- [10] A. Filkins *et al.* (MINERvA), Phys. Rev. D **101**, 11, 112007 (2020), [arXiv:2002.12496].
- [11] D. Ruterbories *et al.* (MINERvA) (2021), [arXiv:2106.16210].
- [12] A. Hiramoto *et al.* (NINJA), Phys. Rev. D **102**, 7, 072006 (2020), [arXiv:2008.03895].
- [13] K. Abe *et al.* (T2K), Phys. Rev. **D87**, 9, 092003 (2013), [arXiv:1302.4908].
- [14] K. Abe *et al.* (T2K), Phys. Rev. **D98**, 012004 (2018), [arXiv:1801.05148].
- [15] K. Abe *et al.* (T2K), Phys. Rev. **D96**, 5, 052001 (2017), [arXiv:1706.04257].
- [16] B. G. Tice *et al.* (MINERvA), Phys. Rev. Lett. **112**, 23, 231801 (2014), [arXiv:1403.2103].
- [17] J. Mousseau *et al.* (MINERvA), Phys. Rev. **D93**, 7, 071101 (2016), [arXiv:1601.06313].
- [18] M. Sajjad Athar and J. G. Morfin, J. Phys. G **48**, 3, 034001 (2021), [arXiv:2006.08603].
- [19] A. Kayis-Topaksu *et al.* (CHORUS), Nucl. Phys. **B798**, 1 (2008), [arXiv:0804.1869].
- [20] O. Samoylov *et al.* (NOMAD), Nucl. Phys. **B876**, 339 (2013), [arXiv:1308.4750].
- [21] D. Mason *et al.* (NuTeV), Phys. Rev. Lett. **99**, 192001 (2007).
- [22] P. Abratenko *et al.* ((MicroBooNE Collaboration)*, MicroBooNE), Phys. Rev. D **104**, 5, 052002 (2021), [arXiv:2101.04228].
- [23] K. Abe *et al.* (T2K), Phys. Rev. Lett. **113**, 24, 241803 (2014), [arXiv:1407.7389].
- [24] K. Abe *et al.* (T2K), Phys. Rev. **D91**, 112010 (2015), [arXiv:1503.08815].
- [25] K. Abe *et al.* (T2K), JHEP **10**, 114 (2020), [arXiv:2002.11986].
- [26] C. Adams *et al.* (MicroBooNE), Eur. Phys. J. **C79**, 3, 248 (2019), [arXiv:1805.06887].
- [27] J. Devan *et al.* (MINERvA), Phys. Rev. **D94**, 11, 112007 (2016), [arXiv:1610.04746].
- [28] L. Ren *et al.* (MINERvA), Phys. Rev. **D95**, 7, 072009 (2017), [Addendum: Phys. Rev. **D97**, no. 1, 019902 (2018)], [arXiv:1701.04857].
- [29] P. Adamson *et al.* (MINOS), Phys. Rev. **D81**, 072002 (2010), [arXiv:0910.2201].
- [30] Q. Wu *et al.* (NOMAD), Phys. Lett. **B660**, 19 (2008), [arXiv:0711.1183].
- [31] Y. Nakajima *et al.* (SciBooNE), Phys. Rev. **D83**, 012005 (2011), [arXiv:1011.2131].
- [32] K. Abe *et al.* (T2K), Phys. Rev. **D90**, 5, 052010 (2014), [arXiv:1407.4256].
- [33] K. Abe *et al.* (T2K), Phys. Rev. **D93**, 7, 072002 (2016), [arXiv:1509.06940].
- [34] K. Abe *et al.* (T2K), PTEP **2019**, 9, 093C02 (2019), [arXiv:1904.09611].
- [35] D. Ruterbories *et al.* (MINERvA), Phys. Rev. **D99**, 1, 012004 (2019), [arXiv:1811.02774].
- [36] C. E. Patrick *et al.* (MINERvA), Phys. Rev. **D97**, 5, 052002 (2018), [arXiv:1801.01197].
- [37] M. F. Carneiro *et al.* (MINERvA), Phys. Rev. Lett. **124**, 12, 121801 (2020), [arXiv:1912.09890].
- [38] T. Cai *et al.* (MINERvA), Phys. Rev. D **101**, 9, 092001 (2020), [arXiv:1910.08658].
- [39] X. G. Lu *et al.* (MINERvA), Phys. Rev. Lett. **121**, 2, 022504 (2018), [arXiv:1805.05486].
- [40] A. A. Aguilar-Arevalo *et al.* (MiniBooNE), Phys. Rev. **D81**, 092005 (2010), [arXiv:1002.2680].
- [41] A. A. Aguilar-Arevalo *et al.* (MiniBooNE), Phys. Rev. **D88**, 3, 032001 (2013), [arXiv:1301.7067].
- [42] K. Abe *et al.* (T2K), Phys. Rev. **D93**, 11, 112012 (2016), [arXiv:1602.03652].
- [43] K. Abe *et al.* (T2K), Phys. Rev. **D97**, 1, 012001 (2018), [arXiv:1708.06771].
- [44] K. Abe *et al.* (T2K), Phys. Rev. D **102**, 1, 012007 (2020), [arXiv:1908.10249].
- [45] K. Abe *et al.* (T2K), Phys. Rev. D **101**, 11, 112004 (2020), [arXiv:2004.05434].
- [46] K. Abe *et al.* (T2K), Phys. Rev. D **101**, 11, 112001 (2020), [arXiv:2002.09323].
- [47] P. Abratenko *et al.* (MicroBooNE), Phys. Rev. D **102**, 11, 112013 (2020), [arXiv:2010.02390].
- [48] P. Abratenko *et al.* (MicroBooNE), Phys. Rev. Lett. **125**, 20, 201803 (2020), [arXiv:2006.00108].
- [49] K. Mahn, C. Marshall and C. Wilkinson, Ann. Rev. Nucl. Part. Sci. **68**, 105 (2018), [arXiv:1803.08848].
- [50] R. Acciarri *et al.* (ArgoNeuT), Phys. Rev. **D90**, 1, 012008 (2014), [arXiv:1405.4261].
- [51] R. Gran *et al.* (K2K), Phys. Rev. **D74**, 052002 (2006), [hep-ex/0603034].
- [52] G. A. Fiorentini *et al.* (MINERvA), Phys. Rev. Lett. **111**, 022502 (2013), [arXiv:1305.2243].
- [53] L. Fields *et al.* (MINERvA), Phys. Rev. Lett. **111**, 2, 022501 (2013), [arXiv:1305.2234].
- [54] T. Walton *et al.* (MINERvA), Phys. Rev. **D91**, 7, 071301 (2015), [arXiv:1409.4497].
- [55] R. Gran *et al.* (MINERvA), Phys. Rev. Lett. **120**, 22, 221805 (2018), [arXiv:1803.09377].
- [56] M. Betancourt *et al.* (MINERvA), Phys. Rev. Lett. **119**, 8, 082001 (2017), [arXiv:1705.03791].
- [57] J. Wolcott *et al.* (MINERvA), Phys. Rev. Lett. **116**, 8, 081802 (2016), [arXiv:1509.05729].
- [58] A. A. Aguilar-Arevalo *et al.* (MiniBooNE), Phys. Rev. Lett. **100**, 032301 (2008), [arXiv:0706.0926].
- [59] A. A. Aguilar-Arevalo *et al.* (MiniBooNE), Phys. Rev. **D82**, 092005 (2010), [arXiv:1007.4730].
- [60] A. A. Aguilar-Arevalo *et al.* (MiniBooNE), Phys. Rev. **D91**, 1, 012004 (2015), [arXiv:1309.7257].
- [61] P. Adamson *et al.* (MINOS), Phys. Rev. **D91**, 1, 012005 (2015), [arXiv:1410.8613].
- [62] V. Lyubushkin *et al.* (NOMAD), Eur. Phys. J. **C63**, 355 (2009), [arXiv:0812.4543].

- [63] L. Wan *et al.* (Super-Kamiokande), Phys. Rev. **D99**, 3, 032005 (2019), [arXiv:1901.05281].
- [64] K. Abe *et al.* (T2K), Phys. Rev. **D91**, 11, 112002 (2015), [arXiv:1503.07452].
- [65] K. Abe *et al.* (T2K), Phys. Rev. **D92**, 11, 112003 (2015), [arXiv:1411.6264].
- [66] K. Abe *et al.* (T2K), Phys. Rev. **D90**, 7, 072012 (2014), [arXiv:1403.3140].
- [67] K. Abe *et al.* (T2K), Phys. Rev. **D98**, 3, 032003 (2018), [arXiv:1802.05078].
- [68] J. Carlson *et al.*, Phys. Rev. **C65**, 024002 (2002), [arXiv:nucl-th/0106047].
- [69] H. Gallagher, G. Garvey and G. P. Zeller, Ann. Rev. Nucl. Part. Sci. **61**, 355 (2011).
- [70] G. T. Garvey *et al.*, Phys. Rept. **580**, 1 (2015), [arXiv:1412.4294].
- [71] O. Palamara (ArgoNeuT), JPS Conf. Proc. **12**, 010017 (2016).
- [72] M. Elkins *et al.* (MINERvA), Phys. Rev. **D100**, 5, 052002 (2019), [arXiv:1901.04892].
- [73] L. A. Ahrens *et al.*, Phys. Rev. **D35**, 785 (1987).
- [74] J. Brunner *et al.* (SKAT), Z. Phys. **C45**, 551 (1990).
- [75] V. V. Ammosov *et al.*, Z. Phys. **C36**, 377 (1987); O. Erriquez *et al.*, Phys. Lett. **70B**, 383 (1977); T. Eichten *et al.*, Phys. Lett. **40B**, 593 (1972).
- [76] C. Wilkinson *et al.*, Phys. Rev. **D90**, 11, 112017 (2014), [arXiv:1411.4482].
- [77] A. S. Meyer *et al.*, Phys. Rev. **D93**, 11, 113015 (2016), [arXiv:1603.03048].
- [78] P. Rodrigues, C. Wilkinson and K. McFarland, Eur. Phys. J. **C76**, 8, 474 (2016), [arXiv:1601.01888].
- [79] R. Acciarri *et al.* (ArgoNeuT), Phys. Rev. Lett. **113**, 26, 261801 (2014), [erratum: Phys. Rev. Lett.114,no.3,039901(2015)], [arXiv:1408.0598].
- [80] R. Acciarri *et al.* (ArgoNeuT), Phys. Rev. D **98**, 5, 052002 (2018), [arXiv:1804.10294].
- [81] R. Acciarri *et al.* (ArgoNeuT), Phys. Rev. **D96**, 1, 012006 (2017), [arXiv:1511.00941].
- [82] A. Rodriguez *et al.* (K2K), Phys. Rev. **D78**, 032003 (2008), [arXiv:0805.0186].
- [83] M. Hasegawa *et al.* (K2K), Phys. Rev. Lett. **95**, 252301 (2005), [hep-ex/0506008].
- [84] C. Mariani *et al.* (K2K), Phys. Rev. **D83**, 054023 (2011), [arXiv:1012.1794].
- [85] S. Nakayama *et al.* (K2K), Phys. Lett. **B619**, 255 (2005), [hep-ex/0408134].
- [86] C. Adams *et al.* (MicroBooNE), Phys. Rev. **D99**, 9, 091102 (2019), [arXiv:1811.02700].
- [87] B. Eberly *et al.* (MINERvA), Phys. Rev. **D92**, 9, 092008 (2015), [arXiv:1406.6415].
- [88] C. L. McGivern *et al.* (MINERvA), Phys. Rev. **D94**, 5, 052005 (2016), [arXiv:1606.07127].
- [89] A. Higuera *et al.* (MINERvA), Phys. Rev. Lett. **113**, 26, 261802 (2014), [arXiv:1409.3835].
- [90] T. Le *et al.* (MINERvA), Phys. Rev. **D100**, 5, 052008 (2019), [arXiv:1906.08300].
- [91] A. Mislivec *et al.* (MINERvA), Phys. Rev. **D97**, 3, 032014 (2018), [arXiv:1711.01178].
- [92] T. Le *et al.* (MINERvA), Phys. Rev. D **100**, 5, 052008 (2019), [arXiv:1906.08300].
- [93] T. Le *et al.* (MINERvA), Phys. Lett. **B749**, 130 (2015), [arXiv:1503.02107].
- [94] O. Altinok *et al.* (MINERvA), Phys. Rev. **D96**, 7, 072003 (2017), [arXiv:1708.03723].
- [95] D. Coplowe *et al.* (MINERvA), Phys. Rev. D **102**, 7, 072007 (2020), [arXiv:2002.05812].
- [96] J. Wolcott *et al.* (MINERvA), Phys. Rev. Lett. **117**, 11, 111801 (2016), [arXiv:1604.01728].
- [97] A. A. Aguilar-Arevalo *et al.* (MiniBooNE), Phys. Rev. **D83**, 052007 (2011), [arXiv:1011.3572].
- [98] A. A. Aguilar-Arevalo *et al.* (MiniBooNE), Phys. Rev. Lett. **103**, 081801 (2009), [arXiv:0904.3159].
- [99] A. A. Aguilar-Arevalo *et al.* (MiniBooNE), Phys. Rev. **D83**, 052009 (2011), [arXiv:1010.3264].
- [100] A. A. Aguilar-Arevalo *et al.* (MiniBooNE), Phys. Rev. **D81**, 013005 (2010), [arXiv:0911.2063].
- [101] A. A. Aguilar-Arevalo *et al.* (MiniBooNE), Phys. Lett. **B664**, 41 (2008), [arXiv:0803.3423].
- [102] P. Adamson *et al.* (MINOS), Phys. Rev. **D94**, 7, 072006 (2016), [arXiv:1608.05702].
- [103] C. T. Kullenberg *et al.* (NOMAD), Phys. Lett. **B682**, 177 (2009), [arXiv:0910.0062].
- [104] M. A. Acero *et al.* (NOvA), Phys. Rev. D **102**, 1, 012004 (2020), [arXiv:1902.00558].
- [105] K. Hiraide *et al.* (SciBooNE), Phys. Rev. **D78**, 112004 (2008), [arXiv:0811.0369].
- [106] Y. Kurimoto *et al.* (SciBooNE), Phys. Rev. **D81**, 033004 (2010), [arXiv:0910.5768].
- [107] Y. Kurimoto *et al.* (SciBooNE), Phys. Rev. **D81**, 111102 (2010), [arXiv:1005.0059].
- [108] K. Abe *et al.* (T2K), Phys. Rev. **D95**, 1, 012010 (2017), [arXiv:1605.07964].
- [109] K. Abe *et al.* (T2K), Phys. Rev. Lett. **117**, 19, 192501 (2016), [arXiv:1604.04406].
- [110] K. Abe *et al.* (T2K), Phys. Rev. D **101**, 1, 012007 (2020), [arXiv:1909.03936].
- [111] K. Abe *et al.* (T2K), Phys. Rev. D **103**, 11, 112009 (2021), [arXiv:2102.03346].
- [112] P. Vilain *et al.* (CHARM-II), Phys. Lett. **B313**, 267 (1993); A compilation of historical coherent pion production data.
- [113] P. Stowell *et al.* (MINERvA), Phys. Rev. **D100**, 7, 072005 (2019), [arXiv:1903.01558].
- [114] C. T. Kullenberg *et al.* (NOMAD), Phys. Lett. **B706**, 268 (2012), [arXiv:1111.3713].
- [115] K. Abe *et al.* (T2K), J. Phys. **G46**, 8, 08LT01 (2019), [arXiv:1902.03848].
- [116] K. Abe *et al.* (T2K), Phys. Rev. D **100**, 11, 112009 (2019), [arXiv:1910.09439].
- [117] C. M. Marshall *et al.* (MINERvA), Phys. Rev. **D94**, 1, 012002 (2016), [arXiv:1604.03920].
- [118] C. M. Marshall *et al.* (MINERvA), Phys. Rev. Lett. **119**, 1, 011802 (2017), [arXiv:1611.02224].
- [119] Z. Wang *et al.* (MINERvA), Phys. Rev. Lett. **117**, 6, 061802 (2016), [arXiv:1606.08890].
- [120] M. Betancourt *et al.*, Phys. Rept. **773-774**, 1 (2018), [arXiv:1805.07378].

53. Plots of Cross Sections and Related Quantities

Updated in 2021. See various sections for details.

53.1	Pseudorapidity Distributions in pp and $\bar{p}p$ Interactions	770
53.2	Average Hadron Multiplicities in Hadronic e^+e^- Annihilation Events	771
53.3	σ and R in e^+e^- Collisions	773
53.4	Annihilation Cross Section Near M_Z	775
53.5	Total Hadronic Cross Sections	776

53.1 Pseudorapidity Distributions in pp and $\bar{p}p$ Interactions

Revised August 2013 by D.R. Ward (Cavendish Lab.).

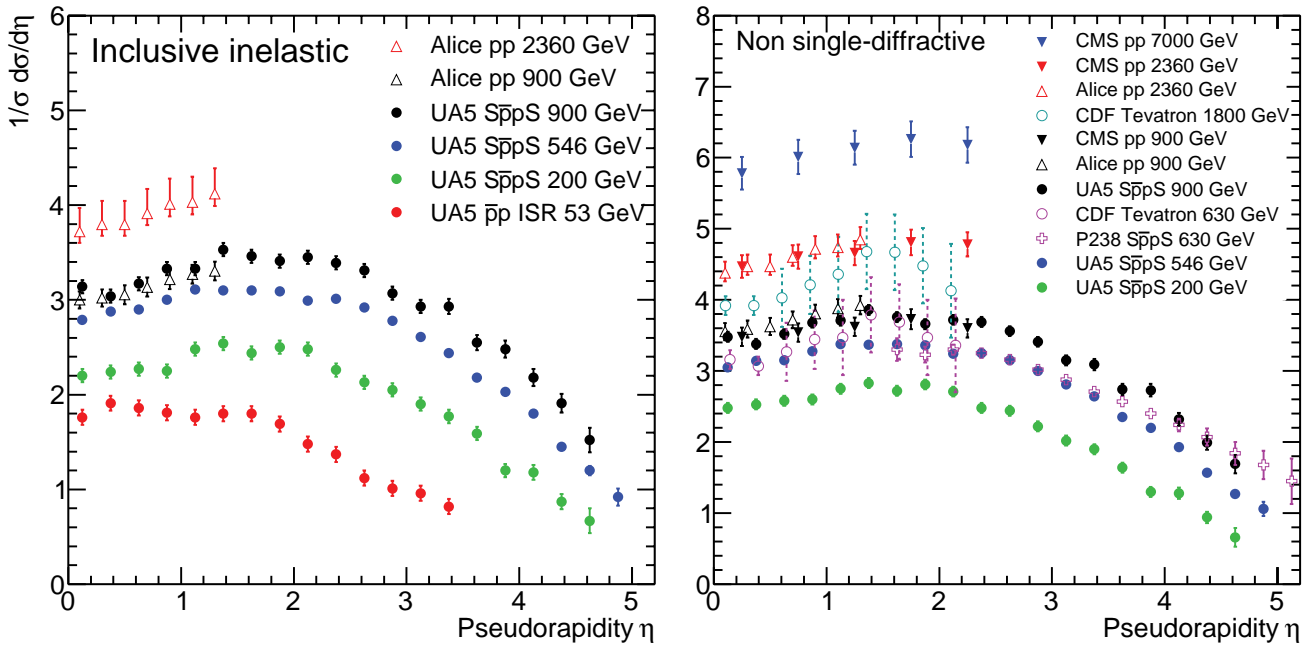
Pseudorapidity Distributions in pp and $\bar{p}p$ Interactions

Figure 53.1: Charged particle pseudorapidity distributions in pp collisions for $53 \text{ GeV} \leq \sqrt{s} \leq 1800 \text{ GeV}$. UA5 data from the S $\bar{p}p$ S are taken from [1], and from the ISR from [2]. The UA5 data are shown for both the full inelastic cross-section and with singly diffractive events excluded. Additional non single-diffractive measurements are available from CDF at the Tevatron [3] and from P238 at the S $\bar{p}p$ S [4]. These may be compared with both inclusive and non single-diffractive measurements in pp collisions at the LHC from ALICE [5] and for non single-diffractive interactions from CMS [6, 7]. (Courtesy of D.R. Ward, Cambridge Univ., 2013)

53.2 Average Hadron Multiplicities in Hadronic e^+e^- Annihilation Events

Revised August 2021 by O. Biebel (Ludwig-Maximilians U.).

Table 53.1: Average hadron multiplicities per hadronic e^+e^- annihilation event at $\sqrt{s} \approx 10, 29\text{--}35, 91,$ and $130\text{--}200$ GeV. The rates given include decay products from resonances with $c\tau < 10$ cm, and include the corresponding anti-particle state. Correlations of the systematic uncertainties were considered for the calculation of the averages. Quoted errors are not increased by scale factor S .

Particle	$\sqrt{s} \approx 10$ GeV	$\sqrt{s} = 29\text{--}35$ GeV	$\sqrt{s} = 91$ GeV	$\sqrt{s} = 130\text{--}200$ GeV	References
Pseudoscalar mesons:					
π^+	6.52 ± 0.11	0.3 ± 0.4	17.02 ± 0.19	21.24 ± 0.39	[8–17]
π^0	3.2 ± 0.3	5.83 ± 0.28	9.42 ± 0.32		[12, 18–23]
K^+	0.953 ± 0.018	1.48 ± 0.09	2.228 ± 0.059	2.82 ± 0.19	[9–17, 24, 25]
K^0	0.91 ± 0.05	1.48 ± 0.07	2.049 ± 0.026	2.10 ± 0.12	[12, 17, 20, 26–36]
η	0.20 ± 0.04	0.61 ± 0.07	1.049 ± 0.080		[12, 18, 19, 22, 23, 37–40]
$\eta(958)$	0.03 ± 0.01	0.26 ± 0.10	0.152 ± 0.020		[20, 39, 41–43]
D^+	$0.194 \pm 0.019^{(a)}$	0.17 ± 0.03	0.175 ± 0.016		[12, 44–47]
D^0	$0.446 \pm 0.032^{(a)}$	0.45 ± 0.07	0.454 ± 0.030		[12, 44–47]
D_s^+	$0.063 \pm 0.014^{(a)}$	$0.45 \pm 0.20^{(b)}$	0.131 ± 0.021		[8, 39, 44, 47–49]
$B^{(c)}$	—	—	$0.134 \pm 0.016^{(d)}$		[46, 50]
B^+	—	—	$0.141 \pm 0.004^{(d)}$		[51]
B_s^0	—	—	$0.054 \pm 0.011^{(d)}$		[52, 53]
Scalar mesons:					
$f_0(980)$	0.024 ± 0.006	$0.05 \pm 0.02^{(e)}$	0.146 ± 0.012		[41, 54–56]
$a_0(980)^\pm$	—	—	$0.27 \pm 0.11^{(f)}$		[43]
Vector mesons:					
$\rho(770)^0$	0.35 ± 0.04	0.81 ± 0.08	1.231 ± 0.098		[9, 12, 55, 57, 58]
$\rho(770)^\pm$	—	—	$2.40 \pm 0.43^{(f)}$		[43]
$\omega(782)$	0.30 ± 0.08	—	1.016 ± 0.065		[40, 42, 43, 57]
$K^*(892)^+$	0.27 ± 0.03	0.64 ± 0.05	0.714 ± 0.055		[9, 12, 33, 57, 59, 60]
$K^*(892)^0$	0.29 ± 0.03	0.56 ± 0.06	0.738 ± 0.024		[9, 12, 36, 57, 58, 61, 62]
$\phi(1020)$	0.044 ± 0.003	0.085 ± 0.011	0.0963 ± 0.0032		[12, 36, 56–58, 61]
$D^*(2010)^+$	$0.177 \pm 0.022^{(a)}$	0.43 ± 0.07	$0.1937 \pm 0.0057^{(g)}$		[12, 44–46, 63, 64]
$D^*(2007)^0$	$0.168 \pm 0.019^{(a)}$	0.27 ± 0.11	—		[12, 44, 45]
$D_s^*(2112)^+$	$0.048 \pm 0.014^{(a)}$	—	$0.101 \pm 0.048^{(h)}$		[48, 65]
$B^*(i)$	—	—	0.288 ± 0.026		[66, 67]
$J/\psi(1S)$	$0.00050 \pm 0.00005^{(a)}$	—	$0.0052 \pm 0.0004^{(j)}$		[68–73]
$\psi(2S)$	—	—	$0.0023 \pm 0.0004^{(j)}$		[71, 73, 74]
$\Upsilon(1S)$	—	—	$0.00014 \pm 0.00007^{(j)}$		[75]
Pseudovector mesons:					
$f_1(1285)$	—	—	0.165 ± 0.051		[76]
$f_1(1420)$	—	—	0.056 ± 0.012		[76]
$\chi_{c1}(3510)$	—	—	$0.0041 \pm 0.0011^{(j)}$		[71, 74]
Tensor mesons:					
$f_2(1270)$	0.09 ± 0.02	0.14 ± 0.04	0.166 ± 0.020		[54–56, 77]
$f_2'(1525)$	—	—	0.012 ± 0.006		[55]
$K_2^*(1430)^+$	—	0.09 ± 0.03	—		[55, 78]
$K_2^*(1430)^0$	—	0.12 ± 0.06	0.084 ± 0.022		[54, 55, 79]
$B^{** (k)}$	—	—	0.118 ± 0.024		[80]
D_{s1}^\pm	—	—	$0.0052 \pm 0.0011^{(l)}$		[81]
$D_{s2}^{*\pm}$	—	—	$0.0083 \pm 0.0031^{(l)}$		[81]
Baryons:					
p	0.266 ± 0.008	0.640 ± 0.050	1.050 ± 0.032	1.41 ± 0.18	[10, 13–17, 24, 25, 77]
Λ	$0.093 \pm 0.006^{(a)}$	0.205 ± 0.010	0.3915 ± 0.0065	0.39 ± 0.03	[17, 20, 34, 36, 77, 82–85]
Σ^0	$0.0221 \pm 0.0018^{(a)}$	—	0.078 ± 0.010		[10, 59, 82, 86–88]
Σ^-	—	—	0.081 ± 0.010		[88, 89]
Σ^+	—	—	0.107 ± 0.011		[87, 88]
Σ^\pm	—	—	0.174 ± 0.009		[84, 88]
Ξ^-	$0.0055 \pm 0.0004^{(a)}$	0.0176 ± 0.0027	0.0262 ± 0.0009		[9, 59, 77, 82–85]
$\Delta(1232)^{++}$	0.040 ± 0.010	—	0.085 ± 0.014		[90–92]
$\Sigma(1385)^-$	0.006 ± 0.002	0.017 ± 0.004	0.0240 ± 0.0017		[59, 82, 84, 85, 93]
$\Sigma(1385)^+$	$0.0062 \pm 0.0011^{(a)}$	0.017 ± 0.004	0.0239 ± 0.0015		[59, 82–85, 93]
$\Sigma(1385)^\pm$	0.0106 ± 0.0020	0.033 ± 0.008	0.0472 ± 0.0027		[59, 82, 84, 85, 93]
$\Xi(1530)^0$	$0.00130 \pm 0.00010^{(a)}$	—	0.00694 ± 0.00049		[59, 82, 83, 85, 94]
Ω^-	$0.00060 \pm 0.00033^{(a)}$	0.014 ± 0.007	0.00124 ± 0.00018		[59, 77, 82, 83, 85, 86]
Λ_c^+	$0.0479 \pm 0.0038^{(a,m)}$	0.110 ± 0.050	0.078 ± 0.017		[47, 49, 77, 83, 95]
Λ_c^0	—	—	0.031 ± 0.016		[96]
Σ_c^0	$0.0025 \pm 0.0004^{(a)}$	—	—		[83]
$\Lambda(1520)$	$0.0046 \pm 0.0004^{(a)}$	—	0.0222 ± 0.0027		[83, 85, 89, 97]

(a) $\sigma_{\text{had}} = 3.33 \pm 0.05 \pm 0.21$ nb (CLEO: [98]) has been used in converting the measured cross sections to average hadron multiplicities.

(b) $B(D_s \rightarrow \eta\pi, \eta'\pi)$ was used (RPP 1994).

- (c) Comprises both charged and neutral B meson states.
- (d) The Standard Model $B(Z \rightarrow b\bar{b}) = 0.217$ was used.
- (e) $x_p = p/p_{\text{beam}} > 0.1$ only.
- (f) Both charge states.
- (g) $B(D^*(2010)^+ \rightarrow D^0\pi^+) \times B(D^0 \rightarrow K^-\pi^+)$ has been used (RPP 2000).
- (h) $B(D_s^* \rightarrow D_S^+\gamma)$, $B(D_s^+ \rightarrow \phi\pi^+)$, $B(\phi \rightarrow K^+K^-)$ have been used (RPP 1998).
- (i) Any charge state (*i.e.*, B_d^* , B_u^* , or B_s^*).
- (j) $B(Z \rightarrow \text{hadrons}) = 0.699$ was used (RPP 1994).
- (k) Any charge state (*i.e.*, B_d^{**} , B_u^{**} , or B_s^{**}).
- (l) Assumes $B(D_{s1}^+ \rightarrow D^{*+}K^0 + D^{*0}K^+) = 100\%$ and $B(D_{s2}^+ \rightarrow D^0K^+) = 45\%$.
- (m) The value was derived from the cross section of $\Lambda_c^+ \rightarrow p\pi K$ using (a) and assuming the branching fraction to be $(5.0 \pm 1.3)\%$ (RPP 2004).

References grouped by collaboration for Table-53.1:

- **RPP**: [12]
- **ALEPH**: [13, 20, 40, 58, 59, 63, 70, 81],
- **ARGUS**: [8, 24, 37, 41, 57, 82, 90, 97],
- **BaBar**: [10, 48, 68, 95],
- **Belle**: [44, 69, 83],
- **CELLO**: [19, 26],
- **CLEO**: [9, 45, 49, 98],
- **Crystal Ball**: [38],
- **DELPHI**: [14, 17, 21, 25, 33, 46, 50–52, 55, 61, 66, 71, 76, 80, 84, 86, 89, 91, 94],
- **HRS**: [27, 54, 78, 93],
- **L3**: [22, 34, 42, 67, 72, 74, 87]
- **MARK II**: [29, 39],
- **JADE**: [18, 28],
- **OPAL**: [15, 23, 35, 43, 47, 53, 56, 60, 62, 64, 65, 73, 75, 79, 85, 88, 92, 96],
- **PLUTO**: [30]
- **SLD**: [16, 36],
- **TASSO**: [31]
- **TPC**: [32].

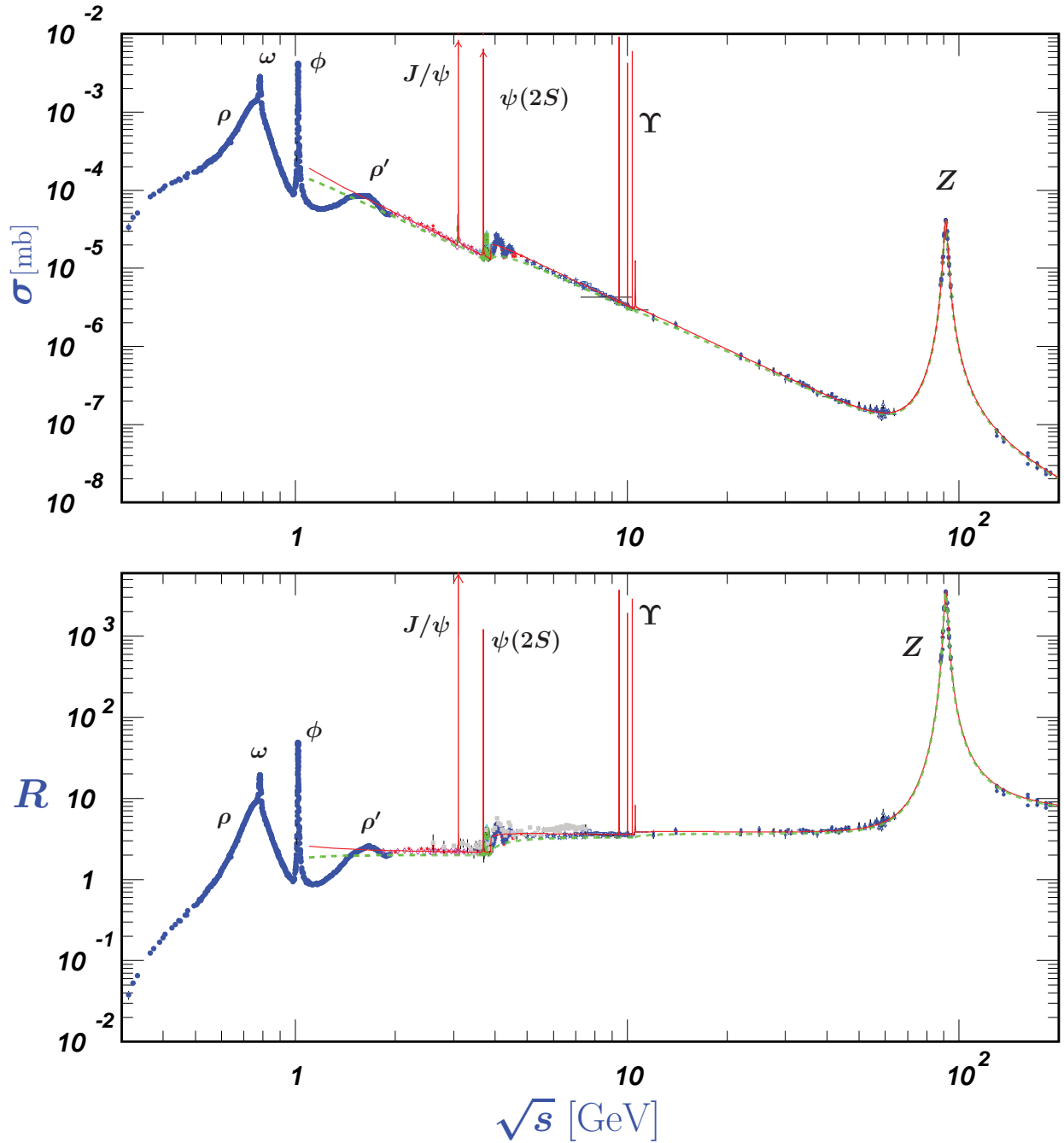
53.3 σ and R in e^+e^- Collisions σ and R in e^+e^- Collisions

Figure 53.2: World data on the total cross section of $e^+e^- \rightarrow \text{hadrons}$ and the ratio $R(s) = \sigma(e^+e^- \rightarrow \text{hadrons}, s) / \sigma(e^+e^- \rightarrow \mu^+\mu^-, s)$. $\sigma(e^+e^- \rightarrow \text{hadrons}, s)$ is the experimental cross section corrected for initial state radiation and electron-positron vertex loops, $\sigma(e^+e^- \rightarrow \mu^+\mu^-, s) = 4\pi\alpha^2(s)/3s$. Data errors are total below 2 GeV and statistical above 2 GeV. The curves are an educative guide: the broken one (green) is a naive quark-parton model prediction, and the solid one (red) is 3-loop pQCD prediction (see “Quantum Chromodynamics” section of this *Review*, Eq. (9.7) or, for more details [99], Breit-Wigner parameterizations of J/ψ , $\psi(2S)$, and $\Upsilon(nS)$, $n = 1, 2, 3, 4$ are also shown. The full list of references to the original data and the details of the R ratio extraction from them can be found in [100]. Corresponding computer-readable data files are available at <http://pdg.lbl.gov/current/xsect/>. (Courtesy of the COMPAS (Protvino) and HEPDATA (Durham) Groups, August 2021. Corrections by P. Janot (CERN) and M. Schmitt (Northwestern U.))

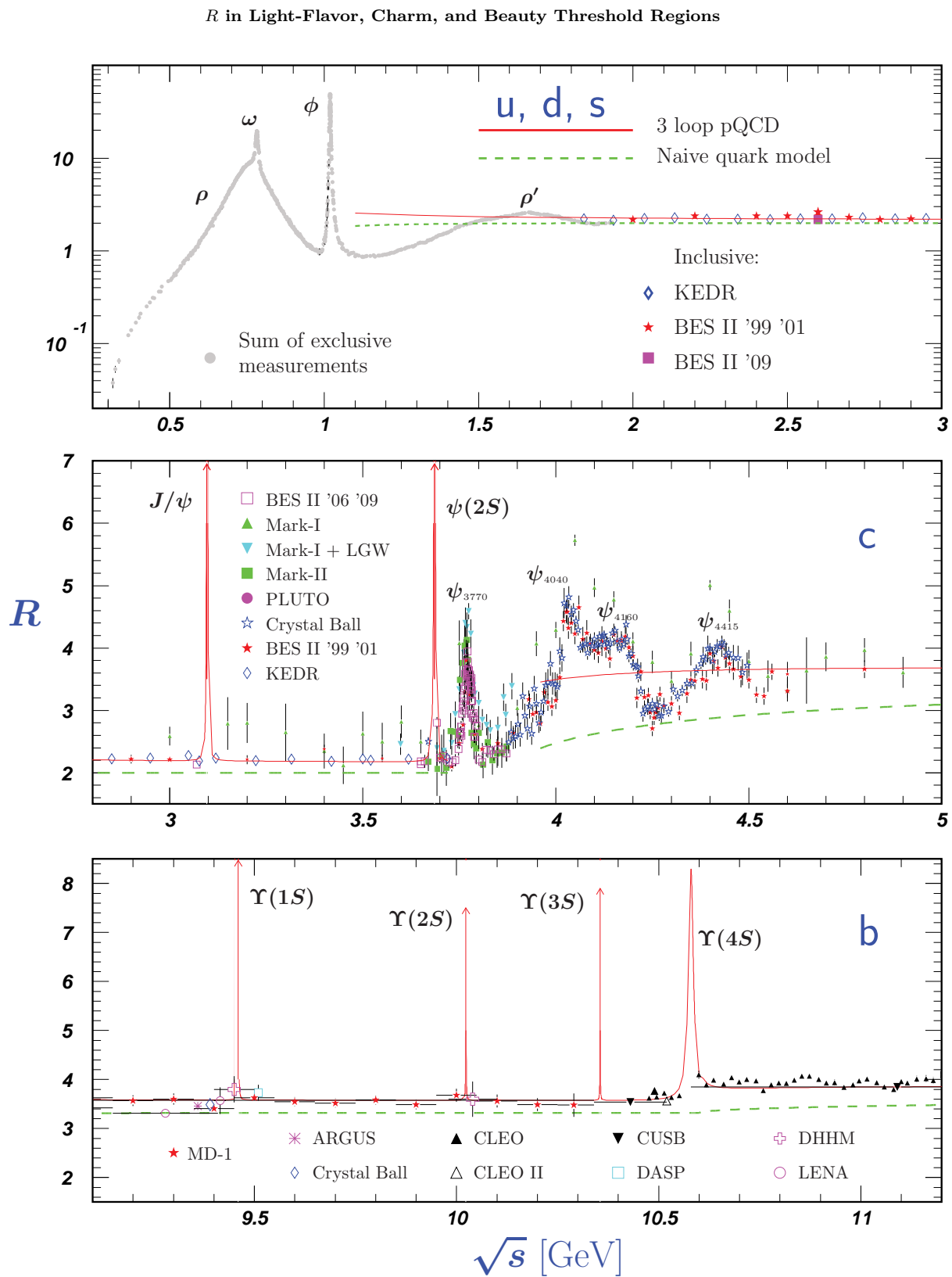


Figure 53.3: R in the light-flavor, charm, and beauty threshold regions. Data errors are total below 2 GeV and statistical above 2 GeV. The curves are the same as in Fig. 53.2. **Note:** CLEO data above $\Upsilon(4S)$ were not fully corrected for radiative effects, and we retain them on the plot only for illustrative purposes with a normalization factor of 0.8. The full list of references to the original data and the details of the R ratio extraction from them can be found in [100]. The computer-readable data are available at <http://pdg.lbl.gov/current/xsect/>. (Courtesy of the COMPAS (Protvino) and HEPDATA (Durham) Groups, August 2021.)

53.4 Annihilation Cross Section Near M_Z

Courtesy of M. Grünewald and the LEP Electroweak Working Group, 2007.

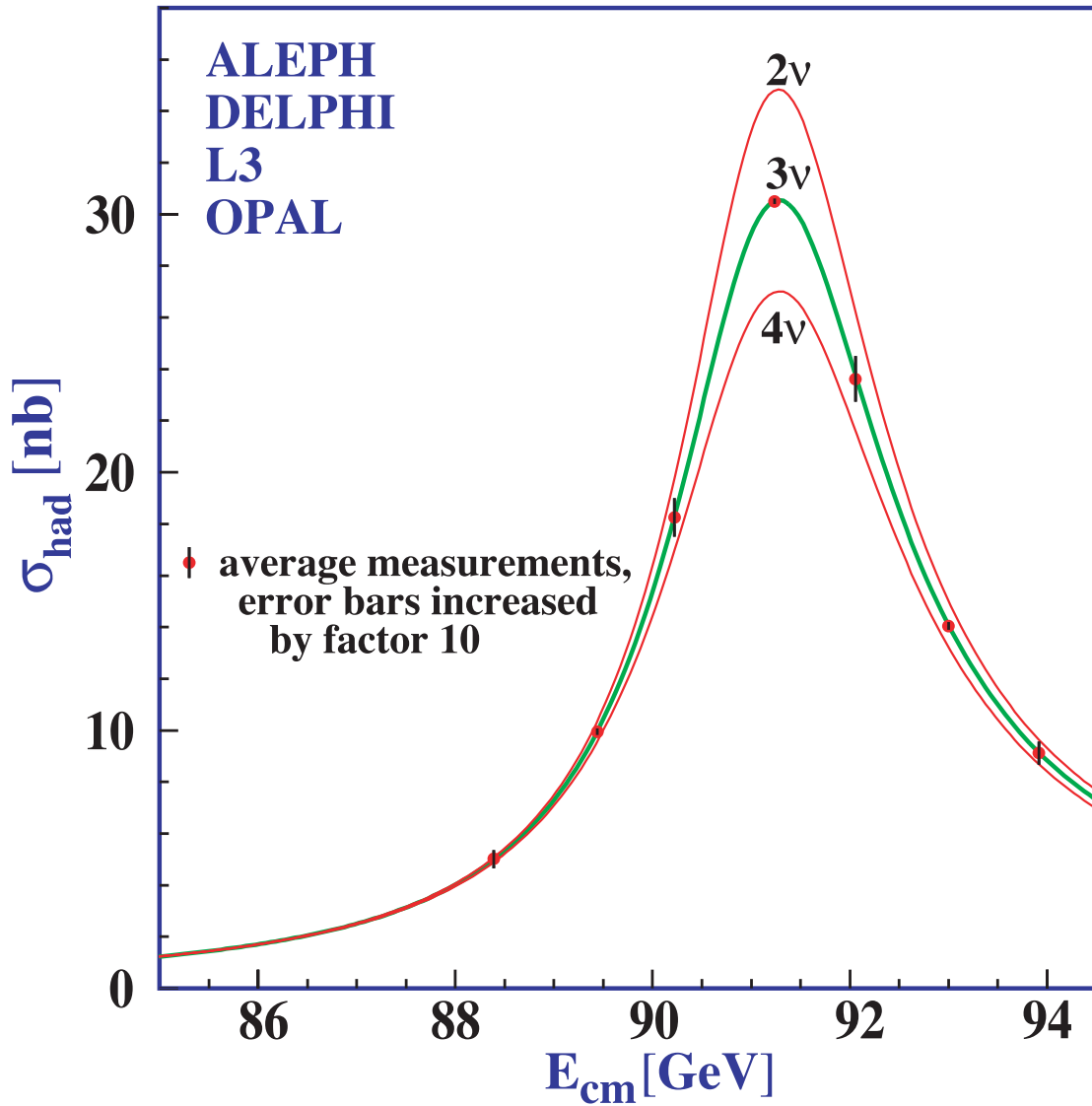


Figure 53.4: Combined data from the ALEPH, DELPHI, L3, and OPAL Collaborations for the cross section in e^+e^- annihilation into hadronic final states as a function of the center-of-mass energy near the Z pole. The curves show the predictions of the Standard Model with two, three, and four species of light neutrinos. The asymmetry of the curve is produced by initial-state radiation. Note that the error bars have been increased by a factor ten for display purposes. References: ALEPH [101], DELPHI [102], L3 [103], OPAL [104], Combination [105],

53.5 Total Hadronic Cross Sections

Revised August 2021 by COMPAS Group (NRC KI – IHEP, Protvino).

There are a significant number of physical quantities extracted from experimental data that are related to the physics of hadronic interactions. Depending on the magnitude of the transverse momenta of particles in the final states, the interactions are either classified as "hard" or "soft". In hard processes, the transverse momenta are comparable in magnitude with the momenta of the initial particles, while in soft processes they are vanishingly small compared to the initial momenta. Soft processes reveal characteristic interference pattern of the scattered states, and are often referred to as diffractive processes. The set of experimentally measured quantities related to diffractive processes include total and elastic cross sections, differential cross sections of elastic scattering and diffraction dissociation processes, as well as secondary quantities such as the slopes of differential cross sections and the ratio of real parts of the scattering amplitude to its imaginary parts (ρ parameter). In this section, plots of total and elastic cross section for various processes are presented. They include the data from purely hadronic collisions such as pp and πp , as well as γp , γd , and $\gamma\gamma^a$.

One of the most important basic notions and tools in general theoretical framework related to the diffractive processes is the notion of the Regge poles, or Reggeons, generalizing a simple one-particle exchange (of Yukawa type) by virtual particles of fixed spin to exchanges by states with "running spin" dependent on the transferred momenta [106,107]. The simplest case of the one-Reggeon exchange amplitude is given by the amplitude (at high c.m. energy \sqrt{s} and fixed (small) transferred momentum squared, t): $T(s, t) = \beta(t)s^{\alpha(t)}$ which qualitatively exhibits many typical features of generic diffractive processes (e.g. the growth of the interaction radius with energy). In practice the single-pole Reggeon model is insufficient for many diffractive processes but serves as a building block for more sophisticated schemes. Up to now no firm results concerning Regge trajectories $\alpha(t)$ and Regge residues $\beta(t)$ are obtained from the first principles of QCD. Therefore one has to rely on general principles of quantum field theory as a guide. These imply, in particular, that both $\alpha(t)$ and $\beta(t)$ are analytic functions with right cuts from some $t_0 > 0$ to positive infinity.

The theoretical requisite for analyzing diffractive phenomena is therefore represented by various model approaches. The more commonly discussed models in the literatures are:

- **Regge-eikonal approach** [108–115]: this approach automatically satisfies the s -channel unitarity condition and generalizes the impact parameter approximation to the relativistic case. The main element of the model is the Born amplitude defined by one or several leading "Pomeronic" Regge trajectories with intercepts higher than 1. To take into account the difference between C -conjugated processes (such as pp and $\bar{p}p$), a term with an Odderon Reggeon is also added, as well as, if one wishes to describe low (5 to 10 GeV) energies, a secondary Reggeon with low intercepts.
- **Regge pole models with minimal corrections due to two-Reggeon exchanges** [116–118]: in this model, contribution of the leading trajectory in the scattering amplitude is supplemented by a two-Reggeon exchange with an arbitrary coefficient chosen from the fitting details.
- **U -matrix (or "resonance") approach** [119,120]: the unitarity respecting approach with the scattering amplitude defined by a " U -matrix".
- **Direct functional modelling of the amplitudes with limited Regge trajectories** [121,122]: this approach appeals to only very general (analytic) properties of the amplitudes leaving aside all dynamical assumptions and mostly aiming at the best phenomenological description of the data.
- **Quasi-classical approach** [123–125]: this model is based on the observation that diffractive processes deal with high quantum numbers, in particular, with large number of virtual quanta.

The ratio $\rho(s) = \text{Re}T(s,0)/\text{Im}T(s,0) = \cot\Phi(s,0)$, where $\Phi(s,0)$ is the phase of the forward scattering amplitude, $T(s,0) = |T(s,0)|\exp(i\Phi(s,0))$, is accessible due to Coulomb-nuclear interference (CNI). There are several different ways to deal with CNI in the literature [126–130]. The value ρ is important for measurements of the total cross-sections as well as for discrimination of different models [131,132]. The phase $\Phi(s,0)$ starts from π at low energies, evolves further down to $\pi/2$, achieves a shallow minimum and then slowly rise up to $\pi/2$ at asymptotic energies.

The total cross-sections results shown in this review exhibit a common feature: starting from a certain energy (unique for each initial state) the cross-sections begin a slow but steady rise which continue up to several tens of TeV. The current data show the upper bound for total hadronic cross-section is well below the Froissart-Martin asymptotic bound [133,134], more than 20000 mb at the LHC energies [135].

For readers who are interested in examples of both total and elastic cross section parametrizations and fits, see previous edition of the *Plots of Cross Sections and Related Quantities* review [136]. For the cross section plots shown in the following pages, the example fits are using parametrizations as described in [136] with the fit range starting at about $\sqrt{s} = 5$ GeV.

^aIn spite of its electromagnetic nature the photon interacts with hadron targets as an effective hadron (via transmutation of γ into virtual vector mesons $\rho^0, \omega, \phi, \dots$).

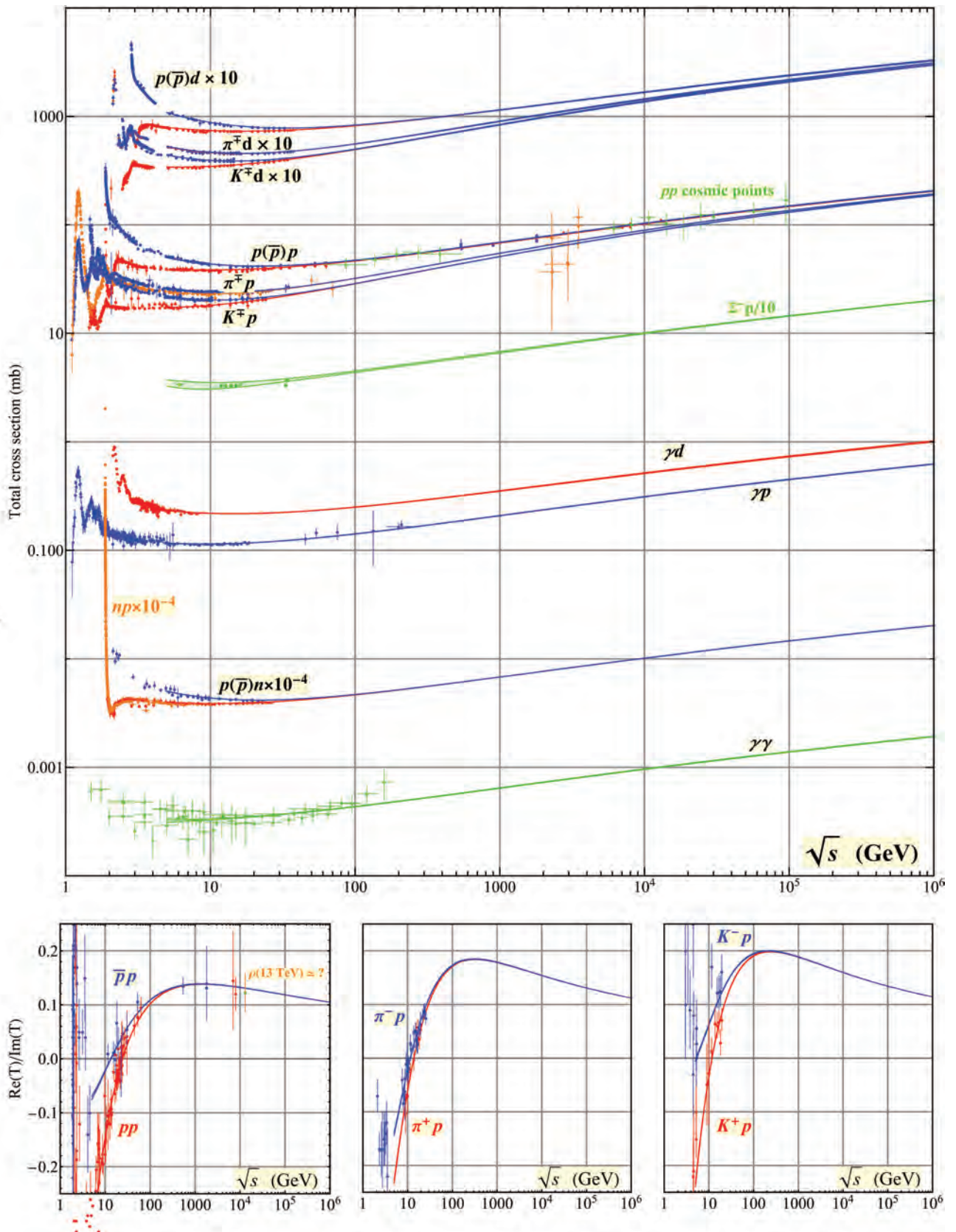


Figure 53.5: Summary of hadronic, γp , γd , and $\gamma\gamma$ total cross sections (top), and ratio of the real to imaginary parts of the forward hadronic amplitudes (bottom). Corresponding computer-readable data files can be found at <https://pdg.lbl.gov/current/xsect/>. (Courtesy of the COMPAS group, NRC KI – IHEP, Protvino, August 2021.)

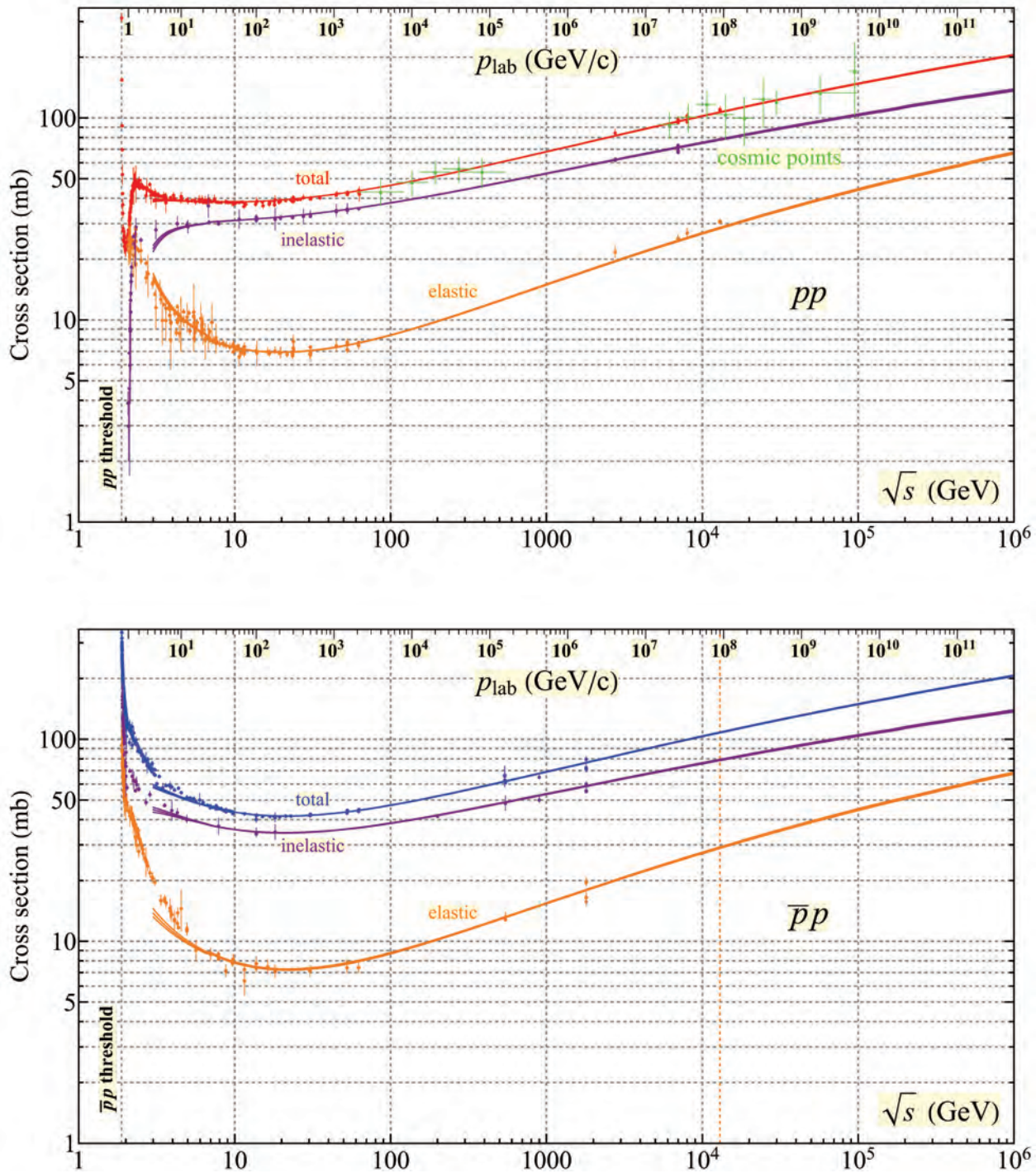


Figure 53.6: Total and elastic cross sections for pp and $\bar{p}p$ collisions as a function of laboratory beam momentum and total center-of-mass energy. σ_{el} is computed using the nuclear part of the elastic scattering amplitude [137]. Corresponding computer-readable data files may be found at <https://pdg.lbl.gov/current/xsect/>. (Courtesy of the COMPAS group, NRC KI – IHEP, Protvino, August 2021.)

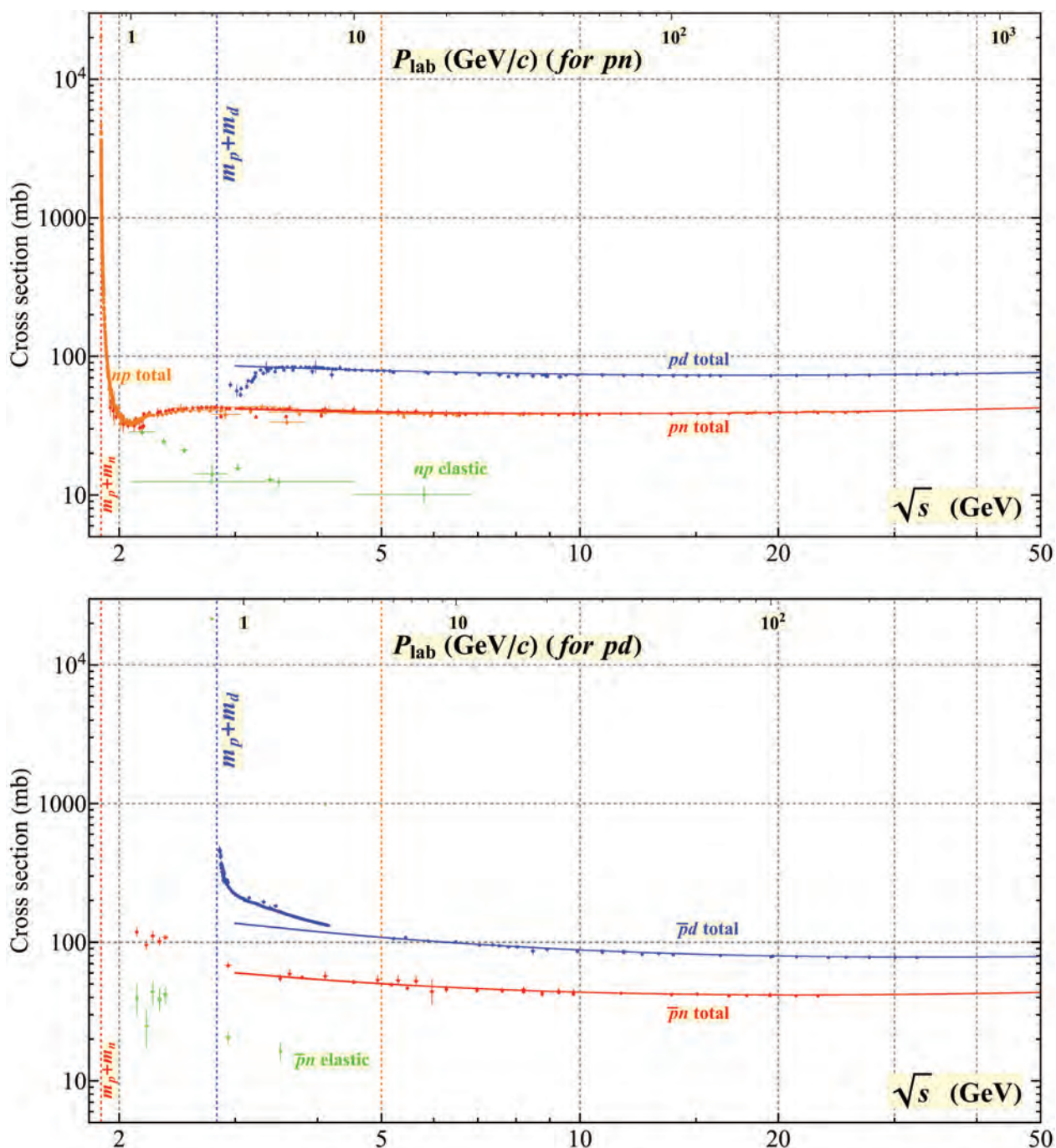


Figure 53.7: Total and elastic cross sections for pd (total only), np , $\bar{p}d$ (total only), and $\bar{p}n$ collisions as a function of laboratory beam momentum and total center-of-mass energy. Corresponding computer-readable data files may be found at <https://pdg.lbl.gov/current/xsect/>. (Courtesy of the COMPAS Group, NRC KI – IHEP, Protvino, August 2021. Corrections by N. Otsuka (IAEA))

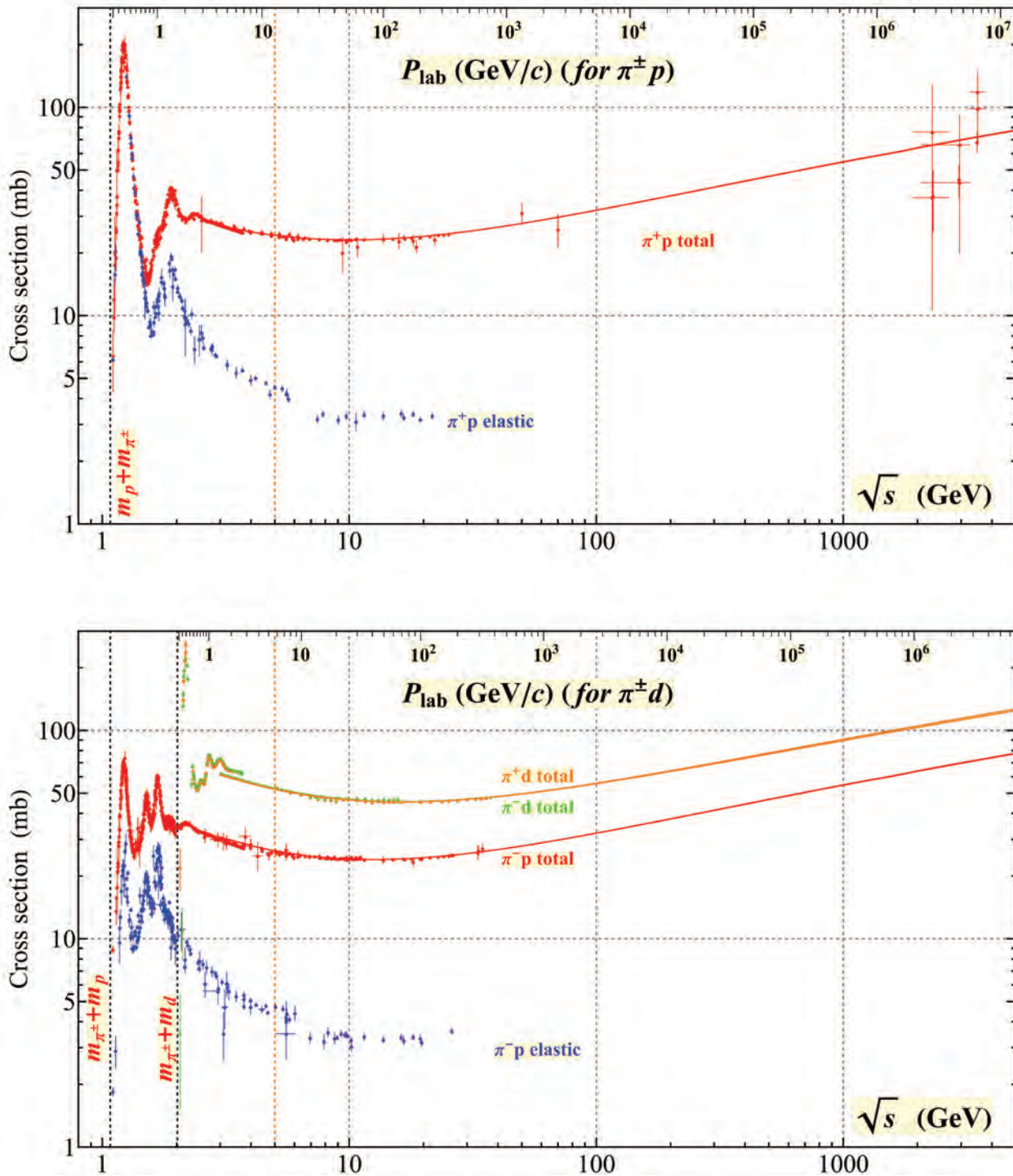


Figure 53.8: Total and elastic cross sections for $\pi^\pm p$ and $\pi^\pm d$ (total only) collisions as a function of laboratory beam momentum and total center-of-mass energy. Corresponding computer-readable data files can be found at <https://pdg.lbl.gov/current/xsect/>. (Courtesy of the COMPAS Group, NRC KI – IHEP, Protvino, August 2021.)

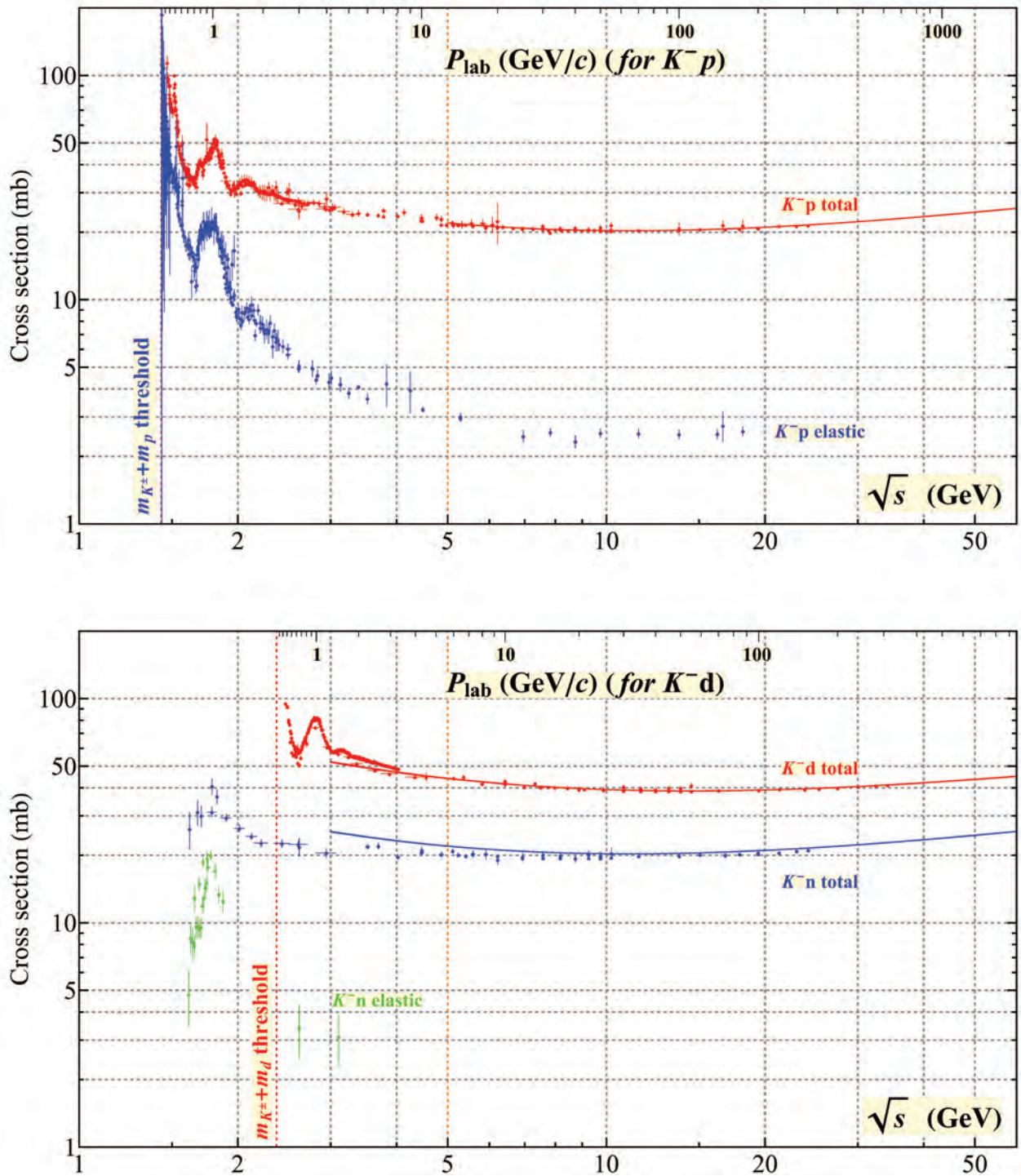


Figure 53.9: Total and elastic cross sections for $K^- p$ and $K^- d$ (total only), and $K^- n$ collisions as a function of laboratory beam momentum and total center-of-mass energy. Corresponding computer-readable data files can be found at <https://pdg.lbl.gov/current/xsect/>. (Courtesy of the COMPAS Group, NRC KI – IHEP, Protvino, August 2021.)

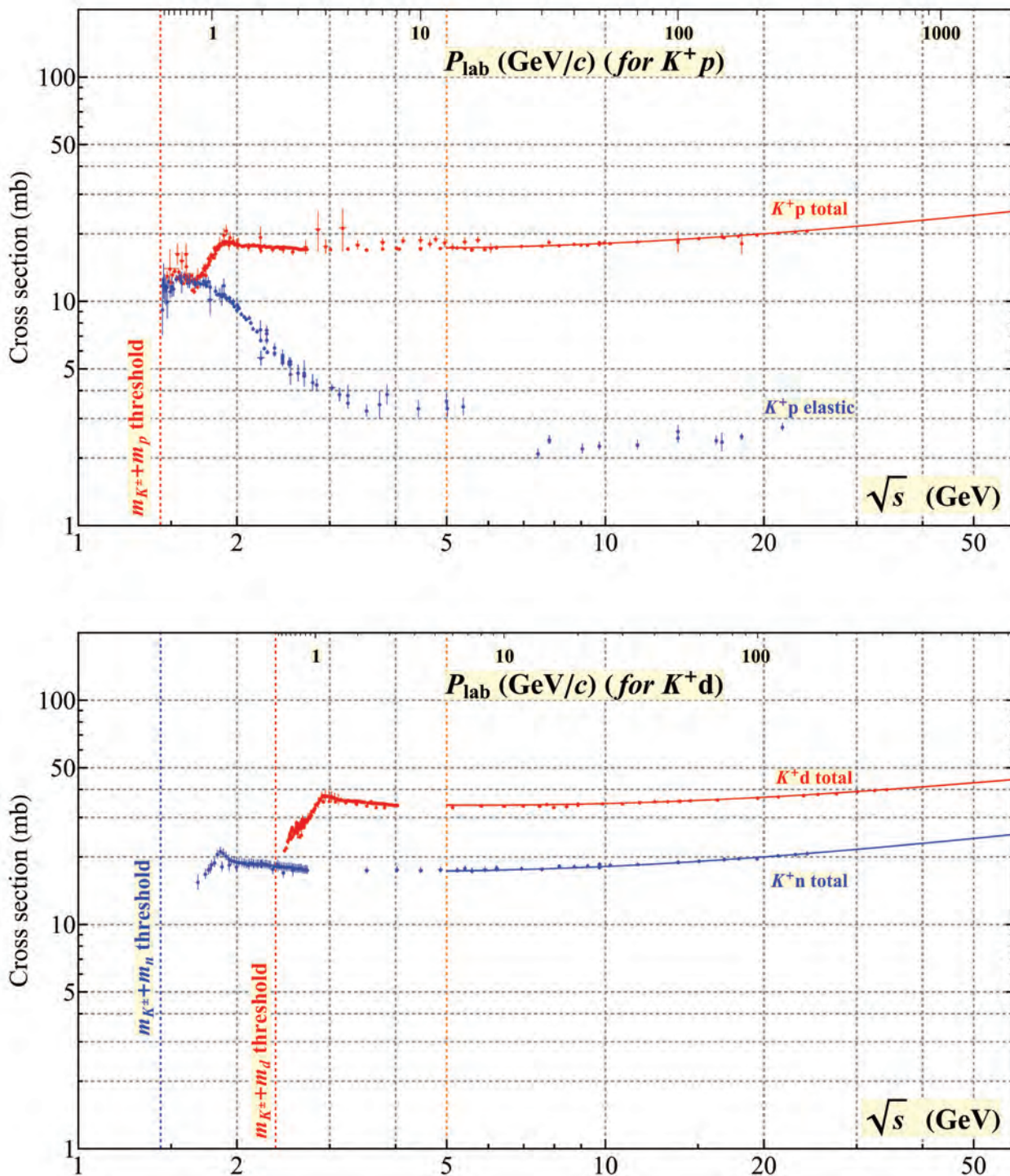


Figure 53.10: Total and elastic cross sections for K^+p and total cross sections for K^+d and K^+n collisions as a function of laboratory beam momentum and total center-of-mass energy. Corresponding computer-readable data files can be found at <https://pdg.lbl.gov/current/xsect/>. (Courtesy of the COMPAS Group, NRC KI – IHEP, Protvino, August 2021.)

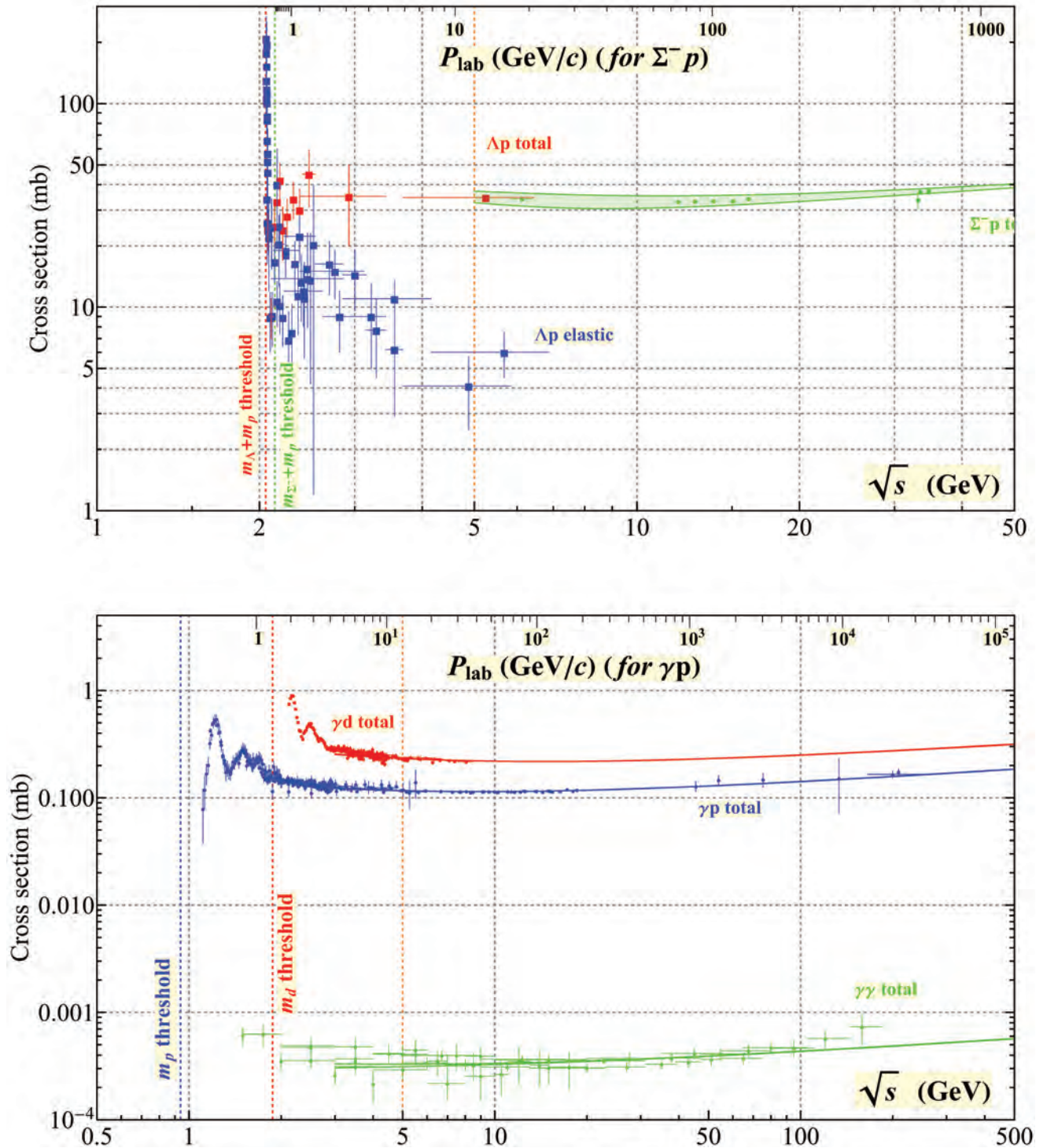


Figure 53.11: Total and elastic cross sections for Δp , total cross section for $\Sigma^- p$, and total hadronic cross sections for γd , γp , and $\gamma\gamma$ collisions as a function of laboratory beam momentum and the total center-of-mass energy. Corresponding computer-readable data files can be found at <https://pdg.lbl.gov/current/xsect/>. (Courtesy of the COMPAS group, NRC KI – IHEP, Protvino, August 2021.)

References

- [1] G. J. Alner *et al.* (UA5), *Z. Phys.* **C33**, 1 (1986).
- [2] K. Alpgard *et al.* (UA5), *Phys. Lett.* **112B**, 183 (1982).
- [3] F. Abe *et al.* (CDF), *Phys. Rev.* **D41**, 2330 (1990), [119(1989)].
- [4] R. Harr *et al.*, *Phys. Lett.* **B401**, 176 (1997), [hep-ex/9703002].
- [5] K. Aamodt *et al.* (ALICE), *Eur. Phys. J.* **C68**, 89 (2010), [arXiv:1004.3034].
- [6] V. Khachatryan *et al.* (CMS), *JHEP* **02**, 041 (2010), [arXiv:1002.0621].
- [7] V. Khachatryan *et al.* (CMS), *Phys. Rev. Lett.* **105**, 022002 (2010), [arXiv:1005.3299].
- [8] H. Albrecht *et al.* (ARGUS), *Z. Phys.* **C54**, 1 (1992).
- [9] S. Behrends *et al.* (CLEO), *Phys. Rev.* **D31**, 2161 (1985).
- [10] J. P. Lees *et al.* (BaBar), *Phys. Rev.* **D88**, 032011 (2013), [arXiv:1306.2895].
- [11] H. Albrecht *et al.*, *Phys. Lett.* **102B**, 291 (1981).
- [12] K. Hikasa *et al.* (Particle Data Group), *Phys. Rev.* **D45**, S1 (1992), [Erratum: *Phys. Rev.*D46,5210(1992)].
- [13] R. Barate *et al.* (ALEPH), *Eur. Phys. J.* **C5**, 205 (1998).
- [14] P. Abreu *et al.* (DELPHI), *Eur. Phys. J.* **C5**, 585 (1998).
- [15] R. Akers *et al.* (OPAL), *Z. Phys.* **C63**, 181 (1994).
- [16] K. Abe *et al.* (SLD), *Phys. Rev.* **D69**, 072003 (2004), [hep-ex/0310017].
- [17] P. Abreu *et al.* (DELPHI), *Eur. Phys. J.* **C18**, 203 (2000), [Erratum: *Eur. Phys. J.*C25,493(2002)], [hep-ex/0103031].
- [18] D. D. Pitzl *et al.* (JADE), *Z. Phys.* **C46**, 1 (1990), [Erratum: *Z. Phys.*C47,676(1990)].
- [19] H. J. Behrend *et al.* (CELLO), *Z. Phys.* **C47**, 1 (1990).
- [20] R. Barate *et al.* (ALEPH), *Eur. Phys. J.* **C16**, 613 (2000).
- [21] W. Adam *et al.* (DELPHI), *Z. Phys.* **C69**, 561 (1996).
- [22] M. Acciarri *et al.* (L3), *Phys. Lett.* **B371**, 126 (1996).
- [23] G. Abbiendi *et al.* (OPAL), *Eur. Phys. J.* **C17**, 373 (2000), [hep-ex/0007017].
- [24] H. Albrecht *et al.* (ARGUS), *Z. Phys.* **C44**, 547 (1989).
- [25] P. Abreu *et al.* (DELPHI), *Nucl. Phys.* **B444**, 3 (1995).
- [26] H. J. Behrend *et al.* (CELLO), *Z. Phys.* **C46**, 397 (1990).
- [27] M. Derrick *et al.*, *Phys. Rev.* **D35**, 2639 (1987).
- [28] W. Bartel *et al.* (JADE), *Z. Phys.* **C20**, 187 (1983).
- [29] H. Schellman *et al.*, *Phys. Rev.* **D31**, 3013 (1985).
- [30] C. Berger *et al.* (PLUTO), *Phys. Lett.* **104B**, 79 (1981).
- [31] M. Althoff *et al.* (TASSO), *Z. Phys.* **C27**, 27 (1985).
- [32] H. Aihara *et al.* (TPC/Two Gamma), *Phys. Rev. Lett.* **53**, 2378 (1984).
- [33] P. Abreu *et al.* (DELPHI), *Z. Phys.* **C65**, 587 (1995).
- [34] M. Acciarri *et al.* (L3), *Phys. Lett.* **B407**, 389 (1997), [Erratum: *Phys. Lett.*B427,409(1998)].
- [35] R. Akers *et al.* (OPAL), *Z. Phys.* **C67**, 389 (1995).
- [36] K. Abe *et al.* (SLD), *Phys. Rev.* **D59**, 052001 (1999), [hep-ex/9805029].
- [37] H. Albrecht *et al.* (ARGUS), *Z. Phys.* **C46**, 15 (1990).
- [38] C. Bieler *et al.* (Crystal Ball), *Z. Phys.* **C49**, 225 (1991).
- [39] G. Wormser *et al.*, *Phys. Rev. Lett.* **61**, 1057 (1988).
- [40] A. Heister *et al.* (ALEPH), *Phys. Lett.* **B528**, 19 (2002), [hep-ex/0201012].
- [41] H. Albrecht *et al.* (ARGUS), *Z. Phys.* **C58**, 199 (1993).
- [42] M. Acciarri *et al.* (L3), *Phys. Lett.* **B393**, 465 (1997).
- [43] K. Ackerstaff *et al.* (OPAL), *Eur. Phys. J.* **C5**, 411 (1998), [hep-ex/9805011].
- [44] R. Seuster *et al.* (Belle), *Phys. Rev.* **D73**, 032002 (2006), [hep-ex/0506068].
- [45] M. Artuso *et al.* (CLEO), *Phys. Rev.* **D70**, 112001 (2004), [hep-ex/0402040].
- [46] P. Abreu *et al.* (DELPHI), *Z. Phys.* **C59**, 533 (1993), [Erratum: *Z. Phys.*C65,709(1995)].
- [47] G. Alexander *et al.* (OPAL), *Z. Phys.* **C72**, 1 (1996).
- [48] B. Aubert *et al.* (BaBar), *Phys. Rev.* **D65**, 091104 (2002), [hep-ex/0201041].
- [49] D. Bortoletto *et al.* (CLEO), *Phys. Rev.* **D37**, 1719 (1988), [Erratum: *Phys. Rev.*D39,1471(1989)].
- [50] P. Abreu *et al.* (DELPHI), *Z. Phys.* **C57**, 181 (1993).
- [51] J. Abdallah *et al.* (DELPHI), *Phys. Lett.* **B576**, 29 (2003), [hep-ex/0311005].
- [52] P. Abreu *et al.* (DELPHI), *Z. Phys.* **C61**, 407 (1994).
- [53] R. Akers *et al.* (OPAL), *Z. Phys.* **C66**, 555 (1995).
- [54] S. Abachi *et al.*, *Phys. Rev. Lett.* **57**, 1990 (1986).
- [55] P. Abreu *et al.* (DELPHI), *Phys. Lett.* **B449**, 364 (1999).
- [56] K. Ackerstaff *et al.* (OPAL), *Eur. Phys. J.* **C4**, 19 (1998), [hep-ex/9802013].
- [57] H. Albrecht *et al.* (ARGUS), *Z. Phys.* **C61**, 1 (1994).
- [58] D. Buskulic *et al.* (ALEPH), *Z. Phys.* **C69**, 379 (1996).
- [59] R. Barate *et al.* (ALEPH), *Phys. Rept.* **294**, 1 (1998).
- [60] P. D. Acton *et al.* (OPAL), *Phys. Lett.* **B305**, 407 (1993).
- [61] P. Abreu *et al.* (DELPHI), *Z. Phys.* **C73**, 61 (1996).
- [62] K. Ackerstaff *et al.* (OPAL), *Phys. Lett.* **B412**, 210 (1997), [hep-ex/9708022].
- [63] R. Barate *et al.* (ALEPH), *Eur. Phys. J.* **C16**, 597 (2000), [hep-ex/9909032].
- [64] K. Ackerstaff *et al.* (OPAL), *Eur. Phys. J.* **C1**, 439 (1998), [hep-ex/9708021].
- [65] K. Ackerstaff *et al.* (OPAL), *Eur. Phys. J.* **C5**, 1 (1998), [hep-ex/9802008].
- [66] P. Abreu *et al.* (DELPHI), *Z. Phys.* **C68**, 353 (1995).
- [67] M. Acciarri *et al.* (L3), *Phys. Lett.* **B345**, 589 (1995).
- [68] B. Aubert *et al.* (BaBar), *Phys. Rev. Lett.* **87**, 162002 (2001), [hep-ex/0106044].
- [69] K. Abe *et al.* (Belle), *Phys. Rev. Lett.* **88**, 052001 (2002), [hep-ex/0110012].
- [70] D. Buskulic *et al.* (ALEPH), *Phys. Lett.* **B295**, 396 (1992).
- [71] P. Abreu *et al.* (DELPHI), *Phys. Lett.* **B341**, 109 (1994).
- [72] M. Acciarri *et al.* (L3), *Phys. Lett.* **B453**, 94 (1999).
- [73] G. Alexander *et al.* (OPAL), *Z. Phys.* **C70**, 197 (1996).
- [74] M. Acciarri *et al.* (L3), *Phys. Lett.* **B407**, 351 (1997).
- [75] G. Alexander *et al.* (OPAL), *Phys. Lett.* **B370**, 185 (1996).
- [76] J. Abdallah *et al.* (DELPHI), *Phys. Lett.* **B569**, 129 (2003), [hep-ex/0309057].
- [77] A. De Angelis, *J. Phys.* **G19**, 1233 (1993).
- [78] S. Abachi *et al.*, *Phys. Lett.* **B199**, 151 (1987).
- [79] R. Akers *et al.* (OPAL), *Z. Phys.* **C68**, 1 (1995).
- [80] P. Abreu *et al.* (DELPHI), *Phys. Lett.* **B345**, 598 (1995).
- [81] A. Heister *et al.* (ALEPH), *Phys. Lett.* **B526**, 34 (2002), [hep-ex/0112010].
- [82] H. Albrecht *et al.* (ARGUS), *Z. Phys.* **C39**, 177 (1988).
- [83] M. Niiyama *et al.* (Belle), *Phys. Rev.* **D97**, 7, 072005 (2018), [arXiv:1706.06791].
- [84] P. Abreu *et al.* (DELPHI), *Z. Phys.* **C67**, 543 (1995).
- [85] G. Alexander *et al.* (OPAL), *Z. Phys.* **C73**, 569 (1997).
- [86] W. Adam *et al.* (DELPHI), *Z. Phys.* **C70**, 371 (1996).
- [87] M. Acciarri *et al.* (L3), *Phys. Lett.* **B479**, 79 (2000), [hep-ex/0002066].

- [88] G. Alexander *et al.* (OPAL), *Z. Phys.* **C73**, 587 (1997).
- [89] P. Abreu *et al.* (DELPHI), *Phys. Lett.* **B475**, 429 (2000), [hep-ex/0103020].
- [90] H. Albrecht *et al.* (ARGUS), *Phys. Lett.* **B230**, 169 (1989).
- [91] P. Abreu *et al.* (DELPHI), *Phys. Lett.* **B361**, 207 (1995).
- [92] G. Alexander *et al.* (OPAL), *Phys. Lett.* **B358**, 162 (1995).
- [93] S. Abachi *et al.*, *Phys. Rev. Lett.* **58**, 2627 (1987), [Erratum: *Phys. Rev. Lett.* 59, 2388 (1987)].
- [94] J. Abdallah *et al.* (DELPHI), *Eur. Phys. J.* **C44**, 299 (2005), [hep-ex/0510023].
- [95] B. Aubert *et al.* (BaBar), *Phys. Rev.* **D75**, 012003 (2007), [hep-ex/0609004].
- [96] P. D. Acton *et al.* (OPAL), *Phys. Lett.* **B281**, 394 (1992).
- [97] H. Albrecht *et al.* (ARGUS), *Phys. Rept.* **276**, 223 (1996).
- [98] R. Giles *et al.* (CLEO), *Phys. Rev.* **D29**, 1285 (1984).
- [99] K. G. Chetyrkin, R. V. Harlander and J. H. Kuhn, *Nucl. Phys.* **B586**, 56 (2000), [Erratum: *Nucl. Phys.* B634, 413 (2002)], [hep-ph/0005139].
- [100] V. V. Ezhela, S. B. Lugovsky and O. V. Zenin (2003), [hep-ph/0312114].
- [101] R. Barate *et al.* (ALEPH), *Eur. Phys. J.* **C14**, 1 (2000).
- [102] P. Abreu *et al.* (DELPHI), *Eur. Phys. J.* **C16**, 371 (2000).
- [103] M. Acciarri *et al.* (L3), *Eur. Phys. J.* **C16**, 1 (2000), [hep-ex/0002046].
- [104] G. Abbiendi *et al.* (OPAL), *Eur. Phys. J.* **C19**, 587 (2001), [hep-ex/0012018].
- [105] S. Schael *et al.* (ALEPH, DELPHI, L3, OPAL, SLD, LEP Electroweak Working Group, SLD Electroweak Group, SLD Heavy Flavour Group), *Phys. Rept.* **427**, 257 (2006), [hep-ex/0509008].
- [106] P. Collins, *An Introduction to Regge Theory and High-Energy Physics*, Cambridge Monographs on Mathematical Physics, Cambridge Univ. Press, Cambridge, UK (2009), ISBN 9780521110358.
- [107] G. Pancheri and Y. N. Srivastava, *Eur. Phys. J.* **C77**, 3, 150 (2017), [arXiv:1610.10038].
- [108] V. A. Petrov and A. Prokudin, *Phys. Rev.* **D87**, 3, 036003 (2013), [arXiv:1212.1924].
- [109] C. Bourrely, J. Soffer and T. T. Wu, *Eur. Phys. J.* **C28**, 97 (2003), [hep-ph/0210264].
- [110] M. M. Block *et al.*, *Phys. Rev.* **D92**, 1, 014030 (2015), [arXiv:1505.04842].
- [111] O. V. Selyugin, *Phys. Rev.* **D91**, 11, 113003 (2015), [Erratum: *Phys. Rev.* D92, no.9, 099901 (2015)], [arXiv:1505.02426].
- [112] L. G. Dakhno and V. A. Nikonov, *Eur. Phys. J.* **A5**, 209 (1999), [hep-ph/9902320].
- [113] A. A. Godizov, *Phys. Lett.* **B735**, 57 (2014), [arXiv:1404.2851].
- [114] E. Gotsman, E. M. Levin and U. Maor, *Phys. Rev.* **D49**, R4321 (1994), [hep-ph/9310257].
- [115] L. A. Harland-Lang, V. A. Khoze and M. G. Ryskin, *Int. J. Mod. Phys.* **A30**, 1542013 (2015).
- [116] A. Donnachie and P. V. Landshoff, *Phys. Lett.* **B727**, 500 (2013), [Erratum: *Phys. Lett.* B750, 669 (2015)], [arXiv:1309.1292].
- [117] E. Martynov, *Phys. Rev.* **D87**, 11, 114018 (2013), [arXiv:1305.3093].
- [118] I. Szanyi, N. Bence and L. Jenkovszky, *J. Phys. G* **46**, 5, 055002 (2019), [arXiv:1808.03588].
- [119] S. M. Troshin and N. E. Tyurin, *Int. J. Mod. Phys.* **A32**, 17, 1750103 (2017), [arXiv:1704.00443].
- [120] V. V. Anisovich, *Phys. Usp.* **58**, 10, 963 (2015).
- [121] D. A. Fagundes, M. J. Menon and P. V. R. G. Silva, *Nucl. Phys.* **A946**, 194 (2016), [arXiv:1509.04108].
- [122] E. Martynov and B. Nicolescu, *Eur. Phys. J.* **C56**, 57 (2008), [arXiv:0712.1685].
- [123] W. Heisenberg, *Z. Phys.* **133**, 65 (1952).
- [124] V. V. Ezhela and O. P. Yushchenko, Submitted to: *Z. Phys. C* (1988).
- [125] H. Nastase and J. Sonnenschein, *Phys. Rev.* **D92**, 105028 (2015), [arXiv:1504.01328].
- [126] H. A. Bethe, *Annals Phys.* **3**, 190 (1958).
- [127] G. B. West and D. R. Yennie, *Phys. Rev.* **172**, 1413 (1968).
- [128] R. Cahn, *Z. Phys. C* **15**, 253 (1982).
- [129] V. Kundrat and M. Lokajicek, *Z. Phys. C* **63**, 619 (1994).
- [130] V. A. Petrov, *Eur. Phys. J. C* **78**, 3, 221 (2018), [Erratum: *Eur. Phys. J. C* 78, 414 (2018)], [arXiv:1801.01815].
- [131] G. Antchev *et al.* (TOTEM), *Eur. Phys. J. C* **79**, 2, 103 (2019), [arXiv:1712.06153].
- [132] V. V. Ezhela, V. A. Petrov and N. P. Tkachenko, *Phys. At. Nucl.* **84**, 3, 298 (2021).
- [133] M. Froissart, *Phys. Rev.* **123**, 1053 (1961).
- [134] A. Martin, *Phys. Rev.* **129**, 1432 (1963).
- [135] V. A. Petrov and V. A. Okorokov, *Int. J. Mod. Phys. A* **33**, 13, 1850077 (2018), [arXiv:1802.01559].
- [136] C. Patrignani *et al.* (Particle Data Group), *Chin. Phys. C* **40**, 10, 100001 (2016).
- [137] V. I. Belousov *et al.*, *Phys. Atom. Nucl.* **79**, 1, 113 (2016), [*Yad. Fiz.* 79, no.1, 55 (2016)].



Particle Properties

Gauge Bosons

54. Mass and width of the W boson (rev.)	789
55. Z boson	791

Charged Leptons

56. Muon anomalous magnetic moment (rev.)	796
57. Muon decay parameters (rev.)	800
58. τ branching fractions (rev.)	803
59. τ -lepton decay parameters (rev.)	806

Quarks

60. Quark masses (rev.)	808
61. Top quark (rev.)	817

Mesons

62. Form factors for semileptonic kaon ($K_{\ell 3}$), radiative pion ($\pi_{\ell 2\gamma}$) & kaon ($K_{\ell 2\gamma}$) decays (rev.)	842
63. Spectroscopy of light meson resonances (new)	845
64. Scalar mesons below 1 GeV (rev.)	858
65. Rare kaon decays (rev.)	865
66. CPT invariance tests in neutral kaon decay (rev.)	871
67. V_{ud} , V_{us} , Cabibbo angle, and CKM unitarity (rev.)	873
68. CP -violation in K_L decays (rev.)	877
69. Review of multibody charm analyses (rev.)	880
70. $D^0-\bar{D}^0$ mixing (rev.)	885
71. D_s^+ branching fractions (rev.)	895
72. Leptonic decays of charged pseudoscalar mesons (rev.)	897
73. Production and decay of b -flavored hadrons (rev.)	908
74. Polarization in B decays (rev.)	919
75. $B^0-\bar{B}^0$ mixing (rev.)	923
76. Semileptonic B decays, V_{cb} and V_{ub} (rev.)	930
77. CKM angles from B hadrons, determination of (rev.)	946
78. Spectroscopy of mesons containing two heavy quarks (rev.)	951
79. Heavy non- $q\bar{q}$ mesons (rev.)	959

Baryons

80. Baryon decay parameters	964
81. N and Δ resonances	965
82. Λ and Σ resonances (rev.)	970
83. Pole structure of the $\Lambda(1405)$ region (rev.)	973
84. Pentaquarks (rev.)	975

Notes in Volume 2

Triple gauge couplings (TGC's)	1146
Anomalous $ZZ\gamma$, $Z\gamma\gamma$, and ZZV couplings	1171
Anomalous W/Z quartic couplings	1173
Neutrino properties (rev.)	1273
Sum of neutrino masses (rev.)	1276
Number of light neutrino types from collider experiments	1282
Neutrinoless double- β decay	1284
Charged kaon mass	1473
Dalitz plot parameters for $K \rightarrow 3\pi$ decays	1482
CP -violation in $K_S \rightarrow 3\pi$	1492
Heavy Flavor Averaging Group (rev.)	1609
Charmonium system (rev.)	1818
Branching ratios of $\psi(2S)$ and $\chi_{c0,1,2}$ (rev.)	1850
Bottomonium system (rev.)	1940
Width determination of the Υ states	1940
Radiative hyperon decays	2122
Ξ resonances	2126



54. Mass and Width of the W Boson

Revised May 2022 by M. Grünwald (University Coll. Dublin) and A. Gurtu (CERN; TIFR Mumbai).

Precision determination of the W mass is of great importance in testing the internal consistency of the Standard Model. From the time of its discovery in 1983, the W boson has been studied and its mass determined in $p\bar{p}$ and e^+e^- interactions; it is currently studied in pp interactions at the LHC. The mass and width definition used here corresponds to a Breit-Wigner with mass-dependent width.

Production of on-shell W bosons at hadron colliders is tagged by the high p_T charged lepton from its leptonic decay modes. Owing to the unknown parton-parton effective energy and missing energy in the longitudinal direction, the hadron collider experiments reconstruct the transverse mass of the W boson, and derive the W mass from comparing the transverse mass distribution with Monte Carlo predictions as a function of the mass m_W . The transverse momentum of the charged lepton itself and the transverse missing energy (arising from the neutrino in W decay) are also sensitive to the W mass and used in its determination. These analyses use the electron and muon decay modes of the W boson.

At the e^+e^- collider LEP, a precise knowledge of the beam energy enables one to determine the $e^+e^- \rightarrow W^+W^-$ cross section as a function of center of mass energy, as well as to reconstruct the W mass precisely from its decay products, even if one of them decays leptonically. Close to the W^+W^- production threshold ($\sqrt{s} = 161$ GeV), the dependence of the W -pair production cross section on m_W is large, and this was used to determine m_W . At higher centre-of-mass energies (172 to 209 GeV) this dependence is much weaker, thus W bosons were directly reconstructed and the mass determined as the invariant mass of the decay products, improving the resolution with a kinematic fit.

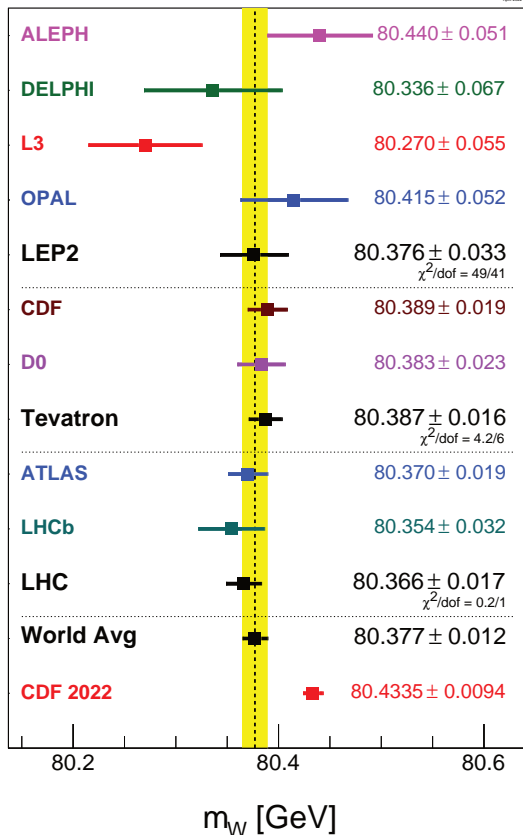


Figure 54.1: Measurements of the W boson mass by the LEP, Tevatron and LHC experiments. The pre-2022 CDF result, used in the world average, is superseded by the new CDF 2022 result.

In order to compute the LEP average W mass, each experiment provided its measured W mass for the $q\bar{q}q\bar{q}$ and $q\bar{q}\ell\nu$, $\ell = e, \mu, \tau$ channels at each center-of-mass energy, along with a detailed break-up of uncertainty contributions: statistical, uncorrelated, partially correlated and fully correlated systematics [1]. These results have been combined to obtain a LEP average W mass of $m_W = 80.376 \pm 0.033$ GeV. Errors on m_W due to uncertainties in the LEP beam energy (9 MeV), and possible effect of color reconnection (CR) and Bose-Einstein correlations (BEC) between quarks from different W bosons (8 MeV) are included. The mass difference between $q\bar{q}q\bar{q}$ and $q\bar{q}\ell\nu$ final states (due to possible CR and BEC effects) is -12 ± 45 MeV. In a similar manner, the results on the total width of the W boson obtained at LEP have been combined, resulting in an average of $\Gamma_W = 2.195 \pm 0.083$ GeV [1].

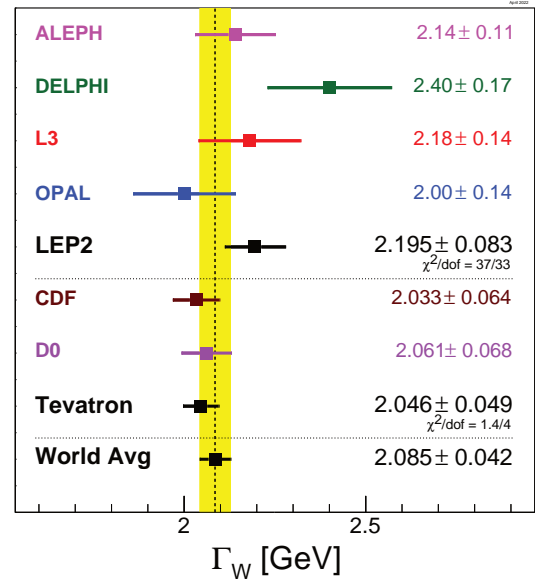


Figure 54.2: Measurements of the W -boson width by the LEP and Tevatron experiments.

The two Tevatron experiments CDF and D0 have also identified common systematic errors. Between the two experiments, uncertainties due to the parton distribution functions (PDF), radiative corrections, and choice of mass (width) in the width (mass) measurements are treated as correlated. An average W width of $\Gamma_W = 2.046 \pm 0.049$ GeV [2] is obtained. Errors of 20 MeV and 7 MeV accounting for PDF and radiative correction uncertainties in this width combination dominate the correlated uncertainties. The CDF and D0 measurements of 80.387 ± 0.019 GeV [3] and 80.375 ± 0.023 GeV [4], respectively, obtained with Run-II data, are the two single most precise determinations of the W boson mass at the Tevatron. Combining the results from Run-I and Run-II of the Tevatron using an improved treatment of correlations, following the procedure used in [5], the results are 80.389 ± 0.019 GeV for CDF and 80.383 ± 0.023 GeV for D0. A combination of all pre-2022 CDF and D0 results yields a Tevatron average of 80.387 ± 0.016 GeV [5], with common uncertainties of 10 MeV (PDF) and 4 MeV (radiative corrections).

Using pp collisions at $\sqrt{s} = 7$ TeV, the ATLAS collaboration has published the first measurement of the W boson mass at the LHC, $m_W = 80.370 \pm 0.019$ GeV [6], which is of similar precision as the best measurements of CDF and D0. The LHCb collaboration has measured the W boson mass in pp collisions at $\sqrt{s} = 13$ TeV at the LHC, $m_W = 80.354 \pm 0.032$ GeV [7]. Combining the results from ATLAS and LHCb using the BLUE procedure [8,9] assuming a correlated uncertainty of 9 MeV (PDF), the LHC average is $m_W = 80.366 \pm 0.017$ GeV.

The results obtained by the experiments at the different accelerators are all in good agreement with each other. Assuming a correlated uncertainty of 7 MeV, a hadron collider average of the

Tevatron and LHC measurements of $m_W = 80.377 \pm 0.013$ GeV is obtained, and a world average of $m_W = 80.377 \pm 0.012$ GeV, combining with the LEP result assuming no correlation, again using the BLUE procedure for these averages.

The LEP, Tevatron and LHC results on mass and width are compared in Fig. 54.1 and Fig. 54.2. The Standard Model prediction from the electroweak fit, including Z-pole data and the measured masses of the top quark and of the Higgs boson, gives a W -boson mass of $m_W = 80.356 \pm 0.006$ GeV (see Section 10, Electroweak Model and Constraints on New Physics, J.Erler and A.Freitas, 2022, this review) and a W -boson width of $\Gamma_W = 2.091 \pm 0.001$ GeV [10], which are in good agreement with the measurements.

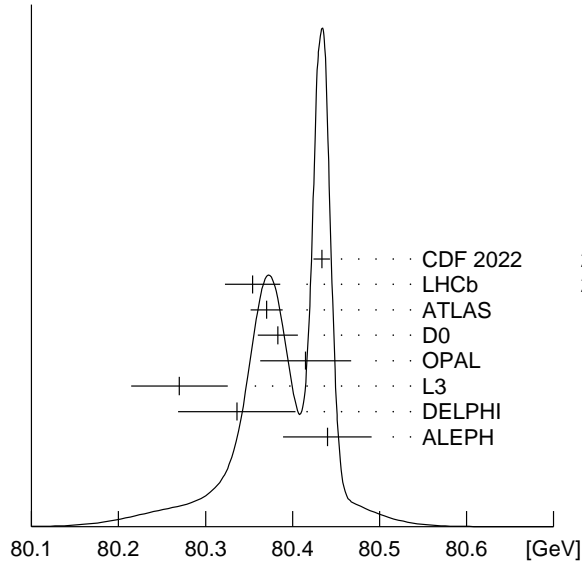


Figure 54.3: Ideogram showing the compatibility of all W -boson mass measurements, replacing the pre-2022 CDF result by the new CDF 2022 result.

In April 2022, after the cut-off of results for this review, the CDF collaboration published a measurement of the W mass based on their full Run-II dataset of 8.8 fb^{-1} , with much reduced uncer-

tainty: $80,433.5 \pm 9.4$ MeV [11]¹. This new CDF Run-II result is of higher precision than our world average of 80.377 ± 0.012 GeV. However, the two determinations disagree significantly, as visible in Fig. 54.1. A probability ideogram comparing the results from Fig. 54.1 is shown in Fig. 54.3 (see Section 5.2 in the Introduction of this review on the construction of ideograms).

For calculating a new world average, replacing the old CDF Run-II result [3] by the new one [11], the uncertainties of all results need to be scaled by a factor of about two in order to achieve a χ^2 per degree of freedom of unity (see Section 5.2 in the Introduction of this review on the definition of the scale factor). The world average quoted above (80.377 ± 0.012 GeV) increases significantly in central value, by up to 40 MeV, while its scaled uncertainty increases by up to 6 MeV, with the exact changes depending on the assumptions made concerning correlated uncertainties. A detailed understanding of the results and their correlations is needed. Corresponding studies are currently being undertaken by the experiments.

References

- [1] S. Schael *et al.* (ALEPH, DELPHI, L3, OPAL, LEP Electroweak Working Group), Phys. Rept. **532**, 119 (2013), [arXiv:1302.3415].
- [2] The Tevatron Electroweak Working Group, for the CDF and D0 Collaborations, March 2010, [arXiv:1003.2826].
- [3] T. Aaltonen *et al.* (CDF), Phys. Rev. Lett. **108**, 151803 (2012), [arXiv:1203.0275].
- [4] V. M. Abazov *et al.* (D0), Phys. Rev. Lett. **108**, 151804 (2012), [arXiv:1203.0293].
- [5] T. A. Aaltonen *et al.* (CDF, D0), Phys. Rev. D **88**, 5, 052018 (2013), [arXiv:1307.7627].
- [6] M. Aaboud *et al.* (ATLAS), Eur. Phys. J. C **78**, 2, 110 (2018), [Erratum: Eur.Phys.J.C 78, 898 (2018)], [arXiv:1701.07240].
- [7] R. Aaij *et al.* (LHCb), JHEP **01**, 166 (2022), [arXiv:2107.10090].
- [8] L. Lyons, D. Gibaut and P. Clifford, Nucl. Instrum. Meth. A **270**, 110 (1988).
- [9] A. Valassi, Nucl. Instrum. Meth. A **500**, 391 (2003).
- [10] J. Haller *et al.*, Eur. Phys. J. C **78**, 8, 675 (2018), [arXiv:1803.01853].
- [11] T. Aaltonen *et al.* (CDF), Science **376**, 6589, 170 (2022).

¹The new result includes the 2.2 fb^{-1} of data used for the previous CDF Run-II result of 80.387 ± 0.019 GeV [3]. Incorporating the improved understanding of PDFs and track reconstruction, the central value of the 2.2 fb^{-1} result is increased by 13.5 MeV to 80,400.5 MeV [11].

55. Z Boson

Revised August 2018 by M. Grünewald (University Coll. Dublin) and A. Gurtu (CERN; TIFR Mumbai).

Precision measurements at the Z -boson resonance using electron–positron colliding beams began in 1989 at the SLC and at LEP. During 1989–95, the four LEP experiments (ALEPH, DELPHI, L3, OPAL) made high-statistics studies of the production and decay properties of the Z . Although the SLD experiment at the SLC collected much lower statistics, it was able to match the precision of LEP experiments in determining the effective electroweak mixing angle $\sin^2\bar{\theta}_W$ and the rates of Z decay to b - and c -quarks, owing to availability of polarized electron beams, small beam size, and stable beam spot.

The Z -boson properties reported in this section may broadly be categorized as:

- The standard ‘lineshape’ parameters of the Z consisting of its mass, M_Z , its total width, Γ_Z , and its partial decay widths, $\Gamma(\text{hadrons})$, and $\Gamma(\ell\bar{\ell})$ where $\ell = e, \mu, \tau, \nu$;
- Z asymmetries in leptonic decays and extraction of Z couplings to charged and neutral leptons;
- The b - and c -quark-related partial widths and charge asymmetries which require special techniques;
- Determination of Z decay modes and the search for modes that violate known conservation laws;
- Average particle multiplicities in hadronic Z decay;
- Z anomalous couplings.

The effective vector and axial-vector coupling constants describing the Z -to-fermion coupling are also measured in $p\bar{p}$ and ep collisions at the Tevatron and at HERA. The corresponding cross-section formulae are given in Section 39 (Cross-section formulae for specific processes) and Section 16 (Structure Functions) in this *Review*. In this minireview, we concentrate on the measurements in e^+e^- collisions at LEP and SLC.

The standard ‘lineshape’ parameters of the Z are determined from an analysis of the production cross sections of these final states in e^+e^- collisions. The $Z \rightarrow \nu\bar{\nu}(\gamma)$ state is identified directly by detecting single photon production and indirectly by subtracting the visible partial widths from the total width. Inclusion in this analysis of the forward-backward asymmetry of charged leptons, $A_{FB}^{(0,\ell)}$, of the τ polarization, $P(\tau)$, and its forward-backward asymmetry, $P(\tau)^{fb}$, enables the separate determination of the effective vector (\bar{g}_V) and axial vector (\bar{g}_A) couplings of the Z to these leptons and the ratio (\bar{g}_V/\bar{g}_A), which is related to the effective electroweak mixing angle $\sin^2\bar{\theta}_W$ (see the ‘Electroweak Model and Constraints on New Physics’ review).

Determination of the b - and c -quark-related partial widths and charge asymmetries involves tagging the b and c quarks for which various methods are employed: requiring the presence of a high momentum prompt lepton in the event with high transverse momentum with respect to the accompanying jet; impact parameter and lifetime tagging using precision vertex measurement with high-resolution detectors; application of neural-network techniques to classify events as b or non- b on a statistical basis using event–shape variables; and using the presence of a charmed meson (D/D^*) or a kaon as a tag.

55.1 Z -parameter determination

LEP was run at energy points on and around the Z mass (88–94 GeV) constituting an energy ‘scan’. The shape of the cross-section variation around the Z peak can be described by a Breit-Wigner *ansatz* with an energy-dependent total width [1–3]. The **three** main properties of this distribution, viz., the **position** of the peak, the **width** of the distribution, and the **height** of the peak, determine respectively the values of M_Z , Γ_Z , and $\Gamma(e^+e^-) \times \Gamma(f\bar{f})$, where $\Gamma(e^+e^-)$ and $\Gamma(f\bar{f})$ are the electron and fermion partial widths of the Z . The quantitative determination of these parameters is done by writing analytic expressions for these cross sections in terms of the parameters, and fitting the calculated cross sections to the measured ones by varying these parameters, taking properly into account all the errors.

Single-photon exchange (σ_γ^0) and γ - Z interference ($\sigma_{\gamma Z}^0$) are included, and the large ($\sim 25\%$) initial-state radiation (ISR) effects are taken into account by convoluting the analytic expressions over a ‘Radiator Function’ [1–5] $H(s, s')$. Thus for the process $e^+e^- \rightarrow f\bar{f}$:

$$\sigma_f(s) = \int H(s, s') \sigma_f^0(s') ds' \quad (55.1)$$

$$\sigma_f^0(s) = \sigma_Z^0 + \sigma_\gamma^0 + \sigma_{\gamma Z}^0 \quad (55.2)$$

$$\sigma_Z^0 = \frac{12\pi}{M_Z^2} \frac{\Gamma(e^+e^-)\Gamma(f\bar{f})}{\Gamma_Z^2} \frac{s \Gamma_Z^2}{(s - M_Z^2)^2 + s^2 \Gamma_Z^2/M_Z^2} \quad (55.3)$$

$$\sigma_\gamma^0 = \frac{4\pi\alpha^2(s)}{3s} Q_f^2 N_c^f \quad (55.4)$$

$$\sigma_{\gamma Z}^0 = -\frac{2\sqrt{2}\alpha(s)}{3} (Q_f G_F N_c^f G_V^e G_V^f) \times \frac{(s - M_Z^2) M_Z^2}{(s - M_Z^2)^2 + s^2 \Gamma_Z^2/M_Z^2} \quad (55.5)$$

where Q_f is the charge of the fermion, $N_c^f = 3$ for quarks and 1 for leptons, and G_V^f is the vector coupling of the Z to the fermion-antifermion pair $f\bar{f}$.

Since $\sigma_{\gamma Z}^0$ is expected to be much less than σ_Z^0 , the LEP Collaborations have generally calculated the interference term in the framework of the Standard Model. This fixing of $\sigma_{\gamma Z}^0$ leads to a tighter constraint on M_Z , and consequently a smaller error on its fitted value. It is possible to relax this constraint and carry out the fit within the S-matrix framework, which is briefly described in the next section.

In the above framework, the QED radiative corrections have been explicitly taken into account by convoluting over the ISR and allowing the electromagnetic coupling constant to run [6]: $\alpha(s) = \alpha/(1 - \Delta\alpha)$. On the other hand, weak radiative corrections that depend upon the assumptions of the electroweak theory and on the values of M_{top} and M_{Higgs} are accounted for by **absorbing them into the couplings**, which are then called the *effective* couplings \mathcal{G}_V and \mathcal{G}_A (or alternatively the effective parameters of the \star scheme of Kennedy and Lynn [7]).

\mathcal{G}_V^f and \mathcal{G}_A^f are complex numbers with small imaginary parts. As experimental data does not allow simultaneous extraction of both real and imaginary parts of the effective couplings, the convention $g_A^f = \text{Re}(\mathcal{G}_A^f)$ and $g_V^f = \text{Re}(\mathcal{G}_V^f)$ is used and the imaginary parts are added in the fitting code [4].

Defining

$$A_f = 2 \frac{g_V^f \cdot g_A^f}{(g_V^f)^2 + (g_A^f)^2} \quad (55.6)$$

the lowest-order expressions for the various lepton-related asymmetries on the Z pole are [8–10] $A_{FB}^{(0,\ell)} = (3/4)A_e A_f$, $P(\tau) = -A_\tau$, $P(\tau)^{fb} = -(3/4)A_e$, $A_{LR} = A_e$. The full analysis takes into account the energy-dependence of the asymmetries. Experimentally A_{LR} is defined as $(\sigma_L - \sigma_R)/(\sigma_L + \sigma_R)$, where $\sigma_{L(R)}$ are the $e^+e^- \rightarrow Z$ production cross sections with left- (right)-handed electrons.

The definition of the partial decay width of the Z to $f\bar{f}$ includes the effects of QED and QCD final-state corrections, as well as the contribution due to the imaginary parts of the couplings:

$$\Gamma(f\bar{f}) = \frac{G_F M_Z^3}{6\sqrt{2}\pi} N_c^f (|\mathcal{G}_A^f|^2 R_A^f + |\mathcal{G}_V^f|^2 R_V^f) + \Delta_{ew/QCD} \quad (55.7)$$

where R_V^f and R_A^f are radiator factors to account for final state QED and QCD corrections, as well as effects due to nonzero fermion masses, and $\Delta_{ew/QCD}$ represents the non-factorizable electroweak/QCD corrections.

55.2 S-matrix approach to the Z

While most experimental analyses of LEP/SLC data have followed the ‘Breit-Wigner’ approach, an alternative S-matrix-based

analysis is also possible. The Z , like all unstable particles, is associated with a complex pole in the S matrix. The pole position is process-independent and gauge-invariant. The mass, \overline{M}_Z , and width, $\overline{\Gamma}_Z$, can be defined in terms of the pole in the energy plane via [11–14]

$$\overline{s} = \overline{M}_Z^2 - i\overline{M}_Z\overline{\Gamma}_Z \quad (55.8)$$

leading to the relations

$$\begin{aligned} \overline{M}_Z &= M_Z / \sqrt{1 + \Gamma_Z^2 / M_Z^2} \\ &\approx M_Z - 34.1 \text{ MeV} \end{aligned} \quad (55.9)$$

$$\begin{aligned} \overline{\Gamma}_Z &= \Gamma_Z / \sqrt{1 + \Gamma_Z^2 / M_Z^2} \\ &\approx \Gamma_Z - 0.9 \text{ MeV}. \end{aligned} \quad (55.10)$$

The LEP collaborations [15] have analyzed their data using the S -matrix approach as defined in Eq. (55.8), in addition to the conventional one. They observe a downward shift in the Z mass as expected.

55.3 Handling the large-angle e^+e^- final state

Unlike other $f\bar{f}$ decay final states of the Z , the e^+e^- final state has a contribution not only from the s -channel but also from the t -channel and s - t interference. The full amplitude is not amenable to fast calculation, which is essential if one has to carry out minimization fits within reasonable computer time. The usual procedure is to calculate the non- s channel part of the cross section separately using the Standard Model programs ALIBABA [16] or TOPAZ0 [17], with the measured value of M_{top} , and $M_{\text{Higgs}} = 150$ GeV, and add it to the s -channel cross section calculated as for other channels. This leads to two additional sources of error in the analysis: firstly, the theoretical calculation in ALIBABA itself is known to be accurate to $\sim 0.5\%$, and secondly, there is uncertainty due to the error on M_{top} and the unknown value of M_{Higgs} (100–1000 GeV). These errors are propagated into the analysis by including them in the systematic error on the e^+e^- final state. As these errors are common to the four LEP experiments, this is taken into account when performing the LEP average.

55.4 Errors due to uncertainty in LEP energy determination

The systematic errors related to the LEP energy measurement, see [18–23], can be classified as:

- The absolute energy scale error;
- Energy-point-to-energy-point errors due to the nonlinear response of the magnets to the exciting currents;
- Energy-point-to-energy-point errors due to possible higher-order effects in the relationship between the dipole field and beam energy;
- Energy reproducibility errors due to various unknown uncertainties in temperatures, tidal effects, corrector settings, RF status, etc.

Precise energy calibration was done outside normal data-taking using the resonant depolarization technique. Run-time energies were determined every 10 minutes by measuring the relevant machine parameters and using a model which takes into account all the known effects, including leakage currents produced by trains in the Geneva area and the tidal effects due to gravitational forces of the Sun and the Moon. The LEP Energy Working Group has provided a covariance matrix from the determination of LEP energies for the different running periods during 1993–1995 [18].

55.5 Choice of fit parameters

The LEP Collaborations have chosen the following primary set of parameters for fitting:

$$M_Z, \Gamma_Z, \sigma_{\text{hadron}}^0, R(\text{lepton}), A_{FB}^{(0,\ell)},$$

where

$$\begin{aligned} R(\text{lepton}) &= \Gamma(\text{hadrons}) / \Gamma(\text{lepton}), \sigma_{\text{hadron}}^0 \\ &= 12\pi\Gamma(e^+e^-)\Gamma(\text{hadrons}) / M_Z^2\Gamma_Z^2. \end{aligned}$$

With a knowledge of these fitted parameters and their covariance matrix, any other parameter can be derived. The main advantage of these parameters is that they form a physics motivated set of parameters with much reduced correlations.

Thus, the most general fit carried out to cross section and asymmetry data determines the **nine parameters**: $M_Z, \Gamma_Z, \sigma_{\text{hadron}}^0, R(e), R(\mu), R(\tau), A_{FB}^{(0,e)}, A_{FB}^{(0,\mu)}, A_{FB}^{(0,\tau)}$. Assumption of lepton universality leads to a **five-parameter fit** determining $M_Z, \Gamma_Z, \sigma_{\text{hadron}}^0, R(\text{lepton}), A_{FB}^{(0,\ell)}$.

55.6 Combining results from LEP and SLC experiments

With a steady increase in statistics over the years and improved understanding of the common systematic errors between LEP experiments, the procedures for combining results have evolved continuously [24]. The Line Shape Sub-group of the LEP Electroweak Working Group investigated the effects of these common errors, and devised a combination procedure for the precise determination of the Z parameters from LEP experiments. Using these procedures, this note also gives the results after combining the final parameter sets from the four experiments, and these are the results quoted as the fit results in the Z listings below. Transformation of variables leads to values of derived parameters like partial decay widths and branching ratios to hadrons and leptons. Finally, transforming the LEP combined nine parameter set to $(M_Z, \Gamma_Z, \sigma_{\text{hadron}}^0, g_A^f, g_V^f, f = e, \mu, \tau)$ using the average values of lepton asymmetry parameters (A_e, A_μ, A_τ) as constraints, leads to the best fitted values of the vector and axial-vector couplings (g_V, g_A) of the charged leptons to the Z .

Brief remarks on the handling of common errors and their magnitudes are given below. The identified common errors are those coming from

- (a) LEP energy-calibration uncertainties, and
- (b) the theoretical uncertainties in (i) the luminosity determination using small angle Bhabha scattering, (ii) estimating the non- s channel contribution to large angle Bhabha scattering, (iii) the calculation of QED radiative effects, and (iv) the parameterization of the cross section in terms of the parameter set used.

55.7 Common LEP energy errors

All the collaborations incorporate in their fit the full LEP energy error matrix as provided by the LEP energy group for their intersection region [18]. The effect of these errors is separated out from that of other errors by carrying out fits with energy errors scaled up and down by $\sim 10\%$ and redoing the fits. From the observed changes in the overall error matrix, the covariance matrix of the common energy errors is determined. Common LEP energy errors lead to uncertainties on M_Z, Γ_Z , and σ_{hadron}^0 of 1.7, 1.2 MeV, and 0.011 nb, respectively.

55.8 Common luminosity errors

BHLUMI 4.04 [25] is used by all LEP collaborations for small-angle Bhabha scattering leading to a common uncertainty in their measured cross sections of 0.061% [26]. BHLUMI does not include a correction for production of light fermion pairs. OPAL explicitly corrects for this effect and reduces their luminosity uncertainty to 0.054%, which is taken fully correlated with the other experiments. The other three experiments among themselves have a common uncertainty of 0.061%.

55.9 Common non- s channel uncertainties

The same standard model programs ALIBABA [16] and TOPAZ0 [17] are used to calculate the non- s channel contribution to the large angle Bhabha scattering [27]. As this contribution is a function of the Z mass, which itself is a variable in the fit, it is parameterized as a function of M_Z by each collaboration to properly track this contribution as M_Z varies in the fit. The common errors on R_e and $A_{FB}^{(0,e)}$ are 0.024 and 0.0014 respectively, and are correlated between them.

55.10 Common theoretical uncertainties: QED

There are large initial-state photon and fermion pair radiation effects near the Z resonance, for which the best currently available evaluations include contributions up to $\mathcal{O}(\alpha^3)$. To estimate the

remaining uncertainties, different schemes are incorporated in the standard model programs ZFITTER [5], TOPAZ0 [17], and MIZA [28]. Comparing the different options leads to error estimates of 0.3 and 0.2 MeV on M_Z and Γ_Z respectively, and of 0.02% on σ_{hadron}^0 .

55.11 Common theoretical uncertainties: parametrization of lineshape and asymmetries

To estimate uncertainties arising from ambiguities in the model-independent parametrization of the differential cross-section near the Z resonance, results from TOPAZ0 and ZFITTER were compared by using ZFITTER to fit the cross sections and asymmetries calculated using TOPAZ0. The resulting uncertainties on M_Z , Γ_Z , σ_{hadron}^0 , $R(\text{lepton})$, and $A_{FB}^{(0,\ell)}$ are 0.1 MeV, 0.1 MeV, 0.001 nb, 0.004, and 0.0001 respectively.

Thus, the overall theoretical errors on M_Z , Γ_Z , σ_{hadron}^0 are 0.3 MeV, 0.2 MeV, and 0.008 nb respectively; on each $R(\text{lepton})$ is 0.004 and on each $A_{FB}^{(0,\ell)}$ is 0.0001. Within the set of three $R(\text{lepton})$'s and the set of three $A_{FB}^{(0,\ell)}$'s, the respective errors are fully correlated.

All the theory-related errors mentioned above utilize Standard Model programs which need the Higgs mass and running electromagnetic coupling constant as inputs; uncertainties on these inputs will also lead to common errors. All LEP collaborations used the same set of inputs for Standard Model calculations: $M_Z = 91.187$ GeV, the Fermi constant $G_F = (1.16637 \pm 0.00001) \times 10^{-5}$ GeV $^{-2}$ [29], $\alpha^{(5)}(M_Z) = 1/128.877 \pm 0.090$ [30], $\alpha_s(M_Z) = 0.119$ [31], $M_{\text{top}} = 174.3 \pm 5.1$ GeV [31] and $M_{\text{Higgs}} = 150$ GeV. The only observable effect, on M_Z , is due to the variation of M_{Higgs} between 100–1000 GeV (due to the variation of the γ/Z interference term which is taken from the Standard Model): M_Z changes by +0.23 MeV per unit change in $\log_{10} M_{\text{Higgs}}/\text{GeV}$, which is not an error but a correction to be applied once M_{Higgs} is determined. The effect is much smaller than the error on M_Z (± 2.1 MeV).

55.12 Methodology of combining the LEP experimental results

The LEP experimental results actually used for combination are slightly modified from those published by the experiments (which are given in the Listings below). This has been done in order to facilitate the procedure by making the inputs more consistent. These modified results are given explicitly in [24]. The main differences compared to the published results are (a) consistent use of ZFITTER 6.23 and TOPAZ0 (the published ALEPH results used ZFITTER 6.10); (b) use of the combined energy-error matrix, which makes a difference of 0.1 MeV on the M_Z and Γ_Z for L3 only as at that intersection the RF modeling uncertainties are the largest.

Thus, nine-parameter sets from all four experiments with their covariance matrices are used together with all the common errors correlations. A grand covariance matrix, V , is constructed and a combined nine-parameter set is obtained by minimizing $\chi^2 = \Delta^T V^{-1} \Delta$, where Δ is the vector of residuals of the combined parameter set to the results of individual experiments. Imposing lepton universality in the combination results in the combined five-parameter set.

55.13 Study of $Z \rightarrow b\bar{b}$ and $Z \rightarrow c\bar{c}$

In the sector of c - and b -physics, the LEP experiments have measured the ratios of partial widths $R_b = \Gamma(Z \rightarrow b\bar{b})/\Gamma(Z \rightarrow \text{hadrons})$, and $R_c = \Gamma(Z \rightarrow c\bar{c})/\Gamma(Z \rightarrow \text{hadrons})$, and the forward-backward (charge) asymmetries $A_{FB}^{b\bar{b}}$ and $A_{FB}^{c\bar{c}}$. The SLD experiment at SLC has measured the ratios R_c and R_b and, utilizing the polarization of the electron beam, was able to obtain the final state coupling parameters A_b and A_c from a measurement of the left-right forward-backward asymmetry of b - and c -quarks. The high precision measurement of R_c at SLD was made possible owing to the small beam size and very stable beam spot at SLC, coupled with a highly precise CCD pixel detector. Several of the analyses have also determined other quantities, in particular the semileptonic branching ratios, $B(b \rightarrow \ell^-)$, $B(b \rightarrow c \rightarrow \ell^+)$, and $B(c \rightarrow \ell^+)$, the average time-integrated $B^0\bar{B}^0$ mixing parameter

$\bar{\chi}$ and the probabilities for a c -quark to fragment into a D^+ , a D_s , a D^{*+} , or a charmed baryon. The latter measurements do not concern properties of the Z boson, and hence they do not appear in the Listing below. However, for completeness, we will report at the end of this minireview their values as obtained fitting the data contained in the Z section. All these quantities are correlated with the electroweak parameters, and since the mixture of b hadrons is different from the one at the $\Upsilon(4S)$, their values might differ from those measured at the $\Upsilon(4S)$.

All the above quantities are correlated to each other since:

- Several analyses (for example the lepton fits) determine more than one parameter simultaneously;
- Some of the electroweak parameters depend explicitly on the values of other parameters (for example R_b depends on R_c);
- Common tagging and analysis techniques produce common systematic uncertainties.

The LEP Electroweak Heavy Flavour Working Group has developed [32] a procedure for combining the measurements taking into account known sources of correlation. The combining procedure determines fourteen parameters: the six parameters of interest in the electroweak sector, R_b , R_c , $A_{FB}^{b\bar{b}}$, $A_{FB}^{c\bar{c}}$, A_b and A_c and, in addition, $B(b \rightarrow \ell^-)$, $B(b \rightarrow c \rightarrow \ell^+)$, $B(c \rightarrow \ell^+)$, $\bar{\chi}$, $f(D^+)$, $f(D_s)$, $f(\text{cbaryon})$ and $P(c \rightarrow D^{*+}) \times B(D^{*+} \rightarrow \pi^+ D^0)$, to take into account their correlations with the electroweak parameters. Before the fit both the peak and off-peak asymmetries are translated to the common energy $\sqrt{s} = 91.26$ GeV using the predicted energy-dependence from ZFITTER [5].

55.14 Summary of the measurements and of the various kinds of analysis

The measurements of R_b and R_c fall into two classes. In the first, named single-tag measurement, a method for selecting b and c events is applied and the number of tagged events is counted. A second technique, named double-tag measurement, has the advantage that the tagging efficiency is directly derived from the data thereby reducing the systematic error on the measurement.

The measurements in the b - and c -sector can be essentially grouped in the following categories:

- Lifetime (and lepton) double-tagging measurements of R_b . These are the most precise measurements of R_b and obviously dominate the combined result. The main sources of systematics come from the charm contamination and from estimating the hemisphere b -tagging efficiency correlation;
- Analyses with $D/D^{*\pm}$ to measure R_c . These measurements make use of several different tagging techniques (inclusive/exclusive double tag, exclusive double tag, reconstruction of all weakly decaying charmed states) and no assumptions are made on the energy-dependence of charm fragmentation;
- A measurement of R_c using single leptons and assuming $B(b \rightarrow c \rightarrow \ell^+)$;
- Lepton fits which use hadronic events with one or more leptons in the final state to measure the asymmetries $A_{FB}^{b\bar{b}}$ and $A_{FB}^{c\bar{c}}$. Each analysis usually gives several other electroweak parameters. The dominant sources of systematics are due to lepton identification, to other semileptonic branching ratios and to the modeling of the semileptonic decay;
- Measurements of $A_{FB}^{b\bar{b}}$ using lifetime tagged events with a hemisphere charge measurement. These measurements dominate the combined result;
- Analyses with $D/D^{*\pm}$ to measure $A_{FB}^{c\bar{c}}$ or simultaneously $A_{FB}^{b\bar{b}}$ and $A_{FB}^{c\bar{c}}$;
- Measurements of A_b and A_c from SLD, using several tagging methods (lepton, kaon, D/D^* , and vertex mass). These quantities are directly extracted from a measurement of the left-right forward-backward asymmetry in $c\bar{c}$ and $b\bar{b}$ production using a polarized electron beam.

55.15 Averaging procedure

All the measurements are provided by the LEP and SLD Collaborations in the form of tables with a detailed breakdown of

the systematic errors of each measurement and its dependence on other electroweak parameters.

The averaging proceeds via the following steps:

- Define and propagate a consistent set of external inputs such as branching ratios, hadron lifetimes, fragmentation models *etc.* All the measurements are checked to ensure that all use a common set of assumptions (for instance, since the QCD corrections for the forward–backward asymmetries are strongly dependent on the experimental conditions, the data are corrected before combining);
- Form the full (statistical and systematic) covariance matrix of the measurements. The systematic correlations between different analyses are calculated from the detailed error breakdown in the measurement tables. The correlations relating several measurements made by the same analysis are also used;
- Take into account any explicit dependence of a measurement on the other electroweak parameters. As an example of this dependence, we illustrate the case of the double-tag measurement of R_b , where c -quarks constitute the main background. The normalization of the charm contribution is not usually fixed by the data and the measurement of R_b depends on the assumed value of R_c , which can be written as:

$$R_b = R_b^{\text{meas}} + a(R_c) \frac{(R_c - R_c^{\text{used}})}{R_c}, \quad (55.11)$$

where R_b^{meas} is the result of the analysis which assumed a value of $R_c = R_c^{\text{used}}$ and $a(R_c)$ is the constant which gives the dependence on R_c ;

- Perform a χ^2 minimization with respect to the combined electroweak parameters.

After the fit the average peak asymmetries $A_{FB}^{c\bar{c}}$ and $A_{FB}^{b\bar{b}}$ are corrected for the energy shift from 91.26 GeV to M_Z and for QED (initial state radiation), γ exchange, and γZ interference effects, to obtain the corresponding pole asymmetries $A_{FB}^{0,c}$ and $A_{FB}^{0,b}$.

This averaging procedure, using the fourteen parameters described above, and applied to the data contained in the Z particle listing below, gives the following results (where the last 8 parameters do not depend directly on the Z):

$$\begin{aligned} R_b^0 &= 0.21629 \pm 0.00066 \\ R_c^0 &= 0.1721 \pm 0.0030 \\ A_{FB}^{0,b} &= 0.0992 \pm 0.0016 \\ A_{FB}^{0,c} &= 0.0707 \pm 0.0035 \\ A_b &= 0.923 \pm 0.020 \\ A_c &= 0.670 \pm 0.027 \end{aligned}$$

$$\begin{aligned} B(b \rightarrow \ell^-) &= 0.1071 \pm 0.0022 \\ B(b \rightarrow c \rightarrow \ell^+) &= 0.0801 \pm 0.0018 \\ B(c \rightarrow \ell^+) &= 0.0969 \pm 0.0031 \\ \bar{\chi} &= 0.1250 \pm 0.0039 \\ f(D^+) &= 0.235 \pm 0.016 \\ f(D_s) &= 0.126 \pm 0.026 \\ f(c_{\text{baryon}}) &= 0.093 \pm 0.022 \end{aligned}$$

$$P(c \rightarrow D^{*+}) \times B(D^{*+} \rightarrow \pi^+ D^0) = 0.1622 \pm 0.0048 \quad (55.12)$$

Among the non–electroweak observables, the B semileptonic branching fraction $B(b \rightarrow \ell^-)$ is of special interest, since the dominant error source on this quantity is the dependence on the semileptonic decay model for $b \rightarrow \ell^-$, with $\Delta B(b \rightarrow \ell^-)_{b \rightarrow \ell^- \text{ model}} = 0.0012$. Extensive studies have been made to understand the size of this error. Among the electroweak quantities, the quark asymmetries with leptons depend also on the semileptonic decay model, while the asymmetries using other

methods usually do not. The fit implicitly requires that the different methods give consistent results and this effectively constrains the decay model, and thus reduces in principle the error from this source in the fit result.

To obtain a conservative estimate of the modelling error, the above fit has been repeated removing all asymmetry measurements. The results of the fit on B -decay related observables are [24]: $B(b \rightarrow \ell^-) = 0.1069 \pm 0.0022$, with $\Delta B(b \rightarrow \ell^-)_{b \rightarrow \ell^- \text{ model}} = 0.0013$, $B(b \rightarrow c \rightarrow \ell^+) = 0.0802 \pm 0.0019$ and $\bar{\chi} = 0.1259 \pm 0.0042$.

References

- [1] R. N. Cahn, Phys. Rev. D **36**, 2666 (1987), [Erratum: Phys.Rev.D 40, 922 (1989)].
- [2] D. Y. Bardin *et al.*, in “LEP Physics Workshop,” 89–127 (1989).
- [3] A. Borrelli *et al.*, Nucl. Phys. B **333**, 357 (1990).
- [4] D. Y. Bardin and G. Passarino (1998), [hep-ph/9803425]; D. Y. Bardin, M. Grunewald and G. Passarino (1999), [hep-ph/9902452].
- [5] D. Bardin *et al.*, Z. Phys. C **44**, 493 (1989); D. Bardin *et al.*, Comput. Phys. Commun. **59**, 303 (1990); D. Y. Bardin *et al.*, Nucl. Phys. B **351**, 1 (1991), [hep-ph/9801208]; D. Y. Bardin *et al.*, Phys. Lett. B **255**, 290 (1991), [hep-ph/9801209]; D. Y. Bardin *et al.* (1992), [hep-ph/9412201]; D. Y. Bardin *et al.*, Comput. Phys. Commun. **133**, 229 (2001), [hep-ph/9908433].
- [6] G. Burgers and F. Jegerlehner, Conf. Proc. C **8902201**, 55 (1989).
- [7] D. Kennedy and B. Lynn, Nucl. Phys. B **322**, 1 (1989).
- [8] M. Consoli, W. Hollik and F. Jegerlehner, in “LEP Physics Workshop,” 7–54 (1989).
- [9] M. Bohm *et al.*, in “LEP Physics Workshop,” 203–234 (1989).
- [10] P. Eberhard *et al.*, in “LEP Physics Workshop,” 235–266 (1989).
- [11] R. G. Stuart, Phys. Lett. B **262**, 113 (1991).
- [12] A. Sirlin, Phys. Rev. Lett. **67**, 2127 (1991).
- [13] A. Leike, T. Riemann and J. Rose, Phys. Lett. B **273**, 513 (1991), [hep-ph/9508390].
- [14] D. Bardin *et al.*, Phys. Lett. B **206**, 539 (1988).
- [15] S. Schael *et al.* (ALEPH, DELPHI, L3, OPAL, LEP Electroweak), Phys. Rept. **532**, 119 (2013), [arXiv:1302.3415].
- [16] W. Beenakker, F. A. Berends and S. van der Marck, Nucl. Phys. B **349**, 323 (1991).
- [17] G. Montagna *et al.*, Nucl. Phys. B **401**, 3 (1993); G. Montagna *et al.*, Comput. Phys. Commun. **76**, 328 (1993); G. Montagna *et al.*, Comput. Phys. Commun. **93**, 120 (1996), [hep-ph/9506329]; G. Montagna *et al.*, Comput. Phys. Commun. **117**, 278 (1999), [hep-ph/9804211].
- [18] R. Assmann *et al.*, Eur. Phys. J. C **6**, 187 (1999).
- [19] R. Assmann *et al.* (Working Group on LEP Energy), Z. Phys. C **66**, 567 (1995).
- [20] L. Arnaudon *et al.* (Working Group on LEP Energy, ALEPH, DELPHI, L3, OPAL), Phys. Lett. B **307**, 187 (1993).
- [21] L. Arnaudon *et al.* (Working Group on LEP energy), in “26th International Conference on High-energy Physics,” (1992).
- [22] L. Arnaudon *et al.* (LEP Polarization), Phys. Lett. B **284**, 431 (1992).
- [23] R. Bailey *et al.*, Conf. Proc. C **900612**, 1765 (1990).
- [24] S. Schael *et al.* (ALEPH, DELPHI, L3, OPAL, SLD, LEP Electroweak Working Group, SLD Electroweak Group, SLD Heavy Flavour Group), Phys. Rept. **427**, 257 (2006), [hep-ex/0509008].
- [25] S. Jadach *et al.*, Comput. Phys. Commun. **102**, 229 (1997); S. Jadach and O. Nicrosini, Event generators for Bhabha scattering, in Physics at LEP2, CERN-96-01 Vol. 2, February 1996.

- [26] B. Ward *et al.*, Phys. Lett. B **450**, 262 (1999), [hep-ph/9811245].
- [27] W. Beenakker and G. Passarino, Phys. Lett. B **425**, 199 (1998), [hep-ph/9710376].
- [28] M. Martinez *et al.*, Z. Phys. C **49**, 645 (1991); M. Martinez and F. Teubert, Z. Phys. **C65**, 267 (1995), updated with results summarized in S. Jadach, B. Pietrzyk, and M. Skrzypek, Phys. Lett. **B456**, 77 (1999) and Reports of the working group on precision calculations for the *Z* resonance, CERN 95-03, ed. D. Bardin, W. Hollik, and G. Passarino, and references therein.
- [29] T. van Ritbergen and R. G. Stuart, Phys. Lett. B **437**, 201 (1998), [hep-ph/9802341]; T. van Ritbergen and R. G. Stuart, Phys. Rev. Lett. **82**, 488 (1999), [hep-ph/9808283].
- [30] S. Eidelman and F. Jegerlehner, Z. Phys. C **67**, 585 (1995), [hep-ph/9502298]; M. Steinhauser, Phys. Lett. B **429**, 158 (1998), [hep-ph/9803313].
- [31] D. E. Groom *et al.* (Particle Data Group), Eur. Phys. J. C **15**, 1 (2000).
- [32] Nucl. Instrum. Meth. A **378**, 101 (1996).

56. Muon Anomalous Magnetic Moment

Revised August 2021 by A. Höcker (CERN) and W.J. Marciano (BNL).

The Dirac equation predicts a muon magnetic moment, $\vec{M} = g_\mu \frac{e}{2m_\mu} \vec{S}$, with gyromagnetic ratio $g_\mu = 2$. Quantum loop effects lead to a small calculable deviation from $g_\mu = 2$, parameterized by the magnetic anomaly¹

$$a_\mu \equiv \frac{g_\mu - 2}{2}. \quad (56.1)$$

That quantity can be accurately measured and, within the Standard Model (SM) framework, precisely predicted. Hence, comparison of experiment and theory tests the SM at its quantum loop level. A deviation in a_μ^{exp} from the SM expectation would signal effects of new physics, with current sensitivity reaching up to mass scales of $\mathcal{O}(\text{TeV})$ [1]. For recent thorough muon $g-2$ reviews, see e.g. Refs. [2–4].

The E821 experiment at Brookhaven National Lab (BNL) studied the precession of μ^+ and μ^- in a constant external magnetic field as they circulated in a confining storage ring. It found² [6]

$$\begin{aligned} a_{\mu^+}^{\text{exp,BNL}} &= 116\,592\,040(60)(50) \times 10^{-11}, \\ a_{\mu^-}^{\text{exp,BNL}} &= 116\,592\,150(80)(30) \times 10^{-11}, \end{aligned} \quad (56.2)$$

where the first errors are statistical and the second systematic. Assuming CPT invariance and taking into account correlations between systematic uncertainties, one finds for their average [5,6]

$$a_\mu^{\text{exp,BNL}} = 116\,592\,089(54)(33) \times 10^{-11}. \quad (56.3)$$

These results represent about a factor of 14 improvement over the classic CERN experiments of the 1970's [7].

Further improvement of the measurement by a factor of four by setting up the E821 storage ring at the Fermilab National Accelerator Laboratory (FNAL), and utilizing a cleaner and more intense muon beam and improved detectors [8] is in progress. A first analysis with positive muons based on a fraction of the data found [9]

$$a_{\mu^+}^{\text{exp,FNAL}} = 116\,592\,040(51)(19) \times 10^{-11}. \quad (56.4)$$

The FNAL result is consistent with the BNL measurement and has comparable statistical as well as improved systematic precision. Their average assuming CPT invariance reads [9]

$$a_\mu^{\text{exp}} = 116\,592\,061(41) \times 10^{-11}, \quad (56.5)$$

providing a relative precision of 0.35 parts per million.

Another muon $g-2$ experiment with similar sensitivity but using an alternative zero-electric-field technique with a low-emittance and low-momentum muon beam is currently under construction at J-PARC in Japan [10].

The SM prediction a_μ^{SM} is generally divided into three parts (see Fig. 56.1 for representative Feynman diagrams)

$$a_\mu^{\text{SM}} = a_\mu^{\text{QED}} + a_\mu^{\text{EW}} + a_\mu^{\text{Had}}. \quad (56.6)$$

In the following discussion we use the numerical estimates provided by the Muon $g-2$ Theory Initiative White Paper [4].

The QED part includes all photonic and leptonic (e, μ, τ) loops starting with the classic $\alpha/2\pi$ Schwinger contribution [11]. It has

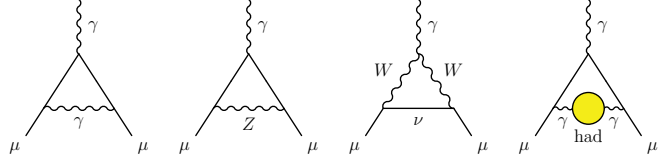


Figure 56.1: Representative diagrams contributing to a_μ^{SM} . From left to right: first order QED (Schwinger term), lowest-order weak, lowest-order hadronic.

been computed through five loops [4, 12, 13]

$$\begin{aligned} a_\mu^{\text{QED}} &= \frac{\alpha}{2\pi} + 0.765\,857\,420(13) \left(\frac{\alpha}{\pi}\right)^2 + 24.050\,509\,85(23) \left(\frac{\alpha}{\pi}\right)^3 \\ &\quad + 130.8782(60) \left(\frac{\alpha}{\pi}\right)^4 + 751.0(9) \left(\frac{\alpha}{\pi}\right)^5 + \dots \end{aligned} \quad (56.7)$$

with little change in the coefficients since our last update of this review. Employing $\alpha^{-1} = 137.035\,999\,046(27)$, obtained from the precise measurements of h/m_{Cs} [14], the Rydberg constant, and m_{Cs}/m_e leads to³ [12]

$$a_\mu^{\text{QED}} = 116\,584\,718.93(0.10) \times 10^{-11}, \quad (56.8)$$

where the small error results mainly from the uncertainties in the estimate of the six loop contribution and in α .

Loop contributions involving heavy W^\pm, Z or Higgs particles are collectively labeled as a_μ^{EW} . They are suppressed by at least a factor of $(\alpha/\pi) \cdot (m_\mu^2/m_W^2) \simeq 4 \times 10^{-9}$. At 1-loop order [18]

$$\begin{aligned} a_\mu^{\text{EW}}[1\text{-loop}] &= \\ &= \frac{G_\mu m_\mu^2}{8\sqrt{2}\pi^2} \left[\frac{5}{3} + \frac{1}{3} (1 - 4\sin^2\theta_W)^2 + \mathcal{O}\left(\frac{m_\mu^2}{M_Z^2}\right) + \mathcal{O}\left(\frac{m_\mu^2}{M_H^2}\right) \right] \\ &= 194.8 \times 10^{-11}, \end{aligned} \quad (56.9)$$

for $\sin^2\theta_W \equiv 1 - M_W^2/M_Z^2 \simeq 0.223$, and where $G_\mu \simeq 1.166 \times 10^{-5} \text{ GeV}^{-2}$ is the Fermi coupling constant. Two-loop corrections are relatively large and negative [19]. For a Higgs boson mass of 125 GeV it amounts to $a_\mu^{\text{EW}}[2\text{-loop}] = -41.2(1.0) \times 10^{-11}$ [19], where the uncertainty stems from quark triangle loops. The 3-loop leading logarithms are negligible, $\mathcal{O}(10^{-12})$ [19, 20]. Overall one finds

$$a_\mu^{\text{EW}} = 153.6(1.0) \times 10^{-11}. \quad (56.10)$$

A recent complete 2-loop numerical evaluation of the electroweak correction [21] when adjusted for appropriate light quark masses confirmed the result in Eq. (56.10).

Hadronic (quark and gluon) loop contributions to a_μ^{SM} give rise to its main uncertainty. One traditionally relies on a data-driven dispersion relation approach to evaluate the lowest-order $\mathcal{O}(\alpha^2)$ hadronic vacuum polarization contribution $a_\mu^{\text{Had}}[\text{LO}]$ from corresponding cross section measurements [22]

$$a_\mu^{\text{Had}}[\text{LO}] = \frac{1}{3} \left(\frac{\alpha}{\pi}\right)^2 \int_{m_\pi^2}^{\infty} ds \frac{K(s)}{s} R^{(0)}(s), \quad (56.11)$$

¹Also referred to as *anomalous magnetic moment* despite being dimensionless.

²The results reported by the experiment have been updated in Eqs. (56.2) and (56.3) to the newest value for the absolute muon-to-proton magnetic ratio $\lambda = 3.183\,345\,142(71)$ [5]. The change induced in a_μ^{exp} with respect to the value of $\lambda = 3.183\,345\,39(10)$ used in Ref. [6] amounts to $+10 \times 10^{-11}$.

³A recent measurement using Rb-87 atoms [15] resulted in $\alpha^{-1} = 137.035\,999\,206(11)$, which exhibits a larger than 5σ discrepancy with the Cs-133 based result. Using this value in Eq. (56.7) leads to a reduction of a_μ^{QED} by 0.14×10^{-11} , which is larger than the quoted uncertainty in Eq. (56.8), but still negligible compared to other uncertainties affecting a_μ^{SM} . This discrepancy impacts, however, the SM prediction of the magnetic anomaly of the electron [13, 16], which differs by respectively -2.4σ and $+1.6\sigma$ from the experimental value [17], depending on whether the Cs-133 or Rb-87 based α value is used.

where $K(s)$ is a QED kernel function [23], and where $R^{(0)}(s)$ denotes the ratio of the bare⁴ cross section for e^+e^- annihilation into hadrons to the pointlike muon-pair cross section at center-of-mass energy \sqrt{s} . The function $K(s) \sim 1/s$ in Eq. (56.11) emphasizes the low-energy part of the integral so that $a_\mu^{\text{Had}}[\text{LO}]$ is dominated by the $\rho(770) \rightarrow \pi^+\pi^-$ resonance.

The analysis of Eq. (56.11) results in the representative value [4, 24–29]

$$a_\mu^{\text{Had}}[\text{LO}] = 6931(40) \times 10^{-11}, \quad (56.12)$$

whose error is dominated by systematic uncertainties in the $e^+e^- \rightarrow$ hadrons cross-section data, and also includes a small uncertainty due to perturbative QCD, which is used at intermediate and large energies in the dispersion integral to predict the contribution from the quark-antiquark continuum. The experimental precision is currently limited by a discrepancy between the most precise $\pi^+\pi^-$ data from the BABAR and KLOE experiments [26, 28].

Alternatively, one can use precise vector spectral functions from $\tau \rightarrow \nu_\tau +$ hadrons decays [30] that can be related to isovector $e^+e^- \rightarrow$ hadrons cross sections by isospin symmetry. Analyses replaced e^+e^- data in the two-pion and four-pion channels by the corresponding isospin-transformed τ data, and applied isospin-violating corrections [31]. Owing to the progress in the precision of the e^+e^- data, the τ data are now less precise and less reliable due to additional theoretical uncertainties, so that recent $a_\mu^{\text{Had}}[\text{LO}]$ evaluations ignored them.

Progress has been achieved on the evaluation of $a_\mu^{\text{Had}}[\text{LO}]$ using lattice QCD, which allows to directly compute the real part of the two-point correlation function without invoking the resonances occurring on the imaginary axis [32–34]. The required sub-percent precision represents a challenge requiring to master systematic and extrapolation uncertainties. A combination of recent lattice QCD evaluations [35, 36] gives [4]

$$a_\mu^{\text{Had}}[\text{LO}] = 7116(184) \times 10^{-11}, \quad (56.13)$$

with an uncertainty that is not yet competitive with the data-driven approach. Another recent lattice QCD calculation with much reduced uncertainty found [37]

$$a_\mu^{\text{Had}}[\text{LO}] = 7075(55) \times 10^{-11}, \quad (56.14)$$

whose error is dominated by systematic uncertainties. It exhibits a 2.1σ tension with the data-driven result, growing up to 3.7σ for the modified observable $a_{\mu,\text{win}}$ that has favourable properties for computation on the lattice⁵ [36, 37, 39]. Because of the complexity and challenges of such a calculation, it is critical that it is confronted with independent lattice results of comparable precision [36, 39, 40].

Higher order hadronic loop contributions are also obtained from dispersion relations using the same $e^+e^- \rightarrow$ hadrons data but with different integration kernels [41]. Recent evaluations found $a_\mu^{\text{Had,Disp}}[\text{NLO}] = (-98.3 \pm 0.7) \times 10^{-11}$ [4, 29] and $a_\mu^{\text{Had,Disp}}[\text{NNLO}] = (12.4 \pm 0.1) \times 10^{-11}$ [42]. In the case of hadronic light-by-light scattering contributions, which enter at NLO, recent studies [3, 4, 43, 44] based on short-distance QCD, dispersion relations and lattice QCD calculations lead to the improved prediction $a_\mu^{\text{Had,LBL}}[\text{NLO}] = 92(18) \times 10^{-11}$ [4].⁶ One

⁴The bare cross section is defined as the measured cross section corrected for initial-state radiation, electron-vertex loop contributions and vacuum-polarization effects in the photon propagator. However, QED effects in the hadron vertex and final state, as photon radiation, are included.

⁵A dispersive approach similar to that for $a_\mu^{\text{Had}}[\text{LO}]$ is used to determine the hadronic contribution to the running of the electromagnetic fine structure constant at the Z -boson mass $\Delta\alpha_{\text{had}}(m_Z)$, which is a critical ingredient of the global electroweak fit. One may therefore ask if the goodness of that fit would break down were $a_\mu^{\text{Had}}[\text{LO}]$ in Eq. (56.12) be brought in compatibility with the result (56.14). However, the difference in the relevant integration kernels (whereas 73% of the contribution to $a_\mu^{\text{Had}}[\text{LO}]$ stems from the $\pi^+\pi^-$ channel, it is only 13% in the case of $\Delta\alpha_{\text{had}}(m_Z)$) allows to absorb large effects in $a_\mu^{\text{Had}}[\text{LO}]$ without creating a significant tension in the electroweak fit. Detailed discussions are available in the literature [38].

⁶A very recent lattice QCD based calculation of $a_\mu^{\text{Had,LBL}}[\text{NLO}]$ [45], not included in [4], gives a consistent result with [4, 44] using a different approach.

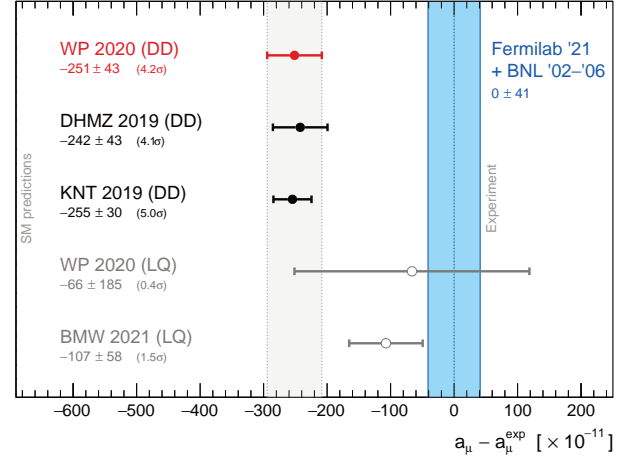


Figure 56.2: Compilation of recent results for a_μ (in units of 10^{-11}), subtracted by the central value of the experimental average (56.3). The light blue vertical band indicates the total experimental uncertainty. The SM predictions shown differ only in the value used for the $a_\mu^{\text{Had}}[\text{LO}]$ contribution. They are taken from: WP 2020 [4] (Eq. (56.16), also indicated by the light grey vertical band), DHMZ 2019 [28], KNT 2019 [29], all three based on the data-driven (DD) $a_\mu^{\text{Had}}[\text{LO}]$ evaluation, and the lattice QCD (LQ) based evaluations WP 2020 [4, 35, 36] and BMW 2021 [37]. Note that the quoted errors in the figure do not include the uncertainty on the subtracted experimental value. To obtain for each theory calculation a result equivalent to Eq. (56.17), the errors from theory and experiment must be added in quadrature.

thus finds for the sum of the three higher order hadronic terms

$$a_\mu^{\text{Had}}[\text{N(N)LO}] = 6(18) \times 10^{-11}, \quad (56.15)$$

where the error is dominated by the hadronic light-by-light scattering uncertainty.

Adding Eqs. (56.8), (56.10), (56.12) and (56.15) gives the representative SM prediction

$$a_\mu^{\text{SM}} = 116\,591\,810(1)(40)(18) \times 10^{-11}, \quad (56.16)$$

whose errors are due to the electroweak, lowest-order hadronic, and higher-order hadronic contributions, respectively. The difference between experiment and theory

$$\Delta a_\mu = a_\mu^{\text{exp}} - a_\mu^{\text{SM}} = 251(41)(43) \times 10^{-11}, \quad (56.17)$$

where the errors are from experiment and theory prediction (with all errors combined in quadrature, taking into account a small anticorrelation [4] between the data-driven lowest and higher order contributions), represents an interesting but not yet conclusive discrepancy of 4.2σ .⁷ The new FNAL measurement has increased the discrepancy with the SM prediction (56.16) from previously 3.7σ . Figure 56.2 represents the difference between experimental and predicted a_μ values based on the most recent data-driven and lattice QCD based evaluations of $a_\mu^{\text{Had}}[\text{LO}]$.

A leading candidate explanation for the deviation observed in Δa_μ has been supersymmetry particle loop contributions. Such a scenario is quite natural, since generically, supersymmetric models predict [1] an additional contribution to a_μ^{SM}

$$a_\mu^{\text{SUSY}} \simeq \pm 130 \times 10^{-11} \cdot \left(\frac{100 \text{ GeV}}{m_{\text{SUSY}}} \right)^2 \tan\beta, \quad (56.18)$$

where m_{SUSY} is a representative supersymmetric mass scale, $\tan\beta \simeq 3\text{--}40$ a potential enhancement factor, and ± 1 corresponds to the sign of the μ term in the supersymmetric Lagrangian. Supersymmetric particles in the mass range 100–500 GeV could be

⁷The probabilistic interpretation of the discrepancy requires caution due to the systematic nature of the a_μ^{SM} uncertainty.

the source of the deviation Δa_μ . If so, those particles should be directly observable at the Large Hadron Collider at CERN. So far, there is however no direct evidence in support of the supersymmetry interpretation.

New physics effects [1] other than supersymmetry could also explain a non-vanishing Δa_μ . A popular scenario involves the “dark photon”, a relatively light hypothetical vector boson from the dark matter sector that couples to our world of particle physics through mixing with the ordinary photon [46–48]. As a result, it couples to ordinary charged particles with strength $\varepsilon \cdot e$ and gives rise to an additional muon magnetic anomaly contribution

$$a_\mu^{\text{dark photon}} = \frac{\alpha}{2\pi} \varepsilon^2 F(m_V/m_\mu), \quad (56.19)$$

where $F(x) = \int_0^1 2z(1-z)^2 / [(1-z)^2 + x^2z] dz$. For values of $\varepsilon \sim 1-2 \times 10^{-3}$ and $m_V \sim 10-100$ MeV, the dark photon, which was originally motivated by cosmology, can provide a viable solution to the muon $g-2$ discrepancy. However, experimental constraints appear to rule out the simplest model in which the dark photon has equal couplings to electrons and muons and decays primarily to e^+e^- pairs [49] or invisible dark particles [50] that give rise to missing event energy. One can expand the dark photon scenario into a more complete theory in which several new particles contribute to the muon $g-2$. Direct searches for a dark photon, therefore, continue to be well motivated, but with primary guidance coming from astrophysics [51].

Recent popular solutions to the muon anomaly discrepancy have also focused on loop contributions induced by relatively light scalar or pseudo scalar particle appendages from physics beyond the SM [52, 53].

References

- [1] A. Czarnecki and W. J. Marciano, Phys. Rev. D **64**, 013014 (2001), [hep-ph/0102122]; M. Davier and W. Marciano, Ann. Rev. Nucl. Part. Sci. **54**, 115 (2004).
- [2] J. P. Miller, E. de Rafael and B. Roberts, Rept. Prog. Phys. **70**, 795 (2007), [hep-ph/0703049]; F. Jegerlehner and A. Nyfeler, Phys. Rept. **477**, 1 (2009), [arXiv:0902.3360]; J. P. Miller *et al.*, Ann. Rev. Nucl. Part. Sci. **62**, 237 (2012).
- [3] F. Jegerlehner, Springer Tracts Mod. Phys. **274**, 1 (2017).
- [4] T. Aoyama *et al.*, Phys. Rept. **887**, 1 (2020), [arXiv:2006.04822].
- [5] P. J. Mohr, D. B. Newell and B. N. Taylor, Rev. Mod. Phys. **88**, 3, 035009 (2016), [arXiv:1507.07956].
- [6] G. Bennett *et al.* (Muon $g-2$), Phys. Rev. Lett. **89**, 101804 (2002), [Erratum: Phys.Rev.Lett. 89, 129903 (2002)], [hep-ex/0208001]; G. Bennett *et al.* (Muon $g-2$), Phys. Rev. Lett. **92**, 161802 (2004), [hep-ex/0401008]; G. Bennett *et al.* (Muon $g-2$), Phys. Rev. D **73**, 072003 (2006), [hep-ex/0602035].
- [7] J. Bailey *et al.* (CERN-Mainz-Daresbury), Nucl. Phys. B **150**, 1 (1979).
- [8] J. Grange *et al.* (Muon $g-2$) (2015), [arXiv:1501.06858].
- [9] B. Abi *et al.* (Muon $g-2$), Phys. Rev. Lett. **126**, 14, 141801 (2021), [arXiv:2104.03281].
- [10] M. Abe *et al.*, PTEP **2019**, 5, 053C02 (2019), [arXiv:1901.03047].
- [11] J. S. Schwinger, Phys. Rev. **73**, 416 (1948).
- [12] T. Aoyama *et al.*, Phys. Rev. Lett. **109**, 111808 (2012), [arXiv:1205.5370]; T. Aoyama *et al.*, Phys. Rev. Lett. **109**, 111807 (2012), [arXiv:1205.5368]; T. Kinoshita and M. Nio, Phys. Rev. D **73**, 013003 (2006), [hep-ph/0507249]; T. Aoyama *et al.*, Phys. Rev. Lett. **99**, 110406 (2007), [arXiv:0706.3496]; T. Kinoshita and M. Nio, Phys. Rev. D **70**, 113001 (2004), [hep-ph/0402206]; T. Kinoshita, Nucl. Phys. B Proc. Suppl. **144**, 206 (2005); T. Kinoshita and M. Nio, Phys. Rev. D **73**, 053007 (2006), [hep-ph/0512330]; S. Laporta, Phys. Lett. B **772**, 232 (2017), [arXiv:1704.06996]; A. Kurz *et al.*, Phys. Rev. D **93**, 5, 053017 (2016), [arXiv:1602.02785]; A. Kataev, in “12th Lomonosov Conference on Elementary Particle Physics,” 345–349 (2006), [hep-ph/0602098]; M. Passera, J. Phys. G **31**, R75 (2005), [hep-ph/0411168].
- [13] T. Aoyama, T. Kinoshita and M. Nio, Atoms **7**, 1, 28 (2019).
- [14] R. H. Parker *et al.*, Science **360**, 191 (2018), [arXiv:1812.04130].
- [15] L. Morel *et al.*, Nature **588**, 7836, 61 (2020).
- [16] T. Aoyama *et al.*, Phys. Rev. D **91**, 3, 033006 (2015), [Erratum: Phys.Rev.D 96, 019901 (2017)], [arXiv:1412.8284].
- [17] D. Hanneke, S. Fogwell and G. Gabrielse, Phys. Rev. Lett. **100**, 120801 (2008), [arXiv:0801.1134]; D. Hanneke, S. F. Hoogerheide and G. Gabrielse, Phys. Rev. A **83**, 052122 (2011), [arXiv:1009.4831].
- [18] R. Jackiw and S. Weinberg, Phys. Rev. D **5**, 2396 (1972); G. Altarelli, N. Cabibbo and L. Maiani, Phys. Lett. B **40**, 415 (1972); I. Bars and M. Yoshimura, Phys. Rev. D **6**, 374 (1972); K. Fujikawa, B. Lee and A. Sanda, Phys. Rev. D **6**, 2923 (1972).
- [19] C. Gnendiger, D. Stöckinger and H. Stöckinger-Kim, Phys. Rev. D **88**, 053005 (2013), [arXiv:1306.5546]; A. Czarnecki, W. J. Marciano and A. Vainshtein, Phys. Rev. D **67**, 073006 (2003), [Erratum: Phys.Rev.D 73, 119901 (2006)], [hep-ph/0212229]; S. Heinemeyer, D. Stockinger and G. Weiglein, Nucl. Phys. B **699**, 103 (2004), [hep-ph/0405255]; T. Gribov and A. Czarnecki, Phys. Rev. D **72**, 053016 (2005), [hep-ph/0509205]; A. Czarnecki, B. Krause and W. J. Marciano, Phys. Rev. Lett. **76**, 3267 (1996), [hep-ph/9512369]; A. Czarnecki, B. Krause and W. J. Marciano, Phys. Rev. D **52**, 2619 (1995), [hep-ph/9506256]; S. Peris, M. Perrotet and E. de Rafael, Phys. Lett. B **355**, 523 (1995), [hep-ph/9505405]; T. Kukkto *et al.*, Nucl. Phys. B **371**, 567 (1992).
- [20] G. Degross and G. Giudice, Phys. Rev. D **58**, 053007 (1998), [hep-ph/9803384].
- [21] T. Ishikawa, N. Nakazawa and Y. Yasui, Phys. Rev. D **99**, 7, 073004 (2019), [arXiv:1810.13445].
- [22] C. Bouchiat and L. Michel, J. Phys. Radium **22**, 2, 121 (1961); M. Gourdin and E. De Rafael, Nucl. Phys. B **10**, 667 (1969).
- [23] S. J. Brodsky and E. De Rafael, Phys. Rev. **168**, 1620 (1968).
- [24] M. Davier *et al.*, Eur. Phys. J. C **77**, 12, 827 (2017), [arXiv:1706.09436].
- [25] A. Keshavarzi, D. Nomura and T. Teubner, Phys. Rev. D **97**, 11, 114025 (2018), [arXiv:1802.02995].
- [26] G. Colangelo, M. Hoferichter and P. Stoffer, JHEP **02**, 006 (2019), [arXiv:1810.00007].
- [27] M. Hoferichter, B.-L. Hoid and B. Kubis, JHEP **08**, 137 (2019), [arXiv:1907.01556].
- [28] M. Davier *et al.*, Eur. Phys. J. C **80**, 3, 241 (2020), [Erratum: Eur.Phys.J.C 80, 410 (2020)], [arXiv:1908.00921].
- [29] A. Keshavarzi, D. Nomura and T. Teubner, Phys. Rev. D **101**, 1, 014029 (2020), [arXiv:1911.00367].
- [30] R. Alemany, M. Davier and A. Hocker, Eur. Phys. J. C **2**, 123 (1998), [hep-ph/9703220].
- [31] M. Davier *et al.*, Eur. Phys. J. C **71**, 1515 (2011), [Erratum: Eur.Phys.J.C 72, 1874 (2012)], [arXiv:1010.4180].
- [32] T. Blum, Phys. Rev. Lett. **91**, 052001 (2003), [hep-lat/0212018].
- [33] D. Bernecker and H. B. Meyer, Eur. Phys. J. A **47**, 148 (2011), [arXiv:1107.4388].
- [34] W. A. Bardeen, R. Gastmans and B. E. Lautrup, Nucl. Phys. B **46**, 319 (1972).
- [35] B. Chakraborty *et al.* (Fermilab Lattice, LATTICE-HQCQD, MILC), Phys. Rev. Lett. **120**, 15, 152001 (2018), [arXiv:1710.11212]; S. Borsanyi *et al.* (Budapest-Marseille-Wuppertal), Phys. Rev. Lett. **121**, 2, 022002 (2018),

- [arXiv:1711.04980]; T. Blum *et al.* (RBC, UKQCD), Phys. Rev. Lett. **121**, 2, 022003 (2018), [arXiv:1801.07224]; D. Giusti *et al.* (ETM), Phys. Rev. **D99**, 11, 114502 (2019), [arXiv:1901.10462]; E. Shintani and Y. Kuramashi, Phys. Rev. **D100**, 3, 034517 (2019), [arXiv:1902.00885]; C. T. H. Davies *et al.* (Fermilab Lattice, LATTICE-HPQCD, MILC), Phys. Rev. **D101**, 3, 034512 (2020), [arXiv:1902.04223]; A. Gérardin *et al.*, Phys. Rev. **D100**, 1, 014510 (2019), [arXiv:1904.03120].
- [36] C. Aubin *et al.*, Phys. Rev. **D101**, 1, 014503 (2020), [arXiv:1905.09307]; D. Giusti and S. Simula, PoS **LATTICE2019**, 104 (2019), [arXiv:1910.03874].
- [37] S. Borsanyi *et al.*, Nature **593**, 7857, 51 (2021), [arXiv:2002.12347].
- [38] A. Crivellin *et al.*, Phys. Rev. Lett. **125**, 9, 091801 (2020), [arXiv:2003.04886]; A. Keshavarzi *et al.*, Phys. Rev. D **102**, 3, 033002 (2020), [arXiv:2006.12666]; E. de Rafael, Phys. Rev. D **102**, 5, 056025 (2020), [arXiv:2006.13880]; B. Malaescu and M. Schott, Eur. Phys. J. C **81**, 1, 46 (2021), [arXiv:2008.08107]; G. Colangelo, M. Hoferichter and P. Stoffer, Phys. Lett. B **814**, 136073 (2021), [arXiv:2010.07943].
- [39] T. Blum *et al.* (RBC, UKQCD), Phys. Rev. Lett. **121**, 2, 022003 (2018), [arXiv:1801.07224].
- [40] C. Lehner and A. S. Meyer, Phys. Rev. D **101**, 074515 (2020), [arXiv:2003.04177].
- [41] B. Krause, Phys. Lett. B **390**, 392 (1997), [hep-ph/9607259].
- [42] A. Kurz *et al.*, Phys. Lett. B **734**, 144 (2014), [arXiv:1403.6400].
- [43] K. Melnikov and A. Vainshtein, Phys. Rev. **D70**, 113006 (2004), [hep-ph/0312226]; P. Masjuan and P. Sánchez-Puertas, Phys. Rev. **D95**, 5, 054026 (2017), [arXiv:1701.05829]; G. Colangelo *et al.*, JHEP **04**, 161 (2017), [arXiv:1702.07347]; M. Hoferichter *et al.*, JHEP **10**, 141 (2018), [arXiv:1808.04823]; A. Gérardin, H. B. Meyer and A. Nyffeler, Phys. Rev. **D100**, 3, 034520 (2019), [arXiv:1903.09471]; J. Bijnens, N. Hermansson-Truedsson and A. Rodríguez-Sánchez, Phys. Lett. **B798**, 134994 (2019), [arXiv:1908.03331]; G. Colangelo *et al.*, JHEP **03**, 101 (2020), [arXiv:1910.13432]; V. Pauk and M. Vanderhaeghen, Eur. Phys. J. C **74**, 8, 3008 (2014), [arXiv:1401.0832]; I. Danilkin and M. Vanderhaeghen, Phys. Rev. **D95**, 1, 014019 (2017), [arXiv:1611.04646]; M. Knecht *et al.*, Phys. Lett. **B787**, 111 (2018), [arXiv:1808.03848]; G. Eichmann, C. S. Fischer and R. Williams, Phys. Rev. **D101**, 5, 054015 (2020), [arXiv:1910.06795]; P. Roig and P. Sánchez-Puertas, Phys. Rev. **D101**, 7, 074019 (2020), [arXiv:1910.02881]; G. Colangelo *et al.*, Phys. Lett. **B735**, 90 (2014), [arXiv:1403.7512].
- [44] T. Blum *et al.*, Phys. Rev. Lett. **124**, 13, 132002 (2020), [arXiv:1911.08123].
- [45] E.-H. Chao *et al.*, Eur. Phys. J. C **81**, 7, 651 (2021), [arXiv:2104.02632].
- [46] P. Fayet, Phys. Rev. D **75**, 115017 (2007), [hep-ph/0702176].
- [47] M. Pospelov, Phys. Rev. D **80**, 095002 (2009), [arXiv:0811.1030].
- [48] D. Tucker-Smith and I. Yavin, Phys. Rev. D **83**, 101702 (2011), [arXiv:1011.4922].
- [49] J. Batley *et al.* (NA48/2), Phys. Lett. B **746**, 178 (2015), [arXiv:1504.00607].
- [50] Y. M. Andreev *et al.* (NA64), Phys. Rev. Lett. **126**, 21, 211802 (2021), [arXiv:2102.01885]; J. P. Lees *et al.* (BaBar), Phys. Rev. Lett. **119**, 13, 131804 (2017), [arXiv:1702.03327].
- [51] J. Alexander *et al.* (2016), [arXiv:1608.08632].
- [52] K.-m. Cheung, C.-H. Chou and O. C. W. Kong, Phys. Rev. D **64**, 111301 (2001), [hep-ph/0103183].
- [53] D. Chang *et al.*, Phys. Rev. D **63**, 091301 (2001), [hep-ph/0009292].

57. Muon Decay Parameters

Revised August 2021 by W. Fetscher (ETH Zurich) and H.-J. Gerber (ETH Zurich).

57.1 Introduction:

All measurements in direct muon decay, $\mu^- \rightarrow e^- + 2$ neutrals, and its inverse, $\nu_\mu + e^- \rightarrow \mu^- + \text{neutral}$, are successfully described by the “ V - A interaction,” which is a particular case of a local, derivative-free, lepton-number-conserving, four-fermion interaction [1]. As shown below, within this framework, the Standard Model assumptions, such as the V - A form and the nature of the neutrals (ν_μ and $\bar{\nu}_e$), and hence the doublet assignments $(\nu_e e^-)_L$ and $(\nu_\mu \mu^-)_L$, have been determined from experiments [2, 3]. All considerations on muon decay are valid for the leptonic tau decays $\tau^- \rightarrow \ell^- + \nu_\tau + \bar{\nu}_\ell$ with the replacements $m_\mu \rightarrow m_\tau$, $m_e \rightarrow m_{e\ell}$, $\ell^- = e^-, \mu^-$.

57.2 Parameters:

The differential decay probability to obtain an e^\pm with (reduced) energy between x and $x + dx$, emitted in the direction \hat{x}_3 at an angle between ϑ and $\vartheta + d\vartheta$ with respect to the muon polarization vector \mathbf{P}_μ , and with its spin parallel to the arbitrary direction $\hat{\zeta}$, neglecting radiative corrections, is given by

$$\frac{d^2\Gamma}{dx d\cos\vartheta} = \frac{m_\mu}{4\pi^3} W_{e\mu}^4 G_F^2 \sqrt{x^2 - x_0^2} \times (F_{\text{IS}}(x) \pm P_\mu \cos\vartheta F_{\text{AS}}(x)) \times [1 + \hat{\zeta} \cdot \mathbf{P}_e(x, \vartheta)]. \quad (57.1)$$

Here, $W_{e\mu} = \max(E_e) = (m_\mu^2 + m_e^2)/2m_\mu$ is the maximum e^\pm energy, $x = E_e/W_{e\mu}$ is the reduced energy, $x_0 = m_e/W_{e\mu} = 9.67 \times 10^{-3}$, and $P_\mu = |\mathbf{P}_\mu|$ is the degree of muon polarization. $\hat{\zeta}$ is the direction in which a perfect polarization-sensitive electron detector is most sensitive. The isotropic part of the spectrum, $F_{\text{IS}}(x)$, the anisotropic part $F_{\text{AS}}(x)$, and the electron polarization, $\mathbf{P}_e(x, \vartheta)$, may be parametrized by the Michel parameter ρ [1], by η [4], by ξ and δ [5, 6], etc. These are bilinear combinations of the coupling constants $g_{\varepsilon\mu}^\gamma$, which occur in the matrix element (given below).

If the masses of the neutrinos as well as x_0^2 are neglected, the energy and angular distribution of the electron in the rest frame of a muon (μ^\pm) measured by a polarization insensitive detector, is given by

$$\frac{d^2\Gamma}{dx d\cos\vartheta} \sim x^2 \cdot \left\{ 3(1-x) + \frac{2\rho}{3}(4x-3) + 3\eta x_0(1-x)/x \pm P_\mu \cdot \xi \cdot \cos\vartheta \left[1 - x + \frac{2\delta}{3}(4x-3) \right] \right\}. \quad (57.2)$$

Here, ϑ is the angle between the electron momentum and the muon spin, and $x \equiv 2E_e/m_\mu$. For the Standard Model coupling, we obtain $\rho = \xi\delta = 3/4$, $\xi = 1$, $\eta = 0$ and the differential decay rate is

$$\frac{d^2\Gamma}{dx d\cos\vartheta} = \frac{G_F^2 m_\mu^5}{192\pi^3} [3 - 2x \pm P_\mu \cos\vartheta(2x-1)] \cdot x^2. \quad (57.3)$$

The coefficient in front of the square bracket is the total decay rate.

If only the neutrino masses are neglected, and if the e^\pm polarization is detected, then the functions in Eq. (57.1) become

$$F_{\text{IS}}(x) = x(1-x) + \frac{2}{9}\rho(4x^2 - 3x - x_0^2) + \eta \cdot x_0(1-x) \quad (57.4a)$$

$$F_{\text{AS}}(x) = \frac{1}{3}\xi \sqrt{x^2 - x_0^2} \times \left[(1-x) + \frac{2}{3}\delta \left\{ (4x-3) + \left(\sqrt{1-x_0^2} - 1 \right) \right\} \right] \quad (57.4b)$$

$$\mathbf{P}_e(x, \vartheta) = P_{T_1} \cdot \hat{x}_1 + P_{T_2} \cdot \hat{x}_2 + P_L \cdot \hat{x}_3 \quad (57.4c)$$

Here \hat{x}_1 , \hat{x}_2 , and \hat{x}_3 are orthogonal unit vectors defined as follows:

$$\begin{aligned} \hat{x}_3 & \text{ is along the } e \text{ momentum } \mathbf{p}_e \\ \frac{\hat{x}_3 \times \mathbf{P}_\mu}{|\hat{x}_3 \times \mathbf{P}_\mu|} = \hat{x}_2 & \text{ is transverse to } \mathbf{p}_e \text{ and perpendicular to "the decay plane"} \\ \hat{x}_2 \times \hat{x}_3 = \hat{x}_1 & \text{ is transverse to } \mathbf{p}_e \text{ and in the decay plane} \end{aligned}$$

The components of \mathbf{P}_e then are given by

$$P_{T_1}(x, \vartheta) = P_\mu \sin\vartheta \cdot F_{T_1}(x) / \{F_{\text{IS}}(x) \pm P_\mu \cos\vartheta \cdot F_{\text{AS}}(x)\} \quad (57.5a)$$

$$P_{T_2}(x, \vartheta) = P_\mu \sin\vartheta \cdot F_{T_2}(x) / \{F_{\text{IS}}(x) \pm P_\mu \cos\vartheta \cdot F_{\text{AS}}(x)\} \quad (57.5b)$$

$$P_L(x, \vartheta) = \frac{\pm F_{\text{IP}}(x) + P_\mu \cos\vartheta \cdot F_{\text{AP}}(x)}{F_{\text{IS}}(x) \pm P_\mu \cos\vartheta \cdot F_{\text{AS}}(x)}, \quad (57.5c)$$

where

$$F_{T_1}(x) = \frac{1}{12} \left\{ -2 \left[\xi'' + 12 \left(\rho - \frac{3}{4} \right) \right] (1-x)x_0 - 3\eta(x^2 - x_0^2) + \eta''(-3x^2 + 4x - x_0^2) \right\} \quad (57.6a)$$

$$F_{T_2}(x) = \frac{1}{3} \sqrt{x^2 - x_0^2} \cdot \left\{ 3 \frac{\alpha'}{A} (1-x) + 2 \frac{\beta'}{A} \sqrt{1-x_0^2} \right\} \quad (57.6b)$$

$$F_{\text{IP}}(x) = \frac{1}{54} \sqrt{x^2 - x_0^2} \cdot \left\{ 9\xi' \left(-2x + 2 + \sqrt{1-x_0^2} \right) + 4\xi \left(\delta - \frac{3}{4} \right) \left(4x - 4 + \sqrt{1-x_0^2} \right) \right\} \quad (57.6c)$$

$$F_{\text{AP}}(x) = \frac{1}{6} \left\{ \xi''(2x^2 - x - x_0^2) + 4 \left(\rho - \frac{3}{4} \right) (4x^2 - 3x - x_0^2) + 2\eta''(1-x)x_0 \right\}. \quad (57.6d)$$

For the experimental values of the parameters ρ , ξ , ξ' , ξ'' , δ , η , η'' , α/A , β/A , α'/A , β'/A , which are not all independent, see the Data Listings below. Experiments in the past have also been analyzed using the parameters a , b , c , a' , b' , c' , α/A , β/A , α'/A , β'/A (and $\eta = (\alpha - 2\beta)/2A$), as defined by Kinoshita and Sirlin [5, 6]. They serve as a model-independent summary of all possible measurements on the decay electron (see Listings below). The relations between the two sets of parameters are

$$\rho - \frac{3}{4} = \frac{3}{4}(-a + 2c)/A \quad (57.7a)$$

$$\eta = (\alpha - 2\beta)/A \quad (57.7b)$$

$$\eta'' = (3\alpha + 2\beta)/A \quad (57.7c)$$

$$\delta - \frac{3}{4} = \frac{9}{4} \cdot \frac{(a' - 2c')/A}{1 - [a + 3a' + 4(b + b') + 6c - 14c']/A} \quad (57.7d)$$

$$1 - \xi \frac{\delta}{\rho} = 4 \frac{[(b + b') + 2(c - c')]/A}{1 - (a - 2c)/A} \quad (57.7e)$$

$$1 - \xi = \left[(a + a') + 4(b + b') + 6(c + c') \right] / A \quad (57.7f)$$

$$1 - \xi'' = (-2a + 20c)/A \quad (57.7g)$$

$$\text{with } A = a + 4b + 6c \quad (57.7h)$$

The differential decay probability to obtain a *left-handed* ν_e with (reduced) energy between y and $y + dy$, neglecting radiative corrections as well as the masses of the electron and of the neutrinos, is given by [7]

$$\frac{d\Gamma}{dy} = \frac{m_\mu^5 G_F^2}{16\pi^3} \cdot Q_L^{\nu_e} \cdot y^2 \left\{ (1-y) - \omega_L \cdot \left(y - \frac{3}{4} \right) \right\}. \quad (57.8)$$

Here, $y = 2 E_{\nu_e}/m_\mu$. $Q_L^{\nu_e}$ and ω_L are parameters. ω_L is the neutrino analog of the spectral shape parameter ρ of Michel. Since in the Standard Model, $Q_L^{\nu_e} = 1$, $\omega_L = 0$, the measurement of $d\Gamma/dy$ has allowed a null-test of the Standard Model (see Listings below).

Table 57.1: Coupling constants $g_{\varepsilon\mu}^\gamma$ and some combinations of them. Ninety-percent confidence level experimental limits. The limits on $|g_{LL}^S|$ and $|g_{LL}^V|$ are from [8–10], and the others from a general analysis of muon decay measurements. Top three rows: [11], fourth row: [12], next three rows: [13], last row: [14]. The experimental uncertainty on the muon polarization in pion decay is included. Note that, by definition, $|g_{\varepsilon\mu}^S| \leq 2$, $|g_{\varepsilon\mu}^V| \leq 1$ and $|g_{\varepsilon\mu}^T| \leq 1/\sqrt{3}$.

$ g_{RR}^S < 0.035$	$ g_{RR}^V < 0.017$	$ g_{RR}^T \equiv 0$
$ g_{LR}^S < 0.050$	$ g_{LR}^V < 0.023$	$ g_{LR}^T < 0.015$
$ g_{RL}^S < 0.420$	$ g_{RL}^V < 0.105$	$ g_{RL}^T < 0.105$
$ g_{LL}^S < 0.550$	$ g_{LL}^V > 0.960$	$ g_{LL}^T \equiv 0$
$ g_{LR}^S + 6g_{LR}^T < 0.143$	$ g_{RL}^S + 6g_{RL}^T < 0.418$	
$ g_{LR}^S + 2g_{LR}^T < 0.108$	$ g_{RL}^S + 2g_{RL}^T < 0.417$	
$ g_{LR}^S - 2g_{LR}^T < 0.070$	$ g_{RL}^S - 2g_{RL}^T < 0.418$	
$Q_{RR} + Q_{LR} < 8.2 \times 10^{-4}$		

57.3 Matrix element:

All results in direct muon decay (energy spectra of the electron and of the neutrinos, polarizations, and angular distributions), and in inverse muon decay (the reaction cross section) at energies well below $m_W c^2$, may be parametrized in terms of amplitudes $g_{\varepsilon\mu}^\gamma$ and the Fermi coupling constant G_F , using the matrix element

$$\frac{4G_F}{\sqrt{2}} \sum_{\substack{\gamma=S,V,T \\ \varepsilon,\mu=R,L}} g_{\varepsilon\mu}^\gamma \langle \bar{e}_\varepsilon | \Gamma^\gamma | (\nu_e)_n \rangle \langle \bar{\nu}_\mu | \Gamma_\gamma | \mu_\mu \rangle \quad (57.9)$$

We use the notation of Fetscher *et al.* [2], who in turn use the sign conventions and definitions of Scheck [15]. Here, $\gamma = S, V, T$ indicates a scalar, vector, or tensor interaction; and $\varepsilon, \mu = R, L$ indicate a right- or left-handed chirality of the electron or muon. The chiralities n and m of the ν_e and $\bar{\nu}_\mu$ are then determined by the values of γ, ε , and μ . The particles are represented by fields of definite chirality [16].

As shown by Langacker and London [17], explicit lepton-number nonconservation still leads to a matrix element equivalent to Eq. (57.9). They conclude that it is not possible, even in principle, to test lepton-number conservation in (leptonic) muon decay if the final neutrinos are massless and are not observed.

The ten complex amplitudes $g_{\varepsilon\mu}^\gamma$ (g_{RR}^T and g_{LL}^T are identically zero) and G_F constitute 19 independent (real) parameters to be determined by experiment. The Standard Model interaction corresponds to one single amplitude g_{LL}^V being unity and all the others being zero.

The (direct) muon decay experiments are compatible with an arbitrary mix of the scalar and vector amplitudes g_{LL}^S and g_{LL}^V – in the extreme even with purely scalar $g_{LL}^S = 2$, $g_{LL}^V = 0$. The decision in favour of the Standard Model comes from the quantitative observation of inverse muon decay, which would be forbidden for pure g_{LL}^S [2].

57.4 Experimental determination of $V-A$:

In order to determine the amplitudes $g_{\varepsilon\mu}^\gamma$ uniquely from experiment, the following set of equations, where the left-hand sides

represent experimental results, has to be solved.

$$a = 16 \left(|g_{RL}^V|^2 + |g_{LR}^V|^2 \right) + \left| g_{RL}^S + 6g_{RL}^T \right|^2 + \left| g_{LR}^S + 6g_{LR}^T \right|^2 \quad (57.10a)$$

$$a' = 16 \left(|g_{RL}^V|^2 - |g_{LR}^V|^2 \right) + \left| g_{RL}^S + 6g_{RL}^T \right|^2 - \left| g_{LR}^S + 6g_{LR}^T \right|^2 \quad (57.10b)$$

$$\alpha = 8 \operatorname{Re} \left\{ g_{RL}^V \left(g_{RL}^{S*} + 6g_{LR}^{T*} \right) + g_{LR}^V \left(g_{RL}^{S*} + 6g_{LR}^{T*} \right) \right\} \quad (57.10c)$$

$$\alpha' = 8 \operatorname{Im} \left\{ -g_{RL}^V \left(g_{LR}^{S*} + 6g_{LR}^{T*} \right) + g_{LR}^V \left(g_{RL}^{S*} + 6g_{RL}^{T*} \right) \right\} \quad (57.10d)$$

$$b = 4 \left(|g_{RR}^V|^2 + |g_{LL}^V|^2 \right) + |g_{RR}^S|^2 + |g_{LL}^S|^2 \quad (57.10e)$$

$$b' = 4 \left(|g_{RR}^V|^2 - |g_{LL}^V|^2 \right) + |g_{RR}^S|^2 - |g_{LL}^S|^2 \quad (57.10f)$$

$$c = \frac{1}{2} \left\{ |g_{RL}^S - 2g_{RL}^T|^2 + |g_{LR}^S - 2g_{LR}^T|^2 \right\} \quad (57.10g)$$

$$c' = \frac{1}{2} \left\{ |g_{RL}^S - 2g_{RL}^T|^2 - |g_{LR}^S - 2g_{LR}^T|^2 \right\} \quad (57.10h)$$

and

$$Q_L^{\nu_e} = 1 - \left\{ \frac{1}{4} |g_{LR}^S|^2 + \frac{1}{4} |g_{LL}^S|^2 + |g_{RR}^V|^2 + |g_{RL}^V|^2 + 3 |g_{LR}^T|^2 \right\}$$

$$\omega_L = \frac{3}{4} \frac{|g_{RR}^S|^2 + 4 |g_{LR}^V|^2 + |g_{RL}^S|^2 + 2 |g_{LR}^T|^2}{|g_{RL}^S|^2 + |g_{RR}^S|^2 + 4 |g_{LL}^V|^2 + 4 |g_{LR}^V|^2 + 12 |g_{RL}^T|^2}. \quad (57.10i)$$

It has been noted earlier by C. Jarlskog [18], that certain experiments observing the decay electron are especially informative if they yield the $V-A$ values. The complete solution is now found as follows. Fetscher *et al.* [2] introduced four probabilities $Q_{\varepsilon\mu}(\varepsilon, \mu = R, L)$ for the decay of a μ -handed muon into an ε -handed electron, and showed that there exist upper bounds on Q_{RR} , Q_{LR} , and Q_{RL} , and a lower bound on Q_{LL} . These probabilities are given in terms of the $g_{\varepsilon\mu}^\gamma$'s by

$$Q_{\varepsilon\mu} = \frac{1}{4} |g_{\varepsilon\mu}^S|^2 + |g_{\varepsilon\mu}^V|^2 + 3(1 - \delta_{\varepsilon\mu}) |g_{\varepsilon\mu}^T|^2 \quad (57.11)$$

where $\delta_{\varepsilon\mu} = 1$ for $\varepsilon = \mu$, and $\delta_{\varepsilon\mu} = 0$ for $\varepsilon \neq \mu$. They are related to the parameters a, b, c, a', b' , and c' by

$$Q_{RR} = 2(b + b')/A \quad (57.12a)$$

$$Q_{LR} = [(a - a') + 6(c - c')]/2A \quad (57.12b)$$

$$Q_{RL} = [(a + a') + 6(c + c')]/2A \quad (57.12c)$$

$$Q_{LL} = 2(b - b')/A \quad (57.12d)$$

with $A = 16$. In the Standard Model, $Q_{LL} = 1$ and the others are zero.

Since the upper bounds on Q_{RR} , Q_{LR} , and Q_{RL} are found to be small, and since the helicity of the ν_μ in pion decay is known from experiment [19, 20] to very high precision to be -1 [21], the cross section S of *inverse* muon decay, normalized to the $V-A$ value, yields [2]

$$|g_{LL}^S|^2 \leq 4(1 - S) \quad (57.13a)$$

and

$$|g_{LL}^V|^2 = S. \quad (57.13b)$$

Thus the Standard Model assumption of a pure $V-A$ leptonic charged weak interaction of e and μ is derived (within errors) from experiments at energies far below the mass of the W^\pm : Eq. (57.13 b) gives a lower limit for $V-A$, and Eqs. (57.12 a, b, c)

and (57.13 a) give upper limits for the other four-fermion interactions. The existence of such upper limits may also be seen from $Q_{RR} + Q_{RL} = (1 - \xi')/2$ (e^+ longitudinal polarization) and $Q_{RR} + Q_{LR} = \frac{1}{2}(1 + \xi/3 - 16\xi\delta/9)$ (decay asymmetry). Table 57.1 gives the current experimental limits on the magnitudes of the $g_{\varepsilon\mu}^\gamma$'s. More stringent limits on the six coupling constants g_{LR}^S , g_{LR}^V , g_{LR}^T , g_{RL}^S , g_{RL}^V , and g_{RL}^T have been derived from upper limits on the neutrino mass [22]. Limits on the “charge retention” coordinates, as used in the older literature (*e.g.*, Ref. [23]), are given by Burkard *et al.* [24].

References

- [1] L. Michel, Proc. Phys. Soc. **A63**, 514 (1950).
- [2] W. Fetscher, H. J. Gerber and K. F. Johnson, Phys. Lett. **B173**, 102 (1986).
- [3] P. Langacker, Comments Nucl. Part. Phys. **19**, 1, 1 (1989).
- [4] C. Bouchiat and L. Michel, Phys. Rev. **106**, 170 (1957).
- [5] T. Kinoshita and A. Sirlin, Phys. Rev. **107**, 593 (1957).
- [6] T. Kinoshita and A. Sirlin, Phys. Rev. **108**, 844 (1957).
- [7] W. Fetscher, Phys. Rev. **D49**, 5945 (1994).
- [8] S. R. Mishra *et al.*, Phys. Lett. **B252**, 170 (1990).
- [9] S. R. Mishra, private communication.
- [10] P. Vilain *et al.* (CHARM-II), Phys. Lett. **B364**, 121 (1995).
- [11] A. Hillairet *et al.* (TWIST), Phys. Rev. **D85**, 092013 (2012), [arXiv:1112.3606].
- [12] R. P. MacDonald *et al.* (TWIST), Phys. Rev. **D78**, 032010 (2008), [arXiv:0807.1125].
- [13] C. A. Gagliardi, R. E. Tribble and N. J. Williams, Phys. Rev. **D72**, 073002 (2005), [hep-ph/0509069].
- [14] R. Bayes *et al.* (TWIST), Phys. Rev. Lett. **106**, 041804 (2011).
- [15] F. Scheck, in *Electroweak and Strong Interactions* (Springer Verlag, 1996).
- [16] K. Mursula and F. Scheck, Nucl. Phys. **B253**, 189 (1985).
- [17] P. Langacker and D. London, Phys. Rev. **D39**, 266 (1989).
- [18] C. Jarlskog, Nucl. Phys. **75**, 659 (1966).
- [19] A. Jodidio *et al.*, Phys. Rev. **D34**, 1967 (1986), [Erratum: Phys. Rev. **D37**, 237 (1988)].
- [20] L. P. Roesch *et al.*, Helv. Phys. Acta **55**, 74 (1982).
- [21] W. Fetscher, Phys. Lett. **140B**, 117 (1984).
- [22] G. Prezeau and A. Kurylov, Phys. Rev. Lett. **95**, 101802 (2005), [hep-ph/0409193].
- [23] S. E. Derenzo, Phys. Rev. **181**, 1854 (1969).
- [24] H. Burkard *et al.*, Phys. Lett. **160B**, 343 (1985).

58. τ Branching Fractions

Revised February 2022 by Sw. Banerjee (Louisville U.) and A. Lusiani (SNS, Pisa; INFN, Pisa).

58.1 τ Branching Fractions

The τ Listings contains 244 entries that correspond to either a τ partial decay fraction into a specific decay mode (branching fraction) or a ratio of two τ partial decay fractions (branching ratio). Experimental information provides values for 147 of these quantities, upper limits for 61 branching fractions to Lepton Family number, Lepton number, or Baryon number violating modes, and 36 additional upper limits for other modes. A total of 170 measurements of τ branching fraction and branching ratio measurements is used for a global fit that determines 129 quantities.

58.2 The constrained fit to τ branching fractions

The τ branching fractions fit uses the reported values, uncertainties and statistical correlations of the τ branching fractions and branching ratios measurements. Asymmetric uncertainties are symmetrized as $\sigma_{\text{symm}}^2 = (\sigma_+^2 + \sigma_-^2)/2$. Additionally, the most precise experimental inputs are treated according to how they depend on external parameters on the basis of their documentation [1]. The τ measurements may depend on parameters such as the τ pair production cross-section in e^+e^- annihilations at the $\Upsilon(4S)$ peak. In some cases, measurements reported in different papers by the same collaboration may depend on common parameters like the estimate of the integrated luminosity or of particle identification efficiencies. For all the significant detected dependencies, the τ measurements and their uncertainties are updated to account for the updated values of the external parameters. The dependencies on common systematic effects are also determined in size and sign, and all the common systematic dependencies of different measurements are used together with the published statistical and systematic uncertainties and correlations in order to compute a single all-inclusive variance and covariance matrix of the experimental inputs of the fit.

The fit procedure parameters correspond to τ quantities that are fit to the experimental measurements while respecting relations described by a series of constraint equations. All the experimental inputs and all the constraint equations are reported in the τ Listings section that follows this review. With respect to the 2016, 2017 and 2018 editions, the fit uses one more experimental measurement, published by the BaBar collaboration in 2018, on $\mathcal{B}(\tau \rightarrow K^- K^0 \nu_\tau)$ [2]. If only a few measurements are correlated, the correlation coefficients are listed in the footnote for each measurement (see for example $\Gamma(\text{particle}^- \geq 0 \text{ neutrals} \geq 0 K^0 \nu_\tau)$ (“1-prong”)/ Γ_{total}). If a large number of measurements are correlated, then the full correlation matrix is listed in the footnote to the measurement that first appears in the τ Listings. Footnotes to the other measurements refer to the first one. For example, the large correlation matrices for the branching fraction or ratio measurements contained in Refs. [3] [4] are listed in Footnotes to the $\Gamma(e^- \bar{\nu}_e \nu_\tau)/\Gamma_{\text{total}}$ and $\Gamma(h^- \nu_\tau)/\Gamma_{\text{total}}$ measurements respectively. The constraints between the τ branching fractions and ratios include coefficients that correspond to physical quantities, like for instance the branching fractions of the η and ω mesons. All quantities are taken from the 2018 edition of the Review of Particle Physics. Their uncertainties are neglected in the fit.

We obtain the branching fraction of $\tau \rightarrow a_1^- (\rightarrow \pi^- \gamma) \nu_\tau$ using the ALEPH estimate for $\mathcal{B}(a_1^- \rightarrow \pi^- \gamma)$ [3], which uses the measurement of $\Gamma(a_1^- \rightarrow \pi^- \gamma)$ [5]. In the fit, we assume that $\mathcal{B}(\tau^- \rightarrow a_1^- \nu_\tau)$ is equal to $\mathcal{B}(\tau^- \rightarrow \pi^- \pi^- \pi^+ \nu_\tau)$ (ex. K^0, ω) + $\mathcal{B}(\tau^- \rightarrow \pi^- 2\pi^0 \nu_\tau)$ (ex. K^0), neglecting the observed but negligible branching fractions to other modes, including $\mathcal{B}(a_1^- \rightarrow \pi^- \gamma)$.

In some cases, constraints describe approximate relations that nevertheless hold within the present experimental precision. For instance, the constraint $\mathcal{B}(\tau \rightarrow K^- K^- K^+ \nu_\tau) = \mathcal{B}(\tau \rightarrow K^- \phi \nu_\tau) \times \mathcal{B}(\phi \rightarrow K^+ K^-)$ is justified within the current experimental evidence.

In the fit, scale factors are applied to the published uncertainties of measurements only if significant inconsistency between different measurements remain after accounting for all relevant uncertainties and correlations. After examining the data and the fit pulls,

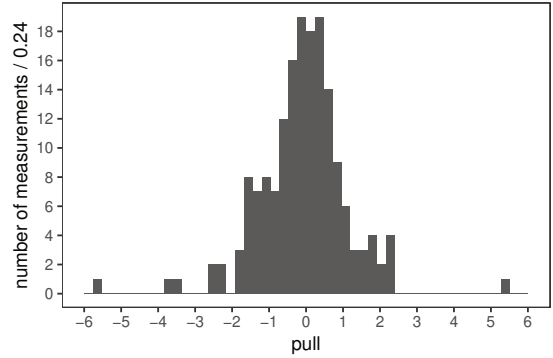


Figure 58.1: Pulls of individual measurements against the respective fitted quantity. No scale factor is used.

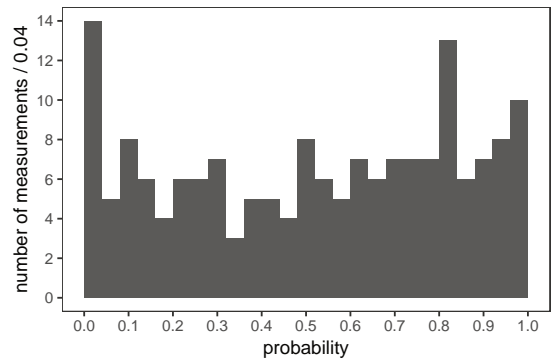


Figure 58.2: Probability of individual measurement pulls against the respective fitted quantity. No scale factor is used.

it has been decided to apply just one scale factor of 5.4 on the measurements of $\mathcal{B}(\tau \rightarrow K^- K^- K^+ \nu_\tau)$. The scale factor has been computed and applied according to the standard PDG procedure. Without the scale factor applied, the χ^2 probability of the fit is about 2%. On a per-measurement basis, the pull distribution in figure 58.1 indicates that just a few measurements have more than 3σ pulls. (The uncertainties to obtain the pulls are computed using the measurements variance matrix and the variance matrix of the result, accounting for the fact that the variance matrix of the result is obtained from the measurement variance with the fit.) The pull probability distribution in figure 58.2 is reasonably flat. With many measurements some entries on the tails of the normal distribution must be expected. There are 170 pulls, one per measurement. They are partially correlated, and the effective number of independent pulls is equal to the number of degrees of freedom of the fit, 125. Only the $\tau \rightarrow K^- K^- K^+ \nu_\tau$ decay mode has a pull that is inconsistent at the level of more than 3σ even if considered as the largest pull in a set of 125. This confirms the choice of adopting just that one scale factor.

After scaling the error, the constrained fit has a χ^2 of 135 for 125 degrees of freedom, corresponding to a χ^2 probability of 26%. We use 170 measurements and 84 constraints on the branching fractions and ratios to determine 129 quantities, consisting of 112 branching fractions and 17 branching ratios. A total of 85 quantities have at least one measurement in the fit. The constraints include the unitarity constraint on the sum of all the exclusive τ decay modes, $\mathcal{B}_{\text{all}} = 1$. If the unitarity constraint is released, the fit result for \mathcal{B}_{all} is consistent with unitarity with $1 - \mathcal{B}_{\text{all}} = (0.00 \pm 0.10)\%$.

For the convenience of summarizing the fit results, we list in the following the values and uncertainties for a set of 46 “basis” decay modes, from which all remaining branching fractions and ratios can be obtained using the constraints. The basis decay modes are not intended to sum up to 1. Since some basis quantities represent multiple branching fractions that are related by constraint equations, they are properly weighted and the unitarity constraint

corresponds to a linear combination whose coefficients are listed in the following. The correlation matrix between the basis modes is reported in the τ Listings.

decay mode	fit result (%)	coefficient
$\mu^- \bar{\nu}_\mu \nu_\tau$	17.3937 ± 0.0384	1.0000
$e^- \bar{\nu}_e \nu_\tau$	17.8175 ± 0.0399	1.0000
$\pi^- \nu_\tau$	10.8164 ± 0.0512	1.0000
$K^- \nu_\tau$	0.6964 ± 0.0096	1.0000
$\pi^- \pi^0 \nu_\tau$	25.4941 ± 0.0893	1.0000
$K^- \pi^0 \nu_\tau$	0.4328 ± 0.0148	1.0000
$\pi^- 2\pi^0 \nu_\tau$ (ex. K^0)	9.2595 ± 0.0964	1.0021
$K^- 2\pi^0 \nu_\tau$ (ex. K^0)	0.0647 ± 0.0218	1.0000
$\pi^- 3\pi^0 \nu_\tau$ (ex. K^0)	1.0429 ± 0.0707	1.0000
$K^- 3\pi^0 \nu_\tau$ (ex. K^0, η)	0.0478 ± 0.0212	1.0000
$h^- 4\pi^0 \nu_\tau$ (ex. K^0, η)	0.1118 ± 0.0391	1.0000
$\pi^- \bar{K}^0 \nu_\tau$	0.8384 ± 0.0138	1.0000
$K^- K^0 \nu_\tau$	0.1486 ± 0.0034	1.0000
$\pi^- \bar{K}^0 \pi^0 \nu_\tau$	0.3817 ± 0.0129	1.0000
$K^- \pi^0 K^0 \nu_\tau$	0.1500 ± 0.0070	1.0000
$\pi^- \bar{K}^0 2\pi^0 \nu_\tau$ (ex. K^0)	0.0263 ± 0.0226	1.0000
$\pi^- K_S^0 K_L^0 \nu_\tau$	0.0235 ± 0.0006	2.0000
$\pi^- K_S^0 K_S^0 \nu_\tau$	0.1081 ± 0.0241	1.0000
$\pi^- \pi^0 K_S^0 K_S^0 \nu_\tau$	0.0018 ± 0.0002	2.0000
$\pi^- \pi^0 K_S^0 K_L^0 \nu_\tau$	0.0325 ± 0.0119	1.0000
$\bar{K}^0 h^- h^- h^+ \nu_\tau$	0.0247 ± 0.0199	1.0000
$\pi^- \pi^- \pi^+ \nu_\tau$ (ex. K^0, ω)	8.9868 ± 0.0513	1.0021
$\pi^- \pi^- \pi^+ \pi^0 \nu_\tau$ (ex. K^0, ω)	2.7404 ± 0.0710	1.0000
$h^- h^- h^+ 2\pi^0 \nu_\tau$ (ex. K^0, ω, η)	0.0981 ± 0.0356	1.0000
$\pi^- K^- K^+ \nu_\tau$	0.1435 ± 0.0027	1.0000
$\pi^- K^- K^+ \pi^0 \nu_\tau$	0.0061 ± 0.0018	1.0000
$\pi^- \pi^0 \eta \nu_\tau$	0.1389 ± 0.0072	1.0000
$K^- \eta \nu_\tau$	0.0155 ± 0.0008	1.0000
$K^- \pi^0 \eta \nu_\tau$	0.0048 ± 0.0012	1.0000
$\pi^- \bar{K}^0 \eta \nu_\tau$	0.0094 ± 0.0015	1.0000
$\pi^- \pi^+ \pi^- \eta \nu_\tau$ (ex. K^0)	0.0220 ± 0.0013	1.0000
$K^- \omega \nu_\tau$	0.0410 ± 0.0092	1.0000
$h^- \pi^0 \omega \nu_\tau$	0.4085 ± 0.0419	1.0000
$K^- \phi \nu_\tau$	0.0044 ± 0.0016	0.8320
$\pi^- \omega \nu_\tau$	1.9494 ± 0.0645	1.0000
$K^- \pi^- \pi^+ \nu_\tau$ (ex. K^0, ω)	0.2927 ± 0.0068	1.0000
$K^- \pi^- \pi^+ \pi^0 \nu_\tau$ (ex. K^0, ω, η)	0.0394 ± 0.0142	1.0000
$2\pi^- 2\pi^0 \nu_\tau$ (ex. K^0)	0.0072 ± 0.0016	1.0000
$2\pi^- \pi^+ 3\pi^0 \nu_\tau$ (ex. K^0, η, ω, f_1)	0.0014 ± 0.0027	1.0000
$3\pi^- 2\pi^+ \nu_\tau$ (ex. K^0, ω, f_1)	0.0775 ± 0.0030	1.0000
$K^- 2\pi^- 2\pi^+ \nu_\tau$ (ex. K^0)	0.0001 ± 0.0001	1.0000
$2\pi^- \pi^+ \omega \nu_\tau$ (ex. K^0)	0.0084 ± 0.0006	1.0000
$3\pi^- 2\pi^+ \pi^0 \nu_\tau$ (ex. K^0, η, ω, f_1)	0.0038 ± 0.0009	1.0000
$K^- 2\pi^- 2\pi^+ \pi^0 \nu_\tau$ (ex. K^0)	0.0001 ± 0.0001	1.0000
$\pi^- f_1 \nu_\tau$ ($f_1 \rightarrow 2\pi^- 2\pi^+$)	0.0052 ± 0.0004	1.0000
$\pi^- 2\pi^0 \eta \nu_\tau$	0.0195 ± 0.0038	1.0000

In defining the fit constraints and in selecting the modes that sum up to one we made some assumptions and choices. We assume that some channels, like $\tau^- \rightarrow \pi^- K^+ \pi^- \geq 0\pi^0 \nu_\tau$ and $\tau^- \rightarrow \pi^+ K^- K^- \geq 0\pi^0 \nu_\tau$, have negligible branching fractions as expected from the Standard Model, even if the experimental limits for these branching fractions are not very stringent. The 95% confidence level upper limits are $\mathcal{B}(\tau^- \rightarrow \pi^- K^+ \pi^- \geq 0\pi^0 \nu_\tau) < 0.25\%$ and $\mathcal{B}(\tau^- \rightarrow \pi^+ K^- K^- \geq 0\pi^0 \nu_\tau) < 0.09\%$, values not so different from measured branching fractions for allowed 3-prong modes containing charged kaons. For decays to final states containing one neutral kaon we assume that the branching fraction with the K_L^0 are the same as the corresponding one with a K_S^0 . On decays with two neutral kaons we assume that the branching fractions with $K_L^0 K_L^0$ are the same as the ones with $K_S^0 K_S^0$.

58.3 BaBar and Belle measure on average lower branching fractions and ratios.

We compare the BaBar and Belle measurements with the results of a fit where all their measurements have been excluded. We find that that BaBar and Belle measure on average lower τ branching fractions and ratios than the other experiments. Figures 58.3 and

58.4 show histograms of the 28 normalized differences between the B -factory measurements and the respective non- B -factory fit results. The normalization is the uncertainty on the difference. The average normalized difference between the two sets of measurements is -0.8σ (-0.7σ for the 16 Belle measurements and -0.8σ for the 12 BaBar measurements).

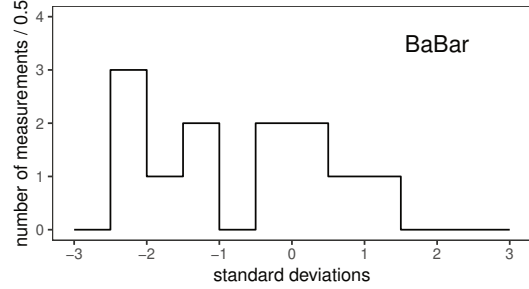


Figure 58.3: Distribution of the normalized difference between 12 measurements of branching fractions and ratios published by the BaBar collaboration and the respective averages computed using only non- B -factory measurements.

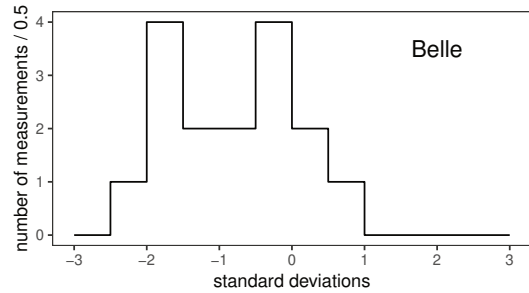


Figure 58.4: Distribution of the normalized difference between 16 measurements of branching fractions and ratios published by the Belle collaboration and the respective averages computed using only non- B -factory measurements.

58.4 Overconsistency of Leptonic Branching Fraction Measurements.

As observed in the previous editions of this review, measurements of the leptonic branching fractions are more consistent with each other than expected from the quoted errors on the individual measurements. The χ^2 is 0.34 for \mathcal{B}_e and 0.08 for \mathcal{B}_μ . Assuming normal errors, the probability of a smaller χ^2 is 1.3% for \mathcal{B}_e and 0.08% for \mathcal{B}_μ .

58.5 Technical implementation of the fit

The fit computes a set of quantities denoted with q_i by minimizing a χ^2 while respecting a series of equality constraints on the q_i . The χ^2 is computed using the measurements m_i and their covariance matrix E_{ij} as $\chi^2 = (m_i - A_{ik} q_k)^t E_{ij}^{-1} (m_j - A_{jl} q_l)$, where the model matrix A_{ij} is used to get the vector of the predicted measurements m'_i from the vector of the fit parameters q_j as $m'_i = A_{ij} q_j$. In this particular implementation the measurements are grouped by the quantity that they measure, and all quantities with at least one measurement correspond to a fit parameter. Therefore, the matrix A_{ij} has one row per measurement m_i and one column per fitted quantity q_j , with unity coefficients for the rows and column that identify a measurement m_i of the quantity q_j , respectively. The constraints are equations involving the fit parameters. The fit does not impose limitations on the functional form of the constraints. In summary, the fit requires:

$$\min [\chi^2(q_k)] = \min [(m_i - A_{ik} q_k)^t E_{ij}^{-1} (m_j - A_{jl} q_l)] \quad (58.1)$$

$$\text{subjected to } f_r(q_s) - c_r = 0 \quad (58.2)$$

where the left term of Eq. 58.2 defines the constraint expressions. Using the method of Lagrange multipliers, a set of equations is

obtained by taking the derivatives with respect to the fitted quantities q_k and the Lagrange multipliers λ_r of the sum of the χ^2 and the constraint expressions multiplied by the Lagrange multipliers λ_r , one for each constraint:

$$\begin{aligned} \min \left[(A_{ik}q_k - m_i)^t E_{ij}^{-1} (A_{jl}q_l - m_j) + 2\lambda_r (f_r(q_s) - c_r) \right] &= \\ &= \min \left[\tilde{\chi}^2(q_k, \lambda_r) \right] , \\ (\partial/\partial q_k, \partial/\partial \lambda_r) \left[\tilde{\chi}^2(q_k, \lambda_r) \right] &= 0 . \end{aligned} \quad (58.3)$$

Eq. 58.3 defines a set of equations for the vector of the unknowns (q_k, λ_r) , some of which may be non-linear, in case of non-linear constraints. An iterative minimization procedure approximates at each step the non-linear constraint expressions by their first order Taylor expansion around the current values of the fitted quantities, \bar{q}_s :

$$f_r(q_s) - c_r = f_r(\bar{q}_s) + \left. \frac{\partial f_r(q_s)}{\partial q_s} \right|_{\bar{q}_s} (q_s - \bar{q}_s) - c_r ,$$

which can be written as

$$B_{rs}q_s - c'_r ,$$

where c'_r are the resulting constant known terms, independent of q_s at first order. After linearization, the differentiation by q_k and λ_r is trivial and leads to a set of linear equations

$$A_{ki}^t E_{ij}^{-1} A_{jl}q_l + B_{kr}^t \lambda_r = A_{ki}^t E_{ij}^{-1} m_j , \quad (58.4)$$

$$B_{rs}q_s = c'_r , \quad (58.5)$$

which can be expressed as

$$F_{ij}u_j = v_i , \quad (58.6)$$

where $u_j = (q_k, \lambda_r)$ and v_i is the vector of the known constant terms running over the index k and then r in the right terms of Eq. 58.4 and Eq. 58.5, respectively. Solving the equation set in Eq. 58.6 by matrix inversion gives the fitted quantities and their variance and covariance matrix, using the measurements and their variance and covariance matrix. The fit procedure starts by computing the linear approximation of the non-linear constraint expressions around the quantities seed values. With an iterative procedure, the unknowns are updated at each step by solving the equations and the equations are then linearized around the updated values, until the variation of the fitted unknowns is reduced below a numerically small threshold.

References

- [1] D. Asner *et al.* (Heavy Flavor Averaging Group) (2010), [arXiv:1010.1589].
- [2] J. P. Lees *et al.* (BaBar), Phys. Rev. **D98**, 3, 032010 (2018), [arXiv:1806.10280].
- [3] S. Schael *et al.* (ALEPH), Phys. Rept. **421**, 191 (2005), [hep-ex/0506072].
- [4] J. Abdallah *et al.* (DELPHI), Eur. Phys. J. **C46**, 1 (2006), [hep-ex/0603044].
- [5] M. Zielinski *et al.*, Phys. Rev. Lett. **52**, 1195 (1984).

59. τ -Lepton Decay Parameters

Revised February 2022 by A. Stahl (RWTH Aachen U.).

The purpose of the measurements of the decay parameters (also known as Michel parameters) of the τ is to determine the structure (spin and chirality) of the current mediating its decays.

59.1 Leptonic Decays:

The Michel parameters are extracted from the energy spectrum of the charged daughter lepton $\ell = e, \mu$ in the decays $\tau \rightarrow \ell \nu_\ell \nu_\tau$. Ignoring radiative corrections, neglecting terms of order $(m_\ell/m_\tau)^2$ and $(m_\tau/\sqrt{s})^2$, and setting the neutrino masses to zero, the spectrum in the laboratory frame reads

$$\frac{d\Gamma}{dx} = \frac{G_{\tau\ell}^2 m_\tau^5}{192 \pi^3} \times \left\{ f_0(x) + \rho f_1(x) + \eta \frac{m_\ell}{m_\tau} f_2(x) - P_\tau [\xi g_1(x) + \xi \delta g_2(x)] \right\} \quad (59.1)$$

with

$$\begin{aligned} f_0(x) &= 2 - 6x^2 + 4x^3 & (59.2) \\ f_1(x) &= -\frac{4}{9} + 4x^2 - \frac{32}{9}x^3 & g_1(x) = -\frac{2}{3} + 4x - 6x^2 + \frac{8}{3}x^3 \\ f_2(x) &= 12(1-x)^2 & g_2(x) = \frac{4}{9} - \frac{16}{3}x + 12x^2 - \frac{64}{9}x^3. \end{aligned}$$

The quantity x is the fractional energy of the daughter lepton ℓ , i.e., $x = E_\ell/E_{\ell, \max} \approx E_\ell/(\sqrt{s}/2)$ and P_τ is the polarization of the tau leptons. The integrated decay width is given by

$$\Gamma = \frac{G_{\tau\ell}^2 m_\tau^5}{192 \pi^3} \left(1 + 4\eta \frac{m_\ell}{m_\tau} \right). \quad (59.3)$$

The situation is similar to muon decays $\mu \rightarrow e \nu_e \nu_\mu$. The generalized matrix element with the couplings $g_{\varepsilon\mu}^2$ and their relations to the Michel parameters ρ , η , ξ , and δ have been described in the ‘‘Note on Muon Decay Parameters’’. The Standard Model expectations are 3/4, 0, 1, and 3/4, respectively. For more details, see Ref. [1].

Additional Michel-parameters can be defined in radiative decays $\tau \rightarrow \ell \nu_\ell \nu_\tau \gamma$, see Ref. [2]. A first measurement is presented in Ref. [3]. The experimental precision does not provide a significant impact on the knowledge about the couplings, yet.

59.2 Hadronic Decays:

In the case of hadronic decays $\tau \rightarrow h \nu_\tau$, with $h = \pi, \rho$, or a_1 , the ansatz is restricted to purely vectorial currents. The matrix element is

$$\frac{G_{\tau h}}{\sqrt{2}} \sum_{\lambda=R,L} g_\lambda \langle \bar{\Psi}_\omega(\nu_\tau) | \gamma^\mu | \Psi_\lambda(\tau) \rangle J_\mu^h \quad (59.4)$$

with the hadronic current J_μ^h . The neutrino chirality ω is uniquely determined from λ . The spectrum depends only on a single parameter ξ_h

$$\frac{d^n \Gamma}{dx_1 dx_2 \dots dx_n} = f(\vec{x}) + \xi_h P_\tau g(\vec{x}), \quad (59.5)$$

with f and g being channel-dependent functions of the n observables $\vec{x} = (x_1, x_2, \dots, x_n)$ (see Ref. [4]). The parameter ξ_h is related to the couplings through

$$\xi_h = |g_L|^2 - |g_R|^2. \quad (59.6)$$

ξ_h is the negative of the chirality of the τ neutrino in these decays. In the Standard Model, $\xi_h = 1$. Also included in the Data Listings for ξ_h are measurements of the neutrino helicity which coincide with ξ_h , if the neutrino is massless (ASNER 00 [5], ACKERSTAFF 97R [6], AKERS 95P [7], ALBRECHT 93C [8], and ALBRECHT 90I [9]).

59.3 Combination of Measurements:

The individual measurements are combined, taking into account the correlations between the parameters. In a first fit, universality between the two leptonic decays, and between all hadronic decays, is assumed. A second fit is made without these assumptions. The results of the two fits are provided as OUR FIT in the Data Listings below in the tables whose title includes ‘‘(e or mu)’’ or ‘‘(all hadronic modes)’’, and ‘‘(e)’’, ‘‘(mu)’’ etc., respectively. The measurements show good agreement with the Standard Model. The χ^2 values with respect to the Standard model predictions are 24.1 for 41 degrees of freedom and 26.8 for 56 degrees of freedom, respectively. The correlations are reduced through this combination to less than 20%, with the exception of ρ and η which are correlated by +23%, for the fit with universality and by +70% for $\tau \rightarrow \mu \nu_\mu \nu_\tau$.

59.4 Model-independent Analysis:

From the Michel parameters, limits can be derived on the couplings $g_{\varepsilon\lambda}^k$ without further model assumptions. In the Standard model $g_{LL}^V = 1$ (leptonic decays), and $g_L = 1$ (hadronic decays) and all other couplings vanish. First, the partial decay widths have to be compared to the Standard Model predictions to derive limits on the normalization of the couplings $A_x = G_{\tau x}^2/G_F^2$ with Fermi’s constant G_F :

$$\begin{aligned} A_e &= 1.0022 \pm 0.0041, \\ A_\mu &= 0.983 \pm 0.017, \\ A_\pi &= 0.9957 \pm 0.0049. \end{aligned} \quad (59.7)$$

Then limits on the couplings (95% CL) can be extracted (see Ref. [10] and Ref. [11]). Without the assumption of universality, the limits given in Table 59.1 are derived.

Table 59.1: Coupling constants $g_{\varepsilon\mu}^\gamma$. 95% confidence level experimental limits. The limits include the quoted values of A_e , A_μ , and A_π and assume $A_\rho = A_{a_1} = 1$.

$\tau \rightarrow e \nu_e \nu_\tau$		
$ g_{RR}^S < 0.70$	$ g_{RR}^V < 0.17$	$ g_{RR}^T \equiv 0$
$ g_{LR}^S < 0.99$	$ g_{LR}^V < 0.13$	$ g_{LR}^T < 0.082$
$ g_{RL}^S < 2.01$	$ g_{RL}^V < 0.52$	$ g_{RL}^T < 0.51$
$ g_{LL}^S < 2.01$	$ g_{LL}^V < 1.004$	$ g_{LL}^T \equiv 0$
$\tau \rightarrow \mu \nu_\mu \nu_\tau$		
$ g_{RR}^S < 0.72$	$ g_{RR}^V < 0.18$	$ g_{RR}^T \equiv 0$
$ g_{LR}^S < 0.95$	$ g_{LR}^V < 0.12$	$ g_{LR}^T < 0.079$
$ g_{RL}^S < 2.01$	$ g_{RL}^V < 0.52$	$ g_{RL}^T < 0.51$
$ g_{LL}^S < 2.01$	$ g_{LL}^V < 1.006$	$ g_{LL}^T \equiv 0$
$\tau \rightarrow \pi \nu_\tau$		
$ g_R^V < 0.15$	$ g_L^V > 0.984$	
$\tau \rightarrow \rho \nu_\tau$		
$ g_R^V < 0.10$	$ g_L^V > 0.995$	
$\tau \rightarrow a_1 \nu_\tau$		
$ g_R^V < 0.16$	$ g_L^V > 0.987$	

59.5 Model-dependent Interpretation:

More stringent limits can be derived assuming specific models. For example, in the framework of a two Higgs doublet model, the measurements correspond to a limit of $m_{H^\pm} > 2.0 \text{ GeV} \times \tan \beta$ on the mass of the charged Higgs boson, or a limit of 500 GeV on the mass of the second W boson in left-right symmetric models for arbitrary mixing (both 95% CL). See Ref. [11] and Ref. [12].

References

- [1] F. Scheck, Phys. Rept. **44**, 187 (1978); W. Fetscher and H.J. Gerber in *Precision Tests of the Standard Model*, edited by P. Langacker, World Scientific, 1993; A. Stahl, *Physics with τ Leptons*, Springer Tracts in Modern Physics, **160**, 1, (2000).
- [2] A. Arbuzov and T. Kopylova, JHEP 109 (2016).
- [3] N. Shimizu *et al.* (Belle), Prog. Theo. Exp. Phys. **2**, 023C01 (2018).
- [4] M. Davier *et al.*, Phys. Lett. B **306**, 411 (1993).
- [5] D. Asner *et al.* (CLEO), Phys. Rev. D **61**, 012002 (2000), [hep-ex/9902022].
- [6] K. Ackerstaff *et al.* (OPAL), Z. Phys. C **75**, 593 (1997).
- [7] R. Akers *et al.* (OPAL), Z. Phys. C **67**, 45 (1995).
- [8] H. Albrecht *et al.* (ARGUS), Z. Phys. C **58**, 61 (1993).
- [9] H. Albrecht *et al.* (ARGUS), Phys. Lett. B **250**, 164 (1990).
- [10] K. Ackerstaff *et al.* (OPAL), Eur. Phys. J. C **8**, 3 (1999), [hep-ex/9808016].
- [11] A. Stahl, Nucl. Phys. B Proc. Suppl. **76**, 173 (1999).
- [12] M.-T. Dova, J. Swain and L. Taylor, Phys. Rev. D **58**, 015005 (1998), [hep-ph/9712384]; T. Hebbeker and W. Lohmann, Z. Phys. C **74**, 399 (1997); A. Pich and J. P. Silva, Phys. Rev. D **52**, 4006 (1995), [hep-ph/9505327].

60. Quark Masses

Revised August 2021 by R.M. Barnett (LBNL), L.P. Lellouch (CNRS & Aix-Marseille U.) and A.V. Manohar (UC San Diego).

60.1 Introduction

This note discusses some of the theoretical issues relevant for the determination of quark masses, which are fundamental parameters of the Standard Model of particle physics. Unlike the leptons, quarks are confined inside hadrons and are not observed as physical particles. Quark masses therefore cannot be measured directly, but must be determined indirectly through their influence on hadronic properties. Although one often speaks loosely of quark masses as one would of the mass of the electron or muon, any quantitative statement about the value of a quark mass must make careful reference to the particular theoretical framework that is used to define it. It is important to keep this *scheme dependence* in mind when using the quark mass values tabulated in the data listings.

Historically, the first determinations of quark masses were performed using quark models. These are usually called constituent quark masses and are of order 350 MeV for the u and d quarks. Constituent quark masses model the effects of dynamical chiral symmetry breaking discussed below, and are not directly related to the quark mass parameters m_q of the QCD Lagrangian of Eq. (60.1). The resulting masses only make sense in the limited context of a particular quark model, and cannot be related to the quark mass parameters, m_q , of the Standard Model. In order to discuss quark masses at a fundamental level, definitions based on quantum field theory must be used, and the purpose of this note is to discuss these definitions and the corresponding determinations of the values of the masses.

60.2 Mass parameters and the QCD Lagrangian

The QCD [1] Lagrangian is

$$\mathcal{L} = \sum_{q=u,d,s,\dots,t} \bar{q}(i\not{D} - m_q)q - \frac{1}{2}\text{tr} G_{\mu\nu}G^{\mu\nu}, \quad (60.1)$$

where the sum runs over the quark flavors u, d, s, c, b and t . $\not{D} = (\partial_\mu - igA_\mu)\gamma^\mu$ is the gauge covariant derivative, A_μ is the SU(3)-valued gluon field, $G_{\mu\nu} = \frac{i}{g}[D_\mu, D_\nu]$ is the gluon field strength, m_q is the mass parameter of quark flavor q , and q is the quark Dirac field. After renormalization, the QCD Lagrangian Eq. (60.1) gives finite values for physical quantities, such as scattering amplitudes. Renormalization is a procedure that invokes a subtraction scheme to render the amplitudes finite, and requires the introduction of a dimensionful scale parameter μ . The mass parameters in the QCD Lagrangian Eq. (60.1) depend on the renormalization scheme used to define the theory, and also on the scale parameter μ . The most commonly used renormalization scheme for QCD perturbation theory is the $\overline{\text{MS}}$ scheme.

The QCD Lagrangian has a chiral symmetry in the limit that the quark masses vanish. This symmetry is spontaneously broken by dynamical chiral symmetry breaking, and explicitly broken by the quark masses. The nonperturbative scale of dynamical chiral symmetry breaking, Λ_χ , is around 1 GeV [2]. It is conventional to call quarks heavy if $m_q > \Lambda_\chi$, so that explicit chiral symmetry breaking dominates (c, b , and t quarks are heavy), and light if $m_q < \Lambda_\chi$, so that spontaneous chiral symmetry breaking dominates (the u and d are light and the s is considered to be light when using SU(3) $_L$ × SU(3) $_R$ chiral perturbation theory). The determination of light- and heavy-quark masses is considered separately in Sec. 60.4 and Sec. 60.5 below.

At high energies or short distances, nonperturbative effects, such as chiral symmetry breaking, become small and one can, in principle, determine quark masses by analyzing mass-dependent effects using QCD perturbation theory. Such computations are conventionally performed using the $\overline{\text{MS}}$ scheme at a scale $\mu \gg \Lambda_\chi$, and give the $\overline{\text{MS}}$ “running” mass $\overline{m}(\mu)$. We use the $\overline{\text{MS}}$ scheme when reporting quark masses; one can readily convert these values into other schemes using perturbation theory.

The μ dependence of $\overline{m}(\mu)$ at short distances can be calculated

using the renormalization group (RG) equation,

$$\mu^2 \frac{d\overline{m}(\mu)}{d\mu^2} = -\gamma(\overline{\alpha}_s(\mu)) \overline{m}(\mu), \quad (60.2)$$

where γ is the anomalous dimension which is now known to four-loop order in perturbation theory [3] [4]. $\overline{\alpha}_s$ is the coupling constant [1] in the $\overline{\text{MS}}$ scheme. Defining the expansion coefficients γ_r by

$$\gamma(\overline{\alpha}_s) \equiv \sum_{r=1}^{\infty} \gamma_r \left(\frac{\overline{\alpha}_s}{4\pi}\right)^r, \quad (60.3)$$

the first four coefficients are given by

$$\begin{aligned} \gamma_1 &= 4, \\ \gamma_2 &= \frac{202}{3} - \frac{20N_L}{9}, \\ \gamma_3 &= 1249 + \left(-\frac{2216}{27} - \frac{160}{3}\zeta(3)\right)N_L - \frac{140}{81}N_L^2, \\ \gamma_4 &= \frac{4603055}{162} + \frac{135680}{27}\zeta(3) - 8800\zeta(5) \\ &\quad + \left(-\frac{91723}{27} - \frac{34192}{9}\zeta(3) + 880\zeta(4) + \frac{18400}{9}\zeta(5)\right)N_L \\ &\quad + \left(\frac{5242}{243} + \frac{800}{9}\zeta(3) - \frac{160}{3}\zeta(4)\right)N_L^2 \\ &\quad + \left(-\frac{332}{243} + \frac{64}{27}\zeta(3)\right)N_L^3, \end{aligned}$$

where N_L is the number of active light quark flavors at the scale μ , i.e. flavors with masses $\leq \mu$, and ζ is the Riemann zeta function ($\zeta(3) \simeq 1.2020569$, $\zeta(4) \simeq 1.0823232$, and $\zeta(5) \simeq 1.0369278$). Eq. (60.2) must be solved in conjunction with the RG equation for $\overline{\alpha}_s(\mu)$ given in [1]. In addition, as the renormalization scale crosses quark mass thresholds one needs to match the scale dependence of \overline{m} below and above the threshold. There are finite threshold corrections; the necessary formulae can be found in Ref. [5].

60.3 Lattice QCD

The use of lattice QCD calculations for *ab initio* determinations of the fundamental parameters of QCD, including the coupling constant and quark masses (except for the top-quark mass) is a very active area of research (see the review on Lattice Quantum Chromodynamics in this *Review*). Here we only briefly recall those features which are required for the determination of quark masses. In order to determine the lattice spacing (a , i.e. the distance between neighboring points of the lattice) and quark masses, one computes a convenient and appropriate set of physical quantities (frequently chosen to be a set of hadronic masses) for a variety of input values of the quark masses in units of the lattice spacing. These input quark masses are then tuned to their true (physical) values by requiring that the calculation correctly reproduces the set of physical quantities being used for the calibration.

The resulting values of the quark masses are bare quark masses, corresponding to a particular discretization of QCD and with the lattice spacing as the ultraviolet cut-off. In order for these results to be useful in phenomenological applications, it is necessary to relate them to renormalized masses defined in some standard renormalization scheme such as $\overline{\text{MS}}$. Provided that both the ultraviolet cut-off a^{-1} and the renormalization scale μ are much greater than Λ_{QCD} , the bare and renormalized masses can be related in perturbation theory. However, in order to avoid uncertainties due to the unknown higher-order coefficients in lattice perturbation theory, most results obtained recently use *nonperturbative renormalization* to relate the bare masses to those defined in renormalization schemes which can be realized directly in lattice QCD (e.g. those obtained from quark and gluon Green functions at specified momenta in the Landau gauge [6] or those defined using finite-volume techniques and the Schrödinger functional [7], but not $\overline{\text{MS}}$ that is only defined for dimensional regularization). These methods require $\mu \gg \Lambda_{\text{QCD}}$ so that unwanted (nonperturbative) corrections proportional to inverse powers of μ , which appear in some

approaches, remain small corrections that can be identified and removed. This condition is also necessary so that matching to other schemes can be performed reliably in perturbation theory. Moreover, these methods require $a^{-1} \gg \mu$ so that cutoff effects are small enough to be extrapolated away. Thus, the calculations are repeated for finer and finer lattice spacings and the continuum limit, $a \rightarrow 0$, of these nonperturbatively renormalized masses is taken to eliminate all cutoff effects. The conversion to the $\overline{\text{MS}}$ scheme is then performed using continuum perturbation theory, which is more readily obtained to higher orders and is usually better behaved than its lattice counterpart.

It is important to note that the final renormalized values for the quark masses must be the same in the continuum limit for any sensible choice of the physical quantities used for calibration, as long as the calculation is performed with a sufficient number of sea-quark flavors and the relevant electromagnetic and strong-isospin breaking corrections for the claimed precision. It is also worth noting that issues surrounding the renormalization of quark masses disappear when considering pairwise ratios of these masses (up to electromagnetic effects for quarks of different charge, which are still smaller than the errors bars quoted on these ratios, e.g. in the $\overline{\text{MS}}$ scheme at a scale of a few GeV). Indeed, if the same scheme and scale are implemented, QCD renormalization factors are identical for all quark flavors, and these factors therefore cancel exactly in quark-mass ratios. In particular, this means that these ratios are scheme and scale independent. Moreover, these ratios may suffer less from the uncertainties in the determination of the lattice scale, in particular in cases where the quantities used to fix the two quarks masses entering the ratio depend on these masses in a similar way, but also because these ratios are dimensionless. Thus, quark-mass ratios are often determined with significantly higher precision using lattice QCD than are the individual masses.

The determination of quark masses using lattice simulations is well established and the current emphasis is on the reduction and control of the systematic uncertainties. With improved algorithms and access to more powerful computing resources, the precision of the results has improved immensely in recent years. Vacuum polarization effects are included with $N_f = 2$, $2 + 1$ or $N_f = 2 + 1 + 1$ flavors of sea quarks. The number 2 here indicates that the up and down quarks are degenerate. The first $+1$ corresponds to the inclusion of strange sea-quark effects and the second $+1$ to those of the charm. Simulations with $2 + 1$ and $2 + 1 + 1$ flavors represent controlled approximations to physical QCD at the low energies considered for quark mass determinations, up to corrections of $O((\Lambda_{\text{QCD}}/m_c)^2/N_c)$ and $O((\Lambda_{\text{QCD}}/m_b)^2/N_c)$, respectively. This is not the case for simulations with $N_f = 2$ or in which vacuum polarization effects are completely neglected (this is the so-called *quenched* approximation) and results obtained in such frameworks will not enter the discussion here.

Particularly pleasing is the observation that different formulations of lattice QCD, with different systematic uncertainties, yield results which are largely consistent with each other. This gives us broad confidence in the estimates of the systematic errors. As the precision of the results approaches (or even exceeds in some cases) 1%, isospin breaking effects, including electromagnetic corrections need to be included and this is beginning to be done as will be discussed below. In particular, a reliable estimate of these effects is required for determining the individual u and d quark masses.

Members of the lattice QCD community have organized a Flavour Lattice Averaging Group (FLAG) which critically reviews quantities computed in lattice QCD relevant to flavor physics, including the determination of quark masses, against stated quality criteria and presents its view of the current status of the results. The latest edition reviews lattice results that have been appeared in print before April 30th 2021 [8]. Since that deadline, there have been no new lattice, quark-mass determinations.

60.4 Light quarks

In this section we review the determination of the masses of the light quarks u , d and s from lattice simulations and then discuss the consequences of the approximate chiral symmetry.

60.4.1 Lattice QCD results

The most reliable determinations of the strange quark mass, m_s , and of the average of the up and down quark masses, $m_{ud} = (m_u + m_d)/2$, are obtained from lattice simulations. As explained in Sec. 60.3 above, the simulations are generally performed with degenerate up and down quarks ($m_u = m_d$) and so it is the average which is obtained directly from the computations. Below we discuss the derivation of m_u and m_d separately, but we start by briefly presenting our estimate of the current status of the latest lattice results in the isospin symmetric limit. The FLAG review [8] bases its summary numbers for these quark masses on references that the review's authors consider to have the most reliable estimates of systematic uncertainties, i.e. [9–15] for $N_f = 2 + 1$ and [16–21] for $N_f = 2 + 1 + 1$ flavors of sea quarks. Note that the $N_f = 2 + 1 + 1$ results [22] did not make the FLAG deadline. Compared to the previous editions of the FLAG [23] and of the present reviews, this corresponds to including the new calculation [15] and to dropping [24], whose simulations do not allow for as good a control over the tuning of m_{ud} as do the other calculations. For $N_f = 2 + 1$ flavors, the FLAG review quotes $\overline{m}_{ud} = (3.381 \pm 0.040)$ MeV, $\overline{m}_s = (92.2 \pm 1.0)$ MeV and $(\overline{m}_s/\overline{m}_{ud}) = 27.42 \pm 0.12$. These numbers are $\overline{m}_{ud} = (3.410 \pm 0.043)$ MeV, $\overline{m}_s = (93.40 \pm 0.57)$ MeV and $(\overline{m}_s/\overline{m}_{ud}) = 27.23 \pm 0.10$ for $N_f = 2 + 1 + 1$ simulations. The masses are given in the $\overline{\text{MS}}$ scheme at a renormalization scale of 2 GeV. These results are not simply the combinations of all the results in quadrature, but include possible correlations between calculations. Since the different collaborations use different formulations of lattice QCD, the (relatively small) variations of the results between the groups provides important information about the reliability of the estimates.

Compared to the previous editions of the FLAG [23] and of the present reviews, the central values of these averages have changed by only a fraction of their error bars, which is not surprising given that they were obtained mostly from the same results. The most notable change is the significant increase in the error of $N_f = 2 + 1$ \overline{m}_s . This is due mainly to the inclusion of [15], whose larger value leads to a $\chi^2/\text{dof} = 1.7$ in the average, which is accounted for by increasing the uncertainties by the usual $\sqrt{\chi^2/\text{dof}}$ scale factor.

Despite being reported in the $\overline{\text{MS}}$ scheme at a renormalization scale of 2 GeV, the results for \overline{m}_{ud} and \overline{m}_s in the two frameworks differ in their renormalization schemes, since $N_f = 2 + 1$ results are renormalized with $N_L = 3$ and $N_f = 2 + 1 + 1$ ones with $N_L = 4$. Thus, for a comparison, one should convert the results to the same scheme. This is not the case for $(\overline{m}_s/\overline{m}_{ud})$, where renormalization factors cancel. The conversion of the $N_f = 2 + 1$ results to the $N_L = 4$ scheme can be performed, for instance, by running them down to the charm threshold in the $N_L = 3$ theory, matching the results to the $N_L = 4$ theory at that scale, and running them back up to 2 GeV with four active flavors. Such a conversion leads to an upward shift in the values of the quark masses of only around 0.3%, well within the quoted errors. There are also nonperturbative contributions to this procedure, of $O((\Lambda_{\text{QCD}}/m_c)^2/N_c) \sim 2\%$. However, lattice QCD studies of these effects have shown that they are typically an order of magnitude smaller on hadronic quantities or on Λ_{QCD} [25, 26]. Given that the total errors on the $N_f = 2 + 1$ results for \overline{m}_{ud} and \overline{m}_s are larger than 1%, we choose to neglect these matching effects and simply to average the results from the two frameworks, yielding as a final lattice QCD estimate in the $\overline{\text{MS}}$ scheme at $\mu = 2$ GeV in the $N_L = 4$ theory:

$$\overline{m}_{ud} = (3.39 \pm 0.04) \text{ MeV}, \quad (60.4)$$

$$\overline{m}_s = (93.1 \pm 0.6) \text{ MeV}, \quad (60.5)$$

and

$$r_s \equiv \frac{\overline{m}_s}{\overline{m}_{ud}} = 27.31 \pm 0.10, \quad (60.6)$$

where the error bars encompass statistical and systematic errors combined in quadrature. In performing these averages, small tensions are found in the results for $\overline{m}_s/\overline{m}_{ud}$, whose weighted av-

erage comes with a $\chi^2/\text{dof} \simeq 1.5$, used to increase error bars in the usual way. As a final error we always quote the largest of the average's error and of the smaller of the errors on the individual flavor averages, to account for possible common systematics.

To obtain the individual values of \overline{m}_u and \overline{m}_d requires the introduction of isospin breaking effects, including electromagnetism. This is now being done completely using lattice field theory, albeit neglecting electromagnetic effects in the sea in most cases (for an exception, see [27] which includes a calculation of the QED contribution to $\Delta M_K^2 = M_{K^0}^2 - M_{K^+}^2$ that is critical for determining $\overline{m}_d - \overline{m}_u$). The effect of this neglect on the u and d quark masses has been estimated in [28], to induce a contribution to the uncertainty that ranges from about 3% in $\overline{m}_u/\overline{m}_d$ to less than 1% in \overline{m}_d . FLAG has also reviewed results for these masses in [8]. Again, they separate results obtained from $N_f = 2 + 1$ and $N_f = 2 + 1 + 1$ simulations. For the former, their number is that of [28], as in the previous review [23], and for the latter, it is the average of the results from [17, 29, 30]. Thus, for $N_f = 2 + 1$ they quote $\overline{m}_u = 2.27(9)$ MeV, $\overline{m}_d = 4.67(9)$ MeV, $(\overline{m}_u/\overline{m}_d) = 0.485(19)$ and, for $N_f = 2 + 1 + 1$, $\overline{m}_u = 2.14(8)$ MeV, $\overline{m}_d = 4.70(5)$ MeV, $(\overline{m}_u/\overline{m}_d) = 0.465(24)$. Compared to the previous editions of the FLAG [23] and of the present reviews, the inclusion of the $N_f = 2 + 1 + 1$ results [17, 30] changes the central values of \overline{m}_u and $\overline{m}_u/\overline{m}_d$ outside error bars, indicating some tension between the results of the newer and older calculations, which is around 2 standard deviations. Here, \overline{m}_u is 0.36 MeV smaller than the value given in [23] and $\overline{m}_u/\overline{m}_d$ is 0.066 units smaller. These reductions make the $N_f = 2 + 1 + 1$ results more compatible with the $N_f = 2 + 1$ ones.

As for the light quark masses in the isospin limit, we average the results obtained with different numbers of sea-quark flavors. Here, only the \overline{m}_u average has a $\chi^2/\text{dof} = 1.2 > 1$, and its error is thus appropriately scaled. Again, we do not allow the errors to become smaller than those on the individual flavor averages because of possible common systematics. Thus, we give as a final lattice QCD estimate in the $\overline{\text{MS}}$ scheme at $\mu = 2$ GeV in the $N_L = 4$ theory:

$$\overline{m}_u = 2.20(8) \text{ MeV}, \quad \overline{m}_d = 4.69(5) \text{ MeV}, \quad r \equiv \frac{\overline{m}_u}{\overline{m}_d} = 0.477(19). \quad (60.7)$$

As a consequence of the newly included $N_f = 2 + 1 + 1$ results [17, 30], the central value of \overline{m}_u has been reduced by 0.12 MeV and that of $\overline{m}_u/\overline{m}_d$ by 0.016 units compared to the previous edition of this review, while the error bar on \overline{m}_u is 20% smaller and that on \overline{m}_d is almost 50% smaller.

It is worth noting that m_u differs from zero by more than 20 times the quoted error, making a scenario in which $m_u = 0$ very unlikely. This is important because there would be no strong CP problem if m_u were to vanish identically.

It should also be emphasized that the results for the light quark masses given in the listings are dominated by the lattice values, since most phenomenological extractions have larger uncertainties.

60.4.2 Chiral Perturbation Theory

For light quarks, one can use the techniques of chiral perturbation theory [31–33] to extract quark mass ratios. The mass term for light quarks in the QCD Lagrangian is

$$\overline{\Psi} M \Psi = \overline{\Psi}_L M \Psi_R + \overline{\Psi}_R M^\dagger \Psi_L, \quad (60.8)$$

where M is the light quark mass matrix,

$$M = \begin{pmatrix} m_u & 0 & 0 \\ 0 & m_d & 0 \\ 0 & 0 & m_s \end{pmatrix}, \quad (60.9)$$

$\Psi = (u, d, s)$, and L and R are the left- and right-chiral components of Ψ given by $\Psi_{L,R} = P_{L,R} \Psi$, $P_L = (1 - \gamma_5)/2$, $P_R = (1 + \gamma_5)/2$. The mass term is the only term in the QCD Lagrangian that mixes left- and right-handed quarks. In the limit $M \rightarrow 0$, there is an independent $\text{SU}(3) \times \text{U}(1)$ flavor symmetry for the left- and right-handed quarks. The vector $\text{U}(1)$ symmetry is baryon number; the axial $\text{U}(1)$ symmetry of the classical theory is

broken in the quantum theory due to the anomaly. The remaining $G_\chi = \text{SU}(3)_L \times \text{SU}(3)_R$ chiral symmetry of the QCD Lagrangian is spontaneously broken to $\text{SU}(3)_V$, which, in the limit $M \rightarrow 0$, leads to eight massless Goldstone bosons, the π 's, K 's, and η .

The symmetry G_χ is only an approximate symmetry, since it is explicitly broken by the quark mass matrix M . The Goldstone bosons acquire masses which can be computed in a systematic expansion in M , in terms of low-energy constants, which are unknown nonperturbative parameters of the effective theory, and are not fixed by the symmetries. One treats the quark mass matrix M as a uniform, external field that transforms under G_χ as $M \rightarrow L M R^\dagger$, where $\Psi_L \rightarrow L \Psi_L$ and $\Psi_R \rightarrow R \Psi_R$ are the $\text{SU}(3)_L$ and $\text{SU}(3)_R$ transformations, and writes down the most general Lagrangian invariant under G_χ . Then one sets M to its given constant value Eq. (60.9), which implements the symmetry breaking. To first order in M one finds that [34]

$$\begin{aligned} m_{\pi^0}^2 &= B(m_u + m_d), \\ m_{\pi^\pm}^2 &= B(m_u + m_d) + \Delta_{\text{em}}, \\ m_{K^0}^2 &= m_{K^+}^2 = B(m_d + m_s), \\ m_{K^\pm}^2 &= B(m_u + m_s) + \Delta_{\text{em}}, \\ m_\eta^2 &= \frac{1}{3} B(m_u + m_d + 4m_s), \end{aligned} \quad (60.10)$$

with two unknown constants B , related to the light quark condensate, and Δ_{em} , the electromagnetic mass difference. From Eq. (60.10), one can determine the quark mass ratios [34]

$$\begin{aligned} \frac{m_u}{m_d} &= \frac{2m_{\pi^0}^2 - m_{\pi^\pm}^2 + m_{K^+}^2 - m_{K^0}^2}{m_{K^0}^2 - m_{K^+}^2 + m_{\pi^\pm}^2} = 0.56, \\ \frac{m_s}{m_d} &= \frac{m_{K^0}^2 + m_{K^+}^2 - m_{\pi^\pm}^2}{m_{K^0}^2 + m_{\pi^\pm}^2 - m_{K^+}^2} = 20.2, \end{aligned} \quad (60.11)$$

to lowest order in chiral perturbation theory, with an error which will be estimated below. Since the mass ratios extracted using chiral perturbation theory use the symmetry transformation property of M under the chiral symmetry G_χ , it is important to use a renormalization scheme for QCD that does not change this transformation law. Any mass-independent subtraction scheme such as $\overline{\text{MS}}$ is suitable. The ratios of quark masses are scale independent in such a scheme (up to electromagnetic corrections), and Eq. (60.11) can be taken to be the ratio of $\overline{\text{MS}}$ masses. Chiral perturbation theory cannot determine the overall scale of the quark masses, since it uses only the symmetry properties of M , and any multiple of M has the same G_χ transformation law as M .

Chiral perturbation theory is a systematic expansion in powers of the light quark masses. The typical expansion parameter is $m_K^2/\Lambda_\chi^2 \sim 0.25$ if one uses $\text{SU}(3)$ chiral symmetry, and $m_\pi^2/\Lambda_\chi^2 \sim 0.02$ if instead one uses $\text{SU}(2)$ chiral symmetry. Electromagnetic effects at the few percent level also break $\text{SU}(2)$ and $\text{SU}(3)$ symmetry. The mass formulæ Eq. (60.10) were derived using $\text{SU}(3)$ chiral symmetry, and are expected to have approximately a 25% uncertainty due to second order corrections. This estimate of the uncertainty yields results consistent with the lattice results summarized in Eq. (60.5)–(60.6).

There is a subtlety which arises when one tries to determine quark mass ratios at second order in chiral perturbation theory. The second order quark mass term [35]

$$(M^\dagger)^{-1} \det M^\dagger \quad (60.12)$$

(which can be generated by instantons) transforms in the same way under G_χ as M . Chiral perturbation theory cannot distinguish between M and $(M^\dagger)^{-1} \det M^\dagger$; one can make the replacement $M \rightarrow M(\lambda) = M + \lambda M (M^\dagger M)^{-1} \det M^\dagger$ in the chiral Lagrangian,

$$\begin{aligned} M(\lambda) &= \text{diag}(m_u(\lambda), m_d(\lambda), m_s(\lambda)) \\ &= \text{diag}(m_u + \lambda m_d m_s, m_d + \lambda m_u m_s, m_s + \lambda m_u m_d), \end{aligned} \quad (60.13)$$

and leave all observables unchanged.

The combination

$$\left(\frac{m_u}{m_d}\right)^2 + \frac{1}{Q^2} \left(\frac{m_s}{m_d}\right)^2 = 1 \quad (60.14)$$

where

$$Q^2 = \frac{m_s^2 - m_{ud}^2}{m_d^2 - m_u^2}, \quad m_{ud} = \frac{1}{2}(m_u + m_d),$$

is insensitive to the transformation in Eq. (60.13). Eq. (60.14) gives an ellipse in the m_u/m_d - m_s/m_d plane. The ellipse is well-determined by chiral perturbation theory, but the location on the ellipse, and the absolute normalization of the quark masses, have larger uncertainties.

A leading-order result for Q in SU(3) chiral perturbation theory can be derived using Eq. (60.10) and the values for the relevant meson masses. This result actually holds to next-to-leading order, yielding $Q \stackrel{\text{NLO}}{=} 24.3$. Phenomenologically, the preferred way to determine Q is from $\eta \rightarrow 3\pi$ decay, giving the smaller value $Q = 22.1(7)$ [36]. Lattice QCD collaborations have also reported determinations of Q . Using $N_f = 2 + 1$ simulations, [28] obtains $Q = 23.4 \pm 0.6$ and [29] determines $Q = 23.8 \pm 1.1$ with $N_f = 2 + 1 + 1$ simulations, which are fully compatible. These results are also compatible with $Q = 22.9 \pm 0.4$, obtained from $Q^2 = (r_s^2 - 1)(1+r)/[4(1-r)]$ and from our lattice averages for r_s and r from Eqs. (60.6) and (60.7), respectively. On the whole, the lattice results are larger than the one from phenomenology [36]. This difference could be due to surprisingly large corrections to the NLO substitution of meson masses by Q in the phenomenological determination, as suggested by the authors of [36].

The absolute normalization of the quark masses cannot be determined using chiral perturbation theory. Other methods, such as lattice simulations discussed above, or spectral function sum rules [37,38] for hadronic correlation functions reviewed next, are necessary.

60.4.3 Sum rules

Sum rule methods have been used extensively to determine quark masses and for illustration we briefly discuss here their application to hadronic τ decays [39]. Other applications involve very similar techniques.

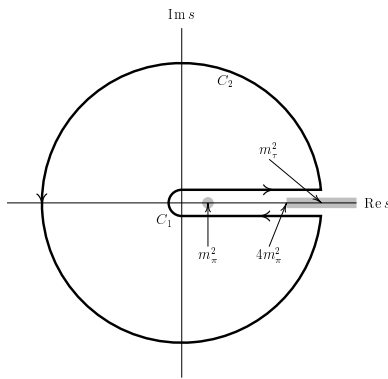


Figure 60.1: The analytic structure of $\Pi(s)$ in the complex s -plane. The contours C_1 and C_2 are the integration contours discussed in the text, and the integral over the closed contour $C_1 + C_2$ vanishes. m_τ^2 has not been drawn to scale; $m_\tau^2 \sim 40(4m_\pi^2)$.

The experimentally measured quantity is R_τ ,

$$\frac{dR_\tau}{ds} = \frac{d\Gamma/ds(\tau^- \rightarrow \text{hadrons} + \nu_\tau(\gamma))}{\Gamma(\tau^- \rightarrow e^- \bar{\nu}_e \nu_\tau(\gamma))} \quad (60.15)$$

the hadronic invariant mass spectrum in semihadronic τ decay, normalized to the leptonic τ decay rate. It is useful to define q as the total momentum of the hadronic final state, so $s = q^2$ is the hadronic invariant mass. The total hadronic τ decay rate R_τ is

then given by integrating dR_τ/ds over the kinematically allowed range $0 \leq s \leq M_\tau^2$.

R_τ can be written as

$$R_\tau = 12\pi \int_0^{M_\tau^2} \frac{ds}{M_\tau^2} \left(1 - \frac{s}{M_\tau^2}\right)^2 \times \left[\left(1 + 2\frac{s}{M_\tau^2}\right) \text{Im} \Pi^T(s) + \text{Im} \Pi^L(s) \right] \quad (60.16)$$

where the hadronic spectral functions $\Pi^{L,T}$ are defined from the time-ordered correlation function of two weak currents ($j^\mu(x)$ and $j^\nu(0)$) by

$$\Pi^{\mu\nu}(q) = i \int d^4x e^{iq \cdot x} \langle 0 | T(j^\mu(x) j^\nu(0)^\dagger) | 0 \rangle, \quad (60.17)$$

$$\Pi^{\mu\nu}(q) = (-g^{\mu\nu} + q^\mu q^\nu) \Pi^T(s) + q^\mu q^\nu \Pi^L(s), \quad (60.18)$$

and the decomposition Eq. (60.17) is the most general possible structure consistent with Lorentz invariance.

By the optical theorem, the imaginary part of $\Pi^{\mu\nu}$ is proportional to the total cross-section for the current to produce all possible states. A detailed analysis including the phase space factors leads to Eq. (60.16). The spectral functions $\Pi^{L,T}(s)$ are analytic in the complex s plane, with singularities along the real axis. There is an isolated pole at $s = m_\pi^2$, and single- and multi-particle singularities for $s \geq 4m_\pi^2$, the two-particle threshold. The discontinuity along the real axis is $\Pi^{L,T}(s + i0^+) - \Pi^{L,T}(s - i0^+) = 2i \text{Im} \Pi^{L,T}(s)$. As a result, Eq. (60.16) can be rewritten with the replacement $\text{Im} \Pi^{L,T}(s) \rightarrow -i \Pi^{L,T}(s)/2$, and the integration being over the contour C_1 . Finally, the contour C_1 can be deformed to $-C_2$ without crossing any singularities, and so leaving the integral unchanged, i.e. the integral over the closed contour $C_1 + C_2$ vanishes. One can derive a series of sum rules analogous to Eq. (60.16) by weighting the differential τ hadronic decay rate by different powers of the hadronic invariant mass [40],

$$R_\tau^{kl} = \int_0^{M_\tau^2} ds \left(1 - \frac{s}{M_\tau^2}\right)^k \left(\frac{s}{M_\tau^2}\right)^l \frac{dR_\tau}{ds}. \quad (60.19)$$

This leads to the final form of the sum rule(s),

$$R_\tau^{kl} = -6\pi i \int_{C_2} \frac{ds}{M_\tau^2} \left(1 - \frac{s}{M_\tau^2}\right)^{2+k} \left(\frac{s}{M_\tau^2}\right)^l \times \left[\left(1 + 2\frac{s}{M_\tau^2}\right) \Pi^T(s) + \Pi^L(s) \right]. \quad (60.20)$$

The manipulations so far are completely rigorous and exact, relying only on the general analytic structure of quantum field theory. The left-hand side of the sum rule Eq. (60.20) is obtained from experiment. The right hand-side can be computed for s far away from any physical cuts using the operator product expansion (OPE) for the time-ordered product of currents in Eq. (60.16), and QCD perturbation theory. The OPE is an expansion in a series of local operators, and is an expansion about the $q \rightarrow \infty$ limit. It gives $\Pi^{L,T}(s)$ as an expansion in powers of $\alpha_s(s)$ and Λ_{QCD}^2/s , and is valid when s is far (in units of Λ_{QCD}^2) from any singularities in the complex s -plane.

The OPE gives $\Pi^{L,T}(s)$ as a series in α_s , quark masses, and various nonperturbative vacuum matrix elements. By computing $\Pi^{L,T}(s)$ theoretically, and comparing with the experimental values of R_τ^{kl} , one determines various parameters such as α_s and the quark masses. The theoretical uncertainties in using Eq. (60.20) arise from neglected higher order corrections (both perturbative and nonperturbative), and because the OPE is no longer valid near the real axis, where $\Pi^{L,T}$ have singularities. The contribution of neglected higher order corrections can be estimated as for any other perturbative computation. The error due to the failure of the OPE is more difficult to estimate. In Eq. (60.20), the OPE fails on the endpoints of C_2 that touch the real axis at $s = M_\tau^2$. The weight factor $(1 - s/M_\tau^2)$ in Eq. (60.20) vanishes at

this point, so the importance of the endpoint can be reduced by choosing larger values of k .

Light quark masses are often determined using QCD sum rules [38], which are similar to the τ sum rules. One takes the correlator of two light-quark-bilinear operators (e.g. an axial vector current), as in Eq. (60.16), and computes their Laplace transforms or moments

$$\mathcal{L}_n(\tau) = \int_0^\infty ds s^n e^{-\tau s} \text{Im } \Pi(s),$$

$$\mathcal{M}_n(Q^2) = \int_0^\infty \frac{ds}{(s+Q^2)^n} \text{Im } \Pi(s)$$

to get Laplace or moment sum rules, respectively. The quark masses are extracted by comparing the theoretical and experimental values of $\mathcal{L}_n(\tau)$ and $\mathcal{M}_n(Q^2)$. Considerable theoretical effort has gone into optimizing n and Q^2 to improve the precision of the resulting light quark masses.

60.5 Heavy quarks

60.5.1 Continuum approaches and results

For heavy quark physics one can exploit the fact that $m_Q \gg \Lambda_{\text{QCD}}$ to construct effective theories (m_Q is the mass of the heavy quark Q). The masses and decay rates of hadrons containing a single heavy quark, such as the B and D mesons can be determined using the heavy quark effective theory (HQET) [41]. The theoretical calculations involve radiative corrections computed in perturbation theory with an expansion in $\alpha_s(m_Q)$ and nonperturbative corrections with an expansion in powers of Λ_{QCD}/m_Q . Due to the asymptotic nature of the QCD perturbation series, the two kinds of corrections are intimately related; an example of this are renormalon effects in the perturbative expansion which are associated with nonperturbative corrections.

Systems containing two heavy quarks such as the Υ or J/ψ are treated using non-relativistic QCD (NRQCD) [42]. The typical momentum and energy transfers in these systems are $\alpha_s m_Q$, and $\alpha_s^2 m_Q$, respectively, so these bound states are sensitive to scales much smaller than m_Q . However, smeared observables, such as the cross-section for $e^+e^- \rightarrow b\bar{b}$ averaged over some range of s that includes several bound state energy levels, are better behaved and only sensitive to scales near m_Q . For this reason, most determinations of the c, b quark masses using perturbative calculations compare smeared observables with experiment [43–45]. The method is similar to that outlined for τ decays. The current correlator in Eq. (60.16) is the electromagnetic current, and the experimental data is the value of $R(s)$ in the threshold region for $e^+e^- \rightarrow Q\bar{Q}$. The theoretical values for the moments are computed using renormalization group improved calculations in non-relativistic QCD.

There are many continuum extractions of the c and b quark masses, some with quoted errors of 10 MeV or smaller. There are systematic effects of comparable size, which are typically not included in these error estimates. Reference [46], for example, shows that even though the error estimate of m_c using the rapid convergence of the α_s perturbation series is only a few MeV, the central value of m_c can differ by a much larger amount depending on which algorithm (all of which are formally equally good) is used to determine m_c from the data. This leads to a systematic error from perturbation theory of around 20 MeV for the c quark and 25 MeV for the b quark. Electromagnetic effects, which also are important at this precision, are often not included. For this reason, we inflate the errors on the continuum extractions of m_c and m_b . The average values of m_c and m_b from continuum determinations are (see Sec. 60.6 for the 1S scheme)

$$\bar{m}_c(\bar{m}_c) = (1.280 \pm 0.025) \text{ GeV},$$

$$\bar{m}_b(\bar{m}_b) = (4.18 \pm 0.03) \text{ GeV}, \quad m_b^{1S} = (4.65 \pm 0.03) \text{ GeV}.$$

60.5.2 Lattice approaches and results

Lattice QCD simulations of a heavy quark Q , described in a relativistic fermion formulation, lead to potentially large discretization errors which are powers of am_Q (modulated by logarithms);

the leading power depends on the formulation of lattice QCD being used and in most cases is quadratic. Clearly those errors can be reduced by performing simulations at smaller lattice spacings a , but also by using *improved* discretizations of the theory, in which the leading discretization errors are systematically eliminated. Recently, with more powerful computing resources, better algorithms and techniques, it has become possible to perform simulations in the charm quark region and beyond, also decreasing the extrapolation which has to be performed to reach the b -quark. It is worth noting that computations using a relativistic fermion formulation for the valence charm with $N_f = 2 + 1$ sea-quark flavors, or with even $N_f = 2 + 1 + 1$ flavors and a relativistic b , suffer from partial-quenching effects. This is because the heavy valence quarks, in those calculations, are absent from the sea. While these effects are not expected to be large, they should be investigated when quoting results below the percent level, especially in the case of $N_f = 2 + 1$ sea-quark flavors. For that reason, we will omit relativistic heavy quark results obtained with $N_f = 2 + 1$ sea-quark flavors from our averages and, more generally focus on $N_f = 2 + 1 + 1$ results. Note that these partial-quenching effects can be and are accounted for systematically in lattice calculations in which the heavy valence quarks are described by HQET or NRQCD.

Traditionally the charm quark mass is obtained by tuning its bare, simulation input value to reproduce the physical mass of charmonium mesons or of the D, D_s mesons (requiring a more precise tuning of the light quark masses). This mass can then be renormalized and matched to the $\overline{\text{MS}}$ scheme using the methods discussed for the light quarks.

An alternative approach for obtaining the $\overline{\text{MS}}$ mass from the tuned bare quark mass was proposed in [47]. Euclidean-time moments of pseudoscalar, two-point functions of $c\bar{c}$ quark-bilinear operators can readily be computed on the lattice and extrapolated to the continuum limit where they can be compared to perturbative calculations of the same quantities at 4-loop order. In this way, both the strong coupling constant and the charm quark mass can be determined with remarkably small errors. As this approach uses the same perturbative expressions for two-point correlators as the continuum determinations discussed above, it suffers from similar perturbation-theory, systematic errors. FLAG [8] has reviewed lattice determinations of the charm quark mass obtained using both approaches. For their $N_f = 2 + 1$ average they retain the results [10, 48–50], with [51] being published after their deadline. As stated above, we focus here on $N_f = 2 + 1 + 1$ results. For these, the quoted average is

$$\bar{m}_c(\bar{m}_c) = 1.278(13) \text{ GeV},$$

based on the results of [16, 17, 19, 22, 52, 53], in good agreement with the continuum result given above, but with a smaller error. Compared to the previous editions of the FLAG [23] and of the present reviews, [53] updates [18] and [22] has appeared, but did not make the FLAG deadline.

It is worth noting that three [17, 18, 53] of the five results entering this average agree, while the two others [19, 52] are over 2 standard deviations larger, a deviation confirmed by [22]. This is taken into account by stretching errors in the usual way, but the total uncertainty on the lattice average of \bar{m}_c will not significantly be reduced until this discrepancy is resolved. It should also be noted that [53] includes QED directly in the lattice calculation, albeit only for valence quarks, while some of the other computations account for these effects using phenomenology. For the moment these effects are still significantly smaller than the quoted error bars, at least when \bar{m}_c is determined using the mass of the J/ψ .

Historically, the main approach to controlling the discretization errors in lattice studies of b quark physics was to perform simulations of effective theories such as HQET and NRQCD. This remains an important technique, both in its own right and in providing additional information for extrapolations from lower masses to the bottom region. Using effective theories, m_b is obtained from what is essentially a computation of the difference of $M_{H_b} - m_b$, where M_{H_b} is the mass of a hadron H_b containing a b -quark. The relative error on m_b is therefore much smaller

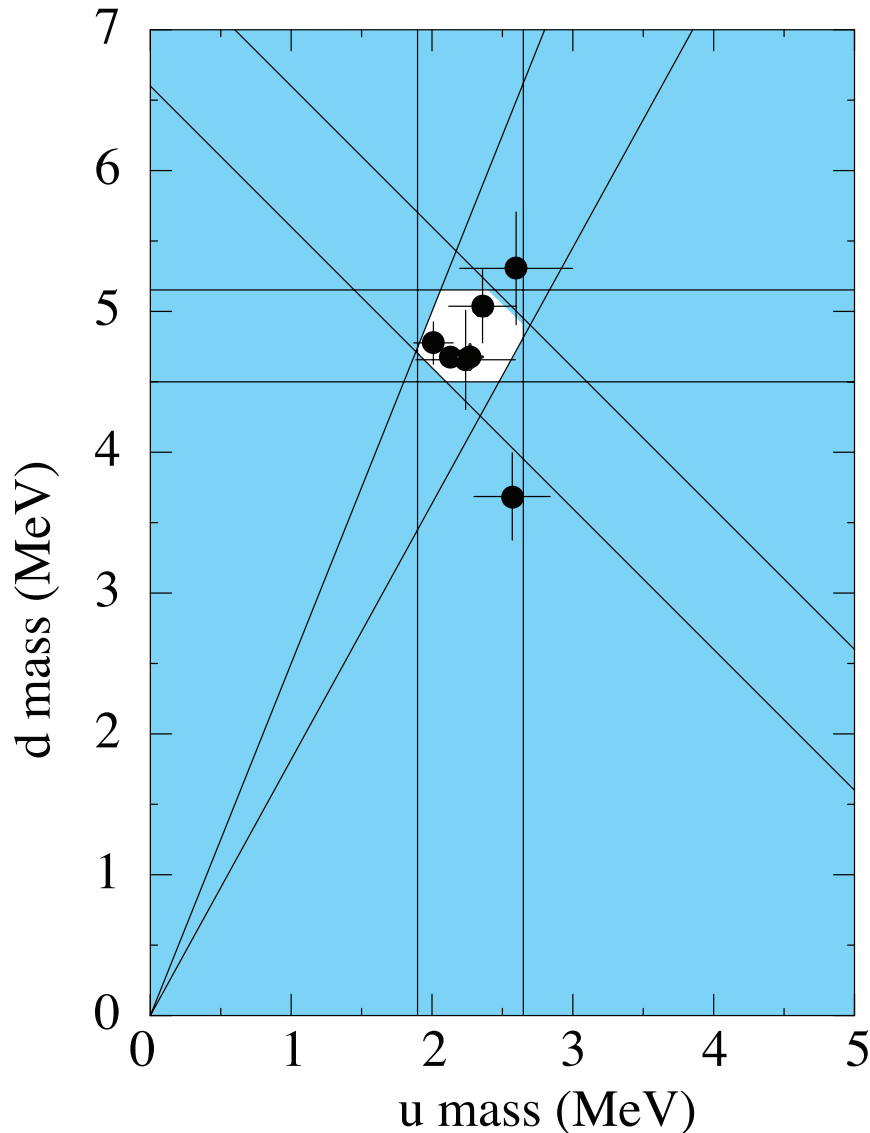


Figure 60.2: The allowed region (shown in white) for up quark and down quark masses renormalized in the $\overline{\text{MS}}$ scheme at 2 GeV. This region was determined in part from papers reporting values for m_u and m_d (data points shown) and in part from an analysis of the allowed ranges of other mass parameters (see Fig. 60.3). The parameter $(m_u + m_d)/2$ yields the two downward-sloping lines, while m_u/m_d yields the two rising lines originating at (0,0). There are two overlapping data points, so one of them is shown as a white diamond (it has very small error bars).

than that for $M_{H_b} - m_b$. The principal systematic errors are the matching of the effective theories to QCD and the presence of power divergences in a^{-1} in the $1/m_b$ corrections which have to be subtracted numerically. A procedure for performing these subtractions fully nonperturbatively was proposed and implemented for the first time in [54].

The most recent lattice QCD determinations of the b quark mass rely on a variety of approaches, including Euclidean-time moments of correlation functions with [55] or without NRQCD [56] and HQET based interpolations [57,58] or extrapolations [17] from above the charm to the b region. Compared to the previous editions of the FLAG [23] and of the present reviews, [56] updates [16] with a significantly reduced error bar. The overall agreement of the results obtained using these very different approaches, which have different systematic errors, is a confirmation that the various groups control these uncertainties. As the range of heavy-quark masses which can be used in numerical simulations increases, results obtained by extrapolating the results to the physical b mass are becoming ever more reliable (see e.g. [17]).

FLAG's compilation [8] of the above $N_f = 2 + 1 + 1$ results yields

$$\overline{m}_b(\overline{m}_b) = 4.203(11) \text{ GeV} ,$$

barely changed from the previous edition. Again, this result is compatible with the average value of continuum results, but with a significantly smaller uncertainty. Note that FLAG [8] also provides an average of $N_f = 2 + 1$ results, taken from [10, 50]. It is about 1.4 combined, standard deviations lower than the result quoted above.

As explained in Sec. 60.3, ratios of quark masses can have significantly smaller errors than the individual masses if they are determined within the same lattice QCD framework (up to small electromagnetic corrections for quarks of different charge). This led HPQCD to leverage their precise determination of m_c [47] to determine m_s and m_{ud} [59], through a precise computation of m_c/m_s [59] and of m_s/m_{ud} [60]. The $N_f = 2 + 1$ calculation [59] was updated using $N_f = 2 + 1 + 1$ simulations in [16]. The ratio m_s/m_c was also computed in [24,48] with $N_f = 2 + 1$ simulations and in [17,19] with $N_f = 2 + 1 + 1$ ones. The results of [19] should be replaced by those of [22] once the latter are published. Based

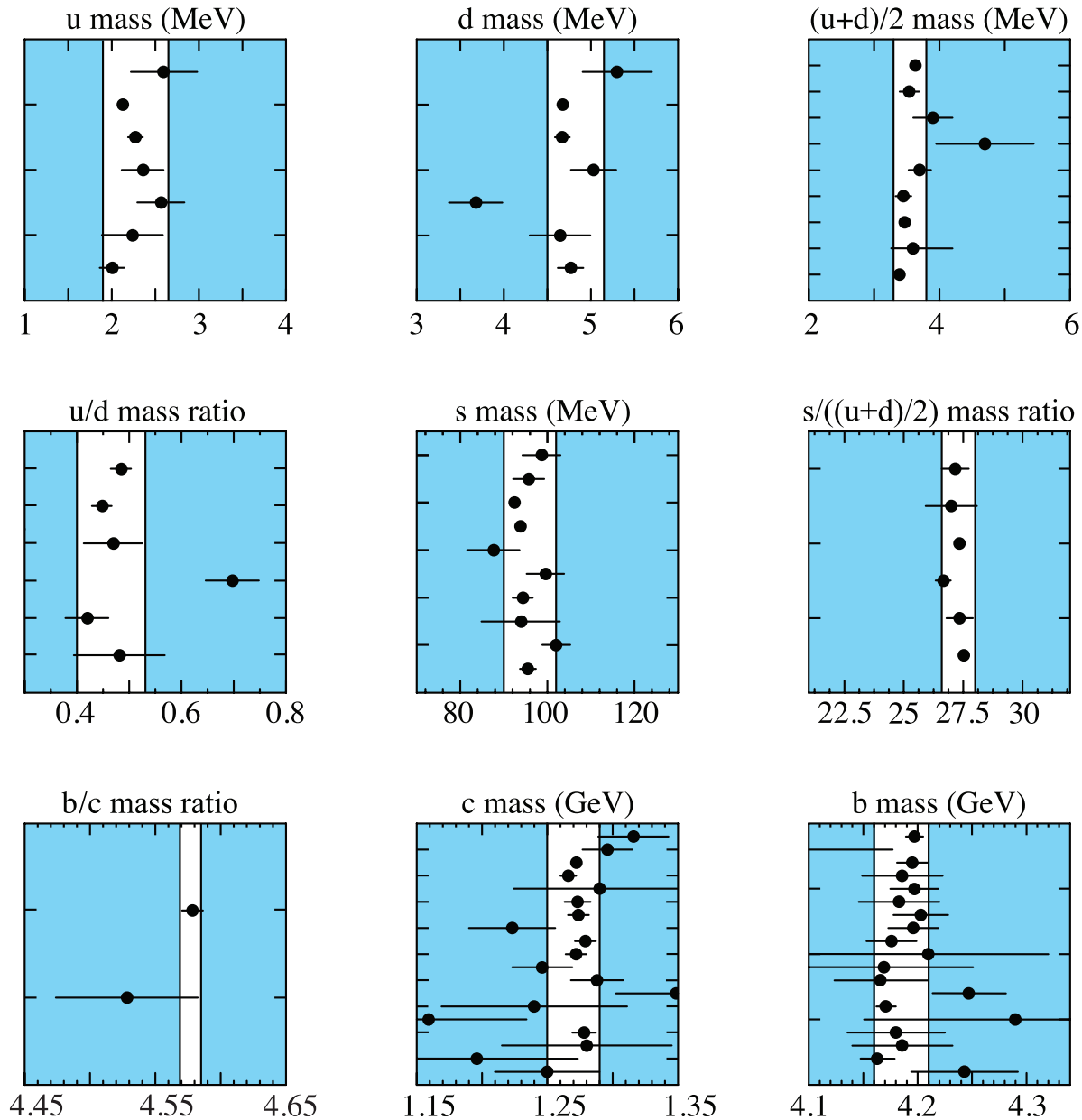


Figure 60.3: The values of each quark mass parameter taken from the Data Listings. The points are in chronological order with the more recent measurements at the top. The shaded regions indicate values excluded by our evaluations; some regions were determined in part through examination of Fig. 60.2.

on [48, 59], FLAG [8] quotes $m_c/m_s = 11.82(16)$ for $N_f = 2 + 1$, and $m_c/m_s = 11.769(35)$ for $N_f = 2 + 1 + 1$, based on [16, 17, 19], where a $\sim 50\%$ stretch of the error bars was applied due to tensions among the results. The latter average is completely dominated by the result of [17] that has a substantially smaller error than the other results. As a final lattice number we give the $N_f = 2 + 1 + 1$ average

$$m_c/m_s = 11.769(35),$$

which is renormalization scheme and scale independent (in the absence of electromagnetic corrections) and is identical to the one given in the last edition of the present review.

The ratio m_b/m_c has also been computed on the lattice. The two $N_f = 2 + 1$ results which satisfy FLAG's criteria are [10, 50]. Here, as explained above, we focus on $N_f = 2 + 1 + 1$ calculations [17, 56, 57]. Amongst these, [56] updates [16], used in the previous edition of the present review, with a substantially reduced error. Averaging these results yields

$$m_b/m_c = 4.579(9),$$

where a scale factor of $\sqrt{\chi^2/\text{dof}} = 1.38$ has been applied to the error bar. Indeed, [57] contributes 3.5 to the total χ^2 . Note that [56] is the only calculation which accounts for QED directly in the lattice simulations, albeit only for valence quarks, and thus must specify the renormalization scheme and scale of its result, which it chooses to be $\overline{\text{MS}}$ at 3 GeV.

60.5.3 Warnings concerning the use of the pole mass

For an observable particle such as the electron, the position of the pole in the propagator is the definition of its mass. In QCD this definition of the quark mass is known as the pole mass. It is known that the on-shell quark propagator has no infrared divergences in perturbation theory [61, 62], so this provides a perturbative definition of the quark mass. However, the pole mass cannot be used to arbitrarily high accuracy because of nonperturbative infrared effects in QCD. In fact the full quark propagator has no pole because the quarks are confined, so that the pole mass cannot be defined outside of perturbation theory. The relation between the pole mass m_Q and the $\overline{\text{MS}}$ mass \overline{m}_Q , used throughout this

review, is known to three loops [63–66]

$$m_Q = \overline{m}_Q(\overline{m}_Q) \left\{ 1 + \frac{4\overline{\alpha}_s(\overline{m}_Q)}{3\pi} \right. \quad (60.21)$$

$$+ \left[-1.0414 \sum_q \left(1 - \frac{4}{3} \frac{\overline{m}_q}{\overline{m}_Q} \right) + 13.4434 \right] \left[\frac{\overline{\alpha}_s(\overline{m}_Q)}{\pi} \right]^2$$

$$\left. + \left[0.6527N_L^2 - 26.655N_L + 190.595 \right] \left[\frac{\overline{\alpha}_s(\overline{m}_Q)}{\pi} \right]^3 \right\},$$

where $\overline{\alpha}_s(\mu)$ is the strong interaction coupling constants in the $\overline{\text{MS}}$ scheme, and the sum over q extends over the N_L flavors lighter than Q . The complete mass dependence of the α_s^2 term can be found in [63]; the mass dependence of the α_s^3 term is not known. For the b -quark, Eq. (60.21) reads

$$m_b = \overline{m}_b(\overline{m}_b) [1 + 0.10 + 0.05 + 0.03], \quad (60.22)$$

where the contributions from the different orders in α_s are shown explicitly. The two and three loop corrections are comparable in size and have the same sign as the one loop term. This is a signal of the asymptotic nature of the perturbation series (there is a renormalon in the pole mass [67]). Such a badly behaved perturbation expansion can be avoided by directly extracting, from data, the mass defined in the $\overline{\text{MS}}$ (used in this review) or other short-distance schemes (see below), without invoking the pole mass as an intermediate step.

60.6 Numerical values and caveats

The quark masses in the particle data listings have been obtained by using a wide variety of methods. Each method involves its own set of approximations and uncertainties. In most cases, the errors are an estimate of the size of neglected higher-order corrections or other uncertainties. The expansion parameters for some of the approximations are not very small (for example, they are $m_K^2/\Lambda_\chi^2 \sim 0.25$ for the SU(3) chiral expansion and $\Lambda_{\text{QCD}}/m_b \sim 0.1$ for the heavy-quark expansion), so an unexpectedly large coefficient in a neglected higher-order term could significantly alter the results. Thus, before using a particular result, it is important to understand the possible limitations of the approach used to obtain it. It is also important to note that the quark mass values can be significantly different in the different schemes.

We have specified all masses in the $\overline{\text{MS}}$ scheme. For light quarks, the renormalization scale has been chosen to be $\mu = 2 \text{ GeV}$. Quoting these masses at smaller values of μ , where perturbative corrections become significantly larger, would introduce unnecessary uncertainties in the results. In fact, as lattice calculations, performed on finer and finer lattices, allow to determine quark masses, fully nonperturbatively, at larger and larger values of μ , it may become advantageous to quote quark mass results at renormalization scales above 2 GeV, where perturbative uncertainties are smaller.

The heavy quark masses obtained using HQET, QCD sum rules, or lattice gauge theory are consistent with each other if they are all converted into the same scheme and scale. For these quarks it is conventional to choose the renormalization scale equal to the quark mass, so we have quoted $\overline{m}_Q(\mu)$ at $\mu = \overline{m}_Q$ for the c and b quarks. Given the small size of the charm quark mass, in the future it may become advantageous to quote its value at larger values of μ so as not to introduce unnecessary perturbative uncertainties (see discussion above). Analyses of inclusive B meson decays have shown that other mass definitions lead to a better behaved perturbation series than for the $\overline{\text{MS}}$ mass, and hence to more accurate mass values [68–71]. Thus, we have chosen to also give values for one of these, the b quark mass in the 1S scheme [68, 69]. Other schemes that have been proposed are the PS-scheme [70], the kinetic scheme [72] and, most recently, the minimal renormalon-subtracted mass (MRS) [71] used in the lattice calculation [17].

If necessary, we have converted values in the original papers to our chosen scheme using two-loop formulae. It is important to realize that our conversions introduce significant additional errors.

In converting to the $\overline{\text{MS}}$ b -quark mass, for example, the three-loop conversions from the 1S and pole masses give values about 35 MeV and 135 MeV lower than the two-loop conversions. The uncertainty in $\alpha_s(M_Z) = 0.1179 \pm 0.0010$ [1] gives an uncertainty of ± 9 MeV and ± 21 MeV respectively in the same conversions. We have not added these additional errors when we do our conversions. The α_s value in the conversion is correlated with the α_s value used in determining the quark mass, so the conversion error is not a simple additional error on the quark mass.

References

- [1] See the review of QCD in this volume.
- [2] A. Manohar and H. Georgi, Nucl. Phys. B **234**, 189 (1984).
- [3] K. Chetyrkin, Phys. Lett. B **404**, 161 (1997), [hep-ph/9703278].
- [4] J. Vermaseren, S. Larin and T. van Ritbergen, Phys. Lett. B **405**, 327 (1997), [hep-ph/9703284].
- [5] K. Chetyrkin, B. A. Kniehl and M. Steinhauser, Nucl. Phys. B **510**, 61 (1998), [hep-ph/9708255].
- [6] G. Martinelli *et al.*, Nucl. Phys. B **445**, 81 (1995), [hep-lat/9411010].
- [7] K. Jansen *et al.*, Phys. Lett. B **372**, 275 (1996), [hep-lat/9512009].
- [8] Y. Aoki *et al.* (2021), [arXiv:2111.09849].
- [9] A. Bazavov *et al.* (MILC), PoS **CD09**, 007 (2009), [arXiv:0910.2966].
- [10] C. McNeile *et al.*, Phys. Rev. D **82**, 034512 (2010), [arXiv:1004.4285].
- [11] A. Bazavov *et al.*, PoS **LATTICE2010**, 083 (2010), [arXiv:1011.1792].
- [12] S. Durr *et al.*, Phys. Lett. B **701**, 265 (2011), [arXiv:1011.2403].
- [13] S. Durr *et al.*, JHEP **08**, 148 (2011), [arXiv:1011.2711].
- [14] T. Blum *et al.* (RBC, UKQCD), Phys. Rev. D **93**, 7, 074505 (2016), [arXiv:1411.7017].
- [15] M. Bruno *et al.* (ALPHA), Eur. Phys. J. C **80**, 2, 169 (2020), [arXiv:1911.08025].
- [16] B. Chakraborty *et al.*, Phys. Rev. D **91**, 5, 054508 (2015), [arXiv:1408.4169].
- [17] A. Bazavov *et al.* (Fermilab Lattice, MILC, TUMQCD), Phys. Rev. D **98**, 5, 054517 (2018), [arXiv:1802.04248].
- [18] A. Lytle *et al.* (HPQCD), Phys. Rev. D **98**, 1, 014513 (2018), [arXiv:1805.06225].
- [19] N. Carrasco *et al.* (European Twisted Mass), Nucl. Phys. B **887**, 19 (2014), [arXiv:1403.4504].
- [20] A. Bazavov *et al.* (Fermilab Lattice, MILC), Phys. Rev. D **90**, 7, 074509 (2014), [arXiv:1407.3772].
- [21] A. Bazavov *et al.*, Phys. Rev. D **98**, 7, 074512 (2018), [arXiv:1712.09262].
- [22] C. Alexandrou *et al.* (2021), [arXiv:2104.13408].
- [23] S. Aoki *et al.* (Flavour Lattice Averaging Group), Eur. Phys. J. C **80**, 2, 113 (2020), [arXiv:1902.08191].
- [24] Y. Maezawa and P. Petreczky, Phys. Rev. D **94**, 3, 034507 (2016), [arXiv:1606.08798].
- [25] M. Bruno *et al.* (ALPHA), Phys. Rev. Lett. **114**, 10, 102001 (2015), [arXiv:1410.8374].
- [26] A. Athenodorou *et al.* (2018), [arXiv:1809.03383].
- [27] S. Borsanyi *et al.*, Science **347**, 1452 (2015), [arXiv:1406.4088].
- [28] Z. Fodor *et al.*, Phys. Rev. Lett. **117**, 8, 082001 (2016), [arXiv:1604.07112].
- [29] D. Giusti *et al.*, Phys. Rev. D **95**, 11, 114504 (2017), [arXiv:1704.06561].
- [30] S. Basak *et al.* (MILC), Phys. Rev. D **99**, 3, 034503 (2019), [arXiv:1807.05556].

- [31] S. Weinberg, *Physica A* **96**, 1-2, 327 (1979).
- [32] J. Gasser and H. Leutwyler, *Annals Phys.* **158**, 142 (1984).
- [33] A. Pich, *Rept. Prog. Phys.* **58**, 563 (1995), [hep-ph/9502366].
- [34] S. Weinberg, *Trans. New York Acad. Sci.* **38**, 185 (1977).
- [35] D. B. Kaplan and A. V. Manohar, *Phys. Rev. Lett.* **56**, 2004 (1986).
- [36] G. Colangelo *et al.*, *Eur. Phys. J. C* **78**, 11, 947 (2018), [arXiv:1807.11937].
- [37] S. Weinberg, *Phys. Rev. Lett.* **18**, 507 (1967).
- [38] M. A. Shifman, A. Vainshtein and V. I. Zakharov, *Nucl. Phys. B* **147**, 385 (1979).
- [39] E. Braaten, S. Narison and A. Pich, *Nucl. Phys. B* **373**, 581 (1992).
- [40] F. Le Diberder and A. Pich, *Phys. Lett. B* **286**, 147 (1992).
- [41] N. Isgur and M. B. Wise, *Phys. Lett. B* **237**, 527 (1990).
- [42] G. T. Bodwin, E. Braaten and G. Lepage, *Phys. Rev. D* **51**, 1125 (1995), [Erratum: *Phys.Rev.D* 55, 5853 (1997)], [hep-ph/9407339].
- [43] A. Hoang, *Phys. Rev. D* **61**, 034005 (2000), [hep-ph/9905550].
- [44] K. Melnikov and A. Yelkhovsky, *Phys. Rev. D* **59**, 114009 (1999), [hep-ph/9805270].
- [45] M. Beneke and A. Signer, *Phys. Lett. B* **471**, 233 (1999), [hep-ph/9906475].
- [46] B. Dehnadi *et al.*, *JHEP* **09**, 103 (2013), [arXiv:1102.2264].
- [47] I. Allison *et al.* (HPQCD), *Phys. Rev. D* **78**, 054513 (2008), [arXiv:0805.2999].
- [48] Y.-B. Yang *et al.*, *Phys. Rev. D* **92**, 3, 034517 (2015), [arXiv:1410.3343].
- [49] K. Nakayama, B. Fahy and S. Hashimoto, *Phys. Rev. D* **94**, 5, 054507 (2016), [arXiv:1606.01002].
- [50] P. Petreczky and J. Weber, *Phys. Rev. D* **100**, 3, 034519 (2019), [arXiv:1901.06424].
- [51] J. Heitger, F. Joswig and S. Kuberski (ALPHA), *JHEP* **05**, 288 (2021), [arXiv:2101.02694].
- [52] C. Alexandrou *et al.*, *Phys. Rev. D* **90**, 7, 074501 (2014), [arXiv:1406.4310].
- [53] D. Hatton *et al.* (HPQCD), *Phys. Rev. D* **102**, 5, 054511 (2020), [arXiv:2005.01845].
- [54] J. Heitger and R. Sommer (ALPHA), *JHEP* **02**, 022 (2004), [hep-lat/0310035].
- [55] B. Colquhoun *et al.*, *Phys. Rev. D* **91**, 7, 074514 (2015), [arXiv:1408.5768].
- [56] D. Hatton *et al.*, *Phys. Rev. D* **103**, 11, 114508 (2021), [arXiv:2102.09609].
- [57] A. Bussone *et al.* (ETM), *Phys. Rev. D* **93**, 11, 114505 (2016), [arXiv:1603.04306].
- [58] P. Gambino, A. Melis and S. Simula, *Phys. Rev. D* **96**, 1, 014511 (2017), [arXiv:1704.06105].
- [59] C. Davies *et al.*, *Phys. Rev. Lett.* **104**, 132003 (2010), [arXiv:0910.3102].
- [60] A. Bazavov *et al.* (MILC), *Rev. Mod. Phys.* **82**, 1349 (2010), [arXiv:0903.3598].
- [61] R. Tarrach, *Nucl. Phys. B* **183**, 384 (1981).
- [62] A. S. Kronfeld, *Phys. Rev. D* **58**, 051501 (1998), [hep-ph/9805215].
- [63] N. Gray *et al.*, *Z. Phys. C* **48**, 673 (1990).
- [64] D. J. Broadhurst, N. Gray and K. Schilcher, *Z. Phys. C* **52**, 111 (1991).
- [65] K. Chetyrkin and M. Steinhauser, *Phys. Rev. Lett.* **83**, 4001 (1999), [hep-ph/9907509].
- [66] K. Melnikov and T. v. Ritbergen, *Phys. Lett. B* **482**, 99 (2000), [hep-ph/9912391].
- [67] M. Beneke and V. M. Braun, *Nucl. Phys. B* **426**, 301 (1994), [hep-ph/9402364].
- [68] A. H. Hoang, Z. Ligeti and A. V. Manohar, *Phys. Rev. Lett.* **82**, 277 (1999), [hep-ph/9809423].
- [69] A. H. Hoang, Z. Ligeti and A. V. Manohar, *Phys. Rev. D* **59**, 074017 (1999), [hep-ph/9811239].
- [70] M. Beneke, *Phys. Lett. B* **434**, 115 (1998), [hep-ph/9804241].
- [71] N. Brambilla *et al.* (TUMQCD), *Phys. Rev. D* **97**, 3, 034503 (2018), [arXiv:1712.04983].
- [72] P. Gambino and N. Uraltsev, *Eur. Phys. J. C* **34**, 181 (2004), [hep-ph/0401063].

61. Top Quark

Revised September 2021 by T.M. Liss (City Coll. of New York), F. Maltoni (CP3 U. catholique de Louvain; Bologna U.) and A. Quadt (Göttingen U.).

61.1 Introduction

In the Standard Model (SM), the left-handed top quark is the $Q = 2/3$, $T_3 = +1/2$ member of the weak-isospin doublet containing the bottom quark, while the right-handed top is an $SU(2)_L$ singlet (see, e.g., the review “Electroweak Model and Constraints on New Physics” here). Its phenomenology is driven by its large mass. Being heavier than a W boson, it is the only quark that decays semi-weakly, i.e., into a real W boson and a b quark. This results in a lifetime that is shorter than the hadronization time. In addition, it is the only quark whose Yukawa coupling to the Higgs boson is of order unity. For these reasons, the top quark plays a special role in the Standard Model and in many extensions thereof. Top quark physics provides a unique laboratory where our understanding of the strong, both in the perturbative and non-perturbative regimes, and electroweak interactions can be tested. An accurate knowledge of its properties (mass, couplings, production cross sections, decay branching ratios, *etc.*) can bring key information on fundamental interactions at the electroweak symmetry-breaking scale and beyond. This review provides a concise discussion of the experimental and theoretical issues involved in the determination of the top-quark properties.

61.2 Top-quark production at the Tevatron and LHC

In hadron collisions, top quarks are produced dominantly in pairs through the processes $q\bar{q} \rightarrow t\bar{t}$ and $gg \rightarrow t\bar{t}$, at leading order in QCD. At the Tevatron ($p\bar{p}$ at 1.96 TeV) approximately 85% of the production cross section is from $q\bar{q}$ annihilation, with the remainder from gluon-gluon fusion. Conversely, at the LHC about 90% (80%) of $t\bar{t}$ production is from gluon-gluon fusion at $\sqrt{s} = 13$ TeV ($\sqrt{s} = 7$ TeV).

Predictions for the top-quark production total cross sections are available at next-to-next-to leading order (NNLO) [1, 2], also including next-to-next-to-leading-log (NNLL) soft gluon resummation. Assuming a top-quark mass of 173.3 GeV/ c^2 , close to the Tevatron + LHC combination [3], the resulting theoretical prediction of the top-quark pair cross-section at NNLO+NNLL accuracy at the Tevatron at $\sqrt{s} = 1.96$ TeV is $\sigma_{t\bar{t}} = 7.16^{+0.11+0.17}_{-0.20-0.12}$ pb where the first uncertainty is from scale dependence and the second from parton distribution functions. At the LHC, assuming a top-quark mass of 172.5 GeV/ c^2 the cross sections are: $\sigma_{t\bar{t}} = 177.3^{+4.6+9.0}_{-6.0-9.0}$ pb at $\sqrt{s} = 7$ TeV, $\sigma_{t\bar{t}} = 252.9^{+6.4+11.7}_{-8.6-11.7}$ pb at $\sqrt{s} = 8$ TeV, $\sigma_{t\bar{t}} = 831.8^{+19.8+35.1}_{-29.2-35.1}$ pb at $\sqrt{s} = 13$ TeV, and $\sigma_{t\bar{t}} = 984.5^{+23.2+41.3}_{-34.7-41.3}$ pb at $\sqrt{s} = 14$ TeV [1].

Electroweak single top-quark production mechanisms, namely from $q\bar{q}' \rightarrow t\bar{b}$ [4], $qb \rightarrow q't$ [5], mediated by virtual s -channel and t -channel W -bosons, and Wt -associated production, through $bg \rightarrow W^-t$, lead to somewhat smaller cross sections. For example, t -channel production, while suppressed by the weak coupling with respect to the strong pair production, is kinematically enhanced, resulting in a sizeable cross section both at Tevatron and LHC energies. At the Tevatron, the t - and s -channel cross sections for top quarks are identical to those for anti-top quarks, while at the LHC they are not, due to the charge-asymmetric initial state. NNLO cross sections for t -channel single top-quark production ($t + \bar{t}$) are calculated for $m_t = 173.2$ GeV/ c^2 to be $2.08^{+0.04+0.08}_{-0.03-0.10}$ pb in $p\bar{p}$ collisions at $\sqrt{s} = 1.96$ TeV, where the first uncertainty is from scale dependence and the second from parton distribution functions. [6]. A calculation at NNLO accuracy for the t -channel cross section at the LHC has first appeared in [7], superseded by more recent calculations [6, 8] which predict ($m_t = 172.5$ GeV/ c^2): $\sigma_{t+\bar{t}} = 64.0^{+0.77}_{-0.38}$ pb at $\sqrt{s} = 7$ TeV, $\sigma_{t+\bar{t}} = 84.6^{+1.0}_{-0.5}$ pb at $\sqrt{s} = 8$ TeV, $\sigma_{t+\bar{t}} = 215^{+2.1}_{-1.3}$ pb at $\sqrt{s} = 13$ TeV, and $\sigma_{t+\bar{t}} = 245^{+2.7}_{-1.3}$ pb at $\sqrt{s} = 14$ TeV, where the quoted uncertainties are from scale variation only. For the s -channel, NNLO approximated calculations yield $1.03^{+0.05}_{-0.05}$ pb for the Tevatron [9]. An NLO calculation gives $4.3^{+0.13+0.14}_{-0.10-0.14}$ pb, $5.2^{+0.15+0.16}_{-0.12-0.16}$ pb,

and $10.3^{+0.29+0.27}_{-0.24-0.27}$ pb for $\sqrt{s} = 7, 8, 13$ TeV at the LHC, respectively, with 64%, 64%, 62%, of top quarks. While negligible at the Tevatron, at LHC energies the Wt -associated production becomes relevant. At $\sqrt{s} = 7, 8, 13$ TeV, an approximate NNLO calculation gives ($t + \bar{t}$), $15.7^{+0.4+1.10}_{-0.4-1.14}$ pb, $22.4^{+0.6+1.40}_{-0.6-1.40}$ pb, $71.7^{+1.8+3.40}_{-1.8-3.40}$ pb, respectively, with an equal proportion of top and anti-top quarks [10].

Assuming $|V_{tb}| \gg |V_{td}|, |V_{ts}|$ (see the review “The CKM Quark-Mixing Matrix” for more information), the cross sections for single top production are proportional to $|V_{tb}|^2$, and no extra hypothesis is needed on the number of quark families or on the unitarity of the CKM matrix in extracting $|V_{tb}|$. Separate measurements of the s - and t -channel processes provide sensitivity to physics beyond the Standard Model [11].

With a mass above the Wb threshold, and $|V_{tb}| \gg |V_{td}|, |V_{ts}|$, the decay width of the top quark is expected to be dominated by the two-body channel $t \rightarrow Wb$. Neglecting terms of order m_b^2/m_t^2 , α_s^2 , and $(\alpha_s/\pi)M_W^2/m_t^2$, the width predicted in the SM at NLO is [12]:

$$\Gamma_t = \frac{G_F m_t^3}{8\pi\sqrt{2}} \left(1 - \frac{M_W^2}{m_t^2}\right)^2 \left(1 + 2\frac{M_W^2}{m_t^2}\right) \left[1 - \frac{2\alpha_s}{3\pi} \left(\frac{2\pi^2}{3} - \frac{5}{2}\right)\right], \quad (61.1)$$

where m_t refers to the top-quark pole mass. The width for a value of $m_t = 173.3$ GeV/ c^2 is 1.35 GeV/ c^2 (we use $\alpha_s(M_Z) = 0.118$) and increases with mass. With its correspondingly short lifetime of about 0.5×10^{-24} s, the top quark is expected to decay before top-flavored hadrons or $t\bar{t}$ -quarkonium-bound states can form [13]. In fact, since the decay time is close to the would-be-resonance binding time, a peak will be visible in e^+e^- scattering at the $t\bar{t}$ threshold [14] and it is in principle present (yet very difficult to measure) in hadron collisions too [15, 16]. The order α_s^2 QCD corrections to Γ_t are also available [17], thereby improving the overall theoretical accuracy to better than 1%.

The final states for the leading pair-production process can be divided into three classes:

- A. $t\bar{t} \rightarrow W^+ b W^- \bar{b} \rightarrow q\bar{q}' b q'' \bar{q}''' \bar{b}$, (45.7%)
- B. $t\bar{t} \rightarrow W^+ b W^- \bar{b} \rightarrow q\bar{q}' b \ell^- \bar{\nu}_\ell \bar{b} + \ell^+ \nu_\ell b q'' \bar{q}''' \bar{b}$, (43.8%)
- C. $t\bar{t} \rightarrow W^+ b W^- \bar{b} \rightarrow \ell^+ \nu_\ell b \ell'^- \bar{\nu}_{\ell'}$. (10.5%)

The quarks in the final state evolve into jets of hadrons. A, B, and C are referred to as the all-hadronic, lepton+jets (ℓ +jets), and dilepton ($\ell\ell$) channels, respectively. Their relative contributions, including hadronic corrections, are given in parentheses assuming lepton universality. While ℓ in the above processes refers to e , μ , or τ , most of the analyses distinguish the e and μ from the τ channel, which is more difficult to reconstruct. Therefore, in what follows, we will use ℓ to refer to e or μ , unless otherwise noted. Here, typically leptonic decays of τ are included. In addition to the quarks resulting from the top-quark decays, extra QCD radiation (quarks and gluons) from the colored particles in the event can lead to extra jets.

The number of jets reconstructed in the detectors depends on the decay kinematics, as well as on the algorithm for reconstructing jets used by the analysis. Information on the transverse momenta, p_T of the neutrinos is obtained from the imbalance in transverse momentum measured in each event (missing p_T , which is here also called missing transverse energy, E_T).

The identification of top quarks in the electroweak single top channel is much more difficult than in the QCD $t\bar{t}$ channel, due to a less distinctive signature and significantly larger backgrounds, mostly due to $t\bar{t}$ and W +jets production.

Fully exclusive predictions via Monte Carlo generators for the $t\bar{t}$ and single top production processes at NLO accuracy in QCD, including top-quark decays and possibly off-shell effects are available [18, 19] through the MC@NLO [20] and POWHEG [21] methods. Very recently, the first Monte Carlo implementation of the NNLO computation has become available [22].

Besides fully inclusive QCD or EW top-quark production, more exclusive final states can be accessed at hadron colliders, whose

cross sections are typically much smaller, yet can provide key information on the properties of the top quark. For all relevant final states (e.g., $t\bar{t}V$, $t\bar{t}VV$ with $V = \gamma, W, Z$, $t\bar{t}H, t\bar{t}+\text{jets}$, $t\bar{t}b\bar{b}$, $t\bar{t}t\bar{t}$) automatic or semi-automatic predictions at NLO accuracy both in QCD and EW expansions, also in the form of event generators are available (see the review “Monte Carlo event generators” for more information).

61.3 Top-quark measurements

Since the discovery of the top quark, direct measurements of $t\bar{t}$ production have been made at six center-of-mass energies in pp or $p\bar{p}$ and in pPb collisions, providing stringent tests of QCD. The first measurements were made in Run I at the Tevatron at $\sqrt{s} = 1.8$ TeV. In Run II at the Tevatron relatively precise measurements were made at $\sqrt{s} = 1.96$ TeV. Finally, beginning in 2010, measurements have been made at the LHC at $\sqrt{s} = 7$ TeV, $\sqrt{s} = 8$ TeV, and $\sqrt{s} = 13$ TeV, and recently also in dedicated low energy runs at $\sqrt{s} = 5.02$ in pp and at 8.16 TeV in pPb collisions.

Production of single top quarks through electroweak interactions has now been measured with good precision at the Tevatron at $\sqrt{s} = 1.96$ TeV, and at the LHC at $\sqrt{s} = 7$ TeV, $\sqrt{s} = 8$ TeV, and also at $\sqrt{s} = 13$ TeV. Measurements at the Tevatron have managed to separate the s - and t -channel production cross sections, and at the LHC, the tW mechanism as well, though the t -channel is measured with best precision to date. The measurements allow an extraction of the CKM matrix element V_{tb} . Also more exclusive production modes and top-quark properties have been measured in single-top production.

With approximately 10 fb^{-1} of Tevatron data, and almost 5 fb^{-1} at 7 TeV, 20 fb^{-1} at 8 TeV and 139 fb^{-1} at 13 TeV at the LHC, many properties of the top quark have been measured with high precision. These include properties related to the production mechanism, such as $t\bar{t}$ spin correlations, forward-backward or charge asymmetries, and differential production cross sections, as well as properties related to the tWb decay vertex, such as the helicity of the W -bosons from the top-quark decay. Also studies of the $t\bar{t}b\bar{b}$, $t\bar{t}t\bar{t}$, $t\bar{t}\gamma$, $t\bar{t}Z$, $t\bar{t}h$, th , tZq or $t\gamma q$ processes and the corresponding vertices as well as contact interactions have been made, some yielding first observations, others strong evidence. Those processes probe genuinely new aspects of the top-quark such as electroweak couplings to neutral gauge bosons or possibly four-top-quark interactions. In addition, many searches for physics beyond the Standard Model are being performed with increasing reach in both production and decay channels.

In the following sections we review the current status of measurements of the characteristics of the top quark.

61.3.1 Top-quark production

61.3.1.1 $t\bar{t}$ production

Fig. 61.1 summarizes the $t\bar{t}$ production cross-section measurements from both, the Tevatron and LHC. Please note that some cross section measurements at the LHC have luminosity-related uncertainties which have improved in the meantime [23]. The latest measurement from DØ [24] ($p\bar{p}$ at $\sqrt{s} = 1.96$ TeV), combining the measurements from the dilepton and lepton plus jets final states in 9.7 fb^{-1} , is 7.26 ± 0.13 (stat.) $^{+0.57}_{-0.50}$ (syst.) pb (7.5%). From CDF the most precise measurement made [25] is in 8.8 fb^{-1} in the dilepton channel requiring at least one b -tag, yielding 7.09 ± 0.84 pb. Both of these measurements assume a top-quark mass of $172.5 \text{ GeV}/c^2$. The dependence of the cross-section measurements on the value chosen for the mass is less than that of the theory calculations because it only affects the determination of the acceptance. In some analyses also the shape of topological variables might be modified.

Combining the recent cross section measurements with older ones in other channels yields $\sigma_{t\bar{t}} = 7.63 \pm 0.50$ pb (6.6%) for CDF, $\sigma_{t\bar{t}} = 7.56 \pm 0.59$ pb (7.8%) for DØ and $\sigma_{t\bar{t}} = 7.60 \pm 0.41$ pb (5.4%) for the Tevatron combination [26]. The contributions to the uncertainty are 0.20 pb from statistical sources, 0.29 pb from systematic sources, and 0.21 pb from the uncertainty on the integrated luminosity. The combined result is in good agreement with the SM expectation of $7.35^{+0.28}_{-0.33}$ pb at NNLO+NNLL in perturbative QCD [1] for a top mass of $172.5 \text{ GeV}/c^2$.

CDF has measured the $t\bar{t}$ production cross section in the dilepton channel with one hadronically decaying tau in 9.0 fb^{-1} , yielding $\sigma_{t\bar{t}} = 8.1 \pm 2.1$ pb. By separately identifying the single-tau and the ditau components, they measure the branching fraction of the top quark into the tau lepton, tau neutrino, and bottom quark to be $(9.6 \pm 2.8)\%$ [27]. CDF has also performed measurements of the $t\bar{t}$ production cross section normalized to the Z production cross section in order to reduce the impact of the luminosity uncertainty [28].

DØ has performed a measurement of differential $t\bar{t}$ cross sections in 9.7 fb^{-1} of lepton+jets data as a function of the transverse momentum, and absolute value of the rapidity of the top quarks as well as of the invariant mass of the $t\bar{t}$ pair [29]. Observed differential cross sections are consistent with SM predictions.

The LHC experiments ATLAS and CMS use similar techniques to measure the $t\bar{t}$ cross section in pp collisions. The most precise measurements come from the dilepton channel, and in particular the $e\mu$ channel. In order to test consistency of the cross-section measurements with some systematic uncertainties cancelling out while testing pQCD and PDFs, cross-section ratios between measurements at 7 TeV and at 8 TeV are performed and quoted in several cases. In other cases, the cross-section ratio between $t\bar{t}$ - and Z -production is determined as that is independent of luminosity uncertainties, but keeps its sensitivity to the ratio of gluon versus quark PDFs. These experimental results should be compared to the theoretical calculations at NNLO+NNLL that yield $7.16^{+0.20}_{-0.23}$ pb for top-quark mass of $173.3 \text{ GeV}/c^2$ [1] at $\sqrt{s} = 1.96$ TeV, $68.2 \pm 4.8^{+1.9}_{-2.3}$ pb [30] for top-quark mass of $172.5 \text{ GeV}/c^2$ at $\sqrt{s} = 5$ TeV, and for top-quark mass of $173.3 \text{ GeV}/c^2$ $\sigma_{t\bar{t}} = 173.6^{+4.5+8.9}_{-5.9-8.9}$ pb at $\sqrt{s} = 7$ TeV, $\sigma_{t\bar{t}} = 247.7^{+6.3+11.5}_{-8.5-11.5}$ pb at $\sqrt{s} = 8$ TeV, and $\sigma_{t\bar{t}} = 816.0^{+19.4+34.4}_{-28.6-34.4}$ pb at $\sqrt{s} = 13$ TeV, at the LHC [1]. In a special run, ATLAS recorded 257 pb^{-1} at $\sqrt{s} = 5.02$ TeV. Using opposite charged dilepton events and counting the number of b -jets, they perform a fit including m_{ll} information to constrain Z +jets background, yielding a result of $\sigma_{t\bar{t}} = 66.0 \pm 4.9$ pb, giving a total uncertainty of 7.5% [31]. CMS has measured the $t\bar{t}$ production cross section at $\sqrt{s} = 5.02$ TeV, accumulating 27.4 pb^{-1} . The measurement is performed by analyzing events with at least one charged lepton. The measured cross section is $\sigma_{t\bar{t}} = 69.5 \pm 8.4$ pb [32], in agreement with the expectation from the Standard Model. Recently, they performed a measurement in opposite-sign $e\mu$ -dilepton events with at least two jets using 304 pb^{-1} . They obtain a Drell-Yan scale factor under the Z -boson mass to estimate the background and extract a cross section using a counting technique of $\sigma_{t\bar{t}} = 60.3 \pm 5.8$ pb. The combination of the two results yields $\sigma_{t\bar{t}} = 62.6 \pm 4.1$ (stat.) ± 3.0 (syst. + lumi.) pb with 7.9% total relative uncertainty [33]. At $\sqrt{s} = 7$ TeV, ATLAS uses 4.6 fb^{-1} of $e\mu$ events in which they select an extremely clean sample and determine the $t\bar{t}$ cross section simultaneously with the efficiency to reconstruct and tag b -jets, yielding $\sigma_{t\bar{t}} = 182.9 \pm 7.1$ pb, corresponding to 3.9% precision [34]. Other measurements by ATLAS at $\sqrt{s} = 7$ TeV, include a measurement in 0.7 fb^{-1} in the lepton+jets channel [35], in the dilepton channel [36], and in 1.02 fb^{-1} in the all-hadronic channel [37], which together yield a combined value of $\sigma_{t\bar{t}} = 177 \pm 3$ (stat.) $^{+8}_{-7}$ (syst.) ± 7 (lumi.) pb (6.2%) assuming $m_t = 172.5 \text{ GeV}/c^2$ [38]. Further analyses in the hadronic τ plus jets channel in 1.67 fb^{-1} [39] and the hadronic τ + lepton channel in 2.05 fb^{-1} [40], and the all-hadronic channel in 4.7 fb^{-1} [41] yield consistent albeit less precise results. Another simultaneous measurement of the $t\bar{t}, W^+W^-$, and $Z/\gamma^* \rightarrow \tau\tau$ cross section using the full 7 TeV dataset with 4.6 fb^{-1} yields $\sigma_{t\bar{t}} = 181 \pm 11$ pb, corresponding to a 6% precision [42]. The most precise measurement from CMS at $\sqrt{s} = 7$ TeV is also obtained in the dilepton channel, where they measure $\sigma_{t\bar{t}} = 161.9 \pm 2.5$ (stat.) $^{+5.1}_{-5.0}$ (syst.) ± 3.6 (lumi.) pb, corresponding to a 4.2% precision [43]. Other measurements at $\sqrt{s} = 7$ TeV from CMS include measurements with 2.3 fb^{-1} in the e/μ +jets channel [44], with 3.5 fb^{-1} in the all-hadronic channel [45], with 2.2 fb^{-1} in the lepton+ τ channel [46], and with 3.9 fb^{-1} in the τ +jets channel [47]. ATLAS and CMS also provide a combined cross section at $\sqrt{s} = 7$ TeV of 173.3 ± 2.3 (stat.) \pm

7.6(stat.) \pm 6.3(lumi.) pb using slightly older results based on 0.7 – 1.1 fb⁻¹ [48]. At $\sqrt{s} = 8$ TeV, ATLAS measures the $t\bar{t}$ cross section with 20.3 fb⁻¹ using $e\mu$ dilepton events, with a simultaneous measurement of the b -tagging efficiency, yielding $\sigma_{t\bar{t}} = 242.9 \pm 1.7(stat.) \pm 5.5(syst.) \pm 5.1(lumi.) \pm 4.2(beam\ energy)$ pb [49] assuming $m_t = 172.5$ GeV/c², which corresponds to a 3.6% precision. In the $\ell + jets$ channel, they measure $\sigma_{t\bar{t}} = 260 \pm 1(stat.)_{-23}^{+20}(syst.) \pm 8(lumi.) \pm 4(beam\ energy)$ pb [50] in 20.3 fb⁻¹ using a likelihood discriminant fit and b -jet identification. Subsequently, ATLAS performed a new analysis in 20.2 fb⁻¹ $\ell + jets$ events. They model the $W + jets$ background using $Z + jets$ data and employ neural networks in three jet-multiplicity and b -jet multiplicity regions for the signal and background separation, yielding $\sigma_{t\bar{t}} = 248.3 \pm 0.7(stat.) \pm 13.4(syst.) \pm 4.7(lumi.)$ pb [51]. ATLAS also performed a cross section measurement in the hadronic $\tau + jets$ channel yielding consistent, albeit less precise results [52]. CMS performs a template fit to the M_{lb} mass distribution using 19.6 fb⁻¹ in the lepton+jets channel yielding $\sigma_{t\bar{t}} = 228.5 \pm 3.8(stat.) \pm 13.7(syst.) \pm 6.0(lumi.)$ pb [53, 54], which corresponds to a 6.7% precision. These 8 TeV measurements are in agreement with QCD predictions up to NLO accuracy. In the $e\mu$ channel, initially using 5.3 fb⁻¹ [54] and then using 19.7 fb⁻¹, the cross sections are extracted using a binned likelihood fit to multi-differential final state distributions related to identified b quark and other jets in the event, yielding $\sigma_{t\bar{t}} = 244.9 \pm 1.4(stat.)_{-5.5}^{+6.3}(syst.) \pm 6.4(lumi.)$ pb [55]. The cross section and its ratio between 7 TeV and 8 TeV measurements are found to be consistent with pQCD calculations. The cross section is also measured in the hadronic $\tau + jets$ channel, yielding $\sigma_{t\bar{t}} = 257 \pm 3(stat.) \pm 24(syst.) \pm 7(lumi.)$ pb [56] and in the all-hadronic final state giving $\sigma_{t\bar{t}} = 275.6 \pm 6.1(stat.) \pm 37.8(syst.) \pm 7.2(lumi.)$ pb [57]. In combination of the most precise $e\mu$ measurements in 5.3 – 20.3 fb⁻¹, ATLAS and CMS together yield at 8 TeV $\sigma_{t\bar{t}} = 241.5 \pm 1.4(stat.) \pm 5.7(syst.) \pm 6.2(lumi.)$ pb [58], which corresponds to a 3.5% precision, challenging the precision of the corresponding theoretical predictions. The LHCb collaboration presented the first observation of top-quark production in the forward region in pp -collisions. The $W + b$ final state with $W \rightarrow \mu\nu$ is reconstructed using muons with a transverse momentum, p_T , larger than 25 GeV in the pseudorapidity range $2.0 < \eta < 4.5$. The b -jets are required to have 50 GeV $< p_T < 100$ GeV and $2.2 < \eta < 4.2$, while the transverse component of the sum of the muon and b -jet momenta must satisfy $p_T > 20$ GeV. The results are based on data corresponding to integrated luminosities of 1.0 and 2.0 fb⁻¹ collected at center-of-mass energies of 7 and 8 TeV by LHCb. The inclusive top quark production cross sections in the fiducial region are $\sigma_{t\bar{t}} = 239 \pm 53(stat.) \pm 38(syst.)$ pb at 7 TeV, and $\sigma_{t\bar{t}} = 289 \pm 43(stat.) \pm 46(syst.)$ pb at 8 TeV [59]. ATLAS and CMS have also measured the $t\bar{t}$ production cross section with Run-II data at $\sqrt{s} = 13$ TeV. In the $e\mu$ events with at least one b -tag, ATLAS uses 78 pb⁻¹ and obtains $\sigma_{t\bar{t}} = 825 \pm 114$ pb [60]. This measurement is updated with lepton identification and trigger efficiencies to give $\sigma_{t\bar{t}} = 829 \pm 50(stat.) \pm 56(syst.) \pm 83(lumi)$ pb [61]. In this note, ATLAS also presents a $t\bar{t}$ cross section measurement in the ee and $\mu\mu$ dilepton channel with one and two b -tags using a counting approach, yielding $\sigma_{t\bar{t}} = 749 \pm 57(stat.) \pm 79(syst.) \pm 74(lumi.)$ pb. The cross section measurement in the $e\mu$ channel counting events with one or with two b -tags is also repeated using 3.2 pb⁻¹ and yields $\sigma_{t\bar{t}} = 818 \pm 8(stat.) \pm 27(syst.) \pm 19(lumi.) \pm 12(beam)$ pb [62], consistent with theoretical QCD calculations at NNLO. In 36.1 fb⁻¹ of $e\mu$ data with one or two b -tags, ATLAS measures the $t\bar{t}$ cross section to $\sigma_{t\bar{t}} = 826.4 \pm 3.6(stat.) \pm 11.5(syst.) \pm 15.7(lumi.) \pm 1.9(beam)$ pb, giving a total of 2.4%. This measurement is also used to determine the top quark pole mass and to derive ratios and double ratios of $t\bar{t}$ and Z cross-sections at different energies as well as absolute and normalised differential cross-sections as functions of single lepton and dilepton kinematic variables [63]. In the $\ell + jets$, using 85 pb⁻¹, the cross-section is extracted by counting the number of events with exactly one electron or muon and at least four jets, at least one of which is identified as originating from a b -quark, yielding $\sigma_{t\bar{t}} = 817 \pm 13(stat.) \pm 103(syst.) \pm 88(lumi.)$ pb, both assuming $m_t = 172.5$ GeV/c² [61].

Very recently, ATLAS measures the inclusive $t\bar{t}$ cross section in 139 fb⁻¹ in the $\ell + jets$ through a profile-likelihood fit to be $\sigma_{t\bar{t}} = 830.4 \pm 0.4(stat.) \pm 36(syst.) \pm 14(lumi)$ pb, with a relative uncertainty of 4.6% [64]. The result is consistent with the theoretical calculations at NNLO order in QCD perturbation theory. CMS uses 43 pb⁻¹ in the $e\mu$ channel to measure $\sigma_{t\bar{t}} = 746 \pm 58(stat.) \pm 53(syst.) \pm 36(lumi)$ pb, in agreement with the expectation from the standard model [65]. Using 2.2 fb⁻¹ in the $e\mu$ channel with at least one b -jet, CMS measures $\sigma_{t\bar{t}} = 815 \pm 9(stat.) \pm 38(syst.) \pm 19(lumi.)$ pb (5.3%), in agreement with the expectation from the Standard Model [66]. Using 35.9 fb⁻¹ of dilepton data, CMS measures the $t\bar{t}$ cross section using a likelihood fit $\sigma_{t\bar{t}} = 803 \pm 2(stat.) \pm 25(syst.) \pm 20(lumi.)$ pb (4.0%), in agreement with the expectation from the SM calculation at NNLO order. This result is also used to extract the top quark mass and the strong coupling constant [67]. Using the same dataset in the dilepton channel with a hadronically decaying τ , they measure $\sigma_{t\bar{t}} = 781 \pm 7(stat.) \pm 62(syst.) \pm 20(lumi.)$ pb (8.3%) [68]. A first measurement of the total inclusive and the normalized differential cross section in the $\ell + jets$ channel is made in 42 pb⁻¹ yielding $\sigma_{t\bar{t}} = 836 \pm 27(stat.) \pm 88(syst.) \pm 100(lumi.)$ pb [69]. In 2.2 fb⁻¹, $\ell + jets$ events are categorized according to the accompanying jet multiplicity. From a likelihood fit to the invariant mass distribution of the isolated lepton and a b -jet, the cross section is measured to be $\sigma_{t\bar{t}} = 888 \pm 2(stat.)_{-28}^{+26}(syst.) \pm 20(lumi)$ pb, in agreement with the SM prediction [70]. This result is also used to extract the top-quark mass. Recently, CMS has used 137 pb⁻¹ in four regions determined by top p_T and b -tag score to measure the cross section in the $\ell + jets$ channel. They employ a combined χ^2 fit considering the migration matrices. Most of the measured differential cross sections are well described by standard model predictions with the exception of some double-differential distributions. They obtain $\sigma_{t\bar{t}} = 791 \pm 1(stat.) \pm 21(syst.) \pm 14(lumi)$ pb (3.2%) [71]. In the all-hadronic channel, CMS uses 2.53 fb⁻¹ of data, yielding a cross section of $\sigma_{t\bar{t}} = 834 \pm 25(stat.)_{-104}^{+118}(syst.) \pm 23(lumi.)$ pb [72]. Also differential cross sections as a function of the leading top quark transverse momentum are measured. As general feature across channels, it is found that the measured top quark p_T spectrum is significantly softer than the NLO+PS theory predictions considered in the corresponding publications. CMS also performed a measurement of top-quark pair production in pPb heavy ion collisions at $\sqrt{s} = 8.16$ TeV in 174 nb⁻¹ of lepton+jets events. They measure a cross section of $\sigma_{t\bar{t}} = 45 \pm 8$ nb, which is consistent with pQCD calculations and with the scaled pp data [73].

In Fig. 61.1, one sees the importance of $p\bar{p}$ at Tevatron energies where the valence antiquarks in the antiprotons contribute to the dominant $q\bar{q}$ production mechanism. At LHC energies, the dominant production mode is gluon-gluon fusion and the pp - $p\bar{p}$ difference nearly disappears. The excellent agreement of these measurements with the theory calculations is a strong validation of QCD and the soft-gluon resummation techniques employed in the calculations. The measurements reach high precision and provide stringent tests of pQCD calculations at NNLO+NNLL level including their respective PDF uncertainties.

Most of these measurements assume a $t \rightarrow Wb$ branching ratio of 100%. CDF and DØ have made direct measurements of the $t \rightarrow Wb$ branching ratio [74]. Comparing the number of events with 0, 1 and 2 tagged b jets in the lepton+jets channel, and also in the dilepton channel, using the known b -tagging efficiency, the ratio $R = B(t \rightarrow Wb) / \sum_{q=d,s,b} B(t \rightarrow Wq)$ can be extracted. In 5.4 fb⁻¹ of data, DØ measures $R = 0.90 \pm 0.04$, 2.5 standard deviations from unity. The currently most precise measurement was made by CMS in 19.7 fb⁻¹ at $\sqrt{s} = 8$ TeV. They find $R = 1.014 \pm 0.003(stat.) \pm 0.032(syst.)$ and $R > 0.955$ at 95% C.L. [75]. A significant deviation of R from unity would imply either non-SM top-quark decay (for example a flavor-changing neutral-current decay), or a fourth generation of quarks. The latter is by other measurements.

Thanks to the large available event samples, the Tevatron and the LHC experiments also performed single-, double- or even triple-differential cross-section measurements in $t\bar{t}$ production. Such measurements are crucial, as they allow even more stringent tests of perturbative QCD as description of the production mech-

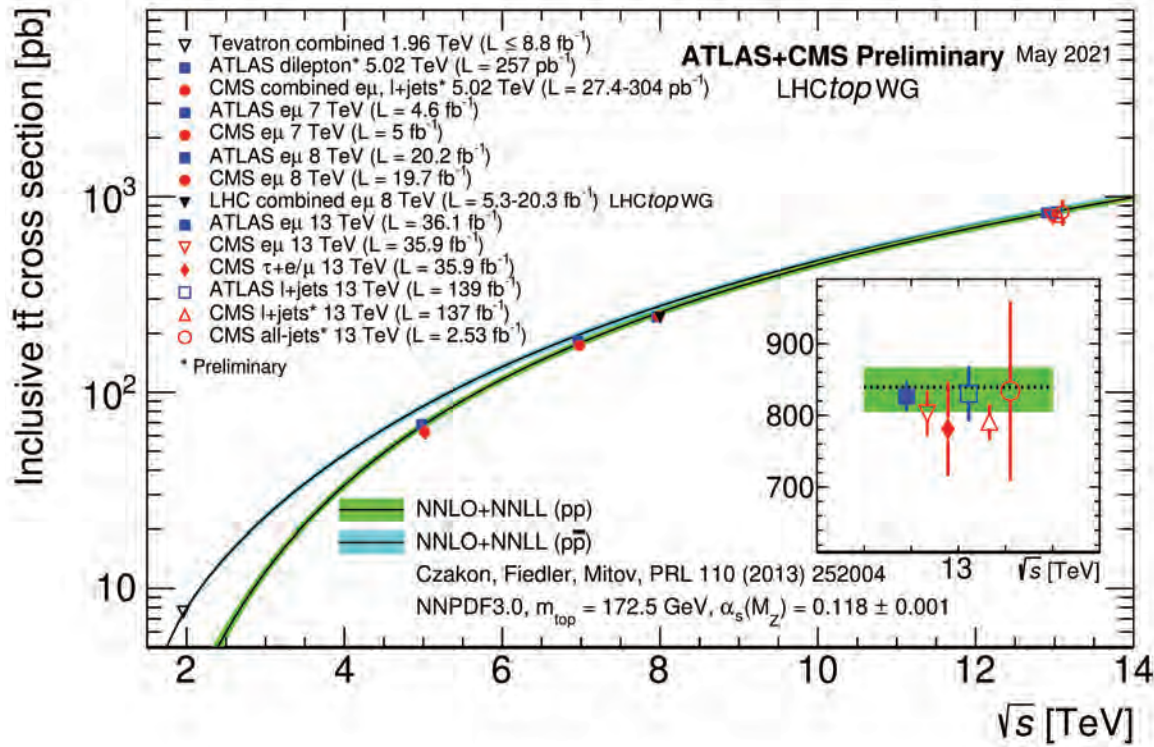


Figure 61.1: Measured and predicted $t\bar{t}$ production cross sections from Tevatron energies in $p\bar{p}$ collisions to LHC energies in pp collisions. The plot is kindly provided by the LHCtopWG working group, see <https://twiki.cern.ch/twiki/bin/view/LHCPhysics/LHCtopWGSummaryPlots>.

anism, allow along with other data the extraction of PDFs in PDF fits, and enhance the sensitivity to possible new physics contributions, especially now that NNLO predictions for the main differential observables in $t\bar{t}$ prediction have become available [76] and later confirmed [2]. Furthermore, such measurements reduce the uncertainty in the description of $t\bar{t}$ production as background in Higgs physics and searches for rare processes or beyond Standard Model physics. Differential cross sections are typically measured by a selection of candidate events, their kinematic reconstruction and subsequent unfolding of the obtained event counts in bins of kinematic distributions in order to correct for detector resolution effects, acceptance and migration effects. In some cases a bin-by-bin unfolding is used, while other analyses use more sophisticated techniques. Experiments at Tevatron and LHC measure the differential cross section with respect to the $t\bar{t}$ invariant mass, $d\sigma/dM_{t\bar{t}}$. The spectra are fully corrected for detector efficiency and resolution effects and are compared to several Monte Carlo simulations as well as selected theoretical calculations. Using 9.45 fb^{-1} , CDF measured $d\sigma/dM_{t\bar{t}}$, in the lepton+jets channel providing sensitivity to a variety of exotic particles decaying into $t\bar{t}$ pairs [77]. In 9.7 fb^{-1} of lepton+jets data, $D\phi$ measured the differential $t\bar{t}$ production cross section with respect to the transverse momentum and absolute rapidity of the top quarks as well as of the invariant mass of the $t\bar{t}$ pair [29], which are all found to be in good agreement with the SM predictions. ATLAS measured the differential $t\bar{t}$ production cross section with respect to the top-quark transverse momentum, and of the mass, transverse momentum and rapidity of the top quark, the antitop quark as well as the $t\bar{t}$ system in up to 4.6 fb^{-1} at $\sqrt{s} = 7 \text{ TeV}$ in the lepton+jets channel [78–80]. It is found that data is softer than all predictions for higher values of the mass of the $t\bar{t}$ system as well as in the tail of the top-quark p_T spectrum beginning at 200 GeV, particularly in the case of the `Alpgen+Herwig` generator. The $M_{t\bar{t}}$ spectrum is not well described by NLO+NNLL calculations and there are also disagreements between the measured rapidity of the $t\bar{t}$ system spectrum and the `MC@NLO+Herwig` and `POWHEG+Herwig`

generators, both evaluated with the CT10 PDF set. All distributions show a preference for HERAPDF1.5 when used for the NLO QCD predictions. In 5.0 fb^{-1} of $\sqrt{s} = 7 \text{ TeV}$ data in the lepton+jets and the dilepton channels, CMS measured normalised differential $t\bar{t}$ cross sections with respect to kinematic properties of the final-state charged leptons and jets associated to b -quarks, as well as those of the top quarks and the $t\bar{t}$ system. The data are compared with several predictions from perturbative QCD calculations and found to be consistent [81]. ATLAS uses 4.6 fb^{-1} of data at 7 TeV and 20.2 fb^{-1} at 8 TeV to measure the differential $t\bar{t}$ cross section in the dilepton final state as a function of the mass, the transverse momentum and the rapidity of the $t\bar{t}$ system [82]. The results are compared with different Monte Carlo generators and theoretical calculations of $t\bar{t}$ production and found to be consistent with the majority of predictions in a wide kinematic range. Using 20.3 fb^{-1} of $t\bar{t}$ events in the lepton+jets channel, ATLAS measures the normalized differential cross sections of $t\bar{t}$ production as a function of the top-quark, $t\bar{t}$ system and event-level kinematic observables [83]. The observables have been chosen to emphasize the $t\bar{t}$ production process and to be sensitive to effects of initial- and final-state radiation, to the different parton distribution functions, and to non-resonant processes and higher-order corrections. The results are in fair agreement with the predictions over a wide kinematic range. Nevertheless, most generators predict a harder top-quark transverse momentum distribution at high values than what is observed in the data. Predictions beyond NLO accuracy improve the agreement with data at high top-quark transverse momenta. Using the current settings in the Monte Carlo programs and parton distribution functions, the rapidity distributions are not well modelled by any generator under consideration. However, the level of agreement is improved when more recent sets of parton distribution functions are used. Using 20.3 fb^{-1} of 8 TeV data, ATLAS performed a dedicated differential $t\bar{t}$ cross-section measurement of highly boosted top quarks in the lepton+jets channel, where the hadronically decaying top quark has a transverse momentum above 300 GeV [84].

Jet substructure techniques are employed to identify top quarks, which are reconstructed with an anti- k_t jet with a radius parameter $R = 1.0$. The predictions of NLO and LO matrix element plus parton shower Monte Carlo generators are found to generally overestimate the measured cross sections. Using 5.0 fb^{-1} of data at 7 TeV and 19.7 fb^{-1} at 8 TeV in the lepton+jets channel, CMS reports measurements of normalized differential cross sections for $t\bar{t}$ production with respect to four kinematic event variables: the missing transverse energy; the scalar sum of the jet transverse momentum (p_T); the scalar sum of the p_T of all objects in the event; and the p_T of leptonically decaying W bosons from top quark decays [85]. No significant deviations from the predictions of several SM event generators are observed. Using the full 19.7 fb^{-1} data in the $e\mu$ channel, CMS measures normalized double-differential cross sections for $t\bar{t}$ production as a function of various pairs of observables characterizing the kinematics of the top quark and $t\bar{t}$ system [86]. The data are compared to calculations using perturbative QCD at NLO and approximate NNLO orders. They are also compared to predictions of Monte Carlo event generators that complement fixed-order computations with parton showers, hadronization, and multiple-parton interactions. Overall agreement is observed with the predictions, which is improved when the latest global sets (as determined here by CMS) of proton parton distribution functions are used. The inclusion of the measured $t\bar{t}$ cross sections in a fit of parametrized parton distribution functions is shown to have significant impact on the gluon distribution [86]. Another analysis at high transverse momentum regime for the top quarks, is performed by the CMS collaboration in 19.7 fb^{-1} at $\sqrt{s} = 8 \text{ TeV}$ [87]. The measurement is performed for events in $e/\mu + jets$ final states where the hadronically decaying top quark is reconstructed as a single large-radius jet and identified as a top candidate using jet substructure techniques. The integrated cross section is measured at particle-level within a fiducial region resembling the detector-level selection as well as at parton-level. At particle-level, the fiducial cross section is measured to be $\sigma_{t\bar{t}} = 0.499 \pm 0.035(\text{stat.} + \text{syst.}) \pm 0.095(\text{theo}) \pm 0.013(\text{lumi})$ pb for $p_T > 400 \text{ GeV}$. At parton-level, it translates to $\sigma_{t\bar{t}} = 1.44 \pm 0.10(\text{stat.} + \text{syst.}) \pm 0.29(\text{theo.}) \pm 0.04(\text{lumi.})$ pb. At parton-level, interactions between incoming partons (quarks or gluons) are considered via a gauge interaction yielding final state partons. While such interactions can be well described theoretically, partons are not visible in the detector. At the particle-level, visible and measurable hadrons, i.e. bound states of quarks and antiquarks, are considered to form jets. The hadronisation process takes us from one level to the other. In 19.7 fb^{-1} at $\sqrt{s} = 8 \text{ TeV}$, CMS repeated those measurements in the lepton+jets and in the dilepton channels [88]. While the overall precision is improved, no significant deviations from the Standard Model are found, yet a softer spectrum for the top quark at high p_T with respect to theoretical available predictions has been observed. This behaviour has been also observed in the all-hadronic final state [89], where a total cross section measurement is performed, yielding $\sigma_{t\bar{t}} = 275.6 \pm 6.1(\text{stat.}) \pm 37.8(\text{syst.}) \pm 7.2(\text{lumi})$ pb. At $\sqrt{s} = 13 \text{ TeV}$, in 3.2 fb^{-1} , ATLAS measured the differential $t\bar{t}$ cross section as a function of the transverse momentum and absolute rapidity of the top quark, and of the transverse momentum, absolute rapidity and invariant mass of the $t\bar{t}$ system [90]. The measured differential cross sections are compared to predictions of NLO generators matched to parton showers and the measurements are found to be consistent with all models within the experimental uncertainties with the exception of the **Powheg-Box+Herwig++** predictions, which differ significantly from the data in both the transverse momentum of the top quark and the mass of the $t\bar{t}$ system. Using 3.2 fb^{-1} of data in the lepton+jets channel, ATLAS measured the differential cross sections of $t\bar{t}$ production in fiducial phase-spaces as a function of top-quark and $t\bar{t}$ system kinematic observables [91]. Two separate selections are applied that each focus on different top-quark momentum regions, referred to as resolved and boosted topologies of the $t\bar{t}$ final state. The measured spectra are corrected for detector effects and are compared to several Monte Carlo simulations by means of calculated χ^2 and p -values.

ATLAS presents a measurement of the boosted top quark dif-

ferential cross section in the all-hadronic decay mode [92]. They require two top-quark candidates, one with $p_T > 500 \text{ GeV}$ and a second with $p_T > 350 \text{ GeV}$, with each candidate reconstructed as an anti- k_T jet with radius parameter $R = 1.0$. The top-quark candidates are separated from the multijet background using the jet substructure and the presence of a b -quark tag in each jet. The observed kinematic distributions are unfolded to recover the differential cross sections in a limited phase-space region and compared with SM predictions, showing agreement. In 36 fb^{-1} , ATLAS measures the single- and double-differential $t\bar{t}$ cross-section in the lepton + jets channel at particle and parton level. Two topologies, resolved and boosted, are considered and the results are presented as a function of several kinematic variables characterising the top and $t\bar{t}$ system and jet multiplicities. Overall, there is good agreement between the theoretical predictions and the data [93]. In 36.1 fb^{-1} of dilepton events, ATLAS measures the differential $t\bar{t}$ cross section as a function of several lepton kinematic variables [63]. The NLO+PS predictions give a good description of several observables. However, **POWHEG** predicts a harder spectrum for lepton p_T variables than observed. In 139 fb^{-1} of data in the $\ell + jets$ channel in a boosted topology with at least one large- R “top-jet” from a hadronic decay with high- p_T , ATLAS employs a parameter sensitive to the top mass to reduce the jet uncertainties and measures the differential $t\bar{t}$ cross section as a function of kinematic variables characterising the $t\bar{t}$ system and also as a function of variables that characterise the additional radiation in the events [94]. The measured distribution of the top-quark transverse momentum, which is measured to be softer than expected, is used to set limits on the Wilson coefficients describing physics beyond the standard model. The modelling of the additional radiation events show some mild disagreements to the data. In the all-hadronic channel with six separately resolved jet, using 36.1 fb^{-1} , ATLAS measures single- and double-differential cross sections at particle and parton level as a function of various kinematic variables [95]. The rapidities of t and $t\bar{t}$ are found to be well modelled while discrepancies between theoretical predictions and data are found in the p_T distributions of the three leading jets, the top and the $t\bar{t}$ system. In 42 pb^{-1} , CMS measures the differential cross section at $\sqrt{s} = 13 \text{ TeV}$ as a function of kinematic properties of the top quarks and the $t\bar{t}$ system, as well as of the jet multiplicity in the event. Several predictions from perturbative QCD calculations are confronted with the data and are found to describe them well [96]. In 2.1 fb^{-1} at $\sqrt{s} = 13 \text{ TeV}$, CMS measures the normalized differential cross sections for $t\bar{t}$ production in the dilepton channels as a function of the kinematic properties of the leptons, jets from bottom quark hadronization, top quarks, and top quark pairs at the particle and parton levels [97]. The results are compared to several Monte Carlo generators that implement calculations up to NLO in perturbative QCD interfaced with parton showering, and also to fixed-order theoretical calculations of top quark pair production up to NNLO, showing agreement. In 2.3 fb^{-1} of events in the lepton+jets channel, CMS measures the differential and double-differential cross sections for the $t\bar{t}$ production as a function of jet multiplicity and of kinematic variables of the top quarks and the $t\bar{t}$ system [98]. The differential cross sections are presented at particle level, within a phase space close to the experimental acceptance, and at parton level in the full phase space. The results are compared to several SM predictions. Using 35.9 fb^{-1} , CMS measures the differential $t\bar{t}$ cross section in the single-lepton decay channel, as a function of a number of kinematic event variables. The data are compared to a variety of state-of-the-art LO and NLO simulations [99]. In 35.8 fb^{-1} , CMS measures the differential and double-differential $t\bar{t}$ cross sections in the $\ell + jets$ channel as a function of kinematic variables of the top quarks and the top quark-antiquark ($t\bar{t}$) system. In addition, kinematic variables and multiplicities of jets associated with the $t\bar{t}$ production are measured. The kinematic variables of the top quarks and the $t\bar{t}$ system are reasonably described in general, though none predict all the measured distributions. In particular, the transverse momentum distribution of the top quarks is more steeply falling than predicted. The kinematic distributions and multiplicities of jets are adequately modeled by certain combinations of NLO calculations and parton

shower models [100]. In the dilepton channel, CMS measures differential $t\bar{t}$ cross sections in 35.9 fb^{-1} as functions of kinematic observables of the top quarks and their decay products, the $t\bar{t}$ system, and the total number of jets in the event. All results are compared with SM predictions from Monte Carlo simulations with NLO accuracy in QCD at matrix-element level interfaced to parton-shower simulations. Where possible, parton-level results are compared to calculations with beyond-NLO precision in QCD. Significant disagreement is observed between data and all predictions for several observables. The measurements are used to constrain the top quark chromomagnetic dipole moment in an effective field theory framework at NLO in QCD and to extract $t\bar{t}$ and leptonic charge asymmetries [101]. In 35.9 fb^{-1} of dilepton events, CMS measures normalised multi-differential $t\bar{t}$ cross sections as a function of the kinematic properties of the top quark and of the $t\bar{t}$ system at parton level in the full phase space. A triple-differential measurement is performed as a function of the invariant mass and rapidity of the $t\bar{t}$ system and the multiplicity of additional jets at particle level. The data are compared to predictions of Monte Carlo event generators that complement NLO QCD calculations with parton showers. The measurement is used to extract the strong coupling constant and the top-quark pole mass and parton distribution functions [102]. In 137 fb^{-1} of $\ell + jets$ data, arranged in four regions according to the top p_T , boosted vs. resolved, and the b -tagging score, CMS measures the single- and double-differential $t\bar{t}$ cross sections [71]. Here also the longitudinal momentum is measured well into the TeV range in one measurement starting in the resolved regime. Most of the measured differential cross sections are well described by standard model predictions with the exception of some double-differential distributions. The top p_T and $m_{t\bar{t}}$ is found to be softer than predicted. In 35.9 fb^{-1} of all-hadronic and $\ell + jets$ events in a boosted topology with at least two large-R jets with a b -tag inside and $p_T > 400 \text{ GeV}$ or one large-R jet, respectively, CMS measures the differential cross section as a function of kinematic variables of individual top quarks or of the $t\bar{t}$ system [103]. The observed absolute cross sections are significantly lower than the predictions from theory, while the normalized differential measurements are well described.

61.3.1.2 Other $t\bar{t}$ production processes

Further cross-section measurements are performed by ATLAS for $t\bar{t}$ +heavy flavour [104] and $t\bar{t}$ +jets production as well as the differential measurement of the jet multiplicity in $t\bar{t}$ events by ATLAS [105] and by CMS [106]. Here, **MC@NLO+Herwig** MC is found to predict too few events at higher jet multiplicities. In addition, CMS measured the cross-section ratio $\sigma_{t\bar{t}b\bar{b}}/\sigma_{t\bar{t}jj}$ using 19.6 fb^{-1} of 8 TeV data [107]. This is of high relevance for top quark production as background to searches, for example for measurements of $t\bar{t}h$ production and ongoing searches for 4-top quark production. Later, ATLAS also measured the $t\bar{t}$ production cross section along with the branching ratios into channels with leptons and quarks using 4.6 fb^{-1} of 7 TeV data [108]. They find agreement with the standard model at the level of a few percent.

Using 139 fb^{-1} of $t\bar{t} \rightarrow$ dilepton events, ATLAS distinguishes in a dedicated analysis muons originating from $W \rightarrow \mu\nu$ decays and those from $W \rightarrow \tau\nu \rightarrow \mu\nu\nu$ decays via their transverse momentum spectrum and the impact parameter of the muon track, that reflects the tau lifetime, yielding high sensitivity. The measured ratio of $R(\tau/\mu) = 0.992 \pm 0.013$ is in agreement with the hypothesis of universal lepton couplings [109].

Using 36 fb^{-1} of dilepton events at 13 TeV, ATLAS also measures differential cross sections with respect to high-resolution variables, constructed to characterize the longitudinal and transverse momentum distributions of the b -hadron within the b -jets [110]. They are used to test the heavy-quark-fragmentation modelling.

Using 137 fb^{-1} of dilepton events at 13 TeV, CMS measures differential cross sections with respect to the mass of the $t\bar{t}$ system and the rapidity difference of the top-quark and antiquark [111]. Exploiting their sensitivity to the top-quark Yukawa coupling yields a best fit value of $Y_t = 1.16^{+0.24}_{-0.35}$, bounding $Y_t < 1.54$ at a 95% confidence level.

In 36.1 fb^{-1} , ATLAS measures the $t\bar{t}b\bar{b}$ cross section in the

dilepton and the $\ell + jets$ channels. Results are presented at particle level in the form of inclusive cross-sections of $t\bar{t}$ final states with three and four b -jets as well as differential cross-sections as a function of global event properties and properties of b -jet pairs. The measured inclusive fiducial cross-sections generally exceed the $t\bar{t}b\bar{b}$ predictions from various NLO matrix element calculations matched to a parton shower, but are compatible within the total uncertainties [112]. In 2.3 fb^{-1} , CMS measures the $t\bar{t}b\bar{b}$ cross section in the dilepton channel [113]. They also determine the cross section ratio $\sigma_{t\bar{t}b\bar{b}}/\sigma_{t\bar{t}jj}$. In 35.9 fb^{-1} , CMS recently measured the cross section $t\bar{t}b\bar{b}$ as well as the cross section ratio $\sigma_{t\bar{t}b\bar{b}}/\sigma_{t\bar{t}jj}$ in the dilepton and the lepton+jets channel [114]. They fit the distribution of the b -tagging discriminant variable of the two jets that do not belong to the $t\bar{t}$ decay. In the same dataset, CMS measures the $t\bar{t}b\bar{b}$ cross section in the all-jet channel by selecting events containing at least eight jets, of which at least two are identified as b -jets. A combination of multivariate analysis techniques is used to reduce the large background from multijet events not containing a top quark pair, and to help discriminate between jets originating from top quark decays and other additional jets. The measured cross sections are found to be larger than theoretical predictions by a factor of 1.5-2.4, corresponding to 1-2 standard deviations [115]. Recently, CMS measured the $t\bar{t} + b\bar{b}$ cross section in 35.9 fb^{-1} of dilepton and $\ell + jets$ events [114]. The cross section is extracted from the cross section ratio $R(t\bar{t} + b\bar{b})$ in order to reduce systematic uncertainties. The assignment of jets to the top or to the additional jets is based on b -tagging scores in the dilepton channel and on a kinematic fit in the $\ell + jets$ channel. Using the same data set in the all-hadronic channel, CMS measured the $t\bar{t} + b\bar{b}$ cross section to $\approx 25\%$ precision employing a multivariate analysis technique and a 2-dimensional likelihood fit [116]. Very recently, CMS also measured the $t\bar{t} + c\bar{c}$ cross section using 41.5 fb^{-1} of events with dileptonic final states [117]. A multi-class neural network is employed to separate $t\bar{t} + b\bar{b}$, $t\bar{t} + c\bar{c}$ and $t\bar{t} + ll$. The results are compatible with the prediction within $1 - 2 \sigma$.

The production of four top-quarks is an interesting test of QCD and at the same time sensitive to the top quark Yukawa coupling and to production mechanisms with new mediators with strong couplings to top quarks. The latest cross section calculation yields $\sigma_{t\bar{t}t\bar{t}} = 12.0 \text{ fb} \pm 20\%$ [118]. Using the full Run-II data set of 139 fb^{-1} , ATLAS measures the four-tops cross section in the two-lepton same sign or three-lepton channel with 13% branching ratio and dominant $t\bar{t}V$ background as $\sigma_{t\bar{t}t\bar{t}} = 24^{+7}_{-6} \text{ fb}$ [119]. Using the same data set in the one-lepton or two-lepton opposite-sign channel with 57% branching ratio and dominant $t\bar{t} +$ heavy flavor background, they measure $\sigma_{t\bar{t}t\bar{t}} = 26^{+17}_{-15} \text{ fb}$ [120]. The combination yields $\sigma_{t\bar{t}t\bar{t}} = 24^{+7}_{-6} \text{ fb}$ [120], corresponding to an observed (expected) significance of 4.7 (2.6) σ significance. CMS measures the four-top cross section in the two-lepton same sign or three-lepton channel in 137 fb^{-1} to $\sigma_{t\bar{t}t\bar{t}} = 12.6^{+5.8}_{-5.2} \text{ fb}$ [121], corresponding to an observed (expected) significance of 2.6 (2.7) σ significance. Using 35.8 fb^{-1} , they also study the one-lepton or two-lepton opposite-sign channel and obtain an upper limit of $\sigma_{t\bar{t}t\bar{t}} < 48 \text{ fb}$ at 95% CL [122]. The results are also interpreted in terms of the top-Yukawa coupling and various scenarios of physics beyond the standard model via effective field theory fits.

61.3.1.3 Single-top production

Single-top quark production was first observed in 2009 by $D\bar{O}$ [123] and CDF [124, 125] at the Tevatron. The production cross section at the Tevatron is roughly half that of the $t\bar{t}$ cross section, but the final state with a single W -boson and typically two jets is less distinct than that for $t\bar{t}$ and much more difficult to distinguish from the background of W +jets and other sources. A comprehensive review of the first observation and the techniques used to extract the signal from the backgrounds can be found in [126].

The dominant production at the Tevatron is through s -channel and t -channel W -boson exchange. Associated production with a W -boson (tW production) has a cross section that is too small to observe at the Tevatron. The t -channel process is $qb \rightarrow q't$, while the s -channel process is $q\bar{q}' \rightarrow t\bar{b}$. The s - and t -channel

productions can be separated kinematically. This is of particular interest because potential physics beyond the Standard Model, such as fourth-generation quarks, heavy W and Z bosons, flavor-changing-neutral-currents [11], or a charged Higgs boson, would affect the s - and t -channels differently. However, the separation is difficult and initial observations and measurements at the Tevatron by both experiments were of combined $s + t$ -channel production. The two experiments combined their measurements for maximum precision with a resulting $s + t$ -channel production cross section of $2.76_{-0.47}^{+0.58}$ pb [127]. The measured value assumes a top-quark mass of $170 \text{ GeV}/c^2$. The mass dependence of the result comes both from the acceptance dependence and from the $t\bar{t}$ background evaluation. Also the shape of discriminating topological variables is sensitive to m_t . The dependence on m_t is therefore not necessarily a simple linear dependence but amounts to only a few tenths of picobarns over the range $170 - 175 \text{ GeV}/c^2$. The measured value agrees well with the theoretical calculation at $m_t = 173 \text{ GeV}/c^2$ of $\sigma_{s+t} = 3.12_{-0.04}^{+0.00}(\text{scale}) \pm 0.18(\text{pdf})$ pb (including both top and anti-top production) [9, 128].

Using the full Run-II data set of up to 9.7 fb^{-1} , CDF and DØ have measured the t -channel single-top quark production to be $\sigma_{t+\bar{t}} = 2.25_{-0.31}^{+0.29}$ pb [129, 130]. In the same publication, they also present the simultaneously measured s - and t -channel cross sections and the $s + t$ combined cross section measurement resulting in $\sigma_{s+t} = 3.30_{-0.40}^{+0.52}$ pb, without assuming the SM ratio of σ_s/σ_t . The modulus of the CKM matrix element obtained from the $s + t$ -channel measurement is $|V_{tb}| = 1.02_{-0.05}^{+0.06}$ and its value is used to set a lower limit of $|V_{tb}| > 0.92$ at 95% C.L. Those results are in good agreement with the theoretical value at the mass $172.5 \text{ GeV}/c^2$ of $\sigma_t = 2.08 \pm 0.13$ pb [128]. It should be noted that the theory citations here list cross sections for t or \bar{t} alone, whereas the experiments measure the sum. At the Tevatron, these cross sections are equal. The theory values quoted here already include this factor of two.

Using datasets of 9.7 fb^{-1} each, CDF and DØ combine their analyses and report the first observation of single-top-quark production in the s -channel, yielding $\sigma_s = 1.29_{-0.24}^{+0.26}$ pb [131]. The probability of observing a statistical fluctuation of the background of the given size is 1.8×10^{-10} , corresponding to a significance of 6.3 standard deviations.

At the LHC, the t -channel cross section is expected to be more than three times as large as s -channel and tW production, combined. Both ATLAS and CMS have measured single top production cross sections at $\sqrt{s} = 7 \text{ TeV}$ in pp collisions (assuming $m_t = 172.5 \text{ GeV}/c^2$ unless noted otherwise). Using 4.59 fb^{-1} of data at $\sqrt{s} = 7 \text{ TeV}$, ATLAS measures the t -channel single-top quark cross section in the lepton plus 2 or 3 jets channel with one b -tag by fitting the distribution of a multivariate discriminant constructed with a neural network, yielding $\sigma_t = 46 \pm 6$ pb, $\sigma_{\bar{t}} = 23 \pm 4$ pb with a ratio $R_t = \sigma_t/\sigma_{\bar{t}} = 2.04 \pm 0.18$ and $\sigma_{t+\bar{t}} = 68 \pm 8$ pb, consistent with SM expectations [132, 133]. CMS follows two approaches in 1.6 fb^{-1} of lepton plus jets events. The first approach exploits the distributions of the pseudorapidity of the recoil jet and reconstructed top-quark mass using background estimates determined from control samples in data. The second approach is based on multivariate analysis techniques that probe the compatibility of the candidate events with the signal. They find $\sigma_{t+\bar{t}}^{\text{t-channel}} = 67.2 \pm 6.1$ pb, and $|V_{tb}| = 1.020 \pm 0.046(\text{exp.}) \pm 0.017(\text{th.})$ [134].

At $\sqrt{s} = 8 \text{ TeV}$, both experiments repeat and refine their measurements. ATLAS uses 20.2 fb^{-1} of data. Total, fiducial and differential cross-sections are measured for both top-quark and top-antiquark production [135]. An artificial neural network is employed to separate signal from background. The fiducial cross-section is measured with a precision of 5.8% (top quark) and 7.8% (top antiquark), respectively. The total cross-sections are measured to be $\sigma_t^{\text{t-channel}}(tq) = 56.7_{-3.8}^{+4.3}$ pb for top-quark production and $\sigma_{\bar{t}}^{\text{t-channel}}(\bar{t}q) = 32.9_{-2.7}^{+3.0}$ pb for top-antiquark production, in agreement with the SM prediction. In addition, the ratio of top-quark to top-antiquark production cross-sections is determined to be $R_t = 1.72 \pm 0.09$. The total cross-section is used to extract the Wtb coupling: $f_{LV} \cdot |V_{tb}| = 1.029 \pm 0.048$,

which corresponds to $|V_{tb}| > 0.92$ at the 95% confidence level, when assuming $f_{LV} = 1$ and restricting the range of $|V_{tb}|$ to the interval $[0, 1]$. The differential cross-sections as a function of the transverse momentum and rapidity of both the top quark and the top antiquark are measured at both the parton and particle levels. The transverse momentum and rapidity differential cross-sections of the accompanying jet from the t -channel scattering are measured at particle level. All measurements are compared to various Monte Carlo predictions as well as to fixed-order QCD calculations where available. The SM predictions provide good descriptions of the data. Using the same dataset, ATLAS probes the Wtb vertex structure from polarization observables in t -channel single-top quark events. The polarization observables are extracted from asymmetries in angular distributions measured with respect to spin quantisation axes appropriately chosen for the top quark and the W -boson. The asymmetry measurements are performed at parton level by correcting the observed angular distributions for detector effects and hadronisation after subtracting the background contributions. The measured top-quark and W -boson polarization values are in agreement with the Standard Model predictions [136]. CMS uses 19.7 fb^{-1} in the electron or muon plus jets channel, exploiting the pseudorapidity distribution of the recoil jet. They find $\sigma_t = 53.8 \pm 1.5(\text{stat.}) \pm 4.4(\text{syst.})$ pb and $\sigma_{\bar{t}} = 27.6 \pm 1.3(\text{stat.}) \pm 3.7(\text{syst.})$ pb, resulting in an inclusive t -channel cross section of $\sigma_{t+\bar{t}} = 83.6 \pm 2.3(\text{stat.}) \pm 7.4(\text{syst.})$ [137]. They measure a cross section ratio of $R_t = \sigma_t/\sigma_{\bar{t}} = 1.95 \pm 0.10(\text{stat.}) \pm 0.19(\text{syst.})$, in agreement with the SM. The CKM matrix element V_{tb} is extracted to be $|V_{tb}| = 0.998 \pm 0.038(\text{exp.}) \pm 0.016(\text{th.})$. Later, CMS has also provided a fiducial cross section measurement for t -channel single top at $\sqrt{s} = 8 \text{ TeV}$ with 19.7 fb^{-1} of data in signal events with exactly one muon or electron and two jets, one of which is associated with a b -hadron [138]. The definition of the fiducial phase space follows closely the constraints imposed by event-selection criteria and detector acceptance. The total fiducial cross section is measured using different generators at next-to-leading order plus parton-shower accuracy. Using as reference the aMC@NLO MC predictions in the four-flavour scheme $\sigma_t^{\text{fid}} = 3.38 \pm 0.25(\text{exp.}) \pm 0.20(\text{th.})$ pb is obtained, in good agreement with the theory predictions. At 13 TeV, ATLAS uses 3.2 fb^{-1} to measure the t -channel cross section. Using a binned maximum-likelihood fit to the discriminant distribution of a neural network, the cross-sections are determined to be $\sigma_t(tq) = 156 \pm 5(\text{stat.}) \pm 27(\text{syst.}) \pm 3(\text{lumi.})$ pb and $\sigma(\bar{t}q) = 91 \pm 4(\text{stat.}) \pm 18(\text{syst.}) \pm 2(\text{lumi.})$ pb [139]. The cross-section ratio is measured to be $R_t = \sigma_t/\sigma_{\bar{t}} = 1.72 \pm 0.09(\text{stat.}) \pm 0.18(\text{syst.})$. All results are in agreement with SM predictions. A measurement of the t -channel single top-quark cross section is also available at 13 TeV with the CMS detector, corresponding to an integrated luminosity of 2.2 fb^{-1} . Fits to the transverse W -mass and the output of an artificial neural network allow the determination of the background and the signal contribution. The measured cross-section is $\sigma_t = 238 \pm 13(\text{stat.}) \pm 29(\text{syst.})$ pb [140]. The CKM matrix element is determined to $|V_{tb}| = 1.05 \pm 0.07(\text{exp.}) \pm 0.02(\text{th.})$. Using 35.9 fb^{-1} of data, CMS performs measurements of the t -channel cross sections of single top quarks and antiquarks in the t channel, and their ratio. Events with one muon or electron are selected, and different categories of jet and b -jet multiplicity and multivariate discriminators are applied to separate the signal from the background, resulting in $\sigma_t(tq) = 130 \pm 1(\text{stat.}) \pm 19(\text{syst.})$ pb and $\sigma_{\bar{t}}(\bar{t}q) = 77 \pm 1(\text{stat.}) \pm 12(\text{syst.})$ pb, respectively, and their ratio is $1.68 \pm 0.02(\text{stat.}) \pm 0.05(\text{syst.})$. The results are in agreement with the predictions from the Standard Model [141]. Recently, CMS used the same dataset to measure the CKM matrix elements from their t -channel single-top quark production cross section. In the standard model hypothesis of CKM unitarity, a lower limit of $|V_{tb}| > 0.970$ is measured at the 95% confidence level. Several theories beyond the standard model are considered, and by releasing all constraints among the involved parameters, the values $|V_{tb}| = 0.988 \pm 0.024$, and $|V_{td}|^2 + |V_{ts}|^2 = 0.06 \pm 0.06$, where the uncertainties include both statistical and systematic components, are measured [142].

The predicted cross section for the tW process at the LHC

$\sqrt{s} = 7$ TeV is 15.6 ± 1.2 pb [10]. This is of interest because it probes the Wtb vertex in a different kinematic region than s - and t -channel production, and because of its similarity to the associated production of a charged-Higgs boson and a top quark. The signal is difficult to extract because of its similarity to the $t\bar{t}$ signature. Furthermore, it is difficult to uniquely define because at NLO a subset of diagrams has the same final state as $t\bar{t}$ and the two interfere [143]. The cross section is calculated using the *diagram removal* technique [144] to define the signal process. In the diagram removal technique the interfering diagrams are removed, at the amplitude level, from the signal definition (an alternative technique, *diagram subtraction* removes these diagrams at the cross-section level and yields similar results [144]). These techniques work provided the selection cuts are defined such that the interference effects are small, which is usually the case.

Both, ATLAS and CMS, also provide evidence for the associated tW production at $\sqrt{s} = 7$ TeV [145, 146]. ATLAS uses 2.05 fb^{-1} in the dilepton plus missing E_T plus jets channel, where a template fit to the final classifier distributions resulting from boosted decision trees as signal to background separation is performed. The result is incompatible with the background-only hypothesis at the 3.3σ (3.4σ expected) level, yielding $\sigma_{tW} = 16.8 \pm 2.9(\text{stat.}) \pm 4.9(\text{ syst.})$ pb and $|V_{tb}| = 1.03^{+0.16}_{-0.19}$ [145]. CMS uses 4.9 fb^{-1} in the dilepton plus jets channel with at least one b -tag. A multivariate analysis based on kinematic properties is utilized to separate the $t\bar{t}$ background from the signal. The observed signal has a significance of 4.0σ and corresponds to a cross section of $\sigma_{tW} = 16^{+5}_{-4}$ pb [146].

Both experiments repeated their tW -analyses at $\sqrt{s} = 8$ TeV. ATLAS uses 20.3 fb^{-1} to select events with two leptons and one central b -jet. The tW signal is separated from the backgrounds using boosted decision trees, each of which combines a number of discriminating variables into one classifier. Production of tW events is observed with a significance of 7.7σ . The cross section is extracted in a profile likelihood fit to the classifier output distributions. The tW cross section, inclusive of decay modes, is measured to be $\sigma_{tW} = 23.0 \pm 1.3(\text{stat.})^{+3.2}_{-3.5}(\text{ syst.}) \pm 1.1(\text{ lumi.})$ pb, yielding a value for the CKM matrix element $|V_{tb}| = 1.01 \pm 0.10$ and a lower limit of 0.80 at the 95% C.L. [147]. A fiducial cross section is also measured. ATLAS and CMS also combine their early measurements and obtain $\sigma_{tW} = 16.3 \pm 4.1$ pb [148], in agreement with the NLO+NNLL expectation. Very recently, ATLAS used 20.2 fb^{-1} in the single-lepton channel with at least three jets to measure the Wt production cross section. A neural network is trained to separate the tW signal from the dominant $t\bar{t}$ background. The cross-section is extracted from a binned profile maximum-likelihood fit to a two-dimensional discriminant built from the neural-network output and the invariant mass of the hadronically decaying W boson. The measured cross section is $\sigma_{tW} = 26 \pm 7$ pb, in good agreement with the Standard Model expectation [149]. CMS uses 12.2 fb^{-1} in events with two leptons and a jet originating from a b -quark. A multivariate analysis based on kinematic properties is utilized to separate the signal and background. The tW associate production signal is observed at the level of 6.1σ , yielding $\sigma_{tW} = 23.4 \pm 5.4$ pb and $|V_{tb}| = 1.03 \pm 0.12(\text{exp.}) \pm 0.04(\text{th.})$ [150]. ATLAS and CMS also combine their early measurements and obtain $\sigma_{tW} = 23.1 \pm 3.6$ pb [148], in agreement with the NLO+NNLL expectation. The product of a form factor with the CKM matrix element V_{tb} is determined to be $|V_{tb}| = 1.02 \pm 0.04(\text{meas.}) \pm 0.02(\text{theo.}) > 0.79$. At 13 TeV in the tW -channel, ATLAS uses 3.2 fb^{-1} of events with two opposite sign isolated leptons and at least one jet; they are separated into signal and control regions based on their jet multiplicity and the number of jets with b -tags. Signal is separated from background in two regions using boosted decision trees. The cross section is extracted by fitting templates to the data distributions, and is measured to be $\sigma_{tW} = 94 \pm 10(\text{stat.})^{+28}_{-22}(\text{ syst.}) \pm 2(\text{ lumi.})$ pb [151]. The measurement is in agreement with the SM prediction. CMS uses 36 fb^{-1} of events with two opposite sign isolated leptons, one tight and one loose jet and one b -tag. Signal and background is separated in categories depending on the number of jets and the subset of b -tagged jets using a boosted decision tree. A maximum likelihood fits yields $\sigma_{tW} = 63.1 \pm 1.8(\text{stat.}) \pm 6.4(\text{ syst.}) \pm 2.1(\text{ lumi.})$ pb [152].

Very recently, CMS uses 36 fb^{-1} in the single-lepton channel, where a boosted decision tree is used to separate the tW signal from the dominant $t\bar{t}$ background, whilst the subleading W +jets and multijet backgrounds are constrained using data-based estimates. This result is the first observation of the tW process in final states containing a muon or electron and jets, with a significance exceeding 5 standard deviations. The cross section is determined to be $\sigma_{tW} = 89 \pm 4(\text{stat.}) \pm 12(\text{ syst.})$ pb, consistent with the Standard Model [153].

The s -channel production cross section is expected to be 4.6 ± 0.3 pb for $m_t = 173 \text{ GeV}/c^2$ at $\sqrt{s} = 7$ TeV [9]. At ATLAS, a search for s -channel single top quark production is performed in 0.7 fb^{-1} at 7 TeV using events containing one lepton, missing transverse energy and two b -jets. Using a cut-based analysis, an observed (expected) upper limit at 95% C.L. on the s -channel cross-section of $\sigma_s < 26.5$ (20.5) pb is obtained [154]. At 8 TeV, ATLAS uses 20.3 fb^{-1} of data with one lepton, large missing transverse momentum and exactly two b -tagged jets. They perform a maximum-likelihood fit of a discriminant based on a Matrix Element Method and optimized in order to separate single top-quark s -channel events from the main background contributions which are top-quark pair production and W boson production in association with heavy flavor jets. They find $\sigma_s = 4.8 \pm 0.8(\text{stat.})^{+1.6}_{-1.3}(\text{ syst.})$ pb with a signal significance of 3.2 standard deviations [155], which provides first evidence for s -channel single-top production at 8 TeV. The signal is extracted through a maximum-likelihood fit to the distribution of a multivariate discriminant defined using boosted decision trees to separate the expected signal contribution from background processes. At 7 TeV and 8 TeV, CMS uses 5.1 fb^{-1} and 19.3 fb^{-1} , respectively, and analyses leptonic decay modes by performing a maximum likelihood fit to a multivariate discriminant defined using a Boosted Decision Tree, yielding cross sections of $\sigma_s = 7.1 \pm 8.1$ pb and $\sigma_s = 13.4 \pm 7.3$ pb, respectively, and a best fit value of 2.0 ± 0.9 for the combined ratio of the measured σ_s values and the ones expected in the Standard Model [156]. The signal significance is 2.5 standard deviations. ATLAS and CMS present the combinations of their single-top-quark production cross-section measurements, using Run-I data corresponding to integrated luminosities of 1.17 to 5.1 fb^{-1} at $\sqrt{s} = 7$ TeV and 12.2 to 20.3 fb^{-1} at $\sqrt{s} = 8$ TeV. These combinations are performed per centre-of-mass energy and for each production mode: t -channel, tW , and s -channel. The combined t -channel cross-sections are 67.5 ± 5.7 pb and 87.7 ± 5.8 pb at $\sqrt{s} = 7$ and 8 TeV, respectively. The combined tW cross-sections are 16.3 ± 4.1 pb and 23.1 ± 3.6 pb at $\sqrt{s} = 7$ and 8 TeV, respectively. For the s -channel cross-section, the combination yields 4.9 ± 1.4 pb at $\sqrt{s} = 8$ TeV. The square of the magnitude of the CKM matrix element V_{tb} multiplied by a form factor f_{LV} is determined for each production mode and centre-of-mass energy, using the ratio of the measured cross-section to its theoretical prediction. All combined measurements are consistent with their corresponding SM predictions [157]. Both, ATLAS and CMS, also measured the electroweak production of single top-quarks in association with a Z -boson, see section 61.3.2.4 of this review.

Fig. 61.2 provides a summary of all single top cross-section measurements at the LHC as a function of the center-of-mass energy. All cross-section measurements are very well described by the theory calculation within their uncertainty.

Thanks to the large statistics now available at the LHC, both CMS and ATLAS experiments also performed differential cross-section measurements in single-top t -channel production [132], [158]. Such measurements are extremely useful as they test our understanding of both QCD and EW top-quark interactions. The CMS collaboration has measured differential single top quark t -channel production cross sections as functions of the transverse momentum and the absolute value of the rapidity of the top quark. The analysis is performed in the leptonic decay channels of the top quark, with either a muon or an electron in the final state, using data collected with the CMS experiment at the LHC at $\sqrt{s} = 8$ TeV and corresponding to an integrated luminosity of 19.7 fb^{-1} . Neural networks are used to discriminate the signal process from the various background contributions. The results

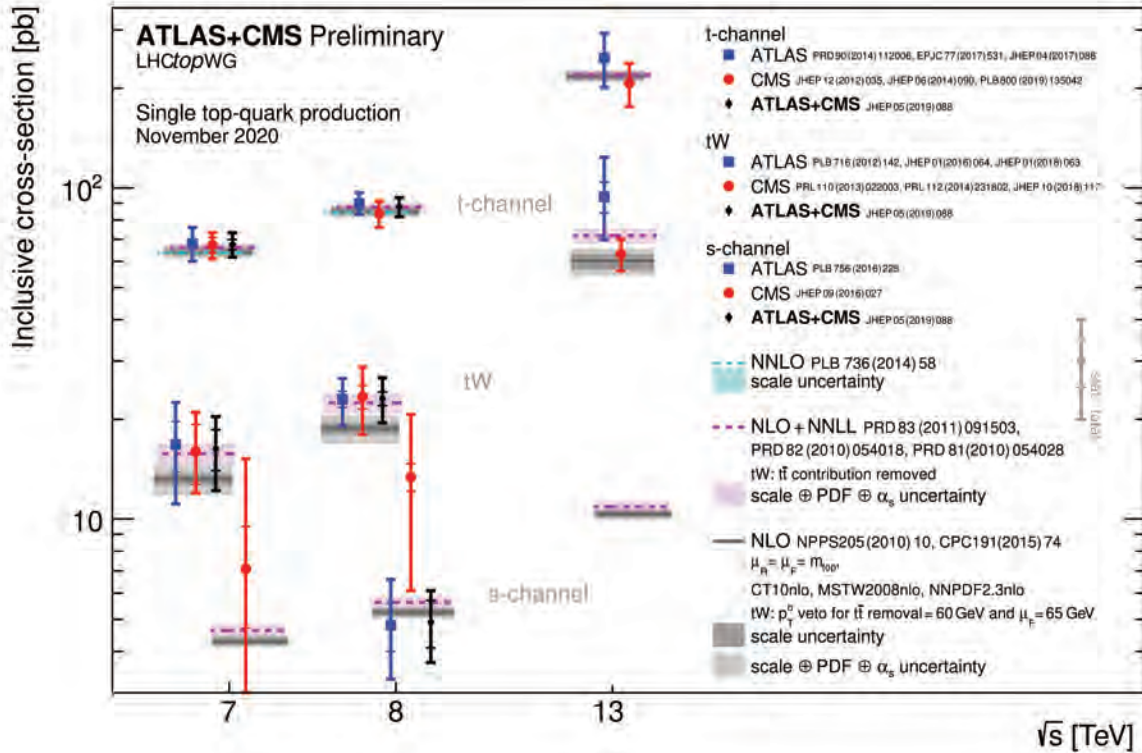


Figure 61.2: Measured and predicted single top production cross sections at LHC energies in pp collisions. The recent CMS measurement of the tW production cross section at 13 TeV in the $l+$ jets channel is not yet shown here. The plot is kindly provided by the LHCTopWG working group, see <https://twiki.cern.ch/twiki/bin/view/LHCPhysics/LHCTopWGSummaryPlots>.

are found to agree with predictions from Monte Carlo generators [158]. Using the same data set and under the assumption that the spin analyzing power of a charged lepton is 100% as predicted in the SM, they are also able to measure the polarization of the top quark $P_t = 0.82 \pm 0.12(\text{stat.}) \pm 0.32(\text{syst.})$ [159]. At 13 TeV, using 35.9 fb^{-1} , CMS measures the differential t -channel cross sections, for the first time in single-top production, and charge ratios for t -channel single top quark production [160]. The results are found to be in agreement with SM predictions using various NLO event generators and sets of parton distribution functions. Additionally, the spin asymmetry, sensitive to the top quark polarization, is determined from the differential distribution of the polarization angle at parton level to be 0.439 ± 0.062 , in agreement with the SM prediction. This disfavors the results obtained at 8 TeV. ATLAS has measured the differential tW cross section in 36.1 fb^{-1} at 13 TeV with respect to the energy of the b -jet, the energy of the system of the two leptons and b -jet, and the transverse mass or mass of combinations of leptons, the b -jet and neutrinos [161]. Using 35.9 fb^{-1} of $e\mu$ events, CMS to measure the differential tW cross section. A fiducial region is defined according to the detector acceptance, and the requirement of exactly one b -tagged jet. The resulting distributions are unfolded to particle-level and compared with predictions calculated at next-to-leading order in perturbative QCD. Within current uncertainties, all the predictions agree with the data [162].

61.3.1.4 Top-Quark Asymmetries

A forward-backward asymmetry in $t\bar{t}$ production at a $p\bar{p}$ collider arises starting at order α_S^3 in QCD from the interference between the Born amplitude $q\bar{q} \rightarrow t\bar{t}$ with 1-loop box production diagrams and between diagrams with initial- and final-state gluon radiation. The asymmetry, A_{FB} , is defined by

$$A_{FB} = \frac{N(\Delta y > 0) - N(\Delta y < 0)}{N(\Delta y > 0) + N(\Delta y < 0)}, \quad (61.2)$$

where $\Delta y = y_t - y_{\bar{t}}$ is the rapidity difference between the top- and the anti-top quark. Calculations at α_S^3 predict a measurable A_{FB} at the Tevatron. The most recent calculations up to order

α_S^4 , including electromagnetic and electroweak corrections, yield a predicted asymmetry of $\approx (9.5 \pm 0.7)\%$ [163]. This is about 10% higher than the previous calculation at NLO [164, 165], and improves the agreement with experiment.

Both CDF and DØ measured asymmetry values in excess of the SM prediction, fueling speculation about exotic production mechanisms (see, for example, [166] and references therein). The first measurement of this asymmetry by DØ in 0.9 fb^{-1} [167] found an asymmetry at the detector level of $(12 \pm 8)\%$. The first CDF measurement in 1.9 fb^{-1} [168] yielded $(24 \pm 14)\%$ at parton level. Both values were higher, though statistically consistent with the SM expectation. With the addition of more data, the uncertainties have been reduced, and the central values, if somewhat smaller, have remained consistent with the first measurements. At the same time, the improved calculations from theory have increased the predicted asymmetry values, improving the agreement between theory and experiment.

CDF and DØ have now combined results using the full Tevatron dataset at $\sqrt{s} = 1.96 \text{ TeV}$ [169]. Three combined asymmetries are reported: $A_{FB}^{t\bar{t}}$ as defined in Eq. 2 for fully-reconstructed $t\bar{t}$ events, a single-lepton asymmetry, A_{FB}^{ℓ} defined as in Eq. 2 but with Δy replaced by the product of the lepton charge and pseudo-rapidity, and a dilepton asymmetry, $A_{FB}^{\ell\ell}$, defined as in Eq. 2 but with Δy replaced by $\Delta\eta$ between the two leptons. The combined results are $A_{FB}^{t\bar{t}} = 0.128 \pm 0.021 \pm 0.014$, $A_{FB}^{\ell} = 0.073 \pm 0.016 \pm 0.012$, and $A_{FB}^{\ell\ell} = 0.108 \pm 0.043 \pm 0.016$, where the first uncertainty is statistical and the second systematic. These are to be compared to SM predictions at NNLO QCD and NLO electroweak of $A_{FB}^{t\bar{t}} = 0.095 \pm 0.007$ [163], $A_{FB}^{\ell} = 0.038 \pm 0.003$, and $A_{FB}^{\ell\ell} = 0.048 \pm 0.004$ [165], respectively. Both experiments have also measured differential asymmetries, in bins of $M_{t\bar{t}}$, Δy , $q_\ell \times \eta_\ell$, and $\Delta\eta_{\ell\ell}$, with consistent results, though the growth of $A_{FB}^{t\bar{t}}$ with increasing $M_{t\bar{t}}$ and Δy appears somewhat more rapid than the SM prediction [169].

At the LHC, where the dominant $t\bar{t}$ production mechanism is the charge-symmetric gluon-gluon fusion, the measurement is

more difficult. For the sub-dominant $q\bar{q}$ production mechanism, the symmetric pp collision does not define a forward and backward direction. Instead, the charge asymmetry, A_C , is defined in terms of a positive versus a negative $t - \bar{t}$ rapidity difference, Δy

$$A_C^{t\bar{t}} = \frac{N(\Delta|y| > 0) - N(\Delta|y| < 0)}{N(\Delta|y| > 0) + N(\Delta|y| < 0)}. \quad (61.3)$$

Both CMS and ATLAS have measured A_C in the LHC dataset. Using lepton+jets events in 4.7 fb^{-1} of data at $\sqrt{s} = 7 \text{ TeV}$, ATLAS measures $A_C^{t\bar{t}} = (0.6 \pm 1.0)\%$ [170]. ATLAS has reported on the same measurement performed at $\sqrt{s} = 8 \text{ TeV}$ with 20.3 fb^{-1} of data, with a result of $A_C^{t\bar{t}} = (0.9 \pm 0.5)\%$ [171]. In the dilepton channel at $\sqrt{s} = 8 \text{ TeV}$, ATLAS measures [172] $A_C^{t\bar{t}} = (2.1 \pm 1.6)\%$, and $A_C^{\ell\ell} = (0.8 \pm 0.6)\%$ (defined in terms of the $\Delta\eta$ of the two leptons) in agreement with the SM predictions of $(1.11 \pm 0.04)\%$ and $(0.64 \pm 0.03)\%$, respectively [165]. Using lepton+jets events CMS has measured A_C at both $\sqrt{s} = 7$ and 8 TeV . They measure $A_C^{t\bar{t}} = (0.4 \pm 1.5)\%$ and $A_C^{\ell\ell} = (0.33 \pm 0.26(\text{stat.}) \pm 0.33(\text{sys.}))\%$ in 5.0 fb^{-1} at $\sqrt{s} = 7 \text{ TeV}$ and in 19.7 fb^{-1} at $\sqrt{s} = 8 \text{ TeV}$, respectively [173, 174]. Both measurements are consistent with the SM expectations of $A_C^{t\bar{t}} = (1.23 \pm 0.05)\%$ at $\sqrt{s} = 7 \text{ TeV}$ and $(1.11 \pm 0.04)\%$ at $\sqrt{s} = 8 \text{ TeV}$ [165], although the uncertainties are still too large for a precision test. In 19.5 fb^{-1} of dilepton events at $\sqrt{s} = 8 \text{ TeV}$, CMS measures $A_C^{t\bar{t}} = (1.1 \pm 1.3)\%$ and $A_C^{\ell\ell} = (0.3 \pm 0.7)\%$ [175], consistent with SM expectations [176].

In their 7 and 8 TeV analyses ATLAS and CMS also provide differential measurements as a function of $M_{t\bar{t}}$ and the transverse momentum p_T and rapidity y of the $t\bar{t}$ system. To reduce model-dependence, the CMS collaboration has performed a measurement in a reduced fiducial phase space [177], with a result of $A_C = (-0.35 \pm 0.72(\text{stat.}) \pm 0.31(\text{sys.}))\%$, in agreement with SM expectations.

To specifically address the dependence of the asymmetry on $M_{t\bar{t}}$, ATLAS has performed a measurement in boosted $t\bar{t}$ events [178]. In 20.3 fb^{-1} of data at $\sqrt{s} = 8 \text{ TeV}$, in events with $M_{t\bar{t}} > 0.75 \text{ TeV}$, and $|(\Delta|y|)| < 2$, ATLAS measures $A_C^{t\bar{t}} = (4.2 \pm 3.2)\%$ compared to a NLO SM prediction of $(1.60 \pm 0.04)\%$. The measurement is also presented in three bins of $M_{t\bar{t}}$, each in agreement, though with large uncertainties, with the SM expectations.

Both ATLAS and CMS have measured asymmetries in the distribution of leptons from $t\bar{t}$ decays. ATLAS, in 4.6 fb^{-1} of $\sqrt{s} = 7 \text{ TeV}$ data, has measured $A_C^{\ell\ell} = (2.4 \pm 1.5(\text{stat.}) \pm 0.9(\text{sys.}))\%$ in dilepton events [179]. Using a neutrino weighting technique in the same dataset to reconstruct the top quarks, ATLAS measures $A_C = (2.1 \pm 2.5(\text{stat.}) \pm 1.7(\text{sys.}))\%$. CMS, in 5.0 fb^{-1} of $\sqrt{s} = 7 \text{ TeV}$ data, uses dilepton events to measure $A_C = (1.0 \pm 1.5(\text{stat.}) \pm 0.6(\text{sys.}))\%$, where a matrix weighting technique is used to reconstruct the top quarks, and $A_C^{\ell\ell} = (0.9 \pm 1.0(\text{stat.}) \pm 0.6(\text{sys.}))\%$ [180]. An earlier result using lepton+jets events from the same CMS dataset found $A_C = (0.4 \pm 1.0 \pm 1.1)\%$ [173]. Combined results from ATLAS and CMS have now been released [181]. At $\sqrt{s} = 7 \text{ TeV}$ the combined result is $A_C = (0.5 \pm 0.7(\text{stat.}) \pm 0.6(\text{sys.}))\%$, and at $\sqrt{s} = 8 \text{ TeV}$ it is $A_C = (0.55 \pm 0.23 \pm 0.25)\%$. These results are all consistent, within their large uncertainties, with the SM expectations of $A_C^{\ell\ell} = (0.70 \pm 0.03)\%$ and $A_C = (1.23 \pm 0.05)\%$ [165].

ATLAS has released a charge asymmetry measurement at $\sqrt{s} = 13 \text{ TeV}$ using the full 139 fb^{-1} dataset. A Bayesian unfolding procedure is used in lepton plus jets events, combining both resolved and boosted topologies, to infer the asymmetry at parton level, correcting for detector resolution and acceptance effects. The inclusive charge asymmetry is measured as $A_C = (0.60 \pm 0.15)\%$ (stat+sys.) [182]. In addition to the inclusive measurement, the result includes differential measurements in five bins of $M_{t\bar{t}}$, and four bins of longitudinal boost. Both inclusive and differential results are found consistent with Standard Model predictions at NNLO in QCD and NLO in electroweak theory.

A model-independent comparison of the Tevatron and LHC results is made difficult by the differing $t\bar{t}$ production mechanisms at work at the two accelerators and by the symmetric nature of

the pp collisions at the LHC. A recent result from the CMS Collaboration [183] in 35.9 fb^{-1} of lepton plus jets events at $\sqrt{s} = 13 \text{ TeV}$, uses a likelihood analysis to separate the $q\bar{q}$ process from production via gluon-gluon and gluon-quark interactions and extract $A_{FB} = (4.8^{+8.8}_{-8.4}(\text{stat.}) \pm 2.8(\text{sys.}))\%$. In addition, given a particular model of BSM physics, a comparison can be obtained through the resulting asymmetry predicted by the model at the two machines, see for example [178].

A new measurement from ATLAS explores a so-called ‘energy asymmetry’ in $t\bar{t}$ production in association with a high- p_T jet ($t\bar{t}j$ production). The energy asymmetry is defined as a difference between the top and anti-top quarks’ energies, and is measured in ATLAS in three bins of the associated high- p_T jet angle, θ_j . Both the energies and jet angle are measured in the $t\bar{t}j$ rest frame. A Bayesian unfolding method corrects for resolution and acceptance effects. The measurement is in agreement with the Standard Model at NLO accuracy [184].

61.3.2 Top-Quark Properties

61.3.2.1 Top-Quark Mass Measurements

The most precisely studied property of the top quark is its mass. The top-quark mass has been measured in the lepton+jets, the dilepton, and the all-jets channel by all four Tevatron and LHC experiments, and now in single-top events at the LHC. The latest and/or most precise results are summarized in Table 61.1. The lepton+jets channel yields the most precise single measurements because of good signal to background ratio (in particular after b -tagging) and the presence of only a single neutrino in the final state. The momentum of a single neutrino can be reconstructed (up to a quadratic ambiguity) via the missing E_T measurement and the constraint that the lepton and neutrino momenta reconstruct to the known W boson mass. In the large data samples available at the LHC, measurements in the dilepton channel can be competitive and certainly complementary to those in the lepton+jets final state.

A large number of techniques have now been applied to measuring the top-quark mass. The original ‘template method’ [185], in which Monte Carlo templates of reconstructed mass distributions are fit to data, has evolved into a precision tool in the lepton+jets channel, where the systematic uncertainty due to the jet energy scale (JES) uncertainty is controlled by a simultaneous, *in situ* fit to the $W \rightarrow jj$ hypothesis [186]. All the latest measurements in the lepton+jets and the all-jets channels use this technique in one way or another. In 20.2 fb^{-1} of data at $\sqrt{s} = 8 \text{ TeV}$ in the lepton+jets channel, ATLAS achieves a total uncertainty of 0.53% with a statistical component of 0.23% [187]. The measurement is based on a 3-dimensional template fit, determining the top-quark mass, the global jet energy scale and a b -to-light jet energy scale factor. The most precise CMS result in the lepton+jets channel uses an ideogram method and comes from a so-called ‘hybrid’ approach in which the prior knowledge about the jet energy scale is incorporated as a Gaussian constraint, with a width determined by the uncertainty on the jet energy corrections. In 19.7 fb^{-1} of $\sqrt{s} = 8 \text{ TeV}$ data, CMS achieves a total uncertainty of 0.30% with a statistical component of 0.09% with the hybrid approach [188]. Using this same method, CMS has released a top-mass measurement from $\sqrt{s} = 13 \text{ TeV}$ data. Using 35.9 fb^{-1} of lepton+jets events they measure the top mass with a precision of 0.36% , with a statistical component of 0.05% [189]. The measurements at $\sqrt{s} = 13 \text{ TeV}$ include, for the first time, an uncertainty due to ‘color reconnection’ [190, 191]. In this same dataset, CMS has extracted a top mass from highly boosted top-quark decays by selecting events in which the hadronic-side top decay is reconstructed as a single jet with $P_T > 400 \text{ GeV}$. The cross section as a function of jet mass is unfolded at the particle level to extract a top mass with a precision of 1.4% [192].

The template method is complemented by the ‘matrix element’ method. This method was first applied by the DØ Collaboration [193], and is similar to a technique originally suggested by Kondo *et al.* [194] and Dalitz and Goldstein [195]. In the matrix element method a probability for each event is calculated as a function of the top-quark mass, using a LO matrix element for the production and decay of $t\bar{t}$ pairs. The *in situ* calibration of dijet pairs to the $W \rightarrow jj$ hypothesis is now also used with the matrix element

technique to constrain the jet energy scale uncertainty. In the lepton+jets channel, $D\bar{O}$ uses the full Tevatron dataset of 9.7 fb^{-1} and yields an uncertainty of about 0.43% [196].

In the dilepton channel, the signal to background is typically very good, but reconstruction of the mass is non-trivial because there are two neutrinos in the final state, yielding a kinematically unconstrained system. A variety of techniques have been developed to handle this. An analytic solution to the problem has been proposed [197], but this has not yet been used in the mass measurement. One of the most precise measurements in the dilepton channel comes from using the invariant mass of the charged lepton and b -quark system ($M_{\ell b}$), which is sensitive to the top-quark mass and avoids the kinematic difficulties of the two-neutrino final state. In 4.6 fb^{-1} of $\sqrt{s} = 7 \text{ TeV}$ data, ATLAS has measured the top-quark mass in the dilepton channel to a precision of 0.53% using a template fit to the $M_{\ell b}$ distribution [198]. Using 19.7 fb^{-1} of data at $\sqrt{s} = 8 \text{ TeV}$, CMS has released [199] a mass measurement in the dilepton channel based on a simultaneous fit to $M_{\ell b}$ and a transverse-mass-like variable M_{T2} [200]. The most precise result in this analysis, which comes from a linear combination of fits with the jet energy scale fixed at its nominal value and one that simultaneously determines the top mass and jet energy scale, has a total uncertainty of 0.54%. At the LHC, because of their precision, these techniques have largely displaced a number of earlier techniques in the dilepton channel, though these techniques are still included, and described, in the combined results from CMS, reported in Ref. [188].

In the neutrino weighting technique, used by CDF to analyze the full Run 2 dilepton dataset of 9.1 fb^{-1} , a weight is assigned by assuming a top-quark mass value and applying energy-momentum conservation to the top-quark decay, resulting in up to four possible pairs of solutions for the neutrino and anti-neutrino momenta. The missing E_T calculated in this way is then compared to the observed missing E_T to assign a weight [205]. The CDF result achieves a precision of 1.8% using a combination of neutrino weighting and an ‘‘alternative mass’’, which is insensitive to the jet energy scale [206]. The alternative mass depends on the angles between the leptons and the leading jets and the lepton four-momenta.

In the all-jets channel there is no ambiguity due to neutrino momenta, but the signal to background is significantly poorer due to the severe QCD multijets background. The emphasis therefore has been on background modeling, and reduction through event selection. The most recent measurement in the all-jets channel, by CMS in 35.9 fb^{-1} of $\sqrt{s} = 13 \text{ TeV}$ data [201], uses an ideogram method and a 2-dimensional simultaneous fit for m_t and the jet energy scale to extract the top-quark mass and achieves a precision of 0.36%. A measurement from ATLAS [202] uses a template fit to the ratio of three-jet (m_t) to two-jet (M_W) mass in the all-hadronic channel, the two-jet denominator provides an *in situ*, fit to the $W \rightarrow jj$ hypothesis. In 20.2 fb^{-1} of data at $\sqrt{s} = 8 \text{ TeV}$, the result has a precision of 0.65%. A measurement from CDF in 9.3 fb^{-1} uses a two-dimensional template fit and achieves a precision of 1.1% [207].

The CMS Collaboration extracted a top-quark mass measurement from single-top events, something not previously done because of the poor signal to background ratio. The mass is extracted from the invariant mass of the muon, bottom quark, and missing transverse energy. The first measurement with 19.7 fb^{-1} of data at $\sqrt{s} = 8 \text{ TeV}$, achieved a precision of 0.71% [208]. A more recent measurement in 35.9 fb^{-1} of data at $\sqrt{s} = 13 \text{ TeV}$ achieves 0.44% precision [203].

A dominant systematic uncertainty in these methods is the understanding of the jet energy scale, and so several techniques have been developed that have little sensitivity to the jet energy scale uncertainty. In addition to Reference [206] mentioned above, these include the measurement of the top-quark mass using the following techniques: Fitting of the lepton p_T spectrum of candidate events [209]; fitting of the transverse decay length of the b -jet (L_{xy}) [210]; fitting the invariant mass of a lepton from the W -decay and a muon from the semileptonic b decay [211, 212], kinematic properties of secondary vertices from b -quark fragmentation [213], the invariant mass of the $J/\psi + \ell$ system in events in

which a b -quark fragments to a J/ψ particle [214], fitting the b -jet energy peak [215], and dilepton kinematics in $e\mu$ events [216].

Several measurements have now been made in which the top-quark mass is extracted from the measured $t\bar{t}$ cross section using the theoretical relationship between the mass and the production cross section. These determinations make use of predictions calculated at higher orders, where the top mass enters as an input parameter defined in a given scheme. At variance with the usual methods, which involve the kinematic properties of the final states and therefore the pole mass, this approach can also directly determine a short-distance mass, such as the $\overline{\text{MS}}$ mass [217]. With an alternative method ATLAS extracted the top-quark pole mass using $t\bar{t}$ events with at least one additional jet, basing the measurement on the relationship between the differential rate of gluon radiation and the mass of the quark [218]. A similar analysis by CMS used the differential cross section as a function of the invariant mass of the $t\bar{t}$ system and the leading jet not associated with the top decays [219].

Each of the experiments has produced a measurement combining its various results. The combined measurement from CMS with up to 19.7 fb^{-1} of data achieves statistical and systematic uncertainties of 0.08% and 0.27%, respectively [188]. The combined measurement from ATLAS, with up to 20.3 fb^{-1} yields statistical and systematic uncertainties of 0.14% and 0.24%, respectively [187]. CDF has combined measurements with up to 9.3 fb^{-1} [220] and achieves a statistical precision of 0.33% and a systematic uncertainty of 0.43%. $D\bar{O}$ achieves a 0.33% statistical+JES and a 0.28% systematic uncertainty by combining results in 9.7 fb^{-1} [221].

Combined measurements from the Tevatron experiments and from the LHC experiments take into account the correlations between different measurements from a single experiment and between measurements from different experiments. The Tevatron average [204], using up to 9.7 fb^{-1} of data, now has a precision of 0.37%. The LHC combination, using up to 4.9 fb^{-1} of data, has a precision of 0.56% [222], where more work on systematic uncertainties is required. A Tevatron-LHC combination has been released, combining the results of all four experiments, using the full Tevatron dataset and the $\sqrt{s} = 7 \text{ TeV}$ LHC data, with a resulting precision of 0.44% [3].

The direct measurements of the top-quark mass, such as those shown in Table 61.1, correspond to the parameter used in the Monte Carlo generators, which is closely related to the pole mass [223]. The relation between the pole mass and short-distance masses, such as $\overline{\text{MS}}$, is affected by non-perturbative effects. Recent calculations evaluate the size of this ambiguity to be below 250 MeV and therefore still smaller than the current measurement uncertainty [224, 225]. ATLAS has recently performed a ‘calibration’ of the top mass parameter in POWHEG + PYTHIA 8 with respect to the so-called ‘MSR’ mass scheme [226]. Using simulated lepton+jets events and the mass distribution of large-radius jets containing the three quarks from the hadronically decaying top quark, they find a mass difference between the Monte Carlo mass and the MSR mass of 80 MeV with large uncertainties [227].

As a result of renormalization at higher-orders in perturbation theory, the top quark mass depends on the scale at which it is evaluated. The CMS collaboration has made the first measurement of the so-called running of the top-quark mass in the $\overline{\text{MS}}$ scheme [228]. The running mass is extracted from a measurement of the differential cross section as a function of the $t\bar{t}$ invariant mass, unfolded back to the parton level, in $e\mu$ final states. The running mass varies by about 15% from $M_{t\bar{t}} = 400 \text{ GeV}$ to $M_{t\bar{t}} \approx 1 \text{ TeV}$, in good agreement with the renormalization group calculation at one-loop level. Compared to the hypothesis of no running, the significance of the measured running is 2.6σ . However, caveats of such an interpretation have been raised as a result of the large theoretical uncertainties [229].

With the discovery of a Higgs boson at the LHC with a mass of about $125 \text{ GeV}/c^2$ [230, 231], the precision measurement of the top-quark mass takes a central role in the question of the stability of the electroweak vacuum because top-quark radiative corrections tend to drive the Higgs quartic coupling, λ , negative, potentially leading to an unstable vacuum. A calculation at NNLO [232]

Table 61.1: Measurements of top-quark mass from Tevatron and LHC. The results are a selection of both published and preliminary (not yet submitted for publication as of September 2021) measurements. For a complete set of published results see the Listings. Statistical uncertainties are listed first, followed by systematic uncertainties.

m_t (GeV/ c^2)	Source	$\int \mathcal{L} dt$ fb $^{-1}$	Ref.	Channel
$172.08 \pm 0.25 \pm 0.41$	ATLAS	20.2	[187]	ℓ +jets+ $\ell\ell$ +All jets
$172.44 \pm 0.13 \pm 0.47$	CMS	19.7	[188]	ℓ +jets+ $\ell\ell$ +All jets
$172.35 \pm 0.16 \pm 0.48$	CMS	19.7	[188]	ℓ +jets
$172.34 \pm 0.20 \pm 0.70$	CMS	35.9	[201]	$\ell\ell$
$173.72 \pm 0.55 \pm 1.01$	ATLAS	20.2	[202]	All jets
$172.25 \pm 0.08 \pm 0.62$	CMS	35.9	[189]	ℓ +jets
$172.6 \pm 0.4 \pm 2.4$	CMS	35.9	[192]	Boosted jets
$172.13 \pm 0.32^{+0.69}_{-0.70}$	CMS	35.9	[203]	Single top
$174.30 \pm 0.35 \pm 0.54$	CDF,DØ (I+II)	≤ 9.7	[204]	publ. or prelim.
$173.34 \pm 0.27 \pm 0.71$	Tevatron+LHC	$\leq 8.7 + \leq 4.9$	[3]	publ. or prelim.

leads to the conclusion of vacuum stability for a Higgs mass satisfying $M_H \geq 129.4 \pm 5.6$ GeV/ c^2 [233]. Given the uncertainty, a Higgs mass of 125 GeV/ c^2 satisfies the limit, but the central values of the Higgs and top-quark masses put the electroweak vacuum squarely in the metastable region. The uncertainty is dominated by the precision of the top-quark mass measurement and its interpretation as the pole mass. For more details, see the Higgs boson review in this volume.

As a test of the *CPT*-symmetry, the mass difference of top- and antitop-quarks $\Delta m_t = m_t - m_{\bar{t}}$, which is expected to be zero, can be measured. CDF measures the mass difference in 8.7 fb $^{-1}$ of 1.96 TeV data in the lepton+jets channel using a template method to find $\Delta m_t = -1.95 \pm 1.11(stat.) \pm 0.59(syst.)$ GeV/ c^2 [234] while DØ uses 3.6 fb $^{-1}$ of lepton+jets events and the matrix element method with at least one *b*-tag. They find $\Delta m_t = 0.8 \pm 1.8(stat.) \pm 0.5(syst.)$ GeV/ c^2 [235]. In 4.7 fb $^{-1}$ of 7 TeV data, ATLAS measures the mass difference in lepton+jets events with a double *b*-tag requirement and hence very low background to find $\Delta m_t = 0.67 \pm 0.61(stat.) \pm 0.41(syst.)$ GeV/ c^2 [236]. CMS measures the top-quark mass difference in 5 fb $^{-1}$ of 7 TeV data in the lepton+jets channel and finds $\Delta m_t = -0.44 \pm 0.46(stat.) \pm 0.27(syst.)$ GeV/ c^2 [237]. They repeat this measurement with 19.6 fb $^{-1}$ of 8 TeV data to find $\Delta m_t = -0.15 \pm 0.19(stat.) \pm 0.09(syst.)$ GeV/ c^2 [238]. Now that the top mass has been measured in single-top events, the mass difference can be measured by tagging the top- or anti-top quark with the lepton charge. In 35.9 fb $^{-1}$ of 13 TeV single-top candidate events CMS measures the mass ratio and difference to be $0.995^{+0.005}_{-0.006}$ and $0.83^{+0.77}_{-1.01}$ GeV, respectively [203]. All measurements are consistent with the SM expectation.

61.3.2.2 Top-Quark Spin Correlations, Polarization, and Width

One of the unique features of the top quark is that it decays before its spin can be flipped by the strong interaction. Thus the top-quark polarization is directly observable via the angular distribution of its decay products and it is possible to define and measure observables sensitive to the top-quark spin and its production mechanism. Although the top- and antitop-quarks produced by strong interactions in hadron collisions are essentially unpolarized, the spins of *t* and \bar{t} are correlated. For QCD production at threshold, the $t\bar{t}$ system is produced in a 3S_1 state with parallel spins for $q\bar{q}$ annihilation or in a 1S_0 state with antiparallel spins for gluon-gluon fusion. The situations at the Tevatron, where the production is primarily from $q\bar{q}$ annihilation, and at the LHC, where the production is primarily from gluon-gluon fusion, are therefore somewhat complementary. However, at the LHC production of $t\bar{t}$ pairs at large invariant mass occurs primarily via fusion of gluons with opposite helicities, and the $t\bar{t}$ pairs so produced have parallel spins as in production at the Tevatron via $q\bar{q}$ annihilation. The direction of the top-quark spin is 100% correlated to the angular distributions of the down-type fermion (charged leptons or *d*-type quarks) in the decay. The joint angular

distribution [239–241]

$$\frac{1}{\sigma} \frac{d^2\sigma}{d(\cos\theta_+)d(\cos\theta_-)} = \frac{1}{4} (1 + B_+ \cos\theta_+ + B_- \cos\theta_- + \kappa \cdot \cos\theta_+ \cdot \cos\theta_-), \quad (61.4)$$

where θ_+ and θ_- are the angles of the daughters in the top-quark rest frame with respect to a particular spin quantization axis (assumed here to be the same for θ_+ and θ_-), is a very sensitive observable. The maximum value for κ , 0.782 at NLO at the Tevatron [242], is found in the off-diagonal basis [239], while at the LHC the value at NLO is 0.326 in the helicity basis [242]. The coefficients B_+ and B_- are near zero in the SM because the top quarks are unpolarized in $t\bar{t}$ production. In place of κ , $A\alpha_+\alpha_-$ is often used, where α_i is the spin analyzing power, and A is the spin correlation coefficient, defined as

$$A = \frac{N(\uparrow\uparrow) + N(\downarrow\downarrow) - N(\uparrow\downarrow) - N(\downarrow\uparrow)}{N(\uparrow\uparrow) + N(\downarrow\downarrow) + N(\uparrow\downarrow) + N(\downarrow\uparrow)}, \quad (61.5)$$

where the first arrow represents the direction of the top-quark spin along a chosen quantization axis, and the second arrow represents the same for the antitop-quark. The spin analyzing power α_i is +0.998 for positively charged leptons, -0.966 for down-type quarks from *W* decays, and -0.393 for bottom quarks [243]. The sign of α flips for the respective antiparticles. The spin correlation could be modified by a new $t\bar{t}$ production mechanism such as through a *Z'* boson, Kaluza-Klein gluons, a dark-matter mediator, or a Higgs boson.

The experiments typically use a Monte Carlo to provide templates for the measured distributions, or alternatively a matrix-element technique, and fit a parameter *f*, representing the fraction of events with the expected Standard Model correlation, with $(1-f)$ the fraction with no correlation. The correlation coefficient is extracted via $A_{\text{meas}} = f \cdot A_{\text{SM}}$. A ‘fraction’ $f > 1$ means that the measured correlation coefficient is larger than the Standard Model expectation.

CDF used 5.1 fb $^{-1}$ in the dilepton channel to measure the correlation coefficient in the beam axis [244]. The measurement was made using the expected distributions of $(\cos\theta_+, \cos\theta_-)$ and $(\cos\theta_b, \cos\theta_{\bar{b}})$ of the charged leptons or the *b*-quarks in the $t\bar{t}$ signal and background templates to calculate a likelihood of observed reconstructed distributions as a function of assumed κ . They determined the 68% confidence interval for the correlation coefficient κ as $-0.52 < \kappa < 0.61$ or $\kappa = 0.04 \pm 0.56$ assuming $m_t = 172.5$ GeV/ c^2 .

CDF also analyzed lepton+jets events in 5.3 fb $^{-1}$ [245] assuming $m_t = 172.5$ GeV/ c^2 . They form three separate templates - the same-spin template, the opposite-spin template, and the background template for the 2-dimensional distributions in $\cos(\theta_t)\cos(\theta_d)$ vs. $\cos(\theta_t)\cos(\theta_b)$. The fit to the data in the helicity basis returns an opposite helicity fraction of $F_{OH} = 0.74 \pm 0.24(stat.) \pm 0.11(syst.)$. Converting this to the spin correlation coefficient yields $\kappa_{\text{helicity}} = 0.48 \pm 0.48(stat.) \pm 0.22(syst.)$. In the beamline basis, they find an opposite spin fraction of

$F_{OS} = 0.86 \pm 0.32(stat.) \pm 0.13(syst.)$ which can be converted into a correlation coefficient of $\kappa_{beam} = 0.72 \pm 0.64(stat.) \pm 0.26(syst.)$.

DØ performed a measurement of the ratio f of events with correlated t and \bar{t} spins to the total number of $t\bar{t}$ events. Combining dilepton and lepton plus jets events, and using a matrix-element technique in 9.7 fb^{-1} of Tevatron data, DØ measures $f = 1.16 \pm 0.21$, corresponding to $A_{exp.} = 0.89 \pm 0.22(stat.+syst.)$ in the off-diagonal basis [246].

In Ref. [247] DØ presents a measurement of top-quark polarization in $t\bar{t}$ production at the Tevatron. In 9.7 fb^{-1} of $p\bar{p}$ collisions, DØ uses lepton angular distributions in lepton+jets events to measure polarization in the beam, helicity, and transverse bases. The measurements are, respectively, 0.081 ± 0.048 , -0.102 ± 0.061 and, 0.040 ± 0.035 , where the beam-basis result is a combination with an earlier DØ result in dilepton events [248]. These results are all consistent near-zero polarization, as predicted in the SM.

Spin correlations have been conclusively measured at the LHC by both the ATLAS and CMS collaborations. In the dominant gluon fusion production mode for $t\bar{t}$ pairs at the LHC, the angular distribution between the two leptons in $t\bar{t}$ decays to dileptons is sensitive to the degree of spin correlation [249].

Measurements have been made at 7, 8, and now 13 TeV. While there is some interest in the \sqrt{s} dependence of the correlations as a test of the production mechanism ($q\bar{q}$ vs gluon-gluon and possible sensitivity to new physics) the earlier measurements at 7 and 8 TeV [250–255] had relatively large uncertainties and have now been overtaken by the high-statistics 13 TeV measurements, which we review here.

The most recent result from ATLAS, in 36.1 fb^{-1} at $\sqrt{s} = 13 \text{ TeV}$, uses $\Delta\phi$, the azimuthal angle between the two charged leptons in $e\mu$ events in an analysis that also measures the differential cross sections in $\Delta\phi$ and $\Delta\eta$ between the two leptons [256]. The result, measured by comparison with NLO Monte Carlo generators, is $f = 1.249 \pm 0.024 \pm 0.061_{-0.090}^{+0.067}$, where the uncertainties are statistical, systematic, and theoretical, is again greater than 1.0. Whereas the previous results were statistically consistent with the Standard Model expectation of 1.0, this result is inconsistent at the level of 2.2σ . The NLO generators are NLO in QCD only (and only at the production level). Including electroweak couplings produces an expected Standard Model distribution consistent with the data, but results in a large scale uncertainty, giving $f = 1.03 \pm 0.13$.

In 35.9 fb^{-1} of data at $\sqrt{s} = 13 \text{ TeV}$, CMS has measured spin correlations in dilepton events using $\Delta\phi$ and found $f = 1.05 \pm 0.03 \pm 0.08_{-0.12}^{+0.09}$ [257], where the uncertainties are statistical, systematic, and theoretical. The correlation is also measured using the coefficient κ in Eq. 61.4 (called $-C_{ij}$ in Reference [257]) using three orthogonal spin quantization axes defined in Ref. [258]. All results are consistent with $f = 1$. Measurements of the coefficients B_i in Eq. 61.4 in this analysis, which are expected to be nearly zero in the SM, yield $B_+ = 0.005 \pm 0.023$ and $B_- = 0.007 \pm 0.023$, consistent with the SM predictions at NLO of $0.004_{-0.0012}^{+0.0017}$ [258]. These results are part of a complete study of the top-quark spin density matrix at $\sqrt{s} = 13 \text{ TeV}$, through the measurement of the coefficients of Eq. 61.4.

In a similar ATLAS measurement at $\sqrt{s} = 8 \text{ TeV}$ [259], the spin-correlation coefficient κ is measured in the helicity basis to be $\kappa = 0.296 \pm 0.093$ in good agreement with the SM expectation of 0.318 (corresponding to a central value of f of 0.931). The polarization coefficients, B , in Eq. 61.4 are measured, also in the helicity basis, to be $B_+ = -0.044 \pm 0.038$ and $B_- = -0.064 \pm 0.040$, consistent with the SM predictions of 0.0030 ± 0.0010 and 0.0034 ± 0.00104 , respectively.

Observation of top-quark spin correlations requires a top-quark lifetime less than the spin decorrelation timescale [260]. The top-quark width, inversely proportional to its lifetime, is expected to be of order $1 \text{ GeV}/c^2$ (Eq. 1). Early measurements made at CDF [261] and CMS [262] established confidence-level intervals for the width, but did not have the sensitivity to make a direct measurement.

The first direct measurement comes from an ATLAS analysis that directly fits reconstructed lepton+jets events in 20.2 fb^{-1} of data at $\sqrt{s} = 8 \text{ TeV}$. They find $\Gamma_t = 1.76 \pm 0.33_{-0.68}^{+0.79} \text{ GeV}/c^2$

[263]. A more recent measurement from ATLAS with 139 fb^{-1} of data at $\sqrt{s} = 13 \text{ TeV}$ [264], uses a template fit to the lepton- b -quark invariant mass in dilepton final states. The result, $\Gamma_t = (1.9 \pm 0.5) \text{ GeV}/c^2$, is the most precise measurement to date.

The total width of the top-quark can also be determined from the partial decay width $\Gamma(t \rightarrow Wb)$ and the branching fraction $B(t \rightarrow Wb)$. DØ obtains $\Gamma(t \rightarrow Wb)$ from the measured t -channel cross section for single top-quark production in 5.4 fb^{-1} , and $B(t \rightarrow Wb)$ is extracted from a measurement of the ratio $R = B(t \rightarrow Wb)/B(t \rightarrow Wq)$ in $t\bar{t}$ events in lepton+jets channels with 0, 1 and 2 b -tags. Assuming $B(t \rightarrow Wq) = 1$, where q includes any kinematically accessible quark, the result is: $\Gamma_t = 2.00_{-0.43}^{+0.47} \text{ GeV}/c^2$ which translates to a top-quark lifetime of $\tau_t = (3.29_{-0.63}^{+0.90}) \times 10^{-25} \text{ s}$. Assuming a high mass fourth generation b' quark and unitarity of the four-generation quark-mixing matrix, they set the first upper limit on $|V_{tb'}| < 0.59$ at 95% C.L. [265]. A similar analysis has performed by CMS in 19.7 fb^{-1} of $\sqrt{s} = 8 \text{ TeV}$ data. It provides a better determination of the total width with respect to the measurement by DØ giving $\Gamma_t = 1.36 \pm 0.02(stat.)_{-0.11}^{+0.14}(syst.) \text{ GeV}/c^2$ [75].

61.3.2.3 W -Boson Helicity in Top-Quark Decay

The Standard Model dictates that the top quark has the same vector-minus-axial-vector ($V - A$) charged-current weak interactions $\left(-i \frac{g}{\sqrt{2}} V_{tb} \gamma^\mu \frac{1}{2}(1 - \gamma_5)\right)$ as all the other fermions. In the SM, the fraction of top-quark decays to longitudinally polarized W bosons is proportional to its Yukawa coupling and hence enhanced with respect to the weak coupling. It is expected to be [266] $\mathcal{F}_0^{\text{SM}} \approx x/(1+x)$, $x = m_t^2/2M_W^2$ ($\mathcal{F}_0^{\text{SM}} \sim 70\%$ for $m_t = 173 \text{ GeV}/c^2$). Fractions of left-handed, right-handed, or longitudinal W bosons are denoted as \mathcal{F}_- , \mathcal{F}_+ , and \mathcal{F}_0 respectively. In the SM, \mathcal{F}_- is expected to be $\approx 30\%$ and $\mathcal{F}_+ \approx 0\%$. Predictions for the W polarization fractions at NNLO in QCD are available [267].

The Tevatron and the LHC experiments use various techniques to measure the helicity of the W boson in top-quark decays, in both the lepton+jets and in dilepton channels in $t\bar{t}$ production.

The first method uses a kinematic fit, similar to that used in the lepton+jets mass analyses, but with the top-quark mass constrained to a fixed value, to improve the reconstruction of final-state observables, and render the under-constrained dilepton channel solvable. Alternatively, in the dilepton channel the final-state momenta can also be obtained through an algebraic solution of the kinematics. The distribution of the helicity angle ($\cos\theta^*$) between the lepton and the b quark in the W rest frame provides the most direct measure of the W helicity. In a simplified version of this approach, the $\cos\theta^*$ distribution is reduced to a forward-backward asymmetry.

The second method (p_T^ℓ) uses the different lepton p_T spectra from longitudinally or transversely polarized W -decays to determine the relative contributions.

A third method uses the invariant mass of the lepton and the b -quark in top-quark decays ($M_{\ell b}^2$) as an observable, which is directly related to $\cos\theta^*$.

At the LHC, top-quark pairs in the dilepton channels are reconstructed by solving a set of six independent kinematic equations in the missing transverse energy in x - and in y -direction, two W -masses, and the two top/antitop-quark masses. In addition, the two jets with the largest p_T in the event are interpreted as b -jets. The pairing of the jets to the charged leptons is based on the minimization of the sum of invariant masses M_{min} . Simulations show that this criterion gives the correct pairing in 68% of the events.

Finally, the Matrix Element Method (MEM) has also been used [194], in which a likelihood is formed from a product of event probabilities calculated from the MEM for a given set of measured kinematic variables and assumed W -helicity fractions.

The results of recent CDF, DØ, ATLAS, and CMS analyses are summarized in Table 61.2. The datasets are now large enough to allow for a simultaneous fit of \mathcal{F}_0 , \mathcal{F}_- and \mathcal{F}_+ , which we denote by ‘3-param’ or \mathcal{F}_0 and \mathcal{F}_+ , which we denote by ‘2-param’ in the table. Results with either \mathcal{F}_0 or \mathcal{F}_+ fixed at its SM value are denoted ‘1-param’. For the simultaneous fits, the correlation

coefficient between the two values is about -0.8 . A complete set of published results can be found in the Listings. All results are in agreement with the SM expectation.

CDF and DØ combined their results based on $2.7 - 5.4 \text{ fb}^{-1}$ [268] for a top-quark mass of $172.5 \text{ GeV}/c^2$. ATLAS presents results from 1.04 fb^{-1} of $\sqrt{s} = 7 \text{ TeV}$ data using a template method for the $\cos\theta^*$ distribution and angular asymmetries from the unfolded $\cos\theta^*$ distribution in the lepton+jets and the dilepton channel [269]. CMS performs a similar measurement based on template fits to the $\cos\theta^*$ distribution with 5.0 fb^{-1} of 7 TeV data in the lepton+jets final state [270]. As the polarization of the W bosons in top-quark decays is sensitive to the Wtb vertex Lorentz structure and anomalous couplings, both experiments also derive limits on anomalous contributions to the Wtb couplings. CMS and ATLAS collaborations have also combined their results from 7 TeV data to obtain values on the helicity fractions as well as limits on anomalous couplings [271].

At 8 TeV , ATLAS came out with a measurement of the W -helicity fractions in 20.2 fb^{-1} in lepton+jets events with at least one b -tag [272]. Using 19.8 fb^{-1} of 8 TeV data, CMS measured the W -helicity in lepton + 4 jet events with two b -tags [273]. In $t\bar{t}$ events with two opposite-sign leptons (electron or muon) in the final state in this dataset, CMS applied six kinematic constraints on the kinematics of the produced particles [274]. Also, using the same dataset a first measurement of the W -boson helicity in top-quark decays was made in electroweak single top production [275], yielding similarly precise and consistent results. The 8 TeV results obtained in $t\bar{t}$ and single-top events by ATLAS and CMS have also been combined recently [276]. These results are in agreement with the standard model predictions at next-to-next-to-leading order in perturbative QCD and represent an improvement in precision of 25 (29)% for F_0 (F_L) with respect to the most precise single measurement. A limit on anomalous right-handed vector (V_R), and left- and right-handed tensor (g_L, g_R) tWb couplings and on corresponding Wilson coefficients is set.

61.3.2.4 Top-Quark Electroweak Charges and Couplings

The top quark is the only quark whose electric charge has not been measured through production at threshold in e^+e^- collisions. Furthermore, it is the only quark whose electromagnetic coupling has not been observed and studied until recently. Since the CDF and DØ analyses on top-quark production did not associate the b , \bar{b} , and W^\pm uniquely to the top or antitop, decays such as $t \rightarrow W^+ \bar{b}, \bar{t} \rightarrow W^- b$ were not excluded. A charge $4/3$ quark of this kind is consistent with current electroweak precision data. The $Z \rightarrow \ell^+ \ell^-$ and $Z \rightarrow b\bar{b}$ data, in particular the discrepancy between A_{LR} from SLC at SLAC and $A_{FB}^{0,b}$ of b -quarks and $A_{FB}^{0,\ell}$ of leptons from LEP at CERN, can be fitted with a top quark of mass $m_t = 270 \text{ GeV}/c^2$, provided that the right-handed b quark mixes with the isospin $+1/2$ component of an exotic doublet of charge $-1/3$ and $-4/3$ quarks, $(Q_1, Q_4)_R$ [278, 279]. Also the third component of the top quark's weak isospin has not been measured so far.

DØ studied the top-quark charge in double-tagged lepton+jets events, CDF did it in single tagged lepton+jets and dilepton events. Assuming the top- and antitop-quarks have equal but opposite electric charge, then reconstructing the charge of the b -quark through jet charge discrimination techniques, the $|Q_{top}| = 4/3$ and $|Q_{top}| = 2/3$ scenarios can be differentiated. For the exotic model of Chang *et al.* [279] with a top-quark charge $|Q_{top}| = 4/3$, CDF excluded the model at 99% C.L. [280] in 5.6 fb^{-1} , while DØ excluded the model at a significance greater than 5 standard deviations using 5.3 fb^{-1} and set an upper limit of 0.46 on the fraction of such quarks in the selected sample [281]. These results indicate that the observed particle is indeed consistent with being a SM $|Q| = 2/3$ quark.

In 2.05 fb^{-1} at $\sqrt{s} = 7 \text{ TeV}$, ATLAS performed a similar analysis, reconstructing the b -quark charge either via a jet-charge technique or via the lepton charge in soft muon decays in combination with a kinematic likelihood fit. They measure the top-quark charge to be $0.64 \pm 0.02(\text{stat.}) \pm 0.08(\text{sys.})$ from the charges of the top-quark decay products in single lepton $t\bar{t}$ events, and hence exclude the exotic scenario with charge $-4/3$ at more than 8σ [282].

In 4.6 fb^{-1} at $\sqrt{s} = 7 \text{ TeV}$, CMS discriminates between the SM and the exotic top-quark charge scenario in the muon+jets final states in $t\bar{t}$ events. They exploit the charge correlation between high- p_t muons from W -boson decays and soft muons from B -hadron decays in b -jets. Using an asymmetry technique, where $A = -1$ represents the exotic $Q = -4/3$ scenario and $A = +1$ the SM $Q = +2/3$ scenario, they find $A_{meas} = 0.97 \pm 0.12(\text{stat.}) \pm 0.31(\text{sys.})$, which agrees with the Standard Model expectation and excludes the exotic scenario at 99.9% C.L. [283].

The electromagnetic or the weak coupling of the top quark can be probed directly by investigating $t\bar{t}$ events with an additional gauge boson, such as $t\bar{t}\gamma$, $t\bar{t}W$, and $t\bar{t}Z$ events. The corresponding coupling can be extracted from the corresponding cross section or extracted from effective field theory (EFT) fits to various measured distributions and differential cross sections.

CDF performed a search for events containing a lepton, a photon, significant missing transverse momentum, and a jet identified as containing a b -quark and at least three jets and large total transverse energy in 6.0 fb^{-1} . They reported evidence for the observation of $t\bar{t}\gamma$ production with a cross section $\sigma_{t\bar{t}\gamma} = 0.18 \pm 0.08 \text{ pb}$ and a ratio of $\sigma_{t\bar{t}\gamma}/\sigma_{t\bar{t}} = 0.024 \pm 0.009$ [284].

ATLAS performed a first measurement of the $t\bar{t}\gamma$ cross section in pp collisions at $\sqrt{s} = 7 \text{ TeV}$ using 4.6 fb^{-1} of data. Events are selected that contain a large transverse momentum electron or muon and a large transverse momentum photon. The production of $t\bar{t}\gamma$ events was observed with a significance of 5.3 standard deviations. The resulting cross section times branching ratio into the single lepton channel for $t\bar{t}\gamma$ production with a photon with transverse momentum above 20 GeV is $\sigma^{fid.}(t\bar{t}\gamma) \times BR = 63 \pm 8(\text{stat.})_{-13}^{+17}(\text{sys.}) \pm 1(\text{lumi.}) \text{ pb}$ per lepton flavour [285], which is consistent with leading-order theoretical calculations.

At 8 TeV , ATLAS has used 20.2 fb^{-1} of data to measure the $t\bar{t}\gamma$ cross section with a photon above 15 GeV and $|\eta| < 2.37$. The fiducial cross section is measured to be $139 \pm 18 \text{ fb}$ [286], in good agreement with the NLO prediction [287]. Using 19.7 fb^{-1} of data at 8 TeV , CMS performed a similar measurement of the $t\bar{t}\gamma$ production cross section in the lepton+jets decay mode with a photon transverse momentum above 25 GeV and $|\eta| < 1.44$. They obtain a normalized cross section $\mathcal{R} = \sigma_{t\bar{t}\gamma}/\sigma_{t\bar{t}} = (5.7 \pm 1.8) \times 10^{-4}$ in e +jets and $(4.7 \pm 1.3) \times 10^{-4}$ in μ +jets. The fiducial $t\bar{t}\gamma$ cross section is obtained by multiplying by the measured $t\bar{t}$ fiducial cross section of $244.9 \pm 1.4(\text{stat.})_{-5.5}^{+6.3}(\text{sys.}) \pm 6.4(\text{lumi.}) \text{ pb}$. Extrapolating to the full phase space, the result is $\sigma_{t\bar{t}\gamma} \times BR = (515 \pm 108) \text{ fb}$, per lepton+jets final state [288], in good agreement with the theoretical prediction.

At $\sqrt{s} = 13 \text{ TeV}$, using 36.1 fb^{-1} of single-lepton and dilepton events with exactly one photon, ATLAS measures the $t\bar{t}\gamma$ cross section. They employ neural network algorithms to separate the signal from the backgrounds. The fiducial cross-sections are measured to be $521 \pm 9(\text{stat.}) \pm 41(\text{sys.}) \text{ fb}$ and $69 \pm 3(\text{stat.}) \pm 4(\text{sys.}) \text{ fb}$ for the single-lepton and dilepton channels, respectively. The differential cross-sections are measured as a function of photon transverse momentum, photon absolute pseudorapidity, and angular distance between the photon and its closest lepton in both channels, as well as azimuthal opening angle and absolute pseudorapidity difference between the two leptons in the dilepton channel. All measurements are in agreement with the theoretical predictions [289]. Very recently, ATLAS uses 139 fb^{-1} of $\sqrt{s} = 13 \text{ TeV}$ $e\mu + \gamma$ events with at least two jets, out of which at least one is b -tagged, to measure the inclusive and differential cross-sections for the production of a top-quark pair in association with a photon. This analysis is sensitive to both processes, $t\bar{t}\gamma + tW\gamma$. The fiducial cross-section is measured to be $39.6_{-2.3}^{+2.7} \text{ fb}$ in good agreement with the dedicated theoretical calculation provided by the authors of refs. [290, 291], which predicts a value of $\sigma_{fid} = 38.50_{-2.18}^{+0.56}(\text{scale})_{-1.18}^{+1.04}(\text{PDF}) \text{ fb}$ for the chosen fiducial phase space. Differential cross-sections as functions of several observables are compared to state-of-the-art Monte Carlo simulations and next-to-leading order theoretical calculations. These include cross-sections as functions of the photon transverse momentum and absolute pseudorapidity and angular variables related to the photon and the leptons and between the two leptons in the event. All measurements are in agreement with the predic-

Table 61.2: Measurement and 95% C.L. upper limits of the W helicity in top-quark decays. The table includes both preliminary, as of September 2021, and published results. A full set of published results is given in the Listings.

W Helicity	Source	$\int \mathcal{L} dt$ (fb^{-1})	Ref.	Method
$\mathcal{F}_0 = 0.722 \pm 0.081$	CDF+DØ Run II	2.7-5.4	[268]	$\cos \theta^*$ 2-param
$\mathcal{F}_0 = 0.682 \pm 0.057$	CDF+DØ Run II	2.7-5.4	[268]	$\cos \theta^*$ 1-param
$\mathcal{F}_0 = 0.726 \pm 0.094$	CDF Run II	8.7	[277]	ME 2-param
$\mathcal{F}_0 = 0.67 \pm 0.07$	ATLAS (7 TeV)	1.0	[269]	$\cos \theta^*$ 3-param
$\mathcal{F}_0 = 0.682 \pm 0.045$	CMS (7 TeV)	5.0	[270]	$\cos \theta^*$ 3-param
$\mathcal{F}_0 = 0.626 \pm 0.059$	ATLAS+CMS (7 TeV)	2.2	[271]	$\cos \theta^*$ 3-param
$\mathcal{F}_0 = 0.709 \pm 0.019$	ATLAS (8 TeV)	20.2	[272]	$\cos \theta^*$ 3-param
$\mathcal{F}_0 = 0.681 \pm 0.026$	CMS (8 TeV)	19.8	[273]	$\cos \theta^*$ 3-param
$\mathcal{F}_0 = 0.653 \pm 0.029$	CMS (8 TeV)	19.7	[274]	$\cos \theta^*$ 3-param
$\mathcal{F}_0 = 0.720 \pm 0.054$	CMS (8 TeV)	19.7	[275]	$\cos \theta^*$ 3-param
$\mathcal{F}_0 = 0.693 \pm 0.014$	ATLAS+CMS (8 TeV)	20	[276]	$\cos \theta^*$ 3-param
$\mathcal{F}_+ = -0.033 \pm 0.046$	CDF+DØ Run II	2.7-5.4	[268]	$\cos \theta^*$ 2-param
$\mathcal{F}_+ = -0.015 \pm 0.035$	CDF+DØ Run II	2.7-5.4	[268]	$\cos \theta^*$ 1-param
$\mathcal{F}_+ = -0.045 \pm 0.073$	CDF Run II	8.7	[277]	ME 2-param
$\mathcal{F}_+ = 0.01 \pm 0.05$	ATLAS (7 TeV)	1.0	[269]	$\cos \theta^*$ 3-param
$\mathcal{F}_+ = 0.008 \pm 0.018$	CMS (7 TeV)	5.0	[270]	$\cos \theta^*$ 3-param
$\mathcal{F}_+ = 0.015 \pm 0.034$	ATLAS+CMS (7 TeV)	2.2	[271]	$\cos \theta^*$ 3-param
$\mathcal{F}_+ = -0.008 \pm 0.014$	ATLAS (8 TeV)	20.2	[272]	$\cos \theta^*$ 3-param
$\mathcal{F}_+ = -0.004 \pm 0.015$	CMS (8 TeV)	19.8	[273]	$\cos \theta^*$ 3-param
$\mathcal{F}_+ = 0.018 \pm 0.027$	CMS (8 TeV)	19.7	[274]	$\cos \theta^*$ 3-param
$\mathcal{F}_+ = -0.018 \pm 0.022$	CMS (8 TeV)	19.7	[275]	$\cos \theta^*$ 3-param
$\mathcal{F}_+ = -0.008 \pm 0.007$	ATLAS+CMS (8 TeV)	20	[276]	$\cos \theta^*$ 3-param

tions [292]. In 35.9 fb^{-1} of lepton-plus-photon-plus-jets events, CMS manages to establish the first evidence for the associated production of a single-top quark and a photon at $\sqrt{s} = 13 \text{ TeV}$. They employ a multivariate discriminant based on topological and kinematic event properties to separate signal from background processes. An excess above the background-only hypothesis is observed, with a significance of 4.4 standard deviations. A fiducial cross section is measured for isolated photons with transverse momentum greater than 25 GeV in the central region of the detector. The measured product of the cross section and branching fraction is $\sigma(pp \rightarrow t\gamma j)B(t \rightarrow \mu\gamma b) = 115 \pm 17(\text{stat}) \pm 30(\text{syst}) \text{ fb}$, which is consistent with the SM prediction [293]. Very recently, CMS used 137 fb^{-1} of data to measure the $t\bar{t}\gamma$ cross section. In the lepton-plus-jets channel, they perform measurements in a fiducial volume defined at the particle level. Events with an isolated, highly energetic lepton, at least three jets from the hadronization of quarks, among which at least one is b -tagged, and one isolated photon are selected. The inclusive fiducial $t\bar{t}\gamma$ cross section, for a photon with transverse momentum greater than 20 GeV and pseudorapidity $|\eta| < 1.4442$, is measured to be $\sigma_{t\bar{t}\gamma} = 800 \pm 7(\text{stat}) \pm 46(\text{syst}) \text{ fb}$, in good agreement with the prediction from the standard model at NLO in QCD [294]. The differential cross sections are also measured as a function of several kinematic observables and interpreted in the framework of the standard model effective field theory (EFT), leading to the most stringent direct limits to date on anomalous electromagnetic dipole moment interactions of the top quark and the photon. Using the same dataset, in the dilepton channel, an inclusive cross section of $174.4 \pm 2.5(\text{stat}) \pm 6.1(\text{syst}) \text{ fb}$ is measured in a signal region with at least one b -tagged jet and exactly one photon with transverse momentum above 20 GeV [295]. In the same analysis, differential cross sections are measured as a function of several kinematic observables of the photon, leptons, and jet, and compared to standard model predictions. The measurements are also interpreted in the standard model effective field theory framework, and limits on the relevant Wilson coefficients are combined with a previous CMS measurement of the same production process using single-lepton events. Using 35.9 fb^{-1} of data with a single muon and a photon, CMS reports first evidence of events consistent with the production of a single top quark in association with a photon. A multivariate discriminant based on topological and kinematic event properties is employed to separate signal from background processes. An excess above the background-only hypothesis is observed, with a significance of 4.4 standard deviations [296]. A precision test of

the vector and axial vector couplings in $t\bar{t}\gamma$ events or searches for possible tensor couplings of top-quarks to photons will only be feasible with an integrated luminosity of several hundred fb^{-1} in the future [297].

ATLAS and CMS have also studied the associate production of top-antitop quark pairs along with an electroweak gauge boson, where in the Standard Model the W -boson is expected to be produced via initial state radiation, while the Z -boson can also be radiated from a final-state top-quark and hence provides sensitivity to the top-quark neutral current weak gauge coupling, which implies a sensitivity to the third component of the top-quark's weak isospin, which has not been measured so far.

CMS performed measurements of the $t\bar{t}W$ and $t\bar{t}Z$ cross section at $\sqrt{s} = 7 \text{ TeV}$ with 5 fb^{-1} , yielding $\sigma_{t\bar{t}V} = 0.43^{+0.17}_{-0.15}(\text{stat.})^{+0.09}_{-0.07}(\text{syst.}) \text{ pb}$ ($V = Z, W$) and $\sigma_{t\bar{t}Z} = 0.28^{+0.14}_{-0.11}(\text{stat.})^{+0.06}_{-0.03}(\text{syst.}) \text{ fb}$, at about 3 standard deviations significance [298] and compatible with the SM expectations of $0.306^{+0.031}_{-0.053} \text{ pb}$ and $0.137^{+0.012}_{-0.016} \text{ pb}$, respectively [299, 300]. ATLAS performed a similar analysis with 4.7 fb^{-1} in the three-lepton channel and set an upper limit of 0.71 pb at 95% C.L. [301].

Using 20.3 fb^{-1} of 8 TeV data, ATLAS performs a simultaneous measurement of the $t\bar{t}W$ and $t\bar{t}Z$ cross section. They observe the $t\bar{t}W$ and $t\bar{t}Z$ production at the 5.0σ and 4.2σ level, respectively, yielding $\sigma_{t\bar{t}W} = 369^{+100}_{-91} \text{ fb}$ and $\sigma_{t\bar{t}Z} = 176^{+58}_{-52} \text{ fb}$ [302]. CMS performs an analysis where signal events are identified by matching reconstructed objects in the detector to specific final state particles from $t\bar{t}W$ and $t\bar{t}Z$ decays using 19.5 fb^{-1} of 8 TeV data. They obtain $\sigma_{t\bar{t}W} = 382^{+117}_{-102} \text{ fb}$ and $\sigma_{t\bar{t}Z} = 242^{+65}_{-55} \text{ fb}$, yielding a significance of 4.8 and 6.4 standard deviation, respectively [303]. These measurements are used to set bounds on five anomalous dimension-six operators that would affect the $t\bar{t}W$ and $t\bar{t}Z$ cross sections.

The most recent measurements in these channels are made at 13 TeV from ATLAS and CMS in multilepton final states. ATLAS made a measurement using 36.1 fb^{-1} of events with two, three or four leptons. In multiple regions, the $t\bar{t}Z$ and $t\bar{t}W$ cross sections are simultaneously measured using a combined fit to all regions, yielding $\sigma_{t\bar{t}Z} = 0.95 \pm 0.08(\text{stat}) \pm 0.10(\text{syst}) \text{ pb}$ and $\sigma_{t\bar{t}W} = 0.87 \pm 0.13(\text{stat}) \pm 0.14(\text{syst}) \text{ pb}$ [304] to be compared with the NLO+NLL (QCD) and NLO (EW) SM predictions, $\sigma_{t\bar{t}W} = 579^{+14\%}_{-9\%} \text{ fb}$ and $\sigma_{t\bar{t}Z} = 811^{+11\%}_{-10\%} \text{ fb}$ [305]. Very recently, ATLAS uses 139 fb^{-1} in three and four lepton events to measure the inclusive and differential $t\bar{t}Z$ cross section. The inclusive cross

section is measured to be $\sigma_{t\bar{t}Z} = 0.99 \pm 0.05(\text{stat.}) \pm 0.08(\text{syst.})$ pb [306], in agreement with the most precise theoretical predictions. The differential measurements are presented as a function of a number of kinematic variables which probe the kinematics of the $t\bar{t}Z$ system. Overall, good agreement is observed between the unfolded data and the predictions. CMS uses 35.9 fb^{-1} of data to measure $\sigma_{t\bar{t}W} = 0.77^{+0.12}_{-0.11}(\text{stat.})^{+0.13}_{-0.12}(\text{syst.})$ pb and $\sigma_{t\bar{t}Z} = 0.99^{+0.09}_{-0.08}(\text{stat.})^{+0.12}_{-0.10}(\text{syst.})$ pb production cross sections, and significances over the background-only hypotheses of 5.5σ and 9.5σ , respectively [307], firmly establishing the observation of these processes. Very recently, CMS measured the inclusive $t\bar{t}Z$ cross section in 77.5 fb^{-1} of events with three or four charged leptons, and the Z boson is detected through its decay to an oppositely charged lepton pair. The production cross section is measured to be $\sigma(t\bar{t}Z) = 0.95 \pm 0.05(\text{stat}) \pm 0.06(\text{syst})$ pb. This measurement includes differential cross sections as functions of the transverse momentum of the Z boson and the angular distribution of the negatively charged lepton from the Z boson decay as well as stringent direct limits on the anomalous tZ couplings [308].

The electroweak couplings can also be probed in single-top production in association with a Z boson. The $pp \rightarrow tZq$ process at the LHC probes both the WWZ coupling in the case where the Z emerges from the t -channel W in single-top production and, in the case where the Z is radiated from the top quark, the tZ coupling. A CMS search at 8 TeV using 19.7 fb^{-1} produced a hint of a tZq signal in tri-lepton events, with a significance compared to the background-only hypothesis of 2.4σ [309]. Very recently, CMS and ATLAS collaborations used 139 fb^{-1} in three-lepton events to measure $tZ(\rightarrow \ell^+\ell^-)q$. CMS obtains $\sigma_{tZq} = 87.9^{+7.5}_{-7.3}(\text{stat})^{+7.3}_{-6.0}(\text{syst})$ fb for $m(\ell\ell) > 30$ GeV [310]. The ratio between the cross sections for the top quark and the top antiquark production in association with a Z boson is measured as $2.37^{+0.56}_{-0.42}(\text{stat})^{+0.27}_{-0.13}(\text{syst.})$. Differential measurements at parton and particle levels are performed for the first time. Additionally, the spin asymmetry, which is sensitive to the top quark polarization, is determined from the differential distribution of the polarization angle at parton level to be $0.58^{+0.15}_{-0.16}(\text{stat}) \pm 0.06(\text{syst.})$, in agreement with SM predictions at next-to-leading order. Using neural networks, ATLAS improves the background rejection and extracts the signal. The measured cross-section for $m(\ell\ell) > 30$ GeV is $97 \pm 13(\text{stat.}) \pm 7(\text{syst.})$ fb, consistent with the Standard Model prediction [311].

Searches for and now also measurements of the associate production of a top-antitop quark pair along with a Higgs boson, $t\bar{t}h$, with various subsequent decays provide sensitivity to the top-Higgs Yukawa coupling. For further details, see the review on ‘‘Higgs’’.

61.3.3 Searches for Physics Beyond the Standard Model

The top quark plays a special role in the SM. Being the only quark with a coupling to the Higgs boson of order one, it provides the most important contributions to the quadratic radiative corrections to the Higgs mass exposing the issue of the naturalness of the SM. It is therefore very common for models where the naturalness problem is addressed to have new physics associated with the top quark. In SUSY, for instance, naturalness predicts the scalar top partners to be the lightest among the squarks and to be accessible at the LHC energies (see the review ‘‘Supersymmetry: Theory’’). In models where the Higgs is a pseudo-Goldstone boson, such as Little Higgs models, naturalness predicts the existence of partners of the top quarks with the same spin and color, but with different electroweak couplings, the so-called vectorial t' . Stops and t' 's are expected to have sizeable branching ratios to top quarks. Another intriguing prediction of SUSY models with universal couplings at the unification scale is that for a top-quark mass close to the measured value, the running of the Yukawa coupling down to 1 TeV naturally leads to the radiative breaking of the electroweak symmetry [312]. In fact, the top quark plays a role in the dynamics of electroweak symmetry breaking in many models [313]. One example is topcolor [314], where a large top-quark mass can be generated through the formation of a dynamic $t\bar{t}$ condensate, X , which is formed by a new strong gauge force coupling preferentially to the third generation. Another example

is topcolor-assisted technicolor [315], predicting the existence of a heavy Z' boson that couples preferentially to the third generation of quarks. If light enough such a state might be directly accessible at the present hadron collider energies, or if too heavy, lead to four-top interactions possibly visible in the $t\bar{t}t\bar{t}$ final state. This final state has been recently observed by CMS [316] and by ATLAS [119].

Current strategies to search for new physics in top quark events at hadron colliders are either tailored to the discovery of specific models or model independent. They can be broadly divided in two classes. In the first class new resonant states are looked for through decay processes involving the top quarks. Current searches for bosonic resonances in $t\bar{t}$ final states, or for direct stop and t' production, or for a charged Higgs in $H^+ \rightarrow t\bar{b}$ fall in the category. On the other hand, if new states are too heavy to be directly produced, they might still give rise to deviations from the SM predictions for the strength and Lorentz form of the top-quark couplings to other SM particles. Accurate SM predictions and measurements are therefore needed and the results be interpreted in the framework of an effective field theory [317–319] as done for example in recent analyses sensitive to the strength and structure of the top quark couplings by the ATLAS [94, 184, 276, 304, 320–323] and CMS [111, 121, 324–330] collaborations. Global effective field theory interpretations based on publicly available measurements in the top quark sector have also appeared [331–337].

61.3.3.1 New Physics in Top Quark Production

Theoretical [338, 339] and experimental efforts have been devoted to the searches of $t\bar{t}$ resonances, both at the Tevatron and at the LHC. Most the analyses have been performed in the hypothesis that resonances are narrow, yet generalizations have been considered for specific scenarios. At the Tevatron, both the CDF and $D\bar{O}$ collaborations have searched for resonant production of $t\bar{t}$ pairs in the lepton+jets channel [340, 341]. In both analyses, the data indicate no evidence of resonant production of $t\bar{t}$ pairs. They place upper limits on the production cross section times branching fraction to $t\bar{t}$ in comparison to the prediction for a narrow ($\Gamma_{Z'} = 0.012M_{Z'}$) leptophobic topcolor Z' boson. Within this model, they exclude Z' bosons with masses below 915 (CDF-full data set) and 835 ($D\bar{O}$, 5 fb^{-1}) GeV/c^2 at the 95% C.L. These limits turn out to be independent of couplings of the $t\bar{t}$ resonance (pure vector, pure axial-vector, or SM-like Z'). A similar analysis has been performed by CDF in the all-hadronic channel using 2.8 fb^{-1} of data [342]. At the LHC, both the CMS and ATLAS collaborations have searched for resonant production of $t\bar{t}$ pairs, employing different techniques and final-state signatures (all-hadronic, lepton+jets, dilepton) at $\sqrt{s} = 7, 8$ and 13 TeV. In the low mass range, from the $t\bar{t}$ threshold to about one TeV/c^2 , standard techniques based on the reconstruction of each of the decay objects (lepton, jets and b -jets, missing E_T) are used to identify the top quarks, while at higher invariant mass, the top quarks are boosted and the decay products more collimated and can appear as large-radius jets with substructure. Dedicated reconstruction techniques have been developed in recent years for boosted top quarks [343] that are currently employed at the LHC. Most of the analyses are model-independent (i.e., no assumption on the quantum numbers of the resonance is made) yet they assume a small width and no signal-background interference. Using lepton+jets and fully hadronic channels in a data set corresponding to an integrated luminosity of 35.9 fb^{-1} at 13 TeV, the CMS collaboration finds no significant deviations from the SM background [344]. In particular, the existence of a leptophobic topcolor particle Z' is excluded at the 95% confidence level for resonances in the mass range $0.6 < M_{Z'} < 3.8 \text{ TeV}/c^2$, $0.5 < M_{Z'} < 5.25 \text{ TeV}/c^2$, and $0.5 < M_{Z'} < 6.65 \text{ TeV}/c^2$ for $\Gamma_{Z'} = 1\%, 10\%, 30\%M_{Z'}$, respectively [345]. Kaluza-Klein excitations of a gluon with $M_{G_{KK}} < 4.55 \text{ TeV}/c^2$ (at 95% confidence level) in the Randall-Sundrum model are also excluded. A dedicated analysis [346] searching for a scalar resonance, set bounds between 400 and 750 GeV in various scenarios. The ATLAS collaboration has performed a search for resonant $t\bar{t}$ production in the lepton+jets channel using 36.1 fb^{-1} of proton-proton (pp) collision data collected at a center-of-mass energy

$\sqrt{s} = 13$ TeV [347]. A search for local excesses in the number of data events compared to the Standard Model expectation in the $t\bar{t}$ invariant mass spectrum is performed. No evidence for a $t\bar{t}$ resonance is found and 95% confidence-level limits on the production rate are determined for massive states predicted in several benchmark models. For instance, a narrow leptophobic topcolor Z' boson with a mass below 3.0 TeV/ c^2 is excluded. A Kaluza-Klein excitation of the graviton is excluded for masses in the range 0.45 TeV/ $c^2 < m_G < 0.65$ TeV/ c^2 . A Kaluza-Klein excitation of the gluon in a Randall-Sundrum model is excluded for masses below 3.8 TeV/ c^2 . ATLAS has also conducted a search for resonances in the all-jet final state at 13 TeV corresponding to an integrated luminosity of 139 fb $^{-1}$ [348]. The $t\bar{t}$ events are reconstructed by selecting two top quarks in their fully hadronic decay modes. A Z' in the topcolor-assisted-technicolor model is excluded at 95% confidence level for masses below 3.9 and 4.7 TeV for the decay widths of 1% and 3%, respectively.

Heavy charged bosons, such as W' or H^+ , can also be searched for in $t\bar{b}$, tj final states (for more information see the review “ W' -boson searches” and “Higgs Bosons: theory and searches”), while heavy fermion resonances, such as vectorial or excited quarks, in final states such as tZ , tH , tW , bW . CMS has performed several searches in this context, the most stringent limits coming from those at $\sqrt{s} = 13$ TeV [349–356]. For instance, a $W' \rightarrow t\bar{b}$ has been searched for in all-hadronic final state in 137 fb $^{-1}$. No evidence has been found for left- and right-handed W' boson and masses below 3.4 TeV/ c^2 are excluded at 95% confidence level [356]. Single production of a vector-like quark decaying to a W boson and a top quark, in fully hadronic final state also been searched in the same data set. No significant deviation from the SM background expectation is observed. The hypotheses of b^* quarks with left-handed, right-handed, and vector-like chiralities are excluded at 95% confidence level for masses below 2.6 , 2.8 , and 3.1 TeV/ c^2 , respectively. These represent the most stringent exclusion limits for the single production of vector-like quarks in this channel. [357] In the same data set, searches for pair production of vector-like T or B quarks in fully hadronic final states have been performed. Lower limits are set on the mass at 95% confidence level equal to 1570 TeV/ c^2 in the case where decays exclusively to a b quark and a Higgs boson, 1390 TeV/ c^2 for when it decays exclusively to a b quark and a Z boson, and 1450 TeV/ c^2 for when it decays equally in these two modes. [358]. ATLAS has performed searches for heavy bosons and fermions decaying to one top quark at $\sqrt{s} = 7$, 8 and 13 TeV. A $W' \rightarrow t\bar{b}$ has been searched for at 13 TeV in lepton+jets in 36.1 fb $^{-1}$. No evidence has been found for a right-handed W' boson with a mass below 3.25 TeV/ c^2 are excluded at 95% [359]. A $H^+ \rightarrow t\bar{b}$ has been searched for at 13 TeV in lepton+jets in 139 fb $^{-1}$. No significant excess above the background-only hypothesis is observed and exclusion limits are derived for the production cross-section times branching ratio as a function of its mass, ranging from 3.6 pb at 200 GeV/ c^2 to 0.036 pb at 2000 GeV/ c^2 at 95% confidence level. [360]. ATLAS has conducted a search for the single and pair production of a new charge $+2/3$ quark (T) decaying via $T \rightarrow Zt$ (and also $-1/3$ quark (B) decaying via $B \rightarrow Zb$) in a dataset corresponding to 139 fb $^{-1}$ luminosity at $\sqrt{s} = 13$ TeV [361]. No significant excess of events above the SM expectation is observed, and upper limits are derived for vector-like quarks of various masses in a two-dimensional plane of branching ratios. Under branching ratio assumptions corresponding to a weak-isospin singlet scenario, a T quark with mass lower than 1.27 TeV/ c^2 (1.2 TeV/ c^2 for a B quark) is excluded at the 95% confidence level. Under branching ratio assumptions corresponding to a particular weak-isospin doublet scenario, a T quark with mass lower than 1.46 TeV/ c^2 (1.32 TeV/ c^2 for a B quark) is excluded at the 95% confidence level. In the same dataset, ATLAS combines the searches for pair-produced vector-like partners of the top and bottom quarks in various decay channels ($T \rightarrow Zt/Wb/Ht$, $B \rightarrow Zb/Wt/Hb$). The observed data are found to be in good agreement with the SM background prediction in all individual searches. Therefore, combined 95% confidence-level upper limits are set on the production cross-section for a range of vector-like quark scenarios, significantly improving upon the reach of the individual searches. Model-independent limits

are set assuming the vector-like quarks decay to SM particles. A singlet T is excluded for masses below 1.31 TeV/ c^2 and a singlet B is excluded for masses below 1.22 TeV/ c^2 . Assuming a weak isospin (T, B) doublet and $|V_{Tb}| \ll |V_{tB}|$, T and B masses below 1.37 TeV/ c^2 are excluded [362].

Vector-like partners of the top and bottom quarks have been searched also in single (electroweak) production, in several decay modes: $T \rightarrow tH$ [363], $T \rightarrow Wb$ [364], $T \rightarrow t(Z \rightarrow \nu\nu)$ [365] and $B \rightarrow bH$ with $H \rightarrow b\bar{b}$ [366] and $H \rightarrow \gamma\gamma$ [367].

In many models top-quark partners preferably decay to top quarks and weakly interacting neutral stable particles, i.e., possibly dark matter candidates, that are not detected. In addition, top quarks could be coupled to states that would mostly decay to dark matter or be invisible. In both cases, an observable especially sensitive to new physics effects in $t\bar{t}$ production is therefore the missing transverse momentum. CMS has presented a differential cross section measurement of top-quark pair and single production with missing transverse energy and corresponding interpretations in the context of dark matter (effective and simplified) models at 8 and 13 TeV [368–371]. The results obtained so far are consistent with the SM expectations. In particular the search performed at 13 TeV [371] is based on 35.9 fb $^{-1}$ of integrated luminosity. Upper limits are derived on the production cross section and interpreted in terms of a simplified model with a scalar/pseudoscalar mediator. Scalar and pseudoscalar mediator particles with masses below 290 and 300 GeV/ c^2 , respectively, are excluded at 95% confidence level, assuming a dark matter particle mass of 1 GeV/ c^2 and mediator couplings to fermions and dark matter particles equal to unity. A generic search for new phenomena with top quark pairs in final states with one isolated electron or muon, multiple jets, and large missing transverse momentum has been performed by ATLAS in a dataset corresponding to 139 fb $^{-1}$ luminosity at $\sqrt{s} = 13$ TeV. No significant excess above the SM background is observed, and limits at 95% confidence level are set in various models. The results exclude top quark masses up to about 1 TeV/ c^2 , and masses of the lightest neutralino up to about 500 GeV/ c^2 . Limits on dark-matter production are set for scalar (pseudoscalar) mediator masses up to about 250 (300) GeV/ c^2 . [372].

ATLAS has also conducted searches for missing transverse momenta in association with single top quarks [373, 374].

Flavor-changing-neutral-currents (FCNC) are hugely suppressed in the SM as non zero contributions only arise at one-loop and are proportional to the splitting between the quark masses. In the case of the top quark $B(t \rightarrow Bq)$ with $B = g, \gamma, Z, H$ and $q = u, c$ are predicted to be order of 10^{-12} ($t \rightarrow cg$) or much smaller [375]. Several observables are accessible at colliders to test and constrain such couplings. CMS has performed several studies on the search for FCNC in top-quark production. They have considered single-top quark production in the t -channel in 5 fb $^{-1}$ integrated luminosity at 7 TeV and 19.7 fb $^{-1}$ integrated luminosity at 8 TeV [376]. Events with the top quark decaying into a muon, neutrino and two or three jets are selected. The upper limits on effective coupling strength can be translated to the 95% upper limits on the corresponding branching ratios $B(t \rightarrow gu) \leq 2.0 \cdot 10^{-5}$, $B(t \rightarrow gc) \leq 4.1 \cdot 10^{-4}$. They have performed a search for a single top quark produced in association with a photon in 19.1 fb $^{-1}$ integrated luminosity at 8 TeV [377]. The event selection requires the presence of one isolated muon and jets in the final state. The upper limits on effective coupling strength can be translated to the 95% upper limits on the corresponding branching ratios $B(t \rightarrow \gamma u) \leq 0.0161\%$, $B(t \rightarrow \gamma c) \leq 0.182\%$. A search for flavor-changing neutral currents in associated production of a top quark with a Higgs boson decaying into $b\bar{b}$ has also been presented by CMS, corresponding to an integrated luminosity of 35.9 fb $^{-1}$ at 13 TeV. Two complementary channels are considered: top quark pair production, with FCNC decay of the top quark or antiquark, and single top associated production. A final state with one isolated lepton and at least three reconstructed jets, among which at least two are identified as b quark jets, is considered. No significant deviation is observed from predicted background and upper limits at 95% confidence level are set on the branching ratios of top quark decays, $B(t \rightarrow uH) < 0.47\%$ and $B(t \rightarrow cH) < 0.47\%$ [378], which are similar to the combined limits on all decay channels ob-

tained with the full data set at 8 TeV [379]. More recently, a search for the signature of flavor-changing neutral current interactions of top quarks and Higgs bosons has been performed, corresponding to an integrated luminosity of 137 fb^{-1} at 13 TeV. Multivariate machine learning techniques have been used to separate signal and standard model background processes. No significant excess above the background prediction is observed, and upper limits on the $t \rightarrow Hq$ branching fractions are derived through a binned fit to the diphoton invariant mass spectrum. The observed 95% confidence level upper limits are found to be 1.9×10^{-4} for $\Gamma(t \rightarrow Hu)$ and 7.3×10^{-4} for $\Gamma(t \rightarrow Hc)$.

ATLAS has presented results on the search for single top-quark production via FCNC's in strong interactions using data collected at $\sqrt{s}=8$ TeV and corresponding to an integrated luminosity of 20.3 fb^{-1} . Flavor-changing-neutral-current events are searched for in which a light quark (u or c) interacts with a gluon to produce a single top quark, either with or without the associated production of another light quark or gluon. Candidate events of top quarks decaying into leptons and jets are selected and classified into signal- and background-like events using a neural network. The observed 95% C.L. limit is $\sigma_{qq \rightarrow t} \times B(t \rightarrow Wb) < 3.4 \text{ pb}$ that can be interpreted as limits on the branching ratios, $B(t \rightarrow ug) < 4 \cdot 10^{-5}$ and $B(t \rightarrow cg) < 1.7 \cdot 10^{-4}$ [380]. ATLAS has set limits on the coupling of a top quark, a photon, and an up or charm quark using 81 fb^{-1} of data 13 TeV. Events with a photon, an electron or muon, a b-tagged jet, and missing transverse momentum are selected. The data are consistent with the background-only hypothesis, and limits are set on the strength of the $tq\gamma$ coupling in an effective field theory. These are also interpreted as 95% CL upper limits on $t \rightarrow u\gamma$ branching ratio via a left-handed (right-handed) interaction of 2.8×10^{-5} (6.1×10^{-5}) and on the $t \rightarrow c\gamma$ branching ratio for of 22×10^{-5} (18×10^{-5}) [381]. Constraints on FCNC couplings of the top quark can also be obtained from searches for anomalous single top-quark production in e^+e^- collisions, via the process $e^+e^- \rightarrow \gamma, Z^* \rightarrow t\bar{q}$ and its charge-conjugate ($q = u, c$), or in $e^\pm p$ collisions, via the process $e^\pm u \rightarrow e^\pm t$. For a leptonic W decay, the topology is at least a high- p_T lepton, a high- p_T jet and missing E_T , while for a hadronic W -decay, the topology is three high- p_T jets. Limits on the cross section for this reaction have been obtained by the LEP collaborations [382] in e^+e^- collisions, and by H1 [383] and ZEUS [384] in $e^\pm p$ collisions. When interpreted in terms of branching ratios in top decay [385, 386], the LEP limits lead to typical 95% C.L. upper bounds of $B(t \rightarrow qZ) < 0.137$. Assuming no coupling to the Z boson, the 95% C.L. limits on the anomalous FCNC coupling $\kappa_\gamma < 0.13$ and < 0.27 by ZEUS and H1, respectively, are stronger than the CDF limit of $\kappa_\gamma < 0.42$, and improve over LEP sensitivity in that domain. The H1 limit is slightly weaker than the ZEUS limit due to an observed excess of five-candidate events over an expected background of 3.2 ± 0.4 . If this excess is attributed to FCNC top-quark production, this leads to a total cross section of $\sigma(ep \rightarrow e + t + X, \sqrt{s} = 319 \text{ GeV}) < 0.25 \text{ pb}$ [383, 387].

61.3.3.2 New Physics in Top-Quark decays

The large sample of top quarks produced at the Tevatron and the LHC allows to measure or set stringent limits on the branching ratios of rare top-quark decays. For example, the existence of a light H^+ can be constrained by looking for $t \rightarrow H^+b$ decay, in particular with tau-leptons in the final state (for more information see the review "Higgs Bosons: theory and searches").

A first class of searches for new physics focuses on the structure of the Wtb vertex. Using up to 2.7 fb^{-1} of data, $D\phi$ has measured the Wtb coupling form factors by combining information from the W -boson helicity in top-quark decays in $t\bar{t}$ events and single top-quark production, allowing to place limits on the left-handed and right-handed vector and tensor couplings [388–390].

ATLAS has published the results of a search for CP -violation in the decay of single top quarks produced in the t -channel where the top quarks are predicted to be highly polarized, using the lepton+jets final state [391]. The data analyzed are from pp collisions at $\sqrt{s} = 7$ TeV and correspond to an integrated luminosity of 4.7 fb^{-1} . In the Standard Model, the couplings at the Wtb vertex are left-handed, right-handed couplings being absent. A forward-backward asymmetry with respect to the normal to

the plane defined by the W -momentum and the top-quark polarization has been used to probe the complex phase of a possibly non-zero value of the right-handed coupling, signaling a source of CP -violation beyond the SM. The measured value of the asymmetry is $0.031 \pm 0.065(\text{stat.})_{-0.031}^{+0.029}(\text{sys.})$ in good agreement with the Standard Model.

A second class of searches focuses on FCNC's in the top-quark decays. Both, CDF and $D\phi$, have provided the first limits for FCNC's in Run I and II. The most recent results from CDF give $B(t \rightarrow qZ) < 3.7\%$ and $B(t \rightarrow q\gamma) < 3.2\%$ at the 95% C.L. [392] while $D\phi$ [393, 394] sets $B(t \rightarrow qZ)(q = u, c \text{ quarks}) < 3.2\%$ at 95% C.L., $B(t \rightarrow gu) < 2.0 \cdot 10^{-4}$, and $B(t \rightarrow gc) < 3.9 \cdot 10^{-3}$ at the 95% C.L. At the LHC, CMS has used a sample at a center-of-mass energy of 8 TeV corresponding to 19.7 fb^{-1} of integrated luminosity to perform a search for flavor changing neutral current top-quark decay $t \rightarrow Zq$. Events with a topology compatible with the decay chain $t\bar{t} \rightarrow Wb + Zq \rightarrow \ell\nu b + \ell\ell q$ are searched for. There is no excess seen in the observed number of events relative to the SM prediction; thus no evidence for flavor changing neutral current in top-quark decays is found. A combination with a previous search at 7 TeV excludes a $t \rightarrow Zq$ branching fraction greater than 0.05% at the 95% confidence level [395]. CMS has also performed a search for the production of a single top quark in association with a Z boson in the same data set at 8 TeV. Final states with three leptons (electrons or muons) and at least one jet are investigated. Exclusion limits at 95% confidence level on the branching fractions are found to be $B(t \rightarrow uZ) < 0.022\%$ and $B(t \rightarrow cZ) < 0.049\%$ [396].

The ATLAS collaboration has also searched for FCNC processes in 36.1 fb^{-1} of $t\bar{t}$ events at a center-of-mass energy of 13 TeV, with one top quark decaying through FCNC ($t \rightarrow qZ$) and the other through the SM dominant mode ($t \rightarrow bW$). Only the decays of the Z boson to charged leptons and leptonic W boson decays were considered as signal, leading to a final state topology characterized by the presence of three isolated leptons, at least two jets and missing transverse energy from the undetected neutrino. No evidence for an FCNC signal was found. An upper limit on the $t \rightarrow qZ$ branching ratio of $B(t \rightarrow Zu(c)) < 1.7(2.4) \times 10^{-4}$ is set at the 95% confidence level [397]. The ATLAS collaboration has also searched for a tqZ coupling, in a study that includes events where a single top quark is produced as $gq \rightarrow tZ$ (with $q = u, c$) and top-quark pair events, with one top quark decaying through the $t \rightarrow qZ$ channel, 139 fb^{-1} of data at 13 TeV. The analysis selects events with three leptons (electrons or muons), a b-tagged jet, possible additional jets and missing transverse momentum. The data are consistent with the background-only hypothesis and 95% confidence-level limits on the branching ratios are set. These are 6.2×10^{-5} (13×10^{-5}) for $t \rightarrow Zu$ ($t \rightarrow Zc$) for a left-handed coupling, and 6.6×10^{-5} (12×10^{-5}) in the case of a right-handed coupling [398].

Another search for FCNCs is the interactions of a top-quark to a Higgs boson and a light parton, tqH , $q = u, c$. The CMS collaboration has performed a search using a sample at a center-of-mass energy of 13 TeV corresponding to 35.9 fb^{-1} of integrated luminosity, [399], combining single top quark FCNC production in association with the Higgs boson ($pp \rightarrow tH$), and top quark pair production with FCNC decay of the top quark ($t \rightarrow qH$). The combined analysis sets an upper limit on the $t \rightarrow u/cH$ branching ratios of $B(t \rightarrow u/cH) < 0.47\%$ at 95% confidence level. The ATLAS collaboration considers $t \rightarrow qH$, $q = u, c$ with 36.1 fb^{-1} of $t\bar{t}$ events at $\sqrt{s} = 13$ TeV. A combined measurement including $H \rightarrow bb$ and $H \rightarrow \tau\tau$ modes yields a 95% C.L. upper limit of 0.11% and 0.12% on the branching ratios of $B(t \rightarrow cH)$ and $B(t \rightarrow uH)$, respectively [400].

61.4 Outlook

Top-quark physics at hadron colliders has developed into precision physics. Various properties of the top quark have been measured with high precision, where the LHC has by now surpassed the Tevatron precision and reach in the majority of relevant observables. Several \sqrt{s} -dependent physics quantities, such as the production cross-section, have been measured at several energies at the Tevatron and the LHC. Up to now, all measurements are consistent with the SM predictions and allow stringent tests of

the underlying production mechanisms by strong and weak interactions. Given the very large event samples available at the LHC, top-quark properties will be further determined in $t\bar{t}$ as well as in electroweak single top-quark production. At the Tevatron, the t - and s -channels for electroweak single top-quark production have been measured separately. At the LHC, quick progress has been achieved in the last years making all three relevant channels measured with more than 5 sigma significance. Furthermore, $t\bar{t}\gamma$, $t\bar{t}Z$, and $t\bar{t}W$ together with $t\bar{t}H$ associated production have started to provide key information on the top-quark electroweak couplings. Corresponding effective field theory (EFT) fits for the coupling extraction are being developed. At the same time various models of physics beyond the SM involving top-quark production are being constrained. While a majority of the Run-II data recorded at 13 TeV has been analysed or is in an advanced stage, the beginning of the Run-III at $\sqrt{s} = 13.6$ to 14 TeV and an expected integrated luminosity of $160 - 200 \text{ fb}^{-1}$, doubling the Run-I plus Run-II data set, is immanent. With the first results to be released, top-quark physics has the potential to shed light on open questions and new aspects of physics at the TeV scale.

CDF note references can be retrieved from

<https://www-cdf.fnal.gov/physics/new/top/top.html>,
and D0 note references from

<https://www-d0.fnal.gov/Run2Physics/WWW/documents/Run2Results.htm>,

and ATLAS note references from

<https://twiki.cern.ch/twiki/bin/view/AtlasPublic/TopPublicResults>,

and CMS note references from

<https://twiki.cern.ch/twiki/bin/view/CMSPublic/PhysicsResultsTOP>,

and plots provided by the LHC Top Working Group from

<https://twiki.cern.ch/twiki/bin/view/LHCPhysics/LHCTopWGSummaryPlots>.

References

- [1] M. Czakon, P. Fiedler and A. Mitov, Phys. Rev. Lett. **110**, 252004 (2013), [arXiv:1303.6254].
- [2] S. Catani *et al.*, JHEP **07**, 100 (2019), [arXiv:1906.06535].
- [3] ATLAS, CMS, CDF, & D0 Collab, [arXiv:1403.4427].
- [4] S. Cortese and R. Petronzio, Phys. Lett. **B253**, 494 (1991).
- [5] S. S. D. Willenbrock and D. A. Dicus, Phys. Rev. **D34**, 155 (1986).
- [6] J. Campbell, T. Neumann and Z. Sullivan, JHEP **02**, 040 (2021), [arXiv:2012.01574].
- [7] M. Brucherseifer, F. Caola and K. Melnikov, Phys. Lett. **B736**, 58 (2014), [arXiv:1404.7116].
- [8] E. L. Berger, J. Gao and H. X. Zhu, JHEP **11**, 158 (2017), [arXiv:1708.09405].
- [9] N. Kidonakis, Phys. Rev. **D81**, 054028 (2010), [arXiv:1001.5034].
- [10] N. Kidonakis, Phys. Rev. **D82**, 054018 (2010), [arXiv:1005.4451].
- [11] T. M. P. Tait and C. P. Yuan, Phys. Rev. **D63**, 014018 (2000), [hep-ph/0007298].
- [12] M. Jezabek and J. H. Kuhn, Nucl. Phys. **B314**, 1 (1989).
- [13] I. I. Y. Bigi *et al.*, Phys. Lett. **B181**, 157 (1986).
- [14] A. H. Hoang *et al.*, Phys. Rev. **D65**, 014014 (2002), [hep-ph/0107144].
- [15] K. Hagiwara, Y. Sumino and H. Yokoya, Phys. Lett. **B666**, 71 (2008), [arXiv:0804.1014].
- [16] B. Fuks *et al.*, Phys. Rev. D **104**, 3, 034023 (2021), [arXiv:2102.11281].
- [17] A. Czarnecki and K. Melnikov, Nucl. Phys. **B544**, 520 (1999), [hep-ph/9806244]; K. G. Chetyrkin *et al.*, Phys. Rev. **D60**, 114015 (1999), [hep-ph/9906273].
- [18] S. Frixione, P. Nason and B. R. Webber, JHEP **08**, 007 (2003), [hep-ph/0305252]; W. Kim and H. Shin, JHEP **07**, 070 (2007), [arXiv:0706.3563]; S. Frixione, P. Nason and G. Ridolfi, JHEP **09**, 126 (2007), [arXiv:0707.3088]; J. M. Campbell *et al.*, JHEP **04**, 114 (2015), [arXiv:1412.1828]; T. Ježo *et al.*, Eur. Phys. J. **C76**, 12, 691 (2016), [arXiv:1607.04538].
- [19] S. Frixione *et al.*, JHEP **03**, 092 (2006), [hep-ph/0512250]; V. Marotta and A. Nadeo, JHEP **08**, 029 (2008), [arXiv:0810.4759]; S. Alioli *et al.*, JHEP **09**, 111 (2009), [Erratum: JHEP02,011(2010)], [arXiv:0907.4076]; E. Re, Eur. Phys. J. **C71**, 1547 (2011), [arXiv:1009.2450]; R. Frederix, E. Re and P. Torrielli, JHEP **09**, 130 (2012), [arXiv:1207.5391]; R. Frederix *et al.*, JHEP **06**, 027 (2016), [arXiv:1603.01178].
- [20] S. Frixione and B. R. Webber, JHEP **06**, 029 (2002), [hep-ph/0204244].
- [21] P. Nason, JHEP **11**, 040 (2004), [hep-ph/0409146].
- [22] J. Mazzitelli *et al.*, Phys. Rev. Lett. **127**, 6, 062001 (2021), [arXiv:2012.14267].
- [23] E. Todesco and J. Wenninger, Phys. Rev. Accel. Beams **20**, 8, 081003 (2017).
- [24] V. M. Abazov *et al.* (D0), Phys. Rev. **D94**, 092004 (2016), [arXiv:1605.06168].
- [25] T. Aaltonen *et al.* (CDF), Phys. Rev. **D88**, 091103 (2013), [arXiv:1304.7961].
- [26] T. A. Aaltonen *et al.* (CDF, D0), Phys. Rev. **D89**, 7, 072001 (2014), [arXiv:1309.7570].
- [27] T. A. Aaltonen *et al.* (CDF), Phys. Rev. **D89**, 9, 091101 (2014), [arXiv:1402.6728].
- [28] T. Aaltonen *et al.* (CDF), Phys. Rev. Lett. **105**, 012001 (2010), [arXiv:1004.3224].
- [29] V. M. Abazov *et al.* (D0), Phys. Rev. **D90**, 9, 092006 (2014), [arXiv:1401.5785].
- [30] M. Czakon and A. Mitov, Comput. Phys. Commun. **185**, 2930 (2014), [arXiv:1112.5675].
- [31] ATLAS Collab., ATLAS-CONF-2021-003.
- [32] A. M. Sirunyan *et al.* (CMS), JHEP **03**, 115 (2018), [arXiv:1711.03143].
- [33] CMS Collab., CMS-PAS-TOP-20-004 (2021).
- [34] G. Aad *et al.* (ATLAS), Eur. Phys. J. **C74**, 10, 3109 (2014), [Addendum: Eur. Phys. J. C76, no.11, 642 (2016)], [arXiv:1406.5375].
- [35] ATLAS Collab., ATLAS-CONF-2011-121 (2011).
- [36] G. Aad *et al.* (ATLAS), JHEP **05**, 059 (2012), [arXiv:1202.4892].
- [37] ATLAS Collab., ATLAS-CONF-2011-140.
- [38] ATLAS Collab., ATLAS-CONF-2012-024.
- [39] G. Aad *et al.* (ATLAS), Eur. Phys. J. **C73**, 3, 2328 (2013), [arXiv:1211.7205].
- [40] G. Aad *et al.* (ATLAS), Phys. Lett. **B717**, 89 (2012), [arXiv:1205.2067].
- [41] ATLAS Collab., ATLAS-CONF-2012-031.
- [42] G. Aad *et al.* (ATLAS), Phys. Rev. **D91**, 5, 052005 (2015), [arXiv:1407.0573].
- [43] S. Chatrchyan *et al.* (CMS), JHEP **11**, 067 (2012), [arXiv:1208.2671].
- [44] S. Chatrchyan *et al.* (CMS), Phys. Lett. **B720**, 83 (2013), [arXiv:1212.6682].
- [45] S. Chatrchyan *et al.* (CMS), JHEP **05**, 065 (2013), [arXiv:1302.0508].
- [46] S. Chatrchyan *et al.* (CMS), Phys. Rev. **D85**, 112007 (2012), [arXiv:1203.6810].
- [47] S. Chatrchyan *et al.* (CMS), Eur. Phys. J. **C73**, 4, 2386 (2013), [arXiv:1301.5755].
- [48] ATLAS & CMS Collab., ATLAS-CONF-2012-134, CMS-PAS-TOP-12-003.

- [49] G. Aad *et al.* (ATLAS), Eur. Phys. J. **C74**, 10, 3109 (2014), [Addendum: Eur. Phys. J.C76,no.11,642(2016)], [arXiv:1406.5375].
- [50] G. Aad *et al.* (ATLAS), Phys. Rev. **D91**, 11, 112013 (2015), [arXiv:1504.04251].
- [51] M. Aaboud *et al.* (ATLAS), Eur. Phys. J. **C78**, 487 (2018), [arXiv:1712.06857].
- [52] M. Aaboud *et al.* (ATLAS), Phys. Rev. **D95**, 7, 072003 (2017), [arXiv:1702.08839].
- [53] V. Khachatryan *et al.* (CMS), Eur. Phys. J. **C77**, 1, 15 (2017), [arXiv:1602.09024].
- [54] S. Chatrchyan *et al.* (CMS), JHEP **02**, 024 (2014), [Erratum: JHEP02,102(2014)], [arXiv:1312.7582].
- [55] V. Khachatryan *et al.* (CMS), JHEP **08**, 029 (2016), [arXiv:1603.02303].
- [56] V. Khachatryan *et al.* (CMS), Phys. Lett. **B739**, 23 (2014), [arXiv:1407.6643].
- [57] V. Khachatryan *et al.* (CMS), Eur. Phys. J. **C76**, 3, 128 (2016), [arXiv:1509.06076].
- [58] ATLAS Collab., ATLAS-CONF-2014-054, CMS Collab., CMS-PAS-TOP-14-016.
- [59] R. Aaij *et al.* (LHCb), Phys. Rev. Lett. **115**, 11, 112001 (2015), [arXiv:1506.00903].
- [60] ATLAS Collab., ATLAS-CONF-2015-033.
- [61] ATLAS collab., ATLAS-CONF-2015-049.
- [62] M. Aaboud *et al.* (ATLAS), Phys. Lett. **B761**, 136 (2016), [Erratum: Phys. Lett.B772,879(2017)], [arXiv:1606.02699].
- [63] G. Aad *et al.* (ATLAS), Eur. Phys. J. C **80**, 6, 528 (2020), [arXiv:1910.08819].
- [64] G. Aad *et al.* (ATLAS), Phys. Lett. B **810**, 135797 (2020), [arXiv:2006.13076].
- [65] V. Khachatryan *et al.* (CMS), Phys. Rev. Lett. **116**, 5, 052002 (2016), [arXiv:1510.05302].
- [66] V. Khachatryan *et al.* (CMS), Eur. Phys. J. **C77**, 172 (2017), [arXiv:1611.04040].
- [67] A. M. Sirunyan *et al.* (CMS), Eur. Phys. J. **C79**, 5, 368 (2019), [arXiv:1812.10505].
- [68] A. M. Sirunyan *et al.* (CMS), JHEP **02**, 191 (2020), [arXiv:1911.13204].
- [69] CMS Collab., CMS-PAS-TOP-15-005.
- [70] A. M. Sirunyan *et al.* (CMS), JHEP **09**, 051 (2017), [arXiv:1701.06228].
- [71] A. Tumasyan *et al.* (CMS) (2021), [arXiv:2108.02803].
- [72] CMS Collab., CMS-PAS-TOP-16-013.
- [73] A. M. Sirunyan *et al.* (CMS), Phys. Rev. Lett. **119**, 24, 242001 (2017), [arXiv:1709.07411].
- [74] V. M. Abazov *et al.* (D0), Phys. Rev. Lett. **107**, 121802 (2011), [arXiv:1106.5436]; D. Acosta *et al.* (CDF), Phys. Rev. Lett. **95**, 102002 (2005), [hep-ex/0505091].
- [75] V. Khachatryan *et al.* (CMS), Phys. Lett. **B736**, 33 (2014), [arXiv:1404.2292].
- [76] M. Czakon, D. Heymes and A. Mitov, Phys. Rev. Lett. **116**, 8, 082003 (2016), [arXiv:1511.00549].
- [77] T. Aaltonen *et al.* (CDF), Phys. Rev. Lett. **110**, 12, 121802 (2013), [arXiv:1211.5363].
- [78] G. Aad *et al.* (ATLAS), Eur. Phys. J. **C73**, 1, 2261 (2013), [arXiv:1207.5644].
- [79] G. Aad *et al.* (ATLAS), Phys. Rev. **D90**, 7, 072004 (2014), [arXiv:1407.0371].
- [80] G. Aad *et al.* (ATLAS), JHEP **06**, 100 (2015), [arXiv:1502.05923].
- [81] S. Chatrchyan *et al.* (CMS), Eur. Phys. J. **C73**, 3, 2339 (2013), [arXiv:1211.2220].
- [82] M. Aaboud *et al.* (ATLAS), Phys. Rev. **D94**, 9, 092003 (2016), [arXiv:1607.07281].
- [83] G. Aad *et al.* (ATLAS), Eur. Phys. J. **C76**, 10, 538 (2016), [arXiv:1511.04716].
- [84] G. Aad *et al.* (ATLAS), Phys. Rev. **D93**, 3, 032009 (2016), [arXiv:1510.03818].
- [85] V. Khachatryan *et al.* (CMS), Phys. Rev. **D94**, 5, 052006 (2016), [arXiv:1607.00837].
- [86] A. M. Sirunyan *et al.* (CMS), Eur. Phys. J. **C77**, 7, 459 (2017), [arXiv:1703.01630].
- [87] V. Khachatryan *et al.* (CMS), Phys. Rev. **D94**, 7, 072002 (2016), [arXiv:1605.00116].
- [88] V. Khachatryan *et al.* (CMS), Eur. Phys. J. **C75**, 11, 542 (2015), [arXiv:1505.04480].
- [89] V. Khachatryan *et al.* (CMS), Eur. Phys. J. **C76**, 3, 128 (2016), [arXiv:1509.06076].
- [90] M. Aaboud *et al.* (ATLAS), Eur. Phys. J. **C77**, 5, 292 (2017), [arXiv:1612.05220].
- [91] M. Aaboud *et al.* (ATLAS), JHEP **11**, 191 (2017), [arXiv:1708.00727].
- [92] M. Aaboud *et al.* (ATLAS), Phys. Rev. **D98**, 1, 012003 (2018), [arXiv:1801.02052].
- [93] G. Aad *et al.* (ATLAS), Eur. Phys. J. C **79**, 12, 1028 (2019), [Erratum: Eur.Phys.J.C 80, 1092 (2020)], [arXiv:1908.07305].
- [94] ATLAS Collab., ATLAS-CONF-2021-031.
- [95] G. Aad *et al.* (ATLAS), JHEP **01**, 033 (2021), [arXiv:2006.09274].
- [96] CMS Collab., CMS-PAS-TOP-15-010.
- [97] A. M. Sirunyan *et al.* (CMS), JHEP **04**, 060 (2018), [arXiv:1708.07638].
- [98] V. Khachatryan *et al.* (CMS), Phys. Rev. **D95**, 9, 092001 (2017), [arXiv:1610.04191].
- [99] A. M. Sirunyan *et al.* (CMS), JHEP **06**, 002 (2018), [arXiv:1803.03991].
- [100] A. M. Sirunyan *et al.* (CMS), Phys. Rev. **D97**, 11, 112003 (2018), [arXiv:1803.08856].
- [101] A. M. Sirunyan *et al.* (CMS), JHEP **02**, 149 (2019), [arXiv:1811.06625].
- [102] A. M. Sirunyan *et al.* (CMS), Eur. Phys. J. C **80**, 7, 658 (2020), [arXiv:1904.05237].
- [103] A. M. Sirunyan *et al.* (CMS), Phys. Rev. D **103**, 5, 052008 (2021), [arXiv:2008.07860].
- [104] G. Aad *et al.* (ATLAS), Eur. Phys. J. **C76**, 1, 11 (2016), [arXiv:1508.06868].
- [105] G. Aad *et al.* (ATLAS), JHEP **01**, 020 (2015), [arXiv:1407.0891].
- [106] S. Chatrchyan *et al.* (CMS), Eur. Phys. J. **C74**, 3014 (2015), [Erratum: Eur. Phys. J.C75,no.5,216(2015)], [arXiv:1404.3171].
- [107] V. Khachatryan *et al.* (CMS), Phys. Lett. **B746**, 132 (2015), [arXiv:1411.5621].
- [108] G. Aad *et al.* (ATLAS), Phys. Rev. **D92**, 7, 072005 (2015), [arXiv:1506.05074].
- [109] G. Aad *et al.* (ATLAS), Nature Phys. **17**, 7, 813 (2021).
- [110] ATLAS Collab., ATLAS-CONF-2020-050.
- [111] A. M. Sirunyan *et al.* (CMS), Phys. Rev. D **102**, 9, 092013 (2020), [arXiv:2009.07123].
- [112] M. Aaboud *et al.* (ATLAS), JHEP **04**, 046 (2019), [arXiv:1811.12113].
- [113] A. M. Sirunyan *et al.* (CMS), Phys. Lett. **B776**, 355 (2018), [arXiv:1705.10141].
- [114] A. M. Sirunyan *et al.* (CMS), JHEP **07**, 125 (2020), [arXiv:2003.06467].

- [115] A. M. Sirunyan *et al.* (CMS) (2019), [arXiv:1909.05306].
- [116] A. M. Sirunyan *et al.* (CMS), Phys. Lett. B **803**, 135285 (2020), [arXiv:1909.05306].
- [117] A. M. Sirunyan *et al.* (CMS), Phys. Lett. B **820**, 136565 (2021), [arXiv:2012.09225].
- [118] R. Frederix, D. Pagani and M. Zaro, JHEP **02**, 031 (2018), [arXiv:1711.02116].
- [119] G. Aad *et al.* (ATLAS), Eur. Phys. J. C **80**, 11, 1085 (2020), [arXiv:2007.14858].
- [120] G. Aad *et al.* (ATLAS) (2021), [arXiv:2106.11683].
- [121] A. M. Sirunyan *et al.* (CMS), Eur. Phys. J. C **80**, 2, 75 (2020), [arXiv:1908.06463].
- [122] A. M. Sirunyan *et al.* (CMS), JHEP **11**, 082 (2019), [arXiv:1906.02805].
- [123] V. M. Abazov *et al.* (D0), Phys. Rev. Lett. **103**, 092001 (2009), [arXiv:0903.0850]; V. M. Abazov *et al.* (D0), Phys. Rev. **D78**, 012005 (2008), [arXiv:0803.0739]; V. M. Abazov *et al.* (D0), Phys. Rev. Lett. **98**, 181802 (2007), [hep-ex/0612052].
- [124] T. Aaltonen *et al.* (CDF), Phys. Rev. Lett. **103**, 092002 (2009), [arXiv:0903.0885]; T. Aaltonen *et al.* (CDF), Phys. Rev. **D81**, 072003 (2010), [arXiv:1001.4577].
- [125] T. Aaltonen *et al.* (CDF), Phys. Rev. **D82**, 112005 (2010), [arXiv:1004.1181].
- [126] A. Heinson and T. R. Junk, Ann. Rev. Nucl. Part. Sci. **61**, 171 (2011), [arXiv:1101.1275].
- [127] Tevatron Electroweak Working Group, (2009), [arXiv:0908.2171].
- [128] N. Kidonakis, Phys. Rev. **D83**, 091503 (2011), [arXiv:1103.2792].
- [129] CDF Collab., CDF conference note 11113 (2014), DØ Collab., DØ conference note 6448 (2014).
- [130] T. A. Aaltonen *et al.* (CDF, D0), Phys. Rev. Lett. **115**, 15, 152003 (2015), [arXiv:1503.05027].
- [131] T. A. Aaltonen *et al.* (CDF, D0), Phys. Rev. Lett. **112**, 231803 (2014), [arXiv:1402.5126].
- [132] G. Aad *et al.* (ATLAS), Phys. Rev. **D90**, 11, 112006 (2014), [arXiv:1406.7844].
- [133] G. Aad *et al.* (ATLAS), Phys. Lett. **B717**, 330 (2012), [arXiv:1205.3130].
- [134] S. Chatrchyan *et al.* (CMS), JHEP **12**, 035 (2012), [arXiv:1209.4533].
- [135] M. Aaboud *et al.* (ATLAS), Eur. Phys. J. **C77**, 8, 531 (2017), [arXiv:1702.02859].
- [136] M. Aaboud *et al.* (ATLAS), JHEP **04**, 124 (2017), [arXiv:1702.08309].
- [137] V. Khachatryan *et al.* (CMS), JHEP **06**, 090 (2014), [arXiv:1403.7366].
- [138] CMS Collab., CMS-PAS-TOP-15-007.
- [139] M. Aaboud *et al.* (ATLAS), JHEP **04**, 086 (2017), [arXiv:1609.03920].
- [140] A. M. Sirunyan *et al.* (CMS), Phys. Lett. **B772**, 752 (2017), [arXiv:1610.00678].
- [141] A. M. Sirunyan *et al.* (CMS), Phys. Lett. B **800**, 135042 (2020), [arXiv:1812.10514].
- [142] A. M. Sirunyan *et al.* (CMS), Phys. Lett. B **808**, 135609 (2020), [arXiv:2004.12181].
- [143] C. D. White *et al.*, JHEP **11**, 074 (2009), [arXiv:0908.0631].
- [144] S. Frixione *et al.*, JHEP **07**, 029 (2008), [arXiv:0805.3067].
- [145] G. Aad *et al.* (ATLAS), Phys. Lett. **B716**, 142 (2012), [arXiv:1205.5764].
- [146] S. Chatrchyan *et al.* (CMS), Phys. Rev. Lett. **110**, 022003 (2013), [arXiv:1209.3489].
- [147] G. Aad *et al.* (ATLAS), JHEP **01**, 064 (2016), [arXiv:1510.03752].
- [148] M. Aaboud *et al.* (ATLAS, CMS), JHEP **05**, 088 (2019), [arXiv:1902.07158].
- [149] G. Aad *et al.* (ATLAS), Eur. Phys. J. C **81**, 8, 720 (2021), [arXiv:2007.01554].
- [150] S. Chatrchyan *et al.* (CMS), Phys. Rev. Lett. **112**, 23, 231802 (2014), [arXiv:1401.2942].
- [151] M. Aaboud *et al.* (ATLAS), JHEP **01**, 063 (2018), [arXiv:1612.07231].
- [152] A. M. Sirunyan *et al.* (CMS), JHEP **10**, 117 (2018), [arXiv:1805.07399].
- [153] A. Tumasyan *et al.* (CMS) (2021), [arXiv:2109.01706].
- [154] ATLAS Collab., ATLAS-CONF-2011-118.
- [155] G. Aad *et al.* (ATLAS), Phys. Lett. **B756**, 228 (2016), [arXiv:1511.05980].
- [156] V. Khachatryan *et al.* (CMS), JHEP **09**, 027 (2016), [arXiv:1603.02555].
- [157] M. Aaboud *et al.* (ATLAS, CMS), JHEP **05**, 088 (2019), [arXiv:1902.07158].
- [158] CMS Collab., CMS-PAS-TOP-14-004.
- [159] CMS Collab., CMS-PAS-TOP-13-001.
- [160] A. M. Sirunyan *et al.* (CMS), Eur. Phys. J. C **80**, 5, 370 (2020), [arXiv:1907.08330].
- [161] M. Aaboud *et al.* (ATLAS), Eur. Phys. J. C **78**, 3, 186 (2018), [arXiv:1712.01602].
- [162] CMS Collab., CMS-PAS-TOP-19-003.
- [163] M. Czakon, P. Fiedler and A. Mitov, Phys. Rev. Lett. **115**, 5, 052001 (2015), [arXiv:1411.3007].
- [164] W. Hollik and D. Pagani, Phys. Rev. **D84**, 093003 (2011), [arXiv:1107.2606].
- [165] W. Bernreuther and Z.-G. Si, Phys. Rev. **D86**, 034026 (2012), [arXiv:1205.6580].
- [166] S. Jung *et al.*, Phys. Rev. **D81**, 015004 (2010), [arXiv:0907.4112].
- [167] V. M. Abazov *et al.* (D0), Phys. Rev. Lett. **100**, 142002 (2008), [arXiv:0712.0851].
- [168] T. Aaltonen *et al.* (CDF), Phys. Rev. Lett. **101**, 202001 (2008), [arXiv:0806.2472].
- [169] T. A. Aaltonen *et al.* (CDF, D0), Phys. Rev. Lett. **120**, 4, 042001 (2018), [arXiv:1709.04894].
- [170] G. Aad *et al.* (ATLAS), JHEP **02**, 107 (2014), [arXiv:1311.6724].
- [171] G. Aad *et al.* (ATLAS), Eur. Phys. J. **C76**, 2, 87 (2016), [Erratum: Eur. Phys. J. **C77**, 564 (2017)], [arXiv:1509.02358].
- [172] G. Aad *et al.* (ATLAS), Phys. Rev. **D94**, 3, 032006 (2016), [arXiv:1604.05538].
- [173] S. Chatrchyan *et al.* (CMS), Phys. Lett. **B717**, 129 (2012), [arXiv:1207.0065].
- [174] V. Khachatryan *et al.* (CMS), Phys. Rev. **D93**, 3, 034014 (2016), [arXiv:1508.03862].
- [175] V. Khachatryan *et al.* (CMS), Phys. Lett. **B760**, 365 (2016), [arXiv:1603.06221].
- [176] M. Czakon *et al.*, Phys. Rev. **D98**, 1, 014003 (2018), [arXiv:1711.03945].
- [177] V. Khachatryan *et al.* (CMS), Phys. Lett. **B757**, 154 (2016), [arXiv:1507.03119].
- [178] G. Aad *et al.* (ATLAS), Phys. Lett. **B756**, 52 (2016), [arXiv:1512.06092].
- [179] G. Aad *et al.* (ATLAS), JHEP **05**, 061 (2015), [arXiv:1501.07383].
- [180] S. Chatrchyan *et al.* (CMS), JHEP **04**, 191 (2014), [arXiv:1402.3803].

- [181] M. Aaboud *et al.* (ATLAS, CMS), JHEP **04**, 033 (2018), [arXiv:1709.05327].
- [182] ATLAS Collab., ATLAS-CONF-2019-026.
- [183] CMS Collab., CMS-PAS-TOP-15-018.
- [184] G. Aad *et al.* (ATLAS) (2021), [arXiv:2110.05453].
- [185] F. Abe *et al.* (CDF), Phys. Rev. **D50**, 2966 (1994).
- [186] A. Abulencia *et al.* (CDF), Phys. Rev. **D73**, 032003 (2006), [hep-ex/0510048].
- [187] M. Aaboud *et al.* (ATLAS), Eur. Phys. J. **C79**, 4, 290 (2019), [arXiv:1810.01772].
- [188] V. Khachatryan *et al.* (CMS), Phys. Rev. **D93**, 7, 072004 (2016), [arXiv:1509.04044].
- [189] A. M. Sirunyan *et al.* (CMS), Eur. Phys. J. **C78**, 11, 891 (2018), [arXiv:1805.01428].
- [190] S. Argyropoulos and T. Sjöstrand, JHEP **11**, 043 (2014), [arXiv:1407.6653].
- [191] J. R. Christiansen and P. Z. Skands, JHEP **08**, 003 (2015), [arXiv:1505.01681].
- [192] A. M. Sirunyan *et al.* (CMS), Phys. Rev. Lett. **124**, 20, 202001 (2020), [arXiv:1911.03800].
- [193] V. M. Abazov *et al.* (D0), Nature **429**, 638 (2004), [hep-ex/0406031].
- [194] K. Kondo, T. Chikamatsu and S. H. Kim, J. Phys. Soc. Jap. **62**, 1177 (1993).
- [195] R. H. Dalitz and G. R. Goldstein, Phys. Rev. **D45**, 1531 (1992); R. H. Dalitz and G. R. Goldstein, Phys. Lett. **B287**, 225 (1992).
- [196] V. M. Abazov *et al.* (D0), Phys. Rev. Lett. **113**, 032002 (2014), [arXiv:1405.1756].
- [197] L. Sonnenschein, Phys. Rev. **D73**, 054015 (2006), [Erratum: Phys. Rev. **D78**, 079902 (2008)], [hep-ph/0603011].
- [198] G. Aad *et al.* (ATLAS), Eur. Phys. J. **C75**, 7, 330 (2015), [arXiv:1503.05427].
- [199] A. M. Sirunyan *et al.* (CMS), Phys. Rev. **D96**, 3, 032002 (2017), [arXiv:1704.06142].
- [200] C. G. Lester and D. J. Summers, Phys. Lett. **B463**, 99 (1999), [hep-ph/9906349].
- [201] A. M. Sirunyan *et al.* (CMS), Eur. Phys. J. **C79**, 4, 313 (2019), [arXiv:1812.10534].
- [202] M. Aaboud *et al.* (ATLAS), JHEP **09**, 118 (2017), [arXiv:1702.07546].
- [203] CMS Collab., CMS-PAS-TOP-19-009.
- [204] The Tevatron Electroweak Working Group and Aaltonen, T., For the CDF and D0 Collab., arXiv:1608.01881, FERMILAB-CONF-16-298-E.
- [205] B. Abbott *et al.* (D0), Phys. Rev. **D60**, 052001 (1999), [hep-ex/9808029]; F. Abe *et al.* (CDF), Phys. Rev. Lett. **82**, 271 (1999), [Erratum: Phys. Rev. Lett. **82**, 2808 (1999)], [hep-ex/9810029].
- [206] T. Aaltonen *et al.* (CDF), Phys. Rev. **D92**, 3, 032003 (2015), [arXiv:1505.00500].
- [207] T. A. Aaltonen *et al.* (CDF), Phys. Rev. **D90**, 9, 091101 (2014), [arXiv:1409.4906].
- [208] A. M. Sirunyan *et al.* (CMS), Eur. Phys. J. **C77**, 5, 354 (2017), [arXiv:1703.02530].
- [209] T. Aaltonen *et al.* (CDF), Phys. Lett. **B698**, 371 (2011), [arXiv:1101.4926].
- [210] CMS Collab., CMS-PAS-TOP-12-030.
- [211] T. Aaltonen *et al.* (CDF), Phys. Rev. **D80**, 051104 (2009), [arXiv:0906.5371].
- [212] ATLAS Collab., ATLAS-CONF-2019-046.
- [213] V. Khachatryan *et al.* (CMS), Phys. Rev. **D93**, 9, 092006 (2016), [arXiv:1603.06536].
- [214] V. Khachatryan *et al.* (CMS), JHEP **12**, 123 (2016), [arXiv:1608.03560].
- [215] CMS Collab., CMS-PAS-TOP-15-002.
- [216] CMS Collab., CMS-PAS-TOP-16-002.
- [217] V. M. Abazov *et al.* (D0), Phys. Rev. Lett. **100**, 192004 (2008), [arXiv:0803.2779]; S. Chatrchyan *et al.* (CMS), Phys. Lett. **B728**, 496 (2014), [Erratum: Phys. Lett. **B738**, 526 (2014)], [arXiv:1307.1907]; V. M. Abazov *et al.* (D0), Phys. Lett. **B703**, 422 (2011), [arXiv:1104.2887]; ATLAS Collab., ATLAS-CONF-2019-041; U. Langenfeld, S. Moch and P. Uwer, Phys. Rev. **D80**, 054009 (2009), [arXiv:0906.5273]; J. Fuster *et al.*, Eur. Phys. J. **C 77**, 11, 794 (2017), [arXiv:1704.00540].
- [218] G. Aad *et al.* (ATLAS) (2019), [arXiv:1905.02302].
- [219] CMS Collab., CMS-PAS-TOP-13-006 (2016).
- [220] CDF Collab., CDF conference note 11080 (2014).
- [221] V. M. Abazov *et al.* (D0), Phys. Rev. **D91**, 11, 112003 (2015), [arXiv:1501.07912].
- [222] CMS Collab., CMS-PAS-TOP-13-005.
- [223] A. H. Hoang, Ann. Rev. Nucl. Part. Sci. **70**, 225 (2020), [arXiv:2004.12915].
- [224] M. Beneke *et al.*, Phys. Lett. **B775**, 63 (2017), [arXiv:1605.03609].
- [225] A. H. Hoang, C. Lepenik and M. Preisser, JHEP **09**, 099 (2017), [arXiv:1706.08526].
- [226] A. H. Hoang *et al.*, Phys. Rev. Lett. **101**, 151602 (2008), [arXiv:0803.4214].
- [227] ATLAS Collab., ATLAS-PHYS-PUB-2021-034.
- [228] A. M. Sirunyan *et al.*, Physics Letters B **803**, 135263 (2020), [arXiv:1909.09193].
- [229] S. Catani *et al.*, JHEP **08**, 08, 027 (2020), [arXiv:2005.00557].
- [230] G. Aad *et al.* (ATLAS), Phys. Lett. **B716**, 1 (2012), [arXiv:1207.7214].
- [231] S. Chatrchyan *et al.* (CMS), Phys. Lett. **B716**, 30 (2012), [arXiv:1207.7235].
- [232] G. Degraasi *et al.*, JHEP **08**, 098 (2012), [arXiv:1205.6497].
- [233] S. Alekhin, A. Djouadi and S. Moch, Phys. Lett. **B716**, 214 (2012), [arXiv:1207.0980].
- [234] T. Aaltonen *et al.* (CDF), Phys. Rev. **D87**, 5, 052013 (2013), [arXiv:1210.6131].
- [235] V. M. Abazov *et al.* (D0), Phys. Rev. **D84**, 052005 (2011), [arXiv:1106.2063].
- [236] G. Aad *et al.* (ATLAS), Phys. Lett. **B728**, 363 (2014), [arXiv:1310.6527].
- [237] S. Chatrchyan *et al.* (CMS), JHEP **06**, 109 (2012), [arXiv:1204.2807].
- [238] S. Chatrchyan *et al.* (CMS), Phys. Lett. **B770**, 50 (2017), [arXiv:1610.09551].
- [239] G. Mahlon and S. J. Parke, Phys. Rev. **D53**, 4886 (1996), [hep-ph/9512264]; G. Mahlon and S. J. Parke, Phys. Lett. **B411**, 173 (1997), [hep-ph/9706304].
- [240] G.R. Goldstein, in *Spin 96: Proceedings of the 12th International Symposium on High Energy Spin Physics*, Amsterdam, 1996, ed. C.W. Jager (World Scientific, Singapore, 1997), p. 328.
- [241] T. Stelzer and S. Willenbrock, Phys. Lett. **B374**, 169 (1996), [hep-ph/9512292].
- [242] W. Bernreuther *et al.*, Nucl. Phys. **B690**, 81 (2004), [hep-ph/0403035].
- [243] A. Brandenburg, Z. G. Si and P. Uwer, Phys. Lett. **B539**, 235 (2002), [hep-ph/0205023].
- [244] CDF Collab., CDF conference note 10719 (2011).
- [245] CDF Collab., CDF conference note 10211 (2010).

- [246] V. M. Abazov *et al.* (D0), Phys. Lett. **B757**, 199 (2016), [arXiv:1512.08818].
- [247] V. M. Abazov *et al.* (D0), Phys. Rev. **D95**, 1, 011101 (2017), [arXiv:1607.07627].
- [248] V. M. Abazov *et al.* (D0), Phys. Rev. **D92**, 052007 (2015), [arXiv:1507.05666].
- [249] G. Mahlon and S. J. Parke, Phys. Rev. **D81**, 074024 (2010), [arXiv:1001.3422].
- [250] G. Aad *et al.* (ATLAS), Phys. Rev. **D90**, 11, 112016 (2014), [arXiv:1407.4314].
- [251] G. Aad *et al.* (ATLAS), Phys. Rev. Lett. **114**, 14, 142001 (2015), [arXiv:1412.4742].
- [252] G. Aad *et al.* (ATLAS), Phys. Rev. **D93**, 1, 012002 (2016), [arXiv:1510.07478].
- [253] S. Chatrchyan *et al.* (CMS), Phys. Rev. Lett. **112**, 18, 182001 (2014), [arXiv:1311.3924].
- [254] V. Khachatryan *et al.* (CMS), Phys. Lett. **B758**, 321 (2016), [arXiv:1511.06170].
- [255] V. Khachatryan *et al.* (CMS), Phys. Rev. **D93**, 5, 052007 (2016), [arXiv:1601.01107].
- [256] M. Aaboud *et al.* (ATLAS), Eur. Phys. J. C **80**, 8, 754 (2020), [arXiv:1903.07570].
- [257] A. M. Sirunyan *et al.* (CMS), Phys. Rev. **D100**, 7, 072002 (2019), [arXiv:1907.03729].
- [258] W. Bernreuther, D. Heisler and Z.-G. Si, JHEP **12**, 026 (2015), [arXiv:1508.05271].
- [259] M. Aaboud *et al.* (ATLAS), JHEP **03**, 113 (2017), [arXiv:1612.07004].
- [260] A. F. Falk and M. E. Peskin, Phys. Rev. **D49**, 3320 (1994), [hep-ph/9308241].
- [261] T. A. Aaltonen *et al.* (CDF), Phys. Rev. Lett. **111**, 20, 202001 (2013), [arXiv:1308.4050].
- [262] CMS Collab., CMS-PAS-TOP-16-019.
- [263] M. Aaboud *et al.* (ATLAS), Eur. Phys. J. **C78**, 2, 129 (2018), [arXiv:1709.04207].
- [264] ATLAS Collab., ATLAS-CONF-2019-038.
- [265] V. M. Abazov *et al.* (D0), Phys. Rev. **D85**, 091104 (2012), [arXiv:1201.4156].
- [266] G. L. Kane, G. A. Ladinsky and C. P. Yuan, Phys. Rev. **D45**, 124 (1992).
- [267] A. Czarnecki, J. G. Korner and J. H. Piclum, Phys. Rev. **D81**, 111503 (2010), [arXiv:1005.2625].
- [268] T. Aaltonen *et al.* (CDF, D0), Phys. Rev. **D85**, 071106 (2012), [arXiv:1202.5272].
- [269] G. Aad *et al.* (ATLAS), JHEP **06**, 088 (2012), [arXiv:1205.2484].
- [270] S. Chatrchyan *et al.* (CMS), JHEP **10**, 167 (2013), [arXiv:1308.3879].
- [271] ATLAS and CMS Collab., ATLAS-CONF-2013-033, CMS-PAS-TOP-12-025.
- [272] M. Aaboud *et al.* (ATLAS), Eur. Phys. J. **C77**, 4, 264 (2017), [Erratum: Eur. Phys. J. C79, no.1, 19(2019)], [arXiv:1612.02577].
- [273] V. Khachatryan *et al.* (CMS), Phys. Lett. **B762**, 512 (2016), [arXiv:1605.09047].
- [274] CMS Collab., CMS-PAS-TOP-14-017.
- [275] V. Khachatryan *et al.* (CMS), JHEP **01**, 053 (2015), [arXiv:1410.1154].
- [276] G. Aad *et al.* (CMS, ATLAS), JHEP **08**, 08, 051 (2020), [arXiv:2005.03799].
- [277] T. Aaltonen *et al.* (CDF), Phys. Rev. **D87**, 3, 031104 (2013), [arXiv:1211.4523].
- [278] D. Choudhury, T. M. P. Tait and C. E. M. Wagner, Phys. Rev. **D65**, 053002 (2002), [hep-ph/0109097].
- [279] D. Chang, W.-F. Chang and E. Ma, Phys. Rev. **D59**, 091503 (1999), [hep-ph/9810531]; D. Chang, W.-F. Chang and E. Ma, Phys. Rev. **D61**, 037301 (2000), [hep-ph/9909537].
- [280] T. Aaltonen *et al.* (CDF), Phys. Rev. **D88**, 3, 032003 (2013), [arXiv:1304.4141].
- [281] V. M. Abazov *et al.* (D0), Phys. Rev. **D90**, 5, 051101 (2014), [Erratum: Phys. Rev. D90, no.7, 079904(2014)], [arXiv:1407.4837].
- [282] G. Aad *et al.* (ATLAS), JHEP **11**, 031 (2013), [arXiv:1307.4568].
- [283] CMS Collab., CMS-PAS-TOP-11-031.
- [284] T. Aaltonen *et al.* (CDF), Phys. Rev. **D84**, 031104 (2011), [arXiv:1106.3970].
- [285] G. Aad *et al.* (ATLAS), Phys. Rev. **D91**, 7, 072007 (2015), [arXiv:1502.00586].
- [286] M. Aaboud *et al.* (ATLAS), JHEP **11**, 086 (2017), [arXiv:1706.03046].
- [287] K. Melnikov, M. Schulze and A. Scharf, Phys. Rev. **D83**, 074013 (2011), [arXiv:1102.1967].
- [288] A. M. Sirunyan *et al.* (CMS), JHEP **10**, 006 (2017), [arXiv:1706.08128].
- [289] M. Aaboud *et al.* (ATLAS), Eur. Phys. J. **C79**, 5, 382 (2019), [arXiv:1812.01697].
- [290] G. Bevilacqua *et al.*, JHEP **10**, 158 (2018), [arXiv:1803.09916].
- [291] G. Bevilacqua *et al.*, JHEP **01**, 188 (2019), [arXiv:1809.08562].
- [292] G. Aad *et al.* (ATLAS), JHEP **09**, 049 (2020), [arXiv:2007.06946].
- [293] A. M. Sirunyan *et al.* (CMS), Phys. Lett. **B779**, 358 (2018), [arXiv:1712.02825].
- [294] A. Tumasyan *et al.* (CMS) (2021), [arXiv:2107.01508].
- [295] CMS Collab., CMS-PAS-TOP-21-004.
- [296] A. M. Sirunyan *et al.* (CMS), Phys. Rev. Lett. **121**, 22, 221802 (2018), [arXiv:1808.02913].
- [297] M. Cepeda *et al.* (HL/HE WG2 group) (2019), [arXiv:1902.00134].
- [298] S. Chatrchyan *et al.* (CMS), Phys. Rev. Lett. **110**, 172002 (2013), [arXiv:1303.3239].
- [299] J. M. Campbell and R. K. Ellis, JHEP **07**, 052 (2012), [arXiv:1204.5678].
- [300] M. V. Garzelli *et al.*, JHEP **11**, 056 (2012), [arXiv:1208.2665].
- [301] ATLAS Collab., ATLAS-CONF-2012-126.
- [302] G. Aad *et al.* (ATLAS), JHEP **11**, 172 (2015), [arXiv:1509.05276].
- [303] V. Khachatryan *et al.* (CMS), JHEP **01**, 096 (2016), [arXiv:1510.01131].
- [304] M. Aaboud *et al.* (ATLAS), Phys. Rev. **D99**, 7, 072009 (2019), [arXiv:1901.03584].
- [305] A. Broggio *et al.*, JHEP **08**, 039 (2019), [arXiv:1907.04343].
- [306] G. Aad *et al.* (ATLAS), Eur. Phys. J. C **81**, 737 (2021), [arXiv:2103.12603].
- [307] A. M. Sirunyan *et al.* (CMS), JHEP **08**, 011 (2018), [arXiv:1711.02547].
- [308] A. M. Sirunyan *et al.* (CMS), JHEP **03**, 056 (2020), [arXiv:1907.11270].
- [309] A. M. Sirunyan *et al.* (CMS), JHEP **07**, 003 (2017), [arXiv:1702.01404].
- [310] CMS Collab., CMS-PAS-TOP-20-010.
- [311] G. Aad *et al.* (ATLAS), JHEP **07**, 124 (2020), [arXiv:2002.07546].
- [312] S. P. Martin 1–98 (1997), [Adv. Ser. Direct. High Energy Phys. 18,1(1998)], [hep-ph/9709356].

- [313] C. T. Hill and E. H. Simmons, Phys. Rept. **381**, 235 (2003), [Erratum: Phys. Rept.390,553(2004)], [hep-ph/0203079].
- [314] C. T. Hill, Phys. Lett. **B266**, 419 (1991).
- [315] C. T. Hill, Phys. Lett. **B345**, 483 (1995), [hep-ph/9411426].
- [316] A. M. Sirunyan *et al.* (CMS) (2019), [arXiv:1908.06463].
- [317] C. Zhang and S. Willenbrock, Phys. Rev. **D83**, 034006 (2011), [arXiv:1008.3869].
- [318] J. A. Aguilar-Saavedra, Nucl. Phys. **B843**, 638 (2011), [Erratum: Nucl. Phys.B851,443(2011)], [arXiv:1008.3562].
- [319] D. Barducci *et al.* (2018), [arXiv:1802.07237].
- [320] M. Aaboud *et al.* (ATLAS), Phys. Rev. D **99**, 5, 052009 (2019), [arXiv:1811.02305].
- [321] Technical report, CERN, Geneva (2019), all figures including auxiliary ones are available at <https://atlas.web.cern.ch/Atlas/GROUPS/PHYSICS/CONFNOTES/ATLAS-CONF-2019-026>, URL <http://cds.cern.ch/record/2682109>.
- [322] Technical report, CERN, Geneva (2021), all figures including auxiliary ones are available at <https://atlas.web.cern.ch/Atlas/GROUPS/PHYSICS/CONFNOTES/ATLAS-CONF-2021-027>, URL <http://cds.cern.ch/record/2773738>.
- [323] Technical report, CERN, Geneva (2021), all figures including auxiliary ones are available at <https://atlas.web.cern.ch/Atlas/GROUPS/PHYSICS/CONFNOTES/ATLAS-CONF-2021-050>, URL <http://cds.cern.ch/record/2782534>.
- [324] A. M. Sirunyan *et al.* (CMS), JHEP **06**, 146 (2020), [arXiv:1912.09540].
- [325] A. M. Sirunyan *et al.* (CMS), Eur. Phys. J. C **79**, 11, 886 (2019), [arXiv:1903.11144].
- [326] Technical report, CERN, Geneva (2021), URL <https://cds.cern.ch/record/2776770>.
- [327] A. M. Sirunyan *et al.* (CMS), JHEP **03**, 095 (2021), [arXiv:2012.04120].
- [328] CMS Collab., CMS-PAS-TOP-18-007 (2020).
- [329] Technical report, CERN, Geneva (2019), URL <https://cds.cern.ch/record/2668721>.
- [330] A. Tumasyan *et al.* (CMS) (2021), [arXiv:2107.13896].
- [331] A. Buckley *et al.*, JHEP **04**, 015 (2016), [arXiv:1512.03360].
- [332] N. P. Hartland *et al.*, JHEP **04**, 100 (2019), [arXiv:1901.05965].
- [333] I. Brivio *et al.* (2019), [arXiv:1910.03606].
- [334] G. Durieux *et al.*, JHEP **12**, 98 (2019), [Erratum: JHEP 01, 195 (2021)], [arXiv:1907.10619].
- [335] J. Ellis *et al.*, JHEP **04**, 279 (2021), [arXiv:2012.02779].
- [336] J. J. Ethier *et al.* (2021), [arXiv:2105.00006].
- [337] V. Miralles *et al.* (2021), [arXiv:2107.13917].
- [338] V. Barger, T. Han and D. G. E. Walker, Phys. Rev. Lett. **100**, 031801 (2008), [hep-ph/0612016].
- [339] R. Frederix and F. Maltoni, JHEP **01**, 047 (2009), [arXiv:0712.2355].
- [340] T. Aaltonen *et al.* (CDF), Phys. Rev. Lett. **110**, 12, 121802 (2013), [arXiv:1211.5363].
- [341] D. Acosta *et al.* (CDF), Phys. Rev. Lett. **94**, 211801 (2005), [hep-ex/0501050].
- [342] T. Aaltonen *et al.* (CDF), Phys. Rev. **D84**, 072003 (2011), [arXiv:1108.4755].
- [343] A. Altheimer *et al.*, J. Phys. **G39**, 063001 (2012), [arXiv:1201.0008].
- [344] A. M. Sirunyan *et al.* (CMS), JHEP **04**, 031 (2019), [arXiv:1810.05905].
- [345] A. M. Sirunyan *et al.* (CMS), JHEP **07**, 001 (2017), [arXiv:1704.03366].
- [346] A. M. Sirunyan *et al.* (CMS), JHEP **04**, 171 (2020), [arXiv:1908.01115].
- [347] M. Aaboud *et al.* (ATLAS), Eur. Phys. J. **C78**, 7, 565 (2018), [arXiv:1804.10823].
- [348] G. Aad *et al.* (ATLAS), JHEP **10**, 061 (2020), [arXiv:2005.05138].
- [349] A. M. Sirunyan *et al.* (CMS), Phys. Lett. **B777**, 39 (2018), [arXiv:1708.08539].
- [350] A. M. Sirunyan *et al.* (CMS), Phys. Lett. **B781**, 574 (2018), [arXiv:1708.01062].
- [351] A. M. Sirunyan *et al.* (CMS), JHEP **08**, 073 (2017), [arXiv:1705.10967].
- [352] A. M. Sirunyan *et al.* (CMS), Phys. Lett. **B772**, 634 (2017), [arXiv:1701.08328].
- [353] V. Khachatryan *et al.* (CMS), Phys. Lett. **B771**, 80 (2017), [arXiv:1612.00999].
- [354] A. M. Sirunyan *et al.* (CMS), JHEP **04**, 136 (2017), [arXiv:1612.05336].
- [355] A. M. Sirunyan *et al.* (CMS), JHEP **05**, 029 (2017), [arXiv:1701.07409].
- [356] A. M. Sirunyan *et al.* (CMS), Phys. Lett. B **820**, 136535 (2021), [arXiv:2104.04831].
- [357] A. M. Sirunyan *et al.* (CMS) (2021), [arXiv:2104.12853].
- [358] A. M. Sirunyan *et al.* (CMS), Phys. Rev. D **102**, 112004 (2020), [arXiv:2008.09835].
- [359] M. Aaboud *et al.* (ATLAS), Phys. Lett. **B788**, 347 (2019), [arXiv:1807.10473].
- [360] G. Aad *et al.* (ATLAS), JHEP **06**, 145 (2021), [arXiv:2102.10076].
- [361] Technical report, CERN, Geneva (2021), all figures including auxiliary ones are available at <https://atlas.web.cern.ch/Atlas/GROUPS/PHYSICS/CONFNOTES/ATLAS-CONF-2021-024>, URL <http://cds.cern.ch/record/2773300>.
- [362] M. Aaboud *et al.* (ATLAS), Phys. Rev. Lett. **121**, 21, 211801 (2018), [arXiv:1808.02343].
- [363] Technical report, CERN, Geneva (2021), all figures including auxiliary ones are available at <https://atlas.web.cern.ch/Atlas/GROUPS/PHYSICS/CONFNOTES/ATLAS-CONF-2021-040>, URL <http://cds.cern.ch/record/2779174>.
- [364] M. Aaboud *et al.* (ATLAS), JHEP **05**, 164 (2019), [arXiv:1812.07343].
- [365] M. Aaboud *et al.* (ATLAS), JHEP **05**, 041 (2019), [arXiv:1812.09743].
- [366] ATLAS Collab., ATLAS-CONF-2021-018 (2021).
- [367] ATLAS Collab., ATLAS-CONF-2018-024 (2018).
- [368] CMS Collab. CMS-PAS-TOP-12-042 (2013).
- [369] V. Khachatryan *et al.* (CMS), JHEP **06**, 121 (2015), [arXiv:1504.03198].
- [370] A. M. Sirunyan *et al.* (CMS), Eur. Phys. J. **C77**, 12, 845 (2017), [arXiv:1706.02581].
- [371] A. M. Sirunyan *et al.* (CMS), JHEP **03**, 141 (2019), [arXiv:1901.01553].
- [372] G. Aad *et al.* (ATLAS), JHEP **04**, 165 (2021), [arXiv:2102.01444].
- [373] G. Aad *et al.* (ATLAS), Eur. Phys. J. C **81**, 860 (2021), [arXiv:2011.09308].
- [374] Technical report, CERN, Geneva (2021), all figures including auxiliary ones are available at <https://atlas.web.cern.ch/Atlas/GROUPS/PHYSICS/CONFNOTES/ATLAS-CONF-2021-036>, URL <http://cds.cern.ch/record/2777863>.
- [375] J. A. Aguilar-Saavedra, Acta Phys. Polon. **B35**, 2695 (2004), [hep-ph/0409342].

- [376] V. Khachatryan *et al.* (CMS), JHEP **02**, 028 (2017), [arXiv:1610.03545].
- [377] CMS Collab., CMS-PAS-TOP-14-003.
- [378] CMS Collab., CMS-PAS-TOP-17-003.
- [379] V. Khachatryan *et al.* (CMS), JHEP **02**, 079 (2017), [arXiv:1610.04857].
- [380] G. Aad *et al.* (ATLAS), Eur. Phys. J. **C76**, 2, 55 (2016), [arXiv:1509.00294].
- [381] G. Aad *et al.* (ATLAS), Phys. Lett. **B800**, 135082 (2020), [arXiv:1908.08461].
- [382] A. Heister *et al.* (ALEPH), Phys. Lett. **B543**, 173 (2002), [hep-ex/0206070]; J. Abdallah *et al.* (DELPHI), Phys. Lett. **B590**, 21 (2004), [hep-ex/0404014]; P. Achard *et al.* (L3), Phys. Lett. **B549**, 290 (2002), [hep-ex/0210041]; G. Abbiendi *et al.* (OPAL), Phys. Lett. **B521**, 181 (2001), [hep-ex/0110009].
- [383] F. D. Aaron *et al.* (H1), Phys. Lett. **B678**, 450 (2009), [arXiv:0904.3876].
- [384] H. Abramowicz *et al.* (ZEUS), Phys. Lett. **B708**, 27 (2012), [arXiv:1111.3901].
- [385] M. Beneke *et al.*, in “1999 CERN Workshop on standard model physics (and more) at the LHC, CERN, Geneva, Switzerland, 25-26 May: Proceedings,” 419–529 (2000), [hep-ph/0003033], URL <http://web.lib.cern.ch/abstract?CERN-TH-2000-100>.
- [386] V. F. Obraztsov, S. R. Slabospitsky and O. P. Yushchenko, Phys. Lett. **B426**, 393 (1998), [hep-ph/9712394].
- [387] T. Carli, D. Dannheim and L. Bellagamba, Mod. Phys. Lett. **A19**, 1881 (2004), [hep-ph/0402012].
- [388] V. M. Abazov *et al.* (D0), Phys. Rev. Lett. **102**, 092002 (2009), [arXiv:0901.0151].
- [389] V.M. Abazov *et al.* (DØ Collab.), DØ conference note 5838 (2009).
- [390] V. M. Abazov *et al.* (D0), Phys. Lett. **B708**, 21 (2012), [arXiv:1110.4592].
- [391] ATLAS Collab., ATLAS-CONF-2013-032.
- [392] T. Aaltonen *et al.* (CDF), Phys. Rev. Lett. **101**, 192002 (2008), [arXiv:0805.2109].
- [393] V. M. Abazov *et al.* (D0), Phys. Lett. **B701**, 313 (2011), [arXiv:1103.4574].
- [394] V. M. Abazov *et al.* (D0), Phys. Lett. **B693**, 81 (2010), [arXiv:1006.3575].
- [395] S. Chatrchyan *et al.* (CMS), Phys. Rev. Lett. **112**, 17, 171802 (2014), [arXiv:1312.4194].
- [396] A. M. Sirunyan *et al.* (CMS), JHEP **07**, 003 (2017), [arXiv:1702.01404].
- [397] M. Aaboud *et al.* (ATLAS), JHEP **07**, 176 (2018), [arXiv:1803.09923].
- [398] M. Aaboud *et al.* (ATLAS), Phys. Rev. D **98**, 11, 112010 (2018), [arXiv:1806.10555].
- [399] A. M. Sirunyan *et al.* (CMS), JHEP **06**, 102 (2018), [arXiv:1712.02399].
- [400] M. Aaboud *et al.* (ATLAS), JHEP **05**, 123 (2019), [arXiv:1812.11568].

62. Form Factors for Semileptonic Kaon ($K_{\ell 3}$), Radiative Pion ($\pi_{\ell 2\gamma}$) and Kaon ($K_{\ell 2\gamma}$) Decays

Revised August 2021 by M.A. Bychkov (Virginia U.) and G. D'Ambrosio (INFN, Napoli).

62.1 $\pi_{\ell 2\gamma}^{\pm}$ and $K_{\ell 2\gamma}^{\pm}$ Form Factors

The radiative decays, $\pi^{\pm} \rightarrow l^{\pm}\nu\gamma$ and $K^{\pm} \rightarrow l^{\pm}\nu\gamma$, with l standing for an e or a μ , and γ for a real or virtual photon ($e^{+}e^{-}$ pair), provide a powerful tool to investigate the hadronic structure of pions and kaons. The structure-dependent part SD_i of the amplitude describes the emission of photons from virtual hadronic states, and is parametrized in terms of form factors V, A , (vector, axial vector), in the standard description [1–4]. Note that in the Listings and some literature, equivalent nomenclature F_V and F_A for the vector and axial form factors is often used. Exotic, non-standard contributions like $i = T, S$ (tensor, scalar) have also been considered. Apart from the SD terms, there is also the Inner Bremsstrahlung amplitude, IB, corresponding to photon radiation from external charged particles and described by Low theorem in terms of the physical decay $\pi^{\pm}(K^{\pm}) \rightarrow l^{\pm}\nu$. Experiments try to optimize their kinematics so as to minimize the IB part of the amplitude.

The SD amplitude in its standard form is given as

$$M(SD_V) = \frac{-eG_F U_{qq'}}{\sqrt{2}m_P} \epsilon^{\mu\nu} V^P \epsilon_{\mu\nu\sigma\tau} k^{\sigma} q^{\tau} \quad (62.1)$$

$$M(SD_A) = \frac{-ieG_F U_{qq'}}{\sqrt{2}m_P} \epsilon^{\mu\nu} \{A^P[(qk - k^2)g_{\mu\nu} - q_{\mu}k_{\nu}] + R^P k^2 g_{\mu\nu}\}, \quad (62.2)$$

which contains an additional axial form factor R^P which only can be accessed if the photon remains virtual. $U_{qq'}$ is the Cabibbo-Kobayashi-Maskawa mixing-matrix element; ϵ^{μ} is the polarization vector of the photon (or the effective vertex, $\epsilon^{\mu} = (e/k^2)\bar{u}(p_-)\gamma^{\mu}v(p_+)$, of the $e^{+}e^{-}$ pair); $\ell^{\nu} = \bar{u}(p_{\nu})\gamma^{\nu}(1 - \gamma_5)v(p_{\ell})$ is the lepton-neutrino current; q and k are the meson and photon four-momenta ($k = p_+ + p_-$ for virtual photons); and P stands for π or K .

For decay processes where the photon is real, the partial decay width can be written in analytical form as a sum of IB, SD, and IB/SD interference terms INT [1, 4]:

$$\begin{aligned} \frac{d^2\Gamma_{P \rightarrow \ell\nu\gamma}}{dxdy} &= \frac{d^2(\Gamma_{IB} + \Gamma_{SD} + \Gamma_{INT})}{dxdy} \\ &= \frac{\alpha}{2\pi} \Gamma_{P \rightarrow \ell\nu} \frac{1}{(1-r)^2} \left\{ \text{IB}(x, y) \right. \\ &+ \frac{1}{r} \left(\frac{m_P}{2f_P} \right)^2 \left[(V+A)^2 \text{SD}^+(x, y) + (V-A)^2 \text{SD}^-(x, y) \right] \\ &\left. + \epsilon_P \frac{m_P}{f_P} \left[(V+A) S_{INT}^+(x, y) + (V-A) S_{INT}^-(x, y) \right] \right\}. \quad (62.3) \end{aligned}$$

Here

$$\begin{aligned} \text{IB}(x, y) &= \left[\frac{1-y+r}{x^2(x+y-1-r)} \right] \\ &\left[x^2 + 2(1-x)(1-r) - \frac{2xr(1-r)}{x+y-1-r} \right] \\ \text{SD}^+(x, y) &= (x+y-1-r) \left[(x+y-1)(1-x) - r \right] \\ \text{SD}^-(x, y) &= (1-y+r) \left[(1-x)(1-y) + r \right] \\ S_{INT}^+(x, y) &= \left[\frac{1-y+r}{x(x+y-1-r)} \right] \left[(1-x)(1-x-y) + r \right] \\ S_{INT}^-(x, y) &= \left[\frac{1-y+r}{x(x+y-1-r)} \right] \left[x^2 - (1-x)(1-x-y) - r \right] \quad (62.4) \end{aligned}$$

where $x = 2E_{\gamma}/m_P$, $y = 2E_{\ell}/m_P$, $r = (m_{\ell}/m_P)^2$, f_P is the meson decay constant, and ϵ_P is +1 for pions and -1 for kaons. The structure dependent terms SD^+ and SD^- are shown in Fig. 1. The SD^- term is maximized in the same kinematic region where overwhelming IB term dominates (along $x+y=1$ diagonal). Thus experimental yields with less background are dominated by SD^+ contribution and proportional to $A^P + V^P$ making simultaneous precise determination of the form factors difficult.

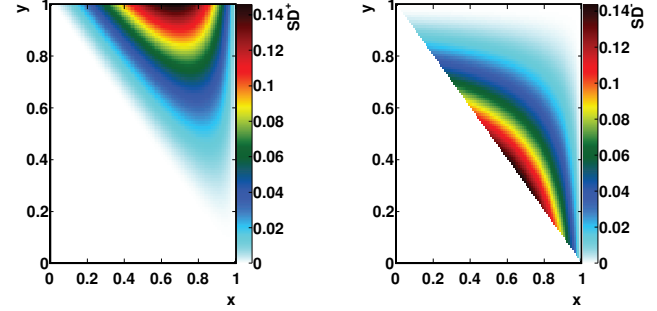


Figure 62.1: Components of the structure dependent terms of the decay width. Left: SD^+ , right: SD^-

Recently, formulas 62.3 and 62.4 have been extended to describe polarized distributions in radiative meson and muon decays [5].

The “helicity” factor r is responsible for the enhancement of the SD over the IB amplitude in the decays $\pi^{\pm} \rightarrow e^{\pm}\nu\gamma$, while $\pi^{\pm} \rightarrow \mu^{\pm}\nu\gamma$ is dominated by IB. Interference terms are important for the decay $K^{\pm} \rightarrow \mu^{\pm}\nu\gamma$ [6], but contribute only a few percent correction to pion decays. However, they provide the basis for determining the signs of V and A . Radiative corrections to the decay $\pi^+ \rightarrow e^+\nu\gamma$ have to be taken into account in the analysis of the precision experiments. They make up to 4% corrections in the total decay rate [7]. In $\pi^{\pm} \rightarrow e^{\pm}\nu e^+e^-$ and $K^{\pm} \rightarrow \ell^{\pm}\nu e^+e^-$ decays, all three form factors, V^P , A^P , and R^P , can be determined [8, 9].

Theoretically, the first non-trivial χPT contributions to A^P and V^P appear at $\mathcal{O}(p^4)$ [4], respectively from Gasser-Leutwyler coefficients, L_i 's, and the anomalous lagrangian:

$$A^P = \frac{4\sqrt{2}M_P}{F_{\pi}} (L_9^r + L_{10}^r), \quad V^P = \frac{\sqrt{2}M_P}{8\pi^2 F_{\pi}}. \quad (62.5)$$

In case of the kaon $A^K = 0.042$ and $V^K = 0.096$. $\mathcal{O}(p^6)$ contributions to A^K can be predicted accurately: they are flat in the momentum dependence and shift the $\mathcal{O}(p^4)$ value to 0.034. $\mathcal{O}(p^6)$ contributions to V^K are model dependent and can be approximated by a form factor linearly dependent on momentum. For example, when looking at the spread of results obtained within two different models, the constant piece of this linear form factor is shifted to 0.078 ± 0.005 [1, 2, 4].

We give the experimental π^{\pm} form factors V^{π} , A^{π} , and R^{π} in the Listings. In the K^{\pm} Listings, we give the extracted sum $A^K + V^K$ and difference $A^K - V^K$, as well as V^K , A^K and R^K . In particular KLOE has measured for the constant piece of the form factor $A^K + V^K = 0.125 \pm 0.007 \pm 0.001$ [10] while ISTRA+, $V^K - A^K = 0.21 \pm 0.04 \pm 0.04$ [11].

The pion vector form factor, V^{π} , is related via CVC (Conserved Vector Current) to the $\pi^0 \rightarrow \gamma\gamma$ decay width. The constant term is given by $|V^{\pi}(0)| = (1/\alpha)\sqrt{2}\Gamma_{\pi^0 \rightarrow \gamma\gamma}/\pi m_{\pi^0}$ [3]. The resulting value, $V^{\pi}(0) = 0.0259(9)$, has been confirmed by calculations based on chiral perturbation theory (χPT) [4], and by two experiments given in the Listings.

A recent experiment by the PIBETA collaboration [12] obtained a $V^{\pi}(0)$ that is in excellent agreement with the CVC hypothesis. It also measured the slope parameter a in $V^{\pi}(s) = V^{\pi}(0)(1+a \cdot s)$, where $s = (1 - 2E_{\gamma}/m_{\pi})$, and E_{γ} is the gamma energy in the pion rest frame: $a = 0.095 \pm 0.058$. A functional dependence on s is expected for all form factors. It becomes non-negligible in the

case of $V^\pi(s)$ when a wide range of photon momenta is recorded; proper treatment in the analysis of K decays is mandatory.

The form factor, R^P , can be related to the electromagnetic radius, r_P , of the meson [2]: $R^P = \frac{1}{3}m_P f_P (r_P^2)$ using PCAC (Partial Conserved Axial vector Current).

In lowest order χPT , the ratio A^π/V^π is related to the pion electric polarizability $\alpha_E = [\alpha/(8\pi^2 m_\pi f_\pi^2)] \times A^\pi/V^\pi$ [13]. Direct experimental and theoretical status of pion polarizability studies currently is not settled. Most recent theoretical predictions from χPT at $\mathcal{O}(p^6)$ [14] and experimental results from COM-PASS collaboration [15] favor a small value of pion polarizability $\alpha_\pi \sim (2 \div 3) \times 10^{-4} \text{ fm}^3$. Dispersive analysis of $\gamma\gamma \rightarrow \pi^+\pi^-$ crosssection [16] and experimental results from MAMI collaboration [17] report a much larger value of $\alpha_\pi \sim 6 \times 10^{-4} \text{ fm}^3$. Precise measurement of the pion form factors by PIBETA collaboration favors smaller values of polarizability $\alpha_\pi = 2.7_{-0.5}^{+0.6} \times 10^{-4} \text{ fm}^3$.

Several searches for the exotic form factors F_T^π , F_T^K (tensor), and F_S^K (scalar) have been pursued in the past. In particular, F_T^π has been brought into focus by experimental as well as theoretical work [18]. New high-statistics data from the PIBETA collaboration have been re-analyzed together with an additional data set optimized for low backgrounds in the radiative pion decay. In particular, lower beam rates have been used in order to reduce the accidental background, thereby making the treatment of systematic uncertainties easier and more reliable. The PIBETA analysis now restricts F_T^π to the range $-5.2 \times 10^{-4} < F_T^\pi < 4.0 \times 10^{-4}$ at a 90% confidence limit [12]. This result is in excellent agreement with the most recent theoretical work [4].

Precision measurements of radiative pion and kaon decays are effective tools to study QCD in the non-perturbative region and are of interest beyond the scope of radiative decays. Meanwhile other processes such as $\pi^+ \rightarrow e^+\nu$ that seem to be better suited to search for new physics at the precision frontier are currently studied. The advantages of such process are the very accurate and reliable theoretical predictions and the more straightforward experimental analysis.

62.2 $K_{\ell 3}^\pm$ and $K_{\ell 3}^0$ Form Factors

Assuming that only the vector current contributes to $K \rightarrow \pi \ell \nu$ decays, we write the matrix element as

$$M \propto f_+(t) \left[(P_K + P_\pi)_\mu \bar{\ell} \gamma_\mu (1 + \gamma_5) \nu \right] + f_-(t) \left[m_\ell \bar{\ell} (1 + \gamma_5) \nu \right], \quad (62.6)$$

where P_K and P_π are the four-momenta of the K and π mesons, m_ℓ is the lepton mass, and f_+ and f_- are dimensionless form factors which can depend only on $t = (P_K - P_\pi)^2$, the square of the four-momentum transfer to the leptons. If time-reversal invariance holds, f_+ and f_- are relatively real. $K_{\mu 3}$ experiments, discussed immediately below, measure f_+ and f_- , while $K_{e 3}$ experiments, discussed further below, are sensitive only to f_+ because the small electron mass makes the f_- term negligible.

62.2.1 $K_{\mu 3}$ Decays

Analyses of $K_{\mu 3}$ data frequently assume a linear dependence of f_+ and f_- on t , *i.e.*,

$$f_\pm(t) = f_\pm(0) \left[1 + \lambda_\pm (t/m_{\pi^+}^2) \right]. \quad (62.7)$$

Most $K_{\mu 3}$ data are adequately described by formula 62.7 for f_+ and a constant f_- (*i.e.*, $\lambda_- = 0$).

There are two equivalent parametrizations commonly used in these analyses: $\lambda_+, \xi(0)$ parametrization and λ_+, λ_0 parametrization.

Older analyses of $K_{\mu 3}$ data often introduce the ratio of the two form factors

$$\xi(t) = f_-(t)/f_+(t). \quad (62.8)$$

The $K_{\mu 3}$ decay distribution is then described by the two parameters λ_+ and $\xi(0)$ (assuming time reversal invariance and $\lambda_- = 0$).

More recent $K_{\mu 3}$ analyses have parametrized in terms of the form factors f_+ and f_0 , which are associated with vector and

scalar exchange, respectively, to the lepton pair. f_0 is related to f_+ and f_- by

$$f_0(t) = f_+(t) + \left[t/(m_K^2 - m_\pi^2) \right] f_-(t). \quad (62.9)$$

Here $f_0(0)$ must equal $f_+(0)$. The earlier assumption that f_+ is linear in t and f_- is constant leads to f_0 linear in t :

$$f_0(t) = f_0(0) \left[1 + \lambda_0 (t/m_{\pi^+}^2) \right]. \quad (62.10)$$

With the assumption that $f_0(0) = f_+(0)$, the two parametrizations, $(\lambda_+, \xi(0))$ and (λ_+, λ_0) are equivalent as long as correlation information is retained. (λ_+, λ_0) correlations tend to be less strong than $(\lambda_+, \xi(0))$ correlations.

Since the 2006 edition of the *Review* [19], we no longer quote results in the $(\lambda_+, \xi(0))$ parametrization. We have removed many older low statistics results from the Listings. See the 2004 version of this note [20] for these older results, and the 1982 version [21] for additional discussion of the $K_{\mu 3}^0$ parameters, correlations, and conversion between parametrizations.

More recent high-statistics experiments have included a quadratic term in the expansion of $f_+(t)$,

$$f_+(t) = f_+(0) \left[1 + \lambda'_+ (t/m_{\pi^+}^2) + \frac{\lambda''_+}{2} (t/m_{\pi^+}^2)^2 \right]. \quad (62.11)$$

If there is a non-vanishing quadratic term, then λ_+ of formula 62.7 represents the average slope, which is then different from λ'_+ . Our convention is to include the factor $\frac{1}{2}$ in the quadratic term, and to use m_{π^+} even for $K_{e 3}^+$ and $K_{\mu 3}^+$ decays. We have converted other's parametrizations to match our conventions, as noted in the beginning of the " $K_{\ell 3}^\pm$ and $K_{\ell 3}^0$ Form Factors" sections of the Listings.

There are two alternatives to the Taylor parametrization: The Pole Parametrization and Dispersive Parametrization.

The pole model describes the t -dependence of $f_+(t)$ and $f_0(t)$ in terms of the exchange of the lightest vector and scalar K^* mesons with masses M_V and M_S , respectively:

$$f_+(t) = f_+(0) \left[\frac{M_V^2}{M_V^2 - t} \right], \quad f_0(t) = f_0(0) \left[\frac{M_S^2}{M_S^2 - t} \right]. \quad (62.12)$$

The Dispersive Parametrization approach, valid in a much wider kinematic range and able to describe at the same time τ -decay data, [22] uses dispersive techniques and the known low-energy K - π phases to parametrize the vector and scalar form factors:

$$f_+(t) = f_+(0) \exp \left[\frac{t}{m_\pi^2} (\Lambda_+ + H(t)) \right]; \quad (62.13)$$

$$f_0(t) = f_+(0) \exp \left[\frac{t}{(m_K^2 - m_\pi^2)} (\ln[C] - G(t)) \right], \quad (62.14)$$

where Λ_+ is the slope of the vector form factor, and $\ln C = \ln[f_0(m_K^2 - m_\pi^2)]$ is the logarithm of the scalar form factor at the Callan-Treiman point. The functions $H(t)$ and $G(t)$ are dispersive integrals.

62.2.2 $K_{e 3}$ Decays

Analysis of $K_{e 3}$ data is simpler than that of $K_{\mu 3}$ because the second term of the matrix element assuming a pure vector current [formula 62.6 above] can be neglected. Here f_+ can be assumed to be linear in t , in which case the linear coefficient λ_+ of formula 62.7 is determined, or quadratic, in which case the linear coefficient λ'_+ and quadratic coefficient λ''_+ of formula 62.11 are determined.

If we remove the assumption of a pure vector current, then the matrix element for the decay, in addition to the terms in formula 62.6, would contain

$$+2m_K f_S \bar{\ell} (1 + \gamma_5) \nu + (2f_T/m_K) (P_K)_\lambda (P_\pi)_\mu \bar{\ell} \sigma_{\lambda\mu} (1 + \gamma_5) \nu, \quad (62.15)$$

where f_S is the scalar form factor, and f_T is the tensor form factor. In the case of the K_{e3} decays where the f_- term can be neglected, experiments have yielded limits on $|f_S/f_+|$ and $|f_T/f_+|$.

For K_{e3} data, we determine best values for the three parametrizations: linear (λ_+), quadratic (λ'_+, λ''_+) and pole (M_V). For $K_{\mu 3}$ data, we determine best values for the three parametrizations: linear (λ_+, λ_0), quadratic ($\lambda'_+, \lambda''_+, \lambda_0$) and pole (M_V, M_S). We then assume $\mu-e$ universality so that we can combine K_{e3} and $K_{\mu 3}$ data, and again determine best values for the three parametrizations: linear (λ_+, λ_0), quadratic ($\lambda'_+, \lambda''_+, \lambda_0$), and pole (M_V, M_S). When there is more than one parameter, fits are done including input correlations. Simple averages suffice in the two K_{e3} cases where there is only one parameter: linear (λ_+) and pole (M_V).

A comprehensive global analysis of the semileptonic kaon decay data and its effect on the CKM unitarity debate can be found in [23, 24]. An update on experimental data including NA48/2 newest results can be found in [25].

Both KTeV and KLOE see an improvement in the quality of their fits relative to linear fits when a quadratic term is introduced, as well as when the pole parametrization is used. The quadratic parametrization has the disadvantage that the quadratic parameter λ''_+ is highly correlated with the linear parameter λ'_+ , in the neighborhood of 95%, and that neither parameter is very well determined. The pole fit has the same number of parameters as the linear fit, but yields slightly better fit probabilities, so that it would be advisable for all experiments to include the pole parametrization as one of their choices.

The "Kaon Particle Listings" show the results with and without assuming $\mu-e$ universality. The "Meson Summary Tables" show all of the results assuming $\mu-e$ universality, but most results not assuming $\mu-e$ universality are given only in the Listings.

References

- [1] D. A. Bryman, P. Depommier and C. Leroy, Phys. Rept. **88**, 151 (1982), see our note on "Decay Constants of Charged Pseudoscalar Mesons" elsewhere in this Review; S. G. Brown and S. A. Bludman, Phys. Rev. **136**, B1160 (1964); P. DeBaenst and J. Pestieau, Nuovo Cimento **A53**, 137 (1968).
- [2] W. T. Chu, T. Ebata and D. M. Scott, Phys. Rev. **166**, 1577 (1968); D. Yu. Bardin and E. A. Ivanov, Sov. J. Part. Nucl. **7**, 286 (1976), [Fiz. Elem. Chast. Atom. Yadra7,726(1976)]; A. Kersch and F. Scheck, Nucl. Phys. **B263**, 475 (1986).
- [3] V.G. Vaks and B.L. Ioffe, Nuovo Cimento **10**, 342 (1958); V.F. Muller, Z. Phys. **173**, 438 (1963).
- [4] C. Q. Geng, I.-L. Ho and T. H. Wu, Nucl. Phys. **B684**, 281 (2004), [hep-ph/0306165]; J. Bijnens and P. Talavera, Nucl. Phys. **B489**, 387 (1997), [hep-ph/9610269]; V. Mateu and J. Portoles, Eur. Phys. J. **C52**, 325 (2007), [arXiv:0706.1039]; R. Unterdorfer and H. Pichl, Eur. Phys. J. **C55**, 273 (2008), [arXiv:0801.2482]; V. Cirigliano *et al.*, Rev. Mod. Phys. **84**, 399 (2012), [arXiv:1107.6001].
- [5] E. Gabrielli and L. Trentadue, Nucl. Phys. **B792**, 48 (2008), [hep-ph/0507191].
- [6] S. Adler *et al.* (E787), Phys. Rev. Lett. **85**, 2256 (2000), [hep-ex/0003019].
- [7] E. A. Kuraev, Yu. M. Bystritsky and E. P. Velicheva, Phys. Rev. **D69**, 114004 (2004), [hep-ph/0310275]; R. Unterdorfer and H. Pichl have treated radiative corrections of the structure terms to lowest order within χPT for the first time. See the reference under [4].
- [8] S. Egli *et al.* (SINDRUM), Phys. Lett. **B175**, 97 (1986).
- [9] A. A. Poblaguev *et al.*, Phys. Rev. Lett. **89**, 061803 (2002), [hep-ex/0204006].
- [10] F. Ambrosino *et al.* (KLOE), Eur. Phys. J. **C64**, 627 (2009), [Erratum: Eur. Phys. J.65,703(2010)], [arXiv:0907.3594].
- [11] V. A. Duk *et al.* (ISTRA+), Phys. Lett. **B695**, 59 (2011), [arXiv:1005.3517].
- [12] D. Pocanic *et al.*, Phys. Rev. Lett. **93**, 181803 (2004), [hep-ex/0312030]; E. Frlez *et al.*, Phys. Rev. Lett. **93**, 181804 (2004), [hep-ex/0312029]; M. Bychkov *et al.*, Phys. Rev. Lett. **103**, 051802 (2009), [arXiv:0804.1815].
- [13] J. F. Donoghue and B. R. Holstein, Phys. Rev. **D40**, 2378 (1989).
- [14] J. Gasser, M. A. Ivanov and M. E. Sainio, Nucl. Phys. **B745**, 84 (2006), [hep-ph/0602234].
- [15] C. Adolph *et al.* (COMPASS), Phys. Rev. Lett. **114**, 062002 (2015), [arXiv:1405.6377].
- [16] L. V. Fil'kov and V. L. Kashevarov, Phys. Rev. **C73**, 035210 (2006), [arXiv:nucl-th/0512047].
- [17] J. Ahrens *et al.*, Eur. Phys. J. **A23**, 113 (2005), [arXiv:nucl-ex/0407011].
- [18] A. A. Poblaguev, Phys. Lett. **B238**, 108 (1990); V. N. Bologotov *et al.*, Phys. Lett. **B243**, 308 (1990); V. M. Belyaev and I. I. Kogan, Phys. Lett. **B280**, 238 (1992); A. V. Chernyshev *et al.*, Mod. Phys. Lett. **A12**, 1669 (1997); A. A. Poblaguev, Phys. Rev. **D68**, 054020 (2003), [hep-ph/0307166]; M. V. Chizhov, Phys. Part. Nucl. Lett. **2**, 193 (2005), [Pisma Fiz. Elem. Chast. Atom. Yadra2005,no.4,7(2005)], [hep-ph/0402105].
- [19] W. Yao *et al.*, Journal of Physics G: Nuclear and Particle Physics **33**, 1 (2006), ISSN 0954-3899.
- [20] S. Eidelman *et al.*, Physics Letters B **592**, 1, 1 (2004), ISSN 0370-2693, review of Particle Physics, URL <https://www.sciencedirect.com/science/article/pii/S0370269304007579>.
- [21] M. Roos *et al.*, Physics Letters B **111**, i (1982), ISSN 0370-2693, URL <https://www.sciencedirect.com/science/article/pii/S0370269382912862>.
- [22] V. Bernard *et al.*, Physics Letters B **638**, 5, 480 (2006), ISSN 0370-2693, URL <https://www.sciencedirect.com/science/article/pii/S0370269306006812>; A. Lai *et al.*, Physics Letters B **647**, 5, 341 (2007), ISSN 0370-2693, URL <https://www.sciencedirect.com/science/article/pii/S0370269307002432>.
- [23] M. Antonelli *et al.* (FlaviaNet Working Group on Kaon Decays), Eur. Phys. J. C **69**, 399 (2010), [arXiv:1005.2323].
- [24] C.-Y. Seng *et al.* (2021), [arXiv:2107.14708].
- [25] J. R. Batley *et al.* (NA48/2), JHEP **10**, 150 (2018), [arXiv:1808.09041].
- [26] L.-M. Chounet, J.-M. Gaillard and M. Gaillard, Physics Reports **4**, 5, 199 (1972), ISSN 0370-1573, URL <https://www.sciencedirect.com/science/article/pii/S037015737290018X>.
- [27] H. W. Fearing, E. Fischbach and J. Smith, Phys. Rev. D **2**, 542 (1970), URL <https://link.aps.org/doi/10.1103/PhysRevD.2.542>.
- [28] N. Cabibbo and A. Maksymowicz, Phys. Lett. **9**, 352 (1964).

63. Spectroscopy of Light Meson Resonances

Written August 2021 by C. Amsler (Stefan Meyer Inst.), S. Eidelman (Budker Inst., Novosibirsk; Novosibirsk U.), A. Masoni (INFN, Cagliari) and G. Venanzoni (INFN, Pisa).

63.1	Introduction	845
63.2	Scalar mesons	845
63.3	Glueballs	847
	63.3.1 Scalar glueballs	847
	63.3.2 Tensor glueballs	848
63.4	Pseudoscalar mesons	848
63.5	Vector mesons	849
	63.5.1 The $\rho(770)$ meson	849
	63.5.2 The $\rho(770)$ excitations	850
63.6	Axial-vector mesons	850
63.7	Hybrid mesons	851
63.8	Tetraquark states	851
63.9	Baryonia	852
63.10	Conclusions	852

63.1 Introduction

According to the constituent quark model, a light meson consists of a color singlet quark-antiquark pair made of the u , d , or s quarks and the \bar{u} , \bar{d} , or \bar{s} antiquarks, grouped into a flavor multiplet of SU(3). However, additional mesons made of bound gluons (glueballs) could exist in the same mass range, suggested by the self coupling of gluons in QCD. Multiquark structures are also possible, such as quark-antiquark pairs with an excited gluon (hybrid mesons). Tetraquarks are compact color singlets of diquark-antidiquark pairs ($qq\bar{q}\bar{q}$) or ‘molecular’ bound states of two mesons ($q\bar{q}q\bar{q}$). More complex systems such as $qqq\bar{q}\bar{q}$ (baryonia) are also predicted.

Fundamentals on the constituent quark model on light and heavy mesons and baryons (including hadrons with charm and bottom quarks), and on predictions from lattice gauge theories, are described in ‘Quark Model’ in this issue of the *Review of Particle Physics*, henceforth called the *Review*. In the present text we describe the experimental spectrum of light mesons and their classifications within the constituent quark model, with emphasis on states exhibiting properties incompatible with $q\bar{q}$ structures. The discussion is driven by the results entered in the database of the *Review*. The spectrum of kaon excitations is much less clear cut and therefore deferred to a future edition, when further data might become available. More detailed discussions on exotic mesons – including those involving the c and b quarks – can be found in Refs. [1–7] and in ‘Heavy Non- $q\bar{q}$ Mesons’ of the *Review*. For more information on the meson (and baryon) spectrum of light (and heavy) quarks we refer to the textbook [8].

Figure 63.1 shows the mass spectrum of $q\bar{q}$ mesons. The mass (vertical axis) increases with orbital excitations ℓ (horizontal axis) and radial excitation n . In the quark model one uses the notation nS , nP , nD ... for the radial excitations ($n = 1$ for the ground states), in contrast to the usual $1s$, $2p$, $3d$... notation in atomic physics. Each box represents an SU(3) nonet containing multiplets of the isospin i , three isovectors, two strange isodoublets, and two isosinglets (one SU(3) singlet and one SU(3) octet). The spin, parity [$P = -(-1)^\ell$] and C -parity [$C = (-1)^{\ell+s}$] take the possible values $J^{PC} = 0^{++}$ (scalar), 0^{-+} (pseudoscalar), 1^{--} (vector), 1^{+-} (axial- or pseudovector), 2^{++} (tensor), etc. Therefore mesons with the *exotic* quantum numbers 0^{--} , 0^{+-} , 1^{-+} , 2^{+-} , 3^{-+} , etc. cannot be $q\bar{q}$ states. Note that the C -parity is defined only for the electrically neutral non-strange nonet members.

The two isosinglets in each nonet mix with an angle θ close to the *ideal* value of 35.3° for the 1^{--} , 1^{+-} , 2^{++} and 3^{--} nonets, in which case the isosinglets decouple to $u\bar{u} + d\bar{d}$ and $s\bar{s}$. The orbital excitations $\ell \geq 1$ consist of four nonets for each value of n , since $j = \ell$ for antiparallel quark spins and $j = \ell - 1, \ell$ or $\ell + 1$ for parallel spins. Since the C -parity is not defined for strange mesons, the K_{1A} and K_{1B} in the axial vector 1^{+-} and 1^{--} nonets of fig. 63.1 are mathematical constructs which mix to give the observed $K_1(1270)$ and $K_1(1400)$ mesons.

As described in more detail below (section 63.2), it is hard to accommodate all the known scalar mesons in the lower $q\bar{q}$ nonets: The light scalar mesons $a_0(980)$, $K_0^*(700)$ (also known as κ), the $f_0(500)$ (also known as σ), and the $f_0(980)$, not shown in the figure, could build the lightest nonet, but could also be two-meson resonances or tetraquarks (section 63.8). Furthermore, the ground state glueball expected below 2 GeV will mix with the $q\bar{q}$ isoscalar scalar mesons (section 63.3.1). The pseudoscalar slot labeled $\eta(1440)$ may consist of two states (section 63.4). The status of vector meson excitations is described in section 63.5. The axial-vector meson $f_1(1420)$ could be replaced in the 1^{+-} nonet by the $f_1(1510)$ which, however, needs confirmation (see the *Listings* and section 63.6). Mesons with exotic quantum numbers are discussed in section 63.7.

63.2 Scalar mesons

Scalar mesons decay dominantly into pairs of pseudoscalar mesons ($\pi\pi$, $K\bar{K}$, $\pi\eta$, $\eta\eta$ or $\eta\eta'$). The widths tend to be large for those decaying into $\pi\pi$, due to the absence of angular momentum barrier and the large available phase space. Identifying broad overlapping states is not straightforward. Furthermore, the onset of the $K\bar{K}$, $\eta\eta$ or $\eta\eta'$ thresholds distorts the line shapes and produces cusps. This requires high statistics data and the use of coupled channel analyses taking into account unitarity and analyticity (see ‘Resonances’ in the *Review*). The SU(3) classification is also not easy, because the ground state scalar glueball and multiquark states are predicted to exist below 2 GeV.

Two isovector scalars are known, the $a_0(980)$ and the $a_0(1450)$. Five isoscalar resonances are established: the very broad $f_0(500)$, the $f_0(980)$, the broad $f_0(1370)$, and the comparatively narrow $f_0(1500)$ and $f_0(1710)$. The strange partners are the $K_0^*(700)$ and the $K_0^*(1430)$. The $f_0(500)$ and $K_0^*(700)$ deserve a separate treatment and can be found in ‘Scalar Mesons below 1 GeV’, which contains more details on the $a_0(980)$ and $f_0(980)$, briefly reviewed in section 63.8.

The $a_0(1450)$ was first reported by the Crystal Barrel experiment in $\bar{p}p$ annihilation with stopped antiprotons [9] (see [10] for a review of Crystal Barrel results). Its mass of about 1450 MeV is not far from that of the $a_2(1320)$ meson. An isovector scalar, possibly the $a_0(1450)$ (albeit at a lower mass of 1317 MeV) is observed by Belle in $\gamma\gamma$ collisions leading to $\eta\pi^0$ [11]. The state interferes destructively with the non-resonant background. Its $\gamma\gamma$ coupling is comparable to that of the $a_2(1320)$, in accord with simple predictions (see *e.g.* [12]). A contribution from $a_0(1450) \rightarrow K\bar{K}$ is also found in the CLEO-c analysis of $D^\pm \rightarrow K^+K^-\pi^\pm$ [13] and $D^0 \rightarrow K_S^0 K^\pm \pi^\mp$ from LHCb [14].

The $f_0(1370)$ and $f_0(1500)$ were observed by Crystal Barrel [15–17] and by WA102 in central production with 450 GeV protons [18, 19]. They decay mostly into 2π and 4π . The $f_0(1500)$ was also observed to decay into $\eta\eta$ [20–22] and $\eta\eta'$ [23]. All data agree that the 4π decay mode represents about half of the $f_0(1500)$ decay width, but is dominant for $f_0(1370)$.

The determination of the $\pi\pi$ coupling of the very broad $f_0(1370)$ is complicated by its interference with the $f_0(500)$ and $f_0(1500)$. Its existence is questioned by COMPASS from $\pi^-p \rightarrow \pi^-\pi^-\pi^+p$ data [24]. In $\bar{B}_s^0 \rightarrow J/\psi(1S)\pi^+\pi^-$ from LHCb a strong scalar contribution from the $f_0(1370)$ was initially observed [25], although new data require the $f_0(500)$ and $f_0(1500)$, without any need for the $f_0(1370)$ [26]. In $\bar{B}^0 \rightarrow J/\psi(1S)\pi^+\pi^-$ the $\pi\pi$ mass spectrum does not show any significant scalar component above ~ 1.2 GeV [27] (an analysis that is however challenged in [28]). $D^0 \rightarrow \pi^+\pi^-\pi^+\pi^-$ data from CLEO-c also require a contribution from $f_0(500)f_0(1370) \rightarrow 4\pi$ [29]. A broad 2π signal is also observed by BaBar around 1400 MeV in the decay $B^\pm \rightarrow \pi^\pm\pi^\pm\pi^\mp$ [30] which is attributed to the $f_0(1370)$, but could also be due to the $f_0(1500)$.

In Refs. [31, 32] the $f_0(1370)$ and $f_0(1710)$ (together with the $f_2(1270)$ and $f_2'(1525)$) are interpreted as bound systems of two vector mesons. This view is challenged in Ref. [33] where in a covariant formalism, *e.g.* the $f_2(1270)$ does not appear as a $\rho\rho$ bound state. Photoproduction data of the $f_2(1270)$ in $\gamma p \rightarrow \pi^0\pi^0 p$ from CLAS [34], as a function of momentum trans-

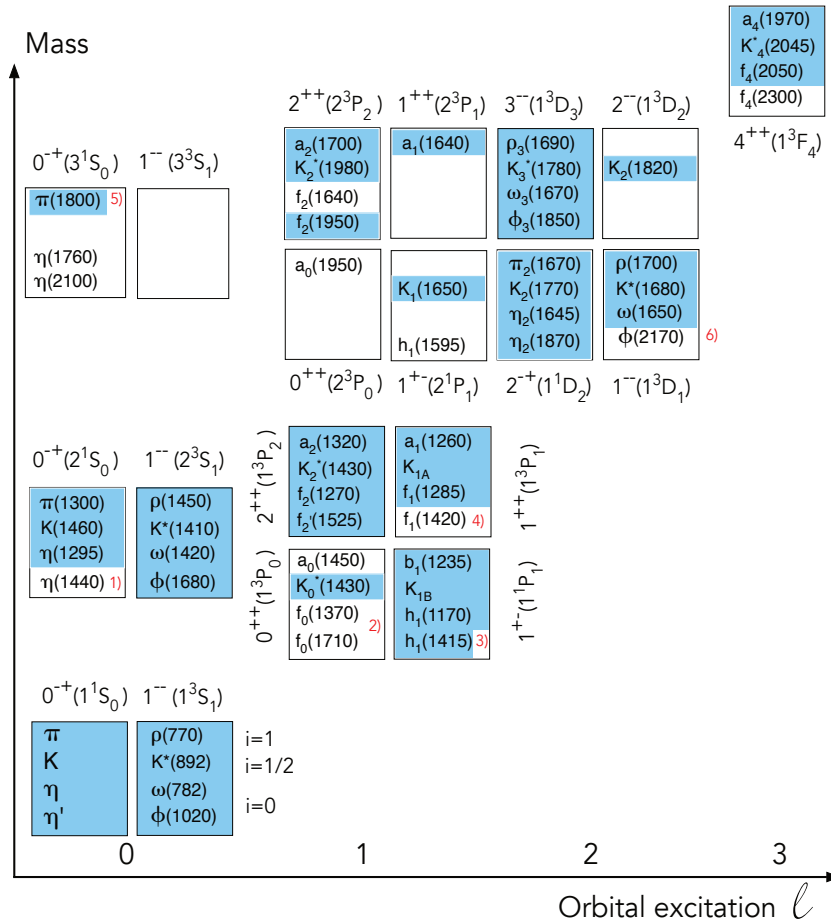


Figure 63.1: The mesons made of the u , d , and s light quarks are organised in $J^{PC}(n^{2s+1}\ell_j)$ nonets with isospin i . The established mesons (which appear in the *Summary Table* of the *Review*) are shown in the dark (blue) areas. The white areas contain those omitted in the *Summary Table* but reported in the *Listings*, or the established ones with a tentative nonet classification. States with the same J^{PC} mix, such as the 2^3S_1 and 1^3D_1 mesons. The states become broad and overlap with increasing masses, which complicates the determination of the resonance parameters *e.g.* mass, width and spin. For a complete list of mesons see the *Listings*.

¹ The $\eta(1440)$ stands for the $\eta(1405)$ and the $\eta(1475)$, section 63.4.

² The classification of the scalar nonet is controversial. Alternative schemes involve the $f_0(1500)$ and the light scalars below 1 GeV, section 63.2.

³ Considered established, but more data would be desirable.

⁴ An alternative to the $f_1(1420)$ is the $f_1(1510)$, section 63.6.

⁵ The $\pi(1800)$ has also been proposed as a hybrid meson, section 63.7.

⁶ The $\phi(2170)$ has also been proposed as a tetraquark state, section 63.8.

fer, also disagree with predictions [35] for the $f_2(1270)$ to be a $\rho\rho$ bound state.

While the $K\bar{K}$ decay branching ratio of the $f_0(1500)$ is small [18] [36], the $f_0(1710)$ decays dominantly into $K\bar{K}$. The $f_0(1710)$ is not observed in $p\bar{p}$ annihilation at rest [36] and only weakly produced in $p\bar{p}$ annihilation in flight [37], with a rate strongly suppressed compared to that of the $f_0(1500)$ ($\sim 7\%$). For comparison, the rate for the $(s\bar{s})$ $f_2'(1525)$ is about 9% that of the $(u\bar{u} + d\bar{d})$ $f_2(1270)$, as expected from the OZI rule [37]. On the other hand the $f_0(1370)$ does not couple strongly to $K\bar{K}$ [18]. This suggests an $n\bar{n}$ structure ($u\bar{u} + d\bar{d}$) for the $f_0(1370)$ and $s\bar{s}$ for the $f_0(1710)$. The $f_0(1500)$ would also qualify as an $n\bar{n}$ state (see 63.3.1), although it is very narrow compared to the other states. Occam's razor principle therefore suggests that the $f_0(1370)$, $a_0(1450)$, and the $f_0(1710)$ are in the same SU(3) flavor nonet, the $f_0(1370)$ and $a_0(1450)$ being the two (mostly) $n\bar{n}$ states, and the $f_0(1710)$ the (dominantly) $s\bar{s}$ one. It is important to note that the spectrum of scalar mesons above the $f_0(1710)$ is not well established: The reported ones in the *Listings* need experimental confirmation and are not included in the *Summary Table*.

According to [38] there is mounting evidence for the existence of two scalar nonets and one glueball below 2 GeV: Table 63.1

shows a proposed classification scheme. The low mass nonet is made of four-quark states which recombine at large distances to become meson-meson resonances, while the ground state 1^3P_0 $q\bar{q}$ nonet lies in the 1400 MeV region, see Ref. [1] for a review and Ref. [39] for the $f_0(500)$. The nature of the $f_0(1500)$ is discussed along this scheme in section 63.3.1.

Other schemes have been proposed, for example a tetraquark for the $f_0(1500)$ [40] or flavor octets for the $f_0(1500)$ and $f_0(1710)$ [3]. In Ref. [41] the $a_0(1450)$, $f_0(1370)$, $f_0(1500)$ and $K_0^*(1430)$ are radial excitations of the scalar nonet below 1 GeV. In Ref. [42] the light and heavy scalar nonets in Table 63.1 are interpreted as mixing of two tetraquark nonets. In the unitarized quark model with coupled $q\bar{q}$ and meson-meson channels, the scalars below 1 GeV are manifestations of bare $q\bar{q}$ confinement states, mass shifted from the 1.4 GeV region and distorted by the strong 3P_0 coupling to S -wave two-meson decay channels [43, 44]. Thus, in these models the light scalar nonet comprising the light and heavy scalar nonets shown in Table 63.1 are manifestations of the same bare input states (see also [45]). Surprisingly for a state decaying strongly into 2π and 4π , the $f_0(1370)$ is assumed to be an $s\bar{s}$ state in Ref. [46]. The $f_0(1500)$ is then a radial excitation and the glueball lies around 1700 MeV.

Table 63.1: Tentative classification of scalar mesons (see the text). The 1^3P_0 ground state $q\bar{q}$ nonet is listed in the bottom half. The third isoscalar $f_0(1500)$ is discussed in section 63.3.1.

	Γ [MeV]	isospin i	structure
$a_0(980)$	~ 50	1	$K\bar{K}, qq\bar{q}\bar{q}$
$f_0(980)$	~ 50	0	$K\bar{K}, qq\bar{q}\bar{q}$
$f_0(500)$	~ 800	0	$\pi\pi, qq\bar{q}\bar{q}$
$K_0^*(700)$	~ 600	$\frac{1}{2}$	$K\pi, qq\bar{q}\bar{q}$
$a_0(1450)$	265	1	$u\bar{d}, d\bar{u}, d\bar{d} - u\bar{u}$
$f_0(1370)$	~ 400	0	$d\bar{d} + u\bar{u}$
$f_0(1710)$	125	0	$s\bar{s}$
$K_0^*(1430)$	294	$\frac{1}{2}$	$u\bar{s}, d\bar{s}, s\bar{u}, s\bar{d}$

63.3 Glueballs

Lattice calculations, QCD sum rules, flux tube, and constituent glue models agree that the lightest glueball has quantum numbers $J^{PC} = 0^{++}$ and the first excited state 2^{++} . Lattice calculations predict for the ground state (0^{++}) a mass around 1600 – 1700 MeV [47–50], while the 2^{++} state lies around 2300 MeV. For more information on lattice calculations see ‘Quark Model’ in the *Review* and fig. 15.3 therein for an example of mass spectrum. These predictions were made in the quenched approximation, neglecting $q\bar{q}$ loops. However quenched predictions and full QCD calculations lead to small mass shifts (see ‘Quark Model’ and fig. 15.15 therein).

Heavier glueballs with quantum numbers $0^{-+}, 2^{-+}, 1^{+-}$, etc. are predicted above 2500 MeV and the lowest exotic ones (with exotic quantum numbers such as 0^{+-} and 2^{+-}) are expected above 4000 MeV [50]. In holographic QCD the 0^{-+} is predicted to be very broad [51] and the 1^{+-} is at least as broad as its width [52]. Calculations of the three lowest scalar and pseudoscalar glueballs masses in pure Yang-Mills theory are in quantitative agreement with lattice results [53]. The lightest glueballs lie in the same mass region as ordinary isoscalar $q\bar{q}$ states, in the mass range of the $1^3P_0(0^{++}), 2^3P_2(2^{++}), 3^3P_2(2^{++})$, and $1^3F_2(2^{++})$ $q\bar{q}$ states. Therefore, mixing of glueballs with nearby $q\bar{q}$ states of the same quantum numbers leads to supernumerary isoscalar state in the $q\bar{q}$ nonets (however, see Ref. [54] discussed in section 63.3.1).

Among the signatures naively expected for glueballs are (i) isoscalar states that do not fit into $q\bar{q}$ nonets, (ii) enhanced production in gluon-rich channels such as central production and radiative $J/\psi(1S)$ decay, (iii) decay branching fractions incompatible with SU(3) predictions for $q\bar{q}$ states, and (iv) reduced $\gamma\gamma$ couplings. However, mixing effects with isoscalar $q\bar{q}$ mesons [47, 55–63] and decay form factors [64] can obscure these simple signatures.

According to SU(3) the decay branching ratios for $q\bar{q}$ mesons and pure glueballs are different, and therefore useful to determine the internal structures of mesons. For pure glueballs with flavor symmetric couplings the decay ratios are $\pi\pi : K\bar{K} : \eta\eta : \eta\eta' = 3 : 4 : 1 : 0$, apart from phase space factors. The partial widths for the decay of a scalar (or a tensor) meson into a pair of pseudoscalar mesons are given in Fig. 63.2 (for a derivation see e.g. [8]).

The decay of a $q\bar{q}$ meson into a pair of mesons involves the creation of a $q\bar{q}$ pair, and SU(3) symmetry assumes that the matrix elements for the creation of $s\bar{s}$, $u\bar{u}$, and $d\bar{d}$ pairs are equal. (The generalization to unequal $s\bar{s}$, $u\bar{u}$, and $d\bar{d}$ couplings is given in Ref. [55].) An excellent fit to the tensor meson decay widths is obtained with $\beta \simeq 0.5$ GeV/c, $\theta_V \simeq 26^\circ$ and $\theta_P \simeq -17^\circ$ [55].

Note that the assumption of flavor symmetric couplings may not apply in models describing the scalar glueball by a dilaton field, which lead to mass dependent couplings [65, 66] (see Ref. [67] which predicts that a scalar glueball above 1 GeV would be unobservably wide).

Another way to determine the flavor contents of neutral mesons is the decay $B \rightarrow J/\psi(1S)X$ which filters out the $d\bar{d}$ content of X , while $B_s^0 \rightarrow J/\psi(1S)X$ selects its $s\bar{s}$ component [68].

63.3.1 Scalar glueballs

One of the three isoscalars, the $f_0(1370)$, $f_0(1500)$ or $f_0(1710)$, appears to be supernumerary. The branching ratios in Fig. 63.2 can be used to deduce the structures of these states, assuming that they are $q\bar{q}$. The comparison of decay branching ratios from Crystal Barrel annihilation and WA102 central collision data shows that the $f_0(1500)$ is compatible with an $n\bar{n}$ structure, while the $f_0(1710)$ is mostly $s\bar{s}$ [12]. However, the close vicinity of the very broad $n\bar{n}$ $f_0(1370)$, its narrow width, enhanced production at low transverse momentum transfer in central collisions [69–71] and absence in $\gamma\gamma$ collisions (see below) favor the $f_0(1500)$ to be the supernumerary non- $q\bar{q}$ state. According to [55, 60] the $f_0(1370)$ and $f_0(1710)$ would be dominantly $q\bar{q}$ states mixing with glue, while the $f_0(1500)$ would be dominantly a glueball mixing with $q\bar{q}$ states. Its suppressed $K\bar{K}$ decay would be due to interferences with the $f_0(1370)$ and $f_0(1710)$. In the analogous mixing scheme of Ref. [72], which uses central production data from WA102 and the hadronic $J/\psi(1S)$ decay data from BES [73, 74], glue is shared between the $f_0(1370)$ (mainly $n\bar{n}$), $f_0(1500)$ (mainly glue) and $f_0(1710)$ (dominantly $s\bar{s}$). This agrees with the analyses [55, 60]. In the mixing scheme of Ref. [75] the QCD spectral sum rule also leads to a large gluonic component in the $f_0(1500)$ (satisfying the observed strong $\pi\pi$ and $f_0(500)f_0(500) \rightarrow 4\pi$ decays).

However, not everybody agrees that the strong $K\bar{K}$ signal is indicative of an $s\bar{s}$ structure for the $f_0(1710)$. The $f_0(1710)$ could still be the glueball, since the two-gluon coupling to $n\bar{n}$ appears to be suppressed by chiral symmetry [76], thus $K\bar{K}$ would be enhanced compared to $\pi\pi$. It was argued that chiral symmetry constraints in a multichannel analysis imply that the $f_0(1710)$ is an unmixed scalar glueball [77]. However, this view is challenged in [78].

The $K\bar{K}$ decay is also naturally enhanced in the extended linear sigma model with a dilaton as glueball [65] and in the holographic model of [66, 79] which both prefer the $f_0(1710)$ as the glueball. For a scalar glueball Ref. [66] finds a strong enhancement of the decays into $K\bar{K}$ and $\eta\eta$, in fairly close agreement with the measured branching ratios of the $f_0(1710)$, while Ref. [79] predicts the (so far not measured) rate into $\eta\eta'$ to be very small.

In $\gamma\gamma$ collisions leading to $K_S K_S$ [80] and $K^+ K^-$ [81] a spin-0 signal is observed at the $f_0(1710)$ mass (together with a dominant spin-2 component), while the $f_0(1500)$ is not observed in $\gamma\gamma \rightarrow K\bar{K}$ nor $\pi^+\pi^-$ [82]. The $f_0(1500)$ is also not observed by Belle in $\gamma\gamma \rightarrow \pi^0\pi^0$, although a shoulder is seen which could also be due to the $f_0(1370)$ [83]. The absence of $f_0(1500)$ signal in the $\pi\pi$ channel in $\gamma\gamma$ collisions does not favor an $n\bar{n}$ interpretation for the $f_0(1500)$. The upper limit for $\Gamma_{2\gamma} (< 1.4$ keV) in $\pi^+\pi^-$ [12]) excludes a large $n\bar{n}$ content, and hence points to a mainly $s\bar{s}$ content [12], which contradicts the small $K\bar{K}$ decay branching ratio of the $f_0(1500)$ [18, 36, 84]. Belle finds that in $\gamma\gamma \rightarrow K_S K_S$ collisions the 1500 MeV region is dominated by the $f_2'(1525)$. The $f_0(1710)$ is also observed with a production rate \times branching ratio compatible with an $s\bar{s}$ state [85]. Note, however, that the $\gamma\gamma$ couplings of glueballs are sensitive to glue mixing with $q\bar{q}$ [72]. Ref. [63] predicts the glueball $\gamma\gamma$ partial width in the few keV range (comparable to that of $q\bar{q}$ mesons) due to couplings of vector mesons to γ via VDM.

Alternative assignments for the scalar glueball have been proposed: In Ref. [57] the gluonic signal is distributed over $f_0(1370)$, $f_0(1500)$ and another broad isoscalar around 1530 MeV, while the gluonic contribution to the $f_0(1710)$ is small. As mentioned already, in Ref. [47, 65, 66] the $f_0(1710)$ is the glueball state, as in Ref. [61], where the $f_0(1500)$ is the $q\bar{q}$ octet state degenerate with the $a_0(1450)$. In the generalized linear sigma model [86] the $a_0(980)$ is dominantly a tetraquark and $a_0(1450)$ a $q\bar{q}$ state. The $f_0(980)$, $f_0(1370)$ and $f_0(1500)$ (or $f_0(1710)$) are dominantly tetraquark, $q\bar{q}$ and glue.

In Ref. [59] the $f_0(500)$ and $f_0(1370)$ are signals from a single broad resonance proposed as the scalar glueball. The ground state scalar nonet then consists of the $f_0(980)$, $a_0(980)$, $K_0^*(1430)$, $f_0(1500)$ and $f_0(1710)$ [62]. The $f_0(980)$ and $f_0(1500)$ mix (similarly to the η and η' in the pseudoscalar nonet), while the $f_0(1500)$ mixes with a glueball in the 500 – 1000 MeV mass range, which is identified as the $f_0(500)$. A reanalysis of the CERN-Munich

Isospin	Decay channel	γ^2
0	$\pi\pi$	$3 \cos^2 \alpha$
	$K\bar{K}$	$(\cos \alpha - \sqrt{2} \sin \alpha)^2$
	$\eta\eta$	$(\cos \alpha \cos^2 \phi - \sqrt{2} \sin \alpha \sin^2 \phi)^2$
	$\eta\eta'$	$\frac{1}{2} \sin^2 2\phi (\cos \alpha + \sqrt{2} \sin \alpha)^2$
1	$\eta\pi$	$2 \cos^2 \phi$
	$\eta'\pi$	$2 \sin^2 \phi$
	$K\bar{K}$	1
$\frac{1}{2}$	$K\pi$	$\frac{3}{2}$
	$K\eta$	$(\sin \phi - \frac{\cos \phi}{\sqrt{2}})^2$
	$K\eta'$	$(\cos \phi + \frac{\sin \phi}{\sqrt{2}})^2$

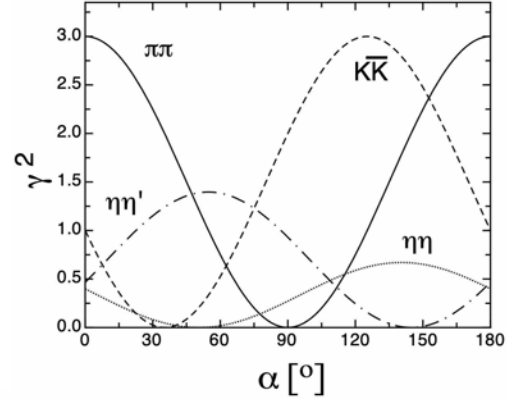


Figure 63.2: Left: SU(3) couplings γ^2 for scalar (or tensor) $q\bar{q}$ meson decays. The angles α and ϕ are defined as $\alpha = 54.7^\circ + \theta$ and $\phi = 54.7^\circ + \theta_P$, where θ is the mixing angle of the decaying isoscalars and θ_P the mixing angle in the 0^{++} (2^{++}) meson nonet. The partial decay width is given by $\Gamma = C \times \gamma^2 \times |F(q)|^2 \times q$, where C is a nonet constant, q the momentum of the decay products and $F(q)$ a form factor which may be taken as $|F(q)|^2 = q^{2\ell} \times \exp(-q^2/8\beta^2)$ with $\beta = 0.5$ GeV/c, and where ℓ is the relative angular momentum between the decay products ($\ell = 0$ for scalars and $\ell = 2$ for tensors). Right: SU(3) couplings as a function of mixing angle α for isoscalar decays for $\theta_P = -17.3^\circ$ (from [55]).

data shows no signal for the $f_0(1370)$ decaying into $\pi\pi$, in contrast to [54, 87]. However, in this scheme the $K_0^*(700)$ and the $a_0(1450)$ are also left out.

In Ref. [88], a large K^+K^- scalar signal reported by Belle in B decays into $KK\bar{K}$ [89], compatible with the $f_0(1500)$, is explained as due to constructive interference of a flavor octet with a broad glueball background. However, the Belle data are inconsistent with the BaBar measurements which show instead a broad scalar at this mass for B decays into both $K^\pm K^\pm K^\mp$ [90] and $K^+K^-\pi^0$ [91].

The $f_0(1500)$ is observed by BESII in $J/\psi(1S) \rightarrow \gamma\pi\pi$ [92] and by BESIII in $J/\psi(1S) \rightarrow \gamma\eta\eta$ [93] with a much smaller rate than for the $f_0(1710)$, which would speak against a glueball interpretation of the former, although the systematic errors are large. Also, the $f_0(1500)$ appears at a lower mass and the $f_0(1710)$ at a higher mass than the accepted values. However, the coupled channel analysis of more data on radiative $J/\psi(1S)$ decay from BESIII [54] (described in the next paragraph) finds comparable contributions from $f_0(1500)$ and $f_0(1710)$ with a preference for $\pi\pi$ decay over $K\bar{K}$ for the former and $K\bar{K}$ over $\pi\pi$ for the latter.

The authors of Ref. [54] have analyzed the high statistics data from $J/\psi(1S)$ radiative decays into $\pi^0\pi^0$, $K_S^0K_S^0$, $\eta\eta$ and $\omega\phi$ from BESIII, including data on $\pi\pi$, $\eta\eta$ and $\eta\eta'$ from the CERN SPS, BNL data on $\pi\pi \rightarrow K_S^0K_S^0$ and $\bar{p}p$ annihilation data from LEAR into various final states. The coupled channel analysis requires ten scalar mesons, the established ones in the *Review* and the four isoscalars $f_0(2020, 2100, 2200, 2330)$ so far omitted from the *Summary Table*. As a new feature, the $f_0(1710)$ splits into two states, one at about 1700 MeV, the former $f_0(1710)$, and a new one around 1770 MeV being mandatory to obtain a good fit. A broad (~ 370 MeV) enhancement is observed in $J/\psi(1S)$ radiative decays around 1865 MeV, attributed to the contribution of glue distributed among the scalar mesons, with a very strong contribution from the new 1770 MeV state [94]. In this model there are no supplementary states as the glue ‘fragments’ between the various isoscalars.

Ref. [95] reports on a very recent re-analysis of the BESIII $J/\psi(1S)$ radiative decay data into $\pi^0\pi^0$ and $K_S^0K_S^0$. A good fit is obtained with only two scalar resonances below 2 GeV, the $f_0(1500)$ and $f_0(1710)$. The latter couples much more strongly to both channels, which points to a sizeable glueball component.

63.3.2 Tensor glueballs

Above the well known $f_2(1270)$ and $f_2'(1525)$ $q\bar{q}$ mesons, the $f_2(1640)$ and $f_2(1950)$ are tentatively assigned to the 2^3P_2 nonet (see Fig. 63.1). The broad $f_2(1950)$ has been observed by several experiments, *e.g.* in central production [19] and in $\bar{p}p$ annihilation in flight [96] and is often identified as the ground state of the

pomeron [97, 98]. Three further isoscalar tensors are established, the $f_2(2010)$, $f_2(2300)$ and $f_2(2340)$, which are in the range of the 1^3F_2 and 3^3P_2 nonets, and in the expected region for the 2^{++} glueball. The large $\phi\phi$ cross section in $\bar{p}p$ just above threshold [99] could be due to the production of the 2^{++} glueball, in accord with earlier observations in π^-N reactions [100, 101] and in central collisions [102].

The $f_2(2010)$, $f_2(2300)$ and $f_2(2340)$ have been observed by BESIII in $J/\psi(1S) \rightarrow \gamma\phi\phi$ [103]. The production rate of a tensor glueball in $J/\psi(1S)$ radiative decay has been calculated in quenched lattice QCD to be large (around 1%) [104] and is claimed by BESIII [103] to be compatible with their rates measured in $J/\psi(1S) \rightarrow f_2(2340)$, $f_2(2340) \rightarrow \eta\eta$ [93], and $f_2(2340) \rightarrow \phi\phi$ [103]. The relatively narrow $f_2(2300)$ with a measured width of 149 MeV [101] is preferred by the holographic QCD model of Ref. [105]. However, the tensor glueball is predicted to be much broader (600–900 MeV) by the holographic model of Ref. [106].

There is no evidence for a narrow meson, $f_J(2220)$ (a tensor candidate) in $\bar{p}p$ annihilation (see the note under the $f_J(2220)$ in the 2004 issue of the *Review*). The measured partial width to $\bar{p}p$ in radiative $J/\psi(1S)$ decay [107] is too large and inconsistent with the upper limit from $\bar{p}p$ annihilation into $\pi\pi$ [108].

63.4 Pseudoscalar mesons

We now deal with the first radial excitations of the 0^{-+} nonet (Fig. 63.1). The $\pi(1300)$ is a very broad resonance (200–600 MeV) decaying into 3π . The $K(1460)$ was recently confirmed with high statistics data from LHCb in $D^0 \rightarrow K3\pi$ decays [109] and has become an established kaon excitation. The first observation of an isoscalar resonance around 1425 MeV – the E -meson – was made in $\bar{p}p$ annihilation at rest into $E\pi^+\pi^-$, $E \rightarrow K\bar{K}\pi$ [110]. This state was reported to decay into $a_0(980)\pi$ and $K^*(892)\bar{K}$ with roughly equal contributions. An isoscalar state, the ι meson, was observed in radiative $J/\psi(1S)$ decay into $K\bar{K}\pi$ [111–113] and $\gamma\rho$ [114], and was considered at that time as a glueball candidate, owing to its strong signal in radiative $J/\psi(1S)$ decay. The E and ι were later assumed to be the same state, called $\eta(1440)$.

The $\eta(1295)$ has been observed in various production mechanisms, in π^-p experiments [115–118], and in $\bar{p}p$ annihilation [84, 119, 120]. In $J/\psi(1S)$ radiative decay, the $\eta(1295)$ signal is also evident in the 0^{-+} $\eta\pi\pi$ wave of the DM2 data [121]. Also BaBar reports a signal around 1295 MeV in B decays into $\eta\pi\pi K$ [122]. Let us therefore assume in the following that the $\eta(1295)$ is one of the isoscalars in this nonet.

However, two isoscalars were later observed in this mass region, the $\eta(1405)$ and $\eta(1475)$. The former decays mainly into $a_0(980)\pi$ (or direct $K\bar{K}\pi$) and the latter mainly into $K^*(892)\bar{K}$. The simultaneous observation of two pseudoscalars is reported in

three production mechanisms: $\pi^- p$ [115, 123], radiative $J/\psi(1S)$ decay [121, 124], and $\bar{p}p$ annihilation at rest [125–128]. All of them give values for the masses, widths, and decay modes that are in reasonable agreement. (However, Ref. [121] favors a state decaying into $K^*(892)\bar{K}$ at a lower mass than the state decaying into $a_0(980)\pi$.) In $J/\psi(1S)$ radiative decay, the $\eta(1405)$ decays into $K\bar{K}\pi$ through $a_0(980)\pi$, and hence a signal is also expected in the $\eta\pi\pi$ mass spectrum. This was indeed observed by MARK III in $\eta\pi^+\pi^-$ [129], which reported a mass of 1400 MeV, in line with the existence of the $\eta(1405)$ decaying into $a_0(980)\pi$. Two states were also reported by BES: Around 1452 MeV BESII observed a $K\bar{K}\pi$ enhancement in $J/\psi(1S) \rightarrow \omega K\bar{K}\pi$ but not in $J/\psi(1S) \rightarrow \phi K\bar{K}\pi$ [130], while BESIII reported a 52 MeV broad state in $\psi(2S) \rightarrow \omega K^* K$ [131], both left without J^{PC} determination.

The $K\bar{K}\pi$ and $\eta\pi\pi$ channels were studied in $\gamma\gamma$ collisions by L3 [132]. (For the 2γ couplings of glueballs and $q\bar{q}$ mesons see [63, 133, 134].) The analysis led to a clear $\eta(1475)$ signal in $K\bar{K}\pi$, decaying into $K^*\bar{K}$, well identified in the untagged data sample, where spin 1 resonances are not allowed. At the same time, L3 did not observe the $\eta(1405)$, neither in $K\bar{K}\pi$ nor in $\eta\pi\pi$ [132]. On the other hand, CLEO-II did not observe any pseudoscalar signal with tagged γ 's in $\gamma\gamma \rightarrow \eta(1475) \rightarrow K_S^0 K^\pm \pi^\mp$ [135], with an upper limit slightly smaller than the signal observed by L3. After the CLEO-II result L3 performed a further analysis with full statistics [136], confirming their previous evidence for the $\eta(1475)$. The CLEO upper limit [135] for $\Gamma_{\gamma\gamma}$, and the L3 results [136], are consistent with the world average for the $\eta(1475)$ width. BaBar [122] also reported the $\eta(1475)$ in B decays into $K\bar{K}^*$ recoiling against a K , while upper limits only were given for the $\eta(1405)$.

Hence, in radiative $J/\psi(1S)$ decay, $\pi^- p$ and $\bar{p}p$ annihilation at rest two isoscalar signals are observed in the 1400–1500 MeV mass region, while the $\eta(1405)$ is not seen in $\gamma\gamma$ interactions nor in B decays. The $\eta(1475)$ could be the first radial excitation of the η' , with the $\eta(1295)$ being the first radial excitation of the η . Ideal mixing, suggested by the $\eta(1295)$ and $\pi(1300)$ mass degeneracy, would then imply that the second isoscalar in the nonet is mainly $s\bar{s}$, and hence couples to $K^*\bar{K}$, in agreement with properties of the $\eta(1475)$. Also, its width agrees with the expected one for the radially excited $s\bar{s}$ state [64, 69]. A study of radial excitations of pseudoscalar mesons [137] also favors the $s\bar{s}$ interpretation of the $\eta(1475)$. However, due to the strong kinematical suppression in $\eta(1405) \rightarrow K^*\bar{K}$ the data are not sufficient to exclude a sizeable $s\bar{s}$ admixture also in the $\eta(1405)$.

The supernumerary isoscalar $\eta(1405)$ would be a candidate for the 0^{-+} glueball in the fluxtube model [138], in which the 0^{++} glueball is also naturally related to a 0^{-+} glueball with mass degeneracy broken in QCD. However, this scenario is not favored by lattice gauge theories which predict the 0^{-+} state above 2 GeV [48, 139] (see ‘Quark model’ in this issue of the *Review*). Nevertheless, the pseudoscalar glueball could lie at a lower mass than predicted from lattice calculation [140], see also Refs. [141–143]. A detailed review of the experimental situation on the pseudoscalar glueball is available in Ref. [144].

Here also, there are alternative explanations. The mere existence of the $\eta(1295)$ is questioned in Refs. [3, 145], in which the authors also propose a single pseudoscalar meson at 1440 MeV, the first radial excitation of the η . According to Ref. [3] the splitting of the 1440 MeV state into $\eta(1405)$ and $\eta(1475)$ is due to nodes in the decay amplitudes, which differ in $\eta\pi\pi$ and $K^*(892)\bar{K}$. The splitting could also be due to a triangle singularity, hence the manifestation of one state only (Fig. 63.3) [146–148]. In Ref. [149], using the triangle singularity approach of [146], the authors conclude that the BESIII results can be reproduced either with the $\eta(1405)$ or the $\eta(1475)$, or by a mixture of these two states.

To summarise this section, the experimental data on the 1400–1500 MeV region span several decades, various production mechanisms and decay modes, with models for data analysis evolving with time. A comprehensive coherent picture of all available data is therefore difficult. We believe that there is sufficient evidence to consider the 0^{-+} nonet with the $\eta(1440)$ in fig. 63.1 as established. Whether one or two different states – $\eta(1405)$ and $\eta(1475)$ – exist is an open question, in which case the $\eta(1405)$ would be

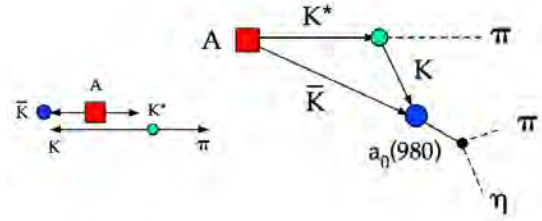


Figure 63.3: Triangle singularity: a state A decays into $K^*\bar{K}$. The K from K^* decay catches up with the \bar{K} and excites the $a_0(980)$ resonance which in turn decays into $\eta\pi$. This mechanism can lead to two distinct peaks (depending on the width of A), one in $K^*\bar{K}$ and the other via rescattering in $\eta\pi\pi$. Similarly, the virtual $K^*\bar{K}$ loop can couple to $f_0(980)$ which, decaying into $\pi\pi$, leads to a peak in the 3π final state.

supernumerary. There is a wide number of experimental results indicating the presence of two separate states but, as mentioned above, data are also consistent with one state only. Theoretical interpretations of the most recent data are not able to lift the ambiguity.

63.5 Vector mesons

In this section we restrict ourselves to the more interesting isovector spectrum which contains broad and overlapping states.

63.5.1 The $\rho(770)$ meson

The determination of the parameters of the $\rho(770)$ is beset with many difficulties because of its large width. The line shape depends on the production process and is not described by a relativistic Breit-Wigner function with a P -wave width, but requires some additional shape parameter. This dependence on parameterization was demonstrated long ago [150]. Bose-Einstein correlations are another source of shifts in the $\rho(770)$ line shape, particularly in multiparticle final-state systems [151].

The same model dependence afflicts any other source of resonance parameters, such as the energy dependence of the phase shift δ_1^1 , or the pole position. It is, therefore, not surprising that a study of $\rho(770)$ dominance in the decays of the η and η' reveals the need for specific dynamical effects, in addition to the $\rho(770)$ pole [152, 153].

The cleanest determination of the $\rho(770)$ mass and width comes from e^+e^- annihilation and τ -lepton decays. ALEPH data [154] showed that the charged $\rho(770)$ parameters measured from τ -lepton decays are consistent with those of the neutral one determined from e^+e^- data [155]. This conclusion is qualitatively supported by the later studies of CLEO [156] and Belle [157]. However, a comparison of the two-pion mass spectrum in τ decays from OPAL [158], CLEO [156], and ALEPH [159, 160], and the $e^+e^- \rightarrow \pi^+\pi^-$ cross section from CMD-2 [161, 162], showed significant discrepancies between the two shapes which can be as high as 10% above the ρ meson mass [163, 164]. This discrepancy remains after measurements of the two-pion cross section in e^+e^- annihilation at KLOE [165–168], SND [169, 170], BaBar [171] and, more recently BESIII [172]. The effect is not accounted for by isospin breaking [173–176], but the accuracy of its calculation may be overestimated [177, 178].

This problem seems to be solved after a recent analysis in [179], which showed that after correcting the τ data for the missing ρ - γ mixing contribution, besides the other known isospin symmetry violating corrections, the $\pi\pi$ isospin 1 part of the hadronic vacuum polarization contribution to the muon $g-2$ is fully compatible between τ based and e^+e^- based evaluations. The global fit of the whole set of the ρ , ω , and ϕ decays, taking into account mixing effects in the hidden local symmetry model, also showed consistency of the data on τ decays to two pions and e^+e^- annihilation [180, 181]. However, because of the progress in e^+e^- data, the τ input is now less precise and less reliable due to additional theoretical uncertainties [182] decreasing the importance of τ decay for the determination of the $\rho(770)$ parameters.

63.5.2 The $\rho(770)$ excitations

In our 1988 edition, we replaced the $\rho(1600)$ entry with two new ones, the $\rho(1450)$ and the $\rho(1700)$, because there was emerging evidence that the 1600-MeV region actually contains two ρ -like resonances. This possibility was pointed out by a theoretical analysis [183] on the consistency of the 2π and 4π electromagnetic form factors and the $\pi\pi$ scattering length. A consistent picture of $e^+e^- \rightarrow 2\pi, 4\pi$ and diffractive photoproduction is obtained with two resonances [184]. The existence of the $\rho(1450)$ was supported by the analysis of $\eta\rho^0$ mass spectra obtained in photoproduction and e^+e^- annihilation [185], as well as that of $e^+e^- \rightarrow \omega\pi$ [186].

The analysis of [184] was further extended by [187, 188] to include new data on 4π -systems produced in e^+e^- annihilation, and in τ decays ($\tau \rightarrow 4\pi$ and $e^+e^- \rightarrow 4\pi$ are related by the Conserved Vector Current hypothesis). These systems were successfully analyzed using interfering contributions from two ρ -like states, and from the tail of the $\rho(770)$ two-body decay. While specific conclusions on $\rho(1450) \rightarrow 4\pi$ were obtained, little could be said about the $\rho(1700)$. Independent evidence for two 1^- states is provided by [189] in 4π electroproduction at $\langle Q^2 \rangle = 1$ (GeV/c)², and by [190] in a high-statistics sample of the $\eta\pi\pi$ system in π^-p charge exchange.

This scenario with two overlapping resonances is supported by other data. DM2 [191] measured the pion form factor in the interval 1.35–2.4 GeV, and observed a deep minimum around 1.6 GeV. The best fit was obtained with the hypothesis of ρ -like resonances at 1420 and 1770 MeV, with widths of about 250 MeV. DM2 [192] found that the $e^+e^- \rightarrow \eta\pi^+\pi^-$ cross section is better fitted with two fully interfering Breit-Wigners, with parameters in fair agreement with those of [184] and [191]. These results can be considered as a confirmation of the $\rho(1450)$.

Decisive evidence for the $\pi\pi$ decay mode of both $\rho(1450)$ and $\rho(1700)$ comes from $\bar{p}p$ annihilation at rest [193]. It has been shown that these resonances possess a $K\bar{K}$ decay mode [84, 194, 195]. This decay mode has also been studied in three-body hadronic B decays [196]. High-statistics studies of the decays $\tau \rightarrow \pi\pi\nu_\tau$ [154, 156], and $\tau \rightarrow 4\pi\nu_\tau$ [197] also require the $\rho(1450)$, but are not sensitive to the $\rho(1700)$, being too close to the τ mass. A recent very-high-statistics study of the $\tau \rightarrow \pi\pi\nu_\tau$ from Belle [157] reports the first observation of both $\rho(1450)$ and $\rho(1700)$ in τ decays. A clear picture of the two $\pi^+\pi^-$ resonances interfering with the $\rho(770)$ in e^+e^- annihilation was also reported by BaBar using the ISR (Initial State Radiation) method [198].

The structure of these ρ states is not yet completely clear. The authors of Refs. [64, 199] claim that $\rho(1450)$ has a mass consistent with radial $2S$, but its decays show characteristics of hybrids, and suggest that this state may be a $2S$ -hybrid mixture. Hybrid states could have a 4π decay mode dominated by the $a_1\pi$ [200]. Such behavior has been observed by [201] in $e^+e^- \rightarrow 4\pi$ in the energy range 1.05–1.38 GeV, and by [197] in $\tau \rightarrow 4\pi$ decays. CLEO [202] and Belle [203] observe the $\rho(1450) \rightarrow \omega\pi$ decay mode in B -meson decays, however, do not find $\rho(1700) \rightarrow \omega\pi^0$. A similar conclusion is made by [204, 205], who studied the process $e^+e^- \rightarrow \omega\pi^0$ and do not observe a statistically significant signal of the $\rho(1700)$. Various decay modes of the $\rho(1450)$ and $\rho(1700)$ are observed in $\bar{p}n$ and $\bar{p}p$ annihilation [206, 207], but no definite conclusions can be drawn. More data should be collected to clarify the nature of the ρ states, particularly in the energy range above 1.6 GeV.

We now list under a separate entry the $\rho(1570)$, the $\phi\pi$ state with $J^{PC} = 1^{--}$ earlier observed by [208] – referred to as $C(1480)$ – and recently confirmed by [209] and [210]. While [211] shows that it may be a threshold effect, Refs. [187] and [212] suggest two independent vector states with this decay mode. The $C(1480)$ has not been seen in the $\bar{p}p$ [213] and e^+e^- [214, 215] experiments. However, the sensitivity of the two latter is an order of magnitude lower than that of [209]. Note that [209] can not exclude that their observation is due to an OZI-suppressed decay mode of the $\rho(1700)$.

Several observations on the $\omega\pi$ system in the 1200 MeV region [216–222] may be interpreted in terms of either $J^P = 1^- \rho(770) \rightarrow \omega\pi$ production [223], or $J^P = 1^+ b_1(1235)$ production [221, 222]. We argue that no special entry for a $\rho(1250)$ is needed. The LASS amplitude analysis [224] showing evidence for $\rho(1270)$ is

preliminary and needs confirmation. However, evidence for the $\rho(1250)$ from a reanalysis of elastic scattering data is claimed in Ref. [225]. For completeness, the relevant observations are listed under the $\rho(1450)$.

Recently Ref. [226] reported a very broad 1^{--} resonance-like K^+K^- state in $J/\psi \rightarrow K^+K^-\pi^0$ decays. Its pole position corresponds to mass of 1576 MeV and width of 818 MeV. Its exotic structure (molecular or multiquark) is suggested [227–229], while in Refs. [230] and [231] this is explained by the interference between the $\rho(1450)$ and $\rho(1700)$. The latter statement is qualitatively supported by BaBar [232] and SND [233]. We quote [226] as $X(1575)$ in the section “Further States.”

Evidence for ρ -like mesons decaying into 6π was first noted by [234] in the analysis of $e^+e^- \rightarrow 6\pi$ [235, 236] and diffractive photoproduction [237]. The authors of Ref. [234] argued that two states at about 2.1 and 1.8 GeV exist: while the former is a candidate for the $\rho(2150)$, the latter could be a manifestation of the $\rho(1700)$ distorted by threshold effects. BaBar reported observations of the new decay modes of the $\rho(2150)$ in the channels $\eta'(958)\pi^+\pi^-$, $f_1(1285)\pi^+\pi^-$ [238] and $\pi^+\pi^-$ [239]. The decay of the $\rho(2150)$ into K^+K^- has been observed by BESIII [240] and confirmed by BaBar [241]. The relativistic quark model [242] predicts the 2^3D_1 state with $J^{PC} = 1^{--}$ at 2.15 GeV which can be identified with the $\rho(2150)$.

Under $\rho(1900)$ we list various observations of irregular behavior of the cross sections near the $N\bar{N}$ threshold. Dips of various width around 1.9 GeV were reported by the E687 Collaboration (a narrow one in the $3\pi^+3\pi^-$ diffractive photoproduction [243, 244]), by the FENICE experiment (a narrow structure in the R value [245]), by BaBar in ISR (a narrow structure in $e^+e^- \rightarrow \phi\pi$ final state [209], but much broader in $e^+e^- \rightarrow 3\pi^+3\pi^-$ and $e^+e^- \rightarrow 2(\pi^+\pi^-\pi^0)$ [246]), by CMD-3 (also a rather broad dip in $e^+e^- \rightarrow 3\pi^+3\pi^-$ [247]). A dedicated scan of the $N\bar{N}$ -threshold region by CMD-3 confirms this effect in the $e^+e^- \rightarrow 3\pi^+3\pi^-$ and $e^+e^- \rightarrow K^+K^-\pi^+\pi^-$ final states, but does not see it in the cross section of $e^+e^- \rightarrow 2\pi^+2\pi^-$ [248]. Most probably, these structures emerge as a threshold effect due to the opening of the $N\bar{N}$ channel [249–251]. A similar enhancement is observed by BESIII in $e^+e^- \rightarrow \Lambda\bar{\Lambda}$ near the $\Lambda\bar{\Lambda}$ threshold [252].

63.6 Axial-vector mesons

The $J^{PC} = 1^{++}$ nonet consists of the isovector $a_1(1260)$, the isoscalars $f_1(1285)$ and $f_1(1420)$, and the K_{1A} , which is a superposition of the physical states $K_1(1270)$ and $K_1(1400)$ with a mixing angle of about 35° [253]. The nonet mixing angle $\theta_{1^{++}}$ is around 23° . The orthogonal combination – the K_{1B} – belongs to the 1^{+-} nonet with a mixing angle $\theta_{1^{+-}}$ of about 28° [253].

The mass region above 1400 MeV is rather complex [254–256]. The $f_1(1420)$ was first reported in π^-p reactions at 4 GeV/c, decaying into $K^*\bar{K}$ [257]. The $f_1(1420) \rightarrow K\bar{K}\pi$ was also observed in a reanalysis of the MARK III data [124], and a $C=+1$ state seen in tagged $\gamma\gamma$ collisions [258]. Axial-vector mesons are not observed in $\bar{p}p$ annihilation at rest in liquid hydrogen, which proceeds dominantly through S -wave annihilation. However, in gaseous hydrogen, P -wave annihilation is enhanced and the $f_1(1420)$ is indeed observed, decaying into $K^*\bar{K}$ [126]. The $f_1(1420)$, decaying into $K\bar{K}\pi$, is also seen in pp central production, together with the $f_1(1285)$. The latter decays via $a_0(980)\pi$, and the former only via $K^*\bar{K}$. The $K_S^0 K_S^0 \pi^0$ decay mode of the $f_1(1420)$ establishes unambiguously $C=+1$. Neither central production [259] nor π^-p interactions at 100 GeV [117] find any evidence for a $\eta\pi\pi$ decay mode of the $f_1(1420)$.

The $f_1(1285)$ has been suggested to be a $K^*\bar{K}$ molecule [260]. However, LHCb has determined the 1^{++} nonet mixing angle to be consistent with a mostly $n\bar{n}$ structure for the $f_1(1285)$ from $\bar{B}^0/\bar{B}^0 \rightarrow J/\psi(1S)f_1(1285)$, independent of the identity of its isoscalar partner [261]. The mixing angle $\theta_{1^{++}} = 24^\circ$ agrees with that of Ref. [253] quoted above. The ratio of \bar{B}^0/\bar{B}_s^0 decay rates also excludes the tetraquark interpretation of the $f_1(1285)$ [261]. This is consistent with earlier determinations assuming that the $f_1(1420)$ is the other isoscalar in the nonet [262].

A resonance candidate decaying into 3π had been reported earlier by COMPASS at 1420 MeV in $\pi^-p \rightarrow \pi^-\pi^-\pi^+p$ [263, 264].

The signal appeared as a clear peak in the $1^{++} f_0(980)\pi$ P -wave and had the expected phase motion of a new resonance, called the $a_1(1420)$. However, the signal appears to originate from a triangle singularity: the decay of the $a_1(1260)$ into $K^*(\rightarrow K\pi)\bar{K}$ is followed by rescattering into the $f_0(980)\pi$ channel, $f_0(980) \rightarrow \pi\pi$ (see the caption of fig. 63.3) [265]. Accordingly, this entry has been removed from the *Listings* in the *Review*.

A similar triangle singularity is proposed for the $f_1(1420)$, resulting from the $K^*\bar{K}$ and $a_0(980)\pi$ decay modes of the $f_1(1285)$ [266]. The $f_1(1420)$ was also suggested to be a hybrid $q\bar{q}g$ meson [267] or a $K^*\bar{K}$ molecule, due to the proximity of the $K^*\bar{K}$ threshold [268]. Indeed, the $f_1(1420)$ is not seen in K^-p [269], which argues against the $f_1(1420)$ being the $s\bar{s}$ member of the 1^{++} nonet. In this case the $s\bar{s}$ partner of the $f_1(1285)$ could be the $f_1(1510)$ which is, however, not well established [270].

The $f_1(1510)$ was seen to decay into $K\bar{K}\pi$ in K^-p interactions at 4 and 11 GeV/c, recoiling against a Λ [269,271], which points to an $s\bar{s}$ state. Evidence was also reported in π^-p interactions, based on the phase motion of the $1^{++} K^*\bar{K}$ wave [256]. A somewhat broader 1^{++} signal is observed in $J/\psi(1S) \rightarrow \gamma\eta\pi^+\pi^-$ [272] and a small signal in $J/\psi(1S) \rightarrow \gamma\eta'\pi^+\pi^-$ [273]. However, there is no evidence for the $f_1(1510)$ in other K^-p experiments [274,275], while the $f_1(1420)$ is observed in K^-p but not in π^-p [274]. The $f_1(1510)$ is not seen in central collisions [276], nor in $\gamma\gamma$ collisions [277], although surprisingly for an assumed $s\bar{s}$ meson, a signal is reported in 4π decays [278]. Given this confusing experimental situation, the meson classification in the 1^{++} nonet is not entirely settled.

63.7 Hybrid mesons

Hybrids may be viewed as $q\bar{q}$ mesons with a vibrating gluon flux tube. In contrast to glueballs, they can have isospin 0 or 1 and be electrically charged. The mass spectrum of hybrids with exotic (non- $q\bar{q}$) quantum numbers was predicted in Ref. [279], while Ref. [280] also deals with non-exotic quantum numbers. The ground-state hybrids with quantum numbers (0^{-+} , 1^{-+} , 1^{-} , and 2^{-+}) are expected around 1.7 to 1.9 GeV. Lattice calculations predict that the hybrid with exotic quantum numbers 1^{-+} lies at a mass of 1.9 ± 0.2 GeV [281,282]. Most hybrids are expected to be rather broad, but some can be as narrow as 100 MeV [283]. They prefer to decay into a pair of S - and P -wave mesons. The lattice study in [284,285], based on full QCD with pion masses around 400 MeV, finds that several of the high-lying states observed in their spectrum show significant overlap with gluon rich source terms interpreted as hybrid states. A very broad 1^{-+} structure is predicted by a recent lattice calculation [286]. The main decay mode is $b_1(1235)\pi$ (a pair of S - and P -wave mesons), while other modes, such as $\rho\pi$, $\eta\pi$ and $\eta'\pi$, are suppressed by at least an order of magnitude. For an experimental and theoretical review on hybrid mesons see [4,287].

There are currently two 1^{-+} candidates, the $\pi_1(1400)$ and $\pi_1(1600)$. The ~ 350 –400 MeV broad $\pi_1(1400)$, was reported in $\pi^-p \rightarrow \eta\pi^-p$ [288,289] and in $\pi^-p \rightarrow \eta\pi^0n$ [290]. It was observed as an interference between the angular momentum $L = 1$ and $L = 2$ $\eta\pi$ amplitudes, leading to a forward/backward asymmetry in the $\eta\pi$ angular distribution. This state had been reported earlier in π^-p reactions [291], but ambiguous solutions in the partial wave analysis were pointed out [292,293]. A resonating 1^{-+} contribution to the $\eta\pi$ P -wave is also required in the Dalitz plot analysis of $\bar{p}n$ annihilation into $\pi^-\pi^0\eta$ [294], and in $\bar{p}p$ annihilation into $\pi^0\pi^0\eta$ [295]. Mass and width are consistent with the results of Ref. [288]. A coupled channel re-analysis of the $\pi^0\pi^0\eta$, $\pi^0\eta\eta$ and $K^+K^-\pi^0$ Crystal Barrel data at 900 MeV/c, supplemented with data from other collaboration in $\pi\pi \rightarrow \pi\pi, K\bar{K}, \eta\eta$ and $\eta\eta'$, leads to a single $1^{-+} \sim 600$ MeV broad state with a pole around 1400 MeV, decaying into $\eta\pi^0$ [296]. Ref. [297] suggested for the production in π^-p that a Deck-generated $\eta\pi$ background from final state rescattering in $\pi_1(1600)$ decay could mimic $\pi_1(1400)$, a mechanism that is, however, absent in $\bar{p}p$ annihilation.

The $\pi_1(1600)$, decaying into $\rho\pi$, was reported by COMPASS with 190 GeV pions hitting a lead target [298,299]. It had already been observed in π^-p interactions in the decay modes $\eta'\pi$ [300], $f_1(1285)\pi$ [301], and $\omega\pi\pi$ [302], $b_1(1235)\pi$, but not $\eta\pi$ [303]. A strong enhancement in the $1^{-+} \eta'\pi$ wave, compared to $\eta\pi$, was

reported at this mass in [304]. The enhancement is also observed by COMPASS in $\pi^-p \rightarrow \eta'\pi$ but in $\eta\pi$ a peak appears at 1400 MeV and in $\eta'\pi$ at 1600 MeV [305]. A coupled channel analysis of the $\eta\pi$ and $\eta'\pi$ COMPASS data leads to a single pole at 1564 ± 89 MeV, with a width of 492 ± 115 MeV [306]. Furthermore, a combined analysis of the COMPASS and Crystal Barrel data at 900 MeV/c leads to compatible results, a single pole around 1623 MeV, with a width of about 455 MeV, although a two-pole scenario cannot be completely excluded [307]. The predicted width from the lattice calculation [286] is compatible with the COMPASS result.

Hybrid candidates with the non-exotic quantum numbers 0^{-+} , 1^{-} , and 2^{-+} have also been reported: the $\pi(1800)$ is somewhat narrow if interpreted as the second radial excitation of the pion. It decays mostly into a pair of S - and P -wave mesons [308,309], in line with expectations for 0^{-+} hybrid mesons. The evidence for 1^{-} hybrids in e^+e^- annihilation and in τ decays has been discussed in [200]. The near degeneracy of the $\eta_2(1645)$ and $\pi_2(1670)$ suggests ideal mixing in the $2^{-+} q\bar{q}$ nonet, and hence, the second isoscalar, presumably the $\eta_2(1870)$, should be mainly $s\bar{s}$. However, the $\eta_2(1870)$ is also observed in $\bar{p}p$ annihilation and decays mainly into $a_2(1320)\pi$ and $f_2(1270)\pi$ [310], with a relative rate compatible with a hybrid state [280]. Evidence for another exotic $\pi_1(2015)$ has been claimed in π^-p interactions [301,302].

Summarizing, there is evidence for a very broad 1^{-+} enhancement in the 1400–1600 MeV region which consists in one or perhaps two exotic states, the lowest one seemingly favored by $\bar{p}p$ annihilation data, the highest one by high energy π^-p data. As isovectors, $\pi_1(1400)$ and $\pi_1(1600)$ cannot be glueballs. The coupling to $\eta\pi$ of the former points to a four-quark state [311], while the $\eta'\pi$ coupling of the latter is favored for hybrid states [312,313]. The mass of $\pi_1(1600)$ is not far below the lattice and flux tube model predictions.

63.8 Tetraquark states

The existence of multi-quark states was suggested a long time ago, based on duality arguments [314,315]. The most prominent tetraquark candidates are the $a_0(980)$ and $f_0(980)$ [316–318]. A remarkable prediction for the existence of low-lying four quarks states is based on color hyperfine splitting. The lowest ground state ($L = 0$) tetraquark multiplet is predicted to be a scalar nonet. The scalar nonet lies just below 1 GeV when one assumes as mass scale the hyperfine color splitting between the ρ and the π (for a simple derivation see [8]). Assuming the classification in Table 63.1 one then gets the nonet structures

$$\begin{aligned} |a_0(980)\rangle &= |us\bar{d}\bar{s}\rangle, \frac{1}{\sqrt{2}}|(u\bar{u} - d\bar{d})s\bar{s}\rangle, |\bar{u}\bar{s}ds\rangle, \\ |f_0(980)\rangle &= \frac{1}{\sqrt{2}}|(u\bar{u} + d\bar{d})s\bar{s}\rangle, \\ |f_0(500)\rangle &= |\bar{u}\bar{d}ud\rangle, \\ |K_0^*(700)\rangle &= |\bar{s}\bar{d}ud\rangle, |\bar{s}\bar{u}ud\rangle \text{ and } |\bar{u}\bar{d}us\rangle, |\bar{u}\bar{d}ds\rangle. \end{aligned}$$

The two isoscalars are expected to mix with the angle φ :

$$\begin{aligned} |f_0(980)\rangle &= \cos\varphi|s\bar{s}\rangle + \sin\varphi|n\bar{n}\rangle, \\ |f_0(500)\rangle &= -\sin\varphi|s\bar{s}\rangle + \cos\varphi|n\bar{n}\rangle. \end{aligned} \quad (63.1)$$

Whether these mesons are really tetraquark states or $q\bar{q}$ mesons, is still an open issue. The $f_0(980)$ is strongly produced in D_s^+ decay [320], which suggests a large $s\bar{s}$ component, due to the Cabibbo-favored $c \rightarrow s$ coupling. However, the mainly $n\bar{n}$ $f_0(1370)$ is also strongly produced in D_s^+ decay, hence additional graphs must contribute [321].

The relative branching ratios for \bar{B}^0 and $\bar{B}_s^0 \rightarrow J/\psi(1S)f_0(500)$ and $J/\psi(1S)f_0(980)$ can be used to probe the $q\bar{q}$ or tetraquark natures of the $f_0(500)$ and $f_0(980)$, as proposed in Refs. [319,322]. LHCb observes the $f_0(980)$ in \bar{B}_s^0 decays, but not the $f_0(500)$ [26], as would be expected for tetraquarks (see Table 63.2). In contrast, LHCb also observes the $f_0(500)$ in \bar{B}^0 decays, but not the $f_0(980)$ with an upper limit eight standard deviations below the predicted value for a tetraquark state [27]. However, these contradicting findings have been challenged by a dispersive analysis [323], using

Table 63.2: Coupling amplitudes for \bar{B}^0 and \bar{B}_s^0 decays into $J/\psi(1S)f_0(500)/f_0(980)$, depending on the $q\bar{q}$ or tetraquark structures of the $f_0(500)$ and $f_0(980)$ (from [319] where illustrative decay diagrams can be found). The angle φ is defined in Eq. 63.1.

		\bar{B}^0		\bar{B}_s^0	
		$f_0(980)$	$f_0(500)$	$f_0(980)$	$f_0(500)$
$q\bar{q}$	$\sin \varphi/\sqrt{2}$	$\cos \varphi/\sqrt{2}$		$\cos \varphi$	$\sin \varphi$
$qq\bar{q}\bar{q}$	$1/\sqrt{2}$	1		$\sqrt{2}$	0

a model independent inclusion of hadronic final state interactions, in which a substantial $f_0(980)$ contribution is nevertheless found in \bar{B}^0 -decays, thus still leaving the tetraquark structure as an open possibility.

The $f_0(980)$ and $a_0(980)$ could also be $K\bar{K}$ molecular states [324–326], being close to the $K\bar{K}$ threshold and decaying strongly into $K\bar{K}$. For $q\bar{q}$ states, the expected $\gamma\gamma$ widths [327, 328] are not significantly larger than for molecular states [327, 329] and both predictions are consistent with data. Radiative decay of the $\phi(1020)$ into $a_0(980)$ and $f_0(980)$ were proposed to disentangle compact (tetraquark) structures from hadronic molecules. Following Refs. [330, 331] the data from KLOE [332, 333], CMD-2 [334] and SND [335] seem to favor these mesons to be tetraquark states. This is also supported by a BESIII analysis of $J/\psi(1S) \rightarrow \gamma\pi^0\pi^0$ data [336] and by a measurement of $a_0(980) - f_0(980)$ mixing at BESIII [337]. In Ref. [38] these states are made of four-quark cores and virtual $K\bar{K}$ clouds at the periphery, a view that is challenged in Ref. [338] showing that radiative ϕ decay data are consistent with molecular structures of light scalars.

As mentioned already, the $f_0(1500)$ [40] and the $f_1(1285)$ [319] have been proposed as tetraquarks, the latter also as $K^*\bar{K}$ molecule [260], together with the $f_1(1420)$ [268].

Another potential candidate for a tetraquark is the $\phi(2170)$. As an excited $q\bar{q}$ state of the $\phi(1020)$, this meson should decay strongly into K^+K^- and $K_S^0K_L^0$, and also $K^*\bar{K}^*$. However, these decays are not observed. Hence, based on its observed decay into $f_0(980)\phi(1020)$ this meson could be $ss\bar{s}\bar{s}$, see Ref. [339] where relative decay rates into various channels are predicted for both $q\bar{q}$ and tetraquark structures of the $f_0(980)$. However Refs. [340, 341] claim that the $\phi(2170)$ may not be a good candidate for the $ss\bar{s}\bar{s}$ state, but could qualify as an $su\bar{s}\bar{u}$ tetraquark [341].

More information on the $a_0(980)$, $f_0(980)$, $f_0(500)$ and $K_0^*(700)$ is provided by ‘Scalar Mesons below 1 GeV’ in the *Review*.

63.9 Baryonia

Nucleon-antinucleon ($N\bar{N}$) bound states and resonances (baryonium) were predicted a long time ago [342, 343], based on the strongly attractive $N\bar{N}$ meson exchange potential, which is obtained from the NN one by multiplying with the G -parity of the exchanged meson. Several candidates had been reported in the seventies by experiments at CERN, BNL and KEK, some of them being indisputably statistically significant (for details on the model and on experiments, see [344, 345] and references therein). Most potential models predict a sequence of deeply bound isoscalar baryonia with quantum numbers $J^{PC} = 2^{++}$, 1^{--} and 0^{++} , the latter being the mostly bound [346, 347]. The $f_2(1565)$ which is observed in $\bar{p}p$ annihilation only [348, 349], is a good candidate for the 2^{++} $\bar{p}p$ bound state.

Enhancements close to the $\bar{p}p$ threshold have also been reported in B decays [350–352]. The strong signal in $J/\psi(1S) \rightarrow \gamma\bar{p}p$ [353–355] could be due to a 0^{++} baryonium [356], but could also be generated by the $N\bar{N}$ final state interaction [357–360]. The strong energy dependence of the cross section in $e^+e^- \rightarrow \bar{p}p$ [361, 362] and $\bar{p}p \rightarrow e^+e^-$ [363] is attributed to the $N\bar{N}$ final state interaction [364] (see also our comments on the $\rho(1900)$ at the end of section 63.5.2). Alternative explanations to baryonia have been proposed for the signals in $B \rightarrow \bar{p}pK$, such as the dynamics of the fragmentation mechanism [351].

63.10 Conclusions

The ground states nonets 1^1S_0 , 1^3S_1 , 1^1P_1 , 1^3P_2 , 1^1D_2 and 1^3D_3 (see fig. 63.1) are complete and established (although more data are desirable for the $h_1(1415)$ in the 1^1P_1 nonet). There are uncertainties and ambiguities in all other nonets. In the pseudoscalar sector the mere existence of the $\eta(1295)$ (possibly the radial excitation of the η) has been questioned. The $\eta(1440)$ consists of two states, one at 1405 MeV, the other at 1475 MeV, which could also be the manifestation of a single state decaying into two different final states. In this case the 1475 one could be the radial excitation of the η' and the 1405 state the pseudoscalar ground state glueball predicted a long time ago by the bag model, although the lattice puts it above 2 GeV. In the 1^{++} nonet two isoscalars – the $f_1(1420)$ and $f_1(1510)$ – compete for the $s\bar{s}$ slot, the former perhaps being exotic, and the latter not being very well established. The first radial excitation 2^3S_1 is complete, but questions have been raised as to the nature of the $\rho(1450)$ and its relation to the $\rho(1700)$. The classification of scalar mesons is not settled with the ones below 1 GeV being tetraquark states or part of the ground state nonet. The nature of the scalars in the 1.5 – 1.8 GeV region is unclear, obscured by the interference with the ground state scalar glueball predicted in this mass region by most theoretical models. For example, the $f_0(1500)$ and the $f_0(1710)$ could be $q\bar{q}$ states ($n\bar{n}$ and $s\bar{s}$, respectively) or made of gluons mixed with $q\bar{q}$. The $f_0(1500)$ or alternatively the $f_0(1710)$ have been proposed as mostly gluonic. Scalar mesons above the $f_0(1710)$ need experimental confirmation. The 1.4 – 1.6 GeV mass region is populated by one or two broad isovector states with exotic (1^{-+}) quantum numbers, the $\pi_1(1400)$ and $\pi_1(1600)$. The mass of latter is not far below theoretical predictions. Above 1.8 GeV mesons are broad and overlap, which complicates the data analyses. This makes the classification difficult, in particular the identification of the 2^{++} glueball.

Acknowledgements

We thank Paolo Gauzzi, Bertram Kopf, Mikhail Mikhasenko and Anton Rebhan for carefully reading the manuscript, and for their detailed and constructive suggestions. We have also benefited from several reviews published earlier in the *Review of Particle Physics*, jointly with Thomas Gutsche, Christoph Hanhart and Stefan Spanier, which have been merged into the current article.

References

- [1] C. Amsler and N. A. Tornqvist, Phys. Rept. **389**, 61 (2004).
- [2] D. V. Bugg, Phys. Rept. **397**, 257 (2004), [hep-ex/0412045].
- [3] E. Klempt and A. Zaitsev, Phys. Rept. **454**, 1 (2007), [arXiv:0708.4016].
- [4] C. A. Meyer and E. S. Swanson, Prog. Part. Nucl. Phys. **82**, 21 (2015), [arXiv:1502.07276].
- [5] R. De Vita, EPJ Web Conf. **66**, 01004 (2014).
- [6] A. Esposito, A. Pilloni and A. D. Polosa, Phys. Rept. **668**, 1 (2017), [arXiv:1611.07920].
- [7] F.-K. Guo *et al.*, Rev. Mod. Phys. **90**, 015004 (2018), [arXiv:1705.00141].
- [8] C. Amsler, *The Quark Structure of Hadrons: An Introduction to the Phenomenology and Spectroscopy*, volume 949 of *Lecture Notes in Physics*, Springer (2018).
- [9] C. Amsler *et al.* (Crystal Barrel), Phys. Lett. **B333**, 277 (1994).
- [10] C. Amsler, Rev. Mod. Phys. **70**, 1293 (1998), [hep-ex/9708025].
- [11] S. Uehara *et al.* (Belle), Phys. Rev. **D80**, 032001 (2009), [arXiv:0906.1464].
- [12] C. Amsler, Phys. Lett. **B541**, 22 (2002), [hep-ph/0206104].
- [13] P. Rubin *et al.* (CLEO), Phys. Rev. **D78**, 072003 (2008), [arXiv:0807.4545].
- [14] R. Aaij *et al.* (LHCb), Phys. Rev. **D93**, 052018 (2016), [arXiv:1509.06628].

- [15] C. Amsler *et al.* (Crystal Barrel), Phys. Lett. **B322**, 431 (1994).
- [16] C. Amsler *et al.* (Crystal Barrel), Phys. Lett. **B342**, 433 (1995).
- [17] A. Abele *et al.* (Crystal Barrel), Phys. Lett. **B380**, 453 (1996).
- [18] D. Barberis *et al.* (WA102), Phys. Lett. **B462**, 462 (1999), [hep-ex/9907055].
- [19] D. Barberis *et al.* (WA102), Phys. Lett. **B471**, 440 (2000), [hep-ex/9912005].
- [20] C. Amsler *et al.* (Crystal Barrel), Phys. Lett. **B353**, 571 (1995).
- [21] C. Amsler *et al.* (Crystal Barrel), Phys. Lett. **B355**, 425 (1995).
- [22] D. Barberis *et al.* (WA102), Phys. Lett. **B479**, 59 (2000), [hep-ex/0003033].
- [23] D. Barberis *et al.*, Physics Letters B **471**, 429 (2000).
- [24] C. Adolph *et al.* (COMPASS), Phys. Rev. **D95**, 032004 (2017), [arXiv:1509.00992].
- [25] R. Aaij *et al.* (LHCb), Phys. Rev. **D86**, 052006 (2012), [arXiv:1204.5643].
- [26] R. Aaij *et al.* (LHCb), Phys. Rev. **D89**, 092006 (2014), [arXiv:1402.6248].
- [27] R. Aaij *et al.* (LHCb), Phys. Rev. **D90**, 012003 (2014), [arXiv:1404.5673].
- [28] F. E. Close and A. Kirk, Phys. Rev. **D91**, 114015 (2015), [arXiv:1503.06942].
- [29] P. d'Argent *et al.*, JHEP **05**, 143 (2017), [arXiv:1703.08505].
- [30] B. Aubert *et al.* (BaBar), Phys. Rev. **D79**, 072006 (2009), [arXiv:0902.2051].
- [31] R. Molina, D. Nicmorus and E. Oset, Phys. Rev. **D78**, 114018 (2008), [arXiv:0809.2233].
- [32] C. García-Recio *et al.*, Phys. Rev. **D87**, 096006 (2013), [arXiv:1304.1021].
- [33] D. Gülmuez, U. G. Meißner and J. A. Oller, Eur. Phys. J. **C77**, 460 (2017), [arXiv:1611.00168].
- [34] M. Carver *et al.* (CLAS), Phys. Rev. Lett. **126**, 082002 (2021), [arXiv:2010.16006].
- [35] J.-J. Xie and E. Oset, Eur. Phys. J. A **51**, 111 (2015), [arXiv:1412.3234].
- [36] A. Abele *et al.* (Crystal Barrel), Phys. Lett. **B385**, 425 (1996).
- [37] C. Amsler *et al.* (Crystal Barrel), Phys. Lett. **B639**, 165 (2006).
- [38] F. E. Close and N. A. Tornqvist, J. Phys. **G28**, R249 (2002), [hep-ph/0204205].
- [39] J. R. Pelaez, Phys. Rept. **658**, 1 (2016), [arXiv:1510.00653].
- [40] L. Zou *et al.*, Phys. Rev. D **99**, 114024 (2019), [arXiv:1901.11205].
- [41] E. Klempt, Physics Letters B **820**, 136512 (2021), [arXiv:2104.09922].
- [42] H. Kim, XVIII Int. Conf. on Hadron Spectroscopy (HADRON2019), Guilin, China [arXiv:1911.09904].
- [43] N. A. Tornqvist, Z. Phys. **C68**, 647 (1995), [hep-ph/9504372].
- [44] E. van Beveren and G. Rupp, Eur. Phys. J. **C22**, 493 (2001), [hep-ex/0106077].
- [45] M. Boglione and M. R. Pennington, Phys. Rev. **D65**, 114010 (2002), [hep-ph/0203149].
- [46] L. S. Celenza *et al.*, Phys. Rev. C **61**, 035201 (2000).
- [47] W.-J. Lee and D. Weingarten, Phys. Rev. **D61**, 014015 (2000), [hep-lat/9910008].
- [48] G. S. Bali *et al.* (UKQCD), Phys. Lett. **B309**, 378 (1993), [hep-lat/9304012].
- [49] C. J. Morningstar and M. J. Peardon, Phys. Rev. **D56**, 4043 (1997), [hep-lat/9704011].
- [50] Y. Chen *et al.*, Phys. Rev. **D73**, 014516 (2006), [hep-lat/0510074].
- [51] J. Leutgeb and A. Rebhan, Phys. Rev. **D101**, 014006 (2020), [arXiv:1909.12352].
- [52] F. Brünner, J. Leutgeb and A. Rebhan, Physics Letters B **788**, 431 (2019).
- [53] M. Q. Huber, C. S. Fischer and H. Sanchis-Alepuz, The European Physical Journal C **80**, 1077 (2020), [arXiv:2004.00415].
- [54] A. Sarantsev *et al.*, Physics Letters B **816**, 136227 (2021), [arXiv:2103.09680].
- [55] C. Amsler and F. E. Close, Phys. Rev. **D53**, 295 (1996), [hep-ph/9507326].
- [56] N. A. Tornqvist and M. Roos, Phys. Rev. Lett. **76**, 1575 (1996), [hep-ph/9511210].
- [57] A. V. Anisovich, V. V. Anisovich and A. V. Sarantsev, Phys. Lett. **B395**, 123 (1997), [hep-ph/9611333].
- [58] M. Boglione and M. R. Pennington, Phys. Rev. Lett. **79**, 1998 (1997), [hep-ph/9703257].
- [59] P. Minkowski and W. Ochs, Eur. Phys. J. **C9**, 283 (1999), [hep-ph/9811518].
- [60] F. E. Close and A. Kirk, Eur. Phys. J. **C21**, 531 (2001), [hep-ph/0103173].
- [61] H.-Y. Cheng, C.-K. Chua and K.-F. Liu, Phys. Rev. **D74**, 094005 (2006), [hep-ph/0607206].
- [62] W. Ochs, J. Phys. **G40**, 043001 (2013), [arXiv:1301.5183].
- [63] S. R. Cotanch and R. A. Williams, Phys. Lett. B **621**, 269 (2005), [arXiv:nucl-th/0505074].
- [64] T. Barnes *et al.*, Phys. Rev. **D55**, 4157 (1997), [hep-ph/9609339].
- [65] S. Janowski, F. Giacosa and D. H. Rischke, Phys. Rev. **D90**, 114005 (2014), [arXiv:1408.4921].
- [66] F. Brünner and A. Rebhan, Phys. Rev. Lett. **115**, 131601 (2015), [arXiv:1504.05815].
- [67] J. Ellis and J. Lánik, Physics Letters B **150**, 289 (1985).
- [68] C.-D. Lu *et al.*, Eur. Phys. J. **A49**, 58 (2013), [arXiv:1301.0225].
- [69] F. E. Close and A. Kirk, Phys. Lett. **B397**, 333 (1997), [hep-ph/9701222].
- [70] F. E. Close, Phys. Lett. **B419**, 387 (1998), [hep-ph/9710450].
- [71] A. Kirk, Phys. Lett. **B489**, 29 (2000), [hep-ph/0008053].
- [72] F. E. Close and Q. Zhao, Phys. Rev. **D71**, 094022 (2005), [hep-ph/0504043].
- [73] M. Ablikim *et al.* (BES), Phys. Lett. **B603**, 138 (2004), [hep-ex/0409007].
- [74] M. Ablikim *et al.* (BES), Phys. Lett. **B607**, 243 (2005), [hep-ex/0411001].
- [75] S. Narison, Nuclear Physics B **509**, 312 (1998).
- [76] M. Chanowitz, Phys. Rev. Lett. **95**, 172001 (2005), [hep-ph/0506125].
- [77] M. Albaladejo and J. A. Oller, Phys. Rev. Lett. **101**, 252002 (2008), [arXiv:0801.4929].
- [78] L. S. Geng and E. Oset, Phys. Rev. **D79**, 074009 (2009), [arXiv:0812.1199].
- [79] F. Brünner and A. Rebhan, Phys. Rev. D **92**, 121902 (2015), [arXiv:1510.07605].
- [80] M. Acciarri *et al.* (L3), Phys. Lett. **B501**, 173 (2001), [hep-ex/0011037].
- [81] K. Abe *et al.* (Belle), Eur. Phys. J. **C32**, 323 (2003), [hep-ex/0309077].

- [82] R. Barate *et al.* (ALEPH), Phys. Lett. **B472**, 189 (2000), [hep-ex/9911022].
- [83] S. Uehara *et al.* (Belle), Phys. Rev. **D78**, 052004 (2008), [arXiv:0805.3387].
- [84] A. Abele *et al.*, Phys. Rev. **D57**, 3860 (1998).
- [85] S. Uehara *et al.* (Belle), PTEP **2013**, 123C01 (2013), [arXiv:1307.7457].
- [86] A. H. Fariborz *et al.*, Phys. Rev. **D90**, 033009 (2014), [arXiv:1407.3870].
- [87] D. V. Bugg, B. S. Zou and A. V. Sarantsev, Nucl. Phys. **B471**, 59 (1996).
- [88] P. Minkowski and W. Ochs, Eur. Phys. J. **C39**, 71 (2005), [hep-ph/0404194].
- [89] A. Garmash *et al.* (Belle), Phys. Rev. **D71**, 092003 (2005), [hep-ex/0412066].
- [90] B. Aubert *et al.* (BaBar), Phys. Rev. **D74**, 032003 (2006), [hep-ex/0605003].
- [91] B. Aubert *et al.* (BaBar), Phys. Rev. Lett. **99**, 161802 (2007), [arXiv:0706.3885].
- [92] M. Ablikim *et al.*, Phys. Lett. **B642**, 441 (2006), [hep-ex/0603048].
- [93] M. Ablikim *et al.* (BESIII), Phys. Rev. **D87**, 092009 (2013), [Erratum: Phys. Rev. **D87**, 119901(2013)], [arXiv:1301.0053].
- [94] E. Klempt and A. Sarantsev, Physics Letters B **826**, 136906 (2022), [arXiv:2112.04348].
- [95] A. Rodas *et al.*, Eur. Phys. J. **C82**, 80 (2022), [arXiv:2110.00027].
- [96] C. Amsler *et al.* (Crystal Barrel), Eur. Phys. J. **C23**, 29 (2002).
- [97] A. A. Godizov, Eur. Phys. J. **C76**, 7, 361 (2016), [arXiv:1604.01689].
- [98] S. Donnachie *et al.*, *Pomeron Physics and QCD*, Cambridge Monographs on Particle Physics, Nuclear Physics and Cosmology, Cambridge University Press, p. 85 (2002).
- [99] C. Evangelista *et al.* (JETSET), Phys. Rev. **D57**, 5370 (1998), [hep-ex/9802016].
- [100] P. S. L. Booth *et al.*, Nucl. Phys. **B273**, 689 (1986).
- [101] A. Etkin *et al.*, Phys. Lett. **B201**, 568 (1988).
- [102] D. Barberis *et al.* (WA102), Phys. Lett. **B432**, 436 (1998), [hep-ex/9805018].
- [103] M. Ablikim *et al.* (BESIII), Phys. Rev. **D93**, 112011 (2016), [arXiv:1602.01523].
- [104] Y.-B. Yang *et al.* (CLQCD Collaboration), Phys. Rev. Lett. **111**, 091601 (2013).
- [105] I. Iatrakis, A. Ramamurti and E. Shuryak, Phys. Rev. **D94**, 045005 (2016), [arXiv:1602.05014].
- [106] F. Brünner, D. Parganlija and A. Rebhan, Phys. Rev. **D91**, 106002 (2015), [Erratum: Phys. Rev. **D93**, 109903 (2016)], [arXiv:1501.07906].
- [107] J. Z. Bai *et al.* (BES), Phys. Rev. Lett. **76**, 3502 (1996).
- [108] C. Amsler *et al.* (Crystal Barrel), Phys. Lett. **B520**, 175 (2001).
- [109] R. Aaij *et al.* (LHCb), Eur. Phys. J. **C78**, 443 (2018), [arXiv:1712.08609].
- [110] P. H. Baillon *et al.*, Nuovo Cim. **A50**, 393 (1967).
- [111] D. L. Scharre *et al.*, Phys. Lett. **97B**, 329 (1980).
- [112] C. Edwards *et al.*, Phys. Rev. Lett. **49**, 259 (1982), [Erratum: Phys. Rev. Lett. **50**, 219(1983)].
- [113] J. E. Augustin *et al.* (DM2), Phys. Rev. **D42**, 10 (1990).
- [114] J. Z. Bai *et al.* (BES), Phys. Lett. **B594**, 47 (2004), [hep-ex/0403008].
- [115] G. S. Adams *et al.* (E852), Phys. Lett. **B516**, 264 (2001), [hep-ex/0107042].
- [116] S. Fukui *et al.*, Phys. Lett. **B267**, 293 (1991).
- [117] D. Alde *et al.* (GAMS), Phys. Atom. Nucl. **60**, 386 (1997), [Yad. Fiz. **60**, 458(1997)].
- [118] J. J. Manak *et al.* (E852), Phys. Rev. **D62**, 012003 (2000), [hep-ex/0001051].
- [119] A. V. Anisovich *et al.*, Nucl. Phys. **A690**, 567 (2001).
- [120] C. Amsler *et al.*, Eur. Phys. J. **C33**, 23 (2004).
- [121] J. E. Augustin *et al.* (DM2), Phys. Rev. **D46**, 1951 (1992).
- [122] B. Aubert *et al.* (BaBar), Phys. Rev. Lett. **101**, 091801 (2008), [arXiv:0804.0411].
- [123] M. G. Rath *et al.*, Phys. Rev. **D40**, 693 (1989).
- [124] Z. Bai *et al.* (MARK-III), Phys. Rev. Lett. **65**, 2507 (1990).
- [125] A. Bertin *et al.* (OBELIX), Phys. Lett. **B361**, 187 (1995).
- [126] A. Bertin *et al.* (OBELIX), Phys. Lett. **B400**, 226 (1997).
- [127] C. Cicalo *et al.* (OBELIX), Phys. Lett. **B462**, 453 (1999).
- [128] F. Nitchitu *et al.* (OBELIX), Phys. Lett. **B545**, 261 (2002).
- [129] T. Bolton *et al.*, Phys. Rev. Lett. **69**, 1328 (1992).
- [130] M. Ablikim *et al.* (BES), Phys. Rev. **D77**, 032005 (2008), [arXiv:0712.1411].
- [131] M. Ablikim *et al.* (BESIII), Phys. Rev. **D87**, 092006 (2013), [arXiv:1303.6360].
- [132] M. Acciarri *et al.* (L3), Phys. Lett. **B501**, 1 (2001), [hep-ex/0011035].
- [133] F. E. Close, G. R. Farrar and Z.-p. Li, Phys. Rev. **D55**, 5749 (1997), [hep-ph/9610280].
- [134] D. M. Li, H. Yu and S. S. Fang, Eur. Phys. J. **C28**, 335 (2003).
- [135] R. Ahohe *et al.* (CLEO), Phys. Rev. **D71**, 072001 (2005), [hep-ex/0501026].
- [136] P. Achard *et al.* (L3), JHEP **03**, 018 (2007).
- [137] T. Gutsche, V. E. Lyubovitskij and M. C. Tichy, Phys. Rev. **D79**, 014036 (2009), [arXiv:0811.0668].
- [138] L. Faddeev, A. J. Niemi and U. Wiedner, Phys. Rev. **D70**, 114033 (2004), [hep-ph/0308240].
- [139] C. J. Morningstar and M. J. Peardon, Phys. Rev. **D60**, 034509 (1999), [hep-lat/9901004].
- [140] H.-Y. Cheng, H.-n. Li and K.-F. Liu, Phys. Rev. **D79**, 014024 (2009), [arXiv:0811.2577].
- [141] G. Li, Q. Zhao and C.-H. Chang, J. Phys. **G35**, 055002 (2008), [hep-ph/0701020].
- [142] T. Gutsche, V. E. Lyubovitskij and M. C. Tichy, Phys. Rev. **D80**, 014014 (2009), [arXiv:0904.3414].
- [143] B. A. Li, Phys. Rev. **D81**, 114002 (2010), [arXiv:0912.2323].
- [144] A. Masoni, C. Cicalo and G. L. Usai, J. Phys. **G32**, R293 (2006).
- [145] E. Klempt, Int. J. Mod. Phys. **A21**, 739 (2006).
- [146] J.-J. Wu *et al.*, Phys. Rev. Lett. **108**, 081803 (2012), [arXiv:1108.3772].
- [147] X.-G. Wu *et al.*, Phys. Rev. **D87**, 014023 (2013), [arXiv:1211.2148].
- [148] M.-C. Du and Q. Zhao, Phys. Rev. **D100**, 036005 (2019), [arXiv:1905.04207].
- [149] F. Aceti *et al.*, Phys. Rev. **D86**, 114007 (2012), [arXiv:1209.6507].
- [150] J. Pisut and M. Roos, Nucl. Phys. **B6**, 325 (1968).
- [151] G. D. Lafferty, Z. Phys. **C60**, 659 (1993).
- [152] A. Abele *et al.* (Crystal Barrel), Phys. Lett. **B402**, 195 (1997).
- [153] M. Benayoun *et al.*, Eur. Phys. J. **C31**, 525 (2003), [arXiv:nucl-th/0306078].
- [154] R. Barate *et al.* (ALEPH), Z. Phys. **C76**, 15 (1997).
- [155] L. M. Barkov *et al.*, Nucl. Phys. **B256**, 365 (1985).

- [156] S. Anderson *et al.* (CLEO), Phys. Rev. **D61**, 112002 (2000), [hep-ex/9910046].
- [157] M. Fujikawa *et al.* (Belle), Phys. Rev. **D78**, 072006 (2008), [arXiv:0805.3773].
- [158] K. Ackerstaff *et al.* (OPAL), Eur. Phys. J. **C7**, 571 (1999), [hep-ex/9808019].
- [159] M. Davier and C.-Z. Yuan, Nucl. Phys. B - Proc. Suppl. **123**, 47 (2003), [hep-ex/0211057].
- [160] S. Schael *et al.* (ALEPH), Phys. Rept. **421**, 191 (2005), [hep-ex/0506072].
- [161] R. R. Akhmetshin *et al.* (CMD-2), Phys. Lett. **B527**, 161 (2002), [hep-ex/0112031].
- [162] R. R. Akhmetshin *et al.* (CMD-2), Phys. Lett. **B578**, 285 (2004), [hep-ex/0308008].
- [163] M. Davier *et al.*, Eur. Phys. J. **C27**, 497 (2003), [hep-ph/0208177].
- [164] M. Davier *et al.*, Eur. Phys. J. **C31**, 503 (2003), [hep-ph/0308213].
- [165] A. Aloisio *et al.* (KLOE), Phys. Lett. **B606**, 12 (2005), [hep-ex/0407048].
- [166] F. Ambrosino *et al.* (KLOE), Phys. Lett. **B670**, 285 (2009), [arXiv:0809.3950].
- [167] F. Ambrosino *et al.* (KLOE), Phys. Lett. **B700**, 102 (2011), [arXiv:1006.5313].
- [168] D. Babusci *et al.* (KLOE), Phys. Lett. B **720**, 336 (2013), [arXiv:1212.4524].
- [169] M. N. Achasov *et al.*, J. Exp. Theor. Phys. **101**, 1053 (2005), [hep-ex/0506076].
- [170] M. N. Achasov *et al.*, J. Exp. Theor. Phys. **103**, 380 (2006), [hep-ex/0605013].
- [171] B. Aubert *et al.* (BaBar), Phys. Rev. Lett. **103**, 231801 (2009), [arXiv:0908.3589].
- [172] M. Ablikim *et al.* (BESIII), Phys. Lett. B **753**, 629 (2016), [Erratum: Phys.Lett.B 812, 135982 (2021)], [arXiv:1507.08188].
- [173] R. Alemany, M. Davier and A. Hocker, Eur. Phys. J. **C2**, 123 (1998), [hep-ph/9703220].
- [174] H. Czyz and J. H. Kuhn, Eur. Phys. J. **C18**, 497 (2001), [hep-ph/0008262].
- [175] V. Cirigliano, G. Ecker and H. Neufeld, Phys. Lett. **B513**, 361 (2001), [hep-ph/0104267].
- [176] V. Cirigliano *et al.*, Eur. Phys. J. **C23**, 121 (2002), [hep-ph/0110153].
- [177] K. Maltman and C. E. Wolfe, Phys. Rev. **D73**, 013004 (2006), [hep-ph/0509224].
- [178] C. E. Wolfe and K. Maltman, Phys. Rev. **D80**, 114024 (2009), [arXiv:0908.2391].
- [179] F. Jegerlehner and R. Szafron, Eur. Phys. J. **C71**, 1632 (2011), [arXiv:1101.2872].
- [180] M. Benayoun *et al.*, Eur. Phys. J. **C72**, 1848 (2012), [arXiv:1106.1315].
- [181] M. Benayoun *et al.*, Eur. Phys. J. C **73**, 2453 (2013), [arXiv:1210.7184].
- [182] M. Davier *et al.*, Eur. Phys. J. C **77**, 827 (2017), [arXiv:1706.09436].
- [183] C. Erkal and M. G. Olsson, Z. Phys. **C31**, 615 (1986).
- [184] A. Donnachie and H. Mirzaie, Z. Phys. **C33**, 407 (1987).
- [185] A. Donnachie and A. B. Clegg, Z. Phys. **C34**, 257 (1987).
- [186] A. Donnachie and A. B. Clegg, Z. Phys. **C51**, 689 (1991).
- [187] A. B. Clegg and A. Donnachie, Z. Phys. **C40**, 313 (1988).
- [188] A. B. Clegg and A. Donnachie, Z. Phys. **C62**, 455 (1994).
- [189] T. J. Killian *et al.*, Phys. Rev. **D21**, 3005 (1980).
- [190] S. Fukui *et al.*, Phys. Lett. **B202**, 441 (1988).
- [191] D. Bisello *et al.* (DM2), Phys. Lett. **B220**, 321 (1989).
- [192] A. Antonelli *et al.* (DM2), Phys. Lett. **B212**, 133 (1988).
- [193] A. Abele *et al.* (Crystal Barrel), Phys. Lett. **B391**, 191 (1997).
- [194] A. Bertin *et al.* (OBELIX), Phys. Lett. **B434**, 180 (1998).
- [195] A. Abele *et al.* (Crystal Barrel), Phys. Lett. **B468**, 178 (1999).
- [196] W.-F. Wang, Phys. Rev. D **103**, 056021 (2021), [arXiv:2012.15039], URL <https://link.aps.org/doi/10.1103/PhysRevD.103.056021>.
- [197] K. W. Edwards *et al.* (CLEO), Phys. Rev. **D61**, 072003 (2000), [hep-ex/9908024].
- [198] J. P. Lees *et al.* (BaBar), Phys. Rev. **D86**, 032013 (2012), [arXiv:1205.2228].
- [199] F. E. Close and P. R. Page, Phys. Rev. **D56**, 1584 (1997), [hep-ph/9701425].
- [200] A. Donnachie and Yu. S. Kalashnikova, Phys. Rev. **D60**, 114011 (1999), [hep-ph/9901334].
- [201] R. R. Akhmetshin *et al.* (CMD-2), Phys. Lett. **B466**, 392 (1999), [hep-ex/9904024].
- [202] J. P. Alexander *et al.* (CLEO), Phys. Rev. **D64**, 092001 (2001), [hep-ex/0103021].
- [203] D. Matvienko *et al.* (Belle), Phys. Rev. **D92**, 012013 (2015), [arXiv:1505.03362].
- [204] R. R. Akhmetshin *et al.* (CMD-2), Phys. Lett. **B562**, 173 (2003), [hep-ex/0304009].
- [205] M. N. Achasov *et al.*, Phys. Rev. D **94**, 112001 (2016), [arXiv:1610.00235].
- [206] A. Abele *et al.* (CRYSTAL BARREL), Eur. Phys. J. **C21**, 261 (2001).
- [207] M. Bargiotti *et al.* (Obelix), Phys. Lett. **B561**, 233 (2003).
- [208] S. I. Bityukov *et al.*, Phys. Lett. **B188**, 383 (1987).
- [209] B. Aubert *et al.* (BaBar), Phys. Rev. **D77**, 092002 (2008), [arXiv:0710.4451].
- [210] M. N. Achasov *et al.*, Eur. Phys. J. C **80**, 1139 (2020).
- [211] N. N. Achasov and G. N. Shestakov, Phys. Atom. Nucl. **59**, 1262 (1996), [Yad. Fiz.59N7,1319(1996)].
- [212] L. G. Landsberg, Sov. J. Nucl. Phys. **55**, 1051 (1992), [Yad. Fiz.55,1896(1992)].
- [213] A. Abele *et al.* (Crystal Barrel), Phys. Lett. **B415**, 280 (1997).
- [214] V. M. Aulchenko *et al.*, JETP Lett. **45**, 145 (1987), [Pisma Zh. Eksp. Teor. Fiz.45,118(1987)].
- [215] D. Bisello *et al.*, Z. Phys. **C52**, 227 (1991).
- [216] P. Frenkiel *et al.*, Nucl. Phys. **B47**, 61 (1972).
- [217] G. Cosme *et al.*, Phys. Lett. **63B**, 352 (1976).
- [218] D. P. Barber *et al.* (LAMP2 Group), Z. Phys. **C4**, 169 (1980).
- [219] D. Aston *et al.*, Phys. Lett. **92B**, 211 (1980), [Erratum: Phys. Lett.95B,461(1980)].
- [220] M. Atkinson *et al.* (Omega Photon), Nucl. Phys. **B243**, 1 (1984).
- [221] J. E. Brau *et al.* (SLAC Hybrid Facility Photon), Phys. Rev. **D37**, 2379 (1988).
- [222] C. Amsler *et al.* (Crystal Barrel), Phys. Lett. **B311**, 362 (1993).
- [223] J. Layssac and F. M. Renard, Nuovo Cim. **A6**, 134 (1971).
- [224] D. Aston *et al.*, Nucl. Phys. Proc. Suppl. **21**, 105 (1991).
- [225] N. Hammoud *et al.*, Phys. Rev. D **102**, 054029 (2020).
- [226] M. Ablikim *et al.* (BES), Phys. Rev. Lett. **97**, 142002 (2006), [hep-ex/0606047].
- [227] G.-J. Ding and M.-L. Yan, Phys. Lett. **B643**, 33 (2006), [hep-ph/0607253].

- [228] F.-K. Guo *et al.*, Nucl. Phys. **A773**, 78 (2006), [hep-ph/0509050].
- [229] A. Zhang, T. Huang and T. G. Steele, Phys. Rev. **D76**, 036004 (2007), [hep-ph/0612146].
- [230] B. A. Li, Phys. Rev. **D76**, 094016 (2007), [hep-ph/0701159].
- [231] X. Liu *et al.*, Phys. Rev. **D75**, 074017 (2007), [hep-ph/0701022].
- [232] J. P. Lees *et al.* (BaBar), Phys. Rev. D **88**, 032013 (2013), [arXiv:1306.3600].
- [233] M. N. Achasov *et al.*, Phys. Rev. D **94**, 112006 (2016), [arXiv:1608.08757].
- [234] A. B. Clegg and A. Donnachie, Z. Phys. **C45**, 677 (1990).
- [235] D. Bisello *et al.*, Phys. Lett. **107B**, 145 (1981).
- [236] A. Castro *et al.*, LAL-88-58(1988), URL <https://doi.org/10.17182/hepdata.38181>.
- [237] M. Atkinson *et al.* (Omega Photon), Z. Phys. **C29**, 333 (1985).
- [238] B. Aubert *et al.* (BaBar), Phys. Rev. **D76**, 092005 (2007), [Erratum: Phys. Rev. D **77**, 119902(2008)], [arXiv:0708.2461].
- [239] J. P. Lees *et al.* (BABAR Collaboration), Phys. Rev. D **86**, 032013 (2012).
- [240] M. Ablikim *et al.* (BESIII Collaboration), Phys. Rev. D **99**, 032001 (2019).
- [241] J. P. Lees *et al.* (BaBar Collaboration), Phys. Rev. D **101**, 012011 (2020).
- [242] S. Godfrey and N. Isgur, Phys. Rev. **D32**, 189 (1985).
- [243] P. L. Frabetti *et al.* (E687), Phys. Lett. **B514**, 240 (2001), [hep-ex/0106029].
- [244] P. L. Frabetti *et al.*, Phys. Lett. **B578**, 290 (2004), [hep-ex/0310041].
- [245] A. Antonelli *et al.* (FENICE), Phys. Lett. **B365**, 427 (1996).
- [246] B. Aubert *et al.* (BaBar), Phys. Rev. **D73**, 052003 (2006), [hep-ex/0602006].
- [247] R. R. Akhmetshin *et al.* (CMD-3), Phys. Lett. **B723**, 82 (2013), [arXiv:1302.0053].
- [248] R. R. Akhmetshin *et al.* (CMD-3), Phys. Lett. B **794**, 64 (2019), [arXiv:1808.00145].
- [249] A. E. Obrazovsky and S. I. Serednyakov, JETP Lett. **99**, 315 (2014), [arXiv:1402.5225].
- [250] J. Haidenbauer *et al.*, Phys. Rev. **D92**, 054032 (2015), [arXiv:1506.08120].
- [251] A. I. Milstein and S. G. Salmikov, Nucl. Phys. A **977**, 60 (2018), [arXiv:1804.01283].
- [252] M. Ablikim *et al.* (BESIII Collaboration), Phys. Rev. D **97**, 032013 (2018), [arXiv:1709.10236].
- [253] H.-Y. Cheng, Phys. Lett. **B707**, 116 (2012), [arXiv:1110.2249].
- [254] S. U. Chung *et al.*, Phys. Rev. Lett. **55**, 779 (1985), [Erratum: Phys. Rev. Lett. **55**, 2093(1985)].
- [255] D. F. Reeves *et al.*, Phys. Rev. **D34**, 1960 (1986).
- [256] A. Birman *et al.*, Phys. Rev. Lett. **61**, 1557 (1988), [Erratum: Phys. Rev. Lett. **62**, 1577(1989)].
- [257] C. Dionisi *et al.* (CERN-College de France-Madrid-Stockholm), Nucl. Phys. **B169**, 1 (1980).
- [258] H. J. Behrend *et al.* (CELLO), Z. Phys. **C42**, 367 (1989).
- [259] T. A. Armstrong *et al.* (WA76), Z. Phys. **C52**, 389 (1991).
- [260] F. Aceti, J.-J. Xie and E. Oset, Phys. Lett. **B750**, 609 (2015), [arXiv:1505.06134].
- [261] R. Aaij *et al.* (LHCb), Phys. Rev. Lett. **112**, 091802 (2014), [arXiv:1310.2145].
- [262] G. Gidal *et al.*, Phys. Rev. Lett. **59**, 2012 (1987).
- [263] C. Adolph *et al.* (COMPASS), Phys. Rev. Lett. **115**, 082001 (2015), [arXiv:1501.05732].
- [264] M. Aghasyan *et al.* (COMPASS), Phys. Rev. **D98**, 092003 (2018), [arXiv:1802.05913].
- [265] G. D. Alexeev *et al.*, Phys. Rev. Lett. **127**, 082501 (2021), [arXiv:2006.05342].
- [266] V. R. Debastiani *et al.*, Phys. Rev. **D95**, 034015 (2017), [arXiv:1611.05383].
- [267] S. Ishida *et al.*, Prog. Theor. Phys. **82**, 119 (1989).
- [268] R. S. Longacre, Phys. Rev. **D42**, 874 (1990).
- [269] D. Aston *et al.*, Phys. Lett. **B201**, 573 (1988).
- [270] F. E. Close and A. Kirk, Z. Phys. **C76**, 469 (1997), [hep-ph/9706543].
- [271] P. Gavillet *et al.*, Z. Phys. **C16**, 119 (1982).
- [272] J. Z. Bai *et al.* (BES), Phys. Lett. **B446**, 356 (1999).
- [273] M. Ablikim *et al.* (BESIII), Phys. Rev. Lett. **106**, 072002 (2011), [arXiv:1012.3510].
- [274] P. F. Ermolov *et al.*, Sov. J. Nucl. Phys. **39**, 738 (1984), [Yad. Fiz. **39**, 1170(1984)].
- [275] E. King *et al.*, Nucl. Phys. Proc. Suppl. **21**, 11 (1991).
- [276] D. Barberis *et al.* (WA102), Phys. Lett. **B413**, 225 (1997), [hep-ex/9707022].
- [277] H. Aihara *et al.* (TPC/Two Gamma), Phys. Rev. **D38**, 1 (1988).
- [278] D. A. Bauer *et al.* (TPC/Two Gamma), Phys. Rev. **D48**, 3976 (1993).
- [279] N. Isgur, R. Kokoski and J. Paton, Phys. Rev. Lett. **54**, 869 (1985).
- [280] F. E. Close and P. R. Page, Nucl. Phys. **B443**, 233 (1995), [hep-ph/9411301].
- [281] P. Lacock *et al.* (UKQCD), Phys. Lett. **B401**, 308 (1997), [hep-lat/9611011].
- [282] C. W. Bernard *et al.* (MILC), Phys. Rev. **D56**, 7039 (1997), [hep-lat/9707008].
- [283] P. R. Page, E. S. Swanson and A. P. Szczepaniak, Phys. Rev. **D59**, 034016 (1999), [hep-ph/9808346].
- [284] J. J. Dudek *et al.*, Phys. Rev. **D83**, 111502 (2011), [arXiv:1102.4299].
- [285] J. J. Dudek *et al.*, Phys. Rev. **D88**, 094505 (2013), [arXiv:1309.2608].
- [286] A. J. Woss *et al.*, Phys. Rev. D **103**, 054502 (2021), [arXiv:2009.10034].
- [287] C. A. Meyer and Y. Van Haarlem, Phys. Rev. C **82**, 025208 (2010).
- [288] D. R. Thompson *et al.* (E852), Phys. Rev. Lett. **79**, 1630 (1997), [hep-ex/9705011].
- [289] S. U. Chung *et al.* (E852), Phys. Rev. **D60**, 092001 (1999), [hep-ex/9902003].
- [290] G. S. Adams *et al.* (E862), Phys. Lett. **B657**, 27 (2007), [hep-ex/0612062].
- [291] D. Alde *et al.*, Phys. Lett. **B205**, 397 (1988).
- [292] Yu. D. Prokoshkin and S. A. Sadovsky, Phys. Atom. Nucl. **58**, 606 (1995), [Yad. Fiz. **58N4**, 662(1995)].
- [293] Yu. D. Prokoshkin and S. A. Sadovsky, Phys. Atom. Nucl. **58**, 853 (1995), [Yad. Fiz. **58**, 921(1995)].
- [294] A. Abele *et al.* (Crystal Barrel), Phys. Lett. **B423**, 175 (1998).
- [295] A. Abele *et al.* (Crystal Barrel), Phys. Lett. **B446**, 349 (1999).
- [296] M. Albrecht *et al.* (Crystal Barrel), Eur. Phys. J. **C80**, 453 (2020), [arXiv:1909.07091].
- [297] A. Donnachie and P. R. Page, Phys. Rev. **D58**, 114012 (1998), [hep-ph/9808225].
- [298] M. Aghasyan *et al.* (COMPASS), Phys. Rev. D **98**, 092003 (2018), [arXiv:1802.05913].

- [299] G. D. Alexeev *et al.*, Phys. Rev. D **105**, 012005 (2022), [arXiv:arXiv:2108.01744].
- [300] E. I. Ivanov *et al.* (E852), Phys. Rev. Lett. **86**, 3977 (2001), [hep-ex/0101058].
- [301] J. Kuhn *et al.* (E852), Phys. Lett. **B595**, 109 (2004), [hep-ex/0401004].
- [302] M. Lu *et al.* (E852), Phys. Rev. Lett. **94**, 032002 (2005), [hep-ex/0405044].
- [303] Yu.P. Gouz *et al.*, Proc. XXVI Int. Conf. on HEP, Dallas (1992).
- [304] G. M. Beladidze *et al.* (VES), Phys. Lett. **B313**, 276 (1993).
- [305] C. Adolph *et al.* (COMPASS), Phys. Lett. B **740**, 303 (2015), [Erratum: Phys.Lett.B 811, 135913 (2020)], [arXiv:1408.4286].
- [306] A. Rodas *et al.* (JPAC), Phys. Rev. Lett. **122**, 042002 (2019), [arXiv:1810.04171].
- [307] B. Kopf *et al.*, Eur. Phys. J. C **81**, 12, 1056 (2021), [arXiv:2008.11566].
- [308] M. Alekseev *et al.* (COMPASS), Phys. Rev. Lett. **104**, 241803 (2010), [arXiv:0910.5842].
- [309] D. V. Amelin *et al.* (VES), Phys. Lett. **B356**, 595 (1995).
- [310] J. Adomeit *et al.* (Crystal Barrel), Z. Phys. **C71**, 227 (1996).
- [311] S. U. Chung, E. Klempt and J. G. Korner, Eur. Phys. J. **A15**, 539 (2002), [hep-ph/0211100].
- [312] F. E. Close and H. J. Lipkin, Phys. Lett. **B196**, 245 (1987).
- [313] F. Iddir and A. S. Safir, Phys. Lett. **B507**, 183 (2001), [hep-ph/0010121].
- [314] G. C. Rossi and G. Veneziano, Nucl. Phys. **B123**, 507 (1977).
- [315] J. L. Rosner, Phys. Rev. Lett. **21**, 950 (1968).
- [316] R. L. Jaffe, Phys. Rev. **D15**, 281 (1977).
- [317] M. G. Alford and R. L. Jaffe, Nucl. Phys. **B578**, 367 (2000), [hep-lat/0001023].
- [318] G. 't Hooft *et al.*, Phys. Lett. **B662**, 424 (2008), [arXiv:0801.2288].
- [319] S. Stone and L. Zhang, Phys. Rev. Lett. **111**, 062001 (2013), [arXiv:1305.6554].
- [320] E. M. Aitala *et al.* (E791), Phys. Rev. Lett. **86**, 765 (2001), [hep-ex/0007027].
- [321] H.-Y. Cheng, Phys. Rev. **D67**, 054021 (2003), [hep-ph/0212361].
- [322] R. Fleischer, R. Knegjens and G. Ricciardi, Eur. Phys. J. **C71**, 1832 (2011), [arXiv:1109.1112].
- [323] J. T. Daub, C. Hanhart and B. Kubis, JHEP **02**, 009 (2016), [arXiv:1508.06841].
- [324] J. D. Weinstein and N. Isgur, Phys. Rev. **D41**, 2236 (1990).
- [325] G. Janssen *et al.*, Phys. Rev. **D52**, 2690 (1995), [arXiv:nucl-th/9411021].
- [326] M. P. Locher, V. E. Markushin and H. Q. Zheng, Eur. Phys. J. **C4**, 317 (1998), [hep-ph/9705230].
- [327] J. A. Oller and E. Oset, AIP Conf. Proc. **432**, 413 (1998), [hep-ph/9710557].
- [328] R. Delbourgo, D.-s. Liu and M. D. Scadron, Phys. Lett. **B446**, 332 (1999), [hep-ph/9811474].
- [329] C. Hanhart *et al.*, Phys. Rev. **D75**, 074015 (2007), [hep-ph/0701214].
- [330] F. E. Close, N. Isgur and S. Kumano, Nucl. Phys. **B389**, 513 (1993), [hep-ph/9301253].
- [331] N. N. Achasov, V. V. Gubin and V. I. Shevchenko, Phys. Rev. **D56**, 203 (1997), [hep-ph/9605245].
- [332] F. Ambrosino *et al.*, Physics Letters B **681**, 5 (2009), [arXiv:0904.2539].
- [333] F. Ambrosino *et al.*, Eur. Phys. J. C **49**, 473 (2007), [hep-ex/0609009].
- [334] R. R. Akhmetshin *et al.* (CMD-2), Phys. Lett. **B462**, 371 (1999), [hep-ex/9907005].
- [335] M. N. Achasov *et al.*, Phys. Lett. **B479**, 53 (2000), [hep-ex/0003031].
- [336] N. N. Achasov *et al.*, Phys. Rev. D **103**, 014010 (2021), [arXiv:2009.04191].
- [337] M. Ablikim *et al.* (BESIII Collaboration), Phys. Rev. Lett. **121**, 022001 (2018), [arXiv:1802.00583].
- [338] Yu. S. Kalashnikova *et al.*, Eur. Phys. J. **A24**, 437 (2005), [hep-ph/0412340].
- [339] H.-W. Ke and X.-Q. Li, Phys. Rev. D **99**, 036014 (2019).
- [340] F.-X. Liu *et al.*, Phys. Rev. D **103**, 016016 (2021).
- [341] S. S. Agaev, K. Azizi and H. Sundu, Phys. Rev. D **101**, 074012 (2020).
- [342] O. D. Dalkarov, V. B. Mandelzweig and I. S. Shapiro, Nucl. Phys. B **21**, 88 (1970).
- [343] G. Rossi and G. Veneziano, Physics Reports **63**, 153 (1980).
- [344] C. Amsler, Adv. Nucl. Phys. **18**, 183 (1987).
- [345] L. Montanet, Phys. Rept. **63**, 201 (1980).
- [346] C. B. Dover and J. M. Richard, Annals Phys. **121**, 70 (1979).
- [347] W. W. Buck, C. B. Dover and J. M. Richard, Annals Phys. **121**, 47 (1979).
- [348] B. May *et al.* (ASTERIX), Z. Phys. **C46**, 203 (1990).
- [349] A. Bertin *et al.* (OBELIX), Phys. Rev. **D57**, 55 (1998).
- [350] K. Abe *et al.* (Belle), Phys. Rev. Lett. **88**, 181803 (2002), [hep-ex/0202017].
- [351] M. Z. Wang *et al.* (Belle), Phys. Lett. **B617**, 141 (2005), [hep-ex/0503047].
- [352] K. Abe *et al.* (Belle), Phys. Rev. Lett. **89**, 151802 (2002), [hep-ex/0205083].
- [353] J. Z. Bai *et al.* (BES), Phys. Rev. Lett. **91**, 022001 (2003), [hep-ex/0303006].
- [354] J. P. Alexander *et al.* (CLEO), Phys. Rev. **D82**, 092002 (2010), [arXiv:1007.2886].
- [355] M. Ablikim *et al.* (BESIII), Phys. Rev. Lett. **108**, 112003 (2012), [arXiv:1112.0942].
- [356] G.-J. Ding and M.-L. Yan, Phys. Rev. **C72**, 015208 (2005), [hep-ph/0502127].
- [357] B. Loiseau and S. Wycech, Phys. Rev. **C72**, 011001 (2005), [hep-ph/0501112].
- [358] A. Sibirtsev *et al.*, Phys. Rev. **D71**, 054010 (2005), [hep-ph/0411386].
- [359] X.-W. Kang, J. Haidenbauer and U.-G. Meissner, JHEP **02**, 113 (2014), [arXiv:1311.1658].
- [360] X.-W. Kang, J. Haidenbauer and U.-G. Meissner, Phys. Rev. **D91**, 074003 (2015), [arXiv:1502.00880].
- [361] J. P. Lees *et al.* (BaBar), Phys. Rev. **D87**, 092005 (2013), [arXiv:1302.0055].
- [362] E. P. Solodov *et al.*, EPJ Web Conf. **212**, 07002 (2019).
- [363] G. Bardin *et al.*, Nucl. Phys. **B411**, 3 (1994).
- [364] J. Haidenbauer, X. W. Kang and U. G. Meissner, Nucl. Phys. **A929**, 102 (2014), [arXiv:1405.1628].

64. Scalar Mesons below 1 GeV

Revised August 2021 by S. Eidelman (Budker Inst., Novosibirsk; Novosibirsk U.), T. Gutsche (Tübingen U.), C. Hanhart (Jülich), R.E. Mitchell (Indiana U.) and S. Spanier (Tennessee U.).

64.1 Introduction

In contrast to the vector and tensor mesons, the identification of the scalar mesons is a long-standing puzzle. Scalar resonances are difficult to resolve because some of them have large decay widths, which cause a strong overlap between resonances and background. In addition, in some cases, several decay channels open up within a short mass interval (*e.g.* at the $K\bar{K}$ and $\eta\eta$ thresholds), producing cusps in the line shapes of the nearby resonances. Furthermore, one expects non- $q\bar{q}$ scalar objects, such as hadronic molecules and multi-quark states, in the mass range of interest (for reviews see, *e.g.*, Refs. [1–5]).

Light scalars are produced, for example, in πN scattering on polarized/unpolarized targets, $p\bar{p}$ annihilation, central hadronic production, $J/\psi(1S)$, B^- , D^- and K -meson decays, $\gamma\gamma$ formation, and ϕ radiative decays. Especially for the lightest scalar mesons simple parameterizations like Breit-Wigner functions and variants thereof fail — this is demonstrated explicitly on the example of the $f_0(500)$ or σ , *e.g.*, in Ref. [6]. Accordingly, more advanced theory tools are necessary to extract the resonance parameters from data. In the analyses available in the literature, fundamental properties of the amplitudes such as unitarity, analyticity, Lorentz invariance, and chiral and flavor symmetry are implemented at different levels of rigor. Especially, chiral symmetry implies the appearance of zeros, the so-called Adler zeros, close to the threshold in elastic S -wave scattering amplitudes involving soft (pseudo) Goldstone bosons [7,8], which may be shifted or removed in associated production processes [9]. Moreover, especially for the lightest non-strange and strange scalar resonance precision extractions of pole parameters get complicated by the presence of both left-hand cuts as well as circular cuts [5]. The methods employed are the K -matrix formalism, the N/D -method, the Dalitz-Tuan ansatz, unitarized quark models with coupled channels, effective chiral field theories and the linear sigma model, *etc.* Dynamics near the lowest two-body thresholds in some analyses are described by crossed channel (t , u) meson exchange or with an effective range parameterization instead of, or in addition to, resonant features in the s -channel. Dispersion theoretical approaches are applied to pin down the location of resonance poles for the low mass states [10–15].

The mass and width of a resonance are found from the position of the nearest pole in the process amplitude (T -matrix or S -matrix) at an unphysical sheet of the complex energy plane, traditionally labeled as

$$\sqrt{s_{\text{Pole}}} = M - i\Gamma/2. \quad (64.1)$$

It is important to note that in general the pole of a Breit-Wigner parameterization does not agree with the S - or T -matrix pole. For a detailed discussion of this issue we refer to the review on *Resonances* in this Review of Particle Physics (RPP).

In this review we present proposed values for the mass parameters of the scalar resonances below 1 GeV. Note that those are labeled as ‘our estimate’ — it is not an average over the quoted analyses, but is chosen to include the bulk of the analyses. An averaging procedure is not justified, since the analyses use overlapping or sometimes even identical data sets so that they are not statistically independent.

On this note, we discuss the light scalars below 1 GeV organized in the *Listings* under the entries $K_0^*(700)$ (or κ) with isospin $I = 1/2$, $a_0(980)$ with $I = 1$, as well as $f_0(500)$ (or σ) and $f_0(980)$ both with $I = 0$. The $I = 2$ $\pi\pi$ and $I = 3/2$ $K\pi$ partial waves do not have any resonances.

64.2 The $K_0^*(700)$, also known as κ ($I = 1/2$)

The $K_0^*(700)$ shows up as a pole in the low energy πK scattering, although its presence and properties are difficult to establish, since it appears to have a very large width ($\Gamma \approx 500$ MeV) and resides close to the $K\pi$ threshold. Hadronic D - and B -meson decays provide additional data points in the vicinity of the $K\pi$ threshold and are discussed in detail in the *Review on Multibody*

Charm Analyses in this RPP. With a few exceptions discussed there, the three- or more-hadron final states are usually treated as non-interacting two-body systems. Precision information from semileptonic D decays, where the strongly interacting two-particle final states could be treated without approximation, is not available. BES II [16] (re-analyzed in [17]) finds a $K_0^*(700)$ -like structure in $J/\psi(1S)$ decays to $\bar{K}^{*0}(892)K^+\pi^-$ where $K_0^*(700)$ recoils against the $K^*(892)$. The decay $\tau^- \rightarrow K_S^0\pi^-\nu_\tau$ can be considered clean with respect to final-state interactions and is studied by Belle [18], with $K_0^*(700)$ parameters fixed to those of Ref. [16].

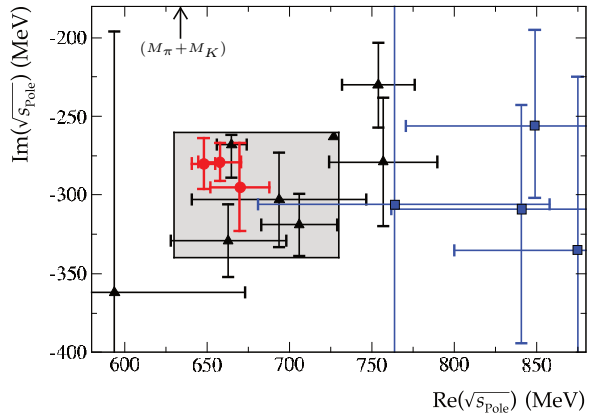


Figure 64.1: Location of the $K_0^*(700)$ (or κ) poles in the complex energy plane. Red circles denote the results of the most sophisticated analyses based on dispersion relations (see text for details), poles extracted from Breit-Wigner fits are shown as blue squares, while all other analyses quoted in the *Listings* are given by black triangles. The corresponding references are given in the listing. The arrow shows the location of the πK thresholds. The grey box indicates the ranges extracted as ‘our estimate’ of the pole locations.

Some authors find a $K_0^*(700)$ pole in their phenomenological analysis (see, *e.g.*, [19–28]), while others do not need to include it in their fits (see, *e.g.*, [29–33]). All works including constraints from chiral symmetry at low energies naturally find a light $K_0^*(700)$ below 800 MeV, see, *e.g.*, [34–39]. The analysis of Ref. [14,40] is based on the Roy-Steiner equations, which include analyticity and crossing symmetry constraints. Ref. [15] uses the Padé method to extract pole parameters after refitting scattering data constrained to satisfy forward dispersion relations. All three arrive at compatible pole positions for the $K_0^*(700)$ that are consistent with the pole parameters deduced from other theoretical methods. Due to their large uncertainties, the pole locations deduced from the Breit-Wigner fits appear to be just about consistent with the other determinations, but the real parts of all those analyses lie systematically too high. Moreover, phase shifts extracted from the Breit-Wigner functions for the $K_0^*(700)$ are very different from the known scalar πK phase shifts. The various poles are shown in Fig. 64.1. The compilation in this figure justifies the pole parameters of the $K_0^*(700)$, which we quote as ‘our estimate’, namely,

$$\sqrt{s_{\text{Pole}}^{\kappa}} = (630 - 730) - i(260 - 340) \text{ MeV}. \quad (64.2)$$

For an extensive discussion about the πK system in general and the κ meson in particular, see Ref. [41].

64.3 The $a_0(980)$ ($I = 1$)

The $a_0(980)$ couples strongly to the channels $\pi\eta$ and $K\bar{K}$. Independent of any model, the $K\bar{K}$ component must be large in the $a_0(980)$ wave function, since the mass of the $a_0(980)$ lies very close to the opening of the $K\bar{K}$ channel, to which it strongly couples [42,43]. This generates a pronounced cusp-like behavior in the resonant amplitude and to reveal its true coupling constants the presence of the $K\bar{K}$ channel cannot be ignored. All listed $a_0(980)$

measurements agree on a mass position value near 980 MeV, but the width deduced from the imaginary part of the pole location has values between 50 and 100 MeV, mostly due to the different models. For example, the analysis of the $p\bar{p}$ annihilation data [42] using a unitary K -matrix description finds a width determined from the T -matrix pole of 92 ± 8 MeV. Note that the width of the $a_0(980)$ line shape is typically smaller than what could be expected from the pole location.

The relative coupling $K\bar{K}/\pi\eta$ is determined indirectly from $f_1(1285)$ [44–46] or $\eta(1410)$ decays [47–49], from the line shape observed in the $\pi\eta$ decay mode [50–53], or from the coupled-channel analysis of the $\pi\pi\eta$ and $K\bar{K}\pi$ final states of $p\bar{p}$ annihilation at rest [42].

There are different recent extractions of the $a_0(980)$ pole location. Refs. [36, 37, 39, 54] use unitarized chiral perturbation theory. Ref. [55] used a similar formalism to extract the pole of the $a_0(980)$, employing the amplitude fixed in Ref. [56]. A dispersion theoretical approach to the isovector scalar $\pi\eta - K\bar{K}$ system is presented in Ref. [57] that may be refined further from studies of heavy meson decays [58]. Those efforts lead to a rather precise determination of the $a_0(980)$ pole location [59]. A value consistent for the mass parameter, but with a larger width, is found in a recent analysis of 1996 LEAR data for $p\bar{p}$ annihilation in flight employing a K -matrix [60]. The poles extracted in Refs. [39, 42, 53, 55, 59, 60] are shown in Fig. 64.2 together with the range of acceptable pole parameters extracted from this compilation, namely,

$$\sqrt{s_{\text{Pole}}^{a_0(980)}} = (960 - 1030) - i(20 - 70) \text{ MeV} \quad (64.3)$$

indicated by the box.

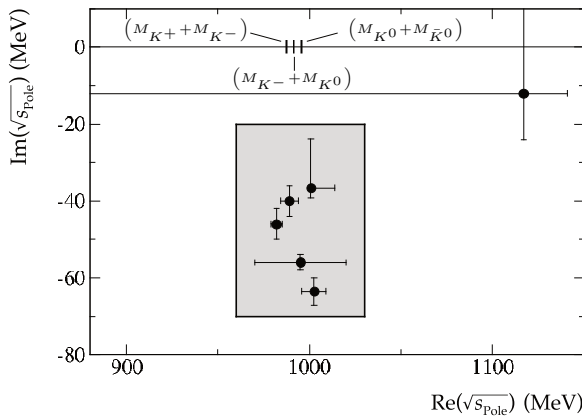


Figure 64.2: Location of the $a_0(980)$ poles from different extractions in the complex energy plane. The corresponding references are given in the *Listings*. Also shown are the thresholds for the K^+K^- and $K^0\bar{K}^0$ channels, relevant for $a_0(980)^0$, and for the K^-K^0 channel, relevant for the $a_0(980)^-$. The grey box indicates the ranges extracted as 'our estimate' of the pole locations.

64.4 The $f_0(500)$, also known as σ -meson ($I = 0$)

For discussions of the $\pi\pi$ S wave below the $K\bar{K}$ threshold and on the long history of the $f_0(500)$, which was suggested in linear sigma models more than 50 years ago, see the review [5]. Information on the $\pi\pi$ S -wave phase shift $\delta_J^I = \delta_0^0$ was already extracted many years ago from πN scattering [61–63], and near the $\pi\pi$ threshold from K_{e4} decays [64]. The kaon decays were later revisited leading to consistent data with very much improved statistics [65, 66]. The reported $\pi\pi \rightarrow K\bar{K}$ cross sections [67–70] have large uncertainties. The πN data have been analyzed in combination with high-statistics data (see entries labeled as RVUE for re-analyses of the data). The $2\pi^0$ invariant mass spectra, extracted from $p\bar{p}$ annihilation at rest into $3\pi^0$ [71, 72] and into $5\pi^0$ [73] and from central pp collision [74] do not show a distinct resonance structure below 900 MeV, but these data are consistently

described with the standard solution for the $\pi\pi$ scalar isoscalar S -wave extracted from high energy $\pi N \rightarrow \pi\pi N$ data [62, 75], which allows for the existence of the broad $f_0(500)$. An enhancement is observed in the $\pi^+\pi^-$ invariant mass near threshold in the decays $D^+ \rightarrow \pi^+\pi^-\pi^+$ [76–78] and $J/\psi(1S) \rightarrow \omega\pi^+\pi^-$ [79, 80], and in $\psi(2S) \rightarrow J/\psi(1S)\pi^+\pi^-$ with very limited phase space [81, 82].

The precise $f_0(500)$ (or σ) pole is difficult to establish because of its large width. The $\pi\pi$ scattering amplitude shows an unusual energy dependence due to the presence of the Adler zero in the unphysical regime close to the threshold [7, 8], required by chiral symmetry. However, most of the analyses listed under $f_0(500)$ agree on a pole position near $(500 - i250)$ MeV. In particular, analyses of $\pi\pi$ data that include unitarity, are consistent with the near threshold $\pi\pi$ data from K_{e4} decays, and the chiral symmetry constraints from Adler zeroes and/or scattering lengths find a light $f_0(500)$, see, e.g., [83, 84].

Precise pole positions with an uncertainty of less than 20 MeV (see our table for the T -matrix pole in the *Listings*) were extracted using the Roy equations, which are twice subtracted dispersion relations derived from crossing symmetry and analyticity. In Ref. [11] the subtraction constants were fixed to the S -wave scattering lengths a_0^0 and a_0^2 derived from matching the Roy equations and two-loop chiral perturbation theory [10]. The only additional relevant input to fix the $f_0(500)$ pole turned out to be the $\pi\pi$ -wave phase shifts at some higher energy point, chosen as 800 MeV. The analysis was improved further in Ref. [13]. Alternatively, in Ref. [12] Roy equations were used as constraints for a fit to the data. In that reference also once-subtracted Roy-like equations, called GKPY equations, were used, since the extrapolation into the complex plane based on the twice-subtracted equations leads to larger uncertainties, mainly due to the limited experimental information on the isospin 2 $\pi\pi$ scattering length. Ref. [85] uses Padé approximants for the analytic continuation. All these extractions find consistent results. Using analyticity and unitarity only to describe data from $K_{2\pi}$ and K_{e4} decays, Ref. [86] finds consistent values for the pole position and the scattering length a_0^0 . The importance of the $\pi\pi$ scattering data for fixing the $f_0(500)$ pole is nicely illustrated by comparing analyses of $p\bar{p} \rightarrow 3\pi^0$ omitting [71, 87] or including [72, 88] information on $\pi\pi$ scattering: while the former analyses find an extremely broad structure above 1 GeV, the latter find $f_0(500)$ masses of the order of 400 MeV.

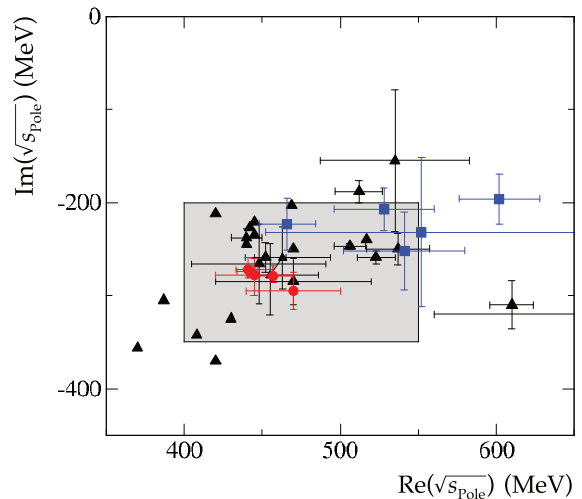


Figure 64.3: Location of the $f_0(500)$ (or σ) poles in the complex energy plane. Circles denote the recent analyses based on Roy(-like) dispersion relations, poles extracted from Breit-Wigner fits are shown as blue squares, while all other analyses are denoted by triangles. The corresponding references are given in the *Listings*. The grey box indicates the ranges extracted as 'our estimate' of the pole locations.

From Fig. 64.3 we read the range of pole positions for the $f_0(500)$, namely,

$$\sqrt{s_{\text{Pole}}^\sigma} = (400 - 550) - i(200 - 350) \text{ MeV} . \quad (64.4)$$

The plot contains the poles from Refs. [24, 35, 37, 39, 52, 54, 61, 72, 78, 81–84, 86, 88–107] as well as the advanced dispersion analyses [10–13, 85]. The extracted $f_0(500)$ pole position is very sensitive to the high accuracy low energy $\pi\pi$ scattering data [65, 66]. In fact, all analyses consistent with those data find poles within the accepted range indicated in the figure. As in case of the $K_0^*(700)$, poles extracted from Breit-Wigner analyses are shown as blue squares. Again we see that those poles have the tendency to appear at higher masses, although here the effect is not as pronounced as in case of the $K_0^*(700)$. One should not take this as an indication that using Breit-Wigners is justified in case of the $f_0(500)$, since $\pi\pi$ phase shifts extracted from Breit-Wigners are in strong discrepancy with the scattering phase shifts.

If one uses just the most advanced dispersive analyses of Refs. [10–13], shown as solid dots in Fig. 64.3 to determine the pole location of the $f_0(500)$, the range narrows down to [5]

$$\sqrt{s_{\text{Pole}}^\sigma} = (449_{-16}^{+22}) - i(275 \pm 12) \text{ MeV} , \quad (64.5)$$

which is labeled as ‘conservative dispersive estimate’ in this reference.

Besides $\pi\pi$, the only other decay channel of the $f_0(500)$ is two photons. Due to the large full width of the $f_0(500)$ an extraction of its two-photon width directly from data is not possible. Thus, the values for $\Gamma(\gamma\gamma)$ quoted in the literature as well as the in *Listings* are based on the expression in the narrow width approximation [108] $\Gamma(\gamma\gamma) \simeq \alpha^2 |g_\gamma|^2 / (4\text{Re}(\sqrt{s_{\text{Pole}}^\sigma}))$, where g_γ is derived from the residue at the $f_0(500)$ pole to two photons and α denotes the electromagnetic fine-structure constant (see also the review on *Resonances* in this issue of the RPP). The explicit form of the expression may vary between different authors due to different definitions of the coupling constant, however, the expression given for $\Gamma(\gamma\gamma)$ is free of ambiguities. According to Refs. [109–112], the data for $f_0(500) \rightarrow \gamma\gamma$ are consistent with what is expected for a two step process of $\gamma\gamma \rightarrow \pi^+\pi^-$ via pion exchange in the t - and u -channel, followed by a final state interaction $\pi^+\pi^- \rightarrow \pi^0\pi^0$. The same conclusion is drawn in Ref. [113], where the bulk part of the $f_0(500) \rightarrow \gamma\gamma$ decay width is dominated by re-scattering. Therefore, it might be difficult to learn anything new about the nature of the $f_0(500)$ from its $\gamma\gamma$ coupling. For the most recent work on $\gamma\gamma \rightarrow \pi\pi$, see Refs. [54, 86–88, 95–108, 111–116]. There are strong indications (*e.g.*, [117–147]) that the $f_0(500)$ pole cannot be classified as a $q\bar{q}$ state.

64.5 The $f_0(980)$ ($I = 0$)

The $f_0(980)$ couples predominantly to the $\pi\pi$ and $K\bar{K}$ channels and its signal overlaps strongly with the background represented mainly by the $f_0(500)$ and the $f_0(1370)$. This can lead to a dip in the $\pi\pi$ spectrum at the $K\bar{K}$ threshold. It changes from a dip into a peak structure in the $\pi^0\pi^0$ invariant mass spectrum of the reaction $\pi^-p \rightarrow \pi^0\pi^0n$ [121], with increasing four momentum transfer to the $\pi^0\pi^0$ system, which means increasing the $a_1(1260)$ exchange contribution in the amplitude, while the π exchange decreases. Also when a $(u\bar{u} + d\bar{d})$ source is switched to a $s\bar{s}$ source, as it appears when moving from $B_d \rightarrow J/\psi(1S)\pi\pi$ to $B_s \rightarrow J/\psi(1S)\pi\pi$, the f_0 signal switches from a dip to a peak [135]. The $f_0(500)$ and the $f_0(980)$ are also observed in the data for radiative ϕ decays ($\phi \rightarrow f_0\gamma$) from SND [122, 123], CMD2 [124], and KLOE [125, 126].

Unitarized chiral perturbation theory was employed to extract the pole of the $f_0(980)$ in Refs. [36, 37, 39, 54, 55]. Two different dispersive analyses were used in Ref. [12] to simultaneously pin down the pole parameters of both the $f_0(500)$ and the $f_0(980)$. The poles extracted in Refs. [12, 13, 39, 55, 60, 91, 148] are shown in Fig. 64.4, together with the range of acceptable pole parameters extracted from this compilation, namely,

$$\sqrt{s_{\text{Pole}}^{f_0(980)}} = (980 - 1010) - i(20 - 35) \text{ MeV} \quad (64.6)$$

indicated by the box. A disclaimer is important here: Both the poles of $a_0(980)$ and of $f_0(980)$ are located very close to the kaon thresholds, with the charged and neutral thresholds being 8 MeV apart — to illustrate this point the pertinent thresholds are shown explicitly in Figs. 64.2 and 64.4. This observation lead to the prediction of an enhanced a_0 – f_0 mixing [149–152]. On the other hand, all analyses employed in the pole determinations quoted above are done assuming isospin symmetry. Future studies need to show the impact of isospin violation on the extraction of the $a_0(980)/f_0(980)$ pole parameters.

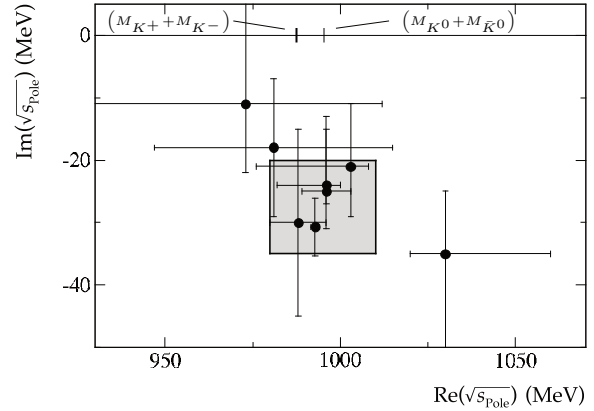


Figure 64.4: Location of the $f_0(980)$ poles from different extractions in the complex energy plane. The corresponding references are given in the *Listings*. Also shown are the thresholds for the K^+K^- and $K^0\bar{K}^0$ channels. The grey box indicates the ranges extracted as ‘our estimate’ of the pole locations.

Analyses of $\gamma\gamma \rightarrow \pi\pi$ data [127–129] underline the importance of the $K\bar{K}$ coupling of the $f_0(980)$, while the resulting two-photon width of the $f_0(980)$ cannot be determined precisely [130]. The prominent appearance of the $f_0(980)$ in the semileptonic D_s decays and decays of B and B_s mesons implies a dominant ($s\bar{s}$) component: those decays occur via weak transitions that alternatively result in $\phi(1020)$ production. Ratios of decay rates of B and/or B_s mesons into $J/\psi(1S)$ plus $f_0(980)$ or $f_0(500)$ were proposed to allow for an extraction of the flavor mixing angle and to probe the tetraquark nature of those mesons within a certain model [131, 132]. The resulting phenomenological fits of the LHCb collaboration [133, 134] lead the authors to conclude that their data are incompatible with a model where $f_0(500)$ and $f_0(980)$ are formed from two quarks and two antiquarks (tetraquarks). However, a dispersive analysis of the same data that allows for a model independent inclusion of the hadronic final state interactions in Ref. [135] puts into question the conclusions of Ref. [133].

64.6 Interpretation of the scalars below 1 GeV

In the literature, many structures are discussed for the light scalar mesons, such as conventional $q\bar{q}$ mesons, compact (qq)($\bar{q}\bar{q}$) structures (tetraquarks), or meson-meson bound states (hadronic molecules). In reality, there can be superpositions of these components, and one often depends on models to determine the dominant one. Although we have seen progress in recent years, this question remains open. Here, we mention some of the present conclusions.

The $f_0(980)$ and $a_0(980)$ are often interpreted as compact tetraquark states [144–147, 153] or $K\bar{K}$ bound states [154]. The insight into their internal structure using two-photon widths [123, 155–161] is not conclusive. The $f_0(980)$ appears as a peak structure in $J/\psi(1S) \rightarrow \phi\pi^+\pi^-$ and in D_s decays without $f_0(500)$ background, while being nearly invisible in $J/\psi(1S) \rightarrow \omega\pi^+\pi^-$. Based on that observation it is suggested that $f_0(980)$ has a large $s\bar{s}$ component, which according to Ref. [162] is surrounded by a virtual $K\bar{K}$ cloud (see also Ref. [163]). Data on radiative decays ($\phi \rightarrow f_0\gamma$ and $\phi \rightarrow a_0\gamma$) from SND, CMD2, and KLOE (see above) are consistent with a prominent role of kaon loops. This

observation is interpreted as evidence for a compact four-quark structure of the light scalars in Ref. [164], while it is claimed to point at a molecular nature in Ref. [165,166]. Details of this controversy are given in the comments [167,168]; see also Ref. [169]. There is now a rather broad consensus that the states $f_0(980)$ and $a_0(980)$, together with the $f_0(500)$ and the $K_0^*(700)$, form a nonet of predominantly four-quark states, where at larger distances the quarks recombine into a pair of pseudoscalar mesons creating a meson cloud (see, *e.g.*, Ref. [170]). Different QCD sum rule studies [171–176] do not agree on a tetraquark configuration for the same particle group.

Models that start directly from chiral Lagrangians, either in non-linear [36, 39, 83, 165] or in linear [177–183] realization, predict the existence of the $f_0(500)$ meson near 500 MeV. Here the $f_0(500)$, $a_0(980)$, $f_0(980)$, and $K_0^*(700)$ (in some models the $K_0^*(1430)$) would form a nonet (not necessarily $q\bar{q}$). In the linear sigma models the lightest pseudoscalars appear as their chiral partners.

In the non-linear approaches of Refs. [36] and [83] the above resonances together with the low mass vector states are generated starting from chiral perturbation theory predictions near the first open channel, and then by extending the predictions to the resonance regions, using unitarity and analyticity.

Ref. [177] uses a framework with explicit resonances that are unitarized and coupled to the light pseudoscalars in a chirally invariant way. Evidence for a dominant non- $q\bar{q}$ nature of the lightest scalar resonances is derived from their mixing scheme. In Ref. [178] the scheme is extended and applied to the decay $\eta' \rightarrow \eta\pi\pi$, which leads to the same conclusions. In Ref. [184] the large N_c behavior of the poles was studied to identify the nature of the resonances generated from scattering equations. This lead to the observation that, while the light vector states behave consistent with what is predicted for $q\bar{q}$ states, the light scalars behave very differently. This finding provides strong support for a dominant non- $q\bar{q}$ nature of the light scalar resonances. Note, the more refined study of Ref. [117] which found, in the case of the $f_0(500)$, indications for a subdominant $q\bar{q}$ component located around 1 GeV in addition to a dominant non- $q\bar{q}$ nature. Additional support for the dominant non- $q\bar{q}$ nature of the $f_0(500)$ is given in Ref. [185], where the connection between the pole of resonances and their Regge trajectories is analyzed. All works including constraints from chiral symmetry at low energies naturally find a light $K_0^*(700)$ below 800 MeV and a $f_0(500)$ below 600 MeV, see, *e.g.*, [34–39]. In these works the $K_0^*(700)$, $f_0(500)$, $f_0(980)$, and $a_0(980)$ appear to form a nonet [35,38]. Additional evidence for this assignment is presented in Ref. [13], where the couplings of the nine states to $q\bar{q}$ sources are compared. The same low mass scalar nonet was also found earlier in the unitarized quark model of Ref. [94].

There are, however, alternative interpretations of the light scalars. For example Ref. [186] (for a more recent, condensed discussion of the idea see Ref. [187]), also builds on chiral symmetry, but expands around an infrared fixed point such that the $f_0(500)$ appears as a QCD dilaton with a mass driven by the QCD scale anomaly. The phenomenology studied in that work appears consistent with this proposal. In Ref. [91,113,188,189] data on $\pi\pi - \bar{K}K$ scattering, as well as $\gamma\gamma \rightarrow \pi\pi$, are analysed and the authors conclude that especially the $f_0(500)$ should have a significant gluon content.

A model independent method to identify hadronic molecules goes back to a proposal by Weinberg [190] (an extension of the formalism to virtual states is provided in Ref. [191]), which was shown to be equivalent to the pole counting arguments of [149–152,192–197] in Ref. [195]. The formalism allows one to extract the amount of molecular component in the wave function from the effective coupling constant of a physical state to a nearby continuum channel. It can be applied to near threshold states only and provides strong evidence that the $f_0(980)$ is predominantly a $\bar{K}K$ molecule, while the situation turns out to be less clear for the $a_0(980)$ (see also Refs. [159,161]). This is in line with the findings of Ref. [55], which reports an important role of the $\pi\eta$ channel to the formation of the $a_0(980)$ in addition to the $\bar{K}K$ channel, while the $f_0(980)$ also in this work appears to be predom-

inantly a $\bar{K}K$ molecule. The relevance of both the $\bar{K}K$ and the $\pi\eta$ channels in a dynamically generated $a_0(980)$ was also pointed out in the description of the $\chi_{c1} \rightarrow \eta\pi^+\pi^-$ and $D_s^+ \rightarrow \pi^+\pi^0\eta$ reactions [198,199]. Further insights into $a_0(980)$ and $f_0(980)$ are expected from their mixing [149]. The corresponding signal predicted in Refs. [150,151] was recently observed at BES III [196]. In order to get a quantitative understanding of those data, in addition to the mixing mechanism itself, some detailed understanding of the production mechanism seems necessary [152].

In the unitarized quark model with coupled $q\bar{q}$ and meson-meson channels, the light scalars are interpreted as additional manifestations of bare $q\bar{q}$ confinement states, strongly mass shifted from the 1.3 - 1.5 GeV region and very distorted due to the strong 3P_0 coupling to S -wave two-meson decay channels [197,200]. Thus, in these models the light scalar nonet comprising the $f_0(500)$, $f_0(980)$, $K_0^*(700)$, and $a_0(980)$, as well as the nonet consisting of the $f_0(1370)$, $f_0(1500)$ (or $f_0(1710)$), $K_0^*(1430)$, and $a_0(1450)$, respectively, are seen as two manifestations of the same bare input states (see also Ref. [201]). It should not remain unmentioned, however, that the heavier nonet lies rather close to the input nonet and that the light scalar one emerges only, once the coupling to the two-meson channels is switched on, again highlighting that the meson-meson interaction is indispensable for the light scalars.

Acknowledgement

The authors would like to thank Claude Amsler, Eberhard Klempt, Mikhail Mikhasenko, and Jose Ramon Pelaez for helpful input and discussions in the preparation of the review.

References

- [1] F. E. Close and N. A. Tornqvist, J. Phys. **G28**, R249 (2002), [hep-ph/0204205].
- [2] C. Amsler and N. A. Tornqvist, Phys. Rept. **389**, 61 (2004).
- [3] D. V. Bugg, Phys. Rept. **397**, 257 (2004), [hep-ex/0412045].
- [4] E. Klempt and A. Zaitsev, Phys. Rept. **454**, 1 (2007), [arXiv:0708.4016].
- [5] J. R. Pelaez, Phys. Rept. **658**, 1 (2016), [arXiv:1510.00653].
- [6] S. Gardner and U.-G. Meissner, Phys. Rev. D **65**, 094004 (2002), [hep-ph/0112281].
- [7] S. L. Adler, Phys. Rev. **137**, B1022 (1965), [,140(1964)].
- [8] S. L. Adler, Phys. Rev. **139**, B1638 (1965), [,152(1965)].
- [9] J. A. Oller, Phys. Rev. **D71**, 054030 (2005), [hep-ph/0411105].
- [10] G. Colangelo, J. Gasser and H. Leutwyler, Nucl. Phys. **B603**, 125 (2001), [hep-ph/0103088].
- [11] I. Caprini, G. Colangelo, and H. Leutwyler, Phys. Rev. Lett. **96**, 132001 (2006).
- [12] R. Garcia-Martin *et al.*, Phys. Rev. Lett. **107**, 072001 (2011), [arXiv:1107.1635].
- [13] B. Moussallam, Eur. Phys. J. **C71**, 1814 (2011), [arXiv:1110.6074].
- [14] S. Descotes-Genon and B. Moussallam, Eur. Phys. J. C **48**, 553 (2006), [hep-ph/0607133].
- [15] J. R. Peláez and A. Rodas, Phys. Rev. Lett. **124**, 17, 172001 (2020), [arXiv:2001.08153].
- [16] M. Ablikim *et al.* (BES), Phys. Lett. **B633**, 681 (2006), [hep-ex/0506055].
- [17] F.-K. Guo *et al.*, Nucl. Phys. **A773**, 78 (2006), [hep-ph/0509050].
- [18] D. Epifanov *et al.* (Belle), Phys. Lett. **B654**, 65 (2007), [arXiv:0706.2231].
- [19] C. Cawfield *et al.* (CLEO), Phys. Rev. **D74**, 031108 (2006), [hep-ex/0606045].
- [20] A. V. Anisovich and A. V. Sarantsev, Phys. Lett. **B413**, 137 (1997), [hep-ph/9705401].
- [21] R. Delbourgo and M. D. Scadron, Int. J. Mod. Phys. **A13**, 657 (1998), [hep-ph/9807504].
- [22] C. M. Shakin and H. Wang, Phys. Rev. **D63**, 014019 (2001).

- [23] M. D. Scadron *et al.*, Nucl. Phys. **A724**, 391 (2003), [hep-ph/0211275].
- [24] D. V. Bugg, Phys. Lett. **B572**, 1 (2003), [Erratum: Phys. Lett. B595,556(2004)].
- [25] M. Ishida, Prog. Theor. Phys. Suppl. **149**, 190 (2003), [hep-ph/0212383].
- [26] H. Q. Zheng *et al.*, Nucl. Phys. **A733**, 235 (2004), [hep-ph/0310293].
- [27] Z. Y. Zhou and H. Q. Zheng, Nucl. Phys. **A775**, 212 (2006), [hep-ph/0603062].
- [28] J. M. Link *et al.* (FOCUS), Phys. Lett. **B653**, 1 (2007), [arXiv:0705.2248].
- [29] S. N. Cherry and M. R. Pennington, Nucl. Phys. **A688**, 823 (2001), [hep-ph/0005208].
- [30] B. Aubert *et al.* (BaBar), Phys. Rev. **D76**, 011102 (2007), [arXiv:0704.3593].
- [31] S. Kopp *et al.* (CLEO), Phys. Rev. **D63**, 092001 (2001), [hep-ex/0011065].
- [32] J. M. Link *et al.* (FOCUS), Phys. Lett. **B535**, 43 (2002), [hep-ex/0203031].
- [33] J. M. Link *et al.* (FOCUS), Phys. Lett. **B621**, 72 (2005), [hep-ex/0503043].
- [34] M. Jamin, J. A. Oller and A. Pich, Nucl. Phys. **B587**, 331 (2000), [hep-ph/0006045].
- [35] D. Black *et al.*, Phys. Rev. **D64**, 014031 (2001), [hep-ph/0012278].
- [36] J. A. Oller, E. Oset and J. R. Pelaez, Phys. Rev. **D59**, 074001 (1999), [Erratum: Phys. Rev. D75,099903(2007)], [hep-ph/9804209].
- [37] J. A. Oller and E. Oset, Phys. Rev. **D60**, 074023 (1999), [hep-ph/9809337].
- [38] J. A. Oller, Nucl. Phys. **A727**, 353 (2003), [hep-ph/0306031].
- [39] J. R. Pelaez, Mod. Phys. Lett. **A19**, 2879 (2004), [hep-ph/0411107].
- [40] J. R. Peláez, A. Rodas and J. Ruiz de Elvira, Eur. Phys. J. **C77**, 2, 91 (2017), [arXiv:1612.07966].
- [41] J. R. Peláez and A. Rodas (2020), [arXiv:2010.11222].
- [42] A. Abele *et al.*, Phys. Rev. **D57**, 3860 (1998).
- [43] M. Bargiotti *et al.* (OBELIX), Eur. Phys. J. **C26**, 371 (2003).
- [44] D. Barberis *et al.* (WA102), Phys. Lett. **B440**, 225 (1998), [hep-ex/9810003].
- [45] M. J. Corden *et al.*, Nucl. Phys. **B144**, 253 (1978).
- [46] C. Defoix *et al.*, Nucl. Phys. **B44**, 125 (1972).
- [47] Z. Bai *et al.* (MARK-III), Phys. Rev. Lett. **65**, 2507 (1990).
- [48] T. Bolton *et al.*, Phys. Rev. Lett. **69**, 1328 (1992).
- [49] C. Amsler *et al.* (Crystal Barrel), Phys. Lett. **B353**, 571 (1995).
- [50] S. M. Flatte, Phys. Lett. **63B**, 224 (1976).
- [51] C. Amsler *et al.* (Crystal Barrel), Phys. Lett. **B333**, 277 (1994).
- [52] G. Janssen *et al.*, Phys. Rev. **D52**, 2690 (1995), [arXiv:nucl-th/9411021].
- [53] D. V. Bugg, Phys. Rev. **D78**, 074023 (2008), [arXiv:0808.2706].
- [54] J. A. Oller and E. Oset, Nucl. Phys. **A620**, 438 (1997), [Erratum: Nucl. Phys. A652,407(1999)], [hep-ph/9702314].
- [55] H. A. Ahmed and C. W. Xiao, Phys. Rev. D **101**, 9, 094034 (2020), [arXiv:2001.08141].
- [56] C. W. Xiao, U. G. Meißner and J. A. Oller, Eur. Phys. J. A **56**, 1, 23 (2020), [arXiv:1907.09072].
- [57] M. Albaladejo and B. Moussallam, Eur. Phys. J. C **75**, 10, 488 (2015), [arXiv:1507.04526].
- [58] M. Albaladejo *et al.*, JHEP **04**, 010 (2017), [arXiv:1611.03502].
- [59] J. Lu and B. Moussallam, Eur. Phys. J. C **80**, 5, 436 (2020), [arXiv:2002.04441].
- [60] M. Albrecht *et al.* (Crystal Barrel), Eur. Phys. J. C **80**, 5, 453 (2020), [arXiv:1909.07091].
- [61] S. D. Protopopescu *et al.*, Phys. Rev. **D7**, 1279 (1973).
- [62] G. Grayer *et al.*, Nucl. Phys. **B75**, 189 (1974).
- [63] H. Becker *et al.* (CERN-Cracow-Munich), Nucl. Phys. **B151**, 46 (1979).
- [64] L. Rosselet *et al.*, Phys. Rev. **D15**, 574 (1977).
- [65] S. Pislak *et al.* (BNL-E865), Phys. Rev. Lett. **87**, 221801 (2001), [Erratum: Phys. Rev. Lett. 105,019901(2010)], [hep-ex/0106071].
- [66] J. R. Batley *et al.* (NA48-2), Eur. Phys. J. **C70**, 635 (2010).
- [67] W. Wetzel *et al.*, Nucl. Phys. **B115**, 208 (1976).
- [68] V. A. Polychronakos *et al.*, Phys. Rev. **D19**, 1317 (1979).
- [69] D. H. Cohen *et al.*, Phys. Rev. **D22**, 2595 (1980).
- [70] A. Etkin *et al.*, Phys. Rev. **D25**, 1786 (1982).
- [71] C. Amsler *et al.*, Phys. Lett. **B342**, 433 (1995).
- [72] C. Amsler *et al.* (Crystal Barrel), Phys. Lett. **B355**, 425 (1995).
- [73] A. Abele *et al.* (Crystal Barrel), Phys. Lett. **B380**, 453 (1996).
- [74] D.M. Alde *et al.*, Phys. Lett. **B397**, 350 (1997).
- [75] R. Kaminski, L. Lesniak and K. Rybicki, Z. Phys. **C74**, 79 (1997), [hep-ph/9606362].
- [76] E. M. Aitala *et al.* (E791), Phys. Rev. Lett. **86**, 770 (2001), [hep-ex/0007028].
- [77] J. M. Link *et al.* (FOCUS), Phys. Lett. **B585**, 200 (2004), [hep-ex/0312040].
- [78] G. Bonvicini *et al.* (CLEO), Phys. Rev. **D76**, 012001 (2007), [arXiv:0704.3954].
- [79] J. E. Augustin *et al.* (DM2), Nucl. Phys. **B320**, 1 (1989).
- [80] M. Ablikim *et al.* (BES), Phys. Lett. **B598**, 149 (2004), [hep-ex/0406038].
- [81] A. Gallegos, J. L. Lucio M. and J. Pestieau, Phys. Rev. **D69**, 074033 (2004), [hep-ph/0311133].
- [82] M. Ablikim *et al.* (BES), Phys. Lett. **B645**, 19 (2007), [hep-ex/0610023].
- [83] A. Dobado and J. R. Pelaez, Phys. Rev. **D56**, 3057 (1997), [hep-ph/9604416].
- [84] I. Caprini, Phys. Rev. **D77**, 114019 (2008), [arXiv:0804.3504].
- [85] P. Masjuan, J. Ruiz de Elvira, J.J. Sanz-Cillero, Phys. Rev. **D90**, 097901 (2014).
- [86] R. Garcia-Martin, J. R. Pelaez and F. J. Yndurain, Phys. Rev. **D76**, 074034 (2007), [hep-ph/0701025].
- [87] V.V. Anisovich *et al.*, Sov. Phys. Usp. **41**, 419 (1998).
- [88] V. V. Anisovich, Int. J. Mod. Phys. **A21**, 3615 (2006), [hep-ph/0510409].
- [89] M. Ablikim *et al.* (BESIII), Phys. Rev. Lett. **118**, 1, 012001 (2017), [arXiv:1606.03847].
- [90] M. Albaladejo and J. A. Oller, Phys. Rev. D **86**, 034003 (2012), [arXiv:1205.6606].
- [91] G. Mennessier, S. Narison and X. G. Wang, Phys. Lett. B **688**, 59 (2010), [arXiv:1002.1402].
- [92] M. Ablikim *et al.* (BES), Phys. Lett. B **598**, 149 (2004), [hep-ex/0406038].
- [93] P. Estabrooks, Phys. Rev. D **19**, 2678 (1979).

- [94] E. van Beveren *et al.*, Z. Phys. **C30**, 615 (1986), [arXiv:0710.4067].
- [95] B. S. Zou and D. V. Bugg, Phys. Rev. **D48**, R3948 (1993).
- [96] N. A. Tornqvist and M. Roos, Phys. Rev. Lett. **76**, 1575 (1996), [hep-ph/9511210].
- [97] R. Kaminski, L. Lesniak and J. P. Maillat, Phys. Rev. **D50**, 3145 (1994), [hep-ph/9403264].
- [98] N. N. Achasov and G. N. Shestakov, Phys. Rev. **D49**, 5779 (1994).
- [99] M. P. Locher, V. E. Markushin and H. Q. Zheng, Eur. Phys. J. **C4**, 317 (1998), [hep-ph/9705230].
- [100] T. Hannah, Phys. Rev. **D60**, 017502 (1999), [hep-ph/9905236].
- [101] R. Kaminski, L. Lesniak and B. Loiseau, Phys. Lett. **B413**, 130 (1997), [hep-ph/9707377].
- [102] R. Kaminski, L. Lesniak and B. Loiseau, Eur. Phys. J. **C9**, 141 (1999), [hep-ph/9810386].
- [103] M. Ishida *et al.*, Prog. Theor. Phys. **104**, 203 (2000), [hep-ph/0005251].
- [104] Y.S. Surovtsev *et al.*, Phys. Rev. **D61**, 054024 (2001).
- [105] M. Ishida *et al.*, Phys. Lett. **B518**, 47 (2001).
- [106] Z. Y. Zhou *et al.*, JHEP **02**, 043 (2005), [hep-ph/0406271].
- [107] D. V. Bugg, J. Phys. **G34**, 151 (2007), [hep-ph/0608081].
- [108] D. Morgan and M. R. Pennington, Z. Phys. **C48**, 623 (1990).
- [109] J. F. Donoghue, B. R. Holstein and Y. C. Lin, Phys. Rev. **D37**, 2423 (1988).
- [110] A. Dobado and J. R. Pelaez, Z. Phys. **C57**, 501 (1993).
- [111] M. R. Pennington, Phys. Rev. Lett. **97**, 011601 (2006).
- [112] M. R. Pennington, Mod. Phys. Lett. **A22**, 1439 (2007), [arXiv:0705.3314].
- [113] G. Mennessier, S. Narison and W. Ochs, Phys. Lett. **B665**, 205 (2008), [arXiv:0804.4452].
- [114] R. Garcia-Martin and B. Moussallam, Eur. Phys. J. **C70**, 155 (2010), [arXiv:1006.5373].
- [115] M. Hoferichter, D. R. Phillips and C. Schat, Eur. Phys. J. **C71**, 1743 (2011), [arXiv:1106.4147].
- [116] L.-Y. Dai and M. R. Pennington, Phys. Rev. **D90**, 3, 036004 (2014), [arXiv:1404.7524].
- [117] J. R. Pelaez and G. Rios, Phys. Rev. Lett. **97**, 242002 (2006), [hep-ph/0610397].
- [118] H.-X. Chen, A. Hosaka and S.-L. Zhu, Phys. Lett. **B650**, 369 (2007), [hep-ph/0609163].
- [119] F. Giacosa, Phys. Rev. **D75**, 054007 (2007), [hep-ph/0611388].
- [120] L. Maiani *et al.*, Eur. Phys. J. **C50**, 609 (2007), [hep-ph/0604018].
- [121] N. N. Achasov and G. N. Shestakov, Phys. Rev. **D58**, 054011 (1998), [hep-ph/9802286].
- [122] M. N. Achasov *et al.*, Phys. Lett. **B479**, 53 (2000), [hep-ex/0003031].
- [123] M. N. Achasov *et al.*, Phys. Lett. **B485**, 349 (2000), [hep-ex/0005017].
- [124] R. R. Akhmetshin *et al.* (CMD-2), Phys. Lett. **B462**, 371 (1999), [hep-ex/9907005].
- [125] A. Aloisio *et al.* (KLOE), Phys. Lett. **B536**, 209 (2002), [hep-ex/0204012].
- [126] F. Ambrosino *et al.* (KLOE), Eur. Phys. J. **C49**, 473 (2007), [hep-ex/0609009].
- [127] M. Boglione and M. R. Pennington, Eur. Phys. J. **C9**, 11 (1999), [hep-ph/9812258].
- [128] T. Mori *et al.* (Belle), Phys. Rev. **D75**, 051101 (2007), [hep-ex/0610038].
- [129] N. N. Achasov and G. N. Shestakov, Phys. Rev. **D77**, 074020 (2008), [arXiv:0712.0885].
- [130] M. R. Pennington *et al.*, Eur. Phys. J. **C56**, 1 (2008), [arXiv:0803.3389].
- [131] R. Fleischer, R. Kneegjens and G. Ricciardi, Eur. Phys. J. **C71**, 1832 (2011), [arXiv:1109.1112].
- [132] S. Stone and L. Zhang, Phys. Rev. Lett. **111**, 6, 062001 (2013), [arXiv:1305.6554].
- [133] R. Aaij *et al.* (LHCb), Phys. Rev. **D90**, 1, 012003 (2014), [arXiv:1404.5673].
- [134] R. Aaij *et al.* (LHCb), Phys. Rev. **D89**, 9, 092006 (2014), [arXiv:1402.6248].
- [135] J. T. Daub, C. Hanhart and B. Kubis, JHEP **02**, 009 (2016), [arXiv:1508.06841].
- [136] D. Barberis *et al.* (WA102), Phys. Lett. **B462**, 462 (1999), [hep-ex/9907055].
- [137] D. Barberis *et al.* (WA102), Phys. Lett. **B479**, 59 (2000), [hep-ex/0003033].
- [138] M. Gaspero, Nucl. Phys. **A562**, 407 (1993).
- [139] A. Adamo *et al.*, Nucl. Phys. **A558**, 13C (1993).
- [140] C. Amsler *et al.* (Crystal Barrel), Phys. Lett. **B322**, 431 (1994).
- [141] A. Abele *et al.* (Crystal Barrel), Eur. Phys. J. **C19**, 667 (2001).
- [142] A. Abele *et al.* (CRYSTAL BARREL), Eur. Phys. J. **C21**, 261 (2001).
- [143] D. Barberis *et al.* (WA102), Phys. Lett. **B471**, 440 (2000), [hep-ex/9912005].
- [144] R. L. Jaffe, Phys. Rev. **D15**, 267 (1977).
- [145] M. G. Alford and R. L. Jaffe, Nucl. Phys. **B578**, 367 (2000), [hep-lat/0001023].
- [146] L. Maiani *et al.*, Phys. Rev. Lett. **93**, 212002 (2004), [hep-ph/0407017].
- [147] L. Maiani, A. D. Polosa and V. Riquer, Phys. Lett. **B651**, 129 (2007), [hep-ph/0703272].
- [148] V. V. Anisovich and A. V. Sarantsev, Int. J. Mod. Phys. **A24**, 2481 (2009).
- [149] N. N. Achasov, S. A. Devyanin and G. N. Shestakov, Phys. Lett. **88B**, 367 (1979).
- [150] J.-J. Wu, Q. Zhao and B. S. Zou, Phys. Rev. **D75**, 114012 (2007), [arXiv:0704.3652].
- [151] C. Hanhart, B. Kubis and J. R. Pelaez, Phys. Rev. **D76**, 074028 (2007), [arXiv:0707.0262].
- [152] L. Roca, Phys. Rev. **D88**, 014045 (2013), [arXiv:1210.4742].
- [153] G. 't Hooft *et al.*, Phys. Lett. **B662**, 424 (2008), [arXiv:0801.2288].
- [154] J. D. Weinstein and N. Isgur, Phys. Rev. **D41**, 2236 (1990).
- [155] T. Barnes, Phys. Lett. **165B**, 434 (1985).
- [156] Z. P. Li, F. E. Close and T. Barnes, Phys. Rev. **D43**, 2161 (1991).
- [157] R. Delbourgo, D.-s. Liu and M. D. Scadron, Phys. Lett. **B446**, 332 (1999), [hep-ph/9811474].
- [158] J. L. Lucio Martinez and M. Napsuciale, Phys. Lett. **B454**, 365 (1999), [hep-ph/9903234].
- [159] C. Hanhart *et al.*, Phys. Rev. **D75**, 074015 (2007), [hep-ph/0701214].
- [160] R. H. Lemmer, Phys. Lett. **B650**, 152 (2007), [hep-ph/0701027].
- [161] T. Branz, T. Gutsche and V. E. Lyubovitskij, Eur. Phys. J. **A37**, 303 (2008), [arXiv:0712.0354].
- [162] A. Deandrea *et al.*, Phys. Lett. **B502**, 79 (2001), [hep-ph/0012120].

- [163] K. M. Ecklund *et al.* (CLEO), Phys. Rev. **D80**, 052009 (2009), [arXiv:0907.3201].
- [164] N. N. Achasov and V. N. Ivanchenko, Nucl. Phys. **B315**, 465 (1989).
- [165] J. A. Oller, Nucl. Phys. **A714**, 161 (2003), [hep-ph/0205121].
- [166] Yu. S. Kalashnikova *et al.*, Eur. Phys. J. **A24**, 437 (2005), [hep-ph/0412340].
- [167] Yu. S. Kalashnikova *et al.*, Phys. Rev. **D78**, 058501 (2008), [arXiv:0711.2902].
- [168] N. N. Achasov and A. V. Kiselev, Phys. Rev. **D78**, 058502 (2008), [arXiv:0806.2993].
- [169] M. Boglione and M. R. Pennington, Eur. Phys. J. **C30**, 503 (2003), [hep-ph/0303200].
- [170] F. Giacosa and G. Pagliara, Phys. Rev. **C76**, 065204 (2007), [arXiv:0707.3594].
- [171] S. Narison, Nucl. Phys. B Proc. Suppl. **96**, 244 (2001).
- [172] H.-J. Lee, Eur. Phys. J. **A30**, 423 (2006), [hep-ph/0512212].
- [173] H.-X. Chen, A. Hosaka and S.-L. Zhu, Phys. Rev. **D76**, 094025 (2007), [arXiv:0707.4586].
- [174] J. Sugiyama *et al.*, Phys. Rev. **D76**, 114010 (2007), [arXiv:0707.2533].
- [175] T. Kojo and D. Jido, Phys. Rev. **D78**, 114005 (2008), [arXiv:0802.2372].
- [176] H.-J. Lee, K. S. Kim and H. Kim, Phys. Rev. D **100**, 3, 034021 (2019), [arXiv:1904.12311].
- [177] D. Black *et al.*, Phys. Rev. **D59**, 074026 (1999), [hep-ph/9808415].
- [178] A. H. Fariborz *et al.*, Phys. Rev. **D90**, 3, 033009 (2014), [arXiv:1407.3870].
- [179] M. D. Scadron, Eur. Phys. J. **C6**, 141 (1999), [hep-ph/9710317].
- [180] M. Ishida, Prog. Theor. Phys. **101**, 661 (1999), [hep-ph/9902260].
- [181] N. A. Tornqvist, Eur. Phys. J. **C11**, 359 (1999), [hep-ph/9905282].
- [182] M. Napsuciale and S. Rodriguez, Phys. Lett. **B603**, 195 (2004), [hep-ph/0403072].
- [183] M. Napsuciale and S. Rodriguez, Phys. Rev. **D70**, 094043 (2004), [hep-ph/0407037].
- [184] J. R. Pelaez, Phys. Rev. Lett. **92**, 102001 (2004), [hep-ph/0309292].
- [185] J. T. Londergan *et al.*, Phys. Lett. **B729**, 9 (2014), [arXiv:1311.7552].
- [186] R. J. Crewther and L. C. Tunstall, Phys. Rev. D **91**, 3, 034016 (2015), [arXiv:1312.3319].
- [187] R. J. Crewther, Universe **6**, 7, 96 (2020), [arXiv:2003.11259].
- [188] R. Kaminski, G. Mennessier and S. Narison, Phys. Lett. B **680**, 148 (2009), [arXiv:0904.2555].
- [189] G. Mennessier, S. Narison and X. G. Wang, Phys. Lett. B **696**, 40 (2011), [arXiv:1009.2773].
- [190] S. Weinberg, Phys. Rev. **130**, 776 (1963).
- [191] I. Matuschek *et al.*, Eur. Phys. J. A **57**, 3, 101 (2021), [arXiv:2007.05329].
- [192] D. Morgan and M. R. Pennington, Phys. Lett. **B258**, 444 (1991), [Erratum: Phys. Lett. B269,477(1991)].
- [193] D. Morgan, Nucl. Phys. **A543**, 632 (1992).
- [194] N. A. Tornqvist, Phys. Rev. **D51**, 5312 (1995), [hep-ph/9403234].
- [195] V. Baru *et al.*, Phys. Lett. **B586**, 53 (2004), [hep-ph/0308129].
- [196] M. Ablikim *et al.* (BESIII), Phys. Rev. **D83**, 032003 (2011), [arXiv:1012.5131].
- [197] N. A. Tornqvist, Z. Phys. **C68**, 647 (1995), [hep-ph/9504372].
- [198] W.-H. Liang, J.-J. Xie and E. Oset, Eur. Phys. J. C **76**, 12, 700 (2016), [arXiv:1609.03864].
- [199] R. Molina *et al.*, Phys. Lett. B **803**, 135279 (2020), [arXiv:1908.11557].
- [200] E. van Beveren and G. Rupp, Eur. Phys. J. **C22**, 493 (2001), [hep-ex/0106077].
- [201] M. Boglione and M. R. Pennington, Phys. Rev. **D65**, 114010 (2002), [hep-ph/0203149].

65. Rare Kaon Decays

Revised August 2021 by L. Littenberg (BNL) and G. Valencia (Monash U.).

65.1 Introduction

There are several useful reviews on rare kaon decays and related topics [1–13]. Activity in rare kaon decays can be divided roughly into four categories:

1. Searches for explicit violations of the Standard Model (SM)
2. The golden modes: $K \rightarrow \pi\nu\bar{\nu}$
3. Other constraints on SM parameters
4. Studies of strong interactions at low energy.

The paradigm of Category 1 is the lepton flavor violating decay $K_L \rightarrow \mu e$. Category 2 includes the two modes that can be calculated with negligible theoretical uncertainty, $K^+ \rightarrow \pi^+\nu\bar{\nu}$ and $K_L \rightarrow \pi^0\nu\bar{\nu}$. These modes can lead to precision determinations of CKM parameters or, in combination with other measurements of these parameters, they can constrain new interactions. They constitute the main focus of the current experimental kaon program. The search for new light particles through the reaction $K \rightarrow \pi X^0$ is a byproduct of these measurements. Category 3 is focused on decays with charged leptons, such as $K_L \rightarrow \pi^0\ell^+\ell^-$ or $K_L \rightarrow \ell^+\ell^-$ where $\ell \equiv e, \mu$. These modes are sensitive to CKM parameters, but they suffer from multiple hadronic uncertainties that can be addressed, at least in part, through a systematic study of the peripheral modes indicated in Fig. 65.1.

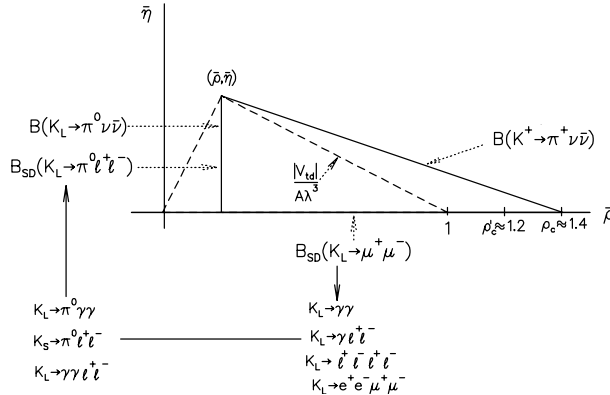


Figure 65.1: Role of rare kaon decays in determining the unitarity triangle. The solid arrows point to auxiliary modes needed to interpret the main results, or potential backgrounds to them.

The interplay between Categories 3-4 and their complementarity to Category 2 is illustrated in the figure. Category 4 includes reactions like $K^+ \rightarrow \pi^+\ell^+\ell^-$ where long distance contributions are dominant and which constitute a testing ground for the ideas

of chiral perturbation theory. Other decays in this category are $K_L \rightarrow \pi^0\gamma\gamma$ and $K_L \rightarrow \ell^+\ell^-\gamma$. The former is important in understanding a CP -conserving contribution to $K_L \rightarrow \pi^0\ell^+\ell^-$, whereas the latter could shed light on long distance contributions to $K_L \rightarrow \mu^+\mu^-$.

65.2 Explicit violations of the Standard Model

Much activity has focussed on searches for lepton flavor violation (LFV). This is motivated by the fact that many extensions of the minimal Standard Model violate lepton flavor and by the potential to access very high energy scales. For example, the tree-level exchange of a LFV vector boson of mass M_X that couples to left-handed fermions with electroweak strength and without mixing angles yields $B(K_L \rightarrow \mu e) = 4.7 \times 10^{-12} (148 \text{ TeV}/M_X)^4$ [2]. This simple dimensional analysis may be used to read from Table 65.1 that the reaction $K_L \rightarrow \mu e$ is already probing scales of over 100 TeV. Table 65.1 summarizes the present experimental situation vis-à-vis LFV. The decays $K_L \rightarrow \mu^\pm e^\mp$ and $K^+ \rightarrow \pi^+ e^\mp \mu^\pm$ (or $K_L \rightarrow \pi^0 e^\mp \mu^\pm$) provide complementary information on potential family number violating interactions, since the former is sensitive to parity-odd couplings and the latter is sensitive to parity-even couplings.

Limits on certain lepton-number violating (LNV) kaon decays also have been obtained, with special interest arising from their role in constraining possible extensions of the neutrino sector [14, 15], and we list those in the table as well. Related searches in μ and τ processes are discussed in our section “Tests of Conservation Laws.”

Table 65.1: Searches for lepton flavor and lepton number violation in K decay

LFV mode	90% CL upper limit	Experiment	Yr./Ref.	Type
$K^+ \rightarrow \pi^+ e^- \mu^+$	1.3×10^{-11}	BNL-865	2005/ [16]	LFV
$K^+ \rightarrow \pi^+ e^+ \mu^-$	6.6×10^{-11}	NA62	2021/ [17]	LFV
$K_L \rightarrow \mu e$	4.7×10^{-12}	BNL-871	1998/ [18]	LFV
$K_L \rightarrow \pi^0 e \mu$	7.6×10^{-11}	KTeV	2008/ [19]	LFV
$K_L \rightarrow \pi^0 \pi^0 e \mu$	1.7×10^{-10}	KTeV	2008/ [19]	LFV
$K^+ \rightarrow \pi^- e^+ e^+$	5.3×10^{-11}	NA62	2022/ [20]	LNV
$K^+ \rightarrow \pi^- \pi^0 e^+ e^+$	8.5×10^{-10}	NA62	2022/ [20]	LNV
$K^+ \rightarrow \pi^- \mu^+ \mu^+$	4.2×10^{-11}	NA62	2019/ [21]	LNV
$K_L \rightarrow e^\pm e^\pm \mu^\mp \mu^\mp$	4.12×10^{-11}	KTeV	2003/ [22]	LNV
$K^+ \rightarrow \pi^- \mu^+ e^+$	4.2×10^{-11}	NA62	2021/ [17]	LNFV

65.3 The golden modes: $K \rightarrow \pi\nu\bar{\nu}$

In the SM, the decay $K^+ \rightarrow \pi^+\nu\bar{\nu}$ is dominated by one-loop diagrams with top-quark intermediate states while long-distance contributions are known to be quite small [23–25]. This permits a precise calculation of this rate in terms of SM parameters. Studies of this process are thus motivated by the possibility of detecting non-SM physics when comparing with the results of global fits [26, 27].

The branching ratio can be written in a compact form that exhibits the different ingredients that go into the calculation [28],

$$B(K^+ \rightarrow \pi^+\nu\bar{\nu}(\gamma)) = \kappa_+(1 + \Delta_{EM}) \left[\left(\frac{\text{Im}(V_{ts}^* V_{td})}{\lambda^5} X_t \right)^2 + \left(\frac{\text{Re}(V_{cs}^* V_{cd})}{\lambda} P_c + \frac{\text{Re}(V_{ts}^* V_{td})}{\lambda^5} X_t \right)^2 \right]. \quad (65.1)$$

The parameters in Eq. 65.1 incorporate the *a priori* unknown hadronic matrix element in terms of the very well-measured K_{e3} rate [23] in κ_+ ; long distance QED corrections in Δ_{EM} [29]; the Inami-Lim function for the short distance top-quark contribution [30] including NLO QCD corrections [31, 32] and the two-loop electroweak correction [28], all in X_t ; and the charm-quark contributions due to short distance effects including NNLO QCD corrections [33, 34] and NLO electroweak corrections via P_c [35], which also includes certain long distance dubbed $\delta P_{c,u}$ [25, 36].

An interesting approximate way to cast this result in terms of the CKM parameters λ , V_{cb} , $\bar{\rho}$ and $\bar{\eta}$ (see our Section on “The Cabibbo-Kobayashi-Maskawa mixing matrix”) [9] is:

$$B(K^+ \rightarrow \pi^+\nu\bar{\nu}) \approx 1.6 \times 10^{-5} |V_{cb}|^4 [(\sigma\bar{\eta})^2 + (\rho_c - \bar{\rho})^2] \quad (65.2)$$

where $\rho_c \approx 1.45$ and $\sigma \equiv \frac{1}{(1 - \frac{1}{2}\lambda^2)^2}$. Thus, $B(K^+ \rightarrow \pi^+\nu\bar{\nu})$ determines an ellipse in the $\bar{\rho}$, $\bar{\eta}$ plane with center $(\rho_c, 0)$ and semiaxes $\approx \frac{1}{|V_{cb}|^2} \sqrt{\frac{B(K^+ \rightarrow \pi^+\nu\bar{\nu})}{1.6 \times 10^{-5}}}$ and $\frac{1}{\sigma|V_{cb}|^2} \sqrt{\frac{B(K^+ \rightarrow \pi^+\nu\bar{\nu})}{1.6 \times 10^{-5}}}$.

BNL-787 observed two candidate events [37, 38] in the clean high π^+ momentum and one event [39] in the low-momentum region. The successor experiment BNL-949 observed one more in the high-momentum region [40] and three more in the low-momentum region [41], yielding a branching ratio of $(1.73_{-1.05}^{+1.15}) \times 10^{-10}$ [42].

The NA62 experiment, performed with in-flight decays at CERN, aims to reach a sensitivity of $\sim 10^{-12}$ per event. NA62 was commissioned in 2015 and has taken data in 2016, 2017 and 2018. They recently published results from the 2016-18 runs [43]. Twenty candidate events were observed, including an estimated background of 7.03, yielding $B(K^+ \rightarrow \pi^+ \nu \bar{\nu}) = (10.6_{-3.4}^{+4.0})_{\text{stat}} \pm 0.9_{\text{sys}} \times 10^{-11}$. NA62 will continue taking data in 2021 with improvements to the detector.

Using the latest CKMfitter input (Dec. 2019) [26], we estimate $B(K^+ \rightarrow \pi^+ \nu \bar{\nu})_{SM} = (8.1 \pm 0.4) \times 10^{-11}$, near the lower end of the measurements of BNL-787/949 and NA62. Current parametric uncertainty in the CKM angles can result in numbers with central values differing from this one by up to 10% [44].

The second golden mode is the neutral counterpart to our preceding discussion: $K_L \rightarrow \pi^0 \nu \bar{\nu}$. It is dominantly CP -violating and free of hadronic uncertainties [23, 45, 46]. In the Standard Model, this mode is dominated by an intermediate top-quark state and does not suffer from the small uncertainty associated with the charm-quark intermediate state that affects $K^+ \rightarrow \pi^+ \nu \bar{\nu}$. The branching ratio is given by Ref. [9]:

$$B(K_L \rightarrow \pi^0 \nu \bar{\nu}) = \kappa_L \left(\frac{\text{Im}(V_{ts}^* V_{td})}{\lambda^5} X_t \right)^2 \approx 7.6 \times 10^{-5} |V_{cb}|^4 \bar{\eta}^2. \quad (65.3)$$

As with the charged mode, the hadronic matrix element can be related to that measured in $K_{\ell 3}$ decay and is parameterized in κ_L .

Our estimate for the branching ratio within the SM, using the latest CKMfitter input (Dec. 2019) [26], is $(2.8 \pm 0.2) \times 10^{-11}$. Similarly to the charged kaon case, parametric uncertainty in the CKM angles can result in a central value that differs from this one by up to almost 20% [44].

Grossman and Nir (GN) [47] pointed out that, in a nearly model-independent manner, the two golden modes satisfy the relation $B(K_L \rightarrow \pi^0 \nu \bar{\nu}) \lesssim 4.3 B(K^+ \rightarrow \pi^+ \nu \bar{\nu})$. Using the BNL 787/949 90% CL bound on $K^+ \rightarrow \pi^+ \nu \bar{\nu}$, GN then predict $B(K_L \rightarrow \pi^0 \nu \bar{\nu}) < 1.46 \times 10^{-9}$. Using instead the latest NA62 result, the GN upper bound becomes $B(K_L \rightarrow \pi^0 \nu \bar{\nu}) < 8.14 \times 10^{-10}$ [13].

The KOTO experiment at J-PARC, whose initial goal is to observe this decay, has been running since 2013 and in 2018 published a 90% CL upper limit of 3.0×10^{-9} [48], based on their 2015 data. They have run every year since, making incremental improvements to the experimental configuration between runs. In 2021 they published a result on the data taken between 2016 and 2018 in which three events were observed in the signal region [49]. Studies revealed two backgrounds previously unanticipated at the current level of sensitivity (7.2×10^{-10} /event), one from halo $K_L \rightarrow \gamma \gamma$ and a larger one from charged kaons produced by K_L interactions in the downstream collimator, followed by $K^\pm \rightarrow \pi^0 e^\pm \nu_e$ where the e^\pm goes backwards and is not observed. These constituted more than 90% of the expected background of 1.22 events. Conservatively assuming the three events were due to background, they extracted a 90% CL upper limit of 4.9×10^{-9} . Subsequent hardware and analysis improvements are expected to greatly reduce these backgrounds in future data collection. An increase of 3-5 in sensitivity is anticipated from runs planned in the next three years.

The current theoretical and experimental situation for the golden modes is summarized in Fig. 65.2. The red area corresponds to the 1σ SM prediction we obtain with the latest input available from CKMfitter (December 2019) [26]. The yellow region shows the result established by the combined BNL-787 and BNL-949 results, whereas the green region marks the new NA62 result for $K^+ \rightarrow \pi^+ \nu \bar{\nu}$. The black shaded region marks the GN exclusion, which lies significantly above the SM expectation leaving a large window for discovery of new physics contributions by

experiments seeking to measure $B(K_L \rightarrow \pi^0 \nu \bar{\nu})$. The 90% CL upper bound on this mode from the KOTO result published in 2018 [48] is shown as a dashed orange line, and is seen to still lie in the GN excluded zone.

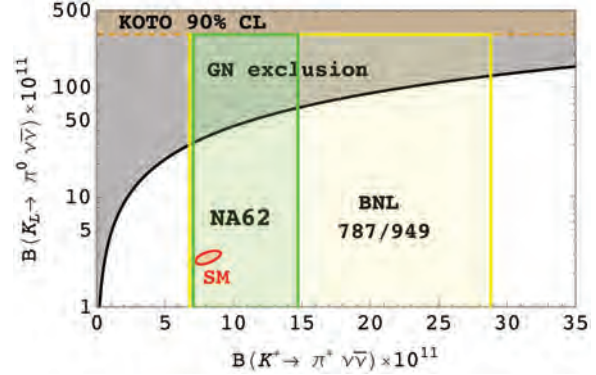


Figure 65.2: Summary of current situation for the golden modes $K \rightarrow \pi \nu \bar{\nu}$. The red ellipse shows the 1σ SM prediction with input from CKMfitter; the green (yellow) region corresponds to the NA62 (BNL787/949) 1σ measurement; and the dashed orange line marks the 90% CL KOTO upper bound. The black shaded region shows the GN exclusion.

Much theoretical work has explored beyond the SM scenarios that can populate this window as well as their correlations with other rare processes outside kaon physics. Although it would be relatively straightforward to establish the existence of new physics by observing deviations from their SM values in the $K \rightarrow \pi \nu \bar{\nu}$ modes, it would take much more extensive global fits to pinpoint the origin of any such deviation. Partial summaries with references focusing on quark flavor physics can be found in Refs. [9, 50–54]. Different possibilities emphasizing an interpretation of these modes as $K \rightarrow \pi + E_{\text{miss}}$ can be found in Refs. [55–57].

There is a subtlety in converting the GN bound extracted from measurements of $K^+ \rightarrow \pi^+ \nu \bar{\nu}$ into an upper bound for $K_L \rightarrow \pi^0 \nu \bar{\nu}$ as applied to KOTO [58]. This is due to a lack of sensitivity of the charged kaon experiments to a kinematic window near the pion mass. New physics appearing through a two body mode $K^+ \rightarrow \pi^+ X^0$, for an invisible X^0 with mass near the pion mass, has a much weaker constraint. The situation is illustrated in Fig. 65.3 which shows the BNL787/949 [42] and NA62 [59] 90% c.l. limits on $K^+ \rightarrow \pi^+ X^0$ as a function of m_{X^0} assuming X^0 is stable. The implied GN bound for $K_L \rightarrow \pi^0 X^0$, $B(K_L \rightarrow \pi^0 X^0) \lesssim 4.3 B(K^+ \rightarrow \pi^+ X^0)$ is shown as a blue line and can be compared with the actual KOTO [48] constraint on $K_L \rightarrow \pi^0 X^0$ in red. Notice that the upper bound derived from NA62 is lower than that derived from BNL787/949 except for a small mass window. For $120 \lesssim m_{X^0} \lesssim 150$ MeV, KOTO already has better sensitivity than that implied by the GN bound in this case. The possibility of new physics in this scenario has generated much theoretical speculation [60–70].

The search for a new light particle X^0 in $K^+ \rightarrow \pi^+ X^0$ has a long tradition covering both long-lived particles (*e.g.*, hyperphoton, axion, familon, *etc.*), and short-lived ones that decay to muon, electron, photon or neutrino pairs. The longstanding 90% CL upper limit on $K^+ \rightarrow \pi^+ X^0$ from BNL787/949 7.3×10^{-11} [40] for the case of massless X^0 has been slightly improved by NA62 to 5×10^{-11} as can be read from Fig. 65.3. These limits can also be reinterpreted in connection with a dark photon [71] or dark Z [72], and in this context NA48/2 also constrained the mode $B(K^\pm \rightarrow \pi^\pm A' \rightarrow \pi^\pm e^+ e^-)$ [73]. Complementary searches for new light particles in kaon experiments use modes with two pions and include the KTeV bound $B(K_L \rightarrow \pi^0 \pi^0 X^0 \rightarrow \pi^0 \pi^0 \mu^+ \mu^-) < 1 \times 10^{-10}$ [74] and the E391a bound $B(K_L \rightarrow \pi^0 \pi^0 X^0 \rightarrow \pi^0 \pi^0 \gamma \gamma) < 2.4 \times 10^{-7}$ [75].

Neutrino pair modes with one extra pion, $K \rightarrow \pi \pi \nu \bar{\nu}$, are similarly dominated by short distance contributions in the SM [76–78]. Even though they are theoretically clean, they occur with very

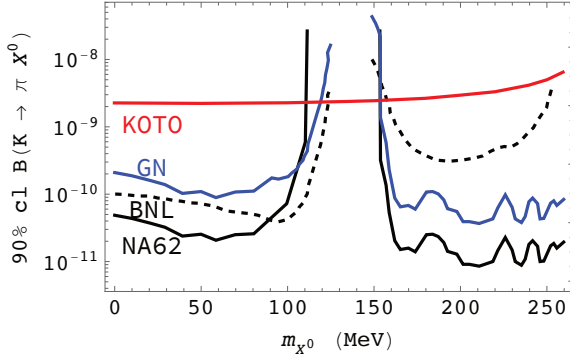


Figure 65.3: Summary of current situation for $K \rightarrow \pi X^0$. The solid (dashed) black line shows the exclusion limit for $K^+ \rightarrow \pi^+ X^0$ from NA62 (BNL787/949) assuming X^0 is stable. The blue line marks the constraint implied for $K_L \rightarrow \pi^0 X^0$ by the Grossman-Nir relation and the red line marks the current KOTO limit on $K^+ \rightarrow \pi^+ X^0$.

low rates with branching ratios of order 10^{-13} . The current best bound comes from KEK-391a, $B(K_L \rightarrow \pi^0 \pi^0 \nu \bar{\nu}) < 8.1 \times 10^{-7}$ at 90% CL [79]. There is also a bound for the charged kaon mode $B(K^+ \rightarrow \pi^+ \pi^0 \nu \bar{\nu}) < 4.3 \times 10^{-5}$ at 90% CL [80] from BNL-787. New physics contributions to these modes are discussed in [81].

65.4 Other constraints on Standard Model parameters

The decay $K_L \rightarrow \mu^+ \mu^-$ has a short distance contribution sensitive to the CKM parameter $\bar{\rho}$, given by [5]:

$$B_{\text{SD}}(K_L \rightarrow \mu^+ \mu^-) \approx 2.7 \times 10^{-4} |V_{cb}|^4 (\rho'_c - \bar{\rho})^2 \quad (65.4)$$

where the three terms correspond to the indirect CP violation, the interference, and the direct CP violation, respectively. The parameter a_S has been extracted by NA48/1 from a measurement of $K_S \rightarrow \pi^0 e^+ e^-$ with the result $|a_S| = 1.06^{+0.26}_{-0.21} \pm 0.07$ [96], as well as from a measurement of $K_S \rightarrow \pi^0 \mu^+ \mu^-$ with the result $|a_S| = 1.54^{+0.40}_{-0.32} \pm 0.06$ [97]. With current constraints on the CKM parameters, and assuming a positive sign for the interference term [95, 98], this implies that $B_{\text{CPV}}(K_L \rightarrow \pi^0 e^+ e^-) \approx (3.1 \pm 0.9) \times 10^{-11}$, where the three contributions to the central value from indirect, interference and direct CP violation are $(1.76, 0.9, 0.45) \times 10^{-11}$ respectively. It should be noted that more recent studies suggest a much larger uncertainty in the value of a_S [99].

$K_L \rightarrow \pi^0 e^+ e^-$ also has a CP -conserving component dominated by a two-photon intermediate state. This component can be decomposed into an absorptive and a dispersive part. The absorptive part can be extracted from the measurement of the low $m_{\gamma\gamma}$ region of the $K_L \rightarrow \pi^0 \gamma\gamma$ spectrum. The rate and the shape of the distribution $d\Gamma/dm_{\gamma\gamma}$ in $K_L \rightarrow \pi^0 \gamma\gamma$ are well described in chiral perturbation theory in terms of three (*a priori*) unknown parameters [100–103].

Both KTeV and NA48 have studied the mode $K_L \rightarrow \pi^0 \gamma\gamma$, reporting similar results. KTeV finds $B(K_L \rightarrow \pi^0 \gamma\gamma) = (1.29 \pm 0.03_{\text{stat}} \pm 0.05_{\text{sys}}) \times 10^{-6}$ [104], while NA48 finds $B(K_L \rightarrow \pi^0 \gamma\gamma) = (1.36 \pm 0.03_{\text{stat}} \pm 0.03_{\text{sys}} \pm 0.03_{\text{norm}}) \times 10^{-6}$ [105]. Both experiments are consistent with a negligible rate in the low $m_{\gamma\gamma}$ region, suggesting a very small CP -conserving component $B_{\text{CP}}(K_L \rightarrow \pi^0 e^+ e^-) \sim \mathcal{O}(10^{-13})$ [95, 103, 105]. There remains some model dependence in the estimate of the dispersive part of the CP -conserving $K_L \rightarrow \pi^0 e^+ e^-$ [95].

The related process, $K_L \rightarrow \pi^0 \gamma e^+ e^-$, is potentially an ad-

ditional background to $K_L \rightarrow \pi^0 e^+ e^-$ in some region of phase space [106]. This process has been observed with a branching ratio of $(1.62 \pm 0.14_{\text{stat}} \pm 0.09_{\text{sys}}) \times 10^{-8}$ [107].

where ρ'_c depends on the charm quark mass and is approximately 1.2. This decay, however, is dominated by a long-distance contribution from a two-photon intermediate state. The absorptive (imaginary) part of the long-distance component is determined by the measured rate for $K_L \rightarrow \gamma\gamma$ to be $B_{\text{abs}}(K_L \rightarrow \mu^+ \mu^-) = (6.64 \pm 0.07) \times 10^{-9}$; and it almost completely saturates the observed rate $B(K_L \rightarrow \mu^+ \mu^-) = (6.84 \pm 0.11) \times 10^{-9}$ [82]. The difference between the observed rate and the absorptive component can be attributed to the (coherent) sum of the short-distance amplitude and the real part of the long-distance amplitude. The latter cannot be derived directly from experiment [83], but can be estimated with certain assumptions [84, 85].

By contrast, the decay $K_L \rightarrow e^+ e^-$ is completely dominated by long distance physics and is easier to estimate. The result, $B(K_L \rightarrow e^+ e^-) \sim 9 \times 10^{-12}$ [83, 86], is in good agreement with the BNL-871 measurement, $(8.7^{+5.7}_{-4.1}) \times 10^{-12}$ [87].

The mode $K_S \rightarrow \mu^+ \mu^-$ has a short distance contribution proportional to the square of the CKM parameter $\bar{\eta}$ entering at the 10^{-13} level [10]. It also has long distance contributions arising from the two photon intermediate state which result in a rate $B(K_S \rightarrow \mu^+ \mu^-)_{\text{LD}} = 5.1 \times 10^{-12}$ [10]. There is a 90% CL limit $B(K_S \rightarrow \mu^+ \mu^-) < 2.1 \times 10^{-10}$ from LHCb [88, 89]. The interplay between $K_L \rightarrow \mu^+ \mu^-$ and $K_S \rightarrow \mu^+ \mu^-$ has been the subject of [90, 91], and it has been pointed out that a measurement of time-dependent interference effects could be used to extract information on CKM angles from $K \rightarrow \mu^+ \mu^-$ measurements [92].

The decay $K_L \rightarrow \pi^0 e^+ e^-$ is sensitive to the CKM parameter η through its CP -violating component. There are both direct and indirect CP -violating amplitudes that can interfere. The direct CP -violating amplitude is short distance dominated and has been calculated in detail within the SM [5]. The indirect CP -violating amplitude can be inferred from a measurement of $K_S \rightarrow \pi^0 e^+ e^-$. The complete CP -violating contribution to the rate can be written as [93–95]:

$$B_{\text{CPV}} \approx \left[15.7 |a_S|^2 \pm 1.4 \left(\frac{|V_{cb}|^2 \bar{\eta}}{10^{-4}} \right) |a_S| + 0.12 \left(\frac{|V_{cb}|^2 \bar{\eta}}{10^{-4}} \right)^2 \right] \times 10^{-12} \quad (65.5)$$

The decay $K_L \rightarrow \pi^0 e^+ e^-$ also has a CP -conserving component dominated by a two-photon intermediate state. This component can be decomposed into an absorptive and a dispersive part. The absorptive part can be extracted from the measurement of the low $m_{\gamma\gamma}$ region of the $K_L \rightarrow \pi^0 \gamma\gamma$ spectrum. The rate and the shape of the distribution $d\Gamma/dm_{\gamma\gamma}$ in $K_L \rightarrow \pi^0 \gamma\gamma$ are well described in chiral perturbation theory in terms of three (*a priori*) unknown parameters [100–103].

Both KTeV and NA48 have studied the mode $K_L \rightarrow \pi^0 \gamma\gamma$, reporting similar results. KTeV finds $B(K_L \rightarrow \pi^0 \gamma\gamma) = (1.29 \pm 0.03_{\text{stat}} \pm 0.05_{\text{sys}}) \times 10^{-6}$ [104], while NA48 finds $B(K_L \rightarrow \pi^0 \gamma\gamma) = (1.36 \pm 0.03_{\text{stat}} \pm 0.03_{\text{sys}} \pm 0.03_{\text{norm}}) \times 10^{-6}$ [105]. Both experiments are consistent with a negligible rate in the low $m_{\gamma\gamma}$ region, suggesting a very small CP -conserving component $B_{\text{CP}}(K_L \rightarrow \pi^0 e^+ e^-) \sim \mathcal{O}(10^{-13})$ [95, 103, 105]. There remains some model dependence in the estimate of the dispersive part of the CP -conserving $K_L \rightarrow \pi^0 e^+ e^-$ [95].

The related process, $K_L \rightarrow \pi^0 \gamma e^+ e^-$, is potentially an additional background to $K_L \rightarrow \pi^0 e^+ e^-$ in some region of phase space [106]. This process has been observed with a branching ratio of $(1.62 \pm 0.14_{\text{stat}} \pm 0.09_{\text{sys}}) \times 10^{-8}$ [107].

The decay $K_L \rightarrow \gamma\gamma e^+ e^-$ constitutes the dominant background to $K_L \rightarrow \pi^0 e^+ e^-$. It was first observed by BNL-845 [108], and subsequently confirmed with a much larger sample by KTeV [109]. It has been estimated that this background will enter at about the 10^{-10} level [110, 111], comparable to or larger than the signal level. Because of this, the observation of $K_L \rightarrow \pi^0 e^+ e^-$ at the SM level will depend on background subtraction with good statistics. Possible alternative strategies are discussed in Ref. [95] and references cited therein.

The 90% CL upper bound for the process $K_L \rightarrow \pi^0 e^+ e^-$ is 2.8×10^{-10} [111]. For the closely related muonic process, the published upper bound is $B(K_L \rightarrow \pi^0 \mu^+ \mu^-) \leq 3.8 \times 10^{-10}$ [112], compared with the SM prediction of $(1.9 \pm 0.5) \times 10^{-11}$. The latter assumes positive interference between the direct- and indirect- CP violating components and includes a CP -conserving component which contributes about 30% of the total [10, 113].

A study of $K_L \rightarrow \pi^0 \mu^+ \mu^-$ has indicated that it might be possible to extract the direct CP -violating contribution by a joint study of the Dalitz plot variables and the components of the μ^+ polarization [114]. The latter tends to be quite substantial so that large statistics may not be necessary.

Combined information from $K_L \rightarrow \pi^0 \ell^+ \ell^-$ as well as $K_L \rightarrow \mu^+ \mu^-$ complements the $K \rightarrow \pi \nu \bar{\nu}$ measurements in constraining physics beyond the SM [115].

65.5 Other long distance dominated modes

The decays $K^+ \rightarrow \pi^+ \ell^+ \ell^-$ ($\ell = e$ or μ) have received considerable attention. The rate and spectrum have been measured for

both the electron and muon modes [116–121]. A review of the theoretical status of these modes can be found in [99, 122].

Ref. [93, 94] has proposed a parameterization inspired by chiral perturbation theory, which provides a successful description of data but indicates the presence of large corrections beyond leading order. More work is needed to fully understand the origin of these large corrections. The mode $K^+ \rightarrow \pi^+\pi^0 e^+ e^-$, analyzed by NA48/2 [123], is also dominated by long distance physics but it has been argued that measuring asymmetries can provide information on the short distance components [124]. The current status of these modes is discussed in [125].

The decay $K^+ \rightarrow \pi^+\gamma\gamma$ can be predicted in terms of one unknown parameter to leading order in χ PT resulting in a correlation between the rate and the diphoton mass spectrum [126]. Certain important corrections at the next order are also known [127]. The rate was first measured by E787 [128], and NA48/2 [129] has obtained a more precise result with a 6% error, as well as the corresponding spectrum fits. The most recent, and precise, result is from NA62 based on a sample of 232 events [130] but is still insufficient to distinguish between the leading order and next order χ PT parameterizations. The NA48 and NA62 results have been combined in [131].

Much information has been recorded by KTeV and NA48 on the rates and spectrum for the Dalitz pair conversion modes $K_L \rightarrow \ell^+\ell^-\gamma$ [132, 133], and $K_L \rightarrow \ell^+\ell^-\ell'^+\ell'^-$ for $\ell, \ell' = e$ or μ [22, 134]. All these results are used to test hadronic models and should eventually help unravel the underlying physics in $K_L \rightarrow \mu^+\mu^-$ [85, 90, 135].

References

- [1] L. Littenberg and G. Valencia, *Ann. Rev. Nucl. Part. Sci.* **43**, 729 (1993), [hep-ph/9303225].
- [2] J. L. Ritchie and S. G. Wojcicki, *Rev. Mod. Phys.* **65**, 1149 (1993).
- [3] B. Winstein and L. Wolfenstein, *Rev. Mod. Phys.* **65**, 1113 (1993).
- [4] A. Pich, *Rept. Prog. Phys.* **58**, 563 (1995), [hep-ph/9502366].
- [5] G. Buchalla, A. J. Buras and M. E. Lautenbacher, *Rev. Mod. Phys.* **68**, 1125 (1996), [hep-ph/9512380].
- [6] G. D'Ambrosio and G. Isidori, *Int. J. Mod. Phys. A* **13**, 1 (1998), [hep-ph/9611284].
- [7] P. Buchholz and B. Renk, *Prog. Part. Nucl. Phys.* **39**, 253 (1997).
- [8] A. R. Barker and S. H. Kettell, *Ann. Rev. Nucl. Part. Sci.* **50**, 249 (2000), [hep-ex/0009024].
- [9] A. J. Buras, F. Schwab and S. Uhlig, *Rev. Mod. Phys.* **80**, 965 (2008), [hep-ph/0405132].
- [10] V. Cirigliano *et al.*, *Rev. Mod. Phys.* **84**, 399 (2012), [arXiv:1107.6001].
- [11] D. Bryman *et al.*, *Ann. Rev. Nucl. Part. Sci.* **61**, 331 (2011).
- [12] T. K. Komatsubara, *Prog. Part. Nucl. Phys.* **67**, 995 (2012), [arXiv:1203.6437].
- [13] A. Ceccucci, *Annual Review of Nuclear and Particle Science* **71**, 1 (2021), URL <https://doi.org/10.1146/annurev-nucl-102419-054905>.
- [14] A. Atre *et al.*, *JHEP* **05**, 030 (2009), [arXiv:0901.3589].
- [15] L. S. Littenberg and R. Shrock, *Phys. Lett.* **B491**, 285 (2000), [hep-ph/0005285].
- [16] A. Sher *et al.*, *Phys. Rev.* **D72**, 012005 (2005), [hep-ex/0502020].
- [17] E. Cortina Gil *et al.* (NA62), *Phys. Rev. Lett.* **127**, 13, 131802 (2021), [arXiv:2105.06759].
- [18] D. Ambrose *et al.* (BNL), *Phys. Rev. Lett.* **81**, 5734 (1998), [hep-ex/9811038].
- [19] E. Abouzaid *et al.* (KTeV), *Phys. Rev. Lett.* **100**, 131803 (2008), [arXiv:0711.3472].
- [20] E. Cortina Gil *et al.* (NA62) (2022), [arXiv:2202.00331].
- [21] E. Cortina Gil *et al.* (NA62), *Phys. Lett.* **B797**, 134794 (2019), [arXiv:1905.07770].
- [22] A. Alavi-Harati *et al.* (KTeV), *Phys. Rev. Lett.* **90**, 141801 (2003), [hep-ex/0212002].
- [23] J. S. Hagelin and L. S. Littenberg, *Prog. Part. Nucl. Phys.* **23**, 1 (1989).
- [24] M. Lu and M. B. Wise, *Phys. Lett.* **B324**, 461 (1994), [hep-ph/9401204].
- [25] A. F. Falk, A. Lewandowski and A. A. Petrov, *Phys. Lett.* **B505**, 107 (2001), [hep-ph/0012099].
- [26] J. Charles *et al.*, *Phys. Rev.* **D84**, 033005 (2011), [arXiv:1106.4041].
- [27] M. Bona *et al.* (UTfit), *JHEP* **03**, 049 (2008), [arXiv:0707.0636].
- [28] J. Brod, M. Gorbahn and E. Stamou, *Phys. Rev.* **D83**, 034030 (2011), [arXiv:1009.0947].
- [29] F. Mescia and C. Smith, *Phys. Rev.* **D76**, 034017 (2007), [arXiv:0705.2025].
- [30] T. Inami and C. S. Lim, *Prog. Theor. Phys.* **65**, 297 (1981), [Erratum: *Prog. Theor. Phys.* **65**, 1772 (1981)].
- [31] G. Buchalla and A. J. Buras, *Nucl. Phys.* **B548**, 309 (1999), [hep-ph/9901288].
- [32] M. Misiak and J. Urban, *Phys. Lett.* **B451**, 161 (1999), [hep-ph/9901278].
- [33] A. J. Buras *et al.*, *Phys. Rev. Lett.* **95**, 261805 (2005), [hep-ph/0508165].
- [34] A. J. Buras *et al.*, *JHEP* **11**, 002 (2006), [Erratum: *JHEP* **11**, 167 (2012)], [hep-ph/0603079].
- [35] J. Brod and M. Gorbahn, *Phys. Rev.* **D78**, 034006 (2008), [arXiv:0805.4119].
- [36] G. Isidori, F. Mescia and C. Smith, *Nucl. Phys.* **B718**, 319 (2005), [hep-ph/0503107].
- [37] S. Adler *et al.* (E787), *Phys. Rev. Lett.* **88**, 041803 (2002), [hep-ex/0111091].
- [38] S. Adler *et al.* (E787), *Phys. Rev. Lett.* **84**, 3768 (2000), [hep-ex/0002015].
- [39] S. S. Adler *et al.* (E787), *Phys. Lett.* **B537**, 211 (2002), [hep-ex/0201037].
- [40] V. V. Anisimovsky *et al.* (E949), *Phys. Rev. Lett.* **93**, 031801 (2004), [hep-ex/0403036].
- [41] A. V. Artamonov *et al.* (E949), *Phys. Rev. Lett.* **101**, 191802 (2008), [arXiv:0808.2459].
- [42] A. V. Artamonov *et al.* (BNL-E949), *Phys. Rev.* **D79**, 092004 (2009), [arXiv:0903.0030].
- [43] E. Cortina Gil *et al.* (NA62), *JHEP* **06**, 093 (2021), [arXiv:2103.15389].
- [44] A. J. Buras *et al.*, *JHEP* **11**, 033 (2015), [arXiv:1503.02693].
- [45] L. S. Littenberg, *Phys. Rev.* **D39**, 3322 (1989).
- [46] G. Buchalla and G. Isidori, *Phys. Lett.* **B440**, 170 (1998), [hep-ph/9806501].
- [47] Y. Grossman and Y. Nir, *Phys. Lett.* **B398**, 163 (1997), [hep-ph/9701313].
- [48] J. K. Ahn *et al.* (KOTO), *Phys. Rev. Lett.* **122**, 021802 (2019), [arXiv:1810.09655].
- [49] J. K. Ahn *et al.* (KOTO), *Phys. Rev. Lett.* **126**, 121801 (2021), [arXiv:2012.07571].
- [50] G. D'Ambrosio and G. Isidori, *Phys. Lett.* **B530**, 108 (2002), [hep-ph/0112135].
- [51] D. Bryman *et al.*, *Int. J. Mod. Phys. A* **21**, 487 (2006), [hep-ph/0505171].
- [52] A. J. Buras, D. Buttazzo and R. Knegjens, *JHEP* **11**, 166 (2015), [arXiv:1507.08672].
- [53] X.-G. He, G. Valencia and K. Wong, *Eur. Phys. J.* **C78**, 472 (2018), [arXiv:1804.07449].

- [54] J. Aebischer, A. J. Buras and J. Kumar, *JHEP* **12**, 097 (2020), [arXiv:2006.01138].
- [55] M. Bordone *et al.*, *Eur. Phys. J.* **C77**, 618 (2017), [arXiv:1705.10729].
- [56] X.-G. He, J. Tandean and G. Valencia, *Phys. Lett.* **B797**, 134842 (2019), [arXiv:1904.04043].
- [57] F. F. Deppisch, K. Fridell and J. Harz, *JHEP* **12**, 186 (2020), [arXiv:2009.04494].
- [58] K. Fuyuto, W.-S. Hou and M. Kohda, *Phys. Rev. Lett.* **114**, 171802 (2015), [arXiv:1412.4397].
- [59] E. Cortina Gil *et al.* (NA62), *JHEP* **03**, 058 (2021), [arXiv:2011.11329].
- [60] T. Kitahara *et al.*, *Phys. Rev. Lett.* **124**, 071801 (2020), [arXiv:1909.11111].
- [61] D. Egana-Ugrinovic, S. Homiller and P. Meade, *Phys. Rev. Lett.* **124**, 191801 (2020), [arXiv:1911.10203].
- [62] P. S. B. Dev, R. N. Mohapatra and Y. Zhang, *Phys. Rev. D* **101**, 075014 (2020), [arXiv:1911.12334].
- [63] M. Fabbrichesi and E. Gabrielli, *Eur. Phys. J. C* **80**, 532 (2020), [arXiv:1911.03755].
- [64] Y. Liao *et al.*, *Phys. Rev. D* **102**, 055005 (2020), [arXiv:2005.00753].
- [65] R. Ziegler, J. Zupan and R. Zwicky, *JHEP* **07**, 229 (2020), [arXiv:2005.00451].
- [66] T. Li, X.-D. Ma and M. A. Schmidt, *Phys. Rev. D* **101**, 055019 (2020), [arXiv:1912.10433].
- [67] X.-G. He *et al.*, *JHEP* **08**, 034 (2020), [arXiv:2005.02942].
- [68] M. Hostert, K. Kaneta and M. Pospelov, *Phys. Rev. D* **102**, 055016 (2020), [arXiv:2005.07102].
- [69] S. Gori, G. Perez and K. Tobioka, *JHEP* **08**, 110 (2020), [arXiv:2005.05170].
- [70] T. B. de Melo *et al.*, *Phys. Rev. D* **103**, 115001 (2021), [arXiv:2102.06262].
- [71] M. Pospelov, *Phys. Rev.* **D80**, 095002 (2009), [arXiv:0811.1030].
- [72] H. Davoudiasl, H.-S. Lee and W. J. Marciano, *Phys. Rev.* **D89**, 095006 (2014), [arXiv:1402.3620].
- [73] J. R. Batley *et al.* (NA48/2), *Phys. Lett.* **B746**, 178 (2015), [arXiv:1504.00607].
- [74] E. Abouzaid *et al.* (KTeV), *Phys. Rev. Lett.* **107**, 201803 (2011), [arXiv:1105.4800].
- [75] Y. C. Tung *et al.* (E391a), *Phys. Rev. Lett.* **102**, 051802 (2009), [arXiv:0810.4222].
- [76] L. S. Littenberg and G. Valencia, *Phys. Lett.* **B385**, 379 (1996), [hep-ph/9512413].
- [77] C.-W. Chiang and F. J. Gilman, *Phys. Rev.* **D62**, 094026 (2000), [hep-ph/0007063].
- [78] C. Q. Geng, I. J. Hsu and Y. C. Lin, *Phys. Rev.* **D50**, 5744 (1994), [hep-ph/9406313].
- [79] R. Ogata *et al.* (E391a), *Phys. Rev.* **D84**, 052009 (2011), [arXiv:1106.3404].
- [80] S. Adler *et al.* (E787), *Phys. Rev.* **D63**, 032004 (2001), [hep-ex/0009055].
- [81] C.-Q. Geng and J. Tandean, *Phys. Rev. D* **102**, 115021 (2020), [arXiv:2009.00608].
- [82] D. Ambrose *et al.* (E871), *Phys. Rev. Lett.* **84**, 1389 (2000).
- [83] G. Valencia, *Nucl. Phys.* **B517**, 339 (1998), [hep-ph/9711377].
- [84] G. D'Ambrosio, G. Isidori and J. Portoles, *Phys. Lett.* **B423**, 385 (1998), [hep-ph/9708326].
- [85] G. Isidori and R. Unterdorfer, *JHEP* **01**, 009 (2004), [hep-ph/0311084].
- [86] D. Gomez Dumm and A. Pich, *Phys. Rev. Lett.* **80**, 4633 (1998), [hep-ph/9801298].
- [87] D. Ambrose *et al.* (BNL E871), *Phys. Rev. Lett.* **81**, 4309 (1998), [hep-ex/9810007].
- [88] R. Aaij *et al.* (LHCb), *Eur. Phys. J.* **C77**, 678 (2017), [arXiv:1706.00758].
- [89] R. Aaij *et al.* (LHCb), *Phys. Rev. Lett.* **125**, 231801 (2020), [arXiv:2001.10354].
- [90] G. D'Ambrosio and T. Kitahara, *Phys. Rev. Lett.* **119**, 201802 (2017), [arXiv:1707.06999].
- [91] V. Chobanova *et al.*, *JHEP* **05**, 024 (2018), [arXiv:1711.11030].
- [92] A. Dery *et al.*, *JHEP* **07**, 103 (2021), [arXiv:2104.06427].
- [93] G. D'Ambrosio *et al.*, *JHEP* **08**, 004 (1998), [hep-ph/9808289].
- [94] C. Dib, I. Dunietz and F. J. Gilman, *Phys. Rev.* **D39**, 2639 (1989).
- [95] G. Buchalla, G. D'Ambrosio and G. Isidori, *Nucl. Phys.* **B672**, 387 (2003), [hep-ph/0308008].
- [96] J. R. Batley *et al.* (NA48/1), *Phys. Lett.* **B576**, 43 (2003), [hep-ex/0309075].
- [97] J. R. Batley *et al.* (NA48/1), *Phys. Lett.* **B599**, 197 (2004), [hep-ex/0409011].
- [98] S. Friot, D. Greynat and E. De Rafael, *Phys. Lett.* **B595**, 301 (2004), [hep-ph/0404136].
- [99] G. D'Ambrosio, D. Greynat and M. Knecht, *JHEP* **02**, 049 (2019), [arXiv:1812.00735].
- [100] G. Ecker, A. Pich and E. de Rafael, *Phys. Lett.* **B237**, 481 (1990).
- [101] L. Cappiello, G. D'Ambrosio and M. Miragliuolo, *Phys. Lett.* **B298**, 423 (1993).
- [102] A. G. Cohen, G. Ecker and A. Pich, *Phys. Lett.* **B304**, 347 (1993).
- [103] F. Gabbiani and G. Valencia, *Phys. Rev.* **D66**, 074006 (2002), [hep-ph/0207189].
- [104] E. Abouzaid *et al.* (KTeV), *Phys. Rev.* **D77**, 112004 (2008), [arXiv:0805.0031].
- [105] A. Lai *et al.* (NA48), *Phys. Lett.* **B536**, 229 (2002), [hep-ex/0205010].
- [106] J. F. Donoghue and F. Gabbiani, *Phys. Rev.* **D56**, 1605 (1997), [hep-ph/9702278].
- [107] E. Abouzaid *et al.* (KTeV), *Phys. Rev.* **D76**, 052001 (2007), [arXiv:0706.4074].
- [108] W. M. Morse *et al.*, *Phys. Rev.* **D45**, 36 (1992).
- [109] A. Alavi-Harati *et al.* (KTeV), *Phys. Rev.* **D64**, 012003 (2001), [hep-ex/0010059].
- [110] H. B. Greenlee, *Phys. Rev.* **D42**, 3724 (1990).
- [111] A. Alavi-Harati *et al.* (KTeV), *Phys. Rev. Lett.* **93**, 021805 (2004), [hep-ex/0309072].
- [112] A. Alavi-Harati *et al.* (KTeV), *Phys. Rev. Lett.* **84**, 5279 (2000), [hep-ex/0001006].
- [113] G. Isidori, C. Smith and R. Unterdorfer, *Eur. Phys. J.* **C36**, 57 (2004), [hep-ph/0404127].
- [114] M. V. Diwan, H. Ma and T. L. Trueman, *Phys. Rev.* **D65**, 054020 (2002), [hep-ph/0112350].
- [115] F. Mescia, C. Smith and S. Trine, *JHEP* **08**, 088 (2006), [hep-ph/0606081].
- [116] R. Appel *et al.* (E865), *Phys. Rev. Lett.* **83**, 4482 (1999), [hep-ex/9907045].
- [117] J. R. Batley *et al.* (NA48/2), *Phys. Lett.* **B677**, 246 (2009), [arXiv:0903.3130].
- [118] S. Adler *et al.* (E787), *Phys. Rev. Lett.* **79**, 4756 (1997), [hep-ex/9708012].
- [119] H. Ma *et al.* (e865), *Phys. Rev. Lett.* **84**, 2580 (2000), [hep-ex/9910047].

- [120] H. K. Park *et al.* (HyperCP), Phys. Rev. Lett. **88**, 111801 (2002), [hep-ex/01110033].
- [121] J. R. Batley *et al.* (NA48/2), Phys. Lett. **B697**, 107 (2011), [arXiv:1011.4817].
- [122] G. D'Ambrosio, D. Greynat and M. Knecht, Phys. Lett. B **797**, 134891 (2019), [arXiv:1906.03046].
- [123] J. R. Batley *et al.* (NA48/2), Phys. Lett. **B788**, 552 (2019), [arXiv:1809.02873].
- [124] L. Cappiello *et al.*, Eur. Phys. J. **C72**, 1872 (2012), [Erratum: Eur. Phys. J. **C72**, 2208 (2012)], [arXiv:1112.5184].
- [125] L. Cappiello, O. Catà and G. D'Ambrosio, Eur. Phys. J. **C78**, 265 (2018), [arXiv:1712.10270].
- [126] G. Ecker, A. Pich and E. de Rafael, Nucl. Phys. **B303**, 665 (1988).
- [127] G. D'Ambrosio and J. Portoles, Phys. Lett. **B386**, 403 (1996), [Erratum: Phys. Lett. **B395**, 389 (1997)], [hep-ph/9606213].
- [128] P. Kitching *et al.* (E787), Phys. Rev. Lett. **79**, 4079 (1997), [hep-ex/9708011].
- [129] J. R. Batley *et al.* (NA48/2), Phys. Lett. **B730**, 141 (2014), [arXiv:1310.5499].
- [130] C. Lazzeroni *et al.* (NA62), Phys. Lett. **B732**, 65 (2014), [arXiv:1402.4334].
- [131] B. Velghe (NA62-RK, NA48/2), Nucl. Part. Phys. Proc. **273-275**, 2720 (2016).
- [132] A. Alavi-Harati *et al.* (KTeV), Phys. Rev. Lett. **87**, 071801 (2001).
- [133] E. Abouzaid *et al.* (KTeV), Phys. Rev. Lett. **99**, 051804 (2007), [hep-ex/0702039].
- [134] V. Fanti *et al.* (NA48), Phys. Lett. **B458**, 553 (1999).
- [135] G. D'Ambrosio, D. Greynat and G. Vulvert, Eur. Phys. J. **C73**, 2678 (2013), [arXiv:1309.5736].

66. CPT Invariance Tests in Neutral Kaon Decay

Revised August 2021 by M. Antonelli (INFN, Frascati), G. D'Ambrosio (INFN, Napoli) and M.S. Sozzi (Pisa U.).

CPT theorem is based on three assumptions: quantum field theory, locality, and Lorentz invariance, and thus it is a fundamental probe of our basic understanding of particle physics. Strangeness oscillation in $K^0 - \bar{K}^0$ system, described by the equation

$$i \frac{d}{dt} \begin{bmatrix} K^0 \\ \bar{K}^0 \end{bmatrix} = [M - i\Gamma/2] \begin{bmatrix} K^0 \\ \bar{K}^0 \end{bmatrix},$$

where M and Γ are hermitian matrices (see PDG review [1], references [2,3], and KLOE paper [4] for notations and previous literature), allows a very accurate test of *CPT* symmetry; indeed since *CPT* requires $M_{11} = M_{22}$ and $\Gamma_{11} = \Gamma_{22}$, the mass and width eigenstates, $K_{S,L}$, have a *CPT*-violating piece, δ , in addition to the usual *CPT*-conserving parameter ϵ :

$$K_{S,L} = \frac{1}{\sqrt{2(1+|\epsilon_{S,L}|^2)}} \left[(1+\epsilon_{S,L}) K^0 \pm (1-\epsilon_{S,L}) \bar{K}^0 \right]$$

$$\epsilon_{S,L} = \frac{-i\Im(M_{12}) - \frac{1}{2}\Im(\Gamma_{12}) \mp \frac{1}{2} [M_{11} - M_{22} - \frac{i}{2}(\Gamma_{11} - \Gamma_{22})]}{m_L - m_S + i(\Gamma_S - \Gamma_L)/2}$$

$$\equiv \epsilon \pm \delta. \quad (66.1)$$

Using the phase convention $\Im(\Gamma_{12}) = 0$, we determine the phase of ϵ to be $\varphi_{SW} \equiv \arctan \frac{2(m_L - m_S)}{\Gamma_S - \Gamma_L}$. Imposing unitarity to an arbitrary combination of K^0 and \bar{K}^0 wave functions, we obtain the Bell-Steinberger relation [5] connecting *CP* and *CPT* violation in the mass matrix to *CP* and *CPT* violation in the decay; in fact, neglecting $\mathcal{O}(\epsilon)$ corrections to the coefficient of the *CPT*-violating parameter, δ , we can write [4]

$$\left[\frac{\Gamma_S + \Gamma_L}{\Gamma_S - \Gamma_L} + i \tan \phi_{SW} \right] \left[\frac{\Re(\epsilon)}{1+|\epsilon|^2} - i\Im(\delta) \right] = \frac{1}{\Gamma_S - \Gamma_L} \sum_f A_L(f) A_S^*(f), \quad (66.2)$$

where $A_{L,S}(f) \equiv A(K_{L,S} \rightarrow f)$. We stress that this relation is phase-convention-independent. The advantage of the neutral kaon system is that only a few decay modes give significant contributions to the r.h.s. in Eq. (66.2); in fact, defining for the hadronic modes

$$\alpha_i \equiv \frac{1}{\Gamma_S} \langle A_L(i) A_S^*(i) \rangle = \eta_i \mathcal{B}(K_S \rightarrow i),$$

$$i = \pi^0 \pi^0, \pi^+ \pi^- (\gamma), 3\pi^0, \pi^0 \pi^+ \pi^- (\gamma), \quad (66.3)$$

the recent data from CPLEAR, KLOE, KTeV, and NA48 have led to the following determinations (the analysis described in Ref. [4] has been updated by using the recent measurements of K_L branching ratios from KTeV [6, 7], NA48 [8, 9], the results described in the *CP* violation in K_L decays minireview, and the KLOE result [10])

$$\alpha_{\pi^+ \pi^-} = ((1.121 \pm 0.010) + i(1.061 \pm 0.010)) \times 10^{-3},$$

$$\alpha_{\pi^0 \pi^0} = ((0.493 \pm 0.005) + i(0.471 \pm 0.005)) \times 10^{-3},$$

$$\alpha_{\pi^+ \pi^- \pi^0} = ((0 \pm 2) + i(0 \pm 2)) \times 10^{-6},$$

$$|\alpha_{\pi^0 \pi^0 \pi^0}| < 1.5 \times 10^{-6} \text{ at } 95\% \text{ CL}. \quad (66.4)$$

The semileptonic contribution to the right-handed side of Eq. (66.2) requires the determination of several observables: we

define [2, 3]

$$\begin{aligned} \mathcal{A}(K^0 \rightarrow \pi^- l^+ \nu) &= \mathcal{A}_0(1 - y), \\ \mathcal{A}(K^0 \rightarrow \pi^+ l^- \nu) &= \mathcal{A}_0^*(1 + y^*)(x_+ - x_-)^*, \\ \mathcal{A}(\bar{K}^0 \rightarrow \pi^+ l^- \nu) &= \mathcal{A}_0^*(1 + y^*), \\ \mathcal{A}(\bar{K}^0 \rightarrow \pi^- l^+ \nu) &= \mathcal{A}_0(1 - y)(x_+ + x_-), \end{aligned} \quad (66.5)$$

where x_+ (x_-) describes the violation of the $\Delta S = \Delta Q$ rule in *CPT*-conserving (violating) decay amplitudes, and y parameterizes *CPT* violation for $\Delta S = \Delta Q$ transitions. Taking advantage of their tagged $K^0(\bar{K}^0)$ beams, CPLEAR has measured $\Im(x_+)$, $\Re(x_-)$, $\Im(\delta)$, and $\Re(\delta)$ [11]. These determinations have been improved in Ref. [4] by including the information $A_S - A_L = 4[\Re(\delta) + \Re(x_-)]$ (valid at first order in the small parameters), where $A_{L,S}$ are the K_L and K_S semileptonic charge asymmetries, respectively, from the PDG [12] and the new KLOE semileptonic measurement [13]. Here we are also including the *T*-violating asymmetry measurement from CPLEAR [14] with a finer binning than appearing in the published article.

Table 66.1: Values, errors, and correlation coefficients for $\Re(\delta)$, $\Im(\delta)$, $\Re(x_-)$, $\Im(x_+)$, and $A_S + A_L$ obtained from a combined fit, including KLOE [4, 13] and CPLEAR [14].

	value	Correlations coefficients			
$\Re(\delta)$	$(4.3 \pm 2.7) \times 10^{-4}$	1			
$\Im(\delta)$	$(-0.9 \pm 0.6) \times 10^{-2}$	-0.40	1		
$\Re(x_-)$	$(-0.22 \pm 0.10) \times 10^{-2}$	-0.14	-0.30	1	
$\Im(x_+)$	$(0.06 \pm 0.19) \times 10^{-2}$	-0.12	-0.02	0.34	1
$A_S + A_L$	$(-0.23 \pm 0.38) \times 10^{-2}$	-0.12	-0.29	0.94	0.18

The value $A_S + A_L$ in Table 66.1 can be directly included in the semileptonic contributions to the Bell Steinberger relations in Eq. (66.2)

$$\begin{aligned} \sum_{\pi l \nu} \langle A_L(\pi l \nu) A_S^*(\pi l \nu) \rangle \\ = 2\Gamma(K_L \rightarrow \pi l \nu) (\Re(\epsilon) - \Re(y) - i(\Im(x_+) + \Im(\delta))) \\ = 2\Gamma(K_L \rightarrow \pi l \nu) ((A_S + A_L)/4 - i(\Im(x_+) + \Im(\delta))). \end{aligned} \quad (66.6)$$

Defining

$$\alpha_{\pi l \nu} \equiv \frac{1}{\Gamma_S} \sum_{\pi l \nu} \langle A_L(\pi l \nu) A_S^*(\pi l \nu) \rangle + 2i \frac{\tau_{KS}}{\tau_{KL}} \mathcal{B}(K_L \rightarrow \pi l \nu) \Im(\delta), \quad (66.7)$$

we find:

$$\alpha_{\pi l \nu} = ((-0.1 \pm 0.2) + i(-0.1 \pm 0.5)) \times 10^{-5}. \quad (66.8)$$

Table 66.2: Summary of results: values, errors, and correlation coefficients for $\Re(\epsilon)$, $\Im(\delta)$, $\Re(\delta)$, and $\Re(x_-)$.

	value	Correlations coefficients			
$\Re(\epsilon)$	$(161.2 \pm 0.5) \times 10^{-5}$	+1			
$\Im(\delta)$	$(-0.3 \pm 1.4) \times 10^{-5}$	+0.08	1		
$\Re(\delta)$	$(2.6 \pm 2.5) \times 10^{-4}$	+0.00	-0.05	1	
$\Re(x_-)$	$(-2.7 \pm 1.0) \times 10^{-3}$	+0.05	0.13	-0.30	1

The analysis of semileptonic decay asymmetries implicitly assumes Lepton Flavour Universality (LFU) of any effect violating *CPT* or $\Delta S = \Delta Q$, through the use of a single set of x, y parameters, consistently with the availability of experimental information on A_S for the electron mode only. The explicit LFU assumption in the input BR measurements has been lifted exploiting the measurement of $BR(K_S \rightarrow \pi \mu \nu)$ Ref. [15], with no effect on the numerical results.

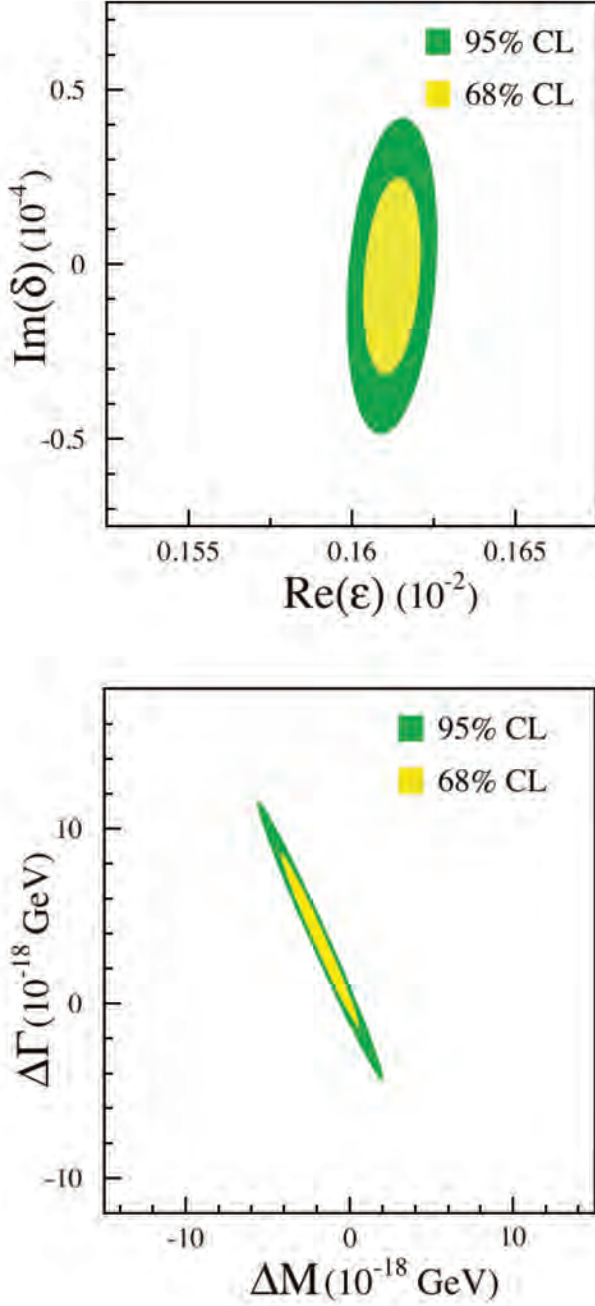


Figure 66.1: Top: allowed region at 68% and 95% C.L. in the $\Re(\epsilon)$, $\Im(\delta)$ plane. Bottom: allowed region at 68% and 95% C.L. in the ΔM , $\Delta\Gamma$ plane.

Inserting the values of the α parameters into Eq. (66.2), we find

$$\begin{aligned}\Re(\epsilon) &= (161.2 \pm 0.5) \times 10^{-5}, \\ \Im(\delta) &= (-0.3 \pm 1.4) \times 10^{-5}.\end{aligned}\quad (66.9)$$

The complete information on Eq. (66.9) is given in Table 66.2.

Now the agreement with CPT conservation, $\Im(\delta) = \Re(\delta) = \Re(x_-) = 0$, is at 18% C.L.

The allowed region in the $\Re(\epsilon) - \Im(\delta)$ plane at 68% CL and 95% C.L. is shown in the top panel of Fig. 66.1.

The process giving the largest contribution to the size of the allowed region is $K_L \rightarrow \pi^+ \pi^-$, through the uncertainty on ϕ_{+-} .

The limits on $\Im(\delta)$ and $\Re(\delta)$ can be used to constrain the $K^0 - \bar{K}^0$ mass and width difference

$$\delta = \frac{i(m_{K^0} - m_{\bar{K}^0}) + \frac{1}{2}(\Gamma_{K^0} - \Gamma_{\bar{K}^0})}{\Gamma_S - \Gamma_L} \cos \phi_{SW} e^{i\phi_{SW}} [1 + \mathcal{O}(\epsilon)].$$

The allowed region in the $\Delta M = (m_{K^0} - m_{\bar{K}^0})$, $\Delta\Gamma = (\Gamma_{K^0} - \Gamma_{\bar{K}^0})$ plane is shown in the bottom panel of Fig. 66.1. As a result, we improve on the previous limits (see for instance, P. Bloch in Ref. [12]) and in the limit $\Gamma_{K^0} - \Gamma_{\bar{K}^0} = 0$ we obtain

$$-4.0 \times 10^{-19} \text{ GeV} < m_{K^0} - m_{\bar{K}^0} < 4.0 \times 10^{-19} \text{ GeV} \quad \text{at 95 \% C.L.}$$

References

- [1] See the “ CP Violation in Meson Decays,” in this *Review*.
- [2] L. Maiani, “ CP And CPT Violation in Neutral Kaon Decays,” L. Maiani, G. Pancheri, and N. Paver, *The Second DAΦNE Physics Handbook*, Vol. 1,2.
- [3] G. D’Ambrosio, G. Isidori and A. Pugliese, in “2nd DAΦNE Physics Handbook:63-96,” 63–96 (1994), [hep-ph/9411389], URL <http://preprints.cern.ch/cgi-bin/setlink?base=preprint&categ=cern&id=th-7504-94>.
- [4] G. D’Ambrosio and G. Isidori (KLOE), *JHEP* **12**, 011 (2006), [hep-ex/0610034].
- [5] J. S. Bell and J. Steinberger, in “Wolfenstein, L. (ed.): CP violation, 42-57. (In Oxford International Symposium Conference on Elementary Particles),” 195–208, 221–222 (1966), (See Book Index).
- [6] T. Alexopoulos *et al.* (KTeV), *Phys. Rev.* **D70**, 092006 (2004), [hep-ex/0406002].
- [7] E. Abouzaid *et al.* (KTeV), *Phys. Rev.* **D83**, 092001 (2011), [arXiv:1011.0127].
- [8] A. Lai *et al.* (NA48), *Phys. Lett.* **B645**, 26 (2007), [hep-ex/0611052]; A. Lai *et al.* (NA48), *Phys. Lett.* **B602**, 41 (2004), [hep-ex/0410059].
- [9] We thanks G. Isidori and M. Palutan for their contribution to the original analysis [4] performed with KLOE data.
- [10] D. Babusci *et al.* (KLOE), *Phys. Lett.* **B723**, 54 (2013), [arXiv:1301.7623].
- [11] A. Angelopoulos *et al.* (CPLEAR), *Phys. Lett.* **B444**, 52 (1998).
- [12] W. M. Yao *et al.* (Particle Data Group), *J. Phys.* **G33**, 1 (2006).
- [13] A. Anastasi *et al.* (KLOE-2), *JHEP* **09**, 021 (2018), [arXiv:1806.08654].
- [14] P. Bloch, M. Fidencaro, private communication of the data in a finer binning format; A. Angelopoulos *et al.* (CPLEAR), *Phys. Lett.* **B444**, 43 (1998).
- [15] D. Babusci *et al.* (KLOE-2), *Phys. Lett. B* **804**, 135378 (2020), [arXiv:1912.05990].

67. V_{ud} , V_{us} the Cabibbo Angle, and CKM Unitarity

Revised August 2021 by E. Blucher (Chicago U.) and W.J. Marciano (BNL).

The Cabibbo-Kobayashi-Maskawa (CKM) [1, 2] three-generation quark mixing matrix written in terms of the Wolfenstein parameters (λ, A, ρ, η) [3] nicely illustrates the orthonormality constraint of unitarity, as well as the central role played by λ .

$$V_{\text{CKM}} = \begin{pmatrix} V_{ud} & V_{us} & V_{ub} \\ V_{cd} & V_{cs} & V_{cb} \\ V_{td} & V_{ts} & V_{tb} \end{pmatrix} = \begin{pmatrix} 1 - \lambda^2/2 & \lambda & A\lambda^3(\rho - i\eta) \\ -\lambda & 1 - \lambda^2/2 & A\lambda^2 \\ A\lambda^3(1 - \rho - i\eta) & -A\lambda^2 & 1 \end{pmatrix} + \mathcal{O}(\lambda^4). \quad (67.1)$$

That cornerstone parameter is a carryover from the two-generation Cabibbo angle, $\lambda = \sin(\theta_{\text{Cabibbo}}) = V_{us}$. Its value is an important component in tests of CKM unitarity.

Up until 2003, the precise value of λ was controversial, with kaon decays (specifically $K \rightarrow \pi e \nu$) branching fractions suggesting [4] $\lambda \simeq 0.220$, while indirect determinations via V_{ud} obtained from nuclear β -decays combined with unitarity preferred a somewhat larger $\lambda \simeq 0.225 - 0.230$. This difference implied a 2 - 2.5 sigma deviation from the first row unitarity requirement

$$|V_{ud}|^2 + |V_{us}|^2 + |V_{ub}|^2 = 1, \quad (67.2)$$

a possible hint [5, 6] of new physics effects. Below, we describe the current status of V_{ud} and V_{us} , and their implication for the unitarity test in Eq. (67.2). (Since $|V_{ub}|^2 \simeq 1.7 \times 10^{-5}$ is negligibly small, it is ignored in this discussion.) Eq. (67.2) is currently the most stringent test of unitarity in the CKM matrix. As we shall see, it is again showing signs of a possible 2 to 3 sigma inconsistency.

67.1 V_{ud}

Precise values of V_{ud} have been obtained from superallowed nuclear, neutron, and pion beta decays. Currently, the best determination of V_{ud} comes from analysis of a set of 15 precisely measured superallowed nuclear beta-decays [5, 6] ($0^+ \rightarrow 0^+$ transitions). Measuring their half-lives, t , and Q values gives the decay rate factors, f , which lead to a precise determination of V_{ud} via [7–12]. Based on several decades of dedicated studies, Hardy and Towner recently updated the average [6]

$$|V_{ud}|^2 = 0.97154(22)(54)_{\text{NS}}/(1 + \Delta_{\text{R}}^{\text{V}}), \quad (67.3)$$

where $\Delta_{\text{R}}^{\text{V}}$ denotes the so-called inner or universal electroweak radiative corrections (RC) to superallowed nuclear beta decays. Note that an additional uncertainty $(54)_{\text{NS}}$ from nuclear structure (NS) [13] has been recently included [6] in that master formula. A dispersion relation (DR) calculational approach [14] to quantum loop corrections, specifically the gamma-W box diagram, gives $\Delta_{\text{R}}^{\text{V}} = 0.02467(22)$. Because of its small uncertainty and more rigorous theoretical footing, we use that value below. A somewhat different approach [15] found $\Delta_{\text{R}}^{\text{V}} = 0.02426(32)$. These recent values are roughly consistent. Both are larger than the 2018 PDG value of 0.02361(38). Implications and possible nuclear physics modifications of those studies are still under scrutiny [13, 16]. Nevertheless, currently the 15 most precisely measured superallowed transitions [12] lead to the DR based weighted average of

$$V_{ud} = 0.97373(11)_{\text{exp.,nucl.}}(9)_{\text{RC}}(27)_{\text{NS}} \text{ (superallowed)}, \quad (67.4)$$

which, assuming unitarity, corresponds to the relatively large $\lambda = 0.2277(13)$. This recent determination of V_{ud} has shifted significantly down compared to the 2018 PDG value of 0.97420(21). In addition, NS uncertainties are now the dominant contribution to the overall uncertainty. Taken at face value, along with current V_{us} determinations (see subsection 67.2), the reduced V_{ud} would seem to violate the first row unitarity requirement and thus suggest the presence of “new physics”.

Measurements of the neutron lifetime, τ_n , and the ratio of axial-vector/vector couplings, $g_A \equiv G_A/G_V$, via neutron decay asymmetries combined with the inner radiative corrections can also be used to determine V_{ud} via the precise formula:

$$|V_{ud}|^2 = \frac{5024.7 \text{ s}}{\tau_n(1 + 3g_A^2)(1 + \Delta_{\text{R}}^{\text{V}})}, \quad (67.5)$$

where $\Delta_{\text{R}}^{\text{V}}$ represents the same inner electroweak radiative corrections [8, 9] as discussed above.

Using the current published world averages [17],

$$\begin{aligned} \tau_n^{\text{ave}} &= 879.4(6) \text{ s} \quad (1.6 \text{ PDG scale factor}) \\ g_A^{\text{ave}} &= 1.2756(13), \quad (2.6 \text{ PDG scale factor}) \end{aligned} \quad (67.6)$$

leads to

$$|V_{ud}| = 0.9737(3)\tau_n(8)g_A(1)_{\text{RC}}, \quad (67.7)$$

for an inner radiative correction of 0.02467(22), while for 0.02426(32) it increases to 0.9739(9). Both central values are similar to the superallowed nuclear beta decay result reported above. Reconciliation with CKM unitarity suggests a shorter neutron lifetime near 878.5 s or a smaller g_A . We note that the most precise recent neutron lifetime update reported [18], $\tau_n = 877.75(34)$ s, has an uncertainty about half as big as the average given in Eq. 67.6. It corresponds to $|V_{ud}| = 0.9746(8)$, a value more in keeping with unitarity expectations; but too large an uncertainty from g_A to be meaningful. Future neutron studies [19] are expected to resolve any current inconsistencies and further reduce the uncertainties in g_A and τ_n making them a potentially better way to determine V_{ud} without the nuclear physics uncertainties.

The PIBETA experiment at PSI measured the very small ($\mathcal{O}(10^{-8})$) branching ratio for $\pi^+ \rightarrow \pi^0 e^+ \nu_e$ with about $\pm 0.6\%$ precision. Its result gives [20]

$$|V_{ud}| = 0.9739(27) \left[\frac{BR(\pi^+ \rightarrow e^+ \nu_e(\gamma))}{1.2325 \times 10^{-4}} \right]^{\frac{1}{2}}, \quad (67.8)$$

which is normalized using the very precisely measured $BR(\pi^+ \rightarrow e^+ \nu_e(\gamma)) = 1.2325(23) \times 10^{-4}$ [7], rather than the theoretical branching ratio of $1.2350(2) \times 10^{-4}$, which if used, would increase $|V_{ud}|$ to 0.9749(27). Theoretical uncertainties in pion beta decay are very small [21], leaving open more than an order of magnitude improvement of its experimental branching ratio before theory uncertainties become a problem. Although challenging, improved measurements of pion beta decay currently under discussion would allow this decay mode to compete with superallowed beta decays and future neutron decay efforts for the most precise direct $|V_{ud}|$ determination.

67.2 V_{us}

$|V_{us}|$ may be directly obtained from kaon decays, hyperon decays, and tau decays. Early determinations most often used $K\ell 3$ decays:

$$I_{K\ell 3} = \frac{G_F^2 M_K^5}{192\pi^3} S_{EW} (1 + \delta_K^\ell + \delta_{SU2}) C^2 |V_{us}|^2 f_+^2(0) I_K^\ell. \quad (67.9)$$

Here, ℓ refers to either e or μ , G_F is the Fermi constant, M_K is the kaon mass, S_{EW} is the short-distance radiative correction, δ_K^ℓ is the mode-dependent long-distance radiative correction, $f_+(0)$ is the calculated form factor at zero momentum transfer for the $\ell\nu$ system, and I_K^ℓ is the phase-space integral, which depends on measured semileptonic form factors. For charged kaon decays, δ_{SU2} is the deviation from one of the ratio of $f_+(0)$ for the charged to neutral kaon decay; it is zero for the neutral kaon. C^2 is 1 (1/2) for neutral (charged) kaon decays. Most early determinations of $|V_{us}|$ were based solely on $K \rightarrow \pi e \nu$ decays; $K \rightarrow \pi \mu \nu$ decays were not used because of large uncertainties in I_K^μ . The experimental measurements are the semileptonic decay widths (based on the semileptonic branching fractions and lifetime) and form factors (allowing calculation of the phase space integrals). Theory is needed for S_{EW} , δ_K^ℓ , δ_{SU2} , and $f_+(0)$.

Many measurements during the last 20 years have resulted in a shift in $|V_{us}|$. Most importantly, the $K \rightarrow \pi e \nu$ branching fractions are significantly different than much earlier PDG averages, probably as a result of inadequate treatment of radiation in older experiments. This effect was first observed by BNL E865 [22] in the charged kaon system and then by KTeV [23,24] in the neutral kaon system; subsequent measurements were made by KLOE [25–28], NA48 [29–31], and ISTRA+ [32]. Current averages (*e.g.*, by the PDG [33] or Flavianet [34]) of the semileptonic branching fractions are based only on recent, high-statistics experiments where the treatment of radiation is clear. In addition to measurements of branching fractions, new measurements of lifetimes [35] and form factors [36–40], have resulted in improved precision for all of the experimental inputs to $|V_{us}|$. Precise measurements of form factors for $K_{\mu 3}$ decay make it possible to use both semileptonic decay modes to extract V_{us} .

Following the analysis of Moulson [41] and the Flavianet group [34, 42], along with recent improvements in the QED radiative corrections [43], one finds [44], after including the isospin violating effect, δ_{SU2} , the values of $|V_{us}|f_+(0)$ in Table 67.1. The average of these measurements, including correlation effects [44] gives

$$f_+(0)|V_{us}| = 0.21635(38)(3) \quad (67.10)$$

where the errors correspond to Kaon experimental parameters and radiative corrections respectively.

Lattice QCD calculations of $f_+(0)$ have been carried out for 2, 2+1, and 2+1+1 quark flavors and range from about 0.96 to 0.97. Here, we illustrate recent FLAG (2020) updated averages [45] for 2+1 and 2+1+1 flavors:

$$\begin{aligned} f_+(0) &= 0.9677(27) \quad N_f = 2 + 1 \\ f_+(0) &= 0.9698(17) \quad N_f = 2 + 1 + 1 \end{aligned} \quad (67.11)$$

One finds from Eq. (67.10) and Eq. (67.11),

$$\begin{aligned} |V_{us}| &= 0.2236(4)_{\text{exp+RC}}(6)_{\text{lattice}} \quad (N_f = 2 + 1, K_{\ell 3} \text{ decays}) \\ &= 0.2231(4)_{\text{exp+RC}}(4)_{\text{lattice}} \quad (N_f = 2 + 1 + 1, K_{\ell 3} \text{ decays}) \end{aligned} \quad (67.12)$$

Table 67.1: $|V_{us}|f_+(0)$ from $K\ell 3$, based on ref. [44]

Decay Mode	$ V_{us} f_+(0)$
$K^\pm e 3$	0.21714 ± 0.00091
$K^\pm \mu 3$	0.21703 ± 0.00114
$K_L e 3$	0.21617 ± 0.00047
$K_L \mu 3$	0.21664 ± 0.00058
$K_S e 3$	0.21530 ± 0.00122
$K_S \mu 3$	0.21265 ± 0.00467
Average (including correlation effects [44])	0.21635 ± 0.00038

A value of V_{us} can also be obtained from a comparison of the radiative inclusive decay rates for $K \rightarrow \mu \nu(\gamma)$ and $\pi \rightarrow \mu \nu(\gamma)$ combined with a lattice gauge theory calculation of f_{K^+}/f_{π^+} via

$$\frac{|V_{us}|f_{K^+}}{|V_{ud}|f_{\pi^+}} = 0.23871(20) \left[\frac{\Gamma(K \rightarrow \mu \nu(\gamma))}{\Gamma(\pi \rightarrow \mu \nu(\gamma))} \right]^{\frac{1}{2}} \quad (67.13)$$

with the small error coming from electroweak radiative corrections [46–48]; these corrections were confirmed by direct lattice calculation of the kaon and pion leptonic decay rates [47, 48]. Employing

$$\frac{\Gamma(K \rightarrow \mu \nu(\gamma))}{\Gamma(\pi \rightarrow \mu \nu(\gamma))} = 1.3367(28), \quad (67.14)$$

which includes $\Gamma(K \rightarrow \mu \nu(\gamma)) = 5.134(11) \times 10^7 s^{-1}$ [41, 49], leads to

$$\frac{|V_{us}|f_{K^+}}{|V_{ud}|f_{\pi^+}} = 0.27600(37). \quad (67.15)$$

Employing the FLAG [45] lattice QCD averages for the isospin broken decay constants

$$\begin{aligned} \frac{f_{K^+}}{f_{\pi^+}} &= 1.1917(37) \quad N_f = 2 + 1 \\ &= 1.1932(21) \quad N_f = 2 + 1 + 1. \end{aligned} \quad (67.16)$$

along with the value of $|V_{ud}|$ in Eq. (67.4) leads to

$$\begin{aligned} |V_{us}| &= 0.2255(8) \quad (N_f = 2 + 1, K_{\mu 2} \text{ decays}) \\ &= 0.2252(5) \quad (N_f = 2 + 1 + 1, K_{\mu 2} \text{ decays}). \end{aligned} \quad (67.17)$$

Together, weighted averages of the $K\ell 3$ (Eq. (67.12)) and $K\mu 2$ (Eq. (67.17)) values give similar results for $N_f = 2+1$ and $2+1+1$ flavors:

$$\begin{aligned} |V_{us}| &= 0.2244(5) \quad N_f = 2 + 1 \\ |V_{us}| &= 0.2243(4) \quad N_f = 2 + 1 + 1. \end{aligned} \quad (67.18)$$

Note that the differences between $K\ell 3$ and $K\mu 2$ values for V_{us} differ by 2 and 3 sigma, respectively, for $N_f = 2+1$ and $2+1+1$ flavors. One should therefore scale the uncertainties in Eq. (67.18) accordingly. For that reason, we allow for a scale factor of 2.7 for both 2+1 and 2+1+1 flavors and average the two values. That approximate procedure leads to $|V_{us}| = 0.2243(8)$ which we use when we consider the first row test of CKM unitarity.

It should be mentioned that hyperon decay fits suggest [50]

$$|V_{us}| = 0.2250(27) \quad (\text{Hyperon Decays}) \quad (67.19)$$

modulo SU(3) breaking effects that could shift that value up or down. We note that a representative effort [51] that incorporates SU(3) breaking found $V_{us} = 0.226(5)$. Strangeness changing tau decays, averaging both inclusive and exclusive measurements, give [52]

$$|V_{us}| = 0.2221(13) \quad (\text{Tau Decays}), \quad (67.20)$$

which differs by about 2 sigma from the kaon determination discussed above, and would, if combined with V_{ud} from super-allowed beta decays, lead to a 4 sigma deviation from unitarity. This discrepancy results mainly from the inclusive tau decay results that rely on Finite Energy Sum Rule techniques and assumptions, as well as experimental uncertainties. Recent investigation of that approach suggests a larger value for V_{us} , which is more in accord with other determinations [53].

Employing the values of V_{ud} and V_{us} with an error scale factor of 2 from Eq. (67.4) and the average obtained after rescaling the errors from Eq. (67.18), respectively, leads to the unitarity consistency check

$$|V_{ud}|^2 + |V_{us}|^2 + |V_{ub}|^2 = 0.9985(6)(4). \quad (67.21)$$

where the first error is the uncertainty from $|V_{ud}|^2$ and the second error is the uncertainty from the average $|V_{us}|^2$ from $N_f = 2+1+1$ and $N_f = 2+1$. One finds about an overall 2 sigma deviation from unitarity. (The deviation increases to 3 sigma if nuclear structure uncertainties are ignored.) That deviation could be due a problem with $|V_{ud}|$ theory (RC or NS), the lattice determination of $f_+(0)$ or new physics.

67.3 CKM Unitarity Constraints

The current 2 sigma experimental disagreement with unitarity, $|V_{ud}|^2 + |V_{us}|^2 + |V_{ub}|^2 = 0.9985(7)$, still provides strong confirmation of Standard Model radiative corrections (which range between 3-4% depending on the nucleus used) at a high significance level [54]. In addition, it implies constraints on ‘‘New Physics’’ effects at both the tree and quantum loop levels. Those effects could be in the form of contributions to nuclear beta decays, K decays and/or muon decays, with the last of these providing normalization via the muon lifetime [55], which is used to obtain the Fermi constant, $G_\mu = 1.1663787(6) \times 10^{-5} \text{GeV}^{-2}$.

In the following examples, we illustrate the implications of CKM unitarity for (1) exotic muon decays [56] (beyond ordinary muon decay $\mu^+ \rightarrow e^+ \nu_e \bar{\nu}_\mu$) and (2) new heavy quark mixing V_{uD} [57]. Other examples in the literature [58, 59] include Z_χ boson quantum loop effects, supersymmetry, leptoquarks, compositeness etc.

67.3.1 Exotic Muon Decays

If additional lepton flavor violating decays such as $\mu^+ \rightarrow e^+ \bar{\nu}_e \nu_\mu$ (wrong neutrinos) occur, they would cause confusion in searches for neutrino oscillations at, for example, muon storage rings/neutrino factories or other neutrino sources from muon decays. Calling the rate for all such decays $\Gamma(\text{exotic } \mu \text{ decays})$, they should be subtracted before the extraction of G_μ and normalization of the CKM matrix. Since that is not done and unitarity works, one has (at one-sided 95% CL)

$$|V_{ud}|^2 + |V_{us}|^2 + |V_{ub}|^2 = 1 - BR(\text{exotic } \mu \text{ decays}) \geq 0.9975 \quad (67.22)$$

or

$$BR(\text{exotic } \mu \text{ decays}) \leq 0.0025. \quad (67.23)$$

This bound is a factor of 10 better than the direct experimental bound on $\mu^+ \rightarrow e^+ \bar{\nu}_e \nu_\mu$.

67.3.2 New Heavy Quark Mixing

Heavy D quarks naturally occur in fourth quark generation models and some heavy quark “new physics” scenarios such as E_6 grand unification. Their mixing with ordinary quarks gives rise to V_{uD} , which is constrained by unitarity (one sided 95% CL)

$$|V_{ud}|^2 + |V_{us}|^2 + |V_{ub}|^2 = 1 - |V_{uD}|^2 \geq 0.9975 \\ |V_{uD}| \leq 0.05. \quad (67.24)$$

A similar constraint applies to heavy neutrino mixing and the couplings $V_{\mu N}$ and V_{eN} .

References

- [1] N. Cabibbo, Phys. Rev. Lett. **10**, 531 (1963).
- [2] M. Kobayashi and T. Maskawa, Prog. Theor. Phys. **49**, 652 (1973).
- [3] L. Wolfenstein, Phys. Rev. Lett. **51**, 1945 (1983).
- [4] S. Eidelman *et al.* (Particle Data Group), Phys. Lett. B **592**, 1-4, 1 (2004).
- [5] I. Towner and J. Hardy, Rept. Prog. Phys. **73**, 046301 (2010).
- [6] J. C. Hardy and I. S. Towner, Phys. Rev. C **102**, 4, 045501 (2020).
- [7] W. J. Marciano and A. Sirlin, Phys. Rev. Lett. **71**, 3629 (1993).
- [8] A. Czarnecki, W. J. Marciano and A. Sirlin, Phys. Rev. D **70**, 093006 (2004), [hep-ph/0406324].
- [9] W. J. Marciano and A. Sirlin, Phys. Rev. Lett. **96**, 032002 (2006), [hep-ph/0510099].
- [10] I. Towner and J. Hardy, Phys. Rev. C **77**, 025501 (2008), [arXiv:0710.3181].
- [11] J. Hardy and I. Towner, Phys. Rev. C **79**, 055502 (2009), [arXiv:0812.1202].
- [12] J. Hardy and I. Towner, Phys. Rev. C **91**, 2, 025501 (2015), [arXiv:1411.5987].
- [13] M. Gorchtein, Phys. Rev. Lett. **123**, 4, 042503 (2019), [arXiv:1812.04229].
- [14] C.-Y. Seng *et al.*, Phys. Rev. Lett. **121**, 24, 241804 (2018), [arXiv:1807.10197].
- [15] A. Czarnecki, W. J. Marciano and A. Sirlin, Phys. Rev. D **100**, 7, 073008 (2019), [arXiv:1907.06737].
- [16] C. Y. Seng, M. Gorchtein and M. J. Ramsey-Musolf, Phys. Rev. D **100**, 1, 013001 (2019), [arXiv:1812.03352].
- [17] P. A. Zyla *et al.* (Particle Data Group), PTEP **2020**, 8, 083C01 (2020).
- [18] F. M. Gonzalez *et al.* (UCN τ) (2021), [arXiv:2106.10375].
- [19] H. Abele, Prog. Part. Nucl. Phys. **60**, 1 (2008).
- [20] D. Pocanic *et al.*, Phys. Rev. Lett. **93**, 181803 (2004), [hep-ex/0312030]; A. Czarnecki, W. J. Marciano and A. Sirlin, Phys. Rev. D **101**, 9, 091301 (2020), [arXiv:1911.04685].
- [21] X. Feng *et al.*, Phys. Rev. Lett. **124**, 19, 192002 (2020), [arXiv:2003.09798].
- [22] A. Sher *et al.*, Phys. Rev. Lett. **91**, 261802 (2003), [hep-ex/0305042].
- [23] T. Alexopoulos *et al.* (KTeV), Phys. Rev. Lett. **93**, 181802 (2004), [hep-ex/0406001].
- [24] T. Alexopoulos *et al.* (KTeV), Phys. Rev. D **70**, 092006 (2004), [hep-ex/0406002].
- [25] F. Ambrosino *et al.* (KLOE), Phys. Lett. B **632**, 43 (2006), [hep-ex/0508027].
- [26] F. Ambrosino *et al.* (KLOE), Phys. Lett. B **638**, 140 (2006), [hep-ex/0603041].
- [27] F. Ambrosino *et al.* (KLOE), Phys. Lett. B **636**, 173 (2006), [hep-ex/0601026].
- [28] B. Sciascia (KLOE), PoS **HEP2005**, 287 (2006), [hep-ex/0510028].
- [29] A. Lai *et al.* (NA48), Phys. Lett. B **602**, 41 (2004), [hep-ex/0410059].
- [30] A. Lai *et al.* (NA48), Phys. Lett. B **645**, 26 (2007), [hep-ex/0611052].
- [31] J. Batley *et al.* (NA48/2), Eur. Phys. J. C **50**, 329 (2007), [Erratum: Eur.Phys.J.C 52, 1021-1023 (2007)], [hep-ex/0702015].
- [32] V. Romanovsky *et al.* (2007), [arXiv:0704.2052].
- [33] K. Olive *et al.* (Particle Data Group), Chin. Phys. C **38**, 090001 (2014).
- [34] M. Antonelli *et al.* (FlaviaNet Working Group on Kaon Decays), Eur. Phys. J. C **69**, 399 (2010), [arXiv:1005.2323]; For a detailed review, see; M. Antonelli *et al.*, Phys. Rept. **494**, 197 (2010), [arXiv:0907.5386].
- [35] F. Ambrosino *et al.* (KLOE), Phys. Lett. B **626**, 15 (2005), [hep-ex/0507088].
- [36] T. Alexopoulos *et al.* (KTeV), Phys. Rev. D **70**, 092007 (2004), [hep-ex/0406003].
- [37] E. Abouzaid *et al.* (KTeV), Phys. Rev. D **74**, 097101 (2006), [hep-ex/0608058].
- [38] F. Ambrosino *et al.* (KLOE), Phys. Lett. B **636**, 166 (2006), [hep-ex/0601038].
- [39] A. Lai *et al.* (NA48), Phys. Lett. B **604**, 1 (2004), [hep-ex/0410065].
- [40] O. Yushchenko *et al.*, Phys. Lett. B **589**, 111 (2004), [hep-ex/0404030].
- [41] M. Moulson, PoS **CKM2016**, 033 (2017), [arXiv:1704.04104].
- [42] E. Passemar, talk at CKM2018, <https://zenodo.org/record/2565480>.
- [43] C.-Y. Seng *et al.* (2021), [arXiv:2103.04843].
- [44] C.-Y. Seng *et al.* (2021), [arXiv:2107.14708].
- [45] S. Aoki *et al.* (Flavour Lattice Averaging Group), Eur. Phys. J. C **80**, 2, 113 (2020), [arXiv:1902.08191]; A. Bazavov *et al.*, Phys. Rev. Lett. **112**, 11, 112001 (2014), [arXiv:1312.1228]; N. Carrasco *et al.*, Phys. Rev. D **93**, 11, 114512 (2016), [arXiv:1602.04113]; A. Bazavov *et al.*, Phys. Rev. D **87**, 073012 (2013), [arXiv:1212.4993]; P. A. Boyle *et al.* (RBC/UKQCD), JHEP **06**, 164 (2015), [arXiv:1504.01692]; A. Bazavov *et al.*, Phys. Rev. D **98**, 7, 074512 (2018), [arXiv:1712.09262]; T. Blum *et al.* (RBC, UKQCD), Phys. Rev. D **93**, 7, 074505 (2016), [arXiv:1411.7017]; R. Dowdall *et al.*, Phys. Rev. D **88**, 074504 (2013), [arXiv:1303.1670]; N. Carrasco *et al.*, Phys. Rev. D **91**, 5, 054507 (2015), [arXiv:1411.7908]; E. Follana *et al.* (HPQCD, UKQCD), Phys. Rev. Lett. **100**, 062002 (2008), [arXiv:0706.1726]; A. Bazavov *et al.* (MILC), PoS **LATTICE2010**, 074 (2010), [arXiv:1012.0868]; S. Durr *et al.*, Phys. Rev. D **81**, 054507 (2010), [arXiv:1001.4692]; S. Dürr *et al.*, Phys. Rev. D **95**, 5, 054513 (2017), [arXiv:1601.05998]; V. Bornyakov *et al.* (QCDSF), Phys. Lett. B **767**, 366 (2017), [arXiv:1612.04798].

- [46] V. Cirigliano and H. Neufeld, Phys. Lett. B **700**, 7 (2011), [arXiv:1102.0563]; W. J. Marciano, Phys. Rev. Lett. **93**, 231803 (2004), [hep-ph/0402299].
- [47] D. Giusti *et al.*, Phys. Rev. Lett. **120**, 7, 072001 (2018), [arXiv:1711.06537].
- [48] M. Di Carlo *et al.*, Phys. Rev. D **100**, 3, 034514 (2019), [arXiv:1904.08731].
- [49] D. Babusci *et al.* (KLOE KLOE-2), Phys. Lett. B **738**, 128 (2014), [arXiv:1407.2028].
- [50] N. Cabibbo, E. C. Swallow and R. Winston, Phys. Rev. Lett. **92**, 251803 (2004), [hep-ph/0307214].
- [51] V. Mateu and A. Pich, JHEP **10**, 041 (2005), [hep-ph/0509045].
- [52] Y. S. Amhis *et al.* (HFLAV) (2019), [arXiv:1909.12524].
- [53] R. J. Hudspith *et al.*, Phys. Lett. B **781**, 206 (2018), [arXiv:1702.01767]; P. Boyle *et al.* (RBC, UKQCD), Phys. Rev. Lett. **121**, 20, 202003 (2018), [arXiv:1803.07228].
- [54] A. Sirlin, Rev. Mod. Phys. **50**, 573 (1978), [Erratum: Rev.Mod.Phys. 50, 905 (1978)].
- [55] D. Webber *et al.* (MuLan), Phys. Rev. Lett. **106**, 041803 (2011), [arXiv:1010.0991].
- [56] K. Babu and S. Pakvasa (2002), [hep-ph/0204236].
- [57] W. Marciano and A. Sirlin, Phys. Rev. Lett. **56**, 22 (1986); P. Langacker and D. London, Phys. Rev. D **38**, 886 (1988).
- [58] W. Marciano and A. Sirlin, Phys. Rev. D **35**, 1672 (1987).
- [59] R. Barbieri *et al.*, Phys. Lett. B **156**, 348 (1985); K. Hagiwara, S. Matsumoto and Y. Yamada, Phys. Rev. Lett. **75**, 3605 (1995), [hep-ph/9507419]; A. Kurylov and M. Ramsey-Musolf, Phys. Rev. Lett. **88**, 071804 (2002), [hep-ph/0109222]; S. Bauman, J. Erler and M. Ramsey-Musolf, Phys. Rev. D **87**, 3, 035012 (2013), [arXiv:1204.0035].

68. CP Violation in K_L^0 Decays

Revised August 2021 by C.-J. Lin (LBNL).

The symmetries C (particle-antiparticle interchange) and P (space inversion) hold for strong and electromagnetic interactions. After the discovery of large C and P violation in the weak interactions, it appeared that the product CP was a good symmetry. In 1964 CP violation was observed in K^0 decays at a level given by the parameter $\epsilon \approx 2.3 \times 10^{-3}$.

A unified treatment of CP violation in K , D , B , and B_s mesons is given in “ CP Violation in Meson Decays” by D. Kirkby and Y. Nir in this *Review*. A more detailed review including a thorough discussion of the experimental techniques used to determine CP violation parameters is given in a book by K. Kleinknecht [1]. Here we give a concise summary of the formalism needed to define the parameters of CP violation in K_L decays, and a description of our fits for the best values of these parameters.

68.1 Formalism for CP violation in Kaon decay

CP violation has been observed in the semi-leptonic decays $K_L^0 \rightarrow \pi^\mp \ell^\pm \nu$, and in the nonleptonic decay $K_L^0 \rightarrow 2\pi$. The experimental numbers that have been measured are

$$A_L = \frac{\Gamma(K_L^0 \rightarrow \pi^- \ell^+ \nu) - \Gamma(K_L^0 \rightarrow \pi^+ \ell^- \nu)}{\Gamma(K_L^0 \rightarrow \pi^- \ell^+ \nu) + \Gamma(K_L^0 \rightarrow \pi^+ \ell^- \nu)} \quad (68.1a)$$

$$\eta_{+-} = A(K_L^0 \rightarrow \pi^+ \pi^-) / A(K_S^0 \rightarrow \pi^+ \pi^-) \\ = |\eta_{+-}| e^{i\phi_{+-}} \quad (68.1b)$$

$$\eta_{00} = A(K_L^0 \rightarrow \pi^0 \pi^0) / A(K_S^0 \rightarrow \pi^0 \pi^0) \\ = |\eta_{00}| e^{i\phi_{00}}. \quad (68.1c)$$

CP violation can occur either in the $K^0 - \bar{K}^0$ mixing or in the decay amplitudes. Assuming CPT invariance, the mass eigenstates of the $K^0 - \bar{K}^0$ system can be written

$$|K_S\rangle = p|K^0\rangle + q|\bar{K}^0\rangle, \quad |K_L\rangle = p|K^0\rangle - q|\bar{K}^0\rangle. \quad (68.2)$$

If CP invariance held, we would have $q = p$ so that K_S would be CP -even and K_L CP -odd. (We define $|\bar{K}^0\rangle$ as $CP|K^0\rangle$). CP violation in $K^0 - \bar{K}^0$ mixing is then given by the parameter ϵ where

$$\frac{p}{q} = \frac{(1 + \tilde{\epsilon})}{(1 - \tilde{\epsilon})}. \quad (68.3)$$

CP violation can also occur in the decay amplitudes

$$A(K^0 \rightarrow \pi\pi(I)) = A_I e^{i\delta_I}, \quad A(\bar{K}^0 \rightarrow \pi\pi(I)) = A_I^* e^{i\delta_I}, \quad (68.4)$$

where I is the isospin of $\pi\pi$, δ_I is the final-state phase shift, and A_I would be real if CP invariance held. The CP -violating observables are usually expressed in terms of ϵ and ϵ' defined by

$$\eta_{+-} = \epsilon + \epsilon', \quad \eta_{00} = \epsilon - 2\epsilon'. \quad (68.5a)$$

One can then show [2]

$$\epsilon = \tilde{\epsilon} + i \left(\text{Im } A_0 / \text{Re } A_0 \right), \quad (68.5b)$$

$$\sqrt{2}\epsilon' = i e^{i(\delta_2 - \delta_0)} (\text{Re } A_2 / \text{Re } A_0) \left(\text{Im } A_2 / \text{Re } A_2 - \text{Im } A_0 / \text{Re } A_0 \right), \quad (68.5c)$$

$$A_L = 2\text{Re } \epsilon / (1 + |\epsilon|^2) \approx 2\text{Re } \epsilon. \quad (68.5d)$$

In Eq. (68.5a), small corrections [3] of order $\epsilon' \times \text{Re } (A_2/A_0)$ are neglected, and Eq. (68.5d) assumes the $\Delta S = \Delta Q$ rule.

The quantities $\text{Im } A_0$, $\text{Im } A_2$, and $\text{Im } \tilde{\epsilon}$ depend on the choice of phase convention, since one can change the phases of K^0 and \bar{K}^0 by a transformation of the strange quark state $|s\rangle \rightarrow |s\rangle e^{i\alpha}$; of course, observables are unchanged. It is possible by a choice of phase convention to set $\text{Im } A_0$ or $\text{Im } A_2$ or $\text{Im } \tilde{\epsilon}$ to zero, but none of these is zero with the usual phase conventions in the Standard Model. The choice $\text{Im } A_0 = 0$ is called the Wu-Yang phase convention [4], in which case $\epsilon = \tilde{\epsilon}$. The value of ϵ' is independent of phase convention, and a nonzero value demonstrates CP violation

in the decay amplitudes, referred to as direct CP violation. The possibility that direct CP violation is essentially zero, and that CP violation occurs only in the mixing matrix, was referred to as the superweak theory [5].

By applying CPT invariance and unitarity the phase of ϵ is given approximately by

$$\phi_\epsilon \approx \tan^{-1} \frac{2(m_{K_L} - m_{K_S})}{\Gamma_{K_S} - \Gamma_{K_L}} \approx 43.52 \pm 0.05^\circ, \quad (68.6a)$$

while Eq. (68.5c) gives the phase of ϵ' to be

$$\phi_{\epsilon'} = \delta_2 - \delta_0 + \frac{\pi}{2} \approx 42.3 \pm 1.5^\circ, \quad (68.6b)$$

where the numerical value is based on an analysis of $\pi - \pi$ scattering using chiral perturbation theory [6]. The approximation in Eq. (68.6a) depends on the assumption that direct CP violation is very small in all K^0 decays. This is expected to be good to a few tenths of a degree, as indicated by the small value of ϵ' and of η_{+-} and η_{00} , the CP -violation parameters in the decays $K_S \rightarrow \pi^+ \pi^- \pi^0$ [7], and $K_S \rightarrow \pi^0 \pi^0 \pi^0$ [8]. The relation in Eq. (68.6a) is exact in the superweak theory, so this is sometimes called the superweak-phase ϕ_{SW} . An important point for the analysis is that $\cos(\phi_{\epsilon'} - \phi_\epsilon) \simeq 1$. The consequence is that only two real quantities need be measured, the magnitude of ϵ and the value of (ϵ'/ϵ) , including its sign. The measured quantity $|\eta_{00}/\eta_{+-}|^2$ is very close to unity so that we can write

$$|\eta_{00}/\eta_{+-}|^2 \approx 1 - 6\text{Re } (\epsilon'/\epsilon) \approx 1 - 6\epsilon'/\epsilon, \quad (68.7a)$$

$$\text{Re}(\epsilon'/\epsilon) \approx \frac{1}{3}(1 - |\eta_{00}/\eta_{+-}|). \quad (68.7b)$$

From the experimental measurements in this edition of the *Review*, and the fits discussed in the next section, one finds

$$|\epsilon| = (2.228 \pm 0.011) \times 10^{-3}, \quad (68.8a)$$

$$\phi_\epsilon = (43.5 \pm 0.5)^\circ, \quad (68.8b)$$

$$\text{Re}(\epsilon'/\epsilon) \approx \epsilon'/\epsilon = (1.66 \pm 0.23) \times 10^{-3}, \quad (68.8c)$$

$$\phi_{+-} = (43.4 \pm 0.5)^\circ, \quad (68.8d)$$

$$\phi_{00} - \phi_{+-} = (0.34 \pm 0.32)^\circ, \quad (68.8e)$$

$$A_L = (3.32 \pm 0.06) \times 10^{-3}. \quad (68.8f)$$

Direct CP violation, as indicated by ϵ'/ϵ , is expected in the Standard Model. However, the numerical value cannot be reliably predicted because of theoretical uncertainties [9]. The value of A_L agrees with Eq. (68.5d). The values of ϕ_{+-} and $\phi_{00} - \phi_{+-}$ are used to set limits on CP violation [see “Tests of Conservation Laws”].

68.2 Fits for K_L^0 CP -violation parameters

In recent years, K_L^0 CP -violation experiments have improved our knowledge of CP -violation parameters,

and their consistency with the expectations of CPT invariance and unitarity. To determine the best values of the CP -violation parameters in $K_L^0 \rightarrow \pi^+ \pi^-$ and $\pi^0 \pi^0$ decay, we make two types of fits, one for the phases ϕ_{+-} and ϕ_{00} jointly with Δm and τ_S , and the other for the amplitudes $|\eta_{+-}|$ and $|\eta_{00}|$ jointly with the $K_L^0 \rightarrow \pi\pi$ branching fractions.

68.2.1 Fits to ϕ_{+-} , ϕ_{00} , $\Delta\phi$, Δm , and τ_S data

These are joint fits to the data on ϕ_{+-} , ϕ_{00} , the phase difference $\Delta\phi = \phi_{00} - \phi_{+-}$, the $K_L^0 - K_S^0$ mass difference Δm , and the K_S^0 mean life τ_S , including the effects of correlations.

Measurements of ϕ_{+-} and ϕ_{00} are highly correlated with Δm and τ_S . Some measurements of τ_S are correlated with Δm . The correlations are given in the footnotes of the ϕ_{+-} and ϕ_{00} sections of the K_L^0 Listings, and the τ_S section of the K_S^0 Listings.

In most cases, the correlations are quoted as 100%, with the value and error of ϕ_{+-} or ϕ_{00} given at a fixed value of Δm and τ_S , with additional terms specifying the dependence of the value on Δm and τ_S . These cases lead to diagonal bands in Figs. 68.1

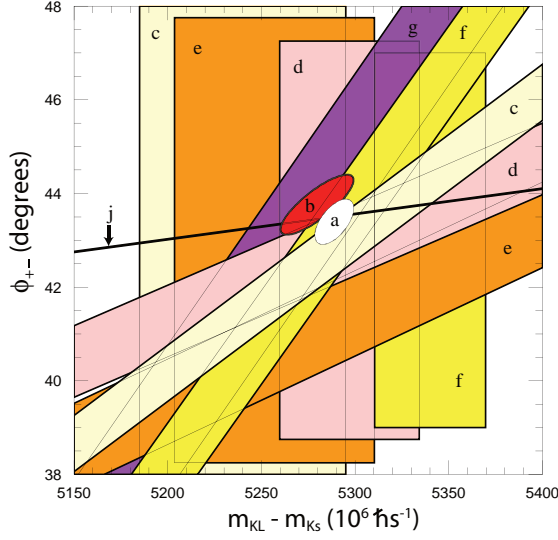


Figure 68.1: ϕ_{+-} vs Δm for experiments which do not assume CPT invariance. Δm measurements appear as vertical bands spanning $\Delta m \pm 1\sigma$, cut near the top and bottom to aid the eye. Most ϕ_{+-} measurements appear as diagonal bands spanning $\phi_{+-} \pm \sigma_\phi$. Data are labeled by letters: “b”–FNAL KTeV, “c”–CERN CPLEAR, “d”–FNAL E773, “e”–FNAL E731, “f”–CERN, “g”–CERN NA31, and are cited in Table 68.1. The narrow band “j” shows ϕ_{SW} . The ellipse “a” shows the $\chi^2 = 1$ contour of the fit result.

and 68.2. The KTeV experiment [10] quotes its results as values of Δm , τ_S , ϕ_ϵ , and $\text{Im}(\epsilon'/\epsilon)$ with correlations, leading to the ellipses labeled “b.” The correlations for the KTeV measurements are given in the $\text{Im}(\epsilon'/\epsilon)$ section of the K_L^0 Listings. For small $|\epsilon'/\epsilon|$, $\phi_{+-} \approx \phi_\epsilon + \text{Im}(\epsilon'/\epsilon)$.

Table 68.1: References, Document ID’s, and sources corresponding to the letter labels in the figures. The data are given in the ϕ_{+-} and Δm sections of the K_L Listings, and the τ_S section of the K_S Listings.

Label	Source	PDG Document ID	Ref.
a	This Review	OUR FIT	
b	FNAL KTeV	ABOUZAID 11	[10]
c	CERN CPLEAR	APOSTOLAKIS 99C	[11]
d	FNAL E773	SCHWINGENHEUER 95	[12]
e	FNAL E731	GIBBONS 93,93C	[13], [14]
f	CERN	GEWENIGER 74B,74C	[15], [16]
g	CERN NA31	CAROSI 90	[17]
h	CERN NA48	LAI 02C	[18]
i	CERN NA31	BERTANZA 97	[19]
j	This Review	SUPERWEAK 16	

The data on τ_S , Δm , and ϕ_{+-} shown in Figs. 68.1 and 68.2 are combined with data on ϕ_{00} and $\phi_{00} - \phi_{+-}$ in two fits, one without assuming CPT , and the other with this assumption. The results without assuming CPT are shown as ellipses labeled “a.” These ellipses are seen to be in good agreement with the superweak phase

$$\phi_{SW} = \tan^{-1} \left(\frac{2\Delta m}{\Delta\Gamma} \right) = \tan^{-1} \left(\frac{2\Delta m \tau_S \tau_L}{\hbar(\tau_L - \tau_S)} \right). \quad (68.9)$$

In Figs. 68.1 and 68.2, ϕ_{SW} is shown as narrow bands labeled “j.”

Table 68.2 column 2, “Fit w/o CPT ,” gives the resulting fitted parameters, while Table 68.3 gives the correlation matrix for this fit. The white ellipses labeled “a” in Figure 68.1 and 68.2 are the $\chi^2 = 1$ contours for this fit.

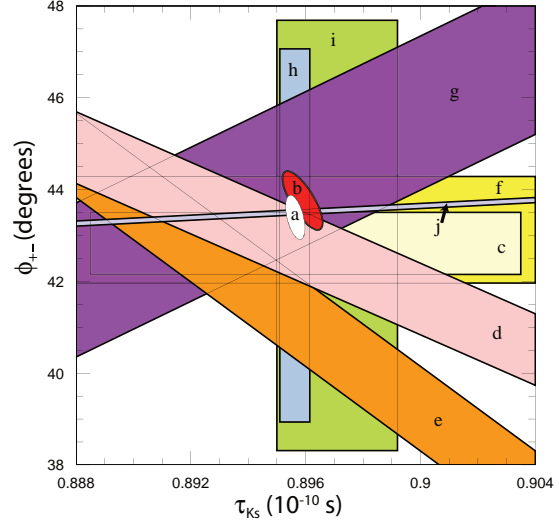


Figure 68.2: ϕ_{+-} vs τ_S . τ_S measurements appear as vertical bands spanning $\tau_S \pm 1\sigma$, some of which are cut near the top and bottom to aid the eye. Most ϕ_{+-} measurements appear as diagonal or horizontal bands spanning $\phi_{+-} \pm \sigma_\phi$. Data are labeled by letters: “b”–FNAL KTeV, “c”–CERN CPLEAR, “d”–FNAL E773, “e”–FNAL E731, “f”–CERN, “g”–CERN NA31, “h”–CERN NA48, “i”–CERN NA31, and are cited in Table 68.1. The narrow band “j” shows ϕ_{SW} . The ellipse “a” shows the fit result’s $\chi^2 = 1$ contour.

For experiments which have dependencies on unseen fit parameters, that is, parameters other than those shown on the x or y axis of the figure, their band positions are evaluated using the fit results and their band widths include the fitted uncertainty in the unseen parameters. This is also true for the ϕ_{SW} bands.

If CPT invariance and unitarity are assumed, then by Eq. (68.6a), the phase of ϵ is constrained to be approximately equal to

$$\phi_{SW} = (43.50258 \pm 0.00021)^\circ + 54.1(\Delta m - 0.5289)^\circ + 32.0(\tau_S - 0.89564) \quad (68.10)$$

where we have linearized the Δm and τ_S dependence of Eq. (68.9). The error ± 0.00021 is due to the uncertainty in τ_L . Here Δm has units $10^{10} \text{ hbar s}^{-1}$ and τ_S has units 10^{-10} s .

If in addition we use the observation that $\text{Re}(\epsilon'/\epsilon) \ll 1$ and $\cos(\phi_{\epsilon'} - \phi_\epsilon) \simeq 1$, as well as the numerical value of $\phi_{\epsilon'}$ given in Eq. (68.6b), then Eqs. 68.5a, which are sketched in Fig 68.3, lead to the constraint

$$\begin{aligned} \phi_{00} - \phi_{+-} &\approx -3 \text{Im} \left(\frac{\epsilon'}{\epsilon} \right) \\ &\approx -3 \text{Re} \left(\frac{\epsilon'}{\epsilon} \right) \tan(\phi_{\epsilon'} - \phi_\epsilon) \\ &\approx 0.006^\circ \pm 0.008^\circ, \end{aligned} \quad (68.11)$$

so that $\phi_{+-} \approx \phi_{00} \approx \phi_\epsilon \approx \phi_{SW}$.

In the fit assuming CPT , we constrain $\phi_\epsilon = \phi_{SW}$ using the linear expression in Eq. (68.10), and constrain $\phi_{00} - \phi_{+-}$ using Eq. (68.11). These constraints are inserted into the Listings with the Document ID of SUPERWEAK 16. Some additional data for which the authors assumed CPT are added to this fit or substitute for other less precise data for which the authors did not make this assumption. See the Listings for details.

The results of this fit are shown in Table 68.2, column 3, “Fit w/ CPT ,” and the correlation matrix is shown in Table 68.4. The Δm precision is improved by the CPT assumption.

68.2.2 Fits for ϵ'/ϵ , $|\eta_{+-}|$, $|\eta_{00}|$, and $B(K_L \rightarrow \pi\pi)$

We list measurements of $|\eta_{+-}|$, $|\eta_{00}|$, $|\eta_{00}/\eta_{+-}|$, and ϵ'/ϵ . Independent information on $|\eta_{+-}|$ and $|\eta_{00}|$ can be obtained from

Table 68.2: Fit results for ϕ_{+-} , Δm , τ_S , ϕ_{00} , $\Delta\phi = \phi_{00} - \phi_{+-}$, and ϕ_ϵ without and with the CPT assumption

Quantity(units)	Fit w/o CPT	Fit w/ CPT
$\phi_{+-}(\circ)$	43.4 ± 0.5 (S=1.2)	43.51 ± 0.05 (S=1.2)
$\Delta m(10^{10} \hbar s^{-1})$	0.5289 ± 0.0010	0.5293 ± 0.0009 (S=1.3)
$\tau_S(10^{-10} \text{s})$	0.89564 ± 0.00033	0.8954 ± 0.0004 (S=1.1)
$\phi_{00}(\circ)$	43.7 ± 0.6 (S=1.2)	43.52 ± 0.05 (S=1.3)
$\Delta\phi(\circ)$	0.34 ± 0.32	0.006 ± 0.014 (S=1.7)
$\phi_\epsilon(\circ)$	43.5 ± 0.5 (S=1.3)	43.52 ± 0.05 (S=1.2)
χ^2	16.4	20.0
# Deg. Free.	14	16

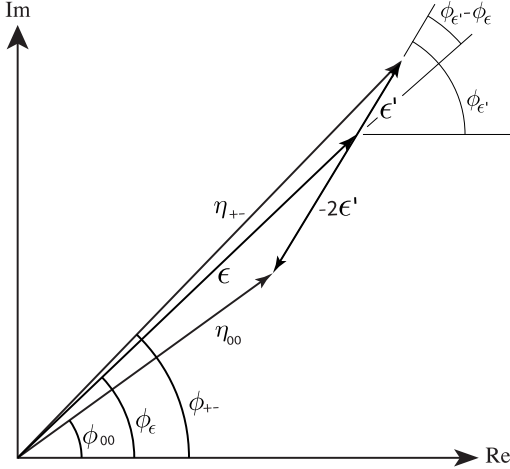


Figure 68.3: Sketch of Eqs. 68.5a. Not to scale

Table 68.3: Correlation matrix for the results of the fit without the CPT assumption

	ϕ_{+-}	Δm	τ_S	ϕ_{00}	$\Delta\phi$	ϕ_ϵ
ϕ_{+-}	1.000	0.596	-0.488	0.827	-0.040	0.976
Δm	0.596	1.000	-0.572	0.487	-0.035	0.580
τ_S	-0.488	-0.572	1.000	-0.423	-0.014	-0.484
ϕ_{00}	0.827	0.487	-0.423	1.000	0.529	0.929
$\Delta\phi$	-0.040	-0.035	-0.014	0.529	1.000	0.178
ϕ_ϵ	0.976	0.580	-0.484	0.929	0.178	1.000

Table 68.4: Correlation matrix for the results of the fit with the CPT assumption

	ϕ_{+-}	Δm	τ_S	ϕ_{00}	$\Delta\phi$	ϕ_ϵ
ϕ_{+-}	1.000	0.972	-0.311	0.957	-0.105	0.995
Δm	0.972	1.000	-0.509	0.958	-0.007	0.977
τ_S	-0.311	-0.509	1.000	-0.306	0.004	-0.312
ϕ_{00}	0.957	0.958	-0.306	1.000	0.189	0.981
$\Delta\phi$	-0.105	-0.007	0.004	0.189	1.000	-0.006
ϕ_ϵ	0.995	0.977	-0.312	0.981	-0.006	1.000

measurements of the K_L^0 and K_S^0 lifetimes (τ_L , τ_S), and branching ratios (B) to $\pi\pi$, using the relations

$$|\eta_{+-}| = \left[\frac{B(K_L^0 \rightarrow \pi^+\pi^-)}{\tau_L} \frac{\tau_S}{B(K_S^0 \rightarrow \pi^+\pi^-)} \right]^{1/2}, \quad (68.12a)$$

$$|\eta_{00}| = \left[\frac{B(K_L^0 \rightarrow \pi^0\pi^0)}{\tau_L} \frac{\tau_S}{B(K_S^0 \rightarrow \pi^0\pi^0)} \right]^{1/2}. \quad (68.12b)$$

For historical reasons, the branching ratio fits and the CP -violation fits are done separately, but we want to include the

influence of $|\eta_{+-}|$, $|\eta_{00}|$, $|\eta_{00}/\eta_{+-}|$, and ϵ'/ϵ measurements on $B(K_L^0 \rightarrow \pi^+\pi^-)$ and $B(K_L^0 \rightarrow \pi^0\pi^0)$ and vice versa. We approximate a global fit to all of these measurements by first performing two independent fits: 1) BRFIT, a fit to the K_L^0 branching ratios, rates, and mean life, and 2) ETAFIT, a fit to the $|\eta_{+-}|$, $|\eta_{00}|$, $|\eta_{+-}/\eta_{00}|$, and ϵ'/ϵ measurements. The results from fit 1, along with the K_S^0 values from this edition, are used to compute values of $|\eta_{+-}|$ and $|\eta_{00}|$, which are included as measurements in the $|\eta_{00}|$ and $|\eta_{+-}|$ sections with a document ID of BRFIT 16. Thus, the fit values of $|\eta_{+-}|$ and $|\eta_{00}|$ given in this edition include both the direct measurements and the results from the branching ratio fit.

The process is reversed in order to include the direct $|\eta|$ measurements in the branching ratio fit. The results from fit 2 above (before including BRFIT 16 values) are used along with the K_L^0 and K_S^0 mean lives and the $K_S^0 \rightarrow \pi\pi$ branching fractions to compute the K_L^0 branching ratio $\Gamma(K_L^0 \rightarrow \pi^0\pi^0)/\Gamma(K_L^0 \rightarrow \pi^+\pi^-)$. This branching ratio value is included as a measurement in the branching ratio section with a document ID of ETAFIT 16. Thus, the K_L^0 branching ratio fit values in this edition include the results of the direct measurement of $|\eta_{+-}|$ and $|\eta_{00}|$ and ϵ'/ϵ . Most individual measurements of $|\eta_{+-}|$ and $|\eta_{00}|$ enter our fits directly via the corresponding measurements of $\Gamma(K_L^0 \rightarrow \pi^+\pi^-)/\Gamma(\text{total})$ and $\Gamma(K_L^0 \rightarrow \pi^0\pi^0)/\Gamma(\text{total})$, and those that do not have too large errors to have any influence on the fitted values of these branching ratios. A more detailed discussion of these fits is given in the 1990 edition of this *Review* [20].

References

- [1] K. Kleinknecht, *Uncovering CP violation: Experimental clarification in the neutral K meson and B meson*, volume 195, Springer Verlag (2003).
- [2] B. Winstein and L. Wolfenstein, *Rev. Mod. Phys.* **65**, 1113 (1993).
- [3] M. S. Sozzi, *Eur. Phys. J.* **C36**, 37 (2004), [hep-ph/0401176].
- [4] T. T. Wu and C.-N. Yang, *Phys. Rev. Lett.* **13**, 380 (1964).
- [5] L. Wolfenstein, *Phys. Rev. Lett.* **13**, 562 (1964); L. Wolfenstein, *Comments Nucl. Part. Phys.* **21**, 5, 275 (1994).
- [6] G. Colangelo, J. Gasser and H. Leutwyler, *Nucl. Phys.* **B603**, 125 (2001), [hep-ph/0103088].
- [7] R. Adler *et al.* (CLEAR), *Phys. Lett.* **B407**, 193 (1997); P. Bloch, *Proceedings of Workshop on K Physics* (Orsay 1996), ed. L. Iconomidou-Fayard, Edition Frontieres, Gif-sur-Yvette, France (1997) p. 307.
- [8] A. Lai *et al.* (NA48), *Phys. Lett.* **B610**, 165 (2005), [hep-ex/0408053].
- [9] G. Buchalla, A. J. Buras and M. E. Lautenbacher, *Rev. Mod. Phys.* **68**, 1125 (1996), [hep-ph/9512380]; S. Bosch *et al.*, *Nucl. Phys.* **B565**, 3 (2000), [hep-ph/9904408]; S. Bertolini, M. Fabbrihesi and J. O. Eeg, *Rev. Mod. Phys.* **72**, 65 (2000), [hep-ph/9802405].
- [10] E. Abouzaid *et al.* (KTeV), *Phys. Rev.* **D83**, 092001 (2011), [arXiv:1011.0127].
- [11] A. Apostolakis *et al.* (CLEAR), *Phys. Lett.* **B458**, 545 (1999).
- [12] B. Schwingerheuer *et al.*, *Phys. Rev. Lett.* **74**, 4376 (1995).
- [13] L. K. Gibbons *et al.*, *Phys. Rev. Lett.* **70**, 1199 (1993).
- [14] L.K. Gibbons, Thesis, RX-1487, Univ. of Chicago, 1993.
- [15] C. Geweniger *et al.*, *Phys. Lett.* **48B**, 487 (1974).
- [16] C. Geweniger *et al.*, *Phys. Lett.* **52B**, 108 (1974).
- [17] R. Carosi *et al.* (NA31), *Phys. Lett.* **B237**, 303 (1990).
- [18] A. Lai *et al.* (NA48), *Phys. Lett.* **B537**, 28 (2002), [hep-ex/0205008].
- [19] L. Bertanza *et al.*, *Z. Phys.* **C73**, 629 (1997).
- [20] J. J. Hernandez *et al.* (Particle Data Group), *Phys. Lett.* **B239**, 1 (1990), [Erratum: *Phys. Lett.* **B253**, 524 (1991)].

69. Review of Multibody Charm Analyses

Revised August 2021 by D.M. Asner (BNL) and J. Rademacker (Bristol U.).

69.1 Overview

The study of multibody charm decays is a vibrant field, with many new experimental results with implications reaching beyond charm, vast and fast-increasing datasets, and new developments in theory and experimental technique. This review is structured as follows. Sec. 69.2 summarises key elements of the theory of multibody charm decays. Sec. 69.3 describes model-independent approaches for precision measurements of mixing and CP violation and the critical role of charm threshold data in this context. Sec. 69.4 reviews applications of the techniques described, and their results. In Sec. 69.5, we conclude.

69.2 Kinematics & Models

The differential decay rate to a point $\mathbf{s} = (s_1, \dots, s_n)$ in n dimensional phase space can be expressed as

$$d\Gamma = |\mathcal{M}(\mathbf{s})|^2 \left| \frac{\partial^n \phi}{\partial (s_1 \dots s_n)} \right| d^n s \quad (69.1)$$

where $|\partial^n \phi / \partial (s_1 \dots s_n)|$ represents the density of states at \mathbf{s} , and \mathcal{M} the matrix element for the decay at that point in phase space, which is 2, 5, 8, ... dimensional for D decays to 3, 4, 5, ... spinless particles. Additional parameters are required to fully describe decays involving particles with non-zero spin in the initial or final state.

For the important case of D decays to three pseudoscalars, the decay kinematics can be represented in a two-dimensional Dalitz plot [1]. This is usually parametrized in terms of $s_{12} \equiv (p_1 + p_2)^2$ and $s_{23} \equiv (p_2 + p_3)^2$, where p_1 , p_2 , and p_3 are the four-momenta of the final state particles. In terms of these variables, phase-space density is constant across the kinematically allowed region, so that any structure seen in the Dalitz plot is a direct consequence of the dynamics encoded in $|\mathcal{M}|^2$. Note that here, because the three-momenta of the decay products are confined to a plane, no parity violating kinematic observables can be constructed (unless they also violate rotational invariance). This is not the case for decays to four or more particles. These can therefore not be unambiguously described in terms of analogously-defined variables s_{ij} , s_{ijk} , which are parity-even. The use of parity-odd observables in four body decays is discussed below.

In the widely-used isobar approach, the matrix element \mathcal{M} is modeled as a sum of interfering decay amplitudes, each proceeding through resonant two-body decays [2–6]. See Refs. [2,7,8] for a review of resonance phenomenology. In most analyses, each resonance is described by a relativistic Breit-Wigner [9] or Flatté [10] lineshape, and the model includes a non-resonant term with a constant phase and magnitude. This approach has well-known theoretical limitations, such as the violation of unitarity and analyticity, which can break the relationship between magnitude and phase across phase space. This motivates the use of more sophisticated descriptions, especially for broad, overlapping resonances (frequently found in S-wave components) where these limitations are particularly problematic. In charm analyses, these approaches have included the K-matrix approach [11] which respects two-body unitarity; the use of LASS scattering data [12]; dispersive methods [13–16]; multi-meson models using chiral Lagrangians [17–20] and methods based on chiral unitarity [21,22]; QCD factorisation [23–26]; and quasi model-independent parametrizations which use generic lineshapes, with minimal theory input and many free parameters, for a subset of resonances [27–32]. An important example, with a rich resonance structure, is $D^0 \rightarrow K_S \pi^+ \pi^-$, which is a key channel in Charge-Parity (CP) violation and charm-mixing analyses. The first analysis by CLEO [33] described the Dalitz plot with approximately 5000 signal events with 10 resonant components. This and analyses by Belle [34] and CDF [35] model the Dalitz plot as a sum of Breit Wigner and Flatté line shapes, and a non-resonant component. BaBar [36] and a more recent Belle analysis [37] on the other hand use a K-matrix description for the $\pi\pi$ S-wave based on [38] and input from LASS scattering data for the $K\pi$ S-wave, with no need to add a non-resonant component to describe the data. This approach is also

followed in the latest analysis of this channel, published jointly by BaBar and Belle [39]. In total 18 resonant components, including four doubly Cabibbo suppressed ones, are required to describe the Dalitz plot with 1.1M $D^0 \rightarrow K_S \pi^+ \pi^-$ events. Belle's and BaBar's data have been re-analyzed by [23] in a QCD factorization framework, using line-shape parametrizations for the S [40,41] and P wave [14] contributions that preserve two-body unitarity and analyticity. The measurements give compatible results for the components they share.

The field of charm amplitude analyses remains very active. Publications since the last update of this review two years ago include Dalitz plot analyses of $D_s^+ \rightarrow K^+ K^- \pi^+$, $K^+ K_S \pi^0$, $K_S^0 \pi^+ \pi^0$, $\pi^+ \pi^- \pi^+$, $D^0 \rightarrow K_S^0 K^+ K^-$ by BES III [31,32,42–44]; $D^0 \rightarrow K^- \pi^+ \eta$ by Belle [45]; a re-analysis of BaBar's $D^0 \rightarrow K_S K^+ K^-$ data in a factorisation approach [26] and of LHCb's $D^+ \rightarrow K^+ K^- K^+$ data [46] in a chiral unitarity approach [22]; four-body amplitude analyses of $D_s^+ \rightarrow \pi^+ \pi^+ \pi^- \eta$, $K^- K^+ \pi^+ \pi^0$, $K_S^0 K^- \pi^+ \pi^+$ by BES III [31,47–49] and of $D^0 \rightarrow K^+ K^- \pi^+ \pi^-$ by LHCb [50]; and the amplitude analysis of the charm baryon decay $\Xi_c^0 \rightarrow \Xi^0 K^+ K^-$ by Belle [51]. Noteworthy is the increasing sophistication of recent amplitude analyses, most of which go substantially beyond the isobar model with Breit Wigner and Flatté lineshapes. However, with the notable exceptions of [15,16,22,46,52], they remain within the isobar framework which describes the decay as a series of two-body processes, and ignores long-range hadronic effects such as re-scattering and does not respect three (or four)-body unitarity and analyticity.

Several groups work on improved models. Dispersive techniques, which respect three-body unitarity and analyticity, have been applied to regions of the $D^+ \rightarrow K^- \pi^+ \pi^+$ and $D^+ \rightarrow K_S \pi^0 \pi^+$ Dalitz plots below the $\eta' K$ threshold [15,16], where they provide a good description of the data with fewer fit parameters than the isobar approach. Ref. [52] uses a unitary coupled channel approach to describe $D^+ \rightarrow K^- \pi^+ \pi^+$, which has no restrictions on the kinematic range, but requires additional parameters to describe the Dalitz plot above the $\eta' K$ threshold. Using an effective chiral Lagrangian, the authors of Ref. [19] provide a description of the annihilation contribution to the decay amplitude which respects three-body unitarity. The approach provides a good description of LHCb $D^+ \rightarrow K^+ K^- K^+$ data, with fewer parameters than an equivalent isobar model [46]. The same channel has more recently been re-analysed by the authors of [22], who argue that the internal emission diagram should dominate and use a chiral unitarity-based approach to achieve a reasonable description of the data with two free parameters.

Limitations in the theoretical description of interfering resonances are the leading source of systematic uncertainty in many analyses. This is set to become increasingly problematic given the statistical precision achievable with the vast, clean charm samples available at the B factories, LHCb, and their upgrades, and BES III. In some cases, the model uncertainty can be removed through model-independent methods, often relying on input from the charm threshold, as discussed below. The authors of [53] expand the scope and applicability of the quasi model-independent approach in amplitude fits. At the same time, increasingly sophisticated models are being developed, and applied to data. The authors of [20] and [54] provide valuable frameworks for sophisticated amplitude analyses.

69.3 Model Independent Methods and the Charm Threshold

The precision measurement of mixing or CP violation parameters such γ/ϕ_3 from multibody charm decays requires as input the phase-differences between the D^0 and \bar{D}^0 amplitudes across phase space, as well as their magnitudes, for each final state of interest. While the magnitudes are fairly easily measured, the phase information requires either amplitude models with reliable phase motion, or model-independent approaches.

Model-independent measurements of the relevant phase differences rely on interference effects in the decays of well-defined coherent superpositions of D^0 and \bar{D}^0 . These are accessible at the charm threshold, where CLEO-c and BES III operate [55–63]. Charm mixing also results in a (time-dependent) $D^0 - \bar{D}^0$ su-

perposition, that can be used to measure the relevant phase information as input to γ/ϕ_3 measurements. This method is particularly powerful in doubly Cabibbo-suppressed decays such as $D^0 \rightarrow K^+\pi^-\pi^+\pi^-$, and when used in combination with threshold data [64,65]. Under some circumstances, with large data sets, the relevant strong phases and γ/ϕ_3 can be extracted simultaneously without external input, for example in simultaneous analysis of the $B^0 \rightarrow DK^+\pi^-$ Dalitz plot and that of the subsequent $D \rightarrow K_S^0\pi^+\pi^-$ decay [66]. However, the global effort to achieve a measurement of γ/ϕ_3 to sub-degree precision will continue to rely critically on input from the charm threshold and BES III's increasing datasets [67]. A particularly noteworthy recent development is the substantial improvement not only in the precision on γ but also on charm mixing parameters achieved through a combined fit of charm mixing, charm threshold, $B \rightarrow DK$ and related data [68].

The model-independent phase information of the charm decay is provided either integrated over the entire phase space of the decay, or in sub-regions/bins. The results can be expressed in terms of one complex parameter $\mathcal{Z} = Re^{-i\delta} = c + is$ per pair of CP -conjugate bins, with magnitude $R \leq 1$. Larger R values lead to higher sensitivity to γ/ϕ_3 . Amplitude models can be used to optimise the binning for sensitivity to γ/ϕ_3 , without introducing a model-dependent bias in the result; novel unbinned approaches are expected to increase the precision on γ in future analyses [69].

CLEO-c data have been analyzed to provide binned \mathcal{Z} for the self-conjugate decays $D^0 \rightarrow K_S\pi^+\pi^-$, $K_S K^+K^-$, $\pi^+\pi^-\pi^+\pi^-$, and $K_S\pi^-\pi^+\pi^0$ and phase space-integrated values for $D^0, \bar{D}^0 \rightarrow K_S K^+K^-$, $K^+\pi^-\pi^0$ and $K^+\pi^-\pi^+\pi^-$ [70–75]. BES III significantly improved the precision for the $K_S\pi^+\pi^-$, $K_S K^+K^-$, $K^+\pi^-\pi^0$ and $K^+\pi^-\pi^+\pi^-$ final states [76–79]. Critically, BES III was able to perform this measurement in four separate bins of $K^+\pi^-\pi^+\pi^-$ phase space. Studies based on recent $D^0 \rightarrow K^\pm\pi^\mp\pi^\pm\pi^\mp$ amplitude models [30] indicate that such a binned analysis could lead to the most precise individual γ measurement [80], especially when combined with LHCb charm mixing data [65,75,81]. For self-conjugate decays such as $D^0 \rightarrow \pi^+\pi^-\pi^0$, analysed with a single pair of bins, \mathcal{Z} is real-valued, and usually expressed in terms of the CP -even fraction $F_+ \equiv \frac{1}{2}(\text{Re}(\mathcal{Z}) + 1)$, defined such that a CP -even eigenstate has $F_+ = 1$, while a CP -odd eigenstate has $F_+ = 0$ [61]. Recent analyses of CLEO-c data reveal that $D^0 \rightarrow \pi^+\pi^-\pi^0$ is compatible with being completely CP -even with $F_+ = 0.973 \pm 0.017$, while $D^0 \rightarrow K^+K^-\pi^0$ has $F_+ = 0.732 \pm 0.055$, $D^0 \rightarrow \pi^+\pi^-\pi^+\pi^-$ has $F_+ = 0.769 \pm 0.023$ and $D^0 \rightarrow K_S\pi^+\pi^-\pi^0$ has 0.238 ± 0.020 [62,72,73].

It is interesting to compare these values with those obtained from amplitude models as a cross-check of the models' phase-motion. $F_+^{4\pi \text{ model}} = 0.729 \pm 0.020$ calculated from Ref. [29]'s $D^0 \rightarrow \pi^+\pi^-\pi^+\pi^-$ model compares well to the measured value given above, as does $|\mathcal{Z}^{K3\pi \text{ model}}| = 0.459 \pm 0.025$ [30] to $\mathcal{Z}^{K3\pi \text{ meas}} = 0.44_{-0.09}^{+0.10} \exp(-i(161^\circ_{-18^\circ}))$ [75,81]. Only for self-conjugate decays or multiple bins does the model provide relevant phase information. The latest bin wise comparisons between model and data for $D^0 \rightarrow K_S\pi^+\pi^-$, $K_S K^+K^-$, $\pi^+\pi^-\pi^+\pi^-$, and $K^\pm\pi^\mp\pi^\pm\pi^\mp$ can be found in [72,76–79] and generally show good agreement, which is a welcome surprise given the preceding discussion on the theoretical shortcomings of such amplitude models.

69.4 Applications of multibody charm analyses

Amplitude analyses provide sensitivity to both relative magnitudes and phases of the interfering decay amplitudes. It is especially this sensitivity to phases that makes amplitude analyses such a uniquely powerful tool for studying a wide range of phenomena. Here we concentrate on their use for CP violation and mixing measurements in charm, and charm inputs to CP violation analyses in B meson decays (properties of light-meson resonances determined in D amplitude analyses are reported in the light-unflavored-meson section of this Review).

69.4.1 Time-integrated searches for CP violation in charm

Comparing the results of amplitude fits for CP -conjugate decay modes provides a measure of CP violation. Recent CP violation searches using this method include amplitude analyses of $D^0 \rightarrow K_S^0 K^\pm\pi^\mp$ and $D^0 \rightarrow K^+K^-\pi^+\pi^-$ by LHCb [82,83], and $D^0 \rightarrow K^+K^-\pi^+\pi^-$, $D^0 \rightarrow \pi^+\pi^-\pi^+\pi^-$ [29,84] using CLEO data.

A widely-used amplitude model-independent technique to search for local CP violation is based on performing a χ^2 comparison of CP -conjugate phase-space distributions. This method was pioneered by BaBar [85] and developed further in [86–88], with results reported by BaBar [85,89] and LHCb in $D^\pm \rightarrow K^+K^-\pi^\pm$ [90,91], CDF in $D^0 \rightarrow K_S\pi^+\pi^-$ [35], and LHCb in $D^+ \rightarrow \pi^-\pi^+\pi^+$, $D^0 \rightarrow K^+K^-\pi^+\pi^-$, $D^0 \rightarrow \pi^+\pi^-\pi^+\pi^-$, and $\Xi_c^+ \rightarrow pK^-\pi^+$ [88,92,93]. Unbinned methods can increase sensitivity [94] and have been applied by LHCb to $D^+ \rightarrow \pi^-\pi^+\pi^+$, $D^0 \rightarrow \pi^+\pi^-\pi^0$, $D^0 \rightarrow \pi^+\pi^-\pi^+\pi^+$, and $\Xi_c^+ \rightarrow pK^-\pi^+$ [92,93,95,96].

An alternative model-independent approach is based on observables in four body decays that are odd under motion reversal (“naive T”) [97–105], which is equivalent to P for scalar particles [105]. One such observable is $C_T = \vec{p}_2 \cdot (\vec{p}_3 \times \vec{p}_4) = (1/m_D)\epsilon_{\alpha\beta\gamma\delta} p_1^\alpha p_2^\beta p_3^\gamma p_4^\delta$, where \vec{p}_i are the decay products' three momenta in the decay's rest frame, and p_i are their four-momenta. Identical particles (as in $D^0 \rightarrow K^+\pi^-\pi^+\pi^-$) are ordered by momentum magnitude. Comparing the P violating asymmetry $A_T \equiv \frac{\Gamma(C_T>0) - \Gamma(C_T<0)}{\Gamma(C_T>0) + \Gamma(C_T<0)}$ with its C -conjugate provides sensitivity to CP violation. Searches for CP violation in this manner have been carried out by BaBar, Belle, FOCUS and LHCb in $D^0 \rightarrow K^+K^-\pi^+\pi^-$ [106–109], $D^+ \rightarrow K^+K_S\pi^+\pi^-$, $D_s^+ \rightarrow K^+K_S\pi^+\pi^-$ [110], $D^0 \rightarrow K_S\pi^+\pi^-\pi^0$ [111], and $D^0 \rightarrow \pi^+\pi^-\pi^+\pi^-$ [96]. The authors of [109] use additional P -odd variables and [108,111]/[96] increase sensitivity by resolving four-body phase space in a binned/unbinned approach.

The results of all measurements described in this section are compatible with CP conservation in charm. Given the discovery of CP violation in $D^0 \rightarrow K^+K^-$, $D^0 \rightarrow \pi^+\pi^-$ decays [112], and the vast data samples about to be collected, one might expect this to change in the foreseeable future.

69.4.2 CP violation in decays of Beauty to Charm

Neutral D mesons originating from $B^- \rightarrow DK^-$ (here denoted as D_{B^-}) are a superposition of D^0 and \bar{D}^0 with a relative phase that depends on the CKM unitarity triangle parameter γ/ϕ_3 ,

$$D_{B^-} \propto D^0 + r_B e^{i(\delta_B - \gamma)} \bar{D}^0,$$

where δ_B is a CP conserving strong phase, and $r_B \sim 0.1$. In the corresponding CP -conjugate expression, γ/ϕ_3 changes sign. An amplitude analysis of the subsequent decay of the D_{B^\pm} to a state accessible to both D^0 and \bar{D}^0 allows the measurement of γ/ϕ_3 [56,113–116]. The method generalizes to similar B hadron decays, such as $B^0 \rightarrow DK^{*0}$. Measurements based on this technique have been reported by BaBar [117,118], Belle [34,119] and LHCb [120–129]. The most precise individual result with an uncertainty of $\sim 5^\circ$ comes from an amplitude model-independent study of $D_{B^-} \rightarrow K_S\pi^+\pi^-$ and $D_{B^-} \rightarrow K_S K^+K^-$ [130], using input from the charm threshold [70,77] as described above. Combining measurements in multiple decay modes from LHCb, CLEO-c and BES III in an amplitude-model independent approach leads to a current uncertainty on γ/ϕ_3 of 4° [68,131].

The interference between mixing and decay in $B^0 \rightarrow D^0 h^0$ with $h^0 = \pi^0, \eta, \omega$ provides sensitivity to β , which can be extracted from the Dalitz plot of the subsequent $D^0 \rightarrow K_S\pi^+\pi^-$ decay [39,132–135]. The combined BaBar/Belle analysis based on this technique resolved the ambiguity in β present in other measurements, such as $B^0 \rightarrow J/\psi K_S$, in favour of the solution compatible with other unitarity triangle constraints [39].

Further details on CP violation in beauty and charm can be found in [55,136].

69.4.3 Charm Mixing and CP violation

Time-dependent amplitude analyses in decays to final states that are accessible to both D^0 and \bar{D}^0 have unique sensitivity to mixing parameters. A Dalitz plot analysis of a self-conjugate

final state, such as $K_S\pi^+\pi^-$ and $K_S K^+K^-$, allows the measurement of the phase difference between the relevant D^0 and \bar{D}^0 decay amplitudes, and thus a direct measurement of x and y , the normalized mass and width difference of the $D^0 - \bar{D}^0$ system's mass eigenstates. This is in contrast to decays like $D^0 \rightarrow K\pi$ [137] which only provide access to the decay-specific parameters x'^2, y' . The phase differences between D^0 and \bar{D}^0 amplitudes across the Dalitz plot affect these measurements in the same way as measurements of γ/ϕ_3 in $B^+ \rightarrow DK^+$, and can be taken into account in an amplitude model-independent way using the same charm threshold results [70,77]. This approach recently resulted the first observation of the mass difference of the neutral charm mass eigenstates by LHCb [138], using a model-independent analysis of $D^0 \rightarrow K_S\pi^+\pi^-$. The “bin flip” technique applied in this measurements exploits that CP -conjugate regions of the $D^0 \rightarrow K_S\pi^+\pi^-$ Dalitz plot have near-identical experimental efficiencies [139]. This measurement is also sensitive to CP violation in mixing and in the interference between mixing and decay, which is discussed further in [55,136]. The most precise values for charm mixing parameters result from a combination of charm data from LHCb and the charm threshold with input from γ -sensitive decays of the type $B^+ \rightarrow D^0 K^+$ [68]. The substantial impact of the latter is noteworthy, as it improves the precision on y by a factor of two compared to the previous world average.

69.5 Summary

Multibody charm decays offer a rich phenomenology, including unique sensitivity to CP violation and charm mixing. This is a highly dynamic field with many new results (some of which we presented here) and rapidly increasing, high quality datasets. These datasets constitute a huge opportunity, but also a challenge to improve the theoretical descriptions of soft hadronic effects in multibody decays. For some measurements, model-independent methods, many relying on input from the charm threshold, provide a way of removing model-induced uncertainties. At the same time, substantial progress in the theoretical description of multibody decays is being made.

References

- [1] R. Dalitz, *Phil. Mag. Ser. 7* **44**, 1068 (1953).
- [2] M. Bauer, B. Stech and M. Wirbel, *Z. Phys. C* **34**, 103 (1987).
- [3] L.-L. Chau and H.-Y. Cheng, *Phys. Rev. D* **36**, 137 (1987), [Addendum: *Phys.Rev.D* 39, 2788–2791 (1989)].
- [4] P. F. Bedaque, A. K. Das and V. Mathur, *Phys. Rev. D* **49**, 269 (1994), [hep-ph/9307296].
- [5] K. Terasaki, *Int. J. Mod. Phys. A* **10**, 3207 (1995).
- [6] F. Buccella, M. Lusignoli and A. Pugliese, *Phys. Lett. B* **379**, 249 (1996), [hep-ph/9601343].
- [7] J. D. Jackson, *Nuovo Cim.* **34**, 1644 (1964).
- [8] See the note on Resonances in this *Review*.
- [9] E. P. Wigner, *Phys. Rev.* **70**, 15 (1946).
- [10] S. M. Flatte, *Phys. Lett. B* **63**, 224 (1976).
- [11] I. Aitchison, *Nucl. Phys. A* **189**, 417 (1972).
- [12] D. Aston *et al.*, *Nucl. Phys. B* **296**, 493 (1988).
- [13] R. Omnes, *Nuovo Cim.* **8**, 316 (1958).
- [14] C. Hanhart, *Phys. Lett. B* **715**, 170 (2012), [arXiv:1203.6839].
- [15] F. Niecknig and B. Kubis, *JHEP* **10**, 142 (2015), [arXiv:1509.03188].
- [16] F. Niecknig and B. Kubis, *Phys. Lett. B* **780**, 471 (2018), [arXiv:1708.00446].
- [17] P. Magalhães and M. Robilotta, *Phys. Rev. D* **92**, 9, 094005 (2015), [arXiv:1504.06346].
- [18] P. Magalhaes *et al.*, *Phys. Rev. D* **84**, 094001 (2011), [arXiv:1105.5120].
- [19] R. Aoude *et al.*, *Phys. Rev. D* **98**, 5, 056021 (2018), [arXiv:1805.11764].
- [20] P. C. Magalhães, A. C. dos Reis and M. R. Robilotta, *Phys. Rev. D* **102**, 7, 076012 (2020), [arXiv:2007.12304].
- [21] J. A. Oller, *Phys. Rev. D* **71**, 054030 (2005), [hep-ph/0411105].
- [22] L. Roca and E. Oset, *Phys. Rev. D* **103**, 3, 034020 (2021), [arXiv:2011.05185].
- [23] J.-P. Dedonder *et al.*, *Phys. Rev. D* **89**, 9, 094018 (2014), [arXiv:1403.2971].
- [24] D. Boito *et al.*, *Phys. Rev. D* **96**, 11, 113003 (2017), [arXiv:1709.09739].
- [25] R. Klein *et al.*, *JHEP* **10**, 117 (2017), [arXiv:1708.02047].
- [26] J. P. Dedonder *et al.*, *Phys. Rev. D* **103**, 11, 114028 (2021), [arXiv:2105.03355].
- [27] E. Aitala *et al.* (E791), *Phys. Rev. D* **73**, 032004 (2006), [Erratum: *Phys. Rev.D* 74, 059901 (2006)], [hep-ex/0507099].
- [28] G. Bonvicini *et al.* (CLEO), *Phys. Rev. D* **78**, 052001 (2008), [arXiv:0802.4214].
- [29] P. d’Argent *et al.*, *JHEP* **05**, 143 (2017), [arXiv:1703.08505].
- [30] R. Aaij *et al.* (LHCb), *Eur. Phys. J. C* **78**, 6, 443 (2018), [arXiv:1712.08609].
- [31] M. Ablikim *et al.* (BESIII), *Phys. Rev. D* **104**, 1, 012016 (2021), [arXiv:2011.08041].
- [32] M. Ablikim *et al.* (BESIII) (2021), [arXiv:2108.10050].
- [33] H. Muramatsu *et al.* (CLEO), *Phys. Rev. Lett.* **89**, 251802 (2002), [Erratum: *Phys. Rev. Lett.* 90, 059901 (2003)], [hep-ex/0207067].
- [34] A. Poluektov *et al.* (Belle), *Phys. Rev. D* **81**, 112002 (2010), [arXiv:1003.3360].
- [35] T. Aaltonen *et al.* (CDF), *Phys. Rev. D* **86**, 032007 (2012), [arXiv:1207.0825].
- [36] P. del Amo Sanchez *et al.* (BaBar), *Phys. Rev. Lett.* **105**, 081803 (2010), [arXiv:1004.5053].
- [37] T. Peng *et al.* (Belle), *Phys. Rev. D* **89**, 9, 091103 (2014), [arXiv:1404.2412].
- [38] V. Anisovich and A. Sarantsev, *Eur. Phys. J. A* **16**, 229 (2003), [hep-ph/0204328].
- [39] I. Adachi *et al.* (BaBar, Belle), *Phys. Rev. Lett.* **121**, 26, 261801 (2018), [arXiv:1804.06152]; I. Adachi *et al.* (BaBar, Belle), *Phys. Rev. D* **98**, 11, 112012 (2018), [arXiv:1804.06153].
- [40] B. El-Bennich *et al.*, *Phys. Rev. D* **79**, 094005 (2009), [Erratum: *Phys. Rev. D* 83, 039903 (2011)], [arXiv:0902.3645].
- [41] J.-P. Dedonder *et al.*, *Acta Phys. Polon. B* **42**, 2013 (2011), [arXiv:1011.0960].
- [42] M. Ablikim *et al.* (BESIII), *JHEP* **2021**, 6, 181 (2021), [arXiv:2103.15098].
- [43] M. Ablikim *et al.* (BESIII) (2020), [arXiv:2006.02800].
- [44] M. Ablikim *et al.* (BESIII), *Phys. Rev. D* **104**, 012006 (2021), [arXiv:2104.09131].
- [45] Y. Q. Chen *et al.* (Belle), *Phys. Rev. D* **102**, 1, 012002 (2020), [arXiv:2003.07759].
- [46] R. Aaij *et al.* (LHCb), *JHEP* **04**, 063 (2019), [arXiv:1902.05884].
- [47] M. Ablikim *et al.* (BESIII) (2021), [arXiv:2106.13536].
- [48] M. Ablikim *et al.* (BESIII), *Phys. Rev. D* **104**, 3, 032011 (2021), [arXiv:2103.02482].
- [49] M. Ablikim *et al.* (BESIII), *Phys. Rev. D* **103**, 9, 092006 (2021), [arXiv:2102.03808].
- [50] R. Aaij *et al.* (LHCb), *JHEP* **02**, 126 (2019), [arXiv:1811.08304].
- [51] J. T. McNeil *et al.* (Belle), *Phys. Rev. D* **103**, 11, 112002 (2021), [arXiv:2012.05607].
- [52] S. X. Nakamura, *Phys. Rev. D* **93**, 1, 014005 (2016), [arXiv:1504.02557].

- [53] F. Krinner *et al.*, Phys. Rev. D **97**, 11, 114008 (2018), [arXiv:1710.09849].
- [54] M. Mikhasenko *et al.* (JPAC), Phys. Rev. D **101**, 3, 034033 (2020), [arXiv:1910.04566].
- [55] See the note on $D^0-\bar{D}^0$ Mixing in this *Review*.
- [56] A. Giri *et al.*, Phys. Rev. D **68**, 054018 (2003), [hep-ph/0303187].
- [57] D. Atwood and A. Soni, Phys. Rev. D **68**, 033003 (2003), [hep-ph/0304085].
- [58] S. Malde and G. Wilkinson, Phys. Lett. B **701**, 353 (2011), [arXiv:1104.2731].
- [59] A. Bondar, A. Poluektov and V. Vorobiev, Phys. Rev. D **82**, 034033 (2010), [arXiv:1004.2350].
- [60] J. Kallen *et al.*, JHEP **10**, 184 (2012), [arXiv:1207.3763].
- [61] M. Nayak *et al.*, Phys. Lett. B **740**, 1 (2015), [arXiv:1410.3964].
- [62] S. Malde *et al.*, Phys. Lett. B **747**, 9 (2015), [arXiv:1504.05878].
- [63] S. Malde, C. Thomas and G. Wilkinson, Phys. Rev. D **91**, 9, 094032 (2015), [arXiv:1502.04560].
- [64] S. Harnew and J. Rademacker, Phys. Lett. B **728**, 296 (2014), [arXiv:1309.0134].
- [65] S. Harnew and J. Rademacker, JHEP **03**, 169 (2015), [arXiv:1412.7254].
- [66] D. Craik, T. Gershon and A. Poluektov, Phys. Rev. D **97**, 5, 056002 (2018), [arXiv:1712.07853].
- [67] M. Ablikim *et al.* (BESIII), Chin. Phys. C **44**, 4, 040001 (2020), [arXiv:1912.05983].
- [68] R. Aaij *et al.* (LHCb) (2021), [arXiv:2110.02350].
- [69] A. Poluektov, Eur. Phys. J. C **78**, 2, 121 (2018), [arXiv:1712.08326].
- [70] J. Libby *et al.* (CLEO), Phys. Rev. D **82**, 112006 (2010), [arXiv:1010.2817].
- [71] R. A. Briere *et al.* (CLEO), Phys. Rev. D **80**, 032002 (2009), [arXiv:0903.1681].
- [72] S. Harnew *et al.*, JHEP **01**, 144 (2018), [arXiv:1709.03467].
- [73] P. Resmi *et al.*, JHEP **01**, 082 (2018), [arXiv:1710.10086].
- [74] J. Insler *et al.* (CLEO), Phys. Rev. D **85**, 092016 (2012), [Erratum: Phys. Rev. D **94**, 099905 (2016)], [arXiv:1203.3804].
- [75] T. Evans *et al.*, Phys. Lett. B **757**, 520 (2016), [Erratum: Phys. Lett. B **765**, 402–403 (2017)], [arXiv:1602.07430].
- [76] M. Ablikim *et al.* (BESIII), Phys. Rev. Lett. **124**, 24, 241802 (2020), [arXiv:2002.12791].
- [77] M. Ablikim *et al.* (BESIII), Phys. Rev. D **101**, 11, 112002 (2020), [arXiv:2003.00091].
- [78] M. Ablikim *et al.* (BESIII), Phys. Rev. D **102**, 5, 052008 (2020), [arXiv:2007.07959].
- [79] M. Ablikim *et al.* (BESIII), JHEP **05**, 164 (2021), [arXiv:2103.05988].
- [80] T. Evans *et al.*, Phys. Lett. B **802**, 135188 (2020), [arXiv:1909.10196].
- [81] R. Aaij *et al.* (LHCb), Phys. Rev. Lett. **116**, 24, 241801 (2016), [arXiv:1602.07224].
- [82] R. Aaij *et al.* (LHCb), Phys. Rev. D **93**, 5, 052018 (2016), [arXiv:1509.06628].
- [83] R. Aaij *et al.* (LHCb), JHEP **02**, 126 (2019), [arXiv:1811.08304].
- [84] M. Artuso *et al.* (CLEO), Phys. Rev. D **85**, 122002 (2012), [arXiv:1201.5716].
- [85] B. Aubert *et al.* (BaBar), Phys. Rev. D **78**, 051102 (2008), [arXiv:0802.4035].
- [86] I. Bediaga *et al.*, Phys. Rev. D **80**, 096006 (2009), [arXiv:0905.4233].
- [87] I. Bediaga *et al.*, Phys. Rev. D **86**, 036005 (2012), [arXiv:1205.3036].
- [88] R. Aaij *et al.* (LHCb), Phys. Lett. B **726**, 623 (2013), [arXiv:1308.3189].
- [89] J. Lees *et al.* (BaBar), Phys. Rev. D **87**, 5, 052010 (2013), [arXiv:1212.1856].
- [90] R. Aaij *et al.* (LHCb), Phys. Rev. D **84**, 112008 (2011), [arXiv:1110.3970].
- [91] R. Aaij *et al.* (LHCb), JHEP **06**, 112 (2013), [arXiv:1303.4906].
- [92] R. Aaij *et al.* (LHCb), Phys. Lett. B **728**, 585 (2014), [arXiv:1310.7953].
- [93] R. Aaij *et al.* (LHCb), Eur. Phys. J. C **80**, 10, 986 (2020), [arXiv:2006.03145].
- [94] M. Williams, Phys. Rev. D **84**, 054015 (2011), [arXiv:1105.5338].
- [95] R. Aaij *et al.* (LHCb), Phys. Lett. B **740**, 158 (2015), [arXiv:1410.4170].
- [96] R. Aaij *et al.* (LHCb), Phys. Lett. B **769**, 345 (2017), [arXiv:1612.03207].
- [97] E. Golowich and G. Valencia, Phys. Rev. D **40**, 112 (1989).
- [98] G. Valencia, Phys. Rev. D **39**, 3339 (1989).
- [99] W. Bensalem and D. London, Phys. Rev. D **64**, 116003 (2001), [hep-ph/0005018].
- [100] I. I. Bigi, in “KAON2001: International Conference on CP Violation,” (2001), [hep-ph/0107102].
- [101] W. Bensalem, A. Datta and D. London, Phys. Rev. D **66**, 094004 (2002), [hep-ph/0208054].
- [102] W. Bensalem, A. Datta and D. London, Phys. Lett. B **538**, 309 (2002), [hep-ph/0205009].
- [103] A. Datta and D. London, Int. J. Mod. Phys. A **19**, 2505 (2004), [hep-ph/0303159].
- [104] M. Gronau and J. L. Rosner, Phys. Rev. D **84**, 096013 (2011), [arXiv:1107.1232].
- [105] G. Durieux and Y. Grossman, Phys. Rev. D **92**, 7, 076013 (2015), [arXiv:1508.03054].
- [106] J. Link *et al.* (FOCUS), Phys. Lett. B **622**, 239 (2005), [hep-ex/0506012].
- [107] P. del Amo Sanchez *et al.* (BaBar), Phys. Rev. D **81**, 111103 (2010), [arXiv:1003.3397].
- [108] R. Aaij *et al.* (LHCb), JHEP **10**, 005 (2014), [arXiv:1408.1299].
- [109] J. Kim *et al.* (Belle), Phys. Rev. D **99**, 1, 011104 (2019), [arXiv:1810.06457].
- [110] J. Lees *et al.* (BaBar), Phys. Rev. D **84**, 031103 (2011), [arXiv:1105.4410].
- [111] K. Prasanth *et al.* (Belle), Phys. Rev. D **95**, 9, 091101 (2017), [arXiv:1703.05721].
- [112] R. Aaij *et al.* (LHCb), Phys. Rev. Lett. **122**, 21, 211803 (2019), [arXiv:1903.08726].
- [113] M. Gronau and D. Wyler, Phys. Lett. B **265**, 172 (1991).
- [114] M. Gronau and D. London, Phys. Lett. B **253**, 483 (1991).
- [115] A. Poluektov *et al.* (Belle), Phys. Rev. D **70**, 072003 (2004), [hep-ex/0406067].
- [116] J. Rademacker and G. Wilkinson, Phys. Lett. B **647**, 400 (2007), [hep-ph/0611272].
- [117] P. del Amo Sanchez *et al.* (BaBar), Phys. Rev. Lett. **105**, 121801 (2010), [arXiv:1005.1096].
- [118] J. Lees *et al.* (BaBar), Phys. Rev. D **84**, 012002 (2011), [arXiv:1104.4472].
- [119] H. Aihara *et al.* (Belle), Phys. Rev. D **85**, 112014 (2012), [arXiv:1204.6561].
- [120] R. Aaij *et al.* (LHCb), Phys. Lett. B **726**, 151 (2013), [arXiv:1305.2050].

- [121] R. Aaij *et al.* (LHCb), Phys. Lett. B **723**, 44 (2013), [arXiv:1303.4646].
- [122] R. Aaij *et al.* (LHCb), Phys. Lett. B **718**, 43 (2012), [arXiv:1209.5869].
- [123] R. Aaij *et al.* (LHCb), JHEP **10**, 097 (2014), [arXiv:1408.2748].
- [124] R. Aaij *et al.* (LHCb), Phys. Lett. B **733**, 36 (2014), [arXiv:1402.2982].
- [125] R. Aaij *et al.* (LHCb), Nucl. Phys. B **888**, 169 (2014), [arXiv:1407.6211].
- [126] R. Aaij *et al.* (LHCb), Phys. Rev. D **91**, 11, 112014 (2015), [arXiv:1504.05442].
- [127] R. Aaij *et al.* (LHCb), JHEP **06**, 131 (2016), [arXiv:1604.01525].
- [128] R. Aaij *et al.* (LHCb), JHEP **12**, 087 (2016), [arXiv:1611.03076].
- [129] R. Aaij *et al.* (LHCb), JHEP **08**, 176 (2018), [Erratum: JHEP 10, 107 (2018)], [arXiv:1806.01202].
- [130] R. Aaij *et al.* (LHCb), JHEP **02**, 169 (2021), [arXiv:2010.08483].
- [131] Y. S. Amhis *et al.* (HFLAV), Eur. Phys. J. **C81**, 226 (2021), updated results and plots available at <https://hflav.web.cern.ch/>, [arXiv:1909.12524].
- [132] A. Bondar, T. Gershon and P. Krokovny, Phys. Lett. B **624**, 1 (2005), [hep-ph/0503174].
- [133] P. Krokovny *et al.* (Belle), Phys. Rev. Lett. **97**, 081801 (2006), [hep-ex/0605023].
- [134] B. Aubert *et al.* (BaBar), Phys. Rev. Lett. **99**, 231802 (2007), [arXiv:0708.1544].
- [135] V. Vorobyev *et al.* (Belle), Phys. Rev. D **94**, 5, 052004 (2016), [arXiv:1607.05813].
- [136] See the note CP violation in the quark sector in this *Review*.
- [137] D. Asner *et al.* (CLEO), Phys. Rev. D **72**, 012001 (2005), [hep-ex/0503045].
- [138] R. Aaij *et al.* (LHCb) (2021), [arXiv:2106.03744].
- [139] A. Di Canto *et al.*, Phys. Rev. D **99**, 1, 012007 (2019), [arXiv:1811.01032].

70. D^0 - \bar{D}^0 Mixing

Revised September 2021 by D.M. Asner (BNL) and A.J. Schwartz (U. of Cincinnati).

The formalism for D^0 - \bar{D}^0 mixing is closely related to that for CP violation; for further details on the latter, see the note “ CP Violation in the Quark Sector” in this *Review*. The time evolution of the D^0 - \bar{D}^0 system is described by the Schrödinger equation

$$i \frac{\partial}{\partial t} \begin{pmatrix} D^0(t) \\ \bar{D}^0(t) \end{pmatrix} = \left(\mathbf{M} - \frac{i}{2} \mathbf{\Gamma} \right) \begin{pmatrix} D^0(t) \\ \bar{D}^0(t) \end{pmatrix}, \quad (70.1)$$

where the \mathbf{M} and $\mathbf{\Gamma}$ matrices are Hermitian, and CPT invariance requires that $M_{11} = M_{22} \equiv M$ and $\Gamma_{11} = \Gamma_{22} \equiv \Gamma$. The off-diagonal elements of \mathbf{M} and $\mathbf{\Gamma}$ are referred to as the dispersive and absorptive parts, respectively, of the mixing. The mass eigenstates D_1 and D_2 of the Hamiltonian $\mathbf{M} - i\mathbf{\Gamma}/2$ are defined as

$$|D_{1,2}\rangle \equiv p|D^0\rangle \pm q|\bar{D}^0\rangle, \quad (70.2)$$

where normalization imposes $|p|^2 + |q|^2 = 1$. If $p = \pm q$, then the mass eigenstates are CP eigenstates and CP is conserved. Our phase convention is $CP|D^0\rangle = -|\bar{D}^0\rangle$, which implies that, in the absence of CP violation, D_2 is CP -even and D_1 is CP -odd.

The eigenvalues of $\mathbf{M} - i\mathbf{\Gamma}/2$ are

$$\omega_{1,2} = \left(M - \frac{i}{2} \Gamma \right) \pm \frac{q}{p} \left(M_{12} - \frac{i}{2} \Gamma_{12} \right) \equiv m_{1,2} - \frac{i}{2} \Gamma_{1,2}, \quad (70.3)$$

where $m_{1,2}$ and $\Gamma_{1,2}$ are real and correspond to the masses and decay widths, respectively, of the $D_{1,2}$ mass eigenstates. As the trace $\Gamma_{11} + \Gamma_{22} = 2\Gamma$ is unchanged by diagonalizing $\mathbf{\Gamma}$, Γ must equal $(\Gamma_1 + \Gamma_2)/2$, the mean decay width. Solving for the eigenstates of the eigenvalues yields

$$\left(\frac{q}{p} \right)^2 = \frac{M_{12}^* - \frac{i}{2} \Gamma_{12}^*}{M_{12} - \frac{i}{2} \Gamma_{12}}. \quad (70.4)$$

If CP is conserved, then $(q/p)^2 = 1$ and M_{12} and Γ_{12} must be real. In this case, the difference in eigenvalues is $\Delta m \equiv m_2 - m_1 = 2M_{12}$ and $\Delta\Gamma \equiv \Gamma_2 - \Gamma_1 = 2\Gamma_{12}$. The signs of Δm and $\Delta\Gamma$ are difficult to predict from theory and thus must be determined experimentally.

We define dimensionless mixing parameters x and y as

$$x \equiv \frac{\Delta m}{\Gamma} \quad (70.5)$$

$$y \equiv \frac{\Delta\Gamma}{2\Gamma}. \quad (70.6)$$

These parameters are measured in several ways. The most precise values are obtained by measuring the time dependence of D^0 decays. For all methods, the initial flavor of the D^0 or \bar{D}^0 when produced must be determined. The most common method used for this is to reconstruct $D^{*+} \rightarrow D^0\pi^+$ or $D^{*-} \rightarrow \bar{D}^0\pi^-$ decays; the charge of the accompanying pion (which has low momentum in the lab frame and is often referred to as the “soft” pion) determines the flavor of the neutral D . BaBar and LHCb have also identified the flavor of the neutral D by reconstructing the semileptonic decays $B^+ \rightarrow \bar{D}^0\ell^+\nu$, $B^0 \rightarrow D^{*-}\ell^+\nu$, $B^- \rightarrow D^0\ell^-\nu$, and $\bar{B}^0 \rightarrow D^{*+}\ell^-\nu$; in this case the charge of the accompanying lepton determines the D flavor. Both experiments have used both tags together to select “double-tagged” $B \rightarrow D^{*\pm}\ell^\mp\nu$, $D^{*\pm} \rightarrow (D^0, \bar{D}^0)\pi^\pm$ decays, which have especially high purity. At e^+e^- collider experiments such as Belle, BaBar, and BESIII, the D flavor can also be determined by fully reconstructing a flavor-specific D decay on the “opposite side” of an event, i.e., recoiling against the signal-side D decay.

At BESIII, where $D\bar{D}$ pairs are produced near their threshold via $e^+e^- \rightarrow \psi(3770) \rightarrow D^0\bar{D}^0$, there is relatively little background and the purity of opposite-side tagging is equivalent to that achieved using $D^{*\pm}$ decays. However, BESIII operates at a symmetric e^+e^- collider, and the $D\bar{D}$ pairs are produced almost at rest in the lab frame. As a consequence, the D 's do

not travel any appreciable distance before decaying, and time-dependent analyses are not possible. To overcome this, measurements of mixing at BESIII utilize the quantum coherence of the initial $\psi(3770) \rightarrow D^0\bar{D}^0$ state and time-integrated measurements [1–5].

70.1 Time-Dependent Analyses

Our notation is as follows: Cabibbo-favored (CF) decay amplitudes are denoted $\bar{A}_f \equiv \langle f|H|\bar{D}^0\rangle$ and $A_{\bar{f}} \equiv \langle \bar{f}|H|D^0\rangle$; i.e, the final state is $f = K^+\ell^-\nu$, $K^+\pi^-$, $K^+\pi^-\pi^0$, etc. Doubly-Cabibbo-suppressed (DCS) decay amplitudes are denoted $A_f \equiv \langle f|H|D^0\rangle$ and $\bar{A}_{\bar{f}} \equiv \langle \bar{f}|H|\bar{D}^0\rangle$.

Starting from a pure $|D^0\rangle$ or $|\bar{D}^0\rangle$ state at $t = 0$, the time-dependent decay rates to “wrong-sign” final states can be written

$$r(t) \equiv |\langle f|H|D^0(t)\rangle|^2 = |\bar{A}_f|^2 \left| \frac{q}{p} \right|^2 |g_+(t)\lambda_f^{-1} + g_-(t)|^2 \quad (70.7)$$

$$\bar{r}(t) \equiv |\langle \bar{f}|H|\bar{D}^0(t)\rangle|^2 = |A_{\bar{f}}|^2 \left| \frac{p}{q} \right|^2 |g_+(t)\lambda_{\bar{f}} + g_-(t)|^2, \quad (70.8)$$

where

$$\lambda_f \equiv \frac{q\bar{A}_f}{pA_f}, \quad \lambda_{\bar{f}} \equiv \frac{q\bar{A}_{\bar{f}}}{pA_{\bar{f}}}, \quad (70.9)$$

and

$$g_{\pm}(t) = \frac{1}{2} \left(e^{-i\omega_1 t} \pm e^{-i\omega_2 t} \right). \quad (70.10)$$

A change in convention for the relative phase of D^0 and \bar{D}^0 would cancel between q/p and \bar{A}_f/A_f or $\bar{A}_{\bar{f}}/A_{\bar{f}}$, leaving λ_f and $\lambda_{\bar{f}}$ unchanged. For multibody final states, these equations apply separately to each point in phase-space. Integrating over regions of phase-space can lead to enhanced sensitivity to CP violation; see the discussion below on multibody decays and the note “Review of Multibody Charm Analyses” in this *Review*. As the mixing parameters x and y are very small, $r(t)$ and $\bar{r}(t)$ are usually expanded to second order in x and y .

70.2 Semileptonic decays

Consider the final state $f = K^+\ell^-\bar{\nu}_\ell$, where $A_f = \bar{A}_{\bar{f}} = 0$ is an excellent approximation in the Standard Model. The final state f is accessible from a D^0 only via mixing,¹ and the decay rate is

$$r(t) = |\bar{A}_f|^2 \left| \frac{q}{p} \right|^2 |g_-(t)|^2 \approx |\bar{A}_f|^2 \left| \frac{q}{p} \right|^2 \left(\frac{x^2 + y^2}{4} \right) (\Gamma t)^2 e^{-\Gamma t}. \quad (70.11)$$

For $\bar{r}(t)$, q/p is replaced by p/q . In the Standard Model, CP violation in charm mixing is small and $|q/p| \approx 1$. In the limit of CP conservation, $r(t) = \bar{r}(t)$, and the time-integrated mixed decay rate relative to the time-integrated unmixed decay rate for semileptonic decays is

$$\frac{\int_0^\infty r(t) dt}{\int_0^\infty |\bar{A}_f|^2 e^{-\Gamma t} dt} = \frac{x^2 + y^2}{2} \equiv R_M. \quad (70.12)$$

Table 70.1 summarizes results for R_M from semileptonic decays. The world average from the Heavy Flavor Averaging Group (HFLAV) [6] is $R_M = (1.30 \pm 2.69) \times 10^{-4}$.

¹There exists a doubly Cabibbo-suppressed amplitude in which the c and \bar{u} quarks exchange a W , and then the resulting d quark (from c) decays semileptonically. We neglect this second-order process.

Table 70.1: Results for $R_M = (x^2 + y^2)/2$ in D^0 semileptonic decays. The HFLAV average assumes statistical and systematic uncertainties are uncorrelated. When a single uncertainty is listed, that corresponds to statistical and systematic uncertainties combined. The measurements with an asterisk (*) have been superseded and thus are not included in the HFLAV average.

Year	Experiment	Final state(s)	$R_M (\times 10^{-3})$	90% C.L. ($\times 10^{-3}$)
2008	Belle (492 fb^{-1}) [7]	$K^{(*)+}e^{-}\bar{\nu}_e$	$0.13 \pm 0.22 \pm 0.20$	< 0.61
2007	BaBar (344 fb^{-1}) [8]	$K^{(*)+}e^{-}\bar{\nu}_e$	$0.04^{+0.70}_{-0.60}$	$(-1.3, 1.2)$
2005	CLEO (9.0 fb^{-1}) [9]	$K^{(*)+}e^{-}\bar{\nu}_e$	$1.6 \pm 2.9 \pm 2.9$	< 7.8
1996	E791 (2×10^{10} evts) [10]	$K^+\ell^-\bar{\nu}_\ell$	$1.1^{+3.0}_{-2.7}{}^{+0.0}_{-0.1}$	< 5.0
HFLAV Average [6]			0.130 ± 0.269	
2005*	Belle (253 fb^{-1}) [11]	$K^{(*)+}e^{-}\bar{\nu}_e$	$0.02 \pm 0.47 \pm 0.14$	< 1.0
2004*	BaBar (87 fb^{-1}) [12]	$K^{(*)+}e^{-}\bar{\nu}_e$	$2.3 \pm 1.2 \pm 0.4$	< 4.2

Table 70.2: Results for R , R_D , and A_D as measured using $D^0 \rightarrow K^\pm \pi^\mp$ decays. When a single uncertainty is listed, that corresponds to statistical and systematic uncertainties combined. The measurements with an asterisk (*) have been superseded and thus are not included in the HFLAV global fit (Section 70.7). The measurements with a dagger (†) are not included in the HFLAV global fit due to much poorer precision.

Year	Experiment	$R (\times 10^{-3})$	$R_D (\times 10^{-3})$	$A_D (\%)$
2018	LHCb ($5.0 \text{ fb}^{-1} D^*$ tag) [13]	—	3.454 ± 0.031	-0.01 ± 0.91
2017	LHCb ($3.0 \text{ fb}^{-1} B+D^*$ double tag) [14]	—	3.48 ± 0.10	-3.15 ± 3.31
2014	Belle (976 fb^{-1}) [15]	3.86 ± 0.06	3.53 ± 0.13	—
2013	CDF (9.6 fb^{-1}) [16]	4.30 ± 0.05	3.51 ± 0.35	—
2007	BaBar (384 fb^{-1}) [17]	$3.53 \pm 0.08 \pm 0.04$	$3.03 \pm 0.16 \pm 0.10$	$-2.1 \pm 5.2 \pm 1.5$
HFLAV Fit Result [18]			3.434 ± 0.019	-0.70 ± 0.36
2013b*	LHCb ($3.0 \text{ fb}^{-1} D^*$ tag) [19]	—	3.568 ± 0.066	-0.7 ± 1.9
2013a*	LHCb (1.0 fb^{-1}) [20]	4.25 ± 0.04	3.52 ± 0.15	—
2008*	CDF (1.5 fb^{-1}) [21]	4.15 ± 0.10	3.04 ± 0.55	—
2006*	Belle (400 fb^{-1}) [22]	$3.77 \pm 0.08 \pm 0.05$	3.64 ± 0.18	2.3 ± 4.7
2005†	FOCUS (234 evts) [23]	$4.29^{+0.63}_{-0.61} \pm 0.27$	$5.17^{+1.47}_{-1.58} \pm 0.76$	$13^{+33}_{-25} \pm 10$
2000†	CLEO (9.0 fb^{-1}) [24]	$3.32^{+0.63}_{-0.65} \pm 0.40$	$4.8 \pm 1.2 \pm 0.4$	$-1^{+16}_{-17} \pm 1$
1998†	E791 (5643 evts) [25]	$6.8^{+3.4}_{-3.3} \pm 0.7$	—	—

70.3 Wrong-sign decays to hadronic non- CP eigenstates

Consider the final state $f = K^+\pi^-$, i.e., A_f and \bar{A}_f are CF, A_f and \bar{A}_f are DCS. Because CF and DCS decays proceed via tree-level amplitudes, and such amplitudes involve only the first two quark generations, direct CP violation is negligible². The ratios of decay amplitudes can be written

$$\frac{A_f}{\bar{A}_f} = -\sqrt{R_D^+} e^{-i\delta_f} \quad \frac{\bar{A}_f}{A_f} = -\sqrt{R_D^-} e^{-i\delta_f}, \quad (70.13)$$

where δ_f is the strong phase difference between the DCS and CF amplitudes. The minus sign originates from the weak phase difference between the amplitudes, specifically, the relative minus sign between V_{us} and V_{cd} (which produces a relative minus sign between $V_{cs}^*V_{ud}$ and $V_{us}^*V_{cd}$). The parameters R_D^+ and R_D^- are the ratios of the DCS decay rate to the CF decay rate. From the relevant CKM matrix elements, one estimates R_D^+ , $R_D^- \sim \tan^4 \theta_c$, where θ_c is the Cabibbo angle.

With the parameterization of Eq. (70.13), Eq. (70.9) becomes

$$\lambda_f^{-1} = \frac{p}{q} \frac{A_f}{\bar{A}_f} = -\sqrt{R_D^+} \left| \frac{p}{q} \right| e^{-i(\delta_f + \phi)} \quad (70.14)$$

$$\lambda_{\bar{f}} = \frac{q}{p} \frac{\bar{A}_f}{A_f} = -\sqrt{R_D^-} \left| \frac{q}{p} \right| e^{-i(\delta_f - \phi)}, \quad (70.15)$$

where $\phi = \text{Arg}(q/p)$. The weak phase ϕ is independent of the final state f and is often referred to as “universal.” For convenience, we define the mean decay rate $R_D \equiv (R_D^+ + R_D^-)/2$, and the decay rate asymmetry $A_D \equiv (R_D^+ - R_D^-)/(R_D^+ + R_D^-)$.

With these definitions, we expand the decay rates in Eqs. (70.7) and (70.8) to second order in the small mixing parameters x and y to obtain [26, 27]:

$$r(t) = \left| \bar{A}_f \right|^2 e^{-\Gamma t} [R_D(1 + A_D) + \sqrt{R_D(1 + A_D)} \left| \frac{q}{p} \right| y'_+(\Gamma t) + \left| \frac{q}{p} \right|^2 \frac{(x'_+{}^2 + y'_+{}^2)}{4} (\Gamma t)^2] \quad (70.16)$$

and

$$\bar{r}(t) = \left| A_f \right|^2 e^{-\Gamma t} [R_D(1 - A_D) + \sqrt{R_D(1 - A_D)} \left| \frac{p}{q} \right| y'_-(\Gamma t) + \left| \frac{p}{q} \right|^2 \frac{(x'_-{}^2 + y'_-{}^2)}{4} (\Gamma t)^2], \quad (70.17)$$

where

$$x'_\pm = x \cos(\delta_f \pm \phi) + y \sin(\delta_f \pm \phi) \quad (70.18)$$

$$y'_\pm = y \cos(\delta_f \pm \phi) - x \sin(\delta_f \pm \phi). \quad (70.19)$$

Defining the “strong-phase-rotated” mixing parameters

$$x' \equiv x \cos \delta_f + y \sin \delta_f \quad (70.20)$$

$$y' \equiv y \cos \delta_f - x \sin \delta_f \quad (70.21)$$

gives

$$x'_\pm = x' \cos \phi \pm y' \sin \phi \quad (70.22)$$

$$y'_\pm = y' \cos \phi \mp x' \sin \phi, \quad (70.23)$$

i.e., x'_\pm and y'_\pm are obtained from x' , y' via an additional “weak-phase rotation.” To summarize, parameters (x', y') are the mixing parameters (x, y) rotated by the strong phase δ_f , and parameters

² For two quark generations, the weak phases can be defined to eliminate all weak-phase differences.

(x'_\pm, y'_\pm) are the parameters (x', y') rotated by the weak phase $+\phi$ for D^0 decays and $-\phi$ for \bar{D}^0 decays. Note that $x'^2 + y'^2 = x'^2_+ + y'^2_+ = x'^2_- + y'^2_- = x^2 + y^2$. In Eqs. (70.16) and (70.17), a fourth term $R_D(1 \pm A_D)(x^2_\pm - y^2_\pm)(\Gamma t)^2/4$ has been dropped, as it is negligible relative to the other terms for the range of decay times measured by experiments.

Comparing Eqs. (70.16) and (70.17), one sees that $r(t) \neq \bar{r}(t)$ and CP is violated if either $A_D \neq 0$, $|q/p| \neq 1$, or $\phi \neq 0$. These three inequalities correspond, respectively, to the three types of CP violation: in the decay amplitudes ($R_D^+ \neq R_D^-$); in the mixing; and due to interference between a mixed decay amplitude (i.e., mixing is followed by decay) and an unmixed decay amplitude. Whereas CP violation in the decay amplitudes is parameterized by A_D , CP violation in mixing is parameterized by $A_M \equiv (|q/p| - |p/q|)/(|q/p| + |p/q|)$.

In the limit of CP conservation, $A_D = 0$, $|q/p| = 1$, and $\phi = 0$. In this case

$$r(t) = \bar{r}(t) = \left| A_{\bar{f}} \right|^2 e^{-\Gamma t} \left[R_D + \sqrt{R_D} y'(\Gamma t) + \frac{x'^2 + y'^2}{4} (\Gamma t)^2 \right], \quad (70.24)$$

and the total number of $D^0 \rightarrow f$ decays divided by the total number of $D^0 \rightarrow \bar{f}$ decays is

$$R = \frac{\int_0^\infty r(t) dt}{\int_0^\infty \left| A_{\bar{f}} \right|^2 e^{-\Gamma t} dt} = R_D + \sqrt{R_D} y' + \frac{x'^2 + y'^2}{2}. \quad (70.25)$$

The ratio R is more straightforward to measure than $r(t)$ or $\bar{r}(t)$, as there is no decay-time dependence. In Table 70.2 we report measurements of R , R_D , and A_D in $D^0 \rightarrow K^+\pi^-$ decays normalized to $D^0 \rightarrow K^-\pi^+$ decays, and results from HFLAV [18] obtained from a global fit to all relevant data that allows for both mixing and CP violation (see Section 70.7). The experiments typically perform a single fit for parameters R_D , x'^2 , and y' ; results for x'^2 and y' are listed in Table 70.3. Allowing for CP violation, the experiments measure parameters (R_D^+, x'^2_+, y'_+) and (R_D^-, x'^2_-, y'_-) [or equivalently (R_D, A_D) instead of (R_D^+, R_D^-)] by separately fitting the $D^0 \rightarrow K^+\pi^-$ and $\bar{D}^0 \rightarrow K^-\pi^+$ event samples.

Extraction of the mixing parameters x and y from measurements of x' and y' requires knowledge of the strong phase difference $\delta_{K\pi}$. This can be determined from the decay rates of $D_\pm \rightarrow K^+\pi^-$, where D_+ (D_-) denotes the CP -even (CP -odd) eigenstate. Since $|D_\pm\rangle = (|D^0\rangle \mp |\bar{D}^0\rangle)/\sqrt{2}$,

$$\sqrt{2} A(D_\pm \rightarrow K^+\pi^-) = A(D^0 \rightarrow K^+\pi^-) \mp A(\bar{D}^0 \rightarrow K^+\pi^-). \quad (70.26)$$

Squaring this amplitude and using Eq. (70.13) yields the relation

$$\cos \delta_{K\pi} = \frac{|A(D_+ \rightarrow K^+\pi^-)|^2 - |A(D_- \rightarrow K^+\pi^-)|^2}{2|A(D^0 \rightarrow K^+\pi^-)||A(\bar{D}^0 \rightarrow K^+\pi^-)|}. \quad (70.27)$$

Measuring the right-hand side is possible if one can identify pure D_+ , D_- , D^0 , and \bar{D}^0 initial states. This is accomplished at CLEOC and BESIII utilizing the processes $e^+e^- \rightarrow \psi(3770) \rightarrow \bar{D}^0 D^0 \rightarrow (f_{CP})(K^+\pi^-)$, or $\psi(3770) \rightarrow \bar{D}^0 D^0 \rightarrow (f_{\bar{D}^0})(K^+\pi^-)$, where f_{CP} denotes a CP -specific final state, and $f_{\bar{D}^0}$ denotes a \bar{D}^0 -flavor-specific final state. In the first case, quantum coherence and CP symmetry ensures that the $K^+\pi^-$ state originates from a neutral D with CP opposite that of f_{CP} . In the second case, at the time when the \bar{D}^0 decays, the opposite side is D^0 . However, it can potentially mix to \bar{D}^0 before decaying to $K^+\pi^-$, and this introduces some dependence on the mixing parameters x and y .

This dependence is seen explicitly in the observable

$$A_{K\pi}^{CP} \equiv \frac{|A(D_- \rightarrow K^-\pi^+)|^2 - |A(D_+ \rightarrow K^-\pi^+)|^2}{|A(D_- \rightarrow K^-\pi^+)|^2 + |A(D_+ \rightarrow K^-\pi^+)|^2}. \quad (70.28)$$

To lowest order in the mixing parameters [28],

$$A_{K\pi}^{CP} = \frac{2\sqrt{R_D} \cos \delta_{K\pi} + y}{1 + R}, \quad (70.29)$$

where R is defined in Eq. (70.25). Such measurements are discussed in Section 70.5.

70.3.1 Wrong-sign decays to multibody final states

For multibody final states, Eqs. (70.13)-(70.25) apply to each point in phase-space. Although x and y do not vary across phase-space, knowledge of the resonant substructure is needed to determine the strong phase difference δ from point to point to extract x and y . Alternatively, experimental knowledge of the strong phase difference between D^0 and \bar{D}^0 decay amplitudes across phase space [39] allow one to determine x and y independent of a decay model of resonant substructure. This phase information can be measured at the charm threshold, where CLEO-c and BESIII took data.

A time-dependent analysis at BaBar [40,41] of $D^0 \rightarrow K^+\pi^-\pi^0$ decays, relative to CF $\bar{D}^0 \rightarrow K^+\pi^-\pi^0$ decays, determined the strong phase variation across the Dalitz plot and reported $x'' = (2.61^{+0.57}_{-0.68} \pm 0.39)\%$ and $y'' = (-0.06^{+0.55}_{-0.64} \pm 0.34)\%$. These mixing parameters are defined as

$$x'' = x \cos \delta_{K\pi\pi^0} + y \sin \delta_{K\pi\pi^0} \quad (70.30)$$

$$y'' = y \cos \delta_{K\pi\pi^0} - x \sin \delta_{K\pi\pi^0}, \quad (70.31)$$

in analogy with x' , y' , and $\delta_{K\pi}$ of Eqs. (70.20) and (70.21). Here, $\delta_{K\pi\pi^0}$ is the strong phase difference between the amplitudes $A(D^0 \rightarrow K^+\pi^-\pi^0)$ and $A(\bar{D}^0 \rightarrow K^+\pi^-\pi^0)$ at a “reference point” of the Dalitz plot. For this analysis, the reference point chosen is $m_{\pi^-\pi^0} = m_{\rho^-}$. The strong phase difference $\delta_{K\pi\pi^0}$ can be determined in a manner similar to that for $\delta_{K\pi}$: by using Eq. (70.27) and quantum-correlated measurements of the branching fractions $B(D_+ \rightarrow K^+\rho^-)$, $B(D_- \rightarrow K^+\rho^-)$, $B(D^0 \rightarrow K^+\rho^-)$, and $B(\bar{D}^0 \rightarrow K^+\rho^-)$ in $e^+e^- \rightarrow \psi(3770)$ events.

For the decay modes D^0 and $\bar{D}^0 \rightarrow K^+\pi^-\pi^+\pi^-$, Belle measured $R = (0.324 \pm 0.008 \pm 0.007)\%$ [42]. Subsequently, a phase-space-integrated analysis from LHCb [43] measured the product of a “coherence factor” $R_D^{K3\pi}$ and the strong-phase-rotated mixing parameter $y'_{K3\pi}$. This measurement resulted in an observation of charm mixing with 8.2σ significance.

Both the sign and magnitude of x and y without strong phases entering or sign ambiguity can be determined by measuring the time-dependent resonant substructure of multibody D^0 decays to self-conjugate final states [37, 38]. For such decays, e.g., $D^0 \rightarrow K_S^0 \pi^+\pi^-$, the DCS and CF decay amplitudes populate the same Dalitz plot, which allows for direct measurement of the strong phase difference. Belle [35, 37], BaBar [36], and CLEO [44] have measured the overall phase difference between $D^0 \rightarrow K^*(892)^-\pi^+$ and $D^0 \rightarrow K^*(892)^+\pi^-$ to be $[173.9 \pm 0.7 \text{ (stat. only)}]^\circ$, $[177.6 \pm 1.1 \text{ (stat. only)}]^\circ$, and $[189 \pm 10 \pm 3^{+15}_{-5}]^\circ$, respectively. These results are close to the 180° expected from Cabibbo factors, i.e., the relative minus sign between $V_{cs}^* V_{ud}$ and $V_{us}^* V_{cd}$; thus they indicate a small strong phase. Three LHCb measurements [31-33] of x , y using $D^0 \rightarrow K_S^0 \pi^+\pi^-$ decays are decay-model independent, as the model of resonances in the intermediate state is replaced by strong-phase measurements from CLEO-c [29] and BESIII [45]. Table 70.4 summarizes results from time-dependent analyses of self-conjugate multibody final states. World average values for the measurements listed are given later, as a result of the HFLAV global fit.

With regard to resonant substructure in $D^0 \rightarrow K_S^0 \pi^+\pi^-$ decays, Belle [35, 37] measured the relative strong phase (statistical errors only) and the ratio R (central values only) of the DCS fit fraction relative to the CF fit fraction for five excited K states: $K^*(892)^+\pi^-$, $K_0^*(1430)^+\pi^-$, $K_2^*(1430)^+\pi^-$, $K^*(1410)^+\pi^-$, and $K^*(1680)^+\pi^-$. Similarly, BaBar [36, 46, 47] reported central values of R for $K^*(892)^+\pi^-$, $K_0^*(1430)^+\pi^-$, and $K_2^*(1430)^+\pi^-$.

Table 70.3: Results for x'^2 and y' , as measured using $D^0 \rightarrow K^\pm \pi^\mp$ decays. When a single uncertainty is listed, that corresponds to statistical and systematic uncertainties combined. The measurements with an asterisk (*) have been superseded and thus are not included in the HFLAV global fit. The measurements with a dagger (\dagger) are not included in the HFLAV global fit due to much poorer precision. All confidence limits and intervals correspond to 95% C.L. The Belle 2006 results restrict x'^2 to the physical region. The BaBar confidence intervals are obtained from the fit, whereas Belle uses a Feldman-Cousins method, and CDF uses a Bayesian method.

Year	Experiment	No CP violation		Allowing for CP violation	
		$x'^2 (\times 10^{-3})$	$y' (\%)$	$x'^2 (\times 10^{-3})$	$y' (\%)$
2018	LHCb (5.0 fb^{-1}) [$D^* \text{ tag}$] [13]	0.039 ± 0.027	0.528 ± 0.052	$\begin{cases} D^0: 0.061 \pm 0.037 \\ \bar{D}^0: 0.016 \pm 0.039 \end{cases}$	$\begin{cases} 0.501 \pm 0.074 \\ 0.554 \pm 0.074 \end{cases}$
2017	LHCb (3.0 fb^{-1}) [$B+D^*$ double tag] [14]	0.028 ± 0.310	0.46 ± 0.37	$\begin{cases} D^0: -0.019 \pm 0.447 \\ \bar{D}^0: 0.079 \pm 0.433 \end{cases}$	$\begin{cases} 0.581 \pm 0.526 \\ 0.332 \pm 0.523 \end{cases}$
2014	Belle (976 fb^{-1}) [15]	0.09 ± 0.22	0.46 ± 0.34	—	—
2013	CDF (9.6 fb^{-1}) [16]	0.08 ± 0.18	0.43 ± 0.43	—	—
2007	BaBar (384 fb^{-1}) [17]	-0.22 ± 0.37	0.97 ± 0.54	$\begin{cases} D^0: -0.24 \pm 0.52 \\ \bar{D}^0: -0.20 \pm 0.50 \end{cases}$	$\begin{cases} 0.98 \pm 0.78 \\ 0.96 \pm 0.75 \end{cases}$
2006	Belle (400 fb^{-1}) [22]	$(0.18^{+0.21}_{-0.23})^*$	$(0.06^{+0.40}_{-0.39})^*$	< 0.72	$-2.8 < y' < 2.1$
2013b*	LHCb (3.0 fb^{-1}) [$D^* \text{ tag}$] [19]	0.055 ± 0.049	0.48 ± 0.10	$\begin{cases} D^0: 0.049 \pm 0.070 \\ \bar{D}^0: 0.060 \pm 0.068 \end{cases}$	$\begin{cases} 0.51 \pm 0.14 \\ 0.45 \pm 0.14 \end{cases}$
2013a*	LHCb (1.0 fb^{-1}) [20]	-0.09 ± 0.13	0.72 ± 0.24	—	—
2008*	CDF (1.5 fb^{-1}) [21]	-0.12 ± 0.35	0.85 ± 0.76	—	—
2005 \dagger	FOCUS (234 evts) [23]	< 8.3	$-7.2 < y' < 4.1$	< 8.0	$-11.2 < y' < 6.7$
2000 \dagger	CLEO (9.0 fb^{-1}) [24]	0.00 ± 0.23	$-2.3^{+1.3}_{-1.4}$	0.00 ± 0.23	$-2.5^{+1.4}_{-1.6}$
1998 \dagger	E791 (5643 evts) [25]	< 17	< 13	—	—

Table 70.4: Results from time-dependent multibody analyses. The errors are statistical, systematic, and, when a third error is listed, due to the decay-model, respectively. The measurement with an asterisk (*) has been superseded and thus is not included in the HFLAV global fit. The measurement with a dagger (\dagger) is not included in the HFLAV global fit due to poorer precision. The 2019 LHCb result utilizes strong-phase measurements from CLEO-c [29] and thus is decay-model independent. This fit determines CP -violating parameters Δx and Δy ; the translation of these parameters to $|q/p|$ and ϕ is given in Ref. [30].

No CP Violation				
Year	Experiment	Final state(s)	$x (\times 10^{-3})$	$y (\times 10^{-3})$
2021	LHCb (5.4 fb^{-1} $D^* \text{ tag}$) [31]	$K_S^0 \pi^+ \pi^-$	$3.97 \pm 0.46 \pm 0.29$	$4.59 \pm 1.20 \pm 0.85$
2019	LHCb (3.0 fb^{-1} $B, D^* \text{ tags}$) [32]	$K_S^0 \pi^+ \pi^-$	$2.7 \pm 1.6 \pm 0.4$	$7.4 \pm 3.6 \pm 1.1$
2016	LHCb (1.0 fb^{-1} $D^* \text{ tag}$) [33]	$K_S^0 \pi^+ \pi^-$	$-8.6 \pm 5.3 \pm 1.7$	$0.3 \pm 4.6 \pm 1.3$
2016	BaBar (468 fb^{-1}) [34]	$\pi^+ \pi^- \pi^0$	$15 \pm 12 \pm 6$	$2 \pm 9 \pm 5$
2014	Belle (921 fb^{-1}) [35]	$K_S^0 \pi^+ \pi^-$	$5.6 \pm 1.9^{+0.3+0.6}_{-0.9-0.9}$	$3.0 \pm 1.5^{+0.4+0.3}_{-0.5-0.6}$
2010	BaBar (469 fb^{-1}) [36]	$\begin{cases} K_S^0 \pi^+ \pi^- \\ K_S^0 K^+ K^- \end{cases}$	$1.6 \pm 2.3 \pm 1.2 \pm 0.8$	$5.7 \pm 2.0 \pm 1.3 \pm 0.7$
2007*	Belle (540 fb^{-1}) [37]	$K_S^0 \pi^+ \pi^-$	$8.0 \pm 2.9^{+0.9+1.0}_{-0.7-1.4}$	$3.3 \pm 2.4^{+0.8+0.6}_{-1.2-0.8}$
2005 \dagger	CLEO (9.0 fb^{-1}) [38]	$K_S^0 \pi^+ \pi^-$	$19^{+32}_{-33} \pm 4 \pm 4$	$-14 \pm 24 \pm 8 \pm 4$
With CP Violation				
Year	Experiment	Final state(s)	$ q/p $	ϕ
2021	LHCb (5.4 fb^{-1}) [31]	$K_S^0 \pi^+ \pi^-$	$\begin{cases} 0.996 \pm 0.052 \\ \Delta x \times 10^3 = \\ -0.27 \pm 0.18 \pm 0.01 \end{cases}$	$\begin{cases} (3.2^{+2.7}_{-2.9})^\circ \\ \Delta y \times 10^3 = \\ 0.20 \pm 0.36 \pm 0.13 \end{cases}$
2019	LHCb (3.0 fb^{-1}) [32]	$K_S^0 \pi^+ \pi^-$	$\begin{cases} 1.05^{+0.22}_{-0.17} \\ \Delta x \times 10^3 = \\ -0.53 \pm 0.70 \pm 0.22 \end{cases}$	$\begin{cases} (-5.2^{+6.3}_{-9.2})^\circ \\ \Delta y \times 10^3 = \\ 0.6 \pm 1.6 \pm 0.3 \end{cases}$
2014	Belle (921 fb^{-1}) [35]	$K_S^0 \pi^+ \pi^-$	$0.90^{+0.16+0.05+0.06}_{-0.15-0.04-0.05}$	$(-6 \pm 11 \pm 3^{+3}_{-4})^\circ$
2007* \dagger	Belle (540 fb^{-1}) [37]	$K_S^0 \pi^+ \pi^-$	$0.86^{+0.30+0.06}_{-0.29-0.03} \pm 0.08$	$(-14^{+16+5+2}_{-18-3-4})^\circ$

\dagger This result allows for all types of CP violation and is superseded by Ref. [35], which assumes no direct CP violation in CF or DCS decays.

The systematic uncertainties on R are not evaluated. Large differences in R are observed among these final states, which indicates significant hadronic effects.

70.4 Decays to CP Eigenstates

When the final state f is a CP eigenstate, there is no distinction between f and \bar{f} . Thus $A_f = A_{\bar{f}}$ and $\bar{A}_{\bar{f}} = \bar{A}_f$. We denote final states with CP eigenvalues ± 1 by f_\pm . Decays to CP eigenstates proceed mainly via singly Cabibbo-suppressed amplitudes. Such amplitudes can contain internal loops and thus involve the third quark generation; in this manner a weak phase would appear in

the decay amplitude, leading to direct CP violation. However, such internal loop amplitudes are suppressed, and the presence of a weak phase is often neglected.

The mixing parameter y may be measured by comparing the rate for D^0 decays to CP eigenstates such as $K^+ K^-$ with the rate to flavor eigenstates such as $K^- \pi^+$ [27]. If decays to $K^+ K^-$ have a shorter effective lifetime than those to $K^- \pi^+$, then $\Gamma_+ > \Gamma_-$, or, since CP violation is very small, $\Gamma_2 > \Gamma_1$ and y is positive. For small mixing ($x, y \ll 1$), the decay rates for $D^0 \rightarrow f_\pm$ and

Table 70.5: Results for y_{CP} and A_Γ from D^0 decays to CP eigenstates. When a single uncertainty is listed, that corresponds to statistical and systematic uncertainties combined. The measurements with an asterisk (*) have been superseded.

Year	Experiment	Final state(s)	y_{CP} (%)	A_Γ ($\times 10^{-3}$)
2021	LHCb (8.4 fb $^{-1}$ B, D^* tags) [48]	$K^+K^- + \pi^+\pi^-$	—	$0.10 \pm 0.11 \pm 0.03$
2021	LHCb (6 fb $^{-1}$ D^* tag) [48]	$K^+K^- + \pi^+\pi^-$	—	$0.27 \pm 0.13 \pm 0.03$
2021	LHCb (6 fb $^{-1}$ D^* tag) [48]	K^+K^-	—	$0.23 \pm 0.15 \pm 0.03$
2021	LHCb (6 fb $^{-1}$ D^* tag) [48]	$\pi^+\pi^-$	—	$0.40 \pm 0.28 \pm 0.04$
2020	Belle (976 fb $^{-1}$) [49]	$K_S^0 \omega$	$0.96 \pm 0.91^{+0.64}_{-0.62}$	—
2020	LHCb (5.4 fb $^{-1}$ B tag) [50]	K^+K^-	—	$-0.43 \pm 0.36 \pm 0.05$
2020	LHCb (5.4 fb $^{-1}$ B tag) [50]	$\pi^+\pi^-$	—	$0.22 \pm 0.70 \pm 0.08$
2019	LHCb (3 fb $^{-1}$ B tag) [51]	$K^+K^- + \pi^+\pi^-$	$0.57 \pm 0.13 \pm 0.09$	—
2017	LHCb (3 fb $^{-1}$ D^* tag) [52]	$K^+K^- + \pi^+\pi^-$	—	$-0.13 \pm 0.28 \pm 0.10$
2017	LHCb (3 fb $^{-1}$ D^* tag) [52]	K^+K^-	—	$-0.30 \pm 0.32 \pm 0.10$
2017	LHCb (3 fb $^{-1}$ D^* tag) [52]	$\pi^+\pi^-$	—	$0.46 \pm 0.58 \pm 0.12$
2016	Belle (976 fb $^{-1}$) [53]	$K^+K^- + \pi^+\pi^-$	$1.11 \pm 0.22 \pm 0.09$	$-0.3 \pm 2.0 \pm 0.7$
2015	LHCb (3 fb $^{-1}$ B tag) [54]	$K^+K^- + \pi^+\pi^-$	—	-1.25 ± 0.73
2015	LHCb (3 fb $^{-1}$ B tag) [54]	K^+K^-	—	$-1.34 \pm 0.77^{+0.26}_{-0.34}$
2015	LHCb (3 fb $^{-1}$ B tag) [54]	$\pi^+\pi^-$	—	$-0.92 \pm 1.45^{+0.25}_{-0.33}$
2015	BES III (2.9 fb $^{-1}$) [55]	$\left\{ \begin{array}{l} K^+K^-, \pi^+\pi^- \\ K_S^0 \pi^0, K_S^0 \pi^0 \pi^0 \\ K_S^0 \eta, K_S^0 \omega \end{array} \right.$	$-2.0 \pm 1.3 \pm 0.7$	—
2014	CDF (9.7 fb $^{-1}$) [56]	$K^+K^- + \pi^+\pi^-$	—	-1.2 ± 1.2
2014	CDF (9.7 fb $^{-1}$) [56]	K^+K^-	—	$-1.9 \pm 1.5 \pm 0.4$
2014	CDF (9.7 fb $^{-1}$) [56]	$\pi^+\pi^-$	—	$-0.1 \pm 1.8 \pm 0.3$
2012	BaBar (468 fb $^{-1}$) [57]	$K^+K^- + \pi^+\pi^-$	$0.72 \pm 0.18 \pm 0.12$	$0.9 \pm 2.6 \pm 0.6$
2009	Belle (673 fb $^{-1}$) [58]	$K_S^0 K^+K^-$	$0.11 \pm 0.61 \pm 0.52$	—
2002	CLEO (9.0 fb $^{-1}$) [59]	$K^+K^- + \pi^+\pi^-$	$-1.2 \pm 2.5 \pm 1.4$	—
2000	FOCUS (1×10^6 evts) [60]	K^+K^-	$3.42 \pm 1.39 \pm 0.74$	—
1999	E791 (2×10^{10} evts) [61]	K^+K^-	$0.73 \pm 2.89 \pm 1.03$	—
HFLAV Average [62]			0.719 ± 0.113	0.089 ± 0.113
2020*	LHCb (5.4 fb $^{-1}$ B tag) [50]	K^+K^-	—	$-0.43 \pm 0.36 \pm 0.05$
2020*	LHCb (5.4 fb $^{-1}$ B tag) [50]	$\pi^+\pi^-$	—	$0.22 \pm 0.70 \pm 0.08$
2013*	LHCb (1.0 fb $^{-1}$ D^* tag) [63]	K^+K^-	—	$-0.35 \pm 0.62 \pm 0.12$
2013*	LHCb (1.0 fb $^{-1}$ D^* tag) [63]	$\pi^+\pi^-$	—	$0.33 \pm 1.06 \pm 0.14$
2011* \ddagger	LHCb (29 pb $^{-1}$ D^* tag) [64]	K^+K^-	$0.55 \pm 0.63 \pm 0.41$	$-5.9 \pm 5.9 \pm 2.1$
2009*	BaBar (384 fb $^{-1}$) [65]	K^+K^-	$1.16 \pm 0.22 \pm 0.18$	—
2008*	BaBar (384 fb $^{-1}$) [66]	$K^+K^- + \pi^+\pi^-$	$1.03 \pm 0.33 \pm 0.19$	$2.6 \pm 3.6 \pm 0.8$
2007*	Belle (540 fb $^{-1}$) [67]	$K^+K^- + \pi^+\pi^-$	$1.31 \pm 0.32 \pm 0.25$	$0.1 \pm 3.0 \pm 1.5$
2003*	BaBar (91 fb $^{-1}$) [68]	$K^+K^- + \pi^+\pi^-$	$0.8 \pm 0.4^{+0.5}_{-0.4}$	—
2001*	Belle (23.4 fb $^{-1}$) [69]	K^+K^-	$-0.5 \pm 1.0^{+0.7}_{-0.8}$	—

 \ddagger This result for y_{CP} is not superseded, but it is not included in the HFLAV average due to having some correlations with the result of Ref. [51] but much worse precision. $\bar{D}^0 \rightarrow f_\pm$ have an approximately exponential time dependence:

$$r_\pm(t) \propto \exp(-\Gamma_\pm t) \quad (70.32)$$

$$\bar{r}_\pm(t) \propto \exp(-\bar{\Gamma}_\pm t), \quad (70.33)$$

where the effective decay widths are given by

$$\Gamma_\pm = \Gamma \left(1 \pm \left| \frac{q}{p} \right| (y \cos \phi - x \sin \phi) \right) \quad (70.34)$$

$$\bar{\Gamma}_\pm = \Gamma \left(1 \pm \left| \frac{p}{q} \right| (y \cos \phi + x \sin \phi) \right). \quad (70.35)$$

Thus, the effective decay rate to a CP eigenstate combining equal numbers of D^0 and \bar{D}^0 decays (e.g., an untagged sample with no production asymmetry) is

$$r_\pm(t) + \bar{r}_\pm(t) \propto e^{-(1 \pm y_{CP})\Gamma t}, \quad (70.36)$$

where

$$y_{CP} = \frac{1}{2} \left(\left| \frac{q}{p} \right| + \left| \frac{p}{q} \right| \right) y \cos \phi - \frac{1}{2} \left(\left| \frac{q}{p} \right| - \left| \frac{p}{q} \right| \right) x \sin \phi \quad (70.37)$$

$$\approx y \cos \phi - A_M x \sin \phi. \quad (70.38)$$

If CP is conserved, $y_{CP} = y$. Most measurements of y_{CP} have used $D^0 \rightarrow K^+K^-$ and $D^0 \rightarrow \pi^+\pi^-$ decays, which are CP -even, measured relative to $D^0 \rightarrow K^-\pi^+$. Belle measured y_{CP} also using $D^0 \rightarrow K_S^0 \omega$ decays [49], which are CP -odd, and $D^0 \rightarrow K_S^0 K^+K^-$ decays [58], which are dominated by the CP -odd final state $K_S^0 \phi$. Table 70.5 summarizes the current status of measurements.In addition to y_{CP} , Belle [53], BaBar [57], CDF [56], and LHCb [48, 64] have reported measurements of the decay-rate asymmetry for CP -even final states:

$$A_\Gamma \equiv \frac{\Gamma_+ - \bar{\Gamma}_+}{\Gamma_+ + \bar{\Gamma}_+} = \frac{(1/\tau_+) - (1/\bar{\tau}_+)}{(1/\tau_+) + (1/\bar{\tau}_+)} = \frac{\bar{\tau}_+ - \tau_+}{\bar{\tau}_+ + \tau_+} \quad (70.39)$$

$$\approx \frac{1}{2} \left(\left| \frac{q}{p} \right| - \left| \frac{p}{q} \right| \right) y \cos \phi - \frac{1}{2} \left(\left| \frac{q}{p} \right| + \left| \frac{p}{q} \right| \right) x \sin \phi \quad (70.40)$$

$$\approx A_M y \cos \phi - x \sin \phi. \quad (70.41)$$

If CP is conserved, $A_\Gamma = 0$.There is a contribution to Eq. (70.41) from direct CP violation, i.e., $|A_f/A_f| \neq 1$ [79, 80]. For $f = K^+K^-$ and $\pi^+\pi^-$, this contribution can be estimated from measurements of $A_{CP}(K^+K^-)$ and $A_{CP}(\pi^+\pi^-)$ (see below) and is much smaller than the current uncertainty on A_M ; thus we neglect it here. We note that, when averaging A_Γ measurements over K^+K^- and $\pi^+\pi^-$ final states, the contribution from direct CP violation cancels, as it has the same magnitude but opposite signs for K^+K^- and $\pi^+\pi^-$ due to U -spin symmetry [80].

Table 70.6: Results for the difference in time-integrated CP asymmetries ΔA_{CP} between $D^0 \rightarrow K^+K^-$ and $D^0 \rightarrow \pi^+\pi^-$ decays. When a single uncertainty is listed, that corresponds to statistical and systematic uncertainties combined. The measurements with an asterisk (*) have been either superseded or combined with subsequent results and thus are not included in the HFLAV global fit.

Year	Experiment	$\Delta A_{CP} (\times 10^{-3})$
2019	LHCb (8.9 fb $^{-1}$ B, D^* tags) [70]	-1.54 ± 0.29
2013	CDF (9.7 fb $^{-1}$ D^* tag) [71]	$-6.2 \pm 2.1 \pm 1.0$
2008	BaBar (386 fb $^{-1}$) [72]	$2.4 \pm 6.2 \pm 2.6$
2008	Belle (540 fb $^{-1}$) [73]	$-8.6 \pm 6.0 \pm 0.7$
2016*	LHCb (3.0 fb $^{-1}$ D^* tag) [74]	$-1.0 \pm 0.8 \pm 0.3$
2014*	LHCb (3.0 fb $^{-1}$ B tag) [75]	$1.4 \pm 1.6 \pm 0.8$
2013*	LHCb (1.0 fb $^{-1}$ B tag) [76]	$4.9 \pm 3.0 \pm 1.4$
2012*	LHCb (0.62 fb $^{-1}$ D^* tag) [77]	$-8.2 \pm 2.1 \pm 1.1$
2012 ‡	Belle (976 fb $^{-1}$) [78]	$-8.7 \pm 4.1 \pm 0.6$

‡ This preliminary result was not published and thus is not included in the HFLAV global fit.

Table 70.7: HFLAV global fit results (see text) [18].

Parameter	No CP Violation	No CP Violation in DCS Decays	All CP Violation Allowed	95% C.L. Interval (CPV Allowed)
x (%)	$0.44^{+0.13}_{-0.15}$	0.409 ± 0.048	$0.409^{+0.048}_{-0.049}$	[0.313, 0.503]
y (%)	0.63 ± 0.07	$0.603^{+0.057}_{-0.056}$	$0.615^{+0.056}_{-0.055}$	[0.509, 0.725]
$\delta_{K\pi}$ ($^\circ$)	$8.9^{+8.9}_{-9.8}$	$5.5^{+8.3}_{-9.9}$	$7.2^{+7.9}_{-9.2}$	[-12.6, 21.8]
R_D (%)	0.344 ± 0.002	0.343 ± 0.002	0.343 ± 0.002	[0.340, 0.347]
A_D (%)	—	—	-0.70 ± 0.36	[-1.40, 0.00]
$ q/p $	—	1.005 ± 0.007	0.995 ± 0.016	[0.96, 1.03]
ϕ ($^\circ$)	—	$-0.18^{+0.28}_{-0.29}$	-2.5 ± 1.2	[-4.91, -0.19]
$\delta_{K\pi\pi}$ ($^\circ$)	$21.8^{+23.5}_{-23.9}$	$22.3^{+21.9}_{-23.0}$	$23.0^{+21.8}_{-22.9}$	[-22.6, 64.9]
$A_{CP}^{\pi\pi}$ (%)	—	0.027 ± 0.137	0.045 ± 0.137	[-0.22, 0.31]
A_{CP}^{KK} (%)	—	-0.133 ± 0.136	-0.113 ± 0.137	[-0.38, 0.15]
x_{12} (%)	—	0.409 ± 0.048	—	[0.314, 0.503]
y_{12} (%)	—	$0.603^{+0.057}_{-0.056}$	—	[0.495, 0.715]
ϕ_{12} ($^\circ$)	—	$0.58^{+0.91}_{-0.90}$	—	[-1.20, 2.42]
$\chi^2/\text{d.o.f.}$	98.68/52 = 1.90	66.27/53 = 1.25	63.64/51 = 1.25	—

The asymmetry A_Γ is an asymmetry in the full decay widths. An asymmetry in partial widths is referred to as A_{CP} and is final-state dependent:

$$A_{CP} \equiv \frac{\Gamma(D^0 \rightarrow f) - \Gamma(\bar{D}^0 \rightarrow \bar{f})}{\Gamma(D^0 \rightarrow f) + \Gamma(\bar{D}^0 \rightarrow \bar{f})}. \quad (70.42)$$

Unlike A_Γ , which is measured by fitting decay time distributions, A_{CP} is measured by fitting for signal yields and (aside from acceptance effects) does not require measuring decay times. For neutral D decays, A_{CP} receives contributions from both direct (in the decay amplitudes) and indirect (due to mixing) processes: $A_{CP}(D^0 \rightarrow f) = A_{CP}^f + A_{CP}^{\text{indirect}}$. The latter indirect contribution depends on the mixing parameters x and y :

$$\begin{aligned} A_{CP}^{\text{indirect}} &= \frac{1}{2} \left(\left| \frac{q}{p} \right| + \left| \frac{p}{q} \right| \right) x \sin \phi - \frac{1}{2} \left(\left| \frac{q}{p} \right| - \left| \frac{p}{q} \right| \right) y \cos \phi \\ &= -A_\Gamma. \end{aligned} \quad (70.43)$$

Numerous measurements of A_{CP} for decays to CP eigenstates are listed in this *Review* [81]. Table 70.6 summarizes the current status of measurements of the difference in A_{CP} for $D^0 \rightarrow K^+K^-$ and $D^0 \rightarrow \pi^+\pi^-$ decays: $\Delta A_{CP} \equiv A_{CP}(K^+K^-) - A_{CP}(\pi^+\pi^-)$. Within the Standard Model, $A_{CP}^{KK} \approx -A_{CP}^{\pi\pi}$ [82], and ΔA_{CP} essentially doubles any direct CP violation present. The difference is also advantageous experimentally, as several systematic uncertainties cancel. As A_{CP}^{indirect} is independent of final state, it subtracts out of ΔA_{CP} . However, at hadron experiments such as LHCb, there are differences in efficiencies between K^+K^- and $\pi^+\pi^-$ such that $\langle t \rangle_{KK} \neq \langle t \rangle_{\pi\pi}$, i.e., the mean decay times slightly differ. This difference retains a small contribution to ΔA_{CP} from A_{CP}^{indirect} [79]. The most recent ΔA_{CP} result from LHCb [70], based on 8.9 fb $^{-1}$ of data, differs from zero with a statistical sig-

nificance of 5.3σ . Thus, this measurement constitutes the first observation of CP violation in charm decays. These CP asymmetries are included in HFLAV's global fit for charm mixing parameters discussed below; the fit shows that the CP violation observed is due to the direct contributions A_{CP}^{KK} and $A_{CP}^{\pi\pi}$.

70.5 Quantum-correlated $D^0\bar{D}^0$ Analyses

Measurements of R_D , $\cos \delta_{K\pi}$, $\sin \delta_{K\pi}$, x , and y can be obtained from a combined fit to time-integrated yields of single-tagged (ST) and double-tagged (DT) $D^0\bar{D}^0$ events produced at the $\psi(3770)$ resonance [83,84]. Single-tagged events are those in which either the D^0 or \bar{D}^0 decay is reconstructed (identified), and the other neutral D decays generically. Double-tagged events are those in which both the D^0 and \bar{D}^0 decay are identified. Due to quantum correlations, the decay of a D^0, \bar{D}^0, D_+ , or D_- projects the other neutral D into a state \bar{D}^0, D^0, D_- , and D_+ , respectively. The CP -specific D_- and D_+ decays (or, neglecting CP violation, D_1 and D_2 decays) include interference between D^0 and \bar{D}^0 amplitudes, and this provides sensitivity to R_D and $\cos \delta_{K\pi}$. The flavor-specific D^0 and \bar{D}^0 decays include interference between D_1 and D_2 amplitudes, and this provides sensitivity to x and y . For details of this method, see Refs. [1–5].

BESIII has reported results using 2.92 fb $^{-1}$ of $e^+e^- \rightarrow \psi(3770)$ data, where the quantum-correlated $D^0\bar{D}^0$ pairs are produced in a $C=-1$ state. They measure $y_{CP} = (-2.0 \pm 1.3 \pm 0.7)\%$ [55] from DT yields using a CP -eigenstate tag for one D and a semileptonic tag for the other; and they measure $A_{CP}^{\pi\pi} = (12.7 \pm 1.3 \pm 0.7)\%$ [28] from DT yields using a CP tag for one D and a $K^\pm\pi^\mp$ tag for the other. For y_{CP} , the CP eigenstates used are K^-K^+ (f_+), $\pi^+\pi^-$ (f_+), $K_S^0\pi^0\pi^0$ (f_+), $K_S^0\pi^0$ (f_-), $K_S^0\eta$ (f_-), and $K_S^0\omega$ (f_-). For $A_{CP}^{\pi\pi}$, additional CP eigenstates included are $\pi^0\pi^0$ (f_+) and $\rho^0\pi^0$ (f_+). Using external inputs for R_D and y from HFLAV [85], and R from the PDG [86], BESIII uses Eq. (70.29)

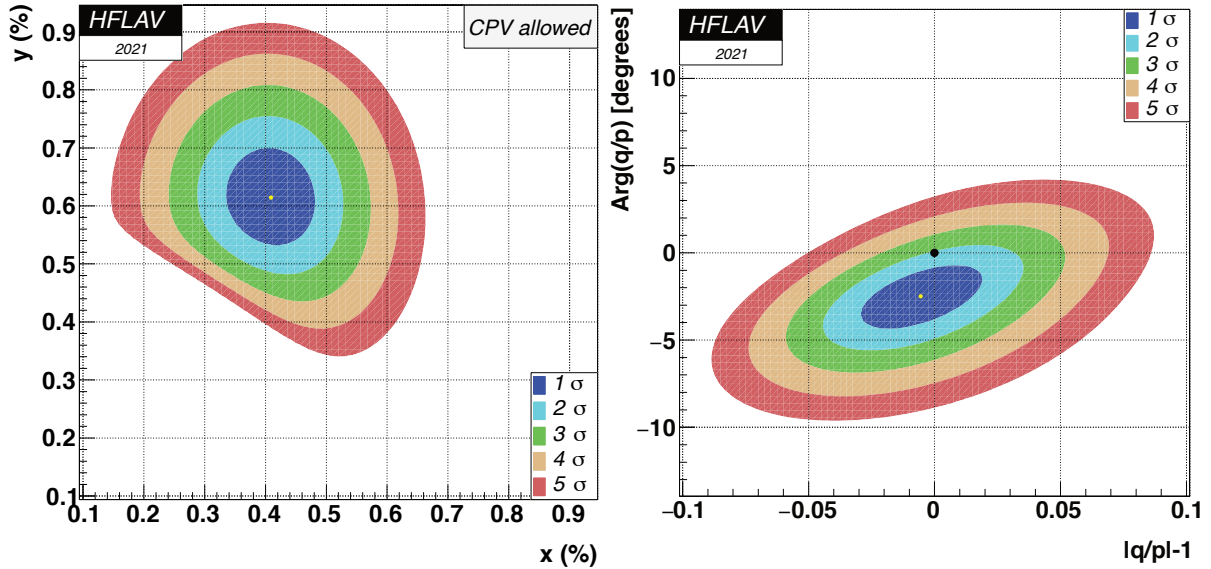


Figure 70.1: Two-dimensional 1σ - 5σ contours for (x, y) (left) and for $(|q/p|, \text{Arg}(q/p))$ (right) as obtained by HFLAV [18], from measurements of $D^0 \rightarrow K^{(*)}\ell\nu, h^+h^-, K^+\pi^-, K^+\pi^-\pi^0, K^+\pi^-\pi^+\pi^-, K_S^0\pi^+\pi^-, K_S^0K^+K^-,$ and $\pi^+\pi^-\pi^0$ decays, and double-tagged branching fractions measured at the $\psi(3770)$ resonance. In the right plot, the black dot denotes the no- CPV point $(0, 0)$.

to determine $\cos\delta_{K\pi} = 1.02 \pm 0.11 \pm 0.06 \pm 0.01$ [28], where the third uncertainty is due to the external inputs.

CLEO-c has reported results using 0.82 fb^{-1} of $e^+e^- \rightarrow \psi(3770)$ data [87–89]. The values for $y, R_M, \cos\delta_{K\pi}$, and $\sin\delta_{K\pi}$ are obtained from a combined fit to the ST (hadronic only) and DT yields. The DT yields include events in which one D is reconstructed in a hadronic mode and the other D is partially reconstructed in either $D \rightarrow K^\mp e^\pm\nu$ or $D \rightarrow K^\mp \mu^\pm\nu$. The CLEO-c analysis obtains $\cos\delta_{K\pi} = 0.81^{+0.22+0.07}_{-0.18-0.05}$ and $\sin\delta_{K\pi} = -0.01 \pm 0.41 \pm 0.04$. These fits allow $\cos\delta_{K\pi}$ and $\sin\delta_{K\pi}$ (and also x^2) to be unphysical. Constraining $\cos\delta_{K\pi}$ and $\sin\delta_{K\pi}$ to the physical range $[-1, +1]$ (i.e., interpreting $\delta_{K\pi}$ as an angle) and also using external inputs for x, y and y_{CP} from HFLAV [90], CLEO-c obtains $\delta_{K\pi} = (18^{+11}_{-17})^\circ$ [89].

70.6 Summary of Experimental Results

The first evidence for D^0 - \bar{D}^0 mixing was obtained in 2007 by Belle [67] and BaBar [17]. These results were confirmed by CDF [91] and, much later, by LHCb [20]. There are now numerous measurements of D^0 - \bar{D}^0 mixing with various levels of sensitivity. For $D^0 \rightarrow K^+\pi^-$ decays, LHCb [19, 20], CDF [16], and Belle [15] each exclude the no-mixing hypothesis by more than five standard deviations. LHCb [43] reported the observation of charm mixing in $D^0 \rightarrow K^+\pi^-\pi^+\pi^-$ decays with 8.2σ significance. However, the strong phase difference for this decay is not known, and thus the mixing parameters x and y cannot be extracted. The most precise measurements of x and y are obtained from a time-dependent Dalitz plot analysis of $D^0 \rightarrow K_S^0\pi^+\pi^-$ decays. This method was originally used at CLEO [92] and subsequently exploited at Belle [35, 37] and BaBar [36] with much higher statistics. BaBar has applied this method also to $D^0 \rightarrow K_S^0K^+K^-$ decays [36]. It has recently been used by LHCb with very high statistics [31] to obtain the most precise values of x and y to date. This measurement resulted in the first observation ($> 5\sigma$ significance) of dispersive mixing, i.e., $x \neq 0$.

The experimental data demonstrate that D^0 and \bar{D}^0 mesons mix. This mixing is presumably dominated by long-distance am-

plitudes, which are difficult to calculate. Under the assumption that the observed mixing is due entirely to non-Standard Model processes, significant constraints on New Physics models can be obtained [93]. A significant limitation to interpreting charm mixing in terms of New Physics is the theoretical uncertainty on Standard Model predictions [94, 95]. We note that the HFLAV global fit results for x and y (see below) indicate that charm mixing is at the upper end of the range of Standard Model predictions.

The current situation would benefit from better knowledge of the strong phase difference $\delta_{K\pi}$ than that currently available from CLEO-c [89] and BESIII [28]. Such knowledge would allow one to extract x and y directly from $D^0 \rightarrow K^+\pi^-$ measurements of x'^2 and y' . Similarly, knowledge of the strong phase difference $\delta_{K\pi\pi\pi}$ would allow one to extract x and y from measurements of x''^2 and y'' obtained using $D^0 \rightarrow K^+\pi^-\pi^+\pi^-$ decays.

With regard to CP violation, by combining four separate measurements from two data sets totalling 8.9 fb^{-1} of data, LHCb observed CP violation in D decays for the first time [70]. The amount of CP violation measured is small, only $\sim 0.15\%$. A theory calculation indicates that this value is consistent with Standard Model expectations [96]; however, new physics contributions cannot be excluded.

70.7 HFLAV Global Fit for Charm Mixing Parameters

The Heavy Flavor Averaging Group (HFLAV) performs a global fit to all relevant mixing measurements to obtain world average values for 10 fitted parameters: $x, y, \delta_{K\pi}, \delta_{K\pi\pi^0}, R_D(K^+\pi^-), A_D(K^+\pi^-), |q/p|, \text{Arg}(q/p) \equiv \phi,$ and the direct CP -violating asymmetries A_{CP}^{KK} and $A_{CP}^{\pi\pi}$. Correlations among observables are taken into account by using the error matrices provided by the experiments. Measurements of $D^0 \rightarrow K^{(*)}\ell^-\bar{\nu}, K^+K^-, \pi^+\pi^-, K^+\pi^-, K^+\pi^-\pi^0, K^+\pi^-\pi^+\pi^-, K_S^0\pi^+\pi^-, K_S^0K^+K^-,$ and $\pi^+\pi^-\pi^0$ decays are used, as well as CLEO-c fitted values of $R_D, x^2, y, \cos\delta,$ and $\sin\delta$ obtained from quantum-correlated branching fractions measured in $e^+e^- \rightarrow \psi(3770) \rightarrow D^0\bar{D}^0$ reactions. There are three observables input to the fit that are

themselves world average values calculated by HFLAV: R_M from $D^0 \rightarrow K^{(*)}\ell^-\bar{\nu}$ decays (Table 70.1), and y_{CP} and A_Γ from $D^0 \rightarrow f_{CP}$ decays (Table 70.5). A measurement by LHCb of R_M using $D^0 \rightarrow K^+\pi^-\pi^+\pi^-$ decays is input separately. Details of the fitting procedure are given in Ref. [6].

The results of the fit as of July, 2021 are listed in Table 70.7. Three separate fits are performed: (a) assuming no CP violation; (b) assuming no CP violation in doubly Cabibbo-suppressed decays; and (c) allowing for all CP violation. The second fit (b) corresponds to the theory expectation [97, 98]; in this case four fitted parameters are reduced to three using the relationship $\tan\phi = (x/y) \cdot (1 - |q/p|^2)/(1 + |q/p|^2)$ [97–99]. Alternatively, one can fit for the three parameters $x_{12} \equiv 2|M_{12}|/\Gamma$, $y_{12} \equiv |\Gamma_{12}|/\Gamma$, and $\phi_{12} \equiv \text{Arg}(M_{12}/\Gamma_{12})$, from which x , y , $|q/p|$, and ϕ can be derived.

Confidence contours in the two dimensions (x, y) and $(|q/p|, \phi)$ resulting from the fit are plotted in Fig. 70.1. These contours are obtained by allowing, for any point in the two-dimensional plane, all other fitted parameters to take their preferred values. The 1σ – 5σ boundaries drawn are the loci of points in which the χ^2 has risen above the minimum by 2.30, 6.18, 11.83, 19.33, and 28.67 units. The fit excludes the no-mixing point $x=y=0$ at more than 11.5σ . The fit is consistent with CP conservation ($|q/p|=1$, $\phi=0$) at the 1.6σ level. The χ^2 of the fit is 63.6 for $61-10=51$ degrees of freedom, which is satisfactory.

One-dimensional likelihood functions for parameters are obtained by allowing, for any value of the parameter, all other fitted parameters to take their preferred values. The resulting likelihood functions give central values, 68.3% C.L. intervals, and 95% C.L. intervals as listed in Table 70.7. The parameter ranges $x \leq 0$ and $y \leq 0$ are excluded at 8.2σ and more than 11.4σ significance, respectively.

From the results of the HFLAV averaging and global fit, we conclude the following: (1) Since CP violation is small and y_{CP} is positive, the CP -even state is shorter-lived, as in the $K^0\bar{K}^0$ system. (2) Since x is positive, the CP -even state is heavier, unlike in the $K^0\bar{K}^0$ system. (3) The strong phase difference $\delta_{K\pi}$ is consistent with the $SU(3)$ expectation of zero, and large values are unlikely (the 95% C.L. interval is $-13^\circ < \delta_{K\pi} < 22^\circ$). (4) While direct CP violation has been observed in D decays, there is no evidence for indirect CP violation, i.e., $|q/p| \neq 1$ or $\phi \neq 0$. Observing such CP violation at the current level of sensitivity would indicate new physics.

70.8 Future Data

Current results are based primarily upon CLEO-c (0.82 fb^{-1} of $e^+e^- \rightarrow \psi(3770)$ data), Belle and BaBar ($\sim 1.4 \text{ ab}^{-1}$ of $e^+e^- \rightarrow \Upsilon(4S)$ data), CDF (9.6 fb^{-1} of $p\bar{p}$ collision data at $\sqrt{s} = 1.96 \text{ TeV}$), and LHCb Runs 1 and 2 ($3.0 \text{ fb}^{-1} + 5.9 \text{ fb}^{-1}$ of pp collision data at $\sqrt{s} = 7, 8, 13 \text{ TeV}$).

BESIII has accumulated 2.9 fb^{-1} of $e^+e^- \rightarrow \psi(3770)$ data and plans to collect up to 20 fb^{-1} in the next few years. These data should provide strong phase measurements that enable improved model-independent determinations of mixing parameters from Belle II and LHCb. In 2019, Belle II began accumulating 50 ab^{-1} of $e^+e^- \rightarrow \Upsilon(4S)$ data [100], which is expected to take approximately ten years to collect. At LHCb, Run 2 was completed in 2018, Run 3 is planned for 2022–24, and Run 4 is planned for 2027–30 [101]. The goal for Runs 3 + 4 is to accumulate an additional 50 fb^{-1} of pp data at $\sqrt{s} \approx 14 \text{ TeV}$ [102]. These data, along with the large e^+e^- dataset from Belle II, should provide more precise measurements of D^0 - \bar{D}^0 mixing and significantly greater sensitivity to direct and indirect CP violation in D^0 decays.

References

- [1] D. M. Asner and W. M. Sun, Phys. Rev. **D73**, 034024 (2006), [Erratum: Phys. Rev. **D77**, 019901 (2008)], [hep-ph/0507238].
- [2] D. Atwood and A. A. Petrov, Phys. Rev. **D71**, 054032 (2005), [hep-ph/0207165].
- [3] M. Gronau, Y. Grossman and J. L. Rosner, Phys. Lett. **B508**, 37 (2001), [hep-ph/0103110].
- [4] Z.-z. Xing, Phys. Rev. **D55**, 196 (1997), [hep-ph/9606422].
- [5] M. Goldhaber and J. L. Rosner, Phys. Rev. **D15**, 1254 (1977).
- [6] Y. S. Amhis *et al.* (HFLAV), Eur. Phys. J. C **81**, 3, 226 (2021), [arXiv:1909.12524].
- [7] U. Bitenc *et al.* (Belle), Phys. Rev. **D77**, 112003 (2008), [arXiv:0802.2952].
- [8] B. Aubert *et al.* (BaBar), Phys. Rev. **D76**, 014018 (2007), [arXiv:0705.0704].
- [9] C. Cawfield *et al.* (CLEO), Phys. Rev. **D71**, 077101 (2005), [hep-ex/0502012].
- [10] E. M. Aitala *et al.* (E791), Phys. Rev. Lett. **77**, 2384 (1996), [hep-ex/9606016].
- [11] U. Bitenc *et al.* (Belle), Phys. Rev. **D72**, 071101 (2005), [hep-ex/0507020].
- [12] B. Aubert *et al.* (BaBar), Phys. Rev. **D70**, 091102 (2004), [hep-ex/0408066].
- [13] R. Aaij *et al.* (LHCb), Phys. Rev. **D97**, 3, 031101 (2018), [arXiv:1712.03220].
- [14] R. Aaij *et al.* (LHCb), Phys. Rev. **D95**, 5, 052004 (2017), [Erratum: Phys. Rev. **D96**, 099907 (2017)], [arXiv:1611.06143].
- [15] B. R. Ko *et al.* (Belle), Phys. Rev. Lett. **112**, 11, 111801 (2014), [Addendum: Phys. Rev. Lett. **112**, 139903 (2014)], [arXiv:1401.3402].
- [16] T. A. Aaltonen *et al.* (CDF), Phys. Rev. Lett. **111**, 23, 231802 (2013), [arXiv:1309.4078].
- [17] B. Aubert *et al.* (BaBar), Phys. Rev. Lett. **98**, 211802 (2007), [hep-ex/0703020].
- [18] Heavy Flavor Averaging Group, https://hflav-eos.web.cern.ch/hflav-eos/charm/CHARM21/results_mix_cp_v.html.
- [19] R. Aaij *et al.* (LHCb), Phys. Rev. Lett. **111**, 25, 251801 (2013), [arXiv:1309.6534].
- [20] R. Aaij *et al.* (LHCb), Phys. Rev. Lett. **110**, 10, 101802 (2013), [arXiv:1211.1230].
- [21] T. Aaltonen *et al.* (CDF), Phys. Rev. Lett. **100**, 121802 (2008), [arXiv:0712.1567].
- [22] L. M. Zhang *et al.* (Belle), Phys. Rev. Lett. **96**, 151801 (2006), [hep-ex/0601029].
- [23] J. M. Link *et al.* (FOCUS), Phys. Lett. **B618**, 23 (2005), [hep-ex/0412034].
- [24] R. Godang *et al.* (CLEO), Phys. Rev. Lett. **84**, 5038 (2000), [hep-ex/0001060].
- [25] E. M. Aitala *et al.* (E791), Phys. Rev. **D57**, 13 (1998), [hep-ex/9608018].
- [26] Y. Nir, Lectures given at 27th SLAC Summer Institute on Particle Physics: “ CP Violation in and Beyond the Standard Model (SSI 99),” Stanford, California, 7–16 July 1999. Published in Trieste 1999, *Particle Physics*, pp. 165–243.
- [27] S. Bergmann *et al.*, Phys. Lett. **B486**, 418 (2000), [hep-ph/0005181].
- [28] M. Ablikim *et al.* (BESIII), Phys. Lett. **B734**, 227 (2014), [arXiv:1404.4691].
- [29] J. Libby *et al.* (CLEO), Phys. Rev. **D82**, 112006 (2010), [arXiv:1010.2817].
- [30] A. Di Canto *et al.*, Phys. Rev. **D99**, 1, 012007 (2019), [arXiv:1811.01032].
- [31] R. Aaij *et al.* (LHCb), Phys. Rev. Lett. **127**, 11, 111801 (2021), [arXiv:2106.03744].
- [32] R. Aaij *et al.* (LHCb), Phys. Rev. Lett. **122**, 23, 231802 (2019), [arXiv:1903.03074].
- [33] R. Aaij *et al.* (LHCb), JHEP **04**, 033 (2016), [arXiv:1510.01664].

- [34] J. P. Lees *et al.* (BaBar), Phys. Rev. **D93**, 11, 112014 (2016), [arXiv:1604.00857].
- [35] T. Peng *et al.* (Belle), Phys. Rev. **D89**, 9, 091103 (2014), [arXiv:1404.2412].
- [36] P. del Amo Sanchez *et al.* (BaBar), Phys. Rev. Lett. **105**, 081803 (2010), [arXiv:1004.5053].
- [37] K. Abe *et al.* (Belle), Phys. Rev. Lett. **99**, 131803 (2007), [arXiv:0704.1000].
- [38] D. M. Asner *et al.* (CLEO), Phys. Rev. **D72**, 012001 (2005), [hep-ex/0503045].
- [39] See “Review of Multibody Charm Analyses” in this *Review*.
- [40] B. Aubert *et al.* (BaBar), Phys. Rev. Lett. **97**, 221803 (2006), [hep-ex/0608006].
- [41] B. Aubert *et al.* (BaBar), Phys. Rev. Lett. **103**, 211801 (2009), [arXiv:0807.4544].
- [42] E. White *et al.* (Belle), Phys. Rev. **D88**, 5, 051101 (2013), [arXiv:1307.5935].
- [43] R. Aaij *et al.* (LHCb), Phys. Rev. Lett. **116**, 24, 241801 (2016), [arXiv:1602.07224].
- [44] H. Muramatsu *et al.* (CLEO), Phys. Rev. Lett. **89**, 251802 (2002), [Erratum: Phys. Rev. Lett. **90**, 059901 (2003)], [hep-ex/0207067].
- [45] M. Ablikim *et al.* (BESIII), Phys. Rev. D **101**, 11, 112002 (2020), [arXiv:2003.00091].
- [46] B. Aubert *et al.* (BaBar), Phys. Rev. Lett. **95**, 121802 (2005), [hep-ex/0504039].
- [47] B. Aubert *et al.* (BaBar), Phys. Rev. **D78**, 034023 (2008), [arXiv:0804.2089].
- [48] R. Aaij *et al.* (LHCb) (2021), [arXiv:2105.09889].
- [49] M. Nayak *et al.* (Belle), Phys. Rev. D **102**, 7, 071102 (2020), [arXiv:1912.10912].
- [50] R. Aaij *et al.* (LHCb), Phys. Rev. **D101**, 1, 012005 (2020), [arXiv:1911.01114].
- [51] R. Aaij *et al.* (LHCb), Phys. Rev. Lett. **122**, 1, 011802 (2019), [arXiv:1810.06874].
- [52] R. Aaij *et al.* (LHCb), Phys. Rev. Lett. **118**, 26, 261803 (2017), [arXiv:1702.06490].
- [53] M. Starič *et al.* (Belle), Phys. Lett. **B753**, 412 (2016), [arXiv:1509.08266].
- [54] R. Aaij *et al.* (LHCb), JHEP **04**, 043 (2015), [arXiv:1501.06777].
- [55] M. Ablikim *et al.* (BESIII), Phys. Lett. **B744**, 339 (2015), [arXiv:1501.01378].
- [56] T. A. Aaltonen *et al.* (CDF), Phys. Rev. **D90**, 11, 111103 (2014), [arXiv:1410.5435].
- [57] J. P. Lees *et al.* (BaBar), Phys. Rev. **D87**, 1, 012004 (2013), [arXiv:1209.3896].
- [58] A. Zupanc *et al.* (Belle), Phys. Rev. **D80**, 052006 (2009), [arXiv:0905.4185].
- [59] S. E. Csorna *et al.* (CLEO), Phys. Rev. **D65**, 092001 (2002), [hep-ex/0111024].
- [60] J. M. Link *et al.* (FOCUS), Phys. Lett. **B485**, 62 (2000), [hep-ex/0004034].
- [61] E. M. Aitala *et al.* (E791), Phys. Rev. Lett. **83**, 32 (1999), [hep-ex/9903012].
- [62] Heavy Flavor Averaging Group, https://hflav-eos.web.cern.ch/hflav-eos/charm/CHARM21/results_mixing.html.
- [63] R. Aaij *et al.* (LHCb), Phys. Rev. Lett. **112**, 4, 041801 (2014), [arXiv:1310.7201].
- [64] R. Aaij *et al.* (LHCb), JHEP **04**, 129 (2012), [arXiv:1112.4698].
- [65] B. Aubert *et al.* (BaBar), Phys. Rev. **D80**, 071103 (2009), [arXiv:0908.0761].
- [66] B. Aubert *et al.* (BaBar), Phys. Rev. **D78**, 011105 (2008), [arXiv:0712.2249].
- [67] M. Starič *et al.* (BELLE), Phys. Rev. Lett. **98**, 211803 (2007), [65(2007)], [hep-ex/0703036].
- [68] B. Aubert *et al.* (BaBar), Phys. Rev. Lett. **91**, 121801 (2003), [hep-ex/0306003].
- [69] K. Abe *et al.* (Belle), Phys. Rev. Lett. **88**, 162001 (2002), [hep-ex/0111026].
- [70] R. Aaij *et al.* (LHCb), Phys. Rev. Lett. **122**, 21, 211803 (2019), [arXiv:1903.08726].
- [71] T. Aaltonen *et al.* (CDF), Phys. Rev. Lett. **109**, 111801 (2012), [arXiv:1207.2158].
- [72] B. Aubert *et al.* (BaBar), Phys. Rev. Lett. **100**, 061803 (2008), [arXiv:0709.2715].
- [73] M. Starič *et al.* (Belle), Phys. Lett. **B670**, 190 (2008), [arXiv:0807.0148].
- [74] R. Aaij *et al.* (LHCb), Phys. Rev. Lett. **116**, 19, 191601 (2016), [arXiv:1602.03160].
- [75] R. Aaij *et al.* (LHCb), JHEP **07**, 041 (2014), [arXiv:1405.2797].
- [76] R. Aaij *et al.* (LHCb), Phys. Lett. **B723**, 33 (2013), [arXiv:1303.2614].
- [77] R. Aaij *et al.* (LHCb), Phys. Rev. Lett. **108**, 111602 (2012), [arXiv:1112.0938].
- [78] B. R. Ko (Belle), in “7th International Workshop on the CKM Unitarity Triangle (CKM 2012) Cincinnati, Ohio, USA, September 28-October 2, 2012,” (2012), [arXiv:1212.5320].
- [79] M. Gersabeck *et al.*, J. Phys. G **39**, 045005 (2012), [arXiv:1111.6515].
- [80] A. L. Kagan and L. Silvestrini, Phys. Rev. D **103**, 5, 053008 (2021), [arXiv:2001.07207].
- [81] See the tabulation of A_{CP} results in the D^0 and D^+ Listings in this *Review*.
- [82] Y. Grossman, A. L. Kagan and Y. Nir, Phys. Rev. D **75**, 036008 (2007), [hep-ph/0609178].
- [83] R.A. Briere *et al.*, (CLEO Collab.), CLNS 01-1742, (2001).
- [84] D. M. Asner *et al.*, (BES-III Collab.), Int. J. Mod. Phys. **A**, 24 (2009).
- [85] Heavy Flavor Averaging Group, https://hflav-eos.web.cern.ch/hflav-eos/charm/CHARM13/results_mix_cpv.html.
- [86] J. Beringer *et al.* (Particle Data Group), Phys. Rev. **D86**, 010001 (2012).
- [87] J. L. Rosner *et al.* (CLEO), Phys. Rev. Lett. **100**, 221801 (2008), [arXiv:0802.2264].
- [88] D. M. Asner *et al.* (CLEO), Phys. Rev. **D78**, 012001 (2008), [arXiv:0802.2268].
- [89] D. M. Asner *et al.* (CLEO), Phys. Rev. **D86**, 112001 (2012), [arXiv:1210.0939].
- [90] Heavy Flavor Averaging Group, https://hflav-eos.web.cern.ch/hflav-eos/charm/March12/results_mix_cpv.html.
- [91] T. Aaltonen *et al.* (CDF), Phys. Rev. Lett. **100**, 121802 (2008), [arXiv:0712.1567].
- [92] D. M. Asner *et al.* (CLEO), Phys. Rev. D **72**, 012001 (2005), [hep-ex/0503045].
- [93] E. Golowich *et al.*, Phys. Rev. **D76**, 095009 (2007), [arXiv:0705.3650].
- [94] G. Isidori *et al.*, Phys. Lett. **B711**, 46 (2012), [arXiv:1111.4987].
- [95] E. Franco, S. Mishima and L. Silvestrini, JHEP **05**, 140 (2012), [arXiv:1203.3131].
- [96] J. Brod, A. L. Kagan and J. Zupan, Phys. Rev. D **86**, 014023 (2012), [arXiv:1111.5000].

- [97] Y. Grossman, Y. Nir and G. Perez, Phys. Rev. Lett. **103**, 071602 (2009), [arXiv:0904.0305].
- [98] A. L. Kagan and M. D. Sokoloff, Phys. Rev. **D80**, 076008 (2009), [arXiv:0907.3917].
- [99] M. Ciuchini *et al.*, Phys. Lett. **B655**, 162 (2007), [hep-ph/0703204].
- [100] W. Altmannshofer *et al.* (Belle-II), PTEP **2019**, 12, 123C01 (2019), [Erratum: PTEP 2020, 029201 (2020)], [arXiv:1808.10567].
- [101] CERN LHC Schedule, <https://lhc-commissioning.web.cern.ch/schedule/LHC-long-term.htm>.
- [102] R. Aaij *et al.* (LHCb) (2018), [arXiv:1808.08865].

71. D_s^+ Branching Fractions

Revised September 2021 by J.L. Rosner (Chicago U.) and C.G. Wohl (LBNL).

Figure 71.1 shows a partial breakdown of the D_s^+ branching fractions. The rest of this note is about how the figure was constructed. The values shown make heavy use of CLEO measurements of inclusive branching fractions [1]. For references to other data cited in the following, see the Listings. An addendum updates branching fractions to two-body final states reported by the BESIII Collaboration in 2020 [2], and the conclusion stresses modes still to be identified.

71.1 Modes with leptons

The bottom $(18.0 \pm 1.0)\%$ of Fig. 71.1 shows the fractions for the modes that include leptons. The measured $K^0 e^+ \nu_e$ and $K^{*0} e^+ \nu_e$ fractions have been doubled to take account of the corresponding $\mu^+ \nu_\mu$ fractions. The sum of the exclusive $X e^+ \nu_e$ fractions is $(6.0 \pm 0.3)\%$, consistent with an inclusive semileptonic measurement of $(6.5 \pm 0.4)\%$. There seems to be little missing here.

71.2 Inclusive hadronic $K\bar{K}$ fractions

The Cabibbo-favored $c \rightarrow s$ decay in D_s^+ decay produces a final state with both an s and an \bar{s} ; and thus modes with a $K\bar{K}$ pair or with an η , ω , η' , or ϕ predominate (as may already be seen in Fig. 71.1 in the semileptonic fractions). We consider the $K\bar{K}$ modes first. A complete picture of the exclusive $K\bar{K}$ charge modes is not yet possible, because branching fractions for many of those modes have not yet been measured. However, CLEO has measured the inclusive K^+ , K^- , K_S^0 , $K^+ K^-$, $K^+ K_S^0$, $K^- K_S^0$, and $2K_S^0$ fractions (these include modes with leptons) [1]. And each of these inclusive fractions with a K_S^0 is equal to the corresponding fraction with a K_L^0 : $f(K^+ K_L^0) = f(K^+ K_S^0)$, $f(2K_L^0) = f(2K_S^0)$, etc. Therefore, of all-inclusive fractions pairing a K^+ , K_S^0 , or K_L^0 with a K^- , K_S^0 , or K_L^0 , we know all but $f(K_S^0 K_L^0)$.

We can get that fraction. The total K_S^0 fraction is

$$f(K_S^0) = f(K^+ K_S^0) + f(K^- K_S^0) + 2f(2K_S^0) + f(K_S^0 K_L^0) + f(\text{single } K_S^0),$$

where $f(\text{single } K_S^0)$ is the sum of the branching fractions for modes such as $K_S^0 \pi^+ 2\pi^0$ with a K_S^0 and no second K . The $K_S^0 \pi^+ 2\pi^0$ mode is in fact the only unmeasured single- K_S^0 mode (throughout, we shall assume that fractions for modes with a K or $K\bar{K}$ and more than three pions are negligible), and we shall take its fraction to be the same as for the $K_S^0 2\pi^+ \pi^-$ mode, $(0.30 \pm 0.11)\%$. Any reasonable deviation from this value would be too small to matter much in the following. Adding the several small single- K_S^0 branching fractions, including those from semileptonic modes, we get $f(\text{single } K_S^0) = (1.7 \pm 0.2)\%$. Using this, we have:

$$\begin{aligned} f(K_S^0 K_L^0) &= f(K_S^0) - f(K^+ K_S^0) - f(K^- K_S^0) \\ &\quad - 2f(2K_S^0) - f(\text{single } K_S^0) \\ &= (19.0 \pm 1.1) - (5.8 \pm 0.5) - (1.9 \pm 0.4) \\ &\quad - 2 \times (1.7 \pm 0.3) - (1.7 \pm 0.2) \\ &= (6.2 \pm 1.4)\%. \end{aligned}$$

Here and below we treat the errors as uncorrelated, although often they are not. However, our main aim is to get numbers for Fig. 71.1; errors are secondary.

There is a check on our result: The ϕ inclusive branching fraction is $(15.7 \pm 1.0)\%$, of which 34%, or $(5.34 \pm 0.34)\%$ of D_s^+ decays, produces a $K_S^0 K_L^0$. Our $f(K_S^0 K_L^0) = (6.2 \pm 1.4)\%$ has to be at least this large—and it is, within the sizable error.

We now have all the inclusive $K\bar{K}$ fractions. We use $f(K^+ \bar{K}^0) = 2f(K^+ K_S^0)$, and likewise for $f(K^- K^0)$. For $K^+ K^-$ and $K_S^0 K_L^0$, we subtract off the contributions from $\phi \ell^+ \nu$ decay to

get the purely hadronic $K\bar{K}$ inclusive fractions:

$$\begin{aligned} f(K^+ K^-, \text{hadronic}) &= (15.8 \pm 0.7) - (2.1 \pm 0.3) \\ &= (13.7 \pm 0.8)\% \\ f(K^+ \bar{K}^0, \text{hadronic}) &= (11.6 \pm 1.0)\% \\ f(K^- K^0, \text{hadronic}) &= (3.8 \pm 0.8)\% \\ f(2K_S^0 + 2K_L^0, \text{hadronic}) &= (3.4 \pm 0.6)\% \\ f(K_S^0 K_L^0, \text{hadronic}) &= (6.2 \pm 1.4) - (1.5 \pm 0.2) \\ &= (4.7 \pm 1.4)\%. \end{aligned}$$

The fractions are shown in Fig. 71.1. They total $(37.2 \pm 2.2)\%$ of

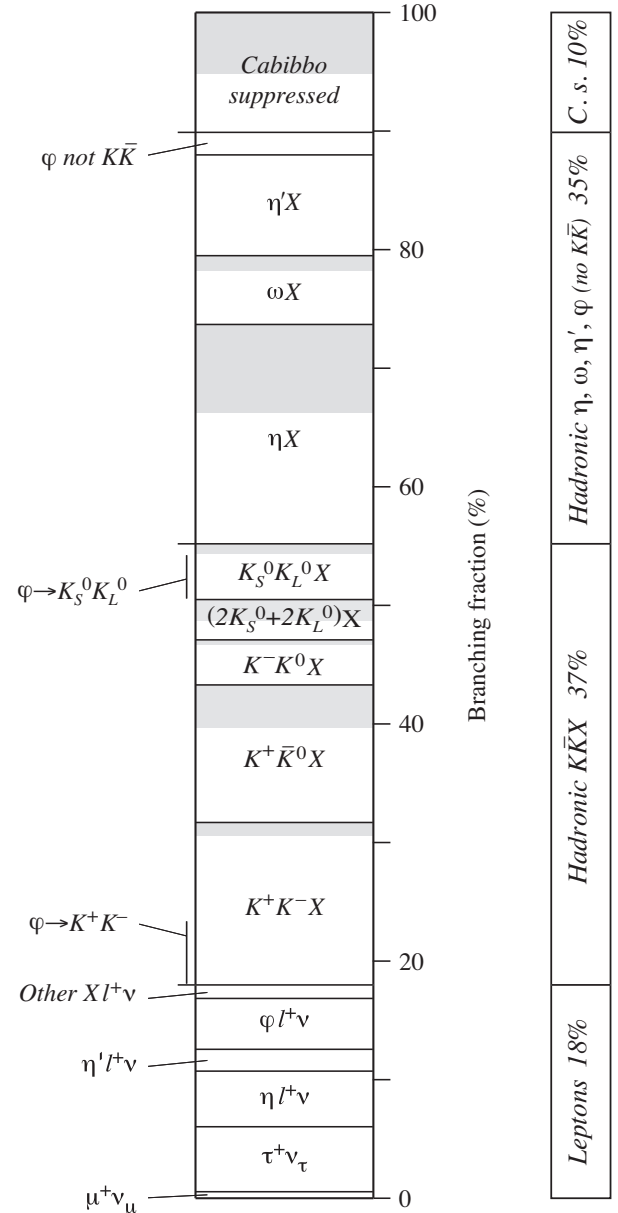


Figure 71.1: A partial breakdown of D_s^+ branching fractions. The hadronic bins in the left column show inclusive fractions. Shading within a bin shows how much of the inclusive fraction is not yet accounted for by adding up all the relevant exclusive fractions. The inclusive hadronic ϕ fraction is spread over three bins, in proportion to its decay fractions into $K^+ K^-$, $K_S^0 K_L^0$, and non- $K\bar{K}$ modes.

D_s^+ decays.

We can add more information to the figure by summing up measured branching fractions for exclusive modes within each bin:

K^+K^- modes—The sum of measured $K^+K^-\pi^+$, $K^+K^-\pi^+\pi^0$, and $K^+K^-2\pi^+\pi^-$ branching fractions is $(12.6 \pm 0.6)\%$. That leaves $(1.1 \pm 1.0)\%$ for the $K^+K^-\pi^+2\pi^0$ mode, which is the only other K^+K^- mode with three or fewer pions. In Fig. 71.1, this unmeasured part of the K^+K^- bin is shaded.

$K^+\bar{K}^0$ modes—Two times the sum of the measured $K^+K_S^0$, $K^+K_S^0\pi^0$, and $K^+K_S^0\pi^+\pi^-$ branching fractions is $(8.0 \pm 0.5)\%$. This leaves $(3.6 \pm 1.1)\%$ for the unmeasured $K^+\bar{K}^0$ modes (there are three such modes with three or fewer pions). This is shaded in the figure.

K^-K^0 modes—Twice the $K^-K_S^02\pi^+$ fraction is $(3.4 \pm 0.2)\%$, which leaves about $(0.4 \pm 0.8)\%$ for $K^-K^02\pi^+\pi^0$, the only other K^-K^0 mode with three or fewer pions.

$2K_S^0+2K_L^0$ modes—The $2K_S^0\pi^+$ and $2K_S^02\pi^+\pi^-$ fractions sum to $(0.86 \pm 0.07)\%$; this times two (for the corresponding $2K_L^0$ modes) is $(1.72 \pm 0.14)\%$. This leaves about $(1.7 \pm 0.7)\%$ for other $2K_S^0+2K_L^0$ modes.

$K_S^0K_L^0$ modes—Most of the $K_S^0K_L^0$ fraction is accounted for by ϕ decays (see below).

71.3 Inclusive hadronic η , ω , η' , and ϕ fractions

These are easier. We start with the inclusive branching fractions, and then, to avoid double counting, subtract: (1) fractions for modes with leptons; (2) η mesons that are included in the inclusive η' fraction; and (3) K^+K^- and $K_S^0K_L^0$ from ϕ decays:

$$f(\eta \text{ hadronic}) = f(\eta \text{ inclusive}) - 0.65 f(\eta' \text{ inclusive}) \\ - f(\eta\ell^+\nu) = (18.5 \pm 3.0)\%$$

$$f(\omega \text{ hadronic}) = f(\omega \text{ inclusive}) - 0.026 f(\eta' \text{ inclusive}) \\ = (5.8 \pm 1.4)\%$$

$$f(\eta' \text{ hadronic}) = f(\eta' \text{ inclusive}) - f(\eta'\ell^+\nu) \\ = (8.5 \pm 1.5)\%$$

$$f(\phi \text{ hadronic, } \not\rightarrow K\bar{K}) = 0.17 [f(\phi \text{ inclusive}) - f(\phi\ell^+\nu)] \\ = (1.9 \pm 0.2)\% .$$

The factors 0.65, 0.026, and 0.17 are the $\eta' \rightarrow \eta$, $\eta' \rightarrow \omega$, and $\phi \not\rightarrow K\bar{K}$ branching fractions. Figure 71.1 shows the results; the sum is $(34.7 \pm 3.6)\%$, which is about equal to the hadronic $K\bar{K}$ total.

Note that the bin marked ϕ near the top of Fig. 71.1 includes neither the $\phi\ell^+\nu$ decays nor the 83% of other ϕ decays that produce a $K\bar{K}$ pair. There is twice as much ϕ in the $K_S^0K_L^0$ bin, and nearly three times as much in the K^+K^- bin. These contributions are indicated in those bins.

Again, we can show how much of each bin is accounted for by measured exclusive branching fractions: η modes—The sum of $\eta\pi^+$, $\eta\pi^+\pi^0$ (nearly all $\eta\rho^+$), and ηK^+ branching fractions is $(11.1 \pm 1.2)\%$, which leaves a good part of the inclusive hadronic η fraction, $(18.5 \pm 3.0)\%$, to be accounted for. This is shaded in the figure. ω modes—The sum of $\omega\pi^+$, $\omega\pi^+\pi^0$, and $\omega2\pi^+\pi^-$ fractions is $(4.6 \pm 0.9)\%$, which is nearly as large as the inclusive hadronic ω fraction, $(5.8 \pm 1.4)\%$. η' modes—The sum of $\eta'\pi^+$, $\eta'\rho^+$, and $\eta'K^+$ fractions is $(9.9 \pm 1.5)\%$, which is larger than but not in serious disagreement with the inclusive hadronic η' fraction, $(8.5 \pm 1.5)\%$.

71.4 Cabibbo-suppressed modes

The sum of the fractions for modes with a $K\bar{K}$, η , ω , η' , or leptons is $(89.9 \pm 4.4)\%$. The remaining $(10.1 \pm 4.4)\%$ is to

Cabibbo-suppressed modes, mainly single- K + pions and multiple-pion modes (see below). However, it should be noted that some small parts of the modes already discussed are Cabibbo-suppressed. For example, the $(1.1 \pm 0.2)\%$ of D_s^+ decays to $K^0\ell\nu$ or $K^{*0}\ell\nu$ is already in the $X\ell\nu$ bin in Fig. 71.1. And the inclusive measurements of η , ω , and η' fractions do not distinguish between (and therefore include both) Cabibbo-allowed and -suppressed modes. We shall not try to make a separation here.

K^0 + pions—Above, we found that $f(\text{single } K_S^0) = (1.7 \pm 0.2)\%$. Subtracting semileptonic fractions with a K_S^0 leaves $(1.3 \pm 0.2)\%$. The hadronic single- K^0 fraction is twice this, about $(2.6 \pm 0.4)\%$. The sum of measured $K^0\pi^+$, $K^0\pi^+\pi^0$, and $K^02\pi^+\pi^-$ fractions is $(1.8 \pm 0.3)\%$, about two-thirds as much.

K^+ + pions—The $K^+\pi^0$ and $K^+\pi^+\pi^-$ fractions sum to $(0.72 \pm 0.05)\%$. The total K^+ fraction wanted here is probably in the 1-to-2% range.

Multi-pions—The $2\pi^+\pi^-$, $\pi^+2\pi^0$, and $3\pi^+2\pi^-$ fractions total $(2.5 \pm 0.2)\%$. Modes not measured might double this.

The sum of the actually measured fractions is, including the semileptonics, $(4.9 \pm 0.3)\%$. The error on our Cabibbo-suppressed total, $(10.1 \pm 4.4)\%$ is too large to know how much we might be missing.

71.5 Addendum: Improved precision in some measurements

The Table compares measurements of branching fractions to pairs of two pseudoscalar mesons used in our 2019 update of the 2018 PDG review with values available in 2021 [2]. They have not changed much but are much better known.

Final state	2019 PDG avg or fit (%)	New BESIII entry in 2021 PDG (%)	2021 PDG avg or fit (%)
$K^+\eta'$	0.18 ± 0.06	0.268 ± 0.025	0.265 ± 0.025
$K^+\eta$	0.177 ± 0.035	0.162 ± 0.012	0.160 ± 0.011
$\eta\pi^+$	1.70 ± 0.09	1.741 ± 0.063	1.68 ± 0.10
$K^+K_S^0$	1.50 ± 0.05	1.502 ± 0.055	1.46 ± 0.04
$K_S^0\pi^+$	0.122 ± 0.006	0.1109 ± 0.005	0.110 ± 0.005
$K^+\pi^0$	0.063 ± 0.021	0.0748 ± 0.0057	0.074 ± 0.0057

Other recent BESIII additions include the measurements $\mathcal{B}(D_s \rightarrow \omega\pi^+, \omega K^+) = (1.77 \pm 0.32 \pm 0.13, 0.87 \pm 0.24 \pm 0.08) \times 10^{-3}$ [3] and $\mathcal{B}(D_s \rightarrow K_{S,L}K^+) = (1.425 \pm 0.038 \pm 0.031, 1.485 \pm 0.039 \pm 0.046)\%$ [4].

71.6 Concluding remarks

The shaded bands in the figure imply that about eight percent of the total D_s decay rate is into ηX , with X still to be accounted for. Unidentified Cabibbo-suppressed modes and the modes $K^+\bar{K}^0 X$ and $(2K_S^0+2K_L^0)X$ respectively correspond to $\sim (5, 3, 2)\%$ of the total. However, one can consider the vast majority of D_s decays to be represented by exclusive final states.

References

- [1] S. Dobbs *et al.* (CLEO), Phys. Rev. D **79**, 112008 (2009), [arXiv:0904.2417].
- [2] M. Ablikim *et al.* (BESIII), JHEP **08**, 146 (2020), [arXiv:2005.05072].
- [3] M. Ablikim *et al.* (BESIII), Phys. Rev. D **99**, 9, 091101 (2019), [arXiv:1811.00392].
- [4] M. Ablikim *et al.* (BESIII), Phys. Rev. D **99**, 11, 112005 (2019), [arXiv:1903.04164].

72. Leptonic Decays of Charged Pseudoscalar Mesons

Revised Sept. 2021 by J.L. Rosner (Chicago U.); written with S.L. Stone (Syracuse U.) and R. Van de Water (FNAL)

72.1 Introduction

This review updates one in Ref. [1]. Extensive use is made of results of the Flavor Lattice Averaging group (FLAG 21), Ref. [2], which have not changed much since the previous compilation [3].

Charged mesons formed from a quark and antiquark can decay to a lepton-neutrino pair when these objects annihilate via a virtual W boson. Figure 72.1 illustrates this process for the purely leptonic decay of a D^+ meson.

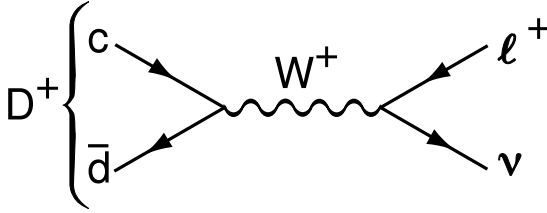


Figure 72.1: The annihilation process for pure D^+ leptonic decays in the standard model.

Similar quark-antiquark annihilations via a virtual W^+ to the $\ell^+\nu$ final states occur for the π^+ , K^+ , D_s^+ , and B^+ mesons. (Whenever pseudoscalar-meson charges are specified in this article, use of the charge-conjugate particles and corresponding decays are also implied.) Let P be any of these pseudoscalar mesons. To lowest order, the decay width is

$$\Gamma^{(0)}(P \rightarrow \ell\nu) = \frac{G_F^2}{8\pi} f_P^2 m_\ell^2 M_P \left(1 - \frac{m_\ell^2}{M_P^2}\right)^2 |V_{q_1 q_2}|^2. \quad (72.1)$$

Here M_P is the P mass, m_ℓ is the ℓ mass, $V_{q_1 q_2}$ is the Cabibbo-Kobayashi-Maskawa (CKM) matrix element between the quarks $q_1 \bar{q}_2$ in P , and G_F is the Fermi coupling constant. The decay constant f_P is proportional to the matrix element of the axial current between the one- P -meson state and the vacuum:

$$\langle 0 | \bar{q}_1 \gamma_\mu \gamma_5 q_2 | P(p) \rangle = i p_\mu f_P, \quad (72.2)$$

and can be thought of as proportional to the “wave function overlap” of the quark and antiquark. In this article, we use the convention in which $f_\pi \approx 130$ MeV. For brevity, we will often denote the purely leptonic decay width in Eq. (72.1) by $\Gamma^{(0)}$.

The decay of P^\pm starts with a spin-0 meson, and ends up with a left-handed neutrino or right-handed antineutrino. By angular momentum conservation, the ℓ^\pm must then also be left-handed or right-handed, respectively. In the $m_\ell = 0$ limit, the decay is forbidden, and can only occur as a result of the finite ℓ mass. This helicity suppression is the origin of the m_ℓ^2 factor in the decay width.

Experimentally, it is difficult to isolate events in which there are *only* a lepton and neutrino in the final state from those with a lepton, neutrino, and soft photon. Thus, radiative contributions must be removed from the experimental measurements *a posteriori* to obtain $\Gamma^{(0)}$. The radiative contributions can be broken into three pieces: the short-distance contribution to leptonic and semileptonic decays mediated by a W^\pm boson that accounts for electroweak corrections not included in the definition of G_F , the long-distance internal bremsstrahlung (IB) contribution, and the contribution from photon emission that depends upon the hadron’s structure. The universal electroweak correction was calculated at $\mathcal{O}(\alpha)$ by Sirlin [4], and increases the purely leptonic decay rate by ~ 1.8 –2.2% depending on the decaying meson. The $\mathcal{O}(\alpha)$ IB contribution was calculated by Kinoshita [5], and again is universal for all leptonic decays at this order. Numerically, the universal long-distance contribution lowers the purely leptonic decay rate by ~ 0.4 –2.4%, where the correction is smallest for pions and largest for $D_{(s)}$ mesons. The structure-dependent contributions have been estimated within various effective theories to increase the purely leptonic rate by one to a few percent [6–11].

In this review, we treat the radiative corrections differently for the light, charm, and bottom meson systems for several reasons. First, the experimental uncertainties on the decay widths vary substantially. Thus, while the inclusion of radiative corrections is essential for the pion, kaon, and D -meson decay widths, which have been measured to (sub)-percent precision, radiative corrections can be neglected (for now) for $B \rightarrow \tau\nu$ decay. Second, the photons are treated differently on the experimental side for the different decay processes. For pions and kaons, the experimental measurements of $\Gamma_{P\ell 2[\gamma]}$ are fully inclusive, while for D mesons, the experiments impose cuts on the energy of any neutral cluster deposited in the calorimeter, which reduce the soft-photon background substantially. Some experiments also remove the QED bremsstrahlung in the leading-logarithmic approximation using the PHOTOS Monte-Carlo generator [12]. Third, the theoretical knowledge of the structure-dependent corrections varies for each meson system.

Once radiative corrections have been accounted for, measurements of purely leptonic decay branching fractions and lifetimes allow an experimental determination of the product $|V_{q_1 q_2}| f_P$. If the decay constant f_P is known to sufficient precision from theory, one can obtain the corresponding CKM element within the standard model. If, on the other hand, one takes the value of $|V_{q_1 q_2}|$ assuming CKM unitarity, one can infer an “experimental measurement” of the decay constant that can then be compared with theory.

The importance of measuring $\Gamma(P \rightarrow \ell\nu)$ depends on the particle being considered. Leptonic decays of charged pseudoscalar mesons occur at tree level within the standard model. Thus one does not expect large new-physics contributions to measurements of $\Gamma(P \rightarrow \ell\nu)$ for the lighter mesons $P = \pi^+, K^+$, and these processes, in principle, provide clean standard-model determinations of $|V_{ud}|$ and $|V_{us}|$. The situation is different for leptonic decays of charm and bottom mesons. The presence of new heavy particles such as charged Higgs bosons or leptoquarks could lead to observable effects in $\Gamma(P \rightarrow \ell\nu)$ for $P = D_{(s)}^+, B^+$ [13–17]. Thus, the determination of $|V_{ub}|$ from $B^+ \rightarrow \tau\nu$ decay, in particular, should be considered a probe of new physics. More generally, the ratio of leptonic decays to $\tau\nu$ over $\mu\nu$ final states probes lepton universality [13, 18].

The determinations of CKM elements from leptonic decays of charged pseudoscalar mesons provide complementary information to those from other decay processes. The decay $P \rightarrow \ell\nu$ proceeds in the standard model via the axial-vector current $\bar{q}_1 \gamma_\mu \gamma_5 q_2$, whereas semileptonic pseudoscalar meson decays $P_1 \rightarrow P_2 \ell\nu$ proceed via the vector current $\bar{q}_1 \gamma_\mu q_2$. Thus the comparison of determinations of $|V_{q_1 q_2}|$ from leptonic and semileptonic decays tests the $V - A$ structure of the standard-model electroweak charged-current interaction. More generally, a small right-handed admixture to the standard-model weak current would lead to discrepancies between $|V_{q_1 q_2}|$ obtained from leptonic pseudoscalar-meson decays, exclusive semileptonic pseudoscalar-meson decays, exclusive semileptonic baryon decays, and inclusive semileptonic decays [19, 20].

Both measurements of the decay rates $\Gamma(P \rightarrow \ell\nu)$ and theoretical calculations of the decay constants f_P for $P = \pi^+, K^+, D_{(s)}^+$ from numerical lattice-QCD calculations are now quite precise. As a result, the elements of the first row of the CKM matrix $|V_{ud}|$ and $|V_{us}|$ can be obtained to sub-percent precision from $\pi^+ \rightarrow \ell\nu$ and $K^+ \rightarrow \ell\nu$, where the limiting error is from continuum theory radiative corrections. The elements of the second row of the CKM matrix $|V_{cd(s)}|$ can be obtained from leptonic decays of charmed pseudoscalar mesons to few-percent precision, where here the limiting error is from experiment. These enable stringent tests of the unitarity of the first and second rows of the CKM matrix.

This review is organized as follows. Because the experimental and theoretical issues associated with measurements of pions and kaons, charmed mesons, and bottom mesons differ, we discuss each one separately. We begin with the pion and kaon system in Sec. 72.2. First, in Sec. 72.2.1, we review current measurements of the experimental decay rates. We provide tables of

branching-ratio measurements and determinations of the product $|V_{ud(s)}|f_{\pi+(K+)}$, as well as average values for these quantities including correlations and other effects needed to combine results. Then, in Sec. 72.2.2, we summarize the status of theoretical calculations of the decay constants. We provide tables of recent lattice-QCD results for $f_{\pi+}$, f_{K+} , and their ratio from calculations including dynamical u , d , s , and (in some cases c) quarks, along with averages including correlations and strong SU(2)-isospin breaking corrections as needed. We next discuss the charmed meson system in Sec. 72.3, again reviewing current experimental rate measurements in Sec. 72.3.1 and theoretical decay-constant calculations in Sec. 72.3.2. Last, we discuss the bottom meson system in Sec. 72.4, following the same organization as the two previous sections. For almost all of the decay constants presented in Secs. 72.2.2, 72.3.2, and 72.4.2, we take as our preferred values the four-flavor averages from the FLAG 21 review [2], which incorporate all lattice-QCD results that appeared before 30 April 2021.

After having established the status of both experimental measurements and theoretical calculations of leptonic charged pseudoscalar-meson decays, we discuss some implications for phenomenology in Sec. 72.5. For each process discussed in Secs. 72.2–72.4, we combine the average $\mathcal{B}(P \rightarrow \ell\nu)$ with the decay constant f_P to infer the associated CKM matrix element. We then compare these results with determinations of the same CKM elements from other processes. We also use the CKM elements obtained from leptonic decays to test the unitarity of the first and second rows of the CKM matrix. Further, as in previous reviews, we combine the experimental $\mathcal{B}(P \rightarrow \ell\nu)$ s with the associated CKM elements obtained from CKM unitarity to infer “experimental” values for the decay constants. The comparison of these values with theory provides a test of lattice and other QCD approaches, assuming that new-physics contributions to these processes are not significant.

72.2 Pions and kaons

72.2.1 Experimental rate measurements

Experimental rate measurements of pion and kaon leptonic decays are fully radiation inclusive. Following Refs. [21, 22], and references therein, we combine the $\mathcal{O}(\alpha)$ radiative corrections to the purely leptonic rate as follows:

$$\Gamma(P \rightarrow \ell\nu[\gamma]) = \Gamma^{(0)}(P \rightarrow \ell\nu) \left[1 + \frac{\alpha}{\pi} C_P \right], \quad (72.3)$$

where $P = \pi, K$. The full expressions for C_π and C_K are given in Eq. (114) of Ref. [8]. In addition to the universal short- [4] and long-distance [5] corrections, C_π and C_K include hadronic-structure dependent contributions [6] through $\mathcal{O}(\alpha p^4)$ in chiral perturbation theory (χ PT), where p is the pion or kaon momentum. The inclusion of radiative corrections to the purely leptonic rates is numerically important given the level of precision achieved on the experimental measurements of the $\pi^\pm \rightarrow \mu^\pm\nu$ and $K^\pm \rightarrow \mu^\pm\nu$ decay widths.

We evaluate $\delta_P \equiv (\alpha/\pi)C_P$ using experimentally-measured meson and lepton masses and coupling constants from the Particle Data Group [23], and taking the low-energy constants (LECs) that parametrize the hadronic contributions from Refs. [8, 24, 25]. Because the finite non-logarithmic parts of the LECs were estimated within the large- N_C approximation assuming that contributions from the lowest-lying resonances dominate, we conservatively assign a 100% uncertainty to the LECs, which leads to a ± 0.9 error in $C_{\pi,K}$.¹ We obtain the following correction factors to the individual charged pion and kaon decay widths:

$$\delta_\pi = 0.0176(21) \quad \text{and} \quad \delta_K = 0.0107(21). \quad (72.4)$$

The error on the ratio of kaon-to-pion leptonic decay widths is under better theoretical control because the hadronic contributions

¹This uncertainty on $C_{\pi,K}$ is smaller than the error estimated by Marciano and Sirlin in Ref. [26], which predates the calculations of the hadronic-structure contributions in Refs. [6, 8, 24, 25]. The hadronic LECs incorporate the large short-distance electroweak logarithm discussed in Ref. [26], and their dependence on the chiral renormalization scale cancels the scale-dependence induced by chiral loops, thereby removing the dominant scale uncertainty of the Marciano–Sirlin analysis [26].

from low-energy constants estimated within the large- N_C framework cancel at lowest order in the chiral expansion. For the ratio, we use the correction factor

$$\delta_{K/\pi} = -0.0069(17), \quad (72.5)$$

where we take the estimated error due to higher-order corrections in the chiral expansion from Ref. [27].

There have been no new measurements of the pion leptonic decay rate since the review of Ref. [28]. The sum of branching fractions for $\pi^- \rightarrow \mu^- \bar{\nu}$ and $\pi^- \rightarrow \mu^- \bar{\nu} \gamma$ is 99.98770(4)% [23]. Together with the lifetime 26.033(5) ns [23] this implies $\Gamma(\pi^- \rightarrow \mu^- \bar{\nu}[\gamma]) = 3.8408(7) \times 10^7 \text{ s}^{-1}$. We then subtract the estimated radiative correction factor δ_π in Eq. (72.4) to obtain the purely leptonic rate $\Gamma^{(0)}(\pi^- \rightarrow \mu^- \bar{\nu})$. Using this rate and the masses from the 2014 PDG review [23] in Eq. (72.1) gives

$$f_{\pi+}|V_{ud}| = (127.13 \pm 0.02 \pm 0.13) \text{ MeV}, \quad (72.6)$$

where the errors are from the experimental rate measurement and the radiative correction factor, respectively.

The uncertainty on $f_{\pi-}|V_{ud}|$ is dominated by that from the theoretical estimate of the hadronic structure-dependent radiative corrections. The first direct lattice-QCD calculation of the radiative corrections to the pion and kaon leptonic decay rates was performed by the RM123-Soton Collaboration [11]. The results for both $\delta_\pi = 0.0153(19)$ and $\delta_K = 0.0088(9)$, which are given in the Gasser-Rusetsky-Scimemi scheme for separating strong and electromagnetic effects [29], are compatible with our chiral-perturbation-theory estimates above and have smaller quoted uncertainties, especially for δ_K . While independent confirmation of these results is needed, they demonstrate a promising approach for reducing the theoretical uncertainties on the pion and kaon leptonic decay rates in the future.

The world average for the $K \rightarrow \mu\nu$ decay rate is obtained from a global fit of several kaon-decay branching ratios and lifetime measurements, and was last updated by the FlaviaNet Working Group on Kaon Decays in 2014 [40]. Thus, the radiation-inclusive branching ratio $\mathcal{B}(K^+ \rightarrow \mu^+ \nu[\gamma]) = 63.58(11)\%$ and lifetime $\tau_{K^\pm} = 12.384(15) \text{ ns}$ are unchanged from our previous review. These measurements imply $\Gamma(K^+ \rightarrow \mu^+ \nu[\gamma]) = 5.134(11) \times 10^7 \text{ s}^{-1}$. As before, we subtract δ_K in Eq. (72.4) from the radiation-inclusive decay width to obtain $\Gamma^{(0)}(K^+ \rightarrow \mu^+ \nu)$. We then use Eq. (72.1) to obtain

$$f_{K+}|V_{us}| = (35.09 \pm 0.04 \pm 0.04) \text{ MeV}, \quad (72.7)$$

where the errors are from the experimental rate measurement and the radiative correction factor, respectively.

Short-distance radiative corrections cancel in the ratio of pion-to-kaon decay rates [41]:

$$\frac{\Gamma_{K\ell 2[\gamma]}}{\Gamma_{\pi\ell 2[\gamma]}} = \frac{|V_{us}|^2 f_{K-}^2}{|V_{ud}|^2 f_{\pi-}^2} \frac{m_K(1 - m_\ell^2/m_K^2)^2}{m_\pi(1 - m_\ell^2/m_\pi^2)^2} (1 + \delta_{K/\pi}), \quad (72.8)$$

where $\delta_{K/\pi}$ is given in Eq. (72.5). The left-hand side of Eq. (72.8) is 1.3367(28), which implies

$$\frac{|V_{us}|f_{K+}}{|V_{ud}|f_{\pi+}} = 0.27599 \pm 0.00029 \pm 0.00024, \quad (72.9)$$

where the first uncertainty is from the branching fractions and the second is from $\delta_{K/\pi}$. Here, the estimated error on the hadronic structure-dependent radiative corrections is commensurate with the experimental error.

In summary, the main experimental results pertaining to charged pion and kaon leptonic decays are

$$|V_{ud}|f_{\pi+} = (127.13 \pm 0.02 \pm 0.13) \text{ MeV}, \quad (72.10)$$

$$|V_{us}|f_{K+} = (35.09 \pm 0.04 \pm 0.04) \text{ MeV}, \quad (72.11)$$

$$\frac{|V_{us}|f_{K+}}{|V_{ud}|f_{\pi+}} = 0.27599 \pm 0.00029 \pm 0.00024, \quad (72.12)$$

where the errors are from the experimental uncertainties in the branching fractions and the theoretical uncertainties in the radiative correction factors δ_P , respectively. All of these values are the same as in our earlier reviews [1, 28, 42].

Table 72.1: Recent published lattice-QCD results for f_{π^+} , f_{K^+} , and their ratio. The upper and lower panels show $(2+1+1)$ -flavor and $(2+1)$ -flavor determinations, respectively. When two errors are shown, they are statistical and systematic, respectively. Results for f_{π} and f_K in the isospin symmetric limit $m_u = m_d$ are noted with a †; they are corrected for isospin breaking via Eq. (72.13) before computing the averages. The 2+1+1 FLAG 21 averages are dominated by the Fermilab/MILC values.

Reference	N_f	f_{π^+} (MeV)	f_{K^+} (MeV)	f_{K^+}/f_{π^+}
CalLat 20 [30]	2+1+1	–	–	1.1942(32)(31)
Fermilab/MILC 17 [31] *	2+1+1	–	–	1.1950(15)($^{+6}_{-18}$)
ETM 14 [32] *	2+1+1	–	154.4(1.5)(1.3)	1.184(12)(11)
Fermilab/MILC 14 [10] * †	2+1+1	–	155.92(13)($^{+42}_{-34}$)	1.1956(10)($^{+26}_{-18}$) † ‡
HPQCD 13 [33] *	2+1+1	–	155.37(20)(27)	1.1916(15)(16)
FLAG 21 average [2]	2+1+1	–	155.7(3)	1.1932(21)
QCDSF/UKQCD 16 [34]	2+1	–	–	1.190(10)(13)
BMW 16 [35]	2+1	–	–	1.178(10)(26)
RBC/UKQCD 14 [36]‡	2+1	130.19(89)	155.51(83)	1.1945(45)
MILC 10 [37]	2+1	129.2(0.4)(1.4)	156.1(4)($^{+6}_{-9}$)	1.197(2)($^{+3}_{-7}$)
BMW 10 [38]‡	2+1	–	–	1.192(7)(6)
HPQCD/UKQCD 07 [39]‡	2+1	132(2)	157(2)	1.189(2)(7)
FLAG 21 average [2]	2+1	130.2(8)	155.7(7)	1.1917(37)

*PDG 2014 value of $f_{\pi^+} = 130.41(21)$ MeV used to set absolute lattice scale.

†Superseded by f_{K^+}/f_{π^+} from Fermilab/MILC 17.

72.2.2 Theoretical decay-constant calculations

Table 72.1 presents recent published results for the charged pion and kaon decay constants and their ratio from numerical lattice-QCD calculations with three ($N_f = 2+1$) or four flavors ($N_f = 2+1+1$) of dynamical quarks. The uncertainties on both the individual decay constants and their ratio are at the sub-percent level. The $SU(3)$ -breaking ratio f_{K^+}/f_{π^+} can be obtained with especially small errors because statistical errors associated with the Monte Carlo calculations are correlated between the numerator and denominator, as are some systematics. The results in Table 72.1 were obtained using several independent sets of gauge-field configurations, and a variety of lattice fermion actions that are sensitive to different systematic uncertainties.² Thus, the good agreement between them indicates that the lattice-QCD uncertainties are controlled and the associated error estimates are reliable.³

Table 72.1 also shows the three- and four-flavor averages for the pion and kaon decay constants and their ratio from the FLAG 21 review [2] in the lines labeled “FLAG 21 average.” There is no four-flavor average for the pion decay constant in Table 72.1 because all of the four-flavor calculations use the quantity $f_{\pi^+} = 130.41(20)$ MeV [23] as an input to fix the absolute lattice scale needed to convert from lattice-spacing units to GeV [10, 32, 33].

All of the results in Table 72.1 were obtained using isospin-symmetric gauge-field configurations, *i.e.*, the dynamical up and down quarks have the same mass. Fortunately, however, the dominant effect of strong-isospin breaking is easily included in lattice-QCD calculations as follows. Because the up-down mass difference $\Delta m_{ud} \equiv (m_u - m_d) \sim -2.5$ MeV [3, 48] is much less than typical hadronic scales, the strong-isospin breaking corrections to physical observables can systematically be expanded in the small parameter $\delta m_{ud} \equiv \Delta m_{ud}/\Lambda_{\text{QCD}}$. The leading strong-isospin-breaking corrections to pseudoscalar-meson decay constants arise from the light *valence* quarks in the initial- and final-state hadrons. (See, *e.g.*, the discussion in Ref. [49], for a detailed discussion of isospin-breaking effects in pion and kaon observables.) Thus, to include the effect of nondegenerate up- and down-quark masses, most recent lattice-QCD calculations of f_{π^+} and f_{K^+} evaluate the masses

of the valence quarks in the pion at the physical m_u and m_d , and the mass of the valence light quark in the kaon at the physical m_u . This procedure yields a correction to the kaon decay constant below 0.5%. Consequently, strong-isospin breaking corrections from the light sea-quark masses — which are suppressed by an additional power of δm_{ud} — can be neglected given present uncertainties.

Some earlier lattice-QCD calculations, however, only provide the decay constants and their ratio in the $SU(2)$ isospin-symmetric limit [36, 38, 39]. The Flavour Lattice Averaging Group corrects these results for strong-isospin breaking using chiral perturbation theory before including them in the averages. The leading strong-isospin-breaking corrections to the pion and kaon decay constants in χ PT can be parametrized as [27, 50]

$$f_{\pi^+} = f_{\pi}, \quad f_{K^+} = f_K \sqrt{1 + \delta_{\text{SU}(2)}}, \quad (72.13)$$

where f_{π} and f_K denote the values of the decay constants in the isospin-symmetric limit. The pion decay constant does not receive corrections linear in $m_u - m_d$ because of the G -parity symmetry of the pion triplet, so at first order the δm_{ud} expansion, strong-isospin breaking corrections are characterized by a single parameter, $\delta_{\text{SU}(2)}$. Next-to-leading order χ PT yields numerical values for $\delta_{\text{SU}(2)}$ of approximately -0.004 . Recent direct lattice-QCD calculations of $\delta_{\text{SU}(2)}$ give larger values of around -0.005 to -0.008 [11, 31–33, 49, 51], but further studies are needed. Thus, to be conservative, FLAG includes an uncertainty of 100% on the χ PT estimate for $\delta_{\text{SU}(2)}$ when correcting those decay-constant values that are quoted in the isospin-symmetric limit.

The errors on the decay-constant results in Table 72.1 obtained from $(2+1)$ -flavor lattice-QCD calculations do not include an estimate of the systematic uncertainty from the omission of charm sea quarks in the calculation. Consequently, when the uncertainty on the $(2+1+1)$ -flavor FLAG average is comparable to or better than that on the $(2+1)$ -flavor FLAG average, we simply use the four-flavor average as our preferred value. This is not possible, however, for the pion decay constant. To account for this, we first estimate the systematic uncertainty on pseudoscalar-meson decay constants associated with the omission of charm sea quarks. We then add this estimate in quadrature to the quoted error on the $(2+1)$ -flavor FLAG average for f_{π^+} to obtain our preferred value.

The error introduced by omitting charm sea quarks can be roughly estimated by expanding the charm-quark determinant in powers of $1/m_c$ [58]; the resulting leading contribution is of order $\alpha_s (\Lambda_{\text{QCD}}/2m_c)^2$ [59]. Taking the $\overline{\text{MS}}$ values $\overline{m}_c(\overline{m}_c) =$

²See the PDG mini-review on “Lattice Quantum Chromodynamics” [43, 44] for a general review of numerical lattice-QCD calculations. Details on the different methods used in modern lattice-QCD calculations are provided in Appendix A of the FLAG “Review[s] of lattice results concerning low energy particle physics” [2, 3, 45, 46].

³See the review by Kronfeld [47] for a summary of the large body of evidence validating the methods employed in modern lattice-QCD calculations.

Table 72.2: Experimental results for $\mathcal{B}(D^+ \rightarrow \mu^+\nu[\gamma])$, $\mathcal{B}(D^+ \rightarrow \tau^+\nu[\gamma])$, and $|V_{cd}|f_{D^+}$. The systematic errors on the inferred values of $|V_{cd}|f_{D^+}$ include those from the D^+ lifetime and mass. The error from radiative corrections is only included in the entries labeled “our average.” In the second CLEO line the τ^+ decays to $\mu^+\nu_\mu\bar{\nu}_\tau$.

Experiment	Mode	\mathcal{B}	$ V_{cd} f_{D^+}$ (MeV)
CLEO-c [52, 53]	$\mu^+\nu$	$(3.93 \pm 0.35 \pm 0.09) \times 10^{-4}$	$46.70 \pm 2.10 \pm 0.55$
CLEO-c [52, 53]	$\mu^+\nu + \tau^+\nu$	$(3.82 \pm 0.32 \pm 0.09) \times 10^{-4}$	$46.00 \pm 1.91 \pm 0.56$
BESIII [54]	$\mu^+\nu$	$(3.71 \pm 0.19 \pm 0.06) \times 10^{-4}$	$45.33 \pm 1.17 \pm 0.38$
Our average	Lines 2+3	$(3.74 \pm 0.17) \times 10^{-4}$	45.50 ± 1.22
CLEO-c [55, 56]	$\tau^+\nu$ ($\pi^+\bar{\nu}$)	$< 1.2 \times 10^{-3}$	
BESIII [57]	$\tau^+\nu$ ($\pi^+\bar{\nu}$)	$(1.20 \pm 0.24 \pm 0.12) \times 10^{-3}$	49.95 ± 2.48
Our average	$\mu^+\nu + \tau^+\nu$		46.17 ± 1.16

1.275 GeV, $\bar{\Lambda}_{\text{QCD}} \sim 340$ MeV from FLAG [45], and $\bar{\alpha}(\bar{m}_c) \sim 0.4$, leads to an estimate of about 0.7% for the contribution to the decay constants from charm sea quarks. We can compare this power-counting estimate of charm sea-quark contributions with the observed differences between the (2+1)- and (2+1+1)-flavor lattice-QCD averages for kaon, $D_{(s)}$ -meson, and $B_{(s)}$ -decay constants in Tables 72.1, 72.4, and 72.6. Looking at Table 72.1, the three- and four-flavor averages for f_{K^+} agree to much better than our simple power-counting estimate. Inspection of Tables 72.4 and 72.6 shows, however, that charm sea-quark effects of this size are still allowed for both $D_{(s)}$ -meson and $B_{(s)}$ -meson decay constants.

Our final preferred theoretical values for the charged pion and kaon decay constants are

$$f_{\pi^+} = 130.2(1.2) \text{ MeV}, \quad f_{K^+} = 155.7(3) \text{ MeV}, \quad \frac{f_{K^+}}{f_{\pi^+}} = 1.193(2), \quad (72.14)$$

where f_{K^+} and f_{K^+}/f_{π^+} are simply the four-flavor FLAG 2021 averages [2], and f_{π^+} is the three-flavor flavor FLAG 2021 average with the error increased by the estimated 0.7% charm sea-quark contribution.

72.3 Charmed mesons

72.3.1 Experimental rate measurements

Measurements have been made of the branching fractions for D^+ and D_s^+ mesons decaying to both $\mu^+\nu$ and $\tau^+\nu$ final states. The CLEO-c and BESIII experiments have made measurements of D^+ decays using e^+e^- collisions at the $\psi(3770)$ resonant energy where D^-D^+ pairs are copiously produced. They fully reconstruct one of the D mesons; for concreteness, we will take this to be the D^- . Counting the number of these events provides the normalization for the branching fraction measurement. The experimental analyses then proceed by identifying a candidate μ^+ and forming the missing-mass squared, $MM^2 = (E_{\text{CM}} - E_{D^-})^2 - (\vec{p}_{\text{CM}} - \vec{p}_{D^-} - \vec{p}_{\mu^+})^2$, where E_{CM} and p_{CM} are the center-of-mass energy (which is known) and momentum (which equals zero in e^+e^- collisions). A peak at zero MM^2 implies the existence of a missing neutrino, and hence the $\mu^+\nu$ decay of the D^+ . CLEO-c does not explicitly identify the muon, so their data consists of a combination of $\mu^+\nu$ and $\tau^+\nu$, $\tau^+ \rightarrow \pi^+\nu$ events. This permits them to do two fits: in one they fit for the individual components, and in the other they fix the ratio of $\tau^+\nu/\mu^+\nu$ events to be that given by the standard-model expectation. Thus, the former measurement should be used for new-physics searches, and the latter for standard-model predictions. Our average uses the fixed-ratio value.

Table 72.2 shows the available measurements of $D^+ \rightarrow \mu^+\nu$, an upper limit on $D^+ \rightarrow \tau^+\nu$ from CLEO-c, and the first measurement of this decay from BESIII. Here there is no change since the previous review [1].

To extract the values of $|V_{cd}|f_{D^+}$ via Eq. (72.1), we use values of $m_{D^+} = 1.86961$ GeV and the well-measured D^+ lifetime of 1.040(7) ps [42], and apply radiative corrections as described below. For calculating the average $\mu^+\nu$ number, we use the CLEO-c result from $\mu^+\nu + \tau^+\nu$.

To obtain the purely leptonic rates $\Gamma^{(0)}(D^+ \rightarrow \mu^+(\tau^+)\nu)$, we

subtract the radiative contributions as in Sec. 72.2.1, but use numerical values for the corrections appropriate for D mesons. First, we reduce both the $\mu^+\nu$ and $\tau^+\nu$ branching fractions in Table 72.2 by 1.8%, which is the universal short-distance electroweak contribution of Sirlin [4] evaluated using the D -meson mass for the factorization scale. We do not adjust the experimental rates by the universal long-distance correction [5]. This is because QED bremsstrahlung contributions have already been subtracted at leading-log order from the measurements in Table 72.2 using Monte-Carlo estimates computed with PHOTOS [12]. The $\mu^+\nu$ rates should also be reduced by the 1% estimate of the structure-dependent contributions from Dobrescu and Kronfeld [17]. This correction accounts for tree-level radiative processes in which the D meson decays into a real photon and an off-shell vector meson, which subsequently decays weakly to a charged lepton and neutrino. It is estimated using Eq. (12) of Burdman *et al.* [7] with the CLEO-c cut on the photon energy from Ref. [70], which is typical of all the measurements. We do not need to apply the structure-dependent correction to the $\mu^+\nu$ branching fractions in Table 72.2, however, because the experiments have already included it in their quoted results. Therefore, in summary, we reduce both the $D^+ \rightarrow \mu^+\nu$ and the $D^+ \rightarrow \tau^+\nu$ rates by 1.8% to account for radiative corrections. It is worth noting, however, that the universal long-distance electromagnetic contribution estimated for point-like charged mesons by Kinoshita [5], which we are not including because IB contributions are already subtracted from the measurements via PHOTOS, would *increase* both rates by about 2.5%.

We now discuss the D_s^+ decay process. Since our previous review [1] there have been several results from BESIII. Measurements of D_s^+ leptonic decay branching fractions by several groups are listed in Table 72.3. We exclude older values obtained by normalizing to D_s^+ decay modes that are not well-defined. Many measurements, for example, used the $\phi\pi^+$ mode. This decay is a subset of the $D_s^+ \rightarrow K^+K^-\pi^+$ channel which has interferences from other modes populating the K^+K^- mass region near the ϕ , the most prominent of which is the $f_0(980)$. Thus, the extraction of the effective $\phi\pi^+$ rate is sensitive to the mass resolution of the experiment and the cuts used to define the ϕ mass region [71].⁴

To find D_s decays in the $\mu^+\nu$ signal channels, the experiments rely on fully reconstructing all of the final state particles except for the neutrino and use a missing-mass technique to infer the existence of the neutrino. CLEO and BESIII use $e^+e^- \rightarrow D_s D_s^*$ collisions at 4170 MeV, while BaBar and Belle use $e^+e^- \rightarrow DK n \pi D_s^*$ collisions at energies near the $\Upsilon(4S)$. CLEO and BESIII do a similar analysis as was done for the D^+ above. BaBar and Belle do a similar MM^2 calculation by using the reconstructed hadrons, the photon from the D_s^{*+} decay and a detected μ^+ . To get the normalization they do a MM^2 fit without the μ^+ and use the signal at the D_s^+ mass squared to determine the total D_s^+ yield.

When selecting the $\tau^+ \rightarrow \pi^+\bar{\nu}$ and $\tau^+ \rightarrow \rho^+\bar{\nu}$ decay modes, CLEO uses both the calculation of the missing-mass and the fact that there should be no extra energy in the event beyond that

⁴We have not included the BaBar result for $\mathcal{B}(D_s^+ \rightarrow \mu^+\nu)$ reported in Ref. [72] because this measurement determined the ratio of the leptonic decay rate to the hadronic decay rate $\Gamma(D_s^+ \rightarrow \ell^+\nu)/\Gamma(D_s^+ \rightarrow \phi\pi^+)$.

Table 72.3: Experimental results for $\mathcal{B}(D_s^+ \rightarrow \mu^+ \nu[\gamma])$, $\mathcal{B}(D_s^+ \rightarrow \tau^+ \nu[\gamma])$, and $|V_{cs}|f_{D_s^+}$. The systematic errors on the inferred values of $|V_{cs}|f_{D_s^+}$ include those from the D_s^+ lifetime and mass. The entries labeled “our average” take into account correlations between systematic errors common to the experiments, and also include errors from radiative corrections.

Experiment	Mode	$\mathcal{B}(\%)$	$ V_{cs} f_{D_s^+}$ (MeV)
CLEO-c [55, 56]	$\mu^+ \nu$	$0.565 \pm 0.045 \pm 0.017$	$247.6 \pm 9.9 \pm 4.1$
BaBar* [61]	$\mu^+ \nu$	$0.602 \pm 0.038 \pm 0.034$	$254.3 \pm 8.0 \pm 7.4$
Belle [62]	$\mu^+ \nu$	$0.531 \pm 0.028 \pm 0.020$	$238.8 \pm 6.3 \pm 4.8$
BESIII [63]	$\mu^+ \nu$	$0.517 \pm 0.075 \pm 0.021$	$238.9 \pm 17.3 \pm 4.9$
BESIII [64]	$\mu^+ \nu$	$0.535 \pm 0.013 \pm 0.016$	$240.9 \pm 2.9 \pm 4.0$
Our average	$\mu^+ \nu$	0.543 ± 0.017	242.6 ± 4.0
CLEO-c [55, 56]	$\tau^+ \nu (\pi^+ \bar{\nu})$	$6.42 \pm 0.81 \pm 0.18$	$267.3 \pm 16.9 \pm 4.2$
CLEO-c [65]	$\tau^+ \nu (\rho^+ \bar{\nu})$	$5.52 \pm 0.57 \pm 0.21$	$247.9 \pm 12.8 \pm 5.0$
CLEO-c [66, 67]	$\tau^+ \nu (e^+ \nu \bar{\nu})$	$5.30 \pm 0.47 \pm 0.22$	$242.9 \pm 10.8 \pm 5.3$
BaBar [61]	$\tau^+ \nu (e^+ (\mu^+) \nu \bar{\nu})$	$5.00 \pm 0.35 \pm 0.49$	$236.9 \pm 8.3 \pm 11.7$
Belle [62]	$\tau^+ \nu (\pi^+ \bar{\nu})$	$6.04 \pm 0.43^{+0.46}_{-0.40}$	$260.3 \pm 9.3^{+10.1}_{-8.8}$
Belle [62]	$\tau^+ \nu (e^+ \nu \bar{\nu})$	$5.37 \pm 0.33^{+0.35}_{-0.31}$	$244.5 \pm 7.5^{+8.2}_{-7.4}$
Belle [62]	$\tau^+ \nu (\mu^+ \nu \bar{\nu})$	$5.86 \pm 0.37^{+0.34}_{-0.59}$	$255.4 \pm 8.0^{+7.6}_{-13.1}$
BESIII [63]	$\tau^+ \nu (\pi^+ \bar{\nu})$	$3.28 \pm 1.83 \pm 0.37$	$193 \pm 54 \pm 11$
BESIII [64]	$\tau^+ \nu (\pi^+ \bar{\nu})$	$5.21 \pm 0.25 \pm 0.17$	$240.8 \pm 5.8 \pm 4.3$
BESIII [68]	$\tau^+ \nu (e^+ \nu_e \bar{\nu})$	$5.27 \pm 0.10 \pm 0.12$	$242.2 \pm 2.3 \pm 3.2$
BESIII [69]	$\tau^+ \nu (\pi^+ \pi^0 \bar{\nu})$	$5.29 \pm 0.25 \pm 0.20$	$242.7 \pm 5.7 \pm 4.0$
Our average	$\tau^+ \nu$	5.33 ± 0.13	244.0 ± 3.1
Our average	$\mu^+ \nu + \tau^+ \nu$		243.5 ± 2.7

*We do not use a previous unpublished BaBar result from a subsample of data that uses a different technique for obtaining the branching fraction normalization [60].

deposited by the measured tagged D_s^- and the τ^+ decay products. The $\tau^+ \rightarrow e^+ \nu \bar{\nu}$ mode, however, uses only extra energy. BaBar and Belle also use the extra energy to discriminate signal from background in their τ^+ measurements. BESIII uses $\tau^+ \rightarrow \pi^+ \bar{\nu}$ decays, where they calculate the MM^2 and discriminate against μ^+ from $D_s^+ \rightarrow \mu^+ \nu$ decays, and more recently $\tau^+ \rightarrow e^+ \nu \bar{\nu}$ and $\tau^+ \rightarrow \pi^+ \pi^0 \bar{\nu}$ decays.

When extracting $|V_{cs}|f_{D_s^+}$ via Eq. (72.1), we first apply the -1.8% universal electroweak correction [4] to all of the $\mu^+ \nu$ and $\tau^+ \nu$ branching fractions in Table 72.3; this is the same as for D^+ mesons. We also decrease the BaBar and Belle $\mu^+ \nu$ branching fractions by the 1% structure-dependent correction [17]. This correction was already included in CLEO and BESIII results for the $\mu^+ \nu$ branching fractions in Table 72.3. We use the masses and lifetimes $m_{D_s^+} = 1.96834(7)$ GeV, $m_{\tau^+} = 1.77686(12)$ GeV, and $\tau_{D_s^+} = 0.504(4)$ ps [42]. The inferred values for $f_{D_s^+}|V_{cs}|$ are in good agreement for the $\mu^+ \nu$ and $\tau^+ \nu$ decay modes.

It is clear from the discussion of radiative corrections in this section that they are less well understood theoretically for D^+ and D_s^+ meson decays than for pions and kaons. We therefore assign a 1.4% systematic uncertainty to the purely leptonic decay rates, which is half the size of the applied radiative corrections. This translates to a 0.7% error on the products of the decay constant times CKM matrix element. Putting everything together, the main experimental results pertaining to charmed meson leptonic decays are (see the bottom lines of Tables 72.2 and 72.3):

$$|V_{cd}|f_{D^+} = 46.17 \pm 1.11 \pm 0.32 = 46.17 \pm 1.16 \text{ MeV} \quad (72.15)$$

$$|V_{cs}|f_{D_s^+} = 243.5 \pm 2.1 \pm 1.7 = 243.5 \pm 2.7 \text{ MeV}, \quad (72.16)$$

where the errors are from the measured branching fractions and the applied radiative corrections, respectively.

72.3.2 Theoretical decay-constant calculations

Table 72.4 presents recent theoretical calculations of charmed heavy-light meson decay constants and their ratio in the isospin-symmetric limit $m_u = m_d$. (As in Sec. 72.2.2, we denote the physical D^+ -meson decay constant by f_{D^+} , and use f_D for the

isospin-symmetric value.) The upper two panels show results from lattice-QCD calculations with three ($N_f = 2 + 1$) or four flavors ($N_f = 2 + 1 + 1$) of dynamical quarks. Although there are fewer available results than for the pion and kaon sector, both f_D and f_{D_s} have been obtained using multiple sets of gauge-field configurations with different lattice fermion actions, providing independent confirmation. For comparison, the bottom panel of Table 72.4 shows QCD-model calculations of the D^- and D_s^- -meson decay constants for which uncertainty estimates are provided. The lattice and non-lattice results agree, but numerical lattice-QCD calculations have now reached significantly greater precision than other approaches. There are no new results quoted from FLAG 21 [2] compared with those in our previous review [1] quoted from FLAG 19 [3].

The lattice-QCD decay-constant results in Table 72.4 were all obtained using isospin-symmetric gauge-field configurations. As discussed in Sec. 72.2.2, however, the leading strong-isospin breaking corrections to heavy-light pseudoscalar-meson decay constants can be accounted for by using the physical down (or up) quark in the D (or B) meson. Strong-isospin breaking corrections to heavy-strange meson decay constants are roughly an order-of-magnitude smaller because there are no light valence quarks involved. Recently, the Fermilab Lattice and MILC Collaborations used this approach to calculate directly the dominant strong-isospin breaking corrections to both f_D and f_B , finding [31]

$$\begin{aligned} f_{D^+} - f_D &= 0.58(1)_{\text{stat}}(7)_{\text{syst}}(1)_{\text{EM scheme}} \text{ MeV}, \\ f_{B^+} - f_B &= -0.53(5)_{\text{stat}}(7)_{\text{syst}}(0)_{\text{EM scheme}} \text{ MeV}. \end{aligned} \quad (72.17)$$

These results agree with independent estimates of the strong-isospin-breaking corrections to heavy-light meson decay constants from Borelized sum rules [85]. Combined with the determinations of f_D and f_B from the same work, Eq. (72.17) implies that the corrections to the SU(3)-flavor breaking ratios are

$$\frac{f_{D_s}}{f_{D^+}} = \frac{f_{D_s}}{f_D} (1 - 0.0027(3)), \quad \frac{f_{B_s}}{f_{B^+}} = \frac{f_{B_s}}{f_B} (1 + 0.0028(5)). \quad (72.18)$$

These estimated strong-isospin-breaking corrections to f_D and f_{D_s}/f_D above are commensurate with the uncertainties on the

Table 72.4: Recent theoretical determinations of f_D , f_{D_s} , and their ratio in the isospin-symmetric limit. The upper panels show results from lattice-QCD calculations with $(2+1+1)$ and $(2+1)$ dynamical quark flavors, respectively. Statistical and systematic errors are quoted separately. The bottom panel shows estimates from QCD sum rules (QCD SR) and the light-front quark model (LFQM). These are not used to obtain our preferred decay-constant values. The $2+1+1$ averages are dominated by the Fermilab/MILC values.

Reference	Method	N_f	f_D (MeV)	f_{D_s} (MeV)	f_{D_s}/f_D
Fermilab/MILC 17 [31]	LQCD	2+1+1	212.1(0.3)(0.5)	249.9(0.3)(0.3)	1.1782(06)(15)*
ETM 14 [32]	LQCD	2+1+1	207.4(3.7)(0.9)	247.2(3.9)(1.4)	1.192(19)(11)
FLAG 21 average [2]	LQCD	2+1+1	212.0(0.7)	249.9(0.5)	1.1783(16)
χ QCD 20A [73]	LQCD	2+1	213(5)	249(7)	1.16(3)
RBC/UKQCD 18A [74] [†]	LQCD	2+1	–	–	1.1740(51)(68)
RBC/UKQCD 17 [75]	LQCD	2+1	208.7(2.8)(^{+2.1} _{-1.8})	246.4(1.3)(^{+1.3} _{-1.9})	1.1667(77)(⁺⁵⁷ ₋₄₃)
χ QCD 14 [76]	LQCD	2+1	–	254(2)(4)	–
HPQCD 12 [77]	LQCD	2+1	208.3(1.0)(3.3)	–	1.187(4)(12)
Fermilab/MILC 11 [78]	LQCD	2+1	218.9(9.2)(6.6)	260.1(8.9)(6.1)	1.188(14)(21)
HPQCD 10 [79]	LQCD	2+1	–	248.0(1.4)(2.1)	–
FLAG 21 average [2]	LQCD	2+1	209.0(2.4)	248.0(1.6)	1.174(7)
Pullin 21 [80]	QCD SR	–	190(15)	226(17)	1.19(7)
Wang 15 [81] [‡]	QCD SR	–	208(10)	240(10)	1.15(6)
Gelhausen 13 [82]	QCD SR	–	201(⁺¹² ₋₁₃)	238(⁺¹³ ₋₂₃)	1.15(^{+0.04} _{-0.05})
Narison 12 [83]	QCD SR	–	204(6)	246(6)	1.21(4)
Lucha 11 [84]	QCD SR	–	206.2(8.9)	245.3(16.3)	1.193(26)

*Ref. [31] provides values for f_D and f_{D_s} in the isospin-symmetric limit, but not for their ratio. Here we infer the central value from those of the individual decay constants, and take the statistical and systematic errors to be the same as for the physical ratio f_{D_s}/f_{D^+} .

[†]Slight difference from preliminary value quoted in 2019 FLAG review.

[‡]Obtained using $m_c^{\overline{\text{MS}}}$; results using m_c^{pole} are also given in the paper.

$(2+1+1)$ -flavor FLAG averages in Table 72.4. Consequently, it is important to account for isospin-breaking effects before combining the theoretical decay constants with the corresponding experimental decay rates.

To obtain the charged D^+ -meson decay constant, we apply the correction in Eq. (72.17) to the $(2+1+1)$ -flavor 2021 FLAG average for the D -meson decay constant in the isospin-symmetric limit. Similarly we use Eq. (72.18) to correct the $(2+1+1)$ -flavor 2021 FLAG average for f_{D_s}/f_D . We take the four-flavor FLAG 2021 average for f_{D_s} directly. Our final preferred theoretical values for the charmed pseudoscalar-meson decay constants are

$$\begin{aligned}
 f_{D^+} &= 212.0(7) \text{ MeV}, \\
 f_{D_s} &= 249.9(5) \text{ MeV}, \\
 \frac{f_{D_s}}{f_{D^+}} &= 1.1783(16).
 \end{aligned}
 \tag{72.19}$$

72.4 Bottom mesons

72.4.1 Experimental rate measurements

The Belle and BaBar collaborations have found evidence for $B^- \rightarrow \tau^- \bar{\nu}$ decay in $e^+e^- \rightarrow B^-B^+$ collisions at the $\Upsilon(4S)$ energy. The analysis relies on reconstructing a hadronic or semileptonic B decay tag, finding a τ candidate in the remaining track and photon candidates, and examining the extra energy in the event which should be close to zero for a real τ^- decay to $e^- \bar{\nu}$ or $\mu^- \bar{\nu}$ opposite a B^+ tag. While the BaBar results have remained unchanged, Belle reanalyzed both samples of their data. The branching fraction using hadronic tags changed from $1.79^{+0.56+0.46}_{-0.49-0.51} \times 10^{-4}$ (2006) [86] to $0.72^{+0.27}_{-0.25} \pm 0.11 \times 10^{-4}$ (2012) [87], while the corresponding change using semileptonic tags was from $1.54^{+0.38+0.29}_{-0.37-0.31}$ to $1.25 \pm 0.28 \pm 0.27$. These changes demonstrate the difficulty of the analysis. The results are listed in Table 72.5. These are unchanged since the previous review [1].

Because there are large backgrounds under the signals for these measurements, as well as substantial systematic errors, the significances of the individual results are still below the 5σ discovery threshold. Belle quotes 4.6σ for their combined hadronic and semileptonic tags, while BaBar quotes 3.3σ and 2.3σ , for hadronic and semileptonic tags. Greater precision is necessary to determine if any effects beyond the standard model are present.

We do not correct the measured branching ratios in Table 72.5 for radiative corrections because the experimental uncertainties

Table 72.5: Experimental results for $\mathcal{B}(B^- \rightarrow \tau^- \bar{\nu})$ and $|V_{ub}|f_{B^+}$. To extract the values of $|V_{ub}|f_{B^+}$ via Eq. (72.1), we use the PDG 2018 value of the B^+ lifetime of 1.638 ± 0.004 ps, and the τ^+ and B^+ masses of 1.77686 and 5.27933 GeV, respectively.

Experiment	Tag	\mathcal{B} (units of 10^{-4})	$ V_{ub} f_{B^+}$ (MeV)
Belle [87]	Hadronic	$0.72^{+0.27}_{-0.25} \pm 0.11$	
Belle [88]	Semileptonic	$1.25 \pm 0.28 \pm 0.27$	
Belle [88]	Average	0.91 ± 0.22	0.72 ± 0.09
BaBar [89]	Hadronic	$1.83^{+0.53}_{-0.49} \pm 0.24$	
BaBar [90]	Semileptonic	$1.7 \pm 0.8 \pm 0.2$	
BaBar [89]	Average	1.79 ± 0.48	1.01 ± 0.14
Our average		1.06 ± 0.20	0.77 ± 0.07

are so large. The relative radiative corrections are expected to be bigger, however, for $B \rightarrow \mu\nu$ leptonic decays because the corrections are no longer helicity suppressed [9], and may be a significant fraction of the purely leptonic rate. More theoretical work is needed to understand radiative corrections to leptonic B decays in anticipation of future measurements with greater precision, and of new decay channels.

72.4.2 Theoretical decay-constant calculations

Table 72.6 presents recent theoretical calculations of bottom heavy-light meson decay constants and their ratio in the isospin-symmetric limit $m_u = m_d$. The upper two panels show results from lattice-QCD calculations with three ($N_f = 2+1$) or four flavors ($N_f = 2+1+1$) of dynamical quarks. For all decay constants, calculations using different gauge-field configurations, light-quark actions, and b -quark actions provide independent confirmation. For comparison, the bottom panel of Table 72.6 shows QCD-model calculations of the B^- and B_s^- -meson decay constants for which uncertainty estimates are provided. These are consistent with the lattice values, but with much larger uncertainties. This table, based on the FLAG 21 averages [2], reflects the latest update of the FLAG 19 averages [3].

The lattice-QCD decay-constant results in Table 72.6 were all obtained using isospin-symmetric gauge-field configurations. Some calculations, however, account for the dominant effect of strong-isospin-breaking by using the correct value for the va-

Table 72.6: Recent theoretical determinations of f_B , f_{B_s} , and their ratio in the isospin-symmetric limit. The upper panels show results from lattice-QCD calculations with $(2+1+1)$ and $(2+1)$ dynamical quark flavors, respectively. When available, statistical and systematic errors are quoted separately. The bottom panel shows estimates from the relativistic potential model (RPM), QCD sum rules, and the light-front quark model, which are not used to obtain our preferred decay-constant values. The $2+1+1$ FLAG 21 averages are dominated by the Fermilab/MILC values.

Reference	Method	N_f	f_B (MeV)	f_{B_s} (MeV)	f_{B_s}/f_B
Fermilab/MILC 17 [31]	LQCD	2+1+1	189.9(1.4)	230.7(1.2)	1.2146(49)
HPQCD 17 [91]*	LQCD	2+1+1	190(4)	229(5)	1.206(5)
ETM 16 [92]	LQCD	2+1+1	193(6)	229(5)	1.184(25)
HPQCD 13 [93]	LQCD	2+1+1	186(4)	224(5)	1.205(7)
FLAG 21 average [2]	LQCD	2+1+1	190.0(1.3)	230.3(1.3)	1.209(5)
Aoki 14 [94] [†]	LQCD	2+1	218.8(6.5)(30.8)	263.5(4.8)(36.7)	1.193(20)(44)
RBC/UKQCD 14 [95] [‡]	LQCD	2+1	195.6(6.4)(13.3)	235.4(5.2)(11.1)	1.223(14)(70)
HPQCD 12 [96]	LQCD	2+1	191(1)(8)	228(3)(10)	1.188(12)(13)
HPQCD 12 [96]	LQCD	2+1	189(3)(3)*	–	–
HPQCD 11 [97]	LQCD	2+1	–	225(3)(3)	–
Fermilab/MILC 11 [78]	LQCD	2+1	196.9(5.5)(7.0)	242.0(5.1)(8.0)	1.229(13)(23)
FLAG 21 average [2]	LQCD	2+1	192.0(4.3)	228.4(3.7)	1.201(16)
Pullin 21 [80]	QCD SR		192 ⁺²⁰ ₋₁₉	225 ⁺²¹ ₋₂₀	1.17(7)
Sun 16 [98] [§]	RPM		219(15)	266(19)	1.21(9)
Wang 15 [81] [§]	QCD SR		194(15)	231(16)	1.19(10)
Baker 13 [99]	QCD SR		186(14)	222(12)	1.19(4)
Lucha 13 [100]	QCD SR		192.0(14.6)	228.0(19.8)	1.184(24)
Gelhausen 13 [82]	QCD SR		207 ⁽⁺¹⁷⁾ ₍₋₉₎	242 ⁽⁺¹⁷⁾ ₍₋₁₂₎	1.17 ⁽⁺³⁾ ₍₋₄₎
Narison 12 [83]	QCD SR		206(7)	234(5)	1.14(3)

* Average of new HPQCD 17 and previous HPQCD 13 results allowing for correlations between the two sets of results.

[†] Obtained with static b quarks (*i.e.*, $m_b \rightarrow \infty$).

[‡] Ref. [95] does not provide results in the isospin-symmetric limit, so we show f_{B^+} and f_{B_s}/f_{B^+} for this work.

[§] Obtained using $m_b^{\overline{\text{MS}}}$; results using m_b^{pole} are also given in the paper.

lence light-quark mass in the B meson (m_u for f_{B^+} and m_d for f_{B^0}). Early estimates of the strong-isospin-breaking correction obtained $f_{B^+} - f_B \sim -2$ MeV [93, 95], which would be significant given the present lattice-QCD uncertainties. It turns out, however, that these calculations inadvertently introduced a spurious sea-quark contribution, and therefore overestimated the size of the effect. A more recent calculation by the Fermilab/MILC Collaboration finds very little evidence for isospin violation ($f_{B^+} - f_B \sim -0.5$ MeV) [31], which is more than two times smaller than the total uncertainties on present lattice-QCD calculations. For this reason, we quote isospin averages in the current review. Our preferred theoretical values for the bottom pseudoscalar-meson decay constants are

$$\begin{aligned} f_B &= 190.0(1.3) \text{ MeV}, \\ f_{B_s} &= 230.0(1.3) \text{ MeV}, \\ \frac{f_{B_s}}{f_B} &= 1.209(5), \end{aligned} \quad (72.20)$$

which are simply the $N_f = 2+1+1$ FLAG 2021 averages [2]. Because the uncertainties on the three-flavor results in Table 72.6 are substantially larger than those on the four-flavor results, including them in the average leaves the central values unchanged, and decreases the errors only slightly.

72.5 Phenomenological implications

72.5.1 $|V_{ud}|$, $|V_{us}|$, and status of first-row unitarity

Using the average values for $f_{\pi^+}|V_{ud}|$, $f_{K^+}|V_{us}|$, and their ratio from Eqs. (72.10)–(72.12) and for f_{π^+} , f_{K^+} , and their ratio from Eq. (72.14), we obtain the following determinations of the CKM matrix elements $|V_{ud}|$, $|V_{us}|$, and their ratio from leptonic decays within the standard model:

$$\begin{aligned} |V_{ud}| &= 0.9764(2)(90)(10), \quad |V_{us}| = 0.2254(3)(4)(3), \\ \frac{|V_{us}|}{|V_{ud}|} &= 0.2313(2)(4)(2), \end{aligned} \quad (72.21)$$

where the errors are from the experimental branching fraction(s), the pseudoscalar decay constant(s), and radiative corrections, re-

spectively. These results enable a test of the unitarity of the first row of the CKM matrix from leptonic decays alone (the contribution from $|V_{ub}|$ is negligible). Using the values of $|V_{ud}|$ and $|V_{us}|$ from Eq. (72.21), we find

$$|V_{ud}|^2 + |V_{us}|^2 + |V_{ub}|^2 - 1 = 0.004(18), \quad (72.22)$$

which is consistent with three-generation unitarity at the few-percent level.

The determinations of $|V_{ud}|$ and $|V_{us}|$ from leptonic decays in Eq. (72.21) can be compared to those obtained from other processes. The result above for $|V_{ud}|$ agrees with the determination from superallowed β -decay (a previous value of $|V_{ud}| = 0.97420(21)$ [101] has been updated to $|V_{ud}| = 0.97373(31)$ [102]) but has a considerably larger error, primarily due to the uncertainty in the theoretical determination of f_{π^+} .

The CKM element $|V_{us}|$ can be determined from semileptonic $K^+ \rightarrow \pi^0 \ell^+ \nu$ decay. Here experimental measurements provide a value for the product $f_+^K \pi(0)|V_{us}|$, where $f_+^K \pi(0)$ is the form factor at zero four-momentum transfer between the initial state kaon and the final state pion. We quote a recent analysis by Seng *et al.* [103] which finds $|V_{us}|f_+^K \pi(0) = 0.21635(38)(3)$, with the first error denoting experiment and the second reflecting uncertainty in higher order corrections. This is not far from the value 0.2165(4) quoted in our 2020 review [40].⁵ Choosing the 2021 $2+1+1$ -flavor FLAG average for $f_+(0)^{K\pi} = 0.9698(17)$ [2] based on the calculations of ETM [107] and Fermilab/MILC [108] gives $|V_{us}| = 0.22309(40)_{\text{exp}}(39)_{\text{LQCD}}(3)_{\text{HO}}$ from semileptonic decay. The determinations of $|V_{us}|$ from leptonic and semileptonic kaon decays are both quite precise, with comparable errors, from but the central values differ by 2.9σ .

Finally, the combination of the ratio $|V_{us}|/|V_{ud}|$ from leptonic decays [Eq. (72.21)] with $|V_{ud}|$ from β decay implies an alternative determination of $|V_{us}| = 0.2253(5)$ which agrees with the value

⁵This was an update of the 2010 Flavianet review [41] that included new measurements of the K_S lifetime [104, 105], $\text{Re}(\epsilon'/\epsilon)$ [105], and $\mathcal{B}(K^\pm \rightarrow \pi^\pm \pi^+ \pi^-)$ [106]. The latter measurement was the primary source of the reduced error on $\mathcal{B}(\text{semileptonic})$, via the constraint that the sum of all branching ratios must equal unity.

from leptonic kaon decay, but disagrees with the semileptonic-decay result at the 2.9σ level.

Given the roughly 3σ tension between $|V_{us}|$ from leptonic and semileptonic kaon decays, it is important to scrutinize the uncertainties on the theoretical and experimental inputs to $|V_{us}|$ and other elements of the first row of the CKM matrix. Seng *et al.* have introduced a new approach for calculating radiative corrections to neutron and nuclear beta decays using dispersion relations [109–112]. These calculations imply a value of $|V_{ud}| = 0.97395(23)$, consistent with the updated analysis of Ref. [102].

An independent calculation of the radiative corrections by Czarnecki and Marciano using QCD sum rules yields similar results [113]. Using this value of $|V_{ud}|$ with the determination of $|V_{us}|$ from leptonic kaon decays in Eq. (72.21), we obtain $|V_{ud}|^2 + |V_{us}|^2 + |V_{ub}|^2 - 1 = -0.0007(5)$, again consistent with first-row unitarity.

Last, we combine the experimental measurement of $f_{\pi^+}|V_{ud}|$ in Eq. (72.10) with $|V_{ud}|$ from superallowed β -decay [102] to infer an “experimental” value for the pion decay constant:

$$f_{\pi^-}^{\text{“exp”}} = 130.56(2)(3)(13) \text{ MeV}, \quad (72.23)$$

where the uncertainties are from the errors on Γ , $|V_{ud}|$, and higher-order corrections, respectively. Many recent (2+1+1)-flavor lattice-QCD calculations use this quantity to set the overall physical scale in their simulations, *e.g.*, Refs. [10, 31–33]. Conversely, comparing $f_{\pi^-}^{\text{“exp”}}$ with the 2021 FLAG (2+1)-flavor average $f_{\pi^+} = 130.2(8)$ MeV, which only includes lattice-QCD results that employ other observables to set the scale [34–39], provides a test of lattice-QCD methods. The values are in good agreement within present uncertainties. We do not quote an “experimental” value for the kaon decay constant because the value of $|V_{us}|$ is less clear given the $\sim 3\sigma$ tension between the values of $|V_{us}|$ obtained from leptonic and semileptonic kaon decays.

72.5.2 $|V_{cd}|$, $|V_{cs}|$, and status of second-row unitarity

Using the average values for $|V_{cd}|f_{D^+}$ and $|V_{cs}|f_{D_s^+}$ from Eqs. (72.15) and (72.16), and for f_{D^+} and $f_{D_s^+}$ from Eq. (72.19), we obtain the following determinations of the CKM matrix elements $|V_{cd}|$ and $|V_{cs}|$ from leptonic decays within the standard model:

$$|V_{cd}| = 0.2178(53)(15)(7) \quad \text{and} \quad |V_{cs}| = 0.9744(84)(16)(20), \quad (72.24)$$

where the errors are from the measured branching fractions, radiative corrections, and decay constants, respectively. These results enable a test of the unitarity of the second row of the CKM matrix. Taking $V_{cb} = 41.0(1.4) \times 10^{-3}$ [1], we obtain

$$|V_{cd}|^2 + |V_{cs}|^2 + |V_{cb}|^2 - 1 = -0.001(22), \quad (72.25)$$

in agreement with three-generation unitarity.

The uncertainty on $|V_{cd}|$ in Eq. (72.24) is limited by the measurement error on the $D^+ \rightarrow \mu^+\nu$ decay rate. For $|V_{cs}|$, however, the experimental and radiative-correction errors are commensurate. The value of $|V_{cs}|$ from leptonic D_s decays decreased substantially from the value of 1.007(17) in an earlier version of this review [28, 114], and is now below unity as expected in the three-generation CKM framework. This change is due to our more consistent treatment of the radiative corrections, which lower the purely leptonic decay rates for $D_s^+ \rightarrow \mu^+\nu$ and $D_s^+ \rightarrow \tau^+\nu$. We emphasize, however, that we have taken a generous uncertainty on these estimates, and that more theoretical work is needed to really pin down the sizes of the radiative corrections to $D_{(s)}$ -meson leptonic decays.

The CKM matrix elements $|V_{cd}|$ and $|V_{cs}|$ can also be obtained from semileptonic $D^+ \rightarrow \pi^0\ell^+\nu$ and $D_s^+ \rightarrow K^0\ell^+\nu$ decays, respectively. Here experimental measurements determine the product of the form factor times the CKM element, and theory provides the value for the form factor at zero four-momentum transfer between the initial $D_{(s)}$ meson and the final pion or kaon.

The latest experimental averages from the Heavy Flavor Averaging Group (HFLAV) are $f_+^{D^+}(0)|V_{cd}| = 0.1426(19)$ and

$f_+^{D_s^+K}(0)|V_{cs}| = 0.7226(34)$ [115]. There are not enough published lattice-QCD calculations of the zero-momentum $D_{(s)}$ -meson semileptonic form factors with $N_f \geq 3$ to permit an average by the FLAG Collaboration. Taking the most precise three-flavor form-factor results $f_+^{D^+\pi}(0) = 0.666(29)$ and $f_+^{D_s^+K}(0) = 0.747(19)$ from the HPQCD Collaboration [116, 117] gives for the CKM matrix elements $|V_{cd}| = 0.2141(97)$ and $|V_{cs}| = 0.967(25)$, in agreement with those from leptonic decays in Eq. (72.24). A newer, four-flavor calculation of the form factors by the ETM Collaboration [118], however, yields a smaller value of $f_+^{D^+\pi}(0) = 0.612(35)$ by 1.2σ and a larger $f_+^{D_s^+K}(0) = 0.765(31)$ by 0.5σ . These imply $|V_{cd}| = 0.233(14)$ and $|V_{cs}| = 0.945(39)$, which are about 1σ above and below the values from leptonic decays in Eq. (72.24), respectively. Independent lattice-QCD calculations of the $D^+ \rightarrow \pi^0\ell^+\nu$ and $D_s^+ \rightarrow K^0\ell^+\nu$ form factors now in progress [119, 120] will help to clarify the picture. In a lattice QCD study of the decay $D \rightarrow K\ell\nu$, the HPQCD Collaboration [121] reports $|V_{cs}| = 0.9663(80)$.

We can combine the experimental measurements of $f_{D^+}|V_{cd}|$ and $f_{D_s^+}|V_{cs}|$ from Tables 72.2 and 72.3 with $|V_{cd}| = 0.2245(8)$ and $|V_{cs}| = 0.97370(14)$ from the PDG 2020 global unitarity-triangle analysis [1] to infer “experimental” values for the decay constants within the standard model. We take the CKM elements from the global fit because they are based on many input quantities, thereby reducing the sensitivity to any one outlying measurement or calculation. We obtain for the decay constants

$$\begin{aligned} f_{D^+}^{\text{“exp”}} &= 208.9(5.0)(3.8)(1.5) \text{ MeV}, \\ f_{D_s^+}^{\text{“exp”}} &= 246.7(2.1)(2.8)(1.7) \text{ MeV}, \\ (f_{D^+}/f_{D_s^+})^{\text{“exp”}} &= 1.181(30)(25)(12). \end{aligned} \quad (72.26)$$

where the uncertainties are from the errors on $\Gamma^{(0)}$, CKM matrix elements, and radiative corrections, respectively. The “experimental” values f_{D^+} ($f_{D_s^+}/f_{D^+}$) are consistent within 1σ with the (2+1+1)-flavor lattice-QCD averages in Eq. (72.19). The CKM matrix element $|V_{cd}|$ is approximately equal to $|V_{us}|$, as first shown by Wolfenstein [122, 123]. Thus, resolving the inconsistencies between determinations of $|V_{us}|$ from leptonic and semileptonic decays discussed in Sec. 72.5.1 may benefit from the constraints observed here.

Last, we can test lepton-flavor universality in charm meson decays by checking the following relationship derived from Eq. (72.1):

$$\frac{\Gamma(D_s^+ \rightarrow \tau^+\nu)}{\Gamma(D_s^+ \rightarrow \mu^+\nu)} = \frac{m_\tau^2 (1 - m_\tau^2/M_{D_s}^2)^2}{m_\mu^2 (1 - m_\mu^2/M_{D_s}^2)^2} = 9.75, \quad (72.27)$$

where the uncertainties from the masses are negligible to the number of digits quoted. The measured ratio of $\tau^+\nu$ to $\mu^+\nu$ rates is 9.82 ± 0.40 , consistent with this standard-model expectation.

72.5.3 $|V_{ub}|$ and other applications

Using the average value for $|V_{ub}|f_{B^+}$ from Table 72.5, and for f_{B^+} from Eq. (72.20), we obtain the following determination of the CKM matrix element $|V_{ub}|$ from leptonic decays within the standard model:

$$|V_{ub}| = 4.05(37)(3) \times 10^{-3}, \quad (72.28)$$

where the errors are from experiment and theory, respectively. One should bear in mind when interpreting Eq. (72.28) that none of the experimental measurements that enter the average for $|V_{ub}|f_{B^+}$ have individually reached the 5σ discovery level (see Sec. 72.4.1). Further, decays involving the third generation of quarks and leptons may be particularly sensitive to new physics associated with electroweak symmetry breaking due to their larger masses [13, 15], so Eq. (72.28) is more likely to be influenced by new physics than the determinations of the elements of the first and second rows of the CKM matrix in the previous sections.

The CKM element $|V_{ub}|$ can also be obtained from semileptonic B -meson decays. For more than a decade, there has remained a persistent 2- 3σ tension between the determinations of $|V_{ub}|$ from exclusive $B \rightarrow \pi\ell\nu$ decay and from inclusive $B \rightarrow X_u\ell\nu$ decay,

where X_u denotes all hadronic states populated by the $bb \rightarrow u$ weak transition [23, 115, 124–127]. The currently most precise determination of $|V_{ub}|^{\text{excl}} = 3.73(14) \times 10^{-3}$ is obtained from a joint z -fit by FLAG [2] of the vector and scalar form factors $f_+^{B\pi}(q^2)$ and $f_0^{B\pi}(q^2)$ calculated in (2+1)-flavor lattice QCD [128–130] and experimental measurements of the differential decay rate from BaBar [131, 132] and Belle [133, 134]. On the other hand, the PDG 2018 inclusive determination obtained using the theoretical frameworks in Refs. [135–137] is $|V_{ub}|^{\text{incl}} = 4.49(28) \times 10^{-3}$ [42, 138]. The value of $|V_{ub}|$ from leptonic $B \rightarrow \tau\nu$ decay in Eq. (72.28) splits the difference between the inclusive and exclusive determinations, and is compatible (within large uncertainties) with both.

Given the large uncertainties on the experimental measurements of $\mathcal{B}(B^- \rightarrow \tau^-\bar{\nu})$, and the more than 2σ disagreement between $|V_{ub}|$ obtained from inclusive and exclusive semileptonic B decays, we do not present an “experimental” value of the decay constant f_{B^+} .

72.6 Concluding remarks

The increasing precision of measurements of leptonic decays of charged pseudoscalar mesons has begun to require control over radiative corrections at a level superior to that presented here. Improvements will be called for both in theory and in experiment (for example, by BESIII and Belle II).

Unitarity of the CKM matrix is in reasonable shape. However, there is a lingering $\sim 3\sigma$ tension between the values of V_{us} determined by semileptonic and leptonic kaon decays. It will be interesting to follow experimental and theoretical developments on this quantity.

Acknowledgements

I thank R. Briere, C. Davies, S. Gottlieb, S. Hajimoto, A. Kronfeld, H.-L. Ma, W. Marciano, and S. Stone for useful discussions on this review, and S. Gottlieb for providing information on the 2021 FLAG lattice averages.

References

- [1] P. A. Zyla *et al.* (Particle Data Group), PTEP **2020**, 8, 083C01 (2020).
- [2] Y. Aoki *et al.* (Flavour Lattice Averaging Group) (2021).
- [3] S. Aoki *et al.* (Flavour Lattice Averaging Group) (2019), [arXiv:1902.08191].
- [4] A. Sirlin, Nucl. Phys. **B196**, 83 (1982).
- [5] T. Kinoshita, Phys. Rev. Lett. **2**, 477 (1959).
- [6] M. Knecht *et al.*, Eur. Phys. J. **C12**, 469 (2000), [hep-ph/9909284].
- [7] G. Burdman, J. T. Goldman and D. Wyler, Phys. Rev. **D51**, 111 (1995), [hep-ph/9405425].
- [8] V. Cirigliano and I. Rosell, JHEP **10**, 005 (2007), [arXiv:0707.4464].
- [9] D. Becirevic, B. Haas and E. Kou, Phys. Lett. **B681**, 257 (2009), [arXiv:0907.1845].
- [10] A. Bazavov *et al.* (Fermilab Lattice and MILC), Phys. Rev. **D90**, 074509 (2014), [arXiv:1407.3772].
- [11] M. Di Carlo *et al.*, Phys. Rev. **D100**, 034514 (2019), [arXiv:1904.08731].
- [12] E. Barberio and Z. Was, Comput. Phys. Commun. **79**, 291 (1994).
- [13] W.-S. Hou, Phys. Rev. **D48**, 2342 (1993).
- [14] A. G. Akeroyd and S. Recksiegel, Phys. Lett. **B554**, 38 (2003), [hep-ph/0210376].
- [15] A. G. Akeroyd and S. Recksiegel, J. Phys. **G29**, 2311 (2003), [hep-ph/0306037].
- [16] A. G. Akeroyd, Prog. Theor. Phys. **111**, 295 (2004), [hep-ph/0308260].
- [17] B. A. Dobrescu and A. S. Kronfeld, Phys. Rev. Lett. **100**, 241802 (2008), [arXiv:0803.0512].
- [18] J. L. Hewett, in “Heavy flavor physics. Proceedings, LISHEP 95, LAFEX International School on High-Energy Physics, session C, cbt Workshop, Rio de Janeiro, Brazil, February 21–23, 1995,” 171–187 (1995), [hep-ph/9505246], URL <http://www-public.slac.stanford.edu/sciDoc/docMeta.aspx?slacPubNumber=SLAC-PUB-6821>.
- [19] A. Crivellin, Phys. Rev. **D81**, 031301 (2010), [arXiv:0907.2461].
- [20] F. U. Bernlochner, Z. Ligeti and S. Turczyk, Phys. Rev. **D90**, 094003 (2014), [arXiv:1408.2516].
- [21] W. J. Marciano, Phys. Rev. Lett. **93**, 231803 (2004), [hep-ph/0402299].
- [22] V. Cirigliano *et al.*, Rev. Mod. Phys. **84**, 399 (2012), [arXiv:1107.6001].
- [23] K. A. Olive *et al.* (Particle Data Group), Chin. Phys. **C38**, 090001 (2014).
- [24] B. Ananthanarayan and B. Moussallam, JHEP **06**, 047 (2004), [hep-ph/0405206].
- [25] S. Descotes-Genon and B. Moussallam, Eur. Phys. J. **C42**, 403 (2005), [hep-ph/0505077].
- [26] W. J. Marciano and A. Sirlin, Phys. Rev. Lett. **71**, 3629 (1993).
- [27] V. Cirigliano and H. Neufeld, Phys. Lett. **B700**, 7 (2011), [arXiv:1102.0563].
- [28] J. L. Rosner, S. Stone and R. S. Van de Water (2015), review prepared for PDG 2015 edition, [arXiv:1509.02220].
- [29] J. Gasser, A. Rusetsky and I. Scimemi, Eur. Phys. J. **C32**, 97 (2003), [hep-ph/0305260].
- [30] N. Miller *et al.*, Phys. Rev. D **102**, 3, 034507 (2020), [arXiv:2005.04795].
- [31] A. Bazavov *et al.*, Phys. Rev. **D98**, 7, 074512 (2018), [arXiv:1712.09262].
- [32] N. Carrasco *et al.* (ETM), Phys. Rev. **D91**, 054507 (2015), [arXiv:1411.7908].
- [33] R. Dowdall *et al.* (HPQCD), Phys. Rev. **D88**, 074504 (2013), [arXiv:1303.1670].
- [34] V. G. Bornyakov *et al.* (QCDSF-UKQCD), Phys. Lett. **B767**, 366 (2017), [arXiv:1612.04798].
- [35] S. Durr *et al.*, Phys. Rev. **D95**, 5, 054513 (2017), [arXiv:1601.05998].
- [36] T. Blum *et al.* (RBC, UKQCD), Phys. Rev. **D93**, 074505 (2016), [arXiv:1411.7017].
- [37] A. Bazavov *et al.* (MILC), PoS **LATTICE2010**, 074 (2010), [arXiv:1012.0868].
- [38] S. Durr *et al.* (BMW), Phys. Rev. **D81**, 054507 (2010), [arXiv:1001.4692].
- [39] E. Follana *et al.* (HPQCD, UKQCD), Phys. Rev. Lett. **100**, 062002 (2008), [arXiv:0706.1726].
- [40] M. Moulson, in “8th International Workshop on the CKM Unitarity Triangle (CKM2014) Vienna, Austria, September 8–12, 2014,” (2014), [arXiv:1411.5252].
- [41] M. Antonelli *et al.* (FlaviaNet Working Group on Kaon Decays), Eur. Phys. J. **C69**, 399 (2010), [arXiv:1005.2323].
- [42] M. Tanabashi *et al.* (Particle Data Group), Phys. Rev. **D98**, 3, 030001 (2018).
- [43] S. Hashimoto, J. Laiho and S. R. Sharpe, “Lattice Quantum Chromodynamics,” <http://pdg.lbl.gov/2019/reviews/rpp2018-rev-lattice-qcd.pdf> (2017), review prepared for PDG 2018 edition.
- [44] S. Hashimoto, J. Laiho and S. R. Sharpe, “Lattice Quantum Chromodynamics,” pdg.lbl.gov/2020/reviews/rpp2020-rev-lattice-qcd.pdf (2020), review prepared for PDG 2020 edition.
- [45] S. Aoki *et al.* (Flavour Lattice Averaging Group), Eur. Phys. J. **C74**, 2890 (2014), [arXiv:1310.8555].

- [46] S. Aoki *et al.*, Eur. Phys. J. **C77**, 2, 112 (2017), [arXiv:1607.00299].
- [47] A. S. Kronfeld, Ann. Rev. Nucl. Part. Sci. **62**, 265 (2012), [arXiv:1203.1204].
- [48] A. V. Manohar, C. T. Sachrajda and R. M. Barnett, “Quark Masses,” <http://pdg.lbl.gov/2019/reviews/rpp2018-rev-quark-masses.pdf> (2018), review prepared for PDG 2018 update.
- [49] G. M. de Divitiis *et al.*, JHEP **04**, 124 (2012), [arXiv:1110.6294].
- [50] J. Gasser and H. Leutwyler, Nucl. Phys. **B250**, 465 (1985).
- [51] G. M. de Divitiis *et al.* (RM123), Phys. Rev. **D87**, 11, 114505 (2013), [arXiv:1303.4896].
- [52] M. Artuso *et al.* (CLEO), Phys. Rev. Lett. **95**, 251801 (2005), [hep-ex/0508057].
- [53] B. I. Eisenstein *et al.* (CLEO), Phys. Rev. **D78**, 052003 (2008), [arXiv:0806.2112].
- [54] M. Ablikim *et al.* (BESIII), Phys. Rev. **D89**, 051104 (2014), [arXiv:1312.0374].
- [55] M. Artuso *et al.* (CLEO), Phys. Rev. Lett. **99**, 071802 (2007), [arXiv:0704.0629].
- [56] J. P. Alexander *et al.* (CLEO), Phys. Rev. **D79**, 052001 (2009), [arXiv:0901.1216].
- [57] M. Ablikim *et al.* (BESIII) (2019), [arXiv:1908.08877].
- [58] M. Nobes (2005), [hep-lat/0501009].
- [59] A. Bazavov *et al.* (Fermilab Lattice, MILC), Phys. Rev. **D93**, 11, 113016 (2016), [arXiv:1602.03560].
- [60] J. P. Lees *et al.* (BaBar) (2010), [arXiv:1003.3063].
- [61] P. del Amo Sanchez *et al.* (BaBar), Phys. Rev. **D82**, 091103 (2010), [Erratum: Phys. Rev. **D91**, no.1, 019901 (2015)], [arXiv:1008.4080].
- [62] A. Zupanc *et al.* (Belle), JHEP **1309**, 139 (2013), [arXiv:1307.6240].
- [63] M. Ablikim *et al.* (BESIII), Phys. Rev. D **94**, 7, 072004 (2016), [arXiv:1608.06732].
- [64] M. Ablikim *et al.* (BESIII) (2021), [arXiv:2102.11734].
- [65] P. Naik *et al.* (CLEO), Phys. Rev. **D80**, 112004 (2009), [arXiv:0910.3602].
- [66] K. M. Ecklund *et al.* (CLEO), Phys. Rev. Lett. **100**, 161801 (2008), [arXiv:0712.1175].
- [67] P. U. E. Onyisi *et al.* (CLEO), Phys. Rev. **D79**, 052002 (2009), [arXiv:0901.1147].
- [68] M. Ablikim *et al.* (BESIII) (2021), [arXiv:2106.02218].
- [69] M. Ablikim *et al.* (BESIII) (2021), [arXiv:2105.07178].
- [70] T. K. Pedlar *et al.* (CLEO), Phys. Rev. **D76**, 072002 (2007), [arXiv:0704.0437].
- [71] J. P. Alexander *et al.* (CLEO), Phys. Rev. Lett. **100**, 161804 (2008), [arXiv:0801.0680].
- [72] B. Aubert *et al.* (BaBar), Phys. Rev. Lett. **98**, 141801 (2007), [hep-ex/0607094].
- [73] Y. Chen *et al.* (χ QCD), Chin. Phys. C **45**, 2, 023109 (2021), [arXiv:2008.05208].
- [74] P. A. Boyle *et al.* (RBC/UKQCD) (2018), [arXiv:1812.08791].
- [75] P. A. Boyle *et al.*, JHEP **12**, 008 (2017), [arXiv:1701.02644].
- [76] Y.-B. Yang *et al.* (χ QCD), Phys. Rev. **D92**, 034517 (2015), [arXiv:1410.3343].
- [77] H. Na *et al.* (HPQCD), Phys. Rev. **D86**, 054510 (2012), [arXiv:1206.4936].
- [78] A. Bazavov *et al.* (Fermilab Lattice and MILC), Phys. Rev. **D85**, 114506 (2012), [arXiv:1112.3051].
- [79] C. T. H. Davies *et al.* (HPQCD), Phys. Rev. **D82**, 114504 (2010), [arXiv:1008.4018].
- [80] B. Pullin and R. Zwicky (2021), [arXiv:2106.13617].
- [81] Z.-G. Wang, Eur. Phys. J. **C75**, 427 (2015), [arXiv:1506.01993].
- [82] P. Gelhausen *et al.*, Phys. Rev. **D88**, 014015 (2013), [arXiv:1305.5432].
- [83] S. Narison, Phys. Lett. **B718**, 1321 (2013), [arXiv:1209.2023].
- [84] W. Lucha, D. Melikhov and S. Simula, Phys. Lett. **B701**, 82 (2011), [arXiv:1101.5986].
- [85] W. Lucha, D. Melikhov and S. Simula, Eur. Phys. J. **C78**, 2, 168 (2018), [Erratum: Eur. Phys. J. **C78**, no.11, 936 (2018)], [arXiv:1702.07537].
- [86] K. Ikado *et al.* (Belle), Phys. Rev. Lett. **97**, 251802 (2006), [hep-ex/0604018].
- [87] I. Adachi *et al.* (Belle), Phys. Rev. Lett. **110**, 131801 (2013), [arXiv:1208.4678].
- [88] B. Kronenbitter *et al.* (Belle), Phys. Rev. **D92**, 051102 (2015), [arXiv:1503.05613].
- [89] J. P. Lees *et al.* (BaBar), Phys. Rev. **D88**, 031102 (2013), [arXiv:1207.0698].
- [90] B. Aubert *et al.* (BaBar), Phys. Rev. **D81**, 051101 (2010), [arXiv:0912.2453].
- [91] C. Hughes, C. T. H. Davies and C. J. Monahan, Phys. Rev. **D97**, 5, 054509 (2018), [arXiv:1711.09981].
- [92] A. Bussone *et al.* (ETM), Phys. Rev. **D93**, 11, 114505 (2016), [arXiv:1603.04306].
- [93] R. Dowdall *et al.* (HPQCD), Phys. Rev. Lett. **110**, 222003 (2013), [arXiv:1302.2644].
- [94] Y. Aoki *et al.*, Phys. Rev. **D91**, 114505 (2015), [arXiv:1406.6192].
- [95] N. H. Christ *et al.* (RBC/UKQCD), Phys. Rev. **D91**, 054502 (2015), [arXiv:1404.4670].
- [96] H. Na *et al.* (HPQCD), Phys. Rev. **D86**, 034506 (2012), [arXiv:1202.4914].
- [97] C. McNeile *et al.* (HPQCD), Phys. Rev. **D85**, 031503 (2012), [arXiv:1110.4510].
- [98] H.-K. Sun and M.-Z. Yang, Phys. Rev. **D95**, 11, 113001 (2017), [arXiv:1609.08958].
- [99] M. J. Baker *et al.*, JHEP **07**, 032 (2014), [arXiv:1310.0941].
- [100] W. Lucha, D. Melikhov and S. Simula, Phys. Rev. **D88**, 056011 (2013), [arXiv:1305.7099].
- [101] J. Hardy and I. S. Towner, PoS **CKM2016**, 028 (2016).
- [102] J. C. Hardy and I. S. Towner, Phys. Rev. C **102**, 4, 045501 (2020).
- [103] C.-Y. Seng *et al.* (2021), [arXiv:2107.14708].
- [104] F. Ambrosino *et al.* (KLOE), Eur. Phys. J. **C71**, 1604 (2011), [arXiv:1011.2668].
- [105] E. Abouzaid *et al.* (KTeV), Phys. Rev. **D83**, 092001 (2011), [arXiv:1011.0127].
- [106] D. Babusci *et al.* (KLOE KLOE-2), Phys. Lett. **B738**, 128 (2014), [arXiv:1407.2028].
- [107] N. Carrasco *et al.*, Phys. Rev. **D93**, 11, 114512 (2016), [arXiv:1602.04113].
- [108] A. Bazavov *et al.* (Fermilab Lattice and MILC), Phys. Rev. Lett. **112**, 112001 (2014), [arXiv:1312.1228].
- [109] C.-Y. Seng *et al.*, Phys. Rev. Lett. **121**, 241804 (2018), [arXiv:1807.10197].
- [110] C. Y. Seng, M. Gorchtein and M. J. Ramsey-Musolf, Phys. Rev. **D100**, 013001 (2019), [arXiv:1812.03352].
- [111] M. Gorchtein, Phys. Rev. Lett. **123**, 042503 (2019), [arXiv:1812.04229].
- [112] C.-Y. Seng and U.-G. Meissner, Phys. Rev. Lett. **122**, 211802 (2019), [arXiv:1903.07969].

- [113] A. Czarnecki, W. J. Marciano and A. Sirlin (2019), [arXiv:1907.06737].
- [114] C. Patrignani *et al.* (Particle Data Group), *Chin. Phys.* **C40**, 10, 100001 (2016).
- [115] Y. Amhis *et al.* (HFLAV), *Eur. Phys. J.* **C77**, 12, 895 (2017), [arXiv:1612.07233].
- [116] H. Na *et al.* (HPQCD), *Phys. Rev.* **D82**, 114506 (2010), [arXiv:1008.4562].
- [117] H. Na *et al.* (HPQCD), *Phys. Rev.* **D84**, 114505 (2011), [arXiv:1109.1501].
- [118] V. Lubicz *et al.* (ETM), *Phys. Rev.* **D96**, 5, 054514 (2017), [erratum: *Phys. Rev.* D99,no.9,099902(2019)], [arXiv:1706.03017].
- [119] B. Chakraborty *et al.*, *EPJ Web Conf.* **175**, 13027 (2018), [arXiv:1710.07334].
- [120] R. Li *et al.* (Fermilab Lattice, MILC), *PoS LATTICE2018*, 269 (2019), [arXiv:1901.08989].
- [121] B. Chakraborty *et al.* ((HPQCD Collaboration)), *Phys. Rev. D* **104**, 3, 034505 (2021), [arXiv:2104.09883].
- [122] L. Wolfenstein, *Phys. Rev. Lett.* **51**, 1945 (1983).
- [123] J. Charles *et al.* (CKMfitter Group), *Eur. Phys. J.* **C41**, 1 (2005), updated results and plots available at: <http://ckmfitter.in2p3.fr>, [hep-ph/0406184].
- [124] M. Antonelli *et al.*, *Phys. Rept.* **494**, 197 (2010), [arXiv:0907.5386].
- [125] J. N. Butler *et al.* (Quark Flavor Physics Working Group), in “Community Summer Study 2013: Snowmass on the Mississippi (CSS2013) Minneapolis, MN, USA, July 29-August 6, 2013,” (2013), [arXiv:1311.1076], URL <http://www.slac.stanford.edu/econf/C1307292/docs/IntensityFrontier/QuarkF1-15.pdf>.
- [126] Y. Amhis *et al.* (Heavy Flavor Averaging Group) (2014), [arXiv:1412.7515].
- [127] A. J. Bevan *et al.* (Belle, BaBar), *Eur. Phys. J.* **C74**, 3026 (2014), [arXiv:1406.6311].
- [128] E. Dalgic *et al.*, *Phys. Rev.* **D73**, 074502 (2006), [Erratum: *Phys. Rev.* D75,119906(2007)], [hep-lat/0601021].
- [129] J. M. Flynn *et al.* (RBC/UKQCD), *Phys. Rev.* **D91**, 074510 (2015), [arXiv:1501.05373].
- [130] J. A. Bailey *et al.* (Fermilab Lattice, MILC), *Phys. Rev.* **D92**, 014024 (2015), [arXiv:1503.07839].
- [131] P. del Amo Sanchez *et al.* (BaBar), *Phys. Rev.* **D83**, 032007 (2011), [arXiv:1005.3288].
- [132] J. P. Lees *et al.* (BaBar), *Phys. Rev.* **D86**, 092004 (2012), [arXiv:1208.1253].
- [133] H. Ha *et al.* (Belle), *Phys. Rev.* **D83**, 071101 (2011), [arXiv:1012.0090].
- [134] A. Sibidanov *et al.* (Belle), *Phys. Rev.* **D88**, 032005 (2013), [arXiv:1306.2781].
- [135] S. W. Bosch *et al.*, *Phys. Rev. Lett.* **93**, 221801 (2004), [hep-ph/0403223].
- [136] J. R. Andersen and E. Gardi, *JHEP* **01**, 097 (2006), [hep-ph/0509360].
- [137] P. Gambino *et al.*, *JHEP* **10**, 058 (2007), [arXiv:0707.2493].
- [138] R. Kowalewski and T. Mannel, “Semileptonic b -Hadron Decays, Determination of V_{cb} , V_{ub} ,” <http://pdg.lbl.gov/2018/reviews/rpp2018-rev-vcb-vub.pdf> (2017), review prepared for PDG 2018 update.

73. Production and Decay of b -flavored Hadrons

Revised September 2021 by P. Eerola (Helsinki U.), M. Kreps (Warwick U.) and Y. Kwon (Yonsei U., Seoul).

The b quark belongs to the third generation of quarks and is the weak-doublet partner of the t quark. The existence of the third-generation quark doublet was proposed in 1973 by Kobayashi and Maskawa [1] in their model of the quark mixing matrix (“CKM” matrix), and confirmed four years later by the first observation of a $b\bar{b}$ meson [2]. In the KM model, CP violation is explained within the Standard Model (SM) by an irreducible phase of the 3×3 unitary matrix. The regular pattern of the three lepton and quark families is one of the most intriguing puzzles in particle physics. The existence of families gives rise to many of the free parameters in the SM, including the fermion masses, and the elements of the CKM matrix.

Since the b quark is the lighter element of the third-generation quark doublet, the decays of b -flavored hadrons occur via generation-changing processes through CKM matrix. Because of this, and the fact that the CKM matrix is close to a 3×3 unitary matrix, many interesting features such as loop and box diagrams, flavor oscillations, as well as large CP asymmetries, can be observed in the weak decays of b -flavored hadrons.

The CKM matrix is parameterized by three real parameters and one complex phase. This complex phase is the source of CP violation in B meson decays in the Standard Model. A crucial milestone was the first observation of CP violation in the B meson system in 2001, by the BaBar [3] and Belle [4] collaborations. They measured a large value for the parameter $\sin 2\beta$ ($= \sin 2\phi_1$) [5], almost four decades after the discovery of a small CP asymmetry in neutral kaons. A more detailed discussion of the CKM matrix and CP violation can be found elsewhere in this Review [6, 7].

The structure of this mini-review is organized as follows. After a discussion of b -quark production and current results on spectroscopy, we discuss lifetimes of b -flavored hadrons. We then discuss some basic properties of B -meson decays, followed by summaries of dominant hadronic, rare hadronic, and electroweak penguin decays of B -mesons. There are separate mini-reviews for $B^0 - \bar{B}^0$ mixing [8] and the extraction of the CKM matrix elements V_{cb} and V_{ub} from B -meson decays [9] in this Review.

73.1 Production and spectroscopy

The bound states of a \bar{b} antiquark and a u , d , s , or c quark are referred to as the B_u (B^+), B_d (B^0), B_s (B_s^0), and B_c (B_c^+) mesons, respectively. The B_c^+ is the heaviest of the ground-state b -flavored mesons, and the most difficult to produce: it was observed for the first time in the semileptonic mode by CDF in 1998 [10], but its mass was accurately determined only in 2006, from the fully reconstructed mode $B_c^+ \rightarrow J/\psi\pi^+$ [11]. Many exclusive decay channels can now be used for the accurate mass measurements, given the large statistics available at the LHC. Currently the most precise measurement is made by LHCb and yields $m(B_c^+) = 6274.47 \pm 0.27 \pm 0.17 \text{ MeV}/c^2$ [12], combining $B_c^+ \rightarrow J/\psi\pi^+$, $B_c^+ \rightarrow J/\psi\pi^+\pi^-\pi^+$, $B_c^+ \rightarrow J/\psi p\bar{p}\pi^+$, $B_c^+ \rightarrow J/\psi D_s^+$, $B_c^+ \rightarrow J/\psi D^0 K^+$ and $B_c^+ \rightarrow B_s^0\pi^+$ decay modes.

The first excited meson is called the B^* meson, while B^{**} is the generic name for the four orbitally excited ($L = 1$) B -meson states that correspond to the P -wave mesons in the charm system, D^{**} . Excited states of the B_s^0 meson are similarly named B_s^* and B_s^{**} .

Of the possible bound $b\bar{b}$ states, the $\Upsilon(nS)$ and $\chi_{bJ}(nP)$ states are well studied. The pseudoscalar ground state η_b has been observed for the first time by BaBar [13] indirectly through the decay $\Upsilon(3S) \rightarrow \gamma\eta_b$, and then confirmed by Babar in $\Upsilon(2S)$ decays [14] and CLEO in $\Upsilon(3S)$ decays [15]. The most accurate mass and width measurements come now from Belle, using decays $\Upsilon(5S) \rightarrow h_b(1P)\pi^+\pi^-$, $h_b(1P) \rightarrow \gamma\eta_b(1S)$ [16] and $\Upsilon(4S) \rightarrow \eta h_b(1P)$, $h_b(1P) \rightarrow \gamma\eta_b(1S)$ [17]. Belle has also reported first evidence for the $\eta_b(2S)$ in the $h_b(2P) \rightarrow \eta_b(2S)\gamma$ transition [16]. In addition, Belle has observed $Z_b(10610)$ and $Z_b(10650)$ states in the processes $\Upsilon(5S) \rightarrow \Upsilon(nS)\pi^+\pi^-$ ($n = 1, 2, 3$) and $\Upsilon(5S) \rightarrow h_b(mP)\pi^+\pi^-$ ($m = 1, 2$) [18]. These Z_b states are observed to decay to $\Upsilon(nS)\pi^\pm$ and $h_b(mP)\pi^\pm$, hence

electrically charged and do not belong to ordinary $q\bar{q}$ mesons. For classification and naming of these and other states, see Ref. [19].

Experimental studies of b decays have been performed in e^+e^- collisions at the $\Upsilon(4S)$ (ARGUS, CLEO, Belle, BaBar) and $\Upsilon(5S)$ (CLEO, Belle) resonances. The $e^+e^- \rightarrow b\bar{b}$ production cross-section at the $\Upsilon(4S)$ ($\Upsilon(5S)$) resonance is about 1.1 nb (0.3 nb). The full data samples of BaBar and Belle are 560 fb^{-1} and 1020 fb^{-1} , respectively, of which 433 fb^{-1} and 710 fb^{-1} are at the $\Upsilon(4S)$ resonance. Since the $\Upsilon(4S)$ decays dominantly to a pair of B mesons (either B^+B^- or $B^0\bar{B}^0$), a precise knowledge of the energy-momentum of one B meson (the ‘tagging B ’) enables deducing the properties of the other B (the ‘signal B ’). This property has been exploited by both BaBar and Belle, in particular, to measure inclusive decay modes as well as final states with missing neutrinos. The Belle II experiment at SuperKEKB has started recording data in 2019, and the experiment has so far collected about 210 fb^{-1} of data by summer 2021. At the Z resonance (SLC, LEP) all species of b -flavored hadrons could be studied for the first time. The $e^+e^- \rightarrow b\bar{b}$ production cross-section at the Z resonance is about 6.6 nb.

High-energy $p\bar{p}$ (Tevatron) and pp collisions (LHC) produce b -flavored hadrons of all species with large cross-sections. At the Tevatron ($\sqrt{s} = 1.96 \text{ TeV}$) the visible cross section $\sigma(p\bar{p} \rightarrow bX, |\eta| < 1)$ is about $30 \mu\text{b}$. CDF and D0 experiments at the Tevatron have accumulated by the end of their running about 10 fb^{-1} each.

At the LHC pp collider at $\sqrt{s} = 7 - 13 \text{ TeV}$, the visible b -hadron cross section at the LHCb experiment with pseudorapidity acceptance $2 < \eta < 5$ has been measured to be $\sim 72 \mu\text{b}$ at 7 TeV and $\sim 144 \mu\text{b}$ at 13 TeV [20] (cross section at 13 TeV corrected in Erratum). LHCb has collected about 1 fb^{-1} at 7 TeV, 2 fb^{-1} at 8 TeV, and close to 5.9 fb^{-1} at 13 TeV during LHC Runs 1 and 2. CMS and ATLAS have collected each about 5 fb^{-1} of data at $\sqrt{s} = 7, 20 \text{ fb}^{-1}$ at 8 TeV and about 150 fb^{-1} at 13 TeV during LHC Runs 1 and 2. The LHCb experiment is undergoing currently major upgrade. The LHC operation is planned to resume in 2022.

In hadron collisions, production happens as $b\bar{b}$ pairs via leading order flavor creation or higher order processes such as gluon-splitting. Single b -quarks can be produced by flavor excitation. The total b -production cross section is an interesting test of our understanding of leading and higher order QCD processes. With a wealth of measurements at LHC and at Tevatron (see Ref. [20] and references therein), and improved calculations [21], there is a reasonable agreement between measurements and predictions.

Each quark of a $b\bar{b}$ pair produced in hadron collisions hadronizes separately and incoherently from the other, but it is still possible to obtain a statistical indication of the charge of a produced b/\bar{b} quark (“flavor tag” or “charge tag”) from the accompanying particles produced in the hadronization process, or from the decay products of the other quark. The momentum spectrum of produced b -quarks typically peaks near the b -quark mass, and extends to much higher momenta, dropping by about a decade for every ten GeV. Typical decay lengths are of the order of a centimeter at 13 TeV pp collisions; the resolution for the decay vertex must be more precise than this to resolve the fast oscillations of B_s^0 mesons.

In e^+e^- colliders, since the B mesons are very slow in the $\Upsilon(4S)$ rest frame, asymmetric beam energies are used to boost the decay products to allow time-dependent measurements that are crucial for the study of CP violation. At KEKB, the boost was $\beta\gamma = 0.43$, while PEP-II used a slightly larger boost, $\beta\gamma = 0.55$. The typical B -meson decay length is dilated from $\approx 20 \mu\text{m}$ to $\approx 200 \mu\text{m}$. At SuperKEKB the boost is lower, $\beta\gamma = 0.28$, which puts more demanding requirements on the track reconstruction precision at Belle II to reach a resolution in decay time measurements similar to Belle. The two B mesons produced in $\Upsilon(4S)$ decay are in a coherent quantum state, which makes it easier than in hadron collisions to infer the charge state of one B meson from observation of the other; however, the coherence also requires determination of the decay time of both mesons, rather than just one, in order to perform time-dependent CP -violation measurements. For B_s^0 , which can be produced at $\Upsilon(5S)$ the situation is less favourable,

as boost is not high enough to provide sufficient time resolution to resolve the fast B_s^0 oscillations.

For the measurement of branching fractions, the initial composition of the data sample must be known. The $\Upsilon(4S)$ resonance decays predominantly to $B^0\bar{B}^0$ and B^+B^- ; the current experimental upper limit for non- $B\bar{B}$ decays of the $\Upsilon(4S)$ is less than 4% at the 95% confidence level (CL) [22]. The observed modes of this category are decays to lower Υ states and a pion pair, η , or η' , measured branching fractions being of order $10^{-4} - 10^{-5}$ [23], and decays to $h_b(1P)\eta$ with branching fraction of order 10^{-3} [17].

The ratio f_+/f_0 of the fractions of charged to neutral B productions from $\Upsilon(4S)$ decays has been measured by CLEO, BaBar, and Belle in various ways. They typically use pairs of isospin-related decays of B^+ and B^0 , such that it can be assumed that $\Gamma(B^+ \rightarrow x^+) = \Gamma(B^0 \rightarrow x^0)$. In this way, the ratio of the number of events observed in these modes is proportional to $(f_+\tau_+)/ (f_0\tau_0)$ [24,25]. BaBar has also performed an independent measurement of f_0 with a different method that does not require isospin symmetry or the value of the lifetime ratio, based on the number of events with one or two reconstructed $B^0 \rightarrow D^{*-}\ell^+\nu$ decays [26]. The combined result, from the current average of τ_+/τ_0 , is $f_+/f_0 = 1.058 \pm 0.024$ [27]. The result is consistent within 2.4σ with equal production of B^+B^- and $B^0\bar{B}^0$ pairs, and we assume $f_+/f_0 = 1$ in this mini-review except where explicitly stated otherwise. This assumption is also supported by the near equality of the B^+ and B^0 masses: our fit yields $m(B^0) = 5279.65 \pm 0.12$ MeV/ c^2 , $m(B^+) = 5279.34 \pm 0.12$ MeV/ c^2 , and $m(B^0) - m(B^+) = 0.31 \pm 0.05$ MeV/ c^2 .

Data collected at the $\Upsilon(5S)$ resonance gave CLEO, Belle and BaBar access to B_s^0 decays. In $\Upsilon(5S)$ decays there are seven possible final states including a pair of non-strange B mesons and 0, 1 or 2 pions, and three with a pair of strange B mesons ($B_s^{*0}\bar{B}_s^{*0}$, $B_s^{*0}\bar{B}_s^0$, and $B_s^0\bar{B}_s^{*0}$). The fraction of events with a pair of B_s^0 mesons over the total number of events with a pair of b -flavored hadrons has been measured to be $f_s[\Upsilon(5S)] = 0.199_{-0.029}^{+0.030}$ [28], of which 88% is $B_s^{*0}\bar{B}_s^{*0}$ events. However, the small boost of B_s^0 mesons produced in this way prevents resolution of their fast oscillations for time-dependent measurements; these are only accessible in hadron collisions (or at the Z peak).

In high-energy collisions, the produced b or \bar{b} quarks can hadronize with different probabilities into the full spectrum of b -hadrons, either in their ground or excited states. The hadronization does not have to be identical in $p\bar{p}$ or pp collisions and in Z decay, because of the different momentum distributions of the b -quark in these processes; the sample used in the $p\bar{p}$ measurements has momenta close to the b mass, rather than $m_Z/2$ in Z decay. The available data from Tevatron and LHC show that the production fractions f_d , f_u , f_s , and f_{baryon} of B^0 , B^+ , B_s^0 , and b baryons, respectively, of weakly decaying b hadrons depend on the kinematics of the produced b hadron. The production fractions of b hadrons are discussed in more detail in the $B^0 - \bar{B}^0$ mixing section in this Review [8].

Excited B -meson states have been thoroughly studied by CLEO, LEP, CUSB, D0 and CDF (an admixture of B mesons) and LHCb (B^{*+} -meson). The current world average of the B^*-B mass difference is 45.21 ± 0.21 MeV/ c^2 . Excited B_s^* -meson states have been observed in $\Upsilon(5S)$ decays by CUSB, CLEO and Belle.

For orbitally excited $B_{(s)}$ meson states, with relative angular momentum $L=1$ of the two quarks, there exist four states $(J, j_q) = (0, 1/2), (1, 1/2), (1, 3/2), (2, 3/2)$, where j_q is the total angular momentum of the light u, d or s quark and J is the total angular momentum of the B meson. These states are collectively called as $B_{(s)}^{**}$ mesons. The $j_q = 1/2$ states are named $B_{(s)0}^*$ ($J=0$) and $B_{(s)1}^*$ ($J=1$) mesons, while the states with $j_q = 3/2$ are named $B_{(s)1}^*$ ($J=1$) and $B_{(s)2}^*$ ($J=2$) mesons. The states with $j_q = 1/2$ can decay through an S -wave transition and are expected to have a large width, but the $j_q = 3/2$ states are narrow D -wave decays. Evidence for B^{**} production has been initially obtained at LEP as a broad $B\pi$ resonance [29] or a B^+K^- enhancement [30]. Detailed results have been obtained for the narrow states $B_1(5721)^{0,+}$ and $B_2(5747)^{0,+}$ at the Tevatron and by

LHCb, and clear enhancements compatible with the higher mass states $B_J(5840)^{0,+}$ and $B_J(5970)^{0,+}$ have been observed [31,32]. Also the narrow B_s^{**} states $B_{s1}(5830)^0$ and $B_{s2}(5840)^0$ have been measured at the CDF [31], LHCb [33], and CMS [34].

Excited states of B_c^+ mesons will provide important information about the strong potential. A $B_c^+\pi^+\pi^-$ resonance has been observed for the first time by ATLAS [35]. The mass of the resonance has been measured precisely by CMS and LHCb as 6871.6 ± 1.1 MeV/ c^2 [36,37]. The resonance may be interpreted as the second S -wave state of the B_c^+ meson, $B_c^+(2S)$, but the quantum numbers are to be confirmed.

Baryon states containing a b quark are labeled according to the same scheme used for non- b baryons, with the addition of a b subscript [19]. The first observed b baryon was the Λ_b^0 (quark composition udb). Thanks to the large samples accumulated at the Tevatron and specially at the LHC many new b baryons have been found. The masses of all these new baryons have been measured to a precision of a few MeV/ c^2 , and found to be in agreement with predictions from Heavy Quark Effective Theory (HQET).

Clear signals of four strongly-decaying baryon states, Σ_b^+ , Σ_b^{*+} (uub), Σ_b^- , Σ_b^{*-} (ddb) have been obtained by CDF [38] and LHCb [39]. LHCb has also observed two new mass peaks in the $\Lambda_b^0\pi^\pm$ systems, consistent with single resonances and named as $\Sigma_b^\pm(6097)$ [39]. The nature of these resonances is, however, not yet clear. The isodoublet of strange b baryons $\Xi_b^0(usb)$ and $\Xi_b^\pm(dsb)$ has been observed by CDF and D0 [40]. Masses, lifetimes, and branching ratios have been accurately measured by LHCb [41] and CDF [42]. LHCb has also measured several parameters sensitive to P and CP violation [43]. Other observed Ξ_b baryons are spin-3/2 states $\Xi_b(5945)^0(\Xi_b^{*0})$ [44,45] and $\Xi_b^*(5955)^-$ [46], a spin-1/2 state $\Xi_b'(5935)^-$ [46], and a resonance state $\Xi_b^-(6227)$ [47]. The doubly-strange bottom baryon Ω_b^- has been observed first by D0 and CDF [48]. Mass and mean life have been measured precisely by LHCb [49] and CDF [42].

The so-called exotic states have raised a lot of interest recently. While many exotic states were seen in the charm sector, in bottom sector there are fewer seen. The D0 Collaboration claimed a narrow state $X(5568)$ decaying into a $B_s^0\pi^\pm$ final state [50]. While this would be an interesting addition to the observed states as the first exotic state with constituent quarks with four different flavours (b, s, u, d), analysis by LHCb yields negative result [51]. Also CMS finds no such a state [52].

73.2 Lifetimes

Precise lifetimes are key in extracting the weak parameters that are important for understanding the role of the CKM matrix in CP violation, such as the determination of V_{cb} and $B_s^0 - \bar{B}_s^0$ mixing parameters. In the naive spectator model, the heavy quark can decay only via the external spectator mechanism, and thus, the lifetimes of all mesons and baryons containing b quarks would be equal. Non-spectator effects, such as the interference between contributing amplitudes, modify this simple picture and give rise to a lifetime hierarchy for b -flavored hadrons similar to the one in the charm sector. However, since the lifetime differences are expected to scale as $1/m_Q^2$, where m_Q is the mass of the heavy quark, the variations in the b system are expected to be only 10% or less [53,54]. We expect:

$$\tau(B^+) \geq \tau(B^0) \approx \tau(B_s^0) > \tau(\Lambda_b^0) \gg \tau(B_c^+) . \quad (73.1)$$

For the B_c^+ , both quarks decay weakly, so the lifetime is much shorter.

Measurements of the lifetimes of the different b -flavored hadrons thus provide a means to determine the importance of non-spectator mechanisms in the b sector. Availability of large samples of fully-reconstructed decays of different b -hadron species has resulted in precise measurements with small statistical and systematic uncertainties ($\sim 1\%$). The world averages given in Table 73.1 have been determined by the Heavy Flavor Averaging Group (HFLAV) [28].

The B_s^0 lifetime in Table 73.1 is defined as $1/\Gamma_s$, where Γ_s is the average width of the light (L) and heavy (H) mass eigenstates, $(\Gamma_L + \Gamma_H)/2$. In the absence of CP violation, the light (heavy) B_s^0

Table 73.1: Summary of the world-average b -hadron lifetime measurements. For the B_s^0 lifetimes, see text below.

Particle	Lifetime [ps]
B^+	1.638 ± 0.004
B^0	1.519 ± 0.004
B_s^0	1.520 ± 0.005
$B_s^0 L$	1.429 ± 0.007
$B_s^0 H$	1.624 ± 0.009
B_c^+	0.510 ± 0.009
A_b^0	1.471 ± 0.009
Ξ_b^-	1.572 ± 0.040
Ξ_b^0	1.480 ± 0.030
Ω_b^-	$1.64^{+0.18}_{-0.17}$

mass eigenstate is the CP -even (CP -odd) eigenstate. Thus, the lifetime of the light (heavy) mass eigenstate can be measured from CP -even (odd) final states. The lifetimes can also be obtained from time-dependent angular analysis of $B_s^0 \rightarrow J/\psi\phi$ decays.

The short B_c^+ lifetime is in good agreement with predictions [55]. With large samples of B_c^+ mesons at the LHC precision on the lifetimes can still improve. The measurement using semileptonic decays gives $\tau_{B_c^+} = 0.509 \pm 0.008 \pm 0.012$ ps [56] while using decays $B_c^+ \rightarrow J/\psi\pi^+$ yields $\tau_{B_c^+} = 0.5134 \pm 0.0110 \pm 0.0057$ ps [57]. Each of these is more precise than the combination of all previous experiments.

The recent A_b^0 lifetime measurements from LHC experiments and CDF are precise and favour lifetime close to the lifetime of B^0 meson, in agreement with theory.

For precision comparisons with theory, lifetime ratios are more sensitive. Experimentally it is found [28]:

$$\frac{\tau_{B^+}}{\tau_{B^0}} = 1.076 \pm 0.004, \quad \frac{\tau_{B_s^0}}{\tau_{B^0}} = 1.001 \pm 0.004,$$

$$\frac{\tau_{A_b^0}}{\tau_{B^0}} = 0.969 \pm 0.006,$$

while recent Heavy Quark Expansion (HQE) predictions give [54]:

$$\frac{\tau_{B^+}}{\tau_{B^0}} = 1.04^{+0.05}_{-0.01} \pm 0.02 \pm 0.01, \quad \frac{\tau_{B_s^0}}{\tau_{B^0}} = 1.001 \pm 0.002,$$

$$\frac{\tau_{A_b^0}}{\tau_{B^0}} = 0.935 \pm 0.054.$$

The ratio of B^+ to B^0 lifetimes has a precision of better than 1%, and is significantly different from 1.0, in agreement with predictions [53]. The ratio of B_s^0 to B^0 lifetimes is expected to be very close to 1.0.

For a detailed discussion on neutral B^0 and B_s^0 oscillation and relevant CP violation measurements see Ref. [8].

73.3 Features of decays

The ground states of b -flavored hadrons decay via weak interactions. In most decays of the b -flavored hadrons, where the b -quark is accompanied by lighter partner quarks (d , u , s , or c), the decay modes are well described by the decay of the b quark (spectator model) [58]. The dominant decay mode of a b quark is $b \rightarrow cW^{*-}$ (referred to as a “tree” or “spectator” decay), where the virtual W materializes either into a pair of leptons $\ell\bar{\nu}$ (“semileptonic decay”), or into a pair of quarks which then hadronizes. The transition $b \rightarrow u$ is suppressed by $|V_{ub}/V_{cb}|^2 \sim (0.1)^2$ relative to $b \rightarrow c$ transitions. The decays in which the spectator quark combines with one of the quarks from W^* to form one of the final state hadrons are suppressed by a factor $\sim (1/3)^2$, because the colors of the two quarks from different sources must match (“color-suppression”).

Semileptonic B decays $B \rightarrow X_c\ell\nu$ and $B \rightarrow X_u\ell\nu$ provide an excellent way to measure the magnitude of the CKM elements $|V_{cb}|$ and $|V_{ub}|$ respectively, because the strong interaction effects are much simplified due to the two leptons in the final state. Both

exclusive and inclusive decays can be used with dominant uncertainties being complementary. For exclusive decay analysis, knowledge of the form factors for the exclusive hadronic system $X_{c(u)}$ is required. For inclusive analysis, it is usually necessary to restrict the available phase-space of the decay products to suppress backgrounds; subsequently uncertainties are introduced in the extrapolation to the full phase-space. Moreover, restriction to a small corner of the phase-space may result in breakdown of the operator-product expansion scheme, thus making theoretical calculations unreliable. A more detailed discussion of B semileptonic decays and the extraction of $|V_{cb}|$ and $|V_{ub}|$ is given elsewhere in this *Review* [9]. While traditionally B^0 and B^+ decays were used, over time also other B hadron studies became available. Most notably, determination of $|V_{ub}|$ using $A_b^0 \rightarrow p\mu^-\bar{\nu}_\mu$ decays by LHCb [59] was more precise than expected. Besides, there have been measurements of inclusive semileptonic decay rates of B_s^0 [60] and B_c^+ [61] mesons. One of the latest additions in this area is the observation of the $B_s^0 \rightarrow K^-\mu^+\nu_\mu$ decays by LHCb using only a fraction of their available data [62].

On the other hand, hadronic B decays are complicated because of strong interaction effects caused by the surrounding cloud of light quarks and gluons. While this complicates the extraction of CKM matrix elements, it also provides a great opportunity to study perturbative and non-perturbative QCD, hadronization, and Final State Interaction (FSI) effects.

Many aspects of B decays can be understood through the Heavy Quark Effective Theory (HQET) [63]. This has been particularly successful for semileptonic decays. For further discussion of HQET, see for instance Ref. [64]. For hadronic decays, one typically uses effective Hamiltonian calculations that rely on a perturbative expansion with Wilson coefficients. In addition, some form of the factorization hypothesis is commonly used, where, in analogy with semileptonic decays, two-body hadronic decays of B mesons are expressed as the product of two independent hadronic currents, one describing the formation of a charm meson (in case of the dominant $b \rightarrow cW^{*-}$ decays), and the other the hadronization of the remaining $\bar{u}d$ (or $\bar{c}s$) system from the virtual W^- . Qualitatively, for B decays with a large energy release, e.g. $b \rightarrow uW^{*-}$ transitions, the $\bar{u}d$ pair (produced as a color singlet) travels fast enough to leave the interaction region without influencing the charm meson. This is known to work well for the dominant spectator decays [65]. There are several common implementations of these ideas for hadronic B decays, the most common of which are QCD factorization (QCDF) [66–69], perturbative QCD (pQCD) [70–74], and soft collinear effective theory (SCET) [75–77].

The transitions $b \rightarrow s$ and $b \rightarrow d$ are flavor-changing neutral-current (FCNC) processes. Although they are not allowed in the SM as a tree-process, they can occur via loop diagrams (denoted “penguin” decays). The rates for $b \rightarrow s$ penguin decays are comparable to the CKM-suppressed $b \rightarrow u$ tree processes. Pure-penguin decays were first established by the observation of $B \rightarrow K^*(892)\gamma$ [78]. Penguin processes involving $b \rightarrow d$ transitions are further suppressed by CKM, and have been observed for $B \rightarrow (\rho/\omega)\gamma$ decays [79, 80]. LHCb has observed a $b \rightarrow d$ penguin transition in the $B^+ \rightarrow \pi^+\mu^+\mu^-$ mode and measured its branching fraction to be $(1.83 \pm 0.24 \pm 0.05) \times 10^{-8}$ [81].

Other decay processes discussed in this *Review* include W -exchange (a W is exchanged between initial-state quarks), penguin annihilation (the gluon from a penguin loop attaches to the spectator quark, similar to an exchange diagram), and pure-annihilation (the initial quarks annihilate to a virtual W , which then decays). Some observed decay modes such as $B^0 \rightarrow D_s^- K^+$, may be interpreted as evidence of a W -exchange process [82]. The evidence for the purely leptonic decay $B^+ \rightarrow \tau^+\nu$ from Belle [83] and BaBar [84] is the first sign of a pure annihilation decay. The average branching fraction is $(1.09 \pm 0.24) \times 10^{-4}$, which is somewhat larger than, though consistent with, the value expected in the SM. A substantial region of parameter space of charged Higgs mass vs. $\tan\beta$ is excluded by the measurements of this mode. A dedicated discussion of purely leptonic decays of charged pseudoscalar mesons is given elsewhere in this *Review* [85].

73.4 Dominant hadronic decays

Most of the hadronic B decays involve $b \rightarrow c$ transition at the quark level, resulting in a charmed hadron or charmonium in the final state. Other types of hadronic decays are very rare and will be discussed separately in the next section. The experimental results on hadronic B decays have steadily improved over the years, and the measurements have reached sufficient precision to challenge our understanding of the dynamics of these decays. With good particle detection and hadron identification capabilities of B -factory detectors, a substantial fraction (roughly on the order of a few per mill) of hadronic B decay events can be fully reconstructed. In particular, good performances for detecting π^0 and other neutral particles helped Belle and BaBar to make comprehensive measurements of the decays $\bar{B}^0 \rightarrow D^{(*)0}h^0$ [86], where h^0 stands for light neutral mesons such as $\pi^0, \eta^{(\prime)}, \rho^0, \omega$. The measurements are being complemented by LHCb, in decays like $\bar{B}^0 \rightarrow D^0\pi^+\pi^-$ [87], where no neutral particles reconstruction is needed. These decays proceed through color-suppressed diagrams, hence they provide useful tests on the factorization models.

Because of the kinematic constraint of $\Upsilon(4S) \rightarrow B\bar{B}$, the energy sum of the final-state particles of a B meson decay is always equal to one half of the total energy in the center of mass frame. As a result, the two variables, ΔE (energy difference) and M_B (B candidate mass with a beam-energy constraint) are very effective for reducing combinatorial background both from $\Upsilon(4S)$ and $e^+e^- \rightarrow q\bar{q}$ continuum events. In particular, the energy-constraint in M_B improves the signal resolution by almost an order of magnitude.

The kinematically clean environment of B meson decays provides an excellent opportunity to search for new states. For instance, quark-level $b \rightarrow c\bar{c}s$ decays have been used to search for new charmonium and charm-strange mesons and study their properties in detail. While narrow charm-strange states $D_{s0}^*(2317)$ [88] and $D_{s1}(2460)$ [89] were discovered by BaBar and CLEO, respectively, the properties of these new states were revealed by studying the B meson decays, $B \rightarrow DD_s^*(2317)$ and $B \rightarrow DD_{s1}(2460)$ by Belle [90] and BaBar [91]. Another example is Dalitz plot analysis of decay $B_s^0 \rightarrow \bar{D}^0 K^- \pi^+$ in which the decay to spin-3 resonance was observed for the first time [92].

Information on B_s^0, B_c^+ and Λ_b^0 decays have been remarkably improved with recent studies of large samples from LHCb. Noticeable additions in B_s include decay modes to $D_s^{(*)+}D_s^{(*)-}, \bar{D}^0\bar{K}^0$, and $J/\psi\bar{K}^*(892)^0$. The $B_s^0 \rightarrow D_s^{(*)+}D_s^{(*)-}$ decays were first observed by CDF [93], followed by Belle [94]. LHCb has improved the precision with $\mathcal{B}(B_s^0 \rightarrow D_s^{(*)+}D_s^{(*)-}) = (3.07 \pm 0.22 \pm 0.33)\%$ [95], which suggests that $B_s^0 \rightarrow D_s^{(*)+}D_s^{(*)-}$ decays do not saturate the CP -even modes of the B_s decays. The $B_s^0 \rightarrow \bar{D}^0\bar{K}^0$ decay occurs mostly via a color-suppressed tree diagram, and has a small theoretical uncertainty in the SM, thus this mode can significantly improve the determination of the CP -violation angle ϕ_s . LHCb has observed this decay and the branching fraction is $(4.3 \pm 0.5 \pm 0.7) \times 10^{-4}$ [96]. The $B_s^0 \rightarrow J/\psi\bar{K}^*(892)^0$ decay can be used to constrain the penguin pollution in determining ϕ_s . LHCb has updated the branching fraction and measured the CP asymmetries of this decay, thereby constraining the penguin pollution in ϕ_s [97], although a much more stringent constraint on penguin pollution can come from $B^0 \rightarrow J/\psi\rho^0$ which has been observed by BaBar [98] and LHCb [99]. The $B_c^+ \rightarrow B_s^0\pi^+$ decay is unique as the only observed mode of b -flavored hadron decays where the partner quark decays (c in this case) while the b quark remains a spectator. LHCb has observed this mode and measured $[\sigma(B_c^+)/\sigma(B_s^0)] \times \mathcal{B}(B_c^+ \rightarrow B_s^0\pi^+) = (2.37 \pm 0.31 \pm 0.11_{-0.13}^{+0.17}) \times 10^{-3}$ [100]. In addition, LHCb [101] and ATLAS [102] have measured $B_c^+ \rightarrow J/\psi D_s^{(*)+}$, which, by comparing with $B_c^+ \rightarrow B_s^0\pi^+$, provides a ratio of exclusive $b \rightarrow c$ and $c \rightarrow s$ decays of B_c^+ . For $\Lambda_b^0 \rightarrow \Lambda_c^+\pi^+\pi^-\pi^-$ [103], not only the total rate is measured, but also structure involving decays through excited Λ_c and Σ_c baryons.

In addition, a variety of exotic particles that do not fit the conventional meson spectroscopy have been discovered in B decays. Belle found the $X(3872)$ state by studying $B^+ \rightarrow J/\psi\pi^+\pi^-K^+$

[104], which was confirmed by CDF [105], D0 [106] and BaBar [107]. Production of $X(3872)$ has been studied by the LHC experiments, LHCb [108], CMS [109] and ATLAS [110].

A charged charmonium-like state $X(4430)^\pm$ that decays to $\psi(2S)\pi^\pm$ was observed by Belle in $B \rightarrow \psi(2S)K\pi^\pm$ [111]. Since it is charged, it could not be an ordinary charmonium state. A high-statistics study by LHCb confirmed the existence of the $X(4430)^\pm$ in decays $B \rightarrow \psi(2S)K\pi^\pm$ [112], demonstrated its resonance character by studying the phase motion, unambiguously determined its spin-parity, and saw evidence for another state. In a Dalitz plot analysis of $\bar{B}^0 \rightarrow J/\psi K^- \pi^+$ [113], Belle has found another state, labeled as $X(4200)^+$ in this Review, adding to the list of exotic charged charmonium-like states. In an amplitude analysis of the decay $\Lambda_b^0 \rightarrow J/\psi p K^-$, LHCb observed exotic structures, labeled as $P_c(4380)^+$ and $P_c(4450)^+$ in this Review, in the $J/\psi p$ channel [114]. The subsequent analysis with significantly increased statistics observed additional state and resolved the peak at 4450 MeV/ c^2 as being due to the two states close in the mass [115]. They are referred to as charmonium-pentaquark states. More detailed discussions of exotic meson-like states and pentaquarks are given elsewhere in this Review [116].

73.5 Rare hadronic decays

All B -meson decays that do not occur through the $b \rightarrow c$ transition are usually called rare B decays. These include both semileptonic and hadronic $b \rightarrow u$ decays that are suppressed at leading order by the small CKM matrix element V_{ub} , as well as higher-order $b \rightarrow s(d)$ processes such as electroweak and gluonic penguin decays. In this section, we review hadronic rare B decays, while electroweak penguin decays and others are discussed in the next.

Charmless B meson decays into two-body hadronic final states such as $B \rightarrow \pi\pi$ and $K\pi$ are experimentally clean, and provide good opportunities to probe new physics and search for indirect and direct CP violations. Since the final state particles in these decays tend to have larger momenta than average B decay products, the event environment is cleaner than for $b \rightarrow c$ decays. Branching fractions are typically around 10^{-5} . Over the past decade, many such modes have been observed not only by e^+e^- collider experiments such as BaBar and Belle, but also by hadron collider experiments such as CDF ($p\bar{p}$) and LHCb (pp). In the latter cases, huge data samples of the modes with all charged final-state particles have been reconstructed by triggering on the impact parameter of the charged tracks. This has also allowed observation of charmless decays of the B_s , in final states such as $\phi\phi$ [117, 118], K^+K^- [119, 120], and $K^-\pi^+$ [120, 121], and of charmless decays of the Λ_b^0 baryon [121]. The large samples available at LHCb experiment allow to perform also time-dependent CP violation measurements [122, 123]. Charmless B_s modes are related to corresponding B^0 modes by U-spin symmetry, and are determined by similar amplitudes. Combining the observables from B_s^0 and B^0 modes is a further way of eliminating hadronic uncertainties and extracting relevant CKM information [124].

Because of relatively high-momenta for final state particles, the dominant source of background in e^+e^- collisions is $q\bar{q}$ continuum events; sophisticated background suppression techniques exploiting event shape variables are essential for these analyses. In hadron collisions, the dominant background comes from QCD or partially reconstructed heavy flavors, and is similarly suppressed by a combination of kinematic and isolation requirements. The results are in general consistent among the experiments.

Most rare decay modes including $B^0 \rightarrow K^+\pi^-$ have contributions from both $b \rightarrow u$ tree and $b \rightarrow sg$ penguin processes. If the size of the two contributions are comparable, the interference between them may result in direct CP violation, seen experimentally as a charge asymmetry in the decay rate measurement. BaBar [125], Belle [126], CDF [119], and LHCb [122] have measured the direct CP violating asymmetry in $B^0 \rightarrow K^+\pi^-$ decays. Direct CP violation has been observed in this decay with a significance of more than 5σ . The world average value of the asymmetry is now rather precise, $A_{CP}(K^+\pi^-) = -0.083 \pm 0.004$. The CP asymmetry in $B^+ \rightarrow K^+\pi^0$ mode has been measured by BaBar [127], Belle [126] and LHCb [128] with the average value $A_{CP}(K^+\pi^0) = 0.017 \pm 0.016$. These two asymmetries differ signif-

icantly, in contrast to a naive expectation based on simplified picture in the SM. For more detailed tests, there are sum rules [129] that relate the decay rates and decay-rate asymmetries between the four $K\pi$ charge states. A crucial ingredient of the sum rule test is $A_{CP}(K^0\pi^0)$. Currently, measured values are reported by both BaBar [130] and Belle [131]. Using the $A_{CP}(K^0\pi^0)$ value of Ref. [131], Belle reports the sum rule test result that is consistent with zero within 1.9σ [126]. With the future improvements via Belle II and upgraded LHCb, the measurements are expected to become precise enough to shape a definite conclusion. The CP asymmetry in the π^+K^- mode has also been measured in B_s^0 decays, by CDF [119] and LHCb [122]. The combined value is $A_{CP}(B_s^0 \rightarrow \pi^+K^-) = 0.221 \pm 0.015$.

In addition to $B_{(s)} \rightarrow K\pi$ modes, significant ($> 3\sigma$) non-zero CP asymmetries have been measured in several other rare decay modes: $A_{CP}(B^+ \rightarrow \rho^0K^+) = 0.37 \pm 0.10$ [132], $A_{CP}(B^+ \rightarrow \eta K^+) = -0.37 \pm 0.08$ [133], $A_{CP}(B^0 \rightarrow \eta K^{*0}) = 0.19 \pm 0.05$ [134], and $A_{CP}(B^+ \rightarrow f_2(1270)K^+) = -0.68^{+0.19}_{-0.17}$ [132]. In at least the first two cases, a large direct CP violation might be expected since the penguin amplitude is suppressed so the tree and penguin amplitudes may have comparable magnitudes. There are also measurements by LHCb of CP asymmetries in several 3-body modes: $A_{CP}(B^+ \rightarrow \pi^+\pi^-\pi^+) = 0.057 \pm 0.013$, $A_{CP}(B^+ \rightarrow K^+\pi^-\pi^+) = 0.027 \pm 0.008$, $A_{CP}(B^+ \rightarrow K^+K^-\pi^+) = -0.122 \pm 0.0021$, and $A_{CP}(B^+ \rightarrow K^+K^-K^+) = -0.033 \pm 0.008$ [135, 136]. Many of these analyses now include Dalitz plot treatments with many intermediate resonances.

BaBar [137] and Belle [126, 138] have observed the decays $B^+ \rightarrow \bar{K}^0K^+$ and $B^0 \rightarrow K^0\bar{K}^0$. The world-average branching fractions are $\mathcal{B}(B^0 \rightarrow K^0\bar{K}^0) = (1.21 \pm 0.16) \times 10^{-6}$ and $\mathcal{B}(B^+ \rightarrow \bar{K}^0K^+) = (1.31 \pm 0.17) \times 10^{-6}$. These are the first observations of hadronic $b \rightarrow d$ transitions, with significance bigger than 5σ for all four measurements. CP asymmetries have been measured for these modes, but with large errors. LHCb has observed $B^0 \rightarrow K^+K^-$ mode which occurs via a weak-annihilation process and is the rarest hadronic B -meson decay thus far observed, with $\mathcal{B}(B^0 \rightarrow K^+K^-) = (7.80 \pm 1.52) \times 10^{-8}$ [139]. $B_s^0 \rightarrow K^+K^-$ decay mode, which occurs mostly via $b \rightarrow s$ penguin process, has been observed by Belle [140], CDF [141] and LHCb [120]. The average branching fraction is $\mathcal{B}(B_s^0 \rightarrow K^+K^-) = (26.6 \pm 2.2) \times 10^{-6}$. Belle has also observed $B_s^0 \rightarrow K^0\bar{K}^0$ [142] which also occurs via $b \rightarrow s$ penguin transition in the SM. This was recently confirmed by LHCb [143]. The average branching fraction is $(1.76 \pm 0.31) \times 10^{-5}$.

The decay $B^0 \rightarrow \pi^+\pi^-$ can be used to extract the CKM angle α (for details see elsewhere in this *Review* [144]). This is complicated by the presence of significant contributions from penguin diagrams. An isospin analysis [145] can be used to untangle the penguin complications. The decay $B^0 \rightarrow \pi^0\pi^0$ is crucial in this analysis. Both BaBar and Belle have observed $B^0 \rightarrow \pi^0\pi^0$, with a mild tension in the measured branching fractions: $(1.83 \pm 0.25) \times 10^{-6}$ for BaBar [125] and $(1.31 \pm 0.26) \times 10^{-6}$ for Belle [146]. It turns out that the amount of penguin pollution in the $B \rightarrow \pi\pi$ system is rather large. In the past few years, measurements in the $B^0 \rightarrow \rho\rho$ system have produced more precise values of α , since penguin amplitudes are generally smaller for decays with vector mesons. An important ingredient in the analysis is the $B^0 \rightarrow \rho^0\rho^0$ branching fraction. The average of measurements from BaBar [147] and Belle [148] yields a branching fraction of $(0.96 \pm 0.15) \times 10^{-6}$. This is only 3% of the $\rho^+\rho^-$ branching fraction, much smaller than the corresponding ratio ($\gtrsim 20\%$) in the $\pi\pi$ system.

Since $B \rightarrow \rho\rho$ has two vector mesons in the final state, the CP eigenvalue of the final state depends on the longitudinal polarization fraction f_L for the decay. Therefore, a measurement of f_L is needed to extract the CKM angle α . Both BaBar and Belle have measured f_L for the decays $\rho^+\rho^-$ [149] and $\rho^+\rho^0$ [150] and in both cases the measurements show $f_L > 0.9$, making a complete angular analysis unnecessary. In $B^0 \rightarrow \rho^0\rho^0$, f_L is measured by BaBar [147], Belle [148] and LHCb [151], with the average value being $0.71^{+0.08}_{-0.09}$.

By analyzing the angular distributions of the B decays to two vector mesons, we can learn a lot about both weak- and strong-

interaction dynamics in B decays. Decays that are penguin-dominated surprisingly have values of f_L near 0.5. The list of such decays has now grown to include $B \rightarrow \phi K^*(892)$, $B \rightarrow \rho K^*(892)$, and $B \rightarrow \omega K^*(892)$. The reasons for this "polarization puzzle" are not fully understood. A detailed description of the angular analysis of B decays to two vector mesons can be found in a separate mini-review [152] in this *Review*.

73.6 Electroweak penguin decays

Electroweak decays are one-loop FCNC decays proceeding through penguin or box Feynman diagrams with final state including real photon or pair of leptons. Such decays were first observed by CLEO experiment when it observed decay $B \rightarrow K^*(892)\gamma$ [78]. Since then significant amount of experimental information was obtained. Branching fractions for these decays are 10^{-5} or less, which makes them excellent candidates for searches for new physics beyond SM. Often several observables are available, which allows for stringent tests of the SM.

Starting with radiative decays, experimentally easiest to study are exclusive decays with a fully reconstructed final state. The best studied decay in this class is $B \rightarrow K^*(892)\gamma$ seen by CLEO, Belle, BaBar experiments [153–155] with world average branching fraction $\mathcal{B}(B^0 \rightarrow K^*(892)^0\gamma) = (41.8 \pm 2.5) \times 10^{-6}$. Decays through several other kaon resonances such as $B \rightarrow K_1(1270)\gamma$, $K_2^*(1430)\gamma$, etc. were studied at B-factories [156–159]. It is worth to mention decay $B^+ \rightarrow K^+\pi^+\pi^-\gamma$ for which besides measurements of the branching fraction [157, 160, 161] one can also use the angular distribution to access photon polarization. Such a measurement was done by the LHCb experiment, which was able to clearly demonstrate that the photon in $B^+ \rightarrow K^+\pi^+\pi^-\gamma$ decay is polarized [162]. Unfortunately given non-trivial hadronic structure, more work is needed before turning this into test of the SM. The exclusive radiative decays $B_s^0 \rightarrow \phi\gamma$ was seen by the Belle and LHCb experiments [163, 164] with an average branching fraction of $(3.4 \pm 0.4) \times 10^{-5}$ and more recently also decay $A_b \rightarrow A\gamma$ was observed by LHCb [165].

Compared to $b \rightarrow s\gamma$, the $b \rightarrow d\gamma$ transitions such as $B \rightarrow \rho\gamma$, are suppressed by the CKM elements ratio $|V_{td}/V_{ts}|^2$. Both Belle and BaBar have observed these decays [79, 80]. The world average $\mathcal{B}(B \rightarrow (\rho, \omega)\gamma) = (1.30 \pm 0.23) \times 10^{-6}$. This can be used to calculate $|V_{td}/V_{ts}|$ [166]; the measured values are $0.195^{+0.025}_{-0.024}$ from Belle [79] and $0.233^{+0.033}_{-0.032}$ from BaBar [80].

The observed radiative penguin branching fractions can constrain a large class of SM extensions [167]. However, due to the uncertainties in the hadronization, only the inclusive $b \rightarrow s\gamma$ rate can be reliably compared with theoretical calculations. This rate can be measured from the endpoint of the inclusive photon spectrum in B decay. By combining the measurements of $B \rightarrow X_s\gamma$ from the CLEO, BaBar, and Belle experiments [168–170], HFLAV obtains the average: $\mathcal{B}(B \rightarrow X_s\gamma) = (3.32 \pm 0.15) \times 10^{-4}$ [28] for $E_\gamma \geq 1.6$ GeV, averaging over B^+ and B^0 . Consistent but less precise results have been reported by ALEPH for inclusive b -hadrons produced at the Z , which includes also contribution from B_s^0 and A_b^0 hadrons. Using the sum of seven exclusive final states, the BaBar experiment measured the branching fraction of inclusive $b \rightarrow d\gamma$ decays to be $(9.2 \pm 2.0 \pm 2.3) \times 10^{-6}$ [171]. The measured branching fraction can be compared to theoretical calculations. Recent calculations of $\mathcal{B}(b \rightarrow s\gamma)$ at NNLO level predict for the $E_\gamma \geq 1.6$ GeV values of $(3.36 \pm 0.23) \times 10^{-4}$ for $b \rightarrow s\gamma$ and $(1.73^{+0.12}_{-0.22}) \times 10^{-5}$ for $b \rightarrow d\gamma$ decays [172].

The CP asymmetry in $b \rightarrow s\gamma$ is extensively studied theoretically both in the SM and beyond [173]. According to the SM, the CP asymmetry in $b \rightarrow s\gamma$ is smaller than 1%, but some non-SM models allow significantly larger CP asymmetry ($\sim 10\%$) without altering the branching fraction. The current world average is $A_{CP} = 0.015 \pm 0.011$, again dominated by BaBar and Belle [174]. In addition to the CP asymmetry, BaBar and Belle also measured the isospin asymmetry $\Delta_{0-} = -0.006 \pm 0.020$ in $b \rightarrow s\gamma$ measured using sum of exclusive decays [174, 175]. An alternative measurement using full reconstruction of the companion B in the hadronic decay modes yields a consistent, but less precise result [176]. Both Belle and BaBar experiments measured the isospin asymmetry in exclusive $B \rightarrow K^*(892)\gamma$ decay with aver-

age of $6.3 \pm 1.7\%$ [154, 155] and therefore providing evidence for the non-zero isospin asymmetry.

In addition, experiments have measured the inclusive photon energy spectrum for $b \rightarrow s\gamma$, and by analyzing the shape of the spectrum they obtain the first and second moments for photon energies. Belle has measured these moments covering the widest range in the photon energy ($1.7 < E_\gamma < 2.8$ GeV) [170]. The measurement by BaBar has slightly smaller range with lower limit at 1.8 GeV [177]. These results can be used to extract non-perturbative HQET parameters that are needed for precise determination of the CKM matrix element V_{ub} (see further discussion elsewhere in this Review [178]).

Additional information on FCNC processes can be obtained from $b \rightarrow s\ell^+\ell^-$ decays. These processes are studied as a function of dilepton invariant mass squared, q^2 . Different q^2 regions are sensitive to different physics. Starting at the very low q^2 decays exhibit sensitivity to the same physics as the radiative decays. Then for the q^2 in region 1.1 to 6.0 GeV²/c⁴ the SM and new physics have best chance to compete. At the high q^2 above the $\psi(2S)$ mass, the interference of SM and new physics is to some extent complementary to that in lower q^2 . Regions around J/ψ and $\psi(2S)$ is normally excluded from measurements as these are dominated by the $b \rightarrow c$ transitions to charmonia. For exclusive decays, theory predictions require calculations of hadronic form factors. With current theory predictions, the most useful are measurements within the q^2 regions 1.1 to 6.0 GeV²/c⁴ and from 16.0 GeV²/c⁴ up to the kinematic limit. From this reason in the listing we provide results mainly in those two regions.

Similar as for radiative decays, also for the $b \rightarrow s\ell^+\ell^-$ decays the inclusive measurements provide some benefits. Both Belle and BaBar performed such measurement without reconstructing hadronic part exclusively and measure a branching fraction of $(5.8 \pm 1.3) \times 10^{-6}$ [179]. Unfortunately this measurement is not trivially possible at hadron colliders and also does not easily allow the angular distributions of the decay products to be exploited. One alternative is to extract information on the inclusive decay as sum of exclusive decays. Such a measurement was performed by Belle [180], but in this case the difficulty lies in extrapolation for the missing hadronic states.

Turning to the exclusive decays, the initial measurements performed by B-factories typically averaged between charged and neutral B mesons as well as between e^+e^- and $\mu^+\mu^-$ final states. The experiments CDF, LHCb, ATLAS and CMS are much better suited for the $\mu^+\mu^-$ final states compared to the e^+e^- final states. As such most measurements at hadron colliders are done only with $\mu^+\mu^-$ pairs and by separating charged and neutral B mesons. The best studied decays are $B^+ \rightarrow K^+\ell^+\ell^-$ and $B^0 \rightarrow K^*(892)^0\ell^+\ell^-$. At hadron colliders other b hadrons are produced and as such CDF and LHCb experiments did observe also $B_s^0 \rightarrow \phi\mu^+\mu^-$ [181, 182], $\Lambda_b^0 \rightarrow \Lambda\mu^+\mu^-$ [181, 183] and $\Lambda_b^0 \rightarrow pK^-\mu^+\mu^-$ decays [184]. The averages of the total branching fractions integrated over whole q^2 regions are $(5.6 \pm 0.6) \times 10^{-7}$ for $B^+ \rightarrow K^+e^+e^-$, $(4.53 \pm 0.35) \times 10^{-7}$ for $B^+ \rightarrow K^+\mu^+\mu^-$, $(1.03^{+0.19}_{-0.17}) \times 10^{-6}$ for $B^0 \rightarrow K^*(892)^0e^+e^-$ and $(0.94 \pm 0.05) \times 10^{-6}$ for $B^0 \rightarrow K^*(892)^0\mu^+\mu^-$ decays [185–189]. The total branching fractions for $B_s^0 \rightarrow \phi\mu^+\mu^-$ and $\Lambda_b^0 \rightarrow \Lambda\mu^+\mu^-$ decays are $(8.2 \pm 1.2) \times 10^{-7}$ [181, 182] and $(1.08 \pm 0.28) \times 10^{-6}$ [181, 183] respectively. With increased precision of $B^0 \rightarrow K^*(892)^0\ell^+\ell^-$ decay, there is a question on what fraction of the seen branching fraction is due to the $K^*(892)^0$ resonance and what fraction is due to the $K\pi$ in s -wave. This has been studied by LHCb which found that the $K\pi$ in s -wave fraction varies between 1% and about 10% depending on the q^2 region [189]. It should be noted, that for all relevant B meson decays the branching fractions so far studied are consistently below the SM expectation.

In the $b \rightarrow s\ell^+\ell^-$ decays angular distributions offer rich source of information. The full angular analysis was performed for decays $B^+ \rightarrow K^+\ell^+\ell^-$, $B^0 \rightarrow K^0\ell^+\ell^-$, $B^+ \rightarrow K^*(892)^+\ell^+\ell^-$, $B^0 \rightarrow K^*(892)^0\ell^+\ell^-$, $B_s^0 \rightarrow \phi\mu^+\mu^-$ and $\Lambda_b^0 \rightarrow \Lambda\mu^+\mu^-$ decays [190–198]. An attempt to increase sensitivity to the NP was made by constructing observables, which have reduced theory uncertainties and measurements of these are done. Most notably the observable called P'_5 [199] shows a discrepancy with the SM

in the q^2 region which is highly sensitive to new physics [192–194]. Measurements of the CP asymmetries [184, 185, 188, 200, 201], the isospin asymmetry [186–188, 200] were also performed. All these measurements are well consistent with the small A_{CP} and small isospin asymmetry expected in the SM [202]. With statistics available at the LHC, the measurement of phase difference between long- and short-distance contribution in $B^+ \rightarrow K^+\mu^+\mu^-$ decays became possible [203].

With the data samples available at LHC, the lepton universality in $b \rightarrow s\ell^+\ell^-$ can be tested. While in the SM decays to electron-positron and muon pairs are expected to be same up to small corrections due to the different masses of leptons, in extensions of the SM this does not have to hold. The angular analysis of $B^0 \rightarrow K^*(892)^0e^+e^-$ decays was performed by LHCb at low dilepton invariant masses [204] and Belle in several regions over whole q^2 range [194]. The LHCb measurement yields the most stringent constraint on the photon polarization. The most notable result on lepton universality test is the ratio of branching fractions between $B^+ \rightarrow K^+\mu^+\mu^-$ and $B^+ \rightarrow K^+e^+e^-$ and between $B^0 \rightarrow K^*(892)^0\mu^+\mu^-$ and $B^0 \rightarrow K^*(892)^0e^+e^-$ decays [186, 205–208]. In both cases, the measurements by LHCb show mild discrepancy from the SM, with significance of 3.1σ for $B^+ \rightarrow K^+\ell^+\ell^-$ and about 2.4σ for $B^0 \rightarrow K^*(892)^0\ell^+\ell^-$. LHCb experiment performed similar test with $\Lambda_b^0 \rightarrow pK^-\ell^+\ell^-$ decays [209].

While $b \rightarrow d\ell^+\ell^-$ decays are further suppressed, they recently became accessible. Signals were observed for $B^+ \rightarrow \pi^+\mu^+\mu^-$ [81], $B^0 \rightarrow \pi^+\pi^-\mu^+\mu^-$ [210] and $\Lambda_b^0 \rightarrow p\pi^-\mu^+\mu^-$ [211] decays. The total branching fractions are only quantities measured and these are about 2×10^{-8} for the meson decays and about 7×10^{-8} for the Λ_b^0 decay.

A closely related process is $B \rightarrow X_s\nu\bar{\nu}$. Since the neutrinos are not detected, the final state is a strange hadron system X_s plus missing energy-momentum. Depending on X_s , the SM branching fraction is $\mathcal{O}(10^{-6})$. New physics effects beyond SM, e.g. those from dark sector models can greatly enhance the yield of X_s plus missing energy. Both BaBar [212] and Belle [213] have searched for these decays and determined the upper limits in the range $\mathcal{O}(10^{-5})$.

Finally the decays $B_{(s)}^0 \rightarrow e^+e^-$ and $\mu^+\mu^-$ are interesting since they only proceed at second order in weak interactions in the SM, but may have large contributions from supersymmetric loops, proportional to $(\tan\beta)^6$. First limits were published 30 years ago and since then experiments at Tevatron, B -factories and LHC gradually improved those and effectively excluded whole models of new physics and significantly constrained allowed parameter space of others. For the decays to $\mu^+\mu^-$, Tevatron experiments pushed the limits down to roughly factor of 5–10 above the SM expectation [214, 215]. The long journey in the search for these decays culminated in 2012, when first evidence for $B_s^0 \rightarrow \mu^+\mu^-$ decay was seen [216]. Subsequently, LHC experiments ATLAS [217], CMS [218] and LHCb [219] observed statistically significant signal for $B_s^0 \rightarrow \mu^+\mu^-$ decay. The average branching fraction is found to be $(2.9 \pm 0.4) \times 10^{-9}$. In experiments at hadron colliders searches for $B^0 \rightarrow \mu^+\mu^-$ decays are performed at the same time. The best limit on $B(B^0 \rightarrow \mu^+\mu^-) < 2.1 \times 10^{-10}$ at 95% C.L. [217]. The limits for the e^+e^- modes are: $< 9.4 \times 10^{-9}$ and $< 2.5 \times 10^{-9}$, respectively, for B_s^0 and B^0 [220]. The searches for decays to $\tau^+\tau^-$ are more challenging with current best limits of $B(B^0 \rightarrow \tau^+\tau^-) < 2.1 \times 10^{-3}$ and $B(B_s^0 \rightarrow \tau^+\tau^-) < 6.8 \times 10^{-3}$ at 95% C.L. [221]. All existing measurements of B^0 and B_s^0 decays to same flavour dilepton pair is consistent with SM expectation [222]. With $B_s^0 \rightarrow \mu^+\mu^-$ decay observed, it was suggested that the effective lifetime is useful further test of the decay [223]. Attempt was made by LHCb and CMS experiments, but its precision is not yet sufficient to provide test of the SM [218, 219]. It will take couple of years until interesting precision is reached. The searches were also performed for lepton flavour violating decays to two leptons with best limits in $e^\pm\mu^\pm$ channel, where limits are $< 1.3 \times 10^{-9}$ for B^0 and $< 6.3 \times 10^{-9}$ for B_s^0 , at 95% confidence level [224].

Several theory groups performed global analysis of electroweak decays concluding that significant tension between data and SM is

present [225]. The tension can be relieved by new physics beyond SM. For more detailed reviews see e.g. Ref. [226].

73.7 Summary and Outlook

The study of B mesons continues to be one of the most productive fields in particle physics. With the two asymmetric B -factory experiments Belle and BaBar, we now have a combined data sample of well over 1 ab^{-1} . CP violation has been firmly established in many decays of B mesons. Evidence for direct CP violation has been observed. Many rare decays resulting from hadronic $b \rightarrow u$ transitions and $b \rightarrow s(d)$ penguin decays have been observed, and the emerging pattern is still full of surprises. Despite the remarkable successes of the B -factory experiments, many fundamental questions in the flavor sector remain unanswered.

At Fermilab, CDF and D0 each has accumulated about 10 fb^{-1} , which is the equivalent of about 10^{12} b -hadrons produced. In spite of the low trigger efficiency of hadronic experiments, a selection of modes have been reconstructed in large quantities, giving a start to a program of studies on B_s and b -flavored baryons, in which a first major step has been the determination of the B_s oscillation frequency.

As Tevatron and B -factories finished their data taking few year ago, the experiments at the LHC have become very active. LHCb has collected about 1 fb^{-1} at 7 TeV, 2 fb^{-1} at 8 TeV, and close to 5.9 fb^{-1} at 13 TeV during LHC Runs 1 and 2. CMS and ATLAS have collected each about 5 fb^{-1} of data at $\sqrt{s} = 7 \text{ TeV}$, 20 fb^{-1} at 8 TeV and about 150 fb^{-1} at 13 TeV during LHC Runs 1 and 2. LHCb, which is dedicated to the studies of b - and c -hadrons, has a data sample that is for many decays larger than the sum of all previous experiments. With it, we are entering to regime of precision physics even for many rare decays, which allows much more detailed measurements.

The Belle II experiment at the SuperKEKB has started recording data in 2019 and has so far collected about 200 fb^{-1} of data (August 2021). The aim to increase sample to $\sim 50 \text{ ab}^{-1}$ will make it possible to explore the indirect evidence of new physics beyond the SM in the heavy-flavor particles (b , c , and τ), in a way that is complementary to the LHC. In the same time period, LHCb Collaboration is working on the upgrade of its detector, installation of which is ongoing. The aim of the upgrade is to increase flexibility of the trigger, which will allow about a factor of five increase in instantaneous luminosity and of about a factor of two in efficiencies on triggering on purely hadronic decays. The plan is to integrate about 50 fb^{-1} of data starting from 2022.

These experiments promise a rich spectrum of rare and precise measurements that have the potential to fundamentally affecting our understanding of the SM and CP -violating phenomena.

References

- [1] M. Kobayashi and T. Maskawa, *Prog. Theor. Phys.* **49**, 652 (1973).
- [2] S. W. Herb *et al.*, *Phys. Rev. Lett.* **39**, 252 (1977).
- [3] B. Aubert *et al.* (BaBar), *Phys. Rev. Lett.* **87**, 091801 (2001), [hep-ex/0107013].
- [4] K. Abe *et al.* (Belle), *Phys. Rev. Lett.* **87**, 091802 (2001), [hep-ex/0107061].
- [5] Currently two different notations (ϕ_1, ϕ_2, ϕ_3) and (α, β, γ) are used in the literature for CKM unitarity angles. In this mini-review, we use the latter notation following the other mini-reviews in this *Review*. The two notations are related by $\phi_1 = \beta$, $\phi_2 = \alpha$ and $\phi_3 = \gamma$.
- [6] See the “ CP Violation in Meson Decays” by D. Kirkby and Y. Nir in this *Review*.
- [7] See the “CKM Quark Mixing Matrix,” by A. Cecucci, Z. Ligeti, and Y. Sakai, in this *Review*.
- [8] See the note on “ $B^0 - \bar{B}^0$ mixing,” by O. Schneider in this *Review*.
- [9] See the “Determination of $|V_{cb}|$ and $|V_{ub}|$,” by R. Kowalewski and T. Mannel in this *Review*.
- [10] F. Abe *et al.* (CDF), *Phys. Rev. Lett.* **81**, 2432 (1998), [hep-ex/9805034]; F. Abe *et al.* (CDF), *Phys. Rev.* **D58**, 112004 (1998), [hep-ex/9804014].
- [11] A. Abulencia *et al.* (CDF), *Phys. Rev. Lett.* **96**, 082002 (2006), [hep-ex/0505076].
- [12] R. Aaij *et al.* (LHCb), *JHEP* **07**, 123 (2020), [arXiv:2004.08163].
- [13] B. Aubert *et al.* (BaBar), *Phys. Rev. Lett.* **101**, 071801 (2008), [Erratum: *Phys. Rev. Lett.*102,029901(2009)], [arXiv:0807.1086].
- [14] B. Aubert *et al.* (BaBar), *Phys. Rev. Lett.* **103**, 161801 (2009), [arXiv:0903.1124].
- [15] G. Bonvicini *et al.* (CLEO), *Phys. Rev.* **D81**, 031104 (2010), [arXiv:0909.5474].
- [16] R. Mizuk *et al.* (Belle), *Phys. Rev. Lett.* **109**, 232002 (2012), [arXiv:1205.6351].
- [17] U. Tamponi *et al.* (Belle), *Phys. Rev. Lett.* **115**, 14, 142001 (2015), [arXiv:1506.08914].
- [18] A. Bondar *et al.* (Belle), *Phys. Rev. Lett.* **108**, 122001 (2012), [arXiv:1110.2251].
- [19] See the note on “Naming scheme for hadrons,” by M. Roos and C.G. Wohl in this *Review*.
- [20] R. Aaij *et al.* (LHCb), *Phys. Rev. Lett.* **118**, 5, 052002 (2017), [Erratum: *Phys. Rev. Lett.*119,no.16,169901(2017)], [arXiv:1612.05140].
- [21] M. Cacciari *et al.*, *JHEP* **10**, 137 (2012), [arXiv:1205.6344]; B. A. Kniehl *et al.*, *Phys. Rev.* **D84**, 094026 (2011), [arXiv:1109.2472]; M. Cacciari, M. L. Mangano and P. Nason, *Eur. Phys. J.* **C75**, 12, 610 (2015), [arXiv:1507.06197].
- [22] B. Barish *et al.* (CLEO), *Phys. Rev. Lett.* **76**, 1570 (1996).
- [23] E. Guido *et al.* (Belle), *Phys. Rev. Lett.* **121**, 062001 (2018), [arXiv:1803.10303]; E. Guido *et al.* (Belle), *Phys. Rev.* **D96**, 052005 (2017), [arXiv:1707.04973]; A. Sokolov *et al.* (Belle), *Phys. Rev.* **D79**, 051103 (2009), [arXiv:0901.1431]; B. Aubert *et al.* (BaBar), *Phys. Rev.* **D78**, 112002 (2008), [arXiv:0807.2014].
- [24] J. P. Alexander *et al.* (CLEO), *Phys. Rev. Lett.* **86**, 2737 (2001), [hep-ex/0006002]; S. B. Athar *et al.* (CLEO), *Phys. Rev.* **D66**, 052003 (2002), [hep-ex/0202033].
- [25] N. C. Hastings *et al.* (Belle), *Phys. Rev.* **D67**, 052004 (2003), [hep-ex/0212033].
- [26] B. Aubert *et al.* (BaBar), *Phys. Rev. Lett.* **95**, 042001 (2005), [hep-ex/0504001].
- [27] Y. Amhis *et al.* (HFLAV), *Eur. Phys. J.* **C77**, 12, 895 (2017), [arXiv:1612.07233].
- [28] Y. S. Amhis *et al.* (HFLAV) (2019), and online update at <https://hflav.web.cern.ch/content/lifetimes-and-oscillation-parameters>, [arXiv:1909.12524].
- [29] P. Abreu *et al.* (DELPHI), *Phys. Lett.* **B345**, 598 (1995).
- [30] R. Akers *et al.* (OPAL), *Z. Phys.* **C66**, 19 (1995).
- [31] T. A. Aaltonen *et al.* (CDF), *Phys. Rev.* **D90**, 1, 012013 (2014), [arXiv:1309.5961].
- [32] R. Aaij *et al.* (LHCb), *JHEP* **04**, 024 (2015), [arXiv:1502.02638].
- [33] R. Aaij *et al.* (LHCb), *Phys. Rev. Lett.* **110**, 15, 151803 (2013), [arXiv:1211.5994].
- [34] A. M. Sirunyan *et al.* (CMS), *Eur. Phys. J.* **C78**, 939 (2018), [arXiv:1809.03578].
- [35] G. Aad *et al.* (ATLAS), *Phys. Rev. Lett.* **113**, 21, 212004 (2014), [arXiv:1407.1032].
- [36] A. Sirunyan *et al.* (CMS), *Phys. Rev. Lett.* **122**, 132001 (2019), [arXiv:1902.00571].
- [37] R. Aaij *et al.* (LHCb), *Phys. Rev. Lett.* **122**, 232001 (2019), [arXiv:1904.00081].
- [38] T. Aaltonen *et al.* (CDF), *Phys. Rev. Lett.* **99**, 202001 (2007), [arXiv:0706.3868]; T. Aaltonen *et al.* (CDF), *Phys. Rev.* **D85**, 092011 (2012), [arXiv:1112.2808].

- [39] R. Aaij *et al.* (LHCb), Phys. Rev. Lett. **122**, 012001 (2019), [arXiv:1809.07752].
- [40] V. M. Abazov *et al.* (D0), Phys. Rev. Lett. **99**, 052001 (2007), [arXiv:0706.1690]; T. Aaltonen *et al.* (CDF), Phys. Rev. Lett. **99**, 052002 (2007), [arXiv:0707.0589].
- [41] R. Aaij *et al.* (LHCb), Phys. Rev. Lett. **113**, 032001 (2014), [arXiv:1405.7223]; R. Aaij *et al.* (LHCb), Phys. Lett. **B736**, 154 (2014), [arXiv:1405.1543]; R. Aaij *et al.* (LHCb), Phys. Rev. **D89**, 3, 032001 (2014), [arXiv:1311.4823]; R. Aaij *et al.* (LHCb), Phys. Rev. Lett. **113**, 24, 242002 (2014), [arXiv:1409.8568]; R. Aaij *et al.* (LHCb), Phys. Rev. Lett. **115**, 24, 241801 (2015), [arXiv:1510.03829]; R. Aaij *et al.* (LHCb), Phys. Rev. Lett. **118**, 7, 071801 (2017), [arXiv:1612.02244]; R. Aaij *et al.* (LHCb), Phys. Lett. **B722**, 265 (2017), [arXiv:1701.05274]; R. Aaij *et al.* (LHCb), Phys. Rev. Lett. **118**, 071801 (2017), [arXiv:1612.02244]; R. Aaij *et al.* (LHCb), JHEP **02**, 98 (2018), [arXiv:1711.05490]; R. Aaij *et al.* (LHCb), Phys. Rev. **D99**, 052006 (2019), [arXiv:1901.07075].
- [42] T. A. Aaltonen *et al.* (CDF), Phys. Rev. **D89**, 7, 072014 (2014), [arXiv:1403.8126].
- [43] R. Aaij *et al.* (LHCb), JHEP **08**, 039 (2018), [arXiv:1805.03941].
- [44] S. Chatrchyan *et al.* (CMS), Phys. Rev. Lett. **108**, 252002 (2012), [arXiv:1204.5955].
- [45] R. Aaij *et al.* (LHCb), JHEP **1605**, 161 (2016), [arXiv:1604.03896].
- [46] R. Aaij *et al.* (LHCb), Phys. Rev. Lett. **114**, 062004 (2015), [arXiv:1411.4849].
- [47] R. Aaij *et al.* (LHCb), Phys. Rev. Lett. **121**, 072002 (2018), [arXiv:1805.09418].
- [48] V. M. Abazov *et al.* (D0), Phys. Rev. Lett. **101**, 232002 (2008), [arXiv:0808.4142]; T. Aaltonen *et al.* (CDF), Phys. Rev. **D80**, 072003 (2009), [arXiv:0905.3123].
- [49] R. Aaij *et al.* (LHCb), Phys. Rev. Lett. **110**, 18, 182001 (2013), [arXiv:1302.1072]; R. Aaij *et al.* (LHCb), Phys. Lett. **B736**, 154 (2014), [arXiv:1405.1543]; R. Aaij *et al.* (LHCb), Phys. Rev. **D93**, 9, 092007 (2016), [arXiv:1604.01412].
- [50] V. M. Abazov *et al.* (D0), Phys. Rev. Lett. **117**, 2, 022003 (2016), [arXiv:1602.07588]; V. M. Abazov *et al.* (D0), Phys. Rev. **D97**, 092004 (2018), [arXiv:1712.10176].
- [51] R. Aaij *et al.* (LHCb), Phys. Rev. Lett. **117**, 15, 152003 (2016), [Addendum: Phys. Rev. Lett. **118**, no.10, 109904 (2017)], [arXiv:1608.00435].
- [52] A. Sirunyan *et al.* (CMS), Phys. Rev. Lett. **120**, 202005 (2018), [arXiv:1712.06144].
- [53] C. Tarantino, Eur. Phys. J. **C33**, S895 (2004), [hep-ph/0310241]; F. Gabbiani, A. I. Onishchenko and A. A. Petrov, Phys. Rev. **D70**, 094031 (2004), [hep-ph/0407004]; F. Gabbiani, A. I. Onishchenko and A. A. Petrov, Phys. Rev. **D68**, 114006 (2003), [hep-ph/0303235].
- [54] A. Lenz, Int. J. Mod. Phys. **A30**, 10, 1543005 (2015), [arXiv:1405.3601].
- [55] C.-H. Chang *et al.*, Phys. Rev. **D64**, 014003 (2001), [hep-ph/0007162]; V. V. Kiselev, A. E. Kovalsky and A. K. Likhoded, Nucl. Phys. **B585**, 353 (2000), [hep-ph/0002127]; A. Yu. Anisimov *et al.*, Phys. Lett. **B452**, 129 (1999), [hep-ph/9812514]; M. Beneke and G. Buchalla, Phys. Rev. **D53**, 4991 (1996), [hep-ph/9601249].
- [56] R. Aaij *et al.* (LHCb), Eur. Phys. J. **C74**, 5, 2839 (2014), [arXiv:1401.6932].
- [57] R. Aaij *et al.* (LHCb), Phys. Lett. **B742**, 29 (2015), [arXiv:1411.6899].
- [58] The B_c is a special case, where a weak decay of the c quark is also possible, but the spectator model still applies.
- [59] R. Aaij *et al.* (LHCb), Nature Phys. **11**, 743 (2015), [arXiv:1504.01568].
- [60] J. P. Lees *et al.* (BaBar), Phys. Rev. **D85**, 011101 (2012), [arXiv:1110.5600]; C. Oswald *et al.* (Belle), Phys. Rev. **D87**, 7, 072008 (2013), [Erratum: Phys. Rev. **D90**, no.11, 119901 (2014)], [arXiv:1212.6400]; C. Oswald *et al.* (Belle), Phys. Rev. **D92**, 7, 072013 (2015), [arXiv:1504.02004].
- [61] T. A. Aaltonen *et al.* (CDF), Phys. Rev. **D93**, 5, 052001 (2016), [arXiv:1601.03819].
- [62] R. Aaij *et al.* (LHCb), Phys. Rev. Lett. **126**, 8, 081804 (2021), [arXiv:2012.05143].
- [63] B. Grinstein, Nucl. Phys. **B339**, 253 (1990); H. Georgi, Phys. Lett. **B240**, 447 (1990); A. F. Falk *et al.*, Nucl. Phys. **B343**, 1 (1990); E. Eichten and B. R. Hill, Phys. Lett. **B234**, 511 (1990).
- [64] "Heavy-Quark and Soft-Collinear Effective Theory" by C.W. Bauer and M. Neubert in this *Review*.
- [65] M. Neubert, "Aspects of QCD Factorization," hep-ph/0110093, *Proceedings of HF9*, Pasadena (2001) and references therein; Z. Ligeti, M. E. Luke and M. B. Wise, Phys. Lett. **B507**, 142 (2001), [hep-ph/0103020].
- [66] M. Beneke *et al.*, Phys. Rev. Lett. **83**, 1914 (1999), [hep-ph/9905312].
- [67] M. Beneke *et al.*, Nucl. Phys. **B591**, 313 (2000), [hep-ph/0006124].
- [68] M. Beneke *et al.*, Nucl. Phys. **B606**, 245 (2001), [hep-ph/0104110].
- [69] M. Beneke and M. Neubert, Nucl. Phys. **B675**, 333 (2003), [hep-ph/0308039].
- [70] Y.-Y. Keum, H.-n. Li and A. I. Sanda, Phys. Lett. **B504**, 6 (2001), [hep-ph/0004004].
- [71] Y. Y. Keum, H.-N. Li and A. I. Sanda, Phys. Rev. **D63**, 054008 (2001), [hep-ph/0004173].
- [72] Y.-Y. Keum and H.-n. Li, Phys. Rev. **D63**, 074006 (2001), [hep-ph/0006001].
- [73] C.-D. Lu, K. Ukai and M.-Z. Yang, Phys. Rev. **D63**, 074009 (2001), [hep-ph/0004213].
- [74] C.-D. Lu and M.-Z. Yang, Eur. Phys. J. **C23**, 275 (2002), [hep-ph/0011238].
- [75] C. W. Bauer, S. Fleming and M. E. Luke, Phys. Rev. **D63**, 014006 (2000), [hep-ph/0005275].
- [76] C. W. Bauer *et al.*, Phys. Rev. **D63**, 114020 (2001), [hep-ph/0011336].
- [77] C. W. Bauer and I. W. Stewart, Phys. Lett. **B516**, 134 (2001), [hep-ph/0107001].
- [78] R. Ammar *et al.* (CLEO), Phys. Rev. Lett. **71**, 674 (1993).
- [79] N. Taniguchi *et al.* (Belle), Phys. Rev. Lett. **101**, 111801 (2008), [Erratum: Phys. Rev. Lett. **101**, 129904 (2008)], [arXiv:0804.4770].
- [80] B. Aubert *et al.* (BaBar), Phys. Rev. **D78**, 112001 (2008), [arXiv:0808.1379].
- [81] R. Aaij *et al.* (LHCb), JHEP **10**, 034 (2015), [arXiv:1509.00414].
- [82] P. Krokovny *et al.* (Belle), Phys. Rev. Lett. **89**, 231804 (2002), [hep-ex/0207077]; B. Aubert *et al.* (BaBar), Phys. Rev. Lett. **98**, 081801 (2007), [hep-ex/0604012].
- [83] B. Kronenbitter *et al.* (Belle), Phys. Rev. **D92**, 5, 051102 (2015), [arXiv:1503.05613]; I. Adachi *et al.* (Belle), Phys. Rev. Lett. **110**, 13, 131801 (2013), [arXiv:1208.4678].
- [84] J. P. Lees *et al.* (BaBar), Phys. Rev. **D88**, 3, 031102 (2013), [arXiv:1207.0698]; B. Aubert *et al.* (BaBar), Phys. Rev. **D81**, 051101 (2010), [arXiv:0912.2453].
- [85] See the "Leptonic decays of charged pseudoscalar mesons," by J. Rosner, S. Stone, and R. Van de Water, in this *Review*.
- [86] J. P. Lees *et al.* (BaBar), Phys. Rev. **D84**, 112007 (2011), [Erratum: Phys. Rev. **D87**, no.3, 039901 (2013)], [arXiv:1107.5751]; S. Blyth *et al.* (Belle), Phys. Rev. **D74**, 092002 (2006), [hep-ex/0607029].

- [87] R. Aaij *et al.* (LHCb), Phys. Rev. D **92**, 3, 032002 (2015), [arXiv:1505.01710].
- [88] B. Aubert *et al.* (BaBar), Phys. Rev. Lett. **90**, 242001 (2003), [hep-ex/0304021].
- [89] D. Besson *et al.* (CLEO), Phys. Rev. **D68**, 032002 (2003), [Erratum: Phys. Rev.D75,119908(2007)], [hep-ex/0305100].
- [90] P. Krokovny *et al.* (Belle), Phys. Rev. Lett. **91**, 262002 (2003), [hep-ex/0308019]; Y. Mikami *et al.* (Belle), Phys. Rev. Lett. **92**, 012002 (2004), [hep-ex/0307052].
- [91] B. Aubert *et al.* (BaBar), Phys. Rev. Lett. **93**, 181801 (2004), [hep-ex/0408041].
- [92] R. Aaij *et al.* (LHCb), Phys. Rev. Lett. **113**, 162001 (2014), [arXiv:1407.7574].
- [93] T. Aaltonen *et al.* (CDF), Phys. Rev. Lett. **108**, 201801 (2012), [arXiv:1204.0536].
- [94] S. Esen *et al.* (Belle), Phys. Rev. **D87**, 3, 031101 (2013), [arXiv:1208.0323].
- [95] R. Aaij *et al.* (LHCb), Phys. Rev. **D93**, 9, 092008 (2016), [arXiv:1602.07543].
- [96] R. Aaij *et al.* (LHCb), Phys. Rev. Lett. **116**, 16, 161802 (2016), [arXiv:1603.02408].
- [97] R. Aaij *et al.* (LHCb), JHEP **11**, 082 (2015), [arXiv:1509.00400].
- [98] B. Aubert *et al.* (BaBar), Phys. Rev. **D76**, 031101 (2007), [arXiv:0704.1266].
- [99] R. Aaij *et al.* (LHCb), Phys. Rev. **D90**, 1, 012003 (2014), [arXiv:1404.5673].
- [100] R. Aaij *et al.* (LHCb), Phys. Rev. Lett. **111**, 18, 181801 (2013), [arXiv:1308.4544].
- [101] R. Aaij *et al.* (LHCb), Phys. Rev. **D87**, 11, 112012 (2013), [Addendum: Phys. Rev.D89,no.1,019901(2014)], [arXiv:1304.4530].
- [102] G. Aad *et al.* (ATLAS), Eur. Phys. J. **C76**, 1, 4 (2016), [arXiv:1507.07099].
- [103] R. Aaij *et al.* (LHCb), Phys. Rev. **D84**, 092001 (2011), [Erratum: Phys. Rev.D85,039904(2012)], [arXiv:1109.6831]; T. Aaltonen *et al.* (CDF), Phys. Rev. **D85**, 032003 (2012), [arXiv:1112.3334].
- [104] S. K. Choi *et al.* (Belle), Phys. Rev. Lett. **91**, 262001 (2003), [hep-ex/0309032].
- [105] D. Acosta *et al.* (CDF), Phys. Rev. Lett. **93**, 072001 (2004), [hep-ex/0312021].
- [106] V. M. Abazov *et al.* (D0), Phys. Rev. Lett. **93**, 162002 (2004), [hep-ex/0405004].
- [107] B. Aubert *et al.* (BaBar), Phys. Rev. **D71**, 071103 (2005), [hep-ex/0406022].
- [108] R. Aaij *et al.* (LHCb), Eur. Phys. J. **C72**, 1972 (2012), [arXiv:1112.5310].
- [109] S. Chatrchyan *et al.* (CMS), JHEP **04**, 154 (2013), [arXiv:1302.3968].
- [110] M. Aaboud *et al.* (ATLAS), JHEP **01**, 117 (2017), [arXiv:1610.09303].
- [111] S. K. Choi *et al.* (Belle), Phys. Rev. Lett. **100**, 142001 (2008), [arXiv:0708.1790]; R. Mizuk *et al.* (Belle), Phys. Rev. **D80**, 031104 (2009), [arXiv:0905.2869].
- [112] R. Aaij *et al.* (LHCb), Phys. Rev. Lett. **112**, 22, 222002 (2014), [arXiv:1404.1903]; R. Aaij *et al.* (LHCb), Phys. Rev. **D92**, 11, 112009 (2015), [arXiv:1510.01951].
- [113] K. Chilikin *et al.* (Belle), Phys. Rev. **D90**, 11, 112009 (2014), [arXiv:1408.6457].
- [114] R. Aaij *et al.* (LHCb), Phys. Rev. Lett. **115**, 072001 (2015), [arXiv:1507.03414].
- [115] R. Aaij *et al.* (LHCb), Phys. Rev. Lett. **122**, 22, 222001 (2019), [arXiv:1904.03947].
- [116] See the “Non- $q\bar{q}$ mesons,” by C. Amsler and C. Hanhart, and “Pentaquarks,” by M. Karliner and T. Skwarnicki, in this *Review*.
- [117] T. Aaltonen *et al.* (CDF), Phys. Rev. Lett. **107**, 261802 (2011), [arXiv:1107.4999].
- [118] R. Aaij *et al.* (LHCb), JHEP **10**, 053 (2015), [arXiv:1508.00788].
- [119] T. A. Aaltonen *et al.* (CDF), Phys. Rev. Lett. **113**, 24, 242001 (2014), [arXiv:1403.5586].
- [120] R. Aaij *et al.* (LHCb), JHEP **10**, 037 (2012), [arXiv:1206.2794].
- [121] T. Aaltonen *et al.* (CDF), Phys. Rev. Lett. **103**, 031801 (2009), [arXiv:0812.4271].
- [122] R. Aaij *et al.* (LHCb), Phys. Rev. D **98**, 3, 032004 (2018), [arXiv:1805.06759].
- [123] R. Aaij *et al.* (LHCb), JHEP **12**, 155 (2019), [arXiv:1907.10003].
- [124] R. Fleischer, Phys. Lett. **B459**, 306 (1999), [hep-ph/9903456]; D. London and J. Matias, Phys. Rev. **D70**, 031502 (2004), [hep-ph/0404009].
- [125] J. P. Lees *et al.* (BaBar), Phys. Rev. **D87**, 5, 052009 (2013), [arXiv:1206.3525].
- [126] Y. T. Duh *et al.* (Belle), Phys. Rev. **D87**, 3, 031103 (2013), [arXiv:1210.1348].
- [127] B. Aubert *et al.* (BaBar), Phys. Rev. **D76**, 091102 (2007), [arXiv:0707.2798].
- [128] R. Aaij *et al.* (LHCb), Phys. Lett. B **726**, 646 (2013), [arXiv:1308.1277].
- [129] M. Gronau and J. L. Rosner, Phys. Rev. **D71**, 074019 (2005), [hep-ph/0503131]; M. Gronau, Phys. Lett. **B627**, 82 (2005), [hep-ph/0508047].
- [130] B. Aubert *et al.* (BaBar), Phys. Rev. D **79**, 052003 (2009), [arXiv:0809.1174].
- [131] M. Fujikawa *et al.* (Belle), Phys. Rev. D **81**, 011101 (2010), [arXiv:0809.4366].
- [132] B. Aubert *et al.* (BaBar), Phys. Rev. **D78**, 012004 (2008), [arXiv:0803.4451]; A. Garmash *et al.* (Belle), Phys. Rev. Lett. **96**, 251803 (2006), [hep-ex/0512066].
- [133] C. T. Hoi *et al.* (Belle), Phys. Rev. Lett. **108**, 031801 (2012), [arXiv:1110.2000]; B. Aubert *et al.* (BaBar), Phys. Rev. **D80**, 112002 (2009), [arXiv:0907.1743].
- [134] B. Aubert *et al.* (BaBar), Phys. Rev. Lett. **97**, 201802 (2006), [hep-ex/0608005]; C. H. Wang *et al.* (Belle), Phys. Rev. **D75**, 092005 (2007), [hep-ex/0701057].
- [135] R. Aaij *et al.* (LHCb), Phys. Rev. **D90**, 11, 112004 (2014), [arXiv:1408.5373].
- [136] C.-L. Hsu *et al.* (Belle), Phys. Rev. D **96**, 3, 031101 (2017), [arXiv:1705.02640].
- [137] B. Aubert *et al.* (BaBar), Phys. Rev. Lett. **97**, 171805 (2006), [hep-ex/0608036].
- [138] K. Abe *et al.* (Belle), Phys. Rev. Lett. **98**, 181804 (2007), [hep-ex/0608049].
- [139] R. Aaij *et al.* (LHCb), Phys. Rev. Lett. **118**, 8, 081801 (2017), [arXiv:1610.08288].
- [140] C. C. Peng *et al.* (Belle), Phys. Rev. **D82**, 072007 (2010), [arXiv:1006.5115].
- [141] T. Aaltonen *et al.* (CDF), Phys. Rev. Lett. **106**, 181802 (2011), [arXiv:1103.5762].
- [142] B. Pal *et al.* (Belle), Phys. Rev. Lett. **116**, 16, 161801 (2016), [arXiv:1512.02145].
- [143] R. Aaij *et al.* (LHCb), Phys. Rev. D **102**, 1, 012011 (2020), [arXiv:2002.08229].
- [144] See the “Determination of CKM angles from B hadrons,” by T. Gershon, M. Kenzie, and K. Trabelsi, in this *Review*.

- [145] M. Gronau and D. London, Phys. Rev. Lett. **65**, 3381 (1990).
- [146] T. Julius *et al.* (Belle), Phys. Rev. **D96**, 3, 032007 (2017), [arXiv:1705.02083].
- [147] B. Aubert *et al.* (BaBar), Phys. Rev. **D78**, 071104 (2008), [arXiv:0807.4977].
- [148] P. Vanhoefer *et al.* (Belle), Phys. Rev. **D89**, 072008 (2014), [Addendum: Phys. Rev.D89,119903(2014)], [arXiv:1212.4015].
- [149] B. Aubert *et al.* (BaBar), Phys. Rev. **D76**, 052007 (2007), [arXiv:0705.2157]; P. Vanhoefer *et al.* (Belle), Phys. Rev. **D93**, 3, 032010 (2016), [Addendum: Phys.Rev.D 94, 099903 (2016)], [arXiv:1510.01245].
- [150] B. Aubert *et al.* (BaBar), Phys. Rev. Lett. **102**, 141802 (2009), [arXiv:0901.3522]; J. Zhang *et al.* (Belle), Phys. Rev. Lett. **91**, 221801 (2003), [hep-ex/0306007].
- [151] R. Aaij *et al.* (LHCb), Phys. Lett. **B747**, 468 (2015), [arXiv:1503.07770].
- [152] See the “Polarization in B Decays,” by A. Gritsan in this *Review*.
- [153] T. E. Coan *et al.* (CLEO), Phys. Rev. Lett. **84**, 5283 (2000), [hep-ex/9912057].
- [154] T. Horiguchi *et al.* (Belle), Phys. Rev. Lett. **119**, 19, 191802 (2017), [arXiv:1707.00394].
- [155] B. Aubert *et al.* (BaBar), Phys. Rev. Lett. **103**, 211802 (2009), [arXiv:0906.2177].
- [156] B. Aubert *et al.* (BaBar), Phys. Rev. **D70**, 091105 (2004), [hep-ex/0409035].
- [157] H. Yang *et al.* (Belle), Phys. Rev. Lett. **94**, 111802 (2005), [hep-ex/0412039].
- [158] S. Nishida *et al.* (Belle), Phys. Lett. **B610**, 23 (2005), [hep-ex/0411065].
- [159] B. Aubert *et al.* (BaBar), Phys. Rev. **D74**, 031102 (2006), [hep-ex/0603054].
- [160] B. Aubert *et al.* (BaBar), Phys. Rev. Lett. **98**, 211804 (2007), [Erratum: Phys. Rev. Lett.100,199905(2008)], [hep-ex/0507031].
- [161] P. del Amo Sanchez *et al.* (BaBar), Phys. Rev. **D93**, 5, 052013 (2016), [arXiv:1512.03579].
- [162] R. Aaij *et al.* (LHCb), Phys. Rev. Lett. **112**, 16, 161801 (2014), [arXiv:1402.6852].
- [163] J. Wicht *et al.* (Belle), Phys. Rev. Lett. **100**, 121801 (2008), [arXiv:0712.2659]; D. Dutta *et al.* (Belle), Phys. Rev. **D91**, 1, 011101 (2015), [arXiv:1411.7771].
- [164] R. Aaij *et al.* (LHCb), Nucl. Phys. **B867**, 1 (2013), [arXiv:1209.0313].
- [165] R. Aaij *et al.* (LHCb), Phys. Rev. Lett. **123**, 3, 031801 (2019), [arXiv:1904.06697].
- [166] A. Ali, E. Lunghi and A. Ya. Parkhomenko, Phys. Lett. **B595**, 323 (2004), [hep-ph/0405075]; P. Ball, G. W. Jones and R. Zwicky, Phys. Rev. **D75**, 054004 (2007), [hep-ph/0612081].
- [167] J. L. Hewett, Phys. Rev. Lett. **70**, 1045 (1993), [hep-ph/9211256].
- [168] S. Chen *et al.* (CLEO), Phys. Rev. Lett. **87**, 251807 (2001), [hep-ex/0108032].
- [169] J. P. Lees *et al.* (BaBar), Phys. Rev. **D86**, 112008 (2012), [arXiv:1207.5772].
- [170] A. Limosani *et al.* (Belle), Phys. Rev. Lett. **103**, 241801 (2009), [arXiv:0907.1384]; T. Saito *et al.* (Belle), Phys. Rev. **D91**, 5, 052004 (2015), [arXiv:1411.7198].
- [171] P. del Amo Sanchez *et al.* (BaBar), Phys. Rev. **D82**, 051101 (2010), [arXiv:1005.4087].
- [172] M. Misiak *et al.*, Phys. Rev. Lett. **114**, 22, 221801 (2015), [arXiv:1503.01789]; M. Czakon *et al.*, JHEP **04**, 168 (2015), [arXiv:1503.01791].
- [173] L. Wolfenstein and Y. L. Wu, Phys. Rev. Lett. **73**, 2809 (1994), [hep-ph/9410253]; G. M. Asatrian and A. Ioanianian, Phys. Rev. **D54**, 5642 (1996), [hep-ph/9603318]; M. Ciuchini, E. Gabrielli and G. F. Giudice, Phys. Lett. **B388**, 353 (1996), [Erratum: Phys. Lett.B393,489(1997)], [hep-ph/9604438]; S. Baek and P. Ko, Phys. Rev. Lett. **83**, 488 (1999), [hep-ph/9812229]; A. L. Kagan and M. Neubert, Phys. Rev. **D58**, 094012 (1998), [hep-ph/9803368]; K. Kierns, A. Soni and G.-H. Wu, Phys. Rev. **D62**, 116004 (2000), [hep-ph/0006280].
- [174] S. Watanuki *et al.* (Belle), Phys. Rev. **D99**, 3, 032012 (2019), [arXiv:1807.04236]; J. P. Lees *et al.* (BaBar), Phys. Rev. **D90**, 9, 092001 (2014), [arXiv:1406.0534].
- [175] B. Aubert *et al.* (BaBar), Phys. Rev. **D72**, 052004 (2005), [hep-ex/0508004].
- [176] B. Aubert *et al.* (BaBar), Phys. Rev. **D77**, 051103 (2008), [arXiv:0711.4889].
- [177] J. P. Lees *et al.* (BaBar), Phys. Rev. Lett. **109**, 191801 (2012), [arXiv:1207.2690].
- [178] See the “Semileptonic b -Hadron Decays, Determination of V_{cb} , V_{ub} ,” by T. Mannel and P. Urquijo in this *Review*.
- [179] M. Iwasaki *et al.* (Belle), Phys. Rev. **D72**, 092005 (2005), [hep-ex/0503044]; J. P. Lees *et al.* (BaBar), Phys. Rev. Lett. **112**, 211802 (2014), [arXiv:1312.5364].
- [180] Y. Sato *et al.* (Belle), Phys. Rev. **D93**, 3, 032008 (2016), [Addendum: Phys. Rev.D93,no.5,059901(2016)], [arXiv:1402.7134].
- [181] T. Aaltonen *et al.* (CDF), Phys. Rev. Lett. **107**, 201802 (2011), [arXiv:1107.3753].
- [182] R. Aaij *et al.* (LHCb), JHEP **07**, 084 (2013), [arXiv:1305.2168]; R. Aaij *et al.* (LHCb), JHEP **09**, 179 (2015), [arXiv:1506.08777].
- [183] R. Aaij *et al.* (LHCb), Phys. Lett. **B725**, 25 (2013), [arXiv:1306.2577].
- [184] R. Aaij *et al.* (LHCb), JHEP **06**, 108 (2017), [arXiv:1703.00256].
- [185] B. Aubert *et al.* (BaBar), Phys. Rev. Lett. **102**, 091803 (2009), [arXiv:0807.4119].
- [186] S. Choudhury *et al.* (BELLE), JHEP **03**, 105 (2021), [arXiv:1908.01848].
- [187] R. Aaij *et al.* (LHCb), JHEP **06**, 133 (2014), [arXiv:1403.8044].
- [188] J. T. Wei *et al.* (Belle), Phys. Rev. Lett. **103**, 171801 (2009), [arXiv:0904.0770].
- [189] R. Aaij *et al.* (LHCb), JHEP **11**, 047 (2016), [Erratum: JHEP 04, 142 (2017)], [arXiv:1606.04731].
- [190] T. Aaltonen *et al.* (CDF), Phys. Rev. Lett. **108**, 081807 (2012), [arXiv:1108.0695].
- [191] R. Aaij *et al.* (LHCb), JHEP **05**, 082 (2014), [arXiv:1403.8045].
- [192] A. M. Sirunyan *et al.* (CMS), Phys. Lett. **B781**, 517 (2018), [arXiv:1710.02846].
- [193] R. Aaij *et al.* (LHCb), Phys. Rev. Lett. **125**, 1, 011802 (2020), [arXiv:2003.04831].
- [194] S. Wehle *et al.* (Belle), Phys. Rev. Lett. **118**, 11, 111801 (2017), [arXiv:1612.05014].
- [195] M. Aaboud *et al.* (ATLAS), JHEP **10**, 047 (2018), [arXiv:1805.04000].
- [196] R. Aaij *et al.* (LHCb), Phys. Rev. Lett. **126**, 16, 161802 (2021), [arXiv:2012.13241].
- [197] R. Aaij *et al.* (LHCb) (2021), [arXiv:2107.13428].
- [198] R. Aaij *et al.* (LHCb), JHEP **09**, 146 (2018), [arXiv:1808.00264].
- [199] S. Descotes-Genon *et al.*, JHEP **01**, 048 (2013), [arXiv:1207.2753].

- [200] J. P. Lees *et al.* (BaBar), Phys. Rev. **D86**, 032012 (2012), [arXiv:1204.3933].
- [201] R. Aaij *et al.* (LHCb), JHEP **09**, 177 (2014), [arXiv:1408.0978].
- [202] J. Lyon and R. Zwicky, Phys. Rev. **D88**, 9, 094004 (2013), [arXiv:1305.4797].
- [203] R. Aaij *et al.* (LHCb), Eur. Phys. J. **C77**, 3, 161 (2017), [arXiv:1612.06764].
- [204] R. Aaij *et al.* (LHCb), JHEP **12**, 081 (2020), [arXiv:2010.06011].
- [205] R. Aaij *et al.* (LHCb), Phys. Rev. Lett. **122**, 19, 191801 (2019), [arXiv:1903.09252].
- [206] R. Aaij *et al.* (LHCb), JHEP **08**, 055 (2017), [arXiv:1705.05802].
- [207] R. Aaij *et al.* (LHCb) (2021), [arXiv:2103.11769].
- [208] A. Abdesselam *et al.* (Belle), Phys. Rev. Lett. **126**, 16, 161801 (2021), [arXiv:1904.02440].
- [209] R. Aaij *et al.* (LHCb) (2019), [arXiv:1912.08139].
- [210] R. Aaij *et al.* (LHCb), Phys. Lett. **B743**, 46 (2015), [arXiv:1412.6433].
- [211] R. Aaij *et al.* (LHCb), JHEP **04**, 029 (2017), [arXiv:1701.08705].
- [212] J. P. Lees *et al.* (BaBar), Phys. Rev. D **87**, 11, 112005 (2013), [arXiv:1303.7465].
- [213] J. Grygier *et al.* (Belle), Phys. Rev. D **96**, 9, 091101 (2017), [Addendum: Phys.Rev.D 97, 099902 (2018)], [arXiv:1702.03224].
- [214] T. Aaltonen *et al.* (CDF), Phys. Rev. Lett. **107**, 191801 (2011), [Addendum: Phys. Rev. Lett.107,no.23,239903(2011)], [arXiv:1107.2304].
- [215] V. M. Abazov *et al.* (D0), Phys. Rev. **D87**, 7, 072006 (2013), [arXiv:1301.4507].
- [216] R. Aaij *et al.* (LHCb), Phys. Rev. Lett. **110**, 2, 021801 (2013), [arXiv:1211.2674].
- [217] M. Aaboud *et al.* (ATLAS), JHEP **04**, 098 (2019), [arXiv:1812.03017].
- [218] A. M. Sirunyan *et al.* (CMS), JHEP **04**, 188 (2020), [arXiv:1910.12127].
- [219] R. Aaij *et al.* (LHCb), Phys. Rev. Lett. **118**, 19, 191801 (2017), [arXiv:1703.05747].
- [220] R. Aaij *et al.* (LHCb), Phys. Rev. Lett. **124**, 21, 211802 (2020), [arXiv:2003.03999].
- [221] R. Aaij *et al.* (LHCb), Phys. Rev. Lett. **118**, 25, 251802 (2017), [arXiv:1703.02508].
- [222] C. Bobeth *et al.*, Phys. Rev. Lett. **112**, 101801 (2014), [arXiv:1311.0903].
- [223] K. De Bruyn *et al.*, Phys. Rev. Lett. **109**, 041801 (2012), [arXiv:1204.1737]; A. J. Buras *et al.*, JHEP **07**, 77 (2013), [arXiv:1303.3820].
- [224] R. Aaij *et al.* (LHCb), JHEP **03**, 078 (2018), [arXiv:1710.04111].
- [225] J. Aebischer *et al.*, Eur. Phys. J. C **80**, 3, 252 (2020), [arXiv:1903.10434]; F. Beaujean, C. Bobeth and D. van Dyk, Eur. Phys. J. **C74**, 2897 (2014), [Erratum: Eur. Phys. J.C74,3179(2014)], [arXiv:1310.2478]; M. Algueró *et al.*, JHEP **07**, 096 (2019), [arXiv:1902.04900]; A. Arbey *et al.*, Phys. Rev. D **100**, 1, 015045 (2019), [arXiv:1904.08399].
- [226] T. Blake, G. Lanfranchi and D. M. Straub, Prog. Part. Nucl. Phys. **92**, 50 (2017), [arXiv:1606.00916]; J. Albrecht, S. Reichert and D. van Dyk, Int. J. Mod. Phys. A **33**, 18n19, 1830016 (2018), [arXiv:1806.05010].

74. Polarization in B Decays

Revised February 2022 by A.V. Gritsan (Johns Hopkins U.).

We review the notation used in polarization measurements in particle production and decay, with a particular emphasis on the B decays and the CP -violating observables in polarization measurements. We look at several examples of vector-vector and vector-tensor B meson decays, while more details about the theory and experimental results in B decays can be found in a separate mini-review [1] in this *Review*.

Figure 74.1 illustrates angular observables in an example of the sequential process $ab \rightarrow X \rightarrow P_1 P_2 \rightarrow (p_{11} p_{12})(p_{21} p_{22})$ [2]. The angular distributions are of particular interest because they are sensitive to spin correlations and reveal properties of particles and their interactions, such as quantum numbers and couplings. In the case of a spin-zero particle X , such as B meson or a Higgs boson, there are no spin correlations in the production mechanism and the decay chain is to be analyzed. The angular distribution of decay products can be expressed as a function of three helicity angles which describe the alignment of the particles in the decay chain. The analyzer of the B -daughter polarization is normally chosen for two-body decays, as the direction of the daughters in the center-of-mass of the parent (e.g., $\rho \rightarrow 2\pi$) [3], and for three-body decays as the normal to the decay plane (e.g., $\omega \rightarrow 3\pi$) [4]. An equivalent set of transversity angles is sometimes used in polarization analyses [5]. The differential decay width depends on complex amplitudes $A_{\lambda_1 \lambda_2}$, corresponding to the X -daughter helicity states λ_i .

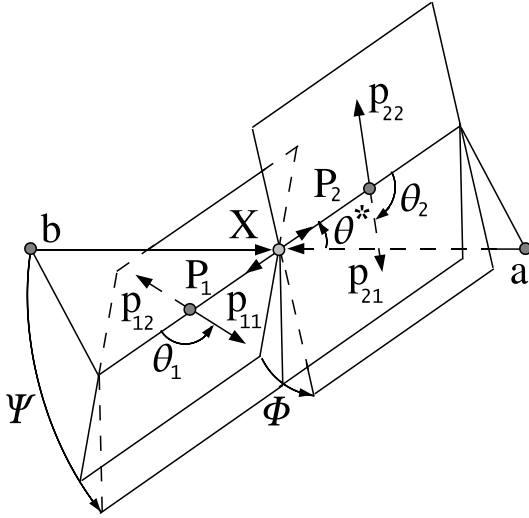


Figure 74.1: Definition of the production and helicity angles in the sequential process $ab \rightarrow X \rightarrow P_1 P_2 \rightarrow (p_{11} p_{12})(p_{21} p_{22})$. The three helicity angles include θ_1 and θ_2 , defined in the rest frame of the two daughters P_1 and P_2 , and Φ , defined in the X frame as the angle between the two decay planes. The two production angles θ^* and Ψ are defined in the X frame, where Ψ is the angle between the production plane and the average of the two decay planes.

In the case of a spin-zero B -meson decay, its daughter helicities are constrained to $\lambda_1 = \lambda_2 = \lambda$. Therefore we simplify amplitude notation as A_λ . Moreover, most B -decay polarization analyses are limited to the case when the spin of one of the B -meson daughters is 1. In that case, there are only three independent amplitudes corresponding to $\lambda = 0$ or ± 1 [6], where the last two can be expressed in terms of parity-even and parity-odd amplitudes $A_{\parallel, \perp} = (A_{+1} \pm A_{-1})/\sqrt{2}$. The overall decay amplitude involves three complex terms proportional to the above amplitudes and the Wigner d functions of helicity angles. The exact angular dependence would depend on the quantum numbers of the B -meson daughters and of their decay products, and can be found in the literature [6, 7]. When both B -meson daughters are tensor mesons and the smaller of the two daughter spins is $J_1 > 1$, this formalism

can be easily extended by introducing the parity-even and parity-odd amplitudes of higher order $A_{\parallel n, \perp n} = (A_{+n} \pm A_{-n})/\sqrt{2}$, with $1 < n \leq J_1$, while the general angular parameterization may be found in Ref. [7]. However, we limit the following discussion to $J_1 = 1$. The differential decay rate would involve six real quantities α_i , including interference terms,

$$\frac{d\Gamma}{\Gamma d \cos \theta_1 d \cos \theta_2 d\Phi} = \sum_i \alpha_i f_i(\cos \theta_1, \cos \theta_2, \Phi), \quad (74.1)$$

where each $f_i(\cos \theta_1, \cos \theta_2, \Phi)$ has unique angular dependence specific to particle quantum numbers, and the α_i parameters are defined as:

$$\alpha_1 = \frac{|A_0|^2}{\Sigma |A_\lambda|^2} = f_L, \quad (74.2)$$

$$\alpha_2 = \frac{|A_\parallel|^2 + |A_\perp|^2}{\Sigma |A_\lambda|^2} = (1 - f_L), \quad (74.3)$$

$$\alpha_3 = \frac{|A_\parallel|^2 - |A_\perp|^2}{\Sigma |A_\lambda|^2} = (1 - f_L - 2f_\perp), \quad (74.4)$$

$$\alpha_4 = \frac{\Im m(A_\perp A_\parallel^*)}{\Sigma |A_\lambda|^2} = \sqrt{f_\perp(1 - f_L - f_\perp)} \sin(\phi_\perp - \phi_\parallel), \quad (74.5)$$

$$\alpha_5 = \frac{\Re e(A_\parallel A_0^*)}{\Sigma |A_\lambda|^2} = \sqrt{f_L(1 - f_L - f_\perp)} \cos(\phi_\parallel), \quad (74.6)$$

$$\alpha_6 = \frac{\Im m(A_\perp A_0^*)}{\Sigma |A_\lambda|^2} = \sqrt{f_\perp f_L} \sin(\phi_\perp), \quad (74.7)$$

where the amplitudes have been expressed with the help of polarization parameters f_L , f_\perp , ϕ_\parallel , and ϕ_\perp defined in Table 74.1. Note that the terms proportional to $\Re e(A_\perp A_\parallel^*)$, $\Im m(A_\parallel A_0^*)$, and $\Re e(A_\perp A_0^*)$ are absent in Eqs. (2-7). However, these terms may appear for some three-body decays of a B -meson daughter, see Ref. [7].

Table 74.1: Rate, polarization, and CP -asymmetry parameters defined for the B -meson decays to mesons with non-zero spin. Numerical examples are shown for the average of the $B^0 \rightarrow \varphi K^*(892)^0$ decay measurements obtained from BABAR [8], Belle [9], and LHCb [10]. The first six parameters are defined under the assumption of no CP violation in decay, while they are averaged between the \bar{B} and B parameters in general. The last six parameters involve differences between the \bar{B} and B meson decay parameters. The phase convention δ_0 is chosen with respect to a single A_{00} amplitude from a reference B decay mode, which is $B^0 \rightarrow \varphi K^*(1430)^0$ for numerical results.

parameter	definition	average
\mathcal{B}	$\Gamma/\Gamma_{\text{total}}$	$(10.1^{+0.6}_{-0.5}) \times 10^{-6}$
f_L	$ A_0 ^2/\Sigma A_\lambda ^2$	0.497 ± 0.017
f_\perp	$ A_\perp ^2/\Sigma A_\lambda ^2$	0.225 ± 0.015
$\phi_\parallel - \pi$	$\arg(A_\parallel/A_0) - \pi$	-0.712 ± 0.058
$\phi_\perp - \pi$	$\arg(A_\perp/A_0) - \pi$	-0.615 ± 0.056
$\delta_0 - \pi$	$\arg(A_{00}/A_0) - \pi$	-0.26 ± 0.10
A_{CP}	$(\bar{\Gamma} - \Gamma)/(\bar{\Gamma} + \Gamma)$	-0.003 ± 0.038
A_{CP}^0	$(\bar{f}_L - f_L)/(\bar{f}_L + f_L)$	-0.007 ± 0.030
A_{CP}^\perp	$(\bar{f}_\perp - f_\perp)/(\bar{f}_\perp + f_\perp)$	-0.014 ± 0.057
$\Delta\phi_\parallel$	$(\bar{\phi}_\parallel - \phi_\parallel)/2$	$+0.051 \pm 0.053$
$\Delta\phi_\perp$	$(\bar{\phi}_\perp - \phi_\perp - \pi)/2$	$+0.075 \pm 0.050$
$\Delta\delta_0$	$(\bar{\delta}_0 - \delta_0)/2$	$+0.13 \pm 0.08$

Overall, six real parameters describe three complex amplitudes A_0 , A_\parallel , and A_\perp . These could be chosen to be the four polarization

parameters f_L , f_\perp , ϕ_\parallel , and ϕ_\perp , one overall size normalization, such as decay rate Γ , or branching fraction \mathcal{B} , and one overall phase δ_0 . The phase convention is arbitrary for an isolated B decay mode. However, for several B decays, the relative phase could produce meaningful and observable effects through interference with other B decays with the same final states, such as for $B \rightarrow VK_J^*$ with $J = 0, 1, 2, 3, 4, \dots$. The phase could be referenced to the single $B \rightarrow VK_0^*$ amplitude A_{00} in such a case, as shown in Table 74.1. Here V stands for any spin-one vector meson.

Moreover, CP violation can be tested in the angular distribution of the decay as the difference between the B and \bar{B} . Each of the six real parameters describing the three complex amplitudes would have a counterpart CP -asymmetry term, corresponding to three direct- CP asymmetries in three amplitudes, and three CP -violating phase differences, equivalent to the phase measurements from the mixing-induced CP asymmetries in the time evolution of B -decays [1]. In Table 74.1 and Ref. [11], these are chosen to be the direct- CP asymmetries in the overall decay rate \mathcal{A}_{CP} , in the f_L fraction \mathcal{A}_{CP}^0 , and in the f_\perp fraction \mathcal{A}_{CP}^\perp , and three weak phase differences:

$$\Delta\phi_\parallel = \frac{1}{2}\arg(\bar{A}_\parallel A_0/A_\parallel \bar{A}_0), \quad (74.8)$$

$$\Delta\phi_\perp = \frac{1}{2}\arg(\bar{A}_\perp A_0/A_\perp \bar{A}_0) - \frac{\pi}{2}, \quad (74.9)$$

$$\Delta\delta_0 = \frac{1}{2}\arg(\bar{A}_{00} A_0/A_{00} \bar{A}_0). \quad (74.10)$$

The $\frac{\pi}{2}$ term in Eq. (74.8) reflects the fact that A_\perp and \bar{A}_\perp differ in phase by π if CP is conserved. The two parameters $\Delta\phi_\parallel$ and $\Delta\phi_\perp$ are equivalent to triple-product asymmetries constructed from the vectors describing the decay angular distribution [12]. The CP -violating phase difference in the reference decay mode [11] is, in the Wolfenstein CKM quark-mixing phase convention,

$$\Delta\phi_{00} = \frac{1}{2}\arg(A_{00}/\bar{A}_{00}). \quad (74.11)$$

This can be measured only together with the mixing-induced phase difference for some of the neutral B -meson decays similar to other mixing-induced CP asymmetry measurements [1].

It may not always be possible to have a phase-reference decay mode which would define δ_0 and $\Delta\delta_0$ parameters. In that case, it may be possible to define the phase difference directly similarly to Eq. (74.11):

$$\Delta\phi_0 = \frac{1}{2}\arg(A_0/\bar{A}_0). \quad (74.12)$$

One can measure the angles of the CKM unitarity triangle, assuming Standard Model contributions to the $\Delta\phi_0$ and B -mixing phases. Examples include measurements of $\beta = \phi_1$ with $B \rightarrow J/\psi K^*$ and $\alpha = \phi_2$ with $B \rightarrow \rho\rho$.

Most of the B decays that arise from tree-level $b \rightarrow c$ transitions have the amplitude hierarchy $|A_0| > |A_+| > |A_-|$ which is expected from analyses based on quark-helicity conservation [13]. The larger the mass of the vector-meson daughters, the weaker the inequality. The B meson decays to heavy vector particles with charm, such as $B \rightarrow J/\psi K^*$, $\psi(2S)K^*$, $\chi_{c1}K^*$, $D^*\rho$, D^*K^* , D^*D^* , and $D^*D_s^*$, show a substantial fraction of the amplitudes corresponding to transverse polarization of the vector mesons ($A_{\pm 1}$), in agreement with the factorization prediction. The detailed amplitude analysis of the $B \rightarrow J/\psi K^*$ decays has been performed by the BABAR [14], Belle [15], CDF [16], CLEO [17], D0 [18], and LHCb [19] collaborations. Most analyses are performed under the assumption of the absence of direct CP violation. The parameter values are given in the particle listing of this *Review*. The difference between the strong phases ϕ_\parallel and ϕ_\perp deviates significantly from zero. The measurements [14, 15] of CP -violating terms similar to those in $B \rightarrow \varphi K^*$ [8] shown in Table 74.1 are consistent with zero.

In addition, the mixing-induced CP -violating asymmetry is measured in the $B^0 \rightarrow J/\psi K^{*0}$ decay [1, 14, 15] where angular analysis allows one to separate CP -eigenstate amplitudes. This allows one to resolve the sign ambiguity of the $\cos 2\beta$ ($\cos 2\phi_1$) term that appears in the time-dependent angular distribution due

to interference of parity-even and parity-odd terms. This analysis relies on the knowledge of discrete ambiguities in the strong phases ϕ_\parallel and ϕ_\perp , as discussed below. The BABAR experiment used a method based on the dependence on the $K\pi$ invariant mass of the interference between the S - and P -waves to resolve the discrete ambiguity in the determination of the strong phases ($\phi_\parallel, \phi_\perp$) in $B \rightarrow J/\psi K^*$ decays [14]. The result is in agreement with the amplitude hierarchy expectation [13]. The CDF [20], D0 [21], and LHCb [22] experiments have studied the $B_s^0 \rightarrow J/\psi(K^+K^-)$, $J/\psi(\pi^+\pi^-)$, $\psi(K^+\pi^-)$ decays and provided the lifetime, polarization, and phase measurements.

The amplitude hierarchy $|A_0| \gg |A_+| \gg |A_-|$ was expected in B decays to light vector particles in both penguin transitions [23, 24] and tree-level transitions [13]. There is confirmation by the BABAR and Belle experiments of predominantly longitudinal polarization in the tree-level $b \rightarrow u$ transition, such as $B^0 \rightarrow \rho^+\rho^-$ [25], $B^+ \rightarrow \rho^0\rho^+$ [26], and $B^+ \rightarrow \omega\rho^+$ [27]; this is consistent with the analysis of the quark helicity conservation [13]. Because the longitudinal amplitude dominates the decay, a detailed amplitude analysis is not possible with current B samples, and limits on the transverse amplitude fraction are obtained. The small branching fractions of $B^0 \rightarrow \rho^0\rho^0, \omega\rho^0, \omega\omega$ [27–30] indicate that $b \rightarrow d$ penguin pollution is small in the charmless, strangeless vector-vector B decays. There is a measurement of large longitudinal polarization in $B^0 \rightarrow \rho^0\rho^0$ [28–30] decays. The fraction of transverse polarization is large in decays to heavier mesons such as $B^0 \rightarrow a_1(1260)^+a_1(1260)^-$ [31].

The interest in the polarization and CP -asymmetry measurements in penguin transition, such as $b \rightarrow s$ decays $B \rightarrow \varphi K^*$, ρK^* , ωK^* , or $B_s^0 \rightarrow \varphi\varphi, K^*K^*$, and $b \rightarrow d$ decay $B \rightarrow K^*\bar{K}^*$, is motivated by their potential sensitivity to physics beyond the Standard Model. The decay amplitudes for $B \rightarrow \varphi K^*$ have been measured by the BABAR, Belle, and LHCb experiments [9–11, 32, 33]. The fractions of longitudinal polarization are $f_L = 0.50 \pm 0.05$ for the $B^+ \rightarrow \varphi K^{*+}$ decay and $f_L = 0.497 \pm 0.017$ for the $B^0 \rightarrow \varphi K^{*0}$ decay. These indicate significant departure from the naive expectation of predominant longitudinal polarization, suggesting other contributions to the decay amplitude, previously neglected, either within the Standard Model, such as penguin annihilation [34] or QCD rescattering [35], or from physics beyond the Standard Model [36]. The complete set of twelve amplitude parameters measured in the $B^0 \rightarrow \varphi K^{*0}$ decay is given in Table 74.1. Several other parameters could be constructed from the above twelve parameters, as suggested in Ref. [37].

The discrete ambiguity in the phase ($\phi_\parallel, \phi_\perp, \Delta\phi_\parallel, \Delta\phi_\perp$) measurements has been resolved by BABAR in favor of $|A_+| \gg |A_-|$ through interference between the S - and P -waves of $K\pi$. The search for vector-tensor and vector-axialvector $B \rightarrow \varphi K_J^{(*)}$ decays with $J = 1, 2, 3, 4$ revealed a large fraction of longitudinal polarization in the decay $B \rightarrow \varphi K_2^*(1430)$ with $f_L = 0.90_{-0.07}^{+0.06}$ [11, 38], but large contribution of transverse amplitude in $B \rightarrow \varphi K_1(1270)$ with $f_L = 0.46_{-0.15}^{+0.13}$ [39].

Like $B \rightarrow \varphi K^*$, the decays $B \rightarrow \rho K^*$ and $B \rightarrow \omega K^*$ may be sensitive to New Physics. Measurements of the longitudinal polarization fraction in $B \rightarrow \rho K^*$ [40] and in both vector-vector and vector-tensor final states of $B \rightarrow \omega K_J^*$ [27] by BABAR and Belle reveal a large fraction of transverse polarization, indicating an anomaly similar to $B \rightarrow \varphi K^*$ except for a different pattern in vector-tensor final states. An angular analysis of the $B^0 \rightarrow \rho^0 K^{*0}$ decay mode by LHCb [41] provides much higher precision and indicates remarkably small longitudinal polarization fraction and a significant direct CP asymmetry observed in angular distributions of $B \rightarrow VV$ decays for the first time. A large transverse polarization is also observed in the $B_s^0 \rightarrow \varphi\varphi$ decay by CDF [42] and LHCb [43], $B_s^0 \rightarrow K^{*0}\bar{K}^{*0}$ decays by LHCb [44], and $B_s^0 \rightarrow \varphi K^{*0}$ decays by LHCb [45]. At the same time, measurement of the polarization in the $b \rightarrow d$ penguin decays $B \rightarrow K^*\bar{K}^*$ indicates a large fraction of longitudinal polarization [44, 46]. The LHCb experiment has also provided the very first polarization results on the tensor-tensor, as well as vector-tensor, decays of the B_s^0 meson in the $(K\pi)(K\pi)$ final state [44]. The polarization pattern in penguin-dominated B -meson decays is not fully understood [34–36].

The three-body semileptonic B -meson decays, such as $B \rightarrow V\ell_1\ell_2$, share many features with the two-body $B \rightarrow VV$ decays. Their differential decay width can be parameterized with the two helicity angles defined in the V and $(\ell_1\ell_2)$ frames and with the azimuthal angle, as defined in Fig. 74.1. However, since the $(\ell_1\ell_2)$ pair does not come from an on-shell particle, the angular distribution is unique to each point in the dilepton mass $m_{\ell\ell}$ spectrum. The polarization measurements as a function of $m_{\ell\ell}$ provide complementary information on physics beyond the Standard Model, as discussed for $B \rightarrow K^*\ell^+\ell^-$ and $B_s \rightarrow \phi\ell^+\ell^-$ decays in Ref. [47]. The data in these modes have been analyzed by the BABAR, Belle, CDF, CMS, and LHCb experiments [48–53].

The examples of the angular distributions and observables in $B \rightarrow K^*\ell^+\ell^-$ are discussed in Ref. [47]. Two angular observables have been measured in this decay in certain ranges of the dilepton mass $m_{\ell\ell}$. One parameter is the fraction of longitudinal polarization F_L , which is determined by the K^* angular distribution and is similar to f_L defined for exclusive two-body decays. The other parameter is the forward-backward asymmetry of the lepton pair A_{FB} , which is the asymmetry of the decay rate with positive and negative values of $\cos\theta_1$. A complete set of observables and angular terms has been adopted by the LHCb collaboration [52] following Ref. [47] with the F_L , A_{FB} , and $S_3 - S_9$ coefficients in the angular distributions. Additional set of optimized observables $P_i^{(\prime)}$ is derived from those, for example $P_2 = 2A_{FB}/(3 - 3F_L)$ and $P_5' = S_5/\sqrt{F_L(1 - F_L)}$. These observables have the advantage that the leading form-factor uncertainties cancel. There have been hints of deviations from SM in the measurement of P_5' and lepton flavor universality [48–53].

In summary, there has been considerable interest in the polarization measurements of B -meson decays because they reveal both weak- and strong-interaction dynamics [34–36, 54]. New measurements will further elucidate the pattern of spin alignment measurements in rare B decays, and further test the Standard Model and strong interaction dynamics, including the non-factorizable contributions to the B -decay amplitudes.

References

- [1] M. Kreps, Y. Kwon, and P. Eerola, “Production and Decay of b -Flavored Hadrons,” mini-review in this *Review*.
- [2] Y. Gao *et al.*, Phys. Rev. D **81**, 075022 (2010), [arXiv:1001.3396].
- [3] M. Jacob and G. Wick, Annals Phys. **7**, 404 (1959).
- [4] S. Berman and M. Jacob, Phys. Rev. **139**, B1023 (1965).
- [5] I. Dunietz *et al.*, Phys. Rev. D **43**, 2193 (1991).
- [6] G. Kramer and W. Palmer, Phys. Rev. D **45**, 193 (1992).
- [7] A. Datta *et al.*, Phys. Rev. D **77**, 114025 (2008), [arXiv:0711.2107].
- [8] B. Aubert *et al.* (BaBar), Phys. Rev. D **78**, 092008 (2008), [arXiv:0808.3586].
- [9] M. Prim *et al.* (Belle), Phys. Rev. D **88**, 7, 072004 (2013), [arXiv:1308.1830].
- [10] R. Aaij *et al.* (LHCb), JHEP **05**, 069 (2014), [arXiv:1403.2888].
- [11] B. Aubert *et al.* (BaBar), Phys. Rev. Lett. **93**, 231804 (2004), [hep-ex/0408017]; B. Aubert *et al.* (BaBar), Phys. Rev. Lett. **98**, 051801 (2007), [hep-ex/0610073]; B. Aubert *et al.* (BaBar), Phys. Rev. D **78**, 092008 (2008), [arXiv:0808.3586].
- [12] G. Valencia, Phys. Rev. D **39**, 3339 (1989); A. Datta and D. London, Int. J. Mod. Phys. A **19**, 2505 (2004), [hep-ph/0303159].
- [13] A. Ali *et al.*, Z. Phys. C **1**, 269 (1979); M. Suzuki, Phys. Rev. D **64**, 117503 (2001), [hep-ph/0106354].
- [14] B. Aubert *et al.* (BaBar), Phys. Rev. D **71**, 032005 (2005), [hep-ex/0411016]; B. Aubert *et al.* (BaBar), Phys. Rev. D **76**, 031102 (2007), [arXiv:0704.0522].
- [15] R. Itoh *et al.* (Belle), Phys. Rev. Lett. **95**, 091601 (2005), [hep-ex/0504030]; M. Prim *et al.* (Belle), Phys. Rev. D **88**, 7, 072004 (2013), [arXiv:1308.1830].
- [16] T. Affolder *et al.* (CDF), Phys. Rev. Lett. **85**, 4668 (2000), [hep-ex/0007034]; D. Acosta *et al.* (CDF), Phys. Rev. Lett. **94**, 101803 (2005), [hep-ex/0412057].
- [17] C. Jessop *et al.* (CLEO), Phys. Rev. Lett. **79**, 4533 (1997), [hep-ex/9702013].
- [18] V. Abazov *et al.* (D0), Phys. Rev. Lett. **102**, 032001 (2009), [arXiv:0810.0037].
- [19] R. Aaij *et al.* (LHCb), Phys. Rev. D **88**, 052002 (2013), [arXiv:1307.2782].
- [20] T. Aaltonen *et al.* (CDF), Phys. Rev. Lett. **100**, 121803 (2008), [arXiv:0712.2348]; T. Aaltonen *et al.* (CDF), Phys. Rev. D **85**, 072002 (2012), [arXiv:1112.1726].
- [21] V. Abazov *et al.* (D0), Phys. Rev. Lett. **98**, 121801 (2007), [hep-ex/0701012]; V. M. Abazov *et al.* (D0), Phys. Rev. D **85**, 032006 (2012), [arXiv:1109.3166].
- [22] R. Aaij *et al.* (LHCb), Phys. Rev. Lett. **108**, 101803 (2012), [arXiv:1112.3183]; R. Aaij *et al.* (LHCb), Phys. Rev. Lett. **114**, 4, 041801 (2015), [arXiv:1411.3104]; R. Aaij *et al.* (LHCb), Phys. Lett. B **747**, 484 (2015), [arXiv:1503.07112]; R. Aaij *et al.* (LHCb), JHEP **11**, 082 (2015), [arXiv:1509.00400]; R. Aaij *et al.* (LHCb), JHEP **08**, 037 (2017), [arXiv:1704.08217].
- [23] H.-Y. Cheng and K.-C. Yang, Phys. Lett. B **511**, 40 (2001), [hep-ph/0104090]; C.-H. Chen, Y.-Y. Keum and H.-n. Li, Phys. Rev. D **66**, 054013 (2002), [hep-ph/0204166].
- [24] A. L. Kagan, Phys. Lett. B **601**, 151 (2004), [hep-ph/0405134]; Y. Grossman, Int. J. Mod. Phys. A **19**, 907 (2004), [hep-ph/0310229].
- [25] B. Aubert *et al.* (BaBar), Phys. Rev. D **76**, 052007 (2007), [arXiv:0705.2157]; P. Vanhove *et al.* (Belle), Phys. Rev. D **93**, 3, 032010 (2016), [Erratum: Phys. Rev. D **94**, 099903 (2016)], [arXiv:1510.01245].
- [26] J. Zhang *et al.* (Belle), Phys. Rev. Lett. **91**, 221801 (2003), [hep-ex/0306007]; B. Aubert *et al.* (BaBar), Phys. Rev. Lett. **102**, 141802 (2009), [arXiv:0901.3522].
- [27] B. Aubert *et al.* (BaBar), Phys. Rev. D **74**, 051102 (2006), [hep-ex/0605017]; B. Aubert *et al.* (BaBar), Phys. Rev. D **79**, 052005 (2009), [arXiv:0901.3703].
- [28] B. Aubert *et al.* (BaBar), Phys. Rev. D **78**, 071104 (2008), [arXiv:0807.4977].
- [29] I. Adachi *et al.* (Belle), Phys. Rev. D **89**, 7, 072008 (2014), [Erratum: Phys. Rev. D **89**, 119903 (2014)], [arXiv:1212.4015].
- [30] R. Aaij *et al.* (LHCb), Phys. Lett. B **747**, 468 (2015), [arXiv:1503.07770].
- [31] B. Aubert *et al.* (BaBar), Phys. Rev. D **80**, 092007 (2009), [arXiv:0907.1776].
- [32] K.-F. Chen *et al.* (Belle), Phys. Rev. Lett. **94**, 221804 (2005), [hep-ex/0503013].
- [33] B. Aubert *et al.* (BaBar), Phys. Rev. Lett. **99**, 201802 (2007), [arXiv:0705.1798].
- [34] A. L. Kagan, Phys. Lett. B **601**, 151 (2004), [hep-ph/0405134]; H.-n. Li and S. Mishima, Phys. Rev. D **71**, 054025 (2005), [hep-ph/0411146]; C.-H. Chen *et al.*, Phys. Rev. D **72**, 054011 (2005), [hep-ph/0507012]; M. Beneke, J. Rohrer and D. Yang, Phys. Rev. Lett. **96**, 141801 (2006), [hep-ph/0512258]; C.-H. Chen and C.-Q. Geng, Phys. Rev. D **75**, 054010 (2007), [hep-ph/0701023]; A. Datta *et al.*, Phys. Rev. D **76**, 034015 (2007), [arXiv:0705.3915]; M. Beneke, J. Rohrer and D. Yang, Nucl. Phys. B **774**, 64 (2007), [hep-ph/0612290]; H.-Y. Cheng and K.-C. Yang, Phys. Rev. D **78**, 094001 (2008), [Erratum: Phys. Rev. D **79**, 039903 (2009)], [arXiv:0805.0329].
- [35] C. W. Bauer *et al.*, Phys. Rev. D **70**, 054015 (2004), [hep-ph/0401188]; P. Colangelo, F. De Fazio and T. Pham, Phys. Lett. B **597**, 291 (2004), [hep-ph/0406162]; M. Ladisa *et al.*, Phys. Rev. D **70**, 114025 (2004), [hep-ph/0409286]; H.-Y. Cheng, C.-K. Chua and A. Soni, Phys. Rev. D **71**, 014030

- (2005), [hep-ph/0409317]; H.-Y. Cheng and K.-C. Yang, Phys. Rev. D **83**, 034001 (2011), [arXiv:1010.3309].
- [36] Y. Grossman, Int. J. Mod. Phys. A **19**, 907 (2004), [hep-ph/0310229]; E. Alvarez *et al.*, Phys. Rev. D **70**, 115014 (2004), [hep-ph/0410096]; P. K. Das and K.-C. Yang, Phys. Rev. D **71**, 094002 (2005), [hep-ph/0412313]; C.-H. Chen and C.-Q. Geng, Phys. Rev. D **71**, 115004 (2005), [hep-ph/0504145]; Y.-D. Yang, R.-M. Wang and G.-R. Lu, Phys. Rev. D **72**, 015009 (2005), [hep-ph/0411211]; K.-C. Yang, Phys. Rev. D **72**, 034009 (2005), [Erratum: Phys. Rev. D **72**, 059901 (2005)], [hep-ph/0506040]; S. Baek *et al.*, Phys. Rev. D **72**, 094008 (2005), [hep-ph/0508149]; C.-S. Huang *et al.*, Phys. Rev. D **73**, 034026 (2006), [hep-ph/0511129]; C.-H. Chen and H. Hatanaka, Phys. Rev. D **73**, 075003 (2006), [hep-ph/0602140]; A. Faessler *et al.*, Phys. Rev. D **75**, 074029 (2007), [hep-ph/0702020].
- [37] D. London, N. Sinha and R. Sinha, Phys. Rev. D **69**, 114013 (2004), [hep-ph/0402214].
- [38] B. Aubert *et al.* (BaBar), Phys. Rev. D **76**, 051103 (2007), [arXiv:0705.0398].
- [39] B. Aubert *et al.* (BaBar), Phys. Rev. Lett. **101**, 161801 (2008), [arXiv:0806.4419].
- [40] J. Zhang *et al.* (Belle), Phys. Rev. Lett. **95**, 141801 (2005), [hep-ex/0408102]; B. Aubert *et al.* (BaBar), Phys. Rev. Lett. **97**, 201801 (2006), [hep-ex/0607057]; P. del Amo Sanchez *et al.* (BaBar), Phys. Rev. D **83**, 051101 (2011), [arXiv:1012.4044]; J. Lees *et al.* (BaBar), Phys. Rev. D **85**, 072005 (2012), [arXiv:1112.3896].
- [41] R. Aaij *et al.* (LHCb), JHEP **05**, 026 (2019), [arXiv:1812.07008].
- [42] T. Aaltonen *et al.* (CDF), Phys. Rev. Lett. **107**, 261802 (2011), [arXiv:1107.4999].
- [43] R. Aaij *et al.* (LHCb), Phys. Lett. B **713**, 369 (2012), [arXiv:1204.2813]; R. Aaij *et al.* (LHCb), Phys. Rev. D **90**, 5, 052011 (2014), [arXiv:1407.2222]; R. Aaij *et al.* (LHCb), JHEP **12**, 155 (2019), [arXiv:1907.10003].
- [44] R. Aaij *et al.* (LHCb), Phys. Lett. B **709**, 50 (2012), [arXiv:1111.4183]; R. Aaij *et al.* (LHCb), JHEP **07**, 166 (2015), [arXiv:1503.05362]; R. Aaij *et al.* (LHCb), JHEP **07**, 032 (2019), [arXiv:1905.06662].
- [45] R. Aaij *et al.* (LHCb), JHEP **11**, 092 (2013), [arXiv:1306.2239].
- [46] B. Aubert *et al.* (BaBar), Phys. Rev. Lett. **100**, 081801 (2008), [arXiv:0708.2248]; B. Aubert *et al.* (BaBar), Phys. Rev. D **79**, 051102 (2009), [arXiv:0901.1223].
- [47] G. Burdman, Phys. Rev. D **52**, 6400 (1995), [hep-ph/9505352]; F. Kruger and J. Matias, Phys. Rev. D **71**, 094009 (2005), [hep-ph/0502060]; E. Lunghi and J. Matias, JHEP **04**, 058 (2007), [hep-ph/0612166]; W. Altmannshofer *et al.*, JHEP **01**, 019 (2009), [arXiv:0811.1214]; J. Matias *et al.*, JHEP **04**, 104 (2012), [arXiv:1202.4266]; S. Descotes-Genon *et al.*, JHEP **01**, 048 (2013), [arXiv:1207.2753].
- [48] B. Aubert *et al.* (BaBar), Phys. Rev. D **79**, 031102 (2009), [arXiv:0804.4412]; J. Lees *et al.* (BaBar), Phys. Rev. D **93**, 5, 052015 (2016), [arXiv:1508.07960].
- [49] J.-T. Wei *et al.* (Belle), Phys. Rev. Lett. **103**, 171801 (2009), [arXiv:0904.0770]; S. Wehle *et al.* (Belle), Phys. Rev. Lett. **118**, 11, 111801 (2017), [arXiv:1612.05014]; A. Abdesselam *et al.* (Belle), Phys. Rev. Lett. **126**, 16, 161801 (2021), [arXiv:1904.02440].
- [50] T. Aaltonen *et al.* (CDF), Phys. Rev. Lett. **108**, 081807 (2012), [arXiv:1108.0695].
- [51] S. Chatrchyan *et al.* (CMS), Phys. Lett. B **727**, 77 (2013), [arXiv:1308.3409]; V. Khachatryan *et al.* (CMS), Phys. Lett. B **753**, 424 (2016), [arXiv:1507.08126]; A. M. Sirunyan *et al.* (CMS), Phys. Lett. B **781**, 517 (2018), [arXiv:1710.02846]; A. M. Sirunyan *et al.* (CMS), JHEP **04**, 124 (2021), [arXiv:2010.13968].
- [52] R. Aaij *et al.* (LHCb), JHEP **08**, 131 (2013), [arXiv:1304.6325]; R. Aaij *et al.* (LHCb), JHEP **04**, 064 (2015), [arXiv:1501.03038]; R. Aaij *et al.* (LHCb), JHEP **02**, 104 (2016), [arXiv:1512.04442]; R. Aaij *et al.* (LHCb), JHEP **11**, 047 (2016), [Erratum: JHEP **04**, 142 (2017)], [arXiv:1606.04731]; R. Aaij *et al.* (LHCb), JHEP **12**, 065 (2016), [arXiv:1609.04736]; R. Aaij *et al.* (LHCb), JHEP **08**, 055 (2017), [arXiv:1705.05802]; R. Aaij *et al.* (LHCb), Phys. Rev. Lett. **125**, 1, 011802 (2020), [arXiv:2003.04831]; R. Aaij *et al.* (LHCb), Phys. Rev. Lett. **126**, 16, 161802 (2021), [arXiv:2012.13241].
- [53] R. Aaij *et al.* (LHCb), JHEP **09**, 179 (2015), [arXiv:1506.08777]; R. Aaij *et al.* (LHCb) (2021), [arXiv:2107.13428].
- [54] C.-H. Chen and H.-N. Li, Phys. Rev. D **71**, 114008 (2005), [hep-ph/0504020].

75. $B^0-\bar{B}^0$ Mixing

Revised March 2022 by O. Schneider (EPFL).

There are two neutral $B^0-\bar{B}^0$ meson systems, $B_d^0-\bar{B}_d^0$ and $B_s^0-\bar{B}_s^0$ (generically denoted $B_q^0-\bar{B}_q^0$, $q = s, d$), which exhibit particle-antiparticle mixing [1]. This mixing phenomenon is described in Ref. [2]. In the following, we adopt the notation introduced in Ref. [2], and assume CPT conservation throughout. In each system, the light (L) and heavy (H) mass eigenstates,

$$|B_{L,H}\rangle = p|B_q^0\rangle \pm q|\bar{B}_q^0\rangle, \quad (75.1)$$

have a mass difference $\Delta m_q = m_H - m_L > 0$, a total decay width difference $\Delta\Gamma_q = \Gamma_L - \Gamma_H$ and an average decay width $\Gamma_q = (\Gamma_L + \Gamma_H)/2$. In the absence of CP violation in the mixing, $|q/p| = 1$, the differences are given by $\Delta m_q = 2|M_{12}|$ and $|\Delta\Gamma_q| = 2|\Gamma_{12}|$, where M_{12} and Γ_{12} are the off-diagonal elements of the mass and decay matrices [2]. The evolution of a pure $|B_q^0\rangle$ or $|\bar{B}_q^0\rangle$ state at $t = 0$ is given by

$$|B_q^0(t)\rangle = g_+(t)|B_q^0\rangle + \frac{q}{p}g_-(t)|\bar{B}_q^0\rangle, \quad (75.2)$$

$$|\bar{B}_q^0(t)\rangle = g_+(t)|\bar{B}_q^0\rangle + \frac{p}{q}g_-(t)|B_q^0\rangle, \quad (75.3)$$

which means that the flavor states remain unchanged (+) or oscillate into each other (-) with time-dependent probabilities proportional to

$$|g_{\pm}(t)|^2 = \frac{e^{-\Gamma_q t}}{2} \left[\cosh\left(\frac{\Delta\Gamma_q}{2} t\right) \pm \cos(\Delta m_q t) \right]. \quad (75.4)$$

In the absence of CP violation, the time-integrated mixing probability $\int |g_-(t)|^2 dt / (\int |g_-(t)|^2 dt + \int |g_+(t)|^2 dt)$ is given by

$$\chi_q = \frac{x_q^2 + y_q^2}{2(x_q^2 + 1)}, \quad \text{where } x_q = \frac{\Delta m_q}{\Gamma_q}, \quad y_q = \frac{\Delta\Gamma_q}{2\Gamma_q}. \quad (75.5)$$

75.1 Standard Model predictions and phenomenology

In the Standard Model, the transitions $B_q^0 \rightarrow \bar{B}_q^0$ and $\bar{B}_q^0 \rightarrow B_q^0$ are due to the weak interaction. They are described, at the lowest order, by box diagrams involving two W bosons and two up-type quarks (see Fig. 75.1), as is the case for $K^0 - \bar{K}^0$ mixing. However, the long range interactions arising from intermediate virtual states are negligible for the neutral B meson systems, because the large B mass is off the region of hadronic resonances. The calculation of the dispersive and absorptive parts of the box diagrams yields the following predictions for the off-diagonal element of the mass and decay matrices [3],

$$M_{12} = -\frac{G_F^2 m_W^2 \eta_B m_{B_q} B_{B_q} f_{B_q}^2}{12\pi^2} S_0(m_t^2/m_W^2) (V_{tq}^* V_{tb})^2, \quad (75.6)$$

$$\begin{aligned} \Gamma_{12} = & \frac{G_F^2 m_b^2 \eta_B' m_{B_q} B_{B_q} f_{B_q}^2}{8\pi} \\ & \times \left[(V_{tq}^* V_{tb})^2 + V_{tq}^* V_{tb} V_{cq}^* V_{cb} \mathcal{O}\left(\frac{m_c^2}{m_b^2}\right) \right. \\ & \left. + (V_{cq}^* V_{cb})^2 \mathcal{O}\left(\frac{m_c^4}{m_b^4}\right) \right], \quad (75.7) \end{aligned}$$

where G_F is the Fermi constant, m_W the W boson mass, and m_i the mass of quark i ; m_{B_q} , f_{B_q} and B_{B_q} are the B_q^0 mass, weak decay constant and bag parameter, respectively. The known function $S_0(x)$ can be approximated very well by $0.784 x_i^{0.76}$ [4], and V_{ij} are the elements of the CKM matrix [5]. The QCD corrections η_B and η_B' are of order unity. The only non-negligible contributions to M_{12} are from box diagrams involving two top quarks. The phases of M_{12} and Γ_{12} satisfy

$$\phi_M - \phi_\Gamma = \pi + \mathcal{O}\left(\frac{m_c^2}{m_b^2}\right), \quad (75.8)$$

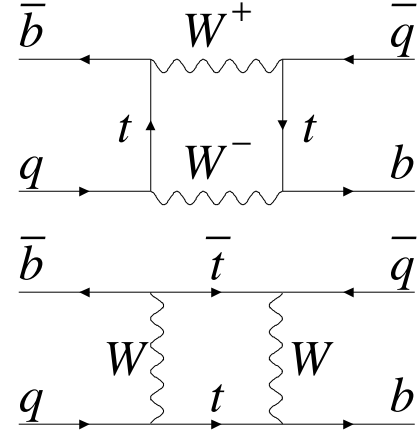


Figure 75.1: Dominant box diagrams for the $B_q^0 \rightarrow \bar{B}_q^0$ transitions ($q = d$ or s). Similar diagrams exist where one or both t quarks are replaced with c or u quarks.

implying that the mass eigenstates have mass and width differences of opposite signs. This means that, like in the $K^0-\bar{K}^0$ system, the heavy state is expected to have a smaller decay width than that of the light state: $\Gamma_H < \Gamma_L$. Hence, $\Delta\Gamma_q = \Gamma_L - \Gamma_H$ is expected to be positive in the Standard Model.

Furthermore, the quantity

$$\left| \frac{\Gamma_{12}}{M_{12}} \right| \simeq \frac{3\pi}{2} \frac{m_b^2}{m_W^2} \frac{1}{S_0(m_t^2/m_W^2)} \sim \mathcal{O}\left(\frac{m_b^2}{m_t^2}\right) \quad (75.9)$$

is small, and a power expansion of $|q/p|^2$ yields

$$\left| \frac{q}{p} \right|^2 = 1 + \left| \frac{\Gamma_{12}}{M_{12}} \right| \sin(\phi_M - \phi_\Gamma) + \mathcal{O}\left(\left| \frac{\Gamma_{12}}{M_{12}} \right|^2\right). \quad (75.10)$$

Therefore, considering both Eqs. (75.8) and (75.9), the CP -violating parameter

$$1 - \left| \frac{q}{p} \right|^2 \simeq \text{Im}\left(\frac{\Gamma_{12}}{M_{12}}\right) \quad (75.11)$$

is expected to be very small: $\sim \mathcal{O}(10^{-3})$ for the $B_d^0-\bar{B}_d^0$ system and $\lesssim \mathcal{O}(10^{-4})$ for the $B_s^0-\bar{B}_s^0$ system [6].

In the approximation of negligible CP violation in mixing, the ratio $\Delta\Gamma_q/\Delta m_q$ is equal to the small quantity $|\Gamma_{12}/M_{12}|$ of Eq. (75.9); it is hence independent of CKM matrix elements, *i.e.*, the same for the $B_d^0-\bar{B}_d^0$ and $B_s^0-\bar{B}_s^0$ systems. Calculations [7] yield $\sim 5 \times 10^{-3}$ with a $\sim 20\%$ uncertainty. Given the published experimental knowledge [8] on the mixing parameter x_q

$$\begin{cases} x_d = 0.769 \pm 0.004 & (B_d^0-\bar{B}_d^0 \text{ system}) \\ x_s = 27.01 \pm 0.10 & (B_s^0-\bar{B}_s^0 \text{ system}) \end{cases}, \quad (75.12)$$

the Standard Model thus predicts that $\Delta\Gamma_d/\Gamma_d$ is very small (below 1%), but $\Delta\Gamma_s/\Gamma_s$ considerably larger ($\sim 10\%$). These width differences are caused by the existence of final states to which both the B_q^0 and \bar{B}_q^0 mesons can decay. Such decays involve $b \rightarrow c\bar{c}q$ quark-level transitions, which are Cabibbo-suppressed if $q = d$ and Cabibbo-allowed if $q = s$.

A complete set of Standard Model predictions for all mixing parameters in both the $B_d^0-\bar{B}_d^0$ and $B_s^0-\bar{B}_s^0$ systems can be found in Refs. [9–11].

75.2 Experimental issues and methods for oscillation analyses

Time-integrated measurements of $B^0-\bar{B}^0$ mixing were published for the first time in 1987 by UA1 [12] and ARGUS [13], and

since then by many other experiments. These measurements are typically based on counting same-sign and opposite-sign lepton pairs from the semileptonic decay of the produced $b\bar{b}$ pairs. Such analyses cannot easily separate the contributions from the different b -hadron species, therefore, the clean environment of $\Upsilon(4S)$ machines (where only B_d^0 and charged B_u mesons are produced) is in principle best suited to measure χ_d .

However, better sensitivity is obtained from time-dependent analyses aiming at the direct measurement of the oscillation frequencies Δm_d and Δm_s , from the proper time distributions of B_d^0 or B_s^0 candidates identified through their decay in (mostly) flavor-specific modes, and suitably tagged as mixed or unmixed. This is particularly true for the $B_s^0\text{-}\bar{B}_s^0$ system, where the large value of x_s implies maximal mixing, *i.e.*, $\chi_s \simeq 1/2$. In such analyses, the B_d^0 or B_s^0 mesons are either fully reconstructed, partially reconstructed from a charm meson, selected from a lepton with the characteristics of a $b \rightarrow \ell^-$ decay, or selected from a reconstructed displaced vertex. At high-energy colliders (LEP, SLC, Tevatron, LHC), the proper time $t = \frac{m_B}{p} L$ is measured from the distance L between the production vertex and the B decay vertex, and from an estimate of the B momentum p . At asymmetric B factories (KEKB, PEP-II), producing $e^+e^- \rightarrow \Upsilon(4S) \rightarrow B_d^0 \bar{B}_d^0$ events with a boost $\beta\gamma$ ($= 0.425, 0.55$), the proper time difference between the two B candidates is estimated as $\Delta t \simeq \frac{\Delta z}{\beta\gamma c}$, where Δz is the spatial separation between the two B decay vertices along the boost direction. In all cases, the good resolution needed on the vertex positions is obtained with silicon detectors.

The average statistical significance \mathcal{S} of a B_q^0 oscillation signal can be approximated as [14]

$$\mathcal{S} \approx \sqrt{N/2} f_{\text{sig}} (1 - 2\eta) e^{-(\Delta m_q \sigma_t)^2/2}, \quad (75.13)$$

where N is the number of selected and tagged candidates, f_{sig} is the fraction of signal in that sample, η is the total mistag probability, and σ_t is the resolution on proper time (or proper time difference). The quantity \mathcal{S} decreases very quickly as Δm_q increases; this dependence is controlled by σ_t , which is therefore a critical parameter for Δm_s analyses. At high-energy colliders, the proper time resolution $\sigma_t \sim \frac{m_B}{(p)} \sigma_L \oplus t \frac{\sigma_p}{p}$ includes a constant contribution due to the decay length resolution σ_L (typically 0.04–0.3 ps), and a term due to the relative momentum resolution σ_p/p (typically 10–20% for partially reconstructed decays), which increases with proper time. At B factories, the boost of the B mesons is estimated from the known beam energies, and the term due to the spatial resolution dominates (typically 1–1.5 ps because of the much smaller B boost).

In order to tag a B_q^0 candidate as mixed or unmixed, it is necessary to determine its flavor both in the initial state and in the final state. The initial and final state mistag probabilities, η_i and η_f , degrade \mathcal{S} by a total factor $(1 - 2\eta) = (1 - 2\eta_i)(1 - 2\eta_f)$. In lepton-based analyses, the final state is tagged by the charge of the lepton from $b \rightarrow \ell^-$ decays; the largest contribution to η_f is then due to $\bar{b} \rightarrow \bar{c} \rightarrow \ell^-$ decays. Alternatively, the charge of a reconstructed charm meson (D^{*-} from B_d^0 or D_s^- from B_s^0), or that of a kaon hypothesized to come from a $b \rightarrow c \rightarrow s$ decay [15], can be used. For fully-inclusive analyses based on topological vertexing, final-state tagging techniques include jet-charge [16] and charge-dipole [17, 18] methods. At high-energy colliders, the methods to tag the initial state (*i.e.*, the state at production), can be divided into two groups: the ones that tag the initial charge of the \bar{b} quark contained in the B_q^0 candidate itself (same-side tag), and the ones that tag the initial charge of the other b quark produced in the event (opposite-side tag). On the same side, the sign of a charged pion, kaon or proton from the primary vertex is correlated with the production state of the B_q^0 meson if that particle is a decay product of a B^{**} state or the first in the fragmentation chain [19, 20]. Jet- and vertex-charge techniques work on both sides and on the opposite side, respectively. Finally, the charge of a lepton from $b \rightarrow \ell^-$, of a kaon from $b \rightarrow c \rightarrow s$ or of a charm hadron from $b \rightarrow c$ [21] can be used as an opposite-side tag, keeping in mind that its performance is degraded due to integrated mixing. At SLC, the beam polarization produced a sizeable forward-backward asymmetry in the $Z \rightarrow b\bar{b}$

decays, and provided another very interesting and effective initial state tag based on the polar angle of the B_q^0 candidate [17]. Initial state tags have also been combined to reach $\eta_i \sim 26\%$ at LEP [20, 22] or 22% at SLD [17] with full efficiency. In the case $\eta_f = 0$, this corresponds to an effective tagging efficiency $Q = \epsilon D^2 = \epsilon(1 - 2\eta)^2$, where ϵ is the tagging efficiency, in the range 23–31%. The equivalent figure achieved by CDF during Tevatron Run I was $\sim 3.5\%$ (see tagging summary on page 160 of Ref. [23]), reflecting the fact that tagging is more difficult at hadron colliders. The CDF and DØ analyses of Tevatron Run II data reached $\epsilon D^2 = (1.8 \pm 0.1)\%$ [24] and $(2.5 \pm 0.2)\%$ [25] for opposite-side tagging, while same-side kaon tagging (for B_s^0 analyses) contributed an additional 3.7–4.8% at CDF [24], and pushed the combined performance to $(4.7 \pm 0.5)\%$ at DØ [26]. LHCb, operating in the forward region at the LHC where the environment is different in terms of track multiplicity and b -hadron production kinematics, has reported $\epsilon D^2 = (2.10 \pm 0.25)\%$ [27] for opposite-side tagging, $(1.80 \pm 0.26)\%$ [28] for same-side kaon tagging, and $(2.11 \pm 0.11)\%$ [29] for same-side pion and proton tagging; the combined figure ranges typically between $(3.73 \pm 0.15)\%$ [30] and $(5.33 \pm 0.25)\%$ [31] depending on the mode in which the tagged B_s^0 meson is reconstructed, and reaches up to $(8.1 \pm 0.6)\%$ [32] for hadronic B_d^0 modes. CMS has recently reported $\epsilon D^2 \sim 10\%$ using opposite-side muon tagging of $B_s^0 \rightarrow J/\psi\phi$ decays [33].

At B factories, the flavor of a B_d^0 meson at production cannot be determined, since the two neutral B mesons produced in a $\Upsilon(4S)$ decay evolve in a coherent P -wave state where they keep opposite flavors at any time. However, as soon as one of them decays, the other follows a time-evolution given by Eqs. (75.2) or (75.3), where t is replaced with Δt (which will take negative values half of the time). Hence, the ‘‘initial state’’ tag of a B can be taken as the final-state tag of the other B . Effective tagging efficiencies of 30% are achieved by BaBar and Belle [34], using different techniques including $b \rightarrow \ell^-$ and $b \rightarrow c \rightarrow s$ tags. It is worth noting that, in this case, mixing of the other B (*i.e.*, the coherent mixing occurring before the first B decay) does not contribute to the mistag probability.

Before the experimental observation of a decay-width difference, oscillation analyses typically neglected $\Delta\Gamma_q$ in Eq. (75.4), and described the time dependence by the functions $\Gamma_q e^{-\Gamma_q t} (1 \pm \cos(\Delta m_q t))/2$ (high-energy colliders) or $\Gamma_d e^{-\Gamma_d |\Delta t|} (1 \pm \cos(\Delta m_d \Delta t))/4$ (asymmetric $\Upsilon(4S)$ machines). As can be seen from Eq. (75.4), a non-zero value of $\Delta\Gamma_q$ would effectively reduce the oscillation amplitude with a small time-dependent factor that would be very difficult to distinguish from time resolution effects. Measurements of Δm_q are usually extracted from the data using a maximum likelihood fit.

75.3 Δm_d and $\Delta\Gamma_d$ measurements

Many $B_q^0\text{-}\bar{B}_d^0$ oscillations analyses have been published [35] by the ALEPH [36], DELPHI [18, 37], L3 [38], OPAL [39, 40], BaBar [41], Belle [42], CDF [19], DØ [25], and LHCb [43–46] collaborations. Although a variety of different techniques have been used, the individual Δm_d results obtained at LEP and Tevatron have remarkably similar precision. Their average is compatible with the more precise measurements at the asymmetric B factories and the LHC. The systematic uncertainties are not negligible; they are often dominated by sample composition, mistag probability, or b -hadron lifetime contributions. Before being combined, the measurements are adjusted on the basis of a common set of input values, including the b -hadron lifetimes and fractions published in this *Review*. Some measurements are statistically correlated. Systematic correlations arise both from common physics sources (fragmentation fractions, lifetimes, branching ratios of b hadrons), and from purely experimental or algorithmic effects (efficiency, resolution, tagging, background description). Combining all measurements [18, 19, 25, 36–46] and accounting for all identified correlations yields $\Delta m_d = 0.5065 \pm 0.0016(\text{stat}) \pm 0.0011(\text{syst}) \text{ ps}^{-1}$ [8], a result dominated by the latest LHCb measurement with $B^0 \rightarrow D^{(*)-} \mu^+ \nu_\mu X$ decays [46].

On the other hand, ARGUS and CLEO have published time-integrated measurements [47–49], which average to $\chi_d = 0.182 \pm 0.015$. Following Ref. [49], the width difference $\Delta\Gamma_d$ could in

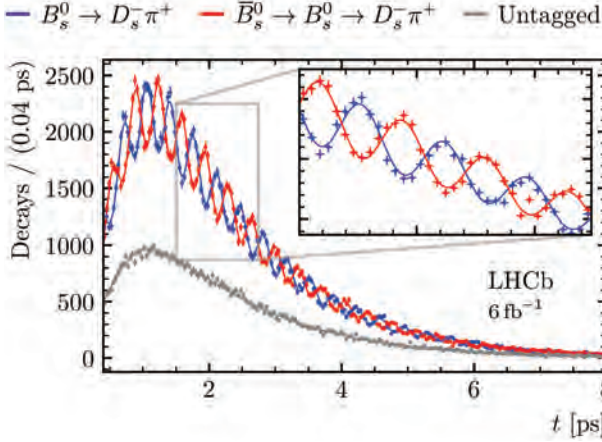


Figure 75.2: Proper time distribution of $B_s^0 \rightarrow D_s^- \pi^+$ candidates tagged as unmixed (blue), tagged as mixed (red) or untagged (grey) in the LHCb experiment, displaying B_s^0 - \bar{B}_s^0 oscillations (from Ref. [59]).

principle be extracted from the measured value of $1/\Gamma_d$ and the above averages for Δm_d and χ_d (see Eq. (75.5)), provided that $\Delta\Gamma_d$ has a negligible impact on the Δm_d and $1/\Gamma_d$ analyses that have assumed $\Delta\Gamma_d = 0$. However, $\Delta\Gamma_d/\Gamma_d$ is too small and the knowledge of χ_d too imprecise to provide useful sensitivity on $\Delta\Gamma_d/\Gamma_d$. Direct time-dependent studies published by DELPHI [18], BaBar [50], Belle [51], LHCb [52], ATLAS [53] and CMS [54] provide stronger constraints, which can be combined to yield [8]

$$\Delta\Gamma_d/\Gamma_d = +0.001 \pm 0.010. \quad (75.14)$$

This determination is compatible both with zero and with the Standard Model prediction of $(3.97 \pm 0.90) \times 10^{-3}$ [11].

Assuming $\Delta\Gamma_d = 0$ and no CP violation in mixing, and using the B_d^0 lifetime average of 1.519 ± 0.004 ps [8], the Δm_d and χ_d results are combined to yield the world average

$$\Delta m_d = 0.5065 \pm 0.0019 \text{ ps}^{-1} \quad (75.15)$$

or, equivalently,

$$\chi_d = 0.1858 \pm 0.0011. \quad (75.16)$$

This Δm_d value provides an estimate of $2|M_{12}|$, and can be used with Eq. (75.6) to extract $|V_{td}|$ within the Standard Model [55]. The main experimental uncertainties on the result come from m_t and Δm_d , but are still completely negligible with respect to the uncertainty due to the hadronic matrix element $f_{B_d} \sqrt{B_{B_d}} = 225 \pm 9$ MeV [56] obtained from three-flavor lattice QCD calculations.

75.4 Δm_s and $\Delta\Gamma_s$ measurements

After many years of intense search at LEP and SLC, B_s^0 - \bar{B}_s^0 oscillations were first observed in 2006 by CDF using 1 fb^{-1} of Tevatron Run II data [24]. LHCb then observed B_s^0 - \bar{B}_s^0 oscillations independently with $B_s^0 \rightarrow D_s^- \pi^+$ [43, 57], $B_s^0 \rightarrow D_s^- \mu^+ \nu X$ [45] and $B_s^0 \rightarrow J/\psi K^+ K^-$ [30] decays, using between 1 and 4.9 fb^{-1} of data collected at the LHC until 2016. More recently measurements based on the full LHC Run 2 data have been published by CMS with $B_s^0 \rightarrow J/\psi \phi$ decays [33], and by LHCb with $B_s^0 \rightarrow D_s^- \pi^+ \pi^- \pi^+$ [58] and $B_s^0 \rightarrow D_s^- \pi^+$ [59] decays. Taking systematic correlations into account, the average [8] of all published measurements of Δm_s [24, 30, 33, 43, 45, 57–59] is

$$\Delta m_s = 17.765 \pm 0.004(\text{stat}) \pm 0.004(\text{syst}) \text{ ps}^{-1}, \quad (75.17)$$

with an impressive precision dominated by the most recent LHCb result (see Fig. 75.2).

The information on $|V_{ts}|$ obtained in the framework of the Standard Model is hampered by the hadronic uncertainty, as in the

B_d^0 case. However, several uncertainties cancel in the frequency ratio

$$\frac{\Delta m_s}{\Delta m_d} = \frac{m_{B_s}}{m_{B_d}} \xi^2 \left| \frac{V_{ts}}{V_{td}} \right|^2, \quad (75.18)$$

where the SU(3) flavor-symmetry breaking factor $\xi = (f_{B_s} \sqrt{B_{B_s}})/(f_{B_d} \sqrt{B_{B_d}})$ is obtained as 1.206 ± 0.017 from a combination of three-flavor lattice QCD calculations [56] dominated by the results of Ref. [60], or as $1.2014^{+0.0065}_{-0.0072}$ from QCD sum rules [61]. Using the measurements of Eqs. (75.15) and (75.17), one can extract

$$\left| \frac{V_{td}}{V_{ts}} \right| = \begin{cases} 0.2053 \pm 0.0004 \pm 0.0029 \text{ (lattice QCD)} \\ 0.2045 \pm 0.0004^{+0.0011}_{-0.0012} \text{ (QCD sum rules)} \end{cases}, \quad (75.19)$$

in good agreement with (but much more precise than) the value obtained from the ratio of the $b \rightarrow d\gamma$ and $b \rightarrow s\gamma$ transition rates observed at the B factories [55].

The CKM matrix can be constrained using experimental results on observables such as Δm_d , Δm_s , $|V_{ub}/V_{cb}|$, ϵ_K , and $\sin(2\beta)$ together with theoretical inputs and unitarity conditions [55, 62, 63]. The constraint from our knowledge on the ratio $\Delta m_s/\Delta m_d$ is more effective in limiting the position of the apex of the CKM unitarity triangle than the one obtained from the Δm_d measurements alone, due to the reduced hadronic uncertainty in Eq. (75.18). We also note that the measured value of Δm_s is consistent with the Standard Model prediction obtained from CKM fits where no experimental information on Δm_s is used, e.g., $17.25 \pm 0.85 \text{ ps}^{-1}$ [62] or $16.54^{+0.50}_{-0.30} \text{ ps}^{-1}$ [63].

Information on $\Delta\Gamma_s$ can be obtained from the study of the proper time distribution of untagged B_s^0 samples [64]. In the case of an inclusive B_s^0 selection [65], or a flavor-specific (semileptonic or hadronic) B_s^0 decay selection [22, 66–68], both the short- and long-lived components are present, and the proper time distribution is a superposition of two exponentials with decay constants $\Gamma_{L,H} = \Gamma_s \pm \Delta\Gamma_s/2$. In principle, this provides sensitivity to both Γ_s and $(\Delta\Gamma_s/\Gamma_s)^2$. Ignoring $\Delta\Gamma_s$ and fitting for a single exponential leads to an estimate of $1/\Gamma_s$ (called effective lifetime) with a relative bias proportional to $(\Delta\Gamma_s/\Gamma_s)^2$. An alternative approach, sensitive to first order in $\Delta\Gamma_s/\Gamma_s$, is to determine the effective lifetime of untagged B_s^0 decays to pure CP eigenstates; measurements exist for $B_s^0 \rightarrow D_s^+ D_s^-$ [67], $B_s^0 \rightarrow K^+ K^-$ [68, 69], $B_s^0 \rightarrow J/\psi \eta$ [70], $B_s^0 \rightarrow J/\psi f_0(980)$ [71], $B_s^0 \rightarrow J/\psi \pi^+ \pi^-$ [54, 72, 73], $B_s^0 \rightarrow J/\psi K_S^0$ [74], and $B_s^0 \rightarrow \mu^+ \mu^-$ [75]. The extraction of $1/\Gamma_s$ and $\Delta\Gamma_s$ from such measurements, discussed in detail in Ref. [76], requires additional information in the form of theoretical assumptions or external inputs on weak phases and hadronic parameters. In what follows, we only use the effective lifetimes of decays to CP -even ($D_s^+ D_s^-$, $J/\psi \eta$) and CP -odd ($J/\psi f_0(980)$, $J/\psi \pi^+ \pi^-$) final states where CP conservation can be assumed.

The best sensitivity to $1/\Gamma_s$ and $\Delta\Gamma_s$ is achieved by the time-dependent measurements of the $B_s^0 \rightarrow J/\psi K^+ K^-$ (including $B_s^0 \rightarrow J/\psi \phi$) and $B_s^0 \rightarrow \psi(2S)\phi$ decay rates performed at CDF [77], DØ [78], ATLAS [79], CMS [33, 80] and LHCb [30, 81–83], where the CP -even and CP -odd amplitudes are separated statistically through a full angular analysis. The LHCb collaboration analyzes the $B_s^0 \rightarrow J/\psi K^+ K^-$ decay considering that the $K^+ K^-$ system can be in a P-wave or S-wave state, and measures the dependence of the strong phase difference between the P-wave and S-wave amplitudes as a function of the $K^+ K^-$ invariant mass [30, 84]; this allows the unambiguous determination of the sign of $\Delta\Gamma_s$, which is found to be positive. All these studies use both untagged and tagged B_s^0 candidates and are optimized for the measurement of the phase $\phi_s^{c\bar{c}s}$ that describes CP violation in the interference between B_s^0 - \bar{B}_s^0 mixing and decay in $b \rightarrow c\bar{c}s$ transitions. The published $B_s^0 \rightarrow J/\psi K^+ K^-$, $J/\psi \phi$ and $\psi(2S)\phi$ analyses [30, 33, 77–83] are combined in a multi-dimensional fit including all measured parameters and their correlations. To account for a tension in the time and angular parameters, scale factors are applied on the combined uncertainty of each parameter where a discrepancy arise. For example, the scale factors on the uncertainties of $\Delta\Gamma_s$, Γ_s and $\phi_s^{c\bar{c}s}$ are 1.72, 2.56 and 1.00, respectively. The averages are then further refined by applying

Table 75.1: $\bar{\chi}$ and b -hadron fractions (see text).

	Z decays [96]	Tevatron [96]	LHC (\sqrt{s}) [97, 98]
$\bar{\chi}$	0.1259 ± 0.0042	0.147 ± 0.011	
$f_u = f_d$	0.408 ± 0.007	0.344 ± 0.021	
f_s	0.100 ± 0.008	0.115 ± 0.013	
f_{baryon}	0.084 ± 0.011	0.198 ± 0.046	
f_s/f_d	0.246 ± 0.023	0.333 ± 0.040	0.239 ± 0.007 (7 TeV) 0.239 ± 0.008 (8 TeV) 0.254 ± 0.008 (13 TeV)

constraints from the effective lifetime measurements with flavor-specific [22,66–68] and pure CP [54,67,70–73] final states, to yield

$$\Delta\Gamma_s = +0.084 \pm 0.005 \text{ ps}^{-1} \text{ and } 1/\Gamma_s = 1.520 \pm 0.005 \text{ ps}, \quad (75.20)$$

or, equivalently,

$$1/\Gamma_L = 1.429 \pm 0.007 \text{ ps} \text{ and } 1/\Gamma_H = 1.624 \pm 0.009 \text{ ps}, \quad (75.21)$$

in good agreement with the Standard Model prediction $\Delta\Gamma_s = +0.091 \pm 0.013 \text{ ps}^{-1}$ [9].

Estimates of $\Delta\Gamma_s/\Gamma_s$ obtained from measurements of the $B_s^0 \rightarrow D_s^{(*)+} D_s^{(*)-}$ branching fractions are not included in the average, since they are based on the questionable [7] assumption that these decays account for all CP -even final states.

75.5 Average b -hadron mixing probability and b -hadron production fractions at high energy

Mixing measurements can significantly improve our knowledge on the fractions f_u, f_d, f_s , and f_{baryon} , defined as the fractions of B_u, B_d^0, B_s^0 , and b -baryons in an unbiased sample of weakly-decaying b hadrons produced in high-energy collisions. Indeed, time-integrated mixing analyses using lepton pairs from $b\bar{b}$ events at high energy measure the quantity

$$\bar{\chi} = f'_d \chi_d + f'_s \chi_s, \quad (75.22)$$

where f'_q ($q = s, d$) is the B_q^0 fraction in a sample of semileptonic b -hadron decays. Assuming that all b hadrons have the same semileptonic decay width implies $f'_q = f_q/(\Gamma_q \tau_b)$, where τ_b is the average b -hadron lifetime. Hence $\bar{\chi}$ measurements performed at LEP [85] and Tevatron [86, 87], together with χ_d given in Eq. (75.16) and the very good approximation $\chi_s = 1/2$ (in fact $\chi_s = 0.499312 \pm 0.000004$ from Eqs. (75.5), (75.17) and (75.20)), provide constraints on f_d and f_s .

The LEP experiments have measured $\mathcal{B}(\bar{b} \rightarrow B_s^0) \times \mathcal{B}(B_s^0 \rightarrow D_s^- \ell^+ \nu_\ell X)$ [88], $\mathcal{B}(b \rightarrow A_b^0) \times \mathcal{B}(A_b^0 \rightarrow A_c^+ \ell^- \bar{\nu}_\ell X)$ [89], and $\mathcal{B}(b \rightarrow \Xi_b^-) \times \mathcal{B}(\Xi_b^- \rightarrow \Xi^- \ell^- \bar{\nu}_\ell X)$ [90] from partially reconstructed final states including a lepton, f_{baryon} from protons identified in b events [91], and the production rate of charged b hadrons [92]. The b -hadron fraction ratios measured at CDF are based on double semileptonic $K^* \mu\mu$ and $\phi\mu\mu$ final states [93] and lepton-charm final states [94]; in addition CDF and DØ have both measured strange b -baryon production [95]. A combination of the available information from LEP and Tevatron yields, under the constraints $f_u = f_d, f_u + f_d + f_s + f_{\text{baryon}} = 1$ and Eq. (75.22), the averages of the first two columns of Table 75.1.

Fraction ratios have been studied by LHCb using fully reconstructed hadronic B_s^0 and B_d^0 decays as well as semileptonic decays of A_b^0, B_s^0, B_d^0 and B_u (see [97] and references therein). ATLAS has measured f_s/f_d using $B_s^0 \rightarrow J/\psi\phi$ and $B^0 \rightarrow J/\psi K^{*0}$ decays [98]. Both CDF and LHCb observe that the ratio $f_{A_b^0}/(f_u + f_d)$ decreases with the transverse momentum of the lepton+charm system, indicating that the b -hadron fractions are not the same in different environments. LHCb also observes that $f_s/(f_u + f_d)$ decreases with transverse momentum. The third column of Table 75.1 displays the LHC measurements of $f_s/f_u = f_s/f_d$, which increase slowly with centre-of-mass energy. The B_c^+ fraction has been measured for the first time by LHCb to be $(0.26 \pm 0.06)\%$ [99].

75.6 CP -violation studies

Evidence for CP violation in B_q^0 - \bar{B}_q^0 mixing has been searched for, both with flavor-specific and inclusive B_q^0 decays, in samples where the initial flavor state is tagged, usually with a lepton from the other b -hadron in the event. In the case of semileptonic (or other flavor-specific) decays, where the final-state tag is also available, the following asymmetry [2]

$$\mathcal{A}_{\text{SL}}^q = \frac{N(\bar{B}_q^0(t) \rightarrow \ell^+ \nu_\ell X) - N(B_q^0(t) \rightarrow \ell^- \bar{\nu}_\ell X)}{N(\bar{B}_q^0(t) \rightarrow \ell^+ \nu_\ell X) + N(B_q^0(t) \rightarrow \ell^- \bar{\nu}_\ell X)} \simeq 1 - |q/p|_q^2 \quad (75.23)$$

has been measured either in time-integrated analyses at CLEO [49, 100], BaBar [101], CDF [102], DØ [103–105] and LHCb [106], or in time-dependent analyses at LEP [40, 107], BaBar [50, 108] and Belle [109]. In the inclusive case, also investigated at LEP [107, 110], no final-state tag is used, and the asymmetry [111]

$$\frac{N(\bar{B}_q^0(t) \rightarrow \text{all}) - N(B_q^0(t) \rightarrow \text{all})}{N(\bar{B}_q^0(t) \rightarrow \text{all}) + N(B_q^0(t) \rightarrow \text{all})} \simeq \mathcal{A}_{\text{SL}}^q \left[\sin^2 \left(\frac{\Delta m_q t}{2} \right) - \frac{x_q}{2} \sin(\Delta m_q t) \right] \quad (75.24)$$

must be measured as a function of the proper time to extract information on CP violation. In addition LHCb has studied the time dependence of the charge asymmetry of $B^0 \rightarrow D^{(*)-} \mu^+ \nu_\mu X$ decays without tagging the initial state [112], which would be equal to

$$\frac{N(D^{(*)-} \mu^+ \nu_\mu X) - N(D^{(*)+} \mu^- \bar{\nu}_\mu X)}{N(D^{(*)-} \mu^+ \nu_\mu X) + N(D^{(*)+} \mu^- \bar{\nu}_\mu X)} = \mathcal{A}_{\text{SL}}^d \frac{1 - \cos(\Delta m_d t)}{2} \quad (75.25)$$

in absence of detection and production asymmetries.

The DØ collaboration measured a like-sign dimuon charge asymmetry in semileptonic b decays that deviates by 2.8σ from the tiny Standard Model prediction and concluded, from a more refined analysis in bins of muon impact parameters, that the overall discrepancy is at the level of 3.6σ [103]. In all other cases, asymmetries compatible with zero (and the Standard Model [10, 11]) have been found, with a precision limited by the available statistics. Several of the analyses at high energy don't disentangle the B_d^0 and B_s^0 contributions, and either quote a mean asymmetry or a measurement of $\mathcal{A}_{\text{SL}}^d$ assuming $\mathcal{A}_{\text{SL}}^s = 0$: we no longer include these in the average. An exception is the dimuon DØ analysis [103], which separates the two contributions by exploiting their dependence on the muon impact parameter cut. The resulting measurements of $\mathcal{A}_{\text{SL}}^d$ and $\mathcal{A}_{\text{SL}}^s$ are then both compatible with the Standard Model. They are also correlated. We therefore perform a two-dimensional average of the measurements of Refs. [49, 50, 100, 101, 103–106, 108, 109, 112] and obtain [8]

$$\mathcal{A}_{\text{SL}}^d = -0.0021 \pm 0.0017 \Leftrightarrow |q/p|_d = 1.0010 \pm 0.0008, \quad (75.26)$$

$$\mathcal{A}_{\text{SL}}^s = -0.0006 \pm 0.0028 \Leftrightarrow |q/p|_s = 1.0003 \pm 0.0014, \quad (75.27)$$

with a correlation coefficient of -0.054 between $\mathcal{A}_{\text{SL}}^d$ and $\mathcal{A}_{\text{SL}}^s$. These results show no evidence of CP violation and are compatible with the very small Standard Model predictions, $\mathcal{A}_{\text{SL}}^{d, \text{SM}} = -(4.73 \pm 0.42) \times 10^{-4}$ and $\mathcal{A}_{\text{SL}}^{s, \text{SM}} = +(2.06 \pm 0.18) \times 10^{-5}$ [9], but have insufficient precision yet to constrain the Standard Model.

CP violation induced by B_s^0 - \bar{B}_s^0 mixing in $b \rightarrow c\bar{c}s$ decays, which is controlled by the small weak phase $\phi_s^{c\bar{c}s}$, has been a field of very active study in the past decade. In addition to the previously mentioned $B_s^0 \rightarrow J/\psi K^+ K^-$ (including $B_s^0 \rightarrow J/\psi\phi$) and $B_s^0 \rightarrow \psi(2S)\phi$ studies, the decay modes $B_s^0 \rightarrow J/\psi\pi^+\pi^-$ (including $B_s^0 \rightarrow J/\psi f_0(980)$) [73, 113] and $B_s^0 \rightarrow D_s^+ D_s^-$ [31] have also been analyzed by LHCb to measure $\phi_s^{c\bar{c}s}$, without the need for an angular analysis. The $J/\psi\pi^+\pi^-$ final state has been shown indeed to be (very close to) a pure CP -odd state [114]. In the $B_s^0 \rightarrow J/\psi\phi$ and $B_s^0 \rightarrow J/\psi K^+ K^-$ analyses, $\phi_s^{c\bar{c}s}$ is obtained together with several other observables, including $\Delta\Gamma_s, \Gamma_s$, the longitudinal and perpendicular ϕ polarisation amplitudes, the S-wave amplitude, and strong phases. In order to account for all correlations, the full sets of measurements provided by the different analyses are

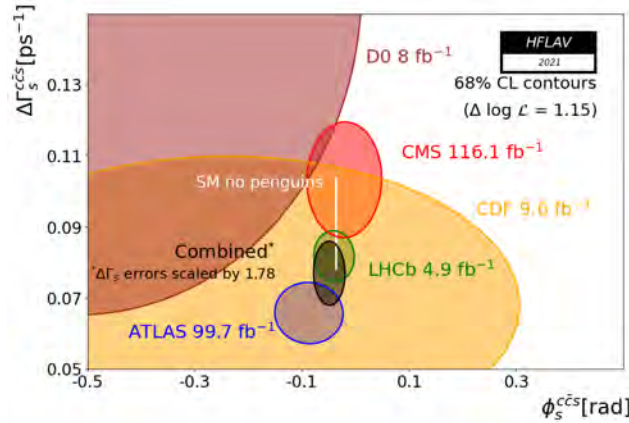


Figure 75.3: 68% CL contours in the $(\phi_s^{c\bar{c}s}, \Delta\Gamma_s)$ plane, showing all measurements from CDF [77], D0 [78], ATLAS [79], CMS [33, 80] and LHCb [30, 31, 73, 81–83, 113]. Their average [8] is represented as the black ellipse, where the combined uncertainty on $\Delta\Gamma_s$ has been multiplied by 1.78. The very thin white rectangle represents the Standard Model predictions of $\phi_s^{c\bar{c}s}$ [63] and $\Delta\Gamma_s$ [9].

combined in a multi-dimensional fit [8] of which $\phi_s^{c\bar{c}s}$ is just one of the free parameters. As already mentioned the $B_s^0 \rightarrow J/\psi\phi$ analyses of ATLAS, CMS and LHCb show a poor overall compatibility, mostly in the lifetime and angular parameters, corresponding approximately 3 standard deviations. Therefore, scale factors are applied on the combined uncertainty of each parameter where a discrepancy arises. For the parameters already in agreement, such as $\phi_s^{c\bar{c}s}$, no scale factor is applied. The combined result based on all published analyses [30, 31, 33, 73, 77–83, 113] is

$$\phi_s^{c\bar{c}s} = -0.049 \pm 0.019. \quad (75.28)$$

A two-dimensional projection of the overall situation in the $(\phi_s^{c\bar{c}s}, \Delta\Gamma_s)$ plane is shown in Fig. 75.3.

The experimental determination of $\phi_s^{c\bar{c}s}$ is still statistically limited. It is consistent with the Standard Model prediction, which is equal to $-2\beta_s = -2\arg(-(V_{ts}V_{tb}^*)/(V_{cs}V_{cb}^*)) = -0.0368_{-0.0009}^{+0.0006}$ [63] assuming negligible Penguin pollution.

75.7 Summary

$B^0-\bar{B}^0$ mixing has been and still is a field of intense study. The mass differences in the $B_d^0-\bar{B}_d^0$ and $B_s^0-\bar{B}_s^0$ systems are known to relative precisions of 0.38% and 0.03%, respectively. The non-zero decay width difference in the $B_s^0-\bar{B}_s^0$ system is well established, with a relative difference of $\Delta\Gamma_s/\Gamma_s = (12.8 \pm 0.7)\%$, meaning that the heavy state of the $B_s^0-\bar{B}_s^0$ system lives $\sim 14\%$ longer than the light state. In contrast, the relative decay width difference in the $B_d^0-\bar{B}_d^0$ system, $\Delta\Gamma_d/\Gamma_d = (0.1 \pm 1.0)\%$, is still consistent with zero. CP violation in $B_d^0-\bar{B}_d^0$ or $B_s^0-\bar{B}_s^0$ mixing has not been observed yet, with precisions on the semileptonic asymmetries below 0.3%. CP violation induced by $B_s^0-\bar{B}_s^0$ mixing in $b \rightarrow c\bar{c}s$ transitions has not yet been observed either, with an uncertainty on the $\phi_s^{c\bar{c}s}$ phase of 19 mrad. All observations so far remain consistent with the Standard Model expectations.

However, the measurements where New Physics might show up are still statistically limited. More results are awaited from the LHC experiments and Belle II, with promising prospects for the investigation of the CP -violating phase $\arg(-M_{12}/\Gamma_{12})$ and an improved determination of $\phi_s^{c\bar{c}s}$.

Mixing studies have clearly reached the stage of precision measurements, where much effort is needed, both on the experimental and theoretical sides, in particular to further reduce the hadronic uncertainties of lattice QCD calculations. In the long term, a stringent check of the consistency of the B_d^0 and B_s^0 mixing amplitudes (magnitudes and phases) with all other measured flavor-physics observables will be possible within the Standard Model,

leading to very tight limits on (or otherwise a long-awaited surprise about) New Physics.

References

- [1] T. D. Lee and C. S. Wu, *Ann. Rev. Nucl. Part. Sci.* **16**, 511 (1966); I. I. Bigi and A. I. Sanda, *Camb. Monogr. Part. Phys. Nucl. Phys. Cosmol.* **9**, 1 (2009), second edition, first published in 2000; G. C. Branco, L. Lavoura and J. P. Silva, *Int. Ser. Monogr. Phys.* **103**, 1 (1999).
- [2] See the review on CP violation in the quark sector by T. Gershon and Y. Nir in this publication.
- [3] A. J. Buras, W. Slominski and H. Steger, *Nucl. Phys.* **B245**, 369 (1984).
- [4] T. Inami and C. S. Lim, *Prog. Theor. Phys.* **65**, 297 (1981), erratum *ibid.* **65**, 1772 (1981); for the power-like approximation, see A. J. Buras and R. Fleischer, page 91 in “Heavy Flavours II,” eds. A. J. Buras and M. Lindner, Singapore World Scientific (1998).
- [5] M. Kobayashi and T. Maskawa, *Prog. Theor. Phys.* **49**, 652 (1973).
- [6] I. I. Bigi *et al.*, in “ CP violation,” ed. C. Jarlskog, Singapore World Scientific (1989).
- [7] A. Lenz and U. Nierste (2011), [arXiv:1102.4274]; A. Lenz and U. Nierste, *JHEP* **06**, 072 (2007), [hep-ph/0612167].
- [8] Y. S. Amhis *et al.* (HFLAV), *Eur. Phys. J.* **C81**, 226 (2021), [arXiv:1909.12524]; the combined results on b -hadron lifetimes and mixing parameters published in this *Review* have been obtained by the B lifetimes and oscillations sub-group of the Heavy Flavor Averaging (HFLAV) group in March 2022 as updates of the averages published in Chapter 4 of the above paper; for more information, see <https://hflav.web.cern.ch/>.
- [9] A. Lenz and G. Tetlalmatzi-Xolocotzi, *JHEP* **07**, 177 (2020), [arXiv:1912.07621].
- [10] T. Jubb *et al.*, *Nucl. Phys.* **B915**, 431 (2017), [arXiv:1603.07770].
- [11] M. Artuso, G. Borissov and A. Lenz, *Rev. Mod. Phys.* **88**, 045002 (2016), [arXiv:1511.09466].
- [12] C. Albajar *et al.* (UA1), *Phys. Lett.* **B186**, 247 (1987), erratum *ibid.* **B197**, 565 (1987).
- [13] H. Albrecht *et al.* (ARGUS), *Phys. Lett.* **B192**, 245 (1987).
- [14] H. G. Moser and A. Roussarie, *Nucl. Instrum. Meth.* **A384**, 491 (1997).
- [15] SLD collab., SLAC-PUB-7228, SLAC-PUB-7229, and SLAC-PUB-7230, *28th Int. Conf. on High Energy Physics*, Warsaw (1996); J. L. Wittlin, *A measurement of the time dependence of $B_d^0-\bar{B}_d^0$ mixing with kaon tagging*, Ph.D. thesis, Massachusetts U., Amherst (2001), URL <http://www.lib.umi.com/dissertations/fullcit?p3027272>.
- [16] ALEPH collab., contrib. 596 to *Int. Europhysics Conf. on High Energy Physics*, Jerusalem (1997).
- [17] K. Abe *et al.* (SLD), *Phys. Rev.* **D67**, 012006 (2003), [hep-ex/0209002].
- [18] J. Abdallah *et al.* (DELPHI), *Eur. Phys. J.* **C28**, 155 (2003), [hep-ex/0303032].
- [19] F. Abe *et al.* (CDF), *Phys. Rev. Lett.* **80**, 2057 (1998), [hep-ex/9712004]; F. Abe *et al.* (CDF), *Phys. Rev.* **D59**, 032001 (1999), [hep-ex/9806026]; F. Abe *et al.* (CDF), *Phys. Rev.* **D60**, 051101 (1999); F. Abe *et al.* (CDF), *Phys. Rev.* **D60**, 072003 (1999), [hep-ex/9903011]; T. Affolder *et al.* (CDF), *Phys. Rev.* **D60**, 112004 (1999), [hep-ex/9907053].
- [20] R. Barate *et al.* (ALEPH), *Eur. Phys. J.* **C4**, 367 (1998); R. Barate *et al.* (ALEPH), *Eur. Phys. J.* **C7**, 553 (1999), [hep-ex/9811018].
- [21] R. Aaij *et al.* (LHCb), *JINST* **10**, P10005 (2015), [arXiv:1507.07892].
- [22] P. Abreu *et al.* (DELPHI), *Eur. Phys. J.* **C16**, 555 (2000), [hep-ex/0107077].

- [23] K. Anikeev *et al.* (2002), [hep-ph/0201071].
- [24] A. Abulencia *et al.* (CDF), Phys. Rev. Lett. **97**, 242003 (2006), [hep-ex/0609040].
- [25] V. M. Abazov *et al.* (DØ), Phys. Rev. **D74**, 112002 (2006), [hep-ex/0609034].
- [26] V. M. Abazov *et al.* (DØ), Phys. Rev. Lett. **101**, 241801 (2008), [arXiv:0802.2255].
- [27] R. Aaij *et al.* (LHCb), Eur. Phys. J. **C72**, 2022 (2012), [arXiv:1202.4979].
- [28] R. Aaij *et al.* (LHCb), JINST **11**, P05010 (2016), [arXiv:1602.07252].
- [29] R. Aaij *et al.* (LHCb), Eur. Phys. J. **C77**, 238 (2017), [arXiv:1610.06019].
- [30] R. Aaij *et al.* (LHCb), Phys. Rev. Lett. **114**, 041801 (2015), [arXiv:1411.3104]; R. Aaij *et al.* (LHCb), Eur. Phys. J. **C79**, 706 (2019), erratum *ibid.* **C80**, 601 (2020), [arXiv:1906.08356].
- [31] R. Aaij *et al.* (LHCb), Phys. Rev. Lett. **113**, 211801 (2014), [arXiv:1409.4619].
- [32] R. Aaij *et al.* (LHCb), Phys. Rev. Lett. **117**, 261801 (2016), [arXiv:1608.06620].
- [33] A. M. Sirunyan *et al.* (CMS), Phys. Lett. **B816**, 136188 (2021), [arXiv:2007.02434].
- [34] B. Aubert *et al.* (BaBar), Phys. Rev. Lett. **94**, 161803 (2005), [hep-ex/0408127]; K. F. Chen *et al.* (Belle), Phys. Rev. **D72**, 012004 (2005), [hep-ex/0504023].
- [35] Throughout this document we omit references of results that have been replaced by new published measurements.
- [36] D. Buskulic *et al.* (ALEPH), Z. Phys. **C75**, 397 (1997).
- [37] P. Abreu *et al.* (DELPHI), Z. Phys. **C76**, 579 (1997).
- [38] M. Acciarri *et al.* (L3), Eur. Phys. J. **C5**, 195 (1998).
- [39] G. Alexander *et al.* (OPAL), Z. Phys. **C72**, 377 (1996); K. Ackerstaff *et al.* (OPAL), Z. Phys. **C76**, 417 (1997), [hep-ex/9707010]; G. Abbiendi *et al.* (OPAL), Phys. Lett. **B493**, 266 (2000), [hep-ex/0010013].
- [40] K. Ackerstaff *et al.* (OPAL), Z. Phys. **C76**, 401 (1997), [hep-ex/9707009].
- [41] B. Aubert *et al.* (BaBar), Phys. Rev. Lett. **88**, 221802 (2002), [hep-ex/0112044]; B. Aubert *et al.* (BaBar), Phys. Rev. **D66**, 032003 (2002), [hep-ex/0201020]; B. Aubert *et al.* (BaBar), Phys. Rev. Lett. **88**, 221803 (2002), [hep-ex/0112045]; B. Aubert *et al.* (BaBar), Phys. Rev. **D67**, 072002 (2003), [hep-ex/0212017]; B. Aubert *et al.* (BaBar), Phys. Rev. **D73**, 012004 (2006), [hep-ex/0507054].
- [42] N. C. Hastings *et al.* (Belle), Phys. Rev. **D67**, 052004 (2003), [hep-ex/0212033]; Y. Zheng *et al.* (Belle), Phys. Rev. **D67**, 092004 (2003), [hep-ex/0211065]; K. Abe *et al.* (Belle), Phys. Rev. **D71**, 072003 (2005), erratum *ibid.* **D71**, 079903 (2005), [hep-ex/0408111].
- [43] R. Aaij *et al.* (LHCb), Phys. Lett. **B709**, 177 (2012), [arXiv:1112.4311].
- [44] R. Aaij *et al.* (LHCb), Phys. Lett. **B719**, 318 (2013), [arXiv:1210.6750].
- [45] R. Aaij *et al.* (LHCb), Eur. Phys. J. **C73**, 2655 (2013), [arXiv:1308.1302].
- [46] R. Aaij *et al.* (LHCb), Eur. Phys. J. **C76**, 412 (2016), [arXiv:1604.03475].
- [47] H. Albrecht *et al.* (ARGUS), Z. Phys. **C55**, 357 (1992); H. Albrecht *et al.* (ARGUS), Phys. Lett. **B324**, 249 (1994).
- [48] J. E. Bartelt *et al.* (CLEO), Phys. Rev. Lett. **71**, 1680 (1993).
- [49] B. H. Behrens *et al.* (CLEO), Phys. Lett. **B490**, 36 (2000), [hep-ex/0005013].
- [50] B. Aubert *et al.* (BaBar), Phys. Rev. Lett. **92**, 181801 (2004), [hep-ex/0311037]; B. Aubert *et al.* (BaBar), Phys. Rev. **D70**, 012007 (2004), [hep-ex/0403002].
- [51] T. Higuchi *et al.*, Phys. Rev. **D85**, 071105 (2012), [arXiv:1203.0930].
- [52] R. Aaij *et al.* (LHCb), JHEP **04**, 114 (2014), [arXiv:1402.2554].
- [53] M. Aaboud *et al.* (ATLAS), JHEP **06**, 081 (2016), [arXiv:1605.07485].
- [54] A. M. Sirunyan *et al.* (CMS), Eur. Phys. J. **C78**, 457 (2018), erratum *ibid.* **C78**, 561 (2018), [arXiv:1710.08949].
- [55] See the review on the CKM quark-mixing matrix by A. Cecucci, Z. Ligeti, and Y. Sakai in this publication.
- [56] S. Aoki *et al.* (Flavour Lattice Averaging Group) (2019), [arXiv:1902.08191].
- [57] R. Aaij *et al.* (LHCb), New J. Phys. **15**, 053021 (2013), [arXiv:1304.4741].
- [58] R. Aaij *et al.* (LHCb), JHEP **03**, 137 (2021), [arXiv:2011.12041].
- [59] R. Aaij *et al.* (LHCb), Nature Phys. **18**, 1 (2022), [arXiv:2104.04421].
- [60] A. Bazavov *et al.* (Fermilab Lattice and MILC), Phys. Rev. **D93**, 113016 (2016), [arXiv:1602.03560].
- [61] D. King, A. Lenz and T. Rauh, JHEP **05**, 034 (2019), [arXiv:1904.00940].
- [62] M. Bona *et al.* (UTfit), JHEP **10**, 081 (2006), [hep-ph/0606167]; updated results at <http://www.utfit.org/>.
- [63] J. Charles *et al.*, Phys. Rev. **D91**, 073007 (2015), [arXiv:1501.05013]; updated results at <http://ckmfitter.in2p3.fr/>.
- [64] K. Hartkorn and H. G. Moser, Eur. Phys. J. **C8**, 381 (1999).
- [65] M. Acciarri *et al.* (L3), Phys. Lett. **B438**, 417 (1998).
- [66] D. Buskulic *et al.* (ALEPH), Phys. Lett. **B377**, 205 (1996); K. Ackerstaff *et al.* (OPAL), Phys. Lett. **B426**, 161 (1998), [hep-ex/9802002]; F. Abe *et al.* (CDF), Phys. Rev. **D59**, 032004 (1999), [hep-ex/9808003]; V. M. Abazov *et al.* (DØ), Phys. Rev. Lett. **114**, 062001 (2015), [arXiv:1410.1568]; T. Aaltonen *et al.* (CDF), Phys. Rev. Lett. **107**, 272001 (2011), [arXiv:1103.1864]; R. Aaij *et al.* (LHCb), Phys. Rev. Lett. **113**, 172001 (2014), [arXiv:1407.5873]; R. Aaij *et al.* (LHCb), Phys. Rev. Lett. **119**, 101801 (2017), [arXiv:1705.03475].
- [67] R. Aaij *et al.* (LHCb), Phys. Rev. Lett. **112**, 111802 (2014), [arXiv:1312.1217].
- [68] R. Aaij *et al.* (LHCb), Phys. Lett. **B736**, 446 (2014), [arXiv:1406.7204].
- [69] R. Aaij *et al.* (LHCb), Phys. Lett. **B707**, 349 (2012), [arXiv:1111.0521].
- [70] R. Aaij *et al.* (LHCb), Phys. Lett. **B762**, 484 (2016), [arXiv:1607.06314].
- [71] T. Aaltonen *et al.* (CDF), Phys. Rev. **D84**, 052012 (2011), [arXiv:1106.3682]; V. M. Abazov *et al.* (DØ), Phys. Rev. **D94**, 012001 (2016), [arXiv:1603.01302].
- [72] R. Aaij *et al.* (LHCb), Phys. Rev. **D87**, 112010 (2013), [arXiv:1304.2600].
- [73] R. Aaij *et al.* (LHCb), Phys. Lett. **B797**, 134789 (2019), [arXiv:1903.05530].
- [74] R. Aaij *et al.* (LHCb), Nucl. Phys. **B873**, 275 (2013), [arXiv:1304.4500].
- [75] R. Aaij *et al.* (LHCb), Phys. Rev. Lett. **128**, 041801 (2022), [arXiv:2108.09284]; R. Aaij *et al.* (LHCb), Phys. Rev. **D105**, 012010 (2022), [arXiv:2108.09283]; A. M. Sirunyan *et al.* (CMS), JHEP **04**, 188 (2020), [arXiv:1910.12127].
- [76] R. Fleischer and R. Knegjens, Eur. Phys. J. **C71**, 1789 (2011), [arXiv:1109.5115].
- [77] T. Aaltonen *et al.* (CDF), Phys. Rev. Lett. **109**, 171802 (2012), [arXiv:1208.2967].
- [78] V. M. Abazov *et al.* (DØ), Phys. Rev. **D85**, 032006 (2012), [arXiv:1109.3166].

- [79] G. Aad *et al.* (ATLAS), Phys. Rev. **D90**, 052007 (2014), [arXiv:1407.1796]; G. Aad *et al.* (ATLAS), JHEP **08**, 147 (2016), [arXiv:1601.03297]; G. Aad *et al.* (ATLAS), Eur. Phys. J. **C81**, 342 (2021), [arXiv:2001.07115].
- [80] V. Khachatryan *et al.* (CMS), Phys. Lett. **B757**, 97 (2016), [arXiv:1507.07527].
- [81] R. Aaij *et al.* (LHCb), Eur. Phys. J. **C81**, 1026 (2021), [arXiv:2105.14738].
- [82] R. Aaij *et al.* (LHCb), JHEP **08**, 037 (2017), [arXiv:1704.08217].
- [83] R. Aaij *et al.* (LHCb), Phys. Lett. **B762**, 253 (2016), [arXiv:1608.04855].
- [84] R. Aaij *et al.* (LHCb), Phys. Rev. Lett. **108**, 241801 (2012), [arXiv:1202.4717].
- [85] S. Schael *et al.* (ALEPH, DELPHI, L3, OPAL, SLD, LEP Electroweak Working Group, SLD Electroweak Group, SLD Heavy Flavour Group), Phys. Rept. **427**, 257 (2006), [hep-ex/0509008]; we use the $\bar{\chi}$ average given in Eq. (5.39).
- [86] D. Acosta *et al.* (CDF), Phys. Rev. **D69**, 012002 (2004), [hep-ex/0309030].
- [87] V. M. Abazov *et al.* (DØ), Phys. Rev. **D74**, 092001 (2006), [hep-ex/0609014].
- [88] P. Abreu *et al.* (DELPHI), Phys. Lett. **B289**, 199 (1992); P. D. Acton *et al.* (OPAL), Phys. Lett. **B295**, 357 (1992); D. Buskulic *et al.* (ALEPH), Phys. Lett. **B361**, 221 (1995).
- [89] P. Abreu *et al.* (DELPHI), Z. Phys. **C68**, 375 (1995); R. Barate *et al.* (ALEPH), Eur. Phys. J. **C2**, 197 (1998).
- [90] D. Buskulic *et al.* (ALEPH), Phys. Lett. **B384**, 449 (1996); J. Abdallah *et al.* (DELPHI), Eur. Phys. J. **C44**, 299 (2005), [hep-ex/0510023].
- [91] R. Barate *et al.* (ALEPH), Eur. Phys. J. **C5**, 205 (1998).
- [92] J. Abdallah *et al.* (DELPHI), Phys. Lett. **B576**, 29 (2003), [hep-ex/0311005].
- [93] F. Abe *et al.* (CDF), Phys. Rev. **D60**, 092005 (1999).
- [94] T. Aaltonen *et al.* (CDF), Phys. Rev. **D77**, 072003 (2008), [arXiv:0801.4375]; T. Affolder *et al.* (CDF), Phys. Rev. Lett. **84**, 1663 (2000), [hep-ex/9909011]; the measurement of f_{baryon}/f_d in the latter paper has been updated based on; T. Aaltonen *et al.* (CDF), Phys. Rev. **D79**, 032001 (2009), [arXiv:0810.3213].
- [95] V. M. Abazov *et al.* (DØ), Phys. Rev. Lett. **99**, 052001 (2007), [arXiv:0706.1690]; V. M. Abazov *et al.* (DØ), Phys. Rev. Lett. **101**, 232002 (2008), [arXiv:0808.4142]; T. Aaltonen *et al.* (CDF), Phys. Rev. **D80**, 072003 (2009), [arXiv:0905.3123].
- [96] Y. S. Amhis *et al.* (HFLAV), *b*-hadron fraction averages computed for the 2020 edition of this Review; for more information, see <https://hflav.web.cern.ch/>.
- [97] R. Aaij *et al.* (LHCb), Phys. Rev. **D104**, 032005 (2021), [arXiv:2103.06810].
- [98] G. Aad *et al.* (ATLAS), Phys. Rev. Lett. **115**, 262001 (2015), [arXiv:1507.08925].
- [99] R. Aaij *et al.* (LHCb), Phys. Rev. **D100**, 112006 (2019), [arXiv:1910.13404].
- [100] D. E. Jaffe *et al.* (CLEO), Phys. Rev. Lett. **86**, 5000 (2001), [hep-ex/0101006].
- [101] J. P. Lees *et al.* (BaBar), Phys. Rev. Lett. **114**, 081801 (2015), [arXiv:1411.1842].
- [102] F. Abe *et al.* (CDF), Phys. Rev. **D55**, 2546 (1997).
- [103] V. M. Abazov *et al.* (DØ), Phys. Rev. **D89**, 012002 (2014), [arXiv:1310.0447].
- [104] V. M. Abazov *et al.* (DØ), Phys. Rev. **D86**, 072009 (2012), [arXiv:1208.5813].
- [105] V. M. Abazov *et al.* (DØ), Phys. Rev. Lett. **110**, 011801 (2013), [arXiv:1207.1769].
- [106] R. Aaij *et al.* (LHCb), Phys. Rev. Lett. **117**, 061803 (2016), erratum *ibid.* **118**, 129903 (2017), [arXiv:1605.09768].
- [107] R. Barate *et al.* (ALEPH), Eur. Phys. J. **C20**, 431 (2001).
- [108] J. P. Lees *et al.* (BaBar), Phys. Rev. Lett. **111**, 101802 (2013), erratum *ibid.* **111**, 159901 (2013), [arXiv:1305.1575].
- [109] E. Nakano *et al.* (Belle), Phys. Rev. **D73**, 112002 (2006), [hep-ex/0505017].
- [110] G. Abbiendi *et al.* (OPAL), Eur. Phys. J. **C12**, 609 (2000), [hep-ex/9901017].
- [111] M. Beneke, G. Buchalla and I. Dunietz, Phys. Lett. **B393**, 132 (1997), [hep-ph/9609357]; I. Dunietz, Eur. Phys. J. **C7**, 197 (1999), [hep-ph/9806521].
- [112] R. Aaij *et al.* (LHCb), Phys. Rev. Lett. **114**, 041601 (2015), [arXiv:1409.8586].
- [113] R. Aaij *et al.* (LHCb), Phys. Lett. **B736**, 186 (2014), [arXiv:1405.4140].
- [114] R. Aaij *et al.* (LHCb), Phys. Rev. **D86**, 052006 (2012), [arXiv:1204.5643].

76. Semileptonic b -Hadron Decays, Determination of V_{cb} , V_{ub}

Revised August 2021 by A.X. El-Khadra (Physics, Illinois U.) and P. Urquijo (School of Phys. U. of Melbourne).

76.1 Introduction

Precision determinations of $|V_{ub}|$ and $|V_{cb}|$ are central to testing the CKM sector of the Standard Model, and complement the measurements of CP asymmetries in B decays. The length of the side of the unitarity triangle opposite the well-measured angle β is proportional to the ratio $|V_{ub}|/|V_{cb}|$; its precise determination is a high priority of the heavy-flavor physics program.

The transitions $b \rightarrow c\ell\bar{\nu}_\ell$ and $b \rightarrow u\ell\bar{\nu}_\ell$ ($\ell = e, \mu$) each provide two avenues for determining these CKM matrix elements, namely through measurements of inclusive decay rates, $\bar{B} \rightarrow X\ell\bar{\nu}_\ell$ with a sum over all possible hadronic states X or of exclusive rates, where the final state hadron is a specific meson ($X = D, D^*, \pi, \rho$ etc.).

Purely leptonic decays, such as $B_c^- \rightarrow \tau\bar{\nu}$, $B^- \rightarrow \tau\bar{\nu}$, and $B^- \rightarrow \mu\bar{\nu}$, provide a third avenue that is theoretically very simple (see the RPP mini-review [1]). However, we do not use this information at present since none of the measurements have reached a competitive level of precision. Hence the results presented here are solely obtained from exclusive and inclusive semileptonic b -hadron decays. This article and the values quoted here update the previous review [2].

The theoretical methods underlying the different determinations of $|V_{qb}|$ are quite mature. The theoretical approach for inclusive determinations uses the fact that the mass m_b of the b quark is large compared to the scale Λ_{QCD} that determines low-energy hadronic physics. Thus the basis for precise calculations is a systematic expansion in powers of Λ/m_b , where $\Lambda \sim 500 - 700$ MeV is a hadronic scale of the order of Λ_{QCD} . Such an expansion can be formulated in the framework of an effective field theory which is described in a separate RPP mini-review [3]. Exclusive determinations rely on non-perturbatively calculated form factors, that encode the low-energy dynamics of the hadronic transition. Here, lattice QCD provides an, in principle, ab-initio method to calculate the non-perturbative QCD contributions to the exclusive decay amplitudes. Thanks to a combination of improved theoretical methods, better algorithms, and large increases in computational power, precise lattice QCD results are now available for the processes that are used in exclusive $|V_{ub}|$ and $|V_{cb}|$ determinations. State-of-the-art lattice QCD calculations are based on gauge-field ensembles that include realistic sea quark effects for degenerate up/down and strange quarks (aka $2 + 1$ -flavor ensembles), and increasingly, also for charm (aka $2 + 1 + 1$ -flavor ensembles). They employ ensembles generated at three (or more) lattice spacings, different spatial volumes, among other parameter variations to allow for quantification of the underlying systematic errors, and include detailed systematic error analyses. This is described in a separate RPP mini-review [4]. The lattice-QCD results discussed in this review are all state-of-the-art with fully quantified uncertainties, and therefore play a central role in exclusive $|V_{qb}|$ determinations. In the case of exclusive $\bar{B} \rightarrow D^{(*)}\ell\bar{\nu}_\ell$ decays, heavy quark symmetry (HQS) and heavy quark effective theory (HQET) yield constraints on the form factors that can be used to improve exclusive $|V_{cb}|$ determinations, especially when lattice QCD form factor results are incomplete, as was the case until very recently for $\bar{B} \rightarrow D^*\ell\bar{\nu}_\ell$. Light-cone sum rules (LCSR) provide another nonperturbative approach to compute form factors. However, while the lattice-QCD results employed in this review have well-quantified uncertainties, LCSR results suffer, in general, from hard-to-quantify systematic errors. The two methods typically provide results in opposite regions of phase space. Lattice-QCD calculations work best at low hadronic recoil or high momentum transfer (q^2) to the leptons, while LCSR calculations provide estimates at high recoil, near $q^2 = 0$.

The measurements discussed in this review are of branching fractions, ratios of branching fractions, and decay kinematic distributions. The determinations of $|V_{cb}|$ and $|V_{ub}|$ also require a measurement of the total decay widths of the corresponding b hadrons, determined from lifetimes, which is the subject of a separate RPP mini-review [5]. The measurements of inclusive

semileptonic decays relevant to this review come primarily from $e^+e^- B$ factories operating at the $\Upsilon(4S)$ resonance, while the measurements of exclusive semileptonic decays come from both the $e^+e^- B$ factories and from the LHCb experiment at CERN.

Semileptonic B -meson decay amplitudes to electrons and muons are well measured and consistent with Standard Model W -boson exchange. As they are expected to be insensitive to the effects of non-Standard-Model physics, they are used to extract $|V_{qb}|$. However, semileptonic decays to tau-lepton final states, such as $\bar{B} \rightarrow D^{(*)}\tau\bar{\nu}_\tau$, may be sensitive to effects from beyond the Standard Model particles due to the large mass of the τ lepton. The currently observed tensions between Standard Model theory and experiment for these decays indicate that semitauonic decays must be studied further.

Many of the numerical results quoted in this review have been provided by the Heavy Flavor Averaging Group (HFLAV) [6].

76.2 Determination of $|V_{cb}|$

Summary: The determination of $|V_{cb}|$ from inclusive decays has a relative uncertainty of about 2%; the limitations arise mainly from our ignorance of higher-order perturbative and non-perturbative corrections. Exclusive $\bar{B} \rightarrow D^*\ell\bar{\nu}_\ell$ decays provide a determination of $|V_{cb}|$ with a relative precision of about 2%, with comparable contributions from theory and experiment to the total uncertainty; the value determined from $\bar{B} \rightarrow D\ell\bar{\nu}_\ell$ decays is consistent and has an uncertainty of 3%. However, as discussed below, recent work has raised questions about determinations based on the CLN parameterization, and we choose to quote a result obtained from a less constraining analysis.

The values obtained from the inclusive and exclusive B decay determinations discussed below are:

$$|V_{cb}| = (42.2 \pm 0.8) \times 10^{-3} \quad (\text{inclusive}) \quad (76.1)$$

$$|V_{cb}| = (39.4 \pm 0.8) \times 10^{-3} \quad (\text{exclusive}). \quad (76.2)$$

An average of these determinations has $p(\chi^2) = 1\%$, so we scale the error by $\sqrt{\chi^2/1} = 2.6$ to find

$$|V_{cb}| = (40.8 \pm 1.4) \times 10^{-3} \quad (\text{average}). \quad (76.3)$$

Given the only marginal consistency, of approximately 2.4σ , this average should be treated with caution.

76.2.1 $|V_{cb}|$ from exclusive decays

Exclusive determinations of $|V_{cb}|$ make use of semileptonic B decays into the ground state charmed mesons D and D^* . The corresponding hadronic matrix elements can be parameterized in terms of six independent form factors, which depend on the variable $w \equiv v \cdot v'$, where v and v' are the four velocities of the initial and final-state hadrons. In the rest frame of the decay this variable corresponds to the Lorentz factor of the final state $D^{(*)}$ meson. Determinations of $|V_{cb}|$ from experimental measurements of $\bar{B} \rightarrow D^{(*)}\ell\bar{\nu}_\ell$ decay rates require precise knowledge of these form factors. Fortunately, lattice QCD results for all relevant form factors, including their recoil dependence, are now available [7–9]. Heavy Quark Symmetry (HQS) [10, 11] predicts that in the infinite mass limit the six form factors collapse into a single one, which is normalized at the “zero recoil point” $w = 1$, the point of maximum momentum transfer to the leptons. Heavy Quark Effective Theory (HQET) provides a framework for obtaining the corrections to the HQS prediction in a systematic expansion in powers of Λ_{QCD}/m_c which is discussed in a separate RPP mini-review [3].

76.2.2 $\bar{B} \rightarrow D^*\ell\bar{\nu}_\ell$

The decay rate for $\bar{B} \rightarrow D^*\ell\bar{\nu}_\ell$, assuming massless leptons, is given by

$$\frac{d\Gamma}{dw}(\bar{B} \rightarrow D^*\ell\bar{\nu}_\ell) = \frac{G_F^2 m_B^5}{48\pi^3} |V_{cb}|^2 |\eta_{\text{EW}}|^2 (w^2 - 1)^{1/2} P(w) |\mathcal{F}(w)|^2, \quad (76.4)$$

where $P(w)$ is a phase space factor,

$$P(w) = r^3(1-r)^2(w+1)^2 \left(1 + \frac{4w}{w+1} \frac{1-2rw+r^2}{(1-r)^2} \right), \quad (76.5)$$

with $r = m_{D^*}/m_B$. The decay amplitude $\mathcal{F}(w)$ can be expressed in terms of the form factors which parametrize the vector and axial vector current matrix elements

$$\begin{aligned} \frac{\langle D^*(v', \epsilon) | \bar{c} \gamma^\mu b | B(v) \rangle}{\sqrt{m_B m_{D^*}}} &= h_V(w) \varepsilon^{\mu\nu\rho\sigma} v_{B,\nu} v_{D^*,\rho} \epsilon_\sigma^*, & (76.6) \\ \frac{\langle D^*(v', \epsilon) | \bar{c} \gamma^\mu \gamma^5 b | B(v) \rangle}{\sqrt{m_B m_{D^*}}} &= i h_{A_1}(w) (1+w) \epsilon^{*\mu} \\ &\quad - i \left[h_{A_2}(w) v_B^\mu + h_{A_3}(w) v_{D^*}^\mu \right] \epsilon^* \cdot v_B, & (76.7) \end{aligned}$$

and the ratios

$$R_1(w) = \frac{h_V(w)}{h_{A_1}(w)}, \quad R_2(w) = \frac{h_{A_3}(w) + r h_{A_2}(w)}{h_{A_1}(w)}, \quad (76.8)$$

as

$$\begin{aligned} P(w) |\mathcal{F}(w)|^2 &= |h_{A_1}(w)|^2 \times \left\{ 2 \frac{r^2 - 2rw + 1}{(1-r)^2} \left[1 + \frac{w-1}{w+1} R_1^2(w) \right] \right. \\ &\quad \left. + \left[1 + \frac{w-1}{1-r} (1 - R_2(w)) \right]^2 \right\}. & (76.9) \end{aligned}$$

Note that \mathcal{F} at $w = 1$ is unity by HQS in the infinite-mass limit [12–15]. The effect of assuming massless leptons is typically very small, but for the muon case can be non-negligible in fits to data at high hadronic recoil.

The factor $\eta_{EW} = 1.0066 \pm 0.0050$ accounts for the leading electroweak corrections to the four-fermion operator mediating the semileptonic decay [16], and includes an estimated uncertainty for missing long-distance QED radiative corrections [17]. At present it is not known if these corrections are or are not already included in the experimental analyses, so this needs to be clarified.

The determination of $|V_{cb}|$ requires knowledge of the normalization, where one commonly uses the zero recoil input, $\mathcal{F}(1)$. Theoretical knowledge of the shapes of the form factors provides crucial compatibility checks between theory and experiment, and improves the precision of the determinations. Model-independent shape parametrizations of the form factors make use of analyticity and unitarity constraints and are expressed in terms of the variable

$$z = \frac{\sqrt{w+1} - \sqrt{2}}{\sqrt{w+1} + \sqrt{2}}, \quad (76.10)$$

originating from a conformal transformation. In terms of this variable the form factors (generically denoted as F) may be written as [18–22]

$$F(z) = \frac{1}{P_F(z)\phi_F(z)} \sum_{n=0}^{\infty} a_n z^n \quad (76.11)$$

where the sum is bounded, $\sum |a_n|^2 < 1$. Furthermore, the function $P_F(z)$ takes into account the resonances in the $(\bar{c}b)$ system below the $\bar{D}B$ threshold, and the weighting functions $\phi_F(z)$ are derived from the unitarity constraint on the corresponding form factor. The values of z relevant to the decay are $0 \leq z \leq 0.06$, hence only very few terms are needed in the series in z . Eq. (76.11) will be referred to as the ‘‘BGL’’ expansion.

The Caprini-Lellouch-Neubert (CLN) parametrization [23] yields a simple form

$$h_{A_1}(w) = h_{A_1}(1) \left[1 - 8\rho^2 z + (53\rho^2 - 15)z^2 - (231\rho^2 - 91)z^3 \right] \quad (76.12)$$

with the slope ρ and normalization $h_{A_1}(1)$ as the only parameters, albeit at the cost of introducing model dependence. Furthermore, the ratios $R_1(w)$ and $R_2(w)$ are expanded in $w - 1$. However, this simple CLN parametrization does not account for higher-order corrections in the $1/m_{c/b}$ expansion, which are now relevant [22, 24–29]. Thus, this report focuses on recent analyses that employ the model-independent BGL expansion. Typical fits include up to three parameters a_n in (76.11) for the different form factors.

Results of the first complete calculation of the $\bar{B} \rightarrow D^* \ell \bar{\nu}_\ell$ form factors at non-zero recoil were recently presented by the Fermilab Lattice and MILC collaborations in Ref. [9]. Preliminary results, obtained by the JLQCD collaboration [30], are reasonably consistent. Prior lattice calculations obtained results for only the form factor at the zero-recoil point, $\mathcal{F}(1)$, [17, 31] with a total uncertainty at the (1-2)% level. The average of the two lattice predictions [32] is

$$\mathcal{F}(1) = 0.904 \pm 0.012, \quad (76.13)$$

Non-lattice estimates based on zero-recoil sum rules for the form factor tend to yield lower central values for $\mathcal{F}(1)$ [33–35]. The sum rules indicate that $\mathcal{F}(1) < 0.92$ [33, 34, 36, 37], while an explicit estimate that includes excited state contributions yields $\mathcal{F}(1) \approx 0.86$ [35, 38]. Lattice-QCD form factors at non-zero recoil provide valuable shape constraints, and hence enable more refined $|V_{cb}|$ determinations. However, since they were not available until very recently, most $|V_{cb}|$ determinations in the literature use the value for $\mathcal{F}(1)$ from Eq. (76.13) as the only quantitative lattice input. We discuss these first, before turning to results for $|V_{cb}|$ which employ the lattice-QCD form factors from Ref. [9].

While Light Cone Sum Rules (LCSR) can provide constraints on the form factors at maximum recoil, the underlying systematic errors are not fully quantified. A recent LCSR calculation [39] quotes uncertainties in the $\lesssim 20\%$ range for the $\bar{B} \rightarrow D^{(*)} \ell \bar{\nu}_\ell$ form factors at $q^2 = 0$. Dispersive methods [40] can also be used to provide additional constraints on form factors calculated in lattice QCD. Very recent work [41, 42] introduces the dispersive matrix method, which includes additional nonperturbative inputs calculable in lattice QCD from two-point correlation functions. A test of this approach for the $D \rightarrow K \ell \nu$ form factors, which can be computed in lattice-QCD over the entire kinematic range, is presented in Ref. [41], while Ref. [42] presents a first lattice-QCD calculation of the needed inputs for the $B \rightarrow D^{(*)}$ transitions. The consistency of the dispersive constraints with the form factor calculations still need to be carefully studied, and the dispersive inputs must be calculated with the same care as the form factors themselves.

Many experiments [43–53] have measured the differential decay rate as a function of w , employing a variety of methods: using either B^+ or B^0 decays, with or without B -tagging, and with or without explicit reconstruction of the transition pion from $D^* \rightarrow D$ decays. In Ref. [6] the experimental measurements were input to a four-dimensional fit for $\eta_{EW} \mathcal{F}(1) |V_{cb}|$, $\rho_{A_1}^2$ and the form-factor ratios $R_1 \propto A_2/A_1$ and $R_2 \propto V/A_1$. The fit has a p -value of 0.9%, so we scale the uncertainty by a factor $\sqrt{\chi^2/23}$ to give $\eta_{EW} \mathcal{F}(1) |V_{cb}| = (35.00 \pm 0.49) \times 10^{-3}$ (CLN).

The leading sources of uncertainty on $\eta_{EW} \mathcal{F}(1) |V_{cb}|$ are due to detection efficiencies and $D^{(*)}$ decay branching fractions. Note that the $\bar{B} \rightarrow D^* \ell \bar{\nu}_\ell$ form factor in the fit is parameterized using the CLN form, which has the drawbacks discussed previously.

Using the value from Eq. (76.13) for $\mathcal{F}(1)$ and accounting for the electroweak correction gives

$$|V_{cb}| = (38.5 \pm 0.5 \pm 0.6) \times 10^{-3} \quad (\bar{B} \rightarrow D^* \ell \bar{\nu}_\ell, \text{ LQCD, CLN}). \quad (76.14)$$

A safer approach is to use the more general BGL form-factor parameterization [19–22, 26]. Two experiments have published analyses with BGL based parametrizations at a given order in the expansion [53, 54]. The Belle analysis [53] is based on an untagged approach in the mode $\bar{B}^0 \rightarrow D^{*+} \ell \bar{\nu}_\ell$ and measures 1- d projections in bins of the hadronic recoil w , and angular variables $\cos \theta_\ell$, $\cos \theta_V$, and χ . The BABAR analysis [54] is based on a hadronic tagged sample, and performs a full 4- d unbinned analysis of neutral and charged B decay modes. Only the BGL form factors are fit in this analysis, not the normalization, which is based on the world average $\bar{B} \rightarrow D^* \ell \bar{\nu}_\ell$ branching fraction.

At present only Ref. [53] publishes the fully-differential decay rate data and associated covariance matrix. The BGL fit results from Ref. [55], $|V_{cb}| = (38.9 \pm 1.0) \times 10^{-3}$, and Ref. [54], $|V_{cb}| = (38.4 \pm 0.9) \times 10^{-3}$, are consistent with result from the fit with the CLN parametrization, Eq. (76.14). Both studies report fit

results at low order in the three BGL expansion terms, ranging from zero-order to second-order in the Belle analysis, and first order for all terms in the BABAR analysis. Studies of the impact of higher order expansions based on the Belle published decay rate data have been reported in Refs. [27, 28], where it is shown that the fit uncertainty on $|V_{cb}|$ increases by approximately 50% with respect to the results reported at lower order. This is due to larger number of degrees of freedom allowed in the higher order expansions, which are not sufficiently constrained without lattice-QCD inputs at nonzero recoil. Belle II has recently provided first preliminary branching fraction measurements of $\bar{B} \rightarrow D^* \ell \bar{\nu}_\ell$ using both tagged and untagged methods [56, 57].

In Ref. [9], BGL expansion fits to the FNAL/MILC lattice QCD form factors show that they are insensitive to truncation effects beyond quadratic order. These form factors were subsequently used in Ref. [9] to extract $|V_{cb}|$ from combined BGL fits to the Belle [53] and synthetic BABAR [54] $\bar{B} \rightarrow D^* \ell \bar{\nu}_\ell$ data, yielding $|V_{cb}| = (38.40 \pm 0.74) \times 10^{-3}$. We note that the determination of $|V_{cb}|$ in Ref. [9] applies the Coulomb factor $(1 + \alpha\pi)$ to the Belle data to account for interactions between the charged final states in the neutral B -meson decay. The p -values for the combined (experiment+lattice QCD) BGL fits reported in Ref. [9] are small, reflecting tensions between the data sets. For a fit combining only the Belle data with the lattice-QCD form factors, Ref. [9] quotes $|V_{cb}| = (38.18 \pm 0.82) \times 10^{-3}$, consistent with the result presented in Eq. (76.15), after accounting for the different values of η_{EW} used in each result. For this review, the method of Ref. [58] was employed in further fits that include the lattice-QCD inputs at non-zero recoil from FNAL/MILC [9] and from JLQCD (preliminary) [30], yielding consistent results at quadratic order. In summary, we adopt the method of Ref. [58], using the recent FNAL/MILC inputs and only the Belle data (given the lack of availability of binned data from the BABAR measurement [54]). The nominal result for $|V_{cb}|$ is therefore

$$|V_{cb}| = (38.7 \pm 1.0) \times 10^{-3} \quad (\bar{B} \rightarrow D^* \ell \bar{\nu}_\ell, \text{LQCD, BGL}), \quad (76.15)$$

where the uncertainty contains contributions from experimental, lattice QCD, and η_{EW} sources. We note that despite the improvements in the experimental data, theoretical inputs, and $|V_{cb}|$ extraction methods, this new exclusive determination of $|V_{cb}|$ is similar in central value to earlier ones, and still in tension with the inclusive determinations discussed in Section 76.2.5 and summarized in Eq. (76.34).

76.2.3 $\bar{B} \rightarrow D \ell \bar{\nu}_\ell$

The differential rate for $\bar{B} \rightarrow D \ell \bar{\nu}_\ell$ is given by

$$\begin{aligned} \frac{d\Gamma}{dw}(\bar{B} \rightarrow D \ell \bar{\nu}_\ell) &= \\ \frac{G_F^2}{48\pi^3} |V_{cb}|^2 (m_B + m_D)^2 m_D^3 (w^2 - 1)^{3/2} (\eta_{EW} \mathcal{G}(w))^2. \end{aligned} \quad (76.16)$$

The form factor is defined in terms of

$$\frac{\langle D(v') | \bar{c} \gamma^\mu b | B(v) \rangle}{\sqrt{m_B m_D}} = h_+(w) (v_B + v_D)^\mu + h_-(w) (v_B - v_D)^\mu \quad (76.17)$$

and reads

$$\mathcal{G}(w) = h_+(w) - \frac{m_B - m_D}{m_B + m_D} h_-(w), \quad (76.18)$$

where $h_+(1)$ is normalized to unity due to HQS and $h_-(1)$ vanishes in the infinite-mass limit. Thus

$$\mathcal{G}(1) = 1 + \mathcal{O}\left(\left(\frac{m_B - m_D}{m_B + m_D}\right)^2 \frac{\Lambda_{\text{QCD}}}{m_c}\right) \quad (76.19)$$

and the corrections to the HQS prediction are of order Λ_{QCD}/m_c in contrast to the case of $\mathcal{F}(1)$. The lattice-QCD result for the normalization, $\mathcal{G}(1)$, obtained in Ref. [7] is

$$\mathcal{G}(1) = 1.054 \pm 0.004 \pm 0.008. \quad (76.20)$$

We first turn to $|V_{cb}|$ extractions that rely on only the normalization $\mathcal{G}(1)$ from Eq. (76.20). The most precise measurements of $\bar{B} \rightarrow D \ell \bar{\nu}_\ell$ [50, 59, 60] dominate the CLN average [6] value, $\eta_{EW} \mathcal{G}(1) |V_{cb}| = (41.53 \pm 0.98) \times 10^{-3}$. Note that this average corresponds to measurements that are fit to the CLN form factor parameterization; the same concerns expressed above for $\bar{B} \rightarrow D^* \ell \bar{\nu}_\ell$ apply here. Using the value from Eq. (76.20) for $\mathcal{G}(1)$ and accounting for the electroweak correction as above gives

$$|V_{cb}| = (39.1 \pm 0.9 \pm 0.4) \times 10^{-3} \quad (\bar{B} \rightarrow D \ell \bar{\nu}_\ell, \text{LQCD, CLN}), \quad (76.21)$$

where the first uncertainty is from experiment, and the second combines the lattice QCD uncertainty in Eq. (76.20) with the electroweak correction.

For the $\bar{B} \rightarrow D \ell \bar{\nu}_\ell$ modes, theoretical input on the shape of the form factor, especially near $w \sim 1$, is especially beneficial to $|V_{cb}|$ determinations, since experimental measurements of the differential decays rate near zero recoil are affected by the more severe phase space suppression, compared to the D^* case. Hence the best $|V_{cb}|$ determinations from exclusive $\bar{B} \rightarrow D \ell \bar{\nu}_\ell$ decays employ lattice-QCD form factors obtained over a range of $w \geq 1$ [7, 8], where Ref. [32] provides a lattice average of the two results. Using the BCL parametrization (z -expansion from Ref. [61]) for the form factors, they can be combined with binned measurements from Belle [60] and BABAR [59]. Only Ref. [60] published the full measurement covariance matrix, while Ref. [59] provides the statistical uncertainty covariance. Nevertheless, Ref. [60] is more precise and dominates the average [32], giving

$$|V_{cb}| = (40.1 \pm 1.0) \times 10^{-3} \quad (\bar{B} \rightarrow D \ell \bar{\nu}_\ell, \text{LQCD, BCL}). \quad (76.22)$$

This result is consistent with the value reported in Ref. [62], which is based on the same experimental and lattice inputs.

The $|V_{cb}|$ averages from $\bar{B} \rightarrow D^* \ell \bar{\nu}_\ell$ and $\bar{B} \rightarrow D \ell \bar{\nu}_\ell$ decays using the BGL (Eq. (76.15)) and BCL (Eq. (76.22)) forms, respectively, are reasonably consistent. The correlations between the lattice uncertainties for $\bar{B} \rightarrow D^* \ell \bar{\nu}_\ell$ and $\bar{B} \rightarrow D \ell \bar{\nu}_\ell$ are discussed in Ref. [32], and considered to be 100% for the statistical uncertainty component. We assume an experimental uncertainty correlation of order 20% and combine the results of Eq. (76.15) and Eq. (76.22), giving

$$|V_{cb}| = (39.4 \pm 0.8) \times 10^{-3} \quad (\text{exclusive}). \quad (76.23)$$

76.2.4 $B_s \rightarrow D_s^{(*)-} \mu^+ \nu_\mu$

Semileptonic decays of B_s mesons are being studied extensively by the LHCb experiment. On the theory side, lattice QCD calculations of the corresponding form factors can proceed using the same methods and gauge-field ensembles as for B -meson decays. In fact, the presence of a strange spectator quark in the B_s -meson decay amplitudes tends to yield smaller statistical and systematic errors in the lattice computation. Nevertheless, to-date there are still fewer lattice-QCD results for B_s -meson form factors available than for the B -meson case, but this situation is quickly changing. For the case of the $B_s \rightarrow D_s$ transition, two lattice QCD calculations of the form factors over a range of recoil momenta have been performed by the HPQCD collaboration, the first on $2 + 1$ -flavor gauge field ensembles (generated by the MILC collaboration) using NRQCD b -quarks [63]. The second calculation uses the $2 + 1 + 1$ -flavor gauge-field ensembles (also generated by MILC), employing the HISQ action for all valence quarks [64]. The all-HISQ approach avoids the need to compute renormalization factors separately, at the cost of requiring an extrapolation to the physical b -quark mass at the lattice spacings used in Ref. [64]. For the $B_s \rightarrow D_s^{*-}$ transition, Ref. [31, 65] provide lattice QCD results for the form factor at zero recoil, where Ref. [65] uses a similar set-up as Ref. [64] and reads

$$\mathcal{F}^{B_s \rightarrow D_s^*}(1) = 0.9020(96)_{\text{stat}}(90)_{\text{sys}}. \quad (76.24)$$

A first lattice QCD calculation of the $B_s \rightarrow D_s^{*-}$ form factors at non-zero recoil, employing ensembles with with 4 flavors of sea quarks, was recently presented in Ref. [66].

LHCb has recently extracted $|V_{cb}|$ from semileptonic B_s^0 decays [67]. The measurement uses both $B_s^0 \rightarrow D_s^- \mu^+ \nu_\mu$ and

$B_s^0 \rightarrow D_s^{*-} \mu^+ \nu_\mu$ decays. The value of $|V_{cb}|$ is determined from the observed yields of B_s^0 decays normalized to those of B^0 decays after correcting for the relative reconstruction and selection efficiencies. The normalization channels are $B^0 \rightarrow D^- \mu^+ \nu_\mu$ and $B^0 \rightarrow D^{*-} \mu^+ \nu_\mu$ decays, where the D^- is reconstructed with the same decay mode of the D_s ($D_{(s)}^- \rightarrow [K^+ K^-]_\phi \pi^-$). The shape of the form factors are extracted using $p_\perp(D_s)$, which is the component of the D_s^- momentum perpendicular to the B_s^0 flight direction. This variable is correlated with q^2 and the helicity angles in the $B_s^0 \rightarrow D_s^{*-} \mu^+ \nu_\mu$ decay. For the $B_s \rightarrow D_s^- \mu^+ \nu_\mu$ decay, for example, $|V_{cb}|$ is related to the measured ratio of signal yields, N_{sig} , and the normalization channel yields, N_{ref} , through the relation

$$\frac{N_{sig}}{N_{ref}} = \xi \frac{f_s}{f_d} \frac{\mathcal{B}(D_s^- \rightarrow K^+ K^- \pi^-)}{\mathcal{B}(D^- \rightarrow K^+ K^- \pi^-)} \frac{1}{\mathcal{B}(B^0 \rightarrow D^- \mu \nu_\mu)} \tau_s \times \int \frac{d\Gamma(B_s \rightarrow D_s \mu \nu_\mu)}{dw} dw,$$

where τ_s is the B_s lifetime, and ξ is the efficiency ratio between the signal and the normalization. The analysis uses the lattice-QCD form factors obtained for $B_s \rightarrow D_s^-$ over the full kinematic range in Ref. [64] and the zero-recoil result for the $B_s \rightarrow D_s^{*-}$ form factor from Ref. [65]. Fits to both the CLN parameterization and a 5-parameter version of BGL were performed. The result for $|V_{cb}|$, updated with the most recent determination of f_s/f_d and $\mathcal{B}(D_s^- \rightarrow K^- K^+ \pi^-)$ from Ref. [68], are $|V_{cb}|_{\text{CLN}} = (40.8 \pm 0.6 \pm 0.9 \pm 1.1) \times 10^{-3}$, and $|V_{cb}|_{\text{BGL}} = (41.7 \pm 0.8 \pm 0.9 \pm 1.1) \times 10^{-3}$, where the first uncertainty is statistical, the second systematic and the third due to the limited knowledge of the external inputs, in particular the constant $f_s/f_d \times \mathcal{B}(D_s^- \rightarrow K^+ K^- \pi^-)$. The results obtained are consistent with the exclusive determinations of $|V_{cb}|$ using the B^0 and B^+ decays but are not used in the overall average in this review at this stage. These channels are important in the measurement of the ratio $|V_{ub}|/|V_{cb}|$, which cancels out the B_s normalisation uncertainties, discussed in Section 76.5.

76.2.5 $|V_{cb}|$ from inclusive decays

Measurements of the total semileptonic branching decay rate, along with moments of the lepton energy and hadronic invariant mass spectra in inclusive semileptonic $b \rightarrow c$ transitions, can be used for a precision determination of $|V_{cb}|$. The total semileptonic decay rate can be calculated quite reliably in terms of non-perturbative parameters that can be extracted from the information contained in the moments.

76.2.6 Inclusive semileptonic rate

The theoretical foundation for the calculation of the total semileptonic rate is the Operator Product Expansion (OPE) which yields the Heavy Quark Expansion (HQE) [69, 70]. Details can be found in the RPP mini-review on Effective Theories [3].

The OPE result for the total rate can be written schematically (details can be found, e.g., in Ref. [71]) as

$$\Gamma = |V_{cb}|^2 \frac{G_F^2 m_b^5(\mu)}{192\pi^3} |\eta_{\text{EW}}|^2 \times \left[z_0^{(0)}(r) + \frac{\alpha_s(\mu)}{\pi} z_0^{(1)}(r) + \left(\frac{\alpha_s(\mu)}{\pi} \right)^2 z_0^{(2)}(r) + \dots \right. \\ \left. + \frac{\mu_\pi^2}{m_b^2} \left(z_2^{(0)}(r) + \frac{\alpha_s(\mu)}{\pi} z_2^{(1)}(r) + \dots \right) \right. \\ \left. + \frac{\mu_G^2}{m_b^2} \left(y_2^{(0)}(r) + \frac{\alpha_s(\mu)}{\pi} y_2^{(1)}(r) + \dots \right) \right. \\ \left. + \frac{\rho_D^3}{m_b^3} \left(z_3^{(0)}(r) + \frac{\alpha_s(\mu)}{\pi} z_3^{(1)}(r) + \dots \right) \right. \\ \left. + \frac{\rho_{LS}^3}{m_b^3} \left(y_3^{(0)}(r) + \frac{\alpha_s(\mu)}{\pi} y_3^{(1)}(r) + \dots \right) + \dots \right] \quad (76.25)$$

where r is the ratio m_c/m_b and the y_i and z_i are perturbatively calculable Wilson coefficients functions that appear at different orders of the heavy mass expansion.

The parameters μ_π^2 , μ_G^2 , ρ_D^3 and ρ_{LS}^3 constitute the non-perturbative input into the heavy quark expansion; they correspond to certain matrix elements to be discussed below. In the same way the HQE can be set up for the moments of distributions of charged-lepton energy, hadronic invariant mass and hadronic energy, e.g.

$$\langle E_e^n \rangle_{E_e > E_{\text{cut}}} = \int_{E_{\text{cut}}}^{E_{\text{max}}} \frac{d\Gamma}{dE_e} E_e^n dE_e \Big/ \int_{E_{\text{cut}}}^{E_{\text{max}}} \frac{d\Gamma}{dE_e} dE_e. \quad (76.26)$$

The coefficients of the HQE are known up to order $1/m_b^5$ at tree level [72–75]. The leading term $z_0^{(i)}$ is the parton model, and is known completely through order α_s^2 [76–78] and now also at α_s^3 [79]. The terms of order $\alpha_s^{n+1} \beta_0^n$ (where β_0 is the first coefficient of the QCD β function, $\beta_0 = (33 - 2n_f)/3$) have been included following the BLM procedure [71, 80–83]. Corrections of order $\alpha_s \mu_\pi^2/m_b^2$ have been computed in Ref. [84] and Ref. [85], while the $\alpha_s \mu_G^2/m_b^2$ terms have been calculated in Ref. [86] and Ref. [87], and the $\alpha_s \rho_D^3/m_b^3$ corrections in Ref. [88].

Starting at order $1/m_b^3$ contributions with an infrared sensitivity to the charm mass, m_c , appear [72, 74, 89, 90]. At order $1/m_b^3$ this “intrinsic charm” contribution manifests as a $\log(m_c)$ in the coefficient of the Darwin term ρ_D^3 . At higher orders, terms such as $1/m_b^3 \times 1/m_c^2$ and $\alpha_s(m_c) 1/m_b^3 \times 1/m_c$ appear, which are comparable in size to the contributions of order $1/m_b^4$.

The HQE parameters are given in terms of forward matrix elements of local operators; the parameters entering the expansion for orders up to $1/m_b^3$ are $(D_\perp^\mu = (g_{\mu\nu} - v_\mu v_\nu) D^\nu)$, where $v = p_B/M_B$ is the four-velocity of the B meson)

$$\begin{aligned} \bar{\Lambda} &= M_B - m_b, \\ \mu_\pi^2 &= -\langle B | \bar{b} (iD_\perp)^2 b | B \rangle, \\ \mu_G^2 &= \langle B | \bar{b} (iD_\perp^\mu) (iD_\perp^\nu) \sigma_{\mu\nu} b | B \rangle, \\ \rho_D^3 &= \langle B | \bar{b} (iD_{\perp\mu}) (ivD) (iD_\perp^\mu) b | B \rangle, \\ \rho_{LS}^3 &= \langle B | \bar{b} (iD_\perp^\mu) (ivD) (iD_\perp^\nu) \sigma_{\mu\nu} b | B \rangle. \end{aligned} \quad (76.27)$$

These parameters still depend on the heavy quark mass. Sometimes the infinite mass limits of these parameters $\bar{\Lambda} \rightarrow \bar{\Lambda}_{\text{HQET}}$, $\mu_\pi^2 \rightarrow -\lambda_1$, $\mu_G^2 \rightarrow 3\lambda_2$, $\rho_D^3 \rightarrow \rho_1$ and $\rho_{LS}^3 \rightarrow 3\rho_2$, are used instead. Beyond $1/m^3$ the number of independent HQE parameters starts to proliferate [91]. In general, there are 13 parameters (at tree level) up to order $1/m^4$ and 31 (at tree level) up to order $1/m^5$, not including $\bar{\Lambda}$. The HQE parameters of the orders $1/m_b^4$ and $1/m_b^5$ have been estimated in Ref. [75, 92], their impact on the $|V_{cb}|$ determination has been studied in Ref. [93]. However, as pointed out in Ref. [94] one may reduce the number of independent parameters in the HQE by exploiting reparametrization invariance, which is a symmetry of the HQE stemming from Lorentz invariance of QCD. For a subset of observables this allows us to reduce the number of parameters to three up to order $1/m^3$ (ρ_{LS}^3 can be absorbed into μ_G^2 by a re-definition) and to 8 up to order $1/m^4$ [95].

The perturbative QCD expansion for the decay rate does not converge, in general. In addition, the expansion coefficients in the rates and spectra depend strongly on the scheme used for m_b (or equivalently on $\bar{\Lambda}$). It is well known (see eg. [96]) that using the pole mass definition for heavy quark masses leads to particularly badly behaved expansions. This motivates the use of “short-distance” mass definitions, such as the kinetic scheme [33] or the $1S$ scheme [97–99]. Both schemes are well suited for the HQE, since they allow the choice of the renormalization scale $\mu \leq m_b$. Furthermore, in both schemes, the masses can be extracted from other observables with sufficient precision, enabling a precise determination of $|V_{cb}|$, despite of the strong quark-mass dependence of the total rate.

The $1S$ scheme eliminates the b quark pole mass by relating it to the perturbative expression for the mass of the $1S$ state of the Υ system. The b quark mass in the $1S$ scheme is half of the perturbatively calculated mass of the $1S$ state of the Υ system. The best determination of the b quark mass in the $1S$ scheme is obtained

from sum rules for $e^+e^- \rightarrow b\bar{b}$ [100]. A second alternative is the so-called “kinetic mass” $m_b^{\text{kin}}(\mu)$, which enters the non-relativistic expression for the kinetic energy of a heavy quark, and is defined using heavy-quark sum rules [33]. The relation between m_b^{kin} and $m_b^{\overline{\text{MS}}}$ is known through three-loop order [101].

Finally, we note that the theoretical description of inclusive decays employed here, is based on the assumption of quark-hadron duality. While there is no evidence of violations of quark-hadron duality, the theoretical uncertainties due to such violations are not well quantified [3].

76.2.7 Determination of HQE Parameters and $|V_{cb}|$

Several experiments have measured moments in $\bar{B} \rightarrow X_c \ell \bar{\nu}_\ell$ decays [102–110] as a function of the minimum lepton momentum. The measurements of the moments of the electron energy spectrum (0th–3rd) and of the squared hadronic mass spectrum (0th–2nd) have statistical uncertainties that are roughly equal to their systematic uncertainties. The 3rd order hadronic mass spectrum moments have also been measured by some experiments, with relatively large statistical uncertainty. The sets of moments measured within each experiment have strong correlations; their use in a global fit requires fully specified statistical and systematic covariance matrices. Measurements of photon energy moments (0th–2nd) in $B \rightarrow X_s \gamma$ decays [111–115] as a function of the minimum accepted photon energy are also used in some fits; the dominant uncertainties on these measurements are statistical.

Global fits [110, 112, 116–121] to the full set of moments have been performed in the 1S and kinetic schemes. The semileptonic moments alone determine a linear combination of m_b and m_c very accurately but leave the orthogonal combination poorly determined (See e.g. [122]); additional input is required to allow a precise determination of m_b . This additional information can come from the radiative $B \rightarrow X_s \gamma$ moments (with the caveat that the OPE for $b \rightarrow s \gamma$ breaks down beyond leading order in Λ_{QCD}/m_b), which provide complementary information on m_b and μ_π^2 , or from precise determinations of the charm quark mass [32, 123]. The values obtained in the kinetic scheme fits [6, 120, 121] with these two constraints are consistent. Based on the charm quark mass constraint $m_c^{\overline{\text{MS}}}(3 \text{ GeV}) = 0.986 \pm 0.013 \text{ GeV}$ [124], a fit in the kinetic scheme [6] obtains

$$|V_{cb}| = (42.19 \pm 0.78) \times 10^{-3} \quad (76.28)$$

$$m_b^{\text{kin}} = (4.554 \pm 0.018) \text{ GeV} \quad (76.29)$$

$$\mu_\pi^2(\text{kin}) = (0.464 \pm 0.076) \text{ GeV}^2, \quad (76.30)$$

where the errors include experimental and theoretical uncertainties. Theoretical uncertainties from higher orders in $1/m$ as well as in α_s are estimated and included in performing the fits. Similar values for the parameters are obtained with a variety of assumptions about the theoretical uncertainties and their correlations. The χ^2/dof is well below unity in all fits, which could suggest that the theoretical uncertainties may be overestimated. However, while one could obtain a satisfactory fit with smaller uncertainties, this would result in unrealistically small uncertainties on the extracted HQE parameters, which are used as input to other calculations (e.g. the determination of $|V_{ub}|$). The mass in the $\overline{\text{MS}}$ scheme corresponding to Eq. (76.29) is $m_b^{\overline{\text{MS}}} = 4.19 \pm 0.04 \text{ GeV}$, where the uncertainty includes a contribution from the translation between mass schemes; this can be compared to the result quoted in the FLAG review [32], $m_b^{\overline{\text{MS}}} = (4.198 \pm 0.012) \text{ GeV}$, which provides a non-trivial cross-check.

A fit to the measured moments in the 1S scheme [6, 112, 119] gives

$$|V_{cb}| = (41.98 \pm 0.45) \times 10^{-3}, \quad (76.31)$$

$$m_b^{1S} = (4.691 \pm 0.037) \text{ GeV}, \quad (76.32)$$

$$\lambda_1(1S) = (-0.362 \pm 0.067) \text{ GeV}^2. \quad (76.33)$$

This fit uses moments measurements from semileptonic and radiative decays and constrains the chromomagnetic operator using the B^*-B and D^*-D mass differences, but does not include the constraint on m_c nor all known higher order corrections.

The fits in the two renormalization schemes give consistent results for $|V_{cb}|$ and, after translation to a common renormalization scheme, for m_b and μ_π^2 . We take the fit in the kinetic scheme [121], which includes higher-order corrections and results in a more conservative uncertainty, as the inclusive determination of $|V_{cb}|$:

$$|V_{cb}| = (42.2 \pm 0.8) \times 10^{-3} \text{ (inclusive)}. \quad (76.34)$$

The precision of the global fit results can be further improved by calculating higher-order perturbative corrections to the coefficients of the HQE parameters. Indeed, a very recent analysis presented in Ref. [125] includes calculations of the third-order corrections to the semi-leptonic $b \rightarrow c \ell \nu$ decay width [79] and mass relations [101, 126] to obtain a value for $|V_{cb}|$ with smaller total uncertainty than in Eq. (76.34). They obtain $|V_{cb}| = (42.16 \pm 0.51) \times 10^{-3}$, as well as an independent determination of $m_b^{\overline{\text{MS}}}$, without direct constraints, $m_b^{\overline{\text{MS}}} = 4.210 \pm 0.022 \text{ GeV}$. Ultimately measurements of higher order moments and moments of additional variables, such as q^2 , will further improve the sensitivity of the fits to higher-order terms in the HQE [95]. The Belle experiment has recently reported new measurements of q^2 moments in inclusive $b \rightarrow c \ell \nu$ decays Ref. [127], but they are not yet included in the global fit.

76.3 Determination of $|V_{ub}|$

Summary: Currently the best determinations of $|V_{ub}|$ are from $\bar{B} \rightarrow \pi \ell \bar{\nu}_\ell$ decays, where combined fits to theory and experimental data as a function of q^2 provide a precision of about 4%; the uncertainties from experiment and theory are comparable in size. Determinations based on inclusive semileptonic B decays are based on different observables and use different strategies to suppress the $b \rightarrow c$ background. Most of the determinations are consistent and provide a precision of about 7%, with comparable contributions to the uncertainty from experiment and theory.

The values obtained from inclusive and exclusive B decay determinations are

$$|V_{ub}| = (4.13 \pm 0.12 \pm_{-0.14}^{+0.13} \pm 0.18) \times 10^{-3} \text{ (inclusive)}, \quad (76.35)$$

$$|V_{ub}| = (3.70 \pm 0.10 \pm 0.12) \times 10^{-3} \text{ (exclusive)}, \quad (76.36)$$

where the last uncertainty on the inclusive result was added by the authors of this review and is discussed below. The exclusive and inclusive determinations are independent, and the dominant uncertainties are on multiplicative factors. The results from the two determinations are compatible to within two standard deviations.

This can be compared to the values derived from $|V_{ub}|/|V_{cb}|$ ratio measurements, described in the next section. Taking the value for this ratio from Eq. (76.56), and $|V_{cb}|$ from Eq. (76.3) we obtain.

$$|V_{ub}| = (3.43 \pm 0.32) \times 10^{-3} \quad (B_s, \Lambda_b), \quad (76.37)$$

We choose to combine only the direct determinations of $|V_{ub}|$, based on the inclusive and exclusive B measurements. In the combination they are weighted by their relative errors, where the uncertainties are treated as normally distributed. The resulting average has $p(\chi^2) = 15\%$, so we scale the error by $\sqrt{\chi^2/1} = 1.4$ to find

$$|V_{ub}| = (3.82 \pm 0.20) \times 10^{-3} \text{ (average)}. \quad (76.38)$$

In a future update we will consider the constraints in the $|V_{ub}|$ - $|V_{cb}|$ plane from the direct determinations together with the LHCb $|V_{ub}|/|V_{cb}|$ results. This will require a better understanding of $|V_{ub}|/|V_{cb}|$ extractions across a more complete range in q^2 , and with finer binning to compare between theory and experiment.

76.3.1 $|V_{ub}|$ from inclusive decays

The theoretical description of inclusive $\bar{B} \rightarrow X_u \ell \bar{\nu}_\ell$ decays is based on the Heavy Quark Expansion and leads to a predicted total decay rate with uncertainties below 5% [98, 128]. However, the total decay rate is hard to measure due to the large background from CKM-favored $\bar{B} \rightarrow X_c \ell \bar{\nu}_\ell$ transitions, and hence the theoretical methods differ from the $\bar{B} \rightarrow X_c \ell \bar{\nu}_\ell$ case. For a calculation of the partial decay rate in regions of phase space where

$\bar{B} \rightarrow X_c \ell \bar{\nu}_\ell$ decays are suppressed one cannot use the HQE as for $b \rightarrow c$, rather one needs to introduce non-perturbative distribution functions, the “shape functions” (SF) [129,130]. Their exact form is not known, but its moments can be related to the HQE parameters known e.g from the $b \rightarrow c$ case.

The shape functions become important when the light-cone momentum component $P_+ \equiv E_X - |P_X|$ is not large compared to Λ_{QCD} , as is the case near the endpoint of the $\bar{B} \rightarrow X_u \ell \bar{\nu}_\ell$ lepton spectrum. Partial rates for $\bar{B} \rightarrow X_u \ell \bar{\nu}_\ell$ are predicted and measured in a variety of kinematic regions that differ in their sensitivity to shape-function effects.

At leading order in $1/m_b$ only a single shape function (SF) appears, which is universal for all heavy-to-light transitions [129,130] and can be extracted in $\bar{B} \rightarrow X_s \gamma$ decays. At subleading order in $1/m_b$, several shape functions appear [131], along with small “resolved photon contributions” specific for $\bar{B} \rightarrow X_s \gamma$ [132–134], and thus the prescriptions that relate directly the partial rates for $\bar{B} \rightarrow X_s \gamma$ and $\bar{B} \rightarrow X_u \ell \bar{\nu}_\ell$ decays [135–143] are limited to leading order in $1/m_b$.

Existing approaches use parametrizations of the leading SF that respect constraints on the normalization and on the first and second moments, which are given in terms of the HQE parameters $\bar{\Lambda} = M_B - m_b$ and μ_π^2 , respectively. The relations between SF moments and the HQE parameters are known to second order in α_s [144]; as a result, measurements of HQE parameters from global fits to $\bar{B} \rightarrow X_c \ell \bar{\nu}_\ell$ and $\bar{B} \rightarrow X_s \gamma$ moments can be used to constrain the SF moments, as well as to provide accurate values of m_b and other parameters for use in determining $|V_{ub}|$. Flexible parametrizations of the SF using orthogonal basis functions [145] or artificial neural networks [146] allow global fits to inclusive B meson decay data [134] that incorporate the known short-distance contributions and renormalization properties of the SF.

HFLAV performs fits on the basis of several approaches, with varying degrees of model dependence. We will consider here the approaches documented in Ref. [147] (BLNP), Ref. [148] (GGOU) and Ref. [149] (DGE).

The triple differential rate in the variables

$$P_\ell = M_B - 2E_\ell, \quad P_- = E_X + |\vec{P}_X|, \quad P_+ = E_X - |\vec{P}_X| \quad (76.39)$$

is

$$\frac{d^3 \Gamma}{dP_+ dP_- dP_\ell} = \frac{G_F^2 |V_{ub}|^2}{16\pi^2} (M_B - P_+) \quad (76.40)$$

$$\left\{ (P_- - P_\ell)(M_B - P_- + P_\ell - P_+) \mathcal{F}_1 \right.$$

$$\left. + (M_B - P_-)(P_- - P_+) \mathcal{F}_2 + (P_- - P_\ell)(P_\ell - P_+) \mathcal{F}_3 \right\}.$$

The “structure functions”, \mathcal{F}_i , can be calculated using factorization theorems that have been proven to subleading order in the $1/m_b$ expansion [150].

The BLNP [147] calculation uses these factorization theorems to write the \mathcal{F}_i terms as functions of perturbatively calculable hard coefficients and jet functions, which are convolved with the (soft) light-cone distribution functions. The calculation of $\mathcal{O}(\alpha_s^2)$ contributions [151,152] is not yet complete and is not included in the $|V_{ub}|$ determination given below.

The leading order term in the $1/m_b$ expansion of the \mathcal{F}_i terms contains a single non-perturbative function and is calculated to subleading order in α_s , while at subleading order in the $1/m_b$ expansion there are several independent non-perturbative functions that have been calculated only at tree level in the α_s expansion.

A distinct approach (GGOU) [148] uses a hard, Wilsonian cut-off that matches the definition of the kinetic mass. The non-perturbative input is similar to what is used in BLNP, but the shape functions are defined differently. In particular, they are defined at finite m_b and depend on the light-cone component k_+ of the b quark momentum and on the momentum transfer q^2 to the leptons. These functions include subleading effects to all orders; as a result they are non-universal, with one shape function corresponding to each structure function in Eq. (76.40). Their k_+ moments can be computed in the OPE.

Going to subleading order in α_s requires the definition of a renormalization scheme for the HQE parameters and for the SF. The relation between the moments of the SF and the forward matrix elements of local operators appearing the HQE is plagued by ultraviolet problems and requires additional renormalization. A scheme for improving this behavior was suggested in Ref. [147] and Ref. [153], which introduce a definition of the quark mass (the so-called shape-function scheme) based on the first moment of the measured $\bar{B} \rightarrow X_s \gamma$ photon energy spectrum. Likewise, the HQE parameters can be defined from measured moments of spectra, corresponding to moments of the SF.

There are various ideas to model the SF, but this requires additional assumptions. One approach (DGE) is the so-called “dressed gluon exponentiation” [149], where the perturbative result is continued into the infrared regime using the renormalon structure obtained in the large β_0 limit, where β_0 has been defined following Eq. (76.25). Other approaches make even stronger assumptions, such as in Ref. [154], which assumes an analytic behavior for the strong coupling in the infrared to perform an extrapolation of perturbation theory.

In order to reduce sensitivity to SF uncertainties, measurements that use a combination of cuts on the leptonic momentum transfer q^2 and the hadronic invariant mass m_X , as suggested in Ref. [155,156], have been made. In general, experimental measurements of $\bar{B} \rightarrow X_u \ell \bar{\nu}_\ell$ into charm-dominated regions (in order to reduce SF uncertainties) are sensitive to the modeling of $\bar{B} \rightarrow X_u \ell \bar{\nu}_\ell$ and $\bar{B} \rightarrow X_c \ell \bar{\nu}_\ell$ decays. The measurements quoted below have used a variety of functional forms to parametrize the leading SF; a specific error budget for one determination is quoted in the next section. In no case is the parametrization uncertainty estimated to be more than a 2% on $|V_{ub}|$.

Weak Annihilation [148,157,158] (WA) can in principle contribute significantly in the high- q^2 region of $\bar{B} \rightarrow X_u \ell \bar{\nu}_\ell$ decays. Estimates based on semileptonic D_s decays [90,155,156,158] lead to a $\sim 2\%$ uncertainty on the total $\bar{B} \rightarrow X_u \ell \bar{\nu}_\ell$ rate from the $\Upsilon(4S)$. The q^2 spectrum of the WA contribution is not well known, but from the OPE it is expected to contribute predominantly at high q^2 . Other theoretical investigations [90,159,160], a direct search [161], and $\mathcal{B}(B^0 \rightarrow X_u \ell \bar{\nu})/\mathcal{B}(B^+ \rightarrow X_u \ell \bar{\nu})$ ratio measurements [162–164] indicate that WA is a small effect, but may become a significant source of uncertainty for $|V_{ub}|$ measurements that accept only a small fraction of the full $\bar{B} \rightarrow X_u \ell \bar{\nu}_\ell$ phase space.

76.3.2 Measurements

We summarize the measurements used in the determination of $|V_{ub}|$ below. Given the improved precision and more rigorous theoretical interpretation of more recent measurements, determinations [165–168] done with LEP data are not considered in this review.

Inclusive electron momentum measurements [169,170] reconstruct a single charged electron to determine a partial decay rate for $\bar{B} \rightarrow X_u \ell \bar{\nu}_\ell$ near the kinematic endpoint. This results in a selection efficiency of order 50% and only modest sensitivity to the modeling of detector response. The inclusive electron momentum spectrum from $B\bar{B}$ events, after subtraction of the $e^+e^- \rightarrow q\bar{q}$ continuum background, is fitted to a model $\bar{B} \rightarrow X_u \ell \bar{\nu}_\ell$ spectrum and several components ($D\ell\bar{\nu}_\ell$, $D^*\ell\bar{\nu}_\ell$, ...) of the $\bar{B} \rightarrow X_c \ell \bar{\nu}_\ell$ background; the dominant uncertainties are related to this subtraction and modelling. The decay rate can be cleanly extracted for $E_e > 2.3$ GeV, but this is deep in the SF region, where theoretical uncertainties are large. More recent measurements have increased the accessed phase space. The resulting $|V_{ub}|$ values for various E_e cuts are given in Table 76.1.

The most recent BABAR measurement [171] is based on the inclusive electron spectrum and determines the partial branching fraction and $|V_{ub}|$ for $E_e > 0.8$ GeV. The analysis shows that the partial branching fraction measurements can have signal model dependence when the kinematic acceptance includes regions dominated by $\bar{B} \rightarrow X_c \ell \bar{\nu}_\ell$ background. The model dependence enters primarily through the partial branching fractions, and arises because the signal yield fit has sensitivity to $\bar{B} \rightarrow X_u \ell \bar{\nu}_\ell$ decays only in regions with good signal to noise.

An untagged “neutrino reconstruction” measurement [172] from

BABAR uses a combination [173] of a high-energy electron with a measurement of the missing momentum vector. This allows $S/B \sim 0.7$ for $E_e > 2.0$ GeV and a $\approx 5\%$ selection efficiency, but at the cost of a smaller accepted phase space for $\bar{B} \rightarrow X_u \ell \bar{\nu}_\ell$ decays and uncertainties associated with the determination of the missing momentum.

The large samples accumulated at the B factories allow studies in which one B meson is fully reconstructed and the recoiling B decays semileptonically [174–177]. The experiments can fully reconstruct a “tag” B candidate in about 0.5% (0.3%) of $B^+ B^-$ ($B^0 \bar{B}^0$) events. An electron or muon with center-of-mass momentum above 1.0 GeV is required amongst the charged tracks not assigned to the tag B and the remaining particles are assigned to the X_u system. The full set of kinematic properties (E_ℓ , m_X , q^2 , etc.) are available for studying the semileptonically decaying B , making possible selections that accept up to 90% of the full $\bar{B} \rightarrow X_u \ell \bar{\nu}_\ell$ rate; however, the sensitivity to $\bar{B} \rightarrow X_u \ell \bar{\nu}_\ell$ decays is still driven by the regions where $\bar{B} \rightarrow X_c \ell \bar{\nu}_\ell$ decays are suppressed. Despite requirements (e.g. on the square of the missing mass) aimed at rejecting events with additional missing particles, undetected or mis-measured particles from $\bar{B} \rightarrow X_c \ell \bar{\nu}_\ell$ decay (e.g., K_L^0 and additional neutrinos) remain an important source of uncertainty.

A new recoil method measurement of partial branching fractions in three phase-space regions, covering about 31% to 86% of the accessible phase space, was performed by Belle [162], where machine learning techniques were used to reduce background levels. The measurement contains substantial decay model updates and supersedes previous measurements from Belle [175, 176]. The measurement of the partial branching fraction obtained in the $E_\ell^B > 1$ GeV region, the most precise one, is used to obtain $|V_{ub}|$ [162]. Belle also reports preliminary measurements of the background subtracted, and unfolded differential decay spectra in bins of m_X , m_X and q^2 , P_+ and E_ℓ [178] for use in global fit analyses. Earlier measurements by BABAR [174] were also performed with cuts on m_X , m_X and q^2 , P_+ and E_ℓ using the recoil method. In each case the experimental systematic uncertainties have significant contributions from the modeling of $\bar{B} \rightarrow X_u \ell \bar{\nu}_\ell$ and $\bar{B} \rightarrow X_c \ell \bar{\nu}_\ell$ decays and from the detector response to charged particles, photons and neutral hadrons. The corresponding $|V_{ub}|$ values are given in Table 76.1.

76.3.3 $|V_{ub}|$ from inclusive partial rates

The measured partial rates and theoretical calculations from BLNP, GGOU and DGE described previously are used to determine $|V_{ub}|$ from all measured partial $\bar{B} \rightarrow X_u \ell \bar{\nu}_\ell$ rates [6]; selected values are given in Table 76.1. The correlations amongst the multiple BABAR recoil-based measurements [174] are fully accounted for in the average. The statistical correlations amongst the other measurements used in the average are small (due to small overlaps among signal events and large differences in S/B ratios) and have been ignored. Correlated systematic and theoretical errors are taken into account, both within an experiment and between experiments. As an illustration of the relative sizes of the uncertainties entering $|V_{ub}|$ we give the error breakdown for the GGOU average: statistical—1.3%; experimental—1.6%; $\bar{B} \rightarrow X_c \ell \bar{\nu}_\ell$ modeling—0.9%; $\bar{B} \rightarrow X_u \ell \bar{\nu}_\ell$ modeling—1.7%; HQE parameters (m_b)—1.8%; higher-order corrections—1.5%; q^2 modeling—1.3%; Weak Annihilation— $^{+0.0}_{-1.1}\%$; SF parametrization—0.1%.

The averages quoted here are based on the following m_b values: $m_b^{SF} = 4.582 \pm 0.023 \pm 0.018$ GeV for BLNP, $m_b^{\text{kin}} = 4.554 \pm 0.018$ GeV for GGOU, and $m_b^{\overline{MS}} = 4.188 \pm 0.043$ GeV for DGE. The m_b^{kin} value is determined in a global fit to moments in the kinetic scheme [6]; this value is translated into m_b^{SF} and $m_b^{\overline{MS}}$ at fixed order in α_s . The second uncertainty quoted on m_b arises from the scheme translation.

Hadronization uncertainties also impact the $|V_{ub}|$ determination. The theoretical expressions are valid at the parton level and do not incorporate any resonant structure (e.g. $\bar{B} \rightarrow \pi \ell \bar{\nu}_\ell$); this must be added to the simulated $\bar{B} \rightarrow X_u \ell \bar{\nu}_\ell$ event samples, since the detailed final state multiplicity and structure impacts the estimates of experimental acceptance and efficiency. The experiments have adopted procedures to input resonant structure

while preserving the appropriate behavior in the kinematic variables (q^2 , E_ℓ , m_X) averaged over the sample, but these prescriptions are *ad hoc* and ultimately require *in situ* calibration. The resulting uncertainties have been estimated to be ~ 1 -2% on $|V_{ub}|$.

All calculations yield compatible $|V_{ub}|$ values and similar error estimates. The arithmetic mean of the values and errors of the HFLAV combinations listed in Table 76.1 is $|V_{ub}| = (4.13 \pm 0.12_{\text{exp}} \text{ } ^{+0.13}_{-0.14} \text{ }_{\text{theo}}) \times 10^{-3}$, although there is a spread of approximately 10% in the evaluations with the three theoretical models. For reasons discussed below, we assign an additional uncertainty due to model dependence that is not reflected in the HFLAV averages. As highlighted in the BABAR analysis [171], model dependence entering measurement procedures can be sizeable, and is not consistently treated across analyses. Many of the analyses shown in Table 76.1 were based on partial branching fraction measurements determined in a single model (i.e. the one used by that analysis when simulating $\bar{B} \rightarrow X_u \ell \bar{\nu}_\ell$ decays), although in some cases simulated events were weighted to match the expected spectra in other models and the differences introduced as systematic uncertainties, e.g. Ref. [176]. The $|V_{ub}|$ value quoted by HFLAV for each model are, typically, derived from this unique partial branching fraction combined with another model-specific partial rate calculation. The model dependence in the partial branching fraction is sensitive to how the model predictions compare in the restricted region with good signal-to-noise, not by how they compare when integrated over the full kinematic range used in the fit. Ideally this effect needs to be accounted for by the experiments; the published information is insufficient to determine it. To account for the range in results using the different theoretical models, we take half of the spread of the averages as an additional systematic uncertainty, denoted Δ_{model} . With this addition, the inclusive $|V_{ub}|$ average is

$$|V_{ub}| = (4.13 \pm 0.12_{\text{exp}} \text{ } ^{+0.13}_{-0.14} \text{ }_{\text{theo}} \pm 0.18_{\Delta_{\text{model}}}) \times 10^{-3} \quad (\text{inclusive}). \quad (76.41)$$

76.3.4 $|V_{ub}|$ from exclusive decays

Exclusive charmless semileptonic decays offer a complementary means of determining $|V_{ub}|$. For the experiments, the specification of the final state provides better background rejection, but the branching fraction to a specific final state is typically only a few percent of that for inclusive decays. For theory, the calculation of the form factors for $\bar{B} \rightarrow X_u \ell \bar{\nu}_\ell$ decays is challenging, but brings in a different set of uncertainties from those encountered in inclusive decays. In this review we focus on $\bar{B} \rightarrow \pi \ell \bar{\nu}_\ell$, as it is the most promising decay mode for both experiment and theory. Measurements of other exclusive $\bar{B} \rightarrow X_u \ell \bar{\nu}_\ell$ decays can be found in Refs. [179–192].

76.3.5 $\bar{B} \rightarrow \pi \ell \bar{\nu}_\ell$ form factor calculations

The relevant form factors for the decay $\bar{B} \rightarrow \pi \ell \bar{\nu}_\ell$ are usually defined as

$$\langle \pi(p_\pi) | V^\mu | B(p_B) \rangle = f_+(q^2) \left[p_B^\mu + p_\pi^\mu - \frac{m_B^2 - m_\pi^2}{q^2} q^\mu \right] + f_0(q^2) \frac{m_B^2 - m_\pi^2}{q^2} q^\mu \quad (76.42)$$

in terms of which the rate becomes (in the limit $m_\ell \rightarrow 0$)

$$\frac{d\Gamma}{dq^2} = \frac{G_F^2 |V_{ub}|^2}{24\pi^3} |p_\pi|^3 |f_+(q^2)|^2, \quad (76.43)$$

where p_π is the pion momentum in the B meson rest frame.

Lattice-QCD calculations of the form factors for the $B \rightarrow \pi \ell \bar{\nu}$ and $B_s \rightarrow K \ell \bar{\nu}$ transitions are available from the Fermilab/MILC [193, 194], HPQCD [195], and RBC/UKQCD [196] collaborations. The lattice form factors are obtained in the large q^2 region, $q_{\text{max}}^2 > q^2 \gtrsim 15$ GeV² and the calculations differ in actions employed for the b quark. While HPQCD [195] is using lattice-nonrelativistic QCD, the results from Fermilab/MILC [193, 194] and RBC/UKQCD [196] are obtained with relativistic b quark actions based on the Fermilab approach [197]. The results agree within the quoted errors. For the $B \rightarrow \pi$

Table 76.1: $|V_{ub}|$ (in units of 10^{-5}) from inclusive $\bar{B} \rightarrow X_u \ell \bar{\nu}_\ell$ measurements. The first uncertainty on $|V_{ub}|$ is experimental, while the second includes both theoretical and HQE parameter uncertainties. The values are generally listed in order of increasing kinematic acceptance, f_u (0.19 to 0.90), except for the BABAR $E_e > 0.8$ GeV measurement; those below the horizontal bar are based on recoil methods.

Ref.	cut (GeV)	BLNP	GGOU	DGE
CLEO [169]	$E_e > 2.1$	422 ± 49	423 ± 49	386 ± 45
BABAR [172]	$E_e - q^2$	471 ± 32	not available	435 ± 29
Belle [170]	$E_e > 1.9$	493 ± 46	495 ± 46	482 ± 45
BABAR [171]	$E_e > 0.8$	441 ± 12	396 ± 10	385 ± 11
BABAR [174]	$q^2 > 8$ $m_X < 1.7$	432 ± 23	433 ± 23	424 ± 22
BABAR [174]	$P_+ < 0.66$	409 ± 25	425 ± 26	417 ± 25
BABAR [174]	$m_X < 1.7$	403 ± 22	410 ± 23	422 ± 23
BABAR [174]	$E_\ell > 1.3$	433 ± 24	444 ± 24	445 ± 24
Belle [162]	$E_\ell > 1$	405 ± 23	415 ± 24	416 ± 24
HFLAV [6]	Combination	428 ± 13	419 ± 12	392 ± 10

form factor $f_+(q^2 = 20 \text{ GeV}^2)$, Ref. [193] quotes uncertainty of 3.4% evaluated at $q^2 = 20 \text{ GeV}^2$, where the leading contribution is due to the chiral-continuum extrapolation fit, which includes statistical and heavy-quark discretization errors.

The extrapolation to small values of q^2 is performed using guidance from analyticity and unitarity. Making use of the heavy-quark limit, stringent constraints on the shape of the form factor can be derived [198], and the conformal mapping of the kinematical variables onto the complex unit disc yields a rapidly converging series in the variable

$$z = \frac{\sqrt{t_+ - t_-} - \sqrt{t_+ - q^2}}{\sqrt{t_+ - t_-} + \sqrt{t_+ - q^2}}, \quad (76.44)$$

where $t_\pm = (M_B \pm m_\pi)^2$. The use of lattice data in combination with experimental measurements of the differential decay rate provides a stringent constraint on the shape of the form factor in addition to precise determination of $|V_{ub}|$ [199].

LCSR calculations provide estimates for the product $f_B f_+(q^2)$, valid in the region $0 < q^2 \lesssim 12 \text{ GeV}$. The determination of $f_+(q^2)$ itself requires knowledge of the decay constant f_B , which is usually obtained by replacing f_B by its two-point QCD (SVZ) sum rule [200] in terms of perturbative and condensate contributions. The advantage of this procedure is the approximate cancellation of various theoretical uncertainties in the ratio $(f_B f_+)/f_B$. The LCSR for $f_B f_+$ is based on the light-cone OPE of the relevant vacuum-to-pion correlation function, calculated in full QCD at finite b -quark mass. The resulting expressions comprise a triple expansion: in the twist, t , of the operators near the light-cone, in α_s , and in the deviation of the pion distribution amplitudes from their asymptotic form, which is fixed from conformal symmetry. The state-of-the-art calculations include the leading twists two, three and four with full one-loop α_s corrections [201,202] and partial two-loop corrections [203]. Higher-twist contributions have been investigated in Ref. [204] and two-particle higher twist contributions are studied in Ref. [39]. Nevertheless, estimates based on LCSR generally suffer from difficult to quantify systematic uncertainties.

A detailed statistical analysis including the various correlations has been performed in Ref. [205], also including unitarity bounds on the form factor. The results obtained are numerically compatible with the lattice QCD calculations of the form factor. For a determination of V_{ub} one may use the partial rate expressed by

the integral

$$\begin{aligned} \Delta\zeta(0, q_{max}^2) &= \frac{G_F^2}{24\pi^3} \int_0^{q_{max}^2} dq^2 p_\pi^3 |f_+(q^2)|^2 \\ &= \frac{1}{|V_{ub}|^2 \tau_{B_0}} \int_0^{q_{max}^2} dq^2 \frac{d\mathcal{B}(B \rightarrow \pi \ell \nu)}{dq^2}, \end{aligned} \quad (76.45)$$

for which the light-cone sum rule gives [205]

$$\Delta\zeta(0, 12 \text{ GeV}^2) = (5.25^{+0.68}_{-0.54}) \text{ ps}^{-1}. \quad (76.46)$$

The uncertainty in this integral is about ten percent, which translates to a theoretical uncertainty of about five percent for the determination of V_{ub} with this method.

76.3.6 $\bar{B} \rightarrow \pi \ell \bar{\nu}_\ell$ measurements

The $\bar{B} \rightarrow \pi \ell \bar{\nu}_\ell$ measurements fall into two broad classes: untagged, in which case the reconstruction of the missing momentum of the event serves as an estimator for the unseen neutrino, and tagged, in which the second B meson in the event is fully reconstructed in either a hadronic or semileptonic decay mode. The tagged measurements have better q^2 resolution, high and uniform acceptance and S/B as high as 10, but lower statistical power. The untagged measurements have higher background (S/B < 1) and make slightly more restrictive kinematic cuts, but still provide statistical power precision on the q^2 dependence of the form factor.

CLEO has analyzed $\bar{B} \rightarrow \pi \ell \bar{\nu}_\ell$ and $\bar{B} \rightarrow \rho \ell \bar{\nu}_\ell$ using an untagged analysis [186–188]. Similar analyses have been done at BABAR [189–192] and Belle [206]. The leading systematic uncertainties in the untagged $\bar{B} \rightarrow \pi \ell \bar{\nu}_\ell$ analyses are associated with modeling the missing momentum reconstruction, with background from $\bar{B} \rightarrow X_u \ell \bar{\nu}_\ell$ decays and $e^+ e^- \rightarrow q \bar{q}$ continuum events, and with varying the form factor used to model $\bar{B} \rightarrow \rho \ell \bar{\nu}_\ell$ decays.

Analyses [181,207] based on reconstructing a B in the $\bar{D}^{(*)} \ell^+ \nu_\ell$ decay mode and looking for a $\bar{B} \rightarrow \pi \ell \bar{\nu}_\ell$ or $\bar{B} \rightarrow \rho \ell \bar{\nu}_\ell$ decay amongst the remaining particles in the event make use of the fact that the B and \bar{B} are back-to-back in the $\Upsilon(4S)$ frame to construct a discriminant variable that provides a signal-to-noise ratio above unity for all q^2 bins. A related technique was discussed in Ref. [208]. BABAR [207] and Belle [179] have also used their samples of B mesons reconstructed in hadronic decay modes to measure exclusive charmless semileptonic decays, resulting in very clean but smaller samples. The dominant systematic uncertainties in the tagged analyses arise from tag calibration.

$|V_{ub}|$ can be obtained from the average $\bar{B} \rightarrow \pi \ell \bar{\nu}_\ell$ branching fraction and the measured q^2 spectrum. Fits to the q^2 spectrum using a theoretically motivated parametrization (e.g. “BCL” from

Ref. [61]) remove most of the model dependence from theoretical uncertainties in the shape of the spectrum. The most sensitive method for determining $|V_{ub}|$ from $\bar{B} \rightarrow \pi \ell \bar{\nu}_\ell$ decays employs a simultaneous fit [6, 193, 198, 199, 209, 210] to measured experimental partial rates and lattice points versus q^2 (or z) to determine $|V_{ub}|$ and the first few coefficients of the expansion of the form factor in z . We quote the result from Ref. [6], which uses as experimental input an average of the measurements in Refs. [179, 189, 192, 206] and an average [211] of the LQCD input from Ref. [193] and Ref. [196]. The probability of the q^2 measurement average is 6%. The average for the total $B^0 \rightarrow \pi^- \ell^+ \nu_\ell$ branching fraction is obtained by summing up the partial branching fractions:

$$\mathcal{B}(B^0 \rightarrow \pi^- \ell^+ \nu_\ell) = (1.50 \pm 0.02_{\text{stat}} \pm 0.06_{\text{syst}}) \times 10^{-4} \quad (76.47)$$

The corresponding value of $|V_{ub}|$ with this approach is found to be

$$|V_{ub}| = (3.70 \pm 0.10 \pm 0.12) \times 10^{-3} \quad (\text{exclusive}), \quad (76.48)$$

where the first uncertainty is experimental and the second is from theory. A consistent result for $|V_{ub}|$ was reported in Ref. [32], which uses the same experimental and lattice-QCD inputs. Adding additional constraints using input from LCSR [203] gives [6] $|V_{ub}| = (3.67 \pm 0.09 \pm 0.12) \times 10^{-3}$ (exclusive, LQCD+LCSR). Other recent LCSR estimates [212, 213] have been used to obtain consistent results for $|V_{ub}|$, albeit with slightly higher central values. Ref. [213] also presents results for $|V_{ub}|$ from joint fits that exclude some of the experimental data in order to bring the exclusive values into agreement with the inclusive ones.

76.3.7 $\bar{B}_s \rightarrow K \ell \bar{\nu}_\ell$

The LHCb experiment have conducted the first observation of the decay $B_s^0 \rightarrow K^- \mu^+ \nu_\mu$ and the measurements of its branching fraction normalised to the $B_s^0 \rightarrow D_s^- \mu^+ \nu_\mu$ decays [214]. The measurement has been performed in two bins of q^2 , derived using the B_s^0 flight direction and the known B_s^0 mass. The analysis uses a BDT classifier to suppress semileptonic b -hadron background. The results of the partial branching fractions have been translated into measurements of $|V_{ub}|/|V_{cb}|$ using form factor calculations from LCSR for $q^2 < 7 \text{ GeV}^2$ [215], and a recent LQCD calculation for $q^2 > 7 \text{ GeV}^2$ [194]. The results are

$$|V_{ub}|/|V_{cb}| = 0.0607 \pm 0.0021 \pm 0.0030, \quad q^2 < 7 \text{ GeV}^2 \quad (76.49)$$

$$|V_{ub}|/|V_{cb}| = 0.0946 \pm 0.0041 \pm 0.0068, \quad q^2 > 7 \text{ GeV}^2 \quad (76.50)$$

where the first uncertainties include also experimental and external input sources, and the latter are due to the form factor calculations. The sizeable discrepancy between the values of $|V_{ub}|/|V_{cb}|$ for the low and high q^2 , requires further investigation. While the experimental measurement has higher purity in the low q^2 region, the theoretical uncertainties in the LCSR results are not fully quantified, unlike the lattice QCD results employed for the high- q^2 region.

76.4 Semileptonic b -baryon decays

Summary: A significant sample of Λ_b^0 baryons is available at the LHCb experiment, and methods have been developed to study their semileptonic decays. Both $\Lambda_b^0 \rightarrow p \mu \bar{\nu}$ and $\Lambda_b^0 \rightarrow \Lambda_c^+ \mu \bar{\nu}$ decays have been measured at LHCb, and the ratio of branching fractions to these two decay modes is used to determine the ratio $|V_{ub}|/|V_{cb}|$.

76.4.1 $\Lambda_b^0 \rightarrow \Lambda_c^+ \mu \bar{\nu}$ and $\Lambda_b^0 \rightarrow p \mu \bar{\nu}$

The $\Lambda_b^0 \rightarrow \Lambda_c^+$ and $\Lambda_b^0 \rightarrow p$ semileptonic transitions are described in terms of six form factors each. The three form factors

corresponding to the vector current can be defined as [216]

$$\begin{aligned} \langle F(p', s') | \bar{q} \gamma_\mu b | \Lambda_b^0(p, s) \rangle = & \bar{u}_F(p', s') \left\{ f_0(q^2) (M_{\Lambda_b^0} - m_F) \frac{q_\mu}{q^2} \right. \\ & + f_+(q^2) \frac{M_{\Lambda_b^0} + m_F}{s_+} \left(p_\mu + p'_\mu - \frac{q_\mu}{q^2} (M_{\Lambda_b^0}^2 - m_F^2) \right) \\ & \left. + f_\perp(q^2) \left(\gamma_\mu - \frac{2m_F}{s_+} p_\mu - \frac{2M_{\Lambda_b^0}}{s_+} p'_\mu \right) \right\} u_{\Lambda_b^0}(p, s), \end{aligned} \quad (76.51)$$

where $F = p$ or Λ_c^+ and where we define $s_\pm = (M_{\Lambda_b^0} \pm m_F)^2 - q^2$. At vanishing momentum transfer, $q^2 \rightarrow 0$, the kinematic constraint $f_0(0) = f_+(0)$ holds. The form factors are defined in such a way that they correspond to time-like (scalar), longitudinal and transverse polarization with respect to the momentum-transfer q^μ for f_0 , f_+ and f_\perp , respectively. Likewise, the expression for the axial-vector current is

$$\begin{aligned} \langle F(p', s') | \bar{q} \gamma_\mu \gamma_5 b | \Lambda_b^0(p, s) \rangle = & -\bar{u}_F(p', s') \gamma_5 \left\{ g_0(q^2) (M_{\Lambda_b^0} + m_F) \frac{q_\mu}{q^2} \right. \\ & + g_+(q^2) \frac{M_{\Lambda_b^0} - m_F}{s_-} \left(p_\mu + p'_\mu - \frac{q_\mu}{q^2} (M_{\Lambda_b^0}^2 - m_F^2) \right) \\ & \left. + g_\perp(q^2) \left(\gamma_\mu + \frac{2m_F}{s_-} p_\mu - \frac{2M_{\Lambda_b^0}}{s_-} p'_\mu \right) \right\} u_{\Lambda_b^0}(p, s), \end{aligned} \quad (76.52)$$

with the kinematic constraint $g_0(0) = g_+(0)$ at $q^2 \rightarrow 0$.

In the heavy-quark limit, where both the b and c quarks are treated as heavy, all the form factors reduce to the Isgur Wise function ξ_B for baryons [216]:

$$f_0 = f_+ = f_\perp = g_0 = g_+ = g_\perp = \xi_B \quad (76.53)$$

With a light baryon in the final state, the form factors are related through the heavy quark symmetries of the Λ_b^0 , reducing the number of independent form factors to two. It should be noted that the differential $\Lambda_b^0 \rightarrow (p/\Lambda_c^+) \mu \bar{\nu}$ decay rates peak at high q^2 , so that the kinematic regions where both lattice QCD calculations and experimental measurements are precise are well matched.

The form factors for Λ_b^0 decays have been studied with lattice QCD [217]. Based on these results the differential rates for both $\Lambda_b^0 \rightarrow \Lambda_c^+ \mu \bar{\nu}$ as well as for $\Lambda_b^0 \rightarrow p \mu \bar{\nu}$ can be predicted in the full phase space. In particular, for the experimentally interesting region they find the ratio of decay rates to be [217]

$$\frac{\mathcal{B}(\Lambda_b^0 \rightarrow p \mu \bar{\nu})_{q^2 > 15 \text{ GeV}^2}}{\mathcal{B}(\Lambda_b^0 \rightarrow \Lambda_c^+ \mu \bar{\nu})_{q^2 > 7 \text{ GeV}^2}} = (1.471 \pm 0.095 \pm 0.109) \left| \frac{V_{ub}}{V_{cb}} \right|^2 \quad (76.54)$$

where the first uncertainty is statistical and the second, systematic.

76.4.2 Measurements at LHCb

The LHCb experiment has measured the branching fractions of the semileptonic decays $\Lambda_b^0 \rightarrow \Lambda_c^+ \mu \bar{\nu}$ and $\Lambda_b^0 \rightarrow p \mu \bar{\nu}$, from which they determine $|V_{ub}|/|V_{cb}|$. This is the first such determination at a hadron collider, the first to use a b baryon decay, and the first observation of $\Lambda_b^0 \rightarrow p \mu \bar{\nu}$. Excellent vertex resolution allows the $p \mu$ and production vertices to be separated, which permits the calculation of the transverse momentum p_\perp of the $p \mu$ pair relative to the Λ_b^0 flight direction. The corrected mass, $m_{\text{corr}} = \sqrt{p_\perp^2 + m_{p\mu}^2} + p_\perp$, peaks at the Λ_b^0 mass for signal decays and provides good discrimination against background combinations. The topologically similar decay $\Lambda_b^0 \rightarrow \Lambda_c^+ \mu \bar{\nu}$ is also measured, which eliminates the need to know the production cross-section or absolute efficiencies. Using vertex and Λ_b^0 mass constraints, q^2 can be determined up to a two-fold ambiguity. The LHCb analysis requires both solutions to be in the high q^2 region to minimise contamination from the low q^2 region. Their result [218],

rescaled [6] to take into account the recent branching fraction measurement [219] $\mathcal{B}(\Lambda_c^+ \rightarrow pK^- \pi^+) = (6.28 \pm 0.32)\%$, is

$$\frac{\mathcal{B}(\Lambda_b^0 \rightarrow p\mu\bar{\nu})_{q^2 > 15\text{GeV}^2}}{\mathcal{B}(\Lambda_b^0 \rightarrow \Lambda_c^+ \mu\bar{\nu})_{q^2 > 7\text{GeV}^2}} = (0.92 \pm 0.04 \pm 0.07) \times 10^{-2} \quad (76.55)$$

The largest systematic uncertainty is from the measured $\mathcal{B}(\Lambda_c^+ \rightarrow pK^- \pi^+)$; uncertainties due to trigger, tracking and the Λ_c^+ selection efficiency are each about 3%.

A recent LHCb analysis [220] measures the normalized q^2 spectrum and finds good agreement with the shape calculated with lattice QCD [217].

The decay rate for $\Lambda_b^0 \rightarrow p\mu\bar{\nu}$ peaks at high q^2 where the calculation of the associated form factors using lattice QCD is under good control. Using the measured ratio from Eq. (76.55) along with the calculated ratio from Ref. [217] (see Eq. (76.54)) results in [6]

$$|V_{ub}|/|V_{cb}| = 0.079 \pm 0.004 \pm 0.004(A_b). \quad (76.56)$$

where the first uncertainty is experimental and the second is from the LQCD calculation.

76.5 The ratio $|V_{ub}|/|V_{cb}|$

The ratio of matrix elements, $|V_{ub}|/|V_{cb}|$, is often required when testing the compatibility of a set of measurements with theoretical predictions. It can be determined from the ratio of branching fractions measured by the LHCb experiment, quoted in the previous sections. It can also be calculated based on the $|V_{ub}|$ and $|V_{cb}|$ values quoted earlier in this review.

The average of the LHCb results extracted at high q^2 from B_s and A_b decays, taken to be uncorrelated, is

$$|V_{ub}|/|V_{cb}| = 0.084 \pm 0.007 \quad (A_b, B_s), \quad (76.57)$$

where the uncertainty has been scaled by a factor $\sqrt{\chi^2/1} = 1.6$.

Given the similarities in the theoretical frameworks used for charmed and charmless decays, we choose to quote separate ratios of $|V_{ub}|/|V_{cb}|$ for inclusive and exclusive B decays, as discussed earlier:

$$|V_{ub}|/|V_{cb}| = 0.098 \pm 0.006 \quad (\text{inclusive}), \quad (76.58)$$

$$|V_{ub}|/|V_{cb}| = 0.094 \pm 0.005 \quad (\text{exclusive}). \quad (76.59)$$

The respective determinations of $|V_{ub}|$ and $|V_{cb}|$ are taken to be uncorrelated in the ratio, although there could be some small cancellations of the uncertainties in both the experimental and the theoretical input. We average the B decay values, along with the B_s and baryonic result in Eq. (76.57), weighting by relative errors. The average has $p(\chi^2) = 4\%$, so we scale the uncertainty by a factor $\sqrt{\chi^2/2} = 1.8$ to find

$$|V_{ub}|/|V_{cb}| = 0.091 \pm 0.005 \quad (\text{average}). \quad (76.60)$$

76.6 Semitauponic decays

Summary: Semileptonic decays to third-generation leptons provide sensitivity to non-Standard Model amplitudes, such as from a charged Higgs boson [221–224] and from leptoquarks [225–231]. The ratios of branching fractions of semileptonic decays involving tau leptons to those involving $\ell = e/\mu$, $R(D^{(*)}) \equiv \mathcal{B}(\bar{B} \rightarrow D^{(*)}\tau\bar{\nu}_\tau)/\mathcal{B}(\bar{B} \rightarrow D^{(*)}\ell\bar{\nu}_\ell)$, are predicted with good precision and consistency in the Standard Model [7–9, 24, 25, 27, 62], using a variety of different strategies. Because this ratio is independent of $|V_{cb}|$, it can, in principle, be computed entirely from within the Standard Model, without using experimental decay rate data. For example, in Ref. [7, 9] the lattice-QCD only ratios are obtained as:

$$\begin{aligned} R(D)^{\text{LQCD, FNAL-MILC}} &= 0.284 \pm 0.014, \\ R(D^*)^{\text{LQCD, FNAL-MILC}} &= 0.265 \pm 0.013. \end{aligned} \quad (76.61)$$

Without constraints from experimental data at large recoil, such SM-theory only evaluations tend to be less precise than those obtained from joint fits that employ experimental data as well as Standard-Model theory inputs (lattice-QCD form factors, HQET

constraints, etc.). Here we use an average of Ref. [25, 62] for $R(D)$ and Ref. [9] for $R(D^*)$, where the uncertainty on $R(D^*)$ is scaled by $\sqrt{\chi^2/1} = 1.2$:

$$\begin{aligned} R(D)^{\text{SM+Exp}} &= 0.299 \pm 0.003, \\ R(D^*)^{\text{LQCD+Exp}} &= 0.2483 \pm 0.0016. \end{aligned} \quad (76.62)$$

Other Standard-Model predictions for $R(D^{(*)})$ [24, 25, 27, 62, 232, 233] using various combinations of experimental data, lattice-QCD form factor inputs, HQET constraints, and LCSR estimates are consistent with the values quoted above. In the case of $R(D^*)$, these predictions have larger uncertainties than the result quoted in Eq. (76.62), as non-zero lattice-QCD form factors for $B \rightarrow D^*$ were not yet available.

Measurements [234–242] of these ratios yield higher values; averaging B -tagged measurements of $R(D)$ and $R(D^*)$ at the $\Upsilon(4S)$ and the LHCb measurements of $R(D^*)$ yields [243]

$$\begin{aligned} R(D)^{\text{meas}} &= 0.339 \pm 0.026 \pm 0.014, \\ R(D^*)^{\text{meas}} &= 0.295 \pm 0.010 \pm 0.010, \end{aligned} \quad (76.63)$$

with a linear correlation of -0.38 . These values exceed the Standard Model predictions of Eq. (76.62) by 1.4σ and 3.3σ , respectively. Not surprisingly, the tensions with respect to the lattice-QCD only prediction of Eq. (76.61) are less significant, at 1.4σ for $R(D)$ and 1.6σ for $R(D^*)$. A variety of new physics models have been proposed to explain this excess, see eg. Ref. [221–228] and recent reviews in Ref. [244–246].

Most models proposed to explain the semitauponic decay excesses tend to, but not always, have very little impact on semileptonic decays involving muons or electrons, so they do not significantly modify the $|V_{ub}|$ or $|V_{cb}|$ determinations discussed previously in this review. Lepton flavor universality in the ratio of electron and muon modes has been confirmed in direct ratio measurements from Belle: $\mathcal{B}(\bar{B} \rightarrow D^*e\bar{\nu}_e)/\mathcal{B}(\bar{B} \rightarrow D^*\mu\bar{\nu}_\mu) = 1.01 \pm 0.03$ [53] and $\Delta\mathcal{B}(B \rightarrow X_{ue}e\bar{\nu}_e)/\Delta\mathcal{B}(B \rightarrow X_{u\mu}\mu\bar{\nu}_\mu) = 0.97 \pm 0.10$ [162]. The uncertainty is dominated by lepton identification uncertainties that do not cancel in the ratio.

76.6.1 Sensitivity of $\bar{B} \rightarrow D^{(*)}\tau\bar{\nu}_\tau$ to additional amplitudes

In addition to the helicity amplitudes present for decays to $e\bar{\nu}_e$ and $\mu\bar{\nu}_\mu$, decays proceeding through $\tau\bar{\nu}_\tau$ include a scalar amplitude H_s . The differential decay rate is given by [247]

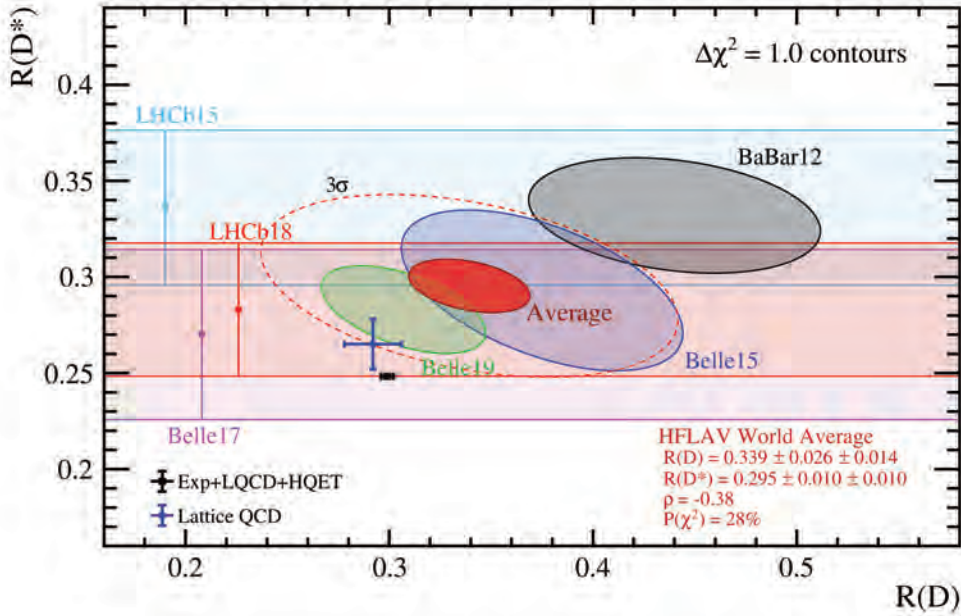
$$\begin{aligned} \frac{d\Gamma}{dq^2} &= \frac{G_F^2 |V_{cb}|^2 |\mathbf{p}_{D^{(*)}}^*|^2}{96\pi^3 m_B^2} \left(1 - \frac{m_\tau^2}{q^2}\right)^2 \\ &\quad \left[(|H_+|^2 + |H_-|^2 + |H_0|^2) \left(1 + \frac{m_\tau^2}{2q^2}\right) + \frac{3m_\tau^2}{2q^2} |H_s|^2 \right], \end{aligned} \quad (76.64)$$

where $|\mathbf{p}_{D^{(*)}}^*|$ is the 3-momentum of the $D^{(*)}$ in the \bar{B} rest frame and the helicity amplitudes H depend on the four-momentum transfer q^2 . All four helicity amplitudes contribute to $\bar{B} \rightarrow D^*\tau\bar{\nu}_\tau$, while only H_0 and H_s contribute to $\bar{B} \rightarrow D\tau\bar{\nu}_\tau$; as a result, new physics contributions can produce larger effects in the latter mode. Semi-leptonic B decays into a τ lepton provide a stringent test of the two-Higgs doublet model of type II (2HD-MII), i.e. where the two Higgs doublets couple separately to up- and down-type quarks. The distinct feature of the 2HDMII is that the contributions of the charged scalars scale as $m_\tau^2/m_{H^\pm}^2$, since the couplings to the charged Higgs particles are proportional to the mass of the lepton. As a consequence, one may expect visible effects in decays into a τ , but only small effects for decays into e and μ . The present data disfavors the 2HDMII, see below.

76.6.2 Measurement of $R(D^{(*)})$

$\bar{B} \rightarrow D^{(*)}\tau\bar{\nu}_\tau$ decays have been studied at the $\Upsilon(4S)$ resonance and in pp collisions. At the $\Upsilon(4S)$, the majority of experimental measurements are based on signatures that consist of a D or D^* meson, an electron or muon (denoted here by ℓ) from the decay $\tau \rightarrow \ell\nu_\tau\bar{\nu}_\ell$, a fully-reconstructed decay of the second B meson in

Figure 76.1: Measurements of $R(D)$ and $R(D^*)$ and their two-dimensional average compared with the average predictions for $R(D)$ and $R(D^*)$. Contours correspond to $\Delta\chi^2 = 1$ i.e., 68% CL for the bands and 39% CL for the ellipses. The average of the Lattice QCD and Experiment-Lattice QCD-HQET predictions and the experimental average deviate from each other by 2.0σ and 4.0σ respectively. The dashed ellipse corresponds to a 3σ contour of the experiment average (99.73% CL).



the event, and multiple missing neutrinos. One analysis reconstructs the τ in a hadronic mode. The analyses that use hadronic B tags separate signal decays from $\bar{B} \rightarrow D^{(*)}\ell\bar{\nu}_\ell$ decays using the lepton momentum and the measured missing mass squared; decays with only a single missing neutrino peak sharply at zero in this variable, while the signal is spread out to positive values. When a semileptonic B tag is used, the discrimination between signal and $\bar{B} \rightarrow D^{(*)}\ell\bar{\nu}_\ell$ decays comes from the calorimeter energy that is not associated with any particle used in the reconstruction of the B meson candidates, the measured missing mass squared and the cosine of the angle between the $D^*\ell$ system and its parent B meson, which is calculated under the assumption that only one particle (a neutrino) is missing. In both these approaches, background from $\bar{B} \rightarrow D^{**}\ell\bar{\nu}_\ell$ decays with one or more unreconstructed particles is challenging to separate from signal, as is background from $\bar{B} \rightarrow D^{(*)}H_c X$ (where H_c is a hadron containing a \bar{c} quark) decays. The leading sources of systematic uncertainty are due to the limited size of simulation samples used in constructing the PDFs, the composition of the D^{**} states, efficiency corrections, and cross-feed (swapping soft particles between the signal and tag B).

The most recent measurement from Belle [240] uses semileptonic B tags and leptonic τ decays to simultaneously measure $R(D^*)$ and $R(D)$. The measurement provides the single most precise determination of these ratios, combining results from charged and neutral B decays, and is compatible with the Standard Model expectation to approximately 1σ .

In addition to the ratio measurements, the Belle experiment has performed polarization measurements of the τ [239] and D^* [248] respectively. The τ polarization measurement uses hadronic B tags and τ^- decays to $\pi^-\nu_\tau$ or $\rho^-\nu_\tau$. The main discriminant variables are the measured missing mass squared and the unassociated calorimeter energy. This measurement provides the first determination of the τ polarization in the $\bar{B} \rightarrow D^*\tau\bar{\nu}_\tau$ decay, $\mathcal{P}_\tau(D^*) = -0.38 \pm 0.51^{+0.21}_{-0.16}$, compatible with the Standard Model expectation [27], $\mathcal{P}_\tau(D^*) = -0.476^{+0.037}_{-0.034}$.

The main uncertainties on the $R(D^*)$ measurement come from the composition of the hadronic B background and from model-

ing of semileptonic B decays and mis-reconstructed D^* mesons. The D^* polarization measurement uses an inclusive tag approach based on Refs. [249, 250], and reconstructs the τ decays in $\ell\nu_\tau\bar{\nu}_\ell$ and $\pi^+\bar{\nu}_\tau$ channels. The main discriminant variables are X_{miss} , a quantity that approximates missing mass but does not depend on tag B reconstruction, the visible energy of the event, and the beam-energy constrained mass, M_{bc} , of the inclusively reconstructed tag side B . This measurement provides the first determination of the D^* longitudinal polarization fraction in the $\bar{B} \rightarrow D^*\tau\bar{\nu}_\tau$ decay, $\mathcal{F}_L(D^*) = -0.38 \pm 0.60^{+0.08}_{-0.04}$, compatible with the Standard Model expectation [251] within 1.7σ .

The LHCb experiment has studied the decay $\bar{B} \rightarrow D^{*+}\tau\bar{\nu}_\tau$ with $D^{*+} \rightarrow D^0\pi^+$, $D^0 \rightarrow K^-\pi^+$ and $\tau \rightarrow \mu\nu_\tau\bar{\nu}_\mu$ in pp collisions. Their analysis [241] takes advantage of the measurable flight lengths of b and c hadrons and τ leptons. A multivariate discriminant is used to select decays where no additional charged particles are consistent with coming from the signal decay vertices. The separation between the primary and B decay vertices is used to calculate the momentum of the B decay products transverse to the B flight direction. The longitudinal component of the B momentum can be estimated based on the visible decay products; this allows a determination of the B rest frame, with modest resolution, and enables the calculation of the same discrimination variables available at the e^+e^- factories. The (rest frame) muon energy, missing mass-squared and q^2 are used in a 3- d fit. The most recent LHCb result [253] on $R(D^*)$ uses three-prong τ decays that take advantage of their excellent vertex resolution to isolate the τ decay from hadronic background. A 3- d fit is performed to determine the signal yield, based on the $\tau\text{-}\nu_\tau$ pair q^2 , the τ lifetime, as well as a boosted decision tree classifier based on isolation, invariant mass and flight distance information. The leading sources of systematic uncertainty are due to the size of the simulation sample used in constructing the fit templates, uncertainties in modelling the background from hadronic $\bar{B} \rightarrow D^{(*)}H_c X$ decays, as well as reconstruction and trigger effects. The result is normalized to $B^0 \rightarrow D^{*+}\pi^-\pi^+$ and found to be 1σ from the Standard Model expectation (using the expectation value quoted here). An analogous measurement of $B_c \rightarrow J/\psi\tau\bar{\nu}_\tau$ was performed by the LHCb measurement [254], in

Table 76.2: Measurements of $R(D)$ and $R(D^*)$, their correlations, ρ , and the combined averages [6].

		$R(D) \times 10^2$	$R(D^*) \times 10^2$	ρ
BABAR [235, 236]	B^0, B^+	$44.0 \pm 5.8 \pm 4.2$	$33.2 \pm 2.4 \pm 1.8$	-0.27
Belle [237]	B^0, B^+	$37.5 \pm 6.4 \pm 2.6$	$29.3 \pm 3.8 \pm 1.5$	-0.49
Belle [239, 252]	B^0, B^+		$27.0 \pm 3.5 \pm_{2.5}^{2.8}$	
Belle [240]	B^0, B^+	$30.7 \pm 3.7 \pm 1.6$	$28.3 \pm 1.8 \pm 1.4$	-0.51
LHCb [241]	B^0		$33.6 \pm 2.7 \pm 3.0$	
LHCb [253]	B^0		$28.3 \pm 1.9 \pm 2.9$	
Average	B^0, B^+	$33.9 \pm 2.6 \pm 1.4$	$29.5 \pm 1.0 \pm 1.0$	-0.38

leptonic τ decays. The result, $R(J/\psi) = 0.71 \pm 0.17 \pm 0.18$, while relatively high is compatible to within 2σ of a recent Standard Model evaluation [255] based on a lattice-QCD calculation [256] of the form factors. Systematic uncertainties are dominated by form factors, as B_c decays are relatively unexplored.

Measurements from BABAR [234–236], Belle [237–240] and LHCb [241, 253] result in values for $R(D)$ and $R(D^*)$ that exceed Standard Model predictions. Table 76.2 lists these values and their average. The simultaneous measurements of $R(D)$ and $R(D^*)$ have linear correlation coefficients of -0.27 (BABAR [235, 236]), -0.49 (Belle hadronic tag [237]) and -0.51 (Belle semileptonic tag [240]); the $R(D)$ and $R(D^*)$ averages have a correlation of -0.38 . Two early untagged Belle measurements [249, 250] are subject to larger systematic uncertainties, with a breakdown of the respective contributions that is inconsistent with the more recent determinations, hence they cannot be reliably combined in the average. All three experiments assume the Standard Model kinematic distributions for $\bar{B} \rightarrow D^{(*)}\tau\bar{\nu}_\tau$ in their determinations of the branching fraction ratios.

The measurement combination in the $R(D) - R(D^*)$ plane is shown in Fig. 76.1, compared with the predictions in Eq. (76.61) (LQCD) and Eq. (76.62) (Experiment+LQCD+HQET). The measurement combination is based on Ref. [6]. The tension between the Standard Model prediction in Eq. (76.62) and the measurements is at the level of 1.4σ ($R(D)$) and 3.3σ ($R(D^*)$); if one considers these deviations together the significance is 4.0σ . This motivates speculation on possible new physics contributions. The measurements reported in Refs. [240, 252, 253] resulted in reduced tensions with the Standard-Model predictions in recent editions of the RPP. The main change in this edition is the availability of lattice-QCD form factors at nonzero recoil, which improves the theory uncertainty on $R(D^*)$ and brings the discrepancy to the level reported in earlier editions. There is some tension in the combination coming from the BABAR measurement, the only measurement to claim a deviation from the Standard Model of more than 3σ , although the p -value of the full combination is an acceptable 28%.

The current discussion of $R(D)$ and $R(D^*)$ may be embedded in the theoretical analysis of the other anomalies that have been observed in semileptonic FCNC ($b \rightarrow s\ell\ell$) transitions. More sophisticated approaches fit the data to a general effective Hamiltonian. Matching this effective Hamiltonian to simplified models, the current situation of the anomalies seems to be compatible with scenarios with an additional Z' or a leptoquark scenario, see eg. [225–231].

76.7 Conclusion

The study of semileptonic B meson decays continues to be an active area for both theory and experiment. The application of HQE calculations to inclusive decays is well established, and fits to moments of $\bar{B} \rightarrow X_c\ell\bar{\nu}_\ell$ decays provide precise values for $|V_{cb}|$ and, in conjunction with input on m_c or from $B \rightarrow X_s\gamma$ decays, provide precise and consistent values for m_b . Recent developments will make use of more types of moments and better theoretical inputs to constrain higher order effects. Further into the future, new nonperturbative methods to compute inclusive decay rates, for example, in lattice QCD [257], may provide interesting new insights.

The determination of $|V_{ub}|$ from inclusive $\bar{B} \rightarrow X_u\ell\bar{\nu}_\ell$ decays is based on multiple calculational approaches and independent

measurements over a variety of kinematic regions, all of which provide consistent results. Further progress in this area is possible, but will require better theoretical control over higher-order terms, improved experimental knowledge of the $\bar{B} \rightarrow X_c\ell\bar{\nu}_\ell$ background and improvements to the modeling of the $\bar{B} \rightarrow X_u\ell\bar{\nu}_\ell$ signal distributions.

In both $b \rightarrow u$ and $b \rightarrow c$ exclusive channels there has been significant recent progress in lattice-QCD calculations, resulting in improved precision on both $|V_{ub}|$ and $|V_{cb}|$. These calculations now provide information on the form factors well away from the high q^2 region, allowing better use of experimental data. For $|V_{cb}|$ recent measurements have provided binned data enabling model-independent fits.

The values from the inclusive and exclusive determinations of $|V_{cb}|$ and $|V_{ub}|$ are only marginally consistent. This is a longstanding puzzle, which the recent improvements have, unfortunately, not yet resolved. The measurement of $|V_{ub}|/|V_{cb}|$ from LHCb based on A_b^0 and B_s decays also do not yet simplify the picture.

Both $|V_{cb}|$ and $|V_{ub}|$ are indispensable inputs into unitarity triangle fits. In particular, knowing $|V_{ub}|$ with good precision allows a test of CKM unitarity in a most direct way, by comparing the length of the $|V_{ub}|$ side of the unitarity triangle with the measurement of $\sin(2\beta)$. This comparison of a “tree” process ($b \rightarrow u$) with a “loop-induced” process ($B^0 - \bar{B}^0$ mixing) provides sensitivity to possible contributions from new physics.

The observation of semileptonic decays into τ leptons has opened a new window to the physics of the third generation. The measurements indicate a tension between the data and Standard-Model predictions, which could be a hint for new physics, manifesting itself as a violation of lepton universality beyond the Standard-Model couplings to the Higgs. It should be noted that none of the most recent measurements alone claim discovery of a deviation from the Standard Model. Combining the data of the semitauonic decays with the anomalies observed in the FCNC $b \rightarrow s\ell\ell$ transitions allows an interpretation in terms of additional Z' or in terms of additional leptoquarks, but the current data does not allow us to draw a definite conclusion.

The authors would like to acknowledge helpful input from D. Ferlewicz, P. Gambino, S. Hashimoto, Z. Ligeti, M. Rotondo, C. Schwanda, and A. Vaquero.

References

- [1] See “Leptonic Decays of Charged Pseudoscalar Mesons” by J.L. Rosner, S.L. Stone, and R. Van de Water in this *Review*.
- [2] M. Tanabashi *et al.* (Particle Data Group), *Phys. Rev. D* **98**, 3, 030001 (2018).
- [3] See “Heavy-Quark and Soft-Collinear Effective Theory” by C.W. Bauer and M. Neubert in this *Review*.
- [4] See “Lattice Quantum Chromodynamics” by S. Hashimoto, J. Laiho, and S.R. Sharpe in this *Review*.
- [5] See “Production and Decay of b -Flavored Hadrons” by P. Eerola, M. Kreps and Y. Kwon in this *Review*.
- [6] Y. S. Amhis *et al.* (HFLAV) (2019), [arXiv:1909.12524].
- [7] J. A. Bailey *et al.* (Fermilab Lattice and MILC), *Phys. Rev. D* **92**, 3, 034506 (2015), [arXiv:1503.07237].
- [8] H. Na *et al.* (HPQCD), *Phys. Rev. D* **92**, 5, 054510 (2015), [Erratum: *Phys. Rev. D* **93**, no.11, 119906 (2016)], [arXiv:1505.03925].

- [9] A. Bazavov *et al.* (Fermilab Lattice, MILC) (2021), [arXiv:2105.14019].
- [10] N. Isgur and M. B. Wise, Phys. Lett. **B232**, 113 (1989); N. Isgur and M. B. Wise, Phys. Lett. **B237**, 527 (1990).
- [11] M. A. Shifman and M. B. Voloshin, Sov. J. Nucl. Phys. **47**, 511 (1988), [Yad. Fiz.47,801(1988)].
- [12] A. V. Manohar and M. B. Wise, Camb. Monogr. Part. Phys. Nucl. Phys. Cosmol. **10**, 1 (2000).
- [13] H. Georgi, Phys. Lett. **B240**, 447 (1990).
- [14] A. F. Falk *et al.*, Nucl. Phys. **B343**, 1 (1990).
- [15] E. Eichten and B. R. Hill, Phys. Lett. **B234**, 511 (1990).
- [16] A. Sirlin, Nucl. Phys. **B196**, 83 (1982).
- [17] J. A. Bailey *et al.* (Fermilab Lattice, MILC), Phys. Rev. **D89**, 11, 114504 (2014), [arXiv:1403.0635].
- [18] C. G. Boyd, B. Grinstein and R. F. Lebed, Phys. Rev. Lett. **74**, 4603 (1995), [hep-ph/9412324].
- [19] C. G. Boyd, B. Grinstein and R. F. Lebed, Phys. Lett. B **353**, 306 (1995), [hep-ph/9504235].
- [20] C. G. Boyd, B. Grinstein and R. F. Lebed, Nucl. Phys. B **461**, 493 (1996), [hep-ph/9508211].
- [21] C. G. Boyd, B. Grinstein and R. F. Lebed, Phys. Rev. D **56**, 6895 (1997), [hep-ph/9705252].
- [22] B. Grinstein and A. Kobach, Phys. Lett. **B771**, 359 (2017), [arXiv:1703.08170].
- [23] I. Caprini, L. Lellouch and M. Neubert, Nucl. Phys. **B530**, 153 (1998), [hep-ph/9712417].
- [24] M. Bordone, M. Jung and D. van Dyk (2019), [arXiv:1908.09398].
- [25] F. U. Bernlochner *et al.*, Phys. Rev. **D95**, 11, 115008 (2017), [Erratum: Phys. Rev.D97,no.5,059902(2018)], [arXiv:1703.05330].
- [26] D. Bigi, P. Gambino and S. Schacht, Phys. Lett. **B769**, 441 (2017), [arXiv:1703.06124].
- [27] P. Gambino, M. Jung and S. Schacht, Phys. Lett. **B795**, 386 (2019), [arXiv:1905.08209].
- [28] F. U. Bernlochner, Z. Ligeti and D. J. Robinson, Phys. Rev. **D100**, 1, 013005 (2019), [arXiv:1902.09553].
- [29] F. U. Bernlochner *et al.*, Phys. Rev. **D96**, 9, 091503 (2017), [arXiv:1708.07134].
- [30] T. Kaneko *et al.* (JLQCD), PoS **LATTICE2019**, 139 (2019), [arXiv:1912.11770].
- [31] J. Harrison, C. Davies and M. Wingate (HPQCD), Phys. Rev. **D97**, 5, 054502 (2018), [arXiv:1711.11013].
- [32] S. Aoki *et al.* (Flavour Lattice Averaging Group) (2019), [arXiv:1902.08191].
- [33] I. I. Y. Bigi *et al.*, Phys. Rev. **D52**, 196 (1995), [hep-ph/9405410].
- [34] A. Kapustin *et al.*, Phys. Lett. **B375**, 327 (1996), [hep-ph/9602262].
- [35] P. Gambino, T. Mannel and N. Uraltsev, Phys. Rev. **D81**, 113002 (2010), [arXiv:1004.2859].
- [36] M. A. Shifman, N. G. Uraltsev and A. I. Vainshtein, Phys. Rev. D **51**, 2217 (1995), [Erratum: Phys.Rev.D 52, 3149 (1995)], [hep-ph/9405207].
- [37] A. Czarnecki, K. Melnikov and N. Uraltsev, Phys. Rev. D **57**, 1769 (1998), [hep-ph/9706311].
- [38] P. Gambino, T. Mannel and N. Uraltsev, JHEP **10**, 169 (2012), [arXiv:1206.2296].
- [39] N. Gubernari, A. Kokulu and D. van Dyk, JHEP **01**, 150 (2019), [arXiv:1811.00983].
- [40] L. Lellouch, Nucl. Phys. B **479**, 353 (1996), [hep-ph/9509358].
- [41] M. Di Carlo *et al.*, Phys. Rev. D **104**, 5, 054502 (2021), [arXiv:2105.02497].
- [42] G. Martinelli, S. Simula and L. Vittorio (2021), [arXiv:2105.07851].
- [43] D. Buskulic *et al.* (ALEPH), Phys. Lett. **B395**, 373 (1997).
- [44] G. Abbiendi *et al.* (OPAL), Phys. Lett. **B482**, 15 (2000), [hep-ex/0003013].
- [45] P. Abreu *et al.* (DELPHI), Phys. Lett. **B510**, 55 (2001), [hep-ex/0104026].
- [46] J. Abdallah *et al.* (DELPHI), Eur. Phys. J. **C33**, 213 (2004), [hep-ex/0401023].
- [47] N. E. Adam *et al.* (CLEO), Phys. Rev. **D67**, 032001 (2003), [hep-ex/0210040].
- [48] B. Aubert *et al.* (BaBar), Phys. Rev. **D77**, 032002 (2008), [arXiv:0705.4008].
- [49] B. Aubert *et al.* (BaBar), Phys. Rev. Lett. **100**, 231803 (2008), [arXiv:0712.3493].
- [50] B. Aubert *et al.* (BaBar), Phys. Rev. **D79**, 012002 (2009), [arXiv:0809.0828].
- [51] W. Dungen *et al.* (Belle), Phys. Rev. **D82**, 112007 (2010), [arXiv:1010.5620].
- [52] A. Abdesselam *et al.* (Belle) (2017), [arXiv:1702.01521].
- [53] A. Abdesselam *et al.* (Belle) (2018), [arXiv:1809.03290].
- [54] J. P. Lees *et al.* (BaBar), Phys. Rev. Lett. **123**, 091801 (2019), [arXiv:1903.10002].
- [55] E. Waheed *et al.* (Belle), Phys. Rev. D **100**, 5, 052007 (2019), [Erratum: Phys.Rev.D 103, 079901 (2021)], [arXiv:1809.03290].
- [56] F. Abudinén *et al.* (Belle-II) (2020), [arXiv:2008.07198].
- [57] F. Abudinén *et al.* (Belle-II) (2020), [arXiv:2008.10299].
- [58] D. Ferlewicz, P. Urquijo and E. Waheed, Phys. Rev. D **103**, 7, 073005 (2021), [arXiv:2008.09341].
- [59] B. Aubert *et al.* (BaBar), Phys. Rev. Lett. **104**, 011802 (2010), [arXiv:0904.4063].
- [60] R. Glattauer *et al.* (Belle), Phys. Rev. **D93**, 3, 032006 (2016), [arXiv:1510.03657].
- [61] C. Bourrely, I. Caprini and L. Lellouch, Phys. Rev. **D79**, 013008 (2009), [Erratum: Phys. Rev.D82,099902(2010)], [arXiv:0807.2722].
- [62] D. Bigi and P. Gambino, Phys. Rev. **D94**, 9, 094008 (2016), [arXiv:1606.08030].
- [63] C. J. Monahan *et al.*, Phys. Rev. D **95**, 11, 114506 (2017), [arXiv:1703.09728].
- [64] E. McLean *et al.*, Phys. Rev. D **101**, 7, 074513 (2020), [arXiv:1906.00701].
- [65] E. McLean *et al.*, Phys. Rev. D **99**, 11, 114512 (2019), [arXiv:1904.02046].
- [66] J. Harrison and C. T. H. Davies (HPQCD) (2021), [arXiv:2105.11433].
- [67] R. Aaij *et al.* (LHCb), Phys. Rev. D **101**, 7, 072004 (2020), [arXiv:2001.03225].
- [68] R. Aaij *et al.* (LHCb), Phys. Rev. D **104**, 3, 032005 (2021), [arXiv:2103.06810].
- [69] A. V. Manohar and M. B. Wise, Phys. Rev. **D49**, 1310 (1994), [hep-ph/9308246].
- [70] I. I. Y. Bigi *et al.*, Phys. Rev. Lett. **71**, 496 (1993), [201(1993)], [hep-ph/9304225]; I. I. Y. Bigi *et al.*, Phys. Lett. **B323**, 408 (1994), [hep-ph/9311339].
- [71] D. Benson *et al.*, Nucl. Phys. **B665**, 367 (2003), [hep-ph/0302262].
- [72] M. Gremm and A. Kapustin, Phys. Rev. **D55**, 6924 (1997), [hep-ph/9603448].
- [73] B. M. Dassingier, T. Mannel and S. Turczyk, JHEP **03**, 087 (2007), [hep-ph/0611168].
- [74] I. I. Bigi, N. Uraltsev and R. Zwicky, Eur. Phys. J. **C50**, 539 (2007), [hep-ph/0511158].

- [75] T. Mannel, S. Turczyk and N. Uraltsev, JHEP **11**, 109 (2010), [arXiv:1009.4622].
- [76] A. Pak and A. Czarnecki, Phys. Rev. **D78**, 114015 (2008), [arXiv:0808.3509].
- [77] S. Biswas and K. Melnikov, JHEP **02**, 089 (2010), [arXiv:0911.4142].
- [78] P. Gambino, JHEP **09**, 055 (2011), [arXiv:1107.3100].
- [79] M. Fael, K. Schönwald and M. Steinhauser, Phys. Rev. D **104**, 1, 016003 (2021), [arXiv:2011.13654].
- [80] P. Gambino and N. Uraltsev, Eur. Phys. J. **C34**, 181 (2004), [hep-ph/0401063].
- [81] V. Aquila *et al.*, Nucl. Phys. **B719**, 77 (2005), [hep-ph/0503083].
- [82] M. E. Luke, M. J. Savage and M. B. Wise, Phys. Lett. B **343**, 329 (1995), [hep-ph/9409287].
- [83] M. E. Luke, M. J. Savage and M. B. Wise, Phys. Lett. B **345**, 301 (1995), [hep-ph/9410387].
- [84] T. Becher, H. Boos and E. Lunghi, JHEP **12**, 062 (2007), [arXiv:0708.0855].
- [85] A. Alberti *et al.*, Nucl. Phys. **B870**, 16 (2013), [arXiv:1212.5082].
- [86] A. Alberti, P. Gambino and S. Nandi, JHEP **01**, 147 (2014), [arXiv:1311.7381].
- [87] T. Mannel, A. A. Pivovarov and D. Rosenthal, Phys. Rev. **D92**, 5, 054025 (2015), [arXiv:1506.08167].
- [88] T. Mannel and A. A. Pivovarov, Phys. Rev. D **100**, 9, 093001 (2019), [arXiv:1907.09187].
- [89] C. Breidenbach *et al.*, Phys. Rev. **D78**, 014022 (2008), [arXiv:0805.0971].
- [90] I. Bigi *et al.*, JHEP **04**, 073 (2010), [arXiv:0911.3322].
- [91] A. Kobach and S. Pal, Phys. Lett. **B772**, 225 (2017), [arXiv:1704.00008].
- [92] J. Heinonen and T. Mannel, Nucl. Phys. **B889**, 46 (2014), [arXiv:1407.4384].
- [93] P. Gambino, K. J. Healey and S. Turczyk, Phys. Lett. **B763**, 60 (2016), [arXiv:1606.06174].
- [94] T. Mannel and K. K. Vos, JHEP **06**, 115 (2018), [arXiv:1802.09409].
- [95] M. Fael, T. Mannel and K. Keri Vos, JHEP **02**, 177 (2019), [arXiv:1812.07472].
- [96] I. I. Y. Bigi *et al.*, Phys. Rev. **D50**, 2234 (1994), [hep-ph/9402360].
- [97] A. H. Hoang, Z. Ligeti and A. V. Manohar, Phys. Rev. Lett. **82**, 277 (1999), [hep-ph/9809423].
- [98] A. H. Hoang, Z. Ligeti and A. V. Manohar, Phys. Rev. **D59**, 074017 (1999), [hep-ph/9811239].
- [99] A. H. Hoang and T. Teubner, Phys. Rev. **D60**, 114027 (1999), [hep-ph/9904468].
- [100] A. Hoang, P. Ruiz-Femenia and M. Stahlhofen, JHEP **10**, 188 (2012), [arXiv:1209.0450].
- [101] M. Fael, K. Schönwald and M. Steinhauser, Phys. Rev. Lett. **125**, 5, 052003 (2020), [arXiv:2005.06487].
- [102] S. E. Csorna *et al.* (CLEO), Phys. Rev. **D70**, 032002 (2004), [hep-ex/0403052].
- [103] A. H. Mahmood *et al.* (CLEO), Phys. Rev. **D70**, 032003 (2004), [hep-ex/0403053].
- [104] B. Aubert *et al.* (BaBar), Phys. Rev. **D69**, 111103 (2004), [hep-ex/0403031].
- [105] B. Aubert *et al.* (BaBar), Phys. Rev. **D69**, 111104 (2004), [hep-ex/0403030].
- [106] C. Schwanda *et al.* (Belle), Phys. Rev. **D75**, 032005 (2007), [hep-ex/0611044].
- [107] P. Urquijo *et al.* (Belle), Phys. Rev. **D75**, 032001 (2007), [hep-ex/0610012].
- [108] J. Abdallah *et al.* (DELPHI), Eur. Phys. J. **C45**, 35 (2006), [hep-ex/0510024].
- [109] D. Acosta *et al.* (CDF), Phys. Rev. **D71**, 051103 (2005), [hep-ex/0502003].
- [110] B. Aubert *et al.* (BaBar), Phys. Rev. **D81**, 032003 (2010), [arXiv:0908.0415].
- [111] A. Limosani *et al.* (Belle), Phys. Rev. Lett. **103**, 241801 (2009), [arXiv:0907.1384].
- [112] C. Schwanda *et al.* (Belle), Phys. Rev. **D78**, 032016 (2008), [arXiv:0803.2158].
- [113] B. Aubert *et al.* (BaBar), Phys. Rev. **D72**, 052004 (2005), [hep-ex/0508004].
- [114] B. Aubert *et al.* (BaBar), Phys. Rev. Lett. **97**, 171803 (2006), [hep-ex/0607071].
- [115] S. Chen *et al.* (CLEO), Phys. Rev. Lett. **87**, 251807 (2001), [hep-ex/0108032].
- [116] M. Battaglia *et al.*, eConf **C0304052**, WG102 (2003), [Phys. Lett. **B556**, 41(2003)], [hep-ph/0210319].
- [117] B. Aubert *et al.* (BaBar), Phys. Rev. Lett. **93**, 011803 (2004), [hep-ex/0404017].
- [118] O. Buchmüller and H. Flächer, hep-ph/0507253 updated in Ref. [258].
- [119] C. W. Bauer *et al.*, Phys. Rev. **D70**, 094017 (2004), updated in Ref. [258], [hep-ph/0408002].
- [120] P. Gambino and C. Schwanda, Phys. Rev. **D89**, 1, 014022 (2014), [arXiv:1307.4551].
- [121] A. Alberti *et al.*, Phys. Rev. Lett. **114**, 6, 061802 (2015), [arXiv:1411.6560].
- [122] M. Antonelli *et al.*, Phys. Rept. **494**, 197 (2010), see section 5.4.2, [arXiv:0907.5386].
- [123] See “Quark Masses” by A.V. Manohar, L.P. Lellouch, and R.M. Barnett in this *Review*.
- [124] K. G. Chetyrkin *et al.*, Phys. Rev. **D80**, 074010 (2009), [arXiv:0907.2110].
- [125] M. Bordone, B. Capdevila and P. Gambino, Phys. Lett. B **822**, 136679 (2021), [arXiv:2107.00604].
- [126] M. Fael, K. Schönwald and M. Steinhauser, Phys. Rev. D **103**, 1, 014005 (2021), [arXiv:2011.11655].
- [127] R. van Tonder *et al.* (Belle) (2021), [arXiv:2109.01685].
- [128] N. Uraltsev, Int. J. Mod. Phys. **A14**, 4641 (1999), [hep-ph/9905520].
- [129] M. Neubert, Phys. Rev. **D49**, 4623 (1994), [hep-ph/9312311]; M. Neubert, Phys. Rev. **D49**, 3392 (1994), [hep-ph/9311325].
- [130] I. I. Y. Bigi *et al.*, Int. J. Mod. Phys. **A9**, 2467 (1994), [hep-ph/9312359].
- [131] C. W. Bauer, M. E. Luke and T. Mannel, Phys. Rev. **D68**, 094001 (2003), [hep-ph/0102089].
- [132] M. Benzke *et al.*, Phys. Rev. Lett. **106**, 141801 (2011), [arXiv:1012.3167].
- [133] A. Gunawardana and G. Paz (2019), [arXiv:1908.02812].
- [134] F. U. Bernlochner *et al.* (SIMBA), Phys. Rev. Lett. **127**, 10, 102001 (2021), [arXiv:2007.04320].
- [135] M. Neubert, Phys. Lett. **B513**, 88 (2001), [hep-ph/0104280].
- [136] M. Neubert, Phys. Lett. **B543**, 269 (2002), [hep-ph/0207002].
- [137] A. K. Leibovich, I. Low and I. Z. Rothstein, Phys. Rev. **D61**, 053006 (2000), [hep-ph/9909404].
- [138] A. K. Leibovich, I. Low and I. Z. Rothstein, Phys. Rev. **D62**, 014010 (2000), [hep-ph/0001028].
- [139] A. K. Leibovich, I. Low and I. Z. Rothstein, Phys. Lett. **B486**, 86 (2000), [hep-ph/0005124].

- [140] A. K. Leibovich, I. Low and I. Z. Rothstein, Phys. Lett. **B513**, 83 (2001), [hep-ph/0105066].
- [141] A. H. Hoang, Z. Ligeti and M. Luke, Phys. Rev. **D71**, 093007 (2005), [hep-ph/0502134].
- [142] B. O. Lange, M. Neubert and G. Paz, JHEP **10**, 084 (2005), [hep-ph/0508178].
- [143] B. O. Lange, JHEP **01**, 104 (2006), [hep-ph/0511098].
- [144] M. Neubert, Phys. Lett. **B612**, 13 (2005), [hep-ph/0412241].
- [145] Z. Ligeti, I. W. Stewart and F. J. Tackmann, Phys. Rev. **D78**, 114014 (2008), [arXiv:0807.1926].
- [146] P. Gambino, K. J. Healey and C. Mondino, Phys. Rev. **D94**, 1, 014031 (2016), [arXiv:1604.07598].
- [147] B. O. Lange, M. Neubert and G. Paz, Phys. Rev. **D72**, 073006 (2005), [hep-ph/0504071].
- [148] P. Gambino *et al.*, JHEP **10**, 058 (2007), [arXiv:0707.2493].
- [149] J. R. Andersen and E. Gardi, JHEP **01**, 097 (2006), [hep-ph/0509360].
- [150] M. Beneke *et al.*, JHEP **06**, 071 (2005), [hep-ph/0411395].
- [151] C. Greub, M. Neubert and B. D. Pecjak, Eur. Phys. J. **C65**, 501 (2010), [arXiv:0909.1609].
- [152] M. Brucherseifer, F. Caola and K. Melnikov, Phys. Lett. **B721**, 107 (2013), [arXiv:1302.0444].
- [153] T. Mannel and S. Recksiegel, Phys. Rev. **D60**, 114040 (1999), [hep-ph/9904475].
- [154] U. Aglietti *et al.*, Eur. Phys. J. **C59**, 831 (2009), [arXiv:0711.0860].
- [155] C. W. Bauer, Z. Ligeti and M. E. Luke, Phys. Rev. **D64**, 113004 (2001), [hep-ph/0107074].
- [156] C. W. Bauer, Z. Ligeti and M. E. Luke, Phys. Lett. **B479**, 395 (2000), [hep-ph/0002161].
- [157] I. I. Y. Bigi and N. G. Uraltsev, Nucl. Phys. **B423**, 33 (1994), [hep-ph/9310285].
- [158] M. B. Voloshin, Phys. Lett. **B515**, 74 (2001), [hep-ph/0106040].
- [159] Z. Ligeti, M. Luke and A. V. Manohar, Phys. Rev. **D82**, 033003 (2010), [arXiv:1003.1351].
- [160] P. Gambino and J. F. Kamenik, Nucl. Phys. **B840**, 424 (2010), [arXiv:1004.0114].
- [161] J. L. Rosner *et al.* (CLEO), Phys. Rev. Lett. **96**, 121801 (2006), [hep-ex/0601027].
- [162] L. Cao *et al.* (Belle), Phys. Rev. D **104**, 1, 012008 (2021), [arXiv:2102.00020].
- [163] B. Aubert *et al.* (BaBar), in “23rd International Symposium on Lepton-Photon Interactions at High Energy (LP07),” (2007), [arXiv:0708.1753].
- [164] J. P. Lees *et al.* (BaBar), Phys. Rev. D **86**, 032004 (2012), [arXiv:1112.0702].
- [165] R. Barate *et al.* (ALEPH), Eur. Phys. J. **C6**, 555 (1999).
- [166] M. Acciarri *et al.* (L3), Phys. Lett. **B436**, 174 (1998).
- [167] G. Abbiendi *et al.* (OPAL), Eur. Phys. J. **C21**, 399 (2001), [hep-ex/0107016].
- [168] P. Abreu *et al.* (DELPHI), Phys. Lett. **B478**, 14 (2000), [hep-ex/0105054].
- [169] A. Bornheim *et al.* (CLEO), Phys. Rev. Lett. **88**, 231803 (2002), [hep-ex/0202019].
- [170] A. Limosani *et al.* (Belle), Phys. Lett. **B621**, 28 (2005), [hep-ex/0504046].
- [171] J. P. Lees *et al.* (BaBar), Phys. Rev. **D95**, 7, 072001 (2017), [arXiv:1611.05624].
- [172] B. Aubert *et al.* (BaBar), Phys. Rev. Lett. **95**, 111801 (2005), [Erratum: Phys. Rev. Lett.97,019903(2006)], [hep-ex/0506036].
- [173] R. V. Kowalewski and S. Menke, Phys. Lett. **B541**, 29 (2002), [hep-ex/0205038].
- [174] J. P. Lees *et al.* (BaBar), Phys. Rev. **D86**, 032004 (2012), [arXiv:1112.0702].
- [175] I. Bizjak *et al.* (Belle), Phys. Rev. Lett. **95**, 241801 (2005), [hep-ex/0505088].
- [176] P. Urquijo *et al.* (Belle), Phys. Rev. Lett. **104**, 021801 (2010), [arXiv:0907.0379].
- [177] B. Aubert *et al.* (BaBar), Phys. Rev. Lett. **96**, 221801 (2006), [hep-ex/0601046].
- [178] L. Cao *et al.* (Belle) (2021), [arXiv:2107.13855].
- [179] A. Sibidanov *et al.* (Belle), Phys. Rev. **D88**, 3, 032005 (2013), [arXiv:1306.2781].
- [180] B. Aubert *et al.* (BaBar), Phys. Rev. Lett. **90**, 181801 (2003), [eConfC0304052,WG117(2003)], [hep-ex/0301001].
- [181] T. Hokuue *et al.* (Belle), Phys. Lett. **B648**, 139 (2007), [hep-ex/0604024].
- [182] B. Aubert *et al.* (BaBar), Phys. Rev. **D79**, 052011 (2009), [arXiv:0808.3524].
- [183] J. P. Lees *et al.* (BaBar), Phys. Rev. **D88**, 7, 072006 (2013), [arXiv:1308.2589].
- [184] J. P. Lees *et al.* (BaBar), Phys. Rev. **D87**, 3, 032004 (2013), [Erratum: Phys. Rev.D87,no.9,099904(2013)], [arXiv:1205.6245].
- [185] C. Schwanda *et al.* (Belle), Phys. Rev. Lett. **93**, 131803 (2004), [hep-ex/0402023].
- [186] N. E. Adam *et al.* (CLEO), Phys. Rev. Lett. **99**, 041802 (2007), [hep-ex/0703041].
- [187] S. B. Athar *et al.* (CLEO), Phys. Rev. **D68**, 072003 (2003), superceded by Ref. [188], [hep-ex/0304019].
- [188] R. Gray *et al.* (CLEO), Phys. Rev. **D76**, 012007 (2007), [Addendum: Phys. Rev.D76,no.3,039901(2007)], [hep-ex/0703042].
- [189] P. del Amo Sanchez *et al.* (BaBar), Phys. Rev. **D83**, 032007 (2011), supercedes Ref. [190], [arXiv:1005.3288].
- [190] B. Aubert *et al.* (BaBar), Phys. Rev. **D72**, 051102 (2005), [hep-ex/0507003].
- [191] P. del Amo Sanchez *et al.* (BaBar), Phys. Rev. **D83**, 052011 (2011), updated in Ref. [192], [arXiv:1010.0987].
- [192] J. P. Lees *et al.* (BaBar), Phys. Rev. **D86**, 092004 (2012), [arXiv:1208.1253].
- [193] J. A. Bailey *et al.* (Fermilab Lattice, MILC), Phys. Rev. **D92**, 1, 014024 (2015), [arXiv:1503.07839].
- [194] A. Bazavov *et al.* (Fermilab Lattice, MILC), Phys. Rev. **D100**, 3, 034501 (2019), [arXiv:1901.02561].
- [195] C. M. Bouchard *et al.*, Phys. Rev. **D90**, 054506 (2014), [arXiv:1406.2279].
- [196] J. M. Flynn *et al.*, Phys. Rev. **D91**, 7, 074510 (2015), [arXiv:1501.05373].
- [197] A. X. El-Khadra, A. S. Kronfeld and P. B. Mackenzie, Phys. Rev. D **55**, 3933 (1997), [hep-lat/9604004].
- [198] T. Becher and R. J. Hill, Phys. Lett. **B633**, 61 (2006), [hep-ph/0509090].
- [199] M. C. Arnesen *et al.*, Phys. Rev. Lett. **95**, 071802 (2005), [hep-ph/0504209].
- [200] M. A. Shifman, A. I. Vainshtein and V. I. Zakharov, Nucl. Phys. **B147**, 385 (1979); M. A. Shifman, A. I. Vainshtein and V. I. Zakharov, Nucl. Phys. **B147**, 448 (1979).
- [201] P. Ball and R. Zwicky, Phys. Rev. **D71**, 014015 (2005), [hep-ph/0406232].
- [202] G. Duplancic *et al.*, JHEP **04**, 014 (2008), [arXiv:0801.1796].
- [203] A. Bharucha, JHEP **05**, 092 (2012), [arXiv:1203.1359].

- [204] A. V. Rusov, Eur. Phys. J. **C77**, 7, 442 (2017), [arXiv:1705.01929].
- [205] I. Sentitemsu Imsong *et al.*, JHEP **02**, 126 (2015), [arXiv:1409.7816].
- [206] H. Ha *et al.* (Belle), Phys. Rev. **D83**, 071101 (2011), [arXiv:1012.0090].
- [207] B. Aubert *et al.* (BaBar), Phys. Rev. Lett. **101**, 081801 (2008), [arXiv:0805.2408].
- [208] W. S. Brower and H. P. Paar, Nucl. Instrum. Meth. **A421**, 411 (1999), [hep-ex/9710029].
- [209] P. Ball, eConf **C070512**, 016 (2007), [arXiv:0705.2290].
- [210] J. M. Flynn and J. Nieves, Phys. Lett. **B649**, 269 (2007), [hep-ph/0703284].
- [211] S. Aoki *et al.*, Eur. Phys. J. **C77**, 2, 112 (2017), [arXiv:1607.00299].
- [212] D. Leljak, B. Melic and D. van Dyk, JHEP **07**, 036 (2021), [arXiv:2102.07233].
- [213] A. Biswas *et al.*, JHEP **07**, 082 (2021), [arXiv:2103.01809].
- [214] R. Aaij *et al.* (LHCb), Phys. Rev. Lett. **126**, 8, 081804 (2021), [arXiv:2012.05143].
- [215] A. Khodjamirian and A. V. Rusov, JHEP **08**, 112 (2017), [arXiv:1703.04765].
- [216] T. Feldmann and M. W. Y. Yip, Phys. Rev. **D85**, 014035 (2012), [Erratum: Phys. Rev. **D86**, 079901(2012)], [arXiv:1111.1844].
- [217] W. Detmold, C. Lehner and S. Meinel, Phys. Rev. **D92**, 3, 034503 (2015), [arXiv:1503.01421].
- [218] R. Aaij *et al.* (LHCb), Nature Phys. **11**, 743 (2015), [arXiv:1504.01568].
- [219] M. Ablikim *et al.* (BESIII), Phys. Rev. Lett. **116**, 5, 052001 (2016), [arXiv:1511.08380].
- [220] R. Aaij *et al.* (LHCb), Phys. Rev. **D96**, 11, 112005 (2017), [arXiv:1709.01920].
- [221] M. Tanaka, Z. Phys. **C67**, 321 (1995), [hep-ph/9411405].
- [222] H. Itoh, S. Komine and Y. Okada, Prog. Theor. Phys. **114**, 179 (2005), [hep-ph/0409228].
- [223] U. Nierste, S. Trine and S. Westhoff, Phys. Rev. **D78**, 015006 (2008), [arXiv:0801.4938].
- [224] M. Tanaka and R. Watanabe, Phys. Rev. **D82**, 034027 (2010), [arXiv:1005.4306].
- [225] A. Datta, M. Duraisamy and D. Ghosh, Phys. Rev. **D86**, 034027 (2012), [arXiv:1206.3760].
- [226] D. Becirevic, N. Kosnik and A. Tayduganov, Phys. Lett. **B716**, 208 (2012), [arXiv:1206.4977].
- [227] S. Fajfer *et al.*, Phys. Rev. Lett. **109**, 161801 (2012), [arXiv:1206.1872].
- [228] A. Crivellin, C. Greub and A. Kokulu, Phys. Rev. **D86**, 054014 (2012), [arXiv:1206.2634].
- [229] M. Bauer and M. Neubert, Phys. Rev. Lett. **116**, 14, 141802 (2016), [arXiv:1511.01900].
- [230] I. Doršner *et al.*, Phys. Rept. **641**, 1 (2016), [arXiv:1603.04993].
- [231] A. Celis *et al.*, Phys. Lett. **B771**, 168 (2017), [arXiv:1612.07757].
- [232] S. Jaiswal, S. Nandi and S. K. Patra, JHEP **12**, 060 (2017), [arXiv:1707.09977].
- [233] M. Bordone *et al.*, Eur. Phys. J. C **80**, 4, 347 (2020), [arXiv:1912.09335].
- [234] B. Aubert *et al.* (BaBar), Phys. Rev. Lett. **100**, 021801 (2008), [arXiv:0709.1698].
- [235] J. P. Lees *et al.* (BaBar), Phys. Rev. Lett. **109**, 101802 (2012), [arXiv:1205.5442].
- [236] J. P. Lees *et al.* (BaBar), Phys. Rev. **D88**, 7, 072012 (2013), [arXiv:1303.0571].
- [237] M. Huschle *et al.* (Belle), Phys. Rev. **D92**, 7, 072014 (2015), [arXiv:1507.03233].
- [238] Y. Sato *et al.* (Belle), Phys. Rev. **D94**, 7, 072007 (2016), [arXiv:1607.07923].
- [239] S. Hirose *et al.* (Belle), Phys. Rev. Lett. **118**, 21, 211801 (2017), [arXiv:1612.00529].
- [240] G. Caria *et al.* (Belle) (2019), [arXiv:1910.05864].
- [241] R. Aaij *et al.* (LHCb), Phys. Rev. Lett. **115**, 11, 111803 (2015), [Erratum: Phys. Rev. Lett. **115**, no.15, 159901(2015)], [arXiv:1506.08614].
- [242] R. Aaij *et al.* (LHCb), Phys. Rev. Lett. **120**, 17, 171802 (2018), [arXiv:1708.08856].
- [243] <http://www.slac.stanford.edu/xorg/hfag/semi/fpcp17/RDRDs.html>.
- [244] M. Blanke, PoS **LeptonPhoton2019**, 015 (2019), [arXiv:1908.09713].
- [245] S. Descotes-Genon, PoS **ALPS2019**, 016 (2020).
- [246] D. London and J. Matias (2021), [arXiv:2110.13270].
- [247] J. G. Korner and G. A. Schuler, Z. Phys. **C46**, 93 (1990).
- [248] A. Abdesselam *et al.* (Belle), in “10th International Workshop on the CKM Unitarity Triangle (CKM 2018) Heidelberg, Germany, September 17-21, 2018,” (2019), [arXiv:1903.03102].
- [249] A. Matyja *et al.* (Belle), Phys. Rev. Lett. **99**, 191807 (2007), [arXiv:0706.4429].
- [250] A. Bozek *et al.* (Belle), Phys. Rev. **D82**, 072005 (2010), [arXiv:1005.2302].
- [251] M. Tanaka and R. Watanabe, Phys. Rev. **D87**, 3, 034028 (2013), [arXiv:1212.1878].
- [252] S. Hirose *et al.* (Belle), Phys. Rev. **D97**, 1, 012004 (2018), [arXiv:1709.00129].
- [253] R. Aaij *et al.* (LHCb), Phys. Rev. **D97**, 7, 072013 (2018), [arXiv:1711.02505].
- [254] R. Aaij *et al.* (LHCb), Phys. Rev. Lett. **120**, 12, 121801 (2018), [arXiv:1711.05623].
- [255] J. Harrison, C. T. H. Davies and A. Lytle (LATTICE-HPQCD), Phys. Rev. Lett. **125**, 22, 222003 (2020), [arXiv:2007.06956].
- [256] J. Harrison, C. T. H. Davies and A. Lytle (HPQCD), Phys. Rev. D **102**, 9, 094518 (2020), [arXiv:2007.06957].
- [257] P. Gambino and S. Hashimoto, Phys. Rev. Lett. **125**, 3, 032001 (2020), [arXiv:2005.13730].
- [258] Y. Amhis *et al.* (HFLAV), Eur. Phys. J. **C77**, 12, 895 (2017), [arXiv:1612.07233].

77. Determination of CKM angles from B hadrons

Revised February 2022 by T. Gershon (Warwick U.), M. Kenzie (Warwick U.) and K. Trabelsi (U. Paris-Saclay, IJCLab).

77.1 Introduction

The Cabibbo–Kobayashi–Maskawa (CKM) description of quark mixing [1, 2] leads to a number of triangle relations between pairs of CKM matrix elements. One of these,

$$V_{ud}V_{ub}^* + V_{cd}V_{cb}^* + V_{td}V_{tb}^* = 0, \quad (77.1)$$

is of particular interest since (i) all its terms are of comparable magnitude, and (ii) its properties can be measured through studies of oscillations and decays of B mesons. As the area of this unitary triangle is a measure of the amount of CP violation in the Standard Model [3], it is of particular interest to determine the values of its angles and to test the consistency of the CKM paradigm with the experimental measurements. The angles are defined as

$$\alpha = \arg \left[-\frac{V_{td}V_{tb}^*}{V_{ud}V_{ub}^*} \right], \quad \beta = \arg \left[-\frac{V_{cd}V_{cb}^*}{V_{td}V_{tb}^*} \right], \quad (77.2)$$

$$\gamma = \arg \left[-\frac{V_{ud}V_{ub}^*}{V_{cd}V_{cb}^*} \right],$$

with an alternative notation $(\phi_2, \phi_1, \phi_3) \equiv (\alpha, \beta, \gamma)$ also widely used in the literature.

In this mini-review, the most precise methods to determine the CKM angles are described, with a particular focus on nontrivial aspects of the combination of results. More detailed discussions of these points can be found in Ref. [4]. A similar mini-review on the side of the unitarity triangle adjacent to the angle γ can be found in Ref. [5]. A detailed overview of the CKM quark-mixing matrix is given in Ref. [6] while CP violation in the quark sector is discussed in Ref. [7].

77.2 β

The relative weak (*i.e.* CP -violating) phase between the amplitude for any CKM-favoured B^0 meson decay to a CP eigenstate and that for the decay following B^0 – \bar{B}^0 oscillation is twice the angle β . The decay-time-dependent CP asymmetry can be expressed as

$$A_{f_{CP}}(t) \equiv \frac{d\Gamma/dt[\bar{B}_{\text{phys}}^0(t) \rightarrow f_{CP}] - d\Gamma/dt[B_{\text{phys}}^0(t) \rightarrow f_{CP}]}{d\Gamma/dt[\bar{B}_{\text{phys}}^0(t) \rightarrow f_{CP}] + d\Gamma/dt[B_{\text{phys}}^0(t) \rightarrow f_{CP}]}, \quad (77.3a)$$

$$= S_f \sin(\Delta m t) - C_f \cos(\Delta m t), \quad (77.3b)$$

where the notation $B_{\text{phys}}^0(t)$ ($\bar{B}_{\text{phys}}^0(t)$) denotes a neutral B meson that decays at time t into the final state f_{CP} , and is known (“tagged”) at time $t = 0$ to have flavour content corresponding to B^0 (\bar{B}^0). In Eq. (77.3b), Δm denotes the mass difference between the two physical eigenstates of the B^0 – \bar{B}^0 system, while the corresponding decay-width difference is assumed to be negligible [8]; moreover CPT symmetry and the absence of CP violation in B^0 – \bar{B}^0 mixing is assumed throughout this mini-review.

In the general case, one can write

$$S_f \equiv \frac{2\text{Im}(\lambda_f)}{1 + |\lambda_f|^2} \quad \text{and} \quad C_f \equiv \frac{1 - |\lambda_f|^2}{1 + |\lambda_f|^2}, \quad (77.4)$$

where the parameter $\lambda_f = \frac{q}{p} \frac{\bar{A}_f}{A_f}$ is defined in terms of p and q , which define the flavour content of the mass eigenstates of the B^0 – \bar{B}^0 system [8], and the amplitudes \bar{A}_f (A_f) for a \bar{B}^0 (B^0) decay to the final state f_{CP} . In the limit that the decay amplitude is dominated by a CKM-favoured transition, as is the case for $B^0 \rightarrow J/\psi K_S^0$ decays, one obtains simple relations: $S_f = -\eta_{CP} \sin(2\beta)$ and $C_f = 0$, where η_{CP} is the CP eigenvalue of the final state [9, 10]. This method has been pursued intensively by experiments. The current world averages, combining results for

several charmonium-kaon final states but dominated by results on $B^0 \rightarrow J/\psi K_S^0$ (CP odd) and $B^0 \rightarrow J/\psi K_L^0$ (CP even), are [4]

$$-\eta_{CP} S_f = 0.699 \pm 0.017, \quad C_f = -0.005 \pm 0.015. \quad (77.5)$$

Despite the large number of signal events in the data, the dominant uncertainties are still statistical. One important source of potential systematic correlation between results from different experiments is that due to “tag-side interference” [11], which is common to measurements exploiting production through the $e^+e^- \rightarrow \Upsilon(4S) \rightarrow B^0\bar{B}^0$ process, including the latest results from BaBar [12] and Belle [13]. It does not, however, affect the results from LHCb [14] that have comparable statistical sensitivity. Another common source of systematic uncertainty is due to knowledge of the value of Δm , but since this quantity has been measured precisely [8] the effect remains small.

The interpretation of the value of $-\eta_{CP} S_f$ from Eq. (77.5) as $\sin(2\beta)$ assumes negligible contributions from subleading amplitudes with a different weak phase to that of the tree diagram (*i.e.* to that of the CKM matrix elements $V_{cb}V_{cs}^*$). This potential additional contribution is often referred to as “penguin pollution”. All existing data, including the value of C_f in Eq. (77.5), as well as several explicit calculations [15–18], are consistent with penguin pollution in B^0 meson decays to charmonium-kaon decays being negligible at the current level of precision. Therefore, the value of $-\eta_{CP} S_f$ is generally converted to $\sin(2\beta)$ without any correction or additional uncertainty being assigned due to this assumption. This gives [4]

$$\beta = (22.2 \pm 0.7)^\circ, \quad (77.6)$$

where only the solution consistent with the Standard Model is reported (methods to resolve the trigonometric ambiguity in the result are discussed below). It is also possible to use data-driven methods, typically based on flavour symmetries plus some additional assumptions, to constrain the effects of penguin pollution [19–21]. In this case it is necessary to consider each charmonium-kaon final state separately, since the penguin pollution to each may differ. The most common approach [19], which relies on experimental information on $B^0 \rightarrow J/\psi \pi^0$ decays, currently gives an additional uncertainty on $\sin(2\beta)$ from $B^0 \rightarrow J/\psi K_S^0$ of around 0.01.

It is possible to avoid the issue of penguin pollution in the measurement of β by using B^0 meson decays to a charm- and light-meson final state, such as $D_{CP} \pi^0$ (where D_{CP} represents a D^0 meson decaying into a CP eigenstate), instead of the charmonium-kaon final states. These decays do have a CKM-suppressed contribution ($V_{ub}V_{cd}^*$ instead of $V_{cb}V_{ud}^*$), which can in principle bias the determination of $\sin(2\beta)$ from S_f , but this can be calculated and is known to be negligible at current precision. The requirement that the neutral D meson decays to a final state that is common to both D^0 and \bar{D}^0 , such as the CP -even eigenstate K^+K^- , reduces the sample size that is available for analysis. Consequently, the world average [4], $\sin(2\beta) = 0.71 \pm 0.09$, with these channels is not as precise as that from the charmonium-kaon states.

Converting experimental results on $\sin(2\beta)$ into constraints on β leads to a trigonometric ambiguity in the range $[0^\circ, 180^\circ]$. This can be resolved with experimental measurements of $\cos(2\beta)$, which can be obtained from decay-time-dependent analyses of B^0 meson decays to multibody (non- CP -eigenstate) final states. Among the charmonium-kaon decays, study of $B^0 \rightarrow J/\psi K^*(892)^0$ with $K^*(892)^0 \rightarrow K_S^0 \pi^0$ is the most promising approach, but due to the limited sample size that has been analysed to date the precision is not sufficient to resolve the ambiguity conclusively. The charm- and light-meson channels such as $B^0 \rightarrow D \pi^0$ with $D \rightarrow K_S^0 \pi^+ \pi^-$ have been shown to provide good statistical power for this purpose, with a joint analysis of BaBar and Belle data giving $\cos(2\beta) = 0.91 \pm 0.25$ [22, 23], sufficient to rule out the alternative solution for β .

77.3 α

In the limit that only tree amplitudes contribute to B^0 meson decays to light mesons, such as $B^0 \rightarrow \pi^+ \pi^-$, then the observables of the decay-time-dependent CP asymmetry of Eq. (77.3) would allow a straight-forward determination of 2α : $S_f = +\eta_{CP} \sin(2\alpha)$

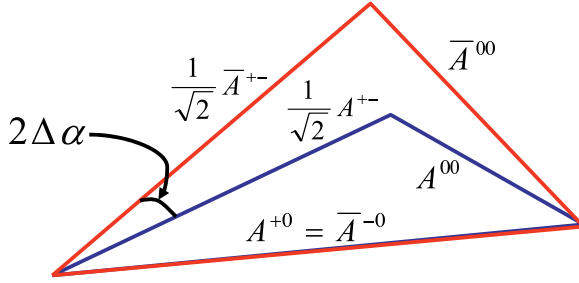


Figure 77.1: Isospin triangles for $B \rightarrow \pi\pi$ decays, reproduced from Ref. [24]. Here, the relative phase between A^{+0} and \bar{A}^{-0} has been rotated away to simplify the picture. The total relative phase probed by $S_{\pi^+\pi^-}$ is arg $\left(\frac{q}{p} \frac{\bar{A}^{+-}}{A^{+-}}\right) = 2\alpha - 2\Delta\alpha$, including contributions from $B^0\text{-}\bar{B}^0$ mixing, the tree-level amplitudes and the correction $\Delta\alpha$, and exploiting the unitarity requirement $\alpha + \beta + \gamma = 180^\circ$.

and $C_f = 0$. In general, however, the determination of α is complicated by the presence of contributions from $b \rightarrow d(u\bar{u})$ neutral-current penguin transitions, which have a similar level of CKM-suppression as the $b \rightarrow u(\bar{u})$ charged-current tree amplitudes but have a different weak phase. Consequently, one obtains instead for $B^0 \rightarrow \pi^+\pi^-$

$$S_{\pi^+\pi^-} = \sqrt{1 - C_{\pi^+\pi^-}^2} \sin(2\alpha - 2\Delta\alpha), \quad (77.7)$$

where $\Delta\alpha$ is the *a priori* unknown penguin contribution.

This contribution from the penguin amplitude can be accounted for in an analysis relating the amplitudes for isospin partner decays, e.g. A^{+-} for $B^0 \rightarrow \pi^+\pi^-$, A^{+0} for $B^+ \rightarrow \pi^+\pi^0$, A^{00} for $B^0 \rightarrow \pi^0\pi^0$ decays and $(\bar{A}^{+-}, \bar{A}^{-0}, \bar{A}^{00})$ for their charge conjugates. The isospin analysis relies on the fact that there is no penguin contribution to A^{+0} and \bar{A}^{-0} , because $\pi^\pm\pi^0$ is a pure isospin-2 state, and the ($\Delta I = \frac{1}{2}$) QCD-penguin amplitudes only contribute to the isospin-0 final state. One therefore obtains the following isospin triangle relations [25]

$$A^{+0} = \frac{1}{\sqrt{2}} A^{+-} + A^{00} \quad \text{and} \quad \bar{A}^{-0} = \frac{1}{\sqrt{2}} \bar{A}^{+-} + \bar{A}^{00}, \quad (77.8)$$

from which it is possible to determine $\Delta\alpha$, as shown in Fig. 77.1.

Since the determination of $\Delta\alpha$ and thus also α requires construction of amplitude-level relations, it is not appropriate to simply average results of α from different experiments. Instead, measurements of each of the observable quantities needed to determine α are input into a combination. For the $B \rightarrow \pi\pi$ system, the inputs are the branching fractions of $B^0 \rightarrow \pi^+\pi^-$, $B^+ \rightarrow \pi^+\pi^0$ and $B^0 \rightarrow \pi^0\pi^0$ decays, the lifetimes of the B^+ and B^0 mesons (which relate the branching fractions to amplitude-level quantities), and the $S_{\pi^+\pi^-}$, $C_{\pi^+\pi^-}$ and $C_{\pi^0\pi^0}$ observables. Potential sources of correlation must be taken into account, but these are predominantly systematic in origin and thus have a small effect on the combination, since the measurements are statistically limited. An exception is that the LHCb measurements of $(S_{\pi^+\pi^-}, C_{\pi^+\pi^-})$ [26, 27] have a significant statistical correlation due to the fact that the time variable of Eq. (77.3) is the difference between production and decay, and hence is in the range $[0, \infty]$. This correlation is largely absent for measurements from BaBar [28] and Belle [29], where the difference between the signal and tagging B meson decay times is measured, and hence $t \in [-\infty, \infty]$. The combination itself can be performed with different statistical approaches; the procedure described in detail in Ref. [30], based on a frequentist treatment, is used here. The knowledge of $C_{\pi^0\pi^0}$ [28, 31] is currently the limiting factor in the precision on α from the $B \rightarrow \pi\pi$ system, and is likely to remain so for some time due to the difficulty to reconstruct this final state.

In general, the isospin triangle construction gives a four-fold ambiguity on $2\Delta\alpha$ (each triangle can face either up or down), leading to an eight-fold ambiguity on α in the range $[0^\circ, 180^\circ]$.

This is reduced if either or both of the triangles are flat, or if the two triangles have sides of identical length. The ambiguities can also be reduced if measurement of the $S_{\pi^0\pi^0}$ (or equivalent) observable is available, since this can be combined with the corresponding $\Delta\alpha$ parameter from the right-hand corner of the triangle in Fig. 77.1 to provide an additional constraint. None of these possibilities are realised in the $B \rightarrow \pi\pi$ system; in particular a decay-time-dependent analysis of $B^0 \rightarrow \pi^0\pi^0$ is extremely challenging experimentally due to the absence of any charged particle originating from the B decay position. Nonetheless, solutions consistent with $\alpha = 0$ can be rejected on physical grounds [24].

The isospin analysis can also be performed with the $B \rightarrow \rho\rho$ system, which contains two vector particles in the final state and so does not have a fixed CP eigenvalue. In principle the analysis can be performed separately for each $\rho\rho$ polarization state, but in practise it is found that the longitudinal polarization fraction, f_L , is close to unity, and hence the final state is approximately CP -even. Compared to $B^0 \rightarrow \pi\pi$, the $\rho\rho$ modes benefit experimentally from a higher branching fraction and smaller penguin contributions, so that the isospin triangles are flatter, reducing the ambiguities. (The value of $\Delta\alpha$ in the $B \rightarrow \rho\rho$ system, obtained from the isospin analysis, has a single solution in $[0, \pi]$ at $(3 \pm 5)^\circ$, while for $B \rightarrow \pi\pi$ there are two solutions at 13° and 27° with $\Delta\alpha \in [7, 33]^\circ$ at 68.3% confidence level (CL). The isospin analysis with either final state has an ambiguity under $\Delta\alpha \leftrightarrow -\Delta\alpha$.) For the BaBar [32] and Belle [33] experiments, the high branching fraction and smaller penguin contribution compensate for the increased difficulty to reconstruct the $\rho\rho$ final state relative to $\pi\pi$. Moreover, in contrast to $S_{\pi^0\pi^0}$, measurement of $S_{\rho^0\rho^0}$ is possible due to the four charged pion final state, following $\rho^0 \rightarrow \pi^+\pi^-$ decay, as has been demonstrated by BaBar [34].

In the $B \rightarrow \rho\pi$ system there are more amplitudes to consider, so that the isospin relation corresponds to a pentagon rather than a triangle and Eq. (77.8) is modified to become

$$\begin{aligned} \sqrt{2}(A^{+0} + A^{0+}) &= A^{+-} + A^{-+} + 2A^{00} \quad \text{and} \\ \sqrt{2}(\bar{A}^{-0} + \bar{A}^{0-}) &= \bar{A}^{+-} + \bar{A}^{-+} + 2\bar{A}^{00}. \end{aligned} \quad (77.9)$$

As in Eq. (77.8), the left-hand sides of these expressions correspond to a pure isospin-2 final state, and therefore the ratio of the right-hand sides gives a pure phase term that, accounting for the $B^0\text{-}\bar{B}^0$ mixing phase that also contributes to the measured quantities, is 2α . The relative amplitudes for B^0 and \bar{B}^0 decays to $\rho^+\pi^-$, $\rho^-\pi^+$ and $\rho^0\pi^0$ can all be determined from a decay-time-dependent analysis of the $\pi^+\pi^-\pi^0$ Dalitz plot, so that study of this channel alone allows determination of α [35]. This analysis in principle leads to a single solution for α in $[0^\circ, 180^\circ]$, but the precision of current measurements [36–38] is limited.

The isospin analysis used to determine α is believed to be valid to high precision, and theoretical uncertainties in the procedure are usually neglected. Nonetheless, it should be noted that the analysis assumes the absence of electroweak penguin amplitudes, which can contribute to $\Delta I = \frac{3}{2}$ transitions with a different weak phase from that of the tree amplitudes [39, 40]. Moreover, isospin-breaking effects such as (π^0, η, η') mixing would impact on the relations of Eq. (77.8). A further complication in the $B \rightarrow \rho\rho$ system is the effect of the non-zero ρ meson width [41]. Estimates of the size of these effects on the determined value of α are typically at the 1° level or less [30]. By contrast, methods to determine α using SU(3) or other flavour symmetries are generally considered to have larger theoretical uncertainties and are not included here.

The world average obtained for the angle α from isospin analysis of $B \rightarrow \pi\pi$, $\rho\pi$ and $\rho\rho$ decays is [4]

$$\alpha = (85.2_{-4.3}^{+4.8})^\circ, \quad (77.10)$$

where the quoted uncertainty is at the 68.3% CL and does not include effects due to isospin-breaking. This world average, together with results split by decay mode, is shown in Fig. 77.2. The combination has a total of 51 experimental inputs from which 24 parameters are determined, and an overall χ^2 of 16.6, which corresponds to a p-value of 94%. Thus, there is excellent overall consistency between the inputs, despite the tension apparent in

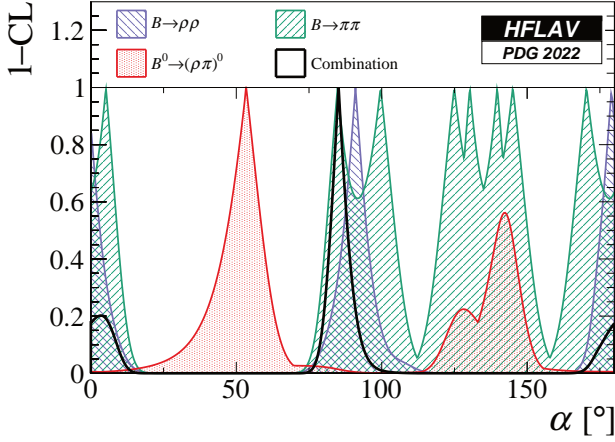


Figure 77.2: World average of α , as well as contributions from individual modes, in terms of 1–CL.

Fig. 77.2 between the results from $B^0 \rightarrow (\rho\pi)^0$ and the others. The combination gives a single best-fit for α in $[0^\circ, 180^\circ]$, but an ambiguous solution exists at $\alpha \leftrightarrow \alpha + 180^\circ$. A secondary minimum close to zero is disfavoured [30].

77.4 γ

The angle γ is the weak phase between Cabibbo-favoured $b \rightarrow c$ and suppressed $b \rightarrow u$ quark transitions and can be determined by exploiting interference between them. Explicitly, the ratio of suppressed to favoured amplitudes is parameterized by

$$r_B e^{i(\delta_B \pm \gamma)} = \frac{A_{\text{sup}}}{A_{\text{fav}}}, \quad (77.11)$$

where r_B is the ratio of amplitude magnitudes, δ_B the strong phase difference and the + or – sign depends on whether the transition involves a \bar{b} or b quark, respectively. Measurement of γ in this way has negligible theoretical uncertainty in the Standard Model [42], and therefore this approach provides a benchmark against which determinations from other methods, typically involving loop diagrams, can be compared.

Interference between these amplitudes is realised in $B^+ \rightarrow DK^+$ decays, where D represents an admixture of D^0 and \bar{D}^0 mesons. The simplest case is that of D decays to CP -eigenstates (GLW method [43, 44]), either CP -even such as K^+K^- ($CP+$) or CP -odd such as $K_S^0\pi^0$ ($CP-$). The normalized decay rate and CP asymmetry are given by

$$R_{CP\pm} = \frac{\Gamma(B^- \rightarrow D_{CP\pm}K^-) + \Gamma(B^+ \rightarrow D_{CP\pm}K^+)}{\Gamma(B^- \rightarrow D^0K^-) + \Gamma(B^+ \rightarrow \bar{D}^0K^+)} \\ = 1 + r_B^2 \pm 2r_B \cos(\delta_B) \cos(\gamma), \quad (77.12a)$$

$$A_{CP\pm} = \frac{\Gamma(B^- \rightarrow D_{CP\pm}K^-) - \Gamma(B^+ \rightarrow D_{CP\pm}K^+)}{\Gamma(B^- \rightarrow D_{CP\pm}K^-) + \Gamma(B^+ \rightarrow D_{CP\pm}K^+)} \\ = \frac{\pm 2r_B \sin(\delta_B) \sin(\gamma)}{1 + r_B^2 \pm 2r_B \cos(\delta_B) \cos(\gamma)}. \quad (77.12b)$$

These relations assume the absence of direct CP violation in the charm system; experimentally allowed deviations from this assumption are too small to cause a significant bias on γ [7, 45]. It is convenient to determine the $R_{CP\pm}$ quantities through a double ratio, normalizing to $B^+ \rightarrow D\pi^+$ decays involving the same final states, since this cancels potential sources of systematic uncertainty due to the branching fractions of the D decays that are used; small possible effects of CP violation in $B^+ \rightarrow D\pi^+$ decays are a source of systematic uncertainty in this procedure. The GLW method can be extended to include final states that are almost CP -eigenstates [46], as is the case in $D \rightarrow \pi^+\pi^-\pi^0$ and $D \rightarrow K^+K^-\pi^0$ decays, via inclusion of a factor encoding the fraction of CP -even (or CP -odd) content, F_{\pm} , which dilutes the sensitivity to γ by reducing the size of the interference terms (the terms linear with r_B) in Eq. (77.12).

For other D decays, the ratio of amplitudes for the D^0 and \bar{D}^0 decays to the final state of interest has to be accounted for in the formalism. The ADS method [47, 48] uses D decays to final states such as $K^\mp\pi^\pm$, which involve interference between Cabibbo-favoured (CF) and doubly-Cabibbo-suppressed (DCS) transitions. The observables in this case are

$$A_{\text{ADS}} = \frac{\Gamma(B^- \rightarrow [K^+\pi^-]_D K^-) - \Gamma(B^+ \rightarrow [K^-\pi^+]_D K^+)}{\Gamma(B^- \rightarrow [K^+\pi^-]_D K^-) + \Gamma(B^+ \rightarrow [K^-\pi^+]_D K^+)} \\ = \frac{2r_B r_D \sin(\delta_B + \delta_D) \sin(\gamma)}{r_B^2 + r_D^2 + 2r_B r_D \cos(\delta_B + \delta_D) \cos(\gamma)}, \quad (77.13a)$$

$$R_{\text{ADS}} = \frac{\Gamma(B^- \rightarrow [K^+\pi^-]_D K^-) + \Gamma(B^+ \rightarrow [K^-\pi^+]_D K^+)}{\Gamma(B^- \rightarrow [K^-\pi^+]_D K^-) + \Gamma(B^+ \rightarrow [K^+\pi^-]_D K^+)} \\ = r_B^2 + r_D^2 + 2r_B r_D \cos(\delta_B + \delta_D) \cos(\gamma), \quad (77.13b)$$

where r_D and δ_D are the amplitude magnitude ratio and strong phase difference between the CF and DCS D decay. An alternative pair of observables, (R_-, R_+) , is also sometimes used, where R_- (R_+) is the ratio of decay rates between the suppressed and favoured transitions for B^- (B^+) decays. The R_- and R_+ observables are statistically independent, while A_{ADS} and R_{ADS} are not (in particular, the uncertainty on A_{ADS} depends on the central value of R_{ADS}). However, the pair (R_-, R_+) has more correlated sources of systematic uncertainty compared to $(A_{\text{ADS}}, R_{\text{ADS}})$. The observables of Eq. (77.13) are therefore usually preferred once a significant signal is established. The ADS method can also be extended to include decays to multibody final states, such as $D \rightarrow K^\pm\pi^\mp\pi^0$ and $D \rightarrow K^\pm\pi^\mp\pi^+\pi^-$, by addition of a coherence factor [49] which appears in the interference terms of Eq. (77.13) and accounts for dilution of the sensitivity due to variation of the decay amplitude across the phase space of the final state. A similar method can be used for singly Cabibbo-suppressed D decays to non- CP eigenstates such as K^*K [50].

For D decays to multibody self-conjugate final states (BPGGSZ method [51, 52]), such as $D \rightarrow K_S^0\pi^+\pi^-$, one can write the partial decay rate as a function of the position in the phase space in terms of the ‘‘Cartesian parameters’’ $x_\pm + iy_\pm = r_B e^{i(\delta_B \pm \gamma)}$:

$$d\Gamma(B^\pm \rightarrow [K_S^0\pi^+\pi^-]_D K^\pm) = A_{(\mp, \pm)}^2 + r_B^2 A_{(\pm, \mp)}^2 \\ + 2A_{(\pm, \mp)} A_{(\mp, \pm)} [x_\pm c_{D(\pm, \mp)} + y_\pm s_{D(\pm, \mp)}], \quad (77.14)$$

where the notation $(+, -)$ is shorthand for the dependence on the Dalitz-plot position — the squared invariant masses of $K_S^0\pi^+$ and $K_S^0\pi^-$ combinations, respectively. The quantities $A_{(+, -)}$ and $A_{(-, +)}$ represent the magnitudes of the D^0 and \bar{D}^0 decay amplitudes at the position $(+, -)$ and are interchangeable with their CP conjugate amplitudes because CP conservation is assumed in the D decay (i.e. $A_{(-, +)} = \bar{A}_{(+, -)}$). The quantities $c_{D(\pm, \mp)}$ and $s_{D(\pm, \mp)}$ are the cosine and sine of the strong phase difference, $\delta_{D(+, -)} = \arg(\bar{A}_{(+, -)}) - \arg(A_{(+, -)})$, between the \bar{D}^0 and D^0 amplitudes. These quantities can be determined from an amplitude model, although this leads to a hard-to-quantify systematic uncertainty associated to the composition of the model. An alternative, ‘‘model-independent’’, approach involves dividing the phase space into appropriate bins. In this case, the analysis benefits from external input on the values of c_D and s_D integrated over each bin. Measurements of these external parameters have been performed for the $D \rightarrow K_S^0\pi^+\pi^-$ decay by the CLEO-c and BES-III collaborations [53–56]. The use of common input values for these parameters in model-independent determinations of γ with the BPGGSZ method by different experiments is a source of correlation between experiments that is currently negligible but will become more significant as the available B meson data samples increase in size.

The discussion above refers to $B^+ \rightarrow DK^+$ decays, but analogous measurements can be made also for additional channels such as $B^+ \rightarrow D^*K^+$ (with $D^* \rightarrow D\pi^0, D\gamma$) and $B^+ \rightarrow DK^{*+}$ (with $K^{*+} \rightarrow K_S^0\pi^+, K^+\pi^0$). In the limit that these can be treated purely as two-body decays, the expressions for $B^+ \rightarrow DK^+$ are modified only by ensuring the r_B and δ_B parameters are specific to each B decay. Moreover, for $B^+ \rightarrow D^*K^+$ decays an effective

shift of the strong phase by π between $D^* \rightarrow D\pi^0$ and $D\gamma$ decays [57] has to be taken into account. In case the finite width of the decaying resonance is non-negligible, as is the case for the $K^*(892)$ state, additional amplitudes can contribute leading to a dilution of the sensitivity, which can be accounted for in the formalism through the introduction of a relevant coherence factor. For the $B^0 \rightarrow DK^{*0}$ decay, full amplitude analysis of the $B^0 \rightarrow DK^+\pi^-$ Dalitz plot provides additional sensitivity compared to the quasi-two-body approach [58, 59].

It is also possible to measure γ using decay-time-dependent analysis of the B_s^0 meson [60]. The weak phase arising in the interference between direct decay of $B_s^0 \rightarrow D_s^\mp K^\pm$ and decay via mixing is $(\gamma - 2\beta_s)$, where β_s is the angle associated with $B_s^0 \rightarrow J/\psi\phi$ decays in a similar way to the relation between β and $B^0 \rightarrow J/\psi K_S^0$ decays described in Sec. 77.2. Sufficient information can be obtained from the tagged, decay-time-dependent rates of $B_s^0 \rightarrow D_s^\mp K^\pm$ decays that this weak phase can be determined, up to an ambiguity, together with the strong phase difference between, and the ratio of the magnitudes of, the suppressed and favoured amplitudes. Since β_s is known to good precision [8], measurements of the decay-time-dependent CP -asymmetry observables in $B_s^0 \rightarrow D_s^\mp K^\pm$ decays can be used to infer constraints on γ . Alternatively, if effects of penguin pollution in $B_s^0 \rightarrow J/\psi\phi$ decays [17, 18] are a concern, as they will become in the future, results from the $B_s^0 \rightarrow D_s^\mp K^\pm$ mode can be combined with an independent precise measurement of γ to provide a penguin-free determination of β_s .

The average for γ requires a non-trivial combination due the complicated relations between the observables and the physics parameters of interest, such as in Eqs. (77.12), (77.13) and (77.14). Moreover, hadronic parameters such as r_B and δ_B defined in Eq. (77.11) are common to all different D decay modes (but differ for each B decay mode). Thus, it is not correct to simply average results for γ obtained by different experiments or in different channels. Instead, measurements of rate asymmetries, rate ratios and the Cartesian parameters are taken as inputs to the combination, from which results are obtained not only for γ but also for the hadronic parameters. Independent measurements of auxiliary parameters such as r_D and δ_D are also treated as inputs to the combination. In some cases the B decay data can help to reduce uncertainties on these auxiliary parameters and therefore a simultaneous fit of charm and beauty data can provide stronger constraints [61]; this approach however is not currently used for the world average.

The precision to which γ can be measured with a particular B decay is approximately inversely proportional to the value of r_B . Thus, results from channels with smaller yields but larger values of r_B , such as $B^0 \rightarrow DK^{*0}$ and $B_s^0 \rightarrow D_s^\mp K^\pm$ ($r_B \approx 0.3$ – 0.4), can have a significant impact on the world average and are included in the combination. By contrast the $B^+ \rightarrow D\pi^+$ mode, for which large samples are available but $r_B \approx 0.005$, has little impact and is also more sensitive to potential systematic biases; hence it is not included. The sensitivity of the world average at present is dominated by results from $B^+ \rightarrow DK^+$, where $r_B \approx 0.1$, in particular results with the GLW [62], ADS [62] and BPGGSZ [63] methods.

The world average obtained for the angle γ , obtained by combining results from $B^+ \rightarrow DK^+$, D^*K^+ , DK^{*+} , $DK^+\pi^+\pi^-$, $B^0 \rightarrow DK^+\pi^-$, $B_s^0 \rightarrow D_s^\mp K^\pm$ and $B_s^0 \rightarrow D_s^\mp K^\pm\pi^+\pi^-$ decays, is [4]

$$\gamma = (65.9_{-3.5}^{+3.3})^\circ, \quad (77.15)$$

where the quoted uncertainty is at the 68.3% CL.

Effects related to charm and kaon mixing and CP violation are generally negligible at the current level of precision, in particular for modes with $r_B \gtrsim 0.1$. An exception is that a dependence of the selection efficiency on the charm decay time can induce a dependence of the observables on charm mixing parameters [64]. Such effects can be important at hadron collider experiments such as LHCb, but can be and are corrected for. Interactions of neutral kaons with detector material can also cause a bias in determination of γ from modes with low values of r_B [65], such as the BPGGSZ method applied to $B^+ \rightarrow D\pi^+$, but are negligible in modes with larger r_B values. A further subtlety is that the

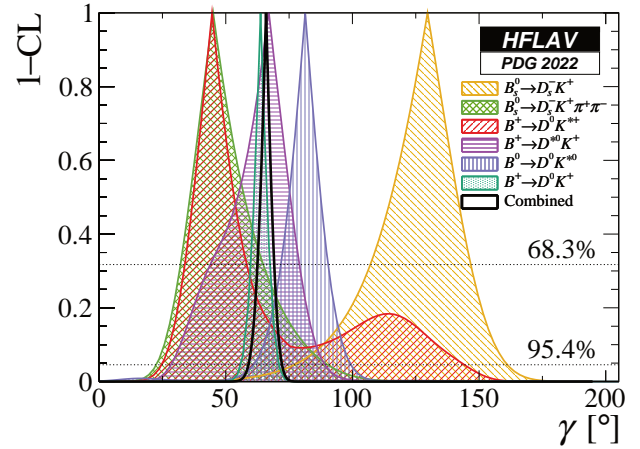


Figure 77.3: World average of $\gamma \equiv \phi_3$, as well as contributions from individual modes, in terms of 1–CL.

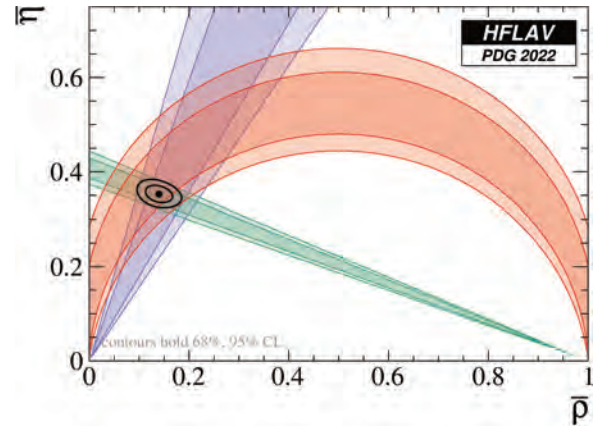


Figure 77.4: Constraints from the measurements of the angles of the CKM unitarity triangle in the $(\bar{\rho}, \bar{\eta})$ plane.

identification of the weak phase between suppressed and favoured amplitudes in $B \rightarrow DK$ decays with γ , as defined in Eq. (77.2), assumes that the 2×2 submatrix of the CKM matrix is real, *i.e.* that $\arg[V_{ud}V_{us}^*/(V_{cd}V_{cs}^*)] = 0$. This is true to an excellent approximation in the Standard Model, and is known experimentally from independent studies of the charm system [45] to contribute negligible bias to current measurements. Nonetheless, in future it will be possible to test directly this assumption by comparing the value of γ obtained from the $B \rightarrow DK$ and $B \rightarrow D\pi$ systems.

Effects from correlated uncertainties between amplitude models and strong phase differences in charm decays are negligible and are not explicitly accounted for in the combination, nor are effects related to charm and kaon mixing and CP violation. This world average, together with results split by decay mode, is shown in Fig. 77.3. The combination has a total of 154 experimental inputs from which 35 parameters are determined, an overall χ^2 of 123.9, which corresponds to a p-value of 36% indicating good agreement between the inputs. The combination gives a single solution for γ in $[0^\circ, 180^\circ]$, but an ambiguous solution exists at $\gamma \Leftrightarrow \gamma + 180^\circ$.

77.5 Summary

Experimental progress has resulted in all three angles of the CKM unitarity triangle being measured with good accuracy, with β known to subdegree precision and both α and γ known to better than 5° . The constraints from these three measurements in the $(\bar{\rho}, \bar{\eta})$ plane are shown in Fig. 77.4; further discussion and comparison with constraints from independent measurements can be found in Ref. [6]. The determinations of all three angles remain statistically limited, but it will be a challenge for experiments to

ensure that this remains the case as the precision improves. Consequently, the correct treatment of sources of correlation between the measurements that go into the world average combinations is becoming increasingly important.

References

- [1] N. Cabibbo, Phys. Rev. Lett. **10**, 531 (1963).
- [2] M. Kobayashi and T. Maskawa, Prog. Theor. Phys. **49**, 652 (1973).
- [3] C. Jarlskog, Phys. Rev. Lett. **55**, 1039 (1985).
- [4] Y. S. Amhis *et al.* (HFLAV), Eur. Phys. J. C **81**, 3, 226 (2021), updated averages are available online at hflav.web.cern.ch, [arXiv:1909.12524].
- [5] See the review on “Semileptonic b -Hadron Decays, Determination of V_{cb} , V_{ub} ” in this *Review*.
- [6] See the review on “Cabibbo-Kobayashi-Maskawa Mixing Matrix,” in this *Review*.
- [7] See the review on “ CP Violation in the Quark Sector,” in this *Review*.
- [8] See the review on “ $B^0-\bar{B}^0$ Mixing” in this *Review*.
- [9] A. Carter and A. Sanda, Phys. Rev. **D23**, 1567 (1981).
- [10] I. Bigi and A. Sanda, Nucl. Phys. **B193**, 85 (1981).
- [11] O. Long *et al.*, Phys. Rev. **D68**, 034010 (2003), [hep-ex/0303030].
- [12] B. Aubert *et al.* (BaBar), Phys. Rev. **D79**, 072009 (2009), [arXiv:0902.1708].
- [13] I. Adachi *et al.*, Phys. Rev. Lett. **108**, 171802 (2012), [arXiv:1201.4643].
- [14] R. Aaij *et al.* (LHCb), Phys. Rev. Lett. **115**, 031601 (2015), [arXiv:1503.07089].
- [15] H.-n. Li and S. Mishima, JHEP **03**, 009 (2007), [hep-ph/0610120].
- [16] M. Jung, Phys. Rev. **D86**, 053008 (2012), [arXiv:1206.2050].
- [17] K. De Bruyn and R. Fleischer, JHEP **1503**, 145 (2015), [arXiv:1412.6834].
- [18] P. Frings, U. Nierste and M. Wiebusch, Phys. Rev. Lett. **115**, 6, 061802 (2015), [arXiv:1503.00859].
- [19] M. Ciuchini, M. Pierini and L. Silvestrini, Phys. Rev. Lett. **95**, 221804 (2005), [hep-ph/0507290].
- [20] S. Faller *et al.*, Phys. Rev. **D79**, 014030 (2009), [arXiv:0809.0842].
- [21] Z. Ligeti and D. Robinson, Phys. Rev. Lett. **115**, 251801 (2015), [arXiv:1507.06671].
- [22] I. Adachi *et al.* (BaBar, Belle), Phys. Rev. Lett. **121**, 261801 (2018), [arXiv:1804.06152].
- [23] I. Adachi *et al.* (BaBar, Belle), Phys. Rev. **D98**, 112012 (2018), [arXiv:1804.06153].
- [24] M. Antonelli *et al.*, Phys. Rept. **494**, 197 (2010), [arXiv:0907.5386].
- [25] M. Gronau and D. London, Phys. Rev. Lett. **65**, 3381 (1990).
- [26] R. Aaij *et al.* (LHCb), Phys. Rev. **D98**, 032004 (2018), [arXiv:1805.06759].
- [27] R. Aaij *et al.* (LHCb), JHEP **03**, 075 (2021), [arXiv:2012.05319].
- [28] J. P. Lees *et al.* (BaBar), Phys. Rev. **D87**, 052009 (2013), [arXiv:1206.3525].
- [29] I. Adachi *et al.* (Belle), Phys. Rev. **D88**, 092003 (2013), [arXiv:1302.0551].
- [30] J. Charles *et al.*, Eur. Phys. J. **C77**, 574 (2017), [arXiv:1705.02981].
- [31] T. Julius *et al.* (Belle), Phys. Rev. **D96**, 032007 (2017), [arXiv:1705.02083].
- [32] B. Aubert *et al.* (BaBar), Phys. Rev. **D76**, 052007 (2007), [arXiv:0705.2157].
- [33] P. Vanhoefer *et al.* (Belle), Phys. Rev. **D93**, 032010 (2016), [Addendum *ibid.*: **D94** 099903 (2016)], [arXiv:1510.01245].
- [34] B. Aubert *et al.* (BaBar), Phys. Rev. **D78**, 071104 (2008), [arXiv:0807.4977].
- [35] A. E. Snyder and H. R. Quinn, Phys. Rev. **D48**, 2139 (1993).
- [36] J. P. Lees *et al.* (BaBar), Phys. Rev. **D88**, 012003 (2013), [arXiv:1304.3503].
- [37] A. Kusaka *et al.* (Belle), Phys. Rev. Lett. **98**, 221602 (2007), [hep-ex/0701015].
- [38] A. Kusaka *et al.* (Belle), Phys. Rev. **D77**, 072001 (2008), [arXiv:0710.4974].
- [39] M. Gronau and J. Zupan, Phys. Rev. **D71**, 074017 (2005), [hep-ph/0502139].
- [40] S. Gardner, Phys. Rev. **D72**, 034015 (2005), [hep-ph/0505071].
- [41] A. Falk *et al.*, Phys. Rev. **D69**, 011502 (2004), [hep-ph/0310242].
- [42] J. Brod and J. Zupan, JHEP **01**, 051 (2014), [arXiv:1308.5663].
- [43] M. Gronau and D. London, Phys. Lett. **B253**, 483 (1991).
- [44] M. Gronau and D. Wyler, Phys. Lett. **B265**, 172 (1991).
- [45] See the review on “ $D^0-\bar{D}^0$ Mixing” in this *Review*.
- [46] M. Nayak *et al.*, Phys. Lett. **B740**, 1 (2015), [arXiv:1410.3964].
- [47] D. Atwood, I. Dunietz and A. Soni, Phys. Rev. Lett. **78**, 3257 (1997), [hep-ph/9612433].
- [48] D. Atwood, I. Dunietz and A. Soni, Phys. Rev. **D63**, 036005 (2001), [hep-ph/0008090].
- [49] D. Atwood and A. Soni, Phys. Rev. **D68**, 033003 (2003), [hep-ph/0304085].
- [50] Y. Grossman, Z. Ligeti and A. Soffer, Phys. Rev. **D67**, 071301 (2003), [hep-ph/0210433].
- [51] A. Giri *et al.*, Phys. Rev. **D68**, 054018 (2003), [hep-ph/0303187].
- [52] A. Bondar, *Proceedings of BINP special analysis meeting on Dalitz analysis*, 24-26 Sep. 2002, unpublished.
- [53] R. Briere *et al.* (CLEO), Phys. Rev. **D80**, 032002 (2009), [arXiv:0903.1681].
- [54] J. Libby *et al.* (CLEO), Phys. Rev. **D82**, 112006 (2010), [arXiv:1010.2817].
- [55] M. Ablikim *et al.* (BESIII), Phys. Rev. Lett. **124**, 24, 241802 (2020), [arXiv:2002.12791].
- [56] M. Ablikim *et al.* (BESIII), Phys. Rev. D **101**, 11, 112002 (2020), [arXiv:2003.00091].
- [57] A. Bondar and T. Gershon, Phys. Rev. **D70**, 091503 (2004), [hep-ph/0409281].
- [58] T. Gershon, Phys. Rev. **D79**, 051301 (2009), [arXiv:0810.2706].
- [59] T. Gershon and M. Williams, Phys. Rev. **D80**, 092002 (2009), [arXiv:0909.1495].
- [60] R. Aleksan, I. Dunietz and B. Kayser, Z. Phys. **C54**, 653 (1992).
- [61] R. Aaij *et al.* (LHCb), JHEP **12**, 141 (2021), [arXiv:2110.02350].
- [62] R. Aaij *et al.* (LHCb), JHEP **04**, 081 (2021), [arXiv:2012.09903].
- [63] R. Aaij *et al.* (LHCb), JHEP **02**, 169 (2021), [arXiv:2010.08483].
- [64] M. Rama, Phys. Rev. **D89**, 014021 (2014), [arXiv:1307.4384].
- [65] M. Bjørn and S. Malde, JHEP **07**, 106 (2019), [arXiv:1904.01129].

78. Spectroscopy of Mesons Containing Two Heavy Quarks

Revised August 2021 by S. Eidelman (Budker Inst., Novosibirsk; Novosibirsk U.), J. J. Hernández-Rey (IFIC, Valencia), C. Lourenço (CERN), R.E. Mitchell (Indiana U.), S. Navas (Granada U.) and C. Patrignani (Bologna U.).

A golden age for heavy quarkonium physics dawned at the turn of this century, initiated by the confluence of exciting advances in quantum chromodynamics (QCD) and an explosion of related experimental activity. The subsequent broad spectrum of breakthroughs, surprises, and continuing puzzles had not been anticipated. Indeed, CLEO-c, BESIII, and the B-factories, later joined by ATLAS, CMS and LHCb, have made a series of groundbreaking observations. For an extensive presentation of the status of heavy quarkonium physics, the reader is referred to several reviews [1–7]. This note focuses on experimental developments in heavy quarkonium spectroscopy with very few theoretical comments. Possible theoretical interpretations of the states not predicted by the quark model are presented in the review “Heavy non- $q\bar{q}$ mesons.” Note that in this review we follow the new naming scheme for hadrons (see the review “Naming scheme for hadrons” in the current edition).

This review covers states discovered since 2003, the year that marked the unexpected discovery of the $X(3872)$ [8]. The $X(3872)$, now called $\chi_{c1}(3872)$, was the first of the mesons containing two heavy quarks that could not be easily accommodated by the $q\bar{q}$ quark model. Its discovery was a watershed event in meson spectroscopy. In earlier versions of this write-up the particles were sorted according to an assumed *conventional* or *unconventional* nature with respect to the quark model. However, since this classification is not always unambiguous, we here follow Ref. [9] and sort the states into three groups, namely states below (*cf.* Table 78.1), above (*cf.* Table 78.2), and near (*cf.* Table 78.3) the lowest open-flavor thresholds.

78.1 States Below Open-Flavor Threshold

Table 78.1 lists properties of recently observed heavy quarkonium states located below the lowest open-flavor thresholds. Those are expected to be (at least prominently) conventional quarkonia. The majority of charmonium ($c\bar{c}$) and bottomonium ($b\bar{b}$) states were established prior to 2003.

78.1.1 Charmonium

The $h_c(1P)$ is the 1^1P_1 charmonium state, the singlet partner of the long-known χ_{cJ} triplet 1^3P_J . After being firmly established in 2005 through the process $\psi(2S) \rightarrow \pi^0 h_c(1P)$ [10], it has since been studied extensively by BESIII using large samples of $\psi(2S)$ decays. Exclusive hadronic decays of the $h_c(1P)$, strongly suppressed relative to the dominant radiative transition $h_c(1P) \rightarrow \gamma \eta_c(1S)$, were first observed in 2019 [11] and 2020 [12].

Belle reported an observation of the $\psi_2(1D)$ decaying to $\gamma \chi_{c1}$ with J^{PC} presumed to be 2^{--} [13]. This state is listed in Table 78.1 as $\psi_2(3823)$. Its existence was confirmed with high significance by BESIII [14]. While the negative C-parity is indeed established by its observed decay channel, the assignment of $J = 2$ was done by matching to the closest quark model state (1^3D_2) and requires experimental confirmation.

The 1^1D_2 state, or the $\eta_{c2}(1D)$, with a mass expected near 3820 MeV, has not yet been observed. Recently Belle performed a search in $B \rightarrow \eta_{c2}(1D)K(\pi)$ decays in the mass range 3795–3845 MeV and found no signal [15]. Thus, the $\eta_{c2}(1D)$ remains the only unobserved conventional charmonium state that does not have open-charm decays.

78.1.2 Bottomonium

The ground state of bottomonium, $\eta_b(1S)$, is well established. After the initial reports from BaBar in radiative decays of the $\Upsilon(3S)$ (observation) [16] and $\Upsilon(2S)$ (evidence) [17], Belle confirmed the existence of the $\eta_b(1S)$ with more than 5σ significance in radiative decays of the newly discovered $h_b(1P)$ [18, 19] and $h_b(2P)$ [18] (see next paragraph), as well as in $\Upsilon(2S)$ radiative decays [20]. Belle has also reported strong evidence for the $\eta_b(2S)$ [18], but it still needs confirmation at the 5σ level. Note that there are hints of tension in the $\eta_b(1S)$ mass as measured in radiative M1 and E1 transitions. In the M1 transition $\Upsilon(2S) \rightarrow$

$\gamma \eta_b(1S)$ Belle measures a mass of $9394.8^{+2.7+4.5}_{-3.1-2.7}$ MeV/ c^2 [20], while in the E1 transitions $h_b(1P, 2P) \rightarrow \gamma \eta_b(1S)$ Belle measures $9402.4 \pm 1.5 \pm 1.8$ MeV/ c^2 [18]. This tension may point to an incomplete understanding of the $\eta_b(1S)$ lineshape in different production mechanisms.

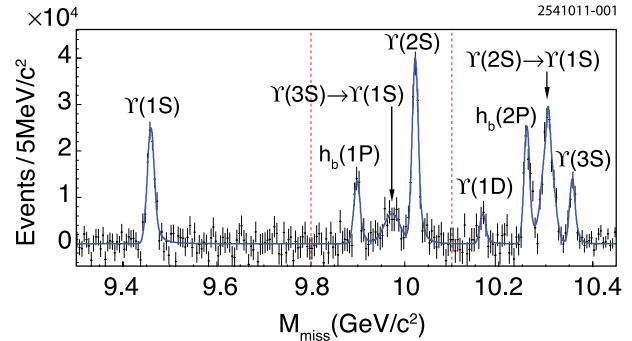


Figure 78.1: From Belle [21], the mass recoiling against $\pi^+\pi^-$ pairs, M_{miss} , in e^+e^- collision data taken near the peak of the $\Upsilon(10860)$ (points with error bars). The smooth combinatorial and $K_S^0 \rightarrow \pi^+\pi^-$ background contributions have been subtracted. The fit to the various labeled signal contributions is overlaid (curve).

The $h_b(1P)$, the bottomonium counterpart of the $h_c(1P)$, and the next excited state, the $h_b(2P)$, were simultaneously discovered by Belle using dipion transitions from the $\Upsilon(10860)$ [21] (Fig. 78.1). The same analysis also showed the $\Upsilon_J(1D)$, the lowest-lying D -wave triplet of the $b\bar{b}$ system, but did not resolve the $J = 1, 2, 3$ components. The search for the $h_b(1P)$ was directly inspired by a CLEO result [22], which found a surprisingly copious production of $e^+e^- \rightarrow \pi^+\pi^-h_c(1P)$ as well as an indication that $\psi(4230) \rightarrow \pi^+\pi^-h_c(1P)$ occurs at a comparable rate with the signature mode $\psi(4230) \rightarrow \pi^+\pi^-J/\psi(1S)$. The presence of $\Upsilon(nS)$ peaks in Fig. 78.1 at rates two orders of magnitude larger than expected, along with separate studies with exclusive decays $\Upsilon(nS) \rightarrow \mu^+\mu^-$, allow precise calibration of the $\pi^+\pi^-$ recoil mass spectrum and very accurate measurements of the $h_b(1P)$ and $h_b(2P)$ masses. Both corresponding hyperfine splittings are consistent with zero within an uncertainty of about 1.5 MeV (lowered to 1.1 MeV for the $h_b(1P)$ in Ref. [23]). Belle later observed the transition $\Upsilon(4S) \rightarrow h_b(1P)\eta$ [19] and the corresponding 1P hyperfine splitting was also found to be compatible with zero at a similar precision level.

Just before Christmas 2011, ATLAS offered the world a beautiful gift, in the form of the discovery of the $\chi_b(3P)$ quarkonium state [24], observed by combining dimuons from $\Upsilon(1S)$ or $\Upsilon(2S)$ decays with photons emitted in the radiative $\chi_b(3P)$ decays (Fig. 78.2, bottom left panel). The new resonance, with a mass of $10530 \pm 5(\text{stat}) \pm 9(\text{syst})$ MeV, was soon confirmed by D0 [25]. Also LHCb observed the $\chi_b(3P)$ peak, using the full Run 1 event sample, corresponding to an integrated luminosity of 3 fb^{-1} [26] (Fig. 78.2, middle left panel). Finally, CMS used 80 fb^{-1} of 13 TeV pp collisions, collected in 2016 and 2017, to show two well-resolved $\chi_{b1}(3P)$ and $\chi_{b2}(3P)$ peaks [27], separated by a mass difference of $10.60 \pm 0.64(\text{stat}) \pm 0.17(\text{syst})$ MeV (Fig. 78.2, top left panel). The remarkable precision of the individual mass measurements, with relative uncertainties as small as 50 ppm, shows that the LHC experiments can provide important results in the field of hadron spectroscopy, especially in the case of heavy particles, which require very high collision energies and large event samples.

78.1.3 B_c System

The B_c^\pm family is quite special because these (charged) quarkonium states consist of two heavy quarks of different flavor. Among other interesting properties, this means that they cannot annihilate into gluons, the excited states only decaying to the pseudoscalar ground state, B_c^\pm , via electromagnetic and pionic transitions.

Table 78.1: New states below the open-flavor thresholds in the $c\bar{c}$, $b\bar{c}$, and $b\bar{b}$ regions, ordered by mass. Masses m and widths Γ represent the PDG21 weighted averages with statistical and systematic uncertainties added in quadrature. In the Production column, the state is always denoted by X . Ellipses (...) indicate inclusively selected event topologies, *i.e.*, additional particles not directly detected by experiment. A question mark (?) indicates an unmeasured value. The Discovery Year column gives the date of the first measurement cited. The Summary Table column indicates whether or not the state appears in the summary tables, usually requiring at least two independent experiments with significance of $>5\sigma$. Refer to the particle listings for references and further information.

PDG Name	Former Name(s)	m (MeV)	Γ (MeV)	$I^G(J^{PC})$	Production	Decay	Discovery Year	Summary Table
$h_c(1P)$		3525.38 ± 0.11	0.7 ± 0.35	$0^-(1^{+-})$	$\psi(2S) \rightarrow \pi^0 X$ $p\bar{p} \rightarrow X$	$\gamma\eta_c(1S)$ hadrons	2004	YES
$\psi_2(3823)$	$X(3823)$	3823.7 ± 0.5	< 5.2	$0^-(2^{--})$	$e^+e^- \rightarrow \pi\pi X$ $B \rightarrow KX$	(see listings) $\gamma\chi_{c1}(1P)$	2013	YES
B_c^+		6274.47 ± 0.32	stable	$0(0^-)$	$e^+e^- \rightarrow \pi^+\pi^- X$ $p\bar{p} \rightarrow X\dots$ $pp \rightarrow X\dots$	$\pi^+\pi^- J/\psi(1S)$ $\pi^+ J/\psi(1S)$ (see listings)	2007	YES
$B_c^+(2S)$		6871.2 ± 1.0	?	$0(0^-)$	$pp \rightarrow X\dots$	$B_c^+\pi^+\pi^-$	2014	YES
$\eta_b(1S)$		9398.7 ± 2.0	10^{+5}_{-4}	$0^+(0^{-+})$	$\Upsilon(2S, 3S) \rightarrow \gamma X$ $h_b(1P, 2P) \rightarrow \gamma X$	hadrons (see listings)	2008	YES
$h_b(1P)$		9899.3 ± 0.8	?	$0^-(1^{+-})$	$\Upsilon(10860) \rightarrow \pi^+\pi^- X$ $\Upsilon(3S) \rightarrow \pi^0 X$ $\Upsilon(4S) \rightarrow \eta X$ $Z_b(10610)^+ \rightarrow \pi^+ X$ $Z_b(10650)^+ \rightarrow \pi^+ X$	$\gamma\eta_b(1S)$	2011	YES
$\eta_b(2S)$		$9999.0^{+4.5}_{-4.0}$	< 24	$0^+(0^{-+})$	$h_b(2P) \rightarrow \gamma X$	hadrons	2012	NO
$\Upsilon_2(1D)$		10163.7 ± 1.4	?	$0^-(2^{--})$	$\Upsilon(3S) \rightarrow \gamma\gamma X$ $\Upsilon(10860) \rightarrow \pi^+\pi^- X$	$\gamma\gamma\Upsilon(1S)$ $\pi^+\pi^-\Upsilon(1S)$	2004	YES
$h_b(2P)$		10259.8 ± 1.2	?	$0^-(1^{+-})$	$\Upsilon(10860) \rightarrow \pi^+\pi^- X$ $Z_b(10610)^+ \rightarrow \pi^+ X$ $Z_b(10650)^+ \rightarrow \pi^+ X$	$\gamma\eta_b(1S, 2S)$	2011	YES
$\chi_{b1}(3P)$		10513.42 ± 0.67	?	$0^+(1^{++})$	$pp \rightarrow X\dots$	$\gamma\Upsilon(1S, 2S, 3S)$	2011	YES
$\chi_{b2}(3P)$		10524.02 ± 0.78	?	$0^+(2^{++})$	$pp \rightarrow X\dots$	$\gamma\Upsilon(3S)$	2011	YES

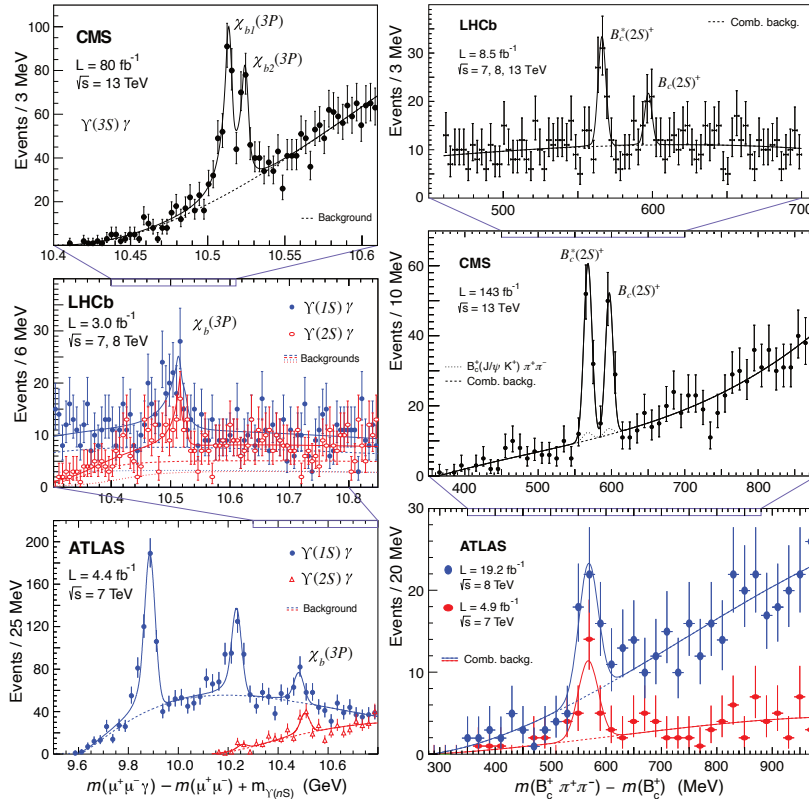


Figure 78.2: (Left Column) Invariant mass distributions measured by the ATLAS [24] (bottom), LHCb [26] (middle) and CMS [27] (top) experiments in their searches for the $\chi_b(3P)$ states through their radiative decays to one of the S-wave bottomonia. (Right Column) Invariant mass distributions measured by the ATLAS [28] (bottom), CMS [29] (middle) and LHCb [30] (top) experiments in their searches for B_c^\pm excited states decaying to the B_c^\pm ground state with the emission of two charged pions.

On the basis of an event sample collected in the Run 1 of the LHC, corresponding to an integrated luminosity of 24 fb^{-1} , adding the 7 and 8 TeV data, the ATLAS Collaboration observed a resonance in the $B_c^+ \pi^+ \pi^-$ invariant mass spectrum [28] (Fig. 78.2, bottom right panel). This peak, observed with a significance of 5.2 standard deviations and a mass of $6842 \pm 4(\text{stat}) \pm 5(\text{syst}) \text{ MeV}$, was immediately recognized as the $B_c(2S)^\pm$ state, the first radial excitation in the B_c^\pm family. Profiting from the much larger Run 2 event sample, collected in the 2015, 2016, 2017 and 2018 running periods and corresponding to 143 fb^{-1} of 13 TeV pp collisions, as well as from a measurement resolution of around 6 MeV, the CMS Collaboration could observe *two* well-resolved peaks, separated by $29.1 \pm 1.5(\text{stat}) \pm 0.7(\text{syst}) \text{ MeV}$ [29] (Fig. 78.2, middle right panel). The existence of two peaks, rather than a single one, is established with a significance of 6.5 standard deviations. The “right peak” has a mass of $6871.0 \pm 1.2(\text{stat}) \pm 0.8(\text{syst}) \pm 0.8(B_c^+)$ MeV, where the last term is the uncertainty in the B_c^+ mass, and is identified as the $B_c(2S)^\pm$ state, which decays directly to the B_c^\pm , emitting two (easy to detect) pions. The CMS observation, reported a couple of months after the end of the LHC Run 2, was soon followed by the corresponding LHCb result [30] (Fig. 78.2, top right panel), which confirmed the existence of the two states and reported a second measurement of the $B_c(2S)^\pm$ mass, $6872.1 \pm 1.3(\text{stat}) \pm 0.1(\text{syst}) \pm 0.8(B_c^+)$ MeV.

The “left peak” is interpreted as being the $B_c^*(2S)^\pm$ signal. It is observed at a mass lower than the real value because the experiments are unable to detect the low-energy photon emitted in the decay chain, $B_c^*(2S)^\pm \rightarrow B_c^{*\pm} \pi^+ \pi^-$ followed by $B_c^{*\pm} \rightarrow B_c^\pm \gamma$ (Fig. 78.3). Its energy, expected to be in the range 40–80 MeV, leads to a very small probability that the photon converts into an e^+e^- pair and the two electrons are reconstructed. The relative ordering of the two peaks is based on a generally-agreed assumption: the $M(B_c^{*\pm}) - M(B_c^\pm)$ mass difference is larger than the $M(B_c^*(2S)^\pm) - M(B_c(2S)^\pm)$ difference. Naturally, these observations provide evidence for the existence of the $B_c^*(1S)^\pm$ state. They also provide measurements of two interesting mass differences, between the masses of the pseudoscalar mesons, $M(B_c(2S)^\pm) - M(B_c(1S)^\pm) = 596.1 \text{ MeV}$, and of the vector mesons, $M(B_c^*(2S)^\pm) - M(B_c^*(1S)^\pm) = 567.0 \text{ MeV}$ (Fig. 78.3).

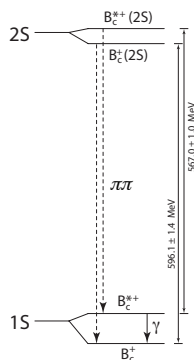


Figure 78.3: Diagram showing the decays mentioned in the text.

78.2 States Above Open-Flavor Threshold

Many states have been discovered both above and near the lowest open-flavor thresholds. They are displayed in Tables 78.2 and 78.3, respectively. With the exception of the $\psi_3(3842)$ and the tensor state located at 3930 MeV (now called $\chi_{c2}(3930)$), which have properties consistent with those expected for the $\psi_3(1^3D_3)$ and $\chi_{c2}(2^3P_2)$, respectively, none of these states can easily be assigned a place in the quark model spectrum of the charmonium or bottomonium families. At the same time, these states also have no universally accepted unconventional interpretation.

78.2.1 Charmonium

Using proton-proton collisions, LHCb observed a narrow state, the $\psi_3(3842)$ resonance, in the decay modes $\psi_3(3842) \rightarrow D^0 \bar{D}^0$

and $D^+ D^-$ [31]. The mass and width of this state are measured to be $3842.71 \pm 0.16 \pm 0.12 \text{ MeV}$ and $2.79 \pm 0.51 \pm 0.35 \text{ MeV}$, respectively. The observed mass and narrow width are consistent with the interpretation of the new state as the unobserved spin-3 $\psi_3(1^3D_3)$ charmonium. Accordingly, the state got the name $\psi_3(3842)$ in the listings, with the remark that the quantum numbers were fixed from the quark model and need to be confirmed.

The $\chi_{c2}(3930)$, which is a natural candidate for the $\chi_{c2}(2^3P_2)$ quark model state, was originally seen by Belle [32] and later confirmed by BaBar [33] in the $\gamma\gamma$ process $e^+e^- \rightarrow e^+e^- D \bar{D}$. This interpretation was strengthened by the more recent LHCb observation of the $\chi_{c2}(3930)$ alongside the $\psi_3(3842)$ in proton-proton collisions [31].

Unlike the $\chi_{c2}(2^3P_2)$, the identification of the $\chi_{c0}(2^3P_0)$ quark model state remains controversial. The original candidate was the $\chi_{c0}(3915)$, discovered by Belle in the $\gamma\gamma$ process $e^+e^- \rightarrow e^+e^- \omega J/\psi(1S)$ [34]. In a subsequent measurement by BaBar, its quantum numbers were determined to be $J^{PC} = 0^{++}$ [35]. However, its identification as the $\chi_{c0}(2^3P_0)$ quark model state was soon challenged [36, 37]. In addition, it was pointed out in Ref. [38] that if the assumption of helicity-2 dominance is abandoned and, instead, one allows for a sizeable helicity-0 component, a $J^{PC} = 2^{++}$ assignment is possible. This could imply that it is the same as the $\chi_{c2}(3930)$ —but to explain the large helicity-0 component a sizable portion of non- $q\bar{q}$ is necessary [38]. A more recent LHCb amplitude analysis of the process $B^+ \rightarrow D^+ D^- K^+$ finds distinct 0^{++} and 2^{++} components decaying to $D^+ D^-$ [39], which are currently identified in the listings as the $\chi_{c0}(3915)$ and $\chi_{c2}(3930)$, respectively.

An alternative candidate for the $\chi_{c0}(2^3P_0)$ (here referred to as the $\chi_{c0}(3860)$) was reported in Ref. [40] with properties more consistent with expectation: its mass is close to the potential model expectations, it decays to $D \bar{D}$, and the preferred quantum numbers are $J^{PC} = 0^{++}$ (this hypothesis is favored over the 2^{++} one with a 2.5σ significance).

In the excited vector charmonium spectrum, the $\psi(4040)$, $\psi(4160)$, and $\psi(4415)$ are prominent in the inclusive e^+e^- hadronic cross section and are naturally identified as the 3^3S_1 , 2^3D_1 , and 4^3S_1 $c\bar{c}$ quark model states, respectively. In addition to these long-established states, however, another set of mesons has been found as peaks in exclusive e^+e^- cross sections. Unlike conventional vector charmonia, they do not appear in the inclusive hadronic cross section and they apparently do not decay to $D \bar{D}$. The PDG summary table currently lists the $\psi(4230)$, $\psi(4360)$, and $\psi(4660)$ within this category. The first of these to be discovered was originally known as the $Y(4260)$ (now the $\psi(4230)$), seen by BaBar [41] and Belle [42, 43] in $e^+e^- \rightarrow \pi^+ \pi^- J/\psi(1S)$ using initial state radiation. In a more recent high-statistics scan of $e^+e^- \rightarrow \pi^+ \pi^- J/\psi(1S)$, BESIII demonstrated that the lineshape in this mass range is highly non-trivial [44]. The latter observation was interpreted by the authors as the presence of two states. However, this lineshape is also consistent with other possible interpretations, such as one assuming a molecular structure for the $\psi(4230)$ [45]. The data of Ref. [44] also called for a significant downward shift of the mass of what was originally called the $Y(4260)$, making it consistent with peaks in other exclusive cross sections, such as $h_c(1P)\pi\pi$ [46]. We thus merged the original $Y(4260)$ (or, more formally, the $\psi(4260)$) with the $\psi(4230)$ in the listings.

BESIII observed the $\chi_{c1}(3872)$, also known as $X(3872)$, in $e^+e^- \rightarrow \gamma \chi_{c1}(3872)$ in the $\psi(4230)$ mass range [47], which could allow for additional insight into the structure of both states (see the review on heavy non- $q\bar{q}$ mesons). BESIII also performed a recent study of the process $e^+e^- \rightarrow \pi^+ \pi^- \psi(2S)$ and found evidence for a lower mass state, possibly the $\psi(4230)$, in addition to the more dominant $\psi(4360)$ [48].

Note that the data of Ref. [44] does not show any indication of the $Y(4008)$ reported by Belle; the data in this region can either be fit with a non-resonant background component or a much wider resonance at lower mass. Also the analysis of the $Y(4008)$ region in Ref. [49] indicates a wide resonance.

Table 78.2: As in Table 78.1, but for new states above the first open-flavor thresholds in the $c\bar{c}$ and $b\bar{b}$ regions, ordered by mass.

PDG Name	Former Name(s)	m (MeV)	Γ (MeV)	$I^G(J^{PC})$	Production	Decay	Discovery Year	Summary Table
ψ_3 (3842)		3842.71 ± 0.20	2.79 ± 0.62	$0^-(3^{--})^*$	$pp \rightarrow X\dots$	$D\bar{D}$	2019	YES
χ_{c0} (3860)		3862^{+48}_{-35}	201^{+177}_{-106}	$0^+(0^{++})$	$e^+e^- \rightarrow J/\psi(1S)X$	$D\bar{D}$	2017	NO
χ_{c0} (3915)	X (3915), Y (3940)	3921.7 ± 1.8	18.8 ± 3.5	$0^+(0/2^{++})$	$B \rightarrow KX$	$\omega J/\psi(1S)$	2004	YES
χ_{c2} (3930)	$\chi_{c2}(2P)$, Z (3930)	3922.5 ± 1.0	35.2 ± 2.2	$0^+(2^{++})$	$e^+e^- \rightarrow e^+e^-X$	$D\bar{D}$	2005	YES
X (3940)		3942^{+9}_{-8}	37^{+27}_{-17}	$??(???)$	$e^+e^- \rightarrow J/\psi(1S)X$	$D\bar{D}^*$	2007	NO
$X(4050)^\pm$	Z_1 (4050)	4051^{+24}_{-43}	82^{+51}_{-28}	$1^-(??^+)$	$\bar{B}^0 \rightarrow K^-X$	$\pi^+\chi_{c1}(1P)$	2008	NO
$X(4055)^\pm$	Z_c (4055)	4054 ± 3	45 ± 13	$1^+(??^-)$	$e^+e^- \rightarrow \pi^-X$	$\pi^+\psi(2S)$	2015	NO
$X(4100)^\pm$		4096^{+27}_{-30}	152^{+83}_{-68}	$1^-(???)$	$\bar{B}^0 \rightarrow K^-X$	$\pi^+\eta_c(1S)$	2018	NO
χ_{c1} (4140)	Y (4140)	4146.5 ± 3.0	19^{+7}_{-5}	$0^+(1^{++})$	$B^+ \rightarrow K^+X$	$\phi J/\psi(1S)$	2009	YES
X (4160)		4156^{+29}_{-25}	139^{+113}_{-65}	$??(???)$	$e^+e^- \rightarrow J/\psi(1S)X$	$D^*\bar{D}^*$	2007	NO
Z_c (4200)		4196^{+35}_{-32}	370^{+99}_{-149}	$1^+(1^{+-})$	$\bar{B}^0 \rightarrow K^-X$	$J/\psi(1S)\pi^+$	2014	NO
ψ (4230)	Y (4230) Y (4260)	4222.7 ± 2.6	49 ± 8	$0^-(1^{--})$	$e^+e^- \rightarrow X$	$\pi^+\pi^-J/\psi(1S)$ $\omega\chi_{c0}(1P)$ $\pi^+\pi^-h_c(1P)$ (see listings)	2015	YES
R_{c0} (4240)	Z_c (4240)	4239^{+48}_{-21}	220^{+118}_{-88}	$1^+(0^{--})$	$\bar{B}^0 \rightarrow K^-X$	$\pi^+\psi(2S)$	2014	NO
$X(4250)^\pm$	Z_2 (4250)	4248^{+185}_{-45}	177^{+321}_{-72}	$1^-(??^+)$	$\bar{B}^0 \rightarrow K^-X$	$\pi^+\chi_{c1}(1P)$	2008	NO
χ_{c1} (4274)	Y (4274)	4286^{+8}_{-9}	51 ± 7	$0^+(1^{++})$	$B^+ \rightarrow K^+X$	$\phi J/\psi(1S)$	2011	YES
X (4350)		$4350.6^{+4.7}_{-5.1}$	13^{+18}_{-10}	$0^+(??^+)$	$e^+e^- \rightarrow e^+e^-X$	$\phi J/\psi(1S)$	2009	NO
ψ (4360)	Y (4360)	4372 ± 9	115 ± 13	$0^-(1^{--})$	$e^+e^- \rightarrow X$	$\pi^+\pi^-\psi(2S)$ $\pi^+\pi^-J/\psi(1S)$	2007	YES
Z_c (4430)		4478^{+15}_{-18}	181 ± 31	$1^+(1^{+-})$	$\bar{B}^0 \rightarrow K^-X$	$\pi^+\psi(2S)$ $\pi^+J/\psi(1S)$	2007	YES
χ_{c0} (4500)	X (4500)	4474 ± 4	77^{+12}_{-10}	$0^+(0^{++})$	$B^+ \rightarrow K^+X$	$\phi J/\psi(1S)$	2017	NO
X (4630)		4626^{+24}_{-111}	174^{+137}_{-78}	$0^+(??^+)$	$B^+ \rightarrow K^+X$	$\phi J/\psi(1S)$	2021	NO
ψ (4660)	Y (4660), X (4630)	4630 ± 6	72^{+14}_{-12}	$0^-(1^{--})$	$e^+e^- \rightarrow X$	$\pi^+\pi^-\psi(2S)$ $A_c^+\bar{A}_c^-$ $D_s^+D_{s1}(2536)$	2007	YES
χ_{c1} (4685)		4684^{+15}_{-17}	126^{+40}_{-44}	$0^+(1^{++})$	$B^+ \rightarrow K^+X$	$\phi J/\psi(1S)$	2021	NO
χ_{c0} (4700)	X (4700)	4694^{+16}_{-5}	87^{+18}_{-10}	$0^+(0^{++})$	$B^+ \rightarrow K^+X$	$\phi J/\psi(1S)$	2017	NO
Υ (10753)		$10752.7^{+5.9}_{-6.0}$	36^{+18}_{-12}	$??(1^{--})$	$e^+e^- \rightarrow X$	$\pi\pi\Upsilon(1S, 2S, 3S)$	2019	NO
Υ (10860)	$\Upsilon(5S)$	$10885.2^{+2.6}_{-1.6}$	37 ± 4	$0^-(1^{--})$	$e^+e^- \rightarrow X$	$B_{(s)}^*(\bar{B}_{(s)}^*)(\pi)$ $\pi\pi\Upsilon(1S, 2S, 3S)$ $\pi^+\pi^-h_b(1P, 2P)$ $\eta\Upsilon(1S, 2S)$ $\pi^+\pi^-\Upsilon(1D)$ (see listings)	1985	YES
Υ (11020)	$\Upsilon(6S)$	11000 ± 4	24^{+8}_{-6}	$0^-(1^{--})$	$e^+e^- \rightarrow X$	$B_{(s)}^*(\bar{B}_{(s)}^*)(\pi)$ $\pi\pi\Upsilon(1S, 2S, 3S)$ $\pi^+\pi^-h_b(1P, 2P)$ (see listings)	1985	YES

*Quantum numbers fixed from the quark model and need confirmation.

Another interesting question is whether a heavier $\pi^+\pi^-\psi(2S)$ state, the $\psi(4660)$, discovered by Belle [50,51] and confirmed by BaBar [52], is identical to the $A_c^+\bar{A}_c^-$ resonance observed by Belle with a nearby mass and width [53]. Most probably it is, the $A_c^+\bar{A}_c^-$ being one more decay mode of the $\psi(4660)$ (see the review on heavy non- $q\bar{q}$ mesons for more detail). Note that this is the interpretation adopted in the particle listings. In addition, Belle reported the first observation of a vector charmonium-like state decaying to $D_s^+D_{s1}(2536)$ with a significance of 5.9σ [54]. Its measured mass and width are $4625.9^{+6.2}_{-6.0} \pm 0.4$ MeV and $49.8^{+13.9}_{-11.5} \pm 4.0$ MeV, respectively, consistent with those of the $\psi(4660)$. Therefore, $D_s^+D_{s1}(2536)$ appears as an additional decay mode of the $\psi(4660)$ in the listings.

A series of isovector states containing $c\bar{c}$ have been found in

B decays to $K\pi(c\bar{c})$, where the isovector state decays to $\pi(c\bar{c})$ and $(c\bar{c})$ stands for $J/\psi(1S)$, $\psi(2S)$, or χ_{c1} . They are manifestly non- $q\bar{q}$ and their discovery implied an expansion of the meson naming scheme. The $Z_c(4430)$, decaying to $\pi\psi(2S)$, is the most well established. Based on a full amplitude analysis of $B^0 \rightarrow K^+\pi^-\psi(2S)$ decays, Belle determined the spin-parity of the $Z_c(4430)$ to be $J^P = 1^+$ [55]. From their study of $B^0 \rightarrow K^+\pi^-J/\psi(1S)$ decays, Belle also found evidence for the decay mode $Z_c(4430) \rightarrow \pi J/\psi(1S)$ [56], which has an order of magnitude lower branching fraction than the discovery mode $Z_c(4430) \rightarrow \pi\psi(2S)$. In the same analysis, Belle reported evidence for one more charged state, dubbed $Z_c(4200)$, decaying to $\pi J/\psi(1S)$. The existence of the $Z_c(4430)$ in $\pi\psi(2S)$, as well as its quantum number assignments, were confirmed by LHCb [57] with a much larger data sample, leading to improved mass and

width values, consistent with earlier measurements; the experiment even reports a resonant behavior of the $Z_c(4430)$ amplitude. The $Z_c(4430)$ was not confirmed (or excluded) by BaBar [58].

Belle also reported an observation of two charged states decaying to $\pi\chi_{c1}$ in an analysis of $B^0 \rightarrow K^+\pi^-\chi_{c1}$ decays [59]. These were originally called the $Z_1(4050)^\pm$ and the $Z_2(4250)^\pm$, but are referred to in Table 78.2 as $X(4050)^\pm$ and $X(4250)^\pm$. These states were not confirmed by BaBar [60]. Belle observes signals with 5.0σ significance for both the $Z_1(4050)^\pm$ and $Z_2(4250)^\pm$, whereas BABAR reports 1.1σ and 2.0σ effects, respectively, setting upper limits that are not inconsistent with Belle's measured rates. The situation remains unresolved.

The decay $B^+ \rightarrow K^+\phi J/\psi(1S)$ appears to be especially rich in resonant substructure. The $Y(4140)$ (now the $\chi_{c1}(4140)$), decaying to $\phi J/\psi(1S)$, was first observed in 2008 by CDF [61, 62], and confirmed by D0 and CMS [63, 64]. However, a second structure, the $Y(4274)$ (now the $\chi_{c1}(4274)$), could not be established unambiguously. Neither of the two states was seen in B decays at Belle [65], LHCb [66] and BaBar [67], or in $\gamma\gamma$ collisions at Belle [68]. The real breakthrough happened when LHCb performed a full amplitude analysis of $B^+ \rightarrow K^+\phi J/\psi(1S)$ with $J/\psi(1S) \rightarrow \mu^+\mu^-$, $\phi \rightarrow K^+K^-$ decays and showed that the data cannot be described in a model that contains only excited kaon states decaying into $K^+\phi$ [69, 70]. They observe two 1^{++} states with masses close to those originally reported by CDF (the $\chi_{c1}(4140)$ and $\chi_{c1}(4274)$), but the width of the one at 4140 MeV is much larger. In addition, they find two significant 0^{++} structures at 4500 and 4700 MeV (the $\chi_{c0}(4500)$ and $\chi_{c0}(4700)$).

78.2.2 Bottomonium

Belle reported a new measurement of the $e^+e^- \rightarrow \Upsilon(nS)\pi^+\pi^-$ ($n = 1, 2, 3$) cross sections at energies from 10.52 to 11.02 GeV [71]. They observed, with a 5.2σ significance, a new structure in the energy dependence of the cross sections. If described by a Breit–Wigner function, its mass and width are $10752.7 \pm 5.9^{+0.7}_{-1.1}$ MeV and $35.5^{+17.6+3.9}_{-11.3-3.3}$ MeV, respectively. The new structure could have a resonant origin and correspond to the not yet observed $\Upsilon(3D)$ state, provided $S-D$ mixing is enhanced, or an exotic state, e.g., a compact tetraquark or hadrobottomium. It could also be a non-resonant effect due to rescattering.

We no longer mention a hypothetical $Y_b(10888)$ state since a new analysis of the $\Upsilon(10860)$ energy range does not show evidence for an additional state with a mass different from that of the $\Upsilon(10860)$ [72]. After the mass of the $\eta_b(1S)$ was shifted upwards by about 10 MeV based on the Belle measurements [18, 19], all of the bottomonium states mentioned above fit into their respective spectroscopies, roughly where expected. An independent experimental confirmation of the shifted masses came from the Belle observation of $\Upsilon(4S) \rightarrow \eta h_b(1P)$ decays [19]. This process turns out to be the strongest observed transition of the $\Upsilon(4S)$ to lower bottomonium states.

78.3 States Near Open-Flavor Threshold

A number of states, listed in Table 78.3, appear near open-flavor thresholds, which is likely an important factor in their theoretical interpretation [73].

78.3.1 Charmonium

The $\chi_{c1}(3872)$, also known as $X(3872)$, is widely studied and seen in many transitions — see Table 78.3. Yet its interpretation remains unsettled (see the heavy non- $q\bar{q}$ review). Its unique experimental features include: it has $J^{PC} = 1^{++}$ [74, 75], yet it is too light to be the $\chi_{c1}(2^3P_1)$ quark model state; its mass is within 200 keV of the $D^0\bar{D}^{*0}$ threshold; it shows substantial isospin-breaking in its decays to $\rho J/\psi(1S)$ and $\pi^0\chi_{c1}$; and it is extremely narrow. Using a large sample of inclusively produced $\chi_{c1}(3872)$ decaying to $\pi^+\pi^-J/\psi(1S)$, LHCb recently determined the decay width of the $\chi_{c1}(3872)$ under two different assumptions [76]. Assuming a Flatté-inspired line shape and exploiting the strong coupling of the $\chi_{c1}(3872)$ to $D^0\bar{D}^{*0}$, LHCb performed the first exploration of the pole structure of the $\chi_{c1}(3872)$, finding a FWHM of $0.22^{+0.06+0.25}_{-0.08-0.17}$ MeV. On the other hand, assuming a Breit–Wigner line shape, its width was found to be $1.39 \pm 0.24 \pm 0.10$ MeV. While the former analysis has a more

firm theoretical foundation, the LHCb detector resolution did not allow for a distinction between the different line shapes.

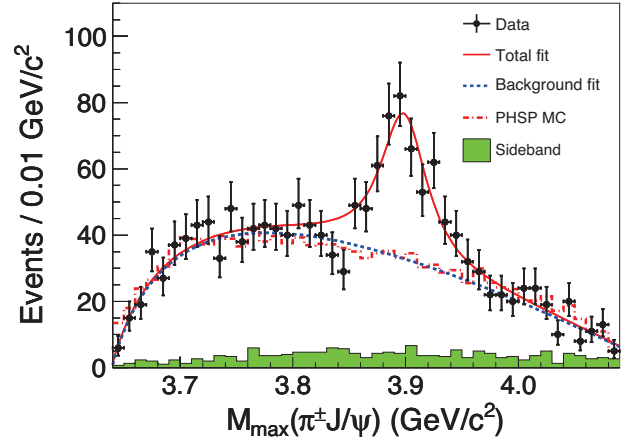


Figure 78.4: The $\pi^\pm J/\psi(1S)$ invariant mass distribution from BESIII [78] e^+e^- collision data taken at a center-of-mass energy near 4260 MeV.

In addition to the Z_c states found in B decays, discussed above, several isovector states with masses near $D\bar{D}^*$ and $D^*\bar{D}$ thresholds appear to be unique to e^+e^- annihilation. In 2013, a state named $Z_c(3900)$ was unearthed in the charmonium region at BESIII [78] and Belle [43] in the process $e^+e^- \rightarrow \pi^\mp Z_c(3900)^\pm$ with $Z_c(3900)^\pm \rightarrow \pi^\pm J/\psi(1S)$. The corresponding spectrum from BESIII is shown in Fig. 78.4. An analysis of CLEO data [79] confirmed this finding and also provided evidence for a neutral partner. A nearby signal was also seen in the $D\bar{D}^*$ channel [80] whose quantum numbers were fixed to 1^{+-} . BESIII reported its neutral partner in both $J/\psi(1S)\pi^0$ [81] and $D\bar{D}^*$ [82] decay modes. The masses extracted from these experiments in different decay modes have differences reaching up to 2σ . However, since the extraction of the mass and width parameters did not allow for an interference with the background and used Breit–Wigner line shapes, which is not justified near thresholds, there might be some additional systematic uncertainty in the mass values. Therefore, in the RPP listings as well as in Table 78.3 both structures appear under the name $Z_c(3900)$. BESIII also reported an observation of another charged state, the $X(4020)^\pm$ (originally called $Z_c(4020)^\pm$), in two decay modes: $h_c\pi^\pm$ [83] and $(D^*\bar{D}^*)^\pm$ [84]. The neutral partners have also been observed by BESIII in the $h_c\pi^0$ [85] and $(D^*\bar{D}^*)^0$ [86] final states. The Z_c states show some remarkable similarities to the Z_b states (discussed below), e.g. they decay dominantly to $D^{(*)}\bar{D}^*$ channels. However, current analyses suggest that the mass of the $Z_c(3900)$ might be somewhat above the $D\bar{D}^*$ threshold. If confirmed, this feature would challenge a possible $D\bar{D}^*$ -molecular interpretation with S -wave interactions only — prominent D -waves can shift molecular poles above threshold (see the discussion in Sec. 78.3.2). Finally, 3.5σ evidence for one more charged charmonium-like state at 4055 MeV decaying into $\psi(2S)\pi^\pm$ was reported by Belle in their analysis of the process $e^+e^- \rightarrow \psi(2S)\pi^+\pi^-$ [51]. This state was confirmed by BESIII, although there appears to be complications in the Dalitz plot requiring further investigation [48].

78.3.2 Bottomonium

New results on the η_b , h_b , and Z_b mostly come from Belle [18, 19, 21, 23, 72, 87–93], all from analyses of 121.4 fb^{-1} of e^+e^- collision data collected near the peak of the $\Upsilon(10860)$ resonance, as well as from an additional 25 fb^{-1} of data collected during the scans of the c.m. energy range 10.63–11.05 GeV. The η_b , h_b , and Z_b appear in the decay chains $\Upsilon(10860) \rightarrow \pi^- Z_b^+$, $Z_b^+ \rightarrow \pi^+(b\bar{b})$, and, when the $b\bar{b}$ forms an $h_b(1P)$, frequently decaying as $h_b(1P) \rightarrow \gamma\eta_b$.

Belle soon noticed that, for events in the peaks of Fig. 78.1, there seemed to be two intermediate charged states, the $Z_b(10610)$ and the $Z_b(10650)$. For example, Fig. 78.5 shows a Dalitz plot for events restricted to the $\Upsilon(2S)$ region of $\pi^+\pi^-$ recoil mass,

Table 78.3: As in Table 78.1, but for new states near the first open-flavor thresholds in the $c\bar{c}$ and $b\bar{b}$ regions, ordered by mass. Updated from Ref. [77] with kind permission, copyright (2011), Springer, and from Ref. [9] with kind permission from the authors.

PDG Name	Former Name(s)	m (MeV)	Γ (MeV)	$I^G(J^{PC})$	Production	Decay	Discovery Year	Summary Table
$\chi_{c1}(3872)$	$X(3872)$	3871.65 ± 0.06	1.19 ± 0.21	$0^+(1^{++})$	$B \rightarrow KX$ $p\bar{p} \rightarrow X\dots$ $pp \rightarrow X\dots$ $e^+e^- \rightarrow \gamma X$	$\pi^+\pi^- J/\psi(1S)$ $3\pi J/\psi(1S)$ $D^{*0}\bar{D}^0$ $\gamma J/\psi(1S)$ $\gamma\psi(2S)$	2003	YES
$Z_c(3900)$		3887.1 ± 2.6	28.4 ± 2.6	$1^+(1^{+-})$	$\psi(4230) \rightarrow \pi^- X$ $\psi(4230) \rightarrow \pi^0 X$	$\pi^0 \chi_{c1}(1P)$ $\pi^+ J/\psi(1S)$ $\pi^0 J/\psi(1S)$ $(D\bar{D}^*)^+$ $(D\bar{D}^*)^0$	2013	YES
$X(4020)$	$Z_c(4020)$	4024.1 ± 1.9	13 ± 5	$1^+(?^{?})$	$\psi(4230, 4360) \rightarrow \pi^- X$ $\psi(4230, 4360) \rightarrow \pi^0 X$	$\pi^+ h_c$ $\pi^0 h_c$ $(D^*\bar{D}^*)^+$ $(D^*\bar{D}^*)^0$	2013	YES
$Z_b(10610)$		10607.2 ± 2.0	18.4 ± 2.4	$1^+(1^{+-})$	$\Upsilon(10860) \rightarrow \pi^- X$ $\Upsilon(10860) \rightarrow \pi^0 X$	$\pi^+ \Upsilon(1S, 2S, 3S)$ $\pi^0 \Upsilon(1S, 2S, 3S)$ $\pi^+ h_b(1P, 2P)$ $(B\bar{B}^*)^+$	2011	YES
$Z_b(10650)$		10652.2 ± 1.5	11.5 ± 2.2	$1^+(1^{+-})$	$\Upsilon(10860) \rightarrow \pi^- X$	$\pi^+ \Upsilon(1S, 2S, 3S)$ $\pi^+ h_b(1P, 2P)$ $(B^*\bar{B}^*)^+$	2011	YES

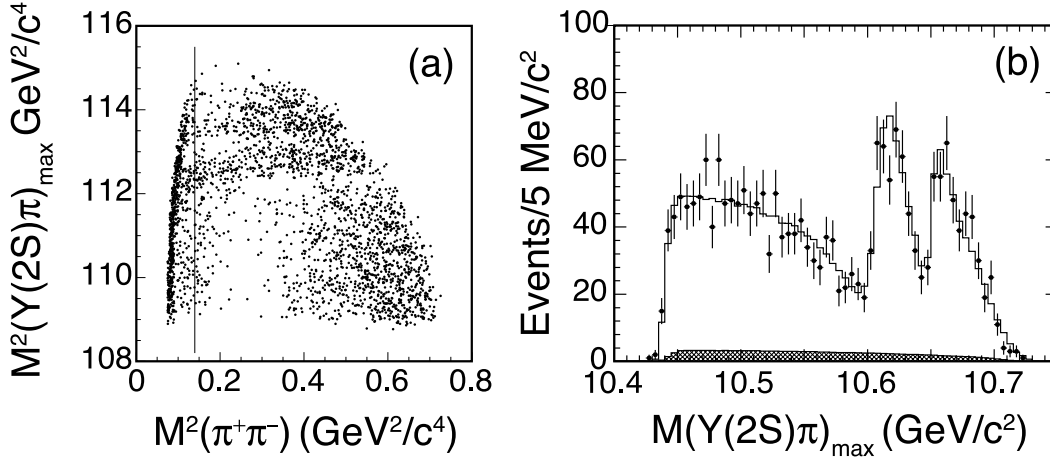


Figure 78.5: From Belle [87] e^+e^- collision data taken near the peak of the $\Upsilon(10860)$ for events with a $\pi^+\pi^-$ -missing mass consistent with an $\Upsilon(2S) \rightarrow \mu^+\mu^-$, (a) the maximum of the two possible single π^\pm -missing-mass-squared combinations vs. the $\pi^+\pi^-$ -mass-squared; and (b) projection of the maximum of the two possible single π^\pm -missing-mass combinations (*points with error bars*) overlaid with a fit (*curve*). Events to the left of the vertical line in (a) are excluded from the amplitude analysis. The hatched histogram in (b) corresponds to the combinatorial background. The two horizontal stripes in (a) and two peaks in (b) correspond to the two Z_b states.

with $\Upsilon(2S) \rightarrow \mu^+\mu^-$ [87]. The two bands observed in the maximum of the two $M[\pi^\pm\Upsilon(2S)]^2$ values also appear in the $\Upsilon(1S)$, $\Upsilon(3S)$, $h_b(1P)$, and $h_b(2P)$ samples. Belle fits all subsamples to resonant plus non-resonant amplitudes, allowing for interference (notably, between $\pi^-Z_b^+$ and $\pi^+Z_b^-$), and finds consistent pairs of Z_b masses for all bottomonium transitions, and comparable strengths of the two states. A recent angular analysis assigned $J^P = 1^+$ for both Z_b states [88], which must also have negative G -parity. Transitions through Z_b to the $h_b(nP)$ saturate the observed $\pi^+\pi^-h_b(nP)$ cross sections. While the two masses of the Z_b states as extracted from Breit–Wigner fits for the various channels are just a few MeV above the $B^*\bar{B}$ and $B^*\bar{B}^*$ thresholds, more refined analyses using only S -waves find pole locations right below the corresponding thresholds either on the physical [94] or the unphysical [95] sheet. Once D -waves are included, the pole of the $Z_b(10650)$ moves above the $B^*\bar{B}^*$ threshold [96]. Regardless of their proximity to the corresponding thresholds, both states predominantly decay into these open-flavor channels [90, 97] with

branching fractions that exceed 80% and 70%, respectively, at 90% CL. This feature provides strong evidence for their molecular nature.

78.4 Concluding Remarks

The discovery of the $\chi_{c1}(3872)$ (also known as the $X(3872)$) in 2003 ushered in an era of tremendous progress in experimental heavy quark meson spectroscopy. As shown in Tables 78.1 to 78.3, more than 40 new states have been reported during this period, many of which were unanticipated. While the states below open-flavor thresholds (Table 78.1) appear to be well-explained by the conventional $q\bar{q}$ quark model, a thorough understanding of the suite of states above (Table 78.2) and near (Table 78.3) open-flavor thresholds remains elusive. After nearly two decades, experimental progress remains rapid with the continuation of BES-III, the commencement of the Belle II program, and the imminent accumulation of additional data at the LHC.

Acknowledgement

The authors would like to express their gratitude to Alex Bondar and Christoph Hanhart for productive discussions during the composition of this review.

References

- [1] N. Brambilla *et al.*, Phys. Rept. **873**, 1 (2020), [arXiv:1907.07583].
- [2] Y.-R. Liu *et al.*, Prog. Part. Nucl. Phys. **107**, 237 (2019), [arXiv:1903.11976].
- [3] S. L. Olsen, T. Skwarnicki and D. Zieminska, Rev. Mod. Phys. **90**, 1, 015003 (2018), [arXiv:1708.04012].
- [4] A. Ali, J. S. Lange and S. Stone, Prog. Part. Nucl. Phys. **97**, 123 (2017), [arXiv:1706.00610].
- [5] F.-K. Guo *et al.*, Rev. Mod. Phys. **90**, 1, 015004 (2018), [arXiv:1705.00141].
- [6] R. F. Lebed, R. E. Mitchell and E. S. Swanson, Prog. Part. Nucl. Phys. **93**, 143 (2017), [arXiv:1610.04528].
- [7] A. E. Bondar, R. V. Mizuk and M. B. Voloshin, Mod. Phys. Lett. A **32**, 04, 1750025 (2017), [arXiv:1610.01102].
- [8] S. K. Choi *et al.* (Belle), Phys. Rev. Lett. **91**, 262001 (2003), [hep-ex/0309032].
- [9] N. Brambilla *et al.*, Eur. Phys. J. **C74**, 10, 2981 (2014), [arXiv:1404.3723].
- [10] J. L. Rosner *et al.* (CLEO), Phys. Rev. Lett. **95**, 102003 (2005), [hep-ex/0505073].
- [11] M. Ablikim *et al.* (BESIII), Phys. Rev. D **99**, 7, 072008 (2019), [arXiv:1810.12023].
- [12] M. Ablikim *et al.* (BESIII), Phys. Rev. D **102**, 112007 (2020), [arXiv:2010.12092].
- [13] V. Bhardwaj *et al.* (Belle), Phys. Rev. Lett. **111**, 3, 032001 (2013), [arXiv:1304.3975].
- [14] M. Ablikim *et al.* (BESIII), Phys. Rev. Lett. **115**, 1, 011803 (2015), [arXiv:1503.08203].
- [15] K. Chilikin *et al.* (Belle) (2020), [arXiv:2003.08335].
- [16] B. Aubert *et al.* (BaBar), Phys. Rev. Lett. **101**, 071801 (2008), [Erratum: Phys.Rev.Lett. 102, 029901 (2009)], [arXiv:0807.1086].
- [17] B. Aubert *et al.* (BaBar), Phys. Rev. Lett. **103**, 161801 (2009), [arXiv:0903.1124].
- [18] R. Mizuk *et al.* (Belle), Phys. Rev. Lett. **109**, 232002 (2012), [arXiv:1205.6351].
- [19] U. Tamponi *et al.* (Belle), Phys. Rev. Lett. **115**, 14, 142001 (2015), [arXiv:1506.08914].
- [20] B. G. Fulson *et al.* (Belle), Phys. Rev. Lett. **121**, 23, 232001 (2018), [arXiv:1807.01201].
- [21] I. Adachi *et al.* (Belle), Phys. Rev. Lett. **108**, 032001 (2012), [arXiv:1103.3419].
- [22] T. K. Pedlar *et al.* (CLEO), Phys. Rev. Lett. **107**, 041803 (2011), [arXiv:1104.2025].
- [23] I. Adachi (Belle), in "8th International Workshop On Heavy Quarkonium (QWG2011) Darmstadt, Germany, October 3-7, 2011," (2011), [arXiv:1110.3934].
- [24] G. Aad *et al.* (ATLAS), Phys. Rev. Lett. **108**, 152001 (2012), [arXiv:1112.5154].
- [25] V. M. Abazov *et al.* (D0), Phys. Rev. D **86**, 031103 (2012), [arXiv:1203.6034].
- [26] R. Aaij *et al.* (LHCb), JHEP **10**, 088 (2014), [arXiv:1409.1408].
- [27] A. M. Sirunyan *et al.* (CMS), Phys. Rev. Lett. **121**, 092002 (2018), [arXiv:1805.11192].
- [28] G. Aad *et al.* (ATLAS), Phys. Rev. Lett. **113**, 212004 (2014), [arXiv:1407.1032].
- [29] A. M. Sirunyan *et al.* (CMS), Phys. Rev. Lett. **122**, 132001 (2019), [arXiv:1902.00571].
- [30] R. Aaij *et al.* (LHCb), Phys. Rev. Lett. **122**, 232001 (2019), [arXiv:1904.00081].
- [31] R. Aaij *et al.* (LHCb), JHEP **07**, 035 (2019), [arXiv:1903.12240].
- [32] S. Uehara *et al.* (Belle), Phys. Rev. Lett. **96**, 082003 (2006), [hep-ex/0512035].
- [33] B. Aubert *et al.* (BaBar), Phys. Rev. D **81**, 092003 (2010), [arXiv:1002.0281].
- [34] K. Abe *et al.* (Belle), Phys. Rev. Lett. **94**, 182002 (2005), [hep-ex/0408126].
- [35] J. P. Lees *et al.* (BaBar), Phys. Rev. **D86**, 072002 (2012), [arXiv:1207.2651].
- [36] F.-K. Guo and U.-G. Meissner, Phys. Rev. **D86**, 091501 (2012), [arXiv:1208.1134].
- [37] S. L. Olsen, Phys. Rev. **D91**, 5, 057501 (2015), [arXiv:1410.6534].
- [38] Z.-Y. Zhou, Z. Xiao and H.-Q. Zhou, Phys. Rev. Lett. **115**, 2, 022001 (2015), [arXiv:1501.00879].
- [39] R. Aaij *et al.* (LHCb), Phys. Rev. D **102**, 112003 (2020), [arXiv:2009.00026].
- [40] K. Chilikin *et al.* (Belle), Phys. Rev. **D95**, 112003 (2017), [arXiv:1704.01872].
- [41] B. Aubert *et al.* (BaBar), Phys. Rev. Lett. **95**, 142001 (2005), [hep-ex/0506081].
- [42] C. Z. Yuan *et al.* (Belle), Phys. Rev. Lett. **99**, 182004 (2007), [arXiv:0707.2541].
- [43] Z. Q. Liu *et al.* (Belle), Phys. Rev. Lett. **110**, 252002 (2013), [arXiv:1304.0121].
- [44] M. Ablikim *et al.* (BESIII), Phys. Rev. Lett. **118**, 9, 092001 (2017), [arXiv:1611.01317].
- [45] M. Cleven *et al.*, Phys. Rev. **D90**, 7, 074039 (2014), [arXiv:1310.2190].
- [46] M. Ablikim *et al.* (BESIII), Phys. Rev. Lett. **118**, 9, 092002 (2017), [arXiv:1610.07044].
- [47] M. Ablikim *et al.* (BESIII), Phys. Rev. Lett. **112**, 9, 092001 (2014), [arXiv:1310.4101].
- [48] M. Ablikim *et al.* (BESIII), Phys. Rev. **D96**, 3, 032004 (2017), [erratum: Phys. Rev.D99,no.1,019903(2019)], [arXiv:1703.08787].
- [49] X. Y. Gao, C. P. Shen and C. Z. Yuan, Phys. Rev. **D95**, 9, 092007 (2017), [arXiv:1703.10351].
- [50] X. L. Wang *et al.* (Belle), Phys. Rev. Lett. **99**, 142002 (2007), [arXiv:0707.3699].
- [51] X. L. Wang *et al.* (Belle), Phys. Rev. **D91**, 112007 (2015), [arXiv:1410.7641].
- [52] J. P. Lees *et al.* (BaBar), Phys. Rev. **D89**, 11, 111103 (2014), [arXiv:1211.6271].
- [53] G. Pakhlova *et al.* (Belle), Phys. Rev. Lett. **101**, 172001 (2008), [arXiv:0807.4458].
- [54] S. Jia *et al.* (Belle), Phys. Rev. **D100**, 11, 111103 (2019), [arXiv:1911.00671].
- [55] K. Chilikin *et al.* (Belle), Phys. Rev. **D88**, 7, 074026 (2013), [arXiv:1306.4894].
- [56] K. Chilikin *et al.* (Belle), Phys. Rev. **D90**, 11, 112009 (2014), [arXiv:1408.6457].
- [57] R. Aaij *et al.* (LHCb), Phys. Rev. Lett. **112**, 22, 222002 (2014), [arXiv:1404.1903].
- [58] B. Aubert *et al.* (BaBar), Phys. Rev. **D79**, 112001 (2009), [arXiv:0811.0564].
- [59] R. Mizuk *et al.* (Belle), Phys. Rev. **D78**, 072004 (2008), [arXiv:0806.4098].
- [60] J. P. Lees *et al.* (BaBar), Phys. Rev. **D85**, 052003 (2012), [arXiv:1111.5919].

- [61] T. Aaltonen *et al.* (CDF), Phys. Rev. Lett. **102**, 242002 (2009), [arXiv:0903.2229].
- [62] T. Aaltonen *et al.* (CDF), Mod. Phys. Lett. **A32**, 26, 1750139 (2017), [arXiv:1101.6058].
- [63] V. M. Abazov *et al.* (D0), Phys. Rev. **D89**, 1, 012004 (2014), [arXiv:1309.6920].
- [64] S. Chatrchyan *et al.* (CMS), Phys. Lett. **B734**, 261 (2014), [arXiv:1309.6920].
- [65] J. Brodzicka, Conf. Proc. **C0908171**, 299 (2009), [299(2009)].
- [66] R. Aaij *et al.* (LHCb), Phys. Rev. **D85**, 091103 (2012), [arXiv:1202.5087].
- [67] J. P. Lees *et al.* (BaBar), Phys. Rev. **D91**, 1, 012003 (2015), [arXiv:1407.7244].
- [68] C. P. Shen *et al.* (Belle), Phys. Rev. Lett. **104**, 112004 (2010), [arXiv:0912.2383].
- [69] R. Aaij *et al.* (LHCb), Phys. Rev. **D95**, 1, 012002 (2017), [arXiv:1606.07898].
- [70] R. Aaij *et al.* (LHCb), Phys. Rev. Lett. **118**, 2, 022003 (2017), [arXiv:1606.07895].
- [71] R. Mizuk *et al.* (Belle), JHEP **10**, 220 (2019), [arXiv:1905.05521].
- [72] D. Santel *et al.* (Belle), Phys. Rev. **D93**, 1, 011101 (2016), [arXiv:1501.01137].
- [73] F.-K. Guo, X.-H. Liu and S. Sakai, Prog. Part. Nucl. Phys. **112**, 103757 (2020), [arXiv:1912.07030].
- [74] R. Aaij *et al.* (LHCb), Phys. Rev. Lett. **110**, 222001 (2013), [arXiv:1302.6269].
- [75] R. Aaij *et al.* (LHCb), Phys. Rev. **D92**, 1, 011102 (2015), [arXiv:1504.06339].
- [76] R. Aaij *et al.* (LHCb), Phys. Rev. D **102**, 9, 092005 (2020), [arXiv:2005.13419].
- [77] N. Brambilla *et al.*, Eur. Phys. J. **C71**, 1534 (2011), [arXiv:1010.5827].
- [78] M. Ablikim *et al.* (BESIII), Phys. Rev. Lett. **110**, 252001 (2013), [arXiv:1303.5949].
- [79] T. Xiao *et al.*, Phys. Lett. **B727**, 366 (2013), [arXiv:1304.3036].
- [80] M. Ablikim *et al.* (BESIII), Phys. Rev. Lett. **112**, 2, 022001 (2014), [arXiv:1310.1163].
- [81] M. Ablikim *et al.* (BESIII), Phys. Rev. Lett. **115**, 11, 112003 (2015), [arXiv:1506.06018].
- [82] M. Ablikim *et al.* (BESIII), Phys. Rev. Lett. **115**, 22, 222002 (2015), [arXiv:1509.05620].
- [83] M. Ablikim *et al.* (BESIII), Phys. Rev. Lett. **111**, 24, 242001 (2013), [arXiv:1309.1896].
- [84] M. Ablikim *et al.* (BESIII), Phys. Rev. Lett. **112**, 13, 132001 (2014), [arXiv:1308.2760].
- [85] M. Ablikim *et al.* (BESIII), Phys. Rev. Lett. **113**, 21, 212002 (2014), [arXiv:1409.6577].
- [86] M. Ablikim *et al.* (BESIII), Phys. Rev. Lett. **115**, 18, 182002 (2015), [arXiv:1507.02404].
- [87] A. Bondar *et al.* (Belle), Phys. Rev. Lett. **108**, 122001 (2012), [arXiv:1110.2251].
- [88] A. Garmash *et al.* (Belle), Phys. Rev. **D91**, 7, 072003 (2015), [arXiv:1403.0992].
- [89] P. Krokovny *et al.* (Belle), Phys. Rev. **D88**, 5, 052016 (2013), [arXiv:1308.2646].
- [90] I. Adachi *et al.* (Belle) (2012), [arXiv:1209.6450].
- [91] K. F. Chen *et al.* (Belle), Phys. Rev. Lett. **100**, 112001 (2008), [arXiv:0710.2577].
- [92] P. Krokovny (Belle Collab.), talk given at Les Rencontres de Physique de la Vallee d'Aoste, La Thuile, Aosta Valley, Italy, 2012.
- [93] A. Abdesselam *et al.* (Belle), Phys. Rev. Lett. **117**, 14, 142001 (2016), [arXiv:1508.06562].
- [94] M. Cleven *et al.*, Eur. Phys. J. **A47**, 120 (2011), [arXiv:1107.0254].
- [95] F. K. Guo *et al.*, Phys. Rev. **D93**, 7, 074031 (2016), [arXiv:1602.00940].
- [96] Q. Wang *et al.*, Phys. Rev. D **98**, 7, 074023 (2018), [arXiv:1805.07453].
- [97] A. Garmash *et al.* (Belle), Phys. Rev. Lett. **116**, 21, 212001 (2016), [arXiv:1512.07419].

79. Heavy Non- $q\bar{q}$ Mesons

Revised June 2021 by S. Eidelman (Budker Inst., Novosibirsk; Novosibirsk U.), T. Gutsche (Tübingen U.), C. Hanhart (Jülich) and R.E. Mitchell (Indiana U.).

The constituent quark model describes the observed meson spectrum as bound $q\bar{q}$ states grouped into SU(N) flavor multiplets (see the ‘Quark Model’ in this issue of the *Review of Particle Physics*). However, the self coupling of gluons in QCD suggests that additional mesons made of bound gluons (glueballs), or $q\bar{q}$ -pairs with an excited gluon (hybrids), may exist. Furthermore, multi-quark color singlet states such as $qq\bar{q}\bar{q}$ (tetraquarks as compact diquark-antidiquark systems and ‘molecular’ bound states of two mesons) or $qqq\bar{q}\bar{q}\bar{q}$ (six-quark, ‘baryonium’ or quasinuclear baryon-antibaryon bound states) have also been predicted. The focus of this review is on the current understanding of exotic states that apparently do not fit into the constituent quark model and contain at least one heavy quark (charm or bottom — the lifetime of the top quark is too short to allow it to hadronise). Light non- $q\bar{q}$ candidates (made of u , d and s quarks) are discussed in ‘Spectroscopy of Light Meson Resonances’ in this *Review*.

The review is split into 3 parts, discussing separately heavy–light systems, heavy–heavy systems, as well as systems with more than two heavy quarks. For a more detailed discussion of the experimental and/or theoretical status on exotic meson candidates in the doubly heavy meson sector we refer to Refs. [1–7]. Reviews with main focus on tetraquarks and molecular states are presented in Ref. [8] and in Ref. [9], respectively.

79.1 Heavy-light systems

Two very narrow states, $D_{s0}^*(2317)^\pm$ and $D_{s1}(2460)^\pm$, were observed at B factories [10, 11]. They lie far below the predicted masses for the two expected broad P -wave $c\bar{s}$ mesons. However, strong cusp effects, due to the nearby DK (DK^*) thresholds, could shift their masses downwards and quench the observed widths, still allowing for a conventional explanation of these states [12]. Such an effect was also claimed for the $a_0(980)$ and $f_0(980)$ mesons, which lie just below the $K\bar{K}$ threshold. In contrast to this picture, many authors favour exotic explanations for these lightest positive parity charmed states, such as four-quark states [13–16] or DK (DK^*) molecules [17–22]. Both states are isoscalars and thus the dominant open decay channels, $D_s^{(*)\pm}\pi^0$, lead to very small widths. For compact structures the hadronic decay is driven by $\eta - \pi^0$ mixing and one finds widths below 10 keV [12, 23]. In contrast to this a hadronic width of typically 100 keV would be the unequivocal signature for a prominent molecular nature of $D_{s0}^*(2317)^\pm$ [19, 21, 22, 24], since meson loops would then contribute significantly. The most refined analysis in the molecular scenario [24], where the parameters of the formalism are constrained by a large bulk of lattice QCD data on singly charmed systems, reports a prediction for the width in the range (104–116) keV. The currently measured upper bound for the width is 3.8 MeV.

It should be stressed that – akin to $q\bar{q}$ mesons – multi-quark states also appear in multiplets. An important probe for the structure of hadrons is therefore the spectra, and in particular the SU(3) flavor multiplets within the different scenarios. For example the tetraquark model advocated in Refs. [16, 25] finds that the $D_{s0}^*(2317)^\pm$ should be degenerate with its non strange-partner state $D_0^*(2300)$ in line with the currently available experimental analyses. However, Ref. [26] showed that the recent LHCb data for $B \rightarrow D\pi\pi$ [27, 28] call for a significantly lighter lightest non-strange scalar charmed meson as soon as constraints from the chiral symmetry of QCD are employed in the analysis. This claim is in line with the recent lattice QCD study of Ref. [29]. In fact, the experimental as well as lattice data turn out to be consistent with the predictions from unitarised chiral perturbation theory pioneered for these systems in Ref. [18]. For more recent calculations see Refs. [24, 30, 31]. Moreover, all these latter calculations predict that there should be in addition a heavier flavor exotic state by about 300 MeV that indeed shows up in the above mentioned LHCb data [31]. Thus, in this picture the structure that appears as $D_0^*(2300)$ in the *Listings* originates from the interplay of two poles, similar to the $\Lambda(1405)$ in the baryon sector, see ‘Pole

structure of the $\Lambda(1405)$ region’ in this *Review*. Two poles in the non-strange scalar sector are also generated in the tetraquark picture of Ref. [16], but in this work the real parts of the poles are located at 2308 MeV and 2666 MeV, in conflict with the data mentioned above. In the refined analysis of Ref. [25] it is shown, however, that the exact pole locations and even the ordering of the higher multiplets depend on the details of the model.

Manifestly exotic candidates around 2.9 GeV were reported in Refs. [32, 33] by LHCb in the $\bar{D}K$ system. Since the strong interactions preserve the quark flavor and the final state contains an \bar{s} as well as a \bar{c} , color neutrality calls for a minimum quark content of $ud\bar{c}\bar{s}$. The explanation for those states include compact tetraquarks [34–36], hadronic molecules with a prominent D^*K^* component [37–39], or kinematic effects such as cusps or triangle singularities without nearby poles [40, 41]. The different pictures are contrasted and observable differences between them are discussed in Ref. [42].

79.2 Heavy-heavy systems

With the discovery of the $\chi_{c1}(3872)^1$ in $B^\pm \rightarrow K^\pm X$ ($X \rightarrow J/\psi \pi^+ \pi^-$) by Belle [43] in 2003, soon confirmed by BaBar [44], many searches for states beyond the standard $q\bar{q}$ quark model were initiated in the charm and bottom sectors. For an updated collection of the currently available experimental information on multi-quark states we refer to ‘Spectroscopy of mesons containing two heavy quarks’ in this *Review*, and in particular to Table 78.2. Moreover, in the decay $\Lambda_b^0 \rightarrow J/\psi K^- p$ the LHCb collaboration has recently reported the observation of new baryons decaying into $J/\psi(1S)p$, which are candidates for heavy pentaquark states [45, 46]. They are discussed in some depth in ‘Pentaquarks’ in this *Review*.

When restricting ourselves to confirmed states we are faced with several states that do not seem to fit into the mass and quantum number schemes of basic $q\bar{q}$ quark models. This is clear for the five established charged states ($Z_c(3900)^\pm$, $Z_c(4020)^\pm$,² and $Z_c(4430)^\pm$ in the charmonium sector, and $Z_b(10610)^\pm$ and $Z_b(10650)^\pm$ in the bottomonium sector). The neutral states ($\chi_{c1}(3872)$, $\psi(4230)$, $\psi(4360)$, and $\psi(4660)$)³ also challenge the quark model since their masses and decay properties are in conflict with expectations.

The quantum numbers of the $\chi_{c1}(3872)$ have been determined by LHCb to be $J^{PC} = 1^{++}$, first by assuming zero angular momentum between the $J/\psi(1S)$ and the dipion [47] and then by relaxing this constraint [48]. The $\chi_{c1}(3872)$ cannot be identified with the $\chi_{c1}(2^3P_1)$ since the latter is predicted to lie about 100 MeV higher in mass [49]. Instead, the $X(3940)$ reported by Belle in $e^+e^- \rightarrow J/\psi X$, decaying into $D^*\bar{D}$ but not into $D\bar{D}$ [50] could be the $\chi_{c1}(2^3P_1)$. The $\chi_{c2}(3930)$ 2^3P_2 tensor partner was reported by Belle at 3931 MeV in $\gamma\gamma$ interactions [51].

The $\chi_{c1}(3872)$ lies within 200 keV of the $D^0\bar{D}^{*0}$ threshold and its width is very small — recent Breit-Wigner analyses by LHCb [52, 53] result in an average value of $\Gamma = (1.19 \pm 0.21)$ MeV as indicated in the *Listings*; employing the formalism of Ref. [54] under the constraint that the $D^*\bar{D}$ decay channel dominates, results in $\Gamma = 0.22^{+0.18}_{-0.19}$ MeV, where the standard convention is applied to use twice the imaginary part of the pole location as width. In the future those values can be refined more by either a direct measurement of the width that should be possible at the planned PANDA experiment [55, 56] or by exploiting the interplay of a triangle singularity and the $\chi_{c1}(3872)$ pole [57–59]. Therefore the most natural explanation for this state is a $1^{++} D\bar{D}^*$ molecule [60], for which strong isospin breaking is predicted [60, 61], since the distance of the pole of the $\chi_{c1}(3872)$ to the $D^0\bar{D}^{*0}$ threshold is significantly smaller than to the $D^+\bar{D}^{*-}$ threshold. Indeed, the comparable rates for $\omega J/\psi$ and $\rho^0 J/\psi$ are

¹ The $\chi_{c1}(3872)$ is also known as the $X(3872)$. According to the PDG naming scheme, which we follow in this review, the primary name for a meson expresses its quantum numbers.

² While the $J^P = 1^+$ quantum numbers are plausible for this state, they are not yet established experimentally. This is why this state appears as $X(4020)$ in both the *Listings* and *Summary Tables*.

³ The $\psi(4230)$, $\psi(4360)$, and $\psi(4660)$ are also known as the $Y(4230)$, $Y(4360)$, and $Y(4660)$, respectively. Before improved mass measurements, the $\psi(4230)$ was originally called the $\psi(4260)$ or $Y(4260)$.

consistent with an interpretation of $\chi_{c1}(3872)$ as an isoscalar $D\bar{D}^*$ molecule, when the different widths of the ρ and ω are taken into account [62]. Similarly, a dominant molecular $D^0\bar{D}^{*0}$ structure in the $\chi_{c1}(3872)$ with further subleading hadronic components is used to explain strong and radiative decays involving $J/\psi(1S)$ and $\psi(2S)$ in the final states [63,64].

A four-quark state $cq\bar{c}\bar{q}'$ is another possible interpretation of the $\chi_{c1}(3872)$ [15] but a charged partner of the $\chi_{c1}(3872)$ has not been observed (e.g. not in $B^- \rightarrow \bar{K}^0 X^-$ nor in $B^0 \rightarrow K^+ X^-$, where $X^- \rightarrow J/\psi \pi^- \pi^0$ [65]) – see [66] for a possible explanation of this non-observation within the tetraquark approach assuming specific diquark correlations and the more recent discussion in Ref. [67]. The claim that $\chi_{c1}(3872)$ must be a compact (tetraquark) state, since it is also produced at very high p_T in $\bar{p}p$ collisions [68] and in high multiplicity final states [69], was challenged in [70] and [71], respectively, which in particular stress the importance of rescattering, see also Refs. [72,73].

A broad structure, originally called $Y(4260)$, decaying into $J/\psi(1S)\pi^+\pi^-$ was reported by BaBar in initial state radiation $e^+e^- \rightarrow (\gamma_{\text{ISR}})Y(4260)$ [74]. A subsequent measurement with significantly improved precision was reported by BESIII [75], and revealed that the original $Y(4260)$ cannot be described with a simple resonant lineshape. Fitting the BESIII data with two Breit-Wigner distributions leads to a narrower and lighter structure (referred to in the *Listings* as the $\psi(4230)$), but also requires a second state at 4320 MeV. However, note that the $D_1(2420)\bar{D}$ molecular model for the $\psi(4230)$ [76] can describe the same data with just one single pole [77]. How many vector states are in the mass range between 4220 MeV and 4400 MeV is not yet settled, but knowing this is crucial to allow for further progress.

There are no charmonium states expected in this mass region with quantum numbers 1^{--} from quark models using the Cornell type of interaction, although this might not be true for some screened versions thereof – for a recent discussion we refer to Ref. [78]. In addition, a charmonium state at this mass is expected to have significant couplings to one or more of the $\bar{D}^{(*)}D^{(*)}$ channels [79,80], a feature that is not observed for the $\psi(4230)$. This state could be a hybrid charmonium with a spin-1 $\bar{c}c$ [81,82] or a spin-0 [83,84] core. However, provided that the observation of $\psi(4230)$ decay into $h_c(1P)\pi\pi$ by BESIII [85] is confirmed, the hybrid hypothesis would be under pressure, since the spin of the heavy quarks (coupled to zero in the $h_c(1P)$) should be conserved in leading order in the expansion in $(\Lambda_{\text{QCD}}/m_c)$. (The individual conservation of the heavy quark spin and the total angular momentum of the light quark cloud is a consequence of the heavy-quark spin symmetry, see ‘Heavy-Quark and Soft-Collinear Effective Theory’ in this issue of the *Review*.) The same criticism applies to the hadrocharmonium interpretation of the $\psi(4230)$, which describes this state as spin-1 quarkonium surrounded by a light quark cloud [86]. To circumvent the spin-symmetry argument, Ref. [87] argues that $\psi(4230)$ and $\psi(4360)$ could be mixtures of two hadrocharmonia with spin-triplet and spin-singlet heavy quark pairs. The same kind of mixing could also be at work for hybrid structures.

A dominant $D_1(2420)\bar{D}$ component in the $\psi(4230)$ [88] explains naturally why $Z_c(3900)^\pm$ (interpreted by the authors as a $\bar{D}D^*$ bound state) is seen in $\psi(4230) \rightarrow \pi^\mp Z_c(3900)^\pm$. A similar mechanism is also found in Ref. [89] linking in addition the $J/\psi(1S)\pi^+\pi^-$ and $\psi(2S)\pi^+\pi^-$ decays of the $\psi(4230)$. Furthermore, a copious production of $\chi_{c1}(3872)$ in $\psi(4230)$ radiative decays was predicted from the prominent $D_1\bar{D}$ component of the $\psi(4230)$ [90], which was confirmed by BESIII [91]. Possible charmonia components both in $\psi(4230)$ and $\chi_{c1}(3872)$ can influence the radiative transition but they are shown to be of subleading order [92]. The $\psi(4360)$ as a $D_1\bar{D}^*$ bound state could be the spin partner of the $\psi(4230)$ [93,94], but a detailed microscopic calculation is still lacking.

The tetraquark picture calls for four ground state vector states – once the parameters of the model are fixed from some candidate states in the negative and positive parity sector, states with other quantum numbers can be predicted. Possible scenarios are for instance discussed in Ref. [95] which builds on a tailor-made spin-spin interaction [96] to describe the $\chi_{c1}(3872)$,

both $Z_c(3900)^\pm$ and $Z_c(4020)^\pm$ and even the $Z(4430)^\pm$ confirmed by Belle [97] and LHCb [98]. This model also explains the copious production of $\chi_{c1}(3872)$ in $\psi(4230)$ radiative decays mentioned above [96,99]. However, tetraquark models (in most cases based on diquark-antidiquark configurations) tend to predict many additional charged and neutral states which have not yet been discovered. In particular, as for the conventional $\bar{q}q$ structures one should expect nearly degenerate isoscalar and isovector states in analogy to the near degeneracy of $\rho(770)$ and $\omega(782)$. The problem and possible explanations are discussed in some detail in Refs. [66,67].

Ref. [100] found a sizeable SU(3) flavor octet contribution when analysing the $\pi\pi$ final state from $\psi(4230) \rightarrow J/\psi(1S)\pi^+\pi^-$, which is consistent with both a molecular and a tetraquark interpretation of $\psi(4230)$, but at odds with a hybrid or a $\bar{c}c$ interpretation.

In the mass range above 4600 MeV, the number of poles is also not yet settled. Experimental signals are seen in the $\psi(2S)\pi\pi$, $A_c^+ \bar{A}_c^-$ and $D_s \bar{D}_{s1}$ final states. In the *Listings* the former two structures go into one node, $\psi(4660)$ due to their proximity in parameter values. Moreover, various theoretical works describe these states in a combined analysis [101–103]. The signal in the hidden strangeness mode around 4630 MeV still calls for confirmation and might be yet another realisation of the same state, but there are already speculations about its nature. While Ref. [104] argues in favor of a $D_s^{(*)}\bar{D}_{s1}(2536)$ or $D_s^{(*)}\bar{D}_{s2}(2573)$ [105] molecular nature, Ref. [106] does not confirm these claims. Ref. [107] identifies the structure as P -wave $[cs][\bar{c}\bar{s}]$ tetraquark state. Other explanations of the $\psi(4660)$ include a $\psi(2S)f_0(980)$ molecule [108] and a $A_c^+ \bar{A}_c^-$ baryonium [101]. Also in this mass range studies of the partner states, driven either by spin or flavor symmetry will be very valuable – see e.g. the predictions in Ref. [109].

The isovector states $Z_c(3900)$ and $Z_c(4020)$, first observed by BESIII [110,111], decay predominantly into $\bar{D}D^*$ and \bar{D}^*D^* , respectively, while the $Z_b(10610)$ and $Z_b(10650)$, first observed by Belle [112,113], decay predominantly into $\bar{B}B^*$ and \bar{B}^*B^* [114], respectively, although all four were discovered in the decay mode heavy quarkonium plus pion. This suggests that these states are close relatives and their interactions are connected via heavy quark flavor symmetry. A molecular interpretation for the bottomonium states was proposed shortly after the discovery of the two Z_b states [115] and also shortly after that of the $Z_c(3900)$ [88]. This picture is confirmed within the meson exchange model of Ref. [116]. Decay patterns of $Z_c(3900)$ and the two Z_b were also shown to be consistent with a molecular interpretation [117–119]. However, some of their properties also appear to be consistent with tetraquark structures [120]. If the molecular picture were correct for the Z_b states, spin symmetry would lead to the existence of spin partner states [121–123], which are still to be found. In Ref. [124] it was shown that the actual pole locations of these partner states would be good probes of one-pion exchange in the molecular potential, which makes the experimental search for those states even more interesting.

The heaviest confirmed charged state in the charmonium sector is the $Z(4430)^\pm$ observed by Belle [97]. It is interpreted as hadrocharmonium [86], $\bar{D}_1 D^*$ molecule [125], as well as tetraquark [96]. Alternatively, in [126,127] the $Z(4430)^\pm$ is explained as a cross-channel effect enhanced by a triangle singularity from open charm states. These works were criticised in Ref. [128] where an alternative triangle consisting of a K^* , a π , and the $\psi(4230)$, is proposed to generate the $Z_c(4430)$. The Argand diagram shows an anticlockwise circle, in line with the experimental analysis [98], while the one of Ref. [127] shows a clockwise motion. By replacing the $\psi(4230)$ by the $\psi(3770)$ and changing the K^* one can also interpret the $Z_c(4200)$ as a kinematic effect [128]. A possible interpretation of $Z_c(3900)$ and $Z_c(4020)$ as crossed channel effects is put forward in Ref. [129]. It remains to be seen, however, if this kind of explanation is also capable of explaining the observations of these lowest Z_c states, also at other total energies.

There is recent evidence for a charged charmonium-like state with strangeness, $Z_{cs}(3985)$, from BESIII [130]. The possible existence of a strange partner to the Z_c near the $D_s\bar{D}^*$ thresholds has been predicted in molecular models [131,132], for

tetraquarks [133,134], for hadrocharmonium structures [134,135], and as a coupled-channel effect [136]. Later on this state is interpreted in Refs. [137,138] as a member of the same multiquark octet and in Refs. [139,140] as a member of the same molecular one as the $Z_c(3900)$. Ref. [138] is also able to describe the recent LHCb data in the $J/\psi(1S)K^-$ system [141], although the extracted total width for their lowest Z_{cs} state is an order of magnitude larger than that found by BESIII. Refs. [142,143] claim that both the molecular components and the compact tetraquark core are relevant to describe the $Z_c(3900)$ and $Z_{cs}(3985)$ resonances. Again, in [144] the $Z_{cs}(3985)$ can be explained as a coupled-channel effect producing the enhancement close to threshold.

It should be stressed that the various scenarios, while describing much of the available data, also make decisive predictions, *e.g.* yet unobserved quantum numbers [95,145]. The forthcoming data on heavy meson spectroscopy from various facilities should provide a much deeper understanding of how QCD forms matter out of quarks and gluons.

There is a very recent report by LHCb [146] on the observation of a narrow peak in the $D^0 D^0 \pi^+$ invariant mass distribution just below the $D^{*+} D^0$ threshold. This structure would possess a minimal $cc\bar{u}\bar{d}$ quark content. An assessment of this state will be discussed in the next issue of this review.

79.3 Systems containing four heavy quarks

Recently LHCb reported the observation of pronounced structures in a double- $J/\psi(1S)$ invariant mass distribution [147] thus pointing at states with $cc\bar{c}\bar{c}$ quarks contents. From quark models the possible existence of bound states like this was discussed already long ago [148,149]. There are now also many model calculations available in the literature. For discussions of those data from the compact tetraquark perspective see Refs. [150–156]. Most of these quark model calculations assign the reported structure to a $cc\bar{c}\bar{c}$ state in the $2S$ multiplet with near-degenerate $J^P = 0^+, 1^+$ and 2^+ configurations. The dominance of a compact tetraquark component in the apparently exotic structure is also supported by the coupled multichannel study of Ref. [157]. For direct analyses of the data within the tetraquark approach, see, *e.g.*, Ref. [158]. Also QCD sum rule studies of the system were published, but do not give consistent results: For example Ref. [159] interprets the structure at 6900 MeV as a hybrid state, Ref. [160] as a tetraquark, and Ref. [161] states that both molecular and tetraquark interpretations are possible. An alternative view on the LHCb double- $J/\psi(1S)$ data is provided in Refs. [162–164] where the analyses are performed using coupled channel T -matrices. In both works the structures in the data emerge from the interplay of thresholds and resonances with the non-trivial prediction that there should exist, if this dynamical picture were correct, a state located very near the double- $J/\psi(1S)$ threshold which can be searched for experimentally.

In contrast to the works above, Ref. [165,166] explains the double- $J/\psi(1S)$ data as cusps without nearby poles. This claim can be tested experimentally: if this explanation were correct, there should not be any narrow near threshold structure in the channel that generates the cusp, for that would call for a non-perturbative interaction in that channel as pointed out in Ref. [167].

Acknowledgement

The authors would like to thank Claude Amsler and Jean-Marc Richard for helpful input and discussions in the preparation of the review.

References

- [1] N. Brambilla *et al.*, Eur. Phys. J. **C71**, 1534 (2011), [arXiv:1010.5827].
- [2] H.-X. Chen *et al.*, Phys. Rept. **639**, 1 (2016), [arXiv:1601.02092].
- [3] A. Ali, J. S. Lange and S. Stone, Prog. Part. Nucl. Phys. **97**, 123 (2017), [arXiv:1706.00610].
- [4] R. F. Lebed, R. E. Mitchell and E. S. Swanson, Prog. Part. Nucl. Phys. **93**, 143 (2017), [arXiv:1610.04528].
- [5] S. L. Olsen, T. Skwarnicki and D. Zieminska, Rev. Mod. Phys. **90**, 1, 015003 (2018), [arXiv:1708.04012].

- [6] Y.-R. Liu *et al.*, Prog. Part. Nucl. Phys. **107**, 237 (2019), [arXiv:1903.11976].
- [7] N. Brambilla *et al.*, Phys. Rept. **873**, 1 (2020), [arXiv:1907.07583].
- [8] A. Esposito, A. Pilloni and A. D. Polosa, Phys. Rept. **668**, 1 (2017), [arXiv:1611.07920].
- [9] F.-K. Guo *et al.*, Rev. Mod. Phys. **90**, 1, 015004 (2018), [arXiv:1705.00141].
- [10] B. Aubert *et al.* (BaBar), Phys. Rev. Lett. **90**, 242001 (2003), [hep-ex/0304021].
- [11] D. Besson *et al.* (CLEO), Phys. Rev. **D68**, 032002 (2003), [Erratum: Phys. Rev. **D75**, 119908(2007)], [hep-ex/0305100].
- [12] S. Godfrey, Phys. Lett. **B568**, 254 (2003), [hep-ph/0305122].
- [13] H.-Y. Cheng and W.-S. Hou, Phys. Lett. **B566**, 193 (2003), [hep-ph/0305038].
- [14] K. Terasaki, Phys. Rev. **D68**, 011501 (2003), [hep-ph/0305213].
- [15] L. Maiani *et al.*, Phys. Rev. **D71**, 014028 (2005), [hep-ph/0412098].
- [16] V. Dmitrasinovic, Phys. Rev. Lett. **94**, 162002 (2005).
- [17] T. Barnes, F. E. Close and H. J. Lipkin, Phys. Rev. **D68**, 054006 (2003), [hep-ph/0305025].
- [18] E. E. Kolomeitsev and M. F. M. Lutz, Phys. Lett. **B582**, 39 (2004), [hep-ph/0307133].
- [19] A. Faessler *et al.*, Phys. Rev. **D76**, 014005 (2007), [arXiv:0705.0254].
- [20] A. Faessler *et al.*, Phys. Rev. **D76**, 114008 (2007), [arXiv:0709.3946].
- [21] M. F. M. Lutz and M. Soyeur, Nucl. Phys. **A813**, 14 (2008), [arXiv:0710.1545].
- [22] L. Liu *et al.*, Phys. Rev. **D87**, 1, 014508 (2013), [arXiv:1208.4535].
- [23] P. Colangelo and F. De Fazio, Phys. Lett. **B570**, 180 (2003), [hep-ph/0305140].
- [24] X.-Y. Guo, Y. Heo and M. F. M. Lutz, Phys. Rev. **D98**, 1, 014510 (2018), [arXiv:1801.10122].
- [25] V. Dmitrasinovic, Phys. Rev. **D86**, 016006 (2012).
- [26] M.-L. Du *et al.*, Phys. Rev. Lett. **126**, 19, 192001 (2021), [arXiv:2012.04599].
- [27] R. Aaij *et al.* (LHCb), Phys. Rev. **D94**, 7, 072001 (2016), [arXiv:1608.01289].
- [28] R. Aaij *et al.* (LHCb), Phys. Rev. **D94**, 7, 072001 (2016), [arXiv:1608.01289].
- [29] L. Gayer *et al.* (Hadron Spectrum), JHEP **07**, 123 (2021), [arXiv:2102.04973].
- [30] M. Albaladejo *et al.*, Phys. Lett. **B767**, 465 (2017), [arXiv:1610.06727].
- [31] M.-L. Du *et al.*, Phys. Rev. **D98**, 9, 094018 (2018), [arXiv:1712.07957].
- [32] R. Aaij *et al.* (LHCb), Phys. Rev. **D102**, 112003 (2020), [arXiv:2009.00026].
- [33] R. Aaij *et al.* (LHCb), Phys. Rev. Lett. **125**, 242001 (2020), [arXiv:2009.00025].
- [34] M. Karliner and J. L. Rosner, Phys. Rev. **D102**, 9, 094016 (2020), [arXiv:2008.05993].
- [35] X.-G. He, W. Wang and R. Zhu, Eur. Phys. J. **C80**, 11, 1026 (2020), [arXiv:2008.07145].
- [36] Z.-G. Wang, Int. J. Mod. Phys. **A35**, 30, 2050187 (2020), [arXiv:2008.07833].
- [37] R. Molina and E. Oset, Phys. Lett. **B811**, 135870 (2020), [arXiv:2008.11171].
- [38] Y. Huang *et al.*, Eur. Phys. J. **C80**, 10, 973 (2020), [arXiv:2008.07959].

- [39] M.-Z. Liu, J.-J. Xie and L.-S. Geng, Phys. Rev. D **102**, 9, 091502 (2020), [arXiv:2008.07389].
- [40] T. J. Burns and E. S. Swanson, Phys. Lett. B **813**, 136057 (2021), [arXiv:2008.12838].
- [41] X.-H. Liu *et al.*, Eur. Phys. J. C **80**, 12, 1178 (2020), [arXiv:2008.07190].
- [42] T. J. Burns and E. S. Swanson, Phys. Rev. D **103**, 1, 014004 (2021), [arXiv:2009.05352].
- [43] S. K. Choi *et al.* (Belle), Phys. Rev. Lett. **91**, 262001 (2003), [hep-ex/0309032].
- [44] B. Aubert *et al.* (BaBar), Phys. Rev. **D71**, 071103 (2005), [hep-ex/0406022].
- [45] R. Aaij *et al.* (LHCb), Phys. Rev. Lett. **115**, 072001 (2015), [arXiv:1507.03414].
- [46] R. Aaij *et al.* (LHCb), Phys. Rev. Lett. **122**, 22, 222001 (2019), [arXiv:1904.03947].
- [47] R. Aaij *et al.* (LHCb), Phys. Rev. Lett. **110**, 222001 (2013), [arXiv:1302.6269].
- [48] R. Aaij *et al.* (LHCb), Phys. Rev. **D92**, 1, 011102 (2015), [arXiv:1504.06339].
- [49] T. Barnes and S. Godfrey, Phys. Rev. **D69**, 054008 (2004), [hep-ph/0311162].
- [50] K. Abe *et al.* (Belle), Phys. Rev. Lett. **98**, 082001 (2007), [hep-ex/0507019].
- [51] S. Uehara *et al.* (Belle), Phys. Rev. Lett. **96**, 082003 (2006), [hep-ex/0512035].
- [52] R. Aaij *et al.* (LHCb), Phys. Rev. D **102**, 9, 092005 (2020), [arXiv:2005.13419].
- [53] R. Aaij *et al.* (LHCb), JHEP **08**, 123 (2020), [arXiv:2005.13422].
- [54] C. Hanhart *et al.*, Phys. Rev. D **76**, 034007 (2007), [arXiv:0704.0605].
- [55] G. Barucca *et al.* (PANDA), Eur. Phys. J. A **55**, 3, 42 (2019), [arXiv:1812.05132].
- [56] G. Barucca *et al.* (PANDA), Eur. Phys. J. A **57**, 6, 184 (2021), [arXiv:2101.11877].
- [57] F.-K. Guo, Phys. Rev. Lett. **122**, 20, 202002 (2019), [arXiv:1902.11221].
- [58] E. Braaten, L.-P. He and K. Inles, Phys. Rev. D **100**, 3, 031501 (2019), [arXiv:1904.12915].
- [59] S. Sakai, H.-J. Jing and F.-K. Guo, Phys. Rev. D **102**, 11, 114041 (2020), [arXiv:2008.10829].
- [60] N. A. Tornqvist, Phys. Lett. **B590**, 209 (2004), [hep-ph/0402237].
- [61] E. S. Swanson, Phys. Lett. **B588**, 189 (2004), [hep-ph/0311229].
- [62] D. Gamermann and E. Oset, Phys. Rev. **D80**, 014003 (2009), [arXiv:0905.0402].
- [63] Y.-b. Dong *et al.*, Phys. Rev. D **77**, 094013 (2008), [arXiv:0802.3610].
- [64] Y. Dong *et al.*, Phys. Rev. D **79**, 094013 (2009), [arXiv:0903.5416].
- [65] B. Aubert *et al.* (BaBar), Phys. Rev. **D71**, 031501 (2005), [hep-ex/0412051].
- [66] L. Maiani, A. D. Polosa and V. Riquer, Phys. Lett. **B778**, 247 (2018), [arXiv:1712.05296].
- [67] L. Maiani, A. D. Polosa and V. Riquer, Phys. Rev. D **102**, 3, 034017 (2020), [arXiv:2005.08764].
- [68] C. Bignamini *et al.*, Phys. Rev. Lett. **103**, 162001 (2009), [arXiv:0906.0882].
- [69] A. Esposito *et al.*, Eur. Phys. J. C **81**, 669 (2021), [arXiv:2006.15044].
- [70] P. Artoisenet and E. Braaten, Phys. Rev. **D81**, 114018 (2010), [arXiv:0911.2016].
- [71] E. Braaten *et al.*, Phys. Rev. D **103**, 7, L071901 (2021), [arXiv:2012.13499].
- [72] F.-K. Guo *et al.*, JHEP **05**, 138 (2014), [arXiv:1403.4032].
- [73] M. Albaladejo *et al.*, Chin. Phys. **C41**, 12, 121001 (2017), [arXiv:1709.09101].
- [74] B. Aubert *et al.* (BaBar), Phys. Rev. Lett. **95**, 142001 (2005), [hep-ex/0506081].
- [75] M. Ablikim *et al.* (BESIII), Phys. Rev. Lett. **118**, 9, 092001 (2017), [arXiv:1611.01317].
- [76] M. Cleven *et al.*, Phys. Rev. **D90**, 7, 074039 (2014), [arXiv:1310.2190].
- [77] C. Hanhart, Int. J. Mod. Phys. Conf. Ser. **46**, 1860004 (2018), [arXiv:1712.01136].
- [78] C. Hanhart and E. Klempt (2019), [arXiv:1906.11971].
- [79] T. Barnes, S. Godfrey and E. S. Swanson, Phys. Rev. D **72**, 054026 (2005), [hep-ph/0505002].
- [80] L.-C. Gui *et al.*, Phys. Rev. D **98**, 1, 016010 (2018), [arXiv:1801.08791].
- [81] F. E. Close and P. R. Page, Phys. Lett. **B628**, 215 (2005), [hep-ph/0507199].
- [82] M. Berwein *et al.*, Phys. Rev. **D92**, 11, 114019 (2015), [arXiv:1510.04299].
- [83] E. Kou and O. Pene, Phys. Lett. **B631**, 164 (2005), [hep-ph/0507119].
- [84] Yu. S. Kalashnikova and A. V. Nefediev, Phys. Rev. **D77**, 054025 (2008), [arXiv:0801.2036].
- [85] M. Ablikim *et al.* (BESIII), Phys. Rev. Lett. **111**, 24, 242001 (2013), [arXiv:1309.1896].
- [86] M. B. Voloshin, Prog. Part. Nucl. Phys. **61**, 455 (2008), [arXiv:0711.4556].
- [87] X. Li and M. B. Voloshin, Mod. Phys. Lett. **A29**, 12, 1450060 (2014), [arXiv:1309.1681].
- [88] Q. Wang, C. Hanhart and Q. Zhao, Phys. Rev. Lett. **111**, 13, 132003 (2013), [arXiv:1303.6355].
- [89] Y. Dong *et al.*, Phys. Rev. D **89**, 3, 034018 (2014), [arXiv:1310.4373].
- [90] F.-K. Guo *et al.*, Phys. Lett. **B725**, 127 (2013), [arXiv:1306.3096].
- [91] M. Ablikim *et al.* (BESIII), Phys. Rev. Lett. **112**, 9, 092001 (2014), [arXiv:1310.4101].
- [92] Y. Dong *et al.*, Phys. Rev. D **90**, 7, 074032 (2014), [arXiv:1404.6161].
- [93] Q. Wang *et al.*, Phys. Rev. **D89**, 3, 034001 (2014), [arXiv:1309.4303].
- [94] V. Baru *et al.*, Phys. Rev. **D91**, 3, 034002 (2015), [arXiv:1501.02924].
- [95] A. Ali *et al.*, Eur. Phys. J. **C78**, 1, 29 (2018), [arXiv:1708.04650].
- [96] L. Maiani *et al.*, Phys. Rev. **D89**, 114010 (2014), [arXiv:1405.1551].
- [97] K. Chilikin *et al.* (Belle), Phys. Rev. **D88**, 7, 074026 (2013), [arXiv:1306.4894].
- [98] R. Aaij *et al.* (LHCb), Phys. Rev. Lett. **112**, 22, 222002 (2014), [arXiv:1404.1903].
- [99] L. Maiani, A. D. Polosa and V. Riquer, Symmetry **13**, 5, 751 (2021), [arXiv:2103.14356].
- [100] Y.-H. Chen *et al.*, Phys. Rev. **D99**, 7, 074016 (2019), [arXiv:1902.10957].
- [101] G. Cotugno *et al.*, Phys. Rev. Lett. **104**, 132005 (2010), [arXiv:0911.2178].
- [102] F.-K. Guo *et al.*, Phys. Rev. **D82**, 094008 (2010), [arXiv:1005.2055].
- [103] L.-Y. Dai, J. Haidenbauer and U. G. Meissner, Phys. Rev. **D96**, 11, 116001 (2017), [arXiv:1710.03142].

- [104] J. He *et al.*, Eur. Phys. J. C **80**, 3, 246 (2020), [arXiv:1912.08420].
- [105] F.-L. Wang and X. Liu, Phys. Rev. D **102**, 9, 094006 (2020), [arXiv:2008.13484].
- [106] H.-W. Ke, X.-H. Liu and X.-Q. Li, Chin. Phys. C **44**, 9, 093104 (2020), [arXiv:2004.03167].
- [107] J.-R. Zhang, Phys. Rev. D **102**, 5, 054006 (2020), [arXiv:2004.10985].
- [108] F.-K. Guo, C. Hanhart and U.-G. Meissner, Phys. Lett. B **665**, 26 (2008), [arXiv:0803.1392].
- [109] F.-K. Guo, C. Hanhart and U.-G. Meissner, Phys. Rev. Lett. **102**, 242004 (2009), [arXiv:0904.3338].
- [110] M. Ablikim *et al.* (BESIII), Phys. Rev. Lett. **110**, 252001 (2013), [arXiv:1303.5949].
- [111] M. Ablikim *et al.* (BESIII), Phys. Rev. Lett. **112**, 2, 022001 (2014), [arXiv:1310.1163].
- [112] P. Krokovny *et al.* (Belle), Phys. Rev. **D88**, 5, 052016 (2013), [arXiv:1308.2646].
- [113] A. Bondar *et al.* (Belle), Phys. Rev. Lett. **108**, 122001 (2012), [arXiv:1110.2251].
- [114] A. Garmash *et al.* (Belle), Phys. Rev. Lett. **116**, 21, 212001 (2016), [arXiv:1512.07419].
- [115] A. E. Bondar *et al.*, Phys. Rev. **D84**, 054010 (2011), [arXiv:1105.4473].
- [116] Z.-M. Ding, H.-Y. Jiang and J. He, Eur. Phys. J. C **80**, 12, 1179 (2020), [arXiv:2011.04980].
- [117] Y. Dong *et al.*, Phys. Rev. D **88**, 1, 014030 (2013), [arXiv:1306.0824].
- [118] F. Goerke *et al.*, Phys. Rev. D **94**, 9, 094017 (2016), [arXiv:1608.04656].
- [119] F. Goerke *et al.*, Phys. Rev. D **96**, 5, 054028 (2017), [arXiv:1707.00539].
- [120] A. Ali *et al.*, Phys. Rev. **D91**, 1, 017502 (2015), [arXiv:1412.2049].
- [121] M. B. Voloshin, Phys. Rev. **D84**, 031502 (2011), [arXiv:1105.5829].
- [122] T. Mehen and J. W. Powell, Phys. Rev. **D84**, 114013 (2011), [arXiv:1109.3479].
- [123] V. Baru *et al.*, JHEP **06**, 158 (2017), [arXiv:1704.07332].
- [124] V. Baru *et al.*, Phys. Rev. **D99**, 9, 094013 (2019), [arXiv:1901.10319].
- [125] T. Branz, T. Gutsche and V. E. Lyubovitskij, Phys. Rev. **D82**, 054025 (2010), [arXiv:1005.3168].
- [126] P. Pakhlov, Phys. Lett. **B702**, 139 (2011), [arXiv:1105.2945].
- [127] P. Pakhlov and T. Uglov, Phys. Lett. **B748**, 183 (2015), [arXiv:1408.5295].
- [128] S. X. Nakamura and K. Tsushima, Phys. Rev. **D100**, 5, 051502 (2019), [arXiv:1901.07385].
- [129] J.-Z. Wang *et al.*, Eur. Phys. J. C **80**, 11, 1040 (2020), [arXiv:2007.02263].
- [130] M. Ablikim *et al.* (BESIII), Phys. Rev. Lett. **126**, 10, 102001 (2021), [arXiv:2011.07855].
- [131] S. H. Lee, M. Nielsen and U. Wiedner, J. Korean Phys. Soc. **55**, 424 (2009), [arXiv:0803.1168].
- [132] J. M. Dias, X. Liu and M. Nielsen, Phys. Rev. D **88**, 9, 096014 (2013), [arXiv:1307.7100].
- [133] D. Ebert, R. N. Faustov and V. O. Galkin, Eur. Phys. J. C **58**, 399 (2008), [arXiv:0808.3912].
- [134] J. Ferretti and E. Santopinto, JHEP **04**, 119 (2020), [arXiv:2001.01067].
- [135] M. B. Voloshin, Phys. Lett. B **798**, 135022 (2019), [arXiv:1901.01936].
- [136] D.-Y. Chen, X. Liu and T. Matsuki, Phys. Rev. Lett. **110**, 23, 232001 (2013), [arXiv:1303.6842].
- [137] L. Meng, B. Wang and S.-L. Zhu, Phys. Rev. D **102**, 11, 111502 (2020), [arXiv:2011.08656].
- [138] P. G. Ortega, D. R. Entem and F. Fernandez, Phys. Lett. B **818**, 136382 (2021), [arXiv:2103.07871].
- [139] Z. Yang *et al.*, Phys. Rev. D **103**, 7, 074029 (2021), [arXiv:2011.08725].
- [140] B. Wang, L. Meng and S.-L. Zhu, Phys. Rev. D **103**, 2, L021501 (2021), [arXiv:2011.10922].
- [141] R. Aaij *et al.* (LHCb), Phys. Rev. Lett. **127**, 8, 082001 (2021), [arXiv:2103.01803].
- [142] R. M. Albuquerque, S. Narison and D. Rabetiarivony, Phys. Rev. D **103**, 7, 074015 (2021), [arXiv:2101.07281].
- [143] Z.-H. Guo and J. A. Oller, Phys. Rev. D **103**, 5, 054021 (2021), [arXiv:2012.11904].
- [144] N. Ikeno, R. Molina and E. Oset, Phys. Lett. B **814**, 136120 (2021), [arXiv:2011.13425].
- [145] M. Cleven *et al.*, Phys. Rev. **D92**, 1, 014005 (2015), [arXiv:1505.01771].
- [146] R. Aaij *et al.* (LHCb) (2021), [arXiv:2109.01038].
- [147] R. Aaij *et al.* (LHCb), Sci. Bull. **65**, 23, 1983 (2020), [arXiv:2006.16957].
- [148] J. P. Ader, J. M. Richard and P. Taxil, Phys. Rev. D **25**, 2370 (1982).
- [149] Y. Iwasaki, Prog. Theor. Phys. **54**, 492 (1975).
- [150] L. Maiani, Sci. Bull. **65**, 1949 (2020), [arXiv:2008.01637].
- [151] K.-T. Chao and S.-L. Zhu, Sci. Bull. **65**, 23, 1952 (2020), [arXiv:2008.07670].
- [152] J.-M. Richard, Sci. Bull. **65**, 1954 (2020), [arXiv:2008.01962].
- [153] R. N. Faustov, V. O. Galkin and E. M. Savchenko, Phys. Rev. D **102**, 11, 114030 (2020), [arXiv:2009.13237].
- [154] J. F. Giron and R. F. Lebed, Phys. Rev. D **102**, 7, 074003 (2020), [arXiv:2008.01631].
- [155] X. Jin *et al.*, Eur. Phys. J. C **80**, 11, 1083 (2020), [arXiv:2006.13745].
- [156] Q.-F. Lü, D.-Y. Chen and Y.-B. Dong, Eur. Phys. J. C **80**, 9, 871 (2020), [arXiv:2006.14445].
- [157] Z.-H. Guo and J. A. Oller, Phys. Rev. D **103**, 3, 034024 (2021), [arXiv:2011.00978].
- [158] M. Karliner and J. L. Rosner, Phys. Rev. D **102**, 11, 114039 (2020), [arXiv:2009.04429].
- [159] B.-D. Wan and C.-F. Qiao, Phys. Lett. B **817**, 136339 (2021), [arXiv:2012.00454].
- [160] B.-C. Yang, L. Tang and C.-F. Qiao, Eur. Phys. J. C **81**, 4, 324 (2021), [arXiv:2012.04463].
- [161] R. M. Albuquerque *et al.*, Phys. Rev. D **102**, 9, 094001 (2020), [arXiv:2008.01569].
- [162] X.-K. Dong *et al.*, Phys. Rev. Lett. **126**, 13, 132001 (2021), [arXiv:2009.07795].
- [163] C. Gong *et al.* (2020), [arXiv:2011.11374].
- [164] Z.-R. Liang, X.-Y. Wu and D.-L. Yao (2021), [arXiv:2104.08589].
- [165] J.-Z. Wang *et al.*, Phys. Rev. D **103**, 7, 071503 (2021), [arXiv:2008.07430].
- [166] J.-Z. Wang, X. Liu and T. Matsuki, Phys. Lett. B **816**, 136209 (2021), [arXiv:2012.03281].
- [167] F.-K. Guo *et al.*, Phys. Rev. D **91**, 5, 051504 (2015), [arXiv:1411.5584].

80. Baryon Decay Parameters

Revised August 2019 by E.D. Commins (UC Berkeley).

80.1 Baryon semileptonic decays

The typical spin-1/2 baryon semileptonic decay is described by a matrix element, the hadronic part of which may be written as:

$$\bar{B}_f \left[f_1(q^2)\gamma_\lambda + i f_2(q^2)\sigma_{\lambda\mu}q^\mu + g_1(q^2)\gamma_\lambda\gamma_5 + g_3(q^2)\gamma_5q_\lambda \right] B_i . \quad (80.1)$$

Here B_i and \bar{B}_f are spinors describing the initial and final baryons, and $q = p_i - p_f$, while the terms in f_1 , f_2 , g_1 , and g_3 account for vector, induced tensor (“weak magnetism”), axial vector, and induced pseudoscalar contributions [1]. Second-class current contributions are ignored here. In the limit of zero momentum transfer, f_1 reduces to the vector coupling constant g_V , and g_1 reduces to the axial-vector coupling constant g_A . The latter coefficients are related by Cabibbo’s theory [2], generalized to six quarks (and three mixing angles) by Kobayashi and Maskawa [3]. The g_3 term is negligible for transitions in which an e^\pm is emitted, and gives a very small correction, which can be estimated by PCAC [4], for μ^\pm modes. Recoil effects include weak magnetism, and are taken into account adequately by considering terms of first order in

$$\delta = \frac{m_i - m_f}{m_i + m_f} , \quad (80.2)$$

where m_i and m_f are the masses of the initial and final baryons.

The experimental quantities of interest are the total decay rate, the lepton-neutrino angular correlation, the asymmetry coefficients in the decay of a polarized initial baryon, and the polarization of the decay baryon in its own rest frame for an unpolarized initial baryon. Formulae for these quantities are derived by standard means [5] and are analogous to formulae for nuclear beta decay [6]. We use the notation of Ref. [6] in the Listings for neutron beta decay. For comparison with experiments at higher q^2 , it is necessary to modify the form factors at $q^2 = 0$ by a “dipole” q^2 dependence, and for high-precision comparisons to apply appropriate radiative corrections [7].

The ratio g_A/g_V may be written as

$$g_A/g_V = |g_A/g_V| e^{i\phi_{AV}} . \quad (80.3)$$

The presence of a “triple correlation” term in the transition probability, proportional to $\text{Im}(g_A/g_V)$ and of the form

$$\sigma_i \cdot (p_\ell \times p_\nu) \quad (80.4)$$

for initial baryon polarization or

$$\sigma_f \cdot (p_\ell \times p_\nu) \quad (80.5)$$

for final baryon polarization, would indicate failure of time-reversal invariance. The phase angle ϕ has been measured precisely only in neutron decay (and in ^{19}Ne nuclear beta decay), and the results are consistent with T invariance.

80.2 Hyperon nonleptonic decays

The amplitude for a spin-1/2 hyperon decaying into a spin-1/2 baryon and a spin-0 meson can be written in the form

$$M = G_F m_\pi^2 \cdot \bar{B}_f (A - B\gamma_5) B_i , \quad (80.6)$$

where A and B are constants [1]. The transition rate is proportional to

$$R = 1 + \gamma \hat{\omega}_f \cdot \hat{\omega}_i + (1 - \gamma)(\hat{\omega}_f \cdot \hat{\mathbf{n}})(\hat{\omega}_i \cdot \hat{\mathbf{n}}) + \alpha(\hat{\omega}_f \cdot \hat{\mathbf{n}} + \hat{\omega}_i \cdot \hat{\mathbf{n}}) + \beta \hat{\mathbf{n}} \cdot (\hat{\omega}_f \times \hat{\omega}_i) , \quad (80.7)$$

where $\hat{\mathbf{n}}$ is a unit vector in the direction of the final baryon momentum, and $\hat{\omega}_i$ and $\hat{\omega}_f$ are unit vectors in the directions of the

initial and final baryon spins. (The sign of the last term in the above equation was incorrect in our 1988 and 1990 editions.) The parameters α , β , and γ are defined as

$$\begin{aligned} \alpha &= 2 \text{Re}(s^*p)/(|s|^2 + |p|^2) , \\ \beta &= 2 \text{Im}(s^*p)/(|s|^2 + |p|^2) , \\ \gamma &= (|s|^2 - |p|^2)/(|s|^2 + |p|^2) , \end{aligned} \quad (80.8)$$

where $s = A$ and $p = |\mathbf{p}_f|B/(E_f + m_f)$; here E_f and \mathbf{p}_f are the energy and momentum of the final baryon. The parameters α , β , and γ satisfy

$$\alpha^2 + \beta^2 + \gamma^2 = 1 \quad (80.9)$$

If the hyperon polarization is \mathbf{P}_Y , the polarization \mathbf{P}_B of the decay baryons is

$$\mathbf{P}_B = \frac{(\alpha + \mathbf{P}_Y \cdot \hat{\mathbf{n}})\hat{\mathbf{n}} + \beta(\mathbf{P}_Y \times \hat{\mathbf{n}}) + \gamma\hat{\mathbf{n}} \times (\mathbf{P}_Y \times \hat{\mathbf{n}})}{1 + \alpha\mathbf{P}_Y \cdot \hat{\mathbf{n}}} . \quad (80.10)$$

Here \mathbf{P}_B is defined in the rest system of the baryon, obtained by a Lorentz transformation along $\hat{\mathbf{n}}$ from the hyperon rest frame, in which $\hat{\mathbf{n}}$ and \mathbf{P}_Y are defined.

An additional useful parameter ϕ is defined by

$$\beta = (1 - \alpha^2)^{1/2} \sin\phi . \quad (80.11)$$

In the Listings, we compile α and ϕ for each decay, since these quantities are most closely related to experiment and are essentially uncorrelated. When necessary, we have changed the signs of reported values to agree with our sign conventions. In the Baryon Summary Table, we give α , ϕ , and Δ (defined below) with errors, and also give the value of γ without error.

Time-reversal invariance requires, in the absence of final-state interactions, that s and p be relatively real, and therefore that $\beta = 0$. However, for the decays discussed here, the final-state interaction is strong. Thus

$$s = |s| e^{i\delta_s} \text{ and } p = |p| e^{i\delta_p} , \quad (80.12)$$

where δ_s and δ_p are the pion-baryon s - and p -wave strong interaction phase shifts. We then have

$$\beta = \frac{-2|s||p|}{|s|^2 + |p|^2} \sin(\delta_s - \delta_p) . \quad (80.13)$$

One also defines $\Delta = -\tan^{-1}(\beta/\alpha)$. If T invariance holds, $\Delta = \delta_s - \delta_p$. For $\Lambda \rightarrow p\pi^-$ decay, the value of Δ may be compared with the s - and p -wave phase shifts in low-energy π^-p scattering, and the results are consistent with T invariance.

See also the note on “Radiative Hyperon Decays” in this *Review*.

References

- [1] E. Commins and P. Bucksbaum, *Weak Interactions of Leptons and Quarks* (1983), ISBN 978-0-521-27370-1, (Cambridge, USA: University Press, 473p).
- [2] N. Cabibbo, Phys. Rev. Lett. **10**, 531 (1963).
- [3] M. Kobayashi and T. Maskawa, Prog. Theor. Phys. **49**, 652 (1973).
- [4] M. Goldberger and S. Treiman, Phys. Rev. **111**, 354 (1958).
- [5] P. Frampton and W.-K. Tung, Phys. Rev. D **3**, 1114 (1971).
- [6] J. Jackson, S. Treiman and H. Wyld, Nucl. Phys. **4**, 206 (1957).
- [7] Y. Yokoo, S. Suzuki and M. Morita, Prog. Theor. Phys. **50**, 1894 (1973).

81. N and Δ Resonances

Revised August 2019 by V.D. Burkert (Jefferson Lab), V. Crede (Florida State U.), U. Thoma (Bonn U.), L. Tiator (KPH, JGU Mainz) and R.L. Workman (George Washington U.).

81.1 Introduction

The excited states of the nucleon have been studied in a large number of formation and production experiments. Until recently, the Breit-Wigner masses and widths, the pole positions, and the elasticities of the N and Δ resonances in the Baryon Summary Table came largely from partial-wave analyses of πN total, elastic, and charge-exchange scattering data. The most comprehensive analyses were carried out by the Karlsruhe-Helsinki (KH80) [1], Carnegie Mellon-Berkeley (CMB80) [2], and George Washington U (GWU) [3] groups. Partial-wave analyses have also been performed on much smaller πN reaction data sets to get ηN , $K\Lambda$, and $K\Sigma$ branching fractions (see the Listings for references). Other branching fractions come from analyses of $\pi N \rightarrow \pi\pi N$ data.

In recent years, a large amount of data on photoproduction of many final states has been accumulated, and these data are beginning to tell us much about the properties of baryon resonances. A survey of data on photoproduction can be found in the proceedings of recent conferences [4] and workshops [5], and in recent reviews [6, 7].

81.2 Naming scheme for baryon resonances

In the past, when nearly all resonance information came from elastic πN scattering, it was common to label resonances with the incoming partial wave $L_{2I,2J}$, as in $\Delta(1232)P_{33}$ and $N(1680)F_{15}$. However, most recent information has come from γN experiments. Therefore, we have replaced $L_{2I,2J}$ with the spin-parity J^P of the state, as in $\Delta(1232)3/2^+$ and $N(1680)5/2^+$; this name gives intrinsic properties of the resonance that are independent of the specific particles and reactions used to study them. This applies equally to all baryons, including Ξ resonances and charm baryons that are not produced in formation experiments. We do not, however, attach the mass or spin-parity to the names of the ground-state (“stable”) baryons $N, \Lambda, \Sigma, \Xi, \Omega, \Lambda_c, \dots$.

81.3 Using the N and Δ listings

Tables 81.1 and 81.2 list all the N and Δ entries in the Baryon Listings and give our evaluation of the overall status and the status channel by channel. Only the established resonances (overall status 3 or 4 stars) are promoted to the Baryon Summary Table. We long ago omitted from the Listings information from old analyses, prior to KH80 and CMB80, which can be found in earlier editions. A rather complete survey of older results was given in our 1982 edition [8].

As a rule, we award an overall status **** or *** only to those resonances which are derived from analyses of data sets that include precision differential cross sections and polarization observables, and are confirmed by independent analyses. All other signals are given ** or * status. New results that are not accompanied by proper error evaluation are less valuable for evaluating star ratings. The following criteria are guidelines for future error analysis.

1. Uncertainties in resonance parameters: The publication should have a detailed discussion on how the uncertainties of parameters were estimated. This requires that the error estimates go beyond the simple fit error as e.g. given by MINUIT, and the robustness of the results should be demonstrated.

2. Fit quality: Concrete measures for the fit quality should be provided. The reduced global χ^2 value of the fit, while useful, is insufficient. Other possibilities include quoting variations of local χ^2 values in kinematic regions where evidence for new resonances, or significantly improved information on resonance parameters, is claimed.

3. Weight factors in observables: Analyses sometimes use weight factors for certain data sets to either increase or reduce their impact on the results. This has been particularly important when polarization observables are involved, which often are sensitive to resonance amplitudes through interferences, but usually have much poorer statistics than differential cross section data. To evaluate sensitivities, the resulting resonance parameters should

be checked against variations of the specific weight factors.

Table 81.1: The status of the N resonances and their decays. Sub-threshold decay modes are omitted. Only resonances with an overall status of *** or **** are included in the main Baryon Summary Table.

Particle	J^P	overall	Status as seen in																		
			$N\gamma$	$N\pi$	$\Delta\pi$	$N\sigma$	$N\eta$	ΛK	ΣK	$N\rho$	$N\omega$	$N\eta'$									
N	$1/2^+$	****																			
$N(1440)$	$1/2^+$	****	****	****	****	****	****	****	****	****	****	****	****	****	****	****	****	****	****	****	****
$N(1520)$	$3/2^-$	****	****	****	****	****	****	****	****	****	****	****	****	****	****	****	****	****	****	****	****
$N(1535)$	$1/2^-$	****	****	****	****	****	****	****	****	****	****	****	****	****	****	****	****	****	****	****	****
$N(1650)$	$1/2^-$	****	****	****	****	****	****	****	****	****	****	****	****	****	****	****	****	****	****	****	****
$N(1675)$	$5/2^-$	****	****	****	****	****	****	****	****	****	****	****	****	****	****	****	****	****	****	****	****
$N(1680)$	$5/2^+$	****	****	****	****	****	****	****	****	****	****	****	****	****	****	****	****	****	****	****	****
$N(1700)$	$3/2^-$	****	****	****	****	****	****	****	****	****	****	****	****	****	****	****	****	****	****	****	****
$N(1710)$	$1/2^+$	****	****	****	****	****	****	****	****	****	****	****	****	****	****	****	****	****	****	****	****
$N(1720)$	$3/2^+$	****	****	****	****	****	****	****	****	****	****	****	****	****	****	****	****	****	****	****	****
$N(1860)$	$5/2^+$	**	*	*	*	*	*	*	*	*	*	*	*	*	*	*	*	*	*	*	*
$N(1875)$	$3/2^-$	**	*	*	*	*	*	*	*	*	*	*	*	*	*	*	*	*	*	*	*
$N(1880)$	$1/2^+$	**	*	*	*	*	*	*	*	*	*	*	*	*	*	*	*	*	*	*	*
$N(1895)$	$1/2^-$	****	****	****	****	****	****	****	****	****	****	****	****	****	****	****	****	****	****	****	****
$N(1900)$	$3/2^+$	****	****	****	****	****	****	****	****	****	****	****	****	****	****	****	****	****	****	****	****
$N(1990)$	$7/2^+$	**	*	*	*	*	*	*	*	*	*	*	*	*	*	*	*	*	*	*	*
$N(2000)$	$5/2^+$	**	*	*	*	*	*	*	*	*	*	*	*	*	*	*	*	*	*	*	*
$N(2040)$	$3/2^+$	*	*	*	*	*	*	*	*	*	*	*	*	*	*	*	*	*	*	*	*
$N(2060)$	$5/2^-$	****	****	****	****	****	****	****	****	****	****	****	****	****	****	****	****	****	****	****	****
$N(2100)$	$1/2^+$	****	****	****	****	****	****	****	****	****	****	****	****	****	****	****	****	****	****	****	****
$N(2120)$	$3/2^-$	****	****	****	****	****	****	****	****	****	****	****	****	****	****	****	****	****	****	****	****
$N(2190)$	$7/2^-$	****	****	****	****	****	****	****	****	****	****	****	****	****	****	****	****	****	****	****	****
$N(2220)$	$9/2^+$	****	****	****	****	****	****	****	****	****	****	****	****	****	****	****	****	****	****	****	****
$N(2250)$	$9/2^-$	****	****	****	****	****	****	****	****	****	****	****	****	****	****	****	****	****	****	****	****
$N(2300)$	$1/2^+$	**	*	*	*	*	*	*	*	*	*	*	*	*	*	*	*	*	*	*	*
$N(2570)$	$5/2^-$	**	*	*	*	*	*	*	*	*	*	*	*	*	*	*	*	*	*	*	*
$N(2600)$	$11/2^-$	****	****	****	****	****	****	****	****	****	****	****	****	****	****	****	****	****	****	****	****
$N(2700)$	$13/2^+$	**	*	*	*	*	*	*	*	*	*	*	*	*	*	*	*	*	*	*	*

**** Existence is certain.
 *** Existence is very likely.
 ** Evidence of existence is fair.
 * Evidence of existence is poor.

Table 81.2: The status of the Δ resonances and their decays. Sub-threshold decay modes are omitted. Only resonances with an overall status of *** or **** are included in the main Baryon Summary Table.

Particle	J^P	overall	Status as seen in							
			$N\gamma$	$N\pi$	$\Delta\pi$	ΣK	$N\rho$	$\Delta\eta$		
$\Delta(1232)$	$3/2^+$	****	****	****	****	****	****	****	****	****
$\Delta(1600)$	$3/2^+$	****	****	****	****	****	****	****	****	****
$\Delta(1620)$	$1/2^-$	****	****	****	****	****	****	****	****	****
$\Delta(1700)$	$3/2^-$	****	****	****	****	****	****	****	****	****
$\Delta(1750)$	$1/2^+$	*	*	*	*	*	*	*	*	*
$\Delta(1900)$	$1/2^-$	****	****	****	****	****	****	****	****	****
$\Delta(1905)$	$5/2^+$	****	****	****	****	****	****	****	****	****
$\Delta(1910)$	$1/2^+$	****	****	****	****	****	****	****	****	****
$\Delta(1920)$	$3/2^+$	****	****	****	****	****	****	****	****	****
$\Delta(1930)$	$5/2^-$	****	****	****	****	****	****	****	****	****
$\Delta(1940)$	$3/2^-$	**	*	*	*	*	*	*	*	*
$\Delta(1950)$	$7/2^+$	****	****	****	****	****	****	****	****	****
$\Delta(2000)$	$5/2^+$	**	*	*	*	*	*	*	*	*
$\Delta(2150)$	$1/2^-$	*	*	*	*	*	*	*	*	*
$\Delta(2200)$	$7/2^-$	****	****	****	****	****	****	****	****	****
$\Delta(2300)$	$9/2^+$	**	*	*	*	*	*	*	*	*
$\Delta(2350)$	$5/2^-$	*	*	*	*	*	*	*	*	*
$\Delta(2390)$	$7/2^+$	*	*	*	*	*	*	*	*	*
$\Delta(2400)$	$9/2^-$	**	*	*	*	*	*	*	*	*
$\Delta(2420)$	$11/2^+$	****	****	****	****	****	****	****	****	****
$\Delta(2750)$	$13/2^-$	**	*	*	*	*	*	*	*	*
$\Delta(2950)$	$15/2^+$	**	*	*	*	*	*	*	*	*

**** Existence is certain.
 *** Existence is very likely.
 ** Evidence of existence is fair.
 * Evidence of existence is poor.

Claims of evidence for new baryon states must be based on a sufficiently complete set of partial waves in the fit. The robustness of signals must be demonstrated, e.g. by examining the effect of

higher partial waves in the fit.

81.4 Properties of resonances

Resonances are defined by poles of the S -matrix, whether in scattering, production or decay matrix elements. These are poles in the complex plane in s , as discussed in the new review on *Resonances*. As is traditional, we quote here the pole positions in the complex energy $w = \sqrt{s}$ plane. Crucially, the position of the pole of the S -matrix is independent of the process, and the production and decay properties factorize. This is the rationale for listing the pole position first for each resonance. These key properties of the S -matrix pole are in contrast to other quantities related to resonance phenomena, such as Breit-Wigner parameters or any K -matrix pole. Breit-Wigner parameters depend on the formalism used, such as angular-momentum barrier factors, or cut-off parameters, and the assumed or modeled background. However, the accurate determination of pole parameters from the analysis of data on the real energy axis is not necessarily simple, or even straightforward. It requires the implementation of the correct analytic structure of the relevant (often coupled) channels.

In principle, there are two ways to extract pole parameters from experimental data: (i) analytic continuation of theoretical single- or multi-channel models into the complex energy plane or (ii) local expansions of the partial-wave T -matrix amplitudes in the complex energy plane in the vicinity of a pole.

At present, poles are usually extracted using the first method [9–14], but considerable effort has been put into the development of alternate approaches, such as the speed plot [15], time delay [16], N/D method [17], regularization procedure [18], or Padé approximation [19].

Methods of the second type are based on the idea to use first or higher-order derivatives in energy to reduce the importance of, or totally eliminate, the background contribution. One either has to model the background contribution and introduce model dependence, or one is faced with numerical derivatives of single-energy data. In both cases, one reaches almost unsurmountable difficulties.

An alternate way to extract pole parameters from partial waves has been proposed by introducing a Laurent+Pietarinen ($L+P$) expansion [20–22]

$$T(W) = \sum_{i=1}^N \frac{Res_i}{W - W_i} + \sum_{j=1}^M \sum_{n=0}^{n_{max}} c_n^j \left(\frac{\alpha_j - \sqrt{x_j - W}}{\alpha_j + \sqrt{x_j - W}} \right)^n, \quad (81.1)$$

where $T(W)$ is a given partial wave amplitude, W_i and Res_i are the N complex pole positions and residues. The background is parameterized with M Pietarinen functions, where α_j are positive range parameters and x_j are real or complex branch points; c_n^j are real expansion coefficients.

The main idea of this procedure is to find the simplest analytic function, with well-defined poles and cuts, regardless of whether they are generated by a theoretical model or some energy-independent procedure. Instead of searching for the function which reproduces the input amplitudes over the complete complex energy plane, on all Riemann sheets, a representation is searched only in a limited complex energy range, near the real axis, which is defined by the radius of convergence of the Laurent decomposition, and which contains the input amplitudes. All details are found in Ref. [21]. Applications of the method can be found in [20–27].

81.5 Photoproduction

A new approach to the nucleon excitation spectrum is provided by dedicated facilities at the Universities of Bonn, Grenoble, and Mainz, and at the national laboratories Jefferson Lab in the US and SPring-8 in Japan. High-precision cross sections and polarization observables for the photoproduction of pseudoscalar mesons provide a data set that is approaching a “complete experiment,” one that fully constrains the four complex amplitudes describing the spin-structure of the reaction [28]. A large number of photoproduction reactions has been studied.

In pseudoscalar meson photoproduction, the four independent helicity amplitudes can be expressed in terms of the four CGLN

[29] amplitudes allowed by Lorentz and gauge invariance. These amplitudes can be expanded in a series of electric and magnetic multipoles. Except for $J = 1/2$, one electric and one magnetic multipole contributes to each J^P combination.

For a given state, these two amplitudes determine the resonance photo-decay helicity amplitudes $A_{1/2}$ and $A_{3/2}$. As described below, this resonance extraction has been carried out either assuming a Breit-Wigner resonance or at the pole.

If a Breit-Wigner parametrization is used, the $N\gamma$ partial width, Γ_γ , is given in terms of the helicity amplitudes $A_{1/2}$ and $A_{3/2}$ by

$$\Gamma_\gamma = \frac{k_{\text{BW}}^2}{\pi} \frac{2m_N}{(2J+1)m_{\text{BW}}} \left(|A_{1/2}|^2 + |A_{3/2}|^2 \right). \quad (81.2)$$

Here m_N and m_{BW} are the nucleon and resonance masses, J is the resonance spin, and k_{BW} is the photon c.m. decay momentum. Most earlier analyses have provided these real quantities $A_{1/2}$ and $A_{3/2}$.

More recent studies have quoted related complex quantities, evaluated at the T -matrix pole. These complex helicity amplitudes, $\tilde{A}_{1/2}$ and $\tilde{A}_{3/2}$, can be cast onto the form

$$\tilde{A}_h = \sqrt{\frac{\pi(2J+1)w_{\text{pole}}}{m_N k_{\text{pole}}^2}} \frac{Res(T_h(\gamma N \rightarrow N b))}{\sqrt{Res(T(N b \rightarrow N b))}} \quad (81.3)$$

where the residues (Res) are evaluated at the pole position, w_{pole} , and $k_{\text{pole}}^2 = (w_{\text{pole}}^2 - m_N^2)^2 / 4w_{\text{pole}}^2$ [30]. For Breit-Wigner amplitudes, $w_{\text{pole}} = m_{\text{BW}}$ and $\tilde{A}_h = A_h$. Similar relations for the photo and electro couplings at the pole position can be found in [31,32].

The determination of eight real numbers from four complex amplitudes (with one overall phase undetermined) requires at least seven independent measurements. At least one further measurement is required to resolve discrete ambiguities that result from the fact that data are proportional to squared amplitudes. Photon beams and nucleon targets can be polarized (with linear or circular polarization P_\perp , P_\odot and \vec{T} , respectively); the recoil polarization of the outgoing baryon \vec{R} can be measured. The experiments can be divided into three classes: (1) the beam and target are polarized (BT); (2) the beam is polarized and the recoil baryon polarization is measured (BR); (3) the target is polarized and the recoil polarization is measured (TR). Different sign conventions are used in the literature, as summarized in [33].

One of the best studied reactions is $\gamma p \rightarrow \Lambda K^+$. Published data include differential cross sections, the beam asymmetry Σ , the target asymmetry T , the recoil polarization P , and the BR double-polarization variables $C_{x'}$, $C_{z'}$, $O_{x'}$, and $O_{z'}$. For the photoproduction of pions and etas, off proton and neutron targets, differential cross sections, single- and double-polarization asymmetries have been measured, mainly for pions.

81.6 Electroproduction

Electroproduction of mesons provides information on the internal structure of resonances. The helicity amplitudes are functions of the (squared) momentum transfer $Q^2 = -(e-e')^2$, where e and e' are the 4-momenta of the incident and scattered electron, and a third amplitude, $S_{1/2}$, measures the resonance response to the longitudinal component of the virtual photon. Most data stem from the reactions $e^- p \rightarrow e^- n \pi^+$ and $e^- p \rightarrow e^- p \pi^0$ but also the reactions $e^- p \rightarrow e^- p \eta$, $e^- p \rightarrow e^- p \pi^+ \pi^-$, and $e^- p \rightarrow e^- \Lambda(\Sigma^0) K^+$ have been studied. The data and their interpretation are reviewed in Refs. [34,35].

The transition to the $\Delta(1232)3/2^+$ is often quantified in terms of the magnetic dipole transition moment M_{1+} (or the magnetic transition form factor $G_{M,As}^*(Q^2)$) [36], and the electric and scalar quadrupole transition moments E_{1+} and S_{1+} . Figure 81.1 shows the strength of the $p \rightarrow \Delta^+$ transition plotted versus the photon virtuality Q^2 . At $Q^2 = 0$, M_{1+} dominates the resonance transition strength. The two amplitudes E_{1+} and S_{1+} imply a quadrupole deformation of the transition to the lowest excited state. The magnitude of $R_{EM} = E_{1+}/M_{1+}$ remains nearly constant, while the magnitude of $R_{SM} = S_{1+}/M_{1+}$ increases rapidly up to 25% at the highest Q^2 value.

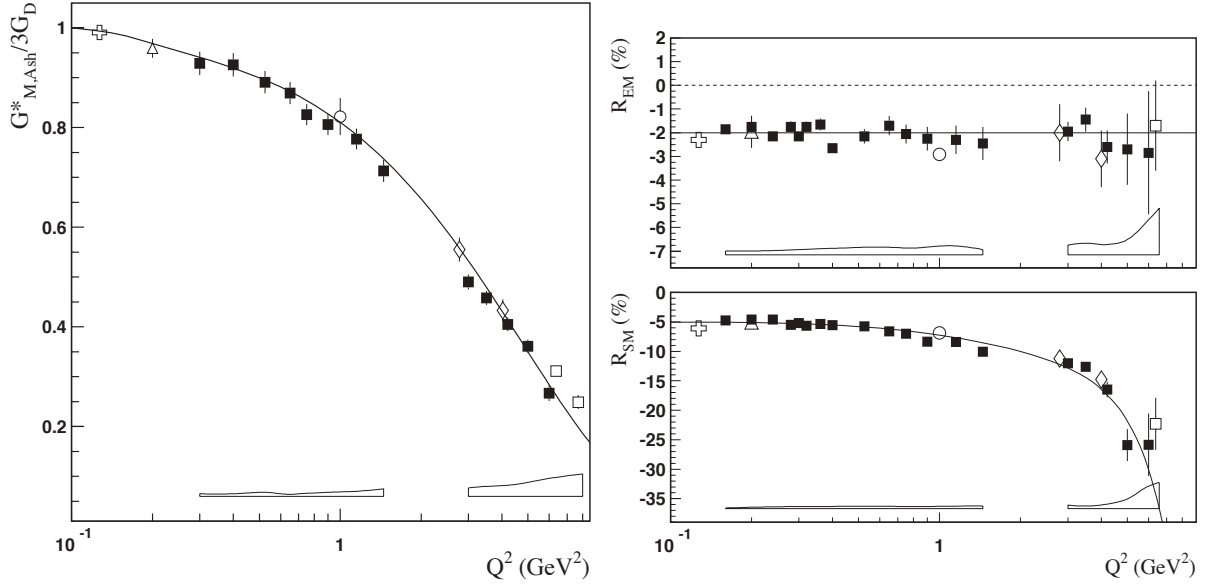


Figure 81.1: Left: The magnetic transition form factor for the $\gamma^*p \rightarrow \Delta^+(1232)$ transition versus the photon virtuality Q^2 . Right: The electric and scalar quadrupole ratios R_{EM} and R_{SM} . The different symbols are results from different experiments at JLab (squares, diamonds, circle) and MAMI (triangle, cross). The boxes near the horizontal axis indicate model uncertainties of the squares. Curves to guide the eyes.

Figure 81.2 shows the transverse and scalar helicity amplitudes for the $N(1440)1/2^+$, $N(1520)3/2^-$, and $N(1535)1/2^-$ resonances from JLab [34]. Similar results have been achieved at Mainz [35]. For the states $N(1440)1/2^+$ and $N(1520)3/2^-$, helicity amplitudes and $\pi\Delta$ and ρp decays were determined at JLab in an analysis of $\pi^+\pi^-p$ electroproduction [37]. The data show distinctly different Q^2 dependencies that indicate different internal structures.

The $N(1520)3/2^-$ helicity amplitudes reveal the dominance of its three-quark nature: the $A_{3/2}$ amplitude is large at the photon point and decreases rapidly $\sim Q^{-5}$ with increasing Q^2 ; $A_{1/2}$ is small at the photon point, increases rapidly with Q^2 and then falls off with $\sim Q^{-3}$. Quantitative agreement with the data is, however, achieved only when meson cloud effects are included.

At high Q^2 , both amplitudes for $N(1440)1/2^+$ are qualitatively described by light front quark models [38]: at short distances the resonance behaves as expected from a radial excitation of the nucleon. On the other hand, $A_{1/2}$ changes sign at about 0.6 GeV^2 . This remarkable behavior has not been observed before for any nucleon form factor or transition amplitude. Obviously, an important change in the structure occurs when the resonance is probed as a function of Q^2 .

The Q^2 dependence of $A_{1/2}$ of the $N(1535)1/2^-$ resonance exhibits the expected Q^{-3} dependence, except for small Q^2 values where meson cloud effects set in.

Figure 81.3 shows the transverse and scalar amplitudes for three states in the 3rd nucleon resonance region, the $\Delta(1620)1/2^-$, the $N(1675)5/2^-$ and $N(1680)5/2^+$. The latter two states have nearly degenerate masses and are parity partners. In the quark model picture, the transverse amplitudes for $N(1675)5/2^-$ on the proton are suppressed due to the Moorhouse selection rule, allowing for a quantitative evaluation of the meson-baryon contributions. The data show significant meson-baryon strength in the $A_{1/2}$ amplitude even at quite high Q^2 , while $A_{3/2}$ drops much faster with Q^2 . $N(1680)5/2^+$ shows qualitatively the features predicted in constituent quark models, a dominant $A_{3/2}$ at the real photon point that drops rapidly with increasing Q^2 , while $A_{1/2}$ becomes the dominant contribution at high Q^2 , indicating a switch of the helicity structure in the resonance transition at short distances.

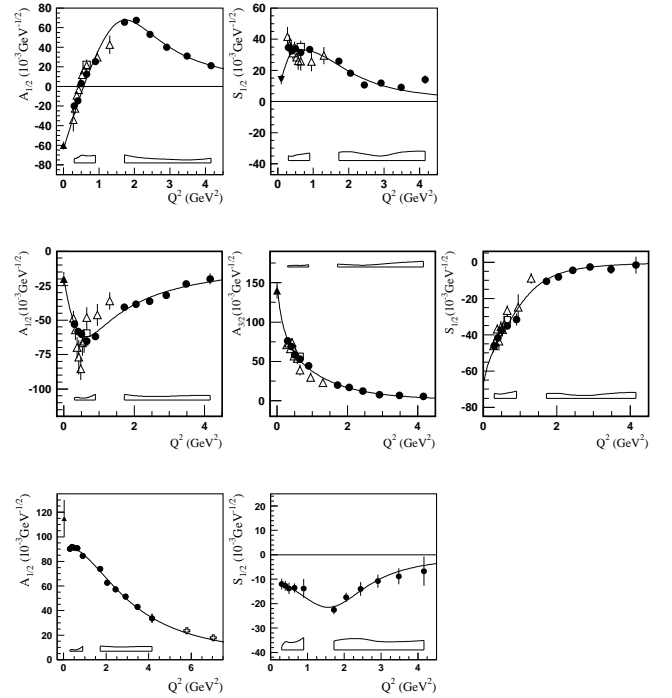


Figure 81.2: Transverse and scalar (longitudinal) helicity amplitudes for $\gamma p \rightarrow N(1440)1/2^+$ (top), $\gamma p \rightarrow N(1520)3/2^-$ (center), and $\gamma p \rightarrow N(1535)1/2^-$ (bottom) as extracted from the JLab/CLAS data in $n\pi^+$ production (full circles), MAMI/A1 data in $p\pi^0$ production (full down triangle), in $p\pi^+\pi^-$ (open triangles), and combined single and double pion production (open squares). The solid triangle is the PDG 2014 value at $Q^2 = 0$. The open boxes are the model uncertainties of the full circles.

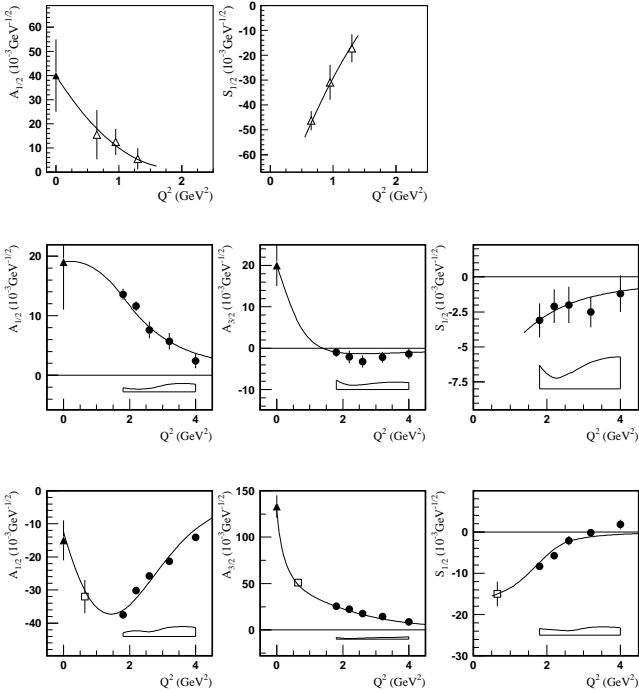


Figure 81.3: Transverse and scalar helicity amplitudes for $\gamma p \rightarrow \Delta(1620)1/2^-$ (top), $\gamma p \rightarrow N(1675)5/2^-$ (center), and $\gamma p \rightarrow N(1680)5/2^+$ (bottom) as extracted from the JLab/CLAS data in $n\pi^+$ production (full circles), $p\pi^+\pi^-$ (open triangles), combined single and double pion production (open square). The solid triangle is the 2014 PDG value at $Q^2 = 0$. The open boxes are the model uncertainties of the full circles. The curves are to guide the eye.

81.7 Partial wave analyses

Several PWA groups are now actively involved in the analysis of the new data. The GWU group maintains a nearly complete database covering reactions from πN and KN elastic scattering to $\gamma N \rightarrow N\pi$, $N\eta$, and $N\eta'$. It is presently the only group determining πN elastic amplitudes from scattering data in sliced energy bins. Given the high-precision of photoproduction data already or soon to be collected, the spectrum of N and Δ resonances will in the near future be better known.

Fits to the data are performed by various groups with the aim to understand the reaction dynamics and to identify N and Δ resonances. For practical reasons, approximations have to be made. We mention several analyses here: (1) The Mainz unitary isobar model [39] focuses on the correct treatment of the low-energy domain. Resonances are added to the unitary amplitude as a sum of Breit-Wigner amplitudes. This model also obtains resonance transition form factors and helicity amplitudes from electroproduction [35]. (2) For $N\pi$ electroproduction, the Yerevan/JLab group uses both the unitary isobar model and the dispersion relation approach developed in [38]. A phenomenological model was developed to extract resonance couplings and partial decay widths from exclusive $\pi^+\pi^-p$ electroproduction [37]. (3) Multichannel analyses using K-matrix parameterizations derive background terms from a chiral Lagrangian - providing a microscopical description of the background - (Giessen [40, 41]) or from phenomenology (KSU [42, 43], Bonn-Gatchina [44]). (4) Several groups (EBAC-Jlab [45, 46], ANL-Osaka [47], Dubna-Mainz-Taipeh [48], Bonn-Jülich [49–51], Valencia [52]) use dynamical reaction models, driven by chiral Lagrangians, which take dispersive parts of intermediate states into account. Several other groups have made important contributions. The Giessen group pioneered multichannel analyses of large data sets on pion- and photo-induced reactions [40, 41]. The Bonn-Gatchina group included recent high-statistics data and reported systematic searches for new baryon resonances in all relevant partial waves. A summary of their re-

sults can be found in [44].

References

- [1] G. Höhler, Pion-Nucleon Scattering, Landolt-Börnstein Vol. I/9b2 (1983), ed. H. Schopper, Springer Verlag.
- [2] R. E. Cutkosky *et al.*, in “VI International Conference on Baryon Resonances,” 19 (1980), Toronto, ed. N. Isgur.
- [3] R. Arndt *et al.*, Phys. Rev. C **74**, 045205 (2006), [arXiv:nucl-th/0605082].
- [4] “Hadron 2011: 14th International Conference on Hadron Spectroscopy”, München, Germany, June, 13 - 17, 2011, published in eConf.
- [5] “NSTAR 2013: 9th International Workshop on the Physics of Excited Nucleons”, 27-30 May 2013, Peñíscola, Spain.
- [6] E. Klempt and J.-M. Richard, Rev. Mod. Phys. **82**, 1095 (2010), [arXiv:0901.2055].
- [7] V. Crede and W. Roberts, Rept. Prog. Phys. **76**, 076301 (2013), [arXiv:1302.7299].
- [8] M. Roos *et al.* (Particle Data Group), Phys. Lett. B **111**, 1 (1982).
- [9] M. Doring *et al.*, Nucl. Phys. A **829**, 170 (2009), [arXiv:0903.4337].
- [10] N. Suzuki *et al.*, Phys. Rev. Lett. **104**, 042302 (2010), [arXiv:0909.1356].
- [11] R. Cutkosky *et al.*, Phys. Rev. D **20**, 2839 (1979).
- [12] R. Arndt *et al.*, Phys. Rev. C **69**, 035213 (2004), [arXiv:nucl-th/0311089].
- [13] M. Batinić *et al.*, Phys. Rev. C **51**, 2310 (1995), [Erratum: Phys.Rev.C 57, 1004–1005 (1998)], [arXiv:nucl-th/9501011]; M. Batinić *et al.*, Phys. Scr. **58**, 15 (1998).
- [14] A. Anisovich *et al.*, Eur. Phys. J. A **48**, 15 (2012), and references therein., [arXiv:1112.4937].
- [15] G. Höhler, PiN Newslett. **1993**, 9, 1 (1993).
- [16] N. Kelkar and M. Nowakowski, Phys. Rev. A **78**, 012709 (2008), and references therein., [arXiv:0805.0608].
- [17] G. F. Chew and S. Mandelstam, Phys. Rev. **119**, 467 (1960).
- [18] S. Ceci *et al.*, Phys. Rev. D **77**, 116007 (2008), [hep-ph/0609236].
- [19] P. Masjuan and J. J. Sanz-Cillero, Eur. Phys. J. C **73**, 2594 (2013), [arXiv:1306.6308].
- [20] A. Švarc *et al.*, Phys. Rev. C **88**, 3, 035206 (2013), [arXiv:1307.4613].
- [21] A. Švarc *et al.*, Phys. Rev. C **89**, 4, 045205 (2014), [arXiv:1401.1947].
- [22] A. Švarc *et al.*, Phys. Lett. B **755**, 452 (2016), [arXiv:1512.07403].
- [23] A. Švarc *et al.*, Phys. Rev. C **89**, 6, 065208 (2014), [arXiv:1404.1544].
- [24] A. Švarc *et al.*, Phys. Rev. C **91**, 1, 015207 (2015), [arXiv:1405.6474].
- [25] L. Tiator *et al.*, Phys. Rev. C **94**, 6, 065204 (2016), [arXiv:1606.00371].
- [26] A. Anisovich *et al.*, Eur. Phys. J. A **53**, 12, 242 (2017), [arXiv:1712.07537].
- [27] A. Anisovich *et al.*, Phys. Rev. Lett. **119**, 6, 062004 (2017), [arXiv:1712.07549].
- [28] C. Fasano, F. Tabakin and B. Saghai, Phys. Rev. C **46**, 2430 (1992).
- [29] G. Chew *et al.*, Phys. Rev. **106**, 1345 (1957).
- [30] R. Workman, L. Tiator and A. Sarantsev, Phys. Rev. C **87**, 6, 068201 (2013), [arXiv:1304.4029].
- [31] N. Suzuki, T. Sato and T.-S. Lee, Phys. Rev. C **82**, 045206 (2010), [arXiv:1006.2196].
- [32] H. Kamano, Phys. Rev. C **88**, 045203 (2013), [arXiv:1305.6678].

- [33] A. Sandorfi *et al.*, AIP Conf. Proc. **1432**, 1, 219 (2012), [arXiv:1108.5411].
- [34] I. Aznauryan and V. Burkert, Prog. Part. Nucl. Phys. **67**, 1 (2012), [arXiv:1109.1720].
- [35] L. Tiator *et al.*, Eur. Phys. J. ST **198**, 141 (2011), [arXiv:1109.6745]; S. Štajner *et al.*, Phys. Rev. Lett. **119**, 2, 022001 (2017).
- [36] W. Ash *et al.*, Phys. Lett. B **24**, 165 (1967).
- [37] V. Mokeev *et al.* (CLAS), Phys. Rev. C **86**, 035203 (2012), [arXiv:1205.3948].
- [38] I. Aznauryan, Phys. Rev. C **67**, 015209 (2003), [arXiv:nucl-th/0206033].
- [39] D. Drechsel, S. Kamalov and L. Tiator, Eur. Phys. J. A **34**, 69 (2007), [arXiv:0710.0306].
- [40] G. Penner and U. Mosel, Phys. Rev. C **66**, 055211 (2002), [arXiv:nucl-th/0207066].
- [41] G. Penner and U. Mosel, Phys. Rev. C **66**, 055212 (2002), [arXiv:nucl-th/0207069].
- [42] D. Manley and E. Saleski, Phys. Rev. D **45**, 4002 (1992).
- [43] M. Shrestha and D. Manley, Phys. Rev. C **86**, 055203 (2012), [arXiv:1208.2710].
- [44] A. Anisovich *et al.*, Eur. Phys. J. A **48**, 15 (2012), [arXiv:1112.4937].
- [45] A. Matsuyama, T. Sato and T.-S. Lee, Phys. Rept. **439**, 193 (2007), [arXiv:nucl-th/0608051].
- [46] T. Sato and T.-S. Lee, J. Phys. G **36**, 073001 (2009), [arXiv:0902.3653].
- [47] H. Kamano *et al.*, Phys. Rev. C **88**, 3, 035209 (2013), [arXiv:1305.4351].
- [48] G. Y. Chen *et al.*, Phys. Rev. C **76**, 035206 (2007), [arXiv:nucl-th/0703096].
- [49] M. Doring *et al.*, Phys. Lett. B **681**, 26 (2009), [arXiv:0903.1781].
- [50] M. Doring *et al.*, Nucl. Phys. A **829**, 170 (2009), [arXiv:0903.4337].
- [51] D. Ronchen *et al.*, Eur. Phys. J. A **49**, 44 (2013), [arXiv:1211.6998].
- [52] S. Sarkar, E. Oset and M. Vicente Vacas, Nucl. Phys. A **750**, 294 (2005), [Erratum: Nucl.Phys.A 780, 90–90 (2006)], [arXiv:nucl-th/0407025].

82. Λ and Σ Resonances

Revised August 2021 by V.D. Burkert (Jefferson Lab), V. Crede (Florida State U.), E. Klempt (Bonn U.), U. Thoma (Bonn U.), L. Tiator (KPH, JGU Mainz) and R.L. Workman (George Washington U.).

82.1 Introduction

For several decades, there has been very little new experimental data bearing on the properties of Λ and Σ resonances. An exception was the study at JLab of the reactions $\gamma p \rightarrow K^+ \Sigma^\pm \pi^\mp$ and $\gamma p \rightarrow K^+ \Sigma^0 \pi^0$ [1], which established the spin and parity of the $\Lambda(1405)$ [2]. There was also from BNL new data on the very low energy region of $K^- p$ scattering [3–7]. Otherwise, the field is starved for data. Recent analyses (see below) have improved what we know about the *properties* of the known Λ and Σ resonances, but the *established* resonances are the same ones that were listed in our 1984 edition [8] except for the $\Sigma(2250)$ which we consider 2-star only due to its unknown spin-parity. The 1990 Review [9] gave a full report of the status of Lambda and Sigma hyperons, and included Argand plots from the partial-wave analyses. The 2018 Review [10] has a short survey of the $\Sigma(1670)$ -region.

In the last few years, four groups have re-analyzed $K^- p$ reactions using more extensive collections of the old data. These analyses justify an update of the status of the Λ and Σ resonances. Although they have not established any new resonances, they have provided at least some evidence for new states and have given a better understanding of the old ones.

Tables 82.1 and 82.2 give our evaluation of the status, both overall and channel by channel, of each Λ and Σ resonance in the Particle Listings. In making these evaluations, we considered, in addition to the four analyses [11–14], the ratings that predated them. The ratings use a 1- to 4-star system. For more details on the evaluation of the overall star ratings, see [15]. The main Summary Table includes only established states with an overall status of 3 or 4 stars; as has already been noted, these are the same fourteen Λ resonances (including $\Lambda(1116)$) and nine Σ resonances instead of the former ten (including $\Sigma(1193)3/2^+$, and $\Sigma(1385)3/2^+$) that had long been in the Table. In addition, there are seven 1-star and two 2-star Λ 's, and fourteen 1-star and three 2-star Σ 's in the Particle Listings.

82.2 New analyses

The new analysis progress was pioneered by the Kent group which collected a large fraction of the available data and performed a comprehensive partial wave analysis [11, 16]. $K^- p$ scattering into a pseudoscalar meson and an octet baryon is governed by two complex amplitudes; hence four quantities need to be measured to fully construct the amplitudes (up to an arbitrary phase per energy and angular bin). Discussions of complete experiments also generally assume perfect data (no experimental uncertainties); realistic uncertainties further complicate the task of amplitude extraction. Here, the available data are limited to the differential cross section and the target or hyperon recoil polarization P ; data on the polarization transfer do not exist. The authors of Ref. [16] overcame this difficulty by using start values for the partial wave amplitudes determined in [17] and/or from an energy-dependent fit and by freezing or releasing sets of amplitudes. The resulting amplitudes were fitted with a unitary multichannel parameterization [11].

The JPAC group presented a coupled-channel fit to the $\bar{K}N$ partial waves derived by the Kent group [13]. The JPAC approach was based on the K -matrix formalism. Special attention was paid to the analytical properties of the amplitudes determined by the square-root unitary branch points and the continuation to the complex angular momentum plane. The fit described the Kent partial waves reasonably well. However, when observables were calculated from their partial-wave amplitudes, significant discrepancies became apparent. The results were therefore not included in the RPP.

The ANL-Osaka group derived the energy-dependent amplitudes in fits to a large subset of the data collected in Ref. [16] and further data sets described in Ref. [18]. Their fits were based on

a phenomenological SU(3) Lagrangian [18]. The two ANL-Osaka models agree on the leading contributions but differ significantly in cases with weaker candidates [12].

Table 82.1: The status of the Λ resonances. Only those with an overall status of *** or **** are included in the main Baryon Summary Table. Decay channels other than $N\bar{K}$ and $\Sigma\pi$ are only given for *** and **** resonances.

Particle	J^P	Overall status	Status as seen in —		
			$N\bar{K}$	$\Sigma\pi$	Other channels
$\Lambda(1116)$	$1/2^+$	****			$N\pi$ (weak decay)
$\Lambda(1380)$	$1/2^-$	**	**	**	
$\Lambda(1405)$	$1/2^-$	****	****	****	
$\Lambda(1520)$	$3/2^-$	****	****	****	$\Lambda\pi\pi, \Lambda\gamma, \Sigma\pi\pi$
$\Lambda(1600)$	$1/2^+$	****	***	****	$\Lambda\pi\pi, \Sigma(1385)\pi$
$\Lambda(1670)$	$1/2^-$	****	****	****	$\Lambda\eta$
$\Lambda(1690)$	$3/2^-$	****	****	***	$\Lambda\pi\pi, \Sigma(1385)\pi$
$\Lambda(1710)$	$1/2^+$	*	*	*	
$\Lambda(1800)$	$1/2^-$	***	***	**	$\Lambda\pi\pi, N\bar{K}^*$
$\Lambda(1810)$	$1/2^+$	***	**	**	$N\bar{K}^*$
$\Lambda(1820)$	$5/2^+$	****	****	****	$\Sigma(1385)\pi$
$\Lambda(1830)$	$5/2^-$	****	****	****	$\Sigma(1385)\pi$
$\Lambda(1890)$	$3/2^+$	****	****	**	$\Sigma(1385)\pi, N\bar{K}^*$
$\Lambda(2000)$	$1/2^-$	*	*	*	
$\Lambda(2050)$	$3/2^-$	*	*	*	
$\Lambda(2070)$	$3/2^+$	*	*	*	
$\Lambda(2080)$	$5/2^-$	*	*	*	
$\Lambda(2085)$	$7/2^+$	**	**	*	
$\Lambda(2100)$	$7/2^-$	****	****	**	$N\bar{K}^*$
$\Lambda(2110)$	$5/2^+$	***	**	**	$N\bar{K}^*$
$\Lambda(2325)$	$3/2^-$	*	*		
$\Lambda(2350)$	$9/2^+$	***	***	*	
$\Lambda(2585)$		*	*		

The Bonn-Gatchina (BnGa) group added further (old) data to those analyzed in Ref. [16]. The data set was fitted in a modified K -matrix approach and the resulting amplitudes were compared with those from Refs. [16, 18]. New resonances were found, other states, mostly one and two-star states could not be confirmed; all resonances were tested for their statistical significance. Additional states with any set of quantum numbers were tested and were found to produce only small improvements in the fit [14]. In Ref. [19], properties of the full set of contributing hyperons were reported.

The star ratings of Λ and Σ resonances given in our earlier editions, and the new results from the Kent, ANL-Osaka and BnGa groups were used to update the star rating of the hyperon resonances. In [19], the overall star rating is directly estimated, for [11] we estimate the star rating from the branching-ratio uncertainties. In [12], two solutions are given but no uncertainties for branching ratios. The overall star ratings are based on the evidence for the resonances in the new analyses as well as their consistency including also the results of earlier analyses given in [20]. For further details see also [15].

We decided to remove the three so-called *bumps* $\Sigma(1480)$, $\Sigma(1560)$, $\Sigma(1670)$, and $\Sigma(1690)$ as well as $\Sigma(1620)$ from production experiments. The entries from $\Sigma(1770)1/2^+$ are now listed under $\Sigma(1660)1/2^+$ and $\Sigma(1880)1/2^+$, the entries from $\Sigma(1730)3/2^+$ and $\Sigma(1840)3/2^+$ are now combined to one $\Sigma(1780)3/2^+$. The one-star $\Sigma(2000)1/2^-$ is combined with a new one-star $\Sigma(2160)1/2^-$ to a single one-star $\Sigma(2110)1/2^-$. Apart from $\Lambda(1380)1/2^-$, four further new resonances were included in the Listings: $\Lambda(2070)3/2^+$, $\Lambda(2080)5/2^-$, $\Sigma(2010)3/2^-$, and $\Sigma(2230)3/2^+$, all with one star.

Table 82.2: The status of the Σ resonances. Only those with an overall status of *** or **** are included in the main Baryon Summary Table. Decay channels other than $N\bar{K}$, $\Lambda\pi$ and $\Sigma\pi$ are only given for *** and **** resonances.

Particle	J^P	Overall status	Status as seen in —				Other channels
			$N\bar{K}$	$\Lambda\pi$	$\Sigma\pi$		
$\Sigma(1193)$	$1/2^+$	****					$N\pi$ (weak decay)
$\Sigma(1385)$	$3/2^+$	****					$\Lambda\gamma$
$\Sigma(1580)$	$3/2^-$	*	*	*	*		
$\Sigma(1620)$	$1/2^-$	*	*	*	*		
$\Sigma(1660)$	$1/2^+$	***	***	***	***		
$\Sigma(1670)$	$3/2^-$	****	****	****	****		
$\Sigma(1750)$	$1/2^-$	***	***	**	***		$\Sigma\eta$
$\Sigma(1775)$	$5/2^-$	****	****	****	**		
$\Sigma(1780)$	$3/2^+$	*	*	*	*		
$\Sigma(1880)$	$1/2^+$	**	**	*			
$\Sigma(1900)$	$1/2^-$	**	**	*	**		
$\Sigma(1910)$	$3/2^-$	***	*	*	**		
$\Sigma(1915)$	$5/2^+$	****	***	***	***		
$\Sigma(1940)$	$3/2^+$	*	*		*		
$\Sigma(2010)$	$3/2^-$	*	*	*			
$\Sigma(2030)$	$7/2^+$	****	****	****	**		$\Delta(1232)\bar{K}$, $N\bar{K}^*$, $\Sigma(1385)\pi$
$\Sigma(2070)$	$5/2^+$	*	*		*		
$\Sigma(2080)$	$3/2^+$	*		*			
$\Sigma(2100)$	$7/2^-$	*	*	*	*		
$\Sigma(2110)$	$1/2^-$	*	*	*	*		
$\Sigma(2230)$	$3/2^+$	*	*	*	*		
$\Sigma(2250)$		**	**	*	*		
$\Sigma(2455)$		*	*				
$\Sigma(2620)$		*	*				
$\Sigma(3000)$		*	*	*			
$\Sigma(3170)$		*					

82.3 Sign conventions for resonance couplings

In terms of the isospin-0 and isospin-1 elastic scattering amplitudes A_0 and A_1 , the amplitude for $K^-p \rightarrow \bar{K}^0n$ scattering is $\pm(A_1 - A_0)/2$, where the sign depends on conventions used in conjunction with the Clebsch-Gordan coefficients (such as, is the baryon or the meson the “first” particle). If this reaction is partial-wave analyzed and if the overall phase is chosen so that, say, the $\Sigma(1775)5/2^- (D_{15})$ amplitude at resonance points along the positive imaginary axis (points “up”), then any Σ at resonance will point “up” and any Λ at resonance will point “down” (along the negative imaginary axis). Thus the phase at resonance determines the isospin. The above ignores background amplitudes in the resonating partial waves.

That is the basic idea. In a similar but somewhat more complicated way, the phases of the $\bar{K}N \rightarrow \Lambda\pi$ and $\bar{K}N \rightarrow \Sigma\pi$ amplitudes for a resonating wave help determine the SU(3) multiplet to which the resonance belongs. Again, a convention has to be adopted for some overall arbitrary phases: which way is “up”? Our convention is that of Levi-Setti [21] and is shown in Fig. 82.1, which also compares experimental results with theoretical predictions for the signs of several resonances. In the Listings, a + or – sign in front of a measurement of an inelastic resonance coupling indicates the sign (the *absence* of a sign means that the sign is not determined, *not* that it is positive). Also other decay modes can be used to assign a hyperon to a SU(3) multiplet [22, 23]. Modern analyses determine properties of resonances at the pole position. In these analyses, the + or – sign is replaced by a phase. Background amplitudes can lead to significant phase shifts, and an additional phase shift due to rescattering is admitted in some analyses. In comparison to quark model predictions [19, 24], three Λ spin doublets can be identified as being mainly SU(3) singlets: the well-known ($\Lambda(1405)1/2^-$, $\Lambda(1520)3/2^-$), the ($\Lambda(2080)5/2^-$, $\Lambda(2100)7/2^-$), and ($\Lambda(2070)3/2^+$, $\Lambda(2110)5/2^+$).

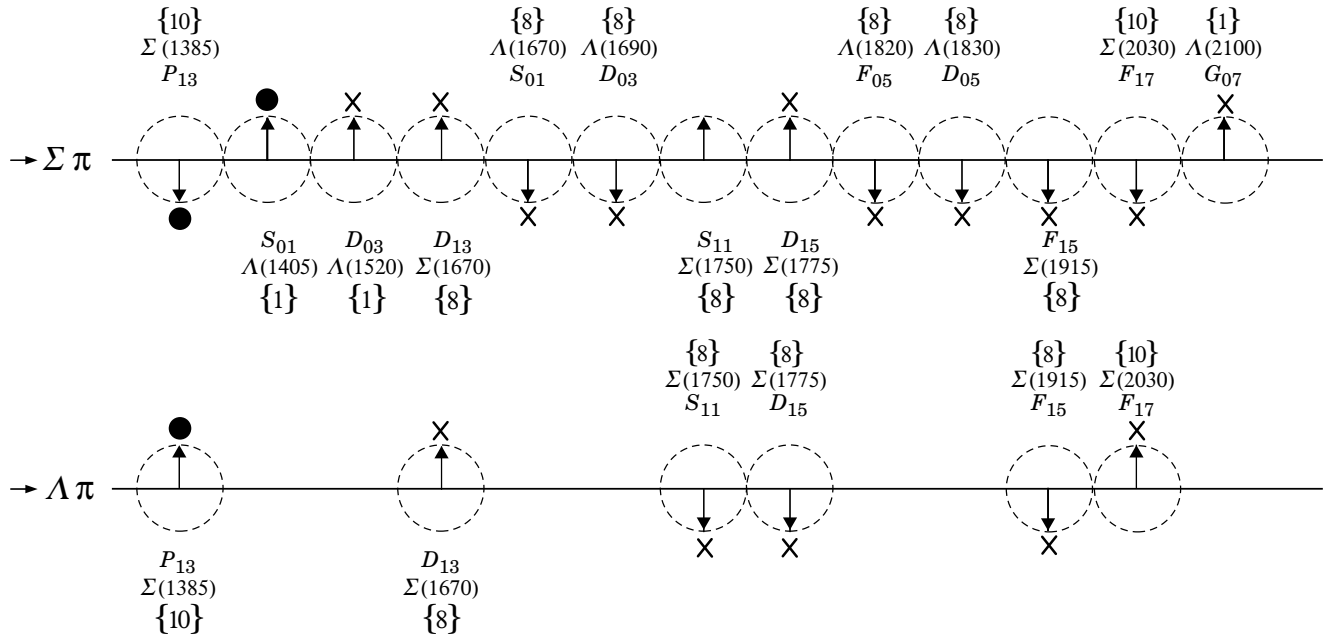


Figure 82.1: The signs of the imaginary parts of resonating amplitudes in the $\bar{K}N \rightarrow \Lambda\pi$ and $\Sigma\pi$ channels. The signs of the $\Sigma(1385)$ and $\Lambda(1405)$, marked with a \bullet , are set by convention, and then the others are determined relative to them. The signs required by the SU(3) assignments of the resonances are shown with an arrow, and the experimentally determined signs are shown with an \times .

82.4 The $\Lambda(1405)$

In coupled-channels calculations based on the chiral SU(3) effective field theory, the strongly attractive forces between $N\bar{K}$

and $\Sigma\pi$ generate five poles, one SU(3) singlet pole, two Λ octet poles and two (or one) octet Σ poles (see Section 83). In quark models, these five states are $\Lambda(1405)$, $\Lambda(1670)$, $\Lambda(1800)$, $\Sigma(1620)$,

and $\Sigma(1750)$. The octet states are found 100 to 150 MeV above the corresponding nucleon resonances. In chiral SU(3) effective field theories, at least three of these states are seen in the 1300 to 1600 MeV mass range. The appearance of two Λ poles in this mass range, a narrow SU(3) octet at ~ 1420 MeV and a wider SU(3) singlet at ~ 1380 MeV, was unexpected. This approach has been pursued by a number of groups; for a summary of the results see our Review 83, “Pole Structure of the $\Lambda(1405)$ Region”. In the Listings, we have introduced the $\Lambda(1380)$ as a new candidate resonance (with two stars), named in accordance with its approximate pole position. The second SU(3) octet Λ state is the well-known $\Lambda(1670)$. The masses of the two associated Σ states are uncertain so far, and no new entries are introduced in the Listings.

In traditional approaches only one resonance was seen in this mass region, the narrow state at 1405 MeV. It was reported to be the SU(3) singlet state a long time ago in Ref. [25], in agreement with the quark-model expectations but in contrast to the findings based on coupled-channels calculations within chiral SU(3) effective field theories. In the Listings, the $\Lambda(1405)$ has been retained with its traditional name. In quark models, this state is identified with the SU(3) singlet state, the two Λ octet states with $\Lambda(1670)$ and $\Lambda(1800)$, and the two Σ states with $\Sigma(1620)$ and $\Sigma(1750)$.

82.5 Uncertainties on masses and widths

The uncertainties quoted on resonance parameters from partial-wave analyses are often only statistical, and the parameters can change beyond these uncertainties when a different parametrization of the waves is used. Furthermore, the different analyses use more or less the same data, so it is not really appropriate to treat the different determinations of the resonance parameters as independent or to average them. In any case, the spread of the masses, widths, and branching fractions from the different analyses is certainly a better indication of the uncertainties than are the quoted uncertainties. In the Listings, we usually give a range reflecting the spread of the values rather than a particular value with error.

82.6 Production experiments

Partial-wave analyses of course separate partial waves, whereas a peak in a cross section or an invariant mass distribution usually cannot be disentangled from background and analyzed for its quantum numbers; and more than one resonance may be contributing to the peak. The $\Sigma(1385)$ and $\Lambda(1405)$ lie below the $\bar{K}N$ threshold and nearly everything about $\Sigma(1385)$ is learned from production experiments. Our knowledge on $\Lambda(1405)$ benefits greatly from photoproduction of the three $\Sigma\pi$ charge states [1,2] and from the precise measurement of the energy shift and width of the kaonic hydrogen atom [26].

Production and formation experiments agree quite well in the case of $\Lambda(1520)$ and results have been combined. Above this mass, no new results on peak hunting have been reported for about 40 years. For these early results, we refer the reader to our earlier editions. In photoproduction with energetic photons [27,28] or at LHCb [29], hyperons are produced abundantly. So far, no attempt has been made to extract hyperon properties from these data. New data on hyperon spectroscopy can be expected from J-PARC [30], JLAB [31], and the forthcoming PANDA experiment [32].

References

- [1] K. Moriya *et al.* (CLAS), Phys. Rev. **C87**, 3, 035206 (2013), [arXiv:1301.5000].
- [2] K. Moriya *et al.* (CLAS), Phys. Rev. Lett. **112**, 8, 082004 (2014), [arXiv:1402.2296].
- [3] A. Starostin *et al.* (Crystal Ball), Phys. Rev. **C64**, 055205 (2001).
- [4] S. Prakhov *et al.*, Phys. Rev. **C69**, 042202 (2004).
- [5] S. Prakhov *et al.* (Crystal Ball), Phys. Rev. **C70**, 034605 (2004).
- [6] R. Manweiler *et al.*, Phys. Rev. **C77**, 015205 (2008).
- [7] S. Prakhov *et al.*, Phys. Rev. **C80**, 025204 (2009), [arXiv:0812.1888].
- [8] C. G. Wohl *et al.* (Particle Data Group), Rev. Mod. Phys. **56**, S1 (1984).
- [9] J. J. Hernandez *et al.* (Particle Data Group), Phys. Lett. **B239**, 1 (1990), [Erratum: Phys. Lett.B253,524(1991)].
- [10] M. Tanabashi *et al.* (Particle Data Group), Phys. Rev. **D98**, 3, 030001 (2018).
- [11] H. Zhang *et al.*, Phys. Rev. **C88**, 3, 035205 (2013), [arXiv:1305.4575].
- [12] H. Kamano *et al.*, Phys. Rev. **C92**, 2, 025205 (2015), [Erratum: Phys. Rev.C95,no.4,049903(2017)], [arXiv:1506.01768].
- [13] C. Fernandez-Ramirez *et al.*, Phys. Rev. **D93**, 3, 034029 (2016), [arXiv:1510.07065].
- [14] M. Matveev *et al.*, Eur. Phys. J. **A55**, 10, 179 (2019), [arXiv:1907.03645].
- [15] E. Klempt *et al.* (Baryon@PDG Group), Eur. Phys. J. A **56**, 10, 261 (2020), [arXiv:2007.04232].
- [16] H. Zhang *et al.*, Phys. Rev. **C88**, 3, 035204 (2013), [arXiv:1305.3598].
- [17] J. Tulpan, PhD Dissertation, Kent State University (2007).
- [18] H. Kamano *et al.*, Phys. Rev. **C90**, 6, 065204 (2014), [arXiv:1407.6839].
- [19] A. V. Sarantsev *et al.*, Eur. Phys. J. **A55**, 10, 180 (2019), [arXiv:1907.13387].
- [20] J. Beringer *et al.* (Particle Data Group), Phys. Rev. **D86**, 010001 (2012).
- [21] R. Levi Setti, Conf. Proc. **C690625**, 339 (1969).
- [22] V. Guzey and M. V. Polyakov, Annalen Phys. **13**, 673 (2004).
- [23] V. Guzey and M. V. Polyakov (2005), [hep-ph/0512355].
- [24] U. Loring, B. C. Metsch and H. R. Petry, Eur. Phys. J. **A10**, 447 (2001), [hep-ph/0103290].
- [25] R. D. Tripp *et al.*, Phys. Rev. Lett. **21**, 1721 (1968).
- [26] M. Bazzi *et al.* (SIDDHARTA), Phys. Lett. **B704**, 113 (2011), [arXiv:1105.3090].
- [27] K. Moriya *et al.* (CLAS), Phys. Rev. **C88**, 045201 (2013), [Addendum: Phys. Rev.C88,no.4,049902(2013)], [arXiv:1305.6776].
- [28] B. Dey *et al.* (CLAS), Phys. Rev. **C89**, 5, 055208 (2014), [Addendum: Phys. Rev.C90,no.1,019901(2014)], [arXiv:1403.2110].
- [29] R. Aaij *et al.* (LHCb), Phys. Rev. Lett. **115**, 072001 (2015), [arXiv:1507.03414].
- [30] K. Hicks and H. Sako, Proposal for J-PARC E45.
- [31] M. Amarian *et al.* (KLF) (2020), [arXiv:2008.08215].
- [32] F. Iazzi (PANDA), AIP Conf. Proc. **1743**, 1, 050006 (2016).

83. Pole Structure of the $\Lambda(1405)$ Region

Revised June 2021 by T. Hyodo (Tokyo Metropolitan U.) and U.-G. Meißner (Bonn U.; Jülich).

The $\Lambda(1405)$ resonance emerges in the meson-baryon scattering amplitude with the strangeness $S = -1$ and isospin $I = 0$. It is the archetype of what is called a dynamically generated resonance, as pioneered by Dalitz and Tuan [1]. The most powerful and systematic approach for the low-energy regime of the strong interactions is chiral perturbation theory (ChPT), see e.g. Ref. [2]. A perturbative calculation is, however, not applicable to this sector because of the existence of the $\Lambda(1405)$ just below the $\bar{K}N$ threshold. In this case, ChPT has to be combined with a non-perturbative resummation technique, just as in the case of the nuclear forces. By solving the Lippmann-Schwinger equation with the interaction kernel determined by ChPT and using a particular regularization, in Ref. [3] a successful description of the low-energy K^-p scattering data as well as the mass distribution of the $\Lambda(1405)$ was achieved (for further developments, see Ref. [4–7] and references therein).

The study of the pole structure was initiated by Ref. [8], which finds two poles of the scattering amplitude in the complex energy plane between the $\bar{K}N$ and $\pi\Sigma$ thresholds. The spectrum in experiments exhibits one effective resonance shape, while the existence of two poles results in the reaction-dependent lineshape [9]. The origin of this two-pole structure is attributed to the two attractive channels of the leading order interaction in the SU(3) basis (singlet and octet) [9] and in the isospin basis ($\bar{K}N$ and $\pi\Sigma$) [10]. It is remarkable that the sign and the strength of the leading order interaction is determined by a low-energy theorem of chiral symmetry, i.e. the so-called Weinberg-Tomozawa term. The two-pole nature of the $\Lambda(1405)$ is qualitatively different from the case of the N(1440) resonance. Two poles of the N(1440) appear on different Riemann sheets of the complex energy plane separated by the $\pi\Delta$ branch point. These poles reflect a single state, with a nearby pole and a more distant shadow pole. In contrast, the two poles in the $\Lambda(1405)$ region on the same Riemann sheet (where $\pi\Sigma$ channels are unphysical and all other channels physical, correspondingly to the one, connected to the real axis between the $\pi\Sigma$ and $\bar{K}N$ thresholds) are generated from two attractive forces mentioned above [9, 10].

Recently, various new experimental results on the $\Lambda(1405)$ have become available [4]. Among these, the most striking measurement is the precise determination of the energy shift and width of kaonic hydrogen by the SIDDHARTA collaboration [11, 12], which provides a quantitative and stringent constraint on the K^-p amplitude at threshold through the improved Deser formula [13]. Systematic studies with error analyses based on the next-to-leading order ChPT interaction including the SIDDHARTA constraint have been performed by various groups [14–18]. All these studies confirm that the new kaonic hydrogen data are compatible with the scattering data above threshold.

The results of the pole positions of $\Lambda(1405)$ in the various approaches are summarized in Table 83.1. We may regard the difference among the calculations as a systematic error, which stems from the various approximations of the Bethe-Salpeter equation, the fitting procedure, and also the inclusion of SU(3) breaking effects such as the choice of the various meson decay constants, and so on. A detailed comparison of the various approaches that enter the table is given in Ref. [19]. A recent analysis including also the $J^P = 1/2^+$ P-wave contribution (and also an explicit $\Sigma(1385)$ $3/2^+$ state) gives results consistent with the findings reported above, with the pole positions at $(1364 - i43)$ MeV and $(1430 - i15)$ MeV, respectively [20].

The main component for the $\Lambda(1405)$ is the pole 1, whose position converges within a relatively small region near the $\bar{K}N$ threshold. On the other hand, the position of the pole 2 shows a sizeable scatter. Detailed studies of the $\pi\Sigma$ spectrum in various reaction processes, together with the precise experimental lineshape (see e.g. the recent precise photoproduction data from the LEPS collaboration [21] and from the CLAS collaboration [22, 23], electroproduction data from the CLAS collaboration [24], and proton-proton collision data from COSY [25] and the HADES collaboration [26]), will shed light on the position of the second pole.

The $\pi\Sigma$ spectra from the CLAS data are analyzed in Ref. [27] and Ref. [18]. It was shown in Ref. [18] that several solutions, which agree with the scattering data, are ruled out if confronted with the recent CLAS data. The remaining solutions are collected as solution #2 and solution #4 in Table 83.1. The HADES data are analyzed in Ref. [28] and Ref. [29]. Although the result of the pole found in Ref. [28] is not compatible with other results, the authors of Ref. [29] invoke the anomalous triangle singularity mechanism to argue that the invariant mass distribution of the $\pi\Sigma$ system is found at lower masses than in other reactions. It is thus desirable to perform more comprehensive analyses of $\pi\Sigma$ spectra together with the systematic error analysis of the scattering data.

Table 83.1: Comparison of the pole positions of $\Lambda(1405)$ in the complex energy plane from next-to-leading order chiral unitary coupled-channel approaches including the SIDDHARTA constraint. The lower two results also include the CLAS photoproduction data.

approach	pole 1 [MeV]	pole 2 [MeV]
Refs. [14, 15], NLO	$1424^{+7}_{-23} - i 26^{+3}_{-14}$	$1381^{+18}_{-6} - i 81^{+19}_{-8}$
Ref. [17], Fit II	$1421^{+3}_{-2} - i 19^{+8}_{-5}$	$1388^{+9}_{-9} - i 114^{+24}_{-25}$
Ref. [18], solution #2	$1434^{+2}_{-2} - i 10^{+2}_{-1}$	$1330^{+4}_{-5} - i 56^{+17}_{-11}$
Ref. [18], solution #4	$1429^{+8}_{-7} - i 12^{+2}_{-3}$	$1325^{+15}_{-15} - i 90^{+12}_{-18}$

References

- [1] R. Dalitz and S. Tuan, Phys. Rev. Lett. **2**, 425 (1959).
- [2] V. Bernard, N. Kaiser and U.-G. Meißner, Int. J. Mod. Phys. E **4**, 193 (1995), [hep-ph/9501384].
- [3] N. Kaiser, P. Siegel and W. Weise, Nucl. Phys. A **594**, 325 (1995), [arXiv:nucl-th/9505043].
- [4] T. Hyodo and D. Jido, Prog. Part. Nucl. Phys. **67**, 55 (2012), [arXiv:1104.4474].
- [5] U.-G. Meißner, Symmetry **12**, 6, 981 (2020), [arXiv:2005.06909].
- [6] M. Mai, Eur. Phys. J. ST **230**, 6, 1593 (2021), [arXiv:2010.00056].
- [7] T. Hyodo and M. Niyama, Prog. Part. Nucl. Phys. **120**, 103868 (2021), [arXiv:2010.07592].
- [8] J. Oller and U.-G. Meißner, Phys. Lett. B **500**, 263 (2001), [hep-ph/0011146].
- [9] D. Jido *et al.*, Nucl. Phys. A **725**, 181 (2003), [arXiv:nucl-th/0303062].
- [10] T. Hyodo and W. Weise, Phys. Rev. C **77**, 035204 (2008), [arXiv:0712.1613].
- [11] M. Bazzi *et al.* (SIDDHARTA), Phys. Lett. B **704**, 113 (2011), [arXiv:1105.3090].
- [12] M. Bazzi *et al.* (SIDDHARTA), Nucl. Phys. A **881**, 88 (2012), [arXiv:1201.4635].
- [13] U.-G. Meißner, U. Raha and A. Rusetsky, Eur. Phys. J. C **35**, 349 (2004), [hep-ph/0402261].
- [14] Y. Ikeda, T. Hyodo and W. Weise, Phys. Lett. B **706**, 63 (2011), [arXiv:1109.3005].
- [15] Y. Ikeda, T. Hyodo and W. Weise, Nucl. Phys. A **881**, 98 (2012), [arXiv:1201.6549].
- [16] M. Mai and U.-G. Meißner, Nucl. Phys. A **900**, 51 (2013), [arXiv:1202.2030].
- [17] Z.-H. Guo and J. Oller, Phys. Rev. C **87**, 3, 035202 (2013), [arXiv:1210.3485].
- [18] M. Mai and U.-G. Meißner, Eur. Phys. J. A **51**, 3, 30 (2015), [arXiv:1411.7884].
- [19] A. Cieplý *et al.*, Nucl. Phys. A **954**, 17 (2016), [arXiv:1603.02531].
- [20] D. Sadasivan, M. Mai and M. Döring, Phys. Lett. B **789**, 329 (2019), [arXiv:1805.04534].

- [21] M. Niiyama *et al.*, Phys. Rev. C **78**, 035202 (2008), [arXiv:0805.4051].
- [22] K. Moriya *et al.* (CLAS), Phys. Rev. C **87**, 3, 035206 (2013), [arXiv:1301.5000].
- [23] K. Moriya *et al.* (CLAS), Phys. Rev. Lett. **112**, 8, 082004 (2014), [arXiv:1402.2296].
- [24] H. Lu *et al.* (CLAS), Phys. Rev. C **88**, 045202 (2013), [arXiv:1307.4411].
- [25] I. Zychor *et al.*, Phys. Lett. B **660**, 167 (2008), [arXiv:0705.1039].
- [26] G. Agakishiev *et al.* (HADES), Phys. Rev. C **87**, 025201 (2013), [arXiv:1208.0205].
- [27] L. Roca and E. Oset, Phys. Rev. C **87**, 5, 055201 (2013), [arXiv:1301.5741].
- [28] M. Hassanvand *et al.*, Phys. Rev. C **87**, 5, 055202 (2013), [Addendum: Phys.Rev.C 88, 019905 (2013)], [arXiv:1210.7725].
- [29] M. Bayar *et al.*, Phys. Rev. C **97**, 3, 035203 (2018), [arXiv:1710.03964].

84. Pentaquarks

Revised September 2021 by M. Karliner (Tel Aviv U.) and T. Skwarnicki (Syracuse U.).

Experimental searches for pentaquark hadrons comprised of light flavors have a long and vivid history. No undisputed candidates had been found in 50 years. The first wave of claimed observations of pentaquark candidates containing a strange antiquark occurred in the early seventies, see e.g. a review in the 1976 edition of Particle Data Group listings for $Z_0(1780)$, $Z_0(1865)$ and $Z_1(1900)$ [1]. The last mention of these candidates can be found in the 1992 edition [2] with the perhaps prophetic comment “the results permit no definite conclusion - the same story for 20 years. [...] The skepticism about baryons not made of three quarks, and lack of any experimental activity in this area, make it likely that another 20 years will pass before the issue is decided.” A decade later, a second wave of observations occurred, possibly motivated by specific theoretical predictions for their existence [3–5]. The evidence for pentaquarks was based on observations of peaks in the invariant mass distributions of their decay products. More data and subsequent more sensitive experiments did not confirm these claims [6]. In the last mention of the best known candidate from that period, $\Theta(1540)^+$, the 2006 Particle Data Group listing [7] included a statement: “The conclusion that pentaquarks in general, and that Θ^+ , in particular, do not exist, appears compelling,” which well reflected the prevailing mood in the particle physics community until a study of $\Lambda_b^0 \rightarrow J/\psi p K^-$ ($J/\psi \rightarrow \mu^+ \mu^-$) decays by LHCb [8] (charge conjugate modes are implied). From an analysis of 3 fb^{-1} Run 1 data at 7 and 8 TeV at the LHC, the LHCb collaboration reported a significant $J/\psi p$ structure in $\Lambda_b^0 \rightarrow J/\psi p K^-$ decays [8]. The exotic character of this structure, with the minimal quark content of $uudc\bar{c}$, was demonstrated in a nearly model-independent way in Ref. [9], where it was shown that the $J/\psi p$ mass ($m_{J/\psi p}$) peak near 4450 MeV was too narrow to be accounted for by $\Lambda^* \rightarrow p K^-$ reflections (Λ^* denotes a generic Λ excitation), reinforcing the results from the earlier model-dependent six-dimensional amplitude analysis of invariant masses and decay angles describing the Λ_b^0 decay in the same data [8]. Even though not apparent from the $m_{J/\psi p}$ distribution, the amplitude analysis also required a second broad $J/\psi p$ state to obtain a good description of the data, which peaked at $4380 \pm 8 \pm 29 \text{ MeV}$ with a width of $205 \pm 18 \pm 86 \text{ MeV}$ and a fit fraction of $(8.4 \pm 0.7 \pm 4.2)\%$.

The LHCb 6 fb^{-1} Run 2 LHC data at 13 TeV, together with the improvements in the data selection for both runs, resulted in a nine-fold increase in the number of reconstructed $\Lambda_b^0 \rightarrow J/\psi p K^-$ decays (246,000 events) [10]. When fit with the same six-dimensional amplitude model, the enlarged data sample gives consistent results for the $P_c(4450)^+$ and $P_c(4380)^+$ parameters, corroborating the compatibility of the data samples. However, the two-state interpretation of the data is contradicted by the observation of new narrow $J/\psi p$ structures which are too faint to have been significant in the Run 1 data analysis. A second horizontal band is observed in the Dalitz plot (Fig. 84.1) near 4312 MeV in the $J/\psi p$ mass.

The 4450 MeV structure also appears to consist of two narrower peaks at 4440 and 4457 MeV. Performing a rigorous six-dimensional amplitude analysis of these faint $J/\psi p$ structures is challenging and has not been accomplished yet. Fortunately, the newly observed peaks are so narrow that it is not necessary to construct an amplitude model to prove that these states are not artifacts of interfering Λ^* resonances, as was previously demonstrated in Ref. [9]. Their masses and widths have been characterized by the LHCb (see Table 84.1) from one-dimensional fits to $J/\psi p$ mass distributions, with different levels of suppression of the Λ^* contributions, which peak at the lower $p K^-$ masses (Fig. 84.1). Such analysis is not sensitive to any broad $J/\psi p$ contributions like $P_c(4380)^+$. The histograms analyzed by the LHCb are available in tabular form at <https://www.hepdata.net/record/89271>.

The fit chosen by the LHCb for the central mass and width values is displayed in Fig. 84.2. The $P_c(4312)^+$ state peaks right below the $\Sigma_c^+ \bar{D}^0$ threshold and has statistical significance over 7.6σ . The $P_c(4457)^+$ state peaks right below the $\Sigma_c^+ \bar{D}^{*0}$ threshold, while the $P_c(4440)^+$ state peaks about 20 MeV below it. The significance of the two-peak versus one-peak hypothesis for the

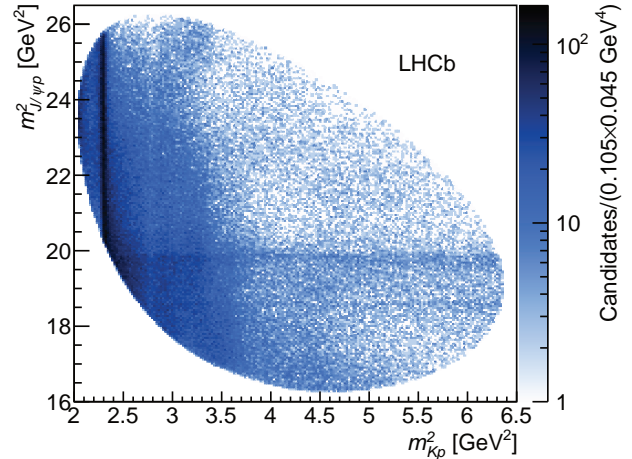


Figure 84.1: Dalitz plot distributions for $\Lambda_b^0 \rightarrow J/\psi p K^-$ decays as observed by LHCb.

4450 MeV structure is over 5.4σ , rendering the single peak interpretation of this region obsolete. The six-dimensional amplitude analysis reported in Ref. [8], which provided evidence for the $P_c(4380)^+$ state, is obsolete since it used the single $P_c(4450)^+$ state and it lacked the $P_c(4312)^+$ state. Furthermore, it used the helicity formalism in which the half-integer spin of the proton was not aligned properly between the different Λ_b decay chains [11, 12]. The newer one-dimensional analysis by LHCb [10] was not sensitive to wide P_c^+ states. The LHCb result from the six-dimensional amplitude analysis of the Cabibbo suppressed channel $\Lambda_b^0 \rightarrow J/\psi p \pi^-$ [13], which contains a statistically marginal evidence for the sum of the P_c^+ and the $Z_c(4200)^-$ contributions, took extensive input from Ref. [8] and, like the $P_c(4380)^+$ state, should be treated with caution until the both amplitude analyses are completed on the enlarged data sets with the modified helicity formalism.

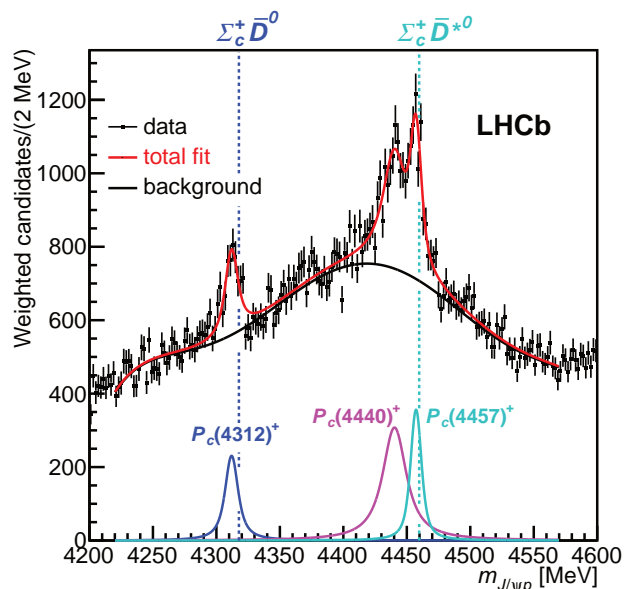


Figure 84.2: Fit to the $J/\psi p$ mass distribution, in which events were weighted to suppress $\Lambda^* \rightarrow p K^-$ backgrounds, of three Breit-Wigner functions and a sixth-order polynomial background. This fit was used to determine the central values of the masses and widths of the P_c^+ states reported by LHCb. The mass thresholds for the $\Sigma_c^+ \bar{D}^0$ and $\Sigma_c^+ \bar{D}^{*0}$ final states are superimposed.

While $\Sigma_c \bar{D}^{(*)}$ states had been predicted [14–17] before the first LHCb results [8], after these results became known, many theo-

Table 84.1: Summary of the narrow P_c^+ properties, interpreted as Breit-Wigner resonances. The central values are based on the fit displayed in Fig. 84.2.

State	M [MeV]	Γ [MeV] (95% CL)	\mathcal{R} [%]
$P_c(4312)^+$	$4311.9 \pm 0.7^{+6.8}_{-0.6}$	$9.8 \pm 2.7^{+3.7}_{-4.5} (< 27)$	$0.30 \pm 0.07^{+0.34}_{-0.09}$
$P_c(4440)^+$	$4440.3 \pm 1.3^{+4.1}_{-4.7}$	$20.6 \pm 4.9^{+8.7}_{-10.1} (< 49)$	$1.11 \pm 0.33^{+0.22}_{-0.10}$
$P_c(4457)^+$	$4457.3 \pm 0.6^{+4.1}_{-1.7}$	$6.4 \pm 2.0^{+5.7}_{-1.9} (< 20)$	$0.53 \pm 0.16^{+0.15}_{-0.13}$

retical groups interpreted the $P_c(4450)^+$ and $P_c(4380)^+$ states in terms of diquarks and triquarks as building blocks of a compact pentaquark [18–24]. In a different strategy, a tentative attempt has been made to treat the full 5-body dynamics, leading to states below the lowest threshold for spontaneous dissociation [25]. In the first implementation of the former approach [18], the pentaquark mass splitting was generated mostly by the change of angular momentum between the sub-components (L) from zero to one, which would also make the heavier state narrower and of opposite parity. Explicit modeling of multi-quark systems [26] questions if centrifugal barrier factor provides enough width suppression via spatial separation of c and \bar{c} quarks at these masses, as the phase space for $J/\psi p$ decay is very large (more than 400 MeV). Also, the observed mass splitting was too small to be only due to the mechanism proposed in Ref. [18] and required fine-tuning of such models. A variation of this model, in which the heavy (cu) diquark couples with heavy \bar{c} to form colored triquark attracting the light diquark (ud), has been re-implemented for the narrow P_c^+ states [27]. In this model, the $P_c(4440)^+$ and $P_c(4457)^+$ states are accommodated via spin-orbit interactions for the $L = 1$ states, while the $P_c(4312)^+$ is one of the $L = 0$ states. However, the mass prediction for the latter is off by (-72 ± 29) MeV [27]. This work was later extended to $SU(3)_F$ [28]. The width dilemma becomes more severe in view of the narrow widths of the newly observed states (Table 84.1), especially for the $L = 0$ $P_c(4312)^+$ state, and requires a different origin of potential barrier between c and \bar{c} than angular momentum [27, 29], which remains a subject of theoretical controversy. Measurement of spin-parity of $P_c(4312)^+$, $P_c(4440)^+$ and $P_c(4457)^+$ will be crucial for testing these and alternative theoretical ideas discussed in the following.

More effective width suppression mechanism is offered by a loosely bound charmed baryon-anticharmed meson molecular model, in which c and \bar{c} can be separated by much larger distances, resulting in a smaller probability of them getting close enough to each other in order to make a J/ψ . Since molecular binding energy cannot be large, such molecules are in S -wave, so their masses must be near the sum of the baryon and meson masses and their spin and parity are inherited from their constituent hadrons [17]. The mass coincidence of the $P_c(4312)^+$ and of $P_c(4457)^+$ states, with the two related thresholds, $\Sigma_c^+ \bar{D}^0$ and $\Sigma_c^+ \bar{D}^{*0}$, provides very strong experimental evidence in favor of this interpretation. Given how close $P_c(4312)^+$ is to the $\Sigma_c^+ \bar{D}^0$ threshold, it might be a virtual rather than a bound state [30]. Since the spins of Σ_c^+ and of \bar{D}^{*0} can be combined in two different ways, the narrow $P_c(4440)^+$ peak also finds natural explanation in this physical picture. It cannot be a virtual state since it is sufficiently below the $\Sigma_c^+ \bar{D}^{*0}$ threshold.

It is worth stressing that other baryon-meson combinations, $\Lambda_c^{(*)+} \bar{D}^{(*)0}$ and $\chi_{cJ} p$ are not expected to bind [14, 31]. Before the first pentaquark observation [8] heavy quark symmetry was used to show that, in addition to the three $\Sigma_c \bar{D}^{(*)0}$ states, one expects four $\Sigma_c^* \bar{D}^{(*)0}$ states, for a total of seven [32]. Indeed, additional states at, or below, the $\Sigma_c^+ \bar{D}$ and $\Sigma_c^+ \bar{D}^*$ thresholds, are expected [33–36]. Since Σ_c^{*+} width is likely around 15 MeV [37], more than the width of either $P_c(4312)^+$ or $P_c(4457)^+$, it is important to keep in mind that a molecule is typically as broad as the constituents¹ [38–40]. For a review on hadronic molecules, see [41, 42].

It is useful to consider the $P_c(4312)^+$, $P_c(4440)^+$ and $P_c(4457)^+$ narrow pentaquarks together with several analogous exotic states with hidden charm and bottom in the meson sector.

This provides additional significant motivation for the molecular model. At least five exotic mesons are close to thresholds of two heavy-light mesons: $X(3872)$ [43–46], $Z_b(10610)$ and $Z_b(10650)$ in the bottomonium sector [47–51] and $Z_c(3900)$ [52–56] and $Z_c(4020)$ [57–59] in the charmonium sector (see Table II in Ref. [60]; for reviews of experimental information see Ref. [61, 62], as well as *Spectroscopy of Mesons Containing Two Heavy Quarks and Heavy Non- $q\bar{q}$ Mesons* in the current Review of Particle Properties). These states share several important features: a) their masses are near thresholds and their spin and parity correspond to S -wave combination of the two mesons; b) they are very narrow, despite very large phase space for decay into quarkonium + pion(s); c) the branching fractions for “fall apart” mode into two mesons are much larger than branching fractions for decay into quarkonium and pion(s). So far, there is no experimental evidence for states at two pseudoscalar thresholds ($D\bar{D}$ and $B\bar{B}$), implying that pseudoscalar exchange is essential for binding in meson-meson systems.

The above provide a strong hint that these states are deuteron-like loosely bound states of two heavy mesons [63–71]. It is then natural to conjecture that similar bound states might exist of two heavy baryons [72, 73], or a meson and a baryon or a baryon and an antibaryon, leading to a rather accurate prediction of the $P_c(4457)^+$ mass as $3/2^- \Sigma_c \bar{D}^*$ molecule (the mass threshold is 4460 MeV for $\Sigma_c^+ D^{*0}$ and 4464 MeV for $\Sigma_c^{*+} D^{*-}$) [17, 60], following similar predictions obtained in a wider framework of doubly heavy baryon-meson hadronic molecules, which might include mixtures of various two-hadron states [14–16, 31]. However, single pion exchange is not possible in $\Sigma_c^+ \bar{D}^0$ system, thus the existence of $P_c(4312)^+$ points to importance of vector or two-pion exchanges in baryon-meson molecules. Two-pion exchange in $D\bar{D}$ system is highly suppressed, because the intermediate state is $D^* \bar{D}^*$, which is 282 MeV heavier than $D\bar{D}$. On the other hand, there is little suppression in the $\Sigma_c \bar{D}$ system, because the dominant intermediate state is $\Lambda_c \bar{D}^*$ which is just 25 MeV lighter than $\Sigma_c \bar{D}$ [74]. In a generic hadronic molecule it is essential that the two hadrons are heavy, in order to minimize the repulsive kinetic energy [72, 73, 75].

Following the initial LHCb discovery [8], several groups carried out a detailed analysis of the P_c^+ states as hadronic molecules [76–85] followed by further analyses [35, 86–110] after the updated LHCb results [10]. Partial widths of all the allowed decay channels for the P_c states have been estimated within a specific model in the molecular picture [111]. The most striking result is that $P_c(4312)$ decays are totally dominated by the $\bar{D}^* \Lambda_c$ channel. This channel is also expected to be very prominent in decays of $P_c(4440)$ and $P_c(4457)$. A recent theoretical analysis reaches an opposite conclusion, on the basis of the data available so far, expecting a rather small signal in the $\bar{D}^{(*)} \Lambda_c$ channels [112]. Obviously, experimental determination of the branching fraction of these channels is of high priority.

The P_c states have also been interpreted as so called hadro-charmonium [113], a bound state of relatively compact charmonium states with light hadronic matter. It was proposed that $P_c(4440)^+$ and $P_c(4457)^+$ are spin-split $\psi(2S)p$ bound states with $J^P = \frac{1}{2}^-$ and $\frac{3}{2}^-$, while $P_c(4312)^+$ is a $\chi_{c0} p$ bound state with $J^P = \frac{1}{2}^+$ [114]. While very interesting from the theoretical point of view, it is not at all clear why the binding energies between charmonia and the nucleon should conspire to produce states so close to the $\Sigma_c \bar{D}$ and $\Sigma_c \bar{D}^*$ thresholds. Moreover, the predicted widths of $P_c(4440)^+$ and $P_c(4457)^+$ are too big by a factor ~ 2 –3. One should also keep in mind that the molecular and hadro-charmonium pictures provide opposite predictions for the parity

¹This feature gets changed if systems are more deeply bound.

of $P_c(4312)^+$. In principle LHCb can check the spin and parity through partial wave analysis, but at present it is not known if systematic uncertainties can be sufficiently reduced to make such an analysis conclusive.

Shortly after the initial experimental discovery it was conjectured that the $P_c(4450)^+$ reflects the presence of a triangle singularity near the $\chi_{c1}p$ threshold [115–118]. These explanations are no longer viable, since the $P_c(4440)^+$ mass is not at any threshold and the $P_c(4312)^+$ and $P_c(4457)^+$ peak slightly below the $\Sigma_c^+\bar{D}^0$ and $\Sigma_c^+\bar{D}^{*0}$ thresholds. The $P_c(4457)^+$ mass is exactly at $\Lambda_c^{*+}\bar{D}^0$ threshold, but LHCb has demonstrated that the observed peaking is narrower in the data than expected from the triangle-diagram when a realistic width of the excited D_s^- state exchanged in the triangle is used (Supplemental Material in Ref. [10]).

More extensive pre-2019 reviews of some of the theoretical issues can be found in Refs. [119, 120]. Two recent relevant reviews are Refs. [121, 122].

So far the P_c^+ states have been observed by only one experiment in only one channel. It is essential to explore other possible experimental channels, such as $P_c \rightarrow \Lambda_c \bar{D}^{(*)}$, $\eta_c p$ [112]. These channels are however much more experimentally challenging than $P_c \rightarrow J/\psi p$. Proposals have also been made to search for heavy pentaquarks in photo-production [123–130]. Ref. [131] discusses photoproduction within the string-junction physical picture of the pentaquarks. Photoproduction is also related to recent work on $J/\psi(\eta_c)N$ scattering on the lattice [132] and on computation of $J/\psi(\eta_c)N$ and $\Upsilon(\eta_b)N$ cross sections [133]. In addition, pentaquark production has been discussed in the context of antiproton-deuterium collisions [134], of heavy ion collisions at LHC [135], in pA collisions [136] and in pion-induced processes [137–139]. The GlueX Collaboration reported negative search results for the P_c^+ states in photo-production at JLAB [140]. Within the large experimental errors and considerable theoretical model dependence these results do not contradict the molecular interpretations of the narrow P_c^+ states, especially in view of the P_c decay being likely dominated by $\Lambda_c \bar{D}^{(*)}$ modes [111, 141]. It has been suggested to determine the pentaquark photo-couplings and branching ratios by measuring the polarization transfer between the incident photon and the outgoing proton in the exclusive photo-production of J/ψ near threshold [142].

As noted in e.g. [17], bottom analogues of the P_c^+ might well exist, but experimental search for such states involves very significant challenges. It is therefore hardly surprising that they have not been observed so far. A detailed discussion is beyond the scope of the current review.

Recently, the LHCb collaboration has obtained a 3.1σ evidence for a $P_c^+ \rightarrow J/\psi p$ state in the four-dimensional amplitude analysis of about 800 $B_s^0 \rightarrow J/\psi p\bar{p}$ ($J/\psi \rightarrow \mu^+\mu^-$) decays [143]. The mass of the state, $4337_{-4}^{+7} \pm 2$ MeV, is not compatible with the $P_c(4312)^+$ state at 3.1 standard deviations. The width is relatively small, $29_{-12}^{+26} \pm 14$ MeV. The present data do not provide sufficient discrimination between various J^P assignments. Its mass is about 19 MeV higher than the $\Sigma_c^+\bar{D}^0$ threshold and about 16 MeV lower than the $\chi_{c0}p$ threshold. At present, no specific explanation for this structure has been proposed, but some intriguing ideas have been raised in Ref. [144]. Since the statistical significance of this evidence is marginal, more data are required before this state is considered experimentally established.

Similarly inconclusive 3.1σ evidence for a $P_{cs}^0 \rightarrow J/\psi \Lambda$ structure was observed by the LHCb collaboration in the six-dimensional amplitude analysis of about 1750 $\Xi_b^- \rightarrow J/\psi \Lambda K^-$ ($J/\psi \rightarrow \mu^+\mu^-$, $\Lambda \rightarrow p\pi^-$) decays [12]. The strange counterparts of P_c^+ states have been predicted in both molecular and compact pentaquark models [15, 98, 100, 145–147]. When interpreted as a single peak, its mass, $4458.8 \pm 2.9_{-1.1}^{+4.7}$ MeV, is 15 MeV above the $\Xi_c^0\bar{D}^0$ threshold and 18 MeV below the $\Xi_c^0\bar{D}^{*0}$ threshold. Its width, $17.3 \pm 6.5_{-5.7}^{+8.0}$ MeV, is relatively narrow, thus plausibly could be interpreted as a loosely bound $\Xi_c^0\bar{D}^{*0}$ state. However, in the latter model two states are expected with J^P equal to $1/2^-$ and $3/2^-$. In fact, the LHCb data are consistent with such hypothesis, under which 4454.9 ± 2.7 MeV ($\Gamma = 7.5 \pm 9.7$ MeV) and 4467.8 ± 3.7 MeV ($\Gamma = 5.2 \pm 5.3$ MeV) mass (width) estimates are obtained

(statistical errors only). It is worth noting, that the $SU(3)$ flavor structure of $\Xi_c^0\bar{D}^{*0}$ states is different from that of $\Sigma_c^+\bar{D}^{*0}$ states, since Ξ_c^0 belongs to the charmed baryon triplet, unlike Σ_c^+ , which together with $\Xi_c^{0'}$, belong to the charmed baryon sextet. More data are required to experimentally establish this structure, clarify its composition, and determine the related quantum numbers.

If $P_{cs}(4459)^0$ indeed is a $\Xi_c^0\bar{D}^{*0}$ molecule, there likely exists another state, corresponding to $\Xi_c^0\bar{D}^*$ [15, 98, 100, 145–147], with a mass shifted upwards by approximately $\Xi_c^0 - \Xi_c$ mass difference [148], i.e. about 108 MeV [37]. Experimental determination whether yet additional $\Xi_c^{(*)}\bar{D}^{(*)0}$ states actually exist will provide a useful testing ground for the various theoretical approaches which have been used to predict them.

In hidden-charm exotics discussed above, the charmed and the anticharmed quarks can form a charmonium and thereby decouple from the light quarks. The molecular model provides an efficient mechanism to suppress such decays, thus making these states narrow. This type of exotic states, should not be confused with exotic hadrons containing two heavy quarks, rather than a heavy quark and a heavy antiquark. Such a decoupling is impossible in exotics which contain two heavy quarks. This has far-reaching consequences.

The first exotic hadron containing two heavy quarks has recently been reported by LHCb [149, 150] and deserves a separate review. Here we briefly discuss only the essential distinction vs. hidden-charm pentaquarks. The reported T_{cc}^+ state has quark content $cc\bar{u}\bar{d}$, $I = 0$ and likely $J^P = 1^+$, and mass about 300 keV below the D^0D^{*+} threshold. Its width is a fraction of an MeV. The phase space available for decay is tiny due to absence of the decoupling mechanism. Therefore the narrow width of T_{cc}^+ is natural in both the compact tetraquark model and in those molecular models which predict the mass very close to the D^0D^{*+} threshold. On the other hand, for sufficiently heavy quarks, e.g. $bb\bar{u}\bar{d}$, such open heavy-flavor exotics are genuine compact tetraquarks which are *stable* under strong interactions; see discussion and references in Refs. [149, 150].

It is quite possible that compact tetraquark states exist also for states with hidden-flavor, but such states are expected to be broader because of the decoupling mechanism. In fact, there is plenty of evidence for them in form of mass structures in $J/\psi\phi$ [151–156], $J/\psi J/\psi$ [157], $Z_c(4430)^+ \rightarrow \psi(2S)\pi^+$ [158–160] and others, although alternative explanations of these structures have been also proposed. Analogous configurations may also exist for pentaquarks, but there is no firm evidence for them yet.

References

- [1] T. G. Trippe *et al.* (Particle Data Group), Rev. Mod. Phys. **48**, S1 (1976), [Erratum: Rev. Mod. Phys.48,497(1976)].
- [2] K. Hikasa *et al.* (Particle Data Group), Phys. Rev. **D45**, S1 (1992), [Erratum: Phys. Rev.D46,5210(1992)].
- [3] M. Praszalowicz, *Skyrmions and Anomalies*, p.112, M. Jezabek Ed., World Scientific Publishing (1987), ISBN 9971503506.
- [4] D. Diakonov, V. Petrov and M. V. Polyakov, Z. Phys. **A359**, 305 (1997), [hep-ph/9703373].
- [5] H. Weigel, Eur. Phys. J. **A2**, 391 (1998), [hep-ph/9804260].
- [6] K. H. Hicks, Eur.Phys.J. **H37**, 1 (2012).
- [7] W. M. Yao *et al.* (Particle Data Group), J. Phys. **G33**, 1 (2006).
- [8] R. Aaij *et al.* (LHCb), Phys. Rev. Lett. **115**, 072001 (2015), [arXiv:1507.03414].
- [9] R. Aaij *et al.* (LHCb), Phys. Rev. Lett. **117**, 8, 082002 (2016), [arXiv:1604.05708].
- [10] R. Aaij *et al.* (LHCb), Phys. Rev. Lett. **122**, 22, 222001 (2019), [arXiv:1904.03947].
- [11] M. Wang *et al.*, Chin. Phys. C **45**, 6, 063103 (2021), [arXiv:2012.03699].
- [12] R. Aaij *et al.* (LHCb), Sci. Bull. **66**, 1391 (2021), [arXiv:2012.10380].

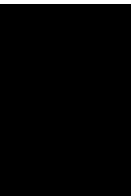
- [13] R. Aaij *et al.* (LHCb), Phys. Rev. Lett. **117**, 8, 082003 (2016), [Addendum: Phys. Rev. Lett.118,119901(2017)], [arXiv:1606.06999].
- [14] Z.-C. Yang *et al.*, Chin. Phys. **C36**, 6 (2012), [arXiv:1105.2901].
- [15] J.-J. Wu *et al.*, Phys. Rev. Lett. **105**, 232001 (2010), [arXiv:1007.0573].
- [16] J.-J. Wu, T. S. H. Lee and B. S. Zou, Phys. Rev. **C85**, 044002 (2012), [arXiv:1202.1036].
- [17] M. Karliner and J. L. Rosner, Phys. Rev. Lett. **115**, 12, 122001 (2015), [arXiv:1506.06386].
- [18] L. Maiani, A. D. Polosa and V. Riquer, Phys. Lett. **B749**, 289 (2015), [arXiv:1507.04980].
- [19] R. F. Lebed, Phys. Lett. **B749**, 454 (2015), [arXiv:1507.05867].
- [20] V. V. Anisovich *et al.* (2015), [arXiv:1507.07652].
- [21] G.-N. Li, X.-G. He and M. He, JHEP **12**, 128 (2015), [arXiv:1507.08252].
- [22] R. Ghosh, A. Bhattacharya and B. Chakrabarti, Phys. Part. Nucl. Lett. **14**, 4, 550 (2017), [arXiv:1508.00356].
- [23] Z.-G. Wang, Eur. Phys. J. **C76**, 2, 70 (2016), [arXiv:1508.01468].
- [24] R. Zhu and C.-F. Qiao, Phys. Lett. **B756**, 259 (2016), [arXiv:1510.08693].
- [25] J. M. Richard, A. Valcarce and J. Vijande, Phys. Lett. **B774**, 710 (2017), [arXiv:1710.08239].
- [26] E. Hiyama *et al.*, Phys. Rev. **C98**, 4, 045208 (2018), [arXiv:1803.11369].
- [27] A. Ali and A. Y. Parkhomenko, Phys. Lett. **B793**, 365 (2019), [arXiv:1904.00446].
- [28] A. Ali *et al.*, JHEP **10**, 256 (2019), [arXiv:1907.06507].
- [29] L. Maiani, A. D. Polosa and V. Riquer, Phys. Lett. **B778**, 247 (2018), [arXiv:1712.05296].
- [30] C. Fernandez-Ramirez *et al.* (JPAC), Phys. Rev. Lett. **123**, 9, 092001 (2019), [arXiv:1904.10021].
- [31] W. L. Wang *et al.*, Phys. Rev. **C84**, 015203 (2011), [arXiv:1101.0453].
- [32] J.-J. Wu *et al.*, Phys. Rev. C **84**, 015202 (2011), [arXiv:1011.2399].
- [33] C. W. Xiao, J. Nieves and E. Oset, Phys. Rev. **D88**, 056012 (2013), [arXiv:1304.5368].
- [34] C. W. Xiao, J. Nieves and E. Oset, Phys. Rev. **D100**, 1, 014021 (2019), [arXiv:1904.01296].
- [35] M.-Z. Liu *et al.*, Phys. Rev. Lett. **122**, 24, 242001 (2019), [arXiv:1903.11560].
- [36] G.-J. Wang *et al.*, Phys. Rev. D **102**, 3, 036012 (2020), [arXiv:1911.09613].
- [37] P. A. Zyla *et al.* (Particle Data Group), PTEP **2020**, 8, 083C01 (2020).
- [38] C. Hanhart, Yu. S. Kalashnikova and A. V. Nefediev, Phys. Rev. **D81**, 094028 (2010), [arXiv:1002.4097].
- [39] A. A. Filin *et al.*, Phys. Rev. Lett. **105**, 019101 (2010), [arXiv:1004.4789].
- [40] F.-K. Guo and U.-G. Meissner, Phys. Rev. **D84**, 014013 (2011), [arXiv:1102.3536].
- [41] F.-K. Guo *et al.*, Rev. Mod. Phys. **90**, 1, 015004 (2018), [arXiv:1705.00141].
- [42] X.-K. Dong, F.-K. Guo and B.-S. Zou (2021), [arXiv:2108.02673].
- [43] S. K. Choi *et al.* (Belle), Phys. Rev. Lett. **91**, 262001 (2003), [hep-ex/0309032].
- [44] D. Acosta *et al.* (CDF), Phys. Rev. Lett. **93**, 072001 (2004), [hep-ex/0312021].
- [45] B. Aubert *et al.* (BaBar), Phys. Rev. **D71**, 071103 (2005), [hep-ex/0406022].
- [46] V. M. Abazov *et al.* (D0), Phys. Rev. Lett. **93**, 162002 (2004), [hep-ex/0405004].
- [47] M. Karliner and H. J. Lipkin (2008), [arXiv:0802.0649].
- [48] K. F. Chen *et al.* (Belle), Phys. Rev. Lett. **100**, 112001 (2008), [arXiv:0710.2577].
- [49] A. Bondar *et al.* (Belle), Phys. Rev. Lett. **108**, 122001 (2012), [arXiv:1110.2251].
- [50] P. Krokovny *et al.* (Belle), Phys. Rev. **D88**, 5, 052016 (2013), [arXiv:1308.2646].
- [51] A. Garmash *et al.* (Belle), Phys. Rev. **D91**, 7, 072003 (2015), [arXiv:1403.0992].
- [52] M. Ablikim *et al.* (BESIII), Phys. Rev. Lett. **110**, 252001 (2013), [arXiv:1303.5949].
- [53] Z. Q. Liu *et al.* (Belle), Phys. Rev. Lett. **110**, 252002 (2013), [arXiv:1304.0121].
- [54] T. Xiao *et al.*, Phys. Lett. **B727**, 366 (2013), [arXiv:1304.3036].
- [55] M. Ablikim *et al.* (BESIII), Phys. Rev. Lett. **112**, 2, 022001 (2014), [arXiv:1310.1163].
- [56] M. Ablikim *et al.* (BESIII), Phys. Rev. Lett. **115**, 11, 112003 (2015), [arXiv:1506.06018].
- [57] M. Ablikim *et al.* (BESIII), Phys. Rev. Lett. **111**, 24, 242001 (2013), [arXiv:1309.1896].
- [58] M. Ablikim *et al.* (BESIII), Phys. Rev. Lett. **113**, 21, 212002 (2014), [arXiv:1409.6577].
- [59] M. Ablikim *et al.* (BESIII), Phys. Rev. Lett. **112**, 13, 132001 (2014), [arXiv:1308.2760].
- [60] M. Karliner, Acta Phys. Polon. **B47**, 117 (2016).
- [61] M. Karliner, J. L. Rosner and T. Skwarnicki, Ann. Rev. Nucl. Part. Sci. **68**, 17 (2018), [arXiv:1711.10626].
- [62] S. L. Olsen, T. Skwarnicki and D. Zieminska, Rev. Mod. Phys. **90**, 1, 015003 (2018), [arXiv:1708.04012].
- [63] M. B. Voloshin and L. B. Okun, JETP Lett. **23**, 333 (1976), [Pisma Zh. Eksp. Teor. Fiz.23,369(1976)].
- [64] A. De Rujula, H. Georgi and S. Glashow, Phys. Rev. Lett. **38**, 317 (1977).
- [65] N. A. Tornqvist, Phys. Rev. Lett. **67**, 556 (1991).
- [66] N. A. Tornqvist, Z. Phys. **C61**, 525 (1994), [hep-ph/9310247].
- [67] N. A. Tornqvist, Phys. Lett. **B590**, 209 (2004), [hep-ph/0402237].
- [68] C. E. Thomas and F. E. Close, Phys. Rev. **D78**, 034007 (2008), [arXiv:0805.3653].
- [69] M. Suzuki, Phys. Rev. **D72**, 114013 (2005), [hep-ph/0508258].
- [70] S. Fleming *et al.*, Phys. Rev. **D76**, 034006 (2007), [hep-ph/0703168].
- [71] T. E. O. Ericson and G. Karl, Phys. Lett. **B309**, 426 (1993).
- [72] M. Karliner, H. J. Lipkin and N. A. Tornqvist, in "Proceedings, 14th International Conference on Hadron spectroscopy (Hadron 2011)," (2011), [arXiv:1109.3472], URL <http://inspirehep.net/record/927616/files/arXiv:1109.3472.pdf>.
- [73] M. Karliner, H. J. Lipkin and N. A. Tornqvist, Nucl. Phys. Proc. Suppl. **225-227**, 102 (2012).
- [74] M. Karliner, "Hidden Charm Molecular Pentaquarks: Some Open Questions," in Proc. Bled Mini-Workshop, Slovenia, July 15-19, 2019, B. Golli *et al.*, Eds., p. 25, <http://www-fi.ijs.si/BledPub/bled2019.pdf>.
- [75] X.-Q. Li and X. Liu, Eur. Phys. J. **C74**, 12, 3198 (2014), [arXiv:1409.3332].

- [76] R. Chen *et al.*, Phys. Rev. Lett. **115**, 13, 132002 (2015), [arXiv:1507.03704].
- [77] H.-X. Chen *et al.*, Phys. Rev. Lett. **115**, 17, 172001 (2015), [arXiv:1507.03717].
- [78] L. Roca, J. Nieves and E. Oset, Phys. Rev. **D92**, 9, 094003 (2015), [arXiv:1507.04249].
- [79] J. He, Phys. Lett. **B753**, 547 (2016), [arXiv:1507.05200].
- [80] H. Huang *et al.*, Eur. Phys. J. **C76**, 11, 624 (2016), [arXiv:1510.04648].
- [81] L. Roca and E. Oset, Eur. Phys. J. **C76**, 11, 591 (2016), [arXiv:1602.06791].
- [82] Q.-F. Lü and Y.-B. Dong, Phys. Rev. **D93**, 7, 074020 (2016), [arXiv:1603.00559].
- [83] Y. Shimizu, D. Suenaga and M. Harada, Phys. Rev. **D93**, 11, 114003 (2016), [arXiv:1603.02376].
- [84] C.-W. Shen *et al.*, Nucl. Phys. **A954**, 393 (2016), [arXiv:1603.04672].
- [85] Y. Yamaguchi *et al.*, Phys. Rev. **D96**, 11, 114031 (2017), [arXiv:1709.00819].
- [86] J. F. Giron, R. F. Lebed and C. T. Peterson, JHEP **05**, 061 (2019), [arXiv:1903.04551].
- [87] R. Chen *et al.*, Phys. Rev. **D100**, 1, 011502 (2019), [arXiv:1903.11013].
- [88] F.-K. Guo *et al.*, Phys. Rev. **D99**, 9, 091501 (2019), [arXiv:1903.11503].
- [89] J. He, Eur. Phys. J. **C79**, 5, 393 (2019), [arXiv:1903.11872].
- [90] H. Huang, J. He and J. Ping (2019), [arXiv:1904.00221].
- [91] Y. Shimizu, Y. Yamaguchi and M. Harada (2019), [arXiv:1904.00587].
- [92] Z.-H. Guo and J. A. Oller, Phys. Lett. **B793**, 144 (2019), [arXiv:1904.00851].
- [93] C.-J. Xiao *et al.*, Phys. Rev. **D100**, 1, 014022 (2019), [arXiv:1904.00872].
- [94] Z.-G. Wang, Int. J. Mod. Phys. A **35**, 01, 2050003 (2020), [arXiv:1905.02892].
- [95] L. Meng *et al.*, Phys. Rev. **D100**, 1, 014031 (2019), [arXiv:1905.04113].
- [96] F. Giannuzzi, Phys. Rev. **D99**, 9, 094006 (2019), [arXiv:1903.04430].
- [97] Q. Wu and D.-Y. Chen, Phys. Rev. D **100**, 11, 114002 (2019), [arXiv:1906.02480].
- [98] C.-W. Shen, J.-J. Wu and B.-S. Zou, Phys. Rev. **D100**, 5, 056006 (2019), [arXiv:1906.03896].
- [99] F. Stancu, Eur. Phys. J. C **79**, 11, 957 (2019), [arXiv:1902.07101].
- [100] C. W. Xiao, J. Nieves and E. Oset, Phys. Lett. B **799**, 135051 (2019), [arXiv:1906.09010].
- [101] M. B. Voloshin, Phys. Rev. **D100**, 3, 034020 (2019), [arXiv:1907.01476].
- [102] S. Sakai, H.-J. Jing and F.-K. Guo, Phys. Rev. D **100**, 7, 074007 (2019), [arXiv:1907.03414].
- [103] Z.-G. Wang and X. Wang, Chin. Phys. C **44**, 103102 (2020), [arXiv:1907.04582].
- [104] Y. Yamaguchi *et al.*, Phys. Rev. D **101**, 9, 091502 (2020), [arXiv:1907.04684].
- [105] Y.-J. Xu *et al.*, Phys. Rev. D **102**, 3, 034028 (2020), [arXiv:1907.05097].
- [106] M. Pavon Valderrama, Phys. Rev. D **100**, 9, 094028 (2019), [arXiv:1907.05294].
- [107] F.-Z. Peng *et al.* (2019), [arXiv:1907.05322].
- [108] M.-Z. Liu *et al.*, Phys. Rev. D **103**, 5, 054004 (2021), [arXiv:1907.06093].
- [109] Y.-W. Pan *et al.*, Phys. Rev. D **102**, 1, 011504 (2020), [arXiv:1907.11220].
- [110] T. J. Burns and E. S. Swanson, Phys. Rev. D **100**, 11, 114033 (2019), [arXiv:1908.03528].
- [111] Y.-H. Lin and B.-S. Zou, Phys. Rev. **D100**, 5, 056005 (2019), [arXiv:1908.05309].
- [112] M.-L. Du *et al.* (2021), [arXiv:2102.07159].
- [113] S. Dubynskiy and M. B. Voloshin, Phys. Lett. **B666**, 344 (2008), [arXiv:0803.2224].
- [114] M. I. Eides, V. Y. Petrov and M. V. Polyakov, Mod. Phys. Lett. A **35**, 18, 2050151 (2020), [arXiv:1904.11616].
- [115] F.-K. Guo *et al.*, Phys. Rev. **D92**, 7, 071502 (2015), [arXiv:1507.04950].
- [116] U.-G. Meissner and J. A. Oller, Phys. Lett. **B751**, 59 (2015), [arXiv:1507.07478].
- [117] X.-H. Liu, Q. Wang and Q. Zhao, Phys. Lett. **B757**, 231 (2016), [arXiv:1507.05359].
- [118] M. Mikhasenko (2015), [arXiv:1507.06552].
- [119] T. J. Burns, Eur. Phys. J. **A51**, 11, 152 (2015), [arXiv:1509.02460].
- [120] H.-X. Chen *et al.*, Phys. Rept. **639**, 1 (2016), [arXiv:1601.02092].
- [121] Y.-R. Liu *et al.*, Prog. Part. Nucl. Phys. **107**, 237 (2019), [arXiv:1903.11976].
- [122] N. Brambilla *et al.*, Phys. Rept. **873**, 1 (2020), [arXiv:1907.07583].
- [123] Y. Huang *et al.*, J. Phys. **G41**, 11, 115004 (2014), [arXiv:1305.4434].
- [124] Q. Wang, X.-H. Liu and Q. Zhao, Phys. Rev. **D92**, 034022 (2015), [arXiv:1508.00339].
- [125] V. Kubarovsky and M. B. Voloshin, Phys. Rev. **D92**, 3, 031502 (2015), [arXiv:1508.00888].
- [126] M. Karliner and J. L. Rosner, Phys. Lett. **B752**, 329 (2016), [arXiv:1508.01496].
- [127] A. N. Hiller Blin *et al.*, Phys. Rev. **D94**, 3, 034002 (2016), [arXiv:1606.08912].
- [128] X. Cao and J.-p. Dai, Phys. Rev. **D100**, 5, 054033 (2019), [arXiv:1904.06015].
- [129] X.-Y. Wang, X.-R. Chen and J. He, Phys. Rev. **D99**, 11, 114007 (2019), [arXiv:1904.11706].
- [130] J.-J. Wu, T. S. H. Lee and B.-S. Zou, Phys. Rev. **C100**, 3, 035206 (2019), [arXiv:1906.05375].
- [131] G. C. Rossi and G. Veneziano (2019), [arXiv:1909.01753].
- [132] U. Skerbis and S. Prelovsek, Phys. Rev. **D99**, 9, 094505 (2019), [arXiv:1811.02285].
- [133] C. W. Xiao and U. G. Meissner, Phys. Rev. **D92**, 11, 114002 (2015), [arXiv:1508.00924].
- [134] M. B. Voloshin, Phys. Rev. **D99**, 9, 093003 (2019), [arXiv:1903.04422].
- [135] R.-Q. Wang *et al.*, Phys. Rev. **C94**, 4, 044913 (2016), [arXiv:1601.02835].
- [136] I. Schmidt and M. Siddikov, Phys. Rev. **D93**, 9, 094005 (2016), [arXiv:1601.05621].
- [137] Q.-F. Lu *et al.*, Phys. Rev. **D93**, 3, 034009 (2016), [arXiv:1510.06271].
- [138] X.-H. Liu and M. Oka, Nucl. Phys. **A954**, 352 (2016), [arXiv:1602.07069].
- [139] X.-Y. Wang *et al.*, Phys. Lett. **B797**, 134862 (2019), [arXiv:1906.04044].
- [140] A. Ali *et al.* (GlueX), Phys. Rev. Lett. **123**, 7, 072001 (2019), [arXiv:1905.10811].
- [141] M.-L. Du *et al.*, Eur. Phys. J. C **80**, 11, 1053 (2020), [arXiv:2009.08345].
- [142] D. Winney *et al.* (JPAC), Phys. Rev. **D100**, 3, 034019 (2019), [arXiv:1907.09393].

- [143] R. Aaij *et al.* (LHCb), Phys. Rev. Lett. **128**, 062001 (2021), [arXiv:2108.04720].
- [144] B. Wang, L. Meng and S.-L. Zhu, JHEP **11**, 108 (2019), [arXiv:1909.13054].
- [145] R. Chen, J. He and X. Liu, Chin. Phys. C **41**, 10, 103105 (2017), [arXiv:1609.03235].
- [146] E. Santopinto and A. Giachino, Phys. Rev. D **96**, 1, 014014 (2017), [arXiv:1604.03769].
- [147] B. Wang, L. Meng and S.-L. Zhu, Phys. Rev. D **101**, 3, 034018 (2020), [arXiv:1912.12592].
- [148] M. Karliner and J. L. Rosner, Sci. Bull. **66**, 13, 1256 (2021), [arXiv:2104.15077].
- [149] R. Aaij *et al.* (LHCb) (2021), [arXiv:2109.01038].
- [150] R. Aaij *et al.* (LHCb) (2021), [arXiv:2109.01056].
- [151] T. Aaltonen *et al.* (CDF), Phys. Rev. Lett. **102**, 242002 (2009), [arXiv:0903.2229].
- [152] T. Aaltonen *et al.* (CDF), Mod. Phys. Lett. A **32**, 26, 1750139 (2017), [arXiv:1101.6058].
- [153] S. Chatrchyan *et al.* (CMS), Phys. Lett. B **734**, 261 (2014), [arXiv:1309.6920].
- [154] R. Aaij *et al.* (LHCb), Phys. Rev. Lett. **118**, 2, 022003 (2017), [arXiv:1606.07895].
- [155] R. Aaij *et al.* (LHCb), Phys. Rev. D **95**, 1, 012002 (2017), [arXiv:1606.07898].
- [156] R. Aaij *et al.* (LHCb), Phys. Rev. Lett. **127**, 8, 082001 (2021), [arXiv:2103.01803].
- [157] R. Aaij *et al.* (LHCb), Sci. Bull. **65**, 23, 1983 (2020), [arXiv:2006.16957].
- [158] S. K. Choi *et al.* (Belle), Phys. Rev. Lett. **100**, 142001 (2008), [arXiv:0708.1790].
- [159] K. Chilikin *et al.* (Belle), Phys. Rev. D **88**, 7, 074026 (2013), [arXiv:1306.4894].
- [160] R. Aaij *et al.* (LHCb), Phys. Rev. Lett. **112**, 22, 222002 (2014), [arXiv:1404.1903].

Hypothetical Particles and Concepts

85. Extra dimensions (rev.)	983
86. W' -boson searches (rev.)	991
87. Z' -boson searches (rev.)	995
88. Supersymmetry: theory (rev.)	1000
89. Supersymmetry: experiment (rev.)	1019
90. Axions and other similar particles (rev.)	1038
91. Quark and lepton compositeness, searches for (rev.)	1055
92. Dynamical electroweak symmetry breaking:	1061
implications of the H^0 (rev.)	
93. Grand unified theories	1076
94. Leptoquarks (rev.)	1090
95. Magnetic monopoles (rev.)	1093



85. Extra Dimensions

Revised August 2021 by Y. Gershtein (Rutgers U.) and A. Pomarol (U. Autònoma de Barcelona; IFAE).

85.1 Introduction

Proposals for a spacetime with more than three spatial dimensions date back to the 1920s, mainly through the work of Kaluza and Klein, in an attempt to unify the forces of nature [1]. Although their initial idea failed, the formalism that they and others developed is still useful nowadays. Around 1980, string theory proposed again to enlarge the number of space dimensions, this time as a requirement for describing a consistent theory of quantum gravity. The extra dimensions were supposed to be compactified at a scale close to the Planck scale, and thus not testable experimentally in the near future.

A different approach was given by Arkani-Hamed, Dimopoulos, and Dvali (ADD) in their seminal paper in 1998 [2], where they showed that the weakness of gravity could be explained by postulating two or more flat extra dimensions in which only gravity could propagate. The size of these extra dimensions should range between roughly a millimeter and $\sim 1/\text{TeV}$, leading to possible observable consequences in current and future experiments. A year later, Randall and Sundrum (RS) [3] found a new possibility using a warped geometry, postulating a five-dimensional Anti-de Sitter (AdS) spacetime with a compactification scale of order $1/\text{TeV}$. The origin of the smallness of the electroweak scale versus the Planck scale was explained by the gravitational redshift factor present in the warped AdS metric. As in the ADD model, originally only gravity was assumed to propagate in the extra dimensions, although it was soon clear that this was not necessary in warped extra dimensions and also the SM gauge fields [4, 5] and SM fermions [6, 7] could propagate in the five-dimensional spacetime.

The physics of warped extra-dimensional models has an alternative interpretation by means of the AdS/CFT correspondence [8–10]. Models with warped extra dimensions are related to four-dimensional strongly-interacting theories, allowing an understanding of the properties of five-dimensional fields as those of four-dimensional composite states [11]. This approach has opened new directions for tackling outstanding questions in particle physics, such as the flavor problem, grand unification, and the origin of electroweak symmetry breaking or supersymmetry breaking.

85.1.1 Experimental Constraints

Constraints on extra-dimensional models arise from astrophysical and cosmological considerations, tabletop experiments exploring gravity at sub-mm distances, and collider experiments. Collider limits on extra-dimensional models are dominated by LHC results, which can be found on the public WWW pages of ATLAS [12] and CMS [13]. This review includes the most recent limits, most of which are published results based on 140 fb^{-1} LHC data collected in 2015–18 at a center-of-mass energy of 13 TeV and legacy results from 20 fb^{-1} of 8 TeV data collected in Run 1. For most of the models, Run 2 results surpass the sensitivity of Run 1.

85.1.2 Kaluza-Klein Theories

Field theories with compact extra dimensions can be written as theories in ordinary four dimensions (4D) by performing a Kaluza-Klein (KK) reduction. As an illustration, consider a simple example, namely a field theory of a complex scalar in flat five-dimensional (5D) spacetime. The action will be given by ¹

$$S_5 = - \int d^4x dy M_5 \left[|\partial_\mu \phi|^2 + |\partial_y \phi|^2 + \lambda_5 |\phi|^4 \right], \quad (85.1)$$

where y refers to the extra (fifth) dimension. A universal scale M_5 has been extracted in front of the action in order to keep the 5D field with the same mass-dimension as in 4D. This theory is perturbative for energies $E \lesssim \ell_5 M_5 / \lambda_5$ where $\ell_5 = 24\pi^3$ [14].

¹Our convention for the metric is $\eta_{MN} = \text{Diag}(-1, 1, 1, 1, 1)$.

Let us now consider that the fifth dimension is compact with the topology of a circle S^1 of radius R , which corresponds to the identification of y with $y + 2\pi R$. In such a case, the 5D complex scalar field can be expanded in a Fourier series:

$$\phi(x, y) = \frac{1}{\sqrt{2\pi R M_5}} \sum_{n=-\infty}^{\infty} e^{iny/R} \phi^{(n)}(x), \quad (85.2)$$

that, inserted in Eq. (85.1) and integrating over y , gives

$$S_5 = S_4^{(0)} + S_4^{(n)}, \quad (85.3)$$

where

$$S_4^{(0)} = - \int d^4x \left[|\partial_\mu \phi^{(0)}|^2 + \lambda_4 |\phi^{(0)}|^4 \right], \quad (85.4)$$

and,

$$S_4^{(n)} = - \int d^4x \sum_{n \neq 0} \left[|\partial_\mu \phi^{(n)}|^2 + \left(\frac{n}{R}\right)^2 |\phi^{(n)}|^2 \right] + \text{quartic interactions}. \quad (85.5)$$

The $n = 0$ mode self-coupling is given by

$$\lambda_4 = \frac{\lambda_5}{2\pi R M_5}. \quad (85.6)$$

The above action corresponds to a 4D theory with a massless scalar $\phi^{(0)}$, referred to as the zero mode, and an infinite tower of massive modes $\phi^{(n)}$ with $n > 0$, known as KK modes. The KK reduction thus allows a treatment of 5D theories as 4D field theories with an infinite number of fields. At energies smaller than $1/R$, the KK modes can be neglected, leaving the zero-mode action of Eq. (85.4). The strength of the interaction of the zero-mode, given by Eq. (85.6), decreases as R increases. Thus, for a large extra dimension $R \gg 1/M_5$, the massless scalar is very weakly coupled.

85.2 Large Extra Dimensions for Gravity

85.2.1 The ADD Scenario

The ADD scenario [2, 15] (for a review see, for example, [16]) assumes a $D = 4 + \delta$ dimensional spacetime, with δ compactified spatial dimensions. The apparent weakness of gravity arises since it propagates in the higher-dimensional space. The SM is assumed to be localized in a 4D subspace, a 3-brane, as can be found in certain string theory constructions [17, 18]. Gravity is described by the Einstein-Hilbert action in $D = 4 + \delta$ spacetime dimensions

$$S_D = - \frac{\bar{M}_D^{2+\delta}}{2} \int d^4x d^\delta y \sqrt{-g} \mathcal{R} + \int d^4x \sqrt{-g_{\text{ind}}} \mathcal{L}_{\text{SM}}, \quad (85.7)$$

where x labels the ordinary four coordinates, y the δ extra coordinates, g refers to the determinant of the D -dimensional metric whose Ricci scalar is defined by \mathcal{R} , and \bar{M}_D is called the reduced Planck scale of the D -dimensional theory. In the second term of Eq. (85.7), which gives the gravitational interactions of SM fields, the D -dimensional metric reduces to the induced metric on the 3-brane where the SM fields propagate. The extra dimensions are assumed to be flat and compactified in a volume V_δ . As an example, consider a toroidal compactification of equal radii R and volume $V_\delta = (2\pi R)^\delta$. After a KK reduction, one finds that the fields that couple to the SM are the spin-2 gravitational field $G_{\mu\nu}(x, y)$ and a tower of spin-0 KK graviscalars [19]. The graviscalars, however, only couple to SM fields through the trace of the energy-momentum tensor, resulting in weaker couplings to the SM fields. The Fourier expansion of the spin-2 field is given by

$$G_{\mu\nu}(x, y) = G_{\mu\nu}^{(0)}(x) + \frac{1}{\sqrt{V_\delta}} \sum_{\vec{n} \neq 0} e^{i\vec{n} \cdot \vec{y}/R} G_{\mu\nu}^{(\vec{n})}(x), \quad (85.8)$$

where $\vec{y} = (y_1, y_2, \dots, y_\delta)$ are the extra-dimensional coordinates and $\vec{n} = (n_1, n_2, \dots, n_\delta)$. Eq. (85.8) contains a massless state,

the 4D graviton $G_{\mu\nu}^{(0)}$, and its KK tower $G_{\mu\nu}^{(\vec{n})}$ with masses $m_{\vec{n}}^2 = |\vec{n}|^2/R^2$. At energies below $1/R$ the action is that of the zero mode

$$S_4^{(0)} = -\frac{\bar{M}_D^{2+\delta}}{2} \int d^4x V_\delta \sqrt{-g^{(0)}} \mathcal{R}^{(0)} + \int d^4x \sqrt{-g_{\text{ind}}^{(0)}} \mathcal{L}_{\text{SM}}, \tag{85.9}$$

where we can identify the 4D reduced Planck mass, $M_P \equiv 1/\sqrt{8\pi G_N} \simeq 2.4 \times 10^{18}$ GeV, as a function of the D -dimensional parameters:

$$M_P^2 = V^\delta \bar{M}_D^{2+\delta} \equiv R^\delta M_D^{2+\delta}. \tag{85.10}$$

Fixing M_D at around the electroweak scale $M_D \sim \text{TeV}$ to avoid introducing a new mass scale in the model, Eq. (85.10) gives a prediction for R :

$$\delta = 1, 2, \dots, 6 \rightarrow R \sim 10^9 \text{ km}, 0.5 \text{ mm}, \dots, 0.1 \text{ MeV}^{-1}. \tag{85.11}$$

The option $\delta = 1$ is clearly ruled out, as it leads to modifications of Newton’s law at solar system distances. However this is not the case for $\delta \geq 2$, and possible observable consequences can be sought in present and future experiments.

Consistency of the model requires a stabilization mechanism for the radii of the extra dimensions, to the values shown in Eq. (85.11). The fact that we need $R \gg 1/M_D$ leads to a new hierarchy problem, the solution of which might require imposing supersymmetry in the extra-dimensional bulk (for the case of two extra dimensions see for example [20]).

85.2.2 Tests of the Gravitational Force Law at Sub-mm Distances

The KK modes of the graviton give rise to deviations from Newton’s law of gravitation for distances $\lesssim R$. Such deviations are usually parameterized by a modified Newtonian potential of the form

$$V(r) = -G_N \frac{m_1 m_2}{r} [1 + \alpha e^{-r/\lambda}]. \tag{85.12}$$

For a 2-torus compactification, $\alpha = 16/3$ and $\lambda = R$. Searches for deviations from Newton’s law of gravitation have been performed in several experiments [21–24]. From Ref. [23] we have the constraint $R < 30\mu\text{m}$ at 95% CL for $\delta = 2$, corresponding to $M_D > 4.0$ TeV. We see then that bounds from Newton’s law deviations are already pushing the scale M_D beyond the TeV for two extra dimensions.

85.2.3 Astrophysical and Cosmological Constraints

The light KK gravitons could be copiously produced in stars, carrying away energy. Ensuring that the graviton luminosity is low enough to preserve the agreement of stellar models with observations provides powerful bounds on the scale M_D . The most stringent bound arises from supernova SN1987A, giving $M_D > 27$ (2.4) TeV for $\delta = 2$ (3) [25]. After a supernova explosion, most of the KK gravitons stay gravitationally trapped in the remnant neutron star. The requirement that neutron stars are not excessively heated by KK decays into photons leads to $M_D > 1700$ (76) TeV for $\delta = 2$ (3) [26].

Cosmological constraints are also quite stringent [27]. To avoid overclosure of the Universe by relic gravitons one needs $M_D > 7$ TeV for $\delta = 2$. Relic KK gravitons decaying into photons contribute to the cosmic diffuse gamma radiation, from which one can derive the bound $M_D > 100$ TeV for $\delta = 2$.

We must mention however that bounds coming from the decays of KK gravitons into photons can be reduced if we assume that KK gravitons decay mainly into other non-SM states. This could happen, for example, if there were other 3-branes with hidden sectors residing on them [15].

85.2.4 Collider Signals

85.2.4.1 Graviton and Other Particle Production

Although each KK graviton has a purely gravitational coupling, suppressed by $1/M_P$, inclusive processes in which one sums over the almost continuous spectrum of available gravitons have cross sections suppressed only by powers of M_D . Processes involving gravitons are therefore detectable in collider experiments if $M_D \sim \text{TeV}$. A number of experimental searches for evidence of

large extra dimensions have been performed at colliders, and interpreted in the context of the ADD model.

One signature arises from direct graviton emission. By making a derivative expansion of Einstein gravity, one can construct an effective theory, valid for energies much lower than M_D , and use it to make predictions for graviton-emission processes at colliders [19, 28, 29]. Gravitons produced in the final state would escape detection, giving rise to missing transverse energy (\cancel{E}_T). The results quoted below are 95% CL lower limits on M_D for a range of values of δ between 2 and 6, with more stringent limits corresponding to lower δ values.

At hadron colliders, experimentally sensitive channels include the jet (j) + \cancel{E}_T and γ + \cancel{E}_T final states. ATLAS (CMS) j + \cancel{E}_T results with 139 (137) fb^{-1} of 13 TeV data provide limits of $M_D > 5.9$ –11.2 TeV [30] ($M_D > 5.5$ –10.7 TeV [31]). For these analyses, both experiments are assuming leading order (LO) cross sections. Since the effective theory is only valid for energies much less than M_D , the results are quoted for the full space, and include the information that suppressing the graviton cross section by a factor M_D^4/\hat{s}^2 for $\sqrt{\hat{s}} > M_D$, where $\sqrt{\hat{s}}$ is the parton-level center-of-mass energy of the hard collision, weakens the limits on M_D by a negligible amount for $\delta = 2$ ($\sim 3\%$ for $\delta = 6$). Less stringent limits are obtained by CMS [32] from analysis of 36 fb^{-1} of 13 TeV data in the γ + \cancel{E}_T final state ($M_D > 2.85$ –2.90 TeV for $\delta = 3$ –6). The analogous ATLAS search [33] uses full Run 2 statistics but does not quote ADD interpretation of the results.

In models in which the ADD scenario is embedded in a string theory at the TeV scale [18], we expect the string scale M_s to be smaller than M_D , and therefore expect production of string resonances at the LHC [34]. A result from CMS analyzing the dijet invariant mass distribution for 137 fb^{-1} of 13 TeV data excludes string resonances that decay predominantly to $q + g$ with masses below 7.9 TeV [35]. ATLAS dijet analysis [36] provides their results in the context of model-independent limits on the cross section times acceptance for generic resonances of a variety of possible widths, from which one can deduce similar lower mass limits ~ 8 TeV for string resonances decaying to $q + g$.

85.2.4.2 Virtual graviton effects

One can also search for virtual graviton effects, the calculation of which however depends on the ultraviolet cut-off of the theory and is therefore very model dependent. In the literature, several different formulations exist [19, 29, 37] for the dimension-eight operator for gravity exchange at tree level:

$$\mathcal{L}_8 = \pm \frac{4}{M_{TT}^4} \left(T_{\mu\nu} T^{\mu\nu} - \frac{1}{\delta + 2} T_\mu^\mu T_\nu^\nu \right), \tag{85.13}$$

where $T_{\mu\nu}$ is the energy-momentum tensor and M_{TT} is related to M_D by some model-dependent coefficient [38]. The relations with the parametrization of Refs. [37] and [19] are, respectively, $M_{TT} = M_S$ and $M_{TT} = (2/\pi)^{1/4} \Lambda_T$. The experimental results below are given as 95% CL lower limits on M_{TT} , including in some cases the possibility of both constructive or destructive interference, depending on the sign chosen in Eq. (9).

The most stringent limits arise from LHC analyses of the dijet angular distribution. Using 35.9 fb^{-1} of 13 TeV data, CMS [39] obtains results that correspond to an approximate limit of $M_{TT} > 9.1$ TeV.

The next most restrictive results come from the analyses of diphoton ($M_{TT} > 6.1$ TeV from ATLAS [40] and $M_{TT} > 7.0$ TeV from CMS [41]) and dilepton mass spectra ($M_{TT} > 6.5$ TeV from CMS [42]). The complete Run 2 (139 fb^{-1}) analysis of ATLAS di-lepton data [43] does not quote the limits on ADD.

At the one-loop level, gravitons can also generate dimension-six operators with coefficients that are also model dependent. Experimental bounds on these operators can also give stringent constraints on M_D [38].

85.2.4.3 Black Hole Production

The physics at energies $\sqrt{s} \sim M_D$ is sensitive to the details of the unknown quantum theory of gravity. Nevertheless, in the transplanckian regime, $\sqrt{s} \gg M_D$, one can rely on a semiclassical description of gravity to obtain predictions. An interesting feature of transplanckian physics is the creation of black holes [44, 45] (for

a review see, for example, [46]). A black hole is expected to be formed in a collision in which the impact parameter is smaller than the Schwarzschild radius [47]:

$$R_S = \frac{1}{M_D} \left[\frac{2^\delta \pi^{\delta-3/2}}{\delta+2} \Gamma\left(\frac{\delta+3}{2}\right) \frac{M_{BH}}{M_D} \right]^{1/(\delta+1)}, \quad (85.14)$$

where M_{BH} is the mass of the black hole, which would roughly correspond to the total energy in the collision. The cross section for black hole production can be estimated to be of the same order as the geometric area $\sigma \sim \pi R_S^2$. For $M_D \sim \text{TeV}$, this gives a production of $\sim 10^7$ black holes at the $\sqrt{s} = 14 \text{ TeV}$ LHC with an integrated luminosity of 30 fb^{-1} [44, 45]. A black hole would provide a striking experimental signature since it is expected to thermally radiate with a Hawking temperature $T_H = (\delta+1)/(4\pi R_S)$, and therefore would evaporate democratically into all SM states. Nevertheless, given the present constraints on M_D , the LHC will not be able to reach energies much above M_D . This implies that predictions based on the semiclassical approximation could receive sizable modifications from model-dependent quantum-gravity effects.

The most stringent limits on microscopic black holes arise from LHC searches which observed no excesses above the SM background in high-multiplicity final states. The results are usually quoted as model-independent limits on the cross section for new physics in the final state and kinematic region analyzed. These results can then be used to provide constraints of models of low-scale gravity and weakly-coupled string theory. In addition, limits are sometimes quoted on particular implementations of models, which are used as benchmarks to illustrate the sensitivity.

A CMS analysis [48] of multi-object final states using 36 fb^{-1} of 13 TeV data, excludes semiclassical black holes below masses of up to 10.1 TeV for $M_D = 2 \text{ TeV}$ and $\delta = 6$. Analogous Run 2 ATLAS analysis [49], using 3.0 fb^{-1} of 13 TeV data, excludes black hole masses up to 9.0 – 9.7 TeV, depending on M_D , for $\delta = 6$. Another ATLAS search [50] for an excess of events with multiple high transverse momentum objects, including charged leptons and jets, using 3.2 fb^{-1} of 13 TeV data, excludes semiclassical black holes below masses of $\sim 8.7 \text{ TeV}$ for $M_D = 2 \text{ TeV}$ and $\delta = 6$.

A complementary approach is to look for jet extinction at high transverse momenta, as we expect hard short distance scattering processes to be highly suppressed at energies above M_D [51]. The CMS analysis [52] of inclusive jet p_T spectrum in 10.7 fb^{-1} of 8 TeV data set a lower limit of 3.3 TeV on the extinction mass scale.

For black hole masses near M_D , the semi-classical approximation is not valid, and one could instead expect quantum black holes (QBH) that decay primarily into two-body final states [53]. LHC Run 2 results at 13 TeV provide lower limits on QBH masses of order 2.3 – 9.4 TeV, depending on the details of the model. Searches that consider interpretations in terms of QBH limits include the CMS multi-object analysis (based on 2.3 fb^{-1} [54]), ATLAS dijet analysis (based on 139 fb^{-1} [36]), and different flavor di-lepton analyses at CMS ($e\mu$, 36 fb^{-1} at 13 TeV [55]) and ATLAS ($e\mu$, $e\tau$, $\mu\tau$, 36.1 fb^{-1} at 13 TeV [56]).

So [36] relies on 139 fb^{-1} and [54] relies on 2.3 fb^{-1} .

In weakly-coupled string models the semiclassical description of gravity fails in the energy range between M_s and M_s/g_s^2 where stringy effects are important. In this regime one expects, instead of black holes, the formation of string balls, made of highly excited long strings, that could be copiously produced at the LHC for $M_s \sim \text{TeV}$ [57], and would evaporate thermally at the Hagedorn temperature giving rise to high-multiplicity events. The same analyses used to search for black holes can be interpreted in the context of string balls. For example, for the case of $\delta = 6$ with $M_s = M_D/1.26 = 3 \text{ TeV}$, the ATLAS multiple high transverse momentum object analysis [49] excludes string balls with masses below 6.5 to 9.0 TeV for values of $0.2 < g_s < 0.8$. The CMS multi-object analysis [48] studies string ball production in two scenarios, both assuming $\delta = 6$. For the constant $g_s = 0.2$ and $1 < M_s < 3.5 \text{ TeV}$ the string ball masses below 7.2 to 9.4 TeV are excluded, while at constant $M_s = 3.6 \text{ TeV}$ and $0.2 < g_s < 0.4$ masses below 7.2 to 8.1 TeV are excluded.

85.3 TeV-Scale Extra Dimensions

85.3.1 Warped Extra Dimensions

The RS model [3] is the most attractive setup of warped extra dimensions at the TeV scale, since it provides an alternative solution to the hierarchy problem. The RS model is based on a 5D theory with the extra dimension compactified in an orbifold, S^1/Z_2 , a circle S^1 with the extra identification of y with $-y$. This corresponds to the segment $y \in [0, \pi R]$, a manifold with boundaries at $y = 0$ and $y = \pi R$. Let us now assume that this 5D theory has a cosmological constant in the bulk Λ , and on the two boundaries Λ_0 and $\Lambda_{\pi R}$:

$$S_5 = - \int d^4x dy \left\{ \sqrt{-g} \left[\frac{1}{2} M_5^3 \mathcal{R} + \Lambda \right] + \sqrt{-g_0} \delta(y) \Lambda_0 + \sqrt{-g_{\pi R}} \delta(y - \pi R) \Lambda_{\pi R} \right\}, \quad (85.15)$$

where g_0 and $g_{\pi R}$ are the values of the determinant of the induced metric on the two respective boundaries. Einstein's equations can be solved, giving in this case the metric

$$ds^2 = a(y)^2 dx^\mu dx^\nu \eta_{\mu\nu} + dy^2, \quad a(y) = e^{-ky}, \quad (85.16)$$

where $k = \sqrt{-\Lambda/6M_5^3}$. Consistency of the solution requires $\Lambda_0 = -\Lambda_{\pi R} = -\Lambda/k$. The metric in Eq. (85.16) corresponds to a 5D AdS space. The factor $a(y)$ is called the “warp” factor and determines how 4D scales change as a function of the position in the extra dimension. In particular, this implies that energy scales for 4D fields localized at the boundary at $y = \pi R$ are redshifted by a factor $e^{-k\pi R}$ with respect to those localized at $y = 0$. For this reason, the boundaries at $y = 0$ and $y = \pi R$ are usually referred to as the ultraviolet (UV) and infrared (IR) boundaries, respectively.

As in the ADD case, we can perform a KK reduction and obtain the low-energy effective theory of the 4D massless graviton. In this case we obtain

$$M_P^2 = \int_0^{\pi R} dy e^{-2ky} M_5^3 = \frac{M_5^3}{2k} (1 - e^{-2k\pi R}). \quad (85.17)$$

Taking $M_5 \sim k \sim M_P$, we can generate an IR-boundary scale of order $ke^{-k\pi R} \sim \text{TeV}$ for an extra dimension of radius $R \simeq 11/k$. Mechanisms to stabilize R to this value have been proposed [58, 59] that, contrary to the ADD case, do not require introducing any new small or large parameter. Therefore a natural solution to the hierarchy problem can be achieved in this framework if the Higgs field, whose vacuum expectation value (VEV) is responsible for electroweak symmetry breaking, is localized at the IR-boundary where the effective mass scales are of order TeV. The radion field is generically heavy in models with a stabilized R . Nevertheless, it has been recently discussed that under some conditions a naturally light radion can arise [60–63]. In these cases the radion is identified with the dilaton, the Nambu-Goldstone boson associated to the spontaneous breaking of scale invariance, and its mass can be naturally below $ke^{-k\pi R} \sim \text{TeV}$. Collider bounds on the radion mass and couplings can be found in [64–66].

In the RS model [3], all the SM fields were assumed to be localized on the IR-boundary. Nevertheless, for the hierarchy problem, only the Higgs field has to be localized there. SM gauge bosons and fermions can propagate in the 5D bulk [4–7] (for a review see, for example, [67, 68]). By performing a KK reduction from the 5D action of a gauge boson, we find [4, 5]

$$\frac{1}{g_4^2} = \int_0^{\pi R} dy \frac{1}{g_5^2} = \frac{\pi R}{g_5^2}, \quad (85.18)$$

where g_D ($D = 4, 5$) is the gauge coupling in D -dimensions. Therefore the 4D gauge couplings can be of order one, as is the case of the SM, if one demands $g_5^2 \sim \pi R$. Using $kR \sim 10$ and $g_4 \sim 0.5$, one obtains the 5D gauge coupling

$$g_5 \sim 4/\sqrt{k}. \quad (85.19)$$

Boundary kinetic terms for the gauge bosons can modify this relation, allowing for larger values of $g_5\sqrt{k}$.

Fermions propagating in a warped extra dimension have 4D massless zero-modes with wavefunctions which vary as $f_0 \sim \exp[(1/2 - c_f)ky]$, where c_fk is their 5D mass [7,69]. Depending on the free parameter c_fk , fermions can be localized either towards the UV-boundary ($c_f > 1/2$) or IR-boundary ($c_f < 1/2$). Since the Higgs boson is localized on the IR-boundary, one can generate exponentially suppressed Yukawa couplings by having the fermion zero-modes localized towards the UV-boundary, generating naturally the light SM fermion spectrum [7]. A large overlap with the wavefunction of the Higgs is needed for the top quark, in order to generate its large mass, thus requiring it to be localized towards the IR-boundary. In conclusion, the large mass hierarchies present in the SM fermion spectrum can be easily obtained in warped models via suitable choices of the order-one parameters c_f [70]. In these scenarios, deviations in flavor physics from the SM predictions are expected to arise from flavor-changing KK gluon couplings [71], putting certain constraints on the parameters of the models and predicting new physics effects to be observed in B -physics processes (see, for example, [72,73]).

The masses of the KK states can also be calculated. One finds [7]

$$m_n \simeq \left(n + \frac{\alpha}{2} - \frac{1}{4} \right) \pi k e^{-\pi k R}, \quad (85.20)$$

where $n = 1, 2, \dots$ and $\alpha = \{c_f - 1/2, 0, 1\}$ for KK fermions, KK gauge bosons and KK gravitons, respectively. Their masses are of order $ke^{-\pi k R} \sim \text{TeV}$ (for this reason we refer to these scenarios as TeV-scale extra dimensions). The first KK state of the gauge bosons would be the lightest, while gravitons are expected to be the heaviest.

85.3.1.1 Models of Electroweak Symmetry Breaking

Theories in warped extra dimensions can be used to implement symmetry breaking at low energies by boundary conditions (for a review see, for example, [74]). For example, for a $U(1)$ gauge symmetry in the 5D bulk, this can be easily achieved by imposing a Dirichlet boundary condition on the IR-boundary for the gauge-boson field, $A_\mu|_{y=\pi R} = 0$. This makes the zero-mode gauge boson get a mass, given by $m_A = g_4 \sqrt{2k/g_5^2} e^{-\pi k R}$. A very different situation occurs if the Dirichlet boundary condition is imposed on the UV-boundary, $A_\mu|_{y=0} = 0$. In this case the zero-mode gauge boson disappears from the spectrum. Finally, if a Dirichlet boundary condition is imposed on the two boundaries, one obtains a massless 4D scalar corresponding to the fifth component of the 5D gauge boson, A_5 . Thus, different scenarios can be implemented by appropriately choosing the 5D bulk gauge symmetry, \mathcal{G}_5 , and the symmetries to which it reduces on the UV and IR-boundary, \mathcal{H}_{UV} and \mathcal{H}_{IR} , respectively. In all cases the KK spectrum comes in representations of the group \mathcal{G}_5 .

Among the most interesting scenarios are those called gauge-Higgs unified models, where the Higgs boson appears as the fifth component of a 5D gauge boson, A_5 . The Higgs mass is protected by the 5D gauge invariance and can only get a nonzero value from non-local one-loop effects [75]. To guarantee the relation $M_W^2 \simeq M_Z^2 \cos^2 \theta_W$, a custodial $SU(2)_V$ symmetry is needed in the bulk and IR-boundary [76]. The simplest realization [77,78] has

$$\begin{aligned} \mathcal{G}_5 &= SU(3)_c \times SO(5) \times U(1)_X, \\ \mathcal{H}_{IR} &= SU(3)_c \times SO(4) \times U(1)_X, \\ \mathcal{H}_{UV} &= G_{SM}. \end{aligned}$$

The Higgs boson gets a potential at the one-loop level that triggers a VEV, breaking the electroweak symmetry. In these models there is a light Higgs boson whose mass can be around 125 GeV, as required by the discovered Higgs boson [79]. This state, as will be explained in Sec. 85.3.2, behaves as a composite pseudo-Nambu-Goldstone boson with couplings that deviate from the SM Higgs [80]. The present experimental determination of the Higgs couplings at the LHC, that agrees with the SM predictions, put important constraints on these scenarios [79]. The lightest KK modes of the model are color fermions with charges $Q = -1/3, 2/3$ and $5/3$ [81].

85.3.1.2 Constraints from Electroweak Precision Tests

Models in which the SM gauge bosons propagate in 1/TeV-sized extra dimensions give generically large corrections to electroweak observables. When the SM fermions are confined on a boundary these corrections are universal and can be parameterized by four quantities: \widehat{S} , \widehat{T} , W and Y , as defined in Ref. [82]. For warped models, where the 5D gauge coupling of Eq. (85.19) is large, the most relevant parameter is \widehat{T} , which gives the bound $m_{KK} \gtrsim 10 \text{ TeV}$ [67]. When a custodial symmetry is imposed [76], the main constraint comes from the \widehat{S} parameter, requiring $m_{KK} \gtrsim 3 \text{ TeV}$, independent of the value of g_5 . Corrections to the $Zb_L\bar{b}_L$ coupling can also be important [67], especially in warped models for electroweak symmetry breaking as the ones described above.

85.3.1.3 Kaluza-Klein Searches

The main prediction of 1/TeV-sized extra dimensions is the presence of a discretized KK spectrum, with masses around the TeV scale, associated with the SM fields that propagate in the extra dimension.

In the RS model [3], only gravity propagates in the 5D bulk. Experimental searches have been performed for the lightest KK graviton through its decay to a variety of SM particle-antiparticle pairs. The results are usually interpreted in the plane of the dimensionless coupling k/M_P versus m_1 , where M_P is the reduced Planck mass defined previously and m_1 is the mass of the lightest KK excitation of the graviton. Since the AdS curvature $\sim k$ cannot exceed the cut-off scale of the model, which is estimated to be $\ell_5^{1/3} M_5$ [38], one must demand $k \ll \sqrt{2\ell_5} M_P \simeq 40 M_P$.

The most stringent limits currently arise from LHC searches for resonances in the dilepton and diphoton final states, using 13 TeV collisions. Best sensitivities are obtained in the $\gamma\gamma$ final state, which is quite powerful since it has a branching fraction twice that of any individual lepton flavor. The CMS analysis [41] of 36 fb⁻¹ of 13 TeV data excludes KK gravitons below 2.3 to 4.6 TeV, depending on the value of the coupling k/M_P , which is varied between 0.01 and 0.2, while ATLAS [83] uses the full 139 fb⁻¹ and provides a lower limit on the KK graviton mass of 4.6 TeV for the coupling parameter 0.1. The CMS [42] dilepton analyses, combining results from the ee and $\mu\mu$ channels, exclude KK gravitons with masses 2.47–4.78 TeV for k/M_P values of 0.01–0.1. The ATLAS [84] analysis of 139 fb⁻¹ of Run 2 data does not include a RS KK graviton interpretation of the results. Less stringent limits on the KK graviton mass can be derived from analyses of the dijet [85,86], HH [87–90], and VV [91–94] final states, where V can represent either a W or Z boson.

In warped extra-dimensional models in which the SM fields propagate in the 5D bulk, the couplings of the KK graviton to $ee/\mu\mu/\gamma\gamma$ are suppressed [95], and the above bounds do not apply. Furthermore, the KK graviton is the heaviest KK state (see Eq. (85.20)), and therefore experimental searches for KK gauge bosons and fermions are more appropriate discovery channels in these scenarios. For the scenarios discussed above in which only the Higgs boson and the top quark are localized close to the IR-boundary, the KK gauge bosons mainly decay into top quarks, longitudinal W/Z bosons, and Higgs bosons. Couplings to light SM fermions are suppressed by a factor $g/\sqrt{g_5^2 k} \sim 0.2$ [7] for the value of Eq. (85.19) that is considered from now on. Searches have been made for evidence of the lightest KK excitation of the gluon, through its decay to $t\bar{t}$ pairs. The searches take into account the natural KK gluon width, which is typically $\sim 15\%$ of its mass. The decay of a heavy particle to $t\bar{t}$ would tend to produce highly boosted top (anti-)quarks in the final state. Products of the subsequent top decays would therefore tend to be close to each other in the detector. In the case of $t \rightarrow Wb \rightarrow jjb$ decays, the three jets could overlap with one another and not be individually reconstructed with the standard jet algorithms, while $t \rightarrow Wb \rightarrow l\nu b$ decays could result in the lepton failing standard isolation requirements due to its proximity to the b -jet; in both cases, the efficiency for properly reconstructing the final state would fall as the mass of the original particle increases. To avoid the loss in sensitivity which would result, a number of techniques, known generally as “top quark tagging” [96,97], have been developed to reconstruct and identify highly boosted top quarks, for example by using a

single “wide” jet to contain all the decay products of a hadronic top decay. The large backgrounds from QCD jets can then be reduced by requiring the “jet mass” be consistent with that of a top quark, and also by examining the substructure of the wide jet for indication that it resulted from the hadronic decay of a top quark. These techniques are key to extending to very high masses the range of accessible resonances decaying to $t\bar{t}$ pairs. The ATLAS search in 139 fb^{-1} of Run 2 data [98] does not provide a KK interpretation. Dedicated analysis from CMS [99] of 36 fb^{-1} of 13 TeV data combines di-lepton, lepton-plus-jet, and all-hadronic $t\bar{t}$ decays and excludes KK gluons with masses below 4.55 TeV. ATLAS uses all-hadronic [100] and lepton-plus-jet [101] final states to exclude KK gluons up to 3.4 and 3.8 TeV respectively with 36 fb^{-1} of 13 TeV data. The results are not directly comparable between the two LHC experiments, since they employ in their respective analyses different implementations of the theoretical model. For masses between 3 and 5 TeV, the cross-section limits are around 20 fb for CMS analysis of 36 fb^{-1} and 30 fb (4 fb) for ATLAS analyses of 36 (139) fb^{-1} .

A gauge boson KK excitation could be also sought through its decay to longitudinal W/Z bosons. Recent analyses from ATLAS [102] (and CMS [103]) with 139 (137) fb^{-1} of 13 TeV data searching for heavy vector resonances decaying to a W or Z boson and a Higgs in the $q\bar{q}b\bar{b}$ final state have set a lower limit on the mass of these KK of 3.2 (3.7) TeV (warped models are equivalent to the Model B considered in the analyses with $g_V \sim g_5\sqrt{k}$). The decay to a pair of intermediate vector bosons has also been exploited to search for KK gravitons in models in which the SM fields propagate in the 5D bulk. The analyses typically reconstruct hadronic W/Z decays using variants of the boosted techniques mentioned previously. An ATLAS analysis [104] combines leptonic and hadronic final states from the KK graviton decay $G^* \rightarrow VV$, where V can represent either a W or Z boson, exclude KK gravitons with masses below 2.3 TeV, for a value of $k/M_P = 1$. CMS VV analysis [105] also provides cross section limits in the context of bulk gravitons; however, a maximum value of $k/M_P = 0.5$ is presented, for which no mass exclusion is possible using the 36 fb^{-1} of 13 TeV data.

The lightest KK states are, in certain models, the partners of the top quark. For example, in 5D composite Higgs models these are colored states with charges $Q = -1/3, 2/3$ and $5/3$ (arising from $SU(2)_L$ doublets with $Y = 7/6, 1/6$), and masses expected to be below the TeV [81]. They can be either singly or pair-produced, and mainly decay into a combination of W/Z with top/bottom quarks [106–109]. An exhaustive review of these searches can be found in Ref. [110]. Of particular note, the $Q = 5/3$ state decays mainly into $W^+t \rightarrow W^+W^+b$, giving a very clean signature of a pair of same-sign leptons in the final state. An analysis by ATLAS [111] searching in the lepton-plus-jets final state for evidence of pair production of the $Q = 5/3$ state provides a lower mass limit of 1.25 TeV. A CMS analysis [112] searching for pair production of the $Q = 5/3$ state using both lepton-plus-jets and same sign lepton final states excludes masses below 1.3 TeV. Both LHC experiments have searched for pair production of vector-like quarks T and B of charges $Q = 2/3$ and $-1/3$ respectively, assuming the allowable decays are $T \rightarrow Wb/Zt/Ht$ and $B \rightarrow Wt/Zb/Hb$. In each case, it is assumed the branching fractions of the three decay modes sum to unity, but the individual branching fractions, which are model-dependent, are allowed to vary within this constraint. Both ATLAS [113] and CMS [114] obtain lower limits on the mass of the T and B vector-like quarks up to 1.5 TeV.

Recent analyses from ATLAS [115] and CMS [116] also search for a single top partner production, the cross section for which is model-dependent [117] but does not carry the kinematic penalty for producing two heavy objects.

85.3.2 Connection with Strongly Coupled Models via the AdS/CFT Correspondence

The AdS/CFT correspondence [8] provides a connection between warped extra-dimensional models and strongly-coupled theories in ordinary 4D. Although the exact connection is only known for certain cases, the AdS/CFT techniques have been very useful to obtain, at the qualitative level, a 4D holographic description of the various phenomena in warped extra-dimensional models [11].

The connection goes as follows. The physics of the bulk AdS₅ models can be interpreted as that of a 4D conformal field theory (CFT) which is strongly coupled. The extra-dimensional coordinate y plays the role of the renormalization scale μ of the CFT by means of the identification $\mu \equiv ke^{-ky}$. Therefore the UV-boundary corresponds in the CFT to a UV cut-off scale at $\Lambda_{UV} = k \sim M_P$, breaking explicitly conformal invariance, while the IR-boundary can be interpreted as a spontaneous breaking of the conformal symmetry at energies $ke^{-k\pi R} \sim \text{TeV}$. Fields localized on the UV-boundary are elementary fields external to the CFT, while fields localized on the IR-boundary and KK states correspond to composite resonances of the CFT. Furthermore, local gauge symmetries in the 5D models, \mathcal{G}_5 , correspond to global symmetries of the CFT, while the UV-boundary symmetry can be interpreted as a gauging of the subgroup \mathcal{H}_{UV} of \mathcal{G}_5 in the CFT. Breaking gauge symmetries by IR-boundary conditions corresponds to the spontaneous breaking $\mathcal{G}_5 \rightarrow \mathcal{H}_{IR}$ in the CFT at energies $\sim ke^{-k\pi R}$. Using this correspondence one can easily derive the 4D massless spectrum of the compactified AdS₅ models. One also has the identification $k^3/M_5^3 \approx 16\pi^2/N^2$ and $g_5^2k \approx 16\pi^2/N^r$ ($r = 1$ or 2 for CFT fields in the fundamental or adjoint representation of the gauge group), where N plays the role of the number of colors of the CFT. Therefore the weak-coupling limit in AdS₅ corresponds to a large- N expansion in the CFT.

Following the above AdS/CFT dictionary one can understand the RS solution to the hierarchy problem from a 4D viewpoint. The equivalent 4D model is a CFT with a TeV mass gap and a Higgs boson emerging as a composite state. In the particular case where the Higgs is the fifth-component of the gauge-boson, A_5 [118], this corresponds to models, similar to those proposed in Ref. [119,120], where the Higgs is a composite pseudo-Nambu-Goldstone boson arising from the spontaneous breaking $\mathcal{G}_5 \rightarrow \mathcal{H}_{IR}$ in the CFT. The AdS/CFT dictionary tells us that KK states must behave as composite resonances. For example, if the SM gauge bosons propagate in the 5D bulk, the lowest KK $SU(2)_L$ -gauge boson must have properties similar to those of the Technirho ρ_T [110] with a coupling to longitudinal W/Z bosons given by $g_5\sqrt{k} \approx g_{\rho T}$, while the coupling to elementary fermions is $g^2/\sqrt{g_5^2k} \approx g^2F_{\rho T}/M_{\rho T}$.

Fermions in compactified AdS₅ also have a simple 4D holographic interpretation. The 4D massless mode described in Sec. 85.3.1 corresponds to an external fermion ψ_i linearly coupled to a fermionic CFT operator \mathcal{O}_i : $\mathcal{L}_{\text{int}} = \lambda_i\bar{\psi}_i\mathcal{O}_i + h.c.$. The dimension of the operator \mathcal{O}_i is related to the 5D fermion mass according to $\text{Dim}[\mathcal{O}_i] = |c_f + 1/2| - 1$. Therefore, by varying c_f one varies $\text{Dim}[\mathcal{O}_i]$, making the coupling λ_i irrelevant ($c_f > 1/2$), marginal ($c_f = 1/2$) or relevant ($c_f < 1/2$). When irrelevant, the coupling is exponentially suppressed at low energies, and then the coupling of ψ_i to the CFT (and eventually to the composite Higgs) is very small. When relevant, the coupling grows in the IR and become as large as g_5 (in units of k), meaning that the fermion is as strongly coupled as the CFT states [77]. In this latter case ψ_i behaves as a composite fermion.

85.3.3 Flat Extra Dimensions

Models with quantum gravity at the TeV scale, as in the ADD scenario, can have extra (flat) dimensions of $1/\text{TeV}$ size, as happens in string scenarios (see, for example, [121]). All SM fields may propagate in these extra dimensions, leading to the possibility of observing their corresponding KK states.

A simple example is to assume that the SM gauge bosons propagate in a flat five-dimensional orbifold S^1/Z_2 of radius R , with the fermions localized on a 4D boundary. The KK gauge bosons behave as sequential SM gauge bosons with a coupling to fermions enhanced by a factor $\sqrt{2}$ [121]. The experimental limits on such sequential gauge bosons could therefore be recast as limits on KK gauge bosons. Such an interpretation of the ATLAS 7 TeV dilepton analysis [122] yielded the bound $1/R > 4.16\text{ TeV}$, while a CMS 8 TeV search with a lepton and missing transverse energy in the final state [123] give $1/R > 3.4\text{ TeV}$. Indirect bounds from LEP2 require however $1/R \gtrsim 6\text{ TeV}$ [82,124], a bound that can considerably improve in the future by high-energy measurements of the dilepton invariant mass spectrum from Drell-Yan processes

at the LHC [125]. More recent LHC limits on leptonically decaying gauge bosons [84, 126–129] are not interpreted as bounds on $1/R$ by the collaborations, but the published results allow for independent derivation of such bounds.

An alternative scenario, known as Universal Extra Dimensions (UED) [130] (for a review see, for example, [131]), assumes that all SM fields propagate universally in a flat orbifold S^1/Z_2 with an extra Z_2 parity, called KK-parity, that interchanges the two boundaries. In this case, the lowest KK state is stable and is a Dark Matter candidate. At colliders, the KK particles would have to be created in pairs, and would then cascade decay to the lightest KK particle, which would be stable and escape detection. The UED mass-spectrum depends not only on the extra-dimensional radius R , but also on the cut-off of the 5D theory Λ , since quantum corrections sensitive to ΛR induce mass-splittings between the KK states. Experimental signatures, such as jets or leptons and \cancel{E}_T , would be similar to those of typical R -parity conserving SUSY searches. An interpretation of the recent LHC experimental SUSY searches for UED models has been presented in Refs. [132, 133]. A lower bound $1/R > 1.4 - 1.5$ TeV was derived for ΛR in the range $5 - 35$ [132]. A recent analysis is given in Ref. [134] where it is shown that the minimal UED model is ruled out when LHC data is combined with Dark Matter relic density data. Extensions to the minimal UED model where boundary terms are included can however be compatible with experiments [134].

Finally, realistic models of electroweak symmetry breaking can also be constructed with flat extra spatial dimensions, similarly to those in the warped case, requiring, however, the presence of sizeable boundary kinetic terms [135]. There is also the possibility of breaking supersymmetry by boundary conditions [136]. Models of this type could explain naturally the presence of a Higgs boson lighter than $M_D \sim$ TeV (see, for example, [137–139]).

References

- [1] For a comprehensive collection of the original papers see, “Modern Kaluza-Klein Theories”, edited by T. Appelquist *et al.*, Addison-Wesley (1987).
- [2] N. Arkani-Hamed, S. Dimopoulos and G. Dvali, Phys. Lett. **B429**, 263 (1998), [hep-ph/9803315].
- [3] L. Randall and R. Sundrum, Phys. Rev. Lett. **83**, 3370 (1999), [hep-ph/9905221].
- [4] H. Davoudiasl, J. L. Hewett and T. G. Rizzo, Phys. Lett. **B473**, 43 (2000), [hep-ph/9911262].
- [5] A. Pomarol, Phys. Lett. **B486**, 153 (2000), [hep-ph/9911294].
- [6] S. Chang *et al.*, Phys. Rev. **D62**, 084025 (2000), [hep-ph/9912498].
- [7] T. Gherghetta and A. Pomarol, Nucl. Phys. **B586**, 141 (2000), [hep-ph/0003129].
- [8] J. M. Maldacena, Int. J. Theor. Phys. **38**, 1113 (1999), [Adv. Theor. Math. Phys. 2, 231 (1998)], [hep-th/9711200].
- [9] E. Witten, Adv. Theor. Math. Phys. **2**, 253 (1998), [hep-th/9802150].
- [10] S. S. Gubser, I. R. Klebanov and A. M. Polyakov, Phys. Lett. **B428**, 105 (1998), [hep-th/9802109].
- [11] N. Arkani-Hamed, M. Porrati and L. Randall, JHEP **08**, 017 (2001), [hep-th/0012148].
- [12] ATLAS public results are available on WWW at <https://twiki.cern.ch/twiki/bin/view/AtlasPublic>.
- [13] CMS public results are available on WWW at <https://cms-results.web.cern.ch/cms-results/public-results/publications>.
- [14] Z. Chacko, M. A. Luty and E. Ponton, JHEP **07**, 036 (2000), [hep-ph/9909248].
- [15] N. Arkani-Hamed, S. Dimopoulos and G. R. Dvali, Phys. Rev. **D59**, 086004 (1999), [hep-ph/9807344].
- [16] R. Rattazzi, hep-ph/0607055 (2006); I. Antoniadis, Yellow report CERN-2002-002 (2002).
- [17] J. D. Lykken, Phys. Rev. **D54**, R3693 (1996), [hep-th/9603133].
- [18] I. Antoniadis *et al.*, Phys. Lett. **B436**, 257 (1998), [hep-ph/9804398].
- [19] G. F. Giudice, R. Rattazzi and J. D. Wells, Nucl. Phys. **B544**, 3 (1999), [hep-ph/9811291].
- [20] N. Arkani-Hamed *et al.*, Phys. Rev. **D62**, 105002 (2000), [hep-ph/9912453].
- [21] E. G. Adelberger *et al.*, Prog. Part. Nucl. Phys. **62**, 102 (2009).
- [22] J. Murata and S. Tanaka, Class. Quant. Grav. **32**, 3, 033001 (2015), [arXiv:1408.3588].
- [23] W.-H. Tan *et al.*, Phys. Rev. Lett. **116**, 13, 131101 (2016).
- [24] J. G. Lee *et al.*, Phys. Rev. Lett. **124**, 101101 (2020), [arXiv:2002.11761].
- [25] C. Hanhart *et al.*, Phys. Lett. **B509**, 1 (2001), [arXiv:astro-ph/0102063].
- [26] S. Hannestad and G. G. Raffelt, Phys. Rev. **D67**, 125008 (2003), [Erratum: Phys. Rev. D69, 029901 (2004)], [hep-ph/0304029].
- [27] L. J. Hall and D. Tucker-Smith, Phys. Rev. **D60**, 085008 (1999), [hep-ph/9904267].
- [28] E. A. Mirabelli, M. Perelstein and M. E. Peskin, Phys. Rev. Lett. **82**, 2236 (1999), [hep-ph/9811337].
- [29] T. Han, J. D. Lykken and R.-J. Zhang, Phys. Rev. **D59**, 105006 (1999), [hep-ph/9811350].
- [30] G. Aad *et al.* (ATLAS), Phys. Rev. D **103**, 112006 (2021), [arXiv:2102.10874].
- [31] A. Tumasyan *et al.* (CMS) (2021), [arXiv:2107.13021].
- [32] A. M. Sirunyan *et al.* (CMS), JHEP **02**, 074 (2019), [arXiv:1810.00196].
- [33] G. Aad *et al.* (ATLAS), JHEP **02**, 226 (2021), [arXiv:2011.05259].
- [34] S. Cullen, M. Perelstein and M. E. Peskin, Phys. Rev. **D62**, 055012 (2000), [hep-ph/0001166].
- [35] A. M. Sirunyan *et al.* (CMS), JHEP **05**, 033 (2020), [arXiv:1911.03947].
- [36] G. Aad *et al.* (ATLAS), JHEP **03**, 145 (2020), [arXiv:1910.08447].
- [37] J. L. Hewett, Phys. Rev. Lett. **82**, 4765 (1999), [hep-ph/9811356].
- [38] G. F. Giudice and A. Strumia, Nucl. Phys. **B663**, 377 (2003), [hep-ph/0301232].
- [39] A. M. Sirunyan *et al.* (CMS), Eur. Phys. J. **C78**, 9, 789 (2018), [arXiv:1803.08030].
- [40] M. Aaboud *et al.* (ATLAS), Phys. Lett. **B775**, 105 (2017), [arXiv:1707.04147].
- [41] A. M. Sirunyan *et al.* (CMS), Phys. Rev. **D98**, 9, 092001 (2018), [arXiv:1809.00327].
- [42] A. M. Sirunyan *et al.*, JHEP **07**, 7 (2021), [arXiv:2103.02708].
- [43] G. Aad *et al.*, JHEP **11**, 005 (2020), [arXiv:2006.12946].
- [44] S. B. Giddings and S. D. Thomas, Phys. Rev. **D65**, 056010 (2002), [hep-ph/0106219].
- [45] S. Dimopoulos and G. L. Landsberg, Phys. Rev. Lett. **87**, 161602 (2001), [hep-ph/0106295].
- [46] P. Kanti, Int. J. Mod. Phys. **A19**, 4899 (2004), [hep-ph/0402168].
- [47] R. C. Myers and M. J. Perry, Annals Phys. **172**, 304 (1986).
- [48] A. M. Sirunyan *et al.* (CMS), JHEP **11**, 042 (2018), [arXiv:1805.06013].
- [49] G. Aad *et al.* (ATLAS), JHEP **03**, 026 (2016), [arXiv:1512.02586].

- [50] M. Aaboud *et al.* (ATLAS), Phys. Lett. **B760**, 520 (2016), [arXiv:1606.02265].
- [51] C. Kilic *et al.*, Phys. Rev. **D89**, 1, 016003 (2014), [arXiv:1207.3525].
- [52] V. Khachatryan *et al.* (CMS), Phys. Rev. **D90**, 3, 032005 (2014), [arXiv:1405.7653].
- [53] P. Meade and L. Randall, JHEP **05**, 003 (2008), [arXiv:0708.3017].
- [54] A. M. Sirunyan *et al.* (CMS), Phys. Lett. **B774**, 279 (2017), [arXiv:1705.01403].
- [55] A. M. Sirunyan *et al.* (CMS), JHEP **04**, 073 (2018), [arXiv:1802.01122].
- [56] M. Aaboud *et al.* (ATLAS), Phys. Rev. **D98**, 9, 092008 (2018), [arXiv:1807.06573].
- [57] S. Dimopoulos and R. Emparan, Phys. Lett. **B526**, 393 (2002), [hep-ph/0108060].
- [58] W. D. Goldberger and M. B. Wise, Phys. Rev. Lett. **83**, 4922 (1999), [hep-ph/9907447].
- [59] J. Garriga and A. Pomarol, Phys. Lett. **B560**, 91 (2003), [hep-th/0212227].
- [60] See talk by R. Rattazzi at Planck 2010, CERN.
- [61] B. Bellazzini *et al.*, Eur. Phys. J. **C74**, 2790 (2014), [arXiv:1305.3919].
- [62] F. Coradeschi *et al.*, JHEP **11**, 057 (2013), [arXiv:1306.4601].
- [63] E. Megias and O. Pujolas, JHEP **08**, 081 (2014), [arXiv:1401.4998].
- [64] K. Blum *et al.*, JHEP **03**, 099 (2015), [arXiv:1410.1873].
- [65] A. Efrati *et al.*, Phys. Rev. **D91**, 5, 055034 (2015), [arXiv:1410.2225].
- [66] F. Abu-Ajamieh, J. S. Lee and J. Terning, JHEP **10**, 050 (2018), [arXiv:1711.02697].
- [67] H. Davoudiasl *et al.*, New J. Phys. **12**, 075011 (2010), [arXiv:0908.1968].
- [68] T. Gherghetta, in “Physics of the large and the small, TASI 09, proceedings of the Theoretical Advanced Study Institute in Elementary Particle Physics, Boulder, Colorado, USA, 1-26 June 2009,” 165–232 (2011), [arXiv:1008.2570].
- [69] Y. Grossman and M. Neubert, Phys. Lett. **B474**, 361 (2000), [hep-ph/9912408].
- [70] S. J. Huber and Q. Shafi, Phys. Lett. **B498**, 256 (2001), [hep-ph/0010195].
- [71] A. Delgado, A. Pomarol and M. Quiros, JHEP **01**, 030 (2000), [hep-ph/9911252].
- [72] K. Agashe, G. Perez and A. Soni, Phys. Rev. **D71**, 016002 (2005), [hep-ph/0408134].
- [73] M. Bauer *et al.*, JHEP **09**, 017 (2010), [arXiv:0912.1625].
- [74] A. Pomarol, Int. J. Mod. Phys. **A24**, 61 (2009), [In *Kane, Gordon (ed.) et al.: Perspectives on LHC physics*, 259 (2008)].
- [75] Y. Hosotani, Phys. Lett. **126B**, 309 (1983).
- [76] K. Agashe *et al.*, JHEP **08**, 050 (2003), [hep-ph/0308036].
- [77] K. Agashe, R. Contino and A. Pomarol, Nucl. Phys. **B719**, 165 (2005), [hep-ph/0412089].
- [78] For a review see, for example, R. Contino, arXiv:1005.4269.
- [79] See, for example, PDG review of Higgs boson in this *Review*.
- [80] G. F. Giudice *et al.*, JHEP **06**, 045 (2007), [hep-ph/0703164].
- [81] R. Contino, L. Da Rold and A. Pomarol, Phys. Rev. **D75**, 055014 (2007), [hep-ph/0612048].
- [82] R. Barbieri *et al.*, Nucl. Phys. **B703**, 127 (2004), [hep-ph/0405040].
- [83] G. Aad *et al.* (ATLAS) (2021), [arXiv:2102.13405].
- [84] G. Aad *et al.* (ATLAS), Phys. Lett. **B796**, 68 (2019), [arXiv:1903.06248].
- [85] A. M. Sirunyan *et al.* (CMS), JHEP **08**, 130 (2018), [arXiv:1806.00843].
- [86] G. Aad *et al.* (ATLAS), Phys. Rev. Lett. **125**, 13, 131801 (2020), [arXiv:2005.02983].
- [87] A. M. Sirunyan *et al.* (CMS), Phys. Rev. Lett. **122**, 12, 121803 (2019), [arXiv:1811.09689].
- [88] M. Aaboud *et al.* (ATLAS), JHEP **01**, 030 (2019), [arXiv:1804.06174].
- [89] A. Tumasyan *et al.* (CMS) (2021), [arXiv:2106.10361].
- [90] G. Aad *et al.* (ATLAS), JHEP **11**, 163 (2020), [arXiv:2007.14811].
- [91] G. Aad *et al.* (ATLAS), JHEP **09**, 091 (2019), [Erratum: JHEP 06, 042 (2020)], [arXiv:1906.08589].
- [92] A. M. Sirunyan *et al.* (CMS) (2019), [arXiv:1906.05977].
- [93] G. Aad *et al.* (ATLAS), Eur. Phys. J. C **80**, 12, 1165 (2020), [arXiv:2004.14636].
- [94] G. Aad *et al.* (ATLAS), Eur. Phys. J. C **81**, 4, 332 (2021), [arXiv:2009.14791].
- [95] K. Agashe *et al.*, Phys. Rev. **D76**, 036006 (2007), [hep-ph/0701186].
- [96] M. Aaboud *et al.* (ATLAS), Eur. Phys. J. C **79**, 5, 375 (2019), [arXiv:1808.07858].
- [97] A. M. Sirunyan *et al.* (CMS), JINST **15**, 06, P06005 (2020), [arXiv:2004.08262].
- [98] G. Aad *et al.* (ATLAS), JHEP **10**, 061 (2020), [arXiv:2005.05138].
- [99] A. M. Sirunyan *et al.* (CMS), JHEP **04**, 031 (2019), [arXiv:1810.05905].
- [100] M. Aaboud *et al.* (ATLAS), Phys. Rev. **D99**, 9, 092004 (2019), [arXiv:1902.10077].
- [101] M. Aaboud *et al.* (ATLAS), Eur. Phys. J. **C78**, 7, 565 (2018), [arXiv:1804.10823].
- [102] G. Aad *et al.* (ATLAS), Phys. Rev. D **102**, 11, 112008 (2020), [arXiv:2007.05293].
- [103] A. M. Sirunyan *et al.* (CMS), Eur. Phys. J. C **81**, 8, 688 (2021), [arXiv:2102.08198].
- [104] M. Aaboud *et al.* (ATLAS), Phys. Rev. **D98**, 5, 052008 (2018), [arXiv:1808.02380].
- [105] A. M. Sirunyan *et al.* (CMS) (2019), [arXiv:1906.00057].
- [106] R. Contino and G. Servant, JHEP **06**, 026 (2008), [arXiv:0801.1679].
- [107] J. A. Aguilar-Saavedra, JHEP **11**, 030 (2009), [arXiv:0907.3155].
- [108] J. Mrazek and A. Wulzer, Phys. Rev. **D81**, 075006 (2010), [arXiv:0909.3977].
- [109] G. Dissertori *et al.*, JHEP **09**, 019 (2010), [arXiv:1005.4414].
- [110] See, for example, PDG review of Technicolor searches in this volume.
- [111] M. Aaboud *et al.* (ATLAS), JHEP **10**, 141 (2017), [arXiv:1707.03347].
- [112] A. M. Sirunyan *et al.* (CMS), JHEP **03**, 082 (2019), [arXiv:1810.03188].
- [113] M. Aaboud *et al.* (ATLAS), Phys. Rev. Lett. **121**, 21, 211801 (2018), [arXiv:1808.02343].
- [114] A. M. Sirunyan *et al.* (CMS), Phys. Rev. D **102**, 112004 (2020), [arXiv:2008.09835].
- [115] M. Aaboud *et al.* (ATLAS), JHEP **05**, 164 (2019), [arXiv:1812.07343].
- [116] A. M. Sirunyan *et al.* (CMS), JHEP **01**, 036 (2020), [arXiv:1909.04721].
- [117] A. De Simone *et al.*, JHEP **04**, 004 (2013), [arXiv:1211.5663].

- [118] R. Contino, Y. Nomura and A. Pomarol, Nucl. Phys. **B671**, 148 (2003), [hep-ph/0306259].
- [119] H. Georgi, D. B. Kaplan and P. Galison, Phys. Lett. **143B**, 152 (1984).
- [120] D. B. Kaplan and H. Georgi, Phys. Lett. **136B**, 183 (1984).
- [121] I. Antoniadis and K. Benakli, Int. J. Mod. Phys. **A15**, 4237 (2000), [hep-ph/0007226].
- [122] G. Aad *et al.* (ATLAS), JHEP **11**, 138 (2012), [arXiv:1209.2535].
- [123] V. Khachatryan *et al.* (CMS), Phys. Rev. **D91**, 9, 092005 (2015), [arXiv:1408.2745].
- [124] K. Cheung and G. L. Landsberg, Phys. Rev. **D65**, 076003 (2002), [hep-ph/0110346].
- [125] M. Farina *et al.*, Phys. Lett. **B772**, 210 (2017), [arXiv:1609.08157].
- [126] M. Aaboud *et al.* (ATLAS), Eur. Phys. J. C **78**, 5, 401 (2018), [arXiv:1706.04786].
- [127] G. Aad *et al.* (ATLAS) (2019), [arXiv:1906.05609].
- [128] A. M. Sirunyan *et al.* (CMS), JHEP **06**, 128 (2018), [arXiv:1803.11133].
- [129] A. M. Sirunyan *et al.* (CMS), JHEP **06**, 120 (2018), [arXiv:1803.06292].
- [130] T. Appelquist, H.-C. Cheng and B. A. Dobrescu, Phys. Rev. **D64**, 035002 (2001), [hep-ph/0012100].
- [131] A. Datta, K. Kong and K. T. Matchev, New J. Phys. **12**, 075017 (2010), [arXiv:1002.4624].
- [132] N. Deutschmann, T. Flacke and J. S. Kim, Phys. Lett. **B771**, 515 (2017), [arXiv:1702.00410].
- [133] J. Beuria *et al.*, Comput. Phys. Commun. **226**, 187 (2018), [arXiv:1702.00413].
- [134] Avnish *et al.*, Phys. Rev. D **103**, 115011 (2021), [arXiv:2012.15137].
- [135] G. Panico, M. Safari and M. Serone, JHEP **02**, 103 (2011), [arXiv:1012.2875].
- [136] J. Scherk and J. H. Schwarz, Phys. Lett. **82B**, 60 (1979).
- [137] A. Pomarol and M. Quiros, Phys. Lett. **B438**, 255 (1998), [hep-ph/9806263].
- [138] I. Antoniadis *et al.*, Nucl. Phys. **B544**, 503 (1999), [hep-ph/9810410].
- [139] R. Barbieri, L. J. Hall and Y. Nomura, Phys. Rev. **D63**, 105007 (2001), [hep-ph/0011311].

86. W' -Boson Searches

Revised October, 2021 by B.A. Dobrescu (FNAL) and S. Willocq (U. Massachusetts).

The W' boson is a massive hypothetical particle of spin 1 and electric charge ± 1 , which is a color singlet and is predicted in various extensions of the Standard Model (SM).

86.1 W' couplings to quarks and leptons

The Lagrangian terms describing the couplings of a W'^+ boson to fermions are given by

$$\frac{W'^+}{\sqrt{2}} \left[\bar{u}_i (C_{qij}^R P_R + C_{qij}^L P_L) \gamma^\mu d_j + \bar{\nu}_i (C_{\ell ij}^R P_R + C_{\ell ij}^L P_L) \gamma^\mu e_j \right]. \quad (86.1)$$

Here, u, d, ν , and e are the SM fermions in the mass eigenstate basis, $i, j = 1, 2, 3$ label the fermion generation, and $P_{R,L} = (1 \pm \gamma_5)/2$. The coefficients $C_{qij}^L, C_{qij}^R, C_{\ell ij}^L$, and $C_{\ell ij}^R$ are complex dimensionless parameters. If $C_{\ell ij}^R \neq 0$, then the i th generation includes a right-handed neutrino. Using this notation, the SM W couplings are $C_q^L = g V_{CKM}$, $C_\ell^L = g \approx 0.63$ and $C_q^R = C_\ell^R = 0$.

Unitarity considerations imply that the W' boson is associated with a spontaneously-broken gauge symmetry. This is true even when it is a composite particle (e.g. ρ^\pm -like bound states [1]) if its mass is much smaller than the compositeness scale, or a Kaluza-Klein mode in theories where the W boson propagates in extra dimensions [2]. The simplest extension of the electroweak gauge group that includes a W' boson is $SU(2)_1 \times SU(2)_2 \times U(1)$, but larger groups are encountered in some theories. A generic property of these gauge theories is that they also include a Z' boson [3]; the W' -to- Z' mass ratio is often a free parameter.

A tree-level mass mixing may be induced between the electrically-charged gauge bosons. Upon diagonalization of their mass matrix, the W -to- Z mass ratio and the couplings of the observed W boson are shifted from the SM values. Their measurements imply that the mixing angle, θ_+ , between the gauge eigenstates must be smaller than about 10^{-2} [4]. In certain theories the mixing is negligible (e.g., due to a new parity [5]), even when the W' mass is near the electroweak scale. Note that $SU(2)$ gauge invariance suppresses the kinetic mixing between the W and W' bosons (in contrast to the case of a Z' boson [3]).

The W' coupling to WZ is fixed by Lorentz and gauge invariances, and to leading order in θ_+ is given by [6]

$$\frac{g \theta_+}{\cos \theta_W} \left[W_\mu'^+ (W_\nu^- Z^{\nu\mu} + Z_\nu W^{-\mu\nu}) + Z^\nu W^{-\mu} W_{\nu\mu}'^+ \right] + \text{H.c.}, \quad (86.2)$$

where $W^{\mu\nu} \equiv \partial^\mu W^\nu - \partial^\nu W^\mu$, etc. The θ_W dependence shown here corrects the one given in Ref. [7], which has been referred to as the Extended Gauge Model by the experimental collaborations. The W' coupling to Wh^0 , where h^0 is the SM Higgs boson, is

$$-\xi_h g_{W'} M_W W_\mu'^+ W^{\mu-} h^0 + \text{H.c.}, \quad (86.3)$$

where $g_{W'}$ is the gauge coupling of the W' boson, and the coefficient ξ_h satisfies $\xi_h \leq 1$ in simple Higgs sectors [6].

In models based on the “left-right symmetric” gauge group [8], $SU(2)_L \times SU(2)_R \times U(1)_{B-L}$, the SM fermions that couple to the W boson transform as doublets under $SU(2)_L$ while the other fermions transform as doublets under $SU(2)_R$. Consequently, the W' boson couples primarily to right-handed fermions; its coupling to left-handed fermions arises due to the θ_+ mixing, so that C_q^L is proportional to the CKM matrix and its elements are much smaller than the diagonal elements of C_q^R . Generically, C_q^R does not need to be proportional to V_{CKM} .

There are many other models based on the $SU(2)_1 \times SU(2)_2 \times U(1)$ gauge symmetry. In the “alternate left-right” model [9], all the couplings shown in Eq. (86.1) vanish, but there are some new fermions such that the W' boson couples to pairs involving a SM fermion and a new fermion. In the “unified SM” [10], the left-handed quarks are doublets under one $SU(2)$, and the left-handed leptons are doublets under a different $SU(2)$, leading to a mostly leptophobic W' boson: $C_{\ell ij}^L \ll C_{qij}^L$ and $C_{\ell ij}^R = C_{qij}^R = 0$. Fermions of different generations may also transform

as doublets under different $SU(2)$ gauge groups [11]. In particular, the couplings to third generation quarks may be enhanced [12].

It is also possible that the W' couplings to SM fermions are highly suppressed. For example, if the quarks and leptons are singlets under one $SU(2)$ [13], then the couplings are proportional to the tiny mixing angle θ_+ . Similar suppressions may arise if some vectorlike fermions mix with the SM fermions [14].

Gauge groups that embed the electroweak symmetry, such as $SU(3)_W \times U(1)$ or $SU(4)_W \times U(1)$, also include one or more W' bosons [15].

86.2 Collider searches

At hadron colliders, W' bosons can be detected through resonant pair production of fermions (f and f') or electroweak bosons with a net electric charge equal to ± 1 . When W' has a width much smaller than its mass ($\Gamma_{W'}/M_{W'} \lesssim 7\%$), the contribution of the s -channel W' exchange to the total rate for $pp \rightarrow f\bar{f}'X$, where X is any final state, may be approximated by the branching fraction $B(W' \rightarrow f\bar{f}')$ times the production cross section [16], which may be written as

$$\sigma(pp \rightarrow W'X) \simeq \frac{\pi}{6s} \sum_{i,j} [(C_{qij}^L)^2 + (C_{qij}^R)^2] w_{ij}(M_{W'}^2/s, M_{W'}). \quad (86.4)$$

The functions w_{ij} include the information about proton structure, and are given to leading order in α_s by

$$w_{ij}(z, \mu) = \int_z^1 \frac{dx}{x} \left[u_i(x, \mu) \bar{d}_j\left(\frac{z}{x}, \mu\right) + \bar{u}_i(x, \mu) d_j\left(\frac{z}{x}, \mu\right) \right], \quad (86.5)$$

where $u_i(x, \mu)$ and $d_i(x, \mu)$ are the parton distributions inside the proton at the factorization scale μ and parton momentum fraction x for the up- and down-type quarks of the i th generation, respectively. QCD corrections to W' production are sizable (they also include quark-gluon initial states), but preserve the above factorization of couplings at next-to-leading order [17].

The most commonly studied W' signal consists of a high-momentum electron or muon and large missing transverse momentum. The signal transverse mass distribution forms a Jacobian peak with its endpoint at $M_{W'}$ (see Fig. 1 (top) of Ref. [18]). Given that the branching fractions for $W' \rightarrow e\nu$ and $W' \rightarrow \mu\nu$ could be very different, the results in these channels should be presented separately. Searches in these channels often implicitly assume that the left-handed couplings vanish (no interference between W and W'), and that the right-handed neutrino is light compared to the W' boson and escapes the detector. An example of parameter values that satisfy these assumptions is $C_q^R = g V_{CKM}$, $C_\ell^R = g$, $C_q^L = C_\ell^L = 0$, which define a model that preserves lepton universality and predicts the same total cross section as the Sequential SM used in many W' searches. However, if a W' boson were discovered and the final state fermions have left-handed helicity, then the effects of $W - W'$ interference could be observed [19], providing information about the W' couplings. The effects of the W' width on interference are discussed in Ref. [20].

In the $e\nu$ channel, the ATLAS and CMS collaborations set limits on the W' production cross section times branching fraction $\sigma \times B$ (and thus indirectly on the W' couplings). These limits are set for $M_{W'}$ in the 0.15–7 TeV range and are based on 139 fb^{-1} at $\sqrt{s} = 13 \text{ TeV}$ [18, 21], with the most stringent limits reproduced in Fig. 86.1. ATLAS sets the strongest mass limit $M_{W'} > 6.0 \text{ TeV}$ in the Sequential SM (all limits in this mini-review are at the 95% CL). The coupling limits are much weaker for $M_{W'} < 150 \text{ GeV}$, a range last explored with the Tevatron at $\sqrt{s} = 1.8 \text{ TeV}$ [22].

In the $\mu\nu$ channel, ATLAS and CMS set rate limits for $M_{W'}$ in the 0.15–7 TeV range [18, 21], with the strongest mass lower limit of 5.6 TeV in the Sequential SM set by CMS [21] using 137 fb^{-1} of $\sqrt{s} = 13 \text{ TeV}$ data, as shown in Fig. 86.1. When combined with the $e\nu$ channel assuming lepton universality, the upper limit on the $\sqrt{s} = 13 \text{ TeV}$ cross section times branching fraction to $\ell\nu$ varies between 0.05 and 2.1 fb for $M_{W'}$ values between 1 and 6 TeV [18]. Only weak limits on $W' \rightarrow \mu\nu$ exist for $M_{W'} < 150 \text{ GeV}$ [25]. Note that masses of the order of the electroweak

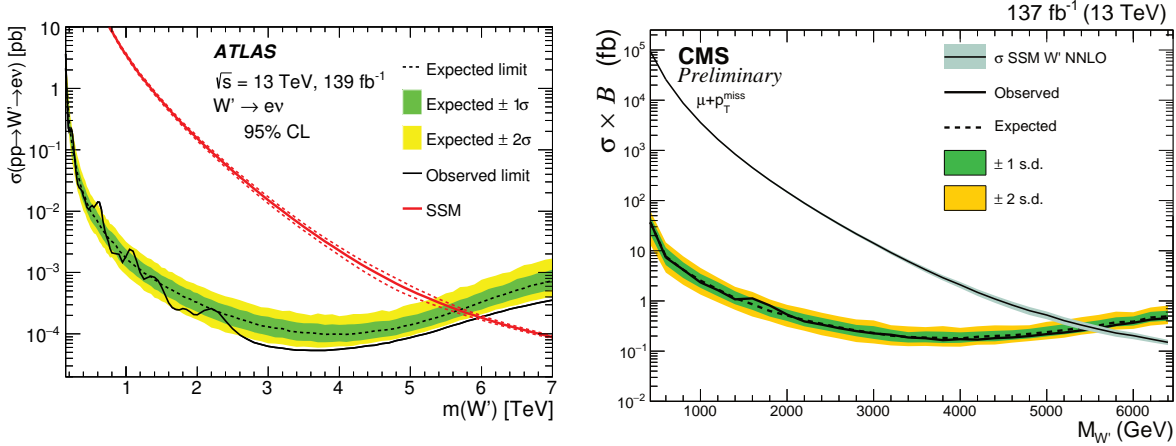


Figure 86.1: Upper limit on $\sigma(pp \rightarrow W'X) \times B(W' \rightarrow \ell\nu)$ in the $e\nu$ channel from ATLAS [18] (left) and the $\mu\nu$ channel from CMS [21] (right). The red (black) line shows the theoretical prediction in the Sequential SM in the $e\nu$ ($\mu\nu$) channel.

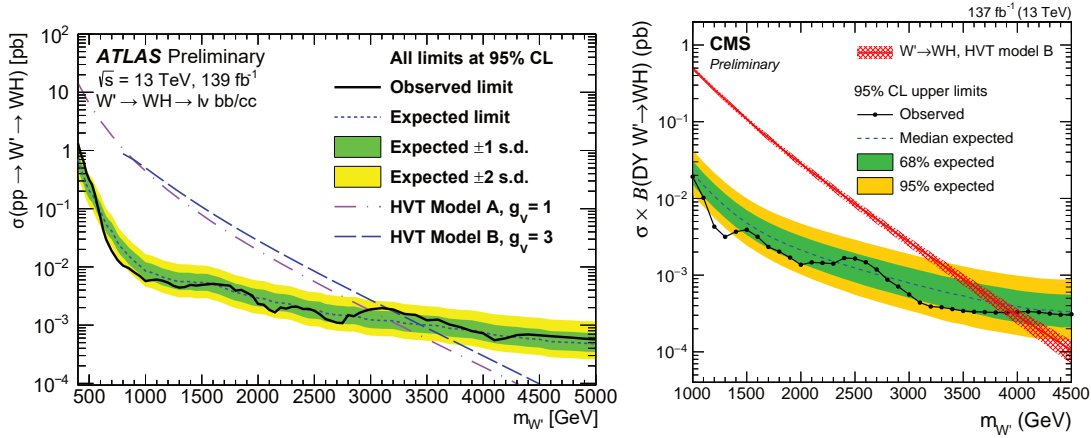


Figure 86.2: Upper limits on W' production cross section times branching fraction into a W and a SM Higgs boson decaying into heavy-flavor quarks, from ATLAS [23] (left) and CMS [24] (right).

scale are interesting from a theoretical point of view, while lepton universality does not necessarily apply to a W' boson.

Searches for $W' \rightarrow \tau\nu$ have been performed at 13 TeV by CMS with 36 fb^{-1} [26], and by ATLAS with 139 fb^{-1} [27]. Limits are set on $\sigma \times B$ for $M_{W'}$ between 0.4 and 6 TeV. A mass lower limit of 5.0 TeV is set in the Sequential SM, and the upper limit on the cross section times branching fraction to $\tau\nu$ at 13 TeV varies between 0.4 and 9 fb for $M_{W'}$ values between 1 and 5 TeV [27].

The W' decay into a charged lepton and a right-handed neutrino, ν_R , may also be followed by the ν_R decay through a virtual W' boson into a charged lepton and two quark jets. The CMS [28] and ATLAS [29] searches in the $eejj$ and $\mu\mu jj$ channels have set limits at $\sqrt{s} = 13 \text{ TeV}$ on the cross section times branching fractions as a function of the ν_R mass and of $M_{W'}$. No requirement is placed on the charge of the lepton pair. A related W' search in the $\tau\tau jj$ channel with hadronic τ decays was also performed by CMS [30].

The $t\bar{b}$ channel is particularly important because a W' boson that couples only to right-handed fermions cannot decay to leptons when the right-handed neutrinos are heavier than $M_{W'}$. Additional motivations are provided by a W' boson with enhanced couplings to the third generation [12], and by a leptophobic W' boson. The usual signature for $W' \rightarrow t\bar{b}$ consists of a leptonically-decaying W boson and two b -jets. Recent studies have also incorporated the fully hadronic decay channel for $M_{W'} \gg m_t$ with the use of jet substructure techniques to tag highly boosted top-jets. For a detailed discussion of this channel, see Ref. [31].

Searches for dijet resonances may be used to set limits on $W' \rightarrow q\bar{q}'$. ATLAS [32] and CMS [33] provide similar coverage in the ~

1.5–8 TeV mass range with 139 and 137 fb^{-1} of data, respectively, collected at $\sqrt{s} = 13 \text{ TeV}$. Interpretation in terms of W' decays with 139 fb^{-1} of 13 TeV data yields a W' mass lower limit of 4.0 TeV in the Sequential SM [32]. For masses in the range $\sim 0.5 - 1.5 \text{ TeV}$, analyses based on jets reconstructed online provide the best sensitivity because they circumvent trigger bandwidth limitations [34, 35]. For W' masses below $\sim 0.5 \text{ TeV}$, the best limits are set in novel analyses exploiting boosted technologies and initial state radiation [36–39]. Cross-section limits for W' masses below $\sim 1.5 \text{ TeV}$ can be derived from the dijet limits on Z' bosons summarized in Ref. [3].

In some theories [5] the W' couplings to SM fermions are suppressed by discrete symmetries. W' production then occurs in pairs, through a photon or Z boson. The decay modes are model-dependent and often involve other new particles. The ensuing collider signals arise from cascade decays and often include missing transverse momentum or boosted multi-jet topologies. An example is a search performed by CMS [40] for W' decays into a vector-like quark and a top or a bottom quark. The final state studied in this analysis involves a boosted SM Higgs boson or Z , as well as a $t\bar{t}$ or $b\bar{b}$ pair, with all heavy particles decaying into jets.

Searches for WZ resonances at the LHC have focused on the process $pp \rightarrow W' \rightarrow WZ$ with the production mainly from $u\bar{d} \rightarrow W'$, assuming SM-like couplings to quarks. ATLAS and CMS have set the upper limits on the $W'WZ$ coupling for $M_{W'}$ in the 0.2–5.0 TeV range with a combination of fully leptonic, semi-leptonic and fully hadronic channels with $\sim 36 \text{ fb}^{-1}$ at 13 TeV [41, 42] (see also Ref. [31]). More recent constraints with

77–139 fb⁻¹ at 13 TeV were also set in individual channels by ATLAS [43, 44] and CMS [24, 45–47]. The strongest lower limit on the W' mass is set by ATLAS [44] in the semi-leptonic channel with a lower limit on $M_{W'}$ of 3.9 TeV [44] in the context of the Heavy Vector Triplet (HVT) weakly-coupled scenario A [48]. A fermiophobic W' boson that couples to WZ may be produced at hadron colliders in association with a Z boson, or via WZ fusion. This would give rise to $(WZ)Z$ and $(WZ)jj$ final states [49]. Results of the search for the latter are reported in Refs. [24, 41, 44, 46].

W' bosons have also been searched for in final states with a W boson and a SM Higgs boson in the channels $W \rightarrow \ell\nu$ or $W \rightarrow q\bar{q}'$ and $h^0 \rightarrow b\bar{b}$ by ATLAS [23, 50] and CMS [24, 51] with 36–139 fb⁻¹ at $\sqrt{s} = 13$ TeV. Cross-section limits are set for W' masses between 0.4 and 5.0 TeV. The ATLAS and CMS 13 TeV analyses with $W \rightarrow \ell\nu$ set the most stringent upper limits on the cross section at low and high $M_{W'}$, respectively, as shown in Fig. 86.2.

At lepton colliders, W' bosons may be produced in pairs via their photon coupling, which is model independent. At LEP-II, although dedicated searches for W' bosons have not been performed, the large cross section for $e^+e^- \rightarrow \gamma^* \rightarrow W'^+W'^-$ and small backgrounds suggest that any W' is ruled out up to the kinematic limit, $M_{W'} < \sqrt{s}/2 \approx 105$ GeV, for most decay modes. Sensitivity to $M_{W'}$ above \sqrt{s} could be achieved [52] using the $e^+e^- \rightarrow \gamma\nu\bar{\nu}$ process via a t -channel W' exchange, if the W' coupling to $e\nu$ is large enough.

86.3 Low-energy constraints

The properties of W' bosons are also constrained by measurements of processes at energies much below $M_{W'}$. The bounds on $W - W'$ mixing [4] are mostly due to the change in W properties compared to the SM. Limits on deviations in the ZWW couplings provide a leading constraint for fermiophobic W' bosons [14].

Constraints arising from low-energy effects of W' exchange are strongly model-dependent. If the W' couplings to quarks are not suppressed, then box diagrams involving a W and a W' boson contribute to neutral meson-mixing. In the case of W' couplings to right-handed quarks as in the left-right symmetric model, the limit from $K_L - K_S$ mixing is severe: $M_{W'} > 2.9$ TeV for $C_q^R = g_{\text{VCKM}}$ [53]. However, if no correlation between the W' and W couplings is assumed, then the limit on $M_{W'}$ may be significantly relaxed [54].

W' exchange also contributes at tree level to various low-energy processes. In particular, it would impact the measurement of the Fermi constant G_F in muon decay, which in turn would change the predictions of many other electroweak processes. A recent test of parity violation in polarized muon decay [55] has set limits of about 600 GeV on $M_{W'}$, assuming W' couplings to right-handed leptons as in left-right symmetric models and a light ν_R . There are also W' contributions to the neutron electric dipole moment, β decays, and other processes [4].

If right-handed neutrinos have Majorana masses, then there are tree-level contributions to neutrinoless double-beta decay, and a limit on $M_{W'}$ versus the ν_R mass may be derived [56]. For ν_R masses below a few GeV, the W' boson contributes to leptonic and semileptonic B meson decays, so that limits may be placed on various combinations of W' parameters [54]. For ν_R masses below ~ 30 MeV, the most stringent constraints on $M_{W'}$ are due to the limits on ν_R emission from supernovae.

References

[1] M. Bando, T. Kugo and K. Yamawaki, Phys. Rept. **164**, 217 (1988).
 [2] H.-C. Cheng *et al.*, Phys. Rev. **D64**, 065007 (2001), [hep-th/0104179].
 [3] See the Section on “ Z' -boson searches” in this *Review*.
 [4] See the particle listings for W' in this *Review*.
 [5] H.-C. Cheng and I. Low, JHEP **09**, 051 (2003), [hep-ph/0308199].
 [6] B. A. Dobrescu and Z. Liu, JHEP **10**, 118 (2015), [arXiv:1507.01923].
 [7] G. Altarelli, B. Mele and M. Ruiz-Altaba, Z. Phys. **C45**, 109 (1989), [Erratum: Z. Phys. **C47**, 676 (1990)].

[8] R. N. Mohapatra and J. C. Pati, Phys. Rev. **D11**, 566 (1975).
 [9] K. S. Babu, X.-G. He and E. Ma, Phys. Rev. **D36**, 878 (1987).
 [10] H. Georgi, E. E. Jenkins and E. H. Simmons, Nucl. Phys. **B331**, 541 (1990).
 [11] X.-y. Li and E. Ma, J. Phys. **G19**, 1265 (1993), [hep-ph/9208210].
 [12] D. J. Muller and S. Nandi, Phys. Lett. **B383**, 345 (1996), [hep-ph/9602390].
 [13] A. Donini *et al.*, Nucl. Phys. **B507**, 51 (1997), [hep-ph/9705450].
 [14] R. S. Chivukula *et al.*, Phys. Rev. **D74**, 075011 (2006), [hep-ph/0607124].
 [15] F. Pisano and V. Pleitez, Phys. Rev. **D46**, 410 (1992), [hep-ph/9206242].
 [16] V. D. Barger and R. J. N. Phillips, *Collider Physics* (1996), ISBN 978-0201149456.
 [17] Z. Sullivan, Phys. Rev. **D66**, 075011 (2002), [hep-ph/0207290].
 [18] G. Aad *et al.* (ATLAS), Phys. Rev. **D100**, 052013 (2019), [arXiv:1906.05609].
 [19] T. G. Rizzo, JHEP **05**, 037 (2007), [arXiv:0704.0235].
 [20] E. Accomando *et al.*, Phys. Rev. **D85**, 115017 (2012), [arXiv:1110.0713].
 [21] CMS Collab., CMS PAS EXO-19-017, Mar. 2021.
 [22] F. Abe *et al.* (CDF), Phys. Rev. Lett. **74**, 2900 (1995).
 [23] ATLAS Collab., ATLAS-CONF-2021-026, Jun. 2021.
 [24] A. Tumasyan *et al.* (CMS) (2021), [arXiv:2109.06055].
 [25] F. Abe *et al.* (CDF), Phys. Rev. Lett. **67**, 2609 (1991).
 [26] A. M. Sirunyan *et al.* (CMS), Phys. Lett. **B792**, 107 (2019), [arXiv:1807.11421].
 [27] ATLAS Collab., ATLAS-CONF-2021-025, Jun. 2021.
 [28] CMS Collab., CMS PAS EXO-20-002, Jul. 2021.
 [29] M. Aaboud *et al.* (ATLAS), Phys. Lett. B **798**, 134942 (2019), [arXiv:1904.12679].
 [30] A. M. Sirunyan *et al.* (CMS), JHEP **03**, 170 (2019), [arXiv:1811.00806].
 [31] K.M. Black *et al.*, “Dynamical electroweak symmetry breaking” in this *Review*.
 [32] G. Aad *et al.* (ATLAS), JHEP **03**, 145 (2020), [arXiv:1910.08447].
 [33] A. M. Sirunyan *et al.* (CMS), JHEP **05**, 033 (2020), [arXiv:1911.03947].
 [34] M. Aaboud *et al.* (ATLAS), Phys. Rev. Lett. **121**, 081801 (2018), [arXiv:1804.03496].
 [35] A. M. Sirunyan *et al.* (CMS), JHEP **08**, 130 (2018), [arXiv:1806.00843].
 [36] M. Aaboud *et al.* (ATLAS), Phys. Lett. **B788**, 316 (2019), [arXiv:1801.08769].
 [37] M. Aaboud *et al.* (ATLAS), Phys. Lett. **B795**, 56 (2019), [arXiv:1901.10917].
 [38] A. M. Sirunyan *et al.* (CMS), Phys. Rev. D **100**, 11, 112007 (2019), [arXiv:1909.04114].
 [39] A. M. Sirunyan *et al.* (CMS), Phys. Rev. Lett. **123**, 23, 231803 (2019), [arXiv:1905.10331].
 [40] CMS Collab., CMS PAS B2G-20-002, Mar. 2021.
 [41] M. Aaboud *et al.* (ATLAS), Phys. Rev. **D98**, 052008 (2018), [arXiv:1808.02380].
 [42] A. M. Sirunyan *et al.* (CMS), Phys. Lett. **B798**, 134952 (2019), [arXiv:1906.00057].
 [43] G. Aad *et al.* (ATLAS), JHEP **09**, 091 (2019), [arXiv:1906.08589].

- [44] G. Aad *et al.* (ATLAS), Eur. Phys. J. C **80**, 12, 1165 (2020), [arXiv:2004.14636].
- [45] A. M. Sirunyan *et al.* (CMS), Eur. Phys. J. C **80**, 3, 237 (2020), [arXiv:1906.05977].
- [46] CMS Collab., CMS PAS B2G-20-008, Mar. 2021.
- [47] CMS Collab., CMS PAS B2G-20-013, Jul. 2021.
- [48] D. Pappadopulo *et al.*, JHEP **09**, 060 (2014), [arXiv:1402.4431].
- [49] H.-J. He *et al.*, Phys. Rev. **D78**, 031701 (2008), [arXiv:0708.2588].
- [50] G. Aad *et al.* (ATLAS), Phys. Rev. D **102**, 11, 112008 (2020), [arXiv:2007.05293].
- [51] A. M. Sirunyan *et al.* (CMS), JHEP **11**, 172 (2018), [arXiv:1807.02826].
- [52] S. Godfrey *et al.*, Phys. Rev. D **61**, 113009 (2000), [hep-ph/0001074].
- [53] Y. Zhang *et al.*, Phys. Rev. **D76**, 091301 (2007), [arXiv:0704.1662].
- [54] P. Langacker and S. U. Sankar, Phys. Rev. **D40**, 1569 (1989).
- [55] J. F. Bueno *et al.* (TWIST), Phys. Rev. **D84**, 032005 (2011), [arXiv:1104.3632].
- [56] G. Prezeau, M. Ramsey-Musolf and P. Vogel, Phys. Rev. D **68**, 034016 (2003), [hep-ph/0303205].

87. Z' -Boson Searches

Revised October 2021 by B.A. Dobrescu (FNAL) and S. Willocq (U. Massachusetts).

The Z' boson is a massive, electrically-neutral and color-singlet hypothetical particle of spin 1. This particle is predicted in many extensions of the Standard Model (SM) and has been the object of extensive phenomenological studies [1].

87.1 Z' boson couplings

The couplings of a Z' boson to the first-generation fermions are given by

$$Z'_\mu \left(g_u^L \bar{u}_L \gamma^\mu u_L + g_d^L \bar{d}_L \gamma^\mu d_L + g_u^R \bar{u}_R \gamma^\mu u_R + g_d^R \bar{d}_R \gamma^\mu d_R + g_e^L \bar{\nu}_L \gamma^\mu \nu_L + g_e^L \bar{e}_L \gamma^\mu e_L + g_e^R \bar{e}_R \gamma^\mu e_R \right), \quad (87.1)$$

where u, d, ν, e are the quark and lepton fields in the mass eigenstate basis, and the coefficients $g_u^L, g_d^L, g_u^R, g_d^R, g_e^L, g_e^R$ are real dimensionless parameters. If the Z' couplings to quarks and leptons are generation-independent, then these seven parameters describe the couplings of the Z' boson to all SM fermions. More generally, however, the Z' couplings to fermions are generation-dependent, in which case Eq. (87.1) may be written with generation indices $i, j = 1, 2, 3$ labeling the quark and lepton fields, and with the seven coefficients promoted to 3×3 Hermitian matrices (e.g., $g_{e,ij}^L \bar{e}_L^i \gamma^\mu e_L^j$, where e_L^2 is the left-handed muon, etc.).

The parameters describing the Z' boson interactions with quarks and leptons are subject to some theoretical constraints. Quantum field theories that include a heavy spin-1 particle are well behaved at high energies only if that particle is a gauge boson associated with a spontaneously broken gauge symmetry. Quantum effects preserve the gauge symmetry only if the couplings of the gauge boson to fermions satisfy the anomaly equations [2]. Furthermore, the fermion charges under the new gauge symmetry are constrained by the requirement that the quarks and leptons get masses from gauge-invariant interactions with the Higgs fields.

The relation between the couplings displayed in Eq. (87.1) and the gauge charges z_f^L and z_f^R of the fermions $f = u, d, \nu, e$ involves the unitary 3×3 matrices V_f^L and V_f^R that transform the gauge eigenstate fermions f_L^i and f_R^i , respectively, into the mass eigenstates. The Z' couplings also depend on the mixings of the new gauge boson in the gauge eigenstate basis (\tilde{Z}'_μ). The main mixings are a kinetic mixing $(-\chi/2)B^{\mu\nu}\tilde{Z}'_{\mu\nu}$ with the hypercharge gauge boson B^μ (χ is a dimensionless parameter), and a mass mixing $\delta M^2 \tilde{Z}'_\mu \tilde{Z}'^\mu$ with the linear combination (\tilde{Z}'_μ) of neutral bosons that couples as the SM Z boson [3]. Since both the kinetic and mass mixings shift the mass and couplings of the Z boson, electroweak measurements impose upper limits on χ and $\delta M^2/(M_{Z'}^2 - M_Z^2)$ of the order of 10^{-3} [4]. Keeping only linear terms in these two small quantities, the couplings of the mass-eigenstate Z' boson are given by

$$g_{f,ij}^L = g_z V_{fii'}^L z_{f,i'}^L (V_f^L)_{i'j}^\dagger + \frac{e}{c_W} \left(\frac{s_W \chi M_{Z'}^2 + \delta M^2}{2s_W (M_{Z'}^2 - M_Z^2)} \sigma_f^3 - \epsilon Q_f \right), \quad (87.2)$$

$$g_{f,ij}^R = g_z V_{fii'}^R z_{f,i'}^R (V_f^R)_{i'j}^\dagger - \frac{e}{c_W} \epsilon Q_f, \quad (87.3)$$

where g_z is the new gauge coupling, Q_f is the electric charge of f , e is the electromagnetic gauge coupling, s_W and c_W are the sine and cosine of the weak mixing angle, $\sigma_f^3 = +1$ for $f = u, \nu$ and $\sigma_f^3 = -1$ for $f = d, e$, and

$$\epsilon = \frac{\chi (M_{Z'}^2 - c_W^2 M_Z^2) + s_W \delta M^2}{M_{Z'}^2 - M_Z^2}. \quad (87.4)$$

The interaction of the Z' boson with a pair of W bosons has

the form

$$\left[i (W_\mu^- Z'_\nu - W_\nu^- Z'_\mu) \partial^\mu W^{+\nu} + \text{H.c.} \right] + i (W_\mu^+ W_\nu^- - W_\nu^+ W_\mu^-) \partial^\mu Z'^\nu \quad (87.5)$$

with a coefficient of order $M_W^2/M_{Z'}^2$ [5]. The Z' also couples to one SM Higgs boson and one Z boson, $Z'_\mu Z^\mu h^0$, with a coefficient of order M_Z .

87.2 Z' models

A simple origin of a Z' boson is a new $U(1)'$ gauge symmetry. In that case, the matrixial equalities $z_u^L = z_d^L$ and $z_\nu^L = z_e^L$ are required by the SM $SU(2)_W$ gauge symmetry. Given that the $U(1)'$ interaction is not asymptotically free, the theory may be well-behaved at high energies (e.g., by embedding $U(1)'$ in a non-Abelian gauge group) only if the charges are commensurate numbers, i.e. any ratio of charges is a rational number. Satisfying the anomaly equations [6] with rational numbers is highly nontrivial, and typically new fermions charged under $U(1)'$ are necessary.

If the couplings are generation-independent ($V_f^{L,R}$ are then unit matrices in Eq. (87.2)) and the mixings of \tilde{Z}' are negligible, then there are five commensurate couplings: $g_u^R, g_d^R, g_e^R, g_q^L$ ($q = u$ or d), g_l^L ($l = \nu$ or e). Four sets of charges are displayed in Table 87.1, each of them spanned by a free parameter x [6]. The first set, labeled $B - xL$, has charges proportional to the baryon number minus x times the lepton number. These charges allow all SM Yukawa couplings to the Higgs doublet which is neutral under $U(1)_{B-xL}$, so that there is no tree-level $\tilde{Z} - \tilde{Z}'$ mixing. For $x = 1$ one recovers the $U(1)_{B-L}$ group, which is non-anomalous in the presence of one “right-handed neutrino” (a chiral fermion that is a singlet under the SM gauge group) per generation. For $x \neq 1$, it is necessary to include some fermions that are vectorlike (i.e. their mass terms are gauge invariant) with respect to the electroweak gauge group and chiral with respect to $U(1)_{B-xL}$. In the particular cases $x = 0$ or $x \gg 1$, the Z' is leptophobic or quark-phobic, respectively.

The second set, $U(1)_{10+x5}$, has charges that commute with the representations of the $SU(5)$ grand unified group. Here x is related to the mixing angle between the two $U(1)$ bosons encountered in the $E_6 \rightarrow SU(5) \times U(1) \times U(1)$ symmetry breaking patterns of grand unified theories [1,7]. With these charges, two Higgs doublets are typically required to generate masses for both up- and down- type fermions. This set leads to $\tilde{Z} - \tilde{Z}'$ mass mixing at tree level, such that for a Z' mass close to the electroweak scale, the measurements at the Z -pole require some fine tuning between the charges and VEVs of the two Higgs doublets. Vectorlike quarks charged under the electroweak gauge group are required (except for $x = -3$) to make this set anomaly free. The particular cases $x = -3, 1, -1/2$ are usually labeled $U(1)_\chi$, $U(1)_\psi$, and $U(1)_\eta$, respectively. Under the third set, $U(1)_{d-xu}$, the weak-doublet quarks are neutral, and the ratio of u_R and d_R charges is $-x$. For $x = 1$, this is the “right-handed” group $U(1)_R$. For $x = 0$, the charges are those of the E_6 -inspired $U(1)_I$ group, which requires new quarks and leptons. Other generation-independent sets of $U(1)'$ charges are given in Ref. [8].

In the absence of new fermions charged under the SM group, the most general generation-independent charge assignment is $U(1)_{q+xu}$, which is a linear combination of hypercharge and $B-L$. Many other anomaly-free solutions exist if generation-dependent charges are allowed. An example is $B - xL_e - yL_\mu + (y-3)L_\tau$, with x, y free parameters. This allows all fermion masses to be generated by Yukawa couplings to a single Higgs doublet, without inducing tree-level flavor-changing neutral current (FCNC) processes. There are also lepton-flavor dependent charges that allow neutrino masses to arise only from operators of high dimensionality [9].

If the $SU(2)_W$ -doublet quarks have generation-dependent $U(1)'$ charges, then the mass eigenstate quarks have flavor off-diagonal couplings to the Z' boson (see Eq. (87.1), and note that $V_u^L (V_d^L)^\dagger$

Table 87.1: Examples of generation-independent $U(1)'$ charges for quarks and leptons. The parameter x is an arbitrary rational number. Gauge anomaly cancellation requires certain new fermions [6].

fermion	$U(1)_{B-xL}$	$U(1)_{10+x5}$	$U(1)_{d-xu}$	$U(1)_{q+xu}$
(u_L, d_L)	1/3	1/3	0	1/3
u_R	1/3	-1/3	$-x/3$	$x/3$
d_R	1/3	$-x/3$	1/3	$(2-x)/3$
(ν_L, e_L)	$-x$	$x/3$	$(-1+x)/3$	-1
e_R	$-x$	-1/3	$x/3$	$-(2+x)/3$

is the CKM matrix). These are severely constrained by measurements of FCNC processes, which in this case are mediated at tree-level by Z' boson exchange [10]. The constraints are relaxed if the first and second generation charges are the same, although they are increasingly tightened by the measurements of B meson properties [11]. If only the $SU(2)_W$ -singlet quarks have generation-dependent $U(1)'$ charges, there is more freedom in adjusting the flavor off-diagonal couplings because the $V_{u,d}^R$ matrices are not observable in the SM.

The anomaly equations for $U(1)'$ could be circumvented only if there is an axion with certain dimension-5 couplings to the gauge bosons. However, such a scenario violates unitarity unless the quantum field theory description breaks down at a scale near $M_{Z'}$ [12]. It is possible, though, that the SM fermions are not charged under the $U(1)'$, but have mass mixing with some vectorlike fermions which are charged under $U(1)'$, implying that the physical fermions have couplings to the Z' [13]. For example, if the only SM quarks that have large mixings with some vectorlike quarks are the b quarks, then the only currently known particles that couple to the Z' would be the physical b quarks.

Z' bosons may also arise from larger gauge groups. These may extend the electroweak group, as in $SU(2) \times SU(2) \times U(1)$, or may embed the electroweak group, as in $SU(3)_W \times U(1)$ [14]. If the larger group is spontaneously broken down to $SU(2)_W \times U(1)_Y \times U(1)'$ at a scale $v_* \gg M_{Z'}/g_z$, then the above discussion applies up to corrections of order $M_{Z'}^2/(g_z v_*)^2$. For $v_* \sim M_{Z'}/g_z$, additional gauge bosons have masses comparable to $M_{Z'}$, including at least a W' boson [14]. If the larger gauge group breaks together with the electroweak symmetry directly to the electromagnetic $U(1)_{em}$, then the left-handed fermion charges are no longer correlated ($z_u^L \neq z_d^L, z_\nu^L \neq z_e^L$) and a $Z'W^+W^-$ coupling is induced.

If the electroweak gauge bosons propagate in extra dimensions, then their Kaluza-Klein (KK) excitations include a series of Z' boson pairs. Each of these pairs can be associated with a different $SU(2) \times U(1)$ gauge group in four dimensions. The properties of the KK particles depend strongly on the extra dimensional theory [15]. For example, in universal extra dimensions there is a parity that forces all couplings of Eq. (87.1) to vanish in the case of the lightest KK bosons, while allowing couplings to pairs of fermions involving a SM and a heavy vectorlike fermion. There are also 4-dimensional gauge theories (*e.g.* little Higgs with T parity) with Z' bosons exhibiting similar properties. By contrast, in a warped extra dimension, the couplings of Eq. (87.1) may be sizable even when SM fields propagate along the extra dimension.

Z' bosons may also be composite particles. For example, in confining gauge theories [16], the ρ -like bound state is a spin-1 boson that may be interpreted as arising from a spontaneously broken gauge symmetry [17].

87.3 Non-resonant Z' signatures at colliders

In the presence of the couplings shown in Eq. (87.1), the Z' boson may be produced in the s -channel at colliders, and would decay to pairs of fermions. The decay width into a pair of electrons is given by

$$\Gamma(Z' \rightarrow e^+e^-) \simeq \left[(g_e^L)^2 + (g_e^R)^2 \right] \frac{M_{Z'}}{24\pi}, \quad (87.6)$$

where small corrections from electroweak loops are not included. The decay width into $q\bar{q}$ is similar, except for an additional color factor of 3, QCD radiative corrections, and fermion mass corrections. Thus, one may compute the Z' branching fractions in terms of the couplings of Eq. (87.1). However, other decay channels, such as WW or a pair of new particles, could have large widths and need to be added to the total decay width.

As mentioned above, there are theories in which the Z' couplings are controlled by a discrete symmetry that forbids decays into a pair of SM particles. Typically, such theories involve several new particles, which may be produced only in pairs and undergo cascade decays through Z' bosons, leading to signals involving missing transverse momentum. Given that the cascade decays depend on the properties of new particles other than the Z' boson (see, *e.g.* Ref. [18]), this case is not discussed further here.

The Z' contribution to the cross sections for $e^+e^- \rightarrow f\bar{f}$ proceeds through an s -channel Z' exchange (when $f = e$, there are also t - and u -channel exchanges). For $M_{Z'} < \sqrt{s}$, the Z' appears as an $f\bar{f}$ resonance in the radiative return process where photon emission tunes the effective center-of-mass energy to $M_{Z'}$. The agreement between the LEP-II measurements and the SM predictions implies that either the Z' couplings are smaller than or of order 10^{-2} , or else $M_{Z'}$ is above 209 GeV, the maximum energy of LEP-II. In the latter case, the Z' exchange may be approximated up to corrections of order $s/M_{Z'}^2$, by the contact interactions

$$\frac{g_z^2}{M_{Z'}^2 - s} \left[\bar{e}\gamma_\mu (z_e^L P_L + z_e^R P_R) e \right] \left[\bar{f}\gamma^\mu (z_f^L P_L + z_f^R P_R) f \right], \quad (87.7)$$

where $P_{L,R}$ are chirality projection operators, and the relation between Z' couplings and charges (see Eq. (87.2) in the limit where the mass and kinetic mixings are neglected) is used, assuming generation-independent charges. The four LEP collaborations have set limits on the coefficients of such operators for all possible chiral structures and for various combinations of fermions [19]. Thus, one may derive bounds on $(M_{Z'}/g_z)|z_e^L z_f^L|^{-1/2}$ and the analogous combinations of LR, RL and RR charges, which are typically on the order of a few TeV. LEP-II limits were derived [6] on the four sets of charges shown in Table 87.1.

Somewhat stronger bounds can be set on $M_{Z'}/g_z$ for specific sets of Z' couplings if the effects of several operators (87.7) are combined. Dedicated analyses by the LEP collaborations have set limits on Z' bosons for particular values of the gauge coupling (see section 3.5 of Ref. [19]). For example, $M_{Z_{SSM}} > 1.76$ TeV for a “sequential” Z' of same couplings as the SM Z boson, while $M_{Z_\chi} > 0.785$ TeV for the Z' associated with $U(1)_\chi$ assuming a unification condition for the gauge coupling.

87.4 Searches at hadron colliders

Z' bosons with couplings to quarks (see Eq. (87.1)) may be produced at hadron colliders in the s -channel and would show up as resonances in the invariant mass distribution of the decay products. The cross section for producing a Z' boson at the LHC, which then decays to some $f\bar{f}$ final state, takes the form [20]

$$\sigma(pp \rightarrow Z'X \rightarrow f\bar{f}X) \simeq \frac{\pi}{6s} \sum_q c_q^f w_q(s, M_{Z'}^2) \quad (87.8)$$

for flavor-diagonal couplings to quarks. Here, we have neglected the interference with the SM contribution to $f\bar{f}$ production, which is a good approximation for a narrow Z' resonance (deviations from the narrow width approximation are discussed in Ref. [21]). The coefficients

$$c_q^f = \left[(g_q^L)^2 + (g_q^R)^2 \right] B(Z' \rightarrow f\bar{f}) \quad (87.9)$$

contain all the dependence on the Z' couplings, while the functions w_q include all the information about parton distributions and QCD corrections [6, 8]. This factorization holds exactly to NLO and the deviations from it induced at NNLO are very small. Note that the w_u and w_d functions are substantially larger than the w_q functions for the other quarks. Eq. (87.8) also applies to

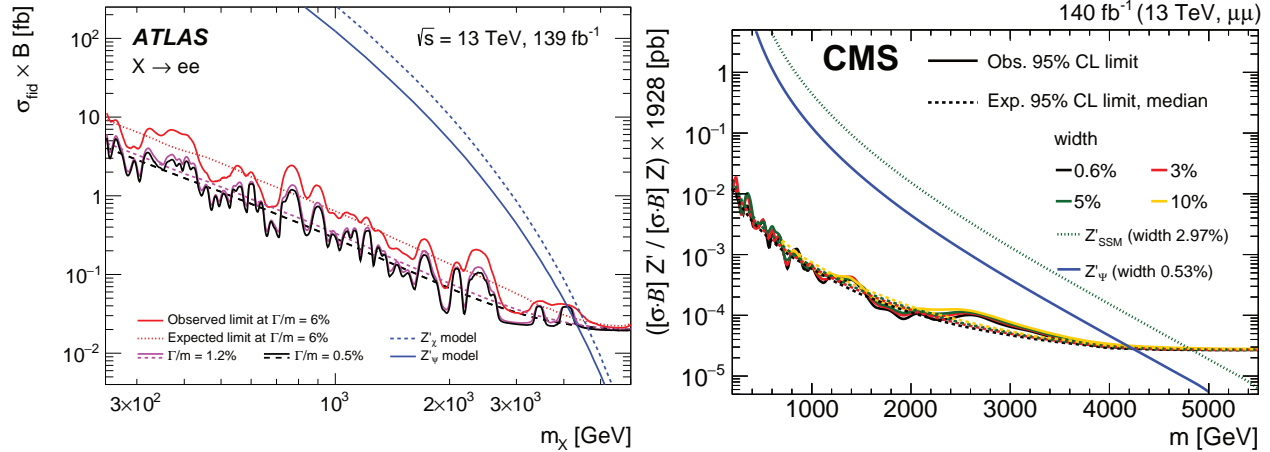


Figure 87.1: Upper limits on the cross section for Z' production times the branching fraction for $Z' \rightarrow e^+e^-$ (left panel, set by ATLAS [22]) or $Z' \rightarrow \mu^+\mu^-$ (right panel, set by CMS [23]) as a function of $M_{Z'}$. The lines labeled by Z'_ψ and Z'_χ are theoretical predictions for the $U(1)_{10+x5}$ models in Table 87.1 with $x = -3$ and $x = +1$, respectively, for g_z fixed by an E_6 unification condition. The Z'_{SSM} line corresponds to Z' couplings equal to those of the Z boson.

the Tevatron, except for changing the pp initial state to $p\bar{p}$, which implies that the $w_q(s, M_{Z'}^2)$ functions are replaced by some other functions $\bar{w}_q((1.96 \text{ TeV})^2, M_{Z'}^2)$.

It is common to present results of Z' searches as limits on the cross section versus $M_{Z'}$ (see for example Fig. 87.1). An alternative is to plot exclusion curves for fixed $M_{Z'}$ values in the $c_u^f - c_d^f$ planes, allowing a simple derivation of the mass limit within any Z' model. CMS upper limits in the $c_u^\ell - c_d^\ell$ plane ($\ell = e$ or μ) for different $M_{Z'}$ are shown in Ref. [23] (for Tevatron limits, see Refs. [8, 24]).

The discovery of a dilepton resonance at the LHC would determine the Z' mass and width. A measurement of the total cross section would define a band in the $c_u^\ell - c_d^\ell$ plane. Angular distributions can be used to measure several combinations of Z' parameters (angular distributions were used in Ref. [25] to improve the Tevatron sensitivity). Even though the original quark direction in a pp collider is unknown, the leptonic forward-backward asymmetry A_{FB}^ℓ can be extracted from the kinematics of the dilepton system, and is sensitive to parity-violating couplings. A fit to the Z' rapidity distribution can distinguish between the couplings to up and down quarks. These measurements, combined with off-peak observables, have the potential to differentiate among various Z' models [26]. In some cases, A_{FB}^ℓ may provide discovery sensitivity that is competitive with the mass distribution [27]. The spin of the Z' boson may be determined from angular distributions [28].

Searches for Z' decays into e^+e^- and $\mu^+\mu^-$ by the ATLAS and CMS collaborations [22, 23] have set 95% C.L. upper cross-section limits as low as 0.02 fb (see Fig. 87.1), with the mass lower limits in specific models as high as 4.9 TeV in a single channel. Cross section limits in the dimuon channel for low mass regions, below 200 GeV but not near the Z mass, have been set at the LHC by CMS [29] and LHCb [30].

The $Z' \rightarrow \tau^+\tau^-$ decay has been searched for with 36 fb^{-1} of 13 TeV data [31], and a limit $M_{Z'} > 2.4 \text{ TeV}$ has been set in the case of a sequential Z' . Limits on heavy scalars in the $\tau^+\tau^-$ final state, set by ATLAS [32] with 139 fb^{-1} and CMS [33] with 36 fb^{-1} at 13 TeV, can be recast into limits on Z' . Limits in the flavor-violating leptonic final states have also been reported by ATLAS [34] and CMS [35] at 13 TeV, for resonances in the $e^\pm\mu^\mp$, $e^\pm\tau^\mp$ and $\mu^\pm\tau^\mp$ channels.

Final states with higher background, jj , $b\bar{b}$ and $t\bar{t}$, are also important as they probe various combinations of Z' couplings to quarks. Besides the improved sensitivity at masses of several TeV, the LHC searches in the dijet channel have been also extended to masses as low as 10 GeV, through the use of new techniques involving boosted topologies and initial state radiation [37]. Limits from such Z' searches in hadronic final states are summarized in Fig. 87.2.

Searches for the $Z' \rightarrow b\bar{b}$ decay have been performed for two production mechanisms. ATLAS [38] and CMS [39] searched for $b\bar{b}$ resonances in 139 fb^{-1} and 137 fb^{-1} of 13 TeV data, respectively, setting limits under the assumption that the Z' boson couples to light quarks and thus is produced in the s -channel. The CMS upper limit on the cross-section times the $Z' \rightarrow b\bar{b}$ branching fraction decreases from 40 fb at $M_{Z'} = 1.8 \text{ TeV}$ to 0.4 fb at $M_{Z'} = 8 \text{ TeV}$. The ATLAS search covered the 1.3 TeV – 5 TeV mass range, setting a lower mass limit of 2.7 TeV for the Z'_{SSM} . Independent of any other couplings, if the Z' couples to the b quark, then it can be produced in association with a $b\bar{b}$ pair, and it decays to a second $b\bar{b}$ pair, which forms a resonance. The cross-section limit for that process, set by ATLAS [40] with 103 fb^{-1} of 13 TeV data, is between 0.1 and 0.2 pb for $M_{Z'}$ in the 1.3 – 3 TeV range. For a vector coupling g_b of Z' to b quarks, *i.e.*, $g_{d33}^L = g_{d33}^R = g_b$ using the notation of Eq. (87.1), the limit is $M_{Z'} > 1.45 \text{ TeV}$ when $g_b = 1$. Searches for the $Z' \rightarrow t\bar{t}$ decay are discussed in Ref. [41].

Heavy resonances decaying into Zh^0 with $Z \rightarrow \ell^+\ell^-$, $\nu\bar{\nu}$ or $q\bar{q}$ and $h^0 \rightarrow b\bar{b}$ have been studied by ATLAS [42, 43] and CMS [44–46] using 13 TeV data. The most stringent constraint on Z' production in the context of the Heavy Vector Triplet (HVT) model weakly-coupled scenario A [47] is set in the semi-leptonic channel, with a mass lower limit of 3.5 TeV [46].

Searches for a Z' boson lighter than the SM Z and which couples to leptons have been performed in the 4-lepton final state. CMS [48] focused on the Z decays into a muon pair followed by the radiation of a Z' boson which decays itself into a muon pair. ATLAS [49] considered the $h^0 \rightarrow ZZ'$ and $h^0 \rightarrow Z'Z'$ processes followed by the leptonic decays of both Z and Z' .

The $pp \rightarrow Z'X \rightarrow W^+W^-X$ process has also been searched for at the LHC. The channel where the Z' boson is produced through its couplings to quarks, and the W bosons decay hadronically, has been explored using boosted techniques to analyze the 13 TeV data [50–53] with a mass lower limit of 3.5 TeV in the HVT model A [51]. The Z' boson may also be produced through its couplings to W bosons [54], which has been explored with the use of forward jets consistent with a vector boson fusion event topology [51, 53]. The latter process provides a test of fermiophobic Z' models.

At the Tevatron, the CDF and DØ collaborations have searched for Z' bosons in the e^+e^- [55], $\mu^+\mu^-$ [56], $e^\pm\mu^\mp$ [57], $\tau^+\tau^-$ [58], $t\bar{t}$ [59], jj [60] and W^+W^- [61] final states. These limits have been mostly superseded by the LHC results.

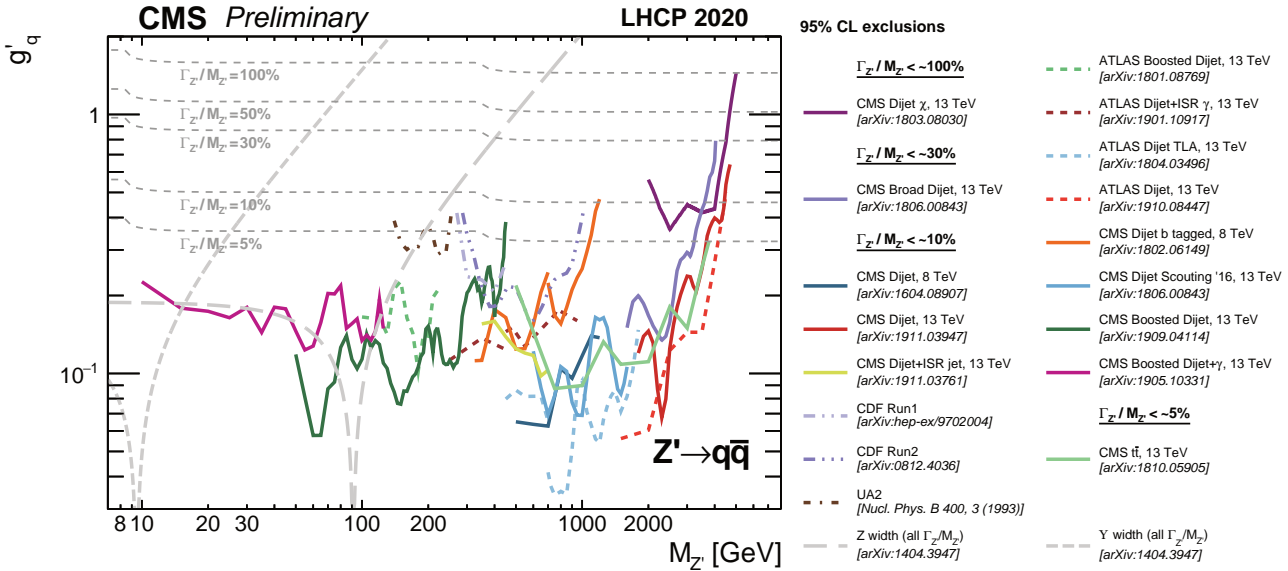


Figure 87.2: Upper limits on the Z' coupling to quarks as a function of $M_{Z'}$ based on various searches performed by the ATLAS, CMS, CDF, and UA2 experiments [36].

87.5 Low-energy constraints

Z' boson properties are also constrained by a variety of low-energy experiments [62]. Polarized electron-nucleon scattering and atomic parity violation are sensitive to electron-quark contact interactions, which get contributions from Z' exchange that can be expressed in terms of the couplings introduced in Eq. (87.1) and $M_{Z'}$. Further corrections to the electron-quark contact interactions are induced in the presence of $\tilde{Z}-\tilde{Z}'$ mixing because of the shifts in the Z couplings to quarks and leptons [3]. Deep-inelastic neutrino-nucleon scattering is similarly affected by Z' bosons. Other low-energy observables are discussed in [4]. Viable models with Z' bosons much lighter than the Z boson have been constructed, despite many additional experimental constraints [63]. Limits on the Z' coupling to leptons in the mass range 0.02–10.2 GeV have been set in e^+e^- collisions by BaBar [64], assuming a dark photon, *i.e.*, a Z' boson whose couplings arise only from the kinetic mixing with the hypercharge gauge boson.

In some models, the lower limits on $M_{Z'}$ set by low-energy data are above 1 TeV. For example, $M_{Z_\chi} > 1.1$ TeV and $M_{Z_\eta} > 0.43$ TeV assuming that the Higgs sectors consist of electroweak doublets and singlets only [4], while the gauge coupling is fixed by an $SO(10)$ unification condition for $U(1)_\chi$ and $U(1)_\eta$. For more general models, see Refs. [1, 6, 65]. The mass bounds from direct searches at the LHC [22, 23] exceed the electroweak constraints by a factor of three or more for the models mentioned here. This conclusion could change if the collider bounds are weakened by exotic decay channels [66].

Although the LHC data are most constraining for many Z' models, one should be careful in assessing the relative reach of various experiments given the freedom in Z' couplings. For example, a Z' coupled to $B-yL_\mu+(y-3)L_\tau$ has implications for the muon $g-2$, neutrino oscillations or τ decays, and would be hard to see in processes involving first-generation fermions. Moreover, the combination of LHC searches and low-energy measurements could allow a precise determination of the Z' parameters [67].

References

- [1] A. Leike, Phys. Rept. **317**, 143 (1999), [hep-ph/9805494].
- [2] T. P. Cheng and L. F. Li, *Gauge Theory of Elementary Particle Physics* (1984), ISBN 9780198519614.
- [3] K. S. Babu, C. F. Kolda and J. March-Russell, Phys. Rev. **D57**, 6788 (1998), [hep-ph/9710441].
- [4] J. Erler *et al.*, JHEP **08**, 017 (2009), [arXiv:0906.2435].
- [5] B. A. Dobrescu and P. J. Fox, JHEP **05**, 047 (2016), [arXiv:1511.02148].
- [6] M. Carena *et al.*, Phys. Rev. **D70**, 093009 (2004), [hep-ph/0408098].
- [7] F. Del Aguila, M. Cvetič and P. Langacker, Phys. Rev. **D52**, 37 (1995), [hep-ph/9501390].
- [8] E. Accomando *et al.*, Phys. Rev. **D83**, 075012 (2011), [arXiv:1010.6058].
- [9] M.-C. Chen, A. de Gouvea and B. A. Dobrescu, Phys. Rev. **D75**, 055009 (2007), [hep-ph/0612017].
- [10] P. Langacker and M. Plumacher, Phys. Rev. **D62**, 013006 (2000), [hep-ph/0001204].
- [11] A. J. Buras, F. De Fazio and J. Girrbach, JHEP **02**, 116 (2013), [arXiv:1211.1896].
- [12] L. E. Ibanez and G. G. Ross, Phys. Lett. **B332**, 100 (1994), [hep-ph/9403338].
- [13] P. J. Fox *et al.*, Phys. Rev. D **84**, 115006 (2011), [arXiv:1104.4127].
- [14] See the Section on “ W' searches” in this Review.
- [15] J. Parsons and A. Pomarol, “Extra dimensions” in this Review.
- [16] K.M. Black *et al.*, “Dynamical electroweak symmetry breaking” in this Review.
- [17] M. Bando, T. Kugo and K. Yamawaki, Phys. Rept. **164**, 217 (1988).
- [18] J. Y. Araz *et al.*, JHEP **02**, 092 (2018), [arXiv:1711.06302].
- [19] S. Schael *et al.* (ALEPH, DELPHI, L3, OPAL, LEP Electroweak), Phys. Rept. **532**, 119 (2013), [arXiv:1302.3415].
- [20] G. Paz and J. Roy, Phys. Rev. **D97**, 075025 (2018), [arXiv:1711.02655].
- [21] E. Accomando *et al.*, JHEP **10**, 153 (2013), [arXiv:1304.6700].
- [22] G. Aad *et al.* (ATLAS), Phys. Lett. **B796**, 68 (2019), [arXiv:1903.06248].
- [23] A. M. Sirunyan *et al.* (CMS), JHEP **07**, 208 (2021), [arXiv:2103.02708].
- [24] A. Abulencia *et al.* (CDF), Phys. Rev. Lett. **95**, 252001 (2005), [hep-ex/0507104].
- [25] A. Abulencia *et al.* (CDF), Phys. Rev. Lett. **96**, 211801 (2006), [hep-ex/0602045].
- [26] F. Petriello and S. Quackenbush, Phys. Rev. **D77**, 115004 (2008), [arXiv:0801.4389].

- [27] E. Accomando *et al.*, JHEP **01**, 127 (2016), [arXiv:1503.02672].
- [28] P. Osland *et al.*, Phys. Rev. **D79**, 115021 (2009), [arXiv:0904.4857].
- [29] A. M. Sirunyan *et al.* (CMS), Phys. Rev. Lett. **124**, 13, 131802 (2020), [arXiv:1912.04776].
- [30] R. Aaij *et al.* (LHCb), JHEP **10**, 156 (2020), [arXiv:2007.03923].
- [31] M. Aaboud *et al.* (ATLAS), JHEP **01**, 055 (2018), [arXiv:1709.07242].
- [32] G. Aad *et al.* (ATLAS), Phys. Rev. Lett. **125**, 5, 051801 (2020), [arXiv:2002.12223].
- [33] A. M. Sirunyan *et al.* (CMS), JHEP **09**, 007 (2018), [arXiv:1803.06553].
- [34] M. Aaboud *et al.* (ATLAS), Phys. Rev. **D98**, 092008 (2018), [arXiv:1807.06573].
- [35] CMS Collab., PAS EXO-19-014, Aug. 2021.
- [36] CMS Collab., <https://twiki.cern.ch/twiki/bin/view/CMSPublic/SummaryPlotsEXO13TeV>.
- [37] A. M. Sirunyan *et al.* (CMS), Phys. Rev. Lett. **123**, 23, 231803 (2019), [arXiv:1905.10331].
- [38] G. Aad *et al.* (ATLAS), JHEP **03**, 145 (2020), [arXiv:1910.08447].
- [39] CMS Collab., CMS PAS EXO-20-008, July 2021.
- [40] G. Aad *et al.* (ATLAS) (2021), [arXiv:2108.09059].
- [41] See the Section on “Dynamical Electroweak Symmetry Breaking” in this *Review*.
- [42] G. Aad *et al.* (ATLAS), Phys. Rev. D **102**, 11, 112008 (2020), [arXiv:2007.05293].
- [43] ATLAS Collab., ATLAS-CONF-2020-043, Jul. 2020.
- [44] A. M. Sirunyan *et al.* (CMS), Eur. Phys. J. **C77**, 636 (2017), [arXiv:1707.01303].
- [45] A. M. Sirunyan *et al.* (CMS), JHEP **01**, 051 (2019), [arXiv:1808.01365].
- [46] A. M. Sirunyan *et al.* (CMS), Eur. Phys. J. C **81**, 8, 688 (2021), [arXiv:2102.08198].
- [47] D. Pappadopulo *et al.*, JHEP **09**, 060 (2014), [arXiv:1402.4431].
- [48] A. M. Sirunyan *et al.* (CMS), Phys. Lett. **B792**, 345 (2019), [arXiv:1808.03684].
- [49] ATLAS Collab., ATLAS-CONF-2021-034, Aug. 2021.
- [50] G. Aad *et al.* (ATLAS), JHEP **09**, 091 (2019), [arXiv:1906.08589].
- [51] G. Aad *et al.* (ATLAS), Eur. Phys. J. C **80**, 12, 1165 (2020), [arXiv:2004.14636].
- [52] A. M. Sirunyan *et al.* (CMS), Eur. Phys. J. C **80**, 3, 237 (2020), [arXiv:1906.05977].
- [53] A. Tumasyan *et al.* (CMS) (2021), [arXiv:2109.06055].
- [54] H.-J. He *et al.*, Phys. Rev. **D78**, 031701 (2008), [arXiv:0708.2588].
- [55] V. M. Abazov *et al.* (D0), Phys. Lett. **B695**, 88 (2011), [arXiv:1008.2023].
- [56] T. Aaltonen *et al.* (CDF), Phys. Rev. Lett. **106**, 121801 (2011), [arXiv:1101.4578].
- [57] A. Abulencia *et al.* (CDF), Phys. Rev. Lett. **96**, 211802 (2006), [hep-ex/0603006].
- [58] D. Acosta *et al.* (CDF), Phys. Rev. Lett. **95**, 131801 (2005), [hep-ex/0506034].
- [59] T. Aaltonen *et al.* (CDF), Phys. Rev. **D84**, 072004 (2011), [arXiv:1107.5063].
- [60] T. Aaltonen *et al.* (CDF), Phys. Rev. **D79**, 112002 (2009), [arXiv:0812.4036].
- [61] T. Aaltonen *et al.* (CDF), Phys. Rev. Lett. **104**, 241801 (2010), [arXiv:1004.4946].
- [62] V. D. Barger *et al.*, Phys. Rev. **D57**, 391 (1998), [hep-ph/9707412].
- [63] R. Harnik, J. Kopp and P. A. N. Machado, JCAP **1207**, 026 (2012), [arXiv:1202.6073].
- [64] J. P. Lees *et al.* (BaBar), Phys. Rev. Lett. **113**, 201801 (2014), [arXiv:1406.2980].
- [65] E. Rojas and J. Erler, JHEP **10**, 063 (2015), [arXiv:1505.03208].
- [66] J. Kang and P. Langacker, Phys. Rev. **D71**, 035014 (2005), [hep-ph/0412190].
- [67] Y. Li, F. Petriello and S. Quackenbush, Phys. Rev. **D80**, 055018 (2009), [arXiv:0906.4132].

88. Supersymmetry, Part I (Theory)

Revised August 2021 by B.C. Allanach (DAMTP, Cambridge U.) and H.E. Haber (UC Santa Cruz).

88.1	Introduction	1000
88.2	Structure of the MSSM	1000
88.2.1	R-parity and the lightest supersymmetric particle	1001
88.2.2	The goldstino and gravitino	1001
88.2.3	Hidden sectors and the structure of SUSY breaking	1002
88.2.4	SUSY and extra dimensions	1002
88.2.5	Split-SUSY	1002
88.3	Parameters of the MSSM	1003
88.3.1	The SUSY-conserving parameters	1003
88.3.2	The SUSY-breaking parameters	1003
88.3.3	MSSM-124	1003
88.4	The supersymmetric-particle spectrum	1004
88.4.1	The charginos and neutralinos	1004
88.4.2	The squarks and sleptons	1004
88.5	The supersymmetric Higgs sector	1005
88.5.1	The tree-level Higgs sector	1005
88.5.2	The radiatively-corrected Higgs sector	1005
88.6	Restricting the MSSM parameter freedom	1006
88.6.1	Gaugino mass relations	1006
88.6.2	Constrained versions of the MSSM: mSUGRA, CMSSM, etc.	1007
88.6.3	Gauge-mediated SUSY breaking	1007
88.6.4	The phenomenological MSSM	1008
88.6.5	Simplified models	1008
88.7	Experimental data confronts the MSSM	1008
88.7.1	Naturalness constraints and the little hierarchy	1009
88.7.2	Indirect constraints on supersymmetric models	1010
88.8	Massive neutrinos in weak-scale SUSY	1010
88.8.1	The supersymmetric seesaw	1011
88.8.2	R-parity-violating SUSY	1011
88.9	Extensions beyond the MSSM	1011

88.1 Introduction

Supersymmetry (SUSY) is a generalization of the space-time symmetries of quantum field theory that transforms fermions into bosons and vice versa [1]. The existence of such a non-trivial extension of the Poincaré symmetry of ordinary quantum field theory was initially surprising, and its form is highly constrained by theoretical principles [2]. SUSY also provides a framework for the unification of particle physics and gravity [3–6] at the Planck energy scale, $M_P \sim 10^{19}$ GeV, where the gravitational interactions become comparable in strength to the gauge interactions. Moreover, supersymmetry can stabilize the hierarchy between the energy scale that characterizes electroweak symmetry breaking, $M_{EW} \sim 100$ GeV, and the Planck scale [7–10] against large radiative corrections. The stability of this large gauge hierarchy with respect to radiative quantum corrections is not possible to maintain in the Standard Model (SM) without an unnatural fine-tuning of the parameters of the fundamental theory at the Planck scale. In contrast, in a supersymmetric extension of the SM, it is possible to maintain the gauge hierarchy while providing a natural framework for elementary scalar fields.

If supersymmetry were an exact symmetry of nature, then particles and their superpartners, which differ in spin by half a unit, would be degenerate in mass. Since superpartners have not (yet) been observed, supersymmetry must be a broken symmetry. Nevertheless, the stability of the gauge hierarchy can still be maintained if the SUSY breaking is soft [11, 12], and the corresponding SUSY-breaking mass parameters are no larger than a few TeV. Whether this is still plausible in light of recent SUSY searches at the LHC (see Sec. 89) will be discussed in Sec. 88.7.

In particular, soft-SUSY-breaking terms of the Lagrangian involve combinations of fields with total mass dimension of three or

less, with some restrictions on the dimension-three terms as elucidated in Ref. [11]. The impact of the soft terms becomes negligible at energy scales much larger than the size of the SUSY-breaking masses. Thus, a theory of weak-scale supersymmetry, where the effective scale of supersymmetry breaking is tied to the scale of electroweak symmetry breaking, provides a natural framework for the origin and the stability of the gauge hierarchy [7–10].

At present, there is no unambiguous experimental evidence for the breakdown of the SM at or below the TeV scale. The expectations for new TeV-scale physics beyond the SM are based primarily on three theoretical arguments. First, in a theory with an elementary scalar field of mass m and interaction strength λ (e.g., a quartic scalar self-coupling, the square of a gauge coupling or the square of a Yukawa coupling), the stability with respect to quantum corrections requires the existence of an energy cutoff roughly of order $(16\pi^2/\lambda)^{1/2}m$, beyond which new physics must enter [13]. A significantly larger energy cutoff would require an unnatural fine-tuning of parameters that govern the effective low-energy theory. Applying this argument to the SM leads to an expectation of new physics at the TeV scale [10].

Second, the unification of the three SM gauge couplings at a very high energy close to the Planck scale is possible if new physics beyond the SM (which modifies the running of the gauge couplings above the electroweak scale) is present. The minimal supersymmetric extension of the SM, where superpartner masses lie below a few TeV, provides an example of successful gauge coupling unification [14].

Third, the existence of dark matter that makes up approximately one quarter of the energy density of the universe, cannot be explained within the SM of particle physics [15]. Remarkably, a stable weakly-interacting massive particle (WIMP) whose mass and interaction rate are governed by new physics associated with the TeV-scale can be consistent with the observed density of dark matter (this is the so-called WIMP miracle, which is reviewed in Ref. [16]). The lightest supersymmetric particle, if stable, is a promising (although not the unique) candidate for the dark matter [17–21]. Further aspects of dark matter can be found in Sec. 27.

88.2 Structure of the MSSM

The minimal supersymmetric extension of the SM (MSSM) consists of the fields of the two-Higgs-doublet extension of the SM and the corresponding superpartners [22, 23]. A particle and its superpartner together form a supermultiplet. The corresponding field content of the supermultiplets of the MSSM and their gauge quantum numbers are shown in Table 88.1. The electric charge $Q = T_3 + \frac{1}{2}Y$ is determined in terms of the third component of the weak isospin (T_3) and the U(1) weak hypercharge (Y).

The gauge supermultiplets consist of the gluons and their gluino fermionic superpartners and the SU(2)×U(1) gauge bosons and their gaugino fermionic superpartners. The matter supermultiplets consist of three generations of left-handed quarks and leptons and their scalar superpartners (squarks and sleptons, collectively referred to as sfermions), and the corresponding antiparticles. The Higgs supermultiplets consist of two complex Higgs doublets, their higgsino fermionic superpartners, and the corresponding antiparticles. The enlarged Higgs sector of the MSSM constitutes the minimal structure needed to guarantee the cancellation of gauge anomalies [25] generated by the higgsino superpartners that can appear as internal lines in triangle diagrams with three external electroweak gauge bosons. Moreover, without a second Higgs doublet, one cannot generate mass for both “up”-type and “down”-type quarks (and charged leptons) in a way consistent with the underlying SUSY [26–28].

In the most elegant treatment of SUSY, spacetime is extended to superspace which consists of the spacetime coordinates and new anticommuting fermionic coordinates θ and θ^\dagger [29, 30]. Each supermultiplet is represented by a superfield that is a function of the superspace coordinates. The fields of a given supermultiplet (which are functions of the spacetime coordinates) are coefficients of the θ and θ^\dagger expansion of the corresponding superfield.

Vector superfields contain the gauge-boson fields and their gaugino superpartners. Chiral superfields contain the spin-0 and spin-

Table 88.1: The fields of the MSSM and their $SU(3)\times SU(2)\times U(1)$ quantum numbers are listed. For simplicity, only one generation of quarks and leptons is exhibited. For each lepton, quark, and Higgs supermultiplet (each denoted by a hatted upper-case letter), there is a corresponding antiparticle multiplet of charge-conjugated fermions and their associated scalar partners [24].

Field Content of the MSSM						
Super-multiplets	Super-field	Bosonic fields	Fermionic partners	SU(3)	SU(2)	U(1)
gluon/gluino	\hat{V}_8	g	\tilde{g}	8	1	0
gauge boson/ gaugino	\hat{V} \hat{V}'	W^\pm, W^0 B	$\tilde{W}^\pm, \tilde{W}^0$ \tilde{B}	1 1	3 1	0 0
slepton/ lepton	\hat{L} \hat{E}^c	$(\tilde{\nu}_L, \tilde{e}_L^-)$ \tilde{e}_R^+	$(\nu, e^-)_L$ e_L^c	1 1	2 1	-1 2
squark/ quark	\hat{Q} \hat{U}^c \hat{D}^c	$(\tilde{u}_L, \tilde{d}_L)$ \tilde{u}_R^* \tilde{d}_R^*	$(u, d)_L$ u_L^c d_L^c	3 3 3	2 1 1	1/3 -4/3 2/3
Higgs boson/ higgsino	\hat{H}_d \hat{H}_u	(H_d^0, H_d^-) (H_u^+, H_u^0)	$(\tilde{H}_d^0, \tilde{H}_d^-)$ $(\tilde{H}_u^+, \tilde{H}_u^0)$	1 1	2 2	-1 1

1/2 fields of the matter or Higgs supermultiplets. A general supersymmetric Lagrangian is determined by three functions of the chiral superfields [4]: the superpotential, the Kähler potential, and the gauge kinetic function (which can be appropriately generalized to accommodate higher derivative terms [31]). Minimal forms for the Kähler potential and gauge kinetic function, which generate canonical kinetic energy terms for all the fields, are required for renormalizable globally supersymmetric theories. A renormalizable superpotential, which is at most cubic in the chiral superfields, yields supersymmetric Yukawa couplings and mass terms. A combination of gauge invariance and SUSY produces couplings of gaugino fields to matter (or Higgs) fields and their corresponding superpartners. The (renormalizable) MSSM Lagrangian is then constructed by including all possible supersymmetric interaction terms (of dimension four or less) that satisfy $SU(3)\times SU(2)\times U(1)$ gauge invariance and $B-L$ conservation (where B =baryon number and L =lepton number). Finally, the most general soft-supersymmetry-breaking terms consistent with these symmetries are added [11, 12, 32].

Although the MSSM is the focus of much of this review, there is some motivation for considering non-minimal supersymmetric extensions of the SM. For example, extra structure is needed to generate non-zero neutrino masses as discussed in Sec. 88.8. In addition, in order to address some theoretical issues and tensions associated with the MSSM, it has been fruitful to introduce one additional singlet Higgs superfield. The resulting next-to-minimal supersymmetric extension of the Standard Model (NMSSM) [33] is considered further in Sec. 88.4–88.7 and 88.9. Finally, one is always free to add additional fields to the SM along with the corresponding superpartners. However, only certain choices for the new fields (*e.g.*, the addition of complete $SU(5)$ multiplets) will preserve the successful gauge coupling unification of the MSSM. Some examples will be briefly mentioned in Sec. 88.9.

88.2.1 R -parity and the lightest supersymmetric particle

The (renormalizable) SM Lagrangian possesses an accidental global $B-L$ symmetry due to the fact that B and L -violating operators composed of SM fields must have dimension $d = 5$ or larger [34]. Consequently, B and L -violating effects are suppressed by $(M_{EW}/M)^{d-4}$, where M is the characteristic mass scale of the physics that generates the corresponding higher dimensional operators. Indeed, values of M of order the grand unification scale or larger may be responsible for the observed (approximate) stability of the proton and suppression of neutrino masses. Unfortunately, these results are not guaranteed in a generic supersymmetric extension of the SM. For example, it is possible to construct gauge invariant supersymmetric dimension-four B and L -violating operators made up of fields of SM particles and their superpartners. Such operators, if simultaneously present in the theory, could yield a proton decay rate many orders of magnitude larger than the current experimental bound. It is for this reason that

$B-L$ conservation is *imposed* on the supersymmetric Lagrangian when defining the MSSM, which is sufficient for eliminating all B and L -violating operators of dimension $d \leq 4$.

As a consequence of the $B-L$ symmetry, the MSSM possesses a multiplicative R -parity invariance, where $R = (-1)^{3(B-L)+2S}$ for a particle of spin S [35]. This implies that all the particles of the SM have even R -parity, whereas the corresponding superpartners have odd R -parity. The conservation of R -parity in scattering and decay processes has a critical impact on supersymmetric phenomenology. For example, any initial state in a scattering experiment will involve ordinary (R -even) particles. Consequently, it follows that supersymmetric particles must be produced in pairs. In general, these particles are highly unstable and decay into lighter states. Moreover, R -parity invariance also implies that the lightest supersymmetric particle (LSP) is absolutely stable, and must eventually be produced at the end of a decay chain initiated by the decay of a heavy unstable supersymmetric particle. In order to be consistent with cosmological constraints, a stable LSP is almost certainly electrically and color neutral [19]. Consequently, the LSP in an R -parity-conserving (RPC) theory is weakly interacting with ordinary matter, *i.e.*, it behaves like a stable heavy neutrino and will escape collider detectors without being directly observed. Thus, the canonical signature for conventional R -parity-conserving supersymmetric theories is missing (transverse) momentum, due to the escape of the LSP. Moreover, as noted in Sec. 88.1 and reviewed in Refs. [20] and [21], the stability of the LSP in R -parity-conserving SUSY makes it a promising candidate for dark matter.

The possibility of relaxing the R -parity invariance of the MSSM (which would generate new B and/or L -violating interactions) will be addressed in Sec. 88.8.2. However, note that in R -parity violating (RPV) models, the LSP is no longer stable and thus would not be a viable candidate for the dark matter (unless its lifetime was significantly longer than the age of the universe). In such scenarios, one has to look elsewhere to explain the origin of dark matter.

88.2.2 The goldstino and gravitino

In the MSSM, SUSY breaking is accomplished by including the most general renormalizable soft-SUSY-breaking terms consistent with the $SU(3)\times SU(2)\times U(1)$ gauge symmetry and R -parity invariance. These terms parameterize our ignorance of the fundamental mechanism of supersymmetry breaking. If supersymmetry breaking occurs spontaneously, then a massless Goldstone fermion called the goldstino ($\tilde{G}_{1/2}$) must exist. The goldstino would then be the LSP, and could play an important role in supersymmetric phenomenology [36].

However, the goldstino degrees of freedom are physical only in models of spontaneously-broken global SUSY. If SUSY is a local symmetry, then the theory must incorporate gravity; the resulting theory is called supergravity [5, 37]. In models of spontaneously-

broken supergravity, the goldstino is “absorbed” by the gravitino (\tilde{G}), the spin-3/2 superpartner of the graviton, via the super-Higgs mechanism [38]. Consequently, the goldstino is removed from the physical spectrum and the gravitino acquires a mass (denoted by $m_{3/2}$). If $m_{3/2}$ is smaller than the mass of the lightest superpartner of the SM particles, then the gravitino is the LSP.

In processes with center-of-mass energy $E \gg m_{3/2}$, one can employ the goldstino-gravitino equivalence theorem [39], which implies that the interactions of the helicity $\pm \frac{1}{2}$ gravitino (whose properties approximate those of the goldstino) dominate those of the helicity $\pm \frac{3}{2}$ gravitino. The interactions of gravitinos with other light fields can be described by a low-energy effective Lagrangian that is determined by fundamental principles [40].

88.2.3 Hidden sectors and the structure of SUSY breaking

It is very difficult (perhaps impossible) to construct a realistic model of spontaneously-broken weak-scale supersymmetry where the supersymmetry breaking arises solely as a consequence of the interactions of the particles of the MSSM. A more successful scheme posits a theory with at least two distinct sectors: a visible sector consisting of the particles of the MSSM [32] and a sector where SUSY breaking is generated. It is often (but not always) assumed that particles of the hidden sector are neutral with respect to the SM gauge group. The effects of the hidden sector supersymmetry breaking are then transmitted to the MSSM by some mechanism (often involving the mediation by particles that comprise an additional messenger sector). Two theoretical scenarios that exhibit this structure are gravity-mediated and gauge-mediated SUSY breaking.

Supergravity models provide a natural mechanism for transmitting the SUSY breaking of the hidden sector to the particle spectrum of the MSSM. In models of gravity-mediated supersymmetry breaking, gravity is the messenger of supersymmetry breaking [41–45]. More precisely, supersymmetry breaking is mediated by effects of gravitational strength (*i.e.* suppressed by inverse powers of the Planck mass). The soft-SUSY-breaking parameters with dimensions of mass arise as model-dependent multiples of the gravitino mass $m_{3/2}$. In this scenario, $m_{3/2}$ is of order the electroweak-symmetry-breaking scale, while the gravitino couplings are roughly gravitational in strength [3, 46].¹

Under certain theoretical assumptions that govern the structure of the Kähler potential (the so-called sequestered form introduced in Ref. [48]), SUSY breaking is due entirely to the super-conformal (super-Weyl) anomaly, which is common to all supergravity models [48]. In particular, gaugino masses are radiatively generated at one-loop, and squark and slepton squared-mass matrices are flavor-diagonal. In sequestered scenarios, sfermion squared-masses arise at two-loops, which implies that gluino and sfermion masses are of the same order of magnitude. This approach is called anomaly-mediated SUSY breaking (AMSB). Indeed, anomaly mediation is more generic than originally conceived, and provides a ubiquitous source of SUSY breaking [49]. However in the simplest formulation of AMSB as applied to the MSSM, the squared-masses of the sleptons are negative (known as the tachyonic slepton problem). It may be possible to cure this otherwise fatal flaw in non-minimal extensions of the MSSM [50]. Alternatively, one can assert that anomaly mediation is not the sole source of SUSY breaking in the sfermion sector. In non-sequestered scenarios, sfermion squared-masses can arise at tree-level, in which case squark masses would be parametrically larger than the loop-suppressed gaugino masses [51].

In gauge-mediated supersymmetry breaking (GMSB), gauge forces transmit the supersymmetry breaking to the MSSM. A typical structure of such models involves a hidden sector where SUSY is broken, a messenger sector consisting of particles (messengers) with nontrivial $SU(3) \times SU(2) \times U(1)$ quantum numbers, and the visible sector consisting of the fields of the MSSM [52–55]. The direct coupling of the messengers to the hidden sector generates a supersymmetry-breaking spectrum in the messenger sector. Supersymmetry breaking is then transmitted to the MSSM via the

virtual exchange of the messenger fields. In models of direct gauge mediation, there is no separate hidden sector. In particular, the sector in which the SUSY breaking originates includes fields that carry nontrivial SM quantum numbers, which allows for the direct transmission of SUSY breaking to the MSSM [56].

In models of gauge-mediated SUSY breaking with a minimal Kähler potential, the gravitino is the LSP [17], as its mass can range from a few eV (in the case of low SUSY breaking scales) up to a few GeV (in the case of high SUSY breaking scales). In particular, the gravitino is a potential dark matter candidate (for a review and guide to the literature, see Ref. [21]). The couplings of the helicity $\pm \frac{1}{2}$ components of \tilde{G} to the particles of the MSSM (which approximate those of the goldstino as previously noted in Sec. 88.2.2) are significantly stronger than gravitational strength and amenable to experimental collider analyses.

The mass ranges of the gravitino in either gravity-mediated or gauge-mediated SUSY breaking are further constrained by cosmological considerations [57, 58]. In particular, there is a danger of over-abundance of gravitinos if it is the dark matter or, if it decays before nucleosynthesis, modifications to the successful predictions of light element abundances. Avoiding these cosmological gravitino problems impose strong constraints on gravity-mediated and gauge-mediated SUSY breaking models.

The concept of a hidden sector is more general than SUSY. Hidden valley models [59] posit the existence of a hidden sector of new particles and interactions that are very weakly coupled to particles of the SM. The impact of a hidden valley on supersymmetric phenomenology at colliders can be significant if the LSP lies in the hidden sector [60].

88.2.4 SUSY and extra dimensions

Approaches to SUSY breaking have also been developed in the context of theories in which the number of spatial dimensions is greater than three. In particular, a number of SUSY-breaking mechanisms have been proposed that are inherently extra-dimensional [61]. The size of the extra dimensions can be significantly larger than M_{P}^{-1} ; in some cases of order $(\text{TeV})^{-1}$ or even larger (see, *e.g.*, Sec. 85 or Ref. [62]).

For example, in one approach the fields of the MSSM live on some brane (a lower-dimensional manifold embedded in a higher-dimensional spacetime), while the sector of the theory that breaks SUSY lives on a second spatially-separated brane. Two examples of this approach are AMSB [48] and gaugino-mediated SUSY breaking [63]. In both cases, SUSY breaking is transmitted through fields that live in the bulk (the higher-dimensional space between the two branes). This setup has some features in common with both gravity-mediated and gauge-mediated SUSY breaking (*e.g.*, hidden and visible sectors and messengers).

Since a higher dimensional theory must be compactified to four spacetime dimensions, one can also generate a source of SUSY breaking by employing boundary conditions on the compactified space that distinguish between fermions and bosons. This is the so-called Scherk-Schwarz mechanism [64]. The phenomenology of such models can be strikingly different from that of the usual MSSM [65].

88.2.5 Split-SUSY

If SUSY is not connected with the origin of the electroweak scale, it may still be possible that some remnant of the superparticle spectrum survives down to the TeV-scale or below. This is the idea of split-SUSY [66, 67], in which scalar superpartners of the quarks and leptons are significantly heavier than 1 TeV, whereas the fermionic superpartners of the gauge and Higgs bosons have masses on the order of 1 TeV or below. With the exception of a single light neutral scalar whose properties are practically indistinguishable from those of the SM Higgs boson, all other Higgs bosons are also assumed to be very heavy. Among the supersymmetric particles, only the fermionic superpartners may be kinematically accessible at the LHC.

In models of split SUSY, the top squark masses cannot be arbitrarily large, as these parameters enter in the radiative corrections to the mass of the observed Higgs boson [68, 69]. In the MSSM, a Higgs boson mass of 125 GeV (see Sec. 11) implies an upper bound on the top squark mass scale in the range of 10 to 10^8 TeV [70–72],

¹However, such a gravitino typically plays no direct role in supersymmetric phenomenology at colliders (except perhaps indirectly in the case where the gravitino is the LSP [47]).

depending on the value of the ratio of the two neutral Higgs field vacuum expectation values, although this mass range can be somewhat extended by varying other relevant MSSM parameters. In some approaches, gaugino masses are one-loop suppressed relative to the sfermion masses, corresponding to the so-called mini-split SUSY spectrum [69, 73]. The higgsino mass scale may or may not be likewise suppressed depending on the details of the model [74].

The SUSY breaking required to produce such a split-SUSY spectrum would destabilize the gauge hierarchy, and thus would not provide an explanation for the scale of electroweak symmetry breaking. Nevertheless, models of split-SUSY can account for the dark matter (which is assumed to be the LSP gaugino or higgsino) and gauge coupling unification, thereby preserving two of the desirable features of weak-scale SUSY. Finally, as a consequence of the very large squark and slepton masses, neutral flavor changing and CP-violating effects, which can be problematic in models with TeV-scale SUSY-breaking masses, are sufficiently reduced to avoid conflict with experimental observations.

88.3 Parameters of the MSSM

The parameters of the MSSM are conveniently described by considering separately the supersymmetry-conserving and the supersymmetry-breaking sectors. A careful discussion of the conventions used here in defining the tree-level MSSM parameters can be found in Refs. [75, 76]. For simplicity, consider first the case of one generation of quarks, leptons, and their scalar superpartners.

88.3.1 The SUSY-conserving parameters

The parameters of the supersymmetry-conserving sector consist of: (i) gauge couplings, g_s , g , and g' , corresponding to the SM gauge group $SU(3) \times SU(2) \times U(1)$ respectively; (ii) a supersymmetry-conserving higgsino mass parameter μ ; and (iii) Higgs-fermion Yukawa couplings, λ_u , λ_d , and λ_e , of one generation of left- and right-handed quarks and leptons, and their superpartners to the Higgs bosons and higgsinos. Because there is no right-handed neutrino/sneutrino in the MSSM as defined here, a Yukawa coupling λ_ν is not included. The complex μ parameter and Yukawa couplings enter via the most general renormalizable R-parity-conserving superpotential,

$$W_{\text{MSSM}} = \lambda_d \hat{H}_d \hat{Q} \hat{D}^c - \lambda_u \hat{H}_u \hat{Q} \hat{U}^c + \lambda_e \hat{H}_d \hat{L} \hat{E}^c + \mu \hat{H}_u \hat{H}_d, \quad (88.1)$$

where the superfields are defined in Table 1 and the gauge group indices are suppressed.

88.3.2 The SUSY-breaking parameters

The supersymmetry-breaking sector contains the following sets of parameters: (i) three complex gaugino Majorana mass parameters, M_3 , M_2 , and M_1 , associated with the $SU(3)$, $SU(2)$, and $U(1)$ subgroups of the SM; (ii) five sfermion squared-mass parameters, M_Q^2 , M_U^2 , M_D^2 , M_L^2 , and M_E^2 , corresponding to the five electroweak gauge multiplets, *i.e.*, superpartners of the left-handed fields $(u, d)_L$, u_L^c , d_L^c , $(\nu, e^-)_L$, and e_L^c , where the superscript c indicates a charge-conjugated fermion field [24]; and (iii) three Higgs-squark-squark and Higgs-slepton-slepton trilinear interaction terms, with complex coefficients $T_U \equiv \lambda_u A_U$, $T_D \equiv \lambda_d A_D$, and $T_E \equiv \lambda_e A_E$ (which define the “ A -parameters”), following the notation employed in Ref. [76]. It is conventional to separate out the factors of the Yukawa couplings in defining the A -parameters (originally motivated by a simple class of gravity-mediated SUSY-breaking models [3, 6]). If the A -parameters are parametrically of the same order (or smaller) relative to other SUSY-breaking mass parameters, then in most cases only the third generation A -parameters are phenomenologically relevant.

Finally, we have (iv) two real squared-mass parameters, $m_{H_d}^2$ and $m_{H_u}^2$ (also called m_1^2 and m_2^2 , respectively, in the literature), and one complex squared-mass parameter, $m_{12}^2 \equiv \mu B$ (the latter defines the “ B -parameter”), which appear in the MSSM tree-level scalar Higgs potential [28],

$$\begin{aligned} V = & (m_{H_d}^2 + |\mu|^2) H_d^\dagger H_d + (m_{H_u}^2 + |\mu|^2) H_u^\dagger H_u \\ & + (m_{12}^2 H_u H_d + \text{h.c.}) \\ & + \frac{1}{8} (g^2 + g'^2) (H_d^\dagger H_d - H_u^\dagger H_u)^2 + \frac{1}{2} g^2 |H_d^\dagger H_u|^2, \end{aligned} \quad (88.2)$$

where the $SU(2)$ -invariant combination, $H_u H_d \equiv H_u^+ H_d^- - H_u^0 H_d^0$. Note that the quartic Higgs couplings are related to the gauge couplings g and g' as a consequence of SUSY. The breaking of the $SU(2) \times U(1)$ electroweak symmetry group to $U(1)_{\text{EM}}$ is only possible after incorporating the SUSY-breaking Higgs squared-mass parameters $m_{H_d}^2$, $m_{H_u}^2$ (which can be negative) and m_{12}^2 . After minimizing the Higgs scalar potential, these three squared-mass parameters can be re-expressed in terms of the two Higgs vacuum expectation values, $\langle H_d^0 \rangle \equiv v_d/\sqrt{2}$ and $\langle H_u^0 \rangle \equiv v_u/\sqrt{2}$, and the CP-odd Higgs mass m_A [cf. Eqs. (88.4) and (88.5) below]. One is always free to rephase the Higgs doublet fields such that v_d and v_u (also called v_1 and v_2 , respectively, in the literature) are both real and positive.

The quantity, $v_d^2 + v_u^2 = 4m_W^2/g^2 = (2G_F^2)^{-1/2} \simeq (246 \text{ GeV})^2$, is fixed by the Fermi constant, G_F , whereas the ratio

$$\tan \beta = v_u/v_d \quad (88.3)$$

is a free parameter such that $0 < \beta < \pi/2$. By employing the tree-level conditions resulting from the minimization of the scalar potential, one can eliminate the diagonal and off-diagonal Higgs squared-masses in favor of $m_Z^2 = \frac{1}{4}(g^2 + g'^2)(v_d^2 + v_u^2)$, the CP-odd Higgs mass m_A and the parameter $\tan \beta$,

$$\sin 2\beta = \frac{2m_{12}^2}{m_{H_d}^2 + m_{H_u}^2 + 2|\mu|^2} = \frac{2m_{12}^2}{m_A^2}, \quad (88.4)$$

$$\frac{1}{2} m_Z^2 = -|\mu|^2 + \frac{m_{H_d}^2 - m_{H_u}^2 \tan^2 \beta}{\tan^2 \beta - 1}. \quad (88.5)$$

One must also guard against the existence of charge and/or color breaking global minima due to non-zero vacuum expectation values for the squark and charged slepton fields. This possibility can be avoided if the A -parameters are not unduly large [42, 77, 78]. Additional constraints must also be respected to avoid the possibility of directions in scalar field space in which the full tree-level scalar potential can become unbounded from below [78]. A computer program has been developed to calculate vacuum stability bounds in general models at the one-loop level [79], and has been applied to the MSSM in Ref. [80].

Note that SUSY-breaking mass terms for the fermionic superpartners of scalar fields and non-holomorphic trilinear scalar interactions (*i.e.*, interactions that mix scalar fields and their complex conjugates) have not been included above in the soft-SUSY-breaking sector. These terms can potentially destabilize the gauge hierarchy [11] in models with a gauge-singlet superfield. The latter is not present in the MSSM; hence as noted in Ref. [12], these so-called non-standard soft-SUSY-breaking terms are benign. The phenomenological impact of non-holomorphic soft SUSY-breaking terms has been reconsidered in Refs. [81–83]. However, in the most common approaches to constructing a fundamental theory of SUSY-breaking, the coefficients of these terms (which have dimensions of mass) are significantly suppressed compared to the TeV-scale [84]. Consequently, we follow the usual approach and omit these terms from further consideration.

88.3.3 MSSM-124

The total number of independent physical parameters that define the MSSM (in its most general form) is quite large, primarily due to the soft-supersymmetry-breaking sector. In particular, in the case of three generations of quarks, leptons, and their superpartners, M_Q^2 , M_U^2 , M_D^2 , M_L^2 , and M_E^2 are hermitian 3×3 matrices, and A_U , A_D , and A_E are complex 3×3 matrices. In addition, M_1 , M_2 , M_3 , B , and μ are in general complex parameters. Finally, as in the SM, the Higgs-fermion Yukawa couplings, λ_f ($f = u, d, \text{ and } e$), are complex 3×3 matrices that are related to the quark and lepton mass matrices via: $M_f = \lambda_f v_f/\sqrt{2}$, where $v_e = v_d$ [with v_u and v_d as defined above Eq. (88.3)].

However, not all these parameters are physical. Some of the MSSM parameters can be eliminated by expressing interaction eigenstates in terms of the mass eigenstates, with an appropriate redefinition of the MSSM fields to remove unphysical degrees of freedom. The analysis of Ref. [85] shows that the MSSM possesses 124 independent real degrees of freedom. Of these, 18

correspond to SM parameters (including the QCD vacuum angle θ_{QCD}), one corresponds to a Higgs sector parameter (the analogue of the SM Higgs mass), and 105 are genuinely new parameters of the model. The latter include: five real parameters and three CP-violating phases in the gaugino/higgsino sector, 21 squark and slepton (sfermion) masses, 36 real mixing angles to define the sfermion mass eigenstates, and 40 CP-violating phases that can appear in sfermion interactions. The most general parameterization of the R-parity-conserving MSSM (without additional theoretical assumptions) will be denoted henceforth as MSSM-124 [86].

88.4 The supersymmetric-particle spectrum

The supersymmetric particles (sparticles) differ in spin by half a unit from their SM partners. The superpartners of the gauge and Higgs bosons are fermions, whose names are obtained by appending “ino” to the end of the corresponding SM particle name. The gluino is the color-octet Majorana fermion partner of the gluon with mass $M_{\tilde{g}} = |M_3|$. The superpartners of the electroweak gauge and Higgs bosons (the gauginos and higgsinos) can mix due to $SU(2) \times U(1)$ breaking effects. As a result, the physical states of definite mass are parameter dependent linear combinations of the charged or neutral gauginos and higgsinos, called charginos and neutralinos, respectively (sometimes collectively called electroweakinos). The neutralinos are Majorana fermions, which can lead to some distinctive phenomenological signatures [87,88]. The superpartners of the quarks and leptons are spin-zero bosons: the squarks, charged sleptons, and sneutrinos, respectively. A complete set of Feynman rules for the sparticles of the MSSM can be found in Ref. [89]. The MSSM Feynman rules also are implicitly contained in a number of amplitude generation and Feynman diagram software packages (see *e.g.*, Refs. [90–92]).

It should be noted that all mass formulae quoted below in this Section are tree-level results. Radiative loop corrections will modify these results and must be included in any precision study of supersymmetric phenomenology [93]. Beyond tree level, the definition of the supersymmetric parameters becomes convention-dependent. For example, one can define physical couplings or running couplings, which differ beyond the tree level. This provides a challenge to any effort that attempts to extract supersymmetric parameters from data. The SUSY Les Houches Accord (SLHA) [76,94] has been adopted, which establishes a set of conventions for specifying generic file structures for supersymmetric model specifications and input parameters, supersymmetric mass and coupling spectra, and decay tables. These provide a universal interface between spectrum calculation programs, decay packages, and high energy physics event generators.

88.4.1 The charginos and neutralinos

The mixing of the charged gauginos (\tilde{W}^\pm) and charged higgsinos (\tilde{H}_d^\pm and \tilde{H}_u^\pm) is described (at tree-level) by a 2×2 complex mass matrix [95,96],

$$M_C \equiv \begin{pmatrix} M_2 & \frac{1}{\sqrt{2}} g v_u \\ \frac{1}{\sqrt{2}} g v_d & \mu \end{pmatrix}. \quad (88.6)$$

To determine the physical chargino states and their masses, one must perform a singular value decomposition [97,98] of the complex matrix M_C :

$$U^* M_C V^{-1} = \text{diag}(M_{\tilde{\chi}_1^\pm}, M_{\tilde{\chi}_2^\pm}), \quad (88.7)$$

where U and V are unitary matrices, and the right-hand side of Eq. (88.7) is the diagonal matrix of (real non-negative) chargino masses. Explicit formulae for the singular value decomposition of M_C can be found in Ref. [99]. The physical chargino states are denoted by $\tilde{\chi}_1^\pm$ and $\tilde{\chi}_2^\pm$. These are linear combinations of the charged gaugino and higgsino states determined by the matrix elements of U and V [95,96]. The chargino masses correspond to the singular values [97] of M_C , *i.e.*, the positive square roots of

the eigenvalues of $M_C^\dagger M_C$:

$$M_{\tilde{\chi}_1^\pm, \tilde{\chi}_2^\pm}^2 = \frac{1}{2} \left\{ |\mu|^2 + |M_2|^2 + 2m_W^2 \mp \sqrt{(|\mu|^2 + |M_2|^2 + 2m_W^2)^2 - 4|\mu M_2 - m_W^2 \sin 2\beta|^2} \right\}, \quad (88.8)$$

in a convention where v_u and v_d are real and positive, and where the states are ordered such that $M_{\tilde{\chi}_1^\pm} \leq M_{\tilde{\chi}_2^\pm}$. The relative phase of μ^* and M_2 is physical and potentially observable [100].

The mixing of the neutral gauginos (\tilde{B} and \tilde{W}^0) and neutral higgsinos (\tilde{H}_d^0 and \tilde{H}_u^0) is described (at tree-level) by a 4×4 complex symmetric mass matrix [95,96],

$$M_N \equiv \begin{pmatrix} M_1 & 0 & -\frac{1}{2} g' v_d & \frac{1}{2} g' v_u \\ 0 & M_2 & \frac{1}{2} g v_d & -\frac{1}{2} g v_u \\ -\frac{1}{2} g' v_d & \frac{1}{2} g v_d & 0 & -\mu \\ \frac{1}{2} g' v_u & -\frac{1}{2} g v_u & -\mu & 0 \end{pmatrix}. \quad (88.9)$$

To determine the physical neutralino states and their masses, one must perform an Autonne-Takagi factorization [97,101] (also called Takagi diagonalization [98,102]) of the complex symmetric matrix M_N :

$$W^T M_N W = \text{diag}(M_{\tilde{\chi}_1^0}, M_{\tilde{\chi}_2^0}, M_{\tilde{\chi}_3^0}, M_{\tilde{\chi}_4^0}), \quad (88.10)$$

where W is a unitary matrix (which is called N^{-1} in Ref. [95]) and the right-hand side of Eq. (88.10) is the diagonal matrix of (real non-negative) neutralino masses. The physical neutralino states are denoted by $\tilde{\chi}_i^0$ (for $i = 1, \dots, 4$), where the states are ordered such that $M_{\tilde{\chi}_1^0} \leq M_{\tilde{\chi}_2^0} \leq M_{\tilde{\chi}_3^0} \leq M_{\tilde{\chi}_4^0}$. The $\tilde{\chi}_i^0$ are the linear combinations of the neutral gaugino and higgsino states determined by the matrix elements of W . The neutralino masses correspond to the singular values of M_N , *i.e.*, the positive square roots of the eigenvalues of $M_N^\dagger M_N$. Exact formulae for these masses can be found in Refs. [103] and [104]. A numerical algorithm for determining the mixing matrix W has been given in Ref. [105].

If a chargino or neutralino state approximates a particular gaugino or higgsino state, it is convenient to employ the corresponding nomenclature. Specifically, if $|M_1|$ and $|M_2|$ are small compared to m_Z and $|\mu|$, then the lightest neutralino $\tilde{\chi}_1^0$ would be nearly a pure photino, $\tilde{\gamma}$, the superpartner of the photon. If $|M_1|$ and m_Z are small compared to $|M_2|$ and $|\mu|$, then the lightest neutralino would be nearly a pure bino, \tilde{B} , the superpartner of the weak hypercharge gauge boson. If $|M_2|$ and m_Z are small compared to $|M_1|$ and $|\mu|$, then the lightest chargino pair and neutralino would constitute a triplet of roughly mass-degenerate pure winos, \tilde{W}^\pm , and \tilde{W}_3^0 , the superpartners of the weak $SU(2)$ gauge bosons. Finally, if $|\mu|$ and m_Z are small compared to $|M_1|$ and $|M_2|$, then the lightest chargino pair and neutralino would be nearly pure higgsino states, the superpartners of the Higgs bosons. Each of the above cases leads to a strikingly different phenomenology.

In the NMSSM, an additional Higgs singlet superfield is added to the MSSM. This superfield comprises two real Higgs scalar degrees of freedom and an associated neutral higgsino degree of freedom. Consequently, there are five neutralino mass eigenstates that are obtained by a Takagi-diagonalization of the 5×5 neutralino mass matrix. In many cases, the fifth neutralino state is dominated by its $SU(2) \times U(1)$ singlet component, and thus is very weakly coupled to the SM particles and their superpartners.

88.4.2 The squarks and sleptons

For a given Dirac fermion f , there are two superpartners, \tilde{f}_L and \tilde{f}_R , where the L and R subscripts simply identify the scalar partners that are related by SUSY to the left-handed and right-handed fermions, $f_{L,R} \equiv \frac{1}{2}(1 \mp \gamma_5)f$, respectively. (There is no $\tilde{\nu}_R$ in the MSSM.) However, $\tilde{f}_L - \tilde{f}_R$ mixing is possible, in which case \tilde{f}_L and \tilde{f}_R are not mass eigenstates. For three generations of squarks, one must diagonalize 6×6 matrices corresponding to the basis $(\tilde{q}_{iL}, \tilde{q}_{iR})$, where $i = 1, 2, 3$ are the generation labels.

For simplicity, only the one-generation case is illustrated in detail below. (The effects of second and third generation squark mixing can be significant and are treated in Ref. [106].)

Using the notation of the third family, the one-generation tree-level squark squared-mass matrix is given by [107],

$$\mathcal{M}^2 = \begin{pmatrix} M_Q^2 + m_q^2 + L_q & m_q X_q^* \\ m_q X_q & M_R^2 + m_q^2 + R_q \end{pmatrix}, \quad (88.11)$$

where

$$X_q \equiv A_q - \mu^* (\cot \beta)^{2T_{3q}}, \quad (88.12)$$

and $T_{3q} = \frac{1}{2} [-\frac{1}{3}]$ for $q = t$ [b]. The diagonal squared-masses are governed by soft-SUSY-breaking squared-masses M_Q^2 and $M_R^2 \equiv M_U^2 [M_D^2]$ for $q = t$ [b], the corresponding quark masses m_t [m_b] and the electroweak correction terms:

$$\begin{aligned} L_q &\equiv (T_{3q} - e_q \sin^2 \theta_W) m_Z^2 \cos 2\beta, \\ R_q &\equiv e_q \sin^2 \theta_W m_Z^2 \cos 2\beta, \end{aligned} \quad (88.13)$$

where $e_q = \frac{2}{3} [-\frac{1}{3}]$ for $q = t$ [b]. The off-diagonal squark squared-masses are proportional to the corresponding quark masses and depend on $\tan \beta$, the soft-SUSY-breaking A -parameters and the higgsino mass parameter μ . Assuming that the A -parameters are parametrically of the same order (or smaller) relative to other SUSY-breaking mass parameters, it then follows that the first and second generation \tilde{q}_L - \tilde{q}_R mixing is smaller than that of the third generation where mixing can be enhanced by factors of m_t and $m_b \tan \beta$.

In the case of third generation \tilde{q}_L - \tilde{q}_R mixing, the mass eigenstates (usually denoted by \tilde{q}_1 and \tilde{q}_2 , with $m_{\tilde{q}_1} < m_{\tilde{q}_2}$) are determined by diagonalizing the 2×2 matrix \mathcal{M}^2 given by Eq. (88.11). The corresponding squared-masses and mixing angle are given by [107]:

$$\begin{aligned} m_{\tilde{q}_{1,2}}^2 &= \frac{1}{2} \left[\text{Tr} \mathcal{M}^2 \mp \sqrt{(\text{Tr} \mathcal{M}^2)^2 - 4 \det \mathcal{M}^2} \right], \\ \sin 2\tilde{\theta}_q &= \frac{2m_q |X_q|}{m_{\tilde{q}_2}^2 - m_{\tilde{q}_1}^2}. \end{aligned} \quad (88.14)$$

The one-generation results above also apply to the charged sleptons, with the obvious substitutions: $q \rightarrow \ell$ with $T_{3\ell} = -\frac{1}{2}$ and $e_\ell = -1$, and the replacement of the SUSY-breaking parameters: $M_Q^2 \rightarrow M_L^2$, $M_R^2 \rightarrow M_E^2$, and $A_q \rightarrow A_\tau$. For the neutral sleptons, $\tilde{\nu}_R$ does not exist in the MSSM, so $\tilde{\nu}_L$ is a mass eigenstate.

In the case of three generations, the SUSY-breaking scalar-squared masses $[M_Q^2, M_U^2, M_D^2, M_L^2, \text{ and } M_E^2]$ and the A -parameters $[A_U, A_D, \text{ and } A_E]$ are now 3×3 matrices as noted in Sec. 88.3.3. The diagonalization of the 6×6 squark mass matrices yields \tilde{f}_{iL} - \tilde{f}_{jR} mixing. In practice, since the \tilde{f}_L - \tilde{f}_R mixing is appreciable only for the third generation, this additional complication can often be neglected (although see Ref. [106] for examples in which the mixing between the second and third generation squarks is relevant).

88.5 The supersymmetric Higgs sector

Consider first the MSSM Higgs sector [27, 28, 108]. Despite the large number of potential CP-violating phases among the MSSM-124 parameters, the tree-level MSSM Higgs potential given by Eq. (88.2) is automatically CP-conserving. This follows from the fact that the only potentially complex parameter (m_{12}^2) of the MSSM Higgs potential can be chosen real and positive by rephasing the Higgs fields, in which case $\tan \beta$ is a real positive parameter. Consequently, the physical neutral Higgs scalars are CP-eigenstates (at tree-level). The MSSM Higgs sector contains five physical spin-zero particles: a charged Higgs boson pair (H^\pm), two CP-even neutral Higgs bosons (denoted by h^0 and H^0 where $m_h < m_H$), and one CP-odd neutral Higgs boson (A^0). The discovery of a SM-like Higgs boson at the LHC with a mass of 125 GeV (see Sec. 11) strongly suggests that this state should be identified with h^0 , although the possibility that the 125 GeV

state should be identified with H^0 cannot yet be completely ruled out [109].

In the NMSSM [33], the scalar component of the singlet Higgs superfield adds two additional neutral states to the Higgs sector. In this model, the tree-level Higgs sector can exhibit explicit CP-violation. If CP is conserved, then the two extra neutral scalar states are CP-even and CP-odd, respectively. These states can potentially mix with the neutral Higgs states of the MSSM. If scalar states exist that are dominantly singlet, then they are weakly coupled to SM gauge bosons and fermions through their small mixing with the MSSM Higgs scalars. Consequently, it is possible that one (or both) of the singlet-dominated states is considerably lighter than the Higgs boson that was observed at the LHC.

88.5.1 The tree-level Higgs sector

The tree-level properties of the Higgs sector are determined by the Higgs potential given by Eq. (88.2). The quartic interaction terms are manifestly supersymmetric (although these are modified by SUSY-breaking effects at the loop level). In general, the quartic couplings arise from two sources: (i) the supersymmetric generalization of the scalar potential (the so-called “ F -terms”), and (ii) interaction terms related by SUSY to the coupling of the scalar fields and the gauge fields, whose coefficients are proportional to the corresponding gauge couplings (the so-called “ D -terms”).

In the MSSM, F -term contributions to the quartic Higgs self-couplings are absent. As a result, the strengths of the MSSM quartic Higgs interactions are fixed in terms of the gauge couplings, as noted below Eq. (88.2). Consequently, all the tree-level MSSM Higgs-sector parameters depend only on two quantities: $\tan \beta$ [defined in Eq. (88.3)] and one Higgs mass usually taken to be m_A . From these two quantities, one can predict the values of the remaining Higgs boson masses, an angle α that measures the mixture of the hypercharge ± 1 scalar fields, H_u^0 and H_d^0 , in the physical CP-even neutral scalars, and the Higgs boson self-couplings. Moreover, the tree-level mass of the lighter CP-even Higgs boson is bounded, $m_h \leq m_Z |\cos 2\beta| \leq m_Z$ [27, 28]. This bound can be substantially modified when radiative corrections are included, as discussed in Sec. 88.5.2.

In the NMSSM, we set $\mu = 0$ in Eq. 88.1 and then add two additional terms to the superpotential,

$$W_{\text{NMSSM}} \ni \lambda \hat{H}_u \hat{H}_d \hat{S} + \frac{1}{3} \kappa \hat{S}^3, \quad (88.15)$$

where \hat{S} is a singlet Higgs superfield. An effective μ term is generated, $\mu_{\text{eff}} = \lambda \langle S \rangle$, where $\langle S \rangle$ is the vacuum expectation value of the scalar field component of \hat{S} . Moreover, due to the term proportional to λ in Eq. 88.15, there is now an F -term contribution to the quartic Higgs self-couplings. Consequently, the tree-level bound for the mass of the lightest CP-even MSSM Higgs boson is modified [110],

$$m_h^2 \leq m_Z^2 \cos^2 2\beta + \frac{1}{2} \lambda^2 v^2 \sin^2 2\beta, \quad (88.16)$$

where $v \equiv (v_u^2 + v_d^2)^{1/2} = 246$ GeV. By requiring that λ remain finite after renormalization-group evolution up to the Planck scale, one finds that λ is constrained to lie below about 0.7–0.8 at the electroweak scale [33] (although larger values of λ have also been considered in Ref. [111]).

The tree-level Higgs-quark and Higgs-lepton interactions of the MSSM are governed by the Yukawa couplings defined by the superpotential given in Eq. (88.1). In particular, the Higgs sector of the MSSM is a Type-II two-Higgs doublet model [112], in which one Higgs doublet (H_d) couples exclusively to the right-handed down-type quark (or lepton) fields and the second Higgs doublet (H_u) couples exclusively to the right-handed up-type quark fields. Consequently, the diagonalization of the fermion mass matrices simultaneously diagonalizes the matrix of Yukawa couplings, resulting in flavor-diagonal tree-level couplings of the neutral Higgs bosons h^0 , H^0 and A^0 to quark and lepton pairs.

88.5.2 The radiatively-corrected Higgs sector

When radiative corrections are incorporated, additional parameters of the supersymmetric model enter via virtual supersymmetric particles that appear in loops. The impact of these corrections

can be significant [113]. The qualitative behavior of these radiative corrections can be most easily seen in the large top-squark mass limit, where in addition, both the splitting of the two diagonal entries and the off-diagonal entries of the top-squark squared-mass matrix [Eq. (88.11)] are small in comparison to the geometric mean of the two top-squark squared-masses, $M_S^2 \equiv M_{t_1} M_{t_2}$. In this case (assuming $m_A > m_Z$), the predicted upper bound for m_h is approximately given by [114]

$$m_h^2 \lesssim m_Z^2 \cos^2 2\beta + \frac{3g^2 m_t^4}{8\pi^2 m_W^2} \left[\ln \left(\frac{M_S^2}{m_t^2} \right) + \frac{X_t^2}{M_S^2} \left(1 - \frac{X_t^2}{12M_S^2} \right) \right], \quad (88.17)$$

where $X_t \equiv A_t - \mu \cot \beta$ [cf. Eq. (88.12)] is proportional to the off-diagonal entry of the top-squark squared-mass matrix (where for simplicity, A_t and μ are taken to be real). The Higgs mass upper limit specified by Eq. (88.17) is saturated when $\tan \beta$ is large (i.e., $\cos^2 2\beta \sim 1$) and $X_t = \sqrt{6} M_S$, which defines the so-called maximal mixing scenario.

A more complete treatment of the radiative corrections shows that Eq. (88.17) somewhat overestimates the true upper bound of m_h . These more refined computations, which incorporate renormalization group improvement, the two loop and the leading three-loop contributions, yield $m_h \lesssim 135$ GeV in the region of large $\tan \beta$ (with an accuracy of a few GeV) for $m_t = 175$ GeV and $M_S \lesssim 2$ TeV [115, 116].

In addition, one-loop radiative corrections can introduce CP-violating effects in the Higgs sector that depend on some of the CP-violating phases among the MSSM-124 parameters [117]. This phenomenon is most easily understood in a scenario where $m_A \ll M_S$ (i.e., all five physical Higgs states are significantly lighter than the SUSY breaking scale). In this case, one can integrate out the heavy superpartners to obtain a low-energy effective theory with two Higgs doublets. The resulting effective two-Higgs doublet model will now contain all possible Higgs self-interaction terms (both CP-conserving and CP-violating) and Higgs-fermion interactions (beyond those of Type-II) that are consistent with electroweak gauge invariance [118].

In the NMSSM with $m_h \simeq 125$ GeV, the dominant radiative correction to Eq. (88.16) is the same as the one given in Eq. (88.17). However, in contrast to the MSSM, one does not need as large a boost from the radiative corrections to achieve a Higgs mass of 125 GeV in certain regimes of the NMSSM parameter space (e.g., $\tan \beta \sim 2$ and $\lambda \sim 0.7$ [119]).

88.6 Restricting the MSSM parameter freedom

In Sections 88.4 and 88.5, we surveyed the parameters that comprise the MSSM-124. However, the MSSM in its most general form is not a phenomenologically viable theory over much of its parameter space. In particular, a generic point of the MSSM-124 parameter space exhibits: (i) no conservation of the separate lepton numbers L_e , L_μ , and L_τ ; (ii) unsuppressed flavor-changing neutral currents (FCNCs); and (iii) new sources of CP violation that are inconsistent with the experimental bounds.

For example, the MSSM contains many new sources of CP violation [120]. Indeed, for TeV-scale sfermion and gaugino masses, some combinations of the complex phases of the gaugino-mass parameters, the A -parameters, and μ must be less than about 10^{-2} – 10^{-3} to avoid generating electric dipole moments for the neutron, electron, and atoms [121–123] in conflict with observed data [124, 125]. The rarity of FCNCs [126–128] places additional constraints on the off-diagonal matrix elements of the squark and slepton soft-SUSY-breaking squared-masses and A -parameters (see Sec. 88.3.3).

The MSSM-124 is also theoretically incomplete as it provides no explanation for the fundamental origin of the supersymmetry-breaking parameters. The successful unification of the MSSM gauge couplings at a grand unified mass scale M_{GUT} , close to the Planck scale [8, 67, 129–131],

$$g_s(M_{\text{GUT}}) = g(M_{\text{GUT}}) = \sqrt{\frac{5}{3}} g'(M_{\text{GUT}}), \quad (88.18)$$

suggests that the high-energy structure of the theory may be

considerably simpler than its low-energy realization.² In a top-down approach, the dynamics that governs the more fundamental theory at high energies is used to derive the effective broken-supersymmetric theory at the TeV scale. A suitable choice for the high energy dynamics is one that yields a TeV-scale theory that satisfies all relevant phenomenological constraints.

In this Section, we examine a number of theoretical frameworks that potentially yield phenomenologically viable regions of the MSSM-124 parameter space. The resulting supersymmetric particle spectrum is then a function of a relatively small number of input parameters. This is accomplished by imposing a simple structure on the soft SUSY-breaking parameters at a common high-energy scale M_X (typically chosen to be the Planck scale, M_P , the grand unified theory scale, M_{GUT} , or the messenger scale, M_{mess}). These serve as initial conditions for the MSSM renormalization group equations (RGEs), which are given in the two-loop approximation in Ref. [132]. Automated programs to compute RGEs for the MSSM and other supersymmetric models of new physics has been developed in Ref. [133]. Solving these equations numerically, one can then derive the low-energy MSSM parameters relevant for phenomenology. A number of software packages exist that numerically calculate the spectrum of supersymmetric particles, consistent with theoretical conditions on SUSY breaking at high energies and some experimental data at low energies [116, 134].

Examples of viable frameworks are provided by models of gravity-mediated, anomaly mediated and gauge-mediated SUSY breaking, to be discussed in more detail below. In some of these approaches, one of the diagonal Higgs squared-mass parameters is driven negative by renormalization group evolution [135]. In such models, electroweak symmetry breaking is generated radiatively, and the resulting electroweak symmetry-breaking scale is intimately tied to the scale of low-energy SUSY breaking.

88.6.1 Gaugino mass relations

One prediction of many supersymmetric grand unified models is the unification of the (tree-level) gaugino mass parameters³ at some high-energy scale, M_X ,

$$M_1(M_X) = M_2(M_X) = M_3(M_X) = m_{1/2}. \quad (88.19)$$

Due to renormalization group running, in the one-loop approximation the effective low-energy gaugino mass parameters (at the electroweak scale) are related,

$$M_3 = (g_s^2/g^2)M_2 \simeq 3.5M_2, \quad M_1 = (5g'^2/3g^2)M_2 \simeq 0.5M_2. \quad (88.20)$$

Eq. (88.20) can arise more generally in gauge-mediated SUSY-breaking models where the gaugino masses are generated at the messenger scale M_{mess} (which typically lies significantly below the unification scale where the gauge couplings unify). In this case, the gaugino mass parameters are proportional to the corresponding squared gauge couplings at the messenger scale.

When Eq. (88.20) is satisfied, the chargino and neutralino masses and mixing angles depend only on three unknown parameters: the gluino mass, μ , and $\tan \beta$. It then follows that the lightest neutralino must be heavier than 46 GeV due to the non-observation of charginos at LEP [137]. If in addition $|\mu| \gg |M_1| \gtrsim m_Z$, then the lightest neutralino is nearly a pure bino, an assumption often made in supersymmetric particle searches at colliders. Although Eq. (88.20) is often assumed in many phenomenological studies, a truly model-independent approach would take the gaugino mass parameters, M_i , to be independent parameters to be determined by experiment. Indeed, an approximately massless neutralino *cannot* be ruled out at present by a model-independent analysis [138].

²Generically, the normalization of the U(1) hypercharges exhibited in Table 88.1 is a matter of convention. In particular, the U(1) hypercharges can be rescaled by absorbing the scaling factor into a redefinition of the hypercharge gauge coupling g' . However, the embedding of the hypercharge U(1) generator into the Lie algebra of a grand unified simple gauge group fixes the normalization of the U(1) hypercharges and results in the rescaled hypercharge gauge coupling shown in Eq. (88.18).

³Non-universal gaugino mass parameters can also be a viable option in grand unified models with non-minimal gauge kinetic functions [136].

It is possible that the tree-level masses for the gauginos are zero. In this case, the gaugino mass parameters arise at one-loop and do not satisfy Eq. (88.20). For example, the gaugino masses in AMSB models arise entirely from a model-independent contribution derived from the super-conformal anomaly [48, 139]. In this case, Eq. (88.20) is replaced (in the one-loop approximation) by:

$$M_i \simeq \frac{b_i g_i^2}{16\pi^2} m_{3/2}, \quad (88.21)$$

where $m_{3/2}$ is the gravitino mass and the b_i are the coefficients of the MSSM gauge beta-functions corresponding to the corresponding U(1), SU(2), and SU(3) gauge groups, $(b_1, b_2, b_3) = (\frac{33}{5}, 1, -3)$. Eq. (88.21) yields $M_1 \simeq 2.8M_2$ and $M_3 \simeq -8.3M_2$, which implies that the lightest chargino pair and neutralino comprise a nearly mass-degenerate triplet of winos, $\tilde{W}^\pm, \tilde{W}^0$ (cf. Table 1), over most of the MSSM parameter space. For example, if $|\mu| \gg m_Z, |M_2|$, then Eq. (88.21) implies that $M_{\tilde{X}^\pm} \simeq M_{\tilde{X}^0} \simeq M_2$ [140]. Alternatively, one can construct an AMSB model where $|\mu|, m_Z \ll M_2$, which yields an LSP that is an approximate higgsino state [141]. In both cases, the corresponding supersymmetric phenomenology differs significantly from the standard phenomenology based on Eq. (88.20) [142, 143].

Finally, it should be noted that the unification of gaugino masses (and scalar masses) can be accidental. In particular, the energy scale where unification takes place may not be directly related to any physical scale. One version of this phenomenon has been called mirage unification and can occur in certain theories of fundamental SUSY breaking [144].

88.6.2 Constrained versions of the MSSM: mSUGRA, CMSSM, etc.

In the minimal supergravity (mSUGRA) framework [3–6, 41–43], the minimal form of the Kähler potential is employed, which yields standard kinetic energy terms for the MSSM fields [45]. As a result, the soft supersymmetry-breaking parameters at the high-energy scale M_X take a particularly simple form in which the scalar squared-masses and the A -parameters are flavor-diagonal and universal [43]:

$$\begin{aligned} M_Q^2(M_X) &= M_U^2(M_X) = M_D^2(M_X) = m_0^2 \mathbf{1}, \\ M_L^2(M_X) &= M_E^2(M_X) = m_0^2 \mathbf{1}, \\ m_1^2(M_X) &= m_2^2(M_X) = m_0^2, \\ A_U(M_X) &= A_D(M_X) = A_E(M_X) = A_0 \mathbf{1}, \end{aligned} \quad (88.22)$$

where $\mathbf{1}$ is a 3×3 identity matrix in generation space. As in the SM, this approach exhibits minimal flavor violation [145, 146], whose unique source is the nontrivial flavor structure of the Higgs-fermion Yukawa couplings. The gaugino masses are also unified according to Eq. (88.19).

Renormalization group evolution is then used to derive the values of the supersymmetric parameters at the low-energy (electroweak) scale. For example, to compute squark masses, one should use the low-energy values for M_Q^2 , M_U^2 , and M_D^2 in Eq. (88.11). Through the renormalization group running with boundary conditions specified in Eq. (88.20) and Eq. (88.22), one can show that the low-energy values of M_Q^2 , M_U^2 , and M_D^2 depend primarily on m_0^2 and $m_{1/2}^2$. A number of useful approximate analytic expressions for superpartner masses in terms of the mSUGRA parameters can be found in Ref. [147].

One can count the number of independent parameters in the mSUGRA framework. In addition to 18 SM parameters (excluding the Higgs mass), one must specify $m_0, m_{1/2}, A_0$, the Planck-scale values for μ and B -parameters (denoted by μ_0 and B_0), and the gravitino mass $m_{3/2}$. Without additional model assumptions, $m_{3/2}$ is independent of the parameters that govern the mass spectrum of the superpartners of the SM [43]. In principle, A_0, B_0, μ_0 , and $m_{3/2}$ can be complex, although in the mSUGRA approach, these parameters are taken to be real for simplicity.

As previously noted, renormalization group evolution is used to compute the low-energy values of the mSUGRA parameters,

which then fixes all the parameters of the low-energy MSSM. In particular, the two Higgs vacuum expectation values (or equivalently, m_Z and $\tan \beta$) can be expressed as a function of the Planck-scale supergravity parameters. The most common procedure is to remove μ_0 and B_0 in favor of m_Z and $\tan \beta$ [the sign of μ_0 , denoted $\text{sgn}(\mu_0)$ below, is not fixed in this process]. In this case, the MSSM spectrum and its interaction strengths are determined by five parameters:

$$m_0, A_0, m_{1/2}, \tan \beta, \text{ and } \text{sgn}(\mu_0), \quad (88.23)$$

and an independent gravitino mass $m_{3/2}$ (in addition to the 18 parameters of the SM). In Ref. [148], this framework was dubbed the constrained minimal supersymmetric extension of the SM (CMSSM). Additional relations such as $B_0 = A_0 - m_0$ and $m_{3/2} = m_0$ comprise the original mSUGRA proposal [41, 45, 149].

One can also relax the universality of scalar masses by decoupling the squared-masses of the Higgs bosons and the squarks/sleptons. This leads to the non-universal Higgs mass models (NUHMs), thereby adding one or two new parameters to the CMSSM depending on whether the diagonal Higgs scalar squared-mass parameters ($m_{H_d}^2$ and $m_{H_u}^2$) are set equal (NUHM1 [150]) or taken to be independent (NUHM2 [151]) at the high energy scale M_X . Clearly, this modification preserves the minimal flavor violation of the mSUGRA approach. Nevertheless, the mSUGRA approach and its NUHM generalizations are probably too simplistic. Theoretical considerations suggest that the universality of Planck-scale soft SUSY-breaking parameters is not generic [152]. In particular, effective operators at the Planck scale exist that do not respect flavor universality, and it is difficult to find a theoretical principle that would forbid them.

In the framework of supergravity, if anomaly mediation is the sole source of SUSY breaking, then the gaugino mass parameters, diagonal scalar squared-mass parameters, and the SUSY-breaking trilinear scalar interaction terms (proportional to $\lambda_f A_F$) are determined in terms of the beta functions of the gauge and Yukawa couplings and the anomalous dimensions of the squark and slepton fields [48, 139, 143]. As noted in Sec. 88.2.3, this approach yields tachyonic sleptons in the MSSM unless additional sources of SUSY breaking are present. In the minimal AMSB (mAMSB) scenario, a universal squared-mass parameter, m_0^2 , is added to the AMSB expressions for the diagonal scalar squared-masses [143]. Thus, the mAMSB spectrum and its interaction strengths are determined by four parameters, $m_0^2, m_{3/2}, \tan \beta$ and $\text{sgn}(\mu_0)$.

The mAMSB scenario appears to be ruled out based on the observed value of the Higgs boson mass, assuming an upper limit on M_S of a few TeV, since the mAMSB constraint on A_F implies that the maximal mixing scenario cannot be achieved [cf. Eq. (88.17)]. Indeed, under the stated assumptions, the mAMSB Higgs mass upper bound lies below the observed Higgs mass value [153]. Thus within the AMSB scenario, either an additional SUSY-breaking contribution to $\lambda_f A_F$ and/or new ingredients beyond the MSSM are required.

88.6.3 Gauge-mediated SUSY breaking

In contrast to models of gravity-mediated SUSY breaking, the flavor universality of the fundamental soft SUSY-breaking squark and slepton squared-mass parameters is guaranteed in gauge-mediated SUSY breaking (GMSB) because the supersymmetry breaking is communicated to the sector of MSSM fields via gauge interactions [53, 55]. In GMSB models, the mass scale of the messenger sector (or its equivalent) is sufficiently below the Planck scale such that the additional SUSY-breaking effects mediated by supergravity can be neglected.

In the minimal GMSB approach, there is one effective mass scale, Λ , that determines all low-energy scalar and gaugino mass parameters through loop effects, while the resulting A -parameters are suppressed. In addition, the minimal form of the Kähler potential is employed. In order that the resulting superpartner masses be of order 1 TeV, one must have $\Lambda \sim \mathcal{O}(100 \text{ TeV})$. The origin of the μ and B -parameters is model-dependent, and lies somewhat outside the ansatz of gauge-mediated SUSY breaking [154].

The simplest GMSB models appear to be ruled out based on the

observed value of the Higgs boson mass. Due to suppressed A parameters, it is difficult to boost the contributions of the radiative corrections in Eq. (88.17) to obtain a Higgs mass as large as 125 GeV. However, this conflict can be alleviated in more complicated GMSB models [155]. To analyze these generalized GMSB models, it has been especially fruitful to develop model-independent techniques that encompass all known GMSB models [156]. These techniques are well-suited for a comprehensive analysis [157] of the phenomenological profile of gauge-mediated SUSY breaking.

The gravitino is the LSP in minimal GMSB models, as noted in Sec. 88.2.3. As a result, the next-to-lightest supersymmetric particle (NLSP) now plays a crucial role in the phenomenology of supersymmetric particle production and decays. Note that unlike the LSP, the NLSP can be charged. In GMSB models, the most likely candidates for the NLSP are $\tilde{\chi}_1^0$ and $\tilde{\tau}_R^\pm$. The NLSP will decay into its superpartner plus a gravitino (e.g., $\tilde{\chi}_1^0 \rightarrow \gamma\tilde{G}$, $\tilde{\chi}_1^0 \rightarrow Z\tilde{G}$, $\tilde{\chi}_1^0 \rightarrow h^0\tilde{G}$ or $\tilde{\tau}_1^\pm \rightarrow \tau^\pm\tilde{G}$), with lifetimes and branching ratios that depend on the model parameters. There are also GMSB scenarios in which there are several nearly degenerate co-NLSPs, any one of which can be produced at the penultimate step of a supersymmetric decay chain [158]. For example, in the slepton co-NLSP case, all three right-handed sleptons are close enough in mass and thus can each play the role of the NLSP.

Different choices for the identity of the NLSP and its decay rate lead to a variety of distinctive supersymmetric phenomenologies [55, 159]. For example, a long-lived $\tilde{\chi}_1^0$ -NLSP that decays outside collider detectors leads to supersymmetric decay chains with missing energy in association with leptons and/or hadronic jets (this case is indistinguishable from the standard phenomenology of the $\tilde{\chi}_1^0$ -LSP). On the other hand, if $\tilde{\chi}_1^0 \rightarrow \gamma\tilde{G}$ is the dominant decay mode, and the decay occurs inside the detector, then nearly all supersymmetric particle decay chains would produce a photon. In contrast, in the case of a $\tilde{\tau}_1^\pm$ -NLSP, the $\tilde{\tau}_1^\pm$ would either be long-lived or would decay inside the detector into a τ -lepton plus missing energy.

A number of attempts have been made to address the origins of the μ and B -parameters in GMSB models based on the field content of the MSSM (see, e.g., Refs. [154, 160]). An alternative approach is to consider GMSB models based on the NMSSM [161]. The vacuum expectation value of the additional singlet Higgs superfield can be used to generate effective μ and B -parameters [162]. Such models provide an alternative GMSB framework for achieving a Higgs mass of 125 GeV, while still being consistent with LHC bounds on supersymmetric particle masses.

88.6.4 The phenomenological MSSM

Any of the theoretical assumptions described in the previous three subsections must be tested experimentally and could turn out to be wrong. To facilitate the exploration of MSSM phenomena in a more model-independent way while respecting the constraints noted at the beginning of this Section, the phenomenological MSSM (pMSSM) has been introduced [163].

The pMSSM is governed by 19 independent real supersymmetric parameters: the three gaugino mass parameters M_1 , M_2 and M_3 , the Higgs sector parameters m_A and $\tan\beta$, the Higgsino mass parameter μ , five sfermion squared-mass parameters for the degenerate first and second generations ($M_{\tilde{Q}}^2$, $M_{\tilde{U}}^2$, $M_{\tilde{D}}^2$, $M_{\tilde{L}}^2$ and $M_{\tilde{E}}^2$), the five corresponding sfermion squared-mass parameters for the third generation, and three third-generation A -parameters (A_t , A_b and A_τ). The first and second generation A -parameters are typically neglected in pMSSM studies, as their phenomenological consequences are negligible in most applications. One counterexample arises when considering the A_μ dependence of the anomalous magnetic moment of the muon, which can be as significant as other contributions due to superpartner mediated radiative corrections [164]. Since its initial proposal, the pMSSM approach has been extended to include a 20th parameter, A_μ [165]. It also has been further extended to include CP-violating SUSY-breaking parameters in Ref. [166].

The 19-parameter pMSSM is often further constrained to expedite scans over the parameter space. For example, in Ref. [167], the number of pMSSM parameters is reduced to ten by assum-

ing one common squark squared-mass parameter for the first two generations, a second common squark squared-mass parameter for the third generation, a common (charged) slepton squared-mass parameter and a common third generation A parameter. In Ref. [168] an eleven parameter pMSSM is defined by allowing for a different stau squared-mass parameter from that of the first two generation charged sleptons. Other applications of the pMSSM approach (with a reduced pMSSM parameter space) to supersymmetric particle searches, and a discussion of the implications for past and future LHC and dark matter studies can be found in Refs. [167, 169, 170].

88.6.5 Simplified models

As Sec. 89 demonstrates, experiments present their searches for supersymmetric particles primarily in terms of simplified models. Simplified models for supersymmetric searches [171] are defined mostly by the empirical objects and kinematic variables involved in the search. Their interpretation by an experimental collaboration usually involves only a small number of supersymmetric particles (often two or three). Other supersymmetric particles are assumed to play no role (this may happen by virtue of them being too heavy to be produced). Experimental bounds from non-observation of a signal are usually presented in terms of the physical masses of the supersymmetric particles involved. Bounds may be presented on the relevant supersymmetric particle masses assuming certain values for the branching ratio of certain supersymmetric particle decays, or as an upper bound on the signal production cross-section as a function of the relevant supersymmetric particle masses.

For example, consider a search for hadronic jets plus missing transverse momentum. One can match such a search to the simplified model of squark pair production followed by the subsequent decay of each squark into a quark (which appears as a jet) and a neutralino LSP that produces the missing transverse momentum, i.e. $\tilde{q}\tilde{q} \rightarrow (q\tilde{\chi}_1^0)(q\tilde{\chi}_1^0)$. Excluded cross-sections resulting from the non-observation of a signal (which in this case could consist of some specified minimum value of missing transverse momentum and at least two hard jets) may be exhibited in the squark mass versus LSP mass plane.

Simplified models have the advantage that they have fewer free parameters than more complete supersymmetric models, whose greater number of free parameters makes it difficult to present excluded regions in any generality. If limits are quoted on supersymmetric particle masses without reference to the signal production cross-section from a simplified model analysis, then there is a potential pitfall—namely, mass limits can differ from those obtained in full models because there may be contributions to the signal coming from processes involving supersymmetric particles other than those assumed. For example, in the $\tilde{q}\tilde{q} \rightarrow q\tilde{\chi}_1^0 q\tilde{\chi}_1^0$ process mentioned above, the simplified model analysis does not account for the interference with tree-level t -channel contributions involving the gluino. Nevertheless, simplified model bounds quoted purely in terms of supersymmetric particle masses may still approximately hold over sizeable regions of parameter space of more complete models, within which the simplified model is embedded. When simplified model limits are phrased as bounds on signal cross-sections, the aforementioned pitfall is sidestepped. Simplified models thus remain an efficient tool for organizing and presenting the results of supersymmetric particle searches. A comparison between supersymmetric particle search constraints in the context of simplified models and the corresponding constraints obtained in the more complete pMSSM can be found in Ref. [172].

88.7 Experimental data confronts the MSSM

At present, there is no significant evidence for weak-scale SUSY from the data analyzed by the LHC experiments. Recent LHC data have been effectively employed in ruling out the existence of colored supersymmetric particles (primarily the gluino and the first generation of squarks) with masses below about 2 TeV (see Fig. 89.13). However, the precise mass limits are very model dependent. For example, as Fig. 89.12 demonstrates, regions of the pMSSM parameter space can be identified in which lighter squarks and gluinos below 1 TeV cannot be definitely ruled out. Under the assumption of gaugino mass unification [cf. Eq. (88.20)],

LHC searches result in a lower bound on neutralino and chargino masses of roughly 200 GeV. It is difficult to place general bounds on neutralino and chargino masses, since the limit in terms of masses from direct searches tends to be particularly model dependent. Nevertheless, one must confront the tension that exists between the theoretical expectations for the magnitude of the SUSY-breaking parameters and the non-observation of supersymmetric phenomena at colliders.

88.7.1 Naturalness constraints and the little hierarchy

In Sec. 88.1, weak-scale SUSY was motivated as a natural solution to the hierarchy problem, which could provide an understanding of the origin of the electroweak symmetry-breaking scale without a significant fine-tuning of the fundamental parameters that govern the MSSM. In this context, the weak scale soft supersymmetry-breaking masses must be generally of the order of 1 TeV or below [173]. This requirement is most easily seen in the determination of m_Z by the scalar potential minimum condition. In light of Eq. (88.5), to avoid the fine-tuning of MSSM parameters, the soft SUSY-breaking squared-masses $m_{H_d}^2$ and $m_{H_u}^2$ and the higgsino squared-mass $|\mu|^2$ should all be roughly of $\mathcal{O}(m_Z^2)$. Many authors have proposed quantitative measures of fine-tuning [173–178]. One of the simplest measures is the one advocated by Barbieri and Giudice [173] (which was also introduced previously in Ref. [174]),

$$\Delta_i \equiv \left| \frac{\partial \ln m_Z^2}{\partial \ln p_i} \right|, \quad \Delta \equiv \max \Delta_i, \quad (88.24)$$

where the p_i are the MSSM parameters at the high-energy scale M_X , which are set by the fundamental SUSY-breaking dynamics. The theory is more fine-tuned as Δ becomes larger. However, different measures of fine-tuning yield quantitatively different results; in particular, calculating minimal fine-tuning based on the high-scale parameters [as defined in Eq. (88.24)] yields a difference by a factor ~ 10 to fine-tuning based on TeV-scale parameters [179, 180].

One can apply the fine-tuning measure to any explicit model of SUSY breaking. For example, in the approaches discussed in Sec. 88.6, the p_i are parameters of the model at the energy scale M_X where the soft SUSY-breaking operators are generated by the dynamics of SUSY breaking. Renormalization group evolution then determines the values of the parameters appearing in Eq. (88.5) at the electroweak scale. In this way, Δ is sensitive to all the SUSY-breaking parameters of the model (see e.g. Ref. [181]). It should be noted that the computation of Δ is often based on Eq. (88.5), which is a tree-level condition. An analysis in Ref. [83], for example, shows that the fine tuning measure can be reduced by as much as a factor of two when loop corrections are included [182].

One way of taking fine-tuning into account in fits to data using Bayesian statistics is to have a prior probability distribution proportional to $1/\Delta$ [183] so that fine-tuning is balanced against the fit to empirical data. In such a Bayesian approach, it is important to choose the prior probability distribution carefully, since prior probability densities that are flat in one set of variables may not be flat in another, more fundamental set. One can in fact derive a different measure of fine-tuning resulting from a Jacobian factor when transforming to other variables.⁴ By comparing the results of several Bayesian fits with different (but reasonable) prior probability distributions, one can assess the robustness of the fit with respect to their variation, mitigating for subjectivity in the interpretation of the fine-tuning measure.

As anticipated, there is a tension between the present experimental lower limits on the masses of colored supersymmetric particles [185, 186] and the expectation that supersymmetry-breaking is associated with the electroweak symmetry-breaking scale. Moreover, this tension is exacerbated [187] by the observed value of the Higgs mass ($m_h \simeq 125$ GeV), which is not far from the MSSM upper bound ($m_h \lesssim 135$ GeV) [which depends on the top-squark

mass and mixing as noted in Sec. 88.5.2]. If M_{SUSY} characterizes the scale of supersymmetric particle masses, then one would crudely expect $\Delta \sim M_{\text{SUSY}}^2/m_Z^2$. For example, if $M_{\text{SUSY}} \sim 1$ TeV then one expects a $\Delta^{-1} \sim 1\%$ fine-tuning of the MSSM parameters to achieve the observed value of m_Z . This separation of the electroweak symmetry-breaking and SUSY-breaking scales is an example of the little hierarchy problem [188, 189].

The fine-tuning parameter Δ can depend quite sensitively on the structure of the SUSY-breaking dynamics, such as the value of M_X and relations among SUSY-breaking parameters in the fundamental high energy theory [190]. For example, in so-called focus point SUSY models [177, 191], all squark masses can be as heavy as 5 TeV *without* significant fine-tuning. This can be attributed to a focusing behavior of the renormalization group evolution when certain relations hold among the high-energy values of the scalar squared-mass SUSY-breaking parameters. Although the focus point region of the CMSSM still yields an uncomfortably high value of Δ due to the observed Higgs mass of 125 GeV, one can achieve moderate values of Δ in models with NUHM2 boundary conditions for the scalar masses [187].

Among the colored superpartners, the third generation squarks typically have the most significant impact on the naturalness constraints [192], while their masses are the least constrained by the LHC data. Hence, in the absence of any relation between third generation squarks and those of the first two generations, the naturalness constraints due to present LHC data can be considerably weaker than those obtained in the CMSSM. Indeed, models with first and second generation squark masses in the multi-TeV range do not necessarily require significant fine tuning. Such models have the added benefit that undesirable FCNCs mediated by squark exchange are naturally suppressed [193]. Other MSSM mass spectra that are compatible with moderate fine tuning have been considered in Refs. [190] and [194].

The lower bounds on squark and gluino masses may not be as large as suggested by the experimental analyses based on the CMSSM or simplified models. For example, mass bounds for the gluino and the first and second generation squarks based on the CMSSM can often be evaded in alternative or extended MSSM models, e.g., compressed SUSY [195] and stealth SUSY [196]. Moreover, the experimental upper limits for the third generation squark masses (which have a more direct impact on the fine-tuning measure) are weaker than the corresponding mass limits for other colored supersymmetric states.

Among the uncolored superpartners, the higgsinos are typically the most impacted by the naturalness constraints. Eq. (88.5) suggests that the masses of the two neutral higgsinos and charged higgsino pair (which are governed by $|\mu|$) should not be significantly larger than m_Z to avoid an unnatural fine-tuning of the supersymmetric parameters, which would imply the existence of light higgsinos (whose masses are not well constrained, as they are difficult to detect directly at the LHC due to their soft decay products). However, it may be possible to avoid the conclusion that $\mu \sim \mathcal{O}(m_Z)$ if additional correlations among the SUSY breaking mass parameters and μ are present. Such a scenario can be realized in models in which the boundary conditions for SUSY breaking are generated by approximately conformal strong dynamics. For example, in the so-called scalar-sequestering model of Ref. [197], values of $|\mu| > 1$ TeV can be achieved while naturally maintaining the observed value of m_Z .

Finally, one can also consider extensions of the MSSM in which the degree of fine-tuning is relaxed. For example, it has already been noted in Sec. 88.5 that it is possible to accommodate the observed Higgs mass more easily in the NMSSM due to contributions to m_h^2 proportional to the parameter λ^2 . This means that we do not have to rely on a large contribution from the radiative corrections to boost the Higgs mass sufficiently above its tree-level bound. This allows for smaller top squark masses, which are more consistent with the demands of naturalness. The reduction of the fine-tuning in various NMSSM models was initially advocated in Ref. [198], and subsequently treated in more detail in Refs. [111, 199]. Naturalness can also be relaxed in extended supersymmetric models with vector-like quarks [200] and in gauge extensions of the MSSM [201].

⁴For example, one may consider the parameters μ and B to be more fundamental than $\tan \beta$ and M_Z . In this case, one would choose a flat prior probability distribution in μ and $m_{H_u}^2$ rather than in $\tan \beta$ and M_Z [176, 184]. The Jacobian factor is then obtained from Eq. (88.4) and Eq. (88.5).

The experimental absence of any new physics beyond the Standard Model at the LHC suggests that the principle of naturalness is presently under significant stress [202]. Nevertheless, one must be very cautious when drawing conclusions about the viability of weak-scale SUSY to explain the origin of electroweak symmetry breaking, since different measures of fine-tuning noted above can lead to different assessments [179, 180]. Moreover, the maximal value of Δ that determines whether weak-scale SUSY is a fine-tuned model (should it be $\Delta \sim 10^7$, 100^7 , 1000^7 ?) is ultimately subjective. Thus, it is premature to conclude that weak-scale SUSY is on the verge of exclusion. It might be possible to sharpen the upper bounds on superpartner masses based on naturalness arguments, which ultimately will either confirm or refute the weak scale SUSY hypothesis [203]. Of course, if evidence for supersymmetric phenomena in the multi-TeV regime were to be established at a future collider facility (with an energy reach beyond the LHC [204]), it would be viewed as a spectacularly successful explanation of the large gauge hierarchy between the (multi-)TeV scale and Planck scale. In this case, the remaining little hierarchy, characterized by the somewhat large value of the fine-tuning parameter Δ discussed above, would be regarded as a less pressing issue.

88.7.2 Indirect constraints on supersymmetric models

While direct empirical searches for supersymmetric particles provide various limits on their properties, indirect constraints can depend more sensitively on details of the whole model. The cold dark matter relic density inferred from cosmological fits to observational data is one such example of an indirect constraint. In supersymmetric models where the LSP is a dark matter candidate, its thermally-produced relic density depends upon the scattering of various supersymmetric particles into dark matter particles and SM particles. The resulting relic density can depend sensitively on masses of the non-LSP supersymmetric particle masses. In a typical model, an appreciable region of the parameter space is ruled out because it yields an overabundance of dark matter (see for example Ref. [205] for a fit to a seven parameter version of the pMSSM). However, subsequent model tweaks such as the introduction of R-parity violating effects can mean that the relic density constraint no longer applies to the LSP because it is unstable.

There are a number of indirect constraints based on low-energy measurements that are sensitive to the effects of new physics via supersymmetric loop effects. For example, the virtual exchange of supersymmetric particles can contribute to the muon anomalous magnetic moment, $a_\mu \equiv \frac{1}{2}(g-2)_\mu$, as reviewed in Ref. [206]. The SM prediction for a_μ , which employs dispersion relations and low energy e^+e^- scattering data to determine the hadronic corrections, exhibits a deviation of 4.2σ from the experimentally observed value [207, 208]. A recent lattice determination [209] of the leading hadronic contribution to the muon magnetic moment yields a smaller deviation from the SM prediction within 1.7σ of the experimental value, although this result has not yet been confirmed by an independent analysis. The 4.2σ deviation is difficult to accommodate in the constrained SUSY models of Sec. 88.6.2 and 88.6.3 given the present sparticle mass bounds [186]. Nevertheless, there are regions of the more general pMSSM parameter space that are consistent with the observed deviation [210].

The precision of the measured value of a_μ is not sensitive to the experimental error associated with the measured value of the fine structure constant, α . In contrast, the comparison of the SM prediction with the experimental measurement of the anomalous magnetic moment of the electron, a_e , depends critically on the value of α . Using the experimentally determined value of α given in Ref. [211] yields a SM prediction for a_e that is 2.4σ above its measured value [212]. However, this previous determination of α is in tension at the 5σ level with a more recent measurement of the fine structure constant [213]. The latter yields a SM prediction for a_e that is 1.6σ below its measured value [213].

Measurements of the fine structure constant, a_e and a_μ jointly constrain the pMSSM parameter space [214] due to shifts originating from supersymmetric loop effects. In particular, if the supersymmetric interpretation of the deviation in the measured value of a_μ from its SM prediction is combined with the experi-

mental limits on the electron electric dipole moment [125], then the resulting upper bounds on MSSM CP-violating phases are even more constraining [215] than previously noted at the beginning of Sec. 88.6.

Flavor anomalies in radiative, leptonic and semi-leptonic b quark decays [216] provide a fertile ground for physics beyond the SM. For example, the rare inclusive decay $b \rightarrow s\gamma$ is a sensitive probe of the virtual effects of new physics beyond the SM. The experimental measurements of $B \rightarrow X_s + \gamma$ [217] are in agreement with the theoretical SM predictions of Ref. [218]. Since supersymmetric loop corrections can contribute an observable shift from the SM predictions, the absence of any significant deviation places useful constraints on the MSSM parameter space [219].

The rare decays $B_s \rightarrow \mu^+\mu^-$ and $B_d \rightarrow \mu^+\mu^-$ are especially sensitive to supersymmetric loop effects, with some loop contributions scaling as $\tan^6\beta$ when $\tan\beta \gg 1$ [220]. At present, a combination [221] of the measurements of these rare decay modes [222] are in slight tension at the 2σ level [223] with the predicted SM rates [224]. Such a tension can be resolved by the aforementioned supersymmetric loop effects [220].

Several tensions exist between SM predictions and measurements of some other experimental observables that probe the $b \rightarrow s\mu^+\mu^-$ transitions. For example, the ratio of branching ratios $R_K = BR(B \rightarrow K\mu^+\mu^-)/BR(B \rightarrow Ke^+e^-)$ exhibits a 3.1σ discrepancy in the bin of di-lepton invariant squared mass between 1 GeV^2 and 6 GeV^2 [225] and in the same invariant mass bin, R_{K^*} displays a 2.5σ discrepancy. In addition, a certain angular distribution parameter (denoted by P'_5) extracted from $B^0 \rightarrow K^{*0}\mu^+\mu^-$ decays [226] deviates from SM predictions by about 4σ . Finally, a 3.6σ deviation is seen in $BR(B_s \rightarrow \phi\mu^+\mu^-)$ [227].

The decays $B^\pm \rightarrow \tau^\pm\nu_\tau$ and $B \rightarrow D^{(*)}\tau^-\bar{\nu}_\tau$ are noteworthy, since in models with extended Higgs sectors such as the MSSM, these processes possess tree-level charged Higgs exchange contributions that can compete with the dominant W -exchange. As Section 72 shows, experimental measurements of $B^\pm \rightarrow \tau^\pm\nu_\tau$ are currently consistent with SM expectations [228]. The BaBar Collaboration measured values of the rates for $\bar{B} \rightarrow D\tau^-\bar{\nu}_\tau$ and $\bar{B} \rightarrow D^*\tau^-\bar{\nu}_\tau$ [229] exhibited a combined 3.4σ discrepancy from the SM predictions, which was also not compatible with the Type-II Higgs Yukawa couplings employed by the MSSM. Subsequent measurements of the LHCb and Belle Collaborations [230] were consistent with the BaBar measurements, although more recent Belle measurements using a semi-leptonic tag are more consistent with SM expectations [231]. The combined difference between the measured and expected values of the $\bar{B} \rightarrow D\tau^-\bar{\nu}_\tau$ and $\bar{B} \rightarrow D^*\tau^-\bar{\nu}_\tau$ decay rates relative to the corresponding SM values has a significance of about three standard deviations [232]. There are a number of additional anomalies in B decay data that have recently attracted some attention, although at present the observed deviations from SM expectations are mostly at the level of about two to three standard deviations (see, e.g., Ref. [223]).

In summary, although there are a few hints of possible deviations from the SM in B decays, none of the discrepancies by themselves are significant enough to conclusively imply the existence of new physics beyond the SM. Moreover, the absence of evidence for deviations in various B -physics observables from their SM predictions can place useful constraints on the MSSM parameter space [128, 185, 233, 234]. On the other hand, if these deviations were eventually confirmed, then it would be possible to accommodate them in a supersymmetric framework with R-parity violation [235]. If R-parity invariance is maintained (for example, in order to preserve the stability of a LSP dark matter candidate), then a supersymmetric explanation of the B physics anomalies would require significant modifications to the SUSY models treated in this review.

Finally, we note that the constraints from precision electroweak observables (see Sec. 10) and measurements of the e'/ϵ anomaly [236], if it persists [237], in the Kaon system are easily accommodated in models of TeV-scale SUSY [168, 238, 239].

88.8 Massive neutrinos in weak-scale SUSY

In the minimal version of the SM and its supersymmetric extension, there are no right-handed neutrinos, and Majorana

mass terms for the left-handed neutrinos are absent. However, given the overwhelming evidence for neutrino masses and mixing (see Sec. 14 and [240]), any viable model of the fundamental particles must provide a mechanism for generating neutrino masses [241]. In extended supersymmetric models, various mechanisms exist for producing massive neutrinos [242]. Although one can devise models for generating massive Dirac neutrinos [243], the most common approaches for incorporating neutrino masses are based on L -violating supersymmetric extensions of the MSSM, which generate massive Majorana neutrinos. Two classes of L -violating supersymmetric models will now be considered.

88.8.1 The supersymmetric seesaw

Neutrino masses can be incorporated into the SM by introducing $SU(3) \times SU(2) \times U(1)$ singlet right-handed neutrinos (ν_R) whose mass parameters are very large, typically near the grand unification scale. In addition, one must also include a standard Yukawa couplings between the lepton doublets, the Higgs doublet, and ν_R . The Higgs vacuum expectation value then induces an off-diagonal ν_L - ν_R mass on the order of the electroweak scale. Diagonalizing the neutrino mass matrix (in the three-generation model) yields three superheavy neutrino states, and three very light neutrino states that are identified with the light neutrinos observed in nature. This is the seesaw mechanism [244].

It is straightforward to construct a supersymmetric generalization of the seesaw model of neutrino masses [245, 246] by promoting the right-handed neutrino field to a superfield $\widehat{N}^c = (\nu_R; \nu_R)$. Integrating out the heavy right-handed neutrino supermultiplet yields a new term in the superpotential [cf. Eq. (88.1)] of the form

$$W_{\text{seesaw}} = \frac{f}{M_R} (\widehat{H}_U \widehat{L}) (\widehat{H}_U \widehat{L}), \quad (88.25)$$

where M_R is the mass scale of the right-handed neutrino sector and f is a dimensionless constant. Note that lepton number is broken by two units by Eq. (88.25), which implies that R-parity invariance is preserved. The supersymmetric analogue of the Majorana neutrino mass term in the sneutrino sector leads to sneutrino-antisneutrino mixing phenomena [246, 247]. The right-handed sneutrino that resides in \widehat{L} also provides an intriguing dark matter candidate [248].

The SUSY Les Houches Accord [76, 94], mentioned at the end of the introduction to Sec. 88.4, has been extended to the supersymmetric seesaw (and other extensions of the MSSM) in Ref. [249].

88.8.2 R-parity-violating SUSY

It is possible to incorporate massive neutrinos in renormalizable supersymmetric models while retaining the minimal particle content of the MSSM by relaxing the assumption of R-parity invariance. The most general R-parity-violating model involving the MSSM spectrum introduces many new parameters to both the SUSY-conserving and the SUSY-breaking sectors [76, 250]. Each new interaction term violates either B or L conservation. For example, starting from the MSSM superpotential given in Eq. (88.1) [suitably generalized to three generations of quarks, leptons and their superpartners], consider the effect of adding the following new terms:

$$W_{\text{RPV}} = (\lambda_L)_{pmn} \widehat{L}_p \widehat{L}_m \widehat{E}_n^c + (\lambda'_L)_{pmn} \widehat{L}_p \widehat{Q}_m \widehat{D}_n^c + (\lambda_B)_{pmn} \widehat{U}_p^c \widehat{D}_m^c \widehat{D}_n^c + (\mu_L)_p \widehat{H}_u \widehat{L}_p, \quad (88.26)$$

where p , m , and n are generation indices, and gauge group indices are suppressed. Eq. (88.26) yields new scalar-fermion Yukawa couplings consisting of all possible combinations involving two SM fermions and one scalar superpartner.

Note that the term in Eq. (88.26) proportional to λ_B violates B , while the other three terms violate L . The L -violating term in Eq. (88.26) proportional to μ_L is the RPV analog of the $\mu \widehat{H}_u \widehat{H}_d$ term of the MSSM superpotential, in which the $Y = -1$ Higgs/higgsino supermultiplet \widehat{H}_d is replaced by the slepton/lepton supermultiplet \widehat{L}_p .

Phenomenological constraints derived from data on various low-energy B - and L -violating processes can be used to establish limits on each of the coefficients $(\lambda_L)_{pmn}$, $(\lambda'_L)_{pmn}$, and $(\lambda_B)_{pmn}$

taken one at a time [250, 251]. If more than one coefficient is simultaneously non-zero, then the limits are in general more complicated [252]. All possible RPV terms cannot be simultaneously present and unsuppressed; otherwise the proton decay rate would be many orders of magnitude larger than the present experimental bound. One way to avoid proton decay is to impose B or L invariance (either one alone would suffice). Otherwise, one must accept the requirement that certain RPV coefficients must be extremely suppressed.

One particularly interesting class of RPV models is one in which B is conserved, but L is violated. It is possible to enforce baryon number conservation (and the stability of the proton), while allowing for lepton-number-violating interactions by imposing a discrete \mathbb{Z}_3 baryon triality symmetry on the low-energy theory [253], in place of the standard \mathbb{Z}_2 R-parity. Since the distinction between the Higgs and matter supermultiplets is lost in RPV models where L is violated, the mixing of sleptons and Higgs bosons, the mixing of neutrinos and neutralinos, and the mixing of charged leptons and charginos are now possible, leading to more complicated mass matrices and mass eigenstates than in the MSSM. The treatment of neutrino masses and mixing in this framework can be found, e.g., in Ref. [254].

Alternatively, one can consider imposing a lepton parity such that all lepton superfields are odd [253, 255]. In this case, only the B -violating term in Eq. (88.26) survives, and L is conserved. Models of this type have been considered in Ref. [256]. Since L is conserved in these models, the mixing of the lepton and Higgs superfields is forbidden. Moreover, neutrino masses (and mixing) are not generated if lepton parity is an exact symmetry. However, one expects that lepton parity cannot be exact due to quantum gravity effects. Remarkably, the standard \mathbb{Z}_2 R-parity and the \mathbb{Z}_3 baryon triality are stable with respect to quantum gravity effects, as they can be identified as residual discrete symmetries that arise from spontaneously broken non-anomalous gauge symmetries [253].

The symmetries employed above to either remove or suppress R-parity violating operators were flavor independent. In contrast, there exist a number of motivated scenarios based on flavor symmetries that can also yield the suppression as required by the experimental data (e.g., see Ref. [257]).

The supersymmetric phenomenology of the RPV models exhibits features that are distinct from that of the MSSM [250]. The LSP is no longer stable, which implies that not all supersymmetric decay chains must yield missing-energy events at colliders. A comprehensive examination of the phenomenology of the MSSM extended by a single R-parity violating coupling at the unification scale and its implications for LHC searches has been given in Ref. [258]. As an example, the sparticle mass bounds obtained in searches for R-parity-conserving SUSY can be considerably relaxed in certain RPV models due to the absence of large missing transverse momentum signatures [259]. This can alleviate some of the tension with naturalness (introduced in Sec. 88.7.1).

Nevertheless, the loss of the missing-energy signature is often compensated by other striking signals (which depend on which R-parity-violating parameters are dominant). For example, supersymmetric particles in RPV models can be singly produced (in contrast to R-parity-conserving models where supersymmetric particles must be produced in pairs). The phenomenology of pair-produced supersymmetric particles is also modified in RPV models due to new decay chains not present in R-parity-conserving SUSY models [250].

In RPV models with lepton number violation (these include weak-scale SUSY models with baryon triality mentioned above), both $\Delta L = 1$ and $\Delta L = 2$ phenomena are allowed, leading to neutrino masses and mixing [260], neutrinoless double-beta decay [261], sneutrino-antisneutrino mixing [262], and resonant s -channel production of sneutrinos in e^+e^- collisions [263] and in charged sleptons in $p\bar{p}$ and pp collisions [264], respectively.

88.9 Extensions beyond the MSSM

Extensions of the MSSM have been proposed to solve a variety of theoretical problems. One such problem involves the μ parameter of the MSSM. Although μ is a SUSY-preserving parameter, it must be of order the effective SUSY-breaking scale of the MSSM

to yield a consistent supersymmetric phenomenology [265]. Any natural solution to the so-called μ -problem must incorporate a symmetry that enforces $\mu = 0$ and a small symmetry-breaking parameter that generates a value of μ that is not parametrically larger than the effective SUSY-breaking scale [266]. A number of proposed mechanisms in the literature (*e.g.*, see Refs. [265–267]) provide concrete examples of a natural solution to the μ -problem of the MSSM.

In extensions of the MSSM, new compelling solutions to the μ -problem are possible. For example, one can replace μ by the vacuum expectation value of a new $SU(3) \times SU(2) \times U(1)$ singlet scalar field, as noted below Eq. 88.15. This is the NMSSM, which yields phenomena that were briefly discussed in Sections 88.4–88.7. The NMSSM superpotential consists only of trilinear terms whose coefficients are dimensionless. There are some advantages to extending the NMSSM further to the ‘USSM’ [102] by adding a new broken $U(1)$ gauge symmetry [268], under which the singlet field is charged.

Alternatively, one can consider a generalized version of the NMSSM (called the GNMSSM in Ref. [199]), where all possible renormalizable terms in the superpotential are allowed, which yield new supersymmetric mass terms (analogous to the μ term of the MSSM). A discussion of the parameters of the GNMSSM can be found in Ref. [76]. Although the GNMSSM does not solve the μ -problem, it does exhibit regions of parameter space in which the degree of fine-tuning is relaxed, as discussed in Sec. 88.7.1.

The generation of the μ term may be connected with the solution to the strong CP problem [269]. Models of this type, which include new gauge singlet fields that are charged under the Peccei-Quinn (PQ) symmetry [270], were first proposed in Ref. [265]. The breaking of the PQ symmetry is thus intimately tied to SUSY breaking, while naturally yielding a value of μ that is of order the electroweak symmetry breaking scale [271].

All supersymmetric models discussed so far in this review possess self-conjugate fermions—the Majorana gluinos and neutralinos. However, it is possible to add additional chiral superfields in the adjoint representation. The spin-1/2 components of these new superfields can pair up with the gauginos to form Dirac gauginos [272, 273]. Such states appear in models of so-called supersoft SUSY breaking [274], in some generalized GMSB models [275], and in R-symmetric SUSY models [276, 277]. Such approaches often lead to improved naturalness and/or significantly relaxed flavor constraints. The implications of models of Dirac gauginos on the observed Higgs boson mass and its properties are addressed in Ref. [278].

For completeness, we briefly note other MSSM extensions considered in the literature. These include an enlarged electroweak gauge group beyond $SU(2) \times U(1)$ [279]; the addition of new Higgs supermultiplets beyond the doublets and singlets of the MSSM/NMSSM [280]; and/or the addition of new (possibly exotic) matter supermultiplets [200, 281, 282] such as vector-like fermions and their superpartners.

References

- [1] *The Supersymmetric World—The Beginnings of the Theory*, World Scientific, Singapore (2000), edited by G. Kane and M. Shifman, contains an early history of supersymmetry and a guide to the original literature.
- [2] R. Haag, J. T. Lopuszanski and M. Sohnius, Nucl. Phys. **B88**, 257 (1975); S. R. Coleman and J. Mandula, Phys. Rev. **159**, 1251 (1967).
- [3] H. P. Nilles, Phys. Rept. **110**, 1 (1984).
- [4] S. Weinberg, *The Quantum Theory of Fields, Volume III: Supersymmetry* (Cambridge University Press, Cambridge, UK, 2000).
- [5] P. Nath, *Supersymmetry, Supergravity, and Unification* (Cambridge University Press, Cambridge, UK, 2017).
- [6] S. P. Martin *A Supersymmetry Primer*, [hep-ph/9709356].
- [7] E. Witten, Nucl. Phys. **B188**, 513 (1981).
- [8] S. Dimopoulos and H. Georgi, Nucl. Phys. **B193**, 150 (1981).
- [9] N. Sakai, Z. Phys. **C11**, 153 (1981).
- [10] L. Susskind, Phys. Rept. **104**, 181 (1984).
- [11] L. Girardello and M. T. Grisaru, Nucl. Phys. **B194**, 65 (1982).
- [12] L. J. Hall and L. Randall, Phys. Rev. Lett. **65**, 2939 (1990); I. Jack and D. R. T. Jones, Phys. Lett. **B457**, 101 (1999), [hep-ph/9903365].
- [13] V. F. Weisskopf, Phys. Rev. **56**, 72 (1939).
- [14] See *e.g.*, N. Polonsky, *Supersymmetry: Structure and phenomena. Extensions of the standard model*, Lect. Notes Phys. **M68**, 1 (2001).
- [15] G. Bertone, D. Hooper and J. Silk, Phys. Rept. **405**, 279 (2005), [hep-ph/0404175].
- [16] D. Hooper, “TASI 2008 Lectures on Dark Matter,” in *The Dawn of the LHC Era, Proceedings of the 2008 Theoretical and Advanced Study Institute in Elementary Particle Physics*, Boulder, Colorado, 2–27 June 2008, edited by Tao Han (World Scientific, Singapore, 2009).
- [17] H. Pagels and J. R. Primack, Phys. Rev. Lett. **48**, 223 (1982).
- [18] H. Goldberg, Phys. Rev. Lett. **50**, 1419 (1983).
- [19] J. R. Ellis *et al.*, Nucl. Phys. **B238**, 453 (1984).
- [20] G. Jungman, M. Kamionkowski, and K. Griest, Phys. Reports **267**, 195 (1996).
- [21] F. D. Steffen, Eur. Phys. J. **C59**, 557 (2009), [arXiv:0811.3347].
- [22] H. E. Haber and G. L. Kane, Phys. Rept. **117**, 75 (1985).
- [23] M. Drees, R. Godbole, and P. Roy, *Theory and Phenomenology of Sparticles* (World Scientific, Singapore, 2005); H. Baer and X. Tata, *Weak Scale Supersymmetry: from Superfields to Scattering Events* (Cambridge University Press, Cambridge, UK, 2006); I.J.R. Aitchison, *Supersymmetry in Particle Physics: an elementary introduction* (Cambridge University Press, Cambridge, UK, 2007).
- [24] Our notation for the charge-conjugated fields follows the notation of P. Langacker, *The Standard Model and Beyond*, 2nd edition (CRC Press, Boca Raton, FL, 2017).
- [25] H. Georgi and S. L. Glashow, Phys. Rev. **D6**, 429 (1972).
- [26] P. Fayet, Nucl. Phys. **B90**, 104 (1975).
- [27] K. Inoue *et al.*, Prog. Theor. Phys. **67**, 1889 (1982).
- [28] J. F. Gunion and H. E. Haber, Nucl. Phys. **B272**, 1 (1986), [Erratum: **B402**, 567 (1993)].
- [29] A. Salam and J. A. Strathdee, Nucl. Phys. **B76**, 477 (1974).
- [30] J. Wess and J. Bagger, *Supersymmetry and Supergravity* (Princeton University Press, Princeton, NJ, 1992).
- [31] I. L. Buchbinder, S. Kuzenko and Z. Yarevskaya, Nucl. Phys. **B411**, 665 (1994); I. Antoniadis, E. Dudas and D. M. Ghilencea, JHEP **03**, 045 (2008), [arXiv:0708.0383].
- [32] D. J. H. Chung *et al.*, Phys. Rept. **407**, 1 (2005), [hep-ph/0312378].
- [33] J. R. Ellis *et al.*, Phys. Rev. **D39**, 844 (1989); U. Ellwanger and C. Hugonie, Eur. Phys. J. **C25**, 297 (2002), [hep-ph/9909260]; U. Ellwanger, C. Hugonie and A. M. Teixeira, Phys. Rept. **496**, 1 (2010), [arXiv:0910.1785]; M. Maniatis, Int. J. Mod. Phys. **A25**, 3505 (2010), [arXiv:0906.0777].
- [34] S. Weinberg, Phys. Rev. Lett. **43**, 1566 (1979); S. Weinberg, Phys. Rev. **D22**, 1694 (1980); F. Wilczek and A. Zee, Phys. Rev. Lett. **43**, 1571 (1979); H. A. Weldon and A. Zee, Nucl. Phys. **B173**, 269 (1980).
- [35] P. Fayet, Phys. Lett. **69B**, 489 (1977); G. R. Farrar and P. Fayet, Phys. Lett. **76B**, 575 (1978).
- [36] P. Fayet, Phys. Lett. **84B**, 421 (1979); P. Fayet, Phys. Lett. **86B**, 272 (1979).
- [37] D.Z. Freedman and A. Van Proeyen, *Supergravity* (Cambridge University Press, Cambridge, UK, 2012); M. Rausch de Traubenberg and M. Valenzuela, *A Supergravity Primer* (World Scientific, Singapore, 2020).

- [38] S. Deser and B. Zumino, *Phys. Rev. Lett.* **38**, 1433 (1977); E. Cremmer *et al.*, *Phys. Lett.* **79B**, 231 (1978).
- [39] R. Casalbuoni *et al.*, *Phys. Lett.* **B215**, 313 (1988); R. Casalbuoni *et al.*, *Phys. Rev.* **D39**, 2281 (1989); A. L. Maroto and J. R. Pelaez, *Phys. Rev.* **D62**, 023518 (2000), [hep-ph/9912212].
- [40] Z. Komargodski and N. Seiberg, *JHEP* **09**, 066 (2009), [arXiv:0907.2441]; I. Antoniadis *et al.*, *Theor. Math. Phys.* **170**, 26 (2012), [*Teor. Mat. Fiz.* **170**, 34 (2012)].
- [41] A.H. Chamseddine, R. Arnowitt, and P. Nath, *Phys. Rev. Lett.* **49**, 970 (1982); R. Barbieri, S. Ferrara and C. A. Savoy, *Phys. Lett.* **119B**, 343 (1982); L. E. Ibanez, *Nucl. Phys.* **B218**, 514 (1983); H. P. Nilles, M. Srednicki and D. Wyler, *Phys. Lett.* **120B**, 346 (1983); H. P. Nilles, M. Srednicki and D. Wyler, *Phys. Lett.* **124B**, 337 (1983); E. Cremmer, P. Fayet and L. Girardello, *Phys. Lett.* **122B**, 41 (1983); N. Ohta, *Prog. Theor. Phys.* **70**, 542 (1983).
- [42] L. Alvarez-Gaumé, J. Polchinski, and M.B. Wise, *Nucl. Phys.* **B221**, 495 (1983).
- [43] L. J. Hall, J. D. Lykken and S. Weinberg, *Phys. Rev.* **D27**, 2359 (1983).
- [44] S. K. Soni and H. A. Weldon, *Phys. Lett.* **126B**, 215 (1983); Y. Kawamura, H. Murayama and M. Yamaguchi, *Phys. Rev.* **D51**, 1337 (1995), [hep-ph/9406245].
- [45] See, *e.g.*, A. Brignole, L.E. Ibáñez, and C. Muñoz, in *Perspectives on Supersymmetry II*, edited by G.L. Kane (World Scientific, Singapore, 2010) pp. 244–268.
- [46] A. B. Lahanas and D. V. Nanopoulos, *Phys. Rept.* **145**, 1 (1987).
- [47] J. L. Feng, A. Rajaraman and F. Takayama, *Phys. Rev. Lett.* **91**, 011302 (2003), [hep-ph/0302215]; J. L. Feng, A. Rajaraman and F. Takayama, *Phys. Rev.* **D68**, 063504 (2003), [hep-ph/0306024]; J. L. Feng, A. Rajaraman and F. Takayama, *Int. J. Mod. Phys.* **D13**, 2355 (2004), [hep-th/0405248].
- [48] L. Randall and R. Sundrum, *Nucl. Phys.* **B557**, 79 (1999), [hep-th/9810155].
- [49] F. D'Eramo, J. Thaler and Z. Thomas, *JHEP* **06**, 151 (2012), [arXiv:1202.1280]; F. D'Eramo, J. Thaler and Z. Thomas, *JHEP* **09**, 125 (2013), [arXiv:1307.3251]; S. P. de Alwis, *Phys. Rev.* **D77**, 105020 (2008), [arXiv:0801.0578]; S. P. de Alwis, *JHEP* **01**, 006 (2013), [arXiv:1206.6775]; K. Harigaya and M. Ibe, *Phys. Rev.* **D90**, 085028 (2014), [arXiv:1409.5029].
- [50] I. Jack, D. R. T. Jones and R. Wild, *Phys. Lett.* **B535**, 193 (2002), [hep-ph/0202101]; B. Murakami and J. D. Wells, *Phys. Rev.* **D68**, 035006 (2003), [hep-ph/0302209]; R. Kitano, G. D. Kribs and H. Murayama, *Phys. Rev.* **D70**, 035001 (2004), [hep-ph/0402215]; R. Hodgson *et al.*, *Nucl. Phys.* **B728**, 192 (2005), [hep-ph/0507193]; D. R. T. Jones and G. G. Ross, *Phys. Lett.* **B642**, 540 (2006), [hep-ph/0609210].
- [51] S. Asai *et al.*, *Phys. Lett.* **B653**, 81 (2007), [arXiv:0705.3086].
- [52] M. Dine, W. Fischler and M. Srednicki, *Nucl. Phys.* **B189**, 575 (1981); S. Dimopoulos and S. Raby, *Nucl. Phys.* **B192**, 353 (1981); S. Dimopoulos and S. Raby, *Nucl. Phys.* **B219**, 479 (1983); M. Dine and W. Fischler, *Phys. Lett.* **110B**, 227 (1982); C. R. Nappi and B. A. Ovrut, *Phys. Lett.* **113B**, 175 (1982); L. Alvarez-Gaume, M. Claudson and M. B. Wise, *Nucl. Phys.* **B207**, 96 (1982).
- [53] M. Dine and A. E. Nelson, *Phys. Rev.* **D48**, 1277 (1993), [hep-ph/9303230]; M. Dine, A. E. Nelson and Y. Shirman, *Phys. Rev.* **D51**, 1362 (1995), [hep-ph/9408384].
- [54] M. Dine *et al.*, *Phys. Rev.* **D53**, 2658 (1996), [hep-ph/9507378].
- [55] G. F. Giudice and R. Rattazzi, *Phys. Rept.* **322**, 419 (1999), [hep-ph/9801271].
- [56] E. Poppitz and S. P. Trivedi, *Phys. Rev.* **D55**, 5508 (1997), [hep-ph/9609529]; H. Murayama, *Phys. Rev. Lett.* **79**, 18 (1997), [hep-ph/9705271]; M. A. Luty and J. Terning, *Phys. Rev.* **D57**, 6799 (1998), [hep-ph/9709306]; K. Agashe, *Phys. Lett.* **B435**, 83 (1998), [hep-ph/9804450]; N. Arkani-Hamed, J. March-Russell and H. Murayama, *Nucl. Phys.* **B509**, 3 (1998), [hep-ph/9701286]; C. Csaki, Y. Shirman and J. Terning, *JHEP* **05**, 099 (2007), [hep-ph/0612241]; M. Ibe and R. Kitano, *Phys. Rev.* **D77**, 075003 (2008), [arXiv:0711.0416].
- [57] S. Weinberg, *Phys. Rev. Lett.* **48**, 1303 (1982); M. Kawasaki, F. Takahashi and T. T. Yanagida, *Phys. Rev. D* **74**, 043519 (2006), [hep-ph/0605297].
- [58] M. Kawasaki *et al.*, *Phys. Rev.* **D78**, 065011 (2008), [arXiv:0804.3745].
- [59] M. J. Strassler and K. M. Zurek, *Phys. Lett.* **B651**, 374 (2007), [hep-ph/0604261]; T. Han *et al.*, *JHEP* **07**, 008 (2008), [arXiv:0712.2041].
- [60] M. J. Strassler [hep-ph/0607160]; K. M. Zurek, *Phys. Rev.* **D79**, 115002 (2009), [arXiv:0811.4429].
- [61] See *e.g.*, M. Quiros, in *Particle Physics and Cosmology: The Quest for Physics Beyond the Standard Model(s), Proceedings of the 2002 Theoretical Advanced Study Institute in Elementary Particle Physics (TASI 2002)*, edited by H.E. Haber and A.E. Nelson (World Scientific, Singapore, 2004) pp. 549–601; C. Csaki, in *ibid.*, pp. 605–698.
- [62] V.A. Rubakov, *Sov. Phys. Usp.* **44**, 871 (2001); J. L. Hewett and M. Spiropulu, *Ann. Rev. Nucl. Part. Sci.* **52**, 397 (2002), [hep-ph/0205106].
- [63] Z. Chacko, M. A. Luty and E. Ponton, *JHEP* **07**, 036 (2000), [hep-ph/9909248]; D. E. Kaplan, G. D. Kribs and M. Schmaltz, *Phys. Rev.* **D62**, 035010 (2000), [hep-ph/9911293]; Z. Chacko *et al.*, *JHEP* **01**, 003 (2000), [hep-ph/9911323].
- [64] J. Scherk and J. H. Schwarz, *Phys. Lett.* **82B**, 60 (1979); J. Scherk and J. H. Schwarz, *Nucl. Phys.* **B153**, 61 (1979).
- [65] R. Barbieri, L. J. Hall and Y. Nomura, *Phys. Rev.* **D66**, 045025 (2002), [hep-ph/0106190]; R. Barbieri, L. J. Hall and Y. Nomura, *Nucl. Phys.* **B624**, 63 (2002), [hep-th/0107004]; I. Garcia Garcia, K. Howe and J. March-Russell, *JHEP* **12**, 005 (2015), [arXiv:1510.07045].
- [66] J. D. Wells, in “11th International Conference on Supersymmetry and the Unification of Fundamental Interactions (SUSY 2003) Tucson, Arizona, June 5-10, 2003,” (2003), [hep-ph/0306127]; J. D. Wells, *Phys. Rev.* **D71**, 015013 (2005), [hep-ph/0411041].
- [67] N. Arkani-Hamed and S. Dimopoulos, *JHEP* **06**, 073 (2005), [hep-th/0405159]; G. F. Giudice and A. Romanino, *Nucl. Phys.* **B699**, 65 (2004), [Erratum: **B706**, 487 (2005)], [hep-ph/0406088].
- [68] G. F. Giudice and A. Strumia, *Nucl. Phys.* **B858**, 63 (2012), [arXiv:1108.6077].
- [69] A. Arvanitaki *et al.*, *JHEP* **02**, 126 (2013), [arXiv:1210.0555]; N. Arkani-Hamed *et al.* (2012), [arXiv:1212.6971].
- [70] E. Bagnaschi *et al.*, *JHEP* **09**, 092 (2014), [arXiv:1407.4081].
- [71] J. Pardo Vega and G. Villadoro, *JHEP* **07**, 159 (2015), [arXiv:1504.05200].
- [72] B. C. Allanach and A. Voigt, *Eur. Phys. J.* **C78**, 573 (2018), [arXiv:1804.09410].
- [73] Y. Kahn, M. McCullough and J. Thaler, *JHEP* **11**, 161 (2013), [arXiv:1308.3490].
- [74] L. J. Hall and Y. Nomura, *JHEP* **01**, 082 (2012), [arXiv:1111.4519]; M. Ibe and T. T. Yanagida, *Phys. Lett.* **B709**, 374 (2012), [arXiv:1112.2462].

- [75] H. E. Haber and L. Stephenson Haskins (2018), *Supersymmetric Theory and Models*, in *Anticipating the Next Discoveries in Particle Physics*, Proceedings of the 2016 Theoretical Advanced Study Institute in Elementary Particle Physics, edited by Rouven Essig and Ian Low (World Scientific, Singapore, 2018) pp. 355-499, [arXiv:1712.05926].
- [76] B. C. Allanach *et al.*, *Comput. Phys. Commun.* **180**, 8 (2009), [arXiv:0801.0045].
- [77] J. M. Frere, D. R. T. Jones and S. Raby, *Nucl. Phys.* **B222**, 11 (1983); J. P. Derendinger and C. A. Savoy, *Nucl. Phys.* **B237**, 307 (1984); J. F. Gunion, H. E. Haber and M. Sher, *Nucl. Phys.* **B306**, 1 (1988); D. Chowdhury *et al.*, *JHEP* **02**, 110 (2014), [Erratum: **03**, 149 (2018)], [arXiv:1310.1932]; W. G. Hollik, *JHEP* **08**, 126 (2016), [arXiv:1606.08356].
- [78] J. A. Casas, A. Lleyda and C. Munoz, *Nucl. Phys.* **B471**, 3 (1996), [hep-ph/9507294].
- [79] J. E. Camargo-Molina *et al.*, *Eur. Phys. J. C* **73**, 10, 2588 (2013), [arXiv:1307.1477].
- [80] N. Blinov and D. E. Morrissey, *JHEP* **03**, 106 (2014), [arXiv:1310.4174].
- [81] C. S. Ün *et al.*, *Phys. Rev.* **D91**, 105033 (2015), [arXiv:1412.1440].
- [82] G. G. Ross, K. Schmidt-Hoberg and F. Staub, *Phys. Lett.* **B759**, 110 (2016), [arXiv:1603.09347].
- [83] G. G. Ross, K. Schmidt-Hoberg and F. Staub, *JHEP* **03**, 021 (2017), [arXiv:1701.03480].
- [84] S. P. Martin, *Phys. Rev.* **D61**, 035004 (2000), [hep-ph/9907550].
- [85] S. Dimopoulos and D. W. Sutter, *Nucl. Phys.* **B452**, 496 (1995), [hep-ph/9504415]; D.W. Sutter, Stanford Ph. D. thesis, arXiv:hep-ph/9704390.
- [86] H.E. Haber, *Nucl. Phys. B (Proc. Suppl.)* **62A-C**, 469 (1998).
- [87] R. M. Barnett, J. F. Gunion and H. E. Haber, *Phys. Lett.* **B315**, 349 (1993), [hep-ph/9306204]; H. Baer, X. Tata and J. Woodside, *Phys. Rev.* **D41**, 906 (1990).
- [88] S. M. Bilenky, N. P. Nedelcheva and E. K. Khristova, *Phys. Lett.* **161B**, 397 (1985); S. M. Bilenky, E. K. Khristova and N. P. Nedelcheva, *Bulg. J. Phys.* **13**, 283 (1986).
- [89] J. Rosiek, *Phys. Rev.* **D41**, 3464 (1990).
- [90] J. Alwall *et al.*, *JHEP* **09**, 028 (2007), [arXiv:0706.2334].
- [91] T. Hahn, *Comput. Phys. Commun.* **140**, 418 (2001), [hep-ph/0012260].
- [92] A. Pukhov *et al.*, INP MSU report 98-41/542 (arXiv:hep-ph/9908288); E. Boos *et al.* [CompHEP Collab.], *Nucl. Instrum. Methods* **A534**, 50 (2004); CompHEP webpage, <https://theory.sinp.msu.ru/dokuwiki/doku.php/comphep/news>.
- [93] D. M. Pierce *et al.*, *Nucl. Phys.* **B491**, 3 (1997), [hep-ph/9606211].
- [94] P. Z. Skands *et al.*, *JHEP* **07**, 036 (2004), [hep-ph/0311123].
- [95] For further details, see *e.g.*, Appendix C of Ref. [22] and Appendix A of Ref. [28].
- [96] J. L. Kneur and G. Moultaka, *Phys. Rev.* **D59**, 015005 (1999), [hep-ph/9807336].
- [97] R.A. Horn and C.R. Johnson, *Matrix Analysis*, 2nd Edition (Cambridge University Press, Cambridge, UK, 2003).
- [98] H. K. Dreiner, H. E. Haber and S. P. Martin, *Phys. Rept.* **494**, 1 (2010), [arXiv:0812.1594].
- [99] H. E. Haber, *Int. J. Mod. Phys. A* **36**, 04, 2130003 (2021), [arXiv:2009.03990].
- [100] S. Pokorski, J. Rosiek and C. A. Savoy, *Nucl. Phys. B* **570**, 81 (2000), [hep-ph/9906206].
- [101] L. Autonne, *Annals de l'Université de Lyon, Nouvelle Série I, Fasc.* **38**, 1 (1915); T. Takagi, *Japan J. Math.* **1**, 83 (1925).
- [102] S. Y. Choi *et al.*, *Nucl. Phys.* **B778**, 85 (2007), [hep-ph/0612218].
- [103] S. Y. Choi *et al.*, *Eur. Phys. J.* **C22**, 563 (2001), [Addendum: *Eur. Phys. J.* **C23**, 769 (2002)], [hep-ph/0108117].
- [104] M. M. El Kheishen, A. A. Aboshousha and A. A. Shafik, *Phys. Rev.* **D45**, 4345 (1992).
- [105] T. Hahn (2006), [arXiv:physics/0607103].
- [106] K.-i. Hikasa and M. Kobayashi, *Phys. Rev.* **D36**, 724 (1987); F. Gabbiani and A. Masiero, *Nucl. Phys.* **B322**, 235 (1989); P. Brax and C. A. Savoy, *Nucl. Phys.* **B447**, 227 (1995), [hep-ph/9503306].
- [107] J. R. Ellis and S. Rudaz, *Phys. Lett.* **128B**, 248 (1983); F. Browning, D. Chang and W.-Y. Keung, *Phys. Rev.* **D64**, 015010 (2001), [hep-ph/0012258]; A. Bartl *et al.*, *Phys. Lett.* **B573**, 153 (2003), [hep-ph/0307317]; A. Bartl *et al.*, *Phys. Rev.* **D70**, 035003 (2004), [hep-ph/0311338].
- [108] J.F. Gunion *et al.*, *The Higgs Hunter's Guide* (Westview Press, Boulder, CO, 2000); M. Carena and H. E. Haber, *Prog. Part. Nucl. Phys.* **50**, 63 (2003), [hep-ph/0208209]; A. Djouadi, *Phys. Rept.* **459**, 1 (2008), [hep-ph/0503173].
- [109] E. Bagnaschi *et al.*, *Eur. Phys. J.* **C79**, 617 (2019), [arXiv:1808.07542].
- [110] H. E. Haber and M. Sher, *Phys. Rev.* **D35**, 2206 (1987).
- [111] L. J. Hall, D. Pinner and J. T. Ruderman, *JHEP* **04**, 131 (2012), [arXiv:1112.2703].
- [112] L. J. Hall and M. B. Wise, *Nucl. Phys.* **B187**, 397 (1981).
- [113] H. E. Haber and R. Hempfling, *Phys. Rev. Lett.* **66**, 1815 (1991); Y. Okada, M. Yamaguchi and T. Yanagida, *Prog. Theor. Phys.* **85**, 1 (1991); J. R. Ellis, G. Ridolfi and F. Zwirner, *Phys. Lett.* **B257**, 83 (1991).
- [114] H. E. Haber, R. Hempfling and A. H. Hoang, *Z. Phys. C* **75**, 539 (1997), [hep-ph/9609331].
- [115] P. Draper and H. Rzehak, *Phys. Rept.* **619**, 1 (2016), [arXiv:1601.01890].
- [116] P. Slavich *et al.*, *Eur. Phys. J. C* **81**, 5, 450 (2021), [arXiv:2012.15629].
- [117] A. Pilaftsis and C. E. M. Wagner, *Nucl. Phys.* **B553**, 3 (1999), [hep-ph/9902371]; D. A. Demir, *Phys. Rev.* **D60**, 055006 (1999), [hep-ph/9901389]; S. Y. Choi, M. Drees and J. S. Lee, *Phys. Lett.* **B481**, 57 (2000), [hep-ph/0002287]; M. Carena *et al.*, *Nucl. Phys.* **B586**, 92 (2000), [hep-ph/0003180]; M. Carena *et al.*, *Phys. Lett.* **B495**, 155 (2000), [hep-ph/0009212]; M. Carena *et al.*, *Nucl. Phys.* **B625**, 345 (2002), [hep-ph/0111245]; M. Frank *et al.*, *JHEP* **02**, 047 (2007), [hep-ph/0611326]; S. Heinemeyer *et al.*, *Phys. Lett.* **B652**, 300 (2007), [arXiv:0705.0746].
- [118] H. E. Haber and J. D. Mason, *Phys. Rev.* **D77**, 115011 (2008), [arXiv:0711.2890].
- [119] M. Carena *et al.*, *Phys. Rev.* **D93**, 035013 (2016), [arXiv:1510.09137].
- [120] S. Khalil, *Int. J. Mod. Phys.* **A18**, 1697 (2003), [hep-ph/0212050].
- [121] W. Fischler, S. Paban and S. D. Thomas, *Phys. Lett.* **B289**, 373 (1992), [hep-ph/9205233].
- [122] A. Masiero and L. Silvestrini, in *Perspectives on Supersymmetry*, edited by G.L. Kane (World Scientific, Singapore, 1998) pp. 423-441.
- [123] M. Pospelov and A. Ritz, *Annals Phys.* **318**, 119 (2005), [hep-ph/0504231].
- [124] J. M. Pendlebury *et al.*, *Phys. Rev.* **D92**, 092003 (2015), [arXiv:1509.04411].
- [125] V. Andreev *et al.* (ACME Collaboration), *Nature* **562**, 355 (2018).
- [126] F. Gabbiani *et al.*, *Nucl. Phys.* **B477**, 321 (1996), [hep-ph/9604387].

- [127] M. J. Ramsey-Musolf and S. Su, Phys. Rept. **456**, 1 (2008), [hep-ph/0612057].
- [128] M. Carena, A. Menon and C. E. M. Wagner, Phys. Rev. **D79**, 075025 (2009), [arXiv:0812.3594].
- [129] M. B. Einhorn and D. R. T. Jones, Nucl. Phys. **B196**, 475 (1982).
- [130] W. J. Marciano and G. Senjanovic, Phys. Rev. **D25**, 3092 (1982).
- [131] R.N. Mohapatra, *Unification and Supersymmetry*, Third Edition (Springer Science, New York, 2003).
- [132] S. P. Martin and M. T. Vaughn, Phys. Rev. **D50**, 2282 (1994), [Erratum: Phys. Rev. **D78**, 039903 (2008)], [hep-ph/9311340]; R. M. Fonseca *et al.*, Nucl. Phys. **B854**, 28 (2012), [arXiv:1107.2670]; F. Staub, Comput. Phys. Commun. **182**, 808 (2011), [arXiv:1002.0840].
- [133] F. Staub, Comput. Phys. Commun. **185**, 1773 (2014), [arXiv:1309.7223]; F. Staub, Adv. High Energy Phys. **2015**, 840780 (2015), [arXiv:1503.04200]; The SARAH homepage is <https://sarah.hepforge.org/>; R. M. Fonseca, Comput. Phys. Commun. **183**, 2298 (2012), [arXiv:1106.5016]; The Susyno homepage is <https://renatofonseca.net/susyno>.
- [134] B. C. Allanach, Comput. Phys. Commun. **143**, 305 (2002), [hep-ph/0104145]; The SOFTSUSY homepage is <http://softsusy.hepforge.org/>; A. Djouadi, J.-L. Kneur and G. Moutaka, Comput. Phys. Commun. **176**, 426 (2007), [hep-ph/0211331]; The Suspect homepage is <http://suspect.in2p3.fr/>; F. E. Paige *et al.* (2003), [hep-ph/0312045]; Isajet may be obtained from <http://www.nhn.ou.edu/~isajet/>; W. Porod, Comput. Phys. Commun. **153**, 275 (2003), [hep-ph/0301101]; Spheno may be obtained from <https://spheno.hepforge.org/>; P. Athron *et al.*, Comput. Phys. Commun. **190**, 139 (2015), [arXiv:1406.2319]; The FlexibleSUSY homepage is <https://flexiblesusy.hepforge.org/>.
- [135] L. E. Ibanez and G. G. Ross, Phys. Lett. **110B**, 215 (1982).
- [136] M. Drees, Phys. Lett. B **158**, 409 (1985); J. R. Ellis *et al.*, Phys. Lett. B **155**, 381 (1985); S. P. Martin, Phys. Rev. D **79**, 095019 (2009), [arXiv:0903.3568].
- [137] J. Abdallah *et al.* (DELPHI Collaboration), Eur. Phys. J. **C31**, 421 (2003), [hep-ex/0311019].
- [138] H. K. Dreiner *et al.*, Eur. Phys. J. **C62**, 547 (2009), [arXiv:0901.3485].
- [139] G. F. Giudice *et al.*, JHEP **12**, 027 (1998), [hep-ph/9810442]; A. Pomarol and R. Rattazzi, JHEP **05**, 013 (1999), [hep-ph/9903448]; D.-W. Jung and J. Y. Lee, JHEP **03**, 123 (2009), [arXiv:0902.0464].
- [140] J. F. Gunion and H. E. Haber, Phys. Rev. **D37**, 2515 (1988); S. Y. Choi, M. Drees and B. Gaissmaier, Phys. Rev. **D70**, 014010 (2004), [hep-ph/0403054].
- [141] H. Baer, V. Barger and D. Sengupta, Phys. Rev. **D98**, 015039 (2018), [arXiv:1801.09730].
- [142] J. L. Feng *et al.*, Phys. Rev. Lett. **83**, 1731 (1999), [hep-ph/9904250]; J. F. Gunion and S. Mrenna, Phys. Rev. **D62**, 015002 (2000), [hep-ph/9906270].
- [143] T. Gherghetta, G. F. Giudice and J. D. Wells, Nucl. Phys. **B559**, 27 (1999), [hep-ph/9904378].
- [144] M. Endo, M. Yamaguchi and K. Yoshioka, Phys. Rev. **D72**, 015004 (2005), [hep-ph/0504036]; K. Choi, K. S. Jeong and K.-i. Okumura, JHEP **09**, 039 (2005), [hep-ph/0504037]; O. Loaiza-Brito *et al.*, AIP Conf. Proc. **805**, 198 (2005), [hep-th/0509158].
- [145] See *e.g.*, G. D'Ambrosio *et al.*, Nucl. Phys. **B645**, 155 (2002).
- [146] C. Smith, Acta Phys. Polon. Supp. **3**, 53 (2010), [arXiv:0909.4444].
- [147] M. Drees and S.P. Martin, in *Electroweak Symmetry Breaking and New Physics at the TeV Scale*, edited by T. Barklow *et al.* (World Scientific, Singapore, 1996) pp. 146–215.
- [148] G. L. Kane *et al.*, Phys. Rev. **D49**, 6173 (1994), [hep-ph/9312272].
- [149] J. R. Ellis *et al.*, Phys. Lett. **B573**, 162 (2003), [hep-ph/0305212]; J. R. Ellis *et al.*, Phys. Rev. **D70**, 055005 (2004), [hep-ph/0405110].
- [150] H. Baer *et al.*, Phys. Rev. **D71**, 095008 (2005), [hep-ph/0412059].
- [151] V. Berezhinsky *et al.*, Astropart. Phys. **5**, 1 (1996), [hep-ph/9508249]; J. R. Ellis *et al.*, Nucl. Phys. **B652**, 259 (2003), [hep-ph/0210205].
- [152] L. E. Ibanez and D. Lust, Nucl. Phys. **B382**, 305 (1992), [hep-th/9202046]; B. de Carlos, J. A. Casas and C. Munoz, Phys. Lett. **B299**, 234 (1993), [hep-ph/9211266]; V. S. Kaplunovsky and J. Louis, Phys. Lett. **B306**, 269 (1993), [hep-th/9303040]; A. Brignole, L. E. Ibanez and C. Munoz, Nucl. Phys. **B422**, 125 (1994), [Erratum: **B436**, 747 (1995)], [hep-ph/9308271].
- [153] A. Arbey *et al.*, Phys. Rev. **D87**, 115020 (2013), [arXiv:1304.0381].
- [154] G. R. Dvali, G. F. Giudice and A. Pomarol, Nucl. Phys. **B478**, 31 (1996), [hep-ph/9603238].
- [155] P. Draper *et al.*, Phys. Rev. **D85**, 095007 (2012), [arXiv:1112.3068].
- [156] P. Meade, N. Seiberg and D. Shih, Prog. Theor. Phys. Suppl. **177**, 143 (2009), [arXiv:0801.3278]; M. Buican *et al.*, JHEP **03**, 016 (2009), [arXiv:0812.3668].
- [157] A. Rajaraman *et al.*, Phys. Lett. **B678**, 367 (2009), [arXiv:0903.0668]; L. M. Carpenter *et al.*, Phys. Rev. **D79**, 035002 (2009), [arXiv:0805.2944].
- [158] S. Ambrosanio, G. D. Kribs and S. P. Martin, Nucl. Phys. **B516**, 55 (1998), [hep-ph/9710217].
- [159] For a review and guide to the literature, see J.F. Gunion and H.E. Haber, in *Perspectives on Supersymmetry II*, edited by G.L. Kane (World Scientific, Singapore, 2010) pp. 420–445.
- [160] T. S. Roy and M. Schmaltz, Phys. Rev. **D77**, 095008 (2008), [arXiv:0708.3593].
- [161] A. de Gouvea, A. Friedland and H. Murayama, Phys. Rev. **D57**, 5676 (1998), [hep-ph/9711264].
- [162] T. Han, D. Marfatia and R.-J. Zhang, Phys. Rev. **D61**, 013007 (2000), [hep-ph/9906508]; Z. Chacko and E. Ponton, Phys. Rev. **D66**, 095004 (2002), [hep-ph/0112190]; A. Delgado, G. F. Giudice and P. Slavich, Phys. Lett. **B653**, 424 (2007), [arXiv:0706.3873]; T. Liu and C. E. M. Wagner, JHEP **06**, 073 (2008), [arXiv:0803.2895].
- [163] A. Djouadi, J.L. Kneur, and G. Moutaka, Comp. Phys. Comm. **176**, 426 (2007); C. F. Berger *et al.*, JHEP **02**, 023 (2009), [arXiv:0812.0980]; B. Allanach *et al.*, Phys. Rev. **D92**, 015006 (2015), [arXiv:1502.05836].
- [164] S. P. Martin and J. D. Wells, Phys. Rev. **D64**, 035003 (2001), [hep-ph/0103067].
- [165] S. S. AbdusSalam *et al.*, Phys. Rev. D **81**, 095012 (2010), [arXiv:0904.2548].
- [166] J. Berger *et al.*, Phys. Rev. **D93**, 035017 (2016), [arXiv:1510.08840].
- [167] K. J. de Vries *et al.*, Eur. Phys. J. **C75**, 422 (2015), [arXiv:1504.03260].
- [168] E. Bagnaschi *et al.*, Eur. Phys. J. **C78**, 256 (2018), [arXiv:1710.11091].
- [169] M. Cahill-Rowley *et al.*, Phys. Rev. **D90**, 095017 (2014), [arXiv:1407.7021]; M. Cahill-Rowley *et al.*, Phys. Rev. **D91**, 055011 (2015), [arXiv:1405.6716].
- [170] G. Bertone *et al.*, JCAP **1604**, 037 (2016), [arXiv:1507.07008].
- [171] N. Arkani-Hamed *et al.* (2007), [hep-ph/0703088]; J. Alwall *et al.*, Phys. Rev. **D79**, 015005 (2009), [arXiv:0809.3264]; J. Alwall, P. Schuster and N. Toro, Phys. Rev. **D79**,

- 075020 (2009), [arXiv:0810.3921]; D. S. M. Alves, E. Izaguirre and J. G. Wacker, Phys. Lett. **B702**, 64 (2011), [arXiv:1008.0407]; D. S. M. Alves, E. Izaguirre and J. G. Wacker, JHEP **10**, 012 (2011), [arXiv:1102.5338]; D. Alves (LHC New Physics Working Group), J. Phys. **G39**, 105005 (2012), [arXiv:1105.2838].
- [172] F. Ambrogio *et al.*, Eur. Phys. J. **C78**, 215 (2018), [arXiv:1707.09036].
- [173] R. Barbieri and G.F. Giudice, Nucl. Phys. **B305**, 63 (1988).
- [174] J. R. Ellis *et al.*, Mod. Phys. Lett. **A1**, 57 (1986).
- [175] G. W. Anderson and D. J. Castano, Phys. Lett. **B347**, 300 (1995), [hep-ph/9409419]; G. W. Anderson and D. J. Castano, Phys. Rev. **D52**, 1693 (1995), [hep-ph/9412322]; G. W. Anderson and D. J. Castano, Phys. Rev. **D53**, 2403 (1996), [hep-ph/9509212]; P. Athron and D. J. Miller, Phys. Rev. **D76**, 075010 (2007), [arXiv:0705.2241].
- [176] M. E. Cabrera, J. A. Casas and R. Ruiz de Austri, JHEP **03**, 075 (2009), [arXiv:0812.0536]; H. Baer *et al.*, Phys. Rev. Lett. **109**, 161802 (2012), [arXiv:1207.3343].
- [177] J. L. Feng, K. T. Matchev and T. Moroi, Phys. Rev. **D61**, 075005 (2000), [hep-ph/9909334].
- [178] D. M. Ghilencea and G. G. Ross, Nucl. Phys. **B868**, 65 (2013), [arXiv:1208.0837].
- [179] H. Baer, V. Barger and D. Mickelson, Phys. Rev. **D88**, 095013 (2013), [arXiv:1309.2984].
- [180] M. van Beekveld, S. Caron and R. Ruiz de Austri, JHEP **01**, 147 (2020), [arXiv:1906.10706].
- [181] G. L. Kane and S. F. King, Phys. Lett. **B451**, 113 (1999), [hep-ph/9810374]; M. Bastero-Gil, G. L. Kane and S. F. King, Phys. Lett. **B474**, 103 (2000), [hep-ph/9910506]; J. A. Casas, J. R. Espinosa and I. Hidalgo, JHEP **01**, 008 (2004), [hep-ph/0310137]; H. Abe, T. Kobayashi and Y. Omura, Phys. Rev. **D76**, 015002 (2007), [hep-ph/0703044]; R. Essig and J.-F. Fortin, JHEP **04**, 073 (2008), [arXiv:0709.0980].
- [182] B. de Carlos and J. A. Casas, Phys. Lett. **B309**, 320 (1993), [hep-ph/9303291]; S. Cassel, D. M. Ghilencea and G. G. Ross, Nucl. Phys. **B825**, 203 (2010), [arXiv:0903.1115]; S. Cassel, D. M. Ghilencea and G. G. Ross, Nucl. Phys. **B835**, 110 (2010), [arXiv:1001.3884].
- [183] B. C. Allanach, Phys. Lett. B **635**, 123 (2006), [hep-ph/0601089].
- [184] B. C. Allanach *et al.*, JHEP **08**, 023 (2007), [arXiv:0705.0487].
- [185] O. Buchmueller *et al.*, Eur. Phys. J. **C74**, 6, 2922 (2014), [arXiv:1312.5250].
- [186] P. Bechtle *et al.*, Eur. Phys. J. **C76**, 96 (2016), [arXiv:1508.05951].
- [187] H. Baer *et al.*, Phys. Rev. **D89**, 115019 (2014), [arXiv:1404.2277].
- [188] R. Barbieri and A. Strumia, in “4th Rencontres du Vietnam: Physics at Extreme Energies (Particle Physics and Astrophysics) Hanoi, Vietnam, July 19-25, 2000,” (2000), [hep-ph/0007265].
- [189] L. Giusti, A. Romanino and A. Strumia, Nucl. Phys. **B550**, 3 (1999), [hep-ph/9811386]; H.-C. Cheng and I. Low, JHEP **09**, 051 (2003), [hep-ph/0308199]; H.-C. Cheng and I. Low, JHEP **08**, 061 (2004), [hep-ph/0405243]; R. Harnik *et al.*, Phys. Rev. **D70**, 015002 (2004), [hep-ph/0311349].
- [190] H. Baer *et al.*, Phys. Rev. **D87**, 035017 (2013), [arXiv:1210.3019]; H. Baer *et al.*, Phys. Rev. **D87**, 115028 (2013), [arXiv:1212.2655]; J. L. Feng, Ann. Rev. Nucl. Part. Sci. **63**, 351 (2013), [arXiv:1302.6587].
- [191] J. L. Feng, K. T. Matchev and T. Moroi, Phys. Rev. Lett. **84**, 2322 (2000), [hep-ph/9908309]; J. L. Feng and F. Wilczek, Phys. Lett. **B631**, 170 (2005), [hep-ph/0507032]; D. Horton and G. G. Ross, Nucl. Phys. **B830**, 221 (2010), [arXiv:0908.0857].
- [192] M. Drees, Phys. Rev. **D33**, 1468 (1986); S. Dimopoulos and G. F. Giudice, Phys. Lett. **B357**, 573 (1995), [hep-ph/9507282]; A. Pomarol and D. Tommasini, Nucl. Phys. **B466**, 3 (1996), [hep-ph/9507462].
- [193] M. Dine, A. Kagan and S. Samuel, Phys. Lett. **B243**, 250 (1990); A. G. Cohen, D. B. Kaplan and A. E. Nelson, Phys. Lett. **B388**, 588 (1996), [hep-ph/9607394].
- [194] C. Brust *et al.*, JHEP **03**, 103 (2012), [arXiv:1110.6670].
- [195] S. P. Martin, Phys. Rev. **D75**, 115005 (2007), [hep-ph/0703097]; S. P. Martin, Phys. Rev. **D78**, 055019 (2008), [arXiv:0807.2820].
- [196] J. Fan, M. Reece and J. T. Ruderman, JHEP **11**, 012 (2011), [arXiv:1105.5135]; J. Fan, M. Reece and J. T. Ruderman, JHEP **07**, 196 (2012), [arXiv:1201.4875].
- [197] H. Murayama, Y. Nomura and D. Poland, Phys. Rev. **D77**, 015005 (2008), [arXiv:0709.0775]; G. Perez, T. S. Roy and M. Schmaltz, Phys. Rev. **D79**, 095016 (2009), [arXiv:0811.3206].
- [198] R. Dermisek and J. F. Gunion, Phys. Rev. Lett. **95**, 041801 (2005), [hep-ph/0502105]; Phys. Rev. **D75**, 095019 (2007); R. Dermisek and J. F. Gunion, Phys. Rev. **D76**, 095006 (2007), [arXiv:0705.4387].
- [199] G. G. Ross and K. Schmidt-Hoberg, Nucl. Phys. **B862**, 710 (2012), [arXiv:1108.1284]; G. G. Ross, K. Schmidt-Hoberg and F. Staub, JHEP **08**, 074 (2012), [arXiv:1205.1509]; A. Kaminska, G. G. Ross and K. Schmidt-Hoberg, JHEP **11**, 209 (2013), [arXiv:1308.4168].
- [200] S. P. Martin and J. D. Wells, Phys. Rev. **D86**, 035017 (2012), [arXiv:1206.2956].
- [201] B. Bellazzini *et al.*, Phys. Rev. **D79**, 095003 (2009), [arXiv:0902.0015].
- [202] M. Dine, Ann. Rev. Nucl. Part. Sci. **65**, 43 (2015), [arXiv:1501.01035].
- [203] H. Baer, V. Barger and M. Savoy, Phys. Rev. **D93**, 035016 (2016), [arXiv:1509.02929].
- [204] M.L. Mangano, editor, *Physics at the FCC-hh, a 100 TeV pp collider*, CERN Yellow Report, CERN-2017-003-M (2017).
- [205] P. Athron *et al.* (GAMBIT), Eur. Phys. J. C **77**, 12, 879 (2017), [arXiv:1705.07917].
- [206] D. Stockinger, J. Phys. **G34**, R45 (2007), [hep-ph/0609168]; P. Athron *et al.*, Eur. Phys. J. **C76**, 62 (2016), [arXiv:1510.08071].
- [207] F. Jegerlehner, Acta Phys. Polon. **B49**, 1157 (2018), [arXiv:1804.07409]; M. Davier *et al.*, Eur. Phys. J. **C80**, 3, 241 (2020), [arXiv:1908.00921].
- [208] B. Abi *et al.* (Muon $g - 2$ Collaboration), Phys. Rev. Lett. **126**, 141801 (2021), [arXiv:2104.03281].
- [209] S. Borsanyi *et al.*, Nature **593**, 51 (2021), [arXiv:2002.12347].
- [210] M. Ibe, T. T. Yanagida and N. Yokozaki, JHEP **08**, 067 (2013), [arXiv:1303.6995].
- [211] D. Hanneke, S. Fogwell and G. Gabrielse, Phys. Rev. Lett. **100**, 120801 (2008), [arXiv:0801.1134].
- [212] R. H. Parker *et al.*, Science **360**, 191 (2018), [arXiv:1812.04130].
- [213] L. Morel *et al.*, Nature **588**, 61 (2020).
- [214] B. Dutta and Y. Mimura, Phys. Lett. **B790**, 563 (2019), [arXiv:1811.10209]; M. Endo and W. Yin, JHEP **08**, 122 (2019), [arXiv:1906.08768]; M. Badziak and K. Sakurai, JHEP **10**, 024 (2019), [arXiv:1908.03607]; S. Li, Y. Xiao and J. M. Yang, Eur. Phys. J. C **82**, 3, 276 (2022), [arXiv:2107.04962].
- [215] T. Ibrahim and P. Nath, Phys. Rev. D **62**, 015004 (2000), [hep-ph/9908443]; R. L. Arnowitt, B. Dutta and Y. Santoso, Phys. Rev. D **64**, 113010 (2001), [hep-ph/0106089]; C. Han (2021), [arXiv:2104.03292].

- [216] J. Albrecht, D. van Dyk and C. Langenbruch, *Prog. Part. Nucl. Phys.* **120**, 103885 (2021), [arXiv:2107.04822].
- [217] A. Limosani *et al.* (Belle Collaboration), *Phys. Rev. Lett.* **103**, 241801 (2009), [arXiv:0907.1384]; J. P. Lees *et al.* (BaBar Collaboration), *Phys. Rev. Lett.* **109**, 191801 (2012), [arXiv:1207.2690]; J. P. Lees *et al.* (BaBar Collaboration), *Phys. Rev.* **D86**, 112008 (2012), [arXiv:1207.5772].
- [218] M. Misiak *et al.*, *Phys. Rev. Lett.* **114**, 221801 (2015), [arXiv:1503.01789]; M. Czakon *et al.*, *JHEP* **04**, 168 (2015), [arXiv:1503.01791]; M. Misiak, A. Rehman and M. Steinhauser, *JHEP* **06**, 175 (2020), [arXiv:2002.01548].
- [219] H. Baer and M. Brhlik, *Phys. Rev.* **D55**, 3201 (1997), [hep-ph/9610224]; M. Ciuchini *et al.*, *Phys. Rev.* **D67**, 075016 (2003), [Erratum: **D68**, 079901 (2003)], [hep-ph/0212397]; T. Hurth, *Rev. Mod. Phys.* **75**, 1159 (2003), [hep-ph/0212304]; F. Mahmoudi, *JHEP* **12**, 026 (2007), [arXiv:0710.3791]; K. A. Olive and L. Velasco-Sevilla, *JHEP* **05**, 052 (2008), [arXiv:0801.0428].
- [220] S. R. Choudhury and N. Gaur, *Phys. Lett.* **B451**, 86 (1999), [hep-ph/9810307]; K. S. Babu and C. F. Kolda, *Phys. Rev. Lett.* **84**, 228 (2000), [hep-ph/9909476]; G. Isidori and A. Retico, *JHEP* **11**, 001 (2001), [hep-ph/0110121]; G. Isidori and A. Retico, *JHEP* **09**, 063 (2002), [hep-ph/0208159].
- [221] W. Altmannshofer and P. Stangl, *Eur. Phys. J. C* **81**, 10, 952 (2021), [arXiv:2103.13370].
- [222] S. Chatrchyan *et al.* (CMS Collaboration), *Phys. Rev. Lett.* **111**, 101804 (2013), [arXiv:1307.5025]; V. Khachatryan *et al.* (CMS and LHCb Collaborations), *Nature* **522**, 68 (2015), [arXiv:1411.4413]; M. Aaboud *et al.* (ATLAS Collaboration), *JHEP* **04**, 098 (2019), [arXiv:1812.03017]; R. Aaij *et al.* (LHCb Collaboration), *Phys. Rev. Lett.* **118**, 191801 (2017), [arXiv:1703.05747].
- [223] J. Aebischer *et al.*, *Eur. Phys. J. C* **80**, 3, 252 (2020), [arXiv:1903.10434].
- [224] C. Bobeth *et al.*, *Phys. Rev. Lett.* **112**, 101801 (2014), [arXiv:1311.0903].
- [225] R. Aaij *et al.* (LHCb Collaboration), *Nature Physics* **18**, 3, 277 (2022), [arXiv:2103.11769].
- [226] R. Aaij *et al.* (LHCb Collaboration), *Phys. Rev. Lett.* **125**, 1, 011802 (2020), [arXiv:2003.04831].
- [227] R. Aaij *et al.* (LHCb), *Phys. Rev. Lett.* **127**, 15, 151801 (2021), [arXiv:2105.14007].
- [228] M. Bona *et al.* (UTfit Collaboration), *Phys. Lett.* **B687**, 61 (2010), [arXiv:0908.3470].
- [229] J. P. Lees *et al.* (BaBar Collaboration), *Phys. Rev. Lett.* **109**, 101802 (2012), [arXiv:1205.5442]; J. P. Lees *et al.* (BaBar Collaboration), *Phys. Rev.* **D88**, 072012 (2013), [arXiv:1303.0571].
- [230] R. Aaij *et al.* (LHCb Collaboration), *Phys. Rev. Lett.* **115**, 111803 (2015), [Erratum: **115**, 159901 (2015)], [arXiv:1506.08614]; R. Aaij *et al.* (LHCb Collaboration), *Phys. Rev. Lett.* **120**, 171802 (2018), [arXiv:1708.08856]; M. Huschle *et al.* (Belle Collaboration), *Phys. Rev.* **D92**, 072014 (2015), [arXiv:1507.03233]; Y. Sato *et al.* (Belle Collaboration), *Phys. Rev.* **D94**, 072007 (2016), [arXiv:1607.07923]; S. Hirose *et al.* (Belle Collaboration), *Phys. Rev. Lett.* **118**, 211801 (2017), [arXiv:1612.00529]; S. Hirose *et al.* (Belle Collaboration), *Phys. Rev.* **D97**, 012004 (2018), [arXiv:1709.00129].
- [231] G. Caria *et al.* (Belle Collaboration), *Phys. Rev. Lett.* **124**, 16, 161803 (2020), [arXiv:1910.05864].
- [232] Y. S. Amhis *et al.* (HFLAV), *Eur. Phys. J. C* **81**, 3, 226 (2021), [arXiv:1909.12524].
- [233] F. Mahmoudi, S. Neshatpour and J. Orloff, *JHEP* **08**, 092 (2012), [arXiv:1205.1845]; A. Arbey *et al.*, *JHEP* **11**, 132 (2017), [arXiv:1707.00426].
- [234] H. Eberl *et al.*, *Phys. Rev. D* **104**, 075025 (2021), [arXiv:2106.15228].
- [235] S. Trifinopoulos, *Eur. Phys. J. C* **78**, 10, 803 (2018), [arXiv:1807.01638]; W. Altmannshofer *et al.*, *Phys. Rev. D* **102**, 1, 015031 (2020), [arXiv:2002.12910]; P. S. Bhupal Dev, A. Soni and F. Xu (2021), [arXiv:2106.15647].
- [236] A. J. Buras, *Acta Phys. Polon.* **B49**, 1043 (2018), [arXiv:1805.11096].
- [237] V. Cirigliano *et al.*, *JHEP* **02**, 032 (2020), [arXiv:1911.01359].
- [238] J. R. Ellis *et al.*, *JHEP* **08**, 083 (2007), [arXiv:0706.0652]; S. Heinemeyer *et al.*, *JHEP* **08**, 087 (2008), [arXiv:0805.2359]; G.-C. Cho *et al.*, *JHEP* **11**, 068 (2011), [arXiv:1104.1769].
- [239] A. J. Buras *et al.*, *Nucl. Phys.* **B592**, 55 (2001), [hep-ph/0007313].
- [240] P. F. de Salas *et al.*, *JHEP* **02**, 071 (2021), [arXiv:2006.11237]; I. Esteban *et al.*, *JHEP* **09**, 178 (2020), [arXiv:2007.14792].
- [241] K. Zuber, *Phys. Rept.* **305**, 295 (1998), [hep-ph/9811267]; S. F. King, *J. Phys.* **G42**, 123001 (2015), [arXiv:1510.02091]; S. F. King, *Prog. Part. Nucl. Phys.* **94**, 217 (2017), [arXiv:1701.04413].
- [242] For a review of neutrino masses in supersymmetry, see *e.g.*, B. Mukhopadhyaya, *Proc. Indian National Science Academy* **A70**, 239 (2004); M. Hirsch and J. W. F. Valle, *New J. Phys.* **6**, 76 (2004), [hep-ph/0405015].
- [243] F. Borzumati and Y. Nomura, *Phys. Rev.* **D64**, 053005 (2001), [hep-ph/0007018].
- [244] P. Minkowski, *Phys. Lett.* **67B**, 421 (1977); M. Gell-Mann, P. Ramond, and R. Slansky, in *Supergravity*, edited by D. Freedman and P. van Nieuwenhuizen (North Holland, Amsterdam, 1979) p. 315; T. Yanagida, *Prog. Theor. Phys.* **64**, 1103 (1980); R. N. Mohapatra and G. Senjanovic, *Phys. Rev. Lett.* **44**, 912 (1980); R. N. Mohapatra and G. Senjanovic, *Phys. Rev.* **D23**, 165 (1981).
- [245] J. Hisano *et al.*, *Phys. Lett.* **B357**, 579 (1995), [hep-ph/9501407]; J. Hisano *et al.*, *Phys. Rev.* **D53**, 2442 (1996), [hep-ph/9510309]; J. A. Casas and A. Ibarra, *Nucl. Phys.* **B618**, 171 (2001), [hep-ph/0103065]; J. R. Ellis *et al.*, *Phys. Rev.* **D66**, 115013 (2002), [hep-ph/0206110]; A. Masiero, S. K. Vempati and O. Vives, *New J. Phys.* **6**, 202 (2004), [hep-ph/0407325]; E. Arganda *et al.*, *Phys. Rev.* **D71**, 035011 (2005), [hep-ph/0407302]; F. R. Joaquim and A. Rossi, *Phys. Rev. Lett.* **97**, 181801 (2006), [hep-ph/0604083]; J. R. Ellis and O. Lebedev, *Phys. Lett.* **B653**, 411 (2007), [arXiv:0707.3419].
- [246] Y. Grossman and H. E. Haber, *Phys. Rev. Lett.* **78**, 3438 (1997), [hep-ph/9702421]; A. Dedes, H. E. Haber and J. Rosiek, *JHEP* **11**, 059 (2007), [arXiv:0707.3718].
- [247] M. Hirsch, H. V. Klapdor-Kleingrothaus and S. G. Kovalenko, *Phys. Lett.* **B398**, 311 (1997), [hep-ph/9701253]; L. J. Hall, T. Moroi and H. Murayama, *Phys. Lett.* **B424**, 305 (1998), [hep-ph/9712515]; K. Choi, K. Hwang and W. Y. Song, *Phys. Rev. Lett.* **88**, 141801 (2002), [hep-ph/0108028]; T. Honkavaara, K. Huitu and S. Roy, *Phys. Rev.* **D73**, 055011 (2006), [hep-ph/0512277].
- [248] T. Faber *et al.*, *Phys. Rev. D* **101**, 5, 055029 (2020), [arXiv:1909.11686].
- [249] L. Basso *et al.*, *Comput. Phys. Commun.* **184**, 698 (2013), [arXiv:1206.4563].
- [250] M. Chemtob, *Prog. Part. Nucl. Phys.* **54**, 71 (2005), [hep-ph/0406029]; R. Barbier *et al.*, *Phys. Rept.* **420**, 1 (2005), [hep-ph/0406039].
- [251] H. Dreiner, in *Perspectives on Supersymmetry II*, edited by G.L. Kane (World Scientific, Singapore, 2010) pp. 565–583.
- [252] B. C. Allanach, A. Dedes and H. K. Dreiner, *Phys. Rev.* **D60**, 075014 (1999), [hep-ph/9906209].

- [253] L. E. Ibanez and G. G. Ross, Nucl. Phys. **B368**, 3 (1992); L. E. Ibanez, Nucl. Phys. **B398**, 301 (1993), [hep-ph/9210211].
- [254] A. Dedes, S. Rimmer and J. Rosiek, JHEP **08**, 005 (2006), [hep-ph/0603225]; B. C. Allanach and C. H. Kom, JHEP **04**, 081 (2008), [arXiv:0712.0852]; H. K. Dreiner *et al.*, Phys. Rev. **D84**, 113005 (2011), [arXiv:1106.4338].
- [255] H. K. Dreiner, C. Luhn and M. Thormeier, Phys. Rev. **D73**, 075007 (2006), [hep-ph/0512163].
- [256] K. Tamvakis, Phys. Lett. **B382**, 251 (1996), [hep-ph/9604343]; G. Eyal and Y. Nir, JHEP **06**, 024 (1999), [hep-ph/9904473]; A. Florez *et al.*, Phys. Rev. **D87**, 095010 (2013), [arXiv:1303.0278].
- [257] C. Csaki, Y. Grossman and B. Heidenreich, Phys. Rev. **D85**, 095009 (2012), [arXiv:1111.1239].
- [258] D. Dercks *et al.*, Eur. Phys. J. **C77**, 856 (2017), [arXiv:1706.09418].
- [259] B. C. Allanach and B. Gripaios, JHEP **05**, 062 (2012), [arXiv:1202.6616]; M. Asano, K. Rolbiecki and K. Sakurai, JHEP **01**, 128 (2013), [arXiv:1209.5778]; N. Chamoun *et al.*, JHEP **08**, 142 (2014), [arXiv:1407.2248].
- [260] J. C. Romao, Nucl. Phys. Proc. Suppl. **81**, 231 (2000), [hep-ph/9907466]; Y. Grossman and S. Rakshit, Phys. Rev. **D69**, 093002 (2004), [hep-ph/0311310].
- [261] R. N. Mohapatra, Phys. Rev. **D34**, 3457 (1986); K. S. Babu and R. N. Mohapatra, Phys. Rev. Lett. **75**, 2276 (1995), [hep-ph/9506354]; M. Hirsch, H. V. Klapdor-Kleingrothaus and S. G. Kovalenko, Phys. Rev. Lett. **75**, 17 (1995); M. Hirsch, H. V. Klapdor-Kleingrothaus and S. G. Kovalenko, Phys. Rev. **D53**, 1329 (1996), [hep-ph/9502385].
- [262] Y. Grossman and H. E. Haber, Phys. Rev. **D59**, 093008 (1999), [hep-ph/9810536].
- [263] S. Dimopoulos and L. J. Hall, Phys. Lett. **B207**, 210 (1988); J. Kalinowski *et al.*, Phys. Lett. **B406**, 314 (1997), [hep-ph/9703436]; J. Erler, J. L. Feng and N. Polonsky, Phys. Rev. Lett. **78**, 3063 (1997), [hep-ph/9612397].
- [264] H. K. Dreiner, P. Richardson and M. H. Seymour, Phys. Rev. **D63**, 055008 (2001), [hep-ph/0007228].
- [265] J. E. Kim and H. P. Nilles, Phys. Lett. **138B**, 150 (1984).
- [266] J. E. Kim and H. P. Nilles, Mod. Phys. Lett. **A9**, 3575 (1994), [hep-ph/9406296].
- [267] G. F. Giudice and A. Masiero, Phys. Lett. **B206**, 480 (1988); J. A. Casas and C. Munoz, Phys. Lett. **B306**, 288 (1993), [hep-ph/9302227]; K. J. Bae *et al.*, Phys. Rev. **D99**, 115027 (2019), [arXiv:1902.10748].
- [268] M. Cvetič *et al.*, Phys. Rev. **D56**, 2861 (1997), [Erratum: **D58**, 119905 (1998)], [hep-ph/9703317].
- [269] R. D. Peccei, Lect. Notes Phys. **741**, 3 (2008), [hep-ph/0607268].
- [270] R. D. Peccei and H. R. Quinn, Phys. Rev. Lett. **38**, 1440 (1977); R. D. Peccei and H. R. Quinn, Phys. Rev. **D16**, 1791 (1977).
- [271] H. Murayama, H. Suzuki and T. Yanagida, Phys. Lett. **B291**, 418 (1992); T. Gherghetta and G. L. Kane, Phys. Lett. **B354**, 300 (1995), [hep-ph/9504420]; K. J. Bae, H. Baer and H. Serce, Phys. Rev. **D91**, 1, 015003 (2015), [arXiv:1410.7500]; H. Baer, V. Barger and D. Sengupta, Phys. Lett. **B790**, 58 (2019), [arXiv:1810.03713].
- [272] P. Fayet, Phys. Lett. **78B**, 417 (1978).
- [273] K. Benakli, Fortsch. Phys. **59**, 1079 (2011), [arXiv:1106.1649].
- [274] P. J. Fox, A. E. Nelson and N. Weiner, JHEP **08**, 035 (2002), [hep-ph/0206096].
- [275] K. Benakli and M. D. Goodsell, Nucl. Phys. **B816**, 185 (2009), [arXiv:0811.4409]; K. Benakli and M. D. Goodsell, Nucl. Phys. **B840**, 1 (2010), [arXiv:1003.4957].
- [276] U. Sarkar and R. Adhikari, Phys. Rev. **D55**, 3836 (1997), [hep-ph/9608209]; R. Fok *et al.*, Phys. Rev. **D87**, 055018 (2013), [arXiv:1208.2784].
- [277] G. D. Kribs, E. Poppitz and N. Weiner, Phys. Rev. **D78**, 055010 (2008), [arXiv:0712.2039].
- [278] K. Benakli, M. D. Goodsell and F. Staub, JHEP **06**, 073 (2013), [arXiv:1211.0552].
- [279] J. L. Hewett and T. G. Rizzo, Phys. Rept. **183**, 193 (1989).
- [280] A. Delgado, G. Nardini and M. Quiros, Phys. Rev. **D86**, 115010 (2012), [arXiv:1207.6596].
- [281] S. F. King, S. Moretti and R. Nevzorov, Phys. Lett. **B634**, 278 (2006), [hep-ph/0511256]; S. F. King, S. Moretti and R. Nevzorov, Phys. Rev. **D73**, 035009 (2006), [hep-ph/0510419].
- [282] H. Kawase, JHEP **12**, 094 (2011), [arXiv:1110.3861]; N. Escudero, C. Munoz and A. M. Teixeira, Phys. Rev. D **73**, 055015 (2006), [hep-ph/0512046]; B. Dutta and Y. Mimura, Phys. Lett. B **790**, 589 (2019), [arXiv:1810.08413]; W. Altmannshofer *et al.*, JHEP **07**, 118 (2021), [arXiv:2104.08293].

89. Supersymmetry, Part II (Experiment)

Revised September 2021 by M. D’Onofrio (Liverpool U.) and F. Moortgat (CERN; Ghent U.).

89.1 Introduction

Supersymmetry (SUSY), a transformation relating fermions to bosons and vice versa [1–9] is one of the most compelling possible extensions of the Standard Model of particle physics (SM).

On theoretical grounds SUSY is motivated as a generalization of space-time symmetries. A low-energy realization of SUSY, *i.e.*, SUSY at the TeV scale, is, however, not a necessary consequence. Instead, low-energy SUSY is motivated by the possible cancellation of quadratic divergences in radiative corrections to the Higgs boson mass [10–15]. Furthermore, it is intriguing that a weakly interacting, (meta)stable supersymmetric particle might make up some or all of the dark matter in the Universe [16–18]. In addition, SUSY predicts that gauge couplings, as measured experimentally at the electroweak scale, unify at an energy scale $\mathcal{O}(10^{16})$ GeV (“GUT scale”) near the Planck scale [19–25].

In the minimal supersymmetric extension to the Standard Model, the so called MSSM [11, 26, 27], a supersymmetry transformation relates every chiral fermion and gauge boson in the SM to a supersymmetric partner with half a unit of spin difference, but otherwise with the same properties (such as mass) and quantum numbers. The MSSM Higgs sector contains two doublets, which give mass to the up-type and down-type quarks, respectively. After electroweak symmetry breaking, five Higgs bosons arise, of which two are charged. The supersymmetric partners of chiral fermions are squarks (\tilde{q}) and sleptons ($\tilde{\ell}, \tilde{\nu}$), and the “gauginos” for gauge bosons. The supersymmetric partners of the Higgs doublets are known as “higgsinos.” The weak gauginos and higgsinos mix, giving rise to charged mass eigenstates called “charginos” ($\tilde{\chi}^{\pm}$), and neutral mass eigenstates called “neutralinos” ($\tilde{\chi}^0$). These are often collectively referred to as electroweakinos (EWkinos). The SUSY partners of the gluons are known as “gluinos” (\tilde{g}). The fact that such particles are not yet observed leads to the conclusion that, if supersymmetry is realized, it is a broken symmetry. A description of SUSY in the form of an effective Lagrangian with only “soft” SUSY breaking terms and SUSY particle masses of the order of *TeV* maintains the cancellation of quadratic divergences of soft SUSY breaking scalar mass squared parameters.

The phenomenology of SUSY is to a large extent defined by the SUSY breaking mechanism and the SUSY breaking scale. These determine the SUSY particle masses, the mass hierarchy, the field contents of physical particles, and their decay modes. In addition, phenomenology crucially depends on whether the multiplicative quantum number of *R*-parity [27], $R = (-1)^{3(B-L)+2S}$, where *B* and *L* are baryon and lepton numbers and *S* is the spin, is conserved or violated. If *R*-parity is conserved, SUSY particles (sparticles), which have odd *R*-parity, are produced in pairs and the decays of each SUSY particle must involve an odd number of lighter SUSY particles. The lightest SUSY particle (LSP) is then stable and often assumed to be a weakly interacting massive particle (WIMP). If *R*-parity is violated, new terms λ_{ijk} , λ'_{ijk} and λ''_{ijk} appear in the superpotential, where *ijk* are generation indices; λ -type couplings appear between lepton superfields only, λ' -type are between quark superfields only, and λ'' -type couplings connect the two. *R*-parity violation implies lepton and/or baryon number violation. More details of the theoretical framework of SUSY are discussed elsewhere in this volume [28].

The discovery of a Higgs boson with a mass around 125 GeV imposes constraints on SUSY models, which are discussed elsewhere [28, 29]. Low-energy data from flavor physics experiments, high-precision electroweak observables as well as astrophysical data also impose strong constraints on the allowed SUSY parameter space. Recent examples of such data include measurements of the rare B-meson decay $B_s \rightarrow \mu^+ \mu^-$ [30–32], measurements of the anomalous magnetic moment of the muon [33, 34], and accurate determinations of the cosmological dark matter relic density constraint [35, 36].

Indirect constraints can be more sensitive to higher SUSY mass scales than experiments searching for direct sparticle production

at colliders, but the interpretation of these results is often strongly model dependent. In contrast, direct searches for sparticle production at collider experiments, which are the main topic of this review, are less subject to interpretation ambiguities and therefore they play a crucial role in the search for SUSY.

89.2 Overview of the experimental search programme

The electron-positron collider LEP was operational at CERN between 1989 and 2000. In the initial phase, center-of-mass energies around the *Z*-peak were probed, but after 1995 the LEP experiments collected a significant amount of luminosity at higher center-of-mass energies, some 235 pb^{-1} per experiment at $\sqrt{s} \geq 204$ GeV, with a maximum \sqrt{s} of 209 GeV. Searches for new physics at e^+e^- colliders benefit from the clean experimental environment and the fact that momentum balance can be measured not only in the plane transverse to the beam, but also in the direction along the beam (up to the beam pipe holes), defined as the longitudinal direction. Searches at LEP are dominated by the data samples taken at the highest center-of-mass energies.

The CDF and D0 experiments at the Tevatron, a proton-antiproton collider at a center-of-mass energy of up to 1.96 TeV, had an extensive search program for supersymmetric particles. CDF and D0 collected integrated luminosities between 10 and 11 fb^{-1} each up to the end of collider operations in 2011.

The electron-proton collider HERA provided collisions to the H1 and ZEUS experiments between 1992 and 2007, at a center-of-mass energy up to 318 GeV. A total integrated luminosity of approximately 0.5 fb^{-1} was collected by each experiment. Since at HERA baryons collide with leptons, SUSY searches at HERA typically look for *R*-parity violating production of single SUSY particles.

The Large Hadron Collider (LHC) at CERN started proton-proton operation at a center-of-mass energy of 7 TeV in 2010. By the end of 2011 the ATLAS and CMS experiments had collected about 5 fb^{-1} of integrated luminosity each, and the LHCb experiment had collected approximately 1 fb^{-1} . In 2012, the LHC operated at a center-of-mass energy of 8 TeV, and ATLAS and CMS collected approximately 20 fb^{-1} each, whereas LHCb collected 2 fb^{-1} . In 2015, the LHC started Run 2, with a center-of-mass energy of 13 TeV. At the end of Run 2 in November 2018, ATLAS and CMS had both collected approximately 140 fb^{-1} , and LHCb had collected almost 6 fb^{-1} .

At the LHC, cross sections of QCD-mediated processes are the largest achievable at colliders, which is reflected in the higher sensitivity for SUSY particles carrying color charge, squarks and gluinos, with respect to LEP, Tevatron and HERA. In particular, proton-proton collisions at the LHC differ from proton-antiproton collisions at the Tevatron in the sense that there are no valence anti-quarks in the proton, and that gluon-initiated processes play a more dominant role. The increased center-of-mass energy of the LHC compared to the Tevatron significantly extends the kinematic reach for SUSY searches. This is reflected foremost in the sensitivity for squarks and gluinos, but also for SUSY particles produced via electroweak processes.

In this review we report results of direct searches for SUSY particles at colliders up to August 2021, mostly covering data analyses at the ATLAS and CMS experiments with reference to results from LEP, HERA and the Tevatron. For more details on LEP and Tevatron constraints, see earlier PDG reviews [37]. Results are categorized depending on the targeted SUSY particles, the nature of their production and decays, and the assumption on *R*-parity. Brief summaries of search techniques and approaches adopted for interpretation of the results are given in Section 89.3 and 89.4, respectively. Sections 89.5–89.9 focus on results for promptly-decaying gluinos and first and second generation squarks, top and bottom squarks, electroweakinos (charginos, neutralinos) and sleptons. Limits obtained for sparticle masses assuming *R*-parity violating models are also reported. Results of dedicated searches for long-lived (LL) SUSY particles are reported in Section 89.10. Finally, Section 89.11 provides examples of global reinterpretations of SUSY searches.

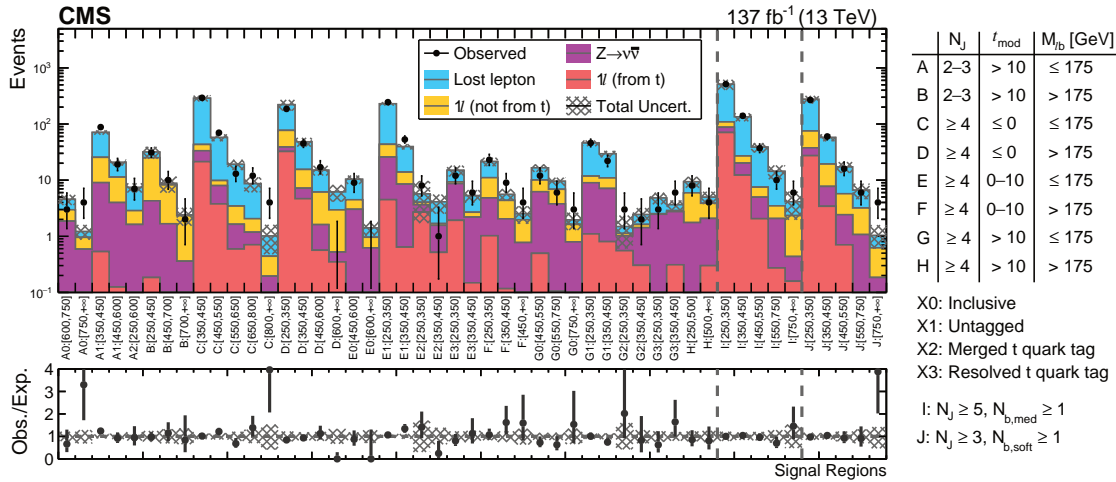


Figure 89.1: Example of multiple signal regions set for a typical SUSY search at the LHC. For definition of regions and acronyms specific for this search, see corresponding paper.

89.3 Experimental search techniques

Large background contributions from Standard Model processes pose challenges to the trigger and analysis. Such backgrounds are dominated by multijet production processes, including, particularly at the LHC, those of top quark production, as well as jet production in association with vector bosons. The proton momentum is shared between its parton constituents, and in each collision only a fraction of the total center-of-mass energy is available in the hard parton-parton scattering. Since the parton momenta in the longitudinal direction are not known on an event-by-event basis, use of momentum conservation constraints in an analysis is restricted to the transverse plane, leading to the definition of transverse variables, such as the missing transverse momentum, and the transverse mass.

Under the assumption of R -parity conservation (RPC), the typical SUSY search signature for squarks and gluinos at hadron colliders contains high- p_T jets, which are produced in the decay chains of heavy squarks and gluinos, and significant missing momentum originating from the two LSPs produced at the end of the decay chains, which escape experimental detection. Electroweakino decays are often characterised by the presence of leptons, for instance from W and Z bosons in the decay chain, plus missing transverse momentum. Standard Model backgrounds with missing transverse momentum include leptonic W/Z -boson decays, associated production of jets and a Z -boson decaying into neutrinos, semi-leptonic heavy-flavor decays to neutrinos, top-quark pair production with one or both W bosons decaying leptonically, and multijet events that may be affected by instrumental effects such as jet mis-measurement.

Selection variables designed to separate the SUSY signal from the Standard Model backgrounds include transverse variables such as H_T , E_T^{miss} , and m_{eff} . The quantities H_T and E_T^{miss} refer to the measured transverse energy and the missing transverse momentum in the event, respectively. They are usually defined as the scalar sum of the transverse jet momenta or of the transverse energies of calorimeter clusters measured in the event (H_T), or the magnitude (E_T^{miss}) of the negative vector sum of transverse momenta of reconstructed objects like jets and leptons in the event (\vec{p}_T^{miss}). The quantity m_{eff} is referred to as the effective mass of the event and is defined as $m_{\text{eff}} = H_T + E_T^{\text{miss}}$. The peak of the m_{eff} distribution for SUSY signal events correlates with the SUSY mass scale, in particular with the mass difference between the primary produced SUSY particle and the LSP [38], whereas the Standard Model backgrounds dominate at low m_{eff} . Additional reduction of multijet backgrounds can be achieved by demanding isolated leptons or photons in the final states; in such events the lepton or photon transverse momentum may be added to H_T or m_{eff} for further signal-background separation. Other kinematic variables and approaches developed to increase the sensitivity to

pair production of heavy sparticles with TeV-scale masses focusing on the kinematics of their decays are the α_T [39–43], *razor* [44], *stransverse mass* (m_{T2}) [45], and *contransverse mass* (m_{CT}) [46] variables. More recently, the topological event reconstruction methods have expanded with the *super-razor* [47] and *recursive jigsaw reconstruction* [48] techniques. Furthermore, the searches for massive SUSY particles frequently attempt to identify their decay into top quarks or vector bosons, which are themselves unstable. If these are produced with a significant boost, jets from their decay will typically overlap, and such topologies are searched for with *jet-substructure* [49] techniques.

Most analyses use simple combinations of selections on kinematic variables (often referred to as *cut-and-count* analyses) and exploit multiple signal regions defined by categorizing events on the basis of several variables and their correlations. An example is provided in Fig. 89.1 from Ref. [50]: 39 signal regions are set to search for top squarks in events with one lepton, jets and missing transverse momentum. Regions depend on jet multiplicities, reconstructed top-quark candidates and thresholds applied to the most discriminant variables used for optimisation.

In recent years, shape analyses or analyses using more sophisticated techniques, e.g. machine learning (ML), have been also developed. ML techniques often allow analyses to better capture the complexity of the events and achieve improved sensitivity with respect to counting experiments. For example, Boosted Decision Trees (BDTs) allow analyses to exploit simultaneously the discriminating power of multiple variables and that of correlations among objects in the events. Deep Neural Networks (NN) are also employed for objects reconstruction and to use directly detector-recorded energies and momenta of produced particles instead of first deriving a restricted set of physical variables. Among others, currently in use are Convolutional NN for image classification techniques, Recurrent NN and Generative Adversarial Networks.

Variables and approaches reported above are also used in searches for R -parity violating (RPV) SUSY models where signal events are often characterised by the presence of multiple leptons and/or jets, and little or no missing transverse momentum. However, if R -parity violating couplings are small, sparticles might be long-lived and may travel macroscopic distances before decaying. Similarly, long lifetimes may be due to small mass splittings, as in the case of pure higgsino/wino scenarios, or to heavy mediators, as in Split SUSY models [51, 52]. The identification of long-lived particles requires dedicated tools and their signatures can be very diverse. At the LHC, customized techniques (also based on NN) have been developed, for example, to reconstruct significantly displaced decay vertices or short track segments, and to identify tracks with atypical properties or unusual ionization, small and localized deposits of energy inside of the calorimeters without associated tracks, or stopped particles that decay out of

time with collisions. For an overview, see Ref. [53].

89.4 Interpretation of search results

Since the mechanism by which SUSY is broken is unknown, a general approach to SUSY via the most general soft SUSY breaking Lagrangian adds a significant number of new free parameters. For the minimal supersymmetric standard model, MSSM, *i.e.*, the model with the minimal particle content, these comprise 105 new real degrees of freedom. A phenomenological analysis of SUSY searches leaving all these parameters free is not feasible. For the practical interpretation of SUSY searches at colliders several approaches are taken to reduce the number of free parameters.

One approach is to assume a SUSY breaking mechanism and lower the number of free parameters through the assumption of additional constraints. Before the start of the LHC, interpretations of experimental results were often performed in constrained models of gravity mediated [54, 55], gauge-mediated [56–58], and anomaly mediated [59, 60] SUSY breaking. The most popular model was the constrained MSSM (CMSSM) [54, 61, 62], which in the literature is also referred to as minimal supergravity, or MSUGRA. These constrained SUSY models are theoretically well motivated and provide a rich spectrum of experimental signatures. However, with universality relations imposed on the soft SUSY breaking parameters, they do not cover all possible kinematic signatures and mass relations of SUSY. Furthermore, LHC Run 1 results, together with other collider and non-collider measurements, limited substantially the allowed SUSY parameter space for these models. This indicates that very constrained models like the CMSSM are no longer good benchmark scenarios to solely characterize the results of SUSY searches at the LHC and efforts have been made to complement them with more flexible approaches.

A broader and more comprehensive subset of the MSSM can be studied via the so-called phenomenological-MSSM, or pMSSM [63–66]. It is derived from the MSSM, using experimental data to eliminate parameters that are free in principle but have already been highly constrained by measurements of *e.g.*, flavor mixing and CP -violation. This effective approach reduces the number of free parameters in the MSSM to typically 19 or even less, making it a practical compromise between the full MSSM and highly constrained models such as the CMSSM.

Even less dependent on fundamental assumptions are interpretations in terms of so-called simplified models [67–70]. Such models assume a limited set of SUSY particle production and decay modes and leave open the possibility to vary masses and other parameters freely. Therefore, simplified models enable comprehensive studies of individual SUSY topologies, and are useful for optimization of the experimental searches over a wide parameter space without limitations on fundamental kinematic properties such as masses, production cross sections, and decay modes.

As a consequence, ATLAS and CMS have adopted simplified models as the primary framework to provide interpretations of their searches. In addition to using simplified models that describe prompt decays of SUSY particles, the experiments are now also focusing more on the use of simplified models that allow for decays of long-lived SUSY particles as they can arise in different SUSY scenarios (see Section 89.10 for further discussion). Today, almost every individual search provides interpretations of their results in one or several simplified models that are characteristic of SUSY topologies probed by the analysis.

While simplified models are very convenient for the interpretation of individual SUSY production and decay topologies, care must be taken when applying these limits to more complex SUSY spectra. In particular, the branching ratio of SUSY particles into a specific final state is often assumed to be 100% and in many of the quoted limits the LSP is assumed to be massless. Therefore, simplified model limits should be seen as an approximation of the constraints that can be placed on sparticle masses in more complex SUSY spectra. Only on a case-by-case basis can it be determined whether the limit of a given simplified model represents a good approximation of the true underlying constraint that can be applied on a sparticle mass in a complex SUSY spectrum. In the following, we will point out explicitly the assumptions that have entered the limits when quoting interpretations from simplified models.

Since none of the searches performed so far have shown significant excess above the SM background prediction, the interpretation of the presented results are exclusion limits on SUSY parameter space. Unless stated differently, all quoted exclusion limits are at 95% confidence level. Finally, we note that many of the recent publications by ATLAS and CMS also present results in terms of model-independent limits such that their discovery potential is statistically quantified independently on a particular model.

89.5 Exclusion limits on gluino, first and second generation squark masses in RPC scenarios

Colored SUSY particles such as squarks and gluinos are produced via the strong interaction and have the highest cross sections at hadron colliders. Limits on squark masses of the order 100 GeV have been set by the LEP experiments [71], in the decay to quark plus neutralino, and for a mass difference between squark and quark plus neutralino of typically at least a few GeV. However, hadron collider experiments are able to set much more stringent mass limits.

The main production mechanisms at hadron colliders are squark-squark, squark-gluino and gluino-gluino production; when “squark” is used “antisquark” is also implied. Pair production usually involves both the s -channel and t -channel parton-parton interactions. However, since there is a negligible amount of bottom and top quark content in the proton, top and bottom squark production proceeds through s -channel diagrams only. Experimental analyses of squark and/or gluino production typically assume the first and second generation squarks to be approximately degenerate in mass. Cross section calculations shown in Fig. 89.2 (from Ref. [72]) assume mass degeneracy of left- and right-handed u , d , s , c squarks. Other sparticle masses are considered decoupled. The LHC experiments have started to also provide simplified model limits on individual first or second generation squarks. Top and bottom squarks have the same production cross section, equivalent to that of a single light squark.

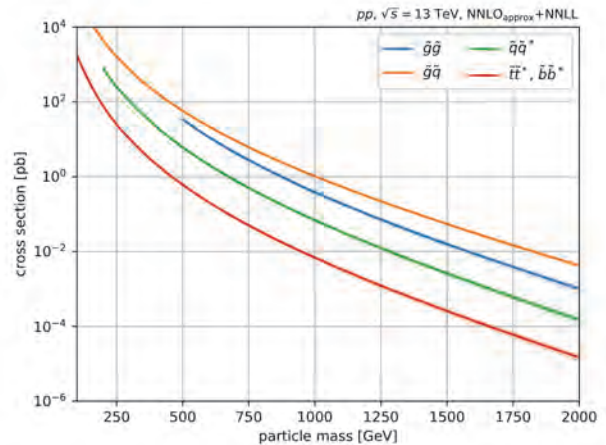


Figure 89.2: Cross sections for pair production of gluinos and squarks as a function of their mass at the LHC for a center-of-mass energy of 13 TeV. They are calculated at approximately next-to-next-to-LO (NNLO) including the resummation of soft gluon emission at the next-to-next-to-leading logarithmic accuracy (NNLO_{approx}+NNLL).

In this section, we focus on results assuming R -parity conservation. Limits set by the Tevatron experiments on the gluino mass assume the framework of the CMSSM, with $\tan\beta = 5$ (CDF) or $\tan\beta = 3$ (D0). Furthermore, the common trilinear term A_0 is set to 0 and the higgsino mass term μ is assumed to be less than 0. The resulting lower mass limits are about 310 GeV for all squark masses, or 390 GeV for the case $m_{\bar{q}} = m_{\bar{g}}$ [73, 74]. These limits have been superseded by those provided by ATLAS and CMS, and the tightest constraints have been set with up to approximately

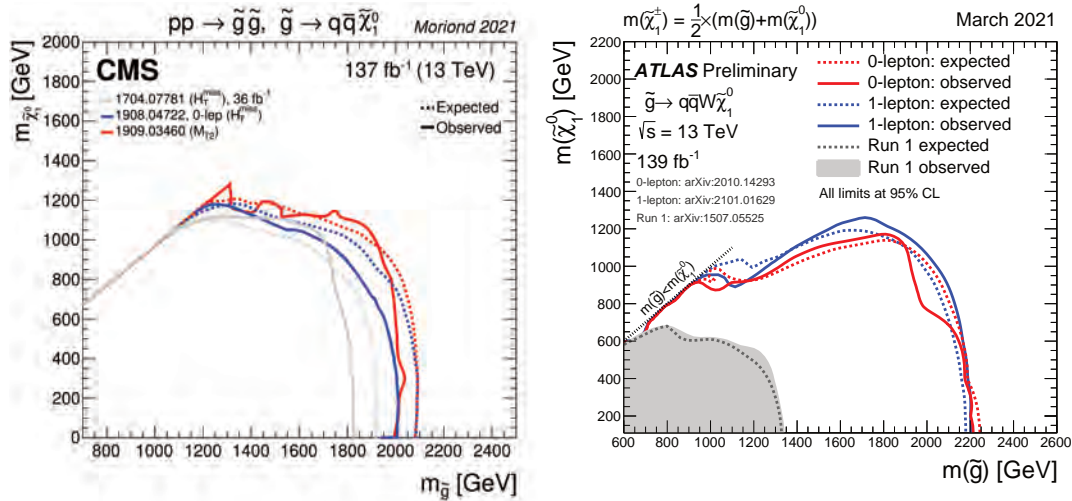


Figure 89.3: Lower mass limits, at 95% C.L., on gluino pair production for various decay chains in the framework of simplified models. Left: $\tilde{g} \rightarrow q\bar{q}\tilde{\chi}_1^0$, result of the CMS collaboration. Right: $\tilde{g} \rightarrow q\bar{q}W\tilde{\chi}_1^0$, result of the ATLAS collaboration.

140 fb⁻¹ of data recorded at the LHC at a center-of-mass energy of 13 TeV.

ATLAS and CMS limits on the gluino mass have been established in the framework of simplified models. Assuming only gluino pair production, three main primary decay chains of the gluino have been considered by the LHC experiments for interpretations of their search results. The first decay chain, $\tilde{g} \rightarrow q\bar{q}\tilde{\chi}_1^0$, assumes gluino mediated production of first and second generation squarks (on-shell or off-shell) which leads to four light flavor quarks in the final state. Therefore, inclusive all-hadronic analyses searching for multijet plus E_T^{miss} final states are utilized to put limits on this simplified model. These limits are derived as a function of the gluino and neutralino (LSP) mass. As shown in Fig. 89.3 (left) the CMS collaboration [75] excludes in this simplified model gluino masses below approximately 2.1 TeV for a light neutralino mass below about 600 GeV. In scenarios where neutralinos are not very light, the efficiency of the analyses is reduced by the fact that jets are less energetic, and there is less missing transverse momentum in the event. This leads to weaker limits when the mass difference $\Delta m = m_{\tilde{g}} - m_{\tilde{\chi}_1^0}$ is reduced. For example, for neutralino masses above about 1.2 TeV no limit on the gluino mass can be set for this decay chain. Therefore, limits on gluino masses are strongly affected by the assumption of the neutralino mass. Similar results for this simplified model have been obtained by ATLAS [76]. A second simplified model postulates a decay chain where $\tilde{g} \rightarrow q\bar{q}W\tilde{\chi}_1^0$, assuming that the intermediate (on-shell or off-shell) squark is left-handed and decays to a chargino and a quark, with the chargino decaying to a W boson and the LSP. This leads to two W bosons and four light flavor quarks plus E_T^{miss} in the final state. Both leptonic and hadronic decays of the W can be considered. In this scenario, the ATLAS collaboration [77, 78] excludes gluino masses below approximately 2.2 TeV for a sufficiently light neutralino and assuming the chargino mass is halfway between the gluino and neutralino mass, see Fig. 89.3 (right). Again, for neutralino masses above about 1.2 TeV, there exists no limit on the gluino mass for this decay chain. Similar results have been obtained by the CMS collaboration [79].

Gluino decays are not limited to first and second generation squarks: another important decay chain of the gluino considered for interpretation in simplified models is $\tilde{g} \rightarrow b\bar{b}\tilde{\chi}_1^0$. In this case the decay is mediated via bottom squarks and thus leads to four jets from b quarks and E_T^{miss} in the final state. For this topology as well, inclusive all-hadronic searches provide the highest sensitivity. However, with four b -quarks in the final state, the use of secondary vertex reconstruction for the identification of jets originating from b -quarks provides a powerful handle on the SM background. Therefore, in addition to a multijet plus E_T^{miss} signa-

ture these searches also require several jets to be tagged as b -jets. As shown in Fig. 89.4 (left), for this simplified model CMS [75] excludes gluino masses below ≈ 2.3 TeV for a sufficiently light neutralino, while for neutralino masses above ≈ 1.5 TeV no limit on the gluino mass can be set. Comparable limits for this simplified model are provided by searches from ATLAS [80].

If kinematically allowed, decays of gluinos to top squarks via $\tilde{g} \rightarrow t\bar{t}$ are also possible. This leads to a “four tops” final state, $ttt\tilde{\chi}_1^0\tilde{\chi}_1^0$, and defines the next important simplified model characterizing gluino pair production, $\tilde{g} \rightarrow t\bar{t}\tilde{\chi}_1^0$. The topology of this decay is very rich in different experimental signatures: as many as four isolated leptons, four b -jets, several light flavor quark jets, and significant missing transverse momentum from the neutrinos in the W decay and from the two neutralinos. As shown in Fig. 89.4 (right), the ATLAS search [80] rules out gluinos with masses below ≈ 2.25 TeV for light neutralinos in this model. For neutralino masses above ≈ 1.2 TeV, no limit can be placed on the gluino mass. The CMS multiple b -jet search [81] obtains similar limits.

Assuming gluinos to be heavier than squarks, squarks will predominantly decay to a quark and a neutralino or chargino, if kinematically allowed. The decay may involve the lightest neutralino (typically the LSP) or chargino, but, depending on the masses and couplings of the gauginos and on the handedness of the squarks, may involve heavier neutralinos or charginos. For pair production of first and second generation squarks, the simplest decay modes involve two jets and missing transverse momentum, with potential extra jets stemming from initial state or final state radiation (ISR/FSR) or from decay modes with longer decay chains (cascades). In cascades, isolated photons or leptons may appear from the decays of sparticles such as neutralinos or charginos. Final states are thus characterized by significant missing transverse momentum, and at least two, and possibly many more high p_T jets, which can be accompanied by one or more isolated objects like photons or leptons, including τ leptons, in the final state.

Limits on first and second generation squark masses set by the Tevatron experiments assume the CMSSM, and amount to lower limits of about 380 GeV for all gluino masses, or 390 GeV for the case $m_{\tilde{q}} = m_{\tilde{g}}$ [73, 74].

At the LHC, limits on squark masses have been set using up to approximately 140 fb⁻¹ of data at 13 TeV. Interpretations in simplified models typically characterize squark pair production with only one decay chain of $\tilde{q} \rightarrow q\tilde{\chi}_1^0$. Here it is assumed that the left and right-handed \tilde{u} , \tilde{d} , \tilde{s} and \tilde{c} squarks are degenerate in mass. Furthermore, it is assumed that the mass of the gluino is very high and thus contributions of the corresponding t -channel diagrams to squark pair production are negligible. Therefore, the total production cross section for this simplified model is eight

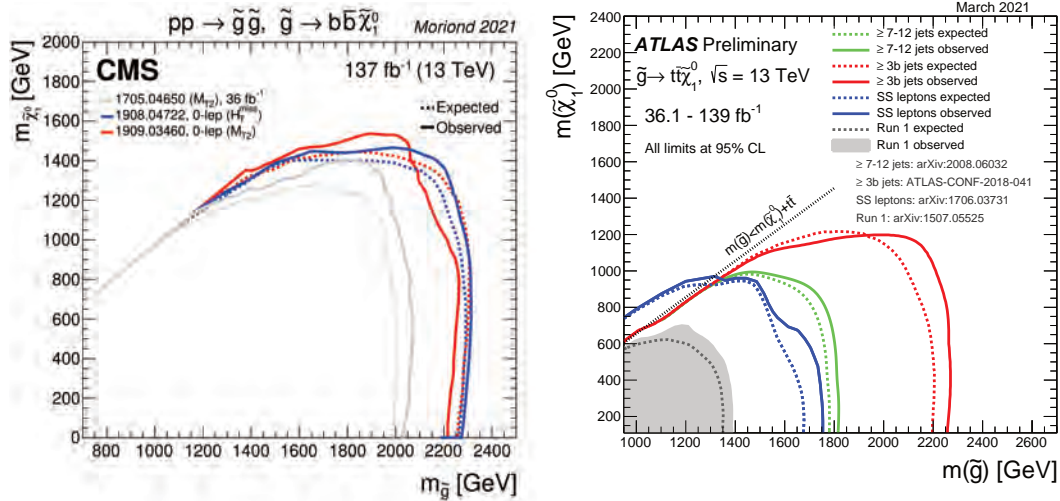


Figure 89.4: Lower mass limits, at 95% C.L., on gluino pair production for various decay chains in the framework of simplified models. Left: $\tilde{g} \rightarrow b\tilde{b}\tilde{\chi}_1^0$. Right: $\tilde{g} \rightarrow t\tilde{t}\tilde{\chi}_1^0$. Results from the CMS and ATLAS collaborations.

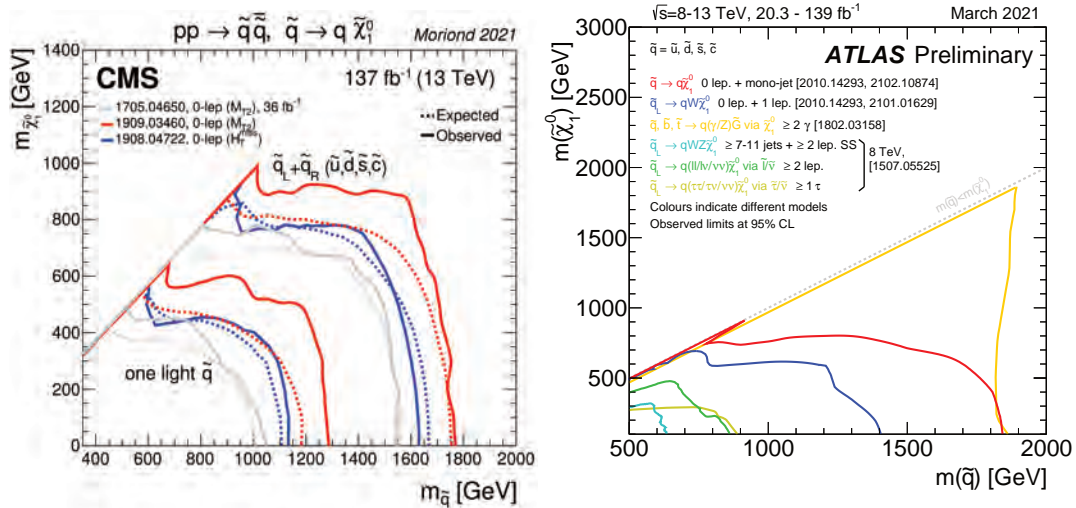


Figure 89.5: Left: 95% C.L. exclusion contours in the framework of simplified models assuming a single decay chain of $\tilde{q} \rightarrow q\tilde{\chi}_1^0$, obtained by the CMS collaboration. Right: Assuming more complicated decay chains including W or Z bosons, obtained by the ATLAS collaboration.

times the production cross section of an individual squark (e.g. \tilde{u}_L). Under these assumptions, CMS obtains a lower squark mass limit of ≈ 1.75 TeV for light neutralinos [81], as shown in Fig. 89.5 (left). The effects of heavy neutralinos on squark limits are similar to those discussed in the gluino case, and only for neutralino masses below ≈ 800 GeV can any squark masses be excluded. Searches for new physics in monojet channels are sensitive to very compressed scenarios, and masses up to 900 GeV are excluded for $\Delta m = m_{\tilde{q}}, m_{\tilde{\chi}_1^0} \approx 5$ GeV [82].

If the assumption of mass degenerate first and second generation squarks is dropped and only the production of a single light squark is assumed, the limits weaken significantly. For example, the CMS limit on degenerate squarks of 1750 GeV for light neutralinos drops to ≈ 1300 GeV for pair production of a single light squark, and for neutralinos heavier than ≈ 600 GeV no squark mass limit can be placed. It should be noted that this limit is not a result of a simple scaling of the above mentioned mass limits assuming eight-fold mass degeneracy but it also takes into account that for an eight times lower production cross section the analyses must probe kinematic regions of phase space that are closer to the ones of SM background production.

The results of the ATLAS searches for more complicated decay

chains, where e.g. intermediate bosons are produced as well [76], can be seen in Fig. 89.5 (right). Depending on the topology, the exclusion limit can reach up to ≈ 2 TeV (this value is only reached in gaugino-mediated simplified models).

For single light squarks ATLAS also reports results of a dedicated search for pair production of scalar partners of charm quarks [83]. Assuming that the scalar-charm state exclusively decays into a charm quark and a neutralino, scalar-charm masses up to 800 GeV are excluded for neutralino masses below 260 GeV.

A summary of the most important squark and gluino mass limits for different interpretation approaches assuming R -parity conservation is shown in Table 89.1. For gluino masses rather similar limits of about 2.3 TeV are obtained from different model assumptions, indicating that the LHC is indeed probing direct gluino production at the TeV scale and beyond. However, for neutralino masses above approximately 1.2 to 1.5 TeV, even in the best case scenarios, ATLAS and CMS searches do not place any limits on the gluino mass. Limits on direct squark production, on the other hand, depend strongly on the chosen model. For neutralino masses above ≈ 600 GeV no limits on any direct squark pair production scenario are placed by the LHC.

Table 89.1: Summary of squark mass and gluino mass limits using different interpretation approaches assuming R -parity conservation. Masses in this table are provided in GeV. Further details about the assumptions and analyses from which these limits are obtained are discussed in the corresponding sections of the text.

Model	Assumption	$m_{\tilde{q}}$	$m_{\tilde{g}}$
Simplified models $\tilde{g}\tilde{g}$			
$\tilde{g} \rightarrow q\bar{q}\tilde{\chi}_1^0$	$m_{\tilde{\chi}_1^0} = 0$	-	≈ 2300
	$m_{\tilde{\chi}_1^0} \gtrsim 1200$	-	no limit
$\tilde{g} \rightarrow b\bar{b}\tilde{\chi}_1^0$	$m_{\tilde{\chi}_1^0} = 0$	-	≈ 2300
	$m_{\tilde{\chi}_1^0} \gtrsim 1500$	-	no limit
$\tilde{g} \rightarrow t\bar{t}\tilde{\chi}_1^0$	$m_{\tilde{\chi}_1^0} = 0$	-	≈ 2250
	$m_{\tilde{\chi}_1^0} \gtrsim 1300$	-	no limit
Simplified models $\tilde{q}\tilde{q}$			
$\tilde{q} \rightarrow q\tilde{\chi}_1^0$	$m_{\tilde{\chi}_1^0} = 0$	≈ 1900	-
	$m_{\tilde{\chi}_1^0} \gtrsim 800$	no limit	-
$\tilde{u}_L \rightarrow q\tilde{\chi}_1^0$	$m_{\tilde{\chi}_1^0} = 0$	≈ 1300	-
	$m_{\tilde{\chi}_1^0} \gtrsim 600$	no limit	-

89.6 Exclusion limits on bottom and top squarks masses in RPC scenarios

Besides placing stringent limits on first and second generation squark masses, the LHC experiments also search for the production of third generation squarks. SUSY at the TeV-scale is often motivated by naturalness arguments, most notably as a solution to cancel quadratic divergences in radiative corrections to the Higgs boson mass. In this context, the most relevant terms for SUSY phenomenology arise from the interplay between the masses of the third generation squarks and the Yukawa coupling of the top quark to the Higgs boson. This motivates a potential constraint on the masses of the top squarks and the left-handed bottom squark. Due to the large top quark mass, significant mixing between \tilde{t}_L and \tilde{t}_R is expected, leading to a lighter mass state \tilde{t}_1 and a heavier mass state \tilde{t}_2 . In the MSSM, the lightest top squark (\tilde{t}_1) can be the lightest squark.

Bottom squarks are expected to decay predominantly to $b\tilde{\chi}_1^0$ giving rise to the characteristic multi b -jet and E_T^{miss} signature. Direct production of bottom squark pairs has been searched for at the Tevatron and at the LHC. Limits from the Tevatron are $m_{\tilde{b}} > 247$ GeV for a massless neutralino [84, 85]. The LHC experiments have surpassed these limits and are well above 1 TeV, and the latest results, shown in Fig. 89.6 (left), are based on up to 140 fb^{-1} of data collected at $\sqrt{s} = 13 \text{ TeV}$. ATLAS has set a lower limit of $m_{\tilde{b}} > 1250$ GeV for massless neutralinos in this model [86] exploiting the two b -jets and missing transverse momentum analysis. For $m_{\tilde{\chi}_1^0} \approx 800$ GeV or higher no limit can be placed on direct bottom squark pair production in this simplified model. Limits from CMS are comparable [81]. Reinterpretations of the monojet analysis results can be used to constrain very compressed scenarios, with exclusion of masses up to 550 GeV in case of $\Delta m = m_{\tilde{b}} - m_{\tilde{\chi}_1^0} \approx 5$ GeV [82]. Further bottom squark decay modes have also been searched for by ATLAS [87–89] and CMS [75, 90, 91], for instance targeting more complex decay chains that include Higgs bosons in the cascade.

The top squark decay modes depend on the SUSY mass spectrum, and on the \tilde{t}_L - \tilde{t}_R mixture of the top squark mass eigenstate. If kinematically allowed, the two-body decays $\tilde{t} \rightarrow t\tilde{\chi}_1^0$ (which requires $m_{\tilde{t}} - m_{\tilde{\chi}_1^0} > m_t$) and $\tilde{t} \rightarrow b\tilde{\chi}_{1\pm}^\pm$ (which requires $m_{\tilde{t}} - m_{\tilde{\chi}_{1\pm}^\pm} > m_b$) are expected to dominate. If not, the top squark decay may proceed either via the two-body decay $\tilde{t} \rightarrow c\tilde{\chi}_1^0$ or through $\tilde{t} \rightarrow bf\bar{f}'\tilde{\chi}_1^0$ (where f and f' denote a fermion-antifermion pair with appropriate quantum numbers). For $m_{\tilde{t}} - m_{\tilde{\chi}_1^0} > m_b$ the latter decay chain represents a four-body decay with a W bo-

son, charged Higgs H , slepton $\tilde{\ell}$, or light flavor squark \tilde{q} , exchange. If the exchanged W boson and/or sleptons are kinematically allowed to be on-shell, the three-body decays $\tilde{t} \rightarrow Wb\tilde{\chi}_1^0$ and/or $\tilde{t} \rightarrow b\nu\tilde{\ell}(\bar{\nu}\ell)$ will become dominant. For further discussion on top squark decays see for example Ref. [92].

Limits from LEP on the \tilde{t}_1 mass are $m_{\tilde{t}} > 96$ GeV in the charm plus neutralino final state, and > 93 GeV in the lepton, b -quark and sneutrino final state [71].

The Tevatron experiments have performed a number of searches for top squarks, often assuming direct pair production. In the $b\bar{b}\nu$ decay channel, and assuming a 100% branching fraction, limits are set as $m_{\tilde{t}} > 210$ GeV for $m_{\tilde{\nu}} < 110$ GeV and $m_{\tilde{t}} - m_{\tilde{\nu}} > 30$ GeV, or $m_{\tilde{t}} > 235$ GeV for $m_{\tilde{\nu}} < 50$ GeV [93, 94]. In the $\tilde{t} \rightarrow c\tilde{\chi}_1^0$ decay mode, a top squark with a mass below 180 GeV is excluded for a neutralino lighter than 95 GeV [95, 96]. In both analyses, no limits on the top squark can be set for heavy sneutrinos or neutralinos. In the $\tilde{t} \rightarrow b\tilde{\chi}_{1\pm}^\pm$ decay channel, searches for a relatively light top squark have been performed in the dilepton final state [97, 98]. The CDF experiment sets limits in the $\tilde{t} - \tilde{\chi}_1^0$ mass plane for various branching fractions of the chargino decay to leptons and for two values of $m_{\tilde{\chi}_{1\pm}^\pm}$. For $m_{\tilde{\chi}_{1\pm}^\pm} = 105.8$ GeV and $m_{\tilde{\chi}_1^0} = 47.6$ GeV, top squarks between 128 and 135 GeV are excluded for W -like leptonic branching fractions of the chargino.

The LHC experiments have improved these limits substantially. As shown in the right plot of Fig. 89.6, limits on the top squark mass assuming a simplified model with a single decay chain of $\tilde{t} \rightarrow t\tilde{\chi}_1^0$ now surpass 1 TeV. The most important searches for this top squark decay topology are dedicated searches requiring zero or one isolated lepton, modest E_T^{miss} , and four or more jets out of which at least one jet must be reconstructed as a b -jet [50, 75, 81, 99–101]. For example, using an all-hadronic analysis, CMS excludes top squarks with masses below about 1300 GeV in this model for light neutralinos, while for $m_{\tilde{\chi}_1^0} > 700$ GeV no limits can be provided [101]. Similar constraints are set by the ATLAS all-hadronic search [99].

Assuming that the top squark decay exclusively proceeds via the chargino mediated decay chain $\tilde{t} \rightarrow b\tilde{\chi}_{1\pm}^\pm$, $\tilde{\chi}_{1\pm}^\pm \rightarrow W^{(*)}\tilde{\chi}_1^0$ yields stop mass exclusion limits that vary strongly with the assumptions made on the $\tilde{t} - \tilde{\chi}_{1\pm}^\pm - \tilde{\chi}_1^0$ mass hierarchy. For example, for $m_{\tilde{\chi}_{1\pm}^\pm} = (m_{\tilde{t}} + m_{\tilde{\chi}_1^0})/2$, a stop mass below ≈ 1150 GeV for a light $\tilde{\chi}_1^0$ is excluded by CMS, while no limit can be placed for $m_{\tilde{\chi}_1^0} > 550$ GeV [50]. These limits, however, can weaken significantly when other assumptions about the mass hierarchy or the decay of the charginos are imposed [50, 102–104].

Other analyses with zero, one or two leptons target this kinematic region [105–111], also providing sensitivity in the case of alternative decay modes of the top squark, *i.e.* including tau sleptons [104, 112, 113] or Higgs and Z bosons in the decay chain [114].

If the decays $\tilde{t} \rightarrow t\tilde{\chi}_1^0$ and $\tilde{t} \rightarrow b\tilde{\chi}_{1\pm}^\pm$, $\tilde{\chi}_{1\pm}^\pm \rightarrow W^{(*)}\tilde{\chi}_1^0$ are kinematically forbidden, the decay chains $\tilde{t} \rightarrow Wb\tilde{\chi}_1^0$ and $\tilde{t} \rightarrow c\tilde{\chi}_1^0$ can become important. The one-lepton ATLAS search provides for the kinematic region $m_{\tilde{t}} - m_{\tilde{\chi}_{1\pm}^\pm} > m_b + m_W$ lower limits on the top squark mass of ≈ 700 GeV for a neutralino lighter than ≈ 570 GeV [100]. For the kinematic region in which even the production of real W bosons is not allowed, ATLAS and CMS improve the Tevatron limit on $\tilde{t} \rightarrow c\tilde{\chi}_1^0$ substantially. Based on a monojet analysis [82] ATLAS excludes top squark masses below $m_{\tilde{\chi}_1^0} \approx 550$ GeV along the kinematic boundary for the $\tilde{t} \rightarrow c\tilde{\chi}_1^0$ decay. The ATLAS monojet analysis also places similar boundaries for the other decay chain relevant in this phase region, $\tilde{t} \rightarrow bf\bar{f}'\tilde{\chi}_1^0$. Other analyses, such as the search in events with one lepton and jets, are also sensitive to this decay mode: the ATLAS one-lepton analysis excludes up to ≈ 650 GeV for $\Delta m = m_{\tilde{t}}, m_{\tilde{\chi}_1^0} \approx 50$ GeV [100]. The CMS collaboration uses the hadronic searches [101, 106, 108] to place constraints on stop decay into charm-quark and excludes $m_{\tilde{t}} \approx 630$ GeV for $\Delta m = m_{\tilde{t}}, m_{\tilde{\chi}_1^0} \approx 50$ GeV [101]. The same constraints are set in case of $\tilde{t} \rightarrow bf\bar{f}'\tilde{\chi}_1^0$, with CMS excluding $m_{\tilde{t}} \approx 640$ GeV for

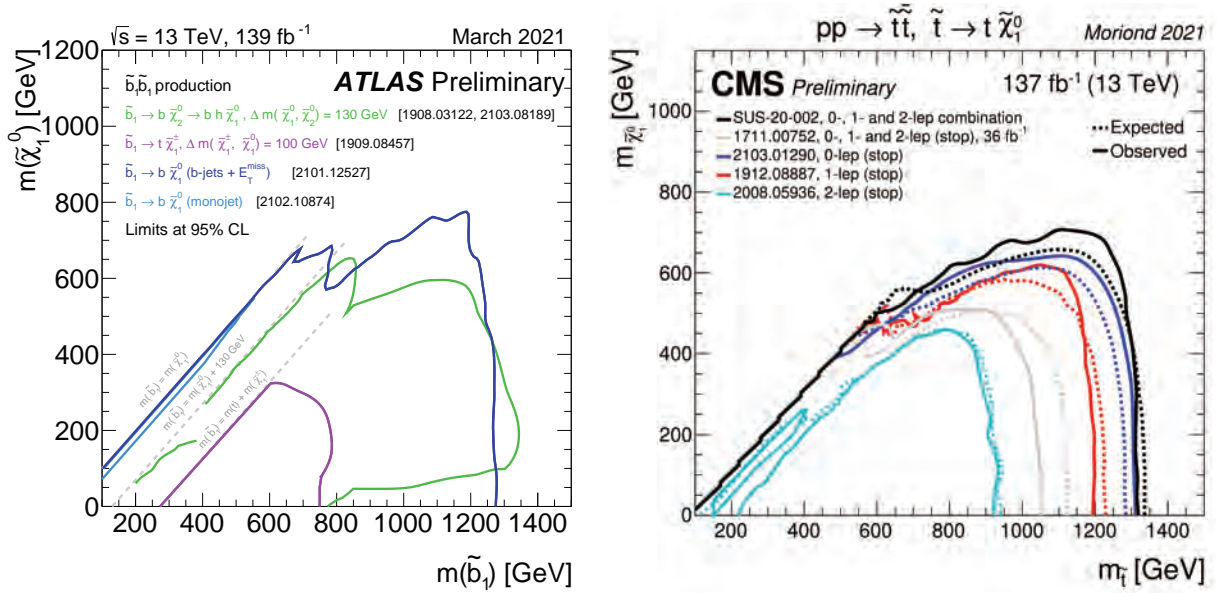


Figure 89.6: Left: A summary of the 95% C.L. exclusion contours in the sbottom-neutralino mass plane for various possible decay chains as obtained in dedicated analyses by ATLAS. Right: The 95% C.L. exclusion contours in the stop-neutralino mass plane defined in the framework of a simplified model assuming a single decay chain of $\tilde{t} \rightarrow t\tilde{\chi}_1^0$ as obtained by CMS.

$$\Delta m = m_{\tilde{t}}, m_{\tilde{\chi}_1^0} \approx 50 \text{ GeV} [101].$$

Table 89.2: Summary of bottom and top squark mass limits using different interpretation approaches assuming R -parity conservation. Masses in this table are provided in GeV. Further details about the assumptions and analyses from which these limits are obtained are discussed in the corresponding sections of the text.

Model	Assumption	$m_{\tilde{q}}$
$\tilde{b} \rightarrow b\tilde{\chi}_1^0$	$m_{\tilde{\chi}_1^0} = 0$	≈ 1250
	$m_{\tilde{\chi}_1^0} > \approx 700$	no limit
$\tilde{t} \rightarrow t\tilde{\chi}_1^0$	$m_{\tilde{\chi}_1^0} = 0$	≈ 1300
	$m_{\tilde{\chi}_1^0} > \approx 600$	no limit
$\tilde{t} \rightarrow b\tilde{\chi}_1^\pm$	$m_{\tilde{\chi}_1^0} = 0$	≈ 1150
	$m_{\tilde{\chi}_1^0} > \approx 550$	no limit
$(m_{\tilde{\chi}_1^\pm} = (m_{\tilde{t}} - m_{\tilde{\chi}_1^0})/2)$	$m_{\tilde{\chi}_1^0} > \approx 550$	no limit
$\tilde{t} \rightarrow Wb\tilde{\chi}_1^0$	$m_{\tilde{\chi}_1^0} < \approx 570$	≈ 700
$(m_W < m_{\tilde{t}} - m_{\tilde{\chi}_1^0} < m_t)$	$\tilde{t} \rightarrow c\tilde{\chi}_1^0$	$m_{\tilde{t}} - m_{\tilde{\chi}_1^0} \approx 50$ ≈ 630
		$m_{\tilde{t}} \approx m_{\tilde{\chi}_1^0}$ ≈ 550
	$\tilde{t} \rightarrow bf f' \tilde{\chi}_1^0$	$m_{\tilde{t}} - m_{\tilde{\chi}_1^0} \approx 50$ ≈ 650
		$m_{\tilde{t}} \approx m_{\tilde{\chi}_1^0}$ ≈ 550
$(m_{\tilde{t}} - m_{\tilde{\chi}_1^0} < m_W)$		

In general, the variety of top squark decay chains in the phase space region where $\tilde{t} \rightarrow t\tilde{\chi}_1^0$ is kinematically forbidden represents a challenge for the experimental search program but more data and refined analyses in Run 2 have further improved the sensitivity in this difficult but important region of SUSY parameter space, and more is expected for future Runs of the LHC. It is also worth mentioning that precision SM measurements can provide important insights to such challenging regions. For instance, analyses of $t\bar{t}$ spin correlations can be used to set constraints on top squark masses close to the top-quark mass. ATLAS [115] excludes the mass region between 150 and 230 GeV for kinematically allowed values of the neutralino mass. CMS [116] results cover a similar mass range.

It should be noted that limits discussed in this section belong

to different top and bottom squark decay channels, different sparticle mass hierarchies, and different simplified decay scenarios. Therefore, care must be taken when interpreting these limits in the context of more complete SUSY models.

89.7 Exclusion limits on squarks and gluinos in RPV scenarios

RPV gluino and squark decays are searched for in a number of final states, generally characterised by the presence of multiple leptons or jets and moderated or no missing transverse momentum. If the couplings are very small, sparticles might be long-lived and dedicated searches for non-prompt decays are reported in Section 89.10.

Searches in multilepton final states [117–121] set lower mass limits of 1 to 1.4 TeV, depending on neutralino mass and lepton flavor, on decays mediated by λ and λ' couplings, assuming prompt decays. Multijet final states have been used to search for fully hadronic gluino decays involving λ'' couplings, by CDF [122], ATLAS [88, 123–126] and CMS [127–129]. Lower gluino mass limits range between 600 and 2000 GeV depending on neutralino mass and flavor content of the final state. More recently, ATLAS [130] searched in events characterised by high jet multiplicity, at least one isolated light lepton and either zero or at least three b -tagged jets, reaching as high as 2.4 TeV in gluino mass.

RPV production of single squarks via a λ' -type coupling has been studied at HERA. In such models, a lower limit on the squark mass of the order of 275 GeV has been set for electromagnetic-strength-like couplings $\lambda' = 0.3$ [131]. At the LHC, prompt [118, 121, 132] R -parity violating squark decays have been searched for with mass limits are very model-dependent.

Dedicated searches for RPV top squarks (at production and/or in decays) have been carried out in the past decades. Production of single top squarks has been searched for at LEP, HERA, and the Tevatron. For example, an analysis from the ZEUS collaboration [133] makes an interpretation of its search result assuming top squarks to be produced via a λ' coupling and decay either to $b\tilde{\chi}_1^\pm$ or R -parity-violating to a lepton and a jet. Limits are set on λ'_{131} as a function of the top squark mass in an MSSM framework with gaugino mass unification at the GUT scale. The search for top squark pair production in the context of RPV supersymmetry has now also become a focus point for searches at the LHC. CMS and ATLAS have performed several searches for top squarks using a variety of multilepton and/or multijet final states and Run 2 data. The λ' -mediated top squark decay $\tilde{t} \rightarrow b\ell$ has been studied

by ATLAS for prompt decays [134], and by ATLAS and CMS for non-prompt decays [135–137], setting limits up to 1.4–1.6 TeV in simplified models for this mode. CMS also searched for the λ' -mediated decay $\tilde{t} \rightarrow b\ell q$, setting lower stop mass limits of 890 GeV (e) or 1000 GeV (μ) [138]. The fully hadronic R -parity violating top squark decays $\tilde{t} \rightarrow bs$, $\tilde{t} \rightarrow ds$, and $\tilde{t} \rightarrow bd$, involving λ'' , have been searched for by ATLAS [118, 124, 139–141], and CMS [142, 143]. Other recent searches target top squarks decaying through cascades into several b - and light-quarks, for example as in [144]. The most recent results set lower top squark mass limits up to 1.35 TeV in top-squark mass [130] if decays include top- and b -quarks [130] lower top squark mass limits are up to 1.35 TeV in top-squark mass. Constraints on masses up to 670 GeV are found if top squarks decays include top- and light-quarks [145].

RPV signatures are often similar to signatures of Stealth SUSY [146–148]. In these scenarios, squarks can decay to a quark and a chargino (neutralino), which can subsequently decay to a singlino \tilde{S} and a W^\pm (photon), with the \tilde{S} decaying to two gluons and a soft gravitino \tilde{G} . A dedicated CMS search [149] excludes squark masses up to 1.05 TeV in the photon channel and up to 550 GeV in the charged lepton channel. Limits have also been placed on top squarks in stealth SUSY scenarios, where the top squark decays to a top quark, a gluon and a \tilde{S} , and the \tilde{S} subsequently decays to a \tilde{G} and two gluons. In such a scenario, top squark masses up to 870 GeV have been excluded [145].

89.8 Exclusion limits on the masses of charginos, neutralinos and sleptons in RPC scenarios

Charginos, neutralinos and sleptons are produced through electroweak interactions and their cross sections depend on the assumptions made for mass and mixing parameters.

Charginos and neutralinos carry no color charge and the mixing of the charged wino and higgsino states (for charginos), and the neutral bino, wino and higgsino states (for neutralinos), is determined by a limited number of parameters. For charginos these are the wino mass parameter M_2 , the higgsino mass parameter μ , and $\tan\beta$, and for neutralinos these are the same parameters plus the bino mass parameter M_1 . If one of the parameters M_1 , M_2 or μ is substantially smaller than the others, the chargino/neutralino composition would be dominated by specific states, which are referred to as bino-like ($M_1 \ll M_2, \mu$), wino-like ($M_2 \ll M_1, \mu$), or higgsino-like ($\mu \ll M_1, M_2$). If gaugino mass unification at the GUT scale is assumed, a relation between M_1 and M_2 at the electroweak scale follows: $M_1 = 5/3 \tan^2\theta_W M_2 \approx 0.5M_2$, with θ_W the weak mixing angle. The largest production rates at hadron machines are obtained when the LSP is bino-like and the lightest chargino and next-to-lightest neutralino are wino-like, forming an approximately mass degenerate SU(2) triplet. If the higgsino mass is much smaller than the gaugino masses, the two lightest neutralinos and the lightest chargino form an approximately mass degenerate Dirac SU(2) doublet, production rates are lower and the mass spectrum is compressed.

In models with slepton and gaugino mass unification at the GUT scale, the superpartner of the right-handed lepton, $\tilde{\ell}_R$, is expected to be lighter than the left-handed one, $\tilde{\ell}_L$. Cross sections depend on the L-R mixing which in turn depends on the mass of the fermion and other parameters. For tau sleptons there may be considerable mixing between the L and R states, leading to a significant mass difference between the lighter $\tilde{\tau}_1$ and the heavier $\tilde{\tau}_2$.

Fig. 89.7 [150, 151] (see also Ref. [72] for further details) shows typical production cross sections at hadron colliders for electroweakinos under various assumptions. For masses of several hundreds of GeV, they are at least two orders of magnitude smaller than for colored SUSY particles. Thanks to the large data samples collected at the LHC, the sensitivity of LEP and Tevatron searches for direct chargino/neutralino or slepton production has been surpassed in several regions of SUSY parameter space.

89.8.1 Exclusion limits on chargino masses

The lightest chargino $\tilde{\chi}_1^\pm$ is searched for either considering pair production, or through associated production of $\tilde{\chi}_1^\pm$ and the next-to-lightest neutralino, $\tilde{\chi}_2^0$, if they are assumed to be degenerate

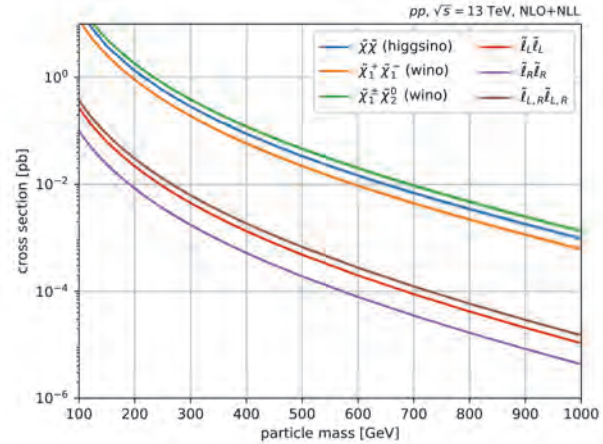


Figure 89.7: Cross sections for pair production of charginos, neutralinos and sleptons calculated for 13 TeV centre-of-mass energy at NLO plus next-to-leading-log (NLL) precision. Wino-like $\tilde{\chi}_1^\pm \tilde{\chi}_2^0$ and $\tilde{\chi}_1^\pm \tilde{\chi}_1^\mp$ productions are calculated in a limit of mass-degenerate $\tilde{\chi}_1^\pm$ and $\tilde{\chi}_2^0$, light bino $\tilde{\chi}_1^0$, and with all the other sparticles assumed to be heavy and decoupled. Higgsino-like cross sections assume mass-degenerate $\tilde{\chi}_1^\pm$, $\tilde{\chi}_2^0$ and $\tilde{\chi}_1^0$. For slepton pair cross sections, left(right)-handed only or 50% mixed states are considered.

in mass. If kinematically allowed, two body decay modes such as $\tilde{\chi}^\pm \rightarrow \tilde{f}\tilde{f}'$ (including $\ell\nu$ and $\tilde{\ell}\nu$) are dominant. If not, three body decays $\tilde{\chi}^\pm \rightarrow f\tilde{f}'\tilde{\chi}_1^0$, mediated through virtual W bosons or sfermions, become dominant. If sfermions are heavy, the W mediation dominates, and $f\tilde{f}'$ are distributed with branching fractions similar to W decay products (barring phase space effects for small mass gaps between $\tilde{\chi}^\pm$ and $\tilde{\chi}_1^0$). If, on the other hand, sleptons are light enough to play a significant role in the decay, leptonic final states will be enhanced.

At LEP, $\tilde{\chi}_1^+ \tilde{\chi}_1^-$ is the dominant production process. Charginos have been searched for in fully-hadronic, semi-leptonic and fully leptonic decay modes [152, 153]. A general lower limit on the lightest chargino mass of 103.5 GeV is derived, except in corners of phase space with low electron sneutrino mass, where destructive interference in chargino production, or two-body decay modes, play a role. The limit is also affected if the mass difference between $\tilde{\chi}_1^\pm$ and $\tilde{\chi}_1^0$ is small; dedicated searches for such scenarios set a lower limit of 92 GeV.

At the Tevatron, charginos have been searched for via associated production of $\tilde{\chi}_1^\pm \tilde{\chi}_2^0$ [154, 155]. Decay modes involving multilepton final states provide the best discrimination against the large multijet background. Analyses have looked for at least three charged isolated leptons, for two leptons with missing transverse momentum, or for two leptons with the same charge. Depending on the $(\tilde{\chi}_1^\pm - \tilde{\chi}_1^0)$ and/or $(\tilde{\chi}_2^0 - \tilde{\chi}_1^0)$ mass differences, leptons may have soft transverse momentum.

At the LHC, the search strategy is similar to that at the Tevatron but it also exploits the large datasets collected to target missing momentum and fully-hadronic final states and consider $\tilde{\chi}_1^+ \tilde{\chi}_1^-$ production only i.e. releasing the assumption of $\tilde{\chi}_1^\pm, \tilde{\chi}_2^0$ mass degeneracy. Furthermore, compressed SUSY spectra are searched for considering low-momentum leptons recoiling against an ISR jet.

Chargino pair production is searched for in the dilepton plus missing momentum final state. In a simplified model interpretation of the results where only the $\tilde{\chi}_1^+ \tilde{\chi}_1^-$ process is considered and assuming mediation of the chargino decay by light sleptons (\tilde{e} and $\tilde{\mu}$), ATLAS [156] and CMS [157] set limits on the chargino mass up to 1 TeV for massless LSPs, but no limits on the chargino mass can be set for $\tilde{\chi}_1^0$ heavier than 480 GeV. Limits are fairly

robust against variation of the slepton mass, unless the mass gap between sparticles becomes small enough that the charged lepton has a too low-momentum to be reconstructed. For decays mediated through $\tilde{\tau}$ or $\tilde{\nu}_\tau$, limits of 630 GeV are set by ATLAS [158] for LSPs not heavier than 200 GeV. The CMS experiment provides similar limits [159].

In case slepton masses are higher than the mass of the chargino, searches are performed for charginos decaying via a W boson. ATLAS sets limits on this kind of simplified models [156] for pure-wino charginos: masses below 420 GeV are excluded for massless LSPs, but no limits are set for LSPs heavier than 120 GeV. Further extension of the sensitivity in the high-mass region is achieved by ATLAS [160] and CMS [161] exploiting the large branching ratio of fully-hadronic final states and the identification of boosted W bosons through large-radius jets and jet substructure information. Considering only wino-like chargino pair production in case of a massless LSP, ATLAS excludes a region between 630 GeV and 760 GeV, while CMS excludes between 290 GeV and 670 GeV. No limits are set for LSP masses above 200 GeV.

Several final states characterised by the presence of missing transverse momentum are studied to set limits on the chargino mass through $\tilde{\chi}_1^\pm \tilde{\chi}_2^0$ associated production. Usually, wino-like $\tilde{\chi}_1^\pm$ and $\tilde{\chi}_2^0$ and bino-like $\tilde{\chi}_1^0$ are assumed with $m_{\tilde{\chi}_1^\pm} = m_{\tilde{\chi}_2^0}$, leaving $m_{\tilde{\chi}_1^\pm}$ and $m_{\tilde{\chi}_1^0}$ free. Again, the branching fraction of leptonic final states is determined by the slepton masses. If the decay is predominantly mediated by a light $\tilde{\ell}_L$, i.e. $\tilde{\ell}_R$ is assumed to be heavy, the three charged-lepton flavors will be produced in equal amounts, and a multi-lepton signature is favored. It is assumed that $\tilde{\ell}_L$ and sneutrino masses are equal, and diagrams with sneutrinos are included. In this scenario, ATLAS [162] and CMS [163] exclude chargino masses below 1450 GeV for massless LSPs; no limits are set for LSP masses above 1 TeV. If the decay is dominated by a light $\tilde{\ell}_R$, the chargino cannot be a pure wino but needs to have a large higgsino component, preferring the decays to tau leptons. Limits are set in various scenarios. If, like for $\tilde{\ell}_L$, a flavor-democratic scenario is assumed (τ -enriched scenario), CMS sets limits of 1150 GeV on the chargino mass for massless LSPs, but under the assumption that both $\tilde{\chi}_1^\pm$ and $\tilde{\chi}_2^0$ decay leads to tau leptons in the final state (τ -dominated scenario), the chargino mass limit deteriorates to 970 GeV for massless LSPs [163]. ATLAS assumes a simplified model in which staus are significantly lighter than the other sleptons in order to search for a similar multi-tau final state, and sets a lower limit on the chargino mass of 760 GeV in this model [158].

If sleptons are heavy, the chargino is assumed to decay to a W boson plus LSP, and the $\tilde{\chi}_2^0$ into Z plus LSP or H plus LSP. Searches for the WZ channel exploit events with either two same-sign leptons or three leptons, or with no leptons (all-hadronic). ATLAS searches in events with three leptons and missing momentum and wino-like chargino masses below 640 GeV are excluded for massless LSPs [164]. Limits are reduced in case of higgsino-like scenarios, with exclusion down to 210 GeV. Searches exploiting all-hadronic final states where boosted, fully-hadronically decaying W , Z and Higgs boson candidates are identified using dedicated algorithm are carried out by ATLAS [160] and CMS [161]. ATLAS excludes wino-like $\tilde{\chi}_2^0$ and $\tilde{\chi}_1^\pm$ masses between 440 GeV and 960 GeV for an LSP mass below 300 GeV. Similar constraints are obtained by CMS.

Interpretations are also provided in a scenario where the $\tilde{\chi}_2^0$ does not decay exclusively into Z plus LSP. CMS [163] excludes chargino masses below 650 GeV for massless LSPs, using events with two leptons of the same sign, or with three or more leptons. No constraints are set for $\tilde{\chi}_1^0$ masses above 300 GeV. Similarly to ATLAS, limits are pushed further utilising fully-hadronic final states [161].

If $\tilde{\chi}_2^0$ decays through a Higgs boson with $m_H = 125$ GeV, searches targeting the WH channel are relevant. Assuming SM-like Higgs decay modes and branching fractions, Higgs bosons in the final state are identified by either two jets originating from bottom quarks ($h \rightarrow b\bar{b}$), two photons ($h \rightarrow \gamma\gamma$), or leptons from the WW , ZZ or $\tau\tau$ decay modes. Searches exploiting the pres-

ence of b -jets are most sensitive in the high-mass chargino region, while analyses targeting photon pair or leptonic decays of the Higgs boson provide the best sensitivity in the region of low masses. CMS [165] sets lower limits on the chargino mass up to 820 GeV for massless LSPs, but vanish for LSP masses above 350 GeV using events with at least one lepton and missing transverse momentum in the final state. Similar sensitivity is achieved by the ATLAS analyses [166–168].

Additional constraints on the chargino mass are placed exploiting all-hadronic analyses. A wino-like (higgsino-like) chargino with mass up to 1060 (900) GeV is excluded by ATLAS [160] when the LSP mass is below 400 (240) GeV and the mass splitting is larger than 400 (450) GeV. CMS [161] excludes wino-like charginos with mass up to 970 GeV for massless LSP.

In both the wino region (a characteristic of anomaly-mediated SUSY breaking models) and the higgsino region of the MSSM, the mass splitting between $\tilde{\chi}_1^\pm$ and $\tilde{\chi}_1^0$ is small. The chargino decay products are very soft and may escape detection. These compressed spectra are hard to detect, and have triggered dedicated search strategies. ATLAS [169] and CMS [170] have performed searches for charginos and neutralinos in a compressed mass spectrum using initial state radiation and two or three low-momentum (soft) leptons. For wino-like charginos, assuming degenerate $\tilde{\chi}_1^\pm$ and $\tilde{\chi}_2^0$, exclusion contours in the chargino-mass versus $\Delta m(\tilde{\chi}_1^\pm - \tilde{\chi}_1^0)$ plane are derived. As an example, such charginos are excluded by CMS (ATLAS) below 280 (240) GeV for $\Delta m(\tilde{\chi}_1^\pm - \tilde{\chi}_1^0) = 10$ GeV. Considering the higgsino model, the masses probed by CMS reach up to 215 GeV for a mass difference of 7.5 GeV and 150 GeV in the highly compressed region with a mass difference of 3 GeV. CMS has also searched for chargino-pair production through vector-boson-fusion [171], also targeting compressed mass spectra. Assuming degenerate $\tilde{\chi}_1^\pm$ and $\tilde{\chi}_2^0$, charginos with a mass below 112 GeV are excluded for $\Delta m(\tilde{\chi}_1^\pm - \tilde{\chi}_1^0) = 1$ GeV. CMS has published further searches for such compressed spectra with a soft tau lepton [172].

89.8.2 Exclusion limits on neutralino masses

In a considerable part of the MSSM parameter space, and in particular when demanding that the LSP carries no electric or color charge, the lightest neutralino $\tilde{\chi}_1^0$ is the LSP. If R -parity is conserved, such a $\tilde{\chi}_1^0$ is stable. Since it is weakly interacting, it will typically escape detectors unseen. Limits on the invisible width of the Z boson apply to neutralinos with a mass below 45.5 GeV, but depend on the Z -neutralino coupling. Such a coupling could be small or even absent; in such a scenario there is no general lower limit on the mass of the lightest neutralino [173]. In models with gaugino mass unification and sfermion mass unification at the GUT scale, a lower limit on the neutralino mass is derived from limits from direct searches, notably for charginos and sleptons, and amounts to 47 GeV [174]. Assuming a constrained model like the CMSSM, this limit increases to 50 GeV at LEP; however the strong constraints now set by the LHC increase such CMSSM-derived $\tilde{\chi}_1^0$ mass limits to well above a few hundred GeV (the latest reinterpretation only uses Run 1 data and indicates 200 GeV [175–177]).

In gauge-mediated SUSY breaking models (GMSB), the LSP is typically a gravitino, and the phenomenology is determined by the nature of the next-to-lightest supersymmetric particle (NLSP). A NLSP neutralino will decay to a gravitino and a SM particle whose nature is determined by the neutralino composition. Final states with two high p_T photons and missing momentum are searched for, and interpreted in gauge mediation models with bino-like neutralinos [178–183].

Assuming the production of at least two neutralinos per event, neutralinos with large non-bino components can also be searched for by their decay in final states with missing momentum plus any two bosons out of the collection γ, Z, H . A number of searches at the LHC have tried to cover the rich phenomenology predicted by the general gauge mediation model (GGM) where $\tilde{\chi}_1^0$ might decay with various BR in the Z and H decay modes [90, 117, 160, 167, 181, 184–193]. As an example, strong constraints for decay modes involving Z and H bosons arise from

full-hadronic searches on higgsino-like scenarios: ATLAS [160] excludes higgsino production with decays into a massless gravitino LSP in a mass range between 450 (500) GeV and 940 (850) GeV assuming $BR = 1$ (0.5) for the Z plus gravitino decay mode. Assuming only H plus gravitino decays, CMS [194] excludes a higgsino mass range between 175 GeV and 1025 GeV.

Heavier neutralinos, in particular $\tilde{\chi}_2^0$, have been searched for in their decays to the lightest neutralino plus a γ , a Z boson or a Higgs boson. Limits on electroweak production of $\tilde{\chi}_2^0$ plus $\tilde{\chi}_1^\pm$ from all-hadronic, same-sign dilepton and trilepton analyses have been discussed in the section on charginos; the assumption of equal mass of $\tilde{\chi}_2^0$ and $\tilde{\chi}_1^\pm$ make the limits on chargino masses apply to $\tilde{\chi}_2^0$ as well. Multilepton analyses have also been used to set limits on $\tilde{\chi}_2^0\tilde{\chi}_3^0$ production; assuming equal mass and decay through light sleptons, limits are set up to 680 GeV for massless LSPs [195]. Again, compressed spectra with small mass differences between the heavier neutralinos and the LSP form the most challenging region.

In $\tilde{\chi}_2^0$ decays to $\tilde{\chi}_1^0$ and a lepton pair, the lepton pair invariant mass distribution may show a structure that can be used to measure the $\tilde{\chi}_2^0 - \tilde{\chi}_1^0$ mass difference in case of a signal [38]. This structure, however, can also be used in the search strategy itself, as demonstrated by ATLAS [196,197] and CMS [90,198].

Fig. 89.8 summarizes some of the most recent results from ATLAS and CMS for chargino pair or chargino and next-to-lightest neutralino pair productions comparing results obtained with various assumptions. The limits on weak gauginos in simplified models are also summarized in Table 89.3. Only results for promptly decaying charginos and neutralinos are included: limits from searches focusing on long-lived particle scenarios are reported in Section 89.10.

Interpretations of the search results outside simplified models, such as in the phenomenological MSSM [199–204], show that the simplified model limits can translate into accurate constraints but must also be interpreted with care. Electroweak gauginos in models that are compatible with the relic density of dark matter in the Universe, for example, have particularly tuned mixing parameters and mass spectra, which are not always captured by the simplified models used.

89.8.3 Exclusion limits on slepton masses

The most model-independent searches for selectrons, smuons and staus originate from the LEP experiments [205]. Smuon production only takes place via s -channel γ^*/Z exchange. Search results are often quoted for $\tilde{\mu}_R$, since it is typically lighter than $\tilde{\mu}_L$ and has a weaker coupling to the Z boson; limits are therefore conservative. Decays are expected to be dominated by $\tilde{\mu}_R \rightarrow \mu\tilde{\chi}_1^0$, leading to two non-back-to-back muons and missing momentum. Slepton mass limits are calculated in the MSSM under the assumption of gaugino mass unification at the GUT scale, and depend on the mass difference between the smuon and $\tilde{\chi}_1^0$. A $\tilde{\mu}_R$ with a mass below 94 GeV is excluded for $m_{\tilde{\mu}_R} - m_{\tilde{\chi}_1^0} > 10$ GeV. The selectron case is similar to the smuon case, except that an additional production mechanism is provided by t -channel neutralino exchange. The \tilde{e}_R lower mass limit is 100 GeV for $m_{\tilde{\chi}_1^0} < 85$ GeV. Due to the t -channel neutralino exchange, $\tilde{e}_R\tilde{e}_L$ pair production was possible at LEP, and a lower limit of 73 GeV was set on the selectron mass regardless of the neutralino mass by scanning over MSSM parameter space [206]. The potentially large mixing between $\tilde{\tau}_L$ and $\tilde{\tau}_R$ not only makes the $\tilde{\tau}_1$ light, but can also make its coupling to the Z boson small. LEP lower limits on the $\tilde{\tau}$ mass range between 87 and 93 GeV depending on the $\tilde{\chi}_1^0$ mass, for $m_{\tilde{\tau}} - m_{\tilde{\chi}_1^0} > 7$ GeV [205].

At the LHC, pair production of sleptons is not only heavily suppressed with respect to pair production of colored SUSY particles but the cross section is also almost two orders of magnitude smaller than the one of pair production of charginos and neutralinos. With the full data sets of Run 1 and Run 2, however, ATLAS and CMS have surpassed the sensitivity of the LEP analyses under certain assumptions.

Table 89.3: Summary of weak gaugino mass limits in simplified models, assuming R -parity conservation. Masses in the table are provided in GeV. Further details about assumptions and corresponding analyses are discussed in the text. Details on constraints for compressed scenarios from soft-lepton searches are not represented in the table.

Assumption	m_χ
$\tilde{\chi}_1^\pm$, all $\Delta m(\tilde{\chi}_1^\pm, \tilde{\chi}_1^0)$	> 92
$\tilde{\chi}_1^\pm$ $\Delta m > 5$, $m_{\tilde{\nu}} > 300$	> 103.5
$\tilde{\chi}_1^\pm$, $m(\tilde{\ell}, \tilde{\nu}) = (m_{\tilde{\chi}_1^\pm} + m_{\tilde{\chi}_1^0})/2$	
$m_{\tilde{\chi}_1^0} \approx 0$	> 1000
$\tilde{\chi}_1^\pm$, $m_{\tilde{\chi}_1^0} > 480$	no LHC limit
$\tilde{\chi}_1^\pm$, $m_{\tilde{\ell}} > m_{\tilde{\chi}_1^\pm}$	
$m_{\tilde{\chi}_1^0} \approx 0$	> 420 and $290 - 760$
$\tilde{\chi}_1^\pm$, $m_{\tilde{\chi}_1^0} > 120$	no LHC limit
$m_{\tilde{\chi}_1^\pm} = m_{\tilde{\chi}_2^0}$, $m_{\tilde{\ell}_L} = (m_{\tilde{\chi}_1^\pm} + m_{\tilde{\chi}_1^0})/2$	
$m_{\tilde{\chi}_1^0} \approx 0$	> 1450
$m_{\tilde{\chi}_1^0} > 1000$	no LHC limit
$m_{\tilde{\chi}_1^\pm} = m_{\tilde{\chi}_2^0}$, $m_{\tilde{\ell}_R} = (m_{\tilde{\chi}_1^\pm} + m_{\tilde{\chi}_1^0})/2$	flavor-democratic
$m_{\tilde{\chi}_1^0} \approx 0$	> 1150
$m_{\tilde{\chi}_1^0} > 700$	no LHC limit
$m_{\tilde{\chi}_1^\pm} = m_{\tilde{\chi}_2^0}$, $m_{\tilde{\tau}} = (m_{\tilde{\chi}_1^\pm} + m_{\tilde{\chi}_1^0})/2$	$\tilde{\tau}$ -dominated
$m_{\tilde{\chi}_1^0} \approx 0$	> 970
$m_{\tilde{\chi}_1^0} > 450$	no LHC limit
$m_{\tilde{\chi}_1^\pm} = m_{\tilde{\chi}_2^0}$, $m_{\tilde{\ell}} > m_{\tilde{\chi}_1^\pm}$, $BF(WZ) = 1$	
$m_{\tilde{\chi}_1^0} \approx 0$	> 960
$m_{\tilde{\chi}_1^0} > 300$	no LHC limit
$m_{\tilde{\chi}_1^\pm} = m_{\tilde{\chi}_2^0}$, $m_{\tilde{\ell}} > m_{\tilde{\chi}_1^\pm}$, $BF(WH) = 1$	
$m_{\tilde{\chi}_1^0} \approx 0$, wino-like $\tilde{\chi}_1^\pm$	> 1060
$m_{\tilde{\chi}_1^0} \approx 0$, higgsino-like $\tilde{\chi}_1^\pm$	> 900
$m_{\tilde{\chi}_1^0} > 400(240)$ no LHC limit wino(higgsino)-like	

ATLAS and CMS have searched for direct production of selectron pairs and smuon pairs at the LHC, with each slepton decaying to its corresponding SM partner lepton and the $\tilde{\chi}_1^0$ LSP. In simplified models, ATLAS [156] and CMS [198] set lower mass limits on sleptons of 700 GeV for degenerate $\tilde{\ell}_L$ and $\tilde{\ell}_R$, for a massless $\tilde{\chi}_1^0$ and assuming equal selectron and smuon masses, as shown in Fig. 89.9. The limits deteriorate with increasing $\tilde{\chi}_1^0$ mass due to decreasing missing momentum and lepton momentum. As a consequence, no limits are set for $\tilde{\chi}_1^0$ masses above 400 GeV. Limits are also derived without the assumption of slepton mass degeneracy [156,207]. A dedicated search for sleptons with small mass difference between $\tilde{\ell}$ and $\tilde{\chi}_1^0$ is performed by ATLAS [208] demanding the presence of ISR jets. Although no sensitivity is achieved for intermediate mass differences between the slepton and the LSP, slepton masses up to 260 GeV are excluded for slepton-LSP mass differences of 10–20 GeV.

ATLAS and CMS have also searched for $\tilde{\tau}$ -pair production. In simplified models, ATLAS excludes $\tilde{\tau}$ masses between 120 and 390 GeV assuming light $\tilde{\chi}_1^0$, combining the production of degenerate left- and right-handed $\tilde{\tau}$ s [209]. The CMS analysis [210] covers lower masses and closes the mass gap with LEP. A recent update from CMS [211] exclude purely left-handed $\tilde{\tau}$ s with masses between 115 and 340 GeV for massless LSP.

In gauge-mediated SUSY breaking models, sleptons can be (co-)NLSPs, *i.e.*, the next-to-lightest SUSY particles and almost degenerate in mass, decaying to a lepton and a gravitino. This decay can either be prompt, or the slepton can have a non-zero lifetime. Combining several analyses, lower mass limits on $\tilde{\mu}_R$ of 96.3 GeV

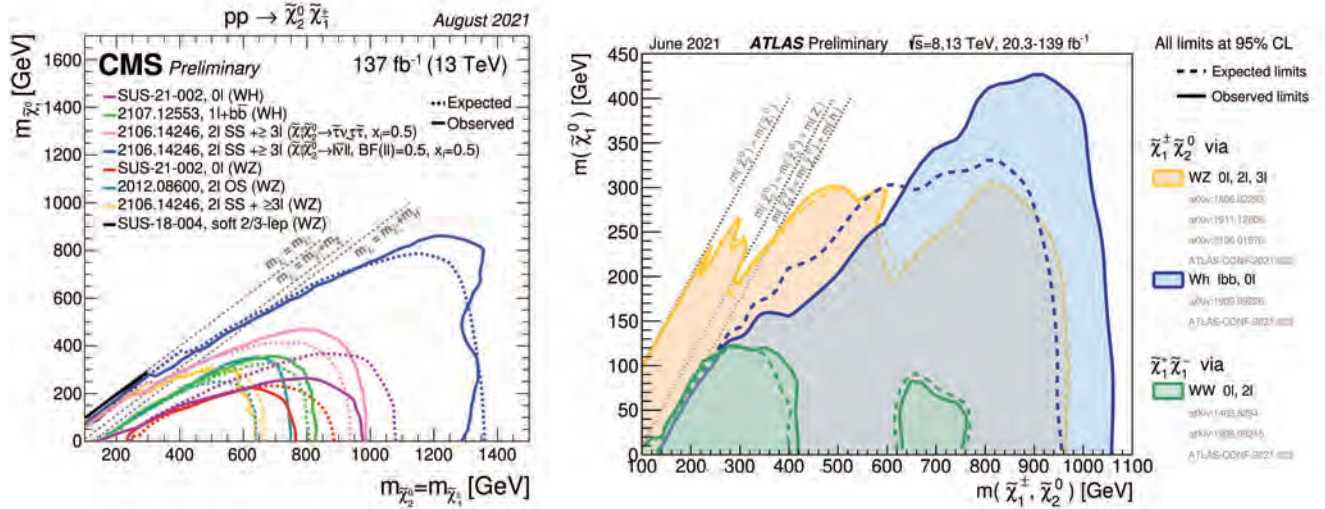


Figure 89.8: LHC exclusion limits on chargino and neutralino masses in a number of simplified models. Left: CMS limits on chargino and neutralino masses for pair production of charginos, pair production of heavier neutralinos, or pair production of chargino and neutralino, under a variety of assumptions including light sleptons mediating the decays. Right: ATLAS limits on chargino and neutralino masses for pair production of chargino and neutralino, under the assumption of decoupled sleptons, and chargino/neutralino decay through on- or off-shell W and Z or H .

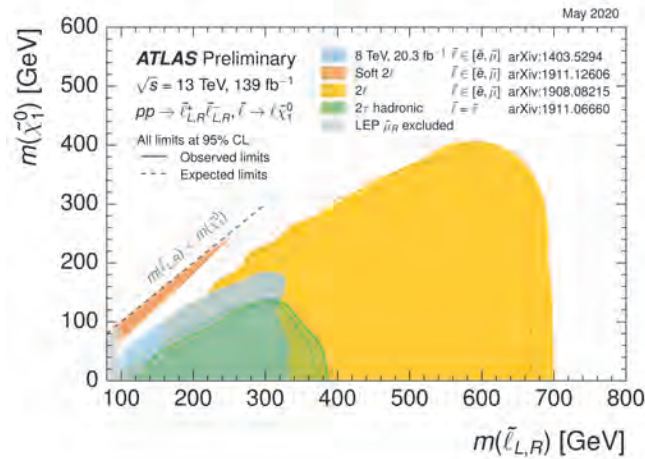


Figure 89.9: LHC exclusion limits on slepton (selectron and smuon) masses, assuming equal masses of selectrons and smuons, degeneracy of $\tilde{\ell}_L$ and $\tilde{\ell}_R$, and a 100% branching fraction for $\tilde{\ell} \rightarrow \tilde{\chi}_1^0 \ell$.

and on \tilde{e}_R of 66 GeV are set for all slepton lifetimes at LEP [212]. In a considerable part of parameter space in these models, the $\tilde{\tau}$ is the NLSP. The LEP experiments have set lower limits on the mass of such a $\tilde{\tau}$ between 87 and 97 GeV, depending on the $\tilde{\tau}$ lifetime. ATLAS and CMS have searched for final states with τ s, jets and missing transverse momentum, and have interpreted the results in GMSB models setting limits on the model parameters [213, 214]. CMS has interpreted a multilepton analysis in terms of limits on gauge mediation models with slepton NLSP [215]. CDF has put limits on gauge mediation models at high $\tan\beta$ and slepton NLSP using an analysis searching for like-charge light leptons and taus [216].

The invisible width of the Z boson puts a lower limit on the sneutrino mass of about 45 GeV. Tighter limits are derived from other searches, notably for gauginos and sleptons, under the assumption of gaugino and sfermion mass universality at the GUT scale, and amount to approximately 94 GeV in the MSSM [217].

The limits on sleptons in simplified models are summarized in Table 89.4.

Table 89.4: Summary of slepton mass limits from LEP and LHC, assuming R -parity conservation and 100% branching fraction for $\tilde{\ell} \rightarrow \tilde{\chi}_1^0 \ell$. Masses in this table are provided in GeV.

Assumption	$m_{\tilde{\ell}}$
$\tilde{\mu}_R, \Delta m(\tilde{\mu}_R, \tilde{\chi}_1^0) > 10$	> 94
$\tilde{e}_R, \Delta m(\tilde{e}_R, \tilde{\chi}_1^0) > 10$	> 94
\tilde{e}_R , any Δm	> 73
$\tilde{\tau}_R, \Delta m(\tilde{\tau}_R, \tilde{\chi}_1^0) > 7$	> 87
$\tilde{\nu}_e, \Delta m(\tilde{e}_R, \tilde{\chi}_1^0) > 10$	> 94
$m_{\tilde{e}_{L,R}} = m_{\tilde{\mu}_{L,R}}, m_{\tilde{\chi}_1^0} \approx 0$	> 700
$m_{\tilde{\chi}_1^0} > \approx 400$	no LHC limit
$m_{\tilde{\tau}_L} = m_{\tilde{\tau}_R}, m_{\tilde{\chi}_1^0} \approx 0$	> 390
$m_{\tilde{\chi}_1^0} > \approx 130$	no LHC limit

89.9 Exclusion limits on the masses of charginos, neutralinos and sleptons in RPV scenarios

In models with R -parity violation, the lightest neutralino can decay even if it is the lightest supersymmetric particle. If the decay involves a non-zero λ coupling, the final state will be a multi-lepton one. Searches for events with four or more isolated charged leptons by ATLAS [117] and CMS [121] are interpreted in such models.

Various searches, including searches for multi-lepton and lepton plus jets events, are interpreted in a model with R -parity violating neutralino decays involving a non-zero λ' coupling [118, 126, 218, 219]. Neutralino decays involving non-zero λ' lead to fully hadronic final states, and searches for multi-jet events and jet-pair resonances are used to set limits, typically on the production of colored particles like top squarks or gluinos, which are assumed to be the primary produced sparticles in these interpretations, as discussed earlier 89.7. For instance, the ATLAS search [130] in events with one lepton and high jet multiplicity excludes up to 320(365) GeV in higgsino (wino) masses. Recent searches [220] also set limits on the production of charginos and neutralinos for a Minimal SUSY model with an approximate $B - L$ symmetry. Charginos and neutralinos with masses between 100 GeV and 1100 GeV are excluded depending on the assumed decay BR into a lepton plus a W, Z or H boson.

Limits also exist on sleptons in R -parity violating models, both from LEP and the Tevatron experiments. From LEP, lower limits

on $\tilde{\mu}_R$ and \tilde{e}_R masses in such models are 97 GeV, and the limits on the stau mass are very close: 96 GeV [221]. CMS has searched for resonant smuon production in a modified CMSSM scenario [222], putting limits on λ'_{211} as a function of $m_0, m_{1/2}$.

Production of pairs of sneutrinos in R -parity violating models has been searched for at LEP [221]. Assuming fully leptonic decays via λ -type couplings, lower mass limits between 85 and 100 GeV are set. At the Tevatron [223, 224] and at the LHC [222, 225–227], searches have focused on scenarios with resonant production of a sneutrino, decaying to $e\mu, \mu\tau$ and $e\tau$ final states. No signal has been seen, and limits have been set on sneutrino masses as a function of the value of relevant RPV couplings. As an example, the LHC experiments exclude a resonant tau sneutrino with a mass below 2.3 TeV for $\lambda_{312} = \lambda_{321} > 0.07$ and $\lambda'_{311} > 0.11$.

89.10 Exclusion limits on long-lived sparticles

Long-lived sparticles arise in many different SUSY models. In particular in co-annihilation scenarios, where the NLSP and LSP are nearly mass-degenerate, this is rather common in order to obtain the correct Dark Matter relic density. Prominent examples are scenarios featuring stau co-annihilation, or models of SUSY breaking, e.g. minimal anomaly-mediated SUSY breaking (AMSB), in which the appropriate Dark Matter density is obtained by co-annihilation of the LSP with an almost degenerate long-lived wino. However, in general, other sparticles can also be long-lived and it is desirable to establish a comprehensive search program for these special long-lived cases, which lead to distinct experimental search signatures. Searches for events with a displaced hadronic vertex, with or without a matched lepton, are for instance interpreted in a model with R -parity violating neutralino decays involving a non-zero λ' coupling [219]. Other signatures interpreted in terms of SUSY models include disappearing tracks, identification of tracks with atypical properties or unusual ionization, small and localized deposits of energy inside of the calorimeters without associated tracks, or stopped particles that decay out of time with collisions. Some examples are reported below.

Past experiments have performed dedicated searches for long-lived SUSY signatures, but given the absence of any experimental evidence for SUSY so far, more effort and focus has gone into such searches at the LHC recently.

If the decay of gluinos is suppressed, for example if squark masses are high, gluinos may live longer than typical hadronization times. It is expected that such gluinos will hadronize to long-living strongly interacting particles known as R-hadrons. In particular, if the suppression of the gluino decay is strong, as in the case that the squark masses are much higher than the TeV scale, these R-hadrons can be (semi-)stable in collider timescales. Searches for such R-hadrons exploit the typical signature of stable charged massive particles in the detector. R-hadrons decaying in the detector are searched for using dE/dx measurements and searches for displaced vertices. As shown in the left plot of Fig. 89.10, the ATLAS experiment excludes semi-stable gluino R-hadrons with masses below 1.9 – 2.3 TeV for all lifetimes in a simplified model where such gluinos always form R-hadrons, and decay into jets and a light neutralino, by combining a number of analyses [124, 228–230]. A combination of CMS searches for long-lived particles, as shown in Fig. 89.11, reaches similar limits [231–235].

Alternatively, since such R-hadrons are strongly interacting, they may be stopped in the calorimeter or in other material, and decay later into energetic jets. These decays are searched for by identifying the jets [236–238] or muons [238] outside the time window associated with bunch-bunch collisions. As shown in Fig. 89.11, the CMS collaboration sets limits on such stopped R-hadrons over 13 orders of magnitude in gluino lifetime, up to masses of 1390 GeV [238]. Recent results from ATLAS [239] sets constraint on the mass of gluino R-hadrons using large out-of-time energy deposits in the calorimeters. Also in this case, masses of up to 1.4 TeV are excluded for gluino lifetimes of $10^{-5} - 10^3$ s.

Top squarks can also be long-lived and hadronize to a R-hadron, for example in the scenario where the top squark is the next-to-lightest SUSY particle (NLSP), with a small mass difference to

the LSP. Searches for massive stable charged particles are sensitive to such top squarks. Tevatron limits are approximately $m_{\tilde{t}} > 300$ GeV [240, 241]. ATLAS sets a limit of 1340 GeV on such top squarks [229], the CMS limits are comparable [233]. Intermediate lifetimes of top squarks decaying through RPV coupling into a quark and a lepton are also targeted by ATLAS and CMS. Limits on top squarks decaying into a quark and a muon are set by ATLAS [242] using events that pass a muon or missing-transverse-momentum trigger and contain a displaced muon track and a displaced vertex. Masses up to 1.7 TeV are excluded for a lifetime of 0.1 ns, and masses below 1.3 TeV are excluded for lifetimes between 0.01 ns and 30 ns. CMS [243] utilizes events with two leptons with transverse impact parameter values between 0.01 and 10 cm not required to form a common vertex to exclude top squarks with masses between 100 and at least 460 GeV for $0.01 < c\tau_0 < 1000$ cm, where $c\tau_0$ is the proper decay length.

In addition to colored sparticles, sparticles like charginos may also be long-lived, especially in scenarios with compressed mass spectra. Charginos decaying in the detectors away from the primary vertex could lead to signatures such as kinked-tracks, or apparently disappearing tracks, since, for example, the pion in $\tilde{\chi}_1^\pm \rightarrow \pi^\pm \tilde{\chi}_1^0$ might be too soft to be reconstructed. At the LHC, searches have been performed for such disappearing tracks, and interpreted within anomaly-mediated SUSY breaking models [244–247]. The right plot of Fig. 89.10 shows constraints for different ATLAS searches on the chargino mass-vs-lifetime plane for an AMSB model ($\tan\beta = 5, \mu > 0$) in which a wino-like $\tilde{\chi}^\pm$ decays to a soft pion and an almost mass-degenerated wino-like $\tilde{\chi}_1^0$ [229, 230, 245–247]. For a similar model, CMS excludes $c\tau$ values between 0.15 and 18 m for a chargino mass of 505 GeV [244], see Fig. 89.11. The most recent ATLAS search [247] provides constraints also for higgsino-like models. Charginos with a lifetime longer than the time needed to pass through the detector appear as charged stable massive particles. Limits have been derived by the LEP experiments [248], by D0 at the Tevatron [241], and by the LHC experiments [229, 249], and such charginos with mass below 1090 GeV are excluded.

In gauge mediation models, NLSP neutralino decays need not be prompt, and experiments have searched for late decays with photons in the final state. CDF has searched for delayed $\tilde{\chi}_1^0 \rightarrow \gamma \tilde{G}$ decays using the timing of photon signals in the calorimeter [250]. CMS has used the same technique at the LHC [251]. Results are given as exclusion contours in the neutralino mass versus lifetime plane, and for example in a GMSB model with a neutralino mass of 300 GeV, $c\tau$ values between 10 and 2000 cm are excluded [251]. D0 has looked at the direction of showers in the electromagnetic calorimeter with a similar goal [252], and ATLAS has searched for photon candidates that do not point back to the primary vertex, as well as for delayed photons [253].

Charged slepton decays may be kinematically suppressed, for example in the scenario of a NLSP slepton with a very small mass difference to the LSP. Such a slepton may appear to be a stable charged massive particle. Interpretation of searches at LEP for such signatures within GMSB models with a stau NLSP or slepton co-NLSP exclude masses up to 99 GeV [248]. Searches for stable charged particles at the Tevatron [240, 241] and at the LHC [229, 233] are also interpreted in terms of limits on stable charged sleptons. The limits obtained at the LHC exclude stable staus with masses below 430 GeV when produced directly in pairs, and below 660 GeV when staus are produced both directly and indirectly in the decay of other particles in a GMSB model. Recent results from ATLAS and CMS set constraints on long-lived charged slepton with intermediate lifetimes. ATLAS searches for charged leptons with large impact parameters and exclude selectron, smuon and stau masses up to 720 GeV, 680 GeV, and 340 GeV, respectively, in case of lifetimes of 0.1 ns. CMS [211] targets long-lived stau with $c\tau$ of about 0.1 mm excluding masses between 115 and 220 GeV for the case that the LSP is nearly massless.

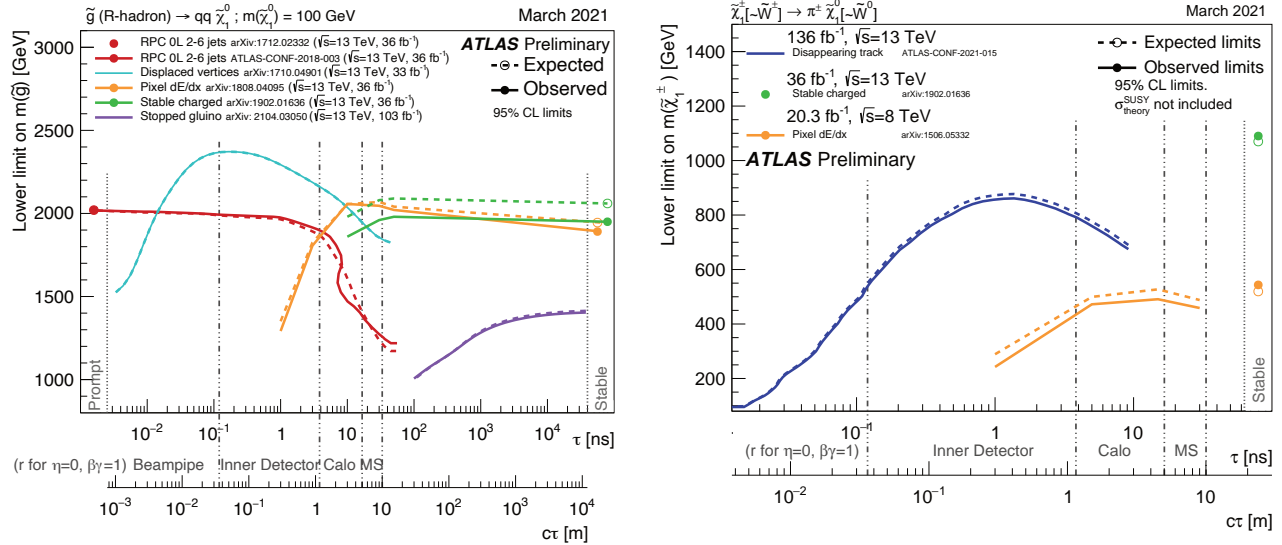


Figure 89.10: Limits at 95% C.L. on the gluino mass in R-hadron models (left), and on the chargino mass in a model where the wino-like chargino is almost degenerate with the LSP (right), as a function of gluino or chargino lifetime, as obtained by ATLAS.

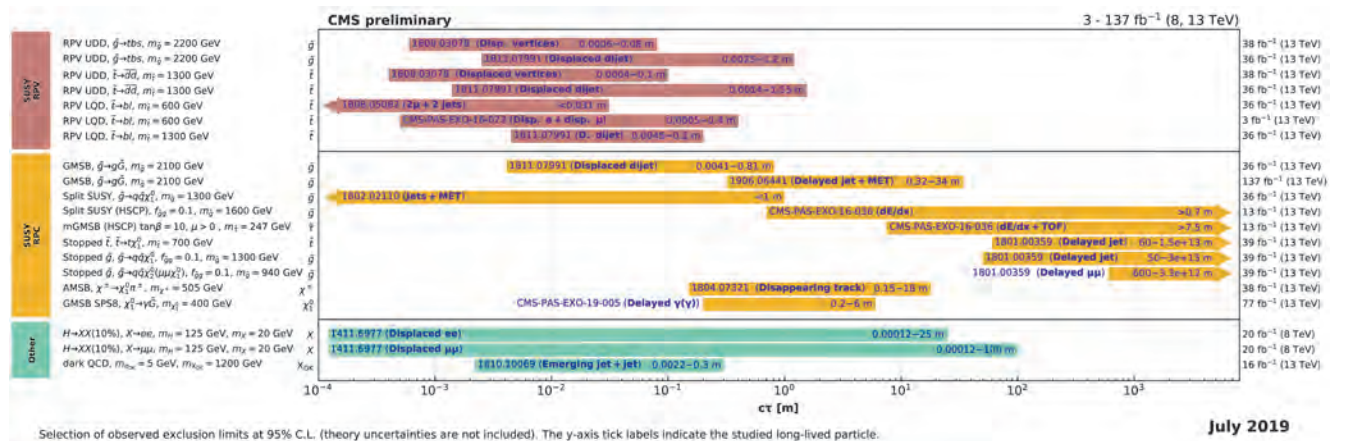


Figure 89.11: Excluded regions, at 95% C.L., in the lifetimes of long-lived particles in several models, as obtained by CMS.

89.11 Global interpretations

Apart from the interpretation of direct searches for sparticle production at colliders in terms of limits on masses of individual SUSY particles, model-dependent interpretations of allowed SUSY parameter space are derived from global SUSY fits. Typically these fits combine the results from collider experiments with indirect constraints on SUSY as obtained from low-energy experiments, flavor physics, high-precision electroweak results, and astrophysical data.

In the pre-LHC era these fits were mainly dominated by indirect constraints. Even for very constrained models like the CMSSM, the allowed parameter space, in terms of squark and gluino masses, ranged from several hundreds of GeV to a few TeV. Furthermore, these global fits indicated that squarks and gluino masses in the range of 500 to 1000 GeV were the preferred region of parameter space, although values as high as a few TeV were allowed with lower probabilities [254–261].

With ATLAS and CMS now probing mass scales around 1 TeV and beyond, the importance of the direct searches for global analyses of allowed SUSY parameter space has increased. For example, imposing the new experimental limits on constrained supergravity models pushes the most likely values of first generation squark and gluino masses significantly beyond 2 TeV, typically resulting in overall values of fit quality much worse than those in the pre-LHC era [175–177, 202, 262–269]. The measured value of m_h pushes the sparticle masses upwards. Although these constrained

models are not yet ruled out, the extended experimental limits impose very tight constraints on the allowed parameter space.

For this reason, the emphasis of global SUSY fits has shifted towards less-constrained SUSY models. Interpretations in the pMSSM [200–204, 249, 262] as well as in simplified models, have been useful to generalize SUSY searches, for example to redesign experimental analyses in order to increase their sensitivity for compressed spectra, where the mass of the LSP is much closer to squark and gluino masses than predicted by the CMSSM. As shown in Table 89.1, for neutralino masses above 0.5–1 TeV the current set of ATLAS and CMS searches, interpreted in simplified models, cannot exclude the existence of squarks or gluinos with masses only marginally above the neutralino mass. However, as these exclusion limits are defined in the context of simplified models, they are only valid for the assumptions in which these models are defined.

As an alternative approach, both ATLAS [200] and CMS [201] have performed an analysis of the impact of their searches on the parameter space of the pMSSM. Fig. 89.12 shows graphically the LHC exclusion power in the pMSSM based on searches performed at $\sqrt{s} = 7$ and 8 TeV. The plot on the left shows the survival probability in the gluino-neutralino mass plane, which is a measure of the parameter space that remains after inclusion of the relevant CMS search results. As can be seen, gluino masses below about 1.2 TeV are almost fully excluded. This result agrees well with the typical exclusion obtained at 8 TeV in simplified mod-

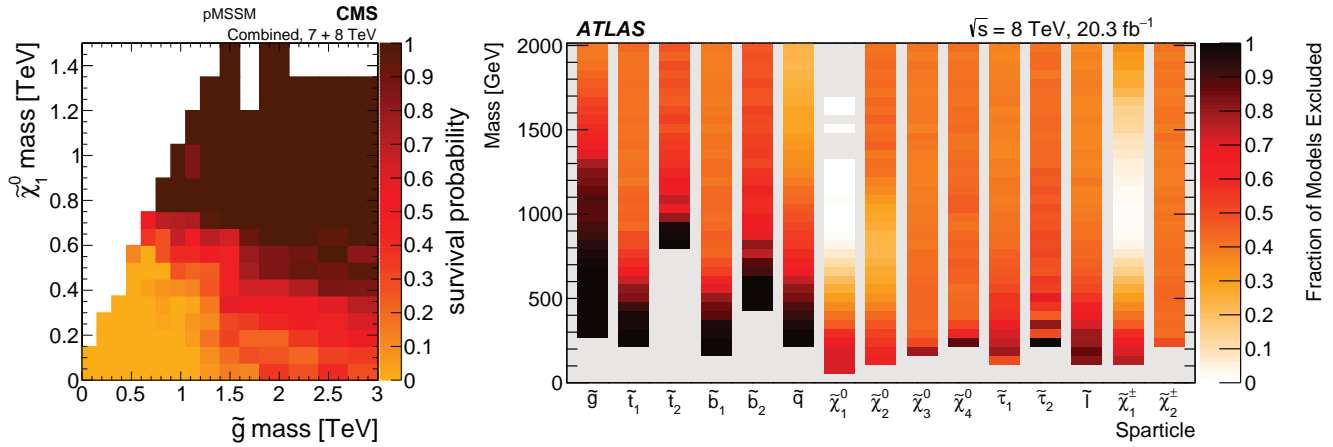


Figure 89.12: The plot on the left shows the survival probability of a pMSSM parameter space model in the gluino-neutralino mass plane after the application of the relevant CMS search results. The plot on the right shows a graphical representation of the ATLAS exclusion power in a pMSSM model. Each vertical bar is a one-dimensional projection of the fraction of models points excluded for each sparticle by ATLAS analyses. The experimental results are obtained from data taken at $\sqrt{s} = 7$ and 8 TeV.

ATLAS SUSY Searches* - 95% CL Lower Limits				ATLAS Preliminary $\sqrt{s} = 13$ TeV					
June 2021									
Model	Signature	$\int \mathcal{L} dt$ [fb^{-1}]	Mass limit	Reference					
Inclusive Searches	$\tilde{g}\tilde{g}, \tilde{g} \rightarrow \tilde{g}\tilde{\chi}_1^0$	0 e, μ mono-jet	2-6 jets 1-3 jets	139 E_{T}^{miss} 36.1	139 E_{T}^{miss} 36.1	\tilde{g} [1x, 6x Degen] \tilde{g} [8x Degen]	1.0 1.85	$m(\tilde{\chi}_1^0) < 400$ GeV $m(\tilde{g}) - m(\tilde{\chi}_1^0) = 5$ GeV	2106.14293 2102.10874
	$\tilde{g}\tilde{g}, \tilde{g} \rightarrow \tilde{g}\tilde{\chi}_1^0$	0 e, μ	2-6 jets	E_{T}^{miss} 139	E_{T}^{miss} 139	\tilde{g}	Forbidden 1.15-1.95	$m(\tilde{\chi}_1^0) = 0$ GeV $m(\tilde{\chi}_1^0) = 1000$ GeV	210.14293 210.14293
	$\tilde{g}\tilde{g}, \tilde{g} \rightarrow \tilde{g}\tilde{\chi}_1^0 W\tilde{\chi}_1^0$	1 e, μ	2-6 jets	E_{T}^{miss} 139	E_{T}^{miss} 139	\tilde{g}	2.2	$m(\tilde{\chi}_1^0) < 600$ GeV	2101.01629
	$\tilde{g}\tilde{g}, \tilde{g} \rightarrow \tilde{g}\tilde{\chi}_1^0 (\tilde{\chi}_1^0 \tilde{\chi}_1^0)$	0 e, μ	2 jets	E_{T}^{miss} 36.1	E_{T}^{miss} 36.1	\tilde{g}	1.2	$m(\tilde{g}) - m(\tilde{\chi}_1^0) = 50$ GeV	1805.11381
	$\tilde{g}\tilde{g}, \tilde{g} \rightarrow \tilde{g}\tilde{\chi}_1^0 WZ\tilde{\chi}_1^0$	0 e, μ	7-11 jets	E_{T}^{miss} 139	E_{T}^{miss} 139	\tilde{g}	1.97	$m(\tilde{\chi}_1^0) < 600$ GeV	2008.06032
	$\tilde{g}\tilde{g}, \tilde{g} \rightarrow \tilde{g}\tilde{\chi}_1^0$	SS e, μ	6 jets	E_{T}^{miss} 139	E_{T}^{miss} 139	\tilde{g}	1.15	$m(\tilde{g}) - m(\tilde{\chi}_1^0) = 200$ GeV	1909.08457
3 γ gen. squarks direct production	$\tilde{b}_1\tilde{b}_1$	0 e, μ	2 b	E_{T}^{miss} 139	E_{T}^{miss} 139	\tilde{b}_1	1.25	$m(\tilde{\chi}_1^0) < 400$ GeV 10 GeV $< \Delta m(\tilde{b}_1, \tilde{\chi}_1^0) < 20$ GeV	2101.12527 2101.12527
	$\tilde{b}_1\tilde{b}_1, \tilde{b}_1 \rightarrow \tilde{b}\tilde{\chi}_1^0 \rightarrow \tilde{b}h\tilde{\chi}_1^0$	0 e, μ	6 b	E_{T}^{miss} 139	E_{T}^{miss} 139	\tilde{b}_1	0.68	$\Delta m(\tilde{\chi}_1^0, \tilde{\chi}_1^0) = 130$ GeV, $m(\tilde{\chi}_1^0) = 100$ GeV $\Delta m(\tilde{\chi}_1^0, \tilde{\chi}_1^0) = 130$ GeV, $m(\tilde{\chi}_1^0) = 0$ GeV	1908.03122 ATLAS-CONF-2020-031
	$\tilde{t}_1\tilde{t}_1, \tilde{t}_1 \rightarrow \tilde{t}\tilde{\chi}_1^0$	0-1 e, μ	≥ 1 jet	E_{T}^{miss} 139	E_{T}^{miss} 139	\tilde{t}_1	1.25	$m(\tilde{\chi}_1^0) = 1$ GeV	2004.14069,2012.03799
	$\tilde{t}_1\tilde{t}_1, \tilde{t}_1 \rightarrow W\tilde{b}\tilde{\chi}_1^0$	1 e, μ	3 jets/1 b	E_{T}^{miss} 139	E_{T}^{miss} 139	\tilde{t}_1	0.65	$m(\tilde{\chi}_1^0) = 500$ GeV	2012.03799
	$\tilde{t}_1\tilde{t}_1, \tilde{t}_1 \rightarrow \tilde{t}\tilde{\chi}_1^0, \tilde{t}_1 \rightarrow \tau\tilde{G}$	1-2 τ	2 jets/1 b	E_{T}^{miss} 139	E_{T}^{miss} 139	\tilde{t}_1	Forbidden 1.4	$m(\tilde{\chi}_1^0) = 800$ GeV	ATLAS-CONF-2021-008
	$\tilde{t}_1\tilde{t}_1, \tilde{t}_1 \rightarrow \tilde{t}\tilde{\chi}_1^0, \tilde{t}_1 \rightarrow \tau\tilde{G}, \tilde{t}_1 \rightarrow \tilde{t}\tilde{\chi}_1^0$	0 e, μ 2 c mono-jet	2 c mono-jet	E_{T}^{miss} 36.1 E_{T}^{miss} 139	E_{T}^{miss} 36.1 E_{T}^{miss} 139	\tilde{t}_1	0.55 0.85	$m(\tilde{\chi}_1^0) = 0$ GeV $m(\tilde{t}_1) - m(\tilde{\chi}_1^0) = 5$ GeV	1805.01649 2102.10874
EW direct	$\tilde{\chi}_1^0\tilde{\chi}_1^0$ via WZ	Multiple l/jets	≥ 1 jet	E_{T}^{miss} 139	E_{T}^{miss} 139	$\tilde{\chi}_1^0$	0.205	$m(\tilde{\chi}_1^0) = 0$, wino-bino $m(\tilde{\chi}_1^0) - m(\tilde{\chi}_1^0) = 5$ GeV, wino-bino	2106.01676, ATLAS-CONF-2021-022 1911.12606
	$\tilde{\chi}_1^0\tilde{\chi}_1^0$ via WW	2 e, μ	6 b	E_{T}^{miss} 139	E_{T}^{miss} 139	$\tilde{\chi}_1^0$	0.42	$m(\tilde{\chi}_1^0) = 0$, wino-bino	1908.08215
	$\tilde{\chi}_1^0\tilde{\chi}_1^0$ via Wh	Multiple l/jets	Multiple l/jets	E_{T}^{miss} 139	E_{T}^{miss} 139	$\tilde{\chi}_1^0$	Forbidden 1.06	$m(\tilde{\chi}_1^0) = 70$ GeV, wino-bino	2004.10894, ATLAS-CONF-2021-022
	$\tilde{\chi}_1^0\tilde{\chi}_1^0$ via $\tilde{t}_1\tilde{t}_1$	2 e, μ	2 τ	E_{T}^{miss} 139	E_{T}^{miss} 139	$\tilde{\chi}_1^0$	0.16-0.3 0.12-0.39	$m(\tilde{\chi}_1^0) = 0.5(m(\tilde{t}_1) + m(\tilde{\chi}_1^0))$	1908.08215 1911.02660
	$\tilde{\chi}_1^0\tilde{\chi}_1^0$ via $\tilde{t}_1\tilde{t}_1$	2 τ	2 τ	E_{T}^{miss} 139	E_{T}^{miss} 139	$\tilde{\chi}_1^0$	0.7	$m(\tilde{\chi}_1^0) = 0$	1908.08215
	$\tilde{t}_1\tilde{t}_1, \tilde{t}_1 \rightarrow \tilde{t}\tilde{\chi}_1^0$	0 e, μ	0 jets	E_{T}^{miss} 139	E_{T}^{miss} 139	\tilde{t}_1	0.256	$m(\tilde{t}_1) - m(\tilde{\chi}_1^0) = 10$ GeV	1908.08215 1911.12606
Long-lived particles	$\tilde{H}, \tilde{H} \rightarrow h\tilde{G}/Z\tilde{G}$	0 e, μ 4 e, μ 0 e, μ	≥ 3 b 0 jets ≥ 2 large jets	E_{T}^{miss} 36.1 E_{T}^{miss} 139 E_{T}^{miss} 139	E_{T}^{miss} 36.1 E_{T}^{miss} 139 E_{T}^{miss} 139	\tilde{H} \tilde{H} \tilde{H}	0.13-0.23 0.55 0.45-0.93	$\text{BR}(\tilde{H} \rightarrow h\tilde{G}) = 1$ $\text{BR}(\tilde{H} \rightarrow Z\tilde{G}) = 1$ $\text{BR}(\tilde{H} \rightarrow Z\tilde{G}) = 1$	1806.04030 2103.11684 ATLAS-CONF-2021-022
	Direct $\tilde{\chi}_1^0\tilde{\chi}_1^0$ prod., long-lived $\tilde{\chi}_1^0$	Disapp. trk	1 jet	E_{T}^{miss} 139	E_{T}^{miss} 139	$\tilde{\chi}_1^0$	0.21 0.66	Pure Wino Pure higgsino	ATLAS-CONF-2021-015 ATLAS-CONF-2021-015
	Stable \tilde{g} R-hadron	Multiple	Multiple	E_{T}^{miss} 36.1	E_{T}^{miss} 36.1	\tilde{g}	2.0 2.05 2.4	$m(\tilde{\chi}_1^0) = 100$ GeV	1902.01636, 1808.04095 1710.04901, 1808.04095
	Metastable \tilde{g} R-hadron, $\tilde{g} \rightarrow \tilde{g}\tilde{\chi}_1^0$	Displ. lep	Multiple	E_{T}^{miss} 139	E_{T}^{miss} 139	\tilde{g}	0.34 0.7	$\tau(\tilde{g}) = 0.1$ ns $\tau(\tilde{g}) = 0.1$ ns	2011.07812 2011.07812
RPV	$\tilde{\chi}_1^0\tilde{\chi}_1^0, \tilde{\chi}_1^0\tilde{\chi}_1^0, \tilde{\chi}_1^0\tilde{\chi}_1^0 \rightarrow Zl\ell\ell$	3 e, μ	0 jets	E_{T}^{miss} 139	E_{T}^{miss} 139	$\tilde{\chi}_1^0$	0.625 1.05	Pure Wino	2011.10543
	$\tilde{\chi}_1^0\tilde{\chi}_1^0, \tilde{\chi}_1^0\tilde{\chi}_1^0 \rightarrow WWZZ\ell\ell\nu\nu$	4 e, μ	0 jets	E_{T}^{miss} 139	E_{T}^{miss} 139	$\tilde{\chi}_1^0$	0.95 1.55	$m(\tilde{\chi}_1^0) = 200$ GeV	2103.11684
	$\tilde{g}\tilde{g}, \tilde{g} \rightarrow \tilde{g}\tilde{\chi}_1^0, \tilde{\chi}_1^0 \rightarrow qq\tilde{q}$	4-5 large jets	Multiple	E_{T}^{miss} 36.1	E_{T}^{miss} 36.1	\tilde{g}	1.3 1.9	Large $A_{1/2}$	1804.03568
	$\tilde{t}_1, \tilde{t}_1 \rightarrow \tilde{t}\tilde{\chi}_1^0, \tilde{\chi}_1^0 \rightarrow sb\tilde{s}$	Multiple	Multiple	E_{T}^{miss} 36.1	E_{T}^{miss} 36.1	\tilde{t}_1	0.55 1.05	$m(\tilde{\chi}_1^0) = 200$ GeV, bino-like $m(\tilde{\chi}_1^0) = 500$ GeV	ATLAS-CONF-2018-003
	$\tilde{t}_1, \tilde{t}_1 \rightarrow \tilde{t}\tilde{\chi}_1^0, \tilde{\chi}_1^0 \rightarrow sb\tilde{s}$	2 jets + 2 b	Multiple	E_{T}^{miss} 139	E_{T}^{miss} 139	\tilde{t}_1	Forbidden 0.95		2010.01015
	$\tilde{t}_1\tilde{t}_1, \tilde{t}_1 \rightarrow b\tilde{s}$	2 e, μ	2 jets + 2 b	E_{T}^{miss} 36.7	E_{T}^{miss} 36.7	\tilde{t}_1	0.42 0.61	$\text{BR}(\tilde{t}_1 \rightarrow b\tilde{s}) > 20\%$	1710.07171
RPV	$\tilde{t}_1\tilde{t}_1, \tilde{t}_1 \rightarrow q\tilde{d}$	2 e, μ	2 b	E_{T}^{miss} 36.1	E_{T}^{miss} 36.1	\tilde{t}_1	0.4-1.45	$\text{BR}(\tilde{t}_1 \rightarrow b\tilde{s}) > 20\%$	1710.05544
	$\tilde{t}_1\tilde{t}_1, \tilde{t}_1 \rightarrow q\tilde{d}$	1 μ	DV	E_{T}^{miss} 136	E_{T}^{miss} 136	\tilde{t}_1	1.0 1.6	$\text{BR}(\tilde{t}_1 \rightarrow q\tilde{d}) = 100\%$, $\cos\phi = 1$	2003.11956
	$\tilde{\chi}_1^0\tilde{\chi}_1^0, \tilde{\chi}_1^0\tilde{\chi}_1^0, \tilde{\chi}_1^0\tilde{\chi}_1^0 \rightarrow t\tilde{b}\tilde{s}, \tilde{\chi}_1^0\tilde{\chi}_1^0 \rightarrow b\tilde{b}\tilde{s}$	1-2 e, μ	≥ 6 jets	E_{T}^{miss} 139	E_{T}^{miss} 139	$\tilde{\chi}_1^0$	0.2-0.32	Pure higgsino	ATLAS-CONF-2021-007

*Only a selection of the available mass limits on new states or phenomena is shown. Many of the limits are based on simplified models, c.f. refs. for the assumptions made.

Figure 89.13: Overview of the current landscape of SUSY searches at the LHC. The plot shows exclusion mass limits of ATLAS for different searches and interpretation assumptions. The corresponding results of the CMS experiment are similar.

els for gluino production. However, as shown in the right plot of Fig. 89.12, when a similar analysis for other sparticles is performed it becomes apparent that exclusions on the pMSSM parameter can be significantly less stringent than simplified model limits might suggest. This is especially apparent for the electroweak sector, where even at rather low masses several of the pMSSM test points still survive the constraint of ATLAS searches at $\sqrt{s} = 7$ and 8 TeV. This again indicates that care must be taken when inter-

preting results from the LHC searches and there are still several scenarios where sparticles below the 1 TeV scale are not excluded, even when considering the most recent results at $\sqrt{s} = 13$ TeV.

Furthermore, the discovery of a Higgs boson with a mass around 125 GeV has triggered many studies regarding the compatibility of SUSY parameter space with this new particle. Much of it is still work in progress and it will be interesting to see how the interplay between the results from direct SUSY searches and more precise

measurements of the properties of the Higgs boson will unfold in the future.

89.12 Summary and Outlook

The absence of any observation of new phenomena at the first run of the LHC at $\sqrt{s} = 7/8$ TeV, and after the second run at $\sqrt{s} = 13$ TeV, places significant constraints on SUSY parameter space. An overview of the current landscape of SUSY searches and limits at the LHC is shown in Figure 89.13, where the ATLAS summary is reported for illustration purposes. Inclusive searches probe production of gluinos at about 2.3 TeV, first and second generation squarks in the range of about 1 to 1.9 TeV, third generation squarks at scales around 600 GeV to 1.2 TeV, electroweak gauginos at scales around 400 – 1100 GeV, and sleptons around 700 GeV. However, depending on the assumptions made on the underlying SUSY spectrum these limits can also weaken considerably.

With the LHC having reached almost its maximum energy of about $\sqrt{s} = 14$ TeV, future sensitivity improvement will have to originate from more data, the improvement of experimental analysis techniques and the focus on special signatures like the ones arising in long-lived sparticle decays. Therefore, it is expected that the current landscape of SUSY searches and corresponding exclusion limits at the LHC, as, for example, shown in Fig. 89.13 from the ATLAS experiment [270] (CMS results are similar [271]), will not change as rapidly anymore as it did in the past, when the LHC underwent several successive increases of collision energy.

The interpretation of results at the LHC has moved away from constrained models like the CMSSM towards a large set of simplified models, or the pMSSM. On the one hand this move is because the LHC limits have put constrained models like the CMSSM under severe pressure, while on the other hand simplified models leave more freedom to vary parameters and form a better representation of the underlying sensitivity of analyses. However, these interpretations in simplified models do not come without a price: the decomposition of a potentially complicated reality in a limited set of individual decay chains can be significantly incomplete. Therefore, quoted limits in simplified models are only valid under the explicit assumptions made in these models. The recent addition of more comprehensive interpretations in the pMSSM will complement those derived from simplified models and, thus, will enable an even more refined understanding of the probed SUSY parameter space.

In this context, the limit range of 1.5 – 2.3 TeV on generic colored SUSY particles only holds for light neutralinos, in the R -parity conserving MSSM. Limits on third generation squarks and electroweak gauginos also only hold for light neutralinos, and under specific assumptions for decay modes and slepton masses.

The next LHC runs, with \sqrt{s} between 13 and 14 TeV and significantly larger integrated luminosities (notably the High-Luminosity LHC), will provide a large data sample for future SUSY searches. As mentioned above, the improvement in sensitivity will largely have to come from a larger data set, and evolution of trigger and analysis techniques, since there will be no significant energy increase at the LHC anymore. Although the sensitivity for colored sparticles will increase somewhat as well, the expanded data set will be particularly beneficial for electroweak gaugino searches, and for the more difficult final states presented by compressed particle spectra, stealth SUSY, long-lived sparticles, or R -parity violating scenarios.

References

- [1] H. Miyazawa, Prog. Theor. Phys. **36**, 6, 1266 (1966).
- [2] Yu. A. Golfand and E. P. Likhtman, JETP Lett. **13**, 323 (1971), [Pisma Zh. Eksp. Teor. Fiz.13,452(1971)].
- [3] J.-L. Gervais and B. Sakita, Nucl. Phys. **B34**, 632 (1971).
- [4] D. V. Volkov and V. P. Akulov, Phys. Lett. **46B**, 109 (1973).
- [5] J. Wess and B. Zumino, Phys. Lett. **49B**, 52 (1974).
- [6] J. Wess and B. Zumino, Nucl. Phys. **B70**, 39 (1974).
- [7] A. Salam and J. A. Strathdee, Nucl. Phys. **B76**, 477 (1974).
- [8] H. P. Nilles, Phys. Rept. **110**, 1 (1984).
- [9] H. E. Haber and G. L. Kane, Phys. Rept. **117**, 75 (1985).
- [10] E. Witten, Nucl. Phys. **B188**, 513 (1981).
- [11] S. Dimopoulos and H. Georgi, Nucl. Phys. **B193**, 150 (1981).
- [12] M. Dine, W. Fischler and M. Srednicki, Nucl. Phys. **B189**, 575 (1981).
- [13] S. Dimopoulos and S. Raby, Nucl. Phys. **B192**, 353 (1981).
- [14] N. Sakai, Z. Phys. **C11**, 153 (1981).
- [15] R. K. Kaul and P. Majumdar, Nucl. Phys. **B199**, 36 (1982).
- [16] H. Goldberg, Phys. Rev. Lett. **50**, 1419 (1983).
- [17] J. R. Ellis *et al.*, Nucl. Phys. **B238**, 453 (1984).
- [18] G. Jungman, M. Kamionkowski and K. Griest, Phys. Rept. **267**, 195 (1996), [hep-ph/9506380].
- [19] S. Dimopoulos, S. Raby and F. Wilczek, Phys. Rev. **D24**, 1681 (1981).
- [20] W. J. Marciano and G. Senjanovic, Phys. Rev. **D25**, 3092 (1982).
- [21] M. B. Einhorn and D. R. T. Jones, Nucl. Phys. **B196**, 475 (1982).
- [22] L. E. Ibanez and G. G. Ross, Phys. Lett. **105B**, 439 (1981).
- [23] U. Amaldi, W. de Boer and H. Furstenau, Phys. Lett. **B260**, 447 (1991).
- [24] P. Langacker and N. Polonsky, Phys. Rev. **D52**, 3081 (1995), [hep-ph/9503214].
- [25] J. R. Ellis, S. Kelley and D. V. Nanopoulos, Phys. Lett. B **260**, 131 (1991).
- [26] P. Fayet, Phys. Lett. **64B**, 159 (1976).
- [27] G. R. Farrar and P. Fayet, Phys. Lett. **76B**, 575 (1978).
- [28] B.C. Allanach and H.E. Haber, *Supersymmetry, Part I (Theory)*, in this Review.
- [29] M. Carena *et al.*, *Status of Higgs Boson Physics*, in this Review.
- [30] A. M. Sirunyan *et al.* (CMS), JHEP **04**, 188 (2020), [arXiv:1910.12127].
- [31] M. Aaboud *et al.* (ATLAS), JHEP **04**, 098 (2019), [arXiv:1812.03017].
- [32] R. Aaij *et al.* (LHCb), Phys. Rev. Lett. **118**, 19, 191801 (2017), [arXiv:1703.05747].
- [33] A. Höcker and W.J. Marciano, *Muon Anomalous Magnetic Moment*, in this Review.
- [34] B. Abi *et al.* (Muon g-2), Phys. Rev. Lett. **126**, 14, 141801 (2021), [arXiv:2104.03281].
- [35] G. Hinshaw *et al.* (WMAP), Astrophys. J. Suppl. **208**, 19 (2013), [arXiv:1212.5226].
- [36] N. Aghanim *et al.* (Planck Collaboration), A&A **641**, A1 (2020).
- [37] K. Nakamura *et al.* (Particle Data Group), J. Phys. **G37**, 075021 (2010).
- [38] I. Hinchliffe *et al.*, Phys. Rev. **D55**, 5520 (1997), [hep-ph/9610544].
- [39] L. Randall and D. Tucker-Smith, Phys. Rev. Lett. **101**, 221803 (2008), [arXiv:0806.1049].
- [40] V. Khachatryan *et al.* (CMS), Phys. Lett. **B698**, 196 (2011), [arXiv:1101.1628].
- [41] S. Chatrchyan *et al.* (CMS), Phys. Rev. Lett. **107**, 221804 (2011), [arXiv:1109.2352].
- [42] S. Chatrchyan *et al.* (CMS), JHEP **01**, 077 (2013), [arXiv:1210.8115].
- [43] S. Chatrchyan *et al.* (CMS), Eur. Phys. J. **C73**, 9, 2568 (2013), [arXiv:1303.2985].
- [44] S. Chatrchyan *et al.* (CMS), Phys. Rev. **D85**, 012004 (2012), [arXiv:1107.1279].
- [45] C. G. Lester and D. J. Summers, Phys. Lett. **B463**, 99 (1999), [hep-ph/9906349].

- [46] D. R. Tovey, JHEP **04**, 034 (2008), [arXiv:0802.2879].
- [47] M. R. Buckley *et al.*, Phys. Rev. **D89**, 5, 055020 (2014), [arXiv:1310.4827].
- [48] P. Jackson, C. Rogan and M. Santoni, Phys. Rev. **D95**, 3, 035031 (2017), [arXiv:1607.08307].
- [49] J. M. Butterworth *et al.*, Phys. Rev. Lett. **100**, 242001 (2008), [arXiv:0802.2470].
- [50] A. M. Sirunyan *et al.* (CMS), JHEP **05**, 032 (2020), [arXiv:1912.08887].
- [51] N. Arkani-Hamed and S. Dimopoulos, JHEP **06**, 073 (2005), [hep-th/0405159].
- [52] G. F. Giudice and A. Romanino, Nucl. Phys. B **699**, 65 (2004), [Erratum: Nucl.Phys.B 706, 487–487 (2005)], [hep-ph/0406088].
- [53] J. Alimena *et al.*, J. Phys. G **47**, 9, 090501 (2020), [arXiv:1903.04497].
- [54] A.H. Chamseddine, R. Arnowitt, and P Nath, Phys. Rev. Lett. **49**, 970 (1982).
- [55] E. Cremmer *et al.*, Nucl. Phys. **B212**, 413 (1983).
- [56] P. Fayet, Phys. Lett. **70B**, 461 (1977).
- [57] M. Dine, A. E. Nelson and Y. Shirman, Phys. Rev. **D51**, 1362 (1995), [hep-ph/9408384].
- [58] P. Meade, N. Seiberg and D. Shih, Prog. Theor. Phys. Suppl. **177**, 143 (2009), [arXiv:0801.3278].
- [59] G. F. Giudice *et al.*, JHEP **12**, 027 (1998), [hep-ph/9810442].
- [60] L. Randall and R. Sundrum, Nucl. Phys. **B557**, 79 (1999), [hep-th/9810155].
- [61] R. L. Arnowitt and P. Nath, Phys. Rev. Lett. **69**, 725 (1992).
- [62] G. L. Kane *et al.*, Phys. Rev. **D49**, 6173 (1994), [hep-ph/9312272].
- [63] A. Djouadi *et al.* (MSSM Working Group), in “GDR (Groupement De Recherche) - Supersymetrie,” (1998), [hep-ph/9901246].
- [64] A. Djouadi, J.-L. Kneur and G. Moultaka, Comput. Phys. Commun. **176**, 426 (2007), [hep-ph/0211331].
- [65] C. F. Berger *et al.*, JHEP **02**, 023 (2009), [arXiv:0812.0980].
- [66] H. Baer *et al.*, in “Workshop on Physics at Current Accelerators and the Supercollider Argonne, Illinois, June 2-5, 1993,” 0703–720 (1993), [hep-ph/9305342], URL http://lss.fnal.gov/cgi-bin/find_paper.pl?other/ssc/sscl-preprint-441.
- [67] R. M. Barnett, H. E. Haber and G. L. Kane, Nucl. Phys. **B267**, 625 (1986).
- [68] H. Baer, D. Karatas and X. Tata, Phys. Lett. **B183**, 220 (1987).
- [69] J. Alwall, P. Schuster and N. Toro, Phys. Rev. **D79**, 075020 (2009), [arXiv:0810.3921].
- [70] J. Alwall *et al.*, Phys. Rev. **D79**, 015005 (2009), [arXiv:0809.3264].
- [71] LEP2 SUSY Working Group, ALEPH, DELPHI, L3 and OPAL experiments, note LEPSUSYWG/04-02.1, <http://lepsusy.web.cern.ch/lepsusy>.
- [72] LHC SUSY cross sections working group, <https://twiki.cern.ch/twiki/bin/view/LHCPhysics/SUSYCrossSections>.
- [73] T. Aaltonen *et al.* (CDF), Phys. Rev. Lett. **102**, 121801 (2009), [arXiv:0811.2512].
- [74] V. M. Abazov *et al.* (D0), Phys. Lett. **B660**, 449 (2008), [arXiv:0712.3805].
- [75] A. M. Sirunyan *et al.* (CMS) (2019), [arXiv:1908.04722].
- [76] ATLAS Collab., ATLAS-CONF-2019-040 (2019).
- [77] G. Aad *et al.* (ATLAS), Eur. Phys. J. C **81**, 7, 600 (2021), [arXiv:2101.01629].
- [78] G. Aad *et al.* (ATLAS), JHEP **02**, 143 (2021), [arXiv:2010.14293].
- [79] A. M. Sirunyan *et al.* (CMS), JHEP **10**, 244 (2019), [arXiv:1908.04722].
- [80] ATLAS Collab., ATLAS-CONF-2018-041 (2018).
- [81] A. M. Sirunyan *et al.* (CMS) (2019), [arXiv:1909.03460].
- [82] G. Aad *et al.* (ATLAS Collaboration), Phys. Rev. D **103**, 112006 (2021), URL <https://link.aps.org/doi/10.1103/PhysRevD.103.112006>.
- [83] M. Aaboud *et al.* (ATLAS), JHEP **09**, 050 (2018), [arXiv:1805.01649].
- [84] T. Aaltonen *et al.* (CDF), Phys. Rev. Lett. **105**, 081802 (2010), [arXiv:1005.3600].
- [85] V. M. Abazov *et al.* (D0), Phys. Lett. **B693**, 95 (2010), [arXiv:1005.2222].
- [86] G. Aad *et al.* (ATLAS), JHEP **05**, 093 (2021), [arXiv:2101.12527].
- [87] G. Aad *et al.* (ATLAS), JHEP **12**, 060 (2019), [arXiv:1908.03122].
- [88] G. Aad *et al.* (ATLAS), JHEP **06**, 046 (2020), [arXiv:1909.08457].
- [89] G. Aad *et al.* (ATLAS), Phys. Rev. D **104**, 3, 032014 (2021), [arXiv:2103.08189].
- [90] A. M. Sirunyan *et al.* (CMS), JHEP **03**, 076 (2018), [arXiv:1709.08908].
- [91] A. M. Sirunyan *et al.* (CMS), Eur. Phys. J. C **80**, 8, 752 (2020), [arXiv:2001.10086].
- [92] C. Boehm, A. Djouadi and Y. Mambrini, Phys. Rev. **D61**, 095006 (2000), [hep-ph/9907428].
- [93] T. Aaltonen *et al.* (CDF), Phys. Rev. **D82**, 092001 (2010), [arXiv:1009.0266].
- [94] V. M. Abazov *et al.* (D0), Phys. Lett. **B696**, 321 (2011), [arXiv:1009.5950].
- [95] T. Aaltonen *et al.* (CDF), JHEP **10**, 158 (2012), [arXiv:1203.4171].
- [96] V. M. Abazov *et al.* (D0), Phys. Lett. **B665**, 1 (2008), [arXiv:0803.2263].
- [97] T. Aaltonen *et al.* (CDF), Phys. Rev. Lett. **104**, 251801 (2010), [arXiv:0912.1308].
- [98] V. M. Abazov *et al.* (D0), Phys. Lett. **B674**, 4 (2009), [arXiv:0901.1063].
- [99] G. Aad *et al.* (ATLAS), Eur. Phys. J. C **80**, 8, 737 (2020), [arXiv:2004.14060].
- [100] G. Aad *et al.* (ATLAS), JHEP **04**, 174 (2021), [arXiv:2012.03799].
- [101] A. M. Sirunyan *et al.* (CMS), Phys. Rev. D **104**, 5, 052001 (2021), [arXiv:2103.01290].
- [102] M. Aaboud *et al.* (ATLAS), JHEP **06**, 108 (2018), [arXiv:1711.11520].
- [103] M. Aaboud *et al.* (ATLAS), Phys. Rev. **D98**, 3, 032008 (2018), [arXiv:1803.10178].
- [104] A. M. Sirunyan *et al.* (CMS), JHEP **02**, 015 (2020), [arXiv:1910.12932].
- [105] G. Aad *et al.* (ATLAS), JHEP **04**, 165 (2021), [arXiv:2102.01444].
- [106] A. M. Sirunyan *et al.* (CMS), Eur. Phys. J. **C77**, 10, 710 (2017), [arXiv:1705.04650].
- [107] A. M. Sirunyan *et al.* (CMS), Phys. Rev. **D96**, 3, 032003 (2017), [arXiv:1704.07781].
- [108] A. M. Sirunyan *et al.* (CMS), JHEP **10**, 005 (2017), [arXiv:1707.03316].
- [109] A. M. Sirunyan *et al.* (CMS), JHEP **10**, 019 (2017), [arXiv:1706.04402].

- [110] A. M. Sirunyan *et al.* (CMS), *Eur. Phys. J. C* **81**, 1, 3 (2021), [arXiv:2008.05936].
- [111] A. M. Sirunyan *et al.* (CMS), *JHEP* **03**, 101 (2019), [arXiv:1901.01288].
- [112] M. Aaboud *et al.* (ATLAS), *Phys. Rev. D* **98**, 3, 032008 (2018), [arXiv:1803.10178].
- [113] G. Aad *et al.* (ATLAS) (2021), [arXiv:2108.07665].
- [114] G. Aad *et al.* (ATLAS), *Eur. Phys. J. C* **80**, 11, 1080 (2020), [arXiv:2006.05880].
- [115] M. Aaboud *et al.* (ATLAS), *Eur. Phys. J. C* **80**, 8, 754 (2020), [arXiv:1903.07570].
- [116] (2018).
- [117] M. Aaboud *et al.* (ATLAS), *Phys. Rev. D* **98**, 3, 032009 (2018), [arXiv:1804.03602].
- [118] M. Aaboud *et al.* (ATLAS), *JHEP* **09**, 084 (2017), [arXiv:1706.03731].
- [119] CMS Collab., CMS-PAS-SUS-19-008 (2019).
- [120] V. Khachatryan *et al.* (CMS), *Phys. Rev. D* **94**, 11, 112009 (2016), [arXiv:1606.08076].
- [121] CMS Collab., CMS-PAS-SUS-13-010 (2013).
- [122] T. Aaltonen *et al.* (CDF), *Phys. Rev. Lett.* **107**, 042001 (2011), [arXiv:1105.2815].
- [123] M. Aaboud *et al.* (ATLAS), *Phys. Lett. B* **785**, 136 (2018), [arXiv:1804.03568].
- [124] ATLAS Collab., ATLAS-CONF-2018-003 (2018).
- [125] ATLAS Collab., ATLAS-CONF-2016-057 (2016).
- [126] M. Aaboud *et al.* (ATLAS), *JHEP* **09**, 088 (2017), [arXiv:1704.08493].
- [127] A. M. Sirunyan *et al.* (CMS), *Phys. Lett. B* **783**, 114 (2018), [arXiv:1712.08920].
- [128] S. Chatrchyan *et al.* (CMS), *Phys. Lett. B* **730**, 193 (2014), [arXiv:1311.1799].
- [129] V. Khachatryan *et al.* (CMS), *Phys. Lett. B* **770**, 257 (2017), [arXiv:1608.01224].
- [130] G. Aad *et al.* (ATLAS) (2021), [arXiv:2106.09609].
- [131] F. D. Aaron *et al.* (H1), *Eur. Phys. J. C* **71**, 1572 (2011), [arXiv:1011.6359].
- [132] ATLAS Collab., ATLAS-CONF-2015-018 (2015).
- [133] S. Chekanov *et al.* (ZEUS), *Eur. Phys. J. C* **50**, 269 (2007), [hep-ex/0611018].
- [134] M. Aaboud *et al.* (ATLAS), *Phys. Rev. D* **97**, 3, 032003 (2018), [arXiv:1710.05544].
- [135] ATLAS Collab., ATLAS-CONF-2019-006 (2019).
- [136] A. M. Sirunyan *et al.* (CMS), *Phys. Rev. D* **99**, 3, 032014 (2019), [arXiv:1808.05082].
- [137] CMS Collab., CMS-PAS-EXO-16-022 (2016).
- [138] V. Khachatryan *et al.* (CMS), *Phys. Lett. B* **760**, 178 (2016), [arXiv:1602.04334].
- [139] M. Aaboud *et al.* (ATLAS), *Eur. Phys. J. C* **78**, 3, 250 (2018), [arXiv:1710.07171].
- [140] G. Aad *et al.* (ATLAS) (2019), [arXiv:1909.08457].
- [141] M. Aaboud *et al.* (ATLAS), *Eur. Phys. J. C* **78**, 3, 250 (2018), [arXiv:1710.07171].
- [142] V. Khachatryan *et al.* (CMS), *Phys. Rev. D* **95**, 1, 012009 (2017), [arXiv:1610.05133].
- [143] V. Khachatryan *et al.* (CMS), *Phys. Lett. B* **747**, 98 (2015), [arXiv:1412.7706].
- [144] G. Aad *et al.* (ATLAS), *Eur. Phys. J. C* **81**, 1, 11 (2021), [Erratum: *Eur. Phys. J. C* **81**, 249 (2021)], [arXiv:2010.01015].
- [145] A. M. Sirunyan *et al.* (CMS), *Phys. Rev. D* **104**, 3, 032006 (2021), [arXiv:2102.06976].
- [146] J. Fan, M. Reece and J. T. Ruderman, *JHEP* **11**, 012 (2011), [arXiv:1105.5135].
- [147] J. Fan, M. Reece and J. T. Ruderman, *JHEP* **07**, 196 (2012), [arXiv:1201.4875].
- [148] J. Fan *et al.*, *JHEP* **07**, 016 (2016), [arXiv:1512.05781].
- [149] V. Khachatryan *et al.* (CMS), *Phys. Lett. B* **743**, 503 (2015), [arXiv:1411.7255].
- [150] B. Fuks *et al.*, *JHEP* **10**, 081 (2012), [arXiv:1207.2159].
- [151] B. Fuks *et al.*, *Eur. Phys. J. C* **73**, 2480 (2013), [arXiv:1304.0790].
- [152] LEP2 SUSY Working Group, ALEPH, DELPHI, L3 and OPAL experiments, note LEPSUSYWG/01-03.1, <http://lepsusy.web.cern.ch/lepsusy>.
- [153] LEP2 SUSY Working Group, ALEPH, DELPHI, L3 and OPAL experiments, note LEPSUSYWG/02-04.1, <http://lepsusy.web.cern.ch/lepsusy>.
- [154] CDF Collab., CDF Note 10636 (2011).
- [155] V. M. Abazov *et al.* (D0), *Phys. Lett. B* **680**, 34 (2009), [arXiv:0901.0646].
- [156] G. Aad *et al.* (ATLAS) (2019), [arXiv:1908.08215].
- [157] A. M. Sirunyan *et al.* (CMS), *JHEP* **11**, 079 (2018), [arXiv:1807.07799].
- [158] M. Aaboud *et al.* (ATLAS), *Eur. Phys. J. C* **78**, 2, 154 (2018), [arXiv:1708.07875].
- [159] A. M. Sirunyan *et al.* (CMS), *JHEP* **11**, 151 (2018), [arXiv:1807.02048].
- [160] G. Aad *et al.* (ATLAS) (2021), [arXiv:2108.07586].
- [161] Technical report, CERN, Geneva (2021), URL <https://cds.cern.ch/record/2779116>.
- [162] M. Aaboud *et al.* (ATLAS), *Eur. Phys. J. C* **78**, 12, 995 (2018), [arXiv:1803.02762].
- [163] A. M. Sirunyan *et al.* (CMS) (2021), [arXiv:2106.14246].
- [164] G. Aad *et al.* (ATLAS) (2021), [arXiv:2106.01676].
- [165] A. Tumasyan *et al.* (CMS), *JHEP* **10**, 045 (2021), [arXiv:2107.12553].
- [166] M. Aaboud *et al.* (ATLAS), *Phys. Rev. D* **100**, 1, 012006 (2019), [arXiv:1812.09432].
- [167] ATLAS Collab., ATLAS-CONF-2019-019 (2019).
- [168] G. Aad *et al.* (ATLAS) (2019), [arXiv:1909.09226].
- [169] ATLAS Collab., ATLAS-CONF-2019-014 (2019).
- [170] (2021).
- [171] A. M. Sirunyan *et al.* (CMS), *JHEP* **08**, 150 (2019), [arXiv:1905.13059].
- [172] A. M. Sirunyan *et al.* (CMS) (2019), [arXiv:1910.01185].
- [173] H. K. Dreiner *et al.*, *Eur. Phys. J. C* **62**, 547 (2009), [arXiv:0901.3485].
- [174] LEP2 SUSY Working Group, ALEPH, DELPHI, L3 and OPAL experiments, note LEPSUSYWG/04-07.1, <http://lepsusy.web.cern.ch/lepsusy>.
- [175] O. Buchmueller *et al.*, *Eur. Phys. J. C* **74**, 6, 2922 (2014), [arXiv:1312.5250].
- [176] C. Strey *et al.*, *JCAP* **1304**, 013 (2013), [arXiv:1212.2636].
- [177] A. Fowlie *et al.*, *Phys. Rev. D* **86**, 075010 (2012), [arXiv:1206.0264].
- [178] LEP2 SUSY Working Group, ALEPH, DELPHI, L3 and OPAL experiments, note LEPSUSYWG/04-09.1, <http://lepsusy.web.cern.ch/lepsusy>.
- [179] T. Aaltonen *et al.* (CDF), *Phys. Rev. Lett.* **104**, 011801 (2010), [arXiv:0910.3606].
- [180] V. M. Abazov *et al.* (D0), *Phys. Rev. Lett.* **105**, 221802 (2010), [arXiv:1008.2133].
- [181] M. Aaboud *et al.* (ATLAS), *Phys. Rev. D* **97**, 9, 092006 (2018), [arXiv:1802.03158].

- [182] A. M. Sirunyan *et al.* (CMS), JHEP **06**, 143 (2019), [arXiv:1903.07070].
- [183] A. M. Sirunyan *et al.* (CMS) (2019), [arXiv:1907.00857].
- [184] M. Aaboud *et al.* (ATLAS), Phys. Rev. **D98**, 9, 092002 (2018), [arXiv:1806.04030].
- [185] M. Aaboud *et al.* (ATLAS), Phys. Rev. **D99**, 1, 012001 (2019), [arXiv:1808.03057].
- [186] G. Aad *et al.* (ATLAS), JHEP **10**, 005 (2020), [arXiv:2004.10894].
- [187] A. M. Sirunyan *et al.* (CMS), JHEP **03**, 166 (2018), [arXiv:1709.05406].
- [188] A. M. Sirunyan *et al.* (CMS), JHEP **03**, 160 (2018), [arXiv:1801.03957].
- [189] A. M. Sirunyan *et al.* (CMS), Eur. Phys. J. **C79**, 5, 444 (2019), [arXiv:1901.06726].
- [190] A. M. Sirunyan *et al.* (CMS), JHEP **01**, 154 (2019), [arXiv:1812.04066].
- [191] A. M. Sirunyan *et al.* (CMS), Phys. Lett. **B780**, 118 (2018), [arXiv:1711.08008].
- [192] A. M. Sirunyan *et al.* (CMS), Phys. Rev. **D97**, 3, 032007 (2018), [arXiv:1709.04896].
- [193] A. M. Sirunyan *et al.* (CMS), Phys. Lett. **B779**, 166 (2018), [arXiv:1709.00384].
- [194] Technical report, CERN, Geneva (2021), URL <https://cds.cern.ch/record/2777125>.
- [195] G. Aad *et al.* (ATLAS), Phys. Rev. **D93**, 5, 052002 (2016), [arXiv:1509.07152].
- [196] M. Aaboud *et al.* (ATLAS), Eur. Phys. J. **C78**, 8, 625 (2018), [arXiv:1805.11381].
- [197] M. Aaboud *et al.* (ATLAS), Eur. Phys. J. **C77**, 3, 144 (2017), [arXiv:1611.05791].
- [198] A. M. Sirunyan *et al.* (CMS), JHEP **04**, 123 (2021), [arXiv:2012.08600].
- [199] A. Arbey, M. Battaglia and F. Mahmoudi, Eur. Phys. J. **C72**, 1847 (2012), [arXiv:1110.3726].
- [200] G. Aad *et al.* (ATLAS), JHEP **10**, 134 (2015), [arXiv:1508.06608].
- [201] V. Khachatryan *et al.* (CMS), JHEP **10**, 129 (2016), [arXiv:1606.03577].
- [202] P. Athron *et al.* (GAMBIT), Eur. Phys. J. **C77**, 12, 879 (2017), [arXiv:1705.07917].
- [203] K. J. de Vries *et al.*, Eur. Phys. J. **C75**, 9, 422 (2015), [arXiv:1504.03260].
- [204] C. Strey *et al.*, JHEP **09**, 081 (2014), [arXiv:1405.0622].
- [205] LEP2 SUSY Working Group, ALEPH, DELPHI, L3 and OPAL experiments, note LEPSUSYWG/04-01.1, <http://lepsusy.web.cern.ch/lepsusy>.
- [206] A. Heister *et al.* (ALEPH), Phys. Lett. **B544**, 73 (2002), [hep-ex/0207056].
- [207] A. M. Sirunyan *et al.* (CMS), Phys. Lett. **B790**, 140 (2019), [arXiv:1806.05264].
- [208] G. Aad *et al.* (ATLAS), Phys. Rev. D **101**, 5, 052005 (2020), [arXiv:1911.12606].
- [209] G. Aad *et al.* (ATLAS), Phys. Rev. D **101**, 3, 032009 (2020), [arXiv:1911.06660].
- [210] A. M. Sirunyan *et al.* (CMS) (2019), [arXiv:1907.13179].
- [211] Technical report, CERN, Geneva (2021), URL <https://cds.cern.ch/record/2777046>.
- [212] LEP2 SUSY Working Group, ALEPH, DELPHI, L3 and OPAL experiments, note LEPSUSYWG/02-09.2, <http://lepsusy.web.cern.ch/lepsusy>.
- [213] M. Aaboud *et al.* (ATLAS), Phys. Rev. **D99**, 1, 012009 (2019), [arXiv:1808.06358].
- [214] S. Chatrchyan *et al.* (CMS), Eur. Phys. J. **C73**, 2493 (2013), [arXiv:1301.3792].
- [215] S. Chatrchyan *et al.* (CMS), Phys. Rev. **D90**, 032006 (2014), [arXiv:1404.5801].
- [216] T. Aaltonen *et al.* (CDF), Phys. Rev. Lett. **110**, 20, 201802 (2013), [arXiv:1302.4491].
- [217] DELPHI Collab., Eur. Phys. J. **C31**, 412 (2003).
- [218] G. Aad *et al.* (ATLAS), Phys. Rev. **D92**, 7, 072004 (2015), [arXiv:1504.05162].
- [219] V. Khachatryan *et al.* (CMS), Phys. Rev. **D91**, 1, 012007 (2015), [arXiv:1411.6530].
- [220] G. Aad *et al.* (ATLAS), Phys. Rev. D **103**, 112003 (2021), [arXiv:2011.10543].
- [221] LEP2 SUSY Working Group, ALEPH, DELPHI, L3 and OPAL experiments, note LEPSUSYWG/02-10.1, <http://lepsusy.web.cern.ch/lepsusy>.
- [222] A. M. Sirunyan *et al.* (CMS), Eur. Phys. J. **C79**, 4, 305 (2019), [arXiv:1811.09760].
- [223] T. Aaltonen *et al.* (CDF), Phys. Rev. Lett. **105**, 191801 (2010), [arXiv:1004.3042].
- [224] V. M. Abazov *et al.* (D0), Phys. Rev. Lett. **105**, 191802 (2010), [arXiv:1007.4835].
- [225] G. Aad *et al.* (ATLAS), Phys. Rev. Lett. **115**, 3, 031801 (2015), [arXiv:1503.04430].
- [226] M. Aaboud *et al.* (ATLAS), Eur. Phys. J. **C76**, 10, 541 (2016), [arXiv:1607.08079].
- [227] V. Khachatryan *et al.* (CMS), Eur. Phys. J. **C76**, 6, 317 (2016), [arXiv:1604.05239].
- [228] M. Aaboud *et al.* (ATLAS), Phys. Rev. **D97**, 5, 052012 (2018), [arXiv:1710.04901].
- [229] M. Aaboud *et al.* (ATLAS), Phys. Rev. **D99**, 9, 092007 (2019), [arXiv:1902.01636].
- [230] G. Aad *et al.* (ATLAS), Eur. Phys. J. **C75**, 9, 407 (2015), [arXiv:1506.05332].
- [231] A. M. Sirunyan *et al.* (CMS), Phys. Lett. **B797**, 134876 (2019), [arXiv:1906.06441].
- [232] A. M. Sirunyan *et al.* (CMS), JHEP **05**, 025 (2018), [arXiv:1802.02110].
- [233] CMS Collab., CMS-PAS-EXO-16-036 (2016).
- [234] A. M. Sirunyan *et al.* (CMS), Phys. Lett. B **806**, 135502 (2020), [arXiv:2004.05153].
- [235] A. M. Sirunyan *et al.* (CMS), Phys. Rev. D **104**, 1, 012015 (2021), [arXiv:2012.01581].
- [236] V. M. Abazov *et al.* (D0), Phys. Rev. Lett. **99**, 131801 (2007), [arXiv:0705.0306].
- [237] G. Aad *et al.* (ATLAS), Phys. Rev. **D88**, 11, 112003 (2013), [arXiv:1310.6584].
- [238] A. M. Sirunyan *et al.* (CMS), JHEP **05**, 127 (2018), [arXiv:1801.00359].
- [239] G. Aad *et al.* (ATLAS), JHEP **07**, 173 (2021), [arXiv:2104.03050].
- [240] T. Aaltonen *et al.* (CDF), Phys. Rev. Lett. **103**, 021802 (2009), [arXiv:0902.1266].
- [241] V. M. Abazov *et al.* (D0), Phys. Rev. **D87**, 5, 052011 (2013), [arXiv:1211.2466].
- [242] G. Aad *et al.* (ATLAS), Phys. Rev. D **102**, 3, 032006 (2020), [arXiv:2003.11956].
- [243] A. Tumasyan *et al.* (CMS) (2021), [arXiv:2110.04809].
- [244] A. M. Sirunyan *et al.* (CMS), JHEP **08**, 016 (2018), [arXiv:1804.07321].
- [245] M. Aaboud *et al.* (ATLAS), JHEP **06**, 022 (2018), [arXiv:1712.02118].
- [246] G. Aad *et al.* (ATLAS), Phys. Rev. **D88**, 11, 112006 (2013), [arXiv:1310.3675].

- [247] Technical report, CERN, Geneva (2021), all figures including auxiliary figures are available at <https://atlas.web.cern.ch/Atlas/GROUPS/PHYSICS/CONFNOTES/ATLAS-CONF-2021-015>, URL <https://cds.cern.ch/record/2759676>.
- [248] LEP2 SUSY Working Group, ALEPH, DELPHI, L3 and OPAL experiments, note LEPSUSYWG/02-05.1, <http://lepsusy.web.cern.ch/lepsusy>.
- [249] V. Khachatryan *et al.* (CMS), Eur. Phys. J. **C75**, 7, 325 (2015), [arXiv:1502.02522].
- [250] T. Aaltonen *et al.* (CDF), Phys. Rev. **D88**, 3, 031103 (2013), [arXiv:1307.0474].
- [251] A. M. Sirunyan *et al.* (CMS) (2019), [arXiv:1909.06166].
- [252] V. M. Abazov *et al.* (D0), Phys. Rev. Lett. **101**, 111802 (2008), [arXiv:0806.2223].
- [253] G. Aad *et al.* (ATLAS), Phys. Rev. **D90**, 11, 112005 (2014), [arXiv:1409.5542].
- [254] O. Buchmueller *et al.*, Eur. Phys. J. **C71**, 1722 (2011), [arXiv:1106.2529].
- [255] E. A. Baltz and P. Gondolo, JHEP **10**, 052 (2004), [hep-ph/0407039].
- [256] B. C. Allanach and C. G. Lester, Phys. Rev. **D73**, 015013 (2006), [hep-ph/0507283].
- [257] R. Ruiz de Austri, R. Trotta and L. Roszkowski, JHEP **05**, 002 (2006), [hep-ph/0602028].
- [258] R. Lafaye *et al.*, Eur. Phys. J. **C54**, 617 (2008), [arXiv:0709.3985].
- [259] M. Shaposhnikov, JHEP **08**, 008 (2008), [arXiv:0804.4542].
- [260] R. Trotta *et al.*, JHEP **12**, 024 (2008), [arXiv:0809.3792].
- [261] P. Bechtle *et al.*, Eur. Phys. J. **C66**, 215 (2010), [arXiv:0907.2589].
- [262] E. Bagnaschi *et al.*, Eur. Phys. J. C **78**, 256, 1 (2018).
- [263] J. Costa *et al.*, Eur. Phys. J. C **78**, 158, 1 (2018).
- [264] E. Bagnaschi *et al.*, Eur. Phys. J. **C77**, 4, 268 (2017), [arXiv:1612.05210].
- [265] E. Bagnaschi *et al.*, Eur. Phys. J. **C77**, 2, 104 (2017), [arXiv:1610.10084].
- [266] L. A. Harland-Lang, V. A. Khoze and M. G. Ryskin, Eur. Phys. J. **C76**, 1, 9 (2016), [arXiv:1508.02718].
- [267] E. A. Bagnaschi *et al.*, Eur. Phys. J. **C75**, 500 (2015), [arXiv:1508.01173].
- [268] O. Buchmueller *et al.*, Eur. Phys. J. **C74**, 12, 3212 (2014), [arXiv:1408.4060].
- [269] M. Citron *et al.*, Phys. Rev. **D87**, 3, 036012 (2013), [arXiv:1212.2886].
- [270] Supersymmetry Physics Results, ATLAS experiment, <http://twiki.cern.ch/twiki/bin/view/AtlasPublic/SupersymmetryPublicResults/>.
- [271] Supersymmetry Physics Results, CMS experiment, <http://cms-results.web.cern.ch/cms-results/public-results/publications/SUS/index.html>.

90. Axions and Other Similar Particles

Revised October 2021 by A. Ringwald (DESY, Hamburg), L. J. Rosenberg (U. Washington) and G. Rybka (U. Washington).

90.1 Introduction

In this section, we list coupling-strength and mass limits for light neutral scalar or pseudoscalar bosons that couple weakly to normal matter and radiation. Such bosons may arise from the spontaneous breaking of a global $U(1)$ symmetry, resulting in a massless Nambu-Goldstone (NG) boson. If there is a small explicit symmetry breaking, either already in the Lagrangian or due to quantum effects such as anomalies, the boson acquires a mass and is called a pseudo-NG boson. Typical examples are axions (a) [1–4] and majorons [5,6], associated, respectively, with a spontaneously broken Peccei-Quinn and lepton-number symmetry.

A common feature of these light bosons ϕ is that their coupling to Standard-Model particles is suppressed by the energy scale that characterizes the symmetry breaking, *i.e.*, the decay constant f . The interaction Lagrangian is

$$\mathcal{L} = f^{-1} J^\mu \partial_\mu \phi, \quad (90.1)$$

where J^μ is the Noether current of the spontaneously broken global symmetry. If f is very large, these new particles interact very weakly. Detecting them would provide a window to physics far beyond what can be probed at accelerators.

Axions are of particular interest because the Peccei-Quinn (PQ) mechanism remains perhaps the most credible scheme to preserve CP -symmetry in QCD. Moreover, the cold dark matter (CDM) of the Universe may well consist of axions and they are searched for in dedicated experiments with a realistic chance of discovery.

Originally it was assumed that the PQ scale f_a was related to the electroweak symmetry-breaking scale $v_{EW} = (\sqrt{2}G_F)^{-1/2} = 247$ GeV. However, the associated “standard” and “variant” axions were quickly excluded—we refer to the Listings for detailed limits. Here we focus on “invisible axions” with $f_a \gg v_{EW}$ as the main possibility.

Axions have a characteristic two-photon vertex, inherited from their mixing with π^0 and η . This coupling allows for the main search strategy based on axion-photon conversion in external magnetic fields [7], an effect that also can be of astrophysical interest. While for axions the product “ $a\gamma\gamma$ interaction strength \times mass” is essentially fixed by the corresponding π^0 properties, one may consider a more general class of axion-like particles (ALPs) where the two parameters (coupling and mass) are independent. A number of experiments explore this more general parameter space. ALPs populating the latter are predicted to arise generically, in addition to the axion, in low-energy effective field theories emerging from string theory [8–15]. The latter often contain also very light Abelian vector bosons under which the Standard-Model particles are not charged: so-called hidden-sector photons, dark photons or paraxions. They share a number of phenomenological features with the axion and ALPs, notably the possibility of hidden photon to photon conversion and of hidden photon dark matter [16–18]. Their physics cases and the current constraints are compiled in Refs. [19–22].

90.2 Theory

90.2.1 Peccei-Quinn mechanism and axions

The QCD Lagrangian includes a CP -violating term $\mathcal{L}_\Theta = -\bar{\Theta} (\alpha_s/8\pi) G^{\mu\nu a} \tilde{G}_{\mu\nu}^a$, where $-\pi \leq \bar{\Theta} \leq +\pi$ is the effective Θ parameter after diagonalizing quark masses, $G_{\mu\nu}^a$ is the color field strength tensor, and $\tilde{G}^{\mu\nu a} \equiv \epsilon^{\mu\nu\lambda\rho} G_{\lambda\rho}^a/2$, with $\epsilon^{0123} = 1$, its dual. This term induces an electric dipole moment (EDM) of the neutron of size $d_n = C_{EDM} e \bar{\Theta}$, where $C_{EDM} = 2.4(1.0) \times 10^{-16}$ cm [23]. Experimental upper bounds on the latter, $|d_n| \leq 1.8 \times 10^{-26}$ e cm [24,25], imply $|\bar{\Theta}| \lesssim 10^{-10}$ even though $\bar{\Theta} = \mathcal{O}(1)$ is otherwise completely satisfactory. The spontaneously broken global Peccei-Quinn symmetry $U(1)_{PQ}$ was introduced to solve this “strong CP problem” [1,2], the axion being the pseudo-NG boson of $U(1)_{PQ}$ [3,4]. This symmetry is broken due to the axion’s anomalous triangle coupling to gluons,

$$\mathcal{L} = \left(\frac{a}{f_a} - \bar{\Theta} \right) \frac{\alpha_s}{8\pi} G^{\mu\nu a} \tilde{G}_{\mu\nu}^a, \quad (90.2)$$

where a is the axion field and f_a the axion decay constant. Color anomaly factors have been absorbed in the normalization of f_a which is defined by this Lagrangian. Thus normalized, f_a is the quantity that enters all low-energy phenomena [26]. Non-perturbative topological fluctuations of the gluon fields in QCD induce a potential for a whose minimum is at $a = \bar{\Theta} f_a$, thereby canceling the $\bar{\Theta}$ term in the QCD Lagrangian and thus restoring CP symmetry.

The resulting axion mass, in units of the PQ scale f_a , is identical to the square root of the topological susceptibility in QCD, $m_a f_a = \sqrt{\chi}$. The latter can be evaluated further [27,28], exploiting the chiral limit (masses of up and down quarks much smaller than the scale of QCD), yielding $m_a f_a = \sqrt{\chi} \approx f_\pi m_\pi$, where $m_\pi = 135$ MeV and $f_\pi \approx 92$ MeV. In more detail one finds, by including $\mathcal{O}(\alpha)$ QED corrections and next-to-next-to-leading order (NNLO) corrections in chiral perturbation theory [29],

$$m_a = 5.691(51) \left(\frac{10^9 \text{ GeV}}{f_a} \right) \text{meV}. \quad (90.3)$$

A direct calculation of the topological susceptibility via QCD lattice simulations finds almost the same central value, albeit with an about five times larger error bar [30].

The axion’s anomalous coupling to gluons induces, at energies below the confinement scale of QCD, a model-independent coupling of the axion to the operator giving rise to the EDM of the nucleon (N),

$$\mathcal{L}_{aN\gamma} = -\frac{i}{2} g_{aN\gamma} a \bar{\Psi}_N \sigma_{\mu\nu} \gamma_5 \Psi_N F^{\mu\nu}, \quad (90.4)$$

where the couplings constants of the neutron (n) and the proton (p) are given by

$$g_{an\gamma} = -g_{ap\gamma} = e \frac{C_{EDM}}{f_a} = (3.7 \pm 1.5) \times 10^{-3} \left(\frac{1}{f_a} \right) \frac{1}{\text{GeV}}. \quad (90.5)$$

This coupling, as a function of the axion mass, is displayed in Fig. 90.1, where the thickness of the yellow band presents the theoretical uncertainty given in Eq. (90.5).

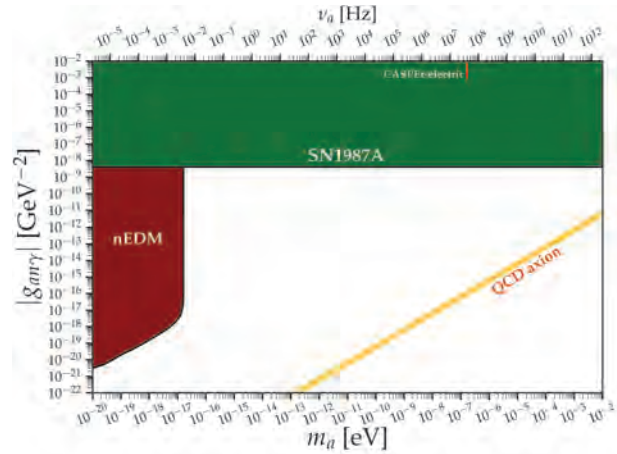


Figure 90.1: Exclusion plot for ALP-EDM coupling as described in the text. Figure courtesy of Ciaran O’Hare [31].

Axions with $f_a \gg v_{EW}$ evade almost all current experimental limits. One generic class of models invokes “hadronic axions” where new heavy quarks carry $U(1)_{PQ}$ charges, leaving ordinary quarks and leptons without tree-level axion couplings. The archetype is the KSVZ model [32,33], where in addition the heavy new quarks are electrically neutral. Another generic class requires at least two Higgs doublets and ordinary quarks and leptons carry PQ charges, the archetype being the DFSZ model [34,35]. All of these models contain at least one electroweak singlet scalar that acquires a vacuum expectation value and thereby breaks the PQ

symmetry. The KSVZ and DFSZ models are frequently used as benchmark examples, but other models exist where both heavy quarks and Higgs doublets carry PQ charges. In supersymmetric models, the axion is part of a supermultiplet and thus inevitably accompanied by a spin-0 saxion and a spin-1/2 axino, which both also have couplings suppressed by f_a and are expected to have large masses due to supersymmetry breaking [36].

90.2.2 Model-dependent axion couplings

Although the generic axion interactions scale approximately with f_π/f_a from the corresponding π^0 couplings, there are non-negligible model-dependent factors and uncertainties. The axion's two-photon interaction plays a key role for many searches,

$$\mathcal{L}_{a\gamma\gamma} = -\frac{g_{a\gamma\gamma}}{4} a F_{\mu\nu} \tilde{F}^{\mu\nu} = g_{a\gamma\gamma} a \mathbf{E} \cdot \mathbf{B}, \quad (90.6)$$

where F is the electromagnetic field-strength tensor and $\tilde{F}^{\mu\nu} \equiv \epsilon^{\mu\nu\lambda\rho} F_{\lambda\rho}/2$, with $\epsilon^{0123} = 1$, its dual. The coupling constant is [37]

$$g_{a\gamma\gamma} = \frac{\alpha}{2\pi f_a} \left(\frac{E}{N} - 1.92(4) \right) = \left(0.203(3) \frac{E}{N} - 0.39(1) \right) \frac{m_a}{\text{GeV}^2}, \quad (90.7)$$

where E and N are the electromagnetic and color anomalies of the axial current associated with the axion. In grand unified models, and notably for DFSZ [34, 35], $E/N = 8/3$, whereas for KSVZ [32, 33] $E/N = 0$ if the electric charge of the new heavy quark is taken to vanish. In general, a broad range of E/N values is possible [38–41], as indicated by the diagonal yellow band in Fig. 90.2, whose width is roughly determined by the boundary values $E/N = 44/3$ and $E/N = 5/3$, respectively. However, this band still does not exhaust all the possibilities. In fact, there exist classes of QCD axion models whose photon couplings populate the entire still-allowed region outside the yellow band in Fig. 90.2 [42–46], motivating axion search efforts over a wide range of masses and couplings.

The two-photon decay width is

$$\Gamma_{a \rightarrow \gamma\gamma} = \frac{g_{a\gamma\gamma}^2 m_a^3}{64\pi} = 1.1 \times 10^{-24} \text{ s}^{-1} \left(\frac{m_a}{\text{eV}} \right)^5. \quad (90.8)$$

The second expression uses Eq. (90.7) with $E/N = 0$. Axions decay faster than the age of the Universe if $m_a \gtrsim 20$ eV.

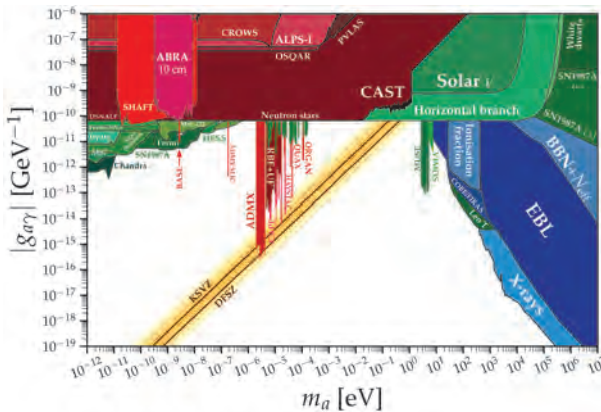


Figure 90.2: Exclusion plot for ALP-photon coupling as described in the text. Figure courtesy of Ciaran O’Hare [31].

The interaction with fermions f has derivative form and is invariant under a shift $a \rightarrow a + a_0$ as behooves a NG boson,

$$\mathcal{L}_{aff} = \frac{C_f}{2f_a} \partial_\mu a \bar{\Psi}_f \gamma^\mu \gamma_5 \Psi_f. \quad (90.9)$$

Here, Ψ_f is the fermion field, m_f its mass, and C_f a model-dependent coefficient. The dimensionless combination $g_{aff} \equiv C_f m_f / f_a$ plays the role of a Yukawa coupling and $\alpha_{aff} \equiv$

$g_{aff}^2/4\pi$ of a “fine-structure constant.” The often-used pseudoscalar form $\mathcal{L}_{aff} = -i(C_f m_f / f_a) a \bar{\Psi}_f \gamma_5 \Psi_f$ need not be equivalent to the appropriate derivative structure, for example when two NG bosons are attached to one fermion line as in axion emission by nucleon bremsstrahlung [47–49].

In hadronic axion models, C_e vanishes at tree level, but is then generated radiatively at one loop [50, 51],

$$C_e \simeq \frac{3\alpha^2}{4\pi^2} \left[\frac{E}{N} \log \left(\frac{f_a}{m_e} \right) - 1.92 \log \left(\frac{A_\chi}{m_e} \right) \right], \quad (90.10)$$

where $A_\chi \simeq 1$ GeV is the chiral symmetry breaking scale. In the DFSZ model [34, 35], the tree-level coupling coefficient to electrons is [50]

$$C_e = \frac{\sin^2 \beta}{3}, \quad (90.11)$$

where $\tan \beta$ is the ratio of the vacuum expectation values of the two Higgs doublets giving masses to the up- and down-type quarks, respectively: $\tan \beta = v_u / v_d$. The resulting prediction for the axion-electron coupling, as a function of the axion mass, for the KSVZ axion ($E/N = 0$), hadronic axions, with $5/3 \leq E/N \leq 44/3$, and the DFSZ axion is displayed in Fig. 90.3. For the DFSZ range we have taken into account the constraint $0.28 \lesssim \tan \beta \lesssim 140$ [52] arising from the requirement of perturbative unitarity of the Yukawa couplings of Standard Model fermions.

For nucleons, $C_{p,n}$ have been determined as [37]

$$\begin{aligned} C_p &= -0.47(3) + 0.88(3)C_u - 0.39(2)C_d - 0.038(5)C_s \\ &\quad - 0.012(5)C_c - 0.009(2)C_b - 0.0035(4)C_t, \\ C_n &= -0.02(3) + 0.88(3)C_d - 0.39(2)C_u - 0.038(5)C_s \\ &\quad - 0.012(5)C_c - 0.009(2)C_b - 0.0035(4)C_t, \end{aligned} \quad (90.12)$$

in terms of the corresponding model-dependent quark couplings C_q , $q = u, d, s, c, b, t$. For hadronic axions, the latter vanish at tree-level, which means that C_n is expected to be much smaller than C_p . In the DFSZ model, $C_u = C_c = C_t = \frac{1}{3} \cos^2 \beta$ and $C_d = C_s = C_b = \frac{1}{3} \sin^2 \beta$, and C_p and C_n , as functions of β ,

$$\begin{aligned} C_p &= -0.435 \sin^2 \beta + (-0.182 \pm 0.025), \\ C_n &= 0.414 \sin^2 \beta + (-0.160 \pm 0.025), \end{aligned} \quad (90.13)$$

The resulting prediction for the axion-neutron coupling, as a function of the axion mass, for the KSVZ axion and the DFSZ axion is displayed in Fig. 90.4.

The axion-pion interaction is given by the Lagrangian [51]

$$\mathcal{L}_{a\pi\pi} = \frac{C_{a\pi}}{f_\pi f_a} \partial_\mu a (\pi^0 \pi^+ \partial_\mu \pi^- + \pi^0 \pi^- \partial_\mu \pi^+ - 2\pi^+ \pi^- \partial_\mu \pi^0), \quad (90.14)$$

where $C_{a\pi} = (1-z)/[3(1+z)]$ in hadronic models and $C_{a\pi} = (1-z)/[3(1+z)] - (1/9) \cos 2\beta$ in the DFSZ model [41], with $z = m_u/m_d = 0.48(3)$ [37].

90.3 Laboratory Searches

90.3.1 Light shining through walls

Searching for “invisible axions” is extremely challenging due to its extraordinarily feeble coupling to normal matter and radiation. Currently, the most promising approaches rely on the axion-two-photon interaction, allowing for axion-photon conversion in external electric or magnetic fields [7]. For the Coulomb field of a charged particle, the conversion is best viewed as a scattering process, $\gamma + Ze \leftrightarrow Ze + a$, called Primakoff effect [53]. In the other extreme of a macroscopic field, usually a large-scale B -field, the momentum transfer is small, the interaction is coherent over a large distance, and the conversion is best viewed as an axion-photon oscillation phenomenon in analogy to neutrino flavor oscillations [54].

Photons propagating through a transverse magnetic field, with incident \mathbf{E}_γ and magnetic field \mathbf{B} parallel, may convert into axions. For $m_a^2 L / 2\omega \ll 2\pi$, where L is the length of the B field

region and ω the photon energy, the resultant axion beam is coherent with the incident photon beam and the conversion probability is $\Pi \sim (1/4)(g_{a\gamma\gamma}BL)^2$. A practical realization uses a laser beam propagating down the bore of a superconducting dipole magnet (like the bending magnets in high-energy accelerators). If another magnet is in line with the first, but shielded by an optical barrier, then photons may be regenerated from the pure axion beam [55, 56]. The overall probability is $P(\gamma \rightarrow A \rightarrow \gamma) = \Pi^2$.

The first such Light-Shining-through-Walls (LSW) experiment was performed by the BFRT (Brookhaven-Fermilab-Rochester-Trieste) collaboration. It utilized two magnets of length $L = 4.4$ m and $B = 3.7$ T and found $|g_{a\gamma\gamma}| < 6.7 \times 10^{-7}$ GeV $^{-1}$ at 95% CL for $m_a < 1$ meV [57, 58]. More recently, several such experiments were performed (see Listings) [59–65]. The current best limit, $|g_{a\gamma\gamma}| < 3.5 \times 10^{-8}$ GeV $^{-1}$ at 95% CL for $m_a \lesssim 0.3$ meV (see Fig. 90.2), has been achieved by the OSQAR (Optical Search for QED Vacuum Birefringence, Axions, and Photon Regeneration) experiment, which exploited two 9 T LHC dipole magnets and an 18.5 W continuous wave laser emitting at the wavelength of 532 nm [65]. The ALPS I (Any Light Particle Search I) experiment achieved a similar sensitivity [63], see Fig. 90.2. Some of these experiments have also reported limits for scalar bosons where the photon \mathbf{E}_γ must be chosen perpendicular to the magnetic field \mathbf{B} .

The concept of resonantly enhanced photon regeneration may open unexplored regions of coupling strength [66–68]. In this scheme, both the production and detection magnets are within Fabry-Perot optical cavities and actively locked in frequency. The $\gamma \rightarrow a \rightarrow \gamma$ rate is enhanced by a factor $\mathcal{F}\mathcal{F}'/\pi^2$ relative to a single-pass experiment, where \mathcal{F} and \mathcal{F}' are the finesse of the two cavities. The resonant enhancement could be of order $10^{(10-12)}$, improving the $g_{a\gamma\gamma}$ sensitivity by $10^{(2.5-3)}$. The experiment ALPS II (Any Light Particle Search II) is based on this concept and aims at an improvement of the current laboratory bound on $g_{a\gamma\gamma}$ by a factor $\sim 10^3$ in the year 2022 [69].

Resonantly enhanced photon regeneration has already been exploited in experiments searching for “radiowaves shining through a shielding” [70–73]. For $m_a \lesssim 10^{-5}$ eV, the upper bound on $g_{a\gamma\gamma}$ established by the CROWS (CERN Resonant Weakly Interacting sub-eV Particle Search) experiment [74] is slightly less stringent than the one set by OSQAR, see Fig. 90.2.

90.3.2 Photon polarization

An alternative to regenerating the lost photons is to use the beam itself to detect conversion: the polarization of light propagating through a transverse B field suffers dichroism and birefringence [75]. Dichroism: The E_{\parallel} component, but not E_{\perp} , is depleted by axion production, causing a small rotation of linearly polarized light. For $m_a^2 L/2\omega \ll 2\pi$, the effect is independent of m_a . For heavier axions, it oscillates and diminishes as m_a increases, and it vanishes for $m_a > \omega$. Birefringence: This effect occurs because there is mixing of virtual axions in the E_{\parallel} state, but not for E_{\perp} . Hence, linearly polarized light will develop elliptical polarization. Higher-order QED also induces vacuum magnetic birefringence (VMB). A search for these effects was performed in the same dipole magnets of the BFRT experiment mentioned before [76]. The dichroic rotation gave a stronger limit than the ellipticity rotation: $|g_{a\gamma\gamma}| < 3.6 \times 10^{-7}$ GeV $^{-1}$ at 95% CL, for $m_a < 5 \times 10^{-4}$ eV. The ellipticity limits are better at higher masses, as they fall off smoothly and do not terminate at m_a .

In 2006, the PVLAS collaboration reported a signature of magnetically induced vacuum dichroism that could be interpreted as the effect of a pseudoscalar with $m_a = 1$ –1.5 meV and $|g_{a\gamma\gamma}| = (1.6$ – $5) \times 10^{-6}$ GeV $^{-1}$ [77]. Later, it turned out that these findings are due to instrumental artifacts [78]. This particle interpretation is also excluded by the above photon regeneration searches that were inspired by the original PVLAS result. The fourth generation setup of the PVLAS experiment has published results on searches for VMB (see Fig. 90.2) and dichroism [79]. The bounds from the non-observation of the latter on $g_{a\gamma\gamma}$ are slightly weaker than the ones from OSQAR.

90.3.3 Long-range forces

New bosons would mediate long-range forces, which are severely constrained by “fifth force” experiments [80]. Those looking for

new mass-spin couplings provide significant constraints on pseudoscalar bosons [81–86], see for example in Fig. 90.4 the limit on the axion-neutron coupling [87] from torsion balance tests of the gravitational inverse square law [88]. Presently, the most restrictive limits are obtained from combining long-range force measurements with stellar cooling arguments [89, 90]. For the moment, any of these limits are far from realistic values expected for the QCD axion. Still, these efforts provide constraints on more general low-mass bosons.

In Ref. [91], a method was proposed that can extend the search for axion-mediated spin-dependent forces by several orders of magnitude. By combining techniques used in nuclear magnetic resonance and short-distance tests of gravity, this method appears to be sensitive to the QCD axion in the μ eV – meV mass range, independent of the cosmic axion abundance, if axions have a CP -violating interaction with nuclei as large as the current experimental bound on the electric dipole moment of the neutron allows. The ARIADNE (Axion Resonant InterAction DetectioN Experiment) is under development and employs this approach to search for axion-mediated spin-dependent short-range interactions between a hyper-polarized 3-He sample and an unpolarized tungsten source mas [92]. The method relies on superconducting magnetic shielding to screen the sample from ordinary magnetic field noise. Experimental tests to demonstrate the requirements of ARIADNE, including characterization of the magnetic field backgrounds, are under way [93, 94].

90.4 Axions from Astrophysical Sources

90.4.1 Stellar energy-loss limits

Low-mass weakly-interacting particles (neutrinos, gravitons, axions, baryonic or leptonic gauge bosons, *etc.*) are produced in hot astrophysical plasma, and can thus transport energy out of stars. The coupling strength of these particles with normal matter and radiation is bounded by the constraint that stellar lifetimes or energy-loss rates are not in conflict with observation [95, 96].

We begin this discussion with our Sun and concentrate first on hadronic axions. They are produced predominantly by the Primakoff process $\gamma + Ze \rightarrow Ze + a$. Integrating over a standard solar model yields the axion luminosity [97]

$$L_a = g_{10}^2 \times 1.85 \times 10^{-3} L_{\odot}, \quad (90.15)$$

where $g_{10} = |g_{a\gamma\gamma}| \times 10^{10}$ GeV. The maximum of the spectrum is at 3.0 keV, the average at 4.2 keV, and the number flux at Earth is $g_{10}^2 \times 3.75 \times 10^{11}$ cm $^{-2}$ s $^{-1}$. The solar photon luminosity is fixed, so energy losses due to the Primakoff process require enhanced nuclear energy production and thus enhanced neutrino fluxes. The all-flavor measurements by SNO (Sudbury Neutrino Observatory), together with a standard solar model, imply $L_a \lesssim 0.10 L_{\odot}$, corresponding to $g_{10} \lesssim 7$ [98], mildly superseding a similar limit from helioseismology (sound speed, surface helium and convective radius) [99]. In Ref. [100], this limit was improved to $g_{10} < 4.1$ (at 3σ), see Fig. 90.2, exploiting a new statistical analysis that combined helioseismology and solar neutrino observations, including theoretical and observational errors, and accounting for tensions between input parameters of solar models, in particular the solar element abundances. Going beyond the hadronic axion, Ref. [98] considered also a non-zero axion-electron coupling and obtained the bound on the latter displayed in Fig. 90.3.

A more restrictive limit derives from globular-cluster (GC) stars that allow for detailed tests of stellar-evolution theory. The stars on the horizontal branch (HB) in the color-magnitude diagram have reached helium burning with a core-averaged energy release of about 80 erg g $^{-1}$ s $^{-1}$, compared to Primakoff axion losses of g_{10}^2 30 erg g $^{-1}$ s $^{-1}$. The accelerated consumption of helium reduces the HB lifetime by about $80/(80+30 g_{10}^2)$. Number counts of HB stars in a large sample of 39 Galactic GCs compared with the number of red giants (that are not much affected by Primakoff losses) give a weak indication of non-standard losses which may be accounted by Primakoff-like axion emission, if the photon coupling is in the range $|g_{a\gamma\gamma}| = (2.9 \pm 1.8) \times 10^{-11}$ GeV $^{-1}$ [101, 102]. Still, the upper bound found in this analysis,

$$|g_{a\gamma\gamma}| < 6.6 \times 10^{-11} \text{ GeV}^{-1} \text{ (95\% CL)}, \quad (90.16)$$

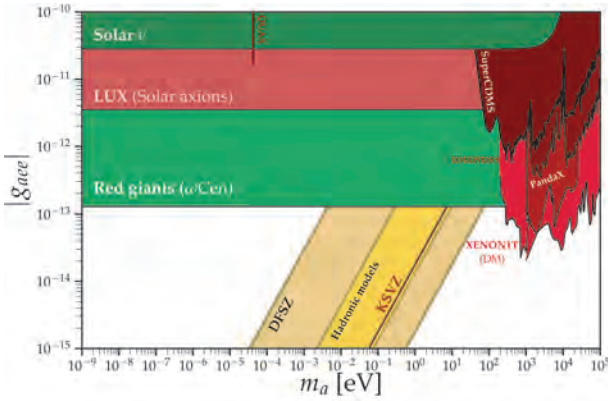


Figure 90.3: Exclusion plot for ALP-electron coupling as described in the text. Figure courtesy of Ciaran O’Hare [31].

represents the strongest limit on $g_{a\gamma\gamma}$ for a wide mass range, see Fig. 90.2. The conservative constraint, Eq. (90.16), on $g_{a\gamma\gamma}$ may be translated to $f_a > 3.4 \times 10^7$ GeV ($m_a < 0.2$ eV), using $E/N = 0$ as in the KSVZ model, or to $f_a > 1.3 \times 10^7$ GeV ($m_a < 0.5$ eV), for the DFSZ axion model, with $E/N = 8/3$, see Fig. 90.2.

If axions couple directly to electrons, the dominant emission processes are atomic axio-recombination and axio-deexcitation, axio-bremsstrahlung in electron-ion or electron-electron collisions, and Compton scattering [103]. Stars in the red giant (RG) branch of the color-magnitude diagram of GCs are particularly sensitive to these processes: they would lead to an extension of the latter to larger brightness. In fact, the RG branch tip – the brightest point of the RG branch – provides the currently most sensitive method to test the axion coupling to electrons. The strongest bounds on it are derived from analyses of the RG branch tip in several globular clusters [104] and in the Galactic globular cluster ω Centauri [105]. The two analyses lead to very similar results,

$$|g_{aee}| < 1.48 \times 10^{-13} \quad (95\% \text{ CL}) \quad \text{and} \quad |g_{aee}| < 1.3 \times 10^{-13} \quad (95\% \text{ CL}), \quad (90.17)$$

respectively, see Fig. 90.3. Reference [104] finds also a small hint for extra cooling, corresponding to $|g_{aee}| = 0.60^{+0.32}_{-0.58} \times 10^{-13}$, while Ref. [105] does not find any evidence for exotic cooling.

Bremsstrahlung is also efficient in white dwarfs (WDs), where the Primakoff and Compton processes are suppressed by the large plasma frequency. A comparison of the predicted and observed luminosity function of WDs can be used to put limits on $|g_{aee}|$ [106, 107]. An analysis based on detailed WD cooling treatment and data on the WD luminosity function (WDLF) of the Galactic disk found that electron couplings above $|g_{aee}| \gtrsim 3 \times 10^{-13}$ are disfavoured [108]. Lower couplings cannot be discarded from the current knowledge of the WDLF of the Galactic disk. On the contrary, features in some WDLFs can be interpreted as suggestions for electron couplings in the range $7.2 \times 10^{-14} \lesssim |g_{aee}| \lesssim 2.2 \times 10^{-13}$ [108–110]. This hypothesis will be further scrutinized by the Large Synoptic Survey Telescope (LSST) which is expected to increase the sample of WDs in the Galactic halo to hundreds of thousands [111]. This will allow for the determination of independent WDLFs from different Galactic populations, greatly reducing the uncertainties related to star formation histories. For pulsationally unstable WDs (ZZ Ceti stars), the period decrease \dot{P}/P is a measure of the cooling speed. The corresponding observations of a handful pulsating WDs imply additional cooling that can be interpreted also in terms of similar axion losses [112–116]. In fact, the combined analysis of these observations gives a good fit for $|g_{aee}| = 2.9 \times 10^{-13}$ and favours the axion (or ALP) interpretation at slightly more than 2σ [41].

Intriguingly, a 3σ preference for the existence of the axion (or an ALP) is found if one combines the hints of excessive cooling of HB stars, RGs and WDs and allows for both a photon and electron coupling [117]. The best fit is obtained for $|g_{a\gamma\gamma}| \sim 1.4 \times 10^{-11}$ GeV $^{-1}$ and $|g_{aee}| \sim 1.5 \times 10^{-13}$, respectively, where the photon coupling is compatible with zero at 1σ , whereas the

electron coupling is non-zero at the level of 3σ [41, 117].

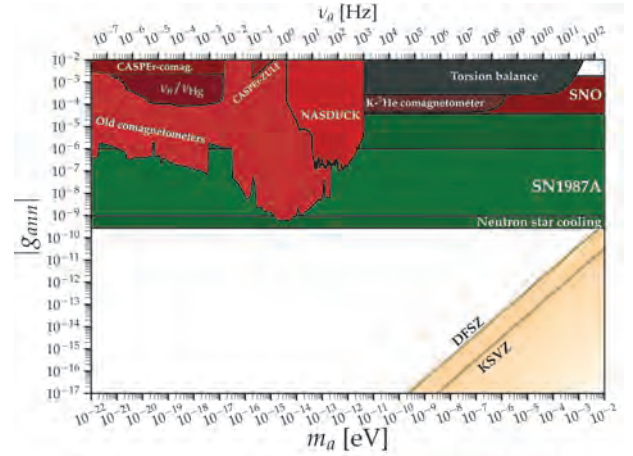


Figure 90.4: Exclusion plot for ALP-neutron coupling as described in the text. Figure courtesy of Ciaran O’Hare [31].

Analogous constraints derive from the measured duration of the neutrino signal of the supernova SN 1987A. Numerical simulations for a variety of cases, including axions and Kaluza-Klein gravitons, reveal that the energy-loss rate of a nuclear medium at the density 3×10^{14} g cm $^{-3}$ and temperature 30 MeV should not exceed about 1×10^{19} erg g $^{-1}$ s $^{-1}$ [118]. The energy-loss rate from nucleon bremsstrahlung, $N + N \rightarrow N + N + a$, is $(C_N/2f_a)^2 (T^4/\pi^2 m_N) F$. Here F is a numerical factor that represents an integral over the dynamical spin-density structure function because axions couple to the nucleon spin. For realistic conditions, even after considerable effort, one is limited to a heuristic estimate leading to $F \approx 1$ [96]. The SN 1987A limits are of particular interest for hadronic axions where the bounds on $|g_{aee}|$ are moot. Using a proton fraction of 0.3, $g_{ann} = 0$, $F = 1$, and $T = 30$ MeV, one finds $f_a > 4 \times 10^8$ GeV and $m_a < 16$ meV [96]. A more detailed numerical calculation [119] with state of the art SN models, again assuming $g_{ann} = 0$, found that a coupling larger than $|g_{app}| \gtrsim 6 \times 10^{-10}$, would shorten significantly the timescale of the neutrino emission. This result is, not surprisingly, rather close to the estimate in Ref. [96]. Improving the calculation of axion emission via nucleon-nucleon bremsstrahlung beyond the basic one-pion exchange approximation appears to loosen the bound [120, 121]. The latter analysis finds a reduction of the axion emissivity by an order of magnitude if one takes into account the non-vanishing mass of the exchanged pion, the contribution from two-pion exchange, effective in-medium nucleon masses and multiple nucleon scattering, leading to a looser bound

$$g_{ann}^2 + 0.61 g_{app}^2 + 0.53 g_{ann} g_{app} < 8.26 \times 10^{-19}, \quad (90.18)$$

see Fig. 90.4. This analysis, however, still neglects another very efficient mechanism for axion production in a SN: the pion production process, $\pi^- + p \rightarrow a + n$, also induced by the axion coupling to nucleons. Pion production was recognized long ago as being competitive with nucleon bremsstrahlung [122–124]. However, only recently it was shown that the pion abundance in the early stages of a SN is much larger than previously expected [125]. Although a complete study of the SN evolution which includes pions self-consistently does not exist at the moment, it was shown in Ref. [126] that pion induced processes dominate over bremsstrahlung and so strengthen the bound on the axion-nucleon coupling. In any case, with the present understanding of SNe (current lack of self-consistent 3D SN simulations) and the sparse data from SN 1987A, the constraint on the axion-nucleon couplings from SN 1987A should be considered more as indicative than as a sharp bound [119].

If axions interact sufficiently strongly they are trapped. Only about three orders of magnitude in g_{aNN} , where $N = n, p$, or m_a are excluded, see Fig. 90.4. For even larger couplings, the axion

flux would have been negligible, yet it would have triggered additional events in the detectors, excluding a further range [127]. A possible gap between these two SN 1987A arguments was discussed as the “hadronic axion window” under the assumption that $g_{a\gamma\gamma}$ was anomalously small [128]. This range is now excluded by hot dark matter (HDM) bounds (see below).

Further bounds on the axion-nucleon coupling can be derived from observations of the cooling of neutron stars, in particular the neutron star (NS) in the supernova remnant Cassiopeia A (Cas A). Its surface temperature measured over 10 years reveals an unusually fast cooling rate. This rapid cooling of the Cas A NS may be explained by NS minimal cooling with neutron superfluidity and proton superconductivity [129,130]. The rapid cooling may also arise from a phase transition of the neutron condensate into a multicomponent state [131]. Recently, Ref. [132] analyzed Cas A NS cooling in the presence of axion emission and obtained

$$g_{app}^2 + 1.6g_{ann}^2 < 1 \times 10^{-18}, \quad (90.19)$$

which is comparable to the SN 1987A bound. Refs. [133,134] put a less stringent bound on a KSVZ type axion, without an attempt to fit a transient behavior of Cas A,

$$f_a > (5 - 10) \times 10^7 \text{ GeV (or } g_{app}^2 < (1 - 6) \times 10^{-17}), \quad (90.20)$$

from the temperatures of Cas A and other NSs. This limit has been confirmed very recently by Ref. [135] focussing again on the CasA NS and finding $f_a > 3 \times 10^7 \text{ GeV}$ (KSVZ) and $f_a > 4.5 \times 10^8 \text{ GeV}$ (DFSZ). The Cas A NS cooling may also be interpreted as a hint for extra cooling caused by the emission of axions from the breaking and re-formation of neutron triplet Cooper pairs [136], requiring a coupling to the neutron of

$$g_{ann}^2 = (1.4 \pm 0.5) \times 10^{-19}, \quad (90.21)$$

corresponding to an axion mass

$$m_a = (2.3 \pm 0.4) \text{ meV}/C_n. \quad (90.22)$$

However, the astrophysical versus instrumental origin of the observed cooling of the CasA NS is still being debated [137]. On the other hand, Ref. [138] considered another hot young NS in the supernova remnant HESS J1731-347. Its high temperature implies that all the neutrino emission processes except neutron-neutron bremsstrahlung must be strongly suppressed, which can be realized with a negligible neutron triplet gap and a large proton singlet gap. In this setup, the bremsstrahlung from neutrons is the dominant channel for axion emission, from which one obtains a limit

$$g_{ann}^2 < 7.7 \times 10^{-20}, \quad (90.23)$$

see Fig. 90.4.

The model-independent axion coupling to the nucleon EDMs, Eq. (90.5), can also be constrained by the non-observation of excess cooling from SN 1987A. Reference [139] presents a determination of the cooling rate due to the axion production process $N + \gamma \rightarrow N + a$, leading to the bound

$$|g_{aN\gamma}| < 4 \times 10^{-9} \text{ GeV}^{-2}, \quad (90.24)$$

see Fig. 90.1.

Finally, let us note that if the interpretation of the various hints for additional cooling of stars, reported in this section in terms of emission of axions with $m_a \sim \text{meV}$, were correct, SNe would lose a large fraction of their energy as axions. This would lead to a diffuse SN axion background in the Universe with an energy density comparable to the extra-galactic background light [140]. However, there is no apparent way of detecting it or the axion burst from the next nearby SN. On the other hand, neutrino detectors such as IceCube, Super-Kamiokande or a future mega-ton water Cherenkov detector will probe exactly the mass region of interest by measuring the neutrino pulse duration of the next Galactic SN [119].

90.4.2 Searches for solar axions and ALPs

Instead of using stellar energy losses to derive axion limits, one can also search directly for these fluxes, notably from the Sun. The main focus has been on ALPs with a two-photon vertex. They are produced by the Primakoff process with a flux given by Eq. (90.15) and an average energy of 4.2 keV, and can be detected at Earth with the reverse process in a macroscopic B -field (“axion helioscope”) [7]. In order to extend the sensitivity in mass towards larger values, one can endow the photon with an effective mass in a gas, $m_\gamma = \omega_{\text{plas}}$, thus matching the axion and photon dispersion relations [141].

An early implementation of these ideas used a conventional dipole magnet, with a conversion volume of variable-pressure gas with a xenon proportional chamber as x-ray detector [142]. The conversion magnet was fixed in orientation and collected data for about 1000 s/day. Axions were excluded for $|g_{a\gamma\gamma}| < 3.6 \times 10^{-9} \text{ GeV}^{-1}$ for $m_a < 0.03 \text{ eV}$, and $|g_{a\gamma\gamma}| < 7.7 \times 10^{-9} \text{ GeV}^{-1}$ for $0.03 < m_a < 0.11 \text{ eV}$ at 95% CL.

Later, the Tokyo axion helioscope used a superconducting magnet on a tracking mount, viewing the Sun continuously. They reported $|g_{a\gamma\gamma}| < 6 \times 10^{-10} \text{ GeV}^{-1}$ for $m_a < 0.3 \text{ eV}$ [143,144]. This experiment was recommissioned and a similar limit for masses around 1 eV was reported [145].

The most recent helioscope CAST (CERN Axion Solar Telescope) uses a decommissioned LHC dipole magnet on a tracking mount. The hardware includes grazing-incidence x-ray optics with solid-state x-ray detectors, as well as novel x-ray Micromegas position-sensitive gaseous detectors. Exploiting an IAXO (see below) pathfinder system, CAST has established the limit

$$|g_{a\gamma\gamma}| < 6.6 \times 10^{-11} \text{ GeV}^{-1} \quad (95\% \text{ CL}), \quad (90.25)$$

for $m_a < 0.02 \text{ eV}$ [146]. To cover larger masses, the magnet bores are filled with a gas at varying pressure. The runs with ^4He cover masses up to about 0.4 eV [147], providing the ^4He limits shown in Fig. 90.2. To cover yet larger masses, ^3He was used to achieve a larger pressure at cryogenic temperatures. Limits up to 1.17 eV allowed CAST to “cross the axion line” for the KSVZ model [148–150], see Fig. 90.2.

Going to yet larger masses in a helioscope search is not well motivated because of the cosmic HDM bound of $m_a \lesssim 1 \text{ eV}$ (see below). Sensitivity to significantly smaller values of $g_{a\gamma\gamma}$ can be achieved with a next-generation axion helioscope with a much larger magnetic-field cross section. Realistic design options for this “International Axion Observatory” (IAXO) have been studied in some detail [151] and its physics potential has been reviewed recently [152]. Such a next-generation axion helioscope may also push the sensitivity in the product of couplings to photons and to electrons, $g_{a\gamma\gamma}g_{aee}$, into a range beyond stellar energy-loss limits and test the hypothesis that WD, RG, and HB cooling is dominated by axion emission [153,154]. As a first step towards IAXO, an intermediate experimental stage called BabyIAXO is currently under preparation at DESY [155].

Other Primakoff searches for solar axions and ALPs have been carried out using crystal detectors, exploiting the coherent conversion of axions into photons when the axion angle of incidence satisfies a Bragg condition with a crystal plane [156–160]. However, none of these limits is more restrictive than the one derived from the constraint on the solar axion luminosity ($L_a \lesssim 0.10 L_\odot$) discussed earlier.

Direct detection experiments searching for dark matter (DM) consisting of weakly interacting massive particles have also the capability to search for solar axions and ALPs. For low masses, $m_a \lesssim 100 \text{ eV}$, the LUX experiment [161] has provided the most stringent bound among those experiments on the axion-electron coupling constant,

$$|g_{aee}| < 3.5 \times 10^{-12} \quad (90\% \text{ CL}), \quad (90.26)$$

see Fig. 90.3, by exploiting the axio-electric effect in liquid xenon. A slightly less stringent limit was set by PandaX-II [162]. However, as obvious from the same figure, this technique has not reached the sensitivity of energy-loss considerations in stars. Recently, the XENON1T collaboration has reported an excess in low

energy electronic recoil data peaking around 2-3 keV [163]. A possible solar axion interpretation is, however, in stark contrast with the constraints from stellar astrophysics [164–166].

90.4.3 Conversion of astrophysical axion fluxes

Large-scale B fields exist in astrophysics that can induce axion-photon oscillations. In practical cases, B is much smaller than in the laboratory, whereas the conversion region L is much larger. Therefore, while the product BL can be large, realistic sensitivities are usually restricted to very low-mass particles, far away from the “axion band” in a plot like Fig. 90.2.

One example is SN 1987A, which would have emitted a burst of ALPs due to the Primakoff production in its core. They would have partially converted into γ -rays in the Galactic B -field. The lack of a gamma-ray signal in the GRS instrument of the SMM satellite in coincidence with the observation of the neutrinos emitted from SN 1987A therefore provides a strong bound on their coupling to photons [167, 168]. This bound has been revisited and the underlying physics has been brought to the current state-of-the-art, as far as modeling of the supernova and the Milky-Way magnetic field are concerned, resulting in the limit [169]

$$|g_{a\gamma\gamma}| < 5.3 \times 10^{-12} \text{ GeV}^{-1}, \text{ for } m_a \lesssim 4.4 \times 10^{-10} \text{ eV}, \quad (90.27)$$

see Fig. 90.2.

Reference [170] reports no evidence of a γ -ray burst in observations of extragalactic SNe with the Fermi Large Area Telescope (LAT). Under the assumption that at least one SN was contained within the LAT field of view, the authors derive an upper bound on the axion photon coupling which is about a factor of 5 weaker than the one from SN 1987A, see Fig. 90.2.

The cumulative emission of ALPs from all past core-collapse SNe would lead to a diffuse gamma-ray flux peaked at energies $\sim 50 - 100$ MeV which can convert in the Galactic magnetic field into photons. Using Fermi-LAT measurements of the diffuse γ -ray flux, Ref. [171] obtains a conservative bound on the photon coupling, $|g_{a\gamma\gamma}| < 5 \times 10^{-10} \text{ GeV}^{-1}$, for $m_a \lesssim 10^{-11} \text{ eV}$, see Fig. 90.2, which can be decreased by nearly three orders of magnitude, if an ALP-nucleon coupling of maximal phenomenologically allowed strength, $|g_{aNN}| \sim 10^{-9}$, is allowed.

We use the first observation of Betelgeuse in hard x rays to perform a novel search for axionlike particles (ALPs). Betelgeuse is not expected to be a standard source of x rays, but light ALPs produced in the stellar core could be converted back into photons in the Galactic magnetic field, producing a detectable flux that peaks in the hard x-ray band ($E_\gamma > 10 \text{ keV}$). Using a 50 ks observation of Betelgeuse by the NuSTAR satellite telescope, we find no significant excess of events above the expected background. Using models of the regular Galactic magnetic field in the direction of Betelgeuse, we set a 95% C.L. upper limit on the ALP-photon coupling of $g_{a\gamma} < (0.5 - 1.8) \times 10^{-11} \text{ GeV}^{-1}$ (depending on magnetic field model) for ALP masses $m_a < (5.5 - 3.5) \times 10^{-11} \text{ eV}$.

Hot, young stars, such as Wolf-Rayet stars, are efficiently producing ALPs with energies $\sim 10 - 100 \text{ keV}$ via the Primakoff effect. Large numbers of those stars are hosted by the Galactic Quintuplet and Westerlund 1 super star clusters (SSCs). The non-observation of hard x-rays originating from axion-photon conversion in the Galactic magnetic field in archival NuSTAR (Nuclear Spectroscopic Telescope Array) data from these SSCs allows to set a bound on the axion-photon coupling [172], $|g_{a\gamma\gamma}| < 3.6 \times 10^{-12} \text{ GeV}^{-1}$, for $m_a \lesssim 5 \times 10^{-11} \text{ eV}$, see Fig. 90.2. A somewhat weaker bound in the same mass range was established exploiting NuSTAR data on Betelgeuse [173].

A hard x-ray excess in data from the nearby Magnificent Seven isolated NSs [174] may be explained by ALPs produced in the core those stars and converted in the surrounding magnetic field, with $|g_{aNN}g_{a\gamma\gamma}| \in (2 \times 10^{-21}, 10^{-18}) \text{ GeV}^{-1}$, for $m_a \lesssim 10^{-5} \text{ eV}$ [175]. The non-observation of an x-ray excess from the magnetic white dwarf RE J0317-853 [176] by Chandra yields the constraint $|g_{aee}g_{a\gamma\gamma}| \lesssim 1.3 \times 10^{-25} \text{ GeV}^{-1}$, for $m_a \ll 10^{-5} \text{ eV}$ [177], which provides a non-trivial constraint on the ratio g_{aee}/g_{aNN} for axion models explaining the Magnificent Seven x-ray excess.

90.4.4 Conversion of astrophysical photon fluxes

Magnetically induced oscillations between photons and ALPs can modify the photon fluxes from distant sources in various ways, featuring (i) frequency-dependent dimming, (ii) modified polarization, and (iii) avoiding absorption by propagation in the form of axions.

For example, dimming of SNe Ia could influence the interpretation in terms of cosmic acceleration [178], although it has become clear that photon-ALP conversion could only be a subdominant effect [179]. Searches for linearly polarized emission from magnetized white dwarfs [180] and changes of the linear polarization from radio galaxies (see, e.g., Ref. [181]) provide limits close to $g_{a\gamma\gamma} \sim 10^{-11} \text{ GeV}^{-1}$, for masses $m_a \lesssim 10^{-7} \text{ eV}$ and $m_a \lesssim 10^{-15} \text{ eV}$, respectively, albeit with uncertainties related to the underlying assumptions. Even stronger limits, $g_{a\gamma\gamma} \lesssim 2 \times 10^{-13} \text{ GeV}^{-1}$, for $m_a \lesssim 10^{-14} \text{ eV}$, have been obtained by exploiting high-precision measurements of quasar polarizations [182].

Remarkably, it appears that the Universe could be too transparent to TeV γ -rays that should be absorbed by pair production on the extra-galactic background light [183–187]. The situation is not conclusive at present [188–191], but the possible role of photon-ALP oscillations in TeV γ -ray astronomy is tantalizing [192–194]. Fortunately, the region in ALP parameter space, $g_{a\gamma\gamma} \sim 10^{-12} - 10^{-10} \text{ GeV}^{-1}$ for $m_a \lesssim 10^{-7} \text{ eV}$ [195], required to explain the anomalous TeV transparency of the Universe, could be conceivably probed by the next generation of laboratory experiments (ALPS II) and helioscopes (IAXO) mentioned above.

This parameter region can also be probed by searching for an irregular behavior of the gamma ray spectrum of distant active galactic nuclei (AGN), expected to arise from photon-ALP mixing in a limited energy range. In this type of studies, the uncertainty in the magnetic field around the source needs to be taken into account. This typically leads to a range of limits on the ALP-photon coupling that depend on the modeling assumptions. The H.E.S.S. collaboration has set a limit of $|g_{a\gamma\gamma}| \lesssim 2.1 \times 10^{-11} \text{ GeV}^{-1}$, for $1.5 \times 10^{-8} \text{ eV} \lesssim m_a \lesssim 6.0 \times 10^{-8} \text{ eV}$, from the non-observation of an irregular behavior of the spectrum of the AGN PKS 2155-304 [196], see Fig. 90.2. The Fermi-LAT collaboration has put an even more stringent limit on the ALP-photon coupling [197] from observations of the gamma ray spectrum of NGC 1275, the central galaxy of the Perseus cluster, see Fig. 90.2. A similar analysis has been carried out in Ref. [198], using Fermi-LAT data of PKS 2155-304, and in Ref. [199], using ARGO-YBJ and Fermi-LAT data of Mrk 421 [199], see Fig. 90.2. However, these constraints were obtained under certain theoretical assumptions about magnetic fields surrounding the sources, not confirmed yet by direct astronomical observations in these particular directions; this introduces large systematic uncertainties in the reported constraints [200].

Evidence for spectral irregularities has been reported in Galactic sources, such as pulsars and supernova remnants, and has been interpreted as hints for ALPs [201, 202] (see also discussion in Ref. [203] and references therein). However, the inferred ALP parameters, $|g_{a\gamma\gamma}| \sim 10^{-10} \text{ GeV}^{-1}$, $m_a \sim \text{neV}$, are in tension with the CAST helioscope bounds. Reference [203] updated the analysis of the pulsar signal region including astrophysical nuisance parameters and correctly deriving confidence intervals on ALP parameters by means of Monte Carlo simulations. The tension with the CAST bounds can be evaded if environmental effects in matter, which would suppress the ALP production in dense astrophysical plasmas like the solar interior, are invoked. If this explanation is correct, the claimed ALP signal would be in reach of the next-generation LSW experiment ALPS II. Other ways to make the CAST bound compatible with photon-ALP conversions in the low-density Galactic medium are invoking photon-ALP-dark photon oscillations [204] or the existence of a number of ‘hidden’ ALPs [205].

At smaller masses, $m_a \lesssim 10^{-12} \text{ eV}$, galaxy clusters become highly efficient at interconverting ALPs and photons at x-ray energies. Constraints on spectral irregularities in the spectra of luminous x-ray sources (Hydra A, M87, NGC 1275, NGC 3862, Seyfert galaxy 2E3140; taken by Chandra and XMM-Newton) located in or behind galaxy clusters then lead to stringent upper

limits on the ALP-photon coupling [206–211], (for the limits exploiting spectra from Hydra and M87 from Refs. [206] and [208], respectively, see Fig. 90.2). Reference [211] recently performed the most sensitive x-ray searches for ALPs to date by employing Chandra’s High-Energy Transmission Gratings that allow for an unsurpassed spectral resolution. New observations of the AGN NGC 1275 then led to the bound

$$|g_{a\gamma\gamma}| < 8 \times 10^{-13} \text{ GeV}^{-1} \quad (99.7\% \text{ CL}) \quad (90.28)$$

for light ALPs, see Fig. 90.2.

90.4.5 Finite density effects

If the QCD axion sector has a discrete, $\mathbb{Z}_{\mathcal{N}}$, shift symmetry, its potential is much shallower, and its mass, in units of its decay constant, $m_a f_a \simeq (3\pi)^{-1/4} \mathcal{N}^{3/4} 2^{-\mathcal{N}/2} m_\pi f_\pi$, is smaller than the one of the canonical QCD axion by an exponential factor $\propto 2^{-\mathcal{N}/2}$ [44, 45]. This opens up the parameter space over which one should search for a QCD axion towards the left of the yellow canonical QCD axion band in Fig. 90.1, Fig. 90.2, Fig. 90.3, and Fig. 90.4. Novel bounds apply to this exceptionally light QCD axion due to finite density effects [212–214]. In fact, in dense stellar media, the minimum of the axion potential may be shifted to π . This has a number of phenomenological consequences that span from the modification of nuclear processes in stars due to $\theta = \mathcal{O}(\pi)$ to modifications in the orbital decay of binary systems (and subsequently in the emitted gravitational waves).

In fact, $\theta \sim 1$ in the solar core would lead to an increased proton-neutron mass difference, which would prohibit the neutrino line corresponding to the ${}^7\text{Be}$ - ${}^7\text{Li}$ mass difference observed by Borexino [215].

Moreover, the fact that the position of the minimum of the axion potential depends on the nuclear density of the medium may also source a long-range force between dense stars [212]. This new long-range force sourced by the axion can be constrained by the measurement of the orbital decay of double pulsar or NS-pulsar binaries [212], Fig. 90.5. The gravitational wave signal of NS-NS mergers or black hole (BH) - NS mergers would also be modified by these axionic long-range forces [212, 213]. A corresponding bound [214] exploiting the gravitational waves observation from the binary NS inspiral GW170817 detected by LIGO (Laser Interferometer Gravitational-Wave Observatory) and Virgo [216] is also plotted in Fig. 90.5.

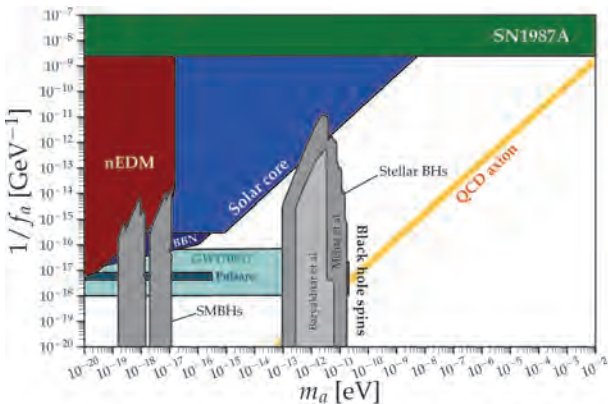


Figure 90.5: Exclusion plot for the QCD axion decay constant as described in the text. Figure courtesy of Ciaran O’Hare [31].

90.4.6 Superradiance of black holes

Light bosonic fields such as axions or ALPs can affect the dynamics and gravitational wave emission of rapidly rotating astrophysical BHs through the superradiance mechanism. When their Compton wavelength is of order of the size of the BH’s ergoregion, they form gravitational bound states around the BH. Their occupation number grows exponentially by extracting energy and angular momentum from the black hole, forming a coherent axion or ALP bound state emitting gravitational waves. When accretion cannot replenish the spin of the BH, superradiance dominates the

BH spin evolution; this is true for both supermassive and stellar mass BHs. The existence of destabilizing light bosonic fields thus leads to exclusion regions in the mass versus spin plot of rotating BHs. Stellar BH spin measurements exploiting well-studied binaries and two independent techniques exclude a mass range $6 \times 10^{-13} \text{ eV} < m_a < 2 \times 10^{-11} \text{ eV}$ at 2σ , which for the axion excludes $3 \times 10^{17} \text{ GeV} < f_a < 1 \times 10^{19} \text{ GeV}$ [12, 217, 218]. These bounds apply when gravitational interactions dominate over the axion self-interaction, which is true for the QCD axion in this mass range. Mehta *et al.* [219, 220] considered superradiance bounds for string theory ALPs with a quartic self-coupling (of either sign) given by $\lambda = m_a^2/f_a^2$, using the bosenova model of Ref. [218]. The analysis can be recast into 95% confidence excluded regions in the plane (m_a, f_a) for ALPs, and are shown in Fig. 90.5 (also compiled in Ref. [45]). These bounds were further extended to massive vector and tensor fields in Ref. [221]. Baryakhtar *et al.* [222] used a more advanced model for the effect of self-interactions on superradiant evolution, and a different (frequentist) statistical methodology, leading to more conservative bounds from stellar mass BHs (region near 10^{-12} eV), see Fig. 90.5. Baryakhtar *et al.* [222] vetoed supermassive BHs (SMBHs) with spins measured at low significance, and thus show no bounds in the SMBH region (near 10^{-18} eV); Mehta *et al.* [219–221] included SMBHs in a (quasi-)Bayesian analysis with a flat prior on the spin.

Long lasting, monochromatic gravitational wave signals, which can be distinguished from ordinary astrophysical sources by their clustering in a narrow frequency range, are expected to be produced by axions or ALPs annihilating to gravitons. Gravitational waves could also be sourced by axions/ALPs transitioning between gravitationally bound levels. Accordingly, the gravitational wave detector Advanced LIGO should be sensitive to the axion in the $m_a \lesssim 10^{-10} \text{ eV}$ region. LIGO measurements of BH spins in binary merger events could also provide statistical evidence for the presence of an axion [223, 224]. Similar signatures could arise for supermassive and intermediate mass BHs for particles with masses $\lesssim 10^{-15} \text{ eV}$. Gravitational waves from such sources could be detected at lower-frequency observatories such as LISA (Laser Interferometer Space Antenna).

90.5 Cosmic Axions

90.5.1 Cosmic axion populations

There are two distinct populations of cosmic relic axion populations: a non-thermal one behaving as CDM, and a thermal one comprising a HDM component, in analogy to massive neutrinos. For $m_a \lesssim 0.01 \text{ eV}$, thermal axions are dominantly produced by processes involving quarks and gluons [225, 226], while, for larger masses, the dominant thermalization process is $\pi + \pi \leftrightarrow \pi + a$ [51, 227, 228]. A number of evaluations exploiting cosmological precision data have found restrictive constraints on a possible HDM fraction that translate into an upper bound on the axion mass, $m_a \lesssim 1 \text{ eV}$, if a LO axion-pion chiral effective field theory (EFT) analysis of the axion-pion thermalization rate is used [229–232]. Recently, it was found that the NLO contribution exceeds the LO contributions for masses below $m_a \lesssim 1.2 (0.12/C_a\pi) \text{ eV}$ [233]. Therefore, in order to assess the reach in sensitivity of future cosmological data sets, one has to improve the EFT description or to compute axion-pion scattering via lattice QCD techniques.

For $m_a \gtrsim 20 \text{ eV}$, axions decay fast on a cosmic time scale, see Eq. (90.8), removing the axion population while injecting photons. This excess radiation provides additional limits on the axion- or ALP-photon coupling up to very large masses [234, 235]. In fact, photons from ALP decays could show up as peaks above known backgrounds in galactic x-ray spectra, could contribute to the extragalactic background light (EBL), could ionize primordial hydrogen and thus contribute to the optical depth after recombination, could spoil the agreement of big bang nucleosynthesis (BBN) with observations. The corresponding up-to-date bounds from Refs. [236, 237] are displayed in Fig. 90.2.

The main cosmological interest in axions derives from their possible role as CDM. In addition to thermal processes, axions are abundantly produced by the misalignment (MIS) mechanism [238–240].

The axion DM abundance crucially depends on the cosmological history. Let us first consider the so called *pre-inflationary PQ symmetry breaking scenario*, in which the PQ symmetry is broken before and during inflation and not restored afterwards. After the breakdown of the PQ symmetry, the axion field relaxes somewhere in the bottom of the “wine-bottle-bottom” potential. Near the QCD epoch, topological fluctuations of the gluon fields such as instantons explicitly break the PQ symmetry. This tilting of the “wine-bottle-bottom” drives the axion field toward the *CP*-conserving minimum, thereby exciting coherent oscillations of the axion field that ultimately represent a condensate of CDM. The fractional cosmic mass density in this homogeneous field mode, created by the MIS mechanism, is [30,241–243],

$$\begin{aligned} \Omega_a^{\text{MIS}} h^2 &\approx 0.12 \left(\frac{f_a}{9 \times 10^{11} \text{ GeV}} \right)^{1.165} F \Theta_i^2 \\ &\approx 0.12 \left(\frac{6 \mu\text{eV}}{m_a} \right)^{1.165} F \Theta_i^2, \end{aligned} \tag{90.29}$$

where h is the present-day Hubble expansion parameter in units of $100 \text{ km s}^{-1} \text{ Mpc}^{-1}$, and $-\pi \leq \Theta_i \leq \pi$ is the initial “misalignment angle” relative to the *CP*-conserving position attained in the causally connected region which evolved into today’s observable Universe. $F = F(\Theta_i, f_a)$ is a factor accounting for anharmonicities in the axion potential. For $F\Theta_i^2 = \mathcal{O}(1)$, m_a should be above $\sim 6 \mu\text{eV}$ in order that the cosmic axion density does not exceed the observed CDM density, $\Omega_{\text{CDM}} h^2 = 0.12$. However, much smaller axion masses (much higher PQ scales) are still possible if entropy is diluted for example by the late decay of a scalar condensate (see for example [244] and references therein) or the initial value Θ_i just happens to be small enough in today’s observable Universe (“anthropic axion window” [245]). In the latter cosmological scenario, however, quantum fluctuations of the axion field during inflation are expected to lead to isocurvature density fluctuations which get imprinted to the temperature fluctuations of the CMB [246,247]. Their non-observation puts severe constraints on the Hubble expansion rate H_I during inflation [248–253], which read, in the simplest cosmological inflationary scenario,

$$H_I \lesssim 5.7 \times 10^8 \text{ GeV} \left(\frac{5 \text{ neV}}{m_a} \right)^{0.4175}, \tag{90.30}$$

if axions represent all of DM. In Ref. [254] an alternative to the MIS mechanism was proposed: the so-called kinetic MIS mechanism. In this case, the axion field is assumed to have an initial velocity which may be generated e.g. by a hypothesized explicit breaking of the axion shift symmetry in the early universe. The amount of QCD axion dark matter generated by the kinetic MIS mechanism can fit the observed dark matter abundance for any $f_a \lesssim 1.5 \times 10^{11} \text{ GeV}$, down to the minimum value allowed by the SN 1987A constraint.

In the *post-inflationary PQ symmetry breaking scenario*, on the other hand, Θ_i will take on different values in different patches of the present Universe. The average contribution is [30,241–243]

$$\Omega_a^{\text{MIS}} h^2 \approx 0.12 \left(\frac{30 \mu\text{eV}}{m_a} \right)^{1.165}. \tag{90.31}$$

The decay of cosmic strings and domain walls gives rise to a further population of CDM axions, whose abundance suffers from significant uncertainties [242, 243, 255–267] which arise from the difficulty in understanding the energy loss process of topological defects and the generated axion spectrum in a quantitative way. In fact, in the present state-of-the-art it is still possible that the CDM contribution from the decay of topological defects is subdominant [260] or overwhelmingly large [264] in comparison to the one from the MIS mechanism. Correspondingly, the plausible range of axion masses providing all of CDM in scenarios with postinflationary PQ symmetry breaking is still rather large, namely [260, 264]

$$m_a \approx 26 \mu\text{eV} - 0.5 \text{ meV}, \tag{90.32}$$

for models with short-lived (requiring unit color anomaly $N = 1$) domain walls, such as the KSVZ model. For models with long-lived ($N > 1$) domain walls, such as an accidental DFSZ model

[268], where the PQ symmetry is broken by higher dimensional Planck suppressed operators, the mass is predicted to be significantly higher [152, 259, 268, 269],

$$m_a \approx (0.58 - 130) \text{ meV}. \tag{90.33}$$

However, the upper part of the predicted range is in conflict with stellar energy-loss limits on the axion.

In this post-inflationary PQ symmetry breakdown scenario, the spatial axion density variations are large at the QCD transition, and they are not erased by free streaming. Gravitationally bound “axion miniclusters” form before and around matter-radiation equality [270–272]. A significant fraction of CDM axions can reside in these bound objects [262, 273]. Remarkably, the minicluster fraction can be bounded by gravitational lensing [274–276], although more simulations are required to understand whether miniclusters are dense enough and survive in sufficient quantities for lensing bounds to apply.

In the above predictions of the fractional cosmic mass density in axions, the exponent, 1.165, arises from the non-trivial temperature dependence of the topological susceptibility $\chi(T) = m_A^2(T) f_A^2$ at temperatures slightly above the QCD quark-hadron phase transition. Lattice QCD calculations of this exponent [30, 277–281], but also Ref. [282], found it to be remarkably close to the prediction of the dilute instanton gas approximation [283] which was previously exploited. Therefore, the state-of-the-art prediction of the axion mass relevant for DM for a fixed initial misalignment angle Θ_i differs from the previous prediction by just a factor of order one.

The non-thermal production mechanisms attributed to axions are generic to light bosonic weakly interacting particles such as ALPs [17]. The relic abundance is set by the epoch when the axion mass becomes significant, $3H(t) \approx m_a(t)$, and ALP field oscillations begin. For ALPs to contribute to the DM density this epoch must precede that of matter radiation equality. For a temperature independent ALP mass this leads to the bound:

$$m_a \gtrsim 7 \times 10^{-28} \text{ eV} \left(\frac{\Omega_m h^2}{0.15} \right)^{1/2} \left(\frac{1 + z_{\text{eq}}}{3.4 \times 10^3} \right)^{3/2}. \tag{90.34}$$

ALPs lighter than this bound are allowed if their cosmic energy density is small, but they are quite distinct from other forms of DM [284]. Ignoring anharmonicities in the ALP potential, and taking the ALP mass to be temperature independent, the relic density in DM ALPs due to the MIS mechanism is given by

$$\begin{aligned} \Omega_{\text{ALP}}^{\text{MIS}} h^2 &= 0.12 \left(\frac{m_a}{4.7 \times 10^{-19} \text{ eV}} \right)^{1/2} \left(\frac{f_a}{10^{16} \text{ GeV}} \right)^2 \times \\ &\left(\frac{\Omega_m h^2}{0.15} \right)^{3/4} \left(\frac{1 + z_{\text{eq}}}{3.4 \times 10^3} \right)^{-3/4} \Theta_i^2. \end{aligned} \tag{90.35}$$

An ALP decay constant near the GUT scale gives the correct relic abundance for *ultralight ALPs* (ULAs) with $m_{\text{ULA}} \approx 10^{-19} \text{ eV}$ [285, 286]. ULAs encompass the entire Earth in a single Compton wavelength, and for large occupation numbers are modelled as a coherent classical field. The coherence time is determined by the mass and virial velocity in the Milky Way, $\tau_{\text{coh}} \sim 1/m_{\text{ULA}} v_{\text{vir}}^2$, with the detailed properties described by a stochastic model with an approximately Rayleigh Jeans distribution [287]. Natural models for ULAs can be found in string and M-theory compactifications [8–15], in field theory with accidental symmetries [288, 289], or new hidden strongly coupled sectors [290, 291].

In addition to the gravitational potential energy, the ULA field also carries gradient energy. On scales where the gradient energy is non-negligible, ULAs acquire an effective pressure and do not behave as CDM. The gradient energy opposes gravitational collapse, leading to a Jeans scale below which perturbations are stable [292]. The Jeans scale suppresses linear cosmological structure formation relative to CDM [293–295]. The Jeans scale at matter-radiation equality in the case that ULAs make up all of

CDM is:

$$k_{J,\text{eq}} = 8.7 \text{ Mpc}^{-1} \left(\frac{1 + z_{\text{eq}}}{3.4 \times 10^3} \right)^{-1/4} \left(\frac{h^2 \Omega_{\text{ALP}}^{\text{MIS}}}{0.12} \right)^{1/4} \times \left(\frac{m_{\text{ULA}}}{10^{-22} \text{ eV}} \right)^{1/2}. \quad (90.36)$$

On non-linear scales the gradient energy leads to the existence of a class of pseudo-solitons known as oscillatons, or axion stars [296]. Axion stars are expected to form in all cosmological scenarios, and for all types of ALPs, including the QCD axion [297–299].

Cosmological and astrophysical observations are consistent with the CDM model, and departures from it are only allowed on the scales of the smallest observed DM structures with $M \sim 10^{6-8} M_{\odot}$. The CMB power spectrum and galaxy auto-correlation power spectrum limit the ULA mass to $m_{\text{ULA}} \gtrsim \mathcal{O}(\text{few}) \times 10^{-24}$ eV from linear theory of structure formation [284, 300]. Analytic models [301] and N -body simulations [302] for non-linear structures show that halo formation is suppressed in ULA models relative to CDM. This leads to constraints on the ULA mass of $m_{\text{ULA}} > 10^{-22}$ eV from observations of high- z galaxies [302–304], and $m_{\text{ULA}} > 2 \times 10^{-20}$ eV from the Lyman-alpha forest flux power spectrum [305]. Including the effects of anharmonicities on structure formation with ALPs can weaken these bounds if the misalignment angle $\Theta_i \approx \pi$ [306]. A comprehensive study of Milky Way satellites by the DES collaboration resulted in the bound $m_{\text{ULA}} > 2.9 \times 10^{-21}$ eV [307]. Cosmological simulations that treat gradient energy in the ULA field beyond the N -body approximation have just recently become available [297, 308–310], and show, among other things, evidence for the formation of axion stars in the centres of ULA halos (various consequences of axion stars are considered in Refs. [311]). These central axion stars have been conjectured to play a role in the apparently cored density profiles of dwarf spheroidal galaxies, and other central galactic regions [297, 312–317]. However, the relationship between the halo mass and the axion star mass [318] leads to problems with this scenario in some galaxies [319–321]. It should be emphasised that many of the conclusions about the role of ULA axion stars in galactic dynamics are based on use of simulation results that do not contain baryons and feedback could be important [322–324].

Inside DM halos the axion gradient energy causes coherence on the de Broglie wavelength and fluctuations on the coherence time [297, 325]. These fluctuations can be thought of as short-lived quasiparticles and lead to relaxation processes that can be described statistically [286, 326] (this relaxation processes also leads to the gravitational condensation of axion stars [298]). The typical relaxation time is:

$$t \sim 10^{10} \text{ years} \left(\frac{m_{\text{ULA}}}{10^{-22} \text{ eV}} \right)^3 \left(\frac{v}{100 \text{ km s}^{-1}} \right)^2 \left(\frac{r}{5 \text{ kpc}} \right)^4, \quad (90.37)$$

where v and r are the velocity and radius of the orbit in the host DM halo.

Relaxation processes such as these are not observed in galaxies, though there are some circumstances where they may be desirable [286]. An absence of observed relaxation can be used to set limits on the ULA mass. An absence of Milky Way disk thickening excludes $m_{\text{ULA}} > 0.6 \times 10^{-22}$ eV [327], while stellar streams give the stronger bound $m_{\text{ULA}} > 1.5 \times 10^{-22}$ eV [328]. The survival of the old star cluster in Eridanus II [329] excludes the range of masses 10^{-21} eV $\lesssim m_{\text{ULA}} \lesssim 10^{-19}$ eV [330]. As in the case of ULA axion stars, current constraints from heating do not fully account for the possible role of baryons.

Finally, one should note that the beyond-CDM physics of ULAs (Jeans scale, relaxation, axion star formation) of course also applies to the QCD axion on smaller length scales. This is of particular interest inside axion miniclusters [270, 271, 298, 299].

90.5.2 Electron recoil searches

In a DM direct detection experiment, a DM ALP featuring a coupling to the electron can be absorbed by the target material, leading to a mono-energetic electronic recoil signal peaked at m_a .

This mechanism allowed the EDELWEISS [331], PandaX [332], SuperCDMS [333] and XENON1T [334] collaborations to put the bounds on the axion-electron coupling displayed in Fig. 90.3 in the keV mass range.

90.5.3 Telescope searches

The two-photon decay is extremely slow for axions with masses in the CDM regime, but could be detectable for eV masses. The signature would be a quasi-monochromatic emission line from galaxies and galaxy clusters. The expected optical line intensity for DFSZ axions is similar to the continuum night emission. A search for optical line emission in two Abell clusters using spectra from the VIMOS (Visible Multi-Object Spectrograph) integral field unit at the Very Large Telescope (VLT) excludes axions and ALPs with a two photon coupling bigger than $\sim 5 \times 10^{-12} \text{ GeV}^{-1}$ in the mass range between 4.5 and 5.5 eV, see Fig. 90.2. Spectral data on the dwarf spheroidal galaxy Leo T from the Multi Unit Spectroscopic Explorer (MUSE) at the VLT improve these constraints by more than an order of magnitude for ALP masses between 2.7 and 5.3 eV [335], see Fig. 90.2.

Very low-mass axions in halos produce a weak quasi-monochromatic radio line. Virial velocities in undisrupted dwarf galaxies are very low, and the axion decay line would therefore be extremely narrow. A search with the Haystack radio telescope on three nearby dwarf galaxies provided a limit $|g_{a\gamma\gamma}| < 1.0 \times 10^{-9} \text{ GeV}^{-1}$ at 96% CL for $298 < m_a < 363 \mu\text{eV}$ [336]. However, this combination of m_a and $g_{a\gamma\gamma}$ does not exclude plausible axion models.

A monochromatic signal is also produced in the conversion of DM axions in the background of slowly varying galactic B -fields [337]. The signal is, however, sensitive to magnetic field power on the scale of the axion mass [338]. Present and future radio telescopes appear to be able to probe ALP DM in the mass range 0.1 – 100 μeV for couplings $g_{a\gamma\gamma} \gtrsim 10^{-13} \text{ GeV}^{-1}$ [338] – unfortunately not reaching down to the benchmark QCD axion sensitivity.

Resonant conversion of QCD axion or ALP DM in NS magnetospheres may give a detectable signal from individual NSs for axion masses in the μeV range [339]. Recent analyses of radio data in the frequency range 1–40 GHz from several NSs have found no evidence for a narrow peak predicted from this mechanism and therefore put bounds on the axion-photon coupling around $10^{-11} \text{ GeV}^{-2}$ for $4 \lesssim m_a \lesssim 160 \text{ GHz}$ [340–342], see Fig. 90.2. However, these limits may still suffer from significant uncertainties because the line intensity is difficult to predict in detail in the complicated environments of NSs [342–345]. Stimulated ALP decays in high radiation environments may be detectable, by next-generation radio telescopes such as the Square Kilometer Array, down to $g_{a\gamma\gamma} \gtrsim 10^{-11} \text{ GeV}^{-1}$, for masses between μeV and 0.1 meV [346]. Furthermore, in condensed ALP dark matter structures such as ALP stars, a parametric instability may lead to an exponential enhancement of the photon flux from ALP-photon conversion by a factor $\sim \exp \left[|g_{a\gamma\gamma}| \int ds \rho_a^{1/2}(s) \right]$, where the integral is along any photon trajectory through the ALP overdensity [347, 348].

Photon propagation on an ULA DM background can induce birefringence that can be compared with upper limits from the CMB [349–351] and may also be probed with other sources such as pulsars [352].

90.5.4 Microwave cavity experiments

Over a large part of the plausible m_a range for CDM, Galactic halo axions may be detected by their resonant conversion into a quasi-monochromatic microwave signal in a high-Q electromagnetic cavity permeated by a strong, static B field [7, 353, 354]. The cavity frequency is tunable, and the signal is maximized when the resonant frequency is the total axion energy, rest mass plus kinetic energy, of $\nu = (m_a/2\pi) [1 + \mathcal{O}(10^{-6})]$, the width above the rest mass representing the axions' virial distribution in the galaxy near Earth. The frequency spectrum may also contain finer structure from axions more recently fallen into the galactic potential and not yet completely virialized [355, 356] or otherwise incompletely thermalized.

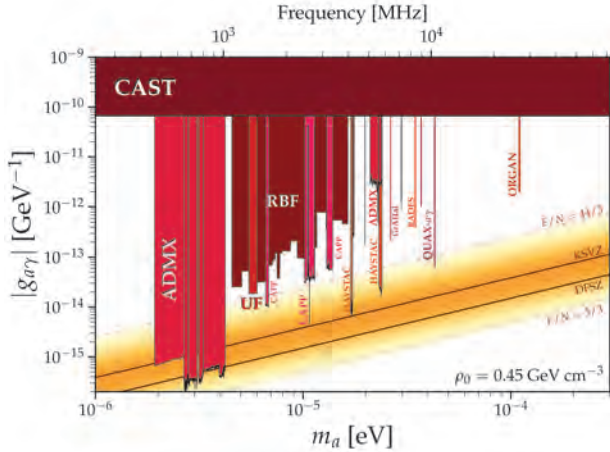


Figure 90.6: Exclusion plot for ALP-photon coupling with closeup on the parameter space of RF cavity experiments as described in the text. Figure courtesy of Ciaran O’Hare [31].

The feasibility of this technique was established in early experiments (RBF (Rochester-Brookhaven-Florida) and UF (University of Florida)) of relatively small sensitive volume, $\mathcal{O}(1)$ liter), with HFET-based microwave amplifiers, setting limits in the range $4.5 < m_a < 16.3 \mu\text{eV}$ [357–359], but lacking by 2–3 orders of magnitude the sensitivity required to detect realistic axions, see Fig. 90.6.

Later, the first generation of ADMX ($B \sim 8$ T, $V \sim 200$ liters) achieved sensitivity to KSVZ axions, assuming they saturate the local DM density and are well virialized, over the mass range 1.9 – $3.3 \mu\text{eV}$ [360]. Should halo axions have a significant narrow component not yet virialized, ADMX was sensitive to DFSZ axions over the entire mass range [361]. The corresponding 90% CL exclusion regions shown in Fig. 90.6 assume a local CDM density of $7.5 \times 10^{-25} \text{ g cm}^{-3}$ (450 MeV cm^{-3}).

Somewhat later, the ADMX experiment commissioned an upgrade [362] that replaced the microwave HFET amplifiers by near-quantum-limited low-noise dc SQUID microwave amplifiers [363] and, more recently, with Josephson parametric amplifiers (related to the earlier dc SQUID amplifiers), also with noise near-quantum-limited [364]. With its large volume and low noise, ADMX has achieved an unprecedented axion DM sensitivity in the mass range between 2.7 and $4.2 \mu\text{eV}$ [365–368], down to the DFSZ benchmark axion-photon coupling over much of the range, see Fig. 90.6. This apparatus is also sensitive to certain other hypothetical light bosons, such as hidden photons or chameleons, over a limited parameter space [17, 369, 370].

ADMX also deployed a testbed experiment to probe higher masses. This experiment – ADMX-Sidecar – sharing the magnet bore and operating in tandem with the main ADMX experiment, searches in three widely spaced frequency ranges (4202–4249 MHz, 5086–5799 MHz and 7173–7203 MHz), using both the TM_{010} and TM_{020} cavity modes, and demonstrating the use of a piezoelectric actuator for cavity tuning in the high-vacuum, high magnetic field, cryogenic environment [371].

The HAYSTAC experiment reported results from a microwave cavity search for DM axions with masses above $20 \mu\text{eV}$. They exclude axions with two-photon coupling $|g_{a\gamma\gamma}| \gtrsim 2 \times 10^{-14} \text{ GeV}^{-1}$ over the range $23.15 \mu\text{eV} < m_a < 24.0 \mu\text{eV}$ [372, 373], a factor of 2.7 above the KSVZ coupling benchmark, see Fig. 90.6. With a Josephson parametric amplifier, this experiment has demonstrated system noise approaching the “standard quantum limit” for the first time in an axion search. More recently, HAYSTAC explored state squeezing to reduce the system noise, where the squeezed quadrature had lower noise relative to that of the “standard quantum limit”, thereby reducing the scan time by a factor of around 2 over a narrow mass range. This resulted in limits on $|g_{a\gamma\gamma}|$ about a factor of 1.4 above the KSVZ benchmark coupling over the axion-mass ranges $16.96 \mu\text{eV} < m_a < 17.12 \mu\text{eV}$

and $17.14 \mu\text{eV} < m_a < 17.28 \mu\text{eV}$ at 90% CL [374] as shown in Fig. 90.6.

The ORGAN experiment aims to probe axions over the relatively high-mass range $60 \mu\text{eV} < m_a < 210 \mu\text{eV}$, which includes axion masses motivated by postinflationary PQ symmetry breaking. ORGAN is based on long, thin cavities with this early generation not being tunable and operating in the TM_{020} mode. In this pathfinding run, it set the limit $|g_{a\gamma\gamma}| < 2 \times 10^{-12} \text{ GeV}^{-1}$ at $110 \mu\text{eV}$ across a narrow mass range 2.5 neV [375], see Fig. 90.6. Another non-tunable experiment is QUAX a - γ , a haloscope of otherwise conventional design sensitivity a factor of approximately 5 above the benchmark KSVZ coupling at two narrowband ranges near 10 GHz [376, 377], see Fig. 90.6. Other cavity detectors are moving into operation, including an experiment with unusual high-aspect-ratio cavities in the CAST bore (CAST-RADES [378]).

CAPP is an ambitious program to search for axions across a wide mass range at high sensitivity. Recently the CAPP-8TB detector has reported results approaching KSVZ sensitivity in the mass range 6.62 – $8.82 \mu\text{eV}$ [379]. A further refinement is searching the higher frequencies allowed by subdividing a cavity into smaller higher-frequency cells. Such a multi-cell cavity system has reported sensitivity around an order-of-magnitude above the KSVZ benchmark coupling in the mass range 13.0 – $13.9 \mu\text{eV}$ [380], see Fig. 90.6. The CAPP-PACE detector has reported limits around KSVZ benchmark sensitivity in the mass range 10.7126 – $10.7186 \mu\text{eV}$ and around an order-of-magnitude above benchmark KSVZ coupling in the mass range 10.16 – $10.37 \mu\text{eV}$ [381], see Fig. 90.6.

90.5.5 New concepts for axion DM direct detection

Other new concepts for searching for axion DM are also being investigated. An alternative to the microwave cavity technique is based on a novel detector architecture consisting of an open, Fabry-Perot resonator and a series of current-carrying wire planes [382]. The Orpheus detector has demonstrated this new technique, excluding DM ALPs with masses between 68.2 and $76.5 \mu\text{eV}$ and axion-photon couplings greater than $4 \times 10^{-7} \text{ GeV}^{-1}$. This technique may be able to probe DM axions in the mass range from 40 to $700 \mu\text{eV}$. “Plasma haloscopes” are under development by the ALPHA collaboration [383]. This concept uses a metamaterial consisting of spaced out wires, inducing an effective photon mass, tunable with wire separation, and sensitive to axion masses 35 – $400 \mu\text{eV}$. Another detector concept exploits the fact that a magnetized mirror would radiate photons in the background of axion DM, which could be collected like in a dish antenna [384]. The proposed MADMAX experiment will place a stack of dielectric layers in a magnetic field in order to resonantly enhance the photon signal, aiming a sensitivity to probe the mass range $40 \mu\text{eV} \lesssim m_a \lesssim 200 \mu\text{eV}$ [385, 386]. Optical dielectric haloscopes with single photon signal detection have been proposed to search for axions in the $50 \text{ meV} - 10 \text{ eV}$ mass range [387]. Absorption of axions on molecular transitions can be sensitive to the axion pseudoscalar coupling g_{aNN} to nucleons or the pseudoscalar coupling g_{aee} to electrons in the $0.5 - 20 \text{ eV}$ range [388]. It has also been pointed out that the coupling induced by an axion field between photonic modes [389, 390] or atomic states [391] separated by an energy equal to the axion mass may be leveraged for axion detection, though the implementation may be challenging. Certain magnetic topological insulators are conjectured to contain axion-polaritons, quasiparticles composed of magnons and the electric field, with magnetically tunable mass in the meV to eV range [392–394]. Axion dark matter leads to resonant photon emission from such materials, which can be detected [395, 396].

In the intermediate mass region, $\text{neV} \lesssim m_a \lesssim 0.1 \mu\text{eV}$, one may exploit a cooled LC circuit and precision magnetometry to search for the oscillating electric current induced by DM axions in a strong magnetic field [397, 398]. A number of small-scale pathfinder experiments have implemented this approach: ABRACADABRA [399, 400] used a nonresonant configuration in a toroidal magnet for a broadband search, ADMX-SLIC [401] used a resonant configuration in a solenoid magnet for a narrowband search, SHAFT [402] used a nonresonant configuration in a toroidal magnet enhanced with a ferromagnetic core, and BASE [403] used antiprotons in a Penning trap as the LC cir-

cuit. The exclusion limits from these experiments are shown in Fig. 90.2; none are yet sensitive to the QCD axion. Future work in this direction is expected to have much more competitive limits [404].

The oscillating Galactic DM axion field induces oscillating nuclear electric dipole moments (EDMs) [139],

$$d_N(t) = g_{aN\gamma} \sqrt{2\rho_{\text{aDM}}} \cos(m_a t)/m_a, \quad (90.38)$$

where $g_{aN\gamma}$ is the coupling of the axion to the nucleon EDM operator, defined in Eq. (90.4). An analysis of the ratio of spin-precession frequencies of stored ultracold neutrons and ^{199}Hg atoms measured by neutron EDM experiments for an axion-induced oscillating neutron EDM revealed no signal consistent with axion DM, excluding a sizeable region of parameter space in the mass region $10^{-24} \text{ eV} \leq m_a \leq 10^{-17} \text{ eV}$ [405], which surpass the limits on anomalous energy loss of SN 1987A by more than seven orders of magnitude, see Fig. 90.1, and are competitive with the ones from the requirement of successful BBN established in [406], see Fig. 90.5.¹ In fact, the oscillating dark matter axion field could increase the neutron-proton mass difference at neutron freeze-out and thus result in the underproduction of ^4He during BBN. The oscillating EDMs cause also the precession of nuclear spins in a nucleon spin polarized sample in the presence of an electric field. The resulting transverse magnetization can be searched for by exploiting magnetic-resonance (MR) techniques, which are most sensitive in the range of low oscillation frequencies corresponding to sub-neV axion masses. The aim of the corresponding Cosmic Axion Spin Precession Experiment (CASPER) [407] is to probe axion DM in the anthropic window, $f_a \gtrsim 10^{15} \text{ GeV}$ ($m_a \lesssim \text{neV}$), motivated from Grand Unification [408–411]. There are two interactions probed through MR: the electric dipole coupling as searched for by CASPER-electric, whose first run has established the limits shown in Fig. 90.1 [412], and an interaction between the axion field gradient and the nuclear spin, which is aimed for by CASPER-wind. In the meantime, the latter has been explored through comagnetometry between a variety of nuclei: $\text{H-}^{12}\text{C}$ in CASPER-ZULF [413,414], Xe-Rb in NASDUCK [415], and $\text{K-}^3\text{He}$ [416,417]. The exclusions from these searches are shown in Fig. 90.4. Sub- μeV ALP masses can also be probed by using the storage ring EDM method proposed in Ref. [418] which exploits a combination of B and E-fields to produce a resonance between the $g-2$ spin precession frequency and the DM ALP field oscillation frequency. This method, however, does not reach the sensitivity to probe the QCD axion prediction for $g_{aN\gamma}$. An eventually non-zero axion electron coupling g_{aee} will lead to an electron spin precession about the axion DM wind [419,420]. The QUAX a-e experiment exploits MR inside a magnetized material [421]. Because of the higher Larmor frequency of the electron, it is sensitive in the classic window. Its first run established the bound in the mass range 42.4 to 43.2 μeV [422], slightly better than the solar ν bound, shown in Fig. 90.3.

90.6 Conclusions

There is a strengthening physics case for very weakly coupled light particles beyond the Standard Model. The elegant solution of the strong CP problem proposed by Peccei and Quinn yields a particularly strong motivation for the axion. In many theoretically appealing ultraviolet completions of the Standard Model axions and ALPs occur automatically. Moreover, they are natural CDM candidates. Perhaps the first hints of their existence have already been seen in the anomalous excessive cooling of stars and the anomalous transparency of the Universe for very high energy gamma rays. Interestingly, a significant portion of previously unexplored, but phenomenologically very interesting and theoretically very well motivated axion and ALP parameter space can be tackled in the foreseeable future by a number of terrestrial experiments searching for axion/ALP DM, for solar axions/ALPs, and for light apparently shining through a wall.

¹These limits are still to the left of the canonical QCD axion line. However, in non-minimal models where the QCD axion is a mediator between strongly interacting hidden sectors enjoying a discrete, \mathbb{Z}_N , shift symmetry, the QCD axion line can be shifted to the left in discrete steps, without any fine tuning [44, 45, 291].

90.7 Acknowledgements

It is a pleasure to thank Masha Baryakhtar, Francesca Calore, Luca Di Luzio, Andrew Geraci, Maurizio Giannotti, Igor Irastorza, David J.E. Marsh, Alessandro Mirizzi, Benjamin Safdi, Ken'ichi Saikawa, Yannis Semertzidis, Guenter Sigl, and Sergey Troitsky for discussions, suggestions, and comments on this review. Particular thanks to Ciaran O'Hare for maintaining a publicly accessible collection of axion plots and providing updates to accommodate this review [31].

References

- [1] R. D. Peccei and H. R. Quinn, Phys. Rev. Lett. **38**, 1440 (1977).
- [2] R. D. Peccei and H. R. Quinn, Phys. Rev. **D16**, 1791 (1977).
- [3] S. Weinberg, Phys. Rev. Lett. **40**, 223 (1978).
- [4] F. Wilczek, Phys. Rev. Lett. **40**, 279 (1978).
- [5] Y. Chikashige, R.N. Mohapatra, and R.D. Peccei, Phys. Lett. **B98**, 265 (1981).
- [6] G. B. Gelmini and M. Roncadelli, Phys. Lett. **99B**, 411 (1981).
- [7] P. Sikivie, Phys. Rev. Lett. **51**, 1415 (1983) and Erratum *ibid.*, **52**, 695 (1984).
- [8] E. Witten, Phys. Lett. **149B**, 351 (1984).
- [9] J. P. Conlon, JHEP **05**, 078 (2006), [hep-th/0602233].
- [10] P. Svrcek and E. Witten, JHEP **06**, 051 (2006), [hep-th/0605206].
- [11] K.-S. Choi *et al.*, Phys. Lett. **B675**, 381 (2009), [arXiv:0902.3070].
- [12] A. Arvanitaki *et al.*, Phys. Rev. **D81**, 123530 (2010), [arXiv:0905.4720].
- [13] B. S. Acharya, K. Bobkov and P. Kumar, JHEP **11**, 105 (2010), [arXiv:1004.5138].
- [14] M. Cicoli, M. Goodsell and A. Ringwald, JHEP **10**, 146 (2012), [arXiv:1206.0819].
- [15] J. Halverson, C. Long and P. Nath, Phys. Rev. **D96**, 5, 056025 (2017), [arXiv:1703.07779].
- [16] A. E. Nelson and J. Scholtz, Phys. Rev. D **84**, 103501 (2011), [arXiv:1105.2812].
- [17] P. Arias *et al.*, JCAP **1206**, 013 (2012), [arXiv:1201.5902].
- [18] P. W. Graham, J. Mardon and S. Rajendran, Phys. Rev. D **93**, 10, 103520 (2016), [arXiv:1504.02102].
- [19] J. Jaeckel and A. Ringwald, Ann. Rev. Nucl. Part. Sci. **60**, 405 (2010), [arXiv:1002.0329].
- [20] A. Ringwald, Phys. Dark Univ. **1**, 116 (2012), [arXiv:1210.5081].
- [21] J. Jaeckel, Frascati Phys. Ser. **56**, 172 (2012), [arXiv:1303.1821].
- [22] A. Caputo *et al.* (2021), [arXiv:2105.04565].
- [23] M. Pospelov and A. Ritz, Nucl. Phys. **B573**, 177 (2000), [hep-ph/9908508].
- [24] C. A. Baker *et al.*, Phys. Rev. Lett. **97**, 131801 (2006), [hep-ex/0602020].
- [25] C. Abel *et al.* (nEDM), Phys. Rev. Lett. **124**, 8, 081803 (2020), [arXiv:2001.11966].
- [26] H. Georgi, D. B. Kaplan and L. Randall, Phys. Lett. **169B**, 73 (1986).
- [27] R. J. Crewther, Phys. Lett. **70B**, 349 (1977).
- [28] P. Di Vecchia and G. Veneziano, Nucl. Phys. **B171**, 253 (1980).
- [29] M. Gorghetto and G. Villadoro, JHEP **03**, 033 (2019), [arXiv:1812.01008].
- [30] S. Borsanyi *et al.*, Nature **539**, 7627, 69 (2016), [arXiv:1606.07494].
- [31] C. O'Hare, "cajohare/axionlimits: Axionlimits," (2020), URL <https://doi.org/10.5281/zenodo.3932430>.

- [32] J. E. Kim, Phys. Rev. Lett. **43**, 103 (1979).
- [33] M. A. Shifman, A. I. Vainshtein and V. I. Zakharov, Nucl. Phys. **B166**, 493 (1980).
- [34] M. Dine, W. Fischler and M. Srednicki, Phys. Lett. **104B**, 199 (1981).
- [35] A. R. Zhitnitsky, Sov. J. Nucl. Phys. **31**, 260 (1980), [Yad. Fiz.31,497(1980)].
- [36] J. E. Kim and G. Carosi, Rev. Mod. Phys. **82**, 557 (2010), [arXiv:0807.3125].
- [37] G. Grilli di Cortona *et al.*, JHEP **01**, 034 (2016), [arXiv:1511.02867].
- [38] J. E. Kim, Phys. Rev. **D58**, 055006 (1998), [hep-ph/9802220].
- [39] L. Di Luzio, F. Mescia and E. Nardi, Phys. Rev. Lett. **118**, 3, 031801 (2017), [arXiv:1610.07593].
- [40] L. Di Luzio, F. Mescia and E. Nardi, Phys. Rev. D **96**, 7, 075003 (2017), [arXiv:1705.05370].
- [41] L. Di Luzio *et al.*, Phys. Rept. **870**, 1 (2020), [arXiv:2003.01100].
- [42] M. Farina *et al.*, JHEP **01**, 095 (2017), [arXiv:1611.09855].
- [43] P. Agrawal *et al.*, JHEP **02**, 006 (2018), [arXiv:1709.06085].
- [44] A. Hook, Phys. Rev. Lett. **120**, 26, 261802 (2018), [arXiv:1802.10093].
- [45] L. Di Luzio *et al.*, JHEP **05**, 184 (2021), [arXiv:2102.00012].
- [46] A. V. Sokolov and A. Ringwald, JHEP **06**, 123 (2021), [arXiv:2104.02574].
- [47] G. Raffelt and D. Seckel, Phys. Rev. Lett. **60**, 1793 (1988).
- [48] M. Carena and R. D. Peccei, Phys. Rev. **D40**, 652 (1989).
- [49] K. Choi, K. Kang and J. E. Kim, Phys. Rev. Lett. **62**, 849 (1989).
- [50] M. Srednicki, Nucl. Phys. **B260**, 689 (1985).
- [51] S. Chang and K. Choi, Phys. Lett. **B316**, 51 (1993), [hep-ph/9306216].
- [52] C.-Y. Chen and S. Dawson, Phys. Rev. **D87**, 055016 (2013), [arXiv:1301.0309].
- [53] D. A. Dicus *et al.*, Phys. Rev. **D18**, 1829 (1978).
- [54] G. Raffelt and L. Stodolsky, Phys. Rev. **D37**, 1237 (1988).
- [55] A. A. Anselm, Yad. Fiz. **42**, 1480 (1985).
- [56] K. van Bibber *et al.*, Phys. Rev. Lett. **59**, 759 (1987).
- [57] G. Ruoso *et al.*, Z. Phys. **C56**, 505 (1992).
- [58] R. Cameron *et al.*, Phys. Rev. **D47**, 3707 (1993).
- [59] M. Fouche *et al.*, Phys. Rev. **D78**, 032013 (2008), [arXiv:0808.2800].
- [60] P. Pugnati *et al.* (OSQAR), Phys. Rev. **D78**, 092003 (2008), [arXiv:0712.3362].
- [61] A. S. Chou *et al.* (GammeV (T-969)), Phys. Rev. Lett. **100**, 080402 (2008), [arXiv:0710.3783].
- [62] A. Afanasev *et al.*, Phys. Rev. Lett. **101**, 120401 (2008), [arXiv:0806.2631].
- [63] K. Ehret *et al.* (ALPS), Phys. Lett. **B689**, 149 (2010), [arXiv:1004.1313].
- [64] P. Pugnati *et al.* (OSQAR), Eur. Phys. J. **C74**, 8, 3027 (2014), [arXiv:1306.0443].
- [65] R. Ballou *et al.* (OSQAR), Phys. Rev. **D92**, 9, 092002 (2015), [arXiv:1506.08082].
- [66] F. Hoogeveen and T. Ziegenhagen, Nucl. Phys. **B358**, 3 (1991).
- [67] P. Sikivie, D. B. Tanner and K. van Bibber, Phys. Rev. Lett. **98**, 172002 (2007), [hep-ph/0701198].
- [68] G. Mueller *et al.*, Phys. Rev. **D80**, 072004 (2009), [arXiv:0907.5387].
- [69] R. Bähre *et al.*, JINST **8**, T09001 (2013), [arXiv:1302.5647].
- [70] F. Hoogeveen, Phys. Lett. **B288**, 195 (1992).
- [71] J. Jaeckel and A. Ringwald, Phys. Lett. **B659**, 509 (2008), [arXiv:0707.2063].
- [72] F. Caspers, J. Jaeckel and A. Ringwald, JINST **4**, P11013 (2009), [arXiv:0908.0759].
- [73] R. Povey, J. Hartnett and M. Tobar, Phys. Rev. **D82**, 052003 (2010), [arXiv:1003.0964].
- [74] M. Betz *et al.*, Phys. Rev. **D88**, 7, 075014 (2013), [arXiv:1310.8098].
- [75] L. Maiani, R. Petronzio and E. Zavattini, Phys. Lett. **B175**, 359 (1986).
- [76] Y. Semertzidis *et al.*, Phys. Rev. Lett. **64**, 2988 (1990).
- [77] E. Zavattini *et al.* (PVLAS), Phys. Rev. Lett. **96**, 110406 (2006), [Erratum: Phys. Rev. Lett.99,129901(2007)], [hep-ex/0507107].
- [78] E. Zavattini *et al.* (PVLAS), Phys. Rev. **D77**, 032006 (2008), [arXiv:0706.3419].
- [79] F. Della Valle *et al.*, Eur. Phys. J. **C76**, 1, 24 (2016), [arXiv:1510.08052].
- [80] E. Fischbach and C. Talmadge, Nature **356**, 207 (1992).
- [81] J. E. Moody and F. Wilczek, Phys. Rev. **D30**, 130 (1984).
- [82] A. N. Youdin *et al.*, Phys. Rev. Lett. **77**, 2170 (1996).
- [83] W.-T. Ni *et al.*, Phys. Rev. Lett. **82**, 2439 (1999).
- [84] D. F. Phillips *et al.*, Phys. Rev. **D63**, 111101 (2001), [arXiv:physics/0008230].
- [85] B. R. Heckel *et al.*, Phys. Rev. Lett. **97**, 021603 (2006), [hep-ph/0606218].
- [86] S. A. Hoedl *et al.*, Phys. Rev. Lett. **106**, 041801 (2011).
- [87] E. G. Adelberger *et al.*, Phys. Rev. Lett. **98**, 131104 (2007), [hep-ph/0611223].
- [88] D. J. Kapner *et al.*, Phys. Rev. Lett. **98**, 021101 (2007), [hep-ph/0611184].
- [89] G. Raffelt, Phys. Rev. **D86**, 015001 (2012), [arXiv:1205.1776].
- [90] C. A. J. O'Hare and E. Vitagliano, Phys. Rev. D **102**, 11, 115026 (2020), [arXiv:2010.03889].
- [91] A. Arvanitaki and A. A. Geraci, Phys. Rev. Lett. **113**, 16, 161801 (2014), [arXiv:1403.1290].
- [92] A. A. Geraci *et al.* (ARIADNE), Springer Proc. Phys. **211**, 151 (2018), [arXiv:1710.05413].
- [93] H. Fossbinder-Elkins *et al.* (2017), [arXiv:1710.08102].
- [94] N. Aggarwal *et al.* (ARIADNE) (2020), [arXiv:2011.12617].
- [95] M. S. Turner, Phys. Rept. **197**, 67 (1990).
- [96] G. G. Raffelt, Lect. Notes Phys. **741**, 51 (2008), [51(2006)], [hep-ph/0611350].
- [97] S. Andriamonje *et al.* (CAST), JCAP **0704**, 010 (2007), [hep-ex/0702006].
- [98] P. Gondolo and G. G. Raffelt, Phys. Rev. **D79**, 107301 (2009), [arXiv:0807.2926].
- [99] H. Schlattl, A. Weiss and G. Raffelt, Astropart. Phys. **10**, 353 (1999), [hep-ph/9807476].
- [100] N. Vinyoles *et al.*, JCAP **1510**, 10, 015 (2015), [arXiv:1501.01639].
- [101] A. Ayala *et al.*, Phys. Rev. Lett. **113**, 19, 191302 (2014), [arXiv:1406.6053].
- [102] O. Straniero *et al.*, in "Proceedings, 11th Patras Workshop on Axions, WIMPs and WISPs (Axion-WIMP 2015): Zaragoza, Spain, June 22-26, 2015," 77–81 (2015).
- [103] J. Redondo, JCAP **1312**, 008 (2013), [arXiv:1310.0823].
- [104] O. Straniero *et al.*, Astron. Astrophys. **644**, A166 (2020), [arXiv:2010.03833].
- [105] F. Capozzi and G. Raffelt, Phys. Rev. D **102**, 8, 083007 (2020), [arXiv:2007.03694].

- [106] G. G. Raffelt, *Phys. Lett.* **166B**, 402 (1986).
- [107] S. I. Blinnikov and N. V. Dunina-Barkovskaya, *Mon. Not. Roy. Astron. Soc.* **266**, 289 (1994).
- [108] M. M. Miller Bertolami *et al.*, *JCAP* **1410**, 10, 069 (2014), [arXiv:1406.7712].
- [109] J. Isern *et al.*, *Astrophys. J.* **682**, L109 (2008), [arXiv:0806.2807].
- [110] J. Isern *et al.*, *J. Phys. Conf. Ser.* **172**, 012005 (2009), [arXiv:0812.3043].
- [111] A. Drlica-Wagner *et al.* (LSST Dark Matter Group) (2019), [arXiv:1902.01055].
- [112] J. Isern *et al.*, *Astron. & Astrophys.* **512**, A86 (2010).
- [113] A. H. Corsico *et al.*, *Mon. Not. Roy. Astron. Soc.* **424**, 2792 (2012), [arXiv:1205.6180].
- [114] A. H. Corsico *et al.*, *JCAP* **1212**, 010 (2012), [arXiv:1211.3389].
- [115] A. H. Córscico *et al.* (2019), [arXiv:1907.00115].
- [116] M. J. Dolan, F. J. Hiskens and R. R. Volkas, *Journal of Cosmology and Astroparticle Physics* **2021**, 09, 010 (2021), URL <https://doi.org/10.1088/1475-7516/2021/09/010>.
- [117] M. Giannotti *et al.*, *JCAP* **1605**, 05, 057 (2016), [arXiv:1512.08108].
- [118] G.G. Raffelt, *Stars as Laboratories for Fundamental Physics*, (Univ. of Chicago Press, Chicago, 1996).
- [119] T. Fischer *et al.*, *Phys. Rev.* **D94**, 8, 085012 (2016), [arXiv:1605.08780].
- [120] J. H. Chang, R. Essig and S. D. McDermott, *JHEP* **09**, 051 (2018), [arXiv:1803.00993].
- [121] P. Carena *et al.*, *JCAP* **10**, 10, 016 (2019), [Erratum: *JCAP* 05, E01 (2020)], [arXiv:1906.11844].
- [122] M. S. Turner, *Phys. Rev. D* **45**, 1066 (1992).
- [123] G. Raffelt and D. Seckel, *Phys. Rev. D* **52**, 1780 (1995), [arXiv:astro-ph/9312019].
- [124] W. Keil *et al.*, *Phys. Rev. D* **56**, 2419 (1997), [arXiv:astro-ph/9612222].
- [125] B. Fore and S. Reddy, *Phys. Rev. C* **101**, 3, 035809 (2020), [arXiv:1911.02632].
- [126] P. Carena *et al.*, *Phys. Rev. Lett.* **126**, 7, 071102 (2021), [arXiv:2010.02943].
- [127] J. Engel, D. Seckel and A. C. Hayes, *Phys. Rev. Lett.* **65**, 960 (1990).
- [128] T. Moroi and H. Murayama, *Phys. Lett.* **B440**, 69 (1998), [hep-ph/9804291].
- [129] D. Page *et al.*, *Phys. Rev. Lett.* **106**, 081101 (2011), [arXiv:1011.6142].
- [130] P. S. Shternin *et al.*, *Mon. Not. Roy. Astron. Soc.* **412**, L108 (2011), [arXiv:1012.0045].
- [131] L. B. Leinson, *Phys. Lett.* **B741**, 87 (2015), [arXiv:1411.6833].
- [132] K. Hamaguchi *et al.*, *Phys. Rev.* **D98**, 10, 103015 (2018), [arXiv:1806.07151].
- [133] J. Keller and A. Sedrakian, *Nucl. Phys.* **A897**, 62 (2013), [arXiv:1205.6940].
- [134] A. Sedrakian, *Phys. Rev.* **D93**, 6, 065044 (2016), [arXiv:1512.07828].
- [135] L. B. Leinson (2021), [arXiv:2105.14745].
- [136] L. B. Leinson, *JCAP* **1408**, 031 (2014), [arXiv:1405.6873].
- [137] B. Posselt and G. G. Pavlov, *Astrophys. J.* **864**, 2, 135 (2018), [arXiv:1808.00531].
- [138] M. V. Beznogov *et al.*, *Phys. Rev.* **C98**, 3, 035802 (2018), [arXiv:1806.07991].
- [139] P. W. Graham and S. Rajendran, *Phys. Rev.* **D88**, 035023 (2013), [arXiv:1306.6088].
- [140] G. G. Raffelt, J. Redondo and N. Viaux Maira, *Phys. Rev.* **D84**, 103008 (2011), [arXiv:1110.6397].
- [141] K. van Bibber *et al.*, *Phys. Rev.* **D39**, 2089 (1989).
- [142] D. M. Lazarus *et al.*, *Phys. Rev. Lett.* **69**, 2333 (1992).
- [143] S. Moriyama *et al.*, *Phys. Lett.* **B434**, 147 (1998), [hep-ex/9805026].
- [144] Y. Inoue *et al.*, *Phys. Lett.* **B536**, 18 (2002), [arXiv:astro-ph/0204388].
- [145] Y. Inoue *et al.*, *Phys. Lett.* **B668**, 93 (2008), [arXiv:0806.2230].
- [146] V. Anastassopoulos *et al.* (CAST), *Nature Phys.* **13**, 584 (2017), [arXiv:1705.02290].
- [147] E. Arik *et al.* (CAST), *JCAP* **0902**, 008 (2009), [arXiv:0810.4482].
- [148] S. Aune *et al.* (CAST), *Phys. Rev. Lett.* **107**, 261302 (2011), [arXiv:1106.3919].
- [149] M. Arik *et al.* (CAST), *Phys. Rev. Lett.* **112**, 9, 091302 (2014), [arXiv:1307.1985].
- [150] M. Arik *et al.* (CAST), *Phys. Rev.* **D92**, 2, 021101 (2015), [arXiv:1503.00610].
- [151] E. Armengaud *et al.*, *JINST* **9**, T05002 (2014), [arXiv:1401.3233].
- [152] E. Armengaud *et al.* (IAXO), *JCAP* **1906**, 06, 047 (2019), [arXiv:1904.09155].
- [153] M. Giannotti *et al.*, *JCAP* **1710**, 10, 010 (2017), [arXiv:1708.02111].
- [154] K. Barth *et al.*, *JCAP* **1305**, 010 (2013), [arXiv:1302.6283].
- [155] A. Abeln *et al.* (BabyIAXO), *JCAP* **2105**, 05, 137 (2021), [arXiv:2010.12076].
- [156] F. T. Avignone, III *et al.* (SOLAX), *Phys. Rev. Lett.* **81**, 5068 (1998), [arXiv:astro-ph/9708008].
- [157] S. Cebrian *et al.*, *Astropart. Phys.* **10**, 397 (1999), [arXiv:astro-ph/9811359].
- [158] A. Morales *et al.* (COSME), *Astropart. Phys.* **16**, 325 (2002), [hep-ex/0101037].
- [159] R. Bernabei *et al.*, *Phys. Lett.* **B515**, 6 (2001).
- [160] Z. Ahmed *et al.* (CDMS), *Phys. Rev. Lett.* **103**, 141802 (2009), [arXiv:0902.4693].
- [161] D. S. Akerib *et al.* (LUX), *Phys. Rev. Lett.* **118**, 26, 261301 (2017), [arXiv:1704.02297].
- [162] X. Zhou *et al.* (PandaX-II) (2020), [arXiv:2008.06485].
- [163] E. Aprile *et al.* (XENON), *Phys. Rev. D* **102**, 7, 072004 (2020), [arXiv:2006.09721].
- [164] L. Di Luzio *et al.*, *Phys. Rev. Lett.* **125**, 13, 131804 (2020), [arXiv:2006.12487].
- [165] C. Gao *et al.*, *Phys. Rev. Lett.* **125**, 13, 131806 (2020), [arXiv:2006.14598].
- [166] J. B. Dent *et al.*, *Phys. Rev. Lett.* **125**, 13, 131805 (2020), [arXiv:2006.15118].
- [167] J. W. Brockway, E. D. Carlson and G. G. Raffelt, *Phys. Lett.* **B383**, 439 (1996), [arXiv:astro-ph/9605197].
- [168] J. A. Grifols, E. Masso and R. Toldra, *Phys. Rev. Lett.* **77**, 2372 (1996), [arXiv:astro-ph/9606028].
- [169] A. Payez *et al.*, *JCAP* **1502**, 02, 006 (2015), [arXiv:1410.3747].
- [170] M. Meyer and T. Petrushevskaya, *Phys. Rev. Lett.* **124**, 23, 231101 (2020), [Erratum: *Phys.Rev.Lett.* 125, 119901 (2020)], [arXiv:2006.06722].
- [171] F. Calore *et al.*, *Phys. Rev. D* **102**, 12, 123005 (2020), [arXiv:2008.11741].
- [172] C. Dessert, J. W. Foster and B. R. Safdi, *Phys. Rev. Lett.* **125**, 26, 261102 (2020), [arXiv:2008.03305].
- [173] M. Xiao *et al.*, *Phys. Rev. Lett.* **126**, 3, 031101 (2021), [arXiv:2009.09059].

- [174] C. Dessert, J. W. Foster and B. R. Safdi, *Astrophys. J.* **904**, 1, 42 (2020), [arXiv:1910.02956].
- [175] M. Buschmann *et al.*, *Phys. Rev. Lett.* **126**, 2, 021102 (2021), [arXiv:1910.04164].
- [176] C. Dessert, A. J. Long and B. R. Safdi, *Phys. Rev. Lett.* **123**, 6, 061104 (2019), [arXiv:1903.05088].
- [177] C. Dessert, A. J. Long and B. R. Safdi (2021), [arXiv:2104.12772].
- [178] C. Csaki, N. Kaloper and J. Terning, *Phys. Rev. Lett.* **88**, 161302 (2002), [hep-ph/0111311].
- [179] A. Mirizzi, G.G. Raffelt, and P.D. Serpico, *Lect. Notes Phys.* **741**, 115 (2008).
- [180] R. Gill and J. S. Heyl, *Phys. Rev.* **D84**, 085001 (2011), [arXiv:1105.2083].
- [181] D. Horns *et al.*, *Phys. Rev.* **D85**, 085021 (2012), [arXiv:1203.2184].
- [182] A. Payez, J. R. Cudell and D. Hutsemekers, *JCAP* **1207**, 041 (2012), [arXiv:1204.6187].
- [183] A. Dominguez, M. A. Sanchez-Conde and F. Prada, *JCAP* **1111**, 020 (2011), [arXiv:1106.1860].
- [184] W. Essey and A. Kusenko, *Astrophys. J.* **751**, L11 (2012), [arXiv:1111.0815].
- [185] D. Horns and M. Meyer, *JCAP* **1202**, 033 (2012), [arXiv:1201.4711].
- [186] G. I. Rubtsov and S. V. Troitsky, *JETP Lett.* **100**, 6, 355 (2014), [*Pisma Zh. Eksp. Teor. Fiz.*100,no.6,397(2014)], [arXiv:1406.0239].
- [187] K. Kohri and H. Kodama, *Phys. Rev.* **D96**, 5, 051701 (2017), [arXiv:1704.05189].
- [188] D. A. Sanchez, S. Fegan and B. Giebels, *Astron. Astrophys.* **554**, A75 (2013), [arXiv:1303.5923].
- [189] J. Biteau and D. A. Williams, *Astrophys. J.* **812**, 1, 60 (2015), [arXiv:1502.04166].
- [190] A. Dominguez and M. Ajello, *Astrophys. J.* **813**, 2, L34 (2015), [arXiv:1510.07913].
- [191] A. Korochkin, G. Rubtsov and S. Troitsky, *JCAP* **12**, 002 (2019), [arXiv:1810.03443].
- [192] A. De Angelis, G. Galanti and M. Roncadelli, *Phys. Rev.* **D84**, 105030 (2011), [Erratum: *Phys. Rev.*D87,no.10,109903(2013)], [arXiv:1106.1132].
- [193] M. Simet, D. Hooper and P. D. Serpico, *Phys. Rev.* **D77**, 063001 (2008), [arXiv:0712.2825].
- [194] M. A. Sanchez-Conde *et al.*, *Phys. Rev.* **D79**, 123511 (2009), [arXiv:0905.3270].
- [195] M. Meyer, D. Horns and M. Raue, *Phys. Rev.* **D87**, 3, 035027 (2013), [arXiv:1302.1208].
- [196] A. Abramowski *et al.* (H.E.S.S.), *Phys. Rev.* **D88**, 10, 102003 (2013), [arXiv:1311.3148].
- [197] M. Ajello *et al.* (Fermi-LAT), *Phys. Rev. Lett.* **116**, 16, 161101 (2016), [arXiv:1603.06978].
- [198] C. Zhang *et al.*, *Phys. Rev.* **D97**, 6, 063009 (2018), [arXiv:1802.08420].
- [199] H.-J. Li *et al.*, *Phys. Rev. D* **103**, 8, 083003 (2021), [arXiv:2008.09464].
- [200] M. Libanov and S. Troitsky, *Phys. Lett. B* **802**, 135252 (2020), [arXiv:1908.03084].
- [201] Z.-Q. Xia *et al.*, *Phys. Rev.* **D97**, 6, 063003 (2018), [arXiv:1801.01646].
- [202] J. Majumdar, F. Calore and D. Horns, *JCAP* **1804**, 04, 048 (2018), [arXiv:1801.08813].
- [203] G. A. Pallathadka *et al.* (2020), [arXiv:2008.08100].
- [204] K. Choi *et al.*, *Phys. Rev. D* **101**, 4, 043007 (2020), [arXiv:1806.09508].
- [205] F. Chadha-Day (2021), [arXiv:2107.12813].
- [206] D. Wouters and P. Brun, *Astrophys. J.* **772**, 44 (2013), [arXiv:1304.0989].
- [207] M. Berg *et al.*, *Astrophys. J.* **847**, 2, 101 (2017), [arXiv:1605.01043].
- [208] M. C. D. Marsh *et al.*, *JCAP* **1712**, 12, 036 (2017), [arXiv:1703.07354].
- [209] J. P. Conlon *et al.*, *JCAP* **1707**, 07, 005 (2017), [arXiv:1704.05256].
- [210] L. Chen and J. P. Conlon, *Mon. Not. Roy. Astron. Soc.* **479**, 2, 2243 (2018), [arXiv:1712.08313].
- [211] C. S. Reynolds *et al.*, *Astrophys. J.* **890**, 1, 59 (2020), [arXiv:1907.05475].
- [212] A. Hook and J. Huang, *JHEP* **06**, 036 (2018), [arXiv:1708.08464].
- [213] J. Huang *et al.*, *Phys. Rev. D* **99**, 6, 063013 (2019), [arXiv:1807.02133].
- [214] J. Zhang *et al.* (2021), [arXiv:2105.13963].
- [215] G. Bellini *et al.* (Borexino), *Phys. Rev. D* **89**, 11, 112007 (2014), [arXiv:1308.0443].
- [216] B. P. Abbott *et al.* (LIGO Scientific, Virgo), *Phys. Rev. Lett.* **119**, 16, 161101 (2017), [arXiv:1710.05832].
- [217] A. Arvanitaki and S. Dubovsky, *Phys. Rev.* **D83**, 044026 (2011), [arXiv:1004.3558].
- [218] A. Arvanitaki, M. Baryakhtar and X. Huang, *Phys. Rev.* **D91**, 8, 084011 (2015), [arXiv:1411.2263].
- [219] V. M. Mehta *et al.* (2020), [arXiv:2011.08693].
- [220] V. M. Mehta *et al.*, *JCAP* **07**, 033 (2021), [arXiv:2103.06812].
- [221] M. J. Stott (2020), [arXiv:2009.07206].
- [222] M. Baryakhtar *et al.*, *Phys. Rev. D* **103**, 9, 095019 (2021), [arXiv:2011.11646].
- [223] A. Arvanitaki *et al.*, *Phys. Rev.* **D95**, 4, 043001 (2017), [arXiv:1604.03958].
- [224] K. K. Y. Ng *et al.*, *Phys. Rev. D* **103**, 6, 063010 (2021), [arXiv:1908.02312].
- [225] E. Masso, F. Rota and G. Zsembinski, *Phys. Rev. D* **66**, 023004 (2002), [hep-ph/0203221].
- [226] P. Graf and F. D. Steffen, *Phys. Rev. D* **83**, 075011 (2011), [arXiv:1008.4528].
- [227] Z. G. Berezhiani, A. S. Sakharov and M. Y. Khlopov, *Sov. J. Nucl. Phys.* **55**, 1063 (1992).
- [228] S. Hannestad, A. Mirizzi and G. Raffelt, *JCAP* **07**, 002 (2005), [hep-ph/0504059].
- [229] S. Hannestad *et al.*, *JCAP* **08**, 001 (2010), [arXiv:1004.0695].
- [230] M. Archidiacono *et al.*, *JCAP* **10**, 020 (2013), [arXiv:1307.0615].
- [231] E. Di Valentino *et al.*, *Phys. Lett. B* **752**, 182 (2016), [arXiv:1507.08665].
- [232] W. Giarè *et al.*, *Mon. Not. Roy. Astron. Soc.* **505**, 2, 2703 (2021), [arXiv:2011.14704].
- [233] L. Di Luzio, G. Martinelli and G. Piazza, *Phys. Rev. Lett.* **126**, 24, 241801 (2021), [arXiv:2101.10330].
- [234] E. Masso and R. Toldra, *Phys. Rev. D* **52**, 1755 (1995), [hep-ph/9503293].
- [235] E. Masso and R. Toldra, *Phys. Rev.* **D55**, 7967 (1997), [hep-ph/9702275].
- [236] D. Cadamuro and J. Redondo, *JCAP* **1202**, 032 (2012), [arXiv:1110.2895].
- [237] P. F. Depta, M. Hufnagel and K. Schmidt-Hoberg, *JCAP* **05**, 009 (2020), [arXiv:2002.08370].
- [238] J. Preskill, M. B. Wise and F. Wilczek, *Phys. Lett.* **B120**, 127 (1983).

- [239] L. F. Abbott and P. Sikivie, Phys. Lett. **B120**, 133 (1983).
- [240] M. Dine and W. Fischler, Phys. Lett. **B120**, 137 (1983).
- [241] K. J. Bae, J.-H. Huh and J. E. Kim, JCAP **0809**, 005 (2008), [arXiv:0806.0497].
- [242] O. Wantz and E. P. S. Shellard, Phys. Rev. **D82**, 123508 (2010), [arXiv:0910.1066].
- [243] G. Ballesteros *et al.*, JCAP **1708**, 08, 001 (2017), [arXiv:1610.01639].
- [244] R. T. Co, F. D'Eramo and L. J. Hall, Phys. Rev. D **94**, 7, 075001 (2016), [arXiv:1603.04439].
- [245] M. Tegmark *et al.*, Phys. Rev. **D73**, 023505 (2006), [arXiv:astro-ph/0511774].
- [246] A. D. Linde, Phys. Lett. **158B**, 375 (1985).
- [247] D. Seckel and M. S. Turner, Phys. Rev. **D32**, 3178 (1985).
- [248] M. Beltran, J. Garcia-Bellido and J. Lesgourgues, Phys. Rev. **D75**, 103507 (2007), [hep-ph/0606107].
- [249] M. P. Hertzberg, M. Tegmark and F. Wilczek, Phys. Rev. **D78**, 083507 (2008), [arXiv:0807.1726].
- [250] J. Hamann *et al.*, JCAP **0906**, 022 (2009), [arXiv:0904.0647].
- [251] P. A. R. Ade *et al.* (Planck), Astron. Astrophys. **571**, A22 (2014), [arXiv:1303.5082].
- [252] P. A. R. Ade *et al.* (Planck), Astron. Astrophys. **594**, A20 (2016), [arXiv:1502.02114].
- [253] B. Bolliet, J. Chluba and R. Battye, Monthly Notices of the Royal Astronomical Society **507**, 3, 3148 (2021), ISSN 0035-8711, URL <https://doi.org/10.1093/mnras/stab1997>.
- [254] R. T. Co, L. J. Hall and K. Harigaya, Phys. Rev. Lett. **124**, 25, 251802 (2020), [arXiv:1910.14152].
- [255] S. Chang, C. Hagmann and P. Sikivie, Phys. Rev. **D59**, 023505 (1999), [hep-ph/9807374].
- [256] C. Hagmann, S. Chang and P. Sikivie, Phys. Rev. **D63**, 125018 (2001), [hep-ph/0012361].
- [257] T. Hiramatsu *et al.*, Phys. Rev. **D83**, 123531 (2011), [arXiv:1012.5502].
- [258] T. Hiramatsu *et al.*, Phys. Rev. **D85**, 105020 (2012), [Erratum: Phys. Rev. **D86**, 089902(2012)], [arXiv:1202.5851].
- [259] M. Kawasaki, K. Saikawa and T. Sekiguchi, Phys. Rev. **D91**, 6, 065014 (2015), [arXiv:1412.0789].
- [260] V. B. Klaer and G. D. Moore, JCAP **1711**, 11, 049 (2017), [arXiv:1708.07521].
- [261] M. Gorghetto, E. Hardy and G. Villadoro, JHEP **07**, 151 (2018), [arXiv:1806.04677].
- [262] M. Buschmann, J. W. Foster and B. R. Safdi, Phys. Rev. Lett. **124**, 16, 161103 (2020), [arXiv:1906.00967].
- [263] M. Hindmarsh *et al.*, Phys. Rev. Lett. **124**, 2, 021301 (2020), [arXiv:1908.03522].
- [264] M. Gorghetto, E. Hardy and G. Villadoro, SciPost Phys. **10**, 050 (2021), [arXiv:2007.04990].
- [265] M. Dine *et al.* (2020), [arXiv:2012.13065].
- [266] M. Hindmarsh *et al.*, Phys. Rev. D **103**, 10, 103534 (2021), [arXiv:2102.07723].
- [267] M. Buschmann *et al.* (2021), [arXiv:2108.05368].
- [268] A. Ringwald and K. Saikawa, Phys. Rev. **D93**, 8, 085031 (2016), [Addendum: Phys. Rev. **D94**, no.4, 049908(2016)], [arXiv:1512.06436].
- [269] T. Hiramatsu *et al.*, JCAP **1301**, 001 (2013), [arXiv:1207.3166].
- [270] C. J. Hogan and M. J. Rees, Phys. Lett. **B205**, 228 (1988).
- [271] E. W. Kolb and I. I. Tkachev, Phys. Rev. Lett. **71**, 3051 (1993), [hep-ph/9303313].
- [272] B. Eggemeier *et al.*, Phys. Rev. Lett. **125**, 4, 041301 (2020), [arXiv:1911.09417].
- [273] A. Vaquero, J. Redondo and J. Stadler (2018), [JCAP1904,no.04,012(2019)], [arXiv:1809.09241].
- [274] E. W. Kolb and I. I. Tkachev, Astrophys. J. **460**, L25 (1996), [arXiv:astro-ph/9510043].
- [275] M. Fairbairn, D. J. E. Marsh and J. Quevillon, Phys. Rev. Lett. **119**, 2, 021101 (2017), [arXiv:1701.04787].
- [276] A. Katz *et al.*, JCAP **1812**, 005 (2018), [arXiv:1807.11495].
- [277] E. Berkowitz, M. I. Buchoff and E. Rinaldi, Phys. Rev. **D92**, 3, 034507 (2015), [arXiv:1505.07455].
- [278] S. Borsanyi *et al.*, Phys. Lett. **B752**, 175 (2016), [arXiv:1508.06917].
- [279] R. Kitano and N. Yamada, JHEP **10**, 136 (2015), [arXiv:1506.00370].
- [280] P. Petreczky, H.-P. Schadler and S. Sharma, Phys. Lett. **B762**, 498 (2016), [arXiv:1606.03145].
- [281] Y. Taniguchi *et al.*, Phys. Rev. **D95**, 5, 054502 (2017), [arXiv:1611.02411].
- [282] M. Dine *et al.*, Phys. Rev. **D96**, 9, 095001 (2017), [arXiv:1705.00676].
- [283] R. D. Pisarski and L. G. Yaffe, Phys. Lett. **97B**, 110 (1980).
- [284] R. Hlozek *et al.*, Phys. Rev. **D91**, 10, 103512 (2015), [arXiv:1410.2896].
- [285] D. J. E. Marsh, Phys. Rept. **643**, 1 (2016), [arXiv:1510.07633].
- [286] L. Hui *et al.*, Phys. Rev. **D95**, 4, 043541 (2017), [arXiv:1610.08297].
- [287] G. P. Centers *et al.* (2019), [arXiv:1905.13650].
- [288] A. G. Dias *et al.*, JHEP **06**, 037 (2014), [arXiv:1403.5760].
- [289] J. E. Kim and D. J. E. Marsh, Phys. Rev. **D93**, 2, 025027 (2016), [arXiv:1510.01701].
- [290] H. Davoudiasl and C. W. Murphy, Phys. Rev. Lett. **118**, 14, 141801 (2017), [arXiv:1701.01136].
- [291] L. Di Luzio *et al.*, JCAP **10**, 001 (2021), [arXiv:2102.01082].
- [292] M. Khlopov, B. A. Malomed and I. B. Zeldovich, Mon. Not. Roy. Astron. Soc. **215**, 575 (1985).
- [293] W. Hu, R. Barkana and A. Gruzinov, Phys. Rev. Lett. **85**, 1158 (2000), [arXiv:astro-ph/0003365].
- [294] L. Amendola and R. Barbieri, Phys. Lett. **B642**, 192 (2006), [hep-ph/0509257].
- [295] D. J. E. Marsh and P. G. Ferreira, Phys. Rev. **D82**, 103528 (2010), [arXiv:1009.3501].
- [296] E. Seidel and W. M. Suen, Phys. Rev. Lett. **66**, 1659 (1991).
- [297] H.-Y. Schive, T. Chiueh and T. Broadhurst, Nature Phys. **10**, 496 (2014), [arXiv:1406.6586].
- [298] D. G. Levkov, A. G. Panin and I. I. Tkachev, Phys. Rev. Lett. **121**, 15, 151301 (2018), [arXiv:1804.05857].
- [299] B. Eggemeier and J. C. Niemeyer, Phys. Rev. D **100**, 6, 063528 (2019), [arXiv:1906.01348].
- [300] R. Hlozek, D. J. E. Marsh and D. Grin, Mon. Not. Roy. Astron. Soc. **476**, 3, 3063 (2018), [arXiv:1708.05681].
- [301] D. J. E. Marsh and J. Silk, Mon. Not. Roy. Astron. Soc. **437**, 3, 2652 (2014), [arXiv:1307.1705].
- [302] H.-Y. Schive *et al.*, Astrophys. J. **818**, 1, 89 (2016), [arXiv:1508.04621].
- [303] B. Bozek *et al.*, Mon. Not. Roy. Astron. Soc. **450**, 1, 209 (2015), [arXiv:1409.3544].
- [304] P. S. Corasaniti *et al.*, Phys. Rev. **D95**, 8, 083512 (2017), [arXiv:1611.05892].
- [305] K. K. Rogers and H. V. Peiris, Phys. Rev. Lett. **126**, 7, 071302 (2021), [arXiv:2007.12705].
- [306] H.-Y. Schive and T. Chiueh, Mon. Not. Roy. Astron. Soc. **473**, 1, L36 (2018), [arXiv:1706.03723].

- [307] E. O. Nadler *et al.* (DES), *Phys. Rev. Lett.* **126**, 091101 (2021), [arXiv:2008.00022].
- [308] B. Schwabe, J. C. Niemeyer and J. F. Engels, *Phys. Rev. D* **94**, 4, 043513 (2016), [arXiv:1606.05151].
- [309] J. Veltmaat and J. C. Niemeyer, *Phys. Rev. D* **94**, 12, 123523 (2016), [arXiv:1608.00802].
- [310] P. Mocz *et al.*, *Mon. Not. Roy. Astron. Soc.* **471**, 4, 4559 (2017), [arXiv:1705.05845].
- [311] D. G. Levkov, A. G. Panin and I. I. Tkachev, *Phys. Rev. Lett.* **118**, 011301 (2017); T. Helfer *et al.*, *JCAP* **1703**, 03, 055 (2017), [arXiv:1609.04724].
- [312] D. J. E. Marsh and A.-R. Pop, *Mon. Not. Roy. Astron. Soc.* **451**, 3, 2479 (2015), [arXiv:1502.03456].
- [313] S.-R. Chen, H.-Y. Schive and T. Chiueh, *Mon. Not. Roy. Astron. Soc.* **468**, 2, 1338 (2017), [arXiv:1606.09030].
- [314] A. X. González-Morales *et al.*, *Mon. Not. Roy. Astron. Soc.* **472**, 2, 1346 (2017), [arXiv:1609.05856].
- [315] I. De Martino *et al.*, *Phys. Dark Univ.* **28**, 100503 (2020), [arXiv:1807.08153].
- [316] T. Broadhurst *et al.*, *Phys. Rev. D* **101**, 8, 083012 (2020), [arXiv:1902.10488].
- [317] D. Wadekar and G. R. Farrar, *Phys. Rev. D* **103**, 123028 (2021), URL <https://link.aps.org/doi/10.1103/PhysRevD.103.123028>.
- [318] H.-Y. Schive *et al.*, *Phys. Rev. Lett.* **113**, 26, 261302 (2014), [arXiv:1407.7762].
- [319] V. H. Robles, J. S. Bullock and M. Boylan-Kolchin, *Mon. Not. Roy. Astron. Soc.* **483**, 1, 289 (2019), [arXiv:1807.06018].
- [320] V. Desjacques and A. Nusser (2019), [arXiv:1905.03450].
- [321] M. Safarzadeh and D. N. Spergel (2019), [arXiv:1906.11848].
- [322] A. Pontzen and F. Governato, *Nature* **506**, 171 (2014), [arXiv:1402.1764].
- [323] P. Mocz *et al.*, *Phys. Rev. Lett.* **123**, 14, 141301 (2019), [arXiv:1910.01653].
- [324] J. Veltmaat, B. Schwabe and J. C. Niemeyer, *Phys. Rev. D* **101**, 8, 083518 (2020), [arXiv:1911.09614].
- [325] J. Veltmaat, J. C. Niemeyer and B. Schwabe, *Phys. Rev. D* **98**, 4, 043509 (2018), [arXiv:1804.09647].
- [326] B. Bar-Or, J.-B. Fouvry and S. Tremaine, *Astrophys. J.* **871**, 1, 28 (2019), [arXiv:1809.07673].
- [327] B. V. Church, P. Mocz and J. P. Ostriker, *MNRAS* **485**, 2861 (2019), [arXiv:1809.04744].
- [328] N. C. Amorisco and A. Loeb (2018), [arXiv:1808.00464].
- [329] T. S. Li *et al.* (DES), *Astrophys. J.* **838**, 1, 8 (2017), [arXiv:1611.05052].
- [330] D. J. E. Marsh and J. C. Niemeyer, *Phys. Rev. Lett.* **123**, 5, 051103 (2019), [arXiv:1810.08543].
- [331] E. Armengaud *et al.* (EDELWEISS), *Phys. Rev. D* **98**, 8, 082004 (2018), [arXiv:1808.02340].
- [332] C. Fu *et al.* (PandaX), *Phys. Rev. Lett.* **119**, 18, 181806 (2017), [arXiv:1707.07921].
- [333] T. Aralis *et al.* (SuperCDMS), *Phys. Rev. D* **101**, 5, 052008 (2020), [Erratum: *Phys. Rev. D* **103**, 039901 (2021)], [arXiv:1911.11905].
- [334] E. Aprile *et al.* (XENON), *Phys. Rev. Lett.* **123**, 25, 251801 (2019), [arXiv:1907.11485].
- [335] M. Regis *et al.*, *Phys. Lett. B* **814**, 136075 (2021), [arXiv:2009.01310].
- [336] B. D. Blout *et al.*, *Astrophys. J.* **546**, 825 (2001), [arXiv:astro-ph/0006310].
- [337] K. Kelley and P. J. Quinn, *Astrophys. J.* **845**, 1, L4 (2017), [arXiv:1708.01399].
- [338] G. Sigl, *Phys. Rev. D* **96**, 10, 103014 (2017), [arXiv:1708.08908].
- [339] A. Hook *et al.*, *Phys. Rev. Lett.* **121**, 24, 241102 (2018), [arXiv:1804.03145].
- [340] J. W. Foster *et al.*, *Phys. Rev. Lett.* **125**, 17, 171301 (2020), [arXiv:2004.00011].
- [341] J. Darling, *Astrophys. J. Lett.* **900**, 2, L28 (2020), [arXiv:2008.11188].
- [342] R. A. Battye *et al.* (2021), [arXiv:2107.01225].
- [343] S. J. Witte *et al.* (2021), [arXiv:2104.07670].
- [344] R. A. Battye *et al.* (2021), [arXiv:2104.08290].
- [345] A. J. Millar *et al.* (2021), [arXiv:2107.07399].
- [346] A. Caputo *et al.*, *JCAP* **1903**, 03, 027 (2019), [arXiv:1811.08436].
- [347] P. Carena, A. Mirizzi and G. Sigl, *Phys. Rev. D* **101**, 10, 103016 (2020), [arXiv:1911.07838].
- [348] D. G. Levkov, A. G. Panin and I. I. Tkachev, *Phys. Rev. D* **102**, 2, 023501 (2020), [arXiv:2004.05179].
- [349] M. A. Fedderke, P. W. Graham and S. Rajendran, *Phys. Rev. D* **100**, 1, 015040 (2019), [arXiv:1903.02666].
- [350] T. Fujita *et al.*, *Phys. Rev. D* **103**, 4, 043509 (2021), [arXiv:2011.11894].
- [351] P. A. R. Ade *et al.* (BICEP/Keck) (2021), [arXiv:2108.03316].
- [352] T. Liu, G. Smoot and Y. Zhao (2019), [arXiv:1901.10981].
- [353] P. Sikivie, *Phys. Rev. D* **32**, 2988 (1985), [Erratum: *Phys. Rev. D* **36**, 974 (1987)].
- [354] R. Bradley *et al.*, *Rev. Mod. Phys.* **75**, 777 (2003).
- [355] P. Sikivie and J. R. Ipser, *Phys. Lett. B* **291**, 288 (1992).
- [356] P. Sikivie, I. I. Tkachev and Y. Wang, *Phys. Rev. Lett.* **75**, 2911 (1995), [arXiv:astro-ph/9504052].
- [357] S. De Panfilis *et al.*, *Phys. Rev. Lett.* **59**, 839 (1987).
- [358] W. Wuensch *et al.*, *Phys. Rev. D* **40**, 3153 (1989).
- [359] C. Hagmann *et al.*, *Phys. Rev. D* **42**, 1297 (1990).
- [360] S. J. Asztalos *et al.* (ADMX), *Phys. Rev. D* **69**, 011101 (2004), [arXiv:astro-ph/0310042].
- [361] L. Duffy *et al.*, *Phys. Rev. Lett.* **95**, 091304 (2005), [arXiv:astro-ph/0505237]; J. Hoskins *et al.*, *Phys. Rev. D* **84**, 121302 (2011), [arXiv:1109.4128].
- [362] S. J. Asztalos *et al.* (ADMX), *Phys. Rev. Lett.* **104**, 041301 (2010), [arXiv:0910.5914].
- [363] S. J. Asztalos *et al.* (ADMX), *Nucl. Instrum. Meth. A* **656**, 39 (2011), [arXiv:1105.4203].
- [364] R. Khatiwada *et al.* (ADMX) (2020), [arXiv:2010.00169].
- [365] N. Du *et al.* (ADMX), *Phys. Rev. Lett.* **120**, 15, 151301 (2018), [arXiv:1804.05750].
- [366] T. Braine *et al.* (ADMX), *Phys. Rev. Lett.* **124**, 10, 101303 (2020), [arXiv:1910.08638].
- [367] C. Bartram *et al.* (ADMX), *Phys. Rev. D* **103**, 3, 032002 (2021), [arXiv:2010.06183].
- [368] C. Bartram *et al.* (ADMX Collaboration), *Phys. Rev. Lett.* **127**, 261803 (2021), URL <https://link.aps.org/doi/10.1103/PhysRevLett.127.261803>.
- [369] G. Rybka *et al.* (ADMX), *Phys. Rev. Lett.* **105**, 051801 (2010), [arXiv:1004.5160].
- [370] A. Wagner *et al.* (ADMX), *Phys. Rev. Lett.* **105**, 171801 (2010), [arXiv:1007.3766].
- [371] C. Boutan *et al.* (ADMX), *Phys. Rev. Lett.* **121**, 26, 261302 (2018), [arXiv:1901.00920].
- [372] B. M. Brubaker *et al.*, *Phys. Rev. Lett.* **118**, 6, 061302 (2017), [arXiv:1610.02580].
- [373] L. Zhong *et al.* (HAYSTAC), *Phys. Rev. D* **97**, 9, 092001 (2018), [arXiv:1803.03690].

- [374] K. M. Backes *et al.* (HAYSTAC), *Nature* **590**, 7845, 238 (2021), [arXiv:2008.01853].
- [375] B. T. McAllister *et al.*, *Phys. Dark Univ.* **18**, 67 (2017), [arXiv:1706.00209].
- [376] D. Alesini *et al.*, *Phys. Rev. D* **99**, 10, 101101 (2019), [arXiv:1903.06547].
- [377] D. Alesini *et al.*, *Phys. Rev. D* **103**, 10, 102004 (2021), [arXiv:2012.09498].
- [378] A. A. Melcón *et al.* (CAST) (2021), [arXiv:2104.13798].
- [379] S. Lee *et al.*, *Phys. Rev. Lett.* **124**, 10, 101802 (2020), [arXiv:2001.05102].
- [380] J. Jeong *et al.*, *Phys. Rev. Lett.* **125**, 22, 221302 (2020), [arXiv:2008.10141].
- [381] O. Kwon *et al.* (CAPP), *Phys. Rev. Lett.* **126**, 19, 191802 (2021), [arXiv:2012.10764].
- [382] G. Rybka *et al.*, *Phys. Rev.* **D91**, 1, 011701 (2015), [arXiv:1403.3121].
- [383] M. Lawson *et al.*, *Phys. Rev. Lett.* **123**, 14, 141802 (2019), [arXiv:1904.11872].
- [384] D. Horns *et al.*, *JCAP* **1304**, 016 (2013), [arXiv:1212.2970].
- [385] A. Caldwell *et al.* (MADMAX Working Group), *Phys. Rev. Lett.* **118**, 9, 091801 (2017), [arXiv:1611.05865].
- [386] P. Brun *et al.* (MADMAX), *Eur. Phys. J.* **C79**, 3, 186 (2019), [arXiv:1901.07401].
- [387] M. Baryakhtar, J. Huang and R. Lasenby, *Phys. Rev.* **D98**, 3, 035006 (2018), [arXiv:1803.11455].
- [388] A. Arvanitaki, S. Dimopoulos and K. Van Tilburg, *Phys. Rev.* **X8**, 4, 041001 (2018), [arXiv:1709.05354].
- [389] C. A. Thomson *et al.*, *Phys. Rev. Lett.* **126**, 8, 081803 (2021), [Erratum: *Phys.Rev.Lett.* 127, 019901 (2021)], [arXiv:1912.07751].
- [390] A. Berlin *et al.*, *JHEP* **07**, 07, 088 (2020), [arXiv:1912.11048].
- [391] P. Sikivie, *Phys. Rev. Lett.* **113**, 20, 201301 (2014), [Erratum: *Phys.Rev.Lett.* 125, 029901 (2020)], [arXiv:1409.2806].
- [392] R. Li *et al.*, *Nature Phys.* **6**, 284 (2010), [arXiv:0908.1537].
- [393] K. Ishiwata, *Phys. Rev. D* **104**, 1, 016004 (2021), [arXiv:2103.02848].
- [394] L. Cao *et al.*, *Phys. Rev. B* **104**, 054421 (2021), URL <https://link.aps.org/doi/10.1103/PhysRevB.104.054421>.
- [395] D. J. E. Marsh *et al.*, *Phys. Rev. Lett.* **123**, 12, 121601 (2019), [arXiv:1807.08810].
- [396] J. Schütte-Engel *et al.*, *JCAP* **08**, 066 (2021), [arXiv:2102.05366].
- [397] P. Sikivie, N. Sullivan, and D. B. Tanner, *Phys. Rev. Lett.* **112**, 131301 (2014).
- [398] Y. Kahn, B. R. Safdi and J. Thaler, *Phys. Rev. Lett.* **117**, 14, 141801 (2016), [arXiv:1602.01086].
- [399] J. L. Ouellet *et al.* (ABRACADABRA), *Phys. Rev. Lett.* **122**, 12, 121802 (2019), [arXiv:1810.12257].
- [400] C. P. Salemi *et al.*, *Phys. Rev. Lett.* **127**, 8, 081801 (2021), [arXiv:2102.06722].
- [401] N. Crisosto *et al.*, *Phys. Rev. Lett.* **124**, 24, 241101 (2020), [arXiv:1911.05772].
- [402] A. V. Gramolin *et al.*, *Nature Phys.* **17**, 1, 79 (2021), [arXiv:2003.03348].
- [403] J. A. Devlin *et al.*, *Phys. Rev. Lett.* **126**, 4, 041301 (2021), [arXiv:2101.11290].
- [404] M. Silva-Feaver *et al.*, *IEEE Trans. Appl. Supercond.* **27**, 4, 1400204 (2017), [arXiv:1610.09344].
- [405] C. Abel *et al.*, *Phys. Rev.* **X7**, 4, 041034 (2017), [arXiv:1708.06367].
- [406] K. Blum *et al.*, *Phys. Lett. B* **737**, 30 (2014), [arXiv:1401.6460].
- [407] D. Budker *et al.*, *Phys. Rev.* **X4**, 2, 021030 (2014), [arXiv:1306.6089].
- [408] M. B. Wise, H. Georgi and S. L. Glashow, *Phys. Rev. Lett.* **47**, 402 (1981).
- [409] A. Ernst, A. Ringwald and C. Tamarit, *JHEP* **02**, 103 (2018), [arXiv:1801.04906].
- [410] L. Di Luzio, A. Ringwald and C. Tamarit, *Phys. Rev.* **D98**, 9, 095011 (2018), [arXiv:1807.09769].
- [411] P. Fileviez Perez, C. Murgui and A. D. Plascencia (2019), [arXiv:1908.01772].
- [412] D. Aybas *et al.*, *Phys. Rev. Lett.* **126**, 14, 141802 (2021), [arXiv:2101.01241].
- [413] T. Wu *et al.*, *Phys. Rev. Lett.* **122**, 19, 191302 (2019), [arXiv:1901.10843].
- [414] A. Garcon *et al.*, *Sci. Adv.* **5**, 10, eaax4539 (2019), [arXiv:1902.04644].
- [415] I. M. Bloch *et al.* (NASDUCK) (2021), [arXiv:2105.04603].
- [416] G. Vasilakis *et al.*, *Physical Review Letters* **103**, 26 (2009), ISSN 1079-7114, URL <http://dx.doi.org/10.1103/PhysRevLett.103.261801>.
- [417] I. M. Bloch *et al.*, *JHEP* **01**, 167 (2020), [arXiv:1907.03767].
- [418] S. P. Chang *et al.*, *Phys. Rev.* **D99**, 8, 083002 (2019), [arXiv:1710.05271].
- [419] L. Krauss *et al.*, *Phys. Rev. Lett.* **55**, 1797 (1985).
- [420] R. Barbieri *et al.*, *Phys. Lett. B* **226**, 357 (1989).
- [421] R. Barbieri *et al.*, *Phys. Dark Univ.* **15**, 135 (2017), [arXiv:1606.02201].
- [422] N. Crescini *et al.* (QUAX), *Phys. Rev. Lett.* **124**, 17, 171801 (2020), [arXiv:2001.08940].

91. Searches for Quark and Lepton Compositeness

Revised October 2021 by K. Hikasa (Tohoku U.), M. Tanabashi (Nagoya U.; KMI, Nagoya U.), K. Terashi (ICEPP, Tokyo U.) and N. Varelas (U. of Illinois at Chicago).

91.1 Limits on contact interactions

If quarks and leptons are made of constituents, then at the scale of constituent binding energies (compositeness scale) there should appear new interactions among them. At energies much below the compositeness scale (Λ), these interactions are suppressed by inverse powers of Λ . The dominant effect of the compositeness of fermion ψ should come from the lowest dimensional interactions with four fermions (contact terms), whose most general flavor-diagonal color-singlet chirally invariant form reads [1, 2]

$$\mathcal{L} = \mathcal{L}_{LL} + \mathcal{L}_{RR} + \mathcal{L}_{LR} + \mathcal{L}_{RL},$$

with

$$\begin{aligned} \mathcal{L}_{LL} &= \frac{g_{\text{contact}}^2}{2\Lambda^2} \sum_{i,j} \eta_{LL}^{ij} (\bar{\psi}_L^i \gamma_\mu \psi_L^i) (\bar{\psi}_L^j \gamma^\mu \psi_L^j), \\ \mathcal{L}_{RR} &= \frac{g_{\text{contact}}^2}{2\Lambda^2} \sum_{i,j} \eta_{RR}^{ij} (\bar{\psi}_R^i \gamma_\mu \psi_R^i) (\bar{\psi}_R^j \gamma^\mu \psi_R^j), \\ \mathcal{L}_{LR} &= \frac{g_{\text{contact}}^2}{2\Lambda^2} \sum_{i,j} \eta_{LR}^{ij} (\bar{\psi}_L^i \gamma_\mu \psi_L^i) (\bar{\psi}_R^j \gamma^\mu \psi_R^j), \\ \mathcal{L}_{RL} &= \frac{g_{\text{contact}}^2}{2\Lambda^2} \sum_{i,j} \eta_{RL}^{ij} (\bar{\psi}_R^i \gamma_\mu \psi_R^i) (\bar{\psi}_L^j \gamma^\mu \psi_L^j), \end{aligned} \quad (91.1)$$

where i, j are the indices of fermion species. Color and other indices are suppressed in Eq. (91.1). Chiral invariance provides a natural explanation why quark and lepton masses are much smaller than their inverse size Λ . Note $\eta_{\alpha\beta}^{ij} = \eta_{\beta\alpha}^{ji}$. Therefore, in order to specify the contact interaction among the same fermion species $i = j$, it is enough to use η_{LL} , η_{RR} and η_{LR} . We will suppress the indices of fermion species hereafter. We may determine the scale Λ unambiguously by using the above form of the effective interactions; the conventional method [1] is to fix its scale by setting $g_{\text{contact}}^2/4\pi = g_{\text{contact}}^2(\Lambda)/4\pi = 1$ for the new strong interaction coupling and by setting the largest magnitude of the coefficients $\eta_{\alpha\beta}$ to be unity. In the following, we denote

$$\begin{aligned} \Lambda &= \Lambda_{LL}^\pm \text{ for } (\eta_{LL}, \eta_{RR}, \eta_{LR}) = (\pm 1, 0, 0), \\ \Lambda &= \Lambda_{RR}^\pm \text{ for } (\eta_{LL}, \eta_{RR}, \eta_{LR}) = (0, \pm 1, 0), \\ \Lambda &= \Lambda_{VV}^\pm \text{ for } (\eta_{LL}, \eta_{RR}, \eta_{LR}) = (\pm 1, \pm 1, \pm 1), \\ \Lambda &= \Lambda_{AA}^\pm \text{ for } (\eta_{LL}, \eta_{RR}, \eta_{LR}) = (\pm 1, \pm 1, \mp 1), \\ \Lambda &= \Lambda_{V-A}^\pm \text{ for } (\eta_{LL}, \eta_{RR}, \eta_{LR}) = (0, 0, \pm 1). \end{aligned} \quad (91.2)$$

Such interactions can arise by interchanging constituents (when the fermions have common constituents), and/or by exchanging the binding quanta (whenever binding quanta couple to constituents of both particles).

Fermion scattering amplitude induced from the contact interaction in Eq. (91.1) interferes with the Standard Model (SM) amplitude destructively or constructively [2]. The sign of interference depends on the sign of $\eta_{\alpha\beta}$ ($\alpha, \beta = L, R$). For instance, in the parton level $qq \rightarrow qq$ scattering cross section in the Λ_{LL}^\pm model, the contact interaction amplitude and the SM gluon exchange amplitude interfere destructively for $\eta_{LL} = +1$, while they interfere constructively for $\eta_{LL} = -1$. In models of quark compositeness, the quark scattering cross sections induced from the contact interactions receive sizable QCD radiative corrections. Ref. [3] provides the exact next-to-leading order (NLO) QCD corrections to the contact interaction induced quark scattering cross sections.

Over the last three decades experiments at the CERN Sp \bar{p} S [4, 5], the Fermilab Tevatron [6, 7], and the CERN LHC [8–12] have searched for quark contact interactions, characterized by the four-fermion effective Lagrangian in Eq. (91.1), using jet final states. These searches have been performed primarily by studying

the angular distribution of the two highest transverse momentum, p_T , jets (dijets), and the inclusive jet p_T spectrum. The variable $\chi = \exp(|y_1 - y_2|)$ is used to measure the dijet angular distribution, where y_1 and y_2 are the rapidities of the two jets with the highest transverse momenta. For collinear massless parton scattering, χ is related to the polar scattering angle θ^* in the partonic center-of-mass frame by $\chi = (1 + |\cos \theta^*|)/(1 - |\cos \theta^*|)$. The choice of χ is motivated by the fact that the angular distribution for Rutherford scattering, which is proportional to $1/(1 - \cos \theta^*)^2$, is independent of χ . In perturbative QCD the χ distributions are relatively uniform and only mildly modified by higher-order QCD or electroweak corrections. Signatures of quark contact interactions exhibit more isotropic angular distribution than QCD and can be identified as an excess at low values of χ . In the inclusive jet cross section measurement, quark contact interaction effects are searched for as deviations from the predictions of perturbative QCD in the tails of the high- p_T jet spectrum [11].

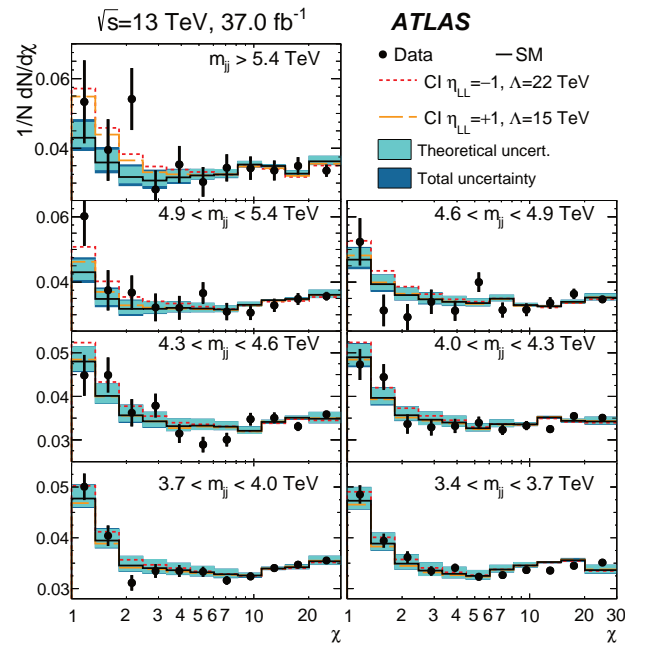


Figure 91.1: Normalized dijet angular distributions in several dijet mass (m_{jj}) ranges. The data distributions are compared to PYTHIA8 predictions with NLO and electroweak corrections applied (solid line) and with the predictions including a contact interaction (CI) term in which only left-handed quarks participate at compositeness scale $\Lambda_{LL}^+ = 15$ TeV (dashed line) and $\Lambda_{LL}^- = 22$ TeV (dotted line). The theoretical uncertainties and the total theoretical and experimental uncertainties in the predictions are displayed as shaded bands around the SM prediction. Figure adopted from Ref. [9].

Recent results from the LHC, using data collected at proton-proton center-of-mass energy of $\sqrt{s} = 13$ TeV, extend previous limits on quark contact interactions. Figure 91.1 shows the normalized dijet angular distributions for several dijet mass ranges measured in ATLAS [9] at $\sqrt{s} = 13$ TeV. The data distributions are compared with SM predictions, estimated using PYTHIA8 [13] with GEANT4-based [14] ATLAS detector simulation and corrected to NLO QCD calculation provided by NLO Jet++ [15] including electroweak corrections [16], and with predictions including a contact interaction term in which only left-handed quarks participate at compositeness scale $\Lambda_{LL}^+ = 15$ TeV ($\Lambda_{LL}^- = 22$ TeV) with destructive (constructive) interference. Over a wide range of χ and dijet mass the data are well described by the SM predictions. Using the dijet angular distributions measured at high dijet masses and $\sqrt{s} = 13$ TeV, the ATLAS [9] and CMS [12] Collaborations have set 95% confidence level (C.L.) lower limits on the contact interaction scale Λ , ranging

from 9.2 to 29.5 TeV for different quark contact interaction models that correspond to various combinations of $(\eta_{LL}, \eta_{RR}, \eta_{LR})$, as summarized in Figure 91.2. The contact interaction scale limits extracted using the dijet angular distributions include the exact NLO QCD corrections to dijet production induced by contact interactions [3]. In proton-proton collisions, the Λ_{LL}^\pm and Λ_{RR}^\pm contact interaction models result in identical tree-level cross sections and NLO QCD corrections and yield the same exclusion limits. For Λ_{VV}^\pm and Λ_{AA}^\pm , the contact interaction predictions are identical at tree level, but exhibit different NLO QCD corrections and yield different exclusion limits.

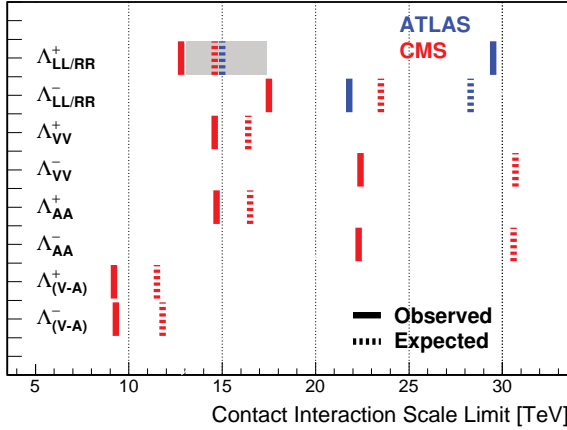


Figure 91.2: Observed (solid lines) and expected (dashed lines) 95% C.L. lower limits on the contact interaction scale Λ for different contact interaction models from ATLAS [9] and CMS [12] using the dijet angular distributions. The contact interaction models used for the dijet angular distributions include the exact NLO QCD corrections to dijet production. The shaded band for the $\Lambda_{LL/RR}^+$ model indicates the range of contact interaction scale that was not excluded in ATLAS [9], due to an observed excess in the data that produced a weaker limit.

If leptons (l) and quarks (q) are composite with common constituents, the interaction of these constituents will manifest itself in the form of a $llqq$ -type four-fermion contact interaction Lagrangian at energies below the compositeness scale Λ . The $llqq$ terms in the contact interaction Lagrangian can be expressed as

$$\begin{aligned}\mathcal{L}_{LL} &= \frac{g_{\text{contact}}^2}{\Lambda^2} \sum_{i,j} \eta_{LL}^{ij} (\bar{q}_L^i \gamma_\mu q_L^i) (\bar{l}_L^j \gamma^\mu l_L^j), \\ \mathcal{L}_{RR} &= \frac{g_{\text{contact}}^2}{\Lambda^2} \sum_{i,j} \eta_{RR}^{ij} (\bar{q}_R^i \gamma_\mu q_R^i) (\bar{l}_R^j \gamma^\mu l_R^j), \\ \mathcal{L}_{LR} &= \frac{g_{\text{contact}}^2}{\Lambda^2} \sum_{i,j} \eta_{LR}^{ij} (\bar{q}_L^i \gamma_\mu q_L^i) (\bar{l}_R^j \gamma^\mu l_R^j), \\ \mathcal{L}_{RL} &= \frac{g_{\text{contact}}^2}{\Lambda^2} \sum_{i,j} \eta_{RL}^{ij} (\bar{q}_R^i \gamma_\mu q_R^i) (\bar{l}_L^j \gamma^\mu l_L^j).\end{aligned}\quad (91.3)$$

Searches on quark-lepton compositeness have been reported from experiments at LEP [17–20], HERA [21, 22], the Tevatron [23, 24], and recently from the ATLAS [25, 26] and CMS [27, 28] experiments at the LHC. The most stringent searches for $llqq$ contact interactions are performed by the LHC experiments using high-mass oppositely-charged lepton pairs produced through the $q\bar{q} \rightarrow l^+l^-$ Drell-Yan process. The contact interaction amplitude of the $u\bar{u} \rightarrow l^+l^-$ process ($l = e$ or μ) interferes with the corresponding SM amplitude constructively (destructively) for $\eta_{\alpha\beta}^{ul} = -1$ ($\eta_{\alpha\beta}^{ul} = +1$). The ATLAS Collaboration has extracted limits on the $llqq$ contact interaction at $\sqrt{s} = 13$ TeV for the right-right ($\eta_{RR} = \pm 1$, $\eta_{LL} = \eta_{LR} = \eta_{RL} = 0$), left-left ($\eta_{LL} = \pm 1$,

$\eta_{RR} = \eta_{LR} = \eta_{RL} = 0$), and left-right ($\eta_{LR} = \eta_{RL} = \pm 1$, $\eta_{RR} = \eta_{LL} = 0$) models. In Ref. [26], ATLAS used a background estimate directly obtained from data. Combining the dielectron and dimuon channels, the 95% C.L. lower limits on the $llqq$ contact interaction scale Λ are 36 TeV (27 TeV) for the right-right model, 36 TeV (26 TeV) for the left-left model, and 33 TeV (29 TeV) for the left-right model, each with constructive (destructive) interference [26]. The CMS Collaboration, using a 140 fb^{-1} dataset at 13 TeV, has set 95% C.L. exclusion limits on the $llqq$ contact interaction scale that range from $\Lambda_{LL} > 23.9$ TeV for the destructive interference to $\Lambda_{RR} > 36.4$ TeV for the constructive interference, for the left-left and the right-right models, respectively [28].

Note that the contact interactions arising from the compositeness of quarks and leptons in Eq. (91.1) can also be regarded as a part of more general dimension six operators in the context of low energy standard model effective field theory (SMEFT). For a complete list of SM gauge invariant dimension six operators, see [29, 30]. A computation of the one loop anomalous dimension matrix for SMEFT operators are found in Refs. [31–33]. See also Refs. [34] and [35] for recent reviews. Consistent SMEFT reinterpretations of top-quark data, and high energy non-resonant dijet and dilepton data are provided, e.g., in Refs. [36–38].

Interactions of hypothetical dark matter candidate particles with SM particles through mediators can also be described as contact interactions at low energy. See “Searches for WIMPs and Other Particles” in this volume for limits on the interactions involving dark matter candidate particles.

91.2 Limits on excited fermions

Another typical consequence of compositeness is the appearance of excited leptons and quarks (l^* and q^*). Phenomenologically, an excited lepton is defined to be a heavy lepton which shares a leptonic quantum number with one of the existing leptons (an excited quark is defined similarly). For example, an excited electron e^* is characterized by a nonzero transition-magnetic coupling with electrons. The smallness of the lepton mass and the success of QED prediction for $g-2$ suggest chirality conservation, *i.e.*, an excited lepton should not couple to both left- and right-handed components of the corresponding lepton [39–41].

Excited leptons may be classified by $SU(2) \times U(1)$ quantum numbers. Typical examples are:

1. Sequential type

$$\begin{pmatrix} \nu^* \\ l^* \end{pmatrix}_L, \quad [\nu_R^*], \quad l_R^*.$$

ν_R^* is necessary if we assume ν^* has a Dirac mass.

2. Mirror type

$$[\nu_L^*], \quad l_L^*, \quad \begin{pmatrix} \nu^* \\ l^* \end{pmatrix}_R.$$

3. Homodoublet type

$$\begin{pmatrix} \nu^* \\ l^* \end{pmatrix}_L, \quad \begin{pmatrix} \nu^* \\ l^* \end{pmatrix}_R.$$

Similar classification can be made for excited quarks.

Excited fermions can be pair produced via their minimal gauge couplings. The couplings of excited leptons with Z are given by

$$\begin{aligned}& \frac{e}{2 \sin \theta_W \cos \theta_W} (-1 + 2 \sin^2 \theta_W) \bar{l}^* \gamma^\mu l^* Z_\mu \\ & + \frac{e}{2 \sin \theta_W \cos \theta_W} \bar{\nu}^* \gamma^\mu \nu^* Z_\mu\end{aligned}$$

in the homodoublet model. The corresponding couplings of excited quarks can be easily obtained. Although form factor effects can be present for the gauge couplings at $q^2 \neq 0$, they are usually neglected.

Excited fermions may also be produced via the contact interactions with ordinary quarks and leptons [42]

$$\begin{aligned}\mathcal{L} &= \frac{g_{\text{contact}}^2}{\Lambda^2} \left[\eta'_{LL} (\bar{\psi}_L \gamma_\mu \psi_L) (\bar{\psi}_L^* \gamma^\mu \psi_L^*) \right. \\ & \left. + (\eta''_{LL} (\bar{\psi}_L \gamma_\mu \psi_L) (\bar{\psi}_L^* \gamma^\mu \psi_L) + \text{h.c.}) + \dots \right].\end{aligned}\quad (91.4)$$

Again, the coefficient is conventionally taken $g_{\text{contact}}^2 = 4\pi$. It is widely assumed $\eta'_{LL} = \eta''_{LL} = 1$, $\eta'_{LR} = \eta''_{LR} = \eta'_{RL} = \eta''_{RL} = \eta'_{RR} = \eta''_{RR} = 0$ in experimental analyses for simplicity.

In addition, transition-magnetic type couplings with a gauge boson are expected. These couplings can be generally parameterized as follows:

$$\begin{aligned} \mathcal{L} = & \frac{\lambda_{\gamma}^{(\psi^*)} e}{2m_{\psi^*}} \bar{\psi}^* \sigma^{\mu\nu} \left(\eta_L \frac{1-\gamma_5}{2} + \eta_R \frac{1+\gamma_5}{2} \right) \psi F_{\mu\nu} \\ & + \frac{\lambda_Z^{(\psi^*)} e}{2m_{\psi^*}} \bar{\psi}^* \sigma^{\mu\nu} \left(\eta_L \frac{1-\gamma_5}{2} + \eta_R \frac{1+\gamma_5}{2} \right) \psi Z_{\mu\nu} \\ & + \frac{\lambda_W^{(l^*)} g}{2m_{l^*}} \bar{l}^* \sigma^{\mu\nu} \frac{1-\gamma_5}{2} \nu W_{\mu\nu} \\ & + \frac{\lambda_W^{(\nu^*)} g}{2m_{\nu^*}} \bar{\nu}^* \sigma^{\mu\nu} \left(\eta_L \frac{1-\gamma_5}{2} + \eta_R \frac{1+\gamma_5}{2} \right) l W_{\mu\nu}^\dagger \\ & + \text{h.c.}, \end{aligned} \quad (91.5)$$

where $g = e/\sin\theta_W$, $\psi = \nu$ or l , $F_{\mu\nu} = \partial_\mu A_\nu - \partial_\nu A_\mu$ is the photon field strength, $Z_{\mu\nu} = \partial_\mu Z_\nu - \partial_\nu Z_\mu$, etc.. The normalization of the coupling is chosen such that

$$\max(|\eta_L|, |\eta_R|) = 1.$$

Chirality conservation requires

$$\eta_L \eta_R = 0. \quad (91.6)$$

These couplings in Eq. (91.5) can arise from $SU(2) \times U(1)$ -invariant higher-dimensional interactions. A well-studied model is the interaction of homodoublet type l^* with the Lagrangian (see [43, 44])

$$\mathcal{L} = \frac{1}{2\Lambda} \bar{L}^* \sigma^{\mu\nu} \left(g_f \frac{\tau^a}{2} W_{\mu\nu}^a + g' f' Y B_{\mu\nu} \right) \frac{1-\gamma_5}{2} L + \text{h.c.}, \quad (91.7)$$

where L denotes the lepton doublet (ν, l), Λ is the compositeness scale, g, g' are $SU(2)$ and $U(1)_Y$ gauge couplings, and $W_{\mu\nu}^a$ and $B_{\mu\nu}$ are the field strengths for $SU(2)$ and $U(1)_Y$ gauge fields. These couplings satisfy the relation

$$\lambda_W = -\sqrt{2} \sin^2 \theta_W (\lambda_Z \cot \theta_W + \lambda_\gamma), \quad (91.8)$$

with $\lambda_{W,Z,\gamma}$ being defined in Eq. (91.5) with $\lambda_{W,Z,\gamma} = \lambda_{W,Z,\gamma}^{(l^*)}$ or $\lambda_{W,Z,\gamma} = \lambda_{W,Z,\gamma}^{(\nu^*)}$. Here $(\eta_L, \eta_R) = (1, 0)$ is assumed. It should be noted that the electromagnetic radiative decay of l^* (ν^*) is forbidden if $f = -f'$ ($f = f'$).

Additional coupling with gluons is possible for excited quarks:

$$\begin{aligned} \mathcal{L} = & \frac{1}{2\Lambda} \bar{Q}^* \sigma^{\mu\nu} \left(g_s f_s \frac{\lambda^a}{2} G_{\mu\nu}^a + g f' \frac{\tau^a}{2} W_{\mu\nu}^a + g' f' Y B_{\mu\nu} \right) \\ & \times \frac{1-\gamma_5}{2} Q + \text{h.c.}, \end{aligned} \quad (91.9)$$

where Q denotes a quark doublet, g_s is the QCD gauge coupling, and $G_{\mu\nu}^a$ the gluon field strength.

If leptons are made of color triplet and antitriplet constituents, we may expect their color-octet partners. Transitions between the octet leptons (l_8) and the ordinary lepton (l) may take place via the dimension-five interactions

$$\mathcal{L} = \frac{1}{2\Lambda} \sum_l \left\{ \bar{l}_8^\alpha g_8 F_{\mu\nu}^\alpha \sigma^{\mu\nu} (\eta_L l_L + \eta_R l_R) + \text{h.c.} \right\} \quad (91.10)$$

where the summation is over charged leptons and neutrinos. The leptonic chiral invariance implies $\eta_L \eta_R = 0$ as before.

Searches for the excited quarks and leptons have been performed over the last decades in experiments at the LEP [45–48], HERA [49, 50], Tevatron [51, 52], and LHC [53–78]. Most stringent constraints, which are described below at 95% confidence level, come from the LHC experiments.

The signature of excited quarks q^* at hadron colliders is characterized by a narrow resonant peak in the reconstructed invariant

mass distribution of the q^* decay products. The decays via the transition-magnetic type operator in Eq. (91.9) are considered for excited quarks in LHC searches, and the final states to search for are dijet (qg) [53, 54, 66–69] or a jet in association with a photon ($q\gamma$) [55, 56, 70, 71] or a weak gauge boson (qW, qZ) [72, 73]. All analyses consider only spin-1/2 excited states of first generation quarks (u^*, d^*) with degenerate masses, expected to be predominantly produced in proton-proton collisions except for the excited b quark searches described below. Only the minimal gauge interactions and the transition-magnetic couplings with the form given in Eq. (91.9) are considered in the production process, and hence the contact interactions in Eq. (91.4) are not considered. The compositeness scale Λ is taken to be the same as the excited quark mass m_{q^*} . The transition-magnetic coupling coefficients f_s, f and f' are assumed to be equal to 1 (denoted by f).

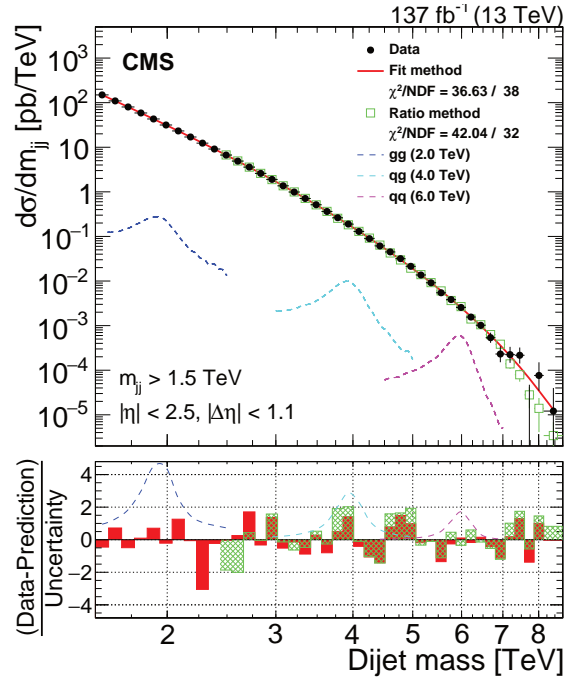


Figure 91.3: Dijet mass distribution measured by CMS using wide jets reconstructed from two highest transverse momentum jets by adding nearby jets within $\Delta R = \sqrt{\Delta\eta^2 + \Delta\phi^2} < 1.1$. The data distribution is compared to a fit representing a smooth background spectrum (solid curve) and the background prediction obtained from the $\Delta\eta_{jj}$ control regions (open squares), denoted as Ratio method, at $m_{jj} > 2.4$ TeV. The excited quark signal with mass of 4.0 TeV (labeled as qq) is shown together with other benchmark signals. Shown at the bottom panel is the difference between the data and the fitted parametrization from the fit method or the data and the background prediction from the Ratio method, divided by the statistical uncertainty of the data. Figure adopted from [69].

With proton-proton collision data recorded at $\sqrt{s} = 13$ TeV at the LHC, the excited quark masses are excluded in dijet resonance searches up to 6.7 TeV in ATLAS using 139 fb^{-1} [54] and 6.3 TeV in CMS using 137 fb^{-1} [69]. Figure 91.3 shows the dijet mass (m_{jj}) distribution measured in CMS [69] by using the two highest p_T jets reconstructed with the anti- k_T algorithm [79] of a distance parameter of 0.4, and by combining nearby jets within $\Delta R = \sqrt{\Delta\eta^2 + \Delta\phi^2} < 1.1$ around the leading two jets. The measured dijet mass spectrum is compared to a fit with smoothly falling background shape (solid curve) at $m_{jj} > 1.5$ TeV and the background prediction obtained from the $\Delta\eta_{jj}$ control regions (open squares), denoted as Ratio method, at $m_{jj} > 2.4$ TeV to look for a narrow resonance. Here $\Delta\eta_{jj}$ is the pseudorapidity separation between the two jets. An excited quark signal with mass of 4.0 TeV is shown in the figure (denoted by qq) as one of the

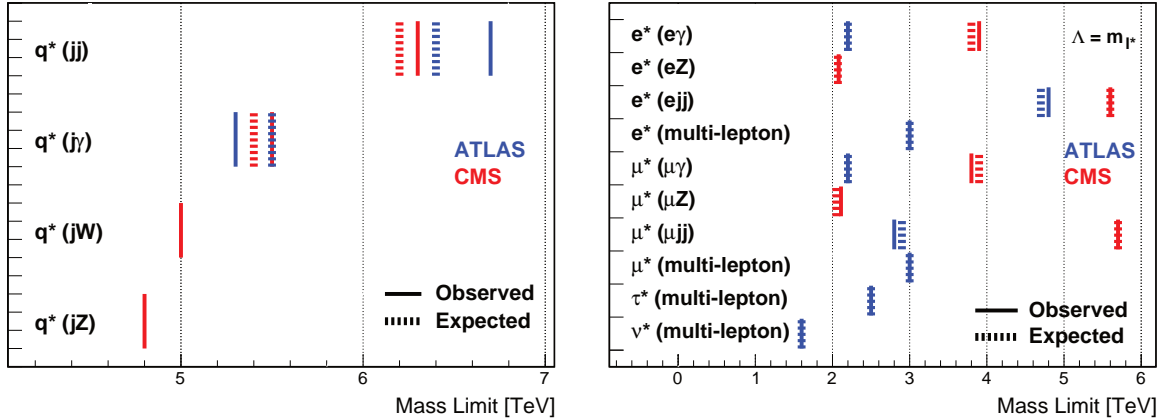


Figure 91.4: 95% C.L. lower mass limits for the excited quarks (left) and excited leptons (right) at ATLAS [54, 56, 62–64] and CMS [69, 71, 73, 76–78] experiments. Shown are the most stringent limits for each final state (denoted in parentheses) of the excited fermions from both experiments. Only first generation quarks (u, d) with transition-magnetic type interactions with $f_s = f = f' = 1$ are considered for the excited quarks. The excited lepton limits are given for the production via contact interactions with $\Lambda = m_{l^*}$.

benchmark signals considered in the analysis.

The photon + jet resonance searches, targeting excited quarks decaying into a quark and a photon ($q^* \rightarrow q + \gamma$), have excluded q^* masses up to 5.3 TeV in ATLAS [56] and 5.5 TeV in CMS [71] using collision data at $\sqrt{s} = 13$ TeV. The W/Z boson + jet final states are examined to look for the $q^* \rightarrow q + W$ and $q + Z$ signal in CMS [73], exploiting jet substructure technique designed to provide sensitivity for highly-boosted hadronically decaying W and Z bosons. The lower mass limit of 5.0 (4.8) TeV is obtained from the $W + \text{jet}$ ($Z + \text{jet}$) search using dataset recorded at $\sqrt{s} = 13$ TeV.

The excited b quarks (b^*) are also considered in the present searches at the LHC. Assuming the similar production processes to the first-generation excited quarks, the b^* has been searched for in final states containing at least one jet identified as originating from a b quark (b -tagging). The searches using two jets including at least one b -tagged jet have been performed at 8 and 13 TeV [54, 57, 58, 67], resulting in b^* lower mass limits of 3.2 TeV in ATLAS using 139 fb^{-1} at $\sqrt{s} = 13$ TeV [54] and 1.6 TeV in CMS using 19.7 fb^{-1} at $\sqrt{s} = 8$ TeV [67]. The CMS Collaboration also performed a search for $b^* \rightarrow b + \gamma$ in events with a b -tagged jet in association with a photon using data at $\sqrt{s} = 13$ TeV [71], and excluded b^* masses up to 1.8 TeV. Excited b quarks with charged-current decay into a W -boson and a top quark ($b^* \rightarrow t + W$) were looked for in both ATLAS and CMS using the full 8 TeV data [59, 74]. ATLAS excluded b^* masses below 1.5 TeV for the b^* with left- and right-handed couplings [59] while CMS excluded the masses below 1.39(1.43) TeV for the left(right)-handed couplings [74].

The excited top quarks (t^*) have also been searched for at the LHC. The CMS Collaboration performed the search for pair-produced t^* quarks with the assumption of the t^* quark decay into a top quark and a gluon, in events with a charged lepton, missing transverse momentum and multiple jets including b -tagged jets at $\sqrt{s} = 8$ TeV [80] and 13 TeV [81]. With 35.9 fb^{-1} data at 13 TeV, CMS excluded the t^* masses below 1.2 TeV for spin 3/2 t^* quarks [81].

Searches for excited leptons l^* are also performed at the LHC using proton-proton collision data recorded at $\sqrt{s} = 7$ and 8 TeV [61–65, 75, 76] as well as at 13 TeV [77]. Considering single l^* production in contact interactions (Eq. (91.4)) and electromagnetic radiative decay to a SM lepton and a photon ($l^* \rightarrow l + \gamma$ where $l = e, \mu$), the excited electron and muon masses are excluded for $\Lambda = m_{l^*}$ up to 3.9 and 3.8 TeV, respectively, using 35.9 fb^{-1} at $\sqrt{s} = 13$ TeV in CMS [77] and 2.2 TeV using 13 fb^{-1} at $\sqrt{s} = 8$ TeV in ATLAS [62].

With the full 20.3 fb^{-1} data at $\sqrt{s} = 8$ TeV, the inclusive search on multi-lepton signatures with 3 or more charged leptons

in ATLAS [63] further constrains the excited charged leptons and neutrinos. Considering both the transition-magnetic (Eq. (91.7)) and contact interaction (Eq. (91.4)) processes, the lower mass limits for the e^* , μ^* , τ^* and ν^* (for every excited neutrino flavor) are obtained to be 3.0, 3.0, 2.5 and 1.6 TeV, respectively, for $\Lambda = m_{e^*}$, m_{μ^*} , m_{τ^*} and m_{ν^*} . The rate of pair-produced excited leptons is independent of Λ for the minimal gauge interaction processes, and it allows to improve search sensitivity with multi-lepton signatures at high Λ , especially for excited neutrinos because the predominant $\nu_l^* \rightarrow l + W$ decays result in a higher acceptance for ≥ 3 charged lepton final states.

Both ATLAS and CMS Collaborations performed searches for singly produced excited leptons. The single excited leptons, both produced and decayed in contact interaction processes (Eq. (91.4)), were searched for in CMS using 77.4 fb^{-1} at 13 TeV [78] and in ATLAS using 20.3 fb^{-1} at 8 TeV [64] using the final states with two leptons and two jets ($q\bar{q} \rightarrow ll^* \rightarrow llq\bar{q}$). The CMS search [78] considered both excited electrons and excited muons, using the invariant mass of the combination of the two leptons and two jets as a discriminating variable to separate signal from background. The ATLAS search [64] considered only excited muons. The single excited electrons, produced in contact interactions and decayed either in contact interaction or charged-current processes, were considered in ATLAS using 36.1 fb^{-1} at 13 TeV [65] in the final states with two electrons and two jets ($q\bar{q} \rightarrow ee^* \rightarrow eeq\bar{q}$) or an electron, missing transverse momentum and a hadronically decaying W -boson candidate ($q\bar{q} \rightarrow ee^* \rightarrow e\nu W$). The excited electron (muon) mass was excluded up to 5.6 (5.7) TeV in CMS [78] at $\Lambda = m_{e^*}$ ($\Lambda = m_{\mu^*}$), which is the best limit to date on the excited electrons (muons).

The CMS Collaboration also performed an excited lepton search in the final states containing a Z boson [76], probing the excited leptons produced in contact interactions and decayed in neutral-current processes ($l^* \rightarrow l + Z$) with $f = f' = 1$ or $f = -f' = 1$. The leptonic and hadronic decays of Z bosons have been considered in the search, and the most stringent limits are obtained from the hadronic Z decay to be 2.08 (2.34) TeV and 2.11 (2.37) TeV for the e^* and μ^* , respectively, with $f = f' = 1$ ($f = -f' = 1$) at $\Lambda = m_{l^*}$.

Figure 91.4 summarizes the most stringent 95% C.L. lower mass limits for excited quarks and leptons obtained from the LHC experiments.

References

- [1] E. Eichten, K. D. Lane and M. E. Peskin, Phys. Rev. Lett. **50**, 811 (1983).
- [2] E. Eichten *et al.*, Rev. Mod. Phys. **56**, 579 (1984), [Addendum: Rev.Mod.Phys. 58, 1065–1073 (1986)].

- [3] J. Gao *et al.*, Phys. Rev. Lett. **106**, 142001 (2011), [arXiv:1101.4611].
- [4] G. Arnison *et al.* (UA1), Phys. Lett. B **177**, 244 (1986).
- [5] J. Appel *et al.* (UA2), Phys. Lett. B **160**, 349 (1985).
- [6] F. Abe *et al.* (CDF), Phys. Rev. Lett. **62**, 613 (1989); F. Abe *et al.* (CDF), Phys. Rev. Lett. **69**, 2896 (1992); F. Abe *et al.* (CDF), Phys. Rev. Lett. **77**, 5336 (1996), [Erratum: Phys.Rev.Lett. **78**, 4307 (1997)], [hep-ex/9609011].
- [7] B. Abbott *et al.* (D0), Phys. Rev. Lett. **80**, 666 (1998), [hep-ex/9707016]; B. Abbott *et al.* (D0), Phys. Rev. Lett. **82**, 2457 (1999), [hep-ex/9807014]; B. Abbott *et al.* (D0), Phys. Rev. D **62**, 031101 (2000), [hep-ex/9912023]; B. Abbott *et al.* (D0), Phys. Rev. D **64**, 032003 (2001), [hep-ex/0012046]; V. Abazov *et al.* (D0), Phys. Rev. Lett. **103**, 191803 (2009), [arXiv:0906.4819].
- [8] G. Aad *et al.* (ATLAS), Phys. Lett. B **694**, 327 (2011), [arXiv:1009.5069]; G. Aad *et al.* (ATLAS), New J. Phys. **13**, 053044 (2011), [arXiv:1103.3864]; G. Aad *et al.* (ATLAS), JHEP **01**, 029 (2013), [arXiv:1210.1718]; G. Aad *et al.* (ATLAS), Phys. Rev. Lett. **114**, 22, 221802 (2015), [arXiv:1504.00357]; G. Aad *et al.* (ATLAS), Phys. Lett. B **754**, 302 (2016), [arXiv:1512.01530].
- [9] M. Aaboud *et al.* (ATLAS), Phys. Rev. D **96**, 5, 052004 (2017), [arXiv:1703.09127].
- [10] V. Khachatryan *et al.* (CMS), Phys. Rev. Lett. **105**, 262001 (2010), [arXiv:1010.4439]; V. Khachatryan *et al.* (CMS), Phys. Rev. Lett. **106**, 201804 (2011), [arXiv:1102.2020]; S. Chatrchyan *et al.* (CMS), JHEP **05**, 055 (2012), [arXiv:1202.5535]; V. Khachatryan *et al.* (CMS), Phys. Lett. B **746**, 79 (2015), [arXiv:1411.2646]; A. M. Sirunyan *et al.* (CMS), JHEP **07**, 013 (2017), [arXiv:1703.09986].
- [11] S. Chatrchyan *et al.* (CMS), Phys. Rev. D **87**, 5, 052017 (2013), [arXiv:1301.5023].
- [12] A. M. Sirunyan *et al.* (CMS), Eur. Phys. J. C **78**, 9, 789 (2018), [arXiv:1803.08030].
- [13] T. Sjostrand, S. Mrenna and P. Z. Skands, Comput. Phys. Commun. **178**, 852 (2008), [arXiv:0710.3820].
- [14] S. Agostinelli *et al.* (GEANT4), Nucl. Instrum. Meth. A **506**, 250 (2003), :GEANT4: a simulation toolkit.
- [15] Z. Nagy, Phys. Rev. Lett. **88**, 122003 (2002), [hep-ph/0110315]; Z. Nagy, Phys. Rev. D **68**, 094002 (2003), [hep-ph/0307268].
- [16] S. Dittmaier, A. Huss and C. Speckner, JHEP **11**, 095 (2012), [arXiv:1210.0438].
- [17] S. Schael *et al.* (ALEPH), Eur. Phys. J. C **49**, 411 (2007), [hep-ex/0609051].
- [18] J. Abdallah *et al.* (DELPHI), Eur. Phys. J. C **45**, 589 (2006), [hep-ex/0512012].
- [19] M. Acciarri *et al.* (L3), Phys. Lett. B **489**, 81 (2000), [hep-ex/0005028].
- [20] K. Ackerstaff *et al.* (OPAL), Phys. Lett. B **391**, 221 (1997); G. Abbiendi *et al.* (OPAL), Eur. Phys. J. C **33**, 173 (2004), [hep-ex/0309053].
- [21] F. Aaron *et al.* (H1), Phys. Lett. B **705**, 52 (2011), [arXiv:1107.2478].
- [22] S. Chekanov *et al.* (ZEUS), Phys. Lett. B **591**, 23 (2004), [hep-ex/0401009].
- [23] F. Abe *et al.* (CDF), Phys. Rev. Lett. **68**, 1463 (1992); F. Abe *et al.* (CDF), Phys. Rev. Lett. **79**, 2198 (1997); T. Affolder *et al.* (CDF), Phys. Rev. Lett. **87**, 231803 (2001), [hep-ex/0107008]; A. Abulencia *et al.* (CDF), Phys. Rev. Lett. **96**, 211801 (2006), [hep-ex/0602045].
- [24] B. Abbott *et al.* (D0), Phys. Rev. Lett. **82**, 4769 (1999), [hep-ex/9812010].
- [25] G. Aad *et al.* (ATLAS), Phys. Rev. D **84**, 011101 (2011), [arXiv:1104.4398]; G. Aad *et al.* (ATLAS), Phys. Lett. B **712**, 40 (2012), [arXiv:1112.4462]; G. Aad *et al.* (ATLAS), Phys. Rev. D **87**, 1, 015010 (2013), [arXiv:1211.1150]; G. Aad *et al.* (ATLAS), Eur. Phys. J. C **74**, 12, 3134 (2014), [arXiv:1407.2410]; M. Aaboud *et al.* (ATLAS), Phys. Lett. B **761**, 372 (2016), [arXiv:1607.03669]; M. Aaboud *et al.* (ATLAS), JHEP **10**, 182 (2017), [arXiv:1707.02424].
- [26] G. Aad *et al.* (ATLAS), JHEP **11**, 005 (2020), [Erratum: JHEP **04**, 142 (2021)], [arXiv:2006.12946].
- [27] S. Chatrchyan *et al.* (CMS), Phys. Rev. D **87**, 3, 032001 (2013), [arXiv:1212.4563]; V. Khachatryan *et al.* (CMS), JHEP **04**, 025 (2015), [arXiv:1412.6302]; A. M. Sirunyan *et al.* (CMS), JHEP **04**, 114 (2019), [arXiv:1812.10443].
- [28] A. M. Sirunyan *et al.* (CMS), JHEP **07**, 208 (2021), [arXiv:2103.02708].
- [29] W. Buchmuller and D. Wyler, Nucl. Phys. B **268**, 621 (1986).
- [30] B. Grzadkowski *et al.*, JHEP **10**, 085 (2010), [arXiv:1008.4884].
- [31] E. E. Jenkins, A. V. Manohar and M. Trott, JHEP **10**, 087 (2013), [arXiv:1308.2627].
- [32] E. E. Jenkins, A. V. Manohar and M. Trott, JHEP **01**, 035 (2014), [arXiv:1310.4838].
- [33] R. Alonso *et al.*, JHEP **04**, 159 (2014), [arXiv:1312.2014].
- [34] I. Brivio and M. Trott, Phys. Rept. **793**, 1 (2019), [arXiv:1706.08945].
- [35] A. V. Manohar (2018), [arXiv:1804.05863].
- [36] D. Barducci *et al.* (2018), [arXiv:1802.07237].
- [37] S. Alte, M. König and W. Shepherd, JHEP **01**, 094 (2018), [arXiv:1711.07484].
- [38] S. Alte, M. König and W. Shepherd, JHEP **07**, 144 (2019), [arXiv:1812.07575].
- [39] F. Renard, Phys. Lett. B **116**, 264 (1982).
- [40] F. del Aguila, A. Mendez and R. Pascual, Phys. Lett. B **140**, 431 (1984).
- [41] M. Suzuki, Phys. Lett. B **143**, 237 (1984).
- [42] U. Baur, M. Spira and P. Zerwas, Phys. Rev. D **42**, 815 (1990).
- [43] K. Hagiwara, D. Zeppenfeld and S. Komamiya, Z. Phys. C **29**, 115 (1985).
- [44] N. Cabibbo, L. Maiani and Y. Srivastava, Phys. Lett. B **139**, 459 (1984).
- [45] D. Decamp *et al.* (ALEPH), Phys. Rept. **216**, 253 (1992); R. Barate *et al.* (ALEPH), Eur. Phys. J. C **4**, 571 (1998).
- [46] P. Abreu *et al.* (DELPHI), Nucl. Phys. B **367**, 511 (1991); J. Abdallah *et al.* (DELPHI), Eur. Phys. J. C **37**, 405 (2004), [hep-ex/0409058].
- [47] O. Adriani *et al.* (L3), Phys. Rept. **236**, 1 (1993); P. Achard *et al.* (L3), Phys. Lett. B **531**, 28 (2002), [hep-ex/0202025]; P. Achard *et al.* (L3), Phys. Lett. B **568**, 23 (2003), [hep-ex/0306016].
- [48] G. Abbiendi *et al.* (OPAL), Phys. Lett. B **544**, 57 (2002), [hep-ex/0206061]; G. Abbiendi *et al.* (OPAL), Phys. Lett. B **602**, 167 (2004), [hep-ex/0412011].
- [49] C. Adloff *et al.* (H1), Phys. Lett. B **525**, 9 (2002), [hep-ex/0110037]; F. Aaron *et al.* (H1), Phys. Lett. B **663**, 382 (2008), [arXiv:0802.1858]; F. Aaron *et al.* (H1), Phys. Lett. B **666**, 131 (2008), [arXiv:0805.4530].
- [50] S. Chekanov *et al.* (ZEUS), Phys. Lett. B **549**, 32 (2002), [hep-ex/0109018].
- [51] D. Acosta *et al.* (CDF), Phys. Rev. Lett. **94**, 101802 (2005), [hep-ex/0410013]; A. Abulencia *et al.* (CDF), Phys. Rev. Lett. **97**, 191802 (2006), [hep-ex/0606043]; T. Aaltonen *et al.* (CDF), Phys. Rev. D **79**, 112002 (2009), [arXiv:0812.4036].

- [52] V. Abazov *et al.* (D0), Phys. Rev. D **73**, 111102 (2006), [hep-ex/0604040]; V. Abazov *et al.* (D0), Phys. Rev. D **77**, 091102 (2008), [arXiv:0801.0877]; V. Abazov *et al.* (D0), Phys. Rev. Lett. **103**, 191803 (2009), [arXiv:0906.4819].
- [53] G. Aad *et al.* (ATLAS), Phys. Lett. B **708**, 37 (2012), [arXiv:1108.6311]; G. Aad *et al.* (ATLAS), JHEP **01**, 029 (2013), [arXiv:1210.1718]; G. Aad *et al.* (ATLAS), Phys. Rev. D **91**, 5, 052007 (2015), [arXiv:1407.1376]; G. Aad *et al.* (ATLAS), Phys. Lett. B **754**, 302 (2016), [arXiv:1512.01530]; M. Aaboud *et al.* (ATLAS), Phys. Rev. D **96**, 5, 052004 (2017), [arXiv:1703.09127].
- [54] G. Aad *et al.* (ATLAS), JHEP **03**, 145 (2020), [arXiv:1910.08447].
- [55] G. Aad *et al.* (ATLAS), Phys. Rev. Lett. **108**, 211802 (2012), [arXiv:1112.3580]; G. Aad *et al.* (ATLAS), Phys. Lett. B **728**, 562 (2014), [arXiv:1309.3230]; G. Aad *et al.* (ATLAS), JHEP **03**, 041 (2016), [arXiv:1512.05910].
- [56] M. Aaboud *et al.* (ATLAS), Eur. Phys. J. C **78**, 2, 102 (2018), [arXiv:1709.10440].
- [57] M. Aaboud *et al.* (ATLAS), Phys. Rev. D **98**, 032016 (2018), [arXiv:1805.09299].
- [58] M. Aaboud *et al.* (ATLAS), Phys. Lett. B **759**, 229 (2016), [arXiv:1603.08791].
- [59] G. Aad *et al.* (ATLAS), JHEP **02**, 110 (2016), [arXiv:1510.02664].
- [60] G. Aad *et al.* (ATLAS), Phys. Lett. B **721**, 171 (2013), [arXiv:1301.1583].
- [61] G. Aad *et al.* (ATLAS), Phys. Rev. D **85**, 072003 (2012), [arXiv:1201.3293].
- [62] G. Aad *et al.* (ATLAS), New J. Phys. **15**, 093011 (2013), [arXiv:1308.1364].
- [63] G. Aad *et al.* (ATLAS), JHEP **08**, 138 (2015), [arXiv:1411.2921].
- [64] G. Aad *et al.* (ATLAS), New J. Phys. **18**, 7, 073021 (2016), [Erratum: New J.Phys. **21**, 109501 (2019)], [arXiv:1601.05627].
- [65] M. Aaboud *et al.* (ATLAS), Eur. Phys. J. C **79**, 9, 803 (2019), [arXiv:1906.03204].
- [66] S. Chatrchyan *et al.* (CMS), Phys. Lett. B **704**, 123 (2011), [arXiv:1107.4771]; S. Chatrchyan *et al.* (CMS), JHEP **01**, 013 (2013), [arXiv:1210.2387]; S. Chatrchyan *et al.* (CMS), Phys. Rev. D **87**, 11, 114015 (2013), [arXiv:1302.4794].
- [67] V. Khachatryan *et al.* (CMS), Phys. Rev. D **91**, 5, 052009 (2015), [arXiv:1501.04198].
- [68] V. Khachatryan *et al.* (CMS), Phys. Rev. Lett. **116**, 7, 071801 (2016), [arXiv:1512.01224]; V. Khachatryan *et al.* (CMS), Phys. Rev. Lett. **117**, 3, 031802 (2016), [arXiv:1604.08907]; A. M. Sirunyan *et al.* (CMS), Phys. Lett. B **769**, 520 (2017), [Erratum: Phys.Lett.B **772**, 882–883 (2017)], [arXiv:1611.03568]; A. M. Sirunyan *et al.* (CMS), JHEP **08**, 130 (2018), [arXiv:1806.00843].
- [69] A. M. Sirunyan *et al.* (CMS), JHEP **05**, 033 (2020), [arXiv:1911.03947].
- [70] V. Khachatryan *et al.* (CMS), Phys. Lett. B **738**, 274 (2014), [arXiv:1406.5171].
- [71] A. M. Sirunyan *et al.* (CMS), Phys. Lett. B **781**, 390 (2018), [arXiv:1711.04652].
- [72] S. Chatrchyan *et al.* (CMS), Phys. Lett. B **722**, 28 (2013), [arXiv:1210.0867]; S. Chatrchyan *et al.* (CMS), Phys. Lett. B **723**, 280 (2013), [arXiv:1212.1910]; V. Khachatryan *et al.* (CMS), JHEP **08**, 173 (2014), [arXiv:1405.1994].
- [73] A. M. Sirunyan *et al.* (CMS), Phys. Rev. D **97**, 7, 072006 (2018), [arXiv:1708.05379].
- [74] V. Khachatryan *et al.* (CMS), JHEP **01**, 166 (2016), [arXiv:1509.08141].
- [75] S. Chatrchyan *et al.* (CMS), Phys. Lett. B **704**, 143 (2011), [arXiv:1107.1773]; S. Chatrchyan *et al.* (CMS), Phys. Lett. B **720**, 309 (2013), [arXiv:1210.2422].
- [76] V. Khachatryan *et al.* (CMS), JHEP **03**, 125 (2016), [arXiv:1511.01407].
- [77] A. M. Sirunyan *et al.* (CMS), JHEP **04**, 015 (2019), [arXiv:1811.03052].
- [78] A. M. Sirunyan *et al.* (CMS), JHEP **05**, 052 (2020), [arXiv:2001.04521].
- [79] M. Cacciari, G. P. Salam and G. Soyez, JHEP **04**, 063 (2008), [arXiv:0802.1189].
- [80] S. Chatrchyan *et al.* (CMS), JHEP **06**, 125 (2014), [arXiv:1311.5357].
- [81] A. M. Sirunyan *et al.* (CMS), Phys. Lett. B **778**, 349 (2018), [arXiv:1711.10949].

92. Dynamical Electroweak Symmetry Breaking: Implications of the H^0

Revised August 2021 by K.M. Black (Wisconsin U.), R. Sekhar Chivukula (UC San Diego) and M. Narain (Brown U.).

92.1 Introduction and Phenomenology

In theories of dynamical electroweak symmetry breaking, the electroweak interactions are broken to electromagnetism by the vacuum expectation value of a composite operator, typically a fermion bilinear. In these theories, the longitudinal components of the massive weak bosons are identified with composite Nambu-Goldstone bosons arising from dynamical symmetry breaking in a strongly-coupled extension of the standard model. Viable theories of dynamical electroweak symmetry breaking must also explain (or at least accommodate) the presence of an additional composite scalar state to be identified with the H^0 scalar boson [1,2] – a state unlike any other observed previously.

Theories of dynamical electroweak symmetry breaking can be classified by the nature of the composite singlet state to be associated with the H^0 and the corresponding dimensional scales f , the analog of the pion decay-constant in QCD, and Λ , the scale of the underlying strong dynamics.¹ Of particular importance is the ratio v/f , where $v^2 = 1/(\sqrt{2}G_F) \approx (246 \text{ GeV})^2$, since this ratio measures the expected size of the deviations of the couplings of a composite Higgs boson from those expected in the standard model. The basic possibilities, and the additional states that they predict, are described below.

92.1.1 Technicolor, $v/f \simeq 1$, $\Lambda \simeq 1 \text{ TeV}$

Technicolor models [7–9] provided the first examples of theories of dynamical electroweak symmetry breaking. These theories incorporate a new asymptotically free gauge theory (“technicolor”) and additional massless fermions (“technifermions” transforming under a vectorial representation of the gauge group). The global chiral symmetry of the fermions is spontaneously broken by the formation of a technifermion condensate, just as the approximate chiral symmetry in QCD is broken down to isospin by the formation of a quark condensate. The $SU(2)_W \times U(1)_Y$ interactions are embedded in the global technifermion chiral symmetries in such a way that the only unbroken gauge symmetry after chiral symmetry breaking is $U(1)_{em}$.² The theories naturally provide the Nambu-Goldstone bosons “eaten” by the W and Z boson. There would also typically be additional heavy states (e.g. vector mesons, analogous to the ρ and ω mesons in QCD) with TeV masses [13,14], and the WW and ZZ scattering amplitudes would be expected to be strong at energies of order 1 TeV.

There are various possibilities for the scalar H^0 in technicolor models. First, the H^0 could be identified as a singlet scalar resonance, analogous to the σ particle expected in pion-scattering in QCD [15,16]. Alternatively, the H^0 could be identified as a dilaton, a (pseudo-)Goldstone boson of scale invariance in theories of “walking technicolor” [17–21].³ Finally, the H^0 could be identified as an additional isosinglet state if the chiral symmetry breaking pattern of the technicolor theory provides for such a state.⁴ In all of these cases, however, one expects large deviations in the couplings of this particle from those of the standard model Higgs boson. Since the couplings observed for the H^0 approximate those of the Higgs boson to the 10% level, models of this kind are very highly constrained.

¹In a strongly interacting theory “Naive Dimensional Analysis” [3,4] implies that, in the absence of fine-tuning, $\Lambda \simeq g^* f$ where $g^* \simeq 4\pi$ is the typical size of a strong coupling in the low-energy theory [5,6]. This estimate is modified in the presence of multiple flavors or colors [7].

²For a review of technicolor models, see [10–12].

³If both the electroweak symmetry and the approximate scale symmetry are broken only by electroweak doublet condensate(s), then the decay-constants for scale and electroweak symmetry breaking may be approximately equal – differing only by terms formally proportional to the amount of explicit scale-symmetry breaking.

⁴In this case, however, the coupling strength of the singlet state to WW and ZZ pairs would be comparable to the couplings to gluon and photon pairs, and these would all arise from loop-level couplings in the underlying technicolor theory [22].

92.1.2 The Higgs doublet as a pseudo-Nambu-Goldstone Boson, $v/f < 1$, $\Lambda > 1 \text{ TeV}$

In technicolor models, the symmetry-breaking properties of the underlying strong dynamics necessarily breaks the electroweak gauge symmetries. An alternative possibility is that the underlying strong dynamics itself does not break the electroweak interactions, and that the entire quartet of bosons in the Higgs doublet (including the state associated with the H^0) are composite (pseudo-) Nambu-Goldstone particles [23–25]. In this case, the underlying dynamics can occur at energies exceeding 1 TeV and additional interactions with the top-quark mass generating sector (and possibly with additional weakly-coupled gauge bosons) cause the vacuum energy to be minimized when the composite Higgs doublet gains a vacuum expectation value [26,27]. In these theories, the couplings of the remaining singlet scalar state would naturally be equal to that of the standard model Higgs boson up to corrections of order $(v/f)^2$ and, therefore, constraints on the size of deviations of the H^0 couplings from that of the standard model Higgs [28] give rise to lower bounds on the scales f and Λ .⁵

The electroweak gauge interactions, as well as the interactions responsible for the top-quark mass, explicitly break the chiral symmetries of the composite Higgs model and lead generically to sizable corrections to the mass-squared of the Higgs-doublet – the so-called “Little Hierarchy Problem” [29]. “Little Higgs” theories [30–33] are examples of composite Higgs models in which the (collective) symmetry-breaking structure is selected so as to suppress these contributions to the Higgs mass-squared.

Composite Higgs models typically require a larger global symmetry of the underlying theory, and hence additional relatively light (compared to Λ) scalar particles, extra electroweak vector bosons (e.g. an additional $SU(2) \times U(1)$ gauge group), and vector-like partners of the top-quark of charge $+2/3$ and possibly also $+5/3$ [34]. In addition to these states, one would expect the underlying dynamics to yield additional scalar and vector resonances with masses of order Λ . If the theory respects a custodial symmetry [35], the couplings of these additional states to the electroweak and Higgs boson will be related – and, for example, one might expect a charged vector resonance to have similar branching ratios to WZ and WH . Different composite Higgs models utilize different mechanisms for arranging for the hierarchy of scales $v < f$ and arranging for a scalar Higgs self-coupling small enough to produce an H^0 of mass of order 125 GeV, for a review see [36]. If the additional states in these models carry color, they can provide additional contributions to Higgs production via gluon fusion [37]. The extent to which Higgs production at the LHC conforms with standard model predictions provides additional constraints (typically lower bounds on the masses of the additional colored states of order 0.7 TeV) on these models.

In addition, if the larger symmetry of the underlying composite Higgs theory does not commute with the standard model gauge group, then the additional states found in those models – especially those related to the top-quark, which tend to have the largest couplings to the electroweak sector – may be *colorless*. For example, in twin Higgs models [38], the top-partners carry no standard model charges. The phenomenology of the additional states in twin Higgs theories is rather different, since lacking color the production of these particles at the LHC will be suppressed – and, their decays may occur only via the electroweak symmetry breaking sector, leading to their being long-lived.

92.1.3 Top-Condensate, Top-Color, Top-Seesaw and related theories, $v/f < 1$, $\Lambda > 1 \text{ TeV}$

A final alternative is to consider a strongly interacting theory with a high (compared to a TeV) underlying dynamical scale that *would* naturally break the electroweak interactions, but whose

⁵In these models v/f is an adjustable parameter, and in the limit $v/f \rightarrow 1$ they reduce, essentially, to the technicolor models discussed in the previous subsection. Our discussion here is consistent with that given there, since we expect corrections to the SM Higgs couplings to be large for $v/f \simeq 1$. Current measurements constrain the couplings of the H^0 to equal those predicted for the Higgs in the standard model to about the 10% level [28], suggesting that f must have values of order a TeV or higher and, therefore, a dynamical scale Λ of at least several TeV.

strength is adjusted (“fine-tuned”) to produce electroweak symmetry breaking at 1 TeV. This alternative is possible if the electroweak (quantum) phase transition is continuous (second order) in the strength of the strong dynamics [39]. If the fine-tuning can be achieved, the underlying strong interactions will produce a light composite Higgs bound state with couplings equal to that of the standard model Higgs boson up to corrections of order $(1 \text{ TeV}/\Lambda)^2$. As in theories in which electroweak symmetry breaking occurs through vacuum alignment, therefore, constraints on the size of deviations of the H^0 couplings from that of the standard model Higgs give rise to lower bounds on the scale Λ . Formally, in the limit $\Lambda \rightarrow \infty$ (a limit which requires arbitrarily fine adjustment of the strength of the high-energy interactions), these theories are equivalent to a theory with a fundamental Higgs boson – and the fine adjustment of the coupling strength is a manifestation of the hierarchy problem of theories with a fundamental scalar particle.

In many of these theories the top-quark itself interacts strongly (at high energies), potentially through an extended color gauge sector [40, 40–44]. In these theories, top-quark condensation (or the condensation of an admixture of the top with additional vector-like quarks) is responsible for electroweak symmetry breaking, and the H^0 is identified with a bound state involving the third generation of quarks. These theories typically include an extra set of massive color-octet vector bosons (top-gluons), and an extra $U(1)$ interaction (giving rise to a top-color Z') which couple preferentially to the third generation and whose masses define the scale Λ of the underlying physics.

92.1.4 Flavor

In addition to the electroweak symmetry breaking dynamics described above, which gives rise to the masses of the W and Z particles, additional interactions must be introduced to produce the masses of the standard model fermions. Two general avenues have been suggested for these new interactions. In “extended technicolor” (ETC) theories [45, 46], the gauge interactions in the underlying strongly interacting theory are extended to incorporate flavor. This extended gauge symmetry is broken down (possibly sequentially, at several different mass scales) to the residual strong interaction responsible for electroweak symmetry breaking. The massive gauge-bosons corresponding to the broken symmetries then mediate interactions between mass operators for the quarks/leptons and the corresponding bilinears of the strongly-interacting fermions, giving rise to the masses of the ordinary fermions after electroweak symmetry breaking.

In the case of “partial compositeness” [47], the additional flavor-dependent interactions arise from mixing between the ordinary quarks and leptons and massive composite fermions in the strongly-interacting underlying theory. Theories incorporating partial compositeness include additional vector-like partners of the ordinary quarks and leptons, typically with masses of order a TeV or less.

In both cases, the effects of flavor interactions on the electroweak properties of the ordinary quarks and leptons are likely to be most pronounced in the third generation of fermions.⁶ The additional particles present in these theories, especially the additional scalars, often couple more strongly to heavier fermions.

Moreover, since the flavor interactions must give rise to quark mixing, we expect that a generic theory of this kind could give rise to large flavor-changing neutral-currents [46]. In ETC theories, these constraints are typically somewhat relaxed if the theory incorporates approximate generational flavor symmetries [48], the theory has a slowly running coupling constant or “walks” [17–21], or if $\Lambda > 1 \text{ TeV}$ [49]. In theories of partial compositeness, the masses of the ordinary fermions depend on the scaling-dimension of the operators corresponding to the composite fermions with which they mix. This leads to a new mechanism for generating the mass-hierarchy of the observed quarks and leptons that, potentially, ameliorates flavor-changing neutral current problems and can provide new contributions to the composite Higgs poten-

tial which allow for $v/f < 1$ [50–54].

Alternatively, one can assume that the underlying flavor dynamics respect flavor symmetries (“minimal” [55, 56] or “next-to-minimal” [57] flavor violation) that suppress flavor-changing neutral currents in the two light generations. Additional considerations apply when extending these arguments to potential explanation of neutrino masses (see, for example, [58, 59]).

92.1.5 Theoretical Considerations

Since the underlying high-energy dynamics in these theories are strongly coupled, there are no reliable calculation techniques that can be applied to analyze their properties. Instead, most phenomenological studies depend on the construction of a “low-energy” effective theory describing additional scalar, fermion, or vector boson degrees of freedom, which incorporates the relevant symmetries and, when available, dynamical principles. In some cases, motivated by the AdS/CFT correspondence [60], the strongly-interacting theories described above have been investigated by analyzing a dual compactified five-dimensional gauge theory. In these cases, the AdS/CFT “dictionary” is used to map the features of the underlying strongly coupled high-energy dynamics onto the low-energy weakly coupled dual theory [61].

More recently, progress has been made in investigating strongly-coupled models using lattice gauge theory [62–65]. These calculations offer the prospect of establishing which strongly coupled theories of electroweak symmetry breaking have a particle with properties consistent with those observed for the H^0 – and for establishing concrete predictions for these theories at the LHC [66].

92.1.6 Summary

The theoretical ideas and models reviewed here motivate searches for a wide variety of new states. Heavy vector bound states decaying to dibosons and additional scalar states appear naturally in both technicolor (92.1.1) and composite higgs models (92.1.2). Composite Higgs models based on collective symmetry breaking naturally include W' , Z' , and vector-like quark states (especially for the third-generation, and potentially including charge $+5/3$ custodial top-partner quarks). Vector-like states are also natural for any theory including partial compositeness in order to address the flavor problem (92.1.4). Top-condensate and related models (92.1.3) predict the existence of colorons which preferentially couple to third-generation quarks. Finally, the new states discussed here also occur in extra-dimensional models [61], which is understandable given that many strongly-coupled theories can be viewed as compactified five-dimensional gauge theories via duality (92.1.5). We turn now to a review the status of experimental searches related to dynamical electroweak symmetry breaking.

92.2 Experimental Searches

As discussed above, the extent to which the couplings of the H^0 conform to the expectations for a standard model Higgs boson constrains the viability of each of these models. Measurements of the H^0 couplings, and their interpretation in terms of effective field theory, are summarized in the H^0 review in this volume. In what follows, we will focus on searches for the additional particles that might be expected to accompany the singlet scalar: extra scalars, fermions, and vector bosons. In some cases, detailed model-specific searches have been made for the particles described above (though generally not yet taking account of the demonstrated existence of the H^0 boson).

In most cases, however, generic searches (e.g. for extra W' or Z' particles, extra scalars in the context of multi-Higgs models, or for fourth-generation quarks) are quoted that can be used – when appropriately translated – to derive bounds on a specific model of interest.

The mass scale of the new particles implied by the interpretations of the low mass of H^0 discussed above, and existing studies from the Tevatron and lower-energy colliders, suggests that only the Large Hadron Collider has any real sensitivity. A number of analyses already carried out by ATLAS and CMS use relevant final states and might have been expected to observe a deviation from standard model expectations – in no case so far has any such deviation been reported. The detailed implications of these

⁶Indeed, from this point of view, the vector-like partners of the top-quark in top-seesaw and little Higgs models can be viewed as incorporating partial compositeness to explain the origin of the top quark’s large mass.

searches in various model frameworks are described below.

Except where otherwise noted, all limits in this section are quoted at a confidence level of 95%. The searches at $\sqrt{s} = 8$ TeV (Run 1) are based on 20.3 fb^{-1} of data recorded by ATLAS, and an integrated luminosity of 19.7 fb^{-1} analyzed by CMS. The datasets collected at $\sqrt{s} = 13$ TeV during Run 2 of the LHC since 2015 are based on analyses with varied integrated luminosities ranging from ~ 2 - 140 fb^{-1} .

92.2.1 Searches for Z' or W' Bosons

Massive vector bosons or particles with similar decay channels would be expected to arise in Little Higgs theories, in theories of Technicolor, or models involving a dilaton, adjusted to produce a light Higgs boson, consistent with the observed H^0 . These particles would be expected to decay to pairs of vector bosons, or to third generation quarks, or to leptons. The generic searches for W' and Z' vector bosons listed below can, therefore, be used to constrain models incorporating a composite Higgs-like boson.

A general review of searches for Z' and W' bosons is also included in this volume [67,68]. In the context of the dynamical electroweak symmetry breaking models, we emphasize their decays to third generation fermions by including a detailed overview, while also briefly summarizing the other searches.

$Z' \rightarrow \ell\ell$:

ATLAS [69] and CMS [70] have both searched for Z' production with $Z' \rightarrow ee$ or $\mu\mu$. No deviation from the standard model prediction was seen in the dielectron and dimuon invariant mass spectra, by either the ATLAS or the CMS analysis, and lower limits on possible Z' boson masses were set. A Z'_{SSM} with couplings equal to the standard model Z' (a “sequential standard model” Z') and a mass below 5.1 TeV was excluded by ATLAS, while CMS set a lower mass limit of 5.15 TeV. The experiments also place limits on the parameters of extra dimension models and in the case of ATLAS on the parameters of a minimal walking technicolor model [17–21], consistent with a 125 GeV Higgs boson [71]. For a general review of searches in these channels see the PDG review of Z prime in this volume [67].

In addition, both experiments have also searched for Z' decaying to a ditau final state [72,73]. An excess in $\tau^+\tau^-$ could have interesting implications for models in which lepton universality is not a requirement and enhanced couplings to the third generation are allowed. This analysis led to lower limits on the mass of a Z'_{SSM} of 2.4 and 2.1 TeV from ATLAS and CMS respectively.

$Z' \rightarrow q\bar{q}$:

The ability to relatively cleanly select $t\bar{t}$ pairs at the LHC together with the existence of enhanced couplings to the third generation in many models makes it worthwhile to search for new particles decaying in this channel. Both ATLAS [74] and CMS [75] have carried out searches for new particles decaying into $t\bar{t}$.

Both the ATLAS and CMS collaborations searched for $t\bar{t}$ in the all hadronic mode [76] [77] in both the resolved and boosted regions. No evidence of resonance production were seen and limits were produced for various models including the Z' boson in topcolor-assisted technicolor which excludes masses less than 3.1 to 3.6 TeV (ATLAS) depending on the details of the model and 3.3, 5.25, and 6.65 TeV for widths of 1, 10 and 30 percent relative to the mass of the resonance.

ATLAS also presented results on the lepton plus jets final state, where the top quark pair decays as $t\bar{t} \rightarrow WbWb$ with one W boson decaying leptonically and the other hadronically; CMS used final states where both, one or neither W decays leptonically and then combined the results. The $t\bar{t}$ invariant mass spectrum was analyzed for any excess, and no evidence for any resonance was seen. ATLAS excluded a narrow ($\Gamma/m = 1.2\%$) leptophobic topcolor Z' boson with masses between 0.7 and 2.1 TeV and with $\Gamma/m = 3\%$ between 0.7 and 3.2 TeV. CMS set limits on leptophobic Z' bosons for three different assumed widths $\Gamma/m = 1.0\%$, $\Gamma/m = 10.0\%$, and $\Gamma/m = 30.0\%$ of 3.9 TeV to 4.0 TeV and exclude RS KK gluons up to 3.3 TeV.

Both ATLAS [78] and CMS [79] have also searched for resonances decaying into $q\bar{q}$, qg or gg using the dijet invariant mass spectrum. Excited quarks are excluded up to masses of 6.7 TeV and model-independent upper limits on cross sections with a

Gaussian signal shape were set. CMS excluded string resonances with masses below 7.9 TeV, scalar diquarks below 7.5 TeV, axigluons and colorons below 6.6 TeV, excited quarks below 6.3 TeV, color-octet scalars below 3.7 TeV, W' bosons below 3.6 TeV, Z' bosons with SM-like couplings below 2.9 TeV and between 3.1 TeV and 3.3 TeV, Randall–Sundrum Gravitons below 2.6 TeV. $W' \rightarrow \ell\nu$:

Both LHC experiments have also searched for massive charged vector bosons. In this section we include a summary of the results, with emphasis on final states with third generation fermions, while the details on other decays are discussed in the mini-review of W' [68]. ATLAS searched for a heavy W' decaying to $e\nu$ or $\mu\nu$ and found no excess over the standard model expectation. A sequential standard model (SSM) W' boson (assuming zero branching ratio to WZ) with mass less than 7 TeV was excluded [80] using the 139 fb^{-1} dataset at $\sqrt{s} = 13$ TeV. Model independent cross-section limits as a function of mass were also set. Based on a smaller dataset, the CMS experiment excluded a SSM W' boson with mass up to 4.1 TeV [81] and presented upper limits on the production of generic W' bosons decaying into this final state using a model-independent approach.

CMS [82] has carried out a complementary search in the $\tau\nu$ final state. As noted above, such searches place limits on models with enhanced couplings to the third generation. No excess was observed and limits between 2.0 and 2.7 TeV were set on the mass of a W' decaying preferentially to the third generation; a W' with universal fermion couplings was also excluded for masses less than 2.7 TeV.

$W' \rightarrow t\bar{b}$:

Heavy new gauge bosons can couple to left-handed fermions like the SM W boson or to right-handed fermions. W' bosons that couple only to right-handed fermions (W'_R) may not have leptonic decay modes, depending on the mass of the right-handed neutrino. For these W' bosons, the $t\bar{b}$ ($t\bar{b} + \bar{t}b$) decay mode is especially important because in many models the W' boson is expected to have enhanced couplings to the third generation of quarks relative to those in the first and second generations. It is also the hadronic decay mode with the best signal-to-background. ATLAS and CMS have performed searches for W' bosons via the $W' \rightarrow t\bar{b}$ decay channel in the lepton+jets and all-hadronic final state.

The CMS lepton+jets search [83–86], $W' \rightarrow t\bar{b} \rightarrow Wbb \rightarrow \ell\nu bb$, proceeded via selecting events with an isolated lepton (electron or muon), and at least two jets, one of which is identified to originate from a b -quark. The mass of the W' boson ($M_{t\bar{b}}$) was reconstructed using the four-momentum vectors of the final state objects ($b\bar{b}\ell\nu$). The distribution of $M_{t\bar{b}}$ is used as the search discriminant. A search [86] using 35.9 fb^{-1} of data, collected at $\sqrt{s} = 13$ TeV, led to an exclusion of W'_R bosons with masses below 3.4 TeV (3.6 TeV) if $M_{W'_R} \gg M_{\nu_R}$ ($M_{W'_R} < M_{\nu_R}$), where M_{ν_R} is the mass of the right-handed neutrino.

The CMS search for $W' \rightarrow t\bar{b}$ decays using the all-hadronic final state focused on W' masses above 1 TeV [85,87]. In this region, the top quark gets a large Lorentz boost and hence the three hadronic products from its decay merge into a single large-radius jet. Deep neural network(DNN) algorithms are used to identify the jet initiated by the bottom quark. Techniques including DNN, which rely on substructure information of the jets [88] are employed to identify boosted all hadronic W boson and top quark [87] decays. The W' candidate mass was computed from back-to-back boosted top-tagged jet and a low mass b -tagged jet. From this all-hadronic search, W' bosons were excluded for masses up to 3.4 TeV [87].

ATLAS has searched for W'_R bosons in the $t\bar{b}$ final state both for lepton+jets [89] and all-hadronic [90] decays of the top. No significant deviations from the standard model were seen in either analysis and limits were set on the $W' \rightarrow t\bar{b}$ cross section times branching ratio and W' bosons with purely right-handed couplings to fermions were excluded for masses below 3.15 TeV when the two channels are combined.

In addition, the above studies also provided upper limits on the W' effective couplings to right- and left-handed fermions.

In Fig. 92.1 (bottom) the upper limits on W' couplings normalized to the SM W boson couplings derived by ATLAS [91] are shown. The top panel of Fig. 92.1 shows the upper limits for arbitrary combinations of left- and right-handed couplings of the W' boson to fermions set using a model independent approach by CMS [86].

92.2.2 Searches for Resonances decaying to Vector Bosons and/or Higgs Bosons

Both the ATLAS and CMS experiments have used the data collected at $\sqrt{s} = 13$ TeV to search for resonances decaying to pairs of bosons. Overall no significant excesses were seen in the full datasets that were analyzed and the results are interpreted in models with heavy vector triplets (HVT) [92], models with strong gravity and extra spatial dimensions, and model independent limits as a function of mass are set. For a full review of models including extra spatial dimensions and the interpretation of many of these results in that context please see the review of extra dimensions in this volume [61].

Utilizing data collected at $\sqrt{s} = 13$ TeV, ATLAS [93] and CMS [94], have both looked for a resonant state decaying into VV (with $V = W$ or Z), VH (with H representing the SM Higgs boson), and HH . ATLAS searches in the $qqqq$, $\nu\nu qq$, $lvqq$, $llqq$, $l\nu l\nu$, $ll\nu\nu$, $lvll$, $llll$, $qqbb$, $\nu\nu bb$, $lvbb$, and $llbb$ final states and combined the results [94]. While CMS analyzed the $qqqq$, $\nu\nu qq$, $lvqq$, $llqq$, $ll\nu\nu$, $\nu\nu bb$, $lvbb$, $llbb$, $bbbb$, $\tau\tau bb$, and $q\tau\tau$ final states.

The combined limits are expressed both as limits on the cross-section as a function resonance mass as well as constraints on the coupling of the heavy boson triplet to quarks, leptons, and the Higgs boson.

$X \rightarrow WZ$:

ATLAS searches for new heavy resonances decaying into WZ in the channels $WZ \rightarrow qqqq$ [95], $lvqq$ [96], and $lvll$ [97]. In the fully leptonic channel, the invariant mass of the WZ pair is obtained by considering all possible four lepton permutations in each event. The dominant background is Standard Model continuum WZ production, ZZ production where one lepton is not identified or falls outside the detector acceptance, and top quark plus vector boson production. No resonant production is seen in data and lower limits on the mass of a HVT decaying into WZ are set at 2260 (2460) GeV assuming a coupling constant of $g_V = 1$ ($g_V = 3$). In the $WZ \rightarrow lvqq$ mode, ATLAS searches in both the cases that the quarks are observed as individual jets (resolved) and where they merge into one jet in the detector (boosted) which probe the low and high p_T regime of the Z boson. No significant excess is seen in either channel and combined lower mass limits are placed at 2900 (3000) GeV for $g_V = 1$ ($g_V = 3$) in the HVT model. In the all hadronic decay mode, ATLAS searches for two high p_T hadronically decaying vector bosons looking for a resonant structure. No excess is seen and limits are placed exclude 1200-3000 (1200-3300) GeV for $g_V = 1$ ($g_V = 3$) in the HVT model.

CMS searches for new heavy resonances in the ZV final state using the semi-leptonic decay channels excluding W' masses up to 1800 GeV in HVT two models with $g_V = 1$ and 3 and in the ZZ channel excludes gravitons up to 1200 GeV. The CMS collaboration searches for $VV \rightarrow qqqq$ [98] in the large R dijet search. The W and Z boson are identified through the mass of the large R jet and substructure variables. No excess is seen and limits are set for charged HVT bosons with masses lower than 3200 (3800) GeV for $g_V = 1$ ($g_V = 3$). Cross-section limits as function of mass are reported for the charged spin-1 resonance interpretation and are placed at 44.4 fb at 1.4 TeV to 0.7 pb at 4 TeV. In the $\nu\nu qq$ final state [99], the CMS collaboration searches for a charged spin 1 resonance decaying into a VZ final state with a Z boson decaying into a pair of neutrinos and the other boson decaying into two collimated quarks reconstructed as a large R -jet. The transverse mass of the VZ candidate is reconstructed and utilized to search for evidence of resonant VZ production. No excess is seen and lower mass limits are placed on the charged resonance at 3100 (3400) GeV for $g_V = 1$ ($g_V = 3$). In the $2l2q$ final state, the CMS collaboration searches for a heavy resonance decaying into ZV [100] looking for events with one large R -jet consistent with the hadronic decay of a vector boson and a Z boson reconstructed in the charged lepton decay channel (e or μ).

Limits are set for a HVT W' with a lower mass of 2270 (2330) for $g_V = 1$ ($g_V = 3$).

$X \rightarrow WW$:

The ATLAS collaboration searches for a new heavy resonance decaying into WW in the channels $WW \rightarrow qqqq$ [95], $lvqq$ [96], and $l\nu\nu$ [101]. In the case where both W 's decay leptonically, ATLAS utilizes the transverse mass of the two lepton and two neutrino final state and searches for an excess in this distribution between 200 GeV and 5 TeV. No excess is seen and a HVT is excluded for masses below 1300 GeV. Vector boson fusion is also considered and cross-section limits as a function of mass are placed ranging from 1.3 pb to 0.006 pb at 200 GeV to 3 TeV, respectively. In the $lvqq$ mode, ATLAS completed a companion analysis to the $WZ \rightarrow$ analysis discussed above and places lower mass limits of 2850 (3150) GeV for $g_V = 1$ ($g_V = 3$) in the HVT model. ATLAS also interprets the all hadronic mode analysis in the hypothesis that $WW \rightarrow qqqq$ and places limits on a HVT boson decaying into WW in the all hadronic mode between 1200 and 2200 (1200 and 2800) GeV for $g_V = 1$ ($g_V = 3$).

The CMS collaboration searches for $VV \rightarrow qqqq$ [98] in the large R dijet search. The W and Z boson are identified through the mass of the large R jet and substructure variables. No excess is seen and limits are set for charged HVT bosons with masses lower than 2700 (2800) GeV for $g_V = 1$ ($g_V = 3$). Cross-section limits as function of mass are reported for the uncharged spin-1 resonance interpretation and are placed at 41.6 fb at 1.4 TeV to 0.6 pb at 4 TeV.

$X \rightarrow VH$:

The ATLAS Collaboration searches for a new heavy resonance decaying into WH and ZH in the $qqbb$ (WH and ZH) [102], $lvbb$ (WH), $\nu\nu bb$ (ZH), $llbb$ (ZH) [103] modes. In the all hadronic mode, ATLAS searches for boosted VH production looking for two large R jets where the larger invariant mass large R jet is interpreted as the Higgs boson decay products while the lesser invariant mass jet is taken to be the hadronically decaying vector boson requiring b -tagging on the Higgs boson subjects. The invariant mass is reconstructed and a search is done for resonant production of ZH . None is found and limits from 1100 to 2500 (1300 to 3800 GeV) are placed for $g_V = 1$ ($g_V = 3$). ATLAS also searches for XH where the W or Z boson decays into $\nu\nu$, lv , and ll . The analysis searches for both resolved and merged (boosted) b -jets from the decay of the Higgs boson and defines the signal regions based on the number of reconstructed charged leptons (0,1,or 2). In the dilepton channel the invariant mass is explicitly reconstructed of the entire diboson system, the single lepton channel reconstructs the diboson final state constraining the lepton and missing transverse momentum utilizing the known W boson mass, while the 0 charged lepton channel reconstructs the transverse mass of the diboson system. No excess is seen in any channel and limits on the production of a HVT are placed at 2800 GeV (2930) GeV for $g_V = 1$ ($g_V = 3$).

The CMS Collaboration searches for a heavy resonance decaying into VH [104] searching for a resonances decaying into a Higgs boson and a hadronically decaying W or Z boson. The search identifies events with two large- R jets using substructure variables and requires one large- R jets is tagged with a pair of b -hadrons clustered in a single jet. The invariant mass of the VH bosons is reconstructed and evidence for resonance production is sought. No excess is seen and limits are placed. With $g_V = 1$ (3) a narrow W' resonance with $m_{W'} < 2470(3150)$ GeV and $m_{Z'} < 1150(1190)$.

The CMS collaboration searches for a heavy resonance decaying into a pair of boosted Higgs boson with $HH \rightarrow b\bar{b}WW^*$ in the single and dilepton channel [105]. Events are categorized according to lepton flavor and multiplicity, along with discriminators that characterize the compatibility with having jets arising from the decay of boosted Higgs and W bosons. The reconstructed Higgs and diHiggs mass distributions are fit and used as the final discriminators. No significant deviations in the 12 sub-categories are seen and 95% confidence limits on spin-0 bosons are set from 24.5 fb at 0.8 TeV to 0.78 fb at 4.5 TeV and spin-2 bosons from

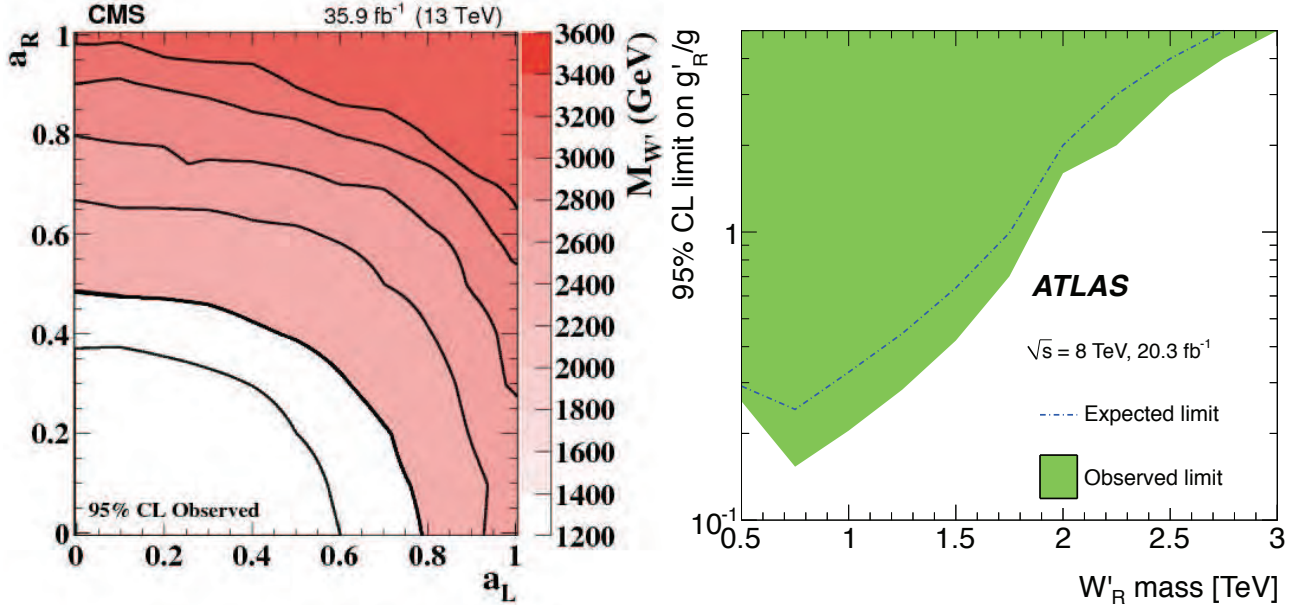


Figure 92.1: Left panel: Observed limits on the W' boson mass as function of the left-handed (a_L) and right-handed (a_R) couplings. Black lines represent contours of equal W' boson mass [86]. Right panel: Observed and expected regions, on the g'/g vs mass of the W' boson plane, that are excluded at 95% CL, for right-handed W' bosons [91] showing the exclusion of the values of a hypothetical right-handed coupling of a heavy W particle.

16.7 fb at 0.8 TeV to 0.67 fb at 4.5 TeV. A similar search in the four b -quark final state is used to set limits range 9.74 to 0.29 fb and 4.94 to 0.19 fb in the spin-0 bosons and spin-2 gravitons (respectively) interpretation with masses of 1-3 TeV [106].

$X \rightarrow H\gamma$ or $V\gamma$:

Both the CMS and ATLAS collaboration search for heavy resonances decaying into either a vector boson and a photon or a Higgs boson or a photon. These searches are motivated generically by the fact that new heavy gauge bosons are generically predicted to decay to either a Higgs boson or a vector boson and a photon by one loop decays [107]. ATLAS searches for a heavy resonances decaying into a Higgs boson and a photon and sets limits from 0.7 to 4 TeV from 11.6 fb to 0.11 fb [108]. ATLAS searches for a heavy resonance decaying into XH where $XH \rightarrow qqbb$ [109] and sets limits from 1 to 4 TeV. CMS searches for a heavy resonance decaying into a W boson and a photon [110] setting limits for narrow resonances range between 0.17 fb at 6.0 TeV and 55 fb at 0.7 TeV.

Summary of Searches with Diboson Final States:

Both ATLAS [93] and CMS [94] provide plots summarizing the various searches results and limits combining. The results are shown in the context of HVT models and models of strong gravity with extra spatial dimensions. No excess is seen in any search and limits on the 4.3 (4.5) TeV (ATLAS) and (CMS). Inclusion of decays directly to fermions increase these limits to 5.3 (5.5) TeV and 5.0 (5.2) TeV from the ATLAS and CMS combinations, respectively. Both collaborations also place varying limits on the coupling strength as a function of HVT boson mass as well.

Searches for Triboson Resonances:

The CMS collaboration presents the first search for massive triboson resonances in both the semi-leptonic [111] and fully hadronic final state [112]. Three boson final states can be produced via the decay of Kaluza-Klein(KK) states decaying via $W_{KK} \rightarrow WR$ with $R \rightarrow WW$ where R is a scalar radion. The search utilizes novel deep neural networks to perform optimal separation between signal and background and searches for evidence of resonance structure in the triboson invariant mass-spectrum. No excesses above SM backgrounds are seen and W_{KK} and radion masses are excluded up to $M_{W_{KK}} = 3.4$ TeV and $M_R = 1$ TeV and up to $M_{W_{KK}} = 3.6$ TeV and $M_R = 0.35$ TeV. $M_{W_{KK}}$ below 3 TeV are excluded for $0.6 < \frac{M_R}{M_{W_{KK}}} < 0.7$ in the semi-

leptonic final state and up to $M_{W_{KK}} = 3.0$ TeV and $M_R = 200$ GeV and up to $M_{W_{KK}} = 1.5$ TeV and $M_R = 1.5$ TeV in the fully hadronic final state.

92.2.3 Vector-like third generation quarks

Vector-like quarks (VLQ) have non-chiral couplings to W bosons, i.e. their left- and right-handed components couple in the same way. They therefore have vectorial couplings to W bosons. Vector-like quarks arise in Little Higgs theories, top-coloron-models, and theories of a composite Higgs boson with partial compositeness. In the following, the notation T quark refers to a vector-like quark with charge $2/3$ and the notation B quark refers to a vector-like quark with charge $-1/3$, the same charges as the SM top and b quarks respectively. The exotic vector-like quarks $X_{5/3}$ and $Y_{-4/3}$ have charges $5/3$, and $-4/3$ respectively. Vector-like quarks couple with SM quarks with Yukawa interactions and may exist as $SU(2)$ singlets (T , and B), doublets $[(X_{5/3}, T), (T, B), (B, Y_{-4/3})]$, or triplets $[(X_{5/3}, T, B), (T, B, Y_{-4/3})]$. At the LHC, VLQs can be pair produced via the dominant gluon-gluon fusion process. VLQs can also be produced singly by their electroweak effective couplings to a weak boson and a standard model quark. The single production rate is expected to dominate over the rate of pair production at large VLQ masses. T quarks can decay to bW , tZ , or tH^0 . Weak isospin singlets are expected to decay to all three final states with (asymptotic) branching fractions of 50%, 25%, 25%, respectively. Weak isospin doublets are expected to decay exclusively to tZ and to tH^0 [113] with equal branching ratios. Analogously, B quarks can decay to tW , bZ , or bH^0 . The $Y_{-4/3}$ and $X_{5/3}$ quarks decay exclusively to bW and to tW . While these are taken as the benchmark scenarios, other representations and decays to exotic new particles are possible [114–116], and hence the final results are interpreted for many allowed branching fraction combinations.

Given the multiple decay modes of the VLQs, the final state signatures of both pair produced and the singly produced VLQs are fairly rich with leptons, jets, b -jets, and missing energy. Depending on the mass of the VLQ, the top quarks and $W/Z/H^0$ bosons may be Lorentz boosted and identified using jet substructure techniques. Thus the searches are performed using lepton+jets signatures, multi-lepton and all-hadronic decays. In addition, T or B quarks with their antiparticles can result in events with same-sign leptons, for example if the decay $T \rightarrow tH \rightarrow bW^+W^-$ is present, followed by leptonic decays of two same-sign W bosons.

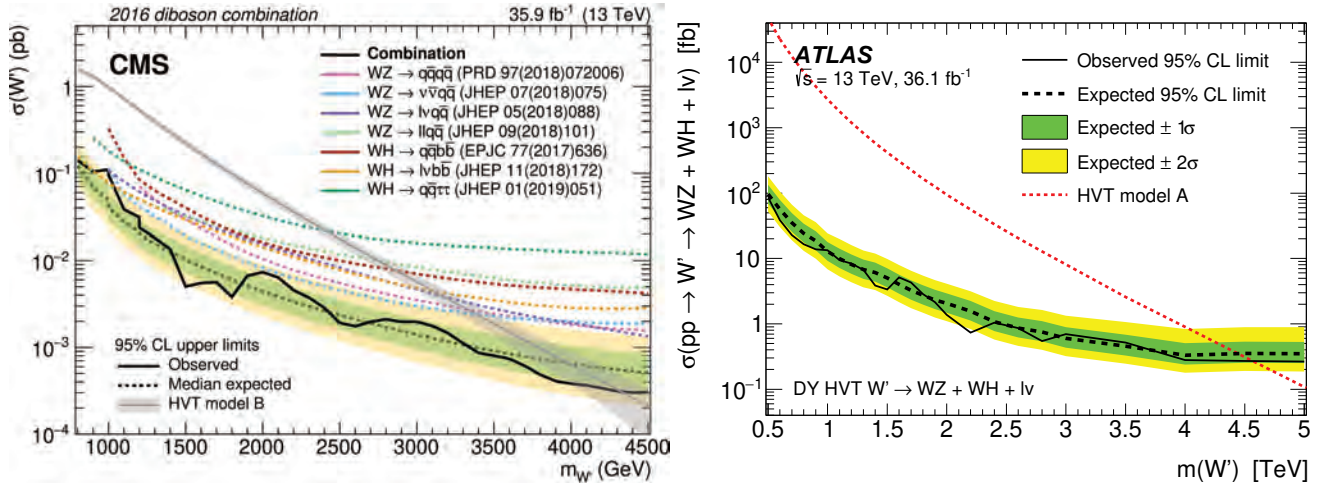


Figure 92.2: Left panel: Observed limits from W' to diboson from CMS [94]. Right panel: Observed limits from W' to diboson decays from ATLAS [93].

In the following subsections, while we describe the searches for each of the decay modes of the VLQs, the same analysis can be re-interpreted to obtain the sensitivity to a combination with varied branching fractions to the different decay modes.

In the following sections, the results obtained for T (B) quarks assuming 100% branching ratio to Wb (Wt) are also applicable to heavy vector-like $Y_{-4/3}$ ($X_{5/3}$) with charge $4/3$ ($5/3$).

92.2.3.1 Searches for T quarks that decay to W , Z and H^0 bosons

$T/Y \rightarrow bW$:

CMS has searched for pair production of heavy T quarks that decay exclusively to bW [117–119]. The analysis selected events with exactly one charged lepton, assuming that the W boson from the second T quark decays hadronically. Under this hypothesis, a 2-constraint kinematic fit can be performed to reconstruct the mass of the T quark as a narrow mass peak with a mass resolution of around 7%. In Refs. [118] and [119], the two-dimensional distribution of reconstructed mass vs S_T was used to test for the signal, where S_T is the scalar sum of the missing p_T and the transverse momenta of the lepton and the leading four jets. This analysis, when combined with the search in the fully hadronic final state [120] excluded new quarks that decay 100% to bW for masses below 0.89 TeV [119]. At times the hadronically-decaying W boson is produced with a large Lorentz boost, leading to the W decay products merged into a large-radius jet. Algorithms such as jet pruning [121] were used to remove contributions from soft, wide angle radiation, from large-radius jets, leading to better discrimination between QCD jets and those arising from decays of the heavy particles. If the mass of the boosted jet was compatible with the W boson mass, then the W boson candidate jet and its subjets were used in the kinematic reconstruction of the T quark. No excess over standard model backgrounds was observed. Upper limits on the production cross section as a function of the mass of T quarks were measured. By comparing them with the predicted cross section for vector like quark pair production, the strong pair production of T quarks was excluded for masses below 1.30 TeV (1.28 TeV expected) [117].

Another “cut-based” search for pair produced T quarks in the all-hadronic final state targeting the Wb decay mode [122], relies on mass reconstruction of two highest p_T Wb combinations using boosted W boson candidates with $p_T > 200$ GeV and b -tagged jets. H_T is used as the signal discriminator, with selected events divided into nine categories based on the multiplicity of W and b -jets in the event. From this search T quarks with pure Wb decays are excluded for masses below 1.04 TeV (1.07 TeV expected).

An analogous search has been carried out by ATLAS [123,124] for the pair production of heavy T quarks. It used the lepton+jets final state with an isolated electron or muon and at least four jets, including a b -jet, and required reconstruction of the T quark

mass. Given that the mass range for the T quark being explored was from a 0.4 TeV to a couple of TeV, the W boson from the T quark may fall in two categories: those with a high boost leading to merged decay products, and others where the two jets from the W boson were resolved. In addition, the selection was optimized to require large angular separation between the high p_T W bosons and the b -jets.

The $T \rightarrow Wb$ candidates were constructed from both the leptonically and hadronically decaying W bosons by pairing them with the two highest p_T b -tagged jets in the event. The pairing of b -jets with W bosons which minimizes the difference between the masses of leptonically decaying T ($m_{lep}(T)$) and the hadronic T ($m_{had}(T)$) was chosen. Finally, $m_{lep}(T)$ was used as the discriminating variable in a signal region defined by high S'_T (here S'_T is defined as the scalar sum of the missing p_T , the p_T of the lepton and jets), and the opening angle between the lepton and the neutrino ($\Delta R(e, \nu)$). With the 36.1 fb^{-1} data collected during Run 2 at $\sqrt{s} = 13$ TeV, assuming 100% branching ratio to the Wb decay, the observed lower limit on the T mass was 1.35 TeV, and in the SU(2) singlet scenario, the lower mass limit was obtained to be 1.17 TeV [123].

A targeted search for a T quark, produced singly in association with a light flavor quark and a b quark and decaying into bW , was carried out by CMS at $\sqrt{s}=13$ TeV and a dataset corresponding to 2.3 fb^{-1} [125]. The analysis used lepton+jets events, with at least one b -tagged jet with large transverse momentum, and a jet in the forward η region. Selected events were required to have $S'_T > 500$ GeV, where S'_T is defined as the scalar sum of the transverse momenta of the lepton, the leading central jet, and the missing transverse momentum. The invariant mass of the T candidate was used as the discriminating variable and was reconstructed using the four-vectors of the leptonically decaying W boson and the leading central jet. No excess over the standard model prediction was observed. As the VLQ width is proportional to the square of the coupling, upper limits were set on the production cross section assuming a narrow width VLQ with coupling greater than 0.5. For Y/T quarks with a coupling of 0.5 and a 100% branching fraction for the decay to bW the excluded masses were in the range from 0.85 to 1.40 TeV [125]. A similar search [126,127] was performed by ATLAS for a singly produced T or $Y_{-4/3}$ quark decaying to Wb using a dataset corresponding to 36.1 fb^{-1} . The search was performed using lepton+jets events with a high p_T b -tagged jet, and at least one forward jet. The reconstructed mass of the $T/Y_{-4/3}$ quark, was used as the discriminating variable and showed no excess above the expectation from SM. Interference effects with the SM background are included in the study. This search led to 95% CL upper limits on the mixing angle $|\sin(\theta_L)|$ (C_L^{Wb}) in the range of 0.18–0.35 (0.25–0.49) for singlet T quark mass between 0.8–1.2 TeV. This search

also provided limits as a function of the $Y_{-4/3}$ quark mass, on the coupling of the $Y_{-4/3}$ quark to bW , and the mixing parameter $|\sin\theta_R|$ (C_R^{Wb}) for a $(B, Y_{-4/3})$ doublet model [126]. For VLQ masses between 0.08–1.8 TeV, the limits on $|\sin(\theta_R)|$ (C_R^{Wb}) are in the range 0.17–0.55 (0.24–0.77), and for $Y_{-4/3}$ quark mass between 0.9–1.25 TeV, the limits on $|\sin\theta_R|$ are around 0.18–0.19 and below the constraints from electroweak precision observables. For $Y_{-4/3}$ quark in the triplets $(T, B, Y_{-4/3})$, limits on $|\sin(\theta_L)|$ (C_L^{Wb}) are between 0.16–0.39 (0.31–0.78) for masses between 0.8 GeV–1.6 TeV [126].

$T \rightarrow tH^0$:

ATLAS has performed a search for $T\bar{T}$ production with $T \rightarrow tH^0$ [124, 128]. Given the dominant decay mode $H^0 \rightarrow b\bar{b}$, these events are characterized by a large number of jets, many of which are b -jets. Thus the event selection required one isolated electron or muon and high jet multiplicity (including b -tagged jets). The sample is categorized by the jet multiplicity (5 and ≥ 6 jets in the 1-lepton channel; 6 and ≥ 7 jets in the 0-lepton channel), b tag multiplicity (2, 3 and ≥ 4) and mass-tagged jet multiplicity (0, 1 and ≥ 2). The distributions of m_{eff} , defined as the scalar sum of the lepton and jet p_T and the missing p_T , for each category were used as the discriminant for the final signal and background separation. No excess of events was found. Weak isospin doublet T quarks were excluded below 1.16 TeV.

A search by ATLAS for pair produced VLQs with an all-hadronic final state signature yields an exclusion of pure decays $T \rightarrow tH^0$ upto a T quark mass of 1.01 TeV [129]. This analysis used a deep neural network technique to identify jets originating from boosted bosons and top-quarks and is described further in subsection 92.2.3.2.

The CMS search for $T\bar{T}$ production, with $T \rightarrow tH^0$ decays has been performed in lepton+jets, multilepton and all-hadronic final states. The lepton+jets analysis [130] emphasizes the presence of a large number of b -tagged jets, and combines it with other kinematic variables in a Boosted Decision Tree (BDT) to enhance signal to background discrimination. The multilepton analysis [130] was optimized for the presence of b -jets and the large hadronic activity. For $\mathcal{B}(T \rightarrow tH^0) = 1$, the combined lepton+jets and multilepton analyses led to a lower limit on T quark masses of 0.71 TeV. A search for $T \rightarrow tH^0$ in all-hadronic decays [131], optimized for a high mass T quark, and based on identifying boosted top quark jets has been carried out by CMS. This search aimed to resolve subjets within the jets arising from boosted top quark decays, including b tagging of the subjets. A likelihood discriminator was defined based on the distributions of H_T and the invariant mass of the two b -jets in the events for signal and background. No excess above background expectations was observed. Assuming 100% branching ratio for $T \rightarrow tH^0$, this analysis led to a lower limit of 0.75 TeV on the mass of the T quark.

Searches for T quarks at $\sqrt{s}=13$ TeV, based on a 2.6 fb $^{-1}$ dataset [132] have been performed by CMS using the lepton+jets final state. This search has been optimized for high mass T quarks by exploiting techniques to identify W or Higgs bosons decaying hadronically with large transverse momenta. The boosted W channel excluded T quarks decaying only to bW with masses below 0.91 TeV, and the boosted tH channel excluded T quarks decaying only to tH for masses below 0.89 TeV.

A CMS search for $T \rightarrow tH^0$ with $H^0 \rightarrow \gamma\gamma$ decays has been performed [133] in pair production of T quarks. To identify the Higgs boson produced in the decay of the heavy T quark, and the subsequent $H^0 \rightarrow \gamma\gamma$ decay, the analysis focused on identification of two photons in events with one or more high p_T lepton+jets or events with no leptons and large hadronic activity. A search for a resonance in the invariant mass distribution of the two photons in events with large hadronic activity defined by the H_T variable showed no excess above the prediction from standard model processes. The analysis resulted in exclusion of T quark masses below 0.54 TeV.

A search for electroweak single production of T quarks decaying to tH^0 using boosted topologies in fully hadronic [134] and lepton+jets [135] in the final states has been performed by CMS.

The electroweak couplings of the T quarks to the SM third generation quarks are highly model dependent, and hence these couplings determine the rates of the single T quark production. In both analyses, T quark invariant mass was reconstructed using the boosted Higgs boson jet and the top quark. Higgs boson jets were identified using jet substructure techniques and subjet b tagging. For the lepton+jets analysis, the top quark was reconstructed from the leptonically decaying W and the b jet, while in the all-hadronic analysis the top quark jet was tagged using substructure analysis. There was no excess of events observed above background. Exclusion limits on the product of the production cross section and the branching fraction ($\sigma(pp \rightarrow Tqt/b) \times \mathcal{B}(T \rightarrow tH^0)$) were derived for the T quark masses in the range 0.70–1.8 TeV. From the lepton+jets analysis, for a mass of 1.0 TeV, values of ($\sigma(pp \rightarrow Tqt/b) \times \mathcal{B}(T \rightarrow tH^0)$) greater than 0.8 and 0.7 pb were excluded assuming left- and right-handed coupling of the T quark to standard model fermions, respectively [135]. For the all-hadronic analysis, upper limits between 0.31 and 0.93 pb were obtained on ($\sigma(pp \rightarrow Tqt/b) \times \mathcal{B}(T \rightarrow tH^0)$) for T quark masses in the range 1.0–1.8 TeV [134].

$T \rightarrow tZ$:

Both ATLAS and CMS searched for T quarks that decay exclusively into tZ in pp collisions at $\sqrt{s} = 13$ TeV. No excesses were found in either search.

ATLAS performed a search [136] optimized for pair production of vector-like top quarks decaying into tZ where the Z boson subsequently decays into neutrino pairs, utilizing 36.1 fb $^{-1}$ of data. The search selected events with one lepton, multiple jets, and significant missing transverse momentum. No significant excesses were found and lower limits on the mass of a vector like top quark were placed, excluding masses below 0.87 TeV (weak-isospin singlet), 1.05 TeV (weak-isospin doublet), and 1.16 TeV (pure tZ mode).

Another search by ATLAS for pair produced T decaying to tZ has been carried out by reconstructing the high transverse momentum Z boson from a pair of opposite-sign same-flavor leptons, using events with two or three charged leptons [137]. The final analysis is based on three final state signatures. In the trilepton events, at least one b -tagged jet is required and S_T is used as the discriminating variable. In events with two leptons, at least 2 b -jets are requested and events with zero or one high p_T top-tagged jet, use H_T as the discriminator. The second dilepton analysis with two top-tagged high p_T jets focuses on hadronically decaying heavy resonances and the invariant mass of the Z boson and the highest p_T b -tagged jet is found to be a good discriminating variable. No excess was observed over the background expectations. The combined analysis yields a lower limit on T quark mass of 1.03 TeV (1.21 TeV) in the singlet (doublet) model or 100% branching ratio for $T \rightarrow tZ$ a lower limit on the T quark mass of 1.34 TeV is obtained.

ATLAS has subsequently carried out a search [138] for singly produced T quarks decaying to tZ where the Z boson decays into neutrino pairs. The search is carried out using 36.1 fb $^{-1}$ of data in events with two different final state signatures: one with jets and significant missing p_T (0L) and the other with a single lepton, jets and missing p_T (1L). Events are divided into signal and dedicated W +jets and $t\bar{t}$ background control regions. The sensitivity to the T quark signal is extracted using distributions of missing p_T for the 1L and the distribution of T quark transverse mass constructed from missing p_T and the high p_T large-radius top-tagged jet, for 0L analysis. There is no excess found over the expected background and lower limits on the production of T singlets are obtained as a function of the left- and right-handed couplings $c_{L,W}$ and $c_{R,W}$ to top quarks and W bosons, where c_W above 0.7 is excluded for T quark mass of 1.4 TeV. The limits on c_W are also recasted into expected and observed 95% CL upper limits for the mixing angle (θ_L) of a singlet T with the top quark.

CMS searched [139] for single production of T quarks decaying into tZ with the Z boson decaying to pairs of charged leptons (electrons and muons) and the top quark decaying hadronically using 35.9 fb $^{-1}$ of data. Limits were placed on T quarks with masses between 0.7 and 1.7 TeV excluding the product of cross section and branching fraction above values of 0.27 to 0.04 pb.

Additionally, limits on the product of cross section and branching fractions for a Z' boson decaying into tZ were set between 0.13 and 0.06 pb for Z' boson masses in the range from 1.5 to 2.5 TeV.

Similar searches by ATLAS for singly produced T decaying to Zt have been performed in final state signatures with two or three charged leptons [137]. The analysis relies on tagging b -jets and high p_T large-radius jets originating from top-quarks. Additional selections are devised to reduce the contributions from pair production of T quarks. For events with dilepton analysis, the discriminating variable is the mass of the T quark formed using the invariant mass of the Z boson candidate and the highest p_T top-tagged jet, while for the trilepton analysis, the variable S_T is used to search for an excess of data over the expected SM background. No excess above the SM expectations is observed. The two final states (dilepton and trileptons) are combined to obtain the final results. For the coupling parameter κ_T between 0.1–1.6, the 95% CL upper limits on the production cross section times branching fraction into Zt is between 0.16–0.18 (0.03–0.05) pb at T quark mass of 0.7 (2) TeV.

The search by the ATLAS experiment for VLQ pair production optimized to search for $T \rightarrow tZ$ decays [140] in a dataset with 139 fb^{-1} of luminosity has been performed in final states with either two leptons or three or more leptons. A multi-class boosted object tagger based on DNN techniques for large-radius jets is used to categorize events according to the number of high p_T boosted H^0 , Z/W , and top quark jets. The discriminant in the signal to evaluate the sensitivity depends on the number of leptons in the event. For the two lepton analysis, the discriminant is the mass of the T quark which is constructed from b and Z candidates, while for the three or more lepton analysis, H_T computed using the p_T of the jets and leptons is used as the discriminant. This analysis excludes T quark masses up to 1.27 GeV (1.46 GeV), for the singlet (doublet) configuration [140].

Combination of $T \rightarrow tZ/tH^0$:

The search performed by the ATLAS experiment for electroweak single production of T quark decaying to tH^0 and tZ uses a dataset corresponding to 139 fb^{-1} of integrated luminosity, and events with a single lepton with multiple jets and b -jets in the final state [141]. The single production channel for VLQs probes κ , the universal coupling constant, which also controls the production cross section and the resonance width of the VLQ. The analysis uses techniques to tag boosted jets, and categorizes events by numbers of jets and b -jets. The event discriminant is the “effective mass” (m_{eff}) observable, defined as the scalar sum of the p_T of all central jets, p_T of leptons and the missing p_T in the event. No significant excess is observed. Limits on the mass of T quark and universal coupling strength (κ) are obtained. For singlet T quarks, values of κ above 0.5 are excluded for all masses below 1.8 TeV. For T quark mass of 1.6 TeV, κ above 0.41 is excluded [141].

A CMS search published in 2020 concentrates on the electroweak production of the T quark with $T \rightarrow tH^0$, and $T \rightarrow tZ$ decays, where subsequently both H^0 and Z Bosons decay hadronically, leading to fully hadronic final states [142]. The search focuses on evidence of T quarks produced in association with a b quark ($qg \rightarrow T\bar{b}q'$) or a top quark ($qg \rightarrow T\bar{t}q$). The production cross sections are model dependent, as the electroweak production depends on the strength of the T quark coupling, TbW (TtZ), for the charged-current (neutral-current) process, at the production vertex. The searches are split into two domains depending on the mass of the T quark and consider a wide range of widths of the T quark from a few percent to about 30% of the T quark mass. The event selection relies primarily on the large number of jets and on efficient identification of jets from b -quarks, in addition to double- b jet decays of the H^0 and Z bosons. The final sensitivity is derived by the search for a resonant peak in the tH^0/Z invariant mass spectrum. For low mass T quark searches, three independent regions based on the b -tagged jet requirements are examined. For T quark masses above 1 TeV, which result in highly Lorentz-boosted top quarks and H^0 or Z boson, large-area jets are used to form the T quark. This search reports upper limits at 95% confidence level on $\sigma B(T \rightarrow tH)$ and $\sigma B(T \rightarrow tZ)$ between 2 pb and 20 fb for T masses between 0.6 to 2.6 TeV in the Tbq and Ttq

production channels. The analysis also reports combined results for $T \rightarrow tH$ and $T \rightarrow tZ$ associated production with a bottom quark and provides constraints on T quarks in the T singlet model for masses below 1.00 TeV. For an expected fractional width of 30%, the expected sensitivity extends to 1.28 TeV, comparable to the most stringent results.

Combination of $T \rightarrow bW/tZ/tH^0$:

Most of the analyses described above target an individual decay mode of the T quark, with 100% branching ratio to either bW , tZ or tH^0 and are optimized accordingly. However, they have varied sensitivity to all three decay modes and the results can be interpreted as a function of branching ratios to each of the three decay modes, assuming the total adds up to unity ($\mathcal{B}(tH) + \mathcal{B}(tZ) + \mathcal{B}(bW) = 1$).

Combinations of analyses have been performed by both ATLAS and CMS. The limits set by ATLAS searches in $W(\ell\nu)b + X$, $H(bb)b + X$, $Z(\nu\bar{\nu})$, $Z(\ell\ell)t/b + X$, dileptons with same-sign charge, trileptons, all-hadronic final states have been combined and the results obtained for various sets of branching fractions for T quark decays to bW , tH^0 and tZ are shown in Fig. 92.3 (left). In the combined analysis, ATLAS sets lower T quarks mass limit of 1.31 TeV for all possible values of the branching fractions to the three decay modes [123, 136, 143]. In Fig. 92.3, exclusion is shown in the plane of $\mathcal{B}(T \rightarrow Ht)$ versus $\mathcal{B}(T \rightarrow Wb)$, for different values of the T quark mass. The default branching ratio values for the weak-isospin singlet and doublet cases are also shown in Fig. 92.3 as yellow circle and star symbols respectively. Assuming a weak isospin (T, B) doublet and $|V_{Tb}| \ll |V_{tB}|$, T quark mass below 1.37 TeV is excluded.

A CMS analysis for pair production of T combines three channels with lepton final states: single lepton, two leptons with the same sign of the electric charge (SS), or at least three leptons (trilepton) [144]. For various combinations of branching fractions for T quark decays to bW , tH^0 and tZ , the combined results exclude T quarks with masses below 1.14–1.3 TeV and are shown in Figure 92.3 (right). Single lepton events are classified into 16 signal categories and 6 background control regions based on multiplicity of b -tagged, high p_T H^0 and W -tagged jets. The discriminating variables are H_T for H^0 -tagged events and the minimum invariant mass constructed from the lepton and the b jet, $\min[M_{b\ell}]$, for zero H^0 -tagged events. For the same-sign dilepton and trilepton analyses, the non-prompt backgrounds due to misidentified jets and leptons are derived from data control regions. In the trilepton analysis the S_T variable is used as the signal discriminator binned in four categories based on the lepton flavor combinations (eee , $e\mu\mu$, $e\mu\mu$, $\mu\mu\mu$). The single lepton analysis is most sensitive for $tHbW$ and $WbWb$ decay modes, within the SS dilepton analysis $tHtH$ and $tHtZ$ have the best efficiency and for trileptons the $tZtZ$ and $tHtZ$ decays modes have the highest efficiency. CMS excludes singlet (doublet) T quark masses below 1.2 (1.28) TeV. Masses below 800 GeV were excluded in previous searches. For T quark masses in the range 0.8–1.8 TeV, cross sections smaller than 30.4–9.4 fb (21.2–6.1 fb) are excluded for the singlet (doublet) scenario.

Another inclusive search for pair produced T in the all-hadronic final state [122] has been performed by CMS using the boosted event shape tagger (BEST) neural network technique to classify jets in six categories W , Z , H^0 , t , b , and light. This search does not focus on a given VLQ mode, but on various combinations of the boson and quark jets in the final state. Anti- k_T jets with a distance parameter of 0.8 are used. The BEST NN algorithm simultaneously classifies jets according to heavy object type. For each of the six particle hypotheses, it boosts each jet constituent into corresponding frame along the jet momentum direction, and calculates event shape and angular variables in the boosted frame, with the expectation that when boosting to the correct rest frame, jet constituents will be isotropic and show the expected N-prong structure of the decaying object in its rest frame. A neural network is trained using the event shape and angular variables in the boosted frame to classify jets according to one of those six possibilities (W , Z , H , t , b , or light). The analysis bins the events into 126 categories depending on the number of W , Z , H , t , b , or light jets in the final state with a maximum of four such objects. For

each category H_T^{AK8} , the scalar sum of p_T of all AK8 jets, is used as the signal discriminator. A scan over a combination of various branching fractions is also performed. This search excludes T quark masses in the range 0.74–1.37 TeV for the tH decay mode in the NN analysis.

An inclusive search for VLQs has been carried out by CMS targeted at heavy T quarks decaying to any combination of bW , tZ , or tH^0 as described in [130]. Selected events have at least one isolated charged lepton. Events were categorized according to number and flavor of the leptons, the number of jets, and the presence of hadronic vector boson and top quark decays that are merged into a single jet. The use of jet substructure to identify hadronic decays significantly increases the acceptance for high T quark masses. No excess above standard model backgrounds was observed. Limits on the pair production cross section of the new quarks are set, combining all event categories, for all combinations of branching fractions into the three final states. For T quarks that exclusively decay to $bW/tZ/tH^0$, masses below 0.70/0.78/0.71 TeV are excluded.

92.2.3.2 Searches for B quarks that decay to W , Z and H^0 bosons

ATLAS and CMS have performed searches for pair production of heavy B quarks which subsequently decay to Wt , bZ or bH^0 . The searches have been carried out in final states with single leptons, dileptons (with same charge or opposite charge), multileptons, as well as in fully hadronic final states.

$B \rightarrow bH^0$:

A search for B pair-produced events has been performed by the CMS experiment [123] using 137 fb^{-1} of data where the B decays into a b/\bar{b} quark and either a H^0 or a Z boson. This search concentrates on final states with fully hadronic signatures, and utilizes different jet multiplicity categories to account for two resolved jets or merged single jets from H^0 or Z boson to $b\bar{b}$ decays, depending on the p_T of the H^0 or Z bosons. Nine final state categories are used, depending on the number of observed jets and the reconstructed event mode. No significant excess over expected background is observed. For the case $\mathcal{B}(B \rightarrow bH) = 100\%(50\%)$, VLQs with masses below 1.57 (1.45) TeV are ruled out.

Using 36.1 fb^{-1} of data, ATLAS has performed a search for pair produced VLQs with all-hadronic final state signature [129]. While this analysis provides exclusion limits for all third generation VLQs, it provides the strongest results for the $B \rightarrow bH^0$ decay mode and excludes decays with $\mathcal{B}(B \rightarrow [\mathcal{H}']) = \infty$ scenario for B masses upto 1.01 TeV. The limits are also cast in a two-dimensional plane of branching ratio values of $B \rightarrow bH^0$ vs. $B \rightarrow Wb$. This analysis required the presence of high p_T jets and multiple b tags. It used a multi-class DNN to classify jets arising from W , Z , H^0 bosons and top-quarks. In addition, the matrix element method was used to compute the likelihood for the event to arise from a particular VLQ final state and to construct the final discriminator. To increase the sensitivity of the analysis, processes with the same number of top quarks, W/Z bosons, and H^0 Higgs bosons are combined into a single hypothesis.

The ATLAS experiment has performed a search for single production of a vector-like B quark decaying to a b -quark and a H^0 boson, with $H^0 \rightarrow b\bar{b}$ decay, using a dataset corresponding to an integrated luminosity of 139 fb^{-1} [145]. The all hadronic final state signature relies on identification of at least 3 b -jets, with an additional soft forward jet from the spectator quark. Large area jets are used to identify boosted H^0 decays. This analysis results in excluding the single production of a VLQ (B , Y) doublet with relative width larger than 5% between masses of 1.0 TeV and 1.76 TeV [145].

$B \rightarrow Wt$:

A search for $B \rightarrow tW$ in B pair produced events has been performed by the ATLAS experiment [123] using lepton+jets events with one hadronically decaying W and one leptonically decaying W utilizing 36.1 fb^{-1} of data at $\sqrt{s} = 13 \text{ TeV}$. The search was optimized for T production decaying into Wb . Since the analysis was optimized for $T \rightarrow Wb$ rather than Wt decays the analysis does not reconstruct the full B mass. As discussed earlier, the

hadronically and leptonically decaying heavy quarks were required to have similar reconstructed masses (within 300 GeV). The interpretation of the $T \rightarrow Wb$ in the context of $B \rightarrow tW$ production led to the exclusion of heavy B like VLQs for masses less than 1.25 TeV and 1.08 TeV, assuming a 100% branching fraction to tW or $SU(2)$ singlet B scenario, respectively.

A similar search by CMS [146], using 19.8 fb^{-1} of $\sqrt{s} = 8 \text{ TeV}$ data, selected events with one lepton and four or more jets, with at least one b -tagged jet, significant missing p_T , and further categorized them based on the number of jets tagged as arising from the decay of boosted W , Z or H^0 bosons. The S_T distributions of the events in different categories showed no excess of events above the expected background and yielded a lower limit on the B quark mass of 0.73 TeV for $BR(B \rightarrow Wt) = 1$.

CMS [132] also searched for pair production of both TT and BB with collisions from 2.5 fb^{-1} of $\sqrt{s} = 13 \text{ TeV}$ data. The analysis searches for events with one high p_T lepton, multiple jets, and highly boosted W or Higgs bosons decaying hadronically. The analysis focuses on pair production and selects events with either a boosted W or Higgs candidate and then proceeds to search for anomalous production in excess of standard model production. Seeing no significant excesses CMS then proceeded to set limits in many different interpretations. The strongest was from the $B \rightarrow Wt$ interpretation leading to excluding heavy vector-like B quarks with mass less than 0.73 TeV.

The all-hadronic inclusive analysis [122] performed by CMS using the BEST NN technique to classify $W/Z/H^0/t/b$ /light jets also gives exclusion limits on B quark production for various combinations of branching fractions for decays to tW , bZ , bH^0 . By considering categories based on various combinations of the boson and quark jets in the final state it excludes B quarks with masses up to 1230 GeV, for B decays to tW with a 100% branching fraction.

Electroweak production of single heavy $B+b$ production has been studied by CMS in the decay to tW with the lepton+jets final state [147]. Single lepton events with hadronic jets, including a forward jet, and missing p_T are selected and divided into 10 different categories based on lepton flavor (e/μ), top-tagged, W -tagged, and $0/1/2$ b -tagged jets. The B quark mass m_{reco} is fully reconstructed from lepton, jets, and missing p_T , where the neutrino four-momentum is computed using the missing p_T and the W mass constraint. For events within the top-tagged category, the high p_T top-tagged hadronic jet and the leptonically decaying W boson are used to compute m_{reco} . The m_{reco} distribution are used as the signal discriminator. In the absence of an excess over the expected SM background, the exclusion limits on the production cross section for B quark masses between 0.7-2 TeV varies between 0.3 to 0.03 pb. In addition, B quarks with left-handed couplings and a relative width of 10, 20, and 30% are excluded for masses below 1.49, 1.59, and 1.66 TeV respectively.

$B \rightarrow bZ$:

As mentioned above, a search for B pair produced events, with final states with fully hadronic signature, using 137 fb^{-1} of data, has been performed by the CMS experiment [123]. In this search, the B decays into a b/\bar{b} quark and either a H^0 or a Z boson. For the case $\mathcal{B}(B \rightarrow bZ) = 100\%(50\%)$, VLQs with masses below 1.39 (1.45) TeV are ruled out by this analysis.

A search by CMS [148] for the pair-production of a heavy B quark and its antiparticle has been performed, where one of the heavy B quark decays to bZ . Events with a Z boson decaying to e^+e^- or $\mu^+\mu^-$ and at least one b jet are selected. The signal from $B \rightarrow bZ$ decays is expected to appear as a local enhancement in the bZ mass distribution. No such enhancement was found and B quarks that decay 100% into bZ are excluded below 0.70 TeV. This analysis also set upper limits on the branching fraction for $B \rightarrow bZ$ decays of 30-100% in the B quark mass range 0.45-0.70 TeV. A complementary search has been carried out by ATLAS for new heavy quarks decaying into a Z boson and a b -quark [149]. Selected dilepton events contain a high transverse momentum Z boson that decays leptonically, together with two b -jets. If the dilepton events have an extra lepton in addition to those from the Z boson, then only one b -jet is required. No significant excess of events above the standard model expectation

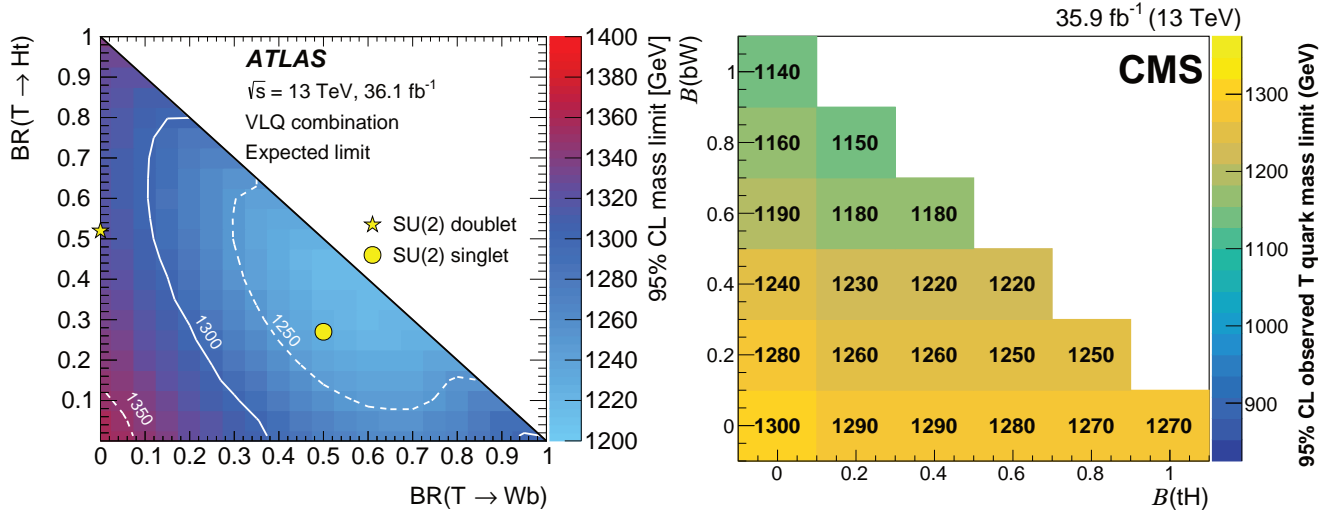


Figure 92.3: Left panel: observed limits on the mass of the T quark in the plane of $B(T \rightarrow tH^0)$ versus $B(T \rightarrow bW)$ from a combination [143] of all ATLAS searches for TT production. The markers indicate the default branching ratios for the SU(2) singlet and doublet scenarios. Right panel: the observed lower limits on the T quark mass (in GeV), from CMS searches after combining all lepton channels [144], for various branching fraction scenarios. $B(T \rightarrow Wb) + B(T \rightarrow tZ) + B(T \rightarrow tH^0) = 1$ is assumed.

was observed, and mass limits were set depending on the assumed branching ratios, as shown in Fig. 92.4. In a weak-isospin singlet scenario, a B quark with mass lower than 0.65 TeV was excluded, while for a particular weak-isospin doublet scenario, a B quark with mass lower than 0.73 TeV was ruled out.

The search by the ATLAS experiment for $B \rightarrow bZ$ decays [140] in final states with either two leptons or three or more leptons using a multi-class boosted object tagger to categorize events according to the number of high p_T boosted H^0 , Z/W , and top quark jets excludes B quark masses up to 1.20 GeV (1.32 GeV), for the singlet (doublet) configuration [140].

In addition to pair production, ATLAS has also searched for the electroweak production of single B quarks, which is accompanied by a b -jet and a light jet [149]. The dilepton selection for double B production was modified for the single B production study by requiring the presence of an additional energetic jet in the forward region. An upper limit of 200 fb was obtained for the process $\sigma(pp \rightarrow B\bar{b}q) \times B(B \rightarrow Zb)$ with a heavy B quark mass at 0.70 TeV. This search indicated that the electroweak mixing parameter X_{Bb} below 0.5 is neither expected nor observed to be excluded for any values of B quark mass.

Combination of $B \rightarrow tW/bZ/bH^0$:

The ATLAS experiment has combined the various analyses targeted for specific decay modes to obtain the most sensitive limit on the pair production of B quarks [123, 124, 143]. Various searches ($W(\ell\nu)t + X, Z(\ell\ell)t/b + X$, same sign charge dilepton events, trilepton events, and all-hadronic) are combined to obtain lower limit on the mass of the B quark [in the plane of $BR(B \rightarrow Wt)$ vs $BR(B \rightarrow bH)$]. The searches were optimized for 100% branching fractions and hence are most sensitive at large $BR(B \rightarrow Wt)$, and also at large $BR(B \rightarrow bH^0)$. For all possible values of branching ratios in the three decay modes tW , bZ , or bH^0 , the lower limits on the B quark mass was found to be 1.03 TeV and shown in Fig. 92.4 (left) as a function of the B quark branching ratios.

CMS combined three channels with lepton final states: single lepton, two leptons with the same sign of the electric charge (SS), or at least three leptons (trilepton) [144]. For various combinations of branching fractions for B quark decays to tW , bH^0 and bZ , the combined results exclude b quarks with masses below 0.91–1.24 TeV and are shown in Figure 92.4 (right); the details are provided earlier in subsection 92.2.3.1. The single lepton analysis is most sensitive for $tHbW$ and $WbWb$ decay modes, within the SS dilepton analysis $tHtH$ and $tHtZ$ have the best efficiency and for trileptons the $tZtZ$ and $tHtZ$ decays modes have the highest efficiency. CMS excludes singlet (doublet) B quark masses below 1.17 (0.94) TeV. Masses below 800 GeV were excluded in previ-

ous searches. For B quark masses in the range 0.8–1.8 TeV, cross sections smaller than 40.6–9.4 fb (101–49.0 fb) are excluded for the singlet (doublet) scenario.

92.2.3.3 Searches for top-partner quark $X_{5/3}$

Searches for a heavy top vector-like quark $X_{5/3}$, with exotic charge $\pm 5/3$, such as that proposed in Refs. [151, 152], have been performed by both ATLAS and CMS [123, 153].

The analyses assumed pair-production or single production of $X_{5/3}$ with $X_{5/3}$ decaying with 100% branching fraction to tW . Searches for $X_{5/3}$ have been performed using two final state signatures: same-sign leptons and lepton+jets.

The analysis based on searching for same-sign leptons, from the two W bosons from one of the $X_{5/3}$, has smaller backgrounds compared to the lepton+jets signature. Requiring same-sign leptons eliminates most of the standard model background processes, leaving those with smaller cross sections: $t\bar{t}W$, $t\bar{t}Z$, WWW , and same-sign WW . In addition, backgrounds from instrumental effects due to charge misidentification were considered. Assuming pair production of $X_{5/3}$, the analysis by CMS using H_T as the discriminating variable restrict the $X_{5/3}$ mass to be higher than 1.16 (1.10) TeV for a right (left) handed chirality particle [153–155]. The limits obtained by ATLAS, by classifying the signal region by number of b -jets, H_T , and missing p_T in the event, led to a lower mass limit on $X_{5/3}$ of 1.19 TeV [156, 157].

Searches for $X_{5/3}$ using leptons+jets final state signatures are based on either full or partial reconstruction of the T mass from the lepton, jets (including b -jets) and missing p_T . The CMS search [153, 158] also utilized jet substructure techniques to identify boosted $X_{5/3}$ topologies. The discriminating variable used was the mass constructed from the lepton and b -tagged jet, $M_{(\ell,b)}$, which corresponds to the visible mass of the leptonically decaying top quark. To optimize the search sensitivity, the events were further separated into categories based on lepton flavor (e, μ), the number of b -tagged jets, the number of W -tagged jets, and the number of t -tagged jets. In the absence of a signal, the CMS analysis excluded $X_{5/3}$ quark masses with right-handed (left-handed) couplings below 1.32 (1.30) TeV [158]. Combining the lepton+jets with the same-sign leptons analyses leads to a slight improvement and excludes $X_{5/3}$ quark masses with right-handed (left-handed) couplings below 1.33 (1.30) TeV.

The ATLAS lepton+jets search for $X_{5/3}$ utilized events with high p_T W bosons and b -jets. The search described earlier for T pair production, with $T \rightarrow Wb$ decays, can be reinterpreted as a search for $X \rightarrow tW$. This analysis excluded $X_{5/3}$ with masses below 1.25 TeV [123].

The single $X_{5/3}$ production cross section depends on the cou-

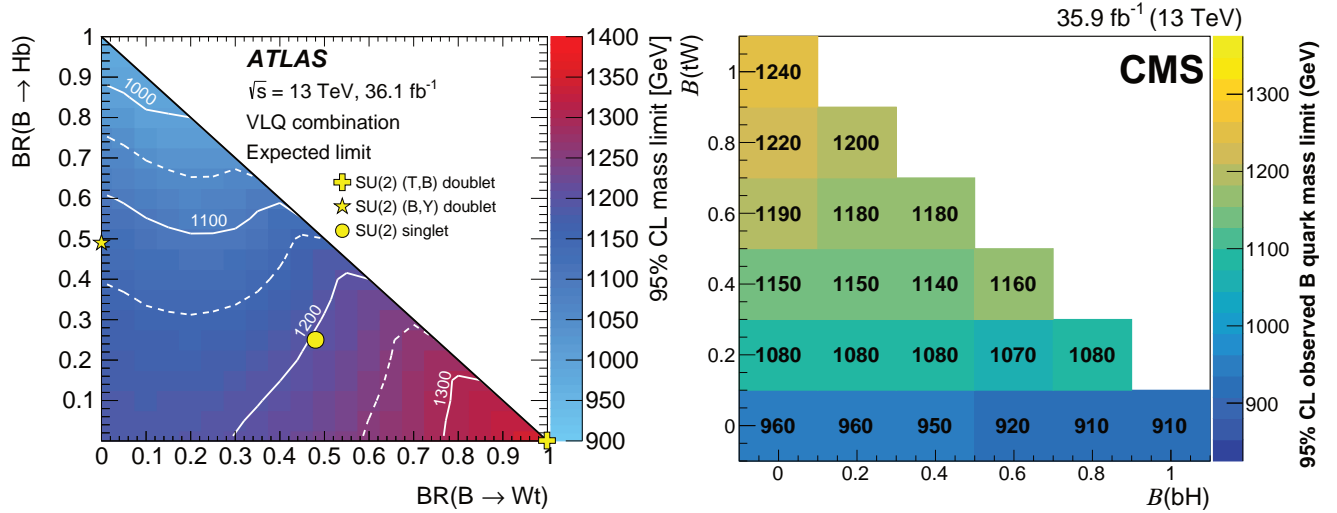


Figure 92.4: Observed limits on the mass of the B quark in the plane of $BR(B \rightarrow bH^0)$ versus $BR(B \rightarrow tW)$ from ATLAS searches [143] on the left panel, and CMS searches [144] on the right panel, for BB production. $B(B \rightarrow \mathcal{H}) + B(B \rightarrow \mathcal{Z}) + B(B \rightarrow \mathcal{W}) = 1$ is assumed. The yellow markers indicate the branching ratios for the $SU(2)$ singlet and doublet scenarios.

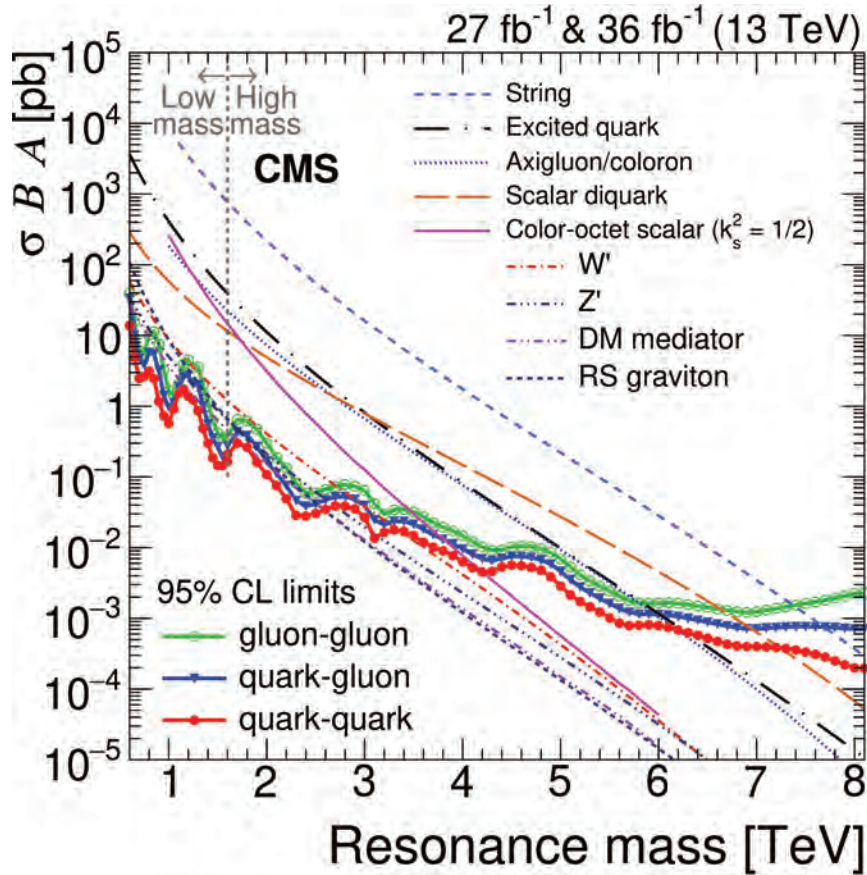


Figure 92.5: Observed 95% C.L. limits on $\sigma \times B \times A$ for string resonances, excited quarks, axigluons, colorons, E6 diquarks, s8 resonances, W' and Z' bosons, and Randall–Sundrum Gravitons g_{KK} from [150].

pling constant λ of the tWX vertex. ATLAS has performed an analysis of same-sign dileptons which includes both the single and pair production. This analysis led to a lower limit on the mass of the $X_{5/3}$ of 0.75 TeV for both values of $\lambda = 0.5$ and 1.0 [159].

Single heavy $X_{5/3} + t$ production has been studied by CMS in the decay to tW with the lepton+jets final state [147]. The description of the analysis is provided earlier in the discussion of $B \rightarrow WtX$ decays, where the reconstructed mass of $X_{5/3}$, m_{reco} distribution is used as the signal discriminator. In the absence of

an excess over the expected SM background, the exclusion limits on the production cross section for $X_{5/3}$ quark masses between 0.7–2 TeV varies between 0.3 to 0.03 pb, depending on the width of $X_{5/3}$ between 1–10%. In addition, $X_{5/3}$ quarks with left-handed couplings and a relative width of 10, 20, and 30% are excluded for masses below 0.92, 1.3, and 1.45 TeV respectively.

92.2.4 Heavy resonances decaying to VLQ

CMS has performed search for VLQ production in the decay of massive resonances such as Z' and W' bosons.

$Z' \rightarrow tT$: Specifically searches are presented by CMS in Refs. [160] and [161] for massive spin-1 Z' resonances decaying to a top quark and a heavy VLQ top quark partner T . The results of this search for a heavy spin-1 resonance are interpreted in the context of two different models. In the G^* model which predicts ten VLQs ($T, B, \tilde{T}, \tilde{B}, T_{5/3}, T_{2/3}, T', B', B_{-1/3}, B_{-4/3}$) with the mass relationship $M(T_{5/3}) = M(T_{2/3}) = M(T)\cos(\phi_L)$. For the benchmark scenario [162], $\cos(\phi_L)=0.84$ and the branching fractions $T \rightarrow tH^0, tZ, Wb$ are 0.25, 0.25 and 0.5 respectively. The ρ^0 model predicts a multiplet of four new VLQs $T, B, X_{2/3}, X_{5/3}$, and in the benchmark scenario [163], the branching fractions $T \rightarrow tH^0, tZ, Wb$ are 0.5, 0.5 and 0 respectively.

Two of the three decays of the $Z' \rightarrow tT$ with $T \rightarrow tH^0, tZ, Wb$ are characterized by the presence of two top quark decays and a boson (H^0/Z). A search [161] by CMS, optimized for $T \rightarrow tH/Zt$ decays was carried out in the lepton+jets final state using a dataset corresponding to an integrated luminosity of 35.9 fb^{-1} . Jet substructure techniques are used to identify (or tag) the high p_T large-radius jets originating from H^0, Z bosons and merged top quarks. The mass of the Z' boson is used as the signal discriminator and constructed using H^0 or Z -tagged dijet, the hadronic and leptonic top quark four vectors. For the leptonic top quark reconstruction ($t \rightarrow b\ell\nu_e$), the neutrino four vector is obtained from the event missing p_T using the W boson mass constraint. While the high p_T hadronic top quark jets from decays of massive Z' bosons are mostly merged and identified by top tagging techniques, those from T decays maybe resolved. The reconstructed Z' candidate events are classified into six different categories requiring the presence of either a H^0 -tagged jet with 2 b -tagged subjects or one b -tagged subjet or a Z -tagged boson, each with either zero or one top-tagged jet. This search does not observe any significant deviation in data over the expectation from standard model backgrounds. Within the context of the G^* model, for a T mass of 1.2 (1.5) TeV, this search excludes G^* [162] resonances with masses between 1.5–2.3 (2.0–2.4) TeV.

The search in the all-hadronic final state is based on a 2.6 fb^{-1} dataset [160], and optimized for $T \rightarrow Wb$ decays. Jet substructure techniques are deployed for tagging jets from high p_T W boson and top quarks. Events are categorized into two groups based on the presence of b -tagged subjects in the top-tagged jet. The multijet background estimation is challenging and determined using side-bands defined by inverting the b -tagging requirement. Upper limits on the cross section for $Z' \rightarrow tT$ are obtained in the range of 0.13–10 pb.

$W' \rightarrow Tb/Bt$: W' bosons are predicted to decay to VLQ third generation partners T, B quarks within composite Higgs and warped extra dimensional models [164]. In the benchmark scenarios of this framework, W' decays to Tb or Bt are equally distributed and the subsequent VLQ decays $T \rightarrow tH$ and $B \rightarrow bH^0$ each are assumed to have a branching fraction of 0.5. The search for $W' \rightarrow Tb/bH^0 \rightarrow tbH^0$ is performed using a sample of 35.9 fb^{-1} by CMS [165] in the final state with all-hadronic decays of both the Higgs boson ($H^0 \rightarrow b\bar{b}$) and the top quark. Both the H^0 boson and the top quark are expected to be boosted in the decay of a heavy W' , and hence jet substructure techniques, including subjet b -tagging and double b -tagging are deployed to identify the H^0 -tagged and the top-tagged jets. The three particle mass m_{tbH^0} , is used as the signal discriminant to observe the W' resonance. There is no excess observed in data above the expected SM background. This search excludes W' production cross section above 0.01–0.43 pb for masses between 1.5–4.0 TeV.

92.2.5 Colorons and Colored Scalars

These particles are associated with top-condensate and top-seesaw models, which involve an enlarged color gauge group. The new particles decay to dijets, $t\bar{t}$, and $b\bar{b}$.

Direct searches for colorons, color-octet scalars and other heavy objects decaying to $q\bar{q}, qg, qg, qg$ have been performed using LHC data from pp collisions at $\sqrt{s}=7, 8$ and 13 TeV. Based on the analysis of dijet events from a data sample corresponding

to a luminosity of 19.6 fb^{-1} , at $\sqrt{s}=8$ TeV, the CMS experiment excluded pair production of colorons with mass between 1.20–3.60 and 3.90–4.08 TeV [166]. Analyses of inclusive 8- and 10-jet final states with low missing transverse momentum by CMS [167], set limits in several benchmark models. Colorons (axiguons) with masses between 0.6 and 0.75 (up to 1.15) TeV were excluded, and gluinos in R -parity violating supersymmetric scenarios were ruled out from 0.6 up to 1.1 TeV.

A search for pair-produced colorons based on an integrated luminosity of 5.0 fb^{-1} at $\sqrt{s}=7$ TeV by CMS excluded colorons with masses between 0.25 TeV and 0.74 TeV, assuming colorons decay 100% into $q\bar{q}$ [168]. This analysis was based on events with at least four jets and two dijet combinations with similar dijet mass. Color-octet scalars (s8) with masses between 1.20–2.79 TeV were excluded by CMS [166], and below 2.7 TeV by ATLAS [169].

These studies have now been extended to take advantage of the increased center-of-mass energy during Run 2 of the LHC. Using 35.9 fb^{-1} of data collected at $\sqrt{s}=13$ TeV, searches for narrow resonances have been performed by CMS. An analysis of the dijet invariant mass spectrum formed using wide jets [150, 170, 171], separated by $\Delta\eta_{jj} \leq 1.3$, led to limits on new particles decaying to parton pairs (qq, qg, gg). Specific exclusions on the masses of colorons and color-octet scalars were obtained and are shown in Fig. 92.5. Exclusions have been obtained for axiguons and colorons below 6.1 TeV, and color-octet scalars below 3.4 TeV.

Additional searches for dijet resonances have been performed by both ATLAS [172–174] and CMS [175, 176], though they have not been interpreted in the context of coloron production.

92.3 Conclusions

As the above analyses have demonstrated, there is already substantial sensitivity to possible new particles predicted to accompany the H^0 in dynamical frameworks of electroweak symmetry breaking. No significant hints of any deviations from the standard model have been observed, and limits typically at the scale of a few hundred GeV to a few TeV are set.

Given the need to better understand the H^0 and to determine in detail how it behaves, such analyses continue to be a major theme of Run 3 of the LHC, and we look forward to increased sensitivity as a result of the higher luminosity at the increased center of mass energy of collisions.

References

- [1] G. Aad *et al.* (ATLAS), Phys. Lett. **B716**, 1 (2012), [arXiv:1207.7214].
- [2] S. Chatrchyan *et al.* (CMS), Phys. Lett. **B716**, 30 (2012), [arXiv:1207.7235].
- [3] S. Weinberg, Physica **A96**, 1-2, 327 (1979).
- [4] A. Manohar and H. Georgi, Nucl. Phys. **B234**, 189 (1984).
- [5] H. Georgi, Nucl. Phys. **B266**, 274 (1986).
- [6] R. S. Chivukula, in “Flavor physics for the millennium. Proceedings, Theoretical Advanced Study Institute in elementary particle physics, TASI 2000, Boulder, USA, June 4-30, 2000,” 731–772 (2000), [hep-ph/0011264].
- [7] R. S. Chivukula, M. J. Dugan and M. Golden, Phys. Rev. **D47**, 2930 (1993), [hep-ph/9206222].
- [8] S. Weinberg, Phys. Rev. **D13**, 974 (1976), [Addendum: Phys. Rev.D19,1277(1979)].
- [9] L. Susskind, Phys. Rev. **D20**, 2619 (1979).
- [10] K. Lane (2002), [hep-ph/0202255].
- [11] C. T. Hill and E. H. Simmons, Phys. Rept. **381**, 235 (2003), [Erratum: Phys. Rept.390,553(2004)], [hep-ph/0203079].
- [12] R. Shrock, in “The origin of mass and strong coupling gauge theories. Proceedings, 5th International Workshop, SCGT’06, Nagoya, Japan November 21-24, 2006,” 227–241 (2007), [hep-ph/0703050].
- [13] E. Eichten *et al.*, Rev. Mod. Phys. **56**, 579 (1984), [Addendum: Rev. Mod. Phys.58,1065(1986)].
- [14] E. Eichten *et al.*, Phys. Rev. **D34**, 1547 (1986).

- [15] R. S. Chivukula and V. Koulovassilopoulos, Phys. Lett. **B309**, 371 (1993), [hep-ph/9304293].
- [16] R. Foadi, M. T. Frandsen and F. Sannino, Phys. Rev. **D87**, 9, 095001 (2013), [arXiv:1211.1083].
- [17] B. Holdom, Phys. Lett. **150B**, 301 (1985).
- [18] K. Yamawaki, M. Bando, and K.-i. Matumoto, Phys. Rev. Lett. **56**, 1335 (1986).
- [19] T. W. Appelquist, D. Karabali and L. C. R. Wijewardhana, Phys. Rev. Lett. **57**, 957 (1986).
- [20] T. Appelquist and L. C. R. Wijewardhana, Phys. Rev. **D35**, 774 (1987).
- [21] T. Appelquist and L. C. R. Wijewardhana, Phys. Rev. **D36**, 568 (1987).
- [22] E. Eichten, K. Lane and A. Martin (2012), [arXiv:1210.5462].
- [23] D. B. Kaplan and H. Georgi, Phys. Lett. **136B**, 183 (1984).
- [24] D. B. Kaplan, H. Georgi and S. Dimopoulos, Phys. Lett. **136B**, 187 (1984).
- [25] G. Ferretti and D. Karateev, JHEP **03**, 077 (2014), [arXiv:1312.5330].
- [26] M. E. Peskin, Nucl. Phys. **B175**, 197 (1980).
- [27] J. Preskill, Nucl. Phys. **B177**, 21 (1981).
- [28] See “Status of Higgs Boson Physics” review in this volume.
- [29] R. Barbieri and A. Strumia, in “4th Rencontres du Vietnam: Physics at Extreme Energies (Particle Physics and Astrophysics) Hanoi, Vietnam, July 19-25, 2000,” (2000), [hep-ph/0007265].
- [30] N. Arkani-Hamed, A. G. Cohen and H. Georgi, Phys. Lett. **B513**, 232 (2001), [hep-ph/0105239].
- [31] N. Arkani-Hamed *et al.*, JHEP **08**, 020 (2002), [hep-ph/0202089].
- [32] N. Arkani-Hamed *et al.*, JHEP **07**, 034 (2002), [hep-ph/0206021].
- [33] M. Schmaltz and D. Tucker-Smith, Ann. Rev. Nucl. Part. Sci. **55**, 229 (2005), [hep-ph/0502182].
- [34] K. Agashe *et al.*, Phys. Lett. **B641**, 62 (2006), [hep-ph/0605341].
- [35] P. Sikivie *et al.*, Nucl. Phys. **B173**, 189 (1980).
- [36] B. Bellazzini, C. Csáki and J. Serra, Eur. Phys. J. **C74**, 5, 2766 (2014), [arXiv:1401.2457].
- [37] R. Essig *et al.*, JHEP **09**, 085 (2017), [arXiv:1707.03399].
- [38] Z. Chacko, H.-S. Goh and R. Harnik, Phys. Rev. Lett. **96**, 231802 (2006), [hep-ph/0506256].
- [39] R. S. Chivukula, A. G. Cohen and K. D. Lane, Nucl. Phys. **B343**, 554 (1990).
- [40] V. A. Miransky, M. Tanabashi and K. Yamawaki, Mod. Phys. Lett. **A4**, 1043 (1989).
- [41] W. A. Bardeen, C. T. Hill and M. Lindner, Phys. Rev. **D41**, 1647 (1990).
- [42] C. T. Hill, Phys. Lett. **B266**, 419 (1991).
- [43] B. A. Dobrescu and C. T. Hill, Phys. Rev. Lett. **81**, 2634 (1998), [hep-ph/9712319].
- [44] R. S. Chivukula *et al.*, Phys. Rev. **D59**, 075003 (1999), [hep-ph/9809470].
- [45] S. Dimopoulos and L. Susskind, Nucl. Phys. **B155**, 237 (1979), [2,930(1979)].
- [46] E. Eichten and K. D. Lane, Phys. Lett. **90B**, 125 (1980).
- [47] D. B. Kaplan, Nucl. Phys. **B365**, 259 (1991).
- [48] T. Appelquist, M. Piai and R. Shrock, Phys. Rev. **D69**, 015002 (2004), [hep-ph/0308061].
- [49] R.S. Chivukula, B.A. Dobrescu, and E.H. Simmons, Phys. Lett. **B401**, 74 (1997).
- [50] Y. Grossman and M. Neubert, Phys. Lett. **B474**, 361 (2000), [hep-ph/9912408].
- [51] S. J. Huber and Q. Shafi, Phys. Lett. **B498**, 256 (2001), [hep-ph/0010195].
- [52] T. Gherghetta and A. Pomarol, Nucl. Phys. **B586**, 141 (2000), [hep-ph/0003129].
- [53] K. Agashe, R. Contino and A. Pomarol, Nucl. Phys. **B719**, 165 (2005), [hep-ph/0412089].
- [54] G. F. Giudice *et al.*, JHEP **06**, 045 (2007), [hep-ph/0703164].
- [55] R. S. Chivukula and H. Georgi, Phys. Lett. **B188**, 99 (1987).
- [56] G. D’Ambrosio *et al.*, Nucl. Phys. **B645**, 155 (2002), [hep-ph/0207036].
- [57] K. Agashe *et al.* (2005), [hep-ph/0509117].
- [58] T. Appelquist and R. Shrock, Phys. Lett. **B548**, 204 (2002), [hep-ph/0204141].
- [59] K. Sakai, Nucl. Phys. **B867**, 429 (2013), [arXiv:1207.4057].
- [60] J. M. Maldacena, Int. J. Theor. Phys. **38**, 1113 (1999), [Adv. Theor. Math. Phys.2,231(1998)], [hep-th/9711200].
- [61] For a review, see C. Csaki, J. Hubisz, and P. Meade, hep-ph/0510275 (2005), and “Extra Dimensions” review in this volume.
- [62] C. Pica, PoS **LATTICE2016**, 015 (2016), [arXiv:1701.07782].
- [63] B. Svetitsky, EPJ Web Conf. **175**, 01017 (2018), [arXiv:1708.04840].
- [64] O. Witzel, PoS **LATTICE2018**, 006 (2019), [arXiv:1901.08216].
- [65] V. Drach, PoS **LATTICE2019**, 242 (2020), [arXiv:2005.01002].
- [66] T. Appelquist *et al.*, Phys. Rev. **D93**, 11, 114514 (2016), [arXiv:1601.04027].
- [67] PDG review on “ Z' -Boson Searches” in this volume.
- [68] PDG review on “ W' -Boson Searches” in this volume.
- [69] M. Aaboud *et al.* (ATLAS), Phys. Lett. **B**, 68 (2019), [arXiv:1903.06248].
- [70] CMS Collaboration, Technical Report CMS-PAS-EXO-19-019, CERN, Geneva (2019), URL <http://cds.cern.ch/record/2684757>.
- [71] G. Aad *et al.* (ATLAS), Phys. Rev. **D90**, 5, 052005 (2014), [arXiv:1405.4123].
- [72] M. Aaboud *et al.* (ATLAS), JHEP **01**, 055 (2018), [arXiv:1709.07242].
- [73] CMS Collaboration, JHEP **0217**, 48 (2017).
- [74] ATLAS Collaboration, ATLAS-CONF-2016-014 (2016).
- [75] CMS Collaboration, JHEP **0717**, 001 (2016).
- [76] M. Aaboud *et al.* (ATLAS), Phys. Rev. D. **99**, 092004 (2019), [arXiv:1902.10077].
- [77] A. M. Sirunyan *et al.* (CMS), JHEP **04**, 031 (2019), [arXiv:1810.05905].
- [78] ATLAS Collaboration, ATLAS-CONF-2019-007 (2019).
- [79] CMS Collaboration, CMS-PAS-EXO-19-012 (2019).
- [80] M. Aaboud *et al.* (ATLAS), Accepted by Phys. Rev. [arXiv:1906.05609].
- [81] V. Khachatryan *et al.* (CMS), Phys. Lett. **B770**, 278 (2017), [arXiv:1612.09274].
- [82] V. Khachatryan *et al.* (CMS), Phys. Lett. **B755**, 196 (2016), [arXiv:1508.04308].
- [83] S. Chatrchyan *et al.* (CMS), JHEP **05**, 108 (2014), [arXiv:1402.2176].
- [84] V. Khachatryan *et al.* (CMS), JHEP **02**, 122 (2016), [arXiv:1509.06051].

- [85] A. M. Sirunyan *et al.* (CMS), JHEP **08**, 029 (2017), [arXiv:1706.04260].
- [86] A. M. Sirunyan *et al.* (CMS), Phys. Lett. **B777**, 39 (2018), [arXiv:1708.08539].
- [87] A. M. Sirunyan *et al.* (CMS), Phys. Lett. B **820**, 136535 (2021), [arXiv:2104.04831].
- [88] CMS Collaboration, Technical Report CMS-PAS-JME-15-002, CERN, Geneva (2016), URL <http://cds.cern.ch/record/2126325>.
- [89] G. Aad *et al.* (ATLAS), Phys. Lett. **B788**, 347 (2019), [arXiv:1807.10473].
- [90] G. Aad *et al.* (ATLAS), Eur. Phys. J. **C75**, 4, 165 (2015), [arXiv:1408.0886].
- [91] G. Aad *et al.* (ATLAS), Phys. Lett. **B743**, 235 (2015), [arXiv:1410.4103].
- [92] D. Pappadopulo *et al.*, JHEP **09**, 060 (2014), [arXiv:1402.4431].
- [93] M. Aaboud *et al.* (ATLAS), Phys. Rev. **D98**, 5, 052008 (2018), [arXiv:1601.04027].
- [94] A. M. Sirunyan *et al.* (CMS), Phys. Lett. **B798**, 134952 (2019), [arXiv:1906.00057].
- [95] M. Aaboud *et al.* (ATLAS), Phys. Lett. **B**, 91 (2017), [arXiv:1708.04445].
- [96] M. Aaboud *et al.* (ATLAS), JHEP **03**, 042 (2018), [arXiv:1710.07235].
- [97] M. Aaboud *et al.* (ATLAS), Phys. Lett. **B**, 68 (2018), [arXiv:1806.10532].
- [98] A. M. Sirunyan *et al.* (CMS), Phys. Rev. **D97**, 072006, [arXiv:1708.05379].
- [99] A. M. Sirunyan *et al.* (CMS), JHEP **07**, 075, [arXiv:1802.09407].
- [100] A. M. Sirunyan *et al.* (CMS), JHEP **09**, 101, [arXiv:1803.10093].
- [101] M. Aaboud *et al.* (ATLAS), Eur. Phys. J. **C**, 78 (2017), [arXiv:1710.01123].
- [102] M. Aaboud *et al.* (ATLAS), Phys. Lett. **B**, 774 (2017), [arXiv:1707.06858].
- [103] M. Aaboud *et al.* (ATLAS), JHEP **B**, 174 (2018), [arXiv:1712.06518].
- [104] A. M. Sirunyan *et al.* (CMS), Eur. Phys. J. **C**, 636, [arXiv:1707.01303].
- [105] CMS Collaboration (CMS), Technical Report CMS-PAS-B2G-20-007 (2021).
- [106] CMS Collaboration (CMS), Technical Report CMS-PAS-B2G-20-004 (2021).
- [107] Eur. Phys. J. **C** **74**, 704 (2017).
- [108] A. Collaboration, PRL **125**, 251802 (2020).
- [109] A. Collaboration, Physics Letters B **779**, 24 (2018).
- [110] C. Collaboration (2021), [arXiv:2106.10509].
- [111] CMS Collaboration (CMS), Technical Report CMS-PAS-B2G-20-001 (2021).
- [112] CMS Collaboration (CMS), Technical Report CMS-PAS-B2G-20-002 (2021).
- [113] F. del Aguila *et al.*, Nucl. Phys. **B334**, 1 (1990).
- [114] J. Serra, Journal of High Energy Physics **2015**, 9 (2015), ISSN 1029-8479, URL [http://dx.doi.org/10.1007/JHEP09\(2015\)176](http://dx.doi.org/10.1007/JHEP09(2015)176).
- [115] A. Anandakrishnan *et al.*, Physical Review D **93**, 7 (2016), ISSN 2470-0029, URL <http://dx.doi.org/10.1103/PhysRevD.93.075009>.
- [116] M. Chala, Physical Review D **96**, 1 (2017), ISSN 2470-0029, URL <http://dx.doi.org/10.1103/PhysRevD.96.015028>.
- [117] A. M. Sirunyan *et al.* (CMS), Phys. Lett. **B779**, 82 (2018), [arXiv:1710.01539].
- [118] CMS Collaboration, Technical Report CMS-PAS-B2G-12-017 (2014).
- [119] V. Khachatryan *et al.* (CMS), Phys. Rev. **D93**, 1, 012003 (2016), [arXiv:1509.04177].
- [120] CMS Collaboration, Technical Report CMS-PAS-B2G-12-013 (2012).
- [121] S. D. Ellis, C. K. Vermilion and J. R. Walsh, Phys. Rev. **D80**, 051501 (2009), [arXiv:0903.5081].
- [122] A. M. Sirunyan *et al.* (CMS), Phys. Rev. D **100**, 7, 072001 (2019), [arXiv:1906.11903].
- [123] M. Aaboud *et al.* (ATLAS), JHEP **10**, 141 (2017), [arXiv:1707.03347].
- [124] G. Aad *et al.* (ATLAS), JHEP **08**, 105 (2015), [arXiv:1505.04306].
- [125] A. M. Sirunyan *et al.* (CMS), Phys. Lett. **B772**, 634 (2017), [arXiv:1701.08328].
- [126] M. Aaboud *et al.* (ATLAS), JHEP **05**, 164 (2019), [arXiv:1812.07343].
- [127] G. Aad *et al.* (ATLAS), Eur. Phys. J. **C76**, 8, 442 (2016), [arXiv:1602.05606].
- [128] ATLAS Collaboration (ATLAS), Technical Report ATLAS-CONF-2016-104 (2016).
- [129] M. Aaboud *et al.* (ATLAS), Phys. Rev. **D98**, 9, 092005 (2018), [arXiv:1808.01771].
- [130] S. Chatrchyan *et al.* (CMS), Phys. Lett. **B729**, 149 (2014), [arXiv:1311.7667].
- [131] V. Khachatryan *et al.* (CMS), JHEP **06**, 080 (2015), [arXiv:1503.01952].
- [132] A. M. Sirunyan *et al.* (CMS), JHEP **11**, 085 (2017), [arXiv:1706.03408].
- [133] CMS Collaboration, cds.cern.ch/record/1709129 (2014).
- [134] A. M. Sirunyan *et al.* (CMS), JHEP **04**, 136 (2017), [arXiv:1612.05336].
- [135] V. Khachatryan *et al.* (CMS), Phys. Lett. **B771**, 80 (2017), [arXiv:1612.00999].
- [136] M. Aaboud *et al.* (ATLAS), JHEP **08**, 052 (2017), [arXiv:1705.10751].
- [137] M. Aaboud *et al.* (ATLAS), Phys. Rev. **D98**, 11, 112010 (2018), [arXiv:1806.10555].
- [138] M. Aaboud *et al.* (ATLAS), JHEP **05**, 041 (2019), [arXiv:1812.09743].
- [139] A. M. Sirunyan *et al.* (CMS), Phys. Lett. **B781**, 574 (2018), [arXiv:1708.01062].
- [140] ATLAS Collaboration (ATLAS), Technical report, CERN, Geneva (2021), URL <https://cds.cern.ch/record/2773300>.
- [141] ATLAS Collaboration (ATLAS), Technical report, CERN, Geneva (2021), URL <https://cds.cern.ch/record/2779174>.
- [142] A. M. Sirunyan *et al.* (CMS), JHEP **01**, 036 (2020), [arXiv:1909.04721].
- [143] M. Aaboud *et al.* (ATLAS), Phys. Rev. Lett. **121**, 21, 211801 (2018), [arXiv:1808.02343].
- [144] A. M. Sirunyan *et al.* (CMS), JHEP **08**, 177 (2018), [arXiv:1805.04758].
- [145] ATLAS Collaboration (ATLAS), Technical report, CERN, Geneva (2021), URL <https://cds.cern.ch/record/2760012>.
- [146] CMS Collaboration, Technical Report CMS-PAS-B2G-12-019 (2012).
- [147] A. M. Sirunyan *et al.* (CMS), Eur. Phys. J. **C79**, 90 (2019), [arXiv:1809.08597].
- [148] V. Khachatryan *et al.* (CMS), Phys. Rev. **D93**, 11, 112009 (2016), [arXiv:1507.07129].

- [149] G. Aad *et al.* (ATLAS), JHEP **11**, 104 (2014), [arXiv:1409.5500].
- [150] A. M. Sirunyan *et al.* (CMS), JHEP **08**, 130 (2018), [arXiv:1806.00843].
- [151] R. Contino and G. Servant, JHEP **06**, 026 (2008), [arXiv:0801.1679].
- [152] J. Mrazek and A. Wulzer, Phys. Rev. **D81**, 075006 (2010), [arXiv:0909.3977].
- [153] A. M. Sirunyan *et al.* (CMS), JHEP **08**, 073 (2017), [arXiv:1705.10967].
- [154] CMS Collaboration, Technical Report CMS-PAS-B2G-16-019 (2017).
- [155] S. Chatrchyan *et al.* (CMS), Phys. Rev. Lett. **112**, 17, 171801 (2014), [arXiv:1312.2391].
- [156] M. Aaboud *et al.* (ATLAS), JHEP **12**, 039 (2018), [arXiv:1807.11883].
- [157] G. Aad *et al.* (ATLAS), Phys. Rev. **D91**, 11, 112011 (2015), [arXiv:1503.05425].
- [158] A. M. Sirunyan *et al.* (CMS), JHEP **03**, 082 (2019), [arXiv:1810.03188].
- [159] G. Aad *et al.* (ATLAS), JHEP **10**, 150 (2015), [arXiv:1504.04605].
- [160] A. M. Sirunyan *et al.* (CMS), JHEP **09**, 053 (2017), [arXiv:1703.06352].
- [161] A. M. Sirunyan *et al.* (CMS), Eur. Phys. J. **C79**, 3, 208 (2019), [arXiv:1812.06489].
- [162] C. Bini, R. Contino and N. Vignaroli, JHEP **01**, 157 (2012), [arXiv:1110.6058].
- [163] D. Greco and D. Liu, JHEP **12**, 126 (2014), [arXiv:1410.2883].
- [164] N. Vignaroli, Phys. Rev. **D89**, 9, 095027 (2014), [arXiv:1404.5558].
- [165] A. M. Sirunyan *et al.* (CMS), JHEP **03**, 127 (2019), [arXiv:1811.07010].
- [166] V. Khachatryan *et al.* (CMS), Phys. Rev. **D91**, 5, 052009 (2015), [arXiv:1501.04198].
- [167] V. Khachatryan *et al.* (CMS), Phys. Lett. **B770**, 257 (2017), [arXiv:1608.01224].
- [168] S. Chatrchyan *et al.* (CMS), Phys. Rev. Lett. **110**, 14, 141802 (2013), [arXiv:1302.0531].
- [169] G. Aad *et al.* (ATLAS), Phys. Rev. **D91**, 5, 052007 (2015), [arXiv:1407.1376].
- [170] A. M. Sirunyan *et al.* (CMS), Phys. Lett. **B769**, 520 (2017), [Erratum: Phys. Lett. **B772**, 882(2017)], [arXiv:1611.03568].
- [171] CMS Collaboration, Technical Report CMS-PAS-EXO-15-001 (2015).
- [172] G. Aad *et al.* (ATLAS), JHEP **06**, 151 (2020), [arXiv:2002.11325].
- [173] G. Aad *et al.* (ATLAS), Phys. Rev. Lett. **125**, 13, 131801 (2020), [arXiv:2005.02983].
- [174] M. Aaboud *et al.* (ATLAS), Phys. Rev. D **96**, 5, 052004 (2017), [arXiv:1703.09127].
- [175] A. M. Sirunyan *et al.* (CMS), Phys. Lett. B **805**, 135448 (2020), [arXiv:1911.03761].
- [176] A. M. Sirunyan *et al.* (CMS), JHEP **05**, 033 (2020), [arXiv:1911.03947].

93. Grand Unified Theories

Revised August 2019 by A. Hebecker (Heidelberg U.) and J. Hisano (KMI, Nagoya U.).

93.1 The standard model

The Standard Model (SM) may be defined as the renormalizable field theory with gauge group $G_{SM} = SU(3)_C \times SU(2)_L \times U(1)_Y$, with 3 generations of fermions in the representation

$$(3, 2)_{1/3} + (\bar{3}, 1)_{-4/3} + (\bar{3}, 1)_{2/3} + (1, 2)_{-1} + (1, 1)_2, \quad (93.1)$$

and a scalar Higgs doublet H transforming as $(1, 2)_1$. Here and below we use boldface numbers to specify the dimension of representations of non-Abelian groups (in this case fundamental and antifundamental) and lower indices for $U(1)$ charges. The fields of Eq. (93.1) should also be familiar as $[Q, u^c, d^c, L, e^c]$, with $Q = (u, d)$ and $L = (\nu, e)$ being the quark and lepton $SU(2)$ -doublets and u^c, d^c, e^c charge conjugate $SU(2)$ -singlets.¹ Especially after the discovery of the Higgs, this model is remarkably complete and consistent with almost all experimental data.

A notable exception are neutrino masses, which are known to be non-zero but are absent in the SM even after the Higgs acquires its vacuum expectation value (VEV). The minimalist attitude is to allow for the dimension-five operator $(HL)^2$ [1], which induces (Majorana) neutrino masses. In the seesaw mechanism [2–4] this operator is generated by integrating out heavy singlet fermions (right-handed (r.h.) neutrinos). Alternatively, neutrinos can have Dirac masses if light singlet neutrinos are added to the SM spectrum.

Conceptual problems of the SM include the absence of a Dark Matter candidate, of a mechanism for generating the baryon asymmetry of the Universe, and of any reason for the observed smallness of the θ parameter of QCD (θ_{QCD}). In addition, the apparently rather complex group-theoretic data of Eq. (93.1) remains unexplained. Together with the abundance of seemingly arbitrary coupling constants, this disfavors the SM as a candidate fundamental theory, even before quantum gravity problems arise at energies near the Planck mass M_P .

To be precise, there are 19 SM parameters which have to be fitted to data: Three gauge couplings² g_3, g_2 and g_1 , 13 parameters associated with the Yukawa couplings (9 charged fermion masses, three mixing angles and one CP phase in the CKM matrix.), the Higgs mass and quartic coupling, and θ_{QCD} . In addition, Majorana neutrinos introduce 3 more masses and 6 mixing angles and phases. As we will see, the paradigm of grand unification addresses mainly the group theoretic data of Eq. (93.1) and the values of the three gauge couplings. In many concrete realizations, it then impacts also the other mentioned issues of the SM, such as the family structure and fermion mass hierarchy.

More specifically, after precision measurements of the Weinberg angle θ_W in the LEP experiments, supersymmetric GUTs (SUSY GUTs) have become the leading candidates in the search for ‘Physics beyond the SM’. Supersymmetry (SUSY) is a symmetry between bosons and fermions which requires the addition of superpartners to the SM spectrum. If SUSY is motivated as a solution to the gauge hierarchy problem (i.e. to the naturalness or fine-tuning problem of the electroweak scale) [5], superpartners have to be present near the weak scale. SUSY GUTs [6] then lead to the prediction of θ_W , in good agreement with subsequent observations [7]. However, the non-discovery of new particles at the LHC puts into question the presence of new physics at the TeV scale in general and in particular of low-scale supersymmetry. Still, SUSY may be present just outside the presently explored energy domain.

The measured Higgs mass (125 GeV) is in principle consistent with this picture, assuming superpartners in the region of roughly 10 TeV. Such heavy superpartners then induce radiative corrections raising the Higgs mass above the Z boson mass m_Z [8, 9]. However, from the vantage point of the hierarchy problem, heavy

superpartners are problematic: They also contribute to SUSY-breaking Higgs mass parameters and thereby to the Higgs potential, tending to raise the Z mass. As a result, the incarnation of SUSY in terms of the minimal supersymmetric SM (MSSM) is becoming questionable. Turning the logic around, one may say that compared to expectations based on the MSSM with superpartner masses below about 1 TeV, the measured Higgs mass value of 125 GeV is somewhat too high [10]. Independently, the LHC has disfavored light colored superpartners (which does not imply that *all* superpartners are heavy). These facts represent new hints for future work on SUSY GUTs or on GUTs without TeV-scale supersymmetry.

93.2 Basic group theory and charge quantization

93.2.1 $SU(4)_C \times SU(2)_L \times SU(2)_R$

Historically, the first attempt at unification was the Pati-Salam model with gauge group $G_{PS} = SU(4)_C \times SU(2)_L \times SU(2)_R$ [11]. It unifies SM fermions in the sense that one generation (plus an extra SM singlet) now comes from the $(4, 2, 1) + (\bar{4}, 1, 2)$ of G_{PS} . This is easy to verify from the breaking pattern $SU(4)_C \rightarrow SU(3)_C \times U(1)_{B-L}$ together with the identification of SM hypercharge as a linear combination between $B - L$ (baryon minus lepton number) and the T_3 generator of $SU(2)_R$. This model explains charge quantization, that is, why all electric charges are integer multiples of some smallest charge in the SM. Concretely, the 4 and $\bar{4}$ of $SU(4)_C$ identify lepton number as the 4th colour and the tracelessness of the diagonal generator implies that quark charges are expressed in terms of $1/N_c$ fractions of lepton charges. However, G_{PS} is not simple (containing three simple factors), and thus it does not predict gauge coupling unification.

93.2.2 $SU(5)$

Since G_{SM} has rank four (two for $SU(3)_C$ and one for $SU(2)_L$ and $U(1)_Y$, respectively), the rank-four group $SU(5)$ is the minimal choice for unification in a simple group [12]. The three SM gauge coupling constants derive from a universal coupling α_G at the GUT scale M_G . Explicitly embedding G_{SM} in $SU(5)$ is straightforward, with $SU(3)_C$ and $SU(2)_L$ corresponding e.g. to the upper-left 3×3 and lower-right 2×2 blocks, respectively, in traceless 5×5 matrices for $SU(5)$ generators of the fundamental representation. The $U(1)_Y$ corresponds to matrices generated by $\text{diag}(-2/3, -2/3, -2/3, 1, 1)$ and hence commutes with $SU(3)_C \times SU(2)_L \subset SU(5)$. It is then easy to derive how one SM generation precisely comes from the $10 + \bar{5}$ of $SU(5)$ (where 10 is the antisymmetric rank-2 tensor):

$$10 : \begin{pmatrix} 0 & u_b^c & -u_g^c & u_r & d_r \\ -u_b^c & 0 & u_r^c & u_g & d_g \\ u_g^c & -u_r^c & 0 & u_b & d_b \\ -u_r & -u_g & -u_b & 0 & e^c \\ -d_r & -d_g & -d_b & -e^c & 0 \end{pmatrix} \quad \text{and} \quad \bar{5} : \begin{pmatrix} d_r^c \\ d_g^c \\ d_b^c \\ e \\ -\nu_e \end{pmatrix}. \quad (93.2)$$

In addition to charge quantization this structure explains why the l.h. quark and lepton states fall in $SU(2)_L$ doublets while the r.h. states are singlets.

Since $SU(5)$ has 24 generators, $SU(5)$ GUTs have 12 new gauge bosons known as X bosons (or X/Y bosons) in addition to the SM. X bosons form an $SU(3)_C$ -triplet and $SU(2)_L$ -doublet. Their interaction connects quarks and leptons such that baryon and lepton numbers are not conserved and nucleon decay is predicted. Furthermore, $U(1)_Y$ hypercharge is automatically quantized since it is embedded in $SU(5)$.

In order to break the electroweak symmetry at the weak scale and give mass to quarks and leptons, Higgs doublets are needed. In the minimal $SU(5)$ model, they can sit in either a 5_H or $\bar{5}_H$. The three additional states are referred to as color-triplet Higgs scalars. Their couplings also violate baryon and lepton numbers, inducing nucleon decay. In order not to violently disagree with the non-observation of nucleon decay, the triplet mass must be greater than $\sim 10^{11}$ GeV [13]. Moreover, in SUSY GUTs [6], in order to cancel anomalies as well as give mass to both up and down quarks, both Higgs multiplets 5_H and $\bar{5}_H$ are required. As we shall discuss later, nucleon decay now constrains the Higgs triplets to have

¹ In our convention the electric charge is $Q = T_3 + Y/2$ and all our spinor fields are left-handed (l.h.).

² Equivalently, the $SU(2)_L$ and $U(1)_Y$ couplings are denoted as $g = g_2$ and $g' = \sqrt{3/5} g_1$. One also uses $\alpha_s = \alpha_3 = (g_3^2/4\pi)$, $\alpha_{EM} = (e^2/4\pi)$ with $e = g \sin \theta_W$ and $\sin^2 \theta_W = (g')^2/(g^2 + (g')^2)$.

mass significantly greater than M_G in the minimal SUSY $SU(5)$ GUT since integrating out the Higgs triplets generates dimension-five baryon-number-violating operators [14]. The mass splitting between doublet and triplet in the $\mathbf{5}_H$ (and $\bar{\mathbf{5}}_H$) comes from their interaction with the $SU(5)$ breaking sector.

93.2.3 $SO(10)$

While $SU(5)$ allows for the minimal GUT models, unification is not complete: Two independent representations, $\mathbf{10}$ and $\bar{\mathbf{5}}$, are required for one SM generation. A further representation, an $SU(5)$ singlet, has to be added to serve as r.h. neutrino in the seesaw mechanism. In this case, the r.h. neutrino masses are not necessarily related to the GUT scale. By contrast, a single $\mathbf{16}$ -dimensional spinor representation of $SO(10)$ accommodates a full SM generation together with an extra singlet, potentially providing a r.h. neutrino [15]. This is most easily understood from the breaking pattern $SO(10) \rightarrow SU(5) \times U(1)_X$ and the associated branching rule³ $\mathbf{16} = \mathbf{10}_{-1} + \bar{\mathbf{5}}_3 + \mathbf{1}_{-4}$. Here the indices refer to charges under the $U(1)_X$ subgroup, which is orthogonal to $SU(5)$ and reflects the fact that $SO(10)$ has rank five. From the above, it is easy to see that $U(1)_X$ charges can be given as $2Y - 5(B - L)$. Intriguingly, all representations of $SO(10)$ are anomaly free in four dimensions (4d). Thus, the absence of anomalies in an $SU(5)$ -GUT or a SM generation can be viewed as deriving from this feature.

We now describe in more detail how one family of quarks and leptons appears in the $\mathbf{16}$. To understand this, recall that the Γ -matrices of the 10d Clifford algebra give rise to five independent, anticommuting ‘creation-annihilation’ operators $\Gamma^{a\pm} = (\Gamma^{2a-1} \pm i\Gamma^{2a})/2$ with $a = 1, \dots, 5$. These correspond to five fermionic harmonic oscillators or ‘spin’ 1/2 systems. The 32-dimensional tensor product of those is reducible since the 10d rotation generators $M_{mn} = -i[\Gamma^m, \Gamma^n]/4$ ($m, n = 1, \dots, 10$) always flip an even number of ‘spins’. This gives rise to the $\mathbf{16}$ as displayed in Table 93.1. Next, one also recalls that the natural embedding of $SU(5)$ in $SO(10)$ relies on ‘pairing up’ the 10 real dimensions to produce 5 complex dimensions, $\mathbb{R}^{10} \equiv \mathbb{C}^5$, similarly to the pairing up of Γ^m s used above. This makes it clear how to associate one $|\pm\rangle$ system to each complex dimension of $SU(5)$, which explains the labeling of the ‘spin’ columns in Table 93.1: The first three and last two ‘spins’ correspond to $SU(3)_C$ and $SU(2)_L$, respectively. In fact, an $SU(3)_C$ rotation just raises one color index and lowers another, changing colors $\{r, g, b\}$, or changes relative phases between the three spin states. Similarly, an $SU(2)_L$ rotation raises one weak index and lowers another, thereby flipping the weak isospin from up to down or vice versa, or changes the relative phase between the two spin states. In this representation $U(1)_Y$ hypercharge is simply given by $Y = -2/3(\sum \text{color spins}) + (\sum \text{weak spins})$. $SU(5)$ rotations corresponding to X bosons then raise (or lower) a color index, while at the same time lowering (or raising) a weak index. It is easy to see that such rotations can mix the states $\{Q, u^c, e^c\}$ and $\{d^c, L\}$ among themselves and ν^c is a singlet. Since $SO(10)$ has 45 generators, additional 21 gauge bosons are introduced including the $U(1)_X$ above. The 20 new $SO(10)$ rotations not in $SU(5)$ are then given by either raising any two spins or lowering them. With these rotations, $\mathbf{1}$ and $\bar{\mathbf{5}}$ are connected with $\mathbf{10}$. The last $SO(10)$ rotation changes phases of states with weight $2(\sum \text{color spins}) + 2(\sum \text{weak spins})$, which corresponds to $U(1)_X$.

$SO(10)$ has two inequivalent maximal subgroups and hence breaking patterns, $SO(10) \rightarrow SU(5) \times U(1)_X$ and $SO(10) \rightarrow SU(4)_C \times SU(2)_L \times SU(2)_R$. In the first case, one can carry on breaking to $G_{SM} \subset SU(5)$ precisely as in the minimal $SU(5)$ case above. Alternatively, one can identify $U(1)_Y$ as an appropriate linear combination of $U(1)_X$ and the $U(1)$ factor from $SU(5)$, leading to the so-called flipped $SU(5)$ [17] as an intermediate step in breaking $SO(10)$ to G_{SM} . In the second case, we have an intermediate Pati-Salam model thanks to the branching rule $\mathbf{16} = (\mathbf{4}, \mathbf{2}, \mathbf{1}) + (\bar{\mathbf{4}}, \mathbf{1}, \mathbf{2})$. Finally, $SO(10)$ can break directly to the SM at M_G . Gauge coupling unification remains intact in

Table 93.1: Quantum numbers of $\mathbf{16}$ -dimensional representation of $SO(10)$.

state	Y	Color	Weak	$SU(5)$	$SO(10)$
ν^c	0	---	--	1	16
e^c	2	---	++	10	
u_r	1/3	+- -	-+		
d_r	1/3	+ - -	+ -		
u_g	1/3	- + -	-+		
d_g	1/3	- + -	+ -		
u_b	1/3	- - +	-+		
d_b	1/3	- - +	+ -		
u^c_r	-4/3	- + +	--		
u^c_g	-4/3	+ - +	--		
u^c_b	-4/3	+ + -	--		
d^c_r	2/3	- + +	++		
d^c_g	2/3	+ - +	++		
d^c_b	2/3	+ + -	++		
ν	-1	+++	-+		
e	-1	+++	+ -		

the case of this ‘direct’ breaking and for the breaking pattern $SO(10) \rightarrow SU(5) \rightarrow G_{SM}$ (with $SU(5)$ broken at M_G). In the case of intermediate-scale Pati-Salam or flipped $SU(5)$ models, gauge coupling predictions are modified. The Higgs multiplets in the minimal $SO(10)$ come from the fundamental representation, $\mathbf{10}_H = \mathbf{5}_H + \bar{\mathbf{5}}_H$. Note, only in $SO(10)$ does the representation type distinguish SM matter from Higgs fields.

93.2.4 Beyond $SO(10)$

Finally, larger symmetry groups can be considered. For example, the exceptional group E_6 has maximal subgroup $SO(10) \times U(1)$ [18]. Its fundamental representation branches as $\mathbf{27} = \mathbf{16}_1 + \mathbf{10}_{-2} + \mathbf{1}_4$. Another maximal subgroup is $SU(3)_C \times SU(3)_L \times SU(3)_R \subset E_6$ with branching rule $\mathbf{27} = (\mathbf{3}, \mathbf{3}, \mathbf{1}) + (\bar{\mathbf{3}}, \mathbf{1}, \bar{\mathbf{3}}) + (\mathbf{1}, \bar{\mathbf{3}}, \mathbf{3})$. Independently of any underlying E_6 , the group $[SU(3)]^3$ with additional permutation symmetry Z_3 interchanging the three factors can be considered. This is known as ‘trinification’ [19]. The $E_6 \rightarrow [SU(3)]^3$ breaking pattern has been used in phenomenological analyses of the heterotic string [20]. However, in larger symmetry groups, such as E_6 , $SU(6)$, etc., there are now many more states which have not been observed and must be removed from the effective low-energy theory.

Intriguingly, the logic by which G_{SM} is a maximal subgroup of $SU(5)$, which together with $U(1)_X$ is a maximal subgroup of $SO(10)$, continues in a very elegant and systematic way up to the largest exceptional group. The resulting famous breaking chain $E_8 \rightarrow E_7 \rightarrow E_6 \rightarrow SO(10) \rightarrow SU(5) \rightarrow G_{SM}$ together with the special role played by E_8 in group and in string theory is a tantalizing hint at deeper structures. However, since all representations of E_8 and E_7 are real and can not lead to 4d chiral fermions, this is necessarily outside the 4d GUT framework.

93.3 GUT breaking and doublet-triplet splitting

In the standard, 4d field-theoretic approach to GUTs, the unified gauge group is broken spontaneously by an appropriate GUT Higgs sector. Scalar potentials (or superpotentials in SUSY GUTs) exist whose vacua spontaneously break $SU(5)$ or $SO(10)$. While these potentials are ad hoc (just like the Higgs potential in the SM), the most naive expectation is that all their dimensional parameters are $O(M_G)$. In the simplest case of $SU(5)$, the $\mathbf{24}$ (adjoint) GUT Higgs develops a VEV along the G_{SM} -singlet direction as $\langle \Phi \rangle \propto \text{diag}(-2/3, -2/3, -2/3, 1, 1)$. In order for $SO(10)$ to break to $SU(5)$, the $\mathbf{16}$ or $\mathbf{126}$, which have a G_{SM} -singlet with non-zero $U(1)_X$ charge, get a VEV.

The masses of doublet and triplet in the $\mathbf{5}_H$ (and $\bar{\mathbf{5}}_H$) generically split due to their coupling to the GUT Higgs. In addition, both the doublet and the triplet masses also get an equal contribution from an $SU(5)$ -invariant GUT-scale mass term. Without any further structure, an extreme fine-tuning between two large effects is then necessary to keep the doublet mass at the electroweak scale. Supersymmetry plays an important role in for-

³ Useful references on group theory in the present context include [16] and refs. therein.

bidding large radiative correction to the doublet mass due to the non-renormalization theorem [5]. However, even in this case we have to fine tune parameters at tree level. This is the doublet-triplet splitting problem which, in the SUSY context, is clearly related the μ -term problem of the MSSM (the smallness of the coefficient of $\mu H_u H_d$).

Several mechanisms for natural doublet-triplet splitting have been suggested under the assumption of supersymmetry, such as the sliding singlet [21], missing partner [22], missing VEV [23], and pseudo-Nambu-Goldstone boson mechanisms [24]. Particular examples of the missing partner mechanism for $SU(5)$ [25], the missing VEV mechanism for $SO(10)$ [26, 27] and the pseudo-Nambu-Goldstone boson mechanism for $SU(6)$ [28] have been shown to be consistent with gauge coupling unification and nucleon decay. From the GUT-scale perspective, one is satisfied if the triplets are naturally heavy and the doublets are massless ($\mu \simeq 0$). There are also several mechanisms for resolving the subsequent issue of why μ is of order the SUSY breaking scale [29].⁴ For a review of the μ problem and some suggested solutions in SUSY GUTs and string theory, see [30–33] and references therein.

In general, GUT-breaking sectors successfully resolving the doublet-triplet splitting problem, dynamically stabilizing all GUT-scale VEVs and allowing for realistic neutrino masses and Yukawa couplings (including the GUT-symmetry violation in the latter) require a number of ingredients. However, for validity of the effective theory, introduction of higher or many representations is limited, otherwise a Landau pole may appear below the Planck scale. In addition, GUTs are only effective theories below the Planck scale in the 4d field-theoretic approach. Since M_G is close to this scale, the effects of higher-dimension operators are not obviously negligible. In particular, operators including the GUT-breaking Higgs may affect low-energy predictions, such as quark and lepton masses.

Thus, especially in the context of GUT breaking and doublet-triplet splitting, models beyond 4d field theory appear attractive. While this is mainly the subject of the next section, some advantages can already be noted: In models with extra dimensions, in particular string constructions, GUT breaking may occur due to boundary conditions in the compactified dimensions [34–37]. No complicated GUT breaking sector is then required. Moreover, boundary conditions can give mass only to the triplet, leaving the doublet massless. This is similar to the ‘missing partner mechanism’ since the effective mass term does not ‘pair up’ the triplets from $\mathbf{5}_H$ and $\bar{\mathbf{5}}_H$ but rather each of them with further fields which are automatically present in the higher-dimensional theory. This can eliminate dimension-five nucleon decay (cf. Sec. 93.6).

93.4 String-theoretic and higher-dimensional unified models

As noted earlier, the GUT scale is dangerously close to the scale of quantum gravity. It may hence be necessary to discuss unified models of particle physics in the latter, more ambitious context. Among the models of quantum gravity, superstring or M-theory stands out as the best-studied and technically most developed proposal, possessing in particular a high level of internal, mathematical consistency. For our purposes, it is sufficient to know that five 10d and one 11d low-energy effective supergravity theories arise in this setting (cf. [38] and refs. therein).

Grand unification is realized most naturally in the context of the two ‘heterotic’ theories with gauge groups $E_8 \times E_8$ and $SO(32)$, respectively [36, 39] (see [40] for some of the more recent results). Justified in part by the intriguing breaking path $E_8 \rightarrow \dots \rightarrow G_{SM}$ mentioned above, the focus has historically largely been on $E_8 \times E_8$. To describe particle physics, solutions of the 10d theory with geometry $\mathbb{R}^{1,3} \times M_6$ are considered, where M_6 is a Calabi-Yau (CY) 3-fold (with 6 real dimensions) [36]. The background solution involves expectation values of higher-dimensional components of the $E_8 \times E_8$ gauge fields. This includes

⁴ The solution of [29] relies on the absence of the fundamental superpotential term $\mu H_u H_d$ (or $\mu \mathbf{5}_H \bar{\mathbf{5}}_H$). This can be ensured either by a discrete R symmetry or by a $U(1)_R$. The latter clashes with typical superpotentials for the GUT breaking sector. However, higher-dimensional or stringy GUTs, where the triplet Higgs is simply projected out, can be consistent with the $U(1)_R$ symmetry.

both Wilson lines [34] and non-vanishing field-strength and leads, in general, to a reduced gauge symmetry and to chirality in the resulting 4d effective theory. The 4d fermions arise from 10d gauginos.

Given an appropriate embedding⁵ of G_{SM} in $E_8 \times E_8$, gauge coupling unification is automatic at leading order. Corrections arise mainly through (string)-loop effects and are similar to the familiar field-theory thresholds of 4d GUTs⁶ [41]. Thus, one may say that coupling unification is a generic prediction in spite of the complete absence⁷ of a 4d GUT at any energy scale. This absence is both an advantage and a weakness. On the up side, GUT breaking and doublet-triplet splitting [43] are more naturally realized and dimension-five nucleon decay is relatively easy to avoid. On the down side, there is no reason to expect full GUT representations in the matter sector and flavor model building is much less tied to the GUT structure than in 4d.

Let us pause to explain the beautiful idea behind the advertised solution of the doublet-triplet splitting problem: One starts with a simply connected CY X and mods out the action of a discrete group G (say \mathbb{Z}_2). In the absence of fixed points, X/G is smooth and has a non-contractible 1-cycle. Furthermore, let G also act on the gauge bundle, according to an embedding $G \rightarrow E_8$. Now the parallel transport around the 1-cycle is tied to a gauge rotation (one says a non-trivial Wilson-line is present). Moreover, this Wilson line can not be continuously turned off since, e.g. in the case of \mathbb{Z}_2 , its square is the unit element of the group. The induced ‘Wilson-line breaking’, which comes on top of the breaking by non-zero field strengths, may remove certain sub-representations (e.g. the triplet of $SU(5) \rightarrow G_{SM}$) while keeping others exactly massless. A simpler and, due to fixed points, singular version of this will appear below in the context of orbifold GUTs.

One technical problem of heterotic constructions is the dependence on the numerous size and shape parameters of M_6 (the so-called moduli), the stabilization of which is poorly understood (see [44] for recent developments). Another is the sheer mathematical complexity of the analysis, involving in particular the study of (non-Abelian) gauge-bundles on CY spaces [45] (see however [46]).

An interesting aspect of heterotic string constructions is represented by orbifold models [35]. Here the internal space is given by a six-torus, modded out by a discrete symmetry group (e.g. T^6/\mathbb{Z}_n). More recent progress is reported in [47, 48], including in particular the systematic exploration of the phenomenological advantages of so-called ‘non-prime’ (referring to n) orbifolds. The symmetry breaking to G_{SM} as well as the survival of Higgs doublets without triplet partners is ensured by the appropriate embedding of the discrete orbifold group in $E_8 \times E_8$. String theory on such spaces, which are locally flat but include singularities, is much more calculable than in the CY case. The orbifold geometries can be viewed as singular limits of CYs.

An even simpler approach to unified models, which includes many of the advantages of full-fledged string constructions, is provided by Orbifold GUTs [37]. These are (mostly) 5d or 6d SUSY field theories with unified gauge group (e.g. $SU(5)$ or $SO(10)$), broken in the process of compactifying to 4d. To give a particularly simple example, consider $SU(5)$ on $\mathbb{R}^{1,3} \times S^1/(\mathbb{Z}_2 \times \mathbb{Z}'_2)$. Here the compact space is an interval of length $\pi R/2$ and the embedding of \mathbb{Z}'_2 in the hypercharge direction of $SU(5)$ realizes the breaking to G_{SM} . Concretely, 5d X bosons are given Dirichlet BCs at one endpoint of the interval and thus have no Kaluza-Klein (KK) zero mode. Their lightest modes have mass $\sim 1/R$, making the KK-scale the effective GUT scale. As an implication, the boundary theory has no $SU(5)$ invariance. Nevertheless, since the $SU(5)$ -symmetric 5d bulk dominates 4d gauge couplings, unification remains a prediction. Many other features but also problems

⁵ All embeddings of G_{SM} in one E_8 factor which are consistent with a breaking-pattern $E_8 \rightarrow SU(5) \rightarrow G_{SM}$ are suitable (cf. for example the natural breaking chain from E_8 to G_{SM} through maximal subgroups mentioned at the end of Sect. 93.3). Other embeddings can change the ratios between the three resulting G_{SM} couplings at the GUT scale by group-theoretic factors. Crucially, due to the single 10d gauge coupling, no continuous tuning is possible.

⁶ Field-theory thresholds of 4d GUTs are discussed in 93.5.

⁷ See however [42].

of 4d GUTs can be circumvented, especially doublet-triplet splitting is easily realized.

With the advent of the string-theory ‘flux landscape’ [49], which is best understood in 10d type-IIB supergravity, the focus in string model building has shifted to this framework. While type II string theories have no gauge group in 10d, brane-stacks support gauge dynamics. A particularly appealing setting (see e.g. [50]) is provided by type IIB models with D7 branes (defining 8d submanifolds). However, in the $SO(10)$ context the **16** is not available and, for $SU(5)$, the top-Yukawa coupling vanishes at leading order [51]. As a crucial insight, this can be overcome on the non-perturbative branch of type IIB, also known as F-theory [52,53]. This setting allows for more general branes, thus avoiding constraints of the Dp -brane framework. GUT breaking can be realized using hypercharge flux (the VEV of the $U(1)_Y$ field strength), an option not available in heterotic models. The whole framework combines the advantages of the heterotic or higher-dimensional unification approach with the more recent progress in understanding moduli stabilization. It thus represents at this moment the most active and promising branch of theory-driven GUT model building (see e.g. [54] and refs. therein).

As a result of the flux-breaking, a characteristic ‘type IIB’ or ‘F-theoretic’ tree-level correction to gauge unification arises [55]. The fact that this correction can be rather significant numerically is occasionally held against the framework of F-theory GUTs. However, at a parametric level, this correction nevertheless behaves like a 4d threshold, i.e., it provides $\mathcal{O}(1)$ additive contributions to the inverse 4d gauge couplings $\alpha_i^{-1}(M_G)$.

A final important issue in string GUTs is the so-called string-scale/GUT-scale problem [56]. It arises since, in heterotic compactifications, the Planck scale and the high-scale value of the gauge coupling unambiguously fix the string-scale to about 10^{18} GeV. As the compactification radius R is raised above the string length, the GUT scale (identified with $1/R$) goes down and the string coupling goes up. Within the domain of perturbative string theory, a gap of about a factor ~ 20 remains between the lowest GUT scale achievable in this way and the phenomenological goal of 2×10^{16} GeV. The situation can be improved by venturing into the non-perturbative regime [56], by considering ‘anisotropic’ geometries with hierarchically different radii R [56,57] or by including GUT scale threshold corrections [58,59].

In F-theory GUTs, the situation is dramatically improved since the gauge theory lives only in four out of the six compact dimensions. This allows for models with a ‘decoupling limit’, where the GUT scale is parametrically below the Planck scale [53]. However, moduli stabilization may not be without problems in such constructions, in part due to a tension between the required large volume and the desirable low SUSY breaking scale.

93.5 Gauge coupling unification

The quantitative unification of the three SM gauge couplings at the energy scale M_G is one of the cornerstones of the GUT paradigm. It is obviously of direct phenomenological relevance. Gauge coupling unification is well understood in the framework of effective field theory (EFT) [60]. In the simplest case, the relevant EFT at energies $\mu \gg M_G$ has a unified gauge symmetry (say $SU(5)$ for definiteness) and a single running gauge coupling $\alpha_G(\mu)$. At energies $\mu \ll M_G$, states with mass $\sim M_G$ (such as X bosons, GUT Higgs, color-triplet Higgs) have to be integrated out. The EFT now has three independent couplings and SM (or SUSY SM) matter content. One-loop renormalization group equations readily allow for an extrapolation to the weak scale,

$$\alpha_i^{-1}(m_Z) = \alpha_G^{-1}(M_G) + \frac{b_i}{2\pi} \log\left(\frac{M_G}{m_Z}\right) + \delta_i, \quad (93.3)$$

($i = 1, 2, 3$). Here we defined δ_i to absorb all sub-leading effects, such as threshold corrections at or near the weak scale (e.g. from superpartners and the additional Higgs bosons in the case of the MSSM) and at the GUT scale, and also higher-order corrections. We will discuss them momentarily.

It is apparent from Eq. (93.3) that the three low-scale couplings can be very different. This is due to the large energy range $m_Z \ll \mu \ll M_G$ and the non-universal β -function coefficients

($b_i^{\text{SM}} = \{41/10, -19/6, -7\}$ or $b_i^{\text{MSSM}} = \{33/5, 1, -3\}$). Incomplete GUT multiplets, such as gauge and Higgs bosons in the SM and also their superpartners and the additional Higgs bosons in the MSSM, contribute to the differences between the β functions. Inverting the argument, one expects that extrapolating the measured couplings to the high scale, we find quantitative unification at $\mu \sim M_G$. While this fails in the SM, it works intriguingly well in the MSSM (cf. Fig. 93.1).

The three equations contained in Eq. (93.3) can be used to determine the three ‘unknowns’ $\alpha_3(m_Z)$, $\alpha_G(M_G)$ and M_G , assuming that all other parameters entering the equations are given. Focusing on the SUSY case and using the $\overline{\text{MS}}$ coupling constants $\alpha_{\text{EM}}^{-1}(m_Z)$ and $\sin^2 \theta_W(m_Z)$ from [62],

$$\alpha_{\text{EM}}^{-1}(m_Z) = 127.955 \pm 0.010, \quad (93.4)$$

$$\sin^2 \theta_W(m_Z) = 0.23122 \pm 0.00003, \quad (93.5)$$

as input, one determines $\alpha_{1,2}^{-1}(m_Z)$, which then gives

$$\alpha_G^{-1}(M_G) \simeq 24.3 \quad \text{and} \quad M_G \simeq 2 \times 10^{16} \text{ GeV}. \quad (93.6)$$

Here we have set $\delta_i = 0$ for simplicity. Crucially, one in addition obtains a prediction for the low-energy observable α_3 ,

$$\alpha_3^{-1}(m_Z) = -\frac{5}{7}\alpha_1^{-1}(m_Z) + \frac{12}{7}\alpha_2^{-1}(m_Z) + \Delta_3, \quad (93.7)$$

where

$$\Delta_3 = \frac{5}{7}\delta_1 - \frac{12}{7}\delta_2 + \delta_3. \quad (93.8)$$

Here we followed the elegant formulation in Ref. [63] of the classical analyses of [7]. Of course, it is a matter of convention which of the three low-energy gauge coupling parameters one ‘predicts’ and indeed, early works on the subject discussed the prediction of $\sin^2 \theta_W$ in terms of α_{EM} and α_3 [64,65].

Remarkably, the leading order result (i.e. Eq. (93.7) with $\delta_i = 0$) is in excellent agreement with experiments [62]:

$$\alpha_3^{\text{LO}}(m_Z) = 0.117 \quad \text{vs.} \quad \alpha_3^{\text{EXP}}(m_Z) = 0.1181 \pm 0.0011. \quad (93.9)$$

However, this near perfection is to some extent accidental. To see this, we now discuss the various contributions to the δ_i (and hence to Δ_3).

The two-loop running correction from the gauge sector $\Delta_3^{(2)}$ and the low-scale threshold correction $\Delta_3^{(l)}$ from superpartners can be summarized as [63]

$$\Delta_3^{(2)} \simeq -0.82 \quad \text{and} \quad \Delta_3^{(l)} \simeq \frac{19}{28\pi} \log\left(\frac{m_{\text{SUSY}}}{m_Z}\right). \quad (93.10)$$

The relevant scale m_{SUSY} can be estimated as [66]

$$m_{\text{SUSY}} \rightarrow m_H^{3/19} m_{\tilde{H}}^{12/19} m_{\tilde{W}}^{4/19} \times \left(\frac{m_{\tilde{W}}}{m_{\tilde{g}}}\right)^{28/19} \left(\frac{m_{\tilde{l}}}{m_{\tilde{q}}}\right)^{3/19}, \quad (93.11)$$

where m_H stands for the masses of non-SM Higgs states and superpartner masses are given in self-evident notation. Detailed analyses including the above effects are best done using appropriate software packages, such as SOFTSUSY [61] (or alternatively SuSpect [67] or SPheno [68]). See also [61] for references to the underlying theoretical two-loop analyses.

To get a very rough feeling for these effects, let us assume that all superpartners are degenerate at $m_{\text{SUSY}} = 1$ TeV, except for heavier gluinos: $m_{\tilde{W}}/m_{\tilde{g}} \simeq 1/3$. This gives $\Delta_3^{(l)} \simeq -0.35 + 0.22 \ln(m_{\text{SUSY}}/m_Z) \simeq 0.18$. The resulting prediction of $\alpha_3(m_Z) \simeq 0.126$ significantly upsets the perfect one-loop agreement found earlier. Before discussing this issue further, it is useful to introduce yet another important type of correction, the high or GUT scale thresholds.

To discuss high scale thresholds, let us set all other corrections to zero for the moment and write down a version of Eq. (93.3)

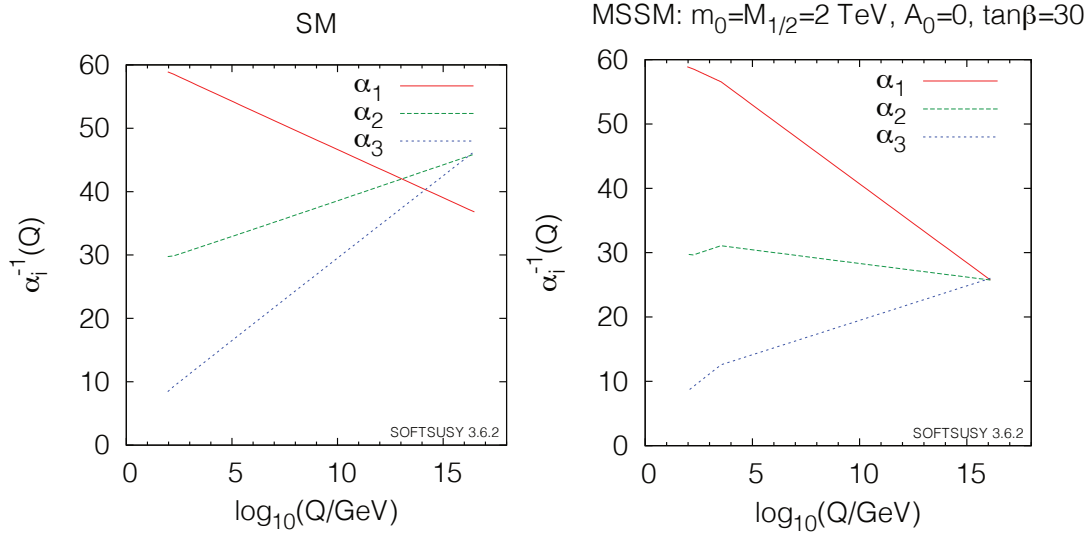


Figure 93.1: Running couplings in SM and MSSM using two-loop RG evolution. The SUSY threshold at 2 TeV is clearly visible on the MSSM side. (We thank Ben Allanach for providing the plots created using SOFTSUSY [61].)

that captures the running near and above the GUT scale more correctly. The threshold correction at one-loop level can be evaluated accurately by the simple step-function approximation for the β functions in the $\overline{\text{DR}}$ scheme⁸ [72],

$$\alpha_i^{-1}(m_Z) = \alpha_G^{-1}(\mu) + \frac{1}{2\pi} \left[b_i^C \ln \frac{\mu}{m_Z} + b_i^X \ln \frac{\mu}{M_C} + b_i^Y \ln \frac{\mu}{M_X} + b_i^\Phi \ln \frac{\mu}{M_\Phi} \right]. \quad (93.12)$$

Here we started the running at some scale $\mu \gg M_G$, including the contribution of the minimal set of states relevant for the transition from the high-scale $SU(5)$ model to the MSSM. These are the color-triplet Higgs multiplets with mass M_C , massive vector multiplets of X -bosons with mass M_X (including GUT Higgs degrees of freedom), and the remaining GUT-Higgs fields and superpartners with mass M_Φ . The coefficients $b_i^{C,X,\Phi}$ can be found in Ref. [73]. Crucially, the b_i in Eq. (93.12) conspire to make the running GUT-universal at high scales, such that the resulting prediction for α_3 does not depend on the value of μ .

To relate this to our previous discussion, we can, for example, define $M_G \equiv M_X$ and then choose $\mu = M_G$ in Eq. (93.12). This gives the high-scale threshold corrections

$$\delta_i^{(h)} = \frac{1}{2\pi} \left[b_i^C \ln \frac{M_G}{M_C} + b_i^\Phi \ln \frac{M_G}{M_\Phi} \right], \quad (93.13)$$

and a corresponding correction $\Delta_3^{(h)}$. To get some intuition for the magnitude, one can furthermore assume $M_\Phi = M_G$, finding (with $b_i^C = \{2/5, 0, 1\}$)

$$\Delta_3^{(h)} = \frac{9}{14\pi} \ln \left(\frac{M_G}{M_C} \right). \quad (93.14)$$

To obtain the desired effect of $-\Delta_3^{(2)} - \Delta_3^{(1)} \simeq +0.64$, the triplet Higgs would have to be by about a factor 20 lighter than the GUT scale. While this is ruled out by nucleon decay in the minimal model [74] as will be discussed Sec. 93.6, it is also clear that threshold corrections of this order of magnitude can, in general, be realized with a certain amount of GUT-scale model building, e.g. in specific $SU(5)$ [25] or $SO(10)$ [26,27] constructions. Corrections can also be much larger or of different sign if, as is required in many fully realistic 4d GUT models, many additional (and in

particular higher) representations are introduced. Thus, there is considerable model building freedom. Nevertheless, a significant constraint from getting the right GUT threshold corrections while keeping the triplet Higgs heavy remains.

The above analysis implicitly assumes universal soft SUSY breaking masses at the GUT scale, which directly affect the spectrum of SUSY particles at the weak scale. In the simplest case we have a universal gaugino mass $M_{1/2}$, a universal mass for squarks and sleptons m_{16} and a universal Higgs mass m_{10} , as motivated by $SO(10)$. In some cases, threshold corrections to gauge coupling unification can be exchanged for threshold corrections to soft SUSY parameters (see [75] and refs. therein). For example, if gaugino masses were not unified at M_G and, in particular, gluinos were lighter than winos at the weak scale (cf. Eq. (93.11)), then it is possible that, due to weak scale threshold corrections, a much smaller or even slightly negative threshold correction at the GUT scale would be consistent with gauge coupling unification [76].

It is also noteworthy that perfect unification can be realized without significant GUT-scale corrections, simply by slightly raising the (universal) SUSY breaking scale. In this case the dark matter abundance produced by thermal processes in the early Universe (if the lightest neutralino is the dark matter particle) is too high. However, even if the gaugino mass in the MSSM is about 1 TeV to explain the dark matter abundance, if the Higgsino and the non-SM Higgs boson masses are about 10-100 TeV, the effective SUSY scale can be raised [77]. This setup is realized in split SUSY [78] or the pure gravity mediation model [79] based on anomaly mediation [80]. Since the squarks and sleptons are much heavier than the gaugino masses in those setups, a gauge hierarchy problem is reintroduced. The facts that no superpartners have so far been seen at the LHC and that the observed Higgs mass favors heavier stop masses than about 1 TeV force one to accept a certain amount of fine-tuning anyway.

For non-SUSY GUTs or GUTs with a very high SUSY breaking scale to fit the data, new light states in incomplete GUT multiplets or multiple GUT breaking scales are required. For example, non-SUSY models $SO(10) \rightarrow SU(4)_C \times SU(2)_L \times SU(2)_R \rightarrow \text{SM}$, with the second breaking scale of order an intermediate scale, determined by light neutrino masses using the see-saw mechanism, can fit the low-energy data for gauge couplings [81] and at the same time survive nucleon decay bounds [82]. Alternatively, one can appeal to string-theoretic corrections discussed in Sec. 93.4 to compensate for a high SUSY breaking scale. This has, for example, been concretely analyzed in the context of F-theory GUTs in [83]. Similarly, one may even wonder whether particularly large GUT threshold corrections could be sufficient to ensure non-SUSY precision unification. Notice here that the gauge coupling unifica-

⁸The $\overline{\text{DR}}$ scheme is frequently used in a supersymmetric regularization [69]. The renormalization transformation of the gauge coupling constants from $\overline{\text{MS}}$ to $\overline{\text{DR}}$ scheme is given in Ref. [70]. For an alternative treatment using holomorphic gauge couplings and NSVZ β -functions see e.g. [71].

tion predicts just one parameter. When introducing new states, typically one can fit the data by choice of their masses. This is not the case in SUSY GUTs with low-scale SUSY breaking scale where the masses are constrained by fine-tuning.

In 5d or 6d orbifold GUTs, certain ‘‘GUT scale’’ threshold corrections come from the Kaluza-Klein modes between the compactification scale, $M_c \sim 1/R$, and the effective cutoff scale M_* . In string theory, this cutoff scale is the string scale. Gauge coupling unification at two loops then constrains the values of M_c and M_* .⁹ Often, one finds M_c to be lower than the 4d GUT scale. Since the X -bosons, responsible for nucleon decay, get mass at the compactification scale, this has significant consequences for nucleon decay.

Finally, it has been shown that non-supersymmetric GUTs in warped 5d orbifolds can be consistent with gauge coupling unification. This assumes (in 4d language) that the r.h. top quark and the Higgs doublets are composite-like objects with a compositeness scale in the TeV range [85].

93.6 Nucleon decay

Quarks and leptons are indistinguishable in any 4d GUT, and both the baryon (B) and lepton number (L) are not conserved. This leads to baryon-number-violating nucleon decay. In addition to baryon-number violation, lepton-number violation is also required for nucleon decay since, in the SM, leptons are the only free fermions which are lighter than nucleons. The lowest-dimension operators relevant for nucleon decay are $(B+L)$ violating dimension-six four-fermion-terms in the SM, and all baryon-violating operators with dimension less than seven preserve $(B-L)$ [1, 86].

In $SU(5)$ GUTs, the dimension-six operators are induced by X boson exchange. These operators are suppressed by $(1/M_X^2)$ (M_X is the X boson mass), and the nucleon lifetime is given by $\tau_N \propto M_X^4/(\alpha_G^2 m_p^5)$ (m_p is proton mass). The dominant decay mode of the proton (and the baryon-violating decay mode of the neutron), via X boson exchange, is $p \rightarrow e^+ \pi^0$ ($n \rightarrow e^+ \pi^-$). In any simple gauge symmetry, with one universal GUT coupling α_G and scale M_X , the nucleon lifetime from gauge boson exchange is calculable. Hence, the GUT scale may be directly observed via the extremely rare decay of the nucleon. Experimental searches for nucleon decay began with the Kolar Gold Mine, Homestake, Soudan, NUSEX, Frejus, HPW, IMB, and Kamiokande detectors [64]. The present experimental bounds on the modes come from Super-Kamiokande. With 306 kton-years of data they find $\tau_p/\text{Br}(p \rightarrow e^+ \pi^0) > 1.67 \times 10^{34}$ years at 90% CL [87]. In addition, Hyper-Kamiokande [88] is planned to reach to $\tau_p/\text{Br}(p \rightarrow e^+ \pi^0) \sim 10^{35}$ years. The hadronic matrix elements for baryon-number-violating operators are evaluated with lattice QCD simulations [89]. In SUSY $SU(5)$ GUTs, the lower bound on the X boson mass from null results in nucleon decay searches is approaching 10^{16} GeV [90], which is close to the GUT scale suggested by gauge coupling unification. On the other hand, the prediction for nucleon decay in non-SUSY GUTs is hard to quantify. The reason is that gauge couplings do not unify with just the SM particle content. Once extra states or large thresholds are included to ensure precision unification, a certain range of unification scales is allowed.

In SUSY GUTs there are additional sources for baryon and/or lepton-number violation – dimension-four and five operators [14]. These arise since, in the SUSY SM, quarks and leptons have scalar partners (squarks and sleptons). Although our notation does not change, when discussing SUSY models our fields are chiral superfields and both fermionic and bosonic matter is implicitly represented by those. In this language, baryon- and/or lepton-number-violating dimension-four and five operators are given as so-called F terms of products of chiral superfields, which contain two fermionic components and the rest scalars or products of scalars. Within the context of $SU(5)$ the dimension-four and five operators have the form

$$(10 \bar{5} \bar{5}) \supset (u^c d^c d^c) + (Q L d^c) + (e^c L L),$$

⁹ It is interesting to note that a ratio $M_*/M_c \sim 100$, needed for gauge coupling unification to work in orbifold GUTs, is typically the maximum value for this ratio consistent with perturbativity [84].

$$(10 \ 10 \ 10 \ \bar{5}) \supset (Q Q Q L) + (u^c u^c d^c e^c) + B\text{- and }L\text{-conserving terms,}$$

respectively.

The dimension-four operators in $(10 \bar{5} \bar{5})$ violate either baryon number or lepton number. The nucleon lifetime is extremely short if both types of dimension-four operators are present in the SUSY SM since squark or slepton exchange induces the dangerous dimension-six SM operators. Even in the case that they violate baryon number or lepton number only but not both, they are constrained by various phenomena [91]. For example, the primordial baryon number in the Universe is washed out unless the dimensionless coupling constants are less than 10^{-7} . Both types of operators can be eliminated by requiring R parity, which distinguishes Higgs from ordinary matter multiplets. R parity [92] or its cousin, matter parity [6, 93], act as $F \rightarrow -F$, $H \rightarrow H$ with $F = \{10, \bar{5}\}$, $H = \{\bar{5}_H, 5_H\}$ in $SU(5)$.¹⁰ In $SU(5)$, the Higgs multiplet $\bar{5}_H$ and the matter multiplets $\bar{5}$ have identical gauge quantum numbers. In E_6 , Higgs and matter multiplets could be unified within the fundamental 27 representation. Only in $SO(10)$ are Higgs and matter multiplets distinguished by their gauge quantum numbers. The Z_4 center of $SO(10)$ distinguishes 10_s from 16_s and can be associated with R parity [94].

The baryon-number violating dimension-five operators have a dimensionful coupling. They are generated by integrating out the color-triplet Higgs with GUT-scale mass in SUSY GUTs such that the coefficient is suppressed by $1/M_G$. Note that both triplet Higgsinos (due to their fermionic nature) and Higgs scalars (due to their mass-enhanced trilinear coupling with matter) contribute to the operators. The dimension-five operators include squarks and/or sleptons. To allow for nucleon decay, these must be converted to light quarks or leptons by exchange of a gaugino or Higgsino in the SUSY SM. The nucleon lifetime is proportional to $M_G^2 m_{\text{SUSY}}^2/m_p^5$, where m_{SUSY} is the SUSY breaking scale. Thus, dimension-five operators may predict a shorter nucleon lifetime than dimension-six operators. Unless accidental cancellations are present, the dominant decay modes from dimension-five operators include a K meson, such as $p \rightarrow K^+ \bar{\nu}$ ($n \rightarrow K^0 \bar{\nu}$). This is due to a simple symmetry argument: The operators are given as $(Q_i Q_j Q_k L_l)$ and $(u_i^c u_j^c d_k^c e_l^c)$, where $i, j, k, l (= 1, 2, 3)$ are family indices and color and weak indices are implicit. They must be invariant under $SU(3)_C$ and $SU(2)_L$ so that their color and weak doublet indices must be anti-symmetrized. Since these operators are given by bosonic superfields, they must be totally symmetric under interchange of all indices. Thus, the first operator vanishes for $i = j = k$ and the second vanishes for $i = j$. Hence a second or third generation member exists in the dominant modes of nucleon decay unless these modes are accidentally suppressed [93].

The Super-Kamiokande bounds on the proton lifetime severely constrain the dimension-five operators. With 306 kton-years of data they find $\tau_p/\text{Br}(p \rightarrow K^+ \bar{\nu}) > 6.61 \times 10^{33}$ years at 90% CL [87]. In the minimal SUSY $SU(5)$, $\tau_p/\text{Br}(p \rightarrow K^+ \bar{\nu})$ is smaller than about 10^{31} years if the triplet Higgs mass is 10^{16} GeV and $m_{\text{SUSY}} = 1$ TeV [95]. The triplet Higgs mass bound from nucleon decay is then in conflict with gauge coupling unification so that this model is considered to be ruled out [74].

Since nucleon decay induced by the triplet Higgs is a severe problem in SUSY GUTs, various proposals for its suppression have been made. First, some accidental symmetry or accidental structure in non-minimal Higgs sectors in $SU(5)$ or $SO(10)$ theories may suppress the dimension-five operators [22, 26, 27, 96]. Symmetries to suppress the dimension-five operators are typically broken by the VEVs responsible for the color-triplet Higgs masses. Consequently, the dimension-five operators are generically generated via the triplet Higgs exchange in SUSY $SU(5)$ GUTs, as mentioned above. In other words, the nucleon decay is suppressed if the Higgs triplets in $\bar{5}_H$ and 5_H do not have a common mass term but, instead, their mass terms involve partners

¹⁰ This forbids the dimension-four operator $(10 \bar{5} \bar{5})$, but allows the Yukawa couplings for quark and lepton masses of the form $(10 \bar{5} \bar{5}_H)$ and $(10 \ 10 \ 5_H)$. It also forbids the dimension-three, lepton-number-violating operator $(\bar{5} \ 5_H) \supset (L H_u)$ as well as the dimension-five, baryon-number-violating operator $(10 \ 10 \ 10 \ 5_H) \supset (Q Q Q H_d) + \dots$

from other $SU(5)$ multiplets. Second, the SUSY breaking scale may be around $\mathcal{O}(10\text{--}100)$ TeV in order to explain the observed Higgs boson mass at the LHC. In this case, nucleon decay is automatically suppressed [78,97,98]. Third, accidental cancellations among diagrams due to a fine-tuned structure of squark and slepton flavor mixing might suppress nucleon decay [99]. Last, we have also implicitly assumed a hierarchical structure for Yukawa matrices in the analysis. It is however possible to fine-tune a hierarchical structure for quarks and leptons which baffles the family structure so that the nucleon decay is suppressed [100]. The upper bound on the proton lifetime from some of these theories is approximately a factor of 10 above the experimental bounds. Future experiments with larger neutrino detectors, such as JUNO [101], Hyper-Kamiokande [88] and DUNE [102], are planned and will have higher sensitivities to nucleon decay.

Are there ways to avoid the stringent predictions for proton decay discussed above? Orbifold GUTs and string theories, see Sec. 93.4, contain grand unified symmetries realized in higher dimensions. In the process of compactification and GUT symmetry breaking, the triplet Higgs states may be removed (projected out of the massless sector of the theory). In such models, the nucleon decay due to dimension-five operators can be severely suppressed or eliminated completely. However, nucleon decay due to dimension-six operators may be enhanced, since the gauge-bosons mediating proton decay obtain mass at the compactification scale, M_c , which is typically less than the 4d GUT scale (cf. Sec. 93.5). Alternatively, the same projections which eliminate the triplet Higgs may rearrange the quark and lepton states such that the massless states of one family come from different higher-dimensional GUT multiplets. This can suppress or completely eliminate even dimension-six proton decay. Thus, enhancement or suppression of dimension-six proton decay is model-dependent. In some complete 5d orbifold GUT models [63,103] the lifetime for the decay $\tau_p/\text{Br}(p \rightarrow e^+ \pi^0)$ can be near the bound of 1×10^{34} years with, however, large model-dependence and/or theoretical uncertainties. In other cases, the modes $p \rightarrow K^+ \bar{\nu}$ and $p \rightarrow K^0 \mu^+$ may be dominant [63]. Thus, interestingly, the observation of nucleon decay may distinguish string or higher-dimensional GUTs from 4d ones.

In orbifold GUTs or string theory, new discrete symmetries consistent with SUSY GUTs can forbid all dimension-three and four baryon- and lepton-number-violating operators. Even the μ term and dimension-five baryon- and lepton-number-violating operators can be forbidden to all orders in perturbation theory [33]. The μ term and dimension-five baryon- and lepton-number-violating operators may then be generated, albeit sufficiently suppressed, via non-perturbative effects. The simplest example of this is a Z_4^R symmetry which is the unique discrete R symmetry consistent with $SO(10)$ [33]. Even though it forbids the dimension-five proton decay operator to the desired level, it allows the required dimension-five neutrino mass term. In this case, proton decay is dominated by dimension-six operators, leading to decays such as $p \rightarrow e^+ \pi^0$.

93.7 Yukawa coupling unification

In the SM, masses and mixings for quarks and leptons come from the Yukawa couplings with the Higgs doublet, but the values of these couplings remain a mystery. GUTs provide at least a partial understanding since each generation is embedded in unified multiplet(s). Specifically, since quarks and leptons are two sides of the same coin, the GUT symmetry relates the Yukawa couplings (and hence the masses) of quarks and leptons.

In $SU(5)$, there are two types of independent renormalizable Yukawa interactions given by $\lambda_{ij} (\mathbf{10}_i \mathbf{10}_j \mathbf{5}_H) + \lambda'_{ij} (\mathbf{10}_i \mathbf{5}_j \mathbf{5}_H)$. These contain the SM interactions $\lambda_{ij} (Q_i u_j^c H_u) + \lambda'_{ij} (Q_i d_j^c H_d + e_i^c L_j H_d)$. Here i, j ($= 1, 2, 3$) are, as before, family indices. Hence, at the GUT scale we have tree-level relations between Yukawa coupling constants for charged lepton and down quark masses, such as $\lambda_b = \lambda_\tau$ in which $\lambda_{b/\tau}$ are the bottom quark / τ lepton Yukawa coupling constants [104,105]. In $SO(10)$, there is only one type of independent renormalizable Yukawa interaction given by $\lambda_{ij} (\mathbf{16}_i \mathbf{16}_j \mathbf{10}_H)$, leading to relations among all Yukawa coupling constants and

quark and lepton masses within one generation [106,107] (such as $\lambda_t = \lambda_b = \lambda_\tau$, with λ_t the top quark Yukawa coupling constant).

In addition to gauge coupling unification, the ratio of bottom quark and τ lepton mass has been a central target in the study of GUTs since it was found that this ratio was almost consistent with observations after including the QCD correction [104]. Today the quark masses and the gauge coupling constants are known precisely such that, as discussed below, the ratio of bottom quark and τ lepton mass has become a target of precision analyses in the GUT context.

93.7.1 The third generation, $b\text{--}\tau$ or $t\text{--}b\text{--}\tau$ unification

Third generation Yukawa couplings are larger than those of the first two generations. Hence, the fermion mass relations predicted from renormalizable GUT interactions which we introduced above are expected to be more reliable. In order to compare them with data, we have to include the radiative correction to these relations from the RG evolution between GUT and fermion mass scale, from integrating out heavy particles at the GUT scale, and from weak scale thresholds.

Since testing Yukawa coupling unification is only possible in models with successful gauge coupling unification, we here focus on SUSY GUTs. In the MSSM, top and bottom quark and τ lepton masses are related to the Yukawa coupling constants at the scale m_Z as

$$\begin{aligned} m_t(m_Z) &= \lambda_t(m_Z) v_u (1 + \delta m_t/m_t), \\ m_{b/\tau}(m_Z) &= \lambda_{b/\tau}(m_Z) v_d (1 + \delta m_{b/\tau}/m_{b/\tau}), \end{aligned}$$

where $\langle H_u^0 \rangle \equiv v_u = \sin \beta v/\sqrt{2}$, $\langle H_d^0 \rangle \equiv v_d = \cos \beta v/\sqrt{2}$, $v_u/v_d \equiv \tan \beta$ and $v \sim 246$ GeV is fixed by the Fermi constant, G_μ . Here, $\delta m_f/m_f$ ($f = t, b, \tau$) represents the threshold correction due to integrating out SUSY partners. For the bottom quark mass, it is found [108] that the dominant corrections come from the gluino-sbottom and from the Higgsino-stop loops,

$$\begin{aligned} \left(\frac{\delta m_b}{m_b}\right)_{g_3} &\sim \frac{g_3^2}{6\pi^2} \frac{m_{\tilde{g}} \mu}{m_{\text{SUSY}}^2} \tan \beta \quad \text{and} \\ \left(\frac{\delta m_b}{m_b}\right)_{\lambda_t} &\sim \frac{\lambda_t^2}{16\pi^2} \frac{A_t \mu}{m_{\text{SUSY}}^2} \tan \beta, \end{aligned} \quad (93.16)$$

where $m_{\tilde{g}}$, μ , and A_t stand for gluino and Higgsino masses and trilinear stop coupling, respectively. Note that Eq. (93.16) only illustrates the structure of the corrections – non-trivial functional dependences on several soft parameters $\sim m_{\text{SUSY}}$ have been suppressed. For the full one-loop correction to the bottom quark mass see, for example, Ref. [109].

Note also that the corrections do not go to zero as SUSY particles become much heavier than m_Z . They may change the bottom quark mass at the $\mathcal{O}(10)\%$ level for $\tan \beta = \mathcal{O}(10)$. The total effect is sensitive to the relative phase between gluino and Higgsino masses since $A_t \sim -m_{\tilde{g}}$ due to the infrared fixed point nature of the RG equation for A_t [110] in settings where SUSY breaking terms come from Planck scale dynamics, such as gravity mediation. The τ lepton mass also receives a similar correction, though only at the few % level. The top quark mass correction, not being proportional to $\tan \beta$, is at most 10% [111].

Including one loop threshold corrections at m_Z and additional RG running, one finds the top, bottom and τ pole masses. In SUSY GUTs, $b\text{--}\tau$ unification has two possible solutions with $\tan \beta \sim 1$ or $\mathcal{O}(10)$. The small $\tan \beta$ solution may be realized in the MSSM if superpartner masses are $\mathcal{O}(10)$ TeV, as suggested by the observed Higgs mass [97]. The large $\tan \beta$ limit such as $\tan \beta \sim 40\text{--}50$ overlaps the $SO(10)$ symmetry relation [111,112]. When $\tan \beta$ is large, there are significant threshold corrections to down quark masses as mentioned above, and Yukawa unification is only consistent with low-energy data in a restricted region of SUSY parameter space, with important consequences for SUSY searches [111,113]. More recent analyses of Yukawa unification after LHC Run-I are found in Ref. [114].

Gauge coupling unification is also successful in the scenario of split supersymmetry [78], in which squarks and sleptons have mass

at a scale $\tilde{m} \gg m_Z$, while gauginos and/or Higgsinos have masses of order the weak scale. Unification of b - τ Yukawa couplings requires $\tan\beta$ to be fine-tuned close to 1 [97]. If by contrast, $\tan\beta \gtrsim 1.5$, b - τ Yukawa unification only works for $\tilde{m} \lesssim 10^4$ GeV. This is because the effective theory between the gaugino mass scale and \tilde{m} includes only one Higgs doublet, as in the standard model. As a result, the large top quark Yukawa coupling tends to increase the ratio λ_b/λ_τ due to the vertex correction, which is absent in supersymmetric theories, as one runs down in energy below \tilde{m} . This is opposite to what happens in the MSSM where the large top quark Yukawa coupling lowers the ratio λ_b/λ_τ [105].

93.7.2 Beyond leading order: three-family models

Simple Yukawa unification is not possible for the first two generations. Indeed, the simplest implementation of $SU(5)$ implies $\lambda_s = \lambda_\mu$, $\lambda_d = \lambda_e$ and hence $\lambda_s/\lambda_d = \lambda_\mu/\lambda_e$. This is an RG-invariant relation which extrapolates to $m_s/m_d = m_\mu/m_e$ at the weak scale, in serious disagreement with data ($m_s/m_d \sim 20$ and $m_\mu/m_e \sim 200$). An elegant solution to this problem was given by Georgi and Jarlskog [115] (for a recent analysis in the SUSY context see [116]).

More generally, we have to recall that in all of the previous discussion of Yukawa couplings, we assumed renormalizable interactions as well as the minimal matter and Higgs content. Since the GUT scale is close to the Planck scale, higher-dimension operators involving the GUT-breaking Higgs may modify the predictions, especially for lower generations. An example is provided by the operators $\mathbf{10} \bar{\mathbf{5}} \bar{\mathbf{5}}_H \mathbf{24}_H$ with $\mathbf{24}_H$ the GUT-breaking Higgs of $SU(5)$. We can fit parameters to the observed fermion masses with these operators, though some fine-tuning is introduced in doing so. The SM Higgs doublet may come in part from higher representations of the GUT group. For example, the $\mathbf{45}$ of $SU(5)$ includes an $SU(2)_L$ doublet with appropriate $U(1)_Y$ charge [115]. This $\mathbf{45}$ can, in turn, come from the $\mathbf{120}$ or $\mathbf{126}$ of $SO(10)$ after its breaking to $SU(5)$ [117, 118]. These fields may also have renormalizable couplings with quarks and leptons. The relations among the Yukawa coupling constants in the SM are modified if the SM Higgs doublet is a linear combination of several such doublets from different $SU(5)$ multiplets. Finally, the SM fermions may not be embedded in GUT multiplets in the minimal way. Indeed, if all quarks and leptons are embedded in $\mathbf{16}$ s of $SO(10)$, the renormalizable interactions with $\mathbf{10}_H$ cannot explain the observed CKM mixing angles. This situation improves when extra matter multiplets, such as $\mathbf{10}$, are introduced: After $U(1)_X$, which distinguishes the $\bar{\mathbf{5}}$ s coming from the $\mathbf{16}$ and the $\mathbf{10}$ of $SO(10)$, is broken (e.g. by a VEV of $\mathbf{16}_H$ or $\mathbf{126}_H$), the r.h. down quarks and l.h. leptons in the SM can be linear combinations of components in $\mathbf{16}$ s and $\mathbf{10}$ s. As a result, $\lambda \neq \lambda'$ in $SU(5)$ [119].

To construct realistic three-family models, some or all of the above effects can be used. Even so, to achieve significant predictions for fermion masses and mixing angles grand unification alone is not sufficient. Other ingredients, for example additional global family symmetries are needed (in particular, non-Abelian symmetries can strongly reduce the number of free parameters). These family symmetries constrain the set of effective higher-dimensional fermion mass operators discussed above. In addition, sequential breaking of the family symmetry can be correlated with the hierarchy of fermion masses [120]. One simple, widely known idea in this context is to ensure that each $\mathbf{10}_i$ enters Yukawa interactions together with a suppression factor ϵ^{3-i} (ϵ being a small parameter). This way one automatically generates a stronger hierarchy in up-type quark Yukawas as compared to down-type quark and lepton Yukawas and no hierarchy for neutrinos, which agrees with observations at the $\mathcal{O}(1)$ -level. Three-family models exist which fit all the data, including neutrino masses and mixing [27, 121].

Finally, a particularly ambitious variant of unification is to require that the fermions of all three generations come from a single representation of a large gauge group. A somewhat weaker assumption is that the flavor group (e.g. $SU(3)$) unifies with the SM gauge group in a simple gauge group at some energy scale $M \geq M_G$. Early work on such ‘flavor-unified GUTs’, see e.g. [119, 122], has been reviewed in [123, 124]. For a selection of more recent papers see [125]. In such settings, Yukawa

couplings are generally determined by gauge couplings together with symmetry breaking VEVs. This is reminiscent of heterotic string GUTs, where all couplings come from the 10d gauge coupling. However, while the $E_8 \rightarrow SU(3) \times E_6$ branching rule $\mathbf{248} = (\mathbf{8}, \mathbf{1}) + (\mathbf{1}, \mathbf{78}) + (\mathbf{3}, \mathbf{27}) + (\bar{\mathbf{3}}, \mathbf{27})$ looks very suggestive in this context, the way in which most modern heterotic models arrive at three generations is actually more complicated.

93.8 Neutrino masses

We see from atmospheric and solar neutrino oscillation observations, along with long baseline accelerator and reactor experiments, that neutrinos have finite masses. By adding three ‘sterile’ neutrinos ν_i^c with Yukawa couplings $\lambda_{\nu,ij}$ ($\nu_i^c L_j H_u$) ($i, j = 1, 2, 3$), one easily obtains three massive Dirac neutrinos with mass $m_\nu = \lambda_\nu v_u$, analogously to quark and charged lepton masses. However, in order to obtain a τ neutrino with mass of order 0.1 eV, one requires the exceedingly small coupling ratio $\lambda_{\nu\tau}/\lambda_\tau \lesssim 10^{-10}$. By contrast, in GUTs the seesaw mechanism *naturally* explains such tiny neutrino masses as follows [2–4]: The sterile neutrinos have no SM gauge quantum numbers so that there is no symmetry other than global lepton number which forbids the Majorana mass term $\frac{1}{2} M_{ij} \nu_i^c \nu_j^c$. Note also that sterile neutrinos can be identified with the r.h. neutrinos necessarily contained in complete families of $SO(10)$ or Pati-Salam models. Since the Majorana mass term violates $U(1)_X$ in $SO(10)$, one might expect $M_{ij} \sim M_G$. The heavy sterile neutrinos can be integrated out, defining an effective low-energy theory with only three light active Majorana neutrinos with the effective dimension-five operator

$$- \mathcal{L}_{eff} = \frac{1}{2} c_{ij} (L_i H_u) (L_j H_u), \quad (93.17)$$

where $c = \lambda_\nu^T M^{-1} \lambda_\nu$. This then leads to a 3×3 Majorana neutrino mass matrix $m = m_\nu^T M^{-1} m_\nu$.

The seesaw mechanism implemented by r.h. neutrinos is sometimes called the type-I seesaw model. There are variant models in which the dimension-five operator for neutrino masses is induced in different ways: In the type-II model, an $SU(2)_L$ triplet Higgs boson Σ is introduced to have couplings ΣL^2 and also ΣH_u^2 [117, 126]. In the type-III model, an $SU(2)_L$ triplet of fermions $\bar{\Sigma}$ with a Yukawa coupling $\bar{\Sigma} L H_u$ is introduced [127]. In these models, the dimension-five operator is induced by integrating out the triplet Higgs boson or fermions. Such models can also be implemented in GUTs by introducing Higgs bosons in the $\mathbf{15}$ or fermions in the $\mathbf{24}$ in $SU(5)$ GUTs or the $\mathbf{126}$ in $SO(10)$ GUTs. Notice that the gauge non-singlet fields in the type-II and III models have masses at the intermediate scale. Thus, gauge coupling unification is not automatic if these variant mechanisms are implemented in SUSY GUTs.

Atmospheric neutrino oscillations discovered by Super-Kamiokande [128] require neutrino masses with $\Delta m_m^2 \sim 2.5 \times 10^{-3}$ eV² with maximal mixing [62], in the simplest scenario of two neutrino dominance. With hierarchical neutrino masses this implies $m_{\nu\tau} = \sqrt{\Delta m_m^2} \sim 0.05$ eV. Next, we can try to relate the neutrino Yukawa coupling to the top quark Yukawa coupling, $\lambda_{\nu\tau} = \lambda_t$ at the GUT scale, as in $SO(10)$ or $SU(4) \times SU(2)_L \times SU(2)_R$ models. This gives $M \sim 10^{14}$ GeV, which is remarkably close to the GUT scale.

Neutrinos pose a special problem for GUTs. The question is why the quark mixing angles in the CKM matrix are small while there are two large lepton mixing angles in the PMNS matrix. Global fits of neutrino masses and mixing angles can, for example, be found in Refs. [129] and [130]. For SUSY GUT models which fit quark and lepton masses, see Ref. [131] for reviews. Finally, for a compilation of the range of SUSY GUT predictions for neutrino mixing, see [132].

93.9 Selected topics

93.9.1 Global symmetries

As we discussed, global symmetries are frequently introduced to control higher-dimension operators in GUT models. This is particularly important in the context of nucleon decay but also plays a role in GUT-based flavor model building and cosmological applications, such as baryogenesis and inflation. However,

we should note that appealing to global symmetries to suppress specific interactions may not be as straightforward as it naively seems. Indeed, there are two possibilities: On the one hand, the relevant symmetry might be gauged at a higher scale. Effects of the VEVs responsible for the spontaneous breaking are then in principle dangerous and need to be quantified. On the other hand, the symmetry might be truly only global. This must e.g. be the case for anomalous symmetries, which are then also violated by field-theoretic non-perturbative effects. The latter can in principle be exponentially small. It is, however, widely believed that global symmetries are always broken in quantum gravity (see e.g. [133]). One then needs to understand which power or functional form the Planck scale suppression of the relevant interaction has. For example, dimension-five baryon number violating operators suppressed by just one unit of the Planck or string scale are completely excluded.

In view of the above, it is also useful to recall that in string models 4d global symmetries generally originate in higher-dimensional gauge symmetries [38, 134]. Here ‘global’ implies that the gauge boson has acquired a Stückelberg-mass. This is a necessity in the anomalous case (Green-Schwarz mechanism [135]) but can also happen to non-anomalous symmetries. One expects no symmetry violation beyond the well-understood non-perturbative effects. Discrete symmetries arise as subgroups of continuous gauge symmetries, such as $\mathbb{Z}_N \subset U(1)$. In particular, non-anomalous subgroups of Stückelberg-massive $U(1)$ s represent unbroken discrete gauge symmetries and as such are non-perturbatively exact (see e.g. [136]). Of course, such discrete gauge symmetries may also arise as remnants of continuous gauge symmetries after conventional 4d spontaneous breaking.

93.9.2 Anomaly constraints vs. GUT paradigm

As emphasized at the very beginning, the fact that the SM fermions of one generation fill out the $\mathbf{10} + \bar{\mathbf{5}}$ of $SU(5)$ appears to provide overwhelming evidence for some form of GUT embedding. However, one should be aware that a counterargument can be made which is related to the issue of ‘charge quantization by anomaly cancellation’ (see [137, 138] for some early papers and [139] for a more detailed reference list): Imagine we only knew that the low-energy gauge group were G_{SM} and the matter content included the $(\mathbf{3}, \mathbf{2})_Y$, i.e. a ‘quark doublet’ with $U(1)$ -charge Y . One can then ask which possibilities exist of adding further matter to ensure the cancellation of all triangle anomalies. It turns out that this problem has only three different, minimal¹¹ solutions [138]. One of those is precisely a single SM generation, with the apparent ‘ $SU(5)$ -ness’ emerging accidentally. Thus, if one randomly picks models from the set of consistent gauge theories, preconditioning on G_{SM} and $(\mathbf{3}, \mathbf{2})_Y$, one may easily end up with ‘ $\mathbf{10} + \bar{\mathbf{5}}$ ’ of an $SU(5)$ that is in no way dynamically present. This is precisely what happens in the context of non-GUT string model building [140].

93.9.3 Magnetic monopoles

In the broken phase of a GUT there are typically localized classical solutions carrying magnetic charge under an unbroken $U(1)$ symmetry [141]. These magnetic monopoles with mass of order M_G/α_G can be produced during a possible GUT phase transition in the early Universe. The flux of magnetic monopoles is experimentally found to be less than $\sim 10^{-16} \text{ cm}^{-2} \text{ s}^{-1} \text{ sr}^{-1}$ [142]. Many more are however predicted, hence the GUT monopole problem. In fact, one of the original motivations for inflation was to solve the monopole problem by exponential expansion after the GUT phase transition [143] and hence dilution of the monopole density. Other possible solutions to the monopole problem include: sweeping them away by domain walls [144], $U(1)$ electromagnetic symmetry breaking at high temperature [145] or GUT symmetry non-restoration [146]. Parenthetically, it was also shown that GUT monopoles can catalyze nucleon decay [147]. A significantly stronger bound on the monopole flux can then be obtained by considering X-ray emission from radio pulsars due

to monopole capture and the subsequent nucleon decay catalysis [148].

Note that the present upper bound on the inflationary vacuum energy density is very close to the GUT scale, $V_{inf}^{1/4} = (1.88 \times 10^{16} \text{ GeV}) \times (r/0.10)^{1/4}$, with the scalar-to-tensor ratio constrained to $r < 0.07$ [149]. This guarantees that reheating does not lead to temperatures above M_G and hence the monopole problem is solved by inflation (unless M_G is unexpectedly low).

93.9.4 Flavor violation

Yukawa interactions of GUT-scale particles with quarks and leptons may leave imprints on the flavor violation induced by SUSY breaking parameters [150]. To understand this, focus first on the MSSM with universal Planck-scale boundary conditions (as e.g. in gravity mediation). Working in a basis where up-quark and lepton Yukawas are diagonal, one finds that the large top-quark Yukawa coupling reduces the l.h. squark mass squareds in the third generation radiatively. It turns out that only the l.h. down-type squark mass matrix has sizable off-diagonal terms in the flavor basis after CKM-rotation. However, in GUTs the color-triplet Higgs has flavor violating interactions from the Yukawa coupling $\lambda_{ij}(\mathbf{10}_i \mathbf{10}_j \mathbf{5}_H)$, such that flavor-violating r.h. slepton mass terms are radiatively generated in addition [151]. In $SU(5)$ extension of the type-I seesaw model, where r.h. neutrinos are introduced as $SU(5)$ singlets with interactions $\lambda''_{ij}(\mathbf{1}_i \bar{\mathbf{5}}_j \mathbf{5}_H)$, the doublet and color-triplet Higgses acquire another type of Yukawa coupling, respectively. They then radiatively generate flavor-violating l.h. slepton [152] and r.h. down squark masses [153]. These flavor-violating SUSY breaking terms induce new contributions to FCNC processes in quark and lepton sectors, such as $\mu \rightarrow e\gamma$ and $K^0-\bar{K}^0$ and $B^0-\bar{B}^0$ mixing. Note that even if the SUSY breaking terms are generated at M_G , the r.h. neutrino Yukawa coupling may induce sizable flavor violation in l.h. slepton masses due to the running between M_G and the right-handed-neutrino mass scale.

EDMs are also induced when both l.h. and r.h. squarks/sleptons have flavor-violating mass terms with relative phases, as discussed for $SO(10)$ in [154] or for $SU(5)$ with r.h. neutrinos in [155]. Thus, such low-energy observables constrain GUT-scale interactions.

93.9.5 From GUT baryogenesis to leptogenesis and B/L -violating transitions

During inflation, any conserved quantum number is extremely diluted. Thus, one expects the observed baryon asymmetry of the Universe to originate at reheating or in the subsequent cosmological evolution. In detail, the situation is slightly more involved: Both baryon number B and lepton number L are global symmetries of the SM. However, $(B+L)$ is anomalous and violated by thermal fluctuations in the early Universe, via so-called sphaleron processes. Moreover, it is violated in GUT models, as is most apparent in proton decay. By contrast, $(B-L)$ is anomaly free and preserved by both the SM as well as $SU(5)$ or $SO(10)$ gauge interactions.

Now, the old idea of GUT baryogenesis [156, 157] is to generate a $(B+L)$ and hence a baryon asymmetry by the out-of-equilibrium decay of the color-triplet Higgs. However such an asymmetry, generated at GUT temperatures, is washed out by sphalerons¹². This can be overcome [159] using lepton-number violating interaction of neutrinos to create a $(B-L)$ from the $(B+L)$ asymmetry, before sphaleron processes become sufficiently fast at $T < 10^{12}$ GeV. This $(B-L)$ asymmetry can then survive the subsequent sphaleron dominated phase. Note that this does not work in the minimal SUSY GUT setting, with the triplet Higgs above the GUT scale. The reason is that a correspondingly high reheating temperature would be required which, as explained above, is ruled out by Planck data.

However, the most widely accepted simple way out of the dilemma is to directly generate a net $(B-L)$ asymmetry dynamically in the early Universe, also using r.h. neutrinos. Indeed, we have seen that neutrino oscillations suggest a new scale of physics

¹¹ Adding extra vector-like sets of fields, e.g. two fermions which only transform under $U(1)$ and have charges Y and $-Y$, is considered to violate minimality.

¹² To be precise, if lepton flavor numbers L_i ($i = 1-3$) are nonzero and $(L_i - L_j) \neq 0$ ($i \neq j$), one may obtain nonzero values for B and L even if $(B-L) = 0$ [158].

of order 10^{14} GeV. This scale is associated with heavy Majorana neutrinos in the seesaw mechanism. If in the early Universe, the decay of the heavy neutrinos is out of equilibrium and violates both lepton number and CP , then a net lepton number may be generated. This lepton number will then be partially converted into baryon number via electroweak processes [160]. This mechanism is called leptogenesis.

If the three heavy Majorana neutrino masses are hierarchical, the net lepton number is produced by decay of the lightest one, and it is proportional to the CP asymmetry in the decay. The CP asymmetry is bounded from above, and the lightest neutrino mass is required to be larger than 10^9 GeV in order to explain the observed baryon asymmetry [161]. This implies that the reheating temperature after inflation should be larger than 10^9 GeV so that the heavy neutrinos are thermally produced¹³. In supersymmetric models, there is a tension between leptogenesis and Big Bang Nucleosynthesis (BBN) if gravitinos decay in the BBN era. The gravitino problem gives a constraint on the reheating temperature $\lesssim 10^{6-10}$ GeV though the precise value depends on the SUSY breaking parameters [163]. Recent reviews of leptogenesis can be found in Ref. [164].

One of the important tests of leptogenesis are searches for neutrinoless double- β ($0\nu\beta\beta$) decays¹⁴. In a $0\nu\beta\beta$ decay, only two electrons but no (anti-)neutrinos are emitted by the decaying nucleus. This is in contrast to ordinary double- β decay. Thus, $0\nu\beta\beta$ decays are lepton-number-violating with $\Delta L = 2$. At the nucleon level, this is described by dimension-nine effective operators for $nn \rightarrow ppee$. These operators may in turn come from SM operators of with dimension less than nine, in combination with SM weak interactions. The lowest one is the dimension-five operator generating the Majorana neutrino mass terms (Eq. (93.17)). Thus, if the lepton-number violating effective interactions come from physics at energies much above the weak scale, the $0\nu\beta\beta$ decay rates are proportional to the Majorana neutrino masses. The latest experimental results are reviewed in [62]. For recent studies of the $0\nu\beta\beta$ decay including SM operators up to mass dimension nine, see [165] and refs. therein.

In addition to L -violation, one can consider $(B-L)$ and B violating phenomena. They are interesting in their own right and may also be relevant to baryogenesis. The relevant operators have higher mass dimension than the familiar dimension-six $(B+L)$ -violating operators (cf. Sec. 93.6). They may be predicted in $SO(10)$ GUTs with an intermediate scale, at which baryogenesis is realized, such as in [166]. First, one may have nucleon decays with $\Delta(B-L) = 2$, such as $n \rightarrow e^-\pi^+$. This is induced by dimension-seven effective operators in the SM, which are suppressed by the SM Higgs VEV or derivatives. Second, there are neutron-antineutron ($n-\bar{n}$) oscillations, which are induced by $\Delta B = 2$ dimension-nine effective operators in the SM. The upper bound on the mean time for $n-\bar{n}$ transitions is directly derived using free neutrons [167]. It is also constrained from the lower limit on the lifetime for neutrons bound in ^{16}O , derived by Super-Kamiokande [168]. Their results are very similar. Super-Kamiokande also searches for dinucleon decays with $\Delta B = 2$, such as $pp \rightarrow \pi^+\pi^+$ and $nn \rightarrow \pi^+\pi^+$ [169].

93.10 Conclusion

Most conservatively, grand unification means that (some of) the SM gauge interactions of $U(1)_Y$, $SU(2)_L$ and $SU(3)_C$ become part of a larger, unifying gauge symmetry at a high energy scale. In most models, especially in the simplest and most appealing variants of $SU(5)$ and $SO(10)$ unification, the statement is much stronger: One expects the three gauge couplings to unify (up to small threshold corrections) at a unique scale, M_G , and the proton to be unstable due to exchange of gauge bosons of the larger symmetry group. Supersymmetric grand unified theories

provide, by far, the most predictive and economical framework allowing for perturbative unification. Many more details than could be discussed in the present article can be found in some of the classic reviews [123,170] and the two books [171] (see also [172] for two recent overviews).

Thus, the three classical pillars of GUTs are gauge coupling unification at $M_G \sim 2 \times 10^{16}$ GeV, low-energy supersymmetry (with a large SUSY desert), and nucleon decay. The first of these may be viewed as predicting the value of the strong coupling – a prediction which has already been verified (see Fig. 93.1). Numerically, this prediction remains intact even if SUSY partner masses are somewhat above the weak scale. However, at the conceptual level a continuously increasing lower bound on the SUSY scale is nevertheless problematic for the GUT paradigm: Indeed, if the independent, gauge-hierarchy-based motivation for SUSY is completely abandoned, the SUSY scale and hence α_3 become simply free parameters and the first two pillars crumble. Thus, it is important to keep pushing bounds on proton decay which, although again not completely universal in all GUT constructions, is arguably a more generic part of the GUT paradigm than low-energy SUSY.

Whether or not Yukawa couplings unify is more model dependent. However, irrespective of possible (partial) Yukawa unification, there certainly exists a very interesting and potentially fruitful interplay between flavor model building and grand unification. Especially in the neutrino sector this is strongly influenced by the developing experimental situation.

Another phenomenological signature of grand unification is the strength of the direct coupling of the QCD axion to photons, relative to its coupling to gluons. It is quantified by the predicted anomaly ratio $E/N = 8/3$ (see [173,174]). This arises in field-theoretic axion models consistent with GUT symmetry (such as DFSZ [175]) and in string-theoretic GUTs [174,176]. In the latter, the axion does not come from the phase of a complex scalar but is a fundamental shift-symmetric real field, coupling through a higher-dimension operator directly to the product of the GUT field-strength and its dual.

It is probably fair to say that, due to limitations of the 4d approach, including especially remaining ambiguities (free parameters or ad hoc assumptions) in models of flavor and GUT breaking, the string theoretic approach has become more important in GUT model building. In this framework, challenges include learning how to deal with the many vacua of the ‘landscape’ as well as, for each vacuum, developing the tools for reliably calculating detailed, phenomenological observables. Finally, due to limitations of space, the present article has barely touched on the interesting cosmological implications of GUTs. They may become more important in the future, especially in the case that a high inflationary energy scale is established observationally.

References

- [1] S. Weinberg, Phys. Rev. Lett. **43**, 1566 (1979).
- [2] P. Minkowski, Phys. Lett. **67B**, 421 (1977).
- [3] T. Yanagida, in *Proceedings of the Workshop on the Unified Theory and the Baryon Number of the Universe*, eds. O. Sawada and A. Sugamoto, KEK report No. 79-18, Tsukuba, Japan, 1979; S. Glashow, Quarks and leptons, published in *Proceedings of the Cargèse Lectures*, M. Levy (ed.), Plenum Press, New York, (1980); M. Gell-Mann, P. Ramond and R. Slansky, in *Supergravity*, ed. P. van Nieuwenhuizen *et al.*, North-Holland, Amsterdam, (1979), p. 315 [arXiv:1306.4669].
- [4] F. Wilczek, eConf **C790823**, 437 (1979); E. Witten, Phys. Lett. **91B**, 81 (1980); R. N. Mohapatra and G. Senjanovic, Phys. Rev. Lett. **44**, 912 (1980), [231(1979)].
- [5] G. 't Hooft, NATO Sci. Ser. B **59**, 135 (1980); M. J. G. Veltman, Acta Phys. Polon. **B12**, 437 (1981); L. Maiani, Gif-sur-Yvette Summer School on Particle Physics, 11th, Gif-sur-Yvette, France, 1979 (Inst. Nat. Phys. Nucl. Phys. Particules, Paris, 1979); E. Witten, Nucl. Phys. **B188**, 513 (1981).
- [6] S. Dimopoulos, S. Raby and F. Wilczek, Phys. Rev. **D24**, 1681 (1981); S. Dimopoulos and H. Georgi, Nucl. Phys.

¹³ This constraint may be avoided in resonant leptogenesis [162], in which the right-handed neutrinos are required to be almost degenerate in mass.

¹⁴ Another important test of leptogenesis would be the observation of CP violation in neutrino oscillations. Strictly speaking, the CP phase in the PMNS matrix does not contribute to ϵ_1 in the seesaw model. Nevertheless, the observation of CP violation in neutrino oscillations would suggest that the seesaw mechanism is associated with a large CP violation, similarly to the quark sector.

- B193**, 150 (1981); L. E. Ibanez and G. G. Ross, *Phys. Lett.* **105B**, 439 (1981); N. Sakai, *Z. Phys.* **C11**, 153 (1981); M. B. Einhorn and D. R. T. Jones, *Nucl. Phys.* **B196**, 475 (1982); W. J. Marciano and G. Senjanovic, *Phys. Rev.* **D25**, 3092 (1982).
- [7] U. Amaldi, W. de Boer and H. Furstenau, *Phys. Lett.* **B260**, 447 (1991); J. R. Ellis, S. Kelley and D. V. Nanopoulos, *Phys. Lett.* **B260**, 131 (1991); P. Langacker and M.-x. Luo, *Phys. Rev.* **D44**, 817 (1991); C. Giunti, C.W. Kim and U.W. Lee, *Mod. Phys. Lett.* **A6**, 1745 (1991); P. Langacker and N. Polonsky, *Phys. Rev.* **D47**, 4028 (1993), [hep-ph/9210235]; M. Carena, S. Pokorski and C. E. M. Wagner, *Nucl. Phys.* **B406**, 59 (1993), [hep-ph/9303202]; See also the review by S. Dimopoulos, S.A. Raby and F. Wilczek, *Physics Today*, p. 25 October (1991).
- [8] Y. Okada, M. Yamaguchi and T. Yanagida, *Prog. Theor. Phys.* **85**, 1 (1991); J. R. Ellis, G. Ridolfi and F. Zwirner, *Phys. Lett.* **B257**, 83 (1991); H. E. Haber and R. Hempfling, *Phys. Rev. Lett.* **66**, 1815 (1991).
- [9] M. Carena *et al.*, *Phys. Lett.* **B355**, 209 (1995), [hep-ph/9504316]; G. Degrandi *et al.*, *Eur. Phys. J.* **C28**, 133 (2003), [hep-ph/0212020]; P. Kant *et al.*, *JHEP* **08**, 104 (2010), [arXiv:1005.5709].
- [10] J. L. Feng *et al.*, *Phys. Rev. Lett.* **111**, 131802 (2013), [arXiv:1306.2318]; S. Heinemeyer (2014), [arXiv:1405.3781]; P. Draper and H. Rzehak, *Phys. Rept.* **619**, 1 (2016), [arXiv:1601.01890].
- [11] J. C. Pati and A. Salam, *Phys. Rev.* **D8**, 1240 (1973); For more discussion on the standard charge assignments in this formalism, see A. Davidson, *Phys. Rev.* **D20**, 776 (1979) and R.N. Mohapatra and R.E. Marshak, *Phys. Lett.* **B91**, 222 (1980); see also J. C. Pati, *Int. J. Mod. Phys. A* **32**, 1741013 (2017), arXiv:1706.09531 for a recent account.
- [12] H. Georgi and S. L. Glashow, *Phys. Rev. Lett.* **32**, 438 (1974).
- [13] J. R. Ellis, M. K. Gaillard and D. V. Nanopoulos, *Phys. Lett.* **80B**, 360 (1979), [Erratum: *Phys. Lett.* **82B**, 464 (1979)]; E. Golowich, *Phys. Rev.* **D24**, 2899 (1981).
- [14] S. Weinberg, *Phys. Rev.* **D26**, 287 (1982); N. Sakai and T. Yanagida, *Nucl. Phys.* **B197**, 533 (1982).
- [15] H. Georgi, *Particles and Fields, Proceedings of the APS Div. of Particles and Fields*, ed. C. Carlson, p. 575 (1975); H. Fritzsch and P. Minkowski, *Annals Phys.* **93**, 193 (1975).
- [16] R. Slansky, *Phys. Rept.* **79**, 1 (1981); H. Georgi, *Front. Phys.* **54**, 1 (1982); R. Feger and T. W. Kephart, *Comput. Phys. Commun.* **192**, 166 (2015), [arXiv:1206.6379]; N. Yamatsu, *PTEP* **2016**, 4, 043B02 (2016), [arXiv:1512.05559].
- [17] S. M. Barr, *Phys. Lett.* **112B**, 219 (1982); J. P. Derendinger, J. E. Kim and D. V. Nanopoulos, *Phys. Lett.* **139B**, 170 (1984); I. Antoniadis *et al.*, *Phys. Lett.* **B194**, 231 (1987); I. Antoniadis *et al.*, *Phys. Lett.* **B231**, 65 (1989).
- [18] F. Gursev, P. Ramond and P. Sikivie, *Phys. Lett.* **60B**, 177 (1976).
- [19] A. de Rujula, H. Georgi and S. L. Glashow, *5th Workshop on Grand Unification*, ed. K. Kang, H. Fried and P. Frampton, World Scientific, Singapore (1984), p. 88; See also earlier paper by Y. Achiman and B. Stech, p. 303, "New Phenomena in Lepton-Hadron Physics," ed. D.E.C. Fries and J. Wess, Plenum, NY (1979).
- [20] B. R. Greene *et al.*, *Nucl. Phys.* **B278**, 667 (1986); B. R. Greene *et al.*, *Nucl. Phys.* **B292**, 606 (1987); B. R. Greene, C. A. Lutken and G. G. Ross, *Nucl. Phys.* **B325**, 101 (1989); J. E. Kim, *Phys. Lett.* **B591**, 119 (2004), [hep-ph/0403196].
- [21] E. Witten, *Phys. Lett.* **105B**, 267 (1981).
- [22] A. Masiero *et al.*, *Phys. Lett.* **115B**, 380 (1982); B. Grinstein, *Nucl. Phys.* **B206**, 387 (1982).
- [23] S. Dimopoulos and F. Wilczek, *Proceedings Erice Summer School*, ed. A. Zichichi (1981); M. Srednicki, *Nucl. Phys.* **B202**, 327 (1982).
- [24] K. Inoue, A. Kakuto and H. Takano, *Prog. Theor. Phys.* **75**, 664 (1986).
- [25] Y. Yamada, *Z. Phys.* **C60**, 83 (1993); J. Hisano *et al.*, *Phys. Lett.* **B342**, 138 (1995), [hep-ph/9406417]; G. Altarelli, F. Feruglio and I. Masina, *JHEP* **11**, 040 (2000), [hep-ph/0007254].
- [26] K. S. Babu and S. M. Barr, *Phys. Rev.* **D48**, 5354 (1993), [hep-ph/9306242]; K. S. Babu and S. M. Barr, *Phys. Rev.* **D50**, 3529 (1994), [hep-ph/9402291]; K. S. Babu, J. C. Pati and Z. Tavartkiladze, *JHEP* **06**, 084 (2010), [arXiv:1003.2625].
- [27] K. S. Babu and R. N. Mohapatra, *Phys. Rev. Lett.* **74**, 2418 (1995), [hep-ph/9410326]; V. Lucas and S. Raby, *Phys. Rev.* **D54**, 2261 (1996), [hep-ph/9601303]; T. Blazek *et al.*, *Phys. Rev.* **D56**, 6919 (1997), [hep-ph/9611217]; S. M. Barr and S. Raby, *Phys. Rev. Lett.* **79**, 4748 (1997), [hep-ph/9705366]; K. S. Babu, J. C. Pati and F. Wilczek, *Nucl. Phys.* **B566**, 33 (2000), [hep-ph/9812538]; R. Dermisek, A. Mafi and S. Raby, *Phys. Rev.* **D63**, 035001 (2001), [hep-ph/0007213].
- [28] R. Barbieri, G. R. Dvali and A. Strumia, *Nucl. Phys.* **B391**, 487 (1993); Z. Berezhiani, C. Csaki and L. Randall, *Nucl. Phys.* **B444**, 61 (1995), [hep-ph/9501336]; Q. Shafi and Z. Tavartkiladze, *Phys. Lett.* **B522**, 102 (2001), [hep-ph/0105140].
- [29] G. F. Giudice and A. Masiero, *Phys. Lett.* **B206**, 480 (1988); J. E. Kim and H. P. Nilles, *Mod. Phys. Lett.* **A9**, 3575 (1994), [hep-ph/9406296].
- [30] L. Randall and C. Csaki, in "Supersymmetry and unification of fundamental interactions. Proceedings, International Workshop, SUSY 95, Palaiseau, France, May 15-19, 1995," 99-109 (1995), [235(1995)], [hep-ph/9508208].
- [31] E. Witten, in "Supersymmetry and unification of fundamental interactions. Proceedings, 10th International Conference, SUSY'02, Hamburg, Germany, June 17-23, 2002," 472-491 (2001), [hep-ph/0201018], URL http://www-library.desy.de/preparch/desy/proc/proc02-02/Proceedings/susy02/special/hertz_pr.ps; M. Dine, Y. Nir and Y. Shadmi, *Phys. Rev.* **D66**, 115001 (2002), [hep-ph/0206268].
- [32] A. Hebecker, J. March-Russell and R. Ziegler, *JHEP* **08**, 064 (2009), [arXiv:0801.4101]; F. Brummer *et al.*, *JHEP* **08**, 011 (2009), [arXiv:0906.2957]; F. Brummer *et al.*, *JHEP* **04**, 006 (2010), [arXiv:1003.0084].
- [33] H. M. Lee *et al.*, *Phys. Lett.* **B694**, 491 (2011), [arXiv:1009.0905]; R. Kappl *et al.*, *Nucl. Phys.* **B847**, 325 (2011), [arXiv:1012.4574]; H. M. Lee *et al.*, *Nucl. Phys.* **B850**, 1 (2011), [arXiv:1102.3595].
- [34] Y. Hosotani, *Phys. Lett.* **126B**, 309 (1983).
- [35] L. J. Dixon *et al.*, *Nucl. Phys.* **B261**, 678 (1985), [678(1985)]; L. J. Dixon *et al.*, *Nucl. Phys.* **B274**, 285 (1986); L. E. Ibanez, H. P. Nilles and F. Quevedo, *Phys. Lett.* **B187**, 25 (1987); L. E. Ibanez *et al.*, *Phys. Lett.* **B191**, 282 (1987).
- [36] P. Candelas *et al.*, *Nucl. Phys.* **B258**, 46 (1985).
- [37] Y. Kawamura, *Prog. Theor. Phys.* **103**, 613 (2000), [hep-ph/9902423]; Y. Kawamura, *Prog. Theor. Phys.* **105**, 999 (2001), [hep-ph/0012125]; G. Altarelli and F. Feruglio, *Phys. Lett.* **B511**, 257 (2001), [hep-ph/0102301]; L. J. Hall and Y. Nomura, *Phys. Rev.* **D64**, 055003 (2001), [hep-ph/0103125]; A. Hebecker and J. March-Russell, *Nucl. Phys.* **B613**, 3 (2001), [hep-ph/0106166]; T. Asaka, W. Buchmuller and L. Covi, *Phys. Lett.* **B523**, 199 (2001), [hep-ph/0108021]; L. J. Hall *et al.*, *Phys. Rev.* **D65**, 035008 (2002), [hep-ph/0108071]; R. Dermisek and A. Mafi, *Phys. Rev.* **D65**, 055002 (2002), [hep-ph/0108139];

- H. D. Kim and S. Raby, *JHEP* **01**, 056 (2003), [hep-ph/0212348].
- [38] L.E. Ibanez and A.M. Uranga, “String theory and particle physics: An introduction to string phenomenology,” Cambridge University Press 2012; K.-S. Choi and J. E. Kim, *Lect. Notes Phys.* **696**, 1 (2006); R. Blumenhagen *et al.*, *Phys. Rept.* **445**, 1 (2007), [hep-th/0610327].
- [39] D. J. Gross *et al.*, *Phys. Rev. Lett.* **54**, 502 (1985).
- [40] V. Braun *et al.*, *JHEP* **05**, 043 (2006), [hep-th/0512177]; V. Bouchard and R. Donagi, *Phys. Lett.* **B633**, 783 (2006), [hep-th/0512149]; L. B. Anderson *et al.*, *Phys. Rev.* **D84**, 106005 (2011), [arXiv:1106.4804].
- [41] L. J. Dixon, V. Kaplunovsky and J. Louis, *Nucl. Phys.* **B355**, 649 (1991).
- [42] G. Aldazabal *et al.*, *Nucl. Phys.* **B452**, 3 (1995), [hep-th/9410206]; Z. Kakushadze *et al.*, *Int. J. Mod. Phys.* **A13**, 2551 (1998), [hep-th/9710149].
- [43] E. Witten, *Nucl. Phys.* **B258**, 75 (1985).
- [44] S. Gukov *et al.*, *Phys. Rev.* **D69**, 086008 (2004), [hep-th/0310159]; G. Curio, A. Krause and D. Lust, *Fortsch. Phys.* **54**, 225 (2006), [hep-th/0502168]; L. B. Anderson *et al.*, *Phys. Rev.* **D83**, 106011 (2011), [arXiv:1102.0011].
- [45] R. Friedman, J. Morgan and E. Witten, *Commun. Math. Phys.* **187**, 679 (1997), [hep-th/9701162].
- [46] R. Blumenhagen, G. Honecker and T. Weigand, *JHEP* **08**, 009 (2005), [hep-th/0507041]; L. B. Anderson *et al.*, *JHEP* **01**, 047 (2014), [arXiv:1307.4787].
- [47] T. Kobayashi, S. Raby and R.-J. Zhang, *Phys. Lett.* **B593**, 262 (2004), [hep-ph/0403065].
- [48] S. Forste *et al.*, *Phys. Rev.* **D70**, 106008 (2004), [hep-th/0406208]; T. Kobayashi, S. Raby and R.-J. Zhang, *Nucl. Phys.* **B704**, 3 (2005), [hep-ph/0409098]; W. Buchmuller *et al.*, *Nucl. Phys.* **B712**, 139 (2005), [hep-ph/0412318]; W. Buchmuller *et al.*, *Phys. Rev. Lett.* **96**, 121602 (2006), [hep-ph/0511035]; W. Buchmuller *et al.*, *Nucl. Phys.* **B785**, 149 (2007), [hep-th/0606187]; O. Lebedev *et al.*, *Phys. Lett.* **B645**, 88 (2007), [hep-th/0611095]; J. E. Kim, J.-H. Kim and B. Kyae, *JHEP* **06**, 034 (2007), [hep-ph/0702278]; O. Lebedev *et al.*, *Phys. Rev.* **D77**, 046013 (2008), [arXiv:0708.2691].
- [49] S. B. Giddings, S. Kachru and J. Polchinski, *Phys. Rev.* **D66**, 106006 (2002), [hep-th/0105097]; S. Kachru *et al.*, *Phys. Rev.* **D68**, 046005 (2003), [hep-th/0301240].
- [50] R. Blumenhagen *et al.*, *Nucl. Phys.* **B815**, 1 (2009), [arXiv:0811.2936].
- [51] R. Blumenhagen *et al.*, *Nucl. Phys.* **B616**, 3 (2001), [hep-th/0107138].
- [52] R. Donagi and M. Wijnholt, *Adv. Theor. Math. Phys.* **15**, 5, 1237 (2011), [arXiv:0802.2969].
- [53] C. Beasley, J. J. Heckman and C. Vafa, *JHEP* **01**, 058 (2009), [arXiv:0802.3391]; C. Beasley, J. J. Heckman and C. Vafa, *JHEP* **01**, 059 (2009), [arXiv:0806.0102].
- [54] T. Weigand, *Class. Quant. Grav.* **27**, 214004 (2010), [arXiv:1009.3497]; J. J. Heckman, *Ann. Rev. Nucl. Part. Sci.* **60**, 237 (2010), [arXiv:1001.0577]; M. Cvetič, I. Garcia-Etxebarria and J. Halverson, *JHEP* **01**, 073 (2011), [arXiv:1003.5337]; A. Maharana and E. Palti, *Int. J. Mod. Phys.* **A28**, 1330005 (2013), [arXiv:1212.0555]; S. Krippendorfer, S. Schafer-Nameki and J.-M. Wong, *JHEP* **11**, 008 (2015), [arXiv:1507.05961].
- [55] R. Donagi and M. Wijnholt, *Adv. Theor. Math. Phys.* **15**, 6, 1523 (2011), [arXiv:0808.2223]; R. Blumenhagen, *Phys. Rev. Lett.* **102**, 071601 (2009), [arXiv:0812.0248]; K.-S. Choi and J. E. Kim, *Phys. Rev.* **D83**, 065016 (2011), [arXiv:1012.0847]; C. Mayrhofer, E. Palti and T. Weigand, *JHEP* **09**, 082 (2013), [arXiv:1303.3589]; G. K. Leon-taris and Q. Shafi, *Phys. Rev.* **D96**, 6, 066023 (2017), [arXiv:1706.08372].
- [56] E. Witten, *Nucl. Phys.* **B471**, 135 (1996), [hep-th/9602070].
- [57] A. Hebecker and M. Trapletti, *Nucl. Phys.* **B713**, 173 (2005), [hep-th/0411131].
- [58] B. Dundee and S. Raby (2008), [arXiv:0808.0992].
- [59] G. G. Ross (2004), [hep-ph/0411057].
- [60] H. Georgi, H. R. Quinn and S. Weinberg, *Phys. Rev. Lett.* **33**, 451 (1974); S. Weinberg, *Phys. Lett.* **91B**, 51 (1980); L. J. Hall, *Nucl. Phys.* **B178**, 75 (1981).
- [61] B. C. Allanach, *Comput. Phys. Commun.* **143**, 305 (2002), [hep-ph/0104145].
- [62] M. Tanabashi *et al.* (Particle Data Group), *Phys. Rev.* **D98**, 3, 030001 (2018).
- [63] M. L. Alciati *et al.*, *JHEP* **03**, 054 (2005), [hep-ph/0501086].
- [64] See talks on proposed and running nucleon decay experiments, and theoretical talks by P. Langacker, p. 131, and W.J. Marciano and A. Sirlin, p. 151, in *The Second Workshop on Grand Unification*, eds. J.P. Leveille *et al.*, Birkhäuser, Boston (1981).
- [65] W.J. Marciano, p. 190, *Eighth Workshop on Grand Unification*, ed. K. Wali, World Scientific Publishing Co., Singapore (1987).
- [66] M.S. Carena *et al.*, in Ref. [7].
- [67] A. Djouadi, J.-L. Kneur and G. Moultaka, *Comput. Phys. Commun.* **176**, 426 (2007), [hep-ph/0211331].
- [68] W. Porod and F. Staub, *Comput. Phys. Commun.* **183**, 2458 (2012), [arXiv:1104.1573].
- [69] W. Siegel, *Phys. Lett.* **94B**, 37 (1980).
- [70] I. Antoniadis, C. Kounnas, and R. Lacaze, *Nucl. Phys.* **B221**, 377 (1983).
- [71] M. A. Shifman, *Int. J. Mod. Phys.* **A11**, 5761 (1996), [hep-ph/9606281]; N. Arkani-Hamed and H. Murayama, *JHEP* **06**, 030 (2000), [hep-th/9707133]; I. Jack, D. R. T. Jones and A. Pickering, *Phys. Lett.* **B435**, 61 (1998), [hep-ph/9805482].
- [72] M.B. Einhorn and D.R.T. Jones in Ref. [6]; I. Antoniadis, C. Kounnas and K. Tamvakis, *Phys. Lett.* **119B**, 377 (1982).
- [73] J. Hisano, H. Murayama and T. Yanagida, *Phys. Rev. Lett.* **69**, 1014 (1992); J. Hisano, H. Murayama and T. Yanagida, *Nucl. Phys.* **B402**, 46 (1993), [hep-ph/9207279].
- [74] H. Murayama and A. Pierce, *Phys. Rev.* **D65**, 055009 (2002), [hep-ph/0108104].
- [75] G. Anderson *et al.*, eConf **C960625**, SUP107 (1996) [hep-ph/9609457].
- [76] L. Roszkowski and M. A. Shifman, *Phys. Rev.* **D53**, 404 (1996), [hep-ph/9503358]; S. Raby, M. Ratz and K. Schmidt-Hoberg, *Phys. Lett.* **B687**, 342 (2010), [arXiv:0911.4249].
- [77] J. Hisano, T. Kuwahara and N. Nagata, *Phys. Lett.* **B723**, 324 (2013), [arXiv:1304.0343].
- [78] N. Arkani-Hamed, A. Delgado and G. F. Giudice, *Nucl. Phys.* **B741**, 108 (2006), [hep-ph/0601041].
- [79] M. Ibe, T. Moroi and T. T. Yanagida, *Phys. Lett.* **B644**, 355 (2007), [hep-ph/0610277].
- [80] G. F. Giudice *et al.*, *JHEP* **12**, 027 (1998), [hep-ph/9810442]; L. Randall and R. Sundrum, *Nucl. Phys.* **B557**, 79 (1999), [hep-th/9810155].
- [81] R. N. Mohapatra and M. K. Parida, *Phys. Rev.* **D47**, 264 (1993), [hep-ph/9204234].
- [82] D.-G. Lee *et al.*, *Phys. Rev.* **D51**, 229 (1995), [hep-ph/9404238].
- [83] L. E. Ibanez *et al.*, *JHEP* **07**, 195 (2012), [arXiv:1206.2655].
- [84] K. R. Dienes, E. Dudas and T. Gherghetta, *Phys. Rev. Lett.* **91**, 061601 (2003), [hep-th/0210294].
- [85] K. Agashe, R. Contino and R. Sundrum, *Phys. Rev. Lett.* **95**, 171804 (2005), [hep-ph/0502222].

- [86] F. Wilczek and A. Zee, Phys. Rev. Lett. **43**, 1571 (1979).
- [87] K. Abe *et al.* (Super-Kamiokande), Phys. Rev. **D95**, 1, 012004 (2017), [arXiv:1610.03597]; S. Mine (Super Kamiokande), J. Phys. Conf. Ser. **718**, 6, 062044 (2016).
- [88] K. Abe *et al.* (Hyper-Kamiokande) (2018), [arXiv:1805.04163].
- [89] Y. Aoki *et al.*, Phys. Rev. **D96**, 1, 014506 (2017), [arXiv:1705.01338].
- [90] J. Hisano, T. Kuwahara and Y. Omura, Nucl. Phys. **B898**, 1 (2015), [Erratum: Nucl. Phys. B907,476(2016)], [arXiv:1503.08561].
- [91] R. Barbier *et al.*, Phys. Rept. **420**, 1 (2005), [hep-ph/0406039]; F. Domingo *et al.*, JHEP **02**, 066 (2019), [arXiv:1810.08228].
- [92] G. R. Farrar and P. Fayet, Phys. Lett. **76B**, 575 (1978).
- [93] S. Dimopoulos, S. Raby and F. Wilczek, Phys. Lett. **112B**, 133 (1982); J. R. Ellis, D. V. Nanopoulos and S. Rudaz, Nucl. Phys. **B202**, 43 (1982).
- [94] C. S. Aulakh *et al.*, Nucl. Phys. **B597**, 89 (2001), [hep-ph/0004031].
- [95] T. Goto and T. Nihei, Phys. Rev. **D59**, 115009 (1999), [hep-ph/9808255].
- [96] G. D. Coughlan *et al.*, Phys. Lett. **160B**, 249 (1985); J. L. Chkareuli and I. G. Gogoladze, Phys. Rev. **D58**, 055011 (1998), [hep-ph/9803335].
- [97] G. F. Giudice and A. Romanino, Nucl. Phys. **B699**, 65 (2004), [Erratum: Nucl. Phys. B706,487(2005)], [hep-ph/0406088].
- [98] J. Hisano *et al.*, JHEP **07**, 038 (2013), [arXiv:1304.3651].
- [99] B. Bajc, P. Fileviez Perez and G. Senjanovic, Phys. Rev. **D66**, 075005 (2002), [hep-ph/0204311].
- [100] K.-S. Choi, Phys. Lett. **B668**, 392 (2008), [arXiv:0807.2766].
- [101] F. An *et al.* (JUNO), J. Phys. **G43**, 3, 030401 (2016), [arXiv:1507.05613].
- [102] R. Acciarri *et al.* (DUNE) (2015), [arXiv:1512.06148].
- [103] L. J. Hall and Y. Nomura, Phys. Rev. **D66**, 075004 (2002), [hep-ph/0205067]; H. D. Kim, S. Raby and L. Schradin, JHEP **05**, 036 (2005), [hep-ph/0411328].
- [104] M.S. Chanowitz, J.R. Ellis and M.K. Gaillard, Nucl. Phys. **B128**, 506 (1977); A. J. Buras *et al.*, Nucl. Phys. **B135**, 66 (1978).
- [105] K. Inoue *et al.*, Prog. Theor. Phys. **67**, 1889 (1982); L. E. Ibanez and C. Lopez, Nucl. Phys. **B233**, 511 (1984).
- [106] H. Georgi and D. V. Nanopoulos, Nucl. Phys. **B159**, 16 (1979); J. A. Harvey, P. Ramond and D. B. Reiss, Phys. Lett. **92B**, 309 (1980); J. A. Harvey, D. B. Reiss and P. Ramond, Nucl. Phys. **B199**, 223 (1982).
- [107] T. Banks, Nucl. Phys. **B303**, 172 (1988); M. Olechowski and S. Pokorski, Phys. Lett. **B214**, 393 (1988); S. Pokorski, Nucl. Phys. Proc. Suppl. **13**, 606 (1990); B. Ananthanarayan, G. Lazarides and Q. Shafi, Phys. Rev. **D44**, 1613 (1991); Q. Shafi and B. Ananthanarayan, ICTP Summer School lectures (1991); S. Dimopoulos, L. J. Hall and S. Raby, Phys. Rev. Lett. **68**, 1984 (1992); S. Dimopoulos, L. J. Hall and S. Raby, Phys. Rev. **D45**, 4192 (1992); G. W. Anderson *et al.*, Phys. Rev. **D47**, R3702 (1993), [hep-ph/9209250]; B. Ananthanarayan, G. Lazarides and Q. Shafi, Phys. Lett. **B300**, 245 (1993); G. Anderson *et al.*, Phys. Rev. **D49**, 3660 (1994), [hep-ph/9308333]; B. Ananthanarayan, Q. Shafi and X. M. Wang, Phys. Rev. **D50**, 5980 (1994), [hep-ph/9311225].
- [108] L. J. Hall, R. Rattazzi and U. Sarid, Phys. Rev. **D50**, 7048 (1994), [hep-ph/9306309]; M. Carena *et al.*, Nucl. Phys. **B426**, 269 (1994), [hep-ph/9402253].
- [109] A. Anandakrishnan, B. C. Bryant and S. Raby, JHEP **05**, 088 (2015), [arXiv:1411.7035].
- [110] M. Lenzagorta and G. G. Ross, Phys. Lett. **B364**, 163 (1995), [hep-ph/9507366].
- [111] K. Tobe and J. D. Wells, Nucl. Phys. **B663**, 123 (2003), [hep-ph/0301015].
- [112] G. Ross and M. Serna, Phys. Lett. **B664**, 97 (2008), [arXiv:0704.1248].
- [113] T. Blazek, R. Dermisek and S. Raby, Phys. Rev. Lett. **88**, 111804 (2002), [hep-ph/0107097]; T. Blazek, R. Dermisek and S. Raby, Phys. Rev. **D65**, 115004 (2002), [hep-ph/0201081]; D. Auto *et al.*, JHEP **06**, 023 (2003), [hep-ph/0302155]; R. Dermisek *et al.*, JHEP **04**, 037 (2003), [hep-ph/0304101]; R. Dermisek *et al.*, JHEP **09**, 029 (2005), [hep-ph/0507233].
- [114] A. Anandakrishnan, S. Raby and A. Wingerter, Phys. Rev. **D87**, 5, 055005 (2013), [arXiv:1212.0542]; M. Adeel Ajaib *et al.*, JHEP **07**, 139 (2013), [arXiv:1303.6964]; Z. Poh and S. Raby, Phys. Rev. **D92**, 1, 015017 (2015), [arXiv:1505.00264]; M. Badziak, M. Olechowski and S. Pokorski, JHEP **10**, 088 (2013), [arXiv:1307.7999].
- [115] H. Georgi and C. Jarlskog, Phys. Lett. **86B**, 297 (1979).
- [116] S. Antusch and M. Spinrath, Phys. Rev. **D79**, 095004 (2009), [arXiv:0902.4644].
- [117] G. Lazarides, Q. Shafi and C. Wetterich, Nucl. Phys. **B181**, 287 (1981).
- [118] T. E. Clark, T.-K. Kuo and N. Nakagawa, Phys. Lett. **115B**, 26 (1982); K. S. Babu and R. N. Mohapatra, Phys. Rev. Lett. **70**, 2845 (1993), [hep-ph/9209215].
- [119] R. Barbieri and D. V. Nanopoulos, Phys. Lett. **91B**, 369 (1980).
- [120] C. D. Froggatt and H. B. Nielsen, Nucl. Phys. **B147**, 277 (1979).
- [121] R. Barbieri *et al.*, Nucl. Phys. **B493**, 3 (1997), [hep-ph/9610449]; T. Blazek, S. Raby and K. Tobe, Phys. Rev. **D60**, 113001 (1999), [hep-ph/9903340]; T. Blazek, S. Raby and K. Tobe, Phys. Rev. **D62**, 055001 (2000), [hep-ph/9912482]; Q. Shafi and Z. Tavartkiladze, Phys. Lett. **B487**, 145 (2000), [hep-ph/9910314]; C. H. Albright and S. M. Barr, Phys. Rev. Lett. **85**, 244 (2000), [hep-ph/0002155]; Z. Berezhiani and A. Rossi, Nucl. Phys. **B594**, 113 (2001), [hep-ph/0003084]; C. H. Albright and S. M. Barr, Phys. Rev. **D64**, 073010 (2001), [hep-ph/0104294]; M.-C. Chen and K. T. Mahanthappa, Int. J. Mod. Phys. **A18**, 5819 (2003), [hep-ph/0305088]; R. Dermisek and S. Raby, Phys. Lett. **B622**, 327 (2005), [hep-ph/0507045].
- [122] H. Georgi, Nucl. Phys. **B156**, 126 (1979); P. H. Frampton, Phys. Lett. **88B**, 299 (1979); P. Frampton and S. Nandi, Phys. Rev. Lett. **43**, 1460 (1979); J.E. Kim, Phys. Rev. Lett. **45**, 1916 (1980), Phys. Rev. **D23**, 2706 (1981) and Phys. Rev. **D26**, 674 (1982); Y. Fujimoto, Phys. Rev. **D26**, 3183 (1982).
- [123] P. Langacker, Phys. Rept. **72**, 185 (1981).
- [124] H. Georgi, Conf. Proc. C **820726**, 705 (1982).
- [125] S. M. Barr, Phys. Rev. **D78**, 055008 (2008), [arXiv:0805.4808]; Y. Goto, Y. Kawamura and T. Miura, Phys. Rev. **D88**, 5, 055016 (2013), [arXiv:1307.2631]; J. E. Kim, JHEP **06**, 114 (2015), [arXiv:1503.03104]; C.H. Albright, R.P. Feger and T.W. Kephart, arXiv:1601.07523; M. Reig, J. W. F. Valle, C. A. Vaquera-Araujo and F. Wilczek, arXiv:1706.03116.
- [126] M. Magg and C. Wetterich, Phys. Lett. **94B**, 61 (1980); J. Schechter and J. W. F. Valle, Phys. Rev. **D22**, 2227 (1980); R. N. Mohapatra and G. Senjanovic, Phys. Rev. **D23**, 165 (1981); G. B. Gelmini and M. Roncadelli, Phys. Lett. **99B**, 411 (1981).
- [127] R. Foot *et al.*, Z. Phys. **C44**, 441 (1989).
- [128] Y. Fukuda *et al.* (Super-Kamiokande), Phys. Rev. Lett. **81**, 1562 (1998), [hep-ex/9807003].

- [129] G. L. Fogli *et al.*, Phys. Rev. **D84**, 053007 (2011), [arXiv:1106.6028].
- [130] T. Schwetz, M. Tortola and J. W. F. Valle, New J. Phys. **13**, 109401 (2011), [arXiv:1108.1376].
- [131] G. Altarelli, Soryushiron Kenkyu Electron. **116**, A29 (2008), [arXiv:0711.0161]; S. F. King and C. Luhn, Rept. Prog. Phys. **76**, 056201 (2013), [arXiv:1301.1340].
- [132] C. H. Albright and M.-C. Chen, Phys. Rev. **D74**, 113006 (2006), [hep-ph/0608137].
- [133] R. Kallosh *et al.*, Phys. Rev. **D52**, 912 (1995), [hep-th/9502069].
- [134] H. Ruegg and M. Ruiz-Altaba, Int. J. Mod. Phys. **A19**, 3265 (2004), [hep-th/0304245].
- [135] M. B. Green and J. H. Schwarz, Phys. Lett. **149B**, 117 (1984).
- [136] L. E. Ibanez and G. G. Ross, Nucl. Phys. **B368**, 3 (1992); M. Berasaluce-Gonzalez *et al.*, JHEP **12**, 113 (2011), [arXiv:1106.4169].
- [137] N.G. Deshpande, OITS-107; C. Q. Geng and R. E. Marshak, Phys. Rev. **D39**, 693 (1989); A. Font, L. E. Ibanez and F. Quevedo, Phys. Lett. **B228**, 79 (1989); K. S. Babu and R. N. Mohapatra, Phys. Rev. Lett. **63**, 938 (1989).
- [138] R. Foot *et al.*, Phys. Rev. **D39**, 3411 (1989).
- [139] M. Nowakowski and A. Pilaftsis, Phys. Rev. **D48**, 259 (1993), [hep-ph/9304312].
- [140] T. P. T. Dijkstra, L. R. Huiszoon and A. N. Schellekens, Phys. Lett. **B609**, 408 (2005), [hep-th/0403196]; F. Gmeiner *et al.*, JHEP **01**, 004 (2006), [hep-th/0510170]; B. Gato-Rivera and A. N. Schellekens, Nucl. Phys. **B883**, 529 (2014), [arXiv:1401.1782].
- [141] G. 't Hooft, Nucl. Phys. **B79**, 276 (1974) A.M. Polyakov, Pis'ma Zh. Eksp. Teor. Fiz. **20**, 430 (1974) [Sov. Phys. JETP Lett. **20**, 194 (1974)]; For a pedagogical introduction, see S. Coleman, in *Aspects of Symmetry*, Selected Erice Lectures, Cambridge University Press, Cambridge, (1985), and P. Goddard and D. Olive, Rept. on Prog. in Phys. **41**, 1357 (1978).
- [142] M. Ambrosio *et al.* (MACRO), Eur. Phys. J. **C25**, 511 (2002), [hep-ex/0207020]; S. Balestra *et al.* (2011), [arXiv:1105.5587]; L. Patrizzii and M. Spurio, Ann. Rev. Nucl. Part. Sci. **65**, 279 (2015), [arXiv:1510.07125].
- [143] For a review, see A.D. Linde, *Particle Physics and Inflationary Cosmology*, Harwood Academic, Switzerland (1990).
- [144] G. R. Dvali, H. Liu and T. Vachaspati, Phys. Rev. Lett. **80**, 2281 (1998), [hep-ph/9710301].
- [145] P. Langacker and S.-Y. Pi, Phys. Rev. Lett. **45**, 1 (1980).
- [146] G. R. Dvali, A. Melfo and G. Senjanovic, Phys. Rev. Lett. **75**, 4559 (1995), [hep-ph/9507230].
- [147] V. Rubakov, Nucl. Phys. **B203**, 311 (1982) and Institute of Nuclear Research Report No. P-0211, Moscow (1981), unpublished; C. G. Callan, Jr., Phys. Rev. **D26**, 2058 (1982); F. Wilczek, Phys. Rev. Lett. **48**, 1146 (1982); S. Dawson and A. N. Schellekens, Phys. Rev. **D27**, 2119 (1983).
- [148] K. Freese, M. S. Turner and D. N. Schramm, Phys. Rev. Lett. **51**, 1625 (1983).
- [149] P. A. R. Ade *et al.* (BICEP2, Keck Array), Phys. Rev. Lett. **116**, 031302 (2016), [arXiv:1510.09217]; N. Aghanim *et al.* (Planck) (2018), [arXiv:1807.06209].
- [150] L. J. Hall, V. A. Kostelecky and S. Raby, Nucl. Phys. **B267**, 415 (1986).
- [151] R. Barbieri and L. J. Hall, Phys. Lett. **B338**, 212 (1994), [hep-ph/9408406]; R. Barbieri, L. J. Hall and A. Strumia, Nucl. Phys. **B445**, 219 (1995), [hep-ph/9501334].
- [152] F. Borzumati and A. Masiero, Phys. Rev. Lett. **57**, 961 (1986); J. Hisano *et al.*, Phys. Lett. **B357**, 579 (1995), [hep-ph/9501407]; J. Hisano *et al.*, Phys. Rev. **D53**, 2442 (1996), [hep-ph/9510309]; J. Hisano and D. Nomura, Phys. Rev. **D59**, 116005 (1999), [hep-ph/9810479].
- [153] T. Moroi, JHEP **03**, 019 (2000), [hep-ph/0002208]; D. Chang, A. Masiero and H. Murayama, Phys. Rev. **D67**, 075013 (2003), [hep-ph/0205111].
- [154] S. Dimopoulos and L. J. Hall, Phys. Lett. **B344**, 185 (1995), [hep-ph/9411273].
- [155] J. Hisano *et al.*, Phys. Lett. **B604**, 216 (2004), [hep-ph/0407169].
- [156] A. Yu. Ignatiev *et al.*, Phys. Lett. **76B**, 436 (1978); M. Yoshimura, Phys. Rev. Lett. **41**, 281 (1978), [Erratum: Phys. Rev. Lett. **42**, 746 (1979)].
- [157] D. Toussaint *et al.*, Phys. Rev. **D19**, 1036 (1979); S. Weinberg, Phys. Rev. Lett. **42**, 850 (1979); M. Yoshimura, Phys. Lett. **88B**, 294 (1979); S. M. Barr, G. Segre and H. A. Weldon, Phys. Rev. **D20**, 2494 (1979); D. V. Nanopoulos and S. Weinberg, Phys. Rev. **D20**, 2484 (1979); A. Yildiz and P. H. Cox, Phys. Rev. **D21**, 906 (1980).
- [158] H. K. Dreiner and G. G. Ross, Nucl. Phys. **B410**, 188 (1993), [hep-ph/9207221].
- [159] M. Fukugita and T. Yanagida, Phys. Rev. Lett. **89**, 131602 (2002), [hep-ph/0203194].
- [160] M. Fukugita and T. Yanagida, Phys. Lett. **B174**, 45 (1986).
- [161] S. Davidson and A. Ibarra, Phys. Lett. **B535**, 25 (2002), [hep-ph/0202239]; K. Hamaguchi, H. Murayama and T. Yanagida, Phys. Rev. **D65**, 043512 (2002), [hep-ph/0109030].
- [162] A. Pilaftsis and T. E. J. Underwood, Phys. Rev. **D72**, 113001 (2005), [hep-ph/0506107].
- [163] M. Kawasaki *et al.*, Phys. Rev. **D78**, 065011 (2008), [arXiv:0804.3745].
- [164] W. Buchmuller, R. D. Peccei and T. Yanagida, Ann. Rev. Nucl. Part. Sci. **55**, 311 (2005), [hep-ph/0502169]; C. S. Fong, E. Nardi and A. Riotto, Adv. High Energy Phys. **2012**, 158303 (2012), [arXiv:1301.3062].
- [165] V. Cirigliano *et al.*, JHEP **12**, 097 (2018), [arXiv:1806.02780].
- [166] K. S. Babu and R. N. Mohapatra, Phys. Rev. **D86**, 035018 (2012), [arXiv:1203.5544]; K. S. Babu and R. N. Mohapatra, Phys. Lett. **B715**, 328 (2012), [arXiv:1206.5701]; K. S. Babu and R. N. Mohapatra, Phys. Rev. Lett. **109**, 091803 (2012), [arXiv:1207.5771].
- [167] M. Baldo-Ceolin *et al.*, Z. Phys. **C63**, 409 (1994).
- [168] K. Abe *et al.* (Super-Kamiokande), Phys. Rev. **D91**, 072006 (2015), [arXiv:1109.4227].
- [169] J. Gustafson *et al.* (Super-Kamiokande), Phys. Rev. **D91**, 7, 072009 (2015), [arXiv:1504.01041].
- [170] K. R. Dienes, Phys. Rept. **287**, 447 (1997), [hep-th/9602045]; P. Nath and P. Fileviez Perez, Phys. Rept. **441**, 191 (2007), [hep-ph/0601023].
- [171] G.G. Ross, "Grand Unified Theories", Benjamin/Cummings, 1984.; S. Raby, Lect. Notes Phys. **939**, 1 (2017).
- [172] P. Nath, Int. J. Mod. Phys. **A33**, 20, 1830017 (2018), [arXiv:1807.05302]; D. Croon *et al.*, Front.in Phys. **7**, 76 (2019), [arXiv:1903.04977].
- [173] A. Ringwald, L.J. Rosenberg and G. Rybka, Review of 'Axions and other Similar Particles' in Ref. [62].
- [174] P. Svrcek and E. Witten, JHEP **06**, 051 (2006), [hep-th/0605206].
- [175] M. Dine, W. Fischler and M. Srednicki, Phys. Lett. **104B**, 199 (1981); A. R. Zhitnitsky, Sov. J. Nucl. Phys. **31**, 260 (1980), [Yad. Fiz. **31**, 497 (1980)].
- [176] J. P. Conlon, JHEP **05**, 078 (2006), [hep-th/0602233].

94. Leptoquarks

Revised August 2021 by S. Rolli (DOE) and M. Tanabashi (Nagoya U.; KMI, Nagoya U.).

Leptoquarks are hypothetical particles carrying both baryon number (B) and lepton number (L). The possible quantum numbers of leptoquark states can be restricted by assuming that their direct interactions with the ordinary Standard Model (SM) fermions are dimensionless and invariant under the SM gauge group. Table 94.1 shows the list of all possible quantum numbers with this assumption [1]. The columns of $SU(3)_C$, $SU(2)_W$, and $U(1)_Y$ in Table 94.1 indicate the QCD representation, the weak isospin representation, and the weak hypercharge, respectively. The spin of a leptoquark state is taken to be 1 (vector leptoquark) or 0 (scalar leptoquark).

Table 94.1: Possible leptoquarks and their quantum numbers.

Spin	$3B + LSU(3)_C$	$SU(2)_W$	$U(1)_Y$	Allowed coupling	
0	-2	$\bar{3}$	1	$1/3$	$\bar{q}_L^c \ell_L$ or $\bar{u}_R^c e_R$
0	-2	$\bar{3}$	1	$4/3$	$\bar{d}_R^c e_R$
0	-2	$\bar{3}$	3	$1/3$	$\bar{q}_L^c \ell_L$
1	-2	$\bar{3}$	2	$5/6$	$\bar{q}_L^c \gamma^\mu e_R$ or $\bar{d}_R^c \gamma^\mu \ell_L$
1	-2	$\bar{3}$	2	$-1/6$	$\bar{u}_R^c \gamma^\mu \ell_L$
0	0	3	2	$7/6$	$\bar{q}_L e_R$ or $\bar{u}_R \ell_L$
0	0	3	2	$1/6$	$\bar{d}_R \ell_L$
1	0	3	1	$2/3$	$\bar{q}_L \gamma^\mu \ell_L$ or $\bar{d}_R \gamma^\mu e_R$
1	0	3	1	$5/3$	$\bar{u}_R \gamma^\mu e_R$
1	0	3	3	$2/3$	$\bar{q}_L \gamma^\mu \ell_L$

If we do not require leptoquark states to couple directly with SM fermions, different assignments of quantum numbers become possible [2,3].

Leptoquark states are expected to exist in various extensions of the SM. The Pati-Salam model [4] is an example predicting the existence of a leptoquark state. Leptoquark states also exist in grand unification theories based on $SU(5)$ [5], $SO(10)$ [6], which includes Pati-Salam color $SU(4)$, and larger gauge groups. Scalar quarks in supersymmetric models with R -parity violation may also have leptoquark-type Yukawa couplings. The bounds on the leptoquark states can therefore be applied to constrain R -parity-violating supersymmetric models. Scalar leptoquarks are expected to exist at the TeV scale in extended technicolor models [7,8] where leptoquark states appear as the bound states of techni-fermions. Compositeness of quarks and leptons also provides examples of models which may have light leptoquark states [9].

Bounds on leptoquark states are obtained both directly and indirectly. Direct limits are from their production cross sections at colliders, while indirect limits are calculated from bounds on leptoquark-induced four-fermion interactions, which are obtained from low-energy experiments, or from collider experiments below threshold. These four-fermion interactions often cause lepton-flavor non-universality in heavy quark decays. Anomalies observed recently in the R_K and R_D ratios [10–12] in the semi-leptonic B decays may be explained in models with TeV scale leptoquarks.

If a leptoquark couples to quarks (leptons) belonging to more than a single generation in the mass eigenbasis, it can induce four-fermion interactions causing flavor-changing neutral currents (lepton-family-number violations). The quantum number assignment of Table 1 allows several leptoquark states to couple to both left- and right-handed quarks simultaneously. Such leptoquark states are called non-chiral and may cause four-fermion interactions affecting the $(\pi \rightarrow e\nu)/(\pi \rightarrow \mu\nu)$ ratio [13]. Non-chiral scalar leptoquarks also contribute to the muon anomalous magnetic moment [14,15]. Since indirect limits provide more stringent constraints on these types of leptoquarks, it is often assumed that a leptoquark state couples only to a single generation of quarks and a single generation of leptons in a chiral interaction, for which indirect limits become much weaker. Additionally, this assumption gives strong constraints on models of leptoquarks.

Refs. [16–18] give extensive lists of the bounds on the leptoquark-induced four-fermion interactions. For the isoscalar scalar and vector leptoquarks S_0 and V_0 , for example, which couple with the first- (second-) generation left-handed quark, and the first-generation left-handed lepton, the bounds $\lambda^2 < 0.07 \times (M_{LQ}/1 \text{ TeV})^2$ for S_0 , and $\lambda^2 < 0.4 \times (M_{LQ}/1 \text{ TeV})^2$ for V_0 ($\lambda^2 < 0.7 \times (M_{LQ}/1 \text{ TeV})^2$ for S_0 , and $\lambda^2 < 0.5 \times (M_{LQ}/1 \text{ TeV})^2$ for V_0) with λ being the leptoquark coupling strength, can be derived from the limits listed in Ref. [19]. The e^+e^- experiments are sensitive to the indirect effects coming from t - and u -channel exchanges of leptoquarks in the $e^+e^- \rightarrow q\bar{q}$ process. The HERA experiments give bounds on the leptoquark-induced four-fermion interaction. For detailed bounds obtained in this way, see the Boson Particle Listings for “Indirect Limits for Leptoquarks” and its references.

Collider experiments provide direct limits on the leptoquark states through limits on the pair- and single-production cross sections. The leading-order cross sections of the parton processes

$$\begin{aligned}
 q + \bar{q} &\rightarrow \text{LQ} + \overline{\text{LQ}} \\
 g + g &\rightarrow \text{LQ} + \overline{\text{LQ}} \\
 e + q &\rightarrow \text{LQ}
 \end{aligned}
 \tag{94.1}$$

may be written as [20]

$$\begin{aligned}
 \hat{\sigma}_{\text{LO}} [q\bar{q} \rightarrow \text{LQ} + \overline{\text{LQ}}] &= \frac{2\alpha_s^2 \pi}{27\hat{s}} \beta^3, \\
 \hat{\sigma}_{\text{LO}} [gg \rightarrow \text{LQ} + \overline{\text{LQ}}] &= \frac{\alpha_s^2 \pi}{96\hat{s}} \\
 &\times \left[\beta(41 - 31\beta^2) + (18\beta^2 - \beta^4 - 17) \log \frac{1+\beta}{1-\beta} \right], \\
 \hat{\sigma}_{\text{LO}} [eq \rightarrow \text{LQ}] &= \frac{\pi\lambda^2}{4} \delta(\hat{s} - M_{\text{LQ}}^2)
 \end{aligned}
 \tag{94.2}$$

for a scalar leptoquark. Here $\sqrt{\hat{s}}$ is the invariant energy of the parton subprocess, and $\beta \equiv \sqrt{1 - 4M_{\text{LQ}}^2/\hat{s}}$. The leptoquark Yukawa coupling is given by λ . Leptoquarks are also produced singly at hadron colliders through $g + q \rightarrow \text{LQ} + \ell$ [21], which allows extending to higher masses the collider reach in the leptoquark search [22], depending on the leptoquark Yukawa coupling. See also Ref. [23] for a comprehensive review on the leptoquark phenomenology in precision experiments and particle colliders.

Leptoquark states which couple only to left- or right-handed quarks are called chiral leptoquarks. Leptoquark states which couple only to the first (second, third) generation are referred as the first- (second-, third-) generation leptoquarks.

The LHC, Tevatron and LEP experiments have been searching for pair production of the leptoquark states, which arises from the leptoquark gauge interaction. Due to the typical decay of the leptoquark into charged and neutral leptons and quarks, the searches are carried on in signatures including high p_T charged leptons, high E_T jets and large missing transverse energy. Additionally, searches for pair produced LQs are often organized by the decay mode of the pair of LQs, via the decay parameter β , which represents the branching fraction into a charge lepton vs a neutrino: $\beta = 1$ for both LQs decaying into a charged lepton, $\beta = 0.5$ for one LQ decaying into a charged lepton and one into a neutrino. The gauge couplings of a scalar leptoquark are determined uniquely according to its quantum numbers in Table 94.1. Since all of the leptoquark states belong to color-triplet representation, the scalar leptoquark pair-production cross section at the Tevatron and LHC can be determined solely as a function of the leptoquark mass without making further assumptions. This is in contrast to the indirect or single-production limits, which give constraints in the leptoquark mass-coupling plane.

Older results from the Tevatron run can be found here: [24–27]. Since the previous version of this review, both ATLAS and CMS have updated their results concerning searches for first, second,

and third generation LQs and leptoquark states which couple only with the i -th generation quarks and the j -th generation leptons ($i \neq j$) without causing conflicts with severe indirect constraints. The datasets were almost all collected at center of mass energy of 13 TeV and corresponding to the latest integrated luminosity collected before the shutdown of the LHC occurring in 2019 and 2020.

It is worthy to note that organizing LQs by flavor quantum number first before organizing them by gauge quantum number is becoming more common and advantageous because it relates more closely to some of the experimental searches being performed. The traditional nomenclature for 1st, 2nd, and 3rd generation LQ encourages only looking for the diagonal elements in a flavor matrix of possibilities, which has been the traditional experimental search strategy.

Current results extend previous mass limits for scalar leptoquarks to > 1435 GeV (first generation, CMS, $\beta = 1$, $\sqrt{s} = 13$ TeV) and > 1270 GeV (first generation, CMS, $\beta = 0.5$, $\sqrt{s} = 13$ TeV) [28]; > 1800 GeV (first generation, ATLAS, $\beta = 1$, $\sqrt{s} = 13$ TeV) [29] and > 1290 GeV (first generation, ATLAS, $\beta = 0.5$, $\sqrt{s} = 13$ TeV) [30]; > 1530 GeV (second generation, CMS, $\beta = 1$, $\sqrt{s} = 13$ TeV) and > 1285 GeV (second generation, CMS, $\beta = 0.5$, $\sqrt{s} = 13$ TeV) [31]; and > 1700 GeV (second generation, ATLAS, $\beta = 1$, $\sqrt{s} = 13$ TeV) [29] and > 1230 GeV (second generation, ATLAS, $\beta = 0.5$, $\sqrt{s} = 13$ TeV) [30]. All limits are presented at 95% C.L.

As for third generation leptoquarks, CMS results are the following: 1) assuming that all leptoquarks decay to a top quark and a τ lepton, the existence of pair produced, third-generation leptoquark up to a mass of 900 GeV ($\beta = 1$, 13 TeV) is excluded at 95% confidence level [32]; 2) assuming that all leptoquarks decay to a bottom quark and a τ lepton, the existence of pair produced, third-generation leptoquark up to a mass of 1020 GeV ($\beta = 1$, 13 TeV) is excluded at 95% confidence level [33]; 3) assuming that all leptoquarks decay to a bottom quark and a τ neutrino, the existence of pair produced, third-generation leptoquark up to a mass of 450 GeV ($\beta = 0$, 7 TeV) is excluded at 95% confidence level [34]. In a recent paper [35] signatures of top quark τ lepton ν bottom and top $\tau \nu$ - not previously explored in dedicated searches, were analyzed in the context of searches for scalar leptoquark of charge $-1/3e$ coupling to a top quark plus a τ lepton ($t\tau$) or a bottom quark plus a neutrino ($b\nu$), or a vector particle of charge $+2/3e$, coupling to $t\nu$ or $b\tau$. These choices are motivated by models that can explain a series of anomalies observed in the measurement of B meson decays. The data are found to be in agreement with the standard model prediction. Lower limits at 95% confidence level are set on the LQ mass in the range 0.98–1.73 TeV, depending on the LQ spin and its coupling λ to a lepton and a quark, and assuming equal couplings for the two LQ decay modes considered. These are the most stringent constraints to date on the existence of leptoquarks in this scenario.

In [36], the ATLAS collaboration has limits on pair production of third generation scalar leptoquarks where all possible decays of the leptoquark into a quark (t , b) and a lepton (τ , ν) of the third generation are considered. The limits are presented as a function of the leptoquark mass and the branching ratio into charged leptons for leptoquark of up-type ($LQ_3^{up} \rightarrow \tau\nu/b\tau$) and down-type ($LQ_3^d \rightarrow b\nu/t\tau$); many results are re-interpretation of previously published ATLAS searches. The collaboration finds that masses below 800 GeV are excluded for both LQ_3^u and LQ_3^d independently of the branching ratio, with masses below about 1 TeV being excluded for the limiting cases of branching ratios equal to zero or unity. In a more recent paper [37] ATLAS present the result of searches for pair production of third-generation scalar leptoquarks decaying into a top quark and a τ -lepton, using 139 fb^{-1} of data collected at 13 TeV. Scalar leptoquarks decaying exclusively into $t\tau$ are excluded up to masses of 1.43 TeV while, for a branching fraction of 50% into $t\tau$, the lower mass limit is 1.22 TeV.

It is also possible to consider leptoquark states which couple only with the i -th generation quarks and the j -th generation leptons ($i \neq j$) without causing conflicts with severe indirect constraints. Such couplings have received renewed attention because they may provide an explanation to anomalies in rare B - meson

decays and the anomalous magnetic moment of the muon. See Ref. [38, 39] and [40] and references therein for collider search strategies and limits on the pair production cross sections of this class of leptoquark states. In this framework, a novel CMS result [41] presents a non-traditional search for pair production of LQs coupled to a top quark and a muon. As no deviation from the Standard Model prediction was observed, scalar LQs decaying exclusively into $top - \mu$ are excluded up to masses of 1420 GeV. In a recent ATLAS paper [42] a search for pair production of scalar leptoquarks, each decaying into either an electron or a muon and a top quark, is presented. This is the first leptoquark search using ATLAS data to investigate top-philic cross-generational couplings that could provide explanations for recently observed anomalies in B meson decays. In the absence of any significant deviation from the background expectation, lower limits on the leptoquark masses are set at 1480 GeV and 1470 GeV for the electron and muon channel, respectively.

The magnetic-dipole-type and the electric-quadrupole-type interactions of a vector leptoquark are not determined even if we fix its gauge quantum numbers as listed in the Table 94.1 [43]. The production of vector leptoquarks depends in general on additional assumptions, where the leptoquark couplings and their pair production cross sections are enhanced relative to the scalar leptoquark contributions. The most stringent limits on vector LQ production are now from CMS [44] where previous searches for squarks and gluinos have been reinterpreted to constrain models of leptoquark production. LQ masses below 1530 GeV are excluded assuming the Yang-Mills case with coupling $\kappa = 1$, or 1115 GeV in the minimal coupling case where $\kappa = 0$, placing the most stringent constraint to date from pair production of vector LQs.

The leptoquark pair-production cross sections in e^+e^- collisions depend on the leptoquark $SU(2) \times U(1)$ quantum numbers and Yukawa coupling with electron [45].

Searches for first generation leptoquark singly produced were performed by the HERA experiments. Since the leptoquark single-production cross section depends on its Yukawa coupling, the leptoquark mass limits from HERA are usually displayed in the mass-coupling plane. For leptoquark Yukawa coupling $\lambda = 0.1$, early ZEUS Collaboration bounds on the first-generation leptoquarks range from 248 to 290 GeV, depending on the leptoquark species [46]. The ZEUS Collaboration has recently released a new paper [47] where data corresponding to a luminosity of around 1 fb^{-1} have been used in the framework of $eeqq$ contact interactions (CI) to set limits on possible high-energy contributions beyond the Standard Model to electron-quark scattering. The analysis of the ep data has been based on simultaneous fits of parton distribution functions including contributions of Contact Interaction (CI) couplings to ep scattering. Several general CI models and scenarios with heavy leptoquarks were considered. As unambiguous deviations from the SM cannot be established, limits for CI compositeness scales and LQ mass scales were set that are in the TeV range. The H1 Collaboration has a comprehensive summary of searches for first generation leptoquarks using the full data sample collected in ep collisions at HERA (446 pb^{-1}). No evidence of production of leptoquarks was observed in final states with a large transverse momentum electron or large missing transverse momentum. For a coupling strength $\lambda = 0.3$, first generation leptoquarks with masses up to 800 GeV are excluded at 95% C.L. [48].

At the LHC, the CMS collaboration performed searches for single production of first and second generation leptoquarks [49], which is complementary to the HERA searches in the high λ region (for coupling strength $\lambda = 1.0$, first generation leptoquarks are excluded for masses up to 1.73 TeV and second generation leptoquark are excluded up to masses of 530 GeV). CMS also recently searched for third generation LQ decaying into τ and bottom in [50]. Assuming unit Yukawa coupling (λ), a third generation scalar leptoquark is excluded for masses below 740 GeV. Limits are also set on λ of the hypothesized leptoquark as a function of its mass. Above $\lambda = 1.4$, the results provide the best upper limit on the mass of a third-generation scalar leptoquark decaying to a τ lepton and a bottom quark.

Searches for LQ will continue with more LHC data, particularly in light of the renewed interest in this type of particle to explain violation of lepton flavor universality and other anomalies, which point to explanations laying outside the Standard Model.

References

- [1] W. Buchmuller, R. Ruckl and D. Wyler, *Phys. Lett. B* **191**, 442 (1987), [Erratum: *Phys.Lett.B* 448, 320–320 (1999)].
- [2] K. Babu, C. F. Kolda and J. March-Russell, *Phys. Lett. B* **408**, 261 (1997), [hep-ph/9705414].
- [3] J. L. Hewett and T. G. Rizzo, *Phys. Rev. D* **58**, 055005 (1998), [hep-ph/9708419].
- [4] J. C. Pati and A. Salam, *Phys. Rev. D* **10**, 275 (1974), [Erratum: *Phys.Rev.D* 11, 703–703 (1975)].
- [5] H. Georgi and S. Glashow, *Phys. Rev. Lett.* **32**, 438 (1974).
- [6] H. Georgi, *AIP Conf. Proc.* **23**, 575 (1975); H. Fritzsch and P. Minkowski, *Annals Phys.* **93**, 193 (1975).
- [7] For a review, see, E. Farhi and L. Susskind, *Phys. Rept.* **74**, 277 (1981).
- [8] K. D. Lane and M. Ramana, *Phys. Rev. D* **44**, 2678 (1991).
- [9] See, for example, B. Schrempp and F. Schrempp, *Phys. Lett.* **153B**, 101 (1985).
- [10] R. Aaij *et al.* (LHCb), *Phys. Rev. Lett.* **120**, 17, 171802 (2018), [arXiv:1708.08856]; R. Aaij *et al.* (LHCb), *Phys. Rev. D* **97**, 7, 072013 (2018), [arXiv:1711.02505].
- [11] R. Aaij *et al.* (LHCb), *JHEP* **08**, 055 (2017), [arXiv:1705.05802]; R. Aaij *et al.* (LHCb), *Phys. Rev. Lett.* **122**, 19, 191801 (2019), [arXiv:1903.09252]; R. Aaij *et al.* (LHCb), *Phys. Rev. Lett.* **125**, 1, 011802 (2020), [arXiv:2003.04831]; R. Aaij *et al.* (LHCb) (2021), [arXiv:2103.11769].
- [12] Y. S. Amhis *et al.* (HFLAV), *Eur. Phys. J. C* **81**, 3, 226 (2021), updated results and plots available at <https://hflav.web.cern.ch/>, [arXiv:1909.12524].
- [13] O. U. Shanker, *Nucl. Phys. B* **204**, 375 (1982).
- [14] U. Mahanta, *Eur. Phys. J. C* **21**, 171 (2001), [hep-ph/0102176].
- [15] K.-M. Cheung, *Phys. Rev. D* **64**, 033001 (2001), [hep-ph/0102238].
- [16] S. Davidson, D. C. Bailey and B. A. Campbell, *Z. Phys. C* **61**, 613 (1994), [hep-ph/9309310].
- [17] M. Leurer, *Phys. Rev. D* **49**, 333 (1994), [hep-ph/9309266]; M. Leurer, *Phys. Rev. D* **50**, 536 (1994), [hep-ph/9312341].
- [18] M. Carpentier and S. Davidson, *Eur. Phys. J. C* **70**, 1071 (2010), [arXiv:1008.0280].
- [19] S. Davidson and A. Saporta, *Phys. Rev. D* **99**, 1, 015032 (2019), [arXiv:1807.10288].
- [20] T. Plehn *et al.*, *Z. Phys. C* **74**, 611 (1997), [hep-ph/9703433]; M. Kramer *et al.*, *Phys. Rev. Lett.* **79**, 341 (1997), [hep-ph/9704322].
- [21] J. Hewett and S. Pakvasa, *Phys. Rev. D* **37**, 3165 (1988); O. J. Eboli and A. V. Olinto, *Phys. Rev. D* **38**, 3461 (1988); A. Dobado, M. J. Herrero and C. Munoz, *Phys. Lett. B* **207**, 97 (1988); V. D. Barger *et al.*, *Phys. Lett. B* **220**, 464 (1989); M. De Montigny and L. Marleau, *Phys. Rev. D* **40**, 2869 (1989), [Erratum: *Phys.Rev.D* 56, 3156 (1997)].
- [22] A. Belyaev *et al.*, *JHEP* **09**, 005 (2005), [hep-ph/0502067].
- [23] I. Doršner *et al.*, *Phys. Rept.* **641**, 1 (2016), [arXiv:1603.04993].
- [24] V. Abazov *et al.* (D0), *Phys. Lett. B* **681**, 224 (2009), [arXiv:0907.1048].
- [25] A. Abulencia *et al.* (CDF), *Phys. Rev. D* **73**, 051102 (2006), [hep-ex/0512055].
- [26] V. Abazov *et al.* (D0), *Phys. Lett. B* **671**, 224 (2009), [arXiv:0808.4023].
- [27] V. M. Abazov *et al.* (D0), *Phys. Lett. B* **693**, 95 (2010), [arXiv:1005.2222].
- [28] A. M. Sirunyan *et al.* (CMS), *Phys. Rev. D* **99**, 5, 052002 (2019), [arXiv:1811.01197].
- [29] G. Aad *et al.* (ATLAS), *JHEP* **10**, 112 (2020), [arXiv:2006.05872].
- [30] M. Aaboud *et al.* (ATLAS), *Eur. Phys. J. C* **79**, 9, 733 (2019), [arXiv:1902.00377].
- [31] A. M. Sirunyan *et al.* (CMS), *Phys. Rev. D* **99**, 3, 032014 (2019), [arXiv:1808.05082].
- [32] A. M. Sirunyan *et al.* (CMS), *Eur. Phys. J. C* **78**, 707 (2018), [arXiv:1803.02864].
- [33] A. M. Sirunyan *et al.* (CMS), *JHEP* **03**, 170 (2019), [arXiv:1811.00806].
- [34] S. Chatrchyan *et al.* (CMS), *JHEP* **12**, 055 (2012), [arXiv:1210.5627].
- [35] A. M. Sirunyan *et al.* (CMS), *Phys. Lett. B* **819**, 136446 (2021), [arXiv:2012.04178].
- [36] M. Aaboud *et al.* (ATLAS), *JHEP* **06**, 144 (2019), [arXiv:1902.08103].
- [37] G. Aad *et al.* (ATLAS), *JHEP* **06**, 179 (2021), [arXiv:2101.11582].
- [38] B. Diaz, M. Schmaltz and Y.-M. Zhong, *JHEP* **10**, 097 (2017), [arXiv:1706.05033].
- [39] M. Schmaltz and Y.-M. Zhong, *JHEP* **01**, 132 (2019), [arXiv:1810.10017].
- [40] D. Müller, *EPJ Web Conf.* **179**, 01015 (2018), [arXiv:1801.03380].
- [41] A. M. Sirunyan *et al.* (CMS), *Phys. Rev. Lett.* **121**, 24, 241802 (2018), [arXiv:1809.05558].
- [42] G. Aad *et al.* (ATLAS), *Eur. Phys. J. C* **81**, 4, 313 (2021), [arXiv:2010.02098].
- [43] J. Blumlein, E. Boos and A. Kryukov, *Z. Phys. C* **76**, 137 (1997), [hep-ph/9610408].
- [44] A. M. Sirunyan *et al.* (CMS), *Phys. Rev. D* **98**, 3, 032005 (2018), [arXiv:1805.10228].
- [45] J. Blumlein and R. Ruckl, *Phys. Lett. B* **304**, 337 (1993).
- [46] S. Chekanov *et al.* (ZEUS), *Phys. Rev. D* **68**, 052004 (2003), [hep-ex/0304008].
- [47] H. Abramowicz *et al.* (ZEUS), *Phys. Rev. D* **99**, 9, 092006 (2019), [arXiv:1902.03048].
- [48] F. Aaron *et al.* (H1), *Phys. Lett. B* **704**, 388 (2011), [arXiv:1107.3716].
- [49] V. Khachatryan *et al.* (CMS), *Phys. Rev. D* **93**, 3, 032005 (2016), [Erratum: *Phys.Rev.D* 95, 039906 (2017)], [arXiv:1509.03750].
- [50] A. Sirunyan *et al.* (CMS), *JHEP* **07**, 115 (2018), [arXiv:1806.03472].

95. Magnetic Monopoles

Revised August 2021 by D. Milstead (Stockholm U.) and E.J. Weinberg (Columbia U.).

95.1 Theory of magnetic monopoles

The symmetry between electric and magnetic fields in the source-free Maxwell's equations naturally suggests that electric charges might have magnetic counterparts, known as magnetic monopoles. Although the greatest interest has been in the super-massive monopoles that are a firm prediction of all grand unified theories, one cannot exclude the possibility of lighter monopoles.

In either case, the magnetic charge is constrained by a quantization condition first found by Dirac [1]. Consider a monopole with magnetic charge Q_M and a Coulomb magnetic field

$$\mathbf{B} = \frac{Q_M}{4\pi} \frac{\hat{\mathbf{r}}}{r^2}. \quad (95.1)$$

Any vector potential \mathbf{A} whose curl is equal to \mathbf{B} must be singular along some line running from the origin to spatial infinity. This Dirac string singularity could potentially be detected through the extra phase that the wavefunction of a particle with electric charge Q_E would acquire if it moved along a loop encircling the string. For the string to be unobservable, this phase must be a multiple of 2π . Requiring that this be the case for any pair of electric and magnetic charges gives the condition that all charges be integer multiples of minimum charges Q_E^{\min} and Q_M^{\min} obeying

$$Q_E^{\min} Q_M^{\min} = 2\pi. \quad (95.2)$$

(For monopoles which also carry an electric charge, called dyons [2], the quantization conditions on their electric charges can be modified. However, the constraints on magnetic charges, as well as those on all purely electric particles, will be unchanged.)

Another way to understand this result is to note that the conserved orbital angular momentum of a point electric charge moving in the field of a magnetic monopole has an additional component, with

$$\mathbf{L} = m\mathbf{r} \times \mathbf{v} - 4\pi Q_E Q_M \hat{\mathbf{r}} \quad (95.3)$$

Requiring the radial component of \mathbf{L} to be quantized in half-integer units yields Eq. 95.2.

If there are unbroken gauge symmetries in addition to the U(1) of electromagnetism, the above analysis must be modified [3, 4]. For example, a monopole could have both a U(1) magnetic charge and a color magnetic charge. The latter could combine with the color charge of a quark to give an additional contribution to the phase factor associated with a loop around the Dirac string, so that the U(1) charge could be the Dirac charge $Q_M^D \equiv 2\pi/e$, the result that would be obtained by substituting the electron charge into Eq. (95.2). On the other hand, for monopoles without color-magnetic charge, one would simply insert the quark electric charges into Eq. 95.2 and conclude that Q_M must be a multiple of $6\pi/e$.

The prediction of GUT monopoles arises from the work of 't Hooft [5] and Polyakov [6], who showed that certain spontaneously broken gauge theories have nonsingular classical solutions that lead to magnetic monopoles in the quantum theory. The simplest example occurs in a theory where the vacuum expectation value of a triplet Higgs field ϕ breaks an SU(2) gauge symmetry down to the U(1) of electromagnetism and gives a mass M_V to two of the gauge bosons. In order to have finite energy, ϕ must approach a vacuum value at infinity. However, there is a continuous family of possible vacua, since the scalar field potential determines only the magnitude v of $\langle\phi\rangle$, but not its orientation in the internal SU(2) space. In the monopole solution, the direction of ϕ in internal space is correlated with the position in physical space; *i.e.*, $\phi^a \sim v\hat{r}^a$. The stability of the solution follows from the fact that this twisting Higgs field cannot be smoothly deformed to a spatially uniform vacuum configuration. Reducing the energetic cost of the spatial variation of ϕ requires a nonzero gauge potential, which turns out to yield the magnetic field corresponding to a charge $Q_M = 4\pi/e$. Numerical solution of the classical field equations shows that the mass of this monopole is

$$M_{\text{mon}} \sim \frac{4\pi M_V}{e^2}. \quad (95.4)$$

The essential ingredient here was the fact that the Higgs fields at spatial infinity could be arranged in a topologically nontrivial configuration. A discussion of the general conditions under which this is possible is beyond the scope of this review, so we restrict ourselves to the two phenomenologically most important cases.

The first is the standard electroweak theory, with SU(2) \times U(1) broken to U(1). There are no topologically nontrivial configurations of the Higgs field, and hence no topologically stable monopole solutions. Although electroweak scale monopoles are thus not required, there have been claims that they might not be ruled out. For example, there have been a variety of proposals in this direction involving modifications of the Lagrangian.

The second case is when any simple Lie group is broken to a subgroup with a U(1) factor, a case that includes all grand unified theories. Here the spectrum of states must include a topologically stable monopole whose mass is determined by the mass scale of the symmetry breaking that allows nontrivial topology. For example, an SU(5) model with

$$\text{SU}(5) \xrightarrow{M_X} \text{SU}(3) \times \text{SU}(2) \times \text{U}(1) \xrightarrow{M_W} \text{SU}(3) \times \text{U}(1) \quad (95.5)$$

has a monopole [7] with $Q_M = 2\pi/e$ and mass

$$M_{\text{mon}} \sim \frac{4\pi M_X}{g^2}, \quad (95.6)$$

where g is the SU(5) gauge coupling. For a unification scale of 10^{16} GeV, these monopoles would have a mass $M_{\text{mon}} \sim 10^{17} - 10^{18}$ GeV.

In theories with several stages of symmetry breaking, monopoles of different mass scales can arise. In an SO(10) theory with

$$\text{SO}(10) \xrightarrow{M_1} \text{SU}(4) \times \text{SU}(2) \times \text{SU}(2) \xrightarrow{M_2} \text{SU}(3) \times \text{SU}(2) \times \text{U}(1) \quad (95.7)$$

there is monopole with $Q_M = 2\pi/e$ and mass $\sim 4\pi M_1/g^2$ and a much lighter monopole with $Q_M = 4\pi/e$ and mass $\sim 4\pi M_2/g^2$ [8].

The central core of a GUT monopole contains the fields of the superheavy gauge bosons that mediate baryon number violation, so one might expect that baryon number conservation could be violated in baryon-monopole scattering. The surprising feature, pointed out by Callan [9] and Rubakov [10], is that these processes are not suppressed by powers of the gauge boson mass. Instead, the cross-sections for catalysis processes such as $p + \text{monopole} \rightarrow e^+ + \pi^0 + \text{monopole}$ are essentially geometric; *i.e.*, $\sigma_{\Delta B} \beta \sim 10^{-27} \text{ cm}^2$, where $\beta = v/c$. Note, however, that this catalysis is model-dependent and is not even a universal property of all GUT monopoles.

95.2 Production and Annihilation

GUT monopoles are far too massive to be produced in any foreseeable accelerator. However, they could have been produced in the early Universe as topological defects arising via the Kibble mechanism [11] in a symmetry-breaking phase transition. Estimates of the initial monopole abundance, and of the degree to which it can be reduced by monopole-antimonopole annihilation, predict a present-day monopole abundance that exceeds by many orders of magnitude the astrophysical and experimental bounds described below [12]. Cosmological inflation and other proposed solutions to this primordial monopole problem generically lead to present-day abundances exponentially smaller than could be plausibly detected, although potentially observable abundances can be obtained in scenarios with carefully tuned parameters.

If monopoles light enough to be produced at colliders exist, one would expect that these could be produced by analogs of the electromagnetic processes that produce pairs of electrically charged particles. Because of the large size of the magnetic charge, this is a strong coupling problem for which perturbation theory cannot be trusted. Indeed, the problem of obtaining reliable quantitative estimates of the production cross-sections remains an open one, on which there is no clear consensus.

95.3 Astrophysical and Cosmological Bounds

If there were no galactic magnetic field, one would expect monopoles in the galaxy to have typical velocities of the order of $10^{-3}c$, comparable to the virial velocity in the galaxy (relevant if the monopoles cluster with the galaxy) and the peculiar velocity of the galaxy with respect to the CMB rest frame (relevant if the monopoles are not bound to the galaxy). This situation is modified by the existence of a galactic magnetic field $B \sim 3\mu\text{G}$. A monopole with the Dirac charge and mass M would be accelerated by this field to a velocity

$$v_{\text{mag}} \sim \begin{cases} c, & M \lesssim 10^{11} \text{ GeV}, \\ 10^{-3}c \left(\frac{10^{17} \text{ GeV}}{M} \right)^{1/2}, & M \gtrsim 10^{11} \text{ GeV}. \end{cases} \quad (95.8)$$

Accelerating these monopoles drains energy from the magnetic field. Parker [13] obtained an upper bound on the flux of monopoles in the galaxy by requiring that the rate of this energy loss be small compared to the time scale on which the galactic field can be regenerated. With reasonable choices for the astrophysical parameters (see Ref. [14] for details), this Parker bound is

$$F < \begin{cases} 10^{-15} \text{ cm}^{-2} \text{ sr}^{-1} \text{ sec}^{-1}, & M \lesssim 10^{17} \text{ GeV}, \\ 10^{-15} \left(\frac{M}{10^{17} \text{ GeV}} \right) \text{ cm}^{-2} \text{ sr}^{-1} \text{ sec}^{-1}, & M \gtrsim 10^{17} \text{ GeV}. \end{cases} \quad (95.9)$$

Applying similar arguments to an earlier seed field that was the progenitor of the current galactic field leads to a tighter bound [15],

$$F < \left[\frac{M}{10^{17} \text{ GeV}} + (3 \times 10^{-6}) \right] 10^{-16} \text{ cm}^{-2} \text{ sr}^{-1} \text{ sec}^{-1}. \quad (95.10)$$

Considering magnetic fields in galactic clusters gives a bound [16] which, although less secure, is about three orders of magnitude lower than the Parker bound.

A flux bound can also be inferred from the total mass of monopoles in the Universe. If the monopole mass density is a fraction Ω_M of the critical density, and the monopoles were uniformly distributed throughout the Universe, there would be a monopole flux

$$F_{\text{uniform}} = 1.3 \times 10^{-16} \Omega_M \left(\frac{10^{17} \text{ GeV}}{M} \right) \left(\frac{v}{10^{-3}c} \right) \text{ cm}^{-2} \text{ sr}^{-1} \text{ sec}^{-1}. \quad (95.11)$$

If we assume that $\Omega_M \sim 0.1$, this gives a stronger constraint than the Parker bound for $M \sim 10^{15}$ GeV. However, monopoles with masses $\sim 10^{17}$ GeV are not ejected by the galactic field and can be gravitationally bound to the galaxy. In this case their flux within the galaxy is increased by about five orders of magnitude for a given value of Ω_M , and the mass density bound only becomes stronger than the Parker bound for $M \sim 10^{18}$ GeV.

A much more stringent flux bound applies to GUT monopoles that catalyze baryon number violation. The essential idea is that compact astrophysical objects would capture monopoles at a rate proportional to the galactic flux. These monopoles would then catalyze proton decay, with the energy released in the decay leading to an observable increase in the luminosity of the object. A variety of bounds, based on neutron stars [17–21], white dwarfs [22], and Jovian planets [23] have been obtained. These depend in the obvious manner on the catalysis cross section, but also on the details of the astrophysical scenarios; *e.g.*, on how much the accumulated density is reduced by monopole-antimonopole annihilation, and on whether monopoles accumulated in the progenitor star survive its collapse to a white dwarf or neutron star. The bounds obtained in this manner lie in the range

$$F \left(\frac{\sigma_{\Delta B \beta}}{10^{-27} \text{ cm}^2} \right) \sim (10^{-18} - 10^{-29}) \text{ cm}^{-2} \text{ sr}^{-1} \text{ sec}^{-1}. \quad (95.12)$$

It is important to remember that not all GUT monopoles catalyze baryon number nonconservation. In particular, the intermediate mass monopoles that arise in some GUTs at later stages

of symmetry-breaking are examples of theoretically motivated monopoles that are exempt from the bound of the above equation.

95.4 Searches for Magnetic Monopoles

To date there have been no confirmed observations of exotic particles possessing magnetic charge. Precision measurements of the properties of known particles have led to tight limits on the values of magnetic charge they may possess. Using the induction method (see below), the electron's magnetic charge has been found to be $Q_e^m < 10^{-24} Q_M^D$ [24] (where Q_M^D is the Dirac charge). Furthermore, measurements of the anomalous magnetic moment of the muon have been used to place a model dependent lower limit of 120 GeV on the monopole mass¹ [25]. Nevertheless, guided mainly by Dirac's argument and the predicted existence of monopoles from spontaneous symmetry breaking mechanisms, searches have been routinely made for monopoles produced at accelerators, in cosmic rays, and bound in matter [26]. Although the resultant limits from such searches are usually made under the assumption of a particle possessing only magnetic charge, most of the searches are also sensitive to dyons.

95.5 Search Techniques

Search strategies are determined by the expected interactions of monopoles as they pass through matter. These would give rise to a number of striking characteristic signatures. Since a complete description of monopole search techniques falls outside of the scope of this minireview, only the most common methods are described below. More comprehensive descriptions of search techniques can be found in Refs. [27, 28].

The induction method exploits the long-ranged electromagnetic interaction of the monopole with the quantum state of a superconducting ring which would lead to a monopole which passes through such a ring inducing a permanent current. The induction technique typically uses Superconducting Quantum Interference Devices (SQUID) technology for detection and is employed for searches for monopoles in cosmic rays and matter. Another approach is to exploit the electromagnetic energy loss of monopoles. Monopoles with Dirac charge would typically lose energy at a rate which is several thousand times larger than that expected from particles possessing the elementary electric charge. Consequently, scintillators, gas chambers and nuclear track detectors (NTDs) have been used in cosmic ray and collider experiments. A further approach, which has been used at colliders, is to search for particles describing a non-helical path in a uniform magnetic field.

95.5.1 Searches for Monopoles Bound in Matter

Monopoles have been sought in a range of bulk materials which it is assumed would have absorbed incident cosmic ray monopoles over a long exposure time of order million years. Materials which have been studied include moon rock, meteorites, manganese modules, and sea water [29, 30]. A stringent upper limit on the monopoles per nucleon ratio of $\sim 10^{-29}$ has been obtained [30].

95.5.2 Searches in Cosmic Rays

Direct searches for monopoles in cosmic rays refer to those experiments in which the passage of the monopole is measured by an active detector. Searches made assuming a catalysis processes in which GUT monopoles could induce nucleon decay are discussed in the next section. To interpret the results of the non-catalysis searches, the cross section for the catalysis process is typically either set to zero [31] or assigned a modest value (1mb) [32].

Although early cosmic ray searches using the induction technique [33] and NTDs [34] observed monopole candidates, none of these apparent observations have been confirmed. Recent experiments have typically employed large scale detectors. The MACRO experiment at the Gran Sasso underground laboratory comprised three different types of detector: liquid scintillator, limited stream tubes, and NTDs, which provided a total acceptance of $\sim 10000 \text{ m}^2$ for an isotropic flux. As shown in Fig. 95.1, this experiment has so far provided the most extensive β -dependent flux limits for GUT monopoles with Dirac charge [32]. Also shown

¹ Where no ambiguity is likely to arise, a reference to a monopole implies a particle possessing Dirac charge.

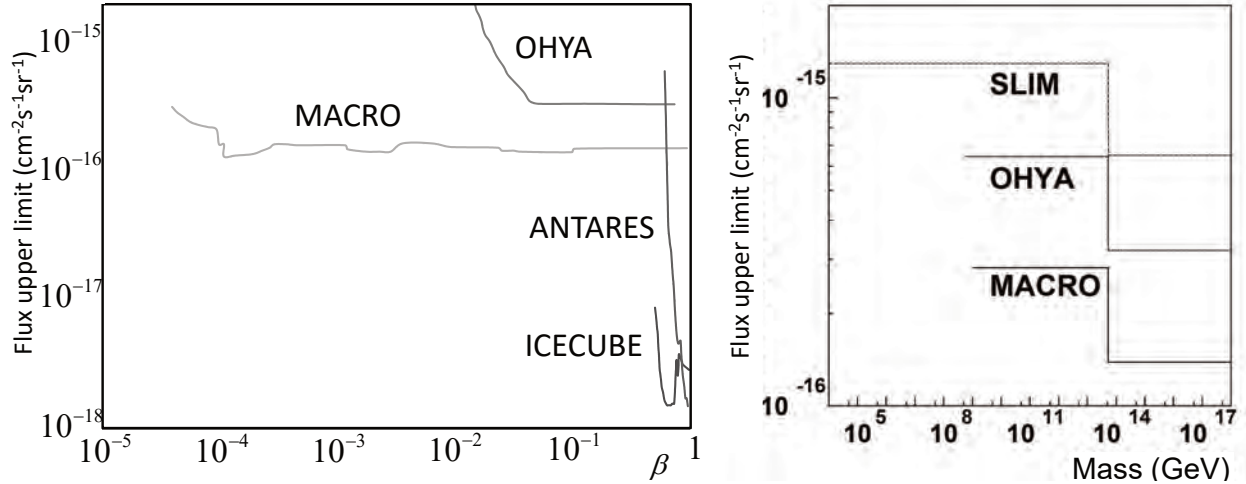


Figure 95.1: Upper flux limits for (left) GUT monopoles as a function of β (right) Monopoles as a function of mass for $\beta > 0.05$.

are limits from an experiment at the OHYA mine in Japan [31], which used a 2000m² array of NTDs.

In Fig. 95.1, upper flux limits are also shown as a function of mass for monopole speed $\beta > 0.05$. In addition to MACRO and OHYA flux limits, results from the SLIM [35] high-altitude experiment are shown. The SLIM experiment provided a good sensitivity to intermediate mass monopoles ($10^5 \lesssim M \lesssim 10^{12}$ GeV). In addition to the results shown in Fig. 95.1, limits as low as $\sim 1.5 \times 10^{-18} \text{ cm}^{-2} \text{ s}^{-1} \text{ sr}^{-1}$ were obtained for monopoles with $\beta > 0.51$ and $\beta > 0.6$ by the IceCube [36] and Antares [37] experiments, respectively. Furthermore, the NoVA experiment [38] has recently set an upper limit on monopole flux of $2 \times 10^{-14} \text{ cm}^{-2} \text{ s}^{-1} \text{ sr}^{-1}$ for speeds $6 \times 10^{-4} < \beta < 10^{-3}$ for masses greater than 5×10^8 GeV. Stringent constraints on the flux of ultra-relativistic monopoles have been obtained at the Pierre Auger Observatory [39] which was sensitive to monopoles with γ values ranging from 10^9 to 10^{12} , leading to flux limits in the range $10^{-15} - 2.5 \times 10^{-21} \text{ cm}^{-2} \text{ s}^{-1} \text{ sr}^{-1}$. The RICE [40] and ANITA-II experiments [41] at the South Pole have also sought ultra-relativistic monopoles with γ values of $10^7 \lesssim \gamma \lesssim 10^{12}$ and $10^9 \lesssim \gamma \lesssim 10^{13}$, respectively, and which produced flux limits as low as $2.5 \times 10^{-21} \text{ cm}^{-2} \text{ s}^{-1} \text{ sr}^{-1}$.

95.5.3 Searches via the Catalysis of Nucleon-Decay

Searches have been performed for evidence of the catalysed decay of a nucleon by a monopole, as predicted by the Callan-Rubakov mechanism. The searches are thus sensitive to the assumed value of the catalysis decay cross section. Searches have been made with the Soudan [42] and Macro [43] experiments, using tracking detectors. Searches at IMB [44], the underwater Lake Baikal experiment [45] and the The IceCube experiment [46] which exploit the Cerenkov effect have also been made. The resulting β -dependent flux limits from these experiments typically vary between $\sim 10^{-18}$ and $\sim 10^{-14} \text{ cm}^{-2} \text{ sr}^{-1} \text{ s}^{-1}$. A recent search for low energy neutrinos (assumed to be produced from induced proton decay in the sun) was made at Super-Kamiokande [47]. A model- and β -dependent of limit of $6.3 \times 10^{-24} (\frac{\beta}{10^{-3}})^2 \text{ cm}^{-2} \text{ sr}^{-1} \text{ s}^{-1}$ was obtained.

95.5.4 Searches at Colliders

Searches have been performed at hadron-hadron, electron-positron and lepton-hadron experiments. Collider searches can be broadly classed as being direct or indirect. In a direct search, evidence of the passage of a monopole through material, such as a charged particle track, is sought. In indirect searches, virtual monopole processes are assumed to influence the production rates of certain final states.

95.5.4.1 Direct Searches at Colliders

Collider experiments typically express their results in terms of upper limits on a production cross section and/or monopole

mass. To calculate these limits, ansatzes are used to model the kinematics of monopole-antimonopole pair production processes since perturbative field theory cannot be used to calculate the rate and kinematic properties of produced monopoles. Limits therefore suffer from a degree of model-dependence, implying that a comparison between the results of different experiments can be problematic, in particular when this concerns excluded mass regions. A conservative approach with as little model-dependence as possible is thus to present representative values of the upper cross-section limits as a function of one half the centre-of-mass energy of the collisions, as shown in Fig. 95.2 for recent results from high energy colliders.

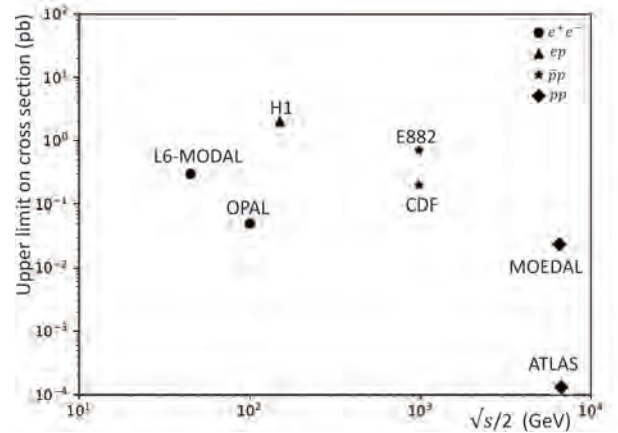


Figure 95.2: Upper limits on the production cross sections of monopoles from various collider-based experiments.

Searches for monopoles produced at the highest available energies in hadron-hadron collisions were made in pp collisions at the LHC by the ATLAS [48, 49] and MoEDAL [50, 51] experiments. The experiments looked for highly ionising particles leaving characteristic energy deposition profiles and stopped monopoles with the induction method, respectively. The charge-dependent mass limits extend up to around 4 TeV. The ATLAS work considers monopoles with $0.5Q_M^D$ and $2Q_M^D$ while MoEDAL quotes limits for monopoles with charges from Q_M^D to $5Q_M^D$. MoEDAL considered monopole-pair production via photon fusion along with, as is commonly used in hadron-hadron collisions, Drell-Yan processes [52]. Tevatron searches have also been carried out by the CDF [53] and E882 [54] experiments. The CDF experiment used a dedicated time-of-flight system whereas the E882 experiment employed the induction technique to search for stopped monopoles in discarded detector material which had been part of the CDF

and D0 detectors using periods of luminosity. Earlier searches at the Tevatron, such as [55], used NTDs and were based on comparatively modest amounts of integrated luminosity. Lower energy hadron-hadron experiments have employed a variety of search techniques including plastic track detectors [56] and searches for trapped monopoles [57].

The only LEP-2 search was made by OPAL [58] which quoted cross section limits for the production of monopoles possessing masses up to around 103 GeV. At LEP-1, searches were made with NTDs deployed around an interaction region. This allowed a range of charges to be sought for masses up to ~ 45 GeV. The L6-MODAL experiment [59] gave limits for monopoles with charges in the range $0.9Q_M^D$ and $3.6Q_M^D$, whilst an earlier search by the MODAL experiment was sensitive to monopoles with charges as low as $0.1Q_M^D$ [60]. The deployment of NTDs around the beam interaction point was also used at earlier e^+e^- colliders such as KEK [61] and PETRA [62]. Searches at e^+e^- facilities have also been made for particles following non-helical trajectories [63, 64].

There has so far been one search for monopole production in lepton-hadron scattering. Using the induction method, monopoles were sought which could have stopped in the aluminium beampipe which had been used by the H1 experiment at HERA [65]. Cross section limits were set for monopoles with charges in the range $Q_M^D - 6Q_M^D$ for masses up to around 140 GeV.

95.5.4.2 Indirect Searches at Colliders

It has been proposed that virtual monopoles can mediate processes which give rise to multi-photon final-states [66, 67]. Photon-based searches were made by the D0 [68] and L3 [69] experiments. The D0 work led to spin-dependent lower mass limits of between 610 and 1580 GeV, while L3 reported a lower mass limit of 510 GeV. However, it should be stressed that uncertainties on the theoretical calculations which were used to derive these limits are difficult to estimate.

References

- [1] P. A. M. Dirac, Proc. Roy. Soc. Lond. **A133**, 821, 60 (1931).
- [2] J. S. Schwinger, Science **165**, 757 (1969).
- [3] F. Englert and P. Windey, Phys. Rev. **D14**, 2728 (1976).
- [4] P. Goddard, J. Nuyts and D. I. Olive, Nucl. Phys. **B125**, 1 (1977).
- [5] G. 't Hooft, Nucl. Phys. **B79**, 276 (1974).
- [6] A. M. Polyakov, JETP Lett. **20**, 194 (1974).
- [7] C. P. Dokos and T. N. Tomaras, Phys. Rev. **D21**, 2940 (1980).
- [8] G. Lazarides and Q. Shafi, Phys. Lett. **94B**, 149 (1980).
- [9] C. G. Callan, Jr., Phys. Rev. **D26**, 2058 (1982).
- [10] V. A. Rubakov, Nucl. Phys. **B203**, 311 (1982).
- [11] T. W. B. Kibble, J. Phys. **A9**, 1387 (1976).
- [12] J. Preskill, Phys. Rev. Lett. **43**, 1365 (1979).
- [13] E. N. Parker, Astrophys. J. **160**, 383 (1970).
- [14] M. S. Turner, E. N. Parker and T. J. Bogdan, Phys. Rev. **D26**, 1296 (1982).
- [15] F. C. Adams *et al.*, Phys. Rev. Lett. **70**, 2511 (1993).
- [16] Y. Rephaeli and M. S. Turner, Phys. Lett. **121B**, 115 (1983).
- [17] E. W. Kolb, S. A. Colgate and J. A. Harvey, Phys. Rev. Lett. **49**, 1373 (1982).
- [18] S. Dimopoulos, J. Preskill and F. Wilczek, Phys. Lett. **119B**, 320 (1982).
- [19] K. Freese, M. S. Turner and D. N. Schramm, Phys. Rev. Lett. **51**, 1625 (1983).
- [20] E. W. Kolb and M. S. Turner, Astrophys. J. **286**, 702 (1984).
- [21] J. A. Harvey, Nucl. Phys. **B236**, 255 (1984).
- [22] K. Freese and E. Krasteva, Phys. Rev. **D59**, 063007 (1999), [arXiv:astro-ph/9804148].
- [23] J. Arafune, M. Fukugita and S. Yanagita, Phys. Rev. **D32**, 2586 (1985).
- [24] L. L. Vant-Hull, Phys. Rev. **173**, 1412 (1968).
- [25] S. Graf, A. Schaefer and W. Greiner, Phys. Lett. **B262**, 463 (1991).
- [26] Review of Particle Physics 2020 (*this paper*), listing on *Searches for Magnetic Monopoles*.
- [27] L. Patrizii and M. Spurio, Ann. Rev. Nucl. Part. Sci. **65**, 279 (2015), [arXiv:1510.07125].
- [28] M. Fairbairn *et al.*, Phys. Rept. **438**, 1 (2007), [hep-ph/0611040].
- [29] J. M. Kovalik and J. L. Kirschvink, Phys. Rev. **A33**, 1183 (1986).
- [30] H. Jeon and M. J. Longo, Phys. Rev. Lett. **75**, 1443 (1995), [Erratum: Phys. Rev. Lett. **76**, 159 (1996)], [hep-ex/9508003].
- [31] S. Orito *et al.*, Phys. Rev. Lett. **66**, 1951 (1991).
- [32] M. Ambrosio *et al.* (MACRO), Eur. Phys. J. **C25**, 511 (2002), [hep-ex/0207020].
- [33] B. Cabrera, Phys. Rev. Lett. **48**, 1378 (1982).
- [34] P. B. Price *et al.*, Phys. Rev. Lett. **35**, 487 (1975).
- [35] S. Balestra *et al.*, Eur. Phys. J. **C55**, 57 (2008), [arXiv:0801.4913].
- [36] M. G. Aartsen *et al.* (IceCube), Eur. Phys. J. **C76**, 3, 133 (2016), [arXiv:1511.01350].
- [37] A. Albert *et al.* (ANTARES), JHEP **07**, 054 (2017), [arXiv:1703.00424].
- [38] M. A. Acero *et al.* (NOvA), Phys. Rev. D **103**, 1, 012007 (2021), [arXiv:2009.04867].
- [39] A. Aab *et al.* (Pierre Auger), Phys. Rev. **D94**, 8, 082002 (2016), [arXiv:1609.04451].
- [40] D. P. Hogan *et al.*, Phys. Rev. **D78**, 075031 (2008), [arXiv:0806.2129].
- [41] M. Detrixhe *et al.* (ANITA-II), Phys. Rev. **D83**, 023513 (2011), [arXiv:1008.1282].
- [42] J. E. Bartelt *et al.*, Phys. Rev. D **36**, 1990 (1987), [Erratum: Phys. Rev. D **40**, 1701 (1989)].
- [43] M. Ambrosio *et al.* (MACRO), Eur. Phys. J. **C26**, 163 (2002), [hep-ex/0207024].
- [44] R. Becker-Szendy *et al.*, Phys. Rev. **D49**, 2169 (1994).
- [45] V. A. Balkanov *et al.* (Baikal), Prog. Part. Nucl. Phys. **40**, 391 (1998), [arXiv:astro-ph/9801044].
- [46] M. G. Aartsen *et al.* (IceCube), Eur. Phys. J. **C74**, 7, 2938 (2014), [Erratum: Eur. Phys. J. **C79**, no. 2, 124 (2019)], [arXiv:1402.3460].
- [47] K. Ueno *et al.* (Super-Kamiokande), Astropart. Phys. **36**, 131 (2012), [arXiv:1203.0940].
- [48] G. Aad *et al.* (ATLAS), Phys. Rev. **D93**, 5, 052009 (2016), [arXiv:1509.08059].
- [49] G. Aad *et al.* (ATLAS), Phys. Rev. Lett. **124**, 3, 031802 (2020), [arXiv:1905.10130].
- [50] B. Acharya *et al.* (MoEDAL), Phys. Rev. Lett. **118**, 6, 061801 (2017), [arXiv:1611.06817].
- [51] B. Acharya *et al.* (MoEDAL), Phys. Rev. Lett. **123**, 2, 021802 (2019), [arXiv:1903.08491].
- [52] S. Baines *et al.*, Eur. Phys. J. **C78**, 11, 966 (2018), [Erratum: Eur. Phys. J. **C79**, no. 2, 166 (2019)], [arXiv:1808.08942].
- [53] A. Abulencia *et al.* (CDF), Phys. Rev. Lett. **96**, 201801 (2006), [hep-ex/0509015].
- [54] G. R. Kalbfleisch *et al.*, Phys. Rev. **D69**, 052002 (2004), [hep-ex/0306045].
- [55] P. B. Price, G.-X. Ren and K. Kinoshita, Phys. Rev. Lett. **59**, 2523 (1987).
- [56] B. Aubert *et al.*, Phys. Lett. **120B**, 465 (1983).
- [57] R. A. Carrigan, F. A. Nezrick and B. P. Strauss, Phys. Rev. **D8**, 3717 (1973).

- [58] G. Abbiendi *et al.* (OPAL), Phys. Lett. **B663**, 37 (2008), [arXiv:0707.0404].
- [59] J. L. Pinfold *et al.*, Phys. Lett. **B316**, 407 (1993).
- [60] K. Kinoshita *et al.*, Phys. Rev. **D46**, R881 (1992).
- [61] K. Kinoshita *et al.*, Phys. Lett. **B228**, 543 (1989).
- [62] P. Musset, M. Price and E. Lohrmann, Phys. Lett. **128B**, 333 (1983).
- [63] T. Gentile *et al.* (CLEO), Phys. Rev. **D35**, 1081 (1987).
- [64] W. Braunschweig *et al.* (TASSO), Z. Phys. **C38**, 543 (1988).
- [65] A. Aktas *et al.* (H1), Eur. Phys. J. **C41**, 133 (2005), [hep-ex/0501039].
- [66] A. De Rujula, Nucl. Phys. **B435**, 257 (1995), [hep-th/9405191].
- [67] I. F. Ginzburg and A. Schiller, Phys. Rev. **D60**, 075016 (1999), [hep-ph/9903314].
- [68] B. Abbott *et al.* (D0), Phys. Rev. Lett. **81**, 524 (1998), [hep-ex/9803023].
- [69] M. Acciarri *et al.* (L3), Phys. Lett. **B345**, 609 (1995).



INDEX

Index

This index is for the complete *Review of Particle Physics* (Volume 1 and 2). Page numbers larger than 1122 refer to the Particle Listings in Volume 2 that can be found in the journal publication and online at <https://pdg.lbl.gov>.

- a* meson resonances
- $a_0(980)$ 34, 1382
 - $a_0(1450)$ 36, 1416
 - $a_0(1950)$ 1456
 - $a_1(1260)$ 35, 1392
 - $a_1(1640)$ 37, 1431
 - $a_2(1320)$ 35, 1402
 - $a_2(1700)$ 38, 1445
 - $a_4(1970)$ [*was* $a_4(2040)$] 39, 1458
- ABC, approximate Bayesian computation 684
- Absolute monochromatic magnitude 134
- Accelerating Universe evidence 471
- Accelerator parameters 543
- Accelerator parameters for neutrino beam lines 548
- Accelerator-based ν detectors 605
- Accelerator-induced radioactivity 648
- Acceptance-rejection method (Von Neumann) 713
- Acoustic oscillations, baryon 478
- Activation function 689
- Active learning 683, 684
- Activity, unit of 646
- AD, automatic differentiation 700
- AdaBoost, adaptive boost 689
- ADAM, Adaptive Momentum Estimation 700
- AdS, anti-de Sitter spacetime 983
- AdS/CFT
- correspondence 983, 1062
 - dictionary 987, 1062
- Advanced acceleration schemes 541
- Age of the Universe 135, 432
- Air shower extensive, EAS 618
- Air showers (cosmic ray) 524
- Aleatoric uncertainty 704
- Algorithms for Monte Carlo 714
- α , fine structure constant 178
- α_s , QCD coupling constant 133
- Amplitudes, Lorentz invariant 743
- AMS, approximate median significance 704
- AMS-02 – alpha magnetic spectrometer, ISS 521
- AMSB, anomaly-mediated SUSY breaking 1002
- Angular-diameter distance, d_A 432
- Anisotropy of CBR 471, 509
- Annihilating dark matter 516
- Anomalous dimension quark mass (\overline{MS}) 808
- Anomaly detection 683, 706
- Anomaly-mediated SUSY breaking, AMSB 1002
- Anthropic approach 435
- Anthropic axion window 1045
- Antineutrino flux from reactor 298
- Antineutrinos, right-handed 897
- Astronomical unit 134
- Astrophysics 483
- Asymmetry formulae in Standard Model 181
- Asymptotic freedom 149
- Asymptotics, total hadronic cross sections behaviour 409
- ATLAS – Thoroidal LHC Apparatus, LHC 208
- Atmospheric
- Cherenkov detectors 620
 - cosmic rays 524
 - fluorescence detector 618
 - Fly’s Eye 618
 - HiRes (high resolution) Fly’s Eye 618
 - Pierre Auger observatory 618
 - Telescope Array 618
 - neutrino flux 293
- Atmospheric pressure 133
- Atomic
- and nuclear properties of materials, table 140
 - mass unit 133
- Atomic weights of elements 137
- Attention 690, 694
- Attenuation length for photons 557
- Auger observatory 525, 618, 1095
- Authors and consultants 12
- Auto-encoder 681, 683
- Averaging of data 16
- Averaging, unconstrained 16
- Avogadro constant 133
- Axial vector couplings, g_V , g_A vector 177
- Axial vector mesons $\ell = 1$; 1^{++} or 1^{+-} 313
- Axial-vector mesons
- K_{1A} - K_{1B} mixing 845, 850
 - $f_1(1285)$, $f_1(1420)$, $f_1(1510)$ 850, 851
- Axion as dark matter 485, 1038
- Axion searches 1038
- Axion stars 1046
- Axion-like particles (ALP) 1038
- Axion-photon mixing 516
- Axions (A^0) and other very light bosons searches 27, 1217
- $B\bar{B}$ mixing 923
- $b\bar{b}$ mesons 81, 1940
- B decay, CP violation in 278, 920
- B decays polarization, note 919
- B mesons
- V_{cb} and V_{ub} CKM Matrix Elements 1780
 - B^* 67, 1781
 - B^0 59, 1675
 - B^\pm 53, 1610
 - B^\pm/B^0 admixture 65, 1750
 - $B^\pm/B^0/B_s^0/B$ -baryon admixture 66, 1772
 - $B_1(5721)$ 68, 1782
 - $B_2^*(5747)$ 68, 1783
 - $B_3^*(5732)$ [*was* B^{**}] 1782
 - $B_J(5840)$ 1783
 - $B_J(5970)$ 68, 1784
 - B_c^+ 70, 1813
 - $B_c(2S)^\pm$ 70, 1817
 - $B_{s1}(5830)^0$ 70, 1811
 - $B_{s2}^*(5840)^0$ 70, 1811
 - $B_{sJ}^*(5850)$ 1811
 - $B_{sJ}(6063)^0$ 1812
 - $B_{sJ}(6114)^0$ 1812
 - B_s^* 69, 1810
 - B_s^0 68, 1786
- b' quark (4^{th} generation), searches for 829
- b -baryon admixture 106, 2179
- b -flavored Hadrons, production and decay 908
- b -quark fragmentation 383, 827
- $b_1(1235)$ meson 35, 1391
- Background
- cosmic microwave, CMB 509
 - cosmic ray radiation 647
 - relic cosmic neutrino 476
 - relic light gravitons 984
- Background cosmology parameters 511
- Backpropagation 684, 700
- Bagging, bootstrap aggregating 688
- Balitsky-Fadin-Kuraev-Lipatov (BFKL) limit 152
- Barkas correction 552
- Baryogenesis 435
- Baryon
- acoustic oscillations 447, 471, 478
 - decay parameters, note on 964
 - density of the Universe 134
 - Hyperon nonleptonic decays 964
 - magnetic moments 321, 326
 - number conservation 116
 - oscillation spectroscopic survey 471
 - resonances, naming scheme 965

resonances, SU(3) classification of	317
semileptonic decays	964
Baryon quick reference table	89
Baryon-to-photon ratio	134, 461
Baryonia	845, 852
$\rho(1900)$	850
$f_2(1565)$	852
Baryons in quark model	317
Batch	700, 702
Bayes' theorem	452, 655
Bayesian	
approach	664
intervals	669
method	660
statistics	669
Bayesian machine learning	705
Bayesian optimization	682, 687
BBN, Big-Bang nucleosynthesis	459
Beam collimation	535, 540
Beam cooling	535
Beam dynamics	533
Beam momentum, c.m. energy and momentum vs	743
Beam-beam interaction	536
Beamstrahlung	536, 538
Becquerel, unit of radioactivity	646
BEPC	543
BEPC-II	543
β function of QCD	149
Beta distribution	658, 715
Beta function	534
β -rays, from radioactive sources	652
Betatron tune	534
Bethe equation	550
Beyond the general relativity physics	516
Beyond the SM physics, BSM	261, 463, 485, 720
Bhabha cross section	555
Bhabha scattering	178
Bi-directional RNN	694
Bias of an estimator	660
Big-Bang cosmology	443
Big-Bang cosmology, note on	430
Big-Bang nucleosynthesis (BBN)	459
Binary classification	679, 680, 686
Binary pulsars, strong-self-gravity	424
Bino	1004
Binomial distribution	658, 714
Biological damage from radiation	646
Birks' law	568
Black holes	
binary	424
coalescing	421
horizon	419
microscopic, searches	985
production	984
strong gravitational fields	418
supermassive	424
Bloch correction	552
BMA, Bayesian model averaging	705
BN, batch normalization	691, 701
Bohr magneton	133
Bohr radius	133, 183
Boiling points of cryogenic gases, table	140
Boltzmann constant k	133
Booklet, Particle Physics, how to get	11
Boosting	688
Bose-Einstein correlations	404, 725, 789
Bosons, Nambu-Goldstone composite	1061
BOSS, baryon oscillation spectroscopic survey	471
Bottleneck	681, 697
Bottom baryons	104, 2161
Bottom mesons	
experimental rate measurements	902
production and decay	908
theoretical decay-constant calculations	902
Bottom mesons (B, B^*)	53, 1610
Bottom, Charmed mesons ($B_c, B_c(2S)$)	70, 1813
Bottom, Strange mesons (B_s, B_s^*, X)	68, 1786
Bottom-changing neutral currents, tests for	117
Bottomonium note	81, 1940
Bragg additivity	554
Brane	463, 984, 1002, 1079
Breit-Wigner parametrization	751
Breit-Wigner distribution	715
Bremsstrahlung	
at very high energies	558
by e^\pm	556
by muons	560
B_s^0 decay, CP violation in	278
BSM, beyond Standard Model	485
Bubble chambers	606
Bubble Universes	435
$c\bar{c}$ mesons (including possibly non- $q\bar{q}$ states)	70, 1818
C (charge conjugation), tests of conservation	110
c -quark fragmentation	383
Cabibbo angle	873
Calorimeter	
electromagnetic (ECAL)	597
hadronic (HCAL)	597
homogeneous	597
sampling	597
CBR – Cosmic background radiation (see CMB)	509
CDM, cold dark matter	483
Central limit theorem	657
CEPC	538
Cepheid variable stars	470
CESR (Cornell)	544
CESR-C (Cornell)	544
CFT, 4d conformal field theory	987
Chandrasekhar mass	134
Change of random variables	656
Channels	685, 690, 702
Characteristic functions	656
Charge conjugation (C) conservation	110
Charge conjugation of $q\bar{q}$ states	313
Charge conservation	113
Charged Higgs bosons (H^\pm and $H^{\pm\pm}$) searches	26, 1196
Chargino mass limits	1026
Charginos	1004
Charm decays, CP violation in	276
Charm mixing and CP violation	881
Charm-changing neutral currents, tests for	117
Charmed baryons ($\Lambda_c^+, \Sigma_c, \Xi_c, \Omega_c^+$)	100, 2136
Charmed baryons, note on	100, 2136
Charmed mesons	
experimental rate measurements	900
theoretical decay-constant calculations	901
Charmed mesons (D, D^*, D_J)	43, 1527
Charmed, Strange mesons (D_s, D_s^*, D_{sJ}, X)	50, 1588
Chemical potential	346, 433
Chemical potential, neutrino	516
Cherenkov detectors	572
at accelerators	
differential	573
ring imaging	573
threshold	572
tracking	572
electromagnetic calorimeters	572
fast paticle counter	572
nonaccelerator	
atmospheric	620
deep underground	621
particle identification PID	572
Cherenkov radiation	561
χ^2 distribution	657, 714
χ_b and χ_c mesons	

$\chi_{b0}(1P)$	82, 1948
$\chi_{b0}(2P)$	84, 1960
$\chi_{b1}(1P)$	82, 1950
$\chi_{b1}(2P)$	84, 1961
$\chi_{b1}(3P)$	84, 1969
$\chi_{b2}(1P)$	83, 1952
$\chi_{b2}(2P)$	84, 1964
$\chi_{b2}(3P)$	85, 1970
$\chi_{c0}(1P)$	73, 1851
$\chi_{c0}(3860)$	1911
$\chi_{c0}(3915)$ [<i>was X(3915)</i>]	79, 1916
$\chi_{c0}(4500)$ [<i>was X(4500)</i>]	1936
$\chi_{c0}(4700)$ [<i>was X(4700)</i>]	1939
$\chi_{c1}(1P)$	74, 1861
$\chi_{c1}(3872)$ [<i>aka X(3872)</i>]	78, 1911
$\chi_{c1}(4140)$ [<i>was X(4140)</i>]	79, 1922
$\chi_{c1}(4274)$ [<i>was X(4274)</i>]	80, 1932
$\chi_{c1}(4685)$	1939
$\chi_{c2}(1P)$	75, 1872
$\chi_{c2}(3930)$	79, 1917
Chiral perturbation theory	341, 810, 859, 865
Chiral superfields	1000
Chromaticity	535
CIPT, countour improved perturbation theory	184
Circular Colliders	533
Circular Higgs factories	538
CKM (Cabibbo-Kobayashi-Maskawa) quark mixing matrix	946
CKM angles	
α	946
β	946
γ	948
from B hadrons determination, note	946
CKM matrix elements	946
CKM quark-mixing matrix, note on	261
CKM unitarity constraints	874
Classical electron radius	133
Classification	676, 679, 683, 686, 687, 691, 697, 705
Clebsch-Gordan coefficients	737, 738
CLIC (CERN) future collider	544
Clustering	681, 697
CMB	
<i>Planck</i> satellite	447, 503, 512
anisotropy	439, 471
anisotropy power spectrum	509
COBE satellite	468, 509
Compton distortion	515
concordance with baryon density	462
cosmic microwave background	509
cosmic variance	510
detectors	633
dipole	509
future Simons observatory	473
lensing	479
LiteBIRD satellite	514
Lorentz-boosted temperature pattern	509
mean temperature, monopole	509
monopole	509
multipoles	509
non-Gaussianity	437, 453, 468, 510
polarization	513
primordial perturbation	511
radiation density of Universe	134
scalar perturbations	511
sky map	509
Solar System motion	509
spectrum	509
tensor perturbations	511
Wilkinson Microwave Anisotropy Probe, <i>WMAP</i>	509
WMAP satellite	503
CMB-Cosmic microwave background	436, 471
CMS – Compact Muon Solenoid, LHC	208
CMSSM, Constrained MSSM	1007, 1021
CNN, convolutional neural network	679, 685, 690, 702
CNO cycle, solar neutrino	292
COBE – COsmic Background Explorer	509
Coherent radio Cherenkov radiation detectors	627
Cold dark matter (CDM)	438
Cold dark matter density	134
Collaboration databases	21
Collaborations	
<i>Planck</i>	470
ALEPH	789
ALICE	397
ALPHA	346
ANITA	629
ARIANNA	629
ATLAS	397, 487, 789, 951, 991
Auger	525
B-factories	951
BaBar	178, 804, 902, 908, 924, 951, 1010
Belle	804, 902, 908, 924, 951, 1010
BERT	1040
BESIII	951
BES III	178
BNL E821	184
CALICE	601
CCFR	608
CDF	789, 908
CJ	366
CLEO	178, 908
CLEO-c	951
CMD-3	178
CMS	179, 487, 951, 991, 997, 1030, 1091
COHERENT	182
COMPASS	843
COMPETE	399, 409
CTA	620
D0	179, 408, 789, 909, 924, 997
DarkSide	631
DELPHI	789, 924
DREAM/RD52	603
DSSV	358
eBOSS	502
ETM	904
Event Horizon Telescope	425
Fermi-LAT	1043
FLAG	904
GlueX	977
GRAND	630
H.E.S.S.	620, 1043
H1	384, 1091
HERA	385, 1025
HFLAV	904
HPQCD	346, 904
HWPF	607
Jefferson lab hall A	182
L3	178, 789, 924
Lattice QCD	811
LEP	789, 791, 996, 1025
LHAASO	525
LHC	789, 997
LHCb	789, 908, 920, 951, 959, 997, 1010
LIGO-Virgo	421
LVC	421
MAGIC	620
MAMI	843
MILC	901
MOSCAB	491
MuLan	178
NEWS-G	491
NEWSdm	491
NEXT	632
NINJA	608
NuTeV	181, 608
OPAL	178, 789, 924
PDG, Particle Data Group	2

PIBETA	842
PVLAS	1040
RBC/UKQCD	936
RD51	580
RM123-Soton	898
RNO-G	630
SLD	186, 793
SND	178
Sp \bar{p}	1055
Telescope Array	525
Tevatron	179, 789, 997, 1025
TOTEM	396
Tunka-Rex	630
UA4	408
VERITAS	620
WMAP	472
ZEUS	187, 384, 1025, 1091
Collider parameters	543
Colliders	533
future	538
present	537
recent	536
Colliders based on Energy Recovery Linacs	539
Collinear and infrared safety	153, 157
Collinear factorization	151
Color confinement	1044
Color factor	149, 159
Color reconnection phenomenon	405, 725, 789
Colorons (axigluons) search	1072
Compact Linear Collider (CLIC)	539
Compactification	1045
Compensation	
intrinsic	602
software	603
Complex ionization history	469
Composite Higgs boson	192, 235
Compton wavelength, electron	133
Concordance cosmology	468
Conditional probability density function	656
Confidence intervals	668
frequentist	669
Gaussian	16
Poisson	671
Confinement	346
-deconfinement quarks-hadrons transition	434
color	1044
harmonic	317
linear	317, 722
Conformal field theory, CFT	987
Conservation laws	110
Consistency of an estimator	660
Constancy of constants tests	423
Constrained fit	803
Constrained fits, procedures for	16
Constrained MSSM, CMSSM	1007, 1021
Constraints, parameter estimation with	663
Consultants	12
Contour-improved perturbation theory (CIPT)	163
Conversion constant	133
Conversion probability for photons to e^+e^-	557
Convolution kernel	690
Convolution, 1×1	690
Convolution, kernel size	690
Convolution, padding	690
Convolution, stride	690
Convolution-transpose	691
Correlation coefficient, definition	656
Correlation matrices	803
Cosmic acceleration, dark energy	499
Cosmic background radiation temperature	509
Cosmic microwave background, CMB	436, 471, 509
Cosmic neutrino background, $C\nu B$	476
Cosmic ray(s)	520
air showers	524
ankle	525, 526
at surface of earth	522
background in counters	647
composition	520
fluorescence detectors FDs	618
fluxes	524
in atmosphere	520
instep	526
knee	525
primary spectra	520
radio detection of air showers	630
second knee	525
secondary neutrinos	523
ultra-high energy	526
ultra-high energy, UHE	628
underground	523
Cosmic topology	470
Cosmological	
constant Λ	134, 430, 443, 499, 511
density parameter, Ω	431
equation of state	431
mass density parameter	430
parameters, note on	467
standard model	517
Cosmological probes	
CMB	515
galaxy peculiar velocities	472
integrated Sachs-Wolfe effect	472
redshift	430
supernovae	470
Cosmology	467, 483
Λ CDM	483
Big-Bang	430, 443, 483
modern	483
outlook for the future	473
Robertson-Walker metric	443
scalar field	444
standard	485
standard early Universe	443
standard neutrino	476
Contour improved perturbation theory, CIPT	184
Coupling between matter and gravity	423
Coupling constant in QCD	133, 149
Coupling unification	1079
Couplings for photon, W , Z	177
Covariance matrix	662
Covariance, definition	656
Coverage	669
CP , tests of conservation	110
CP violation	
and $D^0 - \bar{D}^0$ mixing	885
charm mixing	881
classification of effects	273
in $B\bar{B}$ mixing	926
in B and B_s^0 mixing and decay	278
in B decay	908
in K_L^0 decay	275
in K_L^0 decay, note on	877
in charm	276
in decays of Beauty to Charm	881
in the quark sector, note	271
interference between tree and penguin amplitudes ..	278
overview	110, 271
the CKM matrix	274
the Kobayashi-Maskawa mechanism	274
CPT invariance tests in neutral kaon decay	871
CPT tests of conservation	113
CRF – computer-readable files	770
Critical density in cosmology	430
Critical density of the Universe	134
Critical energy	
for electrons	556

for muons	560	repulsive gravity	500
Cromomagnetic dipole moment	822	Dark energy spectroscopic instrument (DESI)	472, 502
Cross sections and related quantities, plots of	770	Dark matter	438, 469
σ and R in e^+e^- Collisions	773	annihilating	516
e^+e^- annihilation cross section near M_Z	775	CDM cosmology	483
pd , np , $\bar{p}d$, and $\bar{p}n$ collisions	779	density distribution	484
Λp , Σp , γd , γp , and $\gamma\gamma$ collisions	783	detectors	633
$\pi^\pm p$ and $\pi^\pm d$ collisions	780	Gaia satellite	485
K^+p , K^+d and K^+n collisions	782	Galactic halo shape	484
K^-p , K^-d and K^-n collisions	781	genesis, cannibalization	484
Pseudorapidity distribution in pp and $\bar{p}p$ interactions	770	genesis, DM anti-DM asymmetry	484
Average hadron multiplicities		genesis, freeze-in	484
in e^+e^- annihilation events	771	genesis, freeze-out	483
nucleon structure functions	353	genesis, non-thermal production	484
Cross sections, neutrino	765	genesis, primordial black holes	484
Cross sections, relations for	745, 756	laboratory detection	487
Cross-entropy loss	680	missing satellites problem	485
Cross-validation	678	non-baryonic	483
Cryogenic beam vacuum system	539	velocity distribution	485
Cryogenic gases, boiling points, table	140	Dark matter astrophysical detection	
Crystal accelerator	541	cosmic-ray antimatter	493
Cumulative distribution function, definition	655	cosmology	494
Curie, unit of radioactivity	646	gamma rays	492
Curvature	135	multi-wavelength	494
d functions	737	neutrinos	493
D mesons		PBH detection	494
D^0, \bar{D}^0	45, 1543	staller physics	494
D^\pm	43, 1527	Dark matter candidates	
$D(3000)^0$	1587	axions	485
$D^*(2007)^0$	49, 1578	dark photon	486
$D^*(2010)^\pm$	49, 1578	gaugino	1003
$D^*(2640)^\pm$	1585	gravitino	1002
$D_0^*(2300)$ [<i>was</i> $D_0^*(2400)$]	49, 1580	higgsino	1003
$D_0(2550)^0$	1584	sterile neutrinos	485
$D_1^*(2600)^0$ [<i>was</i> $D_1^*(2600)$]	1584	WIMPs	486
$D_1^*(2760)^0$	1586	Dark matter properties	
$D_1(2420)$	49, 1580	darkness	483
$D_1(2430)^0$	49, 1582	mass lower and upper limits	483
$D_2^*(2460)$	49, 1582	self-interactions	483
$D_2(2740)^0$ [<i>was</i> $D(2740)^0$]	1585	stability	483
$D_3^*(2750)$	49, 1586	Data	21
$D_{s0}^*(2317)^\pm$	51, 1601	Data augmentation	686, 703, 704
$D_{s0}(2590)^+$	1605	Data manifold	686
$D_{s1}^*(2700)^\pm$	52, 1606	Data, averaging and fitting procedures	16
$D_{s1}^*(2860)^\pm$	1606	Data, selecting and treatment	15
$D_{s1}(2460)^\pm$	52, 1602	Databases	
$D_{s1}(2536)^\pm$	52, 1604	availability online	20
$D_{s2}^*(2573)$	52, 1605	conferences	21
$D_{s3}^*(2860)^\pm$	52, 1607	experiments	21
$D_{sJ}(3040)^\pm$	1608	high-energy physics	20
$D_s^{*\pm}$	51, 1601	INSPIRE	20
D_s^\pm	50, 1588	Authors	21
$D^0-\bar{D}^0$ mixing, note on	885	Conferences	21
DAΦNE	543	Experiments	21
d_A , angular-diameter distance	471, 516	Jobs	21
Dalitz plot, relations for	744	Literature	20
Damage, biological, from radiation	646	Seminars	21
Dark energy	431, 469, 499	journals	21
cosmic acceleration	499	literature	20
density parameter	134	ADS	20
equation of state parameter	135	arXiv.org	20
equation of state parameter w	471, 499	INSPIRE	20
Euclid satellite	456	MathSciNet	20
experiments	502	ORCID	21
observational probes		particle physics	20
baryon acoustic oscillations, BAO	501	PDGLive, PDG web browser	20
CMB anisotropies	501	Review of Particle Physics (RPP)	20
Type Ia supernovae	501	RPP computer-readable files	20
weak gravitational lensing	501	Day, sidereal	134
parameter, Ω_N	431	dE/dx	549
quintessence	440	Decay parameters, Michel	806
		Decays, kinematics and phase space for	743
		Deceleration parameter, q_0	431

Decision trees	677
Decoder	681, 691, 696, 698
Deep inelastic scattering, DIS	353, 398, 606
Deep learning	690
Deep Sets	685, 696
Deep-inelastic scattering (DIS)	151
Degree of freedom, number of	662
$\Delta B = 1$, weak-neutral currents, tests for	110
$\Delta B = 2$, tests for	110
$\Delta C = 1$, weak-neutral currents, tests for	110
$\Delta C = 2$, tests for	110
Δ resonances	
$\Delta(1232)$	94, 2042
$\Delta(1600)$	94, 2044
$\Delta(1620)$	94, 2045
$\Delta(1700)$	94, 2047
$\Delta(1750)$	2049
$\Delta(1900)$	94, 2049
$\Delta(1905)$	94, 2051
$\Delta(1910)$	95, 2052
$\Delta(1920)$	95, 2054
$\Delta(1930)$	95, 2056
$\Delta(1940)$	2057
$\Delta(1950)$	95, 2058
$\Delta(2000)$	2059
$\Delta(2150)$	2060
$\Delta(2200)$	95, 2061
$\Delta(2300)$	2061
$\Delta(2350)$	2062
$\Delta(2390)$	2062
$\Delta(2400)$	2062
$\Delta(2420)$	95, 2063
$\Delta(2750)$	2064
$\Delta(2950)$	2064
$\Delta(\sim 3000$ Region) Partial-Wave Analyses	2064
$\Delta S = 1$, weak-neutral currents, tests for	110
$\Delta S = \Delta Q$ tests of	110
$\Delta T = 1$, weak-neutral currents, tests for	110
δ -rays	553
DenseNet	692
Density	
of CMB photons	134
of Universe, critical	134
parameter of the Universe Ω_0	134
Density effect in energy loss rate	550
Density estimation	680, 684, 697, 704, 705
Density of materials, table	140
DESI – dark energy spectroscopic instrument	456, 472, 502
Detectors	
bubble chambers	606
calorimeters	
electromagnetic	599
Cherenkov	572, 620
CMB detectors	633
coherent radio Cherenkov radiation	627
Dark matter	633
fluorescence, atmospheric	618
for rare events	630
gas-filled	574
drift chamber	577, 604
high rate effects	578
micro-pattern	578
micro-strip chamber	580
multi-wire proportional chambers, MWPC	577
resistive plate chambers, RPC	584
time-projection chambers, TPC	581
transition radiation, TRD	582
gravitation wave observatory, Virgo	421
hadronic shower	565
ice-based	629
inorganic scintillator	570
Kinetic Inductance Detectors (KIDs)	634
LAr Time projection chambers	586
laser interferometer gravitation observatory, LIGO	421
liquid ionization chamber	605
liquid scintillator	621
low noise readout	593
Low Temperature Detectors (LTDs)	633
low-radioactivity background techniques	638
Magnetic Metallic Calorimeters (MMCs)	635
Neutrino cryogenic detectors	633
neutrino telescopes	623
neutrino, calibration of	652
neutrinos	
accelerator-based	605
bubble chambers	606
Cherenkov	606
emulsion	608
iron tracking calorimeters	606
liquid argon TPC	607
plastic scintillators	607
noble liquid	623
organic scintillator	568
proton decay	621
radio-detection of cosmic ray air showers	630
rare event search	
$0\nu\beta$ decay	632
WIMPs	631
semiconductor	589
hybrid pixels	591
LGAD	592
microstrip	591
monolithic pixels	591
radiation damage	592
Semiconductor Thermistors	634
showers	599
superconducting solenoid magnets for	609
superconducting toroidal magnets for	609
Superconducting Tunnel Junctions (STJs)	634
Transition Edge Sensors (TESs)	635
water Cherenkov	622
wire chambers	586
Deuterium abundance	459
Deuteron mass	133
Deuteron structure function	365
DIEHARD	713
Dielectric constant of gaseous elements, table	141
Dielectric laser accelerator	541
Dielectric suppression of bremsstrahlung	556
Dielectric wakefield accelerators	541
Differentiable simulator	684
Differential Cherenkov detectors	573
Diffraction and high energy soft QCD	392
Diffraction parton distribution	398
Diffraction processes	392
Dirac gauginos	1012
Dirac neutrinos	286
Direct CP asymmetry in B decays	920
Directories, online, people, and organizations	20
DIS, deep inelastic scattering	353, 398
Discriminative model	676, 678, 697
Disk density	134
Dispersion relation	408, 858, 873
Distance ladders	470
Distance-redshift relation	430, 432, 467, 470, 500
Distribution shift	677
Dokshitzer-Gribov-Lipatov-Altarelli-Parisi (DGLAP) equations	152
Domain adaptation	703
Domain shift	677, 703
Donnachie-Landshoff pp -scattering amplitude	393
Dose rate from γ ray sources	648
Dose, radioactivity, unit of absorbed	647
Double PDFs	358
Double- β decay	1284
Doubly charmed baryons	2160

Drell-Yan process	186, 210, 334, 361
Drift chambers	577
Drift velocities of electrons	604
Dropout	679, 690
D_s^+ branching fractions, note on	895
Dual problem	686
Dual readout	603
Dynamic Graph CNN	696
Dynamical electroweak symmetry breaking	1061
e (electron)	28, 1239
e (natural log base)	133
e^- Compton wavelength	133
Early stopping	677, 679, 689, 700, 701
Early Universe	443, 459
Earth	
equatorial radius	134
mass	134
Eddington luminosity	134
Edge	696
Education databases	21
Effective dose of radioactivity	646
Effective field theories (EFTs)	329
Effective number of neutrinos	135
Effective skin depth δ	142
Efficiency of an estimator	660
EFT – effective field theories	329
Elastic cross sections	398
Elastic scattering	392
ELBO, Evidence Lower Bound Objective	680, 697, 698
Electric charge (Q) conservation	113
Electric dipole moment, EDM	111
Electrical resistivity of elements, table	141
Electromagnetic	
calorimeters	599
cascades	559
effects	326
relations	142
showers, lateral distribution	560
showers, longitudinal distribution	559
Electromagnetic field equations	142
Electron	
charge magnitude e	133
critical energy	556
cyclotron frequency/field e/m_e	133
drift velocities	604
mass	133
radius, classical	133
volt eV	133
Electron and photon interactions in matter	555
Electron configuration of element, table	138
Electron-Ion Collider (EIC)	538
Electron-positron collider rings	537
Electron-positron colliders – future	539
Electronic energy loss by heavy particles	549
Electronic structure of the elements	138
Electroweak	
dynamical symmetry breaking	1061
interactions, Standard Model of	177
model and constraints on new physics, review	177
penguin decay	912, 920
Electroweak corrections	154, 162
Electroweak Symmetry Breaking (EWSB)	201
Elements	
electronic structure of	138
ionization energies of	138
Elements, periodic table of	137
Embedding	685
Emission probability	652
Emittance	534
Empirical risk	677
Encoder	681, 691, 696, 698
Encoder-decoder	692, 694
Energy and momentum (c.m.) vs beam momentum	743
Energy density	
of CBR	134
of dark energy	134
of relativistic particles	134
Energy loss	
(fractional) for e^\pm in lead	556
at low energies	551
by electrons	556
by photons	557
density effect	550
higher order corrections	551
rate for heavy charged particles	550
rate for muons at high energies	560
rate in compounds and mixtures	554
rate, form factor corrections	550
rate, most probable	553
rate, restricted	550, 553
scaling with mass	550
Energy Recovery Linac	539
Energy resolution (calorimeter)	597
constant term	598
stochastic term	598
Energy-energy correlation	158
Ensemble methods	688
Entropy density	433, 435
Entropy density / Boltzmann constant	134
e^+e^- annihilation	
cross-section formulae	756
two-photon process	757
Epistemic uncertainty	704
ϵ_0 (permittivity of free space)	133, 142
$\hat{\epsilon}_1, \hat{\epsilon}_2, \hat{\epsilon}_3$ electroweak variables	192
Equivalence principle, experimental tests of	423
Equivalence principle, GR	417
Equivalent noise charge	595
Error function	657
Error propagation	703
Errors, treatment of	16
Established nonets for the meson	314
Estimator	660
η mesons	
η	33, 1354
$\eta(1295)$	35, 1401
$\eta(1405)$	36, 1410
$\eta(1475)$	36, 1420
$\eta(1760)$	1449
$\eta(2225)$	1468
$\eta'(958)$	34, 1373
$\eta_2(1645)$	37, 1432
$\eta_2(1870)$	38, 1453
$\eta_c(1S)$	70, 1818
$\eta_c(2S)$	76, 1883
$\eta_b(1S)$	81, 1940
$\eta_b(2S)$	1954
Event pile up	540
Event shape	158
EWSB, Electroweak Symmetry Breaking	201
Excitation energy	550
Excited fermions searches	1056
Excited leptons searches	1056
Exotic baryons P_c	106, 2181
Exotic muon decays	875
Exotic quantum numbers	845
Expansion of the Universe	431
Expectation value, definition	655
Experiment databases	21
Experimental design optimization	682, 683
Experimental rate measurements	
bottom mesons	902
charmed mesons	900
pions and kaons	898
Experimental sensitivity	673

Experimental tests of gravitational theory	417
Exploding gradient	689, 694, 701
Extensions to the cosmological standard model	468
Extensive air shower, EAS	618
Extra Dimensions	109, 1002, 2243
Extra Dimensions, note on	983
<i>f</i> , <i>F</i> mesons	
$f_0(980)$	34, 1379
$f_0(1370)$	36, 1406
$f_0(1500)$	37, 1421
$f_0(1710)$	38, 1446
$f_0(2020)$	1459
$f_0(2100)$	1462
$f_0(2200)$	1466
$f_0(2330)$	1470
$f_1(1285)$	35, 1398
$f_1(1420)$	36, 1413
$f_1(1510)$	1424
$f_2'(1525)$	37, 1425
$f_2(1270)$	35, 1395
$f_2(1430)$	1416
$f_2(1565)$	1429
$f_2(1640)$	1432
$f_2(1810)$	1451
$f_2(1910)$	1455
$f_2(1950)$	38, 1456
$f_2(2010)$	39, 1459
$f_2(2150)$	1462
$f_2(2300)$	39, 1469
$f_2(2340)$	39, 1470
$f_4(2050)$	39, 1460
$f_4(2300)$	1469
$f_6(2510)$	1472
$f_J(2220)$	1467
$f_0(600)$ [was $f_0(500)$ was σ]	33, 1359
F_2 structure function, plots	365
Factorization scale	151
FCC-ee (Future Circular Collider)	538
FCC-hh (Future Circular Collider)	539
FCNC, flavor-changing neutral currents	833
Feature engineering	681
Feature map	690
Feature vector	677, 689
Fermi constant	178, 1003
Fermi coupling constant $G_F/(hc)^3$	133
Fermi plateau	551
Fermions	
left-handed	1063
right-handed	1063
Feynman's x variable	745
Field equations, electromagnetic	142
Filter	689
Fine tuning	1009
Fine-structure constant, α	133, 178
Fine-structure constant, time variation	516
Fine-tuning	702
Fit to Z electroweak measurements	791
Fit, technical implementation	804
Fits to data	16
Fixed-order perturbation theory (FOPT)	163, 184
Flat extra dimension	987
Flatness of Universe	473
Flavor anomalies	1010
Flavor number scheme (FNS)	152
Flavor symmetric couplings	847
Flavor transitions (oscillations) neutrino	291
Flavor-changing neutral currents, tests for	117
Flavour Lattice Averaging Group (FLAG)	163
Fluctuation amplitude at $8h^{-1}$ Mpc scale	134
Fluctuations in energy loss	553
Fluorescence detector, atmospheric	618
Flux conversion	134
Fly's Eye fluorescence detector	618
FODO cell	534
FOPT, fixed-order perturbation theory	184
Forbidden states in quark model	144
Force, Lorentz	142
Form factors for radiative pion and kaon decays, note on	842
Four-quark states	317, 861
Fourth generation b' quark searches	829
Fragmentation	
functions, scaling violations in	376
heavy-quark	383
in e^+e^- annihilation	375
longitudinal	378
models	379
Fragmentation function	155
Fragmentation functions in	
e^+e^- , ep , and pp collisions, note on	375
Frequentist	
approach	660
confidence intervals	669
statistics	669
Friedman equation	432
Friedmann constraint equation	443
Friedmann-Lemaître equations	430
Further states mesons	1980
g (gluon)	25, 1142
g-2 muon anomalous magnetic moment	798
Galaxy clustering	456, 471
Galaxy power spectrum	471
γ (photon)	25, 1141
γ (Euler constant)	133
Gamma collider	539
Gamma distribution	658, 714
Gamma factory	541
Gamma rays, astrophysical	526
γ -rays, from radioactive sources	652
$\gamma\gamma$ collisions	847
GAN, Generative Adversarial Network	697, 698, 703
Gas electron multiplier (GEM)	579
Gas-filled detectors	
electron drift velocity	575, 604
gas properties	574
high rate effects	578
mobility of ions	576
Townsend coefficient	575
Gauge and Higgs bosons	
H^0 Higgs	26, 1175
W	25, 1142
Z	25, 1156
γ (photon)	25, 1141
g (gluon)	25, 1142
Searches	
graviton	25, 1142
Gauge and Higgs bosons searches	
W' , Z'	27, 1200
axion	27, 1217
charged Higgs H^\pm , $H^{\pm\pm}$	26, 1196
Gauge coupling unification	1079
Gauge hierarchy	1000
Gauge kinetic function	1001
Gauge supermultiplet	1000
Gauge symmetry principle	285
Gauge-mediated supersymmetry breaking, GMSB	1007
Gaugino	1001, 1004
Gaugino mass unification	1006
Gaussian	
n -dimensional ellipsoid	657
(Normal) distribution	658
confidence intervals	670
distribution, MC algorithm	714
distribution, Multivariate	657
General relativity predictions	417

equivalence principle	417	neutrino masses	1083
gravitational waves	418	Pati-Salam model	1076
isotropy of space	423	Yukawa coupling unification	1082
quasi-stationary, weak-field	418	GUTs, grand unified theories	1076
radiative gravity tests	425	g_V, g_A vector, axial vector couplings	177
strong fields, neutron stars, black holes	418		
universality of free fall tests	423	<i>h</i> mesons	
General relativity, GR	417	$h_1(1170)$	35, 1391
General-purpose Monte Carlo generators, (GPMC)	717	$h_1(1415)$ [<i>was</i> $h_1(1380)$]	36, 1412
Generalization	677, 678	$h_1(1595)$	1430
Generalized NMSSM, GNMSSM	1012	$h_b(1P)$	83, 1952
Generative model	677, 678, 697, 705	$h_b(2P)$	84, 1964
Generator of SU(3) transformation	738	$h_c(1P)$	75, 1870
Geometric deep learning	696	H^0 (Higgs boson)	26, 1175
GIM – Glashow-Iliopoulos-Maiani mechanism	214	Hadron colliders	536
Glashow-Iliopoulos-Maiani (GIM) mechanism	113, 214	Hadron colliders – future	540
Global fit in SM	189, 266	Hadron level	156
Glueballs	316, 845, 847	Hadronic	
$\eta(1405)$	849	calorimeters	565
$f_0(1500), f_0(1710)$	847	shower detectors	565
lattice calculations	847	Hadronic Molecules	860
scalar	847	Hadronization corrections	157
tensor	848	Hadronization model	156
Gluino	1001	Half-lives of radioactive nuclides	652
Gluino mass limits	1021	Harrison-Zel’dovich effect	467
Gluino searches	235	<i>h/e</i> ratio	601
Gluon field, SU(3) valued	808	He initialization	701
Gluon induced jets	158	Heavy baryons	320
GMSB, gauge-mediated supersymmetry breaking	1007	Heavy charged lepton searches	30, 1272
GNMSSM, generalized NMSSM	1012	Heavy neutral leptons searches	1307
GNN, graph neural network	685, 696	Heavy Quark Expansion (HQE)	934
Goldstino	1001	Heavy quarks masses	812
GP, Gaussian Process	678, 683, 687	Heavy vector-like quark <i>B</i>	1069
GPMC generators		Heavy vector-like quark <i>T</i>	1066
General-purpose Monte Carlo generators	717	Heavy-quark	
HERWIG	717	effective theory (HQET)	329
PHOTOS	720	expansion for inclusive decays	330
PYTHIA	717	fragmentation	383
SHERPA	717	spin-flavor symmetry	329
uncertainties and tuning	726	Heavy-quark and soft-collinear effective theory, note on	329
GR, general relativity	417	Heavy-quarkonium spectroscopy	951
Gradient boosting	689	Helium-3 abundance	460
Gradient clipping	701	Helium-4 abundance	460
Gradient descent	677, 679, 684, 689, 700	HERA	536
Grand unified theories, GUTs	1076	HERA (DESY) collider parameters	546
Graviscalar searches	983	Hessian	700
Gravitational		HFLAV charm mixing global fit	891
constant G_N	133	Hidden sector	1002
acceleration g_N	133	Hidden state	692
lensing	437, 472, 512	Hidden valley models	1002
radiation	420	Hierarchy problem	984
theory, experimental tests of	417	Higgs and electroweak factories	538
wave speed	421	Higgs boson	
waves in GR	418	ATLAS and CMS total inefficiency	208
Gravitino	1002	double charged search	245
Graviton		in MSSM	236
disperse	426	LHC runs at $\sqrt{s} = 7, 8, 13$ TeV	208
mass	426	mass	203
Randall-Sundrum	1063	mass in electroweak analyses	190
searches	984	mass in Standard Model	177
Graviton searches	25, 1142	new physics models	234
Gravity		non-SM decay channels, searching	217
in extra dimensions	983	quantum numbers	203, 222
tests	421	self coupling	215
Gray, unit of absorbed dose of radiation	646	trilinear self coupling	206
Group normalization	702	vector boson fusion (VBF)	208
GRU, Gated Recurrent Unit	694	width	226
GUTs		Yukawa coupling to fermions	210
baryon-number-violating nucleon decay	1081	Higgs boson physics	201
basic group theory, charge quantization	1076	Higgs production in e^+e^- annihilation	758
breaking	1077	Higgsino	1001
doublet-triplet splitting	1077	High energy diffraction experiments	398
monopoles prediction	1093	High energy diffraction, theoretical description	393

High energy soft QCD and diffraction, note on	392
High intensity beams	535
High-field accelerator magnets	539
High-frequency surface impedance	142
Highlights of this edition of the RPP	6
History of measurements, discussion	18
History plots	19
HL-LHC	537
Holographic model	847, 848
Horizon scale	511
Hot Big-Bang cosmology	459
HQE parameters and V_{cb}	934
HQET – Heavy-quark effective theory	329
HST, Hubble space telescope	470
Hubble	
constant H_0	467, 511
cosmic topology	470
expansion	431
expansion rate	134, 483
flow	502
length c/H_0	134, 432
parameter $H(t)$	430
radius	511
relativistic species	469
scaling factor for expansion rate	134
space telescope HST	470
varying constants	469
Hubble's law	430
Huber loss	678
Hybrid inflation model	445
Hybrid mesons	851
$\pi(1800)$, $\pi_1(2015)$	851
$\pi_1(1400)$, $\pi_1(1600)$	851
$\rho(1450)$	850
Hybrid states	317
Hyperbolic tangent activation	689, 694
Hypercharge	312, 995, 1076
Ice-based detectors	629
ID particle codes for MC	733
Ideal mixing	845
Ideal mixing in quark model	315
Ideograms, criteria for presentation	16
ILC, future International Linear Collider (Japan)	544
Image data	685, 690
Imaging Cherenkov detectors	573
Impedance of free space	142
Impedance, relations for	142
Importance sampling	715
Importance sampling in Monte Carlo calculations	713
Inception	690
Inclusive hadronic reactions	758
Inclusive reactions, kinematics for	745, 758
Inconsistent data, treatment of	16
Independence of random variables	656
Inductive bias	679, 685, 697
Inelastic cross sections	398
Inference	679, 684, 703, 706
Inflation	
CMB photons	443
de Sitter limit $\epsilon \rightarrow 0$	446
effective field theory of	453
Friedman equation	443
future probes of	456
motivation	443
multi-field	454
of early Universe	435, 443, 467
quantum fluctuations	445
reheating	444
slow-roll	444, 510
Inflation models	
R^2 inflation	449
axion monodromy	449
chaotic with power-law potentials	449
D-brane	449
Higgs	450
Hilltop	449
natural	449
pioneering	448
supergravity	451
supersymmetric	450
Inflation primordial perturbations	445
density from single-field	446
gravitational waves	445
metric	445
observational bounds	447
Inflaton	
field fluctuations	446
Higgs scalar field as candidate	451
Inflaton scalar field	419, 435, 445
Information horizon	433
Infrared and collinear safety	153, 157
Initialization	689, 700, 701
Inorganic scintillators	570
Input normalization	701
Instance normalization	702
Integer encoding	685
Integrated Sachs-Wolfe effect	440, 471, 499, 511
Inter-galactic medium clustering	472
Interaction length	597
International Linear Collider (ILC)	538
International System (SI) units	136
INTERNET address for comments	11
Interpretability	677, 691, 695
Introduction	11
Inverse problem	684
Inverse transform method in Monte Carlo	713
Invisible energy (calorimetry)	601
Ion colliders	538
Ionization	
energies of the elements	138
energy loss at minimum, table	140
history of the Universe	469
Ionization yields for charged particles	554
IoU, Intersection over Union	691
Isotropy of space tests	423
$J/\psi(1S)$	71, 1826
Jansky	134
Jet algorithm	
cone	157
sequential recombination	158
Jet definition	157
Jet shape	158
Jet substructure	158
J/ψ radiative decay	848, 849
JS, Jensen-Shannon divergence	699
K factor	156
K stable mesons	
K^0	40, 1488
K^\pm	39, 1473
K_L^0	40, 1493
K_L^0 decay, CP violation in	877
K_S^0	40, 1489
K , K^* meson resonances	
$K(1460)$	42, 1518
$K(1630)$	1519
$K(1830)$	1523
$K(3100)$	1526
$K_1(1270)$	42, 1512
$K_1(1400)$	42, 1513
$K_1(1650)$	42, 1519
$K^*(892)$	42, 1509
$K_0^*(700)$ [<i>was</i> $K_0^*(800)$]	41, 1508
$K^*(1410)$	42, 1514

$K^*(1680)$	42, 1519	$A_b(5920)^0$	105, 2169
$K_0^*(1430)$ [<i>was</i> $\kappa(1350)$]	42, 1515	$A_b(6070)^0$	105, 2170
$K_0^*(1950)$	1523	$A_b(6146)^0$	105, 2170
$K_2^*(1430)$	42, 1516	$A_b(6152)^0$	105, 2170
$K_2^*(1980)$	43, 1523	A_c^-	100, 2136
$K_2(1580)$	1519	$A_c(2595)^+$	101, 2143
$K_2(1770)$	42, 1520	$A_c(2625)^+$	101, 2143
$K_2(1820)$	43, 1522	$A_c(2765)^+$ or $\Sigma_c(2765)$	2144
$K_2(2250)$	1525	$A_c(2860)^+$	101, 2144
$K_3^*(1780)$	42, 1521	$A_c(2880)^+$	101, 2144
$K_3(2320)$	1525	$A_c(2940)^+$	101, 2145
$K_4^*(2045)$	43, 1524	$\Lambda(1405)$ region, pole structure, note on	973
$K_4(2500)$	1525	Λ , cosmological constant	430
$K_5^*(2380)$	1525	Λ CDM, minimal cosmological model	476
k-means clustering	681	CACDM, cold dark matter with dark energy	468
K_L^0 decay, CP violation in	275	MACDM, minimal cosmological model	468
Kähler potential	1001	Landau distribution	553
Kaluza-Klein		Landau-Pomeranchuk-Migdal (LPM) effect	556
excitations	192, 734, 832, 996	Landau-Yuang theorem	222
modes	983, 991, 1081	LAr Time projection chambers, detector	586
reduction	983	LARES – laser relativity satellite	424
searches	986	Large extra dimensions	763, 983
theories	421, 983	Large rapidity gap	392
Kaon decay, CPT invariance tests in neutral	871	Large-scale structure of the Universe	438
KEKB (KEK) collider parameters	544	Last scattering surface, LSS	511
Kernel machines	677	Lattice calculations of spectroscopy	323
Kernel trick	686	Lattice QCD	337, 808, 925, 1045
Kinematic limits		Layer normalization	702
sequential two-body decay	744	LBL, long baseline	289
three-body decays	744	Leaky ReLU	689
Kinematics, decays, and scattering	743	Learning rate	677, 700
Kinetic Inductance Detectors (KIDs)	634	Least squares	662
Kinetic Sunyaev-Zel'dovich effect	440	Left-handed	
KL, Kullback-Leibler divergence	680, 697–699	fermions	1063
Knock-on electrons, energetic	553	leptons	1076
Kobayashi-Maskawa (Cabibbo-) mixing matrix	261	neutrinos	897
KRR, kernel ridge regression	687	quarks	1076
		sleptons	1084
		Left-handed (l.h.)	1076
		Left-handedness of neutrinos	285
		LEP	537
		LEP (CERN)	544
		Lepton	
		conservation, tests of	116
		family number conservation	113
		left-handed	1076
		mixing	287
		Lepton PDF	151
		Lepton-flavor violation, LFV	113
		Leptonic decays of charged pseudoscalar mesons,	
		note on	897
		phenomenological implications	903
		Leptons	
		(see individual entries for e , μ , τ and ν)	28, 1239
		Leptoproduction kinematics	756
		Leptoquark review	1090
		Leptoquark searches	1090
		Lethal dose from penetrating ionizing radiation	647
		LFV – lepton-flavor violation	113
		LHC	537
		LHC (CERN) collider parameters	546
		LHC (CERN) heavy ion collider parameters	547
		LHeC	539
		Light	
		speed in vacuum of	133
		year (deprecated unit)	134
		Light meson spectrum	846
		Light quarks masses	809
		Light unflavored mesons	33, 1349
		Lightest supersymmetric particle, LSP	1001
		LIGO, Laser interferometer gravitational observatory	421
		Likelihood-ratio trick	679, 684, 705
		Limits	668

Linear colliders	536, 538
Linear confinement	317, 722
Linear Higgs factories	538
Linear regression	678
Liquid ionization chambers	605
Lithium-7 abundance	462
Little hierarchy	1009
Local dark matter density	134
Local disk density	134
Local Group velocity with respect to CMB	134
Log-normal distribution	658
Logistic activation	689
Logistic regression	678
Logits	690, 695
Lomonosov satellite. γ -ray burst, high-energy cosmic rays	618
Long baseline neutrino sources (LBL)	289, 1083
Long-lived sparticles masses limits	1030
Longitudinal fragmentation	378
Longitudinal structure function, plots of	365
Lorentz force	142
Lorentz invariant amplitudes	743
Lorentz transformations of four-vectors	743
Loss	677, 678
Low Temperature Detectors (LTDs)	633
Low-radioactivity background techniques	638
LQCD heavy quark masses	341
heavy quarks	339
light quarks masses	340
Monte Carlo method	342
QED	340
scattering amplitudes and resonances	343
status of simulations	344
Wilson fermion action	338
Wilson gauge action	337
LQCD, lattice quantum chromodynamics calculations	337
LSP, lightest supersymmetric particle	1001
LSTM, Long Short-Term Memory	694
Luminosity	533, 535
muon collider	540
circular collider	536
linear collider	538
Luminosity conversion	134
Luminosity distance d_L	432
Lund string model	722
$Ly\alpha$ forest	437
M-theory	1045
Machine learning	676
MAE, mean-absolute error	678
MAF, Masked Autoregressive Flow	699
Magnetic fields, primordial	516
Magnetic Metallic Calorimeters (MMCs)	635
Magnetic monopoles	1084
GUTs prediction	1093
note on	1093
Magnetic monopoles searches	108, 2185
Majorana neutrinos	286
mAMSB, minimal AMSB	1007
Mandelstam variables	745
MAP, maximum a posteriori	679, 684, 705
Marginal probability density function	656
Markov chain	715
Mass attenuation coefficient for photons	557
Mass matrix light quark	810
neutrino	286
Masses heavy quarks	812
light quarks	809
Materials, atomic and nuclear properties of, table	140
Matter supermultiplet	1000
Matter, passage of particles through	549
Maximal mixing scenario	1006
Maximum energy transfer to e^- in single collision	550
Maximum likelihood	661
Maximum-margin classifier	686
Maxwell equations	142
MC – Monte Carlo	733
MDP, Markov decision process	682
Mean energy loss rate in H ₂ liquid, He gas, C, Al, Fe, Sn	550
Mean excitation energy	549, 550
Mean range in H ₂ liquid, He gas, C, Fe, Pb	550
Mean sidereal day	134
Median, definition	655
Meson cloud	861, 967
Meson electromagnetic radius	843
Meson multiplets in quark model	313
Meson nonets (established)	314
Meson quick reference table	88
Meson-meson bound states	860
Mesons Further states	1980
axial vector $\ell = 1; 1^{++}$ or 1^{+-}	313
bottomonium	951
charmonium	951
conventional	951
pseudoscalar $\ell = 0, 0^{-+}$	313
scalar $\ell = 1, 0^{++}$	313, 858
tensor $\ell = 1, 2^{++}$	313
thresholds	951
unconventional	951
vector $\ell = 0, 1^{-}$	313
XYZ	951
Messenger scale	1006
Metric prefixes, commonly used	136
Michel parameters	806
Micro-mesh gaseous structure (MicroMegas)	579
Micro-pattern gas detectors, MPGD	578
MicroMegas, micro-mesh gaseous structure	579
Microwave background	436
Mihheev-Smirnov-Wolfenstein effect for solar neutrinos ..	291
Minimal 7-parameter model, Λ CDM + $\sum m_\nu$	480
cosmological model Λ CDM	476
Minimal AMSB, mAMSB	1007
Minimal supergravity, mSUGRA	1021
Minimal supergravity, mSUGRA	1007
Minimal supersymmetric SM, MSSM	1000
Minimum ionization	550
Minimum ionization loss, table	140
MIP (minimum ionizing particle)	550, 574
Mixing angle, weak ($\sin^2 \hat{\theta}(M_Z)$)	133
Mixing, D^0 - \bar{D}^0 , note on	885
Mixing matrix	288
Mixing, singlet-octet in quark model	323
MLP, multi-layer perceptron	685, 689, 696
Modified gravity	469
Modified minimal subtraction scheme (\overline{MS})	149
Molar volume	133
Molecular states	845, 852
Molière radius	560
Momenta, measurement of, in a magnetic field	610
Monopoles catalysis of nucleon decay	1095
Kibble mechanism	1093
Parker bound	1094
Monte Carlo acceptance-rejection method	713
calculations, importance sampling in	713
codes for radiation protection studies	650
DIEHARD	713
inverse transform method	713
Lagged-Fibonacci-based generator	713
LQCD	342

neutrino event generators	729
particle numbering scheme	733
random number generators	713
RANLUX generator	713
techniques	713
Monte Carlo algorithm for	
χ^2 distribution	714
beta distribution	715
binomial distribution	714
Breit-Wigner distribution	715
exponential decay	714
Gamma distribution	714
Gaussian distribution	714
Poisson distribution	714
sine and cosine of random angle	714
Student's t distribution	714
Monte Carlo dropout	705
Monte Carlo event generators	717
MOSCAB collaboration	491
MPGD, micro-pattern gas detectors	580
MPNN, Message Passing Neural Network	697
MS renormalization scheme	178
\overline{MS} factorization scheme	151
\overline{MS} mass	150
MSE, mean-squared error	678, 705
MSSM current experimental status	1008
MSSM Higgs boson phenomenology	237
MSSM parameters	1003
MSSM, minimal supersymmetric SM	1000
MSSM-124	1003
mSUGRA, minimal supergravity	1007, 1021
μ (muon)	28, 1240
μ_0 (permeability of free space)	133, 142
Multi-arm bandits	682
Multi-class classification	680, 690, 695
Multi-head attention	696
Multi-wire proportional chamber, MWPC	577
Multibody charm analyses, review of	880
Multibody decay kinematics	745
Multinomial distributions	657
Multiple Coulomb scattering	554
Multiple parton-parton interactions, MPI	156, 397, 724
Multiplets, meson in quark model	313
Multiplets, $SU(n)$	739
Multiplexing	635
Multivariate Gaussian distribution	657
Multiverse	435, 455
Muon	
anomalous magnetic moment	184, 798
critical energy	560
energy loss rate at high energies	560
range/energy in rock	523
Muon Anomalous Magnetic Moment	796
Muon collider	540
Muon collider, neutrino radiation hazard	540
Muon decay parameters	800
MWPC, Multi-wire proportional chamber	
maximum wire tension	577
wire stability	577
Møller cross section	555
n (neutron)	90, 1997
N and Δ Resonances	91, 2003
N and Δ Resonances, note on	965
N baryons	
N (~ 3000 Region) Partial-Wave Analyses	2041
$N(1440)$	91, 2003
$N(1520)$	91, 2004
$N(1535)$	91, 2007
$N(1650)$	91, 2009
$N(1675)$	91, 2011
$N(1680)$	91, 2013
$N(1700)$	92, 2015
$N(1710)$	92, 2017
$N(1720)$	92, 2018
$N(1860)$	2021
$N(1875)$	92, 2022
$N(1880)$	92, 2024
$N(1895)$	92, 2025
$N(1900)$	93, 2027
$N(1990)$	2029
$N(2000)$	2030
$N(2040)$	2031
$N(2060)$	93, 2032
$N(2100)$	93, 2033
$N(2120)$	93, 2035
$N(2190)$	93, 2036
$N(2220)$	94, 2038
$N(2250)$	94, 2039
$N(2300)$	2040
$N(2570)$	2040
$N(2600)$	94, 2040
$N(2700)$	2040
N 's and Δ 's note	91, 2003
n -body differential cross sections	743
n -body phase space	743
Nambu-Goldstone bosons	985, 1038
Nambu-Goldstone composite bosons	1061
Names, hadrons	15, 144
Naming scheme for baryon resonances	965
Naturalness	1009
Network-in-network	690
Neural network	677, 679, 689, 697, 700, 701, 705
Neuron	689
Neutral Higgs bosons searches	26, 1187
Neutral-current parameters, values for	181, 191
Neutralinos	1004
Neutralinos mass limits	1027
Neutrino detectors (deep, large, enclosed volume)	621
heavy water	623
liquid scintillator	621
noble	
time-projection chamber	623
table of detectors	621
water-filled	622
Neutrino detectors, cryogenic detectors	633
Neutrino telescopes	
AMANDA, South Pole	624
ANTARES, Med. Sea	624
backgrounds	623
DUMAND, Pacific Ocean	624
effective area	624
GVD, Lake Baikal	624
IceCube, South Pole	624
KM3NeT, Med. Sea	624
NEMO, Med. Sea	624
NESTOR, Med. Sea	624
NT-200, Lake Baikal	624
P-ONE, Pacific Ocean	624
results	626
technical realisation	624
Neutrino(s)	
astrophysical	526, 623
atmospheric	
detectors	621
atmospheric flux	293
beam lines at high-energy proton synchrotrons	548
chemical potential	516
cosmogenic	526
cosmological constraints	476
cross section measurements	765
current temperature	476
density of the Universe	135
Dirac	286
from cosmic rays	520
left-handed	285, 897

Majorana	286
mass density parameter, Ω_ν	467
mass hierarchy	623
mass matrix	286
mass, cosmological limit	472
masses	480
masses, mixing, and oscillations, note on	285
mixing	30, 1288
Monte Carlo event generators	729
neutrinoless double- β decay	307
non-standard	479
oscillation search	291
properties	30, 1273
reactor	
detectors	621
relic background	476
right-handed	285, 1076
see-saw mechanism	286
solar flux	292
solar, pp chain	292
solar, CNO cycle	292
sterile	285, 287, 304
supernova burst	
detectors	621
Neutrinoless double- β decay searches	307
Neutrinos in cosmology, note on	476
Neutron	90, 1997
Neutron mass	133
Neutrons at accelerators	647
Neutrons, from radioactive sources	652
New heavy bosons	
(W' , Z' , leptoquarks, etc.) searches	27, 1200
New Physics (NP) beyond SM	287, 920
NEWS-G collaboration	491
NEWSdm collaboration	491
Newtonian gravitation constant G_N	134
Next-to-lightest supersymmetric particle, NLSP	1008
Next-to-minimal supersymmetric SM, NMSSM	1001
NF, Normalizing Flow	683, 684, 697, 699
NICA	538
NLSP, next-to-lightest supersymmetric particle	1008
NMS, Non-Maximum Suppression	691
NMSSM, next-to-minimal supersymmetric SM	1001
Node	696
Noise	
equivalent noise analysis	594
equivalent noise charge (ENC)	595
in analog signal processing	594
in digital signal processing	596
in timing measurements	596
noise origins	594
Nomenclature for hadrons	144
Non-Gaussianity CMB	437, 453, 468, 510
Non-perturbative corrections	157
Non-standard neutrinos	
interactions beyond weak force	479
sterile neutrinos	479
unstable neutrinos	479
Non $q\bar{q}$ candidates	
$cc\bar{c}$ state	961
Double- $J/\psi(1S)$ invariant mass	961
four heavy quarks	961
heavy-heavy systems	959
heavy-light systems	959
Normal (Gaussian) distribution	658
Normal distribution	657
NP, new heavy quark mixing	875
NP, new physics beyond SM	287
Neutrino properties	30, 1273
Nuclear	
and atomic properties of materials, table	140
interaction length, table	140
magneton	133
Nuclear PDFs	358
Nucleon decay	1081
Nucleosynthesis	436
Nuclides, radioactive, commonly used	652
Number density of baryons	134
Number density of CMB photons	134
Number of degree of freedom	662
Number of neutrino types	
and sum of neutrino masses	30, 1282
Numbering scheme for particles	733
Object detection	691
Observations, the light element abundance	459
Occupational radiation dose, U.S. maximum permissible	647
Octet-singlet mixing in quark model	314
Odderon in soft QCD	407
Ω baryons	
Ω^-	99, 2133
$\Omega(2012)^-$	99, 2134
$\Omega(2250)^-$	100, 2135
$\Omega(2380)^-$	2135
$\Omega(2470)^-$	2135
Ω_b^-	2179
$\Omega_b(6316)^-$	2178
$\Omega_b(6330)^-$	2179
$\Omega_b(6340)^-$	2179
$\Omega_b(6350)^-$	2179
Ω_c^0	103, 2156
$\Omega_c(2770)^0$	103, 2157
$\Omega_c(3000)^0$	103, 2157
$\Omega_c(3050)^0$	103, 2158
$\Omega_c(3065)^0$	103, 2158
$\Omega_c(3090)^0$	103, 2158
$\Omega_c(3120)^0$	104, 2159
Ω_{dm} , dark matter density	469
ω mesons	
$\omega(782)$	34, 1367
$\omega(1420)$	36, 1414
$\omega(1650)$	37, 1433
$\omega_3(1670)$	37, 1434
Ω , cosmological density parameter	431
Ω_{m} , mass density parameter	431
Ω_Λ , scaled cosmological constant	431
Ω_ν , neutrino mass density parameter	467
Ω_{tot} , total energy density of Universe	473
Ω_v , vacuum energy parameter	431
One-hot encoding	685
One-shot learning	702
OOD, out-of-distribution	683
Optimal control	682
Optimization	677
Organic scintillator	568
Other light mesons	1980
Other particle searches	2263
Overfitting	677–679, 681, 700, 701
p (proton)	90, 1987
P (parity), tests of conservation	110
PAE, Probabilistic Auto-Encoder	698
PAMELA – payload for antimatter exploration	
and light nuclei	521
Parameter estimation	660
Parameter estimation with constraints	663
Parametrizing the Universe	467
Paraphotons, searches	1038
Pardethadcal	600
Parity of $q\bar{q}$ states	312
Parsec	134
Partial Conserved Axial Current, PCAC	730, 843
Partial wave analyses, PWA	968
Particle	
ID numbers for MC	733
identification detectors, PID	572

nomenclature	144
symbol style conventions	144
Particle flow	598
Particle flow confusion	599
Particle level	156
Particle nomenclature	15
Particle Physics Booklet, how to get	11
Parton	
density functions	717
distribution function, PDF	398
distributions	356
Parton distribution function (PDF)	151
Parton level	157
Parton shower	156
Parton-shower formalism	719
Passage of particles through matter	549
Pati-Salam model	1076, 1090
$\bar{p}p$ annihilation	845
PBN, primordial black holes	494
P_c , exotic baryons	
$P_c(4312)^+$	106, 2181
$P_c(4380)^+$	106, 2181
$P_c(4440)$	107, 2181
$P_c(4457)^+$	107, 2181
PCA, principle component analysis	681, 698
PCAC, Partial Conserved Axial Current	730, 843
PDF, parton distribution function	398
PdgLive, interactive access to RPP	11
PDGLive, PDG web presentation	20
Peccei-Quinn mechanism and axion	1038
Penguin decays, electroweak	912, 920
Penguin-dominated modes	265
Pentaquarks	
$P_c(4312)^+$	975
$P_c(4440)^+$	975
$P_c(4457)^+$	975
search	975
Pentaquarks	106, 2181
PEP-II (SLAC) collider parameters	544
Periodic table of the elements	137
Permeability μ_0 of free space	142
Permeability of free space μ_0	133
Permittivity ϵ_0 of free space	133
Permittivity ϵ_0 of free space	142
Permutation invariant	685, 696
Perturbation of early Universe	467
Perturbation theory, chiral	859, 865
Phase space, Lorentz invariant	743
Phase space, relations for	743
Phenomenological MSSM, pMSSM	1008, 1021
ϕ mesons	
$\phi(1020)$	34, 1383
$\phi(1680)$	37, 1437
$\phi(2170)$	39, 1465
$\phi_3(1850)$	38, 1453
Photon	
attenuation length	557
coupling	177
cross section in carbon and lead, contributions to	557
pair production cross section	557
structure functions F_2^{γ}	382
to e^+e^- conversion probability	557
total cross sections (C and Pb)	557
ultra-high energy	559
Photon and electron interactions with matter	555
Photon collider	539
Photon detectors	565
Photon PDF	151
Photon-dark photon-paraphoton conversion	1038
Photoproduction	152
Physical constants	133
Physics beyond general relativity	516
π mesons	
π^0	33, 1352
π^\pm	33, 1349
$\pi(1300)$	35, 1402
$\pi_1(1400)$	36, 1409
$\pi_1(1600)$	37, 1430
$\pi_2(1670)$	37, 1435
$\pi_2(1880)$	38, 1454
$\pi_2(2005)$	1459
$\pi_2(2100)$	1461
$\pi(1800)$	38, 1450
π value	133
PID, particle identification detectors	572
Pions and kaons	
experimental rate measurements	898
theoretical decay-constant calculations	899
PixelCNN	699
Planck	
constant h	133
constant, reduced	133
length	134
mass	134
Plasma acceleration	541
Plasma energy	549
pMSSM, phenomenological MSSM	1008
POEMMA – probe of extreme multi-mes. astrophys.	618
Point Net	696
Poisson distribution	658, 714
Polarization in B decays, note on	919
Polarization in penguin-dominated B decays	920
Pole mass	150
Pole structure of the $A(1405)$ region, note on	973
Pomeron effective trajectory	402
Pomeron in soft QCD	401
Pontecorvo-Maki-Nakagawa-Sakata	
mixing matrix (PMNS)	288
Pooling	690
Pooling, average	691
Pooling, max	691
Potentials, electromagnetic	142
Power correction	150
pp -scattering amplitude by Donnachie-Landshoff	393
Precision flavor physics	183
Preconfinement	722
Prefixes, metric, commonly used	136
PReLU, Parametric ReLU	689
Present-day CMB	
dipole amplitude	134
temperature	134
Pressureless matter parameter	134
Primary spectra, cosmic rays	520
Primordial element abundance	459
Primordial helium fraction	135
Primordial magnetic fields	516
Princeton Tritium Observatory for Light, Early universe,	
Massive-neutrino Yield (PTOLEMY)	480
Probability	655
Probability density function, definition	655
Probability, Kolmogorovs definition	655
Production and Decay of b -flavored Hadrons	908
Propagation of errors	656
Properties (atomic and nuclear) of materials, table	140
Properties of resonances	750
Proton	
cyclotron frequency/field e/m_p	133
decay	1081
mass	133
structure function	353
structure function, plots	365
Proton (see p)	90, 1987
Proton decay detectors	621
Proton structure functions	151
Pseudorapidity	392, 746
Pseudoscalar mesons	848

$\eta(1405), \eta(1475)$	848	R-parity conserving, RPC	1001
$\eta(1295)$	848, 849	R-parity violation, RPV	1011
Pseudoscalar mesons $\ell = 0, 0^{-+}$	313	r.h., right-handed	1076
ψ mesons		Rad, unit of absorbed dose of radiation	646
$\psi_2(3823)$ [<i>was</i> $\psi(3823)$; <i>was</i> $X(3823)$]	78, 1910	Radiation	
$\psi_2(3842)$	78, 1911	-dominated epoch	434
$\psi(2S)$	76, 1886	Cherenkov	561
$\psi(3770)$	77, 1903	coherent radio Cherenkov radiation	562
$\psi(4040)$	79, 1919	gravitational	420
$\psi(4160)$	79, 1923	length	556
$\psi(4230)$ [<i>aka</i> $Y(4230)$; <i>was</i> $\psi(4260)$]	80, 1927	length of materials, table	140
$\psi(4360)$ [<i>aka</i> $Y(4360)$; <i>was</i> $X(4360)$]	80, 1933	length, approximate algorithm	556
$\psi(4415)$	81, 1934	protection	646
$\psi(4660)$ [<i>aka</i> $Y(4660)$; <i>was</i> $X(4660)$]	81, 1937	protection instrumentation	649
PTOLEMY, neutrino background direct detection	480	transition	562
Pulsars, binary	424	weighting factor	646
		Radiation damage in silicon detectors	592
QCD		Radiation length	597
Λ parameter	726	Radiative	
$\overline{\text{MS}}$ renormalization scheme	149	corrections in SM	180
β function	149	gravity test, GR prediction	425
color factor	149, 159	Radiative loss by muons	560
coupling constant	149	Radio-detection of cosmic ray air shower	630
jets	157	Radioactive nuclides, half-lives of	652
Lagrangian	149	Radioactive sources, commonly used	652
lagrangian	808	Radioactivity	
Λ parameter	150	accelerator-induced	648
Lattice	337	accelerators prompt neutrons	647
lattice	808, 1045	ambient dose equivalent	646
photon structure functions	382	and radiation protection	646
renormalization group equation (RGE)	149	Becquerel, unit of	646
running coupling	149, 164, 167	biological damage from chronic exposure	646
structure functions	355	Cancer induction	647
Quality factor for biological damage due to radiation	646	cosmic ray background radiation	647
Quantum		dose rate from γ ray sources	648
fluctuations, inflation	445	effective dose	646
gravity theory	983	effective dose limits	647
Quantum numbers in quark model	312	fluence, Φ	646
Quark		kerma, K	646
masses review	32, 1311	lethal dose from	647
masses, note on	808	long-term risk	646
Quark induced jets	158	natural annual background	647
Quark model		personal dosimeters	650
baryon resonances in	317	rem, roentgen equivalent for man	649
ideal mixing in	315	unit of absorbed dose, gray	646
meson multiplets in	313	unit of activity	646
mixing, singlet-octet in	323	weighting factor	646
quantum numbers in	312	Radion searches	985
Quark-antiquark annihilations $c\bar{d} \rightarrow W^+ \rightarrow \ell^+\nu$	897	Randall-Sundrum	
Quark-mixing CKM matrix	261	model	763, 986
Quark-parton model	151	warped geometry	983
Quarks	32, 1311	Randall-Sundrum graviton	1063
and lepton compositeness searches	108, 1055, 2239	Random angle, MC algorithm for sine and cosine of	714
b	32, 1317	Random Forests	688
b' quark (4^{th} generation), searches for	32, 1337	Random number generators	713
c	32, 1315	RANLUX Monte Carlo generator	713
current masses of	179	Rapidity	745
d	32, 1311	Rare event search	
fragmentation in e^+e^- annihilation, heavy	383	$0\nu\beta$ decay	632
Free quark searches	32, 1341	WIMPs	631
left-handed	1076	Rare kaon decay, constraints on CKM parameters	867
model	312	$R_{c0}(4240)$ [<i>was</i> $X(4240)^\pm$]	1931
model assignments	317	Re-ionization of the Universe	471
model, dynamical ingredients	322	Reactor	
properties of	312	antineutrino flux	298
s	32, 1311	antineutrino oscillation	298
t	32, 1319	Readout, detector	593
t' quark (4^{th} generation), searches for	32, 1339	Receptive field	690
u	32, 1311	Recombination scheme	158
Quasi-stationary general relativity	418	Redshift	430
		$z \simeq 1100$, reionization	510
R-CNN, region convolutional neural network	691	age at half reionization	135
R-parity	1001, 1019, 1090	age when acceleration was zero	135

age when optical depth equals unity	135
at half reionization	135
at which optical depth equals unity	135
comoving size of sound horizon at z_*	135
matter-radiation equality	135
when acceleration was zero	135
Redshift distortion	471
Refractive index of materials, table	140
Regge pole approach	392
Regge poles multiple exchange	393
Reggeon field theory	393
Regression	676, 678, 686, 687, 691, 697, 705
Regularization	677, 679, 701, 705
Reionization of the Universe	469
Reionization optical depth	134
Relativistic kinematics	743
Relativistic rise	550
Relativistic transformation of electromagnetic fields	142
ReLU, Rectified Linear Unit	689, 701
Rem, roentgen equivalent for man	646
Renormalization group	
quark mass	808
Renormalization group equation (RGE) of QCD	149, 1006
Renormalization in Standard Model	178
Renormalon	151, 179, 812
Representation learning	681
Representations, $SU(n)$	739
Repulsive gravity, dark energy	500
Resistive plate chambers	565, 584
Resistivity of metals	142
Resistivity, electrical, of elements, table	141
ResNet, Residual Network	692, 694
Resonances	
K -matrix parametrization	751
Breit–Wigner parametrization	751
Chew–Mandelstam function	752
mass, M_R	750
partial-wave decomposition	749
pole position, s_R	750
properties of the S -matrix	747
scattering-length approximation	752
width, Γ_R	750
Resonances, general consideration	747
Restricted energy loss rate	550, 553
Resummation	155
Review of multibody charm analyses	880
Review of Particle Physics overview	11
RG - renormalization group	333, 338
RGE, renormalization group equation	1006
RHIC	537
RHIC (Brookhaven) collider parameters	546
RHIC (Brookhaven) heavy ion collider parameters	547
ρ mesons	
$\rho(770)$	33, 1361
$\rho(1450)$	36, 1417
$\rho(1570)$	1430
$\rho(1700)$	38, 1441
$\rho(1900)$	1455
$\rho(2150)$	1464
$\rho_3(1690)$	38, 1438
$\rho_3(1990)$	1458
$\rho_3(2250)$	1468
$\rho_5(2350)$	1471
ρ parameter	181
Right-handed	
antineutrinos	897
fermions	1063
neutrinos	285, 1076
sleptons	1084
top quark	1081
Right-handed (r.h.)	1076
Risk	677, 704
Risk minimization	677, 678
RL, reinforcement learning	676, 682
RMSprop	700
RNN, recurrent neural network	685, 692
RNNSearch	695
Robertson-Walker metric	430, 443, 467
Robustness of an estimator	660
ROC, receiver operating characteristic curve	677, 679
ROI, region of interest	691
Rotational invariance	686
Rounding errors, treatment of	17
Rounding, PDG rules	17
RPC, R-parity conserving	1001
RPC, resistive plate chambers	584
RPN, Region Proposal Network	691
RPP authors and affiliations	2
RPP criteria for measured data	16
RPV, R-parity violation	1011
Running coupling in QCD	149, 164, 167
Running spectral index, $k_0 = 0.05 \text{ Mpc}^{-1}$	135
Rydberg energy	133
S, T, U electroweak variables	192
S -matrix	
approach to Z	791
for two-body scattering	743
S -matrix properties	747
Sachs-Wolfe effect	439, 511
Sachs-Wolfe effect, integrated	440, 471, 499, 511
Sampling	684
Satellite	
<i>Planck</i> , CMB	447, 503, 509, 512
AMS-02, cosmic-rays	521
COBE, monopole	509
Euclide, dark energy	456
Gaia, density distribution	485
LAGEOS, test of gravity	424
LARES, test of gravity	424
LiteBIRD, inflation, CMB	514
Lomonosov, γ -ray bursts	618
PAMELA, cosmic rays	521
POEMMA, cosmic rays	618
SMM, sun radiation	1043
SPHEREx, inflation	456
WMAP, CMB	503
Scalar field cosmology	444
Scalar mesons	845
$a_0(1450)$	845
$a_0(980)$, $f_0(980)$, $f_0(500)$, $K_0^*(700)$	851
$f_0(1370)$, $f_0(1500)$, $f_0(1710)$	845
nonets	846, 851
SU(3) couplings	847
Scalar mesons $\ell = 1, 0^{++}$	313, 858
Scalar mesons below 1 GeV, note on	858
Scalar spectral index	134
Scale dependence	150
Scale factor, definition of	16
Scaled cosmological constant, Ω_Λ	431
Scaled dot-product attention	695
Scaled Hubble constant	431
Scaling factor for Hubble expansion rate	134
Scaling for cosmological constant	134
Scaling violations in fragmentation functions	376
Scattering, relations for	756
SCET – soft-collinear effective theory	331
Scherk-Schwarz mechanism	1002
Schwarzschild	
radius of a black hole	985
radius of the Earth	134
radius of the Sun	134
Scintillation neutrino detectors	607
Scintillator parameters	568
Sea-level cosmic ray fluxes	522
Searches	

W' bosons	991, 1063
Z' bosons	995, 1063
b' quark fourth generation	829
new light particles in rare K decay	866
axiglons	1063, 1072
axion like particles (ALP)	1042
axions (A^0)	486, 1038
charginos	237
colorons	1072
dark matter	109, 2249
dark photon	218
doubly charged Higgs boson	245
dyons	1094
excited fermions	1056
excited leptons	1056
extra dimensions	486, 983
gluinos	235
graviscalar	983
graviton	984
heavy charged lepton	30, 1272
heavy neutral leptons	1307
heavy non- $q\bar{q}$ mesons	959
leptoquark	1090
light Higgsinos	235
magnetic monopoles	108, 1084, 1093, 2185
neutralino	237
neutrino oscillation or flavor transition	291
neutrinoless double- β decay	307
paraphotons	1038
pentaquarks	975
quark and lepton compositeness	108, 1055, 2239
radion	985
rare events	630
sleptons	237
SM explicit violations	865, 866
solar axions	1042
squarks	235, 237
supersymmetric particle	108, 2187
technicolor	243, 486, 1061, 1090
technifermions	
spontaneously broken chiral symmetry	1061
WIMP	109, 2249
Selection and treatment of data	15
Self-attention	696
Self-supervised learning	680
Semantic segmentation	691
Semiconductor	
detectors	589
materials	590
Semiconductor Thermistors	634
Semileptonic b -hadron decays,	
determination of V_{cb} , V_{ub}	930
Semitaonic decays	939
Sequential data	685, 692
Sequential two-body decay, kinematic limits	744
sfermion	1000
SGD, Stochastic Gradient Descent	700
Shape functions, SF	263, 331
Shared weights	690, 694
Shell correction	551
Shower detectors	599
Showers, electromagnetic	
lateral distribution of	560
longitudinal distribution of	559
SI units, complete set	136
Sidereal day	134
Sievert, unit of radiation dose equivalent	646
σ	33, 1359
Σ baryons	
Σ^+	97, 2090
Σ^-	97, 2093
Σ^0	97, 2092
Σ_b^*	105, 2171
$\Sigma_b(6097)^+$	105, 2172
$\Sigma_b(6097)^-$	105, 2172
Σ_b	105, 2171
$\Sigma(1385)$	97, 2095
$\Sigma(1580)$	2097
$\Sigma(1620)$	2098
$\Sigma(1660)$	97, 2099
$\Sigma(1670)$	98, 2101
$\Sigma(1750)$	98, 2103
$\Sigma(1775)$	98, 2104
$\Sigma(1780)$	2106
$\Sigma(1880)$	2107
$\Sigma(1900)$	2107
$\Sigma(1910)$	98, 2108
$\Sigma(1915)$	98, 2110
$\Sigma(2010)$	2112
$\Sigma(2030)$	98, 2113
$\Sigma(2070)$	2115
$\Sigma(2080)$	2115
$\Sigma(2100)$	2116
$\Sigma(2110)$	2117
$\Sigma(2250)$	2118
$\Sigma(2455)$	2119
$\Sigma(2620)$	2119
$\Sigma(3000)$	2120
$\Sigma(3170)$	2120
$\Sigma_c(2455)$	101, 2145
$\Sigma_c(2520)$	101, 2146
$\Sigma_c(2800)$	101, 2147
Σ baryons ($S = -1$, $I = 1$)	97, 2090
Sign conventions for resonance couplings	971
Silicon detector	589
radiation damage	592
timing measurement	592
Silk damping	512
Simplified models	1008
Simulation-based inference	679, 684, 697, 700, 705
$\sin^2 \theta_W$, weak-mixing angle	190
Singlet-octet mixing in quark model	314
Skip connection	692, 694, 696, 701
Slack variable	686
SLC (SLAC)	537, 544
sleptons	1004
sleptons masses limits	1028
SLHA, SUSY Les Houches accord	1004
Sloan Digital Sky Survey (SDSS)	471
Slow-roll inflation	510
SMM – solar maximum mission satellite	1043
SN1987A	
light gravitons luminosity	984
Sneutrino masses limits	1028
sneutrinos	1004
SNO - sudbury neutrino observatory	1040
Soft supersymmetry breaking	1000
Soft-collinear effective theory (SCET)	331
Softmax	680, 690, 694
Software	21
Solar	
ν experiment	292
ν fluxes	292
ν problem	292
angular velocity around Galactic center	134
circular velocity	134
constant, nominal	134
distance from Galactic center	134
equatorial radius, nominal	134
escape velocity from the Galaxy	134
luminosity, nominal	134
mass	134
photosphere temperature, nominal	134
Schwarzschild radius of	134
standard model	292
velocity with respect to CMB	134

Solid angle	134
Sparticle	1004
Specific heats of elements, table	141
Spectroscopy of mesons	
containing two heavy quarks, note on	951
Speed of light in vacuum c	133
Sphaleron	1084
SPHEREx – spectro-photometer for history	
of epoch reionization, satellite	456
Spherical harmonics	737
Spin polarisation	535
Spin-dependent structure functions	358
Spin-flavor symmetry	329
Split supersymmetry	1002
Splitting functions	152
Spontaneous symmetry breaking	177
SPPC	539
Squark mass limits	1021
squarks	1004
String theory	463
SSM, standard solar model	292
Standard	
cosmological model	468
gravitational acceleration	133
neutrino cosmology	476
particle numbering for MC	733
Solar Model (SSM)	292
Standard Model of electroweak interactions	177
Standard model of particle physics	
as EFT of more fundamental theory	329
Standard model, cosmological	517
Statistical procedures	16
Statistics, note on	660
Status of LQCD simulations	344
Stefan-Boltzmann constant	133
Sterile neutrinos	285, 304
Stopping power for heavy charged projectiles	549
Strangeness-changing neutral currents, tests for	110
String theory	1038
Strong coupling constant	133, 159, 162
Strong fields, neutron stars, black holes in GR	418
Structure functions	353
Student's t distribution	658, 714
SU(n) multiplets	739
SU(3)	
classification of baryon resonances	317
isoscalar factors, note on	738
multiplets	317
representation matrices, note on	738
transformation, generators of	738
SU(5)	321
SU(6) multiplets	317
Sudbury	
neutrino observatory, SNO	1040
Sum of neutrino masses	135
Sum rules	811
Summary tables, organization of	11
Sunyaev-Zel'dovich effect	440, 467, 471, 501, 515
Sunyaev-Zel'dovich effect, kinetic	440
Super tau-charm factories	539
Super-conformal anomaly	1002
Super-Higgs mechanism	1002
Superconducting Tunnel Junctions (STJs)	634
Supergravity	1001, 1002
SuperKEKB (KEK) collider parameters	544
Supermassive GUT monopoles	1093
Supermultiplet	1000
Supernovae	
as cosmological probes	470
Type Ia	470, 480
Type II	470
Superpotential	1001
Superspace	1000
Supersymmetric particle searches	108, 2187
Supersymmetric particle spectrum	1004
Supersymmetry breaking	1002
Supersymmetry, SUSY	1000
Supervised learning	676–678, 683, 686, 697
Survival probability, relations for	743
SUSY Les Houches accord, SLHA	1004
SUSY, supersymmetry	1000
SVM, support vector machine	685, 686
SVR, support vector regression	686, 687
Symmetry breaking	1082
Synchrotron oscillations	535
Synchrotron radiation	143, 535
Synchrotron tune	535
Systematic errors, treatment of	16
SZ, Sunyaev-Zel'dovich effect	515
t (quark)	817
T (time reversal), tests of conservation	110
Tabular data	685
τ lepton	28, 1245
τ branching fractions, note on	803
τ decay parameters, note on	806
Technicolor	108, 2238
electroweak symmetry breaking	1061
Technifermion condensate formation	1061
Telescope Array (TA)	525, 618
Tensor mesons $\ell = 1, 2^{++}$	313, 847, 848
$f_J(2220)$	848
Tensor-to-scalar field perturbations ratio,	135
Testing dataset	677, 679, 681
Tests of conservation laws	120
Tetraquark candidates	
$K_0^*(700)$	861
$X(3872)$	960
$Z(4430)$	960
$\psi(4230)$	960
$a_0(980)$	860
$f_0(500)$	860
$f_0(980)$	860
Tetraquark states	851
$\phi(2170)$	852
$a_0(980), f_0(980)$	851
Tetraquarks	316, 845
Tevatron	536
Tevatron collider parameters	546
Theoretical decay-constant calculations	
Bottom mesons	902
charmed mesons	901
pions and kaons	899
Thermal	
conductivity of elements, table	141
expansion coefficients of elements, table	141
history of the Universe	433
θ_W , Weinberg angle	285
Third generation vector-like quarks	1065
Thomson cross section σ_T	133
Three-body	
decay kinematics	744
decays, kinematic limits	744
phase space	744
Threshold Cherenkov detectors	572
Thrust	158
Time variation of the fine-structure constant	516
Time-projection chambers, TPC	581, 630
Timing	
silicon detectors	592
Timing measurements	596
Top quark t	817
Top quark mass	826
Top quark mass from electroweak analyses	179
Top quark, note on	817
Top-changing neutral currents, tests for	117

Total cross sections	398
Total energy density of Universe, Ω_{tot}	473
Total lepton number conservation	116
TPC, Time-projection chambers	630
Training	677, 679, 683, 689, 706
Training dataset	677–681
Transfer learning	702
Transformation of electromagnetic fields, relativistic	142
Transformer	685, 695, 702
Transition Edge Sensors (TESs)	635
Transition radiation	562
Transition radiation detectors, TRD	582
Translational invariance	685, 690
Transverse variables	746
Trees	685, 687
Triangle singularity	315, 849, 851
Triangles, unitarity, note on	261
Trilepton events	1067
Trilinear coupling	206
Tropical year	134
Two-body	
decay	743
differential cross sections	745
partial decay rate	743
reactions	745
scattering kinematics	743
Two-Higgs-doublet models	240
Two-photon processes in e^+e^- annihilation	758
Type Ia supernovae	470, 480
Type II supernovae	470
U-Net	691
ULA, ultralight axion-like particles	1045
Ultra-high energy cosmic rays	526
Ultralight axion-like particles (ULAs)	1045
Uncertainty quantification	703, 705
Unconstrained averaging	16
Underfitting	677
Underground cosmic rays	523
Underlying event (UE)	156
Unified atomic mass unit	133
Unified theories, grand	1076
Uniform distribution	658
Units and conversion factors	346
Units, electromagnetic	142
Units, SI, complete set	136
Universal approximation	677, 679, 690
Universal Extra Dimension, UED	762, 988
Universality of free fall tests GR	423
Universe	
accelerating evidence	471
age of	432, 473
as a particle detector	480
baryon density of	134, 460
bubble	435
composition	430, 432
cosmological structure	434
critical density of	134
curvature of	431
density fluctuations	437
density parameter of	134
entropy density	435
flatness	473
global description of	467
Hubble expansion of	430, 467
inflation	467
large-scale structure of	432, 438
matter-dominated	436
parametrizing	467
perturbation	467
phase transitions	435
radiation content at early times	434
thermal history of	433, 443
thermodynamic equilibrium	434
Unsupervised learning	676, 677, 680, 683
Υ ($b\bar{b}$) mesons	
$\Upsilon(1S)$	81, 1942
$\Upsilon(2S)$	83, 1954
$\Upsilon_2(1D)$ [<i>was</i> $\Upsilon(1D)$]	83, 1959
$\Upsilon(3S)$	84, 1966
$\Upsilon(4S)$ [<i>was</i> $\Upsilon(10580)$]	85, 1970
$\Upsilon(10753)$	1974
$\Upsilon(10860)$	85, 1975
$\Upsilon(11020)$	86, 1978
Vacuum energy parameter Ω_v	431
VAE, Variational Auto-Encoder	697, 698
Validation dataset	678
Values of particle properties, historical perspective of	19
Vanishing gradient	689, 692, 694, 701
Variance, definition	655
Variational inference	680, 684, 697, 698, 705
Varying constants	
gravitational G_N , fine structure α	469
VBF – vector boson fusion	208
V_{cb} and V_{ub} determination of, note on	930
V_{cb} determination	930
Vector mesons	849
ρ excitations	850
$\rho(1570) - C(1480)$	850
$\rho(1900)$	850
$\rho(770)$	849
Vector mesons $\ell = 0, 1^{--}$	313
Vector superfields	1000
Vector-like quarks, VLQ	1065
VEPP-2000	543
VEPP-4M	543
Virgo, gravitational observatory	421
Virtual graviton process	763
VLQ, vector like quarks	1065
Von Neuman's acceptance-rejection method in MC	713
V_{ub} determination	934
V_{ub}/V_{cb} determination	938
V_{ud} determination	873
$V_{ud}, V_{us}, V_{ub}, V_{cd}, V_{cs}, V_{cb}, V_{td}, V_{ts}, V_{tb}$	261
V_{us} determination	873
W and Z resonant production	757
W boson	25, 1142
ideogram	790
mass	789
width	789
w , dark energy equation of state parameter	431
$W-W'$ mixing	993
Warped extra dimensions	983
Wasserstein distance	683, 697, 699
Wasserstein GAN	699
Wavelength of 1 eV/ c particle	133
WaveNet	699
Weak decay form factors	330
Weak gauge bosons pairs production	757
Weak neutral currents	
tests ($\Delta B = \Delta C = \Delta S = \Delta T = 1$)	110
Weak-field general relativity	418
Weak-mixing angle ($\sin^2 \hat{\theta}(M_Z)$)	133
Weakly supervised learning	679
Weakly-interacting massive particle, WIMP	1000
Weight matrix	689
Weinberg angle θ_W	285
White-dwarf, weak-self-gravity	424
Wien displacement law constant $b = \lambda_m \alpha x T$	133
WIMP	485
miracle	484, 1000
WIMP dark matter searches	109, 2249
WIMP, weakly-interacting massive particle	1000
Wino	1004

WMAP, Wilkinson Microwave Anisotropy Probe	471	$\Xi_b(6227)^-$	106, 2176
Wolfenstein parameters	261, 873, 904	$\Xi_b(6227)^0$	106, 2177
World average of $\alpha_s(M_Z^2)$	163, 166	$\Xi_b'(5935)^-$	106, 2175
W' -boson searches	991, 1072	$\Xi_b(5945)^0$	106, 2176
Wrapped extra dimension	763	$\Xi_b(5955)^-$	106, 2176
X mesons		Ξ_c^+	101, 2148
$X_0(2900)$	1607	Ξ_c^0	102, 2149
$X_1(2900)$	1607	$\Xi_c(2645)$	102, 2152
$X(1835)$	1452	$\Xi_c(2790)$	102, 2152
$X(2370)$	1471	$\Xi_c(2815)$	103, 2153
$X(3872)$ [<i>aka</i> $\chi_{c1}(3872)$]	78, 1911	$\Xi_c(2923)$	2153
$X(3940)$	1918	$\Xi_c(2930)$	2154
$X(4020)^\pm$	79, 1918	$\Xi_c(2970)$	103, 2154
$X(4050)^\pm$	1921	$\Xi_c'^+$	102, 2151
$X(4055)^\pm$	1922	$\Xi_c(3055)$	103, 2155
$X(4100)^\pm$	1922	$\Xi_c(3080)$	103, 2155
$X(4160)$	1926	$\Xi_c(3123)$	2156
$X(4250)^\pm$	1932	$\Xi_c'^0$	102, 2151
$X(4350)$	1932		
$X(4630)$	1937	Year, sidereal	134
$X(5568)^\pm$	1810	Year, tropical	134
x variable (of Feynman's)	745	Young diagrams (tableaux)	739
Xavier initialization	701	Young's modulus of solid elements, table	141
xF_3 structure function, plots of	365	Yukawa coupling	
Ξ baryons		Higgs to fermions direct observation	210
Ξ^-	99, 2123	leptoquark-type	1090
Ξ^0	98, 2121	unification	1082
Ξ_{bc}^0	2177	Z boson	25, 1156
$\Xi(1530)$	99, 2126	branching ratios	792
$\Xi(1620)$	2127	coupling to fermions	179
$\Xi(1690)$	99, 2127	mass	791
$\Xi(1820)$	99, 2128	note on	791
$\Xi(1950)$	99, 2129	width	775, 791
$\Xi(2030)$	99, 2130	Z' -boson searches, note on	995
$\Xi(2120)$	2131	Z' or W' bosons, searches for	1063
$\Xi(2250)$	2131	$Z_c(4200)$ [<i>was</i> $X(4200)^\pm$]	1926
$\Xi(2370)$	2131	$Z_b(10610)$ [<i>was</i> $X(10610)$]	85, 1972
$\Xi(2500)$	2132	$Z_b(10650)$ [<i>was</i> $X(10650)^\pm$]	85, 1973
Ξ_{cc}^{++}	104, 2160	$Z_c(3900)$ [<i>was</i> $X(3900)$]	79, 1915
Ξ_{cc}^+	2160	$Z_c(4430)$ [<i>was</i> $X(4430)^\pm$]	81, 1936
Ξ_b^-	105, 2172	Zeldovich-Sunyaev effect	471
Ξ_b^0	105, 2174	Zero-shot learning	702
$\Xi_b(6100)^-$	106, 2176	Z' -boson searches	1072

VOLUME II: TABLE OF CONTENTS

PARTICLE LISTINGS*

Illustrative key and abbreviations	1127
Gauge and Higgs bosons	
(γ , gluon, graviton, W , Z , Higgs, Axions)	1141
Leptons	
(e , μ , τ , Heavy-charged lepton searches, Neutrino properties, Number of neutrino types Double- β decay, Neutrino mixing, Heavy-neutral lepton searches)	1239
Quarks	
(u , d , s , c , b , t , b' , t' (4^{th} gen.), Free quarks)	1311
Mesons	
Light unflavored (π , ρ , a , b) (η , ω , f , ϕ , h)	1349
Strange (K , K^*)	1473
Charmed (D , D^*)	1527
Charmed, strange (D_s , D_s^* , D_{sJ})	1588
Bottom (B , V_{cb}/V_{ub} , B^* , B_J^*)	1609
Bottom, strange (B_s , B_s^* , B_{sJ}^*)	1786
Bottom, charmed (B_c)	1813
$c\bar{c}$ (η_c , $J/\psi(1S)$, χ_c , h_c , ψ)	1818
$b\bar{b}$ (η_b , Υ , χ_b , h_b)	1940
Other mesons	1980
Baryons	
N	1987
Δ	2042
Λ	2065
Σ	2090
Ξ	2121
Ω	2133
Charmed (Λ_c , Σ_c , Ξ_c , Ω_c)	2136
Doubly charmed (Ξ_{cc})	2160
Bottom (Λ_b , Σ_b , Ξ_b , Ω_b , b -baryon admixture)	2161
Exotic baryons (P_c pentaquarks)	2181
Searches not in Other Sections	
Magnetic monopole searches	2185
Supersymmetric particle searches	2187
Technicolor	2238
Searches for quark and lepton compositeness	2239
Extra dimensions	2243
WIMP and dark matter searches	2249
Other particle searches	2263

*The divider sheets give more detailed indices for each main section of the Particle Listings.

INTRODUCTION TO THE PARTICLE LISTINGS

Illustrative key	1127
Abbreviations	1128

Illustrative Key to the Particle Listings

Name of particle. "Old" name used before 1986 renaming scheme also given if different. See the section "Naming Scheme for Hadrons" for details.

$a_0(1200)$

$$I^G(J^{PC}) = 1^-(0^{++})$$

Particle quantum numbers (where known).

OMITTED FROM SUMMARY TABLE
Evidence not compelling, may be a kinematic effect.

Indicates particle omitted from Particle Physics Summary Table, implying particle's existence is not confirmed.

Quantity tabulated below.

$a_0(1200)$ MASS

Top line gives our best value (and error) of quantity tabulated here, based on weighted average of measurements used. Could also be from fit, best limit, estimate, or other evaluation. See next page for details.

VALUE (MeV)	EVTS	DOCUMENT ID	TECN	CHG	COMMENT
1206 ± 7 OUR AVERAGE					
1210 ± 8 ± 9	3000	FENNER 87	MMS	-	3.5 $\pi^- p$
1198 ± 10		PIERCE 83	ASPK	+	2.1 $K^- p$
1216 ± 11 ± 9	1500	MERRILL 81	HBC	0	3.2 $K^- p$
• • • We do not use the following data for averages, fits, limits, etc. • • •					
1192 ± 16	200	LYNCH 81	HBC	±	2.7 $\pi^- p$
1 Systematic error was added quadratically by us in our 1986 edition.					

General comments on particle.

"Document id" for this result; full reference given below.

Measurement technique. (See abbreviations on next page.)

Footnote number linking measurement to text of footnote.

$a_0(1200)$ WIDTH

Number of events above background.

Measured value used in averages, fits, limits, etc.

Error in measured value (often statistical only; followed by systematic if separately known; the two are combined in quadrature for averaging and fitting.)

Measured value *not used* in averages, fits, limits, etc. See the Introductory Text for explanations.

Arrow points to weighted average.

Shaded pattern extends $\pm 1\sigma$ (scaled by "scale factor" S) from weighted average.

Value and error for each experiment.

VALUE (MeV)	EVTS	DOCUMENT ID	TECN	CHG	COMMENT
41 ± 11 OUR AVERAGE					Error includes scale factor of 1.8. See the ideogram below.
50 ± 8		PIERCE 83	ASPK	+	2.1 $K^- p$
70 +30 -20	200	LYNCH 81	HBC	±	2.7 $\pi^- p$
25 ± 5 ± 7		MERRILL 81	HBC	0	3.2 $K^- p$
• • • We do not use the following data for averages, fits, limits, etc. • • •					
<60		FENNER 87	MMS	-	3.5 $\pi^- p$

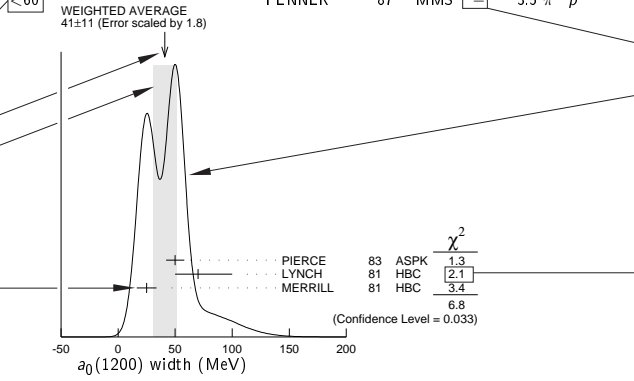
Scale factor > 1 indicates possibly inconsistent data.

Reaction producing particle, or general comments.

"Change bar" indicates result added or changed since previous edition.

Charge(s) of particle(s) detected.

Ideogram to display possibly inconsistent data. Curve is sum of Gaussians, one for each experiment (area of Gaussian = 1/error; width of Gaussian = \pm error). See Introductory Text for discussion.



Contribution of experiment to χ^2 (if no entry present, experiment not used in calculating χ^2 or scale factor because of very large error).

$a_0(1200)$ DECAY MODES

Partial decay mode (labeled by Γ_i).

Mode	Fraction (Γ_i/Γ)	Scale factor/ Confidence level
Γ_1 3π	(65.2 ± 1.3) %	S=1.7
Γ_2 $K\bar{K}$	(34.8 ± 1.3) %	S=1.7
Γ_3 $\eta\pi^\pm$	< 5	$\times 10^{-4}$ CL=95%

Our best value for branching fraction as determined from data averaging, fitting, evaluating, limit selection, etc. This list is basically a compact summary of results in the Branching Ratio section below.

$a_0(1200)$ BRANCHING RATIOS

Branching ratio.

Our best value (and error) of quantity tabulated, as determined from constrained fit (using all significant measured branching ratios for this particle).

Weighted average of measurements of this ratio only.

Footnote (referring to LYNCH 81).

VALUE	DOCUMENT ID	TECN	CHG	COMMENT	Γ_1/Γ
0.652 ± 0.013 OUR FIT				Error includes scale factor of 1.7.	
0.643 ± 0.010 OUR AVERAGE					
0.64 ± 0.01	PIERCE 83	ASPK	+	2.1 $K^- p$	
0.74 ± 0.06	MERRILL 81	HBC	0	3.2 $K^- p$	
• • • We do not use the following data for averages, fits, limits, etc. • • •					
0.48 ± 0.15	² LYNCH 81	HBC	±	2.7 $\pi^- p$	
² Data has questionable background subtraction.					

Γ_2/Γ

Branching ratio in terms of partial decay mode(s) Γ_i above.

VALUE	DOCUMENT ID	TECN	CHG	COMMENT	Γ_2/Γ_1
0.348 ± 0.013 OUR FIT				Error includes scale factor of 1.7.	
0.35 ± 0.05	PIERCE 83	ASPK	+	2.1 $K^- p$	
0.535 ± 0.030 OUR FIT				Error includes scale factor of 1.7.	
0.50 ± 0.03	MERRILL 81	HBC	0	3.2 $K^- p$	

Confidence level for measured upper limit.

VALUE (units 10^{-4})	CL%	DOCUMENT ID	TECN	CHG	COMMENT	$0.71\Gamma_3/\Gamma$
<3.5	95	PIERCE 83	ASPK	+	2.1 $K^- p$	

References, ordered inversely by year, then author.

"Document id" used on data entries above.

Journal, report, preprint, etc. (See abbreviations on next page.)

$a_0(1200)$ REFERENCES

FENNER 87	PRL 55 14	H. Fenner et al.	(SLAC)
PIERCE 83	PL 123B 230	J.H. Pierce	(FNAL) JP
LYNCH 81	PR D24 610	G.R. Lynch et al.	(CLEO Collab.)
MERRILL 81	PRL 47 143	D.W. Merrill et al.	(SACL, CERN)

Partial list of author(s) in addition to first author.

Quantum number determinations in this reference.

Institution(s) of author(s). (See abbreviations on next page.)

Abbreviations Used in the Particle Listings

Indicator of Procedure Used to Obtain Our Result

OUR AVERAGE	From a weighted average of selected data.
OUR FIT	From a constrained or overdetermined multiparameter fit of selected data.
OUR EVALUATION	Not from a direct measurement, but evaluated from measurements of other quantities.
OUR ESTIMATE	Based on the observed range of the data. Not from a formal statistical procedure.
OUR LIMIT	For special cases where the limit is evaluated by us from measured ratios or other data. Not from a direct measurement.

Measurement Techniques

(i.e., Detectors and Methods of Analysis)

A1	A1 Collaboration at MAMI
A2MM	A2 spectrometer at the Mainz Microtron, MAMI
ABRA	ABRACADABRA QCD axion dark matter search
ACCM	ACCMOR Collaboration
ADMX	Axion Dark Matter Experiment
AEMS	Argonne effective mass spectrometer
ALEP	ALEPH – CERN LEP detector
ALPS	Photon regeneration experiment
AMND	AMANDA South Pole neutrino detector
AMY	AMY detector at KEK-TRISTAN
ANAI	Direct DM detection exp. with NaI at Canfranc Underground Lab, Spain
ANIC	ANTARES and IceCube combined analysis
ANIT	Antarctic Impulsive Transient Antenna balloon mission
ANTR	ANTARES underwater neutrino telescope in the Western Mediterranean Sea
APEX	FNAL APEX Collab.
ARG	ARGUS detector at DORIS
ARGD	Fit to semicircular amplitude path on Argand diagram
ASP	Anomalous single-photon detector
ASPK	Automatic spark chambers
ASTE	ASTERIX detector at LEAR
ASTR	Astronomy
ATLS	ATLAS detector at CERN LHC
AUGE	Pierre Auger Observatory
AURG	Resonant-mass gravitational wave AURIGA detector
B787	BNL experiment 787 detector
B791	BNL experiment 791 detector
B845	BNL experiment 845 detector
B852	BNL E-852
B865	BNL E865 detector
B871	BNL experiment 871 detector
B949	BNL E949 detector at AGS
BABR	BaBar Collab.
BAIK	Lake Baikal neutrino telescope
BAKS	Baksan underground scintillation telescope
BC	Bubble chamber
BDMP	Beam dump
BEAT	CERN BEATRICE Collab.
BEBC	Big European bubble chamber at CERN
BEL2	Belle II Collab.
BELL	Belle Collab.
BES	BES Beijing Spectrometer at Beijing Electron-Positron Collider
BES2	BES Beijing Spectrometer at Beijing Electron-Positron Collider
BES3	BES Beijing Spectrometer at Beijing Electron-Positron Collider
BIS2	BIS-2 spectrometer at Serpukhov
BKEI	BENKEI spectrometer system at KEK Proton Synchrotron
BOLO	Bolometer, a cryogenic thermal detector
BONA	Bonanza nonmagnetic detector at DORIS
BORX	BOREXINO
BPWA	Barrelet-zero partial-wave analysis
C100	COSINE-100 experiment in South Korea
CALO	Calorimeter
CASK	CULTASK: CAPPs Ultra Low Temperature Axion Search in Korea
CASP	Cosmic Axion Spin Precession Experiments
CAST	CAST experiment at CERN
CBAL	Crystal Ball detector at SLAC-SPEAR or DORIS
CBAR	Crystal Barrel detector at CERN-LEAR
CBOX	Crystal Box at LAMPF
CBTP	CBELSA/TAPS Collaboration
CC	Cloud chamber
CCFR	Columbia-Chicago-Fermilab-Rochester detector
CDEX	China Dark Matter Experiment

CDF	Collider detector at Fermilab
CDF2	CDF-II Collab.
CDHS	CDHS neutrino detector at CERN
CDM2	CDMS II, Cryogenic Dark Matter Search at Soudan Underground Lab.
CDMS	CDMS Collaboration
CELL	CELLO detector at DESY
CGNT	CoGeNT dark matter search experiment
CHER	Cherenkov detector
CHM2	CHARM-II neutrino detector (glass) at CERN
CHOZ	Nuclear Power Station near Chooz, France
CHRM	CHARM neutrino detector (marble) at CERN
CHRS	CHORUS Collaboration – CERN SPS
CIB	Cosmic Infrared Background
CIBS	CERN-IHEP boson spectrometer
CLAS	Jefferson CLAS Collab.
CLE2	CLEO II detector at CESR
CLE3	CLEO III detector at CESR
CLEC	CLEO-c detector at CESR
CLEO	Cornell magnetic detector at CESR
CMB	Cosmic Microwave Background
CMD	Cryogenic magnetic detector at VEPP-2M, Novosibirsk
CMD2	Cryogenic magnetic detector 2 at VEPP-2M, Novosibirsk
CMD3	Cryogenic magnetic detector 3 at VEPP-2000, Novosibirsk
CMS	CMS detector at CERN LHC
CNTR	Counters
COMB	Combined analysis of data from independent experiments.
COMP	COMPASS experiment at the CERN SPS
CONN	CONNIE: Coherent Neutrino-Nucleus Interaction Experiment
COSM	Cosmology and astrophysics
COSY	COSY-TOF Collaboration
COUP	COUPP (the Chicagoland Observatory for Underground Particle Physics) Collab.
CPLR	CPLEAR Collaboration
CRBT	Crystal Ball and TAPS detector at MAMI
CRES	CRESST cryogenic detector
CRYB	Crystal Ball at BNL
CRYM	Crystal Ball detector at Mainz Microtron MAMI
CSB2	Columbia U. - Stony Brook BGO calorimeter inserted in NaI array
CSME	COSME Collaboration
CUOR	CUORICINO experiment at Gran Sasso Laboratory.
CUSB	Columbia U. - Stony Brook segmented NaI detector at CESR
D0	D0 detector at Fermilab Tevatron Collider
DAMA	DAMA, dark matter detector at Gran Sasso National Lab.
DASP	DESY double-arm spectrometer
DAYA	Daya Bay Collaboration
DBC	Deuterium bubble chamber
DCHZ	Double Chooz Collaboration
DEAP	DEAP-3600 DM search with argon at SNOLAB
DISP	Graviton mass measurement based on dispersion measure
DLCO	DELCO detector at SLAC-SPEAR or SLAC-PEP
DLPH	DELPHI detector at LEP
DM1	Magnetic detector no. 1 at Orsay DCI collider
DM2	Magnetic detector no. 2 at Orsay DCI collider
DMIC	DAMIC Dark Matter in CCD experiment at Fermilab
DMTP	Dark Matter Time Projection Chamber (DMTPC) directional detection experiment
DONU	DONUT Collab.
DPWA	Energy-dependent partial-wave analysis
DRFT	Directional dark matter detector at Boulby Underground Science Facility
DS50	DarkSide-50 Liquid Argon TPC at Gran Sasso National Laboratory
E137	SLAC E137 beam-dump experiment
E621	Fermilab E621 detector
E653	Fermilab E653 detector
E665	Fermilab E665 detector
E687	Fermilab E687 detector
E691	Fermilab E691 detector
E705	Fermilab E705 Spectrometer-Calorimeter
E731	Fermilab E731 Spectrometer-Calorimeter
E756	Fermilab E756 detector
E760	Fermilab E760 detector
E761	Fermilab E761 detector
E771	Fermilab E771 detector
E773	Fermilab E773 Spectrometer-Calorimeter
E789	Fermilab E789 detector
E791	Fermilab E791 detector

Abbreviations Used in the Particle Listings

E799	Fermilab E799 Spectrometer-Calorimeter	K391	KEK E391a detector
E835	Fermilab E835 detector	K470	KEK-E470 Stopping K detector
EDE2	EDELWEISS II dark matter search Collaboration	KAM2	KAMIOKANDE-II underground Cherenkov detector
EDE3	EDELWEISS III dark matter search Collaboration	KAMI	KAMIOKANDE underground Cherenkov detector
EDEL	EDELWEISS dark matter search Collaboration	KAR2	KARMEN2 calorimeter at the ISIS neutron spallation source at Rutherford
EDGS	EDGES: Global EoR (Epoch of Reionization) Signature experiment	KARM	KARMEN calorimeter at the ISIS neutron spallation source at Rutherford
EHS	Four-pi detector at CERN	KEDR	detector operating at VEPP-4M collider (Novosibirsk)
ELEC	Electronic combination	KIMS	Korea Invisible Mass Search experiment at YangYang, Korea
EMC	European muon collaboration detector at CERN	KLND	KamLand Collab. (Japan)
EMUL	Emulsions	KLOE	KLOE detector at DAFNE (the Frascati e+e- collider Italy)
ESR	Electron spin resonance spectroscopy	KOLR	Kolar Gold Field underground detector
FAST	Fiber Active Scintillator Target detector at PSI	KOTO	KOTO experiment with K_L^0 beam at J-PARC
FBC	Freon bubble chamber	KTEV	KTeV Collaboration
FENI	FENICE (at the ADONE collider of Frascati)	L3	L3 detector at LEP
FIT	Fit to previously existing data	LASR	Laser
FLAT	Large Area Telescope onboard the Fermi Gamma-Ray Space Telescope (Fermi-LAT)	LASS	Large-angle superconducting solenoid spectrometer at SLAC
FMPS	Fermilab Multiparticle Spectrometer	LATT	Lattice calculations
FOCS	FNAL E831 FOCUS Collab.	LEBC	Little European bubble chamber at CERN
FRAB	ADONE $B\bar{B}$ group detector	LEGS	BNL LEGS Collab.
FRAG	ADONE $\gamma\gamma$ group detector	LENA	Nonmagnetic lead-glass NaI detector at DORIS
FRAM	ADONE MEA group detector	LEP	From combination of all 4 LEP experiments: ALEPH, DELPHI, L3, OPAL
FREJ	FREJUS Collaboration – modular flash chamber detector (calorimeter)	LEPS	Low-Energy Pion Spectrometer at the Paul Scherrer Institute
FUNK	Finding U(1)'s of a Novel Kind experiment	LGW	Lead Glass Wall collaboration at SPEAR/SLAC
GA24	Hodoscope Cherenkov γ calorimeter (IHEP GAMS-2000) (CERN GAMS-4000)	LHC	Combined analysis of LHC experiments
GALX	GALLEX solar neutrino detector in the Gran Sasso Underground Lab.	LHCb	LHCb detector at CERN LHC
GAM2	IHEP hodoscope Cherenkov γ calorimeter GAMS-2000	L+P	Multichannel L + P model fit
GAM4	CERN hodoscope Cherenkov γ calorimeter GAMS-4000	LSD	Mont Blanc liquid scintillator detector
GAMS	IHEP hodoscope Cherenkov γ calorimeter GAMS-4 π	LSND	Liquid Scintillator Neutrino Detector
GNME	Global Network of Optical Magnetometers for Exotic searches (GNOME)	LSW	Light Shining through a Wall
GNO	Gallium Neutrino Observatory in the Gran Sasso Underground Lab.	LUX	Large Underground Xenon experiment at SURF
GOLI	CERN Goliath spectrometer	MAC	MAC detector at PEP/SLAC
GRAL	GRAAL Collaboration	MAJD	Majorana Demonstrator experiment at SURF
H1	H1 detector at DESY/HERA	MBNE	Fermilab MiniBooNE neutrino experiment
HAWC	High Altitude Water Cherenkov Observatory experiment at Sierra Negra, Mexico	MBR	Molecular beam resonance technique
HBC	Hydrogen bubble chamber	MCBN	Fermilab MicroBooNE neutrino experiment
HDBC	Hydrogen and deuterium bubble chambers	MCRO	MACRO detector in Gran Sasso
HDES	HADES Collaboration at GSI in Darmstadt	MD1	Magnetic detector at VEPP-4, Novosibirsk
HDMO	Heidelberg-Moscow Experiment	MDRP	Millikan drop measurement
HDMS	Heidelberg Dark Matter Search Experiment	MEG	Muon to electron conversion detector at PSI
HEBC	Helium bubble chamber	MGFL	MAGIC and Fermi-LAT Collaborations
HEPT	Helium proportional tubes	MGIC	MAGIC Telescopes gamma-ray observatory
HERA	H1 and ZEUS Collaborations at DESY/HERA	MICA	Underground mica deposits
HERB	HERA-B detector at DESY/HERA	MICR	MICROSCOPE satellite test of weak equivalence principle
HERM	HERMES detector at DESY/HERA	MINS	Fermilab MINOS experiment
HESS	High Energy Stereoscopic System gamma-ray instrument	MIRA	MIRABELLE Liquid-hydrogen bubble chamber
HFR	HighFlow Reactor at the Institut Laue-Langevin	MLEV	Magnetic levitation
HFS	Hyperfine structure	MLS	Modified Laurent Series
HLBC	Heavy-liquid bubble chamber	MMS	Missing mass spectrometer
HOME	Homestake underground scintillation detector	MOEDAL	MoEDAL magnetic monopoles search experiment at LHC
HPGE	High-purity Germanium detector	MPS	Multiparticle spectrometer at BNL
HPS	Heavy Photon Search experiment at JLAB	MPS2	Multiparticle spectrometer upgrade at BNL
HPW	Harvard-Pennsylvania-Wisconsin detector	MPSF	Multiparticle spectrometer at Fermilab
HRS	SLAC high-resolution spectrometer	MPWA	Model-dependent partial-wave analysis
HYBR	Hybrid: bubble chamber + electronics	MRK1	SLAC Mark-I detector
HYCP	HyperCP Collab. (FNAL E-871)	MRK2	SLAC Mark-II detector
HYST	HAYSTAC axion search experiment	MRK3	SLAC Mark-III detector
IACT	Imaging Air Cherenkov Telescope	MRKJ	Mark-J detector at DESY
ICAR	ICARUS experiment at Gran Sasso Laboratory.	MRS	Magnetic resonance spectrometer
ICCB	IceCube neutrino detector at South Pole	MUG2	Muon (g-2)
IGEX	IGEX Collab.	MWPC	Multi-Wire Proportional Chamber
IMB	Irvine-Michigan-Brookhaven underground Cherenkov detector	NA14	CERN NA14
IMB3	Irvine-Michigan-Brookhaven underground Cherenkov detector	NA31	CERN NA31 Spectrometer-Calorimeter
INDU	Magnetic induction	NA32	CERN NA32 Spectrometer
IPWA	Energy-independent partial-wave analysis	NA48	CERN NA48 Collaboration
ISTR	IHEP ISTRA+ spectrometer-calorimeter	NA49	CERN NA49 Collaboration
JADE	JADE detector at DESY	NA60	CERN NA60 Collaboration
JPAC	Joint Physics Analysis Center (JPAC) Collaboration	NA62	CERN NA62 Experiment
K246	KEK E246 detector with polarimeter	NA64	CERN SPS NA64 Experiment
K2K	KEK to Super-Kamiokande	NAGE	NEWAGE, New generation WIMP-search experiment with advanced gaseous tracking
		NAIA	NAIAD (NaI Advanced Detector) dark matter search experiment
		ND	NaI detector at VEPP-2M, Novosibirsk
		NEOS	NEOS Collaboration
		NEWS	NEWS-G direct dark matter search at LSM

Abbreviations Used in the Particle Listings

NICE	Serpukhov nonmagnetic precision spectrometer	TPC	TPC detector at PEP/SLAC
NMR	Nuclear magnetic resonance	TPS	Tagged photon spectrometer at Fermilab
NOMD	NOMAD Collaboration, CERN SPS	TRAP	Penning trap
NOVA	NOvA experiment with Fermilab's NuMI neutrino beam	TWST	TWIST spectrometer at TRIUMF
NTEV	NuTeV Collab. at Fermilab	UA1	UA1 detector at CERN
nTRV	neutron Time-Reversal Violation	UA2	UA2 detector at CERN
NUSX	Mont Blanc NUSEX underground detector	UA5	UA5 detector at CERN
OBLX	OBELIX detector at LEAR	UCNA	UCNA collaboration using polarized ultracold neutrons at LANSCE
OKA	OKA collaboration at U70 accelerator in Protvino, Russia	UKDM	UK Dark Matter Collab.
OLYA	Detector at VEPP-2M and VEPP-4, Novosibirsk	VES	Vertex Spectrometer Facility at 70 GeV IHEP accelerator
OMEG	CERN OMEGA spectrometer	VLBI	Very Long Baseline Interferometer
OPAL	OPAL detector at LEP	VNS	VENUS detector at KEK-TRISTAN
OPER	OPERA experiment with emulsion tracking at Gran Sasso	VRTS	Very Energetic Radiation Imaging Telescope Array System (VERITAS)
OSPK	Optical spark chamber	WA75	CERN WA75 experiment
PIBE	The PIBETA detector at the Paul Scherrer Institute (PSI), Switzerland.	WA82	CERN WA82 experiment
PICA	PICASSO dark matter search experiment	WA89	CERN WA89 experiment
PICO	PICO bubble chamber experiment in SNOLAB underground laboratory	WARP	Liquid argon detector for CDM searches at Gran Sasso
PIE3	π E3 beam-line of Paul Scherrer Institute	WASA	WASA detector at CELSIUS, Uppsala and at COSY, Juelich
PLAS	Plastic detector	WDMX	WISP Dark Matter eXperiment (WISPDIMX) for direct hidden photon search
PLUT	DESY PLUTO detector	WIRE	Wire chamber
PMLA	PAMELA space spectrometer on Resurs-DK1 satellite	X100	XENON100 dark matter search experiment at Gran Sasso National Laboratory
PNDX	PandaX dual-phase liquid xenon dark matter experiment at Jin-Ping	XE10	XENON10 experiment at Gran Sasso National Laboratory
PPTA	Parkes Pulsar Timing Array	XE1T	XENON1T dark matter search experiment at Gran Sasso National Laboratory
PRMX	The PRIMEX detector in Hall B at TJNAF	XEBC	Xenon bubble chamber
PWA	Partial-wave analysis	XMAS	XMASS, liquid xenon scintillation detector at Kamioka Observatory
QUAX	QUAX axion search experiment	YUKA	Graviton mass measurement based on Yukawa potential
RADE	CAST-RADES haloscope search for axions.	ZEP2	ZEPLIN-II dark matter detector
RDK2	NIST rare radioactive decay experiment	ZEP3	ZEPLIN-III dark matter detector at Palmer Underground Lab.
REDE	Resonance depolarization	ZEPL	ZEPLIN-I galactic dark matter detector
RENO	RENO Collaboration	ZEUS	ZEUS detector at DESY/HERA
RICE	Radio Ice Cherenkov Experiment		
RVUE	Review of previous data		
SAGE	US - Russian Gallium Experiment		
SCDM	SuperCDMS experiment at Soudan Underground Lab.		
SELX	FNAL SELEX Collab.		
SENS	Sub-Electron-Noise Skipper CCD Experimental Instrument (SENSEI)		
SFM	CERN split-field magnet		
SHF	SLAC Hybrid Facility Photon Collaboration		
SHFT	Search for Halo Axions with Ferromagnetic Toroids		
SHUK	SHUKET: search for U(1) dark matter with an electromagnetic telescope		
SIGM	Serpukhov CERN-IHEP magnetic spectrometer (SIGMA)		
SILI	Silicon detector		
SIMP	SIMPLE, dark matter detector at Laboratori Nazionali del Sud		
SKAM	Super-Kamiokande Collab.		
SLAX	Solar Axion Experiment in Canfranc Underground Laboratory		
SLD	SLC Large Detector for e^+e^- colliding beams at SLAC		
SLIC	ADMX SLIC (Superconducting LC Circuit Investigating Cold Axions)		
SMPL	SIMPLE, Superheated Instrument for Massive Particle Experiments		
SND	Novosibirsk Spherical neutral detector at VEPP-2M		
SNDR	SINDRUM spectrometer at PSI		
SNO	SNO Collaboration (Sudbury Neutrino Observatory)		
SNO+	SNO+ Collaboration (Sudbury Neutrino Observatory)		
SOU2	Soudan 2 underground detector		
SODU	Soudan underground detector		
SPEC	Spectrometer		
SPED	From maximum of speed plot or resonant amplitude		
SPHR	Bonn SAPHIR Collab.		
SPNX	SPHINX spectrometer at IHEP accelerator		
SPRK	Spark chamber		
SQID	SQUID device		
STRC	Streamer chamber		
SVD2	SVD-2 experiment at IHEP, Protvino		
T2K	T2K Collaboration		
TASS	DESY TASSO detector		
TEVA	Combined analysis of CDF and $D\bar{0}$ experiments		
TEXO	TEXONO Collab., ultra low energy Ge detector at Kuo-Sheng Laboratory		
THEO	Theoretical or heavily model-dependent result		
TNF	TNF-IHEP facility at 70 GeV IHEP accelerator		
TOF	Time-of-flight		
TOPZ	TOPAZ detector at KEK-TRISTAN		

Conferences

Conferences are generally referred to by the location at which they were held (e.g., HAMBURG, TORONTO, CORNELL, BRIGHTON, etc.).

Journals

AA	Astronomy and Astrophysics
ADVP	Advances in Physics
AFIS	Anales de Fisica
AJP	American Journal of Physics
AL	Astronomy Letters
ANP	Annals of Physics
ANPL	Annals of Physics (Leipzig)
ANYAS	Annals of the New York Academy of Sciences
AP	Atomic Physics
APAH	Acta Physica Academiae Scientiarum Hungaricae
APJ	Astrophysical Journal
APJS	Astrophysical Journal Suppl.
APP	Acta Physica Polonica
APS	Acta Physica Slovaca
ARNPS	Annual Review of Nuclear and Particle Science
ARNS	Annual Review of Nuclear Science
ASP	Astroparticle Physics
AST	American Statistician
BAPS	Bulletin of the American Physical Society
BASUP	Bulletin of the Academy of Science, USSR (Physics)
CJNP	Chinese Journal of Nuclear Physics
CJP	Canadian Journal of Physics
CNPP	Comments on Nuclear and Particle Physics
CP	Chinese Physics
CPC	Chinese Physics C
CPL	Chinese Physics Letters
CQG	Classical and Quantum Gravity
CTP	Communications in Theoretical Physics
CZJP	Czechoslovak Journal of Physics
DANS	Doklady Akademii nauk SSSR
DP	Doklady Physics (Magazine)
EPJ	The European Physical Journal
EPJA	The European Physical Journal A
EPJC	The European Physical Journal C
EPL	Europhysics Letters

Abbreviations Used in the Particle Listings

FECAF	Fizika Elementarnykh Chastits i Atomnogo Yadra	ZETFP	Zhurnal Eksperimental'noi i Teoreticheskoi Fiziki, Pis'ma v Redakts
HADJ	Hadronic Journal	ZNAT	Zeitschrift für Naturforschung
IJMP	International Journal of Modern Physics	ZPHY	Zeitschrift für Physik
JAP	Journal of Applied Physics	Institutions	
JCAP	Journal of Cosmology and Astroparticle Physics	AACH	Phys. Inst. der Techn. Hochschule Aachen (Historical, use for general Inst. der Techn. Hochschule)
JETP	English Translation of Soviet Physics ZETF	AACH1	I Phys. Inst. B, RWTH Aachen
JETPL	English Translation of Soviet Physics ZETF Letters	AACH3	III Phys. Inst. A, RWTH Aachen Univ.
JHEP	Journal of High Energy Physics	AACHT	Inst. für Theoretische Teilchenphysik & Kosmologie, RWTH Aachen
JINR	Joint Inst. for Nuclear Research	AARH	Univ. of Aarhus
JINRRC	JINR Rapid Communications	ABO	Åbo Akademi Univ.
JP	Journal of Physics	ADEL	Adelphi Univ.
JPA	Journal of Physics A	ADLD	The Univ. of Adelaide
JPB	Journal of Physics B	AERE	Atomic Energy Research Estab.
JPCRD	Journal of Physical and Chemical Reference Data	AFRR	Armed Forces Radiobiology Res. Inst.
JPCS	Journal of Physics: Conference Series	AHMED	Physical Research Lab. Ahmedabad , Gujarat, India
JPG	Journal of Physics G	AICH	Aichi Univ. of Education
JPSJ	Journal of the Physical Society of Japan	AKIT	Akita Univ.
LHEP	Letters in High Energy Physics	ALAH	Univ. of Alabama (Huntsville)
LNC	Lettere Nuovo Cimento	ALAT	Univ. of Alabama (Tuscaloosa)
MNRAS	Monthly Notices of the Royal Astronomical Society	ALBA	SUNY at Albany
MPL	Modern Physics Letters	ALBE	Univ. of Alberta
MPLA	Modern Physics Letters A	AMES	Ames Lab.
NAST	New Astronomy	AMHT	Amherst College
NAT	Nature	AMST	Univ. van Amsterdam
NATC	Nature Communications (NCAOBW)	ANIK	NIKHEF
NATP	Nature Physics	ANKA	Middle East Technical Univ.; Dept. of Physics; Experimental HEP Lab
NC	Nuovo Cimento	ANL	Argonne National Lab.; High Energy Physics Division, Bldg. 362; Physics Division, Bldg. 203
NIM	Nuclear Instruments and Methods	ANSM	St. Anselm Coll.
NJP	New Journal of Physics	AQUI	Univ. di LAquila
NP	Nuclear Physics	ARCBO	Arecibo Observatory
NPA	Nuclear Physics A	ARIZ	Univ. of Arizona
NPB	Nuclear Physics B	ARZS	Arizona State Univ.
NPBPS	Nuclear Physics B Proceedings Supplement	ASCI	Russian Academy of Sciences
NPPP	Nuclear and Particle Physics Proceedings	AST	Accademia Sinica
PAN	Physics of Atomic Nuclei (formerly SJNP)	ATEN	NCSR " Demokritos "
PD	Physics Doklady (Magazine)	ATHU	Univ. of Athens
PDAT	Physik Daten	AUCK	Univ. of Auckland
PL	Physics Letters	BAKU	Natl. Azerbaijan Academy of Sciences , Inst. of Physics
PLA	Physics Letters A	BANG	Indian Inst. of Science
PLB	Physics Letters B	BANGB	Bangabasi College
PN	Particles and Nuclei	BARC	Univ. Autónoma de Barcelona ; Dept. de Fisica
PPCF	Plasma Physics and Controlled Fusion	BARCE	Univ. Autónoma de Barcelona ; Inst. de Física de Altas Energías
PPN	Physics of Particles and Nuclei (formerly SJPN)	BARI	Univ. e del Politecnico di Bari
PPNL	Physics of Particles and Nuclei Letters	BART	Univ. of Delaware ; Bartol Research Inst.
PPNP	Progress in Particles and Nuclear Physics	BASL	Inst. für Physik der Univ. Basel
PPSL	Proc. of the Physical Society of London	BAYR	Univ. Bayreuth
PR	Physical Review	BCEN	Centre d'Etudes Nucleaires de Bordeaux-Gradignan
PRA	Physical Review A	BCIP	Natl. Inst. for Physics & Nuclear Eng. "Horia Hulubei" (IFIN-HH)
PRAM	Pramana	BELJ	Beijing Univ.
PRC	Physical Review C	BELJT	Inst. of Theoretical Physics
PRD	Physical Review D		
PRL	Physical Review Letters		
PRPL	Physics Reports (Physics Letters C)		
PRSE	Proc. of the Royal Society of Edinburgh		
PRSL	Proc. of the Royal Society of London, Section A		
PS	Physica Scripta		
PTEP	Progress of Theoretical and Experimental Physics		
PTP	Progress of Theoretical Physics		
PTPS	Progress of Theoretical Physics Supplement		
PTRSL	Phil. Trans. Royal Society of London		
RA	Radiochimica Acta		
RMP	Reviews of Modern Physics		
RNC	La Rivista del Nuovo Cimento		
RPP	Reports on Progress in Physics		
RRP	Revue Roumaine de Physique		
SCI	Science		
SCIB	Science Bulletin		
SCPMA	Science China Physics, Mechanics and Astronomy		
SJNP	Soviet Journal of Nuclear Physics		
SJPN	Soviet Journal of Particles and Nuclei		
SPD	Soviet Physics Doklady (Magazine)		
SPU	Soviet Physics - Uspekhi		
SYM	Symmetry		
UFN	Usp. Fiz. Nauk - Russian version of SPU		
YAF	Yadernaya Fizika		
ZETF	Zhurnal Eksperimental'noi i Teoreticheskoi Fiziki		

Abbreviations Used in the Particle Listings

BELG	Inter-University Inst. for High Energies (ULB-VUB)	Brussel , Belgium	CBPF	Centro Brasileiro de Pesquisas Físicas – BIB/CDI/CBPF	Rio de Janeiro , RJ, Brazil
BELL	AT & T Bell Labs	Murray Hill, NJ, USA	CCAC	Allegheny College	Meadville, PA, USA
BERG	Univ. of Bergen	Bergen, Norway	CDEF	Univ. Paris VII, Denis Diderot	Paris, France
BERL	DESY , Deutsches Elektronen-Synchrotron	Zeuthen , Germany	CEA	Cambridge Electron Accelerator (Historical in <i>Review</i>)	Cambridge , MA, USA
BERN	Univ. of Berne	Berne, Switzerland	CEADE	Center for Apl. Studies for Nuclear Physics	Havana, Cuba
BGNA	Univ. di Bologna , & INFN , Sezione di Bologna; Via Irnerio, 46, I-40126 Bologna; Viale C. Berti Pichat, n. 6/2	Bologna, Italy	CEBAF	Jefferson Lab—Thomas Jefferson National Accelerator Facility	Newport News , VA, USA
BHAB	Bhabha Atomic Research Center	Trombay, Bombay, India	CENG	Centre d'Etudes Nucleaires	Grenoble , France
BHEP	Inst. of High Energy Physics	Beijing , China	CERN	CERN , European Organization for Nuclear Research	Genève, Switzerland
BIEL	Univ. Bielefeld	Bielefeld, Germany	CFPA	Univ. of California, (Berkeley)	Berkeley, CA, USA
BING	SUNY at Binghamton	Binghamton, NY, USA	CHIC	Univ. of Chicago	Chicago, IL, USA
BIRK	Birkbeck College , Univ. of London	London, United Kingdom	CIAE	State Nuclear Power Research Inst.	Beijing , China
BIRM	Univ. of Birmingham	Edgbaston, Birmingham, United Kingdom	CINC	Univ. of Cincinnati	Cincinnati, OH, USA
BLSU	Bloomsburg Univ.	Bloomsburg, PA, USA	CINV	CINVESTAV-IPN Centro de Investigacion y de Estudios Avanzados del IPN	México, DF, Mexico
BNL	Brookhaven National Lab.	Upton, NY, USA	CIT	California Inst. of Tech.	Pasadena, CA, USA
BOCH	Ruhr Univ. Bochum	Bochum, Germany	CLER	Univ. de Clermont-Ferrand	Aubière, France
BOHR	Niels Bohr Inst.	Copenhagen Ø, Denmark	CLEV	Cleveland State Univ.	Cleveland, OH, USA
BOIS	Boise State Univ.	Boise, ID, USA	CMNS	Comenius Univ. (FMFI UK)	Bratislava , Slovakia
BOMB	Univ. of Bombay	Bombay, India	CMU	Carnegie Mellon Univ.	Pittsburgh, PA, USA
BONN	Univ. of Bonn	Bonn, Germany	CNEA	Comisión Nacional de Energía Atómica	Buenos Aires, Argentina
BORD	Centre d'Etudes Nucléaires de Bordeaux Gradignan (CENBG)	Gradignan, France	CNRC	Centre for Research in Particle Physics	Ottawa, ON, Canada
BOSE	S.N. Bose National Centre for Basis Sciences	Calcutta, India	COIM	Univ. de Coimbra	Coimbra , Portugal
BOSK	“Rudjer Bošković” Inst.	Zagreb, Croatia	COLO	Univ. of Colorado	Boulder, CO, USA
BOST	Boston Univ.	Boston, MA, USA	COLU	Columbia Univ.	New York, NY, USA
BRAN	Brandeis Univ.	Waltham, MA, USA	CONC	Concordia University	Montreal, PQ, Canada
BRCO	Univ. of British Columbia	Vancouver, BC, Canada	CORN	Cornell Univ.	Ithaca, NY, USA
BRIS	Univ. of Bristol	Bristol, United Kingdom	COSU	Colorado State Univ.	Fort Collins, CO, USA
BROW	Brown Univ.	Providence, RI, USA	CPPM	Centre National de la Recherche Scientifique, Luminy	Marseille , France
BRUN	Brunel Univ.	Uxbridge, Middlesex, United Kingdom	CRAC	Henryk Niewodnicza'nski Inst. of Nuclear Physics	Kraków , Poland
BRUX	Univ. Libre de Bruxelles ; Physique des Particules Élémentaires	Bruxelles, Belgium	CRNL	Chalk River Labs.	Chalk River, ON, Canada
BRUXT	Univ. Libre de Bruxelles ; Physique Théorique	Bruxelles, Belgium	CSOK	Oklahoma Central State Univ.	Edmond, OK, USA
BUCH	Univ. of Bucharest	Bucharest-Magurele, Romania	CST	Univ. of Science and Technology of China	Hefei , Anhui 230026, China
BUDA	Wigner Research Centre for Physics	Budapest , Hungary	CSULB	California State Univ.	Long Beach, CA, USA
BUFF	SUNY at Buffalo	Buffalo, NY, USA	CSUS	California State Univ.	Sacramento, CA, USA
BURE	Inst. des Hautes Etudes Scientifiques	Bures-sur-Yvette , France	CUNY	City College of New York	New York, NY, USA
CAEN	Lab. de Physique Corpusculaire, ENSICAEN	Caen , France	CURCP	Univ. Pierre et Marie Curie (Paris VI), LCP	Paris, France
CAGL	Univ. degli Studi di Cagliari	Monserrato (CA), Italy	CURIN	Univ. Pierre et Marie Curie (Paris VI), LPNHE	Paris, France
CAGLI	INFN , Sezione di Cagliari	Monserrato (CA), Italy	CURIT	Univ. Pierre et Marie Curie (Paris VI), LPTHE	Paris, France
CAIR	Cairo University	Orman, Giza, Cairo, Egypt	DALH	Dalhousie Univ.	Halifax, NS, Canada
CAIW	Carnegie Inst. of Washington	Washington, DC, USA	DALI	Dalian Univ. of Tech.	Dalian, China
CALB	Univ. della Calabria	Cosenza, Italy	DARE	Daresbury Lab	Cheshire, United Kingdom
CALC	Univ. of Calcutta	Calcutta, India	DARM	Tech. Hochschule Darmstadt	Darmstadt, Germany
CAMB	DAMTP	Cambridge, United Kingdom	DELA	Univ. of Delaware ; Dept. of Physics & Astronomy	Newark, DE, USA
CAMP	Univ. Estadual de Campinas (UNICAMP)	Campinas , SP, Brazil	DELH	Univ. of Delhi	Delhi, India
CANB	Australian National Univ.	Canberra, ACT, Australia	DESY	DESY , Deutsches Elektronen-Synchrotron	Hamburg , Germany
CANTB	Inst. de Física de Cantabria (CSIC–Univ. Cantabria)	Santander, Spain	DFAB	Escuela de Ingenieros	Bilbao , Spain
CAPE	University of Cape Town	Rondebosch, Cape Town, South Africa	DOE	Department of Energy	Washington, DC, USA
CARA	Univ. Central de Venezuela	Caracas, Venezuela	DORT	Technische Univ. Dortmund	Dortmund, Germany
CARL	Carleton Univ.	Ottawa, ON, Canada	DUKE	Duke Univ.	Durham, NC, USA
CARLC	Carleton College	Northfield, MN, USA	DURH	Univ. of Durham	Durham, United Kingdom
CASE	Case Western Reserve Univ.	Cleveland, OH, USA	DUUC	University College Dublin	Dublin, Ireland
CAST	China Center of Advanced Science and Technology	Beijing, China	ECT	Europ. Cent. for Theor. Studies in Nucl. Phys.	Trento, Italy
CATA	Univ. di Catania	Catania, Italy	EDIN	Univ. of Edinburgh	Edinburgh, United Kingdom
CATH	Catholic Univ. of America	Washington, DC, USA	EFI	Univ. of Chicago, The Enrico Fermi Inst.	Chicago , IL, USA
CAVE	Cavendish Lab.	Cambridge, United Kingdom	ELMT	Elmhurst College	Elmhurst, IL, USA
CBNM	CBNM	Geel , Belgium			

Abbreviations Used in the Particle Listings

ENSP	l'Ecole Normale Supérieure	Paris, France	HYDER	Indian Inst. of Technology	Hyderabad, India
EOTV	Eötvös University	Budapest, Hungary	HZDR	Helmholtz-Zentrum Dresden-Rossendorf	Dresden, Germany
EPOL	École Polytechnique	Palaiseau, France	IAS	Inst. for Advanced Study	Princeton, NJ, USA
ERLA	Univ. Erlangen-Nurnberg	Erlangen, Germany	IASD	Dublin Inst. for Advanced Studies	Dublin, Ireland
ETH	Eidg. Technische Hochschule	Zürich, Switzerland	IBAR	Ibaraki Univ.	Ibaraki, Japan
FERR	Univ. di Ferrara	Ferrara, Italy	IBM	IBM Corp.	Palo Alto, CA, USA
FIRZ	Univ. degli Studi di Firenze	Sesto Fiorentino, Italy	IBMY	IBM	Yorktown Heights, NY, USA
FISK	Fisk Univ.	Nashville, TN, USA	IBS	Inst. for Boson Studies	Pasadena, CA, USA
FLOR	Univ. of Florida	Gainesville, FL, USA	ICEPP	The Univ. of Tokyo	Tokyo, Japan
FNAL	Fermilab	Batavia, IL, USA	ICRR	Univ. of Tokyo	Chiba, Japan
FOM	FOM , Stichting voor Fundamenteel Onderzoek der Materie	JP Utrecht , The Netherlands	ICTP	Abdus Salam International Centre for Theoretical Physics	Trieste , Italy
FRAN	Frankfurt Inst. for Advanced Studies (FIAS)	Frankfurt am Main, Germany	IFIC	IFIC (Instituto de Física Corpuscular)	Paterna (Valencia) , Spain
FRAS	Lab. Nazionali di Frascati dell'INFN	Frascati (Roma), Italy	IFRJ	Univ. Federal do Rio de Janeiro	Rio de Janeiro, RJ, Brazil
FREIB	Albert-Ludwigs Univ.	Freiburg , Germany	IIT	Illinois Inst. of Tech.	Chicago, IL, USA
FREIE	Freie Univ. Berlin	Berlin, Germany	IITB	Indian Inst. of Tech. IIT Bombay	Powai, Mumbai, India
FRIB	Univ. de Fribourg	Fribourg, Switzerland	IITI	Indian Inst. of Tech. \ef IIT Indore	Simrol, Indore, India
FSU	Florida State Univ.; High Energy Physics	Tallahassee, FL, USA	ILL	Univ. of Illinois at Urbana-Champaign	Urbana, IL, USA
FSUSC	Florida State Univ.; SCS (School of Computational Science)	Tallahassee, FL, USA	ILLC	Univ. of Illinois at Chicago	Chicago, IL, USA
FUKI	Fukui Univ.	Fukui, Japan	ILG	Inst. Laue-Langevin	Grenoble, France
FUKU	Fukushima Univ.	Fukushima, Japan	IND	Indiana Univ.	Bloomington, IN, USA
GENO	Univ. di Genova	Genova, Italy	INEL	E G and G Idaho , Inc.	Idaho Falls, ID, USA
GEOR	E. Andronikashvili Inst. of Physics	Tbilisi, Republic of Georgia	INFN	Ist. Nazionale di Fisica Nucleare (Generic INFN, unknown location)	Various places, Italy
GESC	General Electric Co.	Schenectady, NY, USA	INNS	Univ. of Innsbruck	Innsbruck , Austria
GEVA	Univ. de Genève	Genève, Switzerland	INPK	Henryk Niewodniczański Inst. of Nuclear Physics	Kraków , Poland
GIES	Univ. Giessen	Giessen, Germany	INRM	INR , Inst. for Nucl. Research	Moscow , Russian Federation
GIFU	Gifu Univ.	Gifu, Japan	INUS	KEK , High Energy Accelerator Research Organization	Tokyo, Japan
GLAS	Univ. of Glasgow	Glasgow, United Kingdom	IOAN	Univ. of Ioannina	Ioannina, Greece
GMAS	George Mason Univ.	Fairfax, VA, USA	IOFF	A.F. Ioffe Phys. Tech. Inst.	St. Petersburg , Russian Federation
GOET	Univ. Göttingen	Göttingen, Germany	IOWA	Univ. of Iowa	Iowa City, IA, USA
GOML	Gomel State Univ.	Gomel, Belarus	IPN	IPN , Inst. de Phys. Nucl.	Orsay , France
GRAN	Univ. de Granada	Granada, Spain	IPNP	Univ. Pierre et Marie Curie (Paris VI)	Paris, France
GRAZ	Univ. Graz	Graz, Austria	IRAD	Inst. du Radium (Historical)	Paris , France
GRON	Univ. of Groningen	Groningen, The Netherlands	ISNG	Lab. de Physique Subatomique et de Cosmologie (LPSC)	Grenoble , France
GSCO	Geological Survey of Canada	Ottawa, ON, Canada	ISU	Iowa State Univ.	Ames, IA, USA
GSI	GSI Helmholtzzentrum für Schwerionenforschung GmbH	Darmstadt , Germany	ISUT	Isfahan University of Technology	Isfahan, Iran
GUAN	Univ. de Guanajuato	León, Gto., Mexico	ITEP	ITEP , Inst. of Theor. and Exp. Physics	Moscow , Russian Federation
GUEL	Univ. of Guelph	Guelph, ON, Canada	ITHA	Ithaca College	Ithaca, NY, USA
GWU	George Washington Univ.	Washington, DC, USA	IUPU	Indiana Univ., Purdue Univ. Indianapolis	Indianapolis, IN, USA
HAHN	Hahn-Meitner Inst. Berlin GmbH	Berlin, Germany	JADA	Jadavpur Univ.	Calcutta, India
HAIF	Technion – Israel Inst. of Tech.	Technion, Haifa, Israel	JAGL	Jagiellonian Univ.	Kraków, Poland
HAMB	Univ. Hamburg	Hamburg, Germany	JHU	Johns Hopkins Univ.	Baltimore, MD, USA
HANN	Univ. Hannover	Hannover, Germany	JINR	JINR , Joint Inst. for Nucl. Research	Dubna , Russian Federation
HARC	Houston Advanced Research Ctr.	The Woodlands, TX, USA	JULI	Forschungszentrum Jülich	Jülich, Germany
HARV	Harvard Univ.	Cambridge, MA, USA	JYV	Univ. of Jyväskylä	Jyväskylä, Finland
HARV	Harvard Univ. (LPPC)	Cambridge, MA, USA	KAGO	Univ. of Kagoshima	Kagoshima-shi, Japan
HAWA	Univ. of Hawai'i	Honolulu, HI, USA	KAIST	Korea Advanced Inst. of Science and Technology	Yusung ku, Daejeon, Republic of Korea
HEBR	Hebrew Univ.	Jerusalem, Israel	KANP	Indian Inst. of Tech.	Kanpur , UT, India
HEID	Univ. Heidelberg ; (unspecified division) (Historical in <i>Review</i>)	Heidelberg, Germany	KANS	Univ. of Kansas	Lawrence, KS, USA
HEIDH	Ruprecht-Karls Univ. Heidelberg	Heidelberg, Germany	KARL	Univ. Karlsruhe (Historical in <i>Review</i>)	Karlsruhe, Germany
HEIDP	Univ. Heidelberg ; Physics Inst.	Heidelberg, Germany	KARLE	Karlsruhe Inst. of Technology (KIT); Inst. for Experimental Nuclear Physics	Karlsruhe, Germany
HEIDT	Ruprecht-Karls-Univ. Heidelberg	Heidelberg, Germany	KARLK	Karlsruhe Inst. of Technology (KIT)	EGgenstein-Leopoldshafen, Germany
HELS	Univ. of Helsinki	University of Helsinki, Finland	KARLT	Karlsruhe Inst. of Technology (KIT); Inst. for Theoretical Physics	Karlsruhe, Germany
HINR	Inst. of Nuclear Research (ATOMKI)	Debrecen , Hungary			
HIRO	Hiroshima Univ.	Higashi-Hiroshima, Japan			
HOUS	Univ. of Houston	Houston, TX, USA			
HPC	Hewlett-Packard Corp.	Cupertino, CA, USA			
HSCA	Harvard-Smithsonian Center for Astrophysics	Cambridge, MA, USA			

Abbreviations Used in the Particle Listings

KAZA	Kazakh Inst. of High Energy Physics	Alma Ata, Kazakhstan	LOQM	Queen Mary, Univ. of London	London, United Kingdom
KEK	KEK , High Energy Accelerator Research Organization	Ibaraki-ken, Japan	LOUC	University College London	London, United Kingdom
KENT	Univ. of Kent	Canterbury, United Kingdom	LOUV	Univ. Catholique de Louvain	Louvain-la-Neuve, Belgium
KEYN	Open Univ.	Milton Keynes, United Kingdom	LOWC	Westfield College (Historical, see LOQM (Queen Mary and Westfield joined))	London, United Kingdom
KFTI	Kharkov Inst. of Physics and Tech. (NSC KIPT)	Kharkov, Ukraine	LRL	U.C. Lawrence Radiation Lab. (Old name for LBL)	Berkeley , CA, USA
KIAE	Kurchatov Inst.	Moscow , Russian Federation	LSU	Louisiana State Univ.	Baton Rouge, LA, USA
KIAM	Keldysh Inst. of Applied Math., Acad. Sci., Russia	Moscow, Russian Federation	LUND	Fysiska Institutionen	Lund , Sweden
KIDR	Vinča Inst. of Nuclear Sciences	Belgrade, Serbia	LUND	Lund Univ.	Lund, Sweden
KIEV	Institute for Nuclear Research	Kyiv , Ukraine	LYON	Institute de Physique Nucléaire de Lyon (IPN)	Villeurbanne, France
KINK	Kinki Univ.	Osaka, Japan	MADE	UAM/CSIC , Inst. de Física Teórica	Madrid , Cantoblanco, Spain
KNTY	Univ. of Kentucky	Lexington, KY, USA	MADR	C.I.E.M.A.T	Madrid , Spain
KOBE	Kobe Univ.	Kobe, Japan	MADU	Univ. Autónoma de Madrid	Cantoblanco, Madrid, Spain
KOMAB	Univ. of Tokyo, Komaba	Tokyo, Japan	MAINZ	Johannes-Gutenberg- Univ. ; Inst. für Kernphysik, J.-J.-Becher-Weg 45; Inst. für Physik, Staudingerweg 7	Mainz , Germany
KONAN	Konan Univ.	Kobe, Japan	MANI	Univ. of Manitoba	Winnipeg, MB, Canada
KOSI	Inst. of Experimental Physics SAS	Košice , Slovakia	MARB	Univ. Marburg	Marburg, Germany
KYOT	Kyoto Univ.; Dept. of Physics, Graduate School of Science	Kyoto, Japan	MARS	Centre de Physique des Particules de Marseille	Marseille, France
KYOTU	Kyoto Univ.; Yukawa Inst. for Theor. Physics	Kyoto, Japan	MASA	Univ. of Massachusetts	Amherst , MA, USA
KYUN	Kyungpook National Univ.	Daegu, Republic of Korea	MASB	Univ. of Massachusetts	Boston , MA, USA
KYUSH	Kyushu Univ.; Elementary Particle Theory Group; Exp. Particle Physics Group; Research Center for Advanced Particle Physics	Fukuoka, Japan	MASD	Univ. of Massachusetts	North Dartmouth , MA, USA
LALO	LAL , Laboratoire de l'Accélérateur Linéaire	Orsay , France	MCGI	McGill Univ.	Montreal, QC, Canada
LANC	Lancaster Univ.	Lancaster, United Kingdom	MCHS	Univ. of Manchester	Manchester, United Kingdom
LANL	Los Alamos National Lab. (LANL)	Los Alamos, NM, USA	MCMS	McMaster Univ.	Hamilton, ON, Canada
LAPL	Univ. Nacional de La Plata	La Plata, Argentina	MDRA	Univ. of Madras	Madras, India
LAPP	LAPP , Lab. d'Annecy-le-Vieux de Phys. des Particules	Annecy-le-Vieux , France	MEHTA	Harish-Chandra Research Inst.	Allahabad, India
LASL	U.C. Los Alamos Scientific Lab. (Old name for LANL)	Los Alamos, NM, USA	MEIS	Meisei Univ.	Tokyo, Japan
LATV	Latvian State Univ.	Riga, Latvia	MELB	Univ. of Melbourne	Victoria, Australia
LAUS	EPFL Lausanne	Lausanne, Switzerland	MEUD	Observatoire de Meudon	Meudon, France
LAVL	Univ. Laval	Quebec, QC, Canada	MICH	Univ. of Michigan	Ann Arbor, MI, USA
LBL	Lawrence Berkeley National Lab.	Berkeley, CA, USA	MILA	Univ. di Milano	Milano, Italy
LCGT	Univ. di Torino	Turin, Italy	MILAI	INFN , Sez. di Milano	Milano, Italy
LEBD	Lebedev Physical Inst.	Moscow , Russian Federation	MINN	Univ. of Minnesota	Minneapolis, MN, USA
LECE	Univ. di Lecce	Lecce, Italy	MIPT	Moscow Institute of Physics and Technology	Moscow, Russian Federation
LEED	Univ. of Leeds	Leeds, United Kingdom	MISS	Univ. of Mississippi	University, MS, USA
LEGN	Lab. Naz. di Legnaro	Legnaro , Italy	MISSR	Univ. of Missouri	Rolla, MO, USA
LEHI	Lehigh Univ.	Bethlehem, PA, USA	MIT	MIT Massachusetts Inst. of Technology	Cambridge, MA, USA
LEHM	Lehman College of CUNY	Bronx, NY, USA	MIU	Maharishi International Univ.	Fairfield, IA, USA
LEID	Univ. Leiden	Leiden, The Netherlands	MIYA	Miyazaki Univ.	Miyazaki-shi, Japan
LEMO	Le Moyne Coll.	Syracuse, NY, USA	MONP	Univ. de Montpellier II	Montpellier, France
LENSU	Saint-Petersburg State Univ.	St. Petersburg , Russian Federation	MONS	Univ. of Mons	Mons , Belgium
LEUV	Katholieke Univ. Leuven	Leuven, Belgium	MONT	Univ. de Montréal ; Pavillon René-J.-A.-Lévesque	Montréal, PQ, Canada
LIEG	Univ. de Liège	Liège, Belgium	MONTC	Univ. de Montréal ; Centre de recherches mathématiques	Montréal, PQ, Canada
LINZ	Univ. Linz	Linz, Austria	MOSU	Skobeltsyn Inst. of Nuclear Physics, Lomonosov Moscow State Univ.; Experimental HEP Division; Theoretical HEP Division	Moscow , Russian Federation
LISB	Inst. Nacional de Investigacion Científica	Lisboa CODEX, Portugal	MPCM	Max Planck Inst. für Chemie	Mainz , Germany
LISBT	Centro de Física Teórica de Partículas (CFTP)	Lisboa , Portugal	MPEI	Moscow Physical Engineering Inst.	Moscow, Russian Federation
LIVP	Univ. of Liverpool	Liverpool, United Kingdom	MPIG	Max-Planck -Institute für Astrophysik	Garching, Germany
LJUB	Univerza v Ljubljani	Ljubljana, Slovenia	MPIK	Max-Planck -Inst. für Kernphysik	Heidelberg , Germany
LLL	Lawrence Livermore Lab. (Old name for LLNL)	Livermore, CA, USA	MPIM	Max-Planck -Inst. für Physik	München , Germany
LLNL	Lawrence Livermore National Lab.	Livermore, CA, USA	MRION	Mirion Technologies Canberra	Meriden, CT, USA
LNUDA	Liaoning Normal Univ.	Dalian, China	MSST	Mississippi State University	Mississippi State, MS, USA
LOCK	Lockheed Palo Alto Res. Lab	Palo Alto, CA, USA	MSU	Michigan State Univ.	East Lansing, MI, USA
LOIC	Imperial College of Science Tech. & Medicine	London, United Kingdom	MTHO	Mount Holyoke College	South Hadley, MA, USA
LOKC	Univ. of London , King's College	London, United Kingdom	MULH	Centre Univ. du Haut-Rhin	Mulhouse, France

Abbreviations Used in the Particle Listings

MUNI	Ludwig-Maximilians-Univ. München	Garching, Germany	PARIS	Univ. de Paris (Historical)	Paris , France
MURA	Midwestern Univ. Research Assoc. (Historical in <i>Review</i>)	Stroughton, WI, USA	PARIT	Univ. Paris VII , LPTHE	Paris, France
MURC	Univ. of Murcia	Murcia, Spain	PARM	INFN , Gruppo Collegato di Parma	Parma, Italy
NAAS	North American Aviation Science Center (Historical in <i>Review</i>)	Thousand Oaks, CA, USA	PAST	Institut Pasteur	Paris , France
NAGO	Nagoya Univ.	Nagoya, Japan	PATR	Univ. of Patras	Patras, Greece
NANJ	Nanjing Univ.	Nanjing, China	PAVI	Univ. di Pavia	Pavia, Italy
NAPL	Univ. di Napoli “Federico II”	Napoli, Italy	PAVII	INFN, Sez. di Pavia	Pavia , Italy
NASA	NASA	Greenbelt, MD, USA	PENN	Univ. of Pennsylvania	Philadelphia, PA, USA
NBS	U.S National Bureau of Standards (Old name for NIST)	Gaithersburg, MD, USA	PGIA	INFN, Sezione di Perugia	Perugia, Italy
NBSB	National Inst. Standards Tech.	Boulder, CO, USA	PISA	Univ. di Pisa	Pisa, Italy
NCAR	National Center for Atmospheric Research	Boulder, CO, USA	PISAI	INFN, Sez. di Pisa	Pisa, Italy
NCSU	North Carolina State Univ.	Raleigh , NC, USA	PITT	Univ. of Pittsburgh	Pittsburgh, PA, USA
NDAM	Univ. of Notre Dame	Notre Dame, IN, USA	PLAT	SUNY at Plattsburgh	Plattsburgh, NY, USA
NEAS	Northeastern Univ.	Boston, MA, USA	PLRM	Univ. di Palermo	Palermo, Italy
NEBR	Univ. of Nebraska	Lincoln, NE, USA	PNL	Battelle Memorial Inst.	Richland, WA, USA
NEUC	Univ. de Neuchâtel	Neuchâtel, Switzerland	PNPI	Petersburg Nuclear Physics Inst. of Russian Academy of Sciences	Gatchina, Russian Federation
NICEA	Univ. de Nice	Nice, France	PPA	Princeton-Penn. Proton Accelerator (Historical in <i>Review</i>)	Princeton, NJ, USA
NICEO	Observatoire de Nice	Nice, France	PRAG	Inst. of Physics, ASCR	Prague , Czech Republic
NIHO	Nihon Univ.	Tokyo, Japan	PRIN	Princeton Univ.	Princeton, NJ, USA
NIIG	Niigata Univ.	Niigata, Japan	PSI	Paul Scherrer Institute	Villigen , Switzerland
NIJM	Radboud Univ. Nijmegen	AJ Nijmegen , The Netherlands	PSLL	Physical Science Lab	Las Cruces, NM, USA
NIRS	Nat. Inst. Radiological Sciences	Chiba , Japan	PSU	Penn State Univ.	University Park, PA, USA
NIST	National Institute of Standards & Technology	Gaithersburg, MD, USA	PUCB	Pontificia Univ. Católica do Rio de Janeiro	Rio de Janeiro, RJ, Brazil
NIU	Northern Illinois Univ.	De Kalb, IL, USA	PUEB	Univ. Autonoma de Puebla	Puebla , Pue, Mexico
NJU	Nanjing University	Nanjing, China	PURD	Purdue Univ.	West Lafayette, IN, USA
NMSU	New Mexico State Univ. ; Dept. of Physics, MSC 3D; Part. & Nucl. Phys. Group, Box 30001/Dept.	Las Cruces, NM, USA	QUKI	Queen’s Univ.	Kingston, ON, Canada
NORD	Nordita	Stockholm, Sweden	RAL	STFC Rutherford Appleton Lab.	Chilton, Didcot, Oxfordshire, United Kingdom
NOTT	Univ. of Nottingham	Nottingham, United Kingdom	REGE	Univ. Regensburg	Regensburg, Germany
NOVM	Inst. of Mathematics	Novosibirsk , Russian Federation	REHO	Weizmann Inst. of Science	Rehovot, Israel
NOVO	BINP, Budker Inst. of Nuclear Physics	Novosibirsk , Russian Federation	REZ	Nuclear Physics Inst. AVČR	Řež , Czech Republic
NPOL	Polytechnic of North London	London, United Kingdom	RGSUL	Univ. Federal do Rio Grande do Sul (UFRGS)	Porto Alegre, RS, Brazil
NRL	Naval Research Lab	Washington, DC, USA	RHBL	Royal Holloway, Univ. of London	Egham, Surrey, United Kingdom
NSF	National Science Foundation	Arlington, VA, USA	RHEL	Rutherford High Energy Lab (Old name for RAL)	Chilton, Didcot, Oxon., United Kingdom
NTHU	National Tsing Hua Univ.	Hsinchu, Taiwan	RICE	Rice Univ.	Houston, TX, USA
NTUA	National Tech. Univ. of Athens	Athens, Greece	RIKEN	Riken Nishina Center for Accelerator-Based Science	Saitama, Japan
NWES	Northwestern Univ.	Evanston, IL, USA	RIKK	Rikkyo Univ.	Tokyo, Japan
NYU	New York Univ.	New York, NY, USA	RIS	Rowland Inst. for Science	Cambridge, MA, USA
OBER	Oberlin College	Oberlin, OH, USA	RISC	Rockwell International	Thousand Oaks, CA, USA
OCH	Ochanomizu Univ.	Tokyo, Japan	RISL	Universities Research Reactor	Risley , Warrington, United Kingdom
OHIO	Ohio Univ.	Athens, OH, USA	RISO	Riso National Laboratory	Roskilde, Denmark
OKAY	Okayama Univ.	Okayama, Japan	RITS	Royal Inst. of Technology (KTH)	Stockholm , Sweden
OKLA	Univ. of Oklahoma	Norman, OK, USA	RL	Rutherford High Energy Lab (Old name for RAL)	Chilton, Didcot, Oxon., United Kingdom
OKSU	Oklahoma State Univ.	Stillwater, OK, USA	RMCS	Royal Military Coll. of Science	Swindon, Wilts., United Kingdom
OREG	Univ. of Oregon ; Inst. of Theoretical Science; U.O. Center for High Energy Physics	Eugene, OR, USA	ROCH	Univ. of Rochester	Rochester, NY, USA
ORNL	Oak Ridge National Laboratory	Oak Ridge, TN, USA	ROCK	Rockefeller Univ.	New York, NY, USA
ORSAY	Univ. de Paris Sud 11	Orsay CEDEX, France	ROMA	Univ. di Roma (Historical)	Roma , Italy
ORST	Oregon State Univ.	Corvallis, OR, USA	ROMA2	Univ. di Roma , “Tor Vergata”	Roma, Italy
OSAK	Osaka Univ.	Osaka, Japan	ROMA3	INFN, Sez. di Roma Tre	Roma , Italy
OSKC	Osaka City Univ.	Osaka, Japan	ROMAI	INFN, Sez. di Roma	Roma, Italy
OSLO	Univ. of Oslo	Oslo, Norway	ROSE	Rose-Hulman Inst. of Technology	Terre Haute, IN, USA
OSU	Ohio State Univ.	Columbus, OH, USA	RPI	Rensselaer Polytechnic Inst.	Troy, NY, USA
OTTA	Univ. of Ottawa	Ottawa, ON, Canada	RUTG	Rutgers , the State Univ. of New Jersey	Piscataway, NJ, USA
OXF	University of Oxford	Oxford, United Kingdom	S0GA	Sogang University	Seoul, Republic of Korea
OXFTP	Univ. of Oxford	Oxford, United Kingdom	SACL	CEA Saclay , IRFU	Gif-sur-Yvette, France
PADO	Univ. degli Studi di Padova	Padova, Italy	SACL5	CEA Saclay – IPhT	Gif-sur-Yvette, France
PARIN	LPNHE , IN ² P ³ /CNRS	Paris, France	SACLD	CEA Saclay (Essonne)	Gif-sur-Yvette, France
			SAGA	Saga Univ.	Saga-shi, Japan
			SAHA	Saha Inst. of Nuclear Physics	Bidhan Nagar, Calcutta, India
			SANG	Kyoto Sangyo Univ.	Kyoto-shi, Japan
			SANI	Ist. Superiore di Sanità	Roma , Italy

Abbreviations Used in the Particle Listings

SASK	Univ. of Saskatchewan	Saskatoon, SK, Canada	TEMP	Temple Univ.	Philadelphia, PA, USA
SASSO	Lab. Naz. Gran Sasso dell'INFN	Assergi (AQ), Italy	TENN	Univ. of Tennessee	Knoxville, TN, USA
SAVO	Univ. de Savoie	Chambery, France	TEXA	Univ. of Texas at Austin	Austin, TX, USA
SBER	California State Univ.	San Bernardino , CA, USA	TGAK	Tokyo Gakugei Univ.	Tokyo, Japan
SCHAF	W.J. Schafer Assoc.	Livermore, DA, USA	TGU	Tohoku Gakuin Univ.	Miyagi, Japan
SCIT	Science Univ. of Tokyo	Tokyo, Japan	THES	Aristotle Univ. of Thessaloniki (AUTH)	Thessaloniki, Greece
SCOT	Scottish Univ. Research and Reactor Ctr.	Glasgow, United Kingdom	TINT	Tokyo Inst. of Technology	Tokyo, Japan
SCUC	Univ. of South Carolina	Columbia, SC, USA	TISA	Sagamihara Inst. of Space & Astronautical Sci.	Kanagawa, Japan
SEAT	Seattle Pacific Coll.	Seattle, WA, USA	TMSK	Tomsk Polytechnic Univ.	Tomsk , Russian Federation
SEIB	Austrian Research Center, Seibersdorf LTD.	Seibersdorf, Austria	TMTC	Tokyo Metropolitan Coll. Tech.	Tokyo, Japan
SEOU	Korea Univ.; Dept. of Physics; HEP Group	Seoul, Republic of Korea	TMU	Tokyo Metropolitan Univ.	Tokyo, Japan
SEOUL	Seoul National Univ.; Center for Theoretical Physics; Dept. of Physics & Astronomy, Coll. of Natural Sciences	Seoul, Republic of Korea	TNTO	Univ. of Toronto	Toronto, ON, Canada
SERP	IHEP , Inst. for High Energy Physics	Protvino, Russian Federation	TOHO	Toho Univ.	Chiba, Japan
SETO	Seton Hall Univ.	South Orange, NJ, USA	TOHOK	Tohoku Univ.	Sendai, Japan
SFLA	Univ. of South Florida	Tampa, FL, USA	TOKA	Tokai Univ.	Shimizu, Japan
SFRA	Simon Fraser University	Burnaby, BC, Canada	TOKAH	Tokai Univ.	Hiratsuka, Japan
SFSU	California State Univ.	San Francisco , CA, USA	TOKMS	Univ. of Tokyo ; Meson Sci- ence Laboratory	Tokyo, Japan
SHAMS	Ain Shams University	Abbassia, Cairo, Egypt	TOKU	Univ. of Tokushima	Tokushima-shi, Japan
SHDN	Shandong Univ.	Jinan, Shandong, China	TOKY	Univ. of Tokyo ; High-Energy Physics Theory Group	Tokyo, Japan
SHEF	Univ. of Sheffield	Sheffield, United Kingdom	TOKYC	Univ. of Tokyo ; Dept. of Chemistry	Tokyo, Japan
SHMP	Univ. of Southampton	Southampton, United Kingdom	TORI	Univ. degli Studi di Torino	Torino, Italy
SHRZ	Shiraz Univ.	Shiraz, Iran	TPTI	Uzbek Academy of Sciences	Tashkent , Republic of Uzbek- istan
SIEG	Univ. Siegen	Siegen, Germany	TRIN	Trinity College Dublin	Dublin, Ireland
SILES	Univ. of Silesia	Katowice, Poland	TRIU	TRIUMF	Vancouver, BC, Canada
SIN	Swiss Inst. of Nuclear Re- search (Old name for VILL)	Villigen , Switzerland	TRST	Univ. di Trieste	Trieste, Italy
SING	National Univ. of Singapore	Kent Ridge, Singapore	TRSTI	INFN , Sez. di Trieste	Trieste, Italy
SISSA	Scuola Internazionale Superi- ore di Studi Avanzati	Trieste , Italy	TRSTT	Univ. degli Studi di Trieste	Trieste , Italy
SLAC	SLAC National Accelerator Laboratory	Menlo Park, CA, USA	TSIN	Tsinghua Univ.	Beijing, China
SLOV	Inst. of Physics, Slovak Acad. of Sciences	Bratislava 45, Slovakia	TSUK	Univ. of Tsukuba	Ibaraki-ken, Japan
SMU	Southern Methodist Univ.	Dallas, TX, USA	TTAM	Tamagawa Univ.	Tokyo, Japan
SNSP	Scuola Normale Superiore	Pisa , Italy	TUAT	Tokyo Univ. of Agriculture Tech.	Tokyo, Japan
SOFI	Inst. for Nuclear Research and Nuclear Energy	Sofia , Bulgaria	TUBIN	Univ. Tübingen	Tübingen, Germany
SOFU	Univ. of Sofia "St. Kliment Ohridski"	Sofia, Bulgaria	TUFTS	Tufts Univ.	Medford, MA, USA
SORB	Sorbonne Université	Paris, France	TUM	Tech. Univ. München	Garching, Germany
SPAUL	Univ. de São Paulo	São Paulo, SP, Brazil	TUW	Technische Univ. Wien	Vienna, Austria
SPIFT	Inst. de Física Teórica (IFT)	São Paulo , SP, Brazil	TUZL	Tuzla Univ.	Tuzla, Argentina
SSL	Univ. of California (Berke- ley)	Berkeley, CA, USA	UBA	Univ. de Buenos Aires	Buenos Aires, Argentina
STAN	Stanford Univ.	Stanford, CA, USA	UCB	Univ. of California (Berke- ley)	Berkeley, CA, USA
STEV	Stevens Inst. of Tech.	Hoboken, NJ, USA	UCD	Univ. of California (Davis)	Davis, CA, USA
STFN	Jožef Stefan Institute	Ljubljana , Slovenia	UCI	Univ. of California (Irvine)	Irvine, CA, USA
STLO	St. Louis Univ.	St. Louis, MO, USA	UCLA	Univ. of California (Los Angeles)	Los Angeles, CA, USA
STOH	Stockholm Univ.	Stockholm, Sweden	UCND	Union Carbide Corp.	Oak Ridge, TN, USA
STON	SUNY at Stony Brook	Stony Brook, NY, USA	UCR	Univ. of California (River- side)	Riverside, CA, USA
STRB	Inst. Pluridisciplinaire Hubert Curien (CNRS)	Strasbourg , France	UCSB	Univ. of California (Santa Barbara); Physics Dept., High Energy Physics Experi- ment	Santa Barbara, CA, USA
STUT	Univ. Stuttgart	Stuttgart, Germany	UCSBT	Univ. of California (Santa Barbara); Kavli Inst. for Theoretical Physics	Santa Barbara, CA, USA
STUTM	Max-Planck-Inst.	Stuttgart , Germany	UCSC	Univ. of California (Santa Cruz)	Santa Cruz, CA, USA
SUGI	Sugiyama Jogakuen Univ.	Aichi, Japan	UCSD	Univ. of California (San Diego)	La Jolla, CA, USA
SUNG	Sungkyunkwan Univ.	Suwon, Republic of Korea	UGAZ	Univ. of Gaziantep	Gaziantep, Turkey
SURR	Univ. of Surrey	Guildford, Surrey, United Kingdom	UMD	Univ. of Maryland	College Park, MD, USA
SUSS	Univ. of Sussex	Brighton, United Kingdom	UNAM	Univ. Nac. Autónoma de México (UNAM)	México , DF, Mexico
SVR	Savannah River Labs.	Aiken, SC, USA	UNAM	Univ. Nacional Autónoma de México (UNAM)	México , DF, Mexico
SYDN	Univ. of Sydney	Sydney, NSW, Australia	UNC	Univ. of North Carolina	Greensboro, NC, USA
SYRA	Syracuse Univ.	Syracuse, NY, USA	UNCCH	Univ. of North Carolina at Chapel Hill	Chapel Hill, NC, USA
TAJK	Acad. Sci., Tadjik SSR	Dushanbe , Tadjikistan	UNCS	Union College	Schenectady, NY, USA
TAMU	Texas A&M Univ.	College Station, TX, USA	UNESP	UNESP	Botucatu, Brazil
TATA	Tata Inst. of Fundamental Research	Bombay, India	UNH	Univ. of New Hampshire	Durham, NH, USA
TBIL	Tbilisi State University	Tbilisi, Republic of Georgia	UNM	Univ. of New Mexico	Albuquerque, NM, USA
TELA	Tel-Aviv Univ.	Tel Aviv, Israel			
TELE	Teledyne Brown Engineer- ing	Huntsville, AL, USA			

Abbreviations Used in the Particle Listings

UOEH	Univ. of Occupational and Environmental Health	Kitakyushu , Japan	WATER	Univ. of Waterloo	Waterloo, ON, Canada
UPNJ	Uppsala College	East Orange, NJ, USA	WAUS	Univ. of Western Australia	Perth, WA, Australia
UPPS	Uppsala Univ.	Uppsala , Sweden	WAYN	Wayne State Univ.	Detroit, MI, USA
UPR	Univ. of Puerto Rico	San Juan , PR, USA	WESL	Wesleyan Univ.	Middletown, CT, USA
URI	Univ. of Rhode Island	Kingston, RI, USA	WIEN	Univ. Wien	Vienna, Austria
USC	Univ. of Southern California	Los Angeles, CA, USA	WILL	Coll. of William and Mary	Williamsburg, VA, USA
USF	Univ. of San Francisco	San Francisco, CA, USA	WINR	National Centre for Nuclear Research	Warsaw , Poland
UTAH	Univ. of Utah	Salt Lake City, UT, USA	WISC	Univ. of Wisconsin	Madison, WI, USA
UTRE	Univ. of Utrecht	Utrecht, The Netherlands	WITW	Univ. of the Witwatersrand	Wits, South Africa
UTRO	Norwegian Univ. of Science & Technology	Trondheim, Norway	WMIU	Western Michigan Univ.	Kalamazoo, MI, USA
UVA	Univ. of Virginia	Charlottesville, VA, USA	WONT	The Univ. of Western Ontario	London, ON, Canada
UZINR	Acad. Sci., Ukrainian SSR	Uzhgorod , Ukraine	WOOD	Woodstock College (No longer in existence)	Woodstock, MD, USA
VALE	Univ. de Valencia	Burjassot, Valencia , Spain	WUPP	Bergische Univ. Wuppertal	Wuppertal , Germany
VALP	Valparaiso Univ.	Valparaiso, IN, USA	WURZ	Univ. Würzburg	Würzburg, Germany
VAND	Vanderbilt Univ.	Nashville, TN, USA	WUSL	Washington Univ.	St. Louis, MO, USA
VASS	Vassar College	Poughkeepsie, NY, USA	WYOM	Univ. of Wyoming	Laramie, WY, USA
VICT	Univ. of Victoria	Victoria, BC, Canada	YALE	Yale Univ.	New Haven, CT, USA
VIEN	Inst. für Hochenergiephysik (HEPHY)	Vienna , Austria	YARO	Yaroslavl State Univ.	Yaroslavl, Russian Federation
VILL	Inst. for Part. Phys. and Astrophys. IPA at PSI	Villigen, Switzerland	YCC	Yokohama Coll. of Commerce	Yokohama, Japan
VPI	Virginia Tech.	Blacksburg, VA, USA	YERE	Yerevan Physics Inst.	Yerevan, Armenia
VRIJ	Vrije Univ.	HV Amsterdam , The Netherlands	YOKO	Yokohama National Univ.	Yokohama-shi, Japan
WABR	Eidgenössisches Amt für Messwesen	Waber , Switzerland	YORKC	York Univ.	Toronto, Canada
WARS	Univ. of Warsaw	Warsaw, Poland	ZAGR	Zagreb Univ.	Zagreb, Croatia
WASCR	Waseda Univ.; Cosmic Ray Division	Tokyo, Japan	ZARA	Univ. de Zaragoza	Zaragoza, Spain
WASH	Univ. of Washington ; Elem. Particle Experiment (EPE); Particle Astrophysics (PA)	Seattle, WA, USA	ZEEM	Univ. van Amsterdam	TV Amsterdam, The Netherlands
WASU	Waseda Univ.; Dept. of Physics, High Energy Physics Group	Tokyo, Japan	ZHON	Zhongshan (Sun Yat-Sen) Univ.	Guangzhou, China
			ZHZH	Zhengzhou Univ.	Zhengzhou, Henan, China
			ZURI	Univ. Zürich	Zürich, Switzerland

γ	1141
g (gluon)	1142
graviton	1142
W	1142
Z	1156
H^0	1175
Neutral Higgs Bosons, Searches for	1187
Charged Higgs Bosons (H^\pm and $H^{\pm\pm}$), Searches for	1196
New Heavy Bosons	1200
Axions (A^0) and Other Very Light Bosons	1217

Notes in the Listings

Triple gauge couplings (TGC's)	1146
Anomalous $ZZ\gamma$, $Z\gamma\gamma$, and ZZV couplings	1171
Anomalous W/Z quartic couplings	1173

Related Reviews in Volume 1

54. Mass and width of the W boson (rev.)	789
55. Z boson	791

GAUGE AND HIGGS BOSONS

γ (photon)

$$I(J^{PC}) = 0,1(1^{--})$$

γ MASS

Results prior to 2008 are critiqued in GOLDHABER 10. All experimental results published prior to 2005 are summarized in detail by TU 05.

The following conversions are useful: $1 \text{ eV} = 1.783 \times 10^{-33} \text{ g} = 1.957 \times 10^{-6} m_e$; $\chi_C = (1.973 \times 10^{-7} \text{ m}) \times (1 \text{ eV}/m_\gamma)$.

VALUE (eV)	CL%	DOCUMENT ID	COMMENT
<1 × 10⁻¹⁸		1 RYUTOV 07	MHD of solar wind
••• We do not use the following data for averages, fits, limits, etc. •••			
<2.2 × 10 ⁻¹⁴		2 BONETTI 17	Fast Radio Bursts, FRB 121102
<1.8 × 10 ⁻¹⁴		3 BONETTI 16	Fast Radio Bursts, FRB 150418
<1.9 × 10 ⁻¹⁵		4 RETINO 16	Ampere's Law in solar wind
<2.3 × 10 ⁻⁹	95	5 EGOROV 14	Lensed quasar position
		6 ACCIOLY 10	Anomalous magn. mom.
<1 × 10 ⁻²⁶		7 ADELBERGER 07A	Proca galactic field
no limit feasible		7 ADELBERGER 07A	γ as Higgs particle
<1 × 10 ⁻¹⁹		8 TU 06	Torque on rotating magnetized toroid
<1.4 × 10 ⁻⁷		ACCIOLY 04	Dispersion of GHz radio waves by sun
<2 × 10 ⁻¹⁶		9 FULLEKRUG 04	Speed of 5-50 Hz radiation in atmosphere
<7 × 10 ⁻¹⁹		10 LUO 03	Torque on rotating magnetized toroid
<1 × 10 ⁻¹⁷		11 LAKES 98	Torque on toroid balance
<6 × 10 ⁻¹⁷		12 RYUTOV 97	MHD of solar wind
<8 × 10 ⁻¹⁶	90	13 FISCHBACH 94	Earth magnetic field
<5 × 10 ⁻¹³		14 CHERNIKOV 92	Ampere's Law null test
<1.5 × 10 ⁻⁹	90	15 RYAN 85	Coulomb's Law null test
<3 × 10 ⁻²⁷		16 CHIBISOV 76	Galactic magnetic field
<6 × 10 ⁻¹⁶	99.7	17 DAVIS 75	Jupiter's magnetic field
<7.3 × 10 ⁻¹⁶		HOLLWEG 74	Alfvén waves
<6 × 10 ⁻¹⁷		18 FRANKEN 71	Low freq. res. circuit
<2.4 × 10 ⁻¹³		19 KROLL 71A	Dispersion in atmosphere
<1 × 10 ⁻¹⁴		20 WILLIAMS 71	Tests Coulomb's Law
<2.3 × 10 ⁻¹⁵		GOLDHABER 68	Satellite data

- 1 RYUTOV 07 extends the method of RYUTOV 97 to the radius of Pluto's orbit.
- 2 BONETTI 17 uses frequency-dependent time delays of repeating FRB with well-determined redshift, assuming the DM is caused by expected dispersion in IGM. There are several uncertainties, leading to mass limit $2.2 \times 10^{-14} \text{ eV}$.
- 3 BONETTI 16 uses frequency-dependent time delays of FRB, assuming the DM is caused by expected dispersion in IGM. There are several uncertainties, leading to mass limit $1.8 \times 10^{-14} \text{ eV}$, if indeed the FRB is at the initially reported redshift.
- 4 RETINO 16 looks for deviations from Ampere's law in the solar wind, using Cluster four spacecraft data. Authors quote a range of limits from $1.9 \times 10^{-15} \text{ eV}$ to $7.9 \times 10^{-14} \text{ eV}$ depending on the assumptions of the vector potential from the interplanetary magnetic field.
- 5 EGOROV 14 studies chromatic dispersion of lensed quasar positions ("gravitational rainbows") that could be produced by any of several mechanisms, among them via photon mass. Limit not competitive but obtained on cosmological distance scales.
- 6 ACCIOLY 10 limits come from possible alterations of anomalous magnetic moment of electron and gravitational deflection of electromagnetic radiation. Reported limits are not "claimed" by the authors and in any case are not competitive.
- 7 When trying to measure m one must distinguish between measurements performed on large and small scales. If the photon acquires mass by the Higgs mechanism, the large-scale behavior of the photon might be effectively Maxwellian. If, on the other hand, one postulates the Proca regime for all scales, the very existence of the galactic field implies $m < 10^{-26} \text{ eV}$, as correctly calculated by YAMAGUCHI 59 and CHIBISOV 76.
- 8 TU 06 continues the work of LUO 03, with extended LAKES 98 method, reporting the improved limit $\mu^2 A = (0.7 \pm 1.7) \times 10^{-13} \text{ T/m}$ if $A = 0.2 \mu\text{G}$ out to $4 \times 10^{22} \text{ m}$. Reported result $\mu = (0.9 \pm 1.5) \times 10^{-52} \text{ g}$ reduces to the frequentist mass limit $1.2 \times 10^{-19} \text{ eV}$ (FELDMAN 98).
- 9 FULLEKRUG 04 adopted KROLL 71A method with newer and better Schumann resonance data. Result questionable because assumed frequency shift with photon mass is assumed to be linear. It is quadratic according to theorem by GOLDHABER 71B, KROLL 71, and PARK 71.
- 10 LUO 03 extends LAKES 98 technique to set a limit on $\mu^2 A$, where μ^{-1} is the Compton wavelength χ_C of the massive photon and A is the ambient vector potential. The important departure is that the apparatus rotates, removing sensitivity to the direction of A . They take $A = 10^{12} \text{ Tm}$, due to "cluster level fields." But see comment of GOLDHABER 03 and reply by LUO 03B.
- 11 LAKES 98 reports limits on torque on a toroid Cavendish balance, obtaining a limit on $\mu^2 A < 2 \times 10^{-9} \text{ Tm}^2/\text{m}^2$ via the Maxwell-Proca equations, where μ^{-1} is the characteristic length associated with the photon mass and A is the ambient vector potential in the Lorentz gauge. Assuming $A \approx 1 \times 10^{12} \text{ Tm}$ due to cluster fields he obtains $\mu^{-1} > 2 \times 10^{10} \text{ m}$, corresponding to $\mu < 1 \times 10^{-17} \text{ eV}$. A more conservative limit, using $A \approx (1 \mu\text{G}) \times (600 \text{ pc})$ based on the galactic field, is $\mu^{-1} > 1 \times 10^9 \text{ m}$ or $\mu < 2 \times 10^{-16} \text{ eV}$.
- 12 RYUTOV 97 uses a magnetohydrodynamics argument concerning survival of the Sun's field to the radius of the Earth's orbit. "To reconcile observations to theory, one has to

- reduce [the photon mass] by approximately an order of magnitude compared with" per DAVIS 75. "Secure limit, best by this method" (per GOLDHABER 10).
- 13 FISCHBACH 94 analysis is based on terrestrial magnetic fields; approach analogous to DAVIS 75. Similar result based on a much smaller planet probably follows from more precise B field mapping. "Secure limit, best by this method" (per GOLDHABER 10).
- 14 CHERNIKOV 92, motivated by possibility that photon exhibits mass only below some unknown critical temperature, searches for departure from Ampere's Law at 1.24 K. See also RYAN 85.
- 15 RYAN 85, motivated by possibility that photon exhibits mass only below some unknown critical temperature, sets mass limit at $< (1.5 \pm 1.4) \times 10^{-42} \text{ g}$ based on Coulomb's Law departure limit at 1.36 K. We report the result as frequentist 90% CL (FELDMAN 98).
- 16 CHIBISOV 76 depends in critical way on assumptions such as applicability of virial theorem. Some of the arguments given only in unpublished references.
- 17 DAVIS 75 analysis of Pioneer-10 data on Jupiter's magnetic field. "Secure limit, best by this method" (per GOLDHABER 10).
- 18 FRANKEN 71 method is of dubious validity (KROLL 71A, JACKSON 99, GOLDHABER 10, and references therein).
- 19 KROLL 71A used low frequency Schumann resonances in cavity between the conducting earth and resistive ionosphere, overcoming objections to resonant-cavity methods (JACKSON 99, GOLDHABER 10, and references therein). "Secure limit, best by this method" (per GOLDHABER 10).
- 20 WILLIAMS 71 is landmark test of Coulomb's law. "Secure limit, best by this method" (per GOLDHABER 10).

γ CHARGE

OKUN 06 has argued that schemes in which all photons are charged are inconsistent. He says that if a neutral photon is also admitted to avoid this problem, then other problems emerge, such as those connected with the emission and absorption of charged photons by charged particles. He concludes that in the absence of a self-consistent phenomenological basis, interpretation of experimental data is at best difficult.

VALUE (e)	CHARGE	DOCUMENT ID	TECN	COMMENT
<1 × 10⁻⁴⁶	mixed	1 ALTSCHUL 07B	VLBI	Aharonov-Bohm effect
<1 × 10⁻³⁵	single	2 CAPRINI 05	CMB	Isotropy constraint
••• We do not use the following data for averages, fits, limits, etc. •••				
<1 × 10 ⁻³²	single	1 ALTSCHUL 07B	VLBI	Aharonov-Bohm effect
<3 × 10 ⁻³³	mixed	3 KOBYCHEV 05	VLBI	Smear as function of B-E _γ
<4 × 10 ⁻³¹	single	3 KOBYCHEV 05	VLBI	Deflection as function of B-E _γ
<8.5 × 10 ⁻¹⁷		4 SEMERTZIDIS 03		Laser light deflection in B-field
<3 × 10 ⁻²⁸	single	5 SIVARAM 95	CMB	For $\Omega_M = 0.3$, $h^2 = 0.5$
<5 × 10 ⁻³⁰		6 RAFFELT 94	TOF	Pulsar $f_1 - f_2$
<2 × 10 ⁻²⁸		7 COCCONI 92		VLBA radio telescope resolution
<2 × 10 ⁻³²		COCCONI 88	TOF	Pulsar $f_1 - f_2$ TOF

- 1 ALTSCHUL 07B looks for Aharonov-Bohm phase shift in addition to geometric phase shift in radio interference fringes (VSOP mission).
- 2 CAPRINI 05 uses isotropy of the cosmic microwave background to place stringent limits on possible charge asymmetry of the Universe. Charge limits are set on the photon, neutrino, and dark matter particles. Valid if charge asymmetries produced by different particles are not anticorrelated.
- 3 KOBYCHEV 05 considers a variety of observable effects of photon charge for extragalactic compact radio sources. Best limits if source observed through a foreground cluster of galaxies.
- 4 SEMERTZIDIS 03 reports the first laboratory limit on the photon charge in the last 30 years. Straightforward improvements in the apparatus could attain a sensitivity of 10^{-20} e .
- 5 SIVARAM 95 requires that CMB photon charge density not overwhelm gravity. Result scales as $\Omega_M h^2$.
- 6 RAFFELT 94 notes that COCCONI 88 neglects the fact that the time delay due to dispersion by free electrons in the interstellar medium has the same photon energy dependence as that due to bending of a charged photon in the magnetic field. His limit is based on the assumption that the entire observed dispersion is due to photon charge. It is a factor of 200 less stringent than the COCCONI 88 limit.
- 7 See COCCONI 92 for less stringent limits in other frequency ranges. Also see RAFFELT 94 note.

γ REFERENCES

BONETTI 17	PL B768 326	L. Bonetti et al.	(ORLEANS, CERN)
BONETTI 16	PL B757 548	L. Bonetti et al.	
RETINO 16	ASP 82 49	A. Retino, A.D.A.M. Spallicci, A. Vaivads (CURCP+)	
EGOROV 14	MNRAS 437 L90	P. Egorov et al.	(MOSU, MIPT, INRM)
ACCIOLY 10	PR D82 065026	A. Accioly, J. Helayel-Neto, E. Scatena (LABEX+)	
GOLDHABER 10	RMP 82 939	A.S. Goldhaber, M.M. Nieto (STON, LANL)	
ADELBERGER 07A	PRL 98 010402	E. Adelberger, G. Dvali, A. Gruzinov (WASH, NYU)	
ALTSCHUL 07B	PRL 98 261801	B. Altschul (IND)	
Also	ASP 29 290	B. Altschul (SUC)	
RYUTOV 07	PFCF 49 B429	D.D. Ryutov (LLNL)	
OKUN 06	APP B37 555	L.B. Okun (ITEP)	
TU 06	PL A352 267	L.-C. Tu et al.	
CAPRINI 05	JCAP 0502 006	C. Caprini, P.G. Ferreira (GEVA, OXFTP)	
KOBYCHEV 05	AL 31 147	V.V. Kobychyev, S.B. Popov (KIEV, PADO)	
TU 05	RPP 68 77	L.-C. Tu, J. Luo, G.T. Gillies	
ACCIOLY 04	PR D69 107501	A. Accioly, R. Paszko	
FULLEKRUG 04	PRL 93 043901	M. Fullekrug	
GOLDHABER 03	PRL 91 149101	A.S. Goldhaber, M.M. Nieto	
LUO 03	PRL 90 081801	J. Luo et al.	
LUO 03B	PRL 91 149102	J. Luo et al.	
SEMERTZIDIS 03	PR D67 017701	Y.K. Semertzidis, G.T. Danby, D.M. Lazarus	
JACKSON 99	Classical Electrodynamics (3rd ed., J. Wiley and Sons (1999))	J.D. Jackson	
FELDMAN 98	PR D57 3873	G.J. Feldman, R.D. Cousins	
LAKES 98	PRL 80 1826	R. Lakes (WISC)	
RYUTOV 97	PFCF 39 A73	D.D. Ryutov (LLNL)	
SIVARAM 95	AJP 63 473	C. Sivaram (BANG)	
FISCHBACH 94	PRL 73 514	E. Fischbach et al.	(PURD, JHU+)

Gauge & Higgs Boson Particle Listings

 $\gamma, g, \text{graviton}, W$

RAFFELT	94	PR D50 7729	G. Raffelt	(MPIM)
CHERNIKOV	92	PRL 68 3383	M.A. Chernikov <i>et al.</i>	(ETH)
Also		PRL 69 2999 (erratum)	M.A. Chernikov <i>et al.</i>	(ETH)
COCCONI	92	AJP 60 750	G. Cocconi	(CERN)
COCCONI	88	PL B206 705	G. Cocconi	(CERN)
RYAN	85	PR D32 802	J.J. Ryan, F. Accetta, R.H. Austin	(PRIN)
CHIBISOV	76	SPU 19 624	G.V. Chibisov	(LEBD)
		Translated from UFN 119		
DAVIS	75	PRL 35 1402	L. Davis, A.S. Goldhaber, M.M. Nieto	(CIT, STON+)
HOLLWEG	74	PRL 32 961	J.V. Hollweg	(NCAR)
FRANKEN	71	PRL 26 115	P.A. Franken, G.W. Ampulski	(MICH)
GOLDHABER	71B	RMP 43 277	A.S. Goldhaber, M.M. Nieto	(STON, BOHR, UCSB)
KROLL	71	PRL 26 1395	N.M. Kroll	(SLAC)
KROLL	71A	PRL 27 340	N.M. Kroll	(SLAC)
PARK	71	PRL 26 1393	D. Park, E.R. Williams	(WILC)
WILLIAMS	71	PRL 26 721	E.R. Williams, J.E. Faller, H.A. Hill	(WESL)
GOLDHABER	68	PRL 21 567	A.S. Goldhaber, M.M. Nieto	(STON)
YAMAGUCHI	59	PTPS 11 37	Y. Yamaguchi	

g
or gluon

$$J(J^P) = 0(1^-)$$

SU(3) color octet

Mass $m = 0$. Theoretical value. A mass as large as a few MeV may not be precluded, see YNDURAIN 95.

VALUE	DOCUMENT ID	TECN	COMMENT
• • • We do not use the following data for averages, fits, limits, etc. • • •			
	ABREU	92E DLPH	Spin 1, not 0
	ALEXANDER	91H OPAL	Spin 1, not 0
	BEHREND	82D CELL	Spin 1, not 0
	BERGER	80D PLUT	Spin 1, not 0
	BRANDELIK	80C TASS	Spin 1, not 0

gluon REFERENCES

YNDURAIN	95	PL B345 524	F.J. Yndurain	(MADU)
ABREU	92E	PL B274 498	P. Abreu <i>et al.</i>	(DELPHI Collab.)
ALEXANDER	91H	ZPHY C52 543	G. Alexander <i>et al.</i>	(OPAL Collab.)
BEHREND	82D	PL B110 329	H.J. Behrend <i>et al.</i>	(CELLO Collab.)
BERGER	80D	PL B97 459	C. Berger <i>et al.</i>	(PLUTO Collab.)
BRANDELIK	80C	PL B97 453	R. Brandelik <i>et al.</i>	(TASSO Collab.)

graviton

$$J = 2$$

graviton MASS

It is likely that the graviton is massless. More than fifty years ago Van Dam and Veltman (VANDAM 70), Iwasaki (IWASAKI 70), and Zakharov (ZAKHAROV 70) almost simultaneously showed that in the linear approximation a theory with a finite graviton mass does not approach GR as the mass approaches zero. Attempts have been made to evade this "vDVZ discontinuity" by invoking modified gravity or nonlinear theory by De Rahm (DE-RHAM 17) and others. More recently, the analysis of gravitational wave dispersion has led to bounds that are largely independent of the underlying model, even if not the strongest. We quote the best of these as our best limit.

Experimental limits have been set based on a Yukawa potential (YUKA), dispersion relation (DISP), or other modified gravity theories (MGRV).

The following conversions are useful: $1 \text{ eV} = 1.783 \times 10^{-33} g = 1.957 \times 10^{-6} m_e$; $\chi_C = (1.973 \times 10^{-7} \text{ m}) \times (1 \text{ eV}/m_e)$.

VALUE (eV)	DOCUMENT ID	TECN	COMMENT
• • • We do not use the following data for averages, fits, limits, etc. • • •			
$<1.76 \times 10^{-23}$	1 ABBOTT	21 DISP	LIGO Virgo catalog GWTC-2
$<3.2 \times 10^{-23}$	2 BERNUS	20 YUKA	Planetary ephemeris INPOP19a
$<2 \times 10^{-28}$	3 SHAO	20 DISP	Binary pulsar Galileon radiation
$<4.7 \times 10^{-23}$	4 ABBOTT	19 DISP	LIGO Virgo catalog GWTC-1
$<7 \times 10^{-23}$	5 BERNUS	19 YUKA	Planetary ephemeris INPOP17b
$<3.1 \times 10^{-20}$	6 MIAO	19 DISP	Binary pulsar orbital decay rate
$<1.4 \times 10^{-29}$	7 DESAI	18 YUKA	Gal cluster Abell 1689
$<5 \times 10^{-30}$	8 GUPTA	18 YUKA	Using SPT-SZ
$<3 \times 10^{-30}$	8 GUPTA	18 YUKA	Using Planck all-sky SZ
$<1.3 \times 10^{-29}$	8 GUPTA	18 YUKA	Using redMaPPer SDSS-DR8
$<6 \times 10^{-30}$	9 RANA	18 YUKA	Weak lensing in massive clusters
$<8 \times 10^{-30}$	10 RANA	18 YUKA	SZ effect in massive clusters
$<1.0 \times 10^{-23}$	11 WILL	18 YUKA	Perihelion advances of planets
$<7 \times 10^{-23}$	4 ABBOTT	17 DISP	Combined dispersion limit from three BH mergers
$<1.2 \times 10^{-22}$	4 ABBOTT	16 DISP	Combined dispersion limit from two BH mergers
$<2.9 \times 10^{-21}$	12 ZAKHAROV	16 YUKA	S2 star orbit
$<5 \times 10^{-23}$	13 BRITO	15 MGRV	Spinning black holes bounds
$<6 \times 10^{-32}$	14 GRUZINOV	03 MGRV	Solar System observations
$<6 \times 10^{-32}$	15 CHOUDHURY	04 YUKA	Weak gravitational lensing
$<9.0 \times 10^{-34}$	16 GERSHTEIN	04 MGRV	From Ω_{tot} value assuming RTG
$<8 \times 10^{-20}$	17,18 FINN	02 DISP	Binary pulsar orbital period decrease
$<7 \times 10^{-23}$	TALMADGE	88 YUKA	Solar system planetary astrometric data
$<1.3 \times 10^{-29}$	19 GOLDHABER	74 YUKA	Rich clusters
$<7 \times 10^{-28}$	HARE	73 YUKA	Galaxy
$<8 \times 10^{-4}$	HARE	73 YUKA	2 γ decay

- ABBOTT 21 assumed modified gravitational-wave dispersion to establish a limit on graviton mass, using LIGO-Virgo O1-O3a binary black hole (BBH) events.
- BERNUS 20 use the latest solution of the ephemeris INPOP (19a) in order to improve the constraint in BERNUS 19 on the existence of a Yukawa suppression to the Newtonian potential, generically associated to a gravitons mass.
- SHAO 20 sets limit, 95% CL, based on non-observation of excess gravitational radiation in 14 well-timed binary pulsars in the context of the cubic Galileon model.
- ABBOTT 19, ABBOTT 17, and ABBOTT 16 assumed modified gravitational waves dispersion to establish limits on graviton mass.
- BERNUS 19 use the planetary ephemeris INPOP 17b to constrain the existence of a Yukawa suppression to the Newtonian potential, generically associated to a gravitons mass.
- MIAO 19 90% CL limit is based on orbital period decay rates of 9 binary pulsars using a Bayesian prior uniform in graviton mass. Limit becomes $< 5.2 \times 10^{-21} \text{ eV}$ for a prior uniform in $\ln(m_g)$.
- DESAI 18 limit based on dynamical mass models of galaxy cluster Abell 1689.
- GUPTA 18 obtains graviton mass limits using stacked clusters from 3 disparate surveys.
- RANA 18 limit, 68% CL, obtained using weak lensing mass profiles out to the radius at which the cluster density falls to 200 times the critical density of the Universe. Limit is based on the fractional change between Newtonian and Yukawa accelerations for the 50 most massive galaxy clusters in the Local Cluster Substructure Survey. Limits for other CL's and other density cuts are also given.
- RANA 18 limit, 68% CL, obtained using mass measurements via the SZ effect out to the radius at which the cluster density falls to 500 times the critical density of the Universe for 182 optically confirmed galaxy clusters in an Altacama Cosmology Telescope survey. Limits for other CL's and other density cuts are also given.
- WILL 18 limit from perihelion advances of the planets, notably Earth, Mars, and Saturn. Alternate analysis yields $< 6 \times 10^{-24}$.
- ZAKHAROV 16 constrains range of Yukawa gravity interaction from S2 star orbit about black hole at Galactic center. The limit is $< 2.9 \times 10^{-21} \text{ eV}$ for $\delta = 100$.
- BRITO 13 explore massive graviton (spin-2) fluctuations around rotating black holes.
- GRUZINOV 05 uses the DGP model (DVALI 00) showing that non-perturbative effects restore continuity with Einstein's equations as the graviton mass approaches zero, then bases his limit on Solar System observations.
- CHOUDHURY 04 concludes from a study of weak-lensing data that masses heavier than about the inverse of 100 Mpc seem to be ruled out if the gravitation field has the Yukawa form.
- GERSHTEIN 04 use non-Einstein field relativistic theory of gravity (RTG), with a massive graviton, to obtain the 95% CL mass limit implied by the value of $\Omega_{tot} = 1.02 \pm 0.02$ current at the time of publication.
- FINN 02 analyze the orbital decay rates of PSR B1913+16 and PSR B1534+12 with a possible graviton mass as a parameter. The combined frequentist mass limit is at 90% CL.
- As of 2020, limits on dP/dt are now about 0.1% (see T. Damour, "Experimental tests of gravitational theory," in this Review).
- GOLDHABER 74 establish this limit considering the binding of galactic clusters, corrected to Planck $h_0 = 0.67$.

graviton REFERENCES

ABBOTT	21	PR D103 122002	R. Abbott <i>et al.</i>	(LIGO and Virgo Collabs.)
BERNUS	20	PR D102 021501	L. Bernus <i>et al.</i>	
SHAO	20	PR D102 024069	L. Shao, N. Wex, S.-Y. Zhou	
ABBOTT	19	PR D100 104036	B.P. Abbott <i>et al.</i>	(LIGO and Virgo Collabs.)
BERNUS	19	PRL 123 161103	L. Bernus <i>et al.</i>	
MIAO	19	PR D99 123015	X. Miao, L. Shao, B.-Q. Ma	
DESAI	18	PL B778 325	S. Desai	(HYDER)
GUPTA	18	ANP 299 85	S. Gupta, S. Desai	
RANA	18	PL B761 220	A. Rana <i>et al.</i>	(DELHI)
WILL	18	CQG 35 17LT01	C.M. Will	
ABBOTT	17	PRL 118 221101	B.P. Abbott <i>et al.</i>	(LIGO and Virgo Collabs.)
DE-RHAM	17	RMP 89 025004	C. de Rham <i>et al.</i>	
ABBOTT	16	PRL 116 061102	B.P. Abbott <i>et al.</i>	(LIGO and Virgo Collabs.)
ZAKHAROV	16	JCAP 1605 045	A.F. Zakharov <i>et al.</i>	
BRITO	13	PR D88 023514	R. Brito, V. Cardoso, P. Pani	(LISB, MISS, HSICA+)
GRUZINOV	05	NAST 10 311	A. Gruzinov	(NYU)
CHOUDHURY	04	ASP 21 559	S.R. Choudhury <i>et al.</i>	(DELPHI, MELB)
GERSHTEIN	04	PAN 67 1596	S.S. Gershtein <i>et al.</i>	(SERP)
		Translated from YAF 67		
FINN	02	PR D65 044022	L.S. Finn, P.J. Sutton	
DVALI	00	PL B485 208	G.R. Dvali, G. Gabadadze, M. Porrati	(NYU)
TALMADGE	88	PRL 61 1159	C. Talmadge <i>et al.</i>	(JPL)
GOLDHABER	74	PR D9 1119	A.S. Goldhaber, M.M. Nieto	(LANL, STON)
HARE	73	CJP 51 431	M.G. Hare	(SASK)
IWASAKI	70	PR D2 2255	Y. Iwasaki	
VANDAM	70	NP B22 397	H. van Dam, M. Veltman	(UTRE)
ZAKHAROV	70	JETPL 12 312	V.I. Zakharov <i>et al.</i>	

W

$$J = 1$$

See the related review(s):
Mass and Width of the W Boson

W MASS

The W-mass listed here corresponds to the mass parameter in a Breit-Wigner distribution with mass-dependent width. To obtain the world average, common systematic uncertainties between experiments are properly taken into account. The LEP-2 average W mass based on published results from ALEPH, DELPHI, L3, and OPAL is $80.376 \pm 0.033 \text{ GeV}$ [SCHAEEL 13A]. The combined Tevatron data from CDF and D0 yields an average W mass of $80.387 \pm 0.016 \text{ GeV}$ [AALTONEN 13N]. Assuming a common systematic error of 9 MeV due to PDF uncertainty, the combined LHC data from ATLAS [AABOU 18] and LHCb [AAIJ 22c] yields an average W mass of $80.366 \pm 0.017 \text{ GeV}$ [J. Erler and A. Freitas, "Electroweak Model and Constraints on New Physics" review, PDG 22]. Assuming 7 MeV as the common systematic uncertainty between the LHC

and Tevatron results, the average W mass from the two hadron colliders is estimated to be 80.377 ± 0.013 GeV. Combining this result with the LEP-2 value assuming no correlations, the world average W mass of 80.377 ± 0.012 GeV is obtained [bid]; OUR FIT quotes this value for the W mass.

In April 2022, after the cut-off of results for this review, the CDF collaboration published a determination of the W mass based on their full Run-2 dataset of 8.8 fb^{-1} [AALTONEN 22], with much reduced uncertainty: $80.433.5 \pm 9.4$ MeV. This new CDF result, which includes the data of their previous result [AALTONEN 12E] and thus supersedes it, is of higher precision than our world average quoted above. However, the two determinations disagree significantly. More information is given in M. Grunewald and A. Gurtu, "Mass and Width of the W Boson" review [PDG 22].

VALUE (GeV)	EVTS	DOCUMENT ID	TECN	COMMENT
80.377 ± 0.012 OUR FIT				
80.354 ± 0.023 ± 0.022	2.4M	¹ AAIJ	22C LHCB	$E_{\text{cm}}^{pp} = 13$ TeV
80.370 ± 0.007 ± 0.017	13.7M	² AABOUD	18J ATLS	$E_{\text{cm}}^{pp} = 7$ TeV
80.387 ± 0.012 ± 0.015	1095k	³ AALTONEN	12E CDF	$E_{\text{cm}}^{pp} = 1.96$ TeV
80.375 ± 0.011 ± 0.020	2177k	⁴ ABAZOV	12F D0	$E_{\text{cm}}^{pp} = 1.96$ TeV
80.336 ± 0.055 ± 0.039	10.3k	⁵ ABDALLAH	08A DLPH	$E_{\text{cm}}^{ee} = 161\text{--}209$ GeV
80.415 ± 0.042 ± 0.031	11830	⁶ ABBIENDI	06 OPAL	$E_{\text{cm}}^{ee} = 170\text{--}209$ GeV
80.270 ± 0.046 ± 0.031	9909	⁷ ACHARD	06 L3	$E_{\text{cm}}^{ee} = 161\text{--}209$ GeV
80.440 ± 0.043 ± 0.027	8692	⁸ SCHAEI	06 ALEP	$E_{\text{cm}}^{ee} = 161\text{--}209$ GeV
80.483 ± 0.084	49247	⁹ ABAZOV	02D D0	$E_{\text{cm}}^{pp} = 1.8$ TeV
80.433 ± 0.079	53841	¹⁰ AFFOLDER	01E CDF	$E_{\text{cm}}^{pp} = 1.8$ TeV
• • • We do not use the following data for averages, fits, limits, etc. • • •				
80.520 ± 0.070 ± 0.092		¹¹ ANDREEV	18A H1	$e^{\pm}p$
80.367 ± 0.013 ± 0.022	1677k	¹² ABAZOV	12F D0	$E_{\text{cm}}^{pp} = 1.96$ TeV
80.401 ± 0.021 ± 0.038	500k	¹³ ABAZOV	09AB D0	$E_{\text{cm}}^{pp} = 1.96$ TeV
80.413 ± 0.034 ± 0.034	115k	¹⁴ AALTONEN	07F CDF	$E_{\text{cm}}^{pp} = 1.96$ TeV
82.87 ± 1.82 ± $\begin{smallmatrix} +0.30 \\ -0.16 \end{smallmatrix}$	1500	¹⁵ AKTAS	06 H1	$e^{\pm}p \rightarrow \mathcal{P}_e(\nu_e)X$, $\sqrt{s} \approx 300$ GeV
80.3 ± 2.1 ± 1.2 ± 1.0	645	¹⁶ CHEKANOV	02C ZEUS	$e^-p \rightarrow \nu_e X$, $\sqrt{s} \approx 318$ GeV
81.4 $\begin{smallmatrix} +2.7 \\ -2.6 \end{smallmatrix}$ ± 2.0 $\begin{smallmatrix} +3.3 \\ -3.0 \end{smallmatrix}$	1086	¹⁷ BREITWEG	00D ZEUS	$e^+p \rightarrow \mathcal{P}_e X$, $\sqrt{s} \approx 300$ GeV
80.84 ± 0.22 ± 0.83	2065	¹⁸ ALITTI	92B UA2	See W/Z ratio below
80.79 ± 0.31 ± 0.84		¹⁹ ALITTI	90B UA2	$E_{\text{cm}}^{pp} = 546,630$ GeV
80.0 ± 3.3 ± 2.4	22	²⁰ ABE	89I CDF	$E_{\text{cm}}^{pp} = 1.8$ TeV
82.7 ± 1.0 ± 2.7	149	²¹ ALBAJAR	89 UA1	$E_{\text{cm}}^{pp} = 546,630$ GeV
81.8 $\begin{smallmatrix} +6.0 \\ -5.3 \end{smallmatrix}$ ± 2.6	46	²² ALBAJAR	89 UA1	$E_{\text{cm}}^{pp} = 546,630$ GeV
89 ± 3 ± 6	32	²³ ALBAJAR	89 UA1	$E_{\text{cm}}^{pp} = 546,630$ GeV
81. ± 5.	6	ARNISON	83 UA1	$E_{\text{cm}}^{ee} = 546$ GeV
80. $\begin{smallmatrix} +10. \\ -6. \end{smallmatrix}$	4	BANNER	83B UA2	Repl. by ALITTI 90B

¹ AAIJ 22c analyse W production in the muon decay channel, with the transverse momentum of the muon required to be between 28 and 52 GeV. Analysing the distribution of the muon charge divided by the muon transverse momentum of approximately 2.4 million selected W candidates, a value of $M_W = 80.354 \pm 23(\text{stat.}) \pm 10(\text{exp.}) \pm 17(\text{theo.}) \pm 9(\text{PDF})$ MeV is obtained; we combine the three systematic uncertainties in quadrature.

² AABOUD 18j select $4.61M W^+ \rightarrow \mu^+ \nu_\mu$, $3.40M W^+ \rightarrow e^+ \nu_e$, $3.23M W^- \rightarrow \mu^- \bar{\nu}_\mu$ and $2.49M W^- \rightarrow e^- \bar{\nu}_e$ events in $4.6 \text{ fb}^{-1} pp$ data at 7 TeV. The W mass is determined using the transverse mass and transverse lepton momentum distributions, accounting for correlations. The systematic error includes 0.011 GeV experimental and 0.014 GeV modelling uncertainties.

³ AALTONEN 12E select 470k $W \rightarrow e\nu$ decays and 625k $W \rightarrow \mu\nu$ decays in 2.2 fb^{-1} of Run-II data. The mass is determined using the transverse mass, transverse lepton momentum and transverse missing energy distributions, accounting for correlations. This result supersedes AALTONEN 07F. AALTONEN 14D gives more details on the procedures followed by the authors.

⁴ Combination of results from ABAZOV 12F and ABAZOV 09AB as quoted in ABAZOV 12F.

⁵ ABDALLAH 08A use direct reconstruction of the kinematics of $W^+ W^- \rightarrow q\bar{q}\ell\nu$ and $W^+ W^- \rightarrow q\bar{q}q\bar{q}$ events for energies 172 GeV and above. The W mass was also extracted from the dependence of the WW cross section close to the production threshold and combined appropriately to obtain the final result. The systematic error includes ± 0.025 GeV due to final state interactions and ± 0.009 GeV due to LEP energy uncertainty.

⁶ ABBIENDI 06 use direct reconstruction of the kinematics of $W^+ W^- \rightarrow q\bar{q}\ell\nu_\ell$ and $W^+ W^- \rightarrow q\bar{q}q\bar{q}$ events. The result quoted here is obtained combining this mass value with the results using $W^+ W^- \rightarrow \ell\nu_\ell\ell\nu_\ell$ events in the energy range 183–207 GeV (ABBIENDI 03c) and the dependence of the WW production cross-section on m_W at threshold. The systematic error includes ± 0.009 GeV due to the uncertainty on the LEP beam energy.

⁷ ACHARD 06 use direct reconstruction of the kinematics of $W^+ W^- \rightarrow q\bar{q}\ell\nu_\ell$ and $W^+ W^- \rightarrow q\bar{q}q\bar{q}$ events in the C.M. energy range 189–209 GeV. The result quoted here is obtained combining this mass value with the results obtained from a direct W mass reconstruction at 172 and 183 GeV and with those from the dependence of the WW production cross-section on m_W at 161 and 172 GeV (ACCIARRI 99).

⁸ SCHAEI 06 use direct reconstruction of the kinematics of $W^+ W^- \rightarrow q\bar{q}\ell\nu_\ell$ and $W^+ W^- \rightarrow q\bar{q}q\bar{q}$ events in the C.M. energy range 183–209 GeV. The result quoted

here is obtained combining this mass value with those obtained from the dependence of the W pair production cross-section on m_W at 161 and 172 GeV (BARATE 97 and BARATE 97s respectively). The systematic error includes ± 0.009 GeV due to possible effects of final state interactions in the $q\bar{q}q\bar{q}$ channel and ± 0.009 GeV due to the uncertainty on the LEP beam energy.

⁹ ABAZOV 02d improve the measurement of the W -boson mass including $W \rightarrow e\nu_e$ events in which the electron is close to a boundary of a central electromagnetic calorimeter module. Properly combining the results obtained by fitting $m_T(W)$, $p_T(e)$, and $p_T(\nu)$, this sample provides a mass value of 80.574 ± 0.405 GeV. The value reported here is a combination of this measurement with all previous $D0$ W -boson mass measurements.

¹⁰ AFFOLDER 01E fit the transverse mass spectrum of 30115 $W \rightarrow e\nu_e$ events ($M_W = 80.473 \pm 0.065 \pm 0.092$ GeV) and of 14740 $W \rightarrow \mu\nu_\mu$ events ($M_W = 80.465 \pm 0.100 \pm 0.103$ GeV) obtained in the run IB (1994–95). Combining the electron and muon results, accounting for correlated uncertainties, yields $M_W = 80.470 \pm 0.089$ GeV. They combine this value with their measurement of ABE 95P reported in run IA (1992–93) to obtain the quoted value.

¹¹ ANDREEV 18A obtain this result in a combined electroweak and QCD analysis using all deep-inelastic e^+p and e^-p neutral current and charged current scattering cross sections published by the H1 Collaboration, including data with longitudinally polarized lepton beams.

¹² ABAZOV 12F select 1677k $W \rightarrow e\nu$ decays in 4.3 fb^{-1} of Run-II data. The mass is determined using the transverse mass and transverse lepton momentum distributions, accounting for correlations.

¹³ ABAZOV 09AB study the transverse mass, transverse electron momentum, and transverse missing energy in a sample of 0.5 million $W \rightarrow e\nu$ decays selected in Run-II data. The quoted result combines all three methods, accounting for correlations.

¹⁴ AALTONEN 07F obtain high purity $W \rightarrow e\nu_e$ and $W \rightarrow \mu\nu_\mu$ candidate samples totaling 63,964 and 51,128 events respectively. The W mass value quoted above is derived by simultaneously fitting the transverse mass and the lepton, and neutrino p_T distributions.

¹⁵ AKTAS 06 fit the Q^2 dependence ($300 < Q^2 < 30,000 \text{ GeV}^2$) of the charged-current differential cross section with a propagator mass. The first error is experimental and the second corresponds to uncertainties due to input parameters and model assumptions.

¹⁶ CHEKANOV 02c fit the Q^2 dependence ($200 < Q^2 < 60,000 \text{ GeV}^2$) of the charged-current differential cross sections with a propagator mass fit. The last error is due to the uncertainty on the probability density functions.

¹⁷ BREITWEG 00D fit the Q^2 dependence ($200 < Q^2 < 22500 \text{ GeV}^2$) of the charged-current differential cross sections with a propagator mass fit. The last error is due to the uncertainty on the probability density functions.

¹⁸ ALITTI 92B result has two contributions to the systematic error (± 0.83); one (± 0.81) cancels in m_W/m_Z and one (± 0.17) is noncancelling. These were added in quadrature. We choose the ALITTI 92B value without using the LEP m_Z value, because we perform our own combined fit.

¹⁹ There are two contributions to the systematic error (± 0.84): one (± 0.81) which cancels in m_W/m_Z and one (± 0.21) which is non-cancelling. These were added in quadrature.

²⁰ ABE 89I systematic error dominated by the uncertainty in the absolute energy scale.

²¹ ALBAJAR 89 result is from a total sample of 299 $W \rightarrow e\nu$ events.

²² ALBAJAR 89 result is from a total sample of 67 $W \rightarrow \mu\nu$ events.

VALUE	EVTS	DOCUMENT ID	TECN	COMMENT
0.88145 ± 0.00013		¹ PDG	22	
• • • We do not use the following data for averages, fits, limits, etc. • • •				
0.8821 ± 0.0011 ± 0.0008	28323	² ABBOTT	98N D0	$E_{\text{cm}}^{pp} = 1.8$ TeV
0.88114 ± 0.00154 ± 0.00252	5982	³ ABBOTT	98P D0	$E_{\text{cm}}^{pp} = 1.8$ TeV
0.8813 ± 0.0036 ± 0.0019	156	⁴ ALITTI	92B UA2	$E_{\text{cm}}^{pp} = 630$ GeV

¹ This value was obtained using the world average values of m_Z and m_W as listed in these listings.

² ABBOTT 98N obtain this from a study of 28323 $W \rightarrow e\nu_e$ and 3294 $Z \rightarrow e^+e^-$ decays. Of this latter sample, 2179 events are used to calibrate the electron energy scale.

³ ABBOTT 98P obtain this from a study of 5982 $W \rightarrow e\nu_e$ events. The systematic error includes an uncertainty of ± 0.00175 due to the electron energy scale.

⁴ Scale error cancels in this ratio.

$m_Z - m_W$

VALUE (GeV)	DOCUMENT ID	TECN	COMMENT
10.811 ± 0.012	¹ PDG	22	
• • • We do not use the following data for averages, fits, limits, etc. • • •			
10.4 ± 1.4 ± 0.8	ALBAJAR	89 UA1	$E_{\text{cm}}^{pp} = 546,630$ GeV
11.3 ± 1.3 ± 0.9	ANSARI	87 UA2	$E_{\text{cm}}^{pp} = 546,630$ GeV
¹ This value was obtained using the world average values of m_Z and m_W as listed in these listings.			

$m_{W^+} - m_{W^-}$

Test of CPT invariance.

VALUE (GeV)	EVTS	DOCUMENT ID	TECN	COMMENT
-0.029 ± 0.028 OUR AVERAGE				
-0.029 ± 0.013 ± 0.025	13.7M	¹ AABOUD	18J ATLS	$E_{\text{cm}}^{pp} = 7$ TeV
-0.19 ± 0.58	1722	ABE	90G CDF	$E_{\text{cm}}^{pp} = 1.8$ TeV

¹ AABOUD 18J select $4.61M W^+ \rightarrow \mu^+ \nu_\mu$, $3.40M W^+ \rightarrow e^+ \nu_e$, $3.23M W^- \rightarrow \mu^- \bar{\nu}_\mu$ and $2.49M W^- \rightarrow e^- \bar{\nu}_e$ events in $4.6 \text{ fb}^{-1} pp$ data at 7 TeV. The W mass is determined using the transverse mass and transverse lepton momentum distributions,

Gauge & Higgs Boson Particle Listings

W

accounting for correlations. The systematic error includes 0.007 GeV experimental and 0.024 GeV modelling uncertainties.

W WIDTH

The W width listed here corresponds to the width parameter in a Breit-Wigner distribution with mass-dependent width. To obtain the world average, common systematic uncertainties between experiments are properly taken into account. The LEP-2 average W width based on published results is 2.195 ± 0.083 GeV [SCHAEEL 13A]. The combined Tevatron data yields an average W width of 2.046 ± 0.049 GeV [FERMILAB-TM-2460-E].

OUR FIT uses these average LEP and Tevatron width values and combines them assuming no correlations.

VALUE (GeV)	EVTS	DOCUMENT ID	TECN	COMMENT
2.085 ± 0.042 OUR FIT				
2.028 ± 0.072	5272	¹ ABAZOV	09AK D0	$E_{cm}^{p\bar{p}} = 1.96$ GeV
2.032 ± 0.045 ± 0.057	6055	² AALTONEN	08B CDF	$E_{cm}^{p\bar{p}} = 1.96$ TeV
2.404 ± 0.140 ± 0.101	10.3k	³ ABDALLAH	08A DLPH	$E_{cm}^{e\bar{e}} = 183-209$ GeV
1.996 ± 0.096 ± 0.102	10729	⁴ ABBIENDI	06 OPAL	$E_{cm}^{e\bar{e}} = 170-209$ GeV
2.18 ± 0.11 ± 0.09	9795	⁵ ACHARD	06 L3	$E_{cm}^{e\bar{e}} = 172-209$ GeV
2.14 ± 0.09 ± 0.06	8717	⁶ SCHAEEL	06 ALEP	$E_{cm}^{e\bar{e}} = 183-209$ GeV
2.23 +0.15 -0.14 ± 0.10	294	⁷ ABAZOV	02E D0	$E_{cm}^{p\bar{p}} = 1.8$ TeV
2.05 ± 0.10 ± 0.08	662	⁸ AFFOLDER	00M CDF	$E_{cm}^{p\bar{p}} = 1.8$ TeV
• • • We do not use the following data for averages, fits, limits, etc. • • •				
2.152 ± 0.066	79176	⁹ ABBOTT	00B D0	Extracted value
2.064 ± 0.060 ± 0.059		¹⁰ ABE	95W CDF	Extracted value
2.10 +0.14 -0.13 ± 0.09	3559	¹¹ ALITTI	92 UA2	Extracted value
2.18 +0.26 -0.24 ± 0.04		¹² ALBAJAR	91 UA1	Extracted value

- ABAZOV 09AK obtain this result fitting the high-end tail (100-200 GeV) of the transverse mass spectrum in $W \rightarrow e\nu$ decays.
- AALTONEN 08B obtain this result fitting the high-end tail (90-200 GeV) of the transverse mass spectrum in semileptonic $W \rightarrow e\nu_e$ and $W \rightarrow \mu\nu_\mu$ decays.
- ABDALLAH 08A use direct reconstruction of the kinematics of $W^+W^- \rightarrow q\bar{q}\ell\nu$ and $W^+W^- \rightarrow q\bar{q}q\bar{q}$ events. The systematic error includes ± 0.065 GeV due to final state interactions.
- ABBIENDI 06 use direct reconstruction of the kinematics of $W^+W^- \rightarrow q\bar{q}\ell\nu_\ell$ and $W^+W^- \rightarrow q\bar{q}q\bar{q}$ events. The systematic error includes ± 0.003 GeV due to the uncertainty on the LEP beam energy.
- ACHARD 06 use direct reconstruction of the kinematics of $W^+W^- \rightarrow q\bar{q}\ell\nu_\ell$ and $W^+W^- \rightarrow q\bar{q}q\bar{q}$ events in the C.M. energy range 189-209 GeV. The result quoted here is obtained combining this value of the width with the result obtained from a direct W mass reconstruction at 172 and 183 GeV (ACCIARRI 99).
- SCHAEEL 06 use direct reconstruction of the kinematics of $W^+W^- \rightarrow q\bar{q}\ell\nu_\ell$ and $W^+W^- \rightarrow q\bar{q}q\bar{q}$ events. The systematic error includes ± 0.05 GeV due to possible effects of final state interactions in the $q\bar{q}q\bar{q}$ channel and ± 0.01 GeV due to the uncertainty on the LEP beam energy.
- ABAZOV 02E obtain this result fitting the high-end tail (90-200 GeV) of the transverse-mass spectrum in semileptonic $W \rightarrow e\nu_e$ decays.
- AFFOLDER 00M fit the high transverse mass (100-200 GeV) $W \rightarrow e\nu_e$ and $W \rightarrow \mu\nu_\mu$ events to obtain $\Gamma(W) = 2.04 \pm 0.11(\text{stat}) \pm 0.09(\text{syst})$ GeV. This is combined with the earlier CDF measurement (ABE 95c) to obtain the quoted result.
- ABBOTT 00B measure $R = 10.43 \pm 0.27$ for the $W \rightarrow e\nu_e$ decay channel. They use the SM theoretical predictions for $\sigma(W)/\sigma(Z)$ and $\Gamma(W \rightarrow e\nu_e)$ and the world average for $B(Z \rightarrow ee)$. The value quoted here is obtained combining this result (2.169 \pm 0.070 GeV) with that of ABBOTT 99H.
- ABE 95W measured $R = 10.90 \pm 0.32 \pm 0.29$. They use $m_W = 80.23 \pm 0.18$ GeV, $\sigma(W)/\sigma(Z) = 3.35 \pm 0.03$, $\Gamma(W \rightarrow e\nu) = 225.9 \pm 0.9$ MeV, $\Gamma(Z \rightarrow e^+e^-) = 83.98 \pm 0.18$ MeV, and $\Gamma(Z) = 2.4969 \pm 0.0038$ GeV.
- ALITTI 92 measured $R = 10.4^{+1.0}_{-0.7} \pm 0.3$. The values of $\sigma(Z)$ and $\sigma(W)$ come from $O(\alpha_s^2)$ calculations using $m_W = 80.14 \pm 0.27$ GeV, and $m_Z = 91.175 \pm 0.021$ GeV along with the corresponding value of $\sin^2\theta_W = 0.2274$. They use $\sigma(W)/\sigma(Z) = 3.26 \pm 0.07 \pm 0.05$ and $\Gamma(Z) = 2.487 \pm 0.010$ GeV.
- ALBAJAR 91 measured $R = 9.5^{+1.1}_{-1.0}(\text{stat.} + \text{syst.})$. $\sigma(W)/\sigma(Z)$ is calculated in QCD at the parton level using $m_W = 80.18 \pm 0.28$ GeV and $m_Z = 91.172 \pm 0.031$ GeV along with $\sin^2\theta_W = 0.2322 \pm 0.0014$. They use $\sigma(W)/\sigma(Z) = 3.23 \pm 0.05$ and $\Gamma(Z) = 2.498 \pm 0.020$ GeV. This measurement is obtained combining both the electron and muon channels.

W+ DECAY MODES

W^- modes are charge conjugates of the modes below.

Mode	Fraction (Γ_i/Γ)	Confidence level
Γ_1 $\ell^+\nu$	[a] (10.86 ± 0.09) %	
Γ_2 $e^+\nu$	(10.71 ± 0.16) %	
Γ_3 $\mu^+\nu$	(10.63 ± 0.15) %	
Γ_4 $\tau^+\nu$	(11.38 ± 0.21) %	
Γ_5 hadrons	(67.41 ± 0.27) %	
Γ_6 $\pi^+\gamma$	< 7 × 10 ⁻⁶	95%
Γ_7 $D_s^+\gamma$	< 1.3 × 10 ⁻³	95%

Γ_8 cX	(33.3 ± 2.6) %
Γ_9 $c\bar{s}$	(31 +13 -11) %
Γ_{10} invisible	[b] (1.4 ± 2.9) %
Γ_{11} $\pi^+\pi^+\pi^-$	< 1.01 × 10 ⁻⁶ 95%

[a] ℓ indicates each type of lepton (e , μ , and τ), not sum over them.

[b] This represents the width for the decay of the W boson into a charged particle with momentum below detectability, $p < 200$ MeV.

W PARTIAL WIDTHS

$\Gamma(\text{invisible})$	Γ_{10}		
This represents the width for the decay of the W boson into a charged particle with momentum below detectability, $p < 200$ MeV.			
VALUE (MeV)	DOCUMENT ID	TECN	COMMENT
30 +52 -48 ± 33	¹ BARATE	99I ALEP	$E_{cm}^{e\bar{e}} = 161+172+183$ GeV
• • • We do not use the following data for averages, fits, limits, etc. • • •			
	² BARATE	99L ALEP	$E_{cm}^{e\bar{e}} = 161+172+183$ GeV
¹ BARATE 99I measure this quantity using the dependence of the total cross section σ_{WW} upon a change in the total width. The fit is performed to the WW measured cross sections at 161, 172, and 183 GeV. This partial width is < 139 MeV at 95%CL.			
² BARATE 99L use W -pair production to search for effectively invisible W decays, tagging with the decay of the other W boson to Standard Model particles. The partial width for effectively invisible decay is < 27 MeV at 95%CL.			

W BRANCHING RATIOS

Overall fits are performed to determine the branching ratios of the W boson. Averages on $W \rightarrow e\nu$, $W \rightarrow \mu\nu$, and $W \rightarrow \tau\nu$, and their correlations are obtained by combining results from the four LEP experiments properly taking into account the common systematic uncertainties and their correlations [SCHAEEL 13A]. A first fit determines the three individual leptonic branching ratios $B(W \rightarrow e\nu)$, $B(W \rightarrow \mu\nu)$, and $B(W \rightarrow \tau\nu)$. This fit has a $\chi^2 = 6.3$ for 9 degrees of freedom. The correlation coefficients between the branching fractions are 0.14 ($e-\mu$), -0.20 ($e-\tau$), -0.12 ($\mu-\tau$). A second fit assumes lepton universality and determines the leptonic branching ratio $B(W \rightarrow \ell\nu)$ and the hadronic branching ratio is derived as $B(W \rightarrow \text{hadrons}) = 1 - 3 B(W \rightarrow \ell\nu)$. This fit has a $\chi^2 = 15.4$ for 11 degrees of freedom.

$\Gamma(\ell^+\nu)/\Gamma_{\text{total}}$

ℓ indicates average over e , μ , and τ modes, not sum over modes.

VALUE (units 10 ⁻²)	EVTS	DOCUMENT ID	TECN	COMMENT
10.86 ± 0.09 OUR FIT				
10.86 ± 0.12 ± 0.08	16438	ABBIENDI	07A OPAL	$E_{cm}^{e\bar{e}} = 161-209$ GeV
10.85 ± 0.14 ± 0.08	13600	ABDALLAH	04G DLPH	$E_{cm}^{e\bar{e}} = 161-209$ GeV
10.83 ± 0.14 ± 0.10	11246	ACHARD	04J L3	$E_{cm}^{e\bar{e}} = 161-209$ GeV
10.96 ± 0.12 ± 0.05	16116	SCHAEEL	04A ALEP	$E_{cm}^{e\bar{e}} = 183-209$ GeV

- • • We do not use the following data for averages, fits, limits, etc. • • •
- 11.02 ± 0.52 11858 ¹ ABBOTT 99H D0 $E_{cm}^{p\bar{p}} = 1.8$ TeV
- 10.4 ± 0.8 3642 ² ABE 92I CDF $E_{cm}^{p\bar{p}} = 1.8$ TeV
- ¹ ABBOTT 99H measure $R \equiv [\sigma_W B(W \rightarrow \ell\nu_\ell)]/[\sigma_Z B(Z \rightarrow \ell\ell)] = 10.90 \pm 0.52$ combining electron and muon channels. They use $M_W = 80.39 \pm 0.06$ GeV and the SM theoretical predictions for $\sigma(W)/\sigma(Z)$ and $B(Z \rightarrow \ell\ell)$.
- ² 1216 ± 38 +27 -31 $W \rightarrow \mu\nu$ events from ABE 92I and 2426 $W \rightarrow e\nu$ events of ABE 91C. ABE 92I give the inverse quantity as 9.6 ± 0.7 and we have inverted.

$\Gamma(\mu^+\nu)/\Gamma_{\text{total}}$

VALUE (units 10 ⁻²)	EVTS	DOCUMENT ID	TECN	COMMENT
10.71 ± 0.16 OUR FIT				
10.71 ± 0.25 ± 0.11	2374	ABBIENDI	07A OPAL	$E_{cm}^{e\bar{e}} = 161-209$ GeV
10.55 ± 0.31 ± 0.14	1804	ABDALLAH	04G DLPH	$E_{cm}^{e\bar{e}} = 161-209$ GeV
10.78 ± 0.29 ± 0.13	1576	ACHARD	04J L3	$E_{cm}^{e\bar{e}} = 161-209$ GeV
10.78 ± 0.27 ± 0.10	2142	SCHAEEL	04A ALEP	$E_{cm}^{e\bar{e}} = 183-209$ GeV
• • • We do not use the following data for averages, fits, limits, etc. • • •				
10.61 ± 0.28		¹ ABAZOV	04D TEVA	$E_{cm}^{p\bar{p}} = 1.8$ TeV

¹ ABAZOV 04D take into account all correlations to properly combine the CDF (ABE 95W) and DØ (ABBOTT 00b) measurements of the ratio R in the electron channel. The ratio R is defined as $[\sigma_W \cdot B(W \rightarrow e\nu_e)] / [\sigma_Z \cdot B(Z \rightarrow ee)]$. The combination gives $R^{\text{Tevatron}} = 10.59 \pm 0.23$. σ_W / σ_Z is calculated at next-to-next-to-leading order (3.360 ± 0.051). The branching fraction $B(Z \rightarrow ee)$ is taken from this Review as (3.363 ± 0.004)%.

$\Gamma(\mu^+\nu)/\Gamma_{\text{total}}$

VALUE (units 10 ⁻²)	EVTS	DOCUMENT ID	TECN	COMMENT
10.63 ± 0.15 OUR FIT				
10.78 ± 0.24 ± 0.10	2397	ABBIENDI	07A OPAL	$E_{cm}^{e\bar{e}} = 161-209$ GeV
10.65 ± 0.26 ± 0.08	1998	ABDALLAH	04G DLPH	$E_{cm}^{e\bar{e}} = 161-209$ GeV
10.03 ± 0.29 ± 0.12	1423	ACHARD	04J L3	$E_{cm}^{e\bar{e}} = 161-209$ GeV
10.87 ± 0.25 ± 0.08	2216	SCHAEEL	04A ALEP	$E_{cm}^{e\bar{e}} = 183-209$ GeV

See key on page 1127

Gauge & Higgs Boson Particle Listings

W

$\Gamma(\mu^+\nu)/\Gamma(e^+\nu)$ Γ_3/Γ_2

VALUE	EVTS	DOCUMENT ID	TECN	COMMENT
0.996 ± 0.008 OUR AVERAGE				
1.003 ± 0.010		¹ AABOUD	17Q ATLS	$E_{cm}^{PD} = 7$ TeV
0.980 ± 0.018		² AAIJ	16AJ LHCB	$E_{cm}^{PD} = 8$ TeV
0.993 ± 0.019		SCHAEEL	13A LEP	$E_{cm}^{EE} = 130-209$ GeV
0.89 ± 0.10	13k	³ ABACHI	95D D0	$E_{cm}^{PD} = 1.8$ TeV
1.02 ± 0.08	1216	⁴ ABE	92I CDF	$E_{cm}^{PD} = 1.8$ TeV
1.00 ± 0.14 ± 0.08	67	ALBAJAR	89 UA1	$E_{cm}^{PD} = 546,630$ GeV
1.24 $^{+0.6}_{-0.4}$	14	ARNISON	84D UA1	Repl. by ALBAJAR 89

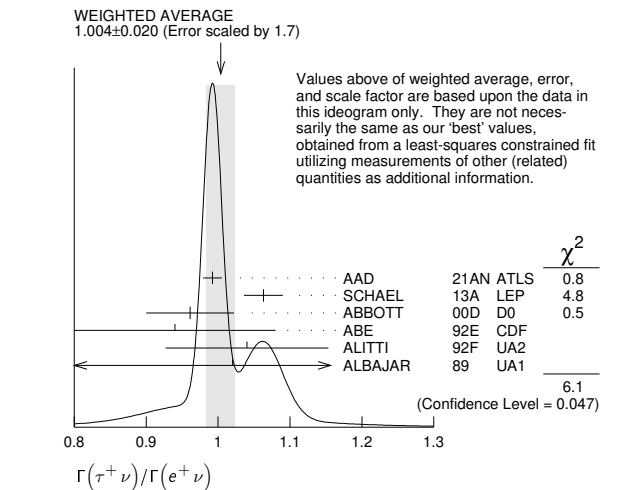
- ¹AABOUD 17Q make a precise determination of $W \rightarrow e\nu$ and $W \rightarrow \mu\nu$ production in the following fiducial phase space: lepton pseudo-rapidity range $|\eta| < 2.5$, lepton and neutrino transverse momenta larger than 25 GeV each, and W transverse mass larger than 25 GeV. They determine the ratio of the W branching fractions $B(W \rightarrow e\nu)/B(W \rightarrow \mu\nu) = 0.9967 \pm 0.0004 \pm 0.0101 = 0.997 \pm 0.010$.
- ²AAIJ 16AJ make precise measurements of forward $W \rightarrow e\nu$ and $W \rightarrow \mu\nu$ production in proton-proton collisions at 8 TeV and determine the ratio of the W branching fractions $B(W \rightarrow e\nu)/B(W \rightarrow \mu\nu) = 1.020 \pm 0.002 \pm 0.019$.
- ³ABACHI 95D obtain this result from the measured $\sigma_W B(W \rightarrow \mu\nu) = 2.09 \pm 0.23 \pm 0.11$ nb and $\sigma_W B(W \rightarrow e\nu) = 2.36 \pm 0.07 \pm 0.13$ nb in which the first error is the combined statistical and systematic uncertainty, the second reflects the uncertainty in the luminosity.
- ⁴ABE 92I obtain $\sigma_W B(W \rightarrow \mu\nu) = 2.21 \pm 0.07 \pm 0.21$ and combine with ABE 91C $\sigma_W B(W \rightarrow e\nu)$ to give a ratio of the couplings from which we derive this measurement.

$\Gamma(\tau^+\nu)/\Gamma_{total}$ Γ_4/Γ

VALUE (units 10^{-2})	EVTS	DOCUMENT ID	TECN	COMMENT
11.38 ± 0.21 OUR FIT				
11.14 ± 0.31 ± 0.17	2177	ABBIENDI	07A OPAL	$E_{cm}^{EE} = 161-209$ GeV
11.46 ± 0.39 ± 0.19	2034	ABDALLAH	04G DLPH	$E_{cm}^{EE} = 161-209$ GeV
11.89 ± 0.40 ± 0.20	1375	ACHARD	04J L3	$E_{cm}^{EE} = 161-209$ GeV
11.25 ± 0.32 ± 0.20	2070	SCHAEEL	04A ALEP	$E_{cm}^{EE} = 183-209$ GeV

$\Gamma(\tau^+\nu)/\Gamma(e^+\nu)$ Γ_4/Γ_2

VALUE	EVTS	DOCUMENT ID	TECN	COMMENT
1.004 ± 0.020 OUR AVERAGE				
0.992 ± 0.007 ± 0.011		¹ AAD	21AN ATLS	$E_{cm}^{PD} = 13$ TeV
1.063 ± 0.027		SCHAEEL	13A LEP	$E_{cm}^{EE} = 130-209$ GeV
0.961 ± 0.061	980	² ABBOTT	00D D0	$E_{cm}^{PD} = 1.8$ TeV
0.94 ± 0.14	179	³ ABE	92E CDF	$E_{cm}^{PD} = 1.8$ TeV
1.04 ± 0.08 ± 0.08	754	⁴ ALITTI	92F UA2	$E_{cm}^{PD} = 630$ GeV
1.02 ± 0.20 ± 0.12	32	ALBAJAR	89 UA1	$E_{cm}^{PD} = 546,630$ GeV
0.995 ± 0.112 ± 0.083	198	ALITTI	91C UA2	Repl. by ALITTI 92F
1.02 ± 0.20 ± 0.10	32	ALBAJAR	87 UA1	Repl. by ALBAJAR 89



- ¹AAD 21AN study $t\bar{t}$ production, with the W bosons in top-quark decay decaying to electrons or taus, with the tau decaying further into a muon. Analyzing the muon impact parameter and its transverse momentum, the contributions from prompt muons (arising from W decay) and non-prompt muons (arising from tau decay) are separated, allowing a measurement of the ratio of the W branching fractions into taus and muons, $R(\tau/\mu) = 0.992 \pm 0.007 \pm 0.011$ where the first error is statistical and the second systematic.
- ²ABBOTT 00D measure $\sigma_W \times B(W \rightarrow \tau\nu_\tau) = 2.22 \pm 0.09 \pm 0.10 \pm 0.10$ nb. Using the ABBOTT 00B result $\sigma_W \times B(W \rightarrow e\nu_e) = 2.31 \pm 0.01 \pm 0.05 \pm 0.10$ nb, they quote the ratio of the couplings from which we derive this measurement.
- ³ABE 92E use two procedures for selecting $W \rightarrow \tau\nu_\tau$ events. The missing E_T trigger leads to $132 \pm 14 \pm 8$ events and the τ trigger to $47 \pm 9 \pm 4$ events. Proper statistical and systematic correlations are taken into account to arrive at $\sigma_B(W \rightarrow \tau\nu) = 2.05 \pm 0.27$

nb. Combined with ABE 91C result on $\sigma_B(W \rightarrow e\nu)$, ABE 92E quote a ratio of the couplings from which we derive this measurement.
⁴This measurement is derived by us from the ratio of the couplings of ALITTI 92F.

$\Gamma(\tau^+\nu)/\Gamma(\mu^+\nu)$ Γ_4/Γ_3

VALUE	DOCUMENT ID	TECN	COMMENT
1.070 ± 0.026	SCHAEEL	13A LEP	$E_{cm}^{EE} = 130-209$ GeV

$\Gamma(\text{hadrons})/\Gamma_{total}$ Γ_5/Γ

OUR FIT value is obtained by a fit to the lepton branching ratio data assuming lepton universality.

VALUE (units 10^{-2})	EVTS	DOCUMENT ID	TECN	COMMENT
67.41 ± 0.27 OUR FIT				
67.41 ± 0.37 ± 0.23	16438	ABBIENDI	07A OPAL	$E_{cm}^{EE} = 161-209$ GeV
67.45 ± 0.41 ± 0.24	13600	ABDALLAH	04G DLPH	$E_{cm}^{EE} = 161-209$ GeV
67.50 ± 0.42 ± 0.30	11246	ACHARD	04J L3	$E_{cm}^{EE} = 161-209$ GeV
67.13 ± 0.37 ± 0.15	16116	SCHAEEL	04A ALEP	$E_{cm}^{EE} = 183-209$ GeV

$\Gamma(\pi^+\gamma)/\Gamma_{total}$ Γ_6/Γ

VALUE	CL%	DOCUMENT ID	COMMENT
$< 1.50 \times 10^{-5}$	95	¹ SIRUNYAN 21I	$E_{cm}^{PD} = 13$ TeV

- ¹SIRUNYAN 21I search for the rare decay of a W boson into a charged pion accompanied by a photon. A signal is not observed, and an upper limit on the branching fraction $B(W \rightarrow \pi\gamma) < 1.50 \times 10^{-5}$ is obtained at 95% C.L.

$\Gamma(\pi^+\gamma)/\Gamma(e^+\nu)$ Γ_6/Γ_2

VALUE	CL%	DOCUMENT ID	TECN	COMMENT
$< 6.4 \times 10^{-5}$	95	AALTONEN	12W CDF	$E_{cm}^{PD} = 1.96$ TeV
$< 7 \times 10^{-4}$	95	ABE	98H CDF	$E_{cm}^{PD} = 1.8$ TeV
$< 4.9 \times 10^{-3}$	95	¹ ALITTI	92D UA2	$E_{cm}^{PD} = 630$ GeV
$< 58 \times 10^{-3}$	95	² ALBAJAR	90 UA1	$E_{cm}^{PD} = 546, 630$ GeV

- ¹ALITTI 92D limit is 3.8×10^{-3} at 90%CL.
- ²ALBAJAR 90 obtain < 0.048 at 90%CL.

$\Gamma(D_s^+\gamma)/\Gamma(e^+\nu)$ Γ_7/Γ_2

VALUE	CL%	DOCUMENT ID	TECN	COMMENT
$< 1.2 \times 10^{-2}$	95	ABE	98P CDF	$E_{cm}^{PD} = 1.8$ TeV

$\Gamma(cX)/\Gamma(\text{hadrons})$ Γ_8/Γ_5

VALUE	EVTS	DOCUMENT ID	TECN	COMMENT
0.49 ± 0.04 OUR AVERAGE				
0.481 ± 0.042 ± 0.032	3005	¹ ABBIENDI	00V OPAL	$E_{cm}^{EE} = 183 + 189$ GeV
0.51 ± 0.05 ± 0.03	746	² BARATE	99M ALEP	$E_{cm}^{EE} = 172 + 183$ GeV

- ¹ABBIENDI 00V tag $W \rightarrow cX$ decays using measured jet properties, lifetime information, and leptons produced in charm decays. From this result, and using the additional measurements of $\Gamma(W)$ and $B(W \rightarrow \text{hadrons})$, $|V_{cs}|$ is determined to be $0.969 \pm 0.045 \pm 0.036$.
- ²BARATE 99M tag c jets using a neural network algorithm. From this measurement $|V_{cs}|$ is determined to be $1.00 \pm 0.11 \pm 0.07$.

$\Gamma(\pi^+\pi^+\pi^-)/\Gamma_{total}$ Γ_{11}/Γ

VALUE (units 10^{-6})	CL%	DOCUMENT ID	TECN	COMMENT
< 1.01	95	¹ SIRUNYAN 19BG	CMS	$E_{cm}^{PD} = 13$ TeV

- ¹SIRUNYAN 19BG search for the rare decay of a W boson into three charged pions. Three pion candidates are required in each event, with transverse momentum larger than 35 GeV, 35 GeV, 18 GeV, respectively, while the transverse momentum of the three-pion system is required to be larger than 40 GeV. Analyzing the three-pion invariant mass, no excess is observed in the W mass region, leading to the 95% C.L. upper limit on the branching fraction.

$R_{c\bar{s}} = \Gamma(c\bar{s})/\Gamma(\text{hadrons})$ Γ_9/Γ_5

VALUE	DOCUMENT ID	TECN	COMMENT
0.46 $^{+0.18}_{-0.14} \pm 0.07$	¹ ABREU	98N DLPH	$E_{cm}^{EE} = 161+172$ GeV

- ¹ABREU 98N tag c and s jets by identifying a charged kaon as the highest momentum particle in a hadronic jet. They also use a lifetime tag to independently identify a c jet, based on the impact parameter distribution of charged particles in a jet. From this measurement $|V_{cs}|$ is determined to be $0.94 $^{+0.32}_{-0.26} \pm 0.13$.$

AVERAGE PARTICLE MULTIPLICITIES IN HADRONIC W DECAY

Summed over particle and antiparticle, when appropriate.

$\langle N_{\pi^\pm} \rangle$

VALUE	DOCUMENT ID	TECN	COMMENT
15.70 ± 0.35	¹ ABREU,P	00F DLPH	$E_{cm}^{EE} = 189$ GeV

- ¹ABREU,P 00F measure $\langle N_{\pi^\pm} \rangle = 31.65 \pm 0.48 \pm 0.76$ and $15.51 \pm 0.38 \pm 0.40$ in the fully hadronic and semileptonic final states respectively. The value quoted is a weighted average without assuming any correlations.

Gauge & Higgs Boson Particle Listings

W

 $\langle N_{K^\pm} \rangle$

VALUE	DOCUMENT ID	TECN	COMMENT
2.20 ± 0.19	¹ ABREU,P	00F	DLPH $E_{cm}^{ee} = 189$ GeV

¹ ABREU,P 00F measure $\langle N_{K^\pm} \rangle = 4.38 \pm 0.42 \pm 0.12$ and $2.23 \pm 0.32 \pm 0.17$ in the fully hadronic and semileptonic final states respectively. The value quoted is a weighted average without assuming any correlations.

 $\langle N_p \rangle$

VALUE	DOCUMENT ID	TECN	COMMENT
0.92 ± 0.14	¹ ABREU,P	00F	DLPH $E_{cm}^{ee} = 189$ GeV

¹ ABREU,P 00F measure $\langle N_p \rangle = 1.82 \pm 0.29 \pm 0.16$ and $0.94 \pm 0.23 \pm 0.06$ in the fully hadronic and semileptonic final states respectively. The value quoted is a weighted average without assuming any correlations.

 $\langle N_{\text{charged}} \rangle$

VALUE	DOCUMENT ID	TECN	COMMENT
19.39 ± 0.08 OUR AVERAGE			
19.38 ± 0.05 ± 0.08	¹ ABBIENDI	06A	OPAL $E_{cm}^{ee} = 189-209$ GeV
19.44 ± 0.17	² ABREU,P	00F	DLPH $E_{cm}^{ee} = 183+189$ GeV
19.3 ± 0.3 ± 0.3	³ ABBIENDI	99N	OPAL $E_{cm}^{ee} = 183$ GeV
19.23 ± 0.74	⁴ ABREU	98c	DLPH $E_{cm}^{ee} = 172$ GeV

¹ ABBIENDI 06A measure $\langle N_{\text{charged}} \rangle = 38.74 \pm 0.12 \pm 0.26$ when both W bosons decay hadronically and $\langle N_{\text{charged}} \rangle = 19.39 \pm 0.11 \pm 0.09$ when one W boson decays semileptonically. The value quoted here is obtained under the assumption that there is no color reconnection between W bosons; the value is a weighted average taking into account correlations in the systematic uncertainties.

² ABREU,P 00F measure $\langle N_{\text{charged}} \rangle = 39.12 \pm 0.33 \pm 0.36$ and $38.11 \pm 0.57 \pm 0.44$ in the fully hadronic final states at 189 and 183 GeV respectively, and $\langle N_{\text{charged}} \rangle = 19.49 \pm 0.31 \pm 0.27$ and $19.78 \pm 0.49 \pm 0.43$ in the semileptonic final states. The value quoted is a weighted average without assuming any correlations.

³ ABBIENDI 99N use the final states $W^+ W^- \rightarrow q\bar{q}\ell\nu_\ell$ to derive this value.

⁴ ABREU 98c combine results from both the fully hadronic as well semileptonic WW final states after demonstrating that the W decay charged multiplicity is independent of the topology within errors.

TRIPLE GAUGE COUPLINGS (TGC'S)

Revised April 2017 by M.W. Grinewald (U. College Dublin) and A. Gurtu (Formerly Tata Inst.).

Fourteen independent couplings, seven each for ZWW and γWW , completely describe the VWW vertices within the most general framework of the electroweak Standard Model (SM) consistent with Lorentz invariance and $U(1)$ gauge invariance. Of each of the seven TGCs, three conserve C and P individually, three violate CP , and one violates C and P individually while conserving CP . Assumption of C and P conservation and electromagnetic gauge invariance reduces the number of independent VWW couplings to five: one common set [1,2] is $(\kappa_\gamma, \kappa_Z, \lambda_\gamma, \lambda_Z, g_1^Z)$, where $\kappa_\gamma = \kappa_Z = g_1^Z = 1$ and $\lambda_\gamma = \lambda_Z = 0$ in the Standard Model at tree level. The parameters κ_Z and λ_Z are related to the other three due to constraints of gauge invariance as follows: $\kappa_Z = g_1^Z - (\kappa_\gamma - 1) \tan^2 \theta_W$ and $\lambda_Z = \lambda_\gamma$, where θ_W is the weak mixing angle. The W magnetic dipole moment, μ_W , and the W electric quadrupole moment, q_W , are expressed as $\mu_W = e(1 + \kappa_\gamma + \lambda_\gamma)/2M_W$ and $q_W = -e(\kappa_\gamma - \lambda_\gamma)/M_W^2$.

Precision measurements of suitable observables at LEP1 has already led to an exploration of much of the TGC parameter space. At LEP2, the VWW coupling arises in W -pair production via s -channel exchange, or in single W production via the radiation of a virtual photon off the incident e^+ or e^- . At the Tevatron and the LHC, hard-photon bremsstrahlung off a produced W or Z signals the presence of a triple-gauge vertex. In order to extract the value of one TGC, the others are generally kept fixed to their SM values. While most analyses use the above gauge constraints in the extraction of TGCs, one analysis of W -pair events also determines the real and imaginary

parts of all 14 couplings using unconstrained single-parameter fits [3]. The results are consistent. Some experiments have determined limits on the couplings under various non-LEP scenarios and assuming different values of the form factor Λ , where the coupling parameters are scaled by $1/(1+s/\Lambda^2)^2$. For practical reasons it is not possible to quote all such determinations in the listings. For that the individual papers may be consulted. Recently, EFT-inspired sets of couplings [4,5], such as $c_{WWW}/\Lambda^2, c_W/\Lambda^2, c_B/\Lambda^2$ which are linearly related to the couplings discussed above, are also determined by the LHC experiments.

References

1. K. Hagiwara *et al.*, Nucl. Phys. **B282**, 253 (1987).
2. G. Gounaris *et al.*, CERN 96-01 p. 525.
3. S. Schael *et al.* (ALEPH Collab.), Phys. Lett. **B614**, 7 (2005).
4. K. Hagiwara *et al.*, Phys. Rev. **D48**, 2182 (1993).
5. C. Degrande *et al.*, Annals Phys. **335** (2013) 21-32.

 g_1^Z

OUR FIT below is taken from [SCHAEL 13A].

VALUE	EVTS	DOCUMENT ID	TECN	COMMENT
0.984 ± 0.018 -0.020 OUR FIT				
0.975 ^{+0.033} _{-0.030}	7872	¹ ABDALLAH	10	DLPH $E_{cm}^{ee} = 189-209$ GeV
1.001 ± 0.027 ± 0.013	9310	² SCHAEL	05A	ALEP $E_{cm}^{ee} = 183-209$ GeV
0.987 ^{+0.034} _{-0.033}	9800	³ ABBIENDI	04D	OPAL $E_{cm}^{ee} = 183-209$ GeV
0.966 ^{+0.034} _{-0.032} ± 0.015	8325	⁴ ACHARD	04D	L3 $E_{cm}^{ee} = 161-209$ GeV
• • • We do not use the following data for averages, fits, limits, etc. • • •				
		⁵ SIRUNYAN	20BA	CMS $E_{cm}^{pp} = 13$ TeV
		⁶ SIRUNYAN	19CL	CMS $E_{cm}^{pp} = 13$ TeV
		⁷ SIRUNYAN	18BZ	CMS $E_{cm}^{pp} = 13$ TeV
		⁸ AABOUD	17S	ATLS $E_{cm}^{pp} = 7+8$ TeV
		⁹ AABOUD	17U	ATLS $E_{cm}^{pp} = 8$ TeV
		¹⁰ KHACHATRY...17O		CMS $E_{cm}^{pp} = 8$ TeV
		¹¹ SIRUNYAN	17X	CMS $E_{cm}^{pp} = 8$ TeV
		¹² AAD	16AR	ATLS $E_{cm}^{pp} = 8$ TeV
		¹³ AAD	16P	ATLS $E_{cm}^{pp} = 8$ TeV
		¹⁴ AAD	14Y	ATLS $E_{cm}^{pp} = 8$ TeV
		¹⁵ AAD	13AL	ATLS $E_{cm}^{pp} = 7$ TeV
		¹⁶ CHATRCHYAN13BF		CMS $E_{cm}^{pp} = 7$ TeV
		¹⁷ AAD	12CD	ATLS $E_{cm}^{pp} = 7$ TeV
		¹⁸ AALTONEN	12AC	CDF $E_{cm}^{pp} = 1.96$ TeV
		¹⁹ ABAZOV	12AG	D0 $E_{cm}^{pp} = 1.96$ TeV
	34	²⁰ ABAZOV	11	D0 $E_{cm}^{pp} = 1.96$ TeV
	334	²¹ AALTONEN	10K	CDF $E_{cm}^{pp} = 1.96$ TeV
1.04 ± 0.09		²² ABAZOV	09AD	D0 $E_{cm}^{pp} = 1.96$ TeV
		²³ ABAZOV	09AJ	D0 $E_{cm}^{pp} = 1.96$ TeV
1.07 ^{+0.08} _{-0.12}	1880	²⁴ ABDALLAH	08C	DLPH Superseded by ABDAL-LAH 10
	13	²⁵ ABAZOV	07Z	D0 $E_{cm}^{pp} = 1.96$ TeV
	2.3	²⁶ ABAZOV	05S	D0 $E_{cm}^{pp} = 1.96$ TeV
0.98 ± 0.07 ± 0.01	2114	²⁷ ABREU	01I	DLPH $E_{cm}^{ee} = 183+189$ GeV
	331	²⁸ ABBOTT	99I	D0 $E_{cm}^{pp} = 1.8$ TeV

¹ ABDALLAH 10 use data on the final states $e^+ e^- \rightarrow jj\ell\nu, jjjj, jjX, \ell X$, at center-of-mass energies between 189-209 GeV at LEP2, where $j = \text{jet}$, $\ell = \text{lepton}$, and X represents missing momentum. The fit is carried out keeping all other parameters fixed at their SM values.

² SCHAEL 05A study single-photon, single- W , and WW -pair production from 183 to 209 GeV. The result quoted here is derived from the WW -pair production sample. Each parameter is determined from a single-parameter fit in which the other parameters assume their Standard Model values.

³ ABBIENDI 04D combine results from $W^+ W^-$ in all decay channels. Only CP -conserving couplings are considered and each parameter is determined from a single-parameter fit in which the other parameters assume their Standard Model values. The 95% confidence interval is $0.923 < g_1^Z < 1.054$.

- 4 ACHARD 04b study W -pair production, single- W production and single-photon production with missing energy from 189 to 209 GeV. The result quoted here is obtained from the W -pair production sample including data from 161 to 183 GeV, ACCIA-RRI 99q. Each parameter is determined from a single-parameter fit in which the other parameters assume their Standard Model values.
- 5 SIRUNYAN 20BA study electroweak production of a W boson in association with two jets, using W decays in the electron or muon channel. The isolated muons (electrons) are required to have a transverse momentum larger than 25 (30) GeV, while the transverse momentum of the two jets has to be larger than 50 and 30 GeV. A total of 2.382 (1.051) million events are selected in the muon (electron) channel, with a Standard Model expectation of 2.39 ± 0.17 (1.054 ± 0.058) million events. Analyzing the transverse momentum distribution of the charged leptons from W decay, the following 95% C.L. limit is obtained: $0.971 < g_1^Z < 1.044$. Combining this result with that from the closely-related electroweak Z -jet-jet production SIRUNYAN 18BZ, the limit becomes: $0.979 < g_1^Z < 1.034$.
- 6 SIRUNYAN 19CL study W and WZ production in lepton + jet events, with one W boson decaying leptonically (electron or muon), and another W or Z boson decaying hadronically, reconstructed as a single massive large-radius jet. In the electron channel 2,456 (2,235) events are selected in the $W(W/Z)$ category, while in the muon channel 3,986 (3,572) events are selected in the $W(W/Z)$ category. Analyzing the di-boson invariant mass distribution, the following 95% C.L. limit is obtained: $0.9939 < g_1^Z < 1.0074$.
- 7 SIRUNYAN 18BZ study $pp \rightarrow Z$ jet jet events at 13 TeV where $Z \rightarrow e^+e^-/\mu^+\mu^-$. Isolated electrons and muons are selected with p_T of the leading/sub-leading lepton $> 30/20$ GeV and $|\eta| < 2.4$, with the di-lepton invariant mass within 15 GeV of the Z mass. The two highest p_T jets are selected with p_T of the leading/sub-leading jet $> 50/30$ GeV respectively and dijet invariant mass > 200 GeV. Templates in the transverse momentum of the Z are utilized to set limits on the triple gauge couplings in the EFT and the LEP parametrizations. The following 95% C.L. limit is obtained: $0.965 < g_1^Z < 1.042$.
- 8 AABOUD 17s analyze electroweak production of a W boson in association with two jets at high dijet invariant mass, with the W boson decaying to electron or muon plus neutrino. In the signal region of dijet mass larger than 1 TeV and leading-jet transverse momentum larger than 600 GeV, 30 events are observed in the data with 39 ± 4 events expected in the Standard Model, yielding the following limit at 95% CL for the form factor cut-off scale $A_{FF} \rightarrow \infty$: $0.87 < g_1^Z < 1.12$.
- 9 AABOUD 17u analyze production of W or WZ boson pairs with one W boson decaying to electron or muon plus neutrino, and the other W or Z boson decaying hadronically. The hadronic decay system is reconstructed as either a resolved two-jet system or as a single large jet. Analyzing the transverse momentum distribution of the hadronic system above 100 GeV yields the following limit at 95% CL for the form factor cut-off scale $A_{FF} \rightarrow \infty$: $0.979 < g_1^Z < 1.024$.
- 10 KHACHATRYAN 17o analyse WZ production where each boson decays into electrons or muons. Events are required to have a tri-lepton invariant mass larger than 100 GeV, with one of the lepton pairs having an invariant mass within 20 GeV of the Z boson mass. The Z transverse momentum spectrum is analyzed to set a 95% C.L. limit of: $0.982 < g_1^Z < 1.035$.
- 11 SIRUNYAN 17x study $pp \rightarrow WW/WZ \rightarrow \ell\nu q\bar{q}$ production at 8 TeV where ℓ is an electron or muon with $p_T > 30$ or 25 GeV respectively. Suitable cuts are put on the p_T of the dijet system and the missing E_T of the event yielding a total of 285 and 204 W events observed in the electron and muon channels. The following 95% C.L. limit is obtained: $0.9913 < g_1^Z < 1.024$.
- 12 AAD 16AR study W production in pp collisions and select 6636 W candidates in decay modes with electrons or muons with an expected background of 1546 ± 157 events. Assuming the LEP formulation and setting the form-factor Λ to infinity, a fit to the transverse momentum distribution of the leading charged lepton, leads to a 95% C.L. range of $0.984 < g_1^Z < 1.027$.
- 13 AAD 16P study WZ production in pp collisions and select 2091 WZ candidates in 4 decay modes with electrons and muons, with an expected background of 1825 ± 7 events. Analyzing the WZ transverse momentum distribution, the resulting 95% C.L. limit is: $0.981 < g_1^Z < 1.029$.
- 14 AAD 14V determine the electroweak Z -dijet cross section in 8 TeV pp collisions. $Z \rightarrow ee$ and $Z \rightarrow \mu\mu$ decays are selected with the di-lepton $p_T > 20$ GeV and mass in the 81–101 GeV range. Minimum two jets are required with $p_T > 55$ and 45 GeV and no additional jets with $p_T > 25$ GeV in the rapidity interval between them. The normalized p_T balance between the Z and the two jets is required to be < 0.15 . This leads to a selection of 900 events with dijet mass > 1 TeV. The number of signal and background events expected is 261 and 592 respectively. A Poisson likelihood method is used on an event by event basis to obtain the 95% CL limit $0.5 < g_1^Z < 1.26$ for a form factor value $\Lambda = \infty$.
- 15 AAD 13AL study W production in pp collisions and select 1325 W candidates in decay modes with electrons or muons with an expected background of 369 ± 61 events. Assuming the LEP formulation and setting the form-factor $\Lambda = \infty$, a fit to the transverse momentum distribution of the leading charged lepton, leads to a 95% C.L. range of $0.961 < g_1^Z < 1.052$. Supersedes AAD 12Ac.
- 16 CHATRCHYAN 13BF determine the W^+W^- production cross section using unlike sign di-lepton (e or μ) events with high p_T . The leptons have $p_T > 20$ GeV/c and are isolated. 1134 candidate events are observed with an expected SM background of 247 ± 34 . The p_T distribution of the leading lepton is fitted to obtain 95% C.L. limits of $0.905 \leq g_1^Z \leq 1.095$.
- 17 AAD 12CD study WZ production in pp collisions and select 317 WZ candidates in three $\ell\nu$ decay modes with an expected background of 68.0 ± 10.0 events. The resulting 95% C.L. range is: $0.943 < g_1^Z < 1.093$. Supersedes AAD 12V.
- 18 AALTONEN 12AC study WZ production in $p\bar{p}$ collisions and select 63 WZ candidates in three $\ell\nu$ decay modes with an expected background of 7.9 ± 1.0 events. Based on the cross section and shape of the Z transverse momentum spectrum, the following 95% C.L. range is reported: $0.92 < g_1^Z < 1.20$ for a form factor of $\Lambda = 2$ TeV.
- 19 ABAZOV 12AG combine new results with already published results on $W\gamma$, WW and WZ production in order to determine the couplings with increased precision, superseding ABAZOV 08R, ABAZOV 11AC, ABAZOV 09AJ, ABAZOV 09AD. The 68% C.L. result for a formfactor cutoff of $\Lambda = 2$ TeV is $g_1^Z = 1.022^{+0.032}_{-0.030}$.
- 20 ABAZOV 11 study the $p\bar{p} \rightarrow 3\ell\nu$ process arising in WZ production. They observe 34 WZ candidates with an estimated background of 6 events. An analysis of the p_T spectrum of the Z boson leads to a 95% C.L. limit of $0.944 < g_1^Z < 1.154$, for a form factor $\Lambda = 2$ TeV.
- 21 AALTONEN 10K study $p\bar{p} \rightarrow W^+W^-$ with $W \rightarrow e/\mu\nu$. The p_T of the leading (second) lepton is required to be > 20 (10) GeV. The final number of events selected is 654 of which 320 ± 47 are estimated to be background. The 95% C.L. interval is $0.76 < g_1^Z < 1.34$ for $\Lambda = 1.5$ TeV and $0.78 < g_1^Z < 1.30$ for $\Lambda = 2$ TeV.
- 22 ABAZOV 09AD study the $p\bar{p} \rightarrow \ell\nu$ 2jet process arising in W and WZ production. They select 12,473 (14,392) events in the electron (muon) channel with an expected di-boson signal of 436 (527) events. The results on the anomalous couplings are derived from an analysis of the p_T spectrum of the 2-jet system and quoted at 68% C.L. and for a form factor of 2 TeV. This measurement is not used for obtaining the mean as it is for a specific form factor. The 95% confidence interval is $0.88 < g_1^Z < 1.20$.
- 23 ABAZOV 09AJ study the $p\bar{p} \rightarrow 2\ell 2\nu$ process arising in WW production. They select 100 events with an expected W signal of 65 events. An analysis of the p_T spectrum of the two charged leptons leads to 95% C.L. limits of $0.86 < g_1^Z < 1.3$, for a form factor $\Lambda = 2$ TeV.
- 24 ABDALLAH 08c determine this triple gauge coupling from the measurement of the spin density matrix elements in $e^+e^- \rightarrow W^+W^- \rightarrow (qq)(\ell\nu)$, where $\ell = e$ or μ . Values of all other couplings are fixed to their standard model values.
- 25 ABAZOV 07Z set limits on anomalous TGCs using the measured cross section and $p_T(Z)$ distribution in WZ production with both the W and the Z decaying leptonically into electrons and muons. Setting the other couplings to their standard model values, the 95% C.L. limit for a form factor scale $\Lambda = 2$ TeV is $0.86 < g_1^Z < 1.35$.
- 26 ABAZOV 05s study $p\bar{p} \rightarrow WZ$ production with a subsequent trilepton decay to $\ell\nu\ell'\bar{\ell}'$ (ℓ and $\ell' = e$ or μ). Three events (estimated background 0.71 ± 0.08 events) with WZ decay characteristics are observed from which they derive limits on the anomalous WWZ couplings. The 95% CL limit for a form factor scale $\Lambda = 1.5$ TeV is $0.51 < g_1^Z < 1.66$, fixing λ_Z and κ_Z to their Standard Model values.
- 27 ABREU 01i combine results from e^+e^- interactions at 189 GeV leading to W^+W^- and $W\nu_e$ final states with results from ABREU 99L at 183 GeV. The 95% confidence interval is $0.84 < g_1^Z < 1.13$.
- 28 ABBOTT 99i perform a simultaneous fit to the $W\gamma$, $WW \rightarrow$ dilepton, $WW/WZ \rightarrow e\nu jj$, $WW/WZ \rightarrow \mu\nu jj$, and $WZ \rightarrow$ trilepton data samples. For $\Lambda = 2.0$ TeV, the 95% CL limits are $0.63 < g_1^Z < 1.57$, fixing λ_Z and κ_Z to their Standard Model values, and assuming Standard Model values for the $WW\gamma$ couplings.

 κ_γ

OUR FIT below is taken from [SCHAE1 13A].

VALUE	EVTS	DOCUMENT ID	TECN	COMMENT
0.982 ± 0.042 OUR FIT				
$1.024^{+0.077}_{-0.081}$	7872	1 ABDALLAH	10 DLPH	$E_{cm}^{ee} = 189\text{--}209$ GeV
$0.971 \pm 0.055 \pm 0.030$	10689	2 SCHAE1	05A ALEP	$E_{cm}^{ee} = 183\text{--}209$ GeV
$0.88^{+0.09}_{-0.08}$	9800	3 ABBIENDI	04D OPAL	$E_{cm}^{ee} = 183\text{--}209$ GeV
$1.013^{+0.067}_{-0.064} \pm 0.026$	10575	4 ACHARD	04D L3	$E_{cm}^{ee} = 161\text{--}209$ GeV
• • • We do not use the following data for averages, fits, limits, etc. • • •				
		5 AABOUD	17U ATLS	$E_{cm}^{pp} = 8$ TeV
		6 SIRUNYAN	17X CMS	$E_{cm}^{pp} = 8$ TeV
		7 CHATRCHYAN	14AB CMS	$E_{cm}^{pp} = 7$ TeV
		8 AAD	13AN ATLS	$E_{cm}^{pp} = 7$ TeV
		9 CHATRCHYAN	13BF CMS	$E_{cm}^{pp} = 7$ TeV
		10 ABAZOV	12AG D0	$E_{cm}^{pp} = 1.96$ TeV
		11 ABAZOV	11AC D0	$E_{cm}^{pp} = 1.96$ TeV
		12 CHATRCHYAN	11M CMS	$E_{cm}^{pp} = 7$ TeV
	334	13 AALTONEN	10K CDF	$E_{cm}^{pp} = 1.96$ TeV
	53	14 AARON	09B H1	$E_{cm}^{ep} = 0.3$ TeV
		15 ABAZOV	09AD D0	$E_{cm}^{pp} = 1.96$ TeV
		16 ABAZOV	09AJ D0	$E_{cm}^{pp} = 1.96$ TeV
		17 ABAZOV	08R D0	$E_{cm}^{pp} = 1.96$ TeV
$0.68^{+0.17}_{-0.15}$	1880	18 ABDALLAH	08c DLPH	Superseded by ABDALLAH 10
	1617	19 AALTONEN	07L CDF	$E_{cm}^{pp} = 1.96$ GeV
	17	20 ABAZOV	06H D0	$E_{cm}^{pp} = 1.96$ TeV
	141	21 ABAZOV	05J D0	$E_{cm}^{pp} = 1.96$ TeV
$1.25^{+0.21}_{-0.20} \pm 0.06$	2298	22 ABREU	01i DLPH	$E_{cm}^{ee} = 183\text{--}189$ GeV
		23 BREITWEG	00 ZEUS	$e^+p \rightarrow e^+W^+X$, $\sqrt{s} \approx 300$ GeV
0.92 ± 0.34	331	24 ABBOTT	99i D0	$E_{cm}^{pp} = 1.8$ TeV

1 ABDALLAH 10 use data on the final states $e^+e^- \rightarrow jj\ell\nu, jjjj, jjX, \ell X$, at center-of-mass energies between 189–209 GeV at LEP2, where $j = \text{jet}$, $\ell = \text{lepton}$, and X represents missing momentum. The fit is carried out keeping all other parameters fixed at their SM values.

2 SCHAE1 05a study single-photon, single- W , and W -pair production from 183 to 209 GeV. Each parameter is determined from a single-parameter fit in which the other parameters assume their Standard Model values.

3 ABBIENDI 04d combine results from W^+W^- in all decay channels. Only CP -conserving couplings are considered and each parameter is determined from a single-parameter fit in which the other parameters assume their Standard Model values. The 95% confidence interval is $0.73 < \kappa_\gamma < 1.07$.

Gauge & Higgs Boson Particle Listings

W

- ⁴ ACHARD 04b study WW -pair production, single- W production and single-photon production with missing energy from 189 to 209 GeV. The result quoted here is obtained including data from 161 to 183 GeV, ACCIARRI 99q. Each parameter is determined from a single-parameter fit in which the other parameters assume their Standard Model values.
- ⁵ AABOUD 17u analyze production of WW or WZ boson pairs with one W boson decaying to electron or muon plus neutrino, and the other W or Z boson decaying hadronically. The hadronic decay system is reconstructed as either a resolved two-jet system or as a single large jet. Analysing the transverse momentum distribution of the hadronic system above 100 GeV yields the following limit at 95% CL for the form factor cut-off scale $\Lambda_{FP} \rightarrow \infty$: $0.939 < \kappa_\gamma < 1.064$.
- ⁶ SIRUNYAN 17x study $pp \rightarrow WW/WZ \rightarrow \ell\nu q\bar{q}$ production at 8 TeV where ℓ is an electron or muon with $p_T > 30$ or 25 GeV respectively. Suitable cuts are put on the p_T of the dijet system and the missing E_T of the event yielding a total of 285 and 204 WW events observed in the electron and muon channels. The following 95% C.L. limit is obtained: $0.956 < \kappa_\gamma < 1.063$.
- ⁷ CHATRCHYAN 14AB measure $W\gamma$ production cross section for $p_T^\gamma > 15$ GeV and $R(\ell\gamma) > 0.7$, which is the separation between the γ and the final state charged lepton (e or μ) in the azimuthal angle-pseudorapidity ($\phi - \eta$) plane. After background subtraction the number of $e\nu\gamma$ and $\mu\nu\gamma$ events is determined to be 3200 ± 325 and 4970 ± 543 respectively, compatible with expectations from the SM. This leads to a 95% CL limit of $0.62 < \kappa_\gamma < 1.29$, assuming other parameters have SM values.
- ⁸ AAD 13AN study $W\gamma$ production in pp collisions. In events with no additional jet, 4449 (6578) W decays to electron (muon) are selected, with an expected background of 1662 ± 262 (2538 ± 362) events. Analysing the photon p_T spectrum above 100 GeV yields a 95% C.L. limit of $0.59 < \kappa_\gamma < 1.46$. Supersedes AAD 12BX.
- ⁹ CHATRCHYAN 13BF determine the W^+W^- production cross section using unlike sign di-lepton (e or μ) events with high p_T . The leptons have $p_T > 20$ GeV/ c and are isolated. 1134 candidate events are observed with an expected SM background of 247 ± 34 . The p_T distribution of the leading lepton is fitted to obtain 95% C.L. limits of $0.79 \leq \kappa_\gamma \leq 1.22$.
- ¹⁰ ABAZOV 12AG combine new results with already published results on $W\gamma$, WW and WZ production in order to determine the couplings with increased precision, superseding ABAZOV 08R, ABAZOV 11AC, ABAZOV 09AJ, ABAZOV 09AD. The 68% C.L. result for a formfactor cutoff of $\Lambda = 2$ TeV is $\kappa_\gamma = 1.048^{+0.106}_{-0.105}$.
- ¹¹ ABAZOV 11AC study $W\gamma$ production in $p\bar{p}$ collisions at 1.96 TeV, with the W decay products containing an electron or a muon. They select 196 (363) events in the electron (muon) mode, with a SM expectation of 190 (372) events. A likelihood fit to the photon E_T spectrum above 15 GeV yields at 95% C.L. the result: $0.6 < \kappa_\gamma < 1.4$ for a formfactor $\Lambda = 2$ TeV.
- ¹² CHATRCHYAN 11M study $W\gamma$ production in pp collisions at $\sqrt{s} = 7$ TeV using 36 pb⁻¹ pp data with the W decaying to electron and muon. The total cross section is measured for photon transverse energy $E_T^\gamma > 10$ GeV and spatial separation from charged leptons in the plane of pseudo rapidity and azimuthal angle $\Delta R(\ell, \gamma) > 0.7$. The number of candidate (background) events is 452 (228 ± 21) for the electron channel and 520 (277 ± 25) for the muon channel. Setting other couplings to their standard model value, they derive a 95% CL limit of $-0.11 < \kappa_\gamma < 2.04$.
- ¹³ AALTONEN 10K study $p\bar{p} \rightarrow W^+W^-$ with $W \rightarrow e/\mu\nu$. The p_T of the leading (second) lepton is required to be > 20 (10) GeV. The final number of events selected is 654 of which 320 ± 47 are estimated to be background. The 95% C.L. interval is $0.37 < \kappa_\gamma < 1.72$ for $\Lambda = 1.5$ TeV and $0.43 < \kappa_\gamma < 1.65$ for $\Lambda = 2$ TeV.
- ¹⁴ AARON 09B study single- W production in ep collisions at 0.3 TeV C.M. energy. They select 53 $W \rightarrow e/\mu$ events with a standard model expectation of 54.1 ± 7.4 events. Fitting the transverse momentum spectrum of the hadronic recoil system they obtain a 95% C.L. limit of $-3.7 < \kappa_\gamma < -1.5$ or $0.3 < \kappa_\gamma < 1.5$, where the ambiguity is due to the quadratic dependence of the cross section to the coupling parameter.
- ¹⁵ ABAZOV 09AD study the $p\bar{p} \rightarrow \ell\nu 2jet$ process arising in WW and WZ production. They select 12,473 (14,392) events in the electron (muon) channel with an expected di-boson signal of 436 (527) events. The results on the anomalous couplings are derived from an analysis of the p_T spectrum of the 2-jet system and quoted at 68% C.L. and for a form factor of 2 TeV. This measurement is not used for obtaining the mean as it is for a specific form factor. The 95% confidence interval is $0.56 < \kappa_\gamma < 1.55$.
- ¹⁶ ABAZOV 09AJ study the $p\bar{p} \rightarrow 2\ell\nu$ process arising in WW production. They select 100 events with an expected WW signal of 65 events. An analysis of the p_T spectrum of the two charged leptons leads to 95% C.L. limits of $0.46 < \kappa_\gamma < 1.83$, for a form factor $\Lambda = 2$ TeV.
- ¹⁷ ABAZOV 08R use 0.7 fb⁻¹ $p\bar{p}$ data at $\sqrt{s} = 1.96$ TeV to select 263 $W\gamma + X$ events, of which 187 constitute signal, with the W decaying into an electron or a muon, which is required to be well separated from a photon with $E_T > 9$ GeV. A likelihood fit to the photon E_T spectrum yields a 95% CL limit $0.49 < \kappa_\gamma < 1.51$ with other couplings fixed to their Standard Model values.
- ¹⁸ ABDALLAH 08c determine this triple gauge coupling from the measurement of the spin density matrix elements in $e^+e^- \rightarrow W^+W^- \rightarrow (q\bar{q})(\ell\nu)$, where $\ell = e$ or μ . Values of all other couplings are fixed to their standard model values.
- ¹⁹ AALTONEN 07L set limits on anomalous TGCs using the $p_T(W)$ distribution in WW and WZ production with the W decaying to an electron or muon and the Z to 2 jets. Setting other couplings to their standard model value, the 95% C.L. limits are $0.54 < \kappa_\gamma < 1.39$ for a form factor scale $\Lambda = 1.5$ TeV.
- ²⁰ ABAZOV 06H study $p\bar{p} \rightarrow WW$ production with a subsequent decay $WW \rightarrow e^+\nu_e e^-\bar{\nu}_e$, $WW \rightarrow e^+\nu_e \mu^+\bar{\nu}_\mu$ or $WW \rightarrow \mu^+\nu_\mu \mu^-\bar{\nu}_\mu$. The 95% C.L. limit for a form factor scale $\Lambda = 1$ TeV is $-0.05 < \kappa_\gamma < 2.29$, fixing $\lambda_\gamma = 0$. With the assumption that the $WW\gamma$ and WZ couplings are equal the 95% C.L. one-dimensional limit ($\Lambda = 2$ TeV) is $0.68 < \kappa < 1.45$.
- ²¹ ABAZOV 05l perform a likelihood fit to the photon E_T spectrum of $W\gamma + X$ events, where the W decays to an electron or muon which is required to be well separated from the photon. For $\Lambda = 2.0$ TeV the 95% CL limits are $0.12 < \kappa_\gamma < 1.96$. In the fit λ_γ is kept fixed to its Standard Model value.
- ²² ABREU 01i combine results from e^+e^- interactions at 189 GeV leading to W^+W^- , $W\nu_e$, and $\nu\bar{\nu}\gamma$ final states with results from ABREU 99L at 183 GeV. The 95% confidence interval is $0.87 < \kappa_\gamma < 1.68$.
- ²³ BREITWEG 00 search for W production in events with large hadronic p_T . For $p_T > 20$ GeV, the upper limit on the cross section gives the 95%CL limit $-3.7 < \kappa_\gamma < 2.5$ (for $\lambda_\gamma = 0$).
- ²⁴ ABBOTT 99i perform a simultaneous fit to the $W\gamma$, $WW \rightarrow$ dilepton, $WW/WZ \rightarrow e\nu jj$, $WW/WZ \rightarrow \mu\nu jj$, and $WZ \rightarrow$ trilepton data samples. For $\Lambda = 2.0$ TeV, the 95%CL limits are $0.75 < \kappa_\gamma < 1.39$.

 λ_γ

OUR FIT below is taken from [SCHAEL 13A].

VALUE	EVTS	DOCUMENT ID	TECN	COMMENT
-0.022 ± 0.019 OUR FIT				
0.002 ± 0.035	7872	1 ABDALLAH	10 DLPH	$E_{cm}^{ee} = 189-209$ GeV
-0.012 ± 0.027 ± 0.011	10689	2 SCHAEL	05A ALEP	$E_{cm}^{ee} = 183-209$ GeV
-0.060 \pm $\begin{smallmatrix} 0.034 \\ -0.033 \end{smallmatrix}$	9800	3 ABBIENDI	04D OPAL	$E_{cm}^{ee} = 183-209$ GeV
-0.021 \pm $\begin{smallmatrix} 0.035 \\ -0.034 \end{smallmatrix}$ ± 0.017	10575	4 ACHARD	04D L3	$E_{cm}^{ee} = 161-209$ GeV
• • • We do not use the following data for averages, fits, limits, etc. • • •				
		5 CHATRCHYAN14AB	CMS	$E_{cm}^{pp} = 7$ TeV
		6 AAD	13AN ATLS	$E_{cm}^{pp} = 7$ TeV
		7 ABAZOV	12AG D0	$E_{cm}^{pp} = 1.96$ TeV
		8 ABAZOV	11AC D0	$E_{cm}^{pp} = 1.96$ TeV
		9 CHATRCHYAN11M	CMS	$E_{cm}^{pp} = 7$ TeV
	53	10 AARON	09B H1	$E_{cm}^{ep} = 0.3$ TeV
0.00 ± 0.06		11 ABAZOV	09AD D0	$E_{cm}^{pp} = 1.96$ TeV
		12 ABAZOV	09AJ D0	$E_{cm}^{pp} = 1.96$ TeV
		13 ABAZOV	08R D0	$E_{cm}^{pp} = 1.96$ TeV
0.16 \pm $\begin{smallmatrix} 0.12 \\ -0.13 \end{smallmatrix}$	1880	14 ABDALLAH	08C DLPH	Superseded by ABDALLAH 10
	1617	15 AALTONEN	07L CDF	$E_{cm}^{pp} = 1.96$ GeV
	17	16 ABAZOV	06H D0	$E_{cm}^{pp} = 1.96$ TeV
	141	17 ABAZOV	05J D0	$E_{cm}^{pp} = 1.96$ TeV
0.05 ± 0.09 ± 0.01	2298	18 ABREU	01I DLPH	$E_{cm}^{ee} = 183-189$ GeV
		19 BREITWEG	00 ZEUS	$e^+p \rightarrow e^+W^+X$, $\sqrt{s} \approx 300$ GeV
0.00 \pm $\begin{smallmatrix} 0.10 \\ -0.09 \end{smallmatrix}$	331	20 ABBOTT	99I D0	$E_{cm}^{pp} = 1.8$ TeV

¹ ABDALLAH 10 use data on the final states $e^+e^- \rightarrow jj\ell\nu$, $jjjj$, jjX , ℓX , at center-of-mass energies between 189–209 GeV at LEP2, where $j = jet$, $\ell = lepton$, and X represents missing momentum. The fit is carried out keeping all other parameters fixed at their SM values.

² SCHAEL 05A study single-photon, single- W , and WW -pair production from 183 to 209 GeV. Each parameter is determined from a single-parameter fit in which the other parameters assume their Standard Model values.

³ ABBIENDI 04d combine results from W^+W^- in all decay channels. Only CP -conserving couplings are considered and each parameter is determined from a single-parameter fit in which the other parameters assume their Standard Model values. The 95% confidence interval is $-0.13 < \lambda_\gamma < 0.01$.

⁴ ACHARD 04b study WW -pair production, single- W production and single-photon production with missing energy from 189 to 209 GeV. The result quoted here is obtained including data from 161 to 183 GeV, ACCIARRI 99q. Each parameter is determined from a single-parameter fit in which the other parameters assume their Standard Model values.

⁵ CHATRCHYAN 14AB measure $W\gamma$ production cross section for $p_T^\gamma > 15$ GeV and $R(\ell\gamma) > 0.7$, which is the separation between the γ and the final state charged lepton (e or μ) in the azimuthal angle-pseudorapidity ($\phi - \eta$) plane. After background subtraction the number of $e\nu\gamma$ and $\mu\nu\gamma$ events is determined to be 3200 ± 325 and 4970 ± 543 respectively, compatible with expectations from the SM. This leads to a 95% CL limit of $-0.050 < \lambda_\gamma < 0.037$, assuming all other parameters have SM values.

⁶ AAD 13AN study $W\gamma$ production in pp collisions. In events with no additional jet, 4449 (6578) W decays to electron (muon) are selected, with an expected background of 1662 ± 262 (2538 ± 362) events. Analysing the photon p_T spectrum above 100 GeV yields a 95% C.L. limit of $-0.065 < \lambda_\gamma < 0.061$. Supersedes AAD 12BX.

⁷ ABAZOV 12AG combine new results with already published results on $W\gamma$, WW and WZ production in order to determine the couplings with increased precision, superseding ABAZOV 08R, ABAZOV 11AC, ABAZOV 09AJ, ABAZOV 09AD. The 68% C.L. result for a formfactor cutoff of $\Lambda = 2$ TeV is $\lambda_\gamma = 0.007^{+0.021}_{-0.022}$.

⁸ ABAZOV 11AC study $W\gamma$ production in $p\bar{p}$ collisions at 1.96 TeV, with the W decay products containing an electron or a muon. They select 196 (363) events in the electron (muon) mode, with a SM expectation of 190 (372) events. A likelihood fit to the photon E_T spectrum above 15 GeV yields at 95% C.L. the result: $-0.08 < \lambda_\gamma < 0.07$ for a formfactor $\Lambda = 2$ TeV.

⁹ CHATRCHYAN 11M study $W\gamma$ production in pp collisions at $\sqrt{s} = 7$ TeV using 36 pb⁻¹ pp data with the W decaying to electron and muon. The total cross section is measured for photon transverse energy $E_T^\gamma > 10$ GeV and spatial separation from charged leptons in the plane of pseudo rapidity and azimuthal angle $\Delta R(\ell, \gamma) > 0.7$. The number of candidate (background) events is 452 (228 ± 21) for the electron channel and 520 (277 ± 25) for the muon channel. Setting other couplings to their standard model value, they derive a 95% CL limit of $-0.18 < \lambda_\gamma < 0.17$.

¹⁰ AARON 09B study single- W production in ep collisions at 0.3 TeV C.M. energy. They select 53 $W \rightarrow e/\mu$ events with a standard model expectation of 54.1 ± 7.4 events. Fitting the transverse momentum spectrum of the hadronic recoil system they obtain a 95% C.L. limit of $-2.5 < \lambda_\gamma < 2.5$.

¹¹ ABAZOV 09AD study the $p\bar{p} \rightarrow \ell\nu 2jet$ process arising in WW and WZ production. They select 12,473 (14,392) events in the electron (muon) channel with an expected di-boson signal of 436 (527) events. The results on the anomalous couplings are derived from an analysis of the p_T spectrum of the 2-jet system and quoted at 68% C.L. and for a form factor of 2 TeV. This measurement is not used for obtaining the mean as it is for a specific form factor. The 95% confidence interval is $-0.10 < \lambda_\gamma < 0.11$.

- ¹² ABAZOV 09AJ study the $p\bar{p} \rightarrow 2\ell 2\nu$ process arising in WW production. They select 100 events with an expected WW signal of 65 events. An analysis of the p_T spectrum of the two charged leptons leads to 95% C.L. limits of $-0.14 < \lambda_\gamma < 0.18$, for a form factor $\Lambda = 2$ TeV.
- ¹³ ABAZOV 08R use $0.7 \text{ fb}^{-1} p\bar{p}$ data at $\sqrt{s} = 1.96$ TeV to select 263 $W\gamma + X$ events, of which 187 constitute signal, with the W decaying into an electron or a muon, which is required to be well separated from a photon with $E_T > 9$ GeV. A likelihood fit to the photon E_T spectrum yields a 95% CL limit $-0.12 < \lambda_\gamma < 0.13$ with other couplings fixed to their Standard Model values.
- ¹⁴ ABDALLAH 08c determine this triple gauge coupling from the measurement of the spin density matrix elements in $e^+e^- \rightarrow W^+W^- \rightarrow (qq)(\ell\nu)$, where $\ell = e$ or μ . Values of all other couplings are fixed to their standard model values.
- ¹⁵ AALTONEN 07L set limits on anomalous TGCs using the $p_T(W)$ distribution in WW and WZ production with the W decaying into an electron or muon and the Z to 2 jets. Setting other couplings to their standard model value, the 95% C.L. limits are $-0.18 < \lambda_\gamma < 0.17$ for a form factor scale $\Lambda = 1.5$ TeV.
- ¹⁶ ABAZOV 06H study $p\bar{p} \rightarrow WW$ production with a subsequent decay $WW \rightarrow e^+\nu_e e^-\bar{\nu}_e$, $WW \rightarrow e^+\nu_e \mu^+\bar{\nu}_\mu$ or $WW \rightarrow \mu^+\nu_\mu \mu^-\bar{\nu}_\mu$. The 95% C.L. limit for a form factor scale $\Lambda = 1$ TeV is $-0.97 < \lambda_\gamma < 1.04$, fixing $\kappa_Z=1$. With the assumption that the $WW\gamma$ and WWZ couplings are equal the 95% C.L. one-dimensional limit ($\Lambda = 2$ TeV) is $-0.29 < \lambda < 0.30$.
- ¹⁷ ABAZOV 05i perform a likelihood fit to the photon E_T spectrum of $W\gamma + X$ events, where the W decays to an electron or muon which is required to be well separated from the photon. For $\Lambda = 2.0$ TeV the 95% CL limits are $-0.20 < \lambda_\gamma < 0.20$. In the fit κ_γ is kept fixed to its Standard Model value.
- ¹⁸ ABREU 01i combine results from e^+e^- interactions at 189 GeV leading to W^+W^- , $W\nu_e\nu_e$, and $\nu\bar{\nu}\gamma$ final states with results from ABREU 99L at 183 GeV. The 95% confidence interval is $-0.11 < \lambda_\gamma < 0.23$.
- ¹⁹ BREITWEG 00 search for W production in events with large hadronic p_T . For $p_T > 20$ GeV, the upper limit on the cross section gives the 95%CL limit $-3.2 < \lambda_\gamma < 3.2$ for κ_γ fixed to its Standard Model value.
- ²⁰ ABBOTT 99i perform a simultaneous fit to the $W\gamma$, $WW \rightarrow$ dilepton, $WW/WZ \rightarrow e\nu jj$, $WW/WZ \rightarrow \mu\nu jj$, and $WZ \rightarrow$ trilepton data samples. For $\Lambda = 2.0$ TeV, the 95%CL limits are $-0.18 < \lambda_\gamma < 0.19$.

κ_Z This coupling is CP-conserving (C- and P- separately conserving).

VALUE	EVTS	DOCUMENT ID	TECN	COMMENT
$0.924 + 0.059 - 0.056 \pm 0.024$	7171	¹ ACHARD	04D L3	$E_{cm}^{ee} = 189\text{--}209$ GeV
• • • We do not use the following data for averages, fits, limits, etc. • • •				
		² SIRUNYAN	20BA CMS	$E_{cm}^{pp} = 13$ TeV
		³ SIRUNYAN	19CL CMS	$E_{cm}^{pp} = 13$ TeV
		⁴ AABOUD	17s ATLS	$E_{cm}^{pp} = 7+8$ TeV
		⁵ KHACHATRYAN...17o	CMS	$E_{cm}^{pp} = 8$ TeV
		⁶ AAD	16AR ATLS	$E_{cm}^{pp} = 8$ TeV
		⁷ AAD	16P ATLS	$E_{cm}^{pp} = 8$ TeV
		⁸ AAD	13AL ATLS	$E_{cm}^{pp} = 7$ TeV
		⁹ AAD	12CD ATLS	$E_{cm}^{pp} = 7$ TeV
		¹⁰ AALTONEN	12AC CDF	$E_{cm}^{pp} = 1.96$ TeV
	34	¹¹ ABAZOV	11 D0	$E_{cm}^{pp} = 1.96$ TeV
	17	¹² ABAZOV	06H D0	$E_{cm}^{pp} = 1.96$ TeV
	2.3	¹³ ABAZOV	05s D0	$E_{cm}^{pp} = 1.96$ TeV

- ¹ ACHARD 04d study WW -pair production, single- W production and single-photon production with missing energy from 189 to 209 GeV. The result quoted here is obtained using the WW -pair production sample. Each parameter is determined from a single-parameter fit in which the other parameters assume their Standard Model values.
- ² SIRUNYAN 20BA study electroweak production of a W boson in association with two jets, using W decays in the electron or muon channel. The isolated muons (electrons) are required to have a transverse momentum larger than 25 (30) GeV, while the transverse momentum of the two jets has to be larger than 50 and 30 GeV. A total of 2.382 (1.051) million events are selected in the muon (electron) channel, with a Standard Model expectation of 2.39 ± 0.17 (1.054 ± 0.058) million events. Analysing the transverse momentum distribution of the charged leptons from W decay, the following 95% C.L. limit is obtained: $0.956 < \kappa_Z < 1.044$. Combining this result with that from the closely-related electroweak Z-jet-jet production SIRUNYAN 18BZ, the limit becomes: $0.957 < \kappa_Z < 1.042$.
- ³ SIRUNYAN 19CL study WW and WZ production in lepton + jet events, with one W boson decaying leptonically (electron or muon), and another W or Z boson decaying hadronically, reconstructed as a single massive large-radius jet. In the electron channel 2,456 (2,235) events are selected in the $WW(WZ)$ category, while in the muon channel 3,996 (3,572) events are selected in the $WW(WZ)$ category. Analysing the di-boson invariant mass distribution, the following 95% C.L. limit is obtained: $0.9921 < \kappa_Z < 1.0082$.
- ⁴ AABOUD 17s analyze electroweak production of a W boson in association with two jets at high dijet invariant mass, with the W boson decaying to electron or muon plus neutrino. In the signal region of dijet mass larger than 1 TeV and leading-jet transverse momentum larger than 600 GeV, 30 events are observed in the data with 39 ± 4 events expected in the Standard Model, yielding the following limit at 95% CL for the form factor cut-off scale $\Lambda_{FF} \rightarrow \infty$: $0.85 < \kappa_Z < 1.16$.
- ⁵ KHACHATRYAN 17o analyse WZ production where each boson decays into electrons or muons. Events are required to have a tri-lepton invariant mass larger than 100 GeV, with one of the lepton pairs having an invariant mass within 20 GeV of the Z boson mass. The Z transverse momentum spectrum is analyzed to set a 95% C.L. limit of: $0.79 < \kappa_Z < 1.25$.
- ⁶ AAD 16AR study WW production in pp collisions and select 6636 WW candidates in decay modes with electrons or muons with an expected background of 1546 ± 157 events. Assuming the LEP formulation and setting the form-factor Λ to infinity, a fit

to the transverse momentum distribution of the leading charged lepton, leads to a 95% C.L. range of $0.975 < \kappa_Z < 1.020$.

- ⁷ AAD 16P study WZ production in pp collisions and select 2091 WZ candidates in 4 decay modes with electrons and muons, with an expected background of 1825 ± 7 events. Analysing the WZ transverse momentum distribution, the resulting 95% C.L. limit is: $0.81 < \kappa_Z < 1.30$.
- ⁸ AAD 13AL study WW production in pp collisions and select 1325 WW candidates in decay modes with electrons or muons with an expected background of 369 ± 61 events. Assuming the LEP formulation and setting the form-factor $\Lambda =$ infinity, a fit to the transverse momentum distribution of the leading charged lepton, leads to a 95% C.L. range of $0.957 < \kappa_Z < 1.043$. Supersedes AAD 12AC.
- ⁹ AAD 12CD study WZ production in pp collisions and select 317 WZ candidates in three $\ell\nu$ decay modes with an expected background of 68.0 ± 10.0 events. The resulting 95% C.L. range is: $0.63 < \kappa_Z < 1.57$. Supersedes AAD 12V.
- ¹⁰ AALTONEN 12AC study WZ production in pp collisions and select 63 WZ candidates in three $\ell\nu$ decay modes with an expected background of 7.9 ± 1.0 events. Based on the cross section and shape of the Z transverse momentum spectrum, the following 95% C.L. range is reported: $0.61 < \kappa_Z < 1.90$ for a form factor of $\Lambda = 2$ TeV.
- ¹¹ ABAZOV 11 study the $p\bar{p} \rightarrow 3\ell\nu$ process arising in WZ production. They observe 34 WZ candidates with an estimated background of 6 events. An analysis of the p_T spectrum of the Z boson leads to a 95% C.L. limit of $0.600 < \kappa_Z < 1.675$, for a form factor $\Lambda = 2$ TeV.
- ¹² ABAZOV 06H study $p\bar{p} \rightarrow WW$ production with a subsequent decay $WW \rightarrow e^+\nu_e e^-\bar{\nu}_e$, $WW \rightarrow e^+\nu_e \mu^+\bar{\nu}_\mu$ or $WW \rightarrow \mu^+\nu_\mu \mu^-\bar{\nu}_\mu$. The 95% C.L. limit for a form factor scale $\Lambda = 2$ TeV is $0.95 < \kappa_Z < 1.55$, fixing $\lambda_\gamma=0$. With the assumption that the $WW\gamma$ and WWZ couplings are equal the 95% C.L. one-dimensional limit ($\Lambda = 2$ TeV) is $0.68 < \kappa < 1.45$.
- ¹³ ABAZOV 05s study $p\bar{p} \rightarrow WZ$ production with a subsequent trilepton decay to $\ell\nu\ell'\bar{\nu}'$ (ℓ and $\ell' = e$ or μ). Three events (estimated background 0.71 ± 0.08 events) with WZ decay characteristics are observed from which they derive limits on the anomalous WZ couplings. The 95% CL limit for a form factor scale $\Lambda = 1$ TeV is $-1.0 < \kappa_Z < 3.4$, fixing λ_Z and g_1^Z to their Standard Model values.

 λ_Z

This coupling is CP-conserving (C- and P- separately conserving).

VALUE	EVTS	DOCUMENT ID	TECN	COMMENT
$-0.088 + 0.060 - 0.057 \pm 0.023$	7171	¹ ACHARD	04D L3	$E_{cm}^{ee} = 189\text{--}209$ GeV
• • • We do not use the following data for averages, fits, limits, etc. • • •				
		² SIRUNYAN	20BA CMS	$E_{cm}^{pp} = 13$ TeV
		³ SIRUNYAN	19CL CMS	$E_{cm}^{pp} = 13$ TeV
		⁴ SIRUNYAN	18BZ CMS	$E_{cm}^{pp} = 13$ TeV
		⁵ AABOUD	17s ATLS	$E_{cm}^{pp} = 7+8$ TeV
		⁶ AABOUD	17u ATLS	$E_{cm}^{pp} = 8$ TeV
		⁷ KHACHATRYAN...17o	CMS	$E_{cm}^{pp} = 8$ TeV
		⁸ SIRUNYAN	17X CMS	$E_{cm}^{pp} = 8$ TeV
		⁹ AAD	16AR ATLS	$E_{cm}^{pp} = 8$ TeV
		¹⁰ AAD	16P ATLS	$E_{cm}^{pp} = 8$ TeV
		¹¹ AAD	14Y ATLS	$E_{cm}^{pp} = 8$ TeV
		¹² AAD	13AL ATLS	$E_{cm}^{pp} = 7$ TeV
		¹³ CHATRCHYAN 13BF	CMS	$E_{cm}^{pp} = 7$ TeV
		¹⁴ AAD	12CD ATLS	$E_{cm}^{pp} = 7$ TeV
		¹⁵ AALTONEN	12AC CDF	$E_{cm}^{pp} = 1.96$ TeV
	34	¹⁶ ABAZOV	11 D0	$E_{cm}^{pp} = 1.96$ TeV
	334	¹⁷ AALTONEN	10K CDF	$E_{cm}^{pp} = 1.96$ TeV
	13	¹⁸ ABAZOV	07Z D0	$E_{cm}^{pp} = 1.96$ TeV
	17	¹⁹ ABAZOV	06H D0	$E_{cm}^{pp} = 1.96$ TeV
	2.3	²⁰ ABAZOV	05s D0	$E_{cm}^{pp} = 1.96$ TeV

- ¹ ACHARD 04d study WW -pair production, single- W production and single-photon production with missing energy from 189 to 209 GeV. The result quoted here is obtained using the WW -pair production sample. Each parameter is determined from a single-parameter fit in which the other parameters assume their Standard Model values.
- ² SIRUNYAN 20BA study electroweak production of a W boson in association with two jets, using W decays in the electron or muon channel. The isolated muons (electrons) are required to have a transverse momentum larger than 25 (30) GeV, while the transverse momentum of the two jets has to be larger than 50 and 30 GeV. A total of 2.382 (1.051) million events are selected in the muon (electron) channel, with a Standard Model expectation of 2.39 ± 0.17 (1.054 ± 0.058) million events. Analysing the transverse momentum distribution of the charged leptons from W decay, the following 95% C.L. limit is obtained: $-0.0088 < \lambda_Z < 0.0095$. Combining this result with that from the closely-related electroweak Z-jet-jet production SIRUNYAN 18BZ, the limit becomes: $-0.0071 < \lambda_Z < 0.0076$.
- ³ SIRUNYAN 19CL study WW and WZ production in lepton + jet events, with one W boson decaying leptonically (electron or muon), and another W or Z boson decaying hadronically, reconstructed as a single massive large-radius jet. In the electron channel 2,456 (2,235) events are selected in the $WW(WZ)$ category, while in the muon channel 3,996 (3,572) events are selected in the $WW(WZ)$ category. Analysing the di-boson invariant mass distribution, the following 95% C.L. limit is obtained: $-0.0065 < \lambda_Z < 0.0066$.
- ⁴ SIRUNYAN 18BZ study $pp \rightarrow Z$ jet jet events at 13 TeV where $Z \rightarrow e^+e^-/\mu^+\mu^-$. Isolated electrons and muons are selected with p_T of the leading/sub-leading lepton $> 30/20$ GeV and $|\eta| < 2.4$, with the di-lepton invariant mass within 15 GeV of the Z mass. The two highest p_T jets are selected with p_T of the leading/sub-leading jet $> 50/30$ GeV respectively and dijet invariant mass > 200 GeV. Templates in the transverse momentum of the Z are utilized to set limits on the triple gauge couplings in the EFT and the LEP parametrizations. The following 95% C.L. limit is obtained $-0.010 < \lambda_Z < 0.010$.

Gauge & Higgs Boson Particle Listings

W

- ⁵ AABOUD 17s analyze electroweak production of a W boson in association with two jets at high dijet invariant mass, with the W boson decaying to electron or muon plus neutrino. In the signal region of dijet mass larger than 1 TeV and leading-jet transverse momentum larger than 600 GeV, 30 events are observed in the data with 39 ± 4 events expected in the Standard Model, yielding the following limit at 95% CL for the form factor cut-off scale $\Lambda_{FF} \rightarrow \infty$: $-0.053 < \lambda_Z < 0.042$.
- ⁶ AABOUD 17u analyze production of WW or WZ boson pairs with one W boson decaying to electron or muon plus neutrino, and the other W or Z boson decaying hadronically. The hadronic decay system is reconstructed as either a resolved two-jet system or as a single large jet. Analysing the transverse momentum distribution of the hadronic system above 100 GeV yields the following limit at 95% CL for the form factor cut-off scale $\Lambda_{FF} \rightarrow \infty$: $-0.013 < \lambda_Z < 0.013$.
- ⁷ KHACHATRYAN 17o analyse WZ production where each boson decays into electrons or muons. Events are required to have a tri-lepton invariant mass larger than 100 GeV, with one of the lepton pairs having an invariant mass within 20 GeV of the Z boson mass. The Z transverse momentum spectrum is analyzed to set a 95% C.L. limit of: $-0.018 < \lambda_Z < 0.016$.
- ⁸ SIRUNYAN 17x study $pp \rightarrow WW/WZ \rightarrow \ell\nu q\bar{q}$ production at 8 TeV where ℓ is an electron or muon with $p_T > 30$ or 25 GeV respectively. Suitable cuts are put on the p_T of the dijet system and the missing E_T of the event yielding a total of 285 and 204 WW events observed in the electron and muon channels. The following 95% C.L. limit is obtained: $-0.011 < \lambda_Z < 0.011$.
- ⁹ AAD 16AR study WW production in pp collisions and select 6636 WW candidates in decay modes with electrons or muons with an expected background of 1546 ± 157 events. Assuming the LEP formulation and setting the form-factor Λ to infinity, a fit to the transverse momentum distribution of the leading charged lepton, leads to a 95% C.L. range of $-0.019 < \lambda_Z < 0.019$.
- ¹⁰ AAD 16P study WZ production in pp collisions and select 2091 WZ candidates in 4 decay modes with electrons and muons, with an expected background of 1825 ± 7 events. Analysing the WZ transverse momentum distribution, the resulting 95% C.L. limit is: $-0.016 < \lambda_Z < 0.016$.
- ¹¹ AAD 14v determine the electroweak Z -dijet cross section in 8 TeV pp collisions. $Z \rightarrow e\bar{e}$ and $Z \rightarrow \mu\bar{\mu}$ decays are selected with the di-lepton $p_T > 20$ GeV and mass in the 81–101 GeV range. Minimum two jets are required with $p_T > 55$ and 45 GeV and no additional jets with $p_T > 25$ GeV in the rapidity interval between them. The normalized p_T balance between the Z and the two jets is required to be < 0.15 . This leads to a selection of 900 events with dijet mass > 1 TeV. The number of signal and background events expected is 261 and 592 respectively. A Poisson likelihood method is used on an event by event basis to obtain the 95% CL limit $-0.15 < \lambda_Z < 0.13$ for a form factor value $\Lambda = \infty$.
- ¹² AAD 13AL study WW production in pp collisions and select 1325 WW candidates in decay modes with electrons or muons with an expected background of 369 ± 61 events. Assuming the LEP formulation and setting the form-factor $\Lambda = \infty$, a fit to the transverse momentum distribution of the leading charged lepton, leads to a 95% C.L. range of $-0.062 < \lambda_Z < 0.059$. Supersedes AAD 12Ac.
- ¹³ CHATRCHYAN 13BF determine the W^+W^- production cross section using unlike sign di-lepton (e or μ) events with high p_T . The leptons have $p_T > 20$ GeV/c and are isolated. 1134 candidate events are observed with an expected SM background of 247 ± 34 . The p_T distribution of the leading lepton is fitted to obtain 95% C.L. limits of $-0.048 \leq \lambda_Z \leq 0.048$.
- ¹⁴ AAD 12CD study WZ production in pp collisions and select 317 WZ candidates in three $\ell\nu$ decay modes with an expected background of 68.0 ± 10.0 events. The resulting 95% C.L. range is: $-0.046 < \lambda_Z < 0.047$. Supersedes AAD 12v.
- ¹⁵ AALTONEN 12AC study WZ production in $p\bar{p}$ collisions and select 63 WZ candidates in three $\ell\nu$ decay modes with an expected background of 7.9 ± 1.0 events. Based on the cross section and shape of the Z transverse momentum spectrum, the following 95% C.L. range is reported: $-0.08 < \lambda_Z < 0.10$ for a form factor of $\Lambda = 2$ TeV.
- ¹⁶ ABAZOV 11 study the $p\bar{p} \rightarrow 3\ell\nu$ process arising in WZ production. They observe 34 WZ candidates with an estimated background of 6 events. An analysis of the p_T spectrum of the Z boson leads to a 95% C.L. limit of $-0.077 < \lambda_Z < 0.093$, for a form factor $\Lambda = 2$ TeV.
- ¹⁷ AALTONEN 10K study $p\bar{p} \rightarrow W^+W^-$ with $W \rightarrow e/\mu\nu$. The p_T of the leading (second) lepton is required to be > 20 (10) GeV. The final number of events selected is 654 of which 320 ± 47 are estimated to be background. The 95% C.L. interval is $-0.16 < \lambda_Z < 0.16$ for $\Lambda = 1.5$ TeV and $-0.14 < \lambda_Z < 0.15$ for $\Lambda = 2$ TeV.
- ¹⁸ ABAZOV 07z set limits on anomalous TGCs using the measured cross section and $p_T(Z)$ distribution in WZ production with both the W and the Z decaying leptonically into electrons and muons. Setting the other couplings to their standard model values, the 95% C.L. limit for a form factor scale $\Lambda = 2$ TeV is $-0.17 < \lambda_Z < 0.21$.
- ¹⁹ ABAZOV 06H study $p\bar{p} \rightarrow WW$ production with a subsequent decay $WW \rightarrow e^+\nu_e e^- \bar{\nu}_e$, $WW \rightarrow e^+\nu_e \mu^+ \bar{\nu}_\mu$ or $WW \rightarrow \mu^+\nu_\mu \mu^- \bar{\nu}_\mu$. The 95% C.L. limit for a form factor scale $\Lambda = 2$ TeV is $-0.39 < \lambda_Z < 0.39$, fixing $\kappa_F=1$. With the assumption that the $WW\gamma$ and WWZ couplings are equal the 95% C.L. one-dimensional limit ($\Lambda = 2$ TeV) is $-0.29 < \lambda < 0.30$.
- ²⁰ ABAZOV 05s study $p\bar{p} \rightarrow WZ$ production with a subsequent trilepton decay to $\ell\nu\ell'\bar{\ell}'$ (ℓ and ℓ' = e or μ). Three events (estimated background 0.71 ± 0.08 events) with WZ decay characteristics are observed from which they derive limits on the anomalous WWZ couplings. The 95% CL limit for a form factor scale $\Lambda = 1.5$ TeV is $-0.48 < \lambda_Z < 0.48$, fixing g_1^Z and κ_Z to their Standard Model values.

 g_1^Z

This coupling is CP -conserving but C - and P -violating.

VALUE	EVTs	DOCUMENT ID	TECN	COMMENT
-0.07 ± 0.09 OUR AVERAGE		Error includes scale factor of 1.1.		
-0.04 ± 0.13	9800	1 ABBIENDI	04D OPAL	$E_{cm}^{ee} = 183-209$ GeV
$0.00 \pm 0.13 \pm 0.05$	7171	2 ACHARD	04D L3	$E_{cm}^{ee} = 189-209$ GeV
-0.44 ± 0.23	1154	3 ACCIARRI	99Q L3	$E_{cm}^{ee} = 161+172+183$ GeV

• • • We do not use the following data for averages, fits, limits, etc. • • •

-0.31 ± 0.23 ⁴ EBOLI 00 THEO LEP1, SLC+ Tevatron

¹ ABBIENDI 04D combine results from W^+W^- in all decay channels. Only CP -conserving couplings are considered and each parameter is determined from a single-parameter fit in

which the other parameters assume their Standard Model values. The 95% confidence interval is $-0.28 < g_2^Z < +0.21$.

² ACHARD 04D study WW -pair production, single- W production and single-photon production with missing energy from 189 to 209 GeV. The result quoted here is obtained using the WW -pair production sample. Each parameter is determined from a single-parameter fit in which the other parameters assume their Standard Model values.

³ ACCIARRI 99Q study W -pair, single- W , and single photon events.

⁴ EBOLI 00 extract this indirect value of the coupling studying the non-universal one-loop contributions to the experimental value of the $Z \rightarrow b\bar{b}$ width ($\Lambda=1$ TeV is assumed).

 g_2^Z

This coupling is CP -violating (C -violating and P -conserving).

VALUE	EVTs	DOCUMENT ID	TECN	COMMENT
-0.30 ± 0.17 OUR AVERAGE				
-0.39 ± 0.19	1880	1 ABDALLAH	08c DLPH	$E_{cm}^{ee} = 189-209$ GeV
-0.02 ± 0.32	1065	2 ABBIENDI	01H OPAL	$E_{cm}^{ee} = 189$ GeV

¹ ABDALLAH 08c determine this triple gauge coupling from the measurement of the spin density matrix elements in $e^+e^- \rightarrow W^+W^- \rightarrow (qq)(\ell\nu)$, where $\ell = e$ or μ . Values of all other couplings are fixed to their standard model values.

² ABBIENDI 01H study W -pair events, with one leptonically and one hadronically decaying W . The coupling is extracted using information from the W production angle together with decay angles from the leptonically decaying W .

 $\tilde{\kappa}_Z$

This coupling is CP -violating (C -conserving and P -violating).

VALUE	EVTs	DOCUMENT ID	TECN	COMMENT
-0.12 ± 0.06 OUR AVERAGE				
-0.09 ± 0.08	1880	1 ABDALLAH	08c DLPH	$E_{cm}^{ee} = 189-209$ GeV
-0.20 ± 0.10	1065	2 ABBIENDI	01H OPAL	$E_{cm}^{ee} = 189$ GeV

• • • We do not use the following data for averages, fits, limits, etc. • • •

³ AABOUD 17s ATLS $E_{cm}^{pp} = 7+8$ TeV

⁴ BLINOV 11 LEP $E_{cm}^{ee} = 183-207$ GeV

¹ ABDALLAH 08c determine this triple gauge coupling from the measurement of the spin density matrix elements in $e^+e^- \rightarrow W^+W^- \rightarrow (qq)(\ell\nu)$, where $\ell = e$ or μ . Values of all other couplings are fixed to their standard model values.

² ABBIENDI 01H study W -pair events, with one leptonically and one hadronically decaying W . The coupling is extracted using information from the W production angle together with decay angles from the leptonically decaying W .

³ AABOUD 17s analyze electroweak production of a W boson in association with two jets at high dijet invariant mass, with the W boson decaying to electron or muon plus neutrino. In the signal region of dijet mass larger than 1 TeV and leading-jet transverse momentum larger than 600 GeV, 30 events are observed in the data with 39 ± 4 events expected in the Standard Model, yielding the following limit at 95% CL for the form factor cut-off scale $\Lambda_{FF} \rightarrow \infty$: $-0.56 < \tilde{\kappa}_Z < 0.56$.

⁴ BLINOV 11 use the LEP-average $e^+e^- \rightarrow W^+W^-$ cross section data for $\sqrt{s} = 183-207$ GeV to determine an upper limit on the TGC $\tilde{\kappa}_Z$. The average values of the cross sections as well as their correlation matrix, and standard model expectations of the cross sections are taken from the LEPWWG note hep-ex/0612034. At 95% confidence level $|\tilde{\kappa}_Z| < 0.13$.

 $\tilde{\lambda}_Z$

This coupling is CP -violating (C -conserving and P -violating).

VALUE	EVTs	DOCUMENT ID	TECN	COMMENT
-0.09 ± 0.07 OUR AVERAGE				
-0.08 ± 0.07	1880	1 ABDALLAH	08c DLPH	$E_{cm}^{ee} = 189-209$ GeV
-0.18 ± 0.24	1065	2 ABBIENDI	01H OPAL	$E_{cm}^{ee} = 189$ GeV

• • • We do not use the following data for averages, fits, limits, etc. • • •

³ AABOUD 17s ATLS $E_{cm}^{pp} = 7+8$ TeV

⁴ BLINOV 11 LEP $E_{cm}^{ee} = 183-207$ GeV

¹ ABDALLAH 08c determine this triple gauge coupling from the measurement of the spin density matrix elements in $e^+e^- \rightarrow W^+W^- \rightarrow (qq)(\ell\nu)$, where $\ell = e$ or μ . Values of all other couplings are fixed to their standard model values.

² ABBIENDI 01H study W -pair events, with one leptonically and one hadronically decaying W . The coupling is extracted using information from the W production angle together with decay angles from the leptonically decaying W .

³ AABOUD 17s analyze electroweak production of a W boson in association with two jets at high dijet invariant mass, with the W boson decaying to electron or muon plus neutrino. In the signal region of dijet mass larger than 1 TeV and leading-jet transverse momentum larger than 600 GeV, 30 events are observed in the data with 39 ± 4 events expected in the Standard Model, yielding the following limit at 95% CL for the form factor cut-off scale $\Lambda_{FF} \rightarrow \infty$: $-0.047 < \tilde{\lambda}_Z < 0.046$.

⁴ BLINOV 11 use the LEP-average $e^+e^- \rightarrow W^+W^-$ cross section data for $\sqrt{s} = 183-207$ GeV to determine an upper limit on the TGC $\tilde{\lambda}_Z$. The average values of the cross sections as well as their correlation matrix, and standard model expectations of the cross sections are taken from the LEPWWG note hep-ex/0612034. At 95% confidence level $|\tilde{\lambda}_Z| < 0.31$.

W ANOMALOUS MAGNETIC MOMENT

The full magnetic moment is given by $\mu_W = e(1+\kappa+\lambda)/2m_W$. In the Standard Model, at tree level, $\kappa=1$ and $\lambda=0$. Some papers have defined $\Delta\kappa = 1-\kappa$ and assume that $\lambda=0$. Note that the electric quadrupole moment is given by $-e(\kappa-\lambda)/m_W^2$. A description of the parameterization of these moments and additional references can be found in HAGIWARA 87

and BAUR 88. The parameter Λ appearing in the theoretical limits below is a regularization cutoff which roughly corresponds to the energy scale where the structure of the W boson becomes manifest.

VALUE ($e/2m_W$)	EVTS	DOCUMENT ID	TECN	COMMENT
$2.22^{+0.20}_{-0.19}$	2298	1 ABREU	01i	DLPH $E_{cm}^e = 183+189$ GeV
• • • We do not use the following data for averages, fits, limits, etc. • • •				
		2 ABE	95G	CDF
		3 ALITTI	92c	UA2
		4 SAMUEL	92	THEO
		5 SAMUEL	91	THEO
		6 GRIFOLS	88	THEO
		7 GROTCHE	87	THEO
		8 VANDERBIJ	87	THEO
		9 GRAU	85	THEO
		10 SUZUKI	85	THEO
		11 HERZOG	84	THEO

- ABREU 01i combine results from e^+e^- interactions at 189 GeV leading to W^+W^- , $W\nu\rho$, and $\nu\bar{\nu}\gamma$ final states with results from ABREU 99L at 183 GeV to determine Δg_Z^2 , $\Delta\kappa_\gamma$, and λ_γ . $\Delta\kappa_\gamma$ and λ_γ are simultaneously floated in the fit to determine μ_W .
- ABE 95G report $-1.3 < \kappa < 3.2$ for $\lambda=0$ and $-0.7 < \lambda < 0.7$ for $\kappa=1$ in $p\bar{p} \rightarrow e\nu_e\gamma X$ and $\mu\nu_\mu\gamma X$ at $\sqrt{s} = 1.8$ TeV.
- ALITTI 92c measure $\kappa = 1^{+2.6}_{-2.2}$ and $\lambda = 0^{+1.7}_{-1.8}$ in $p\bar{p} \rightarrow e\nu\gamma + X$ at $\sqrt{s} = 630$ GeV. At 95%CL they report $-3.5 < \kappa < 5.9$ and $-3.6 < \lambda < 3.5$.
- SAMUEL 92 use preliminary CDF and UA2 data and find $-2.4 < \kappa < 3.7$ at 96%CL and $-3.1 < \lambda < 4.2$ at 95%CL respectively. They use data for $W\gamma$ production and radiative W decay.
- SAMUEL 91 use preliminary CDF data for $p\bar{p} \rightarrow W\gamma X$ to obtain $-11.3 \leq \Delta\kappa \leq 10.9$. Note that their $\kappa = 1 - \Delta\kappa$.
- GRIFOLS 88 uses deviation from ρ parameter to set limit $\Delta\kappa \lesssim 65 (M_W^2/\Lambda^2)$.
- GROTCHE 87 finds the limit $-37 < \Delta\kappa < 73.5$ (90% CL) from the experimental limits on $e^+e^- \rightarrow \nu\bar{\nu}\gamma$ assuming three neutrino generations and $-19.5 < \Delta\kappa < 56$ for four generations. Note their $\Delta\kappa$ has the opposite sign as our definition.
- VANDERBIJ 87 uses existing limits to the photon structure to obtain $|\Delta\kappa| < 33 (m_W/\Lambda)$. In addition VANDERBIJ 87 discusses problems with using the ρ parameter of the Standard Model to determine $\Delta\kappa$.
- GRAU 85 uses the muon anomaly to derive a coupled limit on the anomalous magnetic dipole and electric quadrupole (λ) moments $1.05 > \Delta\kappa \ln(\Lambda/m_W) + \lambda/2 > -2.77$. In the Standard Model $\lambda = 0$.
- SUZUKI 85 uses partial-wave unitarity at high energies to obtain $|\Delta\kappa| \lesssim 190 (m_W/\Lambda)^2$. From the anomalous magnetic moment of the muon, SUZUKI 85 obtains $|\Delta\kappa| \lesssim 2.2 \ln(\Lambda/m_W)$. Finally SUZUKI 85 uses deviations from the ρ parameter and obtains a very qualitative, order-of-magnitude limit $|\Delta\kappa| \lesssim 150 (m_W/\Lambda)^4$ if $|\Delta\kappa| \ll 1$.
- HERZOG 84 consider the contribution of W -boson to muon magnetic moment including anomalous coupling of $WW\gamma$. Obtain a limit $-1 < \Delta\kappa < 3$ for $\Lambda \gtrsim 1$ TeV.

$c_{WWW}/\Lambda^2, c_W/\Lambda^2, c_B/\Lambda^2$

These couplings are used in EFT-based approaches to anomalous couplings. They are linearly related to the couplings discussed above.

VALUE	DOCUMENT ID	TECN	COMMENT
• • • We do not use the following data for averages, fits, limits, etc. • • •			
	1 AAD	21AC ATLS	$E_{cm}^{pp} = 13$ TeV
	2 AAD	21W ATLS	$E_{cm}^{pp} = 13$ TeV
	3 SIRUNYAN	21G CMS	$E_{cm}^{pp} = 13$ TeV
	4 SIRUNYAN	20BA CMS	$E_{cm}^{pp} = 13$ TeV
	5 SIRUNYAN	20BF CMS	$E_{cm}^{pp} = 13$ TeV
	6 AABOUD	19BA ATLS	$E_{cm}^{pp} = 13$ TeV
	7 SIRUNYAN	19AD CMS	$E_{cm}^{pp} = 13$ TeV
	8 SIRUNYAN	19CL CMS	$E_{cm}^{pp} = 13$ TeV
	9 AABOUD	18Q ATLS	$E_{cm}^{pp} = 13$ TeV
	10 SIRUNYAN	18BZ CMS	$E_{cm}^{pp} = 13$ TeV
	11 AABOUD	17s ATLS	$E_{cm}^{pp} = 7+8$ TeV
	12 AABOUD	17t ATLS	$E_{cm}^{pp} = 8$ TeV
	13 KHACHATRYAN...17O	CMS	$E_{cm}^{pp} = 8$ TeV
	14 SIRUNYAN	17X CMS	$E_{cm}^{pp} = 8$ TeV
	15 AAD	16AR ATLS	$E_{cm}^{pp} = 8$ TeV
	16 AAD	16P ATLS	$E_{cm}^{pp} = 8$ TeV
	17 KHACHATRYAN...16BI	CMS	$E_{cm}^{pp} = 8$ TeV

- AAD 21AC study the differential cross-section for the electroweak production of dijets in association with a Z boson, where the Z boson decays to electrons or muons. The number of events selected in the data is 10,870 (12,125) in the electron (muon) channel. Analyzing the distribution of the azimuthal separation of the two jets, the following 95% C.L. limits are derived in units of TeV^{-2} : $-2.7 < c_{WWW}/\Lambda^2 < 5.8$, $-1.6 < \tilde{c}_{WWW}/\Lambda^2 < 2.0$, $-0.19 < c_W/\Lambda^2 < 0.41$, $-0.11 < \tilde{c}_W/\Lambda^2 < 0.14$, $-6.31 < c_{HWB}/\Lambda^2 < 1.01$, $0.23 < \tilde{c}_{HWB}/\Lambda^2 < 2.35$.

- AAD 21W analyze W^+W^- production in association with at least one jet. Events with exactly one oppositely-charged electron-muon pair and at least one hadronic jet of transverse momentum larger than 30 GeV (120 GeV) are selected. In the data, 89,239 (5,825) events are found, with a total Standard-Model expectation of 91600 ± 2500 (5980 ± 150). Analyzing the electron-muon invariant mass distribution, the following limit at 95% C.L. is obtained: $-0.33 < c_{WW}/\Lambda^2 < 0.33$ ($-0.60 < c_W/\Lambda^2 < 0.58$), for a fixed choice of $\Lambda = 1$ TeV.
- SIRUNYAN 21G measure $W\gamma$ production where the W decays into electrons or muons. In the data, 385,224 (395,818) events are selected in the electron (muon) channel, with a total Standard-Model expectation of 396913 ± 54686 (396257 ± 22837) events. Analyzing the photon transverse momentum distribution, the following 95% C.L. limits are derived in units of TeV^{-2} : $-0.90 < c_{WWW}/\Lambda^2 < 0.91$, $-40 < c_B/\Lambda^2 < 41$, $-0.45 < \tilde{c}_{WWW}/\Lambda^2 < 0.45$, $-20 < \tilde{c}_W/\Lambda^2 < 20$.
- SIRUNYAN 20BA study electroweak production of a W boson in association with two jets, using W decays in the electron or muon channel. The isolated muons (electrons) are required to have a transverse momentum larger than 25 (30) GeV, while the transverse momentum of the two jets has to be larger than 50 and 30 GeV. A total of 2,382 (1,051) million events are selected in the muon (electron) channel, with a Standard Model expectation of 2.39 ± 0.17 (1.054 ± 0.058) million events. Analyzing the transverse momentum distribution of the charged leptons from W decay, the following 95% C.L. limits are obtained in units of TeV^{-2} : $-2.3 < c_{WWW}/\Lambda^2 < 2.5$, $-8.8 < c_W/\Lambda^2 < 16$, $-45 < c_B/\Lambda^2 < 46$. Combining these results with those from the closely-related electroweak Z -jet-jet production SIRUNYAN 18BZ, the limits become: $-1.8 < c_{WWW}/\Lambda^2 < 2.0$, $-5.8 < c_W/\Lambda^2 < 10$, $-43 < c_B/\Lambda^2 < 45$.
- SIRUNYAN 20BF study W^+W^- production with the W bosons decaying to electrons or muons. The leading (subleading) lepton is required to have a transverse momentum larger than 25 (20) GeV. Events with a same-flavor di-lepton invariant mass within 15 GeV of the Z mass are rejected, as are event with a third lepton of transverse momentum larger than 10 GeV. In the same- (different-) flavor category a total of 9,604 (20,270) events are selected while the number of expected events is 9640 \pm 490 (20280 \pm 430). Analyzing the different-flavor di-lepton invariant mass distribution, the following 95% C.L. limits are obtained in units of TeV^{-2} : $-1.8 < c_{WWW}/\Lambda^2 < 1.8$, $-3.6 < c_W/\Lambda^2 < 2.8$, $-9.4 < c_B/\Lambda^2 < 8.5$.
- AABOUD 19BA study WW production in decay modes with an electron and a muon. The charged leptons are each required to have a transverse momentum larger than 27 GeV and rapidity less than 2.5. The electron-muon system is required to have a mass larger than 55 GeV and a transverse momentum larger than 30 GeV. The missing transverse energy must be larger than 20 GeV. Events containing a jet with transverse momentum exceeding 35 GeV and rapidity smaller than 4.5 are rejected. A total of 12,659 events are selected in the data, with an expected background of 4240 \pm 477 events. Analyzing the transverse momentum spectrum of the leading charged lepton, the following 95% C.L. limits are derived in units of TeV^{-2} : $-3.4 < c_{WWW}/\Lambda^2 < 3.3$, $-7.4 < c_W/\Lambda^2 < 4.1$, $-21 < c_B/\Lambda^2 < 18$, $-1.6 < \tilde{c}_{WWW}/\Lambda^2 < 1.6$, $-76 < \tilde{c}_W/\Lambda^2 < 76$.
- SIRUNYAN 19AD study inclusive WZ production, with W and Z decaying to electrons or muons. The leading (subleading) charged lepton candidate from the Z boson decay is required to have a transverse momentum larger than 25 GeV (10 GeV). The charged lepton candidate from the W boson decay is required to have a transverse momentum larger than 25 GeV. The invariant mass of the two leptons from Z decay is required to be within 15 GeV of the Z mass, while the invariant mass of the tri-lepton system is required to exceed 100 GeV. A total of 3,831 tri-lepton events are observed, with a fitted SM WZ signal of 3166 ± 62 events and a fitted background of 666 ± 45 events. The approximated WZ invariant mass distribution is analyzed to set 95% C.L. limits as follows: $-4.1 < c_W/\Lambda^2 < 1.1$, $-2.0 < c_{WWW}/\Lambda^2 < 2.1$, $-100 < c_B/\Lambda^2 < 160$, in units of TeV^{-2} .
- SIRUNYAN 19CL study WW and WZ production in lepton + jet events, with one W boson decaying leptonically (electron or muon), and another W or Z boson decaying hadronically, reconstructed as a single massive large-radius jet. In the electron channel 2,456 (2,235) events are selected in the $WW(WZ)$ category, while in the muon channel 3,996 (3572) events are selected in the $WW(WZ)$ category. Analyzing the di-boson invariant mass distribution, the following 95% C.L. limits are obtained in units of TeV^{-2} : $-1.58 < c_{WWW}/\Lambda^2 < 1.59$, $-2.00 < c_W/\Lambda^2 < 2.65$, $-8.78 < c_B/\Lambda^2 < 8.54$.
- AABOUD 18Q study $pp \rightarrow ZZ$ events at $\sqrt{s} = 13$ TeV with $Z \rightarrow e^+e^-$ or $Z \rightarrow \mu^+\mu^-$. The number of events observed in the $4e, 2e2\mu$, and 4μ channels is 249, 465, and 303 respectively. Analyzing the p_T spectrum of the leading Z boson, the following the following 95% C.L. limits are derived in units of TeV^{-4} : $-5.9 < c_{BW}^2/\Lambda^4 < 5.9$, $-3.0 < c_{WW}^2/\Lambda^4 < 3.0$, $-3.3 < c_{BW}^2/\Lambda^4 < 3.3$, $-2.7 < c_{BB}^2/\Lambda^4 < 2.8$.
- SIRUNYAN 18BZ study $pp \rightarrow Z$ jet jet events at 13 TeV where $Z \rightarrow e^+e^-/\mu^+\mu^-$. Isolated electrons and muons are selected with p_T of the leading/sub-leading lepton $> 30/20$ GeV and $|\eta| < 2.4$, with the di-lepton invariant mass within 15 GeV of the Z mass. The two highest p_T jets are selected with p_T of the leading/sub-leading jet $> 50/30$ GeV respectively and dijet invariant mass > 200 GeV. Templates in the transverse momentum of the Z are utilized to set limits on the triple gauge couplings in the EFT and the LEP parametrizations. The following 95% C.L. limits are obtained in units of TeV^{-2} : $-2.6 < c_{WWW}/\Lambda^2 < 2.6$ and $-8.4 < c_W/\Lambda^2 < 10.1$.
- AABOUD 17s analyze electroweak production of a W boson in association with two jets at high dijet invariant mass, with the W boson decaying to electron or muon plus neutrino. In the signal region of dijet mass larger than 1 TeV and leading-jet transverse momentum larger than 600 GeV, 30 events are observed in the data with 39 ± 4 events expected in the Standard Model, yielding the following limits at 95% CL for the form factor cut-off scale $\Lambda_{FF} \rightarrow \infty$: $-33 < c_W/\Lambda^2 < 30$, $-170 < c_B/\Lambda^2 < 160$, $-13 < c_{WWW}/\Lambda^2 < 9$, $-580 < \tilde{c}_W/\Lambda^2 < 580$, $-11 < \tilde{c}_{WWW}/\Lambda^2 < 11$, in units of TeV^{-2} .
- AABOUD 17t analyze production of WW or WZ boson pairs with one W boson decaying to electron or muon plus neutrino, and the other W or Z boson decaying hadronically. The hadronic decay system is reconstructed as either a resolved two-jet system or as a single large jet. Analyzing the transverse momentum distribution of the hadronic system above 100 GeV yields the following limits at 95% CL for the form factor cut-off scale $\Lambda_{FF} \rightarrow \infty$: $-3.1 < c_{WWW}/\Lambda^2 < 3.1$, $-19 < c_B/\Lambda^2 < 20$, $-5.1 < c_W/\Lambda^2 < 5.8$, in units of TeV^{-2} .
- KHACHATRYAN 17O analyse WZ production where each boson decays into electrons or muons. Events are required to have a tri-lepton invariant mass larger than 100 GeV,

Gauge & Higgs Boson Particle Listings

W

with one of the lepton pairs having an invariant mass within 20 GeV of the Z boson mass. The Z transverse momentum spectrum is analyzed to set 95% C.L. limits of: $-260 < c_B/\Lambda^2 < 210$, $-4.2 < c_W/\Lambda^2 < 8.0$, $-4.6 < c_{WW}/\Lambda^2 < 4.2$, in units of TeV^{-2} .

¹⁴ SIRUNYAN 17X study $pp \rightarrow WW/WZ \rightarrow \ell\nu q\bar{q}$ production at 8 TeV where ℓ is an electron or muon with $p_T > 30$ or 25 GeV respectively. Suitable cuts are put on the p_T of the dijet system and the missing E_T of the event yielding a total of 285 and 204 WV events observed in the electron and muon channels. The following 95% C.L. limits in units of TeV^{-2} are obtained: $-2.7 < c_{WW}/\Lambda^2 < 2.7$, $-14 < c_B/\Lambda^2 < 17$, $-2.0 < c_W/\Lambda^2 < 5.7$.

¹⁵ AAD 16AR study WW production in pp collisions and select 6636 WW candidates in decay modes with electrons or muons with an expected background of 1546 ± 157 events. Assuming an EFT formulation, a fit to the transverse momentum distribution of the leading charged lepton, leads to 95% C.L. ranges of: $-4.61 < c_{WW}/\Lambda^2 < 4.60$, $-5.87 < c_W/\Lambda^2 < 10.54$ and $-20.9 < c_B/\Lambda^2 < 26.3$, in units of TeV^{-2} .

¹⁶ AAD 16P study WZ production in pp collisions and select 2091 WZ candidates in 4 decay modes with electrons and muons, with an expected background of 1825 ± 7 events. Analyzing the WZ transverse momentum distribution, the resulting 95% C.L. limits are: $-3.9 < c_{WW}/\Lambda^2 < 4.0$, $-4.3 < c_W/\Lambda^2 < 6.8$, and $-320 < c_B/\Lambda^2 < 210$, in units of TeV^{-2} .

¹⁷ KHACHATRYAN 16BI determine the W^+W^- production cross section using unlike sign di-lepton (e or μ) events with high p_T . The leptons have $p_T > 20$ GeV/c and are isolated. Events are required to have no jets above p_T of 30 GeV/c. 4847 (2233) events are selected with different (same) flavor leptons, with an expected total background of 1179 ± 123 (643 ± 73) events. Analyzing the di-lepton invariant mass spectrum, the following values are obtained: $c_{WW}/\Lambda^2 = 0.1 \pm 3.2$, $c_W/\Lambda^2 = -3.6^{+5.0}_{-4.5}$ and $c_B/\Lambda^2 = -3.2^{+15.0}_{-14.5}$, in units of TeV^{-2} . The limits at 95% C.L. are: $-5.7 < c_{WW}/\Lambda^2 < 5.9$, $-11.4 < c_W/\Lambda^2 < 5.4$ and $-29.2 < c_B/\Lambda^2 < 23.9$, in units of TeV^{-2} .

ANOMALOUS W/Z QUARTIC COUPLINGS

Revised November 2015 by M.W. Gr unewald (U. College Dublin) and A. Gurtu (Formerly Tata Inst.).

Quartic couplings, $WWZZ$, $WWZ\gamma$, $WW\gamma\gamma$, and $ZZ\gamma\gamma$, were studied at LEP and Tevatron at energies at which the Standard Model predicts negligible contributions to multiboson production. Thus, to parametrize limits on these couplings, an effective theory approach is adopted which supplements the Standard Model Lagrangian with higher dimensional operators which include quartic couplings. The LEP collaborations chose the lowest dimensional representation of operators (dimension 6) which presumes the $SU(2) \times U(1)$ gauge symmetry is broken by means other than the conventional Higgs scalar doublet [1–3]. In this representation possible quartic couplings, a_0, a_c, a_n , are expressed in terms of the following dimension-6 operators [1,2];

$$\begin{aligned} L_6^0 &= -\frac{e^2}{16\Lambda^2} a_0 F^{\mu\nu} F_{\mu\nu} \vec{W}^\alpha \cdot \vec{W}_\alpha \\ L_6^c &= -\frac{e^2}{16\Lambda^2} a_c F^{\mu\alpha} F_{\mu\beta} \vec{W}^\beta \cdot \vec{W}_\alpha \\ L_6^n &= -i\frac{e^2}{16\Lambda^2} a_n \epsilon_{ijk} W_{\mu\alpha}^{(i)} W_{\nu}^{(j)} W^{(k)\alpha} F^{\mu\nu} \\ \tilde{L}_6^0 &= -\frac{e^2}{16\Lambda^2} \tilde{a}_0 F^{\mu\nu} \tilde{F}_{\mu\nu} \vec{W}^\alpha \cdot \vec{W}_\alpha \\ \tilde{L}_6^n &= -i\frac{e^2}{16\Lambda^2} \tilde{a}_n \epsilon_{ijk} W_{\mu\alpha}^{(i)} W_{\nu}^{(j)} W^{(k)\alpha} \tilde{F}^{\mu\nu} \end{aligned}$$

where F, W are photon and W fields, L_6^0 and L_6^c conserve C, P separately (\tilde{L}_6^0 conserves only C) and generate anomalous $W^+W^-\gamma\gamma$ and $ZZ\gamma\gamma$ couplings, L_6^n violates CP (\tilde{L}_6^n violates both C and P) and generates an anomalous $W^+W^-Z\gamma$ coupling, and Λ is an energy scale for new physics. For the $ZZ\gamma\gamma$ coupling the CP -violating term represented by L_6^n does not contribute. These couplings are assumed to be real and to vanish at tree level in the Standard Model.

Within the same framework as above, a more recent description of the quartic couplings [3] treats the anomalous parts of the $WW\gamma\gamma$ and $ZZ\gamma\gamma$ couplings separately, leading to two sets parametrized as a_0^V/Λ^2 and a_c^V/Λ^2 , where $V = W$ or Z .

With the discovery of a Higgs at the LHC in 2012, it is then useful to go to the next higher dimensional representation (dimension 8 operators) in which the gauge symmetry is

broken by the conventional Higgs scalar doublet [3,4]. There are 14 operators which can contribute to the anomalous quartic coupling signal. Some of the operators have analogues in the dimension 6 scheme. The CMS collaboration, [5], have used this parametrization, in which the connections between the two schemes are also summarized:

$$\begin{aligned} \mathcal{L}_{AQGC} &= -\frac{e^2 a_0^W}{8 \Lambda^2} F_{\mu\nu} F^{\mu\nu} W^{+a} W_a^- \\ &\quad -\frac{e^2 a_c^W}{16 \Lambda^2} F_{\mu\nu} F^{\mu\alpha} (W^{+\nu} W_a^- + W^{-\nu} W_a^+) \\ &\quad -e^2 g^2 \frac{\kappa_0^W}{\Lambda^2} F_{\mu\nu} Z^{\mu\nu} W^{+a} W_a^- \\ &\quad -\frac{e^2 g^2 \kappa_c^W}{2 \Lambda^2} F_{\mu\nu} Z^{\mu\alpha} (W^{+\nu} W_a^- + W^{-\nu} W_a^+) \\ &\quad + \frac{f_{T,0}}{\Lambda^4} Tr[\widehat{W}_{\mu\nu} \widehat{W}^{\mu\nu}] \times Tr[\widehat{W}_{\alpha\beta} \widehat{W}^{\alpha\beta}] \end{aligned}$$

The energy scale of possible new physics is Λ , and $g = e/\sin(\theta_W)$, e being the unit electric charge and θ_W the Weinberg angle. The field tensors are described in [3,4].

The two dimension 6 operators a_0^W/Λ^2 and a_c^W/Λ^2 are associated with the $WW\gamma\gamma$ vertex. Among dimension 8 operators, κ_0^W/Λ^2 and κ_c^W/Λ^2 are associated with the $WWZ\gamma$ vertex, whereas the parameter $f_{T,0}/\Lambda^4$ contributes to both vertices. There is a relationship between these two dimension 6 parameters and the dimension 8 parameters $f_{M,i}/\Lambda^4$ as follows [3]:

$$\begin{aligned} \frac{a_0^W}{\Lambda^2} &= -\frac{4M_W^2}{g^2} \frac{f_{M,0}}{\Lambda^4} - \frac{8M_W^2}{g'^2} \frac{f_{M,2}}{\Lambda^4} \\ \frac{a_c^W}{\Lambda^2} &= -\frac{4M_W^2}{g^2} \frac{f_{M,1}}{\Lambda^4} - \frac{8M_W^2}{g'^2} \frac{f_{M,3}}{\Lambda^4} \end{aligned}$$

where $g' = e/\cos(\theta_W)$ and M_W is the invariant mass of the W boson. This relation provides a translation between limits on dimension 6 operators $a_{0,c}^W$ and $f_{M,j}/\Lambda^4$. It is further required [4] that $f_{M,0} = 2f_{M,2}$ and $f_{M,1} = 2f_{M,3}$ which suppresses contributions to the $WWZ\gamma$ vertex. The complete set of Lagrangian contributions as presented in [4] corresponds to 19 anomalous couplings in total – $f_{S,i}$, $i = 1, 2$, $f_{M,i}$, $i = 0, \dots, 8$ and $f_{T,i}$, $i = 0, \dots, 9$ – each scaled by $1/\Lambda^4$.

The ATLAS collaboration [6], on the other hand, follows a K-matrix driven approach of Ref. 7 in which the anomalous couplings can be expressed in terms of two parameters α_4 and α_5 , which account for all BSM effects.

It is the early stages in the determination of quartic couplings by the LHC experiments. It is hoped that the two collaborations, ATLAS and CMS, will agree to use at least one common set of parameters to express these limits to enable the reader to make a comparison and allow for a possible LHC combination.

References

1. G. Belanger and F. Boudjema, Phys. Lett. **B288**, 201 (1992).
2. J.W. Stirling and A. Werthenbach, Eur. Phys. J. **C14**, 103 (2000);

- J.W. Stirling and A. Werthenbach, Phys. Lett. **B466**, 369 (1999);
 A. Denner *et al.*, Eur. Phys. J. **C20**, 201 (2001);
 G. Montagna *et al.*, Phys. Lett. **B515**, 197 (2001).
 3. G. Belanger *et al.*, Eur. Phys. J. **C13**, 283 (2000).
 4. O.J.P. Éboli, M.C. Gonzalez-Garcia, and S.M. Lietti, Phys. Rev. **D69**, 095005 (2004);
 O.J.P. Éboli, M.C. Gonzalez-Garcia, and J.K. Mizukoshi, Phys. Rev. **D77**, 073005 (2006).
 5. S. Chatrchyan *et al.*, Phys. Rev. **D90**, 032008 (2014);
 S. Chatrchyan *et al.*, Phys. Rev. Lett. **114**, 051801 (2015).
 6. G. Aad *et al.*, Phys. Rev. Lett. **113**, 141803 (2014).
 7. A. Albateanu, W. Killian, and J. Reuter, JHEP **0811**, 010 (2008).

$a_0/\Lambda^2, a_c/\Lambda^2, a_n/\Lambda^2, \kappa_0^W/\Lambda^2, \kappa_c^W/\Lambda^2, f_{T,0}/\Lambda^4, f_{M,i}/\Lambda^4, \alpha_4, \alpha_5, F_{S,i}/\Lambda^4, F_{M,i}/\Lambda^4, F_{T,i}/\Lambda^4$

Anomalous W quartic couplings are measured by the experiments at LEP, the Tevatron, and the LHC. Some of the recent results from the Tevatron and LHC experiments individually surpass the combined LEP-2 results in precision (see below). As discussed in the review on the "Anomalous W/Z quartic couplings (QGCS)," the measurements are typically done using different operator expansions which then do not allow the results to be compared and averaged. At least one common framework should be agreed upon for the use in the future publications by the experiments.

Some publications from LHC experiments derive limits for various assumed values of the form-factor cutoff Λ_{FF} . The values quoted below are for $\Lambda_{FF} \rightarrow \infty$.

VALUE	DOCUMENT ID	TECN	COMMENT
• • •	We do not use the following data for averages, fits, limits, etc. • • •		
	1 SIRUNYAN	21 CMS	$E_{cm}^{pp} = 13$ TeV
	2 TUMASYAN	21A CMS	$E_{cm}^{pp} = 13$ TeV
	3 TUMASYAN	21B CMS	$E_{cm}^{pp} = 13$ TeV
	4 SIRUNAYN	20 CMS	$E_{cm}^{pp} = 13$ TeV
	5 SIRUNYAN	20AL CMS	$E_{cm}^{pp} = 13$ TeV
	6 SIRUNYAN	20BD CMS	$E_{cm}^{pp} = 13$ TeV
	7 SIRUNYAN	19BM CMS	$E_{cm}^{pp} = 13$ TeV
	8 SIRUNYAN	19BP CMS	$E_{cm}^{pp} = 13$ TeV
	9 SIRUNYAN	19CQ CMS	$E_{cm}^{pp} = 13$ TeV
	10 SIRUNYAN	18CC CMS	$E_{cm}^{pp} = 13$ TeV
	11 AABOUD	17AA ATLS	$E_{cm}^{pp} = 8$ TeV
	12 AABOUD	17AG ATLS	$E_{cm}^{pp} = 8$ TeV
	13 AABOUD	17D ATLS	$E_{cm}^{pp} = 8$ TeV
	14 AABOUD	17J ATLS	$E_{cm}^{pp} = 8$ TeV
	15 AABOUD	17M ATLS	$E_{cm}^{pp} = 8$ TeV
	16 KHACHATRYAN...17AA	CMS	$E_{cm}^{pp} = 8$ TeV
	17 KHACHATRYAN...17M	CMS	$E_{cm}^{pp} = 8$ TeV
	18 SIRUNYAN	17AD CMS	$E_{cm}^{pp} = 13$ TeV
	19 SIRUNYAN	17AR CMS	$E_{cm}^{pp} = 8$ TeV
	20 AABOUD	16E ATLS	$E_{cm}^{pp} = 8$ TeV
	21 AAD	16Q ATLS	$E_{cm}^{pp} = 8$ TeV
	22 KHACHATRYAN...16AX	CMS	$E_{cm}^{pp} = 8$ TeV
	23 AAD	15N ATLS	$E_{cm}^{pp} = 8$ TeV
	24 KHACHATRYAN...15D	CMS	$E_{cm}^{pp} = 8$ TeV
	25 AAD	14AMATLS	
	26 CHATRCHYAN14Q	CMS	
	27 ABAZOV	13D D0	
	28 CHATRCHYAN13AA	CMS	
	29 ABBIENDI	04B OPAL	
	30 ABBIENDI	04L OPAL	
	31 HEISTER	04A ALEP	
	32 ABDALLAH	03I DLPH	
	33 ACHARD	02F L3	

¹ SIRUNYAN 21 study electroweak Z -pair production in association with two jets, with the Z bosons decaying to oppositely-charged electron or muon pairs. Leptons with high transverse momentum are selected, with the di-lepton invariant mass of the two Z boson candidates between 60 GeV and 120 GeV, and the four-lepton invariant mass larger than 180 GeV. A total of 365 events are selected in the data, while the number of expected events is 370 ± 48 . Analyzing the four-lepton invariant mass distribution, the following 95% C.L. limits are derived: $-0.24 < f_{T,0}/\Lambda^4 < 0.22, -0.31 < f_{T,1}/\Lambda^4 < 0.31, -0.63 < f_{T,2}/\Lambda^4 < 0.59, -0.43 < f_{T,8}/\Lambda^4 < 0.43, -0.92 < f_{T,9}/\Lambda^4 < 0.92$, in units of TeV^{-4} .

- ² TUMASYAN 21A study electroweak $Z\gamma$ production in association with two jets, where the Z boson decays to electron or muon pairs and the pair of two jets has high invariant mass, superseding SIRUNYAN 20AL. The number of observed (expected) electron events in the barrel and endcap regions are 375 (349 ± 9) and 174 (166 ± 6) events, respectively, while for muon events the respective numbers are 584 (612 ± 13) and 320 (303 ± 8). Analyzing the $Z\gamma$ invariant mass distribution, the following 95% C.L. limits are derived: $-15.8 < f_{M,0}/\Lambda^4 < 16.0, -35.0 < f_{M,1}/\Lambda^4 < 34.7, -6.55 < f_{M,2}/\Lambda^4 < 6.49, -13.0 < f_{M,3}/\Lambda^4 < 13.0, -13.0 < f_{M,4}/\Lambda^4 < 12.7, -22.2 < f_{M,5}/\Lambda^4 < 21.3, -56.6 < f_{M,7}/\Lambda^4 < 55.9, -0.64 < f_{T,0}/\Lambda^4 < 0.57, -0.81 < f_{T,1}/\Lambda^4 < 0.90, -1.68 < f_{T,2}/\Lambda^4 < 1.54, -0.58 < f_{T,5}/\Lambda^4 < 0.64, -1.30 < f_{T,6}/\Lambda^4 < 1.33, -2.15 < f_{T,7}/\Lambda^4 < 2.43, -0.47 < f_{T,8}/\Lambda^4 < 0.47, -0.91 < f_{T,9}/\Lambda^4 < 0.91$, in units of TeV^{-4} .
- ³ TUMASYAN 21B measure W or Z boson production in association with two photons, using the leptonic decays modes of W and Z with electrons or muons. The number of selected $W \rightarrow e(\mu)\nu$ events is 1987 (2384) and the number of selected $Z \rightarrow ee(\mu\mu)$ events is 110 (272) respectively. Analyzing the transverse momentum of the di-photon system, the following 95% C.L. limits are derived in units of TeV^{-4} : In the W production channel, the observed limits are: $-39.9 < f_{M,2}/\Lambda^4 < 39.5, -63.8 < f_{M,3}/\Lambda^4 < 65.0, -1.30 < f_{T,0}/\Lambda^4 < 1.30, -1.70 < f_{T,1}/\Lambda^4 < 1.66, -3.64 < f_{T,2}/\Lambda^4 < 3.64, -0.52 < f_{T,5}/\Lambda^4 < 0.60, -0.60 < f_{T,6}/\Lambda^4 < 0.68, -1.16 < f_{T,7}/\Lambda^4 < 1.16$. In the Z production channel, the observed limits are: $-5.70 < f_{T,0}/\Lambda^4 < 5.46, -5.70 < f_{T,1}/\Lambda^4 < 5.46, -11.4 < f_{T,2}/\Lambda^4 < 10.9, -2.92 < f_{T,5}/\Lambda^4 < 2.92, -3.80 < f_{T,6}/\Lambda^4 < 3.88, -7.88 < f_{T,7}/\Lambda^4 < 7.72, -1.06 < f_{T,8}/\Lambda^4 < 1.10, -1.82 < f_{T,9}/\Lambda^4 < 1.82$, in units of TeV^{-4} .
- ⁴ SIRUNYAN 20 study WZ and same-sign WW production in association with two jets, using the leptonic decays modes of the W and Z bosons with electrons or muons. Overall, 524 WZ events and 229 WW events are selected, with a Standard Model expectation of 535 ± 52 and 216 ± 21 events, respectively. Analyzing the transverse mass spectrum of the di-boson system and the di-jet invariant mass, the following 95% C.L. limits are derived, not using any unitarization procedure: $-0.25 < f_{T,0}/\Lambda^4 < 0.28, -0.12 < f_{T,1}/\Lambda^4 < 0.14, -0.35 < f_{T,2}/\Lambda^4 < 0.48, -2.7 < f_{M,0}/\Lambda^4 < 2.9, -4.1 < f_{M,1}/\Lambda^4 < 4.2, -5.4 < f_{M,6}/\Lambda^4 < 5.8, -5.7 < f_{M,7}/\Lambda^4 < 6.0, -5.7 < f_{S,0}/\Lambda^4 < 6.1, -16 < f_{S,1}/\Lambda^4 < 17$, in units of TeV^{-4} . The article also reports limits on these couplings by cutting the EFT expansion at the unitarity limit.
- ⁵ SIRUNYAN 20AL study electroweak production of a Z boson and a photon in association with two jets in the electron and muon decay modes of the Z . A signal with a significance of 3.9 standard deviations is observed, compared to a Standard Model expectation of 5.2 standard deviations. Combining with KHACHATRYAN 17AA data at 8 TeV the final observed and expected signal significance is 4.7 and 5.5 standard deviations. Analyzing the Z -photon invariant mass distribution, the following 95% C.L. limits are derived: $-19.5 < f_{M,0}/\Lambda^4 < 20.3, -40.5 < f_{M,1}/\Lambda^4 < 39.5, -8.22 < f_{M,2}/\Lambda^4 < 8.10, -17.7 < f_{M,3}/\Lambda^4 < 17.9, -15.3 < f_{M,4}/\Lambda^4 < 15.8, -25.1 < f_{M,5}/\Lambda^4 < 24.5, -38.9 < f_{M,6}/\Lambda^4 < 40.6, -60.3 < f_{M,7}/\Lambda^4 < 62.5, -0.74 < f_{T,0}/\Lambda^4 < 0.69, -0.98 < f_{T,1}/\Lambda^4 < 0.96, -1.97 < f_{T,2}/\Lambda^4 < 1.86, -0.70 < f_{T,5}/\Lambda^4 < 0.75, -1.64 < f_{T,6}/\Lambda^4 < 1.68, -2.59 < f_{T,7}/\Lambda^4 < 2.82, -0.47 < f_{T,8}/\Lambda^4 < 0.47, -1.27 < f_{T,9}/\Lambda^4 < 1.27$, in units of TeV^{-4} .
- ⁶ SIRUNYAN 20BD study electroweak $W\gamma$ production in association with two jets, where the W boson decays to electron or muon and the two jets have high invariant mass. The number of observed (expected) electron events with the photon in the barrel and endcap regions are 393 (397.1 ± 18.5) and 159 (145.2 ± 10.0) respectively, while for muon events the respective numbers are 565 (537.9 ± 21.4) and 201 (188.2 ± 10.5). Analyzing the $W\gamma$ invariant mass distribution, the following 95% C.L. limits are derived: $-8.1 < f_{M,0}/\Lambda^4 < 8.0, -12 < f_{M,1}/\Lambda^4 < 12, -2.8 < f_{M,2}/\Lambda^4 < 2.8, -4.4 < f_{M,3}/\Lambda^4 < 4.4, -5.0 < f_{M,4}/\Lambda^4 < 5.0, -8.3 < f_{M,5}/\Lambda^4 < 8.3, -16 < f_{M,6}/\Lambda^4 < 16, -21 < f_{M,7}/\Lambda^4 < 20, -0.6 < f_{T,0}/\Lambda^4 < 0.6, -0.4 < f_{T,1}/\Lambda^4 < 0.4, -1.0 < f_{T,2}/\Lambda^4 < 1.2, -0.5 < f_{T,5}/\Lambda^4 < 0.5, -0.4 < f_{T,6}/\Lambda^4 < 0.4, -0.9 < f_{T,7}/\Lambda^4 < 0.9$, in units of TeV^{-4} .
- ⁷ SIRUNYAN 19BM search for the final state $W^+W^-W^\pm$ using W decays to electrons or muons. Two event samples are considered, events with three leptons, or events with two oppositely charged leptons accompanied by two jets. In a kinematic region selected to enhance the effect of anomalous couplings, no events are selected in the data, and 95% C.L. upper limits are obtained as follows: $-1.2 < f_{T,0}/\Lambda^4 < 1.2, -3.3 < f_{T,1}/\Lambda^4 < 3.3, -2.7 < f_{T,2}/\Lambda^4 < 2.6$, in units of TeV^{-4} and without application of a form factor.
- ⁸ SIRUNYAN 19BP study WZ plus 2 jets production, using W and Z decay channels with electrons or muons. In the data, 75 events are selected, with a fitted SM signal of 15.1 ± 1.6 events and a fitted background of 62.4 ± 2.8 events. The transverse mass distribution of the WZ system is analyzed to set the following limits at 95% C.L., in units of TeV^{-4} : $-9.15 < f_{M,0}/\Lambda^4 < 9.15, -9.15 < f_{M,1}/\Lambda^4 < 9.45, -26.5 < f_{S,0}/\Lambda^4 < 27.5, -41.2 < f_{S,1}/\Lambda^4 < 42.8, -0.75 < f_{T,0}/\Lambda^4 < 0.81, -0.49 < f_{T,1}/\Lambda^4 < 0.55, -1.49 < f_{T,2}/\Lambda^4 < 1.85$.
- ⁹ SIRUNYAN 19CQ search for anomalous electroweak production of vector boson pairs in association with two jets. Events are selected by requiring two jets with a large invariant mass and rapidity separation, one or two leptons (electrons or muons), and a W or Z boson decaying hadronically. In the WV (ZV) channel, 347 (47) events are selected in the data, with a total expected background of 352 ± 19 (50.3 ± 5.8) events. Analyzing the mass distribution of the WV or ZV system, the following 95% C.L. limits are obtained: $-2.7 < f_{S,0}/\Lambda^4 < 2.7, -3.4 < f_{S,1}/\Lambda^4 < 3.4, -0.69 < f_{M,0}/\Lambda^4 < 0.70, -2.0 < f_{M,1}/\Lambda^4 < 2.1, -1.3 < f_{M,6}/\Lambda^4 < 1.3, -3.4 < f_{M,7}/\Lambda^4 < 3.4, -0.12 < f_{T,0}/\Lambda^4 < 0.11, -0.12 < f_{T,1}/\Lambda^4 < 0.13, -0.28 < f_{T,2}/\Lambda^4 < 0.28$, in units of TeV^{-4} .
- ¹⁰ SIRUNYAN 18CC study pp collisions at $\sqrt{s} = 13$ TeV leading to a pair of same-sign W pairs decaying leptonically (e or μ) associated with a pair of jets. Isolated leptons

- with $p_T > 25$ (20) GeV for the leading (trailing) lepton, with $|\eta| < 2.5$ (2.4) for e (μ) and jets with $p_T > 30$ GeV, $|\eta| < 5.0$, $|\Delta\eta_{jj}| > 2.5$ and $m_{jj} > 500$ GeV is required. Further cuts are applied to minimize $Z \rightarrow ee$ events, non-prompt leptons and hadronically decaying taus. The number of selected events is 201, with an expected SM signal of 66.9 ± 2.4 and background of 138 ± 13 events. Analysing the dilepton invariant mass spectrum the following 95% C.L. limits are derived: $-7.7 < f_{S,0}/\Lambda^4 < 7.7$, $-21.6 < f_{S,1}/\Lambda^4 < 21.8$, $-6.0 < f_{M,0}/\Lambda^4 < 5.9$, $-8.7 < f_{M,1}/\Lambda^4 < 9.1$, $-11.9 < f_{M,6}/\Lambda^4 < 11.8$, $-13.3 < f_{M,7}/\Lambda^4 < 12.9$, $-0.62 < f_{T,0}/\Lambda^4 < 0.65$, $-0.28 < f_{T,1}/\Lambda^4 < 0.31$, $-0.89 < f_{T,2}/\Lambda^4 < 1.02$.
- 11 AABOUD 17AA analyze $W^\pm W^\pm$ production in association with two jets and W decay modes with electrons or muons. In the kinematic region of VBS the effect of anomalous QGCs is enhanced by requiring the transverse mass of the WW system to be larger than 400 GeV. In the data, 8 events are selected with a total background expected from SM processes of 3.8 ± 0.6 events. Assuming the other QGC coupling to have the SM value of zero, the observed event yield is used to determine 95% CL limits on the QGCs: $-0.14 < \alpha_4 < 0.15$ and $-0.22 < \alpha_5 < 0.22$. Supersedes AAD 14AM.
- 12 AABOUD 17AG determine the $WW\gamma$ and $WZ\gamma$ cross sections in 8 TeV pp interactions by studying the final states $e\nu\mu\nu\gamma$ and $e\nu j j \gamma$ or $\mu\nu j j \gamma$. Upper limits on the production cross sections are derived in a fiducial region optimized for BSM physics. These are used to derive the following 95% C.L. upper limits for quartic couplings assuming the form scale factor, $\Lambda_{FF} = \infty$ (all in units of 10^3 TeV^{-4}): $-0.3 < f_{M,0}/\Lambda^4 < 0.3$, $-0.5 < f_{M,1}/\Lambda^4 < 0.5$, $-1.8 < f_{M,2}/\Lambda^4 < 1.8$, $-1.1 < f_{M,4}/\Lambda^4 < 1.1$, $-1.7 < f_{M,5}/\Lambda^4 < 1.7$, $-0.6 < f_{M,6}/\Lambda^4 < 0.6$, $-1.1 < f_{M,7}/\Lambda^4 < 1.1$, $-0.1 < f_{T,0}/\Lambda^4 < 0.1$, $-0.2 < f_{T,1}/\Lambda^4 < 0.2$, $-0.4 < f_{T,4}/\Lambda^4 < 0.4$, $-1.5 < f_{T,5}/\Lambda^4 < 1.6$, $-1.9 < f_{T,6}/\Lambda^4 < 1.9$, $-4.3 < f_{T,7}/\Lambda^4 < 4.3$.
- 13 AABOUD 17d analyze electroweak diboson (WV , $V = W, Z$) production in association with a high-mass dijet system. In the data, 32 events are selected with an expected total background of 32 ± 12 events. Analysing the transverse mass distribution of the WV system, the following limits are set at 95% C.L.: $-0.024 < \alpha_4 < 0.030$ and $-0.028 < \alpha_5 < 0.033$.
- 14 AABOUD 17j analyze the $Z\gamma$ production in association with a high-mass dijet system, with the Z boson decaying into a pair of electrons, muons, or neutrinos. In the charged lepton (neutrino) channel, events are selected with a dijet mass larger than 500 (600) GeV and a transverse photon energy larger than 250 (150) GeV, with 2 (4) events selected in the data and 0.30 ± 0.08 (1.6 ± 0.5) expected background events. The observed event yield is used to determine 95% CL limits as follows: $-4.1 \times 10^3 < f_{T,9}/\Lambda^4 < 4.2 \times 10^3$, $-1.9 \times 10^3 < f_{T,8}/\Lambda^4 < 2.1 \times 10^3$, $-1.9 \times 10^1 < f_{T,0}/\Lambda^4 < 1.6 \times 10^1$, $-1.6 \times 10^2 < f_{M,0}/\Lambda^4 < 1.8 \times 10^2$, $-3.5 \times 10^2 < f_{M,1}/\Lambda^4 < 3.4 \times 10^2$, $-8.9 \times 10^2 < f_{M,2}/\Lambda^4 < 8.9 \times 10^2$, $-1.7 \times 10^3 < f_{M,3}/\Lambda^4 < 1.7 \times 10^3$, in units of TeV^{-4} and without application of a form factor.
- 15 AABOUD 17M analyze tri-boson $W^\pm W^\pm W^\mp$ production in decay channels with three charged leptons or two like-sign charged leptons with two jets, where the lepton can be an electron or muon. In the data, 24 tri-lepton events and 21 di-lepton plus jets events are selected, compared to a total event yield expected in the SM of 30.8 ± 3.0 and 21.9 ± 2.0 , respectively. Analysing the tri-lepton transverse mass or the transverse momentum sum of the two leptons, two jets and the missing transverse energy, the following limits at 95% CL are derived for the form factor cut-off scale $\Lambda_{FF} \rightarrow \infty$: $-0.13 < f_{S,0}/\Lambda^4 < 0.18$, $-0.21 < f_{S,1}/\Lambda^4 < 0.27$, in units of 10^4 TeV^{-4} , which are converted into the following limits: $-0.49 < \alpha_4 < 0.75$ and $-0.48 < \alpha_5 < 0.62$.
- 16 KHACHATRYAN 17AA analyse electroweak production of $Z\gamma$ in association with two hadronic jets, with the Z boson decaying to electron or muon pairs. Events with photon transverse momentum larger than 60 GeV and di-jet invariant mass larger than 400 GeV are selected. The $Z\gamma$ invariant mass spectrum is analysed to set 95% C.L. limits as follows: $-71 < f_{M,0}/\Lambda^4 < 75$, $-190 < f_{M,1}/\Lambda^4 < 182$, $-32 < f_{M,2}/\Lambda^4 < 31$, $-58 < f_{M,3}/\Lambda^4 < 59$, $-3.8 < f_{T,0}/\Lambda^4 < 3.4$, $-4.4 < f_{T,1}/\Lambda^4 < 4.4$, $-9.9 < f_{T,2}/\Lambda^4 < 9.0$, $-1.8 < f_{T,8}/\Lambda^4 < 1.8$, $-4.0 < f_{T,9}/\Lambda^4 < 4.0$, in units of TeV^{-4} and without application of a form factor.
- 17 KHACHATRYAN 17M analyse electroweak production of $W\gamma$ in association with two hadronic jets, with the W boson decaying to electrons or muons. Events with photon transverse momentum larger than 200 GeV and di-jet invariant mass larger than 200 GeV are selected. The W transverse momentum spectrum is analysed to set 95% C.L. limits as follows: $-77 < f_{M,0}/\Lambda^4 < 74$, $-125 < f_{M,1}/\Lambda^4 < 129$, $-26 < f_{M,2}/\Lambda^4 < 26$, $-43 < f_{M,3}/\Lambda^4 < 44$, $-40 < f_{M,4}/\Lambda^4 < 40$, $-65 < f_{M,5}/\Lambda^4 < 65$, $-129 < f_{M,6}/\Lambda^4 < 129$, $-164 < f_{M,7}/\Lambda^4 < 162$, $-5.4 < f_{T,0}/\Lambda^4 < 5.6$, $-3.7 < f_{T,1}/\Lambda^4 < 4.0$, $-11 < f_{T,2}/\Lambda^4 < 12$, $-3.8 < f_{T,5}/\Lambda^4 < 3.8$, $-2.8 < f_{T,6}/\Lambda^4 < 3.0$, $-7.3 < f_{T,7}/\Lambda^4 < 7.7$, in units of TeV^{-4} and without application of a form factor.
- 18 SIRUANYAN 17AD study pp collisions at $\sqrt{s} = 13$ TeV to determine the cross section of $ZZjj$ with the Z decaying to ee or $\mu\mu$. The ZZ mass distribution is used to set upper limits on the anomalous quartic couplings. The 95% upper limits for the relevant quartic couplings in units of TeV^{-4} are: $-0.46 < f_{T,0}/\Lambda^4 < 0.44$, $-0.61 < f_{T,1}/\Lambda^4 < 0.61$, $-1.2 < f_{T,2}/\Lambda^4 < 1.2$, $-0.84 < f_{T,8}/\Lambda^4 < 0.84$, $-1.8 < f_{T,9}/\Lambda^4 < 1.8$.
- 19 SIRUANYAN 17AR study pp collisions at $\sqrt{s} = 8$ TeV to determine the cross section of $pp \rightarrow W\gamma\gamma$ and $pp \rightarrow Z\gamma\gamma$ where $W \rightarrow \ell\nu$ and $Z \rightarrow \ell^+ \ell^-$, ℓ being an electron or a muon. The number of W events in the e and μ channels is 63 and 108 respectively, and the number of Z events in the e and μ channels is 117 and 141. To increase sensitivity, the transverse momentum of the leading photon is required to be larger than 70 GeV. The 95% C.L. upper limits in units of TeV^{-4} are $-701 < f_{M,2}/\Lambda^4 < 683$, $-1170 < f_{M,3}/\Lambda^4 < 1220$, $-33.5 < f_{T,0}/\Lambda^4 < 34.0$, $-44.3 < f_{T,1}/\Lambda^4 < 44.8$, $-93.8 < f_{T,2}/\Lambda^4 < 93.2$.
- 20 AABOUD 16E study WW production in two-photon mediated pp collisions at 8 TeV where the W boson decays into an electron or muon, probing the $\gamma\gamma WW$ vertex for anomalous quartic gauge couplings. The lepton p_T is required to be larger than 30 GeV. Limits on anomalous couplings are determined from events with p_T larger than 120 GeV where the aQGC effect is enhanced and the SM background reduced; in the data corresponding to an integrated luminosity of 20.2fb^{-1} , 1 event is selected with an expected SM background of 0.37 ± 0.13 events. The 95% C.L. limits without a form-factor cutoff ($\Lambda_{\text{cutoff}} \rightarrow \infty$) are as follows: $-1.7 < a_0^W/\Lambda^2 < 1.7$ and $-6.4 < a_C^W/\Lambda^2 < 6.3$ in units of 10^{-6} GeV^{-2} . In terms of another set of variables: $-6.6 < f_{M,0}/\Lambda^4 < 6.6$ and $-24 < f_{M,1}/\Lambda^4 < 25$ in units of $10^{-11} \text{ GeV}^{-4}$.
- 21 AAD 16Q study $Z\gamma\gamma$ production in pp collisions. In events with no additional jets, 29 (22) Z decays to electron (muon) pairs are selected, with an expected background of 3.3 ± 1.1 (6.5 ± 2.0) events, as well as 19 Z decays to neutrino pairs with an expected background of 8.3 ± 4.4 events. Analysing the photon transverse momentum distribution for $m_{\gamma\gamma}$ above 200 GeV (300 GeV) for lepton (neutrino) events, yields the 95% C.L. limits: $-1.6 \times 10^4 < f_{M,2}/\Lambda^4 < 1.6 \times 10^4$, $-2.9 \times 10^4 < f_{M,3}/\Lambda^4 < 2.7 \times 10^4$, $-0.86 \times 10^2 < f_{T,0}/\Lambda^4 < 1.03 \times 10^2$, $-0.69 \times 10^3 < f_{T,5}/\Lambda^4 < 0.68 \times 10^3$, $-0.74 \times 10^4 < f_{T,9}/\Lambda^4 < 0.74 \times 10^4$ in units of TeV^{-4} and without application of a form factor Λ_{FF} .
- 22 KHACHATRYAN 16AX searches for anomalous $WW\gamma\gamma$ quartic gauge couplings in the two-photon-mediated process $pp \rightarrow ppWW$, assuming the $WW\gamma$ triple gauge boson couplings to be at their Standard Model values. 13 events containing an $e^\pm \mu^\mp$ pair with $p_T(e, \mu) > 30$ GeV are selected in a total luminosity of 19.7 fb^{-1} , with an expected $\gamma\gamma \rightarrow WW$ signal of 5.3 ± 0.1 events and an expected background of 3.9 ± 0.5 events. When combining with the data collected at 7 TeV (KHACHATRYAN 13AA), and not assuming a form factor, the following 1-parameter limits at 95% C.L. are obtained from the $p_T(e, \mu)$ spectrum: $|a_0^W/\Lambda^2| < 1.1 \times 10^{-6} \text{ GeV}^{-2}$ ($a_C^W = 0$), and $|a_C^W/\Lambda^2| < 4.1 \times 10^{-6} \text{ GeV}^{-2}$ ($a_0^W = 0$). In terms of another set of variables: $|f_{M,0}/\Lambda^4| < 4.2 \times 10^{-12} \text{ GeV}^{-4}$, $|f_{M,1}/\Lambda^4| < 16 \times 10^{-12} \text{ GeV}^{-4}$, $|f_{M,2}/\Lambda^4| < 2.1 \times 10^{-12} \text{ GeV}^{-4}$, $|f_{M,3}/\Lambda^4| < 7.8 \times 10^{-12} \text{ GeV}^{-4}$.
- 23 AAD 15N study $W\gamma\gamma$ events in 8 TeV pp interactions, where the W decays into an electron or a muon. The events are characterized by an isolated lepton, a missing transverse energy due to the decay neutrino, and two isolated photons, with the p_T of the lepton and the photons being > 20 GeV. The number of candidate events observed in the electron channel for $N(\text{jet}) \geq 0$ and $N(\text{jet}) = 0$ is 47 and 15, the corresponding numbers for the muon channel being 110 and 53. The backgrounds expected are 30.2 ± 7.4 , 8.7 ± 3.0 , 52.1 ± 12.2 , and 24.4 ± 8.3 respectively. The 95% C.L. limits on the values of the parameters $f_{T,0}/\Lambda^4$, $f_{M,2}/\Lambda^4$ and $f_{M,3}/\Lambda^4$ are $-0.9-0.9 \times 10^2$, $-0.8-0.8 \times 10^4$, and $-1.5-1.4 \times 10^4$ respectively, without application of a form factor Λ_{FF} .
- 24 KHACHATRYAN 15D study vector-boson-scattering tagged by two jets, requiring two same-sign charged leptons arising from $W^\pm W^\pm$ production and decay. The two jets must have a transverse momentum larger than 30 GeV, while the leptons, electrons or muons, must have a transverse momentum > 20 GeV. The dijet mass is required to be > 500 GeV, the dilepton mass > 50 GeV, with additional requirement of differing from the Z mass by > 15 GeV. In the two categories W^+W^+ and W^-W^- , 10 and 2 data events are observed in a data sample corresponding to an integrated luminosity of 19.4 fb^{-1} , with an expected background of 3.1 ± 0.6 and 2.6 ± 0.5 events. Analysing the distribution of the dilepton invariant mass, the following limits at 95% C.L. are obtained, in units of TeV^{-4} : $-38 < f_{S,0}/\Lambda^4 < 40$, $-118 < f_{S,1}/\Lambda^4 < 120$, $-33 < f_{M,0}/\Lambda^4 < 32$, $-44 < f_{M,1}/\Lambda^4 < 47$, $-65 < f_{M,6}/\Lambda^4 < 63$, $-70 < f_{M,7}/\Lambda^4 < 66$, $-4.2 < f_{T,0}/\Lambda^4 < 4.6$, $-1.9 < f_{T,1}/\Lambda^4 < 2.2$, $-5.2 < f_{T,2}/\Lambda^4 < 6.4$.
- 25 AAD 14AM analyze electroweak production of WW jet jet same-charge diboson plus two jets production, with the W bosons decaying to electron or muon, to study the quartic $WWWW$ coupling. In a kinematic region enhancing the electroweak production over the strong production, 34 events are observed in the data while 29.8 ± 2.4 events are expected with a background of 15.9 ± 1.9 events. Assuming the other QGC coupling to have the SM value of zero, the observed event yield is used to determine 95% CL limits on the quartic gauge couplings: $-0.14 < \alpha_4 < 0.16$ and $-0.23 < \alpha_5 < 0.24$.
- 26 KHACHATRYAN 14Q study $WV\gamma$ production in 8 TeV pp collisions, in the single lepton final state, with $W \rightarrow \ell\nu$, $Z \rightarrow \text{dijet}$ or $W \rightarrow \ell\nu$, $W \rightarrow \text{dijet}$, the dijet mass resolution precluding differentiation between the W and Z . p_T and pseudo-rapidity cuts are put on the lepton, the photon and the two jets to minimize backgrounds. The dijet mass is required to be between 70–100 GeV and $|\Delta\eta_{jj}| < 1.4$. The selected number of muon (electron) events are 183 (139), with SM expectation being 194.2 ± 11.5 (147.9 ± 10.7) including signal and background. The photon E_T distribution is used to set limits on the anomalous quartic couplings. The following 95% CL limits are deduced (all in units of TeV^{-2} or TeV^{-4}): $-21 < a_0^W/\Lambda^2 < 20$, $-34 < a_C^W/\Lambda^2 < 32$, $-12 < \kappa_0^W/\Lambda^2 < 10$ and $-18 < \kappa_C^W/\Lambda^2 < 17$; and $-25 < f_{T,0}/\Lambda^4 < 24 \text{ TeV}^{-4}$.
- 27 ABZOV 13D searches for anomalous $WW\gamma\gamma$ quartic gauge couplings in the two-photon-mediated process $pp \rightarrow ppWW$, assuming the $WW\gamma$ triple gauge boson couplings to be at their Standard Model values. 946 events containing an e^+e^- pair with missing energy are selected in a total luminosity of 9.7 fb^{-1} , with an expectation of 983 ± 108 events from Standard-Model processes. The following 1-parameter limits at 95% CL are obtained: $|a_0^W/\Lambda^2| < 4.3 \times 10^{-4} \text{ GeV}^{-2}$ ($a_C^W = 0$), $|a_C^W/\Lambda^2| < 1.5 \times 10^{-3} \text{ GeV}^{-2}$ ($a_0^W = 0$).
- 28 KHACHATRYAN 13AA searches for anomalous $WW\gamma\gamma$ quartic gauge couplings in the two-photon-mediated process $pp \rightarrow ppWW$, assuming the $WW\gamma$ triple gauge boson couplings to be at their Standard Model values. 2 events containing an $e^\pm \mu^\mp$ pair with $p_T(e, \mu) > 30$ GeV are selected in a total luminosity of 5.05 fb^{-1} , with an expected ppW signal of 2.2 ± 0.4 events and an expected background of 0.84 ± 0.15 events. The following 1-parameter limits at 95% CL are obtained from the $p_T(e, \mu)$ spectrum: $|a_0^W/\Lambda^2| < 4.0 \times 10^{-6} \text{ GeV}^{-2}$ ($a_C^W = 0$), $|a_C^W/\Lambda^2| < 1.5 \times 10^{-5} \text{ GeV}^{-2}$ ($a_0^W = 0$).
- 29 ABBIENDI 04B select 187 $e^+e^- \rightarrow W^+W^-\gamma$ events in the C.M. energy range 180–209 GeV, where $E_\gamma > 2.5$ GeV, the photon has a polar angle $|\cos\theta_\gamma| < 0.975$ and is well isolated from the nearest jet and charged lepton, and the effective masses of both fermion-antifermion systems agree with the W mass within $3 \Gamma_W$. The measured differential cross section as a function of the photon energy and photon polar angle is used to extract the 95% CL limits: $-0.020 \text{ GeV}^{-2} < a_0/\Lambda^2 < 0.020 \text{ GeV}^{-2}$, $-0.053 \text{ GeV}^{-2} < a_c/\Lambda^2 < 0.037 \text{ GeV}^{-2}$ and $-0.16 \text{ GeV}^{-2} < a_n/\Lambda^2 < 0.15 \text{ GeV}^{-2}$.
- 30 ABBIENDI 04L select 20 $e^+e^- \rightarrow \nu\bar{\nu}\gamma\gamma$ acoplanar events in the energy range 180–209 GeV and 176 $e^+e^- \rightarrow q\bar{q}\gamma\gamma$ events in the energy range 130–209 GeV. These samples

Gauge & Higgs Boson Particle Listings

W, Z

HERZOG	84	PL 148B 355	F. Herzog	(WIS C)
Also		PL 155B 468 (erratum)	F. Herzog	(WIS C)
ARNIS ON	83	PL 122B 103	G.T.J. Arnison et al.	(UA1 Collab.)
BANNER	83B	PL 122B 476	M. Banner et al.	(UA2 Collab.)



$$J = 1$$

See the related review(s):
Z Boson

Z MASS

OUR FIT is obtained using the fit procedure and correlations as determined by the LEP Electroweak Working Group (see the note "The Z boson" and ref. LEP-SLC 06). The fit is performed using the Z mass and width, the Z hadronic pole cross section, the ratios of hadronic to leptonic partial widths, and the Z pole forward-backward lepton asymmetries. This set is believed to be most free of correlations.

The Z-boson mass listed here corresponds to the mass parameter in a Breit-Wigner distribution with mass dependent width. The value is 34 MeV greater than the real part of the position of the pole (in the energy-squared plane) in the Z-boson propagator. Also the LEP experiments have generally assumed a fixed value of the $\gamma - Z$ interferences term based on the standard model. Keeping this term as free parameter leads to a somewhat larger error on the fitted Z mass. See ACCIARRI 00q and ABBIENDI 04c for a detailed investigation of both these issues.

VALUE (GeV)	EVTS	DOCUMENT ID	TECN	COMMENT
91.1876 ± 0.0021 OUR FIT				
91.1852 ± 0.0030	4.57M	1 ABBIENDI 01A	OPAL	$E_{cm}^{ee} = 88-94$ GeV
91.1863 ± 0.0028	4.08M	2 ABREU 00F	DLPH	$E_{cm}^{ee} = 88-94$ GeV
91.1898 ± 0.0031	3.96M	3 ACCIARRI 00c	L3	$E_{cm}^{ee} = 88-94$ GeV
91.1885 ± 0.0031	4.57M	4 BARATE 00c	ALEP	$E_{cm}^{ee} = 88-94$ GeV
• • • We do not use the following data for averages, fits, limits, etc. • • •				
91.084 ± 0.107		5 ANDREEV 18A	H1	$e^\pm p$
91.1872 ± 0.0033		6 ABBIENDI 04G	OPAL	$E_{cm}^{ee} = \text{LEP1} + 130-209$ GeV
91.272 ± 0.032 ± 0.033		7 ACHARD 04c	L3	$E_{cm}^{ee} = 183-209$ GeV
91.1875 ± 0.0039	3.97M	8 ACCIARRI 00q	L3	$E_{cm}^{ee} = \text{LEP1} + 130-189$ GeV
91.151 ± 0.008		9 MIYABAYASHI 95	TOPZ	$E_{cm}^{ee} = 57.8$ GeV
91.174 ± 0.28 ± 0.93	156	10 ALITTI 92b	UA2	$E_{cm}^{pp} = 630$ GeV
90.9 ± 0.3 ± 0.2	188	11 ABE 89c	CDF	$E_{cm}^{pp} = 1.8$ TeV
91.14 ± 0.12	480	12 ABRAMS 89b	MRK2	$E_{cm}^{ee} = 89-93$ GeV
93.1 ± 1.0 ± 3.0	24	13 ALBAJAR 89	UA1	$E_{cm}^{pp} = 546,630$ GeV

- 1 ABBIENDI 01A error includes approximately 2.3 MeV due to statistics and 1.8 MeV due to LEP energy uncertainty.
- 2 The error includes 1.6 MeV due to LEP energy uncertainty.
- 3 The error includes 1.8 MeV due to LEP energy uncertainty.
- 4 BARATE 00c error includes approximately 2.4 MeV due to statistics, 0.2 MeV due to experimental systematics, and 1.7 MeV due to LEP energy uncertainty.
- 5 ANDREEV 18A obtain this result in a combined electroweak and QCD analysis using all deep-inelastic e^+p and e^-p neutral current and charged current scattering cross sections published by the H1 Collaboration, including data with longitudinally polarized lepton beams.
- 6 ABBIENDI 04G obtain this result using the S-matrix formalism for a combined fit to their cross section and asymmetry data at the Z peak and their data at 130-209 GeV. The authors have corrected the measurement for the 34 MeV shift with respect to the Breit-Wigner fits.
- 7 ACHARD 04c select $e^+e^- \rightarrow Z\gamma$ events with hard initial-state radiation. Z decays to $q\bar{q}$ and muon pairs are considered. The fit results obtained in the two samples are found consistent to each other and combined considering the uncertainty due to ISR modelling as fully correlated.
- 8 ACCIARRI 00q interpret the s-dependence of the cross sections and lepton forward-backward asymmetries in the framework of the S-matrix formalism. They fit to their cross section and asymmetry data at high energies, using the results of S-matrix fits to Z-peak data (ACCIARRI 00c) as constraints. The 130-189 GeV data constrains the γ/Z interference term. The authors have corrected the measurement for the 34.1 MeV shift with respect to the Breit-Wigner fits. The error contains a contribution of ± 2.3 MeV due to the uncertainty on the γ/Z interference.
- 9 MIYABAYASHI 95 combine their low energy total hadronic cross-section measurement with the ACTON 93d data and perform a fit using an S-matrix formalism. As expected, this result is below the mass values obtained with the standard Breit-Wigner parametrization.
- 10 Enters fit through W/Z mass ratio given in the W Particle Listings. The ALITTI 92b systematic error (± 0.93) has two contributions: one (± 0.92) cancels in m_W/m_Z and one (± 0.12) is noncancelling. These were added in quadrature.
- 11 First error of ABE 89 is combination of statistical and systematic contributions; second is mass scale uncertainty.
- 12 ABRAMS 89b uncertainty includes 35 MeV due to the absolute energy measurement.
- 13 ALBAJAR 89 result is from a total sample of 33 $Z \rightarrow e^+e^-$ events.

Z WIDTH

OUR FIT is obtained using the fit procedure and correlations as determined by the LEP Electroweak Working Group (see the note "The Z boson" and ref. LEP-SLC 06).

VALUE (GeV)	EVTS	DOCUMENT ID	TECN	COMMENT
2.4952 ± 0.0023 OUR FIT				
2.4948 ± 0.0041	4.57M	1 ABBIENDI 01A	OPAL	$E_{cm}^{ee} = 88-94$ GeV
2.4876 ± 0.0041	4.08M	2 ABREU 00F	DLPH	$E_{cm}^{ee} = 88-94$ GeV
2.5024 ± 0.0042	3.96M	3 ACCIARRI 00c	L3	$E_{cm}^{ee} = 88-94$ GeV
2.4951 ± 0.0043	4.57M	4 BARATE 00c	ALEP	$E_{cm}^{ee} = 88-94$ GeV
• • • We do not use the following data for averages, fits, limits, etc. • • •				
2.4943 ± 0.0041		5 ABBIENDI 04G	OPAL	$E_{cm}^{ee} = \text{LEP1} + 130-209$ GeV
2.5025 ± 0.0041	3.97M	6 ACCIARRI 00q	L3	$E_{cm}^{ee} = \text{LEP1} + 130-189$ GeV
2.50 ± 0.21 ± 0.06		7 ABREU 96R	DLPH	$E_{cm}^{ee} = 91.2$ GeV
3.8 ± 0.8 ± 1.0	188	8 ABE 89c	CDF	$E_{cm}^{pp} = 1.8$ TeV
2.42 + 0.45 - 0.35	480	9 ABRAMS 89b	MRK2	$E_{cm}^{ee} = 89-93$ GeV
2.7 + 1.2 - 1.0 ± 1.3	24	10 ALBAJAR 89	UA1	$E_{cm}^{pp} = 546,630$ GeV
2.7 ± 2.0 ± 1.0	25	11 ANSARI 87	UA2	$E_{cm}^{pp} = 546,630$ GeV

- 1 ABBIENDI 01A error includes approximately 3.6 MeV due to statistics, 1 MeV due to event selection systematics, and 1.3 MeV due to LEP energy uncertainty.
- 2 The error includes 1.2 MeV due to LEP energy uncertainty.
- 3 The error includes 1.3 MeV due to LEP energy uncertainty.
- 4 BARATE 00c error includes approximately 3.8 MeV due to statistics, 0.9 MeV due to experimental systematics, and 1.3 MeV due to LEP energy uncertainty.
- 5 ABBIENDI 04G obtain this result using the S-matrix formalism for a combined fit to their cross section and asymmetry data at the Z peak and their data at 130-209 GeV. The authors have corrected the measurement for the 1 MeV shift with respect to the Breit-Wigner fits.
- 6 ACCIARRI 00q interpret the s-dependence of the cross sections and lepton forward-backward asymmetries in the framework of the S-matrix formalism. They fit to their cross section and asymmetry data at high energies, using the results of S-matrix fits to Z-peak data (ACCIARRI 00c) as constraints. The 130-189 GeV data constrains the γ/Z interference term. The authors have corrected the measurement for the 0.9 MeV shift with respect to the Breit-Wigner fits.
- 7 ABREU 96R obtain this value from a study of the interference between initial and final state radiation in the process $e^+e^- \rightarrow Z \rightarrow \mu^+\mu^-$.
- 8 ABRAMS 89b uncertainty includes 50 MeV due to the miniSAM background subtraction error.
- 9 ALBAJAR 89 result is from a total sample of 33 $Z \rightarrow e^+e^-$ events.
- 10 Quoted values of ANSARI 87 are from direct fit. Ratio of Z and W production gives either $\Gamma(Z) < (1.09 \pm 0.07) \times \Gamma(W)$, CL = 90% or $\Gamma(Z) = (0.82^{+0.19}_{-0.14} \pm 0.06) \times \Gamma(W)$. Assuming Standard-Model value $\Gamma(W) = 2.65$ GeV then gives $\Gamma(Z) < 2.89 \pm 0.19$ or $= 2.17^{+0.50}_{-0.37} \pm 0.16$.

Z DECAY MODES

Mode	Fraction (Γ_i/Γ)	Scale factor / Confidence level
Γ_1 e^+e^-	[a] (3.3632 ± 0.0042) %	
Γ_2 $\mu^+\mu^-$	[a] (3.3662 ± 0.0066) %	
Γ_3 $\tau^+\tau^-$	[a] (3.3696 ± 0.0083) %	
Γ_4 $\ell^+\ell^-$	[a,b] (3.3658 ± 0.0023) %	
Γ_5 $\mu^+\mu^- \mu^+\mu^-$		
Γ_6 $\ell^+\ell^- \ell^+\ell^-$	[c] (4.55 ± 0.17) × 10 ⁻⁶	
Γ_7 invisible	[a] (20.000 ± 0.055) %	
Γ_8 hadrons	[a] (69.911 ± 0.056) %	
Γ_9 $(u\bar{u} + c\bar{c})/2$	(11.6 ± 0.6) %	
Γ_{10} $(d\bar{d} + s\bar{s} + b\bar{b})/3$	(15.6 ± 0.4) %	
Γ_{11} $c\bar{c}$	(12.03 ± 0.21) %	
Γ_{12} $b\bar{b}$	(15.12 ± 0.05) %	
Γ_{13} $b\bar{b}b\bar{b}$	(3.6 ± 1.3) × 10 ⁻⁴	
Γ_{14} $g\bar{g}g$	< 1.1 %	CL=95%
Γ_{15} $\pi^0\gamma$	< 2.01 × 10 ⁻⁵	CL=95%
Γ_{16} $\eta\gamma$	< 5.1 × 10 ⁻⁵	CL=95%
Γ_{17} $\rho^0\gamma$	< 2.5 × 10 ⁻⁵	CL=95%
Γ_{18} $\omega\gamma$	< 6.5 × 10 ⁻⁴	CL=95%
Γ_{19} $\eta'(958)\gamma$	< 4.2 × 10 ⁻⁵	CL=95%
Γ_{20} $\phi\gamma$	< 9 × 10 ⁻⁷	CL=95%
Γ_{21} $\gamma\gamma$	< 1.46 × 10 ⁻⁵	CL=95%
Γ_{22} $\pi^0\pi^0$	< 1.52 × 10 ⁻⁵	CL=95%
Γ_{23} $\gamma\gamma\gamma$	< 2.2 × 10 ⁻⁶	CL=95%
Γ_{24} $\pi^\pm W^\mp$	[d] < 7 × 10 ⁻⁵	CL=95%
Γ_{25} $\rho^\pm W^\mp$	[d] < 8.3 × 10 ⁻⁵	CL=95%
Γ_{26} $J/\psi(1S)X$	(3.51 + 0.23 - 0.25) × 10 ⁻³	S=1.1
Γ_{27} $J/\psi(1S)\gamma$	< 1.4 × 10 ⁻⁶	CL=95%
Γ_{28} $\psi(2S)X$	(1.60 ± 0.29) × 10 ⁻³	
Γ_{29} $\psi(2S)\gamma$	< 4.5 × 10 ⁻⁶	CL=95%
Γ_{30} $J/\psi(1S)\ell^+\ell^-$		
Γ_{31} $J/\psi(1S)J/\psi(1S)$	< 2.2 × 10 ⁻⁶	CL=95%
Γ_{32} $\chi_{c1}(1P)X$	(2.9 ± 0.7) × 10 ⁻³	
Γ_{33} $\chi_{c2}(1P)X$	< 3.2 × 10 ⁻³	CL=90%

Γ_{34}	$\Upsilon(1S) X + \Upsilon(2S) X + \Upsilon(3S) X$	(1.0 ± 0.5) × 10 ⁻⁴			
Γ_{35}	$\Upsilon(1S) X$	< 4.4	× 10 ⁻⁵	CL=95%	
Γ_{36}	$\Upsilon(1S) \gamma$	< 2.8	× 10 ⁻⁶	CL=95%	
Γ_{37}	$\Upsilon(2S) X$	< 1.39	× 10 ⁻⁴	CL=95%	
Γ_{38}	$\Upsilon(2S) \gamma$	< 1.7	× 10 ⁻⁶	CL=95%	
Γ_{39}	$\Upsilon(3S) X$	< 9.4	× 10 ⁻⁵	CL=95%	
Γ_{40}	$\Upsilon(3S) \gamma$	< 4.8	× 10 ⁻⁶	CL=95%	
Γ_{41}	$\Upsilon(1, 2, 3S) \Upsilon(1, 2, 3S)$	< 1.5	× 10 ⁻⁶	CL=95%	
Γ_{42}	$(D^0/\bar{D}^0) X$	(20.7 ± 2.0) %			
Γ_{43}	$D^\pm X$	(12.2 ± 1.7) %			
Γ_{44}	$D^*(2010)^\pm X$	[d] (11.4 ± 1.3) %			
Γ_{45}	$D_{s1}(2536)^\pm X$	(3.6 ± 0.8) × 10 ⁻³			
Γ_{46}	$D_{sJ}(2573)^\pm X$	(5.8 ± 2.2) × 10 ⁻³			
Γ_{47}	$D^{*0}(2629)^\pm X$	searched for			
Γ_{48}	$B X$				
Γ_{49}	$B^* X$				
Γ_{50}	$B^+ X$	[e] (6.08 ± 0.13) %			
Γ_{51}	$B_s^0 X$	[e] (1.59 ± 0.13) %			
Γ_{52}	$B_c^\pm X$	searched for			
Γ_{53}	$\Lambda_c^+ X$	(1.54 ± 0.33) %			
Γ_{54}	$\Xi_c^0 X$	seen			
Γ_{55}	$\Xi_c^\pm X$	seen			
Γ_{56}	b -baryon X	[e] (1.38 ± 0.22) %			
Γ_{57}	anomalous γ + hadrons	[f] < 3.2	× 10 ⁻³	CL=95%	
Γ_{58}	$e^+ e^- \gamma$	[f] < 5.2	× 10 ⁻⁴	CL=95%	
Γ_{59}	$\mu^+ \mu^- \gamma$	[f] < 5.6	× 10 ⁻⁴	CL=95%	
Γ_{60}	$\tau^+ \tau^- \gamma$	[f] < 7.3	× 10 ⁻⁴	CL=95%	
Γ_{61}	$\ell^+ \ell^- \gamma \gamma$	[g] < 6.8	× 10 ⁻⁶	CL=95%	
Γ_{62}	$q\bar{q} \gamma \gamma$	[g] < 5.5	× 10 ⁻⁶	CL=95%	
Γ_{63}	$\nu\bar{\nu} \gamma \gamma$	[g] < 3.1	× 10 ⁻⁶	CL=95%	
Γ_{64}	$e^\pm \mu^\mp$	LF [d] < 7.5	× 10 ⁻⁷	CL=95%	
Γ_{65}	$e^\pm \tau^\mp$	LF [d] < 5.0	× 10 ⁻⁶	CL=95%	
Γ_{66}	$\mu^\pm \tau^\mp$	LF [d] < 6.5	× 10 ⁻⁶	CL=95%	
Γ_{67}	$p e$	L,B < 1.8	× 10 ⁻⁶	CL=95%	
Γ_{68}	$p \mu$	L,B < 1.8	× 10 ⁻⁶	CL=95%	

[a] This parameter is not directly used in the overall fit but is derived using the fit results; see the note "The Z boson" and ref. LEP-SLC 06 (Physics Reports (Physics Letters C) **427** 257 (2006)).

[b] ℓ indicates each type of lepton (e , μ , and τ), not sum over them.

[c] Here ℓ indicates e or μ .

[d] The value is for the sum of the charge states or particle/antiparticle states indicated.

[e] This value is updated using the product of (i) the $Z \rightarrow b\bar{b}$ fraction from this listing and (ii) the b -hadron fraction in an unbiased sample of weakly decaying b -hadrons produced in Z-decays provided by the Heavy Flavor Averaging Group (HFLAV, http://www.slac.stanford.edu/xorg/hflav/osc/PDG_2009/#FRACZ).

[f] See the Particle Listings below for the γ energy range used in this measurement.

[g] For $m_{\gamma\gamma} = (60 \pm 5)$ GeV.

Z PARTIAL WIDTHS

$\Gamma(e^+ e^-)$ Γ_1
 For the LEP experiments, this parameter is not directly used in the overall fit but is derived using the fit results; see the note "The Z boson" and ref. LEP-SLC 06.

VALUE (MeV)	EVTS	DOCUMENT ID	TECN	COMMENT
83.91 ± 0.12 OUR FIT				
83.66 ± 0.20	137.0k	ABBIENDI	01A OPAL	$E_{cm}^{ee} = 88-94$ GeV
83.54 ± 0.27	117.8k	ABREU	00F DLPH	$E_{cm}^{ee} = 88-94$ GeV
84.16 ± 0.22	124.4k	ACCIARRI	00c L3	$E_{cm}^{ee} = 88-94$ GeV
83.88 ± 0.19		BARATE	00c ALEP	$E_{cm}^{ee} = 88-94$ GeV
82.89 ± 1.20 ± 0.89		¹ ABE	95J SLD	$E_{cm}^{ee} = 91.31$ GeV

¹ABE 95J obtain this measurement from Bhabha events in a restricted fiducial region to improve systematics. They use the values 91.187 and 2.489 GeV for the Z mass and total decay width to extract this partial width.

$\Gamma(\mu^+ \mu^-)$ Γ_2
 This parameter is not directly used in the overall fit but is derived using the fit results; see the note "The Z boson" and ref. LEP-SLC 06.

VALUE (MeV)	EVTS	DOCUMENT ID	TECN	COMMENT
83.99 ± 0.18 OUR FIT				
84.03 ± 0.30	182.8k	ABBIENDI	01A OPAL	$E_{cm}^{ee} = 88-94$ GeV
84.48 ± 0.40	157.6k	ABREU	00F DLPH	$E_{cm}^{ee} = 88-94$ GeV

83.95 ± 0.44	113.4k	ACCIARRI	00c L3	$E_{cm}^{ee} = 88-94$ GeV
84.02 ± 0.28		BARATE	00c ALEP	$E_{cm}^{ee} = 88-94$ GeV

$\Gamma(\tau^+ \tau^-)$ Γ_3
 This parameter is not directly used in the overall fit but is derived using the fit results; see the note "The Z boson" and ref. LEP-SLC 06.

VALUE (MeV)	EVTS	DOCUMENT ID	TECN	COMMENT
84.08 ± 0.22 OUR FIT				
83.94 ± 0.41	151.5k	ABBIENDI	01A OPAL	$E_{cm}^{ee} = 88-94$ GeV
83.71 ± 0.58	104.0k	ABREU	00F DLPH	$E_{cm}^{ee} = 88-94$ GeV
84.23 ± 0.58	103.0k	ACCIARRI	00c L3	$E_{cm}^{ee} = 88-94$ GeV
84.38 ± 0.31		BARATE	00c ALEP	$E_{cm}^{ee} = 88-94$ GeV

$\Gamma(\ell^+ \ell^-)$ Γ_4
 ℓ indicates each type of lepton (e , μ , and τ), not sum over them.

In our fit $\Gamma(\ell^+ \ell^-)$ is defined as the partial Z width for the decay into a pair of massless charged leptons. This parameter is not directly used in the 5-parameter fit assuming lepton universality but is derived using the fit results. See the note "The Z boson" and ref. LEP-SLC 06.

VALUE (MeV)	EVTS	DOCUMENT ID	TECN	COMMENT
83.984 ± 0.086 OUR FIT				
83.82 ± 0.15	471.3k	ABBIENDI	01A OPAL	$E_{cm}^{ee} = 88-94$ GeV
83.85 ± 0.17	379.4k	ABREU	00F DLPH	$E_{cm}^{ee} = 88-94$ GeV
84.14 ± 0.17	340.8k	ACCIARRI	00c L3	$E_{cm}^{ee} = 88-94$ GeV
84.02 ± 0.15	500k	BARATE	00c ALEP	$E_{cm}^{ee} = 88-94$ GeV

$\Gamma(\text{invisible})$ Γ_7
 We use only direct measurements of the invisible partial width using the single photon channel to obtain the average value quoted below. OUR FIT value is obtained as a difference between the total and the observed partial widths assuming lepton universality.

VALUE (MeV)	EVTS	DOCUMENT ID	TECN	COMMENT
499.0 ± 1.5 OUR FIT				
503 ± 16 OUR AVERAGE	Error includes scale factor of 1.2.			
498 ± 12 ± 12	1791	ACCIARRI	98G L3	$E_{cm}^{ee} = 88-94$ GeV
539 ± 26 ± 17	410	AKERS	95c OPAL	$E_{cm}^{ee} = 88-94$ GeV
450 ± 34 ± 34	258	BUSKULIC	93L ALEP	$E_{cm}^{ee} = 88-94$ GeV
540 ± 80 ± 40	52	ADEVA	92 L3	$E_{cm}^{ee} = 88-94$ GeV

• • • We do not use the following data for averages, fits, limits, etc. • • •

498.1 ± 2.6	¹ ABBIENDI	01A OPAL	$E_{cm}^{ee} = 88-94$ GeV
498.1 ± 3.2	¹ ABREU	00F DLPH	$E_{cm}^{ee} = 88-94$ GeV
499.1 ± 2.9	¹ ACCIARRI	00c L3	$E_{cm}^{ee} = 88-94$ GeV
499.1 ± 2.5	¹ BARATE	00c ALEP	$E_{cm}^{ee} = 88-94$ GeV

¹This is an indirect determination of $\Gamma(\text{invisible})$ from a fit to the visible Z decay modes.

$\Gamma(\text{hadrons})$ Γ_8
 This parameter is not directly used in the 5-parameter fit assuming lepton universality, but is derived using the fit results. See the note "The Z boson" and ref. LEP-SLC 06.

VALUE (MeV)	EVTS	DOCUMENT ID	TECN	COMMENT
1744.4 ± 2.0 OUR FIT				
1745.4 ± 3.5	4.10M	ABBIENDI	01A OPAL	$E_{cm}^{ee} = 88-94$ GeV
1738.1 ± 4.0	3.70M	ABREU	00F DLPH	$E_{cm}^{ee} = 88-94$ GeV
1751.1 ± 3.8	3.54M	ACCIARRI	00c L3	$E_{cm}^{ee} = 88-94$ GeV
1744.0 ± 3.4	4.07M	BARATE	00c ALEP	$E_{cm}^{ee} = 88-94$ GeV

Z BRANCHING RATIOS

OUR FIT is obtained using the fit procedure and correlations as determined by the LEP Electroweak Working Group (see the note "The Z boson" and ref. LEP-SLC 06).

$\Gamma(\mu^+ \mu^-)/\Gamma(e^+ e^-)$ Γ_2/Γ_1

VALUE	DOCUMENT ID	TECN	COMMENT
1.0001 ± 0.0024 OUR AVERAGE			
0.9974 ± 0.0050	¹ AABOUD	17q ATLS	$E_{cm}^{pp} = 7$ TeV
1.0009 ± 0.0028	² LEP-SLC	06	$E_{cm}^{ee} = 88-94$ GeV

¹AABOUD 17q make a precise determination of $Z \rightarrow e e$ and $Z \rightarrow \mu \mu$ production in the lepton pseudo-rapidity range $|\eta| < 2.5$ and determine the ratio of the Z branching fractions $B(Z \rightarrow e e)/B(Z \rightarrow \mu \mu) = 1.0026 \pm 0.0013 \pm 0.0048 = 1.0026 \pm 0.0050$.

²This parameter is not directly used in the overall fit but is derived using the fit results; see the note "The Z boson" and ref. LEP-SLC 06.

$\Gamma(\tau^+ \tau^-)/\Gamma(e^+ e^-)$ Γ_3/Γ_1

VALUE	DOCUMENT ID	TECN	COMMENT
1.0020 ± 0.0032 OUR AVERAGE			
1.02 ± 0.06	¹ AAIJ	18AR LHCB	$E_{cm}^{pp} = 8$ TeV
1.0019 ± 0.0032	² LEP-SLC	06	$E_{cm}^{ee} = 88-94$ GeV

¹AAIJ 18AR obtain the result from the ratio of the measured $pp \rightarrow Z + X$ cross sections in the corresponding Z decay channels.

²This parameter is not directly used in the overall fit but is derived using the fit results; see the note "The Z boson" and ref. LEP-SLC 06.

Gauge & Higgs Boson Particle Listings

Z

 $\Gamma(\tau^+ \tau^-)/\Gamma(\mu^+ \mu^-)$ Γ_3/Γ_2

VALUE	DOCUMENT ID	TECN	COMMENT
1.0010 ± 0.0026 OUR AVERAGE			
1.01 ± 0.05	¹ AAIJ	18AR LHCb	$E_{cm}^{pp} = 8$ TeV
1.0010 ± 0.0026	² LEP-SLC	06	$E_{cm}^{ee} = 88-94$ GeV

¹ AAIJ 18AR obtain the result from the ratio of the measured $pp \rightarrow Z + X$ cross sections in the corresponding Z decay channels.

² This parameter is not directly used in the overall fit but is derived using the fit results; see the note "The Z boson" and ref. LEP-SLC 06.

 $\Gamma(\ell^+ \ell^- \ell^+ \ell^-)/\Gamma_{total}$ Γ_6/Γ

Here ℓ indicates either e or μ . The branching fractions in this node are given within the phase-space defined by the requirements that (i) the 4-lepton invariant mass is between 80 GeV and 100 GeV, and (ii) any opposite-sign same-flavor lepton pair has a di-lepton invariant mass larger than 4 GeV.

VALUE (units 10^{-6})	EVTS	DOCUMENT ID	TECN	COMMENT
4.55 ± 0.17 OUR AVERAGE				
4.41 ± 0.13 ± 0.27		¹ AAD	21AQ ATLS	$E_{cm}^{pp} = 13$ TeV
4.70 ± 0.32 ± 0.25		² AABOUD	19N ATLS	$E_{cm}^{pp} = 13$ TeV
4.83 $\pm_{-0.22}^{+0.23+0.35}$	509	³ SIRUNYAN	18BT CMS	$E_{cm}^{pp} = 13$ TeV
4.9 $\pm_{-0.7}^{+0.8+0.4}$	39	⁴ KHACHATRYAN...	16CC CMS	$E_{cm}^{pp} = 13$ TeV
4.31 ± 0.34 ± 0.17	172	AAD	14N ATLS	$E_{cm}^{pp} = 7, 8$ TeV
4.6 $\pm_{-0.9}^{+1.0}$	28	⁵ CHATRCHYAN	12BN CMS	$E_{cm}^{pp} = 7$ TeV

¹ AAD 21AQ analyze differential cross-sections in four-lepton events. Based on the measured cross section in the $Z \rightarrow 4\ell$ channel, a branching fraction of $B(Z \rightarrow 4\ell) = (4.41 \pm 0.13 \pm 0.23 \pm 0.09 \pm 0.12) \times 10^{-6}$ is obtained, where the uncertainties are statistical, systematic, theory and luminosity, respectively.

² AABOUD 19N reports $(4.70 \pm 0.32 \pm 0.21 \pm 0.14) \times 10^{-6}$, where the uncertainties are statistical, systematic, and luminosity. We have combined the latter two in quadrature.

³ SIRUNYAN 18BT report the $Z \rightarrow 4\ell$ branching fraction = $(4.83 \pm_{-0.22}^{+0.23+0.32} \pm 0.08 \pm 0.12) \times 10^{-6}$, where the uncertainties are statistical, systematic, due to theory, and luminosity. The last three have been added in quadrature to obtain the total systematic error.

⁴ KHACHATRYAN 16CC reports $(4.9 \pm_{-0.7-0.2-0.1-0.1}^{+0.8+0.3+0.2+0.1}) \times 10^{-6}$ value, where the uncertainties are statistical, systematic, theory, and due to luminosity. We have combined uncertainties in quadrature.

⁵ CHATRCHYAN 12BN reports $(4.2 \pm_{-0.8}^{+0.9} \pm 0.2) \times 10^{-6}$ value. Their result (both central value and uncertainties) is scaled up by 10% to account for the different phase-space definition used here (see RAINBOLT 19).

 $\Gamma(\text{hadrons})/\Gamma(e^+ e^-)$ Γ_8/Γ_1

VALUE	EVTS	DOCUMENT ID	TECN	COMMENT
20.804 ± 0.050 OUR FIT				
20.902 ± 0.084	137.0k	¹ ABBIENDI	01A OPAL	$E_{cm}^{ee} = 88-94$ GeV
20.88 ± 0.12	117.8k	ABREU	00F DLPH	$E_{cm}^{ee} = 88-94$ GeV
20.816 ± 0.089	124.4k	ACCIARRI	00C L3	$E_{cm}^{ee} = 88-94$ GeV
20.677 ± 0.075		² BARATE	00C ALEP	$E_{cm}^{ee} = 88-94$ GeV
27.0 $\pm_{-8.8}^{+11.7}$	12	³ ABRAMS	89D MRK2	$E_{cm}^{ee} = 89-93$ GeV

¹ ABBIENDI 01A error includes approximately 0.067 due to statistics, 0.040 due to event selection systematics, 0.027 due to the theoretical uncertainty in t-channel prediction, and 0.014 due to LEP energy uncertainty.

² BARATE 00c error includes approximately 0.062 due to statistics, 0.033 due to experimental systematics, and 0.026 due to the theoretical uncertainty in t-channel prediction.

³ ABRAMS 89D have included both statistical and systematic uncertainties in their quoted errors.

 $\Gamma(\text{hadrons})/\Gamma(\mu^+ \mu^-)$ Γ_8/Γ_2

OUR FIT is obtained using the fit procedure and correlations as determined by the LEP Electroweak Working Group (see the note "The Z boson" and ref. LEP-SLC 06).

VALUE	EVTS	DOCUMENT ID	TECN	COMMENT
20.785 ± 0.033 OUR FIT				
20.811 ± 0.058	182.8k	¹ ABBIENDI	01A OPAL	$E_{cm}^{ee} = 88-94$ GeV
20.65 ± 0.08	157.6k	ABREU	00F DLPH	$E_{cm}^{ee} = 88-94$ GeV
20.861 ± 0.097	113.4k	ACCIARRI	00C L3	$E_{cm}^{ee} = 88-94$ GeV
20.799 ± 0.056		² BARATE	00C ALEP	$E_{cm}^{ee} = 88-94$ GeV
18.9 $\pm_{-5.3}^{+7.1}$	13	³ ABRAMS	89D MRK2	$E_{cm}^{ee} = 89-93$ GeV

¹ ABBIENDI 01A error includes approximately 0.050 due to statistics and 0.027 due to event selection systematics.

² BARATE 00c error includes approximately 0.053 due to statistics and 0.021 due to experimental systematics.

³ ABRAMS 89D have included both statistical and systematic uncertainties in their quoted errors.

 $\Gamma(\text{hadrons})/\Gamma(\tau^+ \tau^-)$ Γ_8/Γ_3

OUR FIT is obtained using the fit procedure and correlations as determined by the LEP Electroweak Working Group (see the note "The Z boson" and ref. LEP-SLC 06).

VALUE	EVTS	DOCUMENT ID	TECN	COMMENT
20.764 ± 0.045 OUR FIT				
20.832 ± 0.091	151.5k	¹ ABBIENDI	01A OPAL	$E_{cm}^{ee} = 88-94$ GeV
20.84 ± 0.13	104.0k	ABREU	00F DLPH	$E_{cm}^{ee} = 88-94$ GeV

20.792 ± 0.133 103.0k ACCIARRI 00c L3 $E_{cm}^{ee} = 88-94$ GeV

20.707 ± 0.062 ² BARATE 00c ALEP $E_{cm}^{ee} = 88-94$ GeV

• • • We do not use the following data for averages, fits, limits, etc. • • •

15.2 $\pm_{-3.9}^{+4.8}$ 21 ³ ABRAMS 89D MRK2 $E_{cm}^{ee} = 89-93$ GeV

¹ ABBIENDI 01A error includes approximately 0.055 due to statistics and 0.071 due to event selection systematics.

² BARATE 00c error includes approximately 0.054 due to statistics and 0.033 due to experimental systematics.

³ ABRAMS 89D have included both statistical and systematic uncertainties in their quoted errors.

 $\Gamma(\text{hadrons})/\Gamma(\ell^+ \ell^-)$ Γ_8/Γ_4

ℓ indicates each type of lepton (e, μ , and τ), not sum over them.

VALUE	EVTS	DOCUMENT ID	TECN	COMMENT
20.767 ± 0.025 OUR FIT				
20.823 ± 0.044	471.3k	¹ ABBIENDI	01A OPAL	$E_{cm}^{ee} = 88-94$ GeV
20.730 ± 0.060	379.4k	ABREU	00F DLPH	$E_{cm}^{ee} = 88-94$ GeV
20.810 ± 0.060	340.8k	ACCIARRI	00C L3	$E_{cm}^{ee} = 88-94$ GeV
20.725 ± 0.039	500k	² BARATE	00C ALEP	$E_{cm}^{ee} = 88-94$ GeV

• • • We do not use the following data for averages, fits, limits, etc. • • •

18.9 $\pm_{-3.2}^{+3.6}$ 46 ABRAMS 89B MRK2 $E_{cm}^{ee} = 89-93$ GeV

¹ ABBIENDI 01A error includes approximately 0.034 due to statistics and 0.027 due to event selection systematics.

² BARATE 00c error includes approximately 0.033 due to statistics, 0.020 due to experimental systematics, and 0.005 due to the theoretical uncertainty in t-channel prediction.

• • • We do not use the following data for averages, fits, limits, etc. • • •

18.9 $\pm_{-3.2}^{+3.6}$ 46 ABRAMS 89B MRK2 $E_{cm}^{ee} = 89-93$ GeV

¹ ABBIENDI 01A error includes approximately 0.034 due to statistics and 0.027 due to event selection systematics.

² BARATE 00c error includes approximately 0.033 due to statistics, 0.020 due to experimental systematics, and 0.005 due to the theoretical uncertainty in t-channel prediction.

 $\Gamma((u\bar{u} + c\bar{c})/2)/\Gamma(\text{hadrons})$ Γ_9/Γ_8

This quantity is the branching ratio of $Z \rightarrow$ "up-type" quarks to $Z \rightarrow$ hadrons. Except ACKERSTAFF 97T the values of $Z \rightarrow$ "up-type" and $Z \rightarrow$ "down-type" branchings are extracted from measurements of $\Gamma(\text{hadrons})$, and $\Gamma(Z \rightarrow \gamma + \text{jets})$ where γ is a high-energy (>5 or 7 GeV) isolated photon. As the experiments use different procedures and slightly different values of M_Z , $\Gamma(\text{hadrons})$ and α_s in their extraction procedures, our average has to be taken with caution.

VALUE	DOCUMENT ID	TECN	COMMENT
0.166 ± 0.009 OUR AVERAGE			
0.172 ± 0.011 $\pm_{-0.010}$	¹ ABBIENDI	04E OPAL	$E_{cm}^{ee} = 91.2$ GeV
0.160 ± 0.019 ± 0.019	² ACKERSTAFF	97T OPAL	$E_{cm}^{ee} = 88-94$ GeV
0.137 $\pm_{-0.054}^{+0.038}$	³ ABREU	95x DLPH	$E_{cm}^{ee} = 88-94$ GeV
0.137 ± 0.033	⁴ ADRIANI	93 L3	$E_{cm}^{ee} = 91.2$ GeV

¹ ABBIENDI 04E select photons with energy > 7 GeV and use $\Gamma(\text{hadrons}) = 1744.4 \pm 2.0$ MeV and $\alpha_s = 0.1172 \pm 0.002$ to obtain $\Gamma_u = 300 \pm_{-18}^{+19}$ MeV.

² ACKERSTAFF 97T measure $\Gamma_{u\bar{u}}/(\Gamma_{d\bar{d}} + \Gamma_{u\bar{u}} + \Gamma_{s\bar{s}}) = 0.258 \pm 0.031 \pm 0.032$. To obtain this branching ratio authors use $R_c + R_b = 0.380 \pm 0.010$. This measurement is fully negatively correlated with the measurement of $\Gamma_{d\bar{d},s\bar{s}}/(\Gamma_{d\bar{d}} + \Gamma_{u\bar{u}} + \Gamma_{s\bar{s}})$ given in the next data block.

³ ABREU 95x use $M_Z = 91.187 \pm 0.009$ GeV, $\Gamma(\text{hadrons}) = 1725 \pm 12$ MeV and $\alpha_s = 0.123 \pm 0.005$. To obtain this branching ratio we divide their value of $C_{2/3} = 0.91 \pm_{-0.36}^{+0.25}$ by their value of $(3C_{1/3} + 2C_{2/3}) = 6.66 \pm 0.05$.

⁴ ADRIANI 93 use $M_Z = 91.181 \pm 0.022$ GeV, $\Gamma(\text{hadrons}) = 1742 \pm 19$ MeV and $\alpha_s = 0.125 \pm 0.009$. To obtain this branching ratio we divide their value of $C_{2/3} = 0.92 \pm_{-0.22}^{+0.25}$ by their value of $(3C_{1/3} + 2C_{2/3}) = 6.720 \pm 0.076$.

 $\Gamma((d\bar{d} + s\bar{s} + b\bar{b})/3)/\Gamma(\text{hadrons})$ Γ_{10}/Γ_8

This quantity is the branching ratio of $Z \rightarrow$ "down-type" quarks to $Z \rightarrow$ hadrons. Except ACKERSTAFF 97T the values of $Z \rightarrow$ "up-type" and $Z \rightarrow$ "down-type" branchings are extracted from measurements of $\Gamma(\text{hadrons})$, and $\Gamma(Z \rightarrow \gamma + \text{jets})$ where γ is a high-energy (>5 or 7 GeV) isolated photon. As the experiments use different procedures and slightly different values of M_Z , $\Gamma(\text{hadrons})$ and α_s in their extraction procedures, our average has to be taken with caution.

VALUE	DOCUMENT ID	TECN	COMMENT
0.223 ± 0.006 OUR AVERAGE			
0.218 ± 0.007	¹ ABBIENDI	04E OPAL	$E_{cm}^{ee} = 91.2$ GeV
0.230 ± 0.010 ± 0.010	² ACKERSTAFF	97T OPAL	$E_{cm}^{ee} = 88-94$ GeV
0.243 $\pm_{-0.026}^{+0.036}$	³ ABREU	95x DLPH	$E_{cm}^{ee} = 88-94$ GeV
0.243 ± 0.022	⁴ ADRIANI	93 L3	$E_{cm}^{ee} = 91.2$ GeV

¹ ABBIENDI 04E select photons with energy > 7 GeV and use $\Gamma(\text{hadrons}) = 1744.4 \pm 2.0$ MeV and $\alpha_s = 0.1172 \pm 0.002$ to obtain $\Gamma_d = 381 \pm 12$ MeV.

² ACKERSTAFF 97T measure $\Gamma_{d\bar{d},s\bar{s}}/(\Gamma_{d\bar{d}} + \Gamma_{u\bar{u}} + \Gamma_{s\bar{s}}) = 0.371 \pm 0.016 \pm 0.016$. To obtain this branching ratio authors use $R_c + R_b = 0.380 \pm 0.010$. This measurement is fully negatively correlated with the measurement of $\Gamma_{u\bar{u}}/(\Gamma_{d\bar{d}} + \Gamma_{u\bar{u}} + \Gamma_{s\bar{s}})$ presented in the previous data block.

³ ABREU 95x use $M_Z = 91.187 \pm 0.009$ GeV, $\Gamma(\text{hadrons}) = 1725 \pm 12$ MeV and $\alpha_s = 0.123 \pm 0.005$. To obtain this branching ratio we divide their value of $C_{1/3} = 1.62 \pm_{-0.17}^{+0.24}$ by their value of $(3C_{1/3} + 2C_{2/3}) = 6.66 \pm 0.05$.

⁴ ADRIANI 93 use $M_Z = 91.181 \pm 0.022$ GeV, $\Gamma(\text{hadrons}) = 1742 \pm 19$ MeV and $\alpha_s = 0.125 \pm 0.009$. To obtain this branching ratio we divide their value of $C_{1/3} = 1.63 \pm_{-0.15}^{+0.15}$ by their value of $(3C_{1/3} + 2C_{2/3}) = 6.720 \pm 0.076$.

$R_c = \Gamma(c\bar{c})/\Gamma(\text{hadrons})$ Γ_{11}/Γ_8
OUR FIT is obtained by a simultaneous fit to several c - and b -quark measurements as explained in the note "The Z boson" and ref. LEP-SLC 06.

The Standard Model predicts $R_c = 0.1723$ for $m_t = 174.3$ GeV and $M_H = 150$ GeV.

VALUE	DOCUMENT ID	TECN	COMMENT
0.1721 ± 0.0030 OUR FIT			
0.1744 ± 0.0031 ± 0.0021	¹ ABE	05F SLD	$E_{\text{cm}}^{\text{ee}} = 91.28$ GeV
0.1665 ± 0.0051 ± 0.0081	² ABREU	00 DLPH	$E_{\text{cm}}^{\text{ee}} = 88-94$ GeV
0.1698 ± 0.0069	³ BARATE	00B ALEP	$E_{\text{cm}}^{\text{ee}} = 88-94$ GeV
0.180 ± 0.011 ± 0.013	⁴ ACKERSTAFF	98E OPAL	$E_{\text{cm}}^{\text{ee}} = 88-94$ GeV
0.167 ± 0.011 ± 0.012	⁵ ALEXANDER	96R OPAL	$E_{\text{cm}}^{\text{ee}} = 88-94$ GeV
• • • We do not use the following data for averages, fits, limits, etc. • • •			
0.1623 ± 0.0085 ± 0.0209	⁶ ABREU	95D DLPH	$E_{\text{cm}}^{\text{ee}} = 88-94$ GeV

¹ ABE 05F use hadronic Z decays collected during 1996-98 to obtain an enriched sample of $c\bar{c}$ events using a double tag method. The single c -tag is obtained with a neural network trained to perform flavor discrimination using as input several signatures (corrected secondary vertex mass, vertex decay length, multiplicity and total momentum of the hemisphere). A multitag approach is used, defining 4 regions of the output value of the neural network and R_c is extracted from a simultaneous fit to the count rates of the 4 different tags. The quoted systematic error includes an uncertainty of ± 0.0006 due to the uncertainty on R_b .

² ABREU 00 obtain this result properly combining the measurement from the D^{*+} production rate ($R_c = 0.1610 \pm 0.0104 \pm 0.0077 \pm 0.0043$ (BR)) with that from the overall charm counting ($R_c = 0.1692 \pm 0.0047 \pm 0.0063 \pm 0.0074$ (BR)) in $c\bar{c}$ events. The systematic error includes an uncertainty of ± 0.0054 due to the uncertainty on the charmed hadron branching fractions.

³ BARATE 00B use exclusive decay modes to independently determine the quantities $R_c \times f(c \rightarrow X)$, $X = D^0, D^+, D_s^+$, and A_c . Estimating $R_c \times f(c \rightarrow \Xi_c / \Omega_c) = 0.0034$, they simply sum over all the charm decays to obtain $R_c = 0.1738 \pm 0.0047 \pm 0.0088 \pm 0.0075$ (BR). This is combined with all previous ALEPH measurements (BARATE 98T and BUSKULIC 94G, $R_c = 0.1681 \pm 0.0054 \pm 0.0062$) to obtain the quoted value.

⁴ ACKERSTAFF 98E use an inclusive/exclusive double tag. In one jet $D^{*\pm}$ mesons are exclusively reconstructed in several decay channels and in the opposite jet a slow pion (opposite charge inclusive $D^{*\pm}$) tag is used. The b content of this sample is measured by the simultaneous detection of a lepton in one jet and an inclusively reconstructed $D^{*\pm}$ meson in the opposite jet. The systematic error includes an uncertainty of ± 0.006 due to the external branching ratios.

⁵ ALEXANDER 96R obtain this value via direct charm counting, summing the partial contributions from D^0, D^+, D_s^+ , and A_c^+ , and assuming that strange-charmed baryons account for the 15% of the Λ_c^+ production. An uncertainty of ± 0.005 due to the uncertainties in the charm hadron branching ratios is included in the overall systematics.

⁶ ABREU 95D perform a maximum likelihood fit to the combined p and p_T distributions of single and dilepton samples. The second error includes an uncertainty of ± 0.0124 due to models and branching ratios.

$R_b = \Gamma(b\bar{b})/\Gamma(\text{hadrons})$ Γ_{12}/Γ_8
OUR FIT is obtained by a simultaneous fit to several c - and b -quark measurements as explained in the note "The Z boson" and ref. LEP-SLC 06.

The Standard Model predicts $R_b = 0.21581$ for $m_t = 174.3$ GeV and $M_H = 150$ GeV.

VALUE	DOCUMENT ID	TECN	COMMENT
0.21629 ± 0.00066 OUR FIT			
0.21594 ± 0.00094 ± 0.00075	¹ ABE	05F SLD	$E_{\text{cm}}^{\text{ee}} = 91.28$ GeV
0.2174 ± 0.0015 ± 0.0028	² ACCIARRI	00 L3	$E_{\text{cm}}^{\text{ee}} = 89-93$ GeV
0.2178 ± 0.0011 ± 0.0013	³ ABBIENDI	99B OPAL	$E_{\text{cm}}^{\text{ee}} = 88-94$ GeV
0.21634 ± 0.00067 ± 0.00060	⁴ ABREU	99B DLPH	$E_{\text{cm}}^{\text{ee}} = 88-94$ GeV
0.2159 ± 0.0009 ± 0.0011	⁵ BARATE	97F ALEP	$E_{\text{cm}}^{\text{ee}} = 88-94$ GeV
• • • We do not use the following data for averages, fits, limits, etc. • • •			
0.215 ± 0.0089 ± 0.0067	⁶ ABREU	95D DLPH	$E_{\text{cm}}^{\text{ee}} = 88-94$ GeV
0.219 ± 0.006 ± 0.005	⁷ BUSKULIC	94G ALEP	$E_{\text{cm}}^{\text{ee}} = 88-94$ GeV
0.251 ± 0.049 ± 0.030	⁸ JACOBSEN	91 MRK2	$E_{\text{cm}}^{\text{ee}} = 91$ GeV

¹ ABE 05F use hadronic Z decays collected during 1996-98 to obtain an enriched sample of $b\bar{b}$ events using a double tag method. The single b -tag is obtained with a neural network trained to perform flavor discrimination using as input several signatures (corrected secondary vertex mass, vertex decay length, multiplicity and total momentum of the hemisphere; the key tag is obtained requiring the secondary vertex corrected mass to be above the D -meson mass). ABE 05F obtain $R_b = 0.21604 \pm 0.00098 \pm 0.00074$ where the systematic error includes an uncertainty of ± 0.00012 due to the uncertainty on R_c . The value reported here is obtained properly combining with ABE 98D. The quoted systematic error includes an uncertainty of ± 0.00012 due to the uncertainty on R_c .

² ACCIARRI 00 obtain this result using a double-tagging technique, with a high p_T lepton tag and an impact parameter tag in opposite hemispheres.

³ ABBIENDI 99B tag $Z \rightarrow b\bar{b}$ decays using leptons and/or separated decay vertices. The b -tagging efficiency is measured directly from the data using a double-tagging technique.

⁴ ABREU 99B obtain this result combining in a multivariate analysis several tagging methods (impact parameter and secondary vertex reconstruction, complemented by event shape variables). For R_c different from its Standard Model value of 0.172, R_b varies as $-0.024 \times (R_c - 0.172)$.

⁵ BARATE 97F combine the lifetime-mass hemisphere tag (BARATE 97E) with event shape information and lepton tag to identify $Z \rightarrow b\bar{b}$ candidates. They further use c - and u/d selection tags to identify the background. For R_c different from its Standard Model value of 0.172, R_b varies as $-0.019 \times (R_c - 0.172)$.

⁶ ABREU 95D perform a maximum likelihood fit to the combined p and p_T distributions of single and dilepton samples. The second error includes an uncertainty of ± 0.0023 due to models and branching ratios.

⁷ BUSKULIC 94G perform a simultaneous fit to the p and p_T spectra of both single and dilepton events.

⁸ JACOBSEN 91 tagged $b\bar{b}$ events by requiring coincidence of ≥ 3 tracks with significant impact parameters using vertex detector. Systematic error includes lifetime and decay uncertainties (± 0.014).

$\Gamma(b\bar{b}b\bar{b})/\Gamma(\text{hadrons})$ Γ_{13}/Γ_8

VALUE (units 10^{-4})	DOCUMENT ID	TECN	COMMENT
5.2 ± 1.9 OUR AVERAGE			
3.6 ± 1.7 ± 2.7	¹ ABBIENDI	01G OPAL	$E_{\text{cm}}^{\text{ee}} = 88-94$ GeV
6.0 ± 1.9 ± 1.4	² ABREU	99U DLPH	$E_{\text{cm}}^{\text{ee}} = 88-94$ GeV

¹ ABBIENDI 01G use a sample of four-jet events from hadronic Z decays. To enhance the $b\bar{b}b\bar{b}$ signal, at least three of the four jets are required to have a significantly detached secondary vertex.

² ABREU 99U force hadronic Z decays into 3jets to use all the available phase space and require a b tag for every jet. This decay mode includes primary and secondary $4b$ production, e.g. from gluon splitting to $b\bar{b}$.

$\Gamma(gg g)/\Gamma(\text{hadrons})$ Γ_{14}/Γ_8

VALUE	CL%	DOCUMENT ID	TECN	COMMENT
< 1.6 × 10⁻²	95	¹ ABREU	96S DLPH	$E_{\text{cm}}^{\text{ee}} = 88-94$ GeV

¹ This branching ratio is slightly dependent on the jet-finder algorithm. The value we quote is obtained using the JADE algorithm, while using the DURHAM algorithm ABREU 96S obtain an upper limit of 1.5×10^{-2} .

$\Gamma(\pi^0 \gamma)/\Gamma_{\text{total}}$ Γ_{15}/Γ

VALUE	CL%	DOCUMENT ID	TECN	COMMENT
< 2.01 × 10⁻⁵	95	AALTONEN	14E CDF	$E_{\text{cm}}^{\text{pp}} = 1.96$ TeV
< 5.2 × 10 ⁻⁵	95	¹ ACCIARRI	95G L3	$E_{\text{cm}}^{\text{ee}} = 88-94$ GeV
< 5.5 × 10 ⁻⁵	95	ABREU	94B DLPH	$E_{\text{cm}}^{\text{ee}} = 88-94$ GeV
< 2.1 × 10 ⁻⁴	95	DECAMP	92 ALEP	$E_{\text{cm}}^{\text{ee}} = 88-94$ GeV
< 1.4 × 10 ⁻⁴	95	AKRAWY	91F OPAL	$E_{\text{cm}}^{\text{ee}} = 88-94$ GeV

¹ This limit is for both decay modes $Z \rightarrow \pi^0 \gamma / \gamma \gamma$ which are indistinguishable in ACCIARRI 95G.

$\Gamma(\eta \gamma)/\Gamma_{\text{total}}$ Γ_{16}/Γ

VALUE	CL%	DOCUMENT ID	TECN	COMMENT
< 7.6 × 10 ⁻⁵	95	ACCIARRI	95G L3	$E_{\text{cm}}^{\text{ee}} = 88-94$ GeV
< 8.0 × 10 ⁻⁵	95	ABREU	94B DLPH	$E_{\text{cm}}^{\text{ee}} = 88-94$ GeV
< 5.1 × 10⁻⁵	95	DECAMP	92 ALEP	$E_{\text{cm}}^{\text{ee}} = 88-94$ GeV
< 2.0 × 10 ⁻⁴	95	AKRAWY	91F OPAL	$E_{\text{cm}}^{\text{ee}} = 88-94$ GeV

$\Gamma(\rho^0 \gamma)/\Gamma_{\text{total}}$ Γ_{17}/Γ

VALUE	CL%	EVTS	DOCUMENT ID	TECN	COMMENT
< 2.5 × 10⁻⁵	95	12.5k	¹ AABOUD	18AU ATLS	$E_{\text{cm}}^{\text{pp}} = 13$ TeV

¹ AABOUD 18AU search for the $Z \rightarrow \rho \gamma$ decay mode where the ρ is identified through its decay $\rho \rightarrow \pi^+ \pi^-$. In the data corresponding to 32.3 fb^{-1} , 12,583 events are selected for $635 < m(\pi^+ \pi^-) < 915$ MeV.

$\Gamma(\omega \gamma)/\Gamma_{\text{total}}$ Γ_{18}/Γ

VALUE	CL%	DOCUMENT ID	TECN	COMMENT
< 6.5 × 10⁻⁴	95	ABREU	94B DLPH	$E_{\text{cm}}^{\text{ee}} = 88-94$ GeV

$\Gamma(\eta'(958) \gamma)/\Gamma_{\text{total}}$ Γ_{19}/Γ

VALUE	CL%	DOCUMENT ID	TECN	COMMENT
< 4.2 × 10⁻⁵	95	DECAMP	92 ALEP	$E_{\text{cm}}^{\text{ee}} = 88-94$ GeV

$\Gamma(\phi \gamma)/\Gamma_{\text{total}}$ Γ_{20}/Γ

VALUE	CL%	EVTS	DOCUMENT ID	TECN	COMMENT
< 9 × 10⁻⁷	95	3.3k	¹ AABOUD	18AU ATLS	$E_{\text{cm}}^{\text{pp}} = 13$ TeV
• • • We do not use the following data for averages, fits, limits, etc. • • •					
< 8.3 × 10 ⁻⁶	95	1.0k	² AABOUD	16k ATLS	$E_{\text{cm}}^{\text{pp}} = 13$ TeV

¹ AABOUD 18AU search for the $Z \rightarrow \phi \gamma$ decay mode where the ϕ is identified through its decay $\phi \rightarrow K^+ K^-$. In the data corresponding to 32.3 fb^{-1} , 3,364 events are selected for $1012 < m(K^+ K^-) < 1028$ MeV.

² AABOUD 16k search for the $Z \rightarrow \phi \gamma$ decay mode where the ϕ is identified through its decay into $K^+ K^-$. In the data corresponding to a total luminosity of 2.7 fb^{-1} , 1065 events are selected and their $K^+ K^- \gamma$ invariant mass spectrum is analyzed.

$\Gamma(\gamma \gamma)/\Gamma_{\text{total}}$ Γ_{21}/Γ

This decay would violate the Landau-Yang theorem.

VALUE	CL%	DOCUMENT ID	TECN	COMMENT
< 1.46 × 10⁻⁵	95	AALTONEN	14E CDF	$E_{\text{cm}}^{\text{pp}} = 1.96$ TeV
< 5.2 × 10 ⁻⁵	95	¹ ACCIARRI	95G L3	$E_{\text{cm}}^{\text{ee}} = 88-94$ GeV
< 5.5 × 10 ⁻⁵	95	ABREU	94B DLPH	$E_{\text{cm}}^{\text{ee}} = 88-94$ GeV
< 1.4 × 10 ⁻⁴	95	AKRAWY	91F OPAL	$E_{\text{cm}}^{\text{ee}} = 88-94$ GeV

¹ This limit is for both decay modes $Z \rightarrow \pi^0 \gamma / \gamma \gamma$ which are indistinguishable in ACCIARRI 95G.

$\Gamma(\pi^0 \pi^0)/\Gamma_{\text{total}}$ Γ_{22}/Γ

VALUE	CL%	DOCUMENT ID	TECN	COMMENT
< 1.52 × 10⁻⁵	95	AALTONEN	14E CDF	$E_{\text{cm}}^{\text{pp}} = 1.96$ TeV

Gauge & Higgs Boson Particle Listings

Z

 $\Gamma(\gamma\gamma\gamma)/\Gamma_{\text{total}}$ Γ_{23}/Γ

VALUE	CL%	DOCUMENT ID	TECN	COMMENT
$<2.2 \times 10^{-6}$	95	AAD	16L ATLS	$E_{\text{cm}}^{\text{pp}} = 8 \text{ TeV}$
$<1.0 \times 10^{-5}$	95	1 ACCIARRI	95c L3	$E_{\text{cm}}^{\text{ee}} = 88\text{--}94 \text{ GeV}$
$<1.7 \times 10^{-5}$	95	1 ABREU	94B DLPH	$E_{\text{cm}}^{\text{ee}} = 88\text{--}94 \text{ GeV}$
$<6.6 \times 10^{-5}$	95	AKRAWY	91F OPAL	$E_{\text{cm}}^{\text{ee}} = 88\text{--}94 \text{ GeV}$

¹ Limit derived in the context of composite Z model.

 $\Gamma(\pi^{\pm} W^{\mp})/\Gamma_{\text{total}}$ Γ_{24}/Γ

The value is for the sum of the charge states indicated.

VALUE	CL%	DOCUMENT ID	TECN	COMMENT
$<7 \times 10^{-5}$	95	DECAMP	92 ALEP	$E_{\text{cm}}^{\text{ee}} = 88\text{--}94 \text{ GeV}$

 $\Gamma(\rho^{\pm} W^{\mp})/\Gamma_{\text{total}}$ Γ_{25}/Γ

The value is for the sum of the charge states indicated.

VALUE	CL%	DOCUMENT ID	TECN	COMMENT
$<8.3 \times 10^{-5}$	95	DECAMP	92 ALEP	$E_{\text{cm}}^{\text{ee}} = 88\text{--}94 \text{ GeV}$

 $\Gamma(J/\psi(1S)X)/\Gamma_{\text{total}}$ Γ_{26}/Γ

VALUE (units 10^{-3})	EVTS	DOCUMENT ID	TECN	COMMENT
--------------------------	------	-------------	------	---------

3.51 $^{+0.23}_{-0.25}$ OUR AVERAGE Error includes scale factor of 1.1.

3.21 ± 0.21 $^{+0.19}_{-0.28}$	553	1 ACCIARRI	99F L3	$E_{\text{cm}}^{\text{ee}} = 88\text{--}94 \text{ GeV}$
3.9 $\pm 0.2 \pm 0.3$	511	2 ALEXANDER	96B OPAL	$E_{\text{cm}}^{\text{ee}} = 88\text{--}94 \text{ GeV}$
3.73 $\pm 0.39 \pm 0.36$	153	3 ABREU	94P DLPH	$E_{\text{cm}}^{\text{ee}} = 88\text{--}94 \text{ GeV}$

¹ ACCIARRI 99F combine $\mu^+\mu^-$ and $e^+e^- J/\psi(1S)$ decay channels. The branching ratio for prompt $J/\psi(1S)$ production is measured to be $(2.1 \pm 0.6 \pm 0.4^{+0.4}_{-0.2}(\text{theor.})) \times 10^{-4}$.

² ALEXANDER 96B identify $J/\psi(1S)$ from the decays into lepton pairs. $(4.8 \pm 2.4)\%$ of this branching ratio is due to prompt $J/\psi(1S)$ production (ALEXANDER 96N).

³ Combining $\mu^+\mu^-$ and e^+e^- channels and taking into account the common systematic errors. $(7.7^{+6.3}_{-5.4})\%$ of this branching ratio is due to prompt $J/\psi(1S)$ production.

 $\Gamma(J/\psi(1S)\gamma)/\Gamma_{\text{total}}$ Γ_{27}/Γ

VALUE	CL%	DOCUMENT ID	TECN	COMMENT
-------	-----	-------------	------	---------

$<1.4 \times 10^{-6}$	95	1 SIRUNYAN	19AJ CMS	$E_{\text{cm}}^{\text{pp}} = 13 \text{ TeV}$
$<2.3 \times 10^{-6}$	95	2 AABOUD	18BL ATLS	$E_{\text{cm}}^{\text{pp}} = 13 \text{ TeV}$
$<2.6 \times 10^{-6}$	95	3 AAD	15I ATLS	$E_{\text{cm}}^{\text{pp}} = 8 \text{ TeV}$

¹ SIRUNYAN 19AJ study $Z \rightarrow J/\psi\gamma$ with $J/\psi \rightarrow \mu^+\mu^-$. Candidate events are selected by requiring a pair of oppositely charged muons and a well isolated photon. The leading (subleading) muon is required to have a transverse momentum larger than 20 GeV (4 GeV), while the photon must have a transverse energy larger than 33 GeV. Requiring the invariant mass of the $\mu\mu(\mu\mu\gamma)$ system in the range 3.0 to 3.2 (81 to 101) GeV, selects 183 data events which is consistent with the expected background. The 95% C.L. limit on the Z branching fraction is obtained assuming the J/ψ to be unpolarized.

² AABOUD 18BL study $Z \rightarrow J/\psi\gamma$ in 13 TeV pp interactions. Two triggers were used: isolated photon of $p_T > 35(25)$ GeV and a muon with $p_T > 18(24)$ GeV. The J/ψ is detected via its dimuon decay and it is required that the azimuthal angle between the photon and the J/ψ in the plane transverse to the beam direction is $> \pi/2$. The number of observed/expected background events is $92/89 \pm 6$ in the dimuon mass range 2.9–3.3 GeV leading to the quoted 95% C.L. limit.

³ AAD 15I use events with the highest p_T muon in the pair required to have $p_T > 20$ GeV, the dimuon mass required to be within 0.2 GeV of the $J/\psi(1S)$ mass and its transverse momentum required to be > 36 GeV. The photon is also required to have its $p_T > 36$ GeV.

 $\Gamma(\psi(2S)X)/\Gamma_{\text{total}}$ Γ_{28}/Γ

VALUE (units 10^{-3})	EVTS	DOCUMENT ID	TECN	COMMENT
--------------------------	------	-------------	------	---------

1.60± 0.29 OUR AVERAGE				
1.6 $\pm 0.5 \pm 0.3$	39	1 ACCIARRI	97J L3	$E_{\text{cm}}^{\text{ee}} = 88\text{--}94 \text{ GeV}$
1.6 $\pm 0.3 \pm 0.2$	46.9	2 ALEXANDER	96B OPAL	$E_{\text{cm}}^{\text{ee}} = 88\text{--}94 \text{ GeV}$
1.60 $\pm 0.73 \pm 0.33$	5.4	3 ABREU	94P DLPH	$E_{\text{cm}}^{\text{ee}} = 88\text{--}94 \text{ GeV}$

¹ ACCIARRI 97J measure this branching ratio via the decay channel $\psi(2S) \rightarrow \ell^+\ell^- (\ell = \mu, e)$.

² ALEXANDER 96B measure this branching ratio via the decay channel $\psi(2S) \rightarrow J/\psi\pi^+\pi^-$, with $J/\psi \rightarrow \ell^+\ell^-$.

³ ABREU 94P measure this branching ratio via decay channel $\psi(2S) \rightarrow J/\psi\pi^+\pi^-$, with $J/\psi \rightarrow \mu^+\mu^-$.

 $\Gamma(\psi(2S)\gamma)/\Gamma_{\text{total}}$ Γ_{29}/Γ

VALUE	CL%	DOCUMENT ID	TECN	COMMENT
$<4.5 \times 10^{-6}$	95	1 AABOUD	18BL ATLS	$E_{\text{cm}}^{\text{pp}} = 13 \text{ TeV}$

¹ AABOUD 18BL study $Z \rightarrow \psi(2S)\gamma$ in 13 TeV pp interactions. Two triggers were used: isolated photon of $p_T > 35(25)$ GeV and a muon with $p_T > 18(24)$ GeV. The $\psi(2S)$ is detected via its dimuon decay and it is required that the azimuthal angle between the photon and the $\psi(2S)$ in the plane transverse to the beam direction is $> \pi/2$. The number of observed/expected background events is $43/42 \pm 5$ in the dimuon mass range 3.5–3.9 GeV leading to the quoted 95% C.L. limit.

 $\Gamma(J/\psi(1S)\ell^+\ell^-)/\Gamma(\mu^+\mu^-\mu^+\mu^-)$ Γ_{30}/Γ_5

VALUE	DOCUMENT ID	TECN	COMMENT
0.67$\pm 0.18 \pm 0.05$	1 SIRUNYAN	18Dz CMS	pp at 13 TeV

¹ SIRUNYAN 18Dz observe the decay $Z \rightarrow \Psi\ell^+\ell^-$ in pp collisions at $\sqrt{s} = 13 \text{ TeV}$, where Ψ includes J/ψ as well as $\psi(2S) \rightarrow J/\psi X$, and $\ell^+\ell^-$ represents an electron or muon pair while the J/ψ is detected via its $\mu^+\mu^-$ decay channel. To reduce systematic errors they determine the ratio of the branching fraction of this decay to that of $Z \rightarrow \mu^+\mu^-\mu^+\mu^-$ within phase-space cuts imposed on lepton transverse momentum and pseudo rapidity, dilepton invariant mass, and J/ψ transverse momentum. The number of selected $\Psi\mu^+\mu^- (\Psi e^+e^-)$ candidate events is 29 (18). Analyzing the $\mu^+\mu^-$ and $\mu^+\mu^-\ell^+\ell^-$ invariant mass distributions, a yield of $13.0 \pm 3.9 (11.2 \pm 3.4)$ events for the $\Psi\mu^+\mu^- (\Psi e^+e^-)$ mode is obtained. The ratio of the branching fractions is determined as $0.67 \pm 0.18 \pm 0.05$ within the selected phase-space cuts. Assuming extrapolation to full phase space cancels in the ratio, and using their measured value of $B(Z \rightarrow \mu^+\mu^-\mu^+\mu^-) = (1.20 \pm 0.08) \times 10^{-6}$, they estimate $B(Z \rightarrow J/\psi\ell^+\ell^-) = 8 \times 10^{-7}$.

 $\Gamma(J/\psi(1S)J/\psi(1S))/\Gamma_{\text{total}}$ Γ_{31}/Γ

VALUE	CL%	EVTS	DOCUMENT ID	TECN	COMMENT
$<2.2 \times 10^{-6}$	95	189	1 SIRUNYAN	19BR CMS	$E_{\text{cm}}^{\text{pp}} = 13 \text{ TeV}$

¹ SIRUNYAN 19BR search for Z decays to a pair of J/ψ mesons in the channel $J/\psi \rightarrow \mu^+\mu^-$. The invariant masses of the higher/lower- p_T J/ψ candidates have to be within 0.1/0.15 GeV of the nominal J/ψ mass. A total of 189 events are selected in the 40–140 GeV 4-muon invariant mass range. An un-binned extended maximum likelihood fit leads to the 95% C.L. upper limit, obtained assuming the J/ψ mesons to be unpolarized.

 $\Gamma(\chi_{c1}(1P)X)/\Gamma_{\text{total}}$ Γ_{32}/Γ

VALUE (units 10^{-3})	EVTS	DOCUMENT ID	TECN	COMMENT
2.9± 0.7 OUR AVERAGE				
2.7 $\pm 0.6 \pm 0.5$	33	1 ACCIARRI	97J L3	$E_{\text{cm}}^{\text{ee}} = 88\text{--}94 \text{ GeV}$
5.0 ± 2.1 $^{+1.5}_{-0.9}$	6.4	2 ABREU	94P DLPH	$E_{\text{cm}}^{\text{ee}} = 88\text{--}94 \text{ GeV}$

¹ ACCIARRI 97J measure this branching ratio via the decay channel $\chi_{c1} \rightarrow J/\psi + \gamma$, with $J/\psi \rightarrow \ell^+\ell^- (\ell = \mu, e)$. The $M(\ell^+\ell^-) - M(\ell^+\ell^-)$ mass difference spectrum is fitted with two gaussian shapes for χ_{c1} and χ_{c2} .

² This branching ratio is measured via the decay channel $\chi_{c1} \rightarrow J/\psi + \gamma$, with $J/\psi \rightarrow \mu^+\mu^-$.

 $\Gamma(\chi_{c2}(1P)X)/\Gamma_{\text{total}}$ Γ_{33}/Γ

VALUE	CL%	DOCUMENT ID	TECN	COMMENT
$<3.2 \times 10^{-3}$	90	1 ACCIARRI	97J L3	$E_{\text{cm}}^{\text{ee}} = 88\text{--}94 \text{ GeV}$

¹ ACCIARRI 97J derive this limit via the decay channel $\chi_{c2} \rightarrow J/\psi + \gamma$, with $J/\psi \rightarrow \ell^+\ell^- (\ell = \mu, e)$. The $M(\ell^+\ell^-) - M(\ell^+\ell^-)$ mass difference spectrum is fitted with two gaussian shapes for χ_{c1} and χ_{c2} .

 $\Gamma(\Upsilon(1S)X + \Upsilon(2S)X + \Upsilon(3S)X)/\Gamma_{\text{total}}$ $\Gamma_{34}/\Gamma = (\Gamma_{35} + \Gamma_{37} + \Gamma_{39})/\Gamma$

VALUE (units 10^{-4})	EVTS	DOCUMENT ID	TECN	COMMENT
1.0$\pm 0.4 \pm 0.22$	6.4	1 ALEXANDER	96F OPAL	$E_{\text{cm}}^{\text{ee}} = 88\text{--}94 \text{ GeV}$

¹ ALEXANDER 96F identify the Υ (which refers to any of the three lowest bound states) through its decay into e^+e^- and $\mu^+\mu^-$. The systematic error includes an uncertainty of ± 0.2 due to the production mechanism.

 $\Gamma(\Upsilon(1S)\gamma)/\Gamma_{\text{total}}$ Γ_{35}/Γ

VALUE	CL%	DOCUMENT ID	TECN	COMMENT
$<4.4 \times 10^{-5}$	95	1 ACCIARRI	99F L3	$E_{\text{cm}}^{\text{ee}} = 88\text{--}94 \text{ GeV}$

¹ ACCIARRI 99F search for $\Upsilon(1S)$ through its decay into $\ell^+\ell^- (\ell = e \text{ or } \mu)$.

 $\Gamma(\Upsilon(1S)\gamma)/\Gamma_{\text{total}}$ Γ_{36}/Γ

VALUE	CL%	DOCUMENT ID	TECN	COMMENT
$<2.8 \times 10^{-6}$	95	1 AABOUD	18BL ATLS	$E_{\text{cm}}^{\text{pp}} = 13 \text{ TeV}$

• • • We do not use the following data for averages, fits, limits, etc. • • •

$<3.4 \times 10^{-6}$	95	2 AAD	15I ATLS	$E_{\text{cm}}^{\text{pp}} = 8 \text{ TeV}$
-----------------------	----	-------	----------	---

¹ AABOUD 18BL study $Z \rightarrow \Upsilon(1S)\gamma$ in 13 TeV pp interactions. Two triggers were used: isolated photon of $p_T > 35(25)$ GeV and a muon with $p_T > 18(24)$ GeV. The $\Upsilon(1S)$ is detected via its dimuon decay and it is required that the azimuthal angle between the photon and the $\Upsilon(1S)$ in the plane transverse to the beam direction is $> \pi/2$. The number of observed/expected background events is $115/126 \pm 8$ in the dimuon mass range 9.0–10.0 GeV leading to the quoted 95% C.L. limit.

² AAD 15I use events with the highest p_T muon in the pair required to have $p_T > 20$ GeV, the dimuon mass required to be in the range 8–12 GeV and its transverse momentum required to be > 36 GeV. The photon is also required to have its $p_T > 36$ GeV.

 $\Gamma(\Upsilon(2S)X)/\Gamma_{\text{total}}$ Γ_{37}/Γ

VALUE	CL%	DOCUMENT ID	TECN	COMMENT
$<13.9 \times 10^{-5}$	95	1 ACCIARRI	97R L3	$E_{\text{cm}}^{\text{ee}} = 88\text{--}94 \text{ GeV}$

¹ ACCIARRI 97R search for $\Upsilon(2S)$ through its decay into $\ell^+\ell^- (\ell = e \text{ or } \mu)$.

 $\Gamma(\Upsilon(2S)\gamma)/\Gamma_{\text{total}}$ Γ_{38}/Γ

VALUE	CL%	DOCUMENT ID	TECN	COMMENT
$<1.7 \times 10^{-6}$	95	1 AABOUD	18BL ATLS	$E_{\text{cm}}^{\text{pp}} = 13 \text{ TeV}$

• • • We do not use the following data for averages, fits, limits, etc. • • •

$<6.5 \times 10^{-6}$ 95 2 AAD 15i ATLS $E_{cm}^{pp} = 8$ TeV

¹ AABOUD 18BL study $Z \rightarrow \Upsilon(2S)\gamma$ in 13 TeV pp interactions. Two triggers were used: isolated photon of $p_T > 35(25)$ GeV and a muon with $p_T > 18(24)$ GeV. The $\Upsilon(2S)$ is detected via its dimuon decay and it is required that the azimuthal angle between the photon and the $\Upsilon(2S)$ in the plane transverse to the beam direction is $> \pi/2$. The number of observed/expected background events is $106/121 \pm 8$ in the dimuon mass range 9.5–10.5 GeV leading to the quoted 95% C.L. limit.

² AAD 15i use events with the highest p_T muon in the pair required to have $p_T > 20$ GeV, the dimuon mass required to be in the range 8–12 GeV and it's transverse momentum required to be > 36 GeV. The photon is also required to have it's $p_T > 36$ GeV.

$\Gamma(\Upsilon(3S)X)/\Gamma_{total}$ Γ₃₉/Γ

VALUE	CL%	DOCUMENT ID	TECN	COMMENT
$<9.4 \times 10^{-5}$	95	1 ACCIARRI 97R L3	L3	$E_{cm}^{pp} = 88-94$ GeV

¹ ACCIARRI 97R search for $\Upsilon(3S)$ through its decay into $\ell^+\ell^-$ ($\ell = e$ or μ).

$\Gamma(\Upsilon(3S)\gamma)/\Gamma_{total}$ Γ₄₀/Γ

VALUE	CL%	DOCUMENT ID	TECN	COMMENT
$<4.8 \times 10^{-6}$	95	1 AABOUD 18BL ATLS	ATLS	$E_{cm}^{pp} = 13$ TeV

• • • We do not use the following data for averages, fits, limits, etc. • • •

$<5.4 \times 10^{-6}$ 95 2 AAD 15i ATLS $E_{cm}^{pp} = 8$ TeV

¹ AABOUD 18BL study $Z \rightarrow \Upsilon(3S)\gamma$ in 13 TeV pp interactions. Two triggers were used: isolated photon of $p_T > 35(25)$ GeV and a muon with $p_T > 18(24)$ GeV. The $\Upsilon(3S)$ is detected via its dimuon decay and it is required that the azimuthal angle between the photon and the $\Upsilon(3S)$ in the plane transverse to the beam direction is $> \pi/2$. The number of observed/expected background events is $112/113 \pm 8$ in the dimuon mass range 10.0–11.0 GeV leading to the quoted 95% C.L. limit.

² AAD 15i use events with the highest p_T muon in the pair required to have $p_T > 20$ GeV, the dimuon mass required to be in the range 8–12 GeV and it's transverse momentum required to be > 36 GeV. The photon is also required to have it's $p_T > 36$ GeV.

$\Gamma(\Upsilon(1,2,3S)\Upsilon(1,2,3S))/\Gamma_{total}$ Γ₄₁/Γ

VALUE	CL%	EVTS	DOCUMENT ID	TECN	COMMENT
$<1.5 \times 10^{-6}$	95	106	1 SIRUNYAN 19BR CMS	CMS	$E_{cm}^{pp} = 13$ TeV

¹ SIRUNYAN 19BR search for Z decays to a pair of Υ mesons in the channel $\Upsilon \rightarrow \mu^+\mu^-$. The invariant mass of the Υ candidates has to be in the range of 8.5 to 11 GeV. A total of 106 events are selected in the 20–140 GeV 4-muon invariant mass range. An un-binned extended maximum likelihood fit leads to the 95% C.L. upper limit, obtained assuming the Υ mesons to be unpolarised.

$\Gamma((D^0/\bar{D}^0)X)/\Gamma(\text{hadrons})$ Γ₄₂/Γ₈

VALUE	EVTS	DOCUMENT ID	TECN	COMMENT
$0.296 \pm 0.019 \pm 0.021$	369	1 ABREU 93i DLPH	DLPH	$E_{cm}^{pp} = 88-94$ GeV

¹ The (D^0/\bar{D}^0) states in ABREU 93i are detected by the $K\pi$ decay mode. This is a corrected result (see the erratum of ABREU 93i).

$\Gamma(D^\pm X)/\Gamma(\text{hadrons})$ Γ₄₃/Γ₈

VALUE	EVTS	DOCUMENT ID	TECN	COMMENT
$0.174 \pm 0.016 \pm 0.018$	539	1 ABREU 93i DLPH	DLPH	$E_{cm}^{pp} = 88-94$ GeV

¹ The D^\pm states in ABREU 93i are detected by the $K\pi\pi$ decay mode. This is a corrected result (see the erratum of ABREU 93i).

$\Gamma(D^*(2010)^\pm X)/\Gamma(\text{hadrons})$ Γ₄₄/Γ₈

VALUE	EVTS	DOCUMENT ID	TECN	COMMENT
0.163 ± 0.019 OUR AVERAGE		Error includes scale factor of 1.3.		
$0.155 \pm 0.010 \pm 0.013$	358	1 ABREU 93i DLPH	DLPH	$E_{cm}^{pp} = 88-94$ GeV
0.21 ± 0.04	362	2 DECAMP 91j ALEP	ALEP	$E_{cm}^{pp} = 88-94$ GeV

¹ $D^*(2010)^\pm$ in ABREU 93i are reconstructed from $D^0\pi^\pm$, with $D^0 \rightarrow K^-\pi^+$. The new CLEO II measurement of $B(D^{*\pm} \rightarrow D^0\pi^\pm) = (68.1 \pm 1.6)\%$ is used. This is a corrected result (see the erratum of ABREU 93i).

² DECAMP 91j report $B(D^*(2010)^+ \rightarrow D^0\pi^+) B(D^0 \rightarrow K^-\pi^+) \Gamma(D^*(2010)^\pm X) / \Gamma(\text{hadrons}) = (5.11 \pm 0.34) \times 10^{-3}$. They obtained the above number assuming $B(D^0 \rightarrow K^-\pi^+) = (3.62 \pm 0.34 \pm 0.44)\%$ and $B(D^*(2010)^+ \rightarrow D^0\pi^+) = (55 \pm 4)\%$. We have rescaled their original result of 0.26 ± 0.05 taking into account the new CLEO II branching ratio $B(D^*(2010)^+ \rightarrow D^0\pi^+) = (68.1 \pm 1.6)\%$.

$\Gamma(D_{s1}(2536)^\pm X)/\Gamma(\text{hadrons})$ Γ₄₅/Γ₈

$D_{s1}(2536)^\pm$ is an expected orbitally-excited state of the D_s meson.

VALUE (%)	EVTS	DOCUMENT ID	TECN	COMMENT
$0.52 \pm 0.09 \pm 0.06$	92	1 HEISTER 02b ALEP	ALEP	$E_{cm}^{pp} = 88-94$ GeV

¹ HEISTER 02b reconstruct this meson in the decay modes $D_{s1}(2536)^\pm \rightarrow D^{*\pm}K^0$ and $D_{s1}(2536)^\pm \rightarrow D^{*0}K^\pm$. The quoted branching ratio assumes that the decay width of the $D_{s1}(2536)$ is saturated by the two measured decay modes.

$\Gamma(D_{sJ}(2573)^\pm X)/\Gamma(\text{hadrons})$ Γ₄₆/Γ₈

$D_{sJ}(2573)^\pm$ is an expected orbitally-excited state of the D_s meson.

VALUE (%)	EVTS	DOCUMENT ID	TECN	COMMENT
$0.83 \pm 0.29 \pm 0.07$	64	1 HEISTER 02b ALEP	ALEP	$E_{cm}^{pp} = 88-94$ GeV

¹ HEISTER 02b reconstruct this meson in the decay mode $D_{sJ}^*(2573)^\pm \rightarrow D^0K^\pm$. The quoted branching ratio assumes that the detected decay mode represents 45% of the full decay width.

$\Gamma(D^{*(2629)^\pm X)/\Gamma(\text{hadrons})$ Γ₄₇/Γ₈

$D^{*(2629)^\pm}$ is a predicted radial excitation of the $D^*(2010)^\pm$ meson.

VALUE	DOCUMENT ID	TECN	COMMENT
searched for	1 ABBIENDI 01N OPAL	OPAL	$E_{cm}^{pp} = 88-94$ GeV

¹ ABBIENDI 01N searched for the decay mode $D^{*(2629)^\pm \rightarrow D^{*\pm}\pi^+\pi^-$ with $D^{*\pm} \rightarrow D^0\pi^\pm$, and $D^0 \rightarrow K^-\pi^+$. They quote a 95% CL limit for $Z \rightarrow D^{*(2629)^\pm} \times B(D^{*(2629)^\pm} \rightarrow D^{*\pm}\pi^+\pi^-) < 3.1 \times 10^{-3}$.

$\Gamma(B^*X)/[\Gamma(BX) + \Gamma(B^*X)]$ Γ₄₉/(Γ₄₈+Γ₄₉)

As the experiments assume different values of the b -baryon contribution, our average should be taken with caution.

VALUE	EVTS	DOCUMENT ID	TECN	COMMENT
0.75 ± 0.04 OUR AVERAGE				
$0.760 \pm 0.036 \pm 0.083$		1 ACKERSTAFF 97M OPAL	OPAL	$E_{cm}^{pp} = 88-94$ GeV
$0.771 \pm 0.026 \pm 0.070$		2 BUSKULIC 96D ALEP	ALEP	$E_{cm}^{pp} = 88-94$ GeV
$0.72 \pm 0.03 \pm 0.06$		3 ABREU 95R DLPH	DLPH	$E_{cm}^{pp} = 88-94$ GeV
$0.76 \pm 0.08 \pm 0.06$	1378	4 ACCIARRI 95B L3	L3	$E_{cm}^{pp} = 88-94$ GeV

¹ ACKERSTAFF 97M use an inclusive B reconstruction method and assume a $(13.2 \pm 4.1)\%$ b -baryon contribution. The value refers to a b -flavored meson mixture of B_u, B_d , and B_s .

² BUSKULIC 96D use an inclusive reconstruction of B hadrons and assume a $(12.2 \pm 4.3)\%$ b -baryon contribution. The value refers to a b -flavored mixture of B_u, B_d , and B_s .

³ ABREU 95R use an inclusive B -reconstruction method and assume a $(10 \pm 4)\%$ b -baryon contribution. The value refers to a b -flavored meson mixture of B_u, B_d , and B_s .

⁴ ACCIARRI 95B assume a 9.4% b -baryon contribution. The value refers to a b -flavored mixture of B_u, B_d , and B_s .

$\Gamma(B^+X)/\Gamma(\text{hadrons})$ Γ₅₀/Γ₈

"OUR EVALUATION" is obtained using our current values for $f(\bar{b} \rightarrow B^+)$ and $R_b = \Gamma(b\bar{b})/\Gamma(\text{hadrons})$. We calculate $\Gamma(B^+X)/\Gamma(\text{hadrons}) = R_b \times f(\bar{b} \rightarrow B^+)$. The decay fraction $f(\bar{b} \rightarrow B^+)$ was provided by the Heavy Flavor Averaging Group (HFLAV, <https://hflav.web.cern.ch/>).

VALUE	DOCUMENT ID	TECN	COMMENT
0.0869 ± 0.0019 OUR EVALUATION			
0.0887 ± 0.0030	1 ABDALLAH 03k DLPH	DLPH	$E_{cm}^{pp} = 88-94$ GeV

¹ ABDALLAH 03k measure the production fraction of B^+ mesons in hadronic Z decays $f(B^+) = (40.99 \pm 0.82 \pm 1.11)\%$. The value quoted here is obtained multiplying this production fraction by our value of $R_b = \Gamma(b\bar{b})/\Gamma(\text{hadrons})$.

$\Gamma(B_s^0 X)/\Gamma(\text{hadrons})$ Γ₅₁/Γ₈

"OUR EVALUATION" is obtained using our current values for $f(\bar{b} \rightarrow B_s^0)$ and $R_b = \Gamma(b\bar{b})/\Gamma(\text{hadrons})$. We calculate $\Gamma(B_s^0 X)/\Gamma(\text{hadrons}) = R_b \times f(\bar{b} \rightarrow B_s^0)$. The decay fraction $f(\bar{b} \rightarrow B_s^0)$ was provided by the Heavy Flavor Averaging Group (HFLAV, <https://hflav.web.cern.ch/>).

VALUE	DOCUMENT ID	TECN	COMMENT
0.0227 ± 0.0019 OUR EVALUATION			
seen	1 ABREU 92M DLPH	DLPH	$E_{cm}^{pp} = 88-94$ GeV
seen	2 ACTON 92N OPAL	OPAL	$E_{cm}^{pp} = 88-94$ GeV
seen	3 BUSKULIC 92E ALEP	ALEP	$E_{cm}^{pp} = 88-94$ GeV

¹ ABREU 92M reported value is $\Gamma(B_s^0 X) \times B(B_s^0 \rightarrow D_s \mu \nu_\mu X) \times B(D_s \rightarrow \phi\pi)/\Gamma(\text{hadrons}) = (18 \pm 8) \times 10^{-5}$.

² ACTON 92N find evidence for B_s^0 production using $D_s\ell$ correlations, with $D_s^+ \rightarrow \phi\pi^+$ and $K^*(892)K^+$. Assuming R_b from the Standard Model and averaging over the e and μ channels, authors measure the product branching fraction to be $f(\bar{b} \rightarrow B_s^0) \times B(B_s^0 \rightarrow D_s^-\ell^+\nu_\ell X) \times B(D_s^- \rightarrow \phi\pi^-) = (3.9 \pm 1.1 \pm 0.8) \times 10^{-4}$.

³ BUSKULIC 92E find evidence for B_s^0 production using $D_s\ell$ correlations, with $D_s^+ \rightarrow \phi\pi^+$ and $K^*(892)K^+$. Using $B(D_s^+ \rightarrow \phi\pi^+) = (2.7 \pm 0.7)\%$ and summing up the e and μ channels, the weighted average product branching fraction is measured to be $B(\bar{b} \rightarrow B_s^0) \times B(B_s^0 \rightarrow D_s^-\ell^+\nu_\ell X) = 0.040 \pm 0.011^{+0.010}_{-0.012}$.

$\Gamma(B_c^+ X)/\Gamma(\text{hadrons})$ Γ₅₂/Γ₈

VALUE	DOCUMENT ID	TECN	COMMENT
searched for	1 ACKERSTAFF 98o OPAL	OPAL	$E_{cm}^{pp} = 88-94$ GeV
searched for	2 ABREU 97E DLPH	DLPH	$E_{cm}^{pp} = 88-94$ GeV
searched for	3 BARATE 97H ALEP	ALEP	$E_{cm}^{pp} = 88-94$ GeV

¹ ACKERSTAFF 98o searched for the decay modes $B_c \rightarrow J/\psi\pi^+, J/\psi a_1^+,$ and $J/\psi\ell^+\nu_\ell$ with $J/\psi \rightarrow \ell^+\ell^-, \ell = e, \mu$. The number of candidates (background) for the three decay modes is $2(0.63 \pm 0.2), 0(1.10 \pm 0.22)$, and $1(0.82 \pm 0.19)$ respectively. Interpreting the $2B_c \rightarrow J/\psi\pi^+$ candidates as signal, they report $\Gamma(B_c^+ X) \times B(B_c \rightarrow J/\psi\pi^+)/\Gamma(\text{hadrons}) = (3.8^{+5.0}_{-2.4} \pm 0.5) \times 10^{-5}$. Interpreted as background, the 90% CL bounds are $\Gamma(B_c^+ X) \times B(B_c \rightarrow J/\psi\pi^+)/\Gamma(\text{hadrons}) < 1.06 \times 10^{-4}$, $\Gamma(B_c^+ X) \times B(B_c \rightarrow J/\psi a_1^+)/\Gamma(\text{hadrons}) < 5.29 \times 10^{-4}$, $\Gamma(B_c^+ X) \times B(B_c \rightarrow J/\psi\ell^+\nu_\ell)/\Gamma(\text{hadrons}) < 6.96 \times 10^{-5}$.

² ABREU 97E searched for the decay modes $B_c \rightarrow J/\psi\pi^+, J/\psi\ell^+\nu_\ell$, and $J/\psi(3\pi^+)$, with $J/\psi \rightarrow \ell^+\ell^-, \ell = e, \mu$. The number of candidates (background) for the three decay modes is $1(1.7), 0(0.3)$, and $1(2.3)$ respectively. They report the following 90% CL limits: $\Gamma(B_c^+ X) \times B(B_c \rightarrow J/\psi\pi^+)/\Gamma(\text{hadrons}) < (1.05-0.84) \times 10^{-4}$, $\Gamma(B_c^+ X) \times B(B_c \rightarrow$

Gauge & Higgs Boson Particle Listings

Z

$J/\psi \ell \nu_\ell / \Gamma(\text{hadrons}) < (5.8-5.0) \times 10^{-5}$, $\Gamma(B_c^+ X) * B(B_c \rightarrow J/\psi(3\pi^+)) / \Gamma(\text{hadrons}) < 1.75 \times 10^{-4}$, where the ranges are due to the predicted B_c lifetime (0.4-1.4) ps.

³ BARATE 97H searched for the decay modes $B_c \rightarrow J/\psi \pi^+$ and $J/\psi \ell^+ \nu_\ell$ with $J/\psi \rightarrow \ell^+ \ell^-$, $\ell = e, \mu$. The number of candidates (background) for the two decay modes is 0 (0.44) and 2 (0.81) respectively. They report the following 90% CL limits: $\Gamma(B_c^+ X) * B(B_c \rightarrow J/\psi \pi^+) / \Gamma(\text{hadrons}) < 3.6 \times 10^{-5}$ and $\Gamma(B_c^+ X) * B(B_c \rightarrow J/\psi \ell^+ \nu_\ell) / \Gamma(\text{hadrons}) < 5.2 \times 10^{-5}$.

$\Gamma(\Lambda_c^+ X) / \Gamma(\text{hadrons})$ Γ_{53} / Γ_8

VALUE	DOCUMENT ID	TECN	COMMENT
0.022 ± 0.005 OUR AVERAGE			
0.024 ± 0.005 ± 0.006	¹ ALEXANDER 96R	OPAL	$E_{cm}^{ee} = 88-94$ GeV
0.021 ± 0.003 ± 0.005	² BUSKULIC 96V	ALEP	$E_{cm}^{ee} = 88-94$ GeV

¹ ALEXANDER 96R measure $R_b \times f(b \rightarrow \Lambda_c^+ X) \times B(\Lambda_c^+ \rightarrow p K^- \pi^+) = (0.122 \pm 0.023 \pm 0.010)\%$ in hadronic Z decays; the value quoted here is obtained using our best value $B(\Lambda_c^+ \rightarrow p K^- \pi^+) = (5.0 \pm 1.3)\%$. The first error is the total experiment's error and the second error is the systematic error due to the branching fraction uncertainty.

² BUSKULIC 96V obtain the production fraction of Λ_c^+ baryons in hadronic Z decays $f(b \rightarrow \Lambda_c^+ X) = 0.110 \pm 0.014 \pm 0.006$ using $B(\Lambda_c^+ \rightarrow p K^- \pi^+) = (4.4 \pm 0.6)\%$; we have rescaled using our best value $B(\Lambda_c^+ \rightarrow p K^- \pi^+) = (5.0 \pm 1.3)\%$ obtaining $f(b \rightarrow \Lambda_c^+ X) = 0.097 \pm 0.013 \pm 0.025$ where the first error is their total experiment's error and the second error is the systematic error due to the branching fraction uncertainty. The value quoted here is obtained multiplying this production fraction by our value $R_b = \Gamma(b \bar{b}) / \Gamma(\text{hadrons})$.

$\Gamma(\Xi_c^0 X) / \Gamma(\text{hadrons})$ Γ_{54} / Γ_8

VALUE	DOCUMENT ID	TECN	COMMENT
••• We do not use the following data for averages, fits, limits, etc. •••			
seen	¹ ABDALLAH 05c	DLPH	$E_{cm}^{ee} = 88-94$ GeV

¹ ABDALLAH 05c searched for the charmed strange baryon Ξ_c^0 in the decay channel $\Xi_c^0 \rightarrow \Xi^- \pi^+$ ($\Xi^- \rightarrow \Lambda \pi^-$). The production rate is measured to be $f_{\Xi_c^0} \times B(\Xi_c^0 \rightarrow \Xi^- \pi^+) = (4.7 \pm 1.4 \pm 1.1) \times 10^{-4}$ per hadronic Z decay.

$\Gamma(\Xi_b X) / \Gamma(\text{hadrons})$ Γ_{55} / Γ_8

Here Ξ_b is used as a notation for the strange b -baryon states Ξ_b^- and Ξ_b^0 .

VALUE	DOCUMENT ID	TECN	COMMENT
••• We do not use the following data for averages, fits, limits, etc. •••			
seen	¹ ABDALLAH 05c	DLPH	$E_{cm}^{ee} = 88-94$ GeV
seen	² BUSKULIC 96T	ALEP	$E_{cm}^{ee} = 88-94$ GeV
seen	³ ABREU 95v	DLPH	$E_{cm}^{ee} = 88-94$ GeV

¹ ABDALLAH 05c searched for the beauty strange baryon Ξ_b in the inclusive semileptonic decay channel $\Xi_b \rightarrow \Xi^- \ell^- \bar{\nu}_\ell X$. Evidence for the Ξ_b production is seen from the observation of Ξ^\mp production accompanied by a lepton of the same sign. From the excess of "right-sign" pairs $\Xi^\mp \ell^\mp$ compared to "wrong-sign" pairs $\Xi^\mp \ell^\pm$ the production rate is measured to be $B(b \rightarrow \Xi_b) \times B(\Xi_b \rightarrow \Xi^- \ell^- X) = (3.0 \pm 1.0 \pm 0.3) \times 10^{-4}$ per lepton species, averaged over electrons and muons.

² BUSKULIC 96T investigate Ξ -lepton correlations and find a significant excess of "right-sign" pairs $\Xi^\mp \ell^\mp$ compared to "wrong-sign" pairs $\Xi^\mp \ell^\pm$. This excess is interpreted as evidence for Ξ_b semileptonic decay. The measured product branching ratio is $B(b \rightarrow \Xi_b) \times B(\Xi_b \rightarrow X_c X \ell^- \bar{\nu}_\ell) \times B(X_c \rightarrow \Xi^- X') = (5.4 \pm 1.1 \pm 0.8) \times 10^{-4}$ per lepton species, averaged over electrons and muons, with X_c a charmed baryon.

³ ABREU 95v observe an excess of "right-sign" pairs $\Xi^\mp \ell^\mp$ compared to "wrong-sign" pairs $\Xi^\mp \ell^\pm$ in jets; this excess is interpreted as evidence for the beauty strange baryon Ξ_b production, with $\Xi_b \rightarrow \Xi^- \ell^- \bar{\nu}_\ell X$. They find that the probability for this signal to come from non b -baryon decays is less than 5×10^{-4} and that Λ_b decays can account for less than 10% of these events. The Ξ_b production rate is then measured to be $B(b \rightarrow \Xi_b) \times B(\Xi_b \rightarrow \Xi^- \ell^- X) = (5.9 \pm 2.1 \pm 1.0) \times 10^{-4}$ per lepton species, averaged over electrons and muons.

$\Gamma(b\text{-baryon } X) / \Gamma(\text{hadrons})$ Γ_{56} / Γ_8

"OUR EVALUATION" is obtained using our current values for $f(b \rightarrow b\text{-baryon})$ and $R_b = \Gamma(b \bar{b}) / \Gamma(\text{hadrons})$. We calculate $\Gamma(b\text{-baryon } X) / \Gamma(\text{hadrons}) = R_b \times f(b \rightarrow b\text{-baryon})$. The decay fraction $f(b \rightarrow b\text{-baryon})$ was provided by the Heavy Flavor Averaging Group (<https://hflav.web.cern.ch/>).

VALUE	DOCUMENT ID	TECN	COMMENT
0.0197 ± 0.0032 OUR EVALUATION			
0.0221 ± 0.0015 ± 0.0058	¹ BARATE 98v	ALEP	$E_{cm}^{ee} = 88-94$ GeV

¹ BARATE 98v use the overall number of identified protons in b -hadron decays to measure $f(b \rightarrow b\text{-baryon}) = 0.102 \pm 0.007 \pm 0.027$. They assume $BR(b\text{-baryon} \rightarrow p X) = (58 \pm 6)\%$ and $BR(B_s^0 \rightarrow p X) = (8.0 \pm 4.0)\%$. The value quoted here is obtained multiplying this production fraction by our value of $R_b = \Gamma(b \bar{b}) / \Gamma(\text{hadrons})$.

$\Gamma(\text{anomalous } \gamma + \text{hadrons}) / \Gamma_{\text{total}}$ Γ_{57} / Γ

Limits on additional sources of prompt photons beyond expectations for final-state bremsstrahlung.

VALUE	CL%	DOCUMENT ID	TECN	COMMENT
< 3.2 × 10⁻³	95	¹ AKRAWY 90J	OPAL	$E_{cm}^{ee} = 88-94$ GeV

¹ AKRAWY 90J report $\Gamma(\gamma X) < 8.2$ MeV at 95%CL. They assume a three-body $\gamma q \bar{q}$ distribution and use $E(\gamma) > 10$ GeV.

$\Gamma(e^+ e^- \gamma) / \Gamma_{\text{total}}$ Γ_{58} / Γ

VALUE	CL%	DOCUMENT ID	TECN	COMMENT
< 5.2 × 10⁻⁴	95	¹ ACTON 91B	OPAL	$E_{cm}^{ee} = 91.2$ GeV

¹ ACTON 91B looked for isolated photons with $E > 2\%$ of beam energy (> 0.9 GeV).

$\Gamma(\mu^+ \mu^- \gamma) / \Gamma_{\text{total}}$ Γ_{59} / Γ

VALUE	CL%	DOCUMENT ID	TECN	COMMENT
< 5.6 × 10⁻⁴	95	¹ ACTON 91B	OPAL	$E_{cm}^{ee} = 91.2$ GeV

¹ ACTON 91B looked for isolated photons with $E > 2\%$ of beam energy (> 0.9 GeV).

$\Gamma(\tau^+ \tau^- \gamma) / \Gamma_{\text{total}}$ Γ_{60} / Γ

VALUE	CL%	DOCUMENT ID	TECN	COMMENT
< 7.3 × 10⁻⁴	95	¹ ACTON 91B	OPAL	$E_{cm}^{ee} = 91.2$ GeV

¹ ACTON 91B looked for isolated photons with $E > 2\%$ of beam energy (> 0.9 GeV).

$\Gamma(\ell^+ \ell^- \gamma \gamma) / \Gamma_{\text{total}}$ Γ_{61} / Γ

The value is the sum over $\ell = e, \mu, \tau$.

VALUE	CL%	DOCUMENT ID	TECN	COMMENT
< 6.8 × 10⁻⁶	95	¹ ACTON 93E	OPAL	$E_{cm}^{ee} = 88-94$ GeV

¹ For $m_{\gamma\gamma} = 60 \pm 5$ GeV.

$\Gamma(q \bar{q} \gamma \gamma) / \Gamma_{\text{total}}$ Γ_{62} / Γ

VALUE	CL%	DOCUMENT ID	TECN	COMMENT
< 5.5 × 10⁻⁶	95	¹ ACTON 93E	OPAL	$E_{cm}^{ee} = 88-94$ GeV

¹ For $m_{\gamma\gamma} = 60 \pm 5$ GeV.

$\Gamma(\nu \bar{\nu} \gamma \gamma) / \Gamma_{\text{total}}$ Γ_{63} / Γ

VALUE	CL%	DOCUMENT ID	TECN	COMMENT
< 3.1 × 10⁻⁶	95	¹ ACTON 93E	OPAL	$E_{cm}^{ee} = 88-94$ GeV

¹ For $m_{\gamma\gamma} = 60 \pm 5$ GeV.

$\Gamma(e^\pm \mu^\mp) / \Gamma_{\text{total}}$ Γ_{64} / Γ

Test of lepton family number conservation. The value is for the sum of the charge states indicated.

VALUE	CL%	DOCUMENT ID	TECN	COMMENT
< 7.5 × 10⁻⁷	95	AAD 14AU	ATLS	$E_{cm}^{pp} = 8$ TeV
< 2.5 × 10 ⁻⁶	95	ABREU 97c	DLPH	$E_{cm}^{ee} = 88-94$ GeV
< 1.7 × 10 ⁻⁶	95	AKERS 95w	OPAL	$E_{cm}^{ee} = 88-94$ GeV
< 0.6 × 10 ⁻⁵	95	ADRIANI 93i	L3	$E_{cm}^{ee} = 88-94$ GeV
< 2.6 × 10 ⁻⁵	95	DECAMP 92	ALEP	$E_{cm}^{ee} = 88-94$ GeV

$\Gamma(e^\pm \mu^\mp) / \Gamma(e^+ e^-)$ Γ_{64} / Γ_1

Test of lepton family number conservation. The value is for the sum of the charge states indicated.

VALUE	CL%	DOCUMENT ID	TECN	COMMENT
< 0.07	90	ALBAJAR 89	UA1	$E_{cm}^{pp} = 546,630$ GeV

$\Gamma(e^\pm \tau^\mp) / \Gamma_{\text{total}}$ Γ_{65} / Γ

Test of lepton family number conservation. The value is for the sum of the charge states indicated.

VALUE	CL%	DOCUMENT ID	TECN	COMMENT
< 5.0 × 10⁻⁶	95	AAD 21AV	ATLS	$E_{cm}^{pp} = 13$ TeV
••• We do not use the following data for averages, fits, limits, etc. •••				
< 8.1 × 10 ⁻⁶	95	AAD 21A0	ATLS	$E_{cm}^{pp} = 13$ TeV
< 5.8 × 10 ⁻⁵	95	AABOUD 18CN	ATLS	$E_{cm}^{pp} = 13$ TeV
< 2.2 × 10 ⁻⁵	95	ABREU 97c	DLPH	$E_{cm}^{ee} = 88-94$ GeV
< 9.8 × 10 ⁻⁶	95	AKERS 95w	OPAL	$E_{cm}^{ee} = 88-94$ GeV
< 1.3 × 10 ⁻⁵	95	ADRIANI 93i	L3	$E_{cm}^{ee} = 88-94$ GeV
< 1.2 × 10 ⁻⁴	95	DECAMP 92	ALEP	$E_{cm}^{ee} = 88-94$ GeV

$\Gamma(\mu^\pm \tau^\mp) / \Gamma_{\text{total}}$ Γ_{66} / Γ

Test of lepton family number conservation. The value is for the sum of the charge states indicated.

VALUE	CL%	DOCUMENT ID	TECN	COMMENT
< 6.5 × 10⁻⁶	95	AAD 21AV	ATLS	$E_{cm}^{pp} = 13$ TeV
••• We do not use the following data for averages, fits, limits, etc. •••				
< 9.5 × 10 ⁻⁶	95	AAD 21A0	ATLS	$E_{cm}^{pp} = 13$ TeV
< 1.3 × 10 ⁻⁵	95	AABOUD 18CN	ATLS	$E_{cm}^{pp} = 8, 13$ TeV
< 1.2 × 10 ⁻⁵	95	ABREU 97c	DLPH	$E_{cm}^{ee} = 88-94$ GeV
< 1.7 × 10 ⁻⁵	95	AKERS 95w	OPAL	$E_{cm}^{ee} = 88-94$ GeV
< 1.9 × 10 ⁻⁵	95	ADRIANI 93i	L3	$E_{cm}^{ee} = 88-94$ GeV
< 1.0 × 10 ⁻⁴	95	DECAMP 92	ALEP	$E_{cm}^{ee} = 88-94$ GeV

$\Gamma(p e) / \Gamma_{\text{total}}$ Γ_{67} / Γ

Test of baryon number and lepton number conservations. Charge conjugate states are implied.

VALUE	CL%	DOCUMENT ID	TECN	COMMENT
< 1.8 × 10⁻⁶	95	¹ ABBIENDI 99i	OPAL	$E_{cm}^{ee} = 88-94$ GeV

¹ ABBIENDI 99i give the 95%CL limit on the partial width $\Gamma(Z^0 \rightarrow p e) < 4.6$ KeV and we have transformed it into a branching ratio.

$\Gamma(\rho\mu)/\Gamma_{\text{total}}$ Γ_{68}/Γ
 Test of baryon number and lepton number conservations. Charge conjugate states are implied.

VALUE	CL%	DOCUMENT ID	TECN	COMMENT
$<1.8 \times 10^{-6}$	95	¹ ABBIENDI	99I OPAL	$E_{\text{cm}}^{\text{ee}} = 88\text{--}94$ GeV

¹ ABBIENDI 99I give the 95%CL limit on the partial width $\Gamma(Z^0 \rightarrow \rho\mu) < 4.4$ KeV and we have transformed it into a branching ratio.

AVERAGE PARTICLE MULTIPLICITIES IN HADRONIC Z DECAY

Summed over particle and antiparticle, when appropriate.

$\langle N_\gamma \rangle$

VALUE	DOCUMENT ID	TECN	COMMENT
20.97 ± 0.02 ± 1.15	ACKERSTAFF	98A OPAL	$E_{\text{cm}}^{\text{ee}} = 91.2$ GeV

$\langle N_{\pi^\pm} \rangle$

VALUE	DOCUMENT ID	TECN	COMMENT
17.03 ± 0.16 OUR AVERAGE			
17.007 ± 0.209	ABE	04C SLD	$E_{\text{cm}}^{\text{ee}} = 91.2$ GeV
17.26 ± 0.10 ± 0.88	ABREU	98L DLPH	$E_{\text{cm}}^{\text{ee}} = 91.2$ GeV
17.04 ± 0.31	BARATE	98V ALEP	$E_{\text{cm}}^{\text{ee}} = 91.2$ GeV
17.05 ± 0.43	AKERS	94P OPAL	$E_{\text{cm}}^{\text{ee}} = 91.2$ GeV

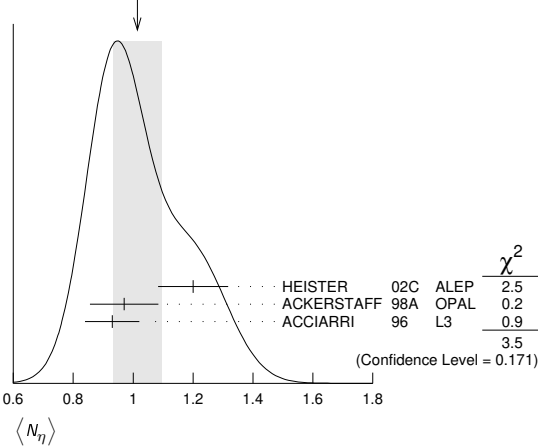
$\langle N_{\rho^0} \rangle$

VALUE	DOCUMENT ID	TECN	COMMENT
9.76 ± 0.26 OUR AVERAGE			
9.55 ± 0.06 ± 0.75	ACKERSTAFF	98A OPAL	$E_{\text{cm}}^{\text{ee}} = 91.2$ GeV
9.63 ± 0.13 ± 0.63	BARATE	97J ALEP	$E_{\text{cm}}^{\text{ee}} = 91.2$ GeV
9.90 ± 0.02 ± 0.33	ACCIARRI	96 L3	$E_{\text{cm}}^{\text{ee}} = 91.2$ GeV
9.2 ± 0.2 ± 1.0	ADAM	96 DLPH	$E_{\text{cm}}^{\text{ee}} = 91.2$ GeV

$\langle N_\eta \rangle$

VALUE	DOCUMENT ID	TECN	COMMENT
1.01 ± 0.08 OUR AVERAGE			Error includes scale factor of 1.3. See the ideogram below.
1.20 ± 0.04 ± 0.11	HEISTER	02C ALEP	$E_{\text{cm}}^{\text{ee}} = 91.2$ GeV
0.97 ± 0.03 ± 0.11	ACKERSTAFF	98A OPAL	$E_{\text{cm}}^{\text{ee}} = 91.2$ GeV
0.93 ± 0.01 ± 0.09	ACCIARRI	96 L3	$E_{\text{cm}}^{\text{ee}} = 91.2$ GeV

WEIGHTED AVERAGE
1.01 ± 0.08 (Error scaled by 1.3)



$\langle N_{\rho^\pm} \rangle$

VALUE	DOCUMENT ID	TECN	COMMENT
2.57 ± 0.15 OUR AVERAGE			
2.59 ± 0.03 ± 0.16	¹ BEDDALL	09	ALEPH archive, $E_{\text{cm}}^{\text{ee}} = 91.2$ GeV
2.40 ± 0.06 ± 0.43	ACKERSTAFF	98A OPAL	$E_{\text{cm}}^{\text{ee}} = 91.2$ GeV

¹ BEDDALL 09 analyse 3.2 million hadronic Z decays as archived by ALEPH collaboration and report a value of $2.59 \pm 0.03 \pm 0.15 \pm 0.04$. The first error is statistical, the second systematic, and the third arises from extrapolation to full phase space. We combine the systematic errors in quadrature.

$\langle N_{\rho^0} \rangle$

VALUE	DOCUMENT ID	TECN	COMMENT
1.24 ± 0.10 OUR AVERAGE			Error includes scale factor of 1.1.
1.19 ± 0.10	ABREU	99J DLPH	$E_{\text{cm}}^{\text{ee}} = 91.2$ GeV
1.45 ± 0.06 ± 0.20	BUSKULIC	96H ALEP	$E_{\text{cm}}^{\text{ee}} = 91.2$ GeV

$\langle N_\omega \rangle$

VALUE	DOCUMENT ID	TECN	COMMENT
1.02 ± 0.06 OUR AVERAGE			
1.00 ± 0.03 ± 0.06	HEISTER	02C ALEP	$E_{\text{cm}}^{\text{ee}} = 91.2$ GeV
1.04 ± 0.04 ± 0.14	ACKERSTAFF	98A OPAL	$E_{\text{cm}}^{\text{ee}} = 91.2$ GeV
1.17 ± 0.09 ± 0.15	ACCIARRI	97D L3	$E_{\text{cm}}^{\text{ee}} = 91.2$ GeV

$\langle N_{\eta'} \rangle$

VALUE	DOCUMENT ID	TECN	COMMENT
0.17 ± 0.05 OUR AVERAGE			Error includes scale factor of 2.4.
0.14 ± 0.01 ± 0.02	ACKERSTAFF	98A OPAL	$E_{\text{cm}}^{\text{ee}} = 91.2$ GeV
0.25 ± 0.04	¹ ACCIARRI	97D L3	$E_{\text{cm}}^{\text{ee}} = 91.2$ GeV
0.068 ± 0.018 ± 0.016	² BUSKULIC	92D ALEP	$E_{\text{cm}}^{\text{ee}} = 91.2$ GeV

• • • We do not use the following data for averages, fits, limits, etc. • • •
¹ ACCIARRI 97D obtain this value averaging over the two decay channels $\eta' \rightarrow \pi^+ \pi^- \eta$ and $\eta' \rightarrow \rho^0 \gamma$.
² BUSKULIC 92D obtain this value for $x > 0.1$.

$\langle N_{f_1(980)} \rangle$

VALUE	DOCUMENT ID	TECN	COMMENT
0.147 ± 0.011 OUR AVERAGE			
0.164 ± 0.021	ABREU	99J DLPH	$E_{\text{cm}}^{\text{ee}} = 91.2$ GeV
0.141 ± 0.007 ± 0.011	ACKERSTAFF	98Q OPAL	$E_{\text{cm}}^{\text{ee}} = 91.2$ GeV

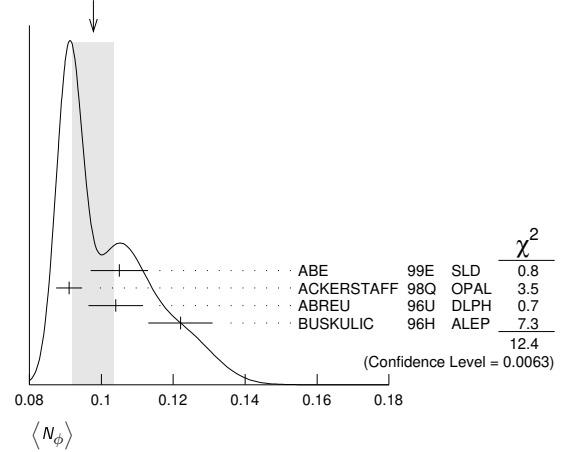
$\langle N_{\rho_0(980)^\pm} \rangle$

VALUE	DOCUMENT ID	TECN	COMMENT
0.27 ± 0.04 ± 0.10	ACKERSTAFF	98A OPAL	$E_{\text{cm}}^{\text{ee}} = 91.2$ GeV

$\langle N_\phi \rangle$

VALUE	DOCUMENT ID	TECN	COMMENT
0.098 ± 0.006 OUR AVERAGE			Error includes scale factor of 2.0. See the ideogram below.
0.105 ± 0.008	ABE	99E SLD	$E_{\text{cm}}^{\text{ee}} = 91.2$ GeV
0.091 ± 0.002 ± 0.003	ACKERSTAFF	98Q OPAL	$E_{\text{cm}}^{\text{ee}} = 91.2$ GeV
0.104 ± 0.003 ± 0.007	ABREU	96U DLPH	$E_{\text{cm}}^{\text{ee}} = 91.2$ GeV
0.122 ± 0.004 ± 0.008	BUSKULIC	96H ALEP	$E_{\text{cm}}^{\text{ee}} = 91.2$ GeV

WEIGHTED AVERAGE
0.098 ± 0.006 (Error scaled by 2.0)



$\langle N_{f_2(1270)} \rangle$

VALUE	DOCUMENT ID	TECN	COMMENT
0.169 ± 0.025 OUR AVERAGE			Error includes scale factor of 1.4.
0.214 ± 0.038	ABREU	99J DLPH	$E_{\text{cm}}^{\text{ee}} = 91.2$ GeV
0.155 ± 0.011 ± 0.018	ACKERSTAFF	98Q OPAL	$E_{\text{cm}}^{\text{ee}} = 91.2$ GeV

$\langle N_{f_1(1285)} \rangle$

VALUE	DOCUMENT ID	TECN	COMMENT
0.165 ± 0.051	¹ ABDALLAH	03H DLPH	$E_{\text{cm}}^{\text{ee}} = 91.2$ GeV

¹ ABDALLAH 03H assume a $K\bar{K}\pi$ branching ratio of $(9.0 \pm 0.4)\%$.

$\langle N_{f_1(1420)} \rangle$

VALUE	DOCUMENT ID	TECN	COMMENT
0.056 ± 0.012	¹ ABDALLAH	03H DLPH	$E_{\text{cm}}^{\text{ee}} = 91.2$ GeV

¹ ABDALLAH 03H assume a $K\bar{K}\pi$ branching ratio of 100%.

$\langle N_{f_2'(1525)} \rangle$

VALUE	DOCUMENT ID	TECN	COMMENT
0.012 ± 0.006	ABREU	99J DLPH	$E_{\text{cm}}^{\text{ee}} = 91.2$ GeV

$\langle N_{K^\pm} \rangle$

VALUE	DOCUMENT ID	TECN	COMMENT
2.24 ± 0.04 OUR AVERAGE			
2.203 ± 0.071	ABE	04C SLD	$E_{\text{cm}}^{\text{ee}} = 91.2$ GeV
2.21 ± 0.05 ± 0.05	ABREU	98L DLPH	$E_{\text{cm}}^{\text{ee}} = 91.2$ GeV
2.26 ± 0.12	BARATE	98V ALEP	$E_{\text{cm}}^{\text{ee}} = 91.2$ GeV
2.42 ± 0.13	AKERS	94P OPAL	$E_{\text{cm}}^{\text{ee}} = 91.2$ GeV

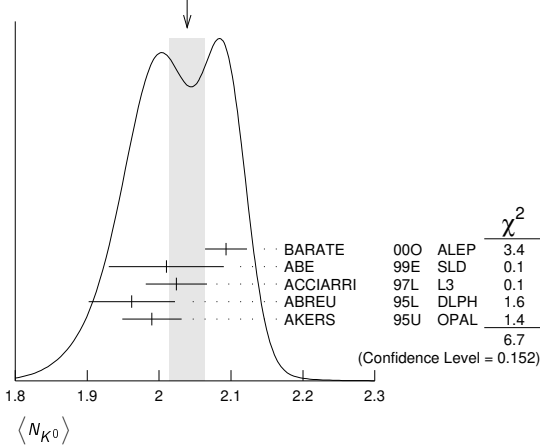
Gauge & Higgs Boson Particle Listings

Z

$\langle N_{K^0} \rangle$

VALUE	DOCUMENT ID	TECN	COMMENT
2.039 ± 0.025 OUR AVERAGE	Error includes scale factor of 1.3. See the ideogram below.		
2.093 ± 0.004 ± 0.029	BARATE	000 ALEP	$E_{cm}^{ee} = 91.2$ GeV
2.01 ± 0.08	ABE	99E SLD	$E_{cm}^{ee} = 91.2$ GeV
2.024 ± 0.006 ± 0.042	ACCIARRI	97L L3	$E_{cm}^{ee} = 91.2$ GeV
1.962 ± 0.022 ± 0.056	ABREU	95L DLPH	$E_{cm}^{ee} = 91.2$ GeV
1.99 ± 0.01 ± 0.04	AKERS	95U OPAL	$E_{cm}^{ee} = 91.2$ GeV

WEIGHTED AVERAGE
2.039 ± 0.025 (Error scaled by 1.3)



$\langle N_{K^*(892)^\pm} \rangle$

VALUE	DOCUMENT ID	TECN	COMMENT
0.72 ± 0.05 OUR AVERAGE			
0.712 ± 0.031 ± 0.059	ABREU	95L DLPH	$E_{cm}^{ee} = 91.2$ GeV
0.72 ± 0.02 ± 0.08	ACTON	93 OPAL	$E_{cm}^{ee} = 91.2$ GeV

$\langle N_{K^*(892)^0} \rangle$

VALUE	DOCUMENT ID	TECN	COMMENT
0.739 ± 0.022 OUR AVERAGE			
0.707 ± 0.041	ABE	99E SLD	$E_{cm}^{ee} = 91.2$ GeV
0.74 ± 0.02 ± 0.02	ACKERSTAFF	97S OPAL	$E_{cm}^{ee} = 91.2$ GeV
0.77 ± 0.02 ± 0.07	ABREU	96U DLPH	$E_{cm}^{ee} = 91.2$ GeV
0.83 ± 0.01 ± 0.09	BUSKULIC	96H ALEP	$E_{cm}^{ee} = 91.2$ GeV
0.97 ± 0.18 ± 0.31	ABREU	93 DLPH	$E_{cm}^{ee} = 91.2$ GeV

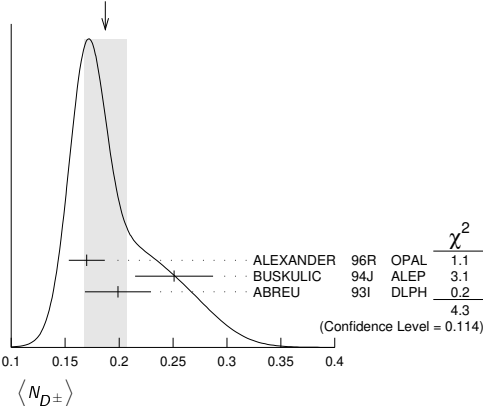
$\langle N_{K_2^*(1430)} \rangle$

VALUE	DOCUMENT ID	TECN	COMMENT
0.073 ± 0.023	ABREU	99J DLPH	$E_{cm}^{ee} = 91.2$ GeV
••• We do not use the following data for averages, fits, limits, etc. •••			
0.19 ± 0.04 ± 0.06	¹ AKERS	95X OPAL	$E_{cm}^{ee} = 91.2$ GeV
¹ AKERS 95X obtain this value for $x < 0.3$.			

$\langle N_{D^\pm} \rangle$

VALUE	DOCUMENT ID	TECN	COMMENT
0.187 ± 0.020 OUR AVERAGE	Error includes scale factor of 1.5. See the ideogram below.		
0.170 ± 0.009 ± 0.014	ALEXANDER	96R OPAL	$E_{cm}^{ee} = 91.2$ GeV
0.251 ± 0.026 ± 0.025	BUSKULIC	94J ALEP	$E_{cm}^{ee} = 91.2$ GeV
0.199 ± 0.019 ± 0.024	¹ ABREU	93I DLPH	$E_{cm}^{ee} = 91.2$ GeV

WEIGHTED AVERAGE
0.187 ± 0.020 (Error scaled by 1.5)



¹ See ABREU 95 (erratum).

$\langle N_{D^0} \rangle$

VALUE	DOCUMENT ID	TECN	COMMENT
0.462 ± 0.026 OUR AVERAGE			
0.465 ± 0.017 ± 0.027	ALEXANDER	96R OPAL	$E_{cm}^{ee} = 91.2$ GeV
0.518 ± 0.052 ± 0.035	BUSKULIC	94J ALEP	$E_{cm}^{ee} = 91.2$ GeV
0.403 ± 0.038 ± 0.044	¹ ABREU	93I DLPH	$E_{cm}^{ee} = 91.2$ GeV

¹ See ABREU 95 (erratum).

$\langle N_{D_s^\pm} \rangle$

VALUE	DOCUMENT ID	TECN	COMMENT
0.131 ± 0.010 ± 0.018	ALEXANDER	96R OPAL	$E_{cm}^{ee} = 91.2$ GeV

$\langle N_{D^*(2010)^\pm} \rangle$

VALUE	DOCUMENT ID	TECN	COMMENT
0.183 ± 0.008 OUR AVERAGE			
0.1854 ± 0.0041 ± 0.0091	¹ ACKERSTAFF	98E OPAL	$E_{cm}^{ee} = 91.2$ GeV
0.187 ± 0.015 ± 0.013	BUSKULIC	94J ALEP	$E_{cm}^{ee} = 91.2$ GeV
0.171 ± 0.012 ± 0.016	² ABREU	93I DLPH	$E_{cm}^{ee} = 91.2$ GeV

¹ ACKERSTAFF 98E systematic error includes an uncertainty of ± 0.0069 due to the branching ratios $B(D^{*+} \rightarrow D^0 \pi^+) = 0.683 \pm 0.014$ and $B(D^0 \rightarrow K^- \pi^+) = 0.0383 \pm 0.0012$.

² See ABREU 95 (erratum).

$\langle N_{D_{s1}(2536)^+} \rangle$

VALUE (units 10^{-3})	DOCUMENT ID	TECN	COMMENT
2.9^{+0.7}_{-0.6} ± 0.2	¹ ACKERSTAFF	97W OPAL	$E_{cm}^{ee} = 91.2$ GeV

¹ ACKERSTAFF 97W obtain this value for $x > 0.6$ and with the assumption that its decay width is saturated by the $D^* K$ final states.

$\langle N_{B^*} \rangle$

VALUE	DOCUMENT ID	TECN	COMMENT
0.28 ± 0.01 ± 0.03	¹ ABREU	95R DLPH	$E_{cm}^{ee} = 91.2$ GeV

¹ ABREU 95R quote this value for a flavor-averaged excited state.

$\langle N_{J/\psi(1S)} \rangle$

VALUE	DOCUMENT ID	TECN	COMMENT
0.0056 ± 0.0003 ± 0.0004	¹ ALEXANDER	96B OPAL	$E_{cm}^{ee} = 91.2$ GeV

¹ ALEXANDER 96B identify $J/\psi(1S)$ from the decays into lepton pairs.

$\langle N_{\psi(2S)} \rangle$

VALUE	DOCUMENT ID	TECN	COMMENT
0.0023 ± 0.0004 ± 0.0003	ALEXANDER	96B OPAL	$E_{cm}^{ee} = 91.2$ GeV

$\langle N_p \rangle$

VALUE	DOCUMENT ID	TECN	COMMENT
1.046 ± 0.026 OUR AVERAGE			
1.054 ± 0.035	ABE	04C SLD	$E_{cm}^{ee} = 91.2$ GeV
1.08 ± 0.04 ± 0.03	ABREU	98L DLPH	$E_{cm}^{ee} = 91.2$ GeV
1.00 ± 0.07	BARATE	98V ALEP	$E_{cm}^{ee} = 91.2$ GeV
0.92 ± 0.11	AKERS	94P OPAL	$E_{cm}^{ee} = 91.2$ GeV

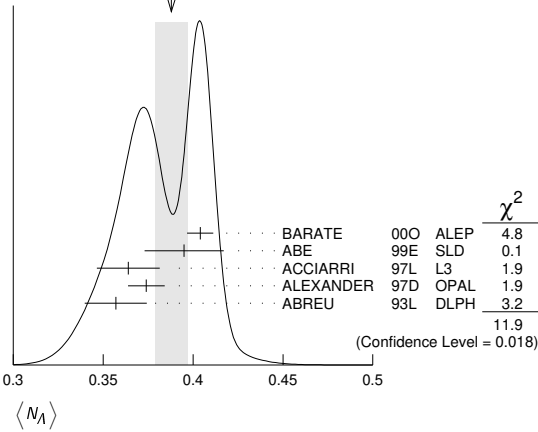
$\langle N_{\Delta(1232)^{++}} \rangle$

VALUE	DOCUMENT ID	TECN	COMMENT
0.087 ± 0.033 OUR AVERAGE	Error includes scale factor of 2.4.		
0.079 ± 0.009 ± 0.011	ABREU	95W DLPH	$E_{cm}^{ee} = 91.2$ GeV
0.22 ± 0.04 ± 0.04	ALEXANDER	95D OPAL	$E_{cm}^{ee} = 91.2$ GeV

$\langle N_\Lambda \rangle$

VALUE	DOCUMENT ID	TECN	COMMENT
0.388 ± 0.009 OUR AVERAGE	Error includes scale factor of 1.7. See the ideogram below.		
0.404 ± 0.002 ± 0.007	BARATE	000 ALEP	$E_{cm}^{ee} = 91.2$ GeV
0.395 ± 0.022	ABE	99E SLD	$E_{cm}^{ee} = 91.2$ GeV
0.364 ± 0.004 ± 0.017	ACCIARRI	97L L3	$E_{cm}^{ee} = 91.2$ GeV
0.374 ± 0.002 ± 0.010	ALEXANDER	97D OPAL	$E_{cm}^{ee} = 91.2$ GeV
0.357 ± 0.003 ± 0.017	ABREU	93L DLPH	$E_{cm}^{ee} = 91.2$ GeV

WEIGHTED AVERAGE
0.388±0.009 (Error scaled by 1.7)



$\langle N_{\Lambda(1520)} \rangle$

VALUE	DOCUMENT ID	TECN	COMMENT
0.0224 ± 0.0027 OUR AVERAGE			
0.029 ± 0.005 ± 0.005	ABREU 00P	DLPH	$E_{cm}^{ee} = 91.2$ GeV
0.0213 ± 0.0021 ± 0.0019	ALEXANDER 97D	OPAL	$E_{cm}^{ee} = 91.2$ GeV

$\langle N_{\Sigma^+} \rangle$

VALUE	DOCUMENT ID	TECN	COMMENT
0.107 ± 0.010 OUR AVERAGE			
0.114 ± 0.011 ± 0.009	ACCIARRI 00J	L3	$E_{cm}^{ee} = 91.2$ GeV
0.099 ± 0.008 ± 0.013	ALEXANDER 97E	OPAL	$E_{cm}^{ee} = 91.2$ GeV

$\langle N_{\Sigma^-} \rangle$

VALUE	DOCUMENT ID	TECN	COMMENT
0.082 ± 0.007 OUR AVERAGE			
0.081 ± 0.002 ± 0.010	ABREU 00P	DLPH	$E_{cm}^{ee} = 91.2$ GeV
0.083 ± 0.006 ± 0.009	ALEXANDER 97E	OPAL	$E_{cm}^{ee} = 91.2$ GeV

$\langle N_{\Sigma^+ + \Sigma^-} \rangle$

VALUE	DOCUMENT ID	TECN	COMMENT
0.181 ± 0.018 OUR AVERAGE			
0.182 ± 0.010 ± 0.016	¹ ALEXANDER 97E	OPAL	$E_{cm}^{ee} = 91.2$ GeV
0.170 ± 0.014 ± 0.061	ABREU 95O	DLPH	$E_{cm}^{ee} = 91.2$ GeV

¹ We have combined the values of $\langle N_{\Sigma^+} \rangle$ and $\langle N_{\Sigma^-} \rangle$ from ALEXANDER 97E adding the statistical and systematic errors of the two final states separately in quadrature. If isospin symmetry is assumed this value becomes $0.174 \pm 0.010 \pm 0.015$.

$\langle N_{\Sigma^0} \rangle$

VALUE	DOCUMENT ID	TECN	COMMENT
0.076 ± 0.010 OUR AVERAGE			
0.095 ± 0.015 ± 0.013	ACCIARRI 00J	L3	$E_{cm}^{ee} = 91.2$ GeV
0.071 ± 0.012 ± 0.013	ALEXANDER 97E	OPAL	$E_{cm}^{ee} = 91.2$ GeV
0.070 ± 0.010 ± 0.010	ADAM 96B	DLPH	$E_{cm}^{ee} = 91.2$ GeV

$\langle N_{(\Sigma^+ + \Sigma^- + \Sigma^0)/3} \rangle$

VALUE	DOCUMENT ID	TECN	COMMENT
0.084 ± 0.005 ± 0.008			
	ALEXANDER 97E	OPAL	$E_{cm}^{ee} = 91.2$ GeV

$\langle N_{\Sigma(1385)^+} \rangle$

VALUE	DOCUMENT ID	TECN	COMMENT
0.0239 ± 0.0009 ± 0.0012			
	ALEXANDER 97D	OPAL	$E_{cm}^{ee} = 91.2$ GeV

$\langle N_{\Sigma(1385)^-} \rangle$

VALUE	DOCUMENT ID	TECN	COMMENT
0.0240 ± 0.0010 ± 0.0014			
	ALEXANDER 97D	OPAL	$E_{cm}^{ee} = 91.2$ GeV

$\langle N_{\Sigma(1385)^+ + \Sigma(1385)^-} \rangle$

VALUE	DOCUMENT ID	TECN	COMMENT
0.046 ± 0.004 OUR AVERAGE			
0.0479 ± 0.0013 ± 0.0026	ALEXANDER 97D	OPAL	$E_{cm}^{ee} = 91.2$ GeV
0.0382 ± 0.0028 ± 0.0045	ABREU 95O	DLPH	$E_{cm}^{ee} = 91.2$ GeV

Error includes scale factor of 1.6.

$\langle N_{\Xi^-} \rangle$

VALUE	DOCUMENT ID	TECN	COMMENT
0.0258 ± 0.0009 OUR AVERAGE			
0.0247 ± 0.0009 ± 0.0025	ABDALLAH 06E	DLPH	$E_{cm}^{ee} = 91.2$ GeV
0.0259 ± 0.0004 ± 0.0009	ALEXANDER 97D	OPAL	$E_{cm}^{ee} = 91.2$ GeV

$\langle N_{\Xi(1530)^0} \rangle$

VALUE	DOCUMENT ID	TECN	COMMENT
0.0059 ± 0.0011 OUR AVERAGE			Error includes scale factor of 2.3.
0.0045 ± 0.0005 ± 0.0006	ABDALLAH 05C	DLPH	$E_{cm}^{ee} = 91.2$ GeV
0.0068 ± 0.0005 ± 0.0004	ALEXANDER 97D	OPAL	$E_{cm}^{ee} = 91.2$ GeV

$\langle N_{\Omega^-} \rangle$

VALUE	DOCUMENT ID	TECN	COMMENT
0.00164 ± 0.00028 OUR AVERAGE			
0.0018 ± 0.0003 ± 0.0002	ALEXANDER 97D	OPAL	$E_{cm}^{ee} = 91.2$ GeV
0.0014 ± 0.0002 ± 0.0004	ADAM 96B	DLPH	$E_{cm}^{ee} = 91.2$ GeV

$\langle N_{\Lambda_c^+} \rangle$

VALUE	DOCUMENT ID	TECN	COMMENT
0.078 ± 0.012 ± 0.012			
	ALEXANDER 96R	OPAL	$E_{cm}^{ee} = 91.2$ GeV

$\langle N_D \rangle$

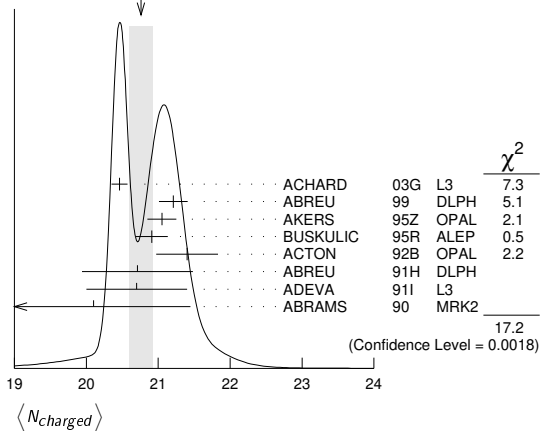
VALUE (units 10^{-6})	DOCUMENT ID	TECN	COMMENT
5.9 ± 1.8 ± 0.5			
	¹ SCHAEEL 06A	ALEP	$E_{cm}^{ee} = 91.2$ GeV

¹ SCHAEEL 06A obtain this anti-deuteron production rate per hadronic Z decay in the anti-deuteron momentum range from 0.62 to 1.03 GeV/c.

$\langle N_{\text{charged}} \rangle$

VALUE	DOCUMENT ID	TECN	COMMENT
20.76 ± 0.16 OUR AVERAGE			Error includes scale factor of 2.1. See the ideogram below.
20.46 ± 0.01 ± 0.11	ACHARD 03G	L3	$E_{cm}^{ee} = 91.2$ GeV
21.21 ± 0.01 ± 0.20	ABREU 99	DLPH	$E_{cm}^{ee} = 91.2$ GeV
21.05 ± 0.20	AKERS 95Z	OPAL	$E_{cm}^{ee} = 91.2$ GeV
20.91 ± 0.03 ± 0.22	BUSKULIC 95R	ALEP	$E_{cm}^{ee} = 91.2$ GeV
21.40 ± 0.43	ACTON 92B	OPAL	$E_{cm}^{ee} = 91.2$ GeV
20.71 ± 0.04 ± 0.77	ABREU 91H	DLPH	$E_{cm}^{ee} = 91.2$ GeV
20.7 ± 0.7	ADEVA 91I	L3	$E_{cm}^{ee} = 91.2$ GeV
20.1 ± 1.0 ± 0.9	ABRAMS 90	MRK2	$E_{cm}^{ee} = 91.1$ GeV

WEIGHTED AVERAGE
20.76±0.16 (Error scaled by 2.1)



Z HADRONIC POLE CROSS SECTION

OUR FIT is obtained using the fit procedure and correlations as determined by the LEP Electroweak Working Group (see the note "The Z boson" and ref. LEP-SLC 06). This quantity is defined as

$$\sigma_h^0 = \frac{12\pi}{M_Z^2} \frac{\Gamma(e^+e^-)\Gamma(\text{hadrons})}{\Gamma_Z^2}$$

It is one of the parameters used in the Z lineshape fit.

VALUE (nb)	EVTS	DOCUMENT ID	TECN	COMMENT
41.541 ± 0.037 OUR FIT				
41.501 ± 0.055	4.10M	¹ ABBIENDI 01A	OPAL	$E_{cm}^{ee} = 88-94$ GeV
41.578 ± 0.069	3.70M	ABREU 00F	DLPH	$E_{cm}^{ee} = 88-94$ GeV
41.535 ± 0.055	3.54M	ACCIARRI 00C	L3	$E_{cm}^{ee} = 88-94$ GeV
41.559 ± 0.058	4.07M	² BARATE 00C	ALEP	$E_{cm}^{ee} = 88-94$ GeV
42 ± 4	450	ABRAMS 89B	MRK2	$E_{cm}^{ee} = 89.2-93.0$ GeV

¹ ABBIENDI 01A error includes approximately 0.031 due to statistics, 0.033 due to event selection systematics, 0.029 due to uncertainty in luminosity measurement, and 0.011 due to LEP energy uncertainty.

² BARATE 00C error includes approximately 0.030 due to statistics, 0.026 due to experimental systematics, and 0.025 due to uncertainty in luminosity measurement.

Z VECTOR COUPLINGS

These quantities are the effective vector couplings of the Z to charged leptons and quarks. Their magnitude is derived from a measurement of the Z lineshape and the forward-backward lepton asymmetries as a function of energy around the Z mass. The relative sign among the vector to axial-vector couplings is obtained from a measurement of the Z asymmetry parameters, A_e , A_μ , and A_τ . By convention the sign of g_A^e is fixed to be negative (and opposite to that of $g^{l'e}$ obtained using ν_e scattering measurements). For the light quarks, the sign of the couplings is assigned consistently with this assumption. The LEP/SLD-based fit values quoted below correspond to global nine- or five-parameter fits to lineshape, lepton forward-backward asymmetry, and A_e , A_μ , and A_τ measurements. See the note "The Z boson" and ref. LEP-SLC 06 for details. Where $p\bar{p}$ and $e\bar{p}$ data is quoted, OUR FIT value corresponds to a weighted average of this with the LEP/SLD fit result.

g_V^e	VALUE	EVTS	DOCUMENT ID	TECN	COMMENT
	-0.03817 ± 0.00047 OUR FIT				
	-0.058 ± 0.016 ± 0.007	5026	1 ACOSTA	05M CDF	$E_{cm}^{pp} = 1.96$ TeV
	-0.0346 ± 0.0023	137.0k	2 ABBIENDI	01o OPAL	$E_{cm}^{ee} = 88-94$ GeV
	-0.0412 ± 0.0027	124.4k	3 ACCIARRI	00c L3	$E_{cm}^{ee} = 88-94$ GeV
	-0.0400 ± 0.0037		BARATE	00c ALEP	$E_{cm}^{ee} = 88-94$ GeV
	-0.0414 ± 0.0020		4 ABE	95J SLD	$E_{cm}^{ee} = 91.31$ GeV

- 1 ACOSTA 05M determine the forward-backward asymmetry of e^+e^- pairs produced via $q\bar{q} \rightarrow Z/\gamma^* \rightarrow e^+e^-$ in 15 M(e^+e^-) effective mass bins ranging from 40 GeV to 600 GeV. These results are used to obtain the vector and axial-vector couplings of the Z to e^+e^- , assuming the quark couplings are as predicted by the standard model. Higher order radiative corrections have not been taken into account.
- 2 ABBIENDI 01o use their measurement of the τ polarization in addition to the lineshape and forward-backward lepton asymmetries.
- 3 ACCIARRI 00c use their measurement of the τ polarization in addition to forward-backward lepton asymmetries.
- 4 ABE 95J obtain this result combining polarized Bhabha results with the A_{FB} measurement of ABE 94c. The Bhabha results alone give $-0.0507 \pm 0.0096 \pm 0.0020$.

g_V^μ	VALUE	EVTS	DOCUMENT ID	TECN	COMMENT
	-0.0367 ± 0.0023 OUR FIT				
	-0.0388 ± 0.0060 ± 0.0064	182.8k	1 ABBIENDI	01o OPAL	$E_{cm}^{ee} = 88-94$ GeV
	-0.0386 ± 0.0073	113.4k	2 ACCIARRI	00c L3	$E_{cm}^{ee} = 88-94$ GeV
	-0.0362 ± 0.0061		BARATE	00c ALEP	$E_{cm}^{ee} = 88-94$ GeV
	-0.0413 ± 0.0060	66143	3 ABBIENDI	01k OPAL	$E_{cm}^{ee} = 89-93$ GeV

- • • We do not use the following data for averages, fits, limits, etc. • • •
- 1 ABBIENDI 01o use their measurement of the τ polarization in addition to the lineshape and forward-backward lepton asymmetries.
- 2 ACCIARRI 00c use their measurement of the τ polarization in addition to forward-backward lepton asymmetries.
- 3 ABBIENDI 01k obtain this from an angular analysis of the muon pair asymmetry which takes into account effects of initial state radiation on an event by event basis and of initial-final state interference.

g_V^τ	VALUE	EVTS	DOCUMENT ID	TECN	COMMENT
	-0.0366 ± 0.0010 OUR FIT				
	-0.0365 ± 0.0023	151.5k	1 ABBIENDI	01o OPAL	$E_{cm}^{ee} = 88-94$ GeV
	-0.0384 ± 0.0026	103.0k	2 ACCIARRI	00c L3	$E_{cm}^{ee} = 88-94$ GeV
	-0.0361 ± 0.0068		BARATE	00c ALEP	$E_{cm}^{ee} = 88-94$ GeV

- 1 ABBIENDI 01o use their measurement of the τ polarization in addition to the lineshape and forward-backward lepton asymmetries.
- 2 ACCIARRI 00c use their measurement of the τ polarization in addition to forward-backward lepton asymmetries.

g_V^l	VALUE	EVTS	DOCUMENT ID	TECN	COMMENT
	-0.03783 ± 0.00041 OUR FIT				
	-0.0358 ± 0.0014	471.3k	1 ABBIENDI	01o OPAL	$E_{cm}^{ee} = 88-94$ GeV
	-0.0397 ± 0.0020	379.4k	2 ABREU	00f DLPH	$E_{cm}^{ee} = 88-94$ GeV
	-0.0397 ± 0.0017	340.8k	3 ACCIARRI	00c L3	$E_{cm}^{ee} = 88-94$ GeV
	-0.0383 ± 0.0018	500k	BARATE	00c ALEP	$E_{cm}^{ee} = 88-94$ GeV

- 1 ABBIENDI 01o use their measurement of the τ polarization in addition to the lineshape and forward-backward lepton asymmetries.
- 2 Using forward-backward lepton asymmetries.
- 3 ACCIARRI 00c use their measurement of the τ polarization in addition to forward-backward lepton asymmetries.

g_V^u	VALUE	EVTS	DOCUMENT ID	TECN	COMMENT
	0.266 ± 0.034 OUR AVERAGE				
	0.270 ± 0.037		1 ANDREEV	18A H1	$e^\pm p$
	0.201 ± 0.112	156k	2 ABAZOV	11D D0	$E_{cm}^{pp} = 1.97$ TeV
	0.24 ± 0.28 ± 0.11		3 LEP-SLC	06	$E_{cm}^{ee} = 88-94$ GeV
	0.399 ± 0.152 ± 0.188	5026	4 ACOSTA	05M CDF	$E_{cm}^{pp} = 1.96$ TeV

• • • We do not use the following data for averages, fits, limits, etc. • • •

0.14 ± 0.09 ± 0.09			5 ABRAMOWICZ16A	ZEUS	
0.144 ± 0.066 ± 0.058			6 ABT	16	
0.27 ± 0.13	1500		7 AKTAS	06 H1	$e^\pm p \rightarrow \mathcal{P}_e(\nu_e)X$, $\sqrt{s} \approx 300$ GeV

- 1 ANDREEV 18A obtain this result in a combined electroweak and QCD analysis using all deep-inelastic e^+p and e^-p neutral current and charged current scattering cross sections published by the H1 Collaboration, including data with longitudinally polarized lepton beams.
- 2 ABAZOV 11D study $p\bar{p} \rightarrow Z/\gamma^* e^+e^-$ events using 5 fb⁻¹ data at $\sqrt{s} = 1.96$ TeV. The candidate events are selected by requiring two isolated electromagnetic showers with $E_T > 25$ GeV, at least one electron in the central region and the di-electron mass in the range 50–1000 GeV. From the forward-backward asymmetry, determined as a function of the di-electron mass, they derive the axial and vector couplings of the u - and d -quarks and the value of $\sin^2\theta_{eff}^l = 0.2309 \pm 0.0008(\text{stat}) \pm 0.0006(\text{syst})$.
- 3 LEP-SLC 06 is a combination of the results from LEP and SLC experiments using light quark tagging. s - and d -quark couplings are assumed to be identical.
- 4 ACOSTA 05M determine the forward-backward asymmetry of e^+e^- pairs produced via $q\bar{q} \rightarrow Z/\gamma^* \rightarrow e^+e^-$ in 15 M(e^+e^-) effective mass bins ranging from 40 GeV to 600 GeV. These results are used to obtain the vector and axial-vector couplings of the Z to the light quarks, assuming the electron couplings are as predicted by the Standard Model. Higher order radiative corrections have not been taken into account.
- 5 ABRAMOWICZ 16A determine the Z⁰ couplings to u - and d -quarks using the ZEUS polarised data from Run II together with the unpolarised data from both ZEUS and H1 Collaborations for Run I and unpolarised H1 data from Run II.
- 6 ABT 16 determine the Z⁰ couplings to u - and d -quarks using the same techniques and data as ABRAMOWICZ 16A but additionally use the published H1 polarised data.
- 7 AKTAS 06 fit the neutral current ($1.5 \leq Q^2 \leq 30,000$ GeV²) and charged current ($1.5 \leq Q^2 \leq 15,000$ GeV²) differential cross sections. In the determination of the u -quark couplings the electron and d -quark couplings are fixed to their standard model values.

g_V^d	VALUE	EVTS	DOCUMENT ID	TECN	COMMENT
	-0.38 ± 0.04 ± 0.05 OUR AVERAGE				
	-0.488 ± 0.092		1 ANDREEV	18A H1	$e^\pm p$
	-0.351 ± 0.251	156k	2 ABAZOV	11D D0	$E_{cm}^{pp} = 1.97$ TeV
	-0.33 ± 0.05 ± 0.07		3 LEP-SLC	06	$E_{cm}^{ee} = 88-94$ GeV
	-0.226 ± 0.635 ± 0.290	5026	4 ACOSTA	05M CDF	$E_{cm}^{pp} = 1.96$ TeV

• • • We do not use the following data for averages, fits, limits, etc. • • •

-0.41 ± 0.25 ± 0.20			5 ABRAMOWICZ16A	ZEUS	
-0.503 ± 0.171 ± 0.103			6 ABT	16	
-0.33 ± 0.33	1500		7 AKTAS	06 H1	$e^\pm p \rightarrow \mathcal{P}_e(\nu_e)X$, $\sqrt{s} \approx 300$ GeV

- 1 ANDREEV 18A obtain this result in a combined electroweak and QCD analysis using all deep-inelastic e^+p and e^-p neutral current and charged current scattering cross sections published by the H1 Collaboration, including data with longitudinally polarized lepton beams.
- 2 ABAZOV 11D study $p\bar{p} \rightarrow Z/\gamma^* e^+e^-$ events using 5 fb⁻¹ data at $\sqrt{s} = 1.96$ TeV. The candidate events are selected by requiring two isolated electromagnetic showers with $E_T > 25$ GeV, at least one electron in the central region and the di-electron mass in the range 50–1000 GeV. From the forward-backward asymmetry, determined as a function of the di-electron mass, they derive the axial and vector couplings of the u - and d -quarks and the value of $\sin^2\theta_{eff}^l = 0.2309 \pm 0.0008(\text{stat}) \pm 0.0006(\text{syst})$.
- 3 LEP-SLC 06 is a combination of the results from LEP and SLC experiments using light quark tagging. s - and d -quark couplings are assumed to be identical.
- 4 ACOSTA 05M determine the forward-backward asymmetry of e^+e^- pairs produced via $q\bar{q} \rightarrow Z/\gamma^* \rightarrow e^+e^-$ in 15 M(e^+e^-) effective mass bins ranging from 40 GeV to 600 GeV. These results are used to obtain the vector and axial-vector couplings of the Z to the light quarks, assuming the electron couplings are as predicted by the Standard Model. Higher order radiative corrections have not been taken into account.
- 5 ABRAMOWICZ 16A determine the Z⁰ couplings to u - and d -quarks using the ZEUS polarised data from Run II together with the unpolarised data from both ZEUS and H1 Collaborations for Run I and unpolarised H1 data from Run II.
- 6 ABT 16 determine the Z⁰ couplings to u - and d -quarks using the same techniques and data as ABRAMOWICZ 16A but additionally use the published H1 polarised data.
- 7 AKTAS 06 fit the neutral current ($1.5 \leq Q^2 \leq 30,000$ GeV²) and charged current ($1.5 \leq Q^2 \leq 15,000$ GeV²) differential cross sections. In the determination of the d -quark couplings the electron and u -quark couplings are fixed to their standard model values.

Z AXIAL-VECTOR COUPLINGS

These quantities are the effective axial-vector couplings of the Z to charged leptons and quarks. Their magnitude is derived from a measurement of the Z lineshape and the forward-backward lepton asymmetries as a function of energy around the Z mass. The relative sign among the vector to axial-vector couplings is obtained from a measurement of the Z asymmetry parameters, A_e , A_μ , and A_τ . By convention the sign of g_A^e is fixed to be negative (and opposite to that of $g^{l'e}$ obtained using ν_e scattering measurements). For the light quarks, the sign of the couplings is assigned consistently with this assumption. The LEP/SLD-based fit values quoted below correspond to global nine- or five-parameter fits to lineshape, lepton forward-backward asymmetry, and A_e , A_μ , and A_τ measurements. See

the note "The Z boson" and ref. LEP-SLC 06 for details. Where $p\bar{p}$ and ep data is quoted, OUR FIT value corresponds to a weighted average of this with the LEP/SLD fit result.

g_A^e				
VALUE	EVTS	DOCUMENT ID	TECN	COMMENT
-0.50111 ± 0.00035 OUR FIT				
-0.528 ± 0.123 ± 0.059	5026	1 ACOSTA	05M CDF	$E_{cm}^{p\bar{p}} = 1.96$ TeV
-0.50062 ± 0.00062	137.0k	2 ABBIENDI	01o OPAL	$E_{cm}^{ee} = 88-94$ GeV
-0.5015 ± 0.0007	124.4k	3 ACCIARRI	00c L3	$E_{cm}^{ee} = 88-94$ GeV
-0.50166 ± 0.00057		BARATE	00c ALEP	$E_{cm}^{ee} = 88-94$ GeV
-0.4977 ± 0.0045		4 ABE	95J SLD	$E_{cm}^{ee} = 91.31$ GeV

- 1 ACOSTA 05M determine the forward-backward asymmetry of e^+e^- pairs produced via $q\bar{q} \rightarrow Z/\gamma^* \rightarrow e^+e^-$ in 15 M(e^+e^-) effective mass bins ranging from 40 GeV to 600 GeV. These results are used to obtain the vector and axial-vector couplings of the Z to e^+e^- , assuming the quark couplings are as predicted by the standard model. Higher order radiative corrections have not been taken into account.
- 2 ABBIENDI 01o use their measurement of the τ polarization in addition to the lineshape and forward-backward lepton asymmetries.
- 3 ACCIARRI 00c use their measurement of the τ polarization in addition to forward-backward lepton asymmetries.
- 4 ABE 95J obtain this result combining polarized Bhabha results with the A_{FB} measurement of ABE 94c. The Bhabha results alone give $-0.4968 \pm 0.0039 \pm 0.0027$.

g_A^μ				
VALUE	EVTS	DOCUMENT ID	TECN	COMMENT
-0.50120 ± 0.00054 OUR FIT				
-0.50117 ± 0.00099	182.8k	1 ABBIENDI	01o OPAL	$E_{cm}^{ee} = 88-94$ GeV
-0.5009 ± 0.0014	113.4k	2 ACCIARRI	00c L3	$E_{cm}^{ee} = 88-94$ GeV
-0.50046 ± 0.00093		BARATE	00c ALEP	$E_{cm}^{ee} = 88-94$ GeV
-0.520 ± 0.015	66143	3 ABBIENDI	01k OPAL	$E_{cm}^{ee} = 89-93$ GeV

- • • We do not use the following data for averages, fits, limits, etc. • • •
- 1 ABBIENDI 01o use their measurement of the τ polarization in addition to the lineshape and forward-backward lepton asymmetries.
- 2 ACCIARRI 00c use their measurement of the τ polarization in addition to forward-backward lepton asymmetries.
- 3 ABBIENDI 01k obtain this from an angular analysis of the muon pair asymmetry which takes into account effects of initial state radiation on an event by event basis and of initial-final state interference.

g_T^{τ}				
VALUE	EVTS	DOCUMENT ID	TECN	COMMENT
-0.50204 ± 0.00064 OUR FIT				
-0.50165 ± 0.00124	151.5k	1 ABBIENDI	01o OPAL	$E_{cm}^{ee} = 88-94$ GeV
-0.5023 ± 0.0017	103.0k	2 ACCIARRI	00c L3	$E_{cm}^{ee} = 88-94$ GeV
-0.50216 ± 0.00100		BARATE	00c ALEP	$E_{cm}^{ee} = 88-94$ GeV

- 1 ABBIENDI 01o use their measurement of the τ polarization in addition to the lineshape and forward-backward lepton asymmetries.
- 2 ACCIARRI 00c use their measurement of the τ polarization in addition to forward-backward lepton asymmetries.

g_A^l				
VALUE	EVTS	DOCUMENT ID	TECN	COMMENT
-0.50123 ± 0.00026 OUR FIT				
-0.50089 ± 0.00045	471.3k	1 ABBIENDI	01o OPAL	$E_{cm}^{ee} = 88-94$ GeV
-0.5007 ± 0.0005	379.4k	ABREU	00f DLPH	$E_{cm}^{ee} = 88-94$ GeV
-0.50153 ± 0.00053	340.8k	2 ACCIARRI	00c L3	$E_{cm}^{ee} = 88-94$ GeV
-0.50150 ± 0.00046	500k	BARATE	00c ALEP	$E_{cm}^{ee} = 88-94$ GeV

- 1 ABBIENDI 01o use their measurement of the τ polarization in addition to the lineshape and forward-backward lepton asymmetries.
- 2 ACCIARRI 00c use their measurement of the τ polarization in addition to forward-backward lepton asymmetries.

g_A^u				
VALUE	EVTS	DOCUMENT ID	TECN	COMMENT
0.519 ± 0.028 -0.033 OUR AVERAGE				
0.548 ± 0.036		1 ANDREEV	18A H1	$e^\pm p$
0.501 ± 0.110	156k	2 ABAZOV	11D D0	$E_{cm}^{p\bar{p}} = 1.97$ TeV
0.47 ± 0.05 -0.33		3 LEP-SLC	06	$E_{cm}^{ee} = 88-94$ GeV
0.441 ± 0.207 -0.173 ± 0.067	5026	4 ACOSTA	05M CDF	$E_{cm}^{p\bar{p}} = 1.96$ TeV

- • • We do not use the following data for averages, fits, limits, etc. • • •
- 5 ABRA MOWICZ16A ZEUS
- 6 ABT 16
- 7 AKTAS 06 H1 $e^\pm p \rightarrow \bar{\nu}_e(\nu_e)X$, $\sqrt{s} \approx 300$ GeV
- 1 ANDREEV 18A obtain this result in a combined electroweak and QCD analysis using all deep-inelastic e^+p and e^-p neutral current and charged current scattering cross sections published by the H1 Collaboration, including data with longitudinally polarized lepton beams.

2 ABAZOV 11D study $p\bar{p} \rightarrow Z/\gamma^* e^+e^-$ events using 5 fb⁻¹ data at $\sqrt{s} = 1.96$ TeV. The candidate events are selected by requiring two isolated electromagnetic showers with $E_T > 25$ GeV, at least one electron in the central region and the di-electron mass in the range 50-1000 GeV. From the forward-backward asymmetry, determined as a function of the di-electron mass, they derive the axial and vector couplings of the u - and d -quarks and the value of $\sin^2\theta_{eff}^e = 0.2309 \pm 0.0008(\text{stat}) \pm 0.0006(\text{syst})$.

- 3 LEP-SLC 06 is a combination of the results from LEP and SLC experiments using light quark tagging. s - and d -quark couplings are assumed to be identical.
- 4 ACOSTA 05M determine the forward-backward asymmetry of e^+e^- pairs produced via $q\bar{q} \rightarrow Z/\gamma^* \rightarrow e^+e^-$ in 15 M(e^+e^-) effective mass bins ranging from 40 GeV to 600 GeV. These results are used to obtain the vector and axial-vector couplings of the Z to the light quarks, assuming the electron couplings are as predicted by the Standard Model. Higher order radiative corrections have not been taken into account.
- 5 ABRA MOWICZ 16A determine the Z⁰ couplings to u - and d -quarks using the ZEUS polarised data from Run II together with the unpolarised data from both ZEUS and H1 Collaborations for Run I and unpolarised H1 data from Run II.
- 6 ABT 16 determine the Z⁰ couplings to u - and d -quarks using the same techniques and data as ABRA MOWICZ 16A but additionally use the published H1 polarised data.
- 7 AKTAS 06 fit the neutral current ($1.5 \leq Q^2 \leq 30,000$ GeV²) and charged current ($1.5 \leq Q^2 \leq 15,000$ GeV²) differential cross sections. In the determination of the u -quark couplings the electron and d -quark couplings are fixed to their standard model values.

g_A^d				
VALUE	EVTS	DOCUMENT ID	TECN	COMMENT
-0.527 ± 0.040 -0.028 OUR AVERAGE				
-0.619 ± 0.108		1 ANDREEV	18A H1	$e^\pm p$
-0.497 ± 0.165	156k	2 ABAZOV	11D D0	$E_{cm}^{p\bar{p}} = 1.97$ TeV
-0.52 ± 0.05 -0.03		3 LEP-SLC	06	$E_{cm}^{ee} = 88-94$ GeV
-0.016 ± 0.346 -0.536 ± 0.091	5026	4 ACOSTA	05M CDF	$E_{cm}^{p\bar{p}} = 1.96$ TeV
-0.56 ± 0.41 -0.15		5 ABRA MOWICZ16A	ZEUS	
-0.409 ± 0.373 -0.213		6 ABT	16	
-0.80 ± 0.24	1500	7 AKTAS	06 H1	$e^\pm p \rightarrow \bar{\nu}_e(\nu_e)X$, $\sqrt{s} \approx 300$ GeV

- 1 ANDREEV 18A obtain this result in a combined electroweak and QCD analysis using all deep-inelastic e^+p and e^-p neutral current and charged current scattering cross sections published by the H1 Collaboration, including data with longitudinally polarized lepton beams.
- 2 ABAZOV 11D study $p\bar{p} \rightarrow Z/\gamma^* e^+e^-$ events using 5 fb⁻¹ data at $\sqrt{s} = 1.96$ TeV. The candidate events are selected by requiring two isolated electromagnetic showers with $E_T > 25$ GeV, at least one electron in the central region and the di-electron mass in the range 50-1000 GeV. From the forward-backward asymmetry, determined as a function of the di-electron mass, they derive the axial and vector couplings of the u - and d -quarks and the value of $\sin^2\theta_{eff}^e = 0.2309 \pm 0.0008(\text{stat}) \pm 0.0006(\text{syst})$.
- 3 LEP-SLC 06 is a combination of the results from LEP and SLC experiments using light quark tagging. s - and d -quark couplings are assumed to be identical.
- 4 ACOSTA 05M determine the forward-backward asymmetry of e^+e^- pairs produced via $q\bar{q} \rightarrow Z/\gamma^* \rightarrow e^+e^-$ in 15 M(e^+e^-) effective mass bins ranging from 40 GeV to 600 GeV. These results are used to obtain the vector and axial-vector couplings of the Z to the light quarks, assuming the electron couplings are as predicted by the Standard Model. Higher order radiative corrections have not been taken into account.
- 5 ABRA MOWICZ 16A determine the Z⁰ couplings to u - and d -quarks using the ZEUS polarised data from Run II together with the unpolarised data from both ZEUS and H1 Collaborations for Run I and unpolarised H1 data from Run II.
- 6 ABT 16 determine the Z⁰ couplings to u - and d -quarks using the same techniques and data as ABRA MOWICZ 16A but additionally use the published H1 polarised data.
- 7 AKTAS 06 fit the neutral current ($1.5 \leq Q^2 \leq 30,000$ GeV²) and charged current ($1.5 \leq Q^2 \leq 15,000$ GeV²) differential cross sections. In the determination of the d -quark couplings the electron and u -quark couplings are fixed to their standard model values.

Z COUPLINGS TO NEUTRAL LEPTONS

Averaging over neutrino species, the invisible Z decay width determines the effective neutrino coupling $g^{\nu e}$. For $g^{\nu e}$ and $g^{\nu\mu}$, $\nu_e e$ and $\nu_\mu e$ scattering results are combined with g_A^e and g_V^e measurements at the Z mass to obtain $g^{\nu e}$ and $g^{\nu\mu}$ following NOVIKOV 93c.

$g^{\nu e}$		
VALUE	DOCUMENT ID	COMMENT
0.50076 ± 0.00076	1 LEP-SLC 06	$E_{cm}^{ee} = 88-94$ GeV

- 1 From invisible Z-decay width.

$g^{\nu\mu}$			
VALUE	DOCUMENT ID	TECN	COMMENT
0.528 ± 0.085	1 VILAIN 94	CHM2	From $\nu_\mu e$ and $\nu_e e$ scattering

- 1 VILAIN 94 derive this value from their value of $g^{\nu\mu}$ and their ratio $g^{\nu e}/g^{\nu\mu} = 1.05 \pm 0.15$
 -0.18 .

Gauge & Higgs Boson Particle Listings

Z

 $g^{\nu\mu}$

VALUE	DOCUMENT ID	TECN	COMMENT
0.502 ± 0.017	1 VILAIN	94 CHM2	From $\nu_\mu e$ scattering

¹VILAIN 94 derive this value from their measurement of the couplings $g_A^{\nu\mu} = -0.503 \pm 0.017$ and $g_V^{\nu\mu} = -0.035 \pm 0.017$ obtained from $\nu_\mu e$ scattering. We have re-evaluated this value using the current PDG values for g_A^e and g_V^e .

Z ASYMMETRY PARAMETERS

For each fermion-antifermion pair coupling to the Z these quantities are defined as

$$A_f = \frac{2g_V^f g_A^f}{(g_V^f)^2 + (g_A^f)^2}$$

where g_V^f and g_A^f are the effective vector and axial-vector couplings. For their relation to the various lepton asymmetries see the note "The Z boson" and ref. LEP-SLC 06.

 A_e

Using polarized beams, this quantity can also be measured as $(\sigma_L - \sigma_R)/(\sigma_L + \sigma_R)$, where σ_L and σ_R are the e^+e^- production cross sections for Z bosons produced with left-handed and right-handed electrons respectively.

VALUE	EVTS	DOCUMENT ID	TECN	COMMENT
0.1515 ± 0.0019 OUR AVERAGE				
0.1454 ± 0.0108 ± 0.0036	144810	1 ABBIENDI	01o OPAL	$E_{cm}^{ee} = 88-94$ GeV
0.1516 ± 0.0021	559000	2 ABE	01B SLD	$E_{cm}^{ee} = 91.24$ GeV
0.1504 ± 0.0068 ± 0.0008		3 HEISTER	01 ALEP	$E_{cm}^{ee} = 88-94$ GeV
0.1382 ± 0.0116 ± 0.0005	105000	4 ABREU	00E DLPH	$E_{cm}^{ee} = 88-94$ GeV
0.1678 ± 0.0127 ± 0.0030	137092	5 ACCIARRI	98H L3	$E_{cm}^{ee} = 88-94$ GeV
0.162 ± 0.041 ± 0.014	89838	6 ABE	97 SLD	$E_{cm}^{ee} = 91.27$ GeV
0.202 ± 0.038 ± 0.008		7 ABE	95J SLD	$E_{cm}^{ee} = 91.31$ GeV

- ¹ABBIENDI 01o fit for A_e and A_τ from measurements of the τ polarization at varying τ production angles. The correlation between A_e and A_τ is less than 0.03.
- ²ABE 01B use the left-right production and left-right forward-backward decay asymmetries in leptonic Z decays to obtain a value of 0.1544 ± 0.0060. This is combined with left-right production asymmetry measurement using hadronic Z decays (ABE 00B) to obtain the quoted value.
- ³HEISTER 01 obtain this result fitting the τ polarization as a function of the polar production angle of the τ .
- ⁴ABREU 00E obtain this result fitting the τ polarization as a function of the polar τ production angle. This measurement is a combination of different analyses (exclusive τ decay modes, inclusive hadronic 1-prong reconstruction, and a neural network analysis).
- ⁵Derived from the measurement of forward-backward τ polarization asymmetry.
- ⁶ABE 97 obtain this result from a measurement of the observed left-right charge asymmetry, $A_{Q^{obs}} = 0.225 \pm 0.056 \pm 0.019$, in hadronic Z decays. If they combine this value of $A_{Q^{obs}}$ with their earlier measurement of A_{LR}^{obs} they determine A_e to be $0.1574 \pm 0.0197 \pm 0.0067$ independent of the beam polarization.
- ⁷ABE 95J obtain this result from polarized Bhabha scattering.

 A_μ

This quantity is directly extracted from a measurement of the left-right forward-backward asymmetry in $\mu^+\mu^-$ production at SLC using a polarized electron beam. This double asymmetry eliminates the dependence on the Z-e-e coupling parameter A_e .

VALUE	EVTS	DOCUMENT ID	TECN	COMMENT
0.142 ± 0.015	16844	1 ABE	01B SLD	$E_{cm}^{ee} = 91.24$ GeV
• • • We do not use the following data for averages, fits, limits, etc. • • •				
0.153 ± 0.012	1.7M	2 AAD	15BT ATLS	$E_{cm}^{pp} = 7$ TeV

- ¹ABE 01B obtain this direct measurement using the left-right production and left-right forward-backward polar angle asymmetries in $\mu^+\mu^-$ decays of the Z boson obtained with a polarized electron beam.
- ²AAD 15BT study $pp \rightarrow Z \rightarrow \ell^+\ell^-$ events where ℓ is an electron or a muon in the dilepton mass region 70–1000 GeV. The background in the Z peak region is estimated to be < 1% for the muon channel. The muon asymmetry parameter is derived from the measured forward-backward asymmetry assuming the value of the quark asymmetry parameter from the SM. For this reason it is not used in the average.

 A_τ

The LEP Collaborations derive this quantity from the measurement of the τ polarization in $Z \rightarrow \tau^+\tau^-$. The SLD Collaboration directly extracts this quantity from its measured left-right forward-backward asymmetry in $Z \rightarrow \tau^+\tau^-$ produced using a polarized e^- beam. This double asymmetry eliminates the dependence on the Z-e-e coupling parameter A_e .

VALUE	EVTS	DOCUMENT ID	TECN	COMMENT
0.143 ± 0.004 OUR AVERAGE				
0.1456 ± 0.0076 ± 0.0057	144810	1 ABBIENDI	01o OPAL	$E_{cm}^{ee} = 88-94$ GeV
0.136 ± 0.015	16083	2 ABE	01B SLD	$E_{cm}^{ee} = 91.24$ GeV
0.1451 ± 0.0052 ± 0.0029		3 HEISTER	01 ALEP	$E_{cm}^{ee} = 88-94$ GeV
0.1359 ± 0.0079 ± 0.0055	105000	4 ABREU	00E DLPH	$E_{cm}^{ee} = 88-94$ GeV
0.1476 ± 0.0088 ± 0.0062	137092	ACCIARRI	98H L3	$E_{cm}^{ee} = 88-94$ GeV

- ¹ABBIENDI 01o fit for A_e and A_τ from measurements of the τ polarization at varying τ production angles. The correlation between A_e and A_τ is less than 0.03.

²ABE 01B obtain this direct measurement using the left-right production and left-right forward-backward polar angle asymmetries in $\tau^+\tau^-$ decays of the Z boson obtained with a polarized electron beam.

³HEISTER 01 obtain this result fitting the τ polarization as a function of the polar production angle of the τ .

⁴ABREU 00E obtain this result fitting the τ polarization as a function of the polar τ production angle. This measurement is a combination of different analyses (exclusive τ decay modes, inclusive hadronic 1-prong reconstruction, and a neural network analysis).

 A_s

The SLD Collaboration directly extracts this quantity by a simultaneous fit to four measured s-quark polar angle distributions corresponding to two states of e^- polarization (positive and negative) and to the K^+K^- and $K^\pm K_S^0$ strange particle tagging modes in the hadronic final states.

VALUE	EVTS	DOCUMENT ID	TECN	COMMENT
0.895 ± 0.066 ± 0.062	2870	1 ABE	00D SLD	$E_{cm}^{ee} = 91.2$ GeV

¹ABE 00D tag $Z \rightarrow s\bar{s}$ events by an absence of B or D hadrons and the presence in each hemisphere of a high momentum K^\pm or K_S^0 .

 A_c

This quantity is directly extracted from a measurement of the left-right forward-backward asymmetry in $c\bar{c}$ production at SLC using polarized electron beam. This double asymmetry eliminates the dependence on the Z-e-e coupling parameter A_e . OUR FIT is obtained by a simultaneous fit to several c- and b-quark measurements as explained in the note "The Z boson" and ref. LEP-SLC 06.

VALUE	DOCUMENT ID	TECN	COMMENT
0.670 ± 0.027 OUR FIT			
0.6712 ± 0.0224 ± 0.0157	1 ABE	05 SLD	$E_{cm}^{ee} = 91.24$ GeV
• • • We do not use the following data for averages, fits, limits, etc. • • •			
0.583 ± 0.055 ± 0.055	2 ABE	02G SLD	$E_{cm}^{ee} = 91.24$ GeV
0.688 ± 0.041	3 ABE	01C SLD	$E_{cm}^{ee} = 91.25$ GeV

- ¹ABE 05 use hadronic Z decays collected during 1996–98 to obtain an enriched sample of $c\bar{c}$ events tagging on the invariant mass of reconstructed secondary decay vertices. The charge of the underlying c-quark is obtained with an algorithm that takes into account the net charge of the vertex as well as the charge of tracks emanating from the vertex and identified as kaons. This yields (9970 events) $A_c = 0.6747 \pm 0.0290 \pm 0.0233$. Taking into account all correlations with earlier results reported in ABE 02G and ABE 01C, they obtain the quoted overall SLD result.
- ²ABE 02G tag b and c quarks through their semileptonic decays into electrons and muons. A maximum likelihood fit is performed to extract simultaneously A_b and A_c .
- ³ABE 01C tag $Z \rightarrow c\bar{c}$ events using two techniques: exclusive reconstruction of D^{*+} , D^+ and D^0 mesons and the soft pion tag for $D^{*+} \rightarrow D^0\pi^+$. The large background from D mesons produced in $b\bar{b}$ events is separated efficiently from the signal using precision vertex information. When combining the A_c values from these two samples, care is taken to avoid double counting of events common to the two samples, and common systematic errors are properly taken into account.

 A_b

This quantity is directly extracted from a measurement of the left-right forward-backward asymmetry in $b\bar{b}$ production at SLC using polarized electron beam. This double asymmetry eliminates the dependence on the Z-e-e coupling parameter A_e . OUR FIT is obtained by a simultaneous fit to several c- and b-quark measurements as explained in the note "The Z boson" and ref. LEP-SLC 06.

VALUE	EVTS	DOCUMENT ID	TECN	COMMENT
0.923 ± 0.020 OUR FIT				
0.9170 ± 0.0147 ± 0.0145	1 ABE	05 SLD	$E_{cm}^{ee} = 91.24$ GeV	
• • • We do not use the following data for averages, fits, limits, etc. • • •				
0.907 ± 0.020 ± 0.024	48028	2 ABE	03F SLD	$E_{cm}^{ee} = 91.24$ GeV
0.919 ± 0.030 ± 0.024		3 ABE	02G SLD	$E_{cm}^{ee} = 91.24$ GeV
0.855 ± 0.088 ± 0.102	7473	4 ABE	99L SLD	$E_{cm}^{ee} = 91.27$ GeV

- ¹ABE 05 use hadronic Z decays collected during 1996–98 to obtain an enriched sample of $b\bar{b}$ events tagging on the invariant mass of reconstructed secondary decay vertices. The charge of the underlying b-quark is obtained with an algorithm that takes into account the net charge of the vertex as well as the charge of tracks emanating from the vertex and identified as kaons. This yields (25917 events) $A_b = 0.9173 \pm 0.0184 \pm 0.0173$. Taking into account all correlations with earlier results reported in ABE 03F, ABE 02G and ABE 99L, they obtain the quoted overall SLD result.
- ²ABE 03F obtain an enriched sample of $b\bar{b}$ events tagging on the invariant mass of a 3-dimensional topologically reconstructed secondary decay. The charge of the underlying b quark is obtained using a self-calibrating track-charge method. For the 1996–1998 data sample they measure $A_b = 0.906 \pm 0.022 \pm 0.023$. The value quoted here is obtained combining the above with the result of ABE 98I (1993–1995 data sample).
- ³ABE 02G tag b and c quarks through their semileptonic decays into electrons and muons. A maximum likelihood fit is performed to extract simultaneously A_b and A_c .
- ⁴ABE 99L obtain an enriched sample of $b\bar{b}$ events tagging with an inclusive vertex mass cut. For distinguishing b and \bar{b} quarks they use the charge of identified K^\pm .

TRANSVERSE SPIN CORRELATIONS IN $Z \rightarrow \tau^+\tau^-$

The correlations between the transverse spin components of $\tau^+\tau^-$ produced in Z decays may be expressed in terms of the vector and axial-vector couplings:

$$C_{TT} = \frac{|g_A^\tau|^2 - |g_V^\tau|^2}{|g_A^\tau|^2 + |g_V^\tau|^2}$$

$$C_{TN} = -2 \frac{|g_A^\tau| |g_V^\tau|}{|g_A^\tau|^2 + |g_V^\tau|^2} \sin(\Phi_{g_V^\tau} - \Phi_{g_A^\tau})$$

C_{TT} refers to the transverse-transverse (within the collision plane) spin correlation and C_{TN} refers to the transverse-normal (to the collision plane) spin correlation.

The longitudinal τ polarization P_τ ($= -A_\tau$) is given by:

$$P_\tau = -2 \frac{|g_V^\tau| |g_A^\tau|}{|g_V^\tau|^2 + |g_A^\tau|^2} \cos(\Phi_{g_V^\tau} - \Phi_{g_A^\tau})$$

Here Φ is the phase and the phase difference $\Phi_{g_V^\tau} - \Phi_{g_A^\tau}$ can be obtained using both the measurements of C_{TN} and P_τ .

C_{TT} VALUE	EVTS	DOCUMENT ID	TECN	COMMENT
1.01 ± 0.12 OUR AVERAGE				
0.87 ± 0.20 ^{+0.10} _{-0.12}	9.1k	ABREU	97G DLPH	$E_{cm}^e = 91.2$ GeV
1.06 ± 0.13 ± 0.05	120k	BARATE	97D ALEP	$E_{cm}^e = 91.2$ GeV

C_{TN} VALUE	EVTS	DOCUMENT ID	TECN	COMMENT
0.08 ± 0.13 ± 0.04				
	120k	1 BARATE	97D ALEP	$E_{cm}^e = 91.2$ GeV

¹ BARATE 97D combine their value of C_{TN} with the world average $P_\tau = -0.140 \pm 0.007$ to obtain $\tan(\Phi_{g_V^\tau} - \Phi_{g_A^\tau}) = -0.57 \pm 0.97$.

FORWARD-BACKWARD $e^+e^- \rightarrow f\bar{f}$ CHARGE ASYMMETRIES

These asymmetries are experimentally determined by tagging the respective lepton or quark flavor in e^+e^- interactions. Details of heavy flavor (c - or b -quark) tagging at LEP are described in the note on "The Z boson" and ref. LEP-SLC 06. The Standard Model predictions for LEP data have been (re)computed using the ZFITTER package (version 6.36) with input parameters $M_Z=91.187$ GeV, $M_{top}=174.3$ GeV, $M_{Higgs}=150$ GeV, $\alpha_s=0.119$, $\alpha^{(5)}(M_Z) = 1/128.877$ and the Fermi constant $G_F = 1.16637 \times 10^{-5}$ GeV⁻² (see the note on "The Z boson" for references). For non-LEP data the Standard Model predictions are as given by the authors of the respective publications.

$A_{FB}^{(0,e)}$ CHARGE ASYMMETRY IN $e^+e^- \rightarrow e^+e^-$

OUR FIT is obtained using the fit procedure and correlations as determined by the LEP Electroweak Working Group (see the note "The Z boson" and ref. LEP-SLC 06). For the Z peak, we report the pole asymmetry defined by $(3/4)A_e^2$ as determined by the nine-parameter fit to cross-section and lepton forward-backward asymmetry data.

ASYMMETRY (%)	STD. MODEL	\sqrt{s} (GeV)	DOCUMENT ID	TECN
1.45 ± 0.25 OUR FIT				
0.89 ± 0.44	1.57	91.2	¹ ABBIENDI 01A	OPAL
1.71 ± 0.49	1.57	91.2	ABREU 00F	DLPH
1.06 ± 0.58	1.57	91.2	ACCIARRI 00C	L3
1.88 ± 0.34	1.57	91.2	² BARATE 00C	ALEP

¹ ABBIENDI 01A error includes approximately 0.38 due to statistics, 0.16 due to event selection systematics, and 0.18 due to the theoretical uncertainty in t -channel prediction.
² BARATE 00C error includes approximately 0.31 due to statistics, 0.06 due to experimental systematics, and 0.13 due to the theoretical uncertainty in t -channel prediction.

$A_{FB}^{(0,\mu)}$ CHARGE ASYMMETRY IN $e^+e^- \rightarrow \mu^+\mu^-$

OUR FIT is obtained using the fit procedure and correlations as determined by the LEP Electroweak Working Group (see the note "The Z boson" and ref. LEP-SLC 06). For the Z peak, we report the pole asymmetry defined by $(3/4)A_e A_\mu$ as determined by the nine-parameter fit to cross-section and lepton forward-backward asymmetry data.

ASYMMETRY (%)	STD. MODEL	\sqrt{s} (GeV)	DOCUMENT ID	TECN
1.69 ± 0.13 OUR FIT				
1.59 ± 0.23	1.57	91.2	¹ ABBIENDI 01A	OPAL
1.65 ± 0.25	1.57	91.2	ABREU 00F	DLPH
1.88 ± 0.33	1.57	91.2	ACCIARRI 00C	L3
1.71 ± 0.24	1.57	91.2	² BARATE 00C	ALEP

• • • We do not use the following data for averages, fits, limits, etc. • • •

9 ± 30	-1.3	20	³ ABREU 95M	DLPH
7 ± 26	-8.3	40	³ ABREU 95M	DLPH
-11 ± 33	-24.1	57	³ ABREU 95M	DLPH
-62 ± 17	-44.6	69	³ ABREU 95M	DLPH
-56 ± 10	-63.5	79	³ ABREU 95M	DLPH
-13 ± 5	-34.4	87.5	³ ABREU 95M	DLPH
-29.0 ± 5.0 ^{+4.8}	-32.1	56.9	⁴ ABE 90I	VNS
-9.9 ± 1.5 ± 0.5	-9.2	35	HEGNER 90	JADE
0.05 ± 0.22	0.026	91.14	⁵ ABRAMS 89D	MRK2
-43.4 ± 17.0	-24.9	52.0	⁶ BACALA 89	AMY
-11.0 ± 16.5	-29.4	55.0	⁶ BACALA 89	AMY
-30.0 ± 12.4	-31.2	56.0	⁶ BACALA 89	AMY
-46.2 ± 14.9	-33.0	57.0	⁶ BACALA 89	AMY
-29 ± 13	-25.9	53.3	ADACHI 88C	TOPZ

+ 5.3 ± 5.0 ± 0.5	-1.2	14.0	ADEVA 88	MRKJ
-10.4 ± 1.3 ± 0.5	-8.6	34.8	ADEVA 88	MRKJ
-12.3 ± 5.3 ± 0.5	-10.7	38.3	ADEVA 88	MRKJ
-15.6 ± 3.0 ± 0.5	-14.9	43.8	ADEVA 88	MRKJ
-1.0 ± 6.0	-1.2	13.9	BRAUNSCH... 88D	TASS
-9.1 ± 2.3 ± 0.5	-8.6	34.5	BRAUNSCH... 88D	TASS
-10.6 ± 2.2 ^{+2.3}	-8.9	35.0	BRAUNSCH... 88D	TASS
-17.6 ± 4.4 ^{+4.3}	-15.2	43.6	BRAUNSCH... 88D	TASS
-4.8 ± 6.5 ± 1.0	-11.5	39	BEHREND 87C	CELL
-18.8 ± 4.5 ± 1.0	-15.4	44	BEHREND 87C	CELL
+ 2.7 ± 4.9	-1.2	13.9	BARTEL 86C	JADE
-11.1 ± 1.8 ± 1.0	-8.6	34.4	BARTEL 86C	JADE
-17.3 ± 4.8 ± 1.0	-13.7	41.5	BARTEL 86C	JADE
-22.8 ± 5.1 ± 1.0	-16.6	44.8	BARTEL 86C	JADE
-6.3 ± 0.8 ± 0.2	-6.3	29	ASH 85	MAC
-4.9 ± 1.5 ± 0.5	-5.9	29	DERRICK 85	HR5
-7.1 ± 1.7	-5.7	29	LEVI 83	MRK2
-16.1 ± 3.2	-9.2	34.2	BRANDELIK 82C	TASS

¹ ABBIENDI 01A error is almost entirely on account of statistics.
² BARATE 00C error is almost entirely on account of statistics.
³ ABREU 95M perform this measurement using radiative muon-pair events associated with high-energy isolated photons.
⁴ ABE 90I measurements in the range $50 \leq \sqrt{s} \leq 60.8$ GeV.
⁵ ABRAMS 89D asymmetry includes both $9 \mu^+ \mu^-$ and $15 \tau^+ \tau^-$ events.
⁶ BACALA 89 systematic error is about 5%.

$A_{FB}^{(0,\tau)}$ CHARGE ASYMMETRY IN $e^+e^- \rightarrow \tau^+\tau^-$

OUR FIT is obtained using the fit procedure and correlations as determined by the LEP Electroweak Working Group (see the note "The Z boson" and ref. LEP-SLC 06). For the Z peak, we report the pole asymmetry defined by $(3/4)A_e A_\tau$ as determined by the nine-parameter fit to cross-section and lepton forward-backward asymmetry data.

ASYMMETRY (%)	STD. MODEL	\sqrt{s} (GeV)	DOCUMENT ID	TECN
1.88 ± 0.17 OUR FIT				
1.45 ± 0.30	1.57	91.2	¹ ABBIENDI 01A	OPAL
2.41 ± 0.37	1.57	91.2	ABREU 00F	DLPH
2.60 ± 0.47	1.57	91.2	ACCIARRI 00C	L3
1.70 ± 0.28	1.57	91.2	² BARATE 00C	ALEP

• • • We do not use the following data for averages, fits, limits, etc. • • •

-32.8 ± 6.4 ^{+6.2}	-32.1	56.9	³ ABE 90I	VNS
-8.1 ± 2.0 ± 0.6	-9.2	35	HEGNER 90	JADE
-18.4 ± 19.2	-24.9	52.0	⁴ BACALA 89	AMY
-17.7 ± 26.1	-29.4	55.0	⁴ BACALA 89	AMY
-45.9 ± 16.6	-31.2	56.0	⁴ BACALA 89	AMY
-49.5 ± 18.0	-33.0	57.0	⁴ BACALA 89	AMY
-20 ± 14	-25.9	53.3	ADACHI 88C	TOPZ
-10.6 ± 3.1 ± 1.5	-8.5	34.7	ADEVA 88	MRKJ
-8.5 ± 6.6 ± 1.5	-15.4	43.8	ADEVA 88	MRKJ
-6.0 ± 2.5 ± 1.0	8.8	34.6	BARTEL 85F	JADE
-11.8 ± 4.6 ± 1.0	14.8	43.0	BARTEL 85F	JADE
-5.5 ± 1.2 ± 0.5	-0.063	29.0	FERNANDEZ 85	MAC
-4.2 ± 2.0	0.057	29	LEVI 83	MRK2
-10.3 ± 5.2	-9.2	34.2	BEHREND 82	CELL
-0.4 ± 6.6	-9.1	34.2	BRANDELIK 82C	TASS

¹ ABBIENDI 01A error includes approximately 0.26 due to statistics and 0.14 due to event selection systematics.
² BARATE 00C error includes approximately 0.26 due to statistics and 0.11 due to experimental systematics.
³ ABE 90I measurements in the range $50 \leq \sqrt{s} \leq 60.8$ GeV.
⁴ BACALA 89 systematic error is about 5%.

$A_{FB}^{(0,\ell)}$ CHARGE ASYMMETRY IN $e^+e^- \rightarrow \ell^+\ell^-$

For the Z peak, we report the pole asymmetry defined by $(3/4)A_e^2$ as determined by the five-parameter fit to cross-section and lepton forward-backward asymmetry data assuming lepton universality. For details see the note "The Z boson" and ref. LEP-SLC 06.

ASYMMETRY (%)	STD. MODEL	\sqrt{s} (GeV)	DOCUMENT ID	TECN
1.71 ± 0.10 OUR FIT				
1.45 ± 0.17	1.57	91.2	¹ ABBIENDI 01A	OPAL
1.87 ± 0.19	1.57	91.2	ABREU 00F	DLPH
1.92 ± 0.24	1.57	91.2	ACCIARRI 00C	L3
1.73 ± 0.16	1.57	91.2	² BARATE 00C	ALEP

¹ ABBIENDI 01A error includes approximately 0.15 due to statistics, 0.06 due to event selection systematics, and 0.03 due to the theoretical uncertainty in t -channel prediction.
² BARATE 00C error includes approximately 0.15 due to statistics, 0.04 due to experimental systematics, and 0.02 due to the theoretical uncertainty in t -channel prediction.

$A_{FB}^{(0,u)}$ CHARGE ASYMMETRY IN $e^+e^- \rightarrow u\bar{u}$

ASYMMETRY (%)	STD. MODEL	\sqrt{s} (GeV)	DOCUMENT ID	TECN
4.0 ± 6.7 ± 2.8				
	7.2	91.2	¹ ACKERSTAFF 97T	OPAL

Gauge & Higgs Boson Particle Listings

Z

¹ACKERSTAFF 97T measure the forward-backward asymmetry of various fast hadrons made of light quarks. Then using SU(2) isospin symmetry and flavor independence for down and strange quarks authors solve for the different quark types.

$A_{FB}^{(0,s)}$ CHARGE ASYMMETRY IN $e^+e^- \rightarrow s\bar{s}$

The s -quark asymmetry is derived from measurements of the forward-backward asymmetry of fast hadrons containing an s quark.

ASYMMETRY (%)	STD. MODEL	\sqrt{s} (GeV)	DOCUMENT ID	TECN
9.8 ± 1.1 OUR AVERAGE				
10.08 ± 1.13 ± 0.40	10.1	91.2	¹ ABREU 00B DLPH	
6.8 ± 3.5 ± 1.1	10.1	91.2	² ACKERSTAFF 97T OPAL	

¹ABREU 00B tag the presence of an s quark requiring a high-momentum-identified charged kaon. The s -quark pole asymmetry is extracted from the charged-kaon asymmetry taking the expected d - and u -quark asymmetries from the Standard Model and using the measured values for the c - and b -quark asymmetries.

²ACKERSTAFF 97T measure the forward-backward asymmetry of various fast hadrons made of light quarks. Then using SU(2) isospin symmetry and flavor independence for down and strange quarks authors solve for the different quark types. The value reported here corresponds then to the forward-backward asymmetry for "down-type" quarks.

$A_{FB}^{(0,c)}$ CHARGE ASYMMETRY IN $e^+e^- \rightarrow c\bar{c}$

OUR FIT, which is obtained by a simultaneous fit to several c - and b -quark measurements as explained in the note "The Z boson" and ref. LEP-SLC 06, refers to the **Z pole** asymmetry. The experimental values, on the other hand, correspond to the measurements carried out at the respective energies.

ASYMMETRY (%)	STD. MODEL	\sqrt{s} (GeV)	DOCUMENT ID	TECN
7.07 ± 0.35 OUR FIT				
6.31 ± 0.93 ± 0.65	6.35	91.26	¹ ABDALLAH 04F DLPH	
5.68 ± 0.54 ± 0.39	6.3	91.25	² ABBIENDI 03P OPAL	
6.45 ± 0.57 ± 0.37	6.10	91.21	³ HEISTER 02H ALEP	
6.59 ± 0.94 ± 0.35	6.2	91.235	⁴ ABREU 99Y DLPH	
6.3 ± 0.9 ± 0.3	6.1	91.22	⁵ BARATE 98O ALEP	
6.3 ± 1.2 ± 0.6	6.1	91.22	⁶ ALEXANDER 97C OPAL	
8.3 ± 3.8 ± 2.7	6.2	91.24	⁷ ADRIANI 92D L3	

• • • We do not use the following data for averages, fits, limits, etc. • • •

3.1 ± 3.5 ± 0.5	-3.5	89.43	¹ ABDALLAH 04F DLPH	
11.0 ± 2.8 ± 0.7	12.3	92.99	¹ ABDALLAH 04F DLPH	
-6.8 ± 2.5 ± 0.9	-3.0	89.51	² ABBIENDI 03P OPAL	
14.6 ± 2.0 ± 0.8	12.2	92.95	² ABBIENDI 03P OPAL	
-12.4 ± 15.9 ± 2.0	-9.6	88.38	³ HEISTER 02H ALEP	
-2.3 ± 2.6 ± 0.2	-3.8	89.38	³ HEISTER 02H ALEP	
-0.3 ± 8.3 ± 0.6	0.9	90.21	³ HEISTER 02H ALEP	
10.6 ± 7.7 ± 0.7	9.6	92.05	³ HEISTER 02H ALEP	
11.9 ± 2.1 ± 0.6	12.2	92.94	³ HEISTER 02H ALEP	
12.1 ± 11.0 ± 1.0	14.2	93.90	³ HEISTER 02H ALEP	
-4.96 ± 3.68 ± 0.53	-3.5	89.434	⁴ ABREU 99Y DLPH	
11.80 ± 3.18 ± 0.62	12.3	92.990	⁴ ABREU 99Y DLPH	
-1.0 ± 4.3 ± 1.0	-3.9	89.37	⁵ BARATE 98O ALEP	
11.0 ± 3.3 ± 0.8	12.3	92.96	⁵ BARATE 98O ALEP	
3.9 ± 5.1 ± 0.9	-3.4	89.45	⁶ ALEXANDER 97C OPAL	
15.8 ± 4.1 ± 1.1	12.4	93.00	⁶ ALEXANDER 97C OPAL	
-12.9 ± 7.8 ± 5.5	-13.6	35	BEHREND 90D CELL	
7.7 ± 13.4 ± 5.0	-22.1	43	BEHREND 90D CELL	
-12.8 ± 4.4 ± 4.1	-13.6	35	ELSEN 90 JADE	
-10.9 ± 12.9 ± 4.6	-23.2	44	ELSEN 90 JADE	
-14.9 ± 6.7	-13.3	35	OULD-SAADAA 89 JADE	

¹ABDALLAH 04F tag b - and c -quarks using semileptonic decays combined with charge flow information from the hemisphere opposite to the lepton. Enriched samples of $c\bar{c}$ and $b\bar{b}$ events are obtained using lifetime information.

²ABBIENDI 03P tag heavy flavors using events with one or two identified leptons. This allows the simultaneous fitting of the b and c quark forward-backward asymmetries as well as the average B^0 - \bar{B}^0 mixing.

³HEISTER 02H measure simultaneously b and c quark forward-backward asymmetries using their semileptonic decays to tag the quark charge. The flavor separation is obtained with a discriminating multivariate analysis.

⁴ABREU 99Y tag $Z \rightarrow b\bar{b}$ and $Z \rightarrow c\bar{c}$ events by an exclusive reconstruction of several D meson decay modes (D^{*+} , D^0 , and D^+ with their charge-conjugate states).

⁵BARATE 98O tag $Z \rightarrow c\bar{c}$ events requiring the presence of high-momentum reconstructed D^{*+} , D^+ , or D^0 mesons.

⁶ALEXANDER 97C identify the b and c events using a D/D^* tag.

⁷ADRIANI 92D use both electron and muon semileptonic decays.

$A_{FB}^{(0,b)}$ CHARGE ASYMMETRY IN $e^+e^- \rightarrow b\bar{b}$

OUR FIT, which is obtained by a simultaneous fit to several c - and b -quark measurements as explained in the note "The Z boson" and ref. LEP-SLC 06, refers to the **Z pole** asymmetry. The experimental values, on the other hand, correspond to the measurements carried out at the respective energies.

ASYMMETRY (%)	STD. MODEL	\sqrt{s} (GeV)	DOCUMENT ID	TECN
9.92 ± 0.16 OUR FIT				
9.58 ± 0.32 ± 0.14	9.68	91.231	¹ ABDALLAH 05 DLPH	
10.04 ± 0.56 ± 0.25	9.69	91.26	² ABDALLAH 04F DLPH	
9.72 ± 0.42 ± 0.15	9.67	91.25	³ ABBIENDI 03P OPAL	
9.77 ± 0.36 ± 0.18	9.69	91.26	⁴ ABBIENDI 02I OPAL	
9.52 ± 0.41 ± 0.17	9.59	91.21	⁵ HEISTER 02H ALEP	
10.00 ± 0.27 ± 0.11	9.63	91.232	⁶ HEISTER 01D ALEP	
7.62 ± 1.94 ± 0.85	9.64	91.235	⁷ ABREU 99Y DLPH	
9.60 ± 0.66 ± 0.33	9.69	91.26	⁸ ACCIARRI 99D L3	
9.31 ± 1.01 ± 0.55	9.65	91.24	⁹ ACCIARRI 98U L3	
9.4 ± 2.7 ± 2.2	9.61	91.22	¹⁰ ALEXANDER 97C OPAL	

• • • We do not use the following data for averages, fits, limits, etc. • • •

6.37 ± 1.43 ± 0.17	5.8	89.449	¹ ABDALLAH 05 DLPH	
10.41 ± 1.15 ± 0.24	12.1	92.990	¹ ABDALLAH 05 DLPH	
6.7 ± 2.2 ± 0.2	5.7	89.43	² ABDALLAH 04F DLPH	
11.2 ± 1.8 ± 0.2	12.1	92.99	² ABDALLAH 04F DLPH	
4.7 ± 1.8 ± 0.1	5.9	89.51	³ ABBIENDI 03P OPAL	
10.3 ± 1.5 ± 0.2	12.0	92.95	³ ABBIENDI 03P OPAL	
5.82 ± 1.53 ± 0.12	5.9	89.50	⁴ ABBIENDI 02I OPAL	
12.21 ± 1.23 ± 0.25	12.0	92.91	⁴ ABBIENDI 02I OPAL	
-13.1 ± 13.5 ± 1.0	3.2	88.38	⁵ HEISTER 02H ALEP	
5.5 ± 1.9 ± 0.1	5.6	89.38	⁵ HEISTER 02H ALEP	
-0.4 ± 6.7 ± 0.8	7.5	90.21	⁵ HEISTER 02H ALEP	
11.1 ± 6.4 ± 0.5	11.0	92.05	⁵ HEISTER 02H ALEP	
10.4 ± 1.5 ± 0.3	12.0	92.94	⁵ HEISTER 02H ALEP	
13.8 ± 9.3 ± 1.1	12.9	93.90	⁵ HEISTER 02H ALEP	
4.36 ± 1.19 ± 0.11	5.8	89.472	⁶ HEISTER 01D ALEP	
11.72 ± 0.97 ± 0.11	12.0	92.950	⁶ HEISTER 01D ALEP	
5.67 ± 7.56 ± 1.17	5.7	89.434	⁷ ABREU 99Y DLPH	
8.82 ± 6.33 ± 1.22	12.1	92.990	⁷ ABREU 99Y DLPH	
6.11 ± 2.93 ± 0.43	5.9	89.50	⁸ ACCIARRI 99D L3	
13.71 ± 2.40 ± 0.44	12.2	93.10	⁸ ACCIARRI 99D L3	
4.95 ± 5.23 ± 0.40	5.8	89.45	⁹ ACCIARRI 98U L3	
11.37 ± 3.99 ± 0.65	12.1	92.99	⁹ ACCIARRI 98U L3	
-8.6 ± 10.8 ± 2.9	5.8	89.45	¹⁰ ALEXANDER 97C OPAL	
-2.1 ± 9.0 ± 2.6	12.1	93.00	¹⁰ ALEXANDER 97C OPAL	
-71 ± 34 ± 8	-58	58.3	SHIMONAKA 91 TOPZ	
-22.2 ± 7.7 ± 3.5	-26.0	35	BEHREND 90D CELL	
-49.1 ± 16.0 ± 5.0	-39.7	43	BEHREND 90D CELL	
-28 ± 11	-23	35	BRAUNSCH... 90 TASS	
-16.6 ± 7.7 ± 4.8	-24.3	35	ELSEN 90 JADE	
-33.6 ± 22.2 ± 5.2	-39.9	44	ELSEN 90 JADE	
3.4 ± 7.0 ± 3.5	-16.0	29.0	BAND 89 MAC	
-72 ± 28 ± 13	-56	55.2	SAGAWA 89 AMY	

¹ABDALLAH 05 obtain an enriched samples of $b\bar{b}$ events using lifetime information. The quark (or antiquark) charge is determined with a neural network using the secondary vertex charge, the jet charge and particle identification.

²ABDALLAH 04F tag b - and c -quarks using semileptonic decays combined with charge flow information from the hemisphere opposite to the lepton. Enriched samples of $c\bar{c}$ and $b\bar{b}$ events are obtained using lifetime information.

³ABBIENDI 03P tag heavy flavors using events with one or two identified leptons. This allows the simultaneous fitting of the b and c quark forward-backward asymmetries as well as the average B^0 - \bar{B}^0 mixing.

⁴ABBIENDI 02I tag $Z^0 \rightarrow b\bar{b}$ decays using a combination of secondary vertex and lepton tags. The sign of the b -quark charge is determined using an inclusive tag based on jet, vertex, and kaon charges.

⁵HEISTER 02H measure simultaneously b and c quark forward-backward asymmetries using their semileptonic decays to tag the quark charge. The flavor separation is obtained with a discriminating multivariate analysis.

⁶HEISTER 01D tag $Z \rightarrow b\bar{b}$ events using the impact parameters of charged tracks complemented with information from displaced vertices, event shape variables, and lepton identification. The b -quark direction and charge is determined using the hemisphere charge method along with information from fast kaon tagging and charge estimators of primary and secondary vertices. The change in the quoted value due to variation of A_{FB}^c and R_b is given as $+0.103 (A_{FB}^c - 0.0651) - 0.440 (R_b - 0.21585)$.

⁷ABREU 99Y tag $Z \rightarrow b\bar{b}$ and $Z \rightarrow c\bar{c}$ events by an exclusive reconstruction of several D meson decay modes (D^{*+} , D^0 , and D^+ with their charge-conjugate states).

⁸ACCIARRI 99D tag $Z \rightarrow b\bar{b}$ events using high p and p_T leptons. The analysis determines simultaneously a mixing parameter $\chi_b = 0.1192 \pm 0.0068 \pm 0.0051$ which is used to correct the observed asymmetry.

⁹ACCIARRI 98U tag $Z \rightarrow b\bar{b}$ events using lifetime and measure the jet charge using the hemisphere charge.

¹⁰ALEXANDER 97C identify the b and c events using a D/D^* tag.

CHARGE ASYMMETRY IN $e^+e^- \rightarrow q\bar{q}$

Summed over five lighter flavors.

Experimental and Standard Model values are somewhat event-selection dependent. Standard Model expectations contain some assumptions on B^0 - \bar{B}^0 mixing and on other electroweak parameters.

ASYMMETRY (%)	STD. MODEL	\sqrt{s} (GeV)	DOCUMENT ID	TECN
---------------	------------	------------------	-------------	------

• • • We do not use the following data for averages, fits, limits, etc. • • •

$-0.76 \pm 0.12 \pm 0.15$		91.2	¹ ABREU	92l	DLPH
$4.0 \pm 0.4 \pm 0.63$	4.0	91.3	² ACTON	92L	OPAL
$9.1 \pm 1.4 \pm 1.6$	9.0	57.9	ADACHI	91	TOPZ
$-0.84 \pm 0.15 \pm 0.04$		91	DECAMP	91B	ALEP
$8.3 \pm 2.9 \pm 1.9$	8.7	56.6	STUART	90	AMY
$11.4 \pm 2.2 \pm 2.1$	8.7	57.6	ABE	89L	VNS
6.0 ± 1.3	5.0	34.8	GREENSHAW	89	JADE
8.2 ± 2.9	8.5	43.6	GREENSHAW	89	JADE

¹ ABREU 92l has 0.14 systematic error due to uncertainty of quark fragmentation.

² ACTON 92L use the weight function method on 259k selected $Z \rightarrow$ hadrons events.

The systematic error includes a contribution of 0.2 due to $B^0\text{-}\bar{B}^0$ mixing effect, 0.4 due to Monte Carlo (MC) fragmentation uncertainties and 0.3 due to MC statistics.

ACTON 92L derive a value of $\sin^2\theta_W^{\text{eff}}$ to be $0.2321 \pm 0.0017 \pm 0.0028$.

CHARGE ASYMMETRY IN $p\bar{p} \rightarrow Z \rightarrow e^+e^-$

ASYMMETRY (%)	STD MODEL	\sqrt{s} (GeV)	DOCUMENT ID	TECN
$5.2 \pm 5.9 \pm 0.4$		91	ABE	91E CDF

• • • We do not use the following data for averages, fits, limits, etc. • • •

ANOMALOUS $ZZ\gamma$, $Z\gamma\gamma$, AND ZZV COUPLINGS

Revised September 2013 by M.W. Grunewald (U. College Dublin and U. Ghent) and A. Gurtu (Formerly Tata Inst.).

In on-shell $Z\gamma$ production, deviations from the Standard Model for the $Z\gamma\gamma^*$ and $Z\gamma Z^*$ couplings may be described in terms of eight parameters, h_i^V ($i = 1, 4; V = \gamma, Z$) [1]. The parameters h_i^γ describe the $Z\gamma\gamma^*$ couplings and the parameters h_i^Z the $Z\gamma Z^*$ couplings. In this formalism h_1^V and h_2^V lead to CP -violating and h_3^V and h_4^V to CP -conserving effects. All these anomalous contributions to the cross section increase rapidly with center-of-mass energy. In order to ensure unitarity, these parameters are usually described by a form-factor representation, $h_i^V(s) = h_{i0}^V/(1 + s/\Lambda^2)^n$, where Λ is the energy scale for the manifestation of a new phenomenon and n is a sufficiently large power. By convention one uses $n = 3$ for $h_{1,3}^V$ and $n = 4$ for $h_{2,4}^V$. Usually limits on h_i^V 's are put assuming some value of Λ , sometimes ∞ .

In on-shell ZZ production, deviations from the Standard Model for the $ZZ\gamma^*$ and ZZZ^* couplings may be described by means of four anomalous couplings f_i^V ($i = 4, 5; V = \gamma, Z$) [2]. As above, the parameters f_i^γ describe the $ZZ\gamma^*$ couplings and the parameters f_i^Z the ZZZ^* couplings. The anomalous couplings f_5^V lead to violation of C and P symmetries while f_4^V introduces CP violation. Also here, formfactors depending on a scale Λ are used.

All these couplings h_i^V and f_i^V are zero at tree level in the Standard Model; they are measured in e^+e^- , $p\bar{p}$ and pp collisions at LEP, Tevatron and LHC.

References

- U. Baur and E.L. Berger, Phys. Rev. **D47**, 4889 (1993).
- K. Hagiwara *et al.*, Nucl. Phys. **B282**, 253 (1987).

h_V^γ

Combining the LEP-2 results taking into account the correlations, the following 95% CL limits are derived [SCHAEEL 13a]:

$$\begin{aligned} -0.12 < h_1^Z < +0.11, & -0.07 < h_2^Z < +0.07, \\ -0.19 < h_3^Z < +0.06, & -0.04 < h_4^Z < +0.13, \\ -0.05 < h_1^\gamma < +0.05, & -0.04 < h_2^\gamma < +0.02, \\ -0.05 < h_3^\gamma < +0.00, & +0.01 < h_4^\gamma < +0.05. \end{aligned}$$

Some of the recent results from the Tevatron and LHC experiments individually surpass the combined LEP-2 results in precision (see below).

VALUE	DOCUMENT ID	TECN	COMMENT
• • • We do not use the following data for averages, fits, limits, etc. • • •			
¹ AAD	16Q ATLS	$E_{\text{cm}}^{\text{pp}} = 8$ TeV	
² KHACHATRYAN..16AE	CMS	$E_{\text{cm}}^{\text{pp}} = 8$ TeV	
³ KHACHATRYAN..15AC	CMS	$E_{\text{cm}}^{\text{pp}} = 8$ TeV	
⁴ CHATRCHYAN14AB	CMS	$E_{\text{cm}}^{\text{pp}} = 7$ TeV	
⁵ AAD	13AN ATLS	$E_{\text{cm}}^{\text{pp}} = 7$ TeV	
⁶ CHATRCHYAN13BI	CMS	$E_{\text{cm}}^{\text{pp}} = 7$ TeV	
⁷ ABAZOV	12s D0	$E_{\text{cm}}^{\text{pp}} = 1.96$ TeV	
⁸ AALTONEN	11s CDF	$E_{\text{cm}}^{\text{pp}} = 1.96$ TeV	
⁹ CHATRCHYAN11M	CMS	$E_{\text{cm}}^{\text{pp}} = 7$ TeV	
¹⁰ ABAZOV	09L D0	$E_{\text{cm}}^{\text{pp}} = 1.96$ TeV	
¹¹ ABAZOV	07M D0	$E_{\text{cm}}^{\text{pp}} = 1.96$ TeV	
¹² ABDALLAH	07C DLPH	$E_{\text{cm}}^{\text{pp}} = 183\text{--}208$ GeV	
¹³ ACHARD	04H L3	$E_{\text{cm}}^{\text{pp}} = 183\text{--}208$ GeV	
¹⁴ ABBIENDI,G	00C OPAL	$E_{\text{cm}}^{\text{pp}} = 189$ GeV	
¹⁵ ABBOTT	98M D0	$E_{\text{cm}}^{\text{pp}} = 1.8$ TeV	
¹⁶ ABREU	98K DLPH	$E_{\text{cm}}^{\text{pp}} = 161, 172$ GeV	

¹ AAD 16Q study $Z\gamma$ production in pp collisions. In events with no additional jets, 10268 (12738) Z decays to electron (muon) pairs are selected, with an expected background of 1291 ± 340 (1537 ± 408) events, as well as 1039 Z decays to neutrino pairs with an expected background of 450 ± 96 events. Analyzing the photon transverse momentum distribution above 250 GeV (400 GeV) for lepton (neutrino) events, yields the 95% C.L. limits: $-7.8 \times 10^{-4} < h_3^Z < 8.6 \times 10^{-4}$, $-3.0 \times 10^{-6} < h_4^Z < 2.9 \times 10^{-6}$, $-9.5 \times 10^{-4} < h_3^\gamma < 9.9 \times 10^{-4}$, $-3.2 \times 10^{-6} < h_4^\gamma < 3.2 \times 10^{-6}$.

² KHACHATRYAN 16AE determine the $Z\gamma \rightarrow \nu\bar{\nu}\gamma$ cross section by selecting events with a photon of $E_T > 145$ GeV and $E_T > 140$ GeV. 630 candidate events are observed with an expected SM background of 269 ± 26 . The E_T spectrum of the photon is used to set 95% C.L. limits as follows: $-1.5 \times 10^{-3} < h_3^Z < 1.6 \times 10^{-3}$, $-3.9 \times 10^{-6} < h_4^Z < 4.5 \times 10^{-6}$, $-1.1 \times 10^{-3} < h_3^\gamma < 0.9 \times 10^{-3}$, $-3.8 \times 10^{-6} < h_4^\gamma < 4.3 \times 10^{-6}$.

³ KHACHATRYAN 15AC study $Z\gamma$ events in 8 TeV pp interactions, where the Z decays into 2 same-flavor, opposite sign leptons (e or μ) and a photon with $p_T > 15$ GeV. The p_T of a lepton is required to be > 20 GeV/c, their effective mass > 50 GeV, and the photon should have a separation $\Delta R > 0.7$ with each lepton. The observed p_T distribution of the photons is used to extract the 95% C.L. limits: $-3.8 \times 10^{-3} < h_3^Z < 3.7 \times 10^{-3}$, $-3.1 \times 10^{-5} < h_4^Z < 3.0 \times 10^{-5}$, $-4.6 \times 10^{-3} < h_3^\gamma < 4.6 \times 10^{-3}$, $-3.6 \times 10^{-5} < h_4^\gamma < 3.5 \times 10^{-5}$.

⁴ CHATRCHYAN 14AB measure $Z\gamma$ production cross section for $p_T^\gamma > 15$ GeV and $R(\ell\gamma) > 0.7$, which is the separation between the γ and the final state charged lepton (e or μ) in the azimuthal angle-pseudorapidity ($\phi - \eta$) plane. The di-lepton mass is required to be > 50 GeV. After background subtraction the number of $e\gamma$ and $\mu\mu\gamma$ events is determined to be 3160 ± 120 and 5030 ± 233 respectively, compatible with expectations from the SM. This leads to a 95% CL limits of $-1 \times 10^{-2} < h_3^\gamma < 1 \times 10^{-2}$, $-9 \times 10^{-5} < h_4^\gamma < 9 \times 10^{-5}$, $-9 \times 10^{-3} < h_3^Z < 9 \times 10^{-3}$, $-8 \times 10^{-5} < h_4^Z < 8 \times 10^{-5}$, assuming h_1^V and h_2^V have SM values, $V = \gamma$ or Z .

⁵ AAD 13AN study $Z\gamma$ production in pp collisions. In events with no additional jet, 1417 (2031) Z decays to electron (muon) pairs are selected, with an expected background of 156 ± 54 (244 ± 64) events, as well as 662 Z decays to neutrino pairs with an expected background of 302 ± 42 events. Analysing the photon p_T spectrum above 100 GeV yields the 95% C.L. limits: $-0.013 < h_3^Z < 0.014$, $-8.7 \times 10^{-5} < h_4^Z < 8.7 \times 10^{-5}$, $-0.015 < h_3^\gamma < 0.016$, $-9.4 \times 10^{-5} < h_4^\gamma < 9.2 \times 10^{-5}$. Supersedes AAD 12Bx.

⁶ CHATRCHYAN 13BI determine the $Z\gamma \rightarrow \nu\bar{\nu}\gamma$ cross section by selecting events with a photon of $E_T > 145$ GeV and a $E_T > 130$ GeV. 73 candidate events are observed with an expected SM background of 30.2 ± 6.5 . The E_T spectrum of the photon is used to set 95% C.L. limits as follows: $|h_3^Z| < 2.7 \times 10^{-3}$, $|h_4^Z| < 1.3 \times 10^{-5}$, $|h_3^\gamma| < 2.9 \times 10^{-3}$, $|h_4^\gamma| < 1.5 \times 10^{-5}$.

⁷ ABAZOV 12s study $Z\gamma$ production in $p\bar{p}$ collisions at $\sqrt{s} = 1.96$ TeV using 6.2 fb^{-1} of data where the Z decays to electron (muon) pairs and the photon has at least 10 GeV of transverse momentum. In data, 304 (308) di-electron (di-muon) events are observed with an expected background of 255 ± 16 (285 ± 24) events. Based on the photon p_T spectrum, and including also earlier data and the $Z \rightarrow \nu\bar{\nu}$ decay mode (from ABAZOV 09L), the following 95% C.L. limits are reported: $|h_{03}^Z| < 0.026$, $|h_{04}^Z| < 0.0013$, $|h_{03}^\gamma| < 0.027$, $|h_{04}^\gamma| < 0.0014$ for a form factor scale of $\Lambda = 1.5$ TeV.

⁸ AALTONEN 11s study $Z\gamma$ events in $p\bar{p}$ interactions at $\sqrt{s} = 1.96$ TeV with integrated luminosity 5.1 fb^{-1} for $Z \rightarrow e^+e^-/\mu^+\mu^-$ and 4.9 fb^{-1} for $Z \rightarrow \nu\bar{\nu}$. For the charged lepton case, the two leptons must be of the same flavor with the transverse momentum/energy of one > 20 GeV and the other > 10 GeV. The isolated photon must have $E_T > 50$ GeV. They observe 91 events with 87.2 ± 7.8 events expected from standard model processes. For the $\nu\bar{\nu}$ case they require solitary photons with $E_T > 25$ GeV and missing $E_T > 25$ GeV and observe 85 events with standard model expectation of 85.9 ± 5.6 events. Taking the form factor $\Lambda = 1.5$ TeV they derive 95% C.L. limits as $|h_3^Z| < 0.022$ and $|h_4^Z| < 0.0009$.

⁹ CHATRCHYAN 11M study $Z\gamma$ production in pp collisions at $\sqrt{s} = 7$ TeV using 36 pb^{-1} pp data, where the Z decays to e^+e^- or $\mu^+\mu^-$. The total cross sections are measured for photon transverse energy $E_T^\gamma > 10$ GeV and spatial separation from charged leptons in the plane of pseudo rapidity and azimuthal angle $\Delta R(\ell,\gamma) > 0.7$ with the dilepton invariant mass requirement of $M_{\ell\ell} > 50$ GeV. The number of $e^+e^- \gamma$ and $\mu^+\mu^- \gamma$ candidates is 81 and 90 with estimated backgrounds of 20.5 ± 2.5 and 27.3 ± 3.2

Gauge & Higgs Boson Particle Listings

Z

- events respectively. The 95% CL limits for $ZZ\gamma$ couplings are $-0.05 < h_3^Z < 0.06$ and $-0.0005 < h_4^Z < 0.0005$, and for $Z\gamma\gamma$ couplings are $-0.07 < h_3^\gamma < 0.07$ and $-0.0005 < h_4^\gamma < 0.0006$.
- ¹⁰ ABAZOV 09L study $Z\gamma, Z \rightarrow \nu\bar{\nu}$ production in $p\bar{p}$ collisions at 1.96 TeV C.M. energy. They select 51 events with a photon of transverse energy E_T larger than 90 GeV, with an expected background of 17 events. Based on the photon E_T spectrum and including also Z decays to charged leptons (from ABAZOV 07M), the following 95% CL limits are reported: $|h_{30}^\gamma| < 0.033$, $|h_{40}^\gamma| < 0.0017$, $|h_{30}^Z| < 0.033$, $|h_{40}^Z| < 0.0017$.
- ¹¹ ABAZOV 07M use 968 $p\bar{p} \rightarrow e^+e^-/\mu^+\mu^-\gamma X$ candidates, at 1.96 TeV center of mass energy, to tag $p\bar{p} \rightarrow Z\gamma$ events by requiring $E_T(\gamma) > 7$ GeV, lepton-gamma separation $\Delta R_{\ell\gamma} > 0.7$, and di-lepton invariant mass > 30 GeV. The cross section is in agreement with the SM prediction. Using these $Z\gamma$ events they obtain 95% C.L. limits on each h_i^V , keeping all others fixed at their SM values. They report: $-0.083 < h_{30}^Z < 0.082$, $-0.0053 < h_{40}^Z < 0.0054$, $-0.085 < h_{30}^\gamma < 0.084$, $-0.0053 < h_{40}^\gamma < 0.0054$, for the form factor scale $\Lambda = 1.2$ TeV.
- ¹² Using data collected at $\sqrt{s} = 183\text{--}208$, ABDALLAH 07c select 1,877 $e^+e^- \rightarrow Z\gamma$ events with $Z \rightarrow q\bar{q}$ or $\nu\bar{\nu}$, 171 $e^+e^- \rightarrow ZZ$ events with $Z \rightarrow q\bar{q}$ or lepton pair (except an explicit τ pair), and 74 $e^+e^- \rightarrow Z\gamma^*$ events with a $q\bar{q}\mu^+\mu^-$ or $q\bar{q}e^+e^-$ signature, to derive 95% CL limits on h_i^V . Each limit is derived with other parameters set to zero. They report: $-0.23 < h_1^Z < 0.23$, $-0.30 < h_2^Z < 0.16$, $-0.14 < h_1^\gamma < 0.14$, $-0.049 < h_3^\gamma < 0.044$.
- ¹³ ACHARD 04H select 3515 $e^+e^- \rightarrow Z\gamma$ events with $Z \rightarrow q\bar{q}$ or $\nu\bar{\nu}$ at $\sqrt{s} = 189\text{--}209$ GeV to derive 95% CL limits on h_i^V . For deriving each limit the other parameters are fixed at zero. They report: $-0.153 < h_1^Z < 0.141$, $-0.087 < h_2^Z < 0.079$, $-0.220 < h_3^Z < 0.112$, $-0.068 < h_4^Z < 0.148$, $-0.057 < h_1^\gamma < 0.057$, $-0.050 < h_2^\gamma < 0.023$, $-0.059 < h_3^\gamma < 0.004$, $-0.004 < h_4^\gamma < 0.042$.
- ¹⁴ ABBIENDI, G 00c study $e^+e^- \rightarrow Z\gamma$ events (with $Z \rightarrow q\bar{q}$ and $Z \rightarrow \nu\bar{\nu}$) at 189 GeV to obtain the central values (and 95% CL limits) of these couplings: $h_1^Z = 0.000 \pm 0.100$ ($-0.190, 0.190$), $h_2^Z = 0.000 \pm 0.068$ ($-0.128, 0.128$), $h_3^Z = -0.074^{+0.102}_{-0.103}$ ($-0.269, 0.119$), $h_4^Z = 0.046 \pm 0.068$ ($-0.084, 0.175$), $h_1^\gamma = 0.000 \pm 0.061$ ($-0.115, 0.115$), $h_2^\gamma = 0.000 \pm 0.041$ ($-0.077, 0.077$), $h_3^\gamma = -0.080^{+0.039}_{-0.041}$ ($-0.164, -0.006$), $h_4^\gamma = 0.064^{+0.033}_{-0.030}$ ($+0.007, +0.134$). The results are derived assuming that only one coupling at a time is different from zero.
- ¹⁵ ABBOTT 98M study $p\bar{p} \rightarrow Z\gamma + X$, with $Z \rightarrow e^+e^-, \mu^+\mu^-, \nu\bar{\nu}$ at 1.8 TeV, to obtain 95% CL limits at $\Lambda = 750$ GeV: $|h_{30}^Z| < 0.36$, $|h_{40}^Z| < 0.05$ (keeping $h_i^\gamma = 0$), and $|h_{30}^\gamma| < 0.37$, $|h_{40}^\gamma| < 0.05$ (keeping $h_i^Z = 0$). Limits on the CP-violating couplings are $|h_{10}^Z| < 0.36$, $|h_{20}^Z| < 0.05$ (keeping $h_i^\gamma = 0$), and $|h_{10}^\gamma| < 0.37$, $|h_{20}^\gamma| < 0.05$ (keeping $h_i^Z = 0$).
- ¹⁶ ABREU 98k determine a 95% CL upper limit on $\sigma(e^+e^- \rightarrow \gamma + \text{invisible particles}) < 2.5$ pb using 161 and 172 GeV data. This is used to set 95% CL limits on $|h_{30}^\gamma| < 0.8$ and $|h_{30}^Z| < 1.3$, derived at a scale $\Lambda = 1$ TeV and with $n = 3$ in the form factor representation.
- f_i^V**
Combining the LEP-2 results taking into account the correlations, the following 95% CL limits are derived [SCHAEEL 13A]:
- $$\begin{aligned} -0.28 < f_4^Z < +0.32, & \quad -0.34 < f_5^Z < +0.35, \\ -0.17 < f_4^\gamma < +0.19, & \quad -0.35 < f_5^\gamma < +0.32. \end{aligned}$$
- Some of the recent results from the Tevatron and LHC experiments individually surpass the combined LEP-2 results in precision (see below).
- | VALUE | DOCUMENT ID | TECN | COMMENT |
|---|------------------|------|-------------------------------------|
| • • • We do not use the following data for averages, fits, limits, etc. • • • | | | |
| 1 | SIRUNYAN 21Q | CMS | $E_{cm}^{pp} = 13$ TeV |
| 2 | AABOUD 19AY | ATLS | $E_{cm}^{pp} = 13$ TeV |
| 3 | AABOUD 18Q | ATLS | $E_{cm}^{pp} = 13$ TeV |
| 4 | SIRUNYAN 18BT | CMS | $E_{cm}^{pp} = 13$ TeV |
| 5 | KHACHATRY...15B | CMS | $E_{cm}^{pp} = 8$ TeV |
| 6 | KHACHATRY...15Bc | CMS | $E_{cm}^{pp} = 7, 8$ TeV |
| 7 | AAD 13z | ATLS | $E_{cm}^{pp} = 7$ TeV |
| 8 | CHATRCHYAN 13B | CMS | $E_{cm}^{pp} = 7$ TeV |
| 9 | SCHAEEL 09 | ALEP | $E_{cm}^{ee} = 192\text{--}209$ GeV |
| 10 | ABAZOV 08k | D0 | $E_{cm}^{pp} = 1.96$ TeV |
| 11 | ABDALLAH 07c | DLPH | $E_{cm}^{ee} = 183\text{--}208$ GeV |
| 12 | ABBIENDI 04c | OPAL | |
| 13 | ACHARD 03D | L3 | |
- ¹ SIRUNYAN 21Q measure ZZ production where both Z bosons decay in the electron or muon channel. Analyzing the four-lepton invariant mass distribution, the following limits are derived at 95% C.L. in units of 10^{-4} : $-6.6 < f_4^Z < 6.0$, $-5.5 < f_5^Z < 7.5$, $-7.8 < f_4^\gamma < 7.1$, $-6.8 < f_5^\gamma < 7.5$. This set of parameters is linearly related to a set of EFT parameters, resulting in the following limits at 95% C.L. in units of TeV^{-4} : $-2.3 < c_{B\bar{W}/\Lambda^4} < 2.5$, $-1.4 < c_{W\bar{W}/\Lambda^4} < 1.2$, $-1.4 < c_{B\bar{W}/\Lambda^4} < 1.3$, $-1.2 < c_{B\bar{B}/\Lambda^4} < 1.2$.
- ² AABOUD 19AY study ZZ production in the $\ell\ell\nu\nu$ decay channel. Events with a pair of isolated high-transverse momentum charged leptons (electron pairs or muon pairs), and with large missing energy, are selected. In the data, 371 (416) di-electron (di-muon) events are found, with a total expected background of 128 ± 8 (143 ± 8) events. Analysing the transverse momentum distribution of the charged dilepton system above 150 GeV, the following 95% C.L. limits are derived in units of 10^{-3} : $-1.2 < f_4^\gamma < 1.2$, $-1.0 < f_5^\gamma < 1.0$, $-1.2 < f_4^Z < 1.2$, $-1.0 < f_5^Z < 1.0$.
- ³ AABOUD 18Q study $pp \rightarrow ZZ$ events at $\sqrt{s} = 13$ TeV with $Z \rightarrow e^+e^-$ or $Z \rightarrow \mu^+\mu^-$. The number of events observed in the $4e, 2e2\mu$, and 4μ channels is 249, 465, and 303 respectively. Analysing the p_T spectrum of the leading Z boson, the following 95% C.L. limits are derived in units of 10^{-4} : $-1.8 < f_4^\gamma < 1.8$, $-1.5 < f_5^\gamma < 1.5$, $-1.8 < f_4^Z < 1.8$, $-1.5 < f_5^Z < 1.5$.
- ⁴ SIRUNYAN 18BT study $ppZZ$ events at $\sqrt{s} = 13$ TeV with $Z \rightarrow e^+e^-$ or $Z \rightarrow \mu^+\mu^-$. The number of events observed in the $4e, 2e2\mu$, and 4μ channels is 220, 543 and 335 respectively. Analysing the 4-lepton invariant mass spectrum, the following 95% C.L. limits are derived in units of 10^{-3} : $-1.2 < f_4^\gamma < 1.3$, $-1.2 < f_5^\gamma < 1.3$, $-1.2 < f_4^Z < 1.3$, $-1.2 < f_5^Z < 1.3$.
- ⁵ KHACHATRYAN 15B study ZZ production in 8 TeV pp collisions. In the decay modes $ZZ \rightarrow 4e, 4\mu, 2e2\mu, 54, 75, 148$ events are observed, with an expected background of $2.2 \pm 0.9, 1.2 \pm 0.6$, and 2.4 ± 1.0 events, respectively. Analysing the 4-lepton invariant mass spectrum in the range from 110 GeV to 1200 GeV, the following 95% C.L. limits are obtained: $|f_4^Z| < 0.004$, $|f_5^Z| < 0.004$, $|f_4^\gamma| < 0.005$, $|f_5^\gamma| < 0.005$.
- ⁶ KHACHATRYAN 15Bc use the cross section measurement of the final state $pp \rightarrow ZZ \rightarrow 2\ell 2\nu$, (ℓ being an electron or a muon) at 7 and 8 TeV to put limits on these triple gauge couplings. Effective mass of the charged lepton pair is required to be in the range 83.5–98.5 GeV and the dilepton $p_T > 45$ GeV. The reduced missing E_T is required to be > 65 GeV, which takes into account the fake missing E_T due to detector effects. The numbers of e^+e^- and $\mu^+\mu^-$ events selected are 35 and 40 at 7 TeV and 176 and 271 at 8 TeV respectively. The production cross sections so obtained are in agreement with SM predictions. The following 95% C.L. limits are set: $-0.0028 < f_4^Z < 0.0032$, $-0.0037 < f_5^Z < 0.0033$, $-0.0029 < f_4^\gamma < 0.0031$, $-0.0033 < f_5^\gamma < 0.0037$. Combining with previous results (KHACHATRYAN 15B and CHATRCHYAN 13B) which include 7 TeV and 8 TeV data on the final states $pp \rightarrow ZZ \rightarrow 2\ell 2\ell'$ where ℓ and ℓ' are an electron or a muon, the best limits are $-0.0022 < f_4^Z < 0.0026$, $-0.0029 < f_5^Z < 0.0026$, $-0.0022 < f_4^\gamma < 0.0026$, $-0.0023 < f_5^\gamma < 0.0023$, $-0.0026 < f_4^Z < 0.0027$.
- ⁷ AAD 13z study ZZ production in pp collisions at $\sqrt{s} = 7$ TeV. In the $ZZ \rightarrow \ell^+\ell^-\ell^+\ell^-$ final state they observe a total of 66 events with an expected background of 0.9 ± 1.3 . In the $ZZ \rightarrow \ell^+\ell^-\nu\nu$ final state they observe a total of 87 events with an expected background of 46.9 ± 5.2 . The limits on anomalous TGCs are determined using the observed and expected numbers of these ZZ events binned in p_T^Z . The 95% C.L. are as follows: for form factor scale $\Lambda = \infty$, $-0.015 < f_4^Z < 0.015$, $-0.013 < f_5^Z < 0.013$, $-0.016 < f_4^\gamma < 0.015$, $-0.013 < f_5^\gamma < 0.013$; for form factor scale $\Lambda = 3$ TeV, $-0.022 < f_4^Z < 0.023$, $-0.019 < f_5^Z < 0.019$, $-0.023 < f_4^\gamma < 0.023$, $-0.020 < f_5^\gamma < 0.019$.
- ⁸ CHATRCHYAN 13B study ZZ production in pp collisions and select 54 ZZ candidates in the Z decay channel with electrons or muons with an expected background of 1.4 ± 0.5 events. The resulting 95% C.L. ranges are: $-0.013 < f_4^Z < 0.015$, $-0.011 < f_5^Z < 0.012$, $-0.012 < f_4^\gamma < 0.014$, $-0.012 < f_5^\gamma < 0.012$.
- ⁹ Using data collected in the center of mass energy range 192–209 GeV, SCHAEEL 09 select 318 $e^+e^- \rightarrow ZZ$ events with 319.4 expected from the standard model. Using this data they derive the following 95% CL limits: $-0.321 < f_4^Z < 0.318$, $-0.534 < f_5^Z < 0.534$, $-0.724 < f_4^\gamma < 0.733$, $-1.194 < f_5^\gamma < 1.190$.
- ¹⁰ ABAZOV 08k search for ZZ and $Z\gamma^*$ events with 1 fb^{-1} $p\bar{p}$ data at $\sqrt{s} = 1.96$ TeV in $(e)e, (\mu\mu), (\mu\mu), (ee), (\mu\mu)$ final states requiring the lepton pair masses to be > 30 GeV. They observe 1 event, which is consistent with an expected signal of 1.71 ± 0.15 events and a background of 0.13 ± 0.03 events. From this they derive the following limits, for a form factor (Λ) value of 1.2 TeV: $-0.28 < f_4^Z < 0.28$, $-0.31 < f_5^Z < 0.29$, $-0.26 < f_4^\gamma < 0.26$, $-0.30 < f_5^\gamma < 0.28$.
- ¹¹ Using data collected at $\sqrt{s} = 183\text{--}208$ GeV, ABDALLAH 07c select 171 $e^+e^- \rightarrow ZZ$ events with $Z \rightarrow q\bar{q}$ or lepton pair (except an explicit τ pair), and 74 $e^+e^- \rightarrow Z\gamma^*$ events with a $q\bar{q}\mu^+\mu^-$ or $q\bar{q}e^+e^-$ signature, to derive 95% CL limits on f_i^V . Each limit is derived with other parameters set to zero. They report: $-0.40 < f_4^Z < 0.42$, $-0.38 < f_5^Z < 0.62$, $-0.23 < f_4^\gamma < 0.25$, $-0.52 < f_5^\gamma < 0.48$.
- ¹² ABBIENDI 04c study ZZ production in e^+e^- collisions in the C.M. energy range 190–209 GeV. They select 340 events with an expected background of 180 events. Including the ABBIENDI 00N data at 183 and 189 GeV (118 events with an expected background of 65 events) they report the following 95% CL limits: $-0.45 < f_4^Z < 0.58$, $-0.94 < f_5^Z < 0.25$, $-0.32 < f_4^\gamma < 0.33$, and $-0.71 < f_5^\gamma < 0.59$.
- ¹³ ACHARD 03D study Z -boson pair production in e^+e^- collisions in the C.M. energy range 200–209 GeV. They select 549 events with an expected background of 432 events. Including the ACCIARRI 99G and ACCIARRI 99o data (183 and 189 GeV respectively, 286 events with an expected background of 241 events) and the 192–202 GeV ACCIARRI 01i results (656 events, expected background of 512 events), they report the following 95% CL limits: $-0.48 \leq f_4^Z \leq 0.46$, $-0.36 \leq f_5^Z \leq 1.03$, $-0.28 \leq f_4^\gamma \leq 0.28$, and $-0.40 \leq f_5^\gamma \leq 0.47$.

ANOMALOUS W/Z QUARTIC COUPLINGS

Revised November 2015 by M.W. Gr unewald (U. College Dublin) and A. Gurtu (Formerly Tata Inst.).

Quartic couplings, $WWZZ$, $WWZ\gamma$, $WW\gamma\gamma$, and $ZZ\gamma\gamma$, were studied at LEP and Tevatron at energies at which the Standard Model predicts negligible contributions to multiboson production. Thus, to parametrize limits on these couplings, an effective theory approach is adopted which supplements the Standard Model Lagrangian with higher dimensional operators which include quartic couplings. The LEP collaborations chose the lowest dimensional representation of operators (dimension 6) which presumes the $SU(2)\times U(1)$ gauge symmetry is broken by means other than the conventional Higgs scalar doublet [1–3]. In this representation possible quartic couplings, a_0, a_c, a_n , are expressed in terms of the following dimension-6 operators [1,2];

$$\begin{aligned} L_6^0 &= -\frac{e^2}{16\Lambda^2} a_0 F^{\mu\nu} F_{\mu\nu} \vec{W}^\alpha \cdot \vec{W}_\alpha \\ L_6^c &= -\frac{e^2}{16\Lambda^2} a_c F^{\mu\alpha} F_{\mu\beta} \vec{W}^\beta \cdot \vec{W}_\alpha \\ L_6^n &= -i\frac{e^2}{16\Lambda^2} a_n \epsilon_{ijk} W_{\mu\alpha}^{(i)} W_\nu^{(j)} W^{(k)\alpha} F^{\mu\nu} \\ \tilde{L}_6^0 &= -\frac{e^2}{16\Lambda^2} \tilde{a}_0 F^{\mu\nu} \tilde{F}_{\mu\nu} \vec{W}^\alpha \cdot \vec{W}_\alpha \\ \tilde{L}_6^n &= -i\frac{e^2}{16\Lambda^2} \tilde{a}_n \epsilon_{ijk} W_{\mu\alpha}^{(i)} W_\nu^{(j)} W^{(k)\alpha} \tilde{F}^{\mu\nu} \end{aligned}$$

where F, W are photon and W fields, L_6^0 and L_6^c conserve C, P separately (\tilde{L}_6^0 conserves only C) and generate anomalous $W^+W^-\gamma\gamma$ and $ZZ\gamma\gamma$ couplings, L_6^n violates CP (\tilde{L}_6^n violates both C and P) and generates an anomalous $W^+W^-Z\gamma$ coupling, and Λ is an energy scale for new physics. For the $ZZ\gamma\gamma$ coupling the CP -violating term represented by L_6^n does not contribute. These couplings are assumed to be real and to vanish at tree level in the Standard Model.

Within the same framework as above, a more recent description of the quartic couplings [3] treats the anomalous parts of the $WW\gamma\gamma$ and $ZZ\gamma\gamma$ couplings separately, leading to two sets parametrized as a_0^V/Λ^2 and a_c^V/Λ^2 , where $V = W$ or Z .

With the discovery of a Higgs at the LHC in 2012, it is then useful to go to the next higher dimensional representation (dimension 8 operators) in which the gauge symmetry is broken by the conventional Higgs scalar doublet [3,4]. There are 14 operators which can contribute to the anomalous quartic coupling signal. Some of the operators have analogues in the dimension 6 scheme. The CMS collaboration, [5], have used this parametrization, in which the connections between the two schemes are also summarized:

$$\begin{aligned} \mathcal{L}_{AQGC} &= -\frac{e^2 a_0^W}{8 \Lambda^2} F_{\mu\nu} F^{\mu\nu} W^{+\alpha} W_\alpha^- \\ &\quad -\frac{e^2 a_c^W}{16 \Lambda^2} F_{\mu\nu} F^{\mu\alpha} (W^{+\nu} W_\alpha^- + W^{-\nu} W_\alpha^+) \\ &\quad -e^2 g^2 \frac{\kappa_0^W}{\Lambda^2} F_{\mu\nu} Z^{\mu\nu} W^{+\alpha} W_\alpha^- \\ &\quad -\frac{e^2 g^2 \kappa_c^W}{2 \Lambda^2} F_{\mu\nu} Z^{\mu\alpha} (W^{+\nu} W_\alpha^- + W^{-\nu} W_\alpha^+) \\ &\quad + \frac{f_{T,0}}{\Lambda^4} Tr[\widehat{W}_{\mu\nu} \widehat{W}^{\mu\nu}] \times Tr[\widehat{W}_{\alpha\beta} \widehat{W}^{\alpha\beta}] \end{aligned}$$

The energy scale of possible new physics is Λ , and $g = e/\sin(\theta_W)$, e being the unit electric charge and θ_W the Weinberg angle. The field tensors are described in [3,4].

The two dimension 6 operators a_0^W/Λ^2 and a_c^W/Λ^2 are associated with the $WW\gamma\gamma$ vertex. Among dimension 8 operators, κ_0^W/Λ^2 and κ_c^W/Λ^2 are associated with the $WWZ\gamma$ vertex, whereas the parameter $f_{T,0}/\Lambda^4$ contributes to both vertices. There is a relationship between these two dimension 6 parameters and the dimension 8 parameters $f_{M,i}/\Lambda^4$ as follows [3]:

$$\begin{aligned} \frac{a_0^W}{\Lambda^2} &= -\frac{4M_W^2}{g^2} \frac{f_{M,0}}{\Lambda^4} - \frac{8M_W^2}{g'^2} \frac{f_{M,2}}{\Lambda^4} \\ \frac{a_c^W}{\Lambda^2} &= -\frac{4M_W^2}{g^2} \frac{f_{M,1}}{\Lambda^4} - \frac{8M_W^2}{g'^2} \frac{f_{M,3}}{\Lambda^4} \end{aligned}$$

where $g' = e/\cos(\theta_W)$ and M_W is the invariant mass of the W boson. This relation provides a translation between limits on dimension 6 operators $a_{0,c}^W$ and $f_{M,j}/\Lambda^4$. It is further required [4] that $f_{M,0} = 2f_{M,2}$ and $f_{M,1} = 2f_{M,3}$ which suppresses contributions to the $WWZ\gamma$ vertex. The complete set of Lagrangian contributions as presented in [4] corresponds to 19 anomalous couplings in total – $f_{S,i}$, $i = 1, 2$, $f_{M,i}$, $i = 0, \dots, 8$ and $f_{T,i}$, $i = 0, \dots, 9$ – each scaled by $1/\Lambda^4$.

The ATLAS collaboration [6], on the other hand, follows a K-matrix driven approach of Ref. 7 in which the anomalous couplings can be expressed in terms of two parameters α_4 and α_5 , which account for all BSM effects.

It is the early stages in the determination of quartic couplings by the LHC experiments. It is hoped that the two collaborations, ATLAS and CMS, will agree to use at least one common set of parameters to express these limits to enable the reader to make a comparison and allow for a possible LHC combination.

References

1. G. Belanger and F. Boudjema, Phys. Lett. **B288**, 201 (1992).
2. J.W. Stirling and A. Werthenbach, Eur. Phys. J. **C14**, 103 (2000); J.W. Stirling and A. Werthenbach, Phys. Lett. **B466**, 369 (1999); A. Denner *et al.*, Eur. Phys. J. **C20**, 201 (2001); G. Montagna *et al.*, Phys. Lett. **B515**, 197 (2001).
3. G. Belanger *et al.*, Eur. Phys. J. **C13**, 283 (2000).
4. O.J.P.  boli, M.C. Gonzalez-Garcia, and S.M. Lietti, Phys. Rev. **D69**, 095005 (2004); O.J.P.  boli, M.C. Gonzalez-Garcia, and J.K. Mizukoshi, Phys. Rev. **D77**, 073005 (2006).
5. S. Chatrchyan *et al.*, Phys. Rev. **D90**, 032008 (2014); S. Chatrchyan *et al.*, Phys. Rev. Lett. **114**, 051801 (2015).
6. G. Aad *et al.*, Phys. Rev. Lett. **113**, 141803 (2014).
7. A. Albateanu, W. Killian, and J. Reuter, JHEP **0811**, 010 (2008).

 $a_0/\Lambda^2, a_c/\Lambda^2$

Combining published and unpublished preliminary LEP results the following 95% CL intervals for the QGCs associated with the $ZZ\gamma\gamma$ vertex are derived (CERN-PH-EP/2005-051 or hep-ex/0511027):

$$\begin{aligned} -0.008 < a_0^Z/\Lambda^2 < +0.021 \\ -0.029 < a_c^Z/\Lambda^2 < +0.039 \end{aligned}$$

Gauge & Higgs Boson Particle Listings

Z

Anomalous Z quartic couplings have also been measured by the Tevatron and LHC experiments. As discussed in the review on "Anomalous W/Z quartic couplings," the coupling parameters in the Anomalous QGC Lagrangian may relate to processes involving only the W or only to the Z or to both. Thus, results on all other AQGCs are reported together in the W listings.

VALUE	DOCUMENT ID	TECN
•••	We do not use the following data for averages, fits, limits, etc. •••	
	1	2
	ABBIENDI 04L	OPAL
	HEISTER 04A	ALEP
	ACHARD 02G	L3

- 1 ABBIENDI 04L select $20 e^+e^- \rightarrow \nu\bar{\nu}\gamma\gamma$ acoplanar events in the energy range 180–209 GeV and $176 e^+e^- \rightarrow q\bar{q}\gamma\gamma$ events in the energy range 130–209 GeV. These samples are used to constrain possible anomalous $W^+W^-\gamma\gamma$ and $ZZ\gamma\gamma$ quartic couplings. Further combining with the $W^+W^-\gamma$ sample of ABBIENDI 04B the following one-parameter 95% CL limits are obtained: $-0.007 < a_0^Z/\Lambda^2 < 0.023 \text{ GeV}^{-2}$, $-0.029 < a_c^Z/\Lambda^2 < 0.029 \text{ GeV}^{-2}$, $-0.020 < a_0^W/\Lambda^2 < 0.020 \text{ GeV}^{-2}$, $-0.052 < a_c^W/\Lambda^2 < 0.037 \text{ GeV}^{-2}$.
- 2 In the CM energy range 183 to 209 GeV HEISTER 04A select $30 e^+e^- \rightarrow \nu\bar{\nu}\gamma\gamma$ events with two acoplanar, high energy and high transverse momentum photons. The photon-photon acoplanarity is required to be $> 5^\circ$, $E_\gamma/\sqrt{s} > 0.025$ (the more energetic photon having energy $> 0.2\sqrt{s}$), $p_{T\gamma}/E_{\text{beam}} > 0.05$ and $|\cos\theta_\gamma| < 0.94$. A likelihood fit to the photon energy and recoil missing mass yields the following one-parameter 95% CL limits: $-0.012 < a_0^Z/\Lambda^2 < 0.019 \text{ GeV}^{-2}$, $-0.041 < a_c^Z/\Lambda^2 < 0.044 \text{ GeV}^{-2}$, $-0.060 < a_0^W/\Lambda^2 < 0.055 \text{ GeV}^{-2}$, $-0.099 < a_c^W/\Lambda^2 < 0.093 \text{ GeV}^{-2}$.
- 3 ACHARD 02G study $e^+e^- \rightarrow Z\gamma\gamma \rightarrow q\bar{q}\gamma\gamma$ events using data at center-of-mass energies from 200 to 209 GeV. The photons are required to be isolated, each with energy $> 5 \text{ GeV}$ and $|\cos\theta| < 0.97$, and the di-jet invariant mass to be compatible with that of the Z boson (74–111 GeV). Cuts on Z velocity ($\beta < 0.73$) and on the energy of the most energetic photon reduce the backgrounds due to non-resonant production of the $q\bar{q}\gamma\gamma$ state and due to ISR respectively, yielding a total of 40 candidate events of which 8.6 are expected to be due to background. The energy spectra of the least energetic photon are fitted for all ten center-of-mass energy values from 130 GeV to 209 GeV (as obtained adding to the present analysis 130–202 GeV data of ACCIARRI 01E, for a total of 137 events with an expected background of 34.1 events) to obtain the fitted values $a_0/\Lambda^2 = 0.00 \pm 0.02 \text{ GeV}^{-2}$ and $a_c/\Lambda^2 = 0.03 \pm 0.01 \text{ GeV}^{-2}$, where the other parameter is kept fixed to its Standard Model value (0). A simultaneous fit to both parameters yields the 95% CL limits $-0.02 \text{ GeV}^{-2} < a_0/\Lambda^2 < 0.03 \text{ GeV}^{-2}$ and $-0.07 \text{ GeV}^{-2} < a_c/\Lambda^2 < 0.05 \text{ GeV}^{-2}$.

Z REFERENCES

AAD 21A0 NATP 17 819	G. Aad et al.	(ATLAS Collab.)
AAD 21A0 JHEP 2107 005	G. Aad et al.	(ATLAS Collab.)
AAD 21AV PRL 127 271801	G. Aad et al.	(ATLAS Collab.)
SIRUNYAN 21Q EPJ C81 200	A.M. Sirunyan et al.	(CMS Collab.)
ABOUD 19AY JHEP 1910 127	M. Aboud et al.	(ATLAS Collab.)
ABOUD 19N JHEP 1904 046	M. Aboud et al.	(ATLAS Collab.)
RAINBOLT 19 PR D99 013004	J.L. Rainbolt, M. Schmitt	(NWES)
SIRUNYAN 19AJ EPJ C79 94	A.M. Sirunyan et al.	(CMS Collab.)
SIRUNYAN 19BR PL B797 134811	A.M. Sirunyan et al.	(CMS Collab.)
ABOUD 18AU JHEP 1807 127	M. Aboud et al.	(ATLAS Collab.)
ABOUD 18BL PL B786 134	M. Aboud et al.	(ATLAS Collab.)
ABOUD 18CN PR D98 092010	M. Aboud et al.	(ATLAS Collab.)
ABOUD 18Q PR D97 032005	M. Aboud et al.	(ATLAS Collab.)
AAJ 18AR JHEP 1809 159	R. Aaij et al.	(LHCb Collab.)
ANDREEV 18A EPJ C78 777	V. Andreev et al.	(HI Collab.)
SIRUNYAN 18BT EPJ C78 165	A.M. Sirunyan et al.	(CMS Collab.)
SIRUNYAN 18DZ PRL 121 141801	A.M. Sirunyan et al.	(CMS Collab.)
ABOUD 17Q EPJ C77 367	M. Aboud et al.	(ATLAS Collab.)
ABOUD 16K PRL 117 111802	M. Aboud et al.	(ATLAS Collab.)
AAD 16L EPJ C76 210	G. Aad et al.	(ATLAS Collab.)
AAD 16Q PR D93 112002	G. Aad et al.	(ATLAS Collab.)
ABRAMOWICZ 16A PR D93 092002	H. Abramowicz et al.	(ZEUS Collab.)
ABT 16 PR D94 052007	I. Abt et al.	(MPIM, OXF, HAMB, DESY)
KHACHATRYAN...16AE PL B760 448	V. Khachatryan et al.	(CMS Collab.)
KHACHATRYAN...16CC PL B763 280	V. Khachatryan et al.	(CMS Collab.)
AAD 15BT JHEP 1509 049	G. Aad et al.	(ATLAS Collab.)
AAD 15I PRL 114 121801	G. Aad et al.	(ATLAS Collab.)
KHACHATRYAN...15AC JHEP 1504 164	V. Khachatryan et al.	(CMS Collab.)
KHACHATRYAN...15B PL B740 250	V. Khachatryan et al.	(CMS Collab.)
KHACHATRYAN...15BC EPJ C75 511	V. Khachatryan et al.	(CMS Collab.)
AAD 14UN PR D90 072010	G. Aad et al.	(ATLAS Collab.)
AAD 14N PRL 112 231806	G. Aad et al.	(ATLAS Collab.)
AALTONEN 14E PRL 112 111803	T. Aaltonen et al.	(CDF Collab.)
CHATRCHYAN 14AB PR D89 092005	S. Chatrchyan et al.	(CMS Collab.)
AAD 13AN PR D87 112003	G. Aad et al.	(ATLAS Collab.)
Also PR D91 119901 (err.)	G. Aad et al.	(ATLAS Collab.)
AAD 13Z JHEP 1303 128	G. Aad et al.	(ATLAS Collab.)
CHATRCHYAN 13B JHEP 1301 063	S. Chatrchyan et al.	(CMS Collab.)
CHATRCHYAN 13BI JHEP 1310 1164	S. Chatrchyan et al.	(CMS Collab.)
SCHAEF 13A PRPL 532 119	S. Schaefer et al.	(CMS Collab.)
AAD 12BX PL B717 49	G. Aad et al.	(ATLAS Collab.)
ABAZOV 12S PR D85 052001	V.M. Abazov et al.	(DO Collab.)
CHATRCHYAN 12BN JHEP 1212 034	S. Chatrchyan et al.	(CMS Collab.)
AALTONEN 11S PRL 107 051802	T. Aaltonen et al.	(CDF Collab.)
ABAZOV 11D PR D84 012007	V.M. Abazov et al.	(DO Collab.)
CHATRCHYAN 11M PL B701 535	S. Chatrchyan et al.	(CMS Collab.)
ABAZOV 09L PRL 102 201802	V.M. Abazov et al.	(DO Collab.)
BEDDALL 09 PL B670 300	A. Beddall, A. Beddall, A. Bingul	(UGAZ)
SCHAEF 09 JHEP 0904 124	S. Schaefer et al.	(ALEPH Collab.)
ABAZOV 08K PRL 100 131801	V.M. Abazov et al.	(DO Collab.)
ABAZOV 07M PL B653 378	V.M. Abazov et al.	(DO Collab.)
ABDALLAH 07C EPJ C51 525	J. Abdallah et al.	(DELPHI Collab.)
ABDALLAH 06E PL B639 179	J. Abdallah et al.	(DELPHI Collab.)
AKTAS 06 PL B632 35	A. Aktas et al.	(HI Collab.)
LEP-SLC 06 PRPL 427 257	ALEPH, DELPHI, L3, OPAL, SLD and working groups	
SCHAEF 06A PL B639 192	S. Schaefer et al.	(ALEPH Collab.)
ABDALLAH 05 EPJ C40 1	J. Abdallah et al.	(DELPHI Collab.)
ABDALLAH 05C EPJ C44 299	J. Abdallah et al.	(DELPHI Collab.)
ABE 05 PRL 94 091801	K. Abe et al.	(SLD Collab.)
ABE 05F PR D71 112004	K. Abe et al.	(SLD Collab.)
ACOSTA 05M PR D71 052002	D. Acosta et al.	(CDF Collab.)
ABBIENDI 04B PL B580 17	G. Abbiendi et al.	(OPAL Collab.)
ABBIENDI 04C EPJ C32 303	G. Abbiendi et al.	(OPAL Collab.)
ABBIENDI 04E PL B586 167	G. Abbiendi et al.	(OPAL Collab.)
ABBIENDI 04G EPJ C33 173	G. Abbiendi et al.	(OPAL Collab.)
ABBIENDI 04L PR D70 032005	G. Abbiendi et al.	(OPAL Collab.)
ABDALLAH 04C EPJ C34 109	J. Abdallah et al.	(DELPHI Collab.)
ABE 04F PR D69 072003	K. Abe et al.	(SLD Collab.)
ACHARD 04C PL B585 42	P. Achard et al.	(L3 Collab.)
ACHARD 04H PL B597 119	P. Achard et al.	(L3 Collab.)
HEISTER 04A PL B602 31	A. Heister et al.	(ALEPH Collab.)
ABBIENDI 03P PL B577 18	G. Abbiendi et al.	(OPAL Collab.)
ABDALLAH 03H PL B569 129	J. Abdallah et al.	(DELPHI Collab.)
ABDALLAH 03K PL B576 29	J. Abdallah et al.	(DELPHI Collab.)
ABE 03F PRL 90 141804	K. Abe et al.	(SLD Collab.)
ACHARD 03D PL B572 133	P. Achard et al.	(L3 Collab.)
ACHARD 03G PL B577 109	P. Achard et al.	(L3 Collab.)
ABBIENDI 02I PL B546 29	G. Abbiendi et al.	(OPAL Collab.)
ABE 02G PRL 88 151801	K. Abe et al.	(SLD Collab.)
ACHARD 02B PL B540 43	P. Achard et al.	(L3 Collab.)
HEISTER 02F PL B526 34	A. Heister et al.	(ALEPH Collab.)
HEISTER 02C PL B528 19	A. Heister et al.	(ALEPH Collab.)
HEISTER 02H EPJ C24 177	A. Heister et al.	(ALEPH Collab.)
ABBIENDI 01A EPJ C19 587	G. Abbiendi et al.	(OPAL Collab.)
ABBIENDI 01G EPJ C18 447	G. Abbiendi et al.	(OPAL Collab.)
ABBIENDI 01K PL B516 1	G. Abbiendi et al.	(OPAL Collab.)
ABBIENDI 01N EPJ C20 445	G. Abbiendi et al.	(OPAL Collab.)
ABBIENDI 01O EPJ C21 1	G. Abbiendi et al.	(OPAL Collab.)
ABE 01B PRL 86 1162	K. Abe et al.	(SLD Collab.)
ABE 01C PR D63 032005	K. Abe et al.	(SLD Collab.)
ACCIARRI 01E PL B505 47	M. Acciari et al.	(L3 Collab.)
ACCIARRI 01I PL B497 23	M. Acciari et al.	(L3 Collab.)
HEISTER 01I EPJ C20 401	A. Heister et al.	(ALEPH Collab.)
HEISTER 01J EPJ C22 201	A. Heister et al.	(ALEPH Collab.)
ABBIENDI 00N PL B476 256	G. Abbiendi et al.	(OPAL Collab.)
ABBIENDI,G 00C EPJ C17 553	G. Abbiendi et al.	(OPAL Collab.)
ABE 00B PRL 84 5945	K. Abe et al.	(SLD Collab.)
ABE 00D PRL 85 5059	K. Abe et al.	(SLD Collab.)
ABREU 00 EPJ C12 225	P. Abreu et al.	(DELPHI Collab.)
ABREU 00E EPJ C14 613	P. Abreu et al.	(DELPHI Collab.)
ABREU 00F EPJ C14 585	P. Abreu et al.	(DELPHI Collab.)
ABREU 00G EPJ C16 371	P. Abreu et al.	(DELPHI Collab.)
ABREU 00P PL B475 429	P. Abreu et al.	(DELPHI Collab.)
ACCIARRI 00 EPJ C13 47	M. Acciari et al.	(L3 Collab.)
ACCIARRI 00C EPJ C11 1	M. Acciari et al.	(L3 Collab.)
ACCIARRI 00J PL B479 79	M. Acciari et al.	(L3 Collab.)
ACCIARRI 00Q PL B489 93	M. Acciari et al.	(L3 Collab.)
BARATE 00B EPJ C16 597	R. Barate et al.	(ALEPH Collab.)
BARATE 00C EPJ C14 1	R. Barate et al.	(ALEPH Collab.)
BARATE 00D EPJ C16 613	R. Barate et al.	(ALEPH Collab.)
ABBIENDI 99B EPJ C8 217	G. Abbiendi et al.	(OPAL Collab.)
ABBIENDI 99I PL B447 157	G. Abbiendi et al.	(OPAL Collab.)
ABE 99E PR D59 052001	K. Abe et al.	(SLD Collab.)
ABE 99L PRL 83 1902	K. Abe et al.	(SLD Collab.)
ABREU 99 EPJ C6 19	P. Abreu et al.	(DELPHI Collab.)
ABREU 99B EPJ C4 415	P. Abreu et al.	(DELPHI Collab.)
ABREU 99I PL B449 364	P. Abreu et al.	(DELPHI Collab.)
ABREU 99U PL B462 425	P. Abreu et al.	(DELPHI Collab.)
ABREU 99Y EPJ C10 219	P. Abreu et al.	(DELPHI Collab.)
ACCIARRI 99D PL B448 152	M. Acciari et al.	(L3 Collab.)
ACCIARRI 99F PL B453 94	M. Acciari et al.	(L3 Collab.)
ACCIARRI 99G PL B450 281	M. Acciari et al.	(L3 Collab.)
ACCIARRI 99O PL B465 363	M. Acciari et al.	(L3 Collab.)
ABBOTT 98M PR D57 3817	B. Abbott et al.	(DO Collab.)
ABE 98B PRL 80 660	K. Abe et al.	(SLD Collab.)
ABE 98L EPJ C81 942	K. Abe et al.	(SLD Collab.)
ABREU 98K PL B423 194	P. Abreu et al.	(DELPHI Collab.)
ABREU 98I EPJ C5 585	P. Abreu et al.	(DELPHI Collab.)
ACCIARRI 98G PL B431 199	M. Acciari et al.	(L3 Collab.)
ACCIARRI 98H PL B429 387	M. Acciari et al.	(L3 Collab.)
ACCIARRI 98J PL B439 225	M. Acciari et al.	(L3 Collab.)
ACKERS TAFF 98A EPJ C5 411	K. Ackersstaff et al.	(OPAL Collab.)
ACKERS TAFF 98E EPJ C1 439	K. Ackersstaff et al.	(OPAL Collab.)
ACKERS TAFF 98B PL B420 157	K. Ackersstaff et al.	(OPAL Collab.)
ACKERS TAFF 98D EPJ C4 19	K. Ackersstaff et al.	(OPAL Collab.)
BARATE 98Q PL B434 415	R. Barate et al.	(ALEPH Collab.)
BARATE 98T EPJ C4 557	R. Barate et al.	(ALEPH Collab.)
BARATE 98V EPJ C5 205	R. Barate et al.	(ALEPH Collab.)
ABE 97 PRL 78 17	K. Abe et al.	(SLD Collab.)
ABREU 97C ZPHY C73 243	P. Abreu et al.	(DELPHI Collab.)
ABREU 97E PL B398 207	P. Abreu et al.	(DELPHI Collab.)
ABREU 97G PL B404 194	P. Abreu et al.	(DELPHI Collab.)
ACCIARRI 97F PL B393 465	M. Acciari et al.	(L3 Collab.)
ACCIARRI 97J PL B407 351	M. Acciari et al.	(L3 Collab.)
ACCIARRI 97L PL B407 389	M. Acciari et al.	(L3 Collab.)
ACCIARRI 97M PL B413 167	M. Acciari et al.	(L3 Collab.)
ACKERS TAFF 97N ZPHY C74 413	K. Ackersstaff et al.	(OPAL Collab.)
ACKERS TAFF 97S PL B412 210	K. Ackersstaff et al.	(OPAL Collab.)
ACKERS TAFF 97T ZPHY C76 387	K. Ackersstaff et al.	(OPAL Collab.)
ACKERS TAFF 97W ZPHY C76 425	K. Ackersstaff et al.	(OPAL Collab.)
ALEXANDER 97C ZPHY C73 379	G. Alexander et al.	(OPAL Collab.)
ALEXANDER 97D ZPHY C73 569	G. Alexander et al.	(OPAL Collab.)
ALEXANDER 97E ZPHY C73 587	G. Alexander et al.	(OPAL Collab.)
BARATE 97F PL B405 191	R. Barate et al.	(ALEPH Collab.)
BARATE 97G PL B401 150	R. Barate et al.	(ALEPH Collab.)
BARATE 97H PL B401 163	R. Barate et al.	(ALEPH Collab.)
BARATE 97J PL B402 213	R. Barate et al.	(ALEPH Collab.)
BARATE 97K ZPHY C74 451	R. Barate et al.	(ALEPH Collab.)
ABREU 96R ZPHY C72 31	P. Abreu et al.	(DELPHI Collab.)
ABREU 96S PL B389 405	P. Abreu et al.	(DELPHI Collab.)
ABREU 96Q ZPHY C73 61	P. Abreu et al.	(DELPHI Collab.)
ACCIARRI 96 PL B371 126	M. Acciari et al.	(L3 Collab.)
ADAM 96 ZPHY C69 561	W. Adam et al.	(DELPHI Collab.)
ADAM 96B ZPHY C70 371	W. Adam et al.	(DELPHI Collab.)
ALEXANDER 96B ZPHY C70 197	G. Alexander et al.	(OPAL Collab.)
ALEXANDER 96F PL B370 185	G. Alexander et al.	(OPAL Collab.)
ALEXANDER 96N PL B384 343	G. Alexander et al.	(OPAL Collab.)
ALEXANDER 96R ZPHY C72 1	G. Alexander et al.	(OPAL Collab.)
BUSKULIC 96D ZPHY C69 393	D. Buskulic et al.	(ALEPH Collab.)
BUSKULIC 96H ZPHY C69 379	D. Buskulic et al.	(ALEPH Collab.)
BUSKULIC 96T PL B384 449	D. Buskulic et al.	(ALEPH Collab.)
BUSKULIC 96Y PL B388 648	D. Buskulic et al.	(ALEPH Collab.)
ABE 95J PRL 74 2880	K. Abe et al.	(SLD Collab.)
ABREU 95 ZPHY C65 709 (erratum)	P. Abreu et al.	(DELPHI Collab.)
ABREU 95D ZPHY C66 323	P. Abreu et al.	(DELPHI Collab.)
ABREU 95L ZPHY C65 587	P. Abreu et al.	(DELPHI Collab.)
ABREU 95M ZPHY C65 603	P. Abreu et al.	(DELPHI Collab.)
ABREU 95O ZPHY C67 543	P. Abreu et al.	(DELPHI Collab.)
ABREU 95R ZPHY C68 353	P. Abreu et al.	(DELPHI Collab.)
ABREU 95S ZPHY C68 541	P. Abreu et al.	(DELPHI Collab.)
ABREU 95W PL B361 207	P. Abreu et al.	(DELPHI Collab.)
ABREU 95X ZPHY C69 1	P. Abreu et al.	(DELPHI Collab.)
ACCIARRI 95B PL B345 589	M. Acciari et al.	(L3 Collab.)
ACCIARRI 95C PL B345 609	M. Acciari et al.	(L3 Collab.)
ACCIARRI 95G PL B353 136	M. Acciari et al.	(L3 Collab.)

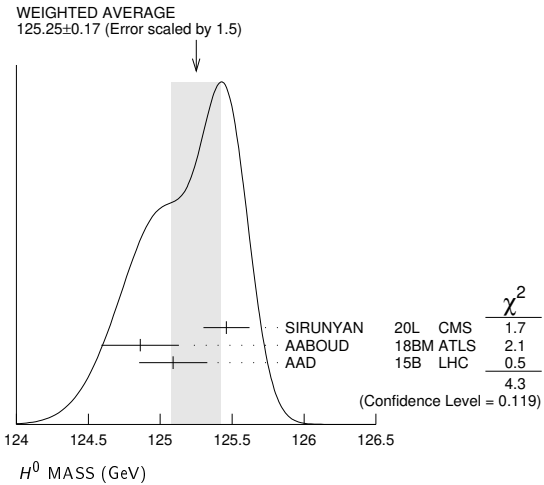
See key on page 1127

Gauge & Higgs Boson Particle Listings

Z, H⁰

AKERS	95C	ZPHY C65 47	R. Akers <i>et al.</i>	(OPAL Collab.)
AKERS	95U	ZPHY C67 389	R. Akers <i>et al.</i>	(OPAL Collab.)
AKERS	95W	ZPHY C67 555	R. Akers <i>et al.</i>	(OPAL Collab.)
AKERS	95X	ZPHY C68 1	R. Akers <i>et al.</i>	(OPAL Collab.)
AKERS	95Z	ZPHY C68 203	R. Akers <i>et al.</i>	(OPAL Collab.)
ALEXANDER	95D	PL B358 162	G. Alexander <i>et al.</i>	(OPAL Collab.)
BUSKULIC	95R	ZPHY C69 15	D. Buskulić <i>et al.</i>	(ALEPH Collab.)
MIYABAYASHI	95	PL B347 171	K. Miyabayashi <i>et al.</i>	(TOPAZ Collab.)
ABE	94C	PRL 73 25	K. Abe <i>et al.</i>	(SLD Collab.)
ABREU	94B	PL B327 386	P. Abreu <i>et al.</i>	(DELPHI Collab.)
ABREU	94P	PL B341 109	P. Abreu <i>et al.</i>	(DELPHI Collab.)
AKERS	94P	ZPHY C63 181	R. Akers <i>et al.</i>	(OPAL Collab.)
BUSKULIC	94G	ZPHY C62 179	D. Buskulić <i>et al.</i>	(ALEPH Collab.)
BUSKULIC	94J	ZPHY C62 1	D. Buskulić <i>et al.</i>	(ALEPH Collab.)
VILAIN	94	PL B320 203	P. Vilain <i>et al.</i>	(CHARM II Collab.)
ABREU	93	PL B298 236	P. Abreu <i>et al.</i>	(DELPHI Collab.)
ABREU	93I	ZPHY C59 533	P. Abreu <i>et al.</i>	(DELPHI Collab.)
ABREU	93L	ZPHY C65 709 (erratum)	P. Abreu <i>et al.</i>	(DELPHI Collab.)
ACTON	93	PL B305 407	P.D. Acton <i>et al.</i>	(DELPHI Collab.)
ACTON	93D	ZPHY C58 219	P.D. Acton <i>et al.</i>	(OPAL Collab.)
ACTON	93E	PL B311 391	P.D. Acton <i>et al.</i>	(OPAL Collab.)
ADRIANI	93	PL B301 136	O. Adriani <i>et al.</i>	(L3 Collab.)
ADRIANI	93I	PL B316 427	O. Adriani <i>et al.</i>	(L3 Collab.)
BUSKULIC	93L	PL B313 520	D. Buskulić <i>et al.</i>	(ALEPH Collab.)
NOVIKOV	93C	PL B298 453	V.A. Novikov, L.B. Okun, M.I. Vysotsky	(ITEP)
ABREU	92I	PL B277 371	P. Abreu <i>et al.</i>	(DELPHI Collab.)
ABREU	92M	PL B289 199	P. Abreu <i>et al.</i>	(DELPHI Collab.)
ACTON	92B	ZPHY C53 539	P.D. Acton <i>et al.</i>	(OPAL Collab.)
ACTON	92L	PL B294 436	P.D. Acton <i>et al.</i>	(OPAL Collab.)
ACTON	92N	PL B295 357	P.D. Acton <i>et al.</i>	(OPAL Collab.)
ADEVA	92	PL B275 209	B. Adeva <i>et al.</i>	(L3 Collab.)
ADRIANI	92D	PL B292 454	O. Adriani <i>et al.</i>	(L3 Collab.)
ALITTI	92B	PL B276 354	J. Alitti <i>et al.</i>	(UA2 Collab.)
BUSKULIC	92D	PL B292 210	D. Buskulić <i>et al.</i>	(ALEPH Collab.)
BUSKULIC	92E	PL B294 145	D. Buskulić <i>et al.</i>	(ALEPH Collab.)
DECAMP	92	PRPL 216 253	D. Decamp <i>et al.</i>	(ALEPH Collab.)
ABE	91E	PRL 67 1502	F. Abe <i>et al.</i>	(CDF Collab.)
ABREU	91H	ZPHY C50 185	P. Abreu <i>et al.</i>	(DELPHI Collab.)
ACTON	91B	PL B273 338	D.P. Acton <i>et al.</i>	(OPAL Collab.)
ADACHI	91	PL B255 613	I. Adachi <i>et al.</i>	(TOPAZ Collab.)
ADEVA	91I	PL B259 199	B. Adeva <i>et al.</i>	(L3 Collab.)
AKRAWY	91F	PL B257 531	M.Z. Akrawy <i>et al.</i>	(OPAL Collab.)
DECAMP	91B	PL B259 377	D. Decamp <i>et al.</i>	(ALEPH Collab.)
DECAMP	91J	PL B266 218	D. Decamp <i>et al.</i>	(ALEPH Collab.)
JACOBSEN	91	PRL 67 3347	R.G. Jacobsen <i>et al.</i>	(Mark II Collab.)
SHIMONAKA	91	PL B268 457	A. Shimonaka <i>et al.</i>	(TOPAZ Collab.)
ABE	90I	ZPHY C48 13	K. Abe <i>et al.</i>	(VENUS Collab.)
ABRAMS	90	PRL 64 1334	G.S. Abrams <i>et al.</i>	(Mark II Collab.)
AKRAWY	90J	PL B246 285	M.Z. Akrawy <i>et al.</i>	(OPAL Collab.)
BEHREND	90D	ZPHY C47 333	H.J. Behrend <i>et al.</i>	(CELLO Collab.)
BRAUNSCH... 90	ZPHY C48 433	W. Braunschweig <i>et al.</i>	(TASSO Collab.)	
ELSEN	90	ZPHY C46 349	E. Elsen <i>et al.</i>	(JADE Collab.)
HEGNER	90	ZPHY C46 547	S. Hegner <i>et al.</i>	(JADE Collab.)
STUART	90	PRL 64 983	D. Stuart <i>et al.</i>	(AMY Collab.)
ABE	89	PRL 62 613	F. Abe <i>et al.</i>	(CDF Collab.)
ABE	89C	PRL 63 720	F. Abe <i>et al.</i>	(CDF Collab.)
ABE	89L	PL B232 425	K. Abe <i>et al.</i>	(VENUS Collab.)
ABRAMS	89B	PRL 63 2173	G.S. Abrams <i>et al.</i>	(Mark II Collab.)
ABRAMS	89D	PRL 63 2780	G.S. Abrams <i>et al.</i>	(Mark II Collab.)
ALBAJAR	89	ZPHY C44 15	C. Albajar <i>et al.</i>	(UA1 Collab.)
BACALA	89	PL B218 112	A. Bacala <i>et al.</i>	(AMY Collab.)
BAND	89	PL B218 369	H.R. Band <i>et al.</i>	(MAC Collab.)
GREENSHAW	89	ZPHY C42 1	T. Greenshaw <i>et al.</i>	(JADE Collab.)
OULD-SAAD	89	ZPHY C44 567	F. Ould-Saada <i>et al.</i>	(JADE Collab.)
SAGAWA	89	PRL 63 2341	H. Sagawa <i>et al.</i>	(AMY Collab.)
ADACHI	88C	PL B208 319	I. Adachi <i>et al.</i>	(TOPAZ Collab.)
ADEVA	88	PR D38 2665	B. Adeva <i>et al.</i>	(Mark-J Collab.)
BRAUNSCH... 88D	ZPHY C40 163	W. Braunschweig <i>et al.</i>	(TASSO Collab.)	
ANSARI	87	PL B186 440	R. Ansari <i>et al.</i>	(UA2 Collab.)
BEHREND	87C	PL B191 209	H.J. Behrend <i>et al.</i>	(CELLO Collab.)
BARTEL	86C	ZPHY C30 371	W. Bartel <i>et al.</i>	(JADE Collab.)
ABO	ZPHY C26 507	W. Bartel <i>et al.</i>	(JADE Collab.)	
ASH	85	PL 108B 140	W. Bartel <i>et al.</i>	(JADE Collab.)
BARTEL	85F	PRL 55 1831	W.W. Ash <i>et al.</i>	(MAC Collab.)
DERRICK	85	PR D31 2352	W. Bartel <i>et al.</i>	(JADE Collab.)
FERNANDEZ	85	PRL 54 1624	M. Derrick <i>et al.</i>	(HRS Collab.)
LEVI	83	PRL 51 1941	E. Fernandez <i>et al.</i>	(MAC Collab.)
BEHREND	82	PL 114B 282	M.E. Levi <i>et al.</i>	(Mark II Collab.)
BRANDELIC	82C	PL 110B 173	H.J. Behrend <i>et al.</i>	(CELLO Collab.)
			R. Brandelik <i>et al.</i>	(TASSO Collab.)

124.79 ± 0.37	6 AABOUD	18BM ATLS	pp, 13 TeV, ZZ* → 4ℓ
124.93 ± 0.40	7 AABOUD	18BM ATLS	pp, 13 TeV, γγ
124.97 ± 0.24	2,8 AABOUD	18BM ATLS	pp, 7, 8, 13 TeV, γγ, ZZ* → 4ℓ
125.26 ± 0.20 ± 0.08	9 SIRUNYAN	17AV CMS	pp, 13 TeV, ZZ* → 4ℓ
125.07 ± 0.25 ± 0.14	3 AAD	15B LHC	pp, 7, 8 TeV, γγ
125.15 ± 0.37 ± 0.15	3 AAD	15B LHC	pp, 7, 8 TeV, ZZ* → 4ℓ
126.02 ± 0.43 ± 0.27	AAD	15B ATLS	pp, 7, 8 TeV, γγ
124.51 ± 0.52 ± 0.04	AAD	15B ATLS	pp, 7, 8 TeV, ZZ* → 4ℓ
125.59 ± 0.42 ± 0.17	AAD	15B CMS	pp, 7, 8 TeV, ZZ* → 4ℓ
125.02 ^{+0.26+0.14} _{-0.27-0.15}	10 KHACHATRYAN	15AM CMS	pp, 7, 8 TeV
125.36 ± 0.37 ± 0.18	2,11 AAD	14W ATLS	pp, 7, 8 TeV
125.98 ± 0.42 ± 0.28	11 AAD	14W ATLS	pp, 7, 8 TeV, γγ
124.51 ± 0.52 ± 0.06	11 AAD	14W ATLS	pp, 7, 8 TeV, ZZ* → 4ℓ
125.6 ± 0.4 ± 0.2	12 CHATRCHYAN	14AA CMS	pp, 7, 8 TeV, ZZ* → 4ℓ
122 ± 7	13 CHATRCHYAN	14K CMS	pp, 7, 8 TeV, ττ
124.70 ± 0.31 ± 0.15	14 KHACHATRYAN	14P CMS	pp, 7, 8 TeV, γγ
125.5 ± 0.2 ^{+0.5} _{-0.6}	2,15 AAD	13AK ATLS	pp, 7, 8 TeV
126.8 ± 0.2 ± 0.7	15 AAD	13AK ATLS	pp, 7, 8 TeV, γγ
124.3 ^{+0.6+0.5} _{-0.5-0.3}	15 AAD	13AK ATLS	pp, 7, 8 TeV, ZZ* → 4ℓ
125.8 ± 0.4 ± 0.4	2,16 CHATRCHYAN	13J CMS	pp, 7, 8 TeV
126.2 ± 0.6 ± 0.2	16 CHATRCHYAN	13J CMS	pp, 7, 8 TeV, ZZ* → 4ℓ
126.0 ± 0.4 ± 0.4	2,17 AAD	12AI ATLS	pp, 7, 8 TeV
125.3 ± 0.4 ± 0.5	2,18 CHATRCHYAN	12N CMS	pp, 7, 8 TeV



- SIRUNYAN 20L result of H⁰ → γγ is combined with that of H⁰ → ZZ* → 4ℓ where ℓ = e, μ (SIRUNYAN 17AV).
- Combined value from γγ and ZZ* → 4ℓ final states.
- ATLAS and CMS data are fitted simultaneously.
- SIRUNYAN 20L use 35.9 fb⁻¹ of pp collisions at E_{cm} = 13 TeV with H⁰ → γγ.
- SIRUNYAN 20L combine 13 TeV results with 7 and 8 TeV results (KHACHATRYAN 15AM).
- AABOUD 18BM use 36.1 fb⁻¹ of pp collisions at E_{cm} = 13 TeV with H⁰ → ZZ* → 4ℓ where ℓ = e, μ.
- AABOUD 18BM use 36.1 fb⁻¹ of pp collisions at E_{cm} = 13 TeV with H⁰ → γγ.
- AABOUD 18BM combine 13 TeV results with 7 and 8 TeV results. Other combined results are summarized in their Fig. 4.
- SIRUNYAN 17AV use 35.9 fb⁻¹ of pp collisions at E_{cm} = 13 TeV with H⁰ → ZZ* → 4ℓ where ℓ = e, μ.
- KHACHATRYAN 15AM use up to 5.1 fb⁻¹ of pp collisions at E_{cm} = 7 TeV and up to 19.7 fb⁻¹ at E_{cm} = 8 TeV.
- AA 14W use 4.5 fb⁻¹ of pp collisions at E_{cm} = 7 TeV and 20.3 fb⁻¹ at 8 TeV.
- CHATRCHYAN 14AA use 5.1 fb⁻¹ of pp collisions at E_{cm} = 7 TeV and 19.7 fb⁻¹ at E_{cm} = 8 TeV.
- CHATRCHYAN 14K use 4.9 fb⁻¹ of pp collisions at E_{cm} = 7 TeV and 19.7 fb⁻¹ at E_{cm} = 8 TeV.
- KHACHATRYAN 14P use 5.1 fb⁻¹ of pp collisions at E_{cm} = 7 TeV and 19.7 fb⁻¹ at E_{cm} = 8 TeV.
- AA 13AK use 4.7 fb⁻¹ of pp collisions at E_{cm} = 7 TeV and 20.7 fb⁻¹ at E_{cm} = 8 TeV. Superseded by AA 14W.
- CHATRCHYAN 13J use 5.1 fb⁻¹ of pp collisions at E_{cm} = 7 TeV and 12.2 fb⁻¹ at E_{cm} = 8 TeV.
- AA 12AI obtain results based on 4.6–4.8 fb⁻¹ of pp collisions at E_{cm} = 7 TeV and 5.8–5.9 fb⁻¹ at E_{cm} = 8 TeV. An excess of events over background with a local significance of 5.9 σ is observed at m_{H⁰} = 126 GeV. See also AA 12DA.
- CHATRCHYAN 12N obtain results based on 4.9–5.1 fb⁻¹ of pp collisions at E_{cm} = 7 TeV and 5.1–5.3 fb⁻¹ at E_{cm} = 8 TeV. An excess of events over background with a local significance of 5.0 σ is observed at about m_{H⁰} = 125 GeV. See also CHATRCHYAN 12BY and CHATRCHYAN 13Y.

H⁰

$$J = 0$$

In the following H⁰ refers to the signal that has been discovered in the Higgs searches. Whereas the observed signal is labeled as a spin 0 particle and is called a Higgs Boson, the detailed properties of H⁰ and its role in the context of electroweak symmetry breaking need to be further clarified. These issues are addressed by the measurements listed below.

Concerning mass limits and cross section limits that have been obtained in the searches for neutral and charged Higgs bosons, see the sections “Searches for Neutral Higgs Bosons” and “Searches for Charged Higgs Bosons (H[±] and H^{±±})”, respectively.

H⁰ MASS

VALUE (GeV)	DOCUMENT ID	TECN	COMMENT
125.25 ± 0.17 OUR AVERAGE	Error includes scale factor of 1.5. See the ideogram below.		
125.46 ± 0.16	1 SIRUNYAN	20L CMS	pp, 13 TeV, γγ, ZZ* → 4ℓ
124.86 ± 0.27	2 AABOUD	18BM ATLS	pp, 13 TeV, γγ, ZZ* → 4ℓ
125.09 ± 0.21 ± 0.11	2,3 AAD	15B LHC	pp, 7, 8 TeV
• • • We do not use the following data for averages, fits, limits, etc. • • •			
125.78 ± 0.26	4 SIRUNYAN	20L CMS	pp, 13 TeV, γγ
125.38 ± 0.14	5 SIRUNYAN	20L CMS	pp, 7, 8, 13 TeV, γγ, ZZ* → 4ℓ

H^0 SPIN AND CP PROPERTIES

The observation of the signal in the $\gamma\gamma$ final state rules out the possibility that the discovered particle has spin 1, as a consequence of the Landau-Yang theorem. This argument relies on the assumptions that the decaying particle is an on-shell resonance and that the decay products are indeed two photons rather than two pairs of boosted photons, which each could in principle be misidentified as a single photon.

Concerning distinguishing the spin 0 hypothesis from a spin 2 hypothesis, some care has to be taken in modelling the latter in order to ensure that the discriminating power is actually based on the spin properties rather than on unphysical behavior that may affect the model of the spin 2 state.

Under the assumption that the observed signal consists of a single state rather than an overlap of more than one resonance, it is sufficient to discriminate between distinct hypotheses in the spin analyses. On the other hand, the determination of the CP properties is in general much more difficult since in principle the observed state could consist of any admixture of CP -even and CP -odd components. As a first step, the compatibility of the data with distinct hypotheses of pure CP -even and pure CP -odd states with different spin assignments has been investigated. In order to treat the case of a possible mixing of different CP states, certain cross section ratios are considered. Those cross section ratios need to be distinguished from the amount of mixing between a CP -even and a CP -odd state, as the cross section ratios depend in addition also on the coupling strengths of the CP -even and CP -odd components to the involved particles. A small relative coupling implies a small sensitivity of the corresponding cross section ratio to effects of CP mixing.

VALUE DOCUMENT ID TECN COMMENT

••• We do not use the following data for averages, fits, limits, etc. •••

VALUE	DOCUMENT ID	TECN	COMMENT
1	AAD	20N ATLS	$H^0 \rightarrow \tau\tau$, VBF, 13 TeV
2	AAD	20Z ATLS	$t\bar{t}H^0, H^0 \rightarrow \gamma\gamma$, 13 TeV
3	SIRUNYAN	20AS CMS	$t\bar{t}H^0, H^0 \rightarrow \gamma\gamma$, 13 TeV
4	SIRUNYAN	19BL CMS	$pp, 7, 8, 13$ TeV, $ZZ^*/ZZ \rightarrow 4\ell$
5	SIRUNYAN	19BZ CMS	$pp \rightarrow H^0 + 2\text{jets}$ (VBF, ggF, VH), $H^0 \rightarrow \tau\tau$, 13 TeV
6	AABOUD	18AJ ATLS	$H^0 \rightarrow ZZ^* \rightarrow 4\ell$ ($\ell = e, \mu$), 13 TeV
7	SIRUNYAN	17AM CMS	$pp \rightarrow H^0 + \geq 2j, H^0 \rightarrow 4\ell$ ($\ell = e, \mu$)
8	AAD	16L ATLS	$H^0 \rightarrow \gamma\gamma$
9	AAD	16BL ATLS	$pp \rightarrow H^0 jjX$ (VBF), $H^0 \rightarrow \tau\tau$, 8 TeV
10	KHACHATRYAN	16AB CMS	$pp \rightarrow WH^0, ZH^0, H^0 \rightarrow b\bar{b}$, 8 TeV
11	AAD	15AX ATLS	$H^0 \rightarrow WW^*$
12	AAD	15CI ATLS	$H^0 \rightarrow ZZ^*, WW^*, \gamma\gamma$
13	AALTONEN	15 TEVA	$p\bar{p} \rightarrow WH^0, ZH^0, H^0 \rightarrow b\bar{b}$
14	AALTONEN	15B CDF	$p\bar{p} \rightarrow WH^0, ZH^0, H^0 \rightarrow b\bar{b}$
15	KHACHATRYAN	15Y CMS	$H^0 \rightarrow 4\ell, WW^*, \gamma\gamma$
16	ABAZOV	14F D0	$p\bar{p} \rightarrow WH^0, ZH^0, H^0 \rightarrow b\bar{b}$
17	CHATRCHYAN	14AA CMS	$H^0 \rightarrow ZZ^*$
18	CHATRCHYAN	14G CMS	$H^0 \rightarrow WW^*$
19	KHACHATRYAN	14P CMS	$H^0 \rightarrow \gamma\gamma$
20	AAD	13AJ ATLS	$H^0 \rightarrow \gamma\gamma, ZZ^* \rightarrow 4\ell, WW^* \rightarrow \ell\nu\ell\nu$
21	CHATRCHYAN	13J CMS	$H^0 \rightarrow ZZ^* \rightarrow 4\ell$

1 AAD 20N test CP invariance in H^0 production via VBF using $H^0 \rightarrow \tau\tau$ decay channel with 36.1 fb^{-1} at $E_{\text{cm}} = 13$ TeV. By using the Optimal Observable method, the data constrain a parameter \bar{d} , which is for the strength of CP violation in an effective field theory, to be $-0.090 \leq \bar{d} \leq 0.035$ at 68% CL (see their Fig. 6).

2 AAD 20Z exclude a CP -mixing angle α , $|\alpha| > 43^\circ$ at 95% CL, where $\alpha = 0$ represents the Standard Model, in 139 fb^{-1} of data at $E_{\text{cm}} = 13$ TeV. The pure CP -odd structure of the top Yukawa coupling ($\alpha = 90^\circ$) is excluded at 3.9σ .

3 SIRUNYAN 20AS exclude the pure CP -odd structure of the top Yukawa coupling at 3.2σ using $t\bar{t}H^0, H^0 \rightarrow \gamma\gamma$ in 137 fb^{-1} of data at $E_{\text{cm}} = 13$ TeV. The fractional contribution of the CP -odd component $f_{\text{CP-odd}}^{t\bar{t}H^0}$ is measured to be 0.00 ± 0.33 .

4 SIRUNYAN 19BL measure the anomalous HVV couplings from on-shell and off-shell production in the 4ℓ final state. Data of 80.2 fb^{-1} at 13 TeV, 19.7 fb^{-1} at 8 TeV, and 5.1 fb^{-1} at 7 TeV are used. See their Tables VI and VII for anomalous HVV couplings of CP -violating and CP -conserving parameters with on- and off-shells.

5 SIRUNYAN 19BZ constrain anomalous HVV couplings of the Higgs boson with data of 35.9 fb^{-1} at $E_{\text{cm}} = 13$ TeV using Higgs boson candidates with two jets produced in VBF, ggF, and VH that decay to $\tau\tau$. See their Table 2 and Fig. 10, which show 68% CL and 95% CL intervals. Combining those with the $H^0 \rightarrow 4\ell$ (SIRUNYAN 19BL, on-shell scenario), results shown in their Tables 3, 4, and Fig. 11 are obtained. A CP -violating parameter is set to be $f_{a3}\cos(\phi_{a3}) = (0.00 \pm 0.27) \times 10^{-3}$ and CP -conserving parameters are $f_{a2}\cos(\phi_{a2}) = (0.08 \pm 1.04) \times 10^{-3}$, $f_{A1}\cos(\phi_{A1}) = (0.00 \pm 0.53) \times 10^{-3}$, and $f_{A1}^Z\cos(\phi_{A1}^Z) = (0.0 \pm 1.1) \times 10^{-3}$.

6 AABOUD 18AJ study the tensor structure of the Higgs boson couplings using an effective Lagrangian using 36.1 fb^{-1} of pp collision data at $E_{\text{cm}} = 13$ TeV. Constraints are set on the non-Standard-Model CP -even and CP -odd couplings to Z bosons and on the CP -odd coupling to gluons. See their Figs. 9 and 10, and Tables 10 and 11.

7 SIRUNYAN 17AM constrain anomalous couplings of the Higgs boson with 5.1 fb^{-1} of pp collisions at $E_{\text{cm}} = 7$ TeV, 19.7 fb^{-1} at $E_{\text{cm}} = 8$ TeV, and 38.6 fb^{-1} at $E_{\text{cm}} = 13$ TeV. See their Table 3 and Fig. 3, which show 68% CL and 95% CL intervals. A CP violation parameter f_{a3} is set to be $f_{a3}\cos(\phi_{a3}) = [-0.38, 0.46]$ at 95% CL ($\phi_{a3} = 0$ or π).

8 AAD 16L study $H^0 \rightarrow \gamma\gamma$ with an effective Lagrangian including CP even and odd terms in 20.3 fb^{-1} of pp collisions at $E_{\text{cm}} = 8$ TeV. The data is consistent with the expectations for the Higgs boson of the Standard Model. Limits on anomalous couplings are also given.

9 AAD 16BL study VBF $H^0 \rightarrow \tau\tau$ with an effective Lagrangian including a CP odd term in 20.3 fb^{-1} of pp collisions at $E_{\text{cm}} = 8$ TeV. The measurement is consistent with

the expectation of the Standard Model. The CP -mixing parameter \bar{d} (a dimensionless coupling $\bar{d} = -(m_W^2/\Lambda^2)f_{\bar{W}W}$) is constrained to the interval of $(-0.11, 0.05)$ at 68% CL under the assumption of $\bar{d} = \bar{d}_B$.

10 KHACHATRYAN 16AB search for anomalous pseudoscalar couplings of the Higgs boson to W and Z with 18.9 fb^{-1} of pp collisions at $E_{\text{cm}} = 8$ TeV. See their Table 5 and Figs 5 and 6 for limits on possible anomalous pseudoscalar coupling parameters.

11 AAD 15AX compare the $J^{CP} = 0^+$ Standard Model assignment with other J^{CP} hypotheses in 20.3 fb^{-1} of pp collisions at $E_{\text{cm}} = 8$ TeV, using the process $H^0 \rightarrow WW^* \rightarrow e\nu\mu\nu$. 2^+ hypotheses are excluded at 84.5–99.4%CL, 0^- at 96.5%CL, 0^+ (field strength coupling) at 70.8%CL. See their Fig. 19 for limits on possible CP mixture parameters.

12 AAD 15CI compare the $J^{CP} = 0^+$ Standard Model assignment with other J^{CP} hypotheses in 4.5 fb^{-1} of pp collisions at $E_{\text{cm}} = 7$ TeV and 20.3 fb^{-1} at $E_{\text{cm}} = 8$ TeV, using the processes $H^0 \rightarrow ZZ^* \rightarrow 4\ell$, $H^0 \rightarrow \gamma\gamma$ and combine with AAD 15AX data. 0^+ (field strength coupling), 0^- and several 2^+ hypotheses are excluded at more than 99.9% CL. See their Tables 7–9 for limits on possible CP mixture parameters.

13 AALTONEN 15 combine AALTONEN 15B and ABAZOV 14F data. An upper limit of 0.36 of the Standard Model production rate at 95% CL is obtained both for a 0^- and a 2^+ state. Assuming the SM event rate, the $J^{CP} = 0^- (2^+)$ hypothesis is excluded at the $5.0\sigma (4.9\sigma)$ level.

14 AALTONEN 15B compare the $J^{CP} = 0^+$ Standard Model assignment with other J^{CP} hypotheses in 9.45 fb^{-1} of $p\bar{p}$ collisions at $E_{\text{cm}} = 1.96$ TeV, using the processes $ZH^0 \rightarrow \ell\ell b\bar{b}$, $WH^0 \rightarrow \ell\nu b\bar{b}$, and $ZH^0 \rightarrow \nu\nu b\bar{b}$. Bounds on the production rates of 0^- and 2^+ (graviton-like) states are set, see their tables II and III.

15 KHACHATRYAN 15Y compare the $J^{CP} = 0^+$ Standard Model assignment with other J^{CP} hypotheses in up to 5.1 fb^{-1} of pp collisions at $E_{\text{cm}} = 7$ TeV and up to 19.7 fb^{-1} at $E_{\text{cm}} = 8$ TeV, using the processes $H^0 \rightarrow 4\ell$, $H^0 \rightarrow WW^*$, and $H^0 \rightarrow \gamma\gamma$. 0^- is excluded at 99.98% CL, and several 2^+ hypotheses are excluded at more than 99% CL. Spin 1 models are excluded at more than 99.999% CL in ZZ^* and WW^* modes. Limits on anomalous couplings and several cross section fractions, treating the case of CP -mixed states, are also given.

16 ABAZOV 14F compare the $J^{CP} = 0^+$ Standard Model assignment with $J^{CP} = 0^-$ and 2^+ (graviton-like coupling) hypotheses in up to 9.7 fb^{-1} of $p\bar{p}$ collisions at $E_{\text{cm}} = 1.96$ TeV. They use kinematic correlations between the decay products of the vector boson and the Higgs boson in the final states $ZH \rightarrow \ell\ell b\bar{b}$, $WH \rightarrow \ell\nu b\bar{b}$, and $ZH \rightarrow \nu\nu b\bar{b}$. The $0^- (2^+)$ hypothesis is excluded at 97.6% CL (99.0% CL). In order to treat the case of a possible mixture of a 0^+ state with another J^{CP} state, the cross section fractions $f_X = \sigma_X/(\sigma_{0^+} + \sigma_X)$ are considered, where $X = 0^-, 2^+$. Values for f_{0^-} (f_{2^+}) above 0.80 (0.67) are excluded at 95% CL under the assumption that the total cross section is that of the SM Higgs boson.

17 CHATRCHYAN 14AA compare the $J^{CP} = 0^+$ Standard Model assignment with various J^{CP} hypotheses in 5.1 fb^{-1} of pp collisions at $E_{\text{cm}} = 7$ TeV and 19.7 fb^{-1} at $E_{\text{cm}} = 8$ TeV. $J^{CP} = 0^-$ and 1^\pm hypotheses are excluded at 99% CL, and several $J = 2$ hypotheses are excluded at 95% CL. In order to treat the case of a possible mixture of a 0^+ state with another J^{CP} state, the cross section fraction $f_{a3} = |a_3|^2 \sigma_3 / (|a_1|^2 \sigma_1 + |a_2|^2 \sigma_2 + |a_3|^2 \sigma_3)$ is considered, where the case $a_3 = 1, a_1 = a_2 = 0$ corresponds to a pure CP -odd state. Assuming $a_2 = 0$, a value for f_{a3} above 0.51 is excluded at 95% CL.

18 CHATRCHYAN 14G compare the $J^{CP} = 0^+$ Standard Model assignment with $J^{CP} = 0^-$ and 2^+ (graviton-like coupling) hypotheses in 4.9 fb^{-1} of pp collisions at $E_{\text{cm}} = 7$ TeV and 19.4 fb^{-1} at $E_{\text{cm}} = 8$ TeV. Varying the fraction of the production of the 2^+ state via gg and $q\bar{q}$, 2^+ hypotheses are disfavored at CL between 83.7 and 99.8%. The 0^- hypothesis is disfavored against 0^+ at the 65.3% CL.

19 KHACHATRYAN 14P compare the $J^{CP} = 0^+$ Standard Model assignment with a 2^+ (graviton-like coupling) hypothesis in 5.1 fb^{-1} of pp collisions at $E_{\text{cm}} = 7$ TeV and 19.7 fb^{-1} at $E_{\text{cm}} = 8$ TeV. Varying the fraction of the production of the 2^+ state via gg and $q\bar{q}$, 2^+ hypotheses are disfavored at CL between 71 and 94%.

20 AAD 13AJ compare the spin 0, CP -even hypothesis with specific alternative hypotheses of spin 0, CP -odd, spin 1, CP -even and CP -odd, and spin 2, CP -even models using the Higgs boson decays $H \rightarrow \gamma\gamma, H \rightarrow ZZ^* \rightarrow 4\ell$ and $WW^* \rightarrow \ell\nu\ell\nu$ and combinations thereof. The data are compatible with the spin 0, CP -even hypothesis, while all other tested hypotheses are excluded at confidence levels above 97.8%.

21 CHATRCHYAN 13J study angular distributions of the lepton pairs in the ZZ^* channel where both Z bosons decay to e or μ pairs. Under the assumption that the observed particle has spin 0, the data are found to be consistent with the pure CP -even hypothesis, while the pure CP -odd hypothesis is disfavored.

 H^0 DECAY WIDTH

The total decay width for a light Higgs boson with a mass in the observed range is not expected to be directly observable at the LHC. For the case of the Standard Model the prediction for the total width is about 4 MeV, which is three orders of magnitude smaller than the experimental mass resolution. There is no indication from the results observed so far that the natural width is broadened by new physics effects to such an extent that it could be directly observable. Furthermore, as all LHC Higgs channels rely on the identification of Higgs decay products, the total Higgs width cannot be measured indirectly without additional assumptions. The different dependence of on-peak and off-peak contributions on the total width in Higgs decays to ZZ^* and interference effects between signal and background in Higgs decays to $\gamma\gamma$ can provide additional information in this context. Constraints on the total width from the combination of on-peak and off-peak contributions in Higgs decays to ZZ^* rely on the assumption of equal on- and off-shell effective couplings. Without an experimental determination of the total width or further theoretical assumptions, only ratios of couplings can be determined at the LHC rather than absolute values of couplings.

VALUE (MeV)	CL%	DOCUMENT ID	TECN	COMMENT
$3.2^{+2.8}_{-2.2}$		1 SIRUNYAN	19BL CMS	$pp, 7, 8, 13$ TeV, $ZZ^*/ZZ \rightarrow 4\ell$

• • • We do not use the following data for averages, fits, limits, etc. • • •

< 14.4	95	2	AABOUD	18BP ATLS	pp , 13 TeV, $ZZ \rightarrow 4\ell, 2\ell 2\nu$
<1100	95	3	SIRUNYAN	17AV CMS	pp , 13 TeV, $ZZ^* \rightarrow 4\ell$
< 26	95	4	KHACHATRYAN	16BA CMS	pp , 7, 8 TeV, WW^*
< 13	95	5	KHACHATRYAN	16BA CMS	pp , 7, 8 TeV, $ZZ^*(^*), WW^*(^*)$
< 22.7	95	6	AAD	15BE ATLS	pp , 8 TeV, $ZZ^*(^*), WW^*(^*)$
<1700	95	7	KHACHATRYAN	15AM CMS	pp , 7, 8 TeV
> 3.5×10^{-9}	95	8	KHACHATRYAN	15BA CMS	pp , 7, 8 TeV, flight distance
< 46	95	9	KHACHATRYAN	15BA CMS	pp , 7, 8 TeV, $ZZ^*(^*) \rightarrow 4\ell$
<5000	95	10	AAD	14W ATLS	pp , 7, 8 TeV, $\gamma\gamma$
<2600	95	10	AAD	14W ATLS	pp , 7, 8 TeV, $ZZ^* \rightarrow 4\ell$
<3400	95	11	CHATRCHYAN	14AA CMS	pp , 7, 8 TeV, $ZZ^* \rightarrow 4\ell$
< 22	95	12	KHACHATRYAN	14D CMS	pp , 7, 8 TeV, $ZZ^*(^*)$
<2400	95	13	KHACHATRYAN	14P CMS	pp , 7, 8 TeV, $\gamma\gamma$

- 1 SIRUNYAN 19BL measure the width and anomalous HVV couplings from on-shell and off-shell production in the 4ℓ final state. Data of 80.2 fb^{-1} at 13 TeV, 19.7 fb^{-1} at 8 TeV, and 5.1 fb^{-1} at 7 TeV are used. The total width for the SM-like couplings is measured to be also [0.08, 9.16] MeV with 95% CL, assuming SM-like couplings for on- and off-shells (see their Table VIII). Constraints on the total width for anomalous HVV interaction cases are found in their Table IX. See their Table X for the Higgs boson signal strength in the off-shell region.
- 2 AABOUD 18BP use 36.1 fb^{-1} at $E_{\text{cm}} = 13 \text{ TeV}$. An observed upper limit on the off-shell Higgs signal strength of 3.8 is obtained at 95% CL using off-shell Higgs boson production in the $ZZ \rightarrow 4\ell$ and $ZZ \rightarrow 2\ell 2\nu$ decay channels ($\ell = e, \mu$). Combining with the on-shell signal strength measurements, the quoted upper limit on the Higgs boson total width is obtained, assuming the ratios of the relevant Higgs-boson couplings to the SM predictions are constant with energy from on-shell production to the high-mass range.
- 3 SIRUNYAN 17AV obtain an upper limit on the width from the $m_{4\ell}$ distribution in $ZZ^* \rightarrow 4\ell$ ($\ell = e, \mu$) decays. Data of 35.9 fb^{-1} pp collisions at $E_{\text{cm}} = 13 \text{ TeV}$ is used. The expected limit is 1.60 GeV.
- 4 KHACHATRYAN 16BA derive constraints on the total width from comparing WW^* production via on-shell and off-shell H^0 using 4.9 fb^{-1} of pp collisions at $E_{\text{cm}} = 7 \text{ TeV}$ and 19.4 fb^{-1} at 8 TeV.
- 5 KHACHATRYAN 16BA combine the WW^* result with $ZZ^*(^*)$ results of KHACHATRYAN 15BA and KHACHATRYAN 14D.
- 6 AAD 15BE derive constraints on the total width from comparing $ZZ^*(^*)$ and $WW^*(^*)$ production via on-shell and off-shell H^0 using 20.3 fb^{-1} of pp collisions at $E_{\text{cm}} = 8 \text{ TeV}$. The K factor for the background processes is assumed to be equal to that for the signal.
- 7 KHACHATRYAN 15AM combine $\gamma\gamma$ and $ZZ^* \rightarrow 4\ell$ results. The expected limit is 2.3 GeV.
- 8 KHACHATRYAN 15BA derive a lower limit on the total width from an upper limit on the decay flight distance $\tau < 1.9 \times 10^{-13} \text{ s}$. 5.1 fb^{-1} of pp collisions at $E_{\text{cm}} = 7 \text{ TeV}$ and 19.7 fb^{-1} at 8 TeV are used.
- 9 KHACHATRYAN 15BA derive constraints on the total width from comparing $ZZ^*(^*)$ production via on-shell and off-shell H^0 with an unconstrained anomalous coupling. 4ℓ final states in 5.1 fb^{-1} of pp collisions at $E_{\text{cm}} = 7 \text{ TeV}$ and 19.7 fb^{-1} at $E_{\text{cm}} = 8 \text{ TeV}$ are used.
- 10 AAD 14W use 4.5 fb^{-1} of pp collisions at $E_{\text{cm}} = 7 \text{ TeV}$ and 20.3 fb^{-1} at 8 TeV. The expected limit is 6.2 GeV.
- 11 CHATRCHYAN 14AA use 5.1 fb^{-1} of pp collisions at $E_{\text{cm}} = 7 \text{ TeV}$ and 19.7 fb^{-1} at $E_{\text{cm}} = 8 \text{ TeV}$. The expected limit is 2.8 GeV.
- 12 KHACHATRYAN 14D derive constraints on the total width from comparing $ZZ^*(^*)$ production via on-shell and off-shell H^0 . 4ℓ and $\ell\ell\nu\nu$ final states in 5.1 fb^{-1} of pp collisions at $E_{\text{cm}} = 7 \text{ TeV}$ and 19.7 fb^{-1} at $E_{\text{cm}} = 8 \text{ TeV}$ are used.
- 13 KHACHATRYAN 14P use 5.1 fb^{-1} of pp collisions at $E_{\text{cm}} = 7 \text{ TeV}$ and 19.7 fb^{-1} at $E_{\text{cm}} = 8 \text{ TeV}$. The expected limit is 3.1 GeV.

H^0 DECAY MODES

Mode	Fraction (Γ_i/Γ)	Confidence level
Γ_1 WW^*		
Γ_2 ZZ^*		
Γ_3 $\gamma\gamma$		
Γ_4 $b\bar{b}$		
Γ_5 e^+e^-	$< 3.6 \times 10^{-4}$	95%
Γ_6 $\mu^+\mu^-$		
Γ_7 $\tau^+\tau^-$		
Γ_8 $Z\gamma$		
Γ_9 $Z\rho(770)$	$< 1.21 \%$	95%
Γ_{10} $Z\phi(1020)$	$< 3.6 \times 10^{-3}$	95%
Γ_{11} $Z\eta_c$		
Γ_{12} ZJ/ψ		
Γ_{13} $\gamma^*\gamma$		
Γ_{14} $J/\psi\gamma$	$< 3.5 \times 10^{-4}$	95%
Γ_{15} $J/\psi J/\psi$	$< 1.8 \times 10^{-3}$	95%
Γ_{16} $\psi(2S)\gamma$	$< 2.0 \times 10^{-3}$	95%
Γ_{17} $\Upsilon(1S)\gamma$	$< 4.9 \times 10^{-4}$	95%
Γ_{18} $\Upsilon(2S)\gamma$	$< 5.9 \times 10^{-4}$	95%
Γ_{19} $\Upsilon(3S)\gamma$	$< 5.7 \times 10^{-4}$	95%
Γ_{20} $\Upsilon(\text{nS})\Upsilon(\text{mS})$	$< 1.4 \times 10^{-3}$	95%
Γ_{21} $\rho(770)\gamma$	$< 8.8 \times 10^{-4}$	95%

Γ_{22} $\phi(1020)\gamma$		$< 4.8 \times 10^{-4}$	95%
Γ_{23} $e\mu$	LF	$< 6.1 \times 10^{-5}$	95%
Γ_{24} $e\tau$	LF	$< 2.2 \times 10^{-3}$	95%
Γ_{25} $\mu\tau$	LF	$< 1.5 \times 10^{-3}$	95%
Γ_{26} invisible		$< 19 \%$	95%
Γ_{27} γ invisible			

H^0 BRANCHING RATIOS

$\Gamma(e^+e^-)/\Gamma_{\text{total}}$	VALUE	CL%	DOCUMENT ID	TECN	COMMENT
--	-------	-----	-------------	------	---------

- $< 3.6 \times 10^{-4}$ 95 1 AAD 20F ATLS pp , 13 TeV
- • • We do not use the following data for averages, fits, limits, etc. • • •
- $< 1.9 \times 10^{-3}$ 95 2 KHACHATRYAN 15H CMS pp , 7, 8 TeV

- 1 AAD 20F use 139 fb^{-1} of pp collisions at $E_{\text{cm}} = 13 \text{ TeV}$. The best-fit value of the $H^0 \rightarrow ee$ branching fraction is $(0.0 \pm 1.7 \pm 0.6) \times 10^{-4}$ for $m_{H^0} = 125 \text{ GeV}$.
- 2 KHACHATRYAN 15H use 5.0 fb^{-1} of pp collisions at $E_{\text{cm}} = 7 \text{ TeV}$ and 19.7 fb^{-1} at 8 TeV.

$\Gamma(Z\rho(770))/\Gamma_{\text{total}}$	VALUE	CL%	DOCUMENT ID	TECN	COMMENT
--	-------	-----	-------------	------	---------

- $< 1.21 \times 10^{-2}$ 95 1 SIRUNYAN 20BK CMS pp , 13 TeV
- 1 SIRUNYAN 20BK search for $H^0 \rightarrow Z\rho, Z \rightarrow e^+e^-/\mu^+\mu^-, \rho \rightarrow \pi^+\pi^-$ with 137 fb^{-1} of pp collision data at $E_{\text{cm}} = 13 \text{ TeV}$. The quoted branching fraction is for the unpolarized decay. See their Table 3 for different polarizations.

$\Gamma(Z\phi(1020))/\Gamma_{\text{total}}$	VALUE	CL%	DOCUMENT ID	TECN	COMMENT
---	-------	-----	-------------	------	---------

- $< 3.6 \times 10^{-3}$ 95 1 SIRUNYAN 20BK CMS pp , 13 TeV
- 1 SIRUNYAN 20BK search for $H^0 \rightarrow Z\phi, Z \rightarrow e^+e^-/\mu^+\mu^-, \phi \rightarrow K^+K^-$ with 137 fb^{-1} of pp collision data at $E_{\text{cm}} = 13 \text{ TeV}$. The quoted branching fraction is for the unpolarized decay. See their Table 4 for different polarizations.

$\Gamma(Z\eta_c)/\Gamma_{\text{total}}$	VALUE	DOCUMENT ID	TECN	COMMENT
---	-------	-------------	------	---------

- • • We do not use the following data for averages, fits, limits, etc. • • •
- 1 AAD 20AE search for $H^0 \rightarrow Z\eta_c$ with two-leptons ($e^+e^-/\mu^+\mu^-$) plus jet events using 139 fb^{-1} of pp collision data at $E_{\text{cm}} = 13 \text{ TeV}$. The upper limit of $\sigma(pp \rightarrow H^0) \cdot B(H^0 \rightarrow Z\eta_c)$ is 110 pb at 95% CL.

$\Gamma(ZJ/\psi)/\Gamma_{\text{total}}$	VALUE	DOCUMENT ID	TECN	COMMENT
---	-------	-------------	------	---------

- • • We do not use the following data for averages, fits, limits, etc. • • •
- 1 AAD 20AE search for $H^0 \rightarrow ZJ/\psi$ with two-leptons ($e^+e^-/\mu^+\mu^-$) plus jet events using 139 fb^{-1} of pp collision data at $E_{\text{cm}} = 13 \text{ TeV}$. The upper limit of $\sigma(pp \rightarrow H^0) \cdot B(H^0 \rightarrow ZJ/\psi)$ is 100 pb at 95% CL.

$\Gamma(J/\psi\gamma)/\Gamma_{\text{total}}$	VALUE	CL%	DOCUMENT ID	TECN	COMMENT
--	-------	-----	-------------	------	---------

- $< 7.6 \times 10^{-4}$ 95 1 SIRUNYAN 19AJ CMS 13 TeV, 35.9 fb^{-1}
- $< 3.5 \times 10^{-4}$ 95 2 AABOUD 18BL ATLS 13 TeV, 36.1 fb^{-1}
- • • We do not use the following data for averages, fits, limits, etc. • • •
- $< 1.5 \times 10^{-3}$ 95 3 KHACHATRYAN 16B CMS 8 TeV
- $< 1.5 \times 10^{-3}$ 95 4 AAD 15I ATLS 8 TeV

- 1 SIRUNYAN 19AJ search for $H^0 \rightarrow J/\psi\gamma, J/\psi \rightarrow \mu^+\mu^-$ with 35.9 fb^{-1} of pp collision data at $E_{\text{cm}} = 13 \text{ TeV}$. The upper limit corresponds to 260 times the SM prediction and by combining the KHACHATRYAN 16B, it is 220 times the SM prediction.
- 2 AABOUD 18BL search for $H^0 \rightarrow J/\psi\gamma, J/\psi \rightarrow \mu^+\mu^-$ with 36.1 fb^{-1} of pp collision data at $E_{\text{cm}} = 13 \text{ TeV}$.
- 3 KHACHATRYAN 16B use 19.7 fb^{-1} of pp collision data at 8 TeV.
- 4 AAD 15I use 19.7 fb^{-1} of pp collision data at 8 TeV.

$\Gamma(J/\psi J/\psi)/\Gamma_{\text{total}}$	VALUE	CL%	DOCUMENT ID	TECN	COMMENT
---	-------	-----	-------------	------	---------

- $< 1.8 \times 10^{-3}$ 95 1 SIRUNYAN 19BR CMS pp at 13 TeV
- 1 SIRUNYAN 19BR search for $H^0 \rightarrow J/\psi J/\psi, J/\psi \rightarrow \mu^+\mu^-$ with 37.5 fb^{-1} of pp collision data at $E_{\text{cm}} = 13 \text{ TeV}$. J/ψ s from the Higgs decay are assumed to be unpolarized. For fully longitudinal (transverse) polarized J/ψ s, limits change by -22% ($+10\%$).

$\Gamma(\psi(2S)\gamma)/\Gamma_{\text{total}}$	VALUE	CL%	DOCUMENT ID	TECN	COMMENT
--	-------	-----	-------------	------	---------

- $< 2.0 \times 10^{-3}$ 95 1 AABOUD 18BL ATLS 13 TeV, 36.1 fb^{-1}
- 1 AABOUD 18BL search for $H^0 \rightarrow \psi(2S)\gamma, \psi(2S) \rightarrow \mu^+\mu^-$ with 36.1 fb^{-1} of pp collision data at $E_{\text{cm}} = 13 \text{ TeV}$.

$\Gamma(\Upsilon(1S)\gamma)/\Gamma_{\text{total}}$	VALUE	CL%	DOCUMENT ID	TECN	COMMENT
--	-------	-----	-------------	------	---------

- $< 4.9 \times 10^{-4}$ 95 1 AABOUD 18BL ATLS 13 TeV, 36.1 fb^{-1}

Gauge & Higgs Boson Particle Listings

 H^0

••• We do not use the following data for averages, fits, limits, etc. •••

$<1.3 \times 10^{-3}$ 95 2 AAD 15i ATLS 8 TeV

¹AABOUD 18BL search for $H^0 \rightarrow \Upsilon(1S)\gamma$, $\Upsilon(1S) \rightarrow \mu^+\mu^-$ with 36.1 fb^{-1} of pp collision data at $E_{\text{cm}} = 13 \text{ TeV}$.

²AAD 15i use 19.7 fb^{-1} of pp collision data at 8 TeV.

$\Gamma(\Upsilon(2S)\gamma)/\Gamma_{\text{total}}$ Γ_{18}/Γ

VALUE	CL%	DOCUMENT ID	TECN	COMMENT
$<5.9 \times 10^{-4}$	95	1 AABOUD	18BL ATLS	13 TeV, 36.1 fb^{-1}

••• We do not use the following data for averages, fits, limits, etc. •••

$<1.9 \times 10^{-3}$ 95 2 AAD 15i ATLS 8 TeV

¹AABOUD 18BL search for $H^0 \rightarrow \Upsilon(2S)\gamma$, $\Upsilon(2S) \rightarrow \mu^+\mu^-$ with 36.1 fb^{-1} of pp collision data at $E_{\text{cm}} = 13 \text{ TeV}$.

²AAD 15i use 19.7 fb^{-1} of pp collision data at 8 TeV.

$\Gamma(\Upsilon(3S)\gamma)/\Gamma_{\text{total}}$ Γ_{19}/Γ

VALUE	CL%	DOCUMENT ID	TECN	COMMENT
$<5.7 \times 10^{-4}$	95	1 AABOUD	18BL ATLS	13 TeV, 36.1 fb^{-1}

••• We do not use the following data for averages, fits, limits, etc. •••

$<1.3 \times 10^{-3}$ 95 2 AAD 15i ATLS 8 TeV

¹AABOUD 18BL search for $H^0 \rightarrow \Upsilon(3S)\gamma$, $\Upsilon(3S) \rightarrow \mu^+\mu^-$ with 36.1 fb^{-1} of pp collision data at $E_{\text{cm}} = 13 \text{ TeV}$.

²AAD 15i use 19.7 fb^{-1} of pp collision data at 8 TeV.

$\Gamma(\Upsilon(nS)\Upsilon(mS))/\Gamma_{\text{total}}$ Γ_{20}/Γ

VALUE	CL%	DOCUMENT ID	TECN	COMMENT
$<1.4 \times 10^{-3}$	95	1 SIRUNYAN	19BR CMS	pp at 13 TeV

¹SIRUNYAN 19BR search for $H^0 \rightarrow \Upsilon(nS)\Upsilon(mS)$ with $\Upsilon(nS), \Upsilon(mS) \rightarrow \mu^+\mu^-$ ($n, m = 1, 2, 3$) for 37.5 fb^{-1} of pp collision data at $E_{\text{cm}} = 13 \text{ TeV}$. Υ s from the Higgs decay are assumed to be unpolarized. For fully longitudinal (transverse) polarized Υ s, limits change by -22% ($+10\%$). The three Υ states selected in a mass range of 8.5–11 GeV are not distinguished.

$\Gamma(\rho(770)\gamma)/\Gamma_{\text{total}}$ Γ_{21}/Γ

VALUE	CL%	DOCUMENT ID	TECN	COMMENT
$<8.8 \times 10^{-4}$	95	1 AABOUD	18AU ATLS	pp , 13 TeV

¹AABOUD 18AU use 35.6 fb^{-1} of pp collision data at 13 TeV.

$\Gamma(\phi(1020)\gamma)/\Gamma_{\text{total}}$ Γ_{22}/Γ

VALUE	CL%	DOCUMENT ID	TECN	COMMENT
$<4.8 \times 10^{-4}$	95	1 AABOUD	18AU ATLS	pp , 13 TeV

••• We do not use the following data for averages, fits, limits, etc. •••

$<1.4 \times 10^{-3}$ 95 2 AABOUD 16K ATLS pp , 13 TeV

¹AABOUD 18AU use 35.6 fb^{-1} of pp collision data at 13 TeV.

²AABOUD 16K use 2.7 fb^{-1} of pp collision data at 13 TeV.

$\Gamma(e\mu)/\Gamma_{\text{total}}$ Γ_{23}/Γ

VALUE	CL%	DOCUMENT ID	TECN	COMMENT
$<6.1 \times 10^{-5}$	95	1 AAD	20F ATLS	pp , 13 TeV

••• We do not use the following data for averages, fits, limits, etc. •••

$<3.5 \times 10^{-4}$ 95 2 KHACHATRYAN...16CD CMS pp , 8 TeV

¹AAD 20F use 139 fb^{-1} of pp collisions at $E_{\text{cm}} = 13 \text{ TeV}$. The best-fit value of the $H^0 \rightarrow e\mu$ branching fraction is $(0.4 \pm 2.9 \pm 0.3) \times 10^{-5}$ for $m_{H^0} = 125 \text{ GeV}$.

²KHACHATRYAN 16CD search for $H^0 \rightarrow e\mu$ in 19.7 fb^{-1} of pp collisions at $E_{\text{cm}} = 8 \text{ TeV}$. The limit constrains the $Y_{e\mu}$ Yukawa coupling to $\sqrt{|Y_{e\mu}|^2 + |Y_{\mu e}|^2} < 5.4 \times 10^{-4}$ at 95% CL (see their Fig. 6).

$\Gamma(e\tau)/\Gamma_{\text{total}}$ Γ_{24}/Γ

VALUE	CL%	DOCUMENT ID	TECN	COMMENT
$<2.2 \times 10^{-3}$	95	1 SIRUNYAN	21Z CMS	pp , 13 TeV

••• We do not use the following data for averages, fits, limits, etc. •••

$<4.7 \times 10^{-3}$ 95 2 AAD 20A ATLS pp , 13 TeV

$<6.1 \times 10^{-3}$ 95 3 SIRUNYAN 18BH CMS pp , 13 TeV

$<10.4 \times 10^{-3}$ 95 4 AAD 17 ATLS pp , 8 TeV

$<6.9 \times 10^{-3}$ 95 5 KHACHATRYAN...16CD CMS pp , 8 TeV

¹SIRUNYAN 21Z search for $H^0 \rightarrow e\tau$ in 137 fb^{-1} of pp collisions at $E_{\text{cm}} = 13 \text{ TeV}$.

The limit constrains the $Y_{e\tau}$ Yukawa coupling to $\sqrt{|Y_{e\tau}|^2 + |Y_{\tau e}|^2} < 1.35 \times 10^{-3}$ at 95% CL (see their Fig. 8).

²AAD 20A search for $H^0 \rightarrow e\tau$ in 36.1 fb^{-1} of pp collisions at $E_{\text{cm}} = 13 \text{ TeV}$. The limit constrains the $Y_{e\tau}$ Yukawa coupling to $\sqrt{|Y_{e\tau}|^2 + |Y_{\tau e}|^2} < 2.0 \times 10^{-3}$ at 95% CL (see their Fig. 5).

³SIRUNYAN 18BH search for $H^0 \rightarrow e\tau$ in 35.9 fb^{-1} of pp collisions at $E_{\text{cm}} = 13 \text{ TeV}$. The limit constrains the $Y_{e\tau}$ Yukawa coupling to $\sqrt{|Y_{e\tau}|^2 + |Y_{\tau e}|^2} < 2.26 \times 10^{-3}$ at 95% CL (see their Fig. 10).

⁴AAD 17 search for $H^0 \rightarrow e\tau$ in 20.3 fb^{-1} of pp collisions at $E_{\text{cm}} = 8 \text{ TeV}$.

⁵KHACHATRYAN 16CD search for $H^0 \rightarrow e\tau$ in 19.7 fb^{-1} of pp collisions at $E_{\text{cm}} = 8 \text{ TeV}$. The limit constrains the $Y_{e\tau}$ Yukawa coupling to $\sqrt{|Y_{e\tau}|^2 + |Y_{\tau e}|^2} < 2.4 \times 10^{-3}$ at 95% CL (see their Fig. 6).

$\Gamma(\mu\tau)/\Gamma_{\text{total}}$ Γ_{25}/Γ

VALUE	CL%	DOCUMENT ID	TECN	COMMENT
$<1.5 \times 10^{-3}$	95	1 SIRUNYAN	21Z CMS	pp , 13 TeV

••• We do not use the following data for averages, fits, limits, etc. •••

$<2.8 \times 10^{-3}$ 95 2 AAD 20A ATLS pp , 13 TeV

$<26 \times 10^{-2}$ 95 3 AAIJ 18AMLHCB pp , 8 TeV

$<2.5 \times 10^{-3}$ 95 4 SIRUNYAN 18BH CMS pp , 13 TeV

$<1.43 \times 10^{-2}$ 95 5 AAD 17 ATLS pp , 8 TeV

$<1.51 \times 10^{-2}$ 95 6 KHACHATRYAN...15Q CMS pp , 8 TeV

¹SIRUNYAN 21Z search for $H^0 \rightarrow \mu\tau$ in 137 fb^{-1} of pp collisions at $E_{\text{cm}} = 13 \text{ TeV}$.

The limit constrains the $Y_{\mu\tau}$ Yukawa coupling to $\sqrt{|Y_{\mu\tau}|^2 + |Y_{\tau\mu}|^2} < 1.11 \times 10^{-3}$ at 95% CL (see their Fig. 8).

²AAD 20A search for $H^0 \rightarrow \mu\tau$ in 36.1 fb^{-1} of pp collisions at $E_{\text{cm}} = 13 \text{ TeV}$. The limit constrains the $Y_{\mu\tau}$ Yukawa coupling to $\sqrt{|Y_{\mu\tau}|^2 + |Y_{\tau\mu}|^2} < 1.5 \times 10^{-3}$ at 95% CL (see their Fig. 5).

³AAIJ 18AM search for $H^0 \rightarrow \mu\tau$ in 2.0 fb^{-1} of pp collisions at $E_{\text{cm}} = 8 \text{ TeV}$. The limit constrains the $Y_{\mu\tau}$ Yukawa coupling to $\sqrt{|Y_{\mu\tau}|^2 + |Y_{\tau\mu}|^2} < 1.7 \times 10^{-2}$ at 95% CL assuming SM production cross sections.

⁴SIRUNYAN 18BH search for $H^0 \rightarrow \mu\tau$ in 35.9 fb^{-1} of pp collisions at $E_{\text{cm}} = 13 \text{ TeV}$. The limit constrains the $Y_{\mu\tau}$ Yukawa coupling to $\sqrt{|Y_{\mu\tau}|^2 + |Y_{\tau\mu}|^2} < 1.43 \times 10^{-3}$ at 95% CL (see their Fig. 10).

⁵AAD 17 search for $H^0 \rightarrow \mu\tau$ in 20.3 fb^{-1} of pp collisions at $E_{\text{cm}} = 8 \text{ TeV}$.

⁶KHACHATRYAN 15Q search for $H^0 \rightarrow \mu\tau$ with τ decaying electronically or hadronically in 19.7 fb^{-1} of pp collisions at $E_{\text{cm}} = 8 \text{ TeV}$. The fit gives $B(H^0 \rightarrow \mu\tau) = (0.84 \pm 0.39)_{-0.37}$ % with a significance of 2.4 σ .

$\Gamma(\text{invisible})/\Gamma_{\text{total}}$ Γ_{26}/Γ

VALUE	CL%	DOCUMENT ID	TECN	COMMENT
<0.26	95	1 AABOUD	19AL ATLS	pp , 7, 8, 13 TeV, $H \rightarrow \text{inv}$

<0.19 95 2 SIRUNYAN 19Bo CMS pp , 7, 8, 13 TeV

••• We do not use the following data for averages, fits, limits, etc. •••

<0.34 95 3 AAD 21F ATLS pp , 13 TeV

<0.29 95 4 SIRUNYAN 21A CMS $pp \rightarrow ZH^0, H^0 \rightarrow \text{inv}$, 13 TeV

<0.278 95 5 TUMASYAN 21D CMS pp , 13 TeV

<0.37 95 6 AABOUD 19AI ATLS $pp \rightarrow qqH^0X, H^0 \rightarrow \text{inv}$, 13 TeV

<0.38 95 7 AABOUD 19AL ATLS pp , 13 TeV, $H \rightarrow \text{inv}$

<0.22 95 8 SIRUNYAN 19AT CMS pp , 13 TeV, $H \rightarrow \text{inv}$

<0.33 95 9 SIRUNYAN 19Bo CMS $pp \rightarrow qqH^0X, H^0 \rightarrow \text{inv}$, 13 TeV

<0.26 95 10 SIRUNYAN 19Bo CMS pp , 13 TeV

<0.67 95 11 AABOUD 18 ATLS $pp \rightarrow H^0ZX, H^0 \rightarrow \text{inv}$, 13 TeV

<0.83 95 12 AABOUD 18CA ATLS $pp \rightarrow H^0W/Z, W/Z \rightarrow jj$, 13 TeV

<0.40 95 13 SIRUNYAN 18BV CMS $pp \rightarrow Z(\ell\ell)H^0, H^0 \rightarrow \text{inv}$, 13 TeV

<0.53 95 14 SIRUNYAN 18S CMS pp , 13 TeV, jet or $V \rightarrow q\bar{q}$, $H^0 \rightarrow \text{inv}$

<0.46 95 15 AABOUD 17BD ATLS $pp \rightarrow gH^0X, qqH^0X, H^0 \rightarrow \text{inv}$, 13 TeV

<0.24 95 16 KHACHATRYAN...17F CMS pp , 7, 8, 13 TeV

<0.28 95 17 AAD 16AF ATLS $pp \rightarrow qqH^0X$, 8 TeV

<0.34 95 18 AAD 16AN LHC pp , 7, 8 TeV

<0.78 95 19 AAD 15BD ATLS $pp \rightarrow H^0W/ZX$, 8 TeV

<0.25 95 20 AAD 15CX ATLS pp , 7, 8 TeV, $H \rightarrow \text{inv}$

<0.75 95 21 AAD 14O ATLS $pp \rightarrow H^0ZX, 7, 8 \text{ TeV}$

<0.58 95 22 CHATRCHYAN14B CMS $pp \rightarrow H^0ZX, qqH^0X$

<0.81 95 23 CHATRCHYAN14B CMS $pp \rightarrow H^0ZX, 7, 8 \text{ TeV}$

<0.65 95 24 CHATRCHYAN14B CMS $pp \rightarrow qqH^0X, 8 \text{ TeV}$

¹AABOUD 19AL combine results of 7, 8 (AAD 15CX), and 13 TeV for H^0 decaying to invisible final states.

²SIRUNYAN 19Bo combine 13 TeV 35.9 fb^{-1} results with 7, 8, 13 TeV (KHACHATRYAN 17F) for H^0 decaying to invisible final states. The quoted limit on the branching ratio is given for $m_{H^0} = 125.09 \text{ GeV}$ and assumes the Standard Model production rates. The branching ratio is obtained to be 0.05 ± 0.03 (stat) ± 0.07 (syst).

³AAD 21F search for an invisibly decaying Higgs boson with an energetic jet ($p_T > 150 \text{ GeV}$) and missing transverse momentum ($> 200 \text{ GeV}$) in 139 fb^{-1} at $E_{\text{cm}} = 13 \text{ TeV}$. The quoted limit on the branching ratio is given for $m_{H^0} = 125 \text{ GeV}$.

⁴SIRUNYAN 21A search for H^0 decaying to invisible final states associated with a Z decaying $ee/\mu\mu$ using 137 fb^{-1} at 13 TeV. The limit is obtained for $m_{H^0} = 125 \text{ GeV}$ and assuming the SM ZH^0 production cross section.

⁵TUMASYAN 21D search for H^0 decaying to invisible final states associated with an energetic jet or a $V, V \rightarrow q\bar{q}$ using 101 fb^{-1} at 13 TeV and the result is combined with SIRUNYAN 18S.

⁶AABOUD 19AI search for $pp \rightarrow qqH^0X$ (VBF) with H^0 decaying to invisible final states using 36.1 fb^{-1} of data. The quoted limit on the branching ratio is given for $m_{H^0} = 125 \text{ GeV}$ and assumes the Standard Model rates for VBF and gluon-fusion production.

⁷AABOUD 19AL combine results of H^0 decaying to invisible final states with VBF(AABOUD 19AI), ZH , and WH productions (AABOUD 18, AABOUD 18CA), which use 36.1 fb^{-1} of data at 13 TeV. The quoted limit is given for $m_{H^0} = 125 \text{ GeV}$ and assumes the Standard Model rates for gluon fusion, VBF, ZH , and WH productions.

- ⁸ SIRUNYAN 19AT perform a combined fit with visible decay using 35.9 fb^{-1} of data at 13 TeV.
- ⁹ SIRUNYAN 19B0 search for $pp \rightarrow qqH^0X$ (VBF) with H^0 decaying to invisible final states using 35.9 fb^{-1} of data. The quoted limit on the branching ratio is given for $m_{H^0} = 125.09 \text{ GeV}$ and assumes the Standard Model production rates.
- ¹⁰ SIRUNYAN 19B0 combine the VBF channel with results of other 13 TeV analyses: SIRUNYAN 18BV and SIRUNYAN 18S. The quoted limit on the branching ratio is given for $m_{H^0} = 125.09 \text{ GeV}$ and assumes the Standard Model production rates.
- ¹¹ ABOUD 18 search for $pp \rightarrow H^0ZX, Z \rightarrow ee, \mu\mu$ with H^0 decaying to invisible final states in 36.1 fb^{-1} at $E_{\text{cm}} = 13 \text{ TeV}$. The quoted limit on the branching ratio is given for $m_{H^0} = 125 \text{ GeV}$ and assumes the Standard Model rate for H^0Z production.
- ¹² ABOUD 18CA search for H^0 decaying to invisible final states using WH, ZH , and ZH productions, where W and Z hadronically decay. The data of 36.1 fb^{-1} at $E_{\text{cm}} = 13 \text{ TeV}$ is used. The quoted limit assumes SM production cross sections with combining the contributions from WH, ZH, ggF and VBF production modes.
- ¹³ SIRUNYAN 18BV search for H^0 decaying to invisible final states associated with a $Z, Z \rightarrow \ell\ell$ using 35.9 fb^{-1} at 13 TeV. The limit is obtained for $m_{H^0} = 125 \text{ GeV}$ and assuming the SM ZH^0 production cross section.
- ¹⁴ SIRUNYAN 18S search for H^0 decaying to invisible final states associated with an energetic jet or a $V, V \rightarrow q\bar{q}$ using 35.9 fb^{-1} at 13 TeV.
- ¹⁵ ABOUD 17BD search for H^0 decaying to invisible final states with ≥ 1 jet and VBF events using 3.2 fb^{-1} of pp collisions at $E_{\text{cm}} = 13 \text{ TeV}$. A cross-section ratio R^{MISS} is used in the measurement. The quoted limit is given for $m_{H^0} = 125 \text{ GeV}$.
- ¹⁶ KHACHATRYAN 17F search for H^0 decaying to invisible final states with gluon fusion, VBF, ZH , and WH productions using 2.3 fb^{-1} of pp collisions at $E_{\text{cm}} = 13 \text{ TeV}$, 19.7 fb^{-1} at 8 TeV, and 5.1 fb^{-1} at 7 TeV. The quoted limit is given for $m_{H^0} = 125 \text{ GeV}$ and assumes the Standard Model rates for gluon fusion, VBF, ZH , and WH productions.
- ¹⁷ AAD 16AF search for $pp \rightarrow qqH^0X$ (VBF) with H^0 decaying to invisible final states in 20.3 fb^{-1} at $E_{\text{cm}} = 8 \text{ TeV}$. The quoted limit on the branching ratio is given for $m_{H^0} = 125 \text{ GeV}$ and assumes the Standard Model rates for VBF and gluon-fusion production.
- ¹⁸ AAD 16AN perform fits to the ATLAS and CMS data at $E_{\text{cm}} = 7$ and 8 TeV. The branching fraction of decays into BSM particles that are invisible or into undetected decay modes is measured for $m_{H^0} = 125.09 \text{ GeV}$.
- ¹⁹ AAD 15BD search for $pp \rightarrow H^0WX$ and $pp \rightarrow H^0ZX$ with W or Z decaying hadronically and H^0 decaying to invisible final states using data at $E_{\text{cm}} = 8 \text{ TeV}$. The quoted limit is given for $m_{H^0} = 125 \text{ GeV}$, assumes the Standard Model rates for the production processes and is based on a combination of the contributions from H^0W, H^0Z and the gluon-fusion process.
- ²⁰ AAD 15CX search for H^0 decaying to invisible final states with VBF, ZH , and WH productions using 20.3 fb^{-1} at 8 TeV, and 4.7 fb^{-1} at 7 TeV. The quoted limit is given for $m_{H^0} = 125.36 \text{ GeV}$ and assumes the Standard Model rates for gluon fusion, VBF, ZH , and WH productions. The upper limit is improved to 0.23 by adding the measured visible decay rates.
- ²¹ AAD 14O search for $pp \rightarrow H^0ZX, Z \rightarrow \ell\ell$, with H^0 decaying to invisible final states in 4.5 fb^{-1} at $E_{\text{cm}} = 7 \text{ TeV}$ and 20.3 fb^{-1} at $E_{\text{cm}} = 8 \text{ TeV}$. The quoted limit on the branching ratio is given for $m_{H^0} = 125.5 \text{ GeV}$ and assumes the Standard Model rate for H^0Z production.
- ²² CHATRCHYAN 14B search for $pp \rightarrow H^0ZX, Z \rightarrow \ell\ell$ and $Z \rightarrow b\bar{b}$, and also $pp \rightarrow qqH^0X$ with H^0 decaying to invisible final states using data at $E_{\text{cm}} = 7$ and 8 TeV. The quoted limit on the branching ratio is obtained from a combination of the limits from H^0Z and qqH^0 . It is given for $m_{H^0} = 125 \text{ GeV}$ and assumes the Standard Model rates for the two production processes.
- ²³ CHATRCHYAN 14B search for $pp \rightarrow H^0ZX$ with H^0 decaying to invisible final states and $Z \rightarrow \ell\ell$ in 4.9 fb^{-1} at $E_{\text{cm}} = 7 \text{ TeV}$ and 19.7 fb^{-1} at $E_{\text{cm}} = 8 \text{ TeV}$, and also with $Z \rightarrow b\bar{b}$ in 18.9 fb^{-1} at $E_{\text{cm}} = 8 \text{ TeV}$. The quoted limit on the branching ratio is given for $m_{H^0} = 125 \text{ GeV}$ and assumes the Standard Model rate for H^0Z production.
- ²⁴ CHATRCHYAN 14B search for $pp \rightarrow qqH^0X$ (vector boson fusion) with H^0 decaying to invisible final states in 19.5 fb^{-1} at $E_{\text{cm}} = 8 \text{ TeV}$. The quoted limit on the branching ratio is given for $m_{H^0} = 125 \text{ GeV}$ and assumes the Standard Model rate for qqH^0 production.

$\Gamma(\gamma\text{invisible})/\Gamma_{\text{total}}$					Γ_{27}/Γ
VALUE	CL%	DOCUMENT ID	TECN	COMMENT	
<0.029	95	1,2 SIRUNYAN	21L CMS	VBF, $H^0Z, H^0 \rightarrow \gamma + \text{invisible}$, 13 TeV	
• • • We do not use the following data for averages, fits, limits, etc. • • •					
<0.035	95	1 SIRUNYAN	21L CMS	VBF, $H^0 \rightarrow \gamma + \text{invisible}$, 13 TeV	
<0.046	95	3 SIRUNYAN	19CG CMS	$pp \rightarrow H^0Z, H^0 \rightarrow \gamma + \text{invisible}, Z \rightarrow \ell\ell$, 13 TeV	

- ¹ SIRUNYAN 21L search for H^0 decaying to an invisible final state plus a γ in the VBF production using 130 fb^{-1} data at $E_{\text{cm}} = 13 \text{ TeV}$. The invisible state is called a dark photon. The quoted limit on the branching ratio is given for $m_{H^0} = 125 \text{ GeV}$ assuming the Standard Model rates.
- ² The result of the VBF production is combined with the $pp \rightarrow H^0Z$ result (SIRUNYAN 19CG).
- ³ SIRUNYAN 19CG search for $pp \rightarrow H^0Z, Z \rightarrow ee, \mu\mu$ with H^0 decaying to invisible final states plus a γ in 137 fb^{-1} at $E_{\text{cm}} = 13 \text{ TeV}$. The quoted limit on the branching ratio is given for $m_{H^0} = 125 \text{ GeV}$ assuming the Standard Model rate for H^0Z production and is obtained in the context of a theoretical model, where the undetected (invisible) particle is massless.

H^0 SIGNAL STRENGTHS IN DIFFERENT CHANNELS

The H^0 signal strength in a particular final state xx is given by the cross section times branching ratio in this channel normalized to the Standard Model (SM) value, $\sigma \cdot \text{B}(H^0 \rightarrow xx) / (\sigma \cdot \text{B}(H^0 \rightarrow xx))_{\text{SM}}$, for the specified mass value of H^0 . For the SM predictions, see DITTMAYER 11, DITTMAYER 12, and HEINEMEYER 13A. Results for fiducial and differential cross sections are also listed below.

Combined Final States

VALUE	DOCUMENT ID	TECN	COMMENT
1.13 ± 0.06 OUR AVERAGE			
$1.11^{+0.09}_{-0.08}$	¹ AAD	20 ATLS	$pp, 13 \text{ TeV}$
1.17 ± 0.10	² SIRUNYAN	19AT CMS	$pp, 13 \text{ TeV}$
$1.09 \pm 0.07 \pm 0.04 \pm 0.03 \pm 0.07_{-0.06}$	^{3,4} AAD	16AN LHC	$pp, 7, 8 \text{ TeV}$
$1.44^{+0.59}_{-0.56}$	⁵ AALTONEN	13M TEVA	$p\bar{p} \rightarrow H^0X, 1.96 \text{ TeV}$
• • • We do not use the following data for averages, fits, limits, etc. • • •			
$1.20 \pm 0.10 \pm 0.06 \pm 0.04 \pm 0.08_{-0.07}$	⁶ SIRUNYAN	19BA CMS	$pp, 13 \text{ TeV}$, differential cross sections
$0.97 \pm 0.09 \pm 0.05 \pm 0.04 \pm 0.07_{-0.03 - 0.06}$	⁴ AAD	16AN ATLS	$pp, 7, 8 \text{ TeV}$
$1.18 \pm 0.10 \pm 0.07 \pm 0.08_{-0.07}$	⁴ AAD	16AN CMS	$pp, 7, 8 \text{ TeV}$
$1.18 \pm 0.10 \pm 0.07 \pm 0.08_{-0.07}$	⁷ AAD	16K ATLS	$pp, 7, 8 \text{ TeV}$
$0.75^{+0.28 + 0.13 + 0.08}_{-0.26 - 0.11 - 0.05}$	⁷ AAD	16K ATLS	$pp, 7 \text{ TeV}$
$1.28 \pm 0.11 \pm 0.08 \pm 0.10_{-0.07 - 0.08}$	⁷ AAD	16K ATLS	$pp, 8 \text{ TeV}$
$1.00 \pm 0.09 \pm 0.07 \pm 0.08_{-0.07}$	⁸ AAD	15P ATLS	$pp, 8 \text{ TeV}$, cross section
$1.33^{+0.14}_{-0.10} \pm 0.15$	⁹ KHACHATRY...	15AM CMS	$pp, 7, 8 \text{ TeV}$
$1.54^{+0.77}_{-0.73}$	¹⁰ AAD	13AK ATLS	$pp, 7$ and 8 TeV
$1.40^{+0.92}_{-0.88}$	¹¹ AALTONEN	13L CDF	$p\bar{p} \rightarrow H^0X, 1.96 \text{ TeV}$
1.4 ± 0.3	¹² ABAZOV	13L D0	$p\bar{p} \rightarrow H^0X, 1.96 \text{ TeV}$
1.2 ± 0.4	¹³ AAD	12AI ATLS	$pp \rightarrow H^0X, 7, 8 \text{ TeV}$
1.5 ± 0.4	¹³ AAD	12AI ATLS	$pp \rightarrow H^0X, 7 \text{ TeV}$
0.87 ± 0.23	¹³ AAD	12AI ATLS	$pp \rightarrow H^0X, 8 \text{ TeV}$
	¹⁴ CHATRCHYAN	12N CMS	$pp \rightarrow H^0X, 7, 8 \text{ TeV}$

- ¹ AAD 20 combine results of up to 79.8 fb^{-1} of data at $E_{\text{cm}} = 13 \text{ TeV}$, assuming $m_{H^0} = 125.09 \text{ GeV}$; $ZZ^*, WW^*, \tau\tau, b\bar{b}, \mu\mu$, invisible, and off-shell analyses (see their Table I). The signal strengths for individual production processes are 1.04 ± 0.09 for gluon fusion, $1.21^{+0.24}_{-0.22}$ for vector boson fusion, $1.30^{+0.40}_{-0.38}$ for WH^0 production, $1.05^{+0.31}_{-0.29}$ for ZH^0 production, and $1.21^{+0.26}_{-0.24}$ for $t\bar{t}H^0 + tH^0$ production (see their Fig. 2 and Table IV). Several results with the simplified template cross section and κ -frameworks are presented: see their Figs. 9–11, Figs 20, 21 and Table VIII for stage-1 simplified template cross sections, their Figs. 12–17 and Tables X–XII for the κ -framework.
- ² SIRUNYAN 19AT combine results of 35.9 fb^{-1} of data at $E_{\text{cm}} = 13 \text{ TeV}$, assuming $m_{H^0} = 125.09 \text{ GeV}$. The signal strengths for individual production processes are $1.22^{+0.14}_{-0.12}$ for gluon fusion, $0.73^{+0.30}_{-0.27}$ for vector boson fusion, $2.18^{+0.58}_{-0.55}$ for WH^0 production, $0.87^{+0.44}_{-0.42}$ for ZH^0 production, and $1.18^{+0.30}_{-0.27}$ for $t\bar{t}H^0$ production. Several results with the simplified template cross section and κ -frameworks are presented: see their Fig. 8 and Table 5 for stage-0 simplified template cross sections, their Figs. 9–18 and Tables 7–11 for the κ -framework.
- ³ AAD 16AN perform fits to the ATLAS and CMS data at $E_{\text{cm}} = 7$ and 8 TeV. The signal strengths for individual production processes are $1.03^{+0.16}_{-0.14}$ for gluon fusion, $1.18^{+0.25}_{-0.23}$ for vector boson fusion, $0.89^{+0.40}_{-0.38}$ for WH^0 production, $0.79^{+0.38}_{-0.36}$ for ZH^0 production, and $2.3^{+0.7}_{-0.6}$ for $t\bar{t}H^0$ production.
- ⁴ AAD 16AN: The uncertainties represent statistics, experimental systematics, theory systematics on the background, and theory systematics on the signal. The quoted signal strengths are given for $m_{H^0} = 125.09 \text{ GeV}$. In the fit, relative branching ratios and relative production cross sections are fixed to those in the Standard Model.
- ⁵ AALTONEN 13M combine all Tevatron data from the CDF and D0 Collaborations with up to 10.0 fb^{-1} and 9.7 fb^{-1} , respectively, of $p\bar{p}$ collisions at $E_{\text{cm}} = 1.96 \text{ TeV}$. The quoted signal strength is given for $m_{H^0} = 125 \text{ GeV}$.
- ⁶ SIRUNYAN 19BA measure differential cross sections for the Higgs boson transverse momentum, the number of jets, the rapidity of the Higgs boson and the transverse momentum of the leading jet using 35.9 fb^{-1} of data at $E_{\text{cm}} = 13 \text{ TeV}$ with $H^0 \rightarrow \gamma\gamma, H^0 \rightarrow ZZ^*$, and $H^0 \rightarrow b\bar{b}$. The total cross section for Higgs boson production is measured to be $61.1 \pm 6.0 \pm 3.7 \text{ pb}$ using $H^0 \rightarrow \gamma\gamma$ and $H^0 \rightarrow ZZ^*$ channels. Several coupling measurements in the κ -framework are performed.
- ⁷ AAD 16K use up to 4.7 fb^{-1} of pp collisions at $E_{\text{cm}} = 7 \text{ TeV}$ and up to 20.3 fb^{-1} at $E_{\text{cm}} = 8 \text{ TeV}$. The third uncertainty in the measurement is theory systematics. The signal strengths for individual production modes are $1.23 \pm 0.14^{+0.09 + 0.16}_{-0.08 - 0.12}$ for gluon fusion, $1.23^{+0.28 + 0.13 + 0.11}_{-0.27 - 0.12 - 0.09}$ for vector boson fusion, $0.80^{+0.31}_{-0.30} \pm 0.17^{+0.10}_{-0.05}$ for W/ZH^0 production, and $1.81^{+0.52 + 0.58 + 0.31}_{-0.50 - 0.55 - 0.12}$ for $t\bar{t}H^0$ production. The quoted signal strengths are given for $m_{H^0} = 125.36 \text{ GeV}$.
- ⁸ AAD 15P measure total and differential cross sections of the process $pp \rightarrow H^0X$ at $E_{\text{cm}} = 8 \text{ TeV}$ with 20.3 fb^{-1} . $\gamma\gamma$ and 4ℓ final states are used. $\sigma(pp \rightarrow H^0X) = 33.0 \pm 5.3 \pm 1.6 \text{ pb}$ is given. See their Figs. 2 and 3 for data on differential cross sections.

Gauge & Higgs Boson Particle Listings

 H^0

- ⁹ KHACHATRYAN 15AM use up to 5.1 fb^{-1} of pp collisions at $E_{\text{cm}} = 7 \text{ TeV}$ and up to 19.7 fb^{-1} at $E_{\text{cm}} = 8 \text{ TeV}$. The third uncertainty in the measurement is theory systematics. Fits to each production mode give the value of $0.85^{+0.19}_{-0.16}$ for gluon fusion, $1.16^{+0.37}_{-0.34}$ for vector boson fusion, $0.92^{+0.38}_{-0.36}$ for WH^0 , ZH^0 production, and $2.90^{+1.08}_{-0.94}$ for $t\bar{t}H^0$ production.
- ¹⁰ AAD 13AK use 4.7 fb^{-1} of pp collisions at $E_{\text{cm}} = 7 \text{ TeV}$ and 20.7 fb^{-1} at $E_{\text{cm}} = 8 \text{ TeV}$. The combined signal strength is based on the $\gamma\gamma$, $ZZ^* \rightarrow 4\ell$, and $WW^* \rightarrow \ell\nu\ell\nu$ channels. The quoted signal strength is given for $m_{H^0} = 125.5 \text{ GeV}$. Reported statistical error value modified following private communication with the experiment.
- ¹¹ AALTONEN 13L combine all CDF results with $9.45\text{--}10.0 \text{ fb}^{-1}$ of $p\bar{p}$ collisions at $E_{\text{cm}} = 1.96 \text{ TeV}$. The quoted signal strength is given for $m_{H^0} = 125 \text{ GeV}$.
- ¹² ABAZOV 13L combine all D0 results with up to 9.7 fb^{-1} of $p\bar{p}$ collisions at $E_{\text{cm}} = 1.96 \text{ TeV}$. The quoted signal strength is given for $m_{H^0} = 125 \text{ GeV}$.
- ¹³ AAD 12AI obtain results based on $4.6\text{--}4.8 \text{ fb}^{-1}$ of pp collisions at $E_{\text{cm}} = 7 \text{ TeV}$ and $5.8\text{--}5.9 \text{ fb}^{-1}$ at $E_{\text{cm}} = 8 \text{ TeV}$. An excess of events over background with a local significance of 5.9σ is observed at $m_{H^0} = 126 \text{ GeV}$. The quoted signal strengths are given for $m_{H^0} = 126 \text{ GeV}$. See also AAD 12DA.
- ¹⁴ CHATRCHYAN 12N obtain results based on $4.9\text{--}5.1 \text{ fb}^{-1}$ of pp collisions at $E_{\text{cm}} = 7 \text{ TeV}$ and $5.1\text{--}5.3 \text{ fb}^{-1}$ at $E_{\text{cm}} = 8 \text{ TeV}$. An excess of events over background with a local significance of 5.0σ is observed at $m_{H^0} = 125 \text{ GeV}$. The combined signal strength is based on the $\gamma\gamma$, ZZ^* , WW^* , $\tau^+\tau^-$, and $b\bar{b}$ channels. The quoted signal strength is given for $m_{H^0} = 125.5 \text{ GeV}$. See also CHATRCHYAN 13Y.

W W* Final State

VALUE	DOCUMENT ID	TECN	COMMENT
1.19±0.12 OUR AVERAGE			
$1.28^{+0.17}_{-0.16}$	1 SIRUNYAN	19AT CMS	pp , 13 TeV
$1.09^{+0.18}_{-0.16}$	2,3 AAD	16AN LHC	pp , 7, 8 TeV
$0.94^{+0.85}_{-0.83}$	4 AALTONEN	13M TEVA	$p\bar{p} \rightarrow H^0 X$, 1.96 TeV
• • • We do not use the following data for averages, fits, limits, etc. • • •			
$2.5^{+0.9}_{-0.8}$	5 AABOUD	19F ATLS	pp , 13 TeV, cross sections
$1.28^{+0.18}_{-0.17}$	6 AAD	19A ATLS	$pp \rightarrow H^0 W/H^0 Z$, $H^0 \rightarrow WW^*$, 13 TeV
$1.22^{+0.23}_{-0.21}$	7 SIRUNYAN	19AX CMS	pp , 13 TeV
$0.90^{+0.23}_{-0.21}$	3 AAD	16AN ATLS	pp , 7, 8 TeV
$1.18 \pm 0.16^{+0.17}_{-0.14}$	8 AAD	16AN CMS	pp , 7, 8 TeV
$1.09^{+0.16}_{-0.15}$	9 AAD	16K ATLS	pp , 7, 8 TeV
$3.0^{+1.3}_{-1.1}$	10 AAD	16AO ATLS	pp , 8 TeV, cross sections
$1.16^{+0.16}_{-0.15}$	11 AAD	16K ATLS	pp , 7, 8 TeV
$0.72 \pm 0.12 \pm 0.10^{+0.12}_{-0.10}$	12 AAD	15AQ ATLS	pp , 7, 8 TeV
$0.99^{+0.31}_{-0.28}$	13 CHATRCHYAN 14G	CMS	pp , 7, 8 TeV
$0.00^{+1.78}_{-0.00}$	14 AAD	13AK ATLS	pp , 7 and 8 TeV
$1.90^{+1.63}_{-1.52}$	15 AALTONEN	13L CDF	$p\bar{p} \rightarrow H^0 X$, 1.96 TeV
1.3 ± 0.5	16 ABAZOV	13L D0	$p\bar{p} \rightarrow H^0 X$, 1.96 TeV
0.5 ± 0.6	17 AAD	12AI ATLS	$pp \rightarrow H^0 X$, 7, 8 TeV
1.9 ± 0.7	17 AAD	12AI ATLS	$pp \rightarrow H^0 X$, 7 TeV
$0.60^{+0.42}_{-0.37}$	17 AAD	12AI ATLS	$pp \rightarrow H^0 X$, 8 TeV
	18 CHATRCHYAN 12N	CMS	$pp \rightarrow H^0 X$, 7, 8 TeV

- ¹ SIRUNYAN 19AT perform a combine fit to 35.9 fb^{-1} of data at $E_{\text{cm}} = 13 \text{ TeV}$.
- ² AAD 16AN perform fits to the ATLAS and CMS data at $E_{\text{cm}} = 7$ and 8 TeV . The signal strengths for individual production processes are 0.84 ± 0.17 for gluon fusion, 1.2 ± 0.4 for vector boson fusion, $1.6^{+1.2}_{-1.0}$ for WH^0 production, $5.9^{+2.6}_{-2.2}$ for ZH^0 production, and $5.0^{+1.8}_{-1.7}$ for $t\bar{t}H^0$ production.
- ³ AAD 16AN: In the fit, relative production cross sections are fixed to those in the Standard Model. The quoted signal strength is given for $m_{H^0} = 125.09 \text{ GeV}$.
- ⁴ AALTONEN 13M combine all Tevatron data from the CDF and D0 Collaborations with up to 10.0 fb^{-1} and 9.7 fb^{-1} , respectively, of $p\bar{p}$ collisions at $E_{\text{cm}} = 1.96 \text{ TeV}$. The quoted signal strength is given for $m_{H^0} = 125 \text{ GeV}$.
- ⁵ AABOUD 19F measure cross-sections times the $H^0 \rightarrow WW^*$ branching fraction in the $H^0 \rightarrow WW^* \rightarrow \nu\mu\nu$ channel using 36.1 fb^{-1} of pp collisions at $E_{\text{cm}} = 13 \text{ TeV}$: $\sigma_{ggF} \times B(H^0 \rightarrow WW^*) = 11.4^{+1.2}_{-1.1} \pm 1.8$ pb and $\sigma_{VBF} \times B(H^0 \rightarrow WW^*) = 0.50^{+0.24}_{-0.22} \pm 0.17$ pb.
- ⁶ AAD 19A use 36.1 fb^{-1} data at 13 TeV . The cross section times branching fraction values are measured to be $0.67^{+0.31}_{-0.27} \pm 0.18$ pb for WH^0 , $H^0 \rightarrow WW^*$ and $0.54^{+0.31}_{-0.24} \pm 0.15$ pb for ZH^0 , $H^0 \rightarrow WW^*$.
- ⁷ SIRUNYAN 19AX measure the signal strengths, cross sections and so on using gluon fusion, VBF and VH^0 production processes with 35.9 fb^{-1} of data. The quoted signal strength is given for $m_{H^0} = 125.09 \text{ GeV}$. Signal strengths for each production process is found in their Fig. 9. Measured cross sections and ratios to the SM predictions in the stage-0 simplified template cross section framework are shown in their Fig. 10. $\kappa_F = 1.52^{+0.48}_{-0.41}$ and $\kappa_V = 1.10 \pm 0.08$ are obtained (see their Fig. 11 (right)).

- ⁸ AAD 16AO measure fiducial total and differential cross sections of gluon fusion process at $E_{\text{cm}} = 8 \text{ TeV}$ with 20.3 fb^{-1} using $H^0 \rightarrow WW^* \rightarrow \nu\nu\mu\nu$. The measured fiducial total cross section is $36.0 \pm 9.7 \text{ fb}$ in their fiducial region (Table 7). See their Fig. 6 for fiducial differential cross sections. The results are given for $m_{H^0} = 125 \text{ GeV}$.
- ⁹ AAD 16K use up to 4.7 fb^{-1} of pp collisions at $E_{\text{cm}} = 7 \text{ TeV}$ and up to 20.3 fb^{-1} at $E_{\text{cm}} = 8 \text{ TeV}$. The quoted signal strength is given for $m_{H^0} = 125.36 \text{ GeV}$.
- ¹⁰ AAD 15AA use 4.5 fb^{-1} of pp collisions at $E_{\text{cm}} = 7 \text{ TeV}$ and 20.3 fb^{-1} at $E_{\text{cm}} = 8 \text{ TeV}$. The signal strength for the gluon fusion and vector boson fusion mode is $1.02 \pm 0.19^{+0.22}_{-0.18}$ and $1.27^{+0.44}_{-0.40} \pm 0.30$, respectively. The quoted signal strengths are given for $m_{H^0} = 125.36 \text{ GeV}$.
- ¹¹ AAD 15AQ use 4.5 fb^{-1} of pp collisions at $E_{\text{cm}} = 7 \text{ TeV}$ and 20.3 fb^{-1} at $E_{\text{cm}} = 8 \text{ TeV}$. The quoted signal strength is given for $m_{H^0} = 125.36 \text{ GeV}$.
- ¹² AAD 15AQ combine their result on W/ZH^0 production with the results of AAD 15AA (gluon fusion and vector boson fusion, slightly updated). The quoted signal strength is given for $m_{H^0} = 125.36 \text{ GeV}$.
- ¹³ CHATRCHYAN 14G use 4.9 fb^{-1} of pp collisions at $E_{\text{cm}} = 7 \text{ TeV}$ and 19.4 fb^{-1} at $E_{\text{cm}} = 8 \text{ TeV}$. The last uncertainty in the measurement is theory systematics. The quoted signal strength is given for $m_{H^0} = 125.6 \text{ GeV}$.
- ¹⁴ AAD 13AK use 4.7 fb^{-1} of pp collisions at $E_{\text{cm}} = 7 \text{ TeV}$ and 20.7 fb^{-1} at $E_{\text{cm}} = 8 \text{ TeV}$. The quoted signal strength is given for $m_{H^0} = 125.5 \text{ GeV}$. Superseded by AAD 15AA.
- ¹⁵ AALTONEN 13L combine all CDF results with $9.45\text{--}10.0 \text{ fb}^{-1}$ of $p\bar{p}$ collisions at $E_{\text{cm}} = 1.96 \text{ TeV}$. The quoted signal strength is given for $m_{H^0} = 125 \text{ GeV}$.
- ¹⁶ ABAZOV 13L combine all D0 results with up to 9.7 fb^{-1} of $p\bar{p}$ collisions at $E_{\text{cm}} = 1.96 \text{ TeV}$. The quoted signal strength is given for $m_{H^0} = 125 \text{ GeV}$.
- ¹⁷ AAD 12AI obtain results based on 4.7 fb^{-1} of pp collisions at $E_{\text{cm}} = 7 \text{ TeV}$ and 5.8 fb^{-1} at $E_{\text{cm}} = 8 \text{ TeV}$. The quoted signal strengths are given for $m_{H^0} = 126 \text{ GeV}$. See also AAD 12DA.
- ¹⁸ CHATRCHYAN 12N obtain results based on 4.9 fb^{-1} of pp collisions at $E_{\text{cm}} = 7 \text{ TeV}$ and 5.1 fb^{-1} at $E_{\text{cm}} = 8 \text{ TeV}$. The quoted signal strength is given for $m_{H^0} = 125.5 \text{ GeV}$. See also CHATRCHYAN 13Y.

ZZ* Final State

VALUE	CL%	DOCUMENT ID	TECN	COMMENT
1.01±0.07 OUR AVERAGE				
$0.94 \pm 0.07^{+0.09}_{-0.08}$		1 SIRUNYAN	21s CMS	pp , 13 TeV
1.01 ± 0.11		2,3 AAD	20AQ ATLS	pp , 13 TeV
$1.29^{+0.26}_{-0.23}$		4,5 AAD	16AN LHC	pp , 7, 8 TeV
• • • We do not use the following data for averages, fits, limits, etc. • • •				
<6.5	95	6 SIRUNYAN	21AE CMS	pp , 13 TeV, couplings
$1.06^{+0.19}_{-0.17}$		2,7 AAD	20AQ ATLS	pp , 13 TeV
$1.28^{+0.21}_{-0.19}$		8 AAD	20BA ATLS	pp , 13 TeV cross sections
<3.8	95	9 AABOUD	19N ATLS	pp , 13 TeV, off-shell
$1.05^{+0.15}_{-0.14}$		10 SIRUNYAN	19AT CMS	pp , 13 TeV
$1.52^{+0.40}_{-0.34}$		11 AABOUD	18AJ ATLS	pp , 13 TeV
$1.04^{+0.32}_{-0.26}$		12 AABOUD	18BP ATLS	pp , 13 TeV, off-shell
$1.46^{+0.35}_{-0.31}$		13 SIRUNYAN	17AV CMS	pp , 13 TeV
$1.44^{+0.34}_{-0.31}$		5 AAD	16AN ATLS	pp , 7, 8 TeV
$0.93^{+0.26}_{-0.23}$		5 AAD	16AN CMS	pp , 7, 8 TeV
$1.43^{+0.40}_{-0.35}$		14 AAD	16K ATLS	pp , 7, 8 TeV
$0.80^{+0.35}_{-0.28}$		15 KHACHATRYAN 16AR	CMS	pp , 7, 8 TeV cross sections
1.2 ± 0.6		16 AAD	15F ATLS	$pp \rightarrow H^0 X$, 7, 8 TeV
1.4 ± 1.1		17 AAD	14AR ATLS	pp , 8 TeV, cross sections
1.1 ± 0.8		18 CHATRCHYAN 14AA	CMS	pp , 7, 8 TeV
$0.73^{+0.45}_{-0.33}$		19 AAD	13AK ATLS	pp , 7 and 8 TeV
1.2 ± 0.6		20 CHATRCHYAN 13J	CMS	$pp \rightarrow H^0 X$, 7, 8 TeV
1.4 ± 1.1		21 AAD	12AI ATLS	$pp \rightarrow H^0 X$, 7, 8 TeV
1.1 ± 0.8		21 AAD	12AI ATLS	$pp \rightarrow H^0 X$, 7 TeV
$1.44^{+0.34}_{-0.31}$		21 AAD	12AI ATLS	$pp \rightarrow H^0 X$, 8 TeV
$0.93^{+0.26}_{-0.23}$		22 CHATRCHYAN 12N	CMS	$pp \rightarrow H^0 X$, 7, 8 TeV

- ¹ SIRUNYAN 21s measure cross sections with the $H^0 \rightarrow ZZ^* \rightarrow 4\ell$ ($\ell = e, \mu$) channel using 137 fb^{-1} data at $E_{\text{cm}} = 13 \text{ TeV}$. Results are given for $m_{H^0} = 125.38 \text{ GeV}$. The signal strengths for individual production processes in their Table 4. Cross sections are given in their Table 6 and Fig. 14, which are based on the simplified template cross section framework (reduced stage-1.2).
- ² AAD 20AQ perform analyses using $H^0 \rightarrow ZZ^* \rightarrow 4\ell$ ($\ell = e, \mu$) with data of 139 fb^{-1} at $E_{\text{cm}} = 13 \text{ TeV}$. Results are given for $m_{H^0} = 125 \text{ GeV}$.
- ³ AAD 20AQ measured the inclusive cross section times branching ratio for $H^0 \rightarrow ZZ^*$ decay ($|y(H^0)| < 2.5$) to be $1.34 \pm 0.12 \text{ pb}$ (with $1.33 \pm 0.08 \text{ pb}$ expected in the SM).
- ⁴ AAD 16AN perform fits to the ATLAS and CMS data at $E_{\text{cm}} = 7$ and 8 TeV . The signal strengths for individual production processes are $1.13^{+0.34}_{-0.31}$ for gluon fusion and $0.1^{+1.1}_{-0.6}$ for vector boson fusion.
- ⁵ AAD 16AN: In the fit, relative production cross sections are fixed to those in the Standard Model. The quoted signal strength is given for $m_{H^0} = 125.09 \text{ GeV}$.

- ⁶ SIRUNYAN 21AE obtains constraints on anomalous couplings to vector bosons (W , Z , and gluon) and top quark using $H^0 \rightarrow ZZ^* \rightarrow 4\ell$ ($\ell = e, \mu$) with data of 137 fb^{-1} at $E_{\text{cm}} = 13 \text{ TeV}$. Their Table 5 and Figs 14–17 show (effective) couplings to gluon and top with combining gluon fusion, $t\bar{t}H^0$ and tH^0 production channels and the result of $t\bar{t}H^0, H^0 \rightarrow \gamma\gamma$ (SIRUNYAN 20AS). Their Tables 6–9 and Figs 18–22 show couplings to W and Z for different assumptions and bases (Higgs and Warsaw).
- ⁷ AAD 20AQ present several results for the channel $H^0 \rightarrow ZZ^* \rightarrow 4\ell$ ($\ell = e, \mu$) with the simplified template cross section with κ -frameworks and the effective field theory (EFT) approach; see their Table 8 and Fig. 10 for simplified template cross sections. $\kappa_V = 1.02 \pm 0.06$ and $\kappa_F = 0.88 \pm 0.16$ are obtained, see their Fig. 12 for the κ -framework. See their Tables 9 and 10 and Figs. 16–18 for the EFT-framework.
- ⁸ AAD 20BA measure the cross section for $pp \rightarrow H^0 \rightarrow ZZ^* \rightarrow 4\ell$ ($\ell = e, \mu$) using 139 fb^{-1} at $E_{\text{cm}} = 13 \text{ TeV}$. They give $\sigma \cdot B = 3.28 \pm 0.30 \pm 0.11 \text{ fb}$ in their fiducial region, where $3.41 \pm 0.18 \text{ fb}$ is expected in the Standard Model for $m_{H^0} = 125 \text{ GeV}$. Various differential cross sections are also given; see their Figs. 19–39. Constraints on Yukawa couplings for bottom and charm quarks are given in their Table 9 and Fig. 41.
- ⁹ AABOUD 19N measure the spectrum of the four-lepton invariant mass $m_{4\ell}$ ($\ell = e$ or μ) using 36.1 fb^{-1} of data at $E_{\text{cm}} = 13 \text{ TeV}$. The quoted signal strength upper limit is obtained from $180 \text{ GeV} < m_{4\ell} < 1200 \text{ GeV}$.
- ¹⁰ SIRUNYAN 19AT perform a combine fit to 35.9 fb^{-1} of data at $E_{\text{cm}} = 13 \text{ TeV}$.
- ¹¹ AABOUD 18AJ perform analyses using $H^0 \rightarrow ZZ^* \rightarrow 4\ell$ ($\ell = e, \mu$) with data of 36.1 fb^{-1} at $E_{\text{cm}} = 13 \text{ TeV}$. Results are given for $m_{H^0} = 125.09 \text{ GeV}$. The inclusive cross section times branching ratio for $H^0 \rightarrow ZZ^* \text{ decay } (|\eta(H^0)| < 2.5)$ is measured to be $1.73^{+0.26}_{-0.24} \text{ pb}$ (with $1.34^{+0.09}_{-0.09} \text{ pb}$ expected in the SM).
- ¹² AABOUD 18BP measure an off-shell Higgs boson production using $ZZ \rightarrow 4\ell$ and $ZZ \rightarrow 2\ell 2\nu$ ($\ell = e, \mu$) decay channels with 36.1 fb^{-1} of data at $E_{\text{cm}} = 13 \text{ TeV}$. The quoted signal strength upper limit is obtained from a combination of these two channels, where $220 \text{ GeV} < m_{4\ell} < 2000 \text{ GeV}$ for $ZZ \rightarrow 4\ell$ and $250 \text{ GeV} < m_{T^{ZZ}} < 2000 \text{ GeV}$ for $ZZ \rightarrow 2\ell 2\nu$ ($m_{T^{ZZ}}$ is defined in their Section 5). See their Table 2 for each measurement.
- ¹³ SIRUNYAN 17AV use 35.9 fb^{-1} of pp collisions at $E_{\text{cm}} = 13 \text{ TeV}$. The quoted signal strength, obtained from the analysis of $H^0 \rightarrow ZZ^* \rightarrow 4\ell$ ($\ell = e, \mu$) decays, is given in their Table 3. The fiducial and differential cross sections are shown in their Fig. 10.
- ¹⁴ AAD 16K use up to 4.7 fb^{-1} of pp collisions at $E_{\text{cm}} = 7 \text{ TeV}$ and up to 20.3 fb^{-1} at $E_{\text{cm}} = 8 \text{ TeV}$. The quoted signal strength is given for $m_{H^0} = 125.36 \text{ GeV}$.
- ¹⁵ KHACHATRYAN 16AR use data of 5.1 fb^{-1} at $E_{\text{cm}} = 7 \text{ TeV}$ and 19.7 fb^{-1} at 8 TeV . The fiducial cross sections for the production of 4 leptons via $H^0 \rightarrow 4\ell$ decays are measured to be $0.56^{+0.67+0.21}_{-0.44-0.06} \text{ fb}$ at 7 TeV and $1.11^{+0.41+0.14}_{-0.35-0.10} \text{ fb}$ at 8 TeV in their fiducial region (Table 2). The differential cross sections at $E_{\text{cm}} = 8 \text{ TeV}$ are also shown in Figs. 4 and 5. The results are given for $m_{H^0} = 125 \text{ GeV}$.
- ¹⁶ AAD 15F use 4.5 fb^{-1} of pp collisions at $E_{\text{cm}} = 7 \text{ TeV}$ and 20.3 fb^{-1} at $E_{\text{cm}} = 8 \text{ TeV}$. The quoted signal strength is given for $m_{H^0} = 125.36 \text{ GeV}$. The signal strength for the gluon fusion production mode is $1.66^{+0.45+0.25}_{-0.41-0.15}$, while the signal strength for the vector boson fusion production mode is $0.26^{+1.60+0.36}_{-0.91-0.23}$.
- ¹⁷ AAD 14AR measure the cross section for $pp \rightarrow H^0 \rightarrow ZZ^* \rightarrow 4\ell$ ($\ell = e, \mu$) using 20.3 fb^{-1} at $E_{\text{cm}} = 8 \text{ TeV}$. They give $\sigma \cdot B = 2.11^{+0.53}_{-0.47} \pm 0.08 \text{ fb}$ in their fiducial region, where $1.30 \pm 0.13 \text{ fb}$ is expected in the Standard Model for $m_{H^0} = 125.4 \text{ GeV}$. Various differential cross sections are also given; see their Fig. 2.
- ¹⁸ CHATRCHYAN 14AA use 5.1 fb^{-1} of pp collisions at $E_{\text{cm}} = 7 \text{ TeV}$ and 19.7 fb^{-1} at $E_{\text{cm}} = 8 \text{ TeV}$. The quoted signal strength is given for $m_{H^0} = 125.6 \text{ GeV}$. The signal strength for the gluon fusion and $t\bar{t}H$ production mode is $0.80^{+0.46}_{-0.36}$, while the signal strength for the vector boson fusion and WH^0, ZH^0 production mode is $1.7^{+2.2}_{-2.1}$.
- ¹⁹ AAD 13AK use 4.7 fb^{-1} of pp collisions at $E_{\text{cm}} = 7 \text{ TeV}$ and 20.7 fb^{-1} at $E_{\text{cm}} = 8 \text{ TeV}$. The quoted signal strength is given for $m_{H^0} = 125.5 \text{ GeV}$.
- ²⁰ CHATRCHYAN 13J obtain results based on $ZZ \rightarrow 4\ell$ final states in 5.1 fb^{-1} of pp collisions at $E_{\text{cm}} = 7 \text{ TeV}$ and 12.2 fb^{-1} at $E_{\text{cm}} = 8 \text{ TeV}$. The quoted signal strength is given for $m_{H^0} = 125.8 \text{ GeV}$. Superseded by CHATRCHYAN 14AA.
- ²¹ AAD 12AI obtain results based on $4.7\text{--}4.8 \text{ fb}^{-1}$ of pp collisions at $E_{\text{cm}} = 7 \text{ TeV}$ and 5.8 fb^{-1} at $E_{\text{cm}} = 8 \text{ TeV}$. The quoted signal strengths are given for $m_{H^0} = 126 \text{ GeV}$. See also AAD 12DA.
- ²² CHATRCHYAN 12N obtain results based on $4.9\text{--}5.1 \text{ fb}^{-1}$ of pp collisions at $E_{\text{cm}} = 7 \text{ TeV}$ and $5.1\text{--}5.3 \text{ fb}^{-1}$ at $E_{\text{cm}} = 8 \text{ TeV}$. An excess of events over background with a local significance of 5.0σ is observed at about $m_{H^0} = 125 \text{ GeV}$. The quoted signal strengths are given for $m_{H^0} = 125.5 \text{ GeV}$. See also CHATRCHYAN 12BY and CHATRCHYAN 13Y.
- ⁹ KHACHATRYAN...16G CMS pp , 8 TeV , diff. x-section
- 10 AAD 14BC ATLS $pp \rightarrow H^0 X$, $7, 8 \text{ TeV}$
- 11 AAD 14BJ ATLS pp , 8 TeV , diff. x-section
- 12 KHACHATRYAN...14P CMS pp , $7, 8 \text{ TeV}$
- 13 AAD 13AK ATLS pp , 7 and 8 TeV
- 14 AALTONEN 13L CDF $p\bar{p} \rightarrow H^0 X$, 1.96 TeV
- 15 ABAZOV 13L D0 $p\bar{p} \rightarrow H^0 X$, 1.96 TeV
- 16 AAD 12AI ATLS $pp \rightarrow H^0 X$, $7, 8 \text{ TeV}$
- 16 AAD 12AI ATLS $pp \rightarrow H^0 X$, 7 TeV
- 16 AAD 12AI ATLS $pp \rightarrow H^0 X$, 8 TeV
- 17 CHATRCHYAN 12N CMS $pp \rightarrow H^0 X$, $7, 8 \text{ TeV}$
- ¹ SIRUNYAN 21o measures cross sections and couplings with the $H^0 \rightarrow \gamma\gamma$ channel using 137 fb^{-1} data at $E_{\text{cm}} = 13 \text{ TeV}$. Results are given for $m_{H^0} = 125.38 \text{ GeV}$. The signal strengths for individual production processes are given in their Fig. 16. Cross sections are given in their Tables 12 and 13 and Figs. 18 and 20, which are based on the simplified template cross section framework (reduced stage-1.2). Results in the κ -framework are given in their Fig. 22.
- ² AABOUD 18BO use 36.1 fb^{-1} of pp collisions at $E_{\text{cm}} = 13 \text{ TeV}$. The signal strengths for the individual production modes are: $0.81^{+0.19}_{-0.18}$ for gluon fusion, $2.0^{+0.6}_{-0.5}$ for vector boson fusion, $0.7^{+0.9}_{-0.8}$ for VH^0 production ($V = W, Z$), and 0.5 ± 0.6 for $t\bar{t}H^0$ and tH^0 production. Other measurements of cross sections and couplings are summarized in their Section 10. The quoted values are given for $m_{H^0} = 125.09 \text{ GeV}$.
- ³ AAD 16AN perform fits to the ATLAS and CMS data at $E_{\text{cm}} = 7$ and 8 TeV . The signal strengths for individual production processes are $1.10^{+0.23}_{-0.22}$ for gluon fusion, 1.3 ± 0.5 for vector boson fusion, $0.5^{+1.3}_{-1.2}$ for WH^0 production, $0.5^{+3.0}_{-2.5}$ for ZH^0 production, and $2.2^{+1.6}_{-1.3}$ for $t\bar{t}H^0$ production.
- ⁴ AAD 16AN: In the fit, relative production cross sections are fixed to those in the Standard Model. The quoted signal strength is given for $m_{H^0} = 125.09 \text{ GeV}$.
- ⁵ AALTONEN 13M combine all Tevatron data from the CDF and D0 Collaborations with up to 10.0 fb^{-1} and 9.7 fb^{-1} , respectively, of $p\bar{p}$ collisions at $E_{\text{cm}} = 1.96 \text{ TeV}$. The quoted signal strength is given for $m_{H^0} = 125 \text{ GeV}$.
- ⁶ SIRUNYAN 19AT perform a combine fit to 35.9 fb^{-1} of data at $E_{\text{cm}} = 13 \text{ TeV}$.
- ⁷ SIRUNYAN 19L measure fiducial and differential cross sections of the process $pp \rightarrow H^0 \rightarrow \gamma\gamma$ at $E_{\text{cm}} = 13 \text{ TeV}$ with 35.9 fb^{-1} . See their Figs. 4–11.
- ⁸ SIRUNYAN 18DS use 35.9 fb^{-1} of $pp \rightarrow H^0$ collisions with $H^0 \rightarrow \gamma\gamma$ at $E_{\text{cm}} = 13 \text{ TeV}$. The Higgs mass is floated in the measurement of a signal strength. The result is $1.18^{+0.12}_{-0.11} \text{ (stat.)} - 0.09 \text{ (syst.)} + 0.07 \text{ (theory)}$, which is largely insensitive to the Higgs mass around 125 GeV .
- ⁹ KHACHATRYAN 16G measure fiducial and differential cross sections of the process $pp \rightarrow H^0 X, H^0 \rightarrow \gamma\gamma$ at $E_{\text{cm}} = 8 \text{ TeV}$ with 19.7 fb^{-1} . See their Figs. 4–6 and Table 1 for data.
- ¹⁰ AAD 14BC use 4.5 fb^{-1} of pp collisions at $E_{\text{cm}} = 7 \text{ TeV}$ and 20.3 fb^{-1} at $E_{\text{cm}} = 8 \text{ TeV}$. The last uncertainty in the measurement is theory systematics. The quoted signal strength is given for $m_{H^0} = 125.4 \text{ GeV}$. The signal strengths for the individual production modes are: 1.32 ± 0.38 for gluon fusion, 0.8 ± 0.7 for vector boson fusion, 1.0 ± 1.6 for WH^0 production, $0.1^{+3.7}_{-0.1}$ for ZH^0 production, and $1.6^{+2.7}_{-1.8}$ for $t\bar{t}H^0$ production.
- ¹¹ AAD 14BJ measure fiducial and differential cross sections of the process $pp \rightarrow H^0 X, H^0 \rightarrow \gamma\gamma$ at $E_{\text{cm}} = 8 \text{ TeV}$ with 20.3 fb^{-1} . See their Table 3 and Figs. 3–12 for data.
- ¹² KHACHATRYAN 14P use 5.1 fb^{-1} of pp collisions at $E_{\text{cm}} = 7 \text{ TeV}$ and 19.7 fb^{-1} at $E_{\text{cm}} = 8 \text{ TeV}$. The last uncertainty in the measurement is theory systematics. The quoted signal strength is given for $m_{H^0} = 124.7 \text{ GeV}$. The signal strength for the gluon fusion and $t\bar{t}H$ production mode is $1.13^{+0.37}_{-0.31}$, while the signal strength for the vector boson fusion and WH^0, ZH^0 production mode is $1.16^{+0.63}_{-0.58}$.
- ¹³ AAD 13AK use 4.7 fb^{-1} of pp collisions at $E_{\text{cm}} = 7 \text{ TeV}$ and 20.7 fb^{-1} at $E_{\text{cm}} = 8 \text{ TeV}$. The quoted signal strength is given for $m_{H^0} = 125.5 \text{ GeV}$.
- ¹⁴ AALTONEN 13L combine all CDF results with $9.45\text{--}10.0 \text{ fb}^{-1}$ of $p\bar{p}$ collisions at $E_{\text{cm}} = 1.96 \text{ TeV}$. The quoted signal strength is given for $m_{H^0} = 125 \text{ GeV}$.
- ¹⁵ ABAZOV 13L combine all D0 results with up to 9.7 fb^{-1} of $p\bar{p}$ collisions at $E_{\text{cm}} = 1.96 \text{ TeV}$. The quoted signal strength is given for $m_{H^0} = 125 \text{ GeV}$.
- ¹⁶ AAD 12AI obtain results based on 4.8 fb^{-1} of pp collisions at $E_{\text{cm}} = 7 \text{ TeV}$ and 5.9 fb^{-1} at $E_{\text{cm}} = 8 \text{ TeV}$. The quoted signal strengths are given for $m_{H^0} = 126 \text{ GeV}$. See also AAD 12DA.
- ¹⁷ CHATRCHYAN 12N obtain results based on 5.1 fb^{-1} of pp collisions at $E_{\text{cm}} = 7 \text{ TeV}$ and 5.3 fb^{-1} at $E_{\text{cm}} = 8 \text{ TeV}$. The quoted signal strength is given for $m_{H^0} = 125.5 \text{ GeV}$. See also CHATRCHYAN 13Y.

 $\gamma\gamma$ Final State

VALUE	DOCUMENT ID	TECN	COMMENT
1.10 ± 0.07 OUR AVERAGE			
1.12 ± 0.09	1 SIRUNYAN 21o CMS	pp , 13 TeV	
$0.9^{+0.15}_{-0.14}$	2 AABOUD 18BO ATLS	pp , 13 TeV, 36.1 fb^{-1}	
$1.14^{+0.19}_{-0.18}$	3,4 AAD 16AN LHC	pp , 7, 8 TeV	
$5.97^{+3.39}_{-3.12}$	5 AALTONEN 13M TEVA	$p\bar{p} \rightarrow H^0 X$, 1.96 TeV	
• • • We do not use the following data for averages, fits, limits, etc. • • •			
$1.20^{+0.18}_{-0.14}$	6 SIRUNYAN 19AT CMS	pp , 13 TeV	
$1.18^{+0.17}_{-0.14}$	7 SIRUNYAN 19L CMS	pp , 13 TeV, diff. x-section	
$1.14^{+0.27}_{-0.25}$	8 SIRUNYAN 18DS CMS	$pp, H^0 \rightarrow \gamma\gamma$, 13 TeV, floated m_{H^0}	
$1.11^{+0.25}_{-0.23}$	4 AAD 16AN ATLS	pp , 7, 8 TeV	
	4 AAD 16AN CMS	pp , 7, 8 TeV	

 $c\bar{c}$ Final State

VALUE	CL%	DOCUMENT ID	TECN	COMMENT
$37 \pm 17^{+11}_{-9}$		1 SIRUNYAN 20AE CMS	pp , 13 TeV	
• • • We do not use the following data for averages, fits, limits, etc. • • •				
<110	95	2 AABOUD 18M ATLS	pp , 13 TeV	
		1 SIRUNYAN 20AE use 35.9 fb^{-1} at of pp collisions at $E_{\text{cm}} = 13 \text{ TeV}$. The measured best fit value of $\sigma(pp \rightarrow VH^0) \cdot B(H^0 \rightarrow c\bar{c})$ is $2.40^{+1.12+0.65}_{-1.11-0.61} \text{ pb}$ (equivalent to $< 4.5 \text{ pb}$ at 95% CL upper limit, i.e. 70 times the standard model), where V is $W \rightarrow \ell\nu, Z \rightarrow \ell\ell$, or $Z \rightarrow \nu\nu$ ($\ell = e, \mu$). The quoted values are given for $m_{H^0} = 125 \text{ GeV}$.		
		2 AABOUD 18M use 36.1 fb^{-1} at of pp collisions at $E_{\text{cm}} = 13 \text{ TeV}$. The upper limit on $\sigma(pp \rightarrow ZH^0) \cdot B(H^0 \rightarrow c\bar{c})$ is 2.7 pb at 95% CL. This corresponds to 110 times the standard model. The quoted values are given for $m_{H^0} = 125 \text{ GeV}$.		

Gauge & Higgs Boson Particle Listings

 H^0 $b\bar{b}$ Final State

VALUE	DOCUMENT ID	TECN	COMMENT
0.98 ± 0.12 OUR AVERAGE			
$1.02^{+0.12}_{-0.11} \pm 0.14_{-0.13}$	1 AAD	21AB ATLS	$pp \rightarrow H^0 W / H^0 Z, H^0 \rightarrow b\bar{b}, 13 \text{ TeV}, 139 \text{ fb}^{-1}$
$0.95 \pm 0.32^{+0.20}_{-0.17}$	2 AAD	21AJ ATLS	VBF, $H^0 \rightarrow b\bar{b}, pp, 13 \text{ TeV}, 126 \text{ fb}^{-1}$
1.06 ± 0.26	3 SIRUNYAN	18DB CMS	$pp \rightarrow H^0 W / H^0 Z, H^0 \rightarrow b\bar{b}, 13 \text{ TeV}, 77.2 \text{ fb}^{-1}$
$0.70^{+0.29}_{-0.27}$	4,5 AAD	16AN LHC	$pp, 7, 8 \text{ TeV}$
$1.59^{+0.69}_{-0.72}$	6 AALTONEN	13M TEVA	$p\bar{p} \rightarrow H^0 X, 1.96 \text{ TeV}$
• • • We do not use the following data for averages, fits, limits, etc. • • •			
$0.95 \pm 0.18^{+0.19}_{-0.18}$	1 AAD	21AB ATLS	$pp \rightarrow H^0 W, H^0 \rightarrow b\bar{b}, 13 \text{ TeV}, 139 \text{ fb}^{-1}$
$1.08 \pm 0.17^{+0.18}_{-0.15}$	1 AAD	21AB ATLS	$pp \rightarrow H^0 Z, H^0 \rightarrow b\bar{b}, 13 \text{ TeV}, 139 \text{ fb}^{-1}$
$0.72^{+0.29+0.26}_{-0.28-0.22}$	7 AAD	21H ATLS	$pp \rightarrow H^0 W / H^0 Z, H^0 \rightarrow b\bar{b}, \text{boosted } W/Z, 13 \text{ TeV}, 139 \text{ fb}^{-1}$
1.3 ± 1.0	8 AAD	21M ATLS	VBF+ $\gamma, H^0 \rightarrow b\bar{b}, pp, 13 \text{ TeV}, 132 \text{ fb}^{-1}$
$3.7 \pm 1.2^{+0.11}_{-0.9}$	9 SIRUNYAN	20BL CMS	boosted $H^0 \rightarrow b\bar{b}, pp, 13 \text{ TeV}$
1.12 ± 0.29	10 AABOUD	19U ATLS	$pp \rightarrow VH^0, H^0 \rightarrow b\bar{b}, 13 \text{ TeV}, \text{cross sections}$
$1.16^{+0.27}_{-0.25}$	11 SIRUNYAN	19AT CMS	$pp, 13 \text{ TeV}$
$0.98^{+0.22}_{-0.21}$	12 AABOUD	18BN ATLS	$pp \rightarrow H^0 W / H^0 Z, H^0 \rightarrow b\bar{b}, 13 \text{ TeV}, 79.8 \text{ fb}^{-1}$
1.01 ± 0.20	13 AABOUD	18BN ATLS	$pp \rightarrow H^0 W / H^0 Z, H^0 \rightarrow b\bar{b}, 7, 8, 13 \text{ TeV}$
1.01 ± 0.20	14 AABOUD	18BN ATLS	$pp \rightarrow H^0 X, \text{ggF}, \text{VBF}, VH^0, t\bar{t}H^0, 7, 8, 13 \text{ TeV}$
$2.5^{+1.4}_{-1.3}$	15,16 AABOUD	18BQ ATLS	$pp \rightarrow H^0 X, \text{VBF}, \text{ggF}, VH^0, t\bar{t}H^0, 13 \text{ TeV}$
$3.0^{+1.7}_{-1.6}$	15,17 AABOUD	18BQ ATLS	$pp \rightarrow H^0 X, \text{VBF}, 13 \text{ TeV}$
$1.19^{+0.40}_{-0.38}$	18 AALTONEN	18C CDF	$p\bar{p} \rightarrow H^0 X, 1.96 \text{ TeV}$
$1.06^{+0.31}_{-0.29}$	19 SIRUNYAN	18AE CMS	$pp \rightarrow H^0 W / H^0 Z, H^0 \rightarrow b\bar{b}, 13 \text{ TeV}$
1.01 ± 0.22	20 SIRUNYAN	18AE CMS	$pp \rightarrow H^0 W / H^0 Z, H^0 \rightarrow b\bar{b}, 7, 8, 13 \text{ TeV}$
1.01 ± 0.22	21 SIRUNYAN	18DB CMS	$pp \rightarrow H^0 W / H^0 Z, H^0 \rightarrow b\bar{b}, 7, 8, 13 \text{ TeV}$
1.04 ± 0.20	22 SIRUNYAN	18DB CMS	$pp \rightarrow H^0 X, \text{ggF}, \text{VBF}, VH^0, t\bar{t}H^0, 7, 8, 13 \text{ TeV}$
$2.3^{+1.8}_{-1.6}$	23 SIRUNYAN	18E CMS	$pp \rightarrow H^0 X, \text{boosted}, 13 \text{ TeV}$
$1.20^{+0.24+0.34}_{-0.23-0.28}$	24 AABOUD	17BA ATLS	$pp \rightarrow H^0 W / ZX, H^0 \rightarrow b\bar{b}, 13 \text{ TeV}, 36.1 \text{ fb}^{-1}$
$0.90 \pm 0.18^{+0.21}_{-0.19}$	25 AABOUD	17BA ATLS	$pp \rightarrow H^0 W / ZX, H^0 \rightarrow b\bar{b}, 7, 8, 13 \text{ TeV}$
$-0.8 \pm 1.3^{+1.8}_{-1.9}$	26 AABOUD	16X ATLS	$pp \rightarrow H^0 X, \text{VBF}, 8 \text{ TeV}$
0.62 ± 0.37	5 AAD	16AN ATLS	$pp, 7, 8 \text{ TeV}$
$0.81^{+0.45}_{-0.43}$	5 AAD	16AN CMS	$pp, 7, 8 \text{ TeV}$
$0.63^{+0.31+0.24}_{-0.30-0.23}$	27 AAD	16K ATLS	$pp, 7, 8 \text{ TeV}$
$0.52 \pm 0.32 \pm 0.24$	28 AAD	15G ATLS	$pp \rightarrow H^0 W / ZX, 7, 8 \text{ TeV}$
$2.8^{+1.6}_{-1.4}$	29 KHACHATRYAN..15Z	CMS	$pp \rightarrow H^0 X, \text{VBF}, 8 \text{ TeV}$
$1.03^{+0.44}_{-0.42}$	30 KHACHATRYAN..15Z	CMS	$pp, 8 \text{ TeV}, \text{combined}$
1.0 ± 0.5	31 CHATRCHYAN14AI	CMS	$pp \rightarrow H^0 W / ZX, 7, 8 \text{ TeV}$
$1.72^{+0.92}_{-0.87}$	32 AALTONEN	13L CDF	$p\bar{p} \rightarrow H^0 X, 1.96 \text{ TeV}$
$1.23^{+1.24}_{-1.17}$	33 ABAZOV	13L D0	$p\bar{p} \rightarrow H^0 X, 1.96 \text{ TeV}$
0.5 ± 2.2	34 AAD	12AI ATLS	$pp \rightarrow H^0 W / ZX, 7 \text{ TeV}$
$0.48^{+0.81}_{-0.70}$	35 AALTONEN	12T TEVA	$p\bar{p} \rightarrow H^0 W / ZX, 1.96 \text{ TeV}$
	36 CHATRCHYAN12N	CMS	$pp \rightarrow H^0 W / ZX, 7, 8 \text{ TeV}$

1 AAD 21AB search for $VH^0, H^0 \rightarrow b\bar{b}$ ($V = W, Z$) using 139 fb^{-1} of pp collision data at $E_{\text{cm}} = 13 \text{ TeV}$. The results are given for $m_{H^0} = 125 \text{ GeV}$. Cross sections are given in their Table 13 and Fig. 7, which are based on the simplified template cross section framework (reduced stage-1.2). Wilson coefficients of the Warsaw-basis operators are given in their Fig. 9.

2 AAD 21AJ present measurements of $H^0 \rightarrow b\bar{b}$ in the VBF production mode. The inclusive VBF cross sections with and without the branching ratio of $H^0 \rightarrow b\bar{b}$ are $2.07 \pm 0.70^{+0.46}_{-0.37} \text{ fb}$ and $3.56 \pm 1.21^{+0.80}_{-0.64} \text{ fb}$, respectively. The latter is obtained assuming the SM value of $B(H^0 \rightarrow b\bar{b}) = 0.5809$ and $m_{H^0} = 125 \text{ GeV}$.

3 SIRUNYAN 18DB search for $VH^0, H^0 \rightarrow b\bar{b}$ ($V = W, Z$) using 77.2 fb^{-1} of pp collision data at $E_{\text{cm}} = 13 \text{ TeV}$. The quoted signal strength corresponds to a significance of 4.4 standard deviations and is given for $m_{H^0} = 125.09 \text{ GeV}$.

4 AAD 16AN perform fits to the ATLAS and CMS data at $E_{\text{cm}} = 7$ and 8 TeV . The signal strengths for individual production processes are 1.0 ± 0.5 for WH^0 production, 0.4 ± 0.4 for ZH^0 production, and 1.1 ± 1.0 for $t\bar{t}H^0$ production.

5 AAD 16AN: In the fit, relative production cross sections are fixed to those in the Standard Model. The quoted signal strength is given for $m_{H^0} = 125.09 \text{ GeV}$.

6 AALTONEN 13M combine all Tevatron data from the CDF and D0 Collaborations with up to 10.0 fb^{-1} and 9.7 fb^{-1} , respectively, of $p\bar{p}$ collisions at $E_{\text{cm}} = 1.96 \text{ TeV}$. The quoted signal strength is given for $m_{H^0} = 125 \text{ GeV}$.

7 AAD 21H present measurements of $H^0 \rightarrow b\bar{b}$ with a boosted vector boson ($p_{\mathcal{T}} > 250 \text{ GeV}$) using 139 fb^{-1} of pp collision data at $E_{\text{cm}} = 13 \text{ TeV}$. Cross sections are given in their Table 6 and Fig. 4, which are based on the simplified template cross section framework (reduced stage-1.2). Wilson coefficients of the Warsaw-basis operators are given in their Fig. 5.

8 AAD 21M search for VBF+ $\gamma, H^0 \rightarrow b\bar{b}$ using 132 fb^{-1} of pp collision data at $E_{\text{cm}} = 13 \text{ TeV}$.

9 SIRUNYAN 20BL search for boosted $H^0 \rightarrow b\bar{b}$ ($p_{\mathcal{T}}(H^0) > 450 \text{ GeV}$) using 137 fb^{-1} of pp collision data at $E_{\text{cm}} = 13 \text{ TeV}$. The quoted signal strength corresponds to a significance of 2.5 standard deviations and is given for $m_{H^0} = 125 \text{ GeV}$. A differential cross section as a function of Higgs boson $p_{\mathcal{T}}$ for ggF is shown in their Fig. 7, assuming the other production modes occur at the expected SM rates. The reported value is $3.7 \pm 1.2^{+0.8+0.8}_{-0.7-0.5}$ where the last uncertainty comes from theoretical modeling. We have combined the systematic uncertainties in quadrature.

10 AABOUD 19U measure cross sections of $pp \rightarrow VH^0, H^0 \rightarrow b\bar{b}$ production as a function of the gauge boson transverse momentum using data of 79.8 fb^{-1} . The kinematic fiducial volumes used is based on the simplified template cross section framework (reduced stage-1). See their Table 3 and Fig. 3.

11 SIRUNYAN 19AT perform a combine fit to 35.9 fb^{-1} of data at $E_{\text{cm}} = 13 \text{ TeV}$.

12 AABOUD 18BN search for $VH^0, H^0 \rightarrow b\bar{b}$ ($V = W, Z$) using 79.8 fb^{-1} of pp collision data at $E_{\text{cm}} = 13 \text{ TeV}$. The quoted signal strength corresponds to a significance of 4.9 standard deviations and is given for $m_{H^0} = 125 \text{ GeV}$.

13 AABOUD 18BN combine results of 79.8 fb^{-1} at $E_{\text{cm}} = 13 \text{ TeV}$ with results of VH^0 at $E_{\text{cm}} = 7$ and 8 TeV .

14 AABOUD 18BN combine results of VH^0 at $E_{\text{cm}} = 7, 8$ and 13 TeV with results of VBF (+gluon fusion) and $t\bar{t}H^0$ at $E_{\text{cm}} = 7, 8$, and 13 TeV to perform a search for the $H^0 \rightarrow b\bar{b}$ decay. The quoted signal strength assumes a SM production strength and corresponds to a significance of 5.4 standard deviations.

15 AABOUD 18BQ search for $H^0 \rightarrow b\bar{b}$ produced through vector-boson fusion (VBF) and VBF+ γ with 30.6 fb^{-1} pp collision data at $E_{\text{cm}} = 13 \text{ TeV}$. The quoted signal strength is given for $m_{H^0} = 125 \text{ GeV}$.

16 The signal strength is measured including all production modes (VBF, ggF, $VH^0, t\bar{t}H^0$).

17 The signal strength is measured for VBF-only and others (ggF, $VH^0, t\bar{t}H^0$) are constrained to Standard Model expectations with uncertainties described in their Section VIII B.

18 AALTONEN 18c use 5.4 fb^{-1} of $p\bar{p}$ collisions at $E_{\text{cm}} = 1.96 \text{ TeV}$. The upper limit at 95% CL on $p\bar{p} \rightarrow H^0 \rightarrow b\bar{b}$ is 33 times the SM prediction, which corresponds to a cross section of 40.6 pb .

19 SIRUNYAN 18AE use 35.9 fb^{-1} of pp collision data at $E_{\text{cm}} = 13 \text{ TeV}$. The quoted signal strength corresponds to 3.3 standard deviations and is given for $m_{H^0} = 125.09 \text{ GeV}$.

20 SIRUNYAN 18AE combine the result of 35.9 fb^{-1} at $E_{\text{cm}} = 13 \text{ TeV}$ with the results obtained from data of up to 5.1 fb^{-1} at $E_{\text{cm}} = 7 \text{ TeV}$ and up to 18.9 fb^{-1} at $E_{\text{cm}} = 8 \text{ TeV}$ (CHATRCHYAN 14AI and KHACHATRYAN 15Z). The quoted signal strength corresponds to 3.8 standard deviations and is given for $m_{H^0} = 125.09 \text{ GeV}$.

21 SIRUNYAN 18DB combine the result of 77.2 fb^{-1} at $E_{\text{cm}} = 13 \text{ TeV}$ with the results obtained from data of up to 5.1 fb^{-1} at $E_{\text{cm}} = 7 \text{ TeV}$ and up to 18.9 fb^{-1} at $E_{\text{cm}} = 8 \text{ TeV}$. The quoted signal strength corresponds to a significance of 4.8 standard deviations and is given for $m_{H^0} = 125.09 \text{ GeV}$.

22 SIRUNYAN 18DB combine results of 77.2 fb^{-1} at $E_{\text{cm}} = 13 \text{ TeV}$ with results of gluon fusion (ggF), VBF and $t\bar{t}H^0$ at $E_{\text{cm}} = 7 \text{ TeV}, 8 \text{ TeV}$ and 13 TeV to perform a search for the $H^0 \rightarrow b\bar{b}$ decay. The quoted signal strength assumes a SM production strength and corresponds to a significance of 5.6 standard deviations and is given for $m_{H^0} = 125.09 \text{ GeV}$.

23 SIRUNYAN 18E use 35.9 fb^{-1} at $E_{\text{cm}} = 13 \text{ TeV}$. The quoted signal strength is given for $m_{H^0} = 125 \text{ GeV}$. They measure $\sigma \cdot B$ for gluon fusion production of $H^0 \rightarrow b\bar{b}$ with $p_{\mathcal{T}} > 450 \text{ GeV}$, $|\eta| < 2.5$ to be $74 \pm 48^{+17}_{-10} \text{ fb}$.

24 AABOUD 17BA use 36.1 fb^{-1} at $E_{\text{cm}} = 13 \text{ TeV}$. The quoted signal strength is given for $m_{H^0} = 125 \text{ GeV}$. They give $\sigma(WH) \cdot B(H^0 \rightarrow b\bar{b}) = 1.08^{+0.54}_{-0.47} \text{ pb}$ and $\sigma(ZH) \cdot B(H^0 \rightarrow b\bar{b}) = 0.57^{+0.26}_{-0.23} \text{ pb}$.

25 AABOUD 17BA combine 7, 8 and 13 TeV analyses. The quoted signal strength is given for $m_{H^0} = 125 \text{ GeV}$.

26 AABOUD 16X search for vector-boson fusion production of H^0 decaying to $b\bar{b}$ in 20.2 fb^{-1} of pp collisions at $E_{\text{cm}} = 8 \text{ TeV}$. The quoted signal strength is given for $m_{H^0} = 125 \text{ GeV}$.

27 AAD 16k use up to 4.7 fb^{-1} of pp collisions at $E_{\text{cm}} = 7 \text{ TeV}$ and up to 20.3 fb^{-1} at $E_{\text{cm}} = 8 \text{ TeV}$. The quoted signal strength is given for $m_{H^0} = 125.36 \text{ GeV}$.

28 AAD 15G use 4.7 fb^{-1} of pp collisions at $E_{\text{cm}} = 7 \text{ TeV}$ and 20.3 fb^{-1} at $E_{\text{cm}} = 8 \text{ TeV}$. The quoted signal strength is given for $m_{H^0} = 125.36 \text{ GeV}$.

29 KHACHATRYAN 15Z search for vector-boson fusion production of H^0 decaying to $b\bar{b}$ in up to 19.8 fb^{-1} of pp collisions at $E_{\text{cm}} = 8 \text{ TeV}$. The quoted signal strength is given for $m_{H^0} = 125 \text{ GeV}$.

30 KHACHATRYAN 15Z combined vector boson fusion, WH^0, ZH^0 production, and $t\bar{t}H^0$ production results. The quoted signal strength is given for $m_{H^0} = 125 \text{ GeV}$.

31 CHATRCHYAN 14AI use up to 5.1 fb^{-1} of pp collisions at $E_{\text{cm}} = 7 \text{ TeV}$ and up to 18.9 fb^{-1} at $E_{\text{cm}} = 8 \text{ TeV}$. The quoted signal strength is given for $m_{H^0} = 125 \text{ GeV}$. See also CHATRCHYAN 14AJ.

See key on page 1127

Gauge & Higgs Boson Particle Listings

 H^0

- ³² AALTONEN 13L combine all CDF results with $9.45\text{--}10.0\text{ fb}^{-1}$ of $p\bar{p}$ collisions at $E_{\text{cm}} = 1.96\text{ TeV}$. The quoted signal strength is given for $m_{H^0} = 125\text{ GeV}$.
- ³³ ABAZOV 13L combine all D0 results with up to 9.7 fb^{-1} of $p\bar{p}$ collisions at $E_{\text{cm}} = 1.96\text{ TeV}$. The quoted signal strength is given for $m_{H^0} = 125\text{ GeV}$.
- ³⁴ AAD 12AI obtain results based on $4.6\text{--}4.8\text{ fb}^{-1}$ of pp collisions at $E_{\text{cm}} = 7\text{ TeV}$. The quoted signal strengths are given in their Fig. 10 for $m_{H^0} = 126\text{ GeV}$. See also Fig. 13 of AAD 12DA.
- ³⁵ AALTONEN 12T combine AALTONEN 12Q, AALTONEN 12R, AALTONEN 12S, ABAZOV 12O, ABAZOV 12P, and ABAZOV 12K. An excess of events over background is observed which is most significant in the region $m_{H^0} = 120\text{--}135\text{ GeV}$, with a local significance of up to 3.3σ . The local significance at $m_{H^0} = 125\text{ GeV}$ is 2.8σ , which corresponds to $(\sigma(H^0 W) + \sigma(H^0 Z)) \cdot \text{B}(H^0 \rightarrow b\bar{b}) = (0.23^{+0.09}_{-0.08})\text{ pb}$, compared to the Standard Model expectation at $m_{H^0} = 125\text{ GeV}$ of $0.12 \pm 0.01\text{ pb}$. Superseded by AALTONEN 13M.
- ³⁶ CHATRCHYAN 12N obtain results based on 5.0 fb^{-1} of pp collisions at $E_{\text{cm}} = 7\text{ TeV}$ and 5.1 fb^{-1} at $E_{\text{cm}} = 8\text{ TeV}$. The quoted signal strength is given for $m_{H^0} = 125.5\text{ GeV}$. See also CHATRCHYAN 13Y.

 $\mu^+ \mu^-$ Final State

VALUE	CL%	DOCUMENT ID	TECN	COMMENT
1.19 ± 0.34	OUR AVERAGE			
1.2 ± 0.6		1 AAD	21 ATLS	pp , 13 TeV
$1.19^{+0.40+0.15}_{-0.39-0.14}$		2 SIRUNYAN	21c CMS	pp , 13 TeV
• • • We do not use the following data for averages, fits, limits, etc. • • •				
$0.69^{+1.25}_{-1.24}$		3 SIRUNYAN	19AT CMS	pp , 13 TeV
0.7 ± 1.0	$^{+0.2}_{-0.1}$	4 SIRUNYAN	19E CMS	pp , 13 TeV, 35.9 fb^{-1}
1.0 ± 1.0	± 0.1	4 SIRUNYAN	19E CMS	pp , 7, 8, 13 TeV
-0.1 ± 1.4		5 AABOUD	17Y ATLS	pp , 7, 8, 13 TeV
-0.1 ± 1.5		5 AABOUD	17Y ATLS	pp , 13 TeV
0.1 ± 2.5		6 AAD	16AN LHC	pp , 7, 8 TeV
-0.6 ± 3.6		6 AAD	16AN ATLS	pp , 7, 8 TeV
0.9 ± 3.6		6 AAD	16AN CMS	pp , 7, 8 TeV
< 7.4	95	7 KHACHATRYAN	15H CMS	$pp \rightarrow H^0 X$, 7, 8 TeV
< 7.0	95	8 AAD	14AS ATLS	$pp \rightarrow H^0 X$, 7, 8 TeV

- ¹ AAD 21 search for $H^0 \rightarrow \mu^+ \mu^-$ using 139 fb^{-1} of pp collision data at $E_{\text{cm}} = 13\text{ TeV}$. The quoted signal strength corresponds to a significance of 2.0 standard deviations and is given for $m_{H^0} = 125.09\text{ GeV}$. The upper limit on the cross section times branching fraction is 2.2 times the SM prediction at 95% CL, which corresponds to the branching fraction upper limit of 4.7×10^{-4} (assuming SM production cross sections).
- ² SIRUNYAN 21 search for $H^0 \rightarrow \mu^+ \mu^-$ using 137 fb^{-1} of pp collision data at $E_{\text{cm}} = 13\text{ TeV}$. The quoted signal strength corresponds to a significance of 3.0 standard deviations and is given for $m_{H^0} = 125.38\text{ GeV}$.
- ³ SIRUNYAN 19AT perform a combine fit to 35.9 fb^{-1} of data at $E_{\text{cm}} = 13\text{ TeV}$.
- ⁴ SIRUNYAN 19E search for $H^0 \rightarrow \mu^+ \mu^-$ using 35.9 fb^{-1} of pp collisions at $E_{\text{cm}} = 13\text{ TeV}$ and combine with results of 7 TeV (5.0 fb^{-1}) and 8 TeV (19.7 fb^{-1}). The upper limit at 95% CL on the signal strength is 2.9, which corresponds to the SM Higgs boson branching fraction to a muon pair of 6.4×10^{-4} .
- ⁵ AABOUD 17Y use 36.1 fb^{-1} of pp collisions at $E_{\text{cm}} = 13\text{ TeV}$, 20.3 fb^{-1} at 8 TeV and 4.5 fb^{-1} at 7 TeV. The quoted signal strength is given for $m_{H^0} = 125\text{ GeV}$.
- ⁶ AAD 16AN: In the fit, relative production cross sections are fixed to those in the Standard Model. The quoted signal strength is given for $m_{H^0} = 125.09\text{ GeV}$.
- ⁷ KHACHATRYAN 15H use 5.0 fb^{-1} of pp collisions at $E_{\text{cm}} = 7\text{ TeV}$ and 19.7 fb^{-1} at 8 TeV. The quoted signal strength is given for $m_{H^0} = 125\text{ GeV}$.
- ⁸ AAD 14AS search for $H^0 \rightarrow \mu^+ \mu^-$ in 4.5 fb^{-1} of pp collisions at $E_{\text{cm}} = 7\text{ TeV}$ and 20.3 fb^{-1} at $E_{\text{cm}} = 8\text{ TeV}$. The quoted signal strength is given for $m_{H^0} = 125.5\text{ GeV}$.

 $\tau^+ \tau^-$ Final State

VALUE	CL%	DOCUMENT ID	TECN	COMMENT
1.15 ± 0.15	OUR AVERAGE			
$1.09^{+0.18+0.26+0.16}_{-0.17-0.22-0.11}$		1 AABOUD	19AQ ATLS	pp , 13 TeV, $H \rightarrow \tau\tau$
$1.24^{+0.29}_{-0.27}$		2 SIRUNYAN	19AF CMS	pp , 13 TeV
$1.11^{+0.24}_{-0.22}$		3,4 AAD	16AN LHC	pp , 7, 8 TeV
$1.68^{+2.28}_{-1.68}$		5 AALTONEN	13M TEVA	$p\bar{p} \rightarrow H^0 X$, 1.96 TeV
• • • We do not use the following data for averages, fits, limits, etc. • • •				
$2.5^{+1.4}_{-1.3}$		6 SIRUNYAN	19AF CMS	$pp \rightarrow H^0 W/H^0 Z$, $H^0 \rightarrow \tau\tau$, 13 TeV
$1.02^{+0.26}_{-0.24}$		7 SIRUNYAN	19AT CMS	pp , 13 TeV
$1.09^{+0.27}_{-0.26}$		8 SIRUNYAN	18Y CMS	pp , 13 TeV
0.98 ± 0.18		9 SIRUNYAN	18Y CMS	pp , 7, 8, 13 TeV
2.3 ± 1.6		10 AAD	16AC ATLS	$pp \rightarrow H^0 W/Z X$, 8 TeV
$1.41^{+0.40}_{-0.36}$		4 AAD	16AN ATLS	pp , 7, 8 TeV
$0.88^{+0.30}_{-0.28}$		4 AAD	16AN CMS	pp , 7, 8 TeV
$1.44^{+0.30+0.29}_{-0.29-0.23}$		11 AAD	16K ATLS	pp , 7, 8 TeV
$1.43^{+0.27+0.32}_{-0.26-0.25} \pm 0.09$		12 AAD	15AH ATLS	$pp \rightarrow H^0 X$, 7, 8 TeV

0.78 ± 0.27		13 CHATRCHYAN	14K CMS	$pp \rightarrow H^0 X$, 7, 8 TeV
$0.00^{+8.44}_{-0.00}$		14 AALTONEN	13L CDF	$p\bar{p} \rightarrow H^0 X$, 1.96 TeV
$3.96^{+4.11}_{-3.38}$		15 ABAZOV	13L D0	$p\bar{p} \rightarrow H^0 X$, 1.96 TeV
$0.4^{+1.6}_{-2.0}$		16 AAD	12AI ATLS	$pp \rightarrow H^0 X$, 7 TeV
$0.09^{+0.76}_{-0.74}$		17 CHATRCHYAN	12N CMS	$pp \rightarrow H^0 X$, 7, 8 TeV

- ¹ AABOUD 19AQ use 36.1 fb^{-1} of data. The first, second and third quoted errors are statistical, experimental systematic and theory systematic uncertainties, respectively. The quoted signal strength is given for $m_{H^0} = 125\text{ GeV}$ and corresponds to 4.4 standard deviations. Combining with 7 TeV and 8 TeV results (AAD 15AH), the observed significance is 6.4 standard deviations. The cross sections in the $H^0 \rightarrow \tau\tau$ decay channel ($m_{H^0} = 125\text{ GeV}$) are measured to $3.77^{+0.60}_{-0.59}$ (stat) $^{+0.87}_{-0.74}$ (syst) pb for the inclusive, $0.28 \pm 0.09^{+0.11}_{-0.09}$ pb for VBF, and $3.1 \pm 1.0^{+1.6}_{-1.3}$ pb for gluon-fusion production. See their Table XI for the cross sections in the framework of simplified template cross sections.
- ² SIRUNYAN 19AF use 35.9 fb^{-1} of data. $H^0 W/Z$ channels are added with a few updates on gluon fusion and vector boson fusion with respect to SIRUNYAN 18Y. The quoted signal strength is given for $m_{H^0} = 125\text{ GeV}$ and corresponds to 5.5 standard deviations. The signal strengths for the individual production modes are: $1.12^{+0.53}_{-0.50}$ for gluon fusion, $1.13^{+0.45}$ for vector boson fusion, $3.39^{+1.68}_{-1.54}$ for WH^0 and $1.23^{+1.62}_{-1.35}$ for ZH^0 . See their Fig. 7 for other couplings (κ_V, κ_f).
- ³ AAD 16AN perform fits to the ATLAS and CMS data at $E_{\text{cm}} = 7$ and 8 TeV. The signal strengths for individual production processes are 1.0 ± 0.6 for gluon fusion, 1.3 ± 0.4 for vector boson fusion, -1.4 ± 1.4 for WH^0 production, $2.2^{+2.2}_{-1.8}$ for ZH^0 production, and $-1.9^{+3.7}_{-3.3}$ for $t\bar{t}H^0$ production.
- ⁴ AAD 16AN: In the fit, relative production cross sections are fixed to those in the Standard Model. The quoted signal strength is given for $m_{H^0} = 125.09\text{ GeV}$.
- ⁵ AALTONEN 13M combine all Tevatron data from the CDF and D0 Collaborations with up to 10.0 fb^{-1} and 9.7 fb^{-1} , respectively, of $p\bar{p}$ collisions at $E_{\text{cm}} = 1.96\text{ TeV}$. The quoted signal strength is given for $m_{H^0} = 125\text{ GeV}$.
- ⁶ SIRUNYAN 19AF use 35.9 fb^{-1} of data. The quoted signal strength is given for $m_{H^0} = 125\text{ GeV}$ and corresponds to 2.3 standard deviations.
- ⁷ SIRUNYAN 19AT perform a combine fit to 35.9 fb^{-1} of data at $E_{\text{cm}} = 13\text{ TeV}$. This combination is based on SIRUNYAN 18Y.
- ⁸ SIRUNYAN 18Y use 35.9 fb^{-1} of pp collisions at $E_{\text{cm}} = 13\text{ TeV}$. The quoted signal strength is given for $m_{H^0} = 125.09\text{ GeV}$ and corresponds to 4.9 standard deviations.
- ⁹ SIRUNYAN 18Y combine the result of 35.9 fb^{-1} at $E_{\text{cm}} = 13\text{ TeV}$ with the results obtained from data of 4.9 fb^{-1} at $E_{\text{cm}} = 7\text{ TeV}$ and 19.7 fb^{-1} at $E_{\text{cm}} = 8\text{ TeV}$ (KHACHATRYAN 15AM). The quoted signal strength is given for $m_{H^0} = 125.09\text{ GeV}$ and corresponds to 5.9 standard deviations.
- ¹⁰ AAD 16AC measure the signal strength with $pp \rightarrow H^0 W/Z X$ processes using 20.3 fb^{-1} of $E_{\text{cm}} = 8\text{ TeV}$. The quoted signal strength is given for $m_{H^0} = 125\text{ GeV}$.
- ¹¹ AAD 16K use up to 4.7 fb^{-1} of pp collisions at $E_{\text{cm}} = 7\text{ TeV}$ and up to 20.3 fb^{-1} at $E_{\text{cm}} = 8\text{ TeV}$. The quoted signal strength is given for $m_{H^0} = 125.36\text{ GeV}$.
- ¹² AAD 15AH use 4.5 fb^{-1} of pp collisions at $E_{\text{cm}} = 7\text{ TeV}$ and 20.3 fb^{-1} at $E_{\text{cm}} = 8\text{ TeV}$. The third uncertainty in the measurement is theory systematics. The signal strength for the gluon fusion mode is $2.0 \pm 0.8^{+1.2}_{-0.8} \pm 0.3$ and that for vector boson fusion and $W/Z H^0$ production modes is $1.24^{+0.49+0.31}_{-0.45-0.29} \pm 0.08$. The quoted signal strength is given for $m_{H^0} = 125.36\text{ GeV}$.
- ¹³ CHATRCHYAN 14K use 4.9 fb^{-1} of pp collisions at $E_{\text{cm}} = 7\text{ TeV}$ and 19.7 fb^{-1} at $E_{\text{cm}} = 8\text{ TeV}$. The quoted signal strength is given for $m_{H^0} = 125\text{ GeV}$. See also CHATRCHYAN 14AJ.
- ¹⁴ AALTONEN 13L combine all CDF results with $9.45\text{--}10.0\text{ fb}^{-1}$ of $p\bar{p}$ collisions at $E_{\text{cm}} = 1.96\text{ TeV}$. The quoted signal strength is given for $m_{H^0} = 125\text{ GeV}$.
- ¹⁵ ABAZOV 13L combine all D0 results with up to 9.7 fb^{-1} of $p\bar{p}$ collisions at $E_{\text{cm}} = 1.96\text{ TeV}$. The quoted signal strength is given for $m_{H^0} = 125\text{ GeV}$.
- ¹⁶ AAD 12AI obtain results based on 4.7 fb^{-1} of pp collisions at $E_{\text{cm}} = 7\text{ TeV}$. The quoted signal strengths are given in their Fig. 10 for $m_{H^0} = 126\text{ GeV}$. See also Fig. 13 of AAD 12DA.
- ¹⁷ CHATRCHYAN 12N obtain results based on 4.9 fb^{-1} of pp collisions at $E_{\text{cm}} = 7\text{ TeV}$ and 5.1 fb^{-1} at $E_{\text{cm}} = 8\text{ TeV}$. The quoted signal strength is given for $m_{H^0} = 125.5\text{ GeV}$. See also CHATRCHYAN 13Y.

 $Z\gamma$ Final State

VALUE	CL%	DOCUMENT ID	TECN	COMMENT
< 3.6	95	1 AAD	20AG ATLS	pp , 13 TeV
• • • We do not use the following data for averages, fits, limits, etc. • • •				
< 7.4	95	2 SIRUNYAN	18DQ CMS	pp , 13 TeV
< 6.6	95	3 AABOUD	17AW ATLS	pp , 13 TeV
< 11	95	4 AAD	14J ATLS	pp , 7, 8 TeV
< 9.5	95	5 CHATRCHYAN	13BK CMS	pp , 7, 8 TeV
• • • We do not use the following data for averages, fits, limits, etc. • • •				
¹ AAD 20AG search for $H^0 \rightarrow Z\gamma$, $Z \rightarrow ee, \mu\mu$ in 139 fb^{-1} of pp collisions at $E_{\text{cm}} = 13\text{ TeV}$. The signal strength is $2.0 \pm 0.9^{+0.4}_{-0.3}$ at $m_{H^0} = 125.09\text{ GeV}$, which corresponds to a significance of 2.2 σ . The upper limit of $\sigma(pp \rightarrow H^0) \cdot \text{B}(H^0 \rightarrow Z\gamma)$ is 305 fb at 95% CL.				
² SIRUNYAN 18DQ search for $H^0 \rightarrow Z\gamma$, $Z \rightarrow ee, \mu\mu$ in 35.9 fb^{-1} of pp collisions at $E_{\text{cm}} = 13\text{ TeV}$. The quoted signal strength (see their Figs. 6 and 7) is given for $m_{H^0} = 125\text{ GeV}$.				
³ AABOUD 17AW search for $H^0 \rightarrow Z\gamma$, $Z \rightarrow ee, \mu\mu$ in 36.1 fb^{-1} of pp collisions at $E_{\text{cm}} = 13\text{ TeV}$. The quoted signal strength is given for $m_{H^0} = 125.09\text{ GeV}$. The upper limit on the branching ratio of $H^0 \rightarrow Z\gamma$ is 1.0% at 95% CL assuming the SM Higgs boson production.				

Gauge & Higgs Boson Particle Listings

 H^0

- 4 AAD 14j search for $H^0 \rightarrow Z\gamma \rightarrow \ell\ell\gamma$ in 4.5 fb⁻¹ of pp collisions at $E_{cm} = 7$ TeV and 20.3 fb⁻¹ at $E_{cm} = 8$ TeV. The quoted signal strength is given for $m_{H^0} = 125.5$ GeV.
- 5 CHATRCHYAN 13BK search for $H^0 \rightarrow Z\gamma \rightarrow \ell\ell\gamma$ in 5.0 fb⁻¹ of pp collisions at $E_{cm} = 7$ TeV and 19.6 fb⁻¹ at $E_{cm} = 8$ TeV. A limit on cross section times branching ratio which corresponds to (4–25) times the expected Standard Model cross section is given in the range $m_{H^0} = 120$ –160 GeV at 95% CL. The quoted limit is given for $m_{H^0} = 125$ GeV, where 10 is expected for no signal.

 $\gamma^*\gamma$ Final State

VALUE	CL%	DOCUMENT ID	TECN	COMMENT
$1.5 \pm 0.5^{+0.2}_{-0.1}$		1 AAD	21i ATLS	pp , 13 TeV, $H^0 \rightarrow \ell\ell\gamma$, 139 fb ⁻¹
• • • We do not use the following data for averages, fits, limits, etc. • • •				
<4.0	95	2 SIRUNYAN	18DQ CMS	$pp \rightarrow H^0 X$, 13 TeV, $H^0 \rightarrow \gamma^*\gamma$
<6.7	95	3 KHACHATRYAN	16B CMS	pp , 8 TeV, $e e \gamma$, $\mu \mu \gamma$
1 AAD 21i search for $H^0 \rightarrow \ell\ell\gamma$ ($\ell = e, \mu$) in 139 fb ⁻¹ of pp collisions at $E_{cm} = 13$ TeV. The mass of dilepton $m_{\ell\ell}$ is smaller than 30 GeV. This region is dominated by the decay through γ^* . The quoted signal strength corresponds to a significance of 3.2 standard deviations and is given for $m_{H^0} = 125.09$ GeV. The cross section times the branching ratio of $H^0 \rightarrow \ell\ell\gamma$ for $m_{\ell\ell} < 30$ GeV is measured to be $8.7 \pm 2.7^{+0.7}_{-0.6}$ fb.				
2 SIRUNYAN 18DQ search for $H^0 \rightarrow \gamma^*\gamma, \gamma^* \rightarrow \mu\mu$ in 35.9 fb ⁻¹ of pp collisions at $E_{cm} = 13$ TeV. The mass of γ^* is smaller than 50 GeV except in J/ψ and Υ mass regions. The quoted signal strength (see their Figs. 6 and 7) is given for $m_{H^0} = 125$ GeV.				
3 KHACHATRYAN 16B search for $H^0 \rightarrow \gamma^*\gamma \rightarrow e^+e^-\gamma$ and $\mu^+\mu^-\gamma$ (with $m(e^+e^-) < 3.5$ GeV and $m(\mu^+\mu^-) < 20$ GeV) in 19.7 fb ⁻¹ of pp collisions at $E_{cm} = 8$ TeV. See their Fig. 6 for limits on individual channels.				

Higgs Yukawa couplings

top Yukawa coupling

VALUE	CL%	DOCUMENT ID	TECN	COMMENT
$[-0.9, -0.7]$ or $[0.7, 1.1]$	95	1 SIRUNYAN	21R CMS	pp , 13 TeV
• • • We do not use the following data for averages, fits, limits, etc. • • •				
<1.7	95	2 SIRUNYAN	20c CMS	pp , 13 TeV
<1.67	95	3 SIRUNYAN	19BY CMS	pp , 13 TeV
<2.1	95	4 SIRUNYAN	18BU CMS	pp , 13 TeV
1 SIRUNYAN 21R constrain the ratio of the top quark Yukawa coupling y_t to its Standard Model value from $t\bar{t}H^0$ and tH^0 production rates using 137 fb ⁻¹ pp collision data at $E_{cm} = 13$ TeV. Assuming a SM Higgs couplings to τ 's, the joint interval $-0.9 < \kappa_t (=y_t/y_t^{SM}) < -0.7$ and $0.7 < \kappa_t < 1.1$ is obtained at 95% CL (see their Fig. 17).				
2 SIRUNYAN 20c search for the production of four top quarks with same-sign and multilepton final states with 137 fb ⁻¹ pp collision data at $E_{cm} = 13$ TeV. The results constrain the ratio of the top quark Yukawa coupling y_t to its Standard Model value by comparing to the central value of a theoretical prediction (see their Refs. [1–2]), yielding $ y_t/y_t^{SM} < 1.7$ at 95% CL. See their Fig. 5.				
3 SIRUNYAN 19BY measure the top quark Yukawa coupling from $t\bar{t}$ kinematic distributions, the invariant mass of the top quark pair and the rapidity difference between t and \bar{t} , in the ℓ -jets final state with 35.8 fb ⁻¹ pp collision data at $E_{cm} = 13$ TeV. The results constrain the ratio of the top quark Yukawa coupling to its the Standard Model to be $1.07^{+0.34}_{-0.43}$ with an upper limit of 1.67 at 95% CL (see their Table III).				
4 SIRUNYAN 18BU search for the production of four top quarks with same-sign and multilepton final states with 35.9 fb ⁻¹ pp collision data at $E_{cm} = 13$ TeV. The results constrain the ratio of the top quark Yukawa coupling y_t to its the Standard Model by comparing to the central value of a theoretical prediction (see their Ref. [16]), yielding $ y_t/y_t^{SM} < 2.1$ at 95% CL.				

OTHER H^0 PRODUCTION PROPERTIES $t\bar{t}H^0$ Production

Signal strength relative to the Standard Model cross section.

VALUE	DOCUMENT ID	TECN	COMMENT
1.10 ± 0.18 OUR AVERAGE			
$0.92 \pm 0.19^{+0.17}_{-0.13}$	1 SIRUNYAN	21R CMS	pp , 13 TeV, $H^0 \rightarrow \tau\tau, WW^*, ZZ^*$
1.2 ± 0.3	2 AABOUD	18AC ATLS	pp , 13 TeV, $H^0 \rightarrow b\bar{b}, \tau\tau, \gamma\gamma, WW^*, ZZ^*$
$1.9^{+0.8}_{-0.7}$	3 AAD	16AN ATLS	pp , 7, 8 TeV
• • • We do not use the following data for averages, fits, limits, etc. • • •			
$1.43^{+0.33+0.21}_{-0.31-0.15}$	4 AAD	20Z ATLS	pp , 13 TeV, $H^0 \rightarrow \gamma\gamma$
$1.38^{+0.36}_{-0.29}$	5 SIRUNYAN	20AS CMS	pp , 13 TeV, $H^0 \rightarrow \gamma\gamma$
$0.72 \pm 0.24 \pm 0.38$	6 SIRUNYAN	19R CMS	pp , 13 TeV, $H^0 \rightarrow b\bar{b}$
$1.6^{+0.5}_{-0.4}$	7 AABOUD	18AC ATLS	pp , 13 TeV, $H^0 \rightarrow \tau\tau, WW^*, ZZ^*$
	8 AABOUD	18BK ATLS	pp , 13 TeV, $H^0 \rightarrow b\bar{b}, \tau\tau, \gamma\gamma, WW^*, ZZ^*$
$0.84^{+0.64}_{-0.61}$	9 AABOUD	18T ATLS	pp , 13 TeV, $H^0 \rightarrow b\bar{b}$
0.9 ± 1.5	10 SIRUNYAN	18BD CMS	pp , 13 TeV, $H^0 \rightarrow b\bar{b}$
$1.23^{+0.45}_{-0.43}$	11 SIRUNYAN	18BQ CMS	pp , 13 TeV, $H^0 \rightarrow \tau\tau, WW^*, ZZ^*$

$1.26^{+0.31}_{-0.26}$	12 SIRUNYAN	18L CMS	pp , 7, 8, 13 TeV, $H^0 \rightarrow b\bar{b}, \tau\tau, \gamma\gamma, WW^*, ZZ^*$
1.7 ± 0.8	13 AAD	16AL ATLS	pp , 7, 8 TeV, $H^0 \rightarrow b\bar{b}, \tau\tau, \gamma\gamma, WW^*$, and ZZ^*
$2.3^{+0.7}_{-0.6}$	3,14 AAD	16AN LHC	pp , 7, 8 TeV
$2.9^{+1.0}_{-0.9}$	3 AAD	16AN CMS	pp , 7, 8 TeV
$1.81^{+0.52+0.58+0.31}_{-0.50-0.55-0.12}$	15 AAD	16K ATLS	pp , 7, 8 TeV
$1.4^{+2.1+0.6}_{-1.4-0.3}$	16 AAD	15 ATLS	pp , 7, 8 TeV
1.5 ± 1.1	17 AAD	15BC ATLS	pp , 8 TeV
$2.1^{+1.4}_{-1.2}$	18 AAD	15T ATLS	pp , 8 TeV
$1.2^{+1.6}_{-1.5}$	19 KHACHATRYAN	15AN CMS	pp , 8 TeV
$2.8^{+1.0}_{-0.9}$	20 KHACHATRYAN	14H CMS	pp , 7, 8 TeV
$9.49^{+6.60}_{-6.28}$	21 AALTONEN	13L CDF	$p\bar{p}$, 1.96 TeV
< 5.8 at 95% CL	22 CHATRCHYAN	13x CMS	pp , 7, 8 TeV, $H^0 \rightarrow b\bar{b}$

- 1 SIRUNYAN 21R search for $t\bar{t}H^0$ in final states with electrons, muons and hadronically decaying τ leptons ($H^0 \rightarrow WW^*, ZZ^*, \tau\tau$) with 137 fb⁻¹ of pp collision data at $E_{cm} = 13$ TeV. The quoted signal strength corresponds to a significance of 4.7 standard deviations and is given for $m_{H^0} = 125$ GeV.
- 2 AABOUD 18AC combine results of $t\bar{t}H^0, H^0 \rightarrow \tau\tau, WW^*(\rightarrow \ell\nu\ell\nu, \ell\nu q\bar{q}), ZZ^*(\rightarrow \ell\nu\nu, \ell\nu q\bar{q})$ with results of $t\bar{t}H^0, H^0 \rightarrow b\bar{b}$ (AABOUD 18T), $\gamma\gamma$ (AABOUD 18B), $ZZ^*(\rightarrow 4\ell)$ (AABOUD 18AJ) in 36.1 fb⁻¹ of pp collisions at $E_{cm} = 13$ TeV. The quoted signal strength is given for $m_{H^0} = 125$ GeV. See their Table 14.
- 3 AAD 16AN: In the fit, relative branching ratios are fixed to those in the Standard Model. The quoted signal strength is given for $m_{H^0} = 125.09$ GeV.
- 4 AAD 20Z measure $\sigma_t\bar{t}H^0 \cdot B(H^0 \rightarrow \gamma\gamma)$ to be $1.64^{+0.38+0.17}_{-0.36-0.14}$ fb in 139 fb⁻¹ of data at $E_{cm} = 13$ TeV.
- 5 SIRUNYAN 20AS measure $\sigma_t\bar{t}H^0 \cdot B(H^0 \rightarrow \gamma\gamma)$ to be $1.56^{+0.34}_{-0.32}$ fb in 137 fb⁻¹ of data at $E_{cm} = 13$ TeV.
- 6 SIRUNYAN 19R search for $t\bar{t}H^0$ production with H^0 decaying to $b\bar{b}$ in 35.9 fb⁻¹ of data at $E_{cm} = 13$ TeV. The quoted signal strength is given for $m_{H^0} = 125$ GeV.
- 7 AABOUD 18AC search for $t\bar{t}H^0$ production with H^0 decaying to $\tau\tau, WW^*(\rightarrow \ell\nu\ell\nu, \ell\nu q\bar{q}), ZZ^*(\rightarrow \ell\nu\nu, \ell\nu q\bar{q})$ in 36.1 fb⁻¹ of pp collisions at $E_{cm} = 13$ TeV. The quoted signal strength is given for $m_{H^0} = 125$ GeV. See their Table 13 and Fig. 13.
- 8 AABOUD 18BK use 79.8 fb⁻¹ data for $t\bar{t}H^0$ production with $H^0 \rightarrow \gamma\gamma$ and $ZZ^* \rightarrow 4\ell$ ($\ell = e, \mu$) and 36.1 fb⁻¹ for other decay channels at $E_{cm} = 13$ TeV. A significance of 5.8 standard deviations is observed for $m_{H^0} = 125.09$ GeV and its signal strength without the uncertainty of the $t\bar{t}H^0$ cross section is $1.32^{+0.28}_{-0.26}$. Combining with results of 7 and 8 TeV (AAD 16K), the significance is 6.3 standard deviations. Assuming Standard Model branching fractions, the total $t\bar{t}H^0$ production cross section at 13 TeV is measured to be $670 \pm 90^{+110}_{-100}$ fb.
- 9 AABOUD 18T search for $t\bar{t}H^0$ production with H^0 decaying to $b\bar{b}$ in 36.1 fb⁻¹ of pp collisions at $E_{cm} = 13$ TeV. The quoted signal strength is given for $m_{H^0} = 125$ GeV.
- 10 SIRUNYAN 18BD search for $t\bar{t}H^0, H^0 \rightarrow b\bar{b}$ in the all-jet final state with 35.9 fb⁻¹ pp collision data at $E_{cm} = 13$ TeV. The quoted signal strength is given for $m_{H^0} = 125$ GeV.
- 11 SIRUNYAN 18BQ search for $t\bar{t}H^0$ in final states with electrons, muons and hadronically decaying τ leptons ($H^0 \rightarrow WW^*, ZZ^*, \tau\tau$) with 35.9 fb⁻¹ of pp collision data at $E_{cm} = 13$ TeV. The quoted signal strength corresponds to a significance of 3.2 standard deviations and is given for $m_{H^0} = 125$ GeV.
- 12 SIRUNYAN 18L use up to 5.1, 19.7 and 35.9 fb⁻¹ of pp collisions at $E_{cm} = 7, 8$, and 13 TeV, respectively. The quoted signal strength corresponds to a significance of 5.2 standard deviations and is given for $m_{H^0} = 125.09$ GeV. H^0 decay channels of $WW^*, ZZ^*, \gamma\gamma, \tau\tau$, and $b\bar{b}$ are used. See their Table 1 and Fig. 2 for results on individual channels.
- 13 AAD 16AL search for $t\bar{t}H^0$ production with H^0 decaying to $\gamma\gamma$ in 4.5 fb⁻¹ of pp collisions at $E_{cm} = 7$ TeV and $b\bar{b}, \tau\tau, \gamma\gamma, WW^*$, and ZZ^* in 20.3 fb⁻¹ at $E_{cm} = 8$ TeV. The quoted signal strength is given for $m_{H^0} = 125$ GeV. This paper combines the results of previous papers, and the new result of this paper only is: $\mu = 1.6 \pm 2.6$.
- 14 AAD 16AN perform fits to the ATLAS and CMS data at $E_{cm} = 7$ and 8 TeV.
- 15 AAD 16K use up to 4.7 fb⁻¹ of pp collisions at $E_{cm} = 7$ TeV and up to 20.3 fb⁻¹ at $E_{cm} = 8$ TeV. The third uncertainty in the measurement is theory systematics. The quoted signal strength is given for $m_{H^0} = 125.36$ GeV.
- 16 AAD 15 search for $t\bar{t}H^0$ production with H^0 decaying to $\gamma\gamma$ in 4.5 fb⁻¹ of pp collisions at $E_{cm} = 7$ TeV and 20.3 fb⁻¹ at $E_{cm} = 8$ TeV. The quoted result on the signal strength is equivalent to an upper limit of 6.7 at 95% CL and is given for $m_{H^0} = 125.4$ GeV.
- 17 AAD 15BC search for $t\bar{t}H^0$ production with H^0 decaying to $b\bar{b}$ in 20.3 fb⁻¹ of pp collisions at $E_{cm} = 8$ TeV. The corresponding upper limit is 3.4 at 95% CL. The quoted signal strength is given for $m_{H^0} = 125$ GeV.
- 18 AAD 15T search for $t\bar{t}H^0$ production with H^0 resulting in multilepton final states (mainly from $WW^*, \tau\tau, ZZ^*$) in 20.3 fb⁻¹ of pp collisions at $E_{cm} = 8$ TeV. The quoted result on the signal strength is given for $m_{H^0} = 125$ GeV and corresponds to an upper limit of 4.7 at 95% CL. The data sample is independent from AAD 15 and AAD 15BC.
- 19 KHACHATRYAN 15AN search for $t\bar{t}H^0$ production with H^0 decaying to $b\bar{b}$ in 19.5 fb⁻¹ of pp collisions at $E_{cm} = 8$ TeV. The quoted result on the signal strength is equivalent to an upper limit of 4.2 at 95% CL and is given for $m_{H^0} = 125$ GeV.
- 20 KHACHATRYAN 14H search for $t\bar{t}H^0$ production with H^0 decaying to $b\bar{b}, \tau\tau, \gamma\gamma, WW^*$, and ZZ^* , in 5.1 fb⁻¹ of pp collisions at $E_{cm} = 7$ TeV and 19.7 fb⁻¹ at $E_{cm} = 8$ TeV. The quoted signal strength is given for $m_{H^0} = 125.6$ GeV.

- 21 AALTONEN 13L combine all CDF results with $9.45\text{--}10.0\text{ fb}^{-1}$ of $p\bar{p}$ collisions at $E_{\text{cm}} = 1.96\text{ TeV}$. The quoted signal strength is given for $m_{H^0} = 125\text{ GeV}$.
- 22 CHATRCHYAN 13x search for $t\bar{t}H^0$ production followed by $H^0 \rightarrow b\bar{b}$, one top decaying to $\ell\nu$ and the other to either $\ell\nu$ or $q\bar{q}$ in 5.0 fb^{-1} and 5.1 fb^{-1} of $p\bar{p}$ collisions at $E_{\text{cm}} = 7$ and 8 TeV . A limit on cross section times branching ratio which corresponds to $(4.0\text{--}8.6)$ times the expected Standard Model cross section is given for $m_{H^0} = 110\text{--}140\text{ GeV}$ at 95% CL. The quoted limit is given for $m_{H^0} = 125\text{ GeV}$, where 5.2 is expected for no signal.

 $H^0 H^0$ Production

The 95% CL limits are for the cross section (CS) and Higgs self coupling (κ_λ) scaling factors both relative to the SM predictions.

CS	κ_λ	CL%	DOCUMENT ID	TECN	COMMENT
< 7.7	-3.3 to 8.5	95	1 SIRUNYAN	21K CMS	13 TeV, $\gamma\gamma b\bar{b}$
< 6.9	-5.0 to 12.0	95	2 AAD	20C ATLS	13 TeV, $b\bar{b}\gamma\gamma$, $b\bar{b}\tau\tau$, $b\bar{b}b\bar{b}$, $b\bar{b}WW^*$, $WW^*\gamma\gamma$, WW^*WW^*
< 40		95	3 AAD	20E ATLS	13 TeV, $H^0 H^0 \rightarrow b\bar{b}\ell\nu\ell\nu$
< 840		95	4 AAD	20X ATLS	13 TeV, VBF, $b\bar{b}b\bar{b}$
< 12.9		95	5 AABOUD	19A ATLS	13 TeV, $b\bar{b}b\bar{b}$
< 300		95	6 AABOUD	19O ATLS	13 TeV, $b\bar{b}WW^*$
< 160		95	7 AABOUD	19T ATLS	13 TeV, WW^*WW^*
< 24	-11 to 17	95	8 SIRUNYAN	19 CMS	13 TeV, $\gamma\gamma b\bar{b}$
< 75		95	9 SIRUNYAN	19AB CMS	13 TeV, $b\bar{b}b\bar{b}$
< 22.2	-11.8 to 18.8	95	10 SIRUNYAN	19BE CMS	13 TeV, $b\bar{b}\gamma\gamma$, $b\bar{b}\tau\tau$, $b\bar{b}b\bar{b}$, $b\bar{b}WW^*$, $b\bar{b}ZZ^*$
< 179		95	11 SIRUNYAN	19H CMS	13 TeV, $b\bar{b}b\bar{b}$
< 230		95	12 AABOUD	18BU ATLS	13 TeV, $\gamma\gamma WW^*$
< 12.7		95	13 AABOUD	18CQ ATLS	13 TeV, $b\bar{b}\tau\tau$
< 22	-8.2 to 13.2	95	14 AABOUD	18CWATLS	13 TeV, $\gamma\gamma b\bar{b}$
< 30		95	15 SIRUNYAN	18A CMS	13 TeV, $b\bar{b}\tau\tau$
< 79		95	16 SIRUNYAN	18F CMS	13 TeV, $b\bar{b}\ell\nu\ell\nu$
< 43		95	17 SIRUNYAN	17CN CMS	8 TeV, $b\bar{b}\tau\tau$, $\gamma\gamma b\bar{b}$, $b\bar{b}b\bar{b}$
< 108		95	18 AABOUD	16I ATLS	13 TeV, $b\bar{b}b\bar{b}$
< 74		95	19 KHACHATRYAN	16BQ CMS	8 TeV, $\gamma\gamma b\bar{b}$
< 70		95	20 AAD	15CE ATLS	8 TeV, $b\bar{b}b\bar{b}$, $b\bar{b}\tau\tau$, $\gamma\gamma b\bar{b}$, $\gamma\gamma WW$

- 1 SIRUNYAN 21K search for non-resonant $H^0 H^0$ production using $H^0 H^0 \rightarrow \gamma\gamma b\bar{b}$ with data of 137 fb^{-1} at $E_{\text{cm}} = 13\text{ TeV}$. The upper limit on the $pp \rightarrow H^0 H^0 \rightarrow \gamma\gamma b\bar{b}$ production cross section at 95% CL is measured to be 0.67 fb , which corresponds to about 7.7 times the SM prediction. The quartic coupling ($VVH^0 H^0$, $V = W, Z$) scaling factor κ_{2V} ($= c_{2V}$) is measured to be $-1.3 < \kappa_{2V} < 3.5$ at 95% CL.
- 2 AAD 20c combine results of up to 36.1 fb^{-1} data at $E_{\text{cm}} = 13\text{ TeV}$ for $pp \rightarrow H^0 H^0 \rightarrow b\bar{b}\gamma\gamma$, $b\bar{b}\tau\tau$, $b\bar{b}b\bar{b}$, $b\bar{b}WW^*$, $WW^*\gamma\gamma$, WW^*WW^* (AABOUD 18CW, AABOUD 18CQ, AABOUD 19A, AABOUD 19O, AABOUD 18BU, and AABOUD 19T).
- 3 AAD 20e search non-resonant for $H^0 H^0$ production using $H^0 H^0 \rightarrow b\bar{b}\ell\nu\ell\nu$, where one of the Higgs bosons decays to $b\bar{b}$ and the other decays to either WW^* , ZZ^* , or $\tau\tau$, with data of 139 fb^{-1} at $E_{\text{cm}} = 13\text{ TeV}$. The upper limit on the $pp \rightarrow H^0 H^0$ production cross section at 95% CL is measured to be 1.2 pb , which corresponds to about 40 times the SM prediction.
- 4 AAD 20x search for $H^0 H^0 \rightarrow b\bar{b}b\bar{b}$ process via VBF with data of 126 fb^{-1} at $E_{\text{cm}} = 13\text{ TeV}$. The upper limit on the SM non-resonant HH production cross section is 1460 fb at 95% CL, which corresponds to 840 times the SM prediction. The quartic coupling ($VVH^0 H^0$, $V = W, Z$) scaling factor κ_{2V} is excluded in the region of $\kappa_{2V} < -0.43$ or $\kappa_{2V} > 2.56$ at 95% CL.
- 5 AABOUD 19a search for $H^0 H^0$ production using $H^0 H^0 \rightarrow b\bar{b}b\bar{b}$ with data of 36.1 fb^{-1} at $E_{\text{cm}} = 13\text{ TeV}$. The upper limit on the $pp \rightarrow H^0 H^0 \rightarrow b\bar{b}b\bar{b}$ production cross section at 95% is measured to be 147 fb , which corresponds to about 12.9 times the SM prediction.
- 6 AABOUD 19o search for $H^0 H^0$ production using $H^0 H^0 \rightarrow b\bar{b}WW^*$ with data of 36.1 fb^{-1} at $E_{\text{cm}} = 13\text{ TeV}$. The upper limit on the $pp \rightarrow H^0 H^0$ production cross section at 95% CL is calculated to be 10 pb from the observed upper limit on the $pp \rightarrow H^0 H^0 \rightarrow b\bar{b}WW^*$ production cross section of 2.5 pb assuming the SM branching fractions. The former corresponds to about 300 times the SM prediction.
- 7 AABOUD 19t search for $H^0 H^0$ production using $H^0 H^0 \rightarrow WW^*WW^*$ with data of 36.1 fb^{-1} at $E_{\text{cm}} = 13\text{ TeV}$. The upper limit on the $pp \rightarrow H^0 H^0$ production cross section at 95% is measured to be 5.3 pb , which corresponds to about 160 times the SM prediction.
- 8 SIRUNYAN 19 search for $H^0 H^0$ production using $H^0 H^0 \rightarrow \gamma\gamma b\bar{b}$ with data of 35.9 fb^{-1} at $E_{\text{cm}} = 13\text{ TeV}$. The upper limit on the $pp \rightarrow H^0 H^0 \rightarrow \gamma\gamma b\bar{b}$ production cross section at 95% CL is measured to be 2.0 fb , which corresponds to about 24 times the SM prediction. The effective Higgs boson self-coupling κ_λ ($= \lambda_{HHH} / \lambda_{HHH}^{\text{SM}}$) is constrained to be $-11 < \kappa_\lambda < 17$ at 95% CL assuming all other Higgs boson couplings are at their SM value.
- 9 SIRUNYAN 19AB search for $H^0 H^0$ production using $H^0 H^0 \rightarrow b\bar{b}b\bar{b}$, where 4 heavy flavor jets from two Higgs bosons are resolved, with data of 35.9 fb^{-1} at $E_{\text{cm}} = 13\text{ TeV}$. The upper limit on the $pp \rightarrow H^0 H^0 \rightarrow b\bar{b}b\bar{b}$ production cross section at 95% is measured to be 847 fb , which corresponds to about 75 times the SM prediction.
- 10 SIRUNYAN 19BE combine results of 13 TeV 35.9 fb^{-1} data: SIRUNYAN 19, SIRUNYAN 18A, SIRUNYAN 19AB, SIRUNYAN 19H, and SIRUNYAN 18F.
- 11 SIRUNYAN 19H search for $H^0 H^0$ production using $H^0 H^0 \rightarrow b\bar{b}b\bar{b}$, where one of $b\bar{b}$ pairs is highly boosted and the other one is resolved, with data of 35.9 fb^{-1} at $E_{\text{cm}} =$

- 13 TeV. The upper limit on the $pp \rightarrow H^0 H^0 \rightarrow b\bar{b}b\bar{b}$ production cross section at 95% is measured to be 1980 fb , which corresponds to about 179 times the SM prediction.
- 12 AABOUD 18BU search for $H^0 H^0$ production using $\gamma\gamma WW^*$ with the final state of $\gamma\gamma\ell\nu j j$ using data of 36.1 fb^{-1} at $E_{\text{cm}} = 13\text{ TeV}$. The upper limit on the $pp \rightarrow H^0 H^0$ production cross section at 95% CL is measured to be 7.7 pb , which corresponds to about 230 times the SM prediction. The upper limit on the $pp \rightarrow H^0 H^0 \rightarrow \gamma\gamma WW^*$ at 95% CL is measured to be 7.5 fb (see their Table 6).
- 13 AABOUD 18CQ search for $H^0 H^0$ production using $H^0 H^0 \rightarrow b\bar{b}\tau\tau$ with data of 36.1 fb^{-1} at $E_{\text{cm}} = 13\text{ TeV}$. The upper limit on the $pp \rightarrow H^0 H^0 \rightarrow b\bar{b}\tau\tau$ production cross section at 95% is measured to be 30.9 fb , which corresponds to about 12.7 times the SM prediction.
- 14 AABOUD 18CW search for $H^0 H^0$ production using $H^0 H^0 \rightarrow \gamma\gamma b\bar{b}$ with data of 36.1 fb^{-1} at $E_{\text{cm}} = 13\text{ TeV}$. The upper limit on the $pp \rightarrow H^0 H^0$ production cross section at 95% is measured to be 0.73 pb , which corresponds to about 22 times the SM prediction. The effective Higgs boson self-coupling κ_λ is constrained to be $-8.2 < \kappa_\lambda < 13.2$ at 95% CL assuming all other Higgs boson couplings are at their SM value.
- 15 SIRUNYAN 18A search for $H^0 H^0$ production using $H^0 H^0 \rightarrow b\bar{b}\tau\tau$ with data of 35.9 fb^{-1} at $E_{\text{cm}} = 13\text{ TeV}$. The upper limit on the $gg \rightarrow H^0 H^0 \rightarrow b\bar{b}\tau\tau$ production cross section is measured to be 75.4 fb , which corresponds to about 30 times the SM prediction. Limits on Higgs-boson trilinear coupling λ_{HHH} and top Yukawa coupling y_t are also given (see their Fig. 6).
- 16 SIRUNYAN 18F search non-resonant for $H^0 H^0$ production using $H^0 H^0 \rightarrow b\bar{b}\ell\nu\ell\nu$, where $\ell\nu\ell\nu$ is either $WW \rightarrow \ell\nu\ell\nu$ or $ZZ \rightarrow \ell\nu\ell\nu$ ($\ell = e, \mu$ or a leptonically decaying τ), with data of 35.9 fb^{-1} at $E_{\text{cm}} = 13\text{ TeV}$. The upper limit on the $H^0 H^0 \rightarrow b\bar{b}\ell\nu\ell\nu$ production cross section at 95% CL is measured to be 72 fb , which corresponds to about 79 times the SM prediction.
- 17 SIRUNYAN 17CN search for $H^0 H^0$ production using $H^0 H^0 \rightarrow b\bar{b}\tau\tau$ with data of 18.3 fb^{-1} at $E_{\text{cm}} = 8\text{ TeV}$. Results are then combined with the published results of the $H^0 H^0 \rightarrow \gamma\gamma b\bar{b}$ and $H^0 H^0 \rightarrow b\bar{b}b\bar{b}$, which use data of up to 19.7 fb^{-1} at $E_{\text{cm}} = 8\text{ TeV}$. The upper limit on the $gg \rightarrow H^0 H^0$ production cross section is measured to be 0.59 pb from $b\bar{b}\tau\tau$, which corresponds to about 59 times the SM prediction (gluon fusion). The combined upper limit is 0.43 pb , which is about 43 times the SM prediction. The quoted values are given for $m_{H^0} = 125\text{ GeV}$.
- 18 AABOUD 16I search for $H^0 H^0$ production using $H^0 H^0 \rightarrow b\bar{b}b\bar{b}$ with data of 3.2 fb^{-1} at $E_{\text{cm}} = 13\text{ TeV}$. The upper limit on the $pp \rightarrow H^0 H^0 \rightarrow b\bar{b}b\bar{b}$ production cross section is measured to be 1.22 pb . This result corresponds to about 108 times the SM prediction (gluon fusion), which is $11.3^{+0.9}_{-1.0}\text{ fb}$ (NNLO+NNLL) including top quark mass effects. The quoted values are given for $m_{H^0} = 125\text{ GeV}$.
- 19 KHACHATRYAN 16BQ search for $H^0 H^0$ production using $H^0 H^0 \rightarrow \gamma\gamma b\bar{b}$ with data of 19.7 fb^{-1} at $E_{\text{cm}} = 8\text{ TeV}$. The upper limit on the $gg \rightarrow H^0 H^0 \rightarrow \gamma\gamma b\bar{b}$ production is measured to be 1.85 fb , which corresponds to about 74 times the SM prediction and is translated into 0.71 pb for $gg \rightarrow H^0 H^0$ production cross section. Limits on Higgs-boson trilinear coupling λ are also given.
- 20 AAD 15CE search for $H^0 H^0$ production using $H^0 H^0 \rightarrow b\bar{b}\tau\tau$ and $H^0 H^0 \rightarrow \gamma\gamma WW$ with data of 20.3 fb^{-1} at $E_{\text{cm}} = 8\text{ TeV}$. These results are then combined with the published results of the $H^0 H^0 \rightarrow \gamma\gamma b\bar{b}$ and $H^0 H^0 \rightarrow b\bar{b}b\bar{b}$, which use data of up to 20.3 fb^{-1} at $E_{\text{cm}} = 8\text{ TeV}$. The upper limits on the $gg \rightarrow H^0 H^0$ production cross section are measured to be 1.6 pb , 11.4 pb , 2.2 pb and 0.62 pb from $b\bar{b}\tau\tau$, $\gamma\gamma WW$, $\gamma\gamma b\bar{b}$ and $b\bar{b}b\bar{b}$, respectively. The combined upper limit is 0.69 pb , which corresponds to about 70 times the SM prediction. The quoted results are given for $m_{H^0} = 125.4\text{ GeV}$. See their Table 4.

 tH^0 production

VALUE	DOCUMENT ID	TECN	COMMENT
$5.7 \pm 2.7 \pm 3.0$	1 SIRUNYAN	21R CMS	pp , 13 TeV
••• We do not use the following data for averages, fits, limits, etc. •••			
	2 AAD	20Z ATLS	pp , 13 TeV
	3 SIRUNYAN	19BK CMS	pp , 13 TeV
	4 KHACHATRYAN	16AU CMS	pp , 8 TeV
1 SIRUNYAN 21R search for tH^0 in final states with electrons, muons and hadronically decaying τ leptons ($H^0 \rightarrow WW^*$, ZZ^* , $\tau\tau$) with 137 fb^{-1} of pp collision data at $E_{\text{cm}} = 13\text{ TeV}$. The quoted signal strength corresponds to a significance of 1.4 standard deviations and is given for $m_{H^0} = 125\text{ GeV}$.			
2 AAD 20Z search for the tH^0 associated production using $H^0 \rightarrow \gamma\gamma$ in 139 fb^{-1} of data at $E_{\text{cm}} = 13\text{ TeV}$. An upper limit on its rate is set to be 12 times the Standard Model at 95% CL ($m_{H^0} = 125.09\text{ GeV}$).			
3 SIRUNYAN 19BK search for the tH^0 associated production using multilepton signatures ($H^0 \rightarrow WW^*$, $H^0 \rightarrow \tau\tau$, $H^0 \rightarrow ZZ^*$) and signatures with a single lepton and a $b\bar{b}$ pair ($H^0 \rightarrow b\bar{b}$) using 35.9 fb^{-1} at $E_{\text{cm}} = 13\text{ TeV}$. Results are combined with $H^0 \rightarrow \gamma\gamma$ (SIRUNYAN 18Ds). The observed 95% CL upper limit on the tH^0 production cross section times $H^0 \rightarrow WW^* + \tau\tau + ZZ^* + b\bar{b} + \gamma\gamma$ branching fraction is 1.94 pb (assuming SM tH^0 production cross section). See their Table X and Fig. 14. The values outside the ranges of $[-0.9, -0.5]$ and $[1.0, 2.1]$ times the standard model top quark Yukawa coupling are excluded at 95% CL.			
4 KHACHATRYAN 16AU search for the tH^0 associated production in 19.7 fb^{-1} at $E_{\text{cm}} = 8\text{ TeV}$. The 95% CL upper limits on the tH^0 associated production cross section is measured to be $600\text{--}1000\text{ fb}$ depending on the assumed $\gamma\gamma$ branching ratios of the Higgs boson. The $\gamma\gamma$ branching ratio is varied to be by a factor of $0.5\text{--}3.0$ of the Standard Model Higgs boson ($m_{H^0} = 125\text{ GeV}$). The results of the signal strengths for a negative Higgs-boson trilinear coupling are given. The results are given for $m_{H^0} = 125\text{ GeV}$.			

 H^0 Production Cross Section in pp Collisions at $\sqrt{s} = 13\text{ TeV}$

Assumes $m_{H^0} = 125\text{ GeV}$

VALUE (pb)	DOCUMENT ID	TECN	COMMENT
56 ± 4 OUR AVERAGE			
$53.5 \pm 4.9 \pm 2.1$	1 AAD	20BA ATLS	pp , 13 TeV, $ZZ^* \rightarrow 4\ell$ ($\ell = e, \mu$)
$61.1 \pm 6.0 \pm 3.7$	2 SIRUNYAN	19BA CMS	pp , 13 TeV, $\gamma\gamma$, $ZZ^* \rightarrow 4\ell$ ($\ell = e, \mu$)

Gauge & Higgs Boson Particle Listings

H⁰

• • • We do not use the following data for averages, fits, limits, etc. • • •

57.0 ^{+6.0+4.0} _{-5.9-3.3}	³ AABOUD	18cg ATLS	$pp, 13 \text{ TeV}, \gamma\gamma, ZZ^* \rightarrow 4\ell (\ell = e, \mu)$
47.9 ^{+9.1} _{-8.6}	³ AABOUD	18cg ATLS	$pp, 13 \text{ TeV}, \gamma\gamma$
68 ⁺¹¹ ₋₁₀	³ AABOUD	18cg ATLS	$pp, 13 \text{ TeV}, ZZ^* \rightarrow 4\ell (\ell = e, \mu)$
69 ⁺¹⁰ ₋₉ ±5	⁴ AABOUD	17co ATLS	$pp, 13 \text{ TeV}, ZZ^* \rightarrow 4\ell$

- 1 AAD 20BA use 139 fb⁻¹ of pp collisions at E_{cm} = 13 TeV with H⁰ → ZZ* → 4ℓ where ℓ = e, μ. The quoted value is given for m_{H⁰} = 125 GeV and assumes the Standard Model branching ratio.
- 2 SIRUNYAN 19BA use 35.9 fb⁻¹ of pp collisions at E_{cm} = 13 TeV.
- 3 AABOUD 18cg use 36.1 fb⁻¹ of pp collisions at E_{cm} = 13 TeV.
- 4 AABOUD 17co use 36.1 fb⁻¹ of pp collisions at E_{cm} = 13 TeV with H⁰ → ZZ* → 4ℓ where ℓ = e, μ for m_{H⁰} = 125 GeV. Differential cross sections for the Higgs boson transverse momentum, Higgs boson rapidity, and other related quantities are measured as shown in their Figs. 8 and 9.

H⁰ REFERENCES

AAD	21	PL B812 135980	G. Aad et al.	(ATLAS Collab.)
AAD	21AB	EPJ C81 178	G. Aad et al.	(ATLAS Collab.)
AAD	21AJ	EPJ C81 537	G. Aad et al.	(ATLAS Collab.)
AAD	21F	PR D103 112006	G. Aad et al.	(ATLAS Collab.)
AAD	21H	PL B816 136204	G. Aad et al.	(ATLAS Collab.)
AAD	21I	PL B819 136412	G. Aad et al.	(ATLAS Collab.)
AAD	21M	JHEP 2103 268	G. Aad et al.	(ATLAS Collab.)
SIRUNYAN	21	PL B812 135992	A. M. Sirunyan et al.	(CMS Collab.)
SIRUNYAN	21A	EPJ C81 13	A. M. Sirunyan et al.	(CMS Collab.)
Also		EPJ C81 333 (errata.)	A. M. Sirunyan et al.	(CMS Collab.)
SIRUNYAN	21AE	PR D104 052004	A. M. Sirunyan et al.	(CMS Collab.)
SIRUNYAN	21C	JHEP 2101 148	A. M. Sirunyan et al.	(CMS Collab.)
SIRUNYAN	21K	JHEP 2103 257	A. M. Sirunyan et al.	(CMS Collab.)
SIRUNYAN	21L	JHEP 2103 011	A. M. Sirunyan et al.	(CMS Collab.)
SIRUNYAN	21O	JHEP 2107 027	A. M. Sirunyan et al.	(CMS Collab.)
SIRUNYAN	21R	EPJ C81 378	A. M. Sirunyan et al.	(CMS Collab.)
SIRUNYAN	21S	EPJ C81 488	A. M. Sirunyan et al.	(CMS Collab.)
SIRUNYAN	21Z	PR D104 032013	A. M. Sirunyan et al.	(CMS Collab.)
TUMASYAN	21D	JHEP 2111 153	A. Tumasyan et al.	(CMS Collab.)
AAD	20	PR D101 012002	G. Aad et al.	(ATLAS Collab.)
AAD	20A	PL B800 135069	G. Aad et al.	(ATLAS Collab.)
AAD	20AE	PRL 125 221802	G. Aad et al.	(ATLAS Collab.)
AAD	20AG	PL B809 135754	G. Aad et al.	(ATLAS Collab.)
AAD	20AQ	EPJ C80 957	G. Aad et al.	(ATLAS Collab.)
Also		EPJ C81 29 (errata.)	G. Aad et al.	(ATLAS Collab.)
Also		EPJ C81 398 (errata.)	G. Aad et al.	(ATLAS Collab.)
AAD	20BA	EPJ C80 942	G. Aad et al.	(ATLAS Collab.)
AAD	20C	PL B800 135103	G. Aad et al.	(ATLAS Collab.)
AAD	20E	PL B801 135145	G. Aad et al.	(ATLAS Collab.)
AAD	20D	PL B801 135148	G. Aad et al.	(ATLAS Collab.)
AAD	20N	PL B805 135426	G. Aad et al.	(ATLAS Collab.)
AAD	20X	JHEP 2007 108	G. Aad et al.	(ATLAS Collab.)
Also		JHEP 2101 145 (errata.)	G. Aad et al.	(ATLAS Collab.)
Also		JHEP 2105 207 (errata.)	G. Aad et al.	(ATLAS Collab.)
AAD	20Z	PRL 125 061802	G. Aad et al.	(ATLAS Collab.)
SIRUNYAN	20AE	JHEP 2003 131	A. M. Sirunyan et al.	(CMS Collab.)
SIRUNYAN	20AS	PRL 125 061801	A. M. Sirunyan et al.	(CMS Collab.)
SIRUNYAN	20BK	JHEP 2011 039	A. M. Sirunyan et al.	(CMS Collab.)
SIRUNYAN	20BL	JHEP 2012 085	A. M. Sirunyan et al.	(CMS Collab.)
SIRUNYAN	20C	EPJ C80 75	A. M. Sirunyan et al.	(CMS Collab.)
SIRUNYAN	20DL	PL B805 135425	A. M. Sirunyan et al.	(CMS Collab.)
AABOUD	19A	JHEP 1901 030	M. Aaboud et al.	(ATLAS Collab.)
AABOUD	19AI	PL B793 499	M. Aaboud et al.	(ATLAS Collab.)
AABOUD	19AL	PRL 122 231801	M. Aaboud et al.	(ATLAS Collab.)
AABOUD	19AQ	PR D99 072001	M. Aaboud et al.	(ATLAS Collab.)
AABOUD	19AF	PL B789 508	M. Aaboud et al.	(ATLAS Collab.)
AABOUD	19N	JHEP 1904 048	M. Aaboud et al.	(ATLAS Collab.)
AABOUD	19O	JHEP 1904 092	M. Aaboud et al.	(ATLAS Collab.)
AABOUD	19T	JHEP 1905 124	M. Aaboud et al.	(ATLAS Collab.)
AABOUD	19U	JHEP 1905 141	M. Aaboud et al.	(ATLAS Collab.)
AAD	19	PL B798 134949	G. Aad et al.	(ATLAS Collab.)
SIRUNYAN	19AB	JHEP 1904 112	A. M. Sirunyan et al.	(CMS Collab.)
SIRUNYAN	19AF	JHEP 1906 093	A. M. Sirunyan et al.	(CMS Collab.)
SIRUNYAN	19AJ	EPJ C79 94	A. M. Sirunyan et al.	(CMS Collab.)
SIRUNYAN	19AT	EPJ C79 421	A. M. Sirunyan et al.	(CMS Collab.)
SIRUNYAN	19AX	PL B791 96	A. M. Sirunyan et al.	(CMS Collab.)
SIRUNYAN	19BA	PL B792 369	A. M. Sirunyan et al.	(CMS Collab.)
SIRUNYAN	19BE	PRL 122 121803	A. M. Sirunyan et al.	(CMS Collab.)
SIRUNYAN	19BK	PR D99 092005	A. M. Sirunyan et al.	(CMS Collab.)
SIRUNYAN	19BL	PR D99 112003	A. M. Sirunyan et al.	(CMS Collab.)
SIRUNYAN	19BO	PL B793 520	A. M. Sirunyan et al.	(CMS Collab.)
SIRUNYAN	19BR	PL B797 134811	A. M. Sirunyan et al.	(CMS Collab.)
SIRUNYAN	19BY	PR D100 072007	A. M. Sirunyan et al.	(CMS Collab.)
SIRUNYAN	19BZ	PR D100 112002	A. M. Sirunyan et al.	(CMS Collab.)
SIRUNYAN	19CG	JHEP 1910 139	A. M. Sirunyan et al.	(CMS Collab.)
SIRUNYAN	19E	PRL 122 021801	A. M. Sirunyan et al.	(CMS Collab.)
SIRUNYAN	19H	JHEP 1901 040	A. M. Sirunyan et al.	(CMS Collab.)
SIRUNYAN	19L	JHEP 1901 183	A. M. Sirunyan et al.	(CMS Collab.)
SIRUNYAN	19R	JHEP 1903 026	A. M. Sirunyan et al.	(CMS Collab.)
AABOUD	18	PL B776 318	M. Aaboud et al.	(ATLAS Collab.)
AABOUD	18AC	PR D97 072003	M. Aaboud et al.	(ATLAS Collab.)
AABOUD	18AJ	JHEP 1803 095	M. Aaboud et al.	(ATLAS Collab.)
AABOUD	18AU	JHEP 1807 127	M. Aaboud et al.	(ATLAS Collab.)
AABOUD	18BK	PL B784 173	M. Aaboud et al.	(ATLAS Collab.)
AABOUD	18BL	PL B786 134	M. Aaboud et al.	(ATLAS Collab.)
AABOUD	18BM	PL B784 345	M. Aaboud et al.	(ATLAS Collab.)
AABOUD	18BN	PL B786 59	M. Aaboud et al.	(ATLAS Collab.)
AABOUD	18BO	PR D98 052005	M. Aaboud et al.	(ATLAS Collab.)
AABOUD	18BP	PL B786 223	M. Aaboud et al.	(ATLAS Collab.)
AABOUD	18BQ	PR D98 052003	M. Aaboud et al.	(ATLAS Collab.)
AABOUD	18BU	EPJ C78 1007	M. Aaboud et al.	(ATLAS Collab.)
AABOUD	18CA	JHEP 1810 180	M. Aaboud et al.	(ATLAS Collab.)
AABOUD	18CO	PL B786 114	M. Aaboud et al.	(ATLAS Collab.)
AABOUD	18CQ	PRL 121 191801	M. Aaboud et al.	(ATLAS Collab.)
AABOUD	18CW	JHEP 1811 040	M. Aaboud et al.	(ATLAS Collab.)
AABOUD	18M	PRL 120 211802	M. Aaboud et al.	(ATLAS Collab.)
AABOUD	18T	PR D97 072016	M. Aaboud et al.	(ATLAS Collab.)
AALJ	18AM	EPJ C78 1008	R. Aaij et al.	(LHCb Collab.)
AALTONEN	18C	PR D98 072002	T. Aaltonen et al.	(CDF Collab.)
SIRUNYAN	18A	PL B778 101	A. M. Sirunyan et al.	(CMS Collab.)
SIRUNYAN	18AE	PL B780 501	A. M. Sirunyan et al.	(CMS Collab.)

SIRUNYAN	18BD	JHEP 1806 101	A. M. Sirunyan et al.	(CMS Collab.)
SIRUNYAN	18BH	JHEP 1806 001	A. M. Sirunyan et al.	(CMS Collab.)
SIRUNYAN	18BQ	JHEP 1808 066	A. M. Sirunyan et al.	(CMS Collab.)
SIRUNYAN	18BU	EPJ C78 140	A. M. Sirunyan et al.	(CMS Collab.)
SIRUNYAN	18BV	EPJ C78 291	A. M. Sirunyan et al.	(CMS Collab.)
SIRUNYAN	18DB	PRL 121 121801	A. M. Sirunyan et al.	(CMS Collab.)
SIRUNYAN	18DQ	JHEP 1811 152	A. M. Sirunyan et al.	(CMS Collab.)
SIRUNYAN	18DS	JHEP 1811 185	A. M. Sirunyan et al.	(CMS Collab.)
SIRUNYAN	18E	PRL 120 071802	A. M. Sirunyan et al.	(CMS Collab.)
SIRUNYAN	18F	JHEP 1801 054	A. M. Sirunyan et al.	(CMS Collab.)
SIRUNYAN	18L	PRL 120 231801	A. M. Sirunyan et al.	(CMS Collab.)
SIRUNYAN	18S	PR D97 092005	A. M. Sirunyan et al.	(CMS Collab.)
SIRUNYAN	18Y	PL B779 283	A. M. Sirunyan et al.	(CMS Collab.)
AABOUD	17AW	JHEP 1710 112	M. Aaboud et al.	(ATLAS Collab.)
AABOUD	17BA	JHEP 1712 024	M. Aaboud et al.	(ATLAS Collab.)
AABOUD	17BD	EPJ C77 765	M. Aaboud et al.	(ATLAS Collab.)
AABOUD	17CO	JHEP 1710 132	M. Aaboud et al.	(ATLAS Collab.)
AABOUD	17Y	PRL 119 051802	M. Aaboud et al.	(ATLAS Collab.)
AAD	17	EPJ C77 70	G. Aad et al.	(ATLAS Collab.)
KHACHATRYAN	17F	JHEP 1702 135	V. Khachatryan et al.	(CMS Collab.)
SIRUNYAN	17AM	PL B775 1	A. M. Sirunyan et al.	(CMS Collab.)
SIRUNYAN	17AV	JHEP 1711 047	A. M. Sirunyan et al.	(CMS Collab.)
SIRUNYAN	17CN	PR D96 072004	A. M. Sirunyan et al.	(CMS Collab.)
AABOUD	16I	PR D94 052002	M. Aaboud et al.	(ATLAS Collab.)
AABOUD	16K	PRL 117 111802	M. Aaboud et al.	(ATLAS Collab.)
AABOUD	16X	JHEP 1611 112	M. Aaboud et al.	(ATLAS Collab.)
AAD	16	PL B753 69	G. Aad et al.	(ATLAS Collab.)
AAD	16AC	PR D93 092005	G. Aad et al.	(ATLAS Collab.)
AAD	16AF	JHEP 1601 172	G. Aad et al.	(ATLAS Collab.)
AAD	16AL	JHEP 1605 160	G. Aad et al.	(ATLAS Collab.)
AAD	16AN	JHEP 1608 045	G. Aad et al.	(ATLAS and CMS Collab.)
AAD	16AO	JHEP 1608 104	G. Aad et al.	(ATLAS Collab.)
AAD	16BL	EPJ C76 658	G. Aad et al.	(ATLAS Collab.)
AAD	16K	EPJ C76 6	G. Aad et al.	(ATLAS Collab.)
KHACHATRYAN	16AB	PL B759 672	V. Khachatryan et al.	(CMS Collab.)
KHACHATRYAN	16AR	JHEP 1604 005	V. Khachatryan et al.	(CMS Collab.)
KHACHATRYAN	16AU	JHEP 1606 177	V. Khachatryan et al.	(CMS Collab.)
KHACHATRYAN	16B	PL B753 341	V. Khachatryan et al.	(CMS Collab.)
KHACHATRYAN	16BA	JHEP 1609 051	V. Khachatryan et al.	(CMS Collab.)
KHACHATRYAN	16BQ	PR D94 052012	V. Khachatryan et al.	(CMS Collab.)
KHACHATRYAN	16CD	PL B753 472	V. Khachatryan et al.	(CMS Collab.)
KHACHATRYAN	16G	EPJ C76 13	V. Khachatryan et al.	(CMS Collab.)
AAD	15	PL B740 222	G. Aad et al.	(ATLAS Collab.)
AAD	15AA	PR D92 012006	G. Aad et al.	(ATLAS Collab.)
AAD	15AH	JHEP 1504 117	G. Aad et al.	(ATLAS Collab.)
AAD	15AJ	JHEP 1508 137	G. Aad et al.	(ATLAS Collab.)
AAD	15AX	EPJ C75 231	G. Aad et al.	(ATLAS Collab.)
AAD	15B	PRL 114 191803	G. Aad et al.	(ATLAS and CMS Collab.)
AAD	15C	EPJ C75 349	G. Aad et al.	(ATLAS Collab.)
AAD	15BD	EPJ C75 337	G. Aad et al.	(ATLAS Collab.)
AAD	15BE	EPJ C75 335	G. Aad et al.	(ATLAS Collab.)
AAD	15CE	PR D92 092004	G. Aad et al.	(ATLAS Collab.)
AAD	15CI	EPJ C75 476	G. Aad et al.	(ATLAS Collab.)
Also		EPJ C76 152 (errata.)	G. Aad et al.	(ATLAS Collab.)
AAD	15CX	JHEP 1511 206	G. Aad et al.	(ATLAS Collab.)
AAD	15F	PR D91 012006	G. Aad et al.	(ATLAS Collab.)
AAD	15G	JHEP 1501 069	G. Aad et al.	(ATLAS Collab.)
AAD	15I	PRL 114 121801	G. Aad et al.	(ATLAS Collab.)
AAD	15P	PRL 115 091801	G. Aad et al.	(ATLAS Collab.)
AAD	15T	PL B749 519	G. Aad et al.	(ATLAS Collab.)
AALTONEN	15	PRL 114 151802	T. Aaltonen et al.	(CDF and DO Collab.)
AALTONEN	15B	PRL 114 141802	T. Aaltonen et al.	(CDF Collab.)
KHACHATRYAN	15AM	EPJ C75 212	V. Khachatryan et al.	(CMS Collab.)
KHACHATRYAN	15AN	EPJ C75 251	V. Khachatryan et al.	(CMS Collab.)
KHACHATRYAN	15BA	PR D92 072010	V. Khachatryan et al.	(CMS Collab.)
KHACHATRYAN	15B	PL B744 184	V. Khachatryan et al.	(CMS Collab.)
KHACHATRYAN	15H	PL B749 337	V. Khachatryan et al.	(CMS Collab.)
KHACHATRYAN	15J	PR D92 012004	V. Khachatryan et al.	(CMS Collab.)
KHACHATRYAN	15Z	PR D92 032008	V. Khachatryan et al.	(CMS Collab.)
AAD	14AR	PL B738 234	G. Aad et al.	(ATLAS Collab.)
AAD	14AS	PL B738 68	G. Aad et al.	(ATLAS Collab.)
AAD	14B	PR D90 112015	G. Aad et al.	(ATLAS Collab.)
AAD	14BJ	JHEP 1409 112	G. Aad et al.	(ATLAS Collab.)
AAD	14J	PL B732 8	G. Aad et al.	(ATLAS Collab.)
AAD	14O	PRL 112 201802	G. Aad et al.	(ATLAS Collab.)
AAD	14W	PR D90 052004	G. Aad et al.	(ATLAS Collab.)
ABAZOV	14F	PRL 113 161802	V. M. Abazov et al.	(DO Collab.)
CHATRCHYAN	14AA	PR D89 092007	S. Chatrchyan et al.	(CMS Collab.)
CHATRCHYAN	14AI	PR D89 012003	S. Chatrchyan et al.	(CMS Collab.)
CHATRCHYAN	14AJ	NATP 10 557	S. Chatrchyan et al.	(CMS Collab.)
CHATRCHYAN	14B	EPJ C74 2980	S. Chatrchyan et al.	(CMS Collab.)
CHATRCHYAN	14G	JHEP 1401 096	S. Chatrchyan et al.	(CMS Collab.)
CHATRCHYAN	14K	JHEP 1405 104	S. Chatrchyan et al.	(CMS Collab.)
KHACHATRYAN	14D	PL B736 64	V. Khachatryan et al.	(CMS Collab.)
KHACHATRYAN	14H	JHEP 1409 087	V. Khachatryan et al.	(CMS Collab.)
KHACHATRYAN	14P	EPJ C74 3076	V. Khachatryan et al.	(CMS Collab.)
AAD	13AJ	PL B726 120	G. Aad et al.	(ATLAS Collab.)
AAD	13AK	PL B726 88	G. Aad et al.	(ATLAS Collab.)
Also		PL B734 406 (errata.)	G. Aad et al.	(ATLAS Collab.)
AALTONEN	13L	PR D88 052013	T. Aaltonen et al.	(CDF Collab.)
AALTONEN	13M	PR D88 052014	T. Aaltonen et al.	(CDF and DO Collab.)
ABAZOV	13L	PR D88 052011	V. M. Abazov et al.	(DO Collab.)
CHATRCHYAN	13BK	PL B726 587	S. Chatrchyan et al.	(CMS Collab.)
CHATRCHYAN	13J	PRL 110 081803	S. Chatrchyan et al.	(CMS Collab.)
CHATRCHYAN	13X	JHEP 1305 145	S. Chatrchyan et al.	(CMS Collab.)
CHATRCHYAN	13Y	JHEP 1306 081	S. Chatrchyan et al.	(CMS Collab.)
HEINEMEYER	13A	arXiv:1307.1347	S. Heinemeyer et al.	(LHC Higgs CS Working Group)
AAD	12AI	PL B716 1	G. Aad et al.	(ATLAS Collab.)
AAD	12DA	SCI 338 1576	G. Aad et al.	(ATLAS Collab.)
AALTONEN	12Q	PRL 109 111803	T. Aaltonen et al.	(CDF Collab.)
AALTONEN	12R	PRL 109 111804	T. Aaltonen et al.	(CDF Collab.)
AALTONEN	12S	PRL 109 111805	T. Aaltonen et al.	(CDF Collab.)
AALTONEN	12T	PRL 109 071804	T. Aaltonen et al.	(CDF and DO Collab.)
ABAZOV	12K	PL B716 285	V. M. Abazov et al.	(DO Collab.)
ABAZOV	12O	PRL 109 121803	V. M. Abazov et al.	(DO Collab.)
ABAZOV	12P	PRL 109 121804	V. M. Abazov et al.	(DO Collab.)
CHATRCHYAN	12BY	SCI 338 1569	S. Chatrchyan et al.	(CMS Collab.)
CHATRCHYAN	12C	PL B		

Neutral Higgs Bosons, Searches for

CONTENTS:

- Mass Limits for Neutral Higgs Bosons in Supersymmetric Models
 - Mass Limits for heavy neutral Higgs bosons (H_2^0, A^0) in the MSSM
 - Mass Limits for H_1^0 (Higgs Boson) in Supersymmetric Models
- Mass Limits for Neutral Higgs Bosons in Extended Higgs Models
 - Mass Limits in General two-Higgs-doublet Models
 - Mass Limits for H^0 with Vanishing Yukawa Couplings
 - Mass Limits for H^0 Decaying to Invisible Final States
 - Mass Limits for Light A^0
 - Other Mass Limits
- Searches for a Higgs Boson with Standard Model Couplings
 - Direct Mass Limits for H^0
 - Indirect Mass Limits for H^0 from Electroweak Analysis

MASS LIMITS FOR NEUTRAL HIGGS BOSONS IN SUPERSYMMETRIC MODELS

The minimal supersymmetric model has two complex doublets of Higgs bosons. The resulting physical states are two scalars [H_1^0 and H_2^0], where we define $m_{H_1^0} < m_{H_2^0}$, a pseudoscalar (A^0), and a charged Higgs pair (H^\pm). H_1^0 and H_2^0 are also called h and H in the literature. There are two free parameters in the Higgs sector which can be chosen to be m_{A^0} and $\tan\beta = v_2/v_1$, the ratio of vacuum expectation values of the two Higgs doublets. Tree-level Higgs masses are constrained by the model to be $m_{H_1^0} \leq m_Z$, $m_{H_2^0} \geq m_Z$, $m_{A^0} \geq m_{H_1^0}$, and $m_{H^\pm} \geq m_W$. However, as described in the review on “Status of Higgs Boson Physics” in this Volume these relations are violated by radiative corrections.

The observed signal at about 125 GeV, see section “ H^0 ”, can be interpreted as one of the neutral Higgs bosons of supersymmetric models. Unless otherwise noted, we identify the lighter scalar H^0 with the Higgs discovered at 125 GeV at the LHC (AAD 12Ai, CHATRCHYAN 12N).

Unless otherwise noted, the experiments in e^+e^- collisions search for the processes $e^+e^- \rightarrow H_1^0 Z^0$ in the channels used for the Standard Model Higgs searches and $e^+e^- \rightarrow H_1^0 A^0$ in the final states $b\bar{b}b\bar{b}$ and $b\bar{b}\tau^+\tau^-$. Unless otherwise stated, the following results assume no invisible H_1^0 or A^0 decays. Unless otherwise noted, the results are given in the m_h^{max} scenario, CARENA 13.

In $p\bar{p}$ and pp collisions the experiments search for a variety of processes, as explicitly specified for each entry. Limits on the A^0 mass arise from these direct searches, as well as from the relations valid in the minimal supersymmetric model between m_{A^0} and $m_{H_1^0}$. As discussed in the review on “Status of Higgs Boson Physics” in this Volume, these relations depend, via potentially large radiative corrections, on the mass of the t quark and on the supersymmetric parameters, in particular those of the stop sector. These indirect limits are weaker for larger t and \bar{t} masses. To include the radiative corrections to the Higgs masses, unless otherwise stated, the listed papers use theoretical predictions incorporating two-loop corrections, and the results are given for the m_h^{mod+} benchmark scenario, see CARENA 13.

Mass Limits for heavy neutral Higgs bosons (H_2^0, A^0) in the MSSM

The limits rely on $pp \rightarrow H_2^0/A^0 \rightarrow \tau^+\tau^-$ and assume that H_2^0 and A^0 are (sufficiently) mass degenerate. The limits depend on $\tan\beta$.

VALUE (GeV)	CL%	DOCUMENT ID	TECN	COMMENT
> 377	95	1 AABOUD	18G ATLS	$\tan\beta = 10$ GeV
> 863	95	1 AABOUD	18G ATLS	$\tan\beta = 20$ GeV
>1157	95	1 AABOUD	18G ATLS	$\tan\beta = 30$ GeV
>1328	95	1 AABOUD	18G ATLS	$\tan\beta = 40$ GeV
>1483	95	1 AABOUD	18G ATLS	$\tan\beta = 50$ GeV
>1613	95	1 AABOUD	18G ATLS	$\tan\beta = 60$ GeV
> 389	95	2 SIRUNYAN	18CX CMS	$\tan\beta = 10$ GeV
> 832	95	2 SIRUNYAN	18CX CMS	$\tan\beta = 20$ GeV
>1148	95	2 SIRUNYAN	18CX CMS	$\tan\beta = 30$ GeV
>1341	95	2 SIRUNYAN	18CX CMS	$\tan\beta = 40$ GeV
>1496	95	2 SIRUNYAN	18CX CMS	$\tan\beta = 50$ GeV
>1613	95	2 SIRUNYAN	18CX CMS	$\tan\beta = 60$ GeV
• • • We do not use the following data for averages, fits, limits, etc. • • •				
		3 AAD	20 ATLS	H^0 properties
		4 AAD	20AA ATLS	$H_2^0/A^0 \rightarrow \tau^+\tau^-$
		5 AAD	20C ATLS	$H_1^0 \rightarrow H^0 H^0$
		6 AAD	20L ATLS	$H_2^0 \rightarrow b\bar{b}$
		7 SIRUNYAN	20AC CMS	$A^0 \rightarrow ZH^0$
		8 SIRUNYAN	20AF CMS	$H_2^0/A^0 \rightarrow t\bar{t}$
		9 SIRUNYAN	20Y CMS	$H_2^0 \rightarrow W^+W^-$
		10 SIRUNYAN	19CR CMS	$H_2^0/A^0 \rightarrow \mu^+\mu^-$
		11 SIRUNYAN	18A CMS	$H_2^0 \rightarrow H^0 H^0$
		12 SIRUNYAN	18BP CMS	$pp \rightarrow H_2^0/A^0 + b + X,$ $H_2^0/A^0 \rightarrow b\bar{b}$
		13 AABOUD	16AA ATLS	$A^0 \rightarrow \tau^+\tau^-$

14	KHACHATRY...16A	CMS	$H_{1,2}^0/A^0 \rightarrow \mu^+\mu^-$	
15	KHACHATRY...16P	CMS	$H_2^0 \rightarrow H^0 H^0, A^0 \rightarrow ZH^0$	
16	KHACHATRY...15AY	CMS	$pp \rightarrow H_{1,2}^0/A^0 + b + X,$ $H_{1,2}^0/A^0 \rightarrow b\bar{b}$	
17	AAD	14AW ATLS	$pp \rightarrow H_{1,2}^0/A^0 + X,$ $H_{1,2}^0/A^0 \rightarrow \tau\tau$	
18	KHACHATRY...14M	CMS	$pp \rightarrow H_{1,2}^0/A^0 + X,$ $H_{1,2}^0/A^0 \rightarrow \tau\tau$	
19	AAD	13O ATLS	$pp \rightarrow H_{1,2}^0/A^0 + X,$ $H_{1,2}^0/A^0 \rightarrow \tau^+\tau^-,$ $\mu^+\mu^-$	
20	AAIJ	13T LHCB	$pp \rightarrow H_{1,2}^0/A^0 + X,$ $H_{1,2}^0/A^0 \rightarrow \tau^+\tau^-$	
21	CHATRCHYAN13AG	CMS	$pp \rightarrow H_{1,2}^0/A^0 + b + X,$ $H_{1,2}^0/A^0 \rightarrow b\bar{b}$	
22	AALTONEN	12AQ TEVA	$p\bar{p} \rightarrow H_{1,2}^0/A^0 + b + X,$ $H_{1,2}^0/A^0 \rightarrow b\bar{b}$	
23	AALTONEN	12X CDF	$p\bar{p} \rightarrow H_{1,2}^0/A^0 + b + X,$ $H_{1,2}^0/A^0 \rightarrow b\bar{b}$	
24	ABAZOV	12G D0	$p\bar{p} \rightarrow H_{1,2}^0/A^0 + X,$ $H_{1,2}^0/A^0 \rightarrow \tau^+\tau^-$	
25	CHATRCHYAN12K	CMS	$pp \rightarrow H_{1,2}^0/A^0 + X,$ $H_{1,2}^0/A^0 \rightarrow \tau^+\tau^-$	
26	ABAZOV	11K D0	$p\bar{p} \rightarrow H_{1,2}^0/A^0 + b + X,$ $H_{1,2}^0/A^0 \rightarrow b\bar{b}$	
27	ABAZOV	11W D0	$p\bar{p} \rightarrow H_{1,2}^0/A^0 + b + X,$ $H_{1,2}^0/A^0 \rightarrow \tau^+\tau^-$	
28	AALTONEN	09AR CDF	$p\bar{p} \rightarrow H_{1,2}^0/A^0 + X,$ $H_{1,2}^0/A^0 \rightarrow \tau^+\tau^-$	
> 90.4		29 ABDALLAH	08B DLPH $E_{cm} \leq 209$ GeV	
> 93.4	95	30 SCHAEEL	06B LEP $E_{cm} \leq 209$ GeV	
		31 ACOSTA	05Q CDF $p\bar{p} \rightarrow H_{1,2}^0/A^0 + X$	
> 85.0	95	32,33 ABBIENDI	04M OPAL $E_{cm} \leq 209$ GeV	
		34 ABBIENDI	03G OPAL $H_1^0 \rightarrow A^0 A^0$	
> 86.5	95	32,35 AKERCHARD	02H L3 $E_{cm} \leq 209$ GeV, $\tan\beta > 0.4$	
		36 AKEROYD	02 RVUE	
> 90.1	95	32,37 HEISTER	02 ALEP $E_{cm} \leq 209$ GeV, $\tan\beta > 0.5$	
1 AABOUD 18G search for production of $H_2^0/A^0 \rightarrow \tau^+\tau^-$ by gluon fusion and b -associated production in 36.1 fb^{-1} of pp collisions at $E_{cm} = 13$ TeV. See their Fig. 10 for excluded regions in the $m_{A^0} - \tan\beta$ plane in several MSSM scenarios.				
2 SIRUNYAN 18CX search for production of $H_{1,2}^0/A^0 \rightarrow \tau^+\tau^-$ by gluon fusion and b -associated production in 35.9 fb^{-1} of pp collisions at $E_{cm} = 13$ TeV. See their Fig. 9 for excluded regions in the $m_{A^0} - \tan(\beta)$ plane in several MSSM scenarios.				
3 AAD 20c combine measurements on H^0 production and decay using data taken in years 2015–2017 (up to 79.8 fb^{-1}) of pp collisions at $E_{cm} = 13$ TeV. See their Fig. 19 for excluded region in the $m_{H^0} - \tan\beta$ parameter space.				
4 AAD 20AA search for $H_2^0/A^0 \rightarrow \tau^+\tau^-$ produced by gluon fusion or b -associated production using 139 fb^{-1} of pp collisions at $E_{cm} = 13$ TeV. See their Fig. 2(c) for excluded region in the $M_{h^{\pm}}^{125}$ scenario of MSSM. Values of $\tan\beta > 8$ (21) are excluded for $m_{A^0} = 1.0$ (1.5) TeV at 95%CL.				
5 AAD 20c combine searches for a scalar resonance decaying to $H^0 H^0$ in 36.1 fb^{-1} of pp collisions at $E_{cm} = 13$ TeV from AABOUD 19A, AABOUD 19O, AABOUD 18CQ, AABOUD 19T, AABOUD 18CW, and AABOUD 18BU. See their Fig. 7(b) for the excluded region in the $m_{H^0} - \tan\beta$ parameter space.				
6 AAD 20L search for b -associated production of H_2^0 decaying to $b\bar{b}$ in 27.8 fb^{-1} of pp collisions at $E_{cm} = 13$ TeV. See their Fig. 9 for excluded regions in $m_{H^0}^{mod+}$ and $m_{H^0}^{mod-}$ scenarios of MSSM.				
7 SIRUNYAN 20AC search for gluon-fusion and b -associated production of A^0 decaying to ZH^0 in 35.9 fb^{-1} of pp collisions at $E_{cm} = 13$ TeV. See their Fig. 6 for excluded regions in the $M_{h^{\pm}}^{125}$ and m_{H^0} scenarios of the MSSM.				
8 SIRUNYAN 20AF search for $H_2^0/A^0 \rightarrow t\bar{t}$ with one or two charged leptons in the final state using kinematic variables in 35.9 fb^{-1} of pp collisions at $E_{cm} = 13$ TeV. See their Fig. 8 for excluded region in the $m_{H^0} - \tan\beta$ scenario of MSSM. Values of $\tan\beta$ below 1.0–1.5 are excluded for $m_{A^0} = 0.4$ –0.75 TeV at 95%CL.				
9 SIRUNYAN 20Y search for gluon-fusion and vector-boson-fusion production of H_2^0 decaying to W^+W^- in the final states $\ell\nu\ell\nu$ and $\ell\nu q\bar{q}$ in 35.9 fb^{-1} of pp collisions at $E_{cm} = 13$ TeV. See their Figs. 8 and 9 for excluded regions in various MSSM scenarios.				
10 SIRUNYAN 19CR search for production of H_2^0/A^0 in gluon fusion and in association with a $b\bar{b}$ pair, decaying to $\mu^+\mu^-$ in 35.9 fb^{-1} of pp collisions at $E_{cm} = 13$ TeV. See their Fig. 5 for the excluded region in the MSSM parameter space in the $m_{H^0}^{mod+}$ and $m_{H^0}^{mod-}$ scenarios.				

Gauge & Higgs Boson Particle Listings

Neutral Higgs Bosons, Searches for

- 11 SIRUNYAN 18A search for production of a scalar resonance decaying to $H^0 H^0 \rightarrow b\bar{b}\tau^+\tau^-$ in 35.9 fb^{-1} of pp collisions at $E_{\text{cm}} = 13 \text{ TeV}$. See their Fig. 5 (lower) for excluded regions in the $m_{A^0} - \tan\beta$ plane in the hMSSM scenario.
- 12 SIRUNYAN 18BP search for production of $H_2^0/A^0 \rightarrow b\bar{b}$ by b -associated production in 35.7 fb^{-1} of pp collisions at $E_{\text{cm}} = 13 \text{ TeV}$. See their Fig. 6 for the limits on cross section times branching ratio for $m_{H_2^0}, m_{A^0} = 0.3\text{--}1.3 \text{ TeV}$, and Fig. 7 for excluded regions in the $m_{A^0} - \tan(\beta)$ plane in several MSSM scenarios.
- 13 AABOUD 16AA search for production of a Higgs boson in gluon fusion and in association with a $b\bar{b}$ pair followed by the decay $A^0 \rightarrow \tau^+\tau^-$ in 3.2 fb^{-1} of pp collisions at $E_{\text{cm}} = 13 \text{ TeV}$. See their Fig. 5(a, b) for limits on cross section times branching ratio for $m_{A^0} = 200\text{--}1200 \text{ GeV}$, and Fig. 5(c, d) for the excluded region in the MSSM parameter space in the $m_h^{\text{mod}+}$ and hMSSM scenarios.
- 14 KHACHATRYAN 16A search for production of a Higgs boson in gluon fusion and in association with a $b\bar{b}$ pair followed by the decay $H_{1,2}^0/A^0 \rightarrow \mu^+\mu^-$ in 5.1 fb^{-1} of pp collisions at $E_{\text{cm}} = 7 \text{ TeV}$ and 19.3 fb^{-1} at $E_{\text{cm}} = 8 \text{ TeV}$. See their Fig. 7 for the excluded region in the MSSM parameter space in the $m_h^{\text{mod}+}$ benchmark scenario and Fig. 9 for limits on cross section times branching ratio.
- 15 KHACHATRYAN 16P search for gluon fusion production of an H_2^0 decaying to $H^0 H^0 \rightarrow b\bar{b}\tau^+\tau^-$ and an A^0 decaying to $ZH^0 \rightarrow \ell^+\ell^-\tau^+\tau^-$ in 19.7 fb^{-1} of pp collisions at $E_{\text{cm}} = 8 \text{ TeV}$. See their Fig. 12 for excluded region in the $\tan\beta - \cos(\beta - \alpha)$ plane for $m_{H_2^0} = m_{A^0} = 300 \text{ GeV}$.
- 16 KHACHATRYAN 15AY search for production of a Higgs boson in association with a b quark in the decay $H_{1,2}^0/A^0 \rightarrow b\bar{b}$ in 19.7 fb^{-1} of pp collisions at $E_{\text{cm}} = 8 \text{ TeV}$ and combine with CHATRCHYAN 13AG 7 TeV data. See their Fig. 6 for the limits on cross section times branching ratio for $m_{A^0} = 100\text{--}900 \text{ GeV}$ and Figs. 7–9 for the excluded region in the MSSM parameter space in various benchmark scenarios.
- 17 AAD 14AW search for production of a Higgs boson followed by the decay $H_{1,2}^0/A^0 \rightarrow \tau^+\tau^-$ in $19.5\text{--}20.3 \text{ fb}^{-1}$ of pp collisions at $E_{\text{cm}} = 8 \text{ TeV}$. See their Fig. 11 for the limits on cross section times branching ratio and their Figs. 9 and 10 for the excluded region in the MSSM parameter space. For $m_{A^0} = 140 \text{ GeV}$, the region $\tan\beta > 5.4$ is excluded at 95% CL in the m_h^{max} scenario.
- 18 KHACHATRYAN 14M search for production of a Higgs boson in gluon fusion and in association with a b quark followed by the decay $H_{1,2}^0/A^0 \rightarrow \tau^+\tau^-$ in 4.9 fb^{-1} of pp collisions at $E_{\text{cm}} = 7 \text{ TeV}$ and 19.7 fb^{-1} at $E_{\text{cm}} = 8 \text{ TeV}$. See their Figs. 7 and 8 for one- and two-dimensional limits on cross section times branching ratio and their Figs. 5 and 6 for the excluded region in the MSSM parameter space. For $m_{A^0} = 140 \text{ GeV}$, the region $\tan\beta > 3.8$ is excluded at 95% CL in the m_h^{max} scenario.
- 19 AAD 13o search for production of a Higgs boson in the decay $H_{1,2}^0/A^0 \rightarrow \tau^+\tau^-$ and $\mu^+\mu^-$ with $4.7\text{--}4.8 \text{ fb}^{-1}$ of pp collisions at $E_{\text{cm}} = 7 \text{ TeV}$. See their Fig. 6 for the excluded region in the MSSM parameter space and their Fig. 7 for the limits on cross section times branching ratio. For $m_{A^0} = 110\text{--}170 \text{ GeV}$, $\tan\beta \gtrsim 10$ is excluded, and for $\tan\beta = 50$, m_{A^0} below 470 GeV is excluded at 95% CL in the m_h^{max} scenario.
- 20 AAIJ 13T search for production of a Higgs boson in the forward region in the decay $H_{1,2}^0/A^0 \rightarrow \tau^+\tau^-$ in 1.0 fb^{-1} of pp collisions at $E_{\text{cm}} = 7 \text{ TeV}$. See their Fig. 2 for the limits on cross section times branching ratio and the excluded region in the MSSM parameter space.
- 21 CHATRCHYAN 13AG search for production of a Higgs boson in association with a b quark in the decay $H_{1,2}^0/A^0 \rightarrow b\bar{b}$ in $2.7\text{--}4.8 \text{ fb}^{-1}$ of pp collisions at $E_{\text{cm}} = 7 \text{ TeV}$. See their Fig. 6 for the excluded region in the MSSM parameter space and Fig. 5 for the limits on cross section times branching ratio. For $m_{A^0} = 90\text{--}350 \text{ GeV}$, upper bounds on $\tan\beta$ of $18\text{--}42$ at 95% CL are obtained in the m_h^{max} scenario with $\mu = +200 \text{ GeV}$.
- 22 AALTONEN 12AQ combine AALTONEN 12X and ABAZOV 11k. See their Table I and Fig. 1 for the limit on cross section times branching ratio and Fig. 2 for the excluded region in the MSSM parameter space.
- 23 AALTONEN 12X search for associated production of a Higgs boson and a b quark in the decay $H_{1,2}^0/A^0 \rightarrow b\bar{b}$, with 2.6 fb^{-1} of $p\bar{p}$ collisions at $E_{\text{cm}} = 1.96 \text{ TeV}$. See their Table III and Fig. 15 for the limit on cross section times branching ratio and Figs. 17, 18 for the excluded region in the MSSM parameter space.
- 24 ABAZOV 12G search for production of a Higgs boson in the decay $H_{1,2}^0/A^0 \rightarrow \tau^+\tau^-$ with 7.3 fb^{-1} of $p\bar{p}$ collisions at $E_{\text{cm}} = 1.96 \text{ TeV}$ and combine with ABAZOV 11w and ABAZOV 11k. See their Figs. 4, 5, and 6 for the excluded region in the MSSM parameter space. For $m_{A^0} = 90\text{--}180 \text{ GeV}$, $\tan\beta \gtrsim 30$ is excluded at 95% CL in the m_h^{max} scenario.
- 25 CHATRCHYAN 12k search for production of a Higgs boson in the decay $H_{1,2}^0/A^0 \rightarrow \tau^+\tau^-$ with 4.6 fb^{-1} of pp collisions at $E_{\text{cm}} = 7 \text{ TeV}$. See their Fig. 3 and Table 4 for the excluded region in the MSSM parameter space. For $m_{A^0} = 160 \text{ GeV}$, the region $\tan\beta > 7.1$ is excluded at 95% CL in the m_h^{max} scenario. Superseded by KHACHATRYAN 14M.
- 26 ABAZOV 11k search for associated production of a Higgs boson and a b quark, followed by the decay $H_{1,2}^0/A^0 \rightarrow b\bar{b}$, in 5.2 fb^{-1} of $p\bar{p}$ collisions at $E_{\text{cm}} = 1.96 \text{ TeV}$. See their Fig. 5/Table 2 for the limit on cross section times branching ratio and Fig. 6 for the excluded region in the MSSM parameter space for $\mu = -200 \text{ GeV}$.
- 27 ABAZOV 11W search for associated production of a Higgs boson and a b quark, followed by the decay $H_{1,2}^0/A^0 \rightarrow \tau\tau$, in 7.3 fb^{-1} of $p\bar{p}$ collisions at $E_{\text{cm}} = 1.96 \text{ TeV}$. See their Fig. 2 for the limit on cross section times branching ratio and for the excluded region in the MSSM parameter space.
- 28 AALTONEN 09AR search for Higgs bosons decaying to $\tau^+\tau^-$ in two doublet models in 1.8 fb^{-1} of $p\bar{p}$ collisions at $E_{\text{cm}} = 1.96 \text{ TeV}$. See their Fig. 2 for the limit on $\sigma \cdot \text{B}(H_{1,2}^0/A^0 \rightarrow \tau^+\tau^-)$ for different Higgs masses, and see their Fig. 3 for the excluded region in the MSSM parameter space.

- 29 ABDALLAH 08B give limits in eight CP -conserving benchmark scenarios and some CP -violating scenarios. See paper for excluded regions for each scenario. Supersedes ABDALLAH 04.
- 30 SCHAEEL 06B make a combined analysis of the LEP data. The quoted limit is for the m_h^{max} scenario with $m_t = 174.3 \text{ GeV}$. In the CP -violating CPX scenario no lower bound on $m_{H_1^0}$ can be set at 95% CL. See paper for excluded regions in various scenarios. See Figs. 2–6 and Tabs. 14–21 for limits on $\sigma(ZH^0) \cdot \text{B}(H^0 \rightarrow b\bar{b}, \tau^+\tau^-)$ and $\sigma(H_1^0 H_2^0) \cdot \text{B}(H_1^0 H_2^0 \rightarrow b\bar{b}, \tau^+\tau^-)$.
- 31 ACOSTA 05Q search for $H_{1,2}^0/A^0$ production in $p\bar{p}$ collisions at $E_{\text{cm}} = 1.8 \text{ TeV}$ with $H_{1,2}^0/A^0 \rightarrow \tau^+\tau^-$. At $m_{A^0} = 100 \text{ GeV}$, the obtained cross section upper limit is above theoretical expectation.
- 32 Search for $e^+e^- \rightarrow H_1^0 A^0$ in the final states $b\bar{b}b\bar{b}$ and $b\bar{b}\tau^+\tau^-$, and $e^+e^- \rightarrow H_1^0 Z$. Universal scalar mass of 1 TeV , $SU(2)$ gaugino mass of 200 GeV , and $\mu = -200 \text{ GeV}$ are assumed, and two-loop radiative corrections incorporated. The limits hold for $m_t = 175 \text{ GeV}$, and for the m_h^{max} scenario.
- 33 ABBIENDI 04M exclude $0.7 < \tan\beta < 1.9$, assuming $m_t = 174.3 \text{ GeV}$. Limits for other MSSM benchmark scenarios, as well as for CP violating cases, are also given.
- 34 ABBIENDI 03G search for $e^+e^- \rightarrow H_1^0 Z$ followed by $H_1^0 \rightarrow A^0 A^0, A^0 \rightarrow c\bar{c}, gg$, or $\tau^+\tau^-$. In the no-mixing scenario, the region $m_{H_1^0} = 45\text{--}85 \text{ GeV}$ and $m_{A^0} = 2\text{--}9.5 \text{ GeV}$ is excluded at 95% CL.
- 35 ACHARD 02H also search for the final state $H_1^0 Z \rightarrow 2A^0 q\bar{q}, A^0 \rightarrow q\bar{q}$. In addition, the MSSM parameter set in the “large- μ ” and “no-mixing” scenarios are examined.
- 36 AKEROYD 02 examine the possibility of a light A^0 with $\tan\beta < 1$. Electroweak measurements are found to be inconsistent with such a scenario.
- 37 HEISTER 02 excludes the range $0.7 < \tan\beta < 2.3$. A wider range is excluded with different stop mixing assumptions. Updates BARATE 01c.

Mass Limits for H_1^0 (Higgs Boson) in Supersymmetric Models

VALUE (GeV)	CL%	DOCUMENT ID	TECN	COMMENT
>89.7		1 ABDALLAH	08B DLPH	$E_{\text{cm}} \leq 209 \text{ GeV}$
>92.8	95	2 SCHAEEL	06B LEP	$E_{\text{cm}} \leq 209 \text{ GeV}$
>84.5	95	3,4 ABBIENDI	04M OPAL	$E_{\text{cm}} \leq 209 \text{ GeV}$
>86.0	95	3,5 ACHARD	02H L3	$E_{\text{cm}} \leq 209 \text{ GeV}, \tan\beta > 0.4$
>89.8	95	3,6 HEISTER	02 ALEP	$E_{\text{cm}} \leq 209 \text{ GeV}, \tan\beta > 0.5$
••• We do not use the following data for averages, fits, limits, etc. •••				
		7 AALTONEN	12AQ TEVA	$p\bar{p} \rightarrow H_{1,2}^0/A^0 + b + X,$ $H_{1,2}^0/A^0 \rightarrow b\bar{b}$

- 1 ABDALLAH 08B give limits in eight CP -conserving benchmark scenarios and some CP -violating scenarios. See paper for excluded regions for each scenario. Supersedes ABDALLAH 04.
- 2 SCHAEEL 06B make a combined analysis of the LEP data. The quoted limit is for the m_h^{max} scenario with $m_t = 174.3 \text{ GeV}$. In the CP -violating CPX scenario no lower bound on $m_{H_1^0}$ can be set at 95% CL. See paper for excluded regions in various scenarios. See Figs. 2–6 and Tabs. 14–21 for limits on $\sigma(ZH^0) \cdot \text{B}(H^0 \rightarrow b\bar{b}, \tau^+\tau^-)$ and $\sigma(H_1^0 H_2^0) \cdot \text{B}(H_1^0 H_2^0 \rightarrow b\bar{b}, \tau^+\tau^-)$.
- 3 Search for $e^+e^- \rightarrow H_1^0 A^0$ in the final states $b\bar{b}b\bar{b}$ and $b\bar{b}\tau^+\tau^-$, and $e^+e^- \rightarrow H_1^0 Z$. Universal scalar mass of 1 TeV , $SU(2)$ gaugino mass of 200 GeV , and $\mu = -200 \text{ GeV}$ are assumed, and two-loop radiative corrections incorporated. The limits hold for $m_t = 175 \text{ GeV}$, and for the m_h^{max} scenario.
- 4 ABBIENDI 04M exclude $0.7 < \tan\beta < 1.9$, assuming $m_t = 174.3 \text{ GeV}$. Limits for other MSSM benchmark scenarios, as well as for CP violating cases, are also given.
- 5 ACHARD 02H also search for the final state $H_1^0 Z \rightarrow 2A^0 q\bar{q}, A^0 \rightarrow q\bar{q}$. In addition, the MSSM parameter set in the “large- μ ” and “no-mixing” scenarios are examined.
- 6 HEISTER 02 excludes the range $0.7 < \tan\beta < 2.3$. A wider range is excluded with different stop mixing assumptions. Updates BARATE 01c.
- 7 AALTONEN 12AQ combine AALTONEN 12X and ABAZOV 11k. See their Table I and Fig. 1 for the limit on cross section times branching ratio and Fig. 2 for the excluded region in the MSSM parameter space.

MASS LIMITS FOR NEUTRAL HIGGS BOSONS IN EXTENDED HIGGS MODELS

This Section covers models which do not fit into either the Standard Model or its simplest minimal Supersymmetric extension (MSSM), leading to anomalous production rates, or nonstandard final states and branching ratios. In particular, this Section covers limits which may apply to generic two-Higgs-doublet models (2HDM), or to special regions of the MSSM parameter space where decays to invisible particles or to photon pairs are dominant (see the review on “Status of Higgs Boson Physics”). Concerning the mass limits for H^0 and A^0 listed below, see the footnotes or the comment lines for details on the nature of the models to which the limits apply.

The observed signal at about 125 GeV , see section “ H^0 ”, can be interpreted as one of the neutral Higgs bosons of an extended Higgs sector.

Mass Limits in General two-Higgs-doublet Models

VALUE (GeV)	CL%	DOCUMENT ID	TECN	COMMENT
••• We do not use the following data for averages, fits, limits, etc. •••				
		1 AAD	21AF ATLS	$H_2^0 \rightarrow ZZ$
		2 AAD	21AI ATLS	$A^0 \rightarrow ZH_2^0$
		3 AAD	20 ATLS	H^0 properties
		4 AAD	20L ATLS	$H_2^0 \rightarrow b\bar{b}$

Gauge & Higgs Boson Particle Listings

Neutral Higgs Bosons, Searches for

5	SIRUNYAN	20AA	CMS	$H_2^0 \rightarrow ZA^0$ or $A^0 \rightarrow ZH_2^0$
6	SIRUNYAN	20Y	CMS	$H_2^0 \rightarrow W^+W^-$
7	SIRUNYAN	19AE	CMS	$A^0 \rightarrow \tau^+\tau^-$
8	SIRUNYAN	19AV	CMS	$A^0 \rightarrow ZH^0$
9	AABOUD	18AH	ATLS	$A^0 \rightarrow ZH_2^0$
10	AABOUD	18AI	ATLS	$A^0 \rightarrow ZH^0$
11	AABOUD	18BF	ATLS	$H_2^0 \rightarrow ZZ$
12	AABOUD	18CE	ATLS	$p\bar{p} \rightarrow H_2^0/A^0 t\bar{t}$, $H_2^0/A^0 \rightarrow t\bar{t}$
13	HALLER	18	RVUE	global fits
14	SIRUNYAN	18BP	CMS	$p\bar{p} \rightarrow H_2^0/A^0 + b + X$, $H_2^0/A^0 \rightarrow b\bar{b}$
15	SIRUNYAN	18ED	CMS	$A^0 \rightarrow ZH^0$
16	AABOUD	17AN	ATLS	$H_2^0, A^0 \rightarrow t\bar{t}$
17	SIRUNYAN	17AX	CMS	$A^0 b\bar{b}, A^0 \rightarrow \mu^+\mu^-$
18	AAD	16AX	ATLS	$H_2^0 \rightarrow ZZ$
19	KHACHATRYAN	16P	CMS	$H_2^0 \rightarrow H^0 H^0, A^0 \rightarrow ZH^0$
20	KHACHATRYAN	16W	CMS	$A^0 b\bar{b}, A^0 \rightarrow \tau^+\tau^-$
21	KHACHATRYAN	16Z	CMS	$H_2^0 \rightarrow ZA^0$ or $A^0 \rightarrow ZH_2^0$
22	AAD	15BK	ATLS	$H_2^0 \rightarrow H^0 H^0$
23	AAD	15S	ATLS	$A^0 \rightarrow ZH^0$
24	KHACHATRYAN	15BB	CMS	$H_2^0, A^0 \rightarrow \gamma\gamma$
25	KHACHATRYAN	15N	CMS	$A^0 \rightarrow ZH^0$
26	AAD	14M	ATLS	$H_2^0 \rightarrow H^\pm W^\mp \rightarrow$ $H^0 W^\pm W^\mp, H^0 \rightarrow b\bar{b}$
27	KHACHATRYAN	14Q	CMS	$H_2^0 \rightarrow H^0 H^0, A^0 \rightarrow ZH^0$
28	AALTONEN	09AR	CDF	$p\bar{p} \rightarrow H_{1,2}^0/A^0 + X$, $H_{1,2}^0/A^0 \rightarrow \tau^+\tau^-$
29	ABBIENDI	05A	OPAL	H_1^0 , Type II model
30	ABDALLAH	05D	DLPH	$H^0 \rightarrow 2$ jets
31	ABDALLAH	04O	DLPH	$Z \rightarrow t\bar{t}H$
32	ABDALLAH	04O	DLPH	$e^+e^- \rightarrow H^0 Z, H^0 A^0$
33	ABBIENDI	02D	OPAL	$e^+e^- \rightarrow b\bar{b}H$
34	ABBIENDI	01E	OPAL	H_1^0 , Type-I model
35	ABBIENDI	99E	OPAL	$\tan\beta > 1$
36	ABREU	95H	DLPH	$Z \rightarrow H^0 Z^*, H^0 A^0$
37	PICH	92	RVUE	Very light Higgs

none 1-55 95

>110.6 95

none 1-44 95

> 68.0 95

1 AAD 21AF search for production of a heavy H_2^0 state decaying to ZZ in the final states $\ell^+\ell^-\ell^+\ell^-$ and $\ell^+\ell^-\nu\bar{\nu}$ in 139 fb⁻¹ of pp collisions at $E_{cm} = 13$ TeV. See their Figs. 6 and 7 for excluded parameter regions of the 2HDM Type I and II.

2 AAD 21AI search for production of an A^0 in gluon-gluon fusion and in association with a $b\bar{b}$, decaying to $ZH_2^0 \rightarrow \ell^+\ell^-b\bar{b}$ or $\ell^+\ell^-W^+W^-$ in 139 fb⁻¹ of pp collisions at $E_{cm} = 13$ TeV. See their Figs. 10 and 14 for excluded regions in the parameter space of various 2HDMs.

3 AAD 20 combine measurements on H^0 production and decay using data taken in years 2015–2017 (up to 79.8 fb⁻¹) of pp collisions at $E_{cm} = 13$ TeV. See their Fig. 18 for excluded regions in various 2HDMs.

4 AAD 20L search for b -associated production of H_2^0 decaying to $b\bar{b}$ in 27.8 fb⁻¹ of pp collisions at $E_{cm} = 13$ TeV. See their Figs. 10 and 11 for excluded regions in the flipped two Higgs doublet model.

5 SIRUNYAN 20AA search for $H_2^0 \rightarrow ZA^0, A^0 \rightarrow b\bar{b}$ or $A^0 \rightarrow ZH_2^0, H_2^0 \rightarrow b\bar{b}$ in 35.9 fb⁻¹ of pp collisions at $E_{cm} = 13$ TeV. See their Figs. 8 and 9 for excluded regions in the parameter space of Type-II two Higgs doublet model.

6 SIRUNYAN 20Y search for gluon-fusion and vector-boson-fusion production of H_2^0 decaying to W^+W^- in the final states $\ell\nu\ell\nu$ and $\ell\nu q\bar{q}$ in 35.9 fb⁻¹ of pp collisions at $E_{cm} = 13$ TeV. See their Fig. 7 for excluded regions in Type I and II two Higgs doublet models.

7 SIRUNYAN 19AE search for a pseudoscalar resonance produced in association with a $b\bar{b}$ pair, decaying to $\tau^+\tau^-$ in 35.9 fb⁻¹ of pp collisions at $E_{cm} = 13$ TeV. See their Fig. 4 for cross section limits for $m_{A^0} = 25$ –70 GeV and comparison with some representative 2HDMs.

8 SIRUNYAN 19AV search for a scalar resonance produced by gluon fusion or b associated production, decaying to $ZH^0 \rightarrow \ell^+\ell^-b\bar{b}$ ($\ell = e, \mu$) or $\nu\bar{\nu}b\bar{b}$ in 35.9 fb⁻¹ of pp collisions at $E_{cm} = 13$ TeV. See their Figs. 6 and 7 for excluded regions in the parameter space of various 2HDMs.

9 AABOUD 18AH search for production of an A^0 in gluon-gluon fusion and in association with a $b\bar{b}$, decaying to $ZH_2^0 \rightarrow \ell^+\ell^-b\bar{b}$ in 36.1 fb⁻¹ of pp collisions at $E_{cm} = 13$ TeV. See their Fig. 6 for excluded regions in the parameter space of various 2HDMs.

10 AABOUD 18AI search for production of an A^0 in gluon-gluon fusion and in association with a $b\bar{b}$, decaying to ZH^0 in the final states $\nu\bar{\nu}b\bar{b}$ and $\ell^+\ell^-b\bar{b}$ in 36.1 fb⁻¹ of pp collisions at $E_{cm} = 13$ TeV. See their Figs. 7 and 8 for excluded regions in the parameter space in various 2HDMs.

11 AABOUD 18BF search for production of a heavy H_2^0 state decaying to ZZ in the final states $\ell^+\ell^-\ell^+\ell^-$ and $\ell^+\ell^-\nu\bar{\nu}$ in 36.1 fb⁻¹ of pp collisions at $E_{cm} = 13$ TeV. See their Figs. 8 and 9 for excluded parameter regions in 2HDM Type I and II.

12 AABOUD 18CE search for the process $p\bar{p} \rightarrow H_2^0/A^0 t\bar{t}$ followed by the decay $H_2^0/A^0 \rightarrow t\bar{t}$ in 36.1 fb⁻¹ of pp collisions at $E_{cm} = 13$ TeV. See their Fig. 12 for limits on cross section times branching ratio, and for lower limits on $\tan\beta$ for $m_{H_2^0}, m_{A^0} = 0.4$ –1.0 TeV in the 2HDM type II.

13 HALLER 18 perform global fits in the framework of two-Higgs-doublet models (type I, II, lepton specific, flipped). See their Fig. 8 for allowed parameter regions from fits to LHC

- H^0 measurements, Fig. 9 bottom and charm decays, Fig. 10 muon anomalous magnetic moment, Fig. 11 electroweak precision data, and Fig. 12 by combination of all data.
- 14 SIRUNYAN 18BP search for production of $H_2^0/A^0 \rightarrow b\bar{b}$ by b -associated production in 35.7 fb⁻¹ of pp collisions at $E_{cm} = 13$ TeV. See their Fig. 6 for the limits on cross section times branching ratio for $m_{H_2^0}, m_{A^0} = 0.3$ –1.3 TeV, and Figs. 8 and 9 for excluded regions in the parameter space of type-II and flipped 2HDMs.
- 15 SIRUNYAN 18ED search for production of an A^0 in gluon-gluon fusion and in association with a $b\bar{b}$, decaying to ZH^0 in the final states $\nu\bar{\nu}b\bar{b}$ or $\ell^+\ell^-b\bar{b}$ in 35.9 fb⁻¹ of pp collisions at $E_{cm} = 13$ TeV. See their Fig. 9 for excluded regions in the parameter space in Type I and II 2HDMs.
- 16 AABOUD 17AN search for production of a heavy H_2^0 and/or A^0 decaying to $t\bar{t}$ in 20.3 fb⁻¹ of pp collisions at $E_{cm} = 8$ TeV. See their Fig. 3 and Table III for excluded parameter regions in Type II Two-Higgs-Doublet-Models.
- 17 SIRUNYAN 17AX search for $A^0 b\bar{b}$ production followed by the decay $A^0 \rightarrow \mu^+\mu^-$ in 19.7 fb⁻¹ of pp collisions at $E_{cm} = 8$ TeV. Limits are set in the range $m_{A^0} = 25$ –60 GeV. See their Fig. 5 for upper limits on $\sigma(A^0 b\bar{b}) \cdot B(A^0 \rightarrow \mu^+\mu^-)$.
- 18 AAD 16AX search for production of a heavy H^0 state decaying to ZZ in the final states $\ell^+\ell^-\ell^+\ell^-$, $\ell^+\ell^-\nu\bar{\nu}$, $\ell^+\ell^-q\bar{q}$, and $\nu\bar{\nu}q\bar{q}$ in 20.3 fb⁻¹ of pp collisions at $E_{cm} = 8$ TeV. See their Figs. 13 and 14 for excluded parameter regions in Type I and II models.
- 19 KHACHATRYAN 16P search for gluon fusion production of an H_2^0 decaying to $H^0 H^0 \rightarrow b\bar{b}\tau^+\tau^-$ and an A^0 decaying to $ZH^0 \rightarrow \ell^+\ell^-\tau^+\tau^-$ in 19.7 fb⁻¹ of pp collisions at $E_{cm} = 8$ TeV. See their Fig. 11 for limits on $\tan\beta$ for $m_{A^0} = 230$ –350 GeV.
- 20 KHACHATRYAN 16W search for $A^0 b\bar{b}$ production followed by the decay $A^0 \rightarrow \tau^+\tau^-$ in 19.7 fb⁻¹ of pp collisions at $E_{cm} = 8$ TeV. See their Fig. 3 for upper limits on $\sigma(A^0 b\bar{b}) \cdot B(A^0 \rightarrow \tau^+\tau^-)$.
- 21 KHACHATRYAN 16Z search for $H_2^0 \rightarrow ZA^0$ followed by $A^0 \rightarrow b\bar{b}$ or $\tau^+\tau^-$, and $A^0 \rightarrow ZH_2^0$ followed by $H_2^0 \rightarrow b\bar{b}$ or $\tau^+\tau^-$, in 19.8 fb⁻¹ of pp collisions at $E_{cm} = 8$ TeV. See their Fig. 4 for cross section limits and Fig. 5 for excluded region in the parameter space.
- 22 AAD 15BK search for production of a heavy H_2^0 decaying to $H^0 H^0$ in the final state $b\bar{b}b\bar{b}$ in 19.5 fb⁻¹ of pp collisions at $E_{cm} = 8$ TeV. See their Figs. 15–18 for excluded regions in the parameter space.
- 23 AAD 15S search for production of A^0 decaying to $ZH^0 \rightarrow \ell^+\ell^-b\bar{b}, \nu\bar{\nu}b\bar{b}$ and $\ell^+\ell^-\tau^+\tau^-$ in 20.3 fb⁻¹ of pp collisions at $E_{cm} = 8$ TeV. See their Figs. 4 and 5 for excluded regions in the parameter space.
- 24 KHACHATRYAN 15BB search for $H_2^0, A^0 \rightarrow \gamma\gamma$ in 19.7 fb⁻¹ of pp collisions at $E_{cm} = 8$ TeV. See their Fig. 10 for excluded regions in the two-Higgs-doublet model parameter space.
- 25 KHACHATRYAN 15N search for production of A^0 decaying to $ZH^0 \rightarrow \ell^+\ell^-b\bar{b}$ in 19.7 fb⁻¹ of pp collisions at $E_{cm} = 8$ TeV. See their Fig. 5 for excluded regions in the $\tan\beta - \cos(\beta - \alpha)$ plane for $m_{A^0} = 300$ GeV.
- 26 AAD 14M search for the decay cascade $H_2^0 \rightarrow H^\pm W^\mp \rightarrow H^0 W^\pm W^\mp, H^0$ decaying to $b\bar{b}$ in 20.3 fb⁻¹ of pp collisions at $E_{cm} = 8$ TeV. See their Table IV for limits in a two-Higgs-doublet model for $m_{H_2^0} = 325$ –1025 GeV and $m_{H^\pm} = 225$ –825 GeV.
- 27 KHACHATRYAN 14Q search for $H_2^0 \rightarrow H^0 H^0$ and $A^0 \rightarrow ZH^0$ in 19.5 fb⁻¹ of pp collisions at $E_{cm} = 8$ TeV. See their Figs. 4 and 5 for limits on cross section times branching ratio for $m_{H_2^0} = 260$ –360 GeV and their Figs. 7–9 for limits in two-Higgs-doublet models.
- 28 AALTONEN 09AR search for Higgs bosons decaying to $\tau^+\tau^-$ in two doublet models in 1.8 fb⁻¹ of $p\bar{p}$ collisions at $E_{cm} = 1.96$ TeV. See their Fig. 2 for the limit on $\sigma \cdot B(H_{1,2}^0/A^0 \rightarrow \tau^+\tau^-)$ for different Higgs masses, and see their Fig. 3 for the excluded region in the MSSM parameter space.
- 29 ABBIENDI 05A search for $e^+e^- \rightarrow H_1^0 A^0$ in general Type-II two-doublet models, with decays $H_1^0, A^0 \rightarrow q\bar{q}, gg, \tau^+\tau^-$, and $H_1^0 \rightarrow A^0 A^0$.
- 30 ABDALLAH 05D search for $e^+e^- \rightarrow H^0 Z$ and $H^0 A^0$ with H^0, A^0 decaying to two jets of any flavor including gg . The limit is for SM $H^0 Z$ production cross section with $B(H^0 \rightarrow jj) = 1$.
- 31 ABDALLAH 04O search for $Z \rightarrow b\bar{b}H^0, b\bar{b}A^0, \tau^+\tau^-H^0$ and $\tau^+\tau^-A^0$ in the final states $4b, b\bar{b}\tau^+\tau^-$, and 4τ . See paper for limits on Yukawa couplings.
- 32 ABDALLAH 04O search for $e^+e^- \rightarrow H^0 Z$ and $H^0 A^0$, with H^0, A^0 decaying to $b\bar{b}, \tau^+\tau^-$, or $H^0 \rightarrow A^0 A^0$ at $E_{cm} = 189$ –208 GeV. See paper for limits on couplings.
- 33 ABBIENDI 02D search for $Z \rightarrow b\bar{b}H_1^0$ and $b\bar{b}A^0$ with $H_1^0/A^0 \rightarrow \tau^+\tau^-$, in the range $4 < m_H < 12$ GeV. See their Fig. 8 for limits on the Yukawa coupling.
- 34 ABBIENDI 01E search for neutral Higgs bosons in general Type-II two-doublet models, at $E_{cm} \leq 189$ GeV. In addition to usual final states, the decays $H_1^0, A^0 \rightarrow q\bar{q}, gg$ are searched for. See their Figs. 15,16 for excluded regions.
- 35 ABBIENDI 99E search for $e^+e^- \rightarrow H^0 A^0$ and $H^0 Z$ at $E_{cm} = 183$ GeV. The limit is with $m_H = m_A$ in general two Higgs-doublet models. See their Fig. 18 for the exclusion limit in the $m_H - m_A$ plane. Updates the results of ACKERSTAFF 98s.
- 36 See Fig. 4 of ABREU 95H for the excluded region in the $m_{H^0} - m_{A^0}$ plane for general two-doublet models. For $\tan\beta > 1$, the region $m_{H^0} + m_{A^0} \lesssim 87$ GeV, $m_{H^0} < 47$ GeV is excluded at 95% CL.
- 37 PICH 92 analyse H^0 with $m_{H^0} < 2m_\mu$ in general two-doublet models. Excluded regions in the space of mass-mixing angles from LEP, beam dump, and π^\pm, η rare decays are shown in Figs. 3,4. The considered mass region is not totally excluded.

Mass Limits for H^0 with Vanishing Yukawa Couplings

These limits assume that H^0 couples to gauge bosons with the same strength as the Standard Model Higgs boson, but has no coupling to quarks and leptons (this is often referred to as “fermiophobic”).

VALUE (GeV)	CL%	DOCUMENT ID	TECN	COMMENT
-------------	-----	-------------	------	---------

••• We do not use the following data for averages, fits, limits, etc. •••

95	1	AALTONEN	13K	CDF	$H^0 \rightarrow WW^{(*)}$
----	---	----------	-----	-----	----------------------------

Gauge & Higgs Boson Particle Listings

Neutral Higgs Bosons, Searches for

none 100-113	95	2	AALTONEN	13L	CDF	$H^0 \rightarrow \gamma\gamma, WW^*, ZZ^*$
none 100-116	95	3	AALTONEN	13M	TEVA	$H^0 \rightarrow \gamma\gamma, WW^*, ZZ^*$
		4	ABAZOV	13G	D0	$H^0 \rightarrow WW^*$
none 100-113	95	5	ABAZOV	13H	D0	$H^0 \rightarrow \gamma\gamma$
		6	ABAZOV	13I	D0	$H^0 \rightarrow WW^*$
		7	ABAZOV	13J	D0	$H^0 \rightarrow WW^*, ZZ^*$
none 100-114	95	8	ABAZOV	13L	D0	$H^0 \rightarrow \gamma\gamma, WW^*, ZZ^*$
none 110-147	95	9	CHATRCHYAN	13AL	CMS	$H^0 \rightarrow \gamma\gamma$
none 110-118, 119.5-121	95	10	AAD	12N	ATLS	$H^0 \rightarrow \gamma\gamma$
none 100-114	95	11	AALTONEN	12AN	CDF	$H^0 \rightarrow \gamma\gamma$
none 110-194	95	12	CHATRCHYAN	12AO	CMS	$H^0 \rightarrow \gamma\gamma, WW^*, ZZ^*$
none 70-106	95	13	AALTONEN	09AB	CDF	$H^0 \rightarrow \gamma\gamma$
none 70-100	95	14	ABAZOV	08U	D0	$H^0 \rightarrow \gamma\gamma$
>105.8	95	15	SCHAEEL	07	ALEP	$e^+e^- \rightarrow H^0 Z, H^0 \rightarrow WW^*$
>104.1	95	16,17	ABDALLAH	04L	DLPH	$e^+e^- \rightarrow H^0 Z, H^0 \rightarrow \gamma\gamma$
>107	95	18	ACHARD	03C	L3	$H^0 \rightarrow WW^*, ZZ^*, \gamma\gamma$
>105.5	95	16,19	ABBIENDI	02F	OPAL	$H^0 \rightarrow \gamma\gamma$
>105.4	95	20	ACHARD	02C	L3	$H^0 \rightarrow \gamma\gamma$
none 60-82	95	21	AFFOLDER	01H	CDF	$p\bar{p} \rightarrow H^0 W/Z, H^0 \rightarrow \gamma\gamma$
> 94.9	95	22	ACCIARRI	00S	L3	$e^+e^- \rightarrow H^0 Z, H^0 \rightarrow \gamma\gamma$
>100.7	95	23	BARATE	00L	ALEP	$e^+e^- \rightarrow H^0 Z, H^0 \rightarrow \gamma\gamma$
> 96.2	95	24	ABBIENDI	99O	OPAL	$e^+e^- \rightarrow H^0 Z, H^0 \rightarrow \gamma\gamma$
> 78.5	95	25	ABBOTT	99B	D0	$p\bar{p} \rightarrow H^0 W/Z, H^0 \rightarrow \gamma\gamma$
		26	ABREU	99P	DLPH	$e^+e^- \rightarrow H^0 \gamma$ and/or $H^0 \rightarrow \gamma\gamma$

- AALTONEN 13K search for $H^0 \rightarrow WW^*$ in 9.7 fb^{-1} of $p\bar{p}$ collisions at $E_{\text{cm}} = 1.96 \text{ TeV}$. A limit on cross section times branching ratio which corresponds to (1.3-6.6) times the expected cross section is given in the range $m_{H^0} = 110-200 \text{ GeV}$ at 95% CL.
- AALTONEN 13L combine all CDF searches with $9.45-10.0 \text{ fb}^{-1}$ of $p\bar{p}$ collisions at $E_{\text{cm}} = 1.96 \text{ TeV}$.
- AALTONEN 13M combine all Tevatron data from the CDF and D0 Collaborations of $p\bar{p}$ collisions at $E_{\text{cm}} = 1.96 \text{ TeV}$.
- ABAZOV 13G search for $H^0 \rightarrow WW^*$ in 9.7 fb^{-1} of $p\bar{p}$ collisions at $E_{\text{cm}} = 1.96 \text{ TeV}$. A limit on cross section times branching ratio which corresponds to (2-9) times the expected cross section is given for $m_{H^0} = 100-200 \text{ GeV}$ at 95% CL.
- ABAZOV 13H search for $H^0 \rightarrow \gamma\gamma$ in 9.6 fb^{-1} of $p\bar{p}$ collisions at $E_{\text{cm}} = 1.96 \text{ TeV}$.
- ABAZOV 13I search for H^0 production in the final state with one lepton and two or more jets plus missing E_T in 9.7 fb^{-1} of $p\bar{p}$ collisions at $E_{\text{cm}} = 1.96 \text{ TeV}$. The search is sensitive to WH^0, ZH^0 and vector-boson fusion Higgs production with $H^0 \rightarrow WW^*$. A limit on cross section times branching ratio which corresponds to (8-30) times the expected cross section is given in the range $m_{H^0} = 100-200 \text{ GeV}$ at 95% CL.
- ABAZOV 13J search for H^0 production in the final states $e\mu\mu, e\mu\mu, \mu\tau\tau, \tau\mu\mu$ in $8.6-9.7 \text{ fb}^{-1}$ of $p\bar{p}$ collisions at $E_{\text{cm}} = 1.96 \text{ TeV}$. The search is sensitive to WH^0, ZH^0 production with $H^0 \rightarrow WW^*, ZZ^*$, decaying to leptonic final states. A limit on cross section times branching ratio which corresponds to (2.4-13.0) times the expected cross section is given in the range $m_{H^0} = 100-200 \text{ GeV}$ at 95% CL.
- ABAZOV 13L combine all D0 results with up to 9.7 fb^{-1} of $p\bar{p}$ collisions at $E_{\text{cm}} = 1.96 \text{ TeV}$.
- CHATRCHYAN 13AL search for $H^0 \rightarrow \gamma\gamma$ in 5.1 fb^{-1} and 5.3 fb^{-1} of pp collisions at $E_{\text{cm}} = 7$ and 8 TeV .
- AAD 12N search for $H^0 \rightarrow \gamma\gamma$ with 4.9 fb^{-1} of pp collisions at $E_{\text{cm}} = 7 \text{ TeV}$ in the mass range $m_{H^0} = 110-150 \text{ GeV}$.
- AALTONEN 12AN search for $H^0 \rightarrow \gamma\gamma$ with 10 fb^{-1} of $p\bar{p}$ collisions at $E_{\text{cm}} = 1.96 \text{ TeV}$ in the mass range $m_{H^0} = 100-150 \text{ GeV}$.
- CHATRCHYAN 12AO use data from CHATRCHYAN 12G, CHATRCHYAN 12E, CHATRCHYAN 12H, CHATRCHYAN 12I, CHATRCHYAN 12D, and CHATRCHYAN 12C.
- AALTONEN 09AB search for $H^0 \rightarrow \gamma\gamma$ in 3.0 fb^{-1} of $p\bar{p}$ collisions at $E_{\text{cm}} = 1.96 \text{ TeV}$ in the mass range $m_{H^0} = 70-150 \text{ GeV}$. Associated $H^0 W, H^0 Z$ production and WW, ZZ fusion are considered.
- ABAZOV 08U search for $H^0 \rightarrow \gamma\gamma$ in $p\bar{p}$ collisions at $E_{\text{cm}} = 1.96 \text{ TeV}$ in the mass range $m_{H^0} = 70-150 \text{ GeV}$. Associated $H^0 W, H^0 Z$ production and WW, ZZ fusion are considered. See their Tab. 1 for the limit on $\sigma \cdot B(H^0 \rightarrow \gamma\gamma)$, and see their Fig. 3 for the excluded region in the $m_{H^0} - B(H^0 \rightarrow \gamma\gamma)$ plane.
- SCHAEEL 07 search for Higgs bosons in association with a fermion pair and decaying to WW^* . The limit is from this search and HEISTER 02L for a H^0 with SM production cross section.
- Search for associated production of a $\gamma\gamma$ resonance with a Z boson, followed by $Z \rightarrow q\bar{q}, \ell^+\ell^-, \text{ or } \nu\bar{\nu}$, at $E_{\text{cm}} \leq 209 \text{ GeV}$. The limit is for a H^0 with SM production cross section.
- Updates ABREU 01F.
- ACHARD 03C search for $e^+e^- \rightarrow ZH^0$ followed by $H^0 \rightarrow WW^* \text{ or } ZZ^*$ at $E_{\text{cm}} = 200-209 \text{ GeV}$ and combine with the ACHARD 02C result. The limit is for a H^0 with SM production cross section. For $B(H^0 \rightarrow WW^*) + B(H^0 \rightarrow ZZ^*) = 1, m_{H^0} > 108.1 \text{ GeV}$ is obtained. See fig. 6 for the limits under different BR assumptions.
- For $B(H^0 \rightarrow \gamma\gamma) = 1, m_{H^0} > 117 \text{ GeV}$ is obtained.
- ACHARD 02C search for associated production of a $\gamma\gamma$ resonance with a Z boson, followed by $Z \rightarrow q\bar{q}, \ell^+\ell^-, \text{ or } \nu\bar{\nu}$, at $E_{\text{cm}} \leq 209 \text{ GeV}$. The limit is for a H^0 with SM production cross section. For $B(H^0 \rightarrow \gamma\gamma) = 1, m_{H^0} > 114 \text{ GeV}$ is obtained.
- AFFOLDER 01H search for associated production of a $\gamma\gamma$ resonance and a W or Z (tagged by two jets, an isolated lepton, or missing E_T). The limit assumes Standard Model values for the production cross section and for the couplings of the H^0 to W and Z bosons. See their Fig. 11 for limits with $B(H^0 \rightarrow \gamma\gamma) < 1$.

- ACCIARRI 00s search for associated production of a $\gamma\gamma$ resonance with a $q\bar{q}, \nu\bar{\nu}$, or $\ell^+\ell^-$ pair in e^+e^- collisions at $E_{\text{cm}} = 189 \text{ GeV}$. The limit is for a H^0 with SM production cross section. For $B(H^0 \rightarrow \gamma\gamma) = 1, m_{H^0} > 98 \text{ GeV}$ is obtained. See their Fig. 5 for limits on $B(H \rightarrow \gamma\gamma) \cdot \sigma(e^+e^- \rightarrow Hf\bar{f}) / \sigma(e^+e^- \rightarrow Hf\bar{f})$ (SM).
- BARATE 00L search for associated production of a $\gamma\gamma$ resonance with a $q\bar{q}, \nu\bar{\nu}$, or $\ell^+\ell^-$ pair in e^+e^- collisions at $E_{\text{cm}} = 88-202 \text{ GeV}$. The limit is for a H^0 with SM production cross section. For $B(H^0 \rightarrow \gamma\gamma) = 1, m_{H^0} > 109 \text{ GeV}$ is obtained. See their Fig. 3 for limits on $B(H \rightarrow \gamma\gamma) \cdot \sigma(e^+e^- \rightarrow Hf\bar{f}) / \sigma(e^+e^- \rightarrow Hf\bar{f})$ (SM).
- ABBIENDI 99o search for associated production of a $\gamma\gamma$ resonance with a $q\bar{q}, \nu\bar{\nu}$, or $\ell^+\ell^-$ pair in e^+e^- collisions at 189 GeV . The limit is for a H^0 with SM production cross section. See their Fig. 4 for limits on $\sigma(e^+e^- \rightarrow H^0 Z^0) \times B(H^0 \rightarrow \gamma\gamma) \times B(X^0 \rightarrow f\bar{f})$ for various masses. Updates the results of ACKERSTAFF 98y.
- ABBOTT 99B search for associated production of a $\gamma\gamma$ resonance and a dijet pair. The limit assumes Standard Model values for the production cross section and for the couplings of the H^0 to W and Z bosons. Limits in the range of $\sigma(H^0 + Z/W) \cdot B(H^0 \rightarrow \gamma\gamma) = 0.80-0.34 \text{ pb}$ are obtained in the mass range $m_{H^0} = 65-150 \text{ GeV}$.
- ABREU 99P search for $e^+e^- \rightarrow H^0 \gamma$ with $H^0 \rightarrow b\bar{b}$ or $\gamma\gamma$, and $e^+e^- \rightarrow H^0 q\bar{q}$ with $H^0 \rightarrow \gamma\gamma$. See their Fig. 4 for limits on $\sigma \times B$. Explicit limits within an effective interaction framework are also given.

Mass Limits for H^0 Decaying to Invisible Final States

These limits are for a neutral scalar H^0 which predominantly decays to invisible final states. Standard Model values are assumed for the couplings of H^0 to ordinary particles unless otherwise stated.

VALUE (GeV)	CL%	DOCUMENT ID	TECN	COMMENT
• • •				We do not use the following data for averages, fits, limits, etc. • • •
		1 AABOUD	19AI ATLS	WW/Z fusion
		2 AAD	15BD ATLS	$pp \rightarrow H^0 WX, H^0 ZX$
		3 AAD	15BH ATLS	jet + missing E_T
		4 AAD	14BA ATLS	secondary vertex
		5 AAD	14O ATLS	$pp \rightarrow H^0 ZX$
		6 CHATRCHYAN	14B CMS	$pp \rightarrow H^0 ZX, qqH^0 X$
		7 AAD	13AG ATLS	secondary vertex
		8 AAD	13AT ATLS	electron jets
		9 CHATRCHYAN	13BJ CMS	
		10 AAD	12AQ ATLS	secondary vertex
		11 AALTONEN	12AB CDF	secondary vertex
		12 AALTONEN	12U CDF	secondary vertex
>108.2	95	13 ABBIENDI	10 OPAL	
>112.3	95	14 ABBIENDI	07 OPAL	large width
>112.1	95	15 ACHARD	05 L3	
>114.1	95	16 ABDALLAH	04B DLPH	
>106.4	95	15 HEISTER	02 ALEP	$E_{\text{cm}} \leq 209 \text{ GeV}$
> 89.2	95	15 BARATE	01C ALEP	$E_{\text{cm}} \leq 202 \text{ GeV}$
		16 ACCIARRI	00M L3	

- AABOUD 19AI search for $H^0_{1,2}$ production by vector boson fusion and decay to invisible final states in 36.1 fb^{-1} of pp collisions at $E_{\text{cm}} = 13 \text{ TeV}$. See their Fig. 6(b) for limits on cross section times branching ratios for $m_{H^0_{1,2}} = 0.1-3 \text{ TeV}$.
- AAD 15BD search for $pp \rightarrow H^0 WX$ and $pp \rightarrow H^0 ZX$ with W or Z decaying hadronically and H^0 decaying to invisible final states in 20.3 fb^{-1} at $E_{\text{cm}} = 8 \text{ TeV}$. See their Fig. 6 for a limit on the cross section times branching ratio for $m_{H^0} = 115-300 \text{ GeV}$.
- AAD 15BH search for events with a jet and missing E_T in 20.3 fb^{-1} of pp collisions at $E_{\text{cm}} = 8 \text{ TeV}$. Limits on $\sigma(H^0) B(H^0 \rightarrow \text{invisible}) < (44-10) \text{ pb}$ (95%CL) is given for $m_{H^0} = 115-300 \text{ GeV}$.
- AAD 14BA search for H^0 production in the decay mode $H^0 \rightarrow X^0 X^0$, where X^0 is a long-lived particle which decays to collimated pairs of $e^+e^-, \mu^+\mu^-, \text{ or } \pi^+\pi^-$ plus invisible particles, in 20.3 fb^{-1} of pp collisions at $E_{\text{cm}} = 8 \text{ TeV}$. See their Figs. 15 and 16 for limits on cross section times branching ratio.
- AAD 14O search for $pp \rightarrow H^0 ZX, Z \rightarrow \ell\ell$, with H^0 decaying to invisible final states in 4.5 fb^{-1} at $E_{\text{cm}} = 7 \text{ TeV}$ and 20.3 fb^{-1} at $E_{\text{cm}} = 8 \text{ TeV}$. See their Fig. 3 for a limit on the cross section times branching ratio for $m_{H^0} = 110-400 \text{ GeV}$.
- CHATRCHYAN 14B search for $pp \rightarrow H^0 ZX, Z \rightarrow \ell\ell$ and $Z \rightarrow b\bar{b}$, and also $pp \rightarrow qqH^0 X$ with H^0 decaying to invisible final states using data at $E_{\text{cm}} = 7$ and 8 TeV . See their Figs. 10, 11 for limits on the cross section times branching ratio for $m_{H^0} = 100-400 \text{ GeV}$.
- AAD 13AG search for H^0 production in the decay mode $H^0 \rightarrow X^0 X^0$, where X^0 is a long-lived particle which decays to $\mu^+\mu^- X^0$, in 1.9 fb^{-1} of pp collisions at $E_{\text{cm}} = 7 \text{ TeV}$. See their Fig. 7 for limits on cross section times branching ratio.
- AAD 13AT search for H^0 production in the decay $H^0 \rightarrow X^0 X^0$, where X^0 eventually decays to clusters of collimated e^+e^- pairs, in 2.04 fb^{-1} of pp collisions at $E_{\text{cm}} = 7 \text{ TeV}$. See their Fig. 3 for limits on cross section times branching ratio.
- CHATRCHYAN 13BJ search for H^0 production in the decay chain $H^0 \rightarrow X^0 X^0, X^0 \rightarrow \mu^+\mu^- X^0$ in 5.3 fb^{-1} of pp collisions at $E_{\text{cm}} = 7 \text{ TeV}$. See their Fig. 2 for limits on cross section times branching ratio.
- AAD 12AQ search for H^0 production in the decay mode $H^0 \rightarrow X^0 X^0$, where X^0 is a long-lived particle which decays mainly to $b\bar{b}$ in the muon detector, in 1.94 fb^{-1} of pp collisions at $E_{\text{cm}} = 7 \text{ TeV}$. See their Fig. 3 for limits on cross section times branching ratio for $m_{H^0} = 120, 140 \text{ GeV}, m_{X^0} = 20, 40 \text{ GeV}$ in the $c\tau$ range of $0.5-35 \text{ m}$.
- AALTONEN 12AB search for H^0 production in the decay $H^0 \rightarrow X^0 X^0$, where X^0 eventually decays to clusters of collimated $\ell^+\ell^-$ pairs, in 5.1 fb^{-1} of $p\bar{p}$ collisions at $E_{\text{cm}} = 1.96 \text{ TeV}$. Cross section limits are provided for a benchmark MSSM model incorporating the parameters given in Table VI.
- AALTONEN 12U search for H^0 production in the decay mode $H^0 \rightarrow X^0 X^0$, where X^0 is a long-lived particle with $c\tau \approx 1 \text{ cm}$ which decays mainly to $b\bar{b}$, in 3.2 fb^{-1} of $p\bar{p}$

collisions at $E_{\text{cm}} = 1.96$ TeV. See their Figs. 9 and 10 for limits on cross section times branching ratio for $m_{H^0} = (130\text{--}170)$ GeV, $m_{X^0} = 20, 40$ GeV.

- 13 ABBIENDI 10 search for $e^+e^- \rightarrow H^0 Z$ with H^0 decaying invisibly. The limit assumes SM production cross section and $B(H^0 \rightarrow \text{invisible}) = 1$.
- 14 ABBIENDI 07 search for $e^+e^- \rightarrow H^0 Z$ with $Z \rightarrow q\bar{q}$ and H^0 decaying to invisible final states. The H^0 width is varied between 1 GeV and 3 TeV. A limit $\sigma \cdot B(H^0 \rightarrow \text{invisible}) < (0.07\text{--}0.57)$ pb (95%CL) is obtained at $E_{\text{cm}} = 206$ GeV for $m_{H^0} = 60\text{--}114$ GeV.
- 15 Search for $e^+e^- \rightarrow H^0 Z$ with H^0 decaying invisibly. The limit assumes SM production cross section and $B(H^0 \rightarrow \text{invisible}) = 1$.
- 16 ACCIARRI 00M search for $e^+e^- \rightarrow ZH^0$ with H^0 decaying invisibly at $E_{\text{cm}} = 183\text{--}189$ GeV. The limit assumes SM production cross section and $B(H^0 \rightarrow \text{invisible}) = 1$. See their Fig. 6 for limits for smaller branching ratios.

Mass Limits for Light A^0

These limits are for a pseudoscalar A^0 in the mass range below $\mathcal{O}(10)$ GeV.

VALUE (GeV)	DOCUMENT ID	TECN	COMMENT
• • •	We do not use the following data for averages, fits, limits, etc. • • •		
1	AAD	20AE ATLS	$H^0 \rightarrow ZA^0$
2	AABOUD	18AP ATLS	$H^0 \rightarrow A^0 A^0$
3	KHACHATRYAN...	17AZ CMS	$H^0 \rightarrow A^0 A^0$
4	ABLIKIM	16E BES3	$J/\psi \rightarrow A^0 \gamma$
5	KHACHATRYAN...	16F CMS	$H^0 \rightarrow A^0 A^0$
6	LEES	15H BABR	$\Upsilon(1S) \rightarrow A^0 \gamma$
7	LEES	13C BABR	$\Upsilon(1S) \rightarrow A^0 \gamma$
8	LEES	13L BABR	$\Upsilon(1S) \rightarrow A^0 \gamma$
9	LEES	13R BABR	$\Upsilon(1S) \rightarrow A^0 \gamma$
10	ABLIKIM	12 BES3	$J/\psi \rightarrow A^0 \gamma$
11	CHATRCHYAN	12V CMS	$A^0 \rightarrow \mu^+ \mu^-$
12	AALTONEN	11P CDF	$t \rightarrow bH^+, H^+ \rightarrow W^+ A^0$
13,14	ABOUZAID	11A KTEV	$K_L \rightarrow \pi^0 \pi^0 A^0, A^0 \rightarrow \mu^+ \mu^-$
15	DEL-AMO-SA...	11J BABR	$\Upsilon(1S) \rightarrow A^0 \gamma$
16	LEES	11H BABR	$\Upsilon(2S, 3S) \rightarrow A^0 \gamma$
17	ANDREAS	10 RVUE	
14,18	HYUN	10 BELL	$B^0 \rightarrow K^* A^0, A^0 \rightarrow \mu^+ \mu^-$
14,19	HYUN	10 BELL	$B^0 \rightarrow \rho^0 A^0, A^0 \rightarrow \mu^+ \mu^-$
20	AUBERT	09P BABR	$\Upsilon(3S) \rightarrow A^0 \gamma$
21	AUBERT	09Z BABR	$\Upsilon(2S) \rightarrow A^0 \gamma$
22	AUBERT	09Z BABR	$\Upsilon(3S) \rightarrow A^0 \gamma$
14,23	TUNG	09 K391	$K_L \rightarrow \pi^0 \pi^0 A^0, A^0 \rightarrow \gamma \gamma$
24	LOVE	08 CLEO	$\Upsilon(1S) \rightarrow A^0 \gamma$
25	BESSON	07 CLEO	$\Upsilon(1S) \rightarrow \eta_b \gamma$
26	PARK	05 HYCP	$\Sigma^+ \rightarrow p A^0, A^0 \rightarrow \mu^+ \mu^-$
27	BALEST	95 CLE2	$\Upsilon(1S) \rightarrow A^0 \gamma$
28	ANTREASIAN	90C CBAL	$\Upsilon(1S) \rightarrow A^0 \gamma$

1 AAD 20AE search for the decay $H^0 \rightarrow ZA^0, Z \rightarrow \ell^+ \ell^-, A^0$ decaying hadronically ($A^0 \rightarrow gg$ or $s\bar{s}$), in 139 fb^{-1} of pp collisions at $E_{\text{cm}} = 13$ TeV. Limit on the product of production cross section and the $H^0 \rightarrow ZA^0$ branching ratio in the range $17\text{--}340$ pb (95% CL) is given for $m_{A^0} = 0.5\text{--}4.0$ GeV, see their Table 1.

2 AABOUD 18AP search for the decay $H^0 \rightarrow A^0 A^0 \rightarrow \mu^+ \mu^- \mu^+ \mu^-$ in 36.1 fb^{-1} of pp collisions at $E_{\text{cm}} = 13$ TeV. See their Fig. 10(b) for limits on $B(H^0 \rightarrow A^0 A^0)$ in the range $m_{A^0} = 1\text{--}2.5, 4.5\text{--}8$ GeV, assuming a type-II two-doublet plus singlet model with $\tan(\beta) = 5$.

3 KHACHATRYAN 17AZ search for the decay $H^0 \rightarrow A^0 A^0 \rightarrow \tau^+ \tau^- \tau^+ \tau^-, \mu^+ \mu^- b\bar{b}$, and $\mu^+ \mu^- \tau^+ \tau^-$ in 19.7 fb^{-1} of pp collisions at $E_{\text{cm}} = 8$ TeV. See their Figs. 4, 5, and 6 for cross section limits in the range $m_{A^0} = 5\text{--}62.5$ GeV. See also their Figs. 7, 8, and 9 for interpretation of the data in terms of models with two Higgs doublets and a singlet.

4 ABLIKIM 16E search for the process $J/\psi \rightarrow A^0 \gamma$ with A^0 decaying to $\mu^+ \mu^-$ and give limits on $B(J/\psi \rightarrow A^0 \gamma) \cdot B(A^0 \rightarrow \mu^+ \mu^-)$ in the range $2.8 \times 10^{-8}\text{--}5.0 \times 10^{-6}$ (90% CL) for $0.212 \leq m_{A^0} \leq 3.0$ GeV. See their Fig. 5.

5 KHACHATRYAN 16F search for the decay $H^0 \rightarrow A^0 A^0 \rightarrow \tau^+ \tau^- \tau^+ \tau^-$ in 19.7 fb^{-1} of pp collisions at $E_{\text{cm}} = 8$ TeV. See their Fig. 8 for cross section limits for $m_{A^0} = 4\text{--}8$ GeV.

6 LEES 15H search for the process $\Upsilon(2S) \rightarrow \Upsilon(1S) \pi^+ \pi^- \rightarrow A^0 \gamma \pi^+ \pi^-$ with A^0 decaying to $c\bar{c}$ and give limits on $B(\Upsilon(1S) \rightarrow A^0 \gamma) \cdot B(A^0 \rightarrow c\bar{c})$ in the range $7.4 \times 10^{-5}\text{--}2.4 \times 10^{-3}$ (90% CL) for $4.00 \leq m_{A^0} \leq 8.95$ and $9.10 \leq m_{A^0} \leq 9.25$ GeV. See their Fig. 6.

7 LEES 13C search for the process $\Upsilon(2S, 3S) \rightarrow \Upsilon(1S) \pi^+ \pi^- \rightarrow A^0 \gamma \pi^+ \pi^-$ with A^0 decaying to $\mu^+ \mu^-$ and give limits on $B(\Upsilon(1S) \rightarrow A^0 \gamma) \cdot B(A^0 \rightarrow \mu^+ \mu^-)$ in the range $(0.3\text{--}9.7) \times 10^{-6}$ (90% CL) for $0.212 \leq m_{A^0} \leq 9.20$ GeV. See their Fig. 5(e) for limits on the $b\text{--}A^0$ Yukawa coupling derived by combining this result with AUBERT 09z.

8 LEES 13L search for the process $\Upsilon(2S) \rightarrow \Upsilon(1S) \pi^+ \pi^- \rightarrow A^0 \gamma \pi^+ \pi^-$ with A^0 decaying to $g\bar{g}$ or $s\bar{s}$ and give limits on $B(\Upsilon(1S) \rightarrow A^0 \gamma) \cdot B(A^0 \rightarrow g\bar{g})$ between 1×10^{-6} and 2×10^{-2} (90% CL) for $0.5 \leq m_{A^0} \leq 9.0$ GeV, and $B(\Upsilon(1S) \rightarrow A^0 \gamma) \cdot B(A^0 \rightarrow s\bar{s})$ between 4×10^{-6} and 1×10^{-3} (90%CL) for $1.5 \leq m_{A^0} \leq 9.0$ GeV. See their Fig. 4.

9 LEES 13R search for the process $\Upsilon(2S) \rightarrow \Upsilon(1S) \pi^+ \pi^- \rightarrow A^0 \gamma \pi^+ \pi^-$ with A^0 decaying to $\tau^+ \tau^-$ and give limits on $B(\Upsilon(1S) \rightarrow A^0 \gamma) \cdot B(A^0 \rightarrow \tau^+ \tau^-)$ in the range $0.9\text{--}13 \times 10^{-5}$ (90% CL) for $3.6 \leq m_{A^0} \leq 9.2$ GeV. See their Fig. 4 for limits on the $b\text{--}A^0$ Yukawa coupling derived by combining this result with AUBERT 09p.

10 ABLIKIM 12 search for the process $\psi(3686) \rightarrow \pi\pi J/\psi, J/\psi \rightarrow A^0 \gamma$ with A^0 decaying to $\mu^+ \mu^-$. It gives mass dependent limits on $B(J/\psi \rightarrow A^0 \gamma) \cdot B(A^0 \rightarrow \mu^+ \mu^-)$ in the range $4 \times 10^{-7}\text{--}2.1 \times 10^{-5}$ (90% C.L.) for $0.212 \leq m_{A^0} \leq 3.0$ GeV. See their Fig. 2.

11 CHATRCHYAN 12V search for A^0 production in the decay $A^0 \rightarrow \mu^+ \mu^-$ with 1.3 fb^{-1} of pp collisions at $E_{\text{cm}} = 7$ TeV. A limit on $\sigma(A^0) \cdot B(A^0 \rightarrow \mu^+ \mu^-)$ in the range $(1.5\text{--}7.5)$ pb is given for $m_{A^0} = (5.5\text{--}8.7)$ and $(11.5\text{--}14)$ GeV at 95% CL.

12 AALTONEN 11P search in 2.7 fb^{-1} of $p\bar{p}$ collisions at $E_{\text{cm}} = 1.96$ TeV for the decay chain $t \rightarrow bH^+, H^+ \rightarrow W^+ A^0, A^0 \rightarrow \tau^+ \tau^-$ with m_{A^0} between 4 and 9 GeV. See their Fig. 4 for limits on $B(t \rightarrow bH^+)$ for $90 < m_{H^+} < 160$ GeV.

13 ABOUZAID 11A search for the decay chain $K_L \rightarrow \pi^0 \pi^0 A^0, A^0 \rightarrow \mu^+ \mu^-$ and give a limit $B(K_L \rightarrow \pi^0 \pi^0 A^0) \cdot B(A^0 \rightarrow \mu^+ \mu^-) < 1.0 \times 10^{-10}$ at 90% CL for $m_{A^0} = 214.3$ MeV.

14 The search was motivated by PARK 05.

15 DEL-AMO-SANCHEZ 11J search for the process $\Upsilon(2S) \rightarrow \Upsilon(1S) \pi^+ \pi^- \rightarrow A^0 \gamma \pi^+ \pi^-$ with A^0 decaying to invisible final states. They give limits on $B(\Upsilon(1S) \rightarrow A^0 \gamma) \cdot B(A^0 \rightarrow \text{invisible})$ in the range $(1.9\text{--}4.5) \times 10^{-6}$ (90% CL) for $0 \leq m_{A^0} \leq 8.0$ GeV, and $(2.7\text{--}37) \times 10^{-6}$ for $8.0 \leq m_{A^0} \leq 9.2$ GeV.

16 LEES 11H search for the process $\Upsilon(2S, 3S) \rightarrow A^0 \gamma$ with A^0 decaying hadronically and give limits on $B(\Upsilon(2S, 3S) \rightarrow A^0 \gamma) \cdot B(A^0 \rightarrow \text{hadrons})$ in the range $1 \times 10^{-6}\text{--}8 \times 10^{-5}$ (90% CL) for $0.3 < m_{A^0} < 7$ GeV. The decay rates for $\Upsilon(2S)$ and $\Upsilon(3S)$ are assumed to be equal up to the phase space factor. See their Fig. 5.

17 ANDREAS 10 μ_e constraints from rare decays and other processes on a light A^0 with $m_{A^0} < 2m_\mu$ and give limits on its coupling to fermions at the level of 10^{-4} times the Standard Model value.

18 HYUN 10 search for the decay chain $B^0 \rightarrow K^* A^0, A^0 \rightarrow \mu^+ \mu^-$ and give a limit on $B(B^0 \rightarrow K^* A^0) \cdot B(A^0 \rightarrow \mu^+ \mu^-)$ in the range $(2.26\text{--}5.53) \times 10^{-8}$ at 90%CL for $m_{A^0} = 212\text{--}300$ MeV. The limit for $m_{A^0} = 214.3$ MeV is 2.26×10^{-8} .

19 HYUN 10 search for the decay chain $B^0 \rightarrow \rho^0 A^0, A^0 \rightarrow \mu^+ \mu^-$ and give a limit on $B(B^0 \rightarrow \rho^0 A^0) \cdot B(A^0 \rightarrow \mu^+ \mu^-)$ in the range $(1.73\text{--}4.51) \times 10^{-8}$ at 90%CL for $m_{A^0} = 212\text{--}300$ MeV. The limit for $m_{A^0} = 214.3$ MeV is 1.73×10^{-8} .

20 AUBERT 09p search for the process $\Upsilon(3S) \rightarrow A^0 \gamma$ with $A^0 \rightarrow \tau^+ \tau^-$ for $4.03 < m_{A^0} < 9.52$ and $9.61 < m_{A^0} < 10.10$ GeV, and give limits on $B(\Upsilon(3S) \rightarrow A^0 \gamma) \cdot B(A^0 \rightarrow \tau^+ \tau^-)$ in the range $(1.5\text{--}16) \times 10^{-5}$ (90% CL).

21 AUBERT 09z search for the process $\Upsilon(2S) \rightarrow A^0 \gamma$ with $A^0 \rightarrow \mu^+ \mu^-$ for $0.212 < m_{A^0} < 9.3$ GeV and give limits on $B(\Upsilon(2S) \rightarrow A^0 \gamma) \cdot B(A^0 \rightarrow \mu^+ \mu^-)$ in the range $(0.3\text{--}8) \times 10^{-6}$ (90% CL).

22 AUBERT 09z search for the process $\Upsilon(3S) \rightarrow A^0 \gamma$ with $A^0 \rightarrow \mu^+ \mu^-$ for $0.212 < m_{A^0} < 9.3$ GeV and give limits on $B(\Upsilon(3S) \rightarrow A^0 \gamma) \cdot B(A^0 \rightarrow \mu^+ \mu^-)$ in the range $(0.3\text{--}5) \times 10^{-6}$ (90% CL).

23 TUNG 09 search for the decay chain $K_L \rightarrow \pi^0 \pi^0 A^0, A^0 \rightarrow \gamma \gamma$ and give a limit on $B(K_L \rightarrow \pi^0 \pi^0 A^0) \cdot B(A^0 \rightarrow \gamma \gamma)$ in the range $(2.4\text{--}10.7) \times 10^{-7}$ at 90%CL for $m_{A^0} = 194.3\text{--}219.3$ MeV. The limit for $m_{A^0} = 214.3$ MeV is 2.4×10^{-7} .

24 LOVE 08 search for the process $\Upsilon(1S) \rightarrow A^0 \gamma$ with $A^0 \rightarrow \mu^+ \mu^-$ (for $m_{A^0} < 2m_\tau$) and $A^0 \rightarrow \tau^+ \tau^-$. Limits on $B(\Upsilon(1S) \rightarrow A^0 \gamma) \cdot B(A^0 \rightarrow \ell^+ \ell^-)$ in the range $10^{-6}\text{--}10^{-4}$ (90% CL) are given.

25 BESSON 07 give a limit $B(\Upsilon(1S) \rightarrow \eta_b \gamma) \cdot B(\eta_b \rightarrow \tau^+ \tau^-) < 0.27\%$ (95% CL), which constrains a possible A^0 exchange contribution to the η_b decay.

26 PARK 05 found three candidate events for $\Sigma^+ \rightarrow p \mu^+ \mu^-$ in the HyperCP experiment. Due to a narrow spread in dimuon mass, they hypothesize the events as a possible signal of a new boson. It can be interpreted as a neutral particle with $m_{A^0} = 214.3 \pm 0.5$ MeV and the branching fraction $B(\Sigma^+ \rightarrow p A^0) \cdot B(A^0 \rightarrow \mu^+ \mu^-) = (3.1^{+2.4}_{-1.9} \pm 1.5) \times 10^{-8}$.

27 BALEST 95 give limits $B(\Upsilon(1S) \rightarrow A^0 \gamma) ; 1.5 \times 10^{-5}$ at 90% CL for $m_{A^0} < 5$ GeV. The limit becomes $< 10^{-4}$ for $m_{A^0} < 7.7$ GeV.

28 ANTREASIAN 90c give limits $B(\Upsilon(1S) \rightarrow A^0 \gamma) ; 5.6 \times 10^{-5}$ at 90% CL for $m_{A^0} < 7.2$ GeV. A^0 is assumed not to decay in the detector.

Other Mass Limits

We use a symbol H^0_1 if mass < 125 GeV or H^0_2 if mass > 125 GeV. The notation H^0 is reserved for the 125 GeV particle.

VALUE (GeV)	CL%	DOCUMENT ID	TECN	COMMENT
• • •	We do not use the following data for averages, fits, limits, etc. • • •			
1	AAD	22A ATLS	$H^0 \rightarrow A^0 A^0$	
2	AAD	21AF ATLS	$H^0_2 \rightarrow Z Z$	
3	AAD	21AI ATLS	$A^0 \rightarrow ZH^0_2$	
4	AAD	21AY ATLS	$H^0_2 \rightarrow \gamma \gamma$	
5	AAD	21AZ ATLS	$A^0_2 \rightarrow H^0 A^0_1$	
6	AAD	21BB ATLS	$A^0_2 \rightarrow H^0 A^0_1$	
7	AAD	21BE ATLS	$A^0_1 \rightarrow \text{invisible}$	
8	ABRATENKO	21 MCBN	$K^+ \rightarrow H^0_1 \pi^+$	
9	SIRUNYAN	21A CMS	$H^0 \rightarrow ZA^0, A^0 \rightarrow \text{invisible}$	
10	TUMASYAN	21F CMS	$H^0_3 \rightarrow H^0 H^0_{1,2}$	
11	AAD	20AA ATLS	$H^0_2/A^0 \rightarrow \tau^+ \tau^-$	
12	AAD	20AI ATLS	$H^0 \rightarrow A^0 A^0$	
13	AAD	20AO ATLS	$H^0 \rightarrow H^0 H^0$	
14	AAD	20C ATLS	$H^0_2 \rightarrow H^0 H^0$	
15	AAD	20L ATLS	$H^0 \rightarrow b\bar{b}$	
16	AAD	20X ATLS	$H^0_2 \rightarrow H^0 H^0$	
17	AAIJ	20AL LHCB	$A^0 \rightarrow \mu^+ \mu^-$	
18	SIRUNYAN	20 CMS	$H^0 \rightarrow A^0 A^0$	
19	SIRUNYAN	20AA CMS	$H^0_2 \rightarrow ZA^0$ or $A^0 \rightarrow ZH^0_2$	
20	SIRUNYAN	20AC CMS	$A^0 \rightarrow ZH^0$	

- 12 AAD 20A search for ZH^0 production followed by the decay $H^0 \rightarrow A^0 A^0 \rightarrow b\bar{b}b\bar{b}$ in 36 fb^{-1} of pp collisions at $E_{\text{cm}} = 13 \text{ TeV}$. The search looks for collimated $A^0 \rightarrow b\bar{b}$ decays and is complementary to AABOUD 18BX. See their Fig. 10 for limits on the product of production cross section and branching ratios in the range $m_{A^0} = 15\text{--}30 \text{ GeV}$.
- 13 AAD 20A search for gluon fusion production of H_2^0 decaying to $H^0 H^0 \rightarrow \tau^+ \tau^- b\bar{b}$ (with hadronically decaying $\tau^+ \tau^-$) using 139 fb^{-1} of pp collisions at $E_{\text{cm}} = 13 \text{ TeV}$. Limit on the product of production cross section times branching ratios in the range $28\text{--}817 \text{ fb}^{-1}$ (95% CL) is given for $m_{A^0} = 1.0\text{--}3.0 \text{ TeV}$, see their Fig. 13.
- 14 AAD 20c combine searches for a scalar resonance decaying to $H^0 H^0$ in 36.1 fb^{-1} of pp collisions at $E_{\text{cm}} = 13 \text{ TeV}$ from AABOUD 19A, AABOUD 19c, AABOUD 18cQ, AABOUD 19T, AABOUD 18cW, and AABOUD 18BU. See their Fig. 5(a) for limits on cross section times branching ratio for $m_{H_2^0} = 0.26\text{--}3 \text{ TeV}$.
- 15 AAD 20L search for b -associated production of H_2^0 decaying to $b\bar{b}$ in 27.8 fb^{-1} of pp collisions at $E_{\text{cm}} = 13 \text{ TeV}$. See their Fig. 8 for limits on the product of cross section and branching ratio for $m_{H_2^0} = 0.45\text{--}1.4 \text{ TeV}$.
- 16 AAD 20x search for vector-boson-fusion production of H_2^0 decaying to $H^0 H^0$ using 126 fb^{-1} of pp collisions at $E_{\text{cm}} = 13 \text{ TeV}$. See their Fig. 5 for limits on the product of cross section and branching ratio for the assumptions of a narrow- and broad-width resonance.
- 17 AAIJ 20AL search for dimuon resonance in the mass range $0.2\text{--}60 \text{ GeV}$ in 5.1 fb^{-1} of pp collisions at $E_{\text{cm}} = 13 \text{ TeV}$, in inclusive and b quark associated production. Displaced decays are searched for masses below 3 GeV . See their Figs. 7–9 for cross section limits and Fig. 10 for limits for mixing angle in two Higgs doublet plus singlet model (at 90% CL).
- 18 SIRUNYAN 20 search for the decay $H^0 \rightarrow A^0 A^0 \rightarrow \tau^+ \tau^- \tau^+ \tau^-$ or $\tau^+ \tau^- \mu^+ \mu^-$ in 35.9 fb^{-1} of pp collisions at $E_{\text{cm}} = 13 \text{ TeV}$. See their Fig. 10 for limits on the product of production cross section (normalized to the SM) and branching ratios in the range $m_{A^0} = 4\text{--}15 \text{ GeV}$.
- 19 SIRUNYAN 20AA search for $H_2^0 \rightarrow Z A^0$, $A^0 \rightarrow b\bar{b}$ or $A^0 \rightarrow Z H_2^0$, $H_2^0 \rightarrow b\bar{b}$ in 35.9 fb^{-1} of pp collisions at $E_{\text{cm}} = 13 \text{ TeV}$. See their Fig. 7 for limits on the product of cross section and branching ratio for $m_{H_2^0} = 0.12\text{--}1 \text{ TeV}$ and $m_{A^0} = 0.03\text{--}1 \text{ TeV}$.
- 20 SIRUNYAN 20AC search for gluon-fusion production of A^0 decaying to $Z H^0$ in 35.9 fb^{-1} of pp collisions at $E_{\text{cm}} = 13 \text{ TeV}$. See their Fig. 5 for limits on the product of cross section and branching ratios for $m_{A^0} = 220\text{--}400 \text{ GeV}$.
- 21 SIRUNYAN 20AD search for lepton-flavor violating decays $H_2^0 \rightarrow \mu\tau$, $e\tau$ of gluon-fusion-produced H_2^0 in 35.9 fb^{-1} of pp collisions at $E_{\text{cm}} = 13 \text{ TeV}$. See their Fig. 5 (9) and Table 5 (6) for limits on production cross section times branching ratio for $m_{H_2^0} = 0.2\text{--}0.9 \text{ TeV}$ for the $\mu\tau$ ($e\tau$) final state.
- 22 SIRUNYAN 20AF search for $H_2^0/A^0 \rightarrow t\bar{t}$ with one or two charged leptons in the final state using kinematic variables in 35.9 fb^{-1} of pp collisions at $E_{\text{cm}} = 13 \text{ TeV}$. See their Figs. 5 and 6 for limits on top Yukawa coupling of H_2^0 and A^0 for $m_{H_2^0}$, $m_{A^0} = 0.4\text{--}0.75 \text{ TeV}$ for various width assumptions.
- 23 SIRUNYAN 20AP search for the decay H^0 or $H_2^0 \rightarrow A^0 A^0 \rightarrow \mu^+ \mu^- \tau^+ \tau^-$ (for $m_{H_2^0} = 300 \text{ GeV}$) with boosted final-state topology in 35.9 fb^{-1} of pp collisions at $E_{\text{cm}} = 13 \text{ TeV}$. See their Fig. 7 for limits on the product of production cross section (normalized to the SM) and branching ratios in the range $m_{A^0} = 3.6\text{--}21 \text{ GeV}$, and Figs. 8 and 9 for its interpretation in terms of models with two Higgs doublets plus a singlet.
- 24 SIRUNYAN 20V search for gluon-fusion and vector-boson-fusion production of H_2^0 decaying to $W^+ W^-$ in the final states $\ell\nu\ell\nu$ and $\ell\nu q\bar{q}$ in 35.9 fb^{-1} of pp collisions at $E_{\text{cm}} = 13 \text{ TeV}$. See their Fig. 6 for limits on the product of cross section and branching ratio for $m_{H_2^0} = 0.2\text{--}3 \text{ TeV}$.
- 25 SIRUNYAN 20Z search for $H_{1,2}^0$ or A^0 production in association with a $t\bar{t}$ pair, decaying to $e^+ e^-$ or $\mu^+ \mu^-$, in 137 fb^{-1} of pp collisions at $E_{\text{cm}} = 13 \text{ TeV}$. See their Fig. 12 for limits on production cross section times branching ratio for $m_{H_{1,2}^0}$, $m_{A^0} = 15\text{--}75 \text{ GeV}$ and $108\text{--}340 \text{ GeV}$.
- 26 AABOUD 19A search for a narrow scalar resonance decaying to $H^0 H^0 \rightarrow b\bar{b}b\bar{b}$ in $27.5\text{--}36.1 \text{ fb}^{-1}$ of pp collisions at $E_{\text{cm}} = 13 \text{ TeV}$. See their Fig. 9(a) for limits on cross section times branching ratios for $m_{H_2^0} = 0.26\text{--}3 \text{ TeV}$.
- 27 AABOUD 19AG search for the decay $H^0 \rightarrow A^0 A^0 \rightarrow \mu^+ \mu^- b\bar{b}$ in 36.7 fb^{-1} of pp collisions at $E_{\text{cm}} = 13 \text{ TeV}$. See their Fig. 6 (a) for limits on the product of production cross section (normalized to the SM) and branching ratios in the range $m_{A^0} = 20\text{--}60 \text{ GeV}$.
- 28 AABOUD 19c search for a scalar resonance decaying to $H^0 H^0 \rightarrow b\bar{b} W W^*$ in 36.1 fb^{-1} of pp collisions at $E_{\text{cm}} = 13 \text{ TeV}$. See their Fig. 12 (left) for limits on cross section times branching ratio for $m_{H_2^0} = 0.5\text{--}3 \text{ TeV}$.
- 29 AABOUD 19T search for a scalar resonance decaying to $H^0 H^0 \rightarrow W W^* W W^*$ in 36.1 fb^{-1} of pp collisions at $E_{\text{cm}} = 13 \text{ TeV}$. See their Fig. 3 for limits on cross section times branching ratio for $m_{H_2^0} = 260\text{--}500 \text{ GeV}$, assuming SM decay rates for the H^0 .
- 30 AABOUD 19v combine published ATLAS data to constrain two-Higgs-doublet plus singlet pseudoscalar model with A_1^0 decaying to invisible final states. See their Fig. 19 for excluded parameter regions.
- 31 AABOUD 19y search for a narrow scalar resonance produced by gluon fusion or b associated production, decaying to $\mu^+ \mu^-$ in 36.1 fb^{-1} of pp collisions at $E_{\text{cm}} = 13 \text{ TeV}$. See their Figs. 4 and 5(a) for cross section limits for $m_{H_2^0} = 0.2\text{--}1.0 \text{ TeV}$.
- 32 AALTONEN 19 search for b associated production of a scalar particle decaying to $b\bar{b}$ in 5.4 fb^{-1} of $p\bar{p}$ collisions at $E_{\text{cm}} = 1.96 \text{ TeV}$. See their Fig. 3 for limits on cross section times branching ratio for $m_{H_{1,2}^0} = 100\text{--}300 \text{ GeV}$.
- 33 SIRUNYAN 19 search for a narrow scalar resonance decaying to $H^0 H^0 \rightarrow \gamma\gamma b\bar{b}$ in 35.9 fb^{-1} of pp collisions at $E_{\text{cm}} = 13 \text{ TeV}$. See their Fig. 9 (left) for limits on cross section times branching ratios for $m_{H_2^0} = 260\text{--}900 \text{ GeV}$.
- 34 SIRUNYAN 19AE search for a scalar resonance produced in association with a $b\bar{b}$ pair, decaying to $\tau^+ \tau^-$ in 35.9 fb^{-1} of pp collisions at $E_{\text{cm}} = 13 \text{ TeV}$. See their Fig. 4 for cross section limits for $m_{A^0} = 25\text{--}70 \text{ GeV}$.
- 35 SIRUNYAN 19AN search for production of A_2^0 decaying to $H^0 A_1^0$ followed by $H^0 \rightarrow b\bar{b}$, $A_1^0 \rightarrow$ invisible in 35.9 fb^{-1} of pp collisions at $E_{\text{cm}} = 13 \text{ TeV}$, in the mass range $m_{A_2^0} = 0.2\text{--}1.6 \text{ TeV}$, $m_{A_1^0} = 0.15\text{--}0.5 \text{ TeV}$. See their Fig. 6 for limits in terms of two-Higgs-doublet plus singlet pseudoscalar model.
- 36 SIRUNYAN 19AV search for a scalar resonance produced by gluon fusion or b -associated production, decaying to $Z H^0 \rightarrow \ell^+ \ell^- b\bar{b}$ ($\ell = e, \mu$) or $\nu\bar{\nu} b\bar{b}$ in 35.9 fb^{-1} of pp collisions at $E_{\text{cm}} = 13 \text{ TeV}$. See their Fig. 5 for cross section limits for $m_{A^0} = 0.22\text{--}1.0 \text{ TeV}$.
- 37 SIRUNYAN 19B search for gluon fusion production of narrow scalar resonance with large transverse momentum, decaying to $b\bar{b}$, in 35.9 fb^{-1} of pp collisions at $E_{\text{cm}} = 13 \text{ TeV}$. See their Figs. 7 and 8 for limits on cross section times branching ratio for the resonance mass of $50\text{--}350 \text{ GeV}$.
- 38 SIRUNYAN 19BB search for the decay $H_1^0 \rightarrow \gamma\gamma$ in 19.7 fb^{-1} of pp collisions at $E_{\text{cm}} = 8 \text{ TeV}$ and 35.9 fb^{-1} at $E_{\text{cm}} = 13 \text{ TeV}$. See their Figs. 4–6 for limits on cross section times branching ratio for $m_{H_1^0} = 80\text{--}110 \text{ GeV}$ (some results in Fig. 5 for $m_{H_1^0} = 70\text{--}110 \text{ GeV}$).
- 39 SIRUNYAN 19BD search for the decay $H^0 \rightarrow A^0 A^0 \rightarrow \mu^+ \mu^- b\bar{b}$ in 35.9 fb^{-1} of pp collisions at $E_{\text{cm}} = 13 \text{ TeV}$. See their Fig. 5 for limits on the product of cross section times branching ratios in the range $m_{A^0} = 20\text{--}62.5 \text{ GeV}$. See also their Figs. 6 and 7 for interpretation of the data in terms of models with two Higgs doublets and a singlet.
- 40 SIRUNYAN 19BE combine searches for $H_2^0 \rightarrow H^0 H^0$ in 35.9 fb^{-1} of pp collisions at $E_{\text{cm}} = 13 \text{ TeV}$ in various H^0 decay modes, from SIRUNYAN 18A, SIRUNYAN 18AF, SIRUNYAN 18cW, SIRUNYAN 19, and SIRUNYAN 19H. See their Fig. 3 for limits on cross section times branching ratios for $m_{H_2^0} = 0.25\text{--}3 \text{ TeV}$.
- 41 SIRUNYAN 19BQ search for production of $H_{1,2}^0$ decaying to $A^0 A^0 \rightarrow \mu^+ \mu^- \mu^+ \mu^-$ in 35.9 fb^{-1} of pp collisions at $E_{\text{cm}} = 13 \text{ TeV}$. See their Fig. 2 for limits on cross section times branching ratio for $m_{H_{1,2}^0} = 90\text{--}150 \text{ GeV}$, $m_{A^0} = 0.25\text{--}3.55 \text{ GeV}$.
- 42 SIRUNYAN 19CR search for production of H_2^0/A^0 in gluon fusion and in association with a $b\bar{b}$ pair, decaying to $\mu^+ \mu^-$ in 35.9 fb^{-1} of pp collisions at $E_{\text{cm}} = 13 \text{ TeV}$. See their Fig. 6 for limits on cross section times branching ratio.
- 43 SIRUNYAN 19H search for a narrow scalar resonance decaying to $H^0 H^0 \rightarrow b\bar{b}b\bar{b}$ in 35.9 fb^{-1} of pp collisions at $E_{\text{cm}} = 13 \text{ TeV}$, where one $b\bar{b}$ pair is resolved and the other not. Limits on cross section times branching ratios for $m_{H_2^0} = 0.75\text{--}1.6 \text{ TeV}$ are obtained and combined with data from SIRUNYAN 18AF. See their Fig. 5 (right).
- 44 AABOUD 18AA search for production of a scalar resonance decaying to $Z\gamma$, with Z decaying hadronically, in 36.1 fb^{-1} of pp collisions at $E_{\text{cm}} = 13 \text{ TeV}$. See their Fig. 8(a) for limits on cross section times branching ratio for $m_{H_2^0} = 1.0\text{--}6.8 \text{ TeV}$.
- 45 AABOUD 18AG search for the decay $H^0 \rightarrow A^0 A^0 \rightarrow \gamma\gamma g\bar{g}$ in 36.7 fb^{-1} of pp collisions at $E_{\text{cm}} = 13 \text{ TeV}$. See their Fig. 2 and Table 6 for cross section limits in the range $m_{A^0} = 20\text{--}60 \text{ GeV}$.
- 46 AABOUD 18AH search for production of an A^0 in gluon-gluon fusion and in association with a $b\bar{b}$, decaying to $Z H_2^0 \rightarrow \ell^+ \ell^- b\bar{b}$ in 36.1 fb^{-1} of pp collisions at $E_{\text{cm}} = 13 \text{ TeV}$. See their Fig. 5 for cross section limits for $m_{A^0} = 230\text{--}800 \text{ GeV}$ and $m_{H_2^0} = 130\text{--}700 \text{ GeV}$.
- 47 AABOUD 18AI search for production of an A^0 in gluon-gluon fusion and in association with a $b\bar{b}$, decaying to $Z H^0$ in the final states $\nu\bar{\nu} b\bar{b}$ and $\ell^+ \ell^- b\bar{b}$ in 36.1 fb^{-1} of pp collisions at $E_{\text{cm}} = 13 \text{ TeV}$. See their Fig. 6 for cross section limits for $m_{A^0} = 0.2\text{--}2 \text{ TeV}$. See also AABOUD 18CC.
- 48 AABOUD 18BF search for production of a heavy H_2^0 state decaying to $Z Z$ in the final states $\ell^+ \ell^- \ell^+ \ell^-$ and $\ell^+ \ell^- \nu\bar{\nu}$ in 36.1 fb^{-1} of pp collisions at $E_{\text{cm}} = 13 \text{ TeV}$. See their Fig. 6 for upper limits on cross section times branching ratio for $m_{H_2^0} = 0.2\text{--}1.2 \text{ TeV}$ assuming ggF or VBF with the NWA. See their Fig. 7 for upper limits on cross section times branching ratio for $m_{H_2^0} = 0.4\text{--}1.0 \text{ TeV}$ assuming ggF, and with several assumptions on its width.
- 49 AABOUD 18BU search for a narrow scalar resonance decaying to $H^0 H^0 \rightarrow \gamma\gamma W W^*$ in 36.1 fb^{-1} of pp collisions at $E_{\text{cm}} = 13 \text{ TeV}$. See their Fig. 4 for limits on cross section times branching ratios for $m_{H_2^0} = 260\text{--}500 \text{ GeV}$.
- 50 AABOUD 18BX search for associated production of $W H^0$ or $Z H^0$ followed by the decay $H^0 \rightarrow A^0 A^0 \rightarrow b\bar{b}b\bar{b}$ in 36.1 fb^{-1} of pp collisions at $E_{\text{cm}} = 13 \text{ TeV}$. See their Fig. 9 for limits on cross section times branching ratios for $m_{A^0} = 20\text{--}60 \text{ GeV}$. See also their Fig. 10 for the dependence of the limit on A^0 lifetime.
- 51 AABOUD 18CQ search for a narrow scalar resonance decaying to $H^0 H^0 \rightarrow b\bar{b}\tau^+ \tau^-$ in 36.1 fb^{-1} of pp collisions at $E_{\text{cm}} = 13 \text{ TeV}$. See their Fig. 2 (above) for limits on cross section times branching ratios for $m_{H_2^0} = 260\text{--}1000 \text{ GeV}$.
- 52 AABOUD 18F search for production of a narrow scalar resonance decaying to $W^+ W^-$ and $Z Z$, followed by hadronic decays of W and Z , in 36.7 fb^{-1} of pp collisions at $E_{\text{cm}} = 13 \text{ TeV}$. See their Fig. 5(c) for limits on cross section times branching ratio for $m_{H_2^0} = 1.2\text{--}3.0 \text{ TeV}$.
- 53 AAIJ 18AM search for gluon-fusion production of $H_{1,2}^0$ decaying to $\mu\tau$ in 2 fb^{-1} of pp collisions at $E_{\text{cm}} = 8 \text{ TeV}$. See their Fig. 2 for limits on cross section times branching ratio for $m_{H_{1,2}^0} = 45\text{--}195 \text{ GeV}$.
- 54 AAIJ 18AQ search for gluon-fusion production of a scalar particle A^0 decaying to $\mu^+ \mu^-$ in 1.99 fb^{-1} of pp collisions at $E_{\text{cm}} = 8 \text{ TeV}$ and 0.98 fb^{-1} at $E_{\text{cm}} = 7 \text{ TeV}$. See

Gauge & Higgs Boson Particle Listings

Neutral Higgs Bosons, Searches for

- their Fig. 4 for limits on cross section times branching ratio for $m_{A^0} = 5.5$ –15 GeV (using the $E_{cm} = 8$ TeV data set).
- 55 AAIJ 18AQ search for the decay $H^0 \rightarrow A^0 A^0$, with one of the A^0 decaying to $\mu^+ \mu^-$, in 1.99 fb^{-1} of pp collisions at $E_{cm} = 8$ TeV and 0.98 fb^{-1} at $E_{cm} = 7$ TeV. See their Fig. 5 (right) for limits on the product of branching ratios for $m_{A^0} = 5.5$ –15 GeV (using the $E_{cm} = 8$ TeV data set).
- 56 SIRUNYAN 18AF search for a narrow scalar resonance decaying to $H^0 H^0 \rightarrow b\bar{b}b\bar{b}$ in 35.9 fb^{-1} of pp collisions at $E_{cm} = 13$ TeV, where both $b\bar{b}$ pairs are not resolved. See their Fig. 9 for limits on cross section times branching ratios for $m_{H_2^0} = 0.75$ –3 TeV.
- 57 SIRUNYAN 18BA search for production of a heavy H_2^0 state decaying to ZZ in the final states $\ell^+ \ell^- \ell^+ \ell^-$, $\ell^+ \ell^- q\bar{q}$, and $\ell^+ \ell^- \nu\bar{\nu}$ in 35.9 fb^{-1} of pp collisions at $E_{cm} = 13$ TeV. See their Figs. 10 and 11 for upper limits on cross section times branching ratio for $m_{H_2^0} = 0.13$ –3 TeV with several assumptions on its width and on the fraction of Vector-Boson-Fusion of the total production cross section.
- 58 SIRUNYAN 18CW search for a narrow scalar resonance decaying to $H^0 H^0 \rightarrow b\bar{b}b\bar{b}$ in 35.9 fb^{-1} of pp collisions at $E_{cm} = 13$ TeV, where both $b\bar{b}$ pairs are resolved. See their Fig. 9 for limits on cross section times branching ratios for $m_{H_2^0} = 260$ –1200 GeV.
- 59 SIRUNYAN 18DK search for production of a scalar resonance decaying to $Z\gamma$, with Z decaying to $\ell^+ \ell^-$ or hadronically, in 35.9 fb^{-1} of pp collisions at $E_{cm} = 13$ TeV. See their Fig. 7 for limits on cross section times branching ratio for $m_{H_2^0} = 0.35$ –4 TeV for different assumptions on the width of the resonance.
- 60 SIRUNYAN 18DT search for the decay $H^0 \rightarrow A^0 A^0 \rightarrow \tau^+ \tau^- b\bar{b}$ in 35.9 fb^{-1} of pp collisions at $E_{cm} = 13$ TeV. See their Fig. 7 for limits on the product of branching ratios in the range $m_{A^0} = 15$ –60 GeV. See also their Fig. 8 for interpretation of the data in terms of models with two Higgs doublets and a singlet.
- 61 SIRUNYAN 18DU search for production of a narrow scalar resonance decaying to $\gamma\gamma$ in 35.9 fb^{-1} (taken in 2016) of pp collisions at $E_{cm} = 13$ TeV. See their Fig. 3 (right) for limits on cross section times branching ratio for $m_{H_2^0} = 0.5$ –5 TeV for several values of its width-to-mass ratio.
- 62 SIRUNYAN 18ED search for production of an A^0 in gluon-gluon fusion and in association with a $b\bar{b}$, decaying to ZH^0 in the final states $\nu\bar{\nu}b\bar{b}$ or $\ell^+ \ell^- b\bar{b}$ in 35.9 fb^{-1} of pp collisions at $E_{cm} = 13$ TeV. See their Fig. 8 for cross section limits for $m_{A^0} = 0.8$ –2 TeV.
- 63 SIRUNYAN 18EE search for the decay $H^0 \rightarrow A^0 A^0 \rightarrow \mu^+ \mu^- \tau^+ \tau^-$ in 35.9 fb^{-1} of pp collisions at $E_{cm} = 13$ TeV. See their Fig. 4 for limits on the product of branching ratios in the range $m_{A^0} = 15$ –62.5 GeV, normalized to the SM production cross section. See also their Fig. 5 for interpretation of the data in terms of models with two Higgs doublets and a singlet.
- 64 SIRUNYAN 18F search for a narrow scalar resonance decaying to $H^0 H^0 \rightarrow W\bar{W}b\bar{b}$ or $ZZb\bar{b}$ in the final state $\ell\ell\nu\nu b\bar{b}$ in 35.9 fb^{-1} of pp collisions at $E_{cm} = 13$ TeV. See their Fig. 7 for limits on cross section times branching ratios for $m_{H_2^0} = 250$ –900 GeV.
- 65 ABOUD 17 search for production of a scalar resonance decaying to $Z\gamma$ in 3.2 fb^{-1} of pp collisions at $E_{cm} = 13$ TeV. See their Fig. 4 for the limits on cross section times branching ratio for $m_{H_2^0} = 0.25$ –3.0 TeV.
- 66 ABOUD 17AP search for production of a scalar resonance decaying to $\gamma\gamma$ in 36.7 fb^{-1} of pp collisions at $E_{cm} = 13$ TeV. See their Fig. 4(a) for limits on fiducial cross section times branching ratio for $m_{H_2^0} = 0.2$ –2.7 TeV with narrow width approximation.
- 67 ABOUD 17AW search for production of a scalar resonance decaying to $Z\gamma$ in 36.1 fb^{-1} of pp collisions at $E_{cm} = 13$ TeV. See their Fig. 7 for limits on cross section times branching ratio for $m_{H_2^0} = 0.25$ –2.4 TeV.
- 68 KHACHATRYAN 17AZ search for the decay $H^0 \rightarrow A^0 A^0 \rightarrow \tau^+ \tau^- \tau^+ \tau^-$, $\mu^+ \mu^- b\bar{b}$, and $\mu^+ \mu^- \tau^+ \tau^-$ in 19.7 fb^{-1} of pp collisions at $E_{cm} = 8$ TeV. See their Figs. 4, 5, and 6 for cross section limits in the range $m_{A^0} = 5$ –62.5 GeV. See also their Figs. 7, 8, and 9 for interpretation of the data in terms of models with two Higgs doublets and a singlet.
- 69 KHACHATRYAN 17D search for production of a scalar resonance decaying to $Z\gamma$ in 19.7 fb^{-1} of pp collisions at $E_{cm} = 8$ TeV and 2.7 fb^{-1} at $E_{cm} = 13$ TeV. See their Figs. 3 and 4 for the limits on cross section times branching ratio for $m_{H_2^0} = 0.2$ –2.0 TeV.
- 70 KHACHATRYAN 17R search for production of a narrow scalar resonance decaying to $\gamma\gamma$ in 12.9 fb^{-1} (taken in 2016) of pp collisions at $E_{cm} = 13$ TeV. See their Fig. 2 for limits on cross section times branching ratio for $m_{H_2^0} = 0.5$ –4.5 TeV for several values of its width-to-mass ratio. Limits from combination with KHACHATRYAN 16M are shown in their Figs. 4 and 6.
- 71 SIRUNYAN 17CN search for a narrow scalar resonance decaying to $H^0 H^0 \rightarrow b\bar{b}\tau^+ \tau^-$ in 18.3 fb^{-1} of pp collisions at $E_{cm} = 8$ TeV. See their Fig. 5 (above) and Table II for limits on the cross section times branching ratios for $m_{H_2^0} = 0.3$ –1 TeV, and Fig. 6 (above) and Table III for the corresponding limits by combining with data from KHACHATRYAN 16BQ and KHACHATRYAN 15R.
- 72 SIRUNYAN 17Y search for production of a scalar resonance decaying to $Z\gamma$ in 19.7 fb^{-1} of pp collisions at $E_{cm} = 8$ TeV and 2.7 fb^{-1} at $E_{cm} = 13$ TeV. See their Figs. 3, 4, and Table 3 for limits on cross section times branching ratio for $m_{H_2^0} = 0.7$ –3.0 TeV, and Fig. 5 for the corresponding limits for $m_{H_2^0} = 0.2$ –3.0 TeV from combination with KHACHATRYAN 17D data.
- 73 ABOUD 16AB search for associated production of WH^0 with the decay $H^0 \rightarrow A^0 A^0 \rightarrow b\bar{b}b\bar{b}$ in 3.2 fb^{-1} of pp collisions at $E_{cm} = 13$ TeV. See their Fig. 8 for limits on cross section times branching ratios for $m_{A^0} = 20$ –60 GeV.
- 74 ABOUD 16AE search for production of a narrow scalar resonance decaying to $W^+ W^-$ and ZZ in 3.2 fb^{-1} of pp collisions at $E_{cm} = 13$ TeV. See their Fig. 4 for limits on cross section times branching ratio for $m_{H_2^0} = 0.5$ –3 TeV.
- 75 ABOUD 16H search for production of a scalar resonance decaying to $\gamma\gamma$ in 3.2 fb^{-1} of pp collisions at $E_{cm} = 13$ TeV. See their Fig. 12 for limits on cross section times branching ratio for $m_{H_2^0} = 0.2$ –2 TeV with different assumptions on the width.
- 76 ABOUD 16I search for a narrow scalar resonance decaying to $H^0 H^0 \rightarrow b\bar{b}b\bar{b}$ in 3.2 fb^{-1} of pp collisions at $E_{cm} = 13$ TeV. See their Fig. 10(c) for limits on cross section times branching ratios for $m_{H_2^0} = 0.5$ –3 TeV.
- 77 AAD 16AX search for production of a heavy H^0 state decaying to ZZ in the final states $\ell^+ \ell^- \ell^+ \ell^-$, $\ell^+ \ell^- \nu\bar{\nu}$, $\ell^+ \ell^- q\bar{q}$, and $\nu\bar{\nu}q\bar{q}$ in 20.3 fb^{-1} of pp collisions at $E_{cm} = 8$ TeV. See their Fig. 12 for upper limits on $\sigma(H^0) \text{B}(H^0 \rightarrow ZZ)$ for m_{H_0} ranging from 140 GeV to 1000 GeV.
- 78 AAD 16C search for production of a heavy H^0 state decaying to $W^+ W^-$ in the final states $\ell\nu\ell\nu$ and $\ell\nu q\bar{q}$ in 20.3 fb^{-1} of pp collisions at $E_{cm} = 8$ TeV. See their Figs. 12, 13, and 16 for upper limits on $\sigma(H^0) \text{B}(H^0 \rightarrow W^+ W^-)$ for m_{H_0} ranging from 300 GeV to 1000 or 1500 GeV with various assumptions on the total width of H^0 .
- 79 AAD 16L search for the decay $H^0 \rightarrow A^0 A^0 \rightarrow \gamma\gamma\gamma\gamma$ in 20.3 fb^{-1} of pp collisions at $E_{cm} = 8$ TeV. See their Fig. 4 (upper right) for limits on cross section times branching ratios (normalized to the SM H^0 cross section) for $m_{A^0} = 10$ –60 GeV.
- 80 AAD 16L search for the decay $H_2^0 \rightarrow A^0 A^0 \rightarrow \gamma\gamma\gamma\gamma$ in 20.3 fb^{-1} of pp collisions at $E_{cm} = 8$ TeV. See their Fig. 4 (lower right) for limits on cross section times branching ratios for $m_{H_2^0} = 600$ GeV and $m_{A^0} = 10$ –245 GeV, and Table 5 for limits for $m_{H_2^0} = 300$ and 900 GeV.
- 81 AALTONEN 16C search for electroweak associated production of $H_1^0 H^\pm$ followed by the decays $H^\pm \rightarrow H_1^0 W^*$, $H_1^0 \rightarrow \gamma\gamma$ for $m_{H_1^0} = 10$ –105 GeV and $m_{H^\pm} = 30$ –300 GeV. See their Fig. 3 for excluded parameter region in a two-doublet model in which H_1^0 has no direct decay to fermions.
- 82 KHACHATRYAN 16BQ search for a narrow scalar resonance decaying to $H^0 H^0 \rightarrow b\bar{b}b\bar{b}$ in 19.7 fb^{-1} of pp collisions at $E_{cm} = 8$ TeV. See their Fig. 6 for limits on the cross section times branching ratios for $m_{H_2^0} = 1.15$ –3 TeV.
- 83 KHACHATRYAN 16BQ search for a resonance decaying to $H^0 H^0 \rightarrow \gamma\gamma b\bar{b}$ in 19.7 fb^{-1} of pp collisions at $E_{cm} = 8$ TeV. See their Fig. 9 for limits on the cross section times branching ratios for $m_{H_2^0} = 0.26$ –1.1 TeV.
- 84 KHACHATRYAN 16F search for the decay $H^0 \rightarrow H_1^0 H_1^0 \rightarrow \tau^+ \tau^- \tau^+ \tau^-$ in 19.7 fb^{-1} of pp collisions at $E_{cm} = 8$ TeV. See their Fig. 8 for cross section limits for $m_{H_1^0} = 4$ –8 GeV.
- 85 KHACHATRYAN 16M search for production of a narrow resonance decaying to $\gamma\gamma$ in 19.7 fb^{-1} of pp collisions at $E_{cm} = 8$ TeV and 3.3 fb^{-1} at $E_{cm} = 13$ TeV. See their Fig. 3 (top) for limits on cross section times branching ratio for $m_{H_2^0} = 0.5$ –4 TeV.
- 86 KHACHATRYAN 16P search for gluon fusion production of an H_2^0 decaying to $H^0 H^0 \rightarrow b\bar{b}\tau^+ \tau^-$ in 19.7 fb^{-1} of pp collisions at $E_{cm} = 8$ TeV. See their Fig. 8 (lower right) for cross section limits for $m_{H_2^0} = 260$ –350 GeV.
- 87 KHACHATRYAN 16P search for gluon fusion production of an A^0 decaying to $ZH^0 \rightarrow \ell^+ \ell^- \tau^+ \tau^-$ in 19.7 fb^{-1} of pp collisions at $E_{cm} = 8$ TeV. See their Fig. 10 for cross section limits for $m_{H_2^0} = 220$ –350 GeV.
- 88 AAD 15BK search for production of a heavy H_2^0 decaying to $H^0 H^0$ in the final state $b\bar{b}b\bar{b}$ in 19.5 fb^{-1} of pp collisions at $E_{cm} = 8$ TeV. See their Fig. 14(c) for $\sigma(H_2^0) \text{B}(H_2^0 \rightarrow H^0 H^0)$ for $m_{H_2^0} = 500$ –1500 GeV with $\Gamma_{H_2^0} = 1$ GeV.
- 89 AAD 15BZ search for the decay $H^0 \rightarrow A^0 A^0 \rightarrow \mu^+ \mu^- \tau^+ \tau^-$ ($m_{H_0} = 125$ GeV) in 20.3 fb^{-1} of pp collisions at $E_{cm} = 8$ TeV. See their Fig. 6 for limits on cross section times branching ratio for $m_{A^0} = 3.7$ –50 GeV.
- 90 AAD 15BZ search for a state H_2^0 via the decay $H_2^0 \rightarrow A^0 A^0 \rightarrow \mu^+ \mu^- \tau^+ \tau^-$ in 20.3 fb^{-1} of pp collisions at $E_{cm} = 8$ TeV. See their Fig. 6 for limits on cross section times branching ratio for $m_{H_2^0} = 100$ –500 GeV and $m_{A^0} = 5$ GeV.
- 91 AAD 15CE search for production of a heavy H_2^0 decaying to $H^0 H^0$ in the final states $b\bar{b}\tau^+ \tau^-$ and $\gamma\gamma WW^*$ in 20.3 fb^{-1} of pp collisions at $E_{cm} = 8$ TeV and combine with data from AAD 15H and AAD 15BK. A limit $\sigma(H_2^0) \text{B}(H_2^0 \rightarrow H^0 H^0) < 2.1$ –0.011 pb (95% CL) is given for $m_{H_2^0} = 260$ –1000 GeV. See their Fig. 6.
- 92 AAD 15H search for production of a heavy H_2^0 decaying to $H^0 H^0$ in the final state $\gamma\gamma b\bar{b}$ in 20.3 fb^{-1} of pp collisions at $E_{cm} = 8$ TeV. A limit of $\sigma(H_2^0) \text{B}(H_2^0 \rightarrow H^0 H^0) < 3.5$ –0.7 pb is given for $m_{H_2^0} = 260$ –500 GeV at 95% CL. See their Fig. 3.
- 93 AAD 15S search for production of A^0 decaying to $ZH^0 \rightarrow \ell^+ \ell^- b\bar{b}$, $\nu\bar{\nu}b\bar{b}$ and $\ell^+ \ell^- \tau^+ \tau^-$ in 20.3 fb^{-1} of pp collisions at $E_{cm} = 8$ TeV. See their Fig. 3 for cross section limits for $m_{A^0} = 200$ –1000 GeV.
- 94 KHACHATRYAN 15AW search for production of a heavy state H_2^0 of an electroweak singlet extension of the Standard Model via the decays of H_2^0 to $W^+ W^-$ and ZZ in up to 5.1 fb^{-1} of pp collisions at $E_{cm} = 7$ TeV and up to 19.7 fb^{-1} at $E_{cm} = 8$ TeV in the range $m_{H_2^0} = 145$ –1000 GeV. See their Figs. 8 and 9 for limits in the parameter space of the model.
- 95 KHACHATRYAN 15BB search for production of a resonance H^0 decaying to $\gamma\gamma$ in 19.7 fb^{-1} of pp collisions at $E_{cm} = 8$ TeV. See their Fig. 7 for limits on cross section times branching ratio for $m_{H_0} = 150$ –850 GeV.
- 96 KHACHATRYAN 15N search for production of A^0 decaying to $ZH^0 \rightarrow \ell^+ \ell^- b\bar{b}$ in 19.7 fb^{-1} of pp collisions at $E_{cm} = 8$ TeV. See their Fig. 3 for limits on cross section times branching ratios for $m_{A^0} = 225$ –600 GeV.
- 97 KHACHATRYAN 15O search for production of a high-mass narrow resonance A^0 decaying to $ZH^0 \rightarrow q\bar{q}\tau^+ \tau^-$ in 19.7 fb^{-1} of pp collisions at $E_{cm} = 8$ TeV. See their Fig. 6 for limits on cross section times branching ratios for $m_{A^0} = 800$ –2500 GeV.
- 98 KHACHATRYAN 15R search for a narrow scalar resonance decaying to $H^0 H^0 \rightarrow b\bar{b}b\bar{b}$ in 17.9 fb^{-1} of pp collisions at $E_{cm} = 8$ TeV. See their Fig. 5 (top) for limits on cross section times branching ratios for $m_{H_2^0} = 0.27$ –1.1 TeV.

Gauge & Higgs Boson Particle Listings

Neutral Higgs Bosons, Searches for

- 99 AAD 14AP search for a second H^0 state decaying to $\gamma\gamma$ in addition to the state at about 125 GeV in 20.3 fb^{-1} of pp collisions at $E_{\text{cm}} = 8$ TeV. See their Fig. 4 for limits on cross section times branching ratio for $m_{H^0} = 65\text{--}600$ GeV.
- 100 AAD 14M search for the decay cascade $H^0_2 \rightarrow H^\pm W^\mp \rightarrow H^0 W^\pm W^\mp, H^0$ decaying to $b\bar{b}$ in 20.3 fb^{-1} of pp collisions at $E_{\text{cm}} = 8$ TeV. See their Table III for limits on cross section times branching ratio for $m_{H^0_2} = 325\text{--}1025$ GeV and $m_{H^\pm} = 225\text{--}925$ GeV.
- 101 CHATRCHYAN 14G search for a second H^0 state decaying to $WW^{(*)}$ in addition to the observed signal at about 125 GeV using 4.9 fb^{-1} of pp collisions at $E_{\text{cm}} = 7$ TeV and 19.4 fb^{-1} at $E_{\text{cm}} = 8$ TeV. See their Fig. 21 (right) for cross section limits in the mass range 110–600 GeV.
- 102 KHACHATRYAN 14P search for a second H^0 state decaying to $\gamma\gamma$ in addition to the observed signal at about 125 GeV using 5.1 fb^{-1} of pp collisions at $E_{\text{cm}} = 7$ TeV and 19.7 fb^{-1} at $E_{\text{cm}} = 8$ TeV. See their Figs. 27 and 28 for cross section limits in the mass range 110–150 GeV.
- 103 AALTONEN 13P search for production of a heavy Higgs boson H^0 that decays into a charged Higgs boson H^\pm and a lighter Higgs boson H^0 via the decay chain $H^0 \rightarrow H^\pm W^\mp, H^\pm \rightarrow W^\pm H^0, H^0 \rightarrow b\bar{b}$ in the final state $\ell\nu$ plus 4 jets in 8.7 fb^{-1} of $p\bar{p}$ collisions at $E_{\text{cm}} = 1.96$ TeV. See their Fig. 4 for limits on cross section times branching ratio in the $m_{H^\pm}\text{--}m_{H^0}$ plane for $m_{H^0} = 126$ GeV.
- 104 CHATRCHYAN 13BJ search for H^0 production in the decay chain $H^0 \rightarrow A^0 A^0, A^0 \rightarrow \mu^+ \mu^-$ in 5.3 fb^{-1} of pp collisions at $E_{\text{cm}} = 7$ TeV. See their Fig. 2 for limits on cross section times branching ratio.
- 105 AALTONEN 11P search in 2.7 fb^{-1} of $p\bar{p}$ collisions at $E_{\text{cm}} = 1.96$ TeV for the decay chain $t \rightarrow bH^+, H^+ \rightarrow W^+ A^0, A^0 \rightarrow \tau^+ \tau^-$ with m_{A^0} between 4 and 9 GeV. See their Fig. 4 for limits on $B(t \rightarrow bH^+)$ for $90 < m_{H^+} < 160$ GeV.
- 106 ABBIENDI 10 search for $e^+ e^- \rightarrow ZH^0$ with the decay chain $H^0 \rightarrow \tilde{\chi}_1^0 \tilde{\chi}_2^0, \tilde{\chi}_2^0 \rightarrow \tilde{\chi}_1^0 + (\gamma \text{ or } Z^*)$, when $\tilde{\chi}_1^0$ and $\tilde{\chi}_2^0$ are nearly degenerate. For a mass difference of 2 (4) GeV, a lower limit on m_{H^0} of 108.4 (107.0) GeV (95% CL) is obtained for SM ZH^0 cross section and $B(H^0 \rightarrow \tilde{\chi}_1^0 \tilde{\chi}_2^0) = 1$.
- 107 SCHAEEL 10 search for the process $e^+ e^- \rightarrow H^0 Z$ followed by the decay chain $H^0 \rightarrow A^0 A^0 \rightarrow \tau^+ \tau^- \tau^+ \tau^-$ with $Z \rightarrow \ell^+ \ell^-, \nu\bar{\nu}$ at $E_{\text{cm}} = 183\text{--}209$ GeV. For a $H^0 Z Z$ coupling equal to the SM value, $B(H^0 \rightarrow A^0 A^0) = B(A^0 \rightarrow \tau^+ \tau^-) = 1$, and $m_{A^0} = 4\text{--}10$ GeV, m_{H^0} up to 107 GeV is excluded at 95% CL.
- 108 ABZOV 09V search for H^0 production followed by the decay chain $H^0 \rightarrow A^0 A^0 \rightarrow \mu^+ \mu^- \mu^+ \mu^-$ or $\mu^+ \mu^- \tau^+ \tau^-$ in 4.2 fb^{-1} of $p\bar{p}$ collisions at $E_{\text{cm}} = 1.96$ TeV. See their Fig. 3 for limits on $\sigma(H^0)\cdot B(H^0 \rightarrow A^0 A^0)$ for $m_{A^0} = 3.6\text{--}19$ GeV.
- 109 ABBIENDI 05A search for $e^+ e^- \rightarrow H^0_1 A^0$ in general Type-II two-doublet models, with decays $H^0_1 A^0 \rightarrow q\bar{q}, g g, \tau^+ \tau^-$, and $H^0_1 \rightarrow A^0 A^0$.
- 110 ABBIENDI 04K search for $e^+ e^- \rightarrow H^0 Z$ with H^0 decaying to two jets of any flavor including $g g$. The limit is for SM production cross section with $B(H^0 \rightarrow jj) = 1$.
- 111 ABDALLAH 04 consider the full combined LEP and LEP2 datasets to set limits on the Higgs coupling to W or Z bosons, assuming SM decays of the Higgs. Results in Fig. 26.
- 112 ACHARD 04B search for $e^+ e^- \rightarrow H^0 Z$ with H^0 decaying to $b\bar{b}, c\bar{c}$, or $g g$. The limit is for SM production cross section with $B(H^0 \rightarrow jj) = 1$.
- 113 ACHARD 04F search for H^0 with anomalous coupling to gauge boson pairs in the processes $e^+ e^- \rightarrow H^0 \gamma, e^+ e^- H^0, H^0 Z$ with decays $H^0 \rightarrow f\bar{f}, \gamma\gamma, Z\gamma$, and $W^* W$ at $E_{\text{cm}} = 189\text{--}209$ GeV. See paper for limits.
- 114 ABBIENDI 03F search for $H^0 \rightarrow$ anything in $e^+ e^- \rightarrow H^0 Z$, using the recoil mass spectrum of $Z \rightarrow e^+ e^-$ or $\mu^+ \mu^-$. In addition, it searched for $Z \rightarrow \nu\bar{\nu}$ and $H^0 \rightarrow e^+ e^-$ or photons. Scenarios with large width or continuum H^0 mass distribution are considered. See their Figs. 11–14 for the results.
- 115 ABBIENDI 03G search for $e^+ e^- \rightarrow H^0_1 Z$ followed by $H^0_1 \rightarrow A^0 A^0, A^0 \rightarrow c\bar{c}, g g$, or $\tau^+ \tau^-$ in the region $m_{H^0_1} = 45\text{--}86$ GeV and $m_{A^0} = 2\text{--}11$ GeV. See their Fig. 7 for the limits.
- 116 Search for associated production of a $\gamma\gamma$ resonance with a Z boson, followed by $Z \rightarrow q\bar{q}, \ell^+ \ell^-,$ or $\nu\bar{\nu}$, at $E_{\text{cm}} \leq 209$ GeV. The limit is for a H^0 with SM production cross section and $B(H^0 \rightarrow f\bar{f})=0$ for all fermions f .
- 117 For $B(H^0 \rightarrow \gamma\gamma)=1, m_{H^0} > 113.1$ GeV is obtained.
- 118 HEISTER 02M search for $e^+ e^- \rightarrow H^0 Z$, assuming that H^0 decays to $q\bar{q}, g g$, or $\tau^+ \tau^-$ only. The limit assumes SM production cross section.
- 119 ABBIENDI 01E search for neutral Higgs bosons in general Type-II two-doublet models, at $E_{\text{cm}} \leq 189$ GeV. In addition to usual final states, the decays $H^0_1 A^0 \rightarrow q\bar{q}, g g$ are searched for. See their Figs. 15, 16 for excluded regions.
- 120 ACCIARRI 00R search for $e^+ e^- \rightarrow H^0 \gamma$ with $H^0 \rightarrow b\bar{b}, Z\gamma$, or $\gamma\gamma$. See their Fig. 3 for limits on σ -B. Explicit limits within an effective interaction framework are also given, for which the Standard Model Higgs search results are used in addition.
- 121 ACCIARRI 00R search for the two-photon type processes $e^+ e^- \rightarrow e^+ e^- H^0$ with $H^0 \rightarrow b\bar{b}$ or $\gamma\gamma$. See their Fig. 4 for limits on $\Gamma(H^0 \rightarrow \gamma\gamma)\cdot B(H^0 \rightarrow \gamma\gamma \text{ or } b\bar{b})$ for $m_{H^0}=70\text{--}170$ GeV.
- 122 GONZALEZ-GARCIA 98B use D0 limit for $\gamma\gamma$ events with missing E_T in $p\bar{p}$ collisions (ABBOTT 98) to constrain possible ZH or WH production followed by unconventional $H \rightarrow \gamma\gamma$ decay which is induced by higher-dimensional operators. See their Figs. 1 and 2 for limits on the anomalous couplings.
- 123 KRAWCZYK 97 analyse the muon anomalous magnetic moment in a two-doublet Higgs model (with type II Yukawa couplings) assuming no $H^0_1 Z Z$ coupling and obtain $m_{H^0_1} \gtrsim 5$ GeV or $m_{A^0} \gtrsim 5$ GeV for $\tan\beta > 50$. Other Higgs bosons are assumed to be much heavier.
- 124 ALEXANDER 96H give $B(Z \rightarrow H^0 \gamma)\cdot B(H^0 \rightarrow q\bar{q}) < 1\text{--}4 \times 10^{-5}$ (95%CL) and $B(Z \rightarrow H^0 \gamma)\cdot B(H^0 \rightarrow b\bar{b}) < 0.7\text{--}2 \times 10^{-5}$ (95%CL) in the range $20 < m_{H^0} < 80$ GeV.

SEARCHES FOR A HIGGS BOSON WITH STANDARD MODEL COUPLINGS

These listings are based on experimental searches for a scalar boson whose couplings to W, Z and fermions are precisely those of the Higgs boson predicted by the three-generation Standard Model with the minimal Higgs sector.

For a review and a bibliography, see the review on “Status of Higgs Boson Physics.”

Indirect Mass Limits for H^0 from Electroweak Analysis

The mass limits shown below apply to a Higgs boson H^0 with Standard Model couplings whose mass is a priori unknown.

For limits obtained before the direct measurement of the top quark mass, see the 1996 (Physical Review **D54** 1 (1996)) Edition of this Review. Other studies based on data available prior to 1996 can be found in the 1998 Edition (The European Physical Journal **C3** 1 (1998)) of this Review.

VALUE (GeV)	DOCUMENT ID	TECN
90^{+21}_{-18}	¹ HALLER	18 RVUE
• • • We do not use the following data for averages, fits, limits, etc. • • •		
91^{+30}_{-23}	² BAAK	12 RVUE
94^{+25}_{-22}	³ BAAK	12A RVUE
91^{+31}_{-24}	⁴ ERLER	10A RVUE
129^{+74}_{-49}	⁵ LEP-SLC	06 RVUE

- ¹ HALLER 18 make Standard Model fits to Z and neutral current parameters, $m_t, m_W,$ and Γ_W measurements available in 2018. The direct mass measurement at the LHC is not used in the fit.
- ² BAAK 12 make Standard Model fits to Z and neutral current parameters, $m_t, m_W,$ and Γ_W measurements available in 2010 (using also preliminary data). The quoted result is obtained from a fit that does not include the limit from the direct Higgs searches. The result including direct search data from LEP2, the Tevatron and the LHC is 120^{+12}_{-5} GeV.
- ³ BAAK 12A make Standard Model fits to Z and neutral current parameters, $m_t, m_W,$ and Γ_W measurements available in 2012 (using also preliminary data). The quoted result is obtained from a fit that does not include the measured mass value of the signal observed at the LHC and also no limits from direct Higgs searches.
- ⁴ ERLER 10A makes Standard Model fits to Z and neutral current parameters, m_t, m_W measurements available in 2009 (using also preliminary data). The quoted result is obtained from a fit that does not include the limits from the direct Higgs searches. With direct search data from LEP2 and Tevatron added to the fit, the 90% CL (99% CL) interval is $115\text{--}148$ ($114\text{--}197$) GeV.
- ⁵ LEP-SLC 06 make Standard Model fits to Z parameters from LEP/SLC and $m_t, m_W,$ and Γ_W measurements available in 2005 with $\Delta\alpha_{\text{had}}^{(5)}(m_Z) = 0.02758 \pm 0.00035$. The 95% CL limit is 285 GeV.

SEARCHES FOR NEUTRAL HIGGS BOSONS REFERENCES

AAD	22A	PR D105 012006	G. Aad et al.	(ATLAS Collab.)
AAD	21AF	EPJ C81 332	G. Aad et al.	(ATLAS Collab.)
AAD	21AI	EPJ C81 396	G. Aad et al.	(ATLAS Collab.)
AAD	21AY	PL B822 136651	G. Aad et al.	(ATLAS Collab.)
AAD	21AZ	JHEP 2110 013	G. Aad et al.	(ATLAS Collab.)
AAD	21BE	JHEP 2111 209	G. Aad et al.	(ATLAS Collab.)
AAD	21BE	EPJ C81 860	G. Aad et al.	(ATLAS Collab.)
ABRATENKO	21	PRL 127 151803	P. Abratenko et al.	(MicroBoONE Collab.)
SIRUNYAN	21A	EPJ C81 13	A.M. Sirunyan et al.	(CMS Collab.)
Also	Also	EPJ C81 333 (errat.)	A.M. Sirunyan et al.	(CMS Collab.)
TUMASYAN	21F	JHEP 2111 057	A. Tumasyan et al.	(CMS Collab.)
AAD	20	PR D101 012002	G. Aad et al.	(ATLAS Collab.)
AAD	20AA	PRL 125 051801	G. Aad et al.	(ATLAS Collab.)
AAD	20AE	PRL 125 221802	G. Aad et al.	(ATLAS Collab.)
AAD	20AI	PR D102 112006	G. Aad et al.	(ATLAS Collab.)
AAD	20AO	JHEP 2011 163	G. Aad et al.	(ATLAS Collab.)
AAD	20C	PL B800 135103	G. Aad et al.	(ATLAS Collab.)
AAD	20L	PR D102 032004	G. Aad et al.	(ATLAS Collab.)
AAD	20X	JHEP 2007 108	G. Aad et al.	(ATLAS Collab.)
Also	Also	JHEP 2101 145 (errat.)	G. Aad et al.	(ATLAS Collab.)
Also	Also	JHEP 2105 207 (errat.)	G. Aad et al.	(ATLAS Collab.)
AAIJ	20AL	JHEP 2010 156	R. Aaij et al.	(LHCb Collab.)
SIRUNYAN	20	PL B800 135087	A.M. Sirunyan et al.	(CMS Collab.)
SIRUNYAN	20AA	JHEP 2003 055	A.M. Sirunyan et al.	(CMS Collab.)
SIRUNYAN	20AC	JHEP 2003 065	A.M. Sirunyan et al.	(CMS Collab.)
SIRUNYAN	20AD	JHEP 2003 103	A.M. Sirunyan et al.	(CMS Collab.)
SIRUNYAN	20AF	JHEP 2004 171	A.M. Sirunyan et al.	(CMS Collab.)
SIRUNYAN	20AP	JHEP 2008 139	A.M. Sirunyan et al.	(CMS Collab.)
SIRUNYAN	20Y	JHEP 2003 034	A.M. Sirunyan et al.	(CMS Collab.)
SIRUNYAN	20Z	JHEP 2003 051	A.M. Sirunyan et al.	(CMS Collab.)
ABOUD	19A	JHEP 1901 030	M. Aaboud et al.	(ATLAS Collab.)
AABOUD	19AG	PL B790 1	M. Aaboud et al.	(ATLAS Collab.)
AABOUD	19AI	PL B793 499	M. Aaboud et al.	(ATLAS Collab.)
AABOUD	19O	JHEP 1904 092	M. Aaboud et al.	(ATLAS Collab.)
AABOUD	19T	JHEP 1905 124	M. Aaboud et al.	(ATLAS Collab.)
AABOUD	19V	JHEP 1905 142	M. Aaboud et al.	(ATLAS Collab.)
AABOUD	19Y	JHEP 1907 117	M. Aaboud et al.	(ATLAS Collab.)
AALTONEN	19	PR D99 052001	T. Aaltonen et al.	(CMS Collab.)
SIRUNYAN	19	PL B788 7	A.M. Sirunyan et al.	(CMS Collab.)
SIRUNYAN	19AE	JHEP 1905 210	A.M. Sirunyan et al.	(CMS Collab.)
SIRUNYAN	19AN	EPJ C79 280	A.M. Sirunyan et al.	(CMS Collab.)
SIRUNYAN	19AV	EPJ C79 564	A.M. Sirunyan et al.	(CMS Collab.)
SIRUNYAN	19B	PR D99 012005	A.M. Sirunyan et al.	(CMS Collab.)
SIRUNYAN	19BB	PL B793 320	A.M. Sirunyan et al.	(CMS Collab.)
SIRUNYAN	19BD	PL B795 398	A.M. Sirunyan et al.	(CMS Collab.)
SIRUNYAN	19BE	PRL 122 121803	A.M. Sirunyan et al.	(CMS Collab.)
SIRUNYAN	19BQ	PL B796 131	A.M. Sirunyan et al.	(CMS Collab.)
SIRUNYAN	19CR	PL B798 134992	A.M. Sirunyan et al.	(CMS Collab.)
SIRUNYAN	19H	JHEP 1901 040	A.M. Sirunyan et al.	(CMS Collab.)
AABOUD	18AA	PR D98 032015	M. Aaboud et al.	(ATLAS Collab.)

Gauge & Higgs Boson Particle Listings

Neutral Higgs Bosons, Searches for, Charged Higgs Bosons (H^\pm and $H^{\pm\pm}$), Searches for

ABOUD 18AG PL B782 750	M. Aboud et al.	(ATLAS Collab.)	CHATRCHYAN 12I JHEP 1203 040	S. Chatrchyan et al.	(CMS Collab.)
ABOUD 18AH PL B783 392	M. Aboud et al.	(ATLAS Collab.)	CHATRCHYAN 12K PL B713 68	S. Chatrchyan et al.	(CMS Collab.)
ABOUD 18AI JHEP 1803 174	M. Aboud et al.	(ATLAS Collab.)	CHATRCHYAN 12N PL B716 30	S. Chatrchyan et al.	(CMS Collab.)
Also JHEP 1811 051 (errat.)	M. Aboud et al.	(ATLAS Collab.)	CHATRCHYAN 12V PRL 109 121801	S. Chatrchyan et al.	(CMS Collab.)
ABOUD 18AP JHEP 1806 166	M. Aboud et al.	(ATLAS Collab.)	AALTONEN 11P PRL 107 031801	T. Aaltonen et al.	(CDF Collab.)
ABOUD 18BF EPJ C78 293	M. Aboud et al.	(ATLAS Collab.)	ABAZOV 11W PL B698 97	V.M. Abazov et al.	(DO Collab.)
ABOUD 18BU EPJ C78 1007	M. Aboud et al.	(ATLAS Collab.)	ABAZOV 11W PRL 107 121801	V.M. Abazov et al.	(DO Collab.)
ABOUD 18BX JHEP 1810 031	M. Aboud et al.	(ATLAS Collab.)	ABOUZAIID 11A PRL 107 201803	E. Abouzaid et al.	(KTeV Collab.)
ABOUD 18CC JHEP 1811 051 (errat.)	M. Aboud et al.	(ATLAS Collab.)	DEL-AMO-SA... 11J PRL 107 021804	P. del Amo Sanchez et al.	(BABAR Collab.)
ABOUD 18CE JHEP 1812 039	M. Aboud et al.	(ATLAS Collab.)	LEES 11H PRL 107 221803	J.P. Lees et al.	(BABAR Collab.)
ABOUD 18CQ PRL 121 191801	M. Aboud et al.	(ATLAS Collab.)	ABBIENDI 10 PL B682 381	G. Abbiendi et al.	(OPAL Collab.)
ABOUD 18CW JHEP 1811 040	M. Aboud et al.	(ATLAS Collab.)	ANDREAS 10 JHEP 1008 003	S. Andreas et al.	(DESY Collab.)
ABOUD 18F PL B777 91	M. Aboud et al.	(ATLAS Collab.)	ERLER 10A PR D81 051301	J. Erler	(UNAM Collab.)
ABOUD 18G JHEP 1801 055	M. Aboud et al.	(ATLAS Collab.)	HYUN 10 PRL 105 091801	H.J. Hyun et al.	(BELLE Collab.)
AAJ 18AM EPJ C78 1008	R. Aaij et al.	(LHCb Collab.)	SCHAEEL 10 JHEP 1005 049	S. Schaeel et al.	(ALEPH Collab.)
AAJ 18AQ JHEP 1809 147	R. Aaij et al.	(LHCb Collab.)	AALTONEN 09AB PRL 103 061803	T. Aaltonen et al.	(CDF Collab.)
HALLER 18 EPJ C78 675	J. Haller et al.	(Gfitter Group)	AALTONEN 09AB PRL 103 201801	T. Aaltonen et al.	(CDF Collab.)
SIRUNYAN 18A PL B778 101	A.M. Sirunyan et al.	(CMS Collab.)	ABAZOV 09V PRL 103 061801	V.M. Abazov et al.	(DO Collab.)
SIRUNYAN 18AF PL B781 244	A.M. Sirunyan et al.	(CMS Collab.)	AUBERT 09P PRL 103 181801	B. Aubert et al.	(BABAR Collab.)
SIRUNYAN 18BA JHEP 1806 127	A.M. Sirunyan et al.	(CMS Collab.)	AUBERT 09P PRL 103 081803	B. Aubert et al.	(BABAR Collab.)
Also JHEP 1903 128 (errat.)	A.M. Sirunyan et al.	(CMS Collab.)	TUNG 09 PRL 102 051802	Y.C. Tung et al.	(KEK E318 Collab.)
SIRUNYAN 18BP JHEP 1808 113	A.M. Sirunyan et al.	(CMS Collab.)	ABAZOV 08U PRL 101 051801	V.M. Abazov et al.	(DO Collab.)
SIRUNYAN 18CW JHEP 1808 152	A.M. Sirunyan et al.	(CMS Collab.)	ABDALLAH 08B EPJ C54 1	J. Abdallah et al.	(DELPHI Collab.)
SIRUNYAN 18CX JHEP 1809 007	A.M. Sirunyan et al.	(CMS Collab.)	Also EPJ C56 165 (errat.)	J. Abdallah et al.	(DELPHI Collab.)
SIRUNYAN 18DK JHEP 1809 148	A.M. Sirunyan et al.	(CMS Collab.)	LOVE 08 PRL 101 151802	W. Love et al.	(CLEO Collab.)
SIRUNYAN 18DT PL B785 462	A.M. Sirunyan et al.	(CMS Collab.)	ABBIENDI 07 EPJ C49 457	G. Abbiendi et al.	(OPAL Collab.)
SIRUNYAN 18DU PR D98 092001	A.M. Sirunyan et al.	(CMS Collab.)	BESSON 07 PRL 98 052002	D. Besson et al.	(CLEO Collab.)
SIRUNYAN 18ED JHEP 1811 172	A.M. Sirunyan et al.	(CMS Collab.)	SCHAEEL 07 EPJ C49 439	S. Schaeel et al.	(ALEPH Collab.)
SIRUNYAN 18EE JHEP 1811 018	A.M. Sirunyan et al.	(CMS Collab.)	LEP-SLC 06 PRPL 427 257	ALEPH, DELPHI, L3, OPAL, SLD and working groups	
SIRUNYAN 18F JHEP 1801 054	A.M. Sirunyan et al.	(CMS Collab.)	SCHAEEL 06B EPJ C47 547	S. Schaeel et al.	(LEP Collabs.)
ABOUD 17 PL B764 11	M. Aboud et al.	(ATLAS Collab.)	ABBIENDI 05A EPJ C40 317	G. Abbiendi et al.	(OPAL Collab.)
ABOUD 17AN PRL 119 191803	M. Aboud et al.	(ATLAS Collab.)	ABDALLAH 05D EPJ C44 147	J. Abdallah et al.	(DELPHI Collab.)
ABOUD 17AP PL B775 105	M. Aboud et al.	(ATLAS Collab.)	ACHARD 05 PL B609 35	P. Achard et al.	(L3 Collab.)
ABOUD 17AW JHEP 1710 112	M. Aboud et al.	(ATLAS Collab.)	ACOSTA 05Q PR D72 072004	D. Acosta et al.	(CDF Collab.)
KHACHATRYAN...17AZ JHEP 1710 076	V. Khachatryan et al.	(CMS Collab.)	PARK 05 PRL 94 021801	H.K. Park et al.	(FNAL HyperCP Collab.)
KHACHATRYAN...17D JHEP 1701 076	V. Khachatryan et al.	(CMS Collab.)	ABBIENDI 04K PL B597 11	G. Abbiendi et al.	(OPAL Collab.)
KHACHATRYAN...17R PL B767 147	V. Khachatryan et al.	(CMS Collab.)	ABBIENDI 04M EPJ C37 49	G. Abbiendi et al.	(OPAL Collab.)
SIRUNYAN 17AX JHEP 1711 010	A.M. Sirunyan et al.	(CMS Collab.)	ABDALLAH 04 EPJ C32 145	J. Abdallah et al.	(DELPHI Collab.)
SIRUNYAN 17CN PR D96 072004	A.M. Sirunyan et al.	(CMS Collab.)	ABDALLAH 04B EPJ C32 475	J. Abdallah et al.	(DELPHI Collab.)
SIRUNYAN 17Y PL B772 363	A.M. Sirunyan et al.	(CMS Collab.)	ABDALLAH 04L EPJ C35 313	J. Abdallah et al.	(DELPHI Collab.)
ABOUD 16AA EPJ C76 585	M. Aboud et al.	(ATLAS Collab.)	ABDALLAH 04O EPJ C38 1	J. Abdallah et al.	(DELPHI Collab.)
ABOUD 16AB EPJ C76 605	M. Aboud et al.	(ATLAS Collab.)	ACHARD 04B PL B583 14	P. Achard et al.	(L3 Collab.)
ABOUD 16AC JHEP 1609 173	M. Aboud et al.	(ATLAS Collab.)	ACHARD 04F PL B589 39	P. Achard et al.	(L3 Collab.)
ABOUD 16H JHEP 1609 001	M. Aboud et al.	(ATLAS Collab.)	ABBIENDI 03F EPJ C31 311	G. Abbiendi et al.	(OPAL Collab.)
ABOUD 16I PR D94 052002	M. Aboud et al.	(ATLAS Collab.)	ABBIENDI 03G EPJ C27 483	G. Abbiendi et al.	(OPAL Collab.)
AAD 16AX EPJ C76 45	G. Aad et al.	(ATLAS Collab.)	ACHARD 03C PL B568 191	P. Achard et al.	(L3 Collab.)
AAD 16C JHEP 1601 032	G. Aad et al.	(ATLAS Collab.)	ABBIENDI 02D EPJ C23 397	G. Abbiendi et al.	(OPAL Collab.)
AAD 16L EPJ C76 210	G. Aad et al.	(ATLAS Collab.)	ABBIENDI 02F PL B544 44	G. Abbiendi et al.	(OPAL Collab.)
AALTONEN 16C PR D93 112010	T. Aaltonen et al.	(CDF Collab.)	ACHARD 02C PL B534 28	P. Achard et al.	(L3 Collab.)
ABLIKIM 16E PR D93 052005	M. Ablikim et al.	(BESIII Collab.)	ACHARD 02H PL B545 30	P. Achard et al.	(L3 Collab.)
KHACHATRYAN...16A PL B752 221	V. Khachatryan et al.	(CMS Collab.)	AKERROYD 02 PR D66 037702	A.G. Akeroyd et al.	
KHACHATRYAN...16BG EPJ C76 371	V. Khachatryan et al.	(CMS Collab.)	HEISTER 02 PL B526 191	A. Heister et al.	(ALEPH Collab.)
KHACHATRYAN...16BQ PR D94 052012	V. Khachatryan et al.	(CMS Collab.)	HEISTER 02L PL B544 16	A. Heister et al.	(ALEPH Collab.)
KHACHATRYAN...16F JHEP 1601 079	V. Khachatryan et al.	(CMS Collab.)	HEISTER 02M PL B544 25	A. Heister et al.	(ALEPH Collab.)
KHACHATRYAN...16G PRL 117 051802	V. Khachatryan et al.	(CMS Collab.)	ABBIENDI 01E EPJ C18 425	G. Abbiendi et al.	(OPAL Collab.)
KHACHATRYAN...16P PL B755 217	V. Khachatryan et al.	(CMS Collab.)	ABREU 01F PL B507 89	P. Abreu et al.	(DELPHI Collab.)
KHACHATRYAN...16W PL B758 296	V. Khachatryan et al.	(CMS Collab.)	AFFOLDER 01H PR D64 092002	T. Affolder et al.	(CDF Collab.)
KHACHATRYAN...16Z PL B759 369	V. Khachatryan et al.	(CMS Collab.)	BARATE 01C PL B499 53	R. Barate et al.	(ALEPH Collab.)
AAD 15BD EPJ C75 337	G. Aad et al.	(ATLAS Collab.)	ACCIARRI 00M PL B485 85	M. Acciarri et al.	(L3 Collab.)
AAD 15BH EPJ C75 299	G. Aad et al.	(ATLAS Collab.)	ACCIARRI 00R PL B489 102	M. Acciarri et al.	(L3 Collab.)
Also EPJ C75 408 (errat.)	G. Aad et al.	(ATLAS Collab.)	ACCIARRI 00S PL B489 115	M. Acciarri et al.	(L3 Collab.)
AAD 15BK EPJ C75 412	G. Aad et al.	(ATLAS Collab.)	BARATE 00L PL B487 241	R. Barate et al.	(ALEPH Collab.)
AAD 15BZ PR D92 052002	G. Aad et al.	(ATLAS Collab.)	ABBIENDI 09E EPJ C7 407	G. Abbiendi et al.	(OPAL Collab.)
AAD 15CE PR D92 092004	G. Aad et al.	(ATLAS Collab.)	ABBIENDI 99O PL B464 311	G. Abbiendi et al.	(OPAL Collab.)
AAD 15H PRL 114 081802	G. Aad et al.	(ATLAS Collab.)	ABBOTT 99B PRL 82 2244	B. Abbott et al.	(DO Collab.)
AAD 15S PL B744 163	G. Aad et al.	(ATLAS Collab.)	ABREU 99P PL B456 431	P. Abreu et al.	(DELPHI Collab.)
KHACHATRYAN...15AW JHEP 1510 144	V. Khachatryan et al.	(CMS Collab.)	ABBOTT 98 PRL 80 442	B. Abbott et al.	(DO Collab.)
KHACHATRYAN...15AY JHEP 1511 071	V. Khachatryan et al.	(CMS Collab.)	ACKERSTAFF 98S EPJ C5 19	K. Ackerstaff et al.	(OPAL Collab.)
KHACHATRYAN...15BB PL B750 494	V. Khachatryan et al.	(CMS Collab.)	ACKERSTAFF 98Y PL B437 218	K. Ackerstaff et al.	(OPAL Collab.)
KHACHATRYAN...15N PL B748 221	V. Khachatryan et al.	(CMS Collab.)	GONZALEZ... 98B PR D57 7045	M.C. Gonzalez-Garcia, S.M. Lletti, S.F. Novas	
KHACHATRYAN...15O PL B748 255	V. Khachatryan et al.	(CMS Collab.)	PDG 98 EPJ C3 1	C. Caso et al.	(PDG Collab.)
KHACHATRYAN...15R PL B749 560	V. Khachatryan et al.	(CMS Collab.)	KRAWCZYK 97 PR D55 6968	M. Krawczyk, J. Zochowski	(WARS Collab.)
LEES 15H PR D91 071102	J.P. Lees et al.	(BABAR Collab.)	ALEXANDER 96H ZPHY C71 1	G. Alexander et al.	(OPAL Collab.)
AAD 14AP PRL 113 171801	G. Aad et al.	(ATLAS Collab.)	PDG 96 PR D54 1	R.M. Barnett et al.	(PDG Collab.)
AAD 14AW JHEP 1411 056	G. Aad et al.	(ATLAS Collab.)	ABREU 95H ZPHY C67 69	P. Abreu et al.	(DELPHI Collab.)
AAD 14BA JHEP 1411 086	G. Aad et al.	(ATLAS Collab.)	BALEST 95 PR D51 2053	R. Balest et al.	(CLEO Collab.)
AAD 14M PR D89 032003	G. Aad et al.	(ATLAS Collab.)	RICH 92 NP B388 31	A. Pich, J. Prades, P. Yepes	(CERN, CP-PM Collab.)
AAD 14O PRL 112 201802	G. Aad et al.	(ATLAS Collab.)	ANTREASYAN 90C PL B251 204	D. Antreasyan et al.	(Crystal Ball Collab.)
CHATRCHYAN 14B EPJ C74 2980	S. Chatrchyan et al.	(CMS Collab.)			
CHATRCHYAN 14G JHEP 1401 096	S. Chatrchyan et al.	(CMS Collab.)			
KHACHATRYAN...14M JHEP 1410 160	V. Khachatryan et al.	(CMS Collab.)			
KHACHATRYAN...14P EPJ C74 3076	V. Khachatryan et al.	(CMS Collab.)			
KHACHATRYAN...14Q PR D90 112013	V. Khachatryan et al.	(CMS Collab.)			
AAD 13AG PL B721 32	G. Aad et al.	(ATLAS Collab.)			
AAD 13AT NJP 15 043009	G. Aad et al.	(ATLAS Collab.)			
AAD 13O JHEP 1302 095	G. Aad et al.	(ATLAS Collab.)			
AAJ 13T JHEP 1305 132	R. Aaij et al.	(LHCb Collab.)			
AALTONEN 13K PR D88 052012	T. Aaltonen et al.	(CDF Collab.)			
AALTONEN 13L PR D88 052013	T. Aaltonen et al.	(CDF Collab.)			
AALTONEN 13M PR D88 052014	T. Aaltonen et al.	(CDF and DO Collabs.)			
AALTONEN 13P PRL 110 121801	T. Aaltonen et al.	(CDF Collab.)			
ABAZOV 13G PR D88 052006	V.M. Abazov et al.	(DO Collab.)			
ABAZOV 13H PR D88 052007	V.M. Abazov et al.	(DO Collab.)			
ABAZOV 13I PR D88 052008	V.M. Abazov et al.	(DO Collab.)			
ABAZOV 13J PR D88 052009	V.M. Abazov et al.	(DO Collab.)			
ABAZOV 13L PR D88 052011	V.M. Abazov et al.	(DO Collab.)			
CARENA 13 EPJ C73 2552	M. Carena et al.	(CMS Collab.)			
CHATRCHYAN 13AG PL B722 207	S. Chatrchyan et al.	(CMS Collab.)			
CHATRCHYAN 13AL PL B725 36	S. Chatrchyan et al.	(CMS Collab.)			
CHATRCHYAN 13BJ PL B726 564	S. Chatrchyan et al.	(CMS Collab.)			
LEES 13C PR D87 031102	J.P. Lees et al.	(BABAR Collab.)			
LEES 13L PR D88 031701	J.P. Lees et al.	(BABAR Collab.)			
LEES 13R PR D88 071102	J.P. Lees et al.	(BABAR Collab.)			
AAD 12AI PL B716 1	G. Aad et al.	(ATLAS Collab.)			
AAD 12AQ PRL 108 251801	G. Aad et al.	(ATLAS Collab.)			
AAD 12N EPJ C72 2157	G. Aad et al.	(ATLAS Collab.)			
AALTONEN 12AB PR D85 092001	T. Aaltonen et al.	(CDF Collab.)			
AALTONEN 12AM PL B717 173	T. Aaltonen et al.	(CDF Collab.)			
AALTONEN 12AQ PR D86 091101	T. Aaltonen et al.	(CDF and DO Collabs.)			
AALTONEN 12U PR D85 012007	T. Aaltonen et al.	(CDF Collab.)			
AALTONEN 12X PR D85 032005	T. Aaltonen et al.	(CDF Collab.)			
ABAZOV 12G PL B710 569	V.M. Abazov et al.	(DO Collab.)			
ABLIIKIM 12 PR D85 092012	M. Ablikim et al.	(BESIII Collab.)			
BAAK 12 EPJ C72 2003	M. Baak et al.	(Gfitter Group)			
BAAK 12A EPJ C72 2205	M. Baak et al.	(Gfitter Group)			
CHATRCHYAN 12AO JHEP 1209 111	S. Chatrchyan et al.	(CMS Collab.)			
CHATRCHYAN 12C JHEP 1203 081	S. Chatrchyan et al.	(CMS Collab.)			
CHATRCHYAN 12D JHEP 1204 036	S. Chatrchyan et al.	(CMS Collab.)			
CHATRCHYAN 12E PL B710 91	S. Chatrchyan et al.	(CMS Collab.)			
CHATRCHYAN 12G PL B710 403	S. Chatrchyan et al.	(CMS Collab.)			
CHATRCHYAN 12H PRL 108 111804	S. Chatrchyan et al.	(CMS Collab.)			

Charged Higgs Bosons (H^\pm and $H^{\pm\pm}$), Searches for

CONTENTS:

- H^\pm (charged Higgs) mass limits for $m_{H^\pm} < m(\text{top})$
- H^\pm (charged Higgs) mass limits for $m_{H^\pm} > m(\text{top})$
- $H^{\pm\pm}$ (doubly-charged Higgs boson) mass limits
 - Limits for $H^{\pm\pm}$ with $T_3 = \pm 1$
 - Limits for $H^{\pm\pm}$ with $T_3 = 0$

H^\pm (charged Higgs) mass limits for $m_{H^\pm} < m(\text{top})$

Unless otherwise stated, LEP limits assume $B(H^+ \rightarrow \tau^+ \nu) + B(H^+ \rightarrow c\bar{s}) = 1$, and hold for all values of $B(H^+ \rightarrow \tau^+ \nu_\mu)$, and assume H^+ weak isospin of $T_3 = +1/2$. In the following, $\tan\beta$ is the ratio of the two vacuum expectation values in two-doublet models (2HDM).

The limits are also applicable to point-like technipions. For a discussion of techniparticles, see the Review of Dynamical Electroweak Symmetry Breaking in this Review.

Limits obtained at the LHC are given in the m_h^{mod-} benchmark scenario, see CARENA 13, and hold for all $\tan\beta$ values.

For limits obtained in hadronic collisions before the observation of the top quark, and based on the top mass values inconsistent with the current

Gauge & Higgs Boson Particle Listings

Charged Higgs Bosons (H^\pm and $H^{\pm\pm}$), Searches for

measurements, see the 1996 (Physical Review **D54** 1 (1996)) Edition of this Review.

Searches in e^+e^- collisions at and above the Z pole have conclusively ruled out the existence of a charged Higgs in the region $m_{H^\pm} \lesssim 45$ GeV, and are meanwhile superseded by the searches in higher energy e^+e^- collisions at LEP. Results that are by now obsolete are therefore not included in this compilation, and can be found in a previous Edition (The European Physical Journal **C15** 1 (2000)) of this Review.

In the following, and unless otherwise stated, results from the LEP experiments (ALEPH, DELPHI, L3, and OPAL) are assumed to derive from the study of the $e^+e^- \rightarrow H^\pm H^\mp$ process. Limits from $b \rightarrow s\gamma$ decays are usually stronger in generic 2HDM models than in Supersymmetric models.

VALUE (GeV)	CL%	DOCUMENT ID	TECN	COMMENT
none 80-140	95	1 AAD	15AF ATLS	$t \rightarrow bH^+$
none 90-155	95	2 KHACHATRYAN 15AX	CMS	$t \rightarrow bH^+, H^+ \rightarrow \tau^+\nu$
> 80	95	3 LEP	13 LEP	$e^+e^- \rightarrow H^\pm H^\mp, E_{cm} \leq 209 \text{ GeV}$
> 76.3	95	4 ABBIENZI	12 OPAL	$e^+e^- \rightarrow H^\pm H^\mp, E_{cm} \leq 209 \text{ GeV}$
> 74.4	95	ABDALLAH	04i DLPH	$E_{cm} \leq 209 \text{ GeV}$
> 76.5	95	ACHARD	03E L3	$E_{cm} \leq 209 \text{ GeV}$
> 79.3	95	HEISTER	02P ALEP	$E_{cm} \leq 209 \text{ GeV}$
•••		We do not use the following data for averages, fits, limits, etc. •••		
		5 AAD	21V ATLS	$\bar{t}bH^+, H^+ \rightarrow t\bar{b}$
		6 SIRUNYAN	21W CMS	$H^+ \rightarrow W^+Z$
		7 AAD	20W ATLS	$H^+ \rightarrow t\bar{b}$
		8 SIRUNYAN	20AO CMS	$H^+ \rightarrow t\bar{b}$
		9 SIRUNYAN	20AV CMS	$H^+ \rightarrow t\bar{b}$
		10 SIRUNYAN	20BE CMS	$t \rightarrow bH^+, H^+ \rightarrow c\bar{s}$
		11 SIRUNYAN	19AH CMS	$H^+ \rightarrow \tau^+\nu$
		12 SIRUNYAN	19BP CMS	$H^+ \rightarrow W^+Z$
		13 SIRUNYAN	19CC CMS	$t \rightarrow bH^+, H^+ \rightarrow W^+A^0, A^0 \rightarrow \mu^+\mu^-$
		14 SIRUNYAN	19CQ CMS	$H^+ \rightarrow W^+Z$
		15 AABOUD	18BW ATLS	$\bar{t}bH^+$ or $t \rightarrow bH^+, H^+ \rightarrow \tau^+\nu$
		16 AABOUD	18CD ATLS	$\bar{t}bH^+, H^+ \rightarrow t\bar{b}$
		17 AABOUD	18CH ATLS	$H^\pm \rightarrow W^\pm Z$
		18 HALLER	18 RVUE	$b \rightarrow s\gamma$
		19 SIRUNYAN	18DO CMS	$t \rightarrow bH^+, H^+ \rightarrow c\bar{b}$
		20 MISIAK	17 RVUE	$b \rightarrow s(d)\gamma$
		21 SIRUNYAN	17AE CMS	$H^\pm \rightarrow W^\pm Z$
		22 AABOUD	16A ATLS	$t(b)H^\pm, H^\pm \rightarrow \tau^+\nu$
		23 AAD	16AJ ATLS	$t(b)H^\pm, H^\pm \rightarrow t\bar{b}$
		24 AAD	16AJ ATLS	$qq \rightarrow H^\pm, H^\pm \rightarrow t\bar{b}$
		25 AAD	15AF ATLS	tH^\pm
		26 AAD	15M ATLS	$H^\pm \rightarrow W^\pm Z$
		27 KHACHATRYAN 15AX	CMS	$tH^+, H^+ \rightarrow t\bar{b}$
		28 KHACHATRYAN 15AX	CMS	$tH^\pm, H^\pm \rightarrow \tau^\pm\nu$
		29 KHACHATRYAN 15BF	CMS	$t \rightarrow bH^+, H^+ \rightarrow c\bar{s}$
		30 AAD	14M ATLS	$H_2^0 \rightarrow H^\pm W^\mp \rightarrow H^0 W^\pm W^\mp, H^0 \rightarrow b\bar{b}$
		31 AALTONEN	14A CDF	$t \rightarrow b\tau\nu$
		32 AAD	13AC ATLS	$t \rightarrow bH^+$
		33 AAD	13V ATLS	$t \rightarrow bH^+, \text{lepton non-universality}$
		34 AAD	12BH ATLS	$t \rightarrow bH^+$
		35 CHATRYAN 12AA	CMS	$t \rightarrow bH^+$
		36 AALTONEN	11P CDF	$t \rightarrow bH^+, H^+ \rightarrow W^+A^0$
>316	95	37 DESCHAMPS	10 RVUE	Type II, flavor physics data
		38 AALTONEN	09AJ CDF	$t \rightarrow bH^+$
		39 ABAZOV	09AC D0	$t \rightarrow bH^+$
		40 ABAZOV	09AG D0	$t \rightarrow bH^+$
		41 ABAZOV	09AI D0	$t \rightarrow bH^+$
		42 ABAZOV	09PD D0	$H^\pm \rightarrow t\bar{b}$
		43 ABULENCIA	06E CDF	$t \rightarrow bH^+$
> 92.0	95	ABBIENZI	04i OPAL	$B(\tau\nu) = 1$
> 76.7	95	44 ABDALLAH	04i DLPH	Type I
		45 ABBIENZI	03i OPAL	$\tau \rightarrow \mu\bar{\nu}_\mu, e\bar{\nu}_\mu$
		46 ABAZOV	02B D0	$t \rightarrow bH^+, H \rightarrow \tau\nu$
		47 BORZUMATI	02 RVUE	
		48 ABBIENZI	01Q OPAL	$B \rightarrow \tau\nu_\tau X$
		49 BARATE	01E ALEP	$B \rightarrow \tau\nu_\tau$
>315	99	50 GAMBINO	01 RVUE	$b \rightarrow s\gamma$
		51 AFFOLDER	00i CDF	$t \rightarrow bH^+, H \rightarrow \tau\nu$
> 59.5	95	ABBIENZI	99E OPAL	$E_{cm} \leq 183 \text{ GeV}$
		52 ABBOTT	99E D0	$t \rightarrow bH^+$
		53 ACKERSTAFF	99D OPAL	$\tau \rightarrow \nu\nu, \mu\nu\nu$
		54 ACCIARRI	97F L3	$B \rightarrow \tau\nu_\tau$
		55 AMMAR	97B CLEO	$\tau \rightarrow \mu\nu\nu$
		56 COARASA	97 RVUE	$B \rightarrow \tau\nu_\tau X$
		57 GUCHAIT	97 RVUE	$t \rightarrow bH^+, H \rightarrow \tau\nu$
		58 MANGANO	97 RVUE	$B_u(c) \rightarrow \tau\nu_\tau$
		59 STAHL	97 RVUE	$\tau \rightarrow \mu\nu\nu$
>244	95	60 ALAM	95 CLE2	$b \rightarrow s\gamma$
		61 BUSKULIC	95 ALEP	$b \rightarrow \tau\nu_\tau X$

- 1 AAD 15AF search for $t\bar{t}$ production followed by $t \rightarrow bH^+, H^+ \rightarrow \tau^+\nu$ in 19.5 fb^{-1} of pp collisions at $E_{cm} = 8 \text{ TeV}$. Upper limits on $B(t \rightarrow bH^+) B(H^+ \rightarrow \tau\nu)$ between 2.3×10^{-3} and 1.3×10^{-2} (95% CL) are given for $m_{H^\pm} = 80-160 \text{ GeV}$. See their Fig. 8 for the excluded regions in different benchmark scenarios of the MSSM. The region $m_{H^\pm} < 140 \text{ GeV}$ is excluded for $\tan\beta > 1$ in the considered scenarios.
- 2 KHACHATRYAN 15AX search for $t\bar{t}$ production followed by $t \rightarrow bH^+, H^+ \rightarrow \tau^+\nu$ in 19.7 fb^{-1} of pp collisions at $E_{cm} = 8 \text{ TeV}$. Upper limits on $B(t \rightarrow bH^+) B(H^+ \rightarrow \tau\nu)$ between 1.2×10^{-2} and 1.5×10^{-3} (95% CL) are given for $m_{H^\pm} = 80-160 \text{ GeV}$. See their Fig. 11 for the excluded regions in different benchmark scenarios of the MSSM. The region $m_{H^\pm} < 155 \text{ GeV}$ is excluded for $\tan\beta > 1$ in the considered scenarios.
- 3 LEP 13 give a limit that refers to the Type II scenario. The limit for $B(H^+ \rightarrow \tau\nu) = 1$ is 94 GeV (95% CL), and for $B(H^+ \rightarrow c\bar{s}) = 1$ the region below 80.5 as well as the region 83-88 GeV is excluded (95% CL). LEP 13 also search for the decay mode $H^+ \rightarrow A^0 W^+$ with $A^0 \rightarrow b\bar{b}$, which is not negligible in Type I models. The limit in Type I models is 72.5 GeV (95% CL) if $m_{A^0} > 12 \text{ GeV}$.
- 4 ABBIENZI 12 also search for the decay mode $H^+ \rightarrow A^0 W^+$ with $A^0 \rightarrow b\bar{b}$.
- 5 AAD 21V search for $\bar{t}bH^+$ associated production followed by $H^+ \rightarrow t\bar{b}$ in 139 fb^{-1} of pp collisions at $E_{cm} = 13 \text{ TeV}$. See their Fig. 6 for upper limits on cross section times branching ratio for $m_{H^\pm} = 0.2-2 \text{ TeV}$. See also their Fig. 7 for the excluded region in the parameter space of the hMSSM and the following MSSM benchmark scenarios: $M_h^{125}, M_h^{25}(\bar{\chi}), M_h^{25}(\bar{\tau}), M_h^{125}$ (alignment), M_h^{125} (CPV).
- 6 SIRUNYAN 21W search for vector boson fusion production of H^+ decaying to $H^+ \rightarrow W^+ Z \rightarrow \ell^+ \nu \ell^+ \ell^-$ in 137 fb^{-1} of pp collisions at $E_{cm} = 13 \text{ TeV}$. See their Fig. 8 for limits on cross section times branching ratio for $m_{H^\pm} = 0.2-3.0 \text{ TeV}$, and also for limits on the fraction of the triplet vev contribution to the W mass in the Georgi-Machacek model.
- 7 AAD 20W search for dijet resonances in events with isolated leptons using 139 fb^{-1} of pp collisions at $E_{cm} = 13 \text{ TeV}$. As a byproduct, $H^+ \rightarrow t\bar{b}$ produced in association with $\bar{t}b$ is searched for. Limits on the product of cross section times branching ratio for $m_{H^\pm} = 0.6-2 \text{ TeV}$ are given in their Fig. 5(c).
- 8 SIRUNYAN 20A search for $H^+ \rightarrow t\bar{b}$ produced in association with $t(b)$ in all jet final states in 35.9 fb^{-1} of pp collisions at $E_{cm} = 13 \text{ TeV}$. See their Fig. 6 for limits on the product of cross section times branching ratio for $m_{H^\pm} = 0.2-3 \text{ TeV}$. Limits for s-channel production are also given for $m_{H^\pm} = 0.8-3 \text{ TeV}$. See also Fig. 7 for the corresponding limits in scenarios in the minimal supersymmetric standard model. Cross section limits from combined results with SIRUNYAN 20AV are given in Fig. 8.
- 9 SIRUNYAN 20AV search for $H^+ \rightarrow t\bar{b}$ produced in association with $t(b)$ in final states with one or two leptons, in 35.9 fb^{-1} of pp collisions at $E_{cm} = 13 \text{ TeV}$. See their Fig. 5 for limits on the product of cross section times branching ratio for $m_{H^\pm} = 0.2-3 \text{ TeV}$, and their Fig. 6 for the corresponding limits in scenarios in the minimal supersymmetric standard model.
- 10 SIRUNYAN 20BE search for $t \rightarrow bH^+$ followed by the decay $H^+ \rightarrow c\bar{s}$ in pair produced top quark events using 35.9 fb^{-1} of pp collisions at $E_{cm} = 13 \text{ TeV}$. Limits on the branching ratio in the range $1.68-0.25\%$ (95%CL) are given for $m_{H^\pm} = 80-160 \text{ GeV}$, see their Fig. 4.
- 11 SIRUNYAN 19AH search for H^+ in the decay of a pair-produced t quark, or in associated $t\bar{b}H^+$ or nonresonant $b\bar{b}H^+ W^+$ production, followed by $H^+ \rightarrow \tau^+\nu$, in 35.9 fb^{-1} of pp collisions at $E_{cm} = 13 \text{ TeV}$. Upper limits on cross section times branching ratio between 6 pb and 5 fb (95% CL) are given for $m_{H^\pm} = 80-3000 \text{ GeV}$ (including the non-resonant production near the top quark mass), see their Fig. 6 (left). See their Fig. 6 (right) for the excluded regions in the m_h^{mod} scenario of the MSSM.
- 12 SIRUNYAN 19BP search for vector boson fusion production of H^+ decaying to $H^+ \rightarrow W^+ Z \rightarrow \ell^+ \nu \ell^+ \ell^-$ in 35.9 fb^{-1} of pp collisions at $E_{cm} = 13 \text{ TeV}$. See their Fig. 7 for limits on cross section times branching ratio for $m_{H^\pm} = 0.3-2.0 \text{ TeV}$, and also for limits on the fraction of the triplet vev contribution to the W mass in the Georgi-Machacek model.
- 13 SIRUNYAN 19CC search for $t \rightarrow bH^+$ from pair produced top quarks, with the decay chain $H^+ \rightarrow W^+ A^0, A^0 \rightarrow \mu^+\mu^-$ in 35.9 fb^{-1} of pp collisions at $E_{cm} = 13 \text{ TeV}$. See their Fig. 2 for limits on the product of branching ratios for $m_{A^0} = 15-75 \text{ GeV}$.
- 14 SIRUNYAN 19CQ search for vector boson fusion production of H^+ decaying to $H^+ \rightarrow W^+ Z \rightarrow \ell^+ \nu q \bar{q}$ or $q \bar{q} \ell^+ \ell^-$ in 35.9 fb^{-1} of pp collisions at $E_{cm} = 13 \text{ TeV}$. See their Fig. 5 for limits on cross section times branching ratio for $m_{H^\pm} = 0.6-2.0 \text{ TeV}$, and also for limits on the triplet vacuum expectation value fraction in the Georgi-Machacek model.
- 15 AABOUD 18BW search for $\bar{t}bH^+$ associated production or the decay $t \rightarrow bH^+$, followed by $H^+ \rightarrow \tau^+\nu$, in 36.1 fb^{-1} of pp collisions at $E_{cm} = 13 \text{ TeV}$. See their Fig. 8(a) for upper limits on cross section times branching ratio for $m_{H^\pm} = 90-2000 \text{ GeV}$, and Fig. 8(b) for limits on $B(t \rightarrow bH^+) B(H^+ \rightarrow \tau^+\nu)$ for $m_{H^\pm} = 90-160 \text{ GeV}$. See also their Fig. 9 for the excluded region in the hMSSM parameter space.
- 16 AABOUD 18CD search for $\bar{t}bH^+$ associated production followed by $H^+ \rightarrow t\bar{b}$ in 36.1 fb^{-1} of pp collisions at $E_{cm} = 13 \text{ TeV}$. See their Fig. 8 for upper limits on cross section times branching ratio for $m_{H^\pm} = 0.2-2 \text{ TeV}$. See also their Fig. 9 for the excluded region in the parameter space of the m_h^{mod} and hMSSM scenarios of the MSSM. The theory predictions overlaid to the experimental limits to determine the excluded m_{H^\pm} range are shown without their respective uncertainty band.
- 17 AABOUD 18CH search for vector boson fusion production of H^\pm decaying to $H^\pm \rightarrow W^\pm Z \rightarrow \ell^\pm \nu \ell^\pm \ell^-$ in 36.1 fb^{-1} of pp collisions at $E_{cm} = 13 \text{ TeV}$. See their Fig. 7 for limits on cross section times branching ratio for $m_{H^\pm} = 0.2-0.9 \text{ TeV}$, and also for limits on the triplet vacuum expectation value fraction in the Georgi-Machacek model.
- 18 HALLER 18 give 95% CL lower limits on m_{H^\pm} of 590 GeV in type II two Higgs doublet model from combined data (including an unpublished BELLE result) for $B(b \rightarrow s\gamma)$.
- 19 SIRUNYAN 18DO search for $t\bar{t}$ production followed by $t \rightarrow bH^+, H^+ \rightarrow c\bar{b}$ in 19.7 fb^{-1} of pp collisions at $E_{cm} = 8 \text{ TeV}$. See their Fig. 3 for upper limits on $B(t \rightarrow bH^+) B(H^+ \rightarrow c\bar{b})$ for $m_{H^\pm} = 90-150 \text{ GeV}$ assuming that $B(H^+ \rightarrow c\bar{b}) = 1$ and $B(t \rightarrow bH^+) + B(t \rightarrow bW^+) = 1$.

Gauge & Higgs Boson Particle Listings

Charged Higgs Bosons (H^\pm and $H^{\pm\pm}$), Searches for

- 20 MISIAK 17 give 95% CL lower limits on m_{H^\pm} between 570 and 800 GeV in type II two Higgs doublet model from combined data (including an unpublished BELLE result) for $B(b \rightarrow s(d)\gamma)$.
- 21 SIRUNYAN 17AE search for vector boson fusion production of H^\pm decaying to $H^\pm \rightarrow W^\pm Z \rightarrow \ell^\pm \nu \ell'^\pm \ell'^\mp$ in 15.2 fb $^{-1}$ of pp collisions at $E_{cm} = 13$ TeV. See their Fig. 3 for limits on cross section times branching ratio for $m_{H^\pm} = 0.2$ -2.0 TeV, and also for limits on the triplet vacuum expectation value fraction in the Georgi-Machacek model.
- 22 AABOUD 16A search for $t(b)$ H^\pm associated production followed by $H^\pm \rightarrow \tau^+ \nu$ in 3.2 fb $^{-1}$ of pp collisions at $E_{cm} = 13$ TeV. Upper limits on $\sigma(t(b) H^\pm) B(H^\pm \rightarrow \tau \nu)$ between 1.9 pb and 15 fb (95% CL) are given for $m_{H^\pm} = 200$ -2000 GeV, see their Fig. 6. See their Fig. 7 for the excluded regions in the hMSSM scenario.
- 23 AAD 16AJ search for $t(b) H^\pm$ associated production followed by $H^\pm \rightarrow tb$ in 20.3 fb $^{-1}$ of pp collisions at $E_{cm} = 8$ TeV. See their Fig. 6 for upper limits on $\sigma(t(b) H^\pm) B(H^\pm \rightarrow tb)$ for $m_{H^\pm} = 200$ -600 GeV.
- 24 AAD 16AJ search for H^\pm production from quark-antiquark annihilation, followed by $H^\pm \rightarrow tb$, in 20.3 fb $^{-1}$ of pp collisions at $E_{cm} = 8$ TeV. See their Fig. 10 for upper limits on $\sigma(H^\pm) B(H^\pm \rightarrow tb)$ for $m_{H^\pm} = 400$ -3000 GeV.
- 25 AAD 15AF search for tH^\pm associated production followed by $H^\pm \rightarrow \tau^\pm \nu$ in 19.5 fb $^{-1}$ of pp collisions at $E_{cm} = 8$ TeV. Upper limits on $\sigma(tH^\pm) B(H^\pm \rightarrow \tau \nu)$ between 760 and 4.5 fb (95% CL) are given for $m_{H^\pm} = 180$ -1000 GeV. See their Fig. 8 for the excluded regions in different benchmark scenarios of the MSSM.
- 26 AAD 15M search for vector boson fusion production of H^\pm decaying to $H^\pm \rightarrow W^\pm Z \rightarrow q\bar{q}\ell^\pm \ell'^\mp$ in 20.3 fb $^{-1}$ of pp collisions at $E_{cm} = 8$ TeV. See their Fig. 2 for limits on cross section times branching ratio for $m_{H^\pm} = 200$ -1000 GeV, and Fig. 3 for limits on triplet vacuum expectation value fraction in the Georgi-Machacek model.
- 27 KHACHATRYAN 15AX search for tH^\pm associated production followed by $H^\pm \rightarrow tb$ in 19.7 fb $^{-1}$ of pp collisions at $E_{cm} = 8$ TeV. Upper limits on $\sigma(tH^\pm) B(H^\pm \rightarrow t\bar{b})$ between 2.0 and 0.13 pb (95% CL) are given for $m_{H^\pm} = 180$ -600 GeV. See their Fig. 11 for the excluded regions in different benchmark scenarios of the MSSM.
- 28 KHACHATRYAN 15AX search for tH^\pm associated production followed by $H^\pm \rightarrow \tau^\pm \nu$ in 19.7 fb $^{-1}$ of pp collisions at $E_{cm} = 8$ TeV. Upper limits on $\sigma(tH^\pm) B(H^\pm \rightarrow \tau \nu)$ between 380 and 25 fb (95% CL) are given for $m_{H^\pm} = 180$ -600 GeV. See their Fig. 11 for the excluded regions in different benchmark scenarios of the MSSM.
- 29 KHACHATRYAN 15BF search for $t\bar{t}$ production followed by $t \rightarrow bH^+, H^+ \rightarrow c\bar{s}$ in 19.7 fb $^{-1}$ of pp collisions at $E_{cm} = 8$ TeV. Upper limits on $B(t \rightarrow bH^+) B(H^+ \rightarrow c\bar{s})$ between 1.2×10^{-2} and 6.5×10^{-2} (95% CL) are given for $m_{H^\pm} = 90$ -160 GeV.
- 30 AAD 14M search for the decay cascade $H_0^2 \rightarrow H^\pm W^\mp \rightarrow H^0 W^\pm W^\mp$, H^0 decaying to $b\bar{b}$ in 20.3 fb $^{-1}$ of pp collisions at $E_{cm} = 8$ TeV. See their Table III for limits on cross section times branching ratio for $m_{H_0^2} = 325$ -1025 GeV and $m_{H^\pm} = 225$ -925 GeV.
- 31 AALTONEN 14A measure $B(t \rightarrow b\tau\nu) = 0.096 \pm 0.028$ using 9 fb $^{-1}$ of $p\bar{p}$ collisions at $E_{cm} = 1.96$ TeV. For $m_{H^\pm} = 80$ -140 GeV, this measured value is translated to a limit $B(t \rightarrow bH^\pm) < 0.059$ at 95% CL assuming $B(H^\pm \rightarrow \tau^+ \nu) = 1$.
- 32 AAD 13AC search for $t\bar{t}$ production followed by $t \rightarrow bH^+, H^+ \rightarrow c\bar{s}$ (flavor unidentified) in 4.7 fb $^{-1}$ of pp collisions at $E_{cm} = 7$ TeV. Upper limits on $B(t \rightarrow bH^+) B(H^+ \rightarrow c\bar{s})$ between 0.05 and 0.01 (95% CL) are given for $m_{H^\pm} = 90$ -150 GeV and $B(H^+ \rightarrow c\bar{s}) = 1$.
- 33 AAD 13V search for $t\bar{t}$ production followed by $t \rightarrow bH^+, H^+ \rightarrow \tau^+ \nu$ through violation of lepton universality with 4.6 fb $^{-1}$ of pp collisions at $E_{cm} = 7$ TeV. Upper limits on $B(t \rightarrow bH^+) B(H^+ \rightarrow \tau^+ \nu)$ between 0.032 and 0.044 (95% CL) are given for $m_{H^\pm} = 90$ -140 GeV and $B(H^+ \rightarrow \tau^+ \nu) = 1$. By combining with AAD 12BH, the limits improve to 0.008 to 0.034 for $m_{H^\pm} = 90$ -160 GeV. See their Fig. 7 for the excluded region in the m_h^{\max} scenario of the MSSM.
- 34 AAD 12BH search for $t\bar{t}$ production followed by $t \rightarrow bH^+, H^+ \rightarrow \tau^+ \nu$ with 4.6 fb $^{-1}$ of pp collisions at $E_{cm} = 7$ TeV. Upper limits on $B(t \rightarrow bH^+) B(H^+ \rightarrow \tau^+ \nu)$ between 0.01 and 0.05 (95% CL) are given for $m_{H^\pm} = 90$ -160 GeV and $B(H^+ \rightarrow \tau^+ \nu) = 1$. See their Fig. 8 for the excluded region in the m_h^{\max} scenario of the MSSM.
- 35 CHATRCHYAN 12AA search for $t\bar{t}$ production followed by $t \rightarrow bH^+, H^+ \rightarrow \tau^+ \nu$ with 2 fb $^{-1}$ of pp collisions at $E_{cm} = 7$ TeV. Upper limits on $B(t \rightarrow bH^+) B(H^+ \rightarrow \tau^+ \nu)$ between 0.019 and 0.041 (95% CL) are given for $m_{H^\pm} = 80$ -160 GeV and $B(H^+ \rightarrow \tau^+ \nu) = 1$.
- 36 AALTONEN 11P search in 2.7 fb $^{-1}$ of $p\bar{p}$ collisions at $E_{cm} = 1.96$ TeV for the decay chain $t \rightarrow bH^+, H^+ \rightarrow W^+ A^0, A^0 \rightarrow \tau^+ \tau^-$ with m_{A^0} between 4 and 9 GeV. See their Fig. 4 for limits on $B(t \rightarrow bH^+) B(H^+ \rightarrow W^+ A^0) B(A^0 \rightarrow \tau^+ \tau^-)$ for $90 < m_{H^\pm} < 160$ GeV.
- 37 DESCHAMPS 10 make Type II two Higgs doublet model fits to weak leptonic and semileptonic decays, $b \rightarrow s\gamma, B, B_s$ mixings, and $Z \rightarrow b\bar{b}$. The limit holds irrespective of $\tan\beta$.
- 38 AALTONEN 09AJ search for $t \rightarrow bH^+, H^+ \rightarrow c\bar{s}$ in $t\bar{t}$ events in 2.2 fb $^{-1}$ of $p\bar{p}$ collisions at $E_{cm} = 1.96$ TeV. Upper limits on $B(t \rightarrow bH^+) B(H^+ \rightarrow c\bar{s})$ between 0.08 and 0.32 (95% CL) are given for $m_{H^\pm} = 60$ -150 GeV and $B(H^+ \rightarrow c\bar{s}) = 1$.
- 39 ABZOV 09AC search for $t \rightarrow bH^+, H^+ \rightarrow \tau^+ \nu$ in $t\bar{t}$ events in 0.9 fb $^{-1}$ of $p\bar{p}$ collisions at $E_{cm} = 1.96$ TeV. Upper limits on $B(t \rightarrow bH^+) B(H^+ \rightarrow \tau^+ \nu)$ between 0.19 and 0.25 (95% CL) are given for $m_{H^\pm} = 80$ -155 GeV and $B(H^+ \rightarrow \tau^+ \nu) = 1$. See their Fig. 4 for an excluded region in a MSSM scenario.
- 40 ABZOV 09AC measure $t\bar{t}$ cross sections in final states with ℓ + jets ($\ell = e, \mu$), $\ell\bar{\ell}$, and $\tau\bar{\ell}$ in 1 fb $^{-1}$ of $p\bar{p}$ collisions at $E_{cm} = 1.96$ TeV, which constrains possible $t \rightarrow bH^+$ branching fractions. Upper limits (95% CL) on $B(t \rightarrow bH^+) B(H^+ \rightarrow \tau^+ \nu)$ between 0.15 and 0.40 (0.48 and 0.57) are given for $B(H^+ \rightarrow \tau^+ \nu) = 1$ ($B(H^+ \rightarrow c\bar{s}) = 1$) for $m_{H^\pm} = 80$ -155 GeV.
- 41 ABZOV 09AI search for $t \rightarrow bH^+$ in $t\bar{t}$ events in 1 fb $^{-1}$ of $p\bar{p}$ collisions at $E_{cm} = 1.96$ TeV. Final states with ℓ + jets ($\ell = e, \mu$), $\ell\bar{\ell}$, and $\tau\bar{\ell}$ are examined. Upper limits on $B(t \rightarrow bH^+) B(H^+ \rightarrow \tau^+ \nu)$ (95% CL) between 0.15 and 0.19 (0.19 and 0.22) are given for $B(H^+ \rightarrow \tau^+ \nu) = 1$ ($B(H^+ \rightarrow c\bar{s}) = 1$) for $m_{H^\pm} = 80$ -155 GeV. For $B(H^+ \rightarrow \tau^+ \nu) = 1$ also a simultaneous extraction of $B(t \rightarrow bH^+)$ and the $t\bar{t}$ cross section is performed,

yielding a limit on $B(t \rightarrow bH^+)$ between 0.12 and 0.26 for $m_{H^\pm} = 80$ -155 GeV. See their Figs. 5-8 for excluded regions in several MSSM scenarios.

- 42 ABZOV 09P search for H^+ production by $q\bar{q}$ annihilation followed by $H^+ \rightarrow t\bar{b}$ decay in 0.9 fb $^{-1}$ of $p\bar{p}$ collisions at $E_{cm} = 1.96$ TeV. Cross section limits in several two-doublet models are given for $m_{H^\pm} = 180$ -300 GeV. A region with $20 \lesssim \tan\beta \lesssim 70$ is excluded (95% CL) for $180 \text{ GeV} \lesssim m_{H^\pm} \lesssim 184 \text{ GeV}$ in type-I models.
- 43 ABULENCIA 06E search for associated $H^0 W$ production in $p\bar{p}$ collisions at $E_{cm} = 1.96$ TeV. A fit is made for $t\bar{t}$ production processes in dilepton, lepton + jets, and lepton + τ final states, with the decays $t \rightarrow W^+ b$ and $t \rightarrow H^+ b$ followed by $H^+ \rightarrow \tau^+ \nu, c\bar{s}, t^* \bar{b}$, or $W^+ H^0$. Within the MSSM the search is sensitive to the region $\tan\beta < 1$ or > 30 in the mass range $m_{H^\pm} = 80$ -160 GeV. See Fig. 2 for the excluded region in a certain MSSM scenario.
- 44 ABDALLAH 04I search for $e^+ e^- \rightarrow H^+ H^-$ with H^\pm decaying to $\tau\nu, cs$, or $W^* A^0$ in Type-I two-Higgs-doublet models.
- 45 ABBIENDI 03 give a limit $m_{H^\pm} > 1.28 \tan\beta \text{ GeV}$ (95%CL) in Type II two-doublet models.
- 46 ABZOV 02B search for a charged Higgs boson in top decays with $H^+ \rightarrow \tau^+ \nu$ at $E_{cm} = 1.8$ TeV. For $m_{H^\pm} = 75$ GeV, the region $\tan\beta > 32.0$ is excluded at 95%CL. The excluded mass region extends to over 140 GeV for $\tan\beta$ values above 100.
- 47 BORZUMATI 02 point out that the decay modes such as $b\bar{b} W, A^0 W$, and supersymmetric ones can have substantial branching fractions in the mass range explored at LEP II and Tevatron.
- 48 ABBIENDI 01Q give a limit $\tan\beta/m_{H^\pm} < 0.53 \text{ GeV}^{-1}$ (95%CL) in Type II two-doublet models.
- 49 BARATE 01E give a limit $\tan\beta/m_{H^\pm} < 0.40 \text{ GeV}^{-1}$ (90% CL) in Type II two-doublet models. An independent measurement of $B \rightarrow \tau\nu X$ gives $\tan\beta/m_{H^\pm} < 0.49 \text{ GeV}^{-1}$ (90% CL).
- 50 GAMBINO 01 use the world average data in the summer of 2001 $B(b \rightarrow s\gamma) = (3.23 \pm 0.42) \times 10^{-4}$. The limit applies for Type-II two-doublet models.
- 51 AFFOLDER 00I search for a charged Higgs boson in top decays with $H^+ \rightarrow \tau^+ \nu$ in $p\bar{p}$ collisions at $E_{cm} = 1.8$ TeV. The excluded mass region extends to over 120 GeV for $\tan\beta$ values above 100 and $B(\tau\nu) = 1$. If $B(t \rightarrow bH^+) \gtrsim 0.6$, m_{H^\pm} up to 160 GeV is excluded. Updates ABE 97L.
- 52 ABBOTT 99E search for a charged Higgs boson in top decays in $p\bar{p}$ collisions at $E_{cm} = 1.8$ TeV, by comparing the observed $t\bar{t}$ cross section (extracted from the data assuming the dominant decay $t \rightarrow bW^+$) with theoretical expectation. The search is sensitive to regions of the domains $\tan\beta \lesssim 1, 50 < m_{H^\pm}(\text{GeV}) \lesssim 120$ and $\tan\beta \gtrsim 40, 50 < m_{H^\pm}(\text{GeV}) \lesssim 160$. See Fig. 3 for the details of the excluded region.
- 53 ACKERSTAFF 99D measure the Michel parameters ρ, ξ, η , and $\xi\delta$ in leptonic τ decays from $Z \rightarrow \tau\tau$. Assuming $e-\mu$ universality, the limit $m_{H^\pm} > 0.97 \tan\beta \text{ GeV}$ (95% CL) is obtained for two-doublet models in which only one doublet couples to leptons.
- 54 ACCIARRI 97F give a limit $m_{H^\pm} > 2.6 \tan\beta \text{ GeV}$ (90% CL) from their limit on the exclusive $B \rightarrow \tau\nu X$ branching ratio.
- 55 AMMAR 97B measure the Michel parameter ρ from $\tau \rightarrow e\nu\nu$ decays and assumes e/μ universality to extract the Michel η parameter from $\tau \rightarrow \mu\nu\nu$ decays. The measurement is translated to a lower limit on m_{H^\pm} in a two-doublet model $m_{H^\pm} > 0.97 \tan\beta \text{ GeV}$ (90% CL).
- 56 COARASA 97 reanalyzed the constraint on the $(m_{H^\pm}, \tan\beta)$ plane derived from the inclusive $B \rightarrow \tau\nu X$ branching ratio in GROSSMAN 95b and BUSKULIC 95. They show that the constraint is quite sensitive to supersymmetric one-loop effects.
- 57 GUCHAIT 97 studies the constraints on m_{H^\pm} set by Tevatron data on $\ell\tau$ final states in $t\bar{t} \rightarrow (Wb)(Hb), W \rightarrow \ell\nu, H \rightarrow \tau\nu$. See Fig. 2 for the excluded region.
- 58 MANGANO 97 reconsiders the limit in ACCIARRI 97F including the effect of the potentially large $B_c \rightarrow \tau\nu X$ background to $B_{\mu\tau} \rightarrow \tau\nu X$ decays. Stronger limits are obtained.
- 59 STAHL 97 fit τ lifetime, leptonic branching ratios, and the Michel parameters and derive limit $m_{H^\pm} > 1.5 \tan\beta \text{ GeV}$ (90% CL) for a two-doublet model. See also STAHL 94.
- 60 ALAM 95 measure the inclusive $b \rightarrow s\gamma$ branching ratio at $T(4S)$ and give $B(b \rightarrow s\gamma) < 4.2 \times 10^{-4}$ (95% CL), which translates to the limit $m_{H^\pm} > [244 + 63/(\tan\beta)]^{1.3}$ GeV in the Type II two-doublet model. Light supersymmetric particles can invalidate this bound.
- 61 BUSKULIC 95 give a limit $m_{H^\pm} > 1.9 \tan\beta \text{ GeV}$ (90% CL) for Type-II models from $B \rightarrow \tau\nu X$ branching ratio, as proposed in GROSSMAN 94.

H^\pm (charged Higgs) mass limits for $m_{H^\pm} > m(\text{top})$

Limits obtained at the LHC are given in the $m_h^{\text{mod-}}$ benchmark scenario, see CARENA 13, and depend on the $\tan\beta$ values.

VALUE (GeV)	CL%	DOCUMENT ID	TECN	COMMENT
> 181	95	1 AABOUD	18BWATLS	$\tan\beta = 10$
> 249	95	1 AABOUD	18BWATLS	$\tan\beta = 20$
> 390	95	1 AABOUD	18BWATLS	$\tan\beta = 30$
> 894	95	1 AABOUD	18BWATLS	$\tan\beta = 40$
>1017	95	1 AABOUD	18BWATLS	$\tan\beta = 50$
>1103	95	1 AABOUD	18BWATLS	$\tan\beta = 60$

- 1 AABOUD 18BW search for $\bar{t}bH^+$ associated production in 36.1 fb $^{-1}$ of pp collisions at $E_{cm} = 13$ TeV. See also their Fig. 9 for the excluded region in the hMSSM parameter space.

$H^{\pm\pm}$ (doubly-charged Higgs boson) mass limits

This section covers searches for a doubly-charged Higgs boson with couplings to lepton pairs. Its weak isospin T_3 is thus restricted to two possibilities depending on lepton chiralities: $T_3(H^{\pm\pm}) = \pm 1$, with the coupling $g_{\ell\ell}$ to $\ell_L^\pm \ell_L^\pm$ and $\ell_R^\pm \ell_R^\pm$ ("left-handed") and $T_3(H^{\pm\pm}) = 0$, with the coupling to $\ell_R^\pm \ell_R^\pm$ and $\ell_L^\pm \ell_L^\pm$ ("right-handed"). These Higgs bosons appear in some left-right symmetric models based on the gauge

Gauge & Higgs Boson Particle Listings
 Charged Higgs Bosons (H^\pm and $H^{\pm\pm}$), Searches for

group $SU(2)_L \times SU(2)_R \times U(1)$, the type-II seesaw model, and the Zee-Babu model. The two cases are listed separately in the following. Unless noted, one of the lepton flavor combinations is assumed to be dominant in the decay.

Limits for $H^{\pm\pm}$ with $T_3 = \pm 1$

VALUE (GeV)	CL%	DOCUMENT ID	TECN	COMMENT
>220	95	1 AABOUD	19k ATLS	$W^\pm W^\pm$
>768	95	2 AABOUD	18bC ATLS	ee
>846	95	2 AABOUD	18bC ATLS	$\mu\mu$
>468	95	3 AAD	15AG ATLS	$e\mu$
>400	95	4 AAD	15AP ATLS	$e\tau$
>400	95	4 AAD	15AP ATLS	$\mu\tau$
>169	95	5 CHATRCHYAN	12AU CMS	$\tau\tau$
>300	95	5 CHATRCHYAN	12AU CMS	$\mu\tau$
>293	95	5 CHATRCHYAN	12AU CMS	$e\tau$
>395	95	5 CHATRCHYAN	12AU CMS	$\mu\mu$
>391	95	5 CHATRCHYAN	12AU CMS	$e\mu$
>382	95	5 CHATRCHYAN	12AU CMS	ee
> 98.1	95	6 ABDALLAH	03 DLPH	$\tau\tau$
> 99.0	95	7 ABBIENDI	02c OPAL	$\tau\tau$
••• We do not use the following data for averages, fits, limits, etc. •••				
>350	95	8 AAD	21u ATLS	$W^\pm W^\pm$
>230	95	9 AAD	21u ATLS	$H^{\pm\pm}H^\mp$ associated production, $H^{\pm\pm} \rightarrow W^\pm W^\pm, H^\pm \rightarrow W^\pm Z$
		10 SIRUNYAN	21w CMS	$W^\pm W^\pm$
		11 SIRUNYAN	19cQ CMS	$W^\pm W^\pm$
		12 SIRUNYAN	18cc CMS	$W^\pm W^\pm$
>551	95	3 AAD	15AG ATLS	ee
>516	95	3 AAD	15AG ATLS	$\mu\mu$
		13 KANEMURA	15 RVUE	$W^{(*)}\pm W^{(*)}\pm$
		14 KHACHATRYAN	15D CMS	$W^\pm W^\pm$
		15 KANEMURA	14 RVUE	$W^{(*)}\pm W^{(*)}\pm$
>330	95	16 AAD	13Y ATLS	$\mu\mu$
>237	95	16 AAD	13Y ATLS	$\mu\tau$
>355	95	17 AAD	12AY ATLS	$\mu\mu$
>398	95	18 AAD	12CQ ATLS	$\mu\mu$
>375	95	18 AAD	12CQ ATLS	$e\mu$
>409	95	18 AAD	12CQ ATLS	ee
>128	95	19 ABAZOV	12A D0	$\tau\tau$
>144	95	19 ABAZOV	12A D0	$\mu\tau$
>245	95	20 AALTONEN	11AF CDF	$\mu\mu$
>210	95	20 AALTONEN	11AF CDF	$e\mu$
>225	95	20 AALTONEN	11AF CDF	ee
>114	95	21 AALTONEN	08AA CDF	$e\tau$
>112	95	21 AALTONEN	08AA CDF	$\mu\tau$
>168	95	22 ABAZOV	08V D0	$\mu\mu$
		23 AKTAS	06A H1	single $H^{\pm\pm}$
>133	95	24 ACOSTA	05L CDF	stable
>118.4	95	25 ABAZOV	04E D0	$\mu\mu$
		26 ABBIENDI	03Q OPAL	$E_{cm} \leq 209$ GeV, single $H^{\pm\pm}$
		27 GORDEEV	97 SPEC	muonium conversion
		28 ASAKA	95 THEO	
> 45.6	95	29 ACTON	92M OPAL	
> 30.4	95	30 ACTON	92M OPAL	
none 6.5–36.6	95	31 SWARTZ	90 MRK2	

1 AABOUD 19k search for pair production of $H^{++}H^{--}$ followed by the decay $H^{\pm\pm} \rightarrow W^\pm W^\pm$ in 36.1 fb^{-1} of pp collisions at $E_{cm} = 13$ TeV. The search is interpreted in a doublet-triplet extension of the scalar sector with a vev of 0.1 GeV, leading to $B(H^{\pm\pm} \rightarrow W^\pm W^\pm) = 1$. See their Fig. 5 for limits on the cross section for $m_{H^{++}}$ between 200 and 700 GeV.

2 See their Figs. 11(b) and 13 for limits with smaller branching ratios.

3 AAD 15AG search for $H^{++}H^{--}$ production in 20.3 fb^{-1} of pp collisions at $E_{cm} = 8$ TeV. The limit assumes 100% branching ratio to the specified final state. See their Fig. 5 for limits for arbitrary branching ratios.

4 AAD 15AP search for $H^{++}H^{--}$ production in 20.3 fb^{-1} of pp collisions at $E_{cm} = 8$ TeV. The limit assumes 100% branching ratio to the specified final state.

5 CHATRCHYAN 12AU search for $H^{++}H^{--}$ production with 4.9 fb^{-1} of pp collisions at $E_{cm} = 7$ TeV. The limit assumes 100% branching ratio to the specified final state. See their Table 6 for limits including associated $H^{++}H^{--}$ production or assuming different scenarios.

6 ABDALLAH 03 search for $H^{++}H^{--}$ pair production either followed by $H^{++} \rightarrow \tau^+\tau^+$, or decaying outside the detector.

7 ABBIENDI 02c searches for pair production of $H^{++}H^{--}$, with $H^{\pm\pm} \rightarrow \ell^\pm \ell^\pm (\ell, \ell' = e, \mu, \tau)$. The limit holds for $\ell = \ell' = \tau$, and becomes stronger for other combinations of leptonic final states. To ensure the decay within the detector, the limit only applies for $g(H\ell\ell) \gtrsim 10^{-7}$.

8 AAD 21u search for pair production of $H^{++}H^{--}$ followed by the decay $H^{\pm\pm} \rightarrow W^\pm W^\pm$ in 139 fb^{-1} of pp collisions at $E_{cm} = 13$ TeV. The search is interpreted in a triplet extension of the SM Higgs sector with a triplet vev of 0.1 GeV, leading to $B(H^{\pm\pm} \rightarrow W^\pm W^\pm) = 1$. See their Fig. 9(a) for limits on the cross section for $m_{H^{++}}$ between 200 and 600 GeV.

9 AAD 21u search for associated production of $H^{\pm\pm}H^\mp$ followed by the decays $H^{\pm\pm} \rightarrow W^\pm W^\pm, H^\pm \rightarrow W^\pm Z$ in 139 fb^{-1} of pp collisions at $E_{cm} = 13$ TeV. $H^{\pm\pm}$ and H^\pm are assumed to be degenerate in mass within 5 GeV. The search is interpreted in a triplet extension of the SM Higgs sector with a triplet vev of 0.1 GeV, leading to $B(H^{\pm\pm} \rightarrow W^\pm W^\pm) = 1$. See their Fig. 9(b) for limits on the cross section for $m_{H^{++}}$ between 200 and 600 GeV.

10 SIRUNYAN 21w search for vector boson fusion production of $H^{\pm\pm}$ decaying to $H^{\pm\pm} \rightarrow W^\pm W^\pm \rightarrow \ell^\pm \nu \ell^\pm \nu$ in 137 fb^{-1} of pp collisions at $E_{cm} = 13$ TeV. See their Fig. 8 for limits on cross section times branching ratio for $m_{H^{++}} = 0.2\text{--}3.0$ TeV.

11 SIRUNYAN 19cQ search for $H^{\pm\pm}$ production by vector boson fusion followed by the decay $H^{\pm\pm} \rightarrow W^\pm W^\pm \rightarrow qq\ell\nu$ in 35.9 fb^{-1} of pp collisions at $E_{cm} = 13$ TeV. See their Fig. 5 for limits on cross section times branching ratio for $m_{H^{\pm\pm}}$ between 0.6 and 2 TeV.

12 SIRUNYAN 18cc search for $H^{\pm\pm}$ production by vector boson fusion followed by the decay $H^{\pm\pm} \rightarrow W^\pm W^\pm$ in 35.9 fb^{-1} of pp collisions at $E_{cm} = 13$ TeV. See their Fig. 3 for limits on cross section times branching ratio for $m_{H^{\pm\pm}}$ between 200 and 1000 GeV.

13 KANEMURA 15 examine the case where H^{++} decays preferentially to $W^{(*)}W^{(*)}$ and estimate that a lower mass limit of ~ 84 GeV can be derived from the same-sign dilepton data of AAD 15AG if H^{++} decays with 100% branching ratio to $W^{(*)}W^{(*)}$.

14 KHACHATRYAN 15D search for $H^{\pm\pm}$ production by vector boson fusion followed by the decay $H^{\pm\pm} \rightarrow W^\pm W^\pm$ in 19.4 fb^{-1} of pp collisions at $E_{cm} = 8$ TeV. See their Fig. 4 for limits on cross section times branching ratio for $m_{H^{++}}$ between 160 and 800 GeV.

15 KANEMURA 14 examine the case where H^{++} decays preferentially to $W^{(*)}W^{(*)}$ and estimate that a lower mass limit of ~ 60 GeV can be derived from the same-sign dilepton data of AAD 12cy.

16 AAD 13y search for $H^{++}H^{--}$ production in a generic search of events with three charged leptons in 4.6 fb^{-1} of pp collisions at $E_{cm} = 7$ TeV. The limit assumes 100% branching ratio to the specified final state.

17 AAD 12ay search for $H^{++}H^{--}$ production with 1.6 fb^{-1} of pp collisions at $E_{cm} = 7$ TeV. The limit assumes 100% branching ratio to the specified final state.

18 AAD 12cq search for $H^{++}H^{--}$ production with 4.7 fb^{-1} of pp collisions at $E_{cm} = 7$ TeV. The limit assumes 100% branching ratio to the specified final state. See their Table 1 for limits assuming smaller branching ratios.

19 ABAZOV 12a search for $H^{++}H^{--}$ production in 7.0 fb^{-1} of $p\bar{p}$ collisions at $E_{cm} = 1.96$ TeV.

20 AALTONEN 11af search for $H^{++}H^{--}$ production in 6.1 fb^{-1} of $p\bar{p}$ collisions at $E_{cm} = 1.96$ TeV.

21 AALTONEN 08aa search for $H^{++}H^{--}$ production in $p\bar{p}$ collisions at $E_{cm} = 1.96$ TeV. The limit assumes 100% branching ratio to the specified final state.

22 ABAZOV 08v search for $H^{++}H^{--}$ production in $p\bar{p}$ collisions at $E_{cm} = 1.96$ TeV. The limit is for $B(H \rightarrow \mu\mu) = 1$. The limit is updated in ABAZOV 12a.

23 AKTAS 06a search for single $H^{\pm\pm}$ production in $e\bar{p}$ collisions at HERA. Assuming that H^{++} only couples to $e^+\mu^+$ with $g_{e\mu} = 0.3$ (electromagnetic strength), a limit $m_{H^{++}} > 141$ GeV (95% CL) is derived. For the case where H^{++} couples to $e\tau$ only the limit is 112 GeV.

24 ACOSTA 05l search for $H^{++}H^{--}$ pair production in $p\bar{p}$ collisions. The limit is valid for $g_{\ell\ell'} < 10^{-8}$ so that the Higgs decays outside the detector.

25 ABAZOV 04e search for $H^{++}H^{--}$ pair production in $H^{\pm\pm} \rightarrow \mu^\pm \mu^\pm$. The limit is valid for $g_{\mu\mu} \gtrsim 10^{-7}$.

26 ABBIENDI 03q searches for single $H^{\pm\pm}$ via direct production in $e^+e^- \rightarrow e^\mp e^\mp H^{\pm\pm}$, and via t-channel exchange in $e^+e^- \rightarrow e^+e^-$. In the direct case, and assuming $B(H^{\pm\pm} \rightarrow \ell^\pm \ell^\pm) = 1$, a 95% CL limit on $h_{ee} < 0.071$ is set for $m_{H^{\pm\pm}} < 160$ GeV (see Fig. 6). In the second case, indirect limits on h_{ee} are set for $m_{H^{\pm\pm}} < 2$ TeV (see Fig. 8).

27 GORDEEV 97 search for muonium-antimuonium conversion and find $G_{MM}/G_F < 0.14$ (90% CL), where G_{MM} is the lepton-flavor violating effective four-fermion coupling. This limit may be converted to $m_{H^{++}} > 210$ GeV if the Yukawa couplings of H^{++} to ee and $\mu\mu$ are as large as the weak gauge coupling. For similar limits on muonium-antimuonium conversion, see the muon Particle Listings.

28 ASAKA 95 point out that H^{++} decays dominantly to four fermions in a large region of parameter space where the limit of ACTON 92M from the search of dilepton modes does not apply.

29 ACTON 92M limit assumes $H^{\pm\pm} \rightarrow \ell^\pm \ell^\pm$ or $H^{\pm\pm}$ does not decay in the detector. Thus the region $g_{\ell\ell} \approx 10^{-7}$ is not excluded.

30 ACTON 92M from $\Delta\Gamma_Z < 40$ MeV.

31 SWARTZ 90 assume $H^{\pm\pm} \rightarrow \ell^\pm \ell^\pm$ (any flavor). The limits are valid for the Higgs-lepton coupling $g(H\ell\ell) \gtrsim 7.4 \times 10^{-7} / [m_{H^\pm}/\text{GeV}]^{1/2}$. The limits improve somewhat for ee and $\mu\mu$ decay modes.

Limits for $H^{\pm\pm}$ with $T_3 = 0$

VALUE (GeV)	CL%	DOCUMENT ID	TECN	COMMENT
> 58	95	1 AABOUD	18bC ATLS	ee
>723	95	1 AABOUD	18bC ATLS	$\mu\mu$
>402	95	2 AAD	15AG ATLS	$e\mu$
>290	95	3 AAD	15AP ATLS	$e\tau$
>290	95	3 AAD	15AP ATLS	$\mu\tau$
> 97.3	95	4 ABDALLAH	03 DLPH	$\tau\tau$
> 97.3	95	5 ACHARD	03F L3	$\tau\tau$
> 98.5	95	6 ABBIENDI	02c OPAL	$\tau\tau$
••• We do not use the following data for averages, fits, limits, etc. •••				
>374	95	2 AAD	15AG ATLS	ee
>438	95	2 AAD	15AG ATLS	$\mu\mu$
>251	95	7 AAD	12AY ATLS	$\mu\mu$
>306	95	8 AAD	12CQ ATLS	$\mu\mu$
>310	95	8 AAD	12CQ ATLS	$e\mu$
>322	95	8 AAD	12CQ ATLS	ee
>113	95	9 ABAZOV	12A D0	$\mu\tau$

Gauge & Higgs Boson Particle Listings

Charged Higgs Bosons (H^\pm and $H^{\pm\pm}$), Searches for, New Heavy Bosons

>205	95	10	AALTONEN	11AF	CDF	$\mu\mu$	15BF JHEP 1512 178	V. Khachatryan et al.	(CMS Collab.)
>190	95	10	AALTONEN	11AF	CDF	$e\mu$	15D PRL 114 051801	V. Khachatryan et al.	(CMS Collab.)
>205	95	10	AALTONEN	11AF	CDF	ee	14M PR D89 032002	G. Aad et al.	(ATLAS Collab.)
>145	95	11	ABAZOV	08V	D0	$\mu\mu$	14 PR D89 091101	T. Aaltonen et al.	(CDF Collab.)
							14 PR D90 115018	S. Kanemura et al.	
							13AC EPJ C73 2465	G. Aad et al.	(ATLAS Collab.)
							13V JHEP 1303 076	G. Aad et al.	(ATLAS Collab.)
							13Y PR D87 052002	G. Aad et al.	(ATLAS Collab.)
							13 EPJ C73 2552	M. Carena et al.	
							13 EPJ C73 2463	LEP Collabs	(ALEPH, DELPHI, L3, OPAL, LEP)
							12AY PR D85 032004	G. Aad et al.	(ATLAS Collab.)
							12BH JHEP 1206 039	G. Aad et al.	(ATLAS Collab.)
							12CQ EPJ C72 2244	G. Aad et al.	(ATLAS Collab.)
							12CY JHEP 1212 007	G. Aad et al.	(ATLAS Collab.)
							12 PRL 108 021801	V.M. Abazov et al.	(DO Collab.)
							12 EPJ C72 2076	G. Abbiendi et al.	(OPAL Collab.)
							12AA JHEP 1207 143	S. Chatrchyan et al.	(CMS Collab.)
							12AU EPJ C72 2189	S. Chatrchyan et al.	(CMS Collab.)
							11AF PRL 107 181801	T. Aaltonen et al.	(CDF Collab.)
							11P PRL 107 031801	T. Aaltonen et al.	(CDF Collab.)
							10 PR D82 073012	O. Deschamps et al.	(CLER, ORSAY, LAPP)
							09AJ PRL 103 101803	T. Aaltonen et al.	(CDF Collab.)
							09AC PR D80 051107	V.M. Abazov et al.	(DO Collab.)
							09AG PR D80 071102	V.M. Abazov et al.	(DO Collab.)
							09AI PL B682 278	V.M. Abazov et al.	(DO Collab.)
							09P PRL 102 191802	V.M. Abazov et al.	(DO Collab.)
							08AA PRL 101 121801	T. Aaltonen et al.	(CDF Collab.)
							08V PRL 101 071803	V.M. Abazov et al.	(DO Collab.)
							06E PRL 96 042003	A. Abulencia et al.	(CDF Collab.)
							06A PL B638 432	A. Aktas et al.	(HI Collab.)
							05L PRL 95 071801	D. Acosta et al.	(CDF Collab.)
							04E PRL 93 141801	V.M. Abazov et al.	(DO Collab.)
							04 EPJ C32 453	G. Abbiendi et al.	(OPAL Collab.)
							04 EPJ C34 399	J. Abdallah et al.	(DELPHI Collab.)
							03 PL B551 35	G. Abbiendi et al.	(OPAL Collab.)
							03 PL B577 93	G. Abbiendi et al.	(OPAL Collab.)
							03 PL B552 127	J. Abdallah et al.	(DELPHI Collab.)
							03E PL B575 208	P. Achard et al.	(L3 Collab.)
							03F PL B576 18	P. Achard et al.	(L3 Collab.)
							02B PRL 88 151803	V.M. Abazov et al.	(DO Collab.)
							02C PL B526 221	G. Abbiendi et al.	(OPAL Collab.)
							02 PL B549 170	F.M. Borzumali, A. Djouadi	
							02P EPJ C61 1	A. Heister et al.	(ALEPH Collab.)
							01E PL B520 1	G. Abbiendi et al.	(OPAL Collab.)
							01E EPJ C19 213	R. Barate et al.	(ALEPH Collab.)
							01 NP B611 338	P. Gambino, M. Misiak	
							01 PR D62 012004	T. Affolder et al.	(CDF Collab.)
							00 EPJ C15 1	D.E. Groom et al.	(PDG Collab.)
							99E EPJ C7 407	G. Abbiendi et al.	(OPAL Collab.)
							99E PRL 82 4975	B. Abbott et al.	(DO Collab.)
							99D EPJ C8 3	K. Ackerstaff et al.	(OPAL Collab.)
							97L PRL 79 357	F. Abe et al.	(CDF Collab.)
							97 PL B396 327	M. Acclari et al.	(L3 Collab.)
							97B PRL 78 4886	R. Ammar et al.	(CLEO Collab.)
							97 PL B406 337	J.A. Coarasa, R.A. Jimenez, J. Sola	
							97 PAN 60 1164	V.A. Gordeev et al.	(PNPI)
							Translated from YAF 60 1291.		
							97 PR D55 7263	M. Guchait, D.P. Roy	(TATA)
							97 PL B410 299	M. Mangano, S. Slabospitsky	
							97 ZPHY C74 73	A. Stahl, H. Voss	(BONN)
							96 PR D54 1	R. M. Barnett et al.	(PDG Collab.)
							95 PRL 74 2885	M.S. Alam et al.	(CLEO Collab.)
							95 PL B345 36	T. Asaka, K.I. Hikasa	(TOHOK)
							95 PL B343 444	D. Buskulic et al.	(ALEPH Collab.)
							95B PL B357 630	Y. Grossman, H. Haber, Y. Nir	
							94 PL B332 373	Y. Grossman, Z. Ligeti	
							94 PL B324 121	A. Stahl	(BONN)
							92M PL B295 347	P.D. Acton et al.	(OPAL Collab.)
							90 PRL 64 2877	M.L. Swartz et al.	(Mark II Collab.)

- 1 See their Figs. 12(b) and 14 for limits with smaller branching ratios.
- 2 AAD 15AG search for $H^{++}H^{--}$ production in 20.3 fb^{-1} of pp collisions at $E_{cm} = 8\text{ TeV}$. The limit assumes 100% branching ratio to the specified final state. See their Fig. 5 for limits for arbitrary branching ratios.
- 3 AAD 15AP search for $H^{++}H^{--}$ production in 20.3 fb^{-1} of pp collisions at $E_{cm} = 8\text{ TeV}$. The limit assumes 100% branching ratio to the specified final state.
- 4 ABDALLAH 03 search for $H^{++}H^{--}$ pair production either followed by $H^{++} \rightarrow \tau^+\tau^+$, or decaying outside the detector.
- 5 ACHARD 03F search for $e^+e^- \rightarrow H^{++}H^{--}$ with $H^{\pm\pm} \rightarrow \ell^\pm\ell^\pm$. The limit holds for $\ell = \ell' = \tau$, and slightly different limits apply for other flavor combinations. The limit is valid for $g_{\ell\ell} \gtrsim 10^{-7}$.
- 6 ABBIENDI 02c searches for pair production of $H^{++}H^{--}$, with $H^{\pm\pm} \rightarrow \ell^\pm\ell^\pm$ ($\ell, \ell' = e, \mu, \tau$), the limit holds for $\ell=\ell'=\tau$, and becomes stronger for other combinations of leptonic final states. To ensure the decay within the detector, the limit only applies for $g(H\ell\ell) \gtrsim 10^{-7}$.
- 7 AAD 12AY search for $H^{++}H^{--}$ production with 1.6 fb^{-1} of pp collisions at $E_{cm} = 7\text{ TeV}$. The limit assumes 100% branching ratio to the specified final state.
- 8 AAD 12CQ search for $H^{++}H^{--}$ production with 4.7 fb^{-1} of pp collisions at $E_{cm} = 7\text{ TeV}$. The limit assumes 100% branching ratio to the specified final state. See their Table 1 for limits assuming smaller branching ratios.
- 9 ABAZOV 12A search for $H^{++}H^{--}$ production in 6.1 fb^{-1} of $p\bar{p}$ collisions at $E_{cm} = 1.96\text{ TeV}$.
- 10 AALTONEN 11AF search for $H^{++}H^{--}$ production in 6.1 fb^{-1} of $p\bar{p}$ collisions at $E_{cm} = 1.96\text{ TeV}$.
- 11 ABAZOV 08V search for $H^{++}H^{--}$ production in $p\bar{p}$ collisions at $E_{cm} = 1.96\text{ TeV}$. The limit is for $B(H \rightarrow \mu\mu) = 1$. The limit is updated in ABAZOV 12A.
- 12 AKTAS 06A search for single $H^{\pm\pm}$ production in ep collisions at HERA. Assuming that H^{++} only couples to $e^+\mu^+$ with $g_{e\mu} = 0.3$ (electromagnetic strength), a limit $m_{H^{++}} > 141\text{ GeV}$ (95% CL) is derived. For the case where H^{++} couples to $e\tau$ only the limit is 112 GeV .
- 13 ACOSTA 05L search for $H^{++}H^{--}$ pair production in $p\bar{p}$ collisions. The limit is valid for $g_{\ell\ell} < 10^{-8}$ so that the Higgs decays outside the detector.
- 14 ABAZOV 04E search for $H^{++}H^{--}$ pair production in $H^{\pm\pm} \rightarrow \mu^\pm\mu^\pm$. The limit is valid for $g_{\mu\mu} \gtrsim 10^{-7}$.
- 15 ABBIENDI 03Q searches for single $H^{\pm\pm}$ via direct production in $e^+e^- \rightarrow e\bar{\nu}e\bar{F}H^{\pm\pm}$, and via t -channel exchange in $e^+e^- \rightarrow e^+e^-$. In the direct case, and assuming $B(H^{\pm\pm} \rightarrow \ell^\pm\ell^\pm) = 1$, a 95% CL limit on $h_{ee} < 0.071$ is set for $m_{H^{\pm\pm}} < 160\text{ GeV}$ (see Fig. 6). In the second case, indirect limits on h_{ee} are set for $m_{H^{\pm\pm}} < 2\text{ TeV}$ (see Fig. 8).
- 16 GORDEEV 97 search for muonium-antimuonium conversion and find $G_{M\bar{M}}/G_F < 0.14$ (90% CL), where $G_{M\bar{M}}$ is the lepton-flavor violating effective four-fermion coupling. This limit may be converted to $m_{H^{++}} > 210\text{ GeV}$ if the Yukawa couplings of H^{++} to ee and $\mu\mu$ are as large as the weak gauge coupling. For similar limits on muonium-antimuonium conversion, see the muon Particle Listings.
- 17 ACTON 92M limit assumes $H^{\pm\pm} \rightarrow \ell^\pm\ell^\pm$ or $H^{\pm\pm}$ does not decay in the detector. Thus the region $g_{\ell\ell} \approx 10^{-7}$ is not excluded.
- 18 ACTON 92M from $\Delta Z < 40\text{ MeV}$.
- 19 SWARTZ 90 assume $H^{\pm\pm} \rightarrow \ell^\pm\ell^\pm$ (any flavor). The limits are valid for the Higgs-lepton coupling $g(H\ell\ell) \gtrsim 7.4 \times 10^{-7} / [m_H/\text{GeV}]^{1/2}$. The limits improve somewhat for ee and $\mu\mu$ decay modes.

H^\pm and $H^{\pm\pm}$ REFERENCES

AAD	21U	JHEP	2106	146	G. Aad et al.	(ATLAS Collab.)
AAD	21V	JHEP	2106	145	G. Aad et al.	(ATLAS Collab.)
SIRUNYAN	21W	EPJ	C81	723	A.M. Sirunyan et al.	(CMS Collab.)
AAD	20W	JHEP	2006	151	G. Aad et al.	(ATLAS Collab.)
SIRUNYAN	20A0	JHEP	2007	126	A.M. Sirunyan et al.	(CMS Collab.)
SIRUNYAN	20AV	JHEP	2001	096	A.M. Sirunyan et al.	(CMS Collab.)
SIRUNYAN	20BE	PR	D102	072001	A.M. Sirunyan et al.	(CMS Collab.)
AABOUD	19K	EPJ	C79	58	M. Aaboud et al.	(ATLAS Collab.)
SIRUNYAN	19AH	JHEP	1907	142	A.M. Sirunyan et al.	(CMS Collab.)
SIRUNYAN	19BP	PL	B795	281	A.M. Sirunyan et al.	(CMS Collab.)
SIRUNYAN	19CC	PRL	123	131802	A.M. Sirunyan et al.	(CMS Collab.)
SIRUNYAN	19CQ	PL	B798	134985	A.M. Sirunyan et al.	(CMS Collab.)
AABOUD	18BC	EPJ	C78	199	M. Aaboud et al.	(ATLAS Collab.)
AABOUD	18BW	JHEP	1809	139	M. Aaboud et al.	(ATLAS Collab.)
AABOUD	18CD	JHEP	1811	085	M. Aaboud et al.	(ATLAS Collab.)
AABOUD	18CH	PL	B787	68	M. Aaboud et al.	(ATLAS Collab.)
HALLER	18	EPJ	C78	675	J. Haller et al.	(Glitter Group)
SIRUNYAN	18CC	PRL	120	081801	A.M. Sirunyan et al.	(CMS Collab.)
SIRUNYAN	18DO	JHEP	1811	115	A.M. Sirunyan et al.	(CMS Collab.)
MISIANK	17	EPJ	C77	201	M. Misiak, M. Steinhauser	
SIRUNYAN	17AE	PRL	119	141802	A.M. Sirunyan et al.	(CMS Collab.)
AABOUD	16A	PL	B759	555	M. Aaboud et al.	(ATLAS Collab.)
AAD	16AJ	JHEP	1603	127	G. Aad et al.	(ATLAS Collab.)
AAD	15AF	JHEP	1503	088	G. Aad et al.	(ATLAS Collab.)
AAD	15AG	JHEP	1503	041	G. Aad et al.	(ATLAS Collab.)
AAD	15AP	JHEP	1508	138	G. Aad et al.	(ATLAS Collab.)
AAD	15M	PRL	114	231801	G. Aad et al.	(ATLAS Collab.)
KANEMURA	15	PTEP	2015	051B02	S. Kanemura et al.	
KHACHATRYAN	15AX	JHEP	1511	018	V. Khachatryan et al.	(CMS Collab.)

New Heavy Bosons ($W', Z', \text{leptoquarks, etc.}$), Searches for

We list here various limits on charged and neutral heavy vector bosons (other than W 's and Z 's), heavy scalar bosons (other than Higgs bosons), vector or scalar leptoquarks, and axigluons. The latest unpublished results are described in "W' Searches" and "Z' Searches" reviews. For recent searches on scalar bosons which could be identified as Higgs bosons, see the listings in the Higgs boson section.

CONTENTS:

- Mass Limits for W' (Heavy Charged Vector Boson Other Than W) in Hadron Collider Experiments
- W_R (Right-Handed W Boson) Mass Limits
- Limit on W_L - W_R Mixing Angle ζ
- Mass Limits for Z' (Heavy Neutral Vector Boson Other Than Z)
 - Limits for Z'_{SM}
 - Limits for Z'_{LR}
 - Limits for Z'_{χ}
 - Limits for Z'_{ψ}
 - Limits for Z'_η
 - Limits for other Z'
 - Searches for Z' with Lepton-Flavor-Violating decays
- Indirect Constraints on Kaluza-Klein Gauge Bosons
- Mass Limits for Leptoquarks from Pair Production
- Mass Limits for Leptoquarks from Single Production
- Indirect Limits for Leptoquarks
- Mass Limits for Diquarks
- Mass Limits for g_A (axigluon) and Other Color-Octet Gauge Bosons
- Mass Limits for Color-Octet Scalar Bosons
- X^0 (Heavy Boson) Searches in Z Decays

See key on page 1127

Gauge & Higgs Boson Particle Listings

New Heavy Bosons

Mass Limits for a Heavy Neutral Boson Coupling to e^+e^-
 Search for X^0 Resonance in e^+e^- Collisions
 Search for X^0 Resonance in $e p$ Collisions
 Search for X^0 Resonance in Two-Photon Process
 Search for X^0 Resonance in $e^+e^- \rightarrow X^0 \gamma$
 Search for X^0 Resonance in $Z \rightarrow f \bar{f} X^0$
 Search for X^0 Resonance in $W X^0$ final state
 Search for X^0 Resonance in Quarkonium Decays

See the related review(s):

[W'-Boson Searches](#)

MASS LIMITS for W' (Heavy Charged Vector Boson Other Than W) in Hadron Collider Experiments

Couplings of W' to quarks and leptons are taken to be identical with those of W . The following limits are obtained from $p\bar{p}$ or $pp \rightarrow W' X$ with W' decaying to the mode indicated in the comments. New decay channels (e.g., $W' \rightarrow WZ$) are assumed to be suppressed. The most recent preliminary results can be found in the "W'-boson searches" review above.

VALUE (GeV)	CL%	DOCUMENT ID	TECN	COMMENT
>6000 (CL = 95%) OUR LIMIT				
none 1000-3400	95	1 SIRUNYAN	21Y CMS	$W' \rightarrow tb$
>3200	95	2 AAD	20AJ ATLS	$W' \rightarrow WH$
>4300	95	3 AAD	20AT ATLS	$W' \rightarrow WZ$
none 1100-4000	95	4 AAD	20T ATLS	$W' \rightarrow q\bar{q}$
none 1800-3600	95	5 SIRUNYAN	20AI CMS	$W' \rightarrow q\bar{q}$
none 1200-3800	95	6 SIRUNYAN	20Q CMS	$W' \rightarrow WZ$
		7 AABOUD	19B ATLS	$W' \rightarrow N\ell \rightarrow \ell\ell j$
		8 AABOUD	19E ATLS	$W' \rightarrow tb$
none 500-3250	95	9 AAD	19c ATLS	$W' \rightarrow \nu\nu, \mu\nu$
>6000	95	10 AAD	19D ATLS	$W' \rightarrow WZ$
none 1300-3600	95	11 SIRUNYAN	19AY CMS	$W' \rightarrow \tau\nu$
none 400-4000	95	12 SIRUNYAN	19CP CMS	$W' \rightarrow WZ, WH, \ell\nu$
>4300	95	13 SIRUNYAN	19I CMS	$W' \rightarrow WH$
>2600	95	14 AABOUD	18AF ATLS	$W' \rightarrow tb$
none 1000-3000	95	15 AABOUD	18AI ATLS	$W' \rightarrow WH$
none 500-2820	95	16 AABOUD	18AK ATLS	$W' \rightarrow WZ$
none 300-3000	95	17 AABOUD	18AL ATLS	$W' \rightarrow WZ$
none 800-3200	95	18 AABOUD	18BG ATLS	$W' \rightarrow \nu\nu, \mu\nu$
>5100	95	19 AABOUD	18CH ATLS	$W' \rightarrow WZ$
none 250-2460	95	20 AABOUD	18F ATLS	$W' \rightarrow WZ$
none 1200-3300	95	21 AABOUD	18K ATLS	$W' \rightarrow \tau\nu$
none 500-3700	95	22 SIRUNYAN	18 CMS	$W' \rightarrow tb$
none 1000-3600	95	23 SIRUNYAN	18AX CMS	$W' \rightarrow WZ$
none 1000-3050	95	24 SIRUNYAN	18AZ CMS	$W' \rightarrow \nu\nu, \mu\nu$
none 400-5200	95	25 SIRUNYAN	18BK CMS	$W' \rightarrow WZ$
none 1000-3400	95	26 SIRUNYAN	18BO CMS	$W' \rightarrow q\bar{q}$
none 600-3300	95	27 SIRUNYAN	18CV CMS	$W' \rightarrow N\ell \rightarrow \ell\ell j$
none 900-4400	95	28 SIRUNYAN	18DJ CMS	$W' \rightarrow WZ$
none 800-2330	95	29 SIRUNYAN	18ED CMS	$W' \rightarrow WH$
>2800	95	30 SIRUNYAN	18P CMS	$W' \rightarrow WZ$
none 1200-3200, 3300-3600	95	31 AABOUD	17AK ATLS	$W' \rightarrow q\bar{q}$
>3600	95	32 AABOUD	17AO ATLS	$W' \rightarrow WH$
none 1100-2500	95	33 AABOUD	17B ATLS	$W' \rightarrow WH$
>2220	95	34 KHACHATRY..17J	CMS	$W' \rightarrow N_\tau \tau \rightarrow \tau\tau jj$
>2300	95	35 KHACHATRY..17W	CMS	$W' \rightarrow q\bar{q}$
none 600-2700	95	36 KHACHATRY..17Z	CMS	$W' \rightarrow \nu\nu, \mu\nu$
>4100	95	37 SIRUNYAN	17A CMS	$W' \rightarrow WZ$
>2200	95	38 SIRUNYAN	17AK CMS	$W' \rightarrow WZ, WH$
>2300	95	39 SIRUNYAN	17H CMS	$W' \rightarrow \tau N$
>2900	95	40 SIRUNYAN	17I CMS	$W' \rightarrow tb$
>2600	95	41 SIRUNYAN	17R CMS	$W' \rightarrow WH$
>2450	95	42 SIRUNYAN	17R CMS	$W' \rightarrow WH$
none 2780-3150	95	43 AABOUD	16AE ATLS	$W' \rightarrow WZ$
>2600	95	44 AABOUD	16V ATLS	$W' \rightarrow \nu\nu, \mu\nu$
>4070	95	45 AAD	16R ATLS	$W' \rightarrow WZ$
>1810	95	46 AAD	16S ATLS	$W' \rightarrow q\bar{q}$
>2600	95	47 KHACHATRY..16AO	CMS	$W' \rightarrow tb$
>2150	95	48 KHACHATRY..16AP	CMS	$W' \rightarrow WH$
none 1000-1600	95	49 KHACHATRY..16BD	CMS	$W' \rightarrow WH \rightarrow b\bar{b}\ell\nu$
none 800-1500	95	50 KHACHATRY..16K	CMS	$W' \rightarrow q\bar{q}$
none 1500-2600	95	51 KHACHATRY..16L	CMS	$W' \rightarrow q\bar{q}$
none 500-1600	95	52 AAD	15AU ATLS	$W' \rightarrow \tau\nu$
none 300-2700	95	53 AAD	15AV ATLS	$W' \rightarrow WZ$
none 400-1590	95	54 AAD	15AZ ATLS	$W' \rightarrow tb$
none 1500-1760	95	55 AAD	15CP ATLS	$W' \rightarrow WZ$
none 300-1490	95	56 AAD	15R ATLS	$W' \rightarrow tb$
none 1300-1500	95	57 AAD	15V ATLS	$W' \rightarrow q\bar{q}$
none 500-1920	95	58 KHACHATRY..15c	CMS	$W' \rightarrow WZ$
none 800-2450	95	59 KHACHATRY..15T	CMS	$W' \rightarrow \nu\nu, \mu\nu$
>1470	95	60 KHACHATRY..14o	CMS	$W' \rightarrow N\ell \rightarrow \ell\ell j$
>3710	95			
none 1000-3010	95			

• • • We do not use the following data for averages, fits, limits, etc. • • •

61 AAD	20AD ATLS	$W' \rightarrow JJ$
62 AAD	20W ATLS	$W' \rightarrow WZ' \rightarrow \ell\nu q\bar{q}$
63 AABOUD	19BB ATLS	$W' \rightarrow N\ell \rightarrow j\ell\ell$
64 SIRUNYAN	19v CMS	$W' \rightarrow Bt, Tb$
65 AABOUD	18AA ATLS	$W' \rightarrow W\gamma$
66 AABOUD	18AD ATLS	$W' \rightarrow HX$
67 AABOUD	18CJ ATLS	$W' \rightarrow WZ, WH, \ell\nu$
68 KHACHATRY..17U	CMS	$W' \rightarrow WH$
69 AAD	15BB ATLS	$W' \rightarrow WH$
70 AALTONEN	15c CDF	$W' \rightarrow tb$
71 KHACHATRY..15v	CMS	$W' \rightarrow q\bar{q}$
>4500	95	
none 300-880	95	
none 1200-1900 and 2000-2200	95	
>3240	95	
none 200-1520	95	
none 1000-1700	95	
none 500-950	95	
none 1100-1680	95	
none 1000-1920	95	
>2900	95	
none 800-1510	95	
none 700-940	95	
none 700-1130	95	
none 200-760	95	
>2550	95	
none 200-1143	95	
>1120	95	
none 180-690	95	
none 600-863	95	
none 285-516	95	
none 280-840	95	
>1000	95	
none 300-800	95	
none 225-536	95	
none 200-480	95	
> 786	95	
none 300-420	95	
> 720	95	
> 610	95	
none 260-600	95	
61 AAD	20AD ATLS	$W' \rightarrow JJ$
62 AAD	20W ATLS	$W' \rightarrow WZ' \rightarrow \ell\nu q\bar{q}$
63 AABOUD	19BB ATLS	$W' \rightarrow N\ell \rightarrow j\ell\ell$
64 SIRUNYAN	19v CMS	$W' \rightarrow Bt, Tb$
65 AABOUD	18AA ATLS	$W' \rightarrow W\gamma$
66 AABOUD	18AD ATLS	$W' \rightarrow HX$
67 AABOUD	18CJ ATLS	$W' \rightarrow WZ, WH, \ell\nu$
68 KHACHATRY..17U	CMS	$W' \rightarrow WH$
69 AAD	15BB ATLS	$W' \rightarrow WH$
70 AALTONEN	15c CDF	$W' \rightarrow tb$
71 KHACHATRY..15v	CMS	$W' \rightarrow q\bar{q}$
AAD	14AI ATLS	$W' \rightarrow \nu\nu, \mu\nu$
AAD	14AT ATLS	$W' \rightarrow W\gamma$
AAD	14S ATLS	$W' \rightarrow WZ$
KHACHATRY..14	CMS	$W' \rightarrow WZ$
KHACHATRY..14A	CMS	$W' \rightarrow WZ$
AAD	13AO ATLS	$W' \rightarrow WZ$
AAD	13D ATLS	$W' \rightarrow q\bar{q}$
CHATRCHYAN 13A	CMS	$W' \rightarrow q\bar{q}$
CHATRCHYAN 13AJ	CMS	$W' \rightarrow WZ$
CHATRCHYAN 13AQ	CMS	$W' \rightarrow \nu\nu, \mu\nu$
CHATRCHYAN 13E	CMS	$W' \rightarrow tb$
CHATRCHYAN 13U	CMS	$W' \rightarrow WZ$
AAD	12AV ATLS	$W' \rightarrow tb$
AAD	12BB ATLS	$W' \rightarrow WZ$
AAD	12CK ATLS	$W' \rightarrow \bar{\tau}q$
AAD	12CR ATLS	$W' \rightarrow \nu\nu, \mu\nu$
AAD	12M ATLS	$W' \rightarrow N\ell \rightarrow \ell\ell j$
AALTONEN	12N CDF	$W' \rightarrow \bar{\tau}q$
CHATRCHYAN 12AF	CMS	$W' \rightarrow WZ$
CHATRCHYAN 12AR	CMS	$W' \rightarrow \bar{\tau}q$
CHATRCHYAN 12BG	CMS	$W' \rightarrow N\ell \rightarrow \ell\ell j$
AALTONEN	11c CDF	$W' \rightarrow \nu\nu$
ABAZOV	11H D0	$W' \rightarrow WZ$
ABAZOV	11L D0	$W' \rightarrow tb$
AALTONEN	10N CDF	$W' \rightarrow WZ$
AALTONEN	09AC CDF	$W' \rightarrow q\bar{q}$
ABAZOV	08c D0	$W' \rightarrow \nu\nu$
ABAZOV	04c D0	$W' \rightarrow q\bar{q}$
ACOSTA	03B CDF	$W' \rightarrow tb$
AFFOLDER	02c CDF	$W' \rightarrow WZ$
AFFOLDER	01i CDF	$W' \rightarrow \nu\nu, \mu\nu$
ABE	97G CDF	$W' \rightarrow q\bar{q}$
ABACHI	96c D0	$W' \rightarrow \nu\nu$
ABACHI	95E D0	$W' \rightarrow \nu\nu, \tau\nu$
RIZZO	93 RVUE	$W' \rightarrow q\bar{q}$

¹ SIRUNYAN 21y search for resonances decaying to tb in pp collisions at $\sqrt{s} = 13$ TeV. See their Fig. 2 for limits on $\sigma \cdot B(W' \rightarrow tb)$.

² AAD 20AJ search for resonances decaying to HW in pp collisions at $\sqrt{s} = 13$ TeV. The quoted limit is for heavy-vector-triplet W' with $g_V = 3$. The limit becomes $M_{W'} > 2900$ GeV for $g_V = 1$. See their Fig. 6 for limits on $\sigma \cdot B$.

³ AAD 20AT search for resonances decaying to WZ in pp collisions at $\sqrt{s} = 13$ TeV. The quoted limit is for heavy-vector-triplet W' with $g_V = 3$. The limit becomes $M_{W'} > 3900$ GeV for $g_V = 1$. See their Fig. 13 for limits on $\sigma \cdot B$.

⁴ AAD 20T search for W' with SM-like couplings in pp collisions at $\sqrt{s} = 13$ TeV. See their Fig. 4(c) for limits on the product of the cross section, acceptance, and branching fraction.

⁵ SIRUNYAN 20AI limit is for W' with SM-like coupling using pp collisions at $\sqrt{s} = 13$ TeV.

⁶ SIRUNYAN 20Q search for resonances decaying to WZ in pp collisions at $\sqrt{s} = 13$ TeV. The quoted limit is for heavy-vector-triplet W' with $g_V = 3$.

⁷ AABOUD 19B search for right-handed W_R in pp collisions at $\sqrt{s} = 13$ TeV. W_R is assumed to decay into ℓ and hypothetical heavy neutrino N , with N decaying to $\ell j j$. See their Figs. 7 and 8 for excluded regions in $M_{W_R} - M_N$ plane.

⁸ AABOUD 19E search for right-handed W' in pp collisions at $\sqrt{s} = 13$ TeV. See their Fig. 8 for limit on $\sigma \cdot B$.

⁹ AAD 19c search for W' with SM-like couplings in pp collisions at $\sqrt{s} = 13$ TeV. Bosonic decays and $W - W'$ interference are neglected. The limits on e and μ separately are 6.0 and 5.1 TeV respectively. See their Fig. 2 for limits on $\sigma \cdot B$.

¹⁰ AAD 19p search for resonances decaying to WZ in pp collisions at $\sqrt{s} = 13$ TeV. The quoted limit is for heavy-vector-triplet W' with $g_V = 3$. The limit becomes $M_{W'} > 3400$ GeV for $g_V = 1$. If we assume $M_{W'} = M_{Z'}$, the limit increases $M_{W'} > 3800$ GeV and $M_{W'} > 3500$ GeV for $g_V = 3$ and $g_V = 1$, respectively. See their Fig. 9 for limits on $\sigma \cdot B$.

¹¹ SIRUNYAN 19AY limits shown for W' with SM-like coupling using pp collisions at $\sqrt{s} = 13$ TeV. $W - W'$ interference and bosonic decays of W' are not included. See their Fig. 5 for limits on $\sigma \cdot B$. Limits in the context of a nonuniversal gauge interaction are shown in Fig. 7. Model independent limits on $\sigma B A e$ can be seen in Fig. 8.

¹² SIRUNYAN 19CP present a statistical combinations of searches for W' decaying to pairs of bosons or leptons in pp collisions at $\sqrt{s} = 13$ TeV. The quoted limit is for heavy-vector-triplet W' with $g_V = 3$. If we assume $M_{W'} = M_{Z'}$, the limit becomes $M_{W'} > 4500$ GeV for $g_V = 3$ and $M_{W'} > 5000$ GeV for $g_V = 1$. See their Figs. 2 and 3 for limits on $\sigma \cdot B$.

Gauge & Higgs Boson Particle Listings

New Heavy Bosons

- 13 SIRUNYAN 19I search for resonances decaying to HW in pp collisions at $\sqrt{s} = 13$ TeV. The quoted limit is for heavy-vector-triplet W' with $g_V = 3$. The limit becomes $M_{W'} > 2800$ GeV if we assume $M_{W'} = M_{Z'}$.
- 14 AABOUD 18AF give the limit above for right-handed W' using pp collisions at $\sqrt{s} = 13$ TeV. These limits also exclude W bosons with left-handed couplings with masses below 2.9 TeV, at the 95% confidence level. $W' \rightarrow \ell\nu_R$ is assumed to be forbidden. See their Fig. 5 for limits on $\sigma \cdot B$ for both cases of left- and right-handed W' .
- 15 AABOUD 18AI search for resonances decaying to HW in pp collisions at $\sqrt{s} = 13$ TeV. The quoted limit is for heavy-vector-triplet W' with $g_V = 3$. The limit becomes $M_{W'} > 2670$ GeV for $g_V = 1$. If we assume $M_{W'} = M_{Z'}$, the limit increases $M_{W'} > 2930$ GeV and $M_{W'} > 2800$ GeV for $g_V = 3$ and $g_V = 1$, respectively. See their Fig. 5 for limits on $\sigma \cdot B$.
- 16 AABOUD 18AL search for resonances decaying to WZ in pp collisions at $\sqrt{s} = 13$ TeV. The limit quoted above is for heavy-vector-triplet W' with $g_V = 3$. The limit becomes $M_{W'} > 2800$ GeV for $g_V = 1$.
- 17 AABOUD 18AL search for resonances decaying to WZ in pp collisions at $\sqrt{s} = 13$ TeV. The limit quoted above is for heavy-vector-triplet W' with $g_V = 3$. The limit becomes $M_{W'} > 2900$ GeV for $g_V = 1$.
- 18 AABOUD 18AG limit is for W' with SM-like couplings using pp collisions at $\sqrt{s} = 13$ TeV. Bosonic decays of W' and $W-W'$ interference are neglected. See Fig. 2 for limits on $\sigma \cdot B$.
- 19 AABOUD 18CH search for resonances decaying to WZ in pp collisions at $\sqrt{s} = 13$ TeV. The limit quoted above is for heavy-vector-triplet W' with $g_V = 3$. The limit becomes $M_{W'} > 2260$ GeV for $g_V = 1$.
- 20 AABOUD 18F search for resonances decaying to WZ in pp collisions at $\sqrt{s} = 13$ TeV. The quoted limit is for heavy-vector-triplet W' with $g_V = 3$. The limit becomes $M_{W'} > 3000$ GeV for $g_V = 1$. If we assume $M_{Z'} = M_{W'}$, the limit increases $M_{W'} > 3500$ GeV and $M_{W'} > 3100$ GeV for $g_V = 3$ and $g_V = 1$, respectively. See their Fig. 5 for limits on $\sigma \cdot B$.
- 21 AABOUD 18K limit is for W' with SM-like coupling using pp collisions at $\sqrt{s} = 13$ TeV. $W-W'$ interference and bosonic decays of W' are not included. See their Fig. 4 for limit on $\sigma \cdot B$.
- 22 SIRUNYAN 18 limit is for right-handed W' using pp collisions at $\sqrt{s} = 13$ TeV. $W' \rightarrow \ell\nu_R$ decay is assumed to be forbidden. The limit becomes $M_{W'} > 3.4$ TeV if $M_{\nu_R} \ll M_{W'}$. See their Fig. 5 for exclusion limits on W' models having both left- and right-handed couplings.
- 23 SIRUNYAN 18AX search for resonances decaying to WZ in pp collisions at $\sqrt{s} = 13$ TeV. The quoted limit is for heavy-vector-triplet W' with $g_V = 3$. See their Fig. 6 for limits on $\sigma \cdot B$.
- 24 SIRUNYAN 18AZ limit is derived for W' with SM-like coupling using pp collisions at $\sqrt{s} = 13$ TeV. No interference with SM W process is considered. The bosonic decays are assumed to be negligible. See their Fig. 6 for limits on $\sigma \cdot B$.
- 25 SIRUNYAN 18BK search for resonances decaying to WZ in pp collisions at $\sqrt{s} = 13$ TeV. The limit quoted above is for heavy-vector-triplet W' with $g_V = 3$. The limit becomes $M_{W'} > 3100$ GeV for $g_V = 1$.
- 26 SIRUNYAN 18BO limit is for W' with SM-like coupling using pp collisions at $\sqrt{s} = 13$ TeV.
- 27 SIRUNYAN 18CV search for right-handed W_R in pp collisions at $\sqrt{s} = 13$ TeV. W_R is assumed to decay into ℓ and hypothetical heavy neutrino N , with N decaying to ℓjj . The quoted limit is for $M_N = M_{W_R}/2$. See their Fig. 6 for excluded regions in the $M_{W_R} - M_N$ plane.
- 28 SIRUNYAN 18DJ search for resonances decaying to WZ in pp collisions at $\sqrt{s} = 13$ TeV. The limit quoted above is for heavy-vector-triplet W' with $g_V = 3$. The limit becomes $M_{W'} > 2270$ GeV for $g_V = 1$.
- 29 SIRUNYAN 18ED search for resonances decaying to HW in pp collisions at $\sqrt{s} = 13$ TeV. The limit above is for heavy-vector-triplet W' with $g_V = 3$. If we assume $M_{W'} = M_{Z'}$, the limit increases $M_{W'} > 2900$ GeV and $M_{W'} > 2800$ GeV for $g_V = 3$ and $g_V = 1$, respectively.
- 30 SIRUNYAN 18P give this limit for a heavy-vector-triplet W' with $g_V = 3$. If they assume $M_{Z'} = M_{W'}$, the limit increases to $M_{W'} > 3800$ GeV.
- 31 AABOUD 17AK search for a new resonance decaying to dijets in pp collisions at $\sqrt{s} = 13$ TeV. The limit above is for a W' boson having axial-vector SM couplings and decaying to quarks with 75% branching fraction.
- 32 AABOUD 17AO search for resonances decaying to HW in pp collisions at $\sqrt{s} = 13$ TeV. The limit quoted above is for a W' in the heavy-vector-triplet model with $g_V = 3$. See their Fig. 4 for limits on $\sigma \cdot B$.
- 33 AABOUD 17B search for resonances decaying to HW ($H \rightarrow b\bar{b}, c\bar{c}; W \rightarrow \ell\nu$) in pp collisions at $\sqrt{s} = 13$ TeV. The quoted limit is for heavy-vector-triplet W' with $g_V = 3$. The limit becomes $M_{W'} > 1750$ GeV for $g_V = 1$. If we assume $M_{W'} = M_{Z'}$, the limit increases $M_{W'} > 2310$ GeV and $M_{W'} > 1730$ GeV for $g_V = 3$ and $g_V = 1$, respectively. See their Fig. 3 for limits on $\sigma \cdot B$.
- 34 KHACHATRYAN 17J search for right-handed W_R in pp collisions at $\sqrt{s} = 13$ TeV. W_R is assumed to decay into τ and hypothetical heavy neutrino N_τ , with N_τ decaying into τjj . The quoted limit is for $M_{N_\tau} = M_{W_R}/2$. The limit becomes $M_{W_R} > 2350$ GeV (1630 GeV) for $M_{W_R}/M_{N_\tau} = 0.8$ (0.2). See their Fig. 4 for excluded regions in the $M_{W_R} - M_{N_\tau}$ plane.
- 35 KHACHATRYAN 17W search for resonances decaying to dijets in pp collisions at $\sqrt{s} = 13$ TeV.
- 36 KHACHATRYAN 17Z limit is for W' with SM-like coupling using pp collisions at $\sqrt{s} = 13$ TeV. The bosonic decays of W' and the interference with SM W process are neglected.
- 37 SIRUNYAN 17A search for resonances decaying to WZ with $WZ \rightarrow \ell\nu q\bar{q}, q\bar{q}q\bar{q}$ in pp collisions at $\sqrt{s} = 13$ TeV. The quoted limit is for heavy-vector-triplet W' with $g_V = 3$. The limit becomes $M_{W'} > 2000$ GeV for $g_V = 1$. If we assume $M_{Z'} = M_{W'}$, the limit increases $M_{W'} > 2400$ GeV and $M_{W'} > 2300$ GeV for $g_V = 3$ and $g_V = 1$, respectively. See their Fig. 6 for limits on $\sigma \cdot B$.
- 38 SIRUNYAN 17AK search for resonances decaying to WZ or HW in pp collisions at $\sqrt{s} = 8$ and 13 TeV. The quoted limit is for heavy-vector-triplet W' with $g_V = 3$. The limit becomes $M_{W'} > 2300$ GeV for $g_V = 1$. If we assume $M_{W'} = M_{Z'}$, the limit increases $M_{W'} > 2400$ GeV for both $g_V = 3$ and $g_V = 1$. See their Fig. 1 and 2 for limits on $\sigma \cdot B$.
- 39 SIRUNYAN 17H search for right-handed W' in pp collisions at $\sqrt{s} = 13$ TeV. W' is assumed to decay into τ and a heavy neutrino N , with N decaying to $\tau q\bar{q}$. The limit above assumes $M_N = M_{W'}/2$.
- 40 SIRUNYAN 17I limit is for a right-handed W' using pp collisions at $\sqrt{s} = 13$ TeV. The limit becomes $M_{W'} > 2400$ GeV for $M_{\nu_R} \ll M_{W'}$.
- 41 SIRUNYAN 17R search for resonances decaying to HW in pp collisions at $\sqrt{s} = 13$ TeV. The quoted limit is for heavy-vector-triplet W' with $g_V = 3$. Mass regions $M_{W'} < 2370$ GeV and $2870 < M_{W'} < 2970$ GeV are excluded for $g_V = 1$. If we assume $M_{Z'} = M_{W'}$, the excluded mass regions are $1000 < M_{W'} < 2500$ GeV and $2760 < M_{W'} < 3300$ GeV for $g_V = 3$; $1000 < M_{W'} < 2430$ GeV and $2810 < M_{W'} < 3130$ GeV for $g_V = 1$. See their Fig. 5 for limits on $\sigma \cdot B$.
- 42 AABOUD 16AE search for resonances decaying to VV ($V = W$ or Z) in pp collisions at $\sqrt{s} = 13$ TeV. Results from $\nu\nu q\bar{q}, \nu\ell q\bar{q}, \ell\ell q\bar{q}$ and $q\bar{q}q\bar{q}$ final states are combined. The quoted limit is for a heavy-vector-triplet W' with $g_V = 3$ and $M_{W'} = M_{Z'}$.
- 43 AABOUD 16V limit is for W' with SM-like coupling using pp collisions at $\sqrt{s} = 13$ TeV. The bosonic decays of W' and the interference with SM W process are neglected.
- 44 AAD 16R search for $W' \rightarrow WZ$ in pp collisions at $\sqrt{s} = 8$ TeV. $\ell\nu\ell'\ell', \ell\ell q\bar{q}, \ell\nu q\bar{q}$, and all hadronic channels are combined. The quoted limit assumes $g_{W'WZ}/g_{WWZ} = (M_W/M_{W'})^2$.
- 45 AAD 16S search for a new resonance decaying to dijets in pp collisions at $\sqrt{s} = 13$ TeV. The limit quoted above is for a W' having SM-like couplings to quarks.
- 46 KHACHATRYAN 16AO limit is for a SM-like right-handed W' using pp collisions at $\sqrt{s} = 8$ TeV. The quoted limit combines $t \rightarrow q\bar{q}b$ and $t \rightarrow \ell\nu b$ events.
- 47 KHACHATRYAN 16AP search for a resonance decaying to HW in pp collisions at $\sqrt{s} = 8$ TeV. Both H and W are assumed to decay to fat jets. The quoted limit is for heavy-vector-triplet W' with $g_V = 3$.
- 48 KHACHATRYAN 16BD search for resonance decaying to HW in pp collisions at $\sqrt{s} = 8$ TeV. The quoted limit is for heavy-vector-triplet (HVT) W' with $g_V = 3$. The HVT model $m_{W'} = m_{Z'} > 1.8$ TeV is also obtained by combining $W'/Z' \rightarrow WH/ZH \rightarrow \ell\nu b\bar{b}, q\bar{q}\tau\tau, q\bar{q}b\bar{b}$, and $q\bar{q}q\bar{q}q\bar{q}$ channels.
- 49 KHACHATRYAN 16K search for resonances decaying to dijets in pp collisions at $\sqrt{s} = 13$ TeV.
- 50 KHACHATRYAN 16L search for resonances decaying to dijets in pp collisions at $\sqrt{s} = 8$ TeV with the data scouting technique, increasing the sensitivity to the low mass resonances.
- 51 KHACHATRYAN 16O limit is for W' having universal couplings. Interferences with the SM amplitudes are assumed to be absent.
- 52 AAD 15AU search for W' decaying into the WZ final state with $W \rightarrow q\bar{q}'$, $Z \rightarrow \ell^+\ell^-$ using pp collisions at $\sqrt{s} = 8$ TeV. The quoted limit assumes $g_{W'WZ}/g_{WWZ} = (M_W/M_{W'})^2$.
- 53 AAD 15AV limit is for a SM like right-handed W' using pp collisions at $\sqrt{s} = 8$ TeV. $W' \rightarrow \ell\nu$ decay is assumed to be forbidden.
- 54 AAD 15AZ search for W' decaying into the WZ final state with $W \rightarrow \ell\nu$, $Z \rightarrow q\bar{q}$ using pp collisions at $\sqrt{s} = 8$ TeV. The quoted limit assumes $g_{W'WZ}/g_{WWZ} = (M_W/M_{W'})^2$.
- 55 AAD 15CP search for W' decaying into the WZ final state with $W \rightarrow q\bar{q}$, $Z \rightarrow q\bar{q}$ using pp collisions at $\sqrt{s} = 8$ TeV. The quoted limit assumes $g_{W'WZ}/g_{WWZ} = (M_W/M_{W'})^2$.
- 56 AAD 15R limit is for a SM like right-handed W' using pp collisions at $\sqrt{s} = 8$ TeV. $W' \rightarrow \ell\nu$ decay is assumed to be forbidden.
- 57 AAD 15V search for new resonance decaying to dijets in pp collisions at $\sqrt{s} = 8$ TeV.
- 58 KHACHATRYAN 15C search for W' decaying via WZ to fully leptonic final states using pp collisions at $\sqrt{s} = 8$ TeV. The quoted limit assumes $g_{W'WZ}/g_{WWZ} = M_W/M_{Z'}$.
- 59 KHACHATRYAN 15T limit is for W' with SM-like coupling which interferes the SM W boson constructively using pp collisions at $\sqrt{s} = 8$ TeV. For W' without interference, the limit becomes > 3280 GeV.
- 60 KHACHATRYAN 14O search for right-handed W_R in pp collisions at $\sqrt{s} = 8$ TeV. W_R is assumed to decay into ℓ and hypothetical heavy neutrino N , with N decaying into ℓjj . The quoted limit is for $M_{\nu_{eR}} = M_{\nu_{\mu R}} = M_{W_R}/2$. See their Fig. 3 and Fig. 5 for excluded regions in the $M_{W_R} - M_\nu$ plane.
- 61 AAD 20AD search for a narrow resonance decaying to a pair of large-radius-jets J_1 and J_2 employing a machine-learning procedure. See their Fig. 3 for limits on $\sigma \cdot B$ depending on assumptions about invariant masses for J_1, J_2 , and $J_1 J_2$.
- 62 AAD 20W search for W' decaying to WZ' in pp collisions at $\sqrt{s} = 13$ TeV. See their Fig. 5(b) for limits on $\sigma \cdot B$ as a function of $m_{Z'}$. The $W' \rightarrow WZ'$ branching fraction was chosen to be 0.5 and the mass difference between the W' and Z' was set to 250 GeV.
- 63 AABOUD 19BB search for right handed W_R in pp collisions at $\sqrt{s} = 13$ TeV. W_R is assumed to decay into ℓ and a boosted hypothetical heavy neutrino N , with N decaying to ℓ and a large radius jet $j = q\bar{q}$. See their Fig. 7 for excluded regions in $M_{W_R} - M_N$ plane.
- 64 SIRUNYAN 19V search for a new resonance decaying to a top quark and a heavy vector-like bottom partner B decaying to Hb (or a bottom quark and a heavy vector-like top partner T decaying to Ht) in pp collisions at $\sqrt{s} = 13$ TeV. See their Fig. 8 for limits on $\sigma \cdot B$.
- 65 AABOUD 18AA search for a narrow charged vector boson decaying to $W\gamma$. See their Fig. 9 for the exclusion limit in $M_{W'} - \sigma \cdot B$ plane.
- 66 AABOUD 18AD search for resonances decaying to HX ($H \rightarrow b\bar{b}, X \rightarrow q\bar{q}'$) in pp collisions at $\sqrt{s} = 13$ TeV. See their Figs. 3-5 for limits on $\sigma \cdot B$.

See key on page 1127

Gauge & Higgs Boson Particle Listings

New Heavy Bosons

- 67 AABOUD 18cJ search for heavy-vector-triplet W' in pp collisions at $\sqrt{s}=13$ TeV. The limit quoted above is for model with $g_V=3$ assuming $M_{W'}=M_{Z'}$. The limit becomes $M_{W'} > 5500$ GeV for model with $g_V=1$.
- 68 KHACHATRYAN 17u search for resonances decaying to HW ($H \rightarrow b\bar{b}$; $W \rightarrow \ell\nu$) in pp collisions at $\sqrt{s}=13$ TeV. The limit on the heavy-vector-triplet model is $M_{Z'} = M_{W'} > 2$ TeV for $g_V=3$, in which constraints from the $Z' \rightarrow HZ$ ($H \rightarrow b\bar{b}$; $Z \rightarrow \ell^+ \ell^-, \nu\bar{\nu}$) are combined. See their Fig.3 and Fig.4 for limits on $\sigma \cdot B$.
- 69 AAD 15bB search for W' decaying into WH with $W \rightarrow \ell\nu$, $H \rightarrow b\bar{b}$. See their Fig. 4 for the exclusion limits in the heavy vector triplet benchmark model parameter space.
- 70 AALTONEN 15c limit is for a SM-like right-handed W' assuming $W' \rightarrow \ell\nu$ decays are forbidden, using $p\bar{p}$ collisions at $\sqrt{s}=1.96$ TeV. See their Fig. 3 for limit on $g_{W'}/g_{WZ}$.
- 71 KHACHATRYAN 15v search new resonance decaying to dijets in pp collisions at $\sqrt{s}=8$ TeV.
- 72 AAD 14At search for a narrow charged vector boson decaying to $W\gamma$. See their Fig. 3a for the exclusion limit in $m_{W'} - \sigma B$ plane.
- 73 AAD 14s search for W' decaying into the WZ final state with $W \rightarrow \ell\nu$, $Z \rightarrow \ell\ell$ using pp collisions at $\sqrt{s}=8$ TeV. The quoted limit assumes $g_{W'WZ}/g_{WWZ} = (M_{W'}/M_{W'})^2$.
- 74 KHACHATRYAN 14 search for W' decaying into WZ final state with $W \rightarrow q\bar{q}$, $Z \rightarrow q\bar{q}$ using pp collisions at $\sqrt{s}=8$ TeV. The quoted limit assumes $g_{W'WZ}/g_{WWZ} = (M_{W'}/M_{W'})^2$.
- 75 KHACHATRYAN 14a search for W' decaying into the WZ final state with $W \rightarrow \ell\nu$, $Z \rightarrow q\bar{q}$, or $W \rightarrow q\bar{q}$, $Z \rightarrow \ell\ell$. pp collisions data at $\sqrt{s}=8$ TeV are used for the search. See their Fig. 13 for the exclusion limit on the number of events in the mass-width plane.
- 76 AAD 13aO search for W' decaying into the WZ final state with $W \rightarrow \ell\nu$, $Z \rightarrow 2j$ using pp collisions at $\sqrt{s}=7$ TeV. The quoted limit assumes $g_{W'WZ}/g_{WWZ} = (M_{W'}/M_{W'})^2$.
- 77 CHATRCHYAN 13aJ search for resonances decaying to WZ pair, using the hadronic decay modes of W and Z , in pp collisions at $\sqrt{s}=7$ TeV. See their Fig. 7 for the limit on the cross section.
- 78 CHATRCHYAN 13aQ limit is for W' with SM-like coupling which interferes with the SM W boson using pp collisions at $\sqrt{s}=7$ TeV.
- 79 CHATRCHYAN 13e limit is for W' with SM-like coupling which interferes with the SM W boson using pp collisions at $\sqrt{s}=7$ TeV. For W' with right-handed coupling, the bound becomes >1850 GeV (>1910 GeV) if W' decays to both leptons and quarks (only to quarks). If both left- and right-handed couplings are present, the limit becomes >1640 GeV.
- 80 CHATRCHYAN 13u search for W' decaying to the WZ final state, with W decaying into jets, in pp collisions at $\sqrt{s}=7$ TeV. The quoted limit assumes $g_{W'WZ}/g_{WWZ} = (M_{W'}/M_{W'})^2$.
- 81 The AAD 12aV quoted limit is for a SM-like right-handed W' using pp collisions at $\sqrt{s}=7$ TeV. $W' \rightarrow \ell\nu$ decay is assumed to be forbidden.
- 82 AAD 12bB use pp collisions data at $\sqrt{s}=7$ TeV. The quoted limit assumes $g_{W'WZ}/g_{WWZ} = (M_{W'}/M_{W'})^2$.
- 83 AAD 12cK search for $p\bar{p} \rightarrow tW'$, $W' \rightarrow \tau q$ events in pp collisions. See their Fig. 5 for the limit on $\sigma \cdot B$.
- 84 AAD 12cR use pp collisions at $\sqrt{s}=7$ TeV.
- 85 AAD 12m search for right-handed W_R in pp collisions at $\sqrt{s}=7$ TeV. W_R is assumed to decay into ℓ and hypothetical heavy neutrino N , with N decaying into ℓj . See their Fig. 4 for the limit in the $m_N - m_{W'}$ plane.
- 86 AALTONEN 12N search for $p\bar{p} \rightarrow tW'$, $W' \rightarrow \tau d$ events in $p\bar{p}$ collisions. See their Fig. 3 for the limit on $\sigma \cdot B$.
- 87 CHATRCHYAN 12aR search for $p\bar{p} \rightarrow tW'$, $W' \rightarrow \tau d$ events in pp collisions. See their Fig. 2 for the limit on $\sigma \cdot B$.
- 88 CHATRCHYAN 12bG search for right-handed W_R in pp collisions $\sqrt{s}=7$ TeV. W_R is assumed to decay into ℓ and hypothetical heavy neutrino N , with N decaying into ℓj . See their Fig. 3 for the limit in the $m_N - m_{W'}$ plane.
- 89 ABZOV 11H use data from $p\bar{p}$ collisions at $\sqrt{s}=1.96$ TeV. The quoted limit is obtained assuming $W'WZ$ coupling strength is the same as the ordinary WWZ coupling strength in the Standard Model.
- 90 ABZOV 11L limit is for W' with SM-like coupling which interferes with the SM W boson, using $p\bar{p}$ collisions at $\sqrt{s}=1.96$ TeV. For W' with right-handed coupling, the bound becomes >885 GeV (>890 GeV) if W' decays to both leptons and quarks (only to quarks). If both left- and right-handed couplings present, the limit becomes >916 GeV.
- 91 AALTONEN 10N use $p\bar{p}$ collision data at $\sqrt{s}=1.96$ TeV. The quoted limit assumes $g_{W'WZ}/g_{WWZ} = (M_{W'}/M_{W'})^2$. See their Fig. 4 for limits in mass-coupling plane.
- 92 AALTONEN 09aC search for new particle decaying to dijets using $p\bar{p}$ collisions at $\sqrt{s}=1.96$ TeV.
- 93 The ACOSTA 03b quoted limit is for $M_{W'} \gg M_{\nu_R}$, using $p\bar{p}$ collisions at $\sqrt{s}=1.8$ TeV. For $M_{W'} < M_{\nu_R}$, $M_{W'}$ between 225 and 566 GeV is excluded.
- 94 The quoted limit is obtained assuming $W'WZ$ coupling strength is the same as the ordinary WWZ coupling strength in the Standard Model, using $p\bar{p}$ collisions at $\sqrt{s}=1.8$ TeV. See their Fig. 2 for the limits on the production cross sections as a function of the W' width.
- 95 AFFOLDER 01i combine a new bound on $W' \rightarrow e\nu$ of 754 GeV, using $p\bar{p}$ collisions at $\sqrt{s}=1.8$ TeV, with the bound of ABE 00 on $W' \rightarrow \mu\nu$ to obtain quoted bound.
- 96 ABE 97g search for new particle decaying to dijets using $p\bar{p}$ collisions at $\sqrt{s}=1.8$ TeV.
- 97 For bounds on W_R with nonzero right-handed mass, see Fig. 5 from ABACHI 96c.
- 98 ABACHI 95E assume that the decay $W' \rightarrow WZ$ is suppressed and that the neutrino from W' decay is stable and has a mass significantly less $m_{W'}$.
- 99 RIZZO 93 analyses CDF limit on possible two-jet resonances. The limit is sensitive to the inclusion of the assumed K factor.

W_R (Right-Handed W Boson) MASS LIMITS

Assuming a light right-handed neutrino, except for BEALL 82, LANGACKER 89b, and COLANGELO 91. $g_R = g_L$ assumed. [Limits in the section MASS LIMITS for W' below are also valid for W_R if $m_{\nu_R} \ll m_{W'}$.] Some limits assume manifest left-right symmetry, i.e., the equality of left- and right Cabibbo-Kobayashi-Maskawa matrices. For a comprehensive review, see LANGACKER 89b. Limits on the $W_L - W_R$ mixing angle ζ are found in the next section. Values in brackets are from cosmological and astrophysical considerations and assume a light right-handed neutrino.

VALUE (GeV)	CL%	DOCUMENT ID	TECN	COMMENT
> 592	90	1 BUENO	11 TWST	μ decay
> 715	90	2 CZAKON	99 RVUE	Electroweak
● ● ● We do not use the following data for averages, fits, limits, etc. ● ● ●				
> 235	90	3 PRIEELS	14 PIE3	μ decay
> 245	90	4 WAUTERS	10 CNTR	^{60}Co β decay
>2500		5 ZHANG	08 THEO	$m_{K_L^0} - m_{K_S^0}$
> 180	90	6 MELCONIAN	07 CNTR	^{37}K β^+ decay
> 290.7	90	7 SCHUMANN	07 CNTR	Polarized neutron decay
[> 3300]	95	8 CYBURT	05 COSM	Nucleosynthesis; light ν_R
> 310	90	9 THOMAS	01 CNTR	β^+ decay
> 137	95	10 ACKERSTAFF	99D OPAL	τ decay
>1400	68	11 BARENBOIM	98 RVUE	Electroweak, $Z-Z'$ mixing
> 549	68	12 BARENBOIM	97 RVUE	μ decay
> 220	95	13 STAHL	97 RVUE	τ decay
> 220	90	14 ALLET	96 CNTR	β^+ decay
> 281	90	15 KUZNETSOV	95 CNTR	Polarized neutron decay
> 282	90	16 KUZNETSOV	94b CNTR	Polarized neutron decay
> 439	90	17 BHATTACH...	93 RVUE	$Z-Z'$ mixing
> 250	90	18 SEVERIUNS	93 CNTR	β^+ decay
		19 IMAZATO	92 CNTR	K^+ decay
> 475	90	20 POLAK	92b RVUE	μ decay
> 240	90	21 AQUINO	91 RVUE	Neutron decay
> 496	90	21 AQUINO	91 RVUE	Neutron and muon decay
> 700		22 COLANGELO	91 THEO	$m_{K_L^0} - m_{K_S^0}$
> 477	90	23 POLAK	91 RVUE	μ decay
[none 540-23000]		24 BARBIERI	89b ASTR	SN 1987A; light ν_R
> 300	90	25 LANGACKER	89b RVUE	General
> 160	90	26 BALKE	88 CNTR	$\mu \rightarrow e\nu\bar{\nu}$
> 406	90	27 JODIDIO	86 ELEC	Any ζ
> 482	90	27 JODIDIO	86 ELEC	$\zeta = 0$
> 800		MOHAPATRA	86 RVUE	$SU(2)_L \times SU(2)_R \times U(1)$
> 400	95	28 STOKER	85 ELEC	Any ζ
> 475	95	28 STOKER	85 ELEC	$\zeta < 0.041$
		29 BERGSMA	83 CHR	$\nu_\mu e \rightarrow \mu\nu e$
> 380	90	30 CARR	83 ELEC	μ^+ decay
>1600		31 BEALL	82 THEO	$m_{K_L^0} - m_{K_S^0}$

- The quoted limit is for manifest left-right symmetric model.
- CZAKON 99 perform a simultaneous fit to charged and neutral sectors.
- PREIEELS 14 limit is from $\mu^+ \rightarrow e^+ \nu\bar{\nu}$ decay parameter ϵ'' , which is determined by the positron polarization measurement.
- WAUTERS 10 limit is from a measurement of the asymmetry parameter of polarized ^{60}Co β decays. The listed limit assumes no mixing.
- ZHANG 08 limit uses a lattice QCD calculation of the relevant hadronic matrix elements, while BEALL 82 limit used the vacuum saturation approximation.
- MELCONIAN 07 measure the neutrino angular asymmetry in β^+ -decays of polarized ^{37}K , stored in a magneto-optical trap. Result is consistent with SM prediction and does not constrain the $W_L - W_R$ mixing angle appreciably.
- SCHUMANN 07 limit is from measurements of the asymmetry $\langle \vec{p}_\nu \cdot \sigma_n \rangle$ in the β decay of polarized neutrons. Zero mixing is assumed.
- CYBURT 05 limit follows by requiring that three light ν_R 's decouple when $T_{dec} > 140$ MeV. For different T_{dec} , the bound becomes $M_{W'} > 3.3$ TeV ($T_{dec} / 140$ MeV) $^{3/4}$.
- THOMAS 01 limit is from measurement of β^+ polarization in decay of polarized ^{12}N . The listed limit assumes no mixing.
- ACKERSTAFF 99d limit is from τ decay parameters. Limit increase to 145 GeV for zero mixing.
- BARENBOIM 98 assumes minimal left-right model with Higgs of $SU(2)_R$ in $SU(2)_L$ doublet. For Higgs in $SU(2)_L$ triplet, $m_{W'} > 1100$ GeV. Bound calculated from effect of corresponding Z_{LR} on electroweak data through $Z-Z_{LR}$ mixing.
- The quoted limit is from μ decay parameters. BARENBOIM 97 also evaluate limit from $K_L - K_S$ mass difference.
- STAHL 97 limit is from fit to τ -decay parameters.
- ALLET 96 measured polarization-asymmetry correlation in ^{12}N β^+ decay. The listed limit assumes zero $L-R$ mixing.
- KUZNETSOV 95 limit is from measurements of the asymmetry $\langle \vec{p}_\nu \cdot \sigma_n \rangle$ in the β decay of polarized neutrons. Zero mixing assumed. See also KUZNETSOV 94b.
- KUZNETSOV 94b limit is from measurements of the asymmetry $\langle \vec{p}_\nu \cdot \sigma_n \rangle$ in the β decay of polarized neutrons. Zero mixing assumed.
- BHATTACHARYA 93 uses $Z-Z'$ mixing limit from LEP '90 data, assuming a specific Higgs sector of $SU(2)_L \times SU(2)_R \times U(1)$ gauge model. The limit is for $m_t=200$ GeV and slightly improves for smaller m_t .
- SEVERIUNS 93 measured polarization-asymmetry correlation in ^{107}In β^+ decay. The listed limit assumes zero $L-R$ mixing. Value quoted here is from SEVERIUNS 94 erratum.
- IMAZATO 92 measure positron asymmetry in $K^+ \rightarrow \mu^+ \nu \mu$ decay and obtain $\epsilon_{\mu}^R > 0.990$ (90% CL). If W_R couples to $u\bar{s}$ with full weak strength ($V_{us}^R=1$), the result corresponds to $m_{W'} > 653$ GeV. See their Fig. 4 for $m_{W'}$ limits for general $|V_{us}^R|^2 = 1 - |V_{ud}^R|^2$.

Gauge & Higgs Boson Particle Listings

New Heavy Bosons

- 20 POLAK 92b limit is from fit to muon decay parameters and is essentially determined by JODIDIO 86 data assuming $\zeta=0$. Supersedes POLAK 91.
- 21 AQUINO 91 limits obtained from neutron lifetime and asymmetries together with unitarity of the CKM matrix. Manifest left-right symmetry assumed. Stronger of the two limits also includes muon decay results.
- 22 COLANGELO 91 limit uses hadronic matrix elements evaluated by QCD sum rule and is less restrictive than BEALL 82 limit which uses vacuum saturation approximation. Manifest left-right symmetry assumed.
- 23 POLAK 91 limit is from fit to muon decay parameters and is essentially determined by JODIDIO 86 data assuming $\zeta=0$. Superseded by POLAK 92b.
- 24 BARBIERI 89b limit holds for $m_{\nu_R} \leq 10$ MeV.
- 25 LANGACKER 89b limit is for any ν_R mass (either Dirac or Majorana) and for a general class of right-handed quark mixing matrices.
- 26 BALKE 88 limit is for $m_{\nu_{eR}} = 0$ and $m_{\nu_{\mu R}} \leq 50$ MeV. Limits come from precise measurements of the muon decay asymmetry as a function of the positron energy.
- 27 JODIDIO 86 is the same TRIUMF experiment as STOKER 85 (and CARR 83); however, it uses a different technique. The results given here are combined results of the two techniques. The technique here involves precise measurement of the end-point e^+ spectrum in the decay of the highly polarized μ^+ .
- 28 STOKER 85 is same TRIUMF experiment as CARR 83. Here they measure the decay e^+ spectrum asymmetry above 46 MeV/c using a muon-spin-rotation technique. Assumed a light right-handed neutrino. Quoted limits are from combining with CARR 83.
- 29 BERGSMAN 83 set limit $m_{W_2}/m_{W_1} > 1.9$ at CL = 90%.
- 30 CARR 83 is TRIUMF experiment with a highly polarized μ^+ beam. Looked for deviation from $V-A$ at the high momentum end of the decay e^+ energy spectrum. Limit from previous world-average muon polarization parameter is $m_{W_R} > 240$ GeV. Assumes a light right-handed neutrino.
- 31 BEALL 82 limit is obtained assuming that W_R contribution to $K_L^0-K_S^0$ mass difference is smaller than the standard one, neglecting the top quark contributions. Manifest left-right symmetry assumed.

Limit on W_L - W_R Mixing Angle ζ

Lighter mass eigenstate $W_1 = W_L \cos \zeta - W_R \sin \zeta$. Light ν_R assumed unless noted. Values in brackets are from cosmological and astrophysical considerations.

VALUE	CL%	DOCUMENT ID	TECN	COMMENT
• • • We do not use the following data for averages, fits, limits, etc. • • •				
-0.020 to 0.017	90	BUENO 11	TWST	$\mu \rightarrow e\nu\bar{\nu}$
< 0.022	90	MACDONALD 08	TWST	$\mu \rightarrow e\nu\bar{\nu}$
< 0.12	95	1 ACKERSTAFF 99d	OPAL	τ decay
< 0.013	90	2 CZAKON 99	RVUE	Electroweak
< 0.0333		3 BARENBOIM 97	RVUE	μ decay
< 0.04	90	4 MISHRA 92	CCFR	νN scattering
-0.0006 to 0.0028	90	5 AQUINO 91	RVUE	
[none 0.00001-0.02]		6 BARBIERI 89b	ASTR	SN 1987A
< 0.040	90	7 JODIDIO 86	ELEC	μ decay
-0.056 to 0.040	90	7 JODIDIO 86	ELEC	μ decay

- 1 ACKERSTAFF 99d limit is from τ decay parameters.
- 2 CZAKON 99 perform a simultaneous fit to charged and neutral sectors.
- 3 The quoted limit is from μ decay parameters. BARENBOIM 97 also evaluate limit from K_L-K_S mass difference.
- 4 MISHRA 92 limit is from the absence of extra large- x , large- y $\bar{\nu}_\mu N \rightarrow \bar{\nu}_\mu X$ events at Tevatron, assuming left-handed ν_L and right-handed $\bar{\nu}_R$ in the neutrino beam. The result gives $\zeta^2(1-2m_{W_1}^2/m_{W_2}^2) < 0.0015$. The limit is independent of ν_R mass.
- 5 AQUINO 91 limits obtained from neutron lifetime and asymmetries together with unitarity of the CKM matrix. Manifest left-right asymmetry is assumed.
- 6 BARBIERI 89b limit holds for $m_{\nu_R} \leq 10$ MeV.
- 7 First JODIDIO 86 result assumes $m_{W_R} = \infty$, second is for unconstrained m_{W_R} .

See the related review(s):

[Z'-Boson Searches](#)

MASS LIMITS for Z' (Heavy Neutral Vector Boson Other Than Z)

Limits for Z'_{SM}

Z'_{SM} is assumed to have couplings with quarks and leptons which are identical to those of Z, and decays only to known fermions. The most recent preliminary results can be found in the "Z'-boson searches" review above.

VALUE (GeV)	CL%	DOCUMENT ID	TECN	COMMENT
>5150 (CL = 95%) OUR LIMIT				
>5150	95	1 SIRUNYAN 21N	CMS	$pp; Z'_{SM} \rightarrow e^+e^-, \mu^+\mu^-$
none 1133-2700	95	2 AAD 20T	ATLS	$pp; Z'_{SM} \rightarrow b\bar{b}$
none 1800-2900, 3100-3300	95	3 SIRUNYAN 20AI	CMS	$pp; Z'_{SM} \rightarrow q\bar{q}$
none 250-5100	95	4 AAD 19L	ATLS	$pp; Z'_{SM} \rightarrow e^+e^-, \mu^+\mu^-$
none 600-2000	95	5 AABOUD 18AB	ATLS	$pp; Z'_{SM} \rightarrow b\bar{b}$
>2420	95	6 AABOUD 18G	ATLS	$pp; Z'_{SM} \rightarrow \tau^+\tau^-$
none 200-4500	95	7 SIRUNYAN 18BB	CMS	$pp; Z'_{SM} \rightarrow e^+e^-, \mu^+\mu^-$
none 600-2700	95	8 SIRUNYAN 18BO	CMS	$pp; Z'_{SM} \rightarrow q\bar{q}$
>4500	95	9 AABOUD 17AT	ATLS	$pp; Z'_{SM} \rightarrow e^+e^-, \mu^+\mu^-$
>2100	95	10 KHACHATRYAN 17H	CMS	$pp; Z'_{SM} \rightarrow \tau^+\tau^-$
>3370	95	11 KHACHATRYAN 17T	CMS	$pp; Z'_{SM} \rightarrow e^+e^-, \mu^+\mu^-$
none 600-2100, 2300-2600	95	12 KHACHATRYAN 17W	CMS	$pp; Z'_{SM} \rightarrow q\bar{q}$

>3360	95	13 AABOUD 16U	ATLS	$pp; Z'_{SM} \rightarrow e^+e^-, \mu^+\mu^-$
>2900	95	14 KHACHATRYAN 15AE	CMS	$pp; Z'_{SM} \rightarrow e^+e^-, \mu^+\mu^-$
none 1200-1700	95	15 KHACHATRYAN 15V	CMS	$pp; Z'_{SM} \rightarrow q\bar{q}$
>2900	95	16 AAD 14V	ATLS	$pp; Z'_{SM} \rightarrow e^+e^-, \mu^+\mu^-$
• • • We do not use the following data for averages, fits, limits, etc. • • •				
		17 BOBOVNIKOV 18	RVUE	$pp; Z'_{SM} \rightarrow W^+W^-$
>1900	95	18 AABOUD 16AA	ATLS	$pp; Z'_{SM} \rightarrow \tau^+\tau^-$
>2020	95	19 AAD 15AM	ATLS	$pp; Z'_{SM} \rightarrow \tau^+\tau^-$
>1400	95	20 AAD 13s	ATLS	$pp; Z'_{SM} \rightarrow \tau^+\tau^-$
>1470	95	21 CHATRCHYAN 13A	CMS	$pp; Z'_{SM} \rightarrow q\bar{q}$
>2590	95	22 CHATRCHYAN 13AF	CMS	$pp; Z'_{SM} \rightarrow e^+e^-, \mu^+\mu^-$
>2220	95	23 AAD 12CC	ATLS	$pp; Z'_{SM} \rightarrow e^+e^-, \mu^+\mu^-$
>1400	95	24 CHATRCHYAN 12O	CMS	$pp; Z'_{SM} \rightarrow \tau^+\tau^-$
>1071	95	25 AALTONEN 11I	CDF	$p\bar{p}; Z'_{SM} \rightarrow \mu^+\mu^-$
>1023	95	26 ABAZOV 11A	D0	$p\bar{p}; Z'_{SM} \rightarrow e^+e^-$
none 247-544	95	27 AALTONEN 10N	CDF	$Z' \rightarrow WW$
none 320-740	95	28 AALTONEN 09AC	CDF	$Z' \rightarrow q\bar{q}$
> 963	95	26 AALTONEN 09T	CDF	$p\bar{p}; Z'_{SM} \rightarrow e^+e^-$
>1403	95	29 ERLER 09	RVUE	Electroweak
>1305	95	30 ABDALLAH 06C	DLPH	e^+e^-
> 399	95	31 ACOSTA 05R	CDF	$p\bar{p}; Z'_{SM} \rightarrow \tau^+\tau^-$
none 400-640	95	32 ABAZOV 04C	D0	$p\bar{p}; Z'_{SM} \rightarrow q\bar{q}$
>1018	95	33 ABBIENDI 04G	OPAL	e^+e^-
> 670	95	34 ABZOV 01B	D0	$p\bar{p}; Z'_{SM} \rightarrow e^+e^-$
>1500	95	35 CHEUNG 01B	RVUE	Electroweak
> 710	95	36 ABREU 00s	DLPH	e^+e^-
> 898	95	37 BARATE 00i	ALEP	e^+e^-
> 809	95	38 ERLER 99	RVUE	Electroweak
> 690	95	39 ABE 97s	CDF	$p\bar{p}; Z'_{SM} \rightarrow e^+e^-, \mu^+\mu^-$
> 398	95	40 VILAIN 94B	CHM2	$\nu_\mu e \rightarrow \nu_\mu e$ and $\bar{\nu}_\mu e \rightarrow \bar{\nu}_\mu e$
> 237	90	41 ALITTI 93	UA2	$p\bar{p}; Z'_{SM} \rightarrow q\bar{q}$
none 260-600	95	42 RIZZO 93	RVUE	$p\bar{p}; Z'_{SM} \rightarrow q\bar{q}$
> 426	90	43 ABE 90f	VNS	e^+e^-

- 1 SIRUNYAN 21N search for resonance decaying to $e^+e^-, \mu^+\mu^-$ in pp collisions at $\sqrt{s} = 13$ TeV.
- 2 AAD 20T search for resonances decaying to $b\bar{b}$ in pp collisions at $\sqrt{s} = 13$ TeV. See their Fig. 7(b) for limits on the product of the cross section, acceptance, b -tagging efficiency, and branching fraction.
- 3 SIRUNYAN 20AI search for resonances decaying into dijets in pp collisions at $\sqrt{s} = 13$ TeV.
- 4 AAD 19L search for resonances decaying to $\ell^+\ell^-$ in pp collisions at $\sqrt{s} = 13$ TeV.
- 5 AABOUD 18AB search for resonances decaying to $b\bar{b}$ in pp collisions at $\sqrt{s} = 13$ TeV.
- 6 AABOUD 18G search for resonances decaying to $\tau^+\tau^-$ in pp collisions at $\sqrt{s} = 13$ TeV.
- 7 SIRUNYAN 18BB search for resonances decaying to $\ell^+\ell^-$ in pp collisions at $\sqrt{s} = 13$ TeV. See their Fig.5 for limits on the Z' coupling strengths with light quarks.
- 8 SIRUNYAN 18BO search for resonances decaying to dijets in pp collisions at $\sqrt{s} = 13$ TeV.
- 9 AABOUD 17AT search for resonances decaying to $\ell^+\ell^-$ in pp collisions at $\sqrt{s} = 13$ TeV.
- 10 KHACHATRYAN 17H search for resonances decaying to $\tau^+\tau^-$ in pp collisions at $\sqrt{s} = 13$ TeV.
- 11 KHACHATRYAN 17T search for resonances decaying to $e^+e^-, \mu^+\mu^-$ in pp collisions at $\sqrt{s} = 8, 13$ TeV.
- 12 KHACHATRYAN 17W search for resonances decaying to dijets in pp collisions at $\sqrt{s} = 13$ TeV.
- 13 AABOUD 16U search for resonances decaying to $\ell^+\ell^-$ in pp collisions at $\sqrt{s} = 13$ TeV.
- 14 KHACHATRYAN 15AE search for resonances decaying to $e^+e^-, \mu^+\mu^-$ in pp collisions at $\sqrt{s} = 8$ TeV.
- 15 KHACHATRYAN 15V search for resonances decaying to dijets in pp collisions at $\sqrt{s} = 8$ TeV.
- 16 AAD 14V search for resonances decaying to $e^+e^-, \mu^+\mu^-$ in pp collisions at $\sqrt{s} = 8$ TeV.
- 17 BOBOVNIKOV 18 use the ATLAS limits on $\sigma(pp \rightarrow Z') \cdot \text{B}(Z' \rightarrow W^+W^-)$ to constrain the Z - Z' mixing parameter ξ . See their Fig. 11 for limits in $M_{Z'} - \xi$ plane.
- 18 AABOUD 16AA search for resonances decaying to $\tau^+\tau^-$ in pp collisions at $\sqrt{s} = 13$ TeV.
- 19 AAD 15AM search for resonances decaying to $\tau^+\tau^-$ in pp collisions at $\sqrt{s} = 8$ TeV.
- 20 AAD 13s search for resonances decaying to $\tau^+\tau^-$ in pp collisions at $\sqrt{s} = 7$ TeV.
- 21 CHATRCHYAN 13A use pp collisions at $\sqrt{s} = 7$ TeV.
- 22 CHATRCHYAN 13AF search for resonances decaying to $e^+e^-, \mu^+\mu^-$ in pp collisions at $\sqrt{s} = 7$ TeV and 8 TeV.
- 23 AAD 12CC search for resonances decaying to $e^+e^-, \mu^+\mu^-$ in pp collisions at $\sqrt{s} = 7$ TeV.
- 24 CHATRCHYAN 12O search for resonances decaying to $\tau^+\tau^-$ in pp collisions at $\sqrt{s} = 7$ TeV.
- 25 AALTONEN 11I search for resonances decaying to $\mu^+\mu^-$ in $p\bar{p}$ collisions at $\sqrt{s} = 1.96$ TeV.
- 26 ABAZOV 11A, AALTONEN 09T, AALTONEN 07H, and ABULENCIA 06L search for resonances decaying to e^+e^- in $p\bar{p}$ collisions at $\sqrt{s} = 1.96$ TeV.
- 27 The quoted limit assumes $g_{WWZ}^{\prime}/g_{WWZ} = (M_W/M_{Z'})^2$. See their Fig. 4 for limits in mass-coupling plane.
- 28 AALTONEN 09AC search for new particle decaying to dijets.
- 29 ERLER 09 give 95% CL limit on the Z - Z' mixing $-0.0026 < \theta < 0.0006$.
- 30 ABDALLAH 06C use data $\sqrt{s} = 130-207$ GeV.

- 31 ACOSTA 05R search for resonances decaying to tau lepton pairs in $\bar{p}p$ collisions at $\sqrt{s} = 1.96$ TeV.
- 32 ABBIENDI 04G give 95% CL limit on $Z-Z'$ mixing $-0.00422 < \theta < 0.00091$. $\sqrt{s} = 91$ to 207 GeV.
- 33 ABAZOV 01B search for resonances in $p\bar{p} \rightarrow e^+e^-$ at $\sqrt{s}=1.8$ TeV. They find $\sigma \cdot B(Z' \rightarrow ee) < 0.06$ pb for $M_{Z'} > 500$ GeV.
- 34 CHEUNG 01B limit is derived from bounds on contact interactions in a global electroweak analysis.
- 35 ABREU 00s uses LEP data at $\sqrt{s}=90$ to 189 GeV.
- 36 BARATE 00i search for deviations in cross section and asymmetries in $e^+e^- \rightarrow$ fermions at $\sqrt{s}=90$ to 183 GeV. Assume $\theta=0$. Bounds in the mass-mixing plane are shown in their Figure 18.
- 37 ERLER 99 give 90%CL limit on the $Z-Z'$ mixing $-0.0041 < \theta < 0.0003$. $\rho_0=1$ is assumed.
- 38 ABE 97s find $\sigma(Z') \times B(e^+e^-, \mu^+\mu^-) < 40$ fb for $m_{Z'} > 600$ GeV at $\sqrt{s} = 1.8$ TeV.
- 39 VILAIN 94B assume $m_t = 150$ GeV.
- 40 ALITTI 93 search for resonances in the two-jet invariant mass. The limit assumes $B(Z' \rightarrow q\bar{q})=0.7$. See their Fig. 5 for limits in the $m_{Z'}-B(q\bar{q})$ plane.
- 41 RIZZO 93 analyses CDF limit on possible two-jet resonances.
- 42 ABE 90f use data for $R, R_{\ell\ell}$, and $A_{\ell\ell}$. They fix $m_{W'} = 80.49 \pm 0.43 \pm 0.24$ GeV and $m_{Z'} = 91.13 \pm 0.03$ GeV.

Limits for Z_{LR}

Z_{LR} is the extra neutral boson in left-right symmetric models. $g_L = g_R$ is assumed unless noted. Values in parentheses assume stronger constraint on the Higgs sector, usually motivated by specific left-right symmetric models (see the Note on the W'). Values in brackets are from cosmological and astrophysical considerations and assume a light right-handed neutrino. Direct search bounds assume decays to Standard Model fermions only, unless noted.

VALUE (GeV)	CL%	DOCUMENT ID	TECN	COMMENT
>1162	95	1 DEL-AGUILA	10 RVUE	Electroweak
> 630	95	2 ABE	97s CDF	$p\bar{p}; Z'_{LR} \rightarrow e^+e^-, \mu^+\mu^-$
••• We do not use the following data for averages, fits, limits, etc. •••				
		3 BOBOVNIKOV 18	RVUE	$p\bar{p}; Z'_{LR} \rightarrow W^+W^-$
> 998	95	4 ERLER 09	RVUE	Electroweak
> 600	95	SCHAEL 07A	ALEP	e^+e^-
> 455	95	5 ABDALLAH 06c	DLPH	e^+e^-
> 518	95	6 ABBIENDI 04g	OPAL	e^+e^-
> 860	95	7 CHEUNG 01b	RVUE	Electroweak
> 380	95	8 ABREU 00s	DLPH	e^+e^-
> 436	95	9 BARATE 00i	ALEP	Repl. by SCHAEL 07A
> 550	95	10 CHAY 00	RVUE	Electroweak
		11 ERLER 00	RVUE	Cs
		12 CASALBUONI 99	RVUE	Cs
(> 1205)	90	13 CZAKON 99	RVUE	Electroweak
> 564	95	14 ERLER 99	RVUE	Electroweak
(> 1673)	95	15 ERLER 99	RVUE	Electroweak
(> 1700)	68	16 BARENBOIM 98	RVUE	Electroweak
> 244	95	17 CONRAD 98	RVUE	$\nu_\mu N$ scattering
> 253	95	18 VILAIN 94b	CHM2	$\nu_\mu e \rightarrow \nu_\mu e$ and $\bar{\nu}_\mu e \rightarrow \bar{\nu}_\mu e$
none 200-600	95	19 RIZZO 93	RVUE	$p\bar{p}; Z_{LR} \rightarrow q\bar{q}$
[> 2000]		WALKER 91	COSM	Nucleosynthesis; light ν_R
none 200-500		20 GRIFOLS 90	ASTR	SN 1987A; light ν_R
none 350-2400		21 BARBIERI 89b	ASTR	SN 1987A; light ν_R

- 1 DEL-AGUILA 10 give 95% CL limit on the $Z-Z'$ mixing $-0.0012 < \theta < 0.0004$.
- 2 ABE 97s find $\sigma(Z') \times B(e^+e^-, \mu^+\mu^-) < 40$ fb for $m_{Z'} > 600$ GeV at $\sqrt{s} = 1.8$ TeV.
- 3 BOBOVNIKOV 18 use the ATLAS limits on $\sigma(p\bar{p} \rightarrow Z') \cdot B(Z' \rightarrow W^+W^-)$ to constrain the $Z-Z'$ mixing parameter ξ . See their Fig. 10 for limits in $M_{Z'}-\xi$ plane.
- 4 ERLER 09 give 95% CL limit on the $Z-Z'$ mixing $-0.0013 < \theta < 0.0006$.
- 5 ABDALLAH 06c give 95% CL limit $|\theta| < 0.0028$. See their Fig. 14 for limit contours in the mass-mixing plane.
- 6 ABBIENDI 04g give 95% CL limit on $Z-Z'$ mixing $-0.00098 < \theta < 0.00190$. See their Fig. 20 for the limit contour in the mass-mixing plane. $\sqrt{s} = 91$ to 207 GeV.
- 7 CHEUNG 01B limit is derived from bounds on contact interactions in a global electroweak analysis.
- 8 ABREU 00s give 95% CL limit on $Z-Z'$ mixing $|\theta| < 0.0018$. See their Fig. 6 for the limit contour in the mass-mixing plane. $\sqrt{s}=90$ to 189 GeV.
- 9 BARATE 00i search for deviations in cross section and asymmetries in $e^+e^- \rightarrow$ fermions at $\sqrt{s}=90$ to 183 GeV. Assume $\theta=0$. Bounds in the mass-mixing plane are shown in their Figure 18.
- 10 CHAY 00 also find $-0.0003 < \theta < 0.0019$. For g_R free, $m_{Z'} > 430$ GeV.
- 11 ERLER 00 discuss the possibility that a discrepancy between the observed and predicted values of $Q_{W'}(Cs)$ is due to the exchange of Z' . The data are better described in a certain class of the Z' models including Z_{LR} and Z_χ .
- 12 CASALBUONI 99 discuss the discrepancy between the observed and predicted values of $Q_{W'}(Cs)$. It is shown that the data are better described in a class of models including the Z_{LR} model.
- 13 CZAKON 99 perform a simultaneous fit to charged and neutral sectors. Assumes manifest left-right symmetric model. Finds $|\theta| < 0.0042$.
- 14 ERLER 99 give 90% CL limit on the $Z-Z'$ mixing $-0.0009 < \theta < 0.0017$.
- 15 ERLER 99 assumes 2 Higgs doublets, transforming as 10 of SO(10), embedded in E_6 .
- 16 BARENBOIM 98 also gives 68% CL limits on the $Z-Z'$ mixing $-0.0005 < \theta < 0.0033$. Assumes Higgs sector of minimal left-right model.
- 17 CONRAD 98 limit is from measurements at CCFR, assuming no $Z-Z'$ mixing.
- 18 VILAIN 94B assume $m_t = 150$ GeV and $\theta=0$. See Fig. 2 for limit contours in the mass-mixing plane.

- 19 RIZZO 93 analyses CDF limit on possible two-jet resonances.
- 20 GRIFOLS 90 limit holds for $m_{\nu_R} \lesssim 1$ MeV. A specific Higgs sector is assumed. See also GRIFOLS 90b, RIZZO 91.
- 21 BARBIERI 89b limit holds for $m_{\nu_R} \leq 10$ MeV. Bounds depend on assumed supernova core temperature.

Limits for Z_χ

Z_χ is the extra neutral boson in $SO(10) \rightarrow SU(5) \times U(1)_\chi$. $g_\chi = e/\cos\theta_W$ is assumed unless otherwise stated. We list limits with the assumption $\rho = 1$ but with no further constraints on the Higgs sector. Values in parentheses assume stronger constraint on the Higgs sector motivated by superstring models. Values in brackets are from cosmological and astrophysical considerations and assume a light right-handed neutrino.

VALUE (GeV)	CL%	DOCUMENT ID	TECN	COMMENT
>4800 (CL = 95%) OUR LIMIT				
none 250-4800	95	1 AAD	19L ATLS	$p\bar{p}; Z'_\chi \rightarrow e^+e^-, \mu^+\mu^-$
>4100	95	2 AABOUD	17AT ATLS	$p\bar{p}; Z'_\chi \rightarrow e^+e^-, \mu^+\mu^-$
••• We do not use the following data for averages, fits, limits, etc. •••				
		3 BOBOVNIKOV 18	RVUE	$p\bar{p}; Z'_\chi \rightarrow W^+W^-$
>3050	95	4 AABOUD	16u ATLS	$p\bar{p}; Z'_\chi \rightarrow e^+e^-, \mu^+\mu^-$
>2620	95	5 AAD	14v ATLS	$p\bar{p}; Z'_\chi \rightarrow e^+e^-, \mu^+\mu^-$
>1970	95	6 AAD	12cc ATLS	$p\bar{p}; Z'_\chi \rightarrow e^+e^-, \mu^+\mu^-$
> 930	95	7 AALTONEN 11i	CDF	$p\bar{p}; Z'_\chi \rightarrow \mu^+\mu^-$
> 903	95	8 ABAZOV 11a	D0	$p\bar{p}; Z'_\chi \rightarrow e^+e^-$
>1022	95	9 DEL-AGUILA 10	RVUE	Electroweak
> 862	95	8 AALTONEN 09t	CDF	$p\bar{p}; Z'_\chi \rightarrow e^+e^-$
> 892	95	10 AALTONEN 09v	CDF	Repl. by AALTONEN 11i
>1141	95	11 ERLER 09	RVUE	Electroweak
> 822	95	8 AALTONEN 07h	CDF	Repl. by AALTONEN 09t
> 680	95	SCHAEL 07a	ALEP	e^+e^-
> 545	95	12 ABDALLAH 06c	DLPH	e^+e^-
> 740		8 ABULENCIA 06L	CDF	Repl. by AALTONEN 07h
> 690	95	13 ABULENCIA 05a	CDF	$p\bar{p}; Z'_\chi \rightarrow e^+e^-, \mu^+\mu^-$
> 781	95	14 ABBIENDI 04g	OPAL	e^+e^-
>2100		15 BARGER 03b	COSM	Nucleosynthesis; light ν_R
> 680	95	16 CHEUNG 01b	RVUE	Electroweak
> 440	95	17 ABREU 00s	DLPH	e^+e^-
> 533	95	18 BARATE 00i	ALEP	Repl. by SCHAEL 07A
> 554	95	19 CHO 00	RVUE	Electroweak
		20 ERLER 00	RVUE	Cs
		21 ROSNER 00	RVUE	Cs
> 545	95	22 ERLER 99	RVUE	Electroweak
(> 1368)	95	23 ERLER 99	RVUE	Electroweak
> 215	95	24 CONRAD 98	RVUE	$\nu_\mu N$ scattering
> 595	95	25 ABE 97s	CDF	$p\bar{p}; Z'_\chi \rightarrow e^+e^-, \mu^+\mu^-$
> 190	95	26 ARIMA 97	VNS	Bhabha scattering
> 262	95	27 VILAIN 94b	CHM2	$\nu_\mu e \rightarrow \nu_\mu e; \bar{\nu}_\mu e \rightarrow \bar{\nu}_\mu e$
[>1470]		28 FARAGGI 91	COSM	Nucleosynthesis; light ν_R
> 231	90	29 ABE 90f	VNS	e^+e^-
> 1140]		30 GONZALEZ... 90b	COSM	Nucleosynthesis; light ν_R
> 2100]		31 GRIFOLS 90	ASTR	SN 1987A; light ν_R

- 1 AAD 19L search for resonances decaying to $\ell^+\ell^-$ in pp collisions at $\sqrt{s} = 13$ TeV.
- 2 AABOUD 17AT search for resonances decaying to $\ell^+\ell^-$ in pp collisions at $\sqrt{s} = 13$ TeV.
- 3 BOBOVNIKOV 18 use the ATLAS limits on $\sigma(p\bar{p} \rightarrow Z') \cdot B(Z' \rightarrow W^+W^-)$ to constrain the $Z-Z'$ mixing parameter ξ . See their Fig. 9 for limits in $M_{Z'}-\xi$ plane.
- 4 AABOUD 16u search for resonances decaying to $\ell^+\ell^-$ in pp collisions at $\sqrt{s} = 13$ TeV.
- 5 AAD 14v search for resonances decaying to $e^+e^-, \mu^+\mu^-$ in pp collisions at $\sqrt{s} = 8$ TeV.
- 6 AAD 12cc search for resonances decaying to $e^+e^-, \mu^+\mu^-$ in pp collisions at $\sqrt{s} = 7$ TeV.
- 7 AALTONEN 11i search for resonances decaying to $\mu^+\mu^-$ in $p\bar{p}$ collisions at $\sqrt{s} = 1.96$ TeV.
- 8 ABAZOV 11a, AALTONEN 09t, AALTONEN 07h, and ABULENCIA 06L search for resonances decaying to e^+e^- in $p\bar{p}$ collisions at $\sqrt{s} = 1.96$ TeV.
- 9 DEL-AGUILA 10 give 95% CL limit on the $Z-Z'$ mixing $-0.0011 < \theta < 0.0007$.
- 10 AALTONEN 09v search for resonances decaying to $\mu^+\mu^-$ in $p\bar{p}$ collisions at $\sqrt{s} = 1.96$ TeV.
- 11 ERLER 09 give 95% CL limit on the $Z-Z'$ mixing $-0.0016 < \theta < 0.0006$.
- 12 ABDALLAH 06c give 95% CL limit $|\theta| < 0.0031$. See their Fig. 14 for limit contours in the mass-mixing plane.
- 13 ABULENCIA 05a search for resonances decaying to electron or muon pairs in $p\bar{p}$ collisions at $\sqrt{s} = 1.96$ TeV.
- 14 ABBIENDI 04g give 95% CL limit on $Z-Z'$ mixing $-0.00099 < \theta < 0.00194$. See their Fig. 20 for the limit contour in the mass-mixing plane. $\sqrt{s} = 91$ to 207 GeV.
- 15 BARGER 03b limit is from the nucleosynthesis bound on the effective number of light neutrino $\delta N_\nu < 1$. The quark-hadron transition temperature $T_C=150$ MeV is assumed. The limit with $T_C=400$ MeV is >4300 GeV.
- 16 CHEUNG 01b limit is derived from bounds on contact interactions in a global electroweak analysis.
- 17 ABREU 00s give 95% CL limit on $Z-Z'$ mixing $|\theta| < 0.0017$. See their Fig. 6 for the limit contour in the mass-mixing plane. $\sqrt{s}=90$ to 189 GeV.
- 18 BARATE 00i search for deviations in cross section and asymmetries in $e^+e^- \rightarrow$ fermions at $\sqrt{s}=90$ to 183 GeV. Assume $\theta=0$. Bounds in the mass-mixing plane are shown in their Figure 18.

Gauge & Higgs Boson Particle Listings

New Heavy Bosons

- ¹⁹ CHO 00 use various electroweak data to constrain Z' models assuming $m_H=100$ GeV. See Fig. 3 for limits in the mass-mixing plane.
- ²⁰ ERLER 00 discuss the possibility that a discrepancy between the observed and predicted values of $Q_W(Cs)$ is due to the exchange of Z' . The data are better described in a certain class of the Z' models including Z_{LR} and Z_χ .
- ²¹ ROSNER 00 discusses the possibility that a discrepancy between the observed and predicted values of $Q_W(Cs)$ is due to the exchange of Z' . The data are better described in a certain class of the Z' models including Z_χ .
- ²² ERLER 99 give 90% CL limit on the Z-Z' mixing $-0.0020 < \theta < 0.0015$.
- ²³ ERLER 99 assumes 2 Higgs doublets, transforming as 10 of SO(10), embedded in E_6 .
- ²⁴ CONRAD 98 limit is from measurements at CCFR, assuming no Z-Z' mixing.
- ²⁵ ABE 97s find $\sigma(Z') \times B(e^+ e^-, \mu^+ \mu^-) < 40$ fb for $m_{Z'} > 600$ GeV at $\sqrt{s} = 1.8$ TeV.
- ²⁶ Z-Z' mixing is assumed to be zero. $\sqrt{s} = 57.77$ GeV.
- ²⁷ VILAIN 94b assume $m_t = 150$ GeV and $\theta = 0$. See Fig. 2 for limit contours in the mass-mixing plane.
- ²⁸ FARAGGI 91 limit assumes the nucleosynthesis bound on the effective number of neutrinos $\Delta N_\nu < 0.5$ and is valid for $m_{\nu_R} < 1$ MeV.
- ²⁹ ABE 90f use data for R , $R_{\ell\ell}$, and $A_{\ell\ell}$. ABE 90f fix $m_W = 80.49 \pm 0.43 \pm 0.24$ GeV and $m_Z = 91.13 \pm 0.03$ GeV.
- ³⁰ Assumes the nucleosynthesis bound on the effective number of light neutrinos ($\delta N_\nu < 1$) and that ν_R is light ($\lesssim 1$ MeV).
- ³¹ GRIFOLS 90 limit holds for $m_{\nu_R} \lesssim 1$ MeV. See also GRIFOLS 90d, RIZZO 91.

Limits for Z_ψ

Z_ψ is the extra neutral boson in $E_6 \rightarrow SO(10) \times U(1)_\psi$. $g_\psi = e/\cos\theta_W$ is assumed unless otherwise stated. We list limits with the assumption $\rho = 1$ but with no further constraints on the Higgs sector. Values in brackets are from cosmological and astrophysical considerations and assume a light right-handed neutrino.

VALUE (GeV)	CL%	DOCUMENT ID	TECN	COMMENT
>4560 (CL = 95%) OUR LIMIT				
>4560	95	1 SIRUNYAN 21N CMS	pp ; $Z'_\psi \rightarrow e^+ e^-, \mu^+ \mu^-$	
none 250-4500	95	2 AAD 19L ATLS	pp ; $Z'_\psi \rightarrow e^+ e^-, \mu^+ \mu^-$	
none 200-3900	95	3 SIRUNYAN 18BB CMS	pp ; $Z'_\psi \rightarrow e^+ e^-, \mu^+ \mu^-$	
>3800	95	4 AABOUD 17AT ATLS	pp ; $Z'_\psi \rightarrow e^+ e^-, \mu^+ \mu^-$	
>2820	95	5 KHACHATRY...17T CMS	pp ; $Z'_\psi \rightarrow e^+ e^-, \mu^+ \mu^-$	
>1100	95	6 CHATRCHYAN 12o CMS	pp ; $Z'_\psi \rightarrow \tau^+ \tau^-$	
• • • We do not use the following data for averages, fits, limits, etc. • • •				
>2740	95	7 BOBOVNIKOV 18 RVUE	pp ; $Z'_\psi \rightarrow W^+ W^-$	
>2570	95	8 AABOUD 16u ATLS	pp ; $Z'_\psi \rightarrow e^+ e^-, \mu^+ \mu^-$	
>2510	95	9 KHACHATRY...15AE CMS	pp ; $Z'_\psi \rightarrow e^+ e^-, \mu^+ \mu^-$	
>2260	95	10 AAD 14v ATLS	pp ; $Z'_\psi \rightarrow e^+ e^-, \mu^+ \mu^-$	
>1790	95	11 CHATRCHYAN 13AF CMS	pp ; $Z'_\psi \rightarrow e^+ e^-, \mu^+ \mu^-$	
>2000	95	12 AAD 12CC ATLS	pp ; $Z'_\psi \rightarrow e^+ e^-, \mu^+ \mu^-$	
> 917	95	13 CHATRCHYAN 12M CMS	Repl. by CHATRCHYAN 13AF	
> 891	95	14 AALTONEN 11i CDF	$p\bar{p}$; $Z'_\psi \rightarrow \mu^+ \mu^-$	
> 476	95	15 ABAZOV 11A D0	$p\bar{p}$; $Z'_\psi \rightarrow e^+ e^-$	
> 851	95	16 DEL-AGUILA 10 RVUE	Electroweak	
> 878	95	17 AALTONEN 09v CDF	Repl. by AALTONEN 11i	
> 147	95	18 ERLER 09 RVUE	Electroweak	
> 822	95	19 AALTONEN 07H CDF	Repl. by AALTONEN 09T	
> 410	95	20 SCHAE 07A ALEP	$e^+ e^-$	
> 475	95	21 ABDALLAH 06C DLPH	$e^+ e^-$	
> 725	95	22 ABULENCIA 06L CDF	Repl. by AALTONEN 07H	
> 675	95	23 ABULENCIA 05A CDF	Repl. by AALTONEN 11i and AALTONEN 09T	
> 366	95	24 ABBIENDI 04G OPAL	$e^+ e^-$	
> 600	95	25 BARGER 03B COSM	Nucleosynthesis; light ν_R	
> 350	95	26 BARATE 00s DLPH	$e^+ e^-$	
> 294	95	27 ABE 97s ALEP	Repl. by SCHAE 07A	
> 137	95	28 CHO 00 RVUE	Electroweak	
> 146	95	29 ERLER 99 RVUE	Electroweak	
> 54	95	30 CONRAD 98 RVUE	$\nu_\mu N$ scattering	
> 590	95	31 ABE 97s CDF	$p\bar{p}$; $Z'_\psi \rightarrow e^+ e^-, \mu^+ \mu^-$	
> 135	95	32 VILAIN 94b CHM2	$\nu_\mu e \rightarrow \nu_\mu e$; $\bar{\nu}_\mu e \rightarrow \bar{\nu}_\mu e$	
> 105	90	33 ABE 90f VNS	$e^+ e^-$	
[> 160]		34 GONZALEZ... 90D COSM	Nucleosynthesis; light ν_R	
[> 2000]		35 GRIFOLS 90D ASTR	SN 1987A; light ν_R	

- ¹ SIRUNYAN 21N search for resonance decaying to $e^+ e^-, \mu^+ \mu^-$ in pp collisions at $\sqrt{s} = 13$ TeV.
- ² AAD 19L search for resonances decaying to $\ell^+ \ell^-$ in pp collisions at $\sqrt{s} = 13$ TeV.
- ³ SIRUNYAN 18BB search for resonances decaying to $\ell^+ \ell^-$ in pp collisions at $\sqrt{s} = 13$ TeV.
- ⁴ AABOUD 17AT search for resonances decaying to $\ell^+ \ell^-$ in pp collisions at $\sqrt{s} = 13$ TeV.
- ⁵ KHACHATRYAN 17T search for resonances decaying to $e^+ e^-, \mu^+ \mu^-$ in pp collisions at $\sqrt{s} = 8, 13$ TeV.
- ⁶ CHATRCHYAN 12o search for resonances decaying to $\tau^+ \tau^-$ in pp collisions at $\sqrt{s} = 7$ TeV.

- ⁷ BOBOVNIKOV 18 use the ATLAS limits on $\sigma(pp \rightarrow Z') B(Z' \rightarrow W^+ W^-)$ to constrain the Z-Z' mixing parameter ξ . See their Fig. 10 for limits in $M_{Z'} - \xi$ plane.
- ⁸ AABOUD 16u search for resonances decaying to $\ell^+ \ell^-$ in pp collisions at $\sqrt{s} = 13$ TeV.
- ⁹ KHACHATRYAN 15AE search for resonances decaying to $e^+ e^-, \mu^+ \mu^-$ in pp collisions at $\sqrt{s} = 8$ TeV.
- ¹⁰ AAD 14v search for resonances decaying to $e^+ e^-, \mu^+ \mu^-$ in pp collisions at $\sqrt{s} = 8$ TeV.
- ¹¹ CHATRCHYAN 13AF search for resonances decaying to $e^+ e^-, \mu^+ \mu^-$ in pp collisions at $\sqrt{s} = 7$ TeV and 8 TeV.
- ¹² AAD 12CC search for resonances decaying to $e^+ e^-, \mu^+ \mu^-$ in pp collisions at $\sqrt{s} = 7$ TeV.
- ¹³ CHATRCHYAN 12M search for resonances decaying to $e^+ e^-$ or $\mu^+ \mu^-$ in pp collisions at $\sqrt{s} = 7$ TeV.
- ¹⁴ AALTONEN 11i search for resonances decaying to $\mu^+ \mu^-$ in $p\bar{p}$ collisions at $\sqrt{s} = 1.96$ TeV.
- ¹⁵ ABAZOV 11A, AALTONEN 09T, AALTONEN 07H, and ABULENCIA 06L search for resonances decaying to $e^+ e^-$ in $p\bar{p}$ collisions at $\sqrt{s} = 1.96$ TeV.
- ¹⁶ DEL-AGUILA 10 give 95% CL limit on the Z-Z' mixing $-0.0019 < \theta < 0.0007$.
- ¹⁷ AALTONEN 09v search for resonances decaying to $\mu^+ \mu^-$ in $p\bar{p}$ collisions at $\sqrt{s} = 1.96$ TeV.
- ¹⁸ ERLER 09 give 95% CL limit on the Z-Z' mixing $-0.0018 < \theta < 0.0009$.
- ¹⁹ ABDALLAH 06c give 95% CL limit $|\theta| < 0.0027$. See their Fig. 14 for limit contours in the mass-mixing plane.
- ²⁰ ABULENCIA 05A search for resonances decaying to electron or muon pairs in $p\bar{p}$ collisions at $\sqrt{s} = 1.96$ TeV.
- ²¹ ABBIENDI 04G give 95% CL limit on Z-Z' mixing $-0.00129 < \theta < 0.00258$. See their Fig. 20 for the limit contour in the mass-mixing plane. $\sqrt{s} = 91$ to 207 GeV.
- ²² BARGER 03B limit is from the nucleosynthesis bound on the effective number of light neutrino $\delta N_\nu < 1$. The quark-hadron transition temperature $T_C=150$ MeV is assumed. The limit with $T_C=400$ MeV is >1100 GeV.
- ²³ ABREU 00s give 95% CL limit on Z-Z' mixing $|\theta| < 0.0018$. See their Fig. 6 for the limit contour in the mass-mixing plane. $\sqrt{s} = 90$ to 189 GeV.
- ²⁴ BARATE 00i search for deviations in cross section and asymmetries in $e^+ e^- \rightarrow$ fermions at $\sqrt{s}=90$ to 183 GeV. Assume $\theta=0$. Bounds in the mass-mixing plane are shown in their Figure 18.
- ²⁵ CHO 00 use various electroweak data to constrain Z' models assuming $m_H=100$ GeV. See Fig. 3 for limits in the mass-mixing plane.
- ²⁶ ERLER 99 give 90% CL limit on the Z-Z' mixing $-0.0013 < \theta < 0.0024$.
- ²⁷ CONRAD 98 limit is from measurements at CCFR, assuming no Z-Z' mixing.
- ²⁸ ABE 97s find $\sigma(Z') \times B(e^+ e^-, \mu^+ \mu^-) < 40$ fb for $m_{Z'} > 600$ GeV at $\sqrt{s} = 1.8$ TeV.
- ²⁹ VILAIN 94b assume $m_t = 150$ GeV and $\theta = 0$. See Fig. 2 for limit contours in the mass-mixing plane.
- ³⁰ ABE 90f use data for R , $R_{\ell\ell}$, and $A_{\ell\ell}$. ABE 90f fix $m_W = 80.49 \pm 0.43 \pm 0.24$ GeV and $m_Z = 91.13 \pm 0.03$ GeV.
- ³¹ Assumes the nucleosynthesis bound on the effective number of light neutrinos ($\delta N_\nu < 1$) and that ν_R is light ($\lesssim 1$ MeV).
- ³² GRIFOLS 90d limit holds for $m_{\nu_R} \lesssim 1$ MeV. See also RIZZO 91.

Limits for Z_η

Z_η is the extra neutral boson in E_6 models, corresponding to $Q_\eta = \sqrt{3/8} Q_\chi - \sqrt{5/8} Q_\psi$. $g_\eta = e/\cos\theta_W$ is assumed unless otherwise stated. We list limits with the assumption $\rho = 1$ but with no further constraints on the Higgs sector. Values in parentheses assume stronger constraint on the Higgs sector motivated by superstring models. Values in brackets are from cosmological and astrophysical considerations and assume a light right-handed neutrino.

VALUE (GeV)	CL%	DOCUMENT ID	TECN	COMMENT
>3900				
	95	1 AABOUD 17AT ATLS	pp ; $Z'_\eta \rightarrow e^+ e^-, \mu^+ \mu^-$	
• • • We do not use the following data for averages, fits, limits, etc. • • •				
	95	2 BOBOVNIKOV 18 RVUE	pp ; $Z'_\eta \rightarrow W^+ W^-$	
>2810	95	3 AABOUD 16u ATLS	pp ; $Z'_\eta \rightarrow e^+ e^-, \mu^+ \mu^-$	
>1870	95	4 AAD 12CC ATLS	pp ; $Z'_\eta \rightarrow e^+ e^-, \mu^+ \mu^-$	
> 938	95	5 AALTONEN 11i CDF	$p\bar{p}$; $Z'_\eta \rightarrow \mu^+ \mu^-$	
> 923	95	6 ABAZOV 11A D0	$p\bar{p}$; $Z'_\eta \rightarrow e^+ e^-$	
> 488	95	7 DEL-AGUILA 10 RVUE	Electroweak	
> 877	95	8 AALTONEN 09T CDF	$p\bar{p}$; $Z'_\eta \rightarrow e^+ e^-$	
> 904	95	9 AALTONEN 09v CDF	Repl. by AALTONEN 11i	
> 427	95	10 ERLER 09 RVUE	Electroweak	
> 891	95	11 AALTONEN 07H CDF	Repl. by AALTONEN 09T	
> 350	95	12 SCHAE 07A ALEP	$e^+ e^-$	
> 360	95	13 ABDALLAH 06C DLPH	$e^+ e^-$	
> 745	95	14 ABULENCIA 06L CDF	Repl. by AALTONEN 07H	
> 720	95	15 ABULENCIA 05A CDF	Repl. by AALTONEN 11i and AALTONEN 09T	
> 515	95	16 ABBIENDI 04G OPAL	$e^+ e^-$	
>1600		17 BARGER 03B COSM	Nucleosynthesis; light ν_R	
> 310	95	18 ABREU 00s DLPH	$e^+ e^-$	
> 329	95	19 BARATE 00i ALEP	Repl. by SCHAE 07A	
> 619	95	20 CHO 00 RVUE	Electroweak	
> 365	95	21 ERLER 99 RVUE	Electroweak	
> 87	95	22 CONRAD 98 RVUE	$\nu_\mu N$ scattering	
> 620	95	23 ABE 97s CDF	$p\bar{p}$; $Z'_\eta \rightarrow e^+ e^-, \mu^+ \mu^-$	
> 100	95	24 VILAIN 94b CHM2	$\nu_\mu e \rightarrow \nu_\mu e$; $\bar{\nu}_\mu e \rightarrow \bar{\nu}_\mu e$	
> 125	90	25 ABE 90f VNS	$e^+ e^-$	
[> 820]		26 GONZALEZ... 90D COSM	Nucleosynthesis; light ν_R	
[> 3300]		27 GRIFOLS 90 ASTR	SN 1987A; light ν_R	
[> 1040]		28 LOPEZ 90 COSM	Nucleosynthesis; light ν_R	

- ¹ AABOUD 17AT search for resonances decaying to $\ell^+ \ell^-$ in pp collisions at $\sqrt{s} = 13$ TeV.

See key on page 1127

Gauge & Higgs Boson Particle Listings
New Heavy Bosons

- 2 BOBOVNIKOV 18 use the ATLAS limits on $\sigma(pp \to Z')\cdot B(Z' \to W^+W^-)$ to constrain the Z - Z' mixing parameter ξ . See their Fig. 9 for limits in $M_{Z'}-\xi$ plane.
3 AABOUD 16U search for resonances decaying to $\ell^+\ell^-$ in pp collisions at $\sqrt{s} = 13$ TeV.
4 AAD 12CC search for resonances decaying to $e^+e^-, \mu^+\mu^-$ in pp collisions at $\sqrt{s} = 7$ TeV.
5 AALTONEN 11I search for resonances decaying to $\mu^+\mu^-$ in $p\bar{p}$ collisions at $\sqrt{s} = 1.96$ TeV.
6 ABAZOV 11A, AALTONEN 09T, AALTONEN 07H, and ABULENCIA 06L search for resonances decaying to e^+e^- in $p\bar{p}$ collisions at $\sqrt{s} = 1.96$ TeV.
7 DEL-AGUILA 10 give 95% CL limit on the Z - Z' mixing $-0.0023 < \theta < 0.0027$.
8 AALTONEN 09V search for resonances decaying to $\mu^+\mu^-$ in $p\bar{p}$ collisions at $\sqrt{s} = 1.96$ TeV.
9 ERLER 09 give 95% CL limit on the Z - Z' mixing $-0.0047 < \theta < 0.0021$.
10 ABDALLAH 06C give 95% CL limit $|\theta| < 0.0092$. See their Fig. 14 for limit contours in the mass-mixing plane.
11 ABULENCIA 05A search for resonances decaying to electron or muon pairs in $p\bar{p}$ collisions at $\sqrt{s} = 1.96$ TeV.
12 ABBIENDI 04G give 95% CL limit on Z - Z' mixing $-0.00447 < \theta < 0.00331$. See their Fig. 20 for the limit contour in the mass-mixing plane. $\sqrt{s} = 91$ to 207 GeV.
13 BARGER 03B limit is from the nucleosynthesis bound on the effective number of light neutrino $\delta N_{\nu} < 1$. The quark-hadron transition temperature $T_C=150$ MeV is assumed. The limit with $T_C=400$ MeV is >3300 GeV.
14 ABREU 00s give 95% CL limit on Z - Z' mixing $|\theta| < 0.0024$. See their Fig. 6 for the limit contour in the mass-mixing plane. $\sqrt{s}=90$ to 189 GeV.
15 BARATE 00i search for deviations in cross section and asymmetries in $e^+e^- \to$ fermions at $\sqrt{s}=90$ to 183 GeV. Assume $\theta=0$. Bounds in the mass-mixing plane are shown in their Figure 18.
16 CHO 00 use various electroweak data to constrain Z' models assuming $m_H=100$ GeV. See Fig. 3 for limits in the mass-mixing plane.
17 ERLER 99 give 90% CL limit on the Z - Z' mixing $-0.0062 < \theta < 0.0011$.
18 CONRAD 98 limit is from measurements at CCFR, assuming no Z - Z' mixing.
19 ABE 97s find $\sigma(Z')\cdot B(e^+e^-, \mu^+\mu^-) < 40$ fb for $m_{Z'} > 600$ GeV at $\sqrt{s}=1.8$ TeV.
20 VILAIN 94B assume $m_t = 150$ GeV and $\theta=0$. See Fig. 2 for limit contours in the mass-mixing plane.
21 ABE 90F use data for $R, R_{\ell\ell}$, and $A_{\ell\ell}$. ABE 90F fix $m_W = 80.49 \pm 0.43 \pm 0.24$ GeV and $m_Z = 91.13 \pm 0.03$ GeV.
22 These authors claim that the nucleosynthesis bound on the effective number of light neutrinos ($\delta N_{\nu} < 1$) constrains Z' masses if ν_R is light ($\lesssim 1$ MeV).
23 GRIFOLS 90 limit holds for $m_{\nu_R} \lesssim 1$ MeV. See also GRIFOLS 90D, RIZZO 91.

Limits for other Z'

Table with columns: VALUE (GeV), CL%, DOCUMENT ID, TECN, COMMENT. Lists various Z' boson limits from different experiments like ATLAS, CMS, etc.

... We do not use the following data for averages, fits, limits, etc. ...

Table listing Z' models and their constraints, including AAD 22 ATLS, 25 AAD 21AQ ATLS, etc.

Main table listing Z' boson decays and constraints from experiments like ATLAS, CMS, LHCb, etc. Columns include document ID, experiment, decay mode, and constraint values.

- 1 SIRUNYAN 21X search for resonances decaying to HZ in pp collisions at $\sqrt{s} = 13$ TeV. The limit quoted above is for heavy-vector-triplet Z' with $g_V = 3$. The limit becomes $M_{Z'} > 3500$ GeV for $g_V = 1$.
2 AAD 20AJ search for resonances decaying to HZ in pp collisions at $\sqrt{s} = 13$ TeV. The quoted limit is for heavy-vector-triplet Z' with $g_V = 3$. The limit becomes $M_{Z'} > 2200$ GeV for $g_V = 1$. See their Fig. 6 for limits on $\sigma\cdot B$.
3 AAD 20AM search for a resonance decaying to $t\bar{t}$ in pp collisions at $\sqrt{s} = 13$ TeV. The quoted limit is for a leptophobic top-color Z' with $\Gamma_{Z'}/M_{Z'} = 0.01$. The limit becomes $M_{Z'} > 4700$ GeV for $\Gamma_{Z'}/M_{Z'} = 0.03$.
4 AAD 20AT search for resonances decaying to WW in pp collisions at $\sqrt{s} = 13$ TeV. The quoted limit is for heavy-vector-triplet Z' with $g_V = 3$. The limit becomes $M_{Z'} > 3500$ GeV for $g_V = 1$. See their Fig. 14 for limits on $\sigma\cdot B$.
5 SIRUNYAN 20q search for resonances decaying to WW in pp collisions at $\sqrt{s} = 13$ TeV. The quoted limit is for heavy-vector-triplet Z' with $g_V = 3$.
6 AABOUD 19As search for a resonance decaying to $t\bar{t}$ in pp collisions at $\sqrt{s} = 13$ TeV. The quoted limit is for a top-color Z' with $\Gamma_{Z'}/M_{Z'} = 0.01$. Limits are also set on Z' masses in simplified Dark Matter models.

Gauge & Higgs Boson Particle Listings

New Heavy Bosons

- 7 AAD 19d search for resonances decaying to WW in pp collisions at $\sqrt{s} = 13$ TeV. The quoted limit is for heavy-vector-triplet Z' with $g_V = 3$. The limit becomes $M_{Z'} > 2900$ GeV for $g_V = 1$. If we assume $M_{Z'} = M_{W'}$, the limit increases $M_{Z'} > 3800$ GeV and $M_{Z'} > 3500$ GeV for $g_V = 3$ and $g_V = 1$, respectively. See their Fig. 9 for limits on $\sigma \cdot B$.
- 8 SIRUNYAN 19AA search for a resonance decaying to $t\bar{t}$ in pp collisions at $\sqrt{s} = 13$ TeV. The quoted limit is for a leptophobic top-color Z' with $\Gamma_{Z'}/M_{Z'} = 0.01$.
- 9 SIRUNYAN 19CP present a statistical combinations of searches for Z' decaying to pairs of bosons or leptons in pp collisions at $\sqrt{s} = 13$ TeV. The quoted limit is for heavy-vector-triplet Z' with $g_V = 3$. If we assume $M_{Z'} = M_{W'}$, the limit becomes $M_{Z'} > 4500$ GeV for $g_V = 3$ and $M_{Z'} > 5000$ GeV for $g_V = 1$. See their Figs. 2 and 3 for limits on $\sigma \cdot B$.
- 10 SIRUNYAN 19I search for resonances decaying to ZW in pp collisions at $\sqrt{s} = 13$ TeV. The quoted limit is for heavy-vector-triplet Z' with $g_V = 3$. The limit becomes $M_{Z'} > 2800$ GeV if we assume $M_{Z'} = M_{W'}$.
- 11 AABOUD 18AB search for resonances decaying to $b\bar{b}$ in pp collisions at $\sqrt{s} = 13$ TeV. The limit quoted above is for a leptophobic Z' with SM-like couplings to quarks. See their Fig. 6 for limits on $\sigma \cdot B$. Additional limits on a Z' axial-vector mediator in a simplified dark-matter model are shown in Fig. 7.
- 12 AABOUD 18AI search for resonances decaying to HZ in pp collisions at $\sqrt{s} = 13$ TeV. The quoted limit is for heavy-vector-triplet Z' with $g_V = 3$. The limit becomes $M_{Z'} > 2650$ GeV for $g_V = 1$. If we assume $M_{W'} = M_{Z'}$, the limit increases $M_{Z'} > 2930$ GeV and $M_{Z'} > 2800$ GeV for $g_V = 3$ and $g_V = 1$, respectively. See their Fig. 5 for limits on $\sigma \cdot B$.
- 13 AABOUD 18AK search for resonances decaying to WW in pp collisions at $\sqrt{s} = 13$ TeV. The limit quoted above is for heavy-vector-triplet Z' with $g_V = 3$. The limit becomes $M_{Z'} > 2750$ GeV for $g_V = 1$.
- 14 AABOUD 18B search for resonances decaying to WW in pp collisions at $\sqrt{s} = 13$ TeV. The quoted limit is for heavy-vector-triplet Z' with $g_V = 1$. See their Fig. 11 for limits on $\sigma \cdot B$.
- 15 AABOUD 18BI search for a resonance decaying to $t\bar{t}$ in pp collisions at $\sqrt{s} = 13$ TeV. The quoted limit is for a top-color assisted TC Z' with $\Gamma_{Z'}/M_{Z'} = 0.01$. The limits for wider resonances are available. See their Fig. 14 for limits on $\sigma \cdot B$.
- 16 AABOUD 18F search for resonances decaying to WW in pp collisions at $\sqrt{s} = 13$ TeV. The quoted limit is for heavy-vector-triplet Z' with $g_V = 3$. The limit becomes $M_{Z'} > 2200$ GeV for $g_V = 1$. If we assume $M_{Z'} = M_{W'}$, the limit increases $M_{Z'} > 3500$ GeV and $M_{Z'} > 3100$ GeV for $g_V = 3$ and $g_V = 1$, respectively. See their Fig. 5 for limits on $\sigma \cdot B$.
- 17 SIRUNYAN 18ED search for resonances decaying to HZ in pp collisions at $\sqrt{s} = 13$ TeV. The limit above is for heavy-vector-triplet Z' with $g_V = 3$. If we assume $M_{Z'} = M_{W'}$, the limit increases $M_{Z'} > 2900$ GeV and $M_{Z'} > 2800$ GeV for $g_V = 3$ and $g_V = 1$, respectively.
- 18 SIRUNYAN 18P give this limit for a heavy-vector-triplet Z' with $g_V = 3$. If we assume $M_{Z'} = M_{W'}$, the limit increases to $M_{Z'} > 3800$ GeV.
- 19 AABOUD 17AK search for a new resonance decaying to dijets in pp collisions at $\sqrt{s} = 13$ TeV. The limit quoted above is for a leptophobic Z' boson having axial-vector coupling strength with quarks $g_q = 0.2$. The limit is 2100 GeV if $g_q = 0.1$.
- 20 AABOUD 17AO search for resonances decaying to HZ in pp collisions at $\sqrt{s} = 13$ TeV. The limit quoted above is for a Z' in the heavy-vector-triplet model with $g_V = 3$. See their Fig. 4 for limits on $\sigma \cdot B$.
- 21 SIRUNYAN 17AK search for resonances decaying to WW or HZ in pp collisions at $\sqrt{s} = 8$ and 13 TeV. The quoted limit is for heavy-vector-triplet Z' with $g_V = 3$. The limit becomes $M_{Z'} > 2200$ GeV for $g_V = 1$. If we assume $M_{Z'} = M_{W'}$, the limit increases $M_{Z'} > 2400$ GeV for both $g_V = 3$ and $g_V = 1$. See their Fig. 1 and 2 for limits on $\sigma \cdot B$.
- 22 SIRUNYAN 17Q search for a resonance decaying to $t\bar{t}$ in pp collisions at $\sqrt{s} = 13$ TeV. The limit quoted above is for a resonance with relative width $\Gamma_{Z'}/M_{Z'} = 0.01$. Limits for wider resonances are available. See their Fig. 6 for limits on $\sigma \cdot B$.
- 23 SIRUNYAN 17R search for resonances decaying to HZ in pp collisions at $\sqrt{s} = 13$ TeV. The quoted limit is for heavy-vector-triplet Z' with $g_V = 3$. Mass regions $M_{Z'} < 1150$ GeV and 1250 GeV $< M_{Z'} < 1670$ GeV are excluded for $g_V = 1$. If we assume $M_{Z'} = M_{W'}$, the excluded mass regions are $1000 < M_{Z'} < 2500$ GeV and $2760 < M_{Z'} < 3300$ GeV for $g_V = 3$; $1000 < M_{Z'} < 2430$ GeV and $2810 < M_{Z'} < 3130$ GeV for $g_V = 1$. See their Fig. 5 for limits on $\sigma \cdot B$.
- 24 AAD 22 search for $b\bar{b}Z'$ productions in pp collisions at $\sqrt{s} = 13$ TeV. Z' is assumed to decay into $b\bar{b}$. See their Fig. 4 for limits on $\sigma \cdot B$.
- 25 AAD 21AQ limits are for a $B-L$ gauge boson model derived from their measurements on four-lepton differential cross sections. See their Fig. 13 for exclusion limits on the $B-L$ breaking Higgs boson mass.
- 26 AAD 21AZ search for DM mediator Z' produced in association with a SM Higgs boson in pp collisions at $\sqrt{s} = 13$ TeV. Z' is assumed to decay invisibly $Z' \rightarrow \chi\chi$. See their Fig. 7 for limits in $M_{Z'} - M_\chi$ plane.
- 27 AAD 21BB search for Z' productions in pp collisions at $\sqrt{s} = 13$ TeV. Z' is assumed to decay into a SM Higgs boson H and an invisible particle A . See their Fig. 7 for limits in $M_{Z'} - M_A$ plane.
- 28 AAD 21d set limits on a dark Higgs model with a spin-1 mediator Z' and a scalar dark Higgs boson s . Dark Higgs s is assumed to decay into WW or ZZ . See their Fig. 4 for limits in $M_{Z'} - M_s$ plane.
- 29 AAD 21k search for $\gamma + \cancel{E}_T$ events in pp collision at $\sqrt{s} = 13$ TeV. See their Fig. 5 for limits on Z' particle invisibly decaying to $\chi\chi$.
- 30 BURAS 21 performed global fit to leptophilic Z' models using a large number of observables.
- 31 CADEDDU 21 obtain limits on Z' coupling $g_{Z'}$ from coherent ν -nucleus scattering data collected by COHERENT experiment. For limits in the $M_{Z'} - g_{Z'}$ plane, see their Figures 3 and 4 for the universal Z' model and Figures 5 and 6 for the $B-L$ model.
- 32 COLARESI 21 obtain limits on Z' coupling from coherent ν -nucleus scattering data collected by a Ge detector at the Dresden-II power reactor. See their Fig. 7 for limits in mass-coupling plane.
- 33 KRIBS 21 set decay-agnostic limits on kinetic mixing parameter between $U(1)_Y$ field and new heavy abelian vector boson (dark photon) field using the HERA ep collision data. See their Fig. 3 for limits in mass-mixing plane.
- 34 TUMASYAN 21D search for energetic jets + \cancel{E}_T events in pp collisions at $\sqrt{s} = 13$ TeV. Z' is assumed to decay into a pair of invisible particles $\chi\chi$. See their Fig. 7 for limits on signal strength in $M_{Z'} - M_\chi$ plane, and Fig. 8 for limits on signal strength in quark and dark matter coupling vs mediator mass.
- 35 AAD 20AF search for resonances decaying to $H\gamma$ in pp collisions at $\sqrt{s} = 13$ TeV. See their Fig. 1c for limits on $\sigma \cdot B$ for the mass range $0.7 < m_{Z'} < 4$ TeV.
- 36 AAD 20T search for Dark Matter mediator Z' decaying invisibly or decaying to $q\bar{q}$ in pp collisions at $\sqrt{s} = 13$ TeV. See their Fig. 5 for limits in $M_{Z'} - g_q$ plane from the inclusive category. See their Fig. 7(a) for limits on the product of the cross section, acceptance, b -tagging efficiency, and branching fraction from the $2b$ -tag category.
- 37 AAD 20W search for a Dark Matter (DM) simplified model Z' produced in association with W in pp collisions at $\sqrt{s} = 13$ TeV. See their Fig. 5 for limits on Z' production cross section.
- 38 AAIJ 20AL search for spin-0 and spin-1 resonances decaying to $\mu^+\mu^-$ in pp collisions at $\sqrt{s} = 13$ TeV in the mass regions $M_{Z'} < 60$ GeV, with non-negligible widths considered above 20 GeV. See their Figs. 7, 8, and 9 for limits on $\sigma \cdot B$.
- 39 ADACHI 20 search for production of Z' in e^+e^- collisions. The Z' is assumed to decay invisibly. See their Fig. 3 and Fig. 5 for limits on Z' coupling and $\sigma(e^+e^- \rightarrow e^+\mu^+\mu^-Z')$.
- 40 SIRUNYAN 20AI search for broad resonances decaying into dijets in pp collisions at $\sqrt{s} = 13$ TeV. See their Fig. 11 for exclusion limits in mass-coupling plane.
- 41 SIRUNYAN 20AQ search for a narrow resonance lighter than 200 GeV decaying to $\mu^+\mu^-$ in pp collisions at $\sqrt{s} = 13$ TeV. See their Fig. 3 for limits on Z' kinetic mixing coefficient.
- 42 SIRUNYAN 20M search for a narrow resonance with a mass between 350 and 700 GeV in pp collisions at $\sqrt{s} = 13$ TeV. See their Fig. 3 for exclusion limits in mass-coupling plane.
- 43 AABOUD 19AJ search in pp collisions at $\sqrt{s} = 13$ TeV for a new resonance decaying to $q\bar{q}$ and produced in association with a high p_T photon. For a leptophobic axial-vector Z' in the mass region 250 GeV $< M_{Z'} < 950$ GeV, the Z' coupling with quarks g_q is constrained below 0.18. See their Fig. 2 for limits in $M_{Z'} - g_q$ plane.
- 44 AABOUD 19D search in pp collisions at $\sqrt{s} = 13$ TeV for a new resonance decaying to $q\bar{q}$ and produced in association with a high- p_T photon or jet. For a leptophobic axial-vector Z' in the mass region 100 GeV $< M_{Z'} < 220$ GeV, the Z' coupling with quarks g_q is constrained below 0.23. See their Fig. 6 for limits in $M_{Z'} - g_q$ plane.
- 45 AABOUD 19V search for Dark Matter simplified Z' decaying invisibly or decaying to fermion pair in pp collisions at $\sqrt{s} = 13$ TeV.
- 46 AAD 19L search for resonances decaying to $t^+\bar{t}^-$ in pp collisions at $\sqrt{s} = 13$ TeV. See their Fig. 4 for limits in the heavy vector triplet model couplings.
- 47 LONG 19 uses the weak charge data of Cesium and proton to constrain mass of Z' in the 3-3.1 models.
- 48 PANDEV 19 obtain limits on Z' induced neutrino non-standard interaction (NSI) parameter ϵ from LHC and IceCube data. See their Fig. 2 for limits in $M_{Z'} - \epsilon$ plane, where $\epsilon = g_q g_\nu v^2 / (2 M_{Z'}^2)$.
- 49 SIRUNYAN 19AL search for a new resonance decaying to a top quark and a heavy vector-like top partner in pp collisions at $\sqrt{s} = 13$ TeV. See their Fig. 8 for limits on Z' production cross section.
- 50 SIRUNYAN 19AN search for a Dark Matter (DM) simplified model Z' decaying to H DM in pp collisions at $\sqrt{s} = 13$ TeV. See their Fig. 7 for limits on the signal strength modifiers.
- 51 SIRUNYAN 19CB search in pp collisions at $\sqrt{s} = 13$ TeV for a new resonance decaying to $q\bar{q}$. For a leptophobic Z' in the mass region 50–300 GeV, the Z' coupling with quarks g'_q is constrained below 0.2. See their Figs. 4 and 5 for limits on g'_q in the mass range $50 < M_{Z'} < 450$ GeV.
- 52 SIRUNYAN 19CD search in pp collisions at $\sqrt{s} = 13$ TeV for a leptophobic Z' produced in association of high p_T ISR photon and decaying to $q\bar{q}$. See their Fig. 2 for limits on the Z' coupling strength g'_q to $q\bar{q}$ in the mass range between 10 and 125 GeV.
- 53 SIRUNYAN 19D search for a narrow neutral vector resonance decaying to $H\gamma$. See their Fig. 3 for exclusion limit in $M_{Z'} - \sigma \cdot B$ plane. Upper limits on the production of $H\gamma$ resonances are set as a function of the resonance mass in the range of 720–3250 GeV.
- 54 AABOUD 18AA search for a narrow neutral vector boson decaying to $H\gamma$. See their Fig. 10 for the exclusion limit in $M_{Z'} - \sigma \cdot B$ plane.
- 55 AABOUD 18CJ search for heavy-vector-triplet Z' in pp collisions at $\sqrt{s} = 13$ TeV. The limit quoted above is for model with $g_V = 3$ assuming $M_{Z'} = M_{W'}$. The limit becomes $M_{Z'} > 5500$ GeV for model with $g_V = 1$.
- 56 AABOUD 18N search for a narrow resonance decaying to $q\bar{q}$ in pp collisions at $\sqrt{s} = 13$ TeV using trigger level analysis to improve the low mass region sensitivity. See their Fig. 5 for limits in the mass-coupling plane in the Z' mass range 450–1800 GeV.
- 57 AAIJ 18AQ search for spin-0 and spin-1 resonances decaying to $\mu^+\mu^-$ in pp collisions at $\sqrt{s} = 7$ and 8 TeV in the mass region near 10 GeV. See their Figs. 4 and 5 for limits on $\sigma \cdot B$.
- 58 SIRUNYAN 18DR searches for $\mu^+\mu^-$ resonances produced in association with b -jets in the pp collision data with $\sqrt{s} = 8$ TeV and 13 TeV. An excess of events near $m_{\mu\mu} = 28$ GeV is observed in the 8 TeV data. See their Fig. 3 for the measured fiducial signal cross sections at $\sqrt{s} = 8$ TeV and the 95% CL upper limits at $\sqrt{s} = 13$ TeV.
- 59 SIRUNYAN 18G search for a new resonance decaying to dijets in pp collisions at $\sqrt{s} = 13$ TeV in the mass range 50–300 GeV. See their Fig. 7 for limits in the mass-coupling plane.
- 60 SIRUNYAN 18I search for a narrow resonance decaying to $b\bar{b}$ in pp collisions at $\sqrt{s} = 8$ TeV using dedicated b -tagged dijet triggers to improve the sensitivity in the low mass region. See their Fig. 3 for limits on $\sigma \cdot B$ in the Z' mass range 325–1200 GeV.
- 61 AABOUD 17B search for resonances decaying to HZ ($H \rightarrow b\bar{b}, c\bar{c}, Z \rightarrow t^+\bar{t}^-, \nu\bar{\nu}$) in pp collisions at $\sqrt{s} = 13$ TeV. The quoted limit is for heavy-vector-triplet Z' with

- $g_V = 3$. The limit becomes $M_{Z'} > 1490$ GeV for $g_V = 1$. If we assume $M_{Z'} = M_{W'}$, the limit increases $M_{Z'} > 2310$ GeV and $M_{Z'} > 1730$ GeV for $g_V = 3$ and $g_V = 1$, respectively. See their Fig.3 for limits on $\sigma \cdot B$.
- 62 KHACHATRYAN 17AX search for lepto-phobic resonances decaying to four leptons in pp collisions at $\sqrt{s} = 8$ TeV.
- 63 KHACHATRYAN 17U search for resonances decaying to HZ ($H \rightarrow b\bar{b}$; $Z \rightarrow \ell^+ \ell^-$, $\nu\bar{\nu}$) in pp collisions at $\sqrt{s} = 13$ TeV. The limit on the heavy-vector-triplet model is $M_{Z'} = M_{W'} > 2$ TeV for $g_V = 3$, in which constraints from the $W' \rightarrow HW$ ($H \rightarrow b\bar{b}$; $W \rightarrow \ell\nu$) are combined. See their Fig.3 and Fig.4 for limits on $\sigma \cdot B$.
- 64 SIRUNYAN 17A search for resonances decaying to WW with $WW \rightarrow \ell\nu q\bar{q}$, $q\bar{q}q\bar{q}$ in pp collisions at $\sqrt{s} = 13$ TeV. The quoted limit is for heavy-vector-triplet Z' with $g_V = 3$. The limit becomes $M_{Z'} > 1600$ GeV for $g_V = 1$. If we assume $M_{Z'} = M_{W'}$, the limit increases $M_{Z'} > 2400$ GeV and $M_{Z'} > 2300$ GeV for $g_V = 3$ and $g_V = 1$, respectively. See their Fig.6 for limits on $\sigma \cdot B$.
- 65 SIRUNYAN 17AP search for resonances decaying into a SM-like Higgs scalar H and a light pseudo scalar A . A is assumed to decay invisibly. See their Fig.9 for limits on $\sigma \cdot B$.
- 66 SIRUNYAN 17T search for a new resonance decaying to dijets in pp collisions at $\sqrt{s} = 13$ TeV in the mass range 100–300 GeV. See their Fig.3 for limits in the mass-coupling plane.
- 67 SIRUNYAN 17V search for a new resonance decaying to a top quark and a heavy vector-like top partner T in pp collisions at $\sqrt{s} = 13$ TeV. See their table 5 for limits on the Z' production cross section for various values of $M_{Z'}$ and M_T in the range of $M_{Z'} = 1500$ –2500 GeV and $M_T = 700$ –1500 GeV.
- 68 AABOUD 16 search for a narrow resonance decaying into $b\bar{b}$ in pp collisions at $\sqrt{s} = 13$ TeV. The limit quoted above is for a leptophobic Z' with SM-like couplings to quarks. See their Fig.6 for limits on $\sigma \cdot B$.
- 69 AAD 16L search for $Z' \rightarrow a\gamma$, $a \rightarrow \gamma\gamma$ in pp collisions at $\sqrt{s} = 8$ TeV. See their Table 6 for limits on $\sigma \cdot B$.
- 70 AAD 16S search for a new resonance decaying to dijets in pp collisions at $\sqrt{s} = 13$ TeV. The limit quoted above is for a leptophobic Z' having coupling strength with quark $g_Q = 0.3$ and is taken from their Figure 3.
- 71 KHACHATRYAN 16AP search for a resonance decaying to HZ in pp collisions at $\sqrt{s} = 8$ TeV. Both H and Z' are assumed to decay to fat jets. The quoted limit is for heavy-vector-triplet Z' with $g_V = 3$.
- 72 KHACHATRYAN 16E search for a leptophobic top-color Z' decaying to $t\bar{t}$ using pp collisions at $\sqrt{s} = 8$ TeV. The quoted limit assumes that $\Gamma_{Z'}/m_{Z'} = 0.012$. Also $m_{Z'} < 2.9$ TeV is excluded for wider topcolor Z' with $\Gamma_{Z'}/m_{Z'} = 0.1$.
- 73 AAD 15A0 search for narrow resonance decaying to $t\bar{t}$ using pp collisions at $\sqrt{s} = 8$ TeV. See Fig. 11 for limit on σB .
- 74 AAD 15AT search for monoton production plus large missing E_T events in pp collisions at $\sqrt{s} = 8$ TeV and give constraints on a Z' model having $Z' u\bar{t}$ coupling. Z' is assumed to decay invisibly. See their Fig. 6 for limits on $\sigma \cdot B$.
- 75 AAD 15CD search for decays of Higgs bosons to 4ℓ states via Z' bosons, $H \rightarrow Z' Z' \rightarrow 4\ell$ or $H \rightarrow Z' Z' \rightarrow 4\ell$. See Fig. 5 for the limit on the signal strength of the $H \rightarrow Z' Z' \rightarrow 4\ell$ process and Fig. 16 for the limit on $H \rightarrow Z' Z' \rightarrow 4\ell$.
- 76 KHACHATRYAN 15F search for monoton production plus large missing E_T events in pp collisions at $\sqrt{s} = 8$ TeV and give constraints on a Z' model having $Z' u\bar{t}$ coupling. Z' is assumed to decay invisibly. See Fig. 3 for limits on σB .
- 77 KHACHATRYAN 15O search for narrow Z' resonance decaying to ZH in pp collisions at $\sqrt{s} = 8$ TeV. See their Fig. 6 for limit on σB .
- 78 AAD 14AT search for a narrow neutral vector boson decaying to $Z\gamma$. See their Fig. 3b for the exclusion limit in $m_{Z'} - \sigma B$ plane.
- 79 KHACHATRYAN 14A search for new resonance in the WW ($\ell\nu q\bar{q}$) and the ZZ ($\ell\ell q\bar{q}$) channels using pp collisions at $\sqrt{s} = 8$ TeV. See their Fig.13 for the exclusion limit on the number of events in the mass-width plane.
- 80 MARTINEZ 14 use various electroweak data to constrain the Z' boson in the 3-3-1 models.
- 81 AAD 13AQ search for a leptophobic top-color Z' decaying to $t\bar{t}$. The quoted limit assumes that $\Gamma_{Z'}/m_{Z'} = 0.012$.
- 82 CHATRCHYAN 13BM search for top-color Z' decaying to $t\bar{t}$ using pp collisions at $\sqrt{s} = 8$ TeV. The quoted limit is for $\Gamma_{Z'}/m_{Z'} = 0.012$.
- 83 CHATRCHYAN 13AP search for top-color leptophobic Z' decaying to $t\bar{t}$ using pp collisions at $\sqrt{s} = 7$ TeV. The quoted limit is for $\Gamma_{Z'}/m_{Z'} = 0.012$.
- 84 AAD 12BV search for narrow resonance decaying to $t\bar{t}$ using pp collisions at $\sqrt{s} = 7$ TeV. See their Fig. 7 for limit on $\sigma \cdot B$.
- 85 AAD 12K search for narrow resonance decaying to $t\bar{t}$ using pp collisions at $\sqrt{s} = 7$ TeV. See their Fig. 5 for limit on $\sigma \cdot B$.
- 86 AALTONEN 12AR search for chromophilic Z' in $p\bar{p}$ collisions at $\sqrt{s} = 1.96$ TeV. See their Fig. 5 for limit on $\sigma \cdot B$.
- 87 AALTONEN 12N search for $p\bar{p} \rightarrow tZ'$, $Z' \rightarrow t\bar{u}$ events in $p\bar{p}$ collisions. See their Fig. 3 for the limit on $\sigma \cdot B$.
- 88 ABAZOV 12R search for top-color Z' boson decaying exclusively to $t\bar{t}$. The quoted limit is for $\Gamma_{Z'}/m_{Z'} = 0.012$.
- 89 CHATRCHYAN 12AI search for $pp \rightarrow tt$ events and give constraints on a Z' model having $Z' t\bar{t}$ coupling. See their Fig. 4 for the limit in mass-coupling plane.
- 90 Search for resonance decaying to $t\bar{t}$. See their Fig. 6 for limit on $\sigma \cdot B$.
- 91 Search for narrow resonance decaying to $t\bar{t}$. See their Fig. 4 for limit on $\sigma \cdot B$.
- 92 Search for narrow resonance decaying to $t\bar{t}$. See their Fig. 3 for limit on $\sigma \cdot B$.
- 93 CHATRCHYAN 11o search for same-sign top production in pp collisions induced by a hypothetical FCNC Z' at $\sqrt{s} = 7$ TeV. See their Fig. 3 for limit in mass-coupling plane.
- 94 Search for narrow resonance decaying to $t\bar{t}$. See their Fig. 3 for limit on $\sigma \cdot B$.
- 95 Search for narrow resonance decaying to $t\bar{t}$. See their Fig. 2 for limit on $\sigma \cdot B$.
- 96 BARGER 03b use the nucleosynthesis bound on the effective number of light neutrino δN_ν . See their Figs. 4–5 for limits in general E_6 motivated models.
- 97 CHO 00 use various electroweak data to constrain Z' models assuming $m_H = 100$ GeV. See Fig. 2 for limits in general E_6 -motivated models.
- 98 CHO 98 study constraints on four-Fermi contact interactions obtained from low-energy electroweak experiments, assuming no Z - Z' mixing.
- 99 Search for Z' decaying to dijets at $\sqrt{s} = 1.8$ TeV. For Z' with electromagnetic strength coupling, no bound is obtained.

Searches for Z' with Lepton-Flavor-Violating decays

The following limits are obtained from $p\bar{p}$ or $pp \rightarrow Z' X$ with Z' decaying to the mode indicated in the comments.

VALUE	DOCUMENT ID	TECN	COMMENT
• • •	We do not use the following data for averages, fits, limits, etc. • • •		
1	AABOUD 18CMATLS		$Z' \rightarrow e\mu, e\tau, \mu\tau$
2	SIRUNYAN 18AT CMS		$Z' \rightarrow e\mu$
3	AABOUD 16P ATLS		$Z' \rightarrow e\mu, e\tau, \mu\tau$
4	KHACHATRYAN 16BE CMS		$Z' \rightarrow e\mu$
5	AAD 15O ATLS		$Z' \rightarrow e\mu, e\tau, \mu\tau$
6	AAD 11H ATLS		$Z' \rightarrow e\mu$
7	AAD 11Z ATLS		$Z' \rightarrow e\mu$
8	ABULENCIA 06M CDF		$Z' \rightarrow e\mu$

- 1 AABOUD 18CM search for a new particle with lepton-flavor violating decay in pp collisions at $\sqrt{s} = 13$ TeV. See their Figs. 4, 5, and 6 for limits on $\sigma \cdot B$.
- 2 SIRUNYAN 18AT search for a narrow resonance Z' decaying into $e\mu$ in pp collisions at $\sqrt{s} = 13$ TeV. See their Fig.5 for limit on $\sigma \cdot B$ in the range of $600 \text{ GeV} < M_{Z'} < 5000$ GeV.
- 3 AABOUD 16P search for new particle with lepton flavor violating decay in pp collisions at $\sqrt{s} = 13$ TeV. See their Figs. 2, 3, and 4 for limits on $\sigma \cdot B$.
- 4 KHACHATRYAN 16BE search for new particle Z' with lepton flavor violating decay in pp collisions at $\sqrt{s} = 8$ TeV in the range of $200 \text{ GeV} < M_{Z'} < 2000$ GeV. See their Fig.4 for limits on $\sigma \cdot B$ and their Table 5 for bounds on various masses.
- 5 AAD 15O search for new particle Z' with lepton flavor violating decay in pp collisions at $\sqrt{s} = 8$ TeV in the range of $500 \text{ GeV} < M_{Z'} < 3000$ GeV. See their Fig. 2 for limits on σB .
- 6 AAD 11H search for new particle Z' with lepton flavor violating decay in pp collisions at $\sqrt{s} = 7$ TeV in the range of $700 \text{ GeV} < M_{Z'} < 1000$ GeV. See their Fig. 3 for limits on $\sigma \cdot B$.
- 7 AAD 11Z search for new particle Z' with lepton flavor violating decay in pp collisions at $\sqrt{s} = 7$ TeV in the range $700 \text{ GeV} < M_{Z'} < 2000$ GeV. See their Fig. 3 for limits on $\sigma \cdot B$.
- 8 ABULENCIA 06M search for new particle Z' with lepton flavor violating decay in $p\bar{p}$ collisions at $\sqrt{s} = 1.96$ TeV in the range of $100 \text{ GeV} < M_{Z'} < 800$ GeV. See their Fig. 4 for limits in the mass-coupling plane.

Indirect Constraints on Kaluza-Klein Gauge Bosons

Bounds on a Kaluza-Klein excitation of the Z boson or photon in $d=1$ extra dimension. These bounds can also be interpreted as a lower bound on $1/R$, the size of the extra dimension. Unless otherwise stated, bounds assume all fermions live on a single brane and all gauge fields occupy the $4+d$ -dimensional bulk. See also the section on “Extra Dimensions” in the “Searches” Listings in this Review.

VALUE (TeV)	CL%	DOCUMENT ID	TECN	COMMENT
• • •	We do not use the following data for averages, fits, limits, etc. • • •			
> 4.7		1 MUECK 02	RVUE	Electroweak
> 3.3	95	2 CORNET 00	RVUE	$e\nu q q'$
>5000		3 DELGADO 00	RVUE	$e\kappa$
> 2.6	95	4 DELGADO 00	RVUE	Electroweak
> 3.3	95	5 RIZZO 00	RVUE	Electroweak
> 2.9	95	6 MARCIANO 99	RVUE	Electroweak
> 2.5	95	7 MASIP 99	RVUE	Electroweak
> 1.6	90	8 NATH 99	RVUE	Electroweak
> 3.4	95	9 STRUMIA 99	RVUE	Electroweak

- 1 MUECK 02 limit is 2σ and is from global electroweak fit ignoring correlations among observables. Higgs is assumed to be confined on the brane and its mass is fixed. For scenarios of bulk Higgs, of brane-SU(2) $_L$ -bulk-U(1) $_\gamma$, and of bulk-SU(2) $_L$ -brane-U(1) $_\gamma$, the corresponding limits are > 4.6 TeV, > 4.3 TeV and > 3.0 TeV, respectively.
- 2 Bound is derived from limits on $e\nu q q'$ contact interaction, using data from HERA and the Tevatron.
- 3 Bound holds only if first two generations of quarks lives on separate branes. If quark mixing is not complex, then bound lowers to 400 TeV from Δm_K .
- 4 See Figs. 1 and 2 of DELGADO 00 for several model variations. Special boundary conditions can be found which permit KK states down to 950 GeV and that agree with the measurement of Q_W (Cs). Quoted bound assumes all Higgs bosons confined to brane; placing one Higgs doublet in the bulk lowers bound to 2.3 TeV.
- 5 Bound is derived from global electroweak analysis assuming the Higgs field is trapped on the matter brane. If the Higgs propagates in the bulk, the bound increases to 3.8 TeV.
- 6 Bound is derived from global electroweak analysis but considering only presence of the KK W bosons.
- 7 Global electroweak analysis used to obtain bound independent of position of Higgs on brane or in bulk.
- 8 Bounds from effect of KK states on G_F , α , $M_{W'}$, and $M_{Z'}$. Hard cutoff at string scale determined using gauge coupling unification. Limits for $d=2,3,4$ rise to 3.5, 5.7, and 7.8 TeV.
- 9 Bound obtained for Higgs confined to the matter brane with $m_H = 500$ GeV. For Higgs in the bulk, the bound increases to 3.5 TeV.

See the related review(s):

Leptoquarks

MASS LIMITS FOR Leptoquarks from Pair Production

These limits rely only on the color or electroweak charge of the leptoquark.

VALUE (GeV)	CL%	DOCUMENT ID	TECN	COMMENT
>1480	95	1 AAD 21AG ATLS		Scalar LQ. $B(\tau e) = 1$
>1470	95	2 AAD 21AG ATLS		Scalar LQ. $B(t\mu) = 1$
>1190	95	3 AAD 21AW ATLS		Scalar LQ. $B(b\tau) = 1$
>1030	95	4 AAD 21AW ATLS		Scalar LQ. $B(t\tau) = 1$
>1760	95	5 AAD 21AW ATLS		Vector LQ. $\kappa = 1$. $B(b\tau) = 1$

Gauge & Higgs Boson Particle Listings

New Heavy Bosons

>1260	95	6	AAD	21s	ATLS	Scalar LQ. $B(b\nu) = 1$
>1430	95	7	AAD	21t	ATLS	Scalar LQ. $B(t\tau) = 1$
> 950	95	8	SIRUNYAN	21j	CMS	Scalar LQ. $B(t\tau)=B(b\nu)=0.5$
>1650	95	9	SIRUNYAN	21j	CMS	Vector LQ. $\kappa=1$, $B(t\nu) = B(b\tau) = 0.5$
>1800	95	10	AAD	20Ak	ATLS	Scalar LQ. $B(eq) = 1$
>1700	95	11	AAD	20Ak	ATLS	Scalar LQ. $B(\mu q) = 1$
>1240	95	12	AAD	20s	ATLS	Scalar LQ. $B(t\nu) = 1$
>1185	95	13	SIRUNYAN	20A	CMS	Scalar LQ. $B(\nu b) = 1$
>1140	95	14	SIRUNYAN	20A	CMS	Scalar LQ. $B(\nu\tau) = 1$
>1140	95	15	SIRUNYAN	20A	CMS	Scalar LQ. $B(\nu q) = 1$ with $q = u, d, s, c$
>1925	95	16	SIRUNYAN	20A	CMS	Vector LQ. $\kappa = 1$. $B(\nu b) = 1$
>1825	95	17	SIRUNYAN	20A	CMS	Vector LQ. $\kappa = 1$. $B(\nu\tau) = 1$
>1980	95	18	SIRUNYAN	20A	CMS	Vector LQ. $\kappa = 1$. $B(\nu q) = 1$ with $q = u, d, s, c$
>1400	95	19	AABOUD	19Ax	ATLS	Scalar LQ. $B(eq) = 1$
>1560	95	20	AABOUD	19Ax	ATLS	Scalar LQ. $B(\mu q) = 1$
>1000	95	21	AABOUD	19x	ATLS	Scalar LQ. $B(t\nu) = 1$
>1030	95	22	AABOUD	19x	ATLS	Scalar LQ. $B(b\tau) = 1$
> 970	95	23	AABOUD	19x	ATLS	Scalar LQ. $B(b\nu) = 1$
> 920	95	24	AABOUD	19x	ATLS	Scalar LQ. $B(t\tau) = 1$
>1530	95	25	SIRUNYAN	19Bi	CMS	Scalar LQ. $B(\mu q)+B(\nu q) = 1$
>1435	95	26	SIRUNYAN	19Bj	CMS	Scalar LQ. $B(eq)+B(\nu q) = 1$
>1020	95	27	SIRUNYAN	19Y	CMS	Scalar LQ. $B(\tau b) = 1$
none 300-900	95	28	SIRUNYAN	18Cz	CMS	Scalar LQ. $B(\tau\tau) = 1$
>1420	95	29	SIRUNYAN	18Ec	CMS	Scalar LQ. $B(\mu t) = 1$
>1190	95	30	SIRUNYAN	18Ec	CMS	Vector LQ. $\mu, \tau, t, \nu b$
>1100	95	31	SIRUNYAN	18U	CMS	Scalar LQ. $B(\nu b) = 1$
> 980	95	32	SIRUNYAN	18U	CMS	Scalar LQ. $B(\nu q) = 1$ with $q = u, d, s, c$
>1020	95	33	SIRUNYAN	18U	CMS	Scalar LQ. $B(\nu\tau) = 1$
>1810	95	34	SIRUNYAN	18U	CMS	Vector LQ. $\kappa=1$. $LQ \rightarrow b\nu$
>1790	95	35	SIRUNYAN	18U	CMS	Vector LQ. $\kappa=1$. $LQ \rightarrow q\nu$ with $q = u, d, s, c$
>1780	95	36	SIRUNYAN	18U	CMS	Vector LQ. $\kappa=1$. $LQ \rightarrow t\nu$
> 740	95	37	KHACHATRY...	17j	CMS	Scalar LQ. $B(\tau b) = 1$
> 850	95	38	SIRUNYAN	17H	CMS	Scalar LQ. $B(\tau b) = 1$
>1050	95	39	AAD	16g	ATLS	Scalar LQ. $B(eq) = 1$
>1000	95	40	AAD	16g	ATLS	Scalar LQ. $B(\mu q) = 1$
> 625	95	41	AAD	16g	ATLS	Scalar LQ. $B(\nu b) = 1$
none 200-640	95	42	AAD	16g	ATLS	Scalar LQ. $B(\nu\tau) = 1$
>1010	95	43	KHACHATRY...	16Af	CMS	Scalar LQ. $B(eq) = 1$
>1080	95	44	KHACHATRY...	16Af	CMS	Scalar LQ. $B(\mu q) = 1$
> 685	95	45	KHACHATRY...	15Aj	CMS	Scalar LQ. $B(\tau\tau) = 1$
> 740	95	46	KHACHATRY...	14T	CMS	Scalar LQ. $B(\tau b) = 1$
• • • We do not use the following data for averages, fits, limits, etc. • • •						
		47	SIRUNYAN	19Bc	CMS	Scalar LQ ($\rightarrow \mu q$) LQ ($\rightarrow X + DM$)
> 534	95	48	AAD	13Ae	ATLS	Third generation
> 525	95	49	CHATRCHYAN	13M	CMS	Third generation
> 660	95	50	AAD	12H	ATLS	First generation
> 685	95	51	AAD	12o	ATLS	Second generation
> 830	95	52	CHATRCHYAN	12Ag	CMS	First generation
> 840	95	53	CHATRCHYAN	12Ag	CMS	Second generation
> 450	95	54	CHATRCHYAN	12Bo	CMS	Third generation
> 376	95	55	AAD	11D	ATLS	Superseded by AAD 12H
> 422	95	56	AAD	11D	ATLS	Superseded by AAD 12o
> 326	95	57	ABAZOV	11V	D0	First generation
> 339	95	58	CHATRCHYAN	11N	CMS	Superseded by CHA-TRCHYAN 12Ag
> 384	95	59	KHACHATRY...	11D	CMS	Superseded by CHA-TRCHYAN 12Ag
> 394	95	60	KHACHATRY...	11E	CMS	Superseded by CHA-TRCHYAN 12Ag
> 247	95	61	ABAZOV	10L	D0	Third generation
> 316	95	62	ABAZOV	09	D0	Second generation
> 299	95	63	ABAZOV	09Af	D0	Superseded by ABAZOV 11V
> 153	95	64	AALTONEN	08P	CDF	Third generation
> 205	95	65	AALTONEN	08Z	CDF	Third generation
> 210	95	66	ABAZOV	08AD	D0	All generations
> 229	95	67	ABAZOV	08AN	D0	Third generation
> 251	95	68	ABAZOV	07J	D0	Superseded by ABAZOV 10L
> 136	95	69	ABAZOV	06A	D0	Superseded by ABAZOV 09
> 226	95	70	ABULENCIA	06T	CDF	Superseded by ABAZOV 08AD
> 256	95	71	ABAZOV	05H	D0	Second generation
> 117	95	72	ACOSTA	05I	CDF	First generation
> 236	95	73	ACOSTA	05P	CDF	First generation
> 99	95	74	ABBIENDI	03R	OPAL	First generation
> 100	95	75	ABBIENDI	03R	OPAL	Second generation
> 98	95	76	ABBIENDI	03R	OPAL	Third generation
> 98	95	77	ABAZOV	02	D0	All generations
> 225	95	78	ABAZOV	01D	D0	First generation
> 85.8	95	79	ABBIENDI	00M	OPAL	Superseded by ABBIENDI 03R
> 85.5	95	80	ABBIENDI	00M	OPAL	Superseded by ABBIENDI 03R
> 82.7	95	81	ABBIENDI	00M	OPAL	Superseded by ABBIENDI 03R
> 200	95	82	ABBOTT	00C	D0	Second generation
> 123	95	83	AFFOLDER	00K	CDF	Second generation
> 148	95	84	AFFOLDER	00K	CDF	Third generation
> 160	95	85	ABBOTT	99J	D0	Second generation
> 225	95	86	ABBOTT	98E	D0	First generation
> 94	95	87	ABBOTT	98J	D0	Third generation
> 202	95	88	ABE	98S	CDF	Second generation
> 242	95	89	GROSS-PILCH.	98		First generation
> 99	95	90	ABE	97F	CDF	Third generation
> 213	95	91	ABE	97X	CDF	First generation
> 45.5	95	92	ABREU	93J	DLPH	First + second generation
> 44.4	95	93	ADRIANI	93M	L3	First generation
> 44.5	95	94	ADRIANI	93M	L3	Second generation
> 45	95	95	DECAMP	92	ALEP	Third generation
none 8.9-22.6	95	96	KIM	90	AMY	First generation
none 10.2-23.2	95	97	KIM	90	AMY	Second generation
none 5-20.8	95	98	BARTEL	87B	JADE	
none 7-20.5	95	99	BEHREND	86B	CELL	

See key on page 1127

Gauge & Higgs Boson Particle Listings
New Heavy Bosons

- 32 SIRUNYAN 18U set limits for scalar and vector leptoquarks decaying to $t\nu$, $b\nu$, and $q\nu$. The limit quoted above assumes scalar leptoquark with $B(q\nu) = 1$. Vector leptoquarks with $\kappa = 1$ are excluded below masses of 1790 GeV.
- 33 SIRUNYAN 18U set limits for scalar and vector leptoquarks decaying to $t\nu$, $b\nu$, and $q\nu$. The limit quoted above assumes scalar leptoquark with $B(\nu t) = 1$. Vector leptoquarks with $\kappa = 1$ are excluded below masses of 1780 GeV.
- 34 SIRUNYAN 18U set limits for scalar and vector leptoquarks decaying to $t\nu$, $b\nu$, and $q\nu$. $\kappa = 1$ and $LQ \rightarrow b\nu$ are assumed.
- 35 SIRUNYAN 18U set limits for scalar and vector leptoquarks decaying to $t\nu$, $b\nu$, and $q\nu$. $\kappa = 1$ and $LQ \rightarrow q\nu$ with $q = u, d, s, c$ are assumed.
- 36 SIRUNYAN 18U set limits for scalar and vector leptoquarks decaying to $t\nu$, $b\nu$, and $q\nu$. $\kappa = 1$ and $LQ \rightarrow t\nu$ are assumed.
- 37 KHACHATRYAN 17J search for scalar leptoquarks decaying to τb using pp collisions at $\sqrt{s} = 13$ TeV. The limit above assumes $B(\tau b) = 1$.
- 38 SIRUNYAN 17H search for scalar leptoquarks using $\tau\tau bb$ events in pp collisions at $\sqrt{s} = 8$ TeV. The limit above assumes $B(\tau b) = 1$.
- 39 AAD 16G search for scalar leptoquarks using $eejj$ events in collisions at $\sqrt{s} = 8$ TeV. The limit above assumes $B(eq) = 1$.
- 40 AAD 16G search for scalar leptoquarks using $\mu\mu jj$ events in collisions at $\sqrt{s} = 8$ TeV. The limit above assumes $B(\mu q) = 1$.
- 41 AAD 16G search for scalar leptoquarks decaying to $b\nu$. The limit above assumes $B(b\nu) = 1$.
- 42 AAD 16G search for scalar leptoquarks decaying to $t\nu$. The limit above assumes $B(t\nu) = 1$.
- 43 KHACHATRYAN 16AF search for scalar leptoquarks using $eejj$ and $e\nu jj$ events in pp collisions at $\sqrt{s} = 8$ TeV. The limit above assumes $B(eq) = 1$. For $B(eq) = 0.5$, the limit becomes 850 GeV.
- 44 KHACHATRYAN 16AF search for scalar leptoquarks using $\mu\mu jj$ and $\mu\nu jj$ events in pp collisions at $\sqrt{s} = 8$ TeV. The limit above assumes $B(\mu q) = 1$. For $B(\mu q) = 0.5$, the limit becomes 760 GeV.
- 45 KHACHATRYAN 15AJ search for scalar leptoquarks using $\tau\tau t$ events in pp collisions at $\sqrt{s} = 8$ TeV. The limit above assumes $B(\tau t) = 1$.
- 46 KHACHATRYAN 14T search for scalar leptoquarks decaying to τb using pp collisions at $\sqrt{s} = 8$ TeV. The limit above assumes $B(\tau b) = 1$. See their Fig. 5 for the exclusion limit as function of $B(\tau b)$.
- 47 SIRUNYAN 19BC search for scalar leptoquark (LQ) pair production in pp collisions at $\sqrt{s} = 13$ TeV. One LQ is assumed to decay to μq , while the other decays to dark matter pair and SM particles. See their Fig. 4 for limits in $M_{LQ} - M_{DM}$ plane.
- 48 AAD 13AE search for scalar leptoquarks using $\tau\tau bb$ events in pp collisions at $E_{cm} = 7$ TeV. The limit above assumes $B(\tau b) = 1$.
- 49 CHATRCHYAN 13M search for scalar and vector leptoquarks decaying to τb in pp collisions at $E_{cm} = 7$ TeV. The limit above is for scalar leptoquarks with $B(\tau b) = 1$.
- 50 AAD 12H search for scalar leptoquarks using $eejj$ and $e\nu jj$ events in pp collisions at $E_{cm} = 7$ TeV. The limit above assumes $B(eq) = 1$. For $B(eq) = 0.5$, the limit becomes 607 GeV.
- 51 AAD 12O search for scalar leptoquarks using $\mu\mu jj$ and $\mu\nu jj$ events in pp collisions at $E_{cm} = 7$ TeV. The limit above assumes $B(\mu q) = 1$. For $B(\mu q) = 0.5$, the limit becomes 594 GeV.
- 52 CHATRCHYAN 12AG search for scalar leptoquarks using $eejj$ and $e\nu jj$ events in pp collisions at $E_{cm} = 7$ TeV. The limit above assumes $B(eq) = 1$. For $B(eq) = 0.5$, the limit becomes 640 GeV.
- 53 CHATRCHYAN 12AG search for scalar leptoquarks using $\mu\mu jj$ and $\mu\nu jj$ events in pp collisions at $E_{cm} = 7$ TeV. The limit above assumes $B(\mu q) = 1$. For $B(\mu q) = 0.5$, the limit becomes 650 GeV.
- 54 CHATRCHYAN 12BO search for scalar leptoquarks decaying to νb in pp collisions at $\sqrt{s} = 7$ TeV. The limit above assumes $B(\nu b) = 1$.
- 55 AAD 11D search for scalar leptoquarks using $eejj$ and $e\nu jj$ events in pp collisions at $E_{cm} = 7$ TeV. The limit above assumes $B(eq) = 1$. For $B(eq) = 0.5$, the limit becomes 319 GeV.
- 56 AAD 11D search for scalar leptoquarks using $\mu\mu jj$ and $\mu\nu jj$ events in pp collisions at $E_{cm} = 7$ TeV. The limit above assumes $B(\mu q) = 1$. For $B(\mu q) = 0.5$, the limit becomes 362 GeV.
- 57 ABZOV 11V search for scalar leptoquarks using $e\nu jj$ events in $p\bar{p}$ collisions at $E_{cm} = 1.96$ TeV. The limit above assumes $B(eq) = 0.5$.
- 58 CHATRCHYAN 11N search for scalar leptoquarks using $e\nu jj$ events in pp collisions at $E_{cm} = 7$ TeV. The limit above assumes $B(eq) = 0.5$.
- 59 KHACHATRYAN 11D search for scalar leptoquarks using $eejj$ events in pp collisions at $E_{cm} = 7$ TeV. The limit above assumes $B(eq) = 1$.
- 60 KHACHATRYAN 11E search for scalar leptoquarks using $\mu\mu jj$ events in pp collisions at $E_{cm} = 7$ TeV. The limit above assumes $B(\mu q) = 1$.
- 61 ABZOV 10L search for pair productions of scalar leptoquark state decaying to νb in $p\bar{p}$ collisions at $E_{cm} = 1.96$ TeV. The limit above assumes $B(\nu b) = 1$.
- 62 ABZOV 09 search for scalar leptoquarks using $\mu\mu jj$ and $\mu\nu jj$ events in $p\bar{p}$ collisions at $E_{cm} = 1.96$ TeV. The limit above assumes $B(\mu q) = 1$. For $B(\mu q) = 0.5$, the limit becomes 270 GeV.
- 63 ABZOV 09AF search for scalar leptoquarks using $eejj$ and $e\nu jj$ events in $p\bar{p}$ collisions at $E_{cm} = 1.96$ TeV. The limit above assumes $B(eq) = 1$. For $B(eq) = 0.5$ the bound becomes 284 GeV.
- 64 AALTONEN 08P search for vector leptoquarks using $\tau^+ \tau^- b\bar{b}$ events in $p\bar{p}$ collisions at $E_{cm} = 1.96$ TeV. Assuming Yang-Mills (minimal) couplings, the mass limit is >317 GeV (251 GeV) at 95% CL for $B(\tau b) = 1$.
- 65 Search for pair production of scalar leptoquark state decaying to τb in $p\bar{p}$ collisions at $E_{cm} = 1.96$ TeV. The limit above assumes $B(\tau b) = 1$.
- 66 Search for scalar leptoquarks using $\nu\nu jj$ events in $p\bar{p}$ collisions at $E_{cm} = 1.96$ TeV. The limit above assumes $B(\nu q) = 1$.
- 67 ABZOV 07J search for pair productions of scalar leptoquark state decaying to νb in $p\bar{p}$ collisions at $E_{cm} = 1.96$ TeV. The limit above assumes $B(\nu b) = 1$.
- 68 ABZOV 06A search for scalar leptoquarks using $\mu\mu jj$ events in $p\bar{p}$ collisions at $E_{cm} = 1.8$ TeV and 1.96 TeV. The limit above assumes $B(\mu q) = 1$. For $B(\mu q) = 0.5$, the limit becomes 204 GeV.
- 69 ABZOV 06L search for scalar leptoquarks using $\nu\nu jj$ events in $p\bar{p}$ collisions at $E_{cm} = 1.8$ TeV and at 1.96 TeV. The limit above assumes $B(\nu q) = 1$.
- 70 ABULENCIA 06T search for scalar leptoquarks using $\mu\mu jj$, $\mu\nu jj$, and $\nu\nu jj$ events in $p\bar{p}$ collisions at $E_{cm} = 1.96$ TeV. The quoted limit assumes $B(\mu q) = 1$. For $B(\mu q) = 0.5$ or 0.1, the bound becomes 208 GeV or 143 GeV, respectively. See their Fig. 4 for the exclusion limit as a function of $B(\mu q)$.
- 71 ABZOV 05H search for scalar leptoquarks using $eejj$ and $e\nu jj$ events in $p\bar{p}$ collisions at $E_{cm} = 1.8$ TeV and 1.96 TeV. The limit above assumes $B(eq) = 1$. For $B(eq) = 0.5$ the bound becomes 234 GeV.
- 72 ACOSTA 05P search for scalar leptoquarks using $eejj$, $e\nu jj$ events in $p\bar{p}$ collisions at $E_{cm} = 1.96$ TeV. The limit above assumes $B(eq) = 1$. For $B(eq) = 0.5$ and 0.1, the bound becomes 205 GeV and 145 GeV, respectively.
- 73 ABBIENDI 03R search for scalar/vector leptoquarks in $e^+ e^-$ collisions at $\sqrt{s} = 189-209$ GeV. The quoted limits are for charge $-4/3$ isospin 0 scalar-leptoquark with $B(\ell q) = 1$. See their table 12 for other cases.
- 74 ABZOV 02 search for scalar leptoquarks using $\nu\nu jj$ events in $p\bar{p}$ collisions at $E_{cm} = 1.8$ TeV. The bound holds for all leptoquark generations. Vector leptoquarks are likewise constrained to lie above 200 GeV.
- 75 ABZOV 01D search for scalar leptoquarks using $e\nu jj$, $eejj$, and $\nu\nu jj$ events in $p\bar{p}$ collisions at $E_{cm} = 1.8$ TeV. The limit above assumes $B(eq) = 1$. For $B(eq) = 0.5$ and 0, the bound becomes 204 and 79 GeV, respectively. Bounds for vector leptoquarks are also given. Supersedes ABBOTT 98E.
- 76 ABBIENDI 00M search for scalar/vector leptoquarks in $e^+ e^-$ collisions at $\sqrt{s} = 183$ GeV. The quoted limits are for charge $-4/3$ isospin 0 scalar-leptoquarks with $B(\ell q) = 1$. See their Table 8 and Figs. 6-9 for other cases.
- 77 ABBOTT 00c search for scalar leptoquarks using $\mu\mu jj$, $\mu\nu jj$, and $\nu\nu jj$ events in $p\bar{p}$ collisions at $E_{cm} = 1.8$ TeV. The limit above assumes $B(\mu q) = 1$. For $B(\mu q) = 0.5$ and 0, the bound becomes 180 and 79 GeV respectively. Bounds for vector leptoquarks are also given.
- 78 AFFOLDER 00k search for scalar leptoquark using $\nu\nu cc$ events in $p\bar{p}$ collisions at $E_{cm} = 1.8$ TeV. The quoted limit assumes $B(\nu c) = 1$. Bounds for vector leptoquarks are also given.
- 79 AFFOLDER 00k search for scalar leptoquark using $\nu\nu bb$ events in $p\bar{p}$ collisions at $E_{cm} = 1.8$ TeV. The quoted limit assumes $B(\nu b) = 1$. Bounds for vector leptoquarks are also given.
- 80 ABBOTT 99J search for leptoquarks using $\mu\nu jj$ events in $p\bar{p}$ collisions at $E_{cm} = 1.8$ TeV. The quoted limit is for a scalar leptoquark with $B(\mu q) = B(\nu q) = 0.5$. Limits on vector leptoquarks range from 240 to 290 GeV.
- 81 ABBOTT 98E search for scalar leptoquarks using $e\nu jj$, $eejj$, and $\nu\nu jj$ events in $p\bar{p}$ collisions at $E_{cm} = 1.8$ TeV. The limit above assumes $B(eq) = 1$. For $B(eq) = 0.5$ and 0, the bound becomes 204 and 79 GeV, respectively.
- 82 ABBOTT 98J search for charge $-1/3$ third generation scalar and vector leptoquarks in $p\bar{p}$ collisions at $E_{cm} = 1.8$ TeV. The quoted limit is for scalar leptoquark with $B(\nu b) = 1$.
- 83 ABE 98s search for scalar leptoquarks using $\mu\mu jj$ events in $p\bar{p}$ collisions at $E_{cm} = 1.8$ TeV. The limit is for $B(\mu q) = 1$. For $B(\mu q) = B(\nu q) = 0.5$, the limit is > 160 GeV.
- 84 GROSS-PILCHER 98 is the combined limit of the CDF and DØ Collaborations as determined by a joint CDF/DØ working group and reported in this FNAL Technical Memo. Original data published in ABE 97x and ABBOTT 98E.
- 85 ABE 97f search for third generation scalar and vector leptoquarks in $p\bar{p}$ collisions at $E_{cm} = 1.8$ TeV. The quoted limit is for scalar leptoquark with $B(\tau b) = 1$.
- 86 ABE 97x search for scalar leptoquarks using $eejj$ events in $p\bar{p}$ collisions at $E_{cm} = 1.8$ TeV. The limit is for $B(eq) = 1$.
- 87 Limit is for charge $-1/3$ isospin-0 leptoquark with $B(\ell q) = 2/3$.
- 88 First and second generation leptoquarks are assumed to be degenerate. The limit is slightly lower for each generation.
- 89 Limits are for charge $-1/3$, isospin-0 scalar leptoquarks decaying to $\ell^- q$ or νq with any branching ratio. See paper for limits for other charge-isospin assignments of leptoquarks.
- 90 KIM 90 assume pair production of charge $2/3$ scalar-leptoquark via photon exchange. The decay of the first (second) generation leptoquark is assumed to be any mixture of $d e^+$ and $u\bar{\nu}$ ($s\mu^+$ and $c\bar{\nu}$). See paper for limits for specific branching ratios.
- 91 BARTEL 87b limit is valid when a pair of charge $2/3$ spinless leptoquarks X is produced with point coupling, and when they decay under the constraint $B(X \rightarrow c\bar{\nu}_\mu) + B(X \rightarrow s\mu^+) = 1$.
- 92 BEHREND 86b assumed that a charge $2/3$ spinless leptoquark, χ , decays either into $s\mu^+$ or $c\bar{\nu}$: $B(X \rightarrow s\mu^+) + B(X \rightarrow c\bar{\nu}) = 1$.

MASS LIMITS for Leptoquarks from Single Production

These limits depend on the q - ℓ -leptoquark coupling g_{LQ} . It is often assumed that $g_{LQ}^2/4\pi = 1/137$. Limits shown are for a scalar, weak isoscalar, charge $-1/3$ leptoquark.

VALUE (GeV)	CL%	DOCUMENT ID	TECN	COMMENT
> 550	95	1 SIRUNYAN 21J	CMS	Third generation
none 150-740	95	2 SIRUNYAN 18BJ	CMS	Third generation
>1755	95	3 KHACHATRYAN 16AG	CMS	First generation
> 660	95	4 KHACHATRYAN 16AG	CMS	Second generation
> 304	95	5 ABRAMOWICZ 21A	ZEUS	First generation
> 73	95	6 ABREU 93J	DLPH	Second generation
● ● ● We do not use the following data for averages, fits, limits, etc. ● ● ●				
		7 TUMASYAN 21D	CMS	First generation
		8 DEY 16	ICCB	$\nu q \rightarrow LQ \rightarrow \nu q$
		9 AARON 11A	H1	Lepton-flavor violation
> 300	95	10 AARON 11B	H1	First generation
		11 ABZOV 07E	D0	Second generation
> 295	95	12 AKTAS 05B	H1	First generation
		13 CHEKANOV 05A	ZEUS	Lepton-flavor violation
> 298	95	14 CHEKANOV 03B	ZEUS	First generation
> 197	95	15 ABBIENDI 02b	OPAL	First generation
		16 CHEKANOV 02	ZEUS	Repl. by CHEKANOV 05A
> 290	95	17 ADLOFF 01c	H1	First generation
> 204	95	18 BREITWEG 01	ZEUS	First generation
		19 BREITWEG 00E	ZEUS	First generation
> 161	95	20 ABREU 99C	DLPH	First generation
> 200	95	21 ADLOFF 99	H1	First generation

Gauge & Higgs Boson Particle Listings

New Heavy Bosons

VALUE (TeV)	CL%	DOCUMENT ID	TECN	COMMENT
> 168	95	22 DERRICK 97 ZEUS	Lepton-flavor violation	
		23 DERRICK 93 ZEUS	First generation	
		1 SIRUNYAN 21j search for single production of charge $-1/3$ scalar leptoquarks decaying to τ^- and $b\nu$, and charge $2/3$ vector leptoquarks decaying to $t\nu$ and $b\tau^+$ in pp collisions at $\sqrt{s} = 13$ TeV. The limit quoted above assumes a scalar leptoquark with $B(\tau^-) = B(b\nu) = 0.5$ and the leptoquark coupling strength $\lambda = 1.5$. The limit becomes $M_{LQ} > 750$ GeV for $\lambda = 2.5$.		
		2 SIRUNYAN 18bj search for single production of charge $2/3$ scalar leptoquarks decaying to τb in pp collisions at $\sqrt{s} = 13$ TeV. The limit above assumes $B(\tau b) = 1$ and the leptoquark coupling strength $\lambda = 1$.		
		3 KHACHATRYAN 16Ag search for single production of charge $\pm 1/3$ scalar leptoquarks using $e e j$ events in pp collisions at $\sqrt{s} = 8$ TeV. The limit above assumes $B(e q) = 1$ and the leptoquark coupling strength $\lambda = 1$.		
		4 KHACHATRYAN 16Ag search for single production of charge $\pm 1/3$ scalar leptoquarks using $\mu \mu j$ events in pp collisions at $\sqrt{s} = 8$ TeV. The limit above assumes $B(\mu q) = 1$ and the leptoquark coupling strength $\lambda = 1$.		
		5 ABRAMOWICZ 12A limit is for a scalar, weak isoscalar, charge $-1/3$ leptoquark coupled with e_R . See their Figs. 12–17 and Table 4 for states with different quantum numbers.		
		6 Limit from single production in Z decay. The limit is for a leptoquark coupling of electromagnetic strength and assumes $B(\ell q) = 2/3$. The limit is 77 GeV if first and second leptoquarks are degenerate.		
		7 TUMASYAN 21D search for energetic jets + \cancel{E}_T events in pp collisions at $\sqrt{s} = 13$ TeV. The branching fraction for the decay of the leptoquark into an electron neutrino and up quark is assumed to be 100% ($\beta = 0$). See their Fig. 12 for exclusion limits in mass-coupling plane.		
		8 DEY 16 use the 2010–2012 IceCube PeV energy data set to constrain the leptoquark production cross section through the $\nu q \rightarrow LQ \rightarrow \nu q$ process. See their Figure 4 for the exclusion limit in the mass-coupling plane.		
		9 AARON 11A search for various leptoquarks with lepton-flavor violating couplings. See their Figs. 2–3 and Tables 1–4 for detailed limits.		
		10 The quoted limit is for a scalar, weak isoscalar, charge $-1/3$ leptoquark coupled with e_R . See their Figs. 3–5 for limits on states with different quantum numbers.		
		11 ABAZOV 07E search for leptoquark single production through qg fusion process in $p\bar{p}$ collisions. See their Fig. 4 for exclusion plot in mass-coupling plane.		
		12 AKTAS 05B limit is for a scalar, weak isoscalar, charge $-1/3$ leptoquark coupled with e_R . See their Fig. 3 for limits on states with different quantum numbers.		
		13 CHEKANOV 05 search for various leptoquarks with lepton-flavor violating couplings. See their Figs. 6–10 and Tables 1–8 for detailed limits.		
		14 CHEKANOV 03B limit is for a scalar, weak isoscalar, charge $-1/3$ leptoquark coupled with e_R . See their Figs. 11–12 and Table 5 for limits on states with different quantum numbers.		
		15 For limits on states with different quantum numbers and the limits in the mass-coupling plane, see their Fig. 4 and Fig. 5.		
		16 CHEKANOV 02 search for various leptoquarks with lepton-flavor violating couplings. See their Figs. 6–7 and Tables 5–6 for detailed limits.		
		17 For limits on states with different quantum numbers and the limits in the mass-coupling plane, see their Fig. 3.		
		18 See their Fig. 14 for limits in the mass-coupling plane.		
		19 BREITWEG 00E search for $F=0$ leptoquarks in e^+p collisions. For limits in mass-coupling plane, see their Fig. 11.		
		20 ABREU 99c limit obtained from process $e\gamma \rightarrow LQ+q$. For limits on vector and scalar states with different quantum numbers and the limits in the coupling-mass plane, see their Fig. 4 and Table 2.		
		21 For limits on states with different quantum numbers and the limits in the mass-coupling plane, see their Fig. 13 and Fig. 14. ADLOFF 99 also search for leptoquarks with lepton-flavor violating couplings. ADLOFF 99 supersedes AID 96b.		
		22 DERRICK 97 search for various leptoquarks with lepton-flavor violating couplings. See their Figs. 8–8 and Table 1 for detailed limits.		
		23 DERRICK 93 search for single leptoquark production in ep collisions with the decay $e q$ and νq . The limit is for leptoquark coupling of electromagnetic strength and assumes $B(e q) = B(\nu q) = 1/2$. The limit for $B(e q) = 1$ is 176 GeV. For limits on states with different quantum numbers, see their Table 3.		

Indirect Limits for Leptoquarks

VALUE (TeV)	CL%	DOCUMENT ID	TECN	COMMENT
• • •		We do not use the following data for averages, fits, limits, etc. • • •		
> 3.1	95	1 CRIVELLIN 21A	RVUE	First generation
		2 AEBISCHER 20	RVUE	B decays
		3 DEPPISCH 20	RVUE	$K \rightarrow \pi\nu\nu$
		4 ABRAMOWICZ19	ZEUS	First generation
		5 MANDAL 19	RVUE	τ, μ, e, K
		6 ZHANG 18A	RVUE	D decays
		7 BARRANCO 16	RVUE	D decays
		8 KUMAR 16	RVUE	neutral K mixing, rare K decays
		9 BESSAA 15	RVUE	$q\bar{q} \rightarrow e^+e^-$
> 14	95	10 SAHOO 15A	RVUE	$B_{s,d} \rightarrow \mu^+\mu^-$
		11 SAKAKI 13	RVUE	$B \rightarrow D^{(*)}\tau\bar{\nu}, B \rightarrow X_S\nu\bar{\nu}$
		12 KOSNIK 12	RVUE	$b \rightarrow s\ell^+\ell^-$
> 2.5	95	13 AARON 11C	H1	First generation
		14 DORSNER 11	RVUE	scalar, weak singlet, charge 4/3
		15 AKTAS 07A	H1	Lepton-flavor violation
> 0.49	95	16 SCHAEEL 07A	ALEP	$e^+e^- \rightarrow q\bar{q}$
		17 SMIRNOV 07	RVUE	$K \rightarrow e\mu, B \rightarrow e\tau$
		18 CHEKANOV 05A	ZEUS	Lepton-flavor violation
> 1.7	96	19 ADLOFF 03	H1	First generation
> 46	90	20 CHANG 03	BELL	Pati-Salam type
> 1.7	95	21 CHEKANOV 02	ZEUS	Repl. by CHEKANOV 05A
> 0.39	95	22 CHEUNG 01B	RVUE	First generation
		23 ACCIARRI 00P	L3	$e^+e^- \rightarrow q\bar{q}$

> 1.5	95	24 ADLOFF 00	H1	First generation
> 0.2	95	25 BARATE 00i	ALEP	Repl. by SCHAEEL 07A
		26 BARGER 00	RVUE	Cs
		27 GABRIELLI 00	RVUE	Lepton flavor violation
> 0.74	95	28 ZARNECKI 00	RVUE	S_1 leptoquark
		29 ABBIENZI 99	OPAL	
> 19.3	95	30 ABE 98v	CDF	$B_s \rightarrow e^+\mu^+\bar{\nu}$, Pati-Salam type
		31 ACCIARRI 98j	L3	$e^+e^- \rightarrow q\bar{q}$
		32 ACKERSTAFF 98v	OPAL	$e^+e^- \rightarrow q\bar{q}, e^+e^- \rightarrow b\bar{b}$
> 0.76	95	33 DEANDREA 97	RVUE	\bar{R}_2 leptoquark
		34 DERRICK 97	ZEUS	Lepton-flavor violation
		35 GROSSMAN 97	RVUE	$B \rightarrow \tau^+\tau^- (X)$
		36 JADACH 97	RVUE	$e^+e^- \rightarrow q\bar{q}$
> 1200		37 KUZNETSOV 95b	RVUE	Pati-Salam type
		38 MIZUKOSHI 95	RVUE	Third generation scalar leptoquark
> 0.3	95	39 BHATTACH... 94	RVUE	Spin-0 leptoquark coupled to $\bar{e}_R t_L$
		40 DAVIDSON 94	RVUE	
> 18		41 KUZNETSOV 94	RVUE	Pati-Salam type
> 0.43	95	42 LEURER 94	RVUE	First generation spin-1 leptoquark
> 0.44	95	42 LEURER 94b	RVUE	First generation spin-0 leptoquark
		43 MAHANTA 94	RVUE	P and T violation
> 1		44 SHANKER 82	RVUE	Nonchiral spin-0 leptoquark
> 125		44 SHANKER 82	RVUE	Nonchiral spin-1 leptoquark
		1 CRIVELLIN 21A set limits on coupling strengths of scalar and vector leptoquarks using $K \rightarrow \pi\nu\nu, K \rightarrow \pi e^+e^-, K^0 - \bar{K}^0$ and $D^0 - \bar{D}^0$ mixings, and weak neutral current measurements. See their Fig. 2 and Fig. 3 for the limits in mass-coupling plane.		
		2 AEBISCHER 20 explain the B decay anomalies using four-fermion operator Wilson coefficients. See their Table 1. These Wilson coefficients may be generated by a U_1 vector leptoquark with U_1 transforming as $(3,1)_{2/3}$ under the SM gauge group. See their Figures 6, 7, 8 for the regions of the LQ parameter space which explains the B anomalies and avoids the indirect low energy constraints.		
		3 DEPPISCH 20 limits on the lepton-number-violating higher-dimensional-operators are derived from $K \rightarrow \pi\nu\nu$ in the standard model effective field theory. These higher-dimensional-operators may be induced from leptoquark-exchange diagrams.		
		4 ABRAMOWICZ 19 obtain a limit on $\lambda/M_{LQ} > 1.16$ TeV $^{-1}$ for weak isotriplet spin-0 leptoquark S_1^{\pm} . We obtain the limit quoted above by converting the limit on λ/M_{LQ} for S_1^{\pm} assuming $\lambda = \sqrt{4\pi}$. See their Table 5 for the limits of leptoquarks with different quantum numbers. These limits are derived from bounds of $e q$ contact interactions.		
		5 MANDAL 19 give bounds on leptoquarks from τ -decays, leptonic dipole moments, lepton-flavor-violating processes, and K decays.		
		6 ZHANG 18A give bounds on leptoquark induced four-fermion interactions from $D \rightarrow K\ell\nu$. The authors inform us that the shape parameter of the vector form factor in both the abstract and the conclusions of ZHANG 18A should be $r_{+1} = 2.16 \pm 0.07$ rather than ± 0.07 . The numbers listed in their Table 7 are correct.		
		7 BARRANCO 16 give bounds on leptoquark induced four-fermion interactions from $D \rightarrow K\ell\nu$ and $D_s \rightarrow \ell\nu$.		
		8 KUMAR 16 give bound on SU(2) singlet scalar leptoquark with charge $-1/3$ from $K^0 - \bar{K}^0$ mixing, $K \rightarrow \pi\nu\bar{\nu}, K_L^0 \rightarrow \mu^+\mu^-,$ and $K_L^0 \rightarrow \mu^+e^{\mp}$ decays.		
		9 BESSAA 15 obtain limit on leptoquark induced four-fermion interactions from the ATLAS and CMS limit on the $\bar{q}q\bar{e}e$ contact interactions.		
		10 SAHOO 15A obtain limit on leptoquark induced four-fermion interactions from $B_{s,d} \rightarrow \mu^+\mu^-$ for $\lambda \simeq O(1)$.		
		11 SAKAKI 13 explain the $B \rightarrow D^{(*)}\tau\bar{\nu}$ anomaly using Wilson coefficients of leptoquark-induced four-fermion operators.		
		12 KOSNIK 12 obtains limits on leptoquark induced four-fermion interactions from $b \rightarrow s\ell^+\ell^-$ decays.		
		13 AARON 11C limit is for weak isotriplet spin-0 leptoquark at strong coupling $\lambda = \sqrt{4\pi}$. For the limits of leptoquarks with different quantum numbers, see their Table 3. Limits are derived from bounds of $e q$ contact interactions.		
		14 DORSNER 11 give bounds on scalar, weak singlet, charge 4/3 leptoquark from K, B, τ decays, meson mixings, LFV, $g-2$ and $Z \rightarrow b\bar{b}$.		
		15 AKTAS 07A search for lepton-flavor violation in ep collision. See their Tables 4–7 for limits on lepton-flavor violating four-fermion interactions induced by various leptoquarks.		
		16 SCHAEEL 07A limit is for the weak-isoscalar spin-0 left-handed leptoquark with the coupling of electromagnetic strength. For the limits of leptoquarks with different quantum numbers, see their Table 35.		
		17 SMIRNOV 07 obtains mass limits for the vector and scalar chiral leptoquark states from $K \rightarrow e\mu, B \rightarrow e\tau$ decays.		
		18 CHEKANOV 05 search for various leptoquarks with lepton-flavor violating couplings. See their Figs. 6–10 and Tables 1–8 for detailed limits.		
		19 ADLOFF 03 limit is for the weak isotriplet spin-0 leptoquark at strong coupling $\lambda = \sqrt{4\pi}$. For the limits of leptoquarks with different quantum numbers, see their Table 3. Limits are derived from bounds on $e^{\pm}q$ contact interactions.		
		20 The bound is derived from $B(B^0 \rightarrow e^{\pm}\mu^{\mp}) < 1.7 \times 10^{-7}$.		
		21 CHEKANOV 02 search for lepton-flavor violation in ep collisions. See their Tables 1–4 for limits on lepton-flavor violating and four-fermion interactions induced by various leptoquarks.		
		22 CHEUNG 01B quoted limit is for a scalar, weak isoscalar, charge $-1/3$ leptoquark with a coupling of electromagnetic strength. The limit is derived from bounds on contact interactions in a global electroweak analysis. For the limits of leptoquarks with different quantum numbers, see Table 5.		
		23 ACCIARRI 00P limit is for the weak isoscalar spin-0 leptoquark with the coupling of electromagnetic strength. For the limits of leptoquarks with different quantum numbers, see their Table 4.		
		24 ADLOFF 00 limit is for the weak isotriplet spin-0 leptoquark at strong coupling, $\lambda = \sqrt{4\pi}$. For the limits of leptoquarks with different quantum numbers, see their Table 2. ADLOFF 00 limits are from the Q^2 spectrum measurement of $e^+p \rightarrow e^+X$.		
		25 BARATE 00i search for deviations in cross section and jet-charge asymmetry in $e^+e^- \rightarrow \bar{q}q$ due to t-channel exchange of a leptoquark at $\sqrt{s}=130$ to 183 GeV. Limits for other scalar and vector leptoquarks are also given in their Table 22.		

See key on page 1127

Gauge & Higgs Boson Particle Listings

New Heavy Bosons

²⁶ BARGER 00 explain the deviation of atomic parity violation in cesium atoms from pre-diction is explained by scalar leptoquark exchange.

²⁷ GABRIELLI 00 calculate various process with lepton flavor violation in leptoquark models.

²⁸ ZARNECKI 00 limit is derived from data of HERA, LEP, and Tevatron and from various low-energy data including atomic parity violation. Leptoquark coupling with electromagnetic strength is assumed.

²⁹ ABBIENDI 99 limits are from $e^+e^- \rightarrow q\bar{q}$ cross section at 130–136, 161–172, 183 GeV. See their Fig. 8 and Fig. 9 for limits in mass-coupling plane.

³⁰ ABE 98v quoted limit is from $B(B_s \rightarrow e^\pm \mu^\mp) < 8.2 \times 10^{-6}$. ABE 98v also obtain a similar limit on $M_{LQ} > 20.4$ TeV from $B(B_d \rightarrow e^\pm \mu^\mp) < 4.5 \times 10^{-6}$. Both bounds assume the non-canonical association of the b quark with electrons or muons under $SU(4)$.

³¹ ACCIARRI 98j limit is from $e^+e^- \rightarrow q\bar{q}$ cross section at $\sqrt{s}=130$ –172 GeV which can be affected by the t - and u -channel exchanges of leptoquarks. See their Fig. 4 and Fig. 5 for limits in the mass-coupling plane.

³² ACKERSTAFF 98v limits are from $e^+e^- \rightarrow q\bar{q}$ and $e^+e^- \rightarrow b\bar{b}$ cross sections at $\sqrt{s}=130$ –172 GeV, which can be affected by the t - and u -channel exchanges of leptoquarks. See their Fig. 21 and Fig. 22 for limits of leptoquarks in mass-coupling plane.

³³ DEANDREA 97 limit is for \bar{R}_2 leptoquark obtained from atomic parity violation (APV). The coupling of leptoquark is assumed to be electromagnetic strength. See Table 2 for limits of the four-fermion interactions induced by various scalar leptoquark exchange. DEANDREA 97 combines APV limit and limits from Tevatron and HERA. See Fig. 1–4 for combined limits of leptoquark in mass-coupling plane.

³⁴ DERRICK 97 search for lepton-flavor violation in ep collision. See their Tables 2–5 for limits on lepton-flavor violating four-fermion interactions induced by various leptoquarks.

³⁵ GROSSMAN 97 estimate the upper bounds on the branching fraction $B \rightarrow \tau^+\tau^- (X)$ from the absence of the B decay with large missing energy. These bounds can be used to constrain leptoquark induced four-fermion interactions.

³⁶ JADACH 97 limit is from $e^+e^- \rightarrow q\bar{q}$ cross section at $\sqrt{s}=172.3$ GeV which can be affected by the t - and u -channel exchanges of leptoquarks. See their Fig. 1 for limits on vector leptoquarks in mass-coupling plane.

³⁷ KUZNETSOV 95B use π, K, B, τ decays and μe conversion and give a list of bounds on the leptoquark mass and the fermion mixing matrix in the Pati-Salam model. The quoted limit is from $K_L \rightarrow \mu e$ decay assuming zero mixing.

³⁸ MIZUKOSHI 95 calculate the one-loop radiative correction to the Z-physics parameters in various scalar leptoquark models. See their Fig. 4 for the exclusion plot of third generation leptoquark models in mass-coupling plane.

³⁹ BHATTACHARYYA 94 limit is from one-loop radiative correction to the leptonic decay width of the Z. $m_H=250$ GeV, $\alpha_s(m_Z)=0.12$, $m_t=180$ GeV, and the electroweak strength of leptoquark coupling are assumed. For leptoquark coupled to $\bar{\nu}_L t_R, \bar{\nu}_L \tau$, and $\bar{\nu}_L t$, see Fig. 2 in BHATTACHARYYA 94b erratum and Fig. 3.

⁴⁰ DAVIDSON 94 gives an extensive list of the bounds on leptoquark-induced four-fermion interactions from π, K, D, B, μ, τ decays and meson mixings, etc. See Table 15 of DAVIDSON 94 for detail.

⁴¹ KUZNETSOV 94 gives mixing independent bound of the Pati-Salam leptoquark from the cosmological limit on $\pi^0 \rightarrow \nu\bar{\nu}$.

⁴² LEURER 94, LEURER 94b limits are obtained from atomic parity violation and apply to any chiral leptoquark which couples to the first generation with electromagnetic strength. For a nonchiral leptoquark, universality in $\pi_{\ell 2}$ decay provides a much more stringent bound.

⁴³ MAHANTA 94 gives bounds of P - and T -violating scalar-leptoquark couplings from atomic and molecular experiments.

⁴⁴ From $(\pi \rightarrow e\nu)/(\pi \rightarrow \mu\nu)$ ratio. SHANKER 82 assumes the leptoquark induced four-fermion coupling $4g^2/M^2 (\bar{\nu}_e L \gamma_\mu U_R) (\bar{d}_R \gamma^\mu e_R)$ with $g=0.004$ for spin-0 leptoquark and $g^2/M^2 (\bar{\nu}_e L \gamma_\mu U_L) (\bar{d}_R \gamma^\mu e_R)$ with $g \approx 0.6$ for spin-1 leptoquark.

MASS LIMITS for Diquarks

VALUE (GeV)	CL%	DOCUMENT ID	TECN	COMMENT
>7200 (CL = 95%) OUR LIMIT				
none 600–7200	95	1 SIRUNYAN 18Bo CMS	E_6	diquark
none 600–6900	95	2 KHACHATRYAN...17W CMS	E_6	diquark
none 1500–6000	95	3 KHACHATRYAN...16K CMS	E_6	diquark
none 500–1600	95	4 KHACHATRYAN...16L CMS	E_6	diquark
none 1200–4700	95	5 KHACHATRYAN...15V CMS	E_6	diquark
••• We do not use the following data for averages, fits, limits, etc. •••				
>3750	95	6 CHATRCHYAN13A CMS	E_6	diquark
none 1000–4280	95	7 CHATRCHYAN13AS CMS		Superseded by KHACHATRYAN 15V
>3520	95	8 CHATRCHYAN11Y CMS		Superseded by CHATRCHYAN 13A
none 970–1080, 1450–1600	95	9 KHACHATRYAN...10 CMS		Superseded by CHATRCHYAN 13A
none 290–630	95	10 AALTONEN 09AC CDF	E_6	diquark
none 290–420	95	11 ABE 97G CDF	E_6	diquark
none 15–31.7	95	12 ABREU 94o DLPH	SUSY E_6	diquark

¹ SIRUNYAN 18Bo search for resonances decaying to dijets in pp collisions at $\sqrt{s}=13$ TeV.

² KHACHATRYAN 17W search for resonances decaying to dijets in pp collisions at $\sqrt{s}=13$ TeV.

³ KHACHATRYAN 16K search for resonances decaying to dijets in pp collisions at $\sqrt{s}=13$ TeV.

⁴ KHACHATRYAN 16L search for resonances decaying to dijets in pp collisions at $\sqrt{s}=8$ TeV with the data scouting technique, increasing the sensitivity to the low mass resonances.

⁵ KHACHATRYAN 15V search for resonances decaying to dijets in pp collisions at $\sqrt{s}=8$ TeV.

⁶ CHATRCHYAN 13A search for new resonance decaying to dijets in pp collisions at $\sqrt{s}=7$ TeV.

⁷ CHATRCHYAN 13AS search for new resonance decaying to dijets in pp collisions at $\sqrt{s}=8$ TeV.

⁸ CHATRCHYAN 11Y search for new resonance decaying to dijets in pp collisions at $\sqrt{s}=7$ TeV.

⁹ KHACHATRYAN 10 search for new resonance decaying to dijets in pp collisions at $\sqrt{s}=7$ TeV.

¹⁰ AALTONEN 09AC search for new narrow resonance decaying to dijets.

¹¹ ABE 97G search for new particle decaying to dijets.

¹² ABREU 94o limit is from $e^+e^- \rightarrow \bar{c}s c s$. Range extends up to 43 GeV if diquarks are degenerate in mass.

MASS LIMITS for g_A (axigluon) and Other Color-Octet Gauge Bosons

Axigluons are massive color-octet gauge bosons in chiral color models and have axial-vector coupling to quarks with the same coupling strength as gluons.

VALUE (GeV)	CL%	DOCUMENT ID	TECN	COMMENT
>6600 (CL = 95%) OUR LIMIT				
none 1800–6600	95	1 SIRUNYAN 20Al CMS	$pp \rightarrow g_A X, g_A \rightarrow 2j$	
none 600–6100	95	2 SIRUNYAN 18Bo CMS	$pp \rightarrow g_A X, g_A \rightarrow 2j$	
none 600–5500	95	3 KHACHATRYAN...17W CMS	$pp \rightarrow g_A X, g_A \rightarrow 2j$	
none 1500–5100	95	4 KHACHATRYAN...16K CMS	$pp \rightarrow g_A X, g_A \rightarrow 2j$	
none 500–1600	95	5 KHACHATRYAN...16L CMS	$pp \rightarrow g_A X, g_A \rightarrow 2j$	
none 1300–3600	95	6 KHACHATRYAN...15V CMS	$pp \rightarrow g_A X, g_A \rightarrow 2j$	
••• We do not use the following data for averages, fits, limits, etc. •••				
>2800	95	7 KHACHATRYAN...17Y CMS	$pp \rightarrow g_A g_A \rightarrow 8j$	
		8 AAD 16W ATLS	$pp \rightarrow g_A X, g_A \rightarrow b\bar{b}b\bar{b}$	
		9 KHACHATRYAN...16E CMS	$pp \rightarrow g_{KK} X, g_{KK} \rightarrow t\bar{t}$	
		10 KHACHATRYAN...15AV CMS	$pp \rightarrow \theta^0 \theta^0 \rightarrow b\bar{b}Zg$	
		11 AALTONEN 13R CDF	$p\bar{p} \rightarrow g_A X, g_A \rightarrow \sigma\sigma, \sigma \rightarrow 2j$	
>3360	95	12 CHATRCHYAN13A CMS	$pp \rightarrow g_A X, g_A \rightarrow 2j$	
none 1000–3270	95	13 CHATRCHYAN13AS CMS		Superseded by KHACHATRYAN 15V
none 250–740	95	14 CHATRCHYAN13AU CMS	$pp \rightarrow 2g_A X, g_A \rightarrow 2j$	
> 775	95	15 ABAZOV 12R D0	$p\bar{p} \rightarrow g_A X, g_A \rightarrow t\bar{t}$	
>2470	95	16 CHATRCHYAN11Y CMS		Superseded by CHATRCHYAN 13A
none 1470–1520	95	17 AALTONEN 10L CDF	$p\bar{p} \rightarrow g_A X, g_A \rightarrow t\bar{t}$	
		18 KHACHATRYAN...10 CMS		Superseded by CHATRCHYAN 13A
none 260–1250	95	19 AALTONEN 09AC CDF	$p\bar{p} \rightarrow g_A X, g_A \rightarrow 2j$	
> 910	95	20 CHOUDHURY 07 RVUE	$p\bar{p} \rightarrow t\bar{t}X$	
> 365	95	21 DONCHESKI 98 RVUE	$\Gamma(Z \rightarrow \text{hadron})$	
none 200–980	95	22 ABE 97G CDF	$p\bar{p} \rightarrow g_A X, g_A \rightarrow 2j$	
none 200–870	95	23 ABE 95N CDF	$p\bar{p} \rightarrow g_A X, g_A \rightarrow q\bar{q}$	
none 240–640	95	24 ABE 93G CDF	$p\bar{p} \rightarrow g_A X, g_A \rightarrow 2j$	
> 50	95	25 CUYPERS 91 RVUE	$\sigma(e^+e^- \rightarrow \text{hadrons})$	
none 120–210	95	26 ABE 90H CDF	$p\bar{p} \rightarrow g_A X, g_A \rightarrow 2j$	
> 29		27 ROBINETT 89 THEO		Partial-wave unitarity
none 150–310	95	28 ALBAJAR 88B UA1	$p\bar{p} \rightarrow g_A X, g_A \rightarrow 2j$	
> 20		BERGSTROM 88 RVUE	$p\bar{p} \rightarrow TX$ via $g_A g$	
> 9		29 CUYPERS 88 RVUE	T decay	
> 25		30 DONCHESKI 88B RVUE	T decay	

¹ SIRUNYAN 20Al search for resonances decaying into dijets in pp collisions at $\sqrt{s}=13$ TeV.

² SIRUNYAN 18Bo search for resonances decaying to dijets in pp collisions at $\sqrt{s}=13$ TeV.

³ KHACHATRYAN 17W search for resonances decaying to dijets in pp collisions at $\sqrt{s}=13$ TeV.

⁴ KHACHATRYAN 16K search for resonances decaying to dijets in pp collisions at $\sqrt{s}=13$ TeV.

⁵ KHACHATRYAN 16L search for resonances decaying to dijets in pp collisions at $\sqrt{s}=8$ TeV with the data scouting technique, increasing the sensitivity to the low mass resonances.

⁶ KHACHATRYAN 15V search for resonances decaying to dijets in pp collisions at $\sqrt{s}=8$ TeV.

⁷ KHACHATRYAN 17Y search for pair production of color-octet gauge boson g_A each decaying to $4j$ in pp collisions at $\sqrt{s}=8$ TeV.

⁸ AAD 16W search for a new resonance decaying to a pair of b and B_H in pp collisions at $\sqrt{s}=8$ TeV. The vector-like quark B_H is assumed to decay to bH . See their Fig. 3 and Fig. 4 for limits on σ - B .

⁹ KHACHATRYAN 16E search for KK gluon decaying to $t\bar{t}$ in pp collisions at $\sqrt{s}=8$ TeV.

¹⁰ KHACHATRYAN 15AV search for pair productions of neutral color-octet weak-triplet scalar particles (θ^0), decaying to $b\bar{b}, Zg$ or γg , in pp collisions at $\sqrt{s}=8$ TeV. The θ^0 particle is often predicted in coloron (G' , color-octet gauge boson) models and appear in the pp collisions through $G' \rightarrow \theta^0 \theta^0$ decays. Assuming $B(\theta^0 \rightarrow b\bar{b})=0.5$, they give limits $m_{\theta^0} > 623$ GeV (426 GeV) for $m_{G'}=2.3 m_{\theta^0}$ ($m_{G'}=5 m_{\theta^0}$).

¹¹ AALTONEN 13R search for new resonance decaying to $\sigma\sigma$, with hypothetical strongly interacting σ particle subsequently decaying to 2 jets, in $p\bar{p}$ collisions at $\sqrt{s}=1.96$ TeV, using data corresponding to an integrated luminosity of 6.6 fb^{-1} . For $50 \text{ GeV} < m_\sigma < m_{g_A}/2$, axigluons in mass range 150–400 GeV are excluded.

¹² CHATRCHYAN 13A search for new resonance decaying to dijets in pp collisions at $\sqrt{s}=7$ TeV.

¹³ CHATRCHYAN 13AS search for new resonance decaying to dijets in pp collisions at $\sqrt{s}=8$ TeV.

¹⁴ CHATRCHYAN 13AU search for the pair produced color-octet vector bosons decaying to $q\bar{q}$ pairs in pp collisions. The quoted limit is for $B(g_A \rightarrow q\bar{q})=1$.

¹⁵ ABAZOV 12R search for massive color octet vector particle decaying to $t\bar{t}$. The quoted limit assumes g_A couplings with light quarks are suppressed by 0.2.

¹⁶ CHATRCHYAN 11Y search for new resonance decaying to dijets in pp collisions at $\sqrt{s}=7$ TeV.

Gauge & Higgs Boson Particle Listings

New Heavy Bosons

- 17 AALTONEN 10L search for massive color octet non-chiral vector particle decaying into $t\bar{t}$ pair with mass in the range $400 \text{ GeV} < M < 800 \text{ GeV}$. See their Fig. 6 for limit in the mass-coupling plane.
- 18 KHACHATRYAN 10 search for new resonance decaying to dijets in pp collisions at $\sqrt{s} = 7 \text{ TeV}$.
- 19 AALTONEN 09AC search for new narrow resonance decaying to dijets.
- 20 CHOUDHURY 07 limit is from the $t\bar{t}$ production cross section measured at CDF.
- 21 DONCHESKI 98 compare α_s derived from low-energy data and that from $\Gamma(Z \rightarrow \text{hadrons})/\Gamma(Z \rightarrow \text{leptons})$.
- 22 ABE 97G search for new particle decaying to dijets.
- 23 ABE 95N assume axigluons decaying to quarks in the Standard Model only.
- 24 ABE 93G assume $\Gamma(g_A) = N\alpha_s m_{g_A}/6$ with $N = 10$.
- 25 CUYPERS 91 compare α_s measured in T decay and that from R at PEP/PETRA energies.
- 26 ABE 90H assumes $\Gamma(g_A) = N\alpha_s m_{g_A}/6$ with $N = 5$ ($\Gamma(g_A) = 0.09 m_{g_A}$). For $N = 10$, the excluded region is reduced to 120–150 GeV.
- 27 ROBINETT 89 result demands partial-wave unitarity of $J = 0$ $t\bar{t} \rightarrow t\bar{t}$ scattering amplitude and derives a limit $m_{g_A} > 0.5 m_t$. Assumes $m_t > 56 \text{ GeV}$.
- 28 ALBAJAR 88B result is from the nonobservation of a peak in two-jet invariant mass distribution. $\Gamma(g_A) < 0.4 m_{g_A}$ assumed. See also BAGGER 88.
- 29 CUYPERS 88 requires $\Gamma(T \rightarrow g g_A) < \Gamma(T \rightarrow g g g)$. A similar result is obtained by DONCHESKI 88.
- 30 DONCHESKI 88B requires $\Gamma(T \rightarrow g q \bar{q})/\Gamma(T \rightarrow g g g) < 0.25$, where the former decay proceeds via axigluon exchange. A more conservative estimate of < 0.5 leads to $m_{g_A} > 21 \text{ GeV}$.

MASS LIMITS for Color-Octet Scalar Bosons

VALUE (GeV)	CL%	DOCUMENT ID	TECN	COMMENT
• • • We do not use the following data for averages, fits, limits, etc. • • •				
none 1800–3700	95	1 SIRUNYAN 20AI CMS		$pp \rightarrow S_8 X, S_8 \rightarrow gg$
none 600–3400	95	2 SIRUNYAN 18BO CMS		$pp \rightarrow S_8 X, S_8 \rightarrow gg$
		3 KHACHATRYAN 15AV CMS		$pp \rightarrow \Theta^0 \Theta^0 \rightarrow b\bar{b} Z g$
none 150–287	95	4 AAD 13K ATLS		$pp \rightarrow S_8 S_8 X, S_8 \rightarrow 2 \text{ jets}$
1 SIRUNYAN 20AI search for resonances decaying into dijets in pp collisions at $\sqrt{s} = 13 \text{ TeV}$. The limit above assumes S_{8gg} coupling $k_s^2 = 1/2$.				
2 SIRUNYAN 18BO search for color octet scalar boson produced through gluon fusion process in pp collisions at $\sqrt{s} = 13 \text{ TeV}$. The limit above assumes S_{8gg} coupling $k_s^2 = 1/2$.				
3 KHACHATRYAN 15AV search for pair productions of neutral color-octet weak-triplet scalar particles (Θ^0), decaying to $b\bar{b}, Zg$ or γg , in pp collisions at $\sqrt{s} = 8 \text{ TeV}$. The Θ^0 particle is often predicted in coloron (G' , color-octet gauge boson) models and appear in the pp collisions through $G' \rightarrow \Theta^0 \Theta^0$ decays. Assuming $B(\Theta^0 \rightarrow b\bar{b}) = 0.5$, they give limits $m_{\Theta^0} > 623 \text{ GeV}$ (426 GeV) for $m_{G'} = 2.3 m_{\Theta^0}$ ($m_{G'} = 5 m_{\Theta^0}$).				
4 AAD 13K search for pair production of color-octet scalar particles in pp collisions at $\sqrt{s} = 7 \text{ TeV}$. Cross section limits are interpreted as mass limits on scalar partners of a Dirac gluino.				

X^0 (Heavy Boson) Searches in Z Decays

Searches for radiative transition of Z to a lighter spin-0 state X^0 decaying to hadrons, a lepton pair, a photon pair, or invisible particles as shown in the comments. The limits are for the product of branching ratios.

VALUE	CL%	DOCUMENT ID	TECN	COMMENT
• • • We do not use the following data for averages, fits, limits, etc. • • •				
		1 RAINBOLT 19 RVUE		$X^0 \rightarrow \ell^+ \ell^-$
		2 SIRUNYAN 19AZ CMS		$X^0 \rightarrow \mu^+ \mu^-$
		3 BARATE 98U ALEP		$X^0 \rightarrow \ell\bar{\ell}, q\bar{q}, gg, \gamma\gamma, \nu\bar{\nu}$
		4 ACCIARRI 97Q L3		$X^0 \rightarrow \text{invisible particle(s)}$
		5 ACTON 93E OPAL		$X^0 \rightarrow \gamma\gamma$
		6 ABREU 92D DLPH		$X^0 \rightarrow \text{hadrons}$
		7 ADRIANI 92F L3		$X^0 \rightarrow \text{hadrons}$
		8 ACTON 91 OPAL		$X^0 \rightarrow \text{anything}$
$< 1.1 \times 10^{-4}$	95	9 ACTON 91B OPAL		$X^0 \rightarrow e^+ e^-$
$< 9 \times 10^{-5}$	95	9 ACTON 91B OPAL		$X^0 \rightarrow \mu^+ \mu^-$
$< 1.1 \times 10^{-4}$	95	9 ACTON 91B OPAL		$X^0 \rightarrow \tau^+ \tau^-$
$< 2.8 \times 10^{-4}$	95	10 ADEVA 91D L3		$X^0 \rightarrow e^+ e^-$
$< 2.3 \times 10^{-4}$	95	10 ADEVA 91D L3		$X^0 \rightarrow \mu^+ \mu^-$
$< 4.7 \times 10^{-4}$	95	11 ADEVA 91D L3		$X^0 \rightarrow \text{hadrons}$
$< 8 \times 10^{-4}$	95	12 AKRAWY 90J OPAL		$X^0 \rightarrow \text{hadrons}$

- 1 RAINBOLT 19 limits are from $B(Z \rightarrow \ell^+ \ell^- X^0)$. See their Figs. 5 and 6 for limits in mass-coupling plane.
- 2 SIRUNYAN 19AZ search for $pp \rightarrow Z \rightarrow X^0 \mu^+ \mu^- \rightarrow \mu^+ \mu^- \mu^+ \mu^-$ events in pp collisions at $\sqrt{s} = 13 \text{ TeV}$. See their Fig. 5 for limits on $\sigma(pp \rightarrow X^0 \mu^+ \mu^-) \cdot B(X^0 \rightarrow \mu^+ \mu^-)$.
- 3 BARATE 98U obtain limits on $B(Z \rightarrow \gamma X^0) \cdot B(X^0 \rightarrow \ell\bar{\ell}, q\bar{q}, gg, \gamma\gamma, \nu\bar{\nu})$. See their Fig. 17.
- 4 See Fig. 4 of ACCIARRI 97Q for the upper limit on $B(Z \rightarrow \gamma X^0; E_\gamma > E_{\text{min}})$ as a function of E_{min} .
- 5 ACTON 93E give $\sigma(e^+ e^- \rightarrow X^0 \gamma) \cdot B(X^0 \rightarrow \gamma\gamma) < 0.4 \text{ pb}$ (95%CL) for $m_{X^0} = 60 \pm 2.5 \text{ GeV}$. If the process occurs via s-channel γ exchange, the limit translates to $\Gamma(X^0) \cdot B(X^0 \rightarrow \gamma\gamma)^2 < 20 \text{ MeV}$ for $m_{X^0} = 60 \pm 1 \text{ GeV}$.
- 6 ABREU 92D give $\sigma_Z \cdot B(Z \rightarrow \gamma X^0) \cdot B(X^0 \rightarrow \text{hadrons}) < (3-10) \text{ pb}$ for $m_{X^0} = 10-78 \text{ GeV}$. A very similar limit is obtained for spin-1 X^0 .

- 7 ADRIANI 92F search for isolated γ in hadronic Z decays. The limit $\sigma_Z \cdot B(Z \rightarrow \gamma X^0) \cdot B(X^0 \rightarrow \text{hadrons}) < (2-10) \text{ pb}$ (95%CL) is given for $m_{X^0} = 25-85 \text{ GeV}$.
- 8 ACTON 91 searches for $Z \rightarrow Z^* X^0, Z^* \rightarrow e^+ e^-, \mu^+ \mu^-, \text{ or } \nu\bar{\nu}$. Excludes any new scalar X^0 with $m_{X^0} < 9.5 \text{ GeV}/c$ if it has the same coupling to ZZ^* as the MSM Higgs boson.
- 9 ACTON 91B limits are for $m_{X^0} = 60-85 \text{ GeV}$.
- 10 ADEVA 91D limits are for $m_{X^0} = 30-89 \text{ GeV}$.
- 11 ADEVA 91D limits are for $m_{X^0} = 30-86 \text{ GeV}$.
- 12 AKRAWY 90J give $\Gamma(Z \rightarrow \gamma X^0) \cdot B(X^0 \rightarrow \text{hadrons}) < 1.9 \text{ MeV}$ (95%CL) for $m_{X^0} = 32-80 \text{ GeV}$. We divide by $\Gamma(Z) = 2.5 \text{ GeV}$ to get product of branching ratios. For nonresonant transitions, the limit is $B(Z \rightarrow \gamma q \bar{q}) < 8.2 \text{ MeV}$ assuming three-body phase space distribution.

MASS LIMITS for a Heavy Neutral Boson Coupling to $e^+ e^-$

VALUE (GeV)	CL%	DOCUMENT ID	TECN	COMMENT
• • • We do not use the following data for averages, fits, limits, etc. • • •				
none 55–61		1 ODAKA 89 VNS		$\Gamma(X^0 \rightarrow e^+ e^-) \cdot B(X^0 \rightarrow \text{had.}) \gtrsim 0.2 \text{ MeV}$
> 45	95	2 DERRICK 86 HRS		$\Gamma(X^0 \rightarrow e^+ e^-) = 6 \text{ MeV}$
> 46.6	95	3 ADEVA 85 MRKJ		$\Gamma(X^0 \rightarrow e^+ e^-) = 10 \text{ keV}$
> 48	95	3 ADEVA 85 MRKJ		$\Gamma(X^0 \rightarrow e^+ e^-) = 4 \text{ MeV}$
		4 BERGER 85B PLUT		
none 39.8–45.5		5 ADEVA 84 MRKJ		$\Gamma(X^0 \rightarrow e^+ e^-) = 10 \text{ keV}$
> 47.8	95	5 ADEVA 84 MRKJ		$\Gamma(X^0 \rightarrow e^+ e^-) = 4 \text{ MeV}$
none 39.8–45.2		5 BEHREND 84c CELL		
> 47	95	5 BEHREND 84c CELL		$\Gamma(X^0 \rightarrow e^+ e^-) = 4 \text{ MeV}$
1 ODAKA 89 looked for a narrow or wide scalar resonance in $e^+ e^- \rightarrow \text{hadrons}$ at $E_{\text{cm}} = 55.0-60.8 \text{ GeV}$.				
2 DERRICK 86 found no deviation from the Standard Model Bhabha scattering at $E_{\text{cm}} = 29 \text{ GeV}$ and set limits on the possible scalar boson $e^+ e^-$ coupling. See their figure 4 for excluded region in the $\Gamma(X^0 \rightarrow e^+ e^-) - m_{X^0}$ plane. Electronic chiral invariance requires a parity doublet of X^0 , in which case the limit applies for $\Gamma(X^0 \rightarrow e^+ e^-) = 3 \text{ MeV}$.				
3 ADEVA 85 first limit is from $2\gamma, \mu^+ \mu^-, \text{ hadrons}$ assuming X^0 is a scalar. Second limit is from $e^+ e^-$ channel. $E_{\text{cm}} = 40-47 \text{ GeV}$. Supersedes ADEVA 84.				
4 BERGER 85B looked for effect of spin-0 boson exchange in $e^+ e^- \rightarrow e^+ e^-$ and $\mu^+ \mu^-$ at $E_{\text{cm}} = 34.7 \text{ GeV}$. See Fig. 5 for excluded region in the $m_{X^0} - \Gamma(X^0)$ plane.				
5 ADEVA 84 and BEHREND 84c have $E_{\text{cm}} = 39.8-45.5 \text{ GeV}$. MARK-J searched X^0 in $e^+ e^- \rightarrow \text{hadrons}, 2\gamma, \mu^+ \mu^-, e^+ e^-$ and CELLO in the same channels plus τ pair. No narrow or broad X^0 is found in the energy range. They also searched for the effect of X^0 with $m_X > E_{\text{cm}}$. The second limits are from Bhabha data and for spin-0 singlet. The same limits apply for $\Gamma(X^0 \rightarrow e^+ e^-) = 2 \text{ MeV}$ if X^0 is a spin-0 doublet. The second limit of BEHREND 84c was read off from their figure 2. The original papers also list limits in other channels.				

Search for X^0 Resonance in $e^+ e^-$ Collisions

The limit is for $\Gamma(X^0 \rightarrow e^+ e^-) \cdot B(X^0 \rightarrow f)$, where f is the specified final state. Spin 0 is assumed for X^0 .

VALUE (keV)	CL%	DOCUMENT ID	TECN	COMMENT
• • • We do not use the following data for averages, fits, limits, etc. • • •				
$< 10^3$	95	1 ABE 93c VNS		$\Gamma(ee)$
$< (0.4-10)$	95	2 ABE 93c VNS		$f = \gamma\gamma$
$< (0.3-5)$	95	3,4 ABE 93D TOPZ		$f = \gamma\gamma$
$< (2-12)$	95	3,4 ABE 93D TOPZ		$f = \text{hadrons}$
$< (4-200)$	95	4,5 ABE 93D TOPZ		$f = ee$
$< (0.1-6)$	95	4,5 ABE 93D TOPZ		$f = \mu\mu$
$< (0.5-8)$	90	6 STERNER 93 AMY		$f = \gamma\gamma$
1 Limit is for $\Gamma(X^0 \rightarrow e^+ e^-) m_{X^0} = 56-63.5 \text{ GeV}$ for $\Gamma(X^0) = 0.5 \text{ GeV}$.				
2 Limit is for $m_{X^0} = 56-61.5 \text{ GeV}$ and is valid for $\Gamma(X^0) \ll 100 \text{ MeV}$. See their Fig. 5 for limits for $\Gamma = 1, 2 \text{ GeV}$.				
3 Limit is for $m_{X^0} = 57.2-60 \text{ GeV}$.				
4 Limit is for $\Gamma(X^0) \ll 100 \text{ MeV}$. See paper for limits for $\Gamma = 1 \text{ GeV}$ and those for $J = 2$ resonances.				
5 Limit is for $m_{X^0} = 56.6-60 \text{ GeV}$.				
6 STERNER 93 limit is for $m_{X^0} = 57-59.6 \text{ GeV}$ and is valid for $\Gamma(X^0) < 100 \text{ MeV}$. See their Fig. 2 for limits for $\Gamma = 1, 3 \text{ GeV}$.				

Search for X^0 Resonance in ep Collisions

VALUE	DOCUMENT ID	TECN	COMMENT
• • • We do not use the following data for averages, fits, limits, etc. • • •			
	1 CHEKANOV 02B ZEUS		$X \rightarrow jj$
1 CHEKANOV 02B search for photoproduction of X decaying into dijets in ep collisions. See their Fig. 5 for the limit on the photoproduction cross section.			

Search for X^0 Resonance in $e^+ e^- \rightarrow X^0 \gamma$

VALUE (GeV)	DOCUMENT ID	TECN	COMMENT
• • • We do not use the following data for averages, fits, limits, etc. • • •			
	1 ABBIENDI 03D OPAL		$X^0 \rightarrow \gamma\gamma$
	2 ABREU 00Z DLPH		X^0 decaying invisibly
	3 ADAM 96c DLPH		X^0 decaying invisibly

See key on page 1127

Gauge & Higgs Boson Particle Listings
New Heavy Bosons

- 1 ABBIENDI 03D measure the e+e- -> gamma gamma cross section at sqrt(s)=181-209 GeV. The upper bound on the production cross section, sigma(e+e- -> X0 gamma) times the branching ratio for X0 -> gamma gamma, is less than 0.03 pb at 95%CL for X0 masses between 20 and 180 GeV. See their Fig. 9b for the limits in the mass-cross section plane.
2 ABREU 00Z is from the single photon cross section at sqrt(s)=183, 189 GeV. The production cross section upper limit is less than 0.3 pb for X0 mass between 40 and 160 GeV. See their Fig. 4 for the limit in mass-cross section plane.
3 ADAM 96c is from the single photon production cross at sqrt(s)=130, 136 GeV. The upper bound is less than 3 pb for X0 masses between 60 and 130 GeV. See their Fig. 5 for the exact bound on the cross section sigma(e+e- -> gamma X0).

Search for X0 Resonance in Z -> f f X0

The limit is for B(Z -> f f X0) * B(X0 -> F) where f is a fermion and F is the specified final state. Spin 0 is assumed for X0.

Table with columns: VALUE, CL%, DOCUMENT ID, TECN, COMMENT. Lists search results for Z -> f f X0 with various experiments and parameters.

- 1 ABREU 96T obtain limit as a function of m_X0. See their Fig. 6.
2 Limit is for m_X0 around 60 GeV.
3 ABREU 96T obtain limit as a function of m_X0. See their Fig. 15.
4 ADRIANI 92F give sigma * B(Z -> q q X0) * B(X0 -> gamma) < (0.75-1.5) pb (95%CL) for m_X0 = 10-70 GeV. The limit is 1 pb at 60 GeV.

Search for X0 Resonance in W X0 final state

The limit is for B(W -> X0 f) * B(X0 -> F) where f is a fermion and F is the specified final state. Spin 0 is assumed for X0.

Table with columns: VALUE (MeV), DOCUMENT ID, TECN, COMMENT. Lists search results for W X0 final state with various experiments and parameters.

Search for X0 Resonance in Quarkonium Decays

Limits are for branching ratios to modes shown. Spin 1 is assumed for X0.

Table with columns: VALUE, CL%, DOCUMENT ID, TECN, COMMENT. Lists search results for quarkonium decays with various experiments and parameters.

Search for X0 Resonance in H(125) Decays

Spin 1 is assumed for X0. See neutral Higgs search listing for pseudoscalar X0.

Table with columns: VALUE, DOCUMENT ID, TECN, COMMENT. Lists search results for H(125) decays with various experiments and parameters.

REFERENCES FOR Searches for New Heavy Bosons (W', Z', leptoquarks, etc.)

AAD 22 PR D105 012001 G. Aad et al. (ATLAS Collab.)
AAD 21AG EPJ C81 313 G. Aad et al. (ATLAS Collab.)
AAD 21AQ JHEP 2107 005 G. Aad et al. (ATLAS Collab.)
AAD 21AW PR D104 112005 G. Aad et al. (ATLAS Collab.)
AAD 21AZ JHEP 2110 013 G. Aad et al. (ATLAS Collab.)
AAD 21BB JHEP 2111 209 G. Aad et al. (ATLAS Collab.)

AAD 21D PRL 126 121802 G. Aad et al. (ATLAS Collab.)
AAD 21K JHEP 2102 226 G. Aad et al. (ATLAS Collab.)
AAD 21S JHEP 2105 093 G. Aad et al. (ATLAS Collab.)
AAD 21T JHEP 2106 179 G. Aad et al. (ATLAS Collab.)
BURAS 21 JHEP 2106 068 A.J. Buras et al. (TUM, CERN, ZURICH)
CADEDDU 21 JHEP 2101 116 M. Cadeddu et al. (CAGLI, CAGL, INFN+)
COLARES1 21 PR D104 072003 J. Colaresi et al. (MRION, FNAL, PNL+)
CRIVELLIN 21J PR D103 115023 A. Crivellin, D. Mueller, L. Schnell (CERN, ZURICH)
KRIBS 21 PRL 126 011801 G.D. Kribs, D. McKeen, N. Raj (OREG, TRIUM)
SIRUNYAN 21A PL B819 136446 A.M. Sirunyan et al. (CMS Collab.)
SIRUNYAN 21N JHEP 2107 208 A.M. Sirunyan et al. (CMS Collab.)
SIRUNYAN 21X EPJ C81 688 A.M. Sirunyan et al. (CMS Collab.)
SIRUNYAN 21Y PL B820 136535 A.M. Sirunyan et al. (CMS Collab.)
TUMASYAN 21D JHEP 2111 153 A. Tumasyan et al. (CMS Collab.)
AAD 20AD PRL 125 131801 G. Aad et al. (ATLAS Collab.)
AAD 20AF PRL 125 251802 G. Aad et al. (ATLAS Collab.)
AAD 20AJ PR D102 112008 G. Aad et al. (ATLAS Collab.)
AAD 20AK JHEP 2010 112 G. Aad et al. (ATLAS Collab.)
AAD 20AM JHEP 2010 061 G. Aad et al. (ATLAS Collab.)
AAD 20AT EPJ C80 1165 G. Aad et al. (ATLAS Collab.)
AAD 20S EPJ C80 737 G. Aad et al. (ATLAS Collab.)
AAD 20T JHEP 2003 145 G. Aad et al. (ATLAS Collab.)
AAD 20W JHEP 2006 151 G. Aad et al. (ATLAS Collab.)
AAJ 20AL JHEP 2010 156 R. Aaij et al. (LHCb Collab.)
ADACHI 20 PRL 124 141801 I. Adachi et al. (BELLE II Collab.)
AEBISCHER 20 EPJ C80 252 J. Aebischer et al. (TUM, LAPTH, UCCS)
DEPPISCH 20 JHEP 2012 186 F.F. Deppisch, K. Fridolf, J. Harz (LOUC, TUC)
SIRUNYAN 20A EPJ C80 3 A.M. Sirunyan et al. (CMS Collab.)
SIRUNYAN 20AI JHEP 2005 033 A.M. Sirunyan et al. (CMS Collab.)
SIRUNYAN 20AM PRL 124 131802 A.M. Sirunyan et al. (CMS Collab.)
SIRUNYAN 20M PL B005 135448 A.M. Sirunyan et al. (CMS Collab.)
SIRUNYAN 20Q EPJ C80 237 A.M. Sirunyan et al. (CMS Collab.)
AABOUD 19AJ PL B795 56 M. Aaboud et al. (ATLAS Collab.)
AABOUD 19AS PR D99 092004 M. Aaboud et al. (ATLAS Collab.)
AABOUD 19AX EPJ C79 733 M. Aaboud et al. (ATLAS Collab.)
AABOUD 19B JHEP 1901 016 M. Aaboud et al. (ATLAS Collab.)
AABOUD 19BB PL B798 134942 M. Aaboud et al. (ATLAS Collab.)
AABOUD 19D PL B788 316 M. Aaboud et al. (ATLAS Collab.)
AABOUD 19E PL B788 347 M. Aaboud et al. (ATLAS Collab.)
AABOUD 19V JHEP 1905 142 M. Aaboud et al. (ATLAS Collab.)
AABOUD 19X JHEP 1906 144 M. Aaboud et al. (ATLAS Collab.)
AAD 19C PR D100 052013 G. Aad et al. (ATLAS Collab.)
AAD 19D JHEP 1909 091 G. Aad et al. (ATLAS Collab.)
Also JHEP 2006 042 (err.) G. Aad et al. (ATLAS Collab.)
AAD 19L PL B796 68 G. Aad et al. (ATLAS Collab.)
ABRAMOWICZ 19 PR D99 092006 H. Abramowicz et al. (ZEUS, SIEG)
LONG 19 NP B943 114629 H.N. Long et al. (VALE, SIEG)
MANDAL 19 JHEP 1912 089 R. Mandal, A. Pich (ITP)
PANDEY 19 JHEP 1911 046 S. Pandey, S. Karmakar, S. Rakshit (NWES)
RAINBOLT 19 PR D99 013004 J.L. Rainbolt, M. Schmitt (CMS Collab.)
SIRUNYAN 19AA JHEP 1904 031 A.M. Sirunyan et al. (CMS Collab.)
SIRUNYAN 19AL EPJ C79 208 A.M. Sirunyan et al. (CMS Collab.)
SIRUNYAN 19AM EPJ C79 280 A.M. Sirunyan et al. (CMS Collab.)
SIRUNYAN 19AY PL B792 107 A.M. Sirunyan et al. (CMS Collab.)
SIRUNYAN 19AZ PL B792 345 A.M. Sirunyan et al. (CMS Collab.)
SIRUNYAN 19BC PL B795 76 A.M. Sirunyan et al. (CMS Collab.)
SIRUNYAN 19BI PR D99 032014 A.M. Sirunyan et al. (CMS Collab.)
SIRUNYAN 19BJ PR D99 052002 A.M. Sirunyan et al. (CMS Collab.)
SIRUNYAN 19CB PR D100 112007 A.M. Sirunyan et al. (CMS Collab.)
SIRUNYAN 19CD PRL 123 231803 A.M. Sirunyan et al. (CMS Collab.)
SIRUNYAN 19CP PL B798 134952 A.M. Sirunyan et al. (CMS Collab.)
SIRUNYAN 19D PRL 122 081804 A.M. Sirunyan et al. (CMS Collab.)
SIRUNYAN 19I JHEP 1901 051 A.M. Sirunyan et al. (CMS Collab.)
SIRUNYAN 19V JHEP 1903 1217 A.M. Sirunyan et al. (CMS Collab.)
SIRUNYAN 19Y JHEP 1903 107 A.M. Sirunyan et al. (CMS Collab.)
AABOUD 18AA PR D98 032015 M. Aaboud et al. (ATLAS Collab.)
AABOUD 18AB PR D98 032016 M. Aaboud et al. (ATLAS Collab.)
AABOUD 18AD PL B779 24 M. Aaboud et al. (ATLAS Collab.)
AABOUD 18AF PL B781 327 M. Aaboud et al. (ATLAS Collab.)
AABOUD 18AI JHEP 1803 174 M. Aaboud et al. (ATLAS Collab.)
Also JHEP 1811 051 (err.) M. Aaboud et al. (ATLAS Collab.)
AABOUD 18AK JHEP 1803 042 M. Aaboud et al. (ATLAS Collab.)
AABOUD 18AL JHEP 1803 009 M. Aaboud et al. (ATLAS Collab.)
AABOUD 18AP JHEP 1806 166 M. Aaboud et al. (ATLAS Collab.)
AABOUD 18B EPJ C78 24 M. Aaboud et al. (ATLAS Collab.)
AABOUD 18C EPJ C78 401 M. Aaboud et al. (ATLAS Collab.)
AABOUD 18BI EPJ C78 565 M. Aaboud et al. (ATLAS Collab.)
AABOUD 18CH PL B787 68 M. Aaboud et al. (ATLAS Collab.)
AABOUD 18CJ PR D98 052008 M. Aaboud et al. (ATLAS Collab.)
AABOUD 18CM PR D98 092008 M. Aaboud et al. (ATLAS Collab.)
AABOUD 18F PL B777 91 M. Aaboud et al. (ATLAS Collab.)
AABOUD 18G JHEP 1801 055 M. Aaboud et al. (ATLAS Collab.)
AABOUD 18H PRL 120 161802 M. Aaboud et al. (ATLAS Collab.)
AABOUD 18N PRL 121 081801 M. Aaboud et al. (ATLAS Collab.)
AAJ 18AQ JHEP 1809 147 R. Aaij et al. (LHCb Collab.)
BOBOVNIKOV 18 PR D98 095029 I.D. Bobovnikov, P. Osland, A.A. Pankov (BER, CGO)
SIRUNYAN 18 PR D98 095029 A.M. Sirunyan et al. (CMS Collab.)
SIRUNYAN 18AT JHEP 1804 073 A.M. Sirunyan et al. (CMS Collab.)
SIRUNYAN 18AX JHEP 1805 088 A.M. Sirunyan et al. (CMS Collab.)
SIRUNYAN 18AZ JHEP 1806 128 A.M. Sirunyan et al. (CMS Collab.)
SIRUNYAN 18BB JHEP 1806 120 A.M. Sirunyan et al. (CMS Collab.)
SIRUNYAN 18BJ JHEP 1807 115 A.M. Sirunyan et al. (CMS Collab.)
SIRUNYAN 18BK JHEP 1807 075 A.M. Sirunyan et al. (CMS Collab.)
SIRUNYAN 18BO JHEP 1808 130 A.M. Sirunyan et al. (CMS Collab.)
SIRUNYAN 18CV JHEP 1805 148 A.M. Sirunyan et al. (CMS Collab.)
SIRUNYAN 18CZ EPJ C78 707 A.M. Sirunyan et al. (CMS Collab.)
SIRUNYAN 18DJ JHEP 1809 101 A.M. Sirunyan et al. (CMS Collab.)
SIRUNYAN 18DR JHEP 1811 161 A.M. Sirunyan et al. (CMS Collab.)
SIRUNYAN 18EC PRL 121 241802 A.M. Sirunyan et al. (CMS Collab.)
SIRUNYAN 18ED JHEP 1811 172 A.M. Sirunyan et al. (CMS Collab.)
SIRUNYAN 18G JHEP 1801 097 A.M. Sirunyan et al. (CMS Collab.)
SIRUNYAN 18I PRL 120 201801 A.M. Sirunyan et al. (CMS Collab.)
SIRUNYAN 18P PR D97 072006 A.M. Sirunyan et al. (CMS Collab.)
SIRUNYAN 18U PR D98 032005 A.M. Sirunyan et al. (CMS Collab.)
ZHANG 18A EPJ C78 695 J. Zhang, C.-X. Yue, C.-H. Li (LNUDA)
AABOUD 17AK PR D96 052004 M. Aaboud et al. (ATLAS Collab.)
AABOUD 17AO PL B774 494 M. Aaboud et al. (ATLAS Collab.)
AABOUD 17AT JHEP 1710 182 M. Aaboud et al. (ATLAS Collab.)
AABOUD 17B PL B765 32 M. Aaboud et al. (ATLAS Collab.)
KHACHATRYAN 17X PL B773 563 V. Khachatryan et al. (CMS Collab.)
KHACHATRYAN 17H JHEP 1702 048 V. Khachatryan et al. (CMS Collab.)
KHACHATRYAN 17J JHEP 1703 077 V. Khachatryan et al. (CMS Collab.)
KHACHATRYAN 17T PL B768 57 V. Khachatryan et al. (CMS Collab.)
KHACHATRYAN 17U PL B768 137 V. Khachatryan et al. (CMS Collab.)
KHACHATRYAN 17W PL B769 520 V. Khachatryan et al. (CMS Collab.)
KHACHATRYAN 17Y PL B770 257 V. Khachatryan et al. (CMS Collab.)
KHACHATRYAN 17Z PL B770 278 V. Khachatryan et al. (CMS Collab.)
SIRUNYAN 17A JHEP 1703 162 A.M. Sirunyan et al. (CMS Collab.)
SIRUNYAN 17AK PL B774 533 A.M. Sirunyan et al. (CMS Collab.)
SIRUNYAN 17AP JHEP 1710 180 A.M. Sirunyan et al. (CMS Collab.)
SIRUNYAN 17H JHEP 1707 121 A.M. Sirunyan et al. (CMS Collab.)
SIRUNYAN 17I JHEP 1708 029 A.M. Sirunyan et al. (CMS Collab.)

Downloaded from https://academic.oup.com/hep/article/2022/8/1665/6666 by CERN Library user on 11 October 2022

Gauge & Higgs Boson Particle Listings

New Heavy Bosons

SIRUNYAN	17Q	JHEP 1707 001	A.M. Sirunyan et al.	(CMS Collab.)	AARON	11B	PL B704 388	F. D. Aaron et al.	(H1 Collab.)
SIRUNYAN	17R	EPJ C76 636	A.M. Sirunyan et al.	(CMS Collab.)	AARON	11C	PL B705 52	F. D. Aaron et al.	(H1 Collab.)
SIRUNYAN	17T	PRL 119 118102	A.M. Sirunyan et al.	(CMS Collab.)	ABAZOV	11A	PL B695 88	V.M. Abazov et al.	(DO Collab.)
SIRUNYAN	17V	JHEP 1709 053	A.M. Sirunyan et al.	(CMS Collab.)	ABAZOV	11H	PRL 107 011801	V.M. Abazov et al.	(DO Collab.)
AABOUD	16	PL B759 229	M. Aboud et al.	(ATLAS Collab.)	ABAZOV	11I	PRL 107 011804	V.M. Abazov et al.	(DO Collab.)
AABOUD	16AA	EPJ C76 585	M. Aboud et al.	(ATLAS Collab.)	ABAZOV	11L	PL B699 145	V.M. Abazov et al.	(DO Collab.)
AABOUD	16AE	JHEP 1609 173	M. Aboud et al.	(ATLAS Collab.)	ABAZOV	11V	PR D84 071104	V.M. Abazov et al.	(DO Collab.)
AABOUD	16E	EPJ C76 541	M. Aboud et al.	(ATLAS Collab.)	BUENO	11	PR D84 032005	J.F. Bueno et al.	(TWIST Collab.)
AABOUD	16U	PL B761 372	M. Aboud et al.	(ATLAS Collab.)	Also	11	PR D85 039908 (err.)	S.F. Chattrchyan et al.	(CMS Collab.)
AABOUD	16V	PL B762 334	M. Aboud et al.	(ATLAS Collab.)	CHATRCHYAN	11N	PL B703 246	S. Chattrchyan et al.	(CMS Collab.)
AAD	16G	EPJ C76 5	G. Aad et al.	(ATLAS Collab.)	CHATRCHYAN	11O	JHEP 1108 005	S. Chattrchyan et al.	(CMS Collab.)
AAD	16L	EPJ C76 210	G. Aad et al.	(ATLAS Collab.)	CHATRCHYAN	11Y	PL B704 123	S. Chattrchyan et al.	(CMS Collab.)
AAD	16R	PL B755 285	G. Aad et al.	(ATLAS Collab.)	DORSNER	11	JHEP 1111 002	I. Dorsner et al.	
AAD	16S	PL B754 302	G. Aad et al.	(ATLAS Collab.)	KHACHATRYAN	11D	PRL 106 201802	V. Khachatryan et al.	(CMS Collab.)
AAD	16W	PL B758 249	G. Aad et al.	(ATLAS Collab.)	KHACHATRYAN	11E	PRL 106 201803	V. Khachatryan et al.	(CMS Collab.)
BARRANCO	16	JP G43 115004	J. Barranco et al.		AALTONEN	10L	PL B691 183	T. Aaltonen et al.	(CDF Collab.)
DEY	16	JHEP 1604 187	U.K. Dey, S. Mohanty		AALTONEN	10N	PRL 104 241801	T. Aaltonen et al.	(CDF Collab.)
KHACHATRYAN	16AF	PR D93 032004	V. Khachatryan et al.	(CMS Collab.)	ABAZOV	10J	PL B693 95	V.M. Abazov et al.	(DO Collab.)
KHACHATRYAN	16AG	PR D93 032005	V. Khachatryan et al.	(CMS Collab.)	DEL-AGUILA	10	JHEP 1009 033	F. del Aguila, J. de Blas, M. Perez-Victoria	(GRAN Collab.)
Also	16H	PR D95 039906 (err.)	V. Khachatryan et al.	(CMS Collab.)	KHACHATRYAN	10	PRL 105 211801	V. Khachatryan et al.	(CMS Collab.)
KHACHATRYAN	16AO	JHEP 1602 122	V. Khachatryan et al.	(CMS Collab.)	Also	10	PRL 106 029902	V. Khachatryan et al.	(CMS Collab.)
KHACHATRYAN	16AP	JHEP 1602 145	V. Khachatryan et al.	(CMS Collab.)	WAUTERS	10	PR C82 055502	F. Wauters et al.	(REZ, TAMU Collab.)
KHACHATRYAN	16BD	EPJ C76 237	V. Khachatryan et al.	(CMS Collab.)	AALTONEN	09AC	PR D79 12002	T. Aaltonen et al.	(CDF Collab.)
KHACHATRYAN	16BE	EPJ C76 317	V. Khachatryan et al.	(CMS Collab.)	AALTONEN	09T	PRL 102 031801	T. Aaltonen et al.	(CDF Collab.)
KHACHATRYAN	16E	PR D93 012001	V. Khachatryan et al.	(CMS Collab.)	AALTONEN	09V	PRL 102 091805	T. Aaltonen et al.	(CDF Collab.)
KHACHATRYAN	16K	PRL 116 071801	V. Khachatryan et al.	(CMS Collab.)	ABAZOV	09	PL B671 224	V.M. Abazov et al.	(DO Collab.)
KHACHATRYAN	16L	PRL 117 031802	V. Khachatryan et al.	(CMS Collab.)	ABAZOV	09AF	PL B681 224	V.M. Abazov et al.	(DO Collab.)
KHACHATRYAN	16O	PL B755 196	V. Khachatryan et al.	(CMS Collab.)	ERLER	09	JHEP 0908 017	J. Erler et al.	
KUMAR	16	PR D94 014022	G. Kumar		AALTONEN	08D	PR D77 051102	T. Aaltonen et al.	(CDF Collab.)
AAD	15AM	JHEP 1507 157	G. Aad et al.	(ATLAS Collab.)	AALTONEN	08P	PR D77 091105	T. Aaltonen et al.	(CDF Collab.)
AAD	15AO	JHEP 1508 148	G. Aad et al.	(ATLAS Collab.)	ABALONEN	08Y	PR 100 221801	T. Aaltonen et al.	(CDF Collab.)
AAD	15AT	EPJ C75 79	G. Aad et al.	(ATLAS Collab.)	AALTONEN	08Z	PL 101 071802	T. Aaltonen et al.	(CDF Collab.)
AAD	15AU	EPJ C75 69	G. Aad et al.	(ATLAS Collab.)	ABAZOV	08AA	PL B668 98	V.M. Abazov et al.	(DO Collab.)
AAD	15AV	EPJ C75 165	G. Aad et al.	(ATLAS Collab.)	ABAZOV	08AD	PL B668 357	V.M. Abazov et al.	(DO Collab.)
AAD	15AZ	EPJ C75 209	G. Aad et al.	(ATLAS Collab.)	ABAZOV	08AN	PRL 101 241802	V.M. Abazov et al.	(DO Collab.)
Also	15B	EPJ C75 370 (err.)	G. Aad et al.	(ATLAS Collab.)	ABAZOV	08C	PRL 100 031804	V.M. Abazov et al.	(DO Collab.)
AAD	15BB	EPJ C75 263	G. Aad et al.	(ATLAS Collab.)	MACDONALD	08	PR D78 032010	R.P. MacDonald et al.	(TWIST Collab.)
AAD	15CD	PR D92 092001	G. Aad et al.	(ATLAS Collab.)	ZHANG	08	NP B802 247	Y. Zhang et al.	(PKG, UMD Collab.)
AAD	15CP	JHEP 1512 055	G. Aad et al.	(ATLAS Collab.)	AALTONEN	07H	PRL 99 171802	T. Aaltonen et al.	(CDF Collab.)
AAD	15O	PRL 115 031801	G. Aad et al.	(ATLAS Collab.)	ABAZOV	07E	PL B647 74	V.M. Abazov et al.	(DO Collab.)
AAD	15R	PL B743 235	G. Aad et al.	(ATLAS Collab.)	ABAZOV	07J	PRL 99 061801	V.M. Abazov et al.	(DO Collab.)
AAD	15S	PR D91 052007	G. Aad et al.	(ATLAS Collab.)	AKTAS	07A	EPJ C52 333	A. Aktas et al.	(H1 Collab.)
AALTONEN	15C	PRL 115 061801	T. Aaltonen et al.	(CDF Collab.)	CHOUDHURY	07	PL B657 69	D. Choudhury et al.	
BESSAA	15	EPJ C75 97	A. Bessaa, S. Davidsson		MELCONIAN	07	PL B649 370	D. Melconian et al.	(TRIUMF Collab.)
KHACHATRYAN	15AE	JHEP 1504 025	V. Khachatryan et al.	(CMS Collab.)	SCHAEI	07A	EPJ C49 411	S. Schaefer et al.	(ALEPH Collab.)
KHACHATRYAN	15AJ	JHEP 1507 042	V. Khachatryan et al.	(CMS Collab.)	SCHUMANN	07	PRL 99 191803	M. Schumann et al.	(HEID, ILLG, KARL+ Collab.)
KHACHATRYAN	15AV	JHEP 1509 201	V. Khachatryan et al.	(CMS Collab.)	SMIRNOV	07	MPL A22 2353	A.D. Smirnov	
KHACHATRYAN	15C	PL B740 83	V. Khachatryan et al.	(CMS Collab.)	ABAZOV	06A	PL B636 183	V.M. Abazov et al.	(DO Collab.)
KHACHATRYAN	15F	PRL 114 101801	V. Khachatryan et al.	(CMS Collab.)	ABAZOV	06L	PL B640 230	V.M. Abazov et al.	(DO Collab.)
KHACHATRYAN	15O	PL B748 255	V. Khachatryan et al.	(CMS Collab.)	ABDALLAH	06C	EPJ C45 589	J. Abdallah et al.	(DELPHI Collab.)
KHACHATRYAN	15T	PR D91 092005	V. Khachatryan et al.	(CMS Collab.)	ABULENCIA	06E	PRL 96 211801	A. Abulencia et al.	(CDF Collab.)
KHACHATRYAN	15V	PR D91 052009	V. Khachatryan et al.	(CMS Collab.)	ABULENCIA	06M	PRL 96 211802	A. Abulencia et al.	(CDF Collab.)
SAHOO	15A	PR D91 094012	S. Sahoo, R. Mohanta		ABULENCIA	06T	PR D73 051102	A. Abulencia et al.	(CDF Collab.)
AAD	14AI	JHEP 1409 037	G. Aad et al.	(ATLAS Collab.)	ABAZOV	05H	PR D71 071104	V.M. Abazov et al.	(DO Collab.)
AAD	14AT	PL B738 428	G. Aad et al.	(ATLAS Collab.)	ABULENCIA	05A	PRL 95 252001	A. Abulencia et al.	(CDF Collab.)
AAD	14S	PL B737 223	G. Aad et al.	(ATLAS Collab.)	ACOSTA	05I	PR D71 112001	D. Acosta et al.	(CDF Collab.)
AAD	14V	PR D90 052005	G. Aad et al.	(ATLAS Collab.)	ACOSTA	05P	PR D72 051107	D. Acosta et al.	(CDF Collab.)
KHACHATRYAN	14	JHEP 1408 173	V. Khachatryan et al.	(CMS Collab.)	ACOSTA	05R	PRL 95 131801	D. Acosta et al.	(CDF Collab.)
KHACHATRYAN	14A	JHEP 1408 174	V. Khachatryan et al.	(CMS Collab.)	AKTAS	05B	PL B629 9	A. Aktas et al.	(H1 Collab.)
KHACHATRYAN	14O	EPJ C74 3149	V. Khachatryan et al.	(CMS Collab.)	CHEKANOV	05	PL B610 212	S. Chekanov et al.	(HERA ZEUS Collab.)
KHACHATRYAN	14T	PL B739 229	V. Khachatryan et al.	(CMS Collab.)	CHEKANOV	05A	EPJ C44 463	S. Chekanov et al.	(ZEUS Collab.)
MARTINEZ	14	PR D90 015028	R. Martinez, F. Ochoa		CYBURT	05	ASP 23 313	R.H. Cyburt et al.	
PREELS	14	PR D90 112003	R. Preiels et al.	(LOUJ, ETH, PSI+ Collab.)	ABAZOV	04A	PRL 92 221801	V.M. Abazov et al.	(DO Collab.)
AAD	13AE	JHEP 1306 033	G. Aad et al.	(ATLAS Collab.)	ABAZOV	04G	PRL 89 111101	V.M. Abazov et al.	(DO Collab.)
AAD	13AO	PR D87 112006	G. Aad et al.	(ATLAS Collab.)	ABBIENDI	04Q	EPJ C33 173	G. Abbiendi et al.	(OPAL Collab.)
AAD	13AQ	PR D88 012004	G. Aad et al.	(ATLAS Collab.)	ABBIENDI	03D	EPJ C26 331	G. Abbiendi et al.	(OPAL Collab.)
AAD	13D	JHEP 1301 029	G. Aad et al.	(ATLAS Collab.)	ABBIENDI	03R	EPJ C31 281	G. Abbiendi et al.	(OPAL Collab.)
AAD	13G	JHEP 1301 116	G. Aad et al.	(ATLAS Collab.)	ACOSTA	03B	PRL 90 081802	D. Acosta et al.	(CDF Collab.)
AAD	13K	EPJ C73 2263	G. Aad et al.	(ATLAS Collab.)	ADLOFF	03	PL B568 35	C. Adloff et al.	(H1 Collab.)
AAD	13S	PL B719 242	G. Aad et al.	(ATLAS Collab.)	BARGER	03B	PR D67 075009	V. Barger, P. Langacker, H. Lee	
AALTONEN	13A	PRL 110 121802	T. Aaltonen et al.	(CDF Collab.)	CHANG	03	PR D68 111101	M.-C. Chang et al.	(BELLE Collab.)
AALTONEN	13AA	PR D88 092004	T. Aaltonen et al.	(CDF Collab.)	CHEKANOV	03B	PR D68 052004	S. Chekanov et al.	(ZEUS Collab.)
AALTONEN	13R	PRL 111 031802	T. Aaltonen et al.	(CDF Collab.)	ABAZOV	02	PRL 88 191801	V.M. Abazov et al.	(DO Collab.)
CHATRCHYAN	13A	JHEP 1301 013	S. Chattrchyan et al.	(CMS Collab.)	ABBIENDI	02B	PL B526 233	G. Abbiendi et al.	(OPAL Collab.)
CHATRCHYAN	13B	PL B720 63	S. Chattrchyan et al.	(CMS Collab.)	CHAY	02C	PRL 88 071106	T. Chay et al.	(OPAL Collab.)
CHATRCHYAN	13AJ	PL B723 280	S. Chattrchyan et al.	(CMS Collab.)	CHEKANOV	02	PR D85 092004	S. Chekanov et al.	(ZEUS Collab.)
CHATRCHYAN	13AP	PR D87 072002	S. Chattrchyan et al.	(CMS Collab.)	CHEKANOV	02	PL B531 9	S. Chekanov et al.	(ZEUS Collab.)
CHATRCHYAN	13AQ	PR D87 072005	S. Chattrchyan et al.	(CMS Collab.)	MUECK	02	PR D65 085037	A. Mueck, A. Pfaffsis, R. Rueckl	
CHATRCHYAN	13AS	PR D87 114015	S. Chattrchyan et al.	(CMS Collab.)	ABAZOV	01B	PRL 87 061802	V.M. Abazov et al.	(DO Collab.)
CHATRCHYAN	13AU	PRL 110 141802	S. Chattrchyan et al.	(CMS Collab.)	ABAZOV	01D	PR D64 092004	V.M. Abazov et al.	(DO Collab.)
CHATRCHYAN	13BM	PRL 111 211804	S. Chattrchyan et al.	(CMS Collab.)	ADLOFF	01C	PL B523 234	C. Adloff et al.	(H1 Collab.)
Also	13P	PRL 112 119903 (err.)	S. Chattrchyan et al.	(CMS Collab.)	AFFOLDER	01	PRL 87 231803	T. Affolder et al.	(CDF Collab.)
CHATRCHYAN	13E	PL B718 1229	S. Chattrchyan et al.	(CMS Collab.)	BREITWEG	01	PR D63 052002	J. Breitweg et al.	(ZEUS Collab.)
CHATRCHYAN	13M	PRL 110 081801	S. Chattrchyan et al.	(CMS Collab.)	CHEUNG	01B	PL B517 167	K. Cheung	
CHATRCHYAN	13U	JHEP 1302 036	S. Chattrchyan et al.	(CMS Collab.)	THOMAS	01	NP A694 559	E. Thomas et al.	
CHATRCHYAN	13V	PR D88 094012	G. Aad et al.	(ATLAS Collab.)	ABBIENDI	00M	EPJ C13 15	G. Abbiendi et al.	(OPAL Collab.)
SAKAKI	13	PR D89 081801	G. Sakaki et al.		ABBOTT	00	PR 84 2088	B. Abbott et al.	(DO Collab.)
AAD	12BV	PR D85 112012	G. Aad et al.	(ATLAS Collab.)	ABE	00	PRL 84 5716	F. Abe et al.	(CDF Collab.)
AAD	12B	JHEP 1209 041	G. Aad et al.	(ATLAS Collab.)	ABREU	00S	PL B485 45	P. Abreu et al.	(DELPHI Collab.)
AAD	12CC	JHEP 1211 138	G. Aad et al.	(ATLAS Collab.)	ABREU	00Z	EPJ C17 53	P. Abreu et al.	(DELPHI Collab.)
AAD	12CK	PR D86 091103	G. Aad et al.	(ATLAS Collab.)	ACCIARRI	00P	PL B489 81	M. Acciarri et al.	(L3 Collab.)
AAD	12CR	EPJ C72 2241	G. Aad et al.	(ATLAS Collab.)	ADLOFF	00	PL B479 358	C. Adloff et al.	(H1 Collab.)
AAD	12H	PL B709 158	G. Aad et al.	(ATLAS Collab.)	AFFOLDER	00K	PRL 85 2056	T. Affolder et al.	(CDF Collab.)
Also	12I	PL B711 442 (err.)	G. Aad et al.	(ATLAS Collab.)	BARATE	00	EPJ C12 183	R. Barate et al.	(ALEPH Collab.)
AAD	12K	EPJ C72 2083	G. Aad et al.	(ATLAS Collab.)	BARGER	00	PL B480 149	V. Barger, K. Cheung	
AAD	12M	EPJ C72 2056	G. Aad et al.	(ATLAS Collab.)	BREITWEG	00E	EPJ C16 253	J. Breitweg et al.	(ZEUS Collab.)
AAD	12O	EPJ C72 2151	G. Aad et al.	(ATLAS Collab.)	CHAY	00	PR D61 035002	J. Chay, K.Y. Lee, S. Nam	
AALTONEN	12AR	PR D86 112002	T. Aaltonen et al.	(CDF Collab.)	CHO	00	MPL B15 311	G. Cho	
AALTONEN	12N	PRL 108 211805	T. Aaltonen et al.	(CDF Collab.)	CORNET	00	PR D61 037701	F. Cornet, M. Relano, J. Rizo	
ABAZOV	12R	PR D85 051101	V.M. Abazov et al.	(DO Collab.)	DELGADO	00	JHEP 0001 030	A. Delgado, A. Pomanol, M. Quins	
ABRAMOWICZ	12A	PR D86 012005	H. Abramowicz et al.	(ZEUS Collab.)	ERLER	00	PRL 84 212	J. Erler, P. Langacker	
CHATRCHYAN	12AF	PRL 109 141801	S. Chattrchyan et al.	(CMS Collab.)	GABRIELLI	00	PR D62 055009	E. Gabrielli	
CHATRCHYAN	12AG	PR D86 052013	S. Chattrchyan et al.	(CMS Collab.)	RIZZO	00	PR D61 016007	T.G. Rizzo, J.D. Wells	
CHATRCHYAN	12AJ	JHEP 1208 110	S. Chattrchyan et al.	(CMS Collab.)	ROSNER	00	PR D61 016006	J.L. Rosner	
CHATRCHYAN	12AQ	JHEP 1209 029	S. Chattrchyan et al.	(CMS Collab.)	ZARNECKI	00	EPJ C17 695	A. Zarnacki	
Also	12B	JHEP 1403 132 (err.)	S. Chattrchyan et al.	(CMS Collab.)	ABBIENDI	99	EPJ C6 1	G. Abbiendi et al.	(OPAL Collab.)
CHATRCHYAN	12AR	PL B717 351	S. Chattrchyan et al.	(CMS Collab.)	ABBOTT	99	PRL 83 2896	B. Abbott et al.	(DO Collab.)
CHATRCHYAN	12BS	PRL 109 261802	S. Chattrchyan et al.	(CMS Collab.)	ABREU	99G	PL B446 62	P. Abreu et al.	(DELPHI Collab.)
CHATRCHYAN	12BL	JHEP 1212 0119	S. Chattrchyan et al.	(CMS Collab.)	ACKERSTAFF	99D	EPJ C8 3	K. Ackersstaff et al.	(OPAL Collab.)
CHATRCHYAN	12BO	JHEP 1212 055	S. Chattrchyan et al.	(CMS Collab.)	ADLOFF	99	EPJ C11 447	C. Adloff et al.	(H1 Collab.)
CHATRCHYAN	12BR	PRL 109 251801	S. Chattrchyan et al.	(CMS Collab.)	Also	99	EPJ C14 553 (err.)	C. Adloff et al.	(H1 Collab.)
CHATRCHYAN	12M	PL B714 158	S. Chattrchyan et al.	(CMS Collab.)	CASALBUONI	99	PL B460 135	R. Casalbuoni et al.	
CHATRCHYAN	12O	PL B716 82	S. Chattrchyan et al.	(CMS Collab.)	CZAKON	99	PL B458 355	M. Czakon, J. Guza, M. Zralek	
KOSNIK	12	PR D86 055004	N. Kosnik	(LALO, STFN Collab.)	ERLER	99	PL B456 68	J. Erler, P. Langacker	
AAD	11D	PR D83 112006	G. Aad et al.	(ATLAS Collab.)	MARCIANO	99	PR D6		

See key on page 1127

Gauge & Higgs Boson Particle Listings
New Heavy Bosons, Axions (A0) and Other Very Light Bosons

Axions (A0) and Other Very Light Bosons, Searches for

See the related review(s): Axions and Other Similar Particles

A0 (Axion) MASS LIMITS from Astrophysics and Cosmology

These bounds depend on model-dependent assumptions (i.e. — on a combination of axion parameters).

Table with columns: VALUE (MeV), DOCUMENT ID, TECN, COMMENT. Lists mass limits for Axions from various experiments like BARROSO, RAFFELT, DICUS, MIKAEELIAN, SATO, VYSOTSKII.

1 Lower bound from 5.5 MeV gamma-ray line from the sun.
2 Lower bound from requiring the red giants' stellar evolution not be disrupted by axion emission.

A0 (Axion) and Other Light Boson (X0) Searches in Hadron Decays

Limits are for branching ratios.

Table with columns: VALUE, CL%, DOCUMENT ID, TECN, COMMENT. Lists branching ratio limits for Axions and other light bosons in hadron decays from experiments like ABRATENKO, CORTINA-GIL, KOTO, etc.

Main table listing particle searches with columns: Author, Year, Publication, Particle, and Collaboration. Includes entries for Acciari et al., Ackerstaff et al., Barate et al., Barendboim et al., Cho et al., Conrad et al., Doncheski et al., Gross-Pilcher et al., Abe et al., F. Abe et al., W. Adam et al., M. Acciari et al., T. Arima et al., G. Barenboim et al., A. Deandrea et al., M. Derrick et al., Y. Grossman et al., S. Adachi et al., S. Abachi et al., F. Abe et al., R. Balest et al., I.A. Kuznetsov et al., J.A. Kuznetsov et al., J.K. Mizukoshi et al., P. Abreu et al., G. Bhattacharyya et al., S. Davidson et al., A.V. Kuznetsov et al., M. Leurer et al., U. Mahanta et al., N. Severijns et al., P. Vilain et al., K. Abe et al., T. Abe et al., F. Abe et al., P. Abreu et al., P.D. Acton et al., O. Adriani et al., J. Alitti et al., G. Bhattacharyya et al., D. Buskulic et al., M. Derrick et al., T.G. Rizzo et al., N. Severijns et al., K.L. Stiermer et al., P. Abreu et al., O. Adriani et al., D. Decamp et al., J. Imazato et al., S.R. Mishra et al., J. Polak et al., D.P. Acton et al., M. Adeva et al., M. Aquino et al., F. Colangelo et al., C. Cuyper et al., A.E. Faraggi et al., J. Polak et al., T.G. Rizzo et al., T.P. Walker et al., K. Abe et al., F. Abe et al., M.Z. Akrawy et al., J.C. Gonzalez-Garcia et al., J.A. Griifols et al., G.N. Kim et al., J.L. Lopez et al., R. Barbieri et al., P. Langacker et al., S. Odaka et al., R.W. Robinett et al., C. Albajar et al., J. Bagger et al., B. Balke et al., L. Bergstrom et al., F. Cuyper et al., M.A. Doncheski et al., W. Bartel et al., H.J. Behrend et al., M. Derrick et al., M. Derrick et al., A. Jodidio et al., R.N. Mohapatra et al., B. Adeva et al., C. Berger et al., D. Storer et al., B. Adeva et al., H.J. Behrend et al., F. Bergsma et al., J. Carr et al., G. Beall et al., O. Shanker et al.

Gauge & Higgs Boson Particle Listings

Axions (A^0) and Other Very Light Bosons

$<(1.5-4) \times 10^{-6}$ 90 38 YAMAZAKI 84 SPEC K decay, $m_{X^0} \ll 100$ MeV
 39 ASANO 82 CNTR Stopped $K^+ \rightarrow \pi^+ X^0$
 40 ASANO 81B CNTR Stopped $K^+ \rightarrow \pi^+ X^0$
 41 ZHITNITSKII 79 Heavy axion

1 ABRATENKO 21 quoted limit is for $m_{X^0} = 150$ MeV and the lifetime $c\tau_{X^0} = 80$ m. See their Fig. 4 for the limits in the range of $m_{X^0} = 10-210$ MeV.
 2 CORTINA-GIL 21 quoted limit is for $m_{X^0} = 370$ MeV. Limits from $O(10^{-5})$ and $O(10^{-6})$ are obtained for $m_{X^0} = 10-370$ MeV (see their Fig. 7).
 3 CORTINA-GIL 21A quoted limit is for $m_{X^0} = 160-250$ MeV. Limits between 5×10^{-11} and 2×10^{-10} are obtained in the range of $m_{X^0} = 0-110$ and $154-260$ MeV, assuming stable or invisibly decaying X^0 . See their Fig. 4 for mass- and lifetime-dependent limits.
 4 CORTINA-GIL 21C quoted limit is for $m_{X^0} = 130-140$ MeV, and limits of $9 \times 10^{-10}-6 \times 10^{-7}$ are obtained in the mass range of $m_{X^0} = 110-155$ MeV, assuming X^0 escapes detection. See their Fig. 6 for mass- and lifetime-dependent limits.
 5 PARK 21 look for dark photons produced by decays of B^0 through off-shell Higgs-dark Higgs mixing. See their Fig. 5 for limits in the range of $m_{X^0} = 0.01-2.62$ GeV.
 6 AHN 19 is an update of AHN 17 from a new data set. See their Fig. 4 for the limits in the range of $m_{X^0} = 0-250$ MeV.
 7 AAIJ 17Aq limit is for $\tau_{X^0} = 10$ ps. See their Fig. 4 for limits in the range of $m_{X^0} = 250-4700$ MeV and $\tau_{X^0} = 0.1-1000$ ps.
 8 AHN 17 limit as a function of m_{X^0} from 0 to 250 MeV is provided in their Fig. 5.
 9 BATLEY 17 limit is for $m_{X^0} = 216$ MeV and $\tau_{X^0} \leq 10$ ps. See their Fig. 4(c) for limits in the range of $m_{X^0} = 211-354$ MeV and longer lifetimes.
 10 WON 16 look for a vector boson coupled to baryon number. Derived limits on $\alpha' < 10^{-3}-10^{-2}$ for $m_{X^0} = 290-520$ MeV at 95% CL. See their Fig. 4 for mass-dependent limits.
 11 AAIJ 15AZ limit is for $\tau_{X^0} = 10$ ps and $m_{X^0} = 214-4350$ MeV. See their Fig. 4 for mass- and lifetime-dependent limits.
 12 ADLARSON 13 limits between 2.0×10^{-5} and 1.5×10^{-6} are obtained for $m_{X^0} = 20-100$ MeV (see their Fig. 8). Angular momentum conservation requires that X^0 has spin ≥ 1 .
 13 BABUSCI 13B limit is for $B(\phi \rightarrow \eta X^0) \cdot B(X^0 \rightarrow e^+ e^-)$ and applies to $m_{X^0} = 410$ MeV. It is derived by analyzing $\eta \rightarrow \pi^0 \pi^0 \pi^0$ and $\pi^- \pi^+ \pi^0$. Limits between 1×10^{-6} and 2×10^{-8} are obtained for $m_{X^0} \leq 450$ MeV (see their Fig. 6).
 14 ARCHILLI 12 analyzed $\eta \rightarrow \pi^+ \pi^- \pi^0$ decays. Derived limits on $\alpha'/\alpha < 2 \times 10^{-5}$ for $m_{X^0} = 50-420$ MeV at 90% CL. See their Fig. 8 for mass-dependent limits.
 15 GNINENKO 12A limit is for $B(\pi^0 \rightarrow \gamma X^0) \cdot B(X^0 \rightarrow e^+ e^-)$ and applies for $m_{X^0} = 90$ MeV and $\tau_{X^0} \approx 1 \times 10^{-8}$ sec. Limits between 10^{-8} and 2×10^{-15} are obtained for $m_{X^0} = 3-120$ MeV and $\tau_{X^0} = 1 \times 10^{-11}-1$ sec. See their Fig. 3 for limits at different masses and lifetimes.
 16 GNINENKO 12B limit is for $B(\eta \rightarrow \gamma X^0) \cdot B(X^0 \rightarrow e^+ e^-)$ and applies for $m_{X^0} = 100$ MeV and $\tau_{X^0} \approx 6 \times 10^{-9}$ sec. Limits between 10^{-5} and 3×10^{-14} are obtained for $m_{X^0} \lesssim 550$ MeV and $\tau_{X^0} = 10^{-10}-10$ sec. See their Fig. 5 for limits at different mass and lifetime and for η' decays.
 17 ADLER 04 limit applies for a mass near 180 MeV. For other masses in the range $m_{X^0} = 150-250$ MeV the limit is less restrictive, but still improves ADLER 02c and ATIYA 93B.
 18 ANISIMOVSKY 04 bound is for $m_{X^0} = 0$.
 19 ADLER 02c bound is for $m_{X^0} < 60$ MeV. See Fig. 2 for limits at higher masses.
 20 The quoted limit is for $m_{X^0} = 0-80$ MeV. See their Fig. 5 for the limit at higher mass. The branching fraction limit assumes pure phase space decay distributions.
 21 ALTEGOER 98 looked for X^0 from π^0 decay which penetrate the shielding and convert to π^0 in the external Coulomb field of a nucleus.
 22 KITCHING 97 limit is for $B(K^+ \rightarrow \pi^+ X^0) \cdot B(X^0 \rightarrow \gamma \gamma)$ and applies for $m_{X^0} \approx 50$ MeV, $\tau_{X^0} < 10^{-10}$ s. Limits are provided for $0 < m_{X^0} < 100$ MeV, $\tau_{X^0} < 10^{-8}$ s.
 23 ADLER 96 looked for a peak in missing-mass distribution. This work is an update of ATIYA 93. The limit is for massless stable X^0 particles and extends to $m_{X^0} = 80$ MeV at the same level. See paper for dependence on finite lifetime.
 24 AMSLER 94B and AMSLER 96B looked for a peak in missing-mass distribution.
 25 MEIJERDREES 94 limit is based on inclusive photon spectrum and is independent of X^0 decay modes. It applies to $\tau(X^0) > 10^{-23}$ sec.
 26 ATIYA 93B looked for a peak in missing mass distribution. The bound applies for stable X^0 of $m_{X^0} = 150-250$ MeV, and the limit becomes stronger (10^{-8}) for $m_{X^0} = 180-240$ MeV.
 27 NG 93 studied the production of X^0 via $\gamma \gamma \rightarrow \pi^0 \rightarrow \gamma X^0$ in the early universe at $T \approx 1$ MeV. The bound on extra neutrinos from nucleosynthesis $\Delta N_\nu < 0.3$ (WALKER 91) is employed. It applies to $m_{X^0} \ll 1$ MeV in order to be relativistic down to nucleosynthesis temperature. See paper for heavier X^0 .
 28 ALLIEGRO 92 limit applies for $m_{X^0} = 150-340$ MeV and is the branching ratio times the decay probability. Limit is $< 1.5 \times 10^{-8}$ at 99% CL.
 29 ATIYA 92 looked for a peak in missing mass distribution. The limit applies to $m_{X^0} = 0-130$ MeV in the narrow resonance limit. See paper for the dependence on lifetime. Covariance requires X^0 to be a vector particle.
 30 BARABASH 92 is a beam dump experiment that searched for a light Higgs. Limits between 1×10^{-12} and 1×10^{-7} are obtained for $3 < m_{X^0} < 40$ MeV.
 31 Limits between 1×10^{-12} and 1 are obtained for $4 < m_{X^0} < 69$ MeV.
 32 Limits between 1×10^{-11} and 5×10^{-3} are obtained for $4 < m_{X^0} < 63$ MeV.
 33 Limits between 1×10^{-14} and 1 are obtained for $3 < m_{X^0} < 82$ MeV.

34 MEIJERDREES 92 limit applies for $\tau_{X^0} = 10^{-23}-10^{-11}$ sec. Limits between 2×10^{-4} and 4×10^{-6} are obtained for $m_{X^0} = 25-120$ MeV. Angular momentum conservation requires that X^0 has spin ≥ 1 .
 35 ATIYA 90b limit is for $B(K^+ \rightarrow \pi^+ X^0) \cdot B(X^0 \rightarrow \gamma \gamma)$ and applies for $m_{X^0} = 50$ MeV, $\tau_{X^0} < 10^{-10}$ s. Limits are also provided for $0 < m_{X^0} < 100$ MeV, $\tau_{X^0} < 10^{-8}$ s.
 36 KORENCHENKO 87 limit assumes $m_{A^0} = 1.7$ MeV, $\tau_{A^0} \lesssim 10^{-12}$ s, and $B(A^0 \rightarrow e^+ e^-) = 1$.
 37 EICHLER 86 looked for $\pi^+ \rightarrow e^+ \nu A^0$ followed by $A^0 \rightarrow e^+ e^-$. Limits on the branching fraction depend on the mass and lifetime of A^0 . The quoted limits are valid when $\tau(A^0) \gtrsim 3 \cdot 10^{-10}$ s if the decays are kinematically allowed.
 38 YAMAZAKI 84 looked for a discrete line in $K^+ \rightarrow \pi^+ X$. Sensitive to wide mass range (5-300 MeV), independent of whether X decays promptly or not.
 39 ASANO 82 at KEK set limits for $B(K^+ \rightarrow \pi^+ X^0)$ for $m_{X^0} < 100$ MeV as $BR < 4 \cdot 10^{-8}$ for $\tau(X^0 \rightarrow n\gamma\text{'s}) > 1 \cdot 10^{-9}$ s, $BR < 1.4 \cdot 10^{-6}$ for $\tau < 1 \cdot 10^{-9}$ s.
 40 ASANO 81B is KEK experiment. Set $B(K^+ \rightarrow \pi^+ X^0) < 3.8 \cdot 10^{-8}$ at CL = 90%.
 41 ZHITNITSKII 79 argue that a heavy axion predicted by YANG 78 ($3 < m < 40$ MeV) contradicts experimental muon anomalous magnetic moments.

A^0 (Axion) Searches in Quarkonium Decays

Decay or transition of quarkonium. Limits are for branching ratio.

VALUE	CL%	DOCUMENT ID	TECN	COMMENT
••• We do not use the following data for averages, fits, limits, etc. •••				
$< 2.8 \times 10^{-8}$	90	1 ABLIKIM 16E BES3	$J/\psi \rightarrow A^0 \gamma (A^0 \rightarrow \mu^+ \mu^-)$	
$< 4 \times 10^{-7}$	90	2 ABLIKIM 12 BES3	$J/\psi \rightarrow A^0 \gamma (A^0 \rightarrow \mu^+ \mu^-)$	
$< 4.0 \times 10^{-5}$	90	3 ANTREASNYAN 90C CBAL	$\Upsilon(1S) \rightarrow A^0 \gamma$	
$< 5 \times 10^{-5}$	90	4 DRUZHININ 87 ND	$\phi \rightarrow A^0 \gamma (A^0 \rightarrow e^+ e^-)$	
$< 2 \times 10^{-3}$	90	5 DRUZHININ 87 ND	$\phi \rightarrow A^0 \gamma (A^0 \rightarrow \gamma \gamma)$	
$< 7 \times 10^{-6}$	90	6 DRUZHININ 87 ND	$\phi \rightarrow A^0 \gamma (A^0 \rightarrow \text{missing})$	
$< 1.4 \times 10^{-5}$	90	7 EDWARDS 82 CBAL	$J/\psi \rightarrow A^0 \gamma$	
1 ABLIKIM 16E limits between $2.8-495.3 \times 10^{-8}$ were obtained for $0.212 \text{ GeV} < m_{A^0} < 3.0 \text{ GeV}$. See their Fig. 5 for mass-dependent limits. 2 ABLIKIM 12 derived limits between $4 \times 10^{-7}-2.1 \times 10^{-5}$ for $0.212 \text{ GeV} < m_{A^0} < 3.0 \text{ GeV}$. See their Fig. 2(c) for mass-dependent limits. 3 ANTREASNYAN 90C assume that A^0 does not decay in the detector. 4 The first DRUZHININ 87 limit is valid when $\tau_{A^0}/m_{A^0} < 3 \times 10^{-13} \text{ s/MeV}$ and $m_{A^0} < 20 \text{ MeV}$. 5 The second DRUZHININ 87 limit is valid when $\tau_{A^0}/m_{A^0} < 5 \times 10^{-13} \text{ s/MeV}$ and $m_{A^0} < 20 \text{ MeV}$. 6 The third DRUZHININ 87 limit is valid when $\tau_{A^0}/m_{A^0} > 7 \times 10^{-12} \text{ s/MeV}$ and $m_{A^0} < 200 \text{ MeV}$. 7 EDWARDS 82 looked for $J/\psi \rightarrow \gamma A^0$ decays by looking for events with a single γ [of energy $\approx 1/2$ the $J/\psi(1S)$ mass], plus nothing else in the detector. The limit is inconsistent with the axion interpretation of the FAISSNER 81B result.				

A^0 (Axion) Searches in Positronium Decays

Decay or transition of positronium. Limits are for branching ratio.

VALUE	CL%	DOCUMENT ID	TECN	COMMENT
••• We do not use the following data for averages, fits, limits, etc. •••				
$< 4.4 \times 10^{-5}$	90	1 BADERT... 02 CNTR	$o\text{-Ps} \rightarrow \gamma X_1 X_2, m_{X_1} + m_{X_2} \leq 900 \text{ keV}$	
$< 2 \times 10^{-4}$	90	2 MAENO 95 CNTR	$o\text{-Ps} \rightarrow A^0 \gamma, m_{A^0} = 850-1013 \text{ keV}$	
$< 3.0 \times 10^{-4}$	90	2 ASAI 94 CNTR	$o\text{-Ps} \rightarrow A^0 \gamma, m_{A^0} = 30-500 \text{ keV}$	
$< 2.8 \times 10^{-5}$	90	3 AKOPYAN 91 CNTR	$o\text{-Ps} \rightarrow A^0 \gamma (A^0 \rightarrow \gamma \gamma), m_{A^0} < 30 \text{ keV}$	
$< 1.1 \times 10^{-6}$	90	4 ASAI 91 CNTR	$o\text{-Ps} \rightarrow A^0 \gamma, m_{A^0} < 800 \text{ keV}$	
$< 3.8 \times 10^{-4}$	90	GNINENKO 90 CNTR	$o\text{-Ps} \rightarrow A^0 \gamma, m_{A^0} < 30 \text{ keV}$	
$< (1-5) \times 10^{-4}$	95	5 TSUCHIYAKI 90 CNTR	$o\text{-Ps} \rightarrow A^0 \gamma, m_{A^0} = 300-900 \text{ keV}$	
$< 6.4 \times 10^{-5}$	90	6 ORITO 89 CNTR	$o\text{-Ps} \rightarrow A^0 \gamma, m_{A^0} < 30 \text{ keV}$	
		7 AMALDI 85 CNTR	Ortho-positronium	
		8 CARBONI 83 CNTR	Ortho-positronium	
1 BADERTSCHER 02 looked for a three-body decay of ortho-positronium into a photon and two penetrating (neutral or milli-charged) particles. 2 The ASAI 94 limit is based on inclusive photon spectrum and is independent of A^0 decay modes. 3 The AKOPYAN 91 limit applies for a short-lived A^0 with $\tau_{A^0} < 10^{-13} m_{A^0} [\text{keV}]$ s. 4 ASAI 91 limit translates to $g_{A^0 e^+ e^-}^2 / 4\pi < 1.1 \times 10^{-11}$ (90% CL) for $m_{A^0} < 800 \text{ keV}$. 5 The TSUCHIYAKI 90 limit is based on inclusive photon spectrum and is independent of A^0 decay modes. 6 ORITO 89 limit translates to $g_{A^0 e^+ e^-}^2 / 4\pi < 6.2 \times 10^{-10}$. Somewhat more sensitive limits are obtained for larger m_{A^0} : $B < 7.6 \times 10^{-6}$ at 100 keV. 7 AMALDI 85 set limits $B(A^0 \gamma) / B(\gamma \gamma \gamma) < (1-5) \times 10^{-6}$ for $m_{A^0} = 900-100 \text{ keV}$ which are about 1/10 of the CARBONI 83 limits. 8 CARBONI 83 looked for ortho-positronium $\rightarrow A^0 \gamma$. Set limit for A^0 electron coupling squared, $(g_{eA^0})^2 / (4\pi) < 6 \cdot 10^{-10} - 7 \cdot 10^{-9}$ for m_{A^0} from 150-900 keV (CL = 99.7%). This is about 1/10 of the bound from $g=2$ experiments.				

A^0 (Axion) Search in Photoproduction

VALUE	DOCUMENT ID	COMMENT
••• We do not use the following data for averages, fits, limits, etc. •••		
	1 BASSOMPIE... 95	$m_{A^0} = 1.8 \pm 0.2 \text{ MeV}$

See key on page 1127

Gauge & Higgs Boson Particle Listings Axions (A^0) and Other Very Light Bosons

¹BASSOMPIERRE 95 is an extension of BASSOMPIERRE 93. They looked for a peak in the invariant mass of e^+e^- pairs in the region $m_{e^+e^-} = 1.8 \pm 0.2$ MeV. They obtained bounds on the production rate A^0 for $\tau(A^0) = 10^{-18}\text{-}10^{-9}$ sec. They also found an excess of events in the range $m_{e^+e^-} = 2.1\text{-}3.5$ MeV.

⁶GAVELA 20 focus on the axion production as an s-channel off shell mediator, and use the Run 2 CMS public data to set limits on the product of the axion couplings to gluons and photons as well as Z bosons as $G_{A\gamma\gamma} G_{Agg} < 2.8 \times 10^{-7} \text{ GeV}^{-2}$ and $G_{AZZ} G_{Agg} < 9.8 \times 10^{-7} \text{ GeV}^{-2}$ for $m_{A^0} \lesssim 200$ GeV. See their Fig.3 for the limits.

A^0 (Axion) Production in Hadron Collisions

Limits are for $\sigma(A^0) / \sigma(\pi^0)$.

VALUE	CL%	EVTS	DOCUMENT ID	TECN	COMMENT
• • • We do not use the following data for averages, fits, limits, etc. • • •					
			1 AAD	21F ATLS	Monojet + missing p_T
			2 AAD	21K ATLS	Mono- γ + missing p_T
			3 AAD	21N ATLS	$\gamma\gamma$ scatt. in Pb+Pb
			4 CARRA	21 ATLS	$p\bar{p} \rightarrow A^0 \rightarrow WW, Z\gamma$
			5 AAIJ	20AL LHCB	$p\bar{p} \rightarrow X^0 \rightarrow \mu^+\mu^-$
			6 GAVELA	20 CMS	$p\bar{p} \rightarrow A^0 \rightarrow \gamma\gamma, ZZ$
			7 SIRUNYAN	19BQ CMS	$X^0 \rightarrow \mu^+\mu^-$
			8 JAIN	07 CNTR	$A^0 \rightarrow e^+e^-$
			9 AHMAD	97 SPEC	e^+ production
			10 LEINBERGER	97 SPEC	$A^0 \rightarrow e^+e^-$
			11 GANZ	96 SPEC	$A^0 \rightarrow e^+e^-$
			12 KAMEL	96 EMUL	^{32}S emulsion, $A^0 \rightarrow e^+e^-$
			13 BLUEMLEIN	92 BDMP	$A^0 N_Z \rightarrow \ell^+ \ell^- N_Z$
			14 MEIJERDREES	92 SPEC	$\pi^- p \rightarrow nA^0, A^0 \rightarrow e^+e^-$
			15 BLUEMLEIN	91 BDMP	$A^0 \rightarrow e^+e^-, 2\gamma$
			16 FAISSNER	89 OSPK	Beam dump, $A^0 \rightarrow e^+e^-$
			17 DEBOER	88 RVUE	$A^0 \rightarrow e^+e^-$
			18 EL-NADI	88 EMUL	$A^0 \rightarrow e^+e^-$
			19 FAISSNER	88 OSPK	Beam dump, $A^0 \rightarrow 2\gamma$
			20 BADIER	86 BDMP	$A^0 \rightarrow e^+e^-$
<2. $\times 10^{-11}$	90	0	21 BERGSM	85 CHR	CERN beam dump
<1. $\times 10^{-13}$	90	0	21 BERGSM	85 CHR	CERN beam dump
		24	22 FAISSNER	83 OSPK	Beam dump, $A^0 \rightarrow 2\gamma$
			23 FAISSNER	83B RVUE	LAMPF beam dump
			24 FRANK	83B RVUE	LAMPF beam dump
			25 HOFFMAN	83 CNTR	$\pi p \rightarrow nA^0$ ($A^0 \rightarrow e^+e^-$)
			26 FETSCHER	82 RVUE	See FAISSNER 81b
		12	27 FAISSNER	81 OSPK	CERN PS ν wideband
		15	28 FAISSNER	81B OSPK	Beam dump, $A^0 \rightarrow 2\gamma$
		8	29 KIM	81 OSPK	26 GeV $pN \rightarrow A^0 X$
		0	30 FAISSNER	80 OSPK	Beam dump, $A^0 \rightarrow e^+e^-$
<1. $\times 10^{-8}$	90		31 JACQUES	80 HLBC	28 GeV protons
<1. $\times 10^{-14}$	90		31 JACQUES	80 HLBC	Beam dump
			32 SOUKAS	80 CALO	28 GeV p beam dump
			33 BECHIS	79 CNTR	
<1. $\times 10^{-8}$	90		34 COTEAU	79 OSPK	Beam dump
<1. $\times 10^{-3}$	95		35 DISHAW	79 CALO	400 GeV $p\bar{p}$
<1. $\times 10^{-8}$	90		ALIBRAN	78 HYBR	Beam dump
<6. $\times 10^{-9}$	95		ASRATYAN	78B CALO	Beam dump
<1.5 $\times 10^{-8}$	90		36 BELLLOTTI	78 HLBC	Beam dump
<5.4 $\times 10^{-14}$	90		36 BELLLOTTI	78 HLBC	$m_{A^0}=1.5$ MeV
<4.1 $\times 10^{-9}$	90		36 BELLLOTTI	78 HLBC	$m_{A^0}=1$ MeV
<1. $\times 10^{-8}$	90		37 BOSETTI	78B HYBR	Beam dump
			38 DONNELLY	78	
<0.5 $\times 10^{-8}$	90		HANSL	78D WIRE	Beam dump
			39 MICELMAC...	78	
			40 VYSOTSKII	78	

¹AAD 21F look for axion production with an energetic jet and large missing p_T , and set a limit on the axion coupling to gluons, $C_G/f_{A^0} < 8 \times 10^{-6} \text{ GeV}^{-1}$ at 95 % CL for $m_{A^0} = 1$ MeV. Using $C_G = \alpha_s/8\pi$, we interpret the limit as $f_{A^0} > 0.4$ TeV for $\alpha_s \approx 0.08$.
²AAD 21K look for axion production with an energetic photon and large missing p_T , and set a limit on the axion coupling to a Z boson and photon, $G_{AZ\gamma} < 5.1 \times 10^{-4} \text{ GeV}^{-1}$ at 95 % CL for $m_{A^0} = 1$ MeV and assuming $G_{A\gamma\gamma} = 0$.
³AAD 21N look for axion production using the measurement of light-by-light scattering based on Pb+Pb collision data. They set the limit on the axion-photon coupling, $G_{A\gamma\gamma} < 5.3 \times 10^{-5}\text{-}3.4 \times 10^{-4} \text{ GeV}^{-1}$ at 95 % CL for $m_{A^0} = 6\text{-}100$ GeV. Here we use $\Lambda_a = G_{A\gamma\gamma}^{-1}$ to translate their limits. See their Fig. 9 for mass-dependent limits.
⁴CARRA 21 is analogous to GAVELA 20, and they use the differential cross sections for W and Z production measured with the ATLAS detector to set limits on the product of the axion couplings to gauge bosons as $G_{AWW} G_{Agg} < 6.2 \times 10^{-7} \text{ GeV}^{-2}$ and $G_{AZ\gamma} G_{Agg} < 3.7 \times 10^{-7} \text{ GeV}^{-2}$ at 95 % CL for $m_{A^0} \lesssim 100$ GeV.
⁵AAIJ 20AL look for a light new boson decaying into a pair of muons using the LHCB data with an integrated luminosity of 5.1 fb⁻¹, and set limits on the cross section over a range of $m_{X^0} = 0.22\text{-}3$ and $20\text{-}60$ GeV. See Figs. 8 and 9 for mass-dependent limits.

⁷SIRUNYAN 19BQ look for the pair production of a new light boson decaying into a pair of muons, and set limits on the product of the production cross section times branching fraction to dimuons squared times acceptance over a range of $m_{X^0} = 0.25\text{-}8.5$ GeV. See the right panel of their Fig. 1 for mass-dependent limits.
⁸JAIN 07 claims evidence for $A^0 \rightarrow e^+e^-$ produced in 207Pb collision on nuclear emulsion (Ag/Br) for $m(A^0) = 7 \pm 1$ or 19 ± 1 MeV and $\tau(A^0) \leq 10^{-13}$ s.
⁹AHMAD 97 reports a result of APEX Collaboration which studied positron production in $^{238}\text{U}_{+232}\text{Ta}$ and $^{238}\text{U}_{+181}\text{Ta}$ collisions, without requiring a coincident electron. No narrow lines were found for $250 < E_{e^+} < 750$ keV.
¹⁰LEINBERGER 97 (ORANGE Collaboration) at GSI looked for a narrow sum-energy e^+e^- line at ~ 635 keV in $^{238}\text{U}_{+181}\text{Ta}$ collision. Limits on the production probability for a narrow sum-energy e^+e^- line are set. See their Table 2.
¹¹GANZ 96 (EPOS II Collaboration) has placed upper bounds on the production cross section of e^+e^- pairs from $^{238}\text{U}_{+181}\text{Ta}$ and $^{238}\text{U}_{+232}\text{Th}$ collisions at GSI. See Table 2 for limits both for back-to-back and isotropic configurations of e^+e^- pairs. These limits rule out the existence of peaks in the e^+e^- sum-energy distribution, reported by an earlier version of this experiment.
¹²KAMEL 96 looked for e^+e^- pairs from the collision of ^{32}S (200 GeV/nucleon) and emulsion. No evidence of mass peaks is found in the region of sensitivity $m_{ee} > 2$ MeV.
¹³BLUEMLEIN 92 is a proton beam dump experiment at Serpukhov with a secondary target to induce Bethe-Heitler production of e^+e^- or $\mu^+\mu^-$ from the produce A^0 . See Fig. 5 for the excluded region in m_{A^0} - x plane. For the standard axion, $0.3 < x < 25$ is excluded at 95% CL. If combined with BLUEMLEIN 91, $0.008 < x < 32$ is excluded.
¹⁴MEIJERDREES 92 give $\Gamma(\pi^- p \rightarrow nA^0) \cdot B(A^0 \rightarrow e^+e^-) / \Gamma(\pi^- p \rightarrow \text{all}) < 10^{-5}$ (90% CL) for $m_{A^0} = 100$ MeV, $\tau_{A^0} = 10^{-11}\text{-}10^{-23}$ sec. Limits ranging from 2.5×10^{-3} to 10^{-7} are given for $m_{A^0} = 25\text{-}136$ MeV.
¹⁵BLUEMLEIN 91 is a proton beam dump experiment at Serpukhov. No candidate event for $A^0 \rightarrow e^+e^-, 2\gamma$ are found. Fig. 6 gives the excluded region in m_{A^0} - x plane ($x = \tan\beta = v_2/v_1$). Standard axion is excluded for $0.2 < m_{A^0} < 3.2$ MeV for most $x > 1$, $0.2\text{-}11$ MeV for most $x < 1$.
¹⁶FAISSNER 89 searched for $A^0 \rightarrow e^+e^-$ in a proton beam dump experiment at SIN. No excess of events was observed over the background. A standard axion with mass $2m_e\text{-}20$ MeV is excluded. Lower limit on f_{A^0} of $\approx 10^4$ GeV is given for $m_{A^0} = 2m_e\text{-}20$ MeV.
¹⁷DEBOER 88 reanalyze EL-NADI 88 data and claim evidence for three distinct states with mass $\sim 1.1, \sim 2.1$, and ~ 9 MeV, lifetimes $10^{-16}\text{-}10^{-15}$ s decaying to e^+e^- and note the similarity of the data with those of a cosmic-ray experiment by Bristol group (B.M. Anand, Proc. of the Royal Society of London, Section A **A22** 183 (1953)). For a criticism see PERKINS 89, who suggests that the events are compatible with π^0 Dalitz decay. DEBOER 89b is a reply which contests the criticism.
¹⁸EL-NADI 88 claim the existence of a neutral particle decaying into e^+e^- with mass 1.60 ± 0.59 MeV, lifetime $(0.15 \pm 0.01) \times 10^{-14}$ s, which is produced in heavy ion interactions with emulsion nuclei at ~ 4 GeV/c/nucleon.
¹⁹FAISSNER 88 is a proton beam dump experiment at SIN. They found no candidate event for $A^0 \rightarrow \gamma\gamma$. A standard axion decaying to 2γ is excluded except for a region $x \geq 1$. Lower limit on f_{A^0} of $10^2\text{-}10^3$ GeV is given for $m_{A^0} = 0.1\text{-}1$ MeV.
²⁰BADIER 86 did not find long-lived A^0 in 300 GeV π^- Beam Dump Experiment that decays into e^+e^- in the mass range $m_{A^0} = (20\text{-}200)$ MeV, which excludes the A^0 decay constant $f(A^0)$ in the interval (60-600) GeV. See their figure 6 for excluded region on $f(A^0)\text{-}m_{A^0}$ plane.
²¹BERGSM 85 look for $A^0 \rightarrow 2\gamma, e^+e^-, \mu^+\mu^-$. First limit above is for $m_{A^0} = 1$ MeV; second is for 200 MeV. See their figure 4 for excluded region on $f_{A^0}\text{-}m_{A^0}$ plane, where f_{A^0} is A^0 decay constant. For Peccei-Quinn PECC 77 $A^0, m_{A^0} < 180$ keV and $\tau > 0.037$ s. (CL = 90%). For the axion of FAISSNER 81b at 250 keV, BERGSM 85 except 15 events but observe zero.
²²FAISSNER 83 observed 19 $1\text{-}\gamma$ and 12 $2\text{-}\gamma$ events where a background of 4.8 and 2.3 respectively is expected. A small-angle peak is observed even if iron wall is set in front of the decay region.
²³FAISSNER 83b extrapolate SIN γ signal to LAMPF ν experimental condition. Resulting 370 γ 's are not at variance with LAMPF upper limit of 450 γ 's. Derived from LAMPF limit that $[d\sigma(A^0)/d\omega \text{ at } 90^\circ] m_{A^0} / \tau_{A^0} < 14 \times 10^{-35} \text{ cm}^2 \text{ sr}^{-1} \text{ MeV ms}^{-1}$. See comment on FRANK 83b.
²⁴FRANK 83b stress the importance of LAMPF data bins with negative net signal. By statistical analysis say that LAMPF and SIN-A0 are at variance when extrapolation by phase-space model is done. They find LAMPF upper limit is 248 not 450 γ 's. See comment on FAISSNER 83b.
²⁵HOFFMAN 83 set CL = 90% limit $d\sigma/dt B(e^+e^-) < 3.5 \times 10^{-32} \text{ cm}^2/\text{GeV}^2$ for $140 < m_{A^0} < 160$ MeV. Limit assumes $\tau(A^0) < 10^{-9}$ s.
²⁶FETSCHER 82 reanalyzes SIN beam-dump data of FAISSNER 81. Claims no evidence for axion since $2\text{-}\gamma$ peak rate remarkably decreases if iron wall is set in front of the decay region.
²⁷FAISSNER 81 see excess μe events. Suggest axion interactions.
²⁸FAISSNER 81b is SIN 590 MeV proton beam dump. Observed 14.5 ± 5.0 events of 2γ decay of long-lived neutral penetrating particle with $m_{2\gamma} \lesssim 1$ MeV. Axion interpretation with $\eta\text{-}A^0$ mixing gives $m_{A^0} = 250 \pm 25$ keV, $\tau_{(2\gamma)} = (7.3 \pm 3.7) \times 10^{-3}$ s from above rate. See critical remarks below in comments of FETSCHER 82, FAISSNER 83, FAISSNER 83b, FRANK 83b, and BERGSM 85. Also see in the next subsection ALEKSEEV 82b, CAVAIGNAC 83, and ANANEV 85.
²⁹KIM 81 analyzed 8 candidates for $A^0 \rightarrow 2\gamma$ obtained by Aachen-Padova experiment at CERN with 26 GeV protons on Be. Estimated axion mass is about 300 keV and lifetime is $(0.86\text{-}5.6) \times 10^{-3}$ s depending on models. Faissner (private communication), says axion production underestimated and mass overestimated. Correct value around 200 keV.

Gauge & Higgs Boson Particle Listings

Axions (A^0) and Other Very Light Bosons

- 30 FAISSNER 80 is SIN beam dump experiment with 590 MeV protons looking for $A^0 \rightarrow e^+e^-$ decay. Assuming $A^0/\pi^0 = 5.5 \times 10^{-7}$, obtained decay rate limit $20/(A^0 \text{ mass}) \text{ MeV/s}$ (CL = 90%), which is about 10^{-7} below theory and interpreted as upper limit to $m_{A^0} < 2m_{e^-}$.
- 31 JACQUES 80 is a BNL beam dump experiment. First limit above comes from nonobservation of excess neutral-current-type events $[\sigma(\text{production})\sigma(\text{interaction})] < 7. \times 10^{-68} \text{ cm}^4$, CL = 90%. Second limit is from nonobservation of axion decays into 2γ 's or e^+e^- , and for axion mass a few MeV.
- 32 SOUKAS 80 at BNL observed no excess of neutral-current-type events in beam dump.
- 33 BECHIS 79 looked for the axion production in low energy electron Bremsstrahlung and the subsequent decay into either 2γ or e^+e^- . No signal found. CL = 90% limits for model parameter(s) are given.
- 34 COTEUS 79 is a beam dump experiment at BNL.
- 35 DISHAW 79 is a calorimetric experiment and looks for low energy tail of energy distributions due to energy lost to weakly interacting particles.
- 36 BELLOTTI 78 first value comes from search for $A^0 \rightarrow e^+e^-$. Second value comes from search for $A^0 \rightarrow 2\gamma$, assuming mass $< 2m_{e^-}$. For any mass satisfying this, limit is above value $\times (\text{mass})^{-4}$. Third value uses data of PL 60B 401 and quotes $\sigma(\text{production})\sigma(\text{interaction}) < 10^{-67} \text{ cm}^4$.
- 37 BOSETTI 78B quotes $\sigma(\text{production})\sigma(\text{interaction}) < 2. \times 10^{-67} \text{ cm}^4$.
- 38 DONNELLY 78 examines data from reactor neutrino experiments of REINES 76 and GURR 74 as well as SLAC beam dump experiment. Evidence is negative.
- 39 MICELMACHER 78 finds no evidence of axion existence in reactor experiments of REINES 76 and GURR 74. (See reference on DONNELLY 78 below).
- 40 VYSOTSKI 78 derived lower limit for the axion mass 25 keV from luminosity of the sun and 200 keV from red supergiants.

A^0 (Axion) Searches in Reactor Experiments

VALUE	DOCUMENT ID	TECN	COMMENT
• • • We do not use the following data for averages, fits, limits, etc. • • •			
	1 CHANG 07		Primakoff or Compton
	2 ALTMANN 95	CNTR	Reactor; $A^0 \rightarrow e^+e^-$
	3 KETOV 86	SPEC	Reactor; $A^0 \rightarrow \gamma\gamma$
	4 KOCH 86	SPEC	Reactor; $A^0 \rightarrow \gamma\gamma$
	5 DATAR 82	CNTR	Light water reactor
	6 VUILLEUMIER 81	CNTR	Reactor; $A^0 \rightarrow 2\gamma$
1 CHANG 07 looked for monochromatic photons from Primakoff or Compton conversion of axions from the Kuo-Sheng reactor due to axion coupling to photon or electron, respectively. The search places model-independent limits on the products $G_{A\gamma\gamma}G_{ANN}$ and $G_{Aee}G_{ANN}$ for $m(A^0)$ less than the MeV range.			
2 ALTMANN 95 looked for A^0 decaying into e^+e^- from the Bugey5 nuclear reactor. They obtain an upper limit on the A^0 production rate of $\omega(A^0)/\omega(\gamma) \times B(A^0 \rightarrow e^+e^-) < 10^{-16}$ for $m_{A^0} = 1.5 \text{ MeV}$ at 90% CL. The limit is weaker for heavier A^0 . In the case of a standard axion, this limit excludes a mass in the range $2m_e < m_{A^0} < 4.8 \text{ MeV}$ at 90% CL. See Fig. 5 of their paper for exclusion limits of axion-like resonances Z^0 in the (m_{X^0}, τ_{X^0}) plane.			
3 KETOV 86 searched for A^0 at the Rovno nuclear power plant. They found an upper limit on the A^0 production probability of $0.8 [100 \text{ keV}/m_{A^0}]^6 \times 10^{-6}$ per fission. In the standard axion model, this corresponds to $m_{A^0} > 150 \text{ keV}$. Not valid for $m_{A^0} \gtrsim 1 \text{ MeV}$.			
4 KOCH 86 searched for $A^0 \rightarrow \gamma\gamma$ at nuclear power reactor Biblis A. They found an upper limit on the A^0 production rate of $\omega(A^0)/\omega(\gamma(M1)) < 1.5 \times 10^{-10}$ (CL=95%). Standard axion with $m_{A^0} = 250 \text{ keV}$ gives 10^{-5} for the ratio. Not valid for $m_{A^0} > 1022 \text{ keV}$.			
5 DATAR 82 looked for $A^0 \rightarrow 2\gamma$ in neutron capture ($np \rightarrow dA^0$) at Tarapur 500 MW reactor. Sensitive to sum of $l = 0$ and $l = 1$ amplitudes. With ZEHNDER 81 ($l = 0$) - ($l = 1$) result, assert nonexistence of standard A^0 .			
6 VUILLEUMIER 81 is at Grenoble reactor. Set limit $m_{A^0} < 280 \text{ keV}$.			

A^0 (Axion) and Other Light Boson (X^0) Searches in Nuclear Transitions

Limits are for branching ratio.

VALUE	CL%	DOCUMENT ID	TECN	COMMENT
• • • We do not use the following data for averages, fits, limits, etc. • • •				
$< 8.5 \times 10^{-6}$	90	1 DERBIN 02	CNTR	^{125m}Te decay
		2 DEBOER 97c	RVUE	M1 transitions
$< 5.5 \times 10^{-10}$	95	3 TSUNODA 95	CNTR	^{252}Cf fission, $A^0 \rightarrow e e$
$< 1.2 \times 10^{-6}$	95	4 MINOWA 93	CNTR	$^{139}\text{La}^* \rightarrow ^{139}\text{La}A^0$
$< 2 \times 10^{-4}$	90	5 HICKS 92	CNTR	^{35}S decay, $A^0 \rightarrow \gamma\gamma$
$< 1.5 \times 10^{-9}$	95	6 ASANUMA 90	CNTR	^{241}Am decay
$< (0.4-10) \times 10^{-3}$	95	7 DEBOER 90	CNTR	$^8\text{Be}^* \rightarrow ^8\text{Be}A^0$, $A^0 \rightarrow e^+e^-$
$< (0.2-1) \times 10^{-3}$	90	8 BINI 89	CNTR	$^{16}\text{O}^* \rightarrow ^{16}\text{O}X^0$, $X^0 \rightarrow e^+e^-$
		9 AVIGNONE 88	CNTR	$\text{Cu}^* \rightarrow \text{Cu}A^0$ ($A^0 \rightarrow 2\gamma$, $A^0 e \rightarrow \gamma e$, $A^0 Z \rightarrow \gamma Z$)
$< 1.5 \times 10^{-4}$	90	10 DATAR 88	CNTR	$^{12}\text{C}^* \rightarrow ^{12}\text{C}A^0$, $A^0 \rightarrow e^+e^-$
$< 5 \times 10^{-3}$	90	11 DEBOER 88c	CNTR	$^{16}\text{O}^* \rightarrow ^{16}\text{O}X^0$, $X^0 \rightarrow e^+e^-$
$< 3.4 \times 10^{-5}$	95	12 DOEHNER 88	SPEC	$^2\text{H}^*$, $A^0 \rightarrow e^+e^-$
$< 4 \times 10^{-4}$	95	13 SAVAGE 88	CNTR	Nuclear decay (isovector)
$< 3 \times 10^{-3}$	95	13 SAVAGE 88	CNTR	Nuclear decay (isoscalar)
$< 10.6 \times 10^{-2}$	90	14 HALLIN 86	SPEC	^6Li isovector decay

< 10.8	90	14 HALLIN 86	SPEC	^{10}B isoscalar decays
< 2.2	90	14 HALLIN 86	SPEC	^{14}N isoscalar decays
$< 4 \times 10^{-4}$	90	15 SAVAGE 86b	CNTR	$^{14}\text{N}^*$
		16 ANANEV 85	CNTR	Li^* , deut* $A^0 \rightarrow 2\gamma$
		17 CAVAI GNAC 83	CNTR	$^{97}\text{Nb}^*$, deut* transition $A^0 \rightarrow 2\gamma$
		18 ALEKSEEV 82b	CNTR	Li^* , deut* transition $A^0 \rightarrow 2\gamma$
		19 LEHMANN 82	CNTR	$\text{Cu}^* \rightarrow \text{Cu}A^0$ ($A^0 \rightarrow 2\gamma$)
		20 ZEHNDER 82	CNTR	Li^* , Nb* decay, n-capt.
		21 ZEHNDER 81	CNTR	$\text{Ba}^* \rightarrow \text{Ba}A^0$ ($A^0 \rightarrow 2\gamma$)
		22 CALAPRICE 79		Carbon

- 1 DERBIN 02 looked for the axion emission in an M1 transition in ^{125m}Te decay. They looked for a possible presence of a shifted energy spectrum in gamma rays due to the undetected axion.
- 2 DEBOER 97c reanalyzed the existent data on Nuclear M1 transitions and find that a 9 MeV boson decaying into e^+e^- would explain the excess of events with large opening angles. See also DEBOER 01 for follow-up experiments.
- 3 TSUNODA 95 looked for axion emission when ^{252}Cf undergoes a spontaneous fission, with the axion decaying into e^+e^- . The bound is for $m_{A^0} = 40 \text{ MeV}$. It improves to 2.5×10^{-5} for $m_{A^0} = 200 \text{ MeV}$.
- 4 MINOWA 93 studied chain process, $^{139}\text{Ce} \rightarrow ^{139}\text{La}^*$ by electron capture and M1 transition of $^{139}\text{La}^*$ to the ground state. It does not assume decay modes of A^0 . The bound applies for $m_{A^0} < 166 \text{ keV}$.
- 5 HICKS 92 bound is applicable for $\tau_{X^0} < 4 \times 10^{-11} \text{ sec}$.
- 6 The ASANUMA 90 limit is for the branching fraction of X^0 emission per ^{241}Am α decay and valid for $\tau_{X^0} < 3 \times 10^{-11} \text{ s}$.
- 7 The DEBOER 90 limit is for the branching ratio $^8\text{Be}^* (18.15 \text{ MeV}, 1^+) \rightarrow ^8\text{Be}A^0$, $A^0 \rightarrow e^+e^-$ for the mass range $m_{A^0} = 4-15 \text{ MeV}$.
- 8 The BINI 89 limit is for the branching fraction of $^{16}\text{O}^*(6.05 \text{ MeV}, 0^+) \rightarrow ^{16}\text{O}X^0$, $X^0 \rightarrow e^+e^-$ for $m_X = 1.5-3.1 \text{ MeV}$. $\tau_{X^0} \lesssim 10^{-11} \text{ s}$ is assumed. The spin-parity of X is restricted to 0^+ or 1^- .
- 9 AVIGNONE 88 looked for the 1115 keV transition $\text{C}^* \rightarrow \text{Cu}A^0$, either from $A^0 \rightarrow 2\gamma$ in-flight decay or from the secondary A^0 interactions by Compton and by Primakoff processes. Limits for axion parameters are obtained for $m_{A^0} < 1.1 \text{ MeV}$.
- 10 DATAR 88 rule out light pseudoscalar particle emission through its decay $A^0 \rightarrow e^+e^-$ in the mass range $1.02-2.5 \text{ MeV}$ and lifetime range $10^{-13}-10^{-8} \text{ s}$. The above limit is for $\tau = 5 \times 10^{-13} \text{ s}$ and $m = 1.7 \text{ MeV}$; see the paper for the $\tau-m$ dependence of the limit.
- 11 The limit is for the branching fraction of $^{16}\text{O}^*(6.05 \text{ MeV}, 0^+) \rightarrow ^{16}\text{O}X^0$, $X^0 \rightarrow e^+e^-$ against internal pair conversion for $m_{X^0} = 1.7 \text{ MeV}$ and $\tau_{X^0} < 10^{-11} \text{ s}$. Similar limits are obtained for $m_{X^0} = 1.3-3.2 \text{ MeV}$. The spin parity of X^0 must be either 0^+ or 1^- . The limit at 1.7 MeV is translated into a limit for the X^0 -nucleon coupling constant: $g_{X^0 NN}^2/4\pi < 2.3 \times 10^{-9}$.
- 12 The DOEHNER 88 limit is for $m_{A^0} = 1.7 \text{ MeV}$, $\tau(A^0) < 10^{-10} \text{ s}$. Limits less than 10^{-4} are obtained for $m_{A^0} = 1.2-2.2 \text{ MeV}$.
- 13 SAVAGE 88 looked for A^0 that decays into e^+e^- in the decay of the $9.17 \text{ MeV } J^P = 2^+$ state in ^{14}N , 17.64 MeV state $J^P = 1^+$ in ^8Be , and the 18.15 MeV state $J^P = 1^+$ in ^8Be . This experiment constrains the isovector coupling of A^0 to hadrons, if $m_{A^0} = (1.1 \rightarrow 2.2) \text{ MeV}$ and the isoscalar coupling of A^0 to hadrons, if $m_{A^0} = (1.1 \rightarrow 2.6) \text{ MeV}$. Both limits are valid only if $\tau(A^0) \lesssim 1 \times 10^{-11} \text{ s}$.
- 14 Limits are for $\Gamma(A^0(1.8 \text{ MeV}))/\Gamma(\pi M1)$; i.e., for 1.8 MeV axion emission normalized to the rate for internal emission of e^+e^- pairs. Valid for $\tau_{A^0} < 2 \times 10^{-11} \text{ s}$. ^6Li isovector decay data strongly disfavor PECCEI 86 model I, whereas the ^{10}B and ^{14}N isoscalar decay data strongly reject PECCEI 86 model II and III.
- 15 SAVAGE 86b looked for A^0 that decays into e^+e^- in the decay of the $9.17 \text{ MeV } J^P = 2^+$ state in ^{14}N . Limit on the branching fraction is valid if $\tau_{A^0} \lesssim 1. \times 10^{-11} \text{ s}$ for $m_{A^0} = (1.1-1.7) \text{ MeV}$. This experiment constrains the iso-vector coupling of A^0 to hadrons.
- 16 ANANEV 85 with IBR-2 pulsed reactor exclude standard A^0 at CL = 95% masses below 470 keV (Li^* decay) and below $2m_e$ for deuteron* decay.
- 17 CAVAI GNAC 83 at Bugey reactor exclude axion at any $m_{97}\text{Nb}^*$ decay and axion with m_{A^0} between 275 and 288 keV (deuteron* decay).
- 18 ALEKSEEV 82 with IBR-2 pulsed reactor exclude standard A^0 at CL = 95% mass-ranges $m_{A^0} < 400 \text{ keV}$ (Li^* decay) and $330 \text{ keV} < m_{A^0} < 2.2 \text{ MeV}$. (deuteron* decay).
- 19 LEHMANN 82 obtained $A^0 \rightarrow 2\gamma$ rate $< 6.2 \times 10^{-5}/\text{s}$ (CL = 95%) excluding m_{A^0} between 100 and 1000 keV.
- 20 ZEHNDER 82 used Gosgen 2.8GW light-water reactor to check A^0 production. No 2γ peak in Li^* , Nb* decay (both single p transition) nor in n capture (combined with previous Ba* negative result) rules out standard A^0 . Set limit $m_{A^0} < 60 \text{ keV}$ for any A^0 .
- 21 ZEHNDER 81 looked for $\text{Ba}^* \rightarrow A^0\text{Ba}$ transition with $A^0 \rightarrow 2\gamma$. Obtained 2γ coincidence rate $< 2.2 \times 10^{-5}/\text{s}$ (CL = 95%) excluding $m_{A^0} > 160 \text{ keV}$ (or 200 keV depending on Higgs mixing). However, see BARROSO 81.
- 22 CALAPRICE 79 saw no axion emission from excited states of carbon. Sensitive to axion mass between 1 and 15 MeV.

A^0 (Axion) Limits from Its Electron Coupling

Limits are for $\tau(A^0 \rightarrow e^+e^-)$.

VALUE (s)	CL%	DOCUMENT ID	TECN	COMMENT
• • • We do not use the following data for averages, fits, limits, etc. • • •				
		1 ANDREEV 21	NA64	$e N \rightarrow e A^0 N$ ($A^0 \rightarrow$ invisibles)

Gauge & Higgs Boson Particle Listings Axions (A^0) and Other Very Light Bosons

none 4×10^{-16} – 4.5×10^{-12}	90	2 ANDREEV	21B NA64	$eN \rightarrow eA^0N$ ($A^0 \rightarrow ee$)
		3 BROSS	91 BDMP	$eN \rightarrow eA^0N$ ($A^0 \rightarrow ee$)
		4 GUO	90 BDMP	$eN \rightarrow eA^0N$ ($A^0 \rightarrow ee$)
		5 BJORKEN	88 CALO	$A \rightarrow e^+e^-$ or 2γ
none 1×10^{-14} – 1×10^{-10}	90	6 BLINOV	88 MD1	$ee \rightarrow eeA^0$ ($A^0 \rightarrow ee$)
none 1×10^{-14} – 1×10^{-11}	90	7 RIORDAN	87 BDMP	$eN \rightarrow eA^0N$ ($A^0 \rightarrow ee$)
none 1×10^{-14} – 9×10^{-11}	90	8 BROWN	86 BDMP	$eN \rightarrow eA^0N$ ($A^0 \rightarrow ee$)
none 6×10^{-14} – 9×10^{-11}	95	9 DAVIER	86 BDMP	$eN \rightarrow eA^0N$ ($A^0 \rightarrow ee$)
none 3×10^{-13} – 1×10^{-7}	90	10 KONAKA	86 BDMP	$eN \rightarrow eA^0N$ ($A^0 \rightarrow ee$)

- ANDREEV 21 look for invisible decays of axions coupled to electrons, and set limits on $g_{Aee} < 4.6 \times 10^{-6}$ – 3.1×10^{-3} for $m_{A^0} = 10^{-3}$ –1 GeV. This limits the axion contribution to the electron g -2 to an order of magnitude less than the current experimental uncertainty. See their Figs. 3 and 4 for mass-dependent limits.
- ANDREEV 21B set limits on g_{Aee} in the range of 6.3×10^{-6} – 1.6×10^{-3} for $m_{A^0} = 2$ –17 MeV at 90% CL. This excludes $6.6 \times 10^{-5} < g_{Aee} < 1 \times 10^{-4}$ at $m_{A^0} = 16.7$ MeV corresponding to the ATOMKI anomaly. See their Fig. 2 for mass-dependent limits.
- The listed BROSS 91 limit is for $m_{A^0} = 1.14$ MeV. $B(A^0 \rightarrow e^+e^-) = 1$ assumed. Excluded domain in the τ_{A^0} - m_{A^0} plane extends up to $m_{A^0} \approx 7$ MeV (see Fig. 5). Combining with electron g -2 constraint, axions coupling only to e^+e^- ruled out for $m_{A^0} < 4.8$ MeV (90% CL).
- GUO 90 use the same apparatus as BROWN 86 and improve the previous limit in the shorter lifetime region. Combined with g -2 constraint, axions coupling only to e^+e^- are ruled out for $m_{A^0} < 2.7$ MeV (90% CL).
- BJORKEN 88 reports limits on axion parameters (f_A, m_A, τ_A) for $m_{A^0} < 200$ MeV from electron beam-dump experiment with production via Primakoff photoproduction, bremsstrahlung from electrons, and resonant annihilation of positrons on atomic electrons.
- BLINOV 88 assume zero spin, $m = 1.8$ MeV and lifetime $< 5 \times 10^{-12}$ s and find $\Gamma(A^0 \rightarrow \gamma\gamma)B(A^0 \rightarrow e^+e^-) < 2$ eV (CL=90%).
- Assumes $A^0\gamma\gamma$ coupling is small and hence Primakoff production is small. Their figure 2 shows limits on axions for $m_{A^0} < 15$ MeV.
- Uses electrons in hadronic showers from an incident 800 GeV proton beam. Limits for $m_{A^0} < 15$ MeV are shown in their figure 3.
- $m_{A^0} = 1.8$ MeV assumed. The excluded domain in the τ_{A^0} - m_{A^0} plane extends up to $m_{A^0} \approx 14$ MeV, see their figure 4.
- The limits are obtained from their figure 3. Also given is the limit on the $A^0\gamma\gamma$ - $A^0e^+e^-$ coupling plane by assuming Primakoff production.

Search for A^0 (Axion) Resonance in Bhabha Scattering

The limit is for $\Gamma(A^0)|B(A^0 \rightarrow e^+e^-)|^2$.

VALUE (10^{-3} eV)	CL%	DOCUMENT ID	TECN	COMMENT
• • • We do not use the following data for averages, fits, limits, etc. • • •				
< 1.3	97	1 HALLIN	92 CNTR	$m_{A^0} = 1.75$ –1.88 MeV
none 0.0016–0.47	90	2 HENDERSON	92c CNTR	$m_{A^0} = 1.5$ –1.86 MeV
< 2.0	90	3 WU	92 CNTR	$m_{A^0} = 1.56$ –1.86 MeV
< 0.013	95	TSERTOS	91 CNTR	$m_{A^0} = 1.832$ MeV
none 0.19–3.3	95	4 WIDMANN	91 CNTR	$m_{A^0} = 1.78$ –1.92 MeV
< 5	97	BAUER	90 CNTR	$m_{A^0} = 1.832$ MeV
none 0.09–1.5	95	5 JUDGE	90 CNTR	$m_{A^0} = 1.832$ MeV, elastic
< 1.9	97	6 TSERTOS	89 CNTR	$m_{A^0} = 1.82$ MeV
<(10–40)	97	6 TSERTOS	89 CNTR	$m_{A^0} = 1.51$ –1.65 MeV
<(1–2.5)	97	6 TSERTOS	89 CNTR	$m_{A^0} = 1.80$ –1.86 MeV
< 31	95	LORENZ	88 CNTR	$m_{A^0} = 1.646$ MeV
< 94	95	LORENZ	88 CNTR	$m_{A^0} = 1.726$ MeV
< 23	95	LORENZ	88 CNTR	$m_{A^0} = 1.782$ MeV
< 19	95	LORENZ	88 CNTR	$m_{A^0} = 1.837$ MeV
< 3.8	97	7 TSERTOS	88 CNTR	$m_{A^0} = 1.832$ MeV
		8 VANKLINKEN	88 CNTR	
		9 MAIER	87 CNTR	
<2500	90	10 MILLS	87 CNTR	$m_{A^0} = 1.8$ MeV
		10 VONWIMMER.87	CNTR	

- HALLIN 92 quote limits on lifetime, 8×10^{-14} – 5×10^{-13} sec depending on mass, assuming $B(A^0 \rightarrow e^+e^-) = 100\%$. They say that TSERTOS 91 overstated their sensitivity by a factor of 3.
- HENDERSON 92c exclude axion with lifetime $\tau_{A^0} = 1.4 \times 10^{-12}$ – 4.0×10^{-10} s, assuming $B(A^0 \rightarrow e^+e^-) = 100\%$. HENDERSON 92c also exclude a vector boson with $\tau = 1.4 \times 10^{-12}$ – 6.0×10^{-10} s.
- WU 92 quote limits on lifetime $> 3.3 \times 10^{-13}$ s assuming $B(A^0 \rightarrow e^+e^-) = 100\%$. They say that TSERTOS 89 overestimate the limit by a factor of $\pi/2$. WU 92 also quote a bound for vector boson, $\tau > 8.2 \times 10^{-13}$ s.
- WIDMANN 91 bound applies exclusively to the case $B(A^0 \rightarrow e^+e^-) = 1$, since the detection efficiency varies substantially as $\Gamma(A^0)_{\text{total}}$ changes. See their Fig. 6.

- JUDGE 90 excludes an elastic pseudoscalar e^+e^- resonance for 4.5×10^{-13} s $< \tau(A^0) < 7.5 \times 10^{-12}$ s (95% CL) at $m_{A^0} = 1.832$ MeV. Comparable limits can be set for $m_{A^0} = 1.776$ –1.856 MeV.
- See also TSERTOS 88B in references.
- The upper limit listed in TSERTOS 88 is too large by a factor of 4. See TSERTOS 88B, footnote 3.
- VANKLINKEN 88 looked for relatively long-lived resonance ($\tau = 10^{-10}$ – 10^{-12} s). The sensitivity is not sufficient to exclude such a narrow resonance.
- MAIER 87 obtained limits $R\Gamma \lesssim 60$ eV (100 eV) at $m_{A^0} \approx 1.64$ MeV (1.83 MeV) for energy resolution $\Delta E_{cm} \approx 3$ keV, where R is the resonance cross section normalized to that of Bhabha scattering, and $\Gamma = \Gamma_{e^+e^-}/\Gamma_{\text{total}}$. For a discussion implying that $\Delta E_{cm} \approx 10$ keV, see TSERTOS 89.
- VONWIMMERSPERG 87 measured Bhabha scattering for $E_{cm} = 1.37$ –1.86 MeV and found a possible peak at 1.73 with $\int \sigma dE_{cm} = 14.5 \pm 6.8$ keV·b. For a comment and a reply, see VANKLINKEN 88B and VONWIMMERSPERG 88. Also see CONNELL 88.

Search for A^0 (Axion) Resonance in $e^+e^- \rightarrow \gamma\gamma$

The limit is for $\Gamma(A^0 \rightarrow e^+e^-)\Gamma(A^0 \rightarrow \gamma\gamma)/\Gamma_{\text{total}}$

VALUE (10^{-3} eV)	CL%	DOCUMENT ID	TECN	COMMENT
• • • We do not use the following data for averages, fits, limits, etc. • • •				
< 0.18	95	VO	94 CNTR	$m_{A^0} = 1.1$ MeV
< 1.5	95	VO	94 CNTR	$m_{A^0} = 1.4$ MeV
<12	95	VO	94 CNTR	$m_{A^0} = 1.7$ MeV
< 6.6	95	1 TRZASKA	91 CNTR	$m_{A^0} = 1.8$ MeV
< 4.4	95	WIDMANN	91 CNTR	$m_{A^0} = 1.78$ –1.92 MeV
		2 FOX	89 CNTR	
< 0.11	95	3 MINOWA	89 CNTR	$m_{A^0} = 1.062$ MeV
<33	97	CONNELL	88 CNTR	$m_{A^0} = 1.580$ MeV
<42	97	CONNELL	88 CNTR	$m_{A^0} = 1.642$ MeV
<73	97	CONNELL	88 CNTR	$m_{A^0} = 1.782$ MeV
<79	97	CONNELL	88 CNTR	$m_{A^0} = 1.832$ MeV
		1 TRZASKA 91		also give limits in the range $(6.6$ – $30) \times 10^{-3}$ eV (95%CL) for $m_{A^0} = 1.6$ –2.0 MeV.
		2 FOX 89		measured positron annihilation with an electron in the source material into two photons and found no signal at 1.062 MeV ($< 9 \times 10^{-5}$ of two-photon annihilation at rest).
		3		Similar limits are obtained for $m_{A^0} = 1.045$ –1.085 MeV.

Search for X^0 (Light Boson) Resonance in $e^+e^- \rightarrow \gamma\gamma\gamma$

The limit is for $\Gamma(X^0 \rightarrow e^+e^-)\Gamma(X^0 \rightarrow \gamma\gamma\gamma)/\Gamma_{\text{total}}$. C invariance forbids spin-0 X^0 coupling to both e^+e^- and $\gamma\gamma\gamma$.

VALUE (10^{-3} eV)	CL%	DOCUMENT ID	TECN	COMMENT
• • • We do not use the following data for averages, fits, limits, etc. • • •				
< 0.2	95	1 VO	94 CNTR	$m_{X^0} = 1.1$ –1.9 MeV
< 1.0	95	2 VO	94 CNTR	$m_{X^0} = 1.1$ MeV
< 2.5	95	2 VO	94 CNTR	$m_{X^0} = 1.4$ MeV
<120	95	2 VO	94 CNTR	$m_{X^0} = 1.7$ MeV
< 3.8	95	3 SKALSEY	92 CNTR	$m_{X^0} = 1.5$ MeV
		1 VO 94		looked for $X^0 \rightarrow \gamma\gamma\gamma$ decaying at rest. The precise limits depend on m_{X^0} . See Fig. 2(b) in paper.
		2 VO 94		looked for $X^0 \rightarrow \gamma\gamma\gamma$ decaying in flight.
		3 SKALSEY 92		also give limits 4.3 for $m_{X^0} = 1.54$ and 7.5 for 1.64 MeV. The spin of X^0 is assumed to be one.

Light Boson (X^0) Search in Nonresonant e^+e^- Annihilation at Rest

Limits are for the ratio of $n\gamma + X^0$ production relative to $\gamma\gamma$.

VALUE (units 10^{-6})	CL%	DOCUMENT ID	TECN	COMMENT
• • • We do not use the following data for averages, fits, limits, etc. • • •				
< 4.2	90	1 MITSUI	96 CNTR	γX^0
< 4	68	2 SKALSEY	95 CNTR	γX^0
<40	68	3 SKALSEY	95 RVUE	γX^0
< 0.18	90	4 ADACHI	94 CNTR	$\gamma\gamma X^0, X^0 \rightarrow \gamma\gamma$
< 0.26	90	5 ADACHI	94 CNTR	$\gamma\gamma X^0, X^0 \rightarrow \gamma\gamma$
< 0.33	90	6 ADACHI	94 CNTR	$\gamma X^0, X^0 \rightarrow \gamma\gamma\gamma$
		1 MITSUI 96		looked for a monochromatic γ . The bound applies for a vector X^0 with $C = -1$ and $m_{X^0} < 200$ keV. They derive an upper bound on eX^0 coupling and hence on the branching ratio $B(o\text{-Ps} \rightarrow \gamma\gamma X^0) < 6.2 \times 10^{-6}$. The bounds weaken for heavier X^0 .
		2 SKALSEY 95		looked for a monochromatic γ without an accompanying γ in e^+e^- annihilation. The bound applies for scalar and vector X^0 with $C = -1$ and $m_{X^0} = 100$ –1000 keV.
		3 SKALSEY 95		reinterpreted the bound on γA^0 decay of $o\text{-Ps}$ by ASAI 91 where 3% of delayed annihilations are not from 3S_1 states. The bound applies for scalar and vector X^0 with $C = -1$ and $m_{X^0} = 0$ –800 keV.
		4 ADACHI 94		looked for a peak in the $\gamma\gamma$ invariant mass distribution in $\gamma\gamma\gamma\gamma$ production from e^+e^- annihilation. The bound applies for $m_{X^0} = 70$ –800 keV.

Gauge & Higgs Boson Particle Listings

Axions (A^0) and Other Very Light Bosons

- 5 ADACHI 94 looked for a peak in the missing-mass mass distribution in $\gamma\gamma$ channel, using $\gamma\gamma\gamma\gamma$ production from e^+e^- annihilation. The bound applies for $m_{X^0} < 800$ keV.
- 6 ADACHI 94 looked for a peak in the missing mass distribution in $\gamma\gamma\gamma$ channel, using $\gamma\gamma\gamma$ production from e^+e^- annihilation. The bound applies for $m_{X^0} = 200$ –900 keV.

Searches for Goldstone Bosons (X^0)

(Including Horizontal Bosons and Majorons.) Limits are for branching ratios.

VALUE	CL%	DOCUMENT ID	TECN	COMMENT
$<4.3 \times 10^{-6}$	90	1 AGUILAR-AR...21A	PIEN	$\pi \rightarrow \mu\nu X^0$, Majoron
$<5.2 \times 10^{-8}$	90	2 AGUILAR-AR...21A	PIEN	$\pi \rightarrow e\nu X^0$, Majoron
$<9 \times 10^{-6}$	90	3 AGUILAR-AR...20	PIEN	$\mu^+ \rightarrow e^+ X^0$, Familon
$<7 \times 10^{-12}$	90	4 BALDINI 20	MEG	$\mu^+ \rightarrow e^+ X^0$ ($X^0 \rightarrow \gamma\gamma$), Familon
$<9 \times 10^{-6}$	90	5 BAYES 15	TWST	$\mu^+ \rightarrow e^+ X^0$, Familon
		6 LATTANZI 13	COSM	Majoron dark matter decay
		7 LESSA 07	RVUE	Meson, ℓ decays to Majoron
		8 DIAZ 98	THEO	$H^0 \rightarrow X^0 X^0, A^0 \rightarrow X^0 X^0 X^0$, Majoron
		9 BOBRAKOV 91		Electron quasi-magnetic interaction
$<3.3 \times 10^{-2}$	95	10 ALBRECHT 90E	ARG	$\tau \rightarrow \mu X^0$, Familon
$<1.8 \times 10^{-2}$	95	10 ALBRECHT 90E	ARG	$\tau \rightarrow e X^0$, Familon
$<6.4 \times 10^{-9}$	90	11 ATIYA 90	B787	$K^+ \rightarrow \pi^+ X^0$, Familon
$<1.4 \times 10^{-5}$	90	12 BALKE 88	CNTR	$\mu^+ \rightarrow e^+ X^0$, Familon
$<1.1 \times 10^{-9}$	90	13 BOLTON 88	CBOX	$\mu^+ \rightarrow e^+ X^0$, Familon
		14 CHANDA 88	ASTR	Sun, Majoron
		15 CHOI 88	ASTR	Majoron, SN 1987A
$<5 \times 10^{-6}$	90	16 PICCIOTTO 88	CNTR	$\pi \rightarrow e\nu X^0$, Majoron
$<1.3 \times 10^{-9}$	90	17 GOLDMAN 87	CNTR	$\mu \rightarrow e\gamma X^0$, Familon
$<3 \times 10^{-4}$	90	18 BRYMAN 86b	RVUE	$\mu \rightarrow e X^0$, Familon
$<1 \times 10^{-10}$	90	19 EICHLER 86	SPEC	$\mu^+ \rightarrow e^+ X^0$, Familon
$<2.6 \times 10^{-6}$	90	20 JODIDIO 86	SPEC	$\mu^+ \rightarrow e^+ X^0$, Familon
		21 BALTRUSAIT...85	MRK3	$\tau \rightarrow \ell X^0$, Familon
		22 DICUS 83	COSM	$\nu(\text{h}\nu) \rightarrow \nu(\text{light}) X^0$

- 1 AGUILAR-AREVALO 21A quoted limit applies to $m_{X^0} = 33.9$ MeV. Limits between 4.3×10^{-6} and 7.5×10^{-5} are obtained for $0 < m_{X^0} < 33.9$ MeV. The lifetime of X^0 is assumed to be long enough. See their Fig. 6 for mass-dependent limits.
- 2 AGUILAR-AREVALO 21A quoted limit applies to $m_{X^0} = 85$ MeV. Limits between 5.2×10^{-8} and 1.4×10^{-6} are obtained for $0 < m_{X^0} < 120$ MeV, which improve the limits of PICCIOTTO 88 by an order of magnitude. The lifetime of X^0 is assumed to be long enough. See their Fig. 4 for mass-dependent limits.
- 3 AGUILAR-AREVALO 20 obtained limits of order 10^{-5} for $m_{X^0} = 47.8$ –95.1 MeV. The quoted limit applies to $m_{X^0} = 75$ MeV. See their Fig. 1 for mass-dependent limits.
- 4 BALDINI 20 obtained limits for $m_{X^0} = 20$ –45 MeV and $\tau_{X^0} < 40$ ps, and supersedes BOLTON 88 for $m_{X^0} = 20$ –40 MeV. See their Fig. 17 for mass-dependent limits.
- 5 BAYES 15 limits are the average over $m_{X^0} = 13$ –80 MeV for the isotropic decay distribution of positrons. See their Fig. 4 and Table II for the mass-dependent limits as well as the dependence on the decay anisotropy. In particular, they find a limit $< 58 \times 10^{-6}$ at 90% CL for massless familons and for the same asymmetry as normal muon decay, a case not covered by JODIDIO 86.
- 6 LATTANZI 13 use WMAP 9 year data as well as X-ray and γ -ray observations to derive limits on decaying majoron dark matter. A limit on the decay width $\Gamma(X^0 \rightarrow \nu\bar{\nu}) < 6.4 \times 10^{-19} \text{ s}^{-1}$ at 95% CL is found if majorons make up all of the dark matter.
- 7 LESSA 07 consider decays of the form Meson $\rightarrow \ell\nu$ Majoron and $\ell \rightarrow \ell'\nu\bar{\nu}$ Majoron and use existing data to derive limits on the neutrino-Majoron Yukawa couplings $g_{\alpha\beta}$ ($\alpha, \beta = e, \mu, \tau$). Their best limits are $|g_{e\alpha}|^2 < 5.5 \times 10^{-6}$, $|g_{\mu\alpha}|^2 < 4.5 \times 10^{-5}$, $|g_{\tau\alpha}|^2 < 5.5 \times 10^{-2}$ at CL = 90%.
- 8 DIAZ 98 studied models of spontaneously broken lepton number with both singlet and triplet Higgses. They obtain limits on the parameter space from invisible decay $Z \rightarrow H^0 A^0 \rightarrow X^0 X^0 X^0 X^0$ and $e^+e^- \rightarrow Z H^0$ with $H^0 \rightarrow X^0 X^0$.
- 9 BOBRAKOV 91 searched for anomalous magnetic interactions between polarized electrons expected from the exchange of a massless pseudoscalar boson (arion). A limit $\chi_e^2 < 2 \times 10^{-4}$ (95%CL) is found for the effective anomalous magneton parametrized as $\chi_e (G_F/8\pi\sqrt{2})^{1/2}$.
- 10 ALBRECHT 90E limits are for $B(\tau \rightarrow \ell X^0)/B(\tau \rightarrow \ell\nu\bar{\nu})$. Valid for $m_{X^0} < 100$ MeV. The limits rise to 7.1% (for μ), 5.0% (for e) for $m_{X^0} = 500$ MeV.
- 11 ATIYA 90 limit is for $m_{X^0} = 0$. The limit $B < 1 \times 10^{-8}$ holds for $m_{X^0} < 95$ MeV. For the reduction of the limit due to finite lifetime of X^0 , see their Fig. 3.
- 12 BALKE 88 limits are for $B(\mu^+ \rightarrow e^+ X^0)$. Valid for $m_{X^0} < 80$ MeV and $\tau_{X^0} > 10^{-8}$ sec.
- 13 BOLTON 88 limit corresponds to $F > 3.1 \times 10^9$ GeV, which does not depend on the chirality property of the coupling.
- 14 CHANDA 88 find $v_T < 10$ MeV for the weak-triplet Higgs vacuum expectation value in Gelmini-Roncadelli model, and $v_S > 5.8 \times 10^6$ GeV in the singlet Majoron model.
- 15 CHOI 88 used the observed neutrino flux from the supernova SN 1987A to exclude the neutrino Majoron Yukawa coupling h in the range $2 \times 10^{-5} < h < 3 \times 10^{-4}$ for the interaction $L_{\text{int}} = \frac{1}{2} i h \bar{\nu}_\nu \gamma_5 \psi_\nu \phi_X$. For several families of neutrinos, the limit applies for $(\sum h_i^2)^{1/4}$.
- 16 PICCIOTTO 88 limit applies when $m_{X^0} < 55$ MeV and $\tau_{X^0} > 2$ ns, and it decreases to 4×10^{-7} at $m_{X^0} = 125$ MeV, beyond which no limit is obtained.

- 17 GOLDMAN 87 limit corresponds to $F > 2.9 \times 10^9$ GeV for the family symmetry breaking scale from the Lagrangian $L_{\text{int}} = (1/F) \bar{\psi}_\mu \gamma^\mu (a + b\gamma_5) \psi_e \theta_\mu \phi_{X^0}$ with $a^2 + b^2 = 1$. This is not as sensitive as the limit $F > 9.9 \times 10^9$ GeV derived from the search for $\mu^+ \rightarrow e^+ X^0$ by JODIDIO 86, but does not depend on the chirality property of the coupling.
- 18 Limits are for $\Gamma(\mu \rightarrow e X^0)/\Gamma(\mu \rightarrow e\nu\bar{\nu})$. Valid when $m_{X^0} = 0$ –93.4, 98.1–103.5 MeV.
- 19 EICHLER 86 looked for $\mu^+ \rightarrow e^+ X^0$ followed by $X^0 \rightarrow e^+ e^-$. Limits on the branching fraction depend on the mass and lifetime of X^0 . The quoted limits are valid when $\tau_{X^0} \lesssim 3. \times 10^{-10}$ s if the decays are kinematically allowed.
- 20 JODIDIO 86 corresponds to $F > 9.9 \times 10^9$ GeV for the family symmetry breaking scale with the parity-conserving effective Lagrangian $L_{\text{int}} = (1/F) \bar{\psi}_\mu \gamma^\mu \psi_e \theta^\mu \phi_{X^0}$.
- 21 BALTRUSAITIS 85 search for light Goldstone boson (X^0) of broken U(1). CL = 95% limits are $B(\tau \rightarrow \mu^+ X^0)/B(\tau \rightarrow \mu^+ \nu\bar{\nu}) < 0.125$ and $B(\tau \rightarrow e^+ X^0)/B(\tau \rightarrow e^+ \nu\bar{\nu}) < 0.04$. Inferred limit for the symmetry breaking scale is $m > 3000$ TeV.
- 22 The primordial heavy neutrino must decay into ν and familon, f_A , early so that the red-shifted decay products are below critical density, see their table. In addition, $K \rightarrow \pi f_A$ and $\mu \rightarrow e f_A$ are unseen. Combining these excludes $m_{\text{heavy}\nu}$ between 5×10^{-5} and 5×10^{-4} MeV (μ decay) and $m_{\text{heavy}\nu}$ between 5×10^{-5} and 0.1 MeV (K -decay).

Majoron Searches in Neutrinoless Double β Decay

Limits are for the half-life of neutrinoless $\beta\beta$ decay with a Majoron emission. No experiment currently claims any such evidence. Only the best or comparable limits for each isotope are reported.

$t_{1/2}(10^{21} \text{ yr})$	CL%	ISOTOPE	TRANSITION	METHOD	DOCUMENT ID
>7200	90	128Te	CNTR		1 BERNATOW... 92
••• We do not use the following data for averages, fits, limits, etc. •••					
>4300	90	136Xe	0 ν 1 χ	EXO-200	2 AL-KHARUSI 21
> 4.4	90	100Mo	0 ν 1 χ	NEMO-3	3 ARNOLD 19
> 37	90	82Se	0 ν 1 χ	NEMO-3	4 ARNOLD 18
> 420	90	76Ge	0 ν 1 χ	GERDA	5 AGOSTINI 15A
> 400	90	100Mo	0 ν 1 χ	NEMO-3	6 ARNOLD 15
>1200	90	136Xe	0 ν 1 χ	EXO-200	7 ALBERT 14A
>2600	90	136Xe	0 ν 1 χ	KamLAND-Zen	8 GANDO 12
> 16	90	130Te	0 ν 1 χ	NEMO-3	9 ARNOLD 11
> 1.9	90	96Zr	2 ν 1 χ	NEMO-3	10 ARGYRADES 10
> 1.52	90	150Nd	0 ν 1 χ	NEMO-3	11 ARGYRADES 09
> 27	90	100Mo	0 ν 1 χ	NEMO-3	12 ARNOLD 06
> 15	90	82Se	0 ν 1 χ	NEMO-3	13 ARNOLD 06
> 14	90	100Mo	0 ν 1 χ	NEMO-3	14 ARNOLD 04
> 12	90	82Se	0 ν 1 χ	NEMO-3	15 ARNOLD 04
> 2.2	90	130Te	0 ν 1 χ	Cryog. det.	16 ARNABOLDI 03
> 0.9	90	130Te	0 ν 2 χ	Cryog. det.	17 ARNABOLDI 03
> 8	90	116Cd	0 ν 1 χ	CdWO ₄ scint.	18 DANEVICH 03
> 0.8	90	116Cd	0 ν 2 χ	CdWO ₄ scint.	19 DANEVICH 03
> 500	90	136Xe	0 ν 1 χ	Liquid Xe Scint.	20 BERNABEI 02D
> 5.8	90	100Mo	0 ν 1 χ	ELEGANT V	21 FUSHIMI 02
> 0.32	90	100Mo	0 ν 1 χ	Liq. Ar ioniz.	22 ASHITKOV 01
> 0.0035	90	160Gd	0 ν 1 χ	¹⁶⁰ Gd ₂ SiO ₅ :Ce	23 DANEVICH 01
> 0.013	90	160Gd	0 ν 2 χ	¹⁶⁰ Gd ₂ SiO ₅ :Ce	24 DANEVICH 01
> 2.3	90	82Se	0 ν 1 χ	NEMO 2	25 ARNOLD 00
> 0.31	90	96Zr	0 ν 1 χ	NEMO 2	26 ARNOLD 00
> 0.63	90	82Se	0 ν 2 χ	NEMO 2	27 ARNOLD 00
> 0.063	90	96Zr	0 ν 2 χ	NEMO 2	27 ARNOLD 00
> 0.16	90	100Mo	0 ν 2 χ	NEMO 2	27 ARNOLD 00
> 2.4	90	82Se	0 ν 1 χ	NEMO 2	28 ARNOLD 98
> 7.2	90	136Xe	0 ν 2 χ	TPC	29 LUESCHER 98
> 7.91	90	76Ge		SPEC	30 GUENTHER 96
> 17	90	76Ge		CNTR	BECK 93

- 1 BERNATOWICZ 92 studied double- β decays of ¹²⁸Te and ¹³⁰Te, and found the ratio $\tau(^{130}\text{Te})/\tau(^{128}\text{Te}) = (3.52 \pm 0.11) \times 10^{-4}$ in agreement with relatively stable theoretical predictions. The bound is based on the requirement that Majoron-emitting decay cannot be larger than the observed double-beta rate of ¹²⁸Te of $(7.7 \pm 0.4) \times 10^{24}$ year. We calculated 90% CL limit as $(7.7-1.28 \times 0.4=7.2) \times 10^{24}$.
- 2 AL-KHARUSI 21 utilize the complete dataset of the EXO-200 experiment, corresponding to an exposure of 234 kg yr, to place a limit on the one Majoron mode of the neutrinoless double beta decay of ¹³⁶Xe. Several limits are reported, the one given here corresponds to a spectral index of 1, resulting in a limit of $g_{\nu\chi} < 0.4$ – 0.9×10^{-5} on the Majoron-neutrino coupling constant. The range reflects the spread of the nuclear matrix elements.
- 3 ARNOLD 19 uses the NEMO-3 tracking calorimeter to determine limits for the Majoron emitting double beta decay, with spectral index $n = 3$. The limit corresponds to the range of the g_{ee} coupling of 0.013–0.035; depending on the nuclear matrix elements used.
- 4 ARNOLD 18 use the NEMO-3 tracking detector. The limit corresponds to $\langle g_{ee} \rangle < 3.2$ – 8.0×10^{-5} ; the range corresponds to different nuclear matrix element calculations.
- 5 AGOSTINI 15A analyze a 20.3 kg yr of data set of the GERDA calorimeter to determine $g_{\nu\chi} < 3.4$ – 8.7×10^{-5} on the Majoron-neutrino coupling constant. The range reflects the spread of the nuclear matrix elements.
- 6 ARNOLD 15 use the NEMO-3 tracking calorimeter with 3.43 kg yr exposure to determine the limit on Majoron emission. The limit corresponds to $g_{\nu\chi} < 1.6$ – 3.0×10^{-4} . The spread reflects different nuclear matrix elements. Supersedes ARNOLD 06.
- 7 ALBERT 14A utilize 100 kg yr of exposure of the EXO-200 tracking calorimeter to place a limit on the $g_{\nu\chi} < 0.8$ – 1.7×10^{-5} on the Majoron-neutrino coupling constant. The range reflects the spread of the nuclear matrix elements.

See key on page 1127

Gauge & Higgs Boson Particle Listings
Axions (A^0) and Other Very Light Bosons

8 GANDO 12 use the KamLAND-Zen detector to obtain the limit on the $0\nu\chi$ decay with Majoron emission. It implies that the coupling constant $g_{\nu\chi} < 0.8\text{--}1.6 \times 10^{-5}$ depending on the nuclear matrix elements used.	< 1.2	95	26 HANNESTAD 07 COSM K, hot dark matter
9 ARNOLD 11 use the NEMO-3 detector to obtain the reported limit on Majoron emission. It implies that the coupling constant $g_{\nu\chi} < 0.6\text{--}1.6 \times 10^{-4}$ depending on the nuclear matrix element used. Supersedes ARNABOLDI 03.	< 0.42	95	27 MELCHIORRI 07A COSM K, hot dark matter
10 ARGYRIADES 10 use the NEMO-3 tracking detector and ^{96}Zr to derive the reported limit. No limit for the Majoron electron coupling is given.	< 1.05	95	28 HANNESTAD 05A COSM K, hot dark matter
11 ARGYRIADES 09 use ^{150}Nd data taken with the NEMO-3 tracking detector. The reported limit corresponds to $\langle g_{\nu\chi} \rangle < 1.7\text{--}3.0 \times 10^{-4}$ using a range of nuclear matrix elements that include the effect of nuclear deformation.	3 to 20		29 MOROI 98 COSM K, hot dark matter
12 ARNOLD 06 use ^{100}Mo data taken with the NEMO-3 tracking detector. The reported limit corresponds to $\langle g_{\nu\chi} \rangle < (0.4\text{--}1.8) \times 10^{-4}$ using a range of matrix element calculations. Superseded by ARNOLD 15.	< 0.007		30 BORISOV 97 ASTR D, neutron star
13 NEMO-3 tracking calorimeter is used in ARNOLD 06. Reported half-life limit for ^{82}Se corresponds to $\langle g_{\nu\chi} \rangle < (0.66\text{--}1.9) \times 10^{-4}$ using a range of matrix element calculations. Supersedes ARNOLD 04.	< 4		31 KACHELRIESS 97 ASTR D, neutron star cooling
14 ARNOLD 04 use the NEMO-3 tracking detector. The limit corresponds to $\langle g_{\nu\chi} \rangle < (0.5\text{--}0.9)10^{-4}$ using the matrix elements of SIMKOVIĆ 99, STOICA 01 and CIVITARESE 03. Superseded by ARNOLD 06.	< (0.5–6) $\times 10^{-3}$		32 KEIL 97 ASTR SN 1987A
15 ARNOLD 04 use the NEMO-3 tracking detector. The limit corresponds to $\langle g_{\nu\chi} \rangle < (0.7\text{--}1.6)10^{-4}$ using the matrix elements of SIMKOVIĆ 99, STOICA 01 and CIVITARESE 03.	< 0.018		33 RAFFELT 95 ASTR D, red giant
16 Supersedes ALESSANDRELLO 00. Array of TeO_2 crystals in high resolution cryogenic calorimeter. Some enriched in ^{130}Te . Derive $\langle g_{\nu\chi} \rangle < 17\text{--}33 \times 10^{-5}$ depending on matrix element.	< 0.010		34 ALTHERR 94 ASTR D, red giants, white dwarfs
17 Supersedes ALESSANDRELLO 00. Cryogenic calorimeter search.	< 0.01		35 CHANG 93 ASTR K, SN 1987A
18 Limit for the $0\nu\chi$ decay with Majoron emission of ^{116}Cd using enriched CdWO_4 scintillators. $\langle g_{\nu\chi} \rangle < 4.6\text{--}8.1 \times 10^{-5}$ depending on the matrix element. Supersedes DANEVICH 00.	< 0.03		WANG 92 ASTR D, white dwarf
19 Limit for the $0\nu 2\chi$ decay of ^{116}Cd . Supersedes DANEVICH 00.	none 3–8		WANG 92C ASTR D, C-O burning
20 BERNABELI 02d obtain limit for $0\nu\chi$ decay with Majoron emission of ^{136}Xe using liquid Xe scintillation detector. They derive $\langle g_{\nu\chi} \rangle < 2.0\text{--}3.0 \times 10^{-5}$ with several nuclear matrix elements.	< 10		36 BERSHADY 91 ASTR D, K, intergalactic light
21 Replaces TANAKA 93. FUSHIMI 02 derive half-life limit for the $0\nu\chi$ decay by means of tracking calorimeter ELEGANT V. Considering various matrix element calculations, a range of limits for the Majoron-neutrino coupling is given: $\langle g_{\nu\chi} \rangle < (6.3\text{--}360) \times 10^{-5}$.	< 1	$\times 10^{-3}$	91C COSM D, K, mass density of the universe, supersymmetry
22 ASHITKOV 01 result for $0\nu\chi$ of ^{100}Mo is less stringent than ARNOLD 00.	none $10^{-3}\text{--}3$		38 RAFFELT 91B ASTR D,K, SN 1987A
23 DANEVICH 01 obtain limit for the $0\nu\chi$ decay with Majoron emission of ^{160}Gd using $\text{Gd}_2\text{SiO}_5\text{:Ce}$ crystal scintillators.	< 0.02		39 RESSELL 91 ASTR K, intergalactic light
24 DANEVICH 01 obtain limit for the $0\nu 2\chi$ decay with 2 Majoron emission of ^{160}Gd .	< 1	$\times 10^{-3}$	BURROWS 90 ASTR D,K, SN 1987A
25 ARNOLD 00 reports limit for the $0\nu\chi$ decay with Majoron emission derived from tracking calorimeter NEMO 2. Using ^{82}Se source: $\langle g_{\nu\chi} \rangle < 1.6 \times 10^{-4}$. Matrix element from GUENTHER 96.	< (1.4–10) $\times 10^{-3}$		40 ENGEL 90 ASTR D,K, SN 1987A
26 Using ^{96}Zr source: $\langle g_{\nu\chi} \rangle < 2.6 \times 10^{-4}$. Matrix element from ARNOLD 99.	< 3.6 $\times 10^{-4}$		41 RAFFELT 90D ASTR D, red giant
27 ARNOLD 00 reports limit for the $0\nu 2\chi$ decay with two Majoron emission derived from tracking calorimeter NEMO 2.	< 12		42 BURROWS 89 ASTR D,K, SN 1987A
28 ARNOLD 98 determine the limit for $0\nu\chi$ decay with Majoron emission of ^{82}Se using the NEMO-2 tracking detector. They derive $\langle g_{\nu\chi} \rangle < 2.3\text{--}4.3 \times 10^{-4}$ with several nuclear matrix elements.	< 1	$\times 10^{-3}$	43 ERICSON 89 ASTR D,K, SN 1987A
29 LUESCHER 98 report a limit for the 0ν decay with Majoron emission of ^{136}Xe using Xe TPC. This result is more stringent than BARABASH 89. Using the matrix elements of ENGEL 88, they obtain a limit on $\langle g_{\nu\chi} \rangle$ of 2.0×10^{-4} .	< 0.07		44 MAYLE 89 ASTR D,K, SN 1987A
30 See Table 1 in GUENTHER 96 for limits on the Majoron coupling in different models.	< 1	$\times 10^{-3}$	CHANDA 88 ASTR D, Sun

Invisible A^0 (Axion) MASS LIMITS from Astrophysics and Cosmology

$v_1 = v_2$ is usually assumed ($v_j =$ vacuum expectation values). For a review of these limits, see RAFFELT 91 and TURNER 90. In the comment lines below, D and K refer to DFSZ and KSVZ axion types, discussed in the above minireview.

VALUE (eV)	CL%	DOCUMENT ID	TECN	COMMENT
> 1.4 $\times 10^{-21}$	95	1	ASTR	Fuzzy DM
< 1.9 $\times 10^4$		2	COSM	warm dark matter
		3	ASTR	SN 1987A, axion-moon coupling
		4	ASTR	Microlensing
none 1.3–2.7 $\times 10^{-13}$		5	ASTR	SN 1987A, Λ decay
> 2 $\times 10^{-20}$	95	6	ASTR	BH superradiance
none 0.8–6.5 $\times 10^{-13}$	95	7	COSM	Lyman- α
> 2 $\times 10^{-17}$		8	ASTR	BH superradiance
		9	COSM	Isocurvature fluctuations
		10	ASTR	Compact binary systems
> 2.1 $\times 10^{-21}$		11	COSM	Fuzzy DM
none 6.4–8.0 $\times 10^{-13}$	95	12	ASTR	BH superradiance
none 2.9–4.6 $\times 10^{-21}$		13	ASTR	BH superradiance
none 10 ⁻²¹ –6 $\times 10^{-20}$		14	ASTR	Fuzzy DM
none 1.1–4 $\times 10^{-13}$	95	15	ASTR	BH superradiance
< 0.06		16	ASTR	K, SN 1987A
< 0.67	95	17	COSM	K, hot dark matter
none 0.7–3 $\times 10^5$		18	COSM	D abundance
<105	90	19	CNTR	D, solar axion
		20	CAST	K, solar axions
< 0.72	95	21	COSM	K, hot dark matter
		22	CAST	K, solar axions
<191	90	23	CNTR	K, solar axions
<334	95	24	HPGE	K, solar axions
< 1.02	95	25	COSM	K, hot dark matter

- BANIK 21 use the subhalo mass function inferred from the analyses of the GD-1 and Pal 5 stellar streams. The limit is strengthened to 2.2×10^{-21} eV when adding dwarf satellite counts.
- BAUMHOLZER 21 study the freeze-in production of axion dark matter through couplings to photons, and set the limit using Lyman- α forest data and the observed number of Milky Way subhalos.
- CROON 21 study the supernova cooling effect of the axion-moon coupling, taking account of semi-Compton scattering and muon-proton bremsstrahlung, as well as the loop-induced axion-photon coupling, and exclude the range of $g_{A\mu\mu} \simeq 7 \times 10^{-3}\text{--}2 \times 10^{-10}$ for $m_{A^0} < 0.5$ GeV. See their Fig. 8 for mass-dependent limits.
- FUJIKURA 21 use the EROS-2 survey and the Subaru HSC observation to set limits on spherically symmetric axion clumps, taking account of the finite lens and source size effects. $f_{A^0} \gtrsim 10^{12}$ GeV can be constrained depending on the fraction of the axion dark matter collapsed into clumps, and the clump densities. See their Figs. 7–10 for the limits.
- MARTINCA MALICH 21 considered axion emission from a supernova core through the Λ hyperon decay, and set the limit on $B(\Lambda \rightarrow nA^0) \lesssim 8 \times 10^{-9}$, or equivalently, $f_{A^0}/C_{sd} \gtrsim 2.6 \times 10^9$ GeV in terms of the flavor-violating axion coupling to the down and strange quarks.
- NG 21 use the binary black holes reported by LIGO and Virgo to determine the black hole spin distribution at formation and the scalar boson mass simultaneously, neglecting the boson self-interaction.
- ROGERS 21 set the limit by using a framework involving Bayesian emulator optimization to accurately forward-model the Lyman- α flux power spectrum, and comparing this with small-scale data to constrain the predicted suppression of cosmic structure growth.
- TSUKADA 21 look for a stochastic GW background produced by extragalactic BH-hidden photon cloud systems through the superradiant instability. They assume a uniform spin distribution at birth of isolated BHs from 0 to 1.
- IRSC 20 used the Lyman- α forest constraint on small-scale isocurvature perturbation to derive limits on the axion mass and decay constant, assuming that the axion makes up all dark matter in the post-inflationary scenario. See their Fig. 1 for other astrophysical limits as well as the limits on the case of the temperature-dependent axion mass.
- PODDAR 20 used the observed decay in orbital period of four compact binary systems to derive a limit on the emission of axions with $m_{A^0} < 1 \times 10^{-19}$ eV, assuming they couple to nucleons and the strong CP phase vanishes at the potential minimum. They exclude $f_{A^0} \lesssim 10^{11}$ GeV for such axions.
- SCHUTZ 20 set a limit on fuzzy dark matter based on the existing limits for warm dark matter derived from the inferred subhalo mass function.
- SUN 20 look for quasimonochromatic gravitational waves emitted from boson clouds around the Cygnus X-1 black hole. The quoted limit assume the black hole age of 5×10^6 years. A mass range of $9.6\text{--}15.5 \times 10^{-13}$ eV is disfavored when repeated induction of bosonova for string axions with decay constant $f_{A^0} \simeq 10^{15}$ GeV prevents the superradiance from being saturated.

Gauge & Higgs Boson Particle Listings

Axions (A^0) and Other Very Light Bosons

- 13 DAVOUDIASL 19 used the observed data of M87* by the Event Horizon Telescope to set the limit. A mass range of $0.85\text{--}4.6 \times 10^{-21}$ eV is disfavored for a spin-1 boson.
- 14 MARSH 19 considered heating of star clusters due to the stochastic oscillations of the core and granular quasiparticles in the outer halo. The limit was derived by requiring the survival of the old star cluster in Eridanus II, where the lower end is set by the validity of diffusion approximation. The effect of tidal stripping is also discussed for lower masses.
- 15 PALOMBA 19 used the LIGO O2 dataset to derive limits on nearly monochromatic gravitational waves emitted by boson clouds formed around a stellar-mass black hole. They exclude boson masses in a range of 1.1×10^{-13} and 4×10^{-13} eV for high initial black hole spin, and 1.2×10^{-13} and 1.8×10^{-13} eV for moderate spin. See their Figs. 2 and 3 for limits based on various values of black hole initial spin, boson cloud age, and distance.
- 16 CHANG 18 update axion bremsstrahlung emission rates in nucleon-nucleon collisions, shifting the excluded mass range to higher values. They rule out the hadronic axion with mass up to a few hundred eV, closing the hadronic axion window. See their Fig. 11 for results based on several different choices of the temperature and density profile of the proto-neutron star.
- 17 ARCHIDIACONO 13A is analogous to HANNESTAD 05A. The limit is based on the CMB temperature power spectrum of the Planck data, the CMB polarization from the WMAP 9-yr data, the matter power spectrum from SDSS-DR7, and the local Hubble parameter measurement by the Carnegie Hubble program.
- 18 CADAMURO 11 use the deuterium abundance to show that the m_{A^0} range 0.7 eV – 300 keV is excluded for axions, complementing HANNESTAD 10.
- 19 DERBIN 11a look for solar axions produced by Compton and bremsstrahlung processes, in the resonant excitation of ^{169}Tm , constraining the axion-electron \times axion-nucleon couplings.
- 20 ANDRIAMONJE 10 search for solar axions produced from ^7Li (478 keV) and $D(p,\gamma)^3\text{He}$ (5.5 MeV) nuclear transitions. They show limits on the axion-photon coupling for two reference values of the axion-nucleon coupling for $m_A < 100$ eV.
- 21 This is an update of HANNESTAD 08 including 7 years of WMAP data.
- 22 ANDRIAMONJE 09 look for solar axions produced from the thermally excited 14.4 keV level of ^{57}Fe . They show limits on the axion-nucleon \times axion-photon coupling assuming $m_A < 0.03$ eV.
- 23 DERBIN 09a look for Primakoff-produced solar axions in the resonant excitation of ^{169}Tm , constraining the axion-photon \times axion-nucleon couplings.
- 24 KEKEZ 09 look at axio-electric effect of solar axions in HPGe detectors. The one-loop axion-electron coupling for hadronic axions is used.
- 25 This is an update of HANNESTAD 07 including 5 years of WMAP data.
- 26 This is an update of HANNESTAD 05A with new cosmological data, notably WMAP (3 years) and baryon acoustic oscillations (BAO). Lyman- α data are left out, in contrast to HANNESTAD 05A and MELCHIORRI 07A, because it is argued that systematic errors are large. It uses Bayesian statistics and marginalizes over a possible neutrino hot dark matter component.
- 27 MELCHIORRI 07A is analogous to HANNESTAD 05A, with updated cosmological data, notably WMAP (3 years). Uses Bayesian statistics and marginalizes over a possible neutrino hot dark matter component. Leaving out Lyman- α data, a conservative limit is 1.4 eV.
- 28 HANNESTAD 05A puts an upper limit on the mass of hadronic axion because in this mass range it would have been thermalized and contribute to the hot dark matter component of the universe. The limit is based on the CMB anisotropy from WMAP, SDSS large scale structure, Lyman α , and the prior Hubble parameter from HST Key Project. A χ^2 statistic is used. Neutrinos are assumed not to contribute to hot dark matter.
- 29 MOROJ 98 points out that a KSVZ axion of this mass range (see CHANG 93) can be a viable hot dark matter of Universe, as long as the model-dependent $g_{A\gamma}$ is accidentally small enough as originally emphasized by KAPLAN 85; see Fig. 1.
- 30 BORISOV 97 bound is on the axion-electron coupling $g_{ae} < 1 \times 10^{-13}$ from the photo-production of axions off of magnetic fields in the outer layers of neutron stars.
- 31 KACHELRIESS 97 bound is on the axion-electron coupling $g_{ae} < 1 \times 10^{-10}$ from the production of axions in strongly magnetized neutron stars. The authors also quote a stronger limit, $g_{ae} < 9 \times 10^{-13}$ which is strongly dependent on the strength of the magnetic field in white dwarfs.
- 32 KEIL 97 uses new measurements of the axial-vector coupling strength of nucleons, as well as a reanalysis of many-body effects and pion-emission processes in the core of the neutron star, to update limits on the invisible-axion mass.
- 33 RAFFELT 95 reexamined the constraints on axion emission from red giants due to the axion-electron coupling. They improve on DEARBORN 86 by taking into proper account degeneracy effects in the bremsstrahlung rate. The limit comes from requiring the red giant core mass at helium ignition not to exceed its standard value by more than 5% (0.025 solar masses).
- 34 ALTHERR 94 bound is on the axion-electron coupling $g_{ae} < 1.5 \times 10^{-13}$, from energy loss via axion emission.
- 35 CHANG 93 updates ENGEL 90 bound with the Kaplan-Manohar ambiguity in $z=m_H/m_A$ (see the Note on the Quark Masses in the Quark Particle Listings). It leaves the window $f_A = 3 \times 10^5\text{--}3 \times 10^6$ GeV open. The constraint from Big-Bang Nucleosynthesis is satisfied in this window as well.
- 36 BERSHADY 91 searched for a line at wave length from 3100–8300 Å expected from 2 γ decays of relic thermal axions in intergalactic light of three rich clusters of galaxies.
- 37 KIM 91c argues that the bound from the mass density of the universe will change drastically for the supersymmetric models due to the entropy production of saxion (scalar component in the axionic chiral multiplet) decay. Note that it is an *upperbound* rather than a lowerbound.
- 38 RAFFELT 91B argue that previous SN 1987A bounds must be relaxed due to corrections to nucleon bremsstrahlung processes.
- 39 RESSELL 91 uses absence of any intracluster line emission to set limit.
- 40 ENGEL 90 rule out $10^{-10} \lesssim g_{AN} \lesssim 10^{-3}$, which for a hadronic axion with EMC motivated axion-nucleon couplings corresponds to 2.5×10^{-3} eV $\lesssim m_{A^0} \lesssim 2.5 \times 10^4$ eV. The constraint is loose in the middle of the range, i.e. for $g_{AN} \sim 10^{-6}$.
- 41 RAFFELT 90D is a re-analysis of DEARBORN 86.
- 42 The region $m_{A^0} \gtrsim 2$ eV is also allowed.
- 43 ERICSON 89 considered various nuclear corrections to axion emission in a supernova core, and found a reduction of the previous limit (MAYLE 88) by a large factor.
- 44 MAYLE 89 limit based on naive quark model couplings of axion to nucleons. Limit based on couplings motivated by EMC measurements is 2–4 times weaker. The limit from axion-electron coupling is weak; see HATSUDA 88b.

- 45 RAFFELT 88b derives a limit for the energy generation rate by exotic processes in helium-burning stars $\epsilon < 100 \text{ erg g}^{-1} \text{ s}^{-1}$, which gives a firmer basis for the axion limits based on red giant cooling.
- 46 RAFFELT 87 also gives a limit $g_{A\gamma} < 1 \times 10^{-10} \text{ GeV}^{-1}$.
- 47 DEARBORN 86 also gives a limit $g_{A\gamma} < 1.4 \times 10^{-11} \text{ GeV}^{-1}$.
- 48 RAFFELT 86 gives a limit $g_{A\gamma} < 1.1 \times 10^{-10} \text{ GeV}^{-1}$ from red giants and $< 2.4 \times 10^{-9} \text{ GeV}^{-1}$ from the sun.
- 49 KAPLAN 85 says $m_{A^0} < 23$ eV is allowed for a special choice of model parameters.
- 50 FUKUGITA 82 gives a limit $g_{A\gamma} < 2.3 \times 10^{-10} \text{ GeV}^{-1}$.

Search for Relic Invisible Axions

Limits are for the dimensionless quantity $[G_{A\gamma\gamma}/m_{A^0}]^2 \rho_A$ where $G_{A\gamma\gamma}$ denotes the axion two-photon coupling, $L_{\text{int}} = -\frac{G_{A\gamma\gamma}}{4} \phi_A F_{\mu\nu} \tilde{F}^{\mu\nu} = G_{A\gamma\gamma} \phi_A \mathbf{E} \cdot \mathbf{B}$, and ρ_A is the axion energy density near the earth, unless otherwise stated. Notice that for QCD axions $G_{A\gamma\gamma}/m_{A^0}$ does not depend on m_{A^0} . For the reference values $m_{A^0} = 1 \mu\text{eV}$, $G_{A\gamma\gamma} = 3.9 \times 10^{-16} \text{ GeV}^{-1}$ (that would apply to KSVZ axions at that mass), and $\rho_A = 300 \text{ MeV}/\text{cm}^3$ one finds $[G_{A\gamma\gamma}/m_{A^0}]^2 \rho_A = 3.5 \times 10^{-43}$.

VALUE	CL%	DOCUMENT ID	TECN	COMMENT
• • • We do not use the following data for averages, fits, limits, etc. • • •				
$< 2.8 \times 10^{-4}$	95	1 ADE	21	CMB $m_{A^0} = 0.16\text{--}4.8 \times 10^{-20}$ eV
$< 1.1 \times 10^{-41}$	90	2 ALESINI	21	QUAX $m_{A^0} = 43 \mu\text{eV}$
$< 1 \times 10^{-44}$	90	3 BARTRAM	21A	ADMX $m_{A^0} = 3.3\text{--}4.2 \mu\text{eV}$
$< 1.6 \times 10^{-29}$	95	4 DEVLIN	21	TRAP $m_{A^0} = 2.7906\text{--}2.7914 \text{ neV}$
$< 1.4 \times 10^{-23}$	95	5 GRAMOLIN	21	SHFT $m_{A^0} = 0.012\text{--}12 \text{ neV}$
$< 7 \times 10^{-43}$	90	6 KWON	21	CASK $m_{A^0} = 10.7126\text{--}10.7186 \mu\text{eV}$
$< 4.6 \times 10^{-40}$	95	7 MELCON	21	RADE $m_{A^0} = 34.6738\text{--}34.6771 \mu\text{eV}$
$< 3.5 \times 10^{-28}$	95	8 SALEMI	21	ABRA $m_{A^0} = 0.41\text{--}8.27 \text{ neV}$
$< 3 \times 10^{-3}$	95	9 THOMSON	21	$m_{A^0} = 7.44\text{--}19.38 \text{ neV}$
$< 1 \times 10^{-2}$	95	9 THOMSON	21	$m_{A^0} = 74.4\text{--}74.5 \mu\text{eV}$
		10 YUAN	21	ASTR $m_{A^0} = 10\text{--}20\text{--}10\text{--}17 \text{ eV}$
$< 1.9 \times 10^{-44}$	90	11 BRAINE	20	ADMX $m_{A^0} = 2.81\text{--}3.31 \mu\text{eV}$
$< 2 \times 10^{-35}$	90	12 CRISOSTO	20	SLIC $m_{A^0} = 180.07\text{--}180.15 \text{ neV}$
$< 4 \times 10^{-37}$	95	13 DARLING	20A	ASTR $m_{A^0} = 4.2\text{--}165.6 \mu\text{eV}$
$< 3.2 \times 10^{-36}$	95	14 FOSTER	20	ASTR $m_{A^0} = 5\text{--}7, 10\text{--}11 \mu\text{eV}$
$< 5.7 \times 10^{-41}$	90	15 JEONG	20	CASK $m_{A^0} = 13.0\text{--}13.9 \mu\text{eV}$
		16 KENNEDY	20	$m_{S^0} = 10\text{--}19\text{--}10\text{--}17 \text{ eV}$
$< 4.8 \times 10^{-42}$	90	17 LEE	20A	CASK $m_{A^0} = 6.62\text{--}6.82 \mu\text{eV}$
$< 2.6 \times 10^{-39}$	95	18 ALESINI	19	QUAX $m_{A^0} = 37.5 \mu\text{eV}$
$< 6 \times 10^{-5}$		19 FUJITA	19	ASTR $m_{A^0} < 10\text{--}21 \text{ eV}$
$< 2 \times 10^{-27}$	95	20 OUELLET	19A	ABRA $m_{A^0} = 0.31\text{--}8.3 \text{ neV}$
$< 7.3 \times 10^{-40}$	90	21 BOUTAN	18	ADMX $m_{A^0} = 17.38\text{--}17.57 \mu\text{eV}$
$< 1.8 \times 10^{-39}$	90	21 BOUTAN	18	ADMX $m_{A^0} = 21.03\text{--}23.98 \mu\text{eV}$
$< 3.4 \times 10^{-39}$	90	21 BOUTAN	18	ADMX $m_{A^0} = 29.67\text{--}29.79 \mu\text{eV}$
$< 1.4 \times 10^{-44}$	90	22 DU	18	ADMX $m_{A^0} = 2.66\text{--}2.81 \mu\text{eV}$
$< 2.87 \times 10^{-42}$	90	23 ZHONG	18	HYST $m_{A^0} = 23.15\text{--}24 \mu\text{eV}$
		24 BRANCA	17	AURG $m_{S^0} = 3.5\text{--}3.9 \text{ peV}$
$< 3 \times 10^{-42}$	90	25 BRUBAKER	17	HYST $m_{A^0} = 23.55\text{--}24.0 \mu\text{eV}$
$< 1.0 \times 10^{-29}$	95	26 CHOI	17	CASK $m_{A^0} = 24.7\text{--}29.1 \mu\text{eV}$
$< 8.6 \times 10^{-42}$	90	27 HOSKINS	16	ADMX $m_{A^0} = 3.36\text{--}3.52$ or $3.55\text{--}3.69 \mu\text{eV}$
		28 BECK	13	$m_{A^0} = 0.11 \text{ meV}$
$< 3.5 \times 10^{-43}$		29 HOSKINS	11	ADMX $m_{A^0} = 3.3\text{--}3.69 \times 10^{-6} \text{ eV}$
$< 2.9 \times 10^{-43}$	90	30 ASZTALOS	10	ADMX $m_{A^0} = 3.34\text{--}3.53 \times 10^{-6} \text{ eV}$
$< 1.9 \times 10^{-43}$	97.7	31 DUFFY	06	ADMX $m_{A^0} = 1.98\text{--}2.17 \times 10^{-6} \text{ eV}$
$< 5.5 \times 10^{-43}$	90	32 ASZTALOS	04	ADMX $m_{A^0} = 1.9\text{--}3.3 \times 10^{-6} \text{ eV}$
		33 KIM	98	THEO
$< 2 \times 10^{-41}$		34 HAGMANN	90	CNTR $m_{A^0} = (5.4\text{--}5.9)10^{-6} \text{ eV}$
$< 6.3 \times 10^{-42}$	95	35 WUENSCH	89	CNTR $m_{A^0} = (4.5\text{--}10.2)10^{-6} \text{ eV}$
$< 5.4 \times 10^{-41}$	95	35 WUENSCH	89	CNTR $m_{A^0} = (11.3\text{--}16.3)10^{-6} \text{ eV}$

- 1 ADE 21 looks for a time-variable global rotation of the CMB polarization induced by the harmonic oscillations of local axion-like dark matter and uses data from the 2012 observing season of the Keck Array, part of the BICEP program. The limits get 25% weaker for $m_{A^0} = 4.8 \times 10^{-20}\text{--}5.7 \times 10^{-19}$ eV. See their Eq. (80) and Fig. 6 for mass-dependent limits.
- 2 ALESINI 21 is an update of ALESINI 19. See their Figs. 5 and 6 for the mass-dependent limits.
- 3 BARTRAM 21A is analogous to DU 18. See their Fig. 4 for mass-dependent limits.
- 4 DEVLIN 21 use the superconducting resonant detection circuit of a cryogenic Penning trap with a single antiproton. See their Fig. 3 for mass-dependent limits.
- 5 GRAMOLIN 21 use two detection channels, each consisting of two stacked toroids to look for the axion-induced oscillating magnetic field. The quoted limit applies at $m_{A^0} = 0.02 \text{ neV}$. See their Fig. 4 for mass-dependent limits.
- 6 KWON 21 is analogous to LEE 20A. They also obtain weaker limits in the range of $m_{A^0} = 10.16\text{--}11.37 \mu\text{eV}$. See their Fig. 4 for mass-dependent limits.
- 7 MELCON 21 use a radio frequency cavity consisting of 5 sub-cavities coupled by inductive irises installed inside the CAST dipole magnet to look for higher axion masses. See their Fig. 9 for mass-dependent limits.

- ⁸SALEMI 21 is an update of OUELLET 19A. See their Fig. 4 for mass-dependent limits.
- ⁹THOMSON 21 use a resonant cavity supporting two spatially overlapping microwave modes, which is sensitive to the axion mass corresponding to the sum or difference of the two resonant frequencies. The original limit was retracted due to a sign error. See their Fig. 2 in the erratum for the corrected limits.
- ¹⁰YUAN 21 use polarimetric observations of Sgr A* taken by the Event Horizon Telescope to search for periodic oscillation of the polarization induced by axion dark matter, assuming a solitonic core near the Galactic center. They obtained limits in the range of $G_{A\gamma\gamma} = 8 \times 10^{-13}$ – 3×10^{-11} GeV $^{-1}$.
- ¹¹BRAINE 20 is analogous to DU 18. See Fig. 4 for their mass-dependent limits.
- ¹²CRISOSTO 20 used a resonant LC circuit to look for lighter axion dark matter. They obtained a similar, slightly weaker limit for $m_{A^0} = 174.98$ – 175.19 and 177.34 – 177.38 neV. See their Fig. 4 for mass-dependent limits.
- ¹³DARLING 20A use VLA data to look for radio-frequency radiation converted from axion dark matter in the magnetosphere of the Galactic Center magnetar PSR J1745-2900. They extended the results of DARLING 20, which used only data with the highest angular resolution, by adding sub-optimal data. They use $\rho_A = 6.5 \times 10^4$ GeV/cm 3 in the vicinity of the magnetar. See their Fig. 2 for mass-dependent limits.
- ¹⁴FOSTER 20 look for radio-frequency radiation converted from axion dark matter in the magnetic field around neutron stars. They use the observed data of isolated local neutron stars and in the Galactic center. The quoted limit applies to $m_{A^0} \approx 7 \mu$ eV. See their Fig. 2 for mass-dependent limits.
- ¹⁵JEONG 20 is analogous to LEE 20A, and they use a double-cell cavity to look for axions with mass $> 10 \mu$ eV. See their Fig. 5 for mass-dependent limits.
- ¹⁶KENNEDY 20 is analogous to BRANCA 17, and they compare the frequency ratios of the Si cavity measured by a Sr optical lattice clock and by a H maser. Assuming the local density of moduli dark matter, $\rho_S = 0.3$ GeV/cm 3 , they obtain a limit $G_{S\gamma\gamma} < 5.8 \times 10^{-24}$ GeV $^{-1}$ at $m_{S^0} = 2 \times 10^{-19}$ eV. See their Fig. 2 for mass-dependent limits as well as limits on the modulus coupling to electrons.
- ¹⁷LEE 20A used a microwave cavity detector at the IBS/CAPP to search for dark matter axions. See Fig. 3 for the mass-dependent limits.
- ¹⁸ALESINI 19 used a superconducting resonant cavity made of NbTi to increase the quality factor. The limit applies to a mass range of 0.2 neV around $m_{A^0} = 37.5 \mu$ eV.
- ¹⁹FUJITA 19 look for photon birefringence under the oscillating axion background using the polarimetric imaging observation of a protoplanetary disk, AB Aur. See their Fig. 2 for a more conservative limit taking account of possible systematic effects.
- ²⁰OUELLET 19A look for the axion-induced oscillating magnetic field generated by a toroidal magnetic field. The quoted limit applies at $m_{A^0} = 8$ neV. See their Fig. 3 for the mass-dependent limits.
- ²¹BOUTAN 18 use a small high frequency cavity installed above the main ADMX cavity to look for heavier axion dark matter. See their Fig. 4 for mass-dependent limits.
- ²²DU 18 is analogous to DUFFY 06. They upgraded a dilution refrigerator to reduce the system noise. The quoted limit is around $m_{A^0} = 2.69 \mu$ eV for the boosted Maxwellian axion line shape. See Fig. 4 for their mass-dependent limits.
- ²³ZHONG 18 is analogous to BRUBAKER 17. The quoted limit applies at $m_{A^0} = 23.76 \mu$ eV. See Fig. 4 for their mass-dependent limits.
- ²⁴BRANCA 17 look for modulations of the fine-structure constant and the electron mass due to moduli dark matter by using the cryogenic resonant-mass AURIGA detector. The limit on the assumed dilatonic coupling implies $G_{S\gamma\gamma} < 1.5 \times 10^{-24}$ GeV $^{-1}$ for the scalar to two-photon coupling. See Fig. 5 for the mass-dependent limits.
- ²⁵BRUBAKER 17 used a microwave cavity detector at the Yale Wright Laboratory to search for dark matter axions. See Fig. 3 for the mass-dependent limits.
- ²⁶CHOI 17 used a microwave cavity detector with toroidal geometry. See Fig. 4 for their mass-dependent limits.
- ²⁷HOSKINS 16 is analogous to DUFFY 06. See Fig. 12 for mass-dependent limits in terms of the local dark matter density.
- ²⁸BECK 13 argues that dark-matter axions passing through Earth may generate a small observable signal in resonant S/N/S Josephson junctions. A measurement by HOFFMANN 04 [Physical Review **B70** 180503 (2004)] is interpreted in terms of subdominant dark matter axions with $m_{A^0} = 0.11$ meV.
- ²⁹HOSKINS 11 is analogous to DUFFY 06. See Fig. 4 for the mass-dependent limit in terms of the local density.
- ³⁰ASZTALOS 10 used the upgraded detector of ASZTALOS 04 to search for halo axions. See their Fig. 5 for the m_{A^0} dependence of the limit.
- ³¹DUFFY 06 used the upgraded detector of ASZTALOS 04, while assuming a smaller velocity dispersion than the isothermal model as in Eq. (8) of their paper. See Fig. 10 of their paper on the axion mass dependence of the limit.
- ³²ASZTALOS 04 looked for a conversion of halo axions to microwave photons in magnetic field. At 90% CL, the KSVZ axion cannot have a local halo density more than 0.45 GeV/cm 3 in the quoted mass range. See Fig. 7 of their paper on the axion mass dependence of the limit.
- ³³KIM 98 calculated the axion-to-photon couplings for various axion models and compared them to the HAGMANN 90 bounds. This analysis demonstrates a strong model dependence of $G_{A\gamma\gamma}$ and hence the bound from relic axion search.
- ³⁴HAGMANN 90 experiment is based on the proposal of SIKIVIE 83.
- ³⁵WUENSCH 89 looks for condensed axions near the earth that could be converted to photons in the presence of an intense electromagnetic field via the Primakoff effect, following the proposal of SIKIVIE 83. The theoretical prediction with $[G_{A\gamma\gamma}/m_{A^0}]^2 = 2 \times 10^{-14}$ MeV $^{-4}$ (the three generation DFSZ model) and $\rho_A = 300$ MeV/cm 3 that makes up galactic halos gives $(G_{A\gamma\gamma}/m_{A^0})^2 \rho_A = 4 \times 10^{-44}$. Note that our definition of $G_{A\gamma\gamma}$ is $(1/4\pi)$ smaller than that of WUENSCH 89.

stated otherwise, i.e., many of these bounds apply to low-mass axion-like particles (ALPs), not to QCD axions.

VALUE (GeV $^{-1}$)	CL%	DOCUMENT ID	TECN	COMMENT
••• We do not use the following data for averages, fits, limits, etc. •••				
$<9.2 \times 10^{-11}$	95	1 BASU	21 ASTR	$m_{A^0} = 3.6 \times 10^{-21}$ eV
$<1.8 \times 10^{-10}$	95	2 BI	21 ASTR	$m_{A^0} = 2-6 \times 10^{-7}$ eV
$<1.6 \times 10^{-10}$	95	3 DOLAN	21A ASTR	$m_{A^0} = 1-570$ keV
$<5 \times 10^{-11}$	95	4 GUO	21 ASTR	$m_{A^0} = 8-23$ neV
$<1.2 \times 10^{-4}$	95	5 HOMMA	21 LASR	$m_{A^0} = 0.4-600$ meV
$<1.2 \times 10^{-11}$	95	6 LI	21B ASTR	$m_{A^0} = 0.5-500$ neV
		7 LLOYD	21 ASTR	Magnetars
$<1 \times 10^{-13}$	95	8 REGIS	21 ASTR	$m_{A^0} = 2.7-5.3$ eV
$<1.8 \times 10^{-11}$	95	9 XIAO	21 ASTR	$m_{A^0} < 3.5 \times 10^{-11}$ eV
$<7 \times 10^{-4}$	95	10 ABUDINEN	20 BEL2	$m_{A^0} = 0.2-1$ GeV
$<2 \times 10^{-4}$	90	11 BANERJEE	20A NA64	$m_{A^0} < 55$ MeV
$<1.0 \times 10^{-11}$	95	12 BUEHLER	20 ASTR	$m_{A^0} < 3$ neV
$<5 \times 10^{-10}$		13 CALORE	20 ASTR	$m_{A^0} \lesssim 10^{-11}$ eV
		14 CARENZA	20 ASTR	Globular clusters
$2-4 \times 10^{-10}$	95	15 DENT	20A ASTR	Solar axions
		16 DEPTA	20 COSM	Axion-like particles
$<3.6 \times 10^{-12}$	95	17 DESSERT	20A ASTR	$m_{A^0} < 5 \times 10^{-11}$ eV
		18 ESTEBAN	20 ANIT	Axion-like particles
$4-6 \times 10^{-10}$	90	19 GAO	20 ASTR	Solar axions
$<2.8 \times 10^{-11}$	95	20 KOROSCHKIN	20 ASTR	$m_{A^0} = 25$ eV
none 6.0×10^{-9} – 1.3×10^{-5}		21 LUCENTE	20A ASTR	$m_{A^0} < 270$ MeV
$<2.6 \times 10^{-11}$	95	22 MEYER	20 FLAT	$m_{A^0} < 3 \times 10^{-10}$ eV
$<8.4 \times 10^{-8}$	99	23 YAMAMOTO	20 COSM	$m_{A^0} < 4 \times 10^{-6}$ eV
$<1 \times 10^{-3}$	95	24 ALONI	19 PRMZ	$m_{A^0} = 0.16$ GeV
$<1.4 \times 10^{-14}$	95	25 CAPUTO	19 ASTR	$m_{A^0} = 5 \times 10^{-24}$ eV
$<9.6 \times 10^{-14}$	95	26 FEDDERKE	19 CMB	$m_{A^0} = 10^{-22}$ eV
$<7 \times 10^{-13}$	95	27 IVANOV	19 ASTR	$m_{A^0} = 5 \times 10^{-23}$ eV
$<4 \times 10^{-11}$	95	28 LIANG	19 ASTR	$m_{A^0} = 1.2 \times 10^{-7}$ eV
		29 FORTIN	18 ASTR	Axion-like particles
$<5.0 \times 10^{-3}$	90	30 YAMAJI	18 LSW	$m_{A^0} = 46-1020$ eV
$<1 \times 10^{-11}$	99.9	31 ZHANG	18 ASTR	$m_{A^0} = 0.6-4$ neV
		32 ADE	17 CMB	Axion-like particles
$<6.6 \times 10^{-11}$	95	33 ANASTASSO...	17 CAST	$m_{A^0} < 0.02$ eV
		34 DOLAN	17 RVUE	Axion-like particles
$<2.51 \times 10^{-4}$	95	35 INADA	17 LSW	$m_{A^0} < 0.1$ eV
$>1.5 \times 10^{-11}$	95	36 KOHRI	17 ASTR	$m_{A^0} = 0.7-50$ neV
$<2.6 \times 10^{-12}$	95	37 MARSH	17 ASTR	$m_{A^0} \leq 10^{-13}$ eV
$<6 \times 10^{-13}$	95	38 TIWARI	17 COSM	$m_{A^0} \leq 10^{-15}$ eV
$<5 \times 10^{-12}$	95	39 AJELLO	16 ASTR	$m_{A^0} = 0.5-5$ meV
$<1.2 \times 10^{-7}$	95	40 DELLA-VALLE	16 LASR	$m_{A^0} = 1.3$ neV
$<7.2 \times 10^{-8}$	95	41 DELLA-VALLE	16 LASR	$m_{A^0} < 0.5$ meV
$<8 \times 10^{-4}$		42 JAECKEL	16 ALPS	$m_{A^0} = 0.1-100$ GeV
$<6 \times 10^{-21}$		43 LEEFER	16	$m_{S^0} < 10^{-18}$ eV
		44 ANASTASSO...	15 CAST	Chameleons
$<1.47 \times 10^{-10}$	95	45 ARIK	15 CAST	$m_{A^0} = 0.39-0.42$ eV
$<3.5 \times 10^{-8}$	95	46 BALLOU	15 LSW	$m_{A^0} < 2 \times 10^{-4}$ eV
		47 BRAX	15 ASTR	$m_{S^0} < 4 \times 10^{-12}$ eV
$<5.42 \times 10^{-4}$	95	48 HASEBE	15 LASR	$m_{A^0} = 0.15$ eV
		49 MILLEA	15 COSM	Axion-like particles
		50 VANTILBURG	15	Dilaton-like dark matter
$<4.1 \times 10^{-10}$	99.7	51 VINYOLES	15 ASTR	$m_{A^0} = 0.6-185$ eV
$<3.3 \times 10^{-10}$	95	52 ARIK	14 CAST	$m_{A^0} = 0.64-1.17$ eV
$<6.6 \times 10^{-11}$	95	53 AYALA	14 ASTR	Globular clusters
$<1.4 \times 10^{-7}$	95	54 DELLA-VALLE	14 LASR	$m_{A^0} = 1$ meV
		55 EJLLI	14 COSM	$m_{A^0} = 2.66-48.8 \mu$ eV
$<8 \times 10^{-8}$	95	56 PUGNAT	14 LSW	$m_{A^0} < 0.3$ meV
$<1 \times 10^{-11}$	95	57 REESMAN	14 ASTR	$m_{A^0} < 1 \times 10^{-10}$ eV
$<2.1 \times 10^{-11}$	95	58 ABRAMOWSKI13A	IACT	$m_{A^0} = 15-60$ neV
$<2.15 \times 10^{-9}$	95	59 ARMENGAUD	13 EDEL	$m_{A^0} < 200$ eV
$<4.5 \times 10^{-8}$	95	60 BETZ	13 LSW	$m_{A^0} = 7.2 \times 10^{-6}$ eV
$<8 \times 10^{-11}$	95	61 FRIEDLAND	13 ASTR	Red giants
$>2 \times 10^{-11}$	95	62 MEYER	13 ASTR	$m_{A^0} < 1 \times 10^{-7}$ eV
$<8.3 \times 10^{-12}$	95	63 WOUTERS	13 ASTR	$m_{A^0} < 7 \times 10^{-12}$ eV
		64 CADAMURO	12 COSM	Axion-like particles
$<2.5 \times 10^{-13}$	95	65 PAYEZ	12 ASTR	$m_{A^0} < 4.2 \times 10^{-14}$ eV
$<2.3 \times 10^{-10}$	95	66 ARIK	11 CAST	$m_{A^0} = 0.39-0.64$ eV
$<6.5 \times 10^{-8}$	95	67 EHRET	10 ALPS	$m_{A^0} < 0.7$ meV
$<2.4 \times 10^{-9}$	95	68 AHMED	09A CDMS	$m_{A^0} < 100$ eV
$<1.2-2.8 \times 10^{-10}$	95	69 ARIK	09 CAST	$m_{A^0} = 0.02-0.39$ eV
		70 CHOU	09	Chameleons
$<7 \times 10^{-10}$	95	71 GONDOLO	09 ASTR	$m_{A^0} < \text{few keV}$

Invisible A^0 (Axion) Limits from Photon Coupling

Limits are for the modulus of the axion-two-photon coupling $G_{A\gamma\gamma}$ defined by $L = -G_{A\gamma\gamma} \phi_A \mathbf{E} \cdot \mathbf{B}$. For scalars S^0 the limit is on the coupling constant in $L = G_{S\gamma\gamma} \phi_S (\mathbf{E}^2 - \mathbf{B}^2)$. The relation between $G_{A\gamma\gamma}$ and m_{A^0} is not used unless

Gauge & Higgs Boson Particle Listings

Axions (A^0) and Other Very Light Bosons

$<1.3 \times 10^{-6}$	95	72 AFANASEV	08	$m_{S^0} < 1 \text{ MeV}$
$<3.5 \times 10^{-7}$	99.7	73 CHOU	08	$m_{A^0} < 0.5 \text{ MeV}$
$<1.1 \times 10^{-6}$	99.7	74 FOUICHE	08	$m_{A^0} < 1 \text{ MeV}$
$<5.6\text{--}13.4 \times 10^{-10}$	95	75 INOUE	08	$m_{A^0} = 0.84\text{--}1.00 \text{ eV}$
$<5 \times 10^{-7}$		76 ZAVATTINI	08	$m_{A^0} < 1 \text{ MeV}$
$<8.8 \times 10^{-11}$	95	77 ANDRIAMONJON	CAST	$m_{A^0} < 0.02 \text{ eV}$
$<1.25 \times 10^{-6}$	95	78 ROBILLIARD	07	$m_{A^0} < 1 \text{ MeV}$
$2\text{--}5 \times 10^{-6}$		79 ZAVATTINI	06	$m_{A^0} = 1\text{--}1.5 \text{ MeV}$
$<1.1 \times 10^{-9}$	95	80 INOUE	02	$m_{A^0} = 0.05\text{--}0.27 \text{ eV}$
$<2.78 \times 10^{-9}$	95	81 MORALES	02B	$m_{A^0} < 1 \text{ keV}$
$<1.7 \times 10^{-9}$	90	82 BERNABEI	01B	$m_{A^0} < 100 \text{ eV}$
$<1.5 \times 10^{-4}$	90	83 ASTIER	00B	NOMD $m_{A^0} < 40 \text{ eV}$
		84 MASSO	00	THEO induced γ coupling
$<2.7 \times 10^{-9}$	95	85 AVIGNONE	98	SLAX $m_{A^0} < 1 \text{ keV}$
$<6.0 \times 10^{-10}$	95	86 MORIYAMA	98	$m_{A^0} < 0.03 \text{ eV}$
$<3.6 \times 10^{-7}$	95	87 CAMERON	93	$m_{A^0} < 10^{-3} \text{ eV}$, optical rotation
$<6.7 \times 10^{-7}$	95	88 CAMERON	93	$m_{A^0} < 10^{-3} \text{ eV}$, photon regeneration
$<3.6 \times 10^{-9}$	99.7	89 LAZARUS	92	$m_{A^0} < 0.03 \text{ eV}$
$<7.7 \times 10^{-9}$	99.7	89 LAZARUS	92	$m_{A^0} = 0.03\text{--}0.11 \text{ eV}$
$<7.7 \times 10^{-7}$	99	90 RUOSO	92	$m_{A^0} < 10^{-3} \text{ eV}$
$<2.5 \times 10^{-6}$		91 SEMERTZIDIS	90	$m_{A^0} < 7 \times 10^{-4} \text{ eV}$

- ¹ BASU 21 searched for birefringence induced by axion dark matter using multiple images of the polarized source in the strongly gravitationally lensed system CLASS B1152+199. They assume the axion makes up all dark matter, and used the axion density in the emitting region, $\rho_A = 20 \text{ GeV/cm}^3$. Limits between $9.2 \times 10^{-11}\text{--}7.7 \times 10^{-8} \text{ GeV}^{-1}$ are obtained for $m_{A^0} = 3.6 \times 10^{-21}\text{--}4.6 \times 10^{-18} \text{ eV}$. See their Fig. 2 for mass-dependent limits.
- ² Bl 21 look for the gamma-ray spectral distortions induced by axion-photon oscillations in the presence of the Galactic magnetic field, using the measurements of sub-TeV gamma-rays from the Crab Nebula by the Tibet AS γ and HAWC experiments, together with MAGIC and HEGRA gamma-ray data. See their Fig. 3 for mass-dependent limits.
- ³ DOLAN 21A study the effect of axion production on the evolution of asymptotic giant branch stars, and use the white-dwarf initial-final mass relation to set the limits. See their Fig. 1 for mass-dependent limits.
- ⁴ GUO 21 is analogous to AJELLO 16, and use the Fermi-LAT and H.E.S.S. II measurements of PG 1553+113 and PKS 2155-304. See their Fig. 6 for mass-dependent limits.
- ⁵ HOMMA 21 look for the production of axion resonance states and their subsequent stimulated decays by combining linearly polarized creation laser pulses and circularly polarized inducing laser pulses. The quoted limit is at $m_{A^0} \approx 0.178 \text{ eV}$. See their Fig. 14 for mass-dependent limits.
- ⁶ Li 21B is analogous to AJELLO 16, and use the spectra of the blazar Mrk 421 measured by ARGON-BJ and Fermi-LAT. They consider ALP-photon mixing in the magnetic fields of both the blazar jet and the Galaxy. The quoted limit applies to $m_{A^0} \approx 1 \times 10^{-9} \text{ eV}$. See their Fig. 5 for mass-dependent limits.
- ⁷ LLOYD 21 is analogous to FORTIN 18, and set limits on the product of the axion couplings to photons and nucleons as $g_{ANN} G_{A\gamma\gamma} \lesssim 4.6 \times 10^{-19} \text{ GeV}^{-1}$ for $m_{A^0} \lesssim 10^{-5} \text{ eV}$ by using the quiescent soft gamma-ray flux upper limits in five magnetars. We use $g_{ANN} = G_{AN} 2m_N$ to translate their limits. See their Table II and Fig. 3 for the limits.
- ⁸ REGIS 21 look for monochromatic photons from axion decay, using the MUSE spectroscopic data on the Leo T dwarf spheroidal galaxy. They assume that axions make up all of dark matter and use the integrated dark matter density along the line of sight determined by observations.
- ⁹ XIAO 21 use X-ray data from Betelgeuse to look for signals from axions produced in the stellar core that were converted to X-rays by the Galactic magnetic field. See their Fig. 1 for the mass-dependent limit.
- ¹⁰ ABDUNINEN 20 look for the process $e^+e^- \rightarrow \gamma A^0 (A^0 \rightarrow \gamma\gamma)$ and set upper limits of around 10^{-3} over the mass range. The quoted limit is at $m_{A^0} = 0.3 \text{ GeV}$. See their Fig. 5 for mass dependent limits.
- ¹¹ BANERJEE 20A look for axions produced from high-energy bremsstrahlung photons through the Primakoff effect with the electric field of the target nuclei. They exclude $G_{A\gamma\gamma} = 2 \times 10^{-4}\text{--}5 \times 10^{-2} \text{ GeV}^{-1}$ for $m_{A^0} < 55 \text{ MeV}$. See their Fig. 5 for mass-dependent limits.
- ¹² BUEHLER 20 look for the γ -ray transparency due to axion-photon oscillations using high-energy photon events from 79 sources in the Second Fermi-LAT Catalog of High-Energy Sources. The quoted limit is for the intergalactic magnetic field strength and coherence length of $B = 1 \text{ nG}$ and $s = 1 \text{ Mpc}$. See their Figs. 4 and 5 for mass-dependent limits and for different magnetic-field parameters.
- ¹³ CALORE 20 use the isotropic diffuse γ -ray background measured by the Fermi-LAT to constrain the γ -ray flux convected in the Galactic magnetic field from axions produced from past core-collapse supernovae. They also derive a limit on a heavier axion with $m_{A^0} \gtrsim \text{keV}$ decaying into two photons of $G_{A\gamma\gamma} \lesssim 5 \times 10^{-11} \text{ GeV}^{-1}$ for $m_{A^0} = 5 \text{ keV}$. See their Figs. 5 and 7 for the limits as well as limits in the presence of axion-nucleon couplings.
- ¹⁴ CARENZA 20 extend the globular cluster bound of AYALA 14 to heavier masses ($m_{A^0} \leq$ a few 100 keV) by taking account of the coalescence process $\gamma + \gamma \rightarrow A^0$ as well as the decay of the ALP inside the stellar core. See their Fig. 4 for mass-dependent limits.
- ¹⁵ DENT 20A is analogous to GAO 20. The quoted limit is from their arXiv:2006.15118v3 (v2 is their published version), using the relativistic Hartree-Fock form factor. The limit is up to two times weaker than the published one. See Fig. 4 in their arXiv version 3 for the correlation between $G_{A\gamma\gamma}$ and g_{Aee} corresponding to the excess reported in APRILE 20.
- ¹⁶ DEPTA 20 correct the underestimated D abundance in MILLEA 15, and derive robust cosmological bounds by allowing the reheating temperature, N_{eff} , and neutrino chemical potential to vary. See their Fig. 6 for mass-dependent limits.

- ¹⁷ DESSERT 20A use the NuSTAR data of the Quintuplet and Westerlund 1 super star clusters to look for X-rays converted in the Galactic magnetic field from the axions produced in stellar cores. See their Fig. 3 for the mass-dependent limits.
- ¹⁸ ESTEBAN 20 show that the two anomalous ANITA events can be explained by the reflected radio pulses that are resonantly produced in the ionosphere via axion-photon conversion for $m_{A^0} \lesssim 1 \times 10^{-7} \text{ eV}$, if an axion clump passes the Earth about once a month. See their Fig. 5 for the region consistent with this interpretation for different values of the axion density inside the clumps.
- ¹⁹ GAO 20 correct the limit of APRILE 20 by including inverse Primakoff scattering in the XENON1T detector. The quoted limit is from their arXiv:2006.14598v4 (v3 is their published version), taking account of the atomic form factor of Xe as pointed out in ABE 20. The limit is weaker by a factor of 1.5-2 than the published one. See Fig. 3 in their arXiv version 4 for correlation between $G_{A\gamma\gamma}$ and g_{Aee} corresponding to the excess reported in APRILE 20.
- ²⁰ KOROCHKIN 20 assume the axion makes up all dark matter, and look for a dip in the observed gamma-ray spectrum of the blazar 1ES 1218+304 by Fermi/LAT and VERITAS due to the extragalactic background light produced by the axion decay. Their analysis favors nonzero axion-induced absorption with $G_{A\gamma\gamma} = 3 \times 10^{-11}\text{--}2 \times 10^{-10} \text{ GeV}^{-1}$ over a range of $m_{A^0} = 2\text{--}18 \text{ eV}$. See their Fig. 1 for mass-dependent limits between $0.25 < m_{A^0} < 25 \text{ eV}$.
- ²¹ LUCENTE 20A study the SN 1987A energy-loss argument on the axion-like particle production. In addition to the Primakoff process, they take account of photon coalescence as well as gravitational trapping that become relevant at $m_{A^0} > 100 \text{ MeV}$. See their Fig. 12 for the mass-dependent limit.
- ²² MEYER 20 look for prompt γ -rays converted in the Galactic magnetic fields from axions produced via the Primakoff process in a sample of 20 extragalactic core-collapse supernovae. The limits assume a progenitor mass of 10 times the solar mass and certain models for the optical emission and the galactic magnetic field. See their Figs. 2 and 6 in the erratum for mass- and model-dependent limits.
- ²³ YAMAMOTO 20 look for X-ray photons converted by the Earth's magnetic field from the axions produced by the two-body decay of dark matter, and set the limits by using the Suzaku data. The quoted limit is for the monochromatic X-ray line from the galactic dark matter with lifetime $\tau = 4.32 \times 10^{17} \text{ sec}$. They also derive limits on the continuum spectrum from the extragalactic component. See their Fig. 7 for the limits.
- ²⁴ ALONI 19 used the data collected by the PRIMEX experiment to derive a limit based on a data-driven method. See their Fig. 2 for mass-dependent limits.
- ²⁵ CAPUTO 19 look for an oscillating variation of the polarization angle of the pulsar J0437-4715, where they assume the local axion energy density $\rho_A = 0.3 \text{ GeV/cm}^3$. See their Fig. 2 for mass-dependent limits for $5 \times 10^{-24} \text{ eV} \leq m_{A^0} \leq 2 \times 10^{-19} \text{ eV}$.
- ²⁶ FEDDERKE 19 look for a uniform reduction of the CMB polarization at large scales, which is induced by the oscillating axion background during CMB decoupling. The quoted limit is based on the assumption that axions make up all of the dark matter. See their Fig. 3 for mass-dependent limits for $m_{A^0} = 10^{-22}\text{--}10^{-19} \text{ eV}$.
- ²⁷ IVANOV 19 look for the axion-induced periodic changes in the polarization angle of parsec-scale jets in active galactic nuclei observed by the MOJAVE program, where they use the axion energy density $\rho_A = 20 \text{ GeV/cm}^3$. See their Fig. 6 for mass-dependent limits for $5 \times 10^{-23} \text{ eV} \leq m_{A^0} \leq 1.2 \times 10^{-21} \text{ eV}$.
- ²⁸ LIANG 19 look for spectral irregularities in the spectrum of 10 bright H.E.S.S. sources in the Galactic plane, assuming photon-ALP mixing in the Galactic magnetic fields. See their Fig. 2 for mass-dependent limits with different Galactic magnetic field models.
- ²⁹ FORTIN 18 studied the conversion of axion-like particles produced in the core of a magnetar to hard X-rays in the magnetosphere. See their Fig. 5 for mass-dependent limits with different values of the magnetar core temperature.
- ³⁰ YAMAJI 18 search for axions with an x-ray LSW at Spring-8, using the Laue-case conversion in a silicon crystal. They also obtain $G_{A\gamma\gamma} < 4.2 \times 10^{-3} \text{ GeV}^{-1}$ for $m_{A^0} < 10 \text{ eV}$. See their Fig. 5 for mass-dependent limits.
- ³¹ ZHANG 18 look for spectral irregularities in the spectrum of PKS 2155-304 measured by Fermi LAT, assuming photon-ALP mixing in the intercluster and Galactic magnetic fields. See their Figs. 2 and 3 for mass-dependent limits with different values of the intercluster magnetic field parameters.
- ³² ADE 17 look for cosmic birefringence from axion-like particles using CMB polarization data taken by the BICEP2 and Keck Array experiments. They set a limit $G_{A\gamma\gamma} H_I < 7.2 \times 10^{-2}$ at 95 %CL for $m_{A^0} < 10^{-28} \text{ eV}$, where H_I is the Hubble parameter during inflation.
- ³³ ANASTASSOPOULOS 17 looked for solar axions by the CAST axion helioscope in the vacuum phase, and supersedes ANDRIAMONJON 07.
- ³⁴ DOLAN 17 update existing limits on $G_{A\gamma\gamma}$ for axion-like particles. The limits from the proton beam dump experiments in their Fig. 2 contained an error, and the corrected version is shown in Fig. 1 of DOLAN 21.
- ³⁵ INADA 17 search for axions with an x-ray LSW at Spring-8. See their Fig. 4 for mass-dependent limits.
- ³⁶ KOHRI 17 attributed to axion-photon oscillations the excess of cosmic infrared background observed by the CIBER experiment. See their Fig. 5 for the region preferred by their scenario.
- ³⁷ MARSH 17 is similar to WOUTERS 13, using Chandra observations of M87. See their Fig. 6 for mass-dependent limits.
- ³⁸ TIWARI 17 use observed limits of the cosmic distance-duality relation to constrain the photon-ALP mixing based on 3D simulations of the magnetic field configuration. The quoted value is for the averaged magnetic field of 1 nG with a coherent length of 1 Mpc. See their Fig. 5 for mass-dependent limits.
- ³⁹ AJELLO 16 look for irregularities in the energy spectrum of the NGC1275 measured by Fermi LAT, assuming photon-ALP mixing in the intra-cluster and Galactic magnetic fields. See their Fig. 2 for mass-dependent limits.
- ⁴⁰ DELLA-VALLE 16 look for the birefringence induced by axion-like particles. See their Fig. 14 for mass-dependent limits.
- ⁴¹ DELLA-VALLE 16 look for the dichroism induced by axion-like particles. See their Fig. 14 for mass-dependent limits.
- ⁴² JAECKEL 16 use the LEP data of $Z \rightarrow 2\gamma$ and $Z \rightarrow 3\gamma$ to constrain the ALP production via $e^+e^- \rightarrow Z \rightarrow A^0 \gamma (A^0 \rightarrow \gamma\gamma)$, assuming the ALP coupling with two hypercharge bosons. See their Fig. 4 for mass-dependent limits.
- ⁴³ LEEFER 16 derived limits by using radio-frequency spectroscopy of dysprosium and atomic clock measurements. See their Fig. 1 for mass-dependent limits as well as limits on Yukawa-type couplings of the scalar to the electron and nucleons.

Gauge & Higgs Boson Particle Listings

Axions (A^0) and Other Very Light Bosons

- 44 ANASTASSOPOULOS 15 search for solar chameleons with CAST and derived limits on the chameleon coupling to photons and matter. See their Fig. 12 for the exclusion region.
- 45 ARIK 15 is analogous to ARIK 09, and search for solar axions for m_{A^0} around 0.2 and 0.4 eV. See their Figs. 1 and 3 for the mass-dependent limits.
- 46 Based on OSQAR photon regeneration experiment. See their Fig. 6 for mass-dependent limits on scalar and pseudoscalar bosons.
- 47 BRAX 15 derived limits on conformal and disformal couplings of a scalar to photons by searching for a chaotic absorption pattern in the X-ray and UV bands of the Hydra A galaxy cluster and a BL lac object, respectively. See their Fig. 8.
- 48 HASEBE 15 look for an axion via a four-wave mixing process at quasi-parallel colliding laser beams. They also derived limits on a scalar coupling to photons $G_{S\gamma\gamma} < 2.62 \times 10^{-4} \text{ GeV}^{-1}$ at $m_{S^0} = 0.15 \text{ eV}$. See their Figs. 11 and 12 for mass-dependent limits.
- 49 MILLEA 15 is similar to CADAMURO 12, including the Planck data and the latest inferences of primordial deuterium abundance. See their Fig. 3 for mass-dependent limits.
- 50 VANTILBURG 15 look for harmonic variations in the dysprosium transition frequency data, induced by coherent oscillations of the fine-structure constant due to dilaton-like dark matter, and set the limits, $G_{S\gamma\gamma} < 6 \times 10^{-27} \text{ GeV}^{-1}$ at $m_{S^0} = 6 \times 10^{-23} \text{ eV}$. See their Fig. 4 for mass-dependent limits between $1 \times 10^{-24} < m_{S^0} < 1 \times 10^{-15} \text{ eV}$.
- 51 VINYOLES 15 performed a global fit analysis based on helioseismology and solar neutrino observations. See their Fig. 9.
- 52 ARIK 14 is similar to ARIK 11. See their Fig. 2 for mass-dependent limits.
- 53 AYALA 14 derived the limit from the helium-burning lifetime of horizontal-branch stars based on number counts in globular clusters.
- 54 DELLA-VALLE 14 use the new PVLAS apparatus to set a limit on vacuum magnetic birefringence induced by axion-like particles. See their Fig. 6 for the mass-dependent limits.
- 55 EJLLI 14 set limits on a product of primordial magnetic field and the axion mass using CMB distortion induced by resonant axion production from CMB photons. See their Fig. 1 for limits applying specifically to the DFSZ and KSVZ axion models.
- 56 PUGNAT 14 is analogous to EHRET 10. See their Fig. 5 for mass-dependent limits on scalar and pseudoscalar bosons.
- 57 REESMAN 14 derive limits by requiring effects of axion-photon interconversion on gamma-ray spectra from distant blazars to be no larger than errors in the best-fit optical depth based on a certain extragalactic background light model. See their Fig. 5 for mass-dependent limits.
- 58 ABRAMOWSKI 13a look for irregularities in the energy spectrum of the BL Lac object PKS 2155-304 measured by H.E.S.S. The limits depend on assumed magnetic field around the source. See their Fig. 7 for mass-dependent limits.
- 59 ARMENGAUD 13 is analogous to AVIGNONE 98. See Fig. 6 for the limit.
- 60 BETZ 13 performed a microwave-based light shining through the wall experiment. See their Fig. 13 for mass-dependent limits.
- 61 FRIEDLAND 13 derived the limit by considering blue-loop suppression of the evolution of red giants with 7-12 solar masses.
- 62 MEYER 13 attributed to axion-photon oscillations the observed excess of very high-energy γ -rays with respect to predictions based on extragalactic background light models. See their Fig. 4 for mass-dependent lower limits for various magnetic field configurations.
- 63 WOUTERS 13 look for irregularities in the X-ray spectrum of the Hydra cluster observed by Chandra. See their Fig. 4 for mass-dependent limits.
- 64 CADAMURO 12 derived cosmological limits on $G_{A\gamma\gamma}$ for axion-like particles. See their Fig. 1 for mass-dependent limits.
- 65 PAYEZ 12 derive limits from polarization measurements of quasar light (see their Fig. 3). The limits depend on assumed magnetic field strength in galaxy clusters. The limits depend on assumed magnetic field and electron density in the local galaxy supercluster.
- 66 ARIK 11 search for solar axions using ^3He buffer gas in CAST, continuing from the ^4He version of ARIK 09. See Fig. 2 for the exact mass-dependent limits.
- 67 ALPS is a photon regeneration experiment. See their Fig. 4 for mass-dependent limits on scalar and pseudoscalar bosons.
- 68 AHMED 09a is analogous to AVIGNONE 98.
- 69 ARIK 09 is the ^4He filling version of the CAST axion helioscope in analogy to INOUE 02 and INOUE 08. See their Fig. 7 for mass-dependent limits.
- 70 CHOU 09 use the GammeV apparatus in the afterglow mode to search for chameleons, (pseudo)scalar bosons with a mass depending on the environment. For pseudoscalars they exclude at 3σ the range $2.6 \times 10^{-7} \text{ GeV}^{-1} < G_{A\gamma\gamma} < 4.2 \times 10^{-6} \text{ GeV}^{-1}$ for vacuum m_{A^0} roughly below 6 meV for density scaling index exceeding 0.8.
- 71 GONDOLQ 09 use the all-flavor measured solar neutrino flux to constrain solar interior temperature and thus energy losses.
- 72 LIPSS photon regeneration experiment, assuming scalar particle s^0 . See Fig. 4 for mass-dependent limits.
- 73 CHOU 08 perform a variable-baseline photon regeneration experiment. See their Fig. 3 for mass-dependent limits. Excludes the PVLAS result of ZAVATTINI 06.
- 74 FOCHE 08 is an update of ROBILLIARD 07. See their Fig. 12 for mass-dependent limits.
- 75 INOUE 08 is an extension of INOUE 02 to larger axion masses, using the Tokyo axion helioscope. See their Fig. 4 for mass-dependent limits.
- 76 ZAVATTINI 08 is an upgrade of ZAVATTINI 06, see their Fig. 8 for mass-dependent limits. They now exclude the parameter range where ZAVATTINI 06 had seen a positive signature.
- 77 ANDRIAMONJE 07 looked for Primakoff conversion of solar axions in 9T superconducting magnet into X-rays. Supersedes ZIOUTAS 05.
- 78 ROBILLIARD 07 perform a photon regeneration experiment with a pulsed laser and pulsed magnetic field. See their Fig. 4 for mass-dependent limits. Excludes the PVLAS result of ZAVATTINI 06 with a CL exceeding 99.9%.
- 79 ZAVATTINI 06 propagate a laser beam in a magnetic field and observe dichroism and birefringence effects that could be attributed to an axion-like particle. This result is now excluded by ROBILLIARD 07, ZAVATTINI 08, and CHOU 08.
- 80 INOUE 02 looked for Primakoff conversion of solar axions in 4T superconducting magnet into X-ray.
- 81 MORALES 02b looked for the coherent conversion of solar axions to photons via the Primakoff effect in Germanium detector.
- 82 BERNABE 01b looked for Primakoff coherent conversion of solar axions into photons via Bragg scattering in NaI crystal in DAMA dark matter detector.

- 83 ASTIER 00b looked for production of axions from the interaction of high-energy photons with the horn magnetic field and their subsequent re-conversion to photons via the interaction with the NOMAD dipole magnetic field.
- 84 MASSO 00 studied limits on axion-proton coupling using the induced axion-photon coupling through the proton loop and CAMERON 93 bound on the axion-photon coupling using optical rotation. They obtained the bound $g_p^2/4\pi < 1.7 \times 10^{-9}$ for the coupling $g_p \vec{p} \vec{\gamma}_5 p \phi_A$.
- 85 AVIGNONE 98 result is based on the coherent conversion of solar axions to photons via the Primakoff effect in a single crystal germanium detector.
- 86 Based on the conversion of solar axions to X-rays in a strong laboratory magnetic field.
- 87 Experiment based on proposal by MAIANI 86.
- 88 Experiment based on proposal by VANBIBBER 87.
- 89 LAZARUS 92 experiment is based on proposal found in VANBIBBER 89.
- 90 RUOSO 92 experiment is based on the proposal by VANBIBBER 87.
- 91 SEMERTZIDIS 90 experiment is based on the proposal of MAIANI 86. The limit is obtained by taking the noise amplitude as the upper limit. Limits extend to $m_{A^0} = 4 \times 10^{-3}$ where $G_{A\gamma\gamma} < 1 \times 10^{-4} \text{ GeV}^{-1}$.

Limit on Invisible A^0 (Axion) Electron Coupling

The limit is for $g_{Aee} \phi_A \bar{e}(i\gamma_5)e$, or equivalently, the dipole-dipole potential

$$-\frac{g_{Aee}^2}{16\pi m_e^2} ((\sigma_1 \cdot \sigma_2) - 3(\sigma_1 \cdot \mathbf{n})(\sigma_2 \cdot \mathbf{n}))/r^3 \text{ where } \mathbf{n} = \mathbf{r}/r \text{ and the sign of the potential was corrected based on DAIDO 17.}$$

VALUE	CL%	DOCUMENT ID	TECN	COMMENT
••• We do not use the following data for averages, fits, limits, etc. •••				
<2.5 × 10 ⁻¹⁰		1 CALORE	21 ASTR	Core-collapse SNe
<3 × 10 ⁻¹²	90	2 LUCENTE	21 ASTR	SN 1987A
<1 × 10 ⁻⁹	90	3 AGOSTINI	20 HPGE	$m_{A^0} = 0.06\text{--}1 \text{ MeV}$
<2 × 10 ⁻¹⁴	90	4 AMARAL	20 SCDM	$m_{A^0} = 1.2\text{--}50 \text{ eV}$
2.6–3.7 × 10 ⁻¹²	90	5 APRILE	20 XE1T	$m_{A^0} = 1 \text{ keV}$
<6 × 10 ⁻¹³	90	6 APRILE	20 XE1T	Solar axions
<1.3 × 10 ⁻¹³	95	7 ARALIS	20 SCDM	$m_{A^0} = 0.04\text{--}500 \text{ keV}$
<1.7 × 10 ⁻¹¹	95	8 CAPOZZI	20 ASTR	Tip of the Red Giant Branch
<1.8 × 10 ⁻⁹		9 CRESCINI	20 QUAX	$m_{A^0} = 42.4\text{--}43.1 \mu\text{eV}$
<1.48 × 10 ⁻¹³	95	10 GHOSH	20A COSM	$m_{A^0} \lesssim 0.5 \text{ MeV}$
<2.48 × 10 ⁻¹¹	90	11 STRANIERO	20 ASTR	Tip of the Red Giant Branch
<4 × 10 ⁻¹³	90	12 WANG	20A CDEX	Solar axions
<1.7 × 10 ⁻¹¹	90	13 WANG	20A CDEX	$m_{A^0} = 1.5 \text{ keV}$
<2.3 × 10 ⁻¹⁴	90	14 ADHIKARI	19B C100	Solar axions
<1.5 × 10 ⁻¹⁰	90	15 APRILE	19D XE1T	$m_{A^0} = 0.186\text{--}1 \text{ keV}$
<1.5 × 10 ⁻¹³	95	16 DESSERT	19 ASTR	Magnetic white dwarf
<1.1 × 10 ⁻¹¹	90	17 TERRANO	19	Torsion pendulum
<4 × 10 ⁻¹³	90	18 ABE	18F XMAS	$m_{A^0} = 40\text{--}120 \text{ keV}$
<4.9 × 10 ⁻¹⁰	95	19 ARMENGAUD	18 EDE3	Solar axions
	90	20 ARMENGAUD	18 EDE3	$m_{A^0} = 0.8\text{--}500 \text{ keV}$
	95	21 CRESCINI	18 QUAX	$m_{A^0} = 58 \mu\text{eV}$
	90	22 FICEK	18 THEO	$m_{A^0} < 10 \text{ keV}$
<4.5 × 10 ⁻¹³	90	23 ABGRALL	17 HPGE	$m_{A^0} = 11.8 \text{ keV}$
<3.5 × 10 ⁻¹²	90	24 AKERIB	17B LUX	Solar axions
<4.2 × 10 ⁻¹³	90	25 AKERIB	17B LUX	$m_{A^0} = 1\text{--}16 \text{ keV}$
<2.3 × 10 ⁻¹³	90	26 APRILE	17B X100	$m_{A^0} = 6 \text{ keV}$
<4 × 10 ⁻⁴	90	27 FICEK	17 THEO	$m_{A^0} < 1 \text{ keV}$
<4.35 × 10 ⁻¹²	90	28 FU	17A PNDX	Solar axions
<4.3 × 10 ⁻¹⁴	90	29 FU	17A PNDX	$m_{A^0} = 2 \text{ keV}$
<5 × 10 ⁻¹³	90	30 LIU	17A CDEX	$m_{A^0} = 13 \text{ keV}$
<2.5 × 10 ⁻¹¹	90	31 LIU	17A CDEX	Solar axions
<0.15	95	32 LUO	17	$m_{A^0} = 300 \text{ eV}$
<3.3 × 10 ⁻¹³	68	33 BATTICH	16 ASTR	White dwarf cooling
<7 × 10 ⁻¹³		34 CORSICO	16 ASTR	White dwarf cooling
<1.39 × 10 ⁻¹¹	90	35 YOON	16 KIMS	Solar axions
<7.4 × 10 ⁻⁹	95	36 TERRANO	15	$m_{A^0} < 30 \mu\text{eV}$
<8 × 10 ⁻¹³	90	37 ABE	14F XMAS	$m_{A^0} = 60 \text{ keV}$
<7.7 × 10 ⁻¹²	90	38 APRILE	14B X100	Solar axions
		39 APRILE	14B X100	$m_{A^0} = 5\text{--}7 \text{ keV}$
< 0.96–8.2 × 10 ⁻⁸	90	40 DERBIN	14 CNTR	$m_{A^0} = 0.1\text{--}1 \text{ MeV}$
<2.8 × 10 ⁻¹³	99	41 MILLER-BER...	14 ASTR	White dwarf cooling
<5.4 × 10 ⁻¹¹	90	42 ABE	13D XMAS	Solar axions
<1.07 × 10 ⁻¹²	90	43 ARMENGAUD	13 EDEL	$m_{A^0} = 12.5 \text{ keV}$
<2.59 × 10 ⁻¹¹	90	44 ARMENGAUD	13 EDEL	Solar axions
		45 BARTH	13 CAST	Solar axions
< 1.4–9.7 × 10 ⁻⁷	90	46 DERBIN	13 CNTR	$m_{A^0} = 0.1\text{--}1 \text{ MeV}$
<1.5 × 10 ⁻⁸	68	47 HECKEL	13	$m_{A^0} \leq 0.1 \mu\text{eV}$
<4.3 × 10 ⁻¹³	95	48 VIAUX	13A ASTR	Low-mass red giants
<7 × 10 ⁻¹³	95	49 CORSICO	12 ASTR	White dwarf cooling
<2.2 × 10 ⁻¹⁰	90	50 DERBIN	12 CNTR	Solar axions
< 0.02–1 × 10 ⁻¹⁰	90	51 AALSETH	11 CNTR	$m_{A^0} = 0.3\text{--}8 \text{ keV}$
<1.4 × 10 ⁻¹²	90	52 AHMED	09A CDMS	$m_{A^0} = 2.5 \text{ keV}$
<4 × 10 ⁻⁹		53 DAVOUDIASL	09 ASTR	Earth cooling

Gauge & Higgs Boson Particle Listings

Axions (A^0) and Other Very Light Bosons

- $<2.7 \times 10^{-8}$ 66 54 NI 94 Induced magnetism
 $<3.6 \times 10^{-7}$ 66 54 CHUI 93 Induced magnetism
 $<2.9 \times 10^{-8}$ 66 55 PAN 92 Torsion pendulum
 $<1.9 \times 10^{-6}$ 95 54 BOBRAKOV 91 Induced magnetism
 $<7 \times 10^{-7}$ 66 56 WINELAND 91 NMR
 $<6.6 \times 10^{-8}$ 66 55 RITTER 90 Torsion pendulum
 95 54 VOROBYOV 88 Induced magnetism
- 1 CALORE 21 consider the production of axions from Galactic and extragalactic SNe via nucleon-nucleon bremsstrahlung and their subsequent decay into electron-positron pairs, and exclude the range of $g_{Aee} \simeq 10^{-19}\text{--}10^{-11}$ at $g_{A\mu\mu} = 10^{-9}$ for $m_{A^0} = 3\text{--}30$ MeV. See their Fig. 7 for the limits.
 - 2 LUCENTE 21 study the axion production in a supernova via electron-proton bremsstrahlung and electron-positron fusion, and exclude the range of $g_{Aee} \simeq 10^{-10}\text{--}10^{-8}$ for $m_{A^0} = 1\text{--}160$ MeV. The quoted limit is at $m_{A^0} = 120$ MeV. See their Fig. 12 for the mass-dependent limits.
 - 3 AGOSTINI 20 is analogous to AHMED 09A. The quoted limit applies to $m_{A^0} = 150$ keV. See their Fig. 3 for mass-dependent limits.
 - 4 AMARAL 20 use a second-generation SuperCDMS high-voltage eV-resolution detector to set limits on dark-matter axion absorption. The quoted limit is for $m_{A^0} \simeq 17$ eV. The local density $\rho_{\chi} = 0.3 \text{ GeV}/\text{cm}^3$ is assumed. See their Fig. 3 for mass-dependent limits.
 - 5 APRILE 20 is an update of APRILE 17B where they look for an absorption signal of axion dark matter. They obtained the limit, $g_{Aee} \lesssim 2 \times 10^{-14}\text{--}1 \times 10^{-12}$ at 90%CL for $m_{A^0} = 1\text{--}200$ keV. They also found an excess over known backgrounds, which favors the mass $m_{A^0} = 2.3 \pm 0.2$ keV with a 3σ significance. See their Fig. 10 for mass-dependent limits.
 - 6 APRILE 20 look for solar axions from the ABC interactions, the Primakoff conversion, and the 14.4 keV M1 transition of ^{57}Fe , and set limits on g_{Aee} , $G_{A\gamma\gamma}$, g_{ANN} , and their products. An excess is observed at low energies between 2 and 3 keV. See their Fig. 8 for correlation between the couplings. The quoted limit applies to the case of vanishing $G_{A\gamma\gamma}$ and g_{ANN} .
 - 7 ARALIS 20 is analogous to AHMED 09A. The quoted limit applies to $m_{A^0} = 0.3$ keV. The limits at masses above 3 keV in their Fig. 9 was later found to be incorrect due to an error in their analysis. See Fig. 2 in ARALIS 21 for the corrected limits.
 - 8 CAPOZZI 20 obtains a limit on the axion-electron coupling from the brightness of the tip of the red-giant branch in ω Centauri. A similar limit of $< 1.6 \times 10^{-13}$ is obtained in NGC 4258.
 - 9 CRESCINI 20 is an update of CRESCINI 18. They assume a local axion dark matter density, $\rho_A = 0.3 \text{ GeV}/\text{cm}^3$. See their Fig. 4 for the limits.
 - 10 GHOSH 20A study thermal production of axion via coupling to leptons in the early universe and estimate its contribution to ΔN_{eff} . The quoted limit is for $\Delta N_{\text{eff}} < 0.5$. See their Fig. 7 for their mass-dependent limits.
 - 11 STRANIERO 20 is analogous to CAPOZZI 20, with 22 galactic globular clusters used to derive the limit.
 - 12 WANG 20A is an update of LIU 17A. See their Fig. 9.
 - 13 WANG 20A is an update of LIU 17A. They assume a local axion dark matter density, $\rho_A = 0.3 \text{ GeV}/\text{cm}^3$. See their Fig. 10 for limits between $0.185 < m_{A^0} < 10$ keV.
 - 14 ADHIKARI 19B is analogous to LIU 17A.
 - 15 APRILE 19D is analogous to APRILE 17B, but they use only ionization signals. The quoted limit applies to $m_{A^0} = 0.7$ keV. See their Fig. 5(e) for mass-dependent limits.
 - 16 DESSERT 19 used the Suzaku observations of a magnetic white dwarf (RE J0317-853) to look for X-ray signatures converted from axions in the surrounding magnetic fields. They obtained the limit, $g_{Aee} \cdot G_{A\gamma\gamma} < 1.6 \times 10^{-24} \text{ GeV}^{-1}$ at 95%CL for $m_{A^0} \lesssim 10^{-5}$ eV. See their Fig. 2 for mass-dependent limits.
 - 17 TERRANO 19 look for the axion-induced oscillating magnetic field acting on the electron spin, using data taken with a rotating torsion pendulum containing polarized electrons. The quoted limit applies to $m_{A^0} = 10^{-23}\text{--}10^{-18}$ eV and assumes a local axion dark matter density, $\rho_A = 0.45 \text{ GeV}/\text{cm}^3$. See their Fig. 5 for mass-dependent limits.
 - 18 ABE 18f is an update of ABE 14f. The quoted limit applies to $m_{A^0} = 60$ keV. See their Fig. 5 for mass-dependent limits.
 - 19 ARMENGAUD 18 is analogous to LIU 17A.
 - 20 ARMENGAUD 18 is analogous to AHMED 09A. See the left panel of Fig. 5 for mass-dependent limits.
 - 21 CRESCINI 18 look for collective excitations of the electron spins caused by dark matter axions. The quoted limit assumes the local dark matter density, $\rho_A = 0.45 \text{ GeV}/\text{cm}^3$.
 - 22 FICEK 18 use the measurements of the hyperfine structure of antiprotonic helium to constrain a dipole-dipole potential between electron and antiproton. See their Fig. 3 for limits on various spin- and velocity-dependent potentials.
 - 23 ABGRALL 17 is analogous to AHMED 09A using the MAJORANA DEMONSTRATOR. See their Fig. 2 for limits between $6 \text{ keV} < m_{A^0} < 97$ keV.
 - 24 AKERIB 17B is analogous to LIU 17A.
 - 25 AKERIB 17B is analogous to AHMED 09A. See their Fig. 7 for mass-dependent limits.
 - 26 APRILE 17B is analogous to AHMED 09A. They found a bug in their code and needed to correct the limits in Fig. 7 of APRILE 14B. See their Fig. 1 for the corrected limits between $1 \text{ keV} < m_{A^0} < 40$ keV.
 - 27 FICEK 17 look for spin-dependent interactions between electrons by comparing precision spectroscopic measurements in ^4He with theoretical calculations. See their Fig. 1 for limits up to $m_{A^0} = 10$ keV.
 - 28 FU 17A is analogous to LIU 17A. See their Fig. 3 for mass-dependent limits.
 - 29 FU 17A is analogous to AHMED 09A. See their Fig. 4 for mass-dependent limits.
 - 30 LIU 17A is analogous to AHMED 09A. See their Fig. 9 for limits between $0.25 \text{ keV} < m_{A^0} < 20$ keV.
 - 31 LIU 17A look for solar axions produced from Compton, bremsstrahlung, atomic-recombination and deexcitation channels, and set a limit for $m_{A^0} < 1$ keV.
 - 32 LUO 17 use a recent measurement of the dipole-dipole interaction between two iron atoms at the nanometer scale and set a limit for $m_{A^0} < 1$ keV. See their Fig. 3 for mass-dependent limits.

- 33 BATTICH 16 is analogous to CORSICO 16 and used the pulsating DB white dwarf PG 1351+489.
- 34 CORSICO 16 studied the cooling rate of the pulsating DA white dwarf L19-2 based on an asteroseismic model.
- 35 YOON 16 look for solar axions with the axio-electric effect in CsI(Tl) crystals and set a limit for $m_{A^0} < 1$ keV.
- 36 TERRANO 15 used a torsion pendulum and rotating attractor with 20-pole electron-spin distributions. See their Fig. 4 for a mass-dependent limit up to $m_{A^0} = 500 \mu\text{eV}$.
- 37 ABE 14f set limits on the axioelectric effect in the XMASS detector assuming the pseudoscalar constitutes all the local dark matter. See their Fig. 3 for limits between $m_{A^0} = 40\text{--}120$ keV.
- 38 APRILE 14B look for solar axions using the XENON100 detector.
- 39 APRILE 14B is analogous to AHMED 09A. Their Fig. 7 was later found to be incorrect due to a bug in their code. See Fig. 1 in APRILE 17B for the corrected limits.
- 40 DERBIN 14 is an update of DERBIN 13 with a BGO scintillating bolometer. See their Fig. 3 for mass-dependent limits.
- 41 MILLER-BERTOLAMI 14 studied the impact of axion emission on white dwarf cooling in a self-consistent way.
- 42 ABE 13d is analogous to DERBIN 12, using the XMASS detector.
- 43 ARMENGAUD 13 is similar to AALSETH 11. See their Fig. 10 for limits between $3 \text{ keV} < m_{A^0} < 100$ keV.
- 44 ARMENGAUD 13 is similar to DERBIN 12, and take account of axio-recombination and axio-deexcitation effects. See their Fig. 12 for mass-dependent limits.
- 45 BARTH 13 search for solar axions produced by axion-electron coupling, and obtained the limit, $g_{Aee} \cdot G_{A\gamma\gamma} < 8.1 \times 10^{-23} \text{ GeV}^{-1}$ at 95%CL.
- 46 DERBIN 13 looked for 5.5 MeV solar axions produced in $p d \rightarrow ^3\text{He} A^0$ in a BGO detector through the axioelectric effect. See their Fig. 4 for mass-dependent limits.
- 47 HECKEL 13 studied the influence of 2 or 4 stationary sources each containing 6.0×10^{24} polarized electrons, on a rotating torsion pendulum containing 9.8×10^{24} polarized electrons. See their Fig. 4 for mass-dependent limits.
- 48 VIAUX 13A constrain axion emission using the observed brightness of the tip of the red-giant branch in the globular cluster M5.
- 49 CORSICO 12 attributed the excessive cooling rate of the pulsating white dwarf R548 to emission of axions with $g_{Aee} \simeq 4.8 \times 10^{-13}$.
- 50 DERBIN 12 look for solar axions with the axio-electric effect in a Si(Li) detector. The solar production is based on Compton and bremsstrahlung processes.
- 51 AALSETH 11 is analogous to AHMED 09A. See their Fig. 4 for mass-dependent limits.
- 52 AHMED 09A assume keV-mass pseudoscalars are the local dark matter and constrain the axio-electric effect in the CDMS detector. See their Fig. 5 for mass-dependent limits.
- 53 DAVOUDI-DIAL 09 use geophysical constraints on Earth cooling by axion emission.
- 54 These experiments measured induced magnetization of a bulk material by the spin-dependent potential generated from other bulk material with aligned electron spins, where the magnetic field is shielded with superconductor. The sign of the limit set by CHUI 93 is opposite to that of the axion-mediated dipole-dipole potential.
- 55 These experiments used a torsion pendulum to measure the potential between two bulk matter objects where the spins are polarized but without a net magnetic field in either of them. The limits reflect the corrected sign of the dipole-dipole potential.
- 56 WINELAND 91 looked for an effect of bulk matter with aligned electron spins on atomic hyperfine splitting using nuclear magnetic resonance.

Invisible A^0 (Axion) Limits from Nucleon Coupling

Limits are for the axion mass in eV.

VALUE (eV)	CL%	DOCUMENT ID	TECN	COMMENT
••• We do not use the following data for averages, fits, limits, etc. •••				
		1 AYBAS 21	CASP	Nucleon EDM
		2 BHUSAL 21	Solar axion	
		3 JIANG 21	NMR	Axion dark matter
		4 ROUSSY 21		Molecular EDM
		5 ZHANG 21B	ASTR	Neutron star inspiral
< 24	90	6 ABDELHAME...20	CNTR	Solar axion
		7 ABDELHAME...20	CNTR	Solar axion
		8 APRILE 20	XE1T	Solar axion
		9 KLIMCHITSK...20		Casimir effect
< 7.3	90	10 WANG 20A	CDEX	Solar axion
< 0.03		11 LEINSON 19	ASTR	Neutron star cooling
< 9.6×10^{-3}	95	12 LLOYD 19	ASTR	γ -rays from NS
		13 SMORRA 19		$\bar{\nu}$ g-factor
		14 WU 19	NMR	Axion dark matter
< 65	95	15 AKHMATOV 18	CNTR	Solar axion
< 6.6	90	16 ARMENGAUD 18	EDE3	Solar axion
< 0.085	90	17 BEZNOGOV 18	ASTR	Neutron star cooling
< 12.7	95	18 GAVRILYUK 18	CNTR	Solar axion
< 0.01		19 HAMAGUCHI 18	ASTR	Neutron star cooling
		20 ABEL 17		Neutron EDM
< 93	90	21 ABGRALL 17	HPGE	Solar axion
< 4	90	22 FU 17A	PNDX	Solar axion
		23 KLIMCHITSK...17A		Casimir effect
<177	90	24 LIU 17A	CDEX	Solar axion
< 0.079	95	25 BERENJI 16	ASTR	γ -rays from NS
<100	95	26 GAVRILYUK 15	CNTR	Solar axion
		27 KLIMCHITSK...15		Casimir-less
		28 BEZERRA 14		Casimir effect
		29 BEZERRA 14A		Casimir effect
		30 BEZERRA 14B		Casimir effect
		31 BEZERRA 14C		Casimir effect
		32 BLUM 14	COSM	^4He abundance

<250	95	33 LEINSON	14	ASTR	Neutron star cooling
<155	90	34 ALESSANDRIA13	CNTR	Solar axion	
< 8.6 × 10 ³	90	35 ARMENGAUD	13	EDEL	Solar axion
< 1.4 × 10 ⁴	90	36 BELLI	12	CNTR	Solar axion
<145	95	37 BELLINI	12b	BORX	Solar axion
		38 DERBIN	11	CNTR	Solar axion
		39 BELLINI	08	CNTR	Solar axion
		40 ADELBERGER	07		Test of Newton's law

1 AYBAS 21 limits the axion couplings to the nucleon EDM and the nucleons as $g_{AN\gamma} < 9.5 \times 10^{-4} \text{ GeV}^{-2}$ and $g_{ANN}/2m_N < 0.28 \text{ GeV}^{-1}$ (95% CL) for $m_{A^0} = 162\text{--}166 \text{ neV}$, based on a measurement of ^{207}Pb solid-state NMR in a polarized ferroelectric crystal. Here m_N is the nucleon mass and g_{ANN} is the dimensionless axion-nucleon coupling. They assume that axions make up all the dark matter with $\rho_A \approx 0.46 \text{ GeV}/\text{cm}^3$. See their Fig. 3 for the limits.

2 BHUSAL 21 looked for 5.5 MeV solar axions produced by $p d \rightarrow {}^3\text{He} A^0$ through the axion-induced dissociation of deuterons by using SNO data, and set a limit on the isovector axion-nucleon coupling, $|g_{aNN}^3| < 2 \times 10^{-5} \text{ GeV}^{-1}$, which is equivalent to $|g_{Ann} - g_{App}| < 4 \times 10^{-5}$ in terms of the dimensionless axion-nucleon couplings.

3 JIANG 21 use the spin-amplifier based on hyperpolarized ^{129}Xe gas to set limits on the axion couplings to nucleons as $g_{ANN}/2m_N < 3.2 \times 10^{-9} \text{ GeV}^{-1}$ (95% CL) at $m_{A^0} = 52.94 \text{ feV}$, and comparable limits in the mass range of 8.3–744 feV. Here m_N is the nucleon mass and g_{ANN} is the dimensionless axion-nucleon coupling. They assume that axions make up all the dark matter with $\rho_A \approx 0.4 \text{ GeV}/\text{cm}^3$. See their Fig. 4b for the limits.

4 ROUSSY 21 look for a time-oscillating EDM of molecular ions HfF^+ induced by axion dark matter couplings to gluons. See their Fig. 3 for limits in the range of $m_{A^0} = 10\text{--}22\text{--}10\text{--}15 \text{ eV}$.

5 ZHANG 21b use the gravitational waves from the binary neutron star inspiral GW170817 to look for a type of axion whose mass is suppressed due to cancellation with additional contributions. They exclude $1.6 \times 10^{16} < f_A < 10^{18} \text{ GeV}$ at 3σ for $m_{A^0} \lesssim 10\text{--}13 \text{ eV}$. See their Fig. 1 for mass-dependent limits.

6 ABDELHAMEED 20 look for the resonant excitation of ^{169}Tm (8.41 keV) by solar axions produced via the Primakoff effect. The mass bound assumes the KSVZ axion model, $S = 0.5$, and $m_U/m_d = 0.56$. They set a limit on the product of axion couplings to photons and nucleons as $G_{A\gamma\gamma} \cdot g_{App} < 1.44 \times 10^{-14} \text{ GeV}^{-1}$ (90% CL).

7 ABDELHAMEED 20 look for the resonant excitation of ^{169}Tm (8.41 keV) by solar axions produced via the axion-electron coupling. They set a limit on the product of axion couplings to electrons and nucleons as $g_{Aee} \cdot g_{App} < 2.81 \times 10^{-16}$ (90% CL).

8 APRILE 20 look for solar axions from the ABC interactions, the Primakoff conversion, and the 14.4 keV M1 transition of ^{57}Fe . An excess is observed at low energies between 2 and 3 keV. See their Fig. 8 for correlation between the couplings.

9 KLIMCHITSKAYA 20 use the measurement of the Casimir force between a Au-coated microsphere and a SiC plate to constrain the force due to two-axion exchange for $17.8 < m_{A^0} < 100 \text{ eV}$. See their Fig. 2 for mass-dependent limits.

10 WANG 20a is an update of LIU 17a. The limit assumes the DFSZ model. See their Fig. 7 for the limit on product of axion couplings to electrons and nucleons.

11 LEINSON 19 is analogous to BEZNOGOV 18, but estimating the axion luminosity based on the Tolman's analytic solution to the Einstein equations of spherical fluids in hydrostatic equilibrium. The dimensionless axion-neutron coupling is constrained as $g_{Ann} < 1.0 \times 10\text{--}10$.

12 LLOYD 19 is analogous to BERENJI 16. They highlight that the limit obtained with this technique strongly depends on the assumed NS core temperature.

13 SMORRA 19 look for spin-precession effects from ultra-light axion dark matter in the \bar{p} spin-flip resonance data. Assuming $\rho_A = 0.4 \text{ GeV}/\text{cm}^3$, they constrain the dimensionless axion-antiproton coupling as $g_{A\bar{p}p} < 2\text{--}9$ at 95% CL for $m_{A^0} = 2 \times 10\text{--}23\text{--}4 \times 10\text{--}17 \text{ eV}$. See the right panel of their Fig. 3.

14 WU 19 look for axion-induced time-oscillating features of the NMR spectrum of acetonitrile- d_2 . Assuming $C_p = C_n$ and $\rho_A = 0.4 \text{ GeV}/\text{cm}^3$, they constrain the dimensionless axion-nucleon coupling as $g_{ANN} < 6 \times 10\text{--}5$ for $m_{A^0} = 10\text{--}21\text{--}1.3 \times 10\text{--}17 \text{ eV}$. Note that the limits for $m_{A^0} < 10\text{--}21 \text{ eV}$ in their Fig. 3(a) should be weaker than those for heavier masses. See ADELBERGER 19 and WU 19c on this issue.

15 AKHMATOV 18 is an update of GAVRILYUK 15.

16 ARMENGAUD 18 is analogous to ALESSANDRIA 13. The quoted limit assumes the DFSZ axion model. See their Fig. 4 for the limit on product of axion couplings to electrons and nucleons.

17 BEZNOGOV 18 constrain the axion-neutron coupling by assuming that thermal evolution of the hot neutron star HESS J1731-347 is dominated by the lowest possible neutrino emission. The quoted limit assumes the KSVZ axion with the effective Peccei-Quinn charge of the neutron $C_n = -0.02$. The dimensionless axion-neutron coupling is constrained as $g_{Ann} < 2.8 \times 10\text{--}10$.

18 GAVRILYUK 18 look for the resonant excitation of ^{83}Kr (9.4 keV) by solar axions produced via the Primakoff effect. The mass bound assumes $m_U/m_d = 0.56$ and $S = 0.5$.

19 HAMAGUCHI 18 studied the axion emission from the neutron star in Cassiopeia A based on the minimal cooling scenario which explains the observed rapid cooling rate. The quoted limit corresponds to $f_A > 5 \times 10^9 \text{ GeV}$ obtained for the KSVZ axion with $C_p = -0.47$ and $C_n = -0.02$.

20 ABEL 17 look for a time-oscillating neutron EDM and an axion-wind spin-precession effect respectively induced by axion dark matter couplings to gluons and nucleons. See their Fig. 4 for limits in the range of $m_{A^0} = 10\text{--}24\text{--}10\text{--}17 \text{ eV}$.

21 ABGRALL 17 limit assumes the hadronic axion model used in ALESSANDRIA 13. See their Fig. 4 for the limit on product of axion couplings to electrons and nucleons.

22 FU 17a look for the 14.4 keV ^{57}Fe solar axions. The limit assumes the DFSZ axion model. See their Fig. 3 for mass-dependent limits on the axion-electron coupling. Notice that in this figure the DFSZ and KSVZ lines should be interchanged.

23 KLIMCHITSKAYA 17a use the differential measurement of the Casimir force between a Ni-coated sphere and Au and Ni sectors of the structured disc to constrain the axion coupling to nucleons for $2.61 \text{ meV} < m_{A^0} < 0.9 \text{ eV}$. See their Figs. 1 and 2 for mass dependent limits.

24 LIU 17 is analogous to ALESSANDRIA 13. The limit assumes the hadronic axion model. See their Fig. 6(b) for the limit on product of axion couplings to electrons and nucleons.

25 BERENJI 16 used the Fermi LAT observations of neutron stars to look for photons from axion decay. They assume the effective Peccei-Quinn charge of the neutron $C_n = 0.1$ and a neutron-star core temperature of 20 MeV.

26 GAVRILYUK 15 look for solar axions emitted by the M1 transition of ^{83}Kr (9.4 keV). The mass bound assumes $m_U/m_d = 0.56$ and $S = 0.5$.

27 KLIMCHITSKAYA 15 use the measurement of differential forces between a test mass and rotating source masses of Au and Si to constrain the force due to two-axion exchange for $1.7 \times 10\text{--}3 < m_{A^0} < 0.9 \text{ eV}$. See their Figs. 1 and 2 for mass dependent limits.

28 BEZERRA 14 use the measurement of the thermal Casimir-Polder force between a Bose-Einstein condensate of ^{87}Rb atoms and a SiO_2 plate to constrain the force mediated by exchange of two pseudoscalars for $0.1 \text{ meV} < m_{A^0} < 0.3 \text{ eV}$. See their Fig. 2 for the mass-dependent limit on pseudoscalar coupling to nucleons.

29 BEZERRA 14a is analogous to BEZERRA 14. They use the measurement of the Casimir pressure between two Au-coated plates to constrain pseudoscalar coupling to nucleons for $1 \times 10\text{--}3 \text{ eV} < m_{A^0} < 15 \text{ eV}$. See their Figs. 1 and 2 for the mass-dependent limit.

30 BEZERRA 14b is analogous to BEZERRA 14. BEZERRA 14b use the measurement of the normal and lateral Casimir forces between sinusoidally corrugated surfaces of a sphere and a plate to constrain pseudoscalar coupling to nucleons for $1 \text{ eV} < m_{A^0} < 20 \text{ eV}$. See their Figs. 1–3 for mass-dependent limits.

31 BEZERRA 14c is analogous to BEZERRA 14. They use the measurement of the gradient of the Casimir force between Au- and Ni-coated surfaces of a sphere and a plate to constrain pseudoscalar coupling to nucleons for $3 \times 10\text{--}5 \text{ eV} < m_{A^0} < 1 \text{ eV}$. See their Figs. 1, 3, and 4 for the mass-dependent limits.

32 BLUM 14 studied effects of an oscillating strong CP phase induced by axion dark matter on the primordial ^4He abundance. See their Fig. 1 for mass-dependent limits.

33 LEINSON 14 attributes the excessive cooling rate of the neutron star in Cassiopeia A to axion emission from the superfluid core, and found $C_n^2 m_{A^0}^2 \approx 5.7 \times 10\text{--}6 \text{ eV}^2$, where C_n is the effective Peccei-Quinn charge of the neutron.

34 ALESSANDRIA 13 used the CUORE experiment to look for 14.4 keV solar axions produced from the M1 transition of thermally excited ^{57}Fe nuclei in the solar core, using the axio-electric effect. The limit assumes the hadronic axion model. See their Fig. 4 for the limit on product of axion couplings to electrons and nucleons.

35 ARMENGAUD 13 is analogous to ALESSANDRIA 13. The limit assumes the hadronic axion model. See their Fig. 8 for the limit on product of axion couplings to electrons and nucleons.

36 BELLI 12 looked for solar axions emitted by the M1 transition of $^7\text{Li}^*$ (478 keV) after the electron capture of ^7Be , using the resonant excitation ^7Li in the LiF crystal. The mass bound assumes $m_U/m_d = 0.55$, $m_U/m_S = 0.029$, and the flavor-singlet axial vector matrix element $S = 0.4$.

37 BELLINI 12b looked for 5.5 MeV solar axions produced in the $p d \rightarrow {}^3\text{He} A^0$. The limit assumes the hadronic axion model. See their Figs. 6 and 7 for mass-dependent limits on product of axion couplings to photons, electrons, and nucleons.

38 DERBIN 11 looked for solar axions emitted by the M1 transition of thermally excited ^{57}Fe nuclei in the Sun, using their possible resonant capture on ^{57}Fe in the laboratory. The mass bound assumes $m_U/m_d = 0.56$ and the flavor-singlet axial vector matrix element $S = 3F - D \approx 0.5$.

39 BELLINI 08 consider solar axions emitted in the M1 transition of $^7\text{Li}^*$ (478 keV) and look for a peak at 478 keV in the energy spectra of the Counting Test Facility (CTF), a Borexino prototype. For $m_{A^0} < 450 \text{ keV}$ they find mass-dependent limits on products of axion couplings to photons, electrons, and nucleons.

40 ADELBERGER 07 use precision tests of Newton's law to constrain a force contribution from the exchange of two pseudoscalars. See their Fig. 5 for limits on the pseudoscalar coupling to nucleons, relevant for m_{A^0} below about 1 meV.

Axion Limits from T-violating Medium-Range Forces

The limit is for the coupling $g = g_p g_s$ in a T-violating potential between nucleons or nucleon and electron of the form $V = \frac{g\hbar^2}{8\pi m_p} (\boldsymbol{\sigma} \cdot \boldsymbol{r}) (\frac{1}{r^2} + \frac{1}{\lambda r}) e^{-r/\lambda}$, where g_p and g_s are dimensionless scalar and pseudoscalar coupling constants and $\lambda = \hbar/(m_A c)$ is the range of the force.

VALUE	DOCUMENT ID	TECN	COMMENT
• • •	We do not use the following data for averages, fits, limits, etc. • • •		
1	AFACH	21	GNME Optical magnetometers
2	DZUBA	18	THEO atomic EDM
3	STADNIK	18	THEO atomic and molecular EDMs
4	CRESCINI	17	SQID paramagnetic GSO crystal
5	AFACH	15	ultracold neutrons
6	STADNIK	15	THEO nucleon spin contributions for nuclei
7	TERRANO	15	torsion pendulum
8	BULATOWICZ	13	NMR polarized ^{129}Xe and ^{131}Xe
9	CHU	13	polarized ^3He
10	TULLNEY	13	SQID polarized ^3He and ^{129}Xe
11	RAFFELT	12	stellar energy loss
12	HOEDL	11	torsion pendulum
13	PETUKHOV	10	polarized ^3He
14	SEREBROV	10	ultracold neutrons
15	IGNATOVICH	09	RVUE ultracold neutrons
16	SEREBROV	09	RVUE ultracold neutrons
17	BAESSLER	07	ultracold neutrons
18	HECKEL	06	torsion pendulum
19	NI	99	paramagnetic Tb F ₃
20	POSPELOV	98	THEO neutron EDM

Gauge & Higgs Boson Particle Listings

Axions (A⁰) and Other Very Light Bosons

21	YOU DIN	96			
22	RITTER	93	torsion pendulum		
23	VENEMA	92	nuclear spin-precession frequencies		
24	WINELAND	91	NMR		
1	AFACH 21		look for axion domain walls coupled to atomic spins by using the global network of optical magnetometers. Assuming that the axion domain walls make up all dark matter, they exclude the effective decay constant below 4×10^5 GeV for m_{A^0} in the range of 10^{-15} – 10^{-11} eV. See their Fig. 4 for the mass-dependent limits.		
2	DZUBA 18		used atomic EDM measurements to derive limits on the product of the pseudoscalar coupling to nucleon and the scalar coupling to electron, which improved on the laboratory bounds for $m_{A^0} > 0.01$ eV. See their Fig. 1 for mass-dependent limits.		
3	STADNIK 18		used atomic and molecular EDM experiments to derive limits on the product of the pseudoscalar couplings to electron and the scalar coupling to nucleon and electron. See their Fig. 2 for mass-dependent limits, which improved on the laboratory bounds for $m_{A^0} > 0.01$ eV.		
4	CRESCINI 17		use the QUAX- $g_p g_S$ experiment to look for variation of a paramagnetic GSO crystal magnetization when rotating lead disks are positioned near the crystal, and find $g = g_p g_S^N < 4.3 \times 10^{-30}$ for $\lambda = 0.1$ – 0.2 m at 95% CL. See their Fig. 6 for limits as a function of λ .		
5	AFACH 15		look for a change of spin precession frequency of ultracold neutrons when a magnetic field with opposite directions is applied, and find $g < 2.2 \times 10^{-27} (\text{m}/\lambda)^2$ at 95% CL for $1 \mu\text{m} < \lambda < 5$ mm. See their Fig. 3 for their limits.		
6	STADNIK 15		studied proton and neutron spin contributions for nuclei and derive the limits $g < 10^{-28}$ – 10^{-23} for $\lambda > 3 \times 10^{-4}$ m using the data of TULLNEY 13. See their Figs. 1 and 2 for λ -dependent limits.		
7	TERRANO 15		used a torsion pendulum and rotating attractor, and derived a restrictive limit on the product of the pseudoscalar coupling to electron and the scalar coupling to nucleons, $g < 9 \times 10^{-29}$ – 5×10^{-26} for $m_{A^0} < 1.5$ – $400 \mu\text{eV}$. See their Fig. 5 for mass-dependent limits.		
8	BULATOWICZ 13		looked for NMR frequency shifts in polarized ^{129}Xe and ^{131}Xe when a zirconia rod is positioned near the NMR cell, and find $g < 1 \times 10^{-19}$ – 1×10^{-24} for $\lambda = 0.01$ – 1 cm. See their Fig. 4 for their limits.		
9	CHU 13		look for a shift of the spin precession frequency of polarized ^3He in the presence of an unpolarized mass, in analogy to YOU DIN 96. See Fig. 3 for limits on g in the approximate m_{A^0} range 0.02–2 MeV.		
10	TULLNEY 13		look for a shift of the precession frequency difference between the colocated ^3He and ^{129}Xe in the presence of an unpolarized mass, and derive limits $g < 3 \times 10^{-29}$ – 2×10^{-22} for $\lambda > 3 \times 10^{-4}$ m. See their Fig. 3 for λ -dependent limits.		
11	RAFFELT 12		show that the pseudoscalar couplings to electron and nucleon and the scalar coupling to nucleon are individually constrained by stellar energy-loss arguments and searches for anomalous monopole-monopole forces, together providing restrictive constraints on g . See their Figs. 2 and 3 for results.		
12	HOEDL 11		use a novel torsion pendulum to study the force by the polarized electrons of an external magnet. In their Fig. 3 they show restrictive limits on g in the approximate m_{A^0} range 0.03–10 MeV.		
13	PETUKHOV 10		use spin relaxation of polarized ^3He and find $g < 3 \times 10^{-23} (\text{cm}/\lambda)^2$ at 95% CL for the force range $\lambda = 10^{-4}$ – 1 cm.		
14	SEREBROV 10		use spin precession of ultracold neutrons close to bulk matter and find $g < 2 \times 10^{-21} (\text{cm}/\lambda)^2$ at 95% CL for the force range $\lambda = 10^{-4}$ – 1 cm.		
15	IGNATOVICH 09		use data on depolarization of ultracold neutrons in material traps. They show λ -dependent limits in their Fig. 1.		
16	SEREBROV 09		uses data on depolarization of ultracold neutrons stored in material traps and finds $g < 2.96 \times 10^{-21} (\text{cm}/\lambda)^2$ for the force range $\lambda = 10^{-3}$ – 1 cm and $g < 3.9 \times 10^{-22} (\text{cm}/\lambda)^2$ for $\lambda = 10^{-4}$ – 10^{-3} cm, each time at 95% CL, significantly improving on BAESSLER 07.		
17	BAESSLER 07		use the observation of quantum states of ultracold neutrons in the Earth's gravitational field to constrain g for an interaction range 1 μm –a few mm. See their Fig. 3 for results.		
18	HECKEL 06		studied the influence of unpolarized bulk matter, including the laboratory's surroundings or the Sun, on a torsion pendulum containing about 9×10^{22} polarized electrons. See their Fig. 4 for limits on g as a function of interaction range.		
19	Ni 99		searched for a T -violating medium-range force acting on paramagnetic Tb F ₃ salt. See their Fig. 1 for the result.		
20	POSPELOV 98		studied the possible contribution of T -violating Medium-Range Force to the neutron electric dipole moment, which is possible when axion interactions violate CP. The size of the force among nucleons must be smaller than gravity by a factor of 2×10^{-10} ($1 \text{ cm}/\lambda_A$), where $\lambda_A = \hbar/m_A c$.		
21	YOU DIN 96		compared the precession frequencies of atomic ^{199}Hg and Cs when a large mass is positioned near the cells, relative to an applied magnetic field. See Fig. 3 for their limits.		
22	RITTER 93		studied the influence of bulk mass with polarized electrons on an unpolarized torsion pendulum, providing limits in the interaction range from 1 to 100 cm.		
23	VENEMA 92		looked for an effect of Earth's gravity on nuclear spin-precession frequencies of ^{199}Hg and ^{201}Hg atoms.		
24	WINELAND 91		looked for an effect of bulk matter with aligned electron spins on atomic hyperfine resonances in stored $^9\text{Be}^+$ ions using nuclear magnetic resonance.		

	3	ANDREEV	21A	NA64	$m_{\gamma'} = 0.1$ – 0.35 GeV
	4	BI	21	ASTR	$m_{\gamma'} = 0.03$ – 0.06 eV
	5	CAZZANIGA	21	NA64	$m_{\gamma'} = 10$ – 390 MeV
	6	DIXIT	21	CNTR	$m_{\gamma'} = 24.86$ μeV
	7	GHOSH	21	RVUE	$m_{\gamma'} = 2$ – 30 μeV
	8	GODFREY	21		$m_{\gamma'} = 0.2637$ – 0.2648 μeV
	9	KOPYLOV	21A	CNTR	$m_{\gamma'} = 9$ – 40 eV
	10	KRIBS	21		$m_{\gamma'} \lesssim 10$ GeV
	11	SCHMIDT	21	THEO	$m_{\gamma'} < 0.6$ GeV
	12	TSAI	21	BDMP	$m_{\gamma'} = 0.78$ GeV
	13	AAIJ	20C	LHCB	$m_{\gamma'} = 214$ MeV
	14	AAIJ	20C	LHCB	$m_{\gamma'} = 218$ – 315 MeV
	15	ABLIKIM	20AB	BES3	$m_{\gamma'} = 0.2$ – 2.1 GeV
	16	AGOSTINI	20	HPGE	$m_{\gamma'} = 60$ keV – 1 MeV
	17	AMARAL	20	SCDM	$m_{\gamma'} = 1.2$ – 50 eV
	18	AN	20	XEIT	$m_{\gamma'} = 200$ eV
	19	ANDRIANAV...	20	FUNK	$m_{\gamma'} = 1.95$ – 8.55 eV
	20	APRILE	20	XEIT	$m_{\gamma'} = 1$ – 200 keV
	21	ARALIS	20	SCDM	$m_{\gamma'} = 0.04$ – 500 keV
	22	ARGUELLES	20	THEO	$m_{\gamma'} = 0.01$ GeV
	23	ARNAUD	20	EDEL	$m_{\gamma'} = 1$ – 40 eV
	24	BANERJEE	20	NA64	$m_{\gamma'} = 1.5$ – 24 MeV
	25	BARAK	20	SENS	$m_{\gamma'} = 1.2$ – 12.8 eV
	26	KRASNIKOV	20	RVUE	$m_{\gamma'} = 16.7$ MeV
	27	SHE	20	CDEX	$m_{\gamma'} = 10$ – 300 eV
	28	SHE	20	CDEX	$m_{\gamma'} = 0.1$ – 4 keV
	29	SIRUNYAN	20AQ	CMS	$m_{\gamma'} = 11.5$ – 75 GeV, 110 – 200 GeV
	30	TOMITA	20		$m_{\gamma'} = 115.79$ – 115.85 μeV
	31	WANG	20A	CDEX	$m_{\gamma'} = 0.185$ – 10 keV
	32	AABOUD	19G	ATLS	$m_{\gamma'} = 20$ – 60 GeV
	33	ABLIKIM	19A	BES3	$m_{\gamma'} = 0.01$ – 2.4 GeV
	34	ABLIKIM	19H	BES3	$m_{\gamma'} = 0.1$ – 2.1 GeV
	35	AGUILAR-AR...	19A	DAMC	$m_{\gamma'} = 1.2$ – 30 eV
	36	APRILE	19D	XEIT	$m_{\gamma'} = 0.186$ – 5 keV
	37	BANERJEE	19	NA64	$m_{\gamma'} = 1$ – 200 MeV
	38	BHOONAH	19	ASTR	$m_{\gamma'} = 10$ – 22 – 10 – 10 eV
	39	BRUN	19	SHUK	$m_{\gamma'} = 20.8$ – 28.3 μeV
	40	CORTINA-GIL	19	NA62	$m_{\gamma'} = 60$ – 110 MeV
	41	DANILOV	19	TEXO	$m_{\gamma'} = 20$ eV – 1 MeV
	42	HOCHBERG	19		$m_{\gamma'} = 0.8$ – 4 eV
	43	KOPYLOV	19	CNTR	$m_{\gamma'} = 9$ – 40 eV
	44	KOVETZ	19	COSM	$m_{\gamma'} = 10$ – 23 – 10 – 13 eV
	45	NGUYEN	19	WDMX	$m_{\gamma'} = 6$ neV – 2.07 μeV
	46	ABE	18F	XMAS	$m_{\gamma'} = 40$ – 120 keV
	47	ADRIAN	18	HPS	$m_{\gamma'} = 19$ – 81 MeV
	48	ANASTASI	18B	KLOE	$m_{\gamma'} = 519$ – 987 MeV
	49	ARMENGAUD	18	EDE3	$m_{\gamma'} = 0.8$ – 500 keV
	50	BANERJEE	18	NA64	$m_{\gamma'} = 1$ – 23 MeV
	51	BANERJEE	18A	NA64	$m_{\gamma'} = 1$ – 100 MeV
	52	KNIRCK	18		$m_{\gamma'} = 0.67$ – 0.92 MeV
	53	ABGRALL	17	HPGE	$m_{\gamma'} = 11.8$ keV
	54	ABLIKIM	17AA	BES3	$m_{\gamma'} = 1.5$ – 3.4 GeV
	55	ANGLOHER	17	CRES	$m_{\gamma'} = 0.3$ – 0.7 keV
	56	BANERJEE	17	NA64	$m_{\gamma'} = 0.002$ – 0.4 GeV
	57	CHANG	17	ASTR	$m_{\gamma'} = 15$ MeV
	58	DUBININA	17	EMUL	$m_{\gamma'} = 1.1$ – 24 MeV
	59	LEES	17E	BABR	$m_{\gamma'} = 4.7$ GeV
	60	AAD	16AG	ATLS	$m_{\gamma'} = 0.1$ – 2 GeV
	61	ANASTASI	16	KLOE	$m_{\gamma'} = 527$ – 987 MeV
	62	KHACHATRY...	16	CMS	$m_{\gamma'} = 2$ GeV
	63	AAD	15CD	ATLS	$m_{\gamma'} = 15$ – 55 GeV
	64	ADARE	15		$m_{\gamma'} = 30$ – 90 MeV
	65	AN	15A		$m_{\gamma'} = 12$ eV – 40 keV
	66	ANASTASI	15	KLOE	$m_{\gamma'} = 2m_{\mu}$ – 1 GeV

Hidden Photons: Kinetic Mixing Parameter Limits

Limits are on the Kinetic mixing parameter χ which is defined by the Lagrangian

$$L = -\frac{1}{4} F_{\mu\nu} F^{\mu\nu} - \frac{1}{4} F'_{\mu\nu} F'^{\mu\nu} - \frac{\chi}{2} F_{\mu\nu} F'^{\mu\nu} + \frac{m^2}{2} A'_\mu A'^\mu,$$

where A_μ and A'_μ are the photon and hidden-photon fields with field strengths $F_{\mu\nu}$ and $F'_{\mu\nu}$, respectively, and $m_{\gamma'}$ is the hidden-photon mass.

VALUE	CL%	DOCUMENT ID	TECN	COMMENT
• • •				We do not use the following data for averages, fits, limits, etc. • • •
		1 LEES	22	BABR $m_{\gamma'} = 1 \times 10^{-3}$ – 3.16 GeV
$<8 \times 10^{-6}$	90	2 ANDREEV	21	NA64 $m_{\gamma'} = 1 \times 10^{-3}$ – 1 GeV

$<1.7 \times 10^{-3}$	90	67 ANASTASI	15A KLOE	$m_{\gamma'} = 5\text{--}320$ MeV
$<4.2 \times 10^{-4}$	90	68 BATLEY	15A NA48	$m_{\gamma'} = 36$ MeV
		69 JAEGLE	15 BELL	$m_{\gamma'} = 0.1\text{--}3.5$ GeV
$<3 \times 10^{-13}$		70 KAZANAS	15 ASTR	$m_{\gamma'} = 2m_e - 100$ MeV
$<6 \times 10^{-12}$		71 SUZUKI	15	$m_{\gamma'} = 1.9\text{--}4.3$ eV
$<2.3 \times 10^{-13}$	99.7	72 VINYOLES	15 ASTR	$m_{\gamma'} = 8$ eV
$<2 \times 10^{-13}$		73 ABE	14F XMAS	$m_{\gamma'} = 40\text{--}120$ keV
$<1.8 \times 10^{-3}$	90	74 AGAKISHIEV	14 HDES	$m_{\gamma'} = 63$ MeV
$<9.0 \times 10^{-4}$	90	75 BABUSCI	14 KLOE	$m_{\gamma'} = 969$ MeV
		76 BATELL	14 BDMP	$m_{\gamma'} = 10^{-3\text{--}1}$ GeV
$<1.3 \times 10^{-7}$	95	77 BLUEMLEIN	14 BDMP	$m_{\gamma'} = 0.6$ GeV
$<3 \times 10^{-18}$		78 FRADETTE	14 COSM	$m_{\gamma'} = 50\text{--}300$ MeV
$<3.5 \times 10^{-4}$	90	79 LEES	14J BABR	$m_{\gamma'} = 0.2$ GeV
$<9 \times 10^{-4}$	95	80 MERKEL	14 A1	$m_{\gamma'} = 40\text{--}300$ MeV
$<3 \times 10^{-15}$		81 AN	13B ASTR	$m_{\gamma'} = 2$ keV
$<7 \times 10^{-14}$		82 AN	13C XE10	$m_{\gamma'} = 100$ eV
$<8 \times 10^{-4}$		83 DIAMOND	13 BDMP	$m_{\gamma'} = 30\text{--}250$ MeV
$<2 \times 10^{-3}$	90	84 GNINENKO	13 BDMP	$m_{\gamma'} = 25\text{--}120$ MeV
$<2.2 \times 10^{-13}$		85 HORVAT	13 HPGE	$m_{\gamma'} = 230$ eV
$<8.06 \times 10^{-5}$	95	86 INADA	13 LSW	$m_{\gamma'} = 0.04$ eV–26 keV
$<2 \times 10^{-10}$	95	87 MIZUMOTO	13	$m_{\gamma'} = 1$ eV
$<1.7 \times 10^{-7}$		88 PARKER	13 LSW	$m_{\gamma'} = 53$ μ eV
$<5.32 \times 10^{-15}$		89 PARKER	13	$m_{\gamma'} = 53$ μ eV
$<1 \times 10^{-15}$		90 REDONDO	13 ASTR	$m_{\gamma'} = 2$ keV
$<8 \times 10^{-8}$	90	91 GNINENKO	12A BDMP	$m_{\gamma'} = 1\text{--}135$ MeV
$<1 \times 10^{-7}$	90	92 GNINENKO	12B CHRM	$m_{\gamma'} = 1\text{--}500$ MeV
$<1 \times 10^{-3}$	90	93 ABRAHAMY...11		$m_{\gamma'} = 175\text{--}250$ MeV
$<9 \times 10^{-8}$	95	94 BLUEMLEIN	11 BDMP	$m_{\gamma'} = 70$ MeV
$<1 \times 10^{-7}$		95 BJORKEN	09 BDMP	$m_{\gamma'} = 2\text{--}400$ MeV
$<5 \times 10^{-9}$		96 BJORKEN	09 ASTR	$m_{\gamma'} = 2\text{--}50$ MeV

1 LEES 22 look for a hidden fermion-fermion bound state decaying into three hidden photons, which subsequently decay into e^+e^- , $\mu^+\mu^-$, or $\pi^+\pi^-$. For the bound-state mass in the range of 0.05–9.5 GeV, limits at the level of $5 \times 10^{-5}\text{--}1 \times 10^{-3}$ are obtained. See their Fig. 6 for mass-dependent limits.

2 ANDREEV 21 is analogous to BANERJEE 18A. The quoted limit applies to $m_{\gamma'} = 1$ MeV. See their Fig. 3 for mass-dependent limits.

3 ANDREEV 21A extends the limits of BANERJEE 19 by taking account of production through the resonant annihilation of secondary positrons with atomic electrons. The quoted limit is at $m_{\gamma'} = 0.23$ GeV, assuming the fermion dark matter of mass $m_{\chi}/3$ and the hidden gauge coupling $\alpha_D = 0.1$. See their Fig. 3 for mass-dependent limits.

4 BI 21 look for the gamma-ray spectral attenuation due to scattering with hidden photons constituting all dark matter, using the measurements of sub-PeV gamma-rays from the Crab Nebula by the Tibet AS γ and HAWC experiments, together with MAGIC and HEGRA gamma-ray data. See their Fig. 4 for mass-dependent limits.

5 CAZZANIGA 21 look for semi-visible decays of hidden photons, $\gamma' \rightarrow \chi_1 \chi_2$ ($\chi_2 \rightarrow \chi_1 e^+ e^-$), where χ_1 and χ_2 are hidden fermions. They exclude $3 \times 10^{-5} \lesssim \chi \lesssim 2 \times 10^{-2}$ assuming the hidden gauge coupling $\alpha_D = 0.1$, and the fermion masses $m_{\chi_1} = m_{\chi_2}/3$, $(m_{\chi_2} - m_{\chi_1})/m_{\chi_1} = 0.4$. See their Fig. 4 for mass-dependent limits.

6 DIXIT 21 look for hidden photon dark matter by using a superconducting transmon qubit dispersively coupled to a high Q storage cavity. The local density $\rho_{\gamma'} = 0.4$ GeV/cm 3 is assumed. See their Fig. 4 for mass-dependent limits.

7 GHOSH 21 use existing haloscope axion search limits to set limits on hidden photon dark matter, considering the polarization of hidden photons. The quoted limit is at $m_{\gamma'} \simeq 3$ μ eV. See their Fig. 1 for mass-dependent limits.

8 GODFREY 21 look for hidden photon dark matter by using a wideband antenna, and set 5σ limits on χ . The local density $\rho_{\gamma'} = 0.38$ GeV/cm 3 is assumed. See their updated Fig. 12 in arXiv:2101.02805v4 for mass-dependent limits in the range of $m_{\gamma'} = 0.207\text{--}1.24$ μ eV.

9 KOPYLOV 21A is an update of KOPYLOV 19, but use Ne gas instead of Ar. The quoted limit applies to $m_{\gamma'} = 12$ eV. See their Fig. 4 for mass-dependent limits.

10 KRIBS 21 used the HERA data on neutral current deep inelastic ep scattering to derive the limits, which become weaker for heavier masses. See their Fig. 3 for mass-dependent limits.

11 SCHMIDT 21 use the microscopic Parton-Hadron-String Dynamics approach to extract limits by comparing the theoretically calculated dilepton spectra with the HADES data on the search for $\gamma' \rightarrow e^+e^-$. See their Fig. 5 for the mass-dependent limits for various allowed surplus of the hidden photon contribution over the standard model yield.

12 TSAI 21 update the limits from the CHARM and NuCal experiments, taking account of additional production channels from proton bremsstrahlung and η meson decays, respectively. Limits between 3×10^{-8} and 1×10^{-4} are obtained for $0.01 < m_{\gamma'} < 0.8$ GeV (see their Fig. 1).

13 AAIJ 20c look for hidden photons produced from the pp collision in the decay channel $\gamma' \rightarrow \mu^+ \mu^-$. For prompt decaying hidden photons, limits at the level of $10^{-4}\text{--}10^{-3}$ are obtained for $m_{\gamma'} = 0.214\text{--}30$ GeV. See their Fig. 2 for mass-dependent limits.

14 AAIJ 20c look for hidden photons produced from the pp collision in the decay channel $\gamma' \rightarrow \mu^+ \mu^-$. For hidden photons with lifetimes of order ps, limits at the level of 10^{-5} are obtained for $m_{\gamma'} = 218\text{--}315$ MeV. See their Fig. 4 for mass-dependent limits.

15 ABLIKIM 20AB search for $J/\psi \rightarrow \eta' \gamma'$ ($\gamma' \rightarrow \gamma \pi^0$), and set the upper limit on the product branching fraction of order 10^{-7} . See their Fig. 7 for mass-dependent limits.

16 AGOSTINI 20 is analogous to ABE 14F. The quoted limit applies to $m_{\gamma'} = 120$ keV. The local density $\rho_{\gamma'} = 0.3$ GeV/cm 3 is assumed. See their Fig. 3 for mass-dependent limits.

17 AMARAL 20 use a second-generation SuperCDMS high-voltage eV-resolution detector to set limits on dark-matter dark photon absorption. The quoted limit is for $m_{\gamma'} \simeq 17$ eV. The local density $\rho_{\gamma'} = 0.3$ GeV/cm 3 is assumed. See their Fig. 3 for mass-dependent limits.

18 AN 20 updates the direct detection limit of AN 13C on solar flux of hidden photons; $\chi < 1.6 \times 10^{-12}$ (eV/ $m_{\gamma'}$) for $m_{\gamma'} < 6$ eV (90% C.L.). For $m_{\gamma'} > 6$ eV, see their Fig. 1 for mass-dependent limits.

19 ANDRIANAVALOMAHEFA 20 is analogous to SUZUKI 15, but uses a mirror that is about one order of magnitude larger than in similar studies in the past. Limits at the level of 10^{-12} are obtained for $m_{\gamma'} = 2.5\text{--}7$ eV. See their Fig. 23 and Table III for mass-dependent limits.

20 APRILE 20 is analogous to ABE 14F, and set limits $\chi \lesssim 10^{-16}\text{--}10^{-12}$. The quoted limit applies to $m_{\gamma'} = 1$ keV. They also found an excess over known backgrounds, which favors the mass $m_{\gamma'} = 2.3 \pm 0.2$ keV with a 3σ significance. See their Fig. 10 for mass-dependent limits.

21 ARALIS 20 is analogous to ABE 14F. The quoted limit applies to $m_{\gamma'} = 0.1$ keV. The local density $\rho_{\gamma'} = 0.3$ GeV/cm 3 is assumed. The limits at masses above 3 keV in their Fig. 10 was later found to be incorrect due to an error in their analysis. See Fig. 3 in ARALIS 21 for the corrected limits.

22 ARGUELLES 20 examine hidden-photon production in atmospheric cosmic-ray showers and its decay in IceCube and Super-Kamiokande. The quoted limit assumes a lifetime of $\tau = 0.1$ km. See their Fig. 16 for mass- and lifetime-dependent limits.

23 ARNAUD 20 look for the absorption signal of hidden photon dark matter in a Ge detector. The quoted limit applies to $m_{\gamma'} \simeq 9$ eV. The local density $\rho_{\gamma'} = 0.3$ GeV/cm 3 is assumed. See their Fig. 3 for mass-dependent limits.

24 BANERJEE 20 is an update of BANERJEE 18. They exclude $8.2 \times 10^{-5} \lesssim \chi \lesssim 1 \times 10^{-2}$ for $m_{\gamma'} = 1.5\text{--}24$ MeV. In particular, they exclude $\chi = 1.2 \times 10^{-4}\text{--}6.8 \times 10^{-4}$ for the 16.7 MeV gauge boson. See their Fig. 5 for mass-dependent limits.

25 BARAK 20 is analogous to AGUILAR-AREVALO 19A, and look for hidden photon dark matter by using the Skipper CCD. The quoted limit applies to $m_{\gamma'} = 12.8$ eV. See their Fig. 4 for mass-dependent limits.

26 KRASNIIKOV 20 showed that the limit of BANERJEE 20 combined with the measured anomalous magnetic moment of the electron exclude the 16.7 MeV gauge boson suggested by the ATOMKI (KRASNAHORKAY 16) experiment if it has pure vector or axial-vector interactions.

27 SHE 20 look for solar hidden photons. The quoted limit applies to $m_{\gamma'} = 180$ eV. See their Fig. 4 for mass-dependent limits.

28 SHE 20 look for hidden photon dark matter and set limits $\chi < 1.3 \times 10^{-15}\text{--}2.8 \times 10^{-14}$ for the quoted mass range. The local density $\rho_{\gamma'} = 0.3$ GeV/cm 3 is assumed. See their Fig. 6 for mass-dependent limits.

29 SIRUNYAN 20AQ look for a narrow resonance decaying into a pair of muons. For $m_{\gamma'} < 45$ GeV, they use dedicated high-rate dimuon triggers to reduce the muon transverse momentum thresholds. The quoted limit applies to $m_{\gamma'} = 50$ GeV, and limits of order 10^{-3} are obtained for the quoted mass range. See their Fig. 3 for mass-dependent limits.

30 TOMITA 20 look for hidden photon dark matter using a planar metal plate and cryogenic receiver and set limits $\chi < 1.8\text{--}4.3 \times 10^{-10}$ for the quoted mass range. The local density $\rho_{\gamma'} = 0.39$ GeV/cm 3 is assumed. See their Fig. 7 for mass-dependent limits.

31 WANG 20A is analogous to ABE 14F. The quoted limit applies to $m_{\gamma'} = 185$ eV. The local density $\rho_{\gamma'} = 0.3$ GeV/cm 3 is assumed. See their Fig. 11 for mass-dependent limits.

32 AABOUD 19G look for $h \rightarrow \gamma' \gamma'$ ($\gamma' \rightarrow \mu^+ \mu^-$) and exclude a kinetic mixing around $10^{-9}\text{--}10^{-8}$ for $B(h \rightarrow \gamma' \gamma') = 0.01$ and 0.1 . See their Fig. 9 for mass-dependent limits.

33 ABLIKIM 19A look for $J/\psi \rightarrow \gamma' \eta$ ($\gamma' \rightarrow e^+ e^-$). Limits between 6×10^{-3} and 5×10^{-2} are obtained (see their Fig. 8).

34 ABLIKIM 19H look for $J/\psi \rightarrow \gamma' \eta'$ ($\gamma' \rightarrow e^+ e^-$). Limits between 3.4×10^{-3} and 2.6×10^{-2} are obtained. See their Fig. 5 for mass-dependent limits.

35 AGUILAR-AREVALO 19A look for the absorption signal of hidden photon dark matter by using a CCD. The quoted limit applies to $m_{\gamma'} = 17$ eV. The local density $\rho_{\gamma'} = 0.3$ GeV/cm 3 is assumed. See their Fig. 4 for mass-dependent limits.

36 APRILE 19D is analogous to ABE 14F. The quoted limit applies to $m_{\gamma'} = 0.7$ keV. See their Fig. 5(f) for mass-dependent limits.

37 BANERJEE 19 is an update of BANERJEE 18A. The quoted limit is at $m_{\gamma'} = 1$ MeV. See their Fig. 3 for mass-dependent limits.

38 BHOONAH 19 examine heating of Galactic Center gas clouds by hidden photon dark matter. The quoted limit applies to $m_{\gamma'} \simeq 10^{-12}$ eV. See their Fig. 2 for mass-dependent limits.

39 BRUN 19 is analogous to SUZUKI 15. The limit is derived under an assumption that hidden photons constitute the local dark matter density $\rho_{\gamma'} = 0.3$ GeV/cm 3 .

40 CORTINA-GIL 19 look for an invisible hidden photon in the reaction $K^+ \rightarrow \pi^+ \pi^0$ ($\pi^0 \rightarrow \gamma \gamma'$). The quoted limit applies to $m_{\gamma'} = 62.5\text{--}65$ MeV. See their Figs. 6 and 7 for mass-dependent limits.

41 DANILOV 19 examined the hidden photon production in nuclear reactors, correctly taking account of the effective photon mass in the reactor and detector. The limit gets weaker

Gauge & Higgs Boson Particle Listings

Axions (A^0) and Other Very Light Bosons

- for $m_{\gamma'}$ less than the effective photon mass in proportion to $1/m_{\gamma'}^2$. See their Fig. 1 for mass-dependent limits.
- 42 HOCHBERG 19 look for the absorption signal of hidden photon dark matter by using superconducting-nanowire single-photon detectors. The quoted limit applies to $m_{\gamma'} \simeq 1$ eV. The local density $\rho_{\gamma'} = 0.3 \text{ GeV/cm}^3$ is assumed. See their Fig. 4 for mass-dependent limits.
- 43 KOPYLOV 19 look for hidden-photon dark matter using a counter with an aluminum cathode and derive limits assuming it constitute all the local dark matter. The quoted limit applies to $m_{\gamma'} = 12$ eV. See their Fig. 7 for mass-dependent limits.
- 44 KOVETZ 19 examine heating of the early Universe plasma by hidden photon dark matter, and derive the limits by requiring that the cosmic mean 21 cm brightness temperature relative to the CMB temperature satisfy $T_{21} > -100$ mK. The quoted limit applies to $m_{\gamma'} \simeq 2 \times 10^{-14}$ eV. See their Fig. 3 for mass-dependent limits.
- 45 NGUYEN 19 look for hidden photon dark matter with a resonant cavity, and set limits $\sim 10^{-12}$ for $m_{\gamma'} = 0.2\text{--}2.07 \mu\text{eV}$. The quoted limit applies to $m_{\gamma'} = 1.3 \mu\text{eV}$. The local density $\rho_{\gamma'} = 0.3 \text{ GeV/cm}^3$ is assumed. See their Fig. 19 for mass-dependent limits.
- 46 ABE 18f is an update of ABE 14f. The quoted limit applies to $m_{\gamma'} \simeq 40$ keV. See their Fig. 5 for mass-dependent limits.
- 47 ADRIAN 18 look for a hidden photon resonance in the reaction $e^- Z \rightarrow e^- Z \gamma'$ ($\gamma' \rightarrow e^+ e^-$). The quoted limit applies to $m_{\gamma'} = 40$ MeV. See their Fig. 4 for mass-dependent limits.
- 48 ANASTASI 18b look for a hidden photon resonance in the reaction $e^+ e^- \rightarrow \gamma' \gamma' \rightarrow \mu^+ \mu^-$. The quoted limit is obtained by combining the result of ANASTASI 16 and it applies to $m_{\gamma'} \simeq 519\text{--}987$ MeV. See their Fig. 9 for mass-dependent limits.
- 49 ARMENGAUD 18 is analogous to ABE 14f. The quoted limits applies to $m_{\gamma'} = 1.6$ keV. See the right panel of Fig. 5 for mass-dependent limits.
- 50 BANERJEE 18 look for hidden photons produced in the reaction $e^- Z \rightarrow e^- Z \gamma'$ ($\gamma' \rightarrow e^+ e^-$), and exclude $9.2 \times 10^{-5} \lesssim \chi \lesssim 1 \times 10^{-2}$ for $m_{\gamma'} = 1\text{--}23$ MeV. They also set a limit on the electron coupling to a 16.7 MeV gauge boson suggested by the ATOMKI (KRASZNAHORKAY 16) experiment. See their Fig. 3 for mass-dependent limits.
- 51 BANERJEE 18a look for invisible decays of hidden photons produced in the reaction $e^- Z \rightarrow e^- Z \gamma'$. The quoted limit is at $m_{\gamma'} = 1$ MeV. See their Fig. 15 for mass-dependent limits.
- 52 KNIRCK 18 is analogous to SUZUKI 15. See their Fig. 5 for mass-dependent limits.
- 53 ABRALL 17 is analogous to ABE 14f using the MAJORANA DEMONSTRATOR. See their Fig. 3 for limits between $6 \text{ keV} < m_{\gamma'} < 97 \text{ keV}$.
- 54 ABLIKIM 17AA look for $e^+ e^- \rightarrow \gamma' \gamma' \rightarrow e^+ e^-$ or $\mu^+ \mu^-$. Limits between 10^{-3} and 10^{-4} are obtained (see their Fig. 3).
- 55 ANGLÖHER 17 is analogous to ABE 14f. The quoted limit is at $m_{\gamma'} = 0.7$ keV. See their Fig. 8 for mass-dependent limits.
- 56 BANERJEE 17 look for invisible decays of hidden photons produced in the reaction $e^- Z \rightarrow e^- Z \gamma'$. The quoted limit applies to $m_{\gamma'} = 2$ MeV. See their Fig. 3 for mass-dependent limits.
- 57 CHANG 17 examine the hidden photon emission from SN1987A, including the effects of finite temperature and density on χ and obtain limits $\chi (m_{\gamma'}/\text{MeV}) \lesssim 3 \times 10^{-9}$ for $m_{\gamma'} < 15$ MeV and $\chi \lesssim 10^{-9}$ for $m_{\gamma'} = 15\text{--}120$ MeV.
- 58 DUBININA 17 look for $\mu^+ \rightarrow e^+ \bar{\nu}_\mu \nu_e \gamma'$ ($\gamma' \rightarrow e^+ e^-$) in a nuclear photoemulsion. The quoted limit applies to $m_{\gamma'} = 1.1$ MeV. Limits between 4.5×10^{-3} and 10^{-2} are obtained (see their Fig. 3).
- 59 LEES 17e look for invisible decays of hidden photons produced in the reaction $e^+ e^- \rightarrow \gamma \gamma'$. See their Fig. 5 for limits in the mass range $m_{\gamma'} \leq 8$ GeV.
- 60 AAD 16AG look for hidden photons promptly decaying into collimated electrons and/or muons, assuming that they are produced in the cascade decays of squarks or the Higgs boson. See their Fig. 10 and Fig.13 for their limits on the cross section times branching fractions.
- 61 ANASTASI 16 look for the decay $\gamma' \rightarrow \pi^+ \pi^-$ in the reaction $e^+ e^- \rightarrow \gamma \gamma'$. Limits between 4.3×10^{-3} and 4.4×10^{-4} are obtained for $527 < m_{\gamma'} < 987$ MeV (see their Fig. 9).
- 62 KHACHATRYAN 16 look for $\gamma' \rightarrow \mu^+ \mu^-$ in a dark SUSY scenario where the SM-like Higgs boson decays into a pair of the visible lightest neutralinos with mass 10 GeV, both of which decay into γ' and a hidden neutralino with mass 1 GeV. See the right panel in their Fig. 2.
- 63 AAD 15CD look for $H \rightarrow Z \gamma' \rightarrow 4\ell$ with the ATLAS detector at LHC and find $\chi < 4\text{--}17 \times 10^{-2}$ for $m_{\gamma'} = 15\text{--}55$ GeV. See their Fig. 6.
- 64 ADARE 15 look for a hidden photon in $\pi^0, \eta^0 \rightarrow \gamma e^+ e^-$ at the PHENIX experiment. See their Fig. 4 for mass-dependent limits.
- 65 AN 15A derived limits from the absence of ionization signals in the XENON10 and XENON100 experiments, assuming hidden photons constitute all the local dark matter. Their best limit is $\chi < 1.3 \times 10^{-15}$ at $m_{\gamma'} = 18$ eV. See their Fig. 1 for mass-dependent limits.
- 66 ANASTASI 15 look for a production of a hidden photon and a hidden Higgs boson with the KLOE detector at DAΦNE, where the hidden photon decays into a pair of muons and the hidden Higgs boson lighter than $m_{\gamma'}$ escape detection. See their Figs. 6 and 7 for mass-dependent limits on a product of the hidden fine structure constant and the kinetic mixing.
- 67 ANASTASI 15A look for the decay $\gamma' \rightarrow e^+ e^-$ in the reaction $e^+ e^- \rightarrow e^+ e^- \gamma'$. Limits between 1.7×10^{-3} and 1×10^{-2} are obtained for $m_{\gamma'} = 5\text{--}320$ MeV (see their Fig. 7).
- 68 BATLEY 15A look for $\pi^0 \rightarrow \gamma \gamma' (\gamma' \rightarrow e^+ e^-)$ at the NA48/2 experiment. Limits between 4.2×10^{-4} and 8.8×10^{-3} are obtained for $m_{\gamma'} = 9\text{--}120$ MeV (see their Fig. 4).
- 69 JAEGLER 15 look for the decay $\gamma' \rightarrow e^+ e^-, \mu^+ \mu^-,$ or $\pi^+ \pi^-$ in the dark Higgsstrahlung channel, $e^+ e^- \rightarrow \gamma' H' (H' \rightarrow \gamma' \gamma')$ at the BELLE experiment. They set limits on a product of the branching fraction and the Born cross section as well as a product of the hidden fine structure constant and the kinetic mixing. See their Figs. 3 and 4.
- 70 KAZANAS 15 set limits by studying the decay of hidden photons $\gamma' \rightarrow e^+ e^-$ inside and near the progenitor star of SN1987A. See their Fig. 6 for mass-dependent limits.
- 71 SUZUKI 15 looked for hidden-photon dark matter with a dish antenna and derived limits assuming they constitute all the local dark matter. Their limits are $\chi < 6 \times 10^{-12}$ for $m_{\gamma'} = 1.9\text{--}4.3$ eV. See their Fig. 7 for mass-dependent limits.
- 72 VINYOLETS 15 performed a global fit analysis based on helioseismology and solar neutrino observations, and set the limits $\chi m_{\gamma'} < 1.8 \times 10^{-12}$ eV for $m_{\gamma'} = 3 \times 10^{-9}\text{--}8$ eV. See their Fig. 11.
- 73 ABE 14f look for the photoelectric-like interaction in the XMASS detector assuming the hidden photon constitutes all the local dark matter. Limits between 2×10^{-13} and 1×10^{-12} are obtained, where the relation $\chi^2 = \alpha'/\alpha$ is used to translate the original bound on the ratio of the hidden and EM fine-structure constants. See their Fig. 3 for mass-dependent limits.
- 74 AGAKISHIEV 14 look for hidden photons $\gamma' \rightarrow e^+ e^-$ at the HADES experiment, and set limits on χ for $m_{\gamma'} = 0.02\text{--}0.6$ GeV. See their Fig. 5 for mass-dependent limits.
- 75 BABUSCI 14 look for the decay $\gamma' \rightarrow \mu^+ \mu^-$ in the reaction $e^+ e^- \rightarrow \mu^+ \mu^- \gamma'$. Limits between 4×10^{-3} and 9.0×10^{-4} are obtained for $520 \text{ MeV} < m_{\gamma'} < 980 \text{ MeV}$ (see their Fig. 7).
- 76 BATELL 14 derived limits from the electron beam dump experiment at SLAC (E-137) by searching for events with recoil electrons by sub-GeV dark matter produced from the decay of the hidden photon. Limits at the level of $10^{-4}\text{--}10^{-1}$ are obtained for $m_{\gamma'} = 10^{-3}\text{--}1$ GeV, depending on the dark matter mass and the hidden gauge coupling (see their Fig. 2).
- 77 BLUEMLEIN 14 analyzed the beam dump data taken at the U-70 accelerator to look for γ' -bremsstrahlung and the subsequent decay into muon pairs and hadrons. See their Fig. 4 for mass-dependent excluded region.
- 78 FRADETTE 14 studied effects of decay of relic hidden photons on BBN and CMB to set constraints on very small values of the kinetic mixing. See their Figs. 4 and 7 for mass-dependent excluded regions.
- 79 LEES 14j look for hidden photons in the reaction $e^+ e^- \rightarrow \gamma \gamma' (\gamma' \rightarrow e^+ e^-, \mu^+ \mu^-)$. Limits at the level of $10^{-4}\text{--}10^{-3}$ are obtained for $0.02 \text{ GeV} < m_{\gamma'} < 10.2 \text{ GeV}$. See their Fig. 4 for mass-dependent limits.
- 80 MERKEL 14 look for $\gamma' \rightarrow e^+ e^-$ at the A1 experiment at the Mainz Microtron (MAMI). See their Fig. 3 for mass-dependent limits.
- 81 AN 13B examined the stellar production of hidden photons, correcting an important error of the production rate of the longitudinal mode which now dominates. See their Fig. 2 for mass-dependent limits based on solar energy loss.
- 82 AN 13C use the solar flux of hidden photons to set a limit on the atomic ionization rate in the XENON10 experiment. They find $\chi m_{\gamma'} < 3 \times 10^{-12}$ eV for $m_{\gamma'} < 1$ eV. See their Fig. 2 for mass-dependent limits.
- 83 DIAMOND 13 analyzed the beam dump data taken at the SLAC millicharge experiment to constrain a hidden photon invisibly decaying into lighter long-lived particles, which undergo elastic scattering off nuclei in the detector. Limits between $8 \times 10^{-4}\text{--}2 \times 10^{-2}$ are obtained. The quoted limit is applied when the dark gauge coupling is set equal to the electromagnetic coupling. See their Fig. 4 for mass-dependent limits.
- 84 GNINENKO 13 used the data taken at the SINDRUM experiment to constrain the decay, $\pi^0 \rightarrow \gamma \gamma' (\gamma' \rightarrow e^+ e^-)$ to derive limits. See their Fig. 2 for their mass-dependent excluded region.
- 85 HORVAT 13 look for hidden-photo-electric effect in HPGe detectors induced by solar hidden photons. See their Fig. 3 for mass-dependent limits.
- 86 INADA 13 search for hidden photons using an intense X-ray beamline at SPRing-8. See their Fig. 4 for mass-dependent limits.
- 87 MIZUMOTO 13 look for solar hidden photons. See their Fig. 5 for mass-dependent limits.
- 88 PARKER 13 look for hidden photons using a cryogenic resonant microwave cavity. See their Fig.5 for mass-dependent limits.
- 89 PARKER 13 derived a limit for the hidden photon CDM with a randomly oriented hidden photon field.
- 90 REDONDO 13 examined the solar emission of hidden photons including the enhancement factor for the longitudinal mode pointed out by AN 13b, and also updated stellar-energy loss arguments. See their Fig.3 for mass-dependent limits, including a review of the currently best limits from other arguments.
- 91 GNINENKO 12a obtained bounds on $B(\pi^0 \rightarrow \gamma \gamma') \cdot B(\gamma' \rightarrow e^+ e^-)$ from the NOMAD and PS191 neutrino experiments, and derived limits between $8 \times 10^{-8}\text{--}2 \times 10^{-4}$. See their Fig.4 for mass-dependent excluded regions.
- 92 GNINENKO 12b used the data taken at the CHARM experiment to constrain the decay, $\eta(\eta') \rightarrow \gamma \gamma' (\gamma' \rightarrow e^+ e^-)$, and derived limits between $1 \times 10^{-7}\text{--}1 \times 10^{-4}$. See their Fig.4 for mass-dependent excluded region.
- 93 ABRAHAM MYAN 11 look for $\gamma' \rightarrow e^+ e^-$ in the electron-nucleon fixed-target experiment at the Jefferson Laboratory (APEX). See their Fig. 5 for mass-dependent limits.
- 94 BLUEMLEIN 11 analyzed the beam dump data taken at the U-70 accelerator to look for $\pi^0 \rightarrow \gamma \gamma' (\gamma' \rightarrow e^+ e^-)$. See their Fig. 5 for mass-dependent limits.
- 95 BJORKEN 09 analyzed the beam dump data taken at E137, E141, and E774 to constrain a hidden photon produced by bremsstrahlung, subsequently decaying into $e^+ e^-$, and derived limits between 10^{-7} and 10^{-2} . See their Fig. 1 for mass-dependent excluded region.
- 96 BJORKEN 09 required the energy loss in the γ' emission from the core of SN1987A not to exceed 10^{53} erg/s, and derived limits between 5×10^{-9} and 2×10^{-6} . See their Fig. 1 for mass-dependent excluded region.

REFERENCES FOR Searches for Axions (A^0) and Other Very Light Bosons

LEES	22	PRL 128 021802	J.P. Lees et al.	(BABAR Collab.)
AAD	21F	PR D103 112006	G. Aad et al.	(ATLAS Collab.)
AAD	21K	JHEP 2102 226	G. Aad et al.	(ATLAS Collab.)
AAD	21N	JHEP 2103 243	G. Aad et al.	(ATLAS Collab.)
Also		JHEP 2111 050 (err.)	G. Aad et al.	(ATLAS Collab.)

See key on page 1127

Gauge & Higgs Boson Particle Listings

Axions (A⁰) and Other Very Light Bosons

ABRATENKO	21	PRL 127 151803	P. Abratenko et al.	(MicroBoONE Collab.)	ALONI	19	PRL 123 071801	D. Aloni et al.	(REHO, MIT, CERN, HAIF)
ADE	21	PR D103 042002	P.A.R. Ade et al.	(BICEP/Keck Collab.)	APRILE	19D	PRL 123 251801	E. Aprile et al.	(XENON1T Collab.)
AFACH	21	NATP 17 1396	S. Afach et al.	(GNOE Collab.)	ARNOLD	19	EPJ C79 440	R. Arnold et al.	(NEMO-3 Collab.)
AQUILAR-AR...	21A	PR D103 052006	A. Aguilar-Arevalo et al.	(PIENU Collab.)	BANERJEE	19	PRL 123 121801	D. Banerjee et al.	(NA64 Collab.)
ALESINI	21	PR D103 102004	D. Alesini et al.	(QUAX Collab.)	BHOONAH	19	PR D100 023001	A. Bhoonah et al.	(SACL)
AL-KHARUSI	21	PR D104 112002	S. Al Kharusi et al.	(EXO-200 Collab.)	BRUN	19	PRL 122 201801	P. Brun, L. Chevalier, C. Flouzat	(SACL)
ANDREEV	21	PRL 126 211802	Yu.M. Andreev et al.	(NA64 Collab.)	CAPUTO	19	PR D100 063515	A. Caputo et al.	(NA62 Collab.)
ANDREEV	21A	PR D104 L091701	Yu.M. Andreev et al.	(NA64 Collab.)	CORTINA-GIL	19	JHEP 1905 182	E. Cortina Gil et al.	(LEBD, INRM+)
ANDREEV	21B	PR D104 111102	Yu.M. Andreev et al.	(NA64 Collab.)	DANILOV	19	PRL 122 041801	M. Danilov, S. Demidov, D. Gorbunov	(EBL)
ARALIS	21	PR D103 039901 (errat.)	T. Aralis et al.	(SuperCDMS Collab.)	DAVOUDIASH	19	PRL 123 021102	H. Davoudiasl, P.B. Denton	(MICH)
AYBAS	21	PRL 126 141802	D. Aybas et al.	(CASPER Collab.)	DESSERT	19	PRL 123 061104	C. Dessert, A.J. Long, B.R. Safdi	(STAN+)
BANIK	21	JCAP 2110 043	N. Banik et al.	(ADMX Collab.)	FEDDERKE	19	PR D100 015040	M.A. Fedderke, P.W. Graham, S. Rajendran	(KEBYT, GEVA, TOHO)
BARRAM	21A	PRL 127 261803	C. Barram et al.	(BIEL, NAGO)	FUJITA	19	PRL 122 191101	T. Fujita, R. Tazaki, K. Toma	(HEBR, MIT, NIST)
BASU	21	PRL 126 191102	A. Basu et al.	(BASE Collab.)	HOCHBERG	19	PRL 123 151802	Y. Hochberg et al.	(NEMO-3 Collab.)
BAUMHOLZ...	21	JCAP 2105 004	S. Baumholzer, V. Brdar, E. Morgante	(MAINZ, FNAL+)	IVANOV	19	JCAP 1902 059	M.M. Ivanov et al.	(INRM)
BHUSAL	21	PRL 126 091601	A. Bhusal, N. Houston, T. Li	(BEIJ)	KOPYLOV	19	JCAP 1907 008	A. Kopylov, I. Orehkov, V. Petukhov	(JHU)
BI	21	PR D103 043018	X.-J. Bi et al.	(BHEP, TSIN)	KOVETZ	19	PR D99 123511	E.D. Kovetz, I. Cholis, D.E. Kaplan	(JHU)
CALORE	21	PR D104 043016	F. Calore et al.	(HEID)	LEINSON	19	JCAP 1911 031	L.B. Leinson	(Y-F, LIANG ET AL.)
CARRA	21	PR D104 092005	S. Carra et al.	(NA64 Collab.)	LIANG	19	JCAP 1906 042	S.J. Liang et al.	(GOET)
CAZZANIGA	21	EPJ C81 959	C. Cazzaniga et al.	(NA62 Collab.)	LLOYD	19	PR D100 063005	D.J.E. Marsh, J.C. Niemeyer	(WISPMIDM Collab.)
CORTINA-GIL	21	PL B816 136259	E. Cortina Gil et al.	(NA62 Collab.)	MARSH	19	PRL 123 051103	L.H. Nguyen, A. Lobanov, D. Horns	(ABRACADABRA Collab.)
CORTINA-GIL	21A	JHEP 2103 058	E. Cortina Gil et al.	(NA62 Collab.)	NGUYEN	19	JCAP 2110 014	J.L. Ouellet et al.	(PALOMBA Collab.)
CORTINA-GIL	21C	JHEP 2102 201	E. Cortina Gil et al.	(NA62 Collab.)	OUELLET	19A	PRL 122 121802	C. Palomba et al.	(CMS Sirunyan et al.)
CROON	21	JHEP 2101 107	D. Croon et al.	(TRIU, WASH, MIT, FNAL)	PALOMBA	19	PRL 123 171101	C. Smorra et al.	(WASH)
DEVILIN	21	PRL 126 041301	J.A. Devlin et al.	(CHIC, RUTG, UCB+)	SIRUNYAN	19BQ	PL B796 131	A.M. Sirunyan et al.	(CASPER-ZULF Collab.)
DIXIT	21	PRL 126 141302	A.V. Dixit et al.	(MELB, BRCO, DESY)	SMORRA	19	NAT 575 310	C. Boutsan et al.	(XMASS Collab.)
DOLAN	21	JHEP 2103 190 (errat.)	M.J. Dolan et al.	(UCD, CSUS, STAN)	TERRANO	19	PRL 122 231301	W. Terrano et al.	(HPS Collab.)
DOLAN	21A	JCAP 2109 010	M.J. Dolan, F.J. Hiskens, R.R. Volkas	(SHAFT Collab.)	WU	19	PRL 122 191302	T. Wu et al.	(CASPER-ZULF Collab.)
FUJIKURA	21	PR D104 123012	K. Fujikura et al.	(BHEP)	WU	19C	PRL 123 169002	T. Wu et al.	(XMASS Collab.)
GHOSH	21	PR D104 092016	S. Ghosh et al.	(UCD, CSUS, STAN)	ABE	18F	PL B787 153	K. Abe et al.	(HPS Collab.)
GODFREY	21	PR D104 012013	B. Godfrey et al.	(SHAFT Collab.)	ADRIAN	18	PR D98 091101	P.H. Adrian et al.	(KLOE-2 Collab.)
GRAMOLIN	21	NATP 17 79	A.V. Gramolin et al.	(BHEP)	AKHMATOV	18	PRM 49 595	Z.A. Akhmatov et al.	(EDELWEISS-III Collab.)
GUO	21	CPL 049 025105	J.-G. Guo et al.	(SAPPHIRES Collab.)	ANASTASI	18B	PL B784 336	A. Anastasi et al.	(NEMO-3 Collab.)
HOMMA	21	JHEP 2112 108	K. Homma et al.	(OREG, TRIU)	ARMENGAUD	18	PR D98 082004	E. Armengaud et al.	(NA64 Collab.)
JIANG	21	NATP 17 1402	M. Jiang et al.	(CAPP-ACTION Collab.)	ARNOLD	18	EPJ C78 821	R. Arnold et al.	(NA64 Collab.)
KOPYLOV	21A	PPN 52 31	A.V. Kopylov, I.V. Orehkov, V.V. Petukhov	(BHEP)	BANERJEE	18	PRL 120 231802	D. Banerjee et al.	(NA64 Collab.)
KRIBS	21	PRL 126 011801	G.D. Kribs, D. McKeen, N. Raj	(DURH, OKLA)	BANERJEE	18A	PR D97 072002	D. Banerjee et al.	(NA64 Collab.)
KWON	21	PRL 126 191802	O. Kwon et al.	(BAR)	BEZNOGOV	18	PR C98 035802	M.V. Beznogov et al.	(ADMX Collab.)
LI	21B	PR D103 083003	H.-J. Li et al.	(CAST-RADES Collab.)	BOUTAN	18	PRL 121 261302	C. Boutsan et al.	(ADMX Collab.)
LLOYD	21	PR D103 023010	S.J. Lloyd et al.	(MIT, ANIK, UTRE, LEUV)	CHANG	18	JHEP 1809 051	J.C. Chang, R. Essig, S.D. McDermott	(QUAX Collab.)
LUCENTE	21	PR D104 103007	G. Lucente, P. Carena	(BELLE Collab.)	CRESINI	18	EPJ C78 703	N. Crescini et al.	(ADMX Collab.)
MARTINCAM...	21	PR D103 121301	J. Martin Camalich et al.	(MUSE Collab.)	DU	18	PRL 120 151301	N. Du et al.	(HAYSTAC Collab.)
MELCON	21	PR D103 083005	A.A. Melcon et al.	(STOH, LOUC)	DZUBA	18	PR D98 033048	V.A. Dzuba et al.	(LHCb Collab.)
NG	21	PRL 126 151102	K.K.Y. Ng et al.	(COLO, MAINZ)	FICEK	18	PRL 120 183002	F. Ficek et al.	(MAJORANA Collab.)
PARK	21	JHEP 2104 191	S.-H. Park et al.	(ABRACADABRA Collab.)	FORTIN	18	JHEP 1806 048	J.-F. Fortin, K. Sinha	(BESIII Collab.)
REGIS	21	PL B814 136075	M. Regis et al.	(FRAN, GSI, WAUS)	GAVRILYUK	18	JETPL 107 589	Yu.M. Gavriluk et al.	(LAVL, OKLA)
ROGERS	21	PRL 126 071302	K.K. Rogers, H.V. Peiris	(WASH)	HAMAGUCHI	18	PR D98 103015	K. Hamaguchi et al.	(TOBY, RIKEN, KEK)
ROUSSY	21	PRL 126 171301	T.S. Roussy et al.	(WASH)	KNIRCK	18	JCAP 1811 031	S. Knirck et al.	(HAYSTAC Collab.)
SALEMI	21	PRL 127 081801	C.P. Salemi et al.	(ROMA, TOKY, WATER)	STADNIK	18	PRL 120 013202	Y.V. Stadnik, V.A. Dzuba, V.V. Flambaum	(LHCb Collab.)
SCHMIDT	21	PR D104 015008	I. Schmidt et al.	(CST)	YAMAJI	18	PL B782 523	T. Yamaji et al.	(MAJORANA Collab.)
THOMSON	21	PRL 126 081803	C.A. Thomson et al.	(LHCb Collab.)	ZHANG	18	PR D97 063009	C. Zhang et al.	(BESIII Collab.)
Also		PRL 127 019901 (errat.)	C.A. Thomson et al.	(LHCb Collab.)	ZHONG	18	PR D97 092001	L. Zhong et al.	(LUX Collab.)
TSAI	21	PRL 126 181801	Y.-D. Tsai, P. deNiverville, M.X. Liu	(LHCb Collab.)	AAJ	17AQ	PR D95 071101	R. Aaij et al.	(KLOE-2 Collab.)
TSUKADA	21	PR D103 083005	L. Tsukada et al.	(LHCb Collab.)	ABEL	17	PR X7 041034	C. Abel et al.	(AURIGA Collab.)
XIAO	21	PRL 126 031101	M. Xiao et al.	(CAE, JINR)	ANGRALL	17	PRL 118 161801	N. Angrall et al.	(YALE, UCB, NIST+)
YUAN	21	JCAP 2103 018	G.-W. Yuan et al.	(JHEP 1701 107)	ABLIKIM	17A	PL B774 252	M. Ablikim et al.	(CAPP-ACTION Collab.)
ZHANG	21B	PRL 127 161101	J. Zhang et al.	(JHEP 1701 107)	ADE	17	PR D96 102003	P.A.R. Ade et al.	(BICEP2/Keck Array Collab.)
AJIJ	20AL	JHEP 2010 156	R. Aaij et al.	(JHEP 1701 107)	AHN	17	PTEP 2017 021C01	J.K. Ahn et al.	(KOTO Collab.)
AJLI	20C	PRL 124 041801	R. Aaij et al.	(JHEP 1701 107)	AKERIB	17B	PRL 118 261301	D.S. Akkerib et al.	(LUX Collab.)
ADDHAMEH...	20	EPJ C80 376	A.H. Abdelhameed et al.	(JHEP 1701 107)	ANASTASSO...	17	NATP 13 584	V. Anastassopoulos et al.	(CAST Collab.)
ABE	20J	PL B815 136174	T. Abe, K. Hamaguchi, N. Nagata	(JHEP 1701 107)	ANGLOHER	17	EPJ C77 299	G. Angloher et al.	(CRESS-TI Collab.)
ABLIKIM	20AB	PR D102 052005	M. Ablikim et al.	(JHEP 1701 107)	APRILE	17B	PR D95 029904	E. Aprile et al.	(XENON100 Collab.)
ABUDINEN	20	PRL 125 161806	F. Abudinen et al.	(JHEP 1701 107)	BANERJEE	17	PRL 118 011802	D. Banerjee et al.	(NA64 Collab.)
AGOSTINI	20	PRL 125 011801	M. Agostini et al.	(JHEP 1701 107)	BATLEY	17	PL B769 67	J.R. Batley et al.	(NA48/2 Collab.)
AQUILAR-AR...	20A	PR D101 052006	A. Aguilar-Arevalo et al.	(JHEP 1701 107)	BRANCA	17	PRL 118 021302	F. Branca et al.	(KIMS Collab.)
AMARAL	20	PR D102 091101	D.M. Amaral et al.	(JHEP 1701 107)	BRUBAKER	17	PRL 118 061302	B.M. Brubaker et al.	(VALE, UCB, NIST+)
AN	20	PR D102 115002	H. An et al.	(JHEP 1701 107)	CHANG	17	JHEP 1701 107	J.H. Chang, R. Essig, S.D. McDermott	(STON)
ANDRIANAV...	20	PR D102 042001	A. Andrianavomaloha et al.	(JHEP 1701 107)	CHOI	17	PR D96 061102	J. Choi et al.	(CAPP-ACTION Collab.)
APRILE	20	PR D102 072004	E. Aprile et al.	(JHEP 1701 107)	CRESINI	17	PL B773 677	N. Crescini et al.	(QUAX-eggs Collab.)
ARALIS	20	PR D101 052008	T. Aralis et al.	(JHEP 1701 107)	DAIDO	17	PL B772 127	R. Daido, F. Takahashi	(JHEP 1701 107)
Also		PR D103 039901 (errat.)	T. Aralis et al.	(JHEP 1701 107)	DOLAN	17	JHEP 1712 094	M.J. Dolan et al.	(MELB, BRCO, DESY)
ARGUELLES	20	JHEP 2002 190	C. Argüelles et al.	(JHEP 1701 107)	Also		JHEP 2103 190 (errat.)	M.J. Dolan et al.	(MELB, BRCO, DESY)
ARNAUD	20	PRL 125 141301	Q. Arnaud et al.	(JHEP 1701 107)	DUBINIINA	17	PAN 80 461	V.V. Dubinina et al.	(Pandax-II Collab.)
BALDINI	20	EPJ C80 858	A.M. Baldini et al.	(JHEP 1701 107)	FICEK	17	PR A95 032505	F. Ficek et al.	(Pandax-II Collab.)
BANERJEE	20	PR D101 071101	D. Banerjee et al.	(JHEP 1701 107)	FU	17A	PRL 119 181806	C. Fu et al.	(Pandax-II Collab.)
BANERJEE	20A	PRL 125 081802	D. Banerjee et al.	(JHEP 1701 107)	INADA	17	PRL 118 071803	I. Inada et al.	(KIMS Collab.)
BARAK	20	PRL 125 171802	L. Barak et al.	(JHEP 1701 107)	KLIMCHITSK...	17A	PR D95 122013	G.L. Klimchitskaya, V.M. Mostepanenko	(KEK, KYOT)
BRINE	20	PRL 124 101303	T. Braine et al.	(JHEP 1701 107)	KOHIRI	17	PR D96 051701	K. Kohri, H. Kodama	(BABAR Collab.)
BUEHLER	20	JCAP 2009 027	R. Buehler et al.	(JHEP 1701 107)	LEES	17E	PRL 119 131804	J.P. Lees et al.	(TINT Collab.)
CALORE	20	PR D102 123005	F. Calore et al.	(JHEP 1701 107)	LIU	17	PL B766 117	X.-H. Liu et al.	(CDEX Collab.)
CAPOZZI	20	PR D102 083007	F. Capozzi, G. Raffelt	(JHEP 1701 107)	LIU	17A	PR D95 052006	S.K. Liu et al.	(CDEX Collab.)
CARENZA	20	PL B809 135709	P. Carena et al.	(JHEP 1701 107)	LUO	17	PR D96 055028	P. Luo et al.	(CDEX Collab.)
CRESINI	20	PRL 124 171801	N. Crescini et al.	(JHEP 1701 107)	MARSH	17	JCAP 1712 036	M.C.D. Marsh et al.	(Technion)
CRIOSTO	20	PRL 124 241101	N. Cristoso et al.	(JHEP 1701 107)	TIWARI	17	PR D95 023005	P. Tiwari	(ATLAS Collab.)
DARLING	20	PRL 125 121103	J. Darling	(JHEP 1701 107)	AAD	16AG	JHEP 1602 062	G. Aad et al.	(ATLAS Collab.)
DARLING	20A	APJ 900 L28	J. Darling	(JHEP 1701 107)	ABLIKIM	16G	PR D93 052005	M. Ablikim et al.	(BESIII Collab.)
DENT	20	PRL 125 131805	J.B. Dent et al.	(JHEP 1701 107)	AJELLO	16	PRL 116 161101	M. Ajello et al.	(Fermi-LAT Collab.)
DEPTA	20	JCAP 2005 009	P.F. Depina, M. Hufnagel, K. Schmidt-Hoberg	(JHEP 1701 107)	ANASTASI	16	PR D97 071801	A. Anastasi et al.	(KLOE-2 Collab.)
DESSERT	20A	PRL 125 261102	C. Dessert, J.W. Foster, B.R. Safdi	(JHEP 1701 107)	BATTICHI	16	JCAP 1608 062	T. Battich et al.	(KLOE-2 Collab.)
ESTEBAN	20	EPJ C80 259	I. Esteban et al.	(JHEP 1701 107)	BERENJI	16	PR D93 045019	B. Berenji et al.	(KLOE-2 Collab.)
FESTER	20	PRL 125 171301	J.W. Foster et al.	(JHEP 1701 107)	CORSICO	16	JCAP 1607 036	A.H. Corsico et al.	(PVLAS Collab.)
GAO	20	PRL 125 131806	C. Gao et al.	(JHEP 1701 107)	DELLA-VALLE	16	EPJ C76 24	F. Della Valle et al.	(ADMX Collab.)
GAVELA	20	PRL 124 051802	M.B. Gavela et al.	(JHEP 1701 107)	HOSKINS	16	PR D94 082001	J. Hoskins et al.	(HEID, DURH)
GHOSH	20A	JCAP 2010 060	D. Ghosh, D. Sachdeva	(JHEP 1701 107)	JAECKEL	16	PL B753 482	J. Jaeckel, M. Spannowsky	(CMS Collab.)
IRSI	20	PR D101 123518	V. Irsic, H. Xiao, M. McQuinn	(JHEP 1701 107)	KHACHATRY...	16	PL B752 146	V. Khachatryan et al.	(CMS Collab.)
JEONG	20	PRL 125 221302	J. Jeong et al.	(JHEP 1701 107)	KRASNAHORAY...	16	PRL 116 042501	A.J. Krasznahorkay et al.	(HINR, ANIK+)
KENNEDY	20	PRL 125 201302	C.J. Kennedy et al.	(JHEP 1701 107)	LEEFER	16	PRL 117 271601	N. Leefler et al.	(MAINZ, BONN, LBL, UCB+)
KLIMCHITSK...	20	PR D101 056013	G.L. Klimchitskaya, P. Kausk, V.M. Mostepanenko	(JHEP 1701 107)	WON	16	PR D94 092006	E. Won et al.	(BELLE Collab.)
KOIRO CHIKIN	20	JCAP 2003 064	A. Korochnik, A. Neranov, D. Semizov	(JHEP 1701 107)	YOUNG	16	JHEP 1606 011	Y.S. Young et al.	(KIMS Collab.)
KRASNIKOVA	20	MPL A35 2050116	N.V. Krasnikova	(JHEP 1701 107)	AAD	15CD	PR D92 022001	G. Aad et al.	(ATLAS Collab.)
LEE	20A	PRL 124 101802	S. Lee et al.	(JHEP 1701 107)	AALJ	15AZ	PRL 115 161802	R. Aaij et al.	(LHCb Collab.)
LUCENTE	20A	JCAP 2012 008	G. Lucente et al.	(JHEP 1701 107)	ADARE	15	PR C91 031901	A. Adare et al.	(PHENIX Collab.)
MEYER	20	PRL 124 231101	M. Meyer, T. Petrushevska	(JHEP 1701 107)	AFACH	15	PL B745 58	S. Afach et al.	(ETH, PSI, CAEN, +)
Also		PRL 125 119901 (errat.)	M. Meyer, T. Petrushevska	(JHEP 1701 107)	AGOSTINI	15A	EPJ C75 416	M. Agostini et al.	(GERDA Collab.)
PODDAR	20	PR D101 083007	T.K. Poddar, S. Mohanty,						

Gauge & Higgs Boson Particle Listings

Axions (A^0) and Other Very Light Bosons

SUZUKI	15	JCAP 1509 042	J. Suzuki et al.	(WASH)	ZIOUTAS	05	PRL 94 121301	K. Zioutas et al.	(CAST Collab.)
TERRANO	15	PRL 115 201801	W.A. Terrano et al.	(WASH)	ADLER	04	PR D70 037102	S. Adler et al.	(BNL E787 Collab.)
VANTILBURG	15	PRL 115 011802	K. Van Tilburg et al.	(WASH)	ANISIMOVSK...	04	PRL 93 031801	V.V. Anisimovsky et al.	(BNL E787 Collab.)
VINYOLES	15	JCAP 1510 015	N. Vinyoles et al.	(XMASS Collab.)	ARNOLD	04	JETPL 80 377	R. Arnold et al.	(NEMO-3 Collab.)
ABE	14F	PRL 113 121301	K. Abe et al.	(XMASS Collab.)	ASZTALOS	04	PR D69 011101	Translated from ZETFP 80 429.	
AGAKISHIEV	14	PL B731 265	G. Agakishiev et al.	(HADES Collab.)	HOFFMANN	04	PR B70 180503	S.J. Asztalos et al.	
ALBERT	14A	PR D90 092004	J.B. Albert et al.	(EXO-200 Collab.)	ARNABOLDI	03	PL B572 167	C. Hoffmann et al.	
APRILE	14B	PR D90 062009	E. Aprile et al.	(XENON100 Collab.)	CIVITARESE	03	NP A729 867	O. Civitaresse, J. Suhonen	
ARIK	14	PRL 112 091302	M. Arik et al.	(CAST Collab.)	DANEVICH	03	PR C68 035501	F.A. Danevich et al.	
AYALA	14	PRL 113 191302	A. Ayala et al.	(KLOE-2 Collab.)	ADLER	02C	PL B537 211	S. Adler et al.	(BNL E787 Collab.)
BABUSCI	14	PL B736 459	D. Babusci et al.	(KLOE-2 Collab.)	BADERT...	02C	PL B542 29	A. Badertscher et al.	
BATELL	14	PRL 113 171802	B. Batell, R. Essig, Z. Surujon	(EFI, STON)	BERNABEI	02D	PL B546 23	R. Bernabei et al.	(DAMA Collab.)
BEZERRA	14	PR D89 035010	V.B. Bezerra et al.		DERBIN	02D	PAN 65 1302	A.V. Derbin et al.	
BEZERRA	14A	EPJ C74 2859	V.B. Bezerra et al.		FUSHIMI	02	PL B531 190	K. Fushimi et al.	(ELEGANT V Collab.)
BEZERRA	14B	PR D90 055013	V.B. Bezerra et al.		INOUE	02	PL B536 18	Y. Inoue et al.	
BEZERRA	14C	PR D89 075002	V.B. Bezerra et al.		MORALES	02B	ASP 166 325	A. Morales et al.	(COSME Collab.)
BLUEMLEIN	14	PL B731 320	J. Bluemlein, J. Brunner	(CPPM, DESY)	ADLER	01	PR D63 032004	S. Adler et al.	(BNL E787 Collab.)
BLUM	14	PL B737 30	K. Blum et al.	(IAS, PRIN)	AMMAR	01B	PRL 87 271801	R. Ammar et al.	(CLEO Collab.)
DELLA-VALLE	14	PR D90 092003	F. Della Valle et al.	(PVLAS Collab.)	ASHITKOV	01	JETPL 74 529	V.D. Ashitkov et al.	
DERBIN	14	EPJ C74 3035	A.V. Derbin et al.		BERNABEI	01B	PL B515 6	R. Bernabei et al.	(DAMA Collab.)
EJILLI	14	PR D90 123527	D. Ejilli		DANEVICH	01	NP A694 375	F.A. Danevich et al.	
FRADLETTE	14	PR D90 035022	A. Fradette et al.	(BABAR Collab.)	DEBOER	01	JP D27 129	F.W.N. de Boer et al.	
LEES	14J	PRL 113 201801	J.P. Lees et al.	(BABAR Collab.)	STOICA	01	NP A594 249	S. Stoica, H.V. Klapdor-Kleingrothaus	
LEINSON	14	JCAP 1408 031	L. Leinson	(A1 at MAMI)	ALESSANDRO...	00	PL B486 13	A. Alessandrello et al.	
MERKEL	14	PRL 112 221802	H. Merkel et al.		ARNOLD	00	NP A678 341	R. Arnold et al.	
MILLER-BER...	14	JCAP 1410 069	M.M. Miller Bertolami et al.	(OSQAR Collab.)	ASTIER	00B	PL B479 371	P. Astier et al.	(NOMAD Collab.)
PUGNAT	14	EPJ C74 3027	R. Pognat et al.	(OSQAR Collab.)	DANEVICH	00	PR C62 045501	F.A. Danevich et al.	
REESMAN	14	JCAP 1408 021	R. Reesman et al.	(OSU)	MASSO	00	PR D61 011701	E. Masso	
ABE	13D	PL B724 46	K. Abe et al.	(XMASS Collab.)	ARNOLD	99	PR A658 299	R. Arnold et al.	(NEMO Collab.)
ABRAMOWSKI	13A	PR D88 102003	A. Abramowski et al.	(H.E.S.S. Collab.)	NI	99	PRL 82 2439	W.-T. Ni et al.	
ADLARSON	13	PL B726 187	P. Adlarson et al.	(WASA-at-COSY Collab.)	SIMKOVIC	99	PR C60 055502	F. Simkovic et al.	
ALESSANDRIA	13B	JCAP 1305 007	F. Alessandria et al.	(CUORE Collab.)	ALTEGOER	98	PL B428 197	J. Altegoer et al.	(NEMO-2 Collab.)
AN	13C	PRL 111 041302	H. An, M. Pospelov, J. Pradler		ARNOLD	98	NP A636 209	R. Arnold et al.	
ARCHIDIACO...	13A	JCAP 1310 020	M. Archidiacono et al.	(EDELWEISS-II Collab.)	AVIGNONE	98	PR B1 5608	F.T. Avignone et al.	(Solar Axion Experiment)
ARMENGAUD	13	JCAP 1311 067	E. Armengaud et al.	(EDELWEISS-II Collab.)	DIAMZ	98	NP B527 44	M.A. Diaz et al.	
BABUSCI	13B	PL B720 111	D. Babusci et al.	(KLOE-2 Collab.)	KIM	98	PR D58 055006	J.E. Kim	
BARTH	13	JCAP 1305 010	K. Barth et al.	(CAST Collab.)	LUESCHER	98	PL B434 407	R. Luescher et al.	
BECK	13	PRL 111 231801	C. Beck	(CROWS Collab.)	MORIYAMA	98	PL B434 147	S. Moriyama et al.	
BETZ	13	PR D88 075014	M. Betz et al.		MORO	98	PL B440 69	T. Mori, H. Murayama	
BULATOWICZ	13	PRL 111 102001	M. Bulatowicz et al.	(DUKE, IND, SJTU)	POSEPPOV	98	PR D58 097703	M. Pospelov	
CHU	13	PR D87 011105	P.-H. Chu et al.		AHMAD	97	PRL 78 618	I. Ahmad et al.	(APEX Collab.)
DERBIN	13	EPJ C73 24190	A.V. Derbin et al.		BORISOV	97	JETP 83 868	A.V. Borisov, V.Y. Grishina	(MOSU)
DIAMOND	13	PRL 111 221803	M.D. Diamond, P. Schuster		DEBOER	97C	JP G23 185	F.W.N. de Boer et al.	
FRIEDLAND	13	PRL 110 061101	A. Friedland, M. Giannotti, M. Wise	(INRM)	KACHELRIESS	97C	PR D56 1313	M. Kachelriess, C. Wilke, G. Wunner	(BOCH)
GNINENKO	13	PR D87 035030	S.N. Gninenko et al.		KEIL	97	PR D56 2419	W. Keil et al.	
HECKEL	13	PRL 111 151802	B.R. Heckel et al.		KIT CHING	97	PRL 79 4079	P. Kit Ching et al.	(BNL E787 Collab.)
HORVAT	13	PL B721 220	R. Horvat et al.		LEINBERGER	97	PL B394 16	U. Leinberger et al.	(ORANGE Collab.)
INADA	13	PL B722 301	T. Inada et al.		ADLER	96	PRL 76 1421	S. Adler et al.	(BNL E787 Collab.)
LATTANZI	13	PR D88 063528	M. Lattanzi et al.		AMSLER	96B	ZPHY C70 219	C. Amstler et al.	(Crystal Barrel Collab.)
MEYER	13	PR D87 035027	M. Meyer, D. Horns, M. Raue		GANZ	96	PL B389 4	R. Ganz et al.	(GS1, HEID, FRAN, JAGL+)
MIZUMOTO	13	JCAP 1307 013	T. Mizumoto et al.		GUNTHER	96	PR D54 3641	M. Gunther et al.	(MPIK, SASSO)
PARKER	13	PR D88 112004	S. Parker et al.		KAMEL	96	PL B368 291	S. Kamel	(SHAMS)
REDOONDO	13	JCAP 1308 034	J. Redondo, G. Raffelt		MITSUI	96	EPL 33 111	T. Mitsui et al.	(TOKY)
TULLNEY	13	PRL 111 108001	K. Tullney et al.		YOUNG	96	PRL 77 2170	A.M. Young et al.	(AMHT, WASH)
VIAUX	13A	PRL 111 231301	N. Viaux et al.	(SACL)	ALTMANN	95	ZPHY C68 221	M. Altmann et al.	(TUM, LAPP, CPPM)
WOUTERS	13	APJ 772 44	D. Wouters, P. Brun	(BESIII Collab.)	BASSOMPIE...	95	PL B355 584	G. Bassompierre et al.	(LAPP, LCGT, LYON)
ABUKIM	12	PR D85 092012	M. Abukim et al.	(KLOE-2 Collab.)	MAENO	95	PL B337 574	T. Maeno et al.	(TOKY)
ARCHILLI	12	PL B706 251	F. Archilli et al.	(DAMA-KIEV)	RAFFELT	95	PR D51 1495	G. Raffelt, A. Weiss	(MPIM, MPFG)
BELLI	12	PL B711 41	P. Belli et al.	(Borexino Collab.)	SKALSEY	95	PR D51 6292	M. Skalsey, R.S. Conti	(MICH)
BELLINI	12B	PR D85 092003	G. Bellini et al.	(MPIM)	TSUNODA	95	EPL 30 273	T. Tsunoda et al.	(TOKY)
CADAMURO	12	JCAP 1202 032	D. Cadamuro et al.	(LAPL, ROSUL, WASH+)	ADACHI	94	PR A49 3201	S. Adachi et al.	(TMU)
CORSICO	12	JCAP 1212 010	A.H. Corsico et al.	(PNPI)	ALTHERR	94	ASP 2 175	T. Altherr, E. Pettigirard, T. del Rio Gaztelurrutia	
DERBIN	12	JETPL 95 339	A.V. Derbin et al.	(KamLAND-Zen Collab.)	AMSLER	94B	PL B333 271	C. Amstler et al.	(Crystal Barrel Collab.)
GANDO	12	PR C86 021601	A. Gando et al.	(INRM)	ASA	94	PL B323 90	S. Asai et al.	(TOKY)
GNINENKO	12A	PR D85 055027	S.N. Gninenko et al.	(INRM)	MEIJERDREES	94	PR D49 4937	M.R. Drees et al.	(BRCO, OREG, TRIU)
GNINENKO	12B	PL B713 244	S.N. Gninenko et al.	(LIEG)	VO	94	PR C49 3521	D.T. Vo et al.	(NTHU)
PAYZE	12	JCAP 1207 041	A. Payze et al.	(LIEG)	ATIYA	93	PRL 70 2521	M.S. Atiya et al.	(ISU, LBL, LLL, UCD)
RAFFELT	12	PR D86 015001	G. Raffelt et al.	(MPIM)	ATIYA	93	PRL 71 305 (erratum)	M.S. Atiya et al.	(BNL E787 Collab.)
AALSETH	11	PRL 106 131301	C.E. Aalseth et al.	(CoGenT Collab.)	ATIYA	93B	PR D48 1	M.S. Atiya et al.	(BNL E787 Collab.)
ABRAHAMY...	11	PRL 107 191804	S. Abrahamyan et al.	(CAST Collab.)	BASSOMPIE...	93	EPL 22 239	G. Bassompierre et al.	(LAPP, TORI, LYON)
ARIK	11	PRL 107 261302	M. Arik et al.	(NEMO-3 Collab.)	BECK	93	PRL 70 2853	M. Beck et al.	(MPIK, KIAE, SASSO)
ARNOLD	11	PRL 107 062504	R. Arnold et al.	(MPIM, AARHUS)	CAMERON	93	PR D47 3707	R.E. Cameron et al.	(ROCH, BNL, FNAL+)
BLUEMLEIN	11	PL B701 155	J. Bluemlein, J. Brunner	(PNPI)	CHANG	93	PL B316 51	S. Chang, K. Choi	
CADAMURO	11	JCAP 1102 003	D. Cadamuro et al.		CHUI	93	PRL 71 3247	T.C.P. Chui, W.T. Ni	(NTHU)
DERBIN	11	PAN 74 596	A.V. Derbin et al.		MINOWA	93	PRL 71 4120	M. Minowa et al.	(TOKY)
DERBIN	11A	PR D83 023505	A.V. Derbin et al.	(WASH)	NG	93	PR D48 2941	K.W. Ng	(AST)
HOEDL	11	PRL 106 041801	S.A. Hoedl et al.		RITTER	93	PRL 70 701	R.C. Ritter et al.	
HOSKINS	11	PR D84 121302	J. Hoskins et al.	(ADMX Collab.)	TANAKA	93	PR D48 5412	J. Tanaka, H. Ejiri	(OSAK)
ANDRIAMON...	10	JCAP 1003 032	S. Andriamonje et al.	(CAST Collab.)	ALLIEGRO	92	PR D68 278	C. Alliegro et al.	(BNL, FNAL, PS+)
ARGYRADES	10	NP A847 168	J. Argyrades et al.	(NEMO-3 Collab.)	ATIYA	92	PRL 69 733	M.S. Atiya et al.	(BNL, LANL, PRIN+)
ASZTALOS	10	PRL 104 041301	S.J. Asztalos et al.	(ADMX Collab.)	BARABASH	92	PL B295 154	L.S. Barabash et al.	(JINR, CERN, SERP+)
EHRET	10	PL B689 149	K. Ehret et al.	(ALPS Collab.)	BERNATOW...	92	PRL 69 2341	T. Bernatowicz et al.	(WUSL, TATA)
HANNESTAD	10	JCAP 1008 001	S. Hannestad et al.		BLUEMLEIN	92	JUMP A7 3835	J. Bluemlein et al.	(BERL, BUDA, JINR+)
PETUKHOV	10	PRL 105 170401	A.K. Petukhov et al.		HALLIN	92	PR D45 3955	A.L. Hallin et al.	(PRIN)
SEREBROV	10	JETPL 91 6	A.P. Serebrov et al.		HENDERSON	92C	PRL 69 1733	S.D. Henderson et al.	(YALE, BNL)
AHMED	09A	PRL 103 141802	Z. Ahmed et al.	(CDMS Collab.)	HICKS	92	PL B276 423	K.H. Hicks, D.E. Alburger	(OHIO, BNL)
ANDRIAMON...	09	JCAP 0912 002	S. Andriamonje et al.	(NEMO-3 Collab.)	LAZARUS	92	PRL 69 2333	D.M. Lazarus et al.	(BNL, ROCH, FNAL)
ARGYRADES	09	PR C80 032501	J. Argyrades et al.	(CAST Collab.)	MEIJERDREES	92	PRL 68 3845	R. Meijer Drees et al.	(SINDRUM I Collab.)
ARIK	09	JCAP 0902 008	M. Arik et al.	(CAST Collab.)	PAN	92	MPL 87 1287	S.S. Pan, W.T. Ni, S.C. Chen	
BJORKEN	09	PR D80 075018	J. Bjorken et al.	(GammeV Collab.)	RUOSO	92	ZPHY C56 505	G. Ruoso et al.	(ROCH, BNL, FNAL, TRST)
CHOU	09	PRL 102 030402	A.S. Chou et al.		SKALSEY	92	PRL 68 456	M. Skalsey, J.J. Kolata	(MICH, NDAM)
DAVOUDIASH...	09	PR D79 095024	H. Davoudiasl, P. Huber		VENEMA	92	PRL 68 135	B.J. Venema et al.	
DERBIN	09A	PL B678 181	A.V. Derbin et al.		WANG	92	MPL A7 1497	J. Wang	(ILL)
GONDOLO	09	PR D79 107301	P. Gondolo, G. Raffelt	(UTAH, MPIM)	WANG	92C	PL B291 97	J. Wang	(ILL)
IGNATOVICH	09	EPJ C64 19	V.K. Ignatovich, Y.N. Pokotilovski	(JINR)	WU	92	PRL 69 1729	X.Y. Wu et al.	(BNL, YALE, CUNY)
KEKEZ	09	PL B671 345	D. Kekez et al.		AKOPYAN	91	PL B272 443	M.V. Akopyan et al.	(INRM)
SEREBROV	09	PR B680 423	A.P. Serebrov et al.	(PNPI)	ASA	91	PRL 66 2440	S. Asai et al.	(ICEPP)
AFANASEV	08	PRL 101 120401	A. Afanasev et al.	(Borexino Collab.)	BERSHADY	91	PRL 66 1398	M.A. Bershad, M.T. Ressell, M.S. Turner	(CHIC+)
BELLINI	08	EPJ C54 61	G. Bellini et al.	(GammeV Collab.)	BLUEMLEIN	91	ZPHY C51 341	J. Bluemlein et al.	(BERL, BUDA, JINR+)
CHOU	08	PRL 100 080402	A.S. Chou et al.		BOBRAKOV	91	JETPL 53 294		

See key on page 1127

Gauge & Higgs Boson Particle Listings
Axions (A⁰) and Other Very Light Bosons

Table with 4 columns: Author(s), Paper ID, Journal Abbreviation, and Other info. Lists numerous axion and boson studies with authors like Engel, Ginoenko, Guo, etc.

OTHER RELATED PAPERS

Summary table of other related papers including Srednicki, Bardeen, and others.

e	1239
μ	1240
τ	1245
Heavy Charged Lepton Searches	1272
Neutrino Properties	1273
Number of Neutrino Types	1282
Double- β Decay	1284
Neutrino Mixing	1288
Heavy Neutral Leptons, Searches for	1307

Notes in the Listings

Neutrino properties (rev.)	1273
Sum of neutrino masses (rev.)	1276
Number of light neutrino types from collider experiments	1282
Neutrinoless double- β decay	1284

Related Reviews in Volume 1

56. Muon anomalous magnetic moment (rev.)	796
57. Muon decay parameters (rev.)	800
58. τ branching fractions (rev.)	803
59. τ -lepton decay parameters (rev.)	806

LEPTONS

e

$$J = \frac{1}{2}$$

e MASS (atomic mass units u)

The primary determination of an electron's mass comes from measuring the ratio of the mass to that of a nucleus, so that the result is obtained in u (atomic mass units). The conversion factor to MeV is more uncertain than the mass of the electron in u; indeed, the recent improvements in the mass determination are not evident when the result is given in MeV. In this datablock we give the result in u, and in the following datablock in MeV.

VALUE (10 ⁻⁶ u)	DOCUMENT ID	TECN	COMMENT
548.5799065 ± 0.00000016	TIESINGA 21	RVUE	2018 CODATA value
• • • We do not use the following data for averages, fits, limits, etc. • • •			
548.57990970 ± 0.000000016	MOHR 16	RVUE	2014 CODATA value
548.57990946 ± 0.00000022	MOHR 12	RVUE	2010 CODATA value
548.57990943 ± 0.00000023	MOHR 08	RVUE	2006 CODATA value
548.57990945 ± 0.00000024	MOHR 05	RVUE	2002 CODATA value
548.5799092 ± 0.00000004	¹ BEIER 02	CNTR	Penning trap
548.5799110 ± 0.0000012	MOHR 99	RVUE	1998 CODATA value
548.5799111 ± 0.0000012	² FARNHAM 95	CNTR	Penning trap
548.579903 ± 0.000013	COHEN 87	RVUE	1986 CODATA value

- ¹ BEIER 02 compares Larmor frequency of the electron bound in a ¹²C⁵⁺ ion with the cyclotron frequency of a single trapped ¹²C⁵⁺ ion.
- ² FARNHAM 95 compares cyclotron frequency of trapped electrons with that of a single trapped ¹²C⁶⁺ ion.

e MASS

The mass is known more precisely in u (atomic mass units) than in MeV. The conversion is: 1 u = 931.494 102 42(28) MeV/c² (2018 CODATA value, TIESINGA 21). The conversion error dominates the uncertainty of the masses given below.

VALUE (MeV)	DOCUMENT ID	TECN	COMMENT
0.51099895000 ± 0.0000000015	TIESINGA 21	RVUE	2018 CODATA value
• • • We do not use the following data for averages, fits, limits, etc. • • •			
0.5109989461 ± 0.0000000031	MOHR 16	RVUE	2014 CODATA value
0.510998928 ± 0.000000011	MOHR 12	RVUE	2010 CODATA value
0.510998910 ± 0.000000013	MOHR 08	RVUE	2006 CODATA value
0.510998918 ± 0.000000044	MOHR 05	RVUE	2002 CODATA value
0.510998901 ± 0.000000020	^{1,2} BEIER 02	CNTR	Penning trap
0.510998902 ± 0.000000021	MOHR 99	RVUE	1998 CODATA value
0.510998903 ± 0.000000020	^{1,3} FARNHAM 95	CNTR	Penning trap
0.510998895 ± 0.000000024	¹ COHEN 87	RVUE	1986 CODATA value
0.5110034 ± 0.0000014	COHEN 73	RVUE	1973 CODATA value

- ¹ Converted to MeV using the 1998 CODATA value of the conversion constant, 931.494013 ± 0.000037 MeV/u.
- ² BEIER 02 compares Larmor frequency of the electron bound in a ¹²C⁵⁺ ion with the cyclotron frequency of a single trapped ¹²C⁵⁺ ion.
- ³ FARNHAM 95 compares cyclotron frequency of trapped electrons with that of a single trapped ¹²C⁶⁺ ion.

$$(m_{e^+} - m_{e^-}) / m_{\text{average}}$$

A test of CPT invariance.

VALUE	CL%	DOCUMENT ID	TECN	COMMENT
< 8 × 10⁻⁹	90	¹ FEE 93	CNTR	Positronium spectroscopy
• • • We do not use the following data for averages, fits, limits, etc. • • •				
< 4 × 10 ⁻²³	90	² DOLGOV 14		From photon mass limit
< 4 × 10 ⁻⁸	90	CHU 84	CNTR	Positronium spectroscopy

- ¹ FEE 93 value is obtained under the assumption that the positronium Rydberg constant is exactly half the hydrogen one.
- ² DOLGOV 14 result is obtained under the assumption that any mass difference between electron and positron would lead to a non-zero photon mass. The PDG 12 limit of 1 × 10⁻¹⁸ eV on the photon mass is in turn used to derive the value quoted here.

$$|q_{e^+} + q_{e^-}|/e$$

A test of CPT invariance. See also similar tests involving the proton.

VALUE	DOCUMENT ID	TECN	COMMENT
< 4 × 10⁻⁸	¹ HUGHES 92	RVUE	
• • • We do not use the following data for averages, fits, limits, etc. • • •			
< 2 × 10 ⁻¹⁸	² SCHAEFER 95	THEO	Vacuum polarization
< 1 × 10 ⁻¹⁸	³ MUELLER 92	THEO	Vacuum polarization

- ¹ HUGHES 92 uses recent measurements of Rydberg-energy and cyclotron-frequency ratios.
- ² SCHAEFER 95 removes model dependency of MUELLER 92.
- ³ MUELLER 92 argues that an inequality of the charge magnitudes would, through higher-order vacuum polarization, contribute to the net charge of atoms.

e MAGNETIC MOMENT ANOMALY

$$\mu_e / \mu_B - 1 = (g-2)/2$$

VALUE (units 10 ⁻⁶)	DOCUMENT ID	TECN	CHG	COMMENT
1159.65218076 ± 0.00000028	OUR AVERAGE			
1159.65218073 ± 0.00000028	HANNEKE 08	MRS		Single electron
1159.6521884 ± 0.0000043	VANDYCK 87	MRS	-	Single electron
• • • We do not use the following data for averages, fits, limits, etc. • • •				
1159.65218128 ± 0.00000018	TIESINGA 21	RVUE		2018 CODATA value
1159.65218091 ± 0.00000026	MOHR 16	RVUE		2014 CODATA value
1159.65218076 ± 0.00000027	MOHR 12	RVUE		2010 CODATA value
1159.65218111 ± 0.00000074	¹ MOHR 08	RVUE		2006 CODATA value
1159.65218085 ± 0.00000076	² ODOM 06	MRS	-	Single electron
1159.6521859 ± 0.0000038	MOHR 05	RVUE		2002 CODATA value
1159.6521869 ± 0.0000041	MOHR 99	RVUE		1998 CODATA value
1159.652193 ± 0.000010	COHEN 87	RVUE		1986 CODATA value
1159.6521879 ± 0.0000043	³ VANDYCK 87	MRS	+	Single positron

- ¹ MOHR 08 average is dominated by ODOM 06.
- ² Superseded by HANNEKE 08 per private communication with Gerald Gabrielse.
- ³ This VANDYCK 87 result is for a positron. We do not take it into account for the average to avoid the assumption of CPT invariance.

$$(g_{e^+} - g_{e^-}) / g_{\text{average}}$$

A test of CPT invariance.

VALUE (units 10 ⁻¹²)	CL%	DOCUMENT ID	TECN	COMMENT
- 0.5 ± 2.1		¹ VANDYCK 87	MRS	Penning trap
• • • We do not use the following data for averages, fits, limits, etc. • • •				
< 12	95	² VASSERMAN 87	CNTR	Assumes m _{e+} = m _{e-}
22 ± 64		SCHWINBERG 81	MRS	Penning trap
• • • We do not use the following data for averages, fits, limits, etc. • • •				
¹ VANDYCK 87 measured (g ₋ /g ₊) - 1 and we converted it.				
² VASSERMAN 87 measured (g ₊ - g ₋)/(g-2). We multiplied by (g-2)/g = 1.2 × 10 ⁻³ .				

e ELECTRIC DIPOLE MOMENT (d)

A nonzero value is forbidden by both T invariance and P invariance.

VALUE (10 ⁻²⁸ ecm)	CL%	DOCUMENT ID	TECN	COMMENT
< 0.11	90	¹ ANDREEV 18	CNTR	ThO molecules
• • • We do not use the following data for averages, fits, limits, etc. • • •				
< 1.3	90	² CAIRCROSS 17	ESR	¹⁸⁰ Hf ¹⁹ F molecules
- 5570 ± 7980 ± 120		KIM 15	CNTR	Gd ₃ Ga ₅ O ₁₂ molecules
< 0.87	90	³ BARON 14	CNTR	ThO molecules
< 6050	90	⁴ ECKEL 12	CNTR	Eu _{0.5} Ba _{0.5} TiO ₃ molecules
< 10.5	90	⁵ HUDSON 11	NMR	YbF molecules
6.9 ± 7.4		REGAN 02	MRS	²⁰⁵ Tl beams
18 ± 12 ± 10		⁶ COMMINS 94	MRS	²⁰⁵ Tl beams
- 27 ± 83		⁶ ABDULLAH 90	MRS	²⁰⁵ Tl beams
- 1400 ± 2400		CHO 89	NMR	TlF molecules
- 150 ± 550 ± 150		MURTHY 89		Cs, no B field
- 5000 ± 11000		LA MOREAUX 87	NMR	¹⁹⁹ Hg
19000 ± 34000	90	SANDARS 75	MRS	Thallium
7000 ± 22000	90	PLAYER 70	MRS	Xenon
< 30000	90	WEISSKOPF 68	MRS	Cesium

- ¹ ANDREEV 18 gives a measurement corresponding to this limit as (4.3 ± 3.1 ± 2.6) × 10⁻³⁰ ecm.
- ² CAIRCROSS 17 gives a measurement corresponding to this limit as (0.09 ± 0.77 ± 0.17) × 10⁻²⁸ ecm.
- ³ BARON 14 gives a measurement corresponding to this limit as (-0.21 ± 0.37 ± 0.25) × 10⁻²⁸ ecm.
- ⁴ ECKEL 12 gives a measurement corresponding to this limit as (-1.07 ± 3.06 ± 1.74) × 10⁻²⁵ ecm.
- ⁵ HUDSON 11 gives a measurement corresponding to this limit as (-2.4 ± 5.7 ± 1.5) × 10⁻²⁸ ecm.
- ⁶ ABDULLAH 90, COMMINS 94, and REGAN 02 use the relativistic enhancement of a valence electron's electric dipole moment in a high-Z atom.

e⁻ MEAN LIFE / BRANCHING FRACTION

A test of charge conservation. See the "Note on Testing Charge Conservation and the Pauli Exclusion Principle" following this section in our 1992 edition (Physical Review **D45** S1 (1992), p. VI.10).

Most of these experiments are one of three kinds: Attempts to observe (a) the 255.5 keV gamma ray produced in e⁻ → ν_eγ, (b) the (K) shell x ray produced when an electron decays without additional energy deposit,

Lepton Particle Listings

e, μ

e.g., $e^- \rightarrow \nu_e \bar{\nu}_e \nu_e$ ("disappearance" experiments), and (c) nuclear de-excitation gamma rays after the electron disappears from an atomic shell and the nucleus is left in an excited state. The last can include both weak boson and photon mediating processes. We use the best $e^- \rightarrow \nu_e \gamma$ limit for the Summary Tables.

Note that we use the mean life rather than the half life, which is often reported.

$e^- \rightarrow \nu_e \gamma$ and astrophysical limits

VALUE (yr)	CL%	DOCUMENT ID	TECN	COMMENT
>6.6 $\times 10^{28}$	90	AGOSTINI 15B	BORX	$e^- \rightarrow \nu \gamma$
••• We do not use the following data for averages, fits, limits, etc. •••				
>1.2 $\times 10^{24}$	90	ABGRALL 17	HPGE	electron decay to invisible
>1.22 $\times 10^{26}$	68	1 Klapdor-K... 07	CNTR	$e^- \rightarrow \nu \gamma$
>4.6 $\times 10^{26}$	90	BACK 02	BORX	$e^- \rightarrow \nu \gamma$
>3.4 $\times 10^{26}$	68	BELLI 00b	DAMA	$e^- \rightarrow \nu \gamma$, liquid Xe
>3.7 $\times 10^{25}$	68	AHARONOV 95b	CNTR	$e^- \rightarrow \nu \gamma$
>2.35 $\times 10^{25}$	68	BALYSH 93	CNTR	$e^- \rightarrow \nu \gamma$, ^{76}Ge detector
>1.5 $\times 10^{25}$	68	AVIGNONE 86	CNTR	$e^- \rightarrow \nu \gamma$
>1 $\times 10^{39}$		2 ORITO 85	ASTR	Astrophysical argument
>3 $\times 10^{23}$	68	BELLOTTI 83b	CNTR	$e^- \rightarrow \nu \gamma$

¹ The authors of A. Derbin et al, arXiv:0704.2047v1 argue that this limit is overestimated by at least a factor of 5.
² ORITO 85 assumes that electromagnetic forces extend out to large enough distances and that the age of our galaxy is 10^{10} years.

Disappearance and nuclear-de-excitation experiments

VALUE (yr)	CL%	DOCUMENT ID	TECN	COMMENT
>6.4 $\times 10^{24}$	68	1 BELLI 99b	DAMA	De-excitation of ^{129}Xe
••• We do not use the following data for averages, fits, limits, etc. •••				
>4.2 $\times 10^{24}$	68	BELLI 99	DAMA	Iodine L-shell disappearance
>2.4 $\times 10^{23}$	90	2 BELLI 99d	DAMA	De-excitation of ^{127}I (in Na)
>4.3 $\times 10^{23}$	68	AHARONOV 95b	CNTR	Ge K-shell disappearance
>2.7 $\times 10^{23}$	68	REUSSER 91	CNTR	Ge K-shell disappearance
>2 $\times 10^{22}$	68	BELLOTTI 83b	CNTR	Ge K-shell disappearance

¹ BELLI 99b limit on charge nonconserving e^- capture involving excitation of the 236.1 keV nuclear state of ^{129}Xe ; the 90% CL limit is 3.7×10^{24} yr. Less stringent limits for other states are also given.
² BELLI 99d limit on charge nonconserving e^- capture involving excitation of the 57.6 keV nuclear state of ^{127}I . Less stringent limits for the other states and for the state of ^{23}Na are also given.

LIMITS ON LEPTON-FLAVOR VIOLATION IN PRODUCTION

Forbidden by lepton family number conservation.

This section was added for the 2008 edition of this Review and is not complete. For a list of further measurements see references in the papers listed below.

$\sigma(e^+e^- \rightarrow e^\pm \tau^\mp) / \sigma(e^+e^- \rightarrow \mu^\pm \mu^-)$

VALUE	CL%	DOCUMENT ID	TECN	COMMENT
<8.9 $\times 10^{-6}$	95	AUBERT 07p	BABR	e^+e^- at $E_{\text{cm}} = 10.58$ GeV
••• We do not use the following data for averages, fits, limits, etc. •••				
<1.8 $\times 10^{-3}$	95	GOMEZ-CAD... 91	MRK2	e^+e^- at $E_{\text{cm}} = 29$ GeV

$\sigma(e^+e^- \rightarrow \mu^\pm \tau^\mp) / \sigma(e^+e^- \rightarrow \mu^\pm \mu^-)$

VALUE	CL%	DOCUMENT ID	TECN	COMMENT
<4.0 $\times 10^{-6}$	95	AUBERT 07p	BABR	e^+e^- at $E_{\text{cm}} = 10.58$ GeV
••• We do not use the following data for averages, fits, limits, etc. •••				
<6.1 $\times 10^{-3}$	95	GOMEZ-CAD... 91	MRK2	e^+e^- at $E_{\text{cm}} = 29$ GeV

e REFERENCES

TIESINGA 21	RMP 93 025010	E. Tiesinga et al.	(NIST)
ANDREEV 18	NAT 562 355	V. Andreev et al.	(ACME Collab.)
ABGRALL 17	PRL 118 161801	N. Abgrall et al.	(MAJORANA Collab.)
CAIRN CROSS 17	PRL 119 153001	W.B. Cairncross et al.	(NIST, COLO)
MOHR 16	RMP 88 035009	P.J. Mohr, D.B. Newell, B.N. Taylor	(NIST)
AGOSTINI 15B	PRL 115 231802	M. Agostini et al.	(Borexino Collab.)
KIM 15	PR D91 102004	Y.J. Kim et al.	(IND, YALE, LANL)
BARON 14	SCIENCE 343 269	J. Baron et al.	(ACME Collab.)
DOLGOV 14	PL B732 244	A.D. Dolgov, V.A. Novikov	
ECKEL 12	PRL 109 193003	S. Eckel, A.O. Sushkov, S.K. Lamoreaux	(YALE)
MOHR 12	RMP 84 1527	P.J. Mohr, B.N. Taylor, D.B. Newell	(NIST)
PDG 12	PR D86 010001	J. Beringer et al.	(PDG Collab.)
HUDSON 11	NAT 473 493	J.J. Hudson et al.	(LOIC)
HANNEKE 08	PRL 100 120801	D. Hanneke, S. Fogwell, G. Gabrielse	(HARV)
MOHR 08	RMP 80 633	P.J. Mohr, B.N. Taylor, D.B. Newell	(NIST)
AUBERT 07p	PR D75 031103	B. Aubert et al.	(BABAR Collab.)
KLAPDOR-K... 07	PL B644 109	H.V. Klapdor-Kleingrothaus, I.V. Krivosheina, I.V. Titkova	(NIST)
ODOM 06	PRL 97 030801	B. Odom et al.	(HARV)
MOHR 05	RMP 77 1	P.J. Mohr, B.N. Taylor	(NIST)
BACK 02	PL B525 29	H.O. Back et al.	(Borexino/SASSO Collab.)
BEIER 02	PRL 88 011603	T. Beier et al.	
REGAN 02	PRL 88 071805	B.C. Regan et al.	
BELLI 00b	PR D61 117301	P. Belli et al.	(DAMA Collab.)
BELLI 99	PL B460 236	P. Belli et al.	(DAMA Collab.)
BELLI 99b	PL B465 315	P. Belli et al.	(DAMA Collab.)
BELLI 99d	PR C60 065901	P. Belli et al.	(DAMA Collab.)
MOHR 99	JPCRD 28 1713	P.J. Mohr, B.N. Taylor	(NIST)
Also	RMP 72 351	P.J. Mohr, B.N. Taylor	(NIST)

AHARONOV 95B	PR D52 3785	Y. Aharonov et al.	(SCUC, PNL, ZARA+)
Also	PL B353 168	Y. Aharonov et al.	(SCUC, PNL, ZARA+)
FARNHAM 95	PRL 75 3598	D.L. Farnham, R.S. van Dyck, P.B. Schwinberg	(WASH)
SCHAEFER 95	PR A51 838	A. Schaefer, J. Reinhardt	(FRAN)
COMMINS 94	PR A50 2960	E.D. Commins et al.	
BALYSH 93	PL B298 278	A. Balysh et al.	(KIAE, MPIK, SASSO)
REE 93	PR A48 192	M.S. Fee et al.	
HUGHES 92	PRL 69 578	R.J. Hughes, B.J. Deutch	(LANL, AARH)
MUELLER 92	PRL 69 3432	B. Müller, M.H. Thoma	(DUKE)
PDG 92	PR D45 5.1	K. Hikasa et al.	(KEK, LBL, BOST+)
GOMEZ-CAD... 91	PRL 66 1007	J.J. Gomez-Cadenas et al.	(SLAC MARK-2 Collab.)
REUSSER 91	PL B255 143	D. Reusser et al.	(NEUC, CIT, PSI)
ABDULLAH 90	PRL 65 2347	K. Abdullah et al.	(LBL, UCB)
CHO 89	PRL 63 2559	D. Cho, K. Sangster, E.A. Hinds	(YALE)
MURTHY 89	PRL 63 965	S.A. Murthy et al.	(AMHT)
COHEN 87	RMP 59 1121	E.R. Cohen, B.N. Taylor	(RISC, NBS)
LAMOREAUX 87	PRL 59 2275	S.K. Lamoreaux et al.	(WASH)
VANDYCK 87	PRL 59 26	R.S. van Dyck, P.B. Schwinberg, H.G. Dehmelt	(WASH)
VASSERMAN 87	PL B198 302	I.B. Vasserma et al.	(NOVO)
Also	PL B187 172	I.B. Vasserma et al.	(NOVO)
AVIGNONE 86	PR D34 97	F.T. Avignone et al.	(PNL, SCUC)
ORITO 85	PRL 54 2457	S. Orto, M. Yoshimura	(TOKY, KEK)
CHU 84	PRL 52 1689	S. Chu, A.P. Mills, J.L. Hall	(BELL, NBS, COLO)
BELLOTTI 83b	PL 124B 435	E. Bellotti et al.	(MILA)
SCHWINBERG 81	PRL 47 1679	P.B. Schwinberg, R.S. van Dyck, H.G. Dehmelt	(WASH)
SANDARS 75	PR A11 473	P.G.H. Sandars, D.M. Sternheimer	(OXF, BNL)
COHEN 73	JPCRD 2 664	E.R. Cohen, B.N. Taylor	(RISC, NBS)
PLAYER 70	JP B3 1620	M.A. Player, P.G.H. Sandars	(OXF)
WEISSKOPF 68	PRL 21 1645	M.C. Weisskopf et al.	(BRAN)

μ

$$J = \frac{1}{2}$$

μ MASS (atomic mass units u)

The muon's mass is obtained from the muon-electron mass ratio as determined from the measurement of Zeeman transition frequencies in muonium ($\mu^+ e^-$ atom). Since the electron's mass is most accurately known in u, the muon's mass is also most accurately known in u. The conversion factor to MeV has approximately the same relative uncertainty as the mass of the muon in u. In this datablock we give the result in u, and in the following datablock in MeV.

VALUE (u)	DOCUMENT ID	TECN	COMMENT
0.1134289259 \pm 0.0000000025	TIESINGA 21	RVUE	2018 CODATA value
••• We do not use the following data for averages, fits, limits, etc. •••			
0.1134289257 \pm 0.0000000025	MOHR 16	RVUE	2014 CODATA value
0.1134289267 \pm 0.0000000029	MOHR 12	RVUE	2010 CODATA value
0.1134289256 \pm 0.0000000029	MOHR 08	RVUE	2006 CODATA value
0.1134289264 \pm 0.0000000030	MOHR 05	RVUE	2002 CODATA value
0.1134289168 \pm 0.0000000034	1 MOHR 99	RVUE	1998 CODATA value
0.113428913 \pm 0.000000017	2 COHEN 87	RVUE	1986 CODATA value

¹ MOHR 99 make use of other 1998 CODATA entries below.
² COHEN 87 make use of other 1986 CODATA entries below.

μ MASS

The mass is known more precisely in u (atomic mass units) than in MeV. The conversion is: $1 \text{ u} = 931.494 102 42(28) \text{ MeV}/c^2$ (2018 CODATA value, TIESINGA 21). The conversion error contributes significantly to the uncertainty of the masses given below.

VALUE (MeV)	DOCUMENT ID	TECN	CHG	COMMENT
105.6583755 \pm 0.00000023	TIESINGA 21	RVUE		2018 CODATA value
••• We do not use the following data for averages, fits, limits, etc. •••				
105.6583745 \pm 0.00000024	MOHR 16	RVUE		2014 CODATA value
105.6583715 \pm 0.00000035	MOHR 12	RVUE		2010 CODATA value
105.6583668 \pm 0.00000038	MOHR 08	RVUE		2006 CODATA value
105.6583692 \pm 0.00000094	MOHR 05	RVUE		2002 CODATA value
105.6583568 \pm 0.00000052	MOHR 99	RVUE		1998 CODATA value
105.658353 \pm 0.0000016	1 COHEN 87	RVUE		1986 CODATA value
105.658386 \pm 0.0000044	2 MARIAM 82	CNTR	+	
105.65836 \pm 0.000026	3 CROWE 72	CNTR		
105.65865 \pm 0.000044	4 CRANE 71	CNTR		

¹ Converted to MeV using the 1998 CODATA value of the conversion constant, $931.494013 \pm 0.000037 \text{ MeV}/u$.

² MARIAM 82 give $m_\mu/m_e = 206.768259(62)$.

³ CROWE 72 give $m_\mu/m_e = 206.7682(5)$.

⁴ CRANE 71 give $m_\mu/m_e = 206.76878(85)$.

μ MEAN LIFE τ

Measurements with an error $> 0.001 \times 10^{-6}$ s have been omitted.

VALUE (10^{-6} s)	DOCUMENT ID	TECN	CHG	COMMENT
2.1969811 \pm 0.0000022	OUR AVERAGE			
2.1969803 \pm 0.0000021 \pm 0.0000007	1 TISHCHENKO 13	CNTR	+	Surface μ^+ at PSI
2.197083 \pm 0.000032 \pm 0.000015	BARCZYK 08	CNTR	+	Muons from π^+ decay at rest
2.197013 \pm 0.000021 \pm 0.000011	CHITWOOD 07	CNTR	+	Surface μ^+ at PSI
2.197078 \pm 0.000073	BARDIN 84	CNTR	+	

2.197025 ± 0.000155	BARDIN	84	CNTR	-
2.19695 ± 0.00006	GIOVANNETTI	84	CNTR	+
2.19711 ± 0.00008	BALANDIN	74	CNTR	+
2.1973 ± 0.0003	DUCLOS	73	CNTR	+

• • • We do not use the following data for averages, fits, limits, etc. • • •
 2.1969803 ± 0.000022 WEBBER 11 CNTR + Surface μ^+ at PSI
¹TISHCHENKO 13 uses 1.6×10^{12} μ^+ events and supersedes WEBBER 11.

$\tau_{\mu^+}/\tau_{\mu^-}$ MEAN LIFE RATIO

A test of CPT invariance.

VALUE	DOCUMENT ID	TECN	COMMENT
1.000024 ± 0.000078	BARDIN	84	CNTR
• • • We do not use the following data for averages, fits, limits, etc. • • •			
1.0008 ± 0.0010	BAILEY	79	CNTR Storage ring
1.000 ± 0.001	MEYER	63	CNTR Mean life μ^+ / μ^-

$(\tau_{\mu^+} - \tau_{\mu^-}) / \tau_{\text{average}}$

A test of CPT invariance. Calculated from the mean-life ratio, above.

VALUE	DOCUMENT ID
(2 ± 8) × 10⁻⁵	OUR EVALUATION

μ/p MAGNETIC MOMENT RATIO

This ratio is used to obtain a precise value of the muon mass and to reduce experimental muon Larmor frequency measurements to the muon magnetic moment anomaly. Measurements with an error > 0.00001 have been omitted. By convention, the minus sign on this ratio is omitted. CODATA values were fitted using their selection of data, plus other data from multiparameter fits.

VALUE	DOCUMENT ID	TECN	CHG	COMMENT
3.183345142 ± 0.000000071	TIESINGA	21	RVUE	2018 CODATA value
• • • We do not use the following data for averages, fits, limits, etc. • • •				
3.183345142 ± 0.000000071	MOHR	16	RVUE	2014 CODATA value
3.183345107 ± 0.000000084	MOHR	12	RVUE	2010 CODATA value
3.183345137 ± 0.000000085	MOHR	08	RVUE	2006 CODATA value
3.183345118 ± 0.000000089	MOHR	05	RVUE	2002 CODATA value
3.18334513 ± 0.000000039	LIU	99	CNTR +	HFS in muonium
3.18334539 ± 0.000000010	MOHR	99	RVUE	1998 CODATA value
3.18334547 ± 0.000000047	COHEN	87	RVUE	1986 CODATA value
3.1833441 ± 0.00000017	KLEMPPT	82	CNTR +	Precession strob
3.1833461 ± 0.00000011	MARIAM	82	CNTR +	HFS splitting
3.1833448 ± 0.00000029	CAMANI	78	CNTR +	See KLEMPPT 82
3.1833403 ± 0.00000044	CASPERSON	77	CNTR +	HFS splitting
3.1833402 ± 0.00000072	COHEN	73	RVUE	1973 CODATA value
3.1833467 ± 0.00000082	CROWE	72	CNTR +	Precession phase

See the related review(s):
Muon Anomalous Magnetic Moment

μ MAGNETIC MOMENT ANOMALY

The parity-violating decay of muons in a storage ring is observed. The difference frequency ω_a between the muon spin precession and the orbital angular frequency ($e/m_\mu c$)(B) is measured, as is the free proton NMR frequency ω_p , thus determining the ratio $R = \omega_a / \omega_p$. Given the magnetic moment ratio $\lambda = \mu_\mu / \mu_p$ (from hyperfine structure in muonium), $(g-2)/2 = R / (\lambda - R)$.

$\mu_\mu / (e\hbar/2m_\mu) - 1 = (g_\mu - 2)/2$

VALUE (units 10 ⁻¹⁰)	DOCUMENT ID	TECN	CHG	COMMENT
11659206.1 ± 4.1	¹ ABI	21	MUG2 ±	Combined FNAL and BNL values
• • • We do not use the following data for averages, fits, limits, etc. • • •				
11659204.0 ± 5.4	ABI	21	MUG2 ±	Storage ring
11659208.0 ± 5.4 ± 3.3	BENNETT	06	MUG2 ±	Average μ^+ and μ^-
11659208 ± 6	BENNETT	04	MUG2 ±	Average μ^+ and μ^-
11659214 ± 8 ± 3	BENNETT	04	MUG2 -	Storage ring
11659203 ± 6 ± 5	BENNETT	04	MUG2 +	Storage ring
11659204 ± 7 ± 5	BENNETT	02	MUG2 +	Storage ring
11659202 ± 14 ± 6	BROWN	01	MUG2 +	Storage ring
11659191 ± 59	BROWN	00	MUG2 +	
11659100 ± 110	² BAILEY	79	CNTR +	Storage ring
11659360 ± 120	² BAILEY	79	CNTR -	Storage ring
11659230 ± 85	² BAILEY	79	CNTR ±	Storage ring
11620000 ± 5000	CHARPAK	62	CNTR +	

¹ ABI 21 combined their value with the previous independent BNL measurement of BENNETT 06. ABI 21 also report that the difference of this combination with the standard model value of $(11659181.0 \pm 4.3) \times 10^{-10}$ (AOYAMA 20) has a significance of 4.2 σ .
² BAILEY 79 values recalculated by HUGHES 99 using the COHEN 87 μ/p magnetic moment. The improved MOHR 99 value does not change the result.

$(g_{\mu^+} - g_{\mu^-}) / g_{\text{average}}$

A test of CPT invariance.

VALUE (units 10 ⁻⁸)	DOCUMENT ID	TECN
-0.11 ± 0.12	BENNETT	04 MUG2
• • • We do not use the following data for averages, fits, limits, etc. • • •		
-2.6 ± 1.6	BAILEY	79 CNTR

μ ELECTRIC DIPOLE MOMENT (d)

A nonzero value is forbidden by both T invariance and P invariance.

VALUE (10 ⁻¹⁹ ecm)	CL%	DOCUMENT ID	TECN	CHG	COMMENT
< 1.8	95	¹ BENNETT	09	MUG2 ±	Storage ring
• • • We do not use the following data for averages, fits, limits, etc. • • •					
-0.1 ± 1.0		² BENNETT	09	MUG2 +	Storage ring
-0.1 ± 0.7		³ BENNETT	09	MUG2 -	Storage ring
-3.7 ± 3.4		⁴ BAILEY	78	CNTR ±	Storage ring
8.6 ± 4.5		BAILEY	78	CNTR +	Storage ring
0.8 ± 4.3		BAILEY	78	CNTR -	Storage ring

¹ This is the combination of the two BENNETT 09 measurements quoted here separately for μ^+ and μ^- . The result is also presented as a measurement of $(0.0 \pm 0.9) \times 10^{-19}$ e cm.
² Also reported as the limit of $|d(\mu^+)| < 2.1 \times 10^{-19}$ e cm at 95% CL.
³ Also reported as the limit of $|d(\mu^-)| < 1.5 \times 10^{-19}$ e cm at 95% CL.
⁴ This is the combination of the two BAILEY 78 results quoted here separately for μ^+ and μ^- . BAILEY 78 uses the convention $d = 1/2 \cdot (d_{\mu^+} - d_{\mu^-})$ and reports 3.7 ± 3.4 . We convert their result to use the same convention as BENNETT 09.

MUON-ELECTRON CHARGE RATIO ANOMALY $q_{\mu^+}/q_{e^-} - 1$

VALUE	DOCUMENT ID	TECN	CHG	COMMENT
(1.1 ± 2.1) × 10⁻⁹	¹ MEYER	00	CNTR +	1s-2s muonium interval

¹ MEYER 00 measure the 1s-2s muonium interval, and then interpret the result in terms of muon-electron charge ratio q_{μ^+}/q_{e^-} .

μ^- DECAY MODES

μ^+ modes are charge conjugates of the modes below.

Mode	Fraction (Γ_i/Γ)	Confidence level
Γ_1 $e^- \bar{\nu}_e \nu_\mu$	≈ 100%	
Γ_2 $e^- \bar{\nu}_e \nu_\mu \gamma$	[a] $(6.0 \pm 0.5) \times 10^{-8}$	
Γ_3 $e^- \bar{\nu}_e \nu_\mu e^+ e^-$	[b] $(3.4 \pm 0.4) \times 10^{-5}$	
Lepton Family number (LF) violating modes		
Γ_4 $e^- \nu_e \bar{\nu}_\mu$	LF [c] < 1.2 %	90%
Γ_5 $e^- \gamma$	LF < 4.2 × 10 ⁻¹³	90%
Γ_6 $e^- e^+ e^-$	LF < 1.0 × 10 ⁻¹²	90%
Γ_7 $e^- 2\gamma$	LF < 7.2 × 10 ⁻¹¹	90%

[a] This only includes events with energy of $e > 45$ MeV and energy of $\gamma > 40$ MeV. Since the $e^- \bar{\nu}_e \nu_\mu$ and $e^- \bar{\nu}_e \nu_\mu \gamma$ modes cannot be clearly separated, we regard the latter mode as a subset of the former.

[b] See the Particle Listings below for the energy limits used in this measurement.

[c] A test of additive vs. multiplicative lepton family number conservation.

μ^- BRANCHING RATIOS

$\Gamma(e^- \bar{\nu}_e \nu_\mu \gamma) / \Gamma_{\text{total}}$		Γ_2 / Γ			
VALUE	EVTS	DOCUMENT ID	TECN	COMMENT	
(6.03 ± 0.14 ± 0.53) × 10⁻⁸	13k	¹ BALDINI	16A	SPEC γ KE > 40 MeV	
• • • We do not use the following data for averages, fits, limits, etc. • • •					
(3.3 ± 1.3) × 10 ⁻³	862	BOGART	67	CNTR γ KE > 14.5 MeV	
(1.4 ± 0.4) × 10 ⁻²		CRITTENDEN	61	CNTR γ KE > 20 MeV	
		CRITTENDEN	61	CNTR γ KE > 10 MeV	
	27	ASHKIN	59	CNTR	
¹ BALDINI 16 measurement refers to $\mu^+ \rightarrow e^+ \nu \bar{\nu} \gamma$ decay and requires energy of $e^+ > 45$ MeV and energy $\gamma > 40$ MeV.					
$\Gamma(e^- \bar{\nu}_e \nu_\mu e^+ e^-) / \Gamma_{\text{total}}$		Γ_3 / Γ			
VALUE (units 10 ⁻⁵)	EVTS	DOCUMENT ID	TECN	CHG	COMMENT
3.4 ± 0.2 ± 0.3	7443	¹ BERTL	85	SPEC +	SINDRUM
• • • We do not use the following data for averages, fits, limits, etc. • • •					
2.2 ± 1.5	7	² CRITTENDEN	61	HLBC +	$E(e^+ e^-) > 10$ MeV
2	1	³ GUREVICH	60	EMUL +	

Lepton Particle Listings

μ

1.5 ± 1.0 3 4 LEE 59 HBC +
 1 BERTL 85 has transverse momentum cut $p_T > 17$ MeV/c. Systematic error was increased by us.
 2 CRITTENDEN 61 count only those decays where total energy of either (e^+ , e^-) combination is > 10 MeV.
 3 GUREVICH 60 interpret their event as either virtual or real photon conversion. e^+ and e^- energies not measured.
 4 In the three LEE 59 events, the sum of energies $E(e^+) + E(e^-) + E(e^+)$ was 51 MeV, 55 MeV, and 33 MeV.

$\Gamma(e^- \nu_e \bar{\nu}_\mu) / \Gamma_{\text{total}}$ Γ_4 / Γ
 Forbidden by the additive conservation law for lepton family number. A multiplicative law predicts this branching ratio to be 1/2. For a review see NEMETHY 81.

VALUE	CL%	DOCUMENT ID	TECN	CHG	COMMENT
< 0.012	90	1 FREEDMAN	93	CNTR +	ν oscillation search
< 0.018	90	KRAKAUER	91B	CALO +	
< 0.05	90	2 BERGSMA	83	CALO	$\bar{\nu}_\mu e^- \rightarrow \mu^- \bar{\nu}_e$
< 0.09	90	JONKER	80	CALO	See BERGSMA 83
-0.001 ± 0.061		WILLIS	80	CNTR +	
0.13 ± 0.15		BLIETSCHAU	78	HLBC ±	Avg. of 4 values
< 0.25	90	EICHTEN	73	HLBC +	

1 FREEDMAN 93 limit on $\bar{\nu}_e$ observation is here interpreted as a limit on lepton family number violation.
 2 BERGSMA 83 gives a limit on the inverse muon decay cross-section ratio $\sigma(\bar{\nu}_\mu e^- \rightarrow \mu^- \bar{\nu}_e) / \sigma(\nu_\mu e^- \rightarrow \mu^- \nu_e)$, which is essentially equivalent to $\Gamma(e^- \nu_e \bar{\nu}_\mu) / \Gamma_{\text{total}}$ for small values like that quoted.

$\Gamma(e^- \gamma) / \Gamma_{\text{total}}$ Γ_5 / Γ
 Forbidden by lepton family number conservation.

VALUE (units 10^{-11})	CL%	DOCUMENT ID	TECN	CHG	COMMENT
< 0.042	90	BALDINI	16	SPEC +	MEG at PSI
< 0.057	90	ADAM	13B	SPEC +	MEG at PSI
< 0.24	90	ADAM	11	SPEC +	MEG at PSI
< 2.8	90	ADAM	10	SPEC +	MEG at PSI
< 1.2	90	AHMED	02	SPEC +	MEGA
< 1.2	90	BROOKS	99	SPEC +	LAMPF
< 4.9	90	BOLTON	88	CBOX +	LAMPF
< 100	90	AZUELOS	83	CNTR +	TRIUMF
< 17	90	KINNISON	82	SPEC +	LAMPF
< 100	90	SCHAAF	80	ELEC +	SIN

$\Gamma(e^- e^+ e^-) / \Gamma_{\text{total}}$ Γ_6 / Γ
 Forbidden by lepton family number conservation.

VALUE (units 10^{-12})	CL%	DOCUMENT ID	TECN	CHG	COMMENT
< 1.0	90	1 BELLGARDT	88	SPEC +	SINDRUM
< 36	90	BARA NOV	91	SPEC +	ARES
< 35	90	BOLTON	88	CBOX +	LAMPF
< 2.4	90	1 BERTL	85	SPEC +	SINDRUM
< 160	90	1 BERTL	84	SPEC +	SINDRUM
< 130	90	1 BOLTON	84	CNTR	LAMPF

1 These experiments assume a constant matrix element.

$\Gamma(e^- 2\gamma) / \Gamma_{\text{total}}$ Γ_7 / Γ
 Forbidden by lepton family number conservation.

VALUE (units 10^{-11})	CL%	DOCUMENT ID	TECN	CHG	COMMENT
< 7.2	90	BOLTON	88	CBOX +	LAMPF
< 1	90	1 BALDINI	20	MEG	PSI
< 840	90	2 AZUELOS	83	CNTR +	TRIUMF
< 5000	90	3 BOWMAN	78	CNTR	DEPOMMIER 77 data

1 BALDINI 20 uses 7.5×10^{14} stopped muons to obtain limits on $\mu \rightarrow eX$ decay mediated by a new light particle X with lifetimes < 40 ps, which decays to $\gamma\gamma$ for X -mass ranges 20-45 MeV. The limit of the order $< 10^{-11}$ at 90% CL is for the mass range 20-30 MeV.
 2 AZUELOS 83 uses the phase space distribution of BOWMAN 78.
 3 BOWMAN 78 assumes an interaction Lagrangian local on the scale of the inverse μ mass.

LIMIT ON $\mu^- \rightarrow e^-$ CONVERSION

Forbidden by lepton family number conservation.

VALUE	CL%	DOCUMENT ID	TECN	CHG	COMMENT
< 7×10^{-11}	90	BADERT...	80	STRC	SIN
< 4×10^{-10}	90	BADERT...	77	STRC	SIN

VALUE	CL%	DOCUMENT ID	TECN	
< 1.6×10^{-8}	90	BRYMAN	72	SPEC

$\sigma(\mu^- \text{Ti} \rightarrow e^- \text{Ti}) / \sigma(\mu^- \text{Ti} \rightarrow \text{capture})$

VALUE	CL%	DOCUMENT ID	TECN	CHG	COMMENT
< 4.3×10^{-12}	90	1 DOHMEN	93	SPEC	SINDRUM II
< 4.6×10^{-12}	90	AHMAD	88	TPC	TRIUMF
< 1.6×10^{-11}	90	BRYMAN	85	TPC	TRIUMF

1 DOHMEN 93 assumes $\mu^- \rightarrow e^-$ conversion leaves the nucleus in its ground state, a process enhanced by coherence and expected to dominate.

$\sigma(\mu^- \text{Pb} \rightarrow e^- \text{Pb}) / \sigma(\mu^- \text{Pb} \rightarrow \text{capture})$

VALUE	CL%	DOCUMENT ID	TECN	CHG	COMMENT
< 4.6×10^{-11}	90	HONECKER	96	SPEC	SINDRUM II
< 4.9×10^{-10}	90	AHMAD	88	TPC	TRIUMF

$\sigma(\mu^- \text{Au} \rightarrow e^- \text{Au}) / \sigma(\mu^- \text{Au} \rightarrow \text{capture})$

VALUE	CL%	DOCUMENT ID	TECN	CHG	COMMENT
< 7×10^{-13}	90	BERTL	06	SPEC	- SINDRUM II

LIMIT ON $\mu^- \rightarrow e^+$ CONVERSION

Forbidden by total lepton number conservation.

$\sigma(\mu^- 32\text{S} \rightarrow e^+ 32\text{Si}^*) / \sigma(\mu^- 32\text{S} \rightarrow \nu_\mu 32\text{P}^*)$

VALUE	CL%	DOCUMENT ID	TECN	CHG	COMMENT
< 9×10^{-10}	90	BADERT...	80	STRC	SIN
< 1.5×10^{-9}	90	BADERT...	78	STRC	SIN

$\sigma(\mu^- 127\text{I} \rightarrow e^+ 127\text{Sb}^*) / \sigma(\mu^- 127\text{I} \rightarrow \text{anything})$

VALUE	CL%	DOCUMENT ID	TECN	CHG	COMMENT
< 3×10^{-10}	90	1 ABELA	80	CNTR	Radiochemical tech.

1 ABELA 80 is upper limit for $\mu^- e^+$ conversion leading to particle-stable states of 127Sb. Limit for total conversion rate is higher by a factor less than 4 (G. Backenstoss, private communication).

$\sigma(\mu^- \text{Cu} \rightarrow e^+ \text{Co}) / \sigma(\mu^- \text{Cu} \rightarrow \nu_\mu \text{Ni})$

VALUE	CL%	DOCUMENT ID	TECN	
< 2.6×10^{-8}	90	BRYMAN	72	SPEC
< 2.2×10^{-7}	90	CONFORTO	62	OSPK

$\sigma(\mu^- \text{Ti} \rightarrow e^+ \text{Ca}) / \sigma(\mu^- \text{Ti} \rightarrow \text{capture})$

VALUE	CL%	EVTS	DOCUMENT ID	TECN	CHG	COMMENT
< 3.6×10^{-11}	90	1	2 KAULARD	98	SPEC	- SINDRUM II
< 1.7×10^{-12}	90	1	2,3 KAULARD	98	SPEC	- SINDRUM II
< 4.3×10^{-12}	90	3	DOHMEN	93	SPEC	SINDRUM II
< 8.9×10^{-11}	90	1	DOHMEN	93	SPEC	SINDRUM II
< 1.7×10^{-10}	90	4	AHMAD	88	TPC	TRIUMF

1 This limit assumes a giant resonance excitation of the daughter Ca nucleus (mean energy and width both 20 MeV).
 2 KAULARD 98 obtained these same limits using the unified classical analysis of FELDMAN 98.
 3 This limit assumes the daughter Ca nucleus is left in the ground state. However, the probability of this is unknown.
 4 Assuming a giant-resonance-excitation model.

LIMIT ON MUONIUM \rightarrow ANTIMUONIUM CONVERSION

Forbidden by lepton family number conservation.

$R_g = G_C / G_F$

The effective Lagrangian for the $\mu^+ e^- \rightarrow \mu^- e^+$ conversion is assumed to be

$$\mathcal{L} = 2^{-1/2} G_C [\bar{\nu}_\mu \gamma_\lambda (1 - \gamma_5) \psi_e] [\bar{\psi}_\mu \gamma_\lambda (1 - \gamma_5) \psi_e] + \text{h.c.}$$

The experimental result is then an upper limit on G_C / G_F , where G_F is the Fermi coupling constant.

VALUE	CL%	EVTS	DOCUMENT ID	TECN	CHG	COMMENT
< 0.0030	90	1	1 WILLMANN	99	SPEC	+ μ^+ at 26 GeV/c
< 0.14	90	1	2 GORDEEV	97	SPEC	+ JINR phasotron
< 0.018	90	0	3 ABELA	96	SPEC	+ μ^+ at 24 MeV
< 6.9	90		NI	93	CBOX	LAMPF
< 0.16	90		MATTHIAS	91	SPEC	LAMPF
< 0.29	90		HUBER	90B	CNTR	TRIUMF
< 20	95		BEER	86	CNTR	TRIUMF
< 42	95		MARSHALL	82	CNTR	

1 WILLMANN 99 quote both probability $P_{MM} < 8.3 \times 10^{-11}$ at 90%CL in a 0.1 T field and $R_g = G_C / G_F$.
 2 GORDEEV 97 quote limits on both $f = G_{MM} / G_F$ and the probability $W_{MM} < 4.7 \times 10^{-7}$ (90% CL).
 3 ABELA 96 quote both probability $P_{MM} < 8 \times 10^{-9}$ at 90% CL and $R_g = G_C / G_F$.

See key on page 1127

Lepton Particle Listings

μ

See the related review(s):
Muon Decay Parameters

μ DECAY PARAMETERS

ρ PARAMETER

(V-A) theory predicts $\rho = 0.75$.

Table with columns: VALUE, EVTS, DOCUMENT ID, TECN, CHG, COMMENT. Includes 'OUR AVERAGE' and data from BAYES, DERENZO, MACDONALD, MUSSER, AMORUSO, FRYBERGER, SHERWOOD, PEOPLES.

- 1 The quoted systematic error includes a contribution of 0.00013 (added in quadrature) from uncertainties on radiative corrections and on the Michel parameter η .
- 2 The quoted systematic error includes a contribution of 0.00011 (added in quadrature) from the dependence on the Michel parameter η .
- 3 The quoted systematic error includes a contribution of 0.00023 (added in quadrature) from the dependence on the Michel parameter η .
- 4 η constrained = 0. These values incorporated into a two parameter fit to ρ and η by DERENZO 69.

η PARAMETER

(V-A) theory predicts $\eta = 0$.

Table with columns: VALUE, EVTS, DOCUMENT ID, TECN, CHG, COMMENT. Includes 'OUR AVERAGE' and data from DANNEBERG, BURKARD, DERENZO, DANNEBERG, BURKARD, BURKARD, FRYBERGER, SHERWOOD, PEOPLES, PLANO.

- 1 Previously we used the global fit result from BURKARD 85B in OUR AVERAGE, we now only include their actual measurement.
- 2 $\alpha = \alpha' = 0$ assumed.
- 3 Global fit to all measured parameters. The fit correlation coefficients are given in BURKARD 85B.
- 4 ρ constrained = 0.75.
- 5 Two parameter fit to ρ and η ; PLANO 60 discounts value for η .

δ PARAMETER

(V-A) theory predicts $\delta = 0.75$.

Table with columns: VALUE, EVTS, DOCUMENT ID, TECN, CHG, COMMENT. Includes 'OUR AVERAGE' and data from BAYES, BALKE, MACDONALD, GAPONENKO, VOSSLER, FRYBERGER, KRUGER, PLANO.

- 1 The quoted systematic error includes a contribution of 0.00006 (added in quadrature) from uncertainties on radiative corrections and on the Michel parameter η .
- 2 BALKE 88 uses $\rho = 0.752 \pm 0.003$.
- 3 VOSSLER 69 has measured the asymmetry below 10 MeV. See comments about radiative corrections in VOSSLER 69.

$(\xi \text{ PARAMETER}) \times (\mu \text{ LONGITUDINAL POLARIZATION})$

(V-A) theory predicts $\xi = 1$, longitudinal polarization = 1.

Table with columns: VALUE, DOCUMENT ID, TECN, CHG, COMMENT. Includes 'OUR AVERAGE' and data from BUENO, BELTRAMI, JAMIESON, IMAZATO, AKHMANOV, GUREVICH, ALI-ZADE, PLANO, BARDON.

- 1 The corresponding 90% confidence limit from IMAZATO 92 is $|\xi P_{\mu}| > 0.990$. This measurement is of K^+ decay, not π^+ decay, so we do not include it in an average, nor do we yet set up a separate data block for K results.
- 2 Depolarization by medium not known sufficiently well.

$\xi \times (\mu \text{ LONGITUDINAL POLARIZATION}) \times \delta / \rho$

Table with columns: VALUE, CL%, DOCUMENT ID, TECN, CHG, COMMENT. Includes 'OUR AVERAGE' and data from BAYES, JODIDIO, STOKER, CARR.

- 1 BAYES 11 obtains the limit > 0.99909 (90% CL) with the constraint that $\xi \times (\mu \text{ LONGITUDINAL POLARIZATION}) \times \delta / \rho \leq 1.0$.
- 2 JODIDIO 86 includes data from CARR 83 and STOKER 85. The value here is from the erratum.
- 3 STOKER 85 find $(\xi P_{\mu} \delta / \rho) > 0.9955$ and > 0.9966 , where the first limit is from new μ spin-rotation data and the second is from combination with CARR 83 data. In V-A theory, $(\delta / \rho) = 1.0$.

$\xi' = \text{LONGITUDINAL POLARIZATION OF } e^{\pm}$

(V-A) theory predicts the longitudinal polarization = ± 1 for e^{\pm} , respectively. We have flipped the sign for e^{-} so our programs can average.

Table with columns: VALUE, EVTS, DOCUMENT ID, TECN, CHG, COMMENT. Includes 'OUR AVERAGE' and data from BURKARD, SCHWARTZ, BLOOM, DUCLOS, BUHLER.

ξ'' PARAMETER

Table with columns: VALUE, EVTS, DOCUMENT ID, TECN, CHG, COMMENT. Includes 'OUR AVERAGE' and data from PRIEELS, BURKARD.

- 1 BURKARD 85 measure $(\xi'' - \xi \xi') / \xi$ and ξ' and set $\xi = 1$.

TRANSVERSE e^+ POLARIZATION IN PLANE OF μ SPIN, e^+ MOMENTUM

Table with columns: VALUE (units 10^{-3}), EVTS, DOCUMENT ID, TECN, CHG, COMMENT. Includes 'OUR AVERAGE' and data from DANNEBERG, BURKARD.

TRANSVERSE e^+ POLARIZATION NORMAL TO PLANE OF μ SPIN, e^+ MOMENTUM

Table with columns: VALUE (units 10^{-3}), EVTS, DOCUMENT ID, TECN, CHG, COMMENT. Includes 'OUR AVERAGE' and data from DANNEBERG, BURKARD.

α/A

Table with columns: VALUE (units 10^{-3}), EVTS, DOCUMENT ID, TECN, CHG, COMMENT. Includes 'OUR AVERAGE' and data from BURKARD.

α'/A

Table with columns: VALUE (units 10^{-3}), EVTS, DOCUMENT ID, TECN, CHG, COMMENT. Includes 'OUR AVERAGE' and data from DANNEBERG, BURKARD.

- 1 Previously we used the global fit result from BURKARD 85B in OUR AVERAGE, we now only include their actual measurement. BURKARD 85B measure e^+ polarizations P_{T1} and P_{T2} versus e^+ energy.
- 2 Global fit to all measured parameters. The fit correlation coefficients are given in BURKARD 85B.

β/A

Table with columns: VALUE (units 10^{-3}), EVTS, DOCUMENT ID, TECN, CHG, COMMENT. Includes 'OUR AVERAGE' and data from BURKARD.

β'/A

Table with columns: VALUE (units 10^{-3}), EVTS, DOCUMENT ID, TECN, CHG, COMMENT. Includes 'OUR AVERAGE' and data from DANNEBERG, BURKARD.

Lepton Particle Listings

μ

••• We do not use the following data for averages, fits, limits, etc. •••

$-1.3 \pm 3.5 \pm 0.6$ 30M ²DANNEBERG 05 CNTR + $7-53$ MeV e^+
 1.5 ± 6.3 ³BURKARD 85B FIT

¹Previously we used the global fit result from BURKARD 85B in OUR AVERAGE, we now only include their actual measurement. BURKARD 85B measure e^+ polarizations P_{T_1} and P_{T_2} versus e^+ energy.

² $\alpha = \alpha' = 0$ assumed.

³Global fit to all measured parameters. The fit correlation coefficients are given in BURKARD 85B.

a/A

This comes from an alternative parameterization to that used in the Summary Table (see the "Note on Muon Decay Parameters" above).

VALUE (units 10^{-3})	CL%	DOCUMENT ID	TECN
<15.9	90	¹ BURKARD 85B FIT	

••• We do not use the following data for averages, fits, limits, etc. •••

¹Global fit to all measured parameters. Correlation coefficients are given in BURKARD 85B.

a'/A

This comes from an alternative parameterization to that used in the Summary Table (see the "Note on Muon Decay Parameters" above).

VALUE (units 10^{-3})	CL%	DOCUMENT ID	TECN
5.3 \pm 4.1		¹ BURKARD 85B FIT	

••• We do not use the following data for averages, fits, limits, etc. •••

¹Global fit to all measured parameters. Correlation coefficients are given in BURKARD 85B.

(b'+b)/A

This comes from an alternative parameterization to that used in the Summary Table (see the "Note on Muon Decay Parameters" above).

VALUE (units 10^{-3})	CL%	DOCUMENT ID	TECN
<1.04	90	¹ BURKARD 85B FIT	

••• We do not use the following data for averages, fits, limits, etc. •••

¹Global fit to all measured parameters. Correlation coefficients are given in BURKARD 85B.

c/A

This comes from an alternative parameterization to that used in the Summary Table (see the "Note on Muon Decay Parameters" above).

VALUE (units 10^{-3})	CL%	DOCUMENT ID	TECN
<6.4	90	¹ BURKARD 85B FIT	

••• We do not use the following data for averages, fits, limits, etc. •••

¹Global fit to all measured parameters. Correlation coefficients are given in BURKARD 85B.

c'/A

This comes from an alternative parameterization to that used in the Summary Table (see the "Note on Muon Decay Parameters" above).

VALUE (units 10^{-3})	CL%	DOCUMENT ID	TECN
3.5 \pm 2.0		¹ BURKARD 85B FIT	

••• We do not use the following data for averages, fits, limits, etc. •••

¹Global fit to all measured parameters. Correlation coefficients are given in BURKARD 85B.

η PARAMETER

($V-A$) theory predicts $\eta = 0$. η affects spectrum of radiative muon decay.

VALUE	DOCUMENT ID	TECN	CHG	COMMENT
0.02 \pm 0.08	OUR AVERAGE			
-0.014 ± 0.090	EICHENBER... 84	ELEC	+	ρ free
$+0.09 \pm 0.14$	BOGART 67	CNTR	+	
-0.035 ± 0.098	EICHENBER... 84	ELEC	+	$\rho=0.75$ assumed

••• We do not use the following data for averages, fits, limits, etc. •••

••• We do not use the following data for averages, fits, limits, etc. •••

μ REFERENCES

ABI	21	PRL 126 141801	B. Abi et al.	(Muon g-2 Collab.)
TIESINGA	21	RMP 93 025010	E. Tiesinga et al.	(NIST)
AOYAMA	20	PRL 807 1	T. Aoyama et al.	(MEG Collab.)
BALDINI	20	EPL C80 858	A.M. Baldini et al.	(MEG Collab.)
BALDINI	16	EPL C76 434	A.M. Baldini et al.	(MEG Collab.)
BALDINI	16A	EPL C76 108	A.M. Baldini et al.	(MEG Collab.)
MOHR	14	RMP 88 035009	P.J. Mohr, D.B. Newell, B.N. Taylor	(NIST)
PRIEELS	14	PR D90 112003	R. Prieels et al.	(LOUV, ETH, PSI+)
ADAM	13B	PRL 110 201801	J. Adam et al.	(MEG Collab.)
TISHCHENKO	13	PR D87 052003	V. Tishchenko et al.	(MuLan Collab.)
MOHR	12	RMP 84 1527	P.J. Mohr, B.N. Taylor, D.B. Newell	(NIST)
ADAM	11	PRL 107 171801	J. Adam et al.	(MEG Collab.)
BAYES	11	PRL 106 041804	R. Bayes et al.	(TWIST Collab.)
Also		PR D85 092013	A. Hillairet et al.	(TWIST Collab.)
BUENO	11	PR D84 032005	J.F. Bueno et al.	(TWIST Collab.)
Also		PR D85 039908 (err.)	J.F. Bueno et al.	(TWIST Collab.)
WEBBER	11	PRL 106 041803	D.M. Webber et al.	(MuLan Collab.)
Also		PRL 106 079901 (err.)	D.M. Webber et al.	(MuLan Collab.)
ADAM	10	NP B834 1	J. Adam et al.	(MEG Collab.)
BENNETT	09	PR D80 052008	G.W. Bennett et al.	(MUG-2 Collab.)
BARCZYK	08	PL B663 172	A. Barczyk et al.	(FAST Collab.)
MACDONALD	08	PR D78 032010	R.P. MacDonald et al.	(TWIST Collab.)
MOHR	08	RMP 80 633	P.J. Mohr, B.N. Taylor, D.B. Newell	(NIST)
CHITWOOD	07	PRL 99 032001	D.B. Chitwood et al.	(MULAN Collab.)
BENNETT	06	PR D73 072003	G.W. Bennett et al.	(MUG-2 Collab.)
BERTL	06	EPL C47 337	W. Bertl et al.	(SINDRUM II Collab.)

JAMIESON	06	PR D74 072007	B. Jamieson et al.	(TWIST Collab.)
DANNEBERG	05	PRL 94 021802	N. Danneberg et al.	(ETH, JAGL, PSI+)
GAPONENKO	05	PR D71 071101	A. Gaponenko et al.	(TWIST Collab.)
MOHR	05	RMP 77 1	P.J. Mohr, B.N. Taylor	(NIST)
MUSSER	05	PRL 94 101805	J.R. Musser et al.	(TWIST Collab.)
AMORUSO	04	EPL C33 233	S. Amoroso et al.	(ICARUS Collab.)
BENNETT	04	PRL 92 161802	G.W. Bennett et al.	(Moon(g-2) Collab.)
AHMED	02	PR D05 112002	M. Ahmed et al.	(MEGA Collab.)
BENNETT	02	PRL 89 101804	G.W. Bennett et al.	(Moon(g-2) Collab.)
BROWN	01	PRL 86 2227	H.N. Brown et al.	(Moon(g-2) Collab.)
BROWN	00	PR D02 091101	H.N. Brown et al.	(BNL/G-2 Collab.)
MEYER	00	PRL 84 1136	V. Meyer et al.	
BROOKS	99	PRL 83 1521	M.L. Brooks et al.	(MEGA/LAMPF Collab.)
HUGHES	99	RMP 71 1533	V.W. Hughes, T. Kinoshita	
LIU	99	PRL 82 711	W. Liu et al.	(LAMPF Collab.)
MOHR	99	JPCRD 28 1713	P.J. Mohr, B.N. Taylor	(NIST)
Also		RMP 72 351	P.J. Mohr, B.N. Taylor	(NIST)
WILLMANN	99	PRL 82 49	L. Willmann et al.	
FELDMAN	98	PR D57 3873	G.J. Feldman, R.D. Cousins	
KALLARD	98	PL B422 334	J. Kallard et al.	(SINDRUM-II Collab.)
GORDEV	97	PAN 60 1164	V.A. Gordev et al.	(PNPI)
Translated from YAF 60		1291.		
ABELA	96	PRL 77 1950	R. Abela et al.	(PSI, ZURI, HEIDH, TBIL+)
HONECKER	96	PRL 76 200	W. Honecker et al.	(SINDRUM II Collab.)
DOHMEN	93	PL B317 631	C. Dohmen et al.	(PSI SINDRUM-II Collab.)
FREEDMAN	93	PR D47 811	S.J. Freedman et al.	(LAMPF E645 Collab.)
NI	93	PR D48 1976	B. Ni et al.	(LAMPF Crystal-Box Collab.)
IMAZATO	92	PRL 69 877	J. Imazato et al.	(KEK, INUS, TOKY+)
BARANOV	91	SJNP 3 302	V.A. Baranov et al.	(JINR)
Translated from YAF 53		1302.		
KRAKAUER	91B	PL B263 534	D.A. Krakauer et al.	(UMD, UCI, LANL)
MATTHIAS	91	PRL 66 2716	B.E. Matthias et al.	(YALE, HEIDP, WILL+)
Also		PRL 67 932 (erratum)	B.E. Matthias et al.	(YALE, HEIDP, WILL+)
HUBER	90B	PR D41 2709	T.M. Huber et al.	(WYOM, VICT, ARIZ+)
AHMAD	88	PR D38 2102	S. Ahmad et al.	(TRIUM, VICT, VPI, BRCO+)
Also		PRL 59 970	S. Ahmad et al.	(TRIUM, VPI, VICT, BRCO+)
BALKE	88	PR D37 587	B. Balke et al.	(LBL, UCB, COLO, NWES+)
BELLEGARDT	88	NP B299 1	U. Bellgardt et al.	(SINDRUM Collab.)
BOLTON	88	PR D38 2077	R.D. Bolton et al.	(RNL, STAN, CHIC+)
Also		PRL 56 2461	R.D. Bolton et al.	(LANL, STAN, CHIC+)
Also		PRL 57 3241	R. Grosnick et al.	(CHIC, LANL, STAN+)
BELTRAMI	87	PL B194 326	I. Beltrami et al.	(ETH, SIN, MAINZ)
COHEN	87	RMP 59 1121	E.R. Cohen, B.N. Taylor	(RISC, NBS)
BEER	86	PRL 57 671	G.A. Beer et al.	(VICT, TRIUM, WYOM)
JODIDIO	86	PR D34 1967	A. Jodidio et al.	(LNL, NWES, TRIUM)
Also		PR D37 237 (erratum)	A. Jodidio et al.	(LBL, NWES, TRIUM)
BERTL	85	NP B260 1	W. Bertl et al.	(SINDRUM Collab.)
BRYMAN	85	PRL 55 465	D.A. Bryman et al.	(TRIUM, CNRC, BRCO+)
BURKARD	85	PL B308 242	H. Burkhardt et al.	(ETH, SIN, MAINZ)
BURKARD	85B	PL 140B 343	H. Burkhardt et al.	(ETH, SIN, MAINZ)
Also		PR D24 2004	F. Corribeau et al.	(ETH, SIN, MAINZ)
Also		PL 129B 260	F. Corribeau et al.	(ETH, SIN, MAINZ)
STOKER	85	PRL 54 1887	D.P. Stoker et al.	(LBL, NWES, TRIUM)
BARDIN	84	PL 137B 135	G. Bardin et al.	(SACL, CERN, BGNA, FIRZ)
BERTL	84	PL 140B 299	W. Bertl et al.	(SINDRUM Collab.)
BOLTON	84	PRL 53 1415	R.D. Bolton et al.	(LANL, CHIC, STAN+)
EICHENBER...	84	NP A412 523	W. Eichenberger, R. Engfer, A. van der Schaff	
GIOVANETTI	84	PR D29 343	K.L. Giovanetti et al.	(WILL)
AZUELOS	83	PRL 51 164	G. Azuelos et al.	(MONT, TRIUM, BRCO)
Also		PRL 39 1113	P. Depommier et al.	(MONT, BRCO, TRIUM)
BERGSMA	83	PL 122B 465	F. Bergsma et al.	(CHARM Collab.)
CARR	83	PRL 51 627	J. Carr et al.	(LBL, NWES, TRIUM)
KINNISON	82	PR D25 2846	W.W. Kinnison et al.	(EFI, STAN, LANL)
Also		PRL 42 556	J.D. Bowman et al.	(LASL, EFI, STAN)
KLEMPPT	82	PR D25 652	E. Klempert et al.	(MAINZ, ETH)
MARIAM	82	PRL 49 993	F.G. Mariam et al.	(YALE, HEIDH, BERN)
MARSHALL	82	PR D25 1174	G.M. Marshall et al.	(BRCO)
NEMETHY	81	CNPP 10 147	P. Nemethy, V.W. Hughes	(LBL, YALE)
ABELA	80	PL 95B 318	R. Abela et al.	(BASL, KARLK, KARLE)
BADERT...	80	LNC 28 401	A. Badertscher et al.	(BERN)
Also		NP A377 406	A. Badertscher et al.	(BERN)
JOEKER	80	PL 92B 203	M. Jonker et al.	(CHARM Collab.)
SCHAAF	80	NP A340 249	A. van der Schaaf et al.	(ZURI, ETH+)
Also		PL 72B 183	H.P. Povel et al.	(ZURI, ETH, SIN)
WILLIS	80	PRL 44 522	S.E. Willis et al.	(YALE, LBL, LASL+)
Also		PRL 45 1370	S.E. Willis et al.	(YALE, LBL, LASL+)
BAILEY	79	NP B150 1	J.M. Bailey	(CERN, DARE, MAINZ)
BADERT...	78	PL 79B 371	A. Badertscher et al.	(BERN)
BAILEY	78	JP G4 345	J.M. Bailey	(DARE, BERN, SHEF, MAINZ, RMCS+)
Also		NP B150 1	J.M. Bailey	(CERN, DARE, MAINZ)
BLIETSCHAU	78	NP B133 205	J. Blietschau et al.	(Gargamelle Collab.)
BOYMAN	78	PRL 41 442	J.D. Bowman et al.	(LASL, IAS, CMU+)
CAMANI	78	PL 77B 326	M. Camani et al.	(ETH, MAINZ)
BADERT...	77	PRL 39 1385	A. Badertscher et al.	(BERN)
CASPERSON	77	PRL 38 956	D.E. Caspersen et al.	(BERN, HEIDH, LASL+)
DEPOMMIER	77	PRL 39 1113	P. Depommier et al.	(MONT, BRCO, TRIUM)
BALANDIN	74	JETP 40 811	M.P. Balandin et al.	(JINR)
Translated from ZETF 67		1631.		
COHEN	73	JPCRD 2 664	E.R. Cohen, B.N. Taylor	(RISC, NBS)
DUCLÓS	73	PL 47B 491	J. Duclós, A. Magnón, J. Picard	(SACL)
EICHTEN	73	PL 46B 201	T. Eichten et al.	(Gargamelle Collab.)
BRYMAN	72	PRL 28 1469	D.A. Bryman et al.	(VPI)
CROWE	72	PR D5 2145	K.M. Crowe et al.	(LBL, WASH)
CRANE	71	PRL 27 474	T. Crane et al.	(YALE)
DERENZO	69	PR 181 1854	S.E. Denzno	(EFI)
VOSSLER	69	NC 63A 423	C. Vossler	(EFI)
AKHMANOV	68	SJNP 6 230	V.V. Akhmanov et al.	(KIAE)
Translated from YAF 6 316.				
FRYBERGER	68	PR 166 1379	D. Fryberger	(EFI)
BOGART	67	PR 156 1405	E. Bogart et al.	(COLU)
SCHWARTZ	67	PR 162 1306	D.H. Schwartz	(EFI)
SHERWOOD	67	PR 156 1475	B.A. Sherwood	(EFI)
PEOPLES	66	Nevis 147 unpub.	J. Peoples	(COLU)
BLOOM	64	PL 8 87	S. Bloom et al.	(CERN)
DUCLÓS	64	PL 9 62	J. Duclós et al.	(CERN)
GUREVICH	64	PL 11 185	I.I. Gurevich et al.	(KIAE)
BUHLER	63	PL 7 368	A. Buhler-Broglin et al.	(CERN)
MEYER	63	PR 132 2693	S.L. Meyer et al.	(COLU)
CHARPAK	62	PL 1 16	G. Charpak et al.	(CERN)
CONFORTO	62	NC 26 261	G. Conforto et al.	(INFN, ROMA, CERN)
ALI-ZADE	61	JETP 13 313	S.A. Ali-Zade, I.I. Gurevich, B.A. Nikolsky	
Translated from ZETF 40		452.		
CRITTENDEN	61	PR 121 1823	R.R. Crittenden, W.D. Walker, J. Ballam	(WIS+)
KRUGER	61	UCRL 9322 unpub.	H. Kruger	(LRL)
GUREVICH	60	JETP 10 225	I.I. Gurevich, B.A. Nikolsky, L.V. Surkova	(ITEP)
Translated from ZETF 37		318.		
PLANO	60	PR 119 1400	R.J. Plano	(COLU)
ASHKIN	59	NC 14 1266	J. Ashkin et al.	(CERN)
BARDON	59	PRL 2 56	M. Bardon, D. Berley, L.M. Lederman	(COLU)
LEE	59	PRL 3 55	J. Lee, N.P. Samios	(COLU)



$$J = \frac{1}{2}$$

$$(\tau_{\tau^+} - \tau_{\tau^-}) / \tau_{\text{average}}$$

Test of CPT invariance.

τ discovery paper was PERL 75. $e^+e^- \rightarrow \tau^+\tau^-$ cross-section threshold behavior and magnitude are consistent with pointlike spin-1/2 Dirac particle. BRANDELIK 78 ruled out pointlike spin-0 or spin-1 particle. FELDMAN 78 ruled out $J = 3/2$. KIRKBY 79 also ruled out $J=\text{integer}$, $J = 3/2$.

VALUE	CL%	DOCUMENT ID	TECN	COMMENT
$< 7.0 \times 10^{-3}$	90	¹ BELOUS	14 BELL	711 fb^{-1} $E_{\text{cm}}^{\text{ee}} = 10.6 \text{ GeV}$

¹BELOUS 14 quote limit on the absolute value of the relative lifetime difference.

τ MASS

VALUE (MeV)	EVTS	DOCUMENT ID	TECN	COMMENT
1776.86 ± 0.12 OUR AVERAGE				
$1776.91 \pm 0.12^{+0.10}_{-0.13}$	1171	¹ ABLIKIM	14D BES3	23.3 pb^{-1} , $E_{\text{cm}}^{\text{ee}} = 3.54\text{--}3.60 \text{ GeV}$
$1776.68 \pm 0.12 \pm 0.41$	682k	² AUBERT	09AK BABR	423 fb^{-1} , $E_{\text{cm}}^{\text{ee}} = 10.6 \text{ GeV}$
$1776.81^{+0.25}_{-0.23} \pm 0.15$	81	ANASHIN	07 KEDR	6.7 pb^{-1} , $E_{\text{cm}}^{\text{ee}} = 3.54\text{--}3.78 \text{ GeV}$
$1776.61 \pm 0.13 \pm 0.35$		² BELOUS	07 BELL	414 fb^{-1} $E_{\text{cm}}^{\text{ee}} = 10.6 \text{ GeV}$
$1775.1 \pm 1.6 \pm 1.0$	13.3k	³ ABBIENDI	00A OPAL	1990–1995 LEP runs
$1778.2 \pm 0.8 \pm 1.2$		ANASTASSOV	97 CLEO	$E_{\text{cm}}^{\text{ee}} = 10.6 \text{ GeV}$
$1776.96^{+0.18+0.25}_{-0.21-0.17}$	65	⁴ BAI	96 BES	$E_{\text{cm}}^{\text{ee}} = 3.54\text{--}3.57 \text{ GeV}$
$1776.3 \pm 2.4 \pm 1.4$	11k	⁵ ALBRECHT	92M ARG	$E_{\text{cm}}^{\text{ee}} = 9.4\text{--}10.6 \text{ GeV}$
1783^{+3}_{-4}	692	⁶ BACINO	78B DLCO	$E_{\text{cm}}^{\text{ee}} = 3.1\text{--}7.4 \text{ GeV}$

••• We do not use the following data for averages, fits, limits, etc. •••
⁷BALEST 93 CLEO Repl. by ANASTASSOV 97
⁸BAI 92 fit $\sigma(e^+e^- \rightarrow \tau^+\tau^-)$ near threshold using $e\mu$ events.

- ¹ABLIKIM 14D fit $\sigma(e^+e^- \rightarrow \tau^+\tau^-)$ at different energies near threshold.
- ²AUBERT 09AK and BELOUS 07 fit τ pseudomass spectrum in $\tau \rightarrow \pi\pi^+\pi^-\nu_\tau$ decays. Result assumes $m_{\nu_\tau} = 0$.
- ³ABBIENDI 00A fit τ pseudomass spectrum in $\tau \rightarrow \pi^\pm \leq 2\pi^0\nu_\tau$ and $\tau \rightarrow \pi^\pm\pi^+\pi^- \leq 1\pi^0\nu_\tau$ decays. Result assumes $m_{\nu_\tau} = 0$.
- ⁴BAI 96 fit $\sigma(e^+e^- \rightarrow \tau^+\tau^-)$ at different energies near threshold.
- ⁵ALBRECHT 92M fit τ pseudomass spectrum in $\tau^- \rightarrow 2\pi^-\pi^+\nu_\tau$ decays. Result assumes $m_{\nu_\tau} = 0$.
- ⁶BACINO 78B value comes from $e^\pm X^\mp$ threshold. Published mass 1782 MeV increased by 1 MeV using the high precision $\psi(2S)$ mass measurement of ZHOLENTZ 80 to eliminate the absolute SPEAR energy calibration uncertainty.
- ⁷BALEST 93 fit spectra of minimum kinematically allowed τ mass in events of the type $e^+e^- \rightarrow \tau^+\tau^- \rightarrow (\pi^+n\pi^0\nu_\tau)(\pi^-m\pi^0\nu_\tau)$ $n \leq 2, m \leq 2, 1 \leq n+m \leq 3$. If $m_{\nu_\tau} \neq 0$, result increases by $(m_{\nu_\tau}^2/1100 \text{ MeV})$.
- ⁸BAI 92 fit $\sigma(e^+e^- \rightarrow \tau^+\tau^-)$ near threshold using $e\mu$ events.

$$(m_{\tau^+} - m_{\tau^-}) / m_{\text{average}}$$

A test of CPT invariance.

VALUE	CL%	DOCUMENT ID	TECN	COMMENT
$< 2.8 \times 10^{-4}$	90	BELOUS	07 BELL	414 fb^{-1} , $E_{\text{cm}}^{\text{ee}} = 10.6 \text{ GeV}$

••• We do not use the following data for averages, fits, limits, etc. •••
 $< 5.5 \times 10^{-4}$ 90 ¹AUBERT 09AK BABR 423 fb^{-1} , $E_{\text{cm}}^{\text{ee}} = 10.6 \text{ GeV}$
 $< 3.0 \times 10^{-3}$ 90 ABBIENDI 00A OPAL 1990–1995 LEP runs
¹AUBERT 09AK quote both the listed upper limit and $(m_{\tau^+} - m_{\tau^-}) / m_{\text{average}} = (-3.4 \pm 1.3 \pm 0.3) \times 10^{-4}$.

τ MEAN LIFE

VALUE (10^{-15} s)	EVTS	DOCUMENT ID	TECN	COMMENT
290.3 ± 0.5 OUR AVERAGE				
$290.17 \pm 0.53 \pm 0.33$	1.1M	BELOUS	14 BELL	711 fb^{-1} $E_{\text{cm}}^{\text{ee}} = 10.6 \text{ GeV}$
$290.9 \pm 1.4 \pm 1.0$		ABDALLAH	04T DLPH	1991–1995 LEP runs
$293.2 \pm 2.0 \pm 1.5$		ACCIARRI	00B L3	1991–1995 LEP runs
$290.1 \pm 1.5 \pm 1.1$		BARATE	97R ALEP	1989–1994 LEP runs
$289.2 \pm 1.7 \pm 1.2$		ALEXANDER	96E OPAL	1990–1994 LEP runs
$289.0 \pm 2.8 \pm 4.0$	57.4k	BALEST	96 CLEO	$E_{\text{cm}}^{\text{ee}} = 10.6 \text{ GeV}$

••• We do not use the following data for averages, fits, limits, etc. •••
 $291.2 \pm 2.0 \pm 1.2$ BARATE 97I ALEP Repl. by BARATE 97R
 291.4 ± 3.0 ABREU 96B DLPH Repl. by ABDALLAH 04T
 290.1 ± 4.0 ACCIARRI 96K L3 Repl. by ACCIARRI 00B
 $297 \pm 9 \pm 5$ 1671 ABE 95Y SLD 1992–1993 SLC runs
 $304 \pm 14 \pm 7$ 4100 BATTLE 92 CLEO $E_{\text{cm}}^{\text{ee}} = 10.6 \text{ GeV}$
 301 ± 29 3780 KLEINWORT 89 JADE $E_{\text{cm}}^{\text{ee}} = 35\text{--}46 \text{ GeV}$
 $288 \pm 16 \pm 17$ 807 AMIDEI 88 MRK2 $E_{\text{cm}}^{\text{ee}} = 29 \text{ GeV}$
 $306 \pm 20 \pm 14$ 695 BRAUNSCH... 88C TASS $E_{\text{cm}}^{\text{ee}} = 36 \text{ GeV}$
 $299 \pm 15 \pm 10$ 1311 ABACHI 87C HRS $E_{\text{cm}}^{\text{ee}} = 29 \text{ GeV}$
 $295 \pm 14 \pm 11$ 5696 ALBRECHT 87P ARG $E_{\text{cm}}^{\text{ee}} = 9.3\text{--}10.6 \text{ GeV}$
 $309 \pm 17 \pm 7$ 3788 BAND 87B MAC $E_{\text{cm}}^{\text{ee}} = 29 \text{ GeV}$
 $325 \pm 14 \pm 18$ 8470 BEBEK 87C CLEO $E_{\text{cm}}^{\text{ee}} = 10.5 \text{ GeV}$
 460 ± 190 102 FELDMAN 82 MRK2 $E_{\text{cm}}^{\text{ee}} = 29 \text{ GeV}$

τ MAGNETIC MOMENT ANOMALY

The q^2 dependence is expected to be small providing no thresholds are nearby.

$$\mu_\tau / (eh/2m_\tau) - 1 = (g_\tau - 2)/2$$

For a theoretical calculation $[(g_\tau - 2)/2 = 117 721(5) \times 10^{-8}]$, see EIDELMAN 07.

VALUE	CL%	DOCUMENT ID	TECN	COMMENT
> -0.052 and < 0.013 (CL = 95%)				OUR LIMIT
> -0.052 and < 0.013	95	¹ ABDALLAH	04k DLPH	$e^+e^- \rightarrow e^+e^-\tau^+\tau^-$ at LEP2

••• We do not use the following data for averages, fits, limits, etc. •••
 < 0.107 95 ²ACHARD 04G L3 $e^+e^- \rightarrow e^+e^-\tau^+\tau^-$ at LEP2
 > -0.007 and < 0.005 95 ³GONZALEZ-S.00 RVUE $e^+e^- \rightarrow \tau^+\tau^-$ and $W \rightarrow \tau\nu_\tau$
 > -0.052 and < 0.058 95 ⁴ACCIARRI 98E L3 1991–1995 LEP runs
 > -0.068 and < 0.065 95 ⁵ACKERSTAFF 98N OPAL 1990–1995 LEP runs
 > -0.004 and < 0.006 95 ⁶ESCRIBANO 97 RVUE $Z \rightarrow \tau^+\tau^-$ at LEP
 < 0.01 95 ⁷ESCRIBANO 93 RVUE $Z \rightarrow \tau^+\tau^-$ at LEP
 < 0.12 90 GRIFOLS 91 RVUE $Z \rightarrow \tau\tau\gamma$ at LEP
 < 0.023 95 ⁸SILVERMAN 83 RVUE $e^+e^- \rightarrow \tau^+\tau^-$ at PETRA

- ¹ABDALLAH 04k limit is derived from $e^+e^- \rightarrow e^+e^-\tau^+\tau^-$ total cross-section measurements at \sqrt{s} between 183 and 208 GeV. In addition to the limits, the authors also quote a value of -0.018 ± 0.017 .
- ²ACHARD 04G limit is derived from $e^+e^- \rightarrow e^+e^-\tau^+\tau^-$ total cross-section measurements at \sqrt{s} between 189 and 206 GeV, and is on the absolute value of the magnetic moment anomaly.
- ³GONZALEZ-SPRINGER 00 use data on tau lepton production at LEP1, SLC, and LEP2, and data from colliders and LEP2 to determine limits. Assume imaginary component is zero.
- ⁴ACCIARRI 98E use $Z \rightarrow \tau^+\tau^-\gamma$ events. In addition to the limits, the authors also quote a value of $0.004 \pm 0.027 \pm 0.023$.
- ⁵ACKERSTAFF 98N use $Z \rightarrow \tau^+\tau^-\gamma$ events. The limit applies to an average of the form factor for off-shell τ 's having p^2 ranging from m_τ^2 to $(M_Z - m_\tau)^2$.
- ⁶ESCRIBANO 97 use preliminary experimental results.
- ⁷ESCRIBANO 93 limit derived from $\Gamma(Z \rightarrow \tau^+\tau^-)$, and is on the absolute value of the magnetic moment anomaly.
- ⁸SILVERMAN 83 limit is derived from $e^+e^- \rightarrow \tau^+\tau^-$ total cross-section measurements for q^2 up to $(37 \text{ GeV})^2$.

τ ELECTRIC DIPOLE MOMENT (d_τ)

A nonzero value is forbidden by both T invariance and P invariance.

The q^2 dependence is expected to be small providing no thresholds are nearby.

$$\text{Re}(d_\tau)$$

VALUE (10^{-16} ecm)	CL%	DOCUMENT ID	TECN	COMMENT
$- 0.22$ to 0.45	95	¹ INAMI	03 BELL	$E_{\text{cm}}^{\text{ee}} = 10.6 \text{ GeV}$

••• We do not use the following data for averages, fits, limits, etc. •••
 < 2.3 90 ²GROZIN 09A RVUE From e EDM limit
 < 3.7 95 ³ABDALLAH 04k DLPH $e^+e^- \rightarrow e^+e^-\tau^+\tau^-$ at LEP2
 < 11.4 95 ⁴ACHARD 04G L3 $e^+e^- \rightarrow e^+e^-\tau^+\tau^-$ at LEP2
 < 4.6 95 ⁵ALBRECHT 00 ARG $E_{\text{cm}}^{\text{ee}} = 10.4 \text{ GeV}$
 > -3.1 and < 3.1 95 ACCIARRI 98E L3 1991–1995 LEP runs
 > -3.8 and < 3.6 95 ⁶ACKERSTAFF 98N OPAL 1990–1995 LEP runs
 < 0.11 95 ^{7,8}ESCRIBANO 97 RVUE $Z \rightarrow \tau^+\tau^-$ at LEP
 < 0.5 95 ⁹ESCRIBANO 93 RVUE $Z \rightarrow \tau^+\tau^-$ at LEP
 < 7 90 GRIFOLS 91 RVUE $Z \rightarrow \tau\tau\gamma$ at LEP
 < 1.6 90 DELAGUILA 90 RVUE $e^+e^- \rightarrow \tau^+\tau^-$ $E_{\text{cm}}^{\text{ee}} = 35 \text{ GeV}$

- ¹INAMI 03 use $e^+e^- \rightarrow \tau^+\tau^-$ events.
- ²GROZIN 09A calculate the contribution to the electron electric dipole moment from the τ electric dipole moment appearing in loops, which is $\Delta d_e = 6.9 \times 10^{-12} d_\tau$. Dividing the REGAN 02 upper limit $|d_e| \leq 1.6 \times 10^{-27} \text{ ecm}$ at CL=90% by 6.9×10^{-12} gives this limit.
- ³ABDALLAH 04k limit is derived from $e^+e^- \rightarrow e^+e^-\tau^+\tau^-$ total cross-section measurements at \sqrt{s} between 183 and 208 GeV and is on the absolute value of d_τ .
- ⁴ACHARD 04G limit is derived from $e^+e^- \rightarrow e^+e^-\tau^+\tau^-$ total cross-section measurements at \sqrt{s} between 189 and 206 GeV, and is on the absolute value of d_τ .
- ⁵ALBRECHT 00 use $e^+e^- \rightarrow \tau^+\tau^-$ events. Limit is on the absolute value of $\text{Re}(d_\tau)$.
- ⁶ACKERSTAFF 98N use $Z \rightarrow \tau^+\tau^-\gamma$ events. The limit applies to an average of the form factor for off-shell τ 's having p^2 ranging from m_τ^2 to $(M_Z - m_\tau)^2$.
- ⁷ESCRIBANO 97 derive the relationship $|d_\tau^W| = \cot \theta_W |d_\tau^W|$ using effective Lagrangian methods, and use a conference result $|d_\tau^W| < 5.8 \times 10^{-18} \text{ ecm}$ at 95% CL (L. Silvestris, ICHEP96) to obtain this result.
- ⁸ESCRIBANO 97 use preliminary experimental results.
- ⁹ESCRIBANO 93 limit derived from $\Gamma(Z \rightarrow \tau^+\tau^-)$, and is on the absolute value of the electric dipole moment.

Lepton Particle Listings

τ

$\text{Im}(d_\tau)$

VALUE ($10^{-16} e cm$)	CL%	DOCUMENT ID	TECN	COMMENT
-0.25 to 0.008	95	¹ INAMI	03 BELL	$E_{cm}^e = 10.6$ GeV
••• We do not use the following data for averages, fits, limits, etc. •••				
< 1.8	95	² ALBRECHT	00 ARG	$E_{cm}^e = 10.4$ GeV

¹INAMI 03 use $e^+e^- \rightarrow \tau^+\tau^-$ events.
²ALBRECHT 00 use $e^+e^- \rightarrow \tau^+\tau^-$ events. Limit is on the absolute value of $\text{Im}(d_\tau)$.

τ WEAK DIPOLE MOMENT (d_τ^W)

A nonzero value is forbidden by CP invariance.

The q^2 dependence is expected to be small providing no thresholds are nearby.

$\text{Re}(d_\tau^W)$

VALUE ($10^{-17} e cm$)	CL%	DOCUMENT ID	TECN	COMMENT
<0.50	95	¹ HEISTER	03F ALEP	1990-1995 LEP runs
••• We do not use the following data for averages, fits, limits, etc. •••				
<3.0	90	¹ ACCIARRI	98C L3	1991-1995 LEP runs
<0.56	95	ACKERSTAFF	97L OPAL	1991-1995 LEP runs
<0.78	95	² AKERS	95F OPAL	Repl. by ACKERSTAFF 97L
<1.5	95	² BUSKULIC	95C ALEP	Repl. by HEISTER 03F
<7.0	95	² ACTON	92F OPAL	Z $\rightarrow \tau^+\tau^-$ at LEP
<3.7	95	² BUSKULIC	92J ALEP	Repl. by BUSKULIC 95C

¹Limit is on the absolute value of the real part of the weak dipole moment.
²Limit is on the absolute value of the real part of the weak dipole moment, and applies for $q^2 = m_Z^2$.

$\text{Im}(d_\tau^W)$

VALUE ($10^{-17} e cm$)	CL%	DOCUMENT ID	TECN	COMMENT
<1.1	95	¹ HEISTER	03F ALEP	1990-1995 LEP runs
••• We do not use the following data for averages, fits, limits, etc. •••				
<1.5	95	ACKERSTAFF	97L OPAL	1991-1995 LEP runs
<4.5	95	² AKERS	95F OPAL	Repl. by ACKERSTAFF 97L

¹HEISTER 03F limit is on the absolute value of the imaginary part of the weak dipole moment.
²Limit is on the absolute value of the imaginary part of the weak dipole moment, and applies for $q^2 = m_Z^2$.

τ WEAK ANOMALOUS MAGNETIC DIPOLE MOMENT (α_τ^W)

Electroweak radiative corrections are expected to contribute at the 10^{-6} level. See BERNABEU 95.

The q^2 dependence is expected to be small providing no thresholds are nearby.

$\text{Re}(\alpha_\tau^W)$

VALUE	CL%	DOCUMENT ID	TECN	COMMENT
<1.1 $\times 10^{-3}$	95	¹ HEISTER	03F ALEP	1990-1995 LEP runs
••• We do not use the following data for averages, fits, limits, etc. •••				
> -0.0024 and < 0.0025	95	² GONZALEZ-S.	.00 RVUE	$e^+e^- \rightarrow \tau^+\tau^-$ and $W \rightarrow \tau\nu_\tau$
<4.5 $\times 10^{-3}$	90	¹ ACCIARRI	98C L3	1991-1995 LEP runs

¹Limit is on the absolute value of the real part of the weak anomalous magnetic dipole moment.
²GONZALEZ-SPRINGBERG 00 use data on tau lepton production at LEP1, SLC, and LEP2, and data from colliders and LEP2 to determine limits. Assume imaginary component is zero.

$\text{Im}(\alpha_\tau^W)$

VALUE	CL%	DOCUMENT ID	TECN	COMMENT
<2.7 $\times 10^{-3}$	95	¹ HEISTER	03F ALEP	1990-1995 LEP runs
••• We do not use the following data for averages, fits, limits, etc. •••				
<9.9 $\times 10^{-3}$	90	¹ ACCIARRI	98C L3	1991-1995 LEP runs

¹Limit is on the absolute value of the imaginary part of the weak anomalous magnetic dipole moment.

τ^- DECAY MODES

τ^\pm modes are charge conjugates of the modes below. " h^\pm " stands for π^\pm or K^\pm . " ℓ " stands for e or μ . "Neutrals" stands for γ 's and/or π^0 's.

Mode	Fraction (Γ_i/Γ)	Scale factor/ Confidence level
------	--------------------------------	-----------------------------------

Modes with one charged particle

Γ_1	particle ≥ 0 neutrals $\geq 0 K_L^0 \nu_\tau$ ("1-prong")	(85.24 \pm 0.06) %
Γ_2	particle ≥ 0 neutrals $\geq 0 K_L^0 \nu_\tau$	(84.58 \pm 0.06) %
Γ_3	$\mu^- \bar{\nu}_\mu \nu_\tau$	[a] (17.39 \pm 0.04) %
Γ_4	$\mu^- \bar{\nu}_\mu \nu_\tau \gamma$	[b] (3.67 \pm 0.08) $\times 10^{-3}$
Γ_5	$e^- \bar{\nu}_e \nu_\tau$	[a] (17.82 \pm 0.04) %

Γ_6	$e^- \bar{\nu}_e \nu_\tau \gamma$	[b] (1.83 \pm 0.05) %
Γ_7	$h^- \geq 0 K_L^0 \nu_\tau$	(12.03 \pm 0.05) %
Γ_8	$h^- \nu_\tau$	(11.51 \pm 0.05) %
Γ_9	$\pi^- \nu_\tau$	[a] (10.82 \pm 0.05) %
Γ_{10}	$K^- \nu_\tau$	[a] (6.96 \pm 0.10) $\times 10^{-3}$
Γ_{11}	$h^- \geq 1$ neutrals ν_τ	(37.01 \pm 0.09) %
Γ_{12}	$h^- \geq 1 \pi^0 \nu_\tau$ (ex. K^0)	(36.51 \pm 0.09) %
Γ_{13}	$h^- \pi^0 \nu_\tau$	(25.93 \pm 0.09) %
Γ_{14}	$\pi^- \pi^0 \nu_\tau$	[a] (25.49 \pm 0.09) %
Γ_{15}	$\pi^- \pi^0$ non- $\rho(770) \nu_\tau$	(3.0 \pm 3.2) $\times 10^{-3}$
Γ_{16}	$K^- \pi^0 \nu_\tau$	[a] (4.33 \pm 0.15) $\times 10^{-3}$
Γ_{17}	$h^- \geq 2 \pi^0 \nu_\tau$	(10.81 \pm 0.09) %
Γ_{18}	$h^- 2 \pi^0 \nu_\tau$	(9.48 \pm 0.10) %
Γ_{19}	$h^- 2 \pi^0 \nu_\tau$ (ex. K^0)	(9.32 \pm 0.10) %
Γ_{20}	$\pi^- 2 \pi^0 \nu_\tau$ (ex. K^0)	[a] (9.26 \pm 0.10) %
Γ_{21}	$\pi^- 2 \pi^0 \nu_\tau$ (ex. K^0), scalar vector	< 9 $\times 10^{-3}$ CL=95%
Γ_{22}	$\pi^- 2 \pi^0 \nu_\tau$ (ex. K^0), scalar vector	< 7 $\times 10^{-3}$ CL=95%
Γ_{23}	$K^- 2 \pi^0 \nu_\tau$ (ex. K^0)	[a] (6.5 \pm 2.2) $\times 10^{-4}$
Γ_{24}	$h^- \geq 3 \pi^0 \nu_\tau$	(1.34 \pm 0.07) %
Γ_{25}	$h^- \geq 3 \pi^0 \nu_\tau$ (ex. K^0)	(1.25 \pm 0.07) %
Γ_{26}	$h^- 3 \pi^0 \nu_\tau$	(1.18 \pm 0.07) %
Γ_{27}	$\pi^- 3 \pi^0 \nu_\tau$ (ex. K^0)	[a] (1.04 \pm 0.07) %
Γ_{28}	$K^- 3 \pi^0 \nu_\tau$ (ex. K^0, η)	[a] (4.8 \pm 2.1) $\times 10^{-4}$
Γ_{29}	$h^- 4 \pi^0 \nu_\tau$ (ex. K^0)	(1.6 \pm 0.4) $\times 10^{-3}$
Γ_{30}	$h^- 4 \pi^0 \nu_\tau$ (ex. K^0, η)	[a] (1.1 \pm 0.4) $\times 10^{-3}$
Γ_{31}	$a_1(1260) \nu_\tau \rightarrow \pi^- \gamma \nu_\tau$	(3.8 \pm 1.5) $\times 10^{-4}$
Γ_{32}	$K^- \geq 0 \pi^0 \geq 0 K^0 \geq 0 \gamma \nu_\tau$	(1.552 \pm 0.029) %
Γ_{33}	$K^- \geq 1 (\pi^0 \text{ or } K^0 \text{ or } \gamma) \nu_\tau$	(8.59 \pm 0.28) $\times 10^{-3}$

Modes with K^0 's

Γ_{34}	K_S^0 (particles) ν_τ	(9.43 \pm 0.28) $\times 10^{-3}$
Γ_{35}	$h^- K^0 \nu_\tau$	(9.87 \pm 0.14) $\times 10^{-3}$
Γ_{36}	$\pi^- K^0 \nu_\tau$	[a] (8.38 \pm 0.14) $\times 10^{-3}$
Γ_{37}	$\pi^- K^0$ (non- $K^*(892)^-$) ν_τ	(5.4 \pm 2.1) $\times 10^{-4}$
Γ_{38}	$K^- K^0 \nu_\tau$	[a] (1.486 \pm 0.034) $\times 10^{-3}$
Γ_{39}	$K^- K^0 \geq 0 \pi^0 \nu_\tau$	(2.99 \pm 0.07) $\times 10^{-3}$
Γ_{40}	$h^- K^0 \pi^0 \nu_\tau$	(5.32 \pm 0.13) $\times 10^{-3}$
Γ_{41}	$\pi^- K^0 \pi^0 \nu_\tau$	[a] (3.82 \pm 0.13) $\times 10^{-3}$
Γ_{42}	$K^0 \rho^- \nu_\tau$	(2.2 \pm 0.5) $\times 10^{-3}$
Γ_{43}	$K^- K^0 \pi^0 \nu_\tau$	[a] (1.50 \pm 0.07) $\times 10^{-3}$
Γ_{44}	$\pi^- K^0 \geq 1 \pi^0 \nu_\tau$	(4.08 \pm 0.25) $\times 10^{-3}$
Γ_{45}	$\pi^- K^0 \pi^0 \pi^0 \nu_\tau$ (ex. K^0)	[a] (2.6 \pm 2.3) $\times 10^{-4}$
Γ_{46}	$K^- K^0 \pi^0 \pi^0 \nu_\tau$	< 1.6 $\times 10^{-4}$ CL=95%
Γ_{47}	$\pi^- K^0 K^0 \nu_\tau$	(1.55 \pm 0.24) $\times 10^{-3}$
Γ_{48}	$\pi^- K_S^0 K_S^0 \nu_\tau$	[a] (2.35 \pm 0.06) $\times 10^{-4}$
Γ_{49}	$\pi^- K_S^0 K_L^0 \nu_\tau$	[a] (1.08 \pm 0.24) $\times 10^{-3}$
Γ_{50}	$\pi^- K_L^0 K_L^0 \nu_\tau$	(2.35 \pm 0.06) $\times 10^{-4}$
Γ_{51}	$\pi^- K^0 K^0 \pi^0 \nu_\tau$	(3.6 \pm 1.2) $\times 10^{-4}$
Γ_{52}	$\pi^- K_S^0 K_S^0 \pi^0 \nu_\tau$	[a] (1.82 \pm 0.21) $\times 10^{-5}$
Γ_{53}	$K^* K^0 \pi^0 \nu_\tau \rightarrow \pi^- K_S^0 K_S^0 \pi^0 \nu_\tau$	(1.08 \pm 0.21) $\times 10^{-5}$
Γ_{54}	$f_1(1285) \pi^- \nu_\tau \rightarrow \pi^- K_S^0 K_S^0 \pi^0 \nu_\tau$	(6.8 \pm 1.5) $\times 10^{-6}$
Γ_{55}	$f_1(1420) \pi^- \nu_\tau \rightarrow \pi^- K_S^0 K_S^0 \pi^0 \nu_\tau$	(2.4 \pm 0.8) $\times 10^{-6}$
Γ_{56}	$\pi^- K^0 K_L^0 \pi^0 \nu_\tau$	[a] (3.2 \pm 1.2) $\times 10^{-4}$
Γ_{57}	$\pi^- K_L^0 K_L^0 \pi^0 \nu_\tau$	(1.82 \pm 0.21) $\times 10^{-5}$
Γ_{58}	$K^- K_S^0 K_S^0 \nu_\tau$	< 6.3 $\times 10^{-7}$ CL=90%
Γ_{59}	$K^- K_S^0 K_S^0 \pi^0 \nu_\tau$	< 4.0 $\times 10^{-7}$ CL=90%
Γ_{60}	$K^0 h^+ h^- h^- \geq 0$ neutrals ν_τ	< 1.7 $\times 10^{-3}$ CL=95%
Γ_{61}	$K^0 h^+ h^- h^- \nu_\tau$	[a] (2.5 \pm 2.0) $\times 10^{-4}$

Modes with three charged particles

Γ_{62}	$h^- h^- h^+ \geq 0$ neutrals $\geq 0 K_L^0 \nu_\tau$	(15.20 \pm 0.06) %
Γ_{63}	$h^- h^- h^+ \geq 0$ neutrals ν_τ (ex. $K_S^0 \rightarrow \pi^+ \pi^-$) ("3-prong")	(14.55 \pm 0.06) %
Γ_{64}	$h^- h^- h^+ \nu_\tau$	(9.80 \pm 0.05) %
Γ_{65}	$h^- h^- h^+ \nu_\tau$ (ex. K^0)	(9.46 \pm 0.05) %
Γ_{66}	$h^- h^- h^+ \nu_\tau$ (ex. K^0, ω)	(9.43 \pm 0.05) %
Γ_{67}	$\pi^- \pi^+ \pi^- \nu_\tau$	(9.31 \pm 0.05) %
Γ_{68}	$\pi^- \pi^+ \pi^- \nu_\tau$ (ex. K^0)	(9.02 \pm 0.05) %
Γ_{69}	$\pi^- \pi^+ \pi^- \nu_\tau$ (ex. K^0), non-axial vector	< 2.4 % CL=95%

See key on page 1127

Lepton Particle Listings

T

Γ ₇₀	$\pi^- \pi^+ \pi^- \nu_\tau$ (ex. K^0, ω)	[a]	$(8.99 \pm 0.05) \%$
Γ ₇₁	$h^- h^- h^+ \geq 1$ neutrals ν_τ		$(5.29 \pm 0.05) \%$
Γ ₇₂	$h^- h^- h^+ \geq 1 \pi^0 \nu_\tau$ (ex. K^0)		$(5.09 \pm 0.05) \%$
Γ ₇₃	$h^- h^- h^+ \pi^0 \nu_\tau$		$(4.76 \pm 0.05) \%$
Γ ₇₄	$h^- h^- h^+ \pi^0 \nu_\tau$ (ex. K^0)		$(4.57 \pm 0.05) \%$
Γ ₇₅	$h^- h^- h^+ \pi^0 \nu_\tau$ (ex. K^0, ω)		$(2.79 \pm 0.07) \%$
Γ ₇₆	$\pi^- \pi^+ \pi^- \pi^0 \nu_\tau$		$(4.62 \pm 0.05) \%$
Γ ₇₇	$\pi^- \pi^+ \pi^- \pi^0 \nu_\tau$ (ex. K^0)		$(4.49 \pm 0.05) \%$
Γ ₇₈	$\pi^- \pi^+ \pi^- \pi^0 \nu_\tau$ (ex. K^0, ω)	[a]	$(2.74 \pm 0.07) \%$
Γ ₇₉	$h^- \rho \pi^0 \nu_\tau$		
Γ ₈₀	$h^- \rho^+ h^- \nu_\tau$		
Γ ₈₁	$h^- \rho^- h^+ \nu_\tau$		
Γ ₈₂	$h^- h^- h^+ \geq 2 \pi^0 \nu_\tau$ (ex. K^0)		$(5.17 \pm 0.31) \times 10^{-3}$
Γ ₈₃	$h^- h^- h^+ 2 \pi^0 \nu_\tau$		$(5.05 \pm 0.31) \times 10^{-3}$
Γ ₈₄	$h^- h^- h^+ 2 \pi^0 \nu_\tau$ (ex. K^0)		$(4.95 \pm 0.31) \times 10^{-3}$
Γ ₈₅	$h^- h^- h^+ 2 \pi^0 \nu_\tau$ (ex. K^0, ω, η)	[a]	$(10 \pm 4) \times 10^{-4}$
Γ ₈₆	$h^- h^- h^+ 3 \pi^0 \nu_\tau$		$(2.13 \pm 0.30) \times 10^{-4}$
Γ ₈₇	$2 \pi^- \pi^+ 3 \pi^0 \nu_\tau$ (ex. K^0)		$(1.95 \pm 0.30) \times 10^{-4}$
Γ ₈₈	$2 \pi^- \pi^+ 3 \pi^0 \nu_\tau$ (ex. $K^0, \eta, f_1(1285)$)		$(1.7 \pm 0.4) \times 10^{-4}$
Γ ₈₉	$2 \pi^- \pi^+ 3 \pi^0 \nu_\tau$ (ex. $K^0, \eta, \omega, f_1(1285)$)	[a]	$(1.4 \pm 2.7) \times 10^{-5}$
Γ ₉₀	$K^- h^+ h^- \geq 0$ neutrals ν_τ		$(6.29 \pm 0.14) \times 10^{-3}$
Γ ₉₁	$K^- h^+ \pi^- \nu_\tau$ (ex. K^0)		$(4.37 \pm 0.07) \times 10^{-3}$
Γ ₉₂	$K^- h^+ \pi^- \pi^0 \nu_\tau$ (ex. K^0)		$(8.6 \pm 1.2) \times 10^{-4}$
Γ ₉₃	$K^- \pi^+ \pi^- \geq 0$ neutrals ν_τ		$(4.77 \pm 0.14) \times 10^{-3}$
Γ ₉₄	$K^- \pi^+ \pi^- \geq 0 \pi^0 \nu_\tau$ (ex. K^0)		$(3.73 \pm 0.13) \times 10^{-3}$
Γ ₉₅	$K^- \pi^+ \pi^- \nu_\tau$		$(3.45 \pm 0.07) \times 10^{-3}$
Γ ₉₆	$K^- \pi^+ \pi^- \nu_\tau$ (ex. K^0)		$(2.93 \pm 0.07) \times 10^{-3}$
Γ ₉₇	$K^- \pi^+ \pi^- \nu_\tau$ (ex. K^0, ω)	[a]	$(2.93 \pm 0.07) \times 10^{-3}$
Γ ₉₈	$K^- \rho^0 \nu_\tau \rightarrow K^- \pi^+ \pi^- \nu_\tau$		$(1.4 \pm 0.5) \times 10^{-3}$
Γ ₉₉	$K^- \pi^+ \pi^- \pi^0 \nu_\tau$		$(1.31 \pm 0.12) \times 10^{-3}$
Γ ₁₀₀	$K^- \pi^+ \pi^- \pi^0 \nu_\tau$ (ex. K^0)		$(7.9 \pm 1.2) \times 10^{-4}$
Γ ₁₀₁	$K^- \pi^+ \pi^- \pi^0 \nu_\tau$ (ex. K^0, η)		$(7.6 \pm 1.2) \times 10^{-4}$
Γ ₁₀₂	$K^- \pi^+ \pi^- \pi^0 \nu_\tau$ (ex. K^0, ω)		$(3.7 \pm 0.9) \times 10^{-4}$
Γ ₁₀₃	$K^- \pi^+ \pi^- \pi^0 \nu_\tau$ (ex. K^0, ω, η)	[a]	$(3.9 \pm 1.4) \times 10^{-4}$
Γ ₁₀₄	$K^- \pi^+ K^- \geq 0$ neut. ν_τ		$< 9 \times 10^{-4}$ CL=95%
Γ ₁₀₅	$K^- K^+ \pi^- \geq 0$ neut. ν_τ		$(1.496 \pm 0.033) \times 10^{-3}$
Γ ₁₀₆	$K^- K^+ \pi^- \nu_\tau$	[a]	$(1.435 \pm 0.027) \times 10^{-3}$
Γ ₁₀₇	$K^- K^+ \pi^- \pi^0 \nu_\tau$	[a]	$(6.1 \pm 1.8) \times 10^{-5}$
Γ ₁₀₈	$K^- K^+ K^- \nu_\tau$		$(2.2 \pm 0.8) \times 10^{-5}$ S=5.4
Γ ₁₀₉	$K^- K^+ K^- \nu_\tau$ (ex. ϕ)		$< 2.5 \times 10^{-6}$ CL=90%
Γ ₁₁₀	$K^- K^+ K^- \pi^0 \nu_\tau$		$< 4.8 \times 10^{-6}$ CL=90%
Γ ₁₁₁	$\pi^- K^+ \pi^- \geq 0$ neut. ν_τ		$< 2.5 \times 10^{-3}$ CL=95%
Γ ₁₁₂	$e^- e^- e^+ \bar{\nu}_e \nu_\tau$		$(2.8 \pm 1.5) \times 10^{-5}$
Γ ₁₁₃	$\mu^- e^- e^+ \bar{\nu}_\mu \nu_\tau$		$< 3.2 \times 10^{-5}$ CL=90%
Γ ₁₁₄	$\pi^- e^- e^+ \nu_\tau$		seen
Γ ₁₁₅	$\pi^- \mu^- \mu^+ \nu_\tau$		$< 1.14 \times 10^{-5}$ CL=90%

Modes with five charged particles

Γ ₁₁₆	$3h^- 2h^+ \geq 0$ neutrals ν_τ (ex. $K_S^0 \rightarrow \pi^- \pi^+$) ("5-prong")		$(9.9 \pm 0.4) \times 10^{-4}$
Γ ₁₁₇	$3h^- 2h^+ \nu_\tau$ (ex. K^0)		$(8.29 \pm 0.31) \times 10^{-4}$
Γ ₁₁₈	$3\pi^- 2\pi^+ \nu_\tau$ (ex. K^0, ω)		$(8.27 \pm 0.31) \times 10^{-4}$
Γ ₁₁₉	$3\pi^- 2\pi^+ \nu_\tau$ (ex. $K^0, \omega, f_1(1285)$)	[a]	$(7.75 \pm 0.30) \times 10^{-4}$
Γ ₁₂₀	$K^- 2\pi^- 2\pi^+ \nu_\tau$ (ex. K^0)	[a]	$(6 \pm 12) \times 10^{-7}$
Γ ₁₂₁	$K^+ 3\pi^- \pi^+ \nu_\tau$		$< 5.0 \times 10^{-6}$ CL=90%
Γ ₁₂₂	$K^+ K^- 2\pi^- \pi^+ \nu_\tau$		$< 4.5 \times 10^{-7}$ CL=90%
Γ ₁₂₃	$3h^- 2h^+ \pi^0 \nu_\tau$ (ex. K^0)		$(1.65 \pm 0.11) \times 10^{-4}$
Γ ₁₂₄	$3\pi^- 2\pi^+ \pi^0 \nu_\tau$ (ex. K^0)		$(1.63 \pm 0.11) \times 10^{-4}$
Γ ₁₂₅	$3\pi^- 2\pi^+ \pi^0 \nu_\tau$ (ex. $K^0, \eta, f_1(1285)$)		$(1.11 \pm 0.10) \times 10^{-4}$
Γ ₁₂₆	$3\pi^- 2\pi^+ \pi^0 \nu_\tau$ (ex. $K^0, \eta, \omega, f_1(1285)$)	[a]	$(3.8 \pm 0.9) \times 10^{-5}$
Γ ₁₂₇	$K^- 2\pi^- 2\pi^+ \pi^0 \nu_\tau$ (ex. K^0)	[a]	$(1.1 \pm 0.6) \times 10^{-6}$
Γ ₁₂₈	$K^+ 3\pi^- \pi^+ \pi^0 \nu_\tau$		$< 8 \times 10^{-7}$ CL=90%
Γ ₁₂₉	$3h^- 2h^+ 2\pi^0 \nu_\tau$		$< 3.4 \times 10^{-6}$ CL=90%

Miscellaneous other allowed modes

Γ ₁₃₀	$(5\pi)^- \nu_\tau$		$(7.8 \pm 0.5) \times 10^{-3}$
Γ ₁₃₁	$4h^- 3h^+ \geq 0$ neutrals ν_τ ("7-prong")		$< 3.0 \times 10^{-7}$ CL=90%

Γ ₁₃₂	$4h^- 3h^+ \nu_\tau$		$< 4.3 \times 10^{-7}$ CL=90%
Γ ₁₃₃	$4h^- 3h^+ \pi^0 \nu_\tau$		$< 2.5 \times 10^{-7}$ CL=90%
Γ ₁₃₄	$X^- (S=-1) \nu_\tau$		$(2.92 \pm 0.04) \%$
Γ ₁₃₅	$K^*(892)^- \geq 0$ neutrals $\geq 0K^0 \nu_\tau$		$(1.42 \pm 0.18) \%$ S=1.4
Γ ₁₃₆	$K^*(892)^- \nu_\tau$		$(1.20 \pm 0.07) \%$ S=1.8
Γ ₁₃₇	$K^*(892)^- \nu_\tau \rightarrow \pi^- \bar{K}^0 \nu_\tau$		$(7.82 \pm 0.26) \times 10^{-3}$
Γ ₁₃₈	$K^*(892)^0 K^- \geq 0$ neutrals ν_τ		$(3.2 \pm 1.4) \times 10^{-3}$
Γ ₁₃₉	$K^*(892)^0 K^- \nu_\tau$		$(2.1 \pm 0.4) \times 10^{-3}$
Γ ₁₄₀	$\bar{K}^*(892)^0 \pi^- \geq 0$ neutrals ν_τ		$(3.8 \pm 1.7) \times 10^{-3}$
Γ ₁₄₁	$\bar{K}^*(892)^0 \pi^- \nu_\tau$		$(2.2 \pm 0.5) \times 10^{-3}$
Γ ₁₄₂	$(\bar{K}^*(892) \pi)^- \nu_\tau \rightarrow \pi^- \bar{K}^0 \pi^0 \nu_\tau$		$(1.0 \pm 0.4) \times 10^{-3}$
Γ ₁₄₃	$K_1(1270)^- \nu_\tau$		$(4.7 \pm 1.1) \times 10^{-3}$
Γ ₁₄₄	$K_1(1400)^- \nu_\tau$		$(1.7 \pm 2.6) \times 10^{-3}$ S=1.7
Γ ₁₄₅	$K^*(1410)^- \nu_\tau$		$(1.5 \pm 1.4) \times 10^{-3}$
Γ ₁₄₆	$K_0^*(1430)^- \nu_\tau$		$< 5 \times 10^{-4}$ CL=95%
Γ ₁₄₇	$K_2^*(1430)^- \nu_\tau$		$< 3 \times 10^{-3}$ CL=95%
Γ ₁₄₈	$a_0(980)^- \geq 0$ neutrals ν_τ		
Γ ₁₄₉	$\eta \pi^- \nu_\tau$		$< 9.9 \times 10^{-5}$ CL=95%
Γ ₁₅₀	$\eta \pi^- \pi^0 \nu_\tau$	[a]	$(1.39 \pm 0.07) \times 10^{-3}$
Γ ₁₅₁	$\eta \pi^- \pi^0 \pi^0 \nu_\tau$	[a]	$(2.0 \pm 0.4) \times 10^{-4}$
Γ ₁₅₂	$\eta K^- \nu_\tau$	[a]	$(1.55 \pm 0.08) \times 10^{-4}$
Γ ₁₅₃	$\eta K^*(892)^- \nu_\tau$		$(1.38 \pm 0.15) \times 10^{-4}$
Γ ₁₅₄	$\eta K^- \pi^0 \nu_\tau$	[a]	$(4.8 \pm 1.2) \times 10^{-5}$
Γ ₁₅₅	$\eta K^- \pi^0$ (non- $K^*(892)$) ν_τ		$< 3.5 \times 10^{-5}$ CL=90%
Γ ₁₅₆	$\eta \bar{K}^0 \pi^- \nu_\tau$	[a]	$(9.4 \pm 1.5) \times 10^{-5}$
Γ ₁₅₇	$\eta \bar{K}^0 \pi^- \pi^0 \nu_\tau$		$< 5.0 \times 10^{-5}$ CL=90%
Γ ₁₅₈	$\eta K^- K^0 \nu_\tau$		$< 9.0 \times 10^{-6}$ CL=90%
Γ ₁₅₉	$\eta \pi^+ \pi^- \pi^- \geq 0$ neutrals ν_τ		$< 3 \times 10^{-3}$ CL=90%
Γ ₁₆₀	$\eta \pi^- \pi^+ \pi^- \nu_\tau$ (ex. K^0)	[a]	$(2.20 \pm 0.13) \times 10^{-4}$
Γ ₁₆₁	$\eta \pi^- \pi^+ \pi^- \nu_\tau$ (ex. $K^0, f_1(1285)$)		$(9.9 \pm 1.6) \times 10^{-5}$
Γ ₁₆₂	$\eta a_1(1260)^- \nu_\tau \rightarrow \eta \pi^- \rho^0 \nu_\tau$		$< 3.9 \times 10^{-4}$ CL=90%
Γ ₁₆₃	$\eta \eta \pi^- \nu_\tau$		$< 7.4 \times 10^{-6}$ CL=90%
Γ ₁₆₄	$\eta \eta \pi^- \pi^0 \nu_\tau$		$< 2.0 \times 10^{-4}$ CL=95%
Γ ₁₆₅	$\eta \eta K^- \nu_\tau$		$< 3.0 \times 10^{-6}$ CL=90%
Γ ₁₆₆	$\eta'(958) \pi^- \nu_\tau$		$< 4.0 \times 10^{-6}$ CL=90%
Γ ₁₆₇	$\eta'(958) \pi^- \pi^0 \nu_\tau$		$< 1.2 \times 10^{-5}$ CL=90%
Γ ₁₆₈	$\eta'(958) K^- \nu_\tau$		$< 2.4 \times 10^{-6}$ CL=90%
Γ ₁₆₉	$\phi \pi^- \nu_\tau$		$(3.4 \pm 0.6) \times 10^{-5}$
Γ ₁₇₀	$\phi K^- \nu_\tau$	[a]	$(4.4 \pm 1.6) \times 10^{-5}$
Γ ₁₇₁	$f_1(1285) \pi^- \nu_\tau$		$(3.9 \pm 0.5) \times 10^{-4}$ S=1.9
Γ ₁₇₂	$f_1(1285) \pi^- \nu_\tau \rightarrow \eta \pi^- \pi^+ \pi^- \nu_\tau$		$(1.18 \pm 0.07) \times 10^{-4}$ S=1.3
Γ ₁₇₃	$f_1(1285) \pi^- \nu_\tau \rightarrow 3\pi^- 2\pi^+ \nu_\tau$	[a]	$(5.2 \pm 0.4) \times 10^{-5}$
Γ ₁₇₄	$\pi(1300)^- \nu_\tau \rightarrow (\rho \pi)^- \nu_\tau \rightarrow (3\pi)^- \nu_\tau$		$< 1.0 \times 10^{-4}$ CL=90%
Γ ₁₇₅	$\pi(1300)^- \nu_\tau \rightarrow ((\pi \pi)_{S\text{-wave}} \pi)^- \nu_\tau \rightarrow (3\pi)^- \nu_\tau$		$< 1.9 \times 10^{-4}$ CL=90%

Lepton Family number (LF), Lepton number (L), or Baryon number (B) violating modes

L means lepton number violation (e.g. $\tau^- \rightarrow e^+ \pi^- \pi^-$). Following common usage, LF means lepton family violation and not lepton number violation (e.g. $\tau^- \rightarrow e^- \pi^+ \pi^-$). B means baryon number violation.

Γ ₁₈₆	$e^- \gamma$	LF	$< 3.3 \times 10^{-8}$ CL=90%
Γ ₁₈₇	$e^- \gamma \gamma$		$< 2.5 \times 10^{-4}$ CL=90%
Γ ₁₈₈	$\mu^- \gamma$	LF	$< 4.2 \times 10^{-8}$ CL=90%
Γ ₁₈₉	$\mu^- \gamma \gamma$		$< 5.8 \times 10^{-4}$ CL=90%
Γ ₁₉₀	$e^- \pi^0$	LF	$< 8.0 \times 10^{-8}$ CL=90%
Γ ₁₉₁	$\mu^- \pi^0$	LF	$< 1.1 \times 10^{-7}$ CL=90%
Γ ₁₉₂	$e^- K_S^0$	LF	$< 2.6 \times 10^{-8}$ CL=90%
Γ ₁₉₃	$\mu^- K_S^0$	LF	$< 2.3 \times 10^{-8}$ CL=90%
Γ ₁₉₄	$e^- \eta$	LF	$< 9.2 \times 10^{-8}$ CL=90%

x36	0																					
x38	0	-15																				
x41	0	-13	2																			
x43	0	-1	-14	-20																		
x45	0	-3	0	-6	0																	
x48	0	-2	3	-4	1	0																
x49	0	-5	0	-4	-1	-10	-1															
x52	0	1	5	-1	6	0	-7	0														
x56	0	-2	0	-2	-1	-4	0	-8	0													
x61	0	-2	0	-2	0	-4	0	-4	0	-2												
x70	-5	-3	3	-2	-1	-4	5	-4	0	-2												
x78	3	1	-1	1	0	2	-1	2	0	1												
x85	2	0	0	0	0	0	0	0	0	0												
x89	0	0	0	0	0	0	0	0	0	-1	0											
x97	-1	-1	0	-1	0	-2	0	-2	0	-1												
x103	-1	-1	0	-1	0	-1	0	-1	0	-1												
x106	-1	-1	1	0	0	-1	2	-1	0	-1												
x107	0	0	0	0	0	0	0	0	0	0												
x119	-1	-1	1	0	0	-1	2	-1	0	0												
x120	0	0	0	0	0	0	0	0	0	0												
x126	0	0	0	0	0	0	0	0	0	0												
x127	0	0	0	0	0	0	0	0	0	0												
x150	-2	-1	0	0	0	-1	0	-1	0	0												
x151	0	0	0	0	0	-1	0	-1	0	0												
x152	0	0	1	0	0	0	1	0	0	0												
x154	0	0	0	0	0	0	0	0	0	0												
x156	0	0	0	0	0	0	0	-1	0	0												
x160	-1	0	1	0	0	-1	1	-1	0	0												
x170	0	0	0	0	0	0	0	0	0	0												
x173	-1	0	1	0	0	0	1	0	0	0												
x178	1	0	0	0	0	-1	0	-1	0	0												
x179	0	0	0	0	0	0	0	0	0	0												
x180	2	-1	0	0	0	-1	0	-1	0	0												
x182	0	0	0	0	0	0	0	0	0	0												
x185	-1	0	1	0	0	0	1	-1	0	0												
x70	-4																					
x78	2	-19																				
x85	0	-1	-8																			
x89	0	-1	-1	0																		
x97	-2	19	-6	0	0																	
x103	-1	-4	-14	-1	0	-1																
x106	-1	15	-4	0	0	0	-1															
x107	0	-1	-1	0	0	0	-3	0														
x119	-1	3	-1	0	-4	-1	0	1	0													
x120	0	0	0	0	0	0	0	0	0	-1												
x126	0	0	0	0	0	0	0	0	0	3												
x127	0	0	0	0	0	0	0	0	0	-1												
x150	-1	0	0	-5	0	0	0	0	0	0												
x151	-1	0	0	0	-11	0	0	0	0	9												
x152	0	2	0	0	0	0	-1	1	0	1												
x154	0	0	0	-1	0	0	0	0	0	0												
x156	0	0	0	0	-2	0	0	0	0	0												
x160	-1	1	-1	0	-8	-1	0	1	0	46												
x170	0	-1	0	0	0	1	0	1	0	0												
x173	0	1	0	0	-2	0	0	1	0	34												
x178	-1	-9	-67	-3	0	-2	10	-2	0	-1												
x179	0	0	12	0	0	-2	-58	0	0	0												
x180	-1	-2	-11	-64	-1	-1	-1	-1	0	0												
x182	0	0	0	0	-16	0	0	0	0	7												
x185	0	1	0	0	-4	0	0	1	0	39												
x61		x70	x78	x85	x89	x97	x103	x106	x107	x119												

x126	0																					
x127	0	-1																				
x150	0	0	0																			
x151	0	2	0	0																		
x152	0	0	0	4	0																	
x154	0	0	0	1	0	1																
x156	0	0	0	2	-1	1	0															
x160	-1	3	-1	0	25	0	0	0														
x170	0	0	0	0	0	0	0	0	0	0												
x173	-1	1	0	0	4	0	0	0	0	20	0											
x178	0	0	0	0	0	0	0	0	0	-1	0											
x179	0	0	0	0	0	0	0	0	0	0	0											
x180	0	0	0	0	0	0	0	0	0	0	0											
x182	0	2	0	0	10	0	0	-1	20	0												
x185	-1	-2	-1	0	17	0	0	0	0	38	0											
x120	x126	x127	x150	x151	x152	x154	x156	x160	x170													
x178	0																					
x179	0	-14																				
x180	0	-4	0																			
x182	3	0	0	0																		
x185	17	0	0	0	14																	
x173	x178	x179	x180	x182																		

See the related review(s):
 τ Branching Fractions

($\Gamma(\tau^+) - \Gamma(\tau^-)$) / ($\Gamma(\tau^+) + \Gamma(\tau^-)$)

$\tau^\pm \rightarrow \pi^\pm K_S^0 \nu_\tau$ (RATE DIFFERENCE) / (RATE SUM)

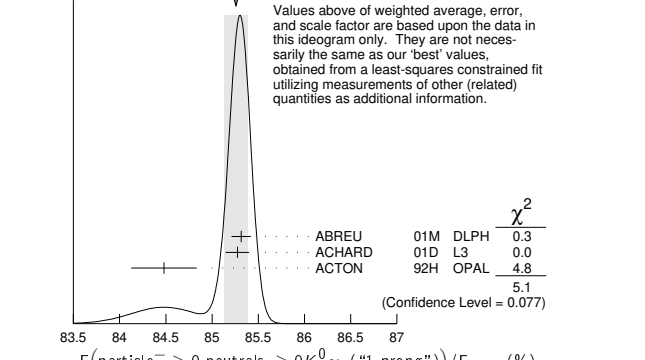
VALUE (%)	DOCUMENT ID	TECN	COMMENT
-0.36 ± 0.23 ± 0.11	LEES	12M BABR	476 fb ⁻¹ E _{cm} ^{ee} = 10.6 GeV

τ^- BRANCHING RATIOS

$\Gamma(\text{particle}^- \geq 0 \text{ neutrals} \geq 0 K_S^0 \nu_\tau \text{ ("1-prong")}) / \Gamma_{\text{total}} = \Gamma_1 / \Gamma$
 $\Gamma_1 / \Gamma = (\Gamma_3 + \Gamma_5 + \Gamma_9 + \Gamma_{10} + \Gamma_{14} + \Gamma_{16} + \Gamma_{20} + \Gamma_{23} + \Gamma_{27} + \Gamma_{28} + \Gamma_{30} + \Gamma_{36} + \Gamma_{38} + \Gamma_{41} + \Gamma_{43} + \Gamma_{45} + \Gamma_{48} + \Gamma_{49} + \Gamma_{50} + \Gamma_{52} + \Gamma_{56} + \Gamma_{57} + 0.7196\Gamma_{150} + 0.7196\Gamma_{152} + 0.7196\Gamma_{154} + 0.7196\Gamma_{156} + 0.339\Gamma_{170} + 0.0835\Gamma_{178} + 0.0835\Gamma_{179} + 0.0835\Gamma_{180}) / \Gamma$

The charged particle here can be e, μ , or hadron. In many analyses, the sum of the topological branching fractions (1, 3, and 5 prongs) is constrained to be unity. Since the 5-prong fraction is very small, the measured 1-prong and 3-prong fractions are highly correlated and cannot be treated as independent quantities in our overall fit. We arbitrarily choose to use the 3-prong fraction in our fit, and leave the 1-prong fraction out. We do, however, use these 1-prong measurements in our average below.

VALUE (%)	EVTS	DOCUMENT ID	TECN	COMMENT
85.24 ± 0.06	OUR FIT			
85.26 ± 0.13	OUR AVERAGE			Error includes scale factor of 1.6. See the ideogram below.
85.316 ± 0.093 ± 0.049	78k	¹ ABREU	01M DLPH	1992–1995 LEP runs
85.274 ± 0.105 ± 0.073		² ACHARD	01D L3	1992–1995 LEP runs
84.48 ± 0.27 ± 0.23		ACTON	92H OPAL	1990–1991 LEP runs
85.45 ^{+0.69} _{-0.73} ± 0.65		DECAMP	92C ALEP	Repl. by SCHAEEL 05c



¹ The correlation coefficients between this measurement and the ABREU 01M measurements of $B(\tau \rightarrow 3\text{-prong})$ and $B(\tau \rightarrow 5\text{-prong})$ are -0.98 and -0.08 respectively.

Downloaded from https://academic.oup.com/ptep/article/2022/8/083C01/66651666 by CERN Library user on 11 October 2022

Lepton Particle Listings

τ

²The correlation coefficients between this measurement and the ACHARD 01D measurements of $B(\tau \rightarrow \text{"3-prong"})$ and $B(\tau \rightarrow \text{"5-prong"})$ are -0.978 and -0.082 respectively.

$$\Gamma(\text{particle}^- \geq 0 \text{ neutrals} \geq 0 K_L^0 \nu_\tau) / \Gamma_{\text{total}} \quad \Gamma_2 / \Gamma$$

$$\Gamma_2 / \Gamma = (\Gamma_3 + \Gamma_5 + \Gamma_9 + \Gamma_{10} + \Gamma_{14} + \Gamma_{16} + \Gamma_{20} + \Gamma_{23} + \Gamma_{27} + \Gamma_{28} + \Gamma_{30} + 0.6534\Gamma_{36} + 0.6534\Gamma_{38} + 0.6534\Gamma_{41} + 0.6534\Gamma_{43} + 0.6534\Gamma_{45} + 0.0942\Gamma_{48} + 0.3069\Gamma_{49} + \Gamma_{50} + 0.0942\Gamma_{52} + 0.3069\Gamma_{56} + \Gamma_{57} + 0.7196\Gamma_{150} + 0.7196\Gamma_{152} + 0.7196\Gamma_{154} + 0.4702\Gamma_{156} + 0.1049\Gamma_{170} + 0.0835\Gamma_{178} + 0.0835\Gamma_{179} + 0.0835\Gamma_{180}) / \Gamma$$

VALUE (%)	EVTS	DOCUMENT ID	TECN	COMMENT
84.58 ± 0.06 OUR FIT				
85.1 ± 0.4 OUR AVERAGE				
● ● ● We use the following data for averages but not for fits. ● ● ●				
85.6 ± 0.6 ± 0.3	3300	¹ ADEVA	91F L3	$E_{\text{cm}}^{\text{ee}} = 88.3\text{--}94.3 \text{ GeV}$
84.9 ± 0.4 ± 0.3		BEHREND	89B CELL	$E_{\text{cm}}^{\text{ee}} = 14\text{--}47 \text{ GeV}$
84.7 ± 0.8 ± 0.6		² AIHARA	87B TPC	$E_{\text{cm}}^{\text{ee}} = 29 \text{ GeV}$
● ● ● We do not use the following data for averages, fits, limits, etc. ● ● ●				
86.4 ± 0.3 ± 0.3		ABACHI	89B HRS	$E_{\text{cm}}^{\text{ee}} = 29 \text{ GeV}$
87.1 ± 1.0 ± 0.7		³ BURCHAT	87 MRK2	$E_{\text{cm}}^{\text{ee}} = 29 \text{ GeV}$
87.2 ± 0.5 ± 0.8		SCHMIDKE	86 MRK2	$E_{\text{cm}}^{\text{ee}} = 29 \text{ GeV}$
84.7 ± 1.1 ± 1.6 -1.3	169	⁴ ALTHOFF	85 TASS	$E_{\text{cm}}^{\text{ee}} = 34.5 \text{ GeV}$
86.1 ± 0.5 ± 0.9		BARTEL	85F JADE	$E_{\text{cm}}^{\text{ee}} = 34.6 \text{ GeV}$
87.8 ± 1.3 ± 3.9		⁵ BERGER	85 PLUT	$E_{\text{cm}}^{\text{ee}} = 34.6 \text{ GeV}$
86.7 ± 0.3 ± 0.6		FERNANDEZ	85 MAC	$E_{\text{cm}}^{\text{ee}} = 29 \text{ GeV}$

- ¹ Not independent of ADEVA 91F $\Gamma(h^- h^+ \geq 0 \text{ neutrals} \geq 0 K_L^0 \nu_\tau) / \Gamma_{\text{total}}$ value.
- ² Not independent of AIHARA 87B $\Gamma(\mu^- \bar{\nu}_\mu \nu_\tau) / \Gamma_{\text{total}}$, $\Gamma(e^- \bar{\nu}_e \nu_\tau) / \Gamma_{\text{total}}$, and $\Gamma(h^- \geq 0 \text{ neutrals} \geq 0 K_L^0 \nu_\tau) / \Gamma_{\text{total}}$ values.
- ³ Not independent of SCHMIDKE 86 value (also not independent of BURCHAT 87 value for $\Gamma(h^- h^+ \geq 0 \text{ neutrals} \geq 0 K_L^0 \nu_\tau) / \Gamma_{\text{total}}$).
- ⁴ Not independent of ALTHOFF 85 $\Gamma(\mu^- \bar{\nu}_\mu \nu_\tau) / \Gamma_{\text{total}}$, $\Gamma(e^- \bar{\nu}_e \nu_\tau) / \Gamma_{\text{total}}$, $\Gamma(h^- \geq 0 \text{ neutrals} \geq 0 K_L^0 \nu_\tau) / \Gamma_{\text{total}}$, and $\Gamma(h^- h^+ \geq 0 \text{ neutrals} \geq 0 K_L^0 \nu_\tau) / \Gamma_{\text{total}}$ values.
- ⁵ Not independent of (1-prong + $0\pi^0$) and (1-prong + $\geq 1\pi^0$) values.

$$\Gamma(\mu^- \bar{\nu}_\mu \nu_\tau) / \Gamma_{\text{total}} \quad \Gamma_3 / \Gamma$$

To minimize the effect of experiments with large systematic errors, we exclude experiments which together would contribute 5% of the weight in the average.

VALUE (%)	EVTS	DOCUMENT ID	TECN	COMMENT
17.39 ± 0.04 OUR FIT				
17.33 ± 0.05 OUR AVERAGE				
17.319 ± 0.070 ± 0.032	54k	¹ SCHAEEL	05c ALEP	1991-1995 LEP runs
17.34 ± 0.09 ± 0.06	31.4k	ABBIENDI	03 OPAL	1990-1995 LEP runs
17.342 ± 0.110 ± 0.067	21.5k	² ACCIARRI	01F L3	1991-1995 LEP runs
17.325 ± 0.095 ± 0.077	27.7k	ABREU	99x DLPH	1991-1995 LEP runs
● ● ● We use the following data for averages but not for fits. ● ● ●				
17.37 ± 0.08 ± 0.18		³ ANASTASSOV	97 CLEO	$E_{\text{cm}}^{\text{ee}} = 10.6 \text{ GeV}$
● ● ● We do not use the following data for averages, fits, limits, etc. ● ● ●				
17.31 ± 0.11 ± 0.05	20.7k	BUSKULIC	96c ALEP	Repl. by SCHAEEL 05c
17.02 ± 0.19 ± 0.24	6586	ABREU	95T DLPH	Repl. by ABREU 99x
17.36 ± 0.27	7941	AKERS	95l OPAL	Repl. by ABBIENDI 03
17.6 ± 0.4 ± 0.4	2148	ADRIANI	93M L3	Repl. by ACCIARRI 01F
17.4 ± 0.3 ± 0.5		⁴ ALBRECHT	93G ARG	$E_{\text{cm}}^{\text{ee}} = 9.4\text{--}10.6 \text{ GeV}$
17.35 ± 0.41 ± 0.37		DECAMP	92c ALEP	1989-1990 LEP runs
17.7 ± 0.8 ± 0.4	568	BEHREND	90 CELL	$E_{\text{cm}}^{\text{ee}} = 35 \text{ GeV}$
17.4 ± 1.0	2197	ADEVA	88 MRKJ	$E_{\text{cm}}^{\text{ee}} = 14\text{--}16 \text{ GeV}$
17.7 ± 1.2 ± 0.7		AIHARA	87B TPC	$E_{\text{cm}}^{\text{ee}} = 29 \text{ GeV}$
18.3 ± 0.9 ± 0.8		BURCHAT	87 MRK2	$E_{\text{cm}}^{\text{ee}} = 29 \text{ GeV}$
18.6 ± 0.8 ± 0.7	558	⁵ BARTEL	86D JADE	$E_{\text{cm}}^{\text{ee}} = 34.6 \text{ GeV}$
12.9 ± 1.7 ± 0.7 -0.5		ALTHOFF	85 TASS	$E_{\text{cm}}^{\text{ee}} = 34.5 \text{ GeV}$
18.0 ± 0.9 ± 0.5	473	⁵ ASH	85B MAC	$E_{\text{cm}}^{\text{ee}} = 29 \text{ GeV}$
18.0 ± 1.0 ± 0.6		⁶ BALTRUSAITIS...	85 MRK3	$E_{\text{cm}}^{\text{ee}} = 3.77 \text{ GeV}$
19.4 ± 1.6 ± 1.7	153	BERGER	85 PLUT	$E_{\text{cm}}^{\text{ee}} = 34.6 \text{ GeV}$
17.6 ± 2.6 ± 2.1	47	BEHREND	83c CELL	$E_{\text{cm}}^{\text{ee}} = 34 \text{ GeV}$
17.8 ± 2.0 ± 1.8		BERGER	81B PLUT	$E_{\text{cm}}^{\text{ee}} = 9\text{--}32 \text{ GeV}$

- ¹ See footnote to SCHAEEL 05c $\Gamma(\tau^- \rightarrow e^- \bar{\nu}_e \nu_\tau) / \Gamma_{\text{total}}$ measurement for correlations with other measurements.
- ² The correlation coefficient between this measurement and the ACCIARRI 01F measurement of $B(\tau^- \rightarrow e^- \bar{\nu}_e \nu_\tau)$ is 0.08.
- ³ The correlation coefficients between this measurement and the ANASTASSOV 97 measurements of $B(e \bar{\nu}_e \nu_\tau)$, $B(\mu \bar{\nu}_\mu \nu_\tau) / B(e \bar{\nu}_e \nu_\tau)$, $B(h^- \nu_\tau)$, and $B(h^- \nu_\tau) / B(e \bar{\nu}_e \nu_\tau)$ are 0.50, 0.58, 0.50, and 0.08 respectively.
- ⁴ Not independent of ALBRECHT 92D $\Gamma(\mu^- \bar{\nu}_\mu \nu_\tau) / \Gamma(e^- \bar{\nu}_e \nu_\tau)$ and ALBRECHT 93G $\Gamma(\mu^- \bar{\nu}_\mu \nu_\tau) \times \Gamma(e^- \bar{\nu}_e \nu_\tau) / \Gamma_{\text{total}}^2$ values.
- ⁵ Modified using $B(e^- \bar{\nu}_e \nu_\tau) / B(\text{"1 prong"})$ and $B(\text{"1 prong"}) := 0.855$.
- ⁶ Error correlated with BALTRUSAITIS 85 $e \bar{\nu} \nu$ value.

VALUE (%)	EVTS	DOCUMENT ID	TECN	COMMENT
0.367 ± 0.008 OUR AVERAGE				
0.363 ± 0.002 ± 0.015	22k	¹ SHIMIZU	18A BELL	$711 \text{ fb}^{-1} E_{\text{cm}}^{\text{ee}} = 10.6 \text{ GeV}$
0.369 ± 0.003 ± 0.010	16k	² LEES	15G BABR	$431 \text{ fb}^{-1} E_{\text{cm}}^{\text{ee}} = 10.6 \text{ GeV}$

$$0.361 \pm 0.016 \pm 0.035 \quad \text{}^3 \text{ BERGFELD } 00 \text{ CLEO } E_{\text{cm}}^{\text{ee}} = 10.6 \text{ GeV}$$

- ● ● We do not use the following data for averages, fits, limits, etc. ● ● ●
- 0.30 ± 0.04 ± 0.05
- 0.23 ± 0.10
- 116
- 10
- ⁴ ALEXANDER 96s OPAL 1991-1994 LEP runs
- ⁵ WU 90 MRK2 $E_{\text{cm}}^{\text{ee}} = 29 \text{ GeV}$

- ¹ SHIMIZU 18A impose requirements on detected γ 's corresponding to a τ -rest-frame energy cutoff $E_\gamma^* > 10 \text{ MeV}$.
- ² LEES 15G impose requirements on detected γ 's corresponding to a τ -rest-frame energy cutoff $E_\gamma^* > 10 \text{ MeV}$.
- ³ BERGFELD 00 impose requirements on detected γ 's corresponding to a τ -rest-frame energy cutoff $E_\gamma^* > 10 \text{ MeV}$. For $E_\gamma^* > 20 \text{ MeV}$, they quote $(3.04 \pm 0.14 \pm 0.30) \times 10^{-3}$.
- ⁴ ALEXANDER 96s impose requirements on detected γ 's corresponding to a τ -rest-frame energy cutoff $E_\gamma > 20 \text{ MeV}$.
- ⁵ WU 90 reports $\Gamma(\mu^- \bar{\nu}_\mu \nu_\tau \gamma) / \Gamma(\mu^- \bar{\nu}_\mu \nu_\tau) = 0.013 \pm 0.006$, which is converted to $\Gamma(\mu^- \bar{\nu}_\mu \nu_\tau \gamma) / \Gamma_{\text{total}}$ using $\Gamma(\mu^- \bar{\nu}_\mu \nu_\tau \gamma) / \Gamma_{\text{total}} = 17.35\%$. Requirements on detected γ 's correspond to a τ rest frame energy cutoff $E_\gamma > 37 \text{ MeV}$.

$$\Gamma(e^- \bar{\nu}_e \nu_\tau) / \Gamma_{\text{total}} \quad \Gamma_5 / \Gamma$$

To minimize the effect of experiments with large systematic errors, we exclude experiments which together would contribute 5% of the weight in the average.

VALUE (%)	EVTS	DOCUMENT ID	TECN	COMMENT
17.82 ± 0.04 OUR FIT				
17.82 ± 0.05 OUR AVERAGE				
17.837 ± 0.072 ± 0.036	5.6k	¹ SCHAEEL	05c ALEP	1991-1995 LEP runs
17.806 ± 0.104 ± 0.076	24.7k	² ACCIARRI	01F L3	1991-1995 LEP runs
17.81 ± 0.09 ± 0.06	33.1k	ABBIENDI	99H OPAL	1991-1995 LEP runs
17.877 ± 0.109 ± 0.110	23.3k	ABREU	99x DLPH	1991-1995 LEP runs
17.76 ± 0.06 ± 0.17		³ ANASTASSOV	97 CLEO	$E_{\text{cm}}^{\text{ee}} = 10.6 \text{ GeV}$
● ● ● We do not use the following data for averages, fits, limits, etc. ● ● ●				
17.78 ± 0.10 ± 0.09	25.3k	ALEXANDER	96D OPAL	Repl. by ABBIENDI 99H
17.79 ± 0.12 ± 0.06	20.6k	BUSKULIC	96c ALEP	Repl. by SCHAEEL 05c
17.51 ± 0.23 ± 0.31	5059	ABREU	95T DLPH	Repl. by ABREU 99x
17.9 ± 0.4 ± 0.4	2892	ADRIANI	93M L3	Repl. by ACCIARRI 01F
17.5 ± 0.3 ± 0.5		⁴ ALBRECHT	93G ARG	$E_{\text{cm}}^{\text{ee}} = 9.4\text{--}10.6 \text{ GeV}$
17.97 ± 0.14 ± 0.23	3970	AKERIB	92 CLEO	Repl. by ANASTASSOV 97
19.1 ± 0.4 ± 0.6	2960	⁵ AMMAR	92 CLEO	$E_{\text{cm}}^{\text{ee}} = 10.5\text{--}10.9 \text{ GeV}$
18.09 ± 0.45 ± 0.45		DECAMP	92c ALEP	Repl. by SCHAEEL 05c
17.0 ± 0.5 ± 0.6	1.7k	ABACHI	90 HRS	$E_{\text{cm}}^{\text{ee}} = 29 \text{ GeV}$
18.4 ± 0.8 ± 0.4	644	BEHREND	90 CELL	$E_{\text{cm}}^{\text{ee}} = 35 \text{ GeV}$
16.3 ± 0.3 ± 3.2		JANSSEN	89 CBAL	$E_{\text{cm}}^{\text{ee}} = 9.4\text{--}10.6 \text{ GeV}$
18.4 ± 1.2 ± 1.0		AIHARA	87B TPC	$E_{\text{cm}}^{\text{ee}} = 29 \text{ GeV}$
19.1 ± 0.8 ± 1.1		BURCHAT	87 MRK2	$E_{\text{cm}}^{\text{ee}} = 29 \text{ GeV}$
16.8 ± 0.7 ± 0.9	515	⁵ BARTEL	86D JADE	$E_{\text{cm}}^{\text{ee}} = 34.6 \text{ GeV}$
20.4 ± 3.0 ± 1.4 -0.9		ALTHOFF	85 TASS	$E_{\text{cm}}^{\text{ee}} = 34.5 \text{ GeV}$
17.8 ± 0.9 ± 0.6	390	⁵ ASH	85B MAC	$E_{\text{cm}}^{\text{ee}} = 29 \text{ GeV}$
18.2 ± 0.7 ± 0.5		⁶ BALTRUSAITIS...	85 MRK3	$E_{\text{cm}}^{\text{ee}} = 3.77 \text{ GeV}$
13.0 ± 1.9 ± 2.9		BERGER	85 PLUT	$E_{\text{cm}}^{\text{ee}} = 34.6 \text{ GeV}$
18.3 ± 2.4 ± 1.9	60	BEHREND	83c CELL	$E_{\text{cm}}^{\text{ee}} = 34 \text{ GeV}$
16.0 ± 1.3	459	⁷ BACINO	78B DLCO	$E_{\text{cm}}^{\text{ee}} = 3.1\text{--}7.4 \text{ GeV}$

¹ Correlation matrix for SCHAEEL 05c branching fractions, in percent:

- (1) $\Gamma(\tau^- \rightarrow e^- \bar{\nu}_e \nu_\tau) / \Gamma_{\text{total}}$
- (2) $\Gamma(\tau^- \rightarrow \mu^- \bar{\nu}_\mu \nu_\tau) / \Gamma_{\text{total}}$
- (3) $\Gamma(\tau^- \rightarrow \pi^- \nu_\tau) / \Gamma_{\text{total}}$
- (4) $\Gamma(\tau^- \rightarrow \pi^- \pi^0 \nu_\tau) / \Gamma_{\text{total}}$
- (5) $\Gamma(\tau^- \rightarrow \pi^- 2\pi^0 \nu_\tau \text{ (ex. } K^0)) / \Gamma_{\text{total}}$
- (6) $\Gamma(\tau^- \rightarrow \pi^- 3\pi^0 \nu_\tau \text{ (ex. } K^0)) / \Gamma_{\text{total}}$
- (7) $\Gamma(\tau^- \rightarrow h^- 4\pi^0 \nu_\tau \text{ (ex. } K^0, \eta)) / \Gamma_{\text{total}}$
- (8) $\Gamma(\tau^- \rightarrow \pi^- \pi^+ \pi^- \nu_\tau \text{ (ex. } K^0, \omega)) / \Gamma_{\text{total}}$
- (9) $\Gamma(\tau^- \rightarrow \pi^- \pi^+ \pi^- \pi^0 \nu_\tau \text{ (ex. } K^0)) / \Gamma_{\text{total}}$
- (10) $\Gamma(\tau^- \rightarrow h^- h^- h^+ 2\pi^0 \nu_\tau \text{ (ex. } K^0)) / \Gamma_{\text{total}}$
- (11) $\Gamma(\tau^- \rightarrow h^- h^- h^+ 3\pi^0 \nu_\tau) / \Gamma_{\text{total}}$
- (12) $\Gamma(\tau^- \rightarrow 3h^- 2h^+ \nu_\tau \text{ (ex. } K^0)) / \Gamma_{\text{total}}$
- (13) $\Gamma(\tau^- \rightarrow 3h^- 2h^+ \pi^0 \nu_\tau \text{ (ex. } K^0)) / \Gamma_{\text{total}}$

(1)	(2)	(3)	(4)	(5)	(6)	(7)	(8)	(9)	(10)	(11)	(12)
(2)	-20										
(3)	-9	-6									
(4)	-16	-12	-2								
(5)	-5	-5	-17	-37							
(6)	0	-4	-15	2	-27						
(7)	-2	-4	-24	-15	20	-47					
(8)	-14	-9	15	-5	-17	-14	-8				
(9)	-13	-12	-25	-30	4	-2	16	-15			
(10)	0	-2	-23	-14	4	10	13	-6	-17		
(11)	1	0	-5	1	4	6	0	-9	-2	-11	
(12)	0	1	9	4	-8	-4	-6	9	-5	-4	-2
(13)	1	-4	-3	-5	3	2	-4	-3	-1	4	-24

- The correlation coefficient between this measurement and the ACCIARRI 01F measurement of $B(\tau^- \rightarrow \mu^- \bar{\nu}_\mu \nu_\tau)$ is 0.08.
- The correlation coefficients between this measurement and the ANASTASSOV 97 measurements of $B(\mu \bar{\nu}_\mu \nu_\tau)$, $B(\mu \bar{\nu}_\mu \nu_\tau)/B(e \bar{\nu}_e \nu_\tau)$, $B(h^- \nu_\tau)$, and $B(h^- \nu_\tau)/B(e \bar{\nu}_e \nu_\tau)$ are 0.50, -0.42, 0.48, and -0.39 respectively.
- Not independent of ALBRECHT 92D $\Gamma(\mu^- \bar{\nu}_\mu \nu_\tau)/\Gamma(e^- \bar{\nu}_e \nu_\tau)$ and ALBRECHT 93G $\Gamma(\mu^- \bar{\nu}_\mu \nu_\tau) \times \Gamma(e^- \bar{\nu}_e \nu_\tau)/\Gamma_{\text{total}}^2$ values.
- Modified using $B(e^- \bar{\nu}_e \nu_\tau)$ and B("1 prong") and B("1 prong") = 0.855.
- Error correlated with BALTRUSAITIS 85 $\Gamma(\mu^- \bar{\nu}_\mu \nu_\tau)/\Gamma_{\text{total}}$.
- BACINO 78B value comes from fit to events with e^\pm and one other nonelectron charged prong.

$\Gamma(\mu^- \bar{\nu}_\mu \nu_\tau)/\Gamma(e^- \bar{\nu}_e \nu_\tau)$ Γ_3/Γ_5
 Standard Model prediction including mass effects is 0.9726.

VALUE (units 10^{-2})	EVTs	DOCUMENT ID	TECN	COMMENT
97.62 ± 0.28 OUR FIT				
97.9 ± 0.4 OUR AVERAGE				
97.96 ± 0.16 ± 0.36	731k	¹ AUBERT	10F BABR	467 fb ⁻¹ $E_{\text{cm}}^{\text{e}} = 10.6$ GeV
97.77 ± 0.63 ± 0.87		² ANASTASSOV	97 CLEO	$E_{\text{cm}}^{\text{e}} = 10.6$ GeV
99.7 ± 3.5 ± 4.0		ALBRECHT	92D ARG	$E_{\text{cm}}^{\text{e}} = 9.4-10.6$ GeV

- Correlation matrix for AUBERT 10F branching fractions:
 - $\Gamma(\tau^- \rightarrow \mu^- \bar{\nu}_\mu \nu_\tau) / \Gamma(\tau^- \rightarrow e^- \bar{\nu}_e \nu_\tau)$
 - $\Gamma(\tau^- \rightarrow \pi^- \nu_\tau) / \Gamma(\tau^- \rightarrow e^- \bar{\nu}_e \nu_\tau)$
 - $\Gamma(\tau^- \rightarrow K^- \nu_\tau) / \Gamma(\tau^- \rightarrow e^- \bar{\nu}_e \nu_\tau)$

(1)	(2)
(2)	0.25
(3)	0.12 0.33
- The correlation coefficients between this measurement and the ANASTASSOV 97 measurements of $B(\mu \bar{\nu}_\mu \nu_\tau)$, $B(e \bar{\nu}_e \nu_\tau)$, $B(h^- \nu_\tau)$, and $B(h^- \nu_\tau)/B(e \bar{\nu}_e \nu_\tau)$ are 0.58, -0.42, 0.07, and 0.45 respectively.

$\Gamma(e^- \bar{\nu}_e \nu_\tau)/\Gamma_{\text{total}}$ Γ_6/Γ

VALUE (%)	EVTs	DOCUMENT ID	TECN	COMMENT
1.83 ± 0.05 OUR AVERAGE				
1.79 ± 0.02 ± 0.10	12k	¹ SHIMIZU	18A BELL	711 fb ⁻¹ $E_{\text{cm}}^{\text{e}} = 10.6$ GeV
1.847 ± 0.015 ± 0.052	18k	² LEES	15G BABR	431 fb ⁻¹ $E_{\text{cm}}^{\text{e}} = 10.6$ GeV
1.75 ± 0.06 ± 0.17		³ BERGFELD	00 CLEO	$E_{\text{cm}}^{\text{e}} = 10.6$ GeV

- SHIMIZU 18A impose requirements on detected γ 's corresponding to a τ -rest-frame energy cutoff $E_\gamma^* > 10$ MeV.
- LEES 15G impose requirements on detected γ 's corresponding to a τ -rest-frame energy cutoff $E_\gamma^* > 10$ MeV.
- BERGFELD 00 impose requirements on detected γ 's corresponding to a τ -rest-frame energy cutoff $E_\gamma^* > 10$ MeV.

$\Gamma(h^- \geq 0K_L^0 \nu_\tau)/\Gamma_{\text{total}}$ Γ_7/Γ
 $\Gamma_7/\Gamma = (\Gamma_9 + \Gamma_{10} + \frac{1}{2}\Gamma_{36} + \frac{1}{2}\Gamma_{38} + \Gamma_{50})/\Gamma$

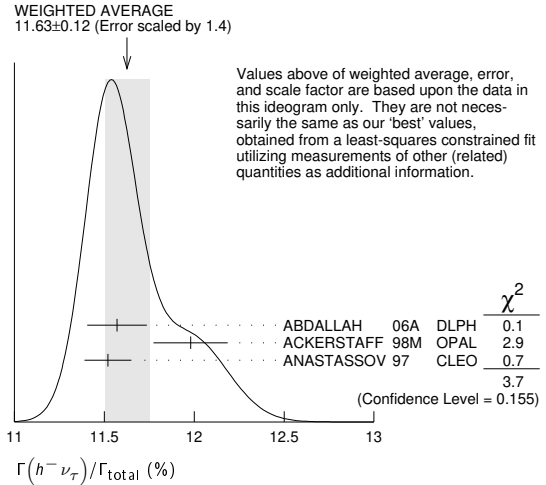
VALUE (%)	EVTs	DOCUMENT ID	TECN	COMMENT
12.03 ± 0.05 OUR FIT				
12.2 ± 0.4 OUR AVERAGE				
12.47 ± 0.26 ± 0.43	2967	¹ ACCIARRI	95 L3	1992 LEP run
12.4 ± 0.7 ± 0.7	283	² ABREU	92N DLPH	1990 LEP run
12.1 ± 0.7 ± 0.5	309	ALEXANDER	91D OPAL	1990 LEP run
••• We use the following data for averages but not for fits. •••				
11.3 ± 0.5 ± 0.8	798	³ FORD	87 MAC	$E_{\text{cm}}^{\text{e}} = 29$ GeV
••• We do not use the following data for averages, fits, limits, etc. •••				
12.44 ± 0.11 ± 0.11	15k	⁴ BUSKULIC	96 ALEP	Repl. by SCHAEEL 05c
11.7 ± 0.6 ± 0.8		⁵ ALBRECHT	92D ARG	$E_{\text{cm}}^{\text{e}} = 9.4-10.6$ GeV
12.98 ± 0.44 ± 0.33		⁶ DECAMP	92C ALEP	Repl. by SCHAEEL 05c
12.3 ± 0.9 ± 0.5	1338	BEHREND	90 CELL	$E_{\text{cm}}^{\text{e}} = 35$ GeV
11.1 ± 1.1 ± 1.4		⁷ BURCHAT	87 MRK2	$E_{\text{cm}}^{\text{e}} = 29$ GeV
12.3 ± 0.6 ± 1.1	328	⁸ BARTEL	86D JADE	$E_{\text{cm}}^{\text{e}} = 34.6$ GeV
13.0 ± 2.0 ± 4.0		BERGER	85 PLUT	$E_{\text{cm}}^{\text{e}} = 34.6$ GeV
11.2 ± 1.7 ± 1.2	34	⁹ BEHREND	83C CELL	$E_{\text{cm}}^{\text{e}} = 34$ GeV

- ACCIARRI 95 with 0.65% added to remove their correction for $\pi^- K_L^0$ backgrounds.
- ABREU 92N with 0.5% added to remove their correction for $K^*(892)^-$ backgrounds.
- FORD 87 result for $B(\pi^- \nu_\tau)$ with 0.67% added to remove their K^- correction and adjusted for 1992 B("1 prong").
- BUSKULIC 96 quote $11.78 \pm 0.11 \pm 0.13$ We add 0.66 to undo their correction for unseen K_L^0 and modify the systematic error accordingly.
- Not independent of ALBRECHT 92D $\Gamma(\mu^- \bar{\nu}_\mu \nu_\tau)/\Gamma(e^- \bar{\nu}_e \nu_\tau)$, $\Gamma(\mu^- \bar{\nu}_\mu \nu_\tau) \times \Gamma(e^- \bar{\nu}_e \nu_\tau)$, and $\Gamma(h^- \geq 0K_L^0 \nu_\tau)/\Gamma(e^- \bar{\nu}_e \nu_\tau)$ values.
- DECAMP 92c quote $B(h^- \geq 0K_L^0 \nu_\tau) = 0(K_S^0 \rightarrow \pi^+ \pi^- \nu_\tau) = 13.32 \pm 0.44 \pm 0.33$. We subtract 0.35 to correct for their inclusion of the K_S^0 decays.
- BURCHAT 87 with 1.1% added to remove their correction for K^- and $K^*(892)^-$ backgrounds.
- BARTEL 86d result for $B(\pi^- \nu_\tau)$ with 0.59% added to remove their K^- correction and adjusted for 1992 B("1 prong").
- BEHREND 83c quote $B(\pi^- \nu_\tau) = 9.9 \pm 1.7 \pm 1.3$ after subtracting 1.3 ± 0.5 to correct for $B(K^- \nu_\tau)$.

$\Gamma(h^- \nu_\tau)/\Gamma_{\text{total}}$ $\Gamma_8/\Gamma = (\Gamma_9 + \Gamma_{10})/\Gamma$

VALUE (%)	EVTs	DOCUMENT ID	TECN	COMMENT
11.51 ± 0.05 OUR FIT				
11.63 ± 0.12 OUR AVERAGE				
11.571 ± 0.120 ± 0.114	19k	¹ ABDALLAH	06A DLPH	1992-1995 LEP runs
11.98 ± 0.13 ± 0.16		ACKERSTAFF	98M OPAL	1991-1995 LEP runs
11.52 ± 0.05 ± 0.12		² ANASTASSOV	97 CLEO	$E_{\text{cm}}^{\text{e}} = 10.6$ GeV

Error includes scale factor of 1.4. See the ideogram below.



¹ Correlation matrix for ABDALLAH 06A branching fractions, in percent:

(1)	$\Gamma(\tau^- \rightarrow h^- \nu_\tau)/\Gamma_{\text{total}}$	(2)	$\Gamma(\tau^- \rightarrow h^- \pi^0 \nu_\tau)/\Gamma_{\text{total}}$	(3)	$\Gamma(\tau^- \rightarrow h^- \geq 1\pi^0 \nu_\tau \text{ (ex. } K^0))/\Gamma_{\text{total}}$	(4)	$\Gamma(\tau^- \rightarrow h^- 2\pi^0 \nu_\tau \text{ (ex. } K^0))/\Gamma_{\text{total}}$	(5)	$\Gamma(\tau^- \rightarrow h^- \geq 3\pi^0 \nu_\tau \text{ (ex. } K^0))/\Gamma_{\text{total}}$	(6)	$\Gamma(\tau^- \rightarrow h^- h^- h^+ \nu_\tau \text{ (ex. } K^0))/\Gamma_{\text{total}}$	(7)	$\Gamma(\tau^- \rightarrow h^- h^- h^+ \pi^0 \nu_\tau \text{ (ex. } K^0))/\Gamma_{\text{total}}$	(8)	$\Gamma(\tau^- \rightarrow h^- h^- h^+ \geq 1\pi^0 \nu_\tau \text{ (ex. } K^0))/\Gamma_{\text{total}}$	(9)	$\Gamma(\tau^- \rightarrow h^- h^- h^+ \geq 2\pi^0 \nu_\tau \text{ (ex. } K^0))/\Gamma_{\text{total}}$	(10)	$\Gamma(\tau^- \rightarrow 3h^- 2h^+ \nu_\tau \text{ (ex. } K^0))/\Gamma_{\text{total}}$	(11)	$\Gamma(\tau^- \rightarrow 3h^- 2h^+ \pi^0 \nu_\tau \text{ (ex. } K^0))/\Gamma_{\text{total}}$
(1)	(2)	(3)	(4)	(5)	(6)	(7)	(8)	(9)	(10)	(11)											
(2)	-34																				
(3)	-47	56																			
(4)	6	-66	15																		
(5)	-6	38	11	-86																	
(6)	-7	-8	15	0	-2																
(7)	-2	-1	-5	-3	3	-53															
(8)	-4	-4	-13	-4	-2	-56	75														
(9)	-1	-1	-4	3	-6	26	-78	-16													
(10)	-1	-1	1	0	0	-2	-3	-1	3												
(11)	0	0	0	0	0	1	0	-5	5	-57											

- The correlation coefficients between this measurement and the ANASTASSOV 97 measurements of $B(\mu \bar{\nu}_\mu \nu_\tau)$, $B(e \bar{\nu}_e \nu_\tau)$, $B(\mu \bar{\nu}_\mu \nu_\tau)/B(e \bar{\nu}_e \nu_\tau)$, and $B(h^- \nu_\tau)/B(e \bar{\nu}_e \nu_\tau)$ are 0.50, 0.48, 0.07, and 0.63 respectively.

$\Gamma(h^- \nu_\tau)/\Gamma(e^- \bar{\nu}_e \nu_\tau)$ $\Gamma_8/\Gamma_5 = (\Gamma_9 + \Gamma_{10})/\Gamma_5$

VALUE (units 10^{-2})	EVTs	DOCUMENT ID	TECN	COMMENT
64.0 ± 0.33 OUR FIT				
64.0 ± 0.7 OUR AVERAGE				
63.33 ± 0.14 ± 0.61	394k	¹ AUBERT	10F BABR	467 fb ⁻¹ $E_{\text{cm}}^{\text{e}} = 10.6$ GeV
64.84 ± 0.41 ± 0.60		² ANASTASSOV	97 CLEO	$E_{\text{cm}}^{\text{e}} = 10.6$ GeV

- Not independent of AUBERT 10F $\Gamma(\tau^- \rightarrow \pi^- \nu_\tau)/\Gamma(\tau^- \rightarrow e^- \bar{\nu}_e \nu_\tau)$ and $\Gamma(\tau^- \rightarrow K^- \nu_\tau)/\Gamma(\tau^- \rightarrow e^- \bar{\nu}_e \nu_\tau)$.
- The correlation coefficients between this measurement and the ANASTASSOV 97 measurements of $B(\mu \bar{\nu}_\mu \nu_\tau)$, $B(e \bar{\nu}_e \nu_\tau)$, $B(\mu \bar{\nu}_\mu \nu_\tau)/B(e \bar{\nu}_e \nu_\tau)$, and $B(h^- \nu_\tau)$ are 0.08, -0.39, 0.45, and 0.63 respectively.

$\Gamma(\pi^- \nu_\tau)/\Gamma_{\text{total}}$ Γ_9/Γ

VALUE (%)	EVTs	DOCUMENT ID	TECN	COMMENT
10.82 ± 0.05 OUR FIT				
10.828 ± 0.070 ± 0.078				
11.06 ± 0.11 ± 0.14	38k	¹ SCHAEEL	05c ALEP	1991-1995 LEP runs
11.7 ± 0.4 ± 1.8	1138	² BUSKULIC	96 ALEP	Repl. by SCHAEEL 05c
		BLOCKER	82D MRK2	$E_{\text{cm}}^{\text{e}} = 3.5-6.7$ GeV

- See footnote to SCHAEEL 05c $\Gamma(\tau^- \rightarrow e^- \bar{\nu}_e \nu_\tau)/\Gamma_{\text{total}}$ measurement for correlations with other measurements.
- Not independent of BUSKULIC 96 $B(h^- \nu_\tau)$ and $B(K^- \nu_\tau)$ values.

Lepton Particle Listings

τ

$\Gamma(\pi^- \nu_\tau)/\Gamma(e^- \bar{\nu}_e \nu_\tau)$ Γ_9/Γ_5

VALUE (units 10^{-2})	EVTS	DOCUMENT ID	TECN	COMMENT
60.71 ± 0.32 OUR FIT				
59.45 ± 0.14 ± 0.61	369k	¹ AUBERT	10F BABR	467 fb ⁻¹ $E_{cm}^{ee} = 10.6$ GeV

¹ See footnote to AUBERT 10F $\Gamma(\tau^- \rightarrow \mu^- \bar{\nu}_\mu \nu_\tau)/\Gamma(\tau^- \rightarrow e^- \bar{\nu}_e \nu_\tau)$ for correlations with other measurements.

$\Gamma(K^- \nu_\tau)/\Gamma_{total}$ Γ_{10}/Γ

VALUE (%)	EVTS	DOCUMENT ID	TECN	COMMENT
0.696 ± 0.010 OUR FIT				
0.685 ± 0.023 OUR AVERAGE				
0.658 ± 0.027 ± 0.029		¹ ABBIENDI	01J OPAL	1990-1995 LEP runs
0.696 ± 0.025 ± 0.014	2032	BARATE	99K ALEP	1991-1995 LEP runs
0.85 ± 0.18	27	ABREU	94K DLPH	LEP 1992 Z data
0.66 ± 0.07 ± 0.09	99	BATTLE	94 CLEO	$E_{cm}^{ee} \approx 10.6$ GeV

- • • We do not use the following data for averages, fits, limits, etc. • • •
- 0.72 ± 0.04 ± 0.04 728 BUSKULIC 96 ALEP Repl. by BARATE 99K
- 0.59 ± 0.18 16 MILLS 84 DLCO $E_{cm}^{ee} = 29$ GeV
- 1.3 ± 0.5 15 BLOCKER 82B MRK2 $E_{cm}^{ee} = 3.9-6.7$ GeV

¹ The correlation coefficient between this measurement and the ABBIENDI 01J $B(\tau^- \rightarrow K^- \geq 0\pi^0 \geq 0K^0 \geq 0\gamma \nu_\tau)$ is 0.60.

$\Gamma(K^- \nu_\tau)/\Gamma(e^- \bar{\nu}_e \nu_\tau)$ Γ_{10}/Γ_5

VALUE (units 10^{-2})	EVTS	DOCUMENT ID	TECN	COMMENT
3.91 ± 0.05 OUR FIT				
3.882 ± 0.032 ± 0.057	25k	¹ AUBERT	10F BABR	467 fb ⁻¹ $E_{cm}^{ee} = 10.6$ GeV

¹ See footnote to AUBERT 10F $\Gamma(\tau^- \rightarrow \mu^- \bar{\nu}_\mu \nu_\tau)/\Gamma(\tau^- \rightarrow e^- \bar{\nu}_e \nu_\tau)$ for correlations with other measurements.

$\Gamma(K^- \nu_\tau)/\Gamma(\pi^- \nu_\tau)$ Γ_{10}/Γ_9

VALUE (units 10^{-2})	DOCUMENT ID	TECN	COMMENT
6.44 ± 0.09 OUR FIT			

- • • We use the following data for averages but not for fits. • • •
- 6.531 ± 0.056 ± 0.093** ¹ AUBERT 10F BABR 467 fb⁻¹ $E_{cm}^{ee} = 10.6$ GeV

¹ Not independent of AUBERT 10F $\Gamma(\tau^- \rightarrow \pi^- \nu_\tau)/\Gamma(\tau^- \rightarrow e^- \bar{\nu}_e \nu_\tau)$ and $\Gamma(\tau^- \rightarrow K^- \nu_\tau)/\Gamma(\tau^- \rightarrow e^- \bar{\nu}_e \nu_\tau)$.

$\Gamma(h^- \geq 1 \text{ neutrals } \nu_\tau)/\Gamma_{total}$ Γ_{11}/Γ

VALUE (%)	DOCUMENT ID	TECN	COMMENT
37.01 ± 0.09 OUR FIT			
• • • We do not use the following data for averages, fits, limits, etc. • • •			
36.14 ± 0.33 ± 0.58	¹ AKERS	94E OPAL	1991-1992 LEP runs
38.4 ± 1.2 ± 1.0	² BURCHAT	87 MRK2	$E_{cm}^{ee} = 29$ GeV
42.7 ± 2.0 ± 2.9	BERGER	85 PLUT	$E_{cm}^{ee} = 34.6$ GeV

¹ Not independent of ACKERSTAFF 98M $B(h^- \pi^0 \nu_\tau)$ and $B(h^- \geq 2\pi^0 \nu_\tau)$.
² BURCHAT 87 quote for $B(\pi^\pm \geq 1 \text{ neutral } \nu_\tau) = 0.378 \pm 0.012 \pm 0.010$. We add 0.006 to account for contribution from $(K^* \nu_\tau)$ which they fixed at BR = 0.013.

$\Gamma(h^- \geq 1\pi^0 \nu_\tau \text{ (ex. } K^0))/\Gamma_{total}$ Γ_{12}/Γ

VALUE (%)	EVTS	DOCUMENT ID	TECN	COMMENT
36.51 ± 0.09 OUR FIT				
• • • We use the following data for averages but not for fits. • • •				
36.641 ± 0.155 ± 0.127	45k	¹ ABDALLAH	06A DLPH	1992-1995 LEP runs

¹ See footnote to ABDALLAH 06A $\Gamma(\tau^- \rightarrow h^- \nu_\tau)/\Gamma_{total}$ measurement for correlations with other measurements.

$\Gamma(h^- \pi^0 \nu_\tau)/\Gamma_{total}$ $\Gamma_{13}/\Gamma = (\Gamma_{14} + \Gamma_{16})/\Gamma$

VALUE (%)	EVTS	DOCUMENT ID	TECN	COMMENT
25.93 ± 0.09 OUR FIT				
25.73 ± 0.16 OUR AVERAGE				
25.67 ± 0.01 ± 0.39	5.4M	FUJIKAWA	08 BELL	72 fb ⁻¹ $E_{cm}^{ee} = 10.6$ GeV
25.740 ± 0.201 ± 0.138	35k	¹ ABDALLAH	06A DLPH	1992-1995 LEP runs
25.89 ± 0.17 ± 0.29		ACKERSTAFF	98M OPAL	1991-1995 LEP runs
25.05 ± 0.35 ± 0.50	6613	ACCIARRI	95 L3	1992 LEP run
25.87 ± 0.12 ± 0.42	51k	² ARTUSO	94 CLEO	$E_{cm}^{ee} = 10.6$ GeV
• • • We do not use the following data for averages, fits, limits, etc. • • •				
25.76 ± 0.15 ± 0.13	31k	BUSKULIC	96 ALEP	Repl. by SCHAEEL 05c
25.98 ± 0.36 ± 0.52		³ AKERS	94E OPAL	Repl. by ACKERSTAFF 98M
22.9 ± 0.8 ± 1.3	283	⁴ ABREU	92N DLPH	$E_{cm}^{ee} = 88.2-94.2$ GeV
23.1 ± 0.4 ± 0.9	1249	⁵ ALBRECHT	92Q ARG	$E_{cm}^{ee} = 10$ GeV
25.02 ± 0.64 ± 0.88	1849	DELCAMP	92C ALEP	1989-1990 LEP runs
22.0 ± 0.8 ± 1.9	779	ANTREASYAN	91 CBAL	$E_{cm}^{ee} = 9.4-10.6$ GeV
22.6 ± 1.5 ± 0.7	1101	BEHREND	90 CELL	$E_{cm}^{ee} = 35$ GeV
23.1 ± 1.9 ± 1.6		BEHREND	84 CELL	$E_{cm}^{ee} = 14,22$ GeV

- See footnote to ABDALLAH 06A $\Gamma(\tau^- \rightarrow h^- \nu_\tau)/\Gamma_{total}$ measurement for correlations with other measurements.
- ARTUSO 94 reports the combined result from three independent methods, one of which (23% of the $\tau^- \rightarrow h^- \pi^0 \nu_\tau$) is normalized to the inclusive one-prong branching fraction, taken as 0.854 ± 0.004 . Renormalization to the present value causes negligible change.
- AKERS 94E quote ($26.25 \pm 0.36 \pm 0.52$) $\times 10^{-2}$; we subtract 0.27% from their number to correct for $\tau^- \rightarrow h^- K_L^0 \nu_\tau$.
- ABREU 92N with 0.5% added to remove their correction for $K^*(892)^-$ backgrounds.
- ALBRECHT 92Q with 0.5% added to remove their correction for $\tau^- \rightarrow K^*(892)^- \nu_\tau$ background.

$\Gamma(\pi^- \pi^0 \nu_\tau)/\Gamma_{total}$ Γ_{14}/Γ

VALUE (%)	EVTS	DOCUMENT ID	TECN	COMMENT
25.49 ± 0.09 OUR FIT				
25.46 ± 0.12 OUR AVERAGE				
25.471 ± 0.097 ± 0.085	81k	¹ SCHAEEL	05c ALEP	1991-1995 LEP runs
• • • We use the following data for averages but not for fits. • • •				
25.36 ± 0.44		² ARTUSO	94 CLEO	$E_{cm}^{ee} = 10.6$ GeV
• • • We do not use the following data for averages, fits, limits, etc. • • •				
25.30 ± 0.15 ± 0.13		³ BUSKULIC	96 ALEP	Repl. by SCHAEEL 05c
21.5 ± 0.4 ± 1.9	4400	^{4,5} ALBRECHT	88L ARG	$E_{cm}^{ee} = 10$ GeV
23.0 ± 1.3 ± 1.7	582	ADLER	87B MRK2	$E_{cm}^{ee} = 3.77$ GeV
25.8 ± 1.7 ± 2.5		⁶ BURCHAT	87 MRK2	$E_{cm}^{ee} = 29$ GeV
22.3 ± 0.6 ± 1.4	629	⁵ YELTON	86 MRK2	$E_{cm}^{ee} = 29$ GeV

- See footnote to SCHAEEL 05c $\Gamma(\tau^- \rightarrow e^- \bar{\nu}_e \nu_\tau)/\Gamma_{total}$ measurement for correlations with other measurements.
- Not independent of ARTUSO 94 $B(h^- \pi^0 \nu_\tau)$ and BATTLE 94 $B(K^- \pi^0 \nu_\tau)$ values.
- Not independent of BUSKULIC 96 $B(h^- \pi^0 \nu_\tau)$ and $B(K^- \pi^0 \nu_\tau)$ values.
- The authors divide by $(\Gamma_3 + \Gamma_5 + \Gamma_9 + \Gamma_{10})/\Gamma = 0.467$ to obtain this result.
- Experiment had no hadron identification. Kaon corrections were made, but insufficient information is given to permit their removal.
- BURCHAT 87 value is not independent of YELTON 86 value. Nonresonant decays included.

$\Gamma(\pi^- \pi^0 \text{ non-}\rho(770)\nu_\tau)/\Gamma_{total}$ Γ_{15}/Γ

VALUE (%)	DOCUMENT ID	TECN	COMMENT
0.3 ± 0.1 ± 0.3	¹ BEHREND	84 CELL	$E_{cm}^{ee} = 14,22$ GeV

¹ BEHREND 84 assume a flat nonresonant mass distribution down to the $\rho(770)$ mass, using events with mass above 1300 to set the level.

$\Gamma(K^- \pi^0 \nu_\tau)/\Gamma_{total}$ Γ_{16}/Γ

VALUE (%)	EVTS	DOCUMENT ID	TECN	COMMENT
0.433 ± 0.015 OUR FIT				
0.426 ± 0.016 OUR AVERAGE				
0.416 ± 0.003 ± 0.018	78k	AUBERT	07AP BABR	230 fb ⁻¹ $E_{cm}^{ee} = 10.6$ GeV
0.471 ± 0.059 ± 0.023	360	ABBIENDI	04J OPAL	1991-1995 LEP runs
0.444 ± 0.026 ± 0.024	923	BARATE	99K ALEP	1991-1995 LEP runs
0.51 ± 0.10 ± 0.07	37	BATTLE	94 CLEO	$E_{cm}^{ee} \approx 10.6$ GeV
• • • We do not use the following data for averages, fits, limits, etc. • • •				
0.52 ± 0.04 ± 0.05	395	BUSKULIC	96 ALEP	Repl. by BARATE 99k

$\Gamma(h^- \geq 2\pi^0 \nu_\tau)/\Gamma_{total}$ Γ_{17}/Γ

VALUE (%)	EVTS	DOCUMENT ID	TECN	COMMENT
10.81 ± 0.09 OUR FIT				
9.91 ± 0.31 ± 0.27				
9.89 ± 0.34 ± 0.55		¹ AKERS	94E OPAL	Repl. by ACKERSTAFF 98M
14.0 ± 1.2 ± 0.6	938	² BEHREND	90 CELL	$E_{cm}^{ee} = 35$ GeV
12.0 ± 1.4 ± 2.5		³ BURCHAT	87 MRK2	$E_{cm}^{ee} = 29$ GeV
13.9 ± 2.0 ± 1.9		⁴ AIHARA	86E TPC	$E_{cm}^{ee} = 29$ GeV

- AKERS 94E not independent of AKERS 94E $B(h^- \geq 1\pi^0 \nu_\tau)$ and $B(h^- \pi^0 \nu_\tau)$ measurements.
- No independent of BEHREND 90 $\Gamma(h^- 2\pi^0 \nu_\tau \text{ (exp. } K^0))$ and $\Gamma(h^- \geq 3\pi^0 \nu_\tau)$.
- Error correlated with BURCHAT 87 $\Gamma(\rho^- \nu_\tau)/\Gamma(\text{total})$ value.
- AIHARA 86E (TPC) quote $B(2\pi^0 \pi^- \nu_\tau) + 1.6B(3\pi^0 \pi^- \nu_\tau) + 1.1B(\pi^0 \eta \pi^- \nu_\tau)$.

$\Gamma(h^- 2\pi^0 \nu_\tau)/\Gamma_{total}$ Γ_{18}/Γ

VALUE (%)	EVTS	DOCUMENT ID	TECN	COMMENT
9.48 ± 0.10 OUR FIT				
• • • We do not use the following data for averages, fits, limits, etc. • • •				
9.48 ± 0.13 ± 0.10	12k	¹ BUSKULIC	96 ALEP	Repl. by SCHAEEL 05c

¹ BUSKULIC 96 quote $9.29 \pm 0.13 \pm 0.10$. We add 0.19 to undo their correction for $\tau^- \rightarrow h^- K^0 \nu_\tau$.

$\Gamma(h^- 2\pi^0 \nu_\tau \text{ (ex. } K^0))/\Gamma_{total}$ Γ_{19}/Γ

VALUE (%)	EVTS	DOCUMENT ID	TECN	COMMENT
9.32 ± 0.10 OUR FIT				
9.17 ± 0.27 OUR AVERAGE				

9.498 ± 0.320 ± 0.275	9.5k	¹ ABDALLAH	06A	DLPH	1992–1995 LEP runs
8.88 ± 0.37 ± 0.42	1060	ACCIARRI	95	L3	1992 LEP run
• • • We use the following data for averages but not for fits. • • •					
8.96 ± 0.16 ± 0.44		² PROCARIO	93	CLEO	$E_{cm}^{ee} \approx 10.6$ GeV
• • • We do not use the following data for averages, fits, limits, etc. • • •					
10.38 ± 0.66 ± 0.82	809	³ DECAMP	92c	ALEP	Repl. by SCHAEEL 05c
5.7 ± 0.5 ± $\frac{+1.7}{-1.0}$	133	⁴ ANTREASIAN	91	CBAL	$E_{cm}^{ee} = 9.4\text{--}10.6$ GeV
10.0 ± 1.5 ± 1.1	333	⁵ BEHREND	90	CELL	$E_{cm}^{ee} = 35$ GeV
8.7 ± 0.4 ± 1.1	815	⁶ BAND	87	MAC	$E_{cm}^{ee} = 29$ GeV
6.2 ± 0.6 ± 1.2		⁷ GAN	87	MRK2	$E_{cm}^{ee} = 29$ GeV
6.0 ± 3.0 ± 1.8		BEHREND	84	CELL	$E_{cm}^{ee} = 14.22$ GeV

¹ See footnote to ABDALLAH 06A $\Gamma(\tau^- \rightarrow h^- \nu_\tau)/\Gamma_{total}$ measurement for correlations with other measurements.

² PROCARIO 93 entry is obtained from $B(h^- 2\pi^0 \nu_\tau)/B(h^- \pi^0 \nu_\tau)$ using ARTUSO 94 result for $B(h^- \pi^0 \nu_\tau)$.

³ We subtract 0.0015 to account for $\tau^- \rightarrow K^*(892)^- \nu_\tau$ contribution.

⁴ ANTREASIAN 91 subtract 0.001 to account for the $\tau^- \rightarrow K^*(892)^- \nu_\tau$ contribution.

⁵ BEHREND 90 subtract 0.002 to account for the $\tau^- \rightarrow K^*(892)^- \nu_\tau$ contribution.

⁶ BAND 87 assume $B(\pi^- 3\pi^0 \nu_\tau) = 0.01$ and $B(\pi^- \pi^0 \eta \nu_\tau) = 0.005$.

⁷ GAN 87 analysis use photon multiplicity distribution.

$\Gamma(h^- 2\pi^0 \nu_\tau \text{ (ex. } K^0)) / \Gamma(h^- \pi^0 \nu_\tau)$ Γ_{19}/Γ_{13}
 $\Gamma_{19}/\Gamma_{13} = (\Gamma_{20} + \Gamma_{23}) / (\Gamma_{14} + \Gamma_{16})$

VALUE (units 10 ⁻²)	DOCUMENT ID	TECN	COMMENT
36.0 ± 0.4 OUR FIT			
34.2 ± 0.6 ± 1.6	¹ PROCARIO	93	CLEO $E_{cm}^{ee} \approx 10.6$ GeV

¹ PROCARIO 93 quote $0.345 \pm 0.006 \pm 0.016$ after correction for 2 kaon backgrounds assuming $B(K^{*-} \nu_\tau) = 1.42 \pm 0.18\%$ and $B(h^- K^0 \pi^0 \nu_\tau) = 0.48 \pm 0.48\%$. We multiply by 0.990 ± 0.010 to remove these corrections to $B(h^- \pi^0 \nu_\tau)$.

$\Gamma(\pi^- 2\pi^0 \nu_\tau \text{ (ex. } K^0)) / \Gamma_{total}$ Γ_{20}/Γ
 VALUE (%) EVTS DOCUMENT ID TECN COMMENT

9.26 ± 0.10 OUR FIT				
9.239 ± 0.086 ± 0.090	31k	¹ SCHAEEL	05c	ALEP 1991–1995 LEP runs
9.21 ± 0.13 ± 0.11		² BUSKULIC	96	ALEP Repl. by SCHAEEL 05c

¹ See footnote to SCHAEEL 05c $\Gamma(\tau^- \rightarrow e^- \bar{\nu}_e \nu_\tau)/\Gamma_{total}$ measurement for correlations with other measurements.

² Not independent of BUSKULIC 96 $B(h^- 2\pi^0 \nu_\tau \text{ (ex. } K^0))$ and $B(K^- 2\pi^0 \nu_\tau \text{ (ex. } K^0))$ values.

$\Gamma(\pi^- 2\pi^0 \nu_\tau \text{ (ex. } K^0), \text{ scalar}) / \Gamma(\pi^- 2\pi^0 \nu_\tau \text{ (ex. } K^0))$ Γ_{21}/Γ_{20}
 VALUE CL% DOCUMENT ID TECN COMMENT

<0.094		¹ BROWDER	00	CLEO $4.7 \text{ fb}^{-1} E_{cm}^{ee} = 10.6$ GeV
--------	--	----------------------	----	---

¹ Model-independent limit from structure function analysis on contribution to $B(\tau^- \rightarrow \pi^- 2\pi^0 \nu_\tau \text{ (ex. } K^0))$ from scalars.

$\Gamma(\pi^- 2\pi^0 \nu_\tau \text{ (ex. } K^0), \text{ vector}) / \Gamma(\pi^- 2\pi^0 \nu_\tau \text{ (ex. } K^0))$ Γ_{22}/Γ_{20}
 VALUE CL% DOCUMENT ID TECN COMMENT

<0.073		¹ BROWDER	00	CLEO $4.7 \text{ fb}^{-1} E_{cm}^{ee} = 10.6$ GeV
--------	--	----------------------	----	---

¹ Model-independent limit from structure function analysis on contribution to $B(\tau^- \rightarrow \pi^- 2\pi^0 \nu_\tau \text{ (ex. } K^0))$ from vectors.

$\Gamma(K^- 2\pi^0 \nu_\tau \text{ (ex. } K^0)) / \Gamma_{total}$ Γ_{23}/Γ
 VALUE (units 10⁻⁴) EVTS DOCUMENT ID TECN COMMENT

6.5 ± 2.2 OUR FIT				
5.8 ± 2.4 OUR AVERAGE				
5.6 ± 2.0 ± 1.5	131	BARATE	99k	ALEP 1991–1995 LEP runs
9 ± 10 ± 3	3	¹ BATTLE	94	CLEO $E_{cm}^{ee} \approx 10.6$ GeV

• • • We do not use the following data for averages, fits, limits, etc. • • •

¹ BATTLE 94 quote $(14 \pm 10 \pm 3) \times 10^{-4}$ or $< 30 \times 10^{-4}$ at 90% CL. We subtract $(5 \pm 2) \times 10^{-4}$ to account for $\tau^- \rightarrow K^- (K^0 \rightarrow \pi^0 \pi^0) \nu_\tau$ background.

$\Gamma(h^- \geq 3\pi^0 \nu_\tau) / \Gamma_{total}$ Γ_{24}/Γ
 $\Gamma_{24}/\Gamma = (\Gamma_{27} + \Gamma_{28} + \Gamma_{30} + 0.15344\Gamma_{41} + 0.15344\Gamma_{43} + 0.0942\Gamma_{48} + 0.0942\Gamma_{52} + 0.3257\Gamma_{150} + 0.3257\Gamma_{152} + 0.3257\Gamma_{154} + 0.0501\Gamma_{156}) / \Gamma$

VALUE (%)	EVTS	DOCUMENT ID	TECN	COMMENT
1.34 ± 0.07 OUR FIT				
1.53 ± 0.40 ± 0.46	186	DECAMP	92c	ALEP Repl. by SCHAEEL 05c
3.2 ± 1.0 ± 1.0		BEHREND	90	CELL $E_{cm}^{ee} = 35$ GeV

• • • We do not use the following data for averages, fits, limits, etc. • • •

$\Gamma(h^- \geq 3\pi^0 \nu_\tau \text{ (ex. } K^0)) / \Gamma_{total}$ Γ_{25}/Γ
 VALUE (%) EVTS DOCUMENT ID TECN COMMENT

1.25 ± 0.07 OUR FIT				
1.403 ± 0.214 ± 0.224	1.1k	¹ ABDALLAH	06A	DLPH 1992–1995 LEP runs

¹ See footnote to ABDALLAH 06A $\Gamma(\tau^- \rightarrow h^- \nu_\tau)/\Gamma_{total}$ measurement for correlations with other measurements.

$\Gamma(h^- 3\pi^0 \nu_\tau) / \Gamma_{total}$ Γ_{26}/Γ
 $\Gamma_{26}/\Gamma = (\Gamma_{27} + \Gamma_{28} + 0.15344\Gamma_{41} + 0.15344\Gamma_{43} + 0.3257\Gamma_{152}) / \Gamma$

VALUE (%)	EVTS	DOCUMENT ID	TECN	COMMENT
1.18 ± 0.07 OUR FIT				
1.21 ± 0.17 OUR AVERAGE				Error includes scale factor of 1.2.
1.70 ± 0.24 ± 0.38	293	ACCIARRI	95	L3 1992 LEP run

• • • We use the following data for averages but not for fits. • • •

1.15 ± 0.08 ± 0.13 ¹ PROCARIO 93 CLEO $E_{cm}^{ee} \approx 10.6$ GeV

• • • We do not use the following data for averages, fits, limits, etc. • • •

1.24 ± 0.09 ± 0.11 2.3k ² BUSKULIC 96 ALEP Repl. by SCHAEEL 05c

0.0 $\frac{+1.4}{-0.1}$ $\frac{+1.1}{-0.1}$ ³ GAN 87 MRK2 $E_{cm}^{ee} = 29$ GeV

¹ PROCARIO 93 entry is obtained from $B(h^- 3\pi^0 \nu_\tau)/B(h^- \pi^0 \nu_\tau)$ using ARTUSO 94 result for $B(h^- \pi^0 \nu_\tau)$.

² BUSKULIC 96 quote $B(h^- 3\pi^0 \nu_\tau \text{ (ex. } K^0)) = 1.17 \pm 0.09 \pm 0.11$. We add 0.07 to remove their correction for K^0 backgrounds.

³ Highly correlated with GAN 87 $\Gamma(\eta \pi^0 \pi^0 \nu_\tau) / \Gamma_{total}$ value. Authors quote $B(\pi^\pm 3\pi^0 \nu_\tau) + 0.67B(\pi^\pm \eta \pi^0 \nu_\tau) = 0.047 \pm 0.010 \pm 0.011$.

$\Gamma(h^- 3\pi^0 \nu_\tau) / \Gamma(h^- \pi^0 \nu_\tau)$ Γ_{26}/Γ_{13}
 $\Gamma_{26}/\Gamma_{13} = (\Gamma_{27} + \Gamma_{28} + 0.15344\Gamma_{41} + 0.15344\Gamma_{43} + 0.3257\Gamma_{152}) / (\Gamma_{14} + \Gamma_{16})$

VALUE (units 10 ⁻²)	DOCUMENT ID	TECN	COMMENT
4.54 ± 0.28 OUR FIT			
4.4 ± 0.3 ± 0.5	¹ PROCARIO	93	CLEO $E_{cm}^{ee} \approx 10.6$ GeV

¹ PROCARIO 93 quote $0.041 \pm 0.003 \pm 0.005$ after correction for 2 kaon backgrounds assuming $B(K^{*-} \nu_\tau) = 1.42 \pm 0.18\%$ and $B(h^- K^0 \pi^0 \nu_\tau) = 0.48 \pm 0.48\%$. We add 0.003 ± 0.003 and multiply the sum by 0.990 ± 0.010 to remove these corrections.

$\Gamma(\pi^- 3\pi^0 \nu_\tau \text{ (ex. } K^0)) / \Gamma_{total}$ Γ_{27}/Γ
 VALUE (%) EVTS DOCUMENT ID TECN COMMENT

1.04 ± 0.07 OUR FIT				
0.977 ± 0.069 ± 0.058	6.1k	¹ SCHAEEL	05c	ALEP 1991–1995 LEP runs

¹ See footnote to SCHAEEL 05c $\Gamma(\tau^- \rightarrow e^- \bar{\nu}_e \nu_\tau)/\Gamma_{total}$ measurement for correlations with other measurements.

$\Gamma(K^- 3\pi^0 \nu_\tau \text{ (ex. } K^0, \eta)) / \Gamma_{total}$ Γ_{28}/Γ
 VALUE (units 10⁻⁴) EVTS DOCUMENT ID TECN COMMENT

4.8 ± 2.1 OUR FIT				
3.7 ± 2.1 ± 1.1	22	BARATE	99k	ALEP 1991–1995 LEP runs
5 ± 13		¹ BUSKULIC	94E	ALEP Repl. by BARATE 99k

• • • We do not use the following data for averages, fits, limits, etc. • • •

¹ BUSKULIC 94E quote $B(K^- \geq 0\pi^0) \geq 0K^0 \nu_\tau - [B(K^- \nu_\tau) + B(K^- \pi^0 \nu_\tau) + B(K^- K^0 \nu_\tau) + B(K^- \pi^0 \pi^0 \nu_\tau) + B(K^- \pi^0 K^0 \nu_\tau)] = (5 \pm 13) \times 10^{-4}$ accounting for common systematic errors in BUSKULIC 94E and BUSKULIC 94F measurements of these modes. We assume $B(K^- \geq 2K^0 \nu_\tau)$ and $B(K^- \geq 4\pi^0 \nu_\tau)$ are negligible.

$\Gamma(h^- 4\pi^0 \nu_\tau \text{ (ex. } K^0)) / \Gamma_{total}$ Γ_{29}/Γ
 $\Gamma_{29}/\Gamma = (\Gamma_{30} + 0.3257\Gamma_{150} + 0.3257\Gamma_{154}) / \Gamma$

VALUE (%)	EVTS	DOCUMENT ID	TECN	COMMENT
0.16 ± 0.04 OUR FIT				
0.16 ± 0.05 ± 0.05		¹ PROCARIO	93	CLEO $E_{cm}^{ee} \approx 10.6$ GeV
0.16 ± 0.04 ± 0.09	232	² BUSKULIC	96	ALEP Repl. by SCHAEEL 05c

• • • We do not use the following data for averages, fits, limits, etc. • • •

¹ PROCARIO 93 quotes $B(h^- 4\pi^0 \nu_\tau)/B(h^- \pi^0 \nu_\tau) = 0.006 \pm 0.002 \pm 0.002$. We multiply by the ARTUSO 94 result for $B(h^- \pi^0 \nu_\tau)$ to obtain $B(h^- 4\pi^0 \nu_\tau)$. PROCARIO 93 assume $B(h^- \geq 5\pi^0 \nu_\tau)$ is small and do not correct for it.

² BUSKULIC 96 quote result for $\tau^- \rightarrow h^- \geq 4\pi^0 \nu_\tau$. We assume $B(h^- \geq 5\pi^0 \nu_\tau)$ is negligible.

$\Gamma(h^- 4\pi^0 \nu_\tau \text{ (ex. } K^0, \eta)) / \Gamma_{total}$ Γ_{30}/Γ
 VALUE (%) EVTS DOCUMENT ID TECN COMMENT

0.11 ± 0.04 OUR FIT				
0.112 ± 0.037 ± 0.035	957	¹ SCHAEEL	05c	ALEP 1991–1995 LEP runs

¹ See footnote to SCHAEEL 05c $\Gamma(\tau^- \rightarrow e^- \bar{\nu}_e \nu_\tau)/\Gamma_{total}$ measurement for correlations with other measurements.

$\Gamma(a_1(1260) \nu_\tau \rightarrow \pi^- \gamma \nu_\tau) / \Gamma_{total}$ $\Gamma_{31}/\Gamma = (0.0021\Gamma_{20} + 0.0021\Gamma_{70}) / \Gamma$
 The uncertainty on $\Gamma(\tau^- \rightarrow a_1(1260) \nu_\tau \rightarrow \pi^- \gamma \nu_\tau) / \Gamma_{total}$ is the sum in quadrature of the uncertainty on the fit result for $\Gamma(\tau^- \rightarrow a_1(1260) \nu_\tau \rightarrow \pi^- \gamma \nu_\tau) / \Gamma_{total}$ and of the uncertainty on $\Gamma(a_1(1260) \rightarrow \pi^- \gamma) / \Gamma_{total} = ((2.1 \pm 0.8) \times 10^{-3})$ as reported in SCHAEEL 05c, which is the coefficient of the relationship that defines $\Gamma(\tau^- \rightarrow a_1(1260) \nu_\tau \rightarrow \pi^- \gamma \nu_\tau) / \Gamma_{total}$ in terms of $\Gamma(\tau^- \rightarrow \pi^- 2\pi^0 \nu_\tau \text{ (ex. } K^0)) / \Gamma_{total}$ and $\Gamma(\tau^- \rightarrow \pi^- \pi^+ \pi^- \nu_\tau \text{ (ex. } K^0, \omega)) / \Gamma_{total}$.

VALUE (units 10 ⁻⁴)	DOCUMENT ID	TECN	COMMENT
3.8 ± 1.5 OUR FIT			
1.552 ± 0.029 OUR FIT			
1.53 ± 0.04 OUR AVERAGE			
1.528 ± 0.039 ± 0.040	¹ ABBIENDI	01j	OPAL 1990–1995 LEP runs

Lepton Particle Listings

τ

1.54 ± 0.24	ABREU	94k	DLPH	LEP 1992 Z data
1.70 ± 0.12 ± 0.19	202	2	BATTLE	94 CLEO $E_{cm}^{ee} \approx 10.6$ GeV
••• We use the following data for averages but not for fits. •••				
1.520 ± 0.040 ± 0.041	4006	3	BARATE	99k ALEP 1991–1995 LEP runs
••• We do not use the following data for averages, fits, limits, etc. •••				
1.70 ± 0.05 ± 0.06	1610	4	BUSKULIC	96 ALEP Repl. by BARATE 99k
1.6 ± 0.4 ± 0.2	35		AIHARA	87B TPC $E_{cm}^{ee} = 29$ GeV
1.71 ± 0.29	53		MILLS	84 DLCO $E_{cm}^{ee} = 29$ GeV

- ¹ The correlation coefficient between this measurement and the ABBIENDI 01J $B(\tau^- \rightarrow K^- \nu_\tau)$ is 0.60.
- ² BATTLE 94 quote $1.60 \pm 0.12 \pm 0.19$. We add 0.10 ± 0.02 to correct for their rejection of $K_S^0 \rightarrow \pi^+ \pi^-$ decays.
- ³ Not independent of BARATE 99k $B(K^- \nu_\tau)$, $B(K^- \pi^0 \nu_\tau)$, $B(K^- 2\pi^0 \nu_\tau)$ (ex. K^0), $B(K^- 3\pi^0 \nu_\tau)$ (ex. K^0), $B(K^- K^0 \nu_\tau)$, and $B(K^- K^0 \pi^0 \nu_\tau)$ values.
- ⁴ Not independent of BUSKULIC 96 $B(K^- \nu_\tau)$, $B(K^- \pi^0 \nu_\tau)$, $B(K^- 2\pi^0 \nu_\tau)$, $B(K^- K^0 \nu_\tau)$, and $B(K^- K^0 \pi^0 \nu_\tau)$ values.

$$\Gamma(K^- \geq 1(\pi^0 \text{ or } K^0 \text{ or } \gamma) \nu_\tau) / \Gamma_{\text{total}} \quad \Gamma_{33} / \Gamma$$

$$\Gamma_{33} / \Gamma = (\Gamma_{16} + \Gamma_{23} + \Gamma_{28} + \Gamma_{38} + \Gamma_{43} + 0.7196\Gamma_{152} + 0.7196\Gamma_{154} + 0.1049\Gamma_{170}) / \Gamma$$

VALUE (%)	EVTS	DOCUMENT ID	TECN	COMMENT
0.859 ± 0.028 OUR FIT				
0.86 ± 0.05 OUR AVERAGE				
••• We use the following data for averages but not for fits. •••				
0.869 ± 0.031 ± 0.034		1	ABBIENDI	01J OPAL 1990–1995 LEP runs
0.69 ± 0.25		2	ABREU	94k DLPH LEP 1992 Z data
••• We do not use the following data for averages, fits, limits, etc. •••				
1.2 ± 0.5	+0.2 -0.4	9	AIHARA	87B TPC $E_{cm}^{ee} = 29$ GeV

- ¹ Not independent of ABBIENDI 01J $B(\tau^- \rightarrow K^- \nu_\tau)$ and $B(\tau^- \rightarrow K^- \geq 0\pi^0 \geq 0K^0 \geq 0\gamma \nu_\tau)$ values.
- ² Not independent of ABREU 94k $B(K^- \nu_\tau)$ and $B(K^- \geq 0 \text{ neutrals } \nu_\tau)$ measurements.

$$\Gamma(K_S^0(\text{particles})^- \nu_\tau) / \Gamma_{\text{total}} \quad \Gamma_{34} / \Gamma$$

$$\Gamma_{34} / \Gamma = (\frac{1}{2}\Gamma_{36} + \frac{1}{2}\Gamma_{38} + \frac{1}{2}\Gamma_{41} + \frac{1}{2}\Gamma_{43} + \frac{1}{2}\Gamma_{45} + \Gamma_{48} + \Gamma_{49} + \Gamma_{52} + \Gamma_{56} + 0.3598\Gamma_{156} + 0.339\Gamma_{170}) / \Gamma$$

VALUE (%)	EVTS	DOCUMENT ID	TECN	COMMENT
0.943 ± 0.028 OUR FIT				
0.918 ± 0.015 OUR AVERAGE				
0.970 ± 0.058 ± 0.062	929		BARATE	98E ALEP 1991–1995 LEP runs
0.97 ± 0.09 ± 0.06	141		AKERS	94G OPAL $E_{cm}^{ee} = 88\text{--}94$ GeV
••• We use the following data for averages but not for fits. •••				
0.915 ± 0.001 ± 0.015	398k	1	RYU	14 BELL $669 \text{ fb}^{-1} E_{cm}^{ee} = 10.6$ GeV

- ¹ Not independent of RYU 14 measurements of $B(\tau^- \rightarrow \pi^- \bar{K}^0 \nu_\tau)$, $B(\tau^- \rightarrow K^- K^0 \nu_\tau)$, $B(\tau^- \rightarrow \pi^- \bar{K}^0 \pi^0 \nu_\tau)$, $B(\tau^- \rightarrow K^- K^0 \pi^0 \nu_\tau)$, $B(\tau^- \rightarrow \pi^- K_S^0 K_S^0 \nu_\tau)$, and $B(\tau^- \rightarrow \pi^- K_S^0 K_L^0 \nu_\tau)$.

$$\Gamma(h^- \bar{K}^0 \nu_\tau) / \Gamma_{\text{total}} \quad \Gamma_{35} / \Gamma = (\Gamma_{36} + \Gamma_{38}) / \Gamma$$

VALUE (%)	EVTS	DOCUMENT ID	TECN	COMMENT
0.987 ± 0.014 OUR FIT				
0.90 ± 0.07 OUR AVERAGE				
0.855 ± 0.036 ± 0.073	1242		COAN	96 CLEO $E_{cm}^{ee} \approx 10.6$ GeV
••• We use the following data for averages but not for fits. •••				
1.01 ± 0.11 ± 0.07	555	1	BARATE	98E ALEP 1991–1995 LEP runs

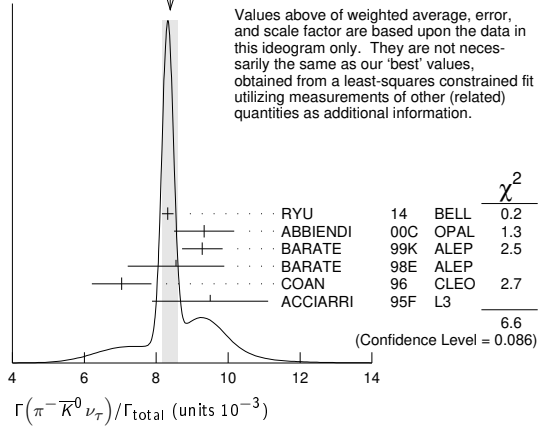
- ¹ Not independent of BARATE 98E $B(\tau^- \rightarrow \pi^- \bar{K}^0 \nu_\tau)$ and $B(\tau^- \rightarrow K^- K^0 \nu_\tau)$ values.

$$\Gamma(\pi^- \bar{K}^0 \nu_\tau) / \Gamma_{\text{total}} \quad \Gamma_{36} / \Gamma$$

VALUE (units 10^{-3})	EVTS	DOCUMENT ID	TECN	COMMENT
8.38 ± 0.14 OUR FIT				
8.39 ± 0.22 OUR AVERAGE				
8.32 ± 0.02 ± 0.16	158k	1	RYU	14 BELL $669 \text{ fb}^{-1} E_{cm}^{ee} = 10.6$ GeV
9.33 ± 0.68 ± 0.49	377		ABBIENDI	00C OPAL 1991–1995 LEP runs
9.28 ± 0.45 ± 0.34	937	2	BARATE	99k ALEP 1991–1995 LEP runs
9.5 ± 1.5 ± 0.6		3	ACCIARRI	95F L3 1991–1993 LEP runs
••• We use the following data for averages but not for fits. •••				
8.55 ± 1.17 ± 0.66	509	4	BARATE	98E ALEP 1991–1995 LEP runs
7.04 ± 0.41 ± 0.72		5	COAN	96 CLEO $E_{cm}^{ee} \approx 10.6$ GeV
••• We do not use the following data for averages, fits, limits, etc. •••				
8.08 ± 0.04 ± 0.26	53k		EPIFANOV	07 BELL Repl. by RYU 14
7.9 ± 1.0 ± 0.9	98	6	BUSKULIC	96 ALEP Repl. by BARATE 99k

- ¹ RYU 14 reconstruct K^0 's using $K_S^0 \rightarrow \pi^+ \pi^-$ decays.
- ² BARATE 99k measure K^0 's by detecting K_L^0 's in their hadron calorimeter.
- ³ ACCIARRI 95F do not identify π^- / K^- and assume $B(K^- K^0 \nu_\tau) = (0.29 \pm 0.12)\%$.
- ⁴ BARATE 98E reconstruct K^0 's using $K_S^0 \rightarrow \pi^+ \pi^-$ decays. Not independent of BARATE 98E $B(K^0 \text{ particles}^- \nu_\tau)$ value.
- ⁵ Not independent of COAN 96 $B(h^- K^0 \nu_\tau)$ and $B(K^- K^0 \nu_\tau)$ measurements.
- ⁶ BUSKULIC 96 measure K^0 's by detecting K_L^0 's in their hadron calorimeter.

WEIGHTED AVERAGE
8.39±0.22 (Error scaled by 1.5)



Values above of weighted average, error, and scale factor are based upon the data in this ideogram only. They are not necessarily the same as our 'best' values, obtained from a least-squares constrained fit utilizing measurements of other (related) quantities as additional information.

$$\Gamma(\pi^- \bar{K}^0 (\text{non-} K^*(892)^- \nu_\tau) / \Gamma_{\text{total}} \quad \Gamma_{37} / \Gamma$$

VALUE (units 10^{-4})	CL%	DOCUMENT ID	TECN	COMMENT
5.4 ± 2.1		1	EPIFANOV	07 BELL $351 \text{ fb}^{-1} E_{cm}^{ee} = 10.6$ GeV
••• We do not use the following data for averages, fits, limits, etc. •••				
<17	95		ACCIARRI	95F L3 1991–1993 LEP runs

- ¹ EPIFANOV 07 quote $B(\tau^- \rightarrow K^*(892)^- \nu_\tau) B(K^*(892)^- \rightarrow K_S^0 \pi^-) / B(\tau^- \rightarrow K_S^0 \pi^- \nu_\tau) = 0.933 \pm 0.027$. We multiply their $B(\tau^- \rightarrow \bar{K}^0 \pi^- \nu_\tau)$ by $[1 - (0.933 \pm 0.027)]$ to obtain this result.

$$\Gamma(K^- K^0 \nu_\tau) / \Gamma_{\text{total}} \quad \Gamma_{38} / \Gamma$$

VALUE (units 10^{-4})	EVTS	DOCUMENT ID	TECN	COMMENT
14.83 ± 0.34 OUR FIT				
14.83 ± 0.35 OUR AVERAGE				
14.78 ± 0.22 ± 0.40	29k	1	LEES	18B BABR $468 \text{ fb}^{-1} E_{cm}^{ee} = 10.6$ GeV
14.80 ± 0.14 ± 0.54	33k	2	RYU	14 BELL $669 \text{ fb}^{-1} E_{cm}^{ee} = 10.6$ GeV
16.2 ± 2.1 ± 1.1	150	3	BARATE	99k ALEP 1991–1995 LEP runs
15.8 ± 4.2 ± 1.7	46	4	BARATE	98E ALEP 1991–1995 LEP runs
15.1 ± 2.1 ± 2.2	111		COAN	96 CLEO $E_{cm}^{ee} \approx 10.6$ GeV
••• We do not use the following data for averages, fits, limits, etc. •••				
26 ± 9 ± 2	13	5	BUSKULIC	96 ALEP Repl. by BARATE 99k

- ¹ LEES 18B reconstructs K_S^0 's using $K_S^0 \rightarrow \pi^+ \pi^-$ decays.
- ² RYU 14 reconstruct K^0 's using $K_S^0 \rightarrow \pi^+ \pi^-$ decays.
- ³ BARATE 99k measure K^0 's by detecting K_L^0 's in their hadron calorimeter.
- ⁴ BARATE 98E reconstruct K^0 's using $K_S^0 \rightarrow \pi^+ \pi^-$ decays.
- ⁵ BUSKULIC 96 measure K^0 's by detecting K_L^0 's in their hadron calorimeter.

$$\Gamma(K^- K^0 \geq 0\pi^0 \nu_\tau) / \Gamma_{\text{total}} \quad \Gamma_{39} / \Gamma = (\Gamma_{38} + \Gamma_{43}) / \Gamma$$

VALUE (%)	EVTS	DOCUMENT ID	TECN	COMMENT
0.299 ± 0.007 OUR FIT				
0.330 ± 0.055 ± 0.039	124		ABBIENDI	00C OPAL 1991–1995 LEP runs

$$\Gamma(h^- \bar{K}^0 \pi^0 \nu_\tau) / \Gamma_{\text{total}} \quad \Gamma_{40} / \Gamma = (\Gamma_{41} + \Gamma_{43}) / \Gamma$$

VALUE (%)	EVTS	DOCUMENT ID	TECN	COMMENT
0.532 ± 0.013 OUR FIT				
0.50 ± 0.06 OUR AVERAGE				
0.562 ± 0.050 ± 0.048	264		COAN	96 CLEO $E_{cm}^{ee} \approx 10.6$ GeV
••• We use the following data for averages but not for fits. •••				
0.446 ± 0.052 ± 0.046	157	1	BARATE	98E ALEP 1991–1995 LEP runs

- ¹ Not independent of BARATE 98E $B(\tau^- \rightarrow \pi^- \bar{K}^0 \pi^0 \nu_\tau)$ and $B(\tau^- \rightarrow K^- K^0 \pi^0 \nu_\tau)$ values.

$$\Gamma(\pi^- \bar{K}^0 \pi^0 \nu_\tau) / \Gamma_{\text{total}} \quad \Gamma_{41} / \Gamma$$

VALUE (%)	EVTS	DOCUMENT ID	TECN	COMMENT
0.382 ± 0.013 OUR FIT				
0.383 ± 0.014 OUR AVERAGE				
0.386 ± 0.004 ± 0.014	27k	1	RYU	14 BELL $669 \text{ fb}^{-1} E_{cm}^{ee} = 10.6$ GeV
0.347 ± 0.053 ± 0.037	299	2	BARATE	99k ALEP 1991–1995 LEP runs
0.294 ± 0.073 ± 0.037	142	3	BARATE	98E ALEP 1991–1995 LEP runs
0.41 ± 0.12 ± 0.03		4	ACCIARRI	95F L3 1991–1993 LEP runs
••• We use the following data for averages but not for fits. •••				
0.417 ± 0.058 ± 0.044		5	COAN	96 CLEO $E_{cm}^{ee} \approx 10.6$ GeV
••• We do not use the following data for averages, fits, limits, etc. •••				
0.32 ± 0.11 ± 0.05	23	6	BUSKULIC	96 ALEP Repl. by BARATE 99k

- ¹ RYU 14 reconstruct K^0 's using $K_S^0 \rightarrow \pi^+ \pi^-$ decays.
- ² BARATE 99k measure K^0 's by detecting K_L^0 's in their hadron calorimeter.
- ³ BARATE 98E reconstruct K^0 's using $K_S^0 \rightarrow \pi^+ \pi^-$ decays.
- ⁴ ACCIARRI 95F do not identify π^- / K^- and assume $B(K^- K^0 \pi^0 \nu_\tau) = (0.05 \pm 0.05)\%$.
- ⁵ Not independent of COAN 96 $B(h^- K^0 \pi^0 \nu_\tau)$ and $B(K^- K^0 \pi^0 \nu_\tau)$ measurements.
- ⁶ BUSKULIC 96 measure K^0 's by detecting K_L^0 's in their hadron calorimeter.

$\Gamma(\overline{K}^0 \rho^- \nu_\tau)/\Gamma_{\text{total}}$	Γ_{42}/Γ
VALUE (%)	
0.22 ± 0.05 OUR AVERAGE	
0.250 ± 0.057 ± 0.044	1 BARATE 99k ALEP 1991–1995 LEP runs
0.188 ± 0.054 ± 0.038	2 BARATE 98E ALEP 1991–1995 LEP runs

1 BARATE 99k measure K^0 's by detecting K_L^0 's in hadron calorimeter. They determine the $\overline{K}^0 \rho^-$ fraction in $\tau^- \rightarrow \pi^- \overline{K}^0 \pi^0 \nu_\tau$ decays to be $(0.72 \pm 0.12 \pm 0.10)$ and multiply their $B(\pi^- \overline{K}^0 \pi^0 \nu_\tau)$ measurement by this fraction to obtain the quoted result.
 2 BARATE 98E reconstruct K^0 's using $K_S^0 \rightarrow \pi^+ \pi^-$ decays. They determine the $\overline{K}^0 \rho^-$ fraction in $\tau^- \rightarrow \pi^- \overline{K}^0 \pi^0 \nu_\tau$ decays to be $(0.64 \pm 0.09 \pm 0.10)$ and multiply their $B(\pi^- \overline{K}^0 \pi^0 \nu_\tau)$ measurement by this fraction to obtain the quoted result.

$\Gamma(K^- K^0 \pi^0 \nu_\tau)/\Gamma_{\text{total}}$	Γ_{43}/Γ
VALUE (units 10 ⁻⁴)	
15.0 ± 0.7 OUR FIT	
14.9 ± 0.7 OUR AVERAGE	
14.96 ± 0.20 ± 0.74	8.3k 1 RYU 14 BELL 669 fb ⁻¹ $E_{\text{cm}}^{\text{ee}} = 10.6$ GeV
14.3 ± 2.5 ± 1.5	78 2 BARATE 99k ALEP 1991–1995 LEP runs
15.2 ± 7.6 ± 2.1	15 3 BARATE 98E ALEP 1991–1995 LEP runs
14.5 ± 3.6 ± 2.0	32 COAN 96 CLEO $E_{\text{cm}}^{\text{ee}} \approx 10.6$ GeV

• • • We do not use the following data for averages, fits, limits, etc. • • •
 10 ± 5 ± 3 5 4 BUSKULIC 96 ALEP Repl. by BARATE 99k
 1 RYU 14 reconstruct K^0 's using $K_S^0 \rightarrow \pi^+ \pi^-$ decays.
 2 BARATE 99k measure K^0 's by detecting K_L^0 's in their hadron calorimeter.
 3 BARATE 98E reconstruct K^0 's using $K_S^0 \rightarrow \pi^+ \pi^-$ decays.
 4 BUSKULIC 96 measure K^0 's by detecting K_L^0 's in their hadron calorimeter.

$\Gamma(\pi^- \overline{K}^0 \geq 1\pi^0 \nu_\tau)/\Gamma_{\text{total}}$	$\Gamma_{44}/\Gamma = (\Gamma_{41} + \Gamma_{45})/\Gamma$
VALUE (%)	
0.408 ± 0.025 OUR FIT	
0.324 ± 0.074 ± 0.066	148
	ABBIENDI 00c OPAL 1991–1995 LEP runs

$\Gamma(\pi^- \overline{K}^0 \pi^0 \pi^0 \nu_\tau \text{ (ex. } K^0))/\Gamma_{\text{total}}$	Γ_{45}/Γ
VALUE (units 10 ⁻³)	
0.26 ± 0.23 OUR FIT	
0.26 ± 0.24	
	1 BARATE 99R ALEP 1991–1995 LEP runs
• • • We do not use the following data for averages, fits, limits, etc. • • •	
<0.66	95 17 2 BARATE 99k ALEP 1991–1995 LEP runs
0.58 ± 0.33 ± 0.14	5 3 BARATE 98E ALEP 1991–1995 LEP runs
1 BARATE 99R combine the BARATE 98E and BARATE 99K measurements to obtain this value. 2 BARATE 99k measure K^0 's by detecting K_L^0 's in their hadron calorimeter. 3 BARATE 98E reconstruct K^0 's using $K_S^0 \rightarrow \pi^+ \pi^-$ decays.	

$\Gamma(K^- K^0 \pi^0 \pi^0 \nu_\tau)/\Gamma_{\text{total}}$	Γ_{46}/Γ
VALUE	
<0.16 × 10⁻³	95
	1 BARATE 99R ALEP 1991–1995 LEP runs
• • • We do not use the following data for averages, fits, limits, etc. • • •	
<0.18 × 10 ⁻³	95 2 BARATE 99k ALEP 1991–1995 LEP runs
<0.39 × 10 ⁻³	95 3 BARATE 98E ALEP 1991–1995 LEP runs
1 BARATE 99R combine the BARATE 98E and BARATE 99K bounds to obtain this value. 2 BARATE 99k measure K^0 's by detecting K_L^0 's in hadron calorimeter. 3 BARATE 98E reconstruct K^0 's by using $K_S^0 \rightarrow \pi^+ \pi^-$ decays.	

$\Gamma(\pi^- K^0 \overline{K}^0 \nu_\tau)/\Gamma_{\text{total}}$	$\Gamma_{47}/\Gamma = (\Gamma_{48} + \Gamma_{49} + \Gamma_{50})/\Gamma$
VALUE (%)	
0.155 ± 0.024 OUR FIT	
• • • We use the following data for averages but not for fits. • • •	
0.153 ± 0.030 ± 0.016	74 1 BARATE 98E ALEP 1991–1995 LEP runs
• • • We do not use the following data for averages, fits, limits, etc. • • •	
0.31 ± 0.12 ± 0.04	2 ACCIARRI 95F L3 1991–1993 LEP runs
1 BARATE 98E obtain this value by adding twice their $B(\pi^- K_S^0 K_S^0 \pi^0 \nu_\tau)$ value to their $B(\pi^- K_S^0 K_L^0 \nu_\tau)$ value. 2 ACCIARRI 95F assume $B(\pi^- K_S^0 K_S^0 \nu) = B(\pi^- K_S^0 K_L^0 \nu) = 1/2 B(\pi^- K_S^0 K_L^0 \nu)$.	

$\Gamma(\pi^- K_S^0 K_S^0 \nu_\tau)/\Gamma_{\text{total}}$	Γ_{48}/Γ
VALUE (units 10 ⁻⁴)	
2.35 ± 0.06 OUR FIT	
2.32 ± 0.06 OUR AVERAGE	
2.33 ± 0.03 ± 0.09	6.7k RYU 14 BELL 669 fb ⁻¹ $E_{\text{cm}}^{\text{ee}} = 10.6$ GeV
2.31 ± 0.04 ± 0.08	5.0k 1 LEES 12Y BABR 468 fb ⁻¹ $E_{\text{cm}}^{\text{ee}} = 10.6$ GeV
2.6 ± 1.0 ± 0.5	6 BARATE 98E ALEP 1991–1995 LEP runs
2.3 ± 0.5 ± 0.3	42 COAN 96 CLEO $E_{\text{cm}}^{\text{ee}} \approx 10.6$ GeV

1 The correlation coefficient between this measurement and the LEES 12Y $\Gamma(\tau^- \rightarrow \pi^- K_S^0 K_S^0 \pi^0 \nu_\tau)/\Gamma_{\text{total}}$ one is 0.0828.

$\Gamma(\pi^- K_S^0 K_L^0 \nu_\tau)/\Gamma_{\text{total}}$	Γ_{49}/Γ
VALUE (units 10 ⁻⁴)	
10.8 ± 2.4 OUR FIT	
10.1 ± 2.3 ± 1.3	68
	BARATE 98E ALEP 1991–1995 LEP runs

$\Gamma(\pi^- K_L^0 K_L^0 \nu_\tau)/\Gamma_{\text{total}}$	$\Gamma_{50}/\Gamma = \Gamma_{48}/\Gamma$
VALUE (units 10 ⁻⁴)	
2.35 ± 0.06 OUR FIT	

$\Gamma(\pi^- K^0 \overline{K}^0 \pi^0 \nu_\tau)/\Gamma_{\text{total}}$	$\Gamma_{51}/\Gamma = (\Gamma_{52} + \Gamma_{56} + \Gamma_{57})/\Gamma$
VALUE (units 10 ⁻⁴)	
3.6 ± 1.2 OUR FIT	

• • • We use the following data for averages but not for fits. • • •
 3.1 ± 2.3 1 BARATE 99R ALEP 1991–1995 LEP runs
 1 BARATE 99R combine BARATE 98E $\Gamma(\pi^- K_S^0 K_S^0 \pi^0 \nu_\tau)/\Gamma_{\text{total}}$ and $\Gamma(\pi^- K_S^0 K_L^0 \pi^0 \nu_\tau)/\Gamma_{\text{total}}$ measurements to obtain this value.

$\Gamma(\pi^- K_S^0 K_S^0 \pi^0 \nu_\tau)/\Gamma_{\text{total}}$	Γ_{52}/Γ
VALUE (units 10 ⁻⁵)	
1.82 ± 0.21 OUR FIT	
1.80 ± 0.21 OUR AVERAGE	
2.00 ± 0.22 ± 0.20	303 RYU 14 BELL 669 fb ⁻¹ $E_{\text{cm}}^{\text{ee}} = 10.6$ GeV
1.60 ± 0.20 ± 0.22	409 1 LEES 12Y BABR 468 fb ⁻¹ $E_{\text{cm}}^{\text{ee}} = 10.6$ GeV

• • • We do not use the following data for averages, fits, limits, etc. • • •
 <20 95 BARATE 98E ALEP 1991–1995 LEP runs
 1 The correlation coefficient between this measurement and the LEES 12Y $\Gamma(\tau^- \rightarrow \pi^- K_S^0 K_S^0 \nu_\tau)/\Gamma_{\text{total}}$ one is 0.0828.

$\Gamma(K^* K^0 \pi^0 \nu_\tau \rightarrow \pi^- K_S^0 K_S^0 \pi^0 \nu_\tau)/\Gamma_{\text{total}}$	Γ_{53}/Γ
VALUE (units 10 ⁻⁶)	
10.8 ± 1.4 ± 1.5	
	RYU 14 BELL 669 fb ⁻¹ $E_{\text{cm}}^{\text{ee}} = 10.6$ GeV

$\Gamma(\tilde{\eta}_1(1285) \pi^- \nu_\tau \rightarrow \pi^- K_S^0 K_S^0 \pi^0 \nu_\tau)/\Gamma_{\text{total}}$	Γ_{54}/Γ
VALUE (units 10 ⁻⁶)	
6.8 ± 1.3 ± 0.7	
	RYU 14 BELL 669 fb ⁻¹ $E_{\text{cm}}^{\text{ee}} = 10.6$ GeV

$\Gamma(\tilde{\eta}_1(1420) \pi^- \nu_\tau \rightarrow \pi^- K_S^0 K_S^0 \pi^0 \nu_\tau)/\Gamma_{\text{total}}$	Γ_{55}/Γ
VALUE (units 10 ⁻⁶)	
2.4 ± 0.5 ± 0.6	
	RYU 14 BELL 669 fb ⁻¹ $E_{\text{cm}}^{\text{ee}} = 10.6$ GeV

$\Gamma(\pi^- K_S^0 K_L^0 \pi^0 \nu_\tau)/\Gamma_{\text{total}}$	Γ_{56}/Γ
VALUE (units 10 ⁻⁴)	
3.2 ± 1.2 OUR FIT	
3.1 ± 1.1 ± 0.5	11
	BARATE 98E ALEP 1991–1995 LEP runs

$\Gamma(\pi^- K_L^0 K_L^0 \pi^0 \nu_\tau)/\Gamma_{\text{total}}$	$\Gamma_{57}/\Gamma = \Gamma_{52}/\Gamma$
VALUE (units 10 ⁻⁵)	
1.82 ± 0.21 OUR FIT	

$\Gamma(K^- K_S^0 K_S^0 \nu_\tau)/\Gamma_{\text{total}}$	Γ_{58}/Γ
VALUE	
<6.3 × 10⁻⁷	90
	LEES 12Y BABR 468 fb ⁻¹ $E_{\text{cm}}^{\text{ee}} = 10.6$ GeV

$\Gamma(K^- K_S^0 K_S^0 \pi^0 \nu_\tau)/\Gamma_{\text{total}}$	Γ_{59}/Γ
VALUE	
<4.0 × 10⁻⁷	90
	LEES 12Y BABR 468 fb ⁻¹ $E_{\text{cm}}^{\text{ee}} = 10.6$ GeV

$\Gamma(K^0 h^+ h^- h^- \geq 0 \text{ neutrals } \nu_\tau)/\Gamma_{\text{total}}$	Γ_{60}/Γ
VALUE (%)	
<0.17	95
	TSCHIRHART 88 HRS $E_{\text{cm}}^{\text{ee}} = 29$ GeV
• • • We do not use the following data for averages, fits, limits, etc. • • •	
<0.27	90
	BELTRAMI 85 HRS $E_{\text{cm}}^{\text{ee}} = 29$ GeV

$\Gamma(K^0 h^+ h^- h^- \nu_\tau)/\Gamma_{\text{total}}$	Γ_{61}/Γ
VALUE (units 10 ⁻⁴)	
2.5 ± 2.0 OUR FIT	
2.3 ± 1.9 ± 0.7	6
	1 BARATE 98E ALEP 1991–1995 LEP runs

1 BARATE 98E reconstruct K^0 's using $K_S^0 \rightarrow \pi^+ \pi^-$ decays.

$\Gamma(h^- h^- h^+ \geq 0 \text{ neutrals } \geq 0 K^0 \nu_\tau)/\Gamma_{\text{total}}$	Γ_{62}/Γ
$\Gamma_{62}/\Gamma = (0.34598\Gamma_{36} + 0.34598\Gamma_{38} + 0.34598\Gamma_{41} + 0.34598\Gamma_{43} + 0.4247\Gamma_{48} + 0.6920\Gamma_{49} + 0.4247\Gamma_{52} + 0.6920\Gamma_{56} + 0.6534\Gamma_{61} + \Gamma_{70} + \Gamma_{78} + \Gamma_{85} + \Gamma_{86} + \Gamma_{97} + \Gamma_{103} + \Gamma_{106} + \Gamma_{107} + 0.2804\Gamma_{150} + 0.2804\Gamma_{152} + 0.2804\Gamma_{154} + 0.2628\Gamma_{156} + 0.7259\Gamma_{170} + 0.9078\Gamma_{178} + 0.9078\Gamma_{179} + 0.9078\Gamma_{180})/\Gamma$	

VALUE (%)	EVTS	DOCUMENT ID	TECN	COMMENT
15.20 ± 0.06 OUR FIT				
14.8 ± 0.4 OUR AVERAGE				
14.4 ± 0.6 ± 0.3		ADEVA	91F L3	$E_{\text{cm}}^{\text{ee}} = 88.3\text{--}94.3$ GeV
15.0 ± 0.4 ± 0.3		BEHREND	89B CELL	$E_{\text{cm}}^{\text{ee}} = 14\text{--}47$ GeV
15.1 ± 0.8 ± 0.6		AIHARA	87B TPC	$E_{\text{cm}}^{\text{ee}} = 29$ GeV

Lepton Particle Listings

T

••• We do not use the following data for averages, fits, limits, etc. •••

13.5 ± 0.3 ± 0.3	ABACHI	89B	HRS	$E_{cm}^{ee} = 29$ GeV
12.8 ± 1.0 ± 0.7	¹ BURCHAT	87	MRK2	$E_{cm}^{ee} = 29$ GeV
12.1 ± 0.5 ± 1.2	RUCKSTUHL	86	DLCO	$E_{cm}^{ee} = 29$ GeV
12.8 ± 0.5 ± 0.8	1420	SCHMIDKE	86	MRK2 $E_{cm}^{ee} = 29$ GeV
15.3 ± 1.1 $^{+1.3}_{-1.6}$	367	ALTHOFF	85	TASS $E_{cm}^{ee} = 34.5$ GeV
13.6 ± 0.5 ± 0.8	BARTEL	85F	JADE	$E_{cm}^{ee} = 34.6$ GeV
12.2 ± 1.3 ± 3.9	² BERGER	85	PLUT	$E_{cm}^{ee} = 34.6$ GeV
13.3 ± 0.3 ± 0.6	FERNANDEZ	85	MAC	$E_{cm}^{ee} = 29$ GeV
24 ± 6	35	BRANDELIK	80	TASS $E_{cm}^{ee} = 30$ GeV
32 ± 5	692	³ BACINO	78B	DLCO $E_{cm}^{ee} = 3.1-7.4$ GeV
35 ± 11	³ BRANDELIK	78	DASP	Assumes V-A decay
18 ± 6.5	33	³ JAROS	78	LGW $E_{cm}^{ee} > 6$ GeV

¹BURCHAT 87 value is not independent of SCHMIDKE 86 value.
²Not independent of BERGER 85 $(\mu^- \bar{\nu}_\mu \nu_\tau)/\Gamma_{total}$, $(e^- \bar{\nu}_e \nu_\tau)/\Gamma_{total}$, $\Gamma(h^- \geq 1 \text{ neutrals } \nu_\tau)/\Gamma_{total}$, and $\Gamma(h^- \geq 0 K^0_L \nu_\tau)/\Gamma_{total}$, and therefore not used in the fit.
³Low energy experiments are not in average or fit because the systematic errors in background subtraction are judged to be large.

$$\Gamma(h^- h^- h^+ \geq 0 \text{ neutrals } \nu_\tau \text{ (ex. } K^0_S \rightarrow \pi^+ \pi^- \text{)})/\Gamma_{total} \quad \Gamma_{63}/\Gamma$$

$$\Gamma_{63}/\Gamma = (\Gamma_{70} + \Gamma_{78} + \Gamma_{85} + \Gamma_{86} + \Gamma_{97} + \Gamma_{103} + \Gamma_{106} + \Gamma_{107} + 0.2804\Gamma_{150} + 0.2804\Gamma_{152} + 0.2804\Gamma_{154} + 0.491\Gamma_{170} + 0.9078\Gamma_{178} + 0.9078\Gamma_{179} + 0.9078\Gamma_{180})/\Gamma$$

VALUE (%)	EVTS	DOCUMENT ID	TECN	COMMENT
14.55 ± 0.06 OUR FIT				
14.61 ± 0.06 OUR AVERAGE				
14.556 ± 0.105 ± 0.076		¹ ACHARD 01D L3	1992-1995 LEP runs	
14.96 ± 0.09 ± 0.22	10.4k	AKERS 95Y OPAL	1991-1994 LEP runs	
••• We use the following data for averages but not for fits. •••				
14.652 ± 0.067 ± 0.086		SCHAELE 05C ALEP	1991-1995 LEP runs	
14.569 ± 0.093 ± 0.048	23k	² ABREU 01M DLPH	1992-1995 LEP runs	
14.22 ± 0.10 ± 0.37		³ BALEST 95C CLEO	$E_{cm}^{ee} \approx 10.6$ GeV	
••• We do not use the following data for averages, fits, limits, etc. •••				
15.26 ± 0.26 ± 0.22		ACTON 92H OPAL	Repl. by AKERS 95Y	
13.3 ± 0.3 ± 0.8		⁴ ALBRECHT 92D ARG	$E_{cm}^{ee} = 9.4-10.6$ GeV	
14.35 $^{+0.40}_{-0.45}$ ± 0.24		DECAMP 92C ALEP	1989-1990 LEP runs	

¹The correlation coefficients between this measurement and the ACHARD 01D measurements of $B(\tau \rightarrow \text{"1-prong"})$ and $B(\tau \rightarrow \text{"5-prong"})$ are -0.978 and -0.19 respectively.
²The correlation coefficients between this measurement and the ABREU 01M measurements of $B(\tau \rightarrow \text{1-prong})$ and $B(\tau \rightarrow \text{5-prong})$ are -0.98 and -0.08 respectively.
³Not independent of BALEST 95C $B(h^- h^- h^+ \nu_\tau)/B(h^- h^- h^+ \pi^0 \nu_\tau)$ values, and BORTOLETTO 93 $B(h^- h^- h^+ 2\pi^0 \nu_\tau)/B(h^- h^- h^+ \geq 0 \text{ neutrals } \nu_\tau)$ value.
⁴This ALBRECHT 92D value is not independent of their $\Gamma(\mu^- \bar{\nu}_\mu \nu_\tau)/\Gamma(e^- \bar{\nu}_e \nu_\tau)/\Gamma_{total}^2$ value.

$$\Gamma(h^- h^- h^+ \nu_\tau)/\Gamma_{total} \quad \Gamma_{64}/\Gamma$$

$$\Gamma_{64}/\Gamma = (0.34598\Gamma_{36} + 0.34598\Gamma_{38} + \Gamma_{70} + \Gamma_{97} + \Gamma_{106} + 0.491\Gamma_{170} + 0.0153\Gamma_{178} + 0.0153\Gamma_{179})/\Gamma$$

VALUE (%)	EVTS	DOCUMENT ID	TECN	COMMENT
9.80 ± 0.05 OUR FIT				
••• We use the following data for averages but not for fits. •••				
7.6 ± 0.1 ± 0.5	7.5k	¹ ALBRECHT 96E ARG	$E_{cm}^{ee} = 9.4-10.6$ GeV	
••• We do not use the following data for averages, fits, limits, etc. •••				
9.92 ± 0.10 ± 0.09		2 BUSKULIC 96 ALEP	Repl. by SCHAELE 05C	
9.49 ± 0.36 ± 0.63		DECAMP 92C ALEP	Repl. by SCHAELE 05C	
8.7 ± 0.7 ± 0.3	694	³ BEHREND 90 CELL	$E_{cm}^{ee} = 35$ GeV	
7.0 ± 0.3 ± 0.7	1566	⁴ BAND 87 MAC	$E_{cm}^{ee} = 29$ GeV	
6.7 ± 0.8 ± 0.9		⁵ BURCHAT 87 MRK2	$E_{cm}^{ee} = 29$ GeV	
6.4 ± 0.4 ± 0.9		⁶ RUCKSTUHL 86 DLCO	$E_{cm}^{ee} = 29$ GeV	
7.8 ± 0.5 ± 0.8	890	SCHMIDKE 86 MRK2	$E_{cm}^{ee} = 29$ GeV	
8.4 ± 0.4 ± 0.7	1255	⁶ FERNANDEZ 85 MAC	$E_{cm}^{ee} = 29$ GeV	
9.7 ± 2.0 ± 1.3		BEHREND 84 CELL	$E_{cm}^{ee} = 14,22$ GeV	

¹ALBRECHT 96E not independent of ALBRECHT 93C $\Gamma(h^- h^- h^+ \nu_\tau \text{ (ex. } K^0) \times \Gamma(\text{particle}^- \geq 0 \text{ neutrals } \geq 0 K^0_L \nu_\tau)/\Gamma_{total}^2$ value.
²BUSKULIC 96 quote $B(h^- h^- h^+ \nu_\tau \text{ (ex. } K^0)) = 9.50 \pm 0.10 \pm 0.11$. We add 0.42 to remove their K^0 correction and reduce the systematic error accordingly.
³BEHREND 90 subtract 0.3% to account for the $\tau^- \rightarrow K^*(892)^- \nu_\tau$ contribution to measured events.
⁴BAND 87 subtract for charged kaon modes; not independent of FERNANDEZ 85 value.
⁵BURCHAT 87 value is not independent of SCHMIDKE 86 value.
⁶Value obtained by multiplying paper's $R = B(h^- h^- h^+ \nu_\tau)/B(\text{3-prong})$ by $B(\text{3-prong}) = 0.143$ and subtracting 0.3% for $K^*(892)$ background.

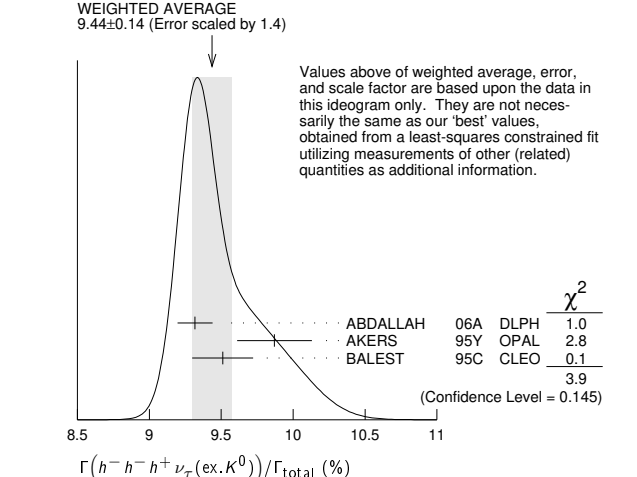
$$\Gamma(h^- h^- h^+ \nu_\tau \text{ (ex. } K^0))/\Gamma_{total} \quad \Gamma_{65}/\Gamma$$

$$\Gamma_{65}/\Gamma = (\Gamma_{70} + \Gamma_{97} + \Gamma_{106} + 0.491\Gamma_{170} + 0.0153\Gamma_{178} + 0.0153\Gamma_{179})/\Gamma$$

VALUE (%)	EVTS	DOCUMENT ID	TECN	COMMENT
9.46 ± 0.05 OUR FIT				
9.44 ± 0.14 OUR AVERAGE				Error includes scale factor of 1.4. See the ideogram below.
9.317 ± 0.090 ± 0.082	12.2k	¹ ABDALLAH 06A DLPH	1992-1995 LEP runs	
9.51 ± 0.07 ± 0.20	37.7k	BALEST 95C CLEO	$E_{cm}^{ee} \approx 10.6$ GeV	

••• We use the following data for averages but not for fits. •••

9.87 ± 0.10 ± 0.24	² AKERS 95Y OPAL	1991-1994 LEP runs	
••• We do not use the following data for averages, fits, limits, etc. •••			
9.50 ± 0.10 ± 0.11	11.2k	³ BUSKULIC 96 ALEP	Repl. by SCHAELE 05C



¹See footnote to ABDALLAH 06A $\Gamma(\tau^- \rightarrow h^- \nu_\tau)/\Gamma_{total}$ measurement for correlations with other measurements.
²Not independent of AKERS 95Y $B(h^- h^- h^+ \geq 0 \text{ neutrals } \nu_\tau \text{ (ex. } K^0_S \rightarrow \pi^+ \pi^-))$ and $B(h^- h^- h^+ \nu_\tau \text{ (ex. } K^0))/B(h^- h^- h^+ \geq 0 \text{ neutrals } \nu_\tau \text{ (ex. } K^0_S \rightarrow \pi^+ \pi^-))$ values.
³Not independent of BUSKULIC 96 $B(h^- h^- h^+ \nu_\tau)$ value.

$$\Gamma(h^- h^- h^+ \nu_\tau \text{ (ex. } K^0))/\Gamma(h^- h^- h^+ \geq 0 \text{ neutrals } \nu_\tau \text{ (ex. } K^0_S \rightarrow \pi^+ \pi^-)) \quad \Gamma_{65}/\Gamma_{63}$$

$$\Gamma_{65}/\Gamma_{63} = (\Gamma_{70} + \Gamma_{97} + \Gamma_{106} + 0.491\Gamma_{170} + 0.0153\Gamma_{178} + 0.0153\Gamma_{179})/(0.424\Gamma_{52} + \Gamma_{70} + \Gamma_{78} + \Gamma_{85} + \Gamma_{97} + \Gamma_{103} + \Gamma_{106} + \Gamma_{107} + 0.2804\Gamma_{150} + 0.2302\Gamma_{151} + 0.2804\Gamma_{152} + 0.2804\Gamma_{154} + 0.1131\Gamma_{156} + 0.3257\Gamma_{160} + 0.491\Gamma_{170} + 0.9078\Gamma_{178} + 0.9078\Gamma_{179} + 0.9078\Gamma_{180} + 0.892\Gamma_{182})$$

VALUE (units 10 ⁻²)	DOCUMENT ID	TECN	COMMENT
64.98 ± 0.31 OUR FIT			
66.0 ± 0.4 ± 1.4	AKERS 95Y OPAL	1991-1994 LEP runs	

$$\Gamma(h^- h^- h^+ \nu_\tau \text{ (ex. } K^0, \omega))/\Gamma_{total} \quad \Gamma_{66}/\Gamma$$

$$\Gamma_{66}/\Gamma = (\Gamma_{70} + \Gamma_{97} + \Gamma_{106} + 0.491\Gamma_{170})/\Gamma$$

VALUE (%)	DOCUMENT ID
9.43 ± 0.05 OUR FIT	

$$\Gamma(\pi^- \pi^+ \pi^- \nu_\tau)/\Gamma_{total} \quad \Gamma_{67}/\Gamma = (0.34598\Gamma_{36} + \Gamma_{70} + 0.0153\Gamma_{178})/\Gamma$$

VALUE (%)	DOCUMENT ID
9.31 ± 0.05 OUR FIT	

$$\Gamma(\pi^- \pi^+ \pi^- \nu_\tau \text{ (ex. } K^0))/\Gamma_{total} \quad \Gamma_{68}/\Gamma = (\Gamma_{70} + 0.0153\Gamma_{178})/\Gamma$$

VALUE (%)	EVTS	DOCUMENT ID	TECN	COMMENT
9.02 ± 0.05 OUR FIT				
8.77 ± 0.13 OUR AVERAGE				Error includes scale factor of 1.1.
8.42 ± 0.00 $^{+0.26}_{-0.25}$	8.9M	¹ LEE 10	BELL	666 fb ⁻¹ $E_{cm}^{ee} = 10.6$ GeV
8.83 ± 0.01 ± 0.13	1.6M	² AUBERT 08	BABR	342 fb ⁻¹ $E_{cm}^{ee} = 10.6$ GeV
9.13 ± 0.05 ± 0.46	43k	³ BRIERE 03	CLE3	$E_{cm}^{ee} = 10.6$ GeV

¹Quoted statistical error is 0.003%. Correlation matrix for LEE 10 branching fractions:
(1) $\Gamma(\tau^- \rightarrow \pi^- \pi^+ \pi^- \nu_\tau \text{ (ex. } K^0))/\Gamma_{total}$
(2) $\Gamma(\tau^- \rightarrow K^- \pi^+ \pi^- \nu_\tau \text{ (ex. } K^0))/\Gamma_{total}$
(3) $\Gamma(\tau^- \rightarrow K^- K^+ \pi^- \nu_\tau)/\Gamma_{total}$
(4) $\Gamma(\tau^- \rightarrow K^- K^+ K^- \nu_\tau)/\Gamma_{total}$

(1)	(2)	(3)
(1)	(2)	(3)
(2)	0.175	
(3)	0.049	0.080
(4)	-0.053	0.035 -0.008

²Correlation matrix for AUBERT 08 branching fractions:
(1) $\Gamma(\tau^- \rightarrow \pi^- \pi^+ \pi^- \nu_\tau \text{ (ex. } K^0))/\Gamma_{total}$
(2) $\Gamma(\tau^- \rightarrow K^- \pi^+ \pi^- \nu_\tau \text{ (ex. } K^0))/\Gamma_{total}$
(3) $\Gamma(\tau^- \rightarrow K^- K^+ \pi^- \nu_\tau)/\Gamma_{total}$
(4) $\Gamma(\tau^- \rightarrow K^- K^+ K^- \nu_\tau)/\Gamma_{total}$

(1)	(2)	(3)
(1)	(2)	(3)
(2)	0.544	
(3)	0.390	0.177
(4)	0.031	0.093 0.087

³47% correlated with BRIERE 03 $\tau^- \rightarrow K^- \pi^+ \pi^- \nu_\tau$ and 71% correlated with $\tau^- \rightarrow K^- K^+ \pi^- \nu_\tau$ because of a common 5% normalization error.

See key on page 1127

Lepton Particle Listings

T

Gamma(pi- pi+ pi- nu_tau (ex. K^0), non-axial vector) / Gamma(pi- pi+ pi- nu_tau (ex. K^0))

Table with columns: VALUE, CL%, DOCUMENT ID, TECN, COMMENT. Row 1: <0.261, 95, ACKERSTAFF 97R OPAL 1992-1994 LEP runs

Model-independent limit from structure function analysis on contribution to B(pi- -> pi- pi+ pi- nu_tau (ex. K^0)) from non-axial vectors.

Gamma(pi- pi+ pi- nu_tau (ex. K^0, omega)) / Gamma_total

Table with columns: VALUE (%), EVTS, DOCUMENT ID, TECN, COMMENT. Row 1: 9.99 +/- 0.05 OUR FIT

See footnote to SCHAEEL 05c Gamma(pi- -> e- nu_e nu_tau) / Gamma_total measurement for correlations with other measurements.

Gamma(h- h- h+ >= 1 neutrals nu_tau) / Gamma_total

Gamma_71 / Gamma = (0.34598 Gamma_41 + 0.34598 Gamma_43 + 0.42477 Gamma_48 + 0.42477 Gamma_52 + Gamma_78 + Gamma_85 + Gamma_86 + Gamma_103 + Gamma_107 + 0.2804 Gamma_150 + 0.2804 Gamma_152 + 0.2804 Gamma_154 + 0.2926 Gamma_156 + 0.892 Gamma_178 + 0.892 Gamma_179 + 0.9078 Gamma_180) / Gamma

Table with columns: VALUE (%), EVTS, DOCUMENT ID, TECN, COMMENT. Row 1: 5.29 +/- 0.05 OUR FIT

- • • We do not use the following data for averages, fits, limits, etc. • • •
5.6 +/- 0.7 +/- 0.3 352 1 BEHREND 90 CELL E_cm^ee = 35 GeV
4.2 +/- 0.5 +/- 0.9 203 2 ALBRECHT 87L ARG E_cm^ee = 10 GeV
6.1 +/- 0.8 +/- 0.9 3 BURCHAT 87 MRK2 E_cm^ee = 29 GeV
7.6 +/- 0.4 +/- 0.9 4,5 RUCKSTUHL 86 DLCO E_cm^ee = 29 GeV
4.7 +/- 0.5 +/- 0.8 530 6 SCHMIDKE 86 MRK2 E_cm^ee = 29 GeV
5.6 +/- 0.4 +/- 0.7 5 FERNANDEZ 85 MAC E_cm^ee = 29 GeV
6.2 +/- 2.3 +/- 1.7 BEHREND 84 CELL E_cm^ee = 14,22 GeV

- 1 BEHREND 90 value is not independent of BEHREND 90 B(3h nu_tau >= 1 neutrals) + B(5-prong).
2 ALBRECHT 87L measure the product of branching ratios B(3 pi+ pi0 nu_tau) B((e nu_e mu nu_tau or pi or K or rho) nu_tau) = 0.029 and use the PDG 86 values for the second branching ratio which sum to 0.69 +/- 0.03 to get the quoted value.
3 BURCHAT 87 value is not independent of SCHMIDKE 86 value.
4 Contributions from kaons and from >1 pi0 are subtracted. Not independent of (3-prong + 0 pi0) and (3-prong + >= 0 pi0) values.
5 Value obtained using paper's R = B(h- h- h+ nu_tau) / B(3-prong) and current B(3-prong) = 0.143.
6 Not independent of SCHMIDKE 86 h- h- h+ nu_tau and h- h- h+ (>= 0 pi0) nu_tau values.

Gamma(h- h- h+ >= 1 pi0 nu_tau (ex. K^0)) / Gamma_total

Table with columns: VALUE (%), EVTS, DOCUMENT ID, TECN, COMMENT. Row 1: 5.09 +/- 0.05 OUR FIT

5.10 +/- 0.12 OUR AVERAGE

- • • We use the following data for averages but not for fits. • • •
5.106 +/- 0.083 +/- 0.103 10.1k 1 ABDALLAH 06A DLPH 1992-1995 LEP runs
5.09 +/- 0.10 +/- 0.23 2 AKERS 95Y OPAL 1991-1994 LEP runs
• • • We do not use the following data for averages, fits, limits, etc. • • •
4.95 +/- 0.29 +/- 0.65 570 DECAMP 92c ALEP Repl. by SCHAEEL 05c

- 1 See footnote to ABDALLAH 06A Gamma(pi- -> h- nu_tau) / Gamma_total measurement for correlations with other measurements.
2 Not independent of AKERS 95Y B(h- h- h+ >= 0 neutrals nu_tau (ex. K_S^0 -> pi+ pi-)) and B(h- h- h+ >= 0 neutrals nu_tau (ex. K_S^0)) / B(h- h- h+ >= 0 neutrals nu_tau (ex. K_S^0 -> pi+ pi-)) values.

Gamma(h- h- h+ pi0 nu_tau) / Gamma_total

Gamma_73 / Gamma = (0.34598 Gamma_41 + 0.34598 Gamma_43 + Gamma_78 + Gamma_103 + Gamma_107 + 0.2302 Gamma_152 + 0.892 Gamma_178 + 0.892 Gamma_179 + 0.0153 Gamma_180) / Gamma

Table with columns: VALUE (%), EVTS, DOCUMENT ID, TECN, COMMENT. Row 1: 4.76 +/- 0.05 OUR FIT

- • • We do not use the following data for averages, fits, limits, etc. • • •
4.45 +/- 0.09 +/- 0.07 6.1k 1 BUSKULIC 96 ALEP Repl. by SCHAEEL 05c
1 BUSKULIC 96 quote B(h- h- h+ pi0 nu_tau (ex. K^0)) = 4.30 +/- 0.09 +/- 0.09. We add 0.15 to remove their K^0 correction and reduce the systematic error accordingly.

Gamma(h- h- h+ pi0 nu_tau (ex. K^0)) / Gamma_total

Gamma_74 / Gamma = (Gamma_78 + Gamma_103 + Gamma_107 + 0.2302 Gamma_152 + 0.892 Gamma_178 + 0.892 Gamma_179 + 0.0153 Gamma_180) / Gamma

Table with columns: VALUE (%), EVTS, DOCUMENT ID, TECN, COMMENT. Row 1: 4.57 +/- 0.05 OUR FIT

- 4.45 +/- 0.14 OUR AVERAGE Error includes scale factor of 1.2.
4.545 +/- 0.106 +/- 0.103 8.9k 1 ABDALLAH 06A DLPH 1992-1995 LEP runs
4.23 +/- 0.06 +/- 0.22 7.2k BALEST 95c CLEO E_cm^ee approx 10.6 GeV

1 See footnote to ABDALLAH 06A Gamma(pi- -> h- nu_tau) / Gamma_total measurement for correlations with other measurements.

Gamma(h- h- h+ pi0 nu_tau (ex. K^0, omega)) / Gamma_total

Gamma_75 / Gamma = (Gamma_78 + Gamma_103 + Gamma_107 + 0.2302 Gamma_152) / Gamma

Table with columns: VALUE (%), DOCUMENT ID. Row 1: 2.79 +/- 0.07 OUR FIT

Gamma(pi- pi+ pi- pi0 nu_tau) / Gamma_total

Table with columns: VALUE (%), DOCUMENT ID. Row 1: 4.62 +/- 0.05 OUR FIT

Gamma(pi- pi+ pi- pi0 nu_tau (ex. K^0)) / Gamma_total

Table with columns: VALUE (%), EVTS, DOCUMENT ID, TECN, COMMENT. Row 1: 4.49 +/- 0.05 OUR FIT

- 4.55 +/- 0.13 OUR AVERAGE Error includes scale factor of 1.6.
4.598 +/- 0.057 +/- 0.064 16k 1 SCHAEEL 05c ALEP 1991-1995 LEP runs
4.19 +/- 0.10 +/- 0.21 2 EDWARDS 00A CLEO 4.7 fb^-1 E_cm^ee = 10.6 GeV

- 1 SCHAEEL 05c quote (4.590 +/- 0.057 +/- 0.064)%. We add 0.008% to remove their correction for pi- -> pi- pi0 omega nu_tau -> pi- pi0 pi+ pi- nu_tau decays. See footnote to SCHAEEL 05c Gamma(pi- -> e- nu_e nu_tau) / Gamma_total measurement for correlations with other measurements.
2 EDWARDS 00A quote (4.19 +/- 0.10) x 10^-2 with a 5% systematic error.

Gamma(pi- pi+ pi- pi0 nu_tau (ex. K^0, omega)) / Gamma_total

Table with columns: VALUE (%), DOCUMENT ID. Row 1: 2.74 +/- 0.07 OUR FIT

Gamma(h- rho pi0 nu_tau) / Gamma(h- h- h+ pi0 nu_tau)

Table with columns: VALUE, EVTS, DOCUMENT ID, TECN, COMMENT. Row 1: 0.30 +/- 0.04 +/- 0.02 393 ALBRECHT 91D ARG E_cm^ee = 9.4-10.6 GeV

Gamma(h- rho+ h- nu_tau) / Gamma(h- h- h+ pi0 nu_tau)

Table with columns: VALUE, EVTS, DOCUMENT ID, TECN, COMMENT. Row 1: 0.10 +/- 0.03 +/- 0.04 142 ALBRECHT 91D ARG E_cm^ee = 9.4-10.6 GeV

Gamma(h- rho- h+ nu_tau) / Gamma(h- h- h+ pi0 nu_tau)

Table with columns: VALUE, EVTS, DOCUMENT ID, TECN, COMMENT. Row 1: 0.26 +/- 0.05 +/- 0.01 370 ALBRECHT 91D ARG E_cm^ee = 9.4-10.6 GeV

Gamma(h- h- h+ >= 2 pi0 nu_tau (ex. K^0)) / Gamma_total

Table with columns: VALUE (%), EVTS, DOCUMENT ID, TECN, COMMENT. Row 1: 0.517 +/- 0.031 OUR FIT

- 0.561 +/- 0.068 +/- 0.095 1.3k 1 ABDALLAH 06A DLPH 1992-1995 LEP runs
1 See footnote to ABDALLAH 06A Gamma(pi- -> h- nu_tau) / Gamma_total measurement for correlations with other measurements.

Gamma(h- h- h+ 2 pi0 nu_tau) / Gamma_total

Table with columns: VALUE (%), DOCUMENT ID. Row 1: 0.505 +/- 0.031 OUR FIT

Gamma(h- h- h+ 2 pi0 nu_tau (ex. K^0)) / Gamma_total

Table with columns: VALUE (%), EVTS, DOCUMENT ID, TECN, COMMENT. Row 1: 0.495 +/- 0.031 OUR FIT

- 0.435 +/- 0.030 +/- 0.035 2.6k 1 SCHAEEL 05c ALEP 1991-1995 LEP runs
• • • We do not use the following data for averages, fits, limits, etc. • • •
0.50 +/- 0.07 +/- 0.07 1.8k BUSKULIC 96 ALEP Repl. by SCHAEEL 05c

- 1 SCHAEEL 05c quote (0.392 +/- 0.030 +/- 0.035)%. We add 0.043% to remove their correction for pi- -> pi- eta pi0 nu_tau -> pi- pi+ pi- 2 pi0 nu_tau and pi- -> K*(892)- eta nu_tau -> K- pi+ pi- 2 pi0 nu_tau decays. See footnote to SCHAEEL 05c Gamma(pi- -> e- nu_e nu_tau) / Gamma_total measurement for correlations with other measurements.

Gamma(h- h- h+ 2 pi0 nu_tau (ex. K^0)) / Gamma(h- h- h+ >= 0 neutrals >= 0 K_S^0 nu_tau)

Gamma_84 / Gamma_62 = (Gamma_85 + 0.2302 Gamma_150 + 0.2302 Gamma_154 + 0.892 Gamma_180) / ((0.34598 Gamma_36 + 0.34598 Gamma_38 + 0.34598 Gamma_41 + 0.34598 Gamma_43 + 0.42477 Gamma_48 + 0.6920 Gamma_49 + 0.8494 Gamma_52 + 0.6920 Gamma_56 + 0.6534 Gamma_61 + Gamma_70 + Gamma_78 + Gamma_85 + Gamma_89 + Gamma_97 + Gamma_103 + Gamma_106 + Gamma_107 + 0.2804 Gamma_150 + 0.2302 Gamma_151 + 0.2804 Gamma_152 + 0.2804 Gamma_154 + 0.3759 Gamma_156 + 0.3257 Gamma_160 + 0.7259 Gamma_170 + 0.9078 Gamma_178 + 0.9078 Gamma_179 + 0.9078 Gamma_180 + 0.892 Gamma_182)

Table with columns: VALUE (units 10^-2), EVTS, DOCUMENT ID, TECN, COMMENT. Row 1: 3.26 +/- 0.20 OUR FIT

Gamma(h- h- h+ 2 pi0 nu_tau (ex. K^0, omega, eta)) / Gamma_total

Table with columns: VALUE (units 10^-4), DOCUMENT ID. Row 1: 10 +/- 4 OUR FIT

Gamma(h- h- h+ 3 pi0 nu_tau) / Gamma_total

Table with columns: VALUE (units 10^-4), CL%, EVTS, DOCUMENT ID, TECN, COMMENT. Row 1: 2.13 +/- 0.30 OUR FIT

Lepton Particle Listings

τ

• • • We do not use the following data for averages, fits, limits, etc. • • •
 < 4.9 95 SCHAEEL 05c ALEP 1991-1995 LEP runs
 $2.85 \pm 0.56 \pm 0.51$ 57 ANDERSON 97 CLEO Repl. by ANAS-TASSOV 01
 11 ± 4 ± 5 440 ¹BUSKULIC 96 ALEP Repl. by SCHAEEL 05c
¹BUSKULIC 96 state their measurement is for $B(h^- h^- h^+ \geq 3\pi^0 \nu_\tau)$. We assume that $B(h^- h^- h^+ \geq 4\pi^0 \nu_\tau)$ is very small.

$\Gamma(2\pi^- \pi^+ 3\pi^0 \nu_\tau (\text{ex. } K^0))/\Gamma_{\text{total}}$ Γ_{87}/Γ
 $\Gamma_{87}/\Gamma = (\Gamma_{89} + 0.2302\Gamma_{151} + 0.3257\Gamma_{160} + 0.892\Gamma_{182})/\Gamma$

VALUE (units 10^{-4})	DOCUMENT ID	TECN	COMMENT
1.95 ± 0.30 OUR FIT			

• • • We use the following data for averages but not for fits. • • •
 $2.07 \pm 0.18 \pm 0.37$ ¹LEES 12X BABR 468 fb^{-1} $E_{\text{cm}}^{ee} = 10.6 \text{ GeV}$
¹Not independent of LEES 12X $\Gamma(\tau^- \rightarrow \eta \pi^- \pi^+ \pi^- \nu_\tau (\text{ex. } K^0))/\Gamma$, $\Gamma(\tau^- \rightarrow \eta \pi^- \pi^0 \pi^0 \nu_\tau)/\Gamma$, $\Gamma(\tau^- \rightarrow \pi^- \omega 2\pi^0 \nu_\tau)/\Gamma$, and $\Gamma(\tau^- \rightarrow f_1(1285) \pi^- \nu_\tau \rightarrow \eta \pi^- \pi^+ \pi^- \nu_\tau)/\Gamma$ values.

$\Gamma(2\pi^- \pi^+ 3\pi^0 \nu_\tau (\text{ex. } K^0, \eta, f_1(1285)))/\Gamma_{\text{total}}$ Γ_{88}/Γ

VALUE (units 10^{-4})	DOCUMENT ID	TECN	COMMENT
$1.69 \pm 0.08 \pm 0.43$	LEES	12X	BABR 468 fb^{-1} $E_{\text{cm}}^{ee} = 10.6 \text{ GeV}$

$\Gamma(2\pi^- \pi^+ 3\pi^0 \nu_\tau (\text{ex. } K^0, \eta, \omega, f_1(1285)))/\Gamma_{\text{total}}$ Γ_{89}/Γ

VALUE (units 10^{-5})	DOCUMENT ID	TECN	COMMENT
1.4 ± 2.7 OUR FIT			
$1.0 \pm 0.8 \pm 3.0$	¹ LEES	12X	BABR 468 fb^{-1} $E_{\text{cm}}^{ee} = 10.6 \text{ GeV}$

¹LEES 12X measurement corresponds to the lower limit of $< 5.8 \times 10^{-5}$ at 90% CL.

$\Gamma(K^- h^+ h^- \geq 0 \text{ neutrals } \nu_\tau)/\Gamma_{\text{total}}$ Γ_{90}/Γ
 $\Gamma_{90}/\Gamma = (0.34598\Gamma_{38} + 0.34598\Gamma_{43} + \Gamma_{97} + \Gamma_{103} + \Gamma_{106} + \Gamma_{107} + 0.2804\Gamma_{152} + 0.491\Gamma_{170} + 0.9078\Gamma_{179})/\Gamma$

VALUE (%)	CL%	DOCUMENT ID	TECN	COMMENT
0.629 ± 0.014 OUR FIT				
< 0.6	90	AIHARA	84c	TPC $E_{\text{cm}}^{ee} = 29 \text{ GeV}$

$\Gamma(K^- h^+ \pi^- \nu_\tau (\text{ex. } K^0))/\Gamma_{\text{total}}$ $\Gamma_{91}/\Gamma = (\Gamma_{97} + \Gamma_{106} + 0.0153\Gamma_{179})/\Gamma$

VALUE (%)	DOCUMENT ID
0.437 ± 0.007 OUR FIT	

$\Gamma(K^- h^+ \pi^- \nu_\tau (\text{ex. } K^0))/\Gamma(\pi^- \pi^+ \pi^- \nu_\tau (\text{ex. } K^0))$ Γ_{91}/Γ_{68}
 $\Gamma_{91}/\Gamma_{68} = (\Gamma_{97} + \Gamma_{106} + 0.0153\Gamma_{179})/(\Gamma_{70} + 0.0153\Gamma_{178})$

VALUE (%)	EVTS	DOCUMENT ID	TECN	COMMENT
4.85 ± 0.08 OUR FIT				
$5.44 \pm 0.21 \pm 0.53$	7.9k	RICHICHI	99	CLEO $E_{\text{cm}}^{ee} = 10.6 \text{ GeV}$

$\Gamma(K^- h^+ \pi^- \pi^0 \nu_\tau (\text{ex. } K^0))/\Gamma_{\text{total}}$ Γ_{92}/Γ
 $\Gamma_{92}/\Gamma = (\Gamma_{103} + \Gamma_{107} + 0.2302\Gamma_{152} + 0.892\Gamma_{179})/\Gamma$

VALUE (units 10^{-4})	DOCUMENT ID
8.6 ± 1.2 OUR FIT	

$\Gamma(K^- h^+ \pi^- \pi^0 \nu_\tau (\text{ex. } K^0))/\Gamma(\pi^- \pi^+ \pi^- \pi^0 \nu_\tau (\text{ex. } K^0))$ Γ_{92}/Γ_{77}
 $\Gamma_{92}/\Gamma_{77} = (\Gamma_{103} + \Gamma_{107} + 0.2302\Gamma_{152} + 0.892\Gamma_{179})/(\Gamma_{78} + 0.892\Gamma_{178} + 0.0153\Gamma_{180})$

VALUE (%)	EVTS	DOCUMENT ID	TECN	COMMENT
1.91 ± 0.26 OUR FIT				
$2.61 \pm 0.45 \pm 0.42$	719	RICHICHI	99	CLEO $E_{\text{cm}}^{ee} = 10.6 \text{ GeV}$

$\Gamma(K^- \pi^+ \pi^- \geq 0 \text{ neutrals } \nu_\tau)/\Gamma_{\text{total}}$ Γ_{93}/Γ
 $\Gamma_{93}/\Gamma = (0.34598\Gamma_{38} + 0.34598\Gamma_{43} + \Gamma_{97} + \Gamma_{103} + 0.2804\Gamma_{152} + 0.9078\Gamma_{179})/\Gamma$

VALUE (%)	EVTS	DOCUMENT ID	TECN	COMMENT
0.477 ± 0.014 OUR FIT				
$0.58 \pm 0.15 \pm 0.12$	20	¹ BAUER	94	TPC $E_{\text{cm}}^{ee} = 29 \text{ GeV}$

• • • We do not use the following data for averages, fits, limits, etc. • • •
 $0.22 \pm 0.16 \pm 0.05$ 9 ²MILLS 85 DLCO $E_{\text{cm}}^{ee} = 29 \text{ GeV}$
¹We multiply 0.58% by 0.20, the relative systematic error quoted by BAUER 94, to obtain the systematic error.
²Error correlated with MILLS 85 ($K K \pi \nu$) value. We multiply 0.22% by 0.23, the relative systematic error quoted by MILLS 85, to obtain the systematic error.

$\Gamma(K^- \pi^+ \pi^- \geq 0 \pi^0 \nu_\tau (\text{ex. } K^0))/\Gamma_{\text{total}}$ Γ_{94}/Γ
 $\Gamma_{94}/\Gamma = (\Gamma_{97} + \Gamma_{103} + 0.2302\Gamma_{152} + 0.9078\Gamma_{179})/\Gamma$

VALUE (%)	DOCUMENT ID	TECN	COMMENT
0.373 ± 0.013 OUR FIT			
0.30 ± 0.05 OUR AVERAGE			

• • • We use the following data for averages but not for fits. • • •
 $0.343 \pm 0.073 \pm 0.031$ ABBIENDI 00D OPAL 1990-1995 LEP runs
 0.275 ± 0.064 ¹BARATE 98 ALEP 1991-1995 LEP runs
¹Not independent of BARATE 98 $\Gamma(\tau^- \rightarrow K^- \pi^+ \pi^- \nu_\tau)/\Gamma_{\text{total}}$ and $\Gamma(\tau^- \rightarrow K^- \pi^+ \pi^- \pi^0 \nu_\tau)/\Gamma_{\text{total}}$ values.

$\Gamma(K^- \pi^+ \pi^- \nu_\tau)/\Gamma_{\text{total}}$ $\Gamma_{95}/\Gamma = (0.34598\Gamma_{38} + \Gamma_{97} + 0.0153\Gamma_{179})/\Gamma$

VALUE (%)	DOCUMENT ID
0.345 ± 0.007 OUR FIT	

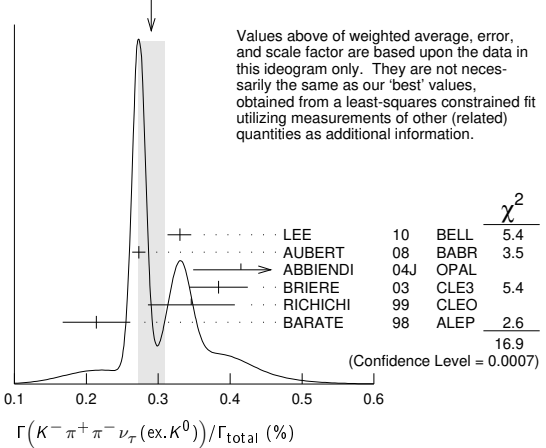
$\Gamma(K^- \pi^+ \pi^- \nu_\tau (\text{ex. } K^0))/\Gamma_{\text{total}}$ $\Gamma_{96}/\Gamma = (\Gamma_{97} + 0.0153\Gamma_{179})/\Gamma$

VALUE (%)	EVTS	DOCUMENT ID	TECN	COMMENT
0.293 ± 0.007 OUR FIT				
0.290 ± 0.018 OUR AVERAGE				Error includes scale factor of 2.4. See the ideogram below.

$0.330 \pm 0.001 \pm 0.016$ 794k ¹LEE 10 BELL 666 fb^{-1} $E_{\text{cm}}^{ee} = 10.6 \text{ GeV}$
 $0.273 \pm 0.002 \pm 0.009$ 70k ²AUBERT 08 BABR 342 fb^{-1} $E_{\text{cm}}^{ee} = 10.6 \text{ GeV}$
 $0.415 \pm 0.053 \pm 0.040$ 269 ABBIENDI 04J OPAL 1991-1995 LEP runs
 $0.384 \pm 0.014 \pm 0.038$ 3.5k ³BRIERE 03 CLE3 $E_{\text{cm}}^{ee} = 10.6 \text{ GeV}$
 $0.214 \pm 0.037 \pm 0.029$ BARATE 98 ALEP 1991-1995 LEP runs

• • • We use the following data for averages but not for fits. • • •
 $0.346 \pm 0.023 \pm 0.056$ 158 ⁴RICHICHI 99 CLEO $E_{\text{cm}}^{ee} = 10.6 \text{ GeV}$
 • • • We do not use the following data for averages, fits, limits, etc. • • •
 $0.360 \pm 0.082 \pm 0.048$ ABBIENDI 00D OPAL 1990-1995 LEP runs

WEIGHTED AVERAGE
 0.290 ± 0.018 (Error scaled by 2.4)



¹ See footnote to LEE 10 $\Gamma(\tau^- \rightarrow \pi^- \pi^+ \pi^- \nu_\tau (\text{ex. } K^0))/\Gamma_{\text{total}}$ measurement for correlations with other measurements. Not independent of LEE 10 $\Gamma(\tau^- \rightarrow K^- \pi^+ \pi^- \nu_\tau (\text{ex. } K^0))/\Gamma(\tau^- \rightarrow \pi^- \pi^+ \pi^- \nu_\tau (\text{ex. } K^0))$ value.
² See footnote to AUBERT 08 $\Gamma(\tau^- \rightarrow \pi^- \pi^+ \pi^- \nu_\tau (\text{ex. } K^0))/\Gamma_{\text{total}}$ measurement for correlations with other measurements.
³ 47% correlated with BRIERE 03 $\tau^- \rightarrow \pi^- \pi^+ \pi^- \nu_\tau$ and 34% correlated with $\tau^- \rightarrow K^- K^+ \pi^- \nu_\tau$ because of a common 5% normalization error.
⁴ Not independent of RICHICHI 99 $\Gamma(\tau^- \rightarrow K^- h^+ \pi^- \nu_\tau (\text{ex. } K^0))/\Gamma(\tau^- \rightarrow \pi^- \pi^+ \pi^- \nu_\tau (\text{ex. } K^0))$, $\Gamma(\tau^- \rightarrow K^- K^+ \pi^- \nu_\tau)/\Gamma(\tau^- \rightarrow \pi^- \pi^+ \pi^- \nu_\tau (\text{ex. } K^0))$ and BALEST 95c $\Gamma(\tau^- \rightarrow h^- h^- h^+ \nu_\tau (\text{ex. } K^0))/\Gamma_{\text{total}}$ values.

$\Gamma(K^- \pi^+ \pi^- \nu_\tau (\text{ex. } K^0))/\Gamma(\pi^- \pi^+ \pi^- \nu_\tau (\text{ex. } K^0))$ Γ_{96}/Γ_{68}
 $\Gamma_{96}/\Gamma_{68} = (\Gamma_{97} + 0.0153\Gamma_{179})/(\Gamma_{70} + 0.0153\Gamma_{178})$

VALUE (units 10^{-2})	EVTS	DOCUMENT ID	TECN	COMMENT
3.25 ± 0.07 OUR FIT				

• • • We use the following data for averages but not for fits. • • •
 $3.92 \pm 0.02 \pm 0.15$ 794k ¹LEE 10 BELL 666 fb^{-1} $E_{\text{cm}}^{ee} = 10.6 \text{ GeV}$
¹Not independent of LEE 10 $\Gamma(\tau^- \rightarrow K^- \pi^+ \pi^- \nu_\tau (\text{ex. } K^0))/\Gamma_{\text{total}}$ and $\Gamma(\tau^- \rightarrow \pi^- \pi^+ \pi^- \nu_\tau (\text{ex. } K^0))/\Gamma_{\text{total}}$ values.

$\Gamma(K^- \pi^+ \pi^- \nu_\tau (\text{ex. } K^0, \omega))/\Gamma_{\text{total}}$ Γ_{97}/Γ

VALUE (units 10^{-3})	DOCUMENT ID
2.93 ± 0.07 OUR FIT	

$\Gamma(K^- \rho^0 \nu_\tau \rightarrow K^- \pi^+ \pi^- \nu_\tau)/\Gamma(K^- \pi^+ \pi^- \nu_\tau (\text{ex. } K^0))$ Γ_{98}/Γ_{96}

VALUE	DOCUMENT ID	TECN	COMMENT
$0.48 \pm 0.14 \pm 0.10$	¹ ASNER	00B	CLEO $E_{\text{cm}}^{ee} = 10.6 \text{ GeV}$

• • • We do not use the following data for averages, fits, limits, etc. • • •
 0.39 ± 0.14 ²BARATE 99R ALEP 1991-1995 LEP runs
¹ASNER 00B assume $\tau^- \rightarrow K^- \pi^+ \pi^- \nu_\tau (\text{ex. } K^0)$ decays proceed only through $K \rho$ and $K^* \pi$ intermediate states. They assume the resonance structure of $\tau^- \rightarrow K^- \pi^+ \pi^- \nu_\tau (\text{ex. } K^0)$ decays is dominated by $K_1(1270)^-$ and $K_1(1400)^-$ resonances, and assume $B(K_1(1270) \rightarrow K^*(892) \pi) = (16 \pm 5)\%$, $B(K_1(1270) \rightarrow K \rho) = (42 \pm 6)\%$, and $B(K_1(1400) \rightarrow K \rho) = 0$.
²BARATE 99R assume $\tau^- \rightarrow K^- \pi^+ \pi^- \nu_\tau (\text{ex. } K^0)$ decays proceed only through $K \rho$ and $K^* \pi$ intermediate states. The quoted error is statistical only.

$$\Gamma(K^-\pi^+\pi^-\pi^0\nu_\tau)/\Gamma_{total} \quad \Gamma_{99}/\Gamma$$

$$\Gamma_{99}/\Gamma = (0.34598\Gamma_{43} + \Gamma_{103} + 0.2302\Gamma_{152} + 0.892\Gamma_{179})/\Gamma$$

VALUE (units 10 ⁻⁴)	DOCUMENT ID
13.1 ± 1.2 OUR FIT	

$$\Gamma(K^-\pi^+\pi^-\pi^0\nu_\tau(ex.K^0))/\Gamma_{total} \quad \Gamma_{100}/\Gamma$$

$$\Gamma_{100}/\Gamma = (\Gamma_{103} + 0.2302\Gamma_{152} + 0.892\Gamma_{179})/\Gamma$$

VALUE (units 10 ⁻⁴)	CL%	DOCUMENT ID	TECN	COMMENT
7.9 ± 1.2 OUR FIT				
7.3 ± 1.2 OUR AVERAGE				

7.4 ± 0.8 ± 1.1		¹ ARMS	05	CLE3	7.6 fb ⁻¹ , E _{cm} ^{ee} = 10.6 GeV
6.1 ± 3.9 ± 1.8		BARATE	98	ALEP	1991-1995 LEP runs
• • • We use the following data for averages but not for fits. • • •					
7.5 ± 2.6 ± 1.8		² RICHICHI	99	CLEO	E _{cm} ^{ee} = 10.6 GeV
• • • We do not use the following data for averages, fits, limits, etc. • • •					
<17		95	ABBIENDI	00D	OPAL 1990-1995 LEP runs

¹ Not independent of ARMS 05 $\Gamma(\tau^- \rightarrow K^-\pi^+\pi^-\pi^0\nu_\tau(ex.K^0, \omega)) / \Gamma_{total}$ and $\Gamma(\tau^- \rightarrow K^-\omega\nu_\tau) / \Gamma_{total}$ values.

² Not independent of RICHICHI 99 $\Gamma(\tau^- \rightarrow K^-h^+\pi^-\nu_\tau(ex.K^0)) / \Gamma(\tau^- \rightarrow \pi^-\pi^+\pi^-\nu_\tau(ex.K^0))$, $\Gamma(\tau^- \rightarrow K^-K^+\pi^-\nu_\tau) / \Gamma(\tau^- \rightarrow \pi^-\pi^+\pi^-\nu_\tau(ex.K^0))$ and BALEST 95c $\Gamma(\tau^- \rightarrow h^-h^-\pi^+\nu_\tau(ex.K^0)) / \Gamma_{total}$ values.

$$\Gamma(K^-\pi^+\pi^-\pi^0\nu_\tau(ex.K^0, \eta))/\Gamma_{total} \quad \Gamma_{101}/\Gamma = (\Gamma_{103} + 0.892\Gamma_{179})/\Gamma$$

VALUE (units 10 ⁻⁴)	DOCUMENT ID
7.6 ± 1.2 OUR FIT	

VALUE (units 10 ⁻⁴)	EVTs	DOCUMENT ID	TECN	COMMENT
3.7 ± 0.5 ± 0.8	833	ARMS	05	CLE3 7.6 fb ⁻¹ , E _{cm} ^{ee} = 10.6 GeV

$$\Gamma(K^-\pi^+\pi^-\pi^0\nu_\tau(ex.K^0, \omega, \eta))/\Gamma_{total} \quad \Gamma_{103}/\Gamma$$

VALUE (units 10 ⁻⁴)	DOCUMENT ID
3.9 ± 1.4 OUR FIT	

VALUE (%)	CL%	DOCUMENT ID	TECN	COMMENT	
<0.09		95	BAUER	94	TPC E _{cm} ^{ee} = 29 GeV

$$\Gamma(K^-K^+\pi^-\nu_\tau)/\Gamma_{total} \quad \Gamma_{104}/\Gamma$$

VALUE (%)	EVTs	DOCUMENT ID	TECN	COMMENT
0.1496 ± 0.0033 OUR FIT				
0.203 ± 0.031 OUR AVERAGE				

0.159 ± 0.053 ± 0.020		ABBIENDI	00D	OPAL 1990-1995 LEP runs
0.15 ± ^{+0.09} / _{-0.07} ± 0.03	4	¹ BAUER	94	TPC E _{cm} ^{ee} = 29 GeV
• • • We use the following data for averages but not for fits. • • •				
0.238 ± 0.042		² BARATE	98	ALEP 1991-1995 LEP runs

¹ We multiply 0.15% by 0.20, the relative systematic error quoted by BAUER 94, to obtain the systematic error.

² Not independent of BARATE 98 $\Gamma(\tau^- \rightarrow K^-K^+\pi^-\nu_\tau) / \Gamma_{total}$ and $\Gamma(\tau^- \rightarrow K^-K^+\pi^-\pi^0\nu_\tau) / \Gamma_{total}$ values.

$$\Gamma(K^-K^+\pi^-\nu_\tau)/\Gamma_{total} \quad \Gamma_{105}/\Gamma = (\Gamma_{106} + \Gamma_{107})/\Gamma$$

VALUE (units 10 ⁻³)	EVTs	DOCUMENT ID	TECN	COMMENT
1.435 ± 0.027 OUR FIT				
1.43 ± 0.07 OUR AVERAGE				

1.55 ± 0.01 ± ^{+0.06} / _{-0.05}	108k	¹ LEE	10	BELL 666 fb ⁻¹ E _{cm} ^{ee} = 10.6 GeV
1.346 ± 0.010 ± 0.036	18k	² AUBERT	08	BABR 342 fb ⁻¹ E _{cm} ^{ee} = 10.6 GeV
1.55 ± 0.06 ± 0.09	932	³ BRIERE	03	CLE3 E _{cm} ^{ee} = 10.6 GeV
1.63 ± 0.21 ± 0.17		BARATE	98	ALEP 1991-1995 LEP runs
• • • We use the following data for averages but not for fits. • • •				
0.87 ± 0.56 ± 0.40		ABBIENDI	00D	OPAL 1990-1995 LEP runs
1.45 ± 0.13 ± 0.28	2.3k	⁴ RICHICHI	99	CLEO E _{cm} ^{ee} = 10.6 GeV
• • • We do not use the following data for averages, fits, limits, etc. • • •				
2.2 ± ^{+1.7} / _{-1.1} ± 0.5	9	⁵ MILLS	85	DLCO E _{cm} ^{ee} = 29 GeV

¹ See footnote to LEE 10 $\Gamma(\tau^- \rightarrow \pi^-\pi^+\pi^-\nu_\tau(ex.K^0)) / \Gamma_{total}$ measurement for correlations with other measurements. Not independent of LEE 10 $\Gamma(\tau^- \rightarrow K^-K^+\pi^-\nu_\tau) / \Gamma(\tau^- \rightarrow \pi^-\pi^+\pi^-\nu_\tau(ex.K^0))$ value.

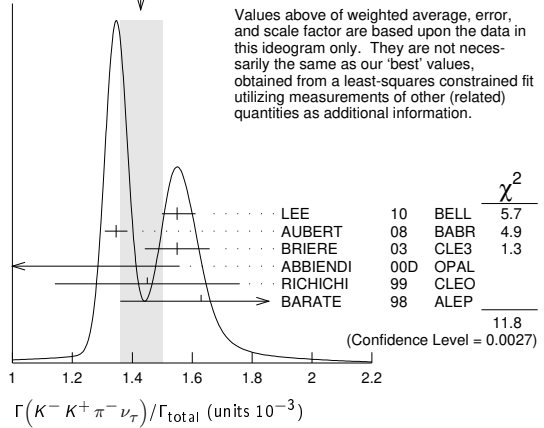
² See footnote to AUBERT 08 $\Gamma(\tau^- \rightarrow \pi^-\pi^+\pi^-\nu_\tau(ex.K^0)) / \Gamma_{total}$ measurement for correlations with other measurements.

³ 71% correlated with BRIERE 03 $\tau^- \rightarrow \pi^-\pi^+\pi^-\nu_\tau$ and 34% correlated with $\tau^- \rightarrow K^-\pi^+\pi^-\nu_\tau$ because of a common 5% normalization error.

⁴ Not independent of RICHICHI 99 $\Gamma(\tau^- \rightarrow K^-K^+\pi^-\nu_\tau) / \Gamma(\tau^- \rightarrow \pi^-\pi^+\pi^-\nu_\tau(ex.K^0))$ and BALEST 95c $\Gamma(\tau^- \rightarrow h^-h^-\pi^+\nu_\tau(ex.K^0)) / \Gamma_{total}$ values.

⁵ Error correlated with MILLS 85 ($K\pi\pi^0\nu$) value. We multiply 0.22% by 0.23, the relative systematic error quoted by MILLS 85, to obtain the systematic error.

WEIGHTED AVERAGE
1.43±0.07 (Error scaled by 2.4)



Values above of weighted average, error, and scale factor are based upon the data in this ideogram only. They are not necessarily the same as our 'best' values, obtained from a least-squares constrained fit utilizing measurements of other (related) quantities as additional information.

$$\Gamma(K^-K^+\pi^-\nu_\tau)/\Gamma(\pi^-\pi^+\pi^-\nu_\tau(ex.K^0)) \quad \Gamma_{106}/\Gamma_{68}$$

$$\Gamma_{106}/\Gamma_{68} = \Gamma_{106}/(\Gamma_{70} + 0.0153\Gamma_{178})$$

VALUE (%)	EVTs	DOCUMENT ID	TECN	COMMENT
1.592 ± 0.030 OUR FIT				
1.83 ± 0.05 OUR AVERAGE				

1.60 ± 0.15 ± 0.30	2.3k	RICHICHI	99	CLEO E _{cm} ^{ee} = 10.6 GeV
• • • We use the following data for averages but not for fits. • • •				
1.84 ± 0.01 ± 0.05	108k	¹ LEE	10	BELL 666 fb ⁻¹ E _{cm} ^{ee} = 10.6 GeV
¹ Not independent of LEE 10 $\Gamma(\tau^- \rightarrow K^-K^+\pi^-\nu_\tau) / \Gamma_{total}$ and $\Gamma(\tau^- \rightarrow \pi^-\pi^+\pi^-\nu_\tau(ex.K^0)) / \Gamma_{total}$ values.				

$$\Gamma(K^-K^+\pi^-\pi^0\nu_\tau)/\Gamma_{total} \quad \Gamma_{107}/\Gamma$$

VALUE (units 10 ⁻⁴)	CL%	EVTs	DOCUMENT ID	TECN	COMMENT
0.61 ± 0.18 OUR FIT					
0.60 ± 0.18 OUR AVERAGE					

0.55 ± 0.14 ± 0.12	48	ARMS	05	CLE3 7.6 fb ⁻¹ , E _{cm} ^{ee} = 10.6 GeV	
7.5 ± 2.9 ± 1.5		BARATE	98	ALEP 1991-1995 LEP runs	
• • • We use the following data for averages but not for fits. • • •					
3.3 ± 1.8 ± 0.7	158	¹ RICHICHI	99	CLEO E _{cm} ^{ee} = 10.6 GeV	
• • • We do not use the following data for averages, fits, limits, etc. • • •					
<27		95	ABBIENDI	00D	OPAL 1990-1995 LEP runs

¹ Not independent of RICHICHI 99 $\Gamma(\tau^- \rightarrow K^-K^+\pi^-\nu_\tau) / \Gamma(\tau^- \rightarrow \pi^-\pi^+\pi^-\nu_\tau(ex.K^0))$ and BALEST 95c $\Gamma(\tau^- \rightarrow h^-h^-\pi^+\nu_\tau(ex.K^0)) / \Gamma_{total}$ values.

$$\Gamma(K^-K^+\pi^-\pi^0\nu_\tau)/\Gamma(\pi^-\pi^+\pi^-\pi^0\nu_\tau(ex.K^0)) \quad \Gamma_{107}/\Gamma_{77}$$

$$\Gamma_{107}/\Gamma_{77} = \Gamma_{107}/(\Gamma_{78} + 0.892\Gamma_{178} + 0.0153\Gamma_{180})$$

VALUE (%)	EVTs	DOCUMENT ID	TECN	COMMENT
0.14 ± 0.04 OUR FIT				
0.79 ± 0.44 ± 0.16	158	¹ RICHICHI	99	CLEO E _{cm} ^{ee} = 10.6 GeV

¹ RICHICHI 99 also quote a 95%CL upper limit of 0.0157 for this measurement.

$$\Gamma(K^-K^+K^-\nu_\tau)/\Gamma_{total} \quad \Gamma_{108}/\Gamma = 0.491\Gamma_{170}/\Gamma$$

VALUE (units 10 ⁻⁵)	CL%	EVTs	DOCUMENT ID	TECN	COMMENT
2.2 ± 0.8 OUR FIT					Error includes scale factor of 5.4.
2.1 ± 0.8 OUR AVERAGE					Error includes scale factor of 5.4.

3.29 ± 0.17 ± ^{+0.19} / _{-0.20}	3.2k	¹ LEE	10	BELL 666 fb ⁻¹ E _{cm} ^{ee} = 10.6 GeV
1.58 ± 0.13 ± 0.12	275	² AUBERT	08	BABR 342 fb ⁻¹ E _{cm} ^{ee} = 10.6 GeV
• • • We do not use the following data for averages, fits, limits, etc. • • •				
< 3.7	90	BRIERE	03	CLE3 E _{cm} ^{ee} = 10.6 GeV
< 19	90	BARATE	98	ALEP 1991-1995 LEP runs

¹ See footnote to LEE 10 $\Gamma(\tau^- \rightarrow \pi^-\pi^+\pi^-\nu_\tau(ex.K^0)) / \Gamma_{total}$ measurement for correlations with other measurements. Not independent of LEE 10 $\Gamma(\tau^- \rightarrow K^-K^+\pi^-\nu_\tau) / \Gamma(\tau^- \rightarrow \pi^-\pi^+\pi^-\nu_\tau(ex.K^0))$ value.

² See footnote to AUBERT 08 $\Gamma(\tau^- \rightarrow \pi^-\pi^+\pi^-\nu_\tau(ex.K^0)) / \Gamma_{total}$ measurement for correlations with other measurements.

$$\Gamma(K^-K^+K^-\nu_\tau)/\Gamma(\pi^-\pi^+\pi^-\nu_\tau(ex.K^0)) \quad \Gamma_{108}/\Gamma_{68}$$

VALUE (units 10 ⁻⁴)	EVTs	DOCUMENT ID	TECN	COMMENT
3.90 ± 0.02 ± ^{+0.22}/_{-0.23}	3.2k	¹ LEE	10	BELL 666 fb ⁻¹ E _{cm} ^{ee} = 10.6 GeV

¹ Not independent of LEE 10 $\Gamma(\tau^- \rightarrow K^-K^+K^-\nu_\tau) / \Gamma_{total}$ and $\Gamma(\tau^- \rightarrow \pi^-\pi^+\pi^-\nu_\tau(ex.K^0)) / \Gamma_{total}$ values.

Lepton Particle Listings

τ

$\Gamma(K^- K^+ K^- \nu_\tau (\text{ex. } \phi))/\Gamma_{\text{total}}$ Γ_{109}/Γ

VALUE	CL%	DOCUMENT ID	TECN	COMMENT
$<2.5 \times 10^{-6}$	90	AUBERT 08	BABR	342 fb^{-1} $E_{\text{cm}}^{\text{ee}} = 10.6 \text{ GeV}$

$\Gamma(K^- K^+ K^- \pi^0 \nu_\tau)/\Gamma_{\text{total}}$ Γ_{110}/Γ

VALUE	CL%	DOCUMENT ID	TECN	COMMENT
$<4.8 \times 10^{-6}$	90	ARMS 05	CLE3	7.6 fb^{-1} , $E_{\text{cm}}^{\text{ee}} = 10.6 \text{ GeV}$

$\Gamma(\pi^- K^+ \pi^- \geq 0 \text{ neut. } \nu_\tau)/\Gamma_{\text{total}}$ Γ_{111}/Γ

VALUE (%)	CL%	DOCUMENT ID	TECN	COMMENT
<0.25	95	BAUER 94	TPC	$E_{\text{cm}}^{\text{ee}} = 29 \text{ GeV}$

$\Gamma(e^- e^- e^+ \bar{\nu}_e \nu_\tau)/\Gamma_{\text{total}}$ Γ_{112}/Γ

VALUE (units 10^{-5})	EVTS	DOCUMENT ID	TECN	COMMENT
$2.8 \pm 1.4 \pm 0.4$	5	ALAM 96	CLEO	$E_{\text{cm}}^{\text{ee}} = 10.6 \text{ GeV}$

$\Gamma(\mu^- e^- e^+ \bar{\nu}_\mu \nu_\tau)/\Gamma_{\text{total}}$ Γ_{113}/Γ

VALUE (units 10^{-5})	CL%	DOCUMENT ID	TECN	COMMENT
<3.2	90	ALAM 96	CLEO	$E_{\text{cm}}^{\text{ee}} = 10.6 \text{ GeV}$

$\Gamma(\pi^- e^- e^+ \nu_\tau)/\Gamma_{\text{total}}$ Γ_{114}/Γ

VALUE (units 10^{-5})	EVTS	DOCUMENT ID	TECN	COMMENT
seen	400	¹ JIN 19	BELL	562 fb^{-1} , $E_{\text{cm}}^{\text{ee}} = 10.6 \text{ GeV}$

• • • We do not use the following data for averages, fits, limits, etc. • • •

$1.46 \pm 0.13 \pm 0.21$	400	¹ JIN 19	BELL	axial-vector, 562 fb^{-1} , $E_{\text{cm}}^{\text{ee}} = 10.6 \text{ GeV}$
$3.01 \pm 0.27 \pm 0.43$	400	¹ JIN 19	BELL	vector, 562 fb^{-1} , $E_{\text{cm}}^{\text{ee}} = 10.6 \text{ GeV}$

¹ JIN 19 measures $B(\tau^- \rightarrow \pi^- e^- e^+ \nu_\tau (m_{\pi^- e^- e^+} > 1.05 \text{ GeV}/c^2)) = (5.90 \pm 0.53 \pm 0.86) \times 10^{-6}$, which is only sensitive to the structure-dependent contribution, and assumes that the decay proceeds with either a pure axial-vector current or a pure vector current to obtain the two respective branching fraction measurements for this mode, which are 100% correlated.

$\Gamma(\pi^- \mu^- \mu^+ \nu_\tau)/\Gamma_{\text{total}}$ Γ_{115}/Γ

VALUE	CL%	DOCUMENT ID	TECN	COMMENT
$<1.14 \times 10^{-5}$	90	JIN 19	BELL	562 fb^{-1} , $E_{\text{cm}}^{\text{ee}} = 10.6 \text{ GeV}$

$\Gamma(3h^- 2h^+ \geq 0 \text{ neutrals } \nu_\tau (\text{ex. } K_S^0 \rightarrow \pi^- \pi^+)(\text{"5-prong"}))/\Gamma_{\text{total}}$ Γ_{116}/Γ

$\Gamma_{116}/\Gamma = (\Gamma_{117} + \Gamma_{123})/\Gamma$

VALUE (%)	EVTS	DOCUMENT ID	TECN	COMMENT
-----------	------	-------------	------	---------

0.099 ± 0.004 OUR FIT
0.107 ± 0.007 OUR AVERAGE Error includes scale factor of 1.1.

$0.170 \pm 0.022 \pm 0.026$		¹ ACHARD 01D	L3	1992-1995 LEP runs
$0.097 \pm 0.005 \pm 0.011$	419	GIBAUT 94B	CLEO	$E_{\text{cm}}^{\text{ee}} = 10.6 \text{ GeV}$
0.102 ± 0.029	13	BYLSMA 87	HRS	$E_{\text{cm}}^{\text{ee}} = 29 \text{ GeV}$

• • • We use the following data for averages but not for fits. • • •

$0.093 \pm 0.009 \pm 0.012$		SCHAEEL 05c	ALEP	1991-1995 LEP runs
$0.115 \pm 0.013 \pm 0.006$	112	² ABREU 01M	DLPH	1992-1995 LEP runs
$0.119 \pm 0.013 \pm 0.008$	119	³ ACKERSTAFF 99E	OPAL	1991-1995 LEP runs

• • • We do not use the following data for averages, fits, limits, etc. • • •

$0.26 \pm 0.06 \pm 0.05$		ACTON 92H	OPAL	$E_{\text{cm}}^{\text{ee}} = 88.2-94.2 \text{ GeV}$
$0.10 \pm 0.05 \pm 0.03$		DECAMP 92c	ALEP	1989-1990 LEP runs
$0.16 \pm 0.13 \pm 0.04$		BEHREND 89B	CELL	$E_{\text{cm}}^{\text{ee}} = 14-47 \text{ GeV}$
$0.3 \pm 0.1 \pm 0.2$		BARTEL 85F	JADE	$E_{\text{cm}}^{\text{ee}} = 34.6 \text{ GeV}$
0.13 ± 0.04	10	BELTRAMI 85	HRS	Repl. by BYLSMA 87
$0.16 \pm 0.08 \pm 0.04$	4	BURCHAT 85	MRK2	$E_{\text{cm}}^{\text{ee}} = 29 \text{ GeV}$
1.0 ± 0.4	10	BEHREND 82	CELL	Repl. by BEHREND 89b

¹ The correlation coefficients between this measurement and the ACHARD 01D measurements of $B(\tau \rightarrow \text{"1-prong"})$ and $B(\tau \rightarrow \text{"3-prong"})$ are -0.082 and -0.19 respectively.

² The correlation coefficients between this measurement and the ABREU 01M measurements of $B(\tau \rightarrow \text{1-prong})$ and $B(\tau \rightarrow \text{3-prong})$ are -0.08 and -0.08 respectively.

³ Not independent of ACKERSTAFF 99E $B(\tau^- \rightarrow 3h^- 2h^+ \nu_\tau (\text{ex. } K^0))$ and $B(\tau^- \rightarrow 3h^- 2h^+ \pi^0 \nu_\tau (\text{ex. } K^0))$ measurements.

$\Gamma(3h^- 2h^+ \nu_\tau (\text{ex. } K^0))/\Gamma_{\text{total}}$ $\Gamma_{117}/\Gamma = (\Gamma_{118} + \Gamma_{120} + 0.0153\Gamma_{185})/\Gamma$

VALUE (units 10^{-4})	EVTS	DOCUMENT ID	TECN	COMMENT
--------------------------	------	-------------	------	---------

8.29 ± 0.31 OUR FIT
8.32 ± 0.35 OUR AVERAGE

$9.7 \pm 1.5 \pm 0.5$	96	¹ ABDALLAH 06A	DLPH	1992-1995 LEP runs
$7.2 \pm 0.9 \pm 1.2$	165	² SCHAEEL 05c	ALEP	1991-1995 LEP runs
$9.1 \pm 1.4 \pm 0.6$	97	ACKERSTAFF 99E	OPAL	1991-1995 LEP runs
$7.7 \pm 0.5 \pm 0.9$	295	GIBAUT 94B	CLEO	$E_{\text{cm}}^{\text{ee}} = 10.6 \text{ GeV}$
$6.4 \pm 2.3 \pm 1.0$	12	ALBRECHT 88B	ARG	$E_{\text{cm}}^{\text{ee}} = 10 \text{ GeV}$
5.1 ± 2.0	7	BYLSMA 87	HRS	$E_{\text{cm}}^{\text{ee}} = 29 \text{ GeV}$

• • • We use the following data for averages but not for fits. • • •

$8.56 \pm 0.05 \pm 0.42$	34k	AUBERT,B 05W	BABR	232 fb^{-1} , $E_{\text{cm}}^{\text{ee}} = 10.6 \text{ GeV}$
--------------------------	-----	--------------	------	--

• • • We do not use the following data for averages, fits, limits, etc. • • •

$8.0 \pm 1.1 \pm 1.3$	58	BUSKULIC 96	ALEP	Repl. by SCHAEEL 05c
6.7 ± 3.0	5	³ BELTRAMI 85	HRS	Repl. by BYLSMA 87

¹ See footnote to ABDALLAH 06A $\Gamma(\tau^- \rightarrow h^- \nu_\tau)/\Gamma_{\text{total}}$ measurement for correlations with other measurements.
² See footnote to SCHAEEL 05c $\Gamma(\tau^- \rightarrow e^- \bar{\nu}_e \nu_\tau)/\Gamma_{\text{total}}$ measurement for correlations with other measurements.
³ The error quoted is statistical only.

$\Gamma(3\pi^- 2\pi^+ \nu_\tau (\text{ex. } K^0, \omega))/\Gamma_{\text{total}}$ $\Gamma_{118}/\Gamma = (\Gamma_{119} + \Gamma_{173})/\Gamma$

VALUE (units 10^{-4})	DOCUMENT ID	TECN	COMMENT
--------------------------	-------------	------	---------

8.27 ± 0.31 OUR FIT
 • • • We use the following data for averages but not for fits. • • •

8.33 ± 0.04 ± 0.43	¹ LEES 12X	BABR	468 fb^{-1} $E_{\text{cm}}^{\text{ee}} = 10.6 \text{ GeV}$
---------------------------	-----------------------	------	--

¹ Not independent of LEES 12X $\Gamma(\tau^- \rightarrow f_1(1285) \pi^- \nu_\tau \rightarrow 3\pi^- 2\pi^+ \nu_\tau)/\Gamma$ and $\Gamma(\tau^- \rightarrow 3\pi^- 2\pi^+ \nu_\tau (\text{ex. } K^0, \omega, f_1(1285)))/\Gamma$ values.

$\Gamma(3\pi^- 2\pi^+ \nu_\tau (\text{ex. } K^0, \omega, f_1(1285)))/\Gamma_{\text{total}}$ Γ_{119}/Γ

VALUE (units 10^{-4})	EVTS	DOCUMENT ID	TECN	COMMENT
--------------------------	------	-------------	------	---------

7.75 ± 0.30 OUR FIT
7.68 ± 0.04 ± 0.40 69k LEES 12X BABR 468 fb^{-1} $E_{\text{cm}}^{\text{ee}} = 10.6 \text{ GeV}$

$\Gamma(K^- 2\pi^- 2\pi^+ \nu_\tau (\text{ex. } K^0))/\Gamma_{\text{total}}$ Γ_{120}/Γ

VALUE (units 10^{-6})	DOCUMENT ID	TECN	COMMENT
--------------------------	-------------	------	---------

0.6 ± 1.2 OUR FIT
0.6 ± 0.5 ± 1.1 ¹LEES 12X BABR 468 fb^{-1} $E_{\text{cm}}^{\text{ee}} = 10.6 \text{ GeV}$
¹ LEES 12X measurement corresponds to the lower limit of $< 2.4 \times 10^{-6}$ at 90% CL.

$\Gamma(K^+ 3\pi^- \pi^+ \nu_\tau)/\Gamma_{\text{total}}$ Γ_{121}/Γ

VALUE	CL%	DOCUMENT ID	TECN	COMMENT
-------	-----	-------------	------	---------

$<5.0 \times 10^{-6}$ 90 LEES 12X BABR 468 fb^{-1} $E_{\text{cm}}^{\text{ee}} = 10.6 \text{ GeV}$

$\Gamma(K^+ K^- 2\pi^- \pi^+ \nu_\tau)/\Gamma_{\text{total}}$ Γ_{122}/Γ

VALUE	CL%	DOCUMENT ID	TECN	COMMENT
-------	-----	-------------	------	---------

$<4.5 \times 10^{-7}$ 90 LEES 12X BABR 468 fb^{-1} $E_{\text{cm}}^{\text{ee}} = 10.6 \text{ GeV}$

$\Gamma(3h^- 2h^+ \pi^0 \nu_\tau (\text{ex. } K^0))/\Gamma_{\text{total}}$ $\Gamma_{123}/\Gamma = (\Gamma_{124} + \Gamma_{127})/\Gamma$

VALUE (units 10^{-4})	EVTS	DOCUMENT ID	TECN	COMMENT
--------------------------	------	-------------	------	---------

1.65 ± 0.11 OUR FIT
1.74 ± 0.27 OUR AVERAGE

$1.6 \pm 1.2 \pm 0.6$	13	¹ ABDALLAH 06A	DLPH	1992-1995 LEP runs
$2.1 \pm 0.7 \pm 0.9$	95	² SCHAEEL 05c	ALEP	1991-1995 LEP runs
$1.7 \pm 0.2 \pm 0.2$	231	ANASTASSOV 01	CLEO	$E_{\text{cm}}^{\text{ee}} = 10.6 \text{ GeV}$
$2.7 \pm 1.8 \pm 0.9$	23	ACKERSTAFF 99E	OPAL	1991-1995 LEP runs

• • • We do not use the following data for averages, fits, limits, etc. • • •

$1.8 \pm 0.7 \pm 1.2$	18	BUSKULIC 96	ALEP	Repl. by SCHAEEL 05c
$1.9 \pm 0.4 \pm 0.4$	31	GIBAUT 94B	CLEO	Repl. by ANASTASSOV 01
5.1 ± 2.2	6	BYLSMA 87	HRS	$E_{\text{cm}}^{\text{ee}} = 29 \text{ GeV}$
6.7 ± 3.0	5	³ BELTRAMI 85	HRS	Repl. by BYLSMA 87

¹ See footnote to ABDALLAH 06A $\Gamma(\tau^- \rightarrow h^- \nu_\tau)/\Gamma_{\text{total}}$ measurement for correlations with other measurements.

² SCHAEEL 05c quote $(1.4 \pm 0.7 \pm 0.9) \times 10^{-4}$. We add 0.7×10^{-4} to remove their correction for $\tau^- \rightarrow \eta \pi^- \pi^+ \pi^- \nu_\tau \rightarrow 3\pi^- 2\pi^+ \pi^0 \nu_\tau$ and $\tau^- \rightarrow K^*(892) \eta \nu_\tau \rightarrow 3\pi^- 2\pi^+ \pi^0 \nu_\tau$ decays. See footnote to SCHAEEL 05c $\Gamma(\tau^- \rightarrow e^- \bar{\nu}_e \nu_\tau)/\Gamma_{\text{total}}$ measurement for correlations with other measurements.

³ The error quoted is statistical only.

$\Gamma(3\pi^- 2\pi^+ \pi^0 \nu_\tau (\text{ex. } K^0))/\Gamma_{\text{total}}$ Γ_{124}/Γ

$\Gamma_{124}/\Gamma = (\Gamma_{126} + 0.2302\Gamma_{160} + 0.892\Gamma_{185})/\Gamma$

VALUE (units 10^{-4})	DOCUMENT ID	TECN	COMMENT
--------------------------	-------------	------	---------

1.63 ± 0.11 OUR FIT
 • • • We use the following data for averages but not for fits. • • •

1.65 ± 0.05 ± 0.09	¹ LEES 12X	BABR	468 fb^{-1} $E_{\text{cm}}^{\text{ee}} = 10.6 \text{ GeV}$
---------------------------	-----------------------	------	--

¹ Not independent of LEES 12X measurements of $\Gamma(\tau^- \rightarrow 2\pi^- \pi^+ \omega \nu_\tau (\text{ex. } K^0))/\Gamma$, $\Gamma(\tau^- \rightarrow \eta \pi^- \pi^+ \pi^- \nu_\tau (\text{ex. } K^0))/\Gamma$, and $\Gamma(\tau^- \rightarrow 3\pi^- 2\pi^+ \pi^0 \nu_\tau (\text{ex. } K^0, \eta, \omega, f_1(1285)))/\Gamma$.

$\Gamma(3\pi^- 2\pi^+ \pi^0 \nu_\tau (\text{ex. } K^0, \eta, f_1(1285)))/\Gamma_{\text{total}}$ Γ_{125}/Γ

VALUE (units 10^{-4})	DOCUMENT ID	TECN	COMMENT
--------------------------	-------------	------	---------

1.11 ± 0.04 ± 0.09 ¹LEES 12X BABR 468 fb^{-1} $E_{\text{cm}}^{\text{ee}} = 10.6 \text{ GeV}$
¹ Not independent of LEES 12X $\Gamma(\tau^- \rightarrow 2\pi^- \pi^+ \omega \nu_\tau (\text{ex. } K^0))/\Gamma$ and $\Gamma(\tau^- \rightarrow 3\pi^- 2\pi^+ \pi^0 \nu_\tau (\text{ex. } K^0, \eta, \omega, f_1(1285)))/\Gamma$ values.

$\Gamma(3\pi^- 2\pi^+ \pi^0 \nu_\tau (\text{ex. } K^0, \eta, \omega, f_1(1285)))/\Gamma_{\text{total}}$ Γ_{126}/Γ

VALUE (units 10^{-4})	EVTS	DOCUMENT ID	TECN	COMMENT
--------------------------	------	-------------	------	---------

0.38 ± 0.09 OUR FIT
0.36 ± 0.03 ± 0.09 7.3k LEES 12X BABR 468 fb^{-1} $E_{\text{cm}}^{\text{ee}} = 10.6 \text{ GeV}$

$\Gamma(K^- 2\pi^- 2\pi^+ \pi^0 \nu_\tau (\text{ex. } K^0))/\Gamma_{\text{total}}$ Γ_{127}/Γ

VALUE (units 10^{-6})	DOCUMENT ID	TECN	COMMENT
--------------------------	-------------	------	---------

1.1 ± 0.6 OUR FIT
1.1 ± 0.4 ± 0.4 ¹LEES 12X BABR 468 fb^{-1} $E_{\text{cm}}^{\text{ee}} = 10.6 \text{ GeV}$
¹ LEES 12X measurement corresponds to the lower limit of $< 1.9 \times 10^{-6}$ at 90% CL.

$\Gamma(K^+ 3\pi^- \pi^+ \pi^0 \nu_\tau)/\Gamma_{total}$					Γ_{128}/Γ
VALUE	CL%	DOCUMENT ID	TECN	COMMENT	
$< 8 \times 10^{-7}$	90	LEES	12X	BABR 468 fb ⁻¹ $E_{cm}^{ee} = 10.6$ GeV	

$\Gamma(3h^- 2h^+ 2\pi^0 \nu_\tau)/\Gamma_{total}$					Γ_{129}/Γ
VALUE	CL%	DOCUMENT ID	TECN	COMMENT	
$< 3.4 \times 10^{-6}$	90	AUBERT,B	06	BABR 232 fb ⁻¹ $E_{cm}^{ee} = 10.6$ GeV	

• • • We do not use the following data for averages, fits, limits, etc. • • •
 $< 1.1 \times 10^{-4}$ 90 GIBAUT 94B CLEO $E_{cm}^{ee} = 10.6$ GeV

$\Gamma((5\pi^-) \nu_\tau)/\Gamma_{total}$					Γ_{130}/Γ
VALUE (%)		DOCUMENT ID	TECN	COMMENT	
0.78 ± 0.05	OUR FIT				

• • • We use the following data for averages but not for fits. • • •
 $0.61 \pm 0.06 \pm 0.08$ 1 GIBAUT 94B CLEO $E_{cm}^{ee} = 10.6$ GeV

1 Not independent of GIBAUT 94B $B(3h^- 2h^+ \nu_\tau)$, PROCARIO 93 $B(h^- 4\pi^0 \nu_\tau)$, and BORTOLETTO 93 $B(2h^- h^+ 2\pi^0 \nu_\tau)/B(\text{"3prong"})$ measurements. Result is corrected for η contributions.

$\Gamma(4h^- 3h^+ \geq 0 \text{ neutrals } \nu_\tau (\text{"7-prong"}))/\Gamma_{total}$					Γ_{131}/Γ
VALUE	CL%	DOCUMENT ID	TECN	COMMENT	
$< 3.0 \times 10^{-7}$	90	AUBERT,B	05F	BABR 232 fb ⁻¹ , $E_{cm}^{ee} = 10.6$ GeV	

• • • We do not use the following data for averages, fits, limits, etc. • • •
 $< 1.8 \times 10^{-5}$ 95 ACKERSTAFF 97J OPAL 1990-1995 LEP runs
 $< 2.4 \times 10^{-6}$ 90 EDWARDS 97B CLEO $E_{cm}^{ee} = 10.6$ GeV
 $< 2.9 \times 10^{-4}$ 90 BYLSMA 87 HRS $E_{cm}^{ee} = 29$ GeV

$\Gamma(4h^- 3h^+ \nu_\tau)/\Gamma_{total}$					Γ_{132}/Γ
VALUE	CL%	DOCUMENT ID	TECN	COMMENT	
$< 4.3 \times 10^{-7}$	90	AUBERT,B	05F	BABR 232 fb ⁻¹ , $E_{cm}^{ee} = 10.6$ GeV	

$\Gamma(4h^- 3h^+ \pi^0 \nu_\tau)/\Gamma_{total}$					Γ_{133}/Γ
VALUE	CL%	DOCUMENT ID	TECN	COMMENT	
$< 2.5 \times 10^{-7}$	90	AUBERT,B	05F	BABR 232 fb ⁻¹ , $E_{cm}^{ee} = 10.6$ GeV	

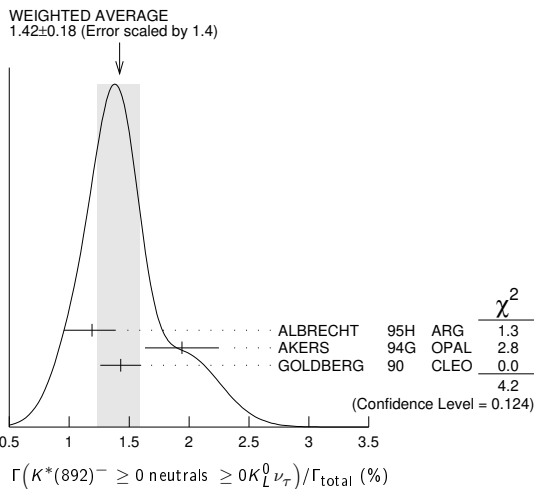
$\Gamma(X^-(S=-1) \nu_\tau)/\Gamma_{total}$					Γ_{134}/Γ
VALUE (%)		DOCUMENT ID	TECN	COMMENT	
2.92 ± 0.04	OUR FIT				

• • • We use the following data for averages but not for fits. • • •
 2.87 ± 0.12 1 BARATE 99R ALEP 1991-1995 LEP runs

1 BARATE 99R perform a combined analysis of all ALEPH LEP 1 data on τ branching fraction measurements for decay modes having total strangeness equal to -1.

$\Gamma(K^*(892)^- \geq 0 \text{ neutrals } \geq 0 K_L^0 \nu_\tau)/\Gamma_{total}$					Γ_{135}/Γ
VALUE (%)	EVTS	DOCUMENT ID	TECN	COMMENT	
1.42 ± 0.18	OUR AVERAGE			Error includes scale factor of 1.4. See the ideogram below.	

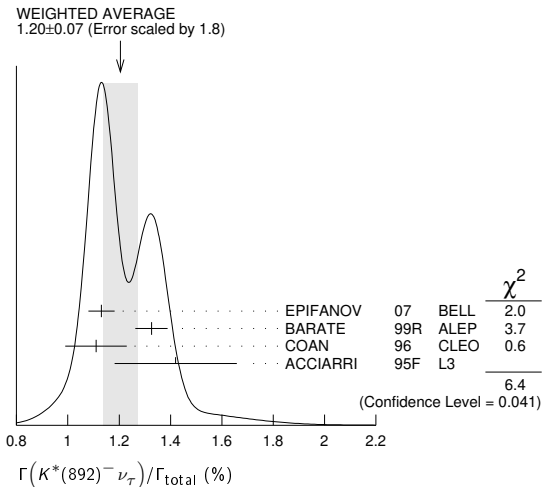
1.19 ± 0.15 $^{+0.13}_{-0.18}$ 104 ALBRECHT 95H ARG $E_{cm}^{ee} = 9.4-10.6$ GeV
 1.94 $\pm 0.27 \pm 0.15$ 74 1 AKERS 94G OPAL $E_{cm}^{ee} = 88-94$ GeV
 1.43 $\pm 0.11 \pm 0.13$ 475 2 GOLDBERG 90 CLEO $E_{cm}^{ee} = 9.4-10.9$ GeV



1 AKERS 94G reject events in which a K_S^0 accompanies the $K^*(892)^-$. We do not correct for them.
 2 GOLDBERG 90 estimates that 10% of observed $K^*(892)$ are accompanied by a π^0 .

$\Gamma(K^*(892)^- \nu_\tau)/\Gamma_{total}$					Γ_{136}/Γ
VALUE (%)	EVTS	DOCUMENT ID	TECN	COMMENT	
1.20 ± 0.07	OUR AVERAGE			Error includes scale factor of 1.8. See the ideogram below.	

1.131 $\pm 0.006 \pm 0.051$ 49k 1 EPIFANOV 07 BELL 351 fb⁻¹ $E_{cm}^{ee} = 10.6$ GeV
 1.326 ± 0.063 BARATE 99R ALEP 1991-1995 LEP runs
 1.11 ± 0.12 2 COAN 96 CLEO $E_{cm}^{ee} \approx 10.6$ GeV
 1.42 $\pm 0.22 \pm 0.09$ 3 ACCIARRI 95F L3 1991-1993 LEP runs
 • • • We do not use the following data for averages, fits, limits, etc. • • •
 1.39 $\pm 0.09 \pm 0.10$ 4 BUSKULIC 96 ALEP Repl. by BARATE 99R
 1.45 $\pm 0.13 \pm 0.11$ 273 5 BUSKULIC 94F ALEP Repl. by BUSKULIC 96
 1.23 ± 0.21 $^{+0.11}_{-0.21}$ 54 6 ALBRECHT 88L ARG $E_{cm}^{ee} = 10$ GeV
 1.9 $\pm 0.3 \pm 0.4$ 44 7 TSCHIRHART 88 HRS $E_{cm}^{ee} = 29$ GeV
 1.5 $\pm 0.4 \pm 0.4$ 15 8 AIHARA 87C TPC $E_{cm}^{ee} = 29$ GeV
 1.3 $\pm 0.3 \pm 0.3$ 31 YELTON 86 MRK2 $E_{cm}^{ee} = 29$ GeV
 1.7 ± 0.7 11 DORFAN 81 MRK2 $E_{cm}^{ee} = 4.2-6.7$ GeV



1 EPIFANOV 07 quote $B(\tau^- \rightarrow K^*(892)^- \nu_\tau) B(K^*(892)^- \rightarrow K_S^0 \pi^-) = (3.77 \pm 0.02(\text{stat}) \pm 0.12(\text{syst}) \pm 0.12(\text{mod})) \times 10^{-3}$. We add the systematic and model uncertainties in quadrature and divide by $B(K^*(892)^- \rightarrow K_S^0 \pi^-) = 0.3333$.
 2 Not independent of COAN 96 $B(\pi^- \bar{K}^0 \nu_\tau)$ and BATTLE 94 $B(K^- \pi^0 \nu_\tau)$ measurements. K final states are consistent with and assumed to originate from $K^*(892)^-$ production.
 3 This result is obtained from their $B(\pi^- \bar{K}^0 \nu_\tau)$ assuming all those decays originate in $K^*(892)^-$ decays.
 4 Not independent of BUSKULIC 96 $B(\pi^- \bar{K}^0 \nu_\tau)$ and $B(K^- \pi^0 \nu_\tau)$ measurements.
 5 BUSKULIC 94F obtain this result from BUSKULIC 94F $B(\bar{K}^0 \pi^- \nu_\tau)$ and BUSKULIC 94E $B(K^- \pi^0 \nu_\tau)$ assuming all of those decays originate in $K^*(892)^-$ decays.
 6 The authors divide by $\Gamma_2/\Gamma = 0.865$ to obtain this result.
 7 Not independent of TSCHIRHART 88 $\Gamma(\tau^- \rightarrow h^- \bar{K}^0 \geq 0 \text{ neutrals } \geq 0 K_L^0 \nu_\tau) / \Gamma$.
 8 Decay π^- identified in this experiment, is assumed in the others.

$\Gamma(K^*(892)^- \nu_\tau)/\Gamma(\pi^- \pi^0 \nu_\tau)$					Γ_{136}/Γ_{14}
VALUE	EVTS	DOCUMENT ID	TECN	COMMENT	
0.075 ± 0.027		1 ABREU 94K	DLPH	LEP 1992 Z data	

1 ABREU 94K quote $B(\tau^- \rightarrow K^*(892)^- \nu_\tau) B(K^*(892)^- \rightarrow K^- \pi^0) / B(\tau^- \rightarrow \rho^- \nu_\tau) = 0.025 \pm 0.009$. We divide by $B(K^*(892)^- \rightarrow K^- \pi^0) = 0.333$ to obtain this result.

$\Gamma(K^*(892)^- \nu_\tau \rightarrow \pi^- \bar{K}^0 \nu_\tau) / \Gamma(\pi^- \bar{K}^0 \nu_\tau)$					Γ_{137}/Γ_{36}
VALUE	EVTS	DOCUMENT ID	TECN	COMMENT	
0.933 ± 0.027	49k	EPIFANOV 07	BELL	351 fb ⁻¹ $E_{cm}^{ee} = 10.6$ GeV	

$\Gamma(K^*(892)^0 K^- \geq 0 \text{ neutrals } \nu_\tau) / \Gamma_{total}$					Γ_{138}/Γ
VALUE (%)	EVTS	DOCUMENT ID	TECN	COMMENT	
$0.32 \pm 0.08 \pm 0.12$	119	GOLDBERG 90	CLEO	$E_{cm}^{ee} = 9.4-10.9$ GeV	

$\Gamma(K^*(892)^0 K^- \nu_\tau) / \Gamma_{total}$					Γ_{139}/Γ
VALUE (%)	EVTS	DOCUMENT ID	TECN	COMMENT	
0.21 ± 0.04	OUR AVERAGE				

0.213 ± 0.048 1 BARATE 98 ALEP 1991-1995 LEP runs
 0.20 $\pm 0.05 \pm 0.04$ 47 ALBRECHT 95H ARG $E_{cm}^{ee} = 9.4-10.6$ GeV

1 BARATE 98 measure the $K^- (\rho^0 \rightarrow \pi^+ \pi^-)$ fraction in $\tau^- \rightarrow K^- \pi^+ \pi^- \nu_\tau$ decays to be $(35 \pm 11)\%$ and derive this result from their measurement of $\Gamma(\tau^- \rightarrow K^- \pi^+ \pi^- \nu_\tau) / \Gamma_{total}$ assuming the intermediate states are all $K^- \rho$ and $K^- K^*(892)^0$.

$\Gamma(\bar{K}^*(892)^0 \pi^- \geq 0 \text{ neutrals } \nu_\tau) / \Gamma_{total}$					Γ_{140}/Γ
VALUE (%)	EVTS	DOCUMENT ID	TECN	COMMENT	
$0.38 \pm 0.11 \pm 0.13$	105	GOLDBERG 90	CLEO	$E_{cm}^{ee} = 9.4-10.9$ GeV	

Lepton Particle Listings

τ

$\Gamma(K^*(892)^0 \pi^- \nu_\tau) / \Gamma_{total}$				Γ_{141} / Γ
VALUE (%)	EVTS	DOCUMENT ID	TECN	COMMENT
0.22 ± 0.05	OUR AVERAGE			
0.209 ± 0.058		1 BARATE	98 ALEP	1991–1995 LEP runs
0.25 ± 0.10 ± 0.05	27	ALBRECHT	95H ARG	$E_{cm}^{ee} = 9.4\text{--}10.6$ GeV

¹ BARATE 98 measure the $K^- K^*(892)^0$ fraction in $\tau^- \rightarrow K^- K^+ \pi^- \nu_\tau$ decays to be $(87 \pm 13)\%$ and derive this result from their measurement of $\Gamma(\tau^- \rightarrow K^- K^+ \pi^- \nu_\tau) / \Gamma_{total}$.

$\Gamma((K^*(892)^0 \pi^-) \nu_\tau \rightarrow \pi^- \bar{K}^0 \pi^0 \nu_\tau) / \Gamma_{total}$				Γ_{142} / Γ
VALUE (%)	EVTS	DOCUMENT ID	TECN	COMMENT
0.10 ± 0.04	OUR AVERAGE			
0.097 ± 0.044 ± 0.036		1 BARATE	99K ALEP	1991–1995 LEP runs
0.106 ± 0.037 ± 0.032		2 BARATE	98E ALEP	1991–1995 LEP runs

¹ BARATE 99K measure K^0 's by detecting K_S^0 's in their hadron calorimeter. They determine the $\bar{K}^0 \rho^-$ fraction in $\tau^- \rightarrow \pi^- \bar{K}^0 \pi^0 \nu_\tau$ decays to be $(0.72 \pm 0.12 \pm 0.10)$ and multiply their $B(\pi^- \bar{K}^0 \pi^0 \nu_\tau)$ measurement by one minus this fraction to obtain the quoted result.
² BARATE 98E reconstruct K^0 's using $K_S^0 \rightarrow \pi^+ \pi^-$ decays. They determine the $\bar{K}^0 \rho^-$ fraction in $\tau^- \rightarrow \pi^- \bar{K}^0 \pi^0 \nu_\tau$ decays to be $(0.64 \pm 0.09 \pm 0.10)$ and multiply their $B(\pi^- \bar{K}^0 \pi^0 \nu_\tau)$ measurement by one minus this fraction to obtain the quoted result.

$\Gamma(K_1(1270)^- \nu_\tau) / \Gamma_{total}$				Γ_{143} / Γ
VALUE (%)	EVTS	DOCUMENT ID	TECN	COMMENT
0.47 ± 0.11	OUR AVERAGE			
0.48 ± 0.11		BARATE	99R ALEP	1991–1995 LEP runs
0.41 $^{+0.41}_{-0.35}$ ± 0.10	5	1 BAUER	94 TPC	$E_{cm}^{ee} = 29$ GeV

¹ We multiply 0.41% by 0.25, the relative systematic error quoted by BAUER 94, to obtain the systematic error.

$\Gamma(K_1(1400)^- \nu_\tau) / \Gamma_{total}$				Γ_{144} / Γ
VALUE (%)	EVTS	DOCUMENT ID	TECN	COMMENT
0.17 ± 0.26	OUR AVERAGE			
0.05 ± 0.17		BARATE	99R ALEP	1991–1995 LEP runs
0.76 $^{+0.40}_{-0.33}$ ± 0.20	11	1 BAUER	94 TPC	$E_{cm}^{ee} = 29$ GeV

¹ We multiply 0.76% by 0.25, the relative systematic error quoted by BAUER 94, to obtain the systematic error.

$[\Gamma(K_1(1270)^- \nu_\tau) + \Gamma(K_1(1400)^- \nu_\tau)] / \Gamma_{total}$				$(\Gamma_{143} + \Gamma_{144}) / \Gamma$
VALUE (%)	EVTS	DOCUMENT ID	TECN	COMMENT
1.17 $^{+0.41}_{-0.37}$ ± 0.29	16	1 BAUER	94 TPC	$E_{cm}^{ee} = 29$ GeV

¹ We multiply 1.17% by 0.25, the relative systematic error quoted by BAUER 94, to obtain the systematic error. Not independent of BAUER 94 $B(K_1(1270)^- \nu_\tau)$ and BAUER 94 $B(K_1(1400)^- \nu_\tau)$ measurements.

$\Gamma(K_1(1270)^- \nu_\tau) / [\Gamma(K_1(1270)^- \nu_\tau) + \Gamma(K_1(1400)^- \nu_\tau)]$				$\Gamma_{143} / (\Gamma_{143} + \Gamma_{144})$
VALUE (%)	EVTS	DOCUMENT ID	TECN	COMMENT
0.69 ± 0.15	OUR AVERAGE			
0.71 ± 0.16 ± 0.11		1 ABBIENDI	00D OPAL	1990–1995 LEP runs
0.66 ± 0.19 ± 0.13		2 ASNER	00B CLEO	$E_{cm}^{ee} = 10.6$ GeV

¹ ABBIENDI 00D assume the resonance structure of $\tau^- \rightarrow K^- \pi^+ \pi^- \nu_\tau$ decays is dominated by the $K_1(1270)^-$ and $K_1(1400)^-$ resonances.
² ASNER 00B assume the resonance structure of $\tau^- \rightarrow K^- \pi^+ \pi^- \nu_\tau$ (ex. K^0) decays is dominated by $K_1(1270)^-$ and $K_1(1400)^-$ resonances.

$\Gamma(K^*(1410)^- \nu_\tau) / \Gamma_{total}$				Γ_{145} / Γ
VALUE (units 10^{-3})	EVTS	DOCUMENT ID	TECN	COMMENT
1.5 $^{+1.4}_{-1.0}$		BARATE	99R ALEP	1991–1995 LEP runs

$\Gamma(K_0^*(1430)^- \nu_\tau) / \Gamma_{total}$				Γ_{146} / Γ
VALUE (units 10^{-3})	CL%	DOCUMENT ID	TECN	COMMENT
< 0.5	95	BARATE	99R ALEP	1991–1995 LEP runs

$\Gamma(K_2^*(1430)^- \nu_\tau) / \Gamma_{total}$				Γ_{147} / Γ	
VALUE (%)	CL%	EVTS	DOCUMENT ID	TECN	COMMENT
< 0.3	95		TSCHIRHART	88 HRS	$E_{cm}^{ee} = 29$ GeV

• • • We do not use the following data for averages, fits, limits, etc. • • •

VALUE (%)	CL%	EVTS	DOCUMENT ID	TECN	COMMENT
< 0.33	95		1 ACCIARRI	95F L3	1991–1993 LEP runs
< 0.9	95	0	DORFAN	81 MRK2	$E_{cm}^{ee} = 4.2\text{--}6.7$ GeV

¹ ACCIARRI 95F quote $B(\tau^- \rightarrow K^*(1430)^- \rightarrow \pi^- \bar{K}^0 \nu_\tau) < 0.11\%$. We divide by $B(K^*(1430)^- \rightarrow \pi^- \bar{K}^0) = 0.33$ to obtain the limit shown.

$\Gamma(a_0(980)^- \geq 0 \text{ neutrals } \nu_\tau) / \Gamma_{total} \times B(a_0(980)^- \rightarrow K^0 K^-)$				$\Gamma_{148} / \Gamma \times B$
VALUE (units 10^{-4})	CL%	DOCUMENT ID	TECN	COMMENT
< 2.8	90	GOLDBERG	90 CLEO	$E_{cm}^{ee} = 9.4\text{--}10.9$ GeV

$\Gamma(\eta \pi^- \nu_\tau) / \Gamma_{total}$				Γ_{149} / Γ	
VALUE (units 10^{-4})	CL%	EVTS	DOCUMENT ID	TECN	COMMENT
< 0.99	95		1 DEL-AMO-SA...	BABR	$470 \text{ fb}^{-1} E_{cm}^{ee} = 10.6$ GeV

• • • We do not use the following data for averages, fits, limits, etc. • • •

VALUE (%)	CL%	EVTS	DOCUMENT ID	TECN	COMMENT
< 6.2	95		BUSKULIC	97C ALEP	1991–1994 LEP runs
< 1.4	95	0	BARTELT	96 CLEO	$E_{cm}^{ee} \approx 10.6$ GeV
< 3.4	95		ARTUSO	92 CLEO	$E_{cm}^{ee} \approx 10.6$ GeV
< 90	95		ALBRECHT	88M ARG	$E_{cm}^{ee} \approx 10$ GeV
< 140	90		BEHREND	88 CELL	$E_{cm}^{ee} = 14\text{--}46.8$ GeV
< 180	95		BARINGER	87 CLEO	$E_{cm}^{ee} = 10.5$ GeV
< 250	90	0	COFFMAN	87 MRK3	$E_{cm}^{ee} = 3.77$ GeV
510 ± 100 ± 120	65		DERRICK	87 HRS	$E_{cm}^{ee} = 29$ GeV
< 100	95		GAN	87B MRK2	$E_{cm}^{ee} = 29$ GeV

¹ DEL-AMO-SANCHEZ 11E also quote $B(\tau^- \rightarrow \eta \pi^- \nu_\tau) = (3.4 \pm 3.4 \pm 2.1) \times 10^{-5}$.

$\Gamma(\eta \pi^- \pi^0 \nu_\tau) / \Gamma_{total}$				Γ_{150} / Γ	
VALUE (units 10^{-3})	CL%	EVTS	DOCUMENT ID	TECN	COMMENT

1.39 ± 0.07 OUR FIT
1.38 ± 0.09 OUR AVERAGE Error includes scale factor of 1.2.
 1.35 ± 0.03 ± 0.07 6.0k INAMI 09 BELL $490 \text{ fb}^{-1} E_{cm}^{ee} = 10.6$ GeV
 1.8 ± 0.4 ± 0.2 BUSKULIC 97C ALEP 1991–1994 LEP runs
 1.7 ± 0.2 ± 0.2 125 ARTUSO 92 CLEO $E_{cm}^{ee} \approx 10.6$ GeV
 • • • We do not use the following data for averages, fits, limits, etc. • • •
 < 11.0 95 ALBRECHT 88M ARG $E_{cm}^{ee} \approx 10$ GeV
 < 21.0 95 BARINGER 87 CLEO $E_{cm}^{ee} = 10.5$ GeV
 42.0 $^{+7.0}_{-12.0}$ ± 16.0 1 GAN 87 MRK2 $E_{cm}^{ee} = 29$ GeV
¹ Highly correlated with GAN 87 $\Gamma(\pi^- 3\pi^0 \nu_\tau) / \Gamma_{total}$ value.

$\Gamma(\eta \pi^- \pi^0 \pi^0 \nu_\tau) / \Gamma_{total}$				Γ_{151} / Γ	
VALUE (units 10^{-4})	CL%	EVTS	DOCUMENT ID	TECN	COMMENT

2.0 ± 0.4 OUR FIT
1.81 ± 0.31 OUR AVERAGE
 2.01 ± 0.34 ± 0.22 381 LEES 12X BABR $468 \text{ fb}^{-1} E_{cm}^{ee} = 10.6$ GeV
 • • • We use the following data for averages but not for fits. • • •
 1.5 ± 0.5 30 1 A NASTASSOV 01 CLEO $E_{cm}^{ee} = 10.6$ GeV
 • • • We do not use the following data for averages, fits, limits, etc. • • •
 1.4 ± 0.6 ± 0.3 15 2 BERGFELD 97 CLEO Repl. by ANASTASSOV 01
 < 4.3 95 ARTUSO 92 CLEO $E_{cm}^{ee} \approx 10.6$ GeV
 < 120 95 ALBRECHT 88M ARG $E_{cm}^{ee} \approx 10$ GeV
¹ Weighted average of BERGFELD 97 and ANASTASSOV 01 value of $(1.5 \pm 0.6 \pm 0.3) \times 10^{-4}$ obtained using η 's reconstructed from $\eta \rightarrow \pi^+ \pi^- \pi^0$ decays.
² BERGFELD 97 reconstruct η 's using $\eta \rightarrow \gamma \gamma$ decays.

$\Gamma(\eta K^- \nu_\tau) / \Gamma_{total}$				Γ_{152} / Γ	
VALUE (units 10^{-4})	CL%	EVTS	DOCUMENT ID	TECN	COMMENT

1.55 ± 0.08 OUR FIT
1.54 ± 0.08 OUR AVERAGE
 1.42 ± 0.11 ± 0.07 690 DEL-AMO-SA...11E BABR $470 \text{ fb}^{-1} E_{cm}^{ee} = 10.6$ GeV
 1.58 ± 0.05 ± 0.09 1.6k INAMI 09 BELL $490 \text{ fb}^{-1} E_{cm}^{ee} = 10.6$ GeV
 2.9 $^{+1.3}_{-1.2}$ ± 0.7 BUSKULIC 97C ALEP 1991–1994 LEP runs
 2.6 ± 0.5 ± 0.5 85 BARTELT 96 CLEO $E_{cm}^{ee} \approx 10.6$ GeV
 • • • We do not use the following data for averages, fits, limits, etc. • • •
 < 4.7 95 ARTUSO 92 CLEO $E_{cm}^{ee} \approx 10.6$ GeV

$\Gamma(\eta K^*(892)^- \nu_\tau) / \Gamma_{total}$				Γ_{153} / Γ
VALUE (units 10^{-4})	EVTS	DOCUMENT ID	TECN	COMMENT

1.38 ± 0.15 OUR AVERAGE
 1.34 ± 0.12 ± 0.09 245 1 INAMI 09 BELL $490 \text{ fb}^{-1} E_{cm}^{ee} = 10.6$ GeV
 2.90 ± 0.80 ± 0.42 25 BISHAI 99 CLEO $E_{cm}^{ee} = 10.6$ GeV
¹ Not independent of INAMI 09 $B(\tau^- \rightarrow \eta K^- \pi^0 \nu_\tau)$ and $B(\tau^- \rightarrow \eta \bar{K}^0 \pi^- \nu_\tau)$ values.

$\Gamma(\eta K^- \pi^0 \nu_\tau) / \Gamma_{total}$				Γ_{154} / Γ
VALUE (units 10^{-4})	EVTS	DOCUMENT ID	TECN	COMMENT

0.48 ± 0.12 OUR FIT
0.48 ± 0.12 OUR AVERAGE
 0.46 ± 0.11 ± 0.04 270 INAMI 09 BELL $490 \text{ fb}^{-1} E_{cm}^{ee} = 10.6$ GeV
 1.77 ± 0.56 ± 0.71 36 BISHAI 99 CLEO $E_{cm}^{ee} = 10.6$ GeV

$\Gamma(\eta K^- \pi^0 (\text{non-}K^*(892)^-) \nu_\tau) / \Gamma_{total}$				Γ_{155} / Γ
VALUE	CL%	DOCUMENT ID	TECN	COMMENT
< 3.5 × 10⁻⁵	90	INAMI	09 BELL	$490 \text{ fb}^{-1} E_{cm}^{ee} = 10.6$ GeV

$\Gamma(\eta K^0 \pi^- \nu_\tau)/\Gamma_{total}$ Γ_{156}/Γ

VALUE (units 10^{-4})	EVTS	DOCUMENT ID	TECN	COMMENT
0.94 ± 0.15 OUR FIT				
0.93 ± 0.15 OUR AVERAGE				
0.88 ± 0.14 ± 0.06	161	¹ INAMI	09 BELL	490 fb ⁻¹ $E_{cm}^{ee} = 10.6$ GeV
2.20 ± 0.70 ± 0.22	15	² BISHAI	99 CLEO	$E_{cm}^{ee} = 10.6$ GeV

¹ We multiply the INAMI 09 measurement $B(\tau^- \rightarrow \eta K_S^0 \pi^- \nu_\tau) = (0.44 \pm 0.07 \pm 0.03) \times 10^{-4}$ by 2 to obtain the listed value.
² We multiply the BISHAI 99 measurement $B(\tau^- \rightarrow \eta K_S^0 \pi^- \nu_\tau) = (1.10 \pm 0.35 \pm 0.11) \times 10^{-4}$ by 2 to obtain the listed value.

$\Gamma(\eta K^0 \pi^- \pi^0 \nu_\tau)/\Gamma_{total}$ Γ_{157}/Γ

VALUE	CL%	DOCUMENT ID	TECN	COMMENT
< 5.0 × 10⁻⁵	90	¹ INAMI	09 BELL	490 fb ⁻¹ $E_{cm}^{ee} = 10.6$ GeV

¹ We multiply the INAMI 09 measurement $B(\tau^- \rightarrow \eta K_S^0 \pi^- \pi^0 \nu_\tau) < 2.5 \times 10^{-5}$ by 2 to obtain the listed value.

$\Gamma(\eta K^- K^0 \nu_\tau)/\Gamma_{total}$ Γ_{158}/Γ

VALUE	CL%	DOCUMENT ID	TECN	COMMENT
< 9.0 × 10⁻⁶	90	¹ INAMI	09 BELL	490 fb ⁻¹ $E_{cm}^{ee} = 10.6$ GeV

¹ We multiply the INAMI 09 measurement $B(\tau^- \rightarrow \eta K^- K_S^0 \nu_\tau) < 4.5 \times 10^{-6}$ by 2 to obtain the listed value.

$\Gamma(\eta \pi^+ \pi^- \pi^0 \nu_\tau)/\Gamma_{total}$ Γ_{159}/Γ

VALUE (%)	CL%	DOCUMENT ID	TECN	COMMENT
< 0.3	90	ABACHI	87B HRS	$E_{cm}^{ee} = 29$ GeV

$\Gamma(\eta \pi^- \pi^+ \pi^- \nu_\tau \text{ (ex. } K^0))/\Gamma_{total}$ Γ_{160}/Γ

VALUE (units 10^{-4})	EVTS	DOCUMENT ID	TECN	COMMENT
2.20 ± 0.13 OUR FIT				
2.23 ± 0.12 OUR AVERAGE				
2.10 ± 0.09 ± 0.13	2.9k	¹ LEES	12X BABR	$\eta \rightarrow \gamma\gamma$
2.37 ± 0.12 ± 0.18	1.4k	¹ LEES	12X BABR	$\eta \rightarrow \pi^+ \pi^- \pi^0$
2.54 ± 0.27 ± 0.25	315	¹ LEES	12X BABR	$\eta \rightarrow 3\pi^0$

• • • We use the following data for averages but not for fits. • • •
 • • • We do not use the following data for averages, fits, limits, etc. • • •
 1.60 ± 0.05 ± 0.11 1.8 k AUBERT 08AE BABR Repl. by LEES 12X
 3.4 ±_{-0.5}^{+0.6} ± 0.6 89 ³ BERGFELD 97 CLEO Repl. by ANASTASSOV 01

¹ LEES 12X uses 468 fb⁻¹ of data taken at $E_{cm}^{ee} = 10.6$ GeV. It gives the average of the three measurements listed here as $(2.25 \pm 0.07 \pm 0.12) \times 10^{-4}$.
² Weighted average of BERGFELD 97 and ANASTASSOV 01 measurements using η 's reconstructed from $\eta \rightarrow \pi^+ \pi^- \pi^0$ and $\eta \rightarrow 3\pi^0$ decays.
³ BERGFELD 97 reconstruct η 's using $\eta \rightarrow \gamma\gamma$ and $\eta \rightarrow 3\pi^0$ decays.

$\Gamma(\eta \pi^- \pi^+ \pi^- \nu_\tau \text{ (ex. } K^0, f_1(1285)))/\Gamma_{total}$ Γ_{161}/Γ

VALUE (units 10^{-4})	DOCUMENT ID	TECN	COMMENT
0.99 ± 0.09 ± 0.13	¹ LEES	12X BABR	468 fb ⁻¹ $E_{cm}^{ee} = 10.6$ GeV

¹ LEES 12X obtain this result by subtracting their $B(\tau^- \rightarrow f_1(1285) \pi^- \nu_\tau \rightarrow \eta \pi^- \pi^+ \pi^- \nu_\tau)$ measurement from their $B(\tau^- \rightarrow \eta \pi^- \pi^+ \pi^- \nu_\tau \text{ (ex. } K^0))$ measurement.

$\Gamma(\eta \rho_1(1260)^- \nu_\tau \rightarrow \eta \pi^- \rho^0 \nu_\tau)/\Gamma_{total}$ Γ_{162}/Γ

VALUE	CL%	DOCUMENT ID	TECN	COMMENT
< 3.9 × 10⁻⁴	90	BERGFELD	97 CLEO	$E_{cm}^{ee} = 10.6$ GeV

$\Gamma(\eta \eta \pi^- \nu_\tau)/\Gamma_{total}$ Γ_{163}/Γ

VALUE	CL%	DOCUMENT ID	TECN	COMMENT
< 7.4 × 10⁻⁶	90	INAMI	09 BELL	490 fb ⁻¹ $E_{cm}^{ee} = 10.6$ GeV

• • • We do not use the following data for averages, fits, limits, etc. • • •
 < 1.1 × 10⁻⁴ 95 ARTUSO 92 CLEO $E_{cm}^{ee} \approx 10.6$ GeV
 < 8.3 × 10⁻³ 95 ALBRECHT 88M ARG $E_{cm}^{ee} \approx 10$ GeV

$\Gamma(\eta \eta \pi^0 \nu_\tau)/\Gamma_{total}$ Γ_{164}/Γ

VALUE (units 10^{-4})	CL%	DOCUMENT ID	TECN	COMMENT
< 2.0	95	ARTUSO	92 CLEO	$E_{cm}^{ee} \approx 10.6$ GeV

• • • We do not use the following data for averages, fits, limits, etc. • • •
 < 90 95 ALBRECHT 88M ARG $E_{cm}^{ee} \approx 10$ GeV

$\Gamma(\eta \eta K^- \nu_\tau)/\Gamma_{total}$ Γ_{165}/Γ

VALUE	CL%	DOCUMENT ID	TECN	COMMENT
< 3.0 × 10⁻⁶	90	INAMI	09 BELL	490 fb ⁻¹ $E_{cm}^{ee} = 10.6$ GeV

$\Gamma(\eta'(958) \pi^- \nu_\tau)/\Gamma_{total}$ Γ_{166}/Γ

VALUE	CL%	DOCUMENT ID	TECN	COMMENT
< 4.0 × 10⁻⁶	90	LEES	12X BABR	468 fb ⁻¹ $E_{cm}^{ee} = 10.6$ GeV

• • • We do not use the following data for averages, fits, limits, etc. • • •
 < 7.2 × 10⁻⁶ 90 AUBERT 08AE BABR 384 fb⁻¹, $E_{cm}^{ee} = 10.6$ GeV
 < 7.4 × 10⁻⁵ 90 BERGFELD 97 CLEO $E_{cm}^{ee} = 10.6$ GeV

$\Gamma(\eta'(958) \pi^- \pi^0 \nu_\tau)/\Gamma_{total}$ Γ_{167}/Γ

VALUE	CL%	DOCUMENT ID	TECN	COMMENT
< 1.2 × 10⁻⁵	90	LEES	12X BABR	468 fb ⁻¹ $E_{cm}^{ee} = 10.6$ GeV

• • • We do not use the following data for averages, fits, limits, etc. • • •
 < 8.0 × 10⁻⁵ 90 BERGFELD 97 CLEO $E_{cm}^{ee} = 10.6$ GeV

$\Gamma(\eta'(958) K^- \nu_\tau)/\Gamma_{total}$ Γ_{168}/Γ

VALUE	CL%	DOCUMENT ID	TECN	COMMENT
< 2.4 × 10⁻⁶	90	LEES	12X BABR	468 fb ⁻¹ $E_{cm}^{ee} = 10.6$ GeV

$\Gamma(\phi \pi^- \nu_\tau)/\Gamma_{total}$ Γ_{169}/Γ

VALUE	CL%	EVTS	DOCUMENT ID	TECN	COMMENT
3.42 ± 0.55 ± 0.25		344	AUBERT	08 BABR	342 fb ⁻¹ $E_{cm}^{ee} = 10.6$ GeV

• • • We do not use the following data for averages, fits, limits, etc. • • •
 < 20 90 ¹ AVERY 97 CLEO $E_{cm}^{ee} = 10.6$ GeV
 < 35 90 ALBRECHT 95H ARG $E_{cm}^{ee} = 9.4$ –10.6 GeV

¹ AVERY 97 limit varies from $(1.2$ – $2.0) \times 10^{-4}$ depending on decay model assumptions.

$\Gamma(\phi K^- \nu_\tau)/\Gamma_{total}$ Γ_{170}/Γ

VALUE (units 10^{-5})	CL%	EVTS	DOCUMENT ID	TECN	COMMENT
4.4 ± 1.6 OUR FIT					
3.70 ± 0.33 OUR AVERAGE					Error includes scale factor of 1.3.

• • • We use the following data for averages but not for fits. • • •
 3.39 ± 0.20 ± 0.28 274 AUBERT 08 BABR 342 fb⁻¹ $E_{cm}^{ee} = 10.6$ GeV
 4.05 ± 0.25 ± 0.26 551 INAMI 06 BELL 401 fb⁻¹ $E_{cm}^{ee} = 10.6$ GeV

• • • We do not use the following data for averages, fits, limits, etc. • • •
 < 6.7 90 ¹ AVERY 97 CLEO $E_{cm}^{ee} = 10.6$ GeV

¹ AVERY 97 limit varies from $(5.4$ – $6.7) \times 10^{-5}$ depending on decay model assumptions.

$\Gamma(f_1(1285) \pi^- \nu_\tau)/\Gamma_{total}$ Γ_{171}/Γ

VALUE (units 10^{-4})	CL%	EVTS	DOCUMENT ID	TECN	COMMENT
3.9 ± 0.5 OUR AVERAGE					Error includes scale factor of 1.9.

4.73 ± 0.28 ± 0.45 3.7k ¹ LEES 12X BABR 468 fb⁻¹ $E_{cm}^{ee} = 10.6$ GeV
 3.60 ± 0.18 ± 0.23 2.5k ² LEES 12X BABR 468 fb⁻¹ $E_{cm}^{ee} = 10.6$ GeV

• • • We do not use the following data for averages, fits, limits, etc. • • •
 3.19 ± 0.18 ± 1.00 1.3 k ³ AUBERT 08AE BABR Repl. by LEES 12X
 3.9 ± 0.7 ± 0.5 1.4 k ⁴ AUBERT,B 05W BABR Repl. by LEES 12X
 5.8 ±_{-1.3}^{+1.4} ± 1.8 54 ⁵ BERGFELD 97 CLEO $E_{cm}^{ee} = 10.6$ GeV

¹ LEES 12X obtain this value by dividing their $B(\tau^- \rightarrow f_1(1285) \pi^- \nu_\tau \rightarrow 3\pi^- 2\pi^+ \nu_\tau)$ measurement by the PDG 12 value of $B(f_1(1285) \rightarrow 2\pi^+ 2\pi^-) = 0.111 \pm_{-0.006}^{+0.007}$.
² LEES 12X obtain this value by dividing their $B(\tau^- \rightarrow f_1(1285) \pi^- \nu_\tau \rightarrow \eta \pi^- \pi^+ \pi^- \nu_\tau)$ measurement by 2/3 of the PDG 12 value of $B(f_1(1285) \rightarrow \eta \pi \pi) = 0.524 \pm_{-0.021}^{+0.019}$.
³ AUBERT 08AE obtain this value by dividing their $B(\tau^- \rightarrow f_1(1285) \pi^- \nu_\tau \rightarrow \eta \pi^- \pi^+ \pi^- \nu_\tau)$ measurement by the PDG 06 value of $B(f_1(1285) \rightarrow \eta \pi^- \pi^+) = 0.35 \pm 0.11$. The quote $(3.19 \pm 0.18 \pm 0.16 \pm 0.99) \times 10^{-4}$ where the final error is due to the uncertainty on $B(f_1(1285) \rightarrow \eta \pi^- \pi^+)$. We combine the two systematic errors in quadrature.
⁴ AUBERT,B 05W use the $f_1(1285) \rightarrow 2\pi^+ 2\pi^-$ decay mode and the PDG 04 value of $B(f_1(1285) \rightarrow 2\pi^+ 2\pi^-) = 0.110 \pm_{-0.006}^{+0.007}$.
⁵ BERGFELD 97 use the $f_1(1285) \rightarrow \eta \pi^+ \pi^-$ decay mode.

$\Gamma(f_1(1285) \pi^- \nu_\tau \rightarrow \eta \pi^- \pi^+ \pi^- \nu_\tau)/\Gamma_{total}$ Γ_{172}/Γ

VALUE (units 10^{-4})	CL%	EVTS	DOCUMENT ID	TECN	COMMENT
1.18 ± 0.07 OUR AVERAGE					Error includes scale factor of 1.3.

1.26 ± 0.06 ± 0.06 2.5k LEES 12X BABR 468 fb⁻¹ $E_{cm}^{ee} = 10.6$ GeV
 1.11 ± 0.06 ± 0.05 1.3 k AUBERT 08AE BABR 384 fb⁻¹, $E_{cm}^{ee} = 10.6$ GeV

$\Gamma(f_1(1285) \pi^- \nu_\tau \rightarrow \eta \pi^- \pi^+ \pi^- \nu_\tau)/\Gamma(\eta \pi^- \pi^+ \pi^- \nu_\tau \text{ (ex. } K^0))$ $\Gamma_{172}/\Gamma_{160}$

VALUE	CL%	DOCUMENT ID	TECN	COMMENT
0.69 ± 0.01 ± 0.05		¹ AUBERT	08AE BABR	384 fb ⁻¹ , $E_{cm}^{ee} = 10.6$ GeV

• • • We do not use the following data for averages, fits, limits, etc. • • •
 0.55 ± 0.14 BERGFELD 97 CLEO $E_{cm}^{ee} = 10.6$ GeV

¹ Not independent of AUBERT 08AE $B(\tau^- \rightarrow f_1(1285) \pi^- \nu_\tau \rightarrow \eta \pi^- \pi^+ \pi^- \nu_\tau)$ and $B(\tau^- \rightarrow \eta \pi^- \pi^+ \pi^- \nu_\tau \text{ (ex. } K^0))$ values.

$\Gamma(f_1(1285) \pi^- \nu_\tau \rightarrow 3\pi^- 2\pi^+ \nu_\tau)/\Gamma_{total}$ Γ_{173}/Γ

VALUE (units 10^{-4})	CL%	EVTS	DOCUMENT ID	TECN	COMMENT
0.52 ± 0.04 OUR FIT					
0.520 ± 0.031 ± 0.037		3.7k	LEES	12X BABR	468 fb ⁻¹ $E_{cm}^{ee} = 10.6$ GeV

$\Gamma(\pi(1300)^- \nu_\tau \rightarrow (\rho \pi)^- \nu_\tau \rightarrow (3\pi)^- \nu_\tau)/\Gamma_{total}$ Γ_{174}/Γ

VALUE	CL%	DOCUMENT ID	TECN	COMMENT
< 1.0 × 10⁻⁴	90	ASNER	00 CLEO	$E_{cm}^{ee} = 10.6$ GeV

Lepton Particle Listings

τ

$\Gamma(\pi(1300)^- \nu_\tau \rightarrow ((\pi\pi)_{S\text{-wave}} \pi)^- \nu_\tau \rightarrow (3\pi)^- \nu_\tau)/\Gamma_{\text{total}}$					Γ_{175}/Γ
VALUE	CL%	DOCUMENT ID	TECN	COMMENT	
$<1.9 \times 10^{-4}$	90	ASNER	00	CLEO $E_{\text{cm}}^{\text{ee}} = 10.6$ GeV	

$\Gamma(h^- \omega \geq 0 \text{ neutrals } \nu_\tau)/\Gamma_{\text{total}}$					Γ_{176}/Γ
$\Gamma_{176}/\Gamma = (\Gamma_{178} + \Gamma_{179} + \Gamma_{180})/\Gamma$					
VALUE (%)	EVTS	DOCUMENT ID	TECN	COMMENT	
2.40 ± 0.08 OUR FIT					
• • • We use the following data for averages but not for fits. • • •					
1.65 ± 0.3 ± 0.2	1513	ALBRECHT	88M	ARG $E_{\text{cm}}^{\text{ee}} \approx 10$ GeV	

$\Gamma(h^- \omega \nu_\tau)/\Gamma_{\text{total}}$					$\Gamma_{177}/\Gamma = (\Gamma_{178} + \Gamma_{179})/\Gamma$
VALUE (%)	EVTS	DOCUMENT ID	TECN	COMMENT	
1.99 ± 0.06 OUR FIT					
1.92 ± 0.07 OUR AVERAGE					
1.91 ± 0.07 ± 0.06	5803	BUSKULIC	97C	ALEP 1991–1994 LEP runs	
1.60 ± 0.27 ± 0.41	139	BARINGER	87	CLEO $E_{\text{cm}}^{\text{ee}} = 10.5$ GeV	
• • • We use the following data for averages but not for fits. • • •					
1.95 ± 0.07 ± 0.11	2223	¹ BALEST	95c	CLEO $E_{\text{cm}}^{\text{ee}} \approx 10.6$ GeV	

¹ Not independent of BALEST 95c $B(\tau^- \rightarrow h^- \omega \nu_\tau)/B(\tau^- \rightarrow h^- h^- h^+ \pi^0 \nu_\tau)$ value.

$[\Gamma(\pi^- \omega \nu_\tau) + \Gamma(K^- \omega \nu_\tau)]/\Gamma(h^- h^- h^+ \pi^0 \nu_\tau \text{ (ex. } K^0))$					$(\Gamma_{178} + \Gamma_{179})/\Gamma_{74}$
$(\Gamma_{178} + \Gamma_{179})/\Gamma_{74} = (\Gamma_{178} + \Gamma_{179})/(\Gamma_{78} + \Gamma_{103} + \Gamma_{107} + 0.2302\Gamma_{152} + 0.892\Gamma_{178} + 0.892\Gamma_{179} + 0.0153\Gamma_{180})$					

VALUE (units 10^{-2})	EVTS	DOCUMENT ID	TECN	COMMENT
43.5 ± 1.4 OUR FIT				
45.3 ± 1.9 OUR AVERAGE				
43.1 ± 3.3	2350	¹ BUSKULIC	96	ALEP LEP 1991–1993 data
46.4 ± 1.6 ± 1.7	2223	² BALEST	95c	CLEO $E_{\text{cm}}^{\text{ee}} \approx 10.6$ GeV
• • • We do not use the following data for averages, fits, limits, etc. • • •				
37 ± 5 ± 2	458	³ ALBRECHT	91D	ARG $E_{\text{cm}}^{\text{ee}} = 9.4$ – 10.6 GeV

¹ BUSKULIC 96 quote the fraction of $\tau \rightarrow h^- h^- h^+ \pi^0 \nu_\tau$ (ex. K^0) decays which originate in a $h^- \omega$ final state = 0.383 ± 0.029. We divide this by the $\omega(782) \rightarrow \pi^+ \pi^- \pi^0$ branching fraction (0.888).

² BALEST 95c quote the fraction of $\tau^- \rightarrow h^- h^- h^+ \pi^0 \nu_\tau$ (ex. K^0) decays which originate in a $h^- \omega$ final state equals 0.412 ± 0.014 ± 0.015. We divide this by the $\omega(782) \rightarrow \pi^+ \pi^- \pi^0$ branching fraction (0.888).

³ ALBRECHT 91D quote the fraction of $\tau^- \rightarrow h^- h^- h^+ \pi^0 \nu_\tau$ decays which originate in a $\pi^- \omega$ final state equals 0.33 ± 0.04 ± 0.02. We divide this by the $\omega(782) \rightarrow \pi^+ \pi^- \pi^0$ branching fraction (0.888).

$\Gamma(\pi^- \omega \nu_\tau)/\Gamma_{\text{total}}$					Γ_{178}/Γ
VALUE (%)		DOCUMENT ID			
1.95 ± 0.06 OUR FIT					

$\Gamma(K^- \omega \nu_\tau)/\Gamma_{\text{total}}$					Γ_{179}/Γ
VALUE (units 10^{-4})	EVTS	DOCUMENT ID	TECN	COMMENT	
4.1 ± 0.9 OUR FIT					
4.1 ± 0.6 ± 0.7	500	ARMS	05	CLE3 7.6 fb^{-1} , $E_{\text{cm}}^{\text{ee}} = 10.6$ GeV	

$\Gamma(h^- \omega \pi^0 \nu_\tau)/\Gamma_{\text{total}}$					Γ_{180}/Γ
VALUE (%)	EVTS	DOCUMENT ID	TECN	COMMENT	
0.41 ± 0.04 OUR FIT					
0.43 ± 0.06 ± 0.05	7283	BUSKULIC	97C	ALEP 1991–1994 LEP runs	

$\Gamma(h^- \omega \pi^0 \nu_\tau)/\Gamma(h^- h^- h^+ \geq 0 \text{ neutrals } \geq 0 K^0 \nu_\tau)$					Γ_{180}/Γ_{62}
$\Gamma_{180}/\Gamma_{62} = \Gamma_{180}/(0.34598\Gamma_{36} + 0.34598\Gamma_{38} + 0.34598\Gamma_{41} + 0.34598\Gamma_{43} + 0.4247\Gamma_{48} + 0.6920\Gamma_{49} + 0.8494\Gamma_{52} + 0.6920\Gamma_{56} + 0.6534\Gamma_{61} + \Gamma_{70} + \Gamma_{78} + \Gamma_{85} + \Gamma_{89} + \Gamma_{97} + \Gamma_{103} + \Gamma_{106} + \Gamma_{107} + 0.2804\Gamma_{150} + 0.2302\Gamma_{151} + 0.2804\Gamma_{152} + 0.2804\Gamma_{154} + 0.3759\Gamma_{156} + 0.3257\Gamma_{160} + 0.7259\Gamma_{170} + 0.9078\Gamma_{178} + 0.9078\Gamma_{179} + 0.9078\Gamma_{180} + 0.892\Gamma_{182})$					
VALUE	EVTS	DOCUMENT ID	TECN	COMMENT	
(2.69 ± 0.28) × 10⁻² OUR FIT					
• • • We use the following data for averages but not for fits. • • •					
0.028 ± 0.003 ± 0.003	430	¹ BORTOLETTO	93	CLEO $E_{\text{cm}}^{\text{ee}} \approx 10.6$ GeV	

¹ Not independent of BORTOLETTO 93 $\Gamma(\tau^- \rightarrow h^- \omega \pi^0 \nu_\tau)/\Gamma(\tau^- \rightarrow h^- h^- h^+ 2\pi^0 \nu_\tau \text{ (ex. } K^0))$ value.

$\Gamma(h^- \omega \pi^0 \nu_\tau)/\Gamma(h^- h^- h^+ 2\pi^0 \nu_\tau \text{ (ex. } K^0))$					Γ_{180}/Γ_{84}
$\Gamma_{180}/\Gamma_{84} = \Gamma_{180}/(\Gamma_{85} + 0.2302\Gamma_{150} + 0.2302\Gamma_{154} + 0.892\Gamma_{180})$					

VALUE (units 10^{-2})	DOCUMENT ID	TECN	COMMENT
82 ± 8 OUR FIT			
81 ± 6 ± 6	BORTOLETTO93	CLEO	$E_{\text{cm}}^{\text{ee}} \approx 10.6$ GeV

$\Gamma(h^- \omega 2\pi^0 \nu_\tau)/\Gamma_{\text{total}}$					Γ_{181}/Γ
VALUE (units 10^{-4})	EVTS	DOCUMENT ID	TECN	COMMENT	
1.4 ± 0.4 ± 0.3	53	ANASTASSOV	01	CLEO $E_{\text{cm}}^{\text{ee}} = 10.6$ GeV	
• • • We do not use the following data for averages, fits, limits, etc. • • •					
1.89 ± 0.74 ± 0.67	19	ANDERSON	97	CLEO Repl. by ANASTASSOV 01	

$\Gamma(\pi^- \omega 2\pi^0 \nu_\tau)/\Gamma_{\text{total}}$					Γ_{182}/Γ
VALUE (units 10^{-4})	EVTS	DOCUMENT ID	TECN	COMMENT	
0.72 ± 0.16 OUR FIT					
0.73 ± 0.12 ± 0.12	1.1k	LEES	12x	BABR 468 fb^{-1} , $E_{\text{cm}}^{\text{ee}} = 10.6$ GeV	

$\Gamma(h^- 2\omega \nu_\tau)/\Gamma_{\text{total}}$					Γ_{183}/Γ
VALUE	CL%	DOCUMENT ID	TECN	COMMENT	
<5.4 × 10⁻⁷	90	AUBERT,B	06	BABR 232 fb^{-1} , $E_{\text{cm}}^{\text{ee}} = 10.6$ GeV	

$\Gamma(2h^- h^+ \omega \nu_\tau)/\Gamma_{\text{total}}$					Γ_{184}/Γ
VALUE (units 10^{-4})	EVTS	DOCUMENT ID	TECN	COMMENT	
1.2 ± 0.2 ± 0.1	110	ANASTASSOV	01	CLEO $E_{\text{cm}}^{\text{ee}} = 10.6$ GeV	

$\Gamma(2\pi^- \pi^+ \omega \nu_\tau \text{ (ex. } K^0))/\Gamma_{\text{total}}$					Γ_{185}/Γ
VALUE (units 10^{-4})	EVTS	DOCUMENT ID	TECN	COMMENT	
0.84 ± 0.06 OUR FIT					
0.84 ± 0.04 ± 0.06	2.4k	LEES	12x	BABR 468 fb^{-1} , $E_{\text{cm}}^{\text{ee}} = 10.6$ GeV	

$\Gamma(e^- \gamma)/\Gamma_{\text{total}}$					Γ_{186}/Γ
Test of lepton family number conservation.					
VALUE	CL%	DOCUMENT ID	TECN	COMMENT	
<3.3 × 10⁻⁸	90	AUBERT	10B	BABR 516 fb^{-1} , $E_{\text{cm}}^{\text{ee}} = 10.6$ GeV	
• • • We do not use the following data for averages, fits, limits, etc. • • •					
<5.6 × 10 ⁻⁸	90	UNO	21	BELL 988 fb^{-1} , $E_{\text{cm}}^{\text{ee}} = 10.6$ GeV	
<1.2 × 10 ⁻⁷	90	HAYASAKA	08	BELL 535 fb^{-1} , $E_{\text{cm}}^{\text{ee}} = 10.6$ GeV	
<1.1 × 10 ⁻⁷	90	AUBERT	06c	BABR 232 fb^{-1} , $E_{\text{cm}}^{\text{ee}} = 10.6$ GeV	
<3.9 × 10 ⁻⁷	90	HAYASAKA	05	BELL 86.7 fb^{-1} , $E_{\text{cm}}^{\text{ee}} = 10.6$ GeV	
<2.7 × 10 ⁻⁶	90	EDWARDS	97	CLEO	
<1.1 × 10 ⁻⁴	90	ABREU	95U	DLPH 1990–1993 LEP runs	
<1.2 × 10 ⁻⁴	90	ALBRECHT	92k	ARG $E_{\text{cm}}^{\text{ee}} = 10$ GeV	
<2.0 × 10 ⁻⁴	90	KEH	88	CBAL $E_{\text{cm}}^{\text{ee}} = 10$ GeV	
<6.4 × 10 ⁻⁴	90	HAYES	82	MRK2 $E_{\text{cm}}^{\text{ee}} = 3.8$ – 6.8 GeV	

$\Gamma(e^- \gamma \gamma)/\Gamma_{\text{total}}$					Γ_{187}/Γ
VALUE	CL%	DOCUMENT ID	TECN	COMMENT	
<2.5 × 10⁻⁴	90	¹ BRYMAN	21	RVUE 516 fb^{-1} , $E_{\text{cm}}^{\text{ee}} = 10.6$ GeV	

¹ BRYMAN 21 reinterprets the upper limit result on $B(\tau^- \rightarrow e^- \gamma)$ and $B(\tau^- \rightarrow \mu^- \gamma)$ by AUBERT 10B, estimating with a simulation the efficiency for this decay mode to be detected as the corresponding AUBERT 10B decay mode.

$\Gamma(\mu^- \gamma)/\Gamma_{\text{total}}$					Γ_{188}/Γ
Test of lepton family number conservation.					
VALUE	CL%	DOCUMENT ID	TECN	COMMENT	
< 4.2 × 10⁻⁸	90	UNO	21	BELL 988 fb^{-1} , $E_{\text{cm}}^{\text{ee}} = 10.6$ GeV	
• • • We do not use the following data for averages, fits, limits, etc. • • •					
< 4.4 × 10 ⁻⁸	90	AUBERT	10B	BABR 516 fb^{-1} , $E_{\text{cm}}^{\text{ee}} = 10.6$ GeV	
< 4.5 × 10 ⁻⁸	90	HAYASAKA	08	BELL 535 fb^{-1} , $E_{\text{cm}}^{\text{ee}} = 10.6$ GeV	
< 6.8 × 10 ⁻⁸	90	AUBERT,B	05A	BABR 232 fb^{-1} , $E_{\text{cm}}^{\text{ee}} = 10.6$ GeV	
< 3.1 × 10 ⁻⁷	90	ABE	04B	BELL 86.3 fb^{-1} , $E_{\text{cm}}^{\text{ee}} = 10.6$ GeV	
< 1.1 × 10 ⁻⁶	90	AHMED	00	CLEO $E_{\text{cm}}^{\text{ee}} = 10.6$ GeV	
< 3.0 × 10 ⁻⁶	90	EDWARDS	97	CLEO	
< 6.2 × 10 ⁻⁵	90	ABREU	95U	DLPH 1990–1993 LEP runs	
< 0.42 × 10 ⁻⁵	90	BEAN	93	CLEO $E_{\text{cm}}^{\text{ee}} = 10.6$ GeV	
< 3.4 × 10 ⁻⁵	90	ALBRECHT	92k	ARG $E_{\text{cm}}^{\text{ee}} = 10$ GeV	
<55 × 10 ⁻⁵	90	HAYES	82	MRK2 $E_{\text{cm}}^{\text{ee}} = 3.8$ – 6.8 GeV	

$\Gamma(\mu^- \gamma \gamma)/\Gamma_{\text{total}}$					Γ_{189}/Γ
VALUE	CL%	DOCUMENT ID	TECN	COMMENT	
<5.8 × 10⁻⁴	90	¹ BRYMAN	21	RVUE 516 fb^{-1} , $E_{\text{cm}}^{\text{ee}} = 10.6$ GeV	

¹ BRYMAN 21 reinterprets the upper limit result on $B(\tau^- \rightarrow e^- \gamma)$ and $B(\tau^- \rightarrow \mu^- \gamma)$ by AUBERT 10B, estimating with a simulation the efficiency for this decay mode to be detected as the corresponding AUBERT 10B decay mode.

$\Gamma(e^- \pi^0)/\Gamma_{\text{total}}$					Γ_{190}/Γ
Test of lepton family number conservation.					
VALUE	CL%	DOCUMENT ID	TECN	COMMENT	
< 8.0 × 10⁻⁸	90	MIYAZAKI	07	BELL 401 fb^{-1} , $E_{\text{cm}}^{\text{ee}} = 10.6$ GeV	
• • • We do not use the following data for averages, fits, limits, etc. • • •					
< 1.3 × 10 ⁻⁷	90	AUBERT	07i	BABR 339 fb^{-1} , $E_{\text{cm}}^{\text{ee}} = 10.6$ GeV	
< 1.9 × 10 ⁻⁷	90	ENARI	05	BELL 154 fb^{-1} , $E_{\text{cm}}^{\text{ee}} = 10.6$ GeV	
< 3.7 × 10 ⁻⁶	90	BONVICINI	97	CLEO $E_{\text{cm}}^{\text{ee}} = 10.6$ GeV	
< 17 × 10 ⁻⁵	90	ALBRECHT	92k	ARG $E_{\text{cm}}^{\text{ee}} = 10$ GeV	
< 14 × 10 ⁻⁵	90	KEH	88	CBAL $E_{\text{cm}}^{\text{ee}} = 10$ GeV	
<210 × 10 ⁻⁵	90	HAYES	82	MRK2 $E_{\text{cm}}^{\text{ee}} = 3.8$ – 6.8 GeV	

Gamma(mu- pi0)/Gamma_total Test of lepton family number conservation. Table with columns: VALUE, CL%, DOCUMENT ID, TECN, COMMENT. Includes data points like <1.1 x 10^-7, 90, AUBERT 07I BABR 339 fb^-1, etc.

Gamma(e- K_S^0)/Gamma_total Test of lepton family number conservation. Table with columns: VALUE, CL%, DOCUMENT ID, TECN, COMMENT. Includes data points like <2.6 x 10^-8, 90, MIYAZAKI 10A BELL 671 fb^-1, etc.

Gamma(mu- K_S^0)/Gamma_total Test of lepton family number conservation. Table with columns: VALUE, CL%, DOCUMENT ID, TECN, COMMENT. Includes data points like <2.3 x 10^-8, 90, MIYAZAKI 10A BELL 671 fb^-1, etc.

Gamma(e- eta)/Gamma_total Test of lepton family number conservation. Table with columns: VALUE, CL%, DOCUMENT ID, TECN, COMMENT. Includes data points like <9.2 x 10^-8, 90, MIYAZAKI 07 BELL 401 fb^-1, etc.

Gamma(mu- eta)/Gamma_total Test of lepton family number conservation. Table with columns: VALUE, CL%, DOCUMENT ID, TECN, COMMENT. Includes data points like <6.5 x 10^-8, 90, MIYAZAKI 07 BELL 401 fb^-1, etc.

Gamma(e- rho^0)/Gamma_total Test of lepton family number conservation. Table with columns: VALUE, CL%, DOCUMENT ID, TECN, COMMENT. Includes data points like <1.8 x 10^-8, 90, MIYAZAKI 11 BELL 854 fb^-1, etc.

Gamma(mu- rho^0)/Gamma_total Test of lepton family number conservation. Table with columns: VALUE, CL%, DOCUMENT ID, TECN, COMMENT. Includes data points like <1.2 x 10^-8, 90, MIYAZAKI 11 BELL 854 fb^-1, etc.

Gamma(e- omega)/Gamma_total Test of lepton family number conservation. Table with columns: VALUE, CL%, DOCUMENT ID, TECN, COMMENT. Includes data points like <4.8 x 10^-8, 90, MIYAZAKI 11 BELL 854 fb^-1, etc.

Gamma(mu- omega)/Gamma_total Test of lepton family number conservation. Table with columns: VALUE, CL%, DOCUMENT ID, TECN, COMMENT. Includes data points like <4.7 x 10^-8, 90, MIYAZAKI 11 BELL 854 fb^-1, etc.

Gamma(e- K*(892)^0)/Gamma_total Test of lepton family number conservation. Table with columns: VALUE, CL%, DOCUMENT ID, TECN, COMMENT. Includes data points like <3.2 x 10^-8, 90, MIYAZAKI 11 BELL 854 fb^-1, etc.

Gamma(mu- K*(892)^0)/Gamma_total Test of lepton family number conservation. Table with columns: VALUE, CL%, DOCUMENT ID, TECN, COMMENT. Includes data points like <5.9 x 10^-8, 90, NISHIO 08 BELL 543 fb^-1, etc.

Gamma(e- K*(892)^0)/Gamma_total Test of lepton family number conservation. Table with columns: VALUE, CL%, DOCUMENT ID, TECN, COMMENT. Includes data points like <3.4 x 10^-8, 90, MIYAZAKI 11 BELL 854 fb^-1, etc.

Gamma(mu- K*(892)^0)/Gamma_total Test of lepton family number conservation. Table with columns: VALUE, CL%, DOCUMENT ID, TECN, COMMENT. Includes data points like <7.0 x 10^-8, 90, MIYAZAKI 11 BELL 854 fb^-1, etc.

Gamma(e- eta'(958))/Gamma_total Test of lepton family number conservation. Table with columns: VALUE, CL%, DOCUMENT ID, TECN, COMMENT. Includes data points like <1.6 x 10^-7, 90, MIYAZAKI 07 BELL 401 fb^-1, etc.

Gamma(mu- eta'(958))/Gamma_total Test of lepton family number conservation. Table with columns: VALUE, CL%, DOCUMENT ID, TECN, COMMENT. Includes data points like <1.3 x 10^-7, 90, MIYAZAKI 07 BELL 401 fb^-1, etc.

Downloaded from https://academic.oup.com/ptep/article/2022/8/083C01/6661666 by CERIN Library user on 11 October 2022

Lepton Particle Listings

T

$\Gamma(e^- \bar{\nu}_0(980) \rightarrow e^- \pi^+ \pi^-)/\Gamma_{\text{total}}$ Γ_{206}/Γ

VALUE	CL%	DOCUMENT ID	TECN	COMMENT
$< 3.2 \times 10^{-8}$	90	MIYAZAKI	09	BELL 671 fb ⁻¹ $E_{\text{cm}}^{\text{ee}} = 10.6$ GeV

$\Gamma(\mu^- \bar{\nu}_0(980) \rightarrow \mu^- \pi^+ \pi^-)/\Gamma_{\text{total}}$ Γ_{207}/Γ

VALUE	CL%	DOCUMENT ID	TECN	COMMENT
$< 3.4 \times 10^{-8}$	90	MIYAZAKI	09	BELL 671 fb ⁻¹ $E_{\text{cm}}^{\text{ee}} = 10.6$ GeV

$\Gamma(e^- \phi)/\Gamma_{\text{total}}$ Γ_{208}/Γ

Test of lepton family number conservation.

VALUE	CL%	DOCUMENT ID	TECN	COMMENT
$< 3.1 \times 10^{-8}$	90	MIYAZAKI	11	BELL 854 fb ⁻¹ $E_{\text{cm}}^{\text{ee}} = 10.6$ GeV
$< 3.1 \times 10^{-8}$	90	AUBERT	09W	BABR 451 fb ⁻¹ $E_{\text{cm}}^{\text{ee}} = 10.6$ GeV
• • • We do not use the following data for averages, fits, limits, etc. • • •				
$< 7.3 \times 10^{-8}$	90	NISHIO	08	BELL 543 fb ⁻¹ $E_{\text{cm}}^{\text{ee}} = 10.6$ GeV
$< 7.3 \times 10^{-7}$	90	YUSA	06	BELL 158 fb ⁻¹ $E_{\text{cm}}^{\text{ee}} = 10.6$ GeV
$< 6.9 \times 10^{-6}$	90	BLISS	98	CLEO $E_{\text{cm}}^{\text{ee}} = 10.6$ GeV

$\Gamma(\mu^- \phi)/\Gamma_{\text{total}}$ Γ_{209}/Γ

Test of lepton family number conservation.

VALUE	CL%	DOCUMENT ID	TECN	COMMENT
$< 8.4 \times 10^{-8}$	90	MIYAZAKI	11	BELL 854 fb ⁻¹ $E_{\text{cm}}^{\text{ee}} = 10.6$ GeV
• • • We do not use the following data for averages, fits, limits, etc. • • •				
$< 1.9 \times 10^{-7}$	90	AUBERT	09W	BABR 451 fb ⁻¹ $E_{\text{cm}}^{\text{ee}} = 10.6$ GeV
$< 1.3 \times 10^{-7}$	90	NISHIO	08	BELL 543 fb ⁻¹ $E_{\text{cm}}^{\text{ee}} = 10.6$ GeV
$< 7.7 \times 10^{-7}$	90	YUSA	06	BELL 158 fb ⁻¹ $E_{\text{cm}}^{\text{ee}} = 10.6$ GeV
$< 7.0 \times 10^{-6}$	90	BLISS	98	CLEO $E_{\text{cm}}^{\text{ee}} = 10.6$ GeV

$\Gamma(e^- e^+ e^-)/\Gamma_{\text{total}}$ Γ_{210}/Γ

Test of lepton family number conservation.

VALUE	CL%	DOCUMENT ID	TECN	COMMENT
$< 2.7 \times 10^{-8}$	90	HAYASAKA	10	BELL 782 fb ⁻¹ $E_{\text{cm}}^{\text{ee}} = 10.6$ GeV
• • • We do not use the following data for averages, fits, limits, etc. • • •				
$< 2.9 \times 10^{-8}$	90	LEES	10A	BABR 468 fb ⁻¹ $E_{\text{cm}}^{\text{ee}} = 10.6$ GeV
$< 3.6 \times 10^{-8}$	90	MIYAZAKI	08	BELL 535 fb ⁻¹ $E_{\text{cm}}^{\text{ee}} = 10.6$ GeV
$< 4.3 \times 10^{-8}$	90	AUBERT	07BK	BABR 376 fb ⁻¹ $E_{\text{cm}}^{\text{ee}} = 10.6$ GeV
$< 2.0 \times 10^{-7}$	90	AUBERT	04J	BABR 91.5 fb ⁻¹ $E_{\text{cm}}^{\text{ee}} = 10.6$ GeV
$< 3.5 \times 10^{-7}$	90	YUSA	04	BELL 87.1 fb ⁻¹ $E_{\text{cm}}^{\text{ee}} = 10.6$ GeV
$< 2.9 \times 10^{-6}$	90	BLISS	98	CLEO $E_{\text{cm}}^{\text{ee}} = 10.6$ GeV
$< 0.33 \times 10^{-5}$	90	¹ BARTELT	94	CLEO Repl. by BLISS 98
$< 1.3 \times 10^{-5}$	90	ALBRECHT	92K	ARG $E_{\text{cm}}^{\text{ee}} = 10$ GeV
$< 2.7 \times 10^{-5}$	90	BOWCOCK	90	CLEO $E_{\text{cm}}^{\text{ee}} = 10.4-10.9$
$< 4.0 \times 10^{-5}$	90	HAYES	82	MRK2 $E_{\text{cm}}^{\text{ee}} = 3.8-6.8$ GeV

¹ BARTELT 94 assume phase space decays.

$\Gamma(e^- \mu^+ \mu^-)/\Gamma_{\text{total}}$ Γ_{211}/Γ

Test of lepton family number conservation.

VALUE	CL%	DOCUMENT ID	TECN	COMMENT
$< 2.7 \times 10^{-8}$	90	HAYASAKA	10	BELL 782 fb ⁻¹ $E_{\text{cm}}^{\text{ee}} = 10.6$ GeV
• • • We do not use the following data for averages, fits, limits, etc. • • •				
$< 3.2 \times 10^{-8}$	90	LEES	10A	BABR 468 fb ⁻¹ $E_{\text{cm}}^{\text{ee}} = 10.6$ GeV
$< 4.1 \times 10^{-8}$	90	MIYAZAKI	08	BELL 535 fb ⁻¹ $E_{\text{cm}}^{\text{ee}} = 10.6$ GeV
$< 3.7 \times 10^{-8}$	90	AUBERT	07BK	BABR 376 fb ⁻¹ $E_{\text{cm}}^{\text{ee}} = 10.6$ GeV
$< 3.3 \times 10^{-7}$	90	AUBERT	04J	BABR 91.5 fb ⁻¹ $E_{\text{cm}}^{\text{ee}} = 10.6$ GeV
$< 2.0 \times 10^{-7}$	90	YUSA	04	BELL 87.1 fb ⁻¹ $E_{\text{cm}}^{\text{ee}} = 10.6$ GeV
$< 1.8 \times 10^{-6}$	90	BLISS	98	CLEO $E_{\text{cm}}^{\text{ee}} = 10.6$ GeV
$< 0.36 \times 10^{-5}$	90	¹ BARTELT	94	CLEO Repl. by BLISS 98
$< 1.9 \times 10^{-5}$	90	ALBRECHT	92K	ARG $E_{\text{cm}}^{\text{ee}} = 10$ GeV
$< 2.7 \times 10^{-5}$	90	BOWCOCK	90	CLEO $E_{\text{cm}}^{\text{ee}} = 10.4-10.9$
$< 33 \times 10^{-5}$	90	HAYES	82	MRK2 $E_{\text{cm}}^{\text{ee}} = 3.8-6.8$ GeV

¹ BARTELT 94 assume phase space decays.

$\Gamma(e^+ \mu^- \mu^-)/\Gamma_{\text{total}}$ Γ_{212}/Γ

Test of lepton family number conservation.

VALUE	CL%	DOCUMENT ID	TECN	COMMENT
$< 1.7 \times 10^{-8}$	90	HAYASAKA	10	BELL 782 fb ⁻¹ $E_{\text{cm}}^{\text{ee}} = 10.6$ GeV
• • • We do not use the following data for averages, fits, limits, etc. • • •				
$< 2.6 \times 10^{-8}$	90	LEES	10A	BABR 468 fb ⁻¹ $E_{\text{cm}}^{\text{ee}} = 10.6$ GeV
$< 2.3 \times 10^{-8}$	90	MIYAZAKI	08	BELL 535 fb ⁻¹ $E_{\text{cm}}^{\text{ee}} = 10.6$ GeV
$< 5.6 \times 10^{-8}$	90	AUBERT	07BK	BABR 376 fb ⁻¹ $E_{\text{cm}}^{\text{ee}} = 10.6$ GeV
$< 1.3 \times 10^{-7}$	90	AUBERT	04J	BABR 91.5 fb ⁻¹ $E_{\text{cm}}^{\text{ee}} = 10.6$ GeV
$< 2.0 \times 10^{-7}$	90	YUSA	04	BELL 87.1 fb ⁻¹ $E_{\text{cm}}^{\text{ee}} = 10.6$ GeV
$< 1.5 \times 10^{-6}$	90	BLISS	98	CLEO $E_{\text{cm}}^{\text{ee}} = 10.6$ GeV
$< 0.35 \times 10^{-5}$	90	¹ BARTELT	94	CLEO Repl. by BLISS 98
$< 1.8 \times 10^{-5}$	90	ALBRECHT	92K	ARG $E_{\text{cm}}^{\text{ee}} = 10$ GeV
$< 1.6 \times 10^{-5}$	90	BOWCOCK	90	CLEO $E_{\text{cm}}^{\text{ee}} = 10.4-10.9$

¹ BARTELT 94 assume phase space decays.

$\Gamma(\mu^- e^+ e^-)/\Gamma_{\text{total}}$ Γ_{213}/Γ

Test of lepton family number conservation.

VALUE	CL%	DOCUMENT ID	TECN	COMMENT
$< 1.8 \times 10^{-8}$	90	HAYASAKA	10	BELL 782 fb ⁻¹ $E_{\text{cm}}^{\text{ee}} = 10.6$ GeV

• • • We do not use the following data for averages, fits, limits, etc. • • •

$< 2.2 \times 10^{-8}$	90	LEES	10A	BABR 468 fb ⁻¹ $E_{\text{cm}}^{\text{ee}} = 10.6$ GeV
$< 2.7 \times 10^{-8}$	90	MIYAZAKI	08	BELL 535 fb ⁻¹ $E_{\text{cm}}^{\text{ee}} = 10.6$ GeV
$< 8.0 \times 10^{-8}$	90	AUBERT	07BK	BABR 376 fb ⁻¹ $E_{\text{cm}}^{\text{ee}} = 10.6$ GeV
$< 2.7 \times 10^{-7}$	90	AUBERT	04J	BABR 91.5 fb ⁻¹ $E_{\text{cm}}^{\text{ee}} = 10.6$ GeV
$< 1.9 \times 10^{-7}$	90	YUSA	04	BELL 87.1 fb ⁻¹ $E_{\text{cm}}^{\text{ee}} = 10.6$ GeV
$< 1.7 \times 10^{-6}$	90	BLISS	98	CLEO $E_{\text{cm}}^{\text{ee}} = 10.6$ GeV
$< 0.34 \times 10^{-5}$	90	¹ BARTELT	94	CLEO Repl. by BLISS 98
$< 1.4 \times 10^{-5}$	90	ALBRECHT	92K	ARG $E_{\text{cm}}^{\text{ee}} = 10$ GeV
$< 2.7 \times 10^{-5}$	90	BOWCOCK	90	CLEO $E_{\text{cm}}^{\text{ee}} = 10.4-10.9$
$< 44 \times 10^{-5}$	90	HAYES	82	MRK2 $E_{\text{cm}}^{\text{ee}} = 3.8-6.8$ GeV

¹ BARTELT 94 assume phase space decays.

$\Gamma(\mu^+ e^- e^-)/\Gamma_{\text{total}}$ Γ_{214}/Γ

Test of lepton family number conservation.

VALUE	CL%	DOCUMENT ID	TECN	COMMENT
$< 1.5 \times 10^{-8}$	90	HAYASAKA	10	BELL 782 fb ⁻¹ $E_{\text{cm}}^{\text{ee}} = 10.6$ GeV

• • • We do not use the following data for averages, fits, limits, etc. • • •

$< 1.8 \times 10^{-8}$	90	LEES	10A	BABR 468 fb ⁻¹ $E_{\text{cm}}^{\text{ee}} = 10.6$ GeV
$< 2.0 \times 10^{-8}$	90	MIYAZAKI	08	BELL 535 fb ⁻¹ $E_{\text{cm}}^{\text{ee}} = 10.6$ GeV
$< 5.8 \times 10^{-8}$	90	AUBERT	07BK	BABR 376 fb ⁻¹ $E_{\text{cm}}^{\text{ee}} = 10.6$ GeV
$< 1.1 \times 10^{-7}$	90	AUBERT	04J	BABR 91.5 fb ⁻¹ $E_{\text{cm}}^{\text{ee}} = 10.6$ GeV
$< 2.0 \times 10^{-7}$	90	YUSA	04	BELL 87.1 fb ⁻¹ $E_{\text{cm}}^{\text{ee}} = 10.6$ GeV
$< 1.5 \times 10^{-6}$	90	BLISS	98	CLEO $E_{\text{cm}}^{\text{ee}} = 10.6$ GeV
$< 0.34 \times 10^{-5}$	90	¹ BARTELT	94	CLEO Repl. by BLISS 98
$< 1.4 \times 10^{-5}$	90	ALBRECHT	92K	ARG $E_{\text{cm}}^{\text{ee}} = 10$ GeV
$< 1.6 \times 10^{-5}$	90	BOWCOCK	90	CLEO $E_{\text{cm}}^{\text{ee}} = 10.4-10.9$

¹ BARTELT 94 assume phase space decays.

$\Gamma(\mu^- \mu^+ \mu^-)/\Gamma_{\text{total}}$ Γ_{215}/Γ

Test of lepton family number conservation.

VALUE	CL%	DOCUMENT ID	TECN	COMMENT
$< 2.1 \times 10^{-8}$	90	HAYASAKA	10	BELL 782 fb ⁻¹ $E_{\text{cm}}^{\text{ee}} = 10.6$ GeV

• • • We do not use the following data for averages, fits, limits, etc. • • •

$< 8.0 \times 10^{-8}$	90	SIRUNYAN	21D	CMS 33.2 fb ⁻¹ , <i>pp</i> at 13 TeV
$< 3.8 \times 10^{-7}$	90	AAD	16BA	ATLS 20.3 fb ⁻¹ , <i>pp</i> at 8 TeV
$< 4.6 \times 10^{-8}$	90	AAIJ	15AI	LHCB 3.0 fb ⁻¹ , <i>pp</i> at 7, 8 TeV
$< 8.0 \times 10^{-8}$	90	¹ AAIJ	13AH	LHCB 1.0 fb ⁻¹ , <i>pp</i> at 7 TeV
$< 3.3 \times 10^{-8}$	90	LEES	10A	BABR 468 fb ⁻¹ $E_{\text{cm}}^{\text{ee}} = 10.6$ GeV
$< 3.2 \times 10^{-8}$	90	MIYAZAKI	08	BELL 535 fb ⁻¹ $E_{\text{cm}}^{\text{ee}} = 10.6$ GeV
$< 5.3 \times 10^{-8}$	90	AUBERT	07BK	BABR 376 fb ⁻¹ $E_{\text{cm}}^{\text{ee}} = 10.6$ GeV
$< 1.9 \times 10^{-7}$	90	AUBERT	04J	BABR 91.5 fb ⁻¹ $E_{\text{cm}}^{\text{ee}} = 10.6$ GeV
$< 2.0 \times 10^{-7}$	90	YUSA	04	BELL 87.1 fb ⁻¹ $E_{\text{cm}}^{\text{ee}} = 10.6$ GeV
$< 1.9 \times 10^{-6}$	90	BLISS	98	CLEO $E_{\text{cm}}^{\text{ee}} = 10.6$ GeV
$< 0.43 \times 10^{-5}$	90	² BARTELT	94	CLEO Repl. by BLISS 98
$< 1.9 \times 10^{-5}$	90	ALBRECHT	92K	ARG $E_{\text{cm}}^{\text{ee}} = 10$ GeV
$< 1.7 \times 10^{-5}$	90	BOWCOCK	90	CLEO $E_{\text{cm}}^{\text{ee}} = 10.4-10.9$
$< 49 \times 10^{-5}$	90	HAYES	82	MRK2 $E_{\text{cm}}^{\text{ee}} = 3.8-6.8$ GeV

¹ Repl. by AAIJ 15AI.² BARTELT 94 assume phase space decays.

$\Gamma(e^- \pi^+ \pi^-)/\Gamma_{\text{total}}$ Γ_{216}/Γ

Test of lepton family number conservation.

VALUE	CL%	DOCUMENT ID	TECN	COMMENT
$< 2.3 \times 10^{-8}$	90	MIYAZAKI	13	BELL 854 fb ⁻¹ $E_{\text{cm}}^{\text{ee}} = 10.6$ GeV

• • • We do not use the following data for averages, fits, limits, etc. • • •

$< 4.4 \times 10^{-8}$	90	MIYAZAKI	10	BELL Repl. by MIYAZAKI 13
$< 7.3 \times 10^{-7}$	90	YUSA	06	BELL 158 fb ⁻¹ $E_{\text{cm}}^{\text{ee}} = 10.6$ GeV
$< 1.2 \times 10^{-7}$	90	AUBERT,BE	05D	BABR 221 fb ⁻¹ , $E_{\text{cm}}^{\text{ee}} = 10.6$ GeV
$< 2.2 \times 10^{-6}$	90	BLISS	98	CLEO $E_{\text{cm}}^{\text{ee}} = 10.6$ GeV
$< 4.4 \times 10^{-6}$	90	¹ BARTELT	94	CLEO Repl. by BLISS 98
$< 2.7 \times 10^{-5}$	90	ALBRECHT	92K	ARG $E_{\text{cm}}^{\text{ee}} = 10$ GeV
$< 6.0 \times 10^{-5}$	90	BOWCOCK	90	CLEO $E_{\text{cm}}^{\text{ee}} = 10.4-10.9$

¹ BARTELT 94 assume phase space decays.

$\Gamma(e^+ \pi^- \pi^-)/\Gamma_{\text{total}}$ Γ_{217}/Γ

Test of lepton number conservation.

VALUE	CL%	DOCUMENT ID	TECN	COMMENT
$< 2.0 \times 10^{-8}$	90	MIYAZAKI	13	BELL 854 fb ⁻¹ $E_{\text{cm}}^{\text{ee}} = 10.6$ GeV

• • • We do not use the following data for averages, fits, limits, etc. • • •

$< 8.8 \times 10^{-8}$	90	MIYAZAKI	10	BELL Repl. by MIYAZAKI 13
$< 2.0 \times 10^{-7}$	90	YUSA	06	BELL 158 fb ⁻¹ $E_{\text{cm}}^{\text{ee}} = 10.6$ GeV
$< 2.7 \times 10^{-7}$	90	AUBERT,BE	05D	BABR 221 fb ⁻¹ , $E_{\text{cm}}^{\text{ee}} = 10.6$ GeV

$<1.9 \times 10^{-6}$	90	BLISS	98	CLEO	$E_{cm}^{ee} = 10.6$ GeV
$<4.4 \times 10^{-6}$	90	¹ BARTELT	94	CLEO	Repl. by BLISS 98
$<1.8 \times 10^{-5}$	90	ALBRECHT	92k	ARG	$E_{cm}^{ee} = 10$ GeV
$<1.7 \times 10^{-5}$	90	BOWCOCK	90	CLEO	$E_{cm}^{ee} = 10.4-10.9$

¹BARTELT 94 assume phase space decays.

$\Gamma(\mu^- \pi^+ \pi^-)/\Gamma_{total}$ Γ₂₁₈/Γ
Test of lepton family number conservation.

VALUE	CL%	DOCUMENT ID	TECN	COMMENT
$<2.1 \times 10^{-8}$	90	MIYAZAKI 13	BELL	$854 \text{ fb}^{-1} E_{cm}^{ee} = 10.6$ GeV
•••				We do not use the following data for averages, fits, limits, etc. •••
$<3.3 \times 10^{-8}$	90	MIYAZAKI 10	BELL	Repl. by MIYAZAKI 13
$<4.8 \times 10^{-7}$	90	YUSA 06	BELL	$158 \text{ fb}^{-1} E_{cm}^{ee} = 10.6$ GeV
$<2.9 \times 10^{-7}$	90	AUBERT,BE 05D	BABR	$221 \text{ fb}^{-1}, E_{cm}^{ee} = 10.6$ GeV
$<8.2 \times 10^{-6}$	90	BLISS 98	CLEO	$E_{cm}^{ee} = 10.6$ GeV
$<7.4 \times 10^{-6}$	90	¹ BARTELT 94	CLEO	Repl. by BLISS 98
$<3.6 \times 10^{-5}$	90	ALBRECHT 92k	ARG	$E_{cm}^{ee} = 10$ GeV
$<3.9 \times 10^{-5}$	90	BOWCOCK 90	CLEO	$E_{cm}^{ee} = 10.4-10.9$

¹BARTELT 94 assume phase space decays.

$\Gamma(\mu^+ \pi^- \pi^-)/\Gamma_{total}$ Γ₂₁₉/Γ
Test of lepton number conservation.

VALUE	CL%	DOCUMENT ID	TECN	COMMENT
$<3.9 \times 10^{-8}$	90	MIYAZAKI 13	BELL	$854 \text{ fb}^{-1} E_{cm}^{ee} = 10.6$ GeV
•••				We do not use the following data for averages, fits, limits, etc. •••
$<3.7 \times 10^{-8}$	90	MIYAZAKI 10	BELL	Repl. by MIYAZAKI 13
$<3.4 \times 10^{-7}$	90	YUSA 06	BELL	$158 \text{ fb}^{-1} E_{cm}^{ee} = 10.6$ GeV
$<7 \times 10^{-8}$	90	AUBERT,BE 05D	BABR	$221 \text{ fb}^{-1}, E_{cm}^{ee} = 10.6$ GeV
$<3.4 \times 10^{-6}$	90	BLISS 98	CLEO	$E_{cm}^{ee} = 10.6$ GeV
$<6.9 \times 10^{-6}$	90	¹ BARTELT 94	CLEO	Repl. by BLISS 98
$<6.3 \times 10^{-5}$	90	ALBRECHT 92k	ARG	$E_{cm}^{ee} = 10$ GeV
$<3.9 \times 10^{-5}$	90	BOWCOCK 90	CLEO	$E_{cm}^{ee} = 10.4-10.9$

¹BARTELT 94 assume phase space decays.

$\Gamma(e^- \pi^+ K^-)/\Gamma_{total}$ Γ₂₂₀/Γ
Test of lepton family number conservation.

VALUE	CL%	DOCUMENT ID	TECN	COMMENT
$<3.7 \times 10^{-8}$	90	MIYAZAKI 13	BELL	$854 \text{ fb}^{-1} E_{cm}^{ee} = 10.6$ GeV
•••				We do not use the following data for averages, fits, limits, etc. •••
$<5.8 \times 10^{-8}$	90	MIYAZAKI 10	BELL	Repl. by MIYAZAKI 13
$<7.2 \times 10^{-7}$	90	YUSA 06	BELL	$158 \text{ fb}^{-1} E_{cm}^{ee} = 10.6$ GeV
$<3.2 \times 10^{-7}$	90	AUBERT,BE 05D	BABR	$221 \text{ fb}^{-1}, E_{cm}^{ee} = 10.6$ GeV
$<6.4 \times 10^{-6}$	90	BLISS 98	CLEO	$E_{cm}^{ee} = 10.6$ GeV
$<7.7 \times 10^{-6}$	90	¹ BARTELT 94	CLEO	Repl. by BLISS 98
$<2.9 \times 10^{-5}$	90	ALBRECHT 92k	ARG	$E_{cm}^{ee} = 10$ GeV
$<5.8 \times 10^{-5}$	90	BOWCOCK 90	CLEO	$E_{cm}^{ee} = 10.4-10.9$

¹BARTELT 94 assume phase space decays.

$\Gamma(e^- \pi^- K^+)/\Gamma_{total}$ Γ₂₂₁/Γ
Test of lepton family number conservation.

VALUE	CL%	DOCUMENT ID	TECN	COMMENT
$<3.1 \times 10^{-8}$	90	MIYAZAKI 13	BELL	$854 \text{ fb}^{-1} E_{cm}^{ee} = 10.6$ GeV
•••				We do not use the following data for averages, fits, limits, etc. •••
$<5.2 \times 10^{-8}$	90	MIYAZAKI 10	BELL	Repl. by MIYAZAKI 13
$<1.6 \times 10^{-7}$	90	YUSA 06	BELL	$158 \text{ fb}^{-1} E_{cm}^{ee} = 10.6$ GeV
$<1.7 \times 10^{-7}$	90	AUBERT,BE 05D	BABR	$221 \text{ fb}^{-1}, E_{cm}^{ee} = 10.6$ GeV
$<3.8 \times 10^{-6}$	90	BLISS 98	CLEO	$E_{cm}^{ee} = 10.6$ GeV
$<4.6 \times 10^{-6}$	90	¹ BARTELT 94	CLEO	Repl. by BLISS 98
$<5.8 \times 10^{-5}$	90	BOWCOCK 90	CLEO	$E_{cm}^{ee} = 10.4-10.9$

¹BARTELT 94 assume phase space decays.

$\Gamma(e^+ \pi^- K^-)/\Gamma_{total}$ Γ₂₂₂/Γ
Test of lepton number conservation.

VALUE	CL%	DOCUMENT ID	TECN	COMMENT
$<3.2 \times 10^{-8}$	90	MIYAZAKI 13	BELL	$854 \text{ fb}^{-1} E_{cm}^{ee} = 10.6$ GeV
•••				We do not use the following data for averages, fits, limits, etc. •••
$<6.7 \times 10^{-8}$	90	MIYAZAKI 10	BELL	Repl. by MIYAZAKI 13
$<1.9 \times 10^{-7}$	90	YUSA 06	BELL	$158 \text{ fb}^{-1} E_{cm}^{ee} = 10.6$ GeV
$<1.8 \times 10^{-7}$	90	AUBERT,BE 05D	BABR	$221 \text{ fb}^{-1}, E_{cm}^{ee} = 10.6$ GeV
$<2.1 \times 10^{-6}$	90	BLISS 98	CLEO	$E_{cm}^{ee} = 10.6$ GeV
$<4.5 \times 10^{-6}$	90	¹ BARTELT 94	CLEO	Repl. by BLISS 98
$<2.0 \times 10^{-5}$	90	ALBRECHT 92k	ARG	$E_{cm}^{ee} = 10$ GeV
$<4.9 \times 10^{-5}$	90	BOWCOCK 90	CLEO	$E_{cm}^{ee} = 10.4-10.9$

¹BARTELT 94 assume phase space decays.

$\Gamma(e^- K_S^0 K_S^0)/\Gamma_{total}$ Γ₂₂₃/Γ
Test of lepton family number conservation.

VALUE	CL%	DOCUMENT ID	TECN	COMMENT
$<7.1 \times 10^{-8}$	90	MIYAZAKI 10A	BELL	$671 \text{ fb}^{-1} E_{cm}^{ee} = 10.6$ GeV
•••				We do not use the following data for averages, fits, limits, etc. •••
$<2.2 \times 10^{-6}$	90	CHEN 02c	CLEO	$E_{cm}^{ee} = 10.6$ GeV

$\Gamma(e^- K^+ K^-)/\Gamma_{total}$ Γ₂₂₄/Γ
Test of lepton family number conservation.

VALUE	CL%	DOCUMENT ID	TECN	COMMENT
$<3.4 \times 10^{-8}$	90	MIYAZAKI 13	BELL	$854 \text{ fb}^{-1} E_{cm}^{ee} = 10.6$ GeV
•••				We do not use the following data for averages, fits, limits, etc. •••
$<5.4 \times 10^{-8}$	90	MIYAZAKI 10	BELL	Repl. by MIYAZAKI 13
$<3.0 \times 10^{-7}$	90	YUSA 06	BELL	$158 \text{ fb}^{-1} E_{cm}^{ee} = 10.6$ GeV
$<1.4 \times 10^{-7}$	90	AUBERT,BE 05D	BABR	$221 \text{ fb}^{-1}, E_{cm}^{ee} = 10.6$ GeV
$<6.0 \times 10^{-6}$	90	BLISS 98	CLEO	$E_{cm}^{ee} = 10.6$ GeV

$\Gamma(e^+ K^- K^-)/\Gamma_{total}$ Γ₂₂₅/Γ
Test of lepton number conservation.

VALUE	CL%	DOCUMENT ID	TECN	COMMENT
$<3.3 \times 10^{-8}$	90	MIYAZAKI 13	BELL	$854 \text{ fb}^{-1} E_{cm}^{ee} = 10.6$ GeV
•••				We do not use the following data for averages, fits, limits, etc. •••
$<6.0 \times 10^{-8}$	90	MIYAZAKI 10	BELL	Repl. by MIYAZAKI 13
$<3.1 \times 10^{-7}$	90	YUSA 06	BELL	$158 \text{ fb}^{-1} E_{cm}^{ee} = 10.6$ GeV
$<1.5 \times 10^{-7}$	90	AUBERT,BE 05D	BABR	$221 \text{ fb}^{-1}, E_{cm}^{ee} = 10.6$ GeV
$<3.8 \times 10^{-6}$	90	BLISS 98	CLEO	$E_{cm}^{ee} = 10.6$ GeV

$\Gamma(\mu^- \pi^+ K^-)/\Gamma_{total}$ Γ₂₂₆/Γ
Test of lepton family number conservation.

VALUE	CL%	DOCUMENT ID	TECN	COMMENT
$< 8.6 \times 10^{-8}$	90	MIYAZAKI 13	BELL	$854 \text{ fb}^{-1} E_{cm}^{ee} = 10.6$ GeV
•••				We do not use the following data for averages, fits, limits, etc. •••
$< 1.6 \times 10^{-7}$	90	MIYAZAKI 10	BELL	Repl. by MIYAZAKI 13
$< 2.7 \times 10^{-7}$	90	YUSA 06	BELL	$158 \text{ fb}^{-1} E_{cm}^{ee} = 10.6$ GeV
$< 2.6 \times 10^{-7}$	90	AUBERT,BE 05D	BABR	$221 \text{ fb}^{-1}, E_{cm}^{ee} = 10.6$ GeV
$< 7.5 \times 10^{-6}$	90	BLISS 98	CLEO	$E_{cm}^{ee} = 10.6$ GeV
$< 8.7 \times 10^{-6}$	90	¹ BARTELT 94	CLEO	Repl. by BLISS 98
$< 11 \times 10^{-5}$	90	ALBRECHT 92k	ARG	$E_{cm}^{ee} = 10$ GeV
$< 7.7 \times 10^{-5}$	90	BOWCOCK 90	CLEO	$E_{cm}^{ee} = 10.4-10.9$

¹BARTELT 94 assume phase space decays.

$\Gamma(\mu^- \pi^- K^+)/\Gamma_{total}$ Γ₂₂₇/Γ
Test of lepton family number conservation.

VALUE	CL%	DOCUMENT ID	TECN	COMMENT
$<4.5 \times 10^{-8}$	90	MIYAZAKI 13	BELL	$854 \text{ fb}^{-1} E_{cm}^{ee} = 10.6$ GeV
•••				We do not use the following data for averages, fits, limits, etc. •••
$<1.0 \times 10^{-7}$	90	MIYAZAKI 10	BELL	Repl. by MIYAZAKI 13
$<7.3 \times 10^{-7}$	90	YUSA 06	BELL	$158 \text{ fb}^{-1} E_{cm}^{ee} = 10.6$ GeV
$<3.2 \times 10^{-7}$	90	AUBERT,BE 05D	BABR	$221 \text{ fb}^{-1}, E_{cm}^{ee} = 10.6$ GeV
$<7.4 \times 10^{-6}$	90	BLISS 98	CLEO	$E_{cm}^{ee} = 10.6$ GeV
$<1.5 \times 10^{-5}$	90	¹ BARTELT 94	CLEO	Repl. by BLISS 98
$<7.7 \times 10^{-5}$	90	BOWCOCK 90	CLEO	$E_{cm}^{ee} = 10.4-10.9$

¹BARTELT 94 assume phase space decays.

$\Gamma(\mu^+ \pi^- K^-)/\Gamma_{total}$ Γ₂₂₈/Γ
Test of lepton number conservation.

VALUE	CL%	DOCUMENT ID	TECN	COMMENT
$<4.8 \times 10^{-8}$	90	MIYAZAKI 13	BELL	$854 \text{ fb}^{-1} E_{cm}^{ee} = 10.6$ GeV
•••				We do not use the following data for averages, fits, limits, etc. •••
$<9.4 \times 10^{-8}$	90	MIYAZAKI 10	BELL	Repl. by MIYAZAKI 13
$<2.9 \times 10^{-7}$	90	YUSA 06	BELL	$158 \text{ fb}^{-1} E_{cm}^{ee} = 10.6$ GeV
$<2.2 \times 10^{-7}$	90	AUBERT,BE 05D	BABR	$221 \text{ fb}^{-1}, E_{cm}^{ee} = 10.6$ GeV
$<7.0 \times 10^{-6}$	90	BLISS 98	CLEO	$E_{cm}^{ee} = 10.6$ GeV
$<2.0 \times 10^{-5}$	90	¹ BARTELT 94	CLEO	Repl. by BLISS 98
$<5.8 \times 10^{-5}$	90	ALBRECHT 92k	ARG	$E_{cm}^{ee} = 10$ GeV
$<4.0 \times 10^{-5}$	90	BOWCOCK 90	CLEO	$E_{cm}^{ee} = 10.4-10.9$

¹BARTELT 94 assume phase space decays.

$\Gamma(\mu^- K_S^0 K_S^0)/\Gamma_{total}$ Γ₂₂₉/Γ

VALUE	CL%	DOCUMENT ID	TECN	COMMENT
$<8.0 \times 10^{-8}$	90	MIYAZAKI 10A	BELL	$671 \text{ fb}^{-1} E_{cm}^{ee} = 10.6$ GeV
•••				We do not use the following data for averages, fits, limits, etc. •••
$<3.4 \times 10^{-6}$	90	CHEN 02c	CLEO	$E_{cm}^{ee} = 10.6$ GeV

Lepton Particle Listings

 τ $\Gamma(\mu^- K^+ K^-)/\Gamma_{\text{total}}$ Γ_{230}/Γ
Test of lepton family number conservation.

VALUE	CL%	DOCUMENT ID	TECN	COMMENT
< 4.4×10^{-8}	90	MIYAZAKI 13	BELL	$854 \text{ fb}^{-1} E_{\text{cm}}^{\text{ee}} = 10.6 \text{ GeV}$
• • • We do not use the following data for averages, fits, limits, etc. • • •				
< 6.8×10^{-8}	90	MIYAZAKI 10	BELL	Repl. by MIYAZAKI 13
< 8.0×10^{-7}	90	YUSA 06	BELL	$158 \text{ fb}^{-1} E_{\text{cm}}^{\text{ee}} = 10.6 \text{ GeV}$
< 2.5×10^{-7}	90	AUBERT,BE 05D	BABR	$221 \text{ fb}^{-1}, E_{\text{cm}}^{\text{ee}} = 10.6 \text{ GeV}$
< 15×10^{-6}	90	BLISS 98	CLEO	$E_{\text{cm}}^{\text{ee}} = 10.6 \text{ GeV}$

 $\Gamma(\mu^+ K^- K^-)/\Gamma_{\text{total}}$ Γ_{231}/Γ
Test of lepton number conservation.

VALUE	CL%	DOCUMENT ID	TECN	COMMENT
< 4.7×10^{-8}	90	MIYAZAKI 13	BELL	$854 \text{ fb}^{-1} E_{\text{cm}}^{\text{ee}} = 10.6 \text{ GeV}$
• • • We do not use the following data for averages, fits, limits, etc. • • •				
< 9.6×10^{-8}	90	MIYAZAKI 10	BELL	Repl. by MIYAZAKI 13
< 4.4×10^{-7}	90	YUSA 06	BELL	$158 \text{ fb}^{-1} E_{\text{cm}}^{\text{ee}} = 10.6 \text{ GeV}$
< 4.8×10^{-7}	90	AUBERT,BE 05D	BABR	$221 \text{ fb}^{-1}, E_{\text{cm}}^{\text{ee}} = 10.6 \text{ GeV}$
< 6.0×10^{-6}	90	BLISS 98	CLEO	$E_{\text{cm}}^{\text{ee}} = 10.6 \text{ GeV}$

 $\Gamma(e^- \pi^0 \pi^0)/\Gamma_{\text{total}}$ Γ_{232}/Γ
Test of lepton family number conservation.

VALUE	CL%	DOCUMENT ID	TECN	COMMENT
< 6.5×10^{-6}	90	BONVICINI 97	CLEO	$E_{\text{cm}}^{\text{ee}} = 10.6 \text{ GeV}$

 $\Gamma(\mu^- \pi^0 \pi^0)/\Gamma_{\text{total}}$ Γ_{233}/Γ
Test of lepton family number conservation.

VALUE	CL%	DOCUMENT ID	TECN	COMMENT
< 14×10^{-6}	90	BONVICINI 97	CLEO	$E_{\text{cm}}^{\text{ee}} = 10.6 \text{ GeV}$

 $\Gamma(e^- \eta \eta)/\Gamma_{\text{total}}$ Γ_{234}/Γ
Test of lepton family number conservation.

VALUE	CL%	DOCUMENT ID	TECN	COMMENT
< 35×10^{-6}	90	BONVICINI 97	CLEO	$E_{\text{cm}}^{\text{ee}} = 10.6 \text{ GeV}$

 $\Gamma(\mu^- \eta \eta)/\Gamma_{\text{total}}$ Γ_{235}/Γ
Test of lepton family number conservation.

VALUE	CL%	DOCUMENT ID	TECN	COMMENT
< 60×10^{-6}	90	BONVICINI 97	CLEO	$E_{\text{cm}}^{\text{ee}} = 10.6 \text{ GeV}$

 $\Gamma(e^- \pi^0 \eta)/\Gamma_{\text{total}}$ Γ_{236}/Γ
Test of lepton family number conservation.

VALUE	CL%	DOCUMENT ID	TECN	COMMENT
< 24×10^{-6}	90	BONVICINI 97	CLEO	$E_{\text{cm}}^{\text{ee}} = 10.6 \text{ GeV}$

 $\Gamma(\mu^- \pi^0 \eta)/\Gamma_{\text{total}}$ Γ_{237}/Γ
Test of lepton family number conservation.

VALUE	CL%	DOCUMENT ID	TECN	COMMENT
< 22×10^{-6}	90	BONVICINI 97	CLEO	$E_{\text{cm}}^{\text{ee}} = 10.6 \text{ GeV}$

 $\Gamma(p e^- e^-)/\Gamma_{\text{total}}$ Γ_{238}/Γ
Test of lepton family number conservation.

VALUE	CL%	DOCUMENT ID	TECN	COMMENT
< 3.0×10^{-8}	90	SAHOO 20	BELL	$921 \text{ fb}^{-1} E_{\text{cm}}^{\text{ee}} = 10.6 \text{ GeV}$

 $\Gamma(\bar{p} e^+ e^-)/\Gamma_{\text{total}}$ Γ_{239}/Γ
Test of lepton family number conservation.

VALUE	CL%	DOCUMENT ID	TECN	COMMENT
< 3.0×10^{-8}	90	SAHOO 20	BELL	$921 \text{ fb}^{-1} E_{\text{cm}}^{\text{ee}} = 10.6 \text{ GeV}$

 $\Gamma(\bar{p} e^+ \mu^-)/\Gamma_{\text{total}}$ Γ_{240}/Γ
Test of lepton family number conservation.

VALUE	CL%	DOCUMENT ID	TECN	COMMENT
< 2.0×10^{-8}	90	SAHOO 20	BELL	$921 \text{ fb}^{-1} E_{\text{cm}}^{\text{ee}} = 10.6 \text{ GeV}$

 $\Gamma(\bar{p} e^- \mu^+)/\Gamma_{\text{total}}$ Γ_{241}/Γ
Test of lepton family number conservation.

VALUE	CL%	DOCUMENT ID	TECN	COMMENT
< 1.8×10^{-8}	90	SAHOO 20	BELL	$921 \text{ fb}^{-1} E_{\text{cm}}^{\text{ee}} = 10.6 \text{ GeV}$

 $\Gamma(p \mu^- \mu^-)/\Gamma_{\text{total}}$ Γ_{242}/Γ
Test of lepton family number conservation.

VALUE	CL%	DOCUMENT ID	TECN	COMMENT
< 4.0×10^{-8}	90	SAHOO 20	BELL	$921 \text{ fb}^{-1} E_{\text{cm}}^{\text{ee}} = 10.6 \text{ GeV}$
• • • We do not use the following data for averages, fits, limits, etc. • • •				
< 4.4×10^{-7}	90	AAIJ 13AH	LHCb	$1.0 \text{ fb}^{-1}, pp \text{ at } 7 \text{ TeV}$

 $\Gamma(\bar{p} \mu^+ \mu^-)/\Gamma_{\text{total}}$ Γ_{243}/Γ
Test of lepton family number conservation.

VALUE	CL%	DOCUMENT ID	TECN	COMMENT
< 1.8×10^{-8}	90	SAHOO 20	BELL	$921 \text{ fb}^{-1} E_{\text{cm}}^{\text{ee}} = 10.6 \text{ GeV}$
• • • We do not use the following data for averages, fits, limits, etc. • • •				
< 3.3×10^{-7}	90	AAIJ 13AH	LHCb	$1.0 \text{ fb}^{-1}, pp \text{ at } 7 \text{ TeV}$

 $\Gamma(\bar{p} \gamma)/\Gamma_{\text{total}}$ Γ_{244}/Γ
Test of lepton number and baryon number conservation.

VALUE	CL%	DOCUMENT ID	TECN	COMMENT
< 3.5×10^{-6}	90	GODANG 99	CLEO	$E_{\text{cm}}^{\text{ee}} = 10.6 \text{ GeV}$
• • • We do not use the following data for averages, fits, limits, etc. • • •				
< 29×10^{-5}	90	ALBRECHT 92k	ARG	$E_{\text{cm}}^{\text{ee}} = 10 \text{ GeV}$

 $\Gamma(\bar{p} \pi^0)/\Gamma_{\text{total}}$ Γ_{245}/Γ
Test of lepton number and baryon number conservation.

VALUE	CL%	DOCUMENT ID	TECN	COMMENT
< 15×10^{-6}	90	GODANG 99	CLEO	$E_{\text{cm}}^{\text{ee}} = 10.6 \text{ GeV}$
• • • We do not use the following data for averages, fits, limits, etc. • • •				
< 66×10^{-5}	90	ALBRECHT 92k	ARG	$E_{\text{cm}}^{\text{ee}} = 10 \text{ GeV}$

 $\Gamma(\bar{p} 2\pi^0)/\Gamma_{\text{total}}$ Γ_{246}/Γ
Test of lepton number and baryon number conservation.

VALUE	CL%	DOCUMENT ID	TECN	COMMENT
< 33×10^{-6}	90	GODANG 99	CLEO	$E_{\text{cm}}^{\text{ee}} = 10.6 \text{ GeV}$

 $\Gamma(\bar{p} \eta)/\Gamma_{\text{total}}$ Γ_{247}/Γ
Test of lepton number and baryon number conservation.

VALUE	CL%	DOCUMENT ID	TECN	COMMENT
< 8.9×10^{-6}	90	GODANG 99	CLEO	$E_{\text{cm}}^{\text{ee}} = 10.6 \text{ GeV}$
• • • We do not use the following data for averages, fits, limits, etc. • • •				
< 130×10^{-5}	90	ALBRECHT 92k	ARG	$E_{\text{cm}}^{\text{ee}} = 10 \text{ GeV}$

 $\Gamma(\bar{p} \pi^0 \eta)/\Gamma_{\text{total}}$ Γ_{248}/Γ
Test of lepton number and baryon number conservation.

VALUE	CL%	DOCUMENT ID	TECN	COMMENT
< 27×10^{-6}	90	GODANG 99	CLEO	$E_{\text{cm}}^{\text{ee}} = 10.6 \text{ GeV}$

 $\Gamma(\Lambda \pi^-)/\Gamma_{\text{total}}$ Γ_{249}/Γ
Test of lepton number and baryon number conservation.

VALUE	CL%	DOCUMENT ID	TECN	COMMENT
< 0.72×10^{-7}	90	MIYAZAKI 06	BELL	$154 \text{ fb}^{-1}, E_{\text{cm}}^{\text{ee}} = 10.6 \text{ GeV}$

 $\Gamma(\bar{\Lambda} \pi^-)/\Gamma_{\text{total}}$ Γ_{250}/Γ
Test of lepton number and baryon number conservation.

VALUE	CL%	DOCUMENT ID	TECN	COMMENT
< 1.4×10^{-7}	90	MIYAZAKI 06	BELL	$154 \text{ fb}^{-1}, E_{\text{cm}}^{\text{ee}} = 10.6 \text{ GeV}$

 $\Gamma(e^- \text{light boson})/\Gamma(e^- \bar{\nu}_e \nu_\tau)$ Γ_{251}/Γ_5
Test of lepton family number conservation.

VALUE	CL%	DOCUMENT ID	TECN	COMMENT
< 0.015	95	¹ ALBRECHT 95g	ARG	$E_{\text{cm}}^{\text{ee}} = 9.4\text{--}10.6 \text{ GeV}$
• • • We do not use the following data for averages, fits, limits, etc. • • •				
< 0.008	95	² BRYMAN 21	RVUE	
< 0.018	95	³ ALBRECHT 90e	ARG	$E_{\text{cm}}^{\text{ee}} = 9.4\text{--}10.6 \text{ GeV}$
< 0.040	95	⁴ BALTRUSAITIS...85	MRK3	$E_{\text{cm}}^{\text{ee}} = 3.77 \text{ GeV}$

¹ ALBRECHT 95g limit holds for bosons with mass < 0.4 GeV. The limit rises to 0.036 for a mass of 1.0 GeV, then falls to 0.006 at the upper mass limit of 1.6 GeV.

² BRYMAN 21 reports indirect limits obtained from the consistency of the world averages of $B(\tau^- \rightarrow e^- \bar{\nu}_e \nu_\tau)$ and $B(\tau^- \rightarrow \mu^- \bar{\nu}_\mu \nu_\tau)$ with their Standard Model predictions, without a simulation of the efficiency as a function of the X mass for the searched decay modes to be detected as the corresponding Standard Model decay modes.

³ ALBRECHT 90e limit applies for spinless boson with mass < 100 MeV, and rises to 0.050 for mass = 500 MeV.

⁴ BALTRUSAITIS 85 limit applies for spinless boson with mass < 100 MeV.

 $\Gamma(\mu^- \text{light boson})/\Gamma(e^- \bar{\nu}_e \nu_\tau)$ Γ_{252}/Γ_5
Test of lepton family number conservation.

VALUE	CL%	DOCUMENT ID	TECN	COMMENT
< 0.026	95	¹ ALBRECHT 95g	ARG	$E_{\text{cm}}^{\text{ee}} = 9.4\text{--}10.6 \text{ GeV}$
• • • We do not use the following data for averages, fits, limits, etc. • • •				
< 0.011	95	² BRYMAN 21	RVUE	
< 0.033	95	³ ALBRECHT 90e	ARG	$E_{\text{cm}}^{\text{ee}} = 9.4\text{--}10.6 \text{ GeV}$
< 0.125	95	⁴ BALTRUSAITIS...85	MRK3	$E_{\text{cm}}^{\text{ee}} = 3.77 \text{ GeV}$

¹ ALBRECHT 95g limit holds for bosons with mass < 1.3 GeV. The limit rises to 0.034 for a mass of 1.4 GeV, then falls to 0.003 at the upper mass limit of 1.6 GeV.

² BRYMAN 21 reports indirect limits obtained from the consistency of the world averages of $B(\tau^- \rightarrow e^- \bar{\nu}_e \nu_\tau)$ and $B(\tau^- \rightarrow \mu^- \bar{\nu}_\mu \nu_\tau)$ with their Standard Model predictions, without a simulation of the efficiency as a function of the X mass for the searched decay modes to be detected as the corresponding Standard Model decay modes.

³ ALBRECHT 90e limit applies for spinless boson with mass < 100 MeV, and rises to 0.071 for mass = 500 MeV.

⁴ BALTRUSAITIS 85 limit applies for spinless boson with mass < 100 MeV.

τ -DECAY PARAMETERS

See the related review(s):

τ -Lepton Decay Parameters

$\rho(e \text{ or } \mu)$ PARAMETER

($V-A$) theory predicts $\rho = 0.75$.

Table with columns: VALUE, EVTS, DOCUMENT ID, TECN, COMMENT. Includes sub-sections for OUR FIT and OUR AVERAGE, listing various experiments like HEISTER, ABREU, ACKERSTAFF, etc.

- 1 Combined fit to ARGUS tau decay parameter measurements in ALBRECHT 98, ALBRECHT 95c, ALBRECHT 93g, and ALBRECHT 94e. ALBRECHT 98 use tau pair events of the type $\tau^- \tau^+ \rightarrow (\ell^- \bar{\nu}_\ell \nu_\tau)(\pi^+ \pi^0 \bar{\nu}_\tau)$, and their charged conjugates.
2 ABE 97o assume $\eta = 0$ in their fit. Letting η vary in the fit gives a ρ value of $0.69 \pm 0.13 \pm 0.05$.
3 Value is from a simultaneous fit for the ρ and η decay parameters to the lepton energy spectrum. Not independent of ALBRECHT 90e $\rho(e \text{ or } \mu)$ value which assumes $\eta = 0$. Result is strongly correlated with ALBRECHT 95c.
4 Combined fit to ARGUS tau decay parameter measurements in ALBRECHT 95c, ALBRECHT 93g, and ALBRECHT 94e.

$\rho(e)$ PARAMETER

($V-A$) theory predicts $\rho = 0.75$.

Table with columns: VALUE, EVTS, DOCUMENT ID, TECN, COMMENT. Includes sub-sections for OUR FIT and OUR AVERAGE, listing various experiments like HEISTER, ABREU, ACKERSTAFF, etc.

- 1 ALBRECHT 98 use tau pair events of the type $\tau^- \tau^+ \rightarrow (\ell^- \bar{\nu}_\ell \nu_\tau)(\pi^+ \pi^0 \bar{\nu}_\tau)$, and their charged conjugates.
2 ALBRECHT 95 use tau pair events of the type $\tau^- \tau^+ \rightarrow (\ell^- \bar{\nu}_\ell \nu_\tau)(h^+ h^- h^+ \pi^0 \bar{\nu}_\tau)$ and their charged conjugates.
3 ALBRECHT 93g use tau pair events of the type $\tau^- \tau^+ \rightarrow (\mu^- \bar{\nu}_\mu \nu_\tau)(e^+ \nu_e \bar{\nu}_\tau)$ and their charged conjugates.

$\rho(\mu)$ PARAMETER

($V-A$) theory predicts $\rho = 0.75$.

Table with columns: VALUE, EVTS, DOCUMENT ID, TECN, COMMENT. Includes sub-sections for OUR FIT and OUR AVERAGE, listing various experiments like HEISTER, ABREU, ACKERSTAFF, etc.

- 1 ALBRECHT 98 use tau pair events of the type $\tau^- \tau^+ \rightarrow (\ell^- \bar{\nu}_\ell \nu_\tau)(\pi^+ \pi^0 \bar{\nu}_\tau)$, and their charged conjugates.

$\xi(e \text{ or } \mu)$ PARAMETER

($V-A$) theory predicts $\xi = 1$.

Table with columns: VALUE, EVTS, DOCUMENT ID, TECN, COMMENT. Includes sub-sections for OUR FIT and OUR AVERAGE, listing various experiments like HEISTER, ABREU, ACKERSTAFF, etc.

- • • We do not use the following data for averages, fits, limits, etc. • • •
0.94 $\pm 0.21 \pm 0.07$ 18k ACCIARRI 96H L3 Repl. by ACCIARRI 98R
0.97 ± 0.14 3 ALBRECHT 95c ARG Repl. by ALBRECHT 98
1.18 $\pm 0.15 \pm 0.16$ BUSKULIC 95D ALEP Repl. by HEISTER 01e
0.90 $\pm 0.15 \pm 0.10$ 3230 4 ALBRECHT 93G ARG $E_{cm}^{ee} = 9.4-10.6$ GeV
1 Combined fit to ARGUS tau decay parameter measurements in ALBRECHT 98, ALBRECHT 95c, ALBRECHT 93g, and ALBRECHT 94e. ALBRECHT 98 use tau pair events of the type $\tau^- \tau^+ \rightarrow (\ell^- \bar{\nu}_\ell \nu_\tau)(\pi^+ \pi^0 \bar{\nu}_\tau)$, and their charged conjugates.
2 ABE 97o assume $\eta = 0$ in their fit. Letting η vary in the fit gives a ξ value of $1.02 \pm 0.36 \pm 0.05$.
3 Combined fit to ARGUS tau decay parameter measurements in ALBRECHT 95c, ALBRECHT 93g, and ALBRECHT 94e. ALBRECHT 95c uses events of the type $\tau^- \tau^+ \rightarrow (\ell^- \bar{\nu}_\ell \nu_\tau)(h^+ h^- h^+ \bar{\nu}_\tau)$ and their charged conjugates.
4 ALBRECHT 93g measurement determines $|\xi|$ for the case $\xi(e) = \xi(\mu)$, but the authors point out that other LEP experiments determine the sign to be positive.

$\xi(e)$ PARAMETER

($V-A$) theory predicts $\xi = 1$.

Table with columns: VALUE, EVTS, DOCUMENT ID, TECN, COMMENT. Includes sub-sections for OUR FIT and OUR AVERAGE, listing various experiments like HEISTER, ABREU, ACKERSTAFF, etc.

- • • We do not use the following data for averages, fits, limits, etc. • • •
1.03 $\pm 0.23 \pm 0.09$ BUSKULIC 95D ALEP Repl. by HEISTER 01e
1 ALBRECHT 98 use tau pair events of the type $\tau^- \tau^+ \rightarrow (\ell^- \bar{\nu}_\ell \nu_\tau)(\pi^+ \pi^0 \bar{\nu}_\tau)$, and their charged conjugates.

$\xi(\mu)$ PARAMETER

($V-A$) theory predicts $\xi = 1$.

Table with columns: VALUE, EVTS, DOCUMENT ID, TECN, COMMENT. Includes sub-sections for OUR FIT and OUR AVERAGE, listing various experiments like HEISTER, ABREU, ACKERSTAFF, etc.

- • • We do not use the following data for averages, fits, limits, etc. • • •
1.23 $\pm 0.22 \pm 0.10$ BUSKULIC 95D ALEP Repl. by HEISTER 01e
1 ALBRECHT 98 use tau pair events of the type $\tau^- \tau^+ \rightarrow (\ell^- \bar{\nu}_\ell \nu_\tau)(\pi^+ \pi^0 \bar{\nu}_\tau)$, and their charged conjugates.

$\eta(e \text{ or } \mu)$ PARAMETER

($V-A$) theory predicts $\eta = 0$.

Table with columns: VALUE, EVTS, DOCUMENT ID, TECN, COMMENT. Includes sub-sections for OUR FIT and OUR AVERAGE, listing various experiments like HEISTER, ABREU, ACKERSTAFF, etc.

- • • We do not use the following data for averages, fits, limits, etc. • • •
0.25 $\pm 0.17 \pm 0.11$ 18k ACCIARRI 96H L3 Repl. by ACCIARRI 98R
-0.04 $\pm 0.15 \pm 0.11$ BUSKULIC 95D ALEP Repl. by HEISTER 01e

$\eta(\mu)$ PARAMETER

($V-A$) theory predicts $\eta = 0$.

Table with columns: VALUE, EVTS, DOCUMENT ID, TECN, COMMENT. Includes sub-sections for OUR FIT and OUR AVERAGE, listing various experiments like HEISTER, ABREU, ACKERSTAFF, etc.

- • • We do not use the following data for averages, fits, limits, etc. • • •
0.17 ± 0.15 OUR AVERAGE Error includes scale factor of 1.2.
0.160 $\pm 0.150 \pm 0.060$ 46k HEISTER 01E ALEP 1991-1995 LEP runs
0.72 $\pm 0.32 \pm 0.15$ ABREU 00L DLPH 1992-1995 runs
-0.59 $\pm 0.82 \pm 0.45$ 1 ABE 97O SLD 1993-1995 SLC runs
0.010 $\pm 0.149 \pm 0.171$ 13k 2 AMMAR 97B CLEO $E_{cm}^{ee} = 10.6$ GeV

Lepton Particle Listings

T

• • • We do not use the following data for averages, fits, limits, etc. • • •
 0.010 ± 0.065 ± 0.001 27k ³ACKERSTAFF 99D OPAL 1990–1995 LEP runs
 –0.24 ± 0.23 ± 0.18 BUSKULIC 95D ALEP Repl. by HEISTER 01E

¹Highly correlated (corr. = 0.92) with ABE 97o $\rho(\mu)$ measurement.
²Highly correlated (corr. = 0.949) with AMMAR 97B $\rho(\mu)$ value.
³ACKERSTAFF 99D result is dominated by a constraint on η from the OPAL measurements of the τ lifetime and $B(\tau^- \rightarrow \mu^- \bar{\nu}_\mu \nu_\tau)$ assuming lepton universality for the total coupling strength.

($\delta\xi$)(e or μ) PARAMETER

(V–A) theory predicts $\langle\delta\xi\rangle = 0.75$.

VALUE	EVTS	DOCUMENT ID	TECN	COMMENT
0.746 ± 0.021 OUR FIT				
0.744 ± 0.022 OUR AVERAGE				
0.776 ± 0.045 ± 0.024	81k	HEISTER 01E ALEP		1991–1995 LEP runs
0.779 ± 0.070 ± 0.028	36k	ABREU 00L DLPH		1992–1995 runs
0.65 ± 0.14 ± 0.07	46k	ACKERSTAFF 99D OPAL		1990–1995 LEP runs
0.70 ± 0.11	54k	ACCIARRI 98R L3		1991–1995 LEP runs
0.63 ± 0.09		¹ ALBRECHT 98 ARG		$E_{cm}^{ee} = 9.5\text{--}10.6$ GeV
0.88 ± 0.27 ± 0.04		² ABE 97o SLD		1993–1995 SLC runs
0.745 ± 0.026 ± 0.009	55k	ALEXANDER 97F CLEO		$E_{cm}^{ee} = 10.6$ GeV
• • • We do not use the following data for averages, fits, limits, etc. • • •				
0.81 ± 0.14 ± 0.06	18k	ACCIARRI 96H L3		Repl. by ACCIARRI 98R
0.65 ± 0.12		³ ALBRECHT 95c ARG		Repl. by ALBRECHT 98
0.88 ± 0.11 ± 0.07		BUSKULIC 95D ALEP		Repl. by HEISTER 01E

¹Combined fit to ARGUS tau decay parameter measurements in ALBRECHT 98, ALBRECHT 95c, ALBRECHT 93g, and ALBRECHT 94E. ALBRECHT 98 use tau pair events of the type $\tau^- \tau^+ \rightarrow (\ell^- \bar{\nu}_\ell \nu_\tau)(\pi^+ \pi^0 \bar{\nu}_\tau)$, and their charged conjugates.
²ABE 97o assume $\eta = 0$ in their fit. Letting η vary in the fit gives a $\langle\delta\xi\rangle$ value of $0.87 \pm 0.27 \pm 0.04$.
³Combined fit to ARGUS tau decay parameter measurements in ALBRECHT 95c, ALBRECHT 93g, and ALBRECHT 94E. ALBRECHT 95c uses events of the type $\tau^- \tau^+ \rightarrow (\ell^- \bar{\nu}_\ell \nu_\tau)(h^+ h^- h^+ \bar{\nu}_\tau)$ and their charged conjugates.

($\delta\xi$)(e) PARAMETER

(V–A) theory predicts $\langle\delta\xi\rangle = 0.75$.

VALUE	EVTS	DOCUMENT ID	TECN	COMMENT
0.734 ± 0.028 OUR FIT				
0.731 ± 0.029 OUR AVERAGE				
0.778 ± 0.066 ± 0.024	44k	HEISTER 01E ALEP		1991–1995 LEP runs
0.85 ± 0.12 ± 0.04	17k	ABREU 00L DLPH		1992–1995 runs
0.72 ± 0.31 ± 0.14	25k	ACKERSTAFF 99D OPAL		1990–1995 LEP runs
0.56 ± 0.14 ± 0.06		¹ ALBRECHT 98 ARG		$E_{cm}^{ee} = 9.5\text{--}10.6$ GeV
0.85 ± 0.43 ± 0.08		ABE 97o SLD		1993–1995 SLC runs
0.720 ± 0.032 ± 0.010	34k	ALEXANDER 97F CLEO		$E_{cm}^{ee} = 10.6$ GeV
• • • We do not use the following data for averages, fits, limits, etc. • • •				
1.11 ± 0.17 ± 0.07		BUSKULIC 95D ALEP		Repl. by HEISTER 01E
¹ ALBRECHT 98 use tau pair events of the type $\tau^- \tau^+ \rightarrow (\ell^- \bar{\nu}_\ell \nu_\tau)(\pi^+ \pi^0 \bar{\nu}_\tau)$, and their charged conjugates.				

($\delta\xi$)(μ) PARAMETER

(V–A) theory predicts $\langle\delta\xi\rangle = 0.75$.

VALUE	EVTS	DOCUMENT ID	TECN	COMMENT
0.778 ± 0.037 OUR FIT				
0.79 ± 0.04 OUR AVERAGE				
0.786 ± 0.066 ± 0.028	46k	HEISTER 01E ALEP		1991–1995 LEP runs
0.86 ± 0.13 ± 0.04	22k	ABREU 00L DLPH		1992–1995 runs
0.63 ± 0.23 ± 0.05	27k	ACKERSTAFF 99D OPAL		1990–1995 LEP runs
0.73 ± 0.18 ± 0.10		¹ ALBRECHT 98 ARG		$E_{cm}^{ee} = 9.5\text{--}10.6$ GeV
0.82 ± 0.32 ± 0.07		ABE 97o SLD		1993–1995 SLC runs
0.786 ± 0.041 ± 0.032	22k	ALEXANDER 97F CLEO		$E_{cm}^{ee} = 10.6$ GeV
• • • We do not use the following data for averages, fits, limits, etc. • • •				
0.71 ± 0.14 ± 0.06		BUSKULIC 95D ALEP		Repl. by HEISTER 01E
¹ ALBRECHT 98 use tau pair events of the type $\tau^- \tau^+ \rightarrow (\ell^- \bar{\nu}_\ell \nu_\tau)(\pi^+ \pi^0 \bar{\nu}_\tau)$, and their charged conjugates.				

$\xi(\pi)$ PARAMETER

(V–A) theory predicts $\xi(\pi) = 1$.

VALUE	EVTS	DOCUMENT ID	TECN	COMMENT
0.993 ± 0.022 OUR FIT				
0.994 ± 0.023 OUR AVERAGE				
0.994 ± 0.020 ± 0.014	27k	HEISTER 01E ALEP		1991–1995 LEP runs
0.81 ± 0.17 ± 0.02		ABE 97o SLD		1993–1995 SLC runs
1.03 ± 0.06 ± 0.04	2.0k	COAN 97 CLEO		$E_{cm}^{ee} = 10.6$ GeV
• • • We do not use the following data for averages, fits, limits, etc. • • •				
0.987 ± 0.057 ± 0.027		BUSKULIC 95D ALEP		Repl. by HEISTER 01E
0.95 ± 0.11 ± 0.05		¹ BUSKULIC 94D ALEP		1990+1991 LEP run
¹ Superseded by BUSKULIC 95D.				

$\xi(\rho)$ PARAMETER

(V–A) theory predicts $\xi(\rho) = 1$.

VALUE	EVTS	DOCUMENT ID	TECN	COMMENT
0.994 ± 0.008 OUR FIT				
0.994 ± 0.009 OUR AVERAGE				
0.987 ± 0.012 ± 0.011	59k	HEISTER 01E ALEP		1991–1995 LEP runs
0.99 ± 0.12 ± 0.04		ABE 97o SLD		1993–1995 SLC runs
0.995 ± 0.010 ± 0.003	66k	ALEXANDER 97F CLEO		$E_{cm}^{ee} = 10.6$ GeV
1.022 ± 0.028 ± 0.030	1.7k	¹ ALBRECHT 94E ARG		$E_{cm}^{ee} = 9.4\text{--}10.6$ GeV

• • • We do not use the following data for averages, fits, limits, etc. • • •
 1.045 ± 0.058 ± 0.032 BUSKULIC 95D ALEP Repl. by HEISTER 01E
 1.03 ± 0.11 ± 0.05 ²BUSKULIC 94D ALEP 1990+1991 LEP run

¹ALBRECHT 94E measure the square of this quantity and use the sign determined by ALBRECHT 90t to obtain the quoted result.
²Superseded by BUSKULIC 95D.

$\xi(a_1)$ PARAMETER

(V–A) theory predicts $\xi(a_1) = 1$.

VALUE	EVTS	DOCUMENT ID	TECN	COMMENT
1.001 ± 0.027 OUR FIT				
1.002 ± 0.028 OUR AVERAGE				
1.000 ± 0.016 ± 0.024	35k	¹ HEISTER 01E ALEP		1991–1995 LEP runs
1.02 ± 0.13 ± 0.03	17.2k	ASNER 00 CLEO		$E_{cm}^{ee} = 10.6$ GeV
1.29 ± 0.26 ± 0.11	7.4k	² ACKERSTAFF 97R OPAL		1992–1994 LEP runs
0.85 ± 0.15 ± 0.05		ALBRECHT 95c ARG		$E_{cm}^{ee} = 9.5\text{--}10.6$ GeV
1.25 ± 0.23 ± 0.15 ± 0.08	7.5k	ALBRECHT 93c ARG		$E_{cm}^{ee} = 9.4\text{--}10.6$ GeV
• • • We do not use the following data for averages, fits, limits, etc. • • •				
1.08 ± 0.46 ± 0.14 ± 0.41 ± 0.25	2.6k	³ AKERS 95P OPAL		Repl. by ACKERSTAFF 97R
0.937 ± 0.116 ± 0.064		BUSKULIC 95D ALEP		Repl. by HEISTER 01E

¹HEISTER 01E quote $1.000 \pm 0.016 \pm 0.013 \pm 0.020$ where the errors are statistical, systematic, and an uncertainty due to the final state model. We combine the systematic error and model uncertainty.
²ACKERSTAFF 97R obtain this result with a model independent fit to the hadronic structure functions. Fitting with the model of Kuhn and Santamaria (ZPHY **C48**, 445 (1990)) gives $0.87 \pm 0.16 \pm 0.04$, and with the model of Isgur *et al.* (PR **D39**, 1357 (1989)) they obtain $1.20 \pm 0.21 \pm 0.14$.
³AKERS 95P obtain this result with a model independent fit to the hadronic structure functions. Fitting with the model of Kuhn and Santamaria (ZPHY **C48**, 445 (1990)) gives $0.87 \pm 0.27^{+0.05}_{-0.06}$, and with the model of Isgur *et al.* (PR **D39**, 1357 (1989)) they obtain $1.10 \pm 0.31^{+0.13}_{-0.14}$.

$\xi(\text{all hadronic modes})$ PARAMETER

(V–A) theory predicts $\xi = 1$.

VALUE	EVTS	DOCUMENT ID	TECN	COMMENT
0.995 ± 0.007 OUR FIT				
0.997 ± 0.007 OUR AVERAGE				
0.992 ± 0.007 ± 0.008	102k	¹ HEISTER 01E ALEP		1991–1995 LEP runs
0.997 ± 0.027 ± 0.011	39k	² ABREU 00L DLPH		1992–1995 runs
1.02 ± 0.13 ± 0.03	17.2k	³ ASNER 00 CLEO		$E_{cm}^{ee} = 10.6$ GeV
1.032 ± 0.031	37k	⁴ ACCIARRI 98R L3		1991–1995 LEP runs
0.93 ± 0.10 ± 0.04		ABE 97o SLD		1993–1995 SLC runs
1.29 ± 0.26 ± 0.11	7.4k	⁵ ACKERSTAFF 97R OPAL		1992–1994 LEP runs
0.995 ± 0.010 ± 0.003	66k	⁶ ALEXANDER 97F CLEO		$E_{cm}^{ee} = 10.6$ GeV
1.03 ± 0.06 ± 0.04	2.0k	⁷ COAN 97 CLEO		$E_{cm}^{ee} = 10.6$ GeV
1.017 ± 0.039		⁸ ALBRECHT 95c ARG		$E_{cm}^{ee} = 9.5\text{--}10.6$ GeV
1.25 ± 0.23 ± 0.15 ± 0.08	7.5k	⁹ ALBRECHT 93c ARG		$E_{cm}^{ee} = 9.4\text{--}10.6$ GeV
• • • We do not use the following data for averages, fits, limits, etc. • • •				
0.970 ± 0.053 ± 0.011	14k	¹⁰ ACCIARRI 96H L3		Repl. by ACCIARRI 98R
1.08 ± 0.46 ± 0.14 ± 0.41 ± 0.25	2.6k	¹¹ AKERS 95P OPAL		Repl. by ACKERSTAFF 97R
1.006 ± 0.032 ± 0.019		¹² BUSKULIC 95D ALEP		Repl. by HEISTER 01E
1.022 ± 0.028 ± 0.030	1.7k	¹³ ALBRECHT 94E ARG		$E_{cm}^{ee} = 9.4\text{--}10.6$ GeV
0.99 ± 0.07 ± 0.04		¹⁴ BUSKULIC 94D ALEP		1990+1991 LEP run
1.14 ± 0.34 ± 0.34 ± 0.17	3.9k	⁹ ALBRECHT 90t ARG		Repl. by ALBRECHT 93c

¹HEISTER 01E quote $0.992 \pm 0.007 \pm 0.006 \pm 0.005$ where the errors are statistical, systematic, and an uncertainty due to the final state model. We combine the systematic error and model uncertainty. They use $\tau \rightarrow \pi\nu_\tau, \tau \rightarrow K\nu_\tau, \tau \rightarrow \rho\nu_\tau$, and $\tau \rightarrow a_1\nu_\tau$ decays.
²ABREU 00L use $\tau^- \rightarrow h^- \geq 0\pi^0 \nu_\tau$ decays.
³ASNER 00 use $\tau^- \rightarrow \pi^- 2\pi^0 \nu_\tau$ decays.
⁴ACCIARRI 98R use $\tau \rightarrow \pi\nu_\tau, \tau \rightarrow K\nu_\tau$, and $\tau \rightarrow \rho\nu_\tau$ decays.
⁵ACKERSTAFF 97R use $\tau \rightarrow a_1\nu_\tau$ decays.
⁶ALEXANDER 97F use $\tau \rightarrow \rho\nu_\tau$ decays.
⁷COAN 97 use $h^+ h^-$ energy correlations.
⁸Combined fit to ARGUS tau decay parameter measurements in ALBRECHT 95c, ALBRECHT 93g, and ALBRECHT 94E.
⁹Uses $\tau \rightarrow a_1\nu_\tau$ decays. Replaced by ALBRECHT 95c.
¹⁰ACCIARRI 96H use $\tau \rightarrow \pi\nu_\tau, \tau \rightarrow K\nu_\tau$, and $\tau \rightarrow \rho\nu_\tau$ decays.
¹¹AKERS 95P use $\tau \rightarrow a_1\nu_\tau$ decays.
¹²BUSKULIC 95D use $\tau \rightarrow \pi\nu_\tau, \tau \rightarrow \rho\nu_\tau$, and $\tau \rightarrow a_1\nu_\tau$ decays.
¹³ALBRECHT 94E measure the square of this quantity and use the sign determined by ALBRECHT 90t to obtain the quoted result. Uses $\tau \rightarrow a_1\nu_\tau$ decays. Replaced by ALBRECHT 95c.
¹⁴BUSKULIC 94D use $\tau \rightarrow \pi\nu_\tau$ and $\tau \rightarrow \rho\nu_\tau$ decays. Superseded by BUSKULIC 95D.

$\overline{\eta}(\mu)$ PARAMETER

(V–A) theory predicts $\overline{\eta}(\mu) = 0$.

VALUE	EVTS	DOCUMENT ID	TECN	COMMENT
-1.3 ± 1.5 ± 0.8				
71k		¹ SHIMIZU 18A BELL		$\tau^- \rightarrow \nu_\tau \mu^- \bar{\nu}_\mu \gamma$
¹ SHIMIZU 18A measurement procedure fits a distribution affected by $\overline{\eta}(\mu), \xi(\mu)$ and $\eta''(\mu)$, floating $\overline{\eta}(\mu)$ and $\xi(\mu)$ and fixing $\eta''(\mu) = 0$. The contribution of $\eta''(\mu)$ is suppressed by m_μ/m_τ .				

(ξκ)(e or μ) PARAMETER

Table with columns: VALUE, EVTS, DOCUMENT ID, TECN, COMMENT. Row 1: 0.5 ± 0.4 ± 0.2, 149k, 1,2 SHIMIZU 18A BELL, τ⁻ → ντ e⁻ ν̄e γ and τ⁻ → ντ μ⁻ ν̄μ γ

1 SHIMIZU 18A measurement procedure fits a distribution of radiative tau decays into both electrons and muons affected by η̄(e or μ), ξκ(e or μ) and η''(e or μ), floating η̄(e or μ) and ξκ(e or μ) and fixing η''(e or μ) = 0. The contribution of η''(e or μ) is suppressed by me/mτ for tau decaying to electrons and by mμ/mτ for tau decaying to muons.

2 Error correlated with SHIMIZU 18A (ξκ)(e) and (ξκ)(μ) values.

(ξκ)(e) PARAMETER

Table with columns: VALUE, EVTS, DOCUMENT ID, TECN, COMMENT. Row 1: -0.4 ± 0.8 ± 0.9, 78k, 1,2 SHIMIZU 18A BELL, τ⁻ → ντ e⁻ ν̄e γ

1 SHIMIZU 18A measurement procedure fits a distribution affected by η̄(e), (ξκ)(e) and η''(e), floating (ξκ)(e) and fixing η̄(e) = 0 and η''(e) = 0. The contribution of η''(e) is suppressed by me/mτ.

2 Error correlated with SHIMIZU 18A (ξκ)(e or μ) value.

(ξκ)(μ) PARAMETER

Table with columns: VALUE, EVTS, DOCUMENT ID, TECN, COMMENT. Row 1: 0.8 ± 0.5 ± 0.3, 71k, 1,2 SHIMIZU 18A BELL, τ⁻ → ντ μ⁻ ν̄μ γ

1 SHIMIZU 18A measurement procedure fits a distribution affected by η̄(μ), ξκ(μ) and η''(μ), floating η̄(μ) and ξκ(μ) and fixing η''(μ) = 0. The contribution of η''(μ) is suppressed by mμ/mτ.

2 Error correlated with SHIMIZU 18A (ξκ)(e or μ) value.

τ REFERENCES

Table listing references for tau decays with columns: Author, Year, Journal, Title, and other details.

Table listing references for tau decays with columns: Author, Year, Journal, Title, and other details.

Lepton Particle Listings

τ , Heavy Charged Lepton Searches

ALBRECHT	92Q	ZPHY C56 339	H. Albrecht et al.	(ARGUS Collab.)
AMMAR	92	PR D45 3976	R. Ammar et al.	(CLEO Collab.)
ARTUSO	92	PRL 69 3278	M. Artuso et al.	(CLEO Collab.)
BAI	92	PRL 69 3021	J.Z. Bai et al.	(BES Collab.)
BATTLE	92	PL B291 488	M. Battle et al.	(CLEO Collab.)
BUSKULIC	92J	PL B297 459	D. Buskulic et al.	(ALEPH Collab.)
DECAMP	92C	ZPHY C54 211	D. Decamp et al.	(ALEPH Collab.)
ADEVA	91F	PL B265 451	B. Adeva et al.	(L3 Collab.)
ALBRECHT	91D	PL B260 259	H. Albrecht et al.	(ARGUS Collab.)
ALEXANDER	91D	PL B266 201	G. Alexander et al.	(OPAL Collab.)
ANTREASYAN	91	PL B259 216	D. Antreasyan et al.	(Crystal Ball Collab.)
GRIFOLS	91	PL B255 611	J.A. Grifols, A. Mendez	(BARC Collab.)
ABACHI	90	PR D41 1414	S. Abachi et al.	(HRS Collab.)
ALBRECHT	90E	PL B246 278	H. Albrecht et al.	(ARGUS Collab.)
ALBRECHT	90I	PL B250 164	H. Albrecht et al.	(ARGUS Collab.)
BEHREND	90	ZPHY C46 537	H.J. Behrend et al.	(CELLO Collab.)
BOWCOCK	90	PR D41 805	T.J.V. Bowcock et al.	(CLEO Collab.)
DELAGUIA	90	PL B252 116	F. del Aguila, M. Sher	(BARC, WILL Collab.)
GOLDBERG	90	PL B251 223	M. Goldberg et al.	(CLEO Collab.)
WU	90	PR D41 2339	D.Y. Wu et al.	(Mark II Collab.)
ABACHI	89B	PL D40 902	S. Abachi et al.	(HRS Collab.)
BEHREND	89B	PL B222 163	H.J. Behrend et al.	(CELLO Collab.)
JANSEN	89	PL B228 273	H. Jansen et al.	(Crystal Ball Collab.)
KLEINWORT	89	ZPHY C42 7	C. Kleinwort et al.	(JADE Collab.)
ADEVA	88	PR D38 2665	B. Adeva et al.	(Mark-J Collab.)
ALBRECHT	88B	PL B202 149	H. Albrecht et al.	(ARGUS Collab.)
ALBRECHT	88L	ZPHY C41 1	H. Albrecht et al.	(ARGUS Collab.)
ALBRECHT	88M	ZPHY C41 405	H. Albrecht et al.	(ARGUS Collab.)
AMIDEI	88	PR D37 1750	D. Amidei et al.	(Mark II Collab.)
BEHREND	88	PL B200 226	H.J. Behrend et al.	(CELLO Collab.)
BRAUNSCHWIG	88C	ZPHY C39 331	W. Braunschweig et al.	(TASSO Collab.)
KEH	88	PL B212 123	S. Keh et al.	(Crystal Ball Collab.)
TSCHIRHART	88	PL B205 407	R. Tschirhart et al.	(HRS Collab.)
ABACHI	87B	PL B197 291	S. Abachi et al.	(HRS Collab.)
ADLER	87B	PRL 59 1527	J. Adler et al.	(Mark III Collab.)
AIHARA	87B	PR D35 1553	H. Aihara et al.	(TPC Collab.)
AIHARA	87C	PRL 59 751	H. Aihara et al.	(TPC Collab.)
ALBRECHT	87L	PL B185 223	H. Albrecht et al.	(ARGUS Collab.)
ALBRECHT	87P	PL B199 580	H. Albrecht et al.	(ARGUS Collab.)
BAND	87	PL B198 297	H.R. Band et al.	(MAC Collab.)
BAND	87B	PRL 59 415	H. Band et al.	(MAC Collab.)
BARINGER	87	PRL 59 1993	P. Baringer et al.	(CLEO Collab.)
BEBEK	87C	PR D36 690	C. Bebek et al.	(CLEO Collab.)
BURCHAT	87	PR D35 27	P.R. Burchat et al.	(Mark II Collab.)
BYLSMA	87	PR D35 2269	B.G. Bylsma et al.	(HRS Collab.)
COFFMAN	87	PR D36 2185	D.M. Coffman et al.	(Mark III Collab.)
DERRICK	87	PL B189 260	M. Derrick et al.	(HRS Collab.)
FORD	87	PR D35 408	W.T. Ford et al.	(MAC Collab.)
FORD	87B	PR D36 1971	W.T. Ford et al.	(MAC Collab.)
GAN	87	PRL 59 411	K.K. Gan et al.	(Mark II Collab.)
GAN	87B	PL B197 561	K.K. Gan et al.	(Mark II Collab.)
AIHARA	86C	PRL 57 1836	H. Aihara et al.	(TPC Collab.)
BARTEL	86D	PL B182 216	W. Bartel et al.	(JADE Collab.)
PDG	86	PL 170B 1	M. Aguilar-Benitez et al.	(CERN, CIT+ Collab.)
RUCKSTUHL	86	PRL 56 2132	W. Ruckstuhl et al.	(DELCO Collab.)
SCHMIDKE	86	PRL 57 527	W.B. Schmidke et al.	(Mark II Collab.)
YELTON	86	PRL 56 812	J.M. Yelton et al.	(Mark II Collab.)
ALTHOFF	85	ZPHY C26 521	M. Althoff et al.	(TASSO Collab.)
ASH	85B	PRL 55 2118	W.W. Ash et al.	(MAC Collab.)
BALTRUSAITIS	85	PRL 55 1842	R.M. Baltrusaitis et al.	(Mark III Collab.)
BARTEL	85F	PL 161B 188	W. Bartel et al.	(JADE Collab.)
BEHREND	85	PR D32 2468	S. Behrends et al.	(CLEO Collab.)
BELTRAMI	85	PRL 54 1775	I. Beltrami et al.	(HRS Collab.)
BERGER	85	ZPHY C28 1	C. Berger et al.	(PLUTO Collab.)
BURCHAT	85	PRL 54 2489	P.R. Burchat et al.	(Mark II Collab.)
FERNANDEZ	85	PRL 54 1624	E. Fernandez et al.	(MAC Collab.)
MILLS	85	PRL 54 624	G.B. Mills et al.	(DELCO Collab.)
AIHARA	84C	PR D30 2436	H. Aihara et al.	(TPC Collab.)
BEHREND	84	ZPHY C23 103	H.J. Behrend et al.	(CELLO Collab.)
MILLS	84	PRL 52 1944	G.B. Mills et al.	(DELCO Collab.)
BEHREND	83C	PL 127B 270	H.J. Behrend et al.	(CELLO Collab.)
SILVERMAN	83	PR D27 1196	D.J. Silverman, G.L. Shaw	(UCI Collab.)
BEHREND	82	PL 114B 282	H.J. Behrend et al.	(CELLO Collab.)
BLOCKER	82B	PRL 49 1596	C.A. Blocker et al.	(Mark II Collab.)
BLOCKER	82D	PL 109B 119	C.A. Blocker et al.	(Mark II Collab.)
FELDMAN	82	PRL 48 66	G.J. Feldman et al.	(Mark II Collab.)
HAYES	82	PR D25 2869	K.G. Hayes et al.	(Mark II Collab.)
BERGER	81B	PL 99B 489	C. Berger et al.	(PLUTO Collab.)
DORFAN	81	PRL 46 215	J.M. Dorfan et al.	(Mark II Collab.)
BRANDELIK	80	PL 92B 199	R. Brandelik et al.	(TASSO Collab.)
ZHOLENTZ	80	PL 96B 214	A.A. Zholents et al.	(NOVO Collab.)
Also		SJNP 34 814	A.A. Zholents et al.	(NOVO Collab.)
Translated from YAF	34	1471		
BACINO	79B	PRL 42 749	W. Bacino et al.	(DELCO Collab.)
KIRKBY	79	SLAC-PUB-2419	J. Kirkby	(SLAC Collab.)
Also		Batavia Lepton Photon Conference.		
BACINO	78B	PRL 41 13	W.J. Bacino et al.	(DELCO Collab.)
Also		Tokyo Conf. 249	J. Kirz	(STON Collab.)
Also		PL 96B 214	A.A. Zholents et al.	(NOVO Collab.)
BRANDELIK	78	PL 73B 109	R. Brandelik et al.	(DASP Collab.)
FELDMAN	78	Tokyo Conf. 777	G.J. Feldman	(SLAC Collab.)
JAROS	78	PRL 40 1120	J. Jaros et al.	(LGW Collab.)
PERL	75	PRL 35 1489	M.L. Perl et al.	(LBL, SLAC Collab.)

OTHER RELATED PAPERS

DAVIER	06	RMP 78 1043	M. Davier, A. Hocker, Z. Zhang	(LALO, PARIN+ Collab.)
RAHAL-CAL	98	JMP A13 695	G. Rahal-Callot	(ETH Collab.)
GENTILE	96	PRPL 274 287	S. Gentile, M. Pohl	(ROMA1, ETH Collab.)
WEINSTEIN	93	ARNPS 43 457	A.J. Weinstein, R. Stroynowski	(CIT, STMU Collab.)
PERL	92	RFP 55 653	M.L. Perl	(SLAC Collab.)
PICH	90	MPL A5 1995	A. Pich	(VALE Collab.)
BARISH	88	PRPL 157 1	B.C. Barish, R. Stroynowski	(CIT Collab.)
GAN	88	JMP A3 531	K.K. Gan, M.L. Perl	(SLAC Collab.)
HAYES	88	PR D38 3351	K.G. Hayes, M.L. Perl	(SLAC Collab.)
PERL	80	ARNPS 30 299	M.L. Perl	(SLAC Collab.)

Heavy Charged Lepton Searches

Charged Heavy Lepton MASS LIMITS

Sequential Charged Heavy Lepton (L^\pm) MASS LIMITS

These experiments assumed that a fourth generation L^\pm decayed to a fourth generation ν_L (or L^0) where ν_L was stable, or that L^\pm decays to a light ν_ℓ via mixing.

See the "Quark and Lepton Compositeness, Searches for" Listings for limits on radiatively decaying excited leptons, i.e. $\ell^* \rightarrow \ell \gamma$. See the "WIMPs and other Particle Searches" section for heavy charged particle search limits in which the charged particle could be a lepton.

VALUE (GeV)	CL%	DOCUMENT ID	TECN	COMMENT
>100.8	95	ACHARD 01B L3		Decay to νW
>101.9	95	ACHARD 01B L3		$m_L - m_{L^0} > 15$ GeV
> 81.5	95	ACKERSTAFF 98c OPAL		Assumed $m_{L^\pm} - m_{L^0} > 8.4$ GeV
> 80.2	95	ACKERSTAFF 98c OPAL		$m_{L^0} > m_{L^\pm}$ and $L^\pm \rightarrow \nu W$
< 48 or > 61	95	¹ ACCIARRI 96G L3		
> 63.9	95	ALEXANDER 96P OPAL		Decay to massless ν 's
> 63.5	95	BUSKULIC 96S ALEP		$m_L - m_{L^0} > 7$ GeV
> 65	95	BUSKULIC 96S ALEP		Decay to massless ν 's
none 10-225		² AHMED 94 CNTR	H1	Collab. at HERA
none 12.6-29.6	95	KIM 91B AMY		Massless ν assumed
> 44.3	95	AKRAWY 90G OPAL		
none 0.5-10	95	³ RILES 90 MRK2		For $(m_{L^0} - m_{L^+}) > 0.25-0.4$ GeV
> 8		⁴ STOKER 89 MRK2		For $(m_{L^+} - m_{L^0}) = 0.4$ GeV
> 12		⁴ STOKER 89 MRK2		For $m_{L^0} = 0.9$ GeV
none 18.4-27.6	95	⁵ ABE 88 VNS		
> 25.5	95	⁶ ADACHI 88B TOPZ		
none 1.5-22.0	95	BEHREND 88c CELL		
> 41	90	⁷ ALBAJAR 87B UA1		
> 22.5	95	⁸ ADEVA 85 MRKJ		
> 18.0	95	⁹ BARTEL 83 JADE		
none 4-14.5	95	¹⁰ BERGER 81B PLUT		
> 15.5	95	¹¹ BRANDELIK 81 TASS		
> 13.		¹² AZIMOV 80		
> 16.	95	¹³ BARBER 80B CNTR		
> 0.490		¹⁴ ROTHE 69 RVUE		

- ¹ ACCIARRI 96G assumes LEP result that the associated neutral heavy lepton mass > 40 GeV.
- ² The AHMED 94 limits are from a search for neutral and charged sequential heavy leptons at HERA via the decay channels $L^- \rightarrow e \gamma$, $L^- \rightarrow \nu W^-$, $L^- \rightarrow e Z$; and $L^0 \rightarrow \nu \gamma$, $L^0 \rightarrow e^- W^+$, $L^0 \rightarrow \nu Z$, where the W decays to $\ell \nu_\ell$, or to jets, and Z decays to $\ell^+ \ell^-$ or jets.
- ³ RILES 90 limits were the result of a special analysis of the data in the case where the mass difference $m_{L^-} - m_{L^0}$ was allowed to be quite small, where L^0 denotes the neutrino into which the sequential charged lepton decays. With a slightly reduced m_{L^\pm} range, the mass difference extends to about 4 GeV.
- ⁴ STOKER 89 (Mark II at PEP) gives bounds on charged heavy lepton (L^+) mass for the generalized case in which the corresponding neutral heavy lepton (L^0) in the SU(2) doublet is not of negligible mass.
- ⁵ ABE 88 search for L^+ and $L^- \rightarrow$ hadrons looking for acoplanar jets. The bound is valid for $m_\nu < 10$ GeV.
- ⁶ ADACHI 88B search for hadronic decays giving acoplanar events with large missing energy. $E_{cm}^{ee} = 52$ GeV.
- ⁷ Assumes associated neutrino is approximately massless.
- ⁸ ADEVA 85 analyze one-isolated-muon data and sensitive to $\tau < 10$ nanosec. Assume $B(\text{lepton}) = 0.30$. $E_{cm} = 40-47$ GeV.
- ⁹ BARTEL 83 limit is from PETRA $e^+ e^-$ experiment with average $E_{cm} = 34.2$ GeV.
- ¹⁰ BERGER 81B is DESY DORIS and PETRA experiment. Looking for $e^+ e^- \rightarrow L^+ L^-$.
- ¹¹ BRANDELIK 81 is DESY-PETRA experiment. Looking for $e^+ e^- \rightarrow L^+ L^-$.
- ¹² AZIMOV 80 estimated probabilities for $M + N$ type events in $e^+ e^- \rightarrow L^+ L^-$ deducing semi-hadronic decay multiplicities of L from $e^+ e^-$ annihilation data at $E_{cm} = (2/3)m_L$. Obtained above limit comparing these with $e^+ e^-$ data (BRANDELIK 80).
- ¹³ BARBER 80B looked for $e^+ e^- \rightarrow L^+ L^-, L \rightarrow \nu^+ X$ with MARK-J at DESY-PETRA.
- ¹⁴ ROTHE 69 examines previous data on μ pair production and π and K decays.

Stable Charged Heavy Lepton (L^\pm) MASS LIMITS

VALUE (GeV)	CL%	DOCUMENT ID	TECN
>102.6	95	ACHARD 01B L3	
> 28.2	95	¹⁵ ADACHI 90c TOPZ	
none 18.5-42.8	95	AKRAWY 90a OPAL	
> 26.5	95	DECAMP 90f ALEP	
none $m_\mu - 36.3$	95	SODERSTROM90 MRK2	

- ¹⁵ ADACHI 90c put lower limits on the mass of stable charged particles with electric charge Q satisfying $2/3 < Q/e < 4/3$ and with spin 0 or 1/2. We list here the special case for a stable charged heavy lepton.

Lepton Particle Listings

Heavy Charged Lepton Searches, Neutrino Properties

Charged Long-Lived Heavy Lepton MASS LIMITS

VALUE (GeV)	CL%	DOCUMENT ID	TECN	CHG	COMMENT
• • • We do not use the following data for averages, fits, limits, etc. • • •					
>574	95	CHATRCHYAN13AB	CMS		Leptons singlet model
>102.0	95	ABBIENDI 03L	OPAL		pair produced in e^+e^-
> 0.1	16	ANSORGE 73B	HBC	-	Long-lived
none 0.55-4.5	17	BUSHNIN 73	CNTR	-	Long-lived
none 0.2-0.92	18	BARNA 68	CNTR	-	Long-lived
none 0.97-1.03	18	BARNA 68	CNTR	-	Long-lived

¹⁶ ANSORGE 73B looks for electron pair production and electron-like Bremsstrahlung.
¹⁷ BUSHNIN 73 is SERPUKHOV 70 GeV p experiment. Masses assume mean life above 7×10^{-10} and 3×10^{-8} respectively. Calculated from cross section (see "Charged Quasi-Stable Lepton Production Differential Cross Section" below) and 30 GeV muon pair production data.
¹⁸ BARNA 68 is SLAC photoproduction experiment.

Doubly-Charged Heavy Lepton MASS LIMITS

VALUE (GeV)	CL%	DOCUMENT ID	TECN	CHG	COMMENT
• • • We do not use the following data for averages, fits, limits, etc. • • •					
none 1-9 GeV	90	19 CLARK	81	SPEC	++

¹⁹ CLARK 81 is FNAL experiment with 209 GeV muons. Bounds apply to $\mu\mu$ which couples with full weak strength to muon. See also section on "Doubly-Charged Lepton Production Cross Section."

Doubly-Charged Lepton Production Cross Section (μN Scattering)

VALUE (cm ²)	EVTS	DOCUMENT ID	TECN	CHG	COMMENT
• • • We do not use the following data for averages, fits, limits, etc. • • •					
<6. $\times 10^{-38}$	0	20 CLARK	81	SPEC	++

²⁰ CLARK 81 is FNAL experiment with 209 GeV muon. Looked for μ^+ nucleon $\rightarrow \bar{\mu}^0 X$, $\bar{\mu}^0 \rightarrow \mu^+ \mu^- \bar{\nu}_\mu$ and $\mu^+ n \rightarrow \mu^+ X, \mu^+ \rightarrow 2\mu^+ \nu_\mu$. Above limits are for $\sigma \times BR$ taken from their mass-dependence plot figure 2.

REFERENCES FOR Heavy Charged Lepton Searches

CHATRCHYAN 13AB	JHEP 1307 122	S. Chatrchyan <i>et al.</i>	(CMS Collab.)
ABBIENDI 03L	PL B572 8	G. Abbiendi <i>et al.</i>	(OPAL Collab.)
ACHARD 01B	PL B517 75	P. Achard <i>et al.</i>	(L3 Collab.)
ACKERSTAFF 98C	EPJ C1 45	K. Ackerstaff <i>et al.</i>	(OPAL Collab.)
ACCIARRI 96G	PL B377 304	M. Acciarri <i>et al.</i>	(L3 Collab.)
ALEXANDER 96P	PL B385 433	G. Alexander <i>et al.</i>	(OPAL Collab.)
BUSKULIC 96S	PL B384 439	D. Buskulic <i>et al.</i>	(ALEPH Collab.)
AHMED 94	PL B340 205	T. Ahmed <i>et al.</i>	(H1 Collab.)
KIM 91B	JMP A6 2583	G.N. Kim <i>et al.</i>	(AMY Collab.)
ADACHI 90C	PL B244 352	I. Adachi <i>et al.</i>	(TOPAZ Collab.)
AKRAWY 90G	PL B240 250	M.Z. Akrawy <i>et al.</i>	(OPAL Collab.)
AKRAWY 90O	PL B252 290	M.Z. Akrawy <i>et al.</i>	(OPAL Collab.)
DECAMP 90F	PL B236 511	D. Decamp <i>et al.</i>	(ALEPH Collab.)
RILES 90	PR D42 1	K. Riles <i>et al.</i>	(Mark II Collab.)
SODERSTROM 90	PRL 64 2980	E. Soderstrom <i>et al.</i>	(Mark II Collab.)
STOKER 89	PR D39 1811	D.P. Stoker <i>et al.</i>	(Mark II Collab.)
ABE 88	PRL 61 915	K. Abe <i>et al.</i>	(VENUS Collab.)
ADACHI 88B	PR D37 1339	I. Adachi <i>et al.</i>	(TOPAZ Collab.)
BEHREND 85C	ZPHY C11 7	H.J. Behrend <i>et al.</i>	(CELLO Collab.)
ALBAJAR 87B	PL B185 241	C. Albajar <i>et al.</i>	(UA1 Collab.)
ADEVA 85	PL 152B 439	B. Adeva <i>et al.</i>	(Mark-J Collab.)
Also	PRPL 109 131	B. Adeva <i>et al.</i>	(Mark-J Collab.)
BARTEL 83	PL 123B 353	W. Bartel <i>et al.</i>	(JADE Collab.)
BERGER 81B	PL 99B 489	C. Berger <i>et al.</i>	(PLUTO Collab.)
BRANDELIK 81	PL 99B 163	R. Brandelik <i>et al.</i>	(TASSO Collab.)
CLARK 81	PRL 46 299	A.R. Clark <i>et al.</i>	(UCB, LBL, FNAL+)
Also	PR D25 2762	W.H. Smith <i>et al.</i>	(LBL, FNAL, PRIN)
AZIMOV 80	JETPL 32 664	Y.I. Azimov, V.A. Khoze	(PNPI)
Translated from	ZETFP 32 677		
BARBER 80B	PRL 45 1904	D.P. Barber <i>et al.</i>	(Mark-J Collab.)
BRANDELIK 80	PL 92B 199	R. Brandelik <i>et al.</i>	(TASSO Collab.)
ANSORGE 73B	PR D7 26	R.E. Ansorge <i>et al.</i>	(CAVE)
BUSHNIN 73	NP B58 476	Y.B. Bushnin <i>et al.</i>	(SERP)
Also	PL 42B 136	S.V. Golovkin <i>et al.</i>	(SERP)
ROTHE 69	NP B10 241	K.W. Rothe, A.M. Wolsky	(PENN)
BARNA 68	PR 173 1391	A. Barna <i>et al.</i>	(SLAC, STAN)

OTHER RELATED PAPERS

PERL 81	SLAC-PUB-2752	M.L. Perl	(SLAC)
Physics in Collision Conference.			

Neutrino Properties

NEUTRINO PROPERTIES

Revised July 2021 by P. Vogel (Caltech) and A. Piepke (University of Alabama).

The Neutrino Properties Listings concern measurements of various properties of neutrinos. Nearly all of the measurements, so far only limits, actually concern superpositions of the mass

eigenstates ν_i , which are in turn related to the weak eigenstates ν_ℓ , via the neutrino mixing matrix

$$|\nu_\ell\rangle = \sum_i U_{\ell i} |\nu_i\rangle.$$

In the analogous case of quark mixing via the CKM matrix, the smallness of the off-diagonal terms (small mixing angles) permits a "dominant eigenstate" approximation. However, the results of neutrino oscillation searches show that the mixing matrix contains two large mixing angles and a third angle that is not exceedingly small. We cannot therefore associate any particular state $|\nu_i\rangle$ with any particular lepton label e, μ or τ . Nevertheless, note that in the standard labeling the $|\nu_1\rangle$ has the largest $|\nu_e\rangle$ component ($\sim 2/3$), $|\nu_2\rangle$ contains $\sim 1/3$ of the $|\nu_e\rangle$ component and $|\nu_3\rangle$ contains only a small $\sim 2.5\%$ $|\nu_e\rangle$ component.

Neutrinos are produced in weak decays with a definite lepton flavor, and are typically detected by the charged current weak interaction again associated with a specific lepton flavor. Hence, the listings for the neutrino mass that follow are separated into the three associated charged lepton categories. Other properties (mean lifetime, magnetic moment, charge and charge radius) are no longer separated this way. If needed, the associated lepton flavor is reported in the footnotes.

Measured quantities (mass-squared, magnetic moments, mean lifetimes, etc.) all depend upon the mixing parameters $|U_{\ell i}|^2$, but to some extent also on experimental conditions (e.g., on energy resolution). Many of these observables, in particular mass-squared, cannot distinguish between Dirac and Majorana neutrinos and are unaffected by CP phases.

Direct neutrino mass measurements are usually based on the analysis of the kinematics of charged particles (leptons, pions) emitted together with neutrinos (flavor states) in various weak decays. The most sensitive neutrino mass measurement to date, involving electron type antineutrinos, is based on fitting the shape of the beta spectrum. The quantity $m_{\nu_e}^{2(eff)} = \sum_i |U_{ei}|^2 m_{\nu_i}^2$ is determined or constrained, where the sum is over all mass eigenvalues m_{ν_i} that are too close together to be resolved experimentally. (The quantity $m_{\nu_e}^{eff} \equiv \sqrt{m_{\nu_e}^{2(eff)}}$ is often denoted $\langle m_\beta \rangle$ in the literature.) If the energy resolution is better than $\Delta m_{ij}^2 \equiv m_{\nu_i}^2 - m_{\nu_j}^2$, the corresponding heavier m_{ν_i} and mixing parameter could be determined by fitting the resulting spectral anomaly (step or kink).

The dependence of m_{ν_e} on the mass of the lightest neutrino is shown in Fig. 14.11 of the *Neutrino Masses, Mixing, and Oscillations* review. In the case of inverted ordering there is a minimum possible value of $m_{\nu_e}^{eff}$, approximately $\sqrt{(\Delta m_{32}^2)} \sim 50$ meV. If $m_{\nu_e}^{eff}$ is found to be larger than this value, it is impossible, based on this information only, to decide which ordering is realized in nature. On the other hand, if the $m_{\nu_e}^{eff}$ is less than ~ 50 meV, only the normal mass ordering is possible.

A limit on $m_{\nu_e}^{2(eff)}$ implies an upper limit on the minimum value m_{min}^2 of $m_{\nu_i}^2$, independent of the mixing parameters U_{ei} :

Lepton Particle Listings

Neutrino Properties

$m_{min}^2 \leq m_{\nu_e}^{2(eff)}$. However, if and when the value of $m_{\nu_e}^{2(eff)}$ is determined then its combination with the results derived from neutrino oscillations that give us the values of the neutrino mass-squared differences $\Delta m_{ij}^2 \equiv m_i^2 - m_j^2$, including eventually also their signs, and the mixing parameters $|U_{ei}|^2$, the individual neutrino mass squares $m_{\nu_j}^2 = m_{\nu_e}^{2(eff)} - \sum_i |U_{ei}|^2 \Delta m_{ij}^2$ can be determined.

So far solar, reactor, atmospheric and accelerator neutrino oscillation experiments can be consistently described using three active neutrino flavors, i.e. two mass splittings and three mixing angles. However, several experiments with radioactive sources, reactors, and accelerators imply the possible existence of one or more non-interacting, i.e. sterile, neutrino species that might be observable since they couple, albeit weakly, to the flavor neutrinos $|\nu_l\rangle$. In that case, the neutrino mixing matrix would be $n \times n$ unitary matrix with $n > 3$.

Combined three neutrino analyses determine the squared mass differences and all three mixing angles to within reasonable accuracy. For given $|\Delta m_{ij}^2|$ a limit on $m_{\nu_e}^{2(eff)}$ from beta decay defines an upper limit on the maximum value m_{max} of m_{ν_i} : $m_{max}^2 \leq m_{\nu_e}^{2(eff)} + \sum_{i < j} |\Delta m_{ij}^2|$. The analysis of the low energy beta decay of tritium, combined with the oscillation results, thus limits *all* active neutrino masses. Traditionally, experimental neutrino mass limits obtained from pion decay $\pi^+ \rightarrow \mu^+ + \nu_\mu$ or the shape of the spectrum of decay products of the τ lepton did not distinguish between flavor and mass eigenstates. These results are reported as limits of the μ and τ based neutrino mass. After the determination of the $|\Delta m_{ij}^2|$'s and the mixing angles θ_{ij} , the corresponding neutrino mass limits are no longer competitive with those derived from low energy beta decays.

The spread of arrival times of the neutrinos from SN1987A, coupled with the measured neutrino energies, provided a time-of-flight limit on a quantity similar to $\langle m_\beta \rangle \equiv \sqrt{m_{\nu_e}^{2(eff)}}$. This statement, clothed in various degrees of sophistication, has been the basis for a very large number of papers. The resulting limits, however, are no longer comparable with the limits from tritium beta decay.

Constraint, or eventually a value, of the sum of the neutrino masses m_{tot} can be determined from the analysis of the cosmic microwave background anisotropy, combined with the galaxy redshift surveys and other data. These limits are reported in a separate table (Sum of Neutrino Masses, m_{tot}). Obviously, m_{tot} represents an upper limit for all m_i values. Note that many reported m_{tot} limits are considerably more stringent than the listed $m_{\nu_e}^{eff}$ limits. Discussion concerning the model dependence of the m_{tot} limit is continuing.

⚡ MASS (electron based)

Those limits given below are for the square root of $m_{\nu_e}^{2(eff)} \equiv \sum_i |U_{ei}|^2 m_{\nu_i}^2$. Limits that come from the kinematics of ${}^3\text{H} \beta\text{-}\tau$ decay are the

square roots of the limits for $m_{\nu_e}^{2(eff)}$. Obtained from the measurements reported in the Listings for "⚡ Mass Squared," below.

VALUE (eV)	CL%	DOCUMENT ID	TECN	COMMENT
< 1.1	90	1 AKER	19	SPEC ${}^3\text{H} \beta$ decay
• • • We do not use the following data for averages, fits, limits, etc. • • •				
< 2.05	95	2 ASEEV	11	SPEC ${}^3\text{H} \beta$ decay
< 5.8	95	3 PAGLIAROLI	10	ASTR SN1987A
< 2.3	95	4 KRAUS	05	SPEC ${}^3\text{H} \beta$ decay
< 21.7	90	5 ARNABOLDI	03A	BOLO ${}^{187}\text{Re} \beta$ decay
< 5.7	95	6 LOREDO	02	ASTR SN1987A
< 2.5	95	7 LOBASHEV	99	SPEC ${}^3\text{H} \beta$ decay
< 2.8	95	8 WEINHEIMER	99	SPEC ${}^3\text{H} \beta$ decay
< 4.35	95	9 BELESEV	95	SPEC ${}^3\text{H} \beta$ decay
< 12.4	95	10 CHING	95	SPEC ${}^3\text{H} \beta$ decay
< 92	95	11 HIDDEMANN	95	SPEC ${}^3\text{H} \beta$ decay
15 $\begin{smallmatrix} +32 \\ -15 \end{smallmatrix}$		HIDDEMANN	95	SPEC ${}^3\text{H} \beta$ decay
< 19.6	95	KERNAN	95	ASTR SN 1987A
< 7.0	95	12 STOEFFL	95	SPEC ${}^3\text{H} \beta$ decay
< 7.2	95	13 WEINHEIMER	93	SPEC ${}^3\text{H} \beta$ decay
< 11.7	95	14 HOLZSCHUH	92B	SPEC ${}^3\text{H} \beta$ decay
< 13.1	95	15 KAWAKAMI	91	SPEC ${}^3\text{H} \beta$ decay
< 9.3	95	16 ROBERTSON	91	SPEC ${}^3\text{H} \beta$ decay
< 14	95	AVIGNONE	90	ASTR SN 1987A
< 16		SPERGEL	88	ASTR SN 1987A
17 to 40		BORIS	87	SPEC ${}^3\text{H} \beta$ decay

1 AKER 19 report a neutrino mass limit, derived from the first month of data collected by the KATRIN tritium endpoint experiment. The analysis of the electron kinematics shows no evidence for neutrino mass. The quoted result is based on a Bayesian analysis of the data. Using the method of Feldman and Cousins, the derived upper limit is < 0.8 eV at 90% C.L.

2 ASEEV 11 report the analysis of the entire beta endpoint data, taken with the Troitsk integrating electrostatic spectrometer between 1997 and 2002 (some of the earlier runs were rejected), using a windowless gaseous tritium source. The fitted value of m_ν , based on the method of Feldman and Cousins, is obtained from the upper limit of the fit for m_ν^2 . Previous analysis problems were resolved by careful monitoring of the tritium gas column density. Supersedes LOBASHEV 99 and BELESEV 95.

3 PAGLIAROLI 10 is critical of the likelihood method used by LOREDO 02.

4 KRAUS 05 is a continuation of the work reported in WEINHEIMER 99. This result represents the final analysis of data taken from 1997 to 2001. Various sources of systematic uncertainties have been identified and quantified. The background has been reduced compared to the initial running period. A spectral anomaly at the endpoint, reported in LOBASHEV 99, was not observed.

5 ARNABOLDI 03A *et al.* report kinematical neutrino mass limit using β -decay of ${}^{187}\text{Re}$. Bolometric AgReO₄ micro-calorimeters are used. Mass bound is substantially weaker than those derived from tritium β -decays but has different systematic uncertainties.

6 LOREDO 02 updates LOREDO 89.

7 LOBASHEV 99 report a new measurement which continues the work reported in BELESEV 95. This limit depends on phenomenological fit parameters used to derive their best fit to m_ν^2 , making an unambiguous interpretation difficult. See the footnote under "⚡ Mass Squared."

8 WEINHEIMER 99 presents two analyses which exclude the spectral anomaly and result in an acceptable m_ν^2 . We report the most conservative limit, but the other is nearly the same. See the footnote under "⚡ Mass Squared."

9 BELESEV 95 (Moscow) use an integral electrostatic spectrometer with adiabatic magnetic collimation and a gaseous tritium sources. A fit to a normal Kurie plot above 18300-18350 eV (to avoid a low-energy anomaly) plus a monochromatic line 7-15 eV below the endpoint yields $m_\nu^2 = -4.1 \pm 10.9$ eV², leading to this Bayesian limit.

10 CHING 95 quotes results previously given by SUN 93; no experimental details are given. A possible explanation for consistently negative values of m_ν^2 is given.

11 HIDDEMANN 95 (Munich) experiment uses atomic tritium embedded in a metal-dioxide lattice. Bayesian limit calculated from the weighted mean $m_\nu^2 = 221 \pm 4244$ eV² from the two runs listed below.

12 STOEFFL 95 (LLNL) result is the Bayesian limit obtained from the m_ν^2 errors given below but with m_ν^2 set equal to 0. The anomalous endpoint accumulation leads to a value of m_ν^2 which is negative by more than 5 standard deviations.

13 WEINHEIMER 93 (Mainz) is a measurement of the endpoint of the tritium β spectrum using an electrostatic spectrometer with a magnetic guiding field. The source is molecular tritium frozen onto an aluminum substrate.

14 HOLZSCHUH 92B (Zurich) result is obtained from the measurement $m_\nu^2 = -24 \pm 48 \pm 61$ (1 σ errors), in eV², using the PDG prescription for conversion to a limit in m_ν .

15 KAWAKAMI 91 (Tokyo) experiment uses tritium-labeled arachidic acid. This result is the Bayesian limit obtained from the m_ν^2 limit with the errors combined in quadrature. This was also done in ROBERTSON 91, although the authors report a different procedure.

16 ROBERTSON 91 (LANL) experiment uses gaseous molecular tritium. The result is in strong disagreement with the earlier claims by the ITPP group [LUBIMOV 80, BORIS 87 (+ BORIS 88 erratum)] that m_ν lies between 17 and 40 eV. However, the probability of a positive m^2 is only 3% if statistical and systematic error are combined in quadrature.

17 See also comment in BORIS 87B and erratum in BORIS 88.

$\bar{\nu}$ MASS SQUARED (electron based)

Given troubling systematics which result in improbably negative estimators of $m_{\nu_e}^{2(\text{eff})} \equiv \sum_i |U_{ei}|^2 m_{\nu_i}^2$, in many experiments, we use only KRAUS 05, LOBASHEV 99, and AKER 19 for our average.

Table with columns: VALUE (eV²), DOCUMENT ID, TECN, COMMENT. Includes 'OUR AVERAGE' and various experimental data points.

- 1 AKER 19 use the first month of data collected by the KATRIN experiment to determine m_nu_e^2. The result is consistent with a neutrino mass of zero and is used to place a limit on m_nu_e.
2 ASEEV 11 report the analysis of the entire beta endpoint data, taken with the Troitsk integrating electrostatic spectrometer between 1997 and 2002, using a windowless gaseous tritium source.
3 KRAUS 05 is a continuation of the work reported in WEINHEIMER 99. This result represents the final analysis of data taken from 1997 to 2001.
4 LOBASHEV 99 report a new measurement which continues the work reported in BELESEV 95. The data were corrected for electron trapping effects in the source, eliminating the dependence of the fitted neutrino mass on the fit interval.
5 WEINHEIMER 99 is a continuation of the work reported in WEINHEIMER 93. Using a lower temperature of the frozen tritium source eliminated the dewetting of the T2 film, which introduced a dependence of the fitted neutrino mass on the fit interval in the earlier work.
6 BELESEV 95 (Moscow) use an integral electrostatic spectrometer with adiabatic collimation and a gaseous tritium sources. This value comes from a fit to a normal Kurie plot above 18300-18350 eV (to avoid a low-energy anomaly), including the effects of an apparent peak 7-15 eV below the endpoint.
7 HIDDEMANN 95 (Munich) experiment uses atomic tritium embedded in a metal-dioxide lattice. They quote measurements from two data sets.
8 STOEFFL 95 (LLNL) uses a gaseous source of molecular tritium. An anomalous pileup of events at the endpoint leads to the negative value for m_nu_e^2. The authors acknowledge that "the negative value for the best fit of m_nu_e^2 has no physical meaning" and discuss possible explanations for this effect.
9 SUN 93 uses a tritiated hydrocarbon source. See also CHING 95.
10 WEINHEIMER 93 (Mainz) is a measurement of the endpoint of the tritium beta spectrum using an electrostatic spectrometer with a magnetic guiding field. The source is molecular tritium frozen onto an aluminum substrate.
11 HOLZSCHUH 92B (Zurich) source is a monolayer of tritiated hydrocarbon.
12 KAWAKAMI 91 (Tokyo) experiment uses tritium-labeled arachidic acid.
13 ROBERTSON 91 (LANL) experiment uses gaseous molecular tritium. The result is in strong disagreement with the earlier claims by the ITEP group [LUBIMOV 80, BORIS 87 (+ BORIS 88 erratum)] that m_nu_e lies between 17 and 40 eV. However, the probability of a positive m_nu_e^2 is only 3% if statistical and systematic error are combined in quadrature.

ν MASS (electron based)

These are measurement of m_nu_nu (in contrast to m_nu_nu_bar, given above). The masses can be different for a Dirac neutrino in the absence of CPT invariance. The possible distinction between nu and nu_bar properties is usually ignored elsewhere in these Listings.

Table with columns: VALUE (eV), CL%, DOCUMENT ID, TECN, COMMENT. Includes data for YASUMI and SPRINGER.

ν MASS (muon based)

Limits given below are for the square root of the $m_{\nu_\mu}^{2(\text{eff})} \equiv \sum_i |U_{\mu i}|^2 m_{\nu_i}^2$.

In some of the COSM papers listed below, the authors did not distinguish between weak and mass eigenstates.

OUR EVALUATION is based on OUR AVERAGE for the pi+ mass and the ASSAMAGAN 96 value for the muon momentum for the pi+ decay at rest. The limit is calculated using the unified classical analysis of FELDMAN 98 for a Gaussian distribution near a physical boundary. WARNING: since m_nu_mu^2(eff) is calculated from the differences of large numbers, it and the corresponding limits are extraordinarily sensitive to small changes in the pion mass, the decay muon momentum, and their errors. For example, the limits obtained using JECKELMANN 94, LENZ 98, and the weighted averages are 0.15, 0.29, and 0.19 MeV, respectively.

Table with columns: VALUE (MeV), CL%, DOCUMENT ID, TECN, COMMENT. Includes 'OUR EVALUATION' and various experimental data points.

- 1 ASSAMAGAN 96 measurement of p_mu from pi+ -> mu+ nu at rest combined with JECKELMANN 94 Solution B pion mass yields m_nu_mu^2 = -0.016 +/- 0.023 with corresponding Bayesian limit listed above. If Solution A is used, m_nu_mu^2 = -0.143 +/- 0.024 MeV^2. Replaces ASSAMAGAN 94.
2 DOLGOV 95 removes earlier assumptions (DOLGOV 93) about thermal equilibrium below T_QCD for wrong-helicity Dirac neutrinos (ENQVIST 93, FULLER 91) to set more stringent limits.
3 ENQVIST 93 bases limit on the fact that thermalized wrong-helicity Dirac neutrinos would speed up expansion of early universe, thus reducing the primordial abundance. FULLER 91 exploits the same mechanism but in the older calculation obtains a larger production rate for these states, and hence a lower limit. Neutrino lifetime assumed to exceed nucleosynthesis time, ~ 1 s.
4 Assumes neutrino lifetime > 1 s. For Dirac neutrinos only. See also ENQVIST 93.
5 ANDERHUB 82 kinematics is insensitive to the pion mass.

ν MASS (tau based)

The limits given below are the square roots of limits for $m_{\nu_\tau}^{2(\text{eff})} \equiv \sum_i |U_{\tau i}|^2 m_{\nu_i}^2$.

In some of the ASTR and COSM papers listed below, the authors did not distinguish between weak and mass eigenstates.

Table with columns: VALUE (MeV), CL%, EVTS, DOCUMENT ID, TECN, COMMENT. Includes data for BARATE, ATHANAS, ACKERSTAFF, AMMAR, ANASTASSOV, FIELDS, SWAIN, ALEXANDER, BOTTINO, HANNESTAD, SOBIE, BUSKULIC, DOLGOV, SIGL, DODELSON, KAWASAKI, PERES, CINABRO, DOLGOV, ENQVIST.

Lepton Particle Listings

Neutrino Properties

< 31	95	19	21	ALBRECHT	92M	ARG	$E_{\text{eff}}^{\nu} = 9.4\text{--}10.6$ GeV
< 0.3			23	FULLER	91	COSM	Nucleosynthesis
< 0.5 or > 25			23	KOLB	91	COSM	Nucleosynthesis
< 0.42			22	LAM	91	COSM	Nucleosynthesis

- ¹ BARATE 98F result based on kinematics of 2939 $\tau^- \rightarrow 2\pi^- \pi^+ \nu_\tau$ and 52 $\tau^- \rightarrow 3\pi^- 2\pi^+ (\pi^0) \nu_\tau$ decays. If possible 2.5% excited a_1 decay is included in 3-prong sample analysis, limit increases to 19.2 MeV.
- ² ATHANAS 00 bound comes from analysis of $\tau^- \rightarrow \pi^- \pi^+ \pi^- \pi^0 \nu_\tau$ decays.
- ³ ACKERSTAFF 98T use $\tau \rightarrow 5\pi^\pm \nu_\tau$ decays to obtain a limit of 43.2 MeV (95%CL). They combine this with ALEXANDER 96M value using $\tau \rightarrow 3h^\pm \nu_\tau$ decays to obtain quoted limit.
- ⁴ AMMAR 98 limit comes from analysis of $\tau^- \rightarrow 3\pi^- 2\pi^+ \nu_\tau$ and $\tau^- \rightarrow 2\pi^- \pi^+ 2\pi^0 \nu_\tau$ decay modes.
- ⁵ ANASTASSOV 97 derive limit by comparing their m_τ measurement (which depends on m_{ν_τ}) to BAL 96 m_τ threshold measurement.
- ⁶ FIELDS 97 limit for a Dirac neutrino. For a Majorana neutrino the mass region < 0.93 or > 31 MeV is excluded. These bounds assume $N_\nu < 4$ from nucleosynthesis; a wider excluded region occurs with a smaller N_ν upper limit.
- ⁷ SWAIN 97 derive their limit from the Standard Model relationships between the tau mass, lifetime, branching fractions for $\tau^- \rightarrow e^- \bar{\nu}_e \nu_\tau$, $\tau^- \rightarrow \mu^- \bar{\nu}_\mu \nu_\tau$, $\tau^- \rightarrow \pi^- \nu_\tau$, and $\tau^- \rightarrow K^- \nu_\tau$, and the muon mass and lifetime by assuming lepton universality and using world average values. Limit is reduced to 48 MeV when the CLEO τ mass measurement (BALEST 93) is included; see CLEO's more recent m_{ν_τ} limit (ANASTASSOV 97). Consideration of mixing with a fourth generation heavy neutrino yields $\sin^2 \theta_L < 0.016$ (95%CL).
- ⁸ ALEXANDER 96M bound comes from analyses of $\tau^- \rightarrow 3\pi^- 2\pi^+ \nu_\tau$ and $\tau^- \rightarrow h^- h^- h^+ \nu_\tau$ decays.
- ⁹ BOTTINO 96 assumes three generations of neutrinos with mixing, finds consistency with massless neutrinos with no mixing based on 1995 data for masses, lifetimes, and leptonic partial widths.
- ¹⁰ HANNESTAD 96c limit is on the mass of a Majorana neutrino. This bound assumes $N_\nu < 4$ from nucleosynthesis. A wider excluded region occurs with a smaller N_ν upper limit. This paper is the corrected version of HANNESTAD 96; see the erratum: HANNESTAD 96b.
- ¹¹ SOBIE 96 derive their limit from the Standard Model relationship between the tau mass, lifetime, and leptonic branching fraction, and the muon mass and lifetime, by assuming lepton universality and using world average values.
- ¹² BUSKULIC 95H bound comes from a two-dimensional fit of the visible energy and invariant mass distribution of $\tau \rightarrow 5\pi(\pi^0) \nu_\tau$ decays. Replaced by BARATE 98F.
- ¹³ DOLGOV 95 removes earlier assumptions (DOLGOV 93) about thermal equilibrium below T_{QCD} for wrong-helicity Dirac neutrinos (ENQVIST 93, FULLER 91) to set more stringent limits. DOLGOV 96 argues that a possible window near 20 MeV is excluded.
- ¹⁴ SIGL 95 exclude massive Dirac or Majorana neutrinos with lifetimes between 10^{-3} and 10^8 seconds if the decay products are predominantly γ or e^+e^- .
- ¹⁵ DODELSON 94 calculate constraints on ν_τ mass and lifetime from nucleosynthesis for 4 generic decay modes. Limits depend strongly on decay mode. Quoted limit is valid for all decay modes of Majorana neutrinos with lifetime greater than about 300s. For Dirac neutrinos limits change to < 0.3 or > 33.
- ¹⁶ KAWASAKI 94 excluded region is for Majorana neutrino with lifetime >1000s. Other limits are given as a function of ν_τ lifetime for decays of the type $\nu_\tau \rightarrow \nu_\mu \phi$ where ϕ is a Nambu-Goldstone boson.
- ¹⁷ PERES 94 used PDG 92 values for parameters to obtain a value consistent with mixing. Reexamination by BOTTINO 96 which included radiative corrections and 1995 PDG parameters resulted in two allowed regions, $m_3 < 70$ MeV and 140 MeV $m_3 < 149$ MeV.
- ¹⁸ CINABRO 93 bound comes from analysis of $\tau^- \rightarrow 3\pi^- 2\pi^+ \nu_\tau$ and $\tau^- \rightarrow 2\pi^- \pi^+ 2\pi^0 \nu_\tau$ decay modes.
- ¹⁹ DOLGOV 93 assumes neutrino lifetime >100s. For Majorana neutrinos, the low mass limit is 0.5 MeV. KAWANO 92 points out that these bounds can be overcome for a Dirac neutrino if it possesses a magnetic moment. See also DOLGOV 96.
- ²⁰ ENQVIST 93 bases limit on the fact that thermalized wrong-helicity Dirac neutrinos would speed up expansion of early universe, thus reducing the primordial abundance. FULLER 91 exploits the same mechanism but in the older calculation obtains a larger production rate for these states, and hence a lower limit. Neutrino lifetime assumed to exceed nucleosynthesis time, ~ 1 s.
- ²¹ ALBRECHT 92M reports measurement of a slightly lower τ mass, which has the effect of reducing the ν_τ mass reported in ALBRECHT 88B. Bound is from analysis of $\tau^- \rightarrow 3\pi^- 2\pi^+ \nu_\tau$ mode.
- ²² Assumes neutrino lifetime >1s. For Dirac neutrinos. See also ENQVIST 93.
- ²³ KOLB 91 exclusion region is for Dirac neutrino with lifetime >1s; other limits are given.

Revised August 2021 by K.A. Olive (University of Minnesota).

Neutrinos decouple from thermal equilibrium in the early universe at temperatures $\mathcal{O}(1)$ MeV. The limits on low mass ($m_\nu \lesssim 1$ MeV) neutrinos apply to m_{tot} given by

$$m_{\text{tot}} = \sum_{\nu} m_{\nu} .$$

Stable neutrinos in this mass range decouple from the thermal bath while still relativistic and make a contribution to the total energy density of the Universe which is given by

$$\rho_\nu = m_{\text{tot}} n_\nu \simeq m_{\text{tot}} (3/11) (3.045/3)^{3/4} n_\gamma ,$$

where the factor 3/11 is the ratio of (light) neutrinos to photons and the factor $(3.045/3)^{3/4}$ corrects for the fact that the effective number of neutrinos in the standard model is 3.045 when taking into account e^+e^- annihilation during neutrino decoupling. Writing $\Omega_\nu = \rho_\nu/\rho_c$, where ρ_c is the critical energy density of the Universe, and using $n_\gamma = 410.7 \text{ cm}^{-3}$, we have

$$\Omega_\nu h^2 \simeq m_{\text{tot}} / (93 \text{ eV}) .$$

While an upper limit to the matter density of $\Omega_m h^2 < 0.12$ would constrain $m_{\text{tot}} < 11$ eV, much stronger constraints are obtained from the observations of the CMB, combined with lensing and baryon acoustic oscillations data. These combine to give an upper limit of around 0.12 eV, and may, in the near future, be able to provide a lower bound on the sum of the neutrino masses. The current lower bound of $m_{\text{tot}} > 0.06$ eV implies a lower limit of $\Omega_\nu h^2 > 6 \times 10^{-4}$. See our review on "Neutrinos in Cosmology" for more details.

SUM OF THE NEUTRINO MASSES, m_{tot}

This is a sum of the neutrino masses, m_{tot} , as defined in the above note, of effectively stable neutrinos, i.e. those with mean lifetimes on cosmological scales. When necessary, we have generalized the results reported so they apply to m_{tot} . For other limits, see SZALAY 76, VYSOTSKY 77, BERNSTEIN 81, FREESE 84, SCHRAMM 84, and COWSIK 85. For more information see a note on "Neutrinos in Cosmology" in this Review.

VALUE (eV)	CL%	DOCUMENT ID	TECN	COMMENT
• • •		We do not use the following data for averages, fits, limits, etc. • • •		
< 0.13	95	1 ABBOTT	21A	COSM DES and Planck
< 0.12	95	2 ALAM	21	COSM
< 0.09	95	3 DI-VALENT...	21	COSM
< 0.16	95	4 GARNY	21	COSM
< 0.06–0.14	95	5 STOCKER	21	COSM Normal mass ordering
< 0.12	95	6 AGHANIM	20	COSM
< 0.15	95	7 CHOUDHURY	20	COSM Normal mass hierarchy
< 0.16	95	8 IVANOV	20	COSM Planck and BOSS
< 0.11	95	9 PALANQUE...	20	COSM Lyman alpha and CMB
< 0.26	95	10 LOUREIRO	19	COSM
< 0.18	95	11 UPADHYE	19	COSM BOSS and CMB
< 0.152	95	12 CHOUDHURY	18	COSM
0.064 \pm 0.061 – 0.005	95	13 SIMPSON	17	COSM
< 0.151	95	14 VAGNOZZI	17	COSM
< 0.14	95	15 YECHE	17	COSM BOSS and XQ-100
< 0.0926	90	16 DIVALENTINO	16	COSM
< 0.18	95	17 HUANG	16	COSM Normal mass hierarchy
< 0.14	95	18 ROSSI	15	COSM
< 0.23	95	19 ADE	14	COSM Planck
0.320 \pm 0.081		20 BATTYE	14	COSM
0.35 \pm 0.10		21 BEUTLER	14	COSM BOSS
0.22 \pm 0.09 – 0.10		22 COSTANZI	14	COSM
< 0.22	95	23 GIUSARMA	14	COSM
0.32 \pm 0.11		24 HOU	14	COSM
< 0.26	95	25 LEISTEDT	14	COSM
< 0.18	95	26 RIEMER-SOR...	14	COSM
< 0.24	68	27 MORESCO	12	COSM
< 0.29	95	28 XIA	12	COSM
< 0.81	95	29 SAITO	11	COSM SDSS
< 0.44	95	30 HANNESTAD	10	COSM
< 0.6	95	31 SEKIGUCHI	10	COSM
< 0.28	95	32 THOMAS	10	COSM
< 1.1		33 ICHIKI	09	COSM

< 1.3	95	34	KOMATSU	09	COSM	WMAP
< 1.2		35	TERENO	09	COSM	
< 0.33		36	VIKHLININ	09	COSM	
< 0.28		37	BERNARDIS	08	COSM	
< 0.17–2.3		38	FOGLI	07	COSM	
< 0.42	95	39	KRISTIANSEN	07	COSM	
< 0.63–2.2		40	ZUNCKEL	07	COSM	
< 0.24	95	41	CIRELLI	06	COSM	
< 0.62	95	42	HANNESTAD	06	COSM	
< 1.2		43	SANCHEZ	06	COSM	
< 0.17	95	41	SELJAK	06	COSM	
< 2.0	95	44	ICHIKAWA	05	COSM	
< 0.75		45	BARGER	04	COSM	
< 1.0		46	CROTTY	04	COSM	
< 0.7		47	SPERGEL	03	COSM	WMAP
< 0.9		48	LEWIS	02	COSM	
< 4.2		49	WANG	02	COSM	CMB
< 2.7		50	FUKUGITA	00	COSM	
< 5.5		51	CROFT	99	ASTR	Ly α power spec
<180			SZALAY	74	COSM	
<132			COWSIK	72	COSM	
<280			MARX	72	COSM	
<400			GERSHTEIN	66	COSM	

- 1 ABBOTT 21A combines Dark Energy Survey (DES) year 3 results with Planck CMB lensing measurements.
- 2 ALAM 21 limit on the sum of neutrino masses by the eBOSS collaboration is based on galaxy, quasar, and Lyman- α 3D clustering data combined with Planck temperature and polarization CMB and supernovae data.
- 3 DI-VALENTINO 21 combines CMB temperature and polarization, SNIa luminosity distances and baryon acoustic oscillations data.
- 4 GARNY 21 employs a model for the Lyman- α flux power spectrum to set a limit using BOSS data. When combined with Planck CMB temperature and polarization data, a 95% CL range 0.10–0.13 eV is found.
- 5 STOCKER 21 use terrestrial and cosmological experiments to set a 95% CL range on the sum of neutrino masses of 0.058–0.139 eV for normal ordering and 0.098–0.174 eV for inverse ordering. They also set an upper limit of 0.037 eV (NO) and 0.042 eV (IO) for the lightest neutrino mass.
- 6 AGHANIM 20 limit on the sum of neutrino masses from Planck data combined with lensing and baryon acoustic oscillations (BAO). Without BAO, the limit relaxes to <0.24 eV. Several other limits are quoted based on different combinations of data.
- 7 CHOUDHURY 20 combines 2018 Planck CMB temperature and polarization data plus lensing, together with baryon acoustic oscillation data from BOSS, MGS, and 6dFGS. Assumes Λ CDM model. The upper limit is 0.17 eV for the inverted hierarchy, and 0.12 eV for degenerate neutrinos. Limits are also derived for extended cosmological models.
- 8 IVANOV 20 combines 2018 Planck CMB data with baryon acoustic oscillation data from BOSS. This study is based on a full-shape likelihood for the redshift-space galaxy power spectrum of the BOSS data.
- 9 PALANQUE-DELABROUILLE 20 combine Lyman alpha and Planck temperature and polarization data. Limit improves to 0.09 eV when CMB lensing and baryon acoustic oscillation data are included.
- 10 LOUREIRO 19 combines data from large scale structure, cosmic microwave background, type Ia supernovae and big bang nucleosynthesis using physically motivated neutrino mass models.
- 11 UPADHYE 19 uses the shape of the BOSS redshift-space galaxy power spectrum in combination with the CMB, and supernovae data. Limit weakens to < 0.54 eV if the dark energy equation of state is allowed to vary.
- 12 CHOUDHURY 18 combines 2015 Planck CMB temperature data, information from the optical depth to reionization from Planck 2016 intermediate results together with baryon acoustic oscillation data from BOSS, MGS, and 6dFGS as well as supernovae Type Ia data from the Pantheon Sample. The limit is strengthened to 0.118 eV when high- l CMB polarization data is also included.
- 13 SIMPSON 17 uses a combination of laboratory and cosmological measurements to determine the light neutrino masses and argue that there is strong evidence for the normal mass ordering.
- 14 Combines temperature anisotropies of the CMB from Planck with data on baryon acoustic oscillations and the optical depth to reionization. Limit is strengthened to 0.118 when high multipole polarization data is included. Updates GIUSARMA 16.
- 15 Constrains the total mass of neutrinos using the Lyman-alpha forest power spectrum with BOSS (mid-resolution), XQ-100 (high-resolution) and CMB. Without the CMB data, the limit relaxes to 0.8 eV. Supersedes PALANQUE-DELABROUILLE 15A.
- 16 Constrains the total mass of neutrinos from Planck CMB data combined with baryon acoustic oscillation and Planck cluster data.
- 17 Constrains the total mass of neutrinos from BAO data from SDSS-III/BOSS combined with CMB data from Planck. Limit quoted for normal mass hierarchy. The limit for the inverted mass hierarchy is 0.20 eV and for the degenerate mass hierarchy it is 0.15 eV.
- 18 ROSSI 15 sets limits on the sum of neutrino masses using BOSS Lyman alpha forest data combined with Planck CMB data and baryon acoustic oscillations.
- 19 Constrains the total mass of neutrinos from Planck CMB data along with WMAP polarization, high l , and BAO data.
- 20 Finite neutrino mass fit to resolve discrepancy between CMB and lensing measurements.
- 21 Fit to the total mass of neutrinos from BOSS data along with WMAP CMB data and data from other BAO constraints and weak lensing.
- 22 Fit to the total mass of neutrinos from Planck CMB data along with BAO.
- 23 Constrains the total mass of neutrinos from Planck CMB data combined with baryon acoustic oscillation data from BOSS and HST data on the Hubble parameter.
- 24 Fit based on the SPT-SZ survey combined with CMB, BAO, and H_0 data.
- 25 Constraints the total mass of neutrinos (marginalizing over the effective number of neutrino species) from CMB, CMB lensing, BAO, and galaxy clustering data.

- 26 Constrains the total mass of neutrinos from Planck CMB data combined with baryon acoustic oscillation data from BOSS, 6dFGS, SDSS, WiggleZ data on the galaxy power spectrum, and HST data on the Hubble parameter. The limit is increased to 0.25 eV if a lower bound to the sum of neutrino masses of 0.04 eV is assumed.
- 27 Constrains the total mass of neutrinos from observational Hubble parameter data with seven-year WMAP data and the most recent estimate of H_0 .
- 28 Constrains the total mass of neutrinos from the CFHTLS combined with seven-year WMAP data and a prior on the Hubble parameter. Limit is relaxed to 0.41 eV when small scales affected by non-linearities are removed.
- 29 Constrains the total mass of neutrinos from the Sloan Digital Sky Survey and the five-year WMAP data.
- 30 Constrains the total mass of neutrinos from the 7-year WMAP data including SDSS and HST data. Limit relaxes to 1.19 eV when CMB data is used alone. Supersedes HANNESTAD 06.
- 31 Constrains the total mass of neutrinos from a combination of CMB data, a recent measurement of H_0 (SHOES), and baryon acoustic oscillation data from SDSS.
- 32 Constrains the total mass of neutrinos from SDSS MegaZ LRG DR7 galaxy clustering data combined with CMB, HST, supernovae and baryon acoustic oscillation data. Limit relaxes to 0.47 eV when the equation of state parameter, $w \neq 1$.
- 33 Constrains the total mass of neutrinos from weak lensing measurements when combined with CMB. Limit improves to 0.54 eV when supernovae and baryon acoustic oscillation observations are included. Assumes Λ CDM model.
- 34 Constrains the total mass of neutrinos from five-year WMAP data. Limit improves to 0.67 eV when supernovae and baryon acoustic oscillation observations are included. Limits quoted assume the Λ CDM model. Supersedes SPERGEL 07.
- 35 Constrains the total mass of neutrinos from weak lensing measurements when combined with CMB. Limit improves to $0.03 < \Sigma m_\nu < 0.54$ eV when supernovae and baryon acoustic oscillation observations are included. The slight preference for massive neutrinos at the two-sigma level disappears when systematic errors are taken into account. Assumes Λ CDM model.
- 36 Constrains the total mass of neutrinos from recent Chandra X-ray observations of galaxy clusters when combined with CMB, supernovae, and baryon acoustic oscillation measurements. Assumes flat universe and constant dark-energy equation of state, w .
- 37 Constraints the total mass of neutrinos from recent CMB and SOSS LRG power spectrum data along with bias mass relations from SDSS, DEEP2, and Lyman-Break Galaxies. It assumes Λ CDM model. Limit degrades to 0.59 eV in a more general w CDM model.
- 38 Constrains the total mass of neutrinos from neutrino oscillation experiments and cosmological data. The most conservative limit uses only WMAP three-year data, while the most stringent limit includes CMB, large-scale structure, supernova, and Lyman-alpha data.
- 39 Constrains the total mass of neutrinos from recent CMB, large scale structure, SNIa, and baryon acoustic oscillation data. The limit relaxes to 1.75 when WMAP data alone is used with no prior. Paper shows results with several combinations of data sets. Supersedes KRISTIANSEN 06.
- 40 Constrains the total mass of neutrinos from the CMB and the large scale structure data. The most conservative limit is obtained when generic initial conditions are allowed.
- 41 Constrains the total mass of neutrinos from recent CMB, large scale structure, Lyman-alpha forest, and SNIa data.
- 42 Constrains the total mass of neutrinos from recent CMB and large scale structure data. See also GOOBAR 06. Superseded by HANNESTAD 10.
- 43 Constrains the total mass of neutrinos from the CMB and the final 2dF Galaxy Redshift Survey.
- 44 Constrains the total mass of neutrinos from the CMB experiments alone, assuming Λ CDM Universe. FUKUGITA 06 show that this result is unchanged by the 3-year WMAP data.
- 45 Constrains the total mass of neutrinos from the power spectrum of fluctuations derived from the Sloan Digital Sky Survey and the 2dF galaxy redshift survey, WMAP and 27 other CMB experiments and measurements by the HST Key project.
- 46 Constrains the total mass of neutrinos from the power spectrum of fluctuations derived from the Sloan Digital Sky Survey, the 2dF galaxy redshift survey, WMAP and ACBAR. The limit is strengthened to 0.6 eV when measurements by the HST Key project and supernovae data are included.
- 47 Constrains the fractional contribution of neutrinos to the total matter density in the Universe from WMAP data combined with other CMB measurements, the 2dFGRS data, and Lyman α data. The limit does not noticeably change if the Lyman α data are not used.
- 48 LEWIS 02 constrains the total mass of neutrinos from the power spectrum of fluctuations derived from the CMB, HST Key project, 2dF galaxy redshift survey, supernovae type Ia, and BBN.
- 49 WANG 02 constrains the total mass of neutrinos from the power spectrum of fluctuations derived from the CMB and other cosmological data sets such as galaxy clustering and the Lyman α forest.
- 50 FUKUGITA 00 is a limit on neutrino masses from structure formation. The constraint is based on the clustering scale σ_8 and the COBE normalization and leads to a conservative limit of 0.9 eV assuming 3 nearly degenerate neutrinos. The quoted limit is on the sum of the light neutrino masses.
- 51 CROFT 99 result based on the power spectrum of the Ly α forest. If $\Omega_{\text{matter}} < 0.5$, the limit is improved to $m_\nu < 2.4 (\Omega_{\text{matter}}/0.17-1)$ eV.

Limits on MASSES of Light Stable Right-Handed ν (with necessarily suppressed interaction strengths)

VALUE (eV)	DOCUMENT ID	TECN	COMMENT
<100–200	1 OLIVE	82	COSM Dirac ν
<200–2000	1 OLIVE	82	COSM Majorana ν

1 Depending on interaction strength G_R where $G_R < G_F$.

Lepton Particle Listings

Neutrino Properties

Limits on MASSES of Heavy Stable Right-Handed ν (with necessarily suppressed interaction strengths)

VALUE (GeV)	DOCUMENT ID	TECN	COMMENT
• • • We do not use the following data for averages, fits, limits, etc. • • •			
> 10	1 OLIVE	82 COSM	$G_R/G_F < 0.1$
> 100	1 OLIVE	82 COSM	$G_R/G_F < 0.01$

1 These results apply to heavy Majorana neutrinos and are summarized by the equation: $m_\nu > 1.2 \text{ GeV} (G_F/G_R)$. The bound saturates, and if G_R is too small no mass range is allowed.

ν CHARGE

$e = \text{electron charge is the unit of values listed below.}$

VALUE (e)	CL%	DOCUMENT ID	TECN	COMMENT
<4 $\times 10^{-35}$	95	1 CAPRINI	05 COSM	charge neutral universe
• • • We do not use the following data for averages, fits, limits, etc. • • •				
<5.4 $\times 10^{-12}$	90	2 ABE	20E XMAS	solar neutrinos
1.7-2.3 $\times 10^{-12}$	68	3 KHAN	20	spectral fit of XENON1T
<3 $\times 10^{-8}$	95	4 DELLA-VALLE	16 LASR	magnetic dichroism
<2.1 $\times 10^{-12}$	90	5 CHEN	14A TEXO	nuclear reactor
<1.5 $\times 10^{-12}$	90	6 STUDENIKIN	14	nuclear reactor
<3.7 $\times 10^{-12}$	90	7 GNINENKO	07 RVUE	nuclear reactor
<2 $\times 10^{-14}$		8 RAFFELT	99 ASTR	red giant luminosity
<6 $\times 10^{-14}$		9 RAFFELT	99 ASTR	solar cooling
<4 $\times 10^{-4}$		10 BABU	94 RVUE	BECB beam dump
<3 $\times 10^{-4}$		11 DAVIDSON	91 RVUE	SLAC e^- beam dump
<2 $\times 10^{-15}$		12 BARBIELLINI	87 ASTR	SN 1987A
<1 $\times 10^{-13}$		13 BERNSTEIN	63 ASTR	solar energy losses

- 1 CAPRINI 05 limit derived from the lack of a charge asymmetry in the universe. Limit assumes that charge asymmetries between particles are not anti-correlated.
- 2 ABE 20E obtains this result by assuming that the low-energy excess events in the XMAS detector are produced by neutrino millicharge which is common for all three neutrino flavors.
- 3 KHAN 20 performed a constrained spectral fit analysis of the excess observed in the electron recoil energy spectrum by the XENON1T experiment. This range of neutrino millicharge values is one of the possible interpretations of these excess events. For the individual flavor constraints at 90% C.L. see the original reference.
- 4 DELLA-VALLE 16 obtain a limit on the charge of neutrinos valid for masses of less than 10 MeV. For heavier neutrinos the limit increases as a power of mass, reaching $10^{-6} e$ for $m = 100 \text{ meV}$.
- 5 CHEN 14A use the Multi-Configuration RPPA method to analyze reactor $\bar{\nu}_e$ scattering on Ge atoms with 300 eV recoil energy threshold to obtain this limit.
- 6 STUDENIKIN 14 uses the limit on μ_ν from BEDA 13 and the 2.8 keV threshold of the electron recoil energy to obtain this limit.
- 7 GNINENKO 07 use limit on $\bar{\nu}_e$ magnetic moment from LI 03b to derive this result. The limit is considerably weaker than the limits on the charge of ν_e and $\bar{\nu}_e$ from various astrophysics considerations.
- 8 This RAFFELT 99 limit applies to all neutrino flavors which are light enough ($<5 \text{ keV}$) to be emitted from globular-cluster red giants.
- 9 This RAFFELT 99 limit is derived from the helioseismological limit on a new energy-loss channel of the Sun, and applies to all neutrino flavors which are light enough ($<1 \text{ keV}$) to be emitted from the sun.
- 10 BABU 94 use COOPER-SARKAR 92 limit on ν magnetic moment to derive quoted result. It applies to ν_τ .
- 11 DAVIDSON 91 use data from early SLAC electron beam dump experiment to derive charge limit as a function of neutrino mass. It applies to ν_τ .
- 12 Exact BARBIELLINI 87 limit depends on assumptions about the intergalactic or galactic magnetic fields and about the direct distance and time through the field. It applies to ν_e .
- 13 The limit applies to all flavors.

ν (MEAN LIFE) / MASS

Measures $[\sum |U_{ej}|^2 \Gamma_j m_j]^{-1}$, where the sum is over mass eigenstates which cannot be resolved experimentally. Some of the limits constrain the radiative decay and are based on the limit of the corresponding photon flux. Other apply to the decay of a heavier neutrino into the lighter one and a Majoron or other invisible particle. Many of these limits apply to any ν within the indicated mass range.

Limits on the radiative decay are either directly based on the limits of the corresponding photon flux, or are derived from the limits on the neutrino magnetic moments. In the later case the transition rate for $\nu_i \rightarrow \nu_j + \gamma$ is constrained by $\Gamma_{ij} = \frac{1}{\tau_{ij}} = \frac{(m_i^2 - m_j^2)^3}{m_i^3} \mu_{ij}^2$, where μ_{ij} is the neutrino transition moment in the mass eigenstates basis. Typically, the limits on lifetime based on the magnetic moments are many orders of magnitude more restrictive than limits based on the nonobservation of photons.

VALUE (s/eV)	CL%	DOCUMENT ID	TECN	COMMENT
> 15.4	90	1 KRAKAUER	91 CNTR	$\nu_\mu, \bar{\nu}_\mu$ at LAMPF
> 7 $\times 10^9$		2 RAFFELT	85 ASTR	
> 300	90	3 REINES	74 CNTR	$\bar{\nu}_e$

• • • We do not use the following data for averages, fits, limits, etc. • • •

> 8.08 $\times 10^{-5}$	90	4 AHARMIM	19 SNO	ν_2 invisible nonradiative decay
> 1.92 $\times 10^{-3}$	90	5 AHARMIM	19 FIT	ν_2 invisible nonradiative decay
6-26 $\times 10^9$	95	6 ESCUDERO	19 COSM	Invisible decay $m_\nu \geq 0.05 \text{ eV}$
> $10^5 - 10^{10}$	95	7 CECCHINI	11 ASTR	$\nu_2 \rightarrow \nu_1$ radiative decay
	90	8 MIRIZZI	07 CMB	radiative decay
	90	9 MIRIZZI	07 CIB	radiative decay
		10 WONG	07 CNTR	Reactor $\bar{\nu}_e$
> 0.11	90	11 XIN	05 CNTR	Reactor ν_e
		12 XIN	05 CNTR	Reactor ν_e
> 0.004	90	13 AHARMIM	04 SNO	quasidegen. ν masses
> 4.4 $\times 10^{-5}$	90	13 AHARMIM	04 SNO	hierarchical ν masses
$\gtrsim 100$	95	14 CECCHINI	04 ASTR	Radiative decay for ν mass $> 0.01 \text{ eV}$
> 0.067	90	15 EGUCHI	04 KLND	quasidegen. ν masses
> 1.1 $\times 10^{-3}$	90	15 EGUCHI	04 KLND	hierarchical ν masses
> 8.7 $\times 10^{-5}$	99	16 BANDYOPA...	03 FIT	nonradiative decay
≥ 4200	90	17 DERBIN	02B CNTR	Solar pp and Be ν
> 2.8 $\times 10^{-5}$	99	18 JOSHIPURA	02B FIT	nonradiative decay
		19 DOLGOV	99 COSM	
		20 BILLER	98 ASTR	$m_\nu = 0.05-1 \text{ eV}$
> 2.8 $\times 10^{15}$	21,22	21,22 BLUDMAN	92 ASTR	$m_\nu < 50 \text{ eV}$
none $10^{-12} - 5 \times 10^4$	23	23 DODELSON	92 ASTR	$m_\nu = 1-300 \text{ keV}$
< 10^{-12} or $> 5 \times 10^4$	23	23 DODELSON	92 ASTR	$m_\nu = 1-300 \text{ keV}$
		24 GRANEK	91 COSM	Decaying L^0
> 6.4	90	25 KRAKAUER	91 CNTR	ν_e at LAMPF
> 1.1 $\times 10^{15}$		26 WALKER	90 ASTR	$m_\nu = 0.03 - \sim 2 \text{ MeV}$
> 6.3 $\times 10^{15}$	22,27	27 CHUPP	89 ASTR	$m_\nu < 20 \text{ eV}$
> 1.7 $\times 10^{15}$	22	22 KOLB	89 ASTR	$m_\nu < 20 \text{ eV}$
	28	28 RAFFELT	89 RVUE	$\bar{\nu}$ (Dirac, Majorana)
	29	29 RAFFELT	89B ASTR	
	30	30 VONFEILIT...	88 ASTR	
> 8.3 $\times 10^{14}$		31 OBERAUER	87	$\bar{\nu}_R$ (Dirac)
> 22	68	31 OBERAUER	87	$\bar{\nu}$ (Majorana)
> 38	68	31 OBERAUER	87	$\bar{\nu}_L$ (Dirac)
> 59	68	31 OBERAUER	87	$\bar{\nu}$ (Dirac)
> 30	68	KETOV	86 CNTR	$\bar{\nu}$ (Dirac)
> 20	68	KETOV	86 CNTR	$\bar{\nu}$ (Majorana)
		32 BINETRUY	84 COSM	$m_\nu \sim 1 \text{ MeV}$
> 0.11	90	33 FRANK	81 CNTR	$\nu \bar{\nu}$ LAMPF
> 2 $\times 10^{21}$		34 STECKER	80 ASTR	$m_\nu = 10-100 \text{ eV}$
> 1.0 $\times 10^{-2}$	90	33 BLIETSCHAU	78 HLBC	ν_μ , CERN GGM
> 1.7 $\times 10^{-2}$	90	33 BLIETSCHAU	78 HLBC	$\bar{\nu}_\mu$, CERN GGM
< 3 $\times 10^{-11}$		35 FALK	78 ASTR	$m_\nu < 10 \text{ MeV}$
> 2.2 $\times 10^{-3}$	90	33 BARNES	77 DBC	ν , ANL 12-ft
		36 COWSIK	77 ASTR	
> 3. $\times 10^{-3}$	90	33 BELLOTTI	76 HLBC	ν , CERN GGM
> 1.3 $\times 10^{-2}$	90	33 BELLOTTI	76 HLBC	$\bar{\nu}$, CERN GGM

- 1 KRAKAUER 91 quotes the limit $\tau/m_{\nu_1} > (0.75a^2 + 21.65a + 26.3) \text{ s/eV}$, where a is a parameter describing the asymmetry in the neutrino decay defined as $dN_\nu/d\cos\theta = (1/2)(1 + a\cos\theta)$. The parameter $a = 0$ for a Majorana neutrino, but can vary from -1 to 1 for a Dirac neutrino. The bound given by the authors is the most conservative (which applies for $a = -1$).
- 2 RAFFELT 85 limit on the radiative decay is from solar x- and γ -ray fluxes. Limit depends on ν flux from pp , now established from GALLEX and SAGE to be > 0.5 of expectation.
- 3 REINES 74 looked for ν of nonzero mass decaying radiatively to a neutral of lesser mass + γ . Used liquid scintillator detector near fission reactor. Finds lab lifetime 6×10^7 s or more. Above value of (mean life)/mass assumes average effective neutrino energy of 0.2 MeV. To obtain the limit 6×10^7 s REINES 74 assumed that the full $\bar{\nu}_e$ reactor flux could be responsible for yielding decays with photon energies in the interval 0.1 MeV - 0.5 MeV. This represents some overestimate so their lower limit is an over-estimate of the lab lifetime (VOGEL 84). If so, OBERAUER 87 may be comparable or better.
- 4 AHARMIM 19 quotes the limit τ/m_{ν_2} for invisible nonradiative decay of ν_2 . They obtained this result by analyzing the entire SNO dataset, allowing for the decay of ν_2 which would cause an energy-dependent distortion of the survival probability of electron-type solar neutrinos.
- 5 AHARMIM 19 quotes the limit τ/m_{ν_2} for invisible nonradiative decay of ν_2 . They obtained this result by combining the τ/m_{ν_2} measurements from SNO and other solar neutrino experiments (Super-Kamiokande, KamLAND, and Borexino ^8B results; Borexino and KamLAND ^7Be results; the combined gallium interaction rate from GNO, GALLEX, and SAGE; and the chlorine interaction rate from Homestake). The quoted limit at 99% CL is $> 1.04 \times 10^{-3}$.
- 6 ESCUDERO 19 sets limits on invisible neutrino decays using Planck 2018 data of $\tau > 1.3-0.3 \times 10^9$ s at 95% C.L. Values in the range $\tau = 2-16 \times 10^9$ s are preferred at 95% C.L. when Planck polarization data is included. Limits scale as $(m_\nu/0.05 \text{ eV})^3$.
- 7 CECCHINI 11 search for radiative decays of solar neutrinos into visible photons during the 2006 total solar eclipse. The range of (mean life)/mass values corresponds to a range of ν_1 masses between 10^{-4} and 0.1 eV .
- 8 MIRIZZI 07 determine a limit on the neutrino radiative decay from analysis of the maximum allowed distortion of the CMB spectrum as measured by the COBE/FIRAS. For the decay $\nu_2 \rightarrow \nu_1$ the lifetime limit is $\lesssim 4 \times 10^{20}$ s for $m_{min} \lesssim 0.14 \text{ eV}$. For transition

- with the $|\Delta m_{31}|$ mass difference the lifetime limit is $\sim 2 \times 10^{19}$ s for $m_{min} \lesssim 0.14$ eV and $\sim 5 \times 10^{20}$ s for $m_{min} \gtrsim 0.14$ eV.
- ⁹ MIRIZZI 07 determine a limit on the neutrino radiative decay from analysis of the cosmic infrared background (CIB) using the Spitzer Observatory data. For transition with the $|\Delta m_{31}|$ mass difference they obtain the lifetime limit $\sim 10^{20}$ s for $m_{min} \lesssim 0.14$ eV.
- ¹⁰ WONG 07 use their limit on the neutrino magnetic moment together with the assumed experimental value of $\Delta m_{23}^2 \sim 2 \times 10^{-3}$ eV² to obtain $\tau_{13}/m_1^3 > 3.2 \times 10^{27}$ s/eV³ for the radiative decay in the case of the inverted mass hierarchy. Similarly to RAFFELT 89 this limit can be violated if electric and magnetic moments are equal to each other. Analogous, but numerically somewhat different limits are obtained for τ_{23} and τ_{21} .
- ¹¹ XIN 05 search for the γ from radiative decay of ν_e produced by the electron capture on ⁵¹Cr. No events were seen and the limit on τ/m_ν was derived. This is a weaker limit on the decay of ν_e than KRAKAUER 91.
- ¹² XIN 05 use their limit on the neutrino magnetic moment of ν_e together with the assumed experimental value of $\Delta m_{23}^2 \sim 2 \times 10^{-3}$ eV² to obtain $\tau_{13}/m_1^3 > 1 \times 10^{23}$ s/eV³ for the radiative decay in the case of the inverted mass hierarchy. Similarly to RAFFELT 89 this limit can be violated if electric and magnetic moments are equal to each other. Analogous, but numerically somewhat different limits are obtained for τ_{23} and τ_{21} . Again, this limit is specific for ν_e .
- ¹³ AHARMIM 04 obtained these results from the solar $\bar{\nu}_e$ flux limit set by the SNO measurement assuming ν_2 decay through nonradiative process $\nu_2 \rightarrow \bar{\nu}_1 X$, where X is a Majoron or other invisible particle. Limits are given for the cases of quasidegenerate and hierarchical neutrino masses.
- ¹⁴ CECCHINI 04 obtained this bound through the observations performed on the occasion of the 21 June 2001 total solar eclipse, looking for visible photons from radiative decays of solar neutrinos. Limit is a τ/m_{ν_2} in $\nu_2 \rightarrow \nu_1 \gamma$. Limit ranges from ~ 100 to 10^7 s/eV for $0.01 < m_{\nu_1} < 0.1$ eV.
- ¹⁵ EGUCHI 04 obtained these results from the solar $\bar{\nu}_e$ flux limit set by the KamLAND measurement assuming ν_2 decay through nonradiative process $\nu_2 \rightarrow \bar{\nu}_1 X$, where X is a Majoron or other invisible particle. Limits are given for the cases of quasidegenerate and hierarchical neutrino masses.
- ¹⁶ The ratio of the lifetime over the mass derived by BANDYOPADHYAY 03 is for ν_2 . They obtained this result using the following solar-neutrino data: total rates measured in Cl and Ga experiments, the Super-Kamiokande's zenith-angle spectra, and SNO's day and night spectra. They assumed that ν_1 is the lowest mass, stable or nearly stable neutrino state and ν_2 decays through nonradiative Majoron emission process, $\nu_2 \rightarrow \bar{\nu}_1 + J$, or through nonradiative process with all the final state particles being sterile. The best fit is obtained in the region of the LMA solution.
- ¹⁷ DERBIN 02b (also BACK 03b) obtained this bound for the radiative decay from the results of background measurements with Counting Test Facility (the prototype of the Borexino detector). The laboratory gamma spectrum is given as $dN_\gamma/d\cos\theta = (1/2)(1 + \alpha\cos\theta)$ with $\alpha=0$ for a Majorana neutrino, and α varying to -1 to 1 for a Dirac neutrino. The listed bound is for the case of $\alpha=0$. The most conservative bound 1.5×10^3 s eV⁻¹ is obtained for the case of $\alpha=-1$.
- ¹⁸ The ratio of the lifetime over the mass derived by JOSHIPURA 02b is for ν_2 . They obtained this result from the total rates measured in all solar neutrino experiments. They assumed that ν_1 is the lowest mass, stable or nearly stable neutrino state and ν_2 decays through nonradiative process like Majoron emission decay, $\nu_2 \rightarrow \nu'_1 + J$ where ν'_1 state is sterile. The exact limit depends on the specific solution of the solar neutrino problem. The quoted limit is for the LMA solution.
- ¹⁹ DOLGOV 99 places limits in the (Majorana) τ -associated ν mass-lifetime plane based on nucleosynthesis. Results would be considerably modified if neutrino oscillations exist.
- ²⁰ BILLER 98 use the observed TeV γ -ray spectra to set limits on the mean life of any radiatively decaying neutrino between 0.05 and 1 eV. Curve shows $\tau_\nu/B_\gamma > 0.15 \times 10^{21}$ s at 0.05 eV, $> 1.2 \times 10^{21}$ s at 0.17 eV, $> 3 \times 10^{21}$ s at 1 eV, where B_γ is the branching ratio to photons.
- ²¹ BLUDMAN 92 sets additional limits by this method for higher mass ranges. Cosmological limits are also obtained.
- ²² Limit on the radiative decay based on nonobservation of γ 's in coincidence with ν 's from SN1987A.
- ²³ DODELSON 92 range is for wrong-helicity keV mass Dirac ν 's from the core of neutron star in SN1987A decaying to ν 's that would have interacted in KAM2 or IMB detectors.
- ²⁴ GRANEK 91 considers heavy neutrino decays to $\gamma\nu_L$ and $3\nu_L$, where $m_{\nu_L} < 100$ keV. Lifetime is calculated as a function of heavy neutrino mass, branching ratio into $\gamma\nu_L$, and m_{ν_L} .
- ²⁵ KRAKAUER 91 quotes the limit for ν_e , $\tau/m_\nu > (0.3a^2 + 9.8a + 15.9)$ s/eV, where a is a parameter describing the asymmetry in the radiative neutrino decay defined as $dN_\gamma/d\cos\theta = (1/2)(1 + a\cos\theta)$ $a=0$ for a Majorana neutrino, but can vary from -1 to 1 for a Dirac neutrino. The bound given by the authors is the most conservative (which applies for $a = -1$).
- ²⁶ WALKER 90 uses SN1987A γ flux limits after 289 days.
- ²⁷ CHUPP 89 should be multiplied by a branching ratio (about 1) and a detection efficiency (about 1/4), and pertains to radiative decay of any neutrino to a lighter or sterile neutrino.
- ²⁸ RAFFELT 89 uses KYULDJIEV 84 to obtain $\tau m^3 > 3 \times 10^{18}$ s eV³ (based on $\bar{\nu}_e e^-$ cross sections). The bound for the radiative decay is not valid if electric and magnetic transition moments are equal for Dirac neutrinos.
- ²⁹ RAFFELT 89b analyze stellar evolution and exclude the region $3 \times 10^{12} < \tau m^3 < 3 \times 10^{21}$ s eV³.
- ³⁰ Model-dependent theoretical analysis of SN1987A neutrinos. Quoted limit is for $[\sum_j |U_{\ell j}|^2 \Gamma_j m_j]^{-1}$, where $\ell = \mu, \tau$. Limit is 3.3×10^{14} s/eV for $\ell = e$.
- ³¹ OBERAUER 87 looks for photons and $e^+ e^-$ pairs from radiative decays of reactor neutrinos.
- ³² BINETRUY 84 finds $\tau < 10^8$ s for neutrinos in a radiation-dominated universe.

- ³³ These experiments look for $\nu_k \rightarrow \nu_j \gamma$ or $\bar{\nu}_k \rightarrow \bar{\nu}_j \gamma$.
- ³⁴ STECKER 80 limit based on UV background; result given is $\tau > 4 \times 10^{22}$ s at $m_\nu = 20$ eV.
- ³⁵ FALK 78 finds lifetime constraints based on supernova energetics.
- ³⁶ COWSIK 77 considers variety of scenarios. For neutrinos produced in the big bang, present limits on optical photon flux require $\tau > 10^{23}$ s for $m_\nu \sim 1$ eV. See also COWSIK 79 and GOLDMAN 79.

ν MAGNETIC MOMENT

The coupling of neutrinos to an electromagnetic field is characterized by a 3×3 matrix λ of the magnetic (μ) and electric (d) dipole moments ($\lambda = \mu - id$). For Majorana neutrinos the matrix λ is antisymmetric and only transition moments are allowed, while for Dirac neutrinos λ is a general 3×3 matrix. In the standard electroweak theory extended to include neutrino masses (see FUJIKAWA 80) $\mu_\nu = 3eG_F m_\nu / (8\pi^2 \sqrt{2}) = 3.2 \times 10^{-19} (m_\nu / \text{eV}) \mu_B$, i.e. it is unobservably small given the known small neutrino masses. In more general models there is no longer a proportionality between neutrino mass and its magnetic moment, even though only massive neutrinos have nonvanishing magnetic moments without fine tuning.

Laboratory bounds on λ are obtained via elastic ν -e scattering, where the scattered neutrino is not observed. The combinations of matrix elements of λ that are constrained by various experiments depend on the initial neutrino flavor and on its propagation between source and detector (e.g., solar ν_e and reactor $\bar{\nu}_e$ do not constrain the same combinations). The listings below therefore identify the initial neutrino flavor.

Other limits, e.g. from various stellar cooling processes, apply to all neutrino flavors. Analogous flavor independent, but weaker, limits are obtained from the analysis of $e^+ e^- \rightarrow \nu \bar{\nu} \gamma$ collider experiments.

VALUE ($10^{-10} \mu_B$)	CL%	DOCUMENT ID	TECN	COMMENT
0.14–0.29	90	1 APRILE 20	XE1T	Solar ν spectrum
< 0.28	90	2 AGOSTINI 17A	BORX	Solar ν spectrum
< 0.29	90	3 BEDA 13	CNTR	Reactor $\bar{\nu}_e$
< 6.8	90	4 AUERBACH 01	LSND	$\nu_e e, \nu_\mu e$ scattering
< 3900	90	5 SCHWIENHO...01	DONU	$\nu_\tau e^- \rightarrow \nu_\tau e^-$
• • • We do not use the following data for averages, fits, limits, etc. • • •				
< 1.8	90	6 ABE 20E	XMAS	Solar ν spectrum
< 0.012	95	7 CAPOZZI 20	ASTR	Tip of the Red-Giant Branch
0.2–0.4	68	8 KHAN 20		Spectral fit of XENON1T
< 0.022	90	9 ARCEO-DIAZ 15	ASTR	Red giants
< 0.1	95	10 CORSICO 14	ASTR	
< 0.05	95	11 MILLER-BER...14b	ASTR	
< 0.045	95	12 VIAUX 13A	ASTR	Globular cluster M5
< 0.32	90	13 BEDA 10	CNTR	Reactor $\bar{\nu}_e$
< 2.2	90	14 DENIZ 10	TEXO	Reactor $\bar{\nu}_e$
< 0.011–0.027		15 KUZNETSOV 09	ASTR	$\nu_L \rightarrow \nu_R$ in SN1987A
< 0.54	90	16 ARPESELLA 08A	BORX	Solar ν spectrum
< 0.58	90	17 BEDA 07	CNTR	Reactor $\bar{\nu}_e$
< 0.74	90	18 WONG 07	CNTR	Reactor $\bar{\nu}_e$
< 0.9	90	19 DARAKTCH... 05		Reactor $\bar{\nu}_e$
< 130	90	20 XIN 05	CNTR	Reactor ν_e
< 37	95	21 GRIFOLS 04	FIT	Solar $\bar{\nu}_e \nu$ (SNO NC)
< 3.6	90	22 LIU 04	SKAM	Solar ν spectrum
< 1.1	90	23 LIU 04	SKAM	Solar ν spectrum (LMA region)
< 5.5	90	24 BACK 03b	CNTR	Solar $p\bar{p}$ and Be ν
< 1.0	90	25 DARAKTCH... 03		Reactor $\bar{\nu}_e$
< 1.3	90	26 LI 03b	CNTR	Reactor $\bar{\nu}_e$
< 2	90	27 GRIMUS 02	FIT	solar + reactor (Majorana ν)
< 80000	90	28 TANIMOTO 00	RVUE	$e^+ e^- \rightarrow \nu \bar{\nu} \gamma$
< 0.01–0.04		29 AYALA 99	ASTR	$\nu_L \rightarrow \nu_R$ in SN1987A
< 1.5	90	30 BEACOM 99	SKAM	Solar ν spectrum
< 0.03		31 RAFFELT 99	ASTR	Red giant luminosity
< 4		32 RAFFELT 99	ASTR	Solar cooling
< 44000	90	33 ABREU 97J	DLPH	$e^+ e^- \rightarrow \nu \bar{\nu} \gamma$ at LEP
< 33000	90	34 ACCIARRI 97Q	L3	$e^+ e^- \rightarrow \nu \bar{\nu} \gamma$ at LEP
< 0.62		34 ELMFORS 97	COSM	Depolarization in early universe plasma
< 27000	95	35 ESCRIBANO 97	RVUE	$\Gamma(Z \rightarrow \nu \nu)$ at LEP
< 30	90	VILAIN 95B	CHM2	$\nu_e e \rightarrow \nu_e e$
< 55000	90	GOULD 94	RVUE	$e^+ e^- \rightarrow \nu \bar{\nu} \gamma$ at LEP
< 1.9	95	36 DERBIN 93	CNTR	Reactor $\bar{\nu}_e \rightarrow \bar{\nu}_e$
< 5400	90	37 COOPER... 92	BEBC	$\nu_\tau e^- \rightarrow \nu_\tau e^-$
< 2.4	90	38 VIDYAKIN 92	CNTR	Reactor $\bar{\nu}_e \rightarrow \bar{\nu}_e$
< 56000	90	39 DESHPANDE 91	RVUE	$e^+ e^- \rightarrow \nu \bar{\nu} \gamma$
< 100	95	39 DORENBOS... 91	CHRM	$\nu_e e \rightarrow \nu_e e$
< 8.5	90	AHRENS 90	CNTR	$\nu_e e \rightarrow \nu_e e$
< 10.8	90	40 KRAKAUER 90	CNTR	LAMPF $\nu_e \rightarrow \nu_e$
< 7.4	90	40 KRAKAUER 90	CNTR	LAMPF $(\nu_\mu, \bar{\nu}_\mu) e$ elast.
< 0.02		41 RAFFELT 90	ASTR	Red giant luminosity
< 0.1		42 RAFFELT 89b	ASTR	Cooling helium stars

Lepton Particle Listings

Neutrino Properties

<40000	90	43 FUKUGITA	88 COSM	Primordial magn. fields
<	.3	44 GROTH	88 RVUE	$e^+ e^- \rightarrow \nu \bar{\nu} \gamma$
<	0.11	42 RAFFELT	88b ASTR	He burning stars
<	0.0006	42 FUKUGITA	87 ASTR	Cooling helium stars
<	0.1–0.2	45 NUSSINOV	87 ASTR	Cosmic EM backgrounds
<	0.85	MORGAN	81 COSM	^4He abundance
<	0.6	BEG	78 ASTR	Stellar plasmons
<	81	46 SUTHERLAND	76 ASTR	Red giants + degenerate dwarfs
<	1	47 KIM	74 RVUE	$\bar{\nu}_\mu e \rightarrow \bar{\nu}_\mu e$
<	14	BERNSTEIN	63 ASTR	Solar cooling
		COWAN	57 CNTR	Reactor $\bar{\nu}$

1 APRILE 20 observed an excess of low-energy events in the XENON1T detector, which could be interpreted as a signal produced by a neutrino magnetic moment with this magnitude.

2 AGOSTINI 17A obtained this limit using the shape of the recoil electron energy spectrum from the Borexino Phase-II 1291.5 live days of solar neutrino data and the constraints on the sum of the solar neutrino fluxes from the radiochemical gallium experiments SAGE, Gallex, and GNO. Without radiochemical constraints, the 90% C.L. limit of $4.0 \times 10^{-11} \mu_B$ is obtained.

3 BEDA 13 report $\bar{\nu}_e e^-$ scattering results, using the Kalinin Nuclear Power Plant and a shielded Ge detector. The recoil electron spectrum is analyzed between 2.5 and 55 keV. Supersedes BEDA 07. Supersedes BEDA 10. This is the most stringent limit on the magnetic moment of reactor $\bar{\nu}_e$.

4 AUERBACH 01 limit is based on the LSND ν_e and ν_μ electron scattering measurements. The limit is slightly more stringent than KRAKAUER 90.

5 SCHWIENHORST 01 quote an experimental sensitivity of 4.9×10^{-7} .

6 ABE 20E observed an excess of low-energy events in the XMASS detector, which could be interpreted as a signal produced by a neutrino magnetic moment with this magnitude.

7 CAPOZZI 20 obtains a limit on the neutrino dipole moment from the brightness of the tip of the red-giant branch in ω Centauri. A similar limit of $\mu_\nu < 1.5 \times 10^{-12} \mu_B$ is obtained in NGC 4258.

8 KHAN 20 performed a constrained spectral fit analysis of the excess observed in the electron recoil energy spectrum by the XENON1T experiment. This range of the μ_B values is one of the possible interpretations of these excess events. For the individual flavor constraints at 90% C.L. see the original reference.

9 ARCEO-DIAZ 15 constrains the neutrino magnetic moment from observation of the tip of the red giant branch in the globular cluster ω -Centauri.

10 CORSICO 14 constrains the neutrino magnetic moment from observations of white dwarf pulsations.

11 MILLER-BERTOLAMI 14b constrains the neutrino magnetic moment from observations of the white dwarf luminosity function of the Galactic disk.

12 VIAUX 13a constrains the neutrino magnetic moment from observations of the globular cluster M5.

13 BEDA 10 report $\bar{\nu}_e e^-$ scattering results, using the Kalinin Nuclear Power Plant and a shielded Ge detector. The recoil electron spectrum is analyzed between 2.9 and 45 keV. Supersedes BEDA 07. Supersedes by BEDA 13.

14 DENIZ 10 observe reactor $\bar{\nu}_e e$ scattering with recoil kinetic energies 3–8 MeV using CsI(Tl) detectors. The observed rate and spectral shape are consistent with the Standard Model prediction, leading to the reported constraint on $\bar{\nu}_e$ magnetic moment.

15 KUZNETSOV 09 obtain a limit on the flavor averaged magnetic moment of Dirac neutrinos from the time averaged neutrino signal of SN1987A. Improves and supersedes the analysis of BARBIERI 88 and AYALA 99.

16 ARPESELLA 08a obtained this limit using the shape of the recoil electron energy spectrum from the Borexino 192 live days of solar neutrino data.

17 BEDA 07 performed search for electromagnetic $\bar{\nu}_e e$ scattering at Kalininskaya nuclear reactor. A Ge detector with active and passive shield was used and the electron recoil spectrum between 3.0 and 61.3 keV analyzed. Supersedes by BEDA 10.

18 WONG 07 performed search for non-standard $\bar{\nu}_e e$ scattering at the Kuo-Sheng nuclear reactor. Ge detector equipped with active anti-Compton shield is used. Most stringent laboratory limit on magnetic moment of reactor $\bar{\nu}_e$. Supersedes LI 03b.

19 DARAKTCHIEVA 05 present the final analysis of the search for non-standard $\bar{\nu}_e e$ scattering component at Bugey nuclear reactor. Full kinematical event reconstruction of both the kinetic energy above 700 keV and scattering angle of the recoil electron, by use of TPC. Most stringent laboratory limit on magnetic moment. Supersedes DARAKTCHIEVA 03.

20 XIN 05 evaluated the ν_e flux at the Kuo-Sheng nuclear reactor and searched for non-standard $\nu_e e$ scattering. Ge detector equipped with active anti-Compton shield was used. This laboratory limit on magnetic moment is considerably less stringent than the limits for reactor $\bar{\nu}_e$, but is specific to ν_e .

21 GRIFOLS 04 obtained this bound using the SNO data of the solar ^8B neutrino flux measured with deuteron breakup. This bound applies to $\mu_{\text{eff}} = (\mu_{21}^2 + \mu_{22}^2 + \mu_{23}^2)^{1/2}$.

22 LIU 04 obtained this limit using the shape of the recoil electron energy spectrum from the Super-Kamiokande-I 1496 days of solar neutrino data. Neutrinos are assumed to have only diagonal magnetic moments, $\mu_{\nu 1} = \mu_{\nu 2}$. This limit corresponds to the oscillation parameters in the vacuum oscillation region.

23 LIU 04 obtained this limit using the shape of the recoil electron energy spectrum from the Super-Kamiokande-I 1496 live-day solar neutrino data, by limiting the oscillation parameter region in the LMA region allowed by solar neutrino experiments plus KamLAND. $\mu_{\nu 1} = \mu_{\nu 2}$ is assumed. In the LMA region, the same limit would be obtained even if neutrinos have off-diagonal magnetic moments.

24 BACK 03b obtained this bound from the results of background measurements with Counting Test Facility (the prototype of the Borexino detector). Standard Solar Model flux was assumed. This μ_ν can be different from the reactor μ_ν in certain oscillation scenarios (see BEACOM 99).

25 DARAKTCHIEVA 03 searched for non-standard $\bar{\nu}_e e$ scattering component at Bugey nuclear reactor. Full kinematical event reconstruction by use of TPC. Supersedes by DARAKTCHIEVA 05.

26 LI 03b used Ge detector in active shield near nuclear reactor to test for nonstandard $\bar{\nu}_e e$ scattering.

27 GRIMUS 02 obtain stringent bounds on all Majorana neutrino transition moments from a simultaneous fit of LMA-MSW oscillation parameters and transition moments to global solar neutrino data + reactor data. Using only solar neutrino data, a 90% CL bound of $6.3 \times 10^{-10} \mu_B$ is obtained.

28 TANIMOTO 00 combined $e^+ e^- \rightarrow \nu \bar{\nu} \gamma$ data from VENUS, TOPAZ, and AMY.

29 AYALA 99 improves the limit of BARBIERI 88.

30 BEACOM 99 obtain the limit using the shape, but not the absolute magnitude which is affected by oscillations, of the solar neutrino spectrum obtained by Superkamiokande (825 days). This μ_ν can be different from the reactor μ_ν in certain oscillation scenarios.

31 RAFFELT 99 is an update of RAFFELT 90. This limit applies to all neutrino flavors which are light enough (< 5 keV) to be emitted from globular-cluster red giants. This limit pertains equally to electric dipole moments and magnetic transition moments, and it applies to both Dirac and Majorana neutrinos.

32 RAFFELT 99 is essentially an update of BERNSTEIN 63, but is derived from the helioseismological limit on a new energy-loss channel of the Sun. This limit applies to all neutrino flavors which are light enough (< 1 keV) to be emitted from the Sun. This limit pertains equally to electric dipole and magnetic transition moments, and it applies to both Dirac and Majorana neutrinos.

33 ACCIARRI 97q result applies to both direct and transition magnetic moments and for $q^2=0$.

34 ELMFORS 97 calculate the rate of depolarization in a plasma for neutrinos with a magnetic moment and use the constraints from a big-bang nucleosynthesis on additional degrees of freedom.

35 Applies to absolute value of magnetic moment.

36 DERBIN 93 determine the cross section for 0.6–2.0 MeV electron energy as $(1.28 \pm 0.63) \times \sigma_{\text{weak}}$. However, the (reactor on – reactor off)/(reactor off) is only $\sim 1/100$.

37 COOPER-SARKAR 92 assume $f_{D_s}/f_\pi = 2$ and D_s, \bar{D}_s production cross section = $2.6 \mu\text{b}$ to calculate ν flux.

38 VIDYAKIN 92 limit is from a $e \bar{\nu}_e$ elastic scattering experiment. No experimental details are given except for the cross section from which this limit is derived. Signal/noise was 1/10. The limit uses $\sin^2 \theta_W = 0.23$ as input.

39 DORENBOSCH 91 corrects an incorrect statement in DORENBOSCH 89 that the ν magnetic moment is $< 1 \times 10^{-9}$ at the 95%CL. DORENBOSCH 89 measures both $\nu_\mu e$ and $\bar{\nu}_e e$ elastic scattering and assume $\mu(\nu) = \mu(\bar{\nu})$.

40 KRAKAUER 90 experiment fully reported in ALLEN 93.

41 RAFFELT 90 limit applies for a diagonal magnetic moment of a Dirac neutrino, or for a transition magnetic moment of a Majorana neutrino. In the latter case, the same analysis gives $< 1.4 \times 10^{-12}$. Limit at 95%CL obtained from δm_C .

42 Significant dependence on details of stellar models.

43 FUKUGITA 88 find magnetic dipole moments of any two neutrino species are bounded by $\mu < 10^{-16} [10^{-9} G/B_0]$ where B_0 is the present-day intergalactic field strength.

44 GROTH 88 combined data from MAC, ASP, CELLO, and Mark J.

45 For $m_\nu = 8\text{--}200$ eV. NUSSINOV 87 examines transition magnetic moments for $\nu_\mu \rightarrow \nu_e$ and obtain $< 3 \times 10^{-15}$ for $m_\nu > 16$ eV and $< 6 \times 10^{-14}$ for $m_\nu > 4$ eV.

46 We obtain above limit from SUTHERLAND 76 using their limit $f < 1/3$.

47 KIM 74 is a theoretical analysis of $\bar{\nu}_\mu$ reaction data.

NEUTRINO CHARGE RADIUS SQUARED

We report limits on the so-called neutrino charge radius squared. While the straight-forward definition of a neutrino charge radius has been proven to be gauge-dependent and, hence, unphysical (LEE 77c), there have been recent attempts to define a physically observable neutrino charge radius (BERNABEU 00, BERNABEU 02). The issue is still controversial (FUJIKAWA 03, BERNABEU 03). A more general interpretation of the experimental results is that they are limits on certain nonstandard contributions to neutrino scattering.

VALUE (10^{-32} cm^2)	CL%	DOCUMENT ID	TECN	COMMENT
– 2.1 to 3.3	90	1 DENIZ	10 TEXO	Reactor $\bar{\nu}_e e$
• • • We do not use the following data for averages, fits, limits, etc. • • •				
– 27.5 to 3	90	2 CADEDDU	18	ν_μ coherent scat. on Csl
– 0.53 to 0.68	90	3 HIRSCH	03	$\nu_\mu e$ scat.
– 8.2 to 9.9	90	4 HIRSCH	03	anomalous $e^+ e^- \rightarrow \nu \bar{\nu} \gamma$
– 2.97 to 4.14	90	5 AUERBACH	01 LSND	$\nu_e e \rightarrow \nu_e e$
– 0.6 to 0.6	90	VILAIN	95b CHM2	$\nu_\mu e$ elastic scat.
0.9 \pm 2.7		ALLEN	93 CNTR	LAMPF $\nu e \rightarrow \nu e$
< 2.3	95	MOURAO	92 ASTR	HOME/KAM2 ν rates
< 7.3	90	6 VIDYAKIN	92 CNTR	Reactor $\bar{\nu} e \rightarrow \bar{\nu} e$
1.1 \pm 2.3		ALLEN	91 CNTR	Repl. by ALLEN 93
– 1.1 \pm 1.0		7 AHRENS	90 CNTR	$\nu_\mu e$ elastic scat.

- 0.3 ± 1.5
- ⁷ DORENBOS... 89 CHR M $\nu_\mu e$ elastic scat.
- ⁸ GRIFOLS 89B ASTR SN 1987A
- ¹ DENIZ 10 observe reactor $\bar{\nu}_e e$ scattering with recoil kinetic energies 3–8 MeV using CsI(Tl) detectors. The observed rate and spectral shape are consistent with the Standard Model prediction, leading to the reported constraint on $\bar{\nu}_e$ charge radius.
- ² CADEDDU 18 use the data of the COHERENT experiment, AKIMOV 18. The limit is $\langle r_{\nu}^2 \rangle$ for ν_μ obtained from the time-dependent data. Weaker limits were obtained for charge radii of ν_e and for transition charge radii. The published value was divided by 2 to conform to the convention of this table.
- ³ Based on analysis of CCFR 98 results. Limit is on $\langle r_{\nu}^2 \rangle + \langle r_{A'}^2 \rangle$. The CHARM II and E734 at BNL results are reanalyzed, and weaker bounds on the charge radius squared than previously published are obtained. The NuTeV result is discussed; when tentatively interpreted as ν_μ charge radius it implies $\langle r_{\nu}^2 \rangle + \langle r_{A'}^2 \rangle = (4.20 \pm 1.64) \times 10^{-33} \text{ cm}^2$.
- ⁴ Results of LEP-2 are interpreted as limits on the axial-vector charge radius squared of a Majorana ν_τ . Slightly weaker limits for both vector and axial-vector charge radius squared are obtained for the Dirac case, and somewhat weaker limits are obtained from the analysis of lower energy data (LEP-1.5 and TRISTAN).
- ⁵ AUERBACH 01 measure $\nu_e e$ elastic scattering with LSND detector. The cross section agrees with the Standard Model expectation, including the charge and neutral current interference. The 90% CL applies to the range shown.
- ⁶ VIDYAKIN 92 limit is from a $e\bar{\nu}$ elastic scattering experiment. No experimental details are given except for the cross section from which this limit is derived. Signal/noise was 1/10. The limit uses $\sin^2 \theta_W = 0.23$ as input.
- ⁷ Result is obtained from reanalysis given in ALLEN 91, followed by our reduction to obtain 1σ errors.
- ⁸ GRIFOLS 89B sets a limit of $\langle r^2 \rangle < 0.2 \times 10^{-32} \text{ cm}^2$ for right-handed neutrinos.

HANNESTAD 06 JCAP 0611 016
KRISTIANSEN 06 PR D74 123005
SANCHEZ 06 MNRAS 366 189
SELJAK 06 JCAP 0610 014
CAPRINI 05 JCAP 0502 006
DARAKTCH... 05 PL B615 153
ICHIKAWA 05 PR D71 043001
KRAUS 05 EPJ C40 447
XIN 05 PR D72 012006
AHARMIM 04 PR D70 030104
BARGER 04 PL B595 55
CECCHINI 04 ASP 21 183
CROTTY 04 PR D69 123007
EGUCHI 04 PRL 92 071301
GRIFOLS 04 PL B587 184
LIU 04 PRL 93 021802
ARNABOLDI 03A PRL 91 161802
BACK 03B PL B563 35
BANDYOPA... 03 PL B555 33
BERNABEU 03 hep-ph/030202
DARAKTCH... 03 PL B564 190
FUJIKAWA 03 hep-ph/0303188
HIRSCH 03 PR D67 033005
LI 03B PRL 90 131802
SPERGEL 03 APJS 148 175
BERNABEU 02 PRL 89 101802
Also PRL 89 229902 (err.)
DERBIN 02B JETPL 76 409

Translated from ZETFP 76 483.
GRIMUS 02 NP B648 376
W. Grimus et al.
JOSHIPURA 02B PR D66 113008
A.S. Joshipura, E. Masso, S. Mohanty
LEWIS 02 PR D66 103511
A. Lewis, S. Bridle
LEEDO 02 PR D65 063002
T.J. Leedo, D.Q. Lamb
WANG 02 PR D65 123001
X. Wang, M. Tegenmark, M. Zaldarriaga
AUERBACH 01 PR D63 112001
L.B. Auerbach et al. (LSND Collab.)
SCHWIENHOR... 01 PL B513 23
R. Schwienhorst et al. (DONUT Collab.)
ATHANAS 00 PR D61 052002
M. Athanas et al. (CLEO Collab.)
BERNABEU 00 PR D62 113012
J. Bernabeu et al.
FUKUGITA 00 PRL 84 1082
M. Fukugita, G.C. Liu, N. Sugiyama
TANIMOTO 00 PL B478 1
N. Tanimoto et al.
AYALA 99 PR D59 111901
A. Ayala, J.C. D'Olivo, M. Torres
BEACOM 99 PRL 83 5222
J.F. Beacom, P. Vogel
CROFT 99 PRL 83 1092
R.A.C. Croft, W. Hu, R. Dave
DOLGOV 99 NP B548 385
A.D. Dolgov et al.
LOBASHEV 99 PR D60 227
V.M. Lobashev et al.
RAFFLET 99 PR D60 219
G.G. Rafflet
WEINHEIMER 99 PL B460 219
Ch. Weinheimer et al.
ACKERSTAFF 98T EPJ C5 229
K. Ackerstaff et al. (OPAL Collab.)
AMMAR 98 PL B431 209
R. Ammar et al. (CLEO Collab.)
BARATE 98F EPJ C2 395
R. Barate et al. (ALEPH Collab.)
BILLER 98 PRL 80 2992
S.D. Biller et al. (WHIPPLe Collab.)
FELDMAN 98 PR D57 3873
G.J. Feldman, R.D. Cousins
LENZ 98 PL B416 50
S. Lenz et al.
ABREU 97J ZPHY C74 577
P. Abreu et al. (DELPHI Collab.)
ACCIARI 97 PL B412 201
M. Acciari et al. (L3 Collab.)
ANASTASSOV 97 PR D55 2559
A. Anastassov et al. (CLEO Collab.)
Also PR D58 119903 (erratum) A. Anastassov et al. (CLEO Collab.)
ELMFOVS 97 NP B503 3
P. Elmfovs et al.
ESCRIBANO 97 PL B395 369
R. Escríbano, E. Masso (BARC, PARIT)
FIELDS 97 ASP 6 169
B.D. Fields, K. Kainulainen, K.A. Olive (NDM+) (NEAS)
SWAIN 97 PR D55 1
J. Swain, L. Taylor
ALEXANDER 96M ZPHY C72 231
G. Alexander et al. (OPAL Collab.)
ASSAMAGAN 96 PR D53 6065
K.A. Assamagan et al. (PSI, ZURI, VILL+)
BAI 96 PR D53 20
J.Z. Bai et al. (BES Collab.)
BOTTINO 96 PR D53 6361
A. Bottino et al.
DOLGOV 96 PL B383 193
A.D. Dolgov, S. Pastor, J.W.F. Valle (IFIC, VALE)
HANNESTAD 96 PR D56 2348
S. Hannestad, J. Madsen (AARH)
HANNESTAD 96B PRL 77 5148 (erratum)
S. Hannestad, J. Madsen (AARH)
HANNESTAD 96C PR D54 7894
S. Hannestad, J. Madsen (AARH)
SOBIE 96 ZPHY C70 383
R.J. Sobie, R.K. Keeler, L. Lawson (VICT)
BELESEV 95 PL B350 263
A.I. Beleshev et al. (INRM, KIAE)
BUSKULIC 95H PL B349 585
D. Buskulic et al. (ALEPH Collab.)
CHING 95 IJMP A10 2841
C.R. Ching et al. (CST, BEIJT, CIAE)
DOLGOV 95 PR D51 4129
A.D. Dolgov, K. Kainulainen, I.Z. Rothstein (MICH+)
HIDDEMANN 95 JP G21 639
K.H. Hiddeemann, H. Daniel, O. Schwentker (TUM)
KERMAN 95 NP B437 243
P.J. Kerman, L.M. Krauss (CASE)
SIGL 95 PR D51 1499
G. Sigl, M.S. Turner (FNAL, EFT)
STOEFFL 95 PR D51 3237
W. Stoeffl, D.J. Decman (LNL)
VILAIN 95B PL B345 115
P. Vilain et al. (CHARM II Collab.)
ASSAMAGAN 94 PL B335 231
K.A. Assamagan et al. (PSI, ZURI, VILL+)
BABU 94 PL B321 140
K.S. Babu, T.M. Gould, I.Z. Rothstein (BART+)
DODELSON 94 PR D49 5068
S. Dodelson, G. Gyuk, M.S. Turner (FNAL, CHIC+)
GOULD 94 PL B333 545
T.M. Gould, I.Z. Rothstein (JHU, MICH)
JECKELMANN 94 PL B335 326
B. Jeckelmann, P.F.A. Goudsmit, H.J. Leisi (WABRN+)
KAWASAKI 94 NP B419 105
M. Kawasaki et al. (OSU)
PERES 94 PR D50 513
O.L.G. Peres, V. Pleitez, R. Zukanovich Funchal
YASUMI 94 PL B334 229
S. Yasumi et al. (KEK, TSUK, KYOT+)
ALLEN 93 PR D47 11
R.C. Allen et al. (UCI, LANL, ANL+)
BALEST 93 PR D47 3671
R. Balest et al. (CLEO Collab.)
CINABRO 93 PRL 70 3700
D. Cinabro et al. (CLEO Collab.)
DERBIN 93 JETPL 57 768
A.V. Derbin et al. (PNPI)

Translated from ZETFP 57 755.
DOLGOV 93 PRL 71 476
A.D. Dolgov, I.Z. Rothstein (MICH)
ENQVIST 93 PL B301 376
K. Enqvist, H. Uibo (NORD)
SUN 93 CJNP 15 261
H.C. Sun et al. (CIAE, CST, BEUT)
WEINHEIMER 93 PL B300 210
C. Weinheimer et al. (MAINZ)
ALBRECHT 92M PL B292 221
H. Albrecht et al. (ARGUS Collab.)
BLUDMAN 92 PR D45 4720
S.A. Bludman (CFPA)
COOPER... 92 PL B280 153
A.M. Cooper-Sarkar et al. (BEBC WA66 Collab.)
DODELSON 92 PRL 68 2572
S. Dodelson, J.A. Frieman, M.S. Turner (FNAL+)
HOLZSCHUH 92B PL B287 381
E. Holzschuh, M. Frisch, W. Kundig (ZURI)
KANANO 92 PR D275 487
D. Kanano et al. (CIT, UCSD, ILL+)
MOURAO 92 PL B285 364
A.M. Mourao, J. Pulido, J.P. Rastbor (LISB, LISB+)
PDG 92 PR D45 51
K. Hikasa et al. (KEK, LBL, BOST+)
VIDYAKIN 92 JETPL 58 206
G.S. Vidyakin et al. (KIAE)

Translated from ZETFP 55 212.
ALLEN 91 PR D43 1
R.C. Allen et al. (UCI, LANL, UMD)
DAVIDSON 91 PR D43 2314
S. Davidson, B.A. Campbell, D. Bailey (ALBE+)
DESHPANDE 91 PR D43 943
N.G. Deshpande, K.V.L. Sarma (OREG, TATA)
DORENBOS... 91 ZPHY C51 142 (erratum) J. Dorenbosch et al. (CHARM Collab.)
FULLER 91 PR D43 3136
G.M. Fuller, R.A. Malaney (UCSD)
GRANEK 91 IJMP A6 2387
H. Granek, B.H.J. McKellar (MELB)
KAWAKAMI 91 PL B256 105
H. Kawakami et al. (INUS, TOHOK, TINT+)
KOLB 91 PRL 67 533
E.W. Kolb et al. (FNAL, CHIC)
KRAKAUER 91 PR D43 381
D.A. Krakauer et al. (LAMPF E225 Collab.)
LI 91 PR D44 3345
W.P. Lam, K.W. Ng (AST)
ROBERTSON 91 PRL 67 957
R.G.H. Robertson et al. (LASL, LLL)
AHRENS 90 PR D41 3297
L.A. Ahrens et al. (BNL, BROW, HIRO+)
AVIGNONE 90 PR D41 682
F.T. Avignone, J.I. Collar (SUCU)
KRAKAUER 90 PL B252 177
D.A. Krakauer et al. (LAMPF E225 Collab.)
RAFFLET 90 PRL 64 2856
G.G. Rafflet (MPIM)

REFERENCES FOR Neutrino Properties

ABBOTT 21A PR D105 023520
T.C.M. Abbott et al. (DES Collab.)
ALAM 21 PR D103 083533
S. Alam et al. (eBOSS Collab.)
DIVALENT... 21 PR D 104 083504
E. Di Valentino, S. Gariazzo, O. Mena (DURH+)
GARMY 21 JCAP 2103 049
M. Garmy et al.
STOCKER 21 PR D103 123508
P. Stocker et al. (GAMBIT Collab.)
ABE 20E PL B809 135782
K. Abe et al. (XMASS Collab.)
AGHANIM 20 AA 641 A6
N. Aghanim et al. (Planck Collab.)
APRILE 20 PR D102 072004
E. Aprile et al. (XENON Collab.)
CAPOZZI 20 PR D102 083007
F. Capozzi, G. Raffelt (MPIM)
CHOUDHURY 20 JCAP 2007 037
S.R. Choudhury, S. Hannestad (IITB, AARH)
IVANOV 20 PR D101 083504
M.M. Ivanov, M. Simonovic, M. Zaldarriaga (NYU+, MPIK)
KHAN 20 PL B809 135782
A.N. Khan (XMASS Collab.)
PALANQUE... 20 JCAP 2004 038
N. Palanque-Desabrouille et al. (SACL+)
AHARMIM 19 PR D99 032013
B. Aharmim et al. (SNO Collab.)
AKER 19 PRL 123 221802
M. Aker et al. (KATRIN Collab.)
Also PR D104 012005
M. Aker et al. (KATRIN Collab.)
ESCUDERO 19 PR D100 103531
M. Escudero, M. Fairbairn (LOK)
LOUREIRO 19 PRL 123 081301
A. Loureiro et al.
UPADHYE 19 JCAP 1905 041
A. Upadhye (WIS C)
AKIMOV 18 arXiv:1804.09459
D. Akimov et al. (COHERENT Collab.)
CADEDDU 18 PR D98 113010
M. Cadeddu et al.
Also PR D101 059902 (err.)
M. Cadeddu et al.
CHOUDHURY 18 JCAP 1809 017
S.R. Choudhury, S. Choubey
AGOSTINI 17A PR D96 091103
M. Agostini et al. (Borexino Collab.)
SIMPSON 17 JCAP 1706 029
F. Simpson et al. (BARC)
VAGNOZZI 17 PR D96 123503
S. Vagnozzi et al.
YECHÉ 17 JCAP 1706 047
C. Yeché et al.
DELLA-VALLE 16 EPJ C76 24
F. Della Valle et al. (PVLAS Collab.)
DIVALENTINO 16 PR D93 083527
E. Di Valentino et al.
GIUSARMA 16 PR D94 083522
E. Giusarma et al.
HUANG 16 EPJ C76 489
Q.-G. Huang, K. Wang, S. Wang
ARCEO-DIAZ 15 ASP 70 1
S. Arceo-Diaz et al.
PALANQUE... 15A JCAP 1511 011
N. Palanque-Desabrouille et al.
ROSSI 15 PR D92 065050
G. Rossi et al.
ADE 14 AA 571 A16
P.A.R. Ade et al. (Planck Collab.)
BATTYE 14 PR D12 051303
R.A. Battye, A. Moss (MCHS, WOTT)
BEUTLER 14 MNRAS 444 3501
F. Beutler et al. (BOSS Collab.)
CHEN 14A PR D90 011301
J.-W. Chen et al. (TEXONO Collab.)
CORISCO 14 JCAP 1408 054
A.H. Corsico
COSTANZI 14 JCAP 1410 081
M. Costanzi et al. (TRST, TRSTI)
GIUSARMA 14 PR D90 043507
E. Giusarma et al.
HOU 14 APJ 782 74
Z. Hou et al.
LEISTEDT 14 PRL 113 041301
B. Leistedt, H.V. Peiris, L. Verde
MILLER-BER... 14B AA 562 A123
M.M. Miller Bertolami (MPIG, LAPL)
RIEMER-SOR... 14 PR D89 103505
S. Riemer-Sørensen, D. Parkinson, T.M. Davis
STUDENIKIN 14 EPL 107 21001
A.I. Studenikin (GEMMA Collab.)
BEDA 13 PPNL 10 139
A.G. Beda et al.
VIAUX 13A PRL 111 231301
N. Viaux et al.
MOROSCO 12 JCAP 1207 053
M. Morosco et al.
XIA 12 JCAP 1206 010
J.-Q. Xia et al.
ASEEV 11 PR D84 112003
V.N. Aseev et al.
CECCHINI 11 ASP 34 486
S. Cecchini et al.
SAITO 11 PR D83 043529
S. Saito, M. Takada, A. Taruya
BEDA 10 PPNL 7 406
A.G. Beda et al. (GEMMA Collab.)
DENIZ 10 PR D81 072001
M. Deniz et al. (TEXONO Collab.)
HANNESTAD 10 JCAP 1008 001
S. Hannestad et al.
PAGLIAROLI 10 ASP 33 287
G. Pagliaroli, F. Rossi-Torres, E. Vissani (INFN+)
SEKIGUCHI 10 JCAP 1003 015
T. Sekiguchi et al.
THOMAS 10 PRL 105 013001
F. Thomas, F.B. Abdalla, O. Lahav (LOUC)
ICHIKI 09 PR D79 023520
K. Ichiki, M. Takada, T. Takahashi
KOMATSU 09 APJS 180 330
E. Komatsu et al.
KUZNETSOV 09 IJMP A24 5977
A.V. Kuznetsov, N.V. Mikheev, A.A. Okrugin (YARO)
TERENO 09 AA 500 657
I. Tereno et al.
VIKHLININ 09 APJ 692 1060
A. Vikhlinin et al.
ARPESELLA 08A PRL 101 091302
C. Arpesella et al. (Borexino Collab.)
BERNARDIS 08 PR D78 083535
F. De Bernardis et al.
BEDA 07 PAN 70 1873
A.G. Beda et al.
Translated from YAF 70 1925.
FOGLI 07 PR D75 053001
G.L. Fogli et al.
GINIENKO 07 PR D75 075014
S.N. Ginienko, N.V. Krasnikov, A. Rubbia
KRISTIANSEN 07 PR D75 083510
J. Kristiansen, O. Elgaroy, H. Dahle
MIRIZZI 07 PR D76 053007
A. Mirizzi, D. Montanino, P.D. Serpico (BOSS Collab.)
SPERGEL 07 APJS 170 377
D.N. Spergel et al.
WONG 07 PR D75 012001
H.T. Wong et al. (TEXONO Collab.)
ZUNCKEL 07 JCAP 0708 004
C. Zunckel, P. Ferreira
CIRELLI 06 JCAP 0612 013
M. Cirelli et al.
FUKUGITA 06 PR D74 027302
M. Fukugita et al.
GOOBAR 06 JCAP 0606 019
A. Goobar et al.

Lepton Particle Listings

Neutrino Properties, Number of Neutrino Types

WALKER	90	PR D41 689	T.P. Walker	(HARV)
CHUPP	89	PRL 62 505	E.L. Chupp, W.T. Vestrand, C. Reppin	(UNH, MPIM)
DORENBOS...	89	ZPHY C41 567	J. Dorenbosch <i>et al.</i>	(CHARM Collab.)
GRIFOLS	89B	PR D40 3819	J.A. Grifols, E. Masso	(BARC)
KOLB	89	PRL 62 509	E.W. Kolb, M.S. Turner	(CHIC, FNAL)
LOREDO	89	ANYAS 571 601	T.J. Loredo, D.Q. Lamb	(CHIC)
RAFFELT	89	PR D39 2066	G.G. Raffelt	(PRIN, UCB)
RAFFELT	89B	APJ 336 61	G. Raffelt, D. Dearborn, J. Silk	(UCB, LLL)
ALBRECHT	88B	PL B202 149	H. Albrecht <i>et al.</i>	(ARGUS Collab.)
BARBIERI	88	PRL 61 27	R. Barbieri, R.N. Mohapatra	(PISA, UMD)
BORIS	88	PRL 61 245 (erratum)	S.D. Boris <i>et al.</i>	(ITEP, ASCI)
FUKUGITA	88	PRL 60 879	M. Fukugita <i>et al.</i>	(KYOTU, MPIM, UCB)
GROTCHE	88	ZPHY C39 553	H. Grotche, R.W. Robinett	(PSU)
RAFFELT	88B	PR D37 549	G.G. Raffelt, D.S.P. Dearborn	(UCB, LLL)
SPERGEL	88	PL B200 366	D.N. Spergel, J.N. Bahcall	(IAS)
VONFEILIT...	88	PL B200 580	F. von Feilitzsch, L. Oberauer	(TUM)
BARBIELLINI	87	NAT 329 21	G. Barbierlini, G. Cocconi	(CERN)
BORIS	87	PRL 58 2019	S.D. Boris <i>et al.</i>	(ITEP, ASCI)
Also		PRL 61 245 (erratum)	S.D. Boris <i>et al.</i>	(ITEP, ASCI)
BORIS	87B	JETPL 45 333	S.D. Boris <i>et al.</i>	(ITEP)
		Translated from ZETFP 45 267		
FUKUGITA	87	PR D36 348	M. Fukugita, S. Yazaki	(KYOTU, TOKY)
NUSINOV	87	PR D36 2278	S. Nussinov, Y. Rephaeli	(TELA)
OBERAUER	87	PL B198 113	L.F. Oberauer, F. von Feilitzsch, R.L. Mossbauer	(LNL)
SPRINGER	87	PR A35 679	P.T. Springer <i>et al.</i>	(LNL)
KETOV	86	JETPL 44 146	S.N. Ketov <i>et al.</i>	(KIAE)
		Translated from ZETFP 44 114		
COWSIK	85	PL 151B 62	R. Cowzik	(TATA)
RAFFELT	85	PR D31 3002	G.G. Raffelt	(MPIM)
BINETRUY	84	PL 134B 174	P. Binetruy, G. Girardi, P. Salati	(LAPP)
FREESE	84	NP B233 167	K. Freese, D.N. Schramm	(CHIC, FNAL)
KYULDJIEV	84	NP B243 387	A.V. Kyuldjiev	(SOFI)
SCHRAMM	84	PL 141B 337	D.N. Schramm, G. Steigman	(FNAL, BART)
VOGEL	84	PR D30 1505	P. Vogel	(ETH, SIN)
ANDERHUB	82	PL 114B 76	H.B. Anderhub <i>et al.</i>	(CHIC, UCSB)
OLIVE	82	PR D25 213	K.A. Olive, M.S. Turner	(CHIC, UCSB)
BERNSTEIN	81	PL 101B 39	J. Bernstein, G. Feinberg	(STEVE, COLU)
FRANK	81	PR D24 2001	J.S. Frank <i>et al.</i>	(LASL, YALE, MIT+)
MORGAN	81	PL 102B 247	J.A. Morgan	(SUSS)
FUJIKAWA	80	PRL 45 963	K. Fujikawa, R. Shrock	(STON)
LUBIMOV	80	PL 94B 266	V.A. Lyubimov <i>et al.</i>	(ITEP)
STECKER	80	PRL 45 1460	F.W. Stecker	(NASA)
COWSIK	79	PR D19 2219	R. Cowzik	(TATA)
GOLDMAN	79	PR D19 2215	T. Goldman, G.J. Stephenson	(LASL)
BEG	78	PR D17 1395	M.A.B. Beg, W.J. Marciano, M. Ruderman	(ROCK+)
BLIETSCHAU	78	NP B133 205	J. Blietschau <i>et al.</i>	(Gangamelle Collab.)
FALK	78	PL 79B 511	S.V. Falk, D.N. Schramm	(CHIC)
BARNES	77	PRL 38 1049	V.E. Barnes <i>et al.</i>	(PURD, ANL)
COWSIK	77	PRL 39 784	R. Cowzik	(MPIM, TATA)
LEE	77C	PR D16 1444	B.W. Lee, R.E. Shrock	(STON)
VYSOTSKY	77	JETPL 26 188	M.L. Vysotsky, A.D. Dolgov, Y.B. Zeldovich	(ITEP)
		Translated from ZETFP 26 200		
BELLOTTI	76	LNC 17 953	E. Bellotti <i>et al.</i>	(MILA)
SUTHERLAND	76	PR D13 2700	P. Sutherland <i>et al.</i>	(PENN, COLU, NYU)
SZALAY	76	AA 49 437	A.S. Szalay, G. Marx	(EOTV)
CLARK	74	PR D9 533	A.R. Clark <i>et al.</i>	(LBL)
KIM	74	PR D9 3050	J.E. Kim, V.S. Mathur, S. Okubo	(ROCH)
REINES	74	PRL 32 180	F. Reines, H.W. Sobel, H.S. Gurr	(UCI)
SZALAY	74	APAH 35 8	A.S. Szalay, G. Marx	(EOTV)
COWSIK	72	PRL 29 669	R. Cowzik, J. McClelland	(UCB)
MARK	72	Nu Conf. Budapest	G. Marx, A.S. Szalay	(EOTV)
GERSHTEIN	66	JETPL 4 120	S.S. Gershtein, Y.B. Zeldovich	(KIAM)
		Translated from ZETFP 4 189		
BERNSTEIN	63	PR 132 1227	J. Bernstein, M. Ruderman, G. Feinberg	(NYU+)
COWAN	57	PR 107 528	C.L. Cowan, F. Reines	(LANL)

Number of Neutrino Types

The neutrinos referred to in this section are those of the Standard $SU(2) \times U(1)$ Electroweak Model possibly extended to allow nonzero neutrino masses. Light neutrinos are those with $m < m_Z/2$. The limits are on the number of neutrino mass eigenstates, including ν_1 , ν_2 , and ν_3 .

THE NUMBER OF LIGHT NEUTRINO TYPES FROM COLLIDER EXPERIMENTS

Revised June 2020 by C.-J. Lin (LBNL). Written by D. Karlen (University of Victoria and TRIUMF).

The most precise measurements of the number of light neutrino types, N_ν , come from studies of Z production in e^+e^- collisions. The invisible partial width, Γ_{inv} , is determined by subtracting the measured visible partial widths, corresponding to Z decays into quarks and charged leptons, from the total Z width. The invisible width is assumed to be due to N_ν light neutrino species each contributing the neutrino partial width Γ_ν as given by the Standard Model. In order to reduce the model dependence, the Standard Model value for the ratio of the neutrino to charged leptonic partial widths, $(\Gamma_\nu/\Gamma_\ell)_{\text{SM}} = 1.991 \pm 0.001$, is used instead of $(\Gamma_\nu)_{\text{SM}}$ to determine the number of light neutrino types:

$$N_\nu = \frac{\Gamma_{\text{inv}}}{\Gamma_\ell} \left(\frac{\Gamma_\ell}{\Gamma_\nu} \right)_{\text{SM}}. \quad (1)$$

The combined result from the four LEP experiments is $N_\nu = 2.984 \pm 0.008$ [1]. Recent analyses applied corrections to the LEP result [1] by including the effect of correlated luminosity systematics and also using an improved Bhabha cross section calculation [2,3] to obtain $N_\nu = 2.9963 \pm 0.0074$.

In the past, when only small samples of Z decays had been recorded by the LEP experiments and by the Mark II at SLC, the uncertainty in N_ν was reduced by using Standard Model fits to the measured hadronic cross sections at several center-of-mass energies near the Z resonance. Since this method is much more dependent on the Standard Model, the approach described above is favored.

Before SLC and LEP, limits on the number of neutrino generations were placed by experiments at lower-energy e^+e^- colliders by measuring the cross section of the process $e^+e^- \rightarrow \nu\bar{\nu}\gamma$. The ASP, CELLO, MAC, MARK J, and VENUS experiments observed a total of 3.9 events above background [4], leading to a 95% CL limit of $N_\nu < 4.8$. This process has a much larger cross section at center-of-mass energies near the Z mass and has been measured at LEP by the ALEPH, DELPHI, L3, and OPAL experiments [5]. These experiments have observed several thousand such events, and the combined result is $N_\nu = 3.00 \pm 0.08$. The same process has also been measured by the LEP experiments at much higher center-of-mass energies, between 130 and 208 GeV, in searches for new physics [6]. Combined with the lower energy data, the result is $N_\nu = 2.92 \pm 0.05$.

Experiments at $p\bar{p}$ colliders also placed limits on N_ν by determining the total Z width from the observed ratio of $W^\pm \rightarrow \ell^\pm \nu$ to $Z \rightarrow \ell^+ \ell^-$ events [7]. This involved a calculation that assumed Standard Model values for the total W width and the ratio of W and Z leptonic partial widths, and used an estimate of the ratio of Z to W production cross sections. Now that the Z width is very precisely known from the LEP experiments, the approach is now one of those used to determine the W width.

References

1. ALEPH, DELPHI, L3, OPAL, and SLD Collaborations, and LEP Electroweak Working Group, and SLD Electroweak Group, and SLD Heavy Flavour Group, Phys. Reports **427**, 257 (2006).
2. P. Janot and S. Jadach, Phys. Lett. **B803**, 135319 (2020).
3. G. Voutsinas *et al.*, Phys. Lett. **B800**, 135068 (2020).
4. VENUS: K. Abe *et al.*, Phys. Lett. **B232**, 431 (1989); ASP: C. Hearty *et al.*, Phys. Rev. **D39**, 3207 (1989); CELLO: H.J. Behrend *et al.*, Phys. Lett. **B215**, 186 (1988); MAC: W.T. Ford *et al.*, Phys. Rev. **D33**, 3472 (1986); MARK J: H. Wu, Ph.D. Thesis, Univ. Hamburg (1986).
5. L3: M. Acciarri *et al.*, Phys. Lett. **B431**, 199 (1998); DELPHI: P. Abreu *et al.*, Z. Phys. **C74**, 577 (1997); OPAL: R. Akers *et al.*, Z. Phys. **C65**, 47 (1995); ALEPH: D. Buskulic *et al.*, Phys. Lett. **B313**, 520 (1993).
6. DELPHI: J. Abdallah *et al.*, Eur. Phys. J. **C38**, 395 (2005); L3: P. Achard *et al.*, Phys. Lett. **B587**, 16 (2004); ALEPH: A. Heister *et al.*, Eur. Phys. J. **C28**, 1 (2003); OPAL: G. Abbiendi *et al.*, Eur. Phys. J. **C18**, 253 (2000).

See key on page 1127

Lepton Particle Listings

Number of Neutrino Types

7. UA1: C. Albajar *et al.*, Phys. Lett. **B198**, 271 (1987);
 UA2: R. Ansari *et al.*, Phys. Lett. **B186**, 440 (1987).

Number from e^+e^- Colliders

Number of Light ν Types

VALUE	DOCUMENT ID	TECN
2.9963±0.0074	1 JANOT 20	
2.9918±0.0081	2 VOUTSINAS 20	
2.9840±0.0082	3 LEP-SLC 06	RVUE
3.00 ±0.05	4 LEP 92	RVUE

• • • We do not use the following data for averages, fits, limits, etc. • • •

- JANOT 20 applies a correction to LEP-SLC 06 using an updated Bhabha cross section calculation. This result also includes a correction to account for correlated luminosity bias as presented in VOUTSINAS 20.
- VOUTSINAS 20 applies a correction to LEP-SLC 06 to account for correlated luminosity bias.
- Combined fit from ALEPH, DELPHI, L3 and OPAL Experiments.
- Simultaneous fits to all measured cross section data from all four LEP experiments.

Number of Light ν Types from Direct Measurement of Invisible Z Width

In the following, the invisible Z width is obtained from studies of single-photon events from the reaction $e^+e^- \rightarrow \nu\bar{\nu}\gamma$. All are obtained from LEP runs in the $E_{\text{CM}}^{\text{e}} = 88\text{--}209$ GeV.

VALUE	DOCUMENT ID	TECN	COMMENT
2.92±0.05 OUR AVERAGE	Error includes scale factor of 1.2.		
2.84±0.10±0.14	ABDALLAH 05B	DLPH	$\sqrt{s} = 180\text{--}209$ GeV
2.98±0.05±0.04	ACHARD 04E	L3	1990-2000 LEP runs
2.86±0.09	HEISTER 03C	ALEP	$\sqrt{s} = 189\text{--}209$ GeV
2.69±0.13±0.11	ABBIENDI,G 00D	OPAL	1998 LEP run
2.89±0.32±0.19	ABREU 97J	DLPH	1993-1994 LEP runs
3.23±0.16±0.10	AKERS 95C	OPAL	1990-1992 LEP runs
2.68±0.20±0.20	BUSKULIC 93L	ALEP	1990-1991 LEP runs
• • • We do not use the following data for averages, fits, limits, etc. • • •			
2.84±0.15±0.14	ABREU 00Z	DLPH	1997-1998 LEP runs
3.01±0.08	ACCIARRI 99R	L3	1991-1998 LEP runs
3.1 ±0.6 ±0.1	ADAM 96C	DLPH	$\sqrt{s} = 130, 136$ GeV

Limits from Astrophysics and Cosmology

Effective Number of Light ν Types

"Light" means here with a mass $<$ about 1 MeV. The quoted values correspond to N_{eff} , where $N_{\text{eff}} = 3.045$ in the Standard Model with $N_{\nu} = 3$. See also reviews on "Big-Bang Nucleosynthesis" and "Neutrinos in Cosmology."

VALUE	CL%	DOCUMENT ID	TECN	COMMENT
• • • We do not use the following data for averages, fits, limits, etc. • • •				
2.99±0.17	68	1 AGHANIM 20	COSM	
2.84±0.15	68	2 FIELDS 20	COSM	BBN
2.88±0.17	68	3 IVANOV 20	COSM	Planck and BOSS
2.3-3.2	95	4 VERDE 17	COSM	
2.88±0.16	68	5 CYBURT 16	COSM	BBN
2.88±0.20	95	6 ROSSI 15	COSM	
3.3 ±0.5	95	7 ADE 14	COSM	Planck
3.78 ^{+0.31} _{-0.30}		8 COSTANZI 14	COSM	
3.29±0.31		9 HOU 14	COSM	
$<$ 3.80	95	10 LEISTEDT 14	COSM	
$<$ 4.10	95	11 MORESCO 12	COSM	
$<$ 5.79	95	12 XIA 12	COSM	
$<$ 4.08	95	MANGANO 11	COSM	BBN
0.9-8.2		13 ICHIKAWA 07	COSM	
3-7	95	14 CIRELLI 06	COSM	
2.7-4.6	95	15 HANNESTAD 06	COSM	
3.6-7.4	95	14 SELJAK 06	COSM	
$<$ 4.4		16 CYBURT 05	COSM	
$<$ 3.3		17 BARGER 03C	COSM	
1.4-6.8		18 CROTTY 03	COSM	
1.9-6.6		18 PIERPAOLI 03	COSM	
2-4		LISI 99	COSM	BBN
$<$ 4.3		OLIVE 99	COSM	BBN
$<$ 4.9		COPI 97		Cosmology
$<$ 3.6		HATA 97B		High D/H quasar abs.
$<$ 4.0		OLIVE 97		BBN; high ^4He and ^7Li
$<$ 4.7		CARDALL 96B		COSM High D/H quasar abs.
$<$ 3.9		FIELDS 96		COSM BBN; high ^4He and ^7Li
$<$ 4.5		KERNAN 96		COSM High D/H quasar abs.
$<$ 3.6		OLIVE 95		BBN; ≥ 3 massless ν
$<$ 3.3		WALKER 91		Cosmology
$<$ 3.4		OLIVE 90		Cosmology
$<$ 4		YANG 84		Cosmology

$<$ 4	YANG 79	Cosmology
$<$ 7	STEIGMAN 77	Cosmology
	PEEBLES 71	Cosmology
$<$ 16	19 SHVARTSMAN69	Cosmology
	HOYLE 64	Cosmology

- AGHANIM 20 best fit on number of neutrino types is based on Planck data combined with lensing and baryon acoustic oscillations (BAO). Without BAO, they find $2.89^{+0.18}_{-0.19}$. Several other values are quoted using different combinations of data.
- FIELDS 20 combines Planck 2018 CMB data with BBN and observations of deuterium and Helium-4.
- IVANOV 20 combines 2018 Planck CMB data with baryon acoustic oscillation data from BOSS. This study is based on a full-shape likelihood for the redshift-space galaxy power spectrum of the BOSS data.
- Uses Planck Data combined with an independent standard measure of distance to the sound horizon to set a limit on the total number of neutrinos. Only CMB and early-time information are used.
- CYBURT 16 combines Planck 2015 CMB data with BBN and observations of deuterium and Helium-4.
- ROSSI 15 sets limits on the number of neutrino types using BOSS Lyman alpha forest data combined with Planck CMB data and baryon acoustic oscillations.
- Fit to the number of neutrino degrees of freedom from Planck CMB data along with WMAP polarization, high L, and BAO data.
- Fit to the number of neutrinos degrees of freedom from Planck CMB data along with BAO, shear and cluster data.
- Fit based on the SPT-SZ survey combined with CMB, BAO, and H_0 data.
- Constrains the number of neutrino degrees of freedom (marginalizing over the total mass) from CMB, CMB lensing, BAO, and galaxy clustering data.
- Limit on the number of light neutrino types from observational Hubble parameter data with seven-year WMAP data, SPT, and the most recent estimate of H_0 . Best fit is 3.45 ± 0.65 .
- Limit on the number of light neutrino types from the CFHTLS combined with seven-year WMAP data and a prior on the Hubble parameter. Best fit is $4.17^{+1.62}_{-1.26}$. Limit is relaxed to $3.98^{+2.02}_{-1.20}$ when small scales affected by non-linearities are removed.
- Constrains the number of neutrino types from recent CMB and large scale structure data. No priors on other cosmological parameters are used.
- Constrains the number of neutrino types from recent CMB, large scale structure, Lyman-alpha forest, and SNIa data. The slight preference for $N_{\nu} > 3$ comes mostly from the Lyman-alpha forest data.
- Constrains the number of neutrino types from recent CMB and large scale structure data. See also HAMANN 07.
- Limit on the number of neutrino types based on ^4He and D/H abundance assuming a baryon density fixed to the WMAP data. Limit relaxes to 4.6 if D/H is not used or to 5.8 if only D/H and the CMB are used. See also CYBURT 01 and CYBURT 03.
- Limit on the number of neutrino types based on combination of WMAP data and big-bang nucleosynthesis. The limit from WMAP data alone is 8.3. See also KNELLER 01. $N_{\nu} \geq 3$ is assumed to compute the limit.
- 95% confidence level range on the number of neutrino flavors from WMAP data combined with other CMB measurements, the 2dFGRS data, and HST data.
- SHVARTSMAN 69 limit inferred from his equations.

Number Coupling with Less Than Full Weak Strength

VALUE	DOCUMENT ID	TECN
• • • We do not use the following data for averages, fits, limits, etc. • • •		
$<$ 20	1 OLIVE 81C	COSM
$<$ 20	1 STEIGMAN 79	COSM

1 Limit varies with strength of coupling. See also WALKER 91.

REFERENCES FOR Limits on Number of Neutrino Types

AGHANIM 20	AA 641 A 6	N. Aghanim <i>et al.</i>	(Planck Collab.)
FIELDS 20	JCAP 2003 010	B. Fields <i>et al.</i>	(ILL, MINN)
Also	JCAP 2011 E02 (errat.)	B. Fields <i>et al.</i>	(ILL, MINN)
IVANOV 20	PR D101 083504	M.M. Ivanov, M. Simonovic, M. Zaldarriaga	(NYU,+)
JANOT 20	PL B803 135319	P. Janot, S. Jadach	(CERN, CRAC)
VOUTSINAS 20	PL B800 135068	G. Voutsinas <i>et al.</i>	(CERN, BOHR)
VERDE 17	JCAP 1704 023	L. Verde <i>et al.</i>	
CYBURT 16	RMP 88 015004	R.H. Cyburt <i>et al.</i>	(MSU, ILL, MINN)
ROSSI 15	PR D92 063505	G. Rossi <i>et al.</i>	
ADE 14	AA 571 A16	P.A.R. Ade <i>et al.</i>	(CERN, CRAC)
COSTANZI 14	JCAP 1410 081	M. Costanzi <i>et al.</i>	(TRST, TRST1)
HOU 14	APJ 782 74	Z. Hou <i>et al.</i>	
LEISTEDT 14	PRL 113 041301	B. Leistedt, H.V. Peiris, L. Verde	
MORESCO 12	JCAP 1207 053	M. Moresco <i>et al.</i>	
XIA 12	JCAP 1206 010	J.-Q. Xia <i>et al.</i>	
MANGANO 11	PL B701 296	G. Mangano, P. Serpico	
HAMANN 07	JCAP 0708 021	J. Hamann <i>et al.</i>	
ICHIKAWA 07	JCAP 0705 007	K. Ichikawa, M. Kawasaki, F. Takahashi	
CIRELLI 06	JCAP 0612 013	M. Cirelli <i>et al.</i>	
HANNESTAD 06	JCAP 0611 016	S. Hannestad, G. Raffelt	
LEP-SLC 06	PRP 427 257	ALEPH, DELPHI, L3, OPAL, SLD and working groups	
SELJAK 06	JCAP 0610 014	U. Seljak, A. Slosar, P. McDonald	(Planck Collab.)
ABDALLAH 05B	EPJ C38 395	J. Abdallah <i>et al.</i>	(DELPHI Collab.)
CYBURT 05	ASP 23 313	R.H. Cyburt <i>et al.</i>	
ACHARD 04E	PL B587 16	P. Achard <i>et al.</i>	(L3 Collab.)
BARGER 03C	PL B566 8	V. Barger <i>et al.</i>	
CROTTY 03	PR D67 123005	P. Crotty, J. Lesgourgues, S. Pastor	
CYBURT 03	PL B567 227	R.H. Cyburt, B.D. Fields, K.A. Olive	
HEISTER 03C	EPJ C28 1	A. Heister <i>et al.</i>	(ALEPH Collab.)
PIERPAOLI 03	MNRAS 342 L63	E. Pierpaoli	
CYBURT 01	ASP 17 87	R.H. Cyburt, B.D. Fields, K.A. Olive	
KNELLER 01	PR D64 123506	J.P. Kneller <i>et al.</i>	
ABBIENDI,G 00D	EPJ C18 253	G. Abbiendi <i>et al.</i>	(OPAL Collab.)

Lepton Particle Listings

Number of Neutrino Types, Double- β Decay

ABREU	00Z	EPJ C17 53	P. Abreu <i>et al.</i>	(DELPHI Collab.)
ACCIARRI	99R	PL B470 268	M. Acciarri <i>et al.</i>	(L3 Collab.)
LISI	99	PR D59 123520	E. Lisi, S. Sarkar, F.L. Villante	
OLIVE	99	ASP 11 403	K.A. Olive, D. Thomas	
ABREU	97J	ZPHY C74 577	P. Abreu <i>et al.</i>	(DELPHI Collab.)
COPI	97	PR D55 3389	C.J. Copi, D.N. Schramm, M.S. Turner	(CHIC)
HATA	97B	PR D55 540	N. Hata <i>et al.</i>	(OSU, PENN)
OLIVE	97	ASP 7 27	K.A. Olive, D. Thomas	(MINN, FLOR)
ADAM	95C	PL B350 471	W. Adam <i>et al.</i>	(DELPHI Collab.)
CARDALL	96B	APJ 472 435	C.Y. Cardall, G.M. Fuller	(UCSD)
FIELDS	96	New Ast 1 77	B.D. Fields <i>et al.</i>	(NDAM, CERN, MINN+)
KERNAN	96	PR D54 3681	P.S. Kerman, S. Sarkar	(CASE, OXFTP)
AKERS	95C	ZPHY C65 47	R. Akers <i>et al.</i>	(OPAL Collab.)
OLIVE	95	PL B354 357	K.A. Olive, G. Steigman	(MINN, OSU)
BUSKULIC	93L	PL B313 520	D. Buskulic <i>et al.</i>	(ALEPH Collab.)
LEP	92	PL B276 247	LEP Collabs.	(LEP, ALEPH, DELPHI, L3, OPAL)
WALKER	91	APJ 376 51	T.P. Walker <i>et al.</i>	(HSCA, OSU, CHIC+)
OLIVE	90	PL B236 454	K.A. Olive <i>et al.</i>	(MINN, CHIC, OSU+)
YANG	84	APJ 281 493	J. Yang <i>et al.</i>	(CHIC, BART)
OLIVE	81C	NP B180 497	K.A. Olive, D.N. Schramm, G. Steigman	(EFL+)
STEIGMAN	79	PRL 43 239	G. Steigman, K.A. Olive, D.N. Schramm	(BART+)
YANG	79	APJ 227 697	J. Yang <i>et al.</i>	(CHIC, YALE, UVA)
STEIGMAN	77	PL 66B 202	G. Steigman, D.N. Schramm, J.E. Gunn	(YALE, CHIC+)
PEEBLES	71	Physical Cosmology	P.Z. Peebles	(PRIN)
		Princeton Univ. Press (1971)		
SHVARTSMAN	69	JETPL 9 184	V.F. Shvartsman	(MOSU)
		Translated from ZETFP 9 315.		
HOYLE	64	NAT 203 1108	F. Hoyle, R.J. Taylor	(CAMB)

Double- β Decay

OMITTED FROM SUMMARY TABLE

NEUTRINOLESS DOUBLE- β DECAY

Revised August 2019 by A. Piepke (University of Alabama) and P. Vogel (Caltech) .

Observation of neutrinoless double-beta ($0\nu\beta\beta$) decay would signal violation of total lepton number conservation. The process can be mediated by an exchange of a light Majorana neutrino, or by an exchange of other particles. However, the existence of $0\nu\beta\beta$ -decay requires a nonvanishing Majorana neutrino mass, no matter what the actual mechanism is. As long as only a limit on the lifetime is available, limits on the effective Majorana neutrino mass, on the lepton-number violating right-handed current or other possible mechanisms mediating $0\nu\beta\beta$ decay can be obtained, independently of the actual mechanism, by assuming that one of these “new physics” possibilities dominates. These limits are listed in the Double- β Decay Listings of the experimental measurements.

In the following we assume that the exchange of light Majorana neutrinos ($m_{\nu_i} \leq 10$ MeV) contributes dominantly to the decay rate. Besides a dependence on the phase space ($G^{0\nu}$) and the nuclear matrix element ($M^{0\nu}$), the observable $0\nu\beta\beta$ -decay rate is proportional then to the square of the effective Majorana mass m_{ee} , $(T_{1/2}^{0\nu})^{-1} = G^{0\nu} \cdot |M^{0\nu}|^2 \cdot m_{ee}^2$, with $m_{ee}^2 = |\sum_i U_{ei}^2 m_{\nu_i}|^2$. The sum contains, in general, complex CP-phases in U_{ei}^2 , i.e., cancellations may occur. For three neutrino flavors there are two physical phases for Majorana neutrinos (η_1, η_2) and one for Dirac neutrinos (δ_{CP}). The relevant Majorana phases affect only processes to which lepton-number changing amplitudes contribute. Given the general 3×3 mixing matrix for Majorana neutrinos, one can construct other analogous lepton number violating quantities, $m_{\ell\ell'} = \sum_i U_{ei} U_{\ell i} m_{\nu_i} (\ell \text{ or } \ell' \neq e)$. However, these are currently much less constrained than m_{ee} .

Nuclear structure calculations are needed to deduce m_{ee} from the decay rate. While $G^{0\nu}$ can be calculated accurately,

the computation of $M^{0\nu}$ is subject to uncertainty. Comparing different nuclear model evaluations indicates a factor ~ 2 -3 spread in the calculated nuclear matrix elements. Nuclear structure calculation consistently overestimate Gamow-Teller (axial current) matrix elements. This inability of the nuclear models to reproduce Gamow-Teller decay rates is often parametrized in form of a modified coupling constant g_A . Many nuclear theorists interpret this shortcoming as evidence that important physics is missing in the modeling of weak nuclear transitions. It is not clear how these observed uncertainties impact $0\nu\beta\beta$ -matrix elements. Nevertheless, this constitutes an additional element of uncertainty. Recent work, [1] shows how the discrepancy between experimental and theoretical axial current matrix elements might be resolved. However, application of this approach to the $0\nu\beta\beta$ decay remains to be accomplished. The particle physics quantities to be determined are thus nuclear model-dependent, so the half-life measurements are listed first. Where possible, we reference the nuclear matrix elements used in the subsequent analysis. Since rates for the conventional $2\nu\beta\beta$ decay serve to constrain the nuclear theory models, results for this process are also given.

Oscillation experiments utilizing atmospheric, accelerator, solar, and reactor produced neutrinos and anti-neutrinos show that at least some neutrinos are massive. However, so far the inverted mass ordering (i.e., whether $\Delta m_{31}^2 < 0$) is disfavored only by 2-3 σ compared to the normal mass ordering (when $\Delta m_{31}^2 > 0$), while the absolute neutrino mass values or the properties of neutrinos under CPT-conjugation (Dirac or Majorana) remain undetermined. All confirmed oscillation experiments can be consistently described using three interacting neutrino species with two mass splittings and three mixing angles. (For values of the mixing angles and mass square differences see the corresponding tables.)

Based on the 3-neutrino analysis:
 $m_{ee}^2 = |\cos^2 \theta_{13} \cos^2 \theta_{12} m_1 + e^{2i(\eta_2 - \eta_1)} \cos^2 \theta_{13} \sin^2 \theta_{12} m_2 + e^{-2i(\eta_1 + \delta_{CP})} \sin^2 \theta_{13} m_3|^2$, valid for both mass orderings. Given the present knowledge of the neutrino oscillation parameters one can derive a relation between the effective Majorana mass and the mass of the lightest neutrino, as illustrated in Figure 14.11 in the Neutrino Masses, Mixing and Oscillations review. The three mass orderings allowed by the oscillation data: normal ($m_1 < m_2 \ll m_3$), inverted ($m_3 \ll m_1 < m_2$), and degenerate ($m_1 \approx m_2 \approx m_3$), result in different projections. The width of the colored bands reflects the uncertainty introduced by the unknown Majorana and Dirac phases as well as the experimental errors of the oscillation parameters. The latter causes only minor broadening of the bands. Because of the overlap of the different mass scenarios, a measurement of m_{ee} would not reveal which mass ordering is applicable, provided the value of m_{ee} is in the overlapping range.

Analogous plots depict the relation of m_{ee} with the summed neutrino mass $m_{tot} = m_1 + m_2 + m_3$, constrained by observational cosmology, and m_{ee} as a function of the average mass

See key on page 1127

Lepton Particle Listings

Double- β Decay

$m_{\nu_e}^{eff} = [\sum |U_{ei}|^2 m_{\nu_i}^2]^{1/2}$ determined through the analysis of the electron energy distribution in low energy beta decays. (See Fig. 1 of [2].) The oscillation data thus allow to test whether observed values of m_{ee} and m_{tot} or $m_{\nu_e}^{eff}$ are consistent within the 3 neutrino framework. The rather large intrinsic width of the $\beta\beta$ -decay constraints essentially does not allow to positively identify the mass ordering, and thus the sign of Δm_{31}^2 , even in combination with these other observables. Naturally, if a value of $0 < m_{ee} \leq 0.01$ eV is ever established, then the normal mass ordering becomes the only possible scenario.

It should be noted that systematic uncertainties of the nuclear matrix elements and possible quenching of the axial current matrix elements are sometimes not folded into the mass limits reported by $\beta\beta$ -decay experiments. Taking this additional uncertainty into account would further widen the projections. The plots are based on a 3-neutrino analysis. If it turns out that additional, i.e. sterile light neutrinos exist, the allowed regions would be modified substantially.

If neutrinoless double-beta decay is observed, it will be possible to fix a range of absolute values of the masses m_{ν_i} . Unlike the direct neutrino mass measurements, however, a limit on m_{ee} does not allow one to constrain the individual mass values m_{ν_i} , even when the mass differences Δm_{ij}^2 are known.

Neutrino oscillation data imply the existence of a lower limit ~ 0.014 eV for the Majorana neutrino mass for the inverted mass ordering pattern, while m_{ee} could, by fine tuning, vanish in the case of the normal mass ordering. Several new double-beta searches have been proposed to probe the interesting m_{ee} mass range, with the prospect of full coverage of the inverted mass ordering region within the next decade.

The $0\nu\beta\beta$ decay mechanism discussed so far is not the only way in which the decay can occur. Numerous other possible scenarios have been proposed, however, all of them requiring new physics. It will be a challenging task to decide which mechanism was responsible once $0\nu\beta\beta$ decay is observed. LHC experiments may reveal corresponding signatures for new physics of lepton number violation. If lepton-number violating right-handed weak current interactions exist, its strength can be characterized by the phenomenological coupling constants η and λ (η describes the coupling between the right-handed lepton current and left-handed quark current while λ describes the coupling when both currents are right-handed). The $0\nu\beta\beta$ decay rate then depends on $\langle\eta\rangle = \eta \sum_i U_{ei} V_{ei}$ and $\langle\lambda\rangle = \lambda \sum_i U_{ei} V_{ei}$ that vanish for massless or unmixed neutrinos ($V_{\ell j}$ is a matrix analogous to $U_{\ell j}$ but describing the mixing with the hypothetical right-handed neutrinos). The observation of the single electron spectra could, in principle, allow to distinguish this mechanism of $0\nu\beta\beta$ from the light Majorana neutrino exchange driven mode. The limits on $\langle\eta\rangle$ and $\langle\lambda\rangle$ are listed in a separate table. The reader is cautioned that a number of earlier experiments did not distinguish between η and λ . In addition, see the section on Majoron searches for additional limits set by these experiments.

References

1. P. Gysbers *et al.*, Nature Phys. **15**, 5 (2019); [arXiv:1903.00047].
2. M.J. Dolinski, A.W.P. Poon and W. Rodejohann, Ann. Rev. Nucl. Part. Sci. **49**, 219 (2019); [arXiv:1902.04097].

Half-life 0ν double- β decay

In most cases the transitions $(Z,A) \rightarrow (Z+2,A) + 2e^-$ to the 0^+ ground state of the final nucleus are listed. We also list transitions that decrease the nuclear charge ($2e^+$, e^+ CC and double EC) and transitions to an excited state of the final nucleus (0^+_{\neq} , 2^+ , and 2^+_{\neq}). In the following Listings only the best or comparable limits for the half-lives of each transition are reported and only those with about $T_{1/2} > 10^{23}$ years that are relevant for particle physics.

$t_{1/2}(10^{23}$ yr)	CL%	ISOTOPE	TRANSITION	METHOD	DOCUMENT ID
• • • We do not use the following data for averages, fits, limits, etc. • • •					
> 59	90	^{130}Te	$g.s. \rightarrow 0^+_1$	CUORE	¹ ADAMS 21A
> 15	90	^{100}Mo		CUPID-Mo	² ARMENGAUD 21
> 39.9	90	^{76}Ge	$g.s. \rightarrow 0^+_1$	MAJORANA-Dem	³ ARNQUIST 21
> 21.2	90	^{76}Ge	$g.s. \rightarrow 2^+_1$	MAJORANA-Dem	⁴ ARNQUIST 21
> 9.7	90	^{76}Ge	$g.s. \rightarrow 2^+_2$	MAJORANA-Dem	⁵ ARNQUIST 21
> 320	90	^{130}Te		CUORE	⁶ ADAMS 20A
>1800	90	^{76}Ge		GERDA	⁷ AGOSTINI 20B
> 900	90	^{76}Ge		GERDA	⁸ AGOSTINI 19
> 14	90	^{130}Te	$g.s. \rightarrow 0^+_1$	CUORE-0	⁹ ALDUINO 19
> 0.95	90	^{100}Mo		AMORE	¹⁰ ALENKOV 19
> 270	90	^{76}Ge		MAJORANA	¹¹ ALVIS 19
> 350	90	^{136}Xe		EXO-200	¹² ANTON 19
> 35	90	^{82}Se		CUPID-0	¹³ AZZOLINI 19
> 2.4	90	^{136}Xe		PANDAX-II	¹⁴ NI 19
> 190	90	^{76}Ge		MAJORANA	¹⁵ AALSETH 18
> 800	90	^{76}Ge		GERDA	¹⁶ AGOSTINI 18
> 180	90	^{136}Xe		EXO-200	¹⁷ ALBERT 18
> 150	90	^{130}Te		CUORE	¹⁸ ALDUINO 18
> 2.5	90	^{82}Se		NEMO-3	¹⁹ ARNOLD 18
> 24	90	^{82}Se		CUPID-0	²⁰ AZZOLINI 18
> 0.81	90	^{82}Se	$g.s. \rightarrow 0^+_1$	CUPID-0	²¹ AZZOLINI 18A
> 2.2	90	^{116}Cd		AURORA	²² BARABASH 18
> 530	90	^{76}Ge		GERDA	²³ AGOSTINI 17
> 1.1	90	^{134}Xe		EXO-200	²⁴ ALBERT 17C
> 1	90	^{116}Cd		NEMO-3	²⁵ ARNOLD 17
> 40	90	^{130}Te		CUORE(CINO)	²⁶ ALDUINO 16
> 260	90	^{136}Xe	$g.s. \rightarrow 2^+_1$	KamLAND-Zen	²⁷ ASAKURA 16
> 260	90	^{136}Xe	$g.s. \rightarrow 2^+_2$	KamLAND-Zen	²⁸ ASAKURA 16
> 240	90	^{136}Xe	$g.s. \rightarrow 0^+_1$	KamLAND-Zen	²⁹ ASAKURA 16
>1070	90	^{136}Xe		KamLAND-Zen	³⁰ GANDO 16
> 11	90	^{100}Mo		NEMO-3	³¹ ARNOLD 15
> 110	90	^{136}Xe		EXO-200	³² ALBERT 14B
> 9.4	90	^{130}Te	$g.s. \rightarrow 0^+_1$	CUORICINO	³³ ANDREOTTI 12
> 3.6	90	^{82}Se		NEMO-3	³⁴ BARABASH 11A
> 30	90	^{130}Te		CUORICINO	³⁵ ARNABOLDI 08
> 0.58	90	^{48}Ca		CaF ₂ scint.	³⁶ UMEHARA 08
> 0.89	90	^{100}Mo	$g.s. \rightarrow 0^+_1$	NEMO-3	³⁷ ARNOLD 07
> 1.6	90	^{100}Mo	$g.s. \rightarrow 2^+_1$	NEMO-3	³⁸ ARNOLD 07
> 1	90	^{82}Se		NEMO-3	³⁹ ARNOLD 05A
> 1.1	90	^{128}Te		Cryog. det.	⁴⁰ ARNABOLDI 03
> 1.7	90	^{116}Cd		$^{116}\text{CdWO}_4$ scint.	⁴¹ DANEVICH 03
> 157	90	^{76}Ge		Enriched HPGe	⁴² AALSETH 02B
> 190	90	^{76}Ge		Enriched HPGe	⁴³ KLAPDOR-K... 01

¹ADAMS 21A et al. used 101.76 kg yr of ^{130}Te exposure of the CUORE (LNGS) bolometric detector to place a limit on the decay to the first excited state of ^{130}Xe , superseding ALDUINO 19 as the most restrictive bound on this particular decay.

²ARMENGAUD 21 use the CUPID-Mo 4.2 kg array of enriched $\text{Li}_2^{100}\text{MoO}_4$ scintillating bolometers, with 1.17 kg-yr exposure, to set this limit.

³ARNQUIST 21 use the MAJORANA demonstrator to set this limit for the $0\nu\beta\beta$ decay to the first excited 0^+ state, with a 41.9 kg yr isotopic exposure. The median sensitivity is 39.9×10^{23} yr.

⁴ARNQUIST 21 use the MAJORANA demonstrator to set this limit for the $0\nu\beta\beta$ decay to the first excited 2^+ state, with a 41.9 kg yr isotopic exposure. The median sensitivity is 21.2×10^{23} yr.

⁵ARNQUIST 21 use the MAJORANA demonstrator to set this limit for the $0\nu\beta\beta$ decay to the second excited 2^+ state, with a 41.9 kg yr isotopic exposure. The median sensitivity is 18.6×10^{23} yr.

Lepton Particle Listings

Double- β Decay

- 6 ADAMS 20A use the CUORE detector to search for the $0\nu\beta\beta$ decay of ^{130}Te . The exposure was 372.5 kg-yr of TeO_2 corresponding to 103.6 kg-yr of ^{130}Te . The exclusion sensitivity is 1.7×10^{25} yr. Supersedes ALDUINO 18.
- 7 AGOSTINI 20b present the final data set of the GERDA experiment, searching for $0\nu\beta\beta$ decay of ^{76}Ge with isotopically enriched, high resolution Ge detectors. A final exposure of 127.2 kg-yr is reported. The experiment reports the lowest background and longest half life limit ever achieved by any double beta decay experiment. The reported experiment sensitivity equals the limit. Supersedes AGOSTINI 19.
- 8 AGOSTINI 19 use 82.4 kg-yr of data, collected by the GERDA experiment, to search for the $0\nu\beta\beta$ decay of ^{76}Ge . High resolution Ge-calorimeters, made from isotopically enriched Ge, are used. A median sensitivity of 1.1×10^{26} yr is reported. Supersedes AGOSTINI 18.
- 9 ALDUINO 19 use the combined data of the CUORICINO and CUORE-0 experiments to place a lower limit on the half life of the $0\nu\beta\beta$ decay of ^{130}Te to the first excited 0^+ state of ^{130}Xe . Supersedes ANDREOTTI 12.
- 10 ALENKOV 19 report the $0\nu\beta\beta$ decay half-life limit based on the 52.1 kg-d exposure of ^{100}Mo , of a cryogenic dual heat and light detector in the Yangyang underground laboratory. The median sensitivity is 1.1×10^{23} years.
- 11 ALVIS 19 use the MAJORANA Demonstrator with enriched in ^{76}Ge detectors to set this limit on $0\nu\beta\beta$ half-life of ^{76}Ge . The exposure is 26.0 kg yr. The sensitivity is 4.8×10^{25} yr.
- 12 ANTON 19 uses the complete dataset of the EXO-200 detector to search for the $0\nu\beta\beta$ decay. The exposure is 234.1 kg yr. The median sensitivity is 5.0×10^{25} yr. Supersedes ALBERT 18 and ALBERT 14b.
- 13 AZZOLINI 19 use the CPID-0 scintillating cryogenic bolometer to set this limit on $0\nu\beta\beta$ half-life of ^{82}Se . The exposure is 5.29 kg yr. The sensitivity is 5×10^{24} yr.
- 14 NI 19 use the PandaX-II dual phase TPC at CJPL to search for the $0\nu\beta\beta$ decay of ^{136}Xe . The half-life limit 2.4×10^{23} yr is obtained from 22.2 kg yr exposure with a sensitivity of 1.9×10^{23} yr.
- 15 AALSETH 18 uses the MAJORANA Demonstrator to search for the $0\nu\beta\beta$ decay. The exposure is 9.95 kg-year. The median sensitivity is 2.1×10^{25} yr.
- 16 AGOSTINI 18 uses the GERDA detector to search for the $0\nu\beta\beta$ decay. The exposure is 46.7 kg-year. The median sensitivity is 5.8×10^{25} yr. Supersedes AGOSTINI 17.
- 17 ALBERT 18 uses the EXO-200 detector to search for the $0\nu\beta\beta$ decay. The exposure is 177.6 kg-year. The median sensitivity is 3.7×10^{25} years.
- 18 ALDUINO 18 uses the CUORE detector to search for the $0\nu\beta\beta$ decay of ^{130}Te . The exposure is 86.3 kg-year of natural TeO_2 corresponding to 24.0 kg-year for ^{130}Te . The median sensitivity is 0.7×10^{25} yr. The limit is obtained combining the new data from CUORE with those of CUORE0 (9.8 kg-year of ^{130}Te) and Cuoricino (19.8 kg-year of ^{130}Te).
- 19 ARNOLD 18 use the NEMO-3 tracking detector to place a limit on the $0\nu\beta\beta$ decay of ^{82}Se . This is a slightly weaker limit than in BARABASH 11A, using the same detector. Supersedes ARNOLD 05A.
- 20 AZZOLINI 18 uses CUPID-0 detector, a novel scintillating cryogenic calorimeter, operated in the LNGS. This results replaces BARABASH 11A (NEMO-3) as the most stringent limit on the $0\nu\beta\beta$ -decay of ^{82}Se .
- 21 AZZOLINI 18A data collected by CUPID-0 based on scintillating bolometers is used to derive a new most stringent limit on the $0\nu\beta\beta$ -decay of ^{82}Se to the 0_1^+ state of ^{82}Kr .
- 22 BARABASH 18 use 1.162 kg of $^{116}\text{CdWO}_4$ scintillating crystals to obtain this limit. Supersedes DANEVICH 03 with analogous source and is more sensitive than ARNOLD 17.
- 23 AGOSTINI 17 result corresponds to data collected with GERDA phase 1 and first release of phase 2 for a total of 343 mol-yr exposure. Supersedes AGOSTINI 13A. The median sensitivity is 4.0×10^{25} yr.
- 24 ALBERT 17c uses the EXO-200 detector that contains $19.098 \pm 0.014\%$ admixture of ^{134}Xe to search for the 0ν and $2\nu\beta\beta$ decay modes. The exposure is 29.6 kg-year. The median sensitivity is 1.9×10^{21} years.
- 25 ARNOLD 17 use the NEMO-3 tracking calorimeter, containing 410 g of enriched ^{116}Cd exposed for 5.26 yr, to determine the half-life limit. Supersedes BARABASH 11A.
- 26 ALDUINO 16 report result obtained with 9.8 kg y of data collected with the CUORE-0 bolometer, combined with data from the CUORICINO. Supersedes ALFONSO 15.
- 27 ASAKURA 16 use the KamLAND-Zen liquid scintillator calorimeter (^{136}Xe 89.5 kg yr) to place a limit on the $0\nu\beta\beta$ -decay into the first excited state of the daughter nuclide.
- 28 ASAKURA 16 use the KamLAND-Zen liquid scintillator calorimeter (^{136}Xe 89.5 kg yr) to place a limit on the $0\nu\beta\beta$ -decay into the second excited state of the daughter nuclide.
- 29 ASAKURA 16 use the KamLAND-Zen liquid scintillator calorimeter (^{136}Xe 89.5 kg yr) to place a limit on the $0\nu\beta\beta$ -decay into the third excited state of the daughter nuclide.
- 30 GANDO 16 use the the KamLAND detector to search for the 0ν decay of ^{136}Xe . With a significant background reduction, the combination of results of the first (270.7 days) and the second phase (263.8 days) of the experiment leads to about six fold improvement over the previous limit. Supersedes GANDO 13A. The sensitivity is 5.6×10^{25} yr.
- 31 ARNOLD 15 use the NEMO-3 tracking calorimeter with 34.3 kg yr exposure to determine the limit of $0\nu\beta\beta$ -half life of ^{100}Mo . Supersedes ARNOLD 2005A and BARABASH 11A.
- 32 ALBERT 14b use 100 kg yr of exposure of the EXO-200 tracking calorimeter to place a lower limit on the $0\nu\beta\beta$ -half life of ^{136}Xe . Supersedes AUGER 12.
- 33 ANDREOTTI 12 use high resolution TeO_2 bolometric calorimeter to search for the $0\nu\beta\beta$ decay of ^{130}Te leading to the excited 0_1^+ state at 1793.5 keV.
- 34 BARABASH 11A use the NEMO-3 detector to measure $2\nu\beta\beta$ rates and place limits on $0\nu\beta\beta$ half lives for various nuclides. Supersedes ARNOLD 05A, ARNOLD 04, ARNOLD 98, and ELLIOTT 92.

- 35 Supersedes ARNOLDI 04. Bolometric TeO_2 detector array CUORICINO is used for high resolution search for $0\nu\beta\beta$ decay. The half-life limit is derived from 3.09 kg yr ^{130}Te exposure.
- 36 UMEHARA 08 use CaF_2 scintillation calorimeter to search for double beta decay of ^{48}Ca . Limit is significantly more stringent than quoted sensitivity: 18×10^{21} years.
- 37 Limit on 0ν -decay to the first excited 0_1^+ -state of daughter nucleus using NEMO-3 tracking calorimeter. Supersedes DASSIE 95.
- 38 Limit on 0ν -decay to the first excited 2^+ -state of daughter nucleus using NEMO-3 tracking calorimeter.
- 39 NEMO-3 tracking calorimeter is used in ARNOLD 05A to place limit on $0\nu\beta\beta$ half-life of ^{82}Se . Detector contains 0.93 kg of enriched ^{82}Se . Supersedes ARNOLD 04.
- 40 Supersedes ALESSANDRELLO 00. Array of TeO_2 crystals in high resolution cryogenic calorimeter. Some enriched in ^{128}Te . Ground state to ground state decay.
- 41 Limit on $0\nu\beta\beta$ decay of ^{116}Cd using enriched CdWO_4 scintillators. Supersedes DANEVICH 00.
- 42 AALSETH 02b limit is based on 117 mol-yr of data using enriched Ge detectors. Background reduction by means of pulse shape analysis is applied to part of the data set. Reported limit is slightly less restrictive than that in KLAPDOR-KLEINGROTHAUS 01 However, it excludes part of the allowed half-life range reported in KLAPDOR-KLEINGROTHAUS 01b for the same nuclide. The analysis has been criticized in KLAPDOR-KLEINGROTHAUS 04b. The criticism was addressed and disputed in AALSETH 04.
- 43 KLAPDOR-KLEINGROTHAUS 01 is a continuation of the work published in BAUDIS 99. Isotopically enriched Ge detectors are used in calorimetric measurement. The most stringent bound is derived from the data set in which pulse-shape analysis has been used to reduce background. Exposure time is 35.5 kg y. Supersedes BAUDIS 99 as most stringent result.

Half-life measurements of the two-neutrino double- β decay

The measured half-life values for the transitions $(Z,A) \rightarrow (Z+2,A) + 2e^- + 2\bar{\nu}_e$ to the 0^+ ground state of the final nucleus are listed. We also list the transitions to an excited state of the final nucleus (0_i^+ , etc.). We report only the measurements with the smallest (or comparable) uncertainty for each transition.

$t_{1/2}(10^{21} \text{ yr})$	ISOTOPE	TRANSITION	METHOD	DOCUMENT ID
0.771 \pm 0.008 \pm 0.012 -0.006 -0.015	^{130}Te		CUORE	1 ADAMS 21
0.00712 \pm 0.00018 0.00014 \pm 0.00010	^{100}Mo		CUPID-Mo	2 ARMENGAUD 20
18 \pm 5 \pm 1	^{124}Xe	$2\nu\text{DEC}$	XENON1T	3 APRILE 19E
0.00680 \pm 0.00001 \pm 0.00038 -0.00040	^{100}Mo		NEMO-3	4 ARNOLD 19
0.0860 \pm 0.0003 \pm 0.0019 -0.0013	^{82}Se		CUPID-0	5 AZZOLINI 19B
0.0939 \pm 0.0017 \pm 0.0058	^{82}Se		NEMO-3	6 ARNOLD 18
0.0263 \pm 0.0011 -0.0012	^{116}Cd		AURORA	7 BARABASH 18
> 0.87	^{134}Xe		EXO-200	8 ALBERT 17C
0.82 \pm 0.02 \pm 0.06	^{130}Te		CUORE-0	9 ALDUINO 17
0.00690 \pm 0.00015 \pm 0.00037	^{100}Mo		CUPID	10 ARMENGAUD 17
0.0274 \pm 0.0004 \pm 0.0018	^{116}Cd		NEMO-3	11 ARNOLD 17
0.064 \pm 0.007 \pm 0.012 -0.006 -0.009	^{48}Ca		NEMO-3	12 ARNOLD 16
0.00934 \pm 0.00022 \pm 0.00062 -0.00060	^{150}Nd		NEMO-3	13 ARNOLD 16A
1.926 \pm 0.094	^{76}Ge		GERDA	14 AGOSTINI 15A
0.00693 \pm 0.00004	^{100}Mo		NEMO-3	15 ARNOLD 15
2.165 \pm 0.016 \pm 0.059	^{136}Xe		EXO-200	16 ALBERT 14
9.2 \pm 5.5 \pm 1.3 -2.6	^{78}Kr		BAKSAN	17 GAVRILYAK 13
2.38 \pm 0.02 \pm 0.14	^{136}Xe		KamLAND-Zen	18 GANDO 12A
0.7 \pm 0.09 \pm 0.11	^{130}Te		NEMO-3	19 ARNOLD 11
0.0235 \pm 0.0014 \pm 0.0016	^{96}Zr		NEMO-3	20 ARGYRADES 10
0.69 \pm 0.10 -0.08 \pm 0.07	^{100}Mo	$0^+ \rightarrow 0_1^+$	Ge coinc.	21 BELLI 10
0.57 \pm 0.13 -0.09 \pm 0.08	^{100}Mo	$0^+ \rightarrow 0_1^+$	NEMO-3	22 ARNOLD 07
0.096 \pm 0.003 \pm 0.010	^{82}Se		NEMO-3	23 ARNOLD 05A
0.029 \pm 0.004 -0.003	^{116}Cd		CdWO_4 scint.	24 DANEVICH 03

- 1 ADAMS 21 use 102.7 kg yr of ^{130}Te exposure, collected by the CUORE bolometric detector at LNGS, to perform the most precise measurement of $2\nu\beta\beta$ decay of this nuclide to date. The dataset is more than 10-times that used by the CUORE-0 experiment. Supersedes ALDUINO 17.
- 2 ARMENGAUD 20 use the $\text{Li}_2^{100}\text{MoO}_4$ scintillating bolometers to determine the half-life of the $2\nu\beta\beta$ decay of ^{100}Mo . The total exposure was 42.235 kg-d. The single-state dominance for this decay is favored at $> 3\sigma$.
- 3 APRILE 19E report first measurement of two-neutrino double electron capture in ^{124}Xe using the XENON1T detector with a 0.73 t-yr exposure. An excess of 126 ± 29 events is observed at 64.3 ± 0.6 keV decay energy, corresponding to $\sqrt{\Delta\chi^2} = 4.4$ with respect to the background-only hypothesis.
- 4 ARNOLD 19 use the NEMO-3 tracking calorimeter with 34.3 kg y exposure to determine the $2\nu\beta\beta$ half-life of ^{100}Mo . Supersedes ARNOLD 15.

See key on page 1127

Lepton Particle Listings

Double-β Decay

- ⁵ AZZOLINI 19B use the CUPID-0 experiment, utilizing ZnSe bolometers and an exposure of 9.95 kg-yr of Zn⁸²Se, to determine the half-life of the 2νββ decay of ⁸²Se. The analysis provides evidence for single state dominance showing that the higher state dominance is disfavored at the level of 5.5 σ.
- ⁶ ARNOLD 18 use the NEMO-3 tracking detector to determine the 2νββ half-life of ⁸²Se. 0.93 kg of ⁸²Se was observed for 5.25 y. The half-life value was obtained based on the single-state-dominance (SSD) hypothesis, preferred in this case by about 2 σ. Supersedes ARNOLD 05A.
- ⁷ BARABASH 18 use 1.162 kg of ¹¹⁶CdWO₄ scintillating crystals to obtain this value. Supersedes DANEVICH 03 with analogous source and agrees with ARNOLD 17 with the NEMO-3 detector.
- ⁸ ALBERT 17C uses the EXO-200 detector that contains 19.098 ± 0.014% admixture of ¹³⁴Xe to search for the 2νββ decay mode. The exposure is 29.6 kg-year. The median sensitivity is 1.2 × 10²¹ years.
- ⁹ ALDUINO 17 use the CUORE-0 detector containing 10.8 kg of ¹³⁰Te in 52 crystals of TeO₂. The exposure was 9.3 kg yr of ¹³⁰Te. This is a more accurate rate determination than in ARNOLD 11 and BARABASH 11A.
- ¹⁰ ARMENGAUD 17 use 185.9 ± 0.1 g crystal of Li₂¹⁰⁰MoO₄ to determine the ¹⁰⁰Mo 2νββ half-life. The exposure was of 1303 ± 26 hours only, using novel technique.
- ¹¹ ARNOLD 17 use the NEMO-3 tracking calorimeter, containing 410 grams of enriched ¹¹⁶Cd exposed for 5.26 years, to determine the half-life value.
- ¹² ARNOLD 16 use the NEMO-3 detector and a source of 6.99 g of ⁴⁸Ca. The half-life is based on 36.7 g year exposure. It is consistent, although somewhat longer, than the previous determinations of the half-life. Supersedes BARABASH 11A.
- ¹³ ARNOLD 16A use the NEMO-3 tracking calorimeter, containing 36.6 g of ¹⁵⁰Nd exposed for 1918.5 days, to determine the half-life. Supersedes ARGYRIADES 09.
- ¹⁴ AGOSTINI 15A use 17.9 kg yr exposure of the GERDA calorimeter to derive an improved measurement of the 2νββ decay half life of ⁷⁶Ge.
- ¹⁵ ARNOLD 15 use the NEMO-3 tracking calorimeter with 34.3 kg yr exposure to determine the 2νββ-half life of ¹⁰⁰Mo. Supersedes ARNOLD 05A and ARNOLD 04.
- ¹⁶ ALBERT 14 use the EXO-200 tracking detector for a re-measurement of the 2νββ-half life of ¹³⁶Xe. A nuclear matrix element of 0.0218 ± 0.0003 MeV⁻¹ is derived from this data. Supersedes ACKERMAN 11.
- ¹⁷ GAVRILYAK 13 use a proportional counter filled with Kr gas to search for the 2ν2K decay of ⁷⁸Kr. Data with the enriched and depleted Kr were used to determine signal and background. A 2.5σ excess of events obtained with the enriched sample is interpreted as an indication for the presence of this decay.
- ¹⁸ GANDO 12A use a modification of the existing KamLAND detector. The ββ decay source/detector is 13 tons of enriched ¹³⁶Xe-loaded scintillator contained in an inner balloon. The 2νββ decay rate is derived from the fit to the spectrum between 0.5 and 4.8 MeV. This result is in agreement with ACKERMAN 11.
- ¹⁹ ARNOLD 11 use enriched ¹³⁰Te in the NEMO-3 detector to measure the 2νββ decay rate. This result is in agreement with, but more accurate than ARNABOLDI 03.
- ²⁰ ARGYRIADES 10 use 9.4 ± 0.2 g of ⁹⁶Zr in NEMO-3 detector and identify its 2νββ decay. The result is in agreement and supersedes ARNOLD 99.
- ²¹ BELLI 10 use enriched ¹⁰⁰Mo with 4 HP Ge detectors to record the 590.8 and 539.5 keV γ rays from the decay of the 0₁⁺ state in ¹⁰⁰Ru both in singles and coincidences. This result confirms the measurement of KIDD 09 and ARNOLD 07 and supersedes them.
- ²² First exclusive measurement of 2ν-decay to the first excited 0₁⁺-state of daughter nucleus. ARNOLD 07 use the NEMO-3 tracking calorimeter to detect all particles emitted in decay. Result agrees with the inclusive (0ν + 2ν) measurement of DEBRAECKELEER 01.
- ²³ ARNOLD 05A use the NEMO-3 tracking detector to determine the 2νββ half-life of ⁸²Se with high statistics and low background (389 days of data taking). Supersedes ARNOLD 04.
- ²⁴ DANEVICH 03 is calorimetric measurement of 2νββ ground state decay of ¹¹⁶Cd using enriched CdWO₄ scintillators. Agrees with EJIRI 95 and ARNOLD 96. Supersedes DANEVICH 00.

$\langle m_{ee} \rangle$. The Effective Weighted Sum of Majorana Neutrino Masses Contributing to Neutrinoless Double-β Decay

$\langle m_{ee} \rangle = |\sum U_{ei}^2 m_{\nu_i}|$, $i = 1, 2, 3$. It is assumed that ν_i are Majorana particles and that the transition is dominated by the known (light) neutrinos. Note that U_{ei}^2 and not $|U_{ei}|^2$ occur in the sum, and that consequently cancellations are possible. The experiments obtain the limits on $\langle m_{\nu} \rangle$ from the measured ones on $T_{1/2}$ using a range of nuclear matrix elements (NME), which is reflected in the spread of $\langle m_{\nu} \rangle$. Different experiments may choose different NME. All assume $g_A = 1.27$. In the following Listings, only the best or comparable limits for each isotope are reported. When not mentioned explicitly the transition is between ground states, but transitions between excited states are also reported.

VALUE (eV)	ISOTOPE	METHOD	DOCUMENT ID
< 0.31–0.54	¹⁰⁰ Mo	CUPID-Mo	1 ARMENGAUD 21
< 0.075–0.35	¹³⁰ Te	CUORE	2 ADAMS 20A
< 0.079–0.180	⁷⁶ Ge	GERDA	3 AGOSTINI 20B
< 0.07–0.16	⁷⁶ Ge	GERDA	4 AGOSTINI 19
< 1.2–2.1	¹⁰⁰ Mo	AMORE	5 ALENKOV 19
< 0.200–0.433	⁷⁶ Ge	MAJORANA	6 ALVIS 19
< 0.093–0.286	¹³⁶ Xe	EXO-200	7 ANTON 19
< 0.311–0.638	⁸² Se	CUPID-0	8 AZZOLINI 19
< 1.3–3.5	¹³⁶ Xe	PANDAX-II	9 NI 19

• • • We do not use the following data for averages, fits, limits, etc. • • •

< 0.24–0.52	⁷⁶ Ge	MAJORANA Dem	10 AALSETH 18
< 0.12–0.26	⁷⁶ Ge	GERDA	11 AGOSTINI 18
< 0.15–0.40	¹³⁶ Xe	EXO-200	12 ALBERT 18
< 0.11–0.52	¹³⁰ Te	CUORE	13 ALDUINO 18
< 1.2–3.0	⁸² Se	NEMO-3	14 ARNOLD 18
< 0.376–0.770	⁸² Se	CUPID-0	15 AZZOLINI 18
< 1.0–1.7	¹¹⁶ Cd	AURORA	16 BARABASH 18
< 0.15–0.33	⁷⁶ Ge	GERDA	17 AGOSTINI 17
< 1.4–2.5	¹¹⁶ Cd	NEMO-3	18 ARNOLD 17
< 0.27–0.76	¹³⁰ Te	CUORE(CINO)	19 ALDUINO 16
< 1.6–5.3	¹⁵⁰ Nd	NEMO-3	20 ARNOLD 16A
< 0.061–0.165	¹³⁶ Xe	KamLAND-Zen	21 GANDO 16
< 0.33–0.62	¹⁰⁰ Mo	NEMO-3	22 ARNOLD 15
< 0.19–0.45	¹³⁶ Xe	EXO-200	23 ALBERT 14B
< 0.89–2.43	⁸² Se	NEMO-3	24 BARABASH 11A
< 7.2–19.5	⁹⁶ Zr	NEMO-3	25 ARGYRIADES 10
< 3.5–22	⁴⁸ Ca	CaF ₂ scint.	26 UMEHARA 08
< 0.2–1.1	¹³⁰ Te	Cryog. det.	27 ARNABOLDI 05
< 0.37–1.9	¹³⁰ Te	Cryog. det.	28 ARNABOLDI 04
< 1.5–1.7	¹¹⁶ Cd	¹¹⁶ CdWO ₄ scint.	29 DANEVICH 03
< 0.350	⁷⁶ Ge	Enriched HPGe	30 KLAPDOR-K. 01
< 8.3	⁴⁸ Ca	CaF ₂ scint.	YOU 91

- ¹ ARMENGAUD 21 use the CUPID-Mo demonstrator, with 1.17 kg-yr exposure of ¹⁰⁰Mo, to set this limit. The range reflects the estimated uncertainty of the calculated nuclear matrix elements.
- ² ADAMS 20A use the data of CUORE (372.5 kg-yr exposure of TeO₂) to obtain this limit.
- ³ AGOSTINI 20B use the final data set of the GERDA experiment, representing an exposure of 127.2 kg-yr to derive an upper limit for $\langle m_{\beta\beta} \rangle$. Isotopically enriched Ge detectors were used. The range reflects the variability of the theoretically calculated nuclear matrix elements. Supersedes AGOSTINI 19.
- ⁴ AGOSTINI 19 use 82.4 kg-yr of data collected by the isotopically enriched ⁷⁶Ge detectors of the GERDA experiment to derive an upper limit for $\langle m_{\beta\beta} \rangle$. The range reflects the variability of the theoretically calculated nuclear matrix elements. Supersedes AGOSTINI 18.
- ⁵ ALENKOV 19 report the range of the effective masses $\langle m_{\beta\beta} \rangle$ corresponding to the 0νββ decay half-life limit. It is based on the 52.1 kg-d exposure of ¹⁰⁰Mo, in the Yangyang underground laboratory. The median sensitivity is 1.1 × 10²³ years. The range of $\langle m_{\beta\beta} \rangle$ reflects the uncertainty of nuclear matrix elements.
- ⁶ ALVIS 19 use the MAJORANA Demonstrator with enriched ⁷⁶Ge detectors to set this limit. The exposure is 26.0 kg yr. The sensitivity is 4.8 × 10²⁵ yr.
- ⁷ ANTON 19 uses the complete dataset of the EXO-200 experiment to obtain these limits. The spread reflect the uncertainty in the nuclear matrix elements. Supersedes ALBERT 18 and ALBERT 14B.
- ⁸ AZZOLINI 19 use the CPID-0 scintillating cryogenic bolometer to set this limit. The exposure is 5.29 kg yr. The sensitivity is 5 × 10²⁴ yr.
- ⁹ NI 19 use the PandaX-II dual phase TPC at CJPL to search for the 0νββ decay of ¹³⁶Xe with 22.2 kg yr exposure. The range in the $m_{\beta\beta}$ limit of 1.3–3.5 eV reflects the range of the calculated nuclear matrix elements. The sensitivity is 1.9 × 10²³ yr.
- ¹⁰ AALSETH 18 uses the MAJORANA Demonstrator detector to establish this limit.
- ¹¹ AGOSTINI 18 uses the GERDA detector to establish this limit.
- ¹² ALBERT 18 uses the EXO-200 experiment to obtain this limit.
- ¹³ ALDUINO 18 use the combined data of CUORE, CUORE0, and Cuoricino to obtain this limit.
- ¹⁴ ARNOLD 18 use the NEMO-3 tracking detector to constrain the 0νββ decay of ⁸²Se. The limit on $\langle m_{\beta\beta} \rangle$ is obtained assuming light neutrino exchange; the range reflects different calculations of the nuclear matrix elements. This is a somewhat weaker limit than in BARABASH 11A using the same detector.
- ¹⁵ AZZOLINI 18 uses data collected by the CUPID-0 scintillating cryogenic calorimeter, operated in the LNGS, to derive a range of limits on $\langle m_{\nu} \rangle$. The reported range reflects the spread of the nuclear matrix element calculations considered in this work. Use $g_A = 1.269$.
- ¹⁶ BARABASH 18 use 1.162 kg of ¹¹⁶CdWO₄ scintillating crystals to obtain these limits. The spread reflects the estimated uncertainty in the nuclear matrix element. Supersedes DANEVICH 03.
- ¹⁷ AGOSTINI 17 is based on 343 mol yr of data from GERDA phase 1 and phase 2 first part and the corresponding limit on $T_{1/2}$ using the different nuclear matrix elements mentioned by the authors. Supersedes AGOSTINI 13A.
- ¹⁸ ARNOLD 17 utilize NEMO-3 data, taken with enriched ¹¹⁶Cd to limit the effective Majorana neutrino mass. The reported range results from the use of different nuclear matrix elements. Supersedes BARABASH 11A.
- ¹⁹ ALDUINO 16 place a limit on the effective Majorana neutrino mass using the combined data of the CUORE-0 and CUORICINO experiments. The range reflects the authors' evaluation of the variability of the nuclear matrix elements. Supersedes ALFONSO 15.
- ²⁰ ARNOLD 16A limit is derived from data taken with the NEMO-3 detector and ¹⁵⁰Nd. A range of nuclear matrix elements that include the effect of nuclear deformation have been used. Supersedes ARGYRIADES 09.
- ²¹ GANDO 16 result is based on the 2016 KamLAND-Zen half-life limit. The stated range reflects different nuclear matrix elements, an unquenched $g_A = 1.27$ is used. Supersedes GANDO 13A.
- ²² ARNOLD 15 use the NEMO-3 tracking calorimeter with 34.3 kg yr exposure to determine the neutrino mass limit based on the 0νββ-half life of ¹⁰⁰Mo. The spread range reflects different nuclear matrix elements. Supersedes ARNOLD 14 and BARABASH 11A.
- ²³ ALBERT 14B is based on 100 kg yr of exposure of the EXO-200 tracking calorimeter. The mass range reflects the nuclear matrix element calculations. Supersedes AUGER 12.

Lepton Particle Listings

Double- β Decay, Neutrino Mixing

- ²⁴ BARABASH 11A limit is based on NEMO-3 data for ⁸²Se. The reported range reflects different nuclear matrix elements. Supersedes ARNOLD 05A and ARNOLD 04.
- ²⁵ ARGYRIADES 10 use ⁹⁶Zr and the NEMO-3 tracking detector to obtain the reported mass limit. The range reflects the fluctuation of the nuclear matrix elements considered.
- ²⁶ Limit was obtained using CaF₂ scintillation calorimeter to search for double beta decay of ⁴⁸Ca. Reported range of limits reflects spread of QRPA and SM matrix element calculations used. Supersedes OGAWA 04.
- ²⁷ Supersedes ARNABOLDI 04. Reported range of limits due to use of different nuclear matrix element calculations.
- ²⁸ Supersedes ARNABOLDI 03. Reported range of limits due to use of different nuclear matrix element calculations.
- ²⁹ Limit for $\langle m_{\nu} \rangle$ is based on the nuclear matrix elements of STAUDT 90 and ARNOLD 96. Supersedes DANEVICH 00.
- ³⁰ KLAPDOR-KLEINGROTHAUS 01 uses the calculation by STAUDT 90. Using several other models in the literature could worsen the limit up to 1.2eV. This is the most stringent experimental bound on m_{ν} . It supersedes BAUDIS 99B.

Limits on Lepton-Number Violating (V+A) Current Admixture

For reasons given in the discussion at the beginning of this section, we list only results from 1989 and later. $\langle \lambda \rangle = \lambda \sum U_{ej} V_{ej}$ and $\langle \eta \rangle = \eta \sum U_{ej} V_{ej}$, where the sum is over the number of neutrino generations. This sum vanishes for massless or unmixed neutrinos. In the following Listings, only best or comparable limits or lifetimes for each isotope are reported.

$\langle \lambda \rangle$ (10^{-6})	CL%	$\langle \eta \rangle$ (10^{-8})	CL%	ISOTOPE	METHOD	DOCUMENT ID
< 2.2-2.6	90	< 1.7-2.1	90	⁸² Se	NEMO-3	1 ARNOLD 18
< 1.8-22	90	< 1.6-21	90	¹¹⁶ Cd	AURORA	2 BARABASH 18
< 0.9-1.3	90	< 0.5-0.8	90	¹⁰⁰ Mo	NEMO-3	3 ARNOLD 14
<120	90			¹⁰⁰ Mo	0 ⁺ → 2 ⁺	4 ARNOLD 07
0.692 ± 0.058 -0.056	68	0.305 ± 0.026 -0.025	68	⁷⁶ Ge	Enriched HPGe	5 KLAPDOR-K...06A
< 2.5	90			¹⁰⁰ Mo	0 ν , NEMO-3	6 ARNOLD 05A
< 3.8	90			⁸² Se	0 ν , NEMO-3	7 ARNOLD 05A
< 1.5-2.0	90			¹⁰⁰ Mo	0 ν , NEMO-3	8 ARNOLD 04
< 3.2-3.8	90			⁸² Se	0 ν , NEMO-3	9 ARNOLD 04
< 1.6-2.4	90	< 0.9-5.3	90	¹³⁰ Te	Cryog. det.	10 ARNABOLDI 03
< 2.2	90	<2.5	90	¹¹⁶ Cd	¹¹⁶ CdWO ₄ scint.	11 DANEVICH 03
< 3.2-4.7	90	< 2.4-2.7	90	¹⁰⁰ Mo	ELEGANT V	12 EJIRI 01
< 1.1	90	<0.64	90	⁷⁶ Ge	Enriched HPGe	13 GUENTHER 97
< 4.4	90	<2.3	90	¹³⁶ Xe	TPC	14 VUILLEUMIER 93
		<5.3		¹²⁸ Te	Geochem	15 BERNATOW... 92

- ¹ ARNOLD 18 use the NEMO03 tracking detector, with 0.93 kg of ⁸²Se mass and 5.25 y exposure to obtain the limits for the hypothetical right-handed currents. Supersedes ARNOLD 05A.
- ² BARABASH 18 use 1.162 kg of ¹¹⁶CdWO₄ scintillating crystals to obtain this limits for the hypothetical right-handed currents in the 0 $\nu\beta\beta$ decay of ¹¹⁶Cd.
- ³ ARNOLD 14 is based on 34.7 kg yr of exposure of the NEMO-3 tracking calorimeter. The reported range limit on $\langle \lambda \rangle$ and $\langle \eta \rangle$ reflects the nuclear matrix element uncertainty in ¹⁰⁰Mo.
- ⁴ ARNOLD 07 use NEMO-3 half life limit for 0 ν -decay of ¹⁰⁰Mo to the first excited 2⁺-state of daughter nucleus to limit the right-right handed admixture of weak currents $\langle \lambda \rangle$. This limit is not competitive when compared to the decay to the ground state.
- ⁵ Re-analysis of data originally published in KLAPDOR-KLEINGROTHAUS 04A. Modified pulse shape analysis leads the authors to claim 6 σ statistical evidence for observation of 0 ν -decay. Authors use matrix element of MUTO 89 to determine $\langle \lambda \rangle$ and $\langle \eta \rangle$. Uncertainty of nuclear matrix element is not reflected in stated errors.
- ⁶ ARNOLD 05A derive limit for $\langle \lambda \rangle$ based on ¹⁰⁰Mo data collected with NEMO-3 detector. No limit for $\langle \eta \rangle$ is given. Supersedes ARNOLD 04.
- ⁷ ARNOLD 05A derive limit for $\langle \lambda \rangle$ based on ⁸²Se data collected with NEMO-3 detector. No limit for $\langle \eta \rangle$ is given. Supersedes ARNOLD 04.
- ⁸ ARNOLD 04 use the matrix elements of SUHONEN 94 to obtain a limit for $\langle \lambda \rangle$, no limit for $\langle \eta \rangle$ is given. This limit is more stringent than the limit in EJIRI 01 for the same nucleus.
- ⁹ ARNOLD 04 use the matrix elements of TOMODA 91 and SUHONEN 91 to obtain a limit for $\langle \lambda \rangle$, no limit for $\langle \eta \rangle$ is given.
- ¹⁰ Supersedes ALESSANDRELLO 00. Cryogenic calorimeter search. Reported a range reflecting uncertainty in nuclear matrix element calculations.
- ¹¹ Limits for $\langle \lambda \rangle$ and $\langle \eta \rangle$ are based on nuclear matrix elements of STAUDT 90. Supersedes DANEVICH 00.
- ¹² The range of the reported $\langle \lambda \rangle$ and $\langle \eta \rangle$ values reflects the spread of the nuclear matrix elements. On axis value assuming $\langle m_{\nu} \rangle = 0$ and $\langle \lambda \rangle = \langle \eta \rangle = 0$, respectively.
- ¹³ GUENTHER 97 limits use the matrix elements of STAUDT 90. Supersedes BALYSH 95 and BALYSH 92.
- ¹⁴ VUILLEUMIER 93 uses the matrix elements of MUTO 89. Based on a half-life limit 2.6×10^{23} y at 90%CL.
- ¹⁵ BERNATOWICZ 92 takes the measured geochemical decay width as a limit on the 0 ν width, and uses the SUHONEN 91 coefficients to obtain the least restrictive limit on η . Further details of the experiment are given in BERNATOWICZ 93.

Double- β Decay REFERENCES

ADAMS 21	PRL 126 171801	D.Q. Adams <i>et al.</i>	(CUORE Collab.)
ADAMS 21A	EPJ C81 567	D.Q. Adams <i>et al.</i>	(CUORE Collab.)
ARMENGAUD 21	PRL 126 181802	E. Armengaud <i>et al.</i>	(CUPIID-Mo Collab.)
ARNQUIST 21	PR C103 015501	I.J. Arnuquist <i>et al.</i>	(MAJORANA Collab.)
ADAMS 20A	PRL 124 122501	D.Q. Adams <i>et al.</i>	(CUORE Collab.)
AGOSTINI 20B	PRL 125 252502	M. Agostini <i>et al.</i>	(GERDA Collab.)
ARMENGAUD 20	EPJ C80 674	E. Armengaud <i>et al.</i>	(CUPIID-Mo Collab.)
AGOSTINI 19	SCI 365 1445	M. Agostini <i>et al.</i>	(GERDA Collab.)
ALDUINO 19	EPJ C79 795	C. Alduino <i>et al.</i>	(CUORE Collab.)
ALENKOV 19	EPJ C79 791	V. Alenkov <i>et al.</i>	(AMORE Collab.)
ALVIS 19	PR C100 025501	S.I. Alvis <i>et al.</i>	(MAJORANA Collab.)
ANTON 19	PRL 123 161802	G. Anton <i>et al.</i>	(EXO-200 Collab.)
APRILE 19E	NAT 568 532	E. Aprile <i>et al.</i>	(XENON1T Collab.)
ARNOLD 19	EPJ C79 440	R. Arnold <i>et al.</i>	(NEMO-3 Collab.)
AZZOLINI 19	PRL 123 032501	O. Azzolini <i>et al.</i>	(CUPIID-0 Collab.)
AZZOLINI 19B	PRL 123 262501	O. Azzolini <i>et al.</i>	(CUPIID-0 Collab.)
NI 19	CP C43 113001	K. Ni <i>et al.</i>	(Pandax-II Collab.)
AALSETH 18	PRL 120 132502	C.E. Aalseth <i>et al.</i>	(MAJORANA Collab.)
AGOSTINI 18	PRL 120 132503	M. Agostini <i>et al.</i>	(GERDA Collab.)
ALBERT 18	PRL 120 072701	J.B. Albert <i>et al.</i>	(EXO-200 Collab.)
ALDUINO 18	PRL 120 132501	C. Alduino <i>et al.</i>	(CUORE Collab.)
ARNOLD 18	EPJ C78 821	R. Arnold <i>et al.</i>	(NEMO-3 Collab.)
AZZOLINI 18	PRL 120 232502	O. Azzolini <i>et al.</i>	(CUPIID-0 Collab.)
AZZOLINI 18A	EPJ C78 888	O. Azzolini <i>et al.</i>	(CUPIID-0 Collab.)
BARABASH 18	PR D98 092007	A.S. Barabash <i>et al.</i>	(AURORA Collab.)
AGOSTINI 17	NAT 544 47	M. Agostini <i>et al.</i>	(GERDA Collab.)
ALBERT 17C	PR D96 092001	J.B. Albert <i>et al.</i>	(EXO-200 Collab.)
ALDUINO 17	EPJ C77 13	C. Alduino <i>et al.</i>	(CUORE Collab.)
ARMENGAUD 17	EPJ C77 785	E. Armengaud <i>et al.</i>	(CUPIID Collab.)
ARNOLD 17	PR D95 012007	R. Arnold <i>et al.</i>	(NEMO-3 Collab.)
ALDUINO 16	PR C93 045503	C. Alduino <i>et al.</i>	(CUORE Collab.)
ARNOLD 16	PR D93 112008	R. Arnold <i>et al.</i>	(NEMO-3 Collab.)
ARNOLD 16A	PR D94 072003	R. Arnold <i>et al.</i>	(NEMO-3 Collab.)
ASAKURA 16	NP A946 371	K. Asakura <i>et al.</i>	(KamLAND-Zen Collab.)
GANDO 16	PRL 117 082503	A. Gando <i>et al.</i>	(KamLAND-Zen Collab.)
AGOSTINI 15A	EPJ C75 416	M. Agostini <i>et al.</i>	(GERDA Collab.)
ALFONSO 15	PRL 115 102502	K. Alfonso <i>et al.</i>	(CUORE Collab.)
ARNOLD 15	PR D92 072011	R. Arnold <i>et al.</i>	(NEMO-3 Collab.)
ALBERT 14	PR C89 015502	J. Albert <i>et al.</i>	(EXO-200 Collab.)
ALBERT 14B	NAT 510 229	J.B. Albert <i>et al.</i>	(EXO-200 Collab.)
ARNOLD 14	PR D89 111101	R. Arnold <i>et al.</i>	(NEMO-3 Collab.)
AGOSTINI 13A	PRL 111 122503	M. Agostini <i>et al.</i>	(GERDA Collab.)
GANDO 13A	PRL 110 062502	A. Gando <i>et al.</i>	(KamLAND-Zen Collab.)
GAVRILYAK 13	PR C87 035011	Yu.M. Gavriluk <i>et al.</i>	(NEMO-3 Collab.)
ANDREOTTI 12	PR C85 045503	E. Andreotti <i>et al.</i>	(CUORICINO Collab.)
AUGER 12	PRL 109 032505	M. Auger <i>et al.</i>	(EXO-200 Collab.)
GANDO 12A	PR C85 045504	A. Gando <i>et al.</i>	(KamLAND-Zen Collab.)
ACKERMAN 11	PRL 107 121501	N. Ackerman <i>et al.</i>	(EXO Collab.)
ARNOLD 11	PRL 107 062504	R. Arnold <i>et al.</i>	(NEMO-3 Collab.)
BARABASH 11A	PAN 74 312	A.S. Barabash <i>et al.</i>	(NEMO-3 Collab.)
Translated from YAF 74 330.			
ARGYRIADES 10	NP A847 168	J. Argyriades <i>et al.</i>	(NEMO-3 Collab.)
BELLI 10	NP A846 143	P. Belli <i>et al.</i>	(DAMA-1NR Collab.)
ARGYRIADES 09	PR C80 032501	J. Argyriades <i>et al.</i>	(NEMO-3 Collab.)
KIDD 09	NP A821 251	M. Kidd <i>et al.</i>	(CUORICINO Collab.)
ARNABOLDI 08	PR C78 035502	C. Arnaboldi <i>et al.</i>	(CUORICINO Collab.)
UMEHARA 08	PR C78 035501	S. Uehara <i>et al.</i>	(NEMO-3 Collab.)
ARNOLD 07	NP A781 209	R. Arnold <i>et al.</i>	(NEMO-3 Collab.)
KLAPDOR-K...06A	MPL A21 1547	H.V. Klapdor-Kleingrothaus, I.V. Krivosheina	(CUORICINO Collab.)
ARNABOLDI 05A	PRL 95 142501	C. Arnaboldi <i>et al.</i>	(CUORICINO Collab.)
ARNOLD 05A	PRL 95 182302	R. Arnold <i>et al.</i>	(NEMO-3 Collab.)
AALSETH 04	PR D70 078302	C.E. Aalseth <i>et al.</i>	(NEMO-3 Collab.)
ARNABOLDI 04	PL B584 260	C. Arnaboldi <i>et al.</i>	(NEMO-3 Collab.)
ARNOLD 04	JETPL 80 377	R. Arnold <i>et al.</i>	(NEMO-3 Collab.)
Translated from ZETFP 80 429.			
KLAPDOR-K...04A	PL B586 198	H.V. Klapdor-Kleingrothaus <i>et al.</i>	(NEMO-3 Collab.)
KLAPDOR-K...04B	PR D70 078301	H.V. Klapdor-Kleingrothaus, A. Dietz, I.V. Krivosheina	(NEMO-3 Collab.)
OGAWA 04	NP A730 215	I. Ogawa <i>et al.</i>	(NEMO-3 Collab.)
ARNABOLDI 03	PL B557 167	C. Arnaboldi <i>et al.</i>	(NEMO-3 Collab.)
DANEVICH 03	PR C68 035501	F.A. Danevich <i>et al.</i>	(IGEX Collab.)
AALSETH 02B	PR D65 092007	C.E. Aalseth <i>et al.</i>	(NEMO-3 Collab.)
DEBRAECKEL...01	PRL 86 3510	L. De Braeckeleer <i>et al.</i>	(NEMO-3 Collab.)
EJIRI 01	PR C63 065501	H. Ejiri <i>et al.</i>	(NEMO-3 Collab.)
KLAPDOR-K...01	EPJ A12 147	H.V. Klapdor-Kleingrothaus <i>et al.</i>	(NEMO-3 Collab.)
KLAPDOR-K...01B	MPL A16 2409	H.V. Klapdor-Kleingrothaus <i>et al.</i>	(NEMO-3 Collab.)
ALESSAND...00	PL B486 13	A. Alessandrello <i>et al.</i>	(NEMO-3 Collab.)
DANEVICH 00	PR C62 045501	F.A. Danevich <i>et al.</i>	(NEMO-3 Collab.)
ARNOLD 99	NP A658 299	R. Arnold <i>et al.</i>	(NEMO-3 Collab.)
BAUDIS 99	PR D59 022001	L. Baudis <i>et al.</i>	(Heidelberg-Moscow Collab.)
BAUDIS 99B	PRL 83 41	L. Baudis <i>et al.</i>	(Heidelberg-Moscow Collab.)
ARNOLD 98	NP A636 209	R. Arnold <i>et al.</i>	(NEMO-3 Collab.)
GUENTHER 97	PR D55 54	M. Guenther <i>et al.</i>	(Heidelberg-Moscow Collab.)
ARNOLD 96	ZPHY C72 239	R. Arnold <i>et al.</i>	(BCEN, CAEN, JINR+ Collab.)
BALYSH 95	PL B356 450	A. Balysh <i>et al.</i>	(Heidelberg-Moscow Collab.)
DASSIE 95	PR D51 2090	D. Dassie <i>et al.</i>	(NEMO-3 Collab.)
EJIRI 95	JPSJ 64 339	H. Ejiri <i>et al.</i>	(OSAK, KIEV Collab.)
SUHONEN 94	PR C49 3055	J. Suhonen, O. Civitarese	(WUSL, TATA Collab.)
BERNATOW...93	PR C47 806	T. Bernatowicz <i>et al.</i>	(WUSL, TATA Collab.)
VUILLEUMIER 93	PR D48 1009	J.C. Vuilleumier <i>et al.</i>	(NEUC, CIT, VILL Collab.)
BALYSH 92	PL B283 32	A. Balysh <i>et al.</i>	(MPIK, KIAE, SASSO Collab.)
BERNATOW...92	PRL 69 2341	T. Bernatowicz <i>et al.</i>	(WUSL, TATA Collab.)
ELLIOTT 92	PR C46 1535	S.R. Elliott <i>et al.</i>	(UCI Collab.)
SUHONEN 91	NP A535 509	J. Suhonen, S.B. Khadkikar, A. Faessler	(JYV+ Collab.)
TOMODA 91	IPP 54 53	T. Tomoda	(JYV+ Collab.)
YOU 91	PL B265 53	K. You <i>et al.</i>	(BHEP, CAST+ Collab.)
STAUDT 90	EPL 13 31	A. Staudt, K. Muto, H.V. Klapdor-Kleingrothaus	(TINT, MPIK Collab.)
MUTO 89	ZPHY A334 187	K. Muto, E. Bender, H.V. Klapdor	(TINT, MPIK Collab.)

Neutrino Mixing

With the possible exceptions of "short-baseline anomalies," such as LSND, all neutrino data can be described within the framework of a 3×3 mixing matrix between the mass eigenstates ν_1 , ν_2 , and ν_3 , leading to the flavor eigenstates ν_e , ν_μ , and ν_τ , as described in the review "Neutrino masses, mixing and oscillations."

The Listings are divided in the following sections:

(A) Neutrino fluxes and event ratios: shows measurements which correspond to various oscillation tests for Accelerator, Reactor, Atmospheric, and Solar neutrino experiments. Typically, ratios involve a measurement in a realm sensitive to oscillations compared to one for which no oscillation effect is expected.

(B) Neutrino mixing parameters: shows measurements of $\sin^2(\theta_{12})$, $\sin^2(\theta_{23})$, $\sin^2(\theta_{13})$, Δm_{21}^2 , Δm_{32}^2 , and δ_{CP} as extracted from the measured data in the quoted publications in the frame of the three-neutrino mixing scheme. The quoted averages are not the result of a global fit, as in the review "Neutrino masses, mixing, and oscillations," and, as a consequence, might slightly differ from them. In some cases, measurements depend on the mass order (normal when $\Delta m_{32}^2 > 0$ or inverted when $\Delta m_{32}^2 < 0$) or octant of θ_{23} (lower when $\theta_{23} < 45^\circ$ or upper when $\theta_{23} > 45^\circ$).

(C) Other neutrino mixing results:

The LSND anomaly [AGUILAR 01], reported a signal which is consistent with $\bar{\nu}_\mu \rightarrow \bar{\nu}_e$ oscillations. In a three neutrino framework, this would be a measurement of θ_{12} and Δm_{21}^2 . This does not appear to be consistent with the interpretation of other neutrino data. It has been interpreted as evidence for a 4th "sterile" neutrino. The following listings include results which might be relevant towards understanding this observation. They include searches for $\nu_\mu \rightarrow \nu_e$, $\bar{\nu}_\mu \rightarrow \bar{\nu}_e$, sterile neutrino oscillations, and others.

(A) Neutrino fluxes and event ratios

Events (observed/expected) from accelerator ν_μ experiments.

Some neutrino oscillation experiments compare the flux in two or more detectors. This is usually quoted as the ratio of the event rate in the far detector to the expected rate based on an extrapolation from the near detector in the absence of oscillations.

VALUE	DOCUMENT ID	TECN	COMMENT
• • • We do not use the following data for averages, fits, limits, etc. • • •			
1.01 ± 0.10	1 ABE	14B T2K	ν_e rate in T2K near detect.
0.71 ± 0.08	2 AHN	06A K2K	K2K to Super-K
0.64 ± 0.05	3 MICHAEL	06 MINS	All charged current events
0.71 ^{+0.08} _{-0.09}	4 ALIU	05 K2K	KEK to Super-K
0.70 ^{+0.10} _{-0.11}	5 AHN	03 K2K	KEK to Super-K

- ¹ The rate of ν_e from μ decay was measured to be 0.68 ± 0.30 compared to the predicted flux. From K decay 1.10 ± 0.14 compared to the predicted flux.
- ² Based on the observation of 112 events when 158.1 ± 9.2 were expected without oscillations. Including not only the number of events but also the shape of the energy distribution, the evidence for oscillation is at the level of about 4.3σ . Supersedes ALIU 05.
- ³ This ratio is based on the observation of 215 events compared to an expectation of 336 ± 14 without oscillations. See also ADAMSON 08.
- ⁴ This ratio is based on the observation of 107 events at the far detector 250 km away from KEK, and an expectation of 151 ± 10 .
- ⁵ This ratio is based on the observation of 56 events with an expectation of 80.1 ± 6.2 .

Events (observed/expected) from reactor $\bar{\nu}_e$ experiments.

The quoted values are the ratios of the measured reactor $\bar{\nu}_e$ event rate at the quoted distances, and the rate expected without oscillations. The expected rate is based on the experimental data for the most significant reactor fuels (^{235}U , ^{239}Pu , ^{241}Pu) and on calculations for ^{238}U .

A recent re-evaluation of the spectral conversion of electron to $\bar{\nu}_e$ in MUELLER 11 results in an upward shift of the reactor $\bar{\nu}_e$ spectrum by 3% and, thus, might require revisions to the ratios listed in this table.

VALUE	DOCUMENT ID	TECN	COMMENT
• • • We do not use the following data for averages, fits, limits, etc. • • •			
0.948 ± 0.008 ± 0.033	1 ALMAZAN	20 RHF	RHF reactor at ILL
0.952 ± 0.027	2 ADEY	19 DAYA	DayaBay, Ling Ao/Ao II reactors
	3 AN	16 DAYA	DayaBay, Ling Ao/Ao II reactors
1.08 ± 0.21 ± 0.16	4 DENIZ	10 TEXO	Kuo-Sheng reactor, 28 m
0.658 ± 0.044 ± 0.047	5 ARAKI	05 KLND	Japanese react. ~180 km
0.611 ± 0.085 ± 0.041	6 EGUCHI	03 KLND	Japanese react. ~180 km
1.01 ± 0.024 ± 0.053	7 BOEHM	01	Palo Verde react. 0.75–0.89 km
1.01 ± 0.028 ± 0.027	8 APOLLONIO	99 CHOZ	Chooz reactors 1 km
0.987 ± 0.006 ± 0.037	9 GREENWOOD	96	Savannah River, 18.2 m
0.988 ± 0.004 ± 0.05	ACHKAR	95 CNTR	Bugey reactor, 15 m
0.994 ± 0.010 ± 0.05	ACHKAR	95 CNTR	Bugey reactor, 40 m
0.915 ± 0.132 ± 0.05	ACHKAR	95 CNTR	Bugey reactor, 95 m
0.987 ± 0.014 ± 0.027	10 DECLAIS	94 CNTR	Bugey reactor, 15 m
0.985 ± 0.018 ± 0.034	KUVSHINN...	91 CNTR	Rovno reactor
1.05 ± 0.02 ± 0.05	VUILLEUMIER	82	Gösgen reactor
0.955 ± 0.035 ± 0.110	11 KWON	81	$\bar{\nu}_e p \rightarrow e^+ n$
0.89 ± 0.15	11 BOEHM	80	$\bar{\nu}_e p \rightarrow e^+ n$

- ¹ ALMAZAN 20 use the RHF research reactor at ILL to compare their measured anti-neutrino event rate to the calculation by HUBER 11. Reported $0.948 \pm 0.008 \pm 0.023 \pm 0.023$ measurement with uncertainties from statistics, systematic, and model. Note that this result is obtained for highly enriched ^{235}U reactor fuel while most other reactor experiments utilize a low-enrichment mix of fissile nuclides.
- ² ADEY 19 present a re-analysis of 1230 days of Daya Bay near detector data with reduced systematic uncertainties on the neutron detection efficiency. Note that ADEY 19 report the measured to predicted antineutrino ratio using the reactor model of MUELLER 11 (Huber-Mueller model). The ratio using the older ILL-Vogel model is $1.001 \pm 0.015 \pm 0.027$.
- ³ AN 16 use 217 days of data (338k events) to determine the neutrino flux ratio relative to the prediction of Mueller-Huber and ILL-Vogel models (see AN 16 for details). The reported flux ratios were corrected for θ_{13} oscillation effect. The flux measurement is consistent with results from previous short-baseline reactor experiments. The measured inverse beta decay yield is $(1.55 \pm 0.04) \times 10^{-18} \text{ cm}^2/(\text{GW day})$ or $\sigma_f = (5.92 \pm 0.14) \times 10^{-43} \text{ cm}^2/\text{fission}$. About 4σ excess of events was observed in the 4–6 MeV prompt energy region.
- ⁴ DENIZ 10 observe reactor $\bar{\nu}_e e$ scattering with recoil kinetic energies 3–8 MeV using CsI(Tl) detectors. The observed rate is consistent with the Standard Model prediction, leading to a constraint on $\sin^2\theta_{W} = 0.251 \pm 0.031(\text{stat}) \pm 0.024(\text{sys})$.
- ⁵ Updated result of KamLAND, including the data used in EGUCHI 03. Note that the survival probabilities for different periods are not directly comparable because the effective baseline varies with power output of the reactor sources involved, and there were large variations in the reactor power production in Japan in 2003.
- ⁶ EGUCHI 03 observe reactor neutrino disappearance at ~180 km baseline to various Japanese nuclear power reactors.
- ⁷ BOEHM 01 search for neutrino oscillations at 0.75 and 0.89 km distance from the Palo Verde reactors.
- ⁸ APOLLONIO 99, APOLLONIO 98 search for neutrino oscillations at 1.1 km fixed distance from Chooz reactors. They use $\bar{\nu}_e p \rightarrow e^+ n$ in Gd-loaded scintillator target. APOLLONIO 99 supersedes APOLLONIO 98. See also APOLLONIO 03 for detailed description.
- ⁹ GREENWOOD 96 search for neutrino oscillations at 18 m and 24 m from the reactor at Savannah River.
- ¹⁰ DECLAIS 94 result based on integral measurement of neutrons only. Result is ratio of measured cross section to that expected in standard V-A theory. Replaced by ACHKAR 95.
- ¹¹ KWON 81 represents an analysis of a larger set of data from the same experiment as BOEHM 80.

Atmospheric neutrinos

Neutrinos and antineutrinos produced in the atmosphere induce μ -like and e -like events in underground detectors. The ratio of the numbers of the two kinds of events is defined as μ/e . It has the advantage that systematic effects, such as flux uncertainty, tend to cancel, for both experimental and theoretical values of the ratio. The "ratio of the ratios" of experimental to theoretical μ/e , $R(\mu/e)$, or that of experimental to theoretical μ/total , $R(\mu/\text{total})$ with $\text{total} = \mu + e$, is reported below. If the actual value is not unity, the value obtained in a given experiment may depend on the experimental conditions. In addition, the measured "up-down asymmetry" for μ ($N_{up}(\mu)/N_{down}(\mu)$) or e ($N_{up}(e)/N_{down}(e)$) is reported. The expected "up-down asymmetry" is nearly unity if there is no neutrino oscillation.

$R(\mu/e) = (\text{Measured Ratio } \mu/e) / (\text{Expected Ratio } \mu/e)$

VALUE	DOCUMENT ID	TECN	COMMENT
• • • We do not use the following data for averages, fits, limits, etc. • • •			
0.658 ± 0.016 ± 0.035	1 ASHIE	05 SKAM	sub-GeV
0.702 ^{+0.032} _{-0.030} ± 0.101	2 ASHIE	05 SKAM	multi-GeV
0.69 ± 0.10 ± 0.06	3 SANCHEZ	03 SOU2	Calorimeter raw data
	4 FUKUDA	96B KAMI	Water Cherenkov

Lepton Particle Listings

Neutrino Mixing

$1.00 \pm 0.15 \pm 0.08$	5	DAUM	95	FREJ	Calorimeter
$0.60 \pm 0.06 \pm 0.05$	6	FUKUDA	94	KAMI	sub-GeV
$0.57 \pm 0.08 \pm 0.07$	7	FUKUDA	94	KAMI	multi-GeV
	8	BECKER-SZ...	92B	IMB	Water Cherenkov

¹ ASHIE 05 results are based on an exposure of 92 kton yr during the complete Super-Kamiokande I running period. The analyzed data sample consists of fully-contained single-ring e -like events with $0.1 \text{ GeV}/c < p_e$ and μ -like events $0.2 \text{ GeV}/c < p_\mu$, both having a visible energy $< 1.33 \text{ GeV}$. These criteria match the definition used by FUKUDA 94.

² ASHIE 05 results are based on an exposure of 92 kton yr during the complete Super-Kamiokande I running period. The analyzed data sample consists of fully-contained single-ring events with visible energy $> 1.33 \text{ GeV}$ and partially-contained events. All partially-contained events are classified as μ -like.

³ SANCHEZ 03 result is based on an exposure of 5.9 kton yr, and updates ALLISON 99 result. The analyzed data sample consists of fully-contained e -flavor and μ -flavor events having lepton momentum $> 0.3 \text{ GeV}/c$.

⁴ FUKUDA 96b studied neutron background in the atmospheric neutrino sample observed in the Kamiokande detector. No evidence for the background contamination was found.

⁵ DAUM 95 results are based on an exposure of 2.0 kton yr which includes the data used by BERGER 90b. This ratio is for the contained and semicontained events. DAUM 95 also report $R(\mu/e) = 0.99 \pm 0.13 \pm 0.08$ for the total neutrino induced data sample which includes upward going stopping muons and horizontal muons in addition to the contained and semicontained events.

⁶ FUKUDA 94 result is based on an exposure of 7.7 kton yr and updates the HIRATA 92 result. The analyzed data sample consists of fully-contained e -like events with $0.1 < p_e < 1.33 \text{ GeV}/c$ and fully-contained μ -like events with $0.2 < p_\mu < 1.5 \text{ GeV}/c$.

⁷ FUKUDA 94 analyzed the data sample consisting of fully contained events with visible energy $> 1.33 \text{ GeV}$ and partially contained μ -like events.

⁸ BECKER-SZENDY 92b reports the fraction of nonshowering events (mostly muons from atmospheric neutrinos) as $0.36 \pm 0.02 \pm 0.02$, as compared with expected fraction $0.51 \pm 0.01 \pm 0.05$. After cutting the energy range to the Kamiokande limits, BEIER 92 finds $R(\mu/e)$ very close to the Kamiokande value.

 $R(\nu_\mu) = (\text{Measured Flux of } \nu_\mu) / (\text{Expected Flux of } \nu_\mu)$

VALUE	DOCUMENT ID	TECN	COMMENT
• • •			We do not use the following data for averages, fits, limits, etc. • • •
0.84 ± 0.12	1	ADAMSON	06 MINS MINOS atmospheric
$0.72 \pm 0.026 \pm 0.13$	2	AMBROSIO	01 MCRO upward through-going
$0.57 \pm 0.05 \pm 0.15$	3	AMBROSIO	00 MCRO upgoing partially contained
$0.71 \pm 0.05 \pm 0.19$	4	AMBROSIO	00 MCRO downgoing partially contained + upgoing stopping
$0.74 \pm 0.036 \pm 0.046$	5	AMBROSIO	98 MCRO Streamer tubes
	6	CASPER	91 IMB Water Cherenkov
	7	AGLIETTA	89 NUSX
0.95 ± 0.22	8	BOLIEV	81 Baksan
0.62 ± 0.17		CROUCH	78 Case Western /UCI

¹ ADAMSON 06 uses a measurement of 107 total neutrinos compared to an expected rate of 127 ± 13 without oscillations.

² AMBROSIO 01 result is based on the upward through-going muon tracks with $E_\mu > 1 \text{ GeV}$. The data came from three different detector configurations, but the statistics is largely dominated by the full detector run, from May 1994 to December 2000. The total live time, normalized to the full detector configuration, is 6.17 years. The first error is the statistical error, the second is the systematic error, dominated by the theoretical error in the predicted flux.

³ AMBROSIO 00 result is based on the upgoing partially contained event sample. It came from 4.1 live years of data taking with the full detector, from April 1994 to February 1999. The average energy of atmospheric muon neutrinos corresponding to this sample is 4 GeV. The first error is statistical, the second is the systematic error, dominated by the 25% theoretical error in the rate (20% in the flux and 15% in the cross section, added in quadrature). Within statistics, the observed deficit is uniform over the zenith angle.

⁴ AMBROSIO 00 result is based on the combined samples of downgoing partially contained events and upgoing stopping events. These two subsamples could not be distinguished due to the lack of timing information. The result came from 4.1 live years of data taking with the full detector, from April 1994 to February 1999. The average energy of atmospheric muon neutrinos corresponding to this sample is 4 GeV. The first error is statistical, the second is the systematic error, dominated by the 25% theoretical error in the rate (20% in the flux and 15% in the cross section, added in quadrature). Within statistics, the observed deficit is uniform over the zenith angle.

⁵ AMBROSIO 98 result is for all nadir angles and updates AHLEN 95 result. The lower cutoff on the muon energy is 1 GeV. In addition to the statistical and systematic errors, there is a Monte Carlo flux error (theoretical error) of ± 0.13 . With a neutrino oscillation hypothesis, the fit either to the flux or zenith distribution independently yields $\sin^2 2\theta = 1.0$ and $\Delta(m^2) \sim$ a few times 10^{-3} eV^2 . However, the fit to the observed zenith distribution gives a maximum probability for χ^2 of only 5% for the best oscillation hypothesis.

⁶ CASPER 91 correlates showering/nonshowering signature of single-ring events with parent atmospheric-neutrino flavor. They find nonshowering ($\approx \nu_\mu$ induced) fraction is $0.41 \pm 0.03 \pm 0.02$, as compared with expected 0.51 ± 0.05 (syst).

⁷ AGLIETTA 89 finds no evidence for any anomaly in the neutrino flux. They define $\rho = (\text{measured number of } \nu_e\text{'s})/(\text{measured number of } \nu_\mu\text{'s})$. They report $\rho(\text{measured}) = \rho(\text{expected}) = 0.96 \pm 0.32 \pm 0.28$.

⁸ From this data BOLIEV 81 obtain the limit $\Delta(m^2) \leq 6 \times 10^{-3} \text{ eV}^2$ for maximal mixing, $\nu_\mu \leftrightarrow \nu_\mu$ type oscillation.

 $R(\mu/\text{total}) = (\text{Measured Ratio } \mu/\text{total}) / (\text{Expected Ratio } \mu/\text{total})$

VALUE	DOCUMENT ID	TECN	COMMENT
• • •			We do not use the following data for averages, fits, limits, etc. • • •
$1.1 \pm 0.07 \pm 0.11$	1	CLARK	97 IMB multi-GeV

¹ CLARK 97 obtained this result by an analysis of fully contained and partially contained events in the IMB water-Cherenkov detector with visible energy $> 0.95 \text{ GeV}$.

 $N_{\text{up}}(\mu)/N_{\text{down}}(\mu)$

VALUE	DOCUMENT ID	TECN	COMMENT
• • •			We do not use the following data for averages, fits, limits, etc. • • •
0.71 ± 0.06	1	ADAMSON	12B MINS contained-vertex muons
$0.551 \pm 0.035 \pm 0.004$	2	ASHIE	05 SKAM multi-GeV

¹ ADAMSON 12b reports the atmospheric neutrino results obtained with MINOS far detector in 2,553 live days (an exposure of 37.9 kton-yr). This result is obtained with a sample of high resolution contained-vertex muons. The quoted error is statistical only.

² ASHIE 05 results are based on an exposure of 92 kton yr during the complete Super-Kamiokande I running period. The analyzed data sample consists of fully-contained single-ring μ -like events with visible energy $> 1.33 \text{ GeV}$ and partially-contained events. All partially-contained events are classified as μ -like. Upward-going events are those with $-1 < \cos(\text{zenith angle}) < -0.2$ and downward-going events are those with $0.2 < \cos(\text{zenith angle}) < 1$. The μ -like up-down ratio for the multi-GeV data deviates from 1 (the expectation for no atmospheric ν_μ oscillations) by more than 12 standard deviations.

 $N_{\text{up}}(e)/N_{\text{down}}(e)$

VALUE	DOCUMENT ID	TECN	COMMENT
• • •			We do not use the following data for averages, fits, limits, etc. • • •
$0.961 \pm 0.086 \pm 0.016$	1	ASHIE	05 SKAM multi-GeV

¹ ASHIE 05 results are based on an exposure of 92 kton yr during the complete Super-Kamiokande I running period. The analyzed data sample consists of fully-contained single-ring e -like events with visible energy $> 1.33 \text{ GeV}$. Upward-going events are those with $-1 < \cos(\text{zenith angle}) < -0.2$ and downward-going events are those with $0.2 < \cos(\text{zenith angle}) < 1$. The e -like up-down ratio for the multi-GeV data is consistent with 1 (the expectation for no atmospheric ν_e oscillations).

 $R(\text{up/down}; \mu) = (\text{Measured up/down}; \mu) / (\text{Expected up/down}; \mu)$

VALUE	DOCUMENT ID	TECN	COMMENT
• • •			We do not use the following data for averages, fits, limits, etc. • • •
$0.62 \pm 0.05 \pm 0.02$	1	ADAMSON	12B MINS contained-vertex muons
$0.62 \pm 0.19 \pm 0.02$	2	ADAMSON	06 MINS atmospheric ν with far detector

¹ ADAMSON 12b reports the atmospheric neutrino results obtained with MINOS far detector in 2,553 live days (an exposure of 37.9 kton-yr). This result is obtained with a sample of high resolution contained-vertex muons. The expected ratio is calculated with no neutrino oscillation.

² ADAMSON 06 result is obtained with the MINOS far detector with an exposure of 4.54 kton yr. The expected ratio is calculated with no neutrino oscillation.

 $N(\mu^+)/N(\mu^-)$

VALUE	DOCUMENT ID	TECN	COMMENT
• • •			We do not use the following data for averages, fits, limits, etc. • • •
$0.46 \pm 0.05 \pm 0.04$	1,2	ADAMSON	12B MINS contained-vertex muons
$0.63 \pm 0.09 \pm 0.08$	1,3	ADAMSON	12B MINS ν -induced rock-muons

¹ ADAMSON 12b reports the atmospheric neutrino results obtained with MINOS far detector in 2,553 live days (an exposure of 37.9 kton-yr). The muon charge ratio $N(\mu^+)/N(\mu^-)$ represents the $\bar{\nu}_\mu/\nu_\mu$ ratio.

² This result is obtained with a charge-separated sample of high resolution contained-vertex muons. The quoted error is statistical only.

³ This result is obtained with a charge-separated sample of high resolution neutrino-induced rock-muons. The quoted error is statistical only.

 $R(\mu^+/\mu^-) = (\text{Measured } N(\mu^+)/N(\mu^-)) / (\text{Expected } N(\mu^+)/N(\mu^-))$

VALUE	DOCUMENT ID	TECN	COMMENT
• • •			We do not use the following data for averages, fits, limits, etc. • • •
$0.93 \pm 0.09 \pm 0.09$	1,2	ADAMSON	12B MINS contained-vertex muons
$1.29 \pm 0.19 \pm 0.16$	1,3	ADAMSON	12B MINS ν -induced rock-muons
$1.03 \pm 0.08 \pm 0.08$	1,4	ADAMSON	12B MINS contained
$1.39 \pm 0.35 \pm 0.08 \pm 0.46 \pm 0.14$	5	ADAMSON	07 MINS Upward and horizontal μ with far detector
$0.96 \pm 0.38 \pm 0.27 \pm 0.15$	6	ADAMSON	06 MINS atmospheric ν with far detector

¹ ADAMSON 12b reports the atmospheric neutrino results obtained with MINOS far detector in 2,553 live days (an exposure of 37.9 kton-yr). The muon charge ratio $N(\mu^+)/N(\mu^-)$ represents the $\bar{\nu}_\mu/\nu_\mu$ ratio. As far as the same oscillation parameters are used for ν_s and $\bar{\nu}_s$, the expected $\bar{\nu}_\mu/\nu_\mu$ ratio is almost entirely independent of any input oscillations.

See key on page 1127

Lepton Particle Listings

Neutrino Mixing

- ²This result is obtained with a charge-separated sample of high resolution contained-vertex muons.
- ³This result is obtained with a charge-separated sample of high resolution neutrino-induced rock-muons.
- ⁴The charge-separated samples of high resolution contained-vertex muons and neutrino-induced rock-muons are combined to obtain this result which is consistent with unity.
- ⁵ADAMSON 07 result is obtained with the MINOS far detector in 854.24 live days, based on neutrino-induced upward-going and horizontal muons. This result is consistent with CPT conservation.
- ⁶ADAMSON 06 result is obtained with the MINOS far detector with an exposure of 4.54 kton yr, based on contained events. The expected ratio is calculated by assuming the same oscillation parameters for neutrinos and antineutrinos.

Solar neutrinos

Solar neutrinos are produced by thermonuclear fusion reactions in the Sun. Radiochemical experiments measure particular combinations of fluxes from various neutrino-producing reactions, whereas water-Cherenkov experiments mainly measure a flux of neutrinos from decay of ⁸B. Solar neutrino fluxes are composed of all active neutrino species, ν_e , ν_μ , and ν_τ . In addition, some other mechanisms may cause antineutrino components in solar neutrino fluxes. Each measurement method is sensitive to a particular component or a combination of components of solar neutrino fluxes.

ν_e Capture Rates from Radiochemical Experiments

1 SNU (Solar Neutrino Unit) = 10^{-36} captures per atom per second.

VALUE (SNU)	DOCUMENT ID	TECN	COMMENT
● ● ● We do not use the following data for averages, fits, limits, etc. ● ● ●			
73.4 ^{+6.1} / _{-6.0} ^{+3.7} / _{-4.1}	1 KAETHER	10	GALX reanalysis
67.6 ^{+4.0} / _{-3.2}	2 KAETHER	10	GNO+GALX reanalysis combined
65.4 ^{+3.1} / _{-3.0} ^{+2.6} / _{-2.8}	3 ABDURASHITOV 09	SAGE	⁷¹ Ga → ⁷¹ Ge
62.9 ^{+5.5} / _{-5.3} ^{+2.5} / _{-2.5}	4 ALTMANN	05	GNO ⁷¹ Ga → ⁷¹ Ge
69.3 ^{+4.1} / _{-3.6}	5 ALTMANN	05	GNO + GALX combined
77.5 ^{+6.2} / _{-4.7} ^{+4.3} / _{-4.7}	6 HAMPEL	99	GALX ⁷¹ Ga → ⁷¹ Ge
2.56 ± 0.16 ± 0.16	7 CLEVELAND	98	HOME ³⁷ Cl → ³⁷ Ar

- ¹KAETHER 10 reports the reanalysis results of a complete GALLEX data (GALLEX I-II+III+IV, reported in HAMPEL 99) based on the event selection with a new pulse shape analysis, which provides a better background reduction than the rise time analysis adopted in HAMPEL 99.
- ²Combined result of GALLEX I-II+III+IV reanalysis and GNO I-II+III (ALTMANN 05).
- ³ABDURASHITOV 09 reports a combined analysis of 168 extractions of the SAGE solar neutrino experiment during the period January 1990 through December 2007, and updates the ABDURASHITOV 02 result. The data are consistent with the assumption that the solar neutrino production rate is constant in time. Note that a ~ 15% systematic uncertainty in the overall normalization may be added to the ABDURASHITOV 09 result, because calibration experiments for gallium solar neutrino measurements using intense ⁵¹Cr (twice by GALLEX and once by SAGE) and ³⁷Ar (by SAGE) result in an average ratio of 0.87 ± 0.05 of the observed to calculated rates.
- ⁴ALTMANN 05 reports the complete result from the GNO solar neutrino experiment (GNO I-II+III), which is the successor project of GALLEX. Experimental technique of GNO is essentially the same as that of GALLEX. The run data cover the period 20 May 1998 through 9 April 2003.
- ⁵Combined result of GALLEX I-II+III+IV (HAMPEL 99) and GNO I-II+III.
- ⁶HAMPEL 99 report the combined result for GALLEX I-II+III+IV (65 runs in total), which update the HAMPEL 96 result. The GALLEX IV result (12 runs) is 118.4 ± 17.8 ± 6.6 SNU. (HAMPEL 99 discuss the consistency of partial results with the mean.) The GALLEX experimental program has been completed with these runs. The total run data cover the period 14 May 1991 through 23 January 1997. A total of 300 ⁷¹Ge events were observed. Note that a ~ 15% systematic uncertainty in the overall normalization may be added to the HAMPEL 99 result, because calibration experiments for gallium solar neutrino measurements using intense ⁵¹Cr (twice by GALLEX and once by SAGE) and ³⁷Ar (by SAGE) result in an average ratio of 0.87 ± 0.05 of the observed to calculated rates.
- ⁷CLEVELAND 98 is a detailed report of the ³⁷Cl experiment at the Homestake Mine. The average solar neutrino-induced ³⁷Ar production rate from 108 runs between 1970 and 1994 updates the DAVIS 89 result.

ϕ_{ES} (⁸B)

⁸B solar-neutrino flux measured via νe elastic scattering. This process is sensitive to all active neutrino flavors, but with reduced sensitivity to ν_μ , ν_τ due to the cross-section difference, $\sigma(\nu_{\mu,\tau} e) \approx 0.16\sigma(\nu_e e)$. If the ⁸B solar-neutrino flux involves nonelectron flavor active neutrinos, their contribution to the flux is ~ 0.16 times of ν_e .

VALUE ($10^6 \text{ cm}^{-2}\text{s}^{-1}$)	DOCUMENT ID	TECN	COMMENT
● ● ● We do not use the following data for averages, fits, limits, etc. ● ● ●			
2.57 ^{+0.17} / _{-0.18} ^{+0.07} / _{-0.07}	1 AGOSTINI	20A	BORX average flux
2.53 ^{+0.31} / _{-0.28} ^{+0.13} / _{-0.10}	2 ANDERSON	19	SNO+ Water phase; average flux

2.57 ^{+0.17} / _{-0.18} ^{+0.07} / _{-0.07}	3 AGOSTINI	18B	BORX average flux
2.345 ± 0.014 ± 0.036	4 ABE	16c	SKAM SK-I+II+III+IV average flux
2.308 ± 0.020 ^{+0.039} / _{-0.040}	5 ABE	16c	SKAM SK-IV average flux
2.250 ^{+0.030} / _{-0.029} ± 0.038	5 ABE	16c	SKAM SK-IV day flux
2.364 ± 0.029 ± 0.040	5 ABE	16c	SKAM SK-IV night flux
2.404 ± 0.039 ± 0.053	6 ABE	16c	SKAM SK-III average flux
2.41 ± 0.05 ^{+0.16} / _{-0.15}	7 ABE	11	SKAM SK-II average flux
2.38 ± 0.02 ± 0.08	8 ABE	11	SKAM SK-I average flux
2.77 ± 0.26 ± 0.32	9 ABE	11B	KLND average flux
2.4 ± 0.4 ± 0.1	10 BELLINI	10A	BORX average flux
1.77 ^{+0.24} / _{-0.21} ^{+0.09} / _{-0.10}	11 AHARMIM	08	SNO Phase III
2.38 ± 0.05 ^{+0.16} / _{-0.15}	12 CRAVENS	08	SKAM average flux
2.35 ± 0.02 ± 0.08	13 HOSAKA	06	SKAM average flux
2.35 ± 0.22 ± 0.15	14 AHARMIM	05A	SNO Salty D ₂ O; ⁸ B shape not constrained
2.34 ± 0.23 ^{+0.15} / _{-0.14}	14 AHARMIM	05A	SNO Salty D ₂ O; ⁸ B shape not constrained
2.39 ^{+0.24} / _{-0.23} ± 0.12	15 AHMAD	02	SNO average flux
2.39 ± 0.34 ^{+0.16} / _{-0.14}	16 AHMAD	01	SNO average flux
2.80 ± 0.19 ± 0.33	17 FUKUDA	96	KAMI average flux
2.70 ± 0.27	17 FUKUDA	96	KAMI day flux
2.87 ^{+0.27} / _{-0.26}	17 FUKUDA	96	KAMI night flux

- ¹AGOSTINI 20A obtained this result from the $\nu_e e$ elastic scattering rate over the period between January 2008 and December 2016. Use the same data as AGOSTINI 18B, but the analysis technique is significantly improved.
- ²ANDERSON 19 reports this result from the $\nu_e e$ elastic scattering rate using a 69.2 kton-day (or 114.7 days) of exposure from May through December, 2017 during the SNO+ detector's water commissioning phase. The events over the reconstructed electron kinetic energy range of 5–15 MeV were analyzed.
- ³AGOSTINI 18B obtained this result from the $\nu_e e$ elastic scattering rate over the period between January 2008 and December 2016.
- ⁴ABE 16c reports the combined results of the four phases of the Super-Kamiokande average flux measurements. Here the revised Super-Kamiokande-III result is used.
- ⁵ABE 16c reports the Super-Kamiokande-IV results for 1664 live days from September 2008 to February 2014. The analysis threshold is total electron energy of 4.0 MeV.
- ⁶ABE 16c revised the Super-Kamiokande-III average flux value reported in ABE 11. Super-Kamiokande-III results are for 548 live days from August 4, 2006 to August 18, 2008. The analysis threshold is 5.0 MeV, but the event sample in the 5.0–6.5 MeV total electron energy range has a total live time of 298 days.
- ⁷ABE 11 recalculated the Super-Kamiokande-II results using ⁸B spectrum of WINTER 06A.
- ⁸ABE 11 recalculated the Super-Kamiokande-I results using ⁸B spectrum of WINTER 06A.
- ⁹ABE 11B use a 123 kton-day exposure of the KamLAND liquid scintillation detector to measure the ⁸B solar neutrino flux. They utilize $\nu - e$ elastic scattering above a reconstructed-energy threshold of 5.5 MeV, corresponding to 5 MeV electron recoil energy. 299 electron recoil candidate events are reported, of which 157 ± 23.6 are assigned to background.
- ¹⁰BELLINI 10A reports the Borexino result with 3 MeV energy threshold for scattered electrons. The data correspond to 345.3 live days with a target mass of 100 t, between July 15, 2007 and August 23, 2009.
- ¹¹AHARMIM 08 reports the results from SNO Phase III measurement using an array of ³He proportional counters to measure the rate of NC interactions in heavy water, over the period between November 27, 2004 and November 28, 2006, corresponding to 385.17 live days. A simultaneous fit was made for the number of NC events detected by the proportional counters and the numbers of NC, CC, and ES events detected by the PMTs, where the spectral distributions of the ES and CC events were not constrained to the ⁸B shape.
- ¹²CRAVENS 08 reports the Super-Kamiokande-II results for 791 live days from December 2002 to October 2005. The photocathode coverage of the detector is 19% (reduced from 40% of that of Super-Kamiokande-I due to an accident in 2001). The analysis threshold for the average flux is 7 MeV.
- ¹³HOSAKA 06 reports the final results for 1496 live days with Super-Kamiokande-I between May 31, 1996 and July 15, 2001, and replace FUKUDA 02 results. The analysis threshold is 5 MeV except for the first 280 live days (6.5 MeV).
- ¹⁴AHARMIM 05A measurements were made with dissolved NaCl (0.195% by weight) in heavy water over the period between July 26, 2001 and August 28, 2003, corresponding to 391.4 live days, and update AHMED 04A. The CC, ES, and NC events were statistically separated. In one method, the ⁸B energy spectrum was not constrained. In the other method, the constraint of an undistorted ⁸B energy spectrum was added for comparison with AHMAD 02 results.
- ¹⁵AHMAD 02 reports the ⁸B solar-neutrino flux measured via νe elastic scattering above the kinetic energy threshold of 5 MeV. The data correspond to 306.4 live days with SNO between November 2, 1999 and May 28, 2001, and updates AHMAD 01 results.
- ¹⁶AHMAD 01 reports the ⁸B solar-neutrino flux measured via νe elastic scattering above the kinetic energy threshold of 6.75 MeV. The data correspond to 241 live days with SNO between November 2, 1999 and January 15, 2001.
- ¹⁷FUKUDA 96 results are for a total of 2079 live days with Kamiokande II and III from January 1987 through February 1995, covering the entire solar cycle 22, with threshold $E_e > 9.3 \text{ MeV}$ (first 449 days), $> 7.5 \text{ MeV}$ (middle 794 days), and $> 7.0 \text{ MeV}$ (last 836 days). These results update the HIRATA 90 result for the average ⁸B solar-neutrino flux and HIRATA 91 result for the day-night variation in the ⁸B solar-neutrino flux. The total

Lepton Particle Listings

Neutrino Mixing

data sample was also analyzed for short-term variations: within experimental errors, no strong correlation of the solar-neutrino flux with the sunspot numbers was found.

ϕ_{CC} (^8B)

^8B solar-neutrino flux measured with charged-current reaction which is sensitive exclusively to ν_e .

VALUE ($10^6 \text{ cm}^{-2}\text{s}^{-1}$)	DOCUMENT ID	TECN	COMMENT
• • • We do not use the following data for averages, fits, limits, etc. • • •			
$1.67^{+0.05+0.07}_{-0.04-0.08}$	1 AHARMIM	08	SNO Phase III
$1.68 \pm 0.06^{+0.08}_{-0.09}$	2 AHARMIM	05A	SNO Salty D_2O ; ^8B shape not const.
$1.72 \pm 0.05 \pm 0.11$	2 AHARMIM	05A	SNO Salty D_2O ; ^8B shape constrained
$1.76^{+0.06}_{-0.05} \pm 0.09$	3 AHMAD	02	SNO average flux
$1.75 \pm 0.07^{+0.12}_{-0.11} \pm 0.05$	4 AHMAD	01	SNO average flux

¹AHARMIM 08 reports the results from SNO Phase III measurement using an array of ³He proportional counters to measure the rate of NC interactions in heavy water, over the period between November 27, 2004 and November 28, 2006, corresponding to 385.17 live days. A simultaneous fit was made for the number of NC events detected by the proportional counters and the numbers of NC, CC, and ES events detected by the PMTs, where the spectral distributions of the ES and CC events were not constrained to the ^8B shape.

²AHARMIM 05A measurements were made with dissolved NaCl (0.195% by weight) in heavy water over the period between July 26, 2001 and August 28, 2003, corresponding to 391.4 live days, and update AHMED 04A. The CC, ES, and NC events were statistically separated. In one method, the ^8B energy spectrum was not constrained. In the other method, the constraint of an undistorted ^8B energy spectrum was added for comparison with AHMAD 02 results.

³AHMAD 02 reports the SNO result of the ^8B solar-neutrino flux measured with charged-current reaction on deuterium, $\nu_e d \rightarrow pp e^-$, above the kinetic energy threshold of 5 MeV. The data correspond to 306.4 live days with SNO between November 2, 1999 and May 28, 2001, and updates AHMAD 01 results. The complete description of the SNO Phase I data set is given in AHARMIM 07.

⁴AHMAD 01 reports the first SNO result of the ^8B solar-neutrino flux measured with the charged-current reaction on deuterium, $\nu_e d \rightarrow pp e^-$, above the kinetic energy threshold of 6.75 MeV. The data correspond to 241 live days with SNO between November 2, 1999 and January 15, 2001.

ϕ_{NC} (^8B)

^8B solar neutrino flux measured with neutral-current reaction, which is equally sensitive to ν_e , ν_μ , and ν_τ .

VALUE ($10^6 \text{ cm}^{-2}\text{s}^{-1}$)	DOCUMENT ID	TECN	COMMENT
• • • We do not use the following data for averages, fits, limits, etc. • • •			
$5.25 \pm 0.16^{+0.11}_{-0.13}$	1 AHARMIM	13	SNO All three phases combined
$5.140^{+0.160+0.132}_{-0.158-0.117}$	2 AHARMIM	10	SNO Phase I+II, low threshold
$5.54^{+0.33+0.36}_{-0.31-0.34}$	3 AHARMIM	08	SNO Phase III, prop. counter + PMT
$4.94 \pm 0.21^{+0.38}_{-0.34}$	4 AHARMIM	05A	SNO Salty D_2O ; ^8B shape not const.
$4.81 \pm 0.19^{+0.28}_{-0.27}$	4 AHARMIM	05A	SNO Salty D_2O ; ^8B shape constrained
$5.09^{+0.44+0.46}_{-0.43-0.43}$	5 AHMAD	02	SNO average flux; ^8B shape const.
$6.42 \pm 1.57^{+0.55}_{-0.58}$	5 AHMAD	02	SNO average flux; ^8B shape not const.

¹AHARMIM 13 obtained this result from a combined analysis of the data from all three phases, SNO-I, II, and III. The measurement of the ^8B flux mostly comes from the NC signal, however, CC contribution is included in the fit.

²AHARMIM 10 reports this result from a joint analysis of SNO Phase I+II data with the "effective electron kinetic energy" threshold of 3.5 MeV. This result is obtained with a "binned-histogram unconstrained fit" where binned probability distribution functions of the neutrino signal observables were used without any model constraints on the shape of the neutrino spectrum.

³AHARMIM 08 reports the results from SNO Phase III measurement using an array of ³He proportional counters to measure the rate of NC interactions in heavy water, over the period between November 27, 2004 and November 28, 2006, corresponding to 385.17 live days. A simultaneous fit was made for the number of NC events detected by the proportional counters and the numbers of NC, CC, and ES events detected by the PMTs, where the spectral distributions of the ES and CC events were not constrained to the ^8B shape.

⁴AHARMIM 05A measurements were made with dissolved NaCl (0.195% by weight) in heavy water over the period between July 26, 2001 and August 28, 2003, corresponding to 391.4 live days, and update AHMED 04A. The CC, ES, and NC events were statistically separated. In one method, the ^8B energy spectrum was not constrained. In the other method, the constraint of an undistorted ^8B energy spectrum was added for comparison with AHMAD 02 results.

⁵AHMAD 02 reports the first SNO result of the ^8B solar-neutrino flux measured with the neutral-current reaction on deuterium, $\nu_e d \rightarrow np \nu_e$, above the neutral-current reaction threshold of 2.2 MeV. The data correspond to 306.4 live days with SNO between November 2, 1999 and May 28, 2001. The complete description of the SNO Phase I data set is given in AHARMIM 07.

$\phi_{\nu_\mu+\nu_\tau}$ (^8B)

Nonelectron-flavor active neutrino component (ν_μ and ν_τ) in the ^8B solar-neutrino flux.

VALUE ($10^6 \text{ cm}^{-2}\text{s}^{-1}$)	DOCUMENT ID	TECN	COMMENT
• • • We do not use the following data for averages, fits, limits, etc. • • •			
$3.26 \pm 0.25^{+0.40}_{-0.35}$	1 AHARMIM	05A	SNO From ϕ_{NC} , ϕ_{CC} , and ϕ_{ES} ; ^8B shape not const.
$3.09 \pm 0.22^{+0.30}_{-0.27}$	1 AHARMIM	05A	SNO From ϕ_{NC} , ϕ_{CC} , and ϕ_{ES} ; ^8B shape constrained
$3.41 \pm 0.45^{+0.48}_{-0.45}$	2 AHMAD	02	SNO From ϕ_{NC} , ϕ_{CC} , and ϕ_{ES}
3.69 ± 1.13	3 AHMAD	01	Derived from SNO+SuperKam, water Cherenkov

¹AHARMIM 05A measurements were made with dissolved NaCl (0.195% by weight) in heavy water over the period between July 26, 2001 and August 28, 2003, corresponding to 391.4 live days, and update AHMED 04A. The CC, ES, and NC events were statistically separated. In one method, the ^8B energy spectrum was not constrained. In the other method, the constraint of an undistorted ^8B energy spectrum was added for comparison with AHMAD 02 results.

²AHMAD 02 deduced the nonelectron-flavor active neutrino component (ν_μ and ν_τ) in the ^8B solar-neutrino flux, by combining the charged-current result, the ν_e elastic-scattering result and the neutral-current result. The complete description of the SNO Phase I data set is given in AHARMIM 07.

³AHMAD 01 deduced the nonelectron-flavor active neutrino component (ν_μ and ν_τ) in the ^8B solar-neutrino flux, by combining the SNO charged-current result (AHMAD 01) and the Super-Kamiokande ν_e elastic-scattering result (FUKUDA 01).

Total Flux of Active pp Solar Neutrinos

Total flux of active neutrinos (ν_e, ν_μ, ν_τ).

VALUE ($10^{10} \text{ cm}^{-2}\text{s}^{-1}$)	DOCUMENT ID	TECN	COMMENT
• • • We do not use the following data for averages, fits, limits, etc. • • •			
$6.1 \pm 0.5^{+0.3}_{-0.5}$	1 AGOSTINI	18B	BORX Use $\nu_e e$ scattering rate

¹AGOSTINI 18B obtained this result from the measured $\nu_e e$ elastic scattering rate over the period between December 2011 and May 2016, assuming the MSW-LMA oscillation parameters derived by ESTEBAN 17. Assuming a high-metallicity standard solar model, the electron neutrino survival probability for the pp solar neutrino is calculated to be 0.57 ± 0.09 .

Total Flux of Active ^7Be Solar Neutrinos

Total flux of active neutrinos (ν_e, ν_μ, ν_τ).

VALUE ($10^9 \text{ cm}^{-2}\text{s}^{-1}$)	DOCUMENT ID	TECN	COMMENT
• • • We do not use the following data for averages, fits, limits, etc. • • •			
$4.99 \pm 0.11^{+0.06}_{-0.08}$	1 AGOSTINI	18B	BORX Use $\nu_e e$ scattering rate

¹AGOSTINI 18B obtained this result from the measured $\nu_e e$ elastic scattering rate over the period between December 2011 and May 2016, assuming the MSW-LMA oscillation parameters derived by ESTEBAN 17. Assuming a high-metallicity standard solar model, the electron neutrino survival probability for the ^7Be solar neutrino is calculated to be 0.53 ± 0.05 .

Total Flux of Active pep Solar Neutrinos

Total flux of active neutrinos (ν_e, ν_μ, ν_τ).

VALUE ($10^8 \text{ cm}^{-2}\text{s}^{-1}$)	DOCUMENT ID	TECN	COMMENT
• • • We do not use the following data for averages, fits, limits, etc. • • •			
$1.27 \pm 0.19^{+0.08}_{-0.12}$	1 AGOSTINI	18B	BORX Use $\nu_e e$ scattering rate

¹AGOSTINI 18B obtained this result from the measured $\nu_e e$ elastic scattering rate over the period between December 2011 and May 2016, assuming the MSW-LMA oscillation parameters derived by ESTEBAN 17 and a high-metallicity standard solar model. The electron neutrino survival probability for the pep solar neutrino is calculated to be 0.43 ± 0.11 .

Total Flux of Active ^8B Solar Neutrinos

Total flux of active neutrinos (ν_e, ν_μ , and ν_τ).

VALUE ($10^6 \text{ cm}^{-2}\text{s}^{-1}$)	DOCUMENT ID	TECN	COMMENT
• • • We do not use the following data for averages, fits, limits, etc. • • •			
$5.95^{+0.75+0.28}_{-0.71-0.30}$	1 ANDERSON	19	SNO+ Water phase; $\nu_e e$ scattering rate
$5.68^{+0.39+0.03}_{-0.41-0.03}$	2 AGOSTINI	18B	BORX From $\nu_e e$ scattering rate
$5.25 \pm 0.16^{+0.11}_{-0.13}$	3 AHARMIM	13	SNO All three phases combined
$5.046^{+0.159+0.107}_{-0.152-0.123}$	4 AHARMIM	10	SNO From ϕ_{NC} in Phase I+II, low threshold
$5.54^{+0.33+0.36}_{-0.31-0.34}$	5 AHARMIM	08	SNO ϕ_{NC} in Phase III

See key on page 1127

Lepton Particle Listings

Neutrino Mixing

4.94 ± 0.21 ^{+0.38} / _{-0.34}	⁶ AHARMIM	05A	SNO	From ϕ_{NC} ; ⁸ B shape not const.
4.81 ± 0.19 ^{+0.28} / _{-0.27}	⁶ AHARMIM	05A	SNO	From ϕ_{NC} ; ⁸ B shape constrained
5.09 ^{+0.44} / _{-0.43} ^{+0.46} / _{-0.43}	⁷ AHMAD	02	SNO	Direct measurement from ϕ_{NC}
5.44 ± 0.99	⁸ AHMAD	01		Derived from SNO+SuperKam, water Cherenkov

0.063 ± 0.042 ± 0.037	⁴ CRAVENS	08	SKAM	Based on ϕ_{ES}
0.021 ± 0.020 ^{+0.012} / _{-0.013}	⁵ HOSAKA	06	SKAM	Based on ϕ_{ES}
0.017 ± 0.016 ^{+0.012} / _{-0.013}	⁶ HOSAKA	06	SKAM	Fitted in the LMA region
-0.056 ± 0.074 ± 0.053	⁷ AHARMIM	05A	SNO	From salty SNO ϕ_{CC}
-0.037 ± 0.063 ± 0.032	⁷ AHARMIM	05A	SNO	From salty SNO ϕ_{CC} ; const. of no ϕ_{NC} asymmetry
0.14 ± 0.063 ^{+0.015} / _{-0.014}	⁸ AHMAD	02B	SNO	Derived from SNO ϕ_{CC}
0.07 ± 0.049 ^{+0.013} / _{-0.012}	⁹ AHMAD	02B	SNO	Const. of no ϕ_{NC} asymmetry

- ANDERSON 19 reports this result from the measured ν_e elastic scattering rate using a 69.2 kton-day (or 114.7 days) of exposure from May through December, 2017 during the SNO+ detector's water commissioning phase, assuming the neutrino mixing parameters given in PDG 16 and a standard solar model given in BAHCALL 05.
- AGOSTINI 18B obtained this result from the measured ν_e elastic scattering rate over the period between January 2008 and December 2016, assuming the MSW-LMA oscillation parameters derived by ESTEBAN 17. Assuming a high-metallicity standard solar model, the electron neutrino survival probability for the ⁸B solar neutrino is calculated to be 0.37 ± 0.08.
- AHARMIM 13 obtained this result from a combined analysis of the data from all three phases, SNO-I, II, and III. The measurement of the ⁸B flux mostly comes from the NC signal, however, CC contribution is included in the fit.
- AHARMIM 10 reports this result from a joint analysis of SNO Phase I+II data with the "effective electron kinetic energy" threshold of 3.5 MeV. This result is obtained with the assumption of unitarity, which relates the NC, CC, and ES rates. The data were fit with the free parameters directly describing the total ⁸B neutrino flux and the energy-dependent ν_e survival probability.
- AHARMIM 08 reports the results from SNO Phase III measurement using an array of ³He proportional counters to measure the rate of NC interactions in heavy water, over the period between November 27, 2004 and November 28, 2006, corresponding to 385.17 live days. A simultaneous fit was made for the number of NC events detected by the proportional counters and the numbers of NC, CC, and ES events detected by the PMTs, where the spectral distributions of the ES and CC events were not constrained to the ⁸B shape.
- AHARMIM 05A measurements were made with dissolved NaCl (0.195% by weight) in heavy water over the period between July 26, 2001 and August 28, 2003, corresponding to 391.4 live days, and update AHMED 04A. The CC, ES, and NC events were statistically separated. In one method, the ⁸B energy spectrum was not constrained. In the other method, the constraint of an undistorted ⁸B energy spectrum was added for comparison with AHMAD 02 results.
- AHMAD 02 determined the total flux of active ⁸B solar neutrinos by directly measuring the neutral-current reaction, $\nu_e d \rightarrow np \nu_e$, which is equally sensitive to $\nu_e, \nu_\mu,$ and ν_τ . The complete description of the SNO Phase I data set is given in AHARMIM 07.
- AHMAD 01 deduced the total flux of active ⁸B solar neutrinos by combining the SNO charged-current result (AHMAD 01) and the Super-Kamiokande ν_e elastic-scattering result (FUKUDA 01).

Total Flux of Active CNO Solar Neutrinos

Total flux of active neutrinos (ν_e, ν_μ, ν_τ).

VALUE ($10^8 \text{ cm}^{-2} \text{ s}^{-1}$)	CL%	DOCUMENT ID	TECN	COMMENT
• • •				We do not use the following data for averages, fits, limits, etc. • • •
<7.9	95	¹ AGOSTINI	18B	BORX Use ν_e e scattering rate
				¹ AGOSTINI 18B obtained this result from an upper limit of the ν_e e elastic scattering rate for the CNO neutrinos over the period between December 2011 and May 2016, assuming the MSW-LMA oscillation parameters derived by ESTEBAN 17.

Total Flux of Active hep Solar Neutrinos

Total flux of active neutrinos (ν_e, ν_μ, ν_τ).

VALUE ($10^5 \text{ cm}^{-2} \text{ s}^{-1}$)	CL%	DOCUMENT ID	TECN	COMMENT
• • •				We do not use the following data for averages, fits, limits, etc. • • •
<1.8	90	¹ AGOSTINI	20A	BORX Use ν_e e scattering and $^{12}\text{C}(\nu, \nu')^{12}\text{C}^*$
<0.3	90	² AHARMIM	20	SNO CC, NC, ν_e e scattering
<2.2	90	³ AGOSTINI	18B	BORX Use ν_e e scattering rate
				¹ AGOSTINI 20A obtained this result from an upper limit of the ν_e e elastic scattering rate and NC-mediated inelastic scattering on carbon nuclei with 15.1 MeV deexcitation γ -ray for the hep neutrino. The dataset corresponds to an effective exposure of 0.745 kt-yr from November 2009 to October 2017. A FADC DAQ system, optimized for the acquisition of high-energy events was used for data collection. The MSW-LMA oscillation parameters derived by ESTEBAN 17 were assumed.
				² AHARMIM 20 uses the entire SNO dataset, corresponding to 2.47 kton-yr of exposure after fiducialization. With the D ₂ O target, SNO was sensitive to charged current, neutral current, and elastic scattering channels.
				³ AGOSTINI 18B obtained this result from an upper limit of the ν_e e elastic scattering rate for the hep neutrino using the dataset corresponding to an exposure of 0.8 kt-yr and assuming the MSW-LMA oscillation parameters derived by ESTEBAN 17.

Day-Night Asymmetry (⁸B)

$$A = (\phi_{\text{night}} - \phi_{\text{day}}) / \phi_{\text{average}}$$

VALUE	DOCUMENT ID	TECN	COMMENT
0.033 ± 0.010 ± 0.005	¹ ABE	16c	SKAM SK combined; Based on ϕ_{ES}
• • •			We do not use the following data for averages, fits, limits, etc. • • •
0.036 ± 0.016 ± 0.006	² ABE	16c	SKAM SK-IV; Based on ϕ_{ES}
0.032 ± 0.011 ± 0.005	³ RENSHAW	14	SKAM Based on ϕ_{ES}

- ABE 16c reports the combined day-night flux asymmetry results of the four phases of the Super-Kamiokande measurements. Amplitude fit method is used. See footnote to RENSHAW 14.
- ABE 16c reports the Super-Kamiokande-IV results for 1664 live days from September 2008 to February 2014. The analysis threshold for day-night flux asymmetry is recoil electron energy of 4.49 MeV (total electron energy of 5.0 MeV). Amplitude fit method is used. See footnote to RENSHAW 14.
- RENSHAW 14 obtains this result by using the "amplitude fit" introduced in SMY 04. The data from the Super-Kamiokande(SK)-I, -II, -III, and 1306 live days of the SK-IV measurements are used. The analysis threshold is recoil-electron kinetic energy of 4.5 MeV for SK-III, and SK-IV except for 250 live days in SK-III (6.0 MeV). The analysis threshold for SK-I and SK-II is the same as in the previous reports. (Note that in the previous SK solar-neutrino results, the analysis threshold is quoted as recoil-electron total energy.) This day-night asymmetry result is consistent with neutrino oscillations for $4 \times 10^{-5} \text{ eV}^2 < \Delta m_{21}^2 < 7 \times 10^{-5} \text{ eV}^2$ and large mixing values of θ_{12} at the 68% CL.
- CRAVENS 08 reports the Super-Kamiokande-II results for 791 live days from December 2002 to October 2005. The photocathode coverage of the detector is 19% (reduced from 40% of that of Super-Kamiokande-I due to an accident in 2001). The analysis threshold for the day and night fluxes is 7.5 MeV except for the first 159 live days (8.0 MeV).
- HOSAKA 06 reports the final results for 1496 live days with Super-Kamiokande-I between May 31, 1996 and July 15, 2001, and replace FUKUDA 02 results. The analysis threshold is 5 MeV except for the first 280 live days (6.5 MeV).
- This result with reduced statistical uncertainty is obtained by assuming two-neutrino oscillations within the LMA (large mixing angle) region and by fitting the time variation of the solar neutrino flux measured via ν_e elastic scattering to the variations expected from neutrino oscillations. For details, see SMY 04. There is an additional small systematic error of ±0.0004 coming from uncertainty of oscillation parameters.
- AHARMIM 05A measurements were made with dissolved NaCl (0.195% by weight) in heavy water over the period between July 26, 2001 and August 28, 2003, with 176.5 days of the live time recorded during the day and 214.9 days during the night. This result is obtained with the spectral distribution of the CC events not constrained to the ⁸B shape.
- AHMAD 02B results are based on the charged-current interactions recorded between November 2, 1999 and May 28, 2001, with the day and night live times of 128.5 and 177.9 days, respectively. The complete description of the SNO Phase I data set is given in AHARMIM 07.
- AHMAD 02B results are derived from the charged-current interactions, neutral-current interactions, and ν_e elastic scattering, with the total flux of active neutrinos constrained to have no asymmetry. The data were recorded between November 2, 1999 and May 28, 2001, with the day and night live times of 128.5 and 177.9 days, respectively. The complete description of the SNO Phase I data set is given in AHARMIM 07.

ϕ_{ES} (⁷Be)

⁷Be solar-neutrino flux measured via ν_e elastic scattering. This process is sensitive to all active neutrino flavors, but with reduced sensitivity to ν_μ, ν_τ due to the cross-section difference, $\sigma(\nu_{\mu,\tau} e) \sim 0.2 \sigma(\nu_e e)$. If the ⁷Be solar-neutrino flux involves nonelectron flavor active neutrinos, their contribution to the flux is ~ 0.2 times that of ν_e .

VALUE ($10^9 \text{ cm}^{-2} \text{ s}^{-1}$)	DOCUMENT ID	TECN	COMMENT
• • •			We do not use the following data for averages, fits, limits, etc. • • •
3.26 ± 0.52	¹ GANDO	15	KLND average flux
3.10 ± 0.15	² BELLINI	11A	BORX average flux

- GANDO 15 uses 165.4 kton-day exposure of the KamLAND liquid scintillator detector to measure the 862 keV ⁷Be solar neutrino flux via $\nu - e$ elastic scattering
- BELLINI 11A reports the ⁷Be solar neutrino flux measured via $\nu - e$ elastic scattering. The data correspond to 740.7 live days between May 16, 2007 and May 8, 2010, and also correspond to 153.6 ton-year fiducial exposure. BELLINI 11A measured the 862 keV ⁷Be solar neutrino flux, which is an 89.6% branch of the ⁷Be solar neutrino flux, to be $(2.78 \pm 0.13) \times 10^9 \text{ cm}^{-2} \text{ s}^{-1}$. Supercedes ARPESELLA 08A.

ϕ_{ES} ($p\bar{p}p$)

$p\bar{p}p$ solar-neutrino flux measured via ν_e elastic scattering. This process is sensitive to all active neutrino flavors, but with reduced sensitivity to ν_μ, ν_τ due to the cross section difference, $\sigma(\nu_{\mu,\tau} e) \sim 0.2 \sigma(\nu_e e)$. If the $p\bar{p}p$ solar-neutrino flux involves non-electron flavor active neutrinos, their contribution to the flux is ~ 0.2 times that of ν_e .

VALUE ($10^8 \text{ cm}^{-2} \text{ s}^{-1}$)	DOCUMENT ID	TECN	COMMENT
• • •			We do not use the following data for averages, fits, limits, etc. • • •
1.0 ± 0.2	¹ BELLINI	12A	BORX average flux

- BELLINI 12A reports 1.44 MeV $p\bar{p}p$ solar-neutrino flux measured via ν_e elastic scattering. The data were collected between January 13, 2008 and May 9, 2010, corresponding to 20,4009 ton-day fiducial exposure. The listed flux value is calculated from the observed

Lepton Particle Listings

Neutrino Mixing

rate of pep solar neutrino interactions in Borexino ($3.1 \pm 0.6 \pm 0.3$ counts/(day-100 ton)) and the corresponding rate expected for no neutrino flavor oscillations (4.47 ± 0.05 counts/(day-100 ton)), using the SSM prediction for the pep solar neutrino flux of $(1.441 \pm 0.012) \times 10^6 \text{ cm}^{-2} \text{ s}^{-1}$.

$\phi_{ES}(\text{CNO})$

CNO solar-neutrino flux measured via ν_e elastic scattering. This process is sensitive to all active neutrino flavors, but with reduced sensitivity to ν_μ, ν_τ due to the cross section difference, $\sigma(\nu_{\mu,\tau} e) \sim 0.2 \sigma(\nu_e e)$. If the CNO solar-neutrino flux involves non-electron flavor active neutrinos, their contribution to the flux is ~ 0.2 times that of ν_e .

VALUE ($10^8 \text{ cm}^{-2} \text{ s}^{-1}$)	CL%	DOCUMENT ID	TECN	COMMENT
---	-----	-------------	------	---------

• • • We do not use the following data for averages, fits, limits, etc. • • •

<7.7	90	¹ BELLINI	12A	BORX MSW-LMA solution assumed
------	----	----------------------	-----	-------------------------------

¹BELLINI 12A reports an upper limit of the CNO solar neutrino flux measured via ν_e elastic scattering. The data were collected between January 13, 2008 and May 9, 2010, corresponding to 20,409 ton-day fiducial exposure.

$\phi_{ES}(pp)$

pp solar-neutrino flux measured via ν_e elastic scattering. This process is sensitive to all active neutrino flavors, but with reduced sensitivity to ν_μ, ν_τ due to the cross section difference, $\sigma(\nu_{\mu,\tau} e) \sim 0.3 \sigma(\nu_e e)$. If the pp solar-neutrino flux involves non-electron flavor active neutrinos, their contribution to the flux is ~ 0.3 times of ν_e .

VALUE ($10^{10} \text{ cm}^{-2} \text{ s}^{-1}$)	DOCUMENT ID	TECN	COMMENT
--	-------------	------	---------

• • • We do not use the following data for averages, fits, limits, etc. • • •

4.4±0.5		¹ BELLINI	14A	BORX average flux
---------	--	----------------------	-----	-------------------

¹BELLINI 14A reports pp solar-neutrino flux measured via ν_e elastic scattering. The data were collected between January 2012 and May 2013, corresponding to 408 days of data. The pp neutrino interaction rate in Borexino is measured to be $144 \pm 13 \pm 10$ counts/(day-100 ton) by fitting the measured energy spectrum of events in the 165–590 keV recoil electron kinetic energy window with the expected signal + background spectrum. The listed flux value $\phi_{ES}(pp)$ is calculated from the observed rate and the number of $(3.307 \pm 0.003) \times 10^{31}$ electrons for 100 tons of the Borexino scintillator, and the $\nu_e e$ integrated cross section over the pp neutrino spectrum, $\sigma(\nu_e e) = 11.38 \times 10^{-46} \text{ cm}^2$.

$\phi_{CC}(pp)$

pp solar-neutrino flux measured with charged-current reaction which is sensitive exclusively to ν_e .

VALUE ($10^{10} \text{ cm}^{-2} \text{ s}^{-1}$)	DOCUMENT ID	TECN	COMMENT
--	-------------	------	---------

• • • We do not use the following data for averages, fits, limits, etc. • • •

3.38±0.47		¹ ABDURASHI... 09	FIT	Fit existing solar- ν data
-----------	--	------------------------------	-----	--------------------------------

¹ABDURASHITOV 09 reports the pp solar-neutrino flux derived from the Ga solar neutrino capture rate by subtracting contributions from $^8\text{B}, ^7\text{Be}, pep$ and CNO solar neutrino fluxes determined by other solar neutrino experiments as well as neutrino oscillation parameters determined from available world neutrino oscillation data.

$\phi_{ES}(\text{hep})$

hep solar-neutrino flux measured via ν_e elastic scattering. This process is sensitive to all active neutrino flavors, but with reduced sensitivity to ν_μ, ν_τ due to the cross-section difference, $\sigma(\nu_{\mu,\tau} e) \sim 0.16 \sigma(\nu_e e)$. If the hep solar-neutrino flux involves nonelectron flavor active neutrinos, their contribution to the flux is ~ 0.16 times of ν_e .

VALUE ($10^3 \text{ cm}^{-2} \text{ s}^{-1}$)	CL%	DOCUMENT ID	TECN	COMMENT
---	-----	-------------	------	---------

• • • We do not use the following data for averages, fits, limits, etc. • • •

<73	90	¹ HOSAKA	06	SKAM
-----	----	---------------------	----	------

¹HOSAKA 06 result is obtained from the recoil electron energy window of 18–21 MeV, and updates FUKUDA 01 result.

$\phi_{\bar{\nu}_e}(\text{}^8\text{B})$

Searches are made for electron antineutrino flux from the Sun. Flux limits listed here are derived relative to the BS05(OP) Standard Solar Model ^8B solar neutrino flux ($5.69 \times 10^6 \text{ cm}^{-2} \text{ s}^{-1}$), with an assumption that solar $\bar{\nu}_e$ s follow an unoscillated ^8B neutrino spectrum.

VALUE (%)	CL%	DOCUMENT ID	TECN	COMMENT
-----------	-----	-------------	------	---------

• • • We do not use the following data for averages, fits, limits, etc. • • •

<0.0072	90	¹ AGOSTINI	21	BORX $E_{\bar{\nu}_e} > 1.8 \text{ MeV}$
<0.013	90	² BELLINI	11	BORX $E_{\bar{\nu}_e} > 1.8 \text{ MeV}$
<1.9	90	³ BALATA	06	CNTR $1.8 < E_{\bar{\nu}_e} < 20.0 \text{ MeV}$
<0.72	90	AHARMIM	04	SNO $4.0 < E_{\bar{\nu}_e} < 14.8 \text{ MeV}$
<0.022	90	EGUCHI	04	KLND $8.3 < E_{\bar{\nu}_e} < 14.8 \text{ MeV}$
<0.7	90	GANDO	03	SKAM $8.0 < E_{\bar{\nu}_e} < 20.0 \text{ MeV}$
<1.7	90	AGLIETTA	96	LSD $7 < E_{\bar{\nu}_e} < 17 \text{ MeV}$

¹AGOSTINI 21 derived this result relative to the Standard Solar Model ^8B solar neutrino flux, under an assumption of high solar metallicity, of $5.46 (1 \pm 0.12) \times 10^6 \text{ cm}^{-2} \text{ s}^{-1}$ (see VINYOLES 17).

²Superseded by AGOSTINI 21.

³BALATA 06 obtained this result from the search for $\bar{\nu}_e$ interactions with Counting Test Facility (the prototype of the Borexino detector).

(B) Three-neutrino mixing parameters

$\sin^2(\theta_{12})$

If an experiment reports $\sin^2(2\theta_{12})$ we convert the value to $\sin^2(\theta_{12})$.

VALUE	DOCUMENT ID	TECN	COMMENT
-------	-------------	------	---------

0.307+0.013 -0.012	¹ ABE	16c	FIT KamLAND+global solar; 3ν
-------------------------------------	------------------	-----	----------------------------------

• • • We do not use the following data for averages, fits, limits, etc. • • •

0.318±0.016	² SALAS	21	FIT global fit
0.304±0.012	³ ESTEBAN	20A	FIT Global fit
0.320+0.020 -0.016	DE-SALAS	18	FIT Global fit
0.310±0.014	⁴ ABE	16c	FIT SKAM+SNO; 3ν
0.334+0.027 -0.023	⁵ ABE	16c	FIT SK-I+II+III+IV; 3ν
0.327+0.026 -0.031	⁶ ABE	16c	FIT SK-IV; 3ν
0.323±0.016	⁷ FORERO	14	FIT 3ν
0.304+0.013 -0.012	⁸ GONZALEZ...	14	FIT Either mass ordering; global fit
0.299+0.014 -0.014	^{9,10} AHARMIM	13	FIT global solar: 2ν
0.307+0.016 -0.013	^{10,11} AHARMIM	13	FIT global solar: 3ν
0.304+0.022 -0.018	^{10,12} AHARMIM	13	FIT KamLAND + global solar: 3ν
0.304+0.014 -0.013	¹³ GANDO	13	FIT KamLAND + global solar + SBL + accelerator: 3ν
0.304+0.014 -0.013	¹⁴ GANDO	13	FIT KamLAND + global solar: 3ν
0.325+0.039 -0.039	¹⁵ GANDO	13	FIT KamLAND: 3ν
0.30+0.02 -0.01	¹⁶ ABE	11	FIT KamLAND + global solar: 2ν
0.30+0.02 -0.01	¹⁷ ABE	11	FIT global solar: 2ν
0.31+0.03 -0.02	¹⁸ ABE	11	FIT KamLAND + global solar: 3ν
0.31+0.03 -0.03	¹⁹ ABE	11	FIT global solar: 3ν
0.314+0.015 -0.012	²⁰ BELLINI	11A	FIT KamLAND + global solar: 2ν
0.319+0.017 -0.015	²¹ BELLINI	11A	FIT global solar: 2ν
0.311+0.016 -0.016	²² GANDO	11	FIT KamLAND + solar: 3ν
0.304+0.046 -0.042	²³ GANDO	11	FIT KamLAND: 3ν
0.314+0.018 -0.014	^{24,25} AHARMIM	10	FIT KamLAND + global solar: 2ν
0.314+0.017 -0.020	^{24,26} AHARMIM	10	FIT global solar: 2ν
0.319+0.019 -0.016	^{24,27} AHARMIM	10	FIT KamLAND + global solar: 3ν
0.319+0.023 -0.024	^{24,28} AHARMIM	10	FIT global solar: 3ν
0.36+0.05 -0.04	²⁹ ABE	08A	FIT KamLAND
0.32±0.03	³⁰ ABE	08A	FIT KamLAND + global fit
0.32±0.02	³¹ AHARMIM	08	FIT KamLAND + global solar
0.31+0.04 -0.04	³² HOSAKA	06	FIT KamLAND + global solar
0.31+0.04 -0.03	³³ HOSAKA	06	FIT SKAM+SNO+KamLAND
0.31+0.03 -0.04	³⁴ HOSAKA	06	FIT SKAM+SNO
0.31+0.02 -0.03	³⁵ AHARMIM	05A	FIT KamLAND + global solar
0.25–0.39	³⁶ AHARMIM	05A	FIT global solar
0.29±0.03	³⁷ ARAKI	05	FIT KamLAND + global solar
0.29+0.03 -0.02	³⁸ AHMED	04A	FIT KamLAND + global solar
0.23–0.37	³⁹ AHMED	04A	FIT global solar
0.31+0.04 -0.04	⁴⁰ SMY	04	FIT KamLAND + global solar
0.29+0.04 -0.04	⁴¹ SMY	04	FIT global solar
0.32+0.06 -0.05	⁴² SMY	04	FIT SKAM + SNO
0.19–0.33	⁴³ AHMAD	02B	FIT global solar
0.19–0.39	⁴⁴ FUKUDA	02	FIT global solar

¹ABE 16c obtained this result by a three-neutrino oscillation analysis, with a constraint of $\sin^2(\theta_{13}) = 0.0219 \pm 0.0014$ coming from reactor neutrino experiments, using all solar data and KamLAND data. $CP T$ invariance is assumed.

²SALAS 21 reports results of a global fit to neutrino oscillation data available at the time of the Neutrino 2020 conference.

³ESTEBAN 20A reports results of a global fit to neutrino oscillation data available at the time of the Neutrino2020 conference.

- ⁴ ABE 16c obtained this result by a three-neutrino oscillation analysis, with a constraint of $\sin^2(\theta_{13}) = 0.0219 \pm 0.0014$ coming from reactor neutrino experiments, using Super-Kamiokande (I+II+III+IV) and SNO data.
- ⁵ ABE 16c obtained this result by a three-neutrino oscillation analysis, with a constraint of $\sin^2(\theta_{13}) = 0.0219 \pm 0.0014$ coming from reactor neutrino experiments, by combining the four phases of the Super-Kamiokande solar data.
- ⁶ ABE 16c obtained this result by a three-neutrino oscillation analysis, with a constraint of $\sin^2(\theta_{13}) = 0.0219 \pm 0.0014$ coming from reactor neutrino experiments, using the Super-Kamiokande-IV data.
- ⁷ FORERO 14 performs a global fit to neutrino oscillations using solar, reactor, long-baseline accelerator, and atmospheric neutrino data.
- ⁸ GONZALEZ-GARCIA 14 result comes from a frequentist global fit. The corresponding Bayesian global fit to the same data results are reported in BERGSTROM 15 as $0.304^{+0.013}_{-0.012}$ for normal and $0.305^{+0.012}_{-0.013}$ for inverted mass ordering.
- ⁹ AHARMIM 13 obtained this result by a two-neutrino oscillation analysis using global solar neutrino data.
- ¹⁰ AHARMIM 13 global solar neutrino data include SNO's all-phases-combined analysis results on the total active ^8B neutrino flux and energy-dependent ν_e survival probability parameters, measurements of Cl (CLEVELAND 98), Ga (ABDURASHITOV 09 which contains combined analysis with GNO (ALTMANN 05 and Ph.D. thesis of F. Kaether)), and ^7Be (BELLINI 11A) rates, and ^8B solar-neutrino recoil electron measurements of SK-I (HOSAKA 06) zenith, SK-II (CRAVENS 08) and SK-III (ABE 11) day/night spectra, and Borexino (BELLINI 10A) spectra.
- ¹¹ AHARMIM 13 obtained this result by a three-neutrino oscillation analysis with the value of Δm_{32}^2 fixed to $2.45 \times 10^{-3} \text{ eV}^2$, using global solar neutrino data.
- ¹² AHARMIM 13 obtained this result by a three-neutrino oscillation analysis with the value of Δm_{32}^2 fixed to $2.45 \times 10^{-3} \text{ eV}^2$, using global solar neutrino and KamLAND (GANDO 11) data. *CPT* invariance is assumed.
- ¹³ GANDO 13 obtained this result by a three-neutrino oscillation analysis using KamLAND, global solar neutrino, short-baseline (SBL) reactor, and accelerator data, assuming *CPT* invariance. Supersedes GANDO 11.
- ¹⁴ GANDO 13 obtained this result by a three-neutrino oscillation analysis using KamLAND and global solar neutrino data, assuming *CPT* invariance. Supersedes GANDO 11.
- ¹⁵ GANDO 13 obtained this result by a three-neutrino oscillation analysis using KamLAND data. Supersedes GANDO 11.
- ¹⁶ ABE 11 obtained this result by a two-neutrino oscillation analysis using solar neutrino data including Super-Kamiokande, SNO, Borexino (ARPESELLA 08A), Homestake, GALLEX/GNO, SAGE, and KamLAND data. *CPT* invariance is assumed.
- ¹⁷ ABE 11 obtained this result by a two-neutrino oscillation analysis using solar neutrino data including Super-Kamiokande, SNO, Borexino (ARPESELLA 08A), Homestake, GALLEX/GNO, and SAGE data.
- ¹⁸ ABE 11 obtained this result by a three-neutrino oscillation analysis with the value of Δm_{32}^2 fixed to $2.4 \times 10^{-3} \text{ eV}^2$, using solar neutrino data including Super-Kamiokande, SNO, Borexino (ARPESELLA 08A), Homestake, GALLEX/GNO, SAGE, and KamLAND data. The normal neutrino mass ordering and *CPT* invariance are assumed.
- ¹⁹ ABE 11 obtained this result by a three-neutrino oscillation analysis with the value of Δm_{32}^2 fixed to $2.4 \times 10^{-3} \text{ eV}^2$, using solar neutrino data including Super-Kamiokande, SNO, Borexino (ARPESELLA 08A), Homestake, and GALLEX/GNO data. The normal neutrino mass ordering is assumed.
- ²⁰ BELLINI 11A obtained this result by a two-neutrino oscillation analysis using KamLAND, Homestake, SAGE, Gallex, GNO, Kamiokande, Super-Kamiokande, SNO, and Borexino (BELLINI 11A) data and the SSM flux prediction in SERENELLI 11 (Astrophysical Journal **743** 24 (2011)) with the exception that the ^8B flux was left free. *CPT* invariance is assumed.
- ²¹ BELLINI 11A obtained this result by a two-neutrino oscillation analysis using Homestake, SAGE, Gallex, GNO, Kamiokande, Super-Kamiokande, SNO, and Borexino (BELLINI 11A) data and the SSM flux prediction in SERENELLI 11 (Astrophysical Journal **743** 24 (2011)) with the exception that the ^8B flux was left free.
- ²² GANDO 11 obtain this result with three-neutrino fit using the KamLAND + solar data. Superseded by GANDO 13.
- ²³ GANDO 11 obtain this result with three-neutrino fit using the KamLAND data only. Superseded by GANDO 13.
- ²⁴ AHARMIM 10 global solar neutrino data include SNO's low-energy-threshold analysis survival probability day/night curves, SNO Phase III integral rates (AHARMIM 08), Cl (CLEVELAND 98), SAGE (ABDURASHITOV 09), Gallex/GNO (HAMPEL 99, ALTMANN 05), Borexino (ARPESELLA 08A), SK-I zenith (HOSAKA 06), and SK-II day/night spectra (CRAVENS 08).
- ²⁵ AHARMIM 10 obtained this result by a two-neutrino oscillation analysis using global solar neutrino data and KamLAND data (ABE 08A). *CPT* invariance is assumed.
- ²⁶ AHARMIM 10 obtained this result by a two-neutrino oscillation analysis using global solar neutrino data.
- ²⁷ AHARMIM 10 obtained this result by a three-neutrino oscillation analysis with the value of Δm_{31}^2 fixed to $2.3 \times 10^{-3} \text{ eV}^2$, using global solar neutrino data and KamLAND data (ABE 08A). *CPT* invariance is assumed.
- ²⁸ AHARMIM 10 obtained this result by a three-neutrino oscillation analysis with the value of Δm_{31}^2 fixed to $2.3 \times 10^{-3} \text{ eV}^2$, using global solar neutrino data.
- ²⁹ ABE 08A obtained this result by a rate + shape + time combined geoneutrino and reactor two-neutrino fit for Δm_{21}^2 and $\tan^2\theta_{12}$, using KamLAND data only. Superseded by GANDO 11.
- ³⁰ ABE 08A obtained this result by means of a two-neutrino fit using KamLAND, Homestake, SAGE, GALLEX, GNO, SK (zenith angle and E-spectrum), the SNO χ^2 -map, and solar flux data. *CPT* invariance is assumed. Superseded by GANDO 11.
- ³¹ The result given by AHARMIM 08 is $\theta = (34.4^{+1.3}_{-1.2})^\circ$. This result is obtained by a two-neutrino oscillation analysis using solar neutrino data including those of Borexino (ARPESELLA 08A) and Super-Kamiokande-I (HOSAKA 06), and KamLAND data (ABE 08A). *CPT* invariance is assumed.
- ³² HOSAKA 06 obtained this result by a two-neutrino oscillation analysis using SK ν_e data, CC data from other solar neutrino experiments, and KamLAND data (ARAKI 05). *CPT* invariance is assumed.
- ³³ HOSAKA 06 obtained this result by a two-neutrino oscillation analysis using the data from Super-Kamiokande, SNO (AHMAD 02 and AHMAD 02B), and KamLAND (ARAKI 05) experiments. *CPT* invariance is assumed.
- ³⁴ HOSAKA 06 obtained this result by a two-neutrino oscillation analysis using the Super-Kamiokande and SNO (AHMAD 02 and AHMAD 02B) solar neutrino data.
- ³⁵ The result given by AHARMIM 05A is $\theta = (33.9 \pm 1.6)^\circ$. This result is obtained by a two-neutrino oscillation analysis using SNO pure deuterium and salt phase data, SK ν_e data, Cl and Ga CC data, and KamLAND data (ARAKI 05). *CPT* invariance is assumed. AHARMIM 05A also quotes $\theta = (33.9^{+2.4}_{-2.2})^\circ$ as the error enveloping the 68% CL two-dimensional region. This translates into $\sin^2 2\theta = 0.86^{+0.05}_{-0.06}$.
- ³⁶ AHARMIM 05A obtained this result by a two-neutrino oscillation analysis using the data from all solar neutrino experiments. The listed range of the parameter envelops the 95% CL two-dimensional region shown in figure 35a of AHARMIM 05A. AHARMIM 05A also quotes $\tan^2\theta = 0.45^{+0.09}_{-0.08}$ as the error enveloping the 68% CL two-dimensional region. This translates into $\sin^2 2\theta = 0.86^{+0.05}_{-0.07}$.
- ³⁷ ARAKI 05 obtained this result by a two-neutrino oscillation analysis using KamLAND and solar neutrino data. *CPT* invariance is assumed. The 1σ error shown here is translated from the number provided by the KamLAND collaboration, $\tan^2\theta = 0.40^{+0.05}_{-0.05}$. The corresponding number quoted in ARAKI 05 is $\tan^2\theta = 0.40^{+0.10}_{-0.07}$ ($\sin^2 2\theta = 0.82 \pm 0.07$), which envelops the 68% CL two-dimensional region.
- ³⁸ The result given by AHMED 04A is $\theta = (32.5^{+1.7}_{-1.6})^\circ$. This result is obtained by a two-neutrino oscillation analysis using solar neutrino and KamLAND data (EGUCHI 03). *CPT* invariance is assumed. AHMED 04A also quotes $\theta = (32.5^{+2.4}_{-2.3})^\circ$ as the error enveloping the 68% CL two-dimensional region. This translates into $\sin^2 2\theta = 0.82 \pm 0.06$.
- ³⁹ AHMED 04A obtained this result by a two-neutrino oscillation analysis using the data from all solar neutrino experiments. The listed range of the parameter envelops the 95% CL two-dimensional region shown in Fig. 5(a) of AHMED 04A. The best-fit point is $\Delta(m^2) = 6.5 \times 10^{-5} \text{ eV}^2$, $\tan^2\theta = 0.40$ ($\sin^2 2\theta = 0.82$).
- ⁴⁰ The result given by SMY 04 is $\tan^2\theta = 0.44 \pm 0.08$. This result is obtained by a two-neutrino oscillation analysis using solar neutrino and KamLAND data (IANNI 03). *CPT* invariance is assumed.
- ⁴¹ SMY 04 obtained this result by a two-neutrino oscillation analysis using the data from all solar neutrino experiments. The 1σ errors are read from Fig. 6(a) of SMY 04.
- ⁴² SMY 04 obtained this result by a two-neutrino oscillation analysis using the Super-Kamiokande and SNO (AHMAD 02 and AHMAD 02B) solar neutrino data. The 1σ errors are read from Fig. 6(a) of SMY 04.
- ⁴³ AHMAD 02B obtained this result by a two-neutrino oscillation analysis using the data from all solar neutrino experiments. The listed range of the parameter envelops the 95% CL two-dimensional region shown in Fig. 4(b) of AHMAD 02B. The best fit point is $\Delta(m^2) = 5.0 \times 10^{-5} \text{ eV}^2$ and $\tan\theta = 0.34$ ($\sin^2 2\theta = 0.76$).
- ⁴⁴ FUKUDA 02 obtained this result by a two-neutrino oscillation analysis using the data from all solar neutrino experiments. The listed range of the parameter envelops the 95% CL two-dimensional region shown in Fig. 4 of FUKUDA 02. The best fit point is $\Delta(m^2) = 6.9 \times 10^{-5} \text{ eV}^2$ and $\tan^2\theta = 0.38$ ($\sin^2 2\theta = 0.80$).

 Δm_{21}^2

VALUE (10^{-5} eV^2)	DOCUMENT ID	TECN	COMMENT
7.53 ± 0.18	1	GANDO 13	FIT KamLAND + global solar + SBL + accelerator: 3ν
$7.50^{+0.22}_{-0.20}$	2	SALAS 21	FIT global fit
$7.42^{+0.21}_{-0.20}$	3	ESTEBAN 20A	FIT Global fit
$7.55^{+0.20}_{-0.16}$	DE-SALAS 18	FIT	Global fit
$7.49^{+0.19}_{-0.18}$	4	ABE 16c	FIT KamLAND+global solar; 3ν
$4.8^{+1.3}_{-0.6}$	5	ABE 16c	FIT SKAM+SNO; 3ν
$4.8^{+1.5}_{-0.8}$	6	ABE 16c	FIT SK-I+II+III+IV; 3ν
$3.2^{+2.8}_{-0.2}$	7	ABE 16c	FIT SK-IV; 3ν
$7.6^{+0.19}_{-0.18}$	8	FORERO 14	FIT 3ν
$7.50^{+0.19}_{-0.17}$	9	GONZALEZ...	14 FIT Either mass ordering; global fit
$5.13^{+1.29}_{-0.96}$	10,11	AHARMIM 13	FIT global solar: 2ν
$5.13^{+1.49}_{-0.98}$	11,12	AHARMIM 13	FIT global solar: 3ν
$7.46^{+0.20}_{-0.19}$	11,13	AHARMIM 13	FIT KamLAND + global solar: 3ν
$7.53^{+0.19}_{-0.18}$	14	GANDO 13	FIT KamLAND + global solar: 3ν
$7.54^{+0.19}_{-0.18}$	15	GANDO 13	FIT KamLAND: 3ν
7.6 ± 0.2	16	ABE 11	FIT KamLAND + global solar: 2ν

• • • We do not use the following data for averages, fits, limits, etc. • • •

Lepton Particle Listings

Neutrino Mixing

6.2 ^{+1.1} _{-1.9}	17 ABE	11 FIT	global solar: 2ν
7.7 ± 0.3	18 ABE	11 FIT	KamLAND + global solar: 3ν
6.0 ^{+2.2} _{-2.5}	19 ABE	11 FIT	global solar: 3ν
7.50 ^{+0.16} _{-0.24}	20 BELLINI	11A FIT	KamLAND + global solar: 2ν
5.2 ^{+1.5} _{-0.9}	21 BELLINI	11A FIT	global solar: 2ν
7.50 ^{+0.19} _{-0.20}	22 GANDO	11 FIT	KamLAND + solar: 3ν
7.49 ± 0.20	23 GANDO	11 FIT	KamLAND: 3ν
7.59 ^{+0.20} _{-0.21}	24,25 AHARMIM	10 FIT	KamLAND + global solar: 2ν
5.89 ^{+2.13} _{-2.16}	24,26 AHARMIM	10 FIT	global solar: 2ν
7.59 ± 0.21	24,27 AHARMIM	10 FIT	KamLAND + global solar: 3ν
6.31 ^{+2.49} _{-2.58}	24,28 AHARMIM	10 FIT	global solar: 3ν
7.58 ^{+0.14} _{-0.13} ± 0.15	29 ABE	08A FIT	KamLAND
7.59 ± 0.21	30 ABE	08A FIT	KamLAND + global solar
7.59 ^{+0.19} _{-0.21}	31 AHARMIM	08 FIT	KamLAND + global solar
8.0 ± 0.3	32 HOSAKA	06 FIT	KamLAND + global solar
8.0 ± 0.3	33 HOSAKA	06 FIT	SKAM+SNO+KamLAND
6.3 ^{+3.7} _{-1.5}	34 HOSAKA	06 FIT	SKAM+SNO
5-12	35 HOSAKA	06 FIT	SKAM day/night in the LMA region
8.0 ^{+0.4} _{-0.3}	36 AHARMIM	05A FIT	KamLAND + global solar LMA
3.3-14.4	37 AHARMIM	05A FIT	global solar
7.9 ^{+0.4} _{-0.3}	38 ARAKI	05 FIT	KamLAND + global solar
7.1 ^{+1.0} _{-0.3}	39 AHMED	04A FIT	KamLAND + global solar
3.2-13.7	40 AHMED	04A FIT	global solar
7.1 ^{+0.6} _{-0.5}	41 SMY	04 FIT	KamLAND + global solar
6.0 ^{+1.7} _{-1.6}	42 SMY	04 FIT	global solar
6.0 ^{+2.5} _{-1.6}	43 SMY	04 FIT	SKAM + SNO
2.8-12.0	44 AHMAD	02B FIT	global solar
3.2-19.1	45 FUKUDA	02 FIT	global solar

- ¹ GANDO 13 obtained this result by a three-neutrino oscillation analysis using KamLAND, global solar neutrino, short-baseline (SBL) reactor, and accelerator data, assuming CPT invariance. Supersedes GANDO 11.
- ² SALAS 21 reports results of a global fit to neutrino oscillation data available at the time of the Neutrino 2020 conference.
- ³ ESTEBAN 20A reports results of a global fit to neutrino oscillation data available at the time of the Neutrino2020 conference.
- ⁴ ABE 16c obtained this result by a three-neutrino oscillation analysis, with a constraint of $\sin^2(\theta_{13}) = 0.0219 \pm 0.0014$ coming from reactor neutrino experiments, using all solar data and KamLAND data. CPT invariance is assumed.
- ⁵ ABE 16c obtained this result by a three-neutrino oscillation analysis, with a constraint of $\sin^2(\theta_{13}) = 0.0219 \pm 0.0014$ coming from reactor neutrino experiments, using Super-Kamiokande (I+II+III+IV) and SNO data.
- ⁶ ABE 16c obtained this result by a three-neutrino oscillation analysis, with a constraint of $\sin^2(\theta_{13}) = 0.0219 \pm 0.0014$ coming from reactor neutrino experiments, by combining the four phases of the Super-Kamiokande solar data.
- ⁷ ABE 16c obtained this result by a three-neutrino oscillation analysis, with a constraint of $\sin^2(\theta_{13}) = 0.0219 \pm 0.0014$ coming from reactor neutrino experiments, using the Super-Kamiokande-IV data.
- ⁸ FORERO 14 performs a global fit to Δm_{21}^2 using solar, reactor, long-baseline accelerator, and atmospheric neutrino data.
- ⁹ GONZALEZ-GARCIA 14 result comes from a frequentist global fit. The corresponding Bayesian global fit to the same data results are reported in BERGSTROM 15 as $(7.50_{-0.19}^{+0.17}) \times 10^{-5} \text{ eV}^2$ for normal and $(7.50_{-0.17}^{+0.18}) \times 10^{-5} \text{ eV}^2$ for inverted mass ordering.
- ¹⁰ AHARMIM 13 obtained this result by a two-neutrino oscillation analysis using global solar neutrino data.
- ¹¹ AHARMIM 13 global solar neutrino data include SNO's all-phases-combined analysis results on the total active ^8B neutrino flux and energy-dependent ν_e survival probability parameters, measurements of Cl (CLEVELAND 98), Ga (ABDURASHITOV 09 which contains combined analysis with GNO (ALTMANN 05 and Ph.D. thesis of F. Kaether)), and ^7Be (BELLINI 11A) rates, and ^8B solar-neutrino recoil electron measurements of SK-I (HOSAKA 06) zenith, SK-II (CRAVENS 08), and SK-III (ABE 11) day/night spectra, and Borexino (BELLINI 10A) spectra.
- ¹² AHARMIM 13 obtained this result by a three-neutrino oscillation analysis with the value of Δm_{31}^2 fixed to $2.45 \times 10^{-3} \text{ eV}^2$, using global solar neutrino data.
- ¹³ AHARMIM 13 obtained this result by a three-neutrino oscillation analysis with the value of Δm_{31}^2 fixed to $2.45 \times 10^{-3} \text{ eV}^2$, using global solar neutrino and KamLAND data (GANDO 11). CPT invariance is assumed.
- ¹⁴ GANDO 13 obtained this result by a three-neutrino oscillation analysis using KamLAND and global solar neutrino data, assuming CPT invariance. Supersedes GANDO 11.
- ¹⁵ GANDO 13 obtained this result by a three-neutrino oscillation analysis using KamLAND data. Supersedes GANDO 11.

- ¹⁶ ABE 11 obtained this result by a two-neutrino oscillation analysis using solar neutrino data including Super-Kamiokande, SNO, Borexino (ARPESELLA 08A), Homestake, GALLEX/GNO, SAGE, and KamLAND data. CPT invariance is assumed.
- ¹⁷ ABE 11 obtained this result by a two-neutrino oscillation analysis using solar neutrino data including Super-Kamiokande, SNO, Borexino (ARPESELLA 08A), Homestake, GALLEX/GNO, and SAGE data.
- ¹⁸ ABE 11 obtained this result by a three-neutrino oscillation analysis with the value of Δm_{32}^2 fixed to $2.4 \times 10^{-3} \text{ eV}^2$, using solar neutrino data including Super-Kamiokande, SNO, Borexino (ARPESELLA 08A), Homestake, GALLEX/GNO, SAGE, and KamLAND data. The normal neutrino mass ordering and CPT invariance are assumed.
- ¹⁹ ABE 11 obtained this result by a three-neutrino oscillation analysis with the value of Δm_{32}^2 fixed to $2.4 \times 10^{-3} \text{ eV}^2$, using solar neutrino data including Super-Kamiokande, SNO, Borexino (ARPESELLA 08A), Homestake, and GALLEX/GNO data. The normal neutrino mass ordering is assumed.
- ²⁰ BELLINI 11A obtained this result by a two-neutrino oscillation analysis using KamLAND, Homestake, SAGE, Gallex, GNO, Kamiokande, Super-Kamiokande, SNO, and Borexino (BELLINI 11A) data and the SSM flux prediction in SERENELLI 11 (Astrophysical Journal **743** 24 (2011)) with the exception that the ^8B flux was left free. CPT invariance is assumed.
- ²¹ BELLINI 11A obtained this result by a two-neutrino oscillation analysis using Homestake, SAGE, Gallex, GNO, Kamiokande, Super-Kamiokande, SNO, and Borexino (BELLINI 11A) data and the SSM flux prediction in SERENELLI 11 (Astrophysical Journal **743** 24 (2011)) with the exception that the ^8B flux was left free.
- ²² GANDO 11 obtain this result with three-neutrino fit using the KamLAND + solar data. Superseded by GANDO 13.
- ²³ GANDO 11 obtain this result with three-neutrino fit using the KamLAND data only. Supersedes ABE 08A.
- ²⁴ AHARMIM 10 global solar neutrino data include SNO's low-energy-threshold analysis survival probability day/night curves, SNO Phase III integral rates (AHARMIM 08), Cl (CLEVELAND 98), SAGE (ABDURASHITOV 09), Gallex/GNO (HAMPEL 99, ALTMANN 05), Borexino (ARPESELLA 08A), SK-I zenith (HOSAKA 06), and SK-II day/night spectra (CRAVENS 08).
- ²⁵ AHARMIM 10 obtained this result by a two-neutrino oscillation analysis using global solar neutrino data and KamLAND data (ABE 08A). CPT invariance is assumed.
- ²⁶ AHARMIM 10 obtained this result by a two-neutrino oscillation analysis using global solar neutrino data.
- ²⁷ AHARMIM 10 obtained this result by a three-neutrino oscillation analysis with the value of Δm_{31}^2 fixed to $2.3 \times 10^{-3} \text{ eV}^2$, using global solar neutrino data and KamLAND data (ABE 08A). CPT invariance is assumed.
- ²⁸ AHARMIM 10 obtained this result by a three-neutrino oscillation analysis with the value of Δm_{31}^2 fixed to $2.3 \times 10^{-3} \text{ eV}^2$, using global solar neutrino data.
- ²⁹ ABE 08a obtained this result by a rate + shape + time combined geoneutrino and reactor two-neutrino fit for Δm_{21}^2 and $\tan^2\theta_{12}$, using KamLAND data only. Superseded by GANDO 11.
- ³⁰ ABE 08a obtained this result by means of a two-neutrino fit using KamLAND, Homestake, SAGE, GALLEX, GNO, SK (zenith angle and E-spectrum), the SNO χ^2 -map, and solar flux data. CPT invariance is assumed. Superseded by GANDO 11.
- ³¹ AHARMIM 08 obtained this result by a two-neutrino oscillation analysis using all solar neutrino data including those of Borexino (ARPESELLA 08A) and Super-Kamiokande-I (HOSAKA 06), and KamLAND data (ABE 08A). CPT invariance is assumed.
- ³² HOSAKA 06 obtained this result by a two-neutrino oscillation analysis using solar neutrino and KamLAND data (ARAKI 05). CPT invariance is assumed.
- ³³ HOSAKA 06 obtained this result by a two-neutrino oscillation analysis using the data from Super-Kamiokande, SNO (AHMAD 02 and AHMAD 02B), and KamLAND (ARAKI 05) experiments. CPT invariance is assumed.
- ³⁴ HOSAKA 06 obtained this result by a two-neutrino oscillation analysis using the Super-Kamiokande and SNO (AHMAD 02 and AHMAD 02B) solar neutrino data.
- ³⁵ HOSAKA 06 obtained this result from the consistency between the observed and expected day-night flux asymmetry amplitude. The listed 68% CL range is derived from the 1σ boundary of the amplitude fit to the data. Oscillation parameters are constrained to be in the LMA region. The mixing angle is fixed at $\tan^2\theta = 0.44$ because the fit depends only very weakly on it.
- ³⁶ AHARMIM 05a obtained this result by a two-neutrino oscillation analysis using solar neutrino and KamLAND data (ARAKI 05). CPT invariance is assumed. AHARMIM 05a also quotes $\Delta(m^2) = (8.0_{-0.4}^{+0.6}) \times 10^{-5} \text{ eV}^2$ as the error enveloping the 68% CL two-dimensional region.
- ³⁷ AHARMIM 05a obtained this result by a two-neutrino oscillation analysis using the data from all solar neutrino experiments. The listed range of the parameter envelops the 95% CL two-dimensional region shown in figure 35a of AHARMIM 05a. AHARMIM 05a also quotes $\Delta(m^2) = (6.5_{-2.3}^{+4.4}) \times 10^{-5} \text{ eV}^2$ as the error enveloping the 68% CL two-dimensional region.
- ³⁸ ARAKI 05 obtained this result by a two-neutrino oscillation analysis using KamLAND and solar neutrino data. CPT invariance is assumed. The 1σ error shown here is provided by the KamLAND collaboration. The error quoted in ARAKI 05, $\Delta(m^2) = (7.9_{-0.5}^{+0.6}) \times 10^{-5}$, envelops the 68% CL two-dimensional region.
- ³⁹ AHMED 04a obtained this result by a two-neutrino oscillation analysis using solar neutrino and KamLAND data (EGUCHI 03). CPT invariance is assumed. AHMED 04a also quotes $\Delta(m^2) = (7.1_{-0.6}^{+1.2}) \times 10^{-5} \text{ eV}^2$ as the error enveloping the 68% CL two-dimensional region.
- ⁴⁰ AHMED 04a obtained this result by a two-neutrino oscillation analysis using the data from all solar neutrino experiments. The listed range of the parameter envelops the 95% CL two-dimensional region shown in Fig. 5(a) of AHMED 04a. The best-fit point is $\Delta(m^2) = 6.5 \times 10^{-5} \text{ eV}^2$, $\tan^2\theta = 0.40$ ($\sin^2 2\theta = 0.82$).

See key on page 1127

Lepton Particle Listings

Neutrino Mixing

- ⁴¹ SMY 04 obtained this result by a two-neutrino oscillation analysis using solar neutrino and KamLAND data (IANNI 03). *CPT* invariance is assumed.
- ⁴² SMY 04 obtained this result by a two-neutrino oscillation analysis using the data from all solar neutrino experiments. The 1σ errors are read from Fig. 6(a) of SMY 04.
- ⁴³ SMY 04 obtained this result by a two-neutrino oscillation analysis using the Super-Kamiokande and SNO (AHMAD 02 and AHMAD 02B) solar neutrino data. The 1σ errors are read from Fig. 6(a) of SMY 04.
- ⁴⁴ AHMAD 02B obtained this result by a two-neutrino oscillation analysis using the data from all solar neutrino experiments. The listed range of the parameter envelopes the 95% CL two-dimensional region shown in Fig. 4(b) of AHMAD 02B. The best fit point is $\Delta(m^2) = 5.0 \times 10^{-5} \text{ eV}^2$ and $\tan\theta = 0.34$ ($\sin^2 2\theta = 0.76$).
- ⁴⁵ FUKUDA 02 obtained this result by a two-neutrino oscillation analysis using the data from all solar neutrino experiments. The listed range of the parameter envelopes the 95% CL two-dimensional region shown in Fig. 4 of FUKUDA 02. The best fit point is $\Delta(m^2) = 6.9 \times 10^{-5} \text{ eV}^2$ and $\tan^2\theta = 0.38$ ($\sin^2 2\theta = 0.80$).

$\sin^2(\theta_{23})$

The reported limits below correspond to the projection onto the $\sin^2(\theta_{23})$ axis of the 90% CL contours in the $\sin^2(\theta_{23}) - \Delta m_{32}^2$ plane presented by the authors. Unless otherwise specified, the limits are 90% CL and the reported uncertainties are 68% CL.

If an experiment reports $\sin^2(2\theta_{23})$ we convert the value to $\sin^2(\theta_{23})$.

VALUE	DOCUMENT ID	TECN	COMMENT
0.539 ± 0.022 OUR FIT			Error includes scale factor of 1.1. Assuming inverted mass ordering
0.546 ± 0.021 OUR FIT			Assuming normal mass ordering
0.53 ^{+0.03} / _{-0.04}	1 ABE	20F T2K	Both mass orderings
0.43 ^{+0.20} / _{-0.04}	2 ADAMSON	20A MINS	Normal mass ordering
0.42 ^{+0.07} / _{-0.03}	2 ADAMSON	20A MINS	Inverted mass ordering
0.56 ^{+0.04} / _{-0.03}	3 ACERO	19 NOVA	Normal mass order; octant II for θ_{23}
0.56 ^{+0.04} / _{-0.03}	3,4 ACERO	19 NOVA	Inverted mass order; octant II for θ_{23}
0.51 ^{+0.07} / _{-0.09}	5 AARTSEN	18A ICCB	Normal mass ordering
0.588 ^{+0.031} / _{-0.064}	6 ABE	18B SKAM	Normal mass ordering, θ_{13} constrained
0.575 ^{+0.036} / _{-0.073}	6 ABE	18B SKAM	Inverted mass ordering, θ_{13} constrained
• • • We do not use the following data for averages, fits, limits, etc. • • •			
0.51 ^{+0.06} / _{-0.07}	7 ABE	21A T2K	ν_μ disappearance
0.43 ^{+0.21} / _{-0.05}	7 ABE	21A T2K	$\bar{\nu}_\mu$ disappearance
0.574 ± 0.014	8 SALAS	21 FIT	Normal mass ordering, global fit
0.578 ^{+0.010} / _{-0.017}	8 SALAS	21 FIT	Inverted mass ordering, global fit
0.455	9 AARTSEN	20 ICCB	For both mass orderings
0.573 ^{+0.016} / _{-0.020}	10 ESTEBAN	20A FIT	Normal mass ordering, global fit
0.575 ^{+0.016} / _{-0.019}	10 ESTEBAN	20A FIT	Inverted mass ordering, global fit
0.58 ^{+0.04} / _{-0.13}	11 AARTSEN	19c ICCB	
0.48 ^{+0.04} / _{-0.03}	3,4 ACERO	19 NOVA	Normal mass order; octant I for θ_{23}
0.47 ^{+0.04} / _{-0.03}	3,4 ACERO	19 NOVA	Inverted mass order; octant I for θ_{23}
0.49 ^{+0.30} / _{-0.28}	AGAFONOVA	19 OPER	
0.50 ^{+0.20} / _{-0.19}	12 ALBERT	19 ANTR	Atmospheric ν , deep sea telescope
0.587 ^{+0.036} / _{-0.069}	13 ABE	18B SKAM	3ν osc: normal mass ordering, θ_{13} free
0.551 ^{+0.044} / _{-0.075}	13 ABE	18B SKAM	3ν osc: inverted mass ordering, θ_{13} free
0.526 ^{+0.032} / _{-0.036}	14 ABE	18G T2K	Normal mass ordering, θ_{13} constrained
0.530 ^{+0.030} / _{-0.034}	14 ABE	18G T2K	Inverted mass ordering, θ_{13} constrained
0.56 ± 0.04	15 ACERO	18 NOVA	Normal mass order; octant II for θ_{23}
0.47 ± 0.04	15 ACERO	18 NOVA	Normal mass order; octant I for θ_{23}
0.547 ^{+0.020} / _{-0.030}	DE-SALAS	18 FIT	Normal mass ordering, global fit
0.551 ^{+0.018} / _{-0.030}	DE-SALAS	18 FIT	Inverted mass order, global fit
0.532 ^{+0.061} / _{-0.087}	16 ABE	17A T2K	Normal mass ordering
0.534 ^{+0.061} / _{-0.087}	16 ABE	17A T2K	Inverted mass ordering
0.51 ^{+0.08} / _{-0.07}	ABE	17C T2K	Normal mass ordering with neutrinos
0.42 ^{+0.25} / _{-0.07}	ABE	17C T2K	Normal mass ordering with antineutrinos
0.52 ^{+0.075} / _{-0.09}	ABE	17C T2K	normal mass ordering with neutrinos and antineutrinos
0.55 ^{+0.05} / _{-0.09}	16 ABE	17F T2K	Normal mass ordering

0.55 ^{+0.05} / _{-0.08}	16 ABE	17F T2K	Inverted mass ordering
0.404 ^{+0.022} / _{-0.030}	17 ADAMSON	17A NOVA	Normal mass ordering; octant I for θ_{23}
0.624 ^{+0.022} / _{-0.030}	17 ADAMSON	17A NOVA	Normal mass ordering; octant II for θ_{23}
0.398 ^{+0.030} / _{-0.022}	17 ADAMSON	17A NOVA	Inverted mass ordering; octant I for θ_{23}
0.618 ^{+0.022} / _{-0.030}	17 ADAMSON	17A NOVA	Inverted mass ordering; octant II for θ_{23}
0.45 ^{+0.19} / _{-0.07}	18 ABE	16D T2K	3ν osc; normal mass ordering; $\bar{\nu}$ beam
0.38 to 0.65	19 ADAMSON	16A NOVA	normal mass ordering
0.37 to 0.64	19 ADAMSON	16A NOVA	Inverted mass ordering
0.53 ^{+0.09} / _{-0.12}	20 AARTSEN	15A ICCB	Normal mass ordering
0.51 ^{+0.09} / _{-0.11}	20 AARTSEN	15A ICCB	Inverted mass ordering
0.514 ^{+0.055} / _{-0.056}	21 ABE	14 T2K	3ν osc.; normal mass ordering
0.511 ± 0.055	21 ABE	14 T2K	3ν osc.; inverted mass ordering
0.41 ^{+0.23} / _{-0.06}	22 ADAMSON	14 MINS	Normal mass ordering
0.41 ^{+0.26} / _{-0.07}	22 ADAMSON	14 MINS	Inverted mass ordering
0.567 ^{+0.032} / _{-0.128}	23 FORERO	14 FIT	Normal mass ordering
0.573 ^{+0.025} / _{-0.043}	23 FORERO	14 FIT	Inverted mass ordering
0.452 ^{+0.052} / _{-0.028}	24 GONZALEZ...	14 FIT	Normal mass ordering; global fit
0.579 ^{+0.025} / _{-0.037}	24 GONZALEZ...	14 FIT	Inverted mass ordering; global fit
0.24 to 0.76	25 AARTSEN	13B ICCB	DeepCore, 2ν oscillation
0.514 ± 0.082	26 ABE	13G T2K	3ν osc.; normal mass ordering
0.388 ^{+0.051} / _{-0.053}	27 ADAMSON	13B MINS	Beam + Atmospheric; identical ν & $\bar{\nu}$
0.3 to 0.7	28 ABE	12A T2K	Off-axis beam
0.28 to 0.72	29 ADAMSON	12 MINS	$\bar{\nu}$ beam
0.25 to 0.75	30,31 ADAMSON	12B MINS	MINOS atmospheric
0.27 to 0.73	30,32 ADAMSON	12B MINS	MINOS pure atmospheric ν
0.21 to 0.79	30,32 ADAMSON	12B MINS	MINOS pure atmospheric $\bar{\nu}$
0.15 to 0.85	33 ADRIAN-MAR.	12 ANTR	Atmospheric ν with deep sea telescope
0.39 to 0.61	34 ABE	11C SKAM	Super-Kamiokande
0.34 to 0.66	ADAMSON	11 MINS	2ν osc.; maximal mixing
0.31 ^{+0.10} / _{-0.07}	35 ADAMSON	11B MINS	$\bar{\nu}$ beam
0.41 to 0.59	36 WENDELL	10 SKAM	3ν osc. with solar terms; $\theta_{13} = 0$
0.39 to 0.61	37 WENDELL	10 SKAM	3ν osc.; normal mass ordering
0.37 to 0.63	38 WENDELL	10 SKAM	3ν osc.; inverted mass ordering
0.31 to 0.69	ADAMSON	08A MINS	MINOS
0.05 to 0.95	39 ADAMSON	06 MINS	Atmospheric ν with far detector
0.18 to 0.82	40 AHN	06A K2K	KEK to Super-K
0.23 to 0.77	41 MICHAEL	06 MINS	MINOS
0.18 to 0.82	42 ALIU	05 K2K	KEK to Super-K
0.18 to 0.82	43 ALLISON	05 SOU2	
0.36 to 0.64	44 ASHIE	05 SKAM	Super-Kamiokande
0.28 to 0.72	45 AMBROSIO	04 MCRO	MACRO
0.34 to 0.66	46 ASHIE	04 SKAM	L/E distribution
0.08 to 0.92	47 AHN	03 K2K	KEK to Super-K
0.13 to 0.87	48 AMBROSIO	03 MCRO	MACRO
0.26 to 0.74	49 AMBROSIO	03 MCRO	MACRO
0.15 to 0.85	50 SANCHEZ	03 SOU2	Soudan-2 Atmospheric
0.28 to 0.72	51 AMBROSIO	01 MCRO	Upward μ
0.29 to 0.71	52 AMBROSIO	01 MCRO	Upward μ
0.13 to 0.87	53 FUKUDA	99c SKAM	Upward μ
0.23 to 0.77	54 FUKUDA	99d SKAM	Upward μ
0.08 to 0.92	55 FUKUDA	99d SKAM	Stop μ / through
0.29 to 0.71	56 FUKUDA	98c SKAM	Super-Kamiokande
0.08 to 0.92	57 HATAKEYAMA	98 KAMI	Kamiokande
0.24 to 0.76	58 HATAKEYAMA	98 KAMI	Kamiokande
0.20 to 0.80	59 FUKUDA	94 KAMI	Kamiokande

- ¹ ABE 20F results are based on data collected between 2009 and 2018 in (anti)neutrino mode and include a neutrino beam exposure of 1.49×10^{21} (1.64×10^{21}) protons on target. Supersedes ABE 18G.
- ² ADAMSON 20A uses the complete dataset from MINOS and MINOS+ experiments. The data were collected using a total exposure of 23.76×10^{20} protons on target and 60.75 kton-yr exposure to atmospheric neutrinos. Supersedes ADAMSON 14.
- ³ ACERO 19 is based on a sample size of 12.33×10^{20} protons on target. The fit combines both antineutrino and neutrino data to extract the oscillation parameters. The results favor the normal mass ordering by 1.9σ and θ_{23} values in octant II by 1.6σ . Supersedes ACERO 18.
- ⁴ Errors are from normal mass ordering and θ_{13} octant II fits.
- ⁵ AARTSEN 18A uses three years (April 2012 – May 2015) of neutrino data from full sky with reconstructed energies between 5.6 and 56 GeV, measured with the low-energy subdetector DeepCore of the IceCube neutrino telescope. AARTSEN 18A also reports the best fit result for the inverted mass ordering as $\Delta m_{32}^2 = -2.32 \times 10^{-3} \text{ eV}^2$ and $\sin^2(\theta_{23}) = 0.51$. Uncertainties for the inverted mass ordering fits were not provided. Supersedes AARTSEN 15A.
- ⁶ ABE 18b uses 328 kton-years of Super-Kamiokande I-IV atmospheric neutrino data to obtain this result. The fit is performed over the three parameters, Δm_{32}^2 , $\sin^2(\theta_{23})$, and

- δ , while the solar parameters and $\sin^2(\theta_{13})$ are fixed to $\Delta m_{21}^2 = (7.53 \pm 0.18) \times 10^{-5} \text{ eV}^2$, $\sin^2(\theta_{12}) = 0.304 \pm 0.014$, and $\sin^2(\theta_{13}) = 0.0219 \pm 0.0012$.
- 7 ABE 21A results are based on 1.49×10^{21} POT in neutrino mode and 1.64×10^{21} POT in antineutrino mode.
 - 8 SALAS 21 reports results of a global fit to neutrino oscillation data available at the time of the Neutrino 2020 conference.
 - 9 AARTSEN 20 uses the data taken between May 2012 and April 2014 with the low-energy subdetector DeepCore of the IceCube neutrino telescope. The reconstructed energy range is between 4 (5) and 90 (80) GeV for the main (confirmatory) analysis. Though the observed best-fit is in the lower octant for both mass orderings, a substantial range of $\sin^2(\theta_{23}) > 0.5$ is still compatible with the observed data for both mass orderings.
 - 10 ESTEBAN 20A reports results of a global fit to neutrino oscillation data available at the time of the Neutrino2020 conference.
 - 11 AARTSEN 19c uses three years (April 2012 – May 2015) of neutrino data from full sky with reconstructed energies between 5.6 and 56 GeV, measured with the low-energy subdetector DeepCore of the IceCube neutrino telescope. AARTSEN 19c adopts looser event selection criteria to prioritize the efficiency of selecting neutrino events, different from tighter event selection criteria which closely follow the criteria used by AARTSEN 18A to measure the ν_μ disappearance.
 - 12 ALBERT 19 measured the oscillation parameters of atmospheric neutrinos with the ANTARES deep sea neutrino telescope using the data taken from 2007 to 2016 (2830 days of total live time). Supersedes ADRIAN-MARTINEZ 12.
 - 13 ABE 18b uses 328 kton-years of Super-Kamiokande I-IV atmospheric neutrino data to obtain this result. The fit is performed over the four parameters, Δm_{32}^2 , $\sin^2\theta_{23}$, $\sin^2\theta_{13}$, and δ , while the solar parameters are fixed to $\Delta m_{21}^2 = (7.53 \pm 0.18) \times 10^{-5} \text{ eV}^2$ and $\sin^2\theta_{12} = 0.304 \pm 0.014$.
 - 14 ABE 18c data prefers normal mass ordering is with a posterior probability of 87%. Supersedes ABE 17F.
 - 15 ACERO 18 performs a joint fit to the data for ν_μ disappearance and ν_e appearance. The overall best fit favors normal mass ordering and θ_{23} in octant II. No 1σ confidence intervals are presented for the inverted mass ordering scenarios. Superseded by ACERO 19.
 - 16 Errors are from the projections of the 68% contour on 2D plot of Δm^2 versus $\sin^2(\theta_{23})$. ABE 17f supersedes ABE 17A. Superseded by ABE 18g.
 - 17 Superseded by ACERO 18.
 - 18 ABE 16d reports oscillation results using $\bar{\nu}_\mu$ disappearance in an off-axis beam.
 - 19 ADAMSON 16a obtains $\sin^2(\theta_{23})$ in the 68% C.L. range [0.38, 0.65] ([0.37, 0.64]), with two statistically degenerate best-fit values of 0.44 and 0.59 (0.44 and 0.59) for normal (inverted) mass ordering. Superseded by ADAMSON 17A.
 - 20 AARTSEN 15A obtains this result by a three-neutrino oscillation analysis using 10–100 GeV muon neutrino sample from a total of 953 days of measurement with the low-energy subdetector DeepCore of the IceCube neutrino telescope. Superseded by AARTSEN 18A.
 - 21 ABE 14 results are based on ν_μ disappearance using three-neutrino oscillation fit. The confidence intervals are derived from one dimensional profiled likelihoods. Superseded by ABE 17A.
 - 22 ADAMSON 14 uses a complete set of accelerator and atmospheric data. The analysis combines the ν_μ disappearance and ν_e appearance data using three-neutrino oscillation fit. The fit results are obtained for normal and inverted mass ordering assumptions. The best fit is for first θ_{23} octant and inverted mass ordering.
 - 23 FORERO 14 performs a global fit to neutrino oscillations using solar, reactor, long-baseline accelerator, and atmospheric neutrino data.
 - 24 GONZALEZ-GARCIA 14 result comes from a frequentist global fit. The corresponding Bayesian global fit to the same data results are reported in BERGSTROM 15 as 68% CL intervals of 0.433–0.496 or 0.530–0.594 for normal and 0.514–0.612 for inverted mass ordering.
 - 25 AARTSEN 13B obtained this result by a two-neutrino oscillation analysis using 20–100 GeV muon neutrino sample from a total of 318.9 days of live-time measurement with the low-energy subdetector DeepCore of the IceCube neutrino telescope.
 - 26 The best fit value is $\sin^2(\theta_{23}) = 0.514 \pm 0.082$. Superseded by ABE 14.
 - 27 ADAMSON 13b obtained this result from ν_μ and $\bar{\nu}_\mu$ disappearance using ν_μ (10.71×10^{20} POT) and $\bar{\nu}_\mu$ (3.36×10^{20} POT) beams, and atmospheric (37.88kton-years) data from MINOS The fit assumed two-flavor neutrino hypothesis and identical ν_μ and $\bar{\nu}_\mu$ oscillation parameters. Superseded by ADAMSON 14.
 - 28 ABE 12A obtained this result by a two-neutrino oscillation analysis. The best-fit point is $\sin^2(2\theta_{23}) = 0.98$.
 - 29 ADAMSON 12 is a two-neutrino oscillation analysis using antineutrinos. The best fit value is $\sin^2(2\theta_{23}) = 0.95^{+0.10}_{-0.11} \pm 0.01$.
 - 30 ADAMSON 12b obtained this result by a two-neutrino oscillation analysis of the L/E distribution using 37.9 kton-yr atmospheric neutrino data with the MINOS far detector.
 - 31 The best fit point is $\Delta m^2 = 0.0019 \text{ eV}^2$ and $\sin^2 2\theta = 0.99$. The 90% single-parameter confidence interval at the best fit point is $\sin^2 2\theta > 0.86$.
 - 32 The data are separated into pure samples of ν_s and $\bar{\nu}_s$, and separate oscillation parameters for ν_s and $\bar{\nu}_s$ are fit to the data. The best fit point is $(\Delta m^2, \sin^2 2\theta) = (0.0022 \text{ eV}^2, 0.99)$ and $(\Delta \bar{m}^2, \sin^2 2\bar{\theta}) = (0.0016 \text{ eV}^2, 1.00)$. The quoted result is taken from the 90% C.L. contour in the $(\Delta m^2, \sin^2 2\theta)$ plane obtained by minimizing the four parameter log-likelihood function with respect to the other oscillation parameters.
 - 33 ADRIAN-MARTINEZ 12 measured the oscillation parameters of atmospheric neutrinos with the ANTARES deep sea neutrino telescope using the data taken from 2007 to 2010 (863 days of total live time). Superseded by ALBERT 19.
 - 34 ABE 11c obtained this result by a two-neutrino oscillation analysis using the Super-Kamiokande-I+II+III atmospheric neutrino data. ABE 11c also reported results under a two-neutrino disappearance model with separate mixing parameters between ν and $\bar{\nu}$, and obtained $\sin^2 2\theta > 0.93$ for ν and $\sin^2 2\theta > 0.83$ for $\bar{\nu}$ at 90% C.L.
 - 35 ADAMSON 11b obtained this result by a two-neutrino oscillation analysis of antineutrinos in an antineutrino enhanced beam with 1.71×10^{20} protons on target. This result is consistent with the neutrino measurements of ADAMSON 11 at 2% C.L.
 - 36 WENDELL 10 obtained this result ($\sin^2\theta_{23} = 0.407\text{--}0.583$) by a three-neutrino oscillation analysis using the Super-Kamiokande-I+II+III atmospheric neutrino data, assuming $\theta_{13} = 0$ but including the solar oscillation parameters Δm_{21}^2 and $\sin^2\theta_{12}$ in the fit.
 - 37 WENDELL 10 obtained this result ($\sin^2\theta_{23} = 0.43\text{--}0.61$) by a three-neutrino oscillation analysis with one mass scale dominance ($\Delta m_{21}^2 = 0$) using the Super-Kamiokande-I+II+III atmospheric neutrino data, and updates the HOSAKA 06a result.
 - 38 WENDELL 10 obtained this result ($\sin^2\theta_{23} = 0.44\text{--}0.63$) by a three-neutrino oscillation analysis with one mass scale dominance ($\Delta m_{21}^2 = 0$) using the Super-Kamiokande-I+II+III atmospheric neutrino data, and updates the HOSAKA 06a result.
 - 39 ADAMSON 06 obtained this result by a two-neutrino oscillation analysis of the L/E distribution using 4.54 kton yr atmospheric neutrino data with the MINOS far detector.
 - 40 Supersedes ALIU 05.
 - 41 MICHAEL 06 best fit is for maximal mixing. See also ADAMSON 08.
 - 42 The best fit is for maximal mixing.
 - 43 ALLISON 05 result is based upon atmospheric neutrino interactions including upward-stopping muons, with an exposure of 5.9 kton yr. From a two-flavor oscillation analysis the best-fit point is $\Delta m^2 = 0.0017 \text{ eV}^2$ and $\sin^2(2\theta) = 0.97$.
 - 44 ASHIE 05 obtained this result by a two-neutrino oscillation analysis using 92 kton yr atmospheric neutrino data from the complete Super-Kamiokande I running period.
 - 45 AMBROSIO 04 obtained this result, without using the absolute normalization of the neutrino flux, by combining the angular distribution of upward through-going muon tracks with $E_\mu > 1 \text{ GeV}$, N_{low} and N_{high} , and the numbers of InDown + UpStop and InUp events. Here, N_{low} and N_{high} are the number of events with reconstructed neutrino energies $< 30 \text{ GeV}$ and $> 130 \text{ GeV}$, respectively. InDown and InUp represent events with downward and upward-going tracks starting inside the detector due to neutrino interactions, while UpStop represents entering upward-going tracks which stop in the detector. The best fit is for maximal mixing.
 - 46 ASHIE 04 obtained this result from the L(flight length)/E(estimated neutrino energy) distribution of ν_μ disappearance probability, using the Super-Kamiokande-I 1489 live-day atmospheric neutrino data.
 - 47 There are several islands of allowed region from this K2K analysis, extending to high values of Δm^2 . We only include the one that overlaps atmospheric neutrino analyses. The best fit is for maximal mixing.
 - 48 AMBROSIO 03 obtained this result on the basis of the ratio $R = N_{low}/N_{high}$, where N_{low} and N_{high} are the number of upward through-going muon events with reconstructed neutrino energy $< 30 \text{ GeV}$ and $> 130 \text{ GeV}$, respectively. The data came from the full detector run started in 1994. The method of FELDMAN 98 is used to obtain the limits.
 - 49 AMBROSIO 03 obtained this result by using the ratio R and the angular distribution of the upward through-going muons. R is given in the previous note and the angular distribution is reported in AMBROSIO 01. The method of FELDMAN 98 is used to obtain the limits. The best fit is to maximal mixing.
 - 50 SANCHEZ 03 is based on an exposure of 5.9 kton yr. The result is obtained using a likelihood analysis of the neutrino L/E distribution for a selection μ flavor sample while the e-flavor sample provides flux normalization. The method of FELDMAN 98 is used to obtain the allowed region. The best fit is $\sin^2(2\theta) = 0.97$.
 - 51 AMBROSIO 01 result is based on the angular distribution of upward through-going muon tracks with $E_\mu > 1 \text{ GeV}$. The data came from three different detector configurations, but the statistics is largely dominated by the full detector run, from May 1994 to December 2000. The total live time, normalized to the full detector configuration is 6.17 years. The best fit is obtained outside the physical region. The method of FELDMAN 98 is used to obtain the limits. The best fit is for maximal mixing.
 - 52 AMBROSIO 01 result is based on the angular distribution and normalization of upward through-going muon tracks with $E_\mu > 1 \text{ GeV}$. See the previous footnote.
 - 53 FUKUDA 99c obtained this result from a total of 537 live days of upward through-going muon data in Super-Kamiokande between April 1996 to January 1998. With a threshold of $E_\mu > 1.6 \text{ GeV}$, the observed flux is $(1.74 \pm 0.07 \pm 0.02) \times 10^{-13} \text{ cm}^{-2}\text{s}^{-1}\text{sr}^{-1}$. The best fit is $\sin^2(2\theta) = 0.95$.
 - 54 FUKUDA 99b obtained this result from a simultaneous fitting to zenith angle distributions of upward-stopping and through-going muons. The flux of upward-stopping muons of minimum energy of 1.6 GeV measured between April 1996 and January 1998 is $(0.39 \pm 0.04 \pm 0.02) \times 10^{-13} \text{ cm}^{-2}\text{s}^{-1}\text{sr}^{-1}$. This is compared to the expected flux of $(0.73 \pm 0.16 \text{ (theoretical error)}) \times 10^{-13} \text{ cm}^{-2}\text{s}^{-1}\text{sr}^{-1}$. The best fit is to maximal mixing.
 - 55 FUKUDA 99d obtained this result from the zenith dependence of the upward-stopping/through-going flux ratio. The best fit is to maximal mixing.
 - 56 FUKUDA 98c obtained this result by an analysis of 33.0 kton yr atmospheric neutrino data. The best fit is for maximal mixing.
 - 57 HATAKEYAMA 98 obtained this result from a total of 2456 live days of upward-going muon data in Kamiokande between December 1985 and May 1995. With a threshold of $E_\mu > 1.6 \text{ GeV}$, the observed flux of upward through-going muons is $(1.94 \pm 0.10^{+0.07}_{-0.06}) \times 10^{-13} \text{ cm}^{-2}\text{s}^{-1}\text{sr}^{-1}$. This is compared to the expected flux of $(2.46 \pm 0.54 \text{ (theoretical error)}) \times 10^{-13} \text{ cm}^{-2}\text{s}^{-1}\text{sr}^{-1}$. The best fit is for maximal mixing.
 - 58 HATAKEYAMA 98 obtained this result from a combined analysis of Kamiokande contained events (FUKUDA 94) and upward going muon events. The best fit is $\sin^2(2\theta) = 0.95$.
 - 59 FUKUDA 94 obtained the result by a combined analysis of sub- and multi-GeV atmospheric neutrino events in Kamiokande. The best fit is for maximal mixing.

See key on page 1127

Lepton Particle Listings

Neutrino Mixing

Δm_{32}^2

The sign of Δm_{32}^2 is not known at this time. If given, values are shown separately for the normal and inverted mass ordering. Unless otherwise specified, the ranges below correspond to the projection onto the Δm_{32}^2 axis of the 90% CL contours in the $\sin^2(2\theta_{23}) - \Delta m_{32}^2$ plane presented by the authors. If uncertainties are reported with the value, they correspond to one standard deviation uncertainty.

VALUE (10^{-3} eV^2)	DOCUMENT ID	TECN	COMMENT
-2.536 ± 0.034 OUR FIT	Assuming inverted ordering		
2.453 ± 0.033 OUR FIT	Assuming normal ordering		
2.45 ± 0.07	1 ABE	20F T2K	Normal mass ordering, θ_{13} constrained
-2.51 ± 0.07	1,2 ABE	20F T2K	Inverted mass ordering, θ_{13} constrained
2.40 $^{+0.08}_{-0.09}$	3 ADAMSON	20A MINS	Accel., atmospheric, normal mass ordering
-2.45 $^{+0.08}_{-0.07}$	3 ADAMSON	20A MINS	Accel., atmospheric, inverted mass ordering
2.48 $^{+0.11}_{-0.06}$	4 ACERO	19 NOVA	Normal mass ordering, octant II for θ_{23}
-2.54 $^{+0.06}_{-0.11}$	4 ACERO	19 NOVA	Inverted mass ordering, octant II for θ_{23}
2.31 $^{+0.11}_{-0.13}$	5 AARTSEN	18A ICCB	Normal mass ordering
2.50 $^{+0.13}_{-0.20}$	6 ABE	18B SKAM	Normal mass ordering, θ_{13} constrained
-2.58 $^{+0.08}_{-0.37}$	6 ABE	18B SKAM	Inverted mass ordering, θ_{13} constrained
2.471 $^{+0.068}_{-0.070}$	7 ADEY	18A DAYA	Normal mass ordering
-2.575 $^{+0.068}_{-0.070}$	7 ADEY	18A DAYA	Inverted mass ordering
2.63 ± 0.14	8 BAK	18 RENO	Normal mass ordering
-2.73 ± 0.14	8 BAK	18 RENO	Inverted mass ordering
● ● ● We do not use the following data for averages, fits, limits, etc. ● ● ●			
2.47 $^{+0.08}_{-0.09}$	9 ABE	21A T2K	ν_μ disappearance
2.50 $^{+0.18}_{-0.13}$	9 ABE	21A T2K	$\bar{\nu}_\mu$ disappearance
2.517 $^{+0.026}_{-0.028}$	10 ESTEBAN	20A FIT	Normal mass ordering, global fit
-2.498 $^{+0.028}_{-0.028}$	10 ESTEBAN	20A FIT	Inverted mass ordering, global fit
2.55 $^{+0.12}_{-0.11}$	11 AARTSEN	19c ICCB	
< 4.1 at 90% CL	AGAFONOVA	19 OPER	
2.0 $^{+0.4}_{-0.3}$	12 ALBERT	19 ANTR	Atmospheric ν , deep sea telescope
2.50 $^{+0.13}_{-0.31}$	13 ABE	18B SKAM	3ν osc: normal mass ordering, θ_{13} free
-2.28 $^{+0.33}_{-0.13}$	13 ABE	18B SKAM	3ν osc: inverted mass ordering, θ_{13} free
2.463 $^{+0.071}_{-0.070}$	14 ABE	18G T2K	Normal mass ordering, θ_{13} constrained
-2.507 ± 0.070	14,15 ABE	18G T2K	Inverted mass ordering, θ_{13} constrained
2.44 $^{+0.08}_{-0.07}$	16 ACERO	18 NOVA	Normal mass order, octant II for θ_{23}
2.45 $^{+0.07}_{-0.08}$	16,17 ACERO	18 NOVA	Normal mass order; octant I for θ_{23}
2.7 $^{+0.7}_{-0.6}$	18 AGAFONOVA	18 OPER	OPERA ν_τ appearance
2.42 ± 0.03	DE-SALAS	18 FIT	Normal mass ordering, global fit
-2.50 $^{+0.03}_{-0.04}$	DE-SALAS	18 FIT	Inverted mass order, global fit
2.57 $^{+0.21}_{-0.23}$ $^{+0.12}_{-0.13}$	19 SEO	18 RENO	Normal mass ordering
-2.67 $^{+0.23}_{-0.21}$ $^{+0.13}_{-0.12}$	19 SEO	18 RENO	Inverted mass ordering
2.53 $^{+0.15}_{-0.13}$	ABE	17C T2K	Normal mass ordering with neutrinos
2.55 $^{+0.33}_{-0.27}$	ABE	17C T2K	Normal mass ordering with antineutrinos
2.55 $^{+0.08}_{-0.08}$	ABE	17C T2K	Normal mass ordering with neutrinos and antineutrinos
-2.63 $^{+0.08}_{-0.08}$	ABE	17C T2K	Inverted mass ordering with neutrinos and antineutrinos
2.54 ± 0.08	20 ABE	17F T2K	Normal mass ordering; $\nu+\bar{\nu}$
-2.51 ± 0.08	20 ABE	17F T2K	Inverted mass ordering; $\nu+\bar{\nu}$
2.67 ± 0.11	21 ADAMSON	17A NOVA	3ν osc; normal mass ordering
-2.72 ± 0.11	21 ADAMSON	17A NOVA	3ν osc; inverted mass ordering
2.45 ± 0.06 ± 0.06	22 AN	17A DAYA	Normal mass ordering
-2.56 ± 0.06 ± 0.06	22 AN	17A DAYA	Inverted mass ordering
2.51 $^{+0.29}_{-0.25}$	23 ABE	16D T2K	3ν osc.; normal mass ordering; $\bar{\nu}$ beam
2.52 $^{+0.20}_{-0.18}$	24 ADAMSON	16A NOVA	3ν osc; normal mass ordering

-2.56 ± 0.19	24 ADAMSON	16A NOVA	3ν osc; inverted mass ordering
2.56 $^{+0.21}_{-0.23}$ $^{+0.12}_{-0.13}$	25 CHOI	16 RENO	3ν osc; normal mass ordering
-2.69 $^{+0.23}_{-0.21}$ $^{+0.13}_{-0.12}$	25 CHOI	16 RENO	3ν osc; inverted mass ordering
2.72 $^{+0.19}_{-0.20}$	26 AARTSEN	15A ICCB	Normal mass ordering
-2.73 $^{+0.21}_{-0.18}$	26 AARTSEN	15A ICCB	Inverted mass ordering
2.0-5.0	27 AGAFONOVA	15A OPER	90% CL, 5 events
2.37 ± 0.11	28 AN	15 DAYA	3ν osc.; normal mass ordering
-2.47 ± 0.11	28 AN	15 DAYA	3ν osc.; inverted mass ordering
2.51 ± 0.10	29 ABE	14 T2K	3ν osc.; normal mass ordering
-2.56 ± 0.10	29 ABE	14 T2K	3ν osc.; inverted mass ordering
2.37 ± 0.09	30 ADAMSON	14 MINS	Accel., atmospheric, normal mass ordering
-2.41 $^{+0.09}_{-0.12}$	30 ADAMSON	14 MINS	Accel., atmospheric, inverted mass ordering
2.54 $^{+0.19}_{-0.20}$	31 AN	14 DAYA	3ν osc.; normal mass ordering
-2.64 $^{+0.20}_{-0.19}$	31 AN	14 DAYA	3ν osc.; inverted mass ordering
2.48 $^{+0.05}_{-0.07}$	32 FORERO	14 FIT	3ν ; normal mass ordering
-2.38 $^{+0.06}_{-0.05}$	32 FORERO	14 FIT	3ν ; inverted mass ordering
2.457 ± 0.047	33,34 GONZALEZ...	14 FIT	Normal mass ordering; global fit
-2.449 $^{+0.047}_{-0.048}$	33 GONZALEZ...	14 FIT	Inverted mass ordering; global fit
2.3 $^{+0.6}_{-0.5}$	35 AARTSEN	13B ICCB	DeepCore, 2ν oscillation
2.44 $^{+0.17}_{-0.15}$	36 ABE	13G T2K	3ν osc.; normal mass ordering
2.41 $^{+0.09}_{-0.10}$	37 ADAMSON	13B MINS	2ν osc.; beam + atmospheric; identical ν & $\bar{\nu}$
2.2-3.1	38 ABE	12A T2K	off-axis beam
2.62 $^{+0.31}_{-0.28}$ ± 0.09	39 ADAMSON	12 MINS	$\bar{\nu}$ beam
1.35-2.55	40,41 ADAMSON	12B MINS	MINOS atmospheric
1.4-5.6	40,42 ADAMSON	12B MINS	MINOS pure atmospheric ν
0.9-2.5	40,42 ADAMSON	12B MINS	MINOS pure atmospheric $\bar{\nu}$
1.8-5.0	43 ADRIAN-MAR.	12 ANTR	Atmospheric ν with deep sea telescope
1.3-4.0	44 ABE	11C SKAM	atmospheric $\bar{\nu}$
2.32 $^{+0.12}_{-0.08}$	ADAMSON	11 MINS	2ν oscillation; maximal mixing
3.36 $^{+0.46}_{-0.40}$	45 ADAMSON	11B MINS	$\bar{\nu}$ beam
< 3.37	46 ADAMSON	11C MINS	MINOS
1.9-2.6	47 WENDELL	10 SKAM	3ν osc.; normal mass ordering
-1.7- - 2.7	47 WENDELL	10 SKAM	3ν osc.; inverted mass ordering
2.43 ± 0.13	ADAMSON	08A MINS	MINOS
0.07-50	48 ADAMSON	06 MINS	atmospheric ν with far detector
1.9-4.0	49,50 AHN	06A K2K	KEK to Super-K
2.2-3.8	51 MICHAEL	06 MINS	MINOS
1.9-3.6	49 ALIU	05 K2K	KEK to Super-K
0.3-1.2	52 ALLISON	05 SOU2	
1.5-3.4	53 ASHIE	05 SKAM	atmospheric neutrino
0.6-8.0	54 AMBROSIO	04 MCRO	MACRO
1.9 to 3.0	55 ASHIE	04 SKAM	L/E distribution
1.5-3.9	56 AHN	03 K2K	KEK to Super-K
0.25-9.0	57 AMBROSIO	03 MCRO	MACRO
0.6-7.0	58 AMBROSIO	03 MCRO	MACRO
0.15-15	59 SANCHEZ	03 SOU2	Soudan-2 Atmospheric
0.6-15	60 AMBROSIO	01 MCRO	upward μ
1.0-6.0	61 AMBROSIO	01 MCRO	upward μ
1.0-50	62 FUKUDA	99C SKAM	upward μ
1.5-15.0	63 FUKUDA	99D SKAM	upward μ
0.7-18	64 FUKUDA	99D SKAM	stop μ / through
0.5-6.0	65 FUKUDA	98C SKAM	Super-Kamiokande
0.55-50	66 HATAKEYAMA	98 KAMI	Kamiokande
4-23	67 HATAKEYAMA	98 KAMI	Kamiokande
5-25	68 FUKUDA	94 KAMI	Kamiokande

1 ABE 20F results are based on data collected between 2009 and 2018 in (anti)neutrino mode and include a neutrino beam exposure of 1.49×10^{21} (1.64×10^{21}) protons on target. Supersedes ABE 18c.

2 ABE 20F reports $\Delta m_{13}^2 = (2.43 \pm 0.07) \times 10^{-3} \text{ eV}^2$ for inverted mass ordering. We convert to Δm_{32}^2 using PDG 20 value of $\Delta m_{21}^2 = (7.53 \pm 0.18) \times 10^{-5} \text{ eV}^2$.

3 ADAMSON 20A uses the complete dataset from MINOS and MINOS+ experiments. The data were collected using a total exposure of 23.76×10^{20} protons on target and 60.75 kton-yr exposure to atmospheric neutrinos. Supersedes ADAMSON 14.

4 ACERO 19 is based on a sample size of 12.33×10^{20} protons on target. The fit combines both antineutrino and neutrino data to extract the oscillation parameters. The results favor the normal mass ordering by 1.9 σ and θ_{23} values in octant II by 1.6 σ . Supersedes ACERO 18.

5 AARTSEN 18A uses three years (April 2012 - May 2015) of neutrino data from full sky with reconstructed energies between 5.6 and 56 GeV, measured with the low-energy subdetector DeepCore of the IceCube neutrino telescope. AARTSEN 18A also reports the best fit values for the inverted mass ordering as $\Delta m_{32}^2 = -2.32 \times 10^{-3} \text{ eV}^2$ and $\sin^2(\theta_{23}) = 0.51$. Uncertainties for the inverted mass ordering fits were not provided. Supersedes AARTSEN 15A.

Lepton Particle Listings

Neutrino Mixing

- ⁶ ABE 18b uses 328 kton-years of Super-Kamiokande I-IV atmospheric neutrino data to obtain this result. The fit is performed over the three parameters, Δm_{32}^2 , $\sin^2(\theta_{23})$, and δ , while the solar parameters and $\sin^2(\theta_{13})$ are fixed to $\Delta m_{21}^2 = (7.53 \pm 0.18) \times 10^{-5} \text{ eV}^2$, $\sin^2(\theta_{12}) = 0.304 \pm 0.014$, and $\sin^2(\theta_{13}) = 0.0219 \pm 0.0012$.
- ⁷ ADEY 18a reports results from analysis of 1958 days of data taking with the Daya-Bay experiment, with $3.9 \times 10^6 \bar{\nu}_e$ candidates. The fit to the data gives $\Delta m_{ee}^2 = (2.522^{+0.068}_{-0.070}) \times 10^{-3} \text{ eV}^2$. Solar oscillation parameters are fixed in the analysis using the global averages, $\sin^2(\theta_{12}) = 0.307^{+0.013}_{-0.012}$, $\Delta m_{21}^2 = (7.53 \pm 0.18) \times 10^{-5} \text{ eV}^2$, from PDG 18. Supersedes AN 17a.
- ⁸ BAK 18 reports results of the RENO experiment using about 2200 live-days of data taken with detectors placed at 410.6 and 1445.7 m from reactors of the Hanbit Nuclear Power Plant. We convert the results to Δm_{32}^2 using the PDG 18 values of $\sin^2\theta_{12} = 0.307^{+0.013}_{-0.012}$ and $\Delta m_{21}^2 = (7.53 \pm 0.18) \times 10^{-5} \text{ eV}^2$. Supersedes SEO 18.
- ⁹ ABE 21a results are based on 1.49×10^{21} POT in neutrino mode and 1.64×10^{21} POT in antineutrino mode.
- ¹⁰ ESTEBAN 20a reports results of a global fit to neutrino oscillation data available at the time of the Neutrino2020 conference.
- ¹¹ AARTSEN 19c uses three years (April 2012 – May 2015) of neutrino data from full sky with reconstructed energies between 5.6 and 56 GeV, measured with the low-energy sub-detector DeepCore of the IceCube neutrino telescope. AARTSEN 19c adopts looser event selection criteria to prioritize the efficiency of selecting neutrino events, different from tighter event selection criteria which closely follow the criteria used by AARTSEN 18a to measure the ν_μ disappearance.
- ¹² ALBERT 19 measured the oscillation parameters of atmospheric neutrinos with the ANTARES deep sea neutrino telescope using the data taken from 2007 to 2016 (2830 days of total live time). Supersedes ADRIAN-MARTINEZ 12.
- ¹³ ABE 18b uses 328 kton-years of Super-Kamiokande I-IV atmospheric neutrino data to obtain this result. The fit is performed over the four parameters, Δm_{32}^2 , $\sin^2\theta_{23}$, $\sin^2\theta_{13}$, and δ , while the solar parameters are fixed to $\Delta m_{21}^2 = (7.53 \pm 0.18) \times 10^{-5} \text{ eV}^2$ and $\sin^2\theta_{12} = 0.304 \pm 0.014$.
- ¹⁴ ABE 18c data prefers normal ordering with a posterior probability of 87%. Supersedes ABE 17f.
- ¹⁵ ABE 18c reports $\Delta m_{13}^2 = (2.432 \pm 0.070) \times 10^{-3} \text{ eV}^2$ for inverted mass ordering. We convert to Δm_{32}^2 using PDG 18 value of $\Delta m_{21}^2 = (7.53 \pm 0.18) \times 10^{-5} \text{ eV}^2$.
- ¹⁶ ACERO 18 performs a joint fit to the data for ν_μ disappearance and ν_e appearance. The overall best fit favors normal mass ordering and θ_{23} in octant II. No 1σ confidence intervals are presented for the inverted mass ordering scenarios. Superseded by ACERO 19.
- ¹⁷ The error for octant I is taken from the result for octant II.
- ¹⁸ AGAFONOVA 18 assumes maximal θ_{23} mixing.
- ¹⁹ SEO 18 reports result of the RENO experiment from a rate and shape analysis of 500 days of data. A simultaneous fit to θ_{13} and Δm_{ee}^2 yields $\Delta m_{ee}^2 = (2.62^{+0.21+0.12}_{-0.23-0.13}) \times 10^{-3} \text{ eV}^2$. We convert the results to Δm_{32}^2 using the PDG 18 values of $\sin^2\theta_{12}$ and Δm_{21}^2 . SEO 18 is a detailed description of the results published in CHOI 16, which it supersedes. Superseded by BAK 18.
- ²⁰ ABE 17f confidence intervals are obtained using a frequentist analysis including θ_{13} constraint from reactor experiments. Bayesian intervals based on Markov Chain Monte Carlo method are also provided by the authors. Superseded by ABE 18c.
- ²¹ Superseded by ACERO 18.
- ²² AN 17a report results from combined rate and spectral shape analysis of 1230 days of data taken with the Daya Bay reactor experiment. The data set contains more than 2.5×10^6 inverse beta-decay events with neutron capture on Gd. The fit to the data gives $\Delta_{ee}^2 = (2.50 \pm 0.06 \pm 0.06) \times 10^{-3} \text{ eV}^2$. Superseded by ADEY 18a.
- ²³ ABE 16d reports oscillation results using $\bar{\nu}_\mu$ disappearance in an off-axis beam.
- ²⁴ Superseded by ADAMSON 17a.
- ²⁵ CHOI 16 reports result of the RENO experiment from a rate and shape analysis of 500 days of data. A simultaneous fit to θ_{13} and Δm_{ee}^2 yields $\Delta m_{ee}^2 = (2.62^{+0.21+0.12}_{-0.23-0.13}) \times 10^{-3} \text{ eV}^2$. We convert the results to Δm_{32}^2 using PDG 18 values of $\sin^2(\theta_{12})$ and Δm_{21}^2 .
- ²⁶ AARTSEN 15a obtains this result by a three-neutrino oscillation analysis using 10–100 GeV muon neutrino sample from a total of 953 days of measurements with the low-energy sub-detector DeepCore of the IceCube neutrino telescope. Superseded by AARTSEN 18a.
- ²⁷ AGAFONOVA 15a result is based on $5 \nu_\mu \rightarrow \nu_\tau$ appearance candidates with an expected background of 0.25 ± 0.05 events. The best fit is for $\Delta m_{32}^2 = 3.3 \times 10^{-3} \text{ eV}^2$.
- ²⁸ AN 15 uses all eight identical detectors, with four placed near the reactor cores and the remaining four at the far hall to determine prompt energy spectra. The results correspond to the exposure of $6.9 \times 10^5 \text{ GW}_{th}\text{-ton-days}$. They derive $\Delta m_{ee}^2 = (2.42 \pm 0.11) \times 10^{-3} \text{ eV}^2$. Assuming the normal (inverted) ordering, the fitted $\Delta m_{32}^2 = (2.37 \pm 0.11) \times 10^{-3} \text{ eV}^2$ ($(2.47 \pm 0.11) \times 10^{-3} \text{ eV}^2$). Superseded by AN 17a.
- ²⁹ ABE 14 results are based on ν_μ disappearance using three-neutrino oscillation fit. The confidence intervals are derived from one dimensional profiled likelihoods. In ABE 14 the inverted mass ordering result is reported as $\Delta m_{13}^2 = (2.48 \pm 0.10) \times 10^{-3} \text{ eV}^2$ which we converted to Δm_{32}^2 by adding PDG 14 value of $\Delta m_{21}^2 = (7.53 \pm 0.18) \times 10^{-5} \text{ eV}^2$. Superseded by ABE 17c.
- ³⁰ ADAMSON 14 uses a complete set of accelerator and atmospheric data. The analysis combines The analysis combines the ν_μ disappearance and ν_e appearance data using three-neutrino oscillation fit. The fit results are obtained for normal and inverted mass ordering assumptions.
- ³¹ AN 14 uses six identical detectors, with three placed near the reactor cores (flux-weighted baselines of 512 and 561 m) and the remaining three at the far hall (at the flux averaged distance of 1579 m from all six reactor cores) to determine prompt energy spectra and derive $\Delta m_{ee}^2 = (2.59^{+0.19}_{-0.20}) \times 10^{-3} \text{ eV}^2$. Assuming the normal (inverted) ordering, the fitted $\Delta m_{32}^2 = (2.54^{+0.19}_{-0.20}) \times 10^{-3} \text{ eV}^2$ ($(2.64^{+0.19}_{-0.20}) \times 10^{-3} \text{ eV}^2$). Superseded by AN 15.
- ³² FORERO 14 performs a global fit to Δm_{31}^2 using solar, reactor, long-baseline accelerator, and atmospheric neutrino data.
- ³³ GONZALEZ-GARCIA 14 result comes from a frequentist global fit. The corresponding Bayesian global fit to the same data results are reported in BERGSTROM 15 as $(2.460 \pm 0.046) \times 10^{-3} \text{ eV}^2$ for normal and $(2.445^{+0.047}_{-0.045}) \times 10^{-3} \text{ eV}^2$ for inverted mass ordering.
- ³⁴ The value for normal mass ordering is actually a measurement of Δm_{31}^2 which differs from Δm_{32}^2 by a much smaller value of Δm_{21}^2 .
- ³⁵ AARTSEN 13b obtained this result by a two-neutrino oscillation analysis using 20–100 GeV muon neutrino sample from a total of 318.9 days of live-time measurement with the low-energy sub-detector DeepCore of the IceCube neutrino telescope.
- ³⁶ Based on the observation of 58 ν_μ events with 205 ± 17 (syst) expected in the absence of neutrino oscillations. Superseded by ABE 14.
- ³⁷ ADAMSON 13b obtained this result from ν_μ and $\bar{\nu}_\mu$ disappearance using ν_μ (10.71×10^{20} POT) and $\bar{\nu}_\mu$ (3.36×10^{20} POT) beams, and atmospheric (37.88 kton-years) data from MINOS. The fit assumed two-flavor neutrino hypothesis and identical ν_μ and $\bar{\nu}_\mu$ oscillation parameters.
- ³⁸ ABE 12a obtained this result by a two-neutrino oscillation analysis. The best-fit point is $\Delta m_{32}^2 = 2.65 \times 10^{-3} \text{ eV}^2$.
- ³⁹ ADAMSON 12 is a two-neutrino oscillation analysis using antineutrinos.
- ⁴⁰ ADAMSON 12b obtained this result by a two-neutrino oscillation analysis of the L/E distribution using 37.9 kton-yr atmospheric neutrino data with the MINOS far detector.
- ⁴¹ The 90% single-parameter confidence interval at the best fit point is $\Delta m^2 = 0.0019 \pm 0.0004 \text{ eV}^2$.
- ⁴² The data are separated into pure samples of ν_s and $\bar{\nu}_s$, and separate oscillation parameters for ν_s and $\bar{\nu}_s$ are fit to the data. The best fit point is $(\Delta m^2, \sin^2 2\theta) = (0.0022 \text{ eV}^2, 0.99)$ and $(\Delta \bar{m}^2, \sin^2 2\bar{\theta}) = (0.0016 \text{ eV}^2, 1.00)$. The quoted result is taken from the 90% C.L. contour in the $(\Delta m^2, \sin^2 2\theta)$ plane obtained by minimizing the four parameter log-likelihood function with respect to the other oscillation parameters.
- ⁴³ ADRIAN-MARTINEZ 12 measured the oscillation parameters of atmospheric neutrinos with the ANTARES deep sea neutrino telescope using the data taken from 2007 to 2010 (863 days of total live time). Superseded by ALBERT 19.
- ⁴⁴ ABE 11c obtained this result by a two-neutrino oscillation analysis with separate mixing parameters between neutrinos and antineutrinos, using the Super-Kamiokande-I+II+III atmospheric neutrino data. The corresponding 90% CL neutrino oscillation parameter range obtained from this analysis is $\Delta m^2 = 1.7\text{--}3.0 \times 10^{-3} \text{ eV}^2$.
- ⁴⁵ ADAMSON 11b obtained this result by a two-neutrino oscillation analysis of antineutrinos in an antineutrino enhanced beam with 1.71×10^{20} protons on target. This result is consistent with the neutrino measurements of ADAMSON 11 at 2% C.L.
- ⁴⁶ ADAMSON 11c obtains this result based on a study of antineutrinos in a neutrino beam and assumes maximal mixing in the two-flavor approximation.
- ⁴⁷ WENDELL 10 obtained this result by a three-neutrino oscillation analysis with one mass scale dominance ($\Delta m_{21}^2 = 0$) using the Super-Kamiokande-I+II+III atmospheric neutrino data, and updates the HOSAKA 06a result.
- ⁴⁸ ADAMSON 06 obtained this result by a two-neutrino oscillation analysis of the L/E distribution using 4.54 kton yr atmospheric neutrino data with the MINOS far detector.
- ⁴⁹ The best fit in the physical region is for $\Delta m^2 = 2.8 \times 10^{-3} \text{ eV}^2$.
- ⁵⁰ Supersedes ALIU 05.
- ⁵¹ MICHAEL 06 best fit is $2.74 \times 10^{-3} \text{ eV}^2$. See also ADAMSON 08.
- ⁵² ALLISON 05 result is based on an atmospheric neutrino observation with an exposure of 5.9 kton yr. From a two-flavor oscillation analysis the best-fit point is $\Delta m^2 = 0.0017 \text{ eV}^2$ and $\sin^2 2\theta = 0.97$.
- ⁵³ ASHIE 05 obtained this result by a two-neutrino oscillation analysis using 92 kton yr atmospheric neutrino data from the complete Super-Kamiokande I running period. The best fit is for $\Delta m^2 = 2.1 \times 10^{-3} \text{ eV}^2$.
- ⁵⁴ AMBROSIO 04 obtained this result, without using the absolute normalization of the neutrino flux, by combining the angular distribution of upward through-going muon tracks with $E_\mu > 1 \text{ GeV}$, N_{low} and N_{high} , and the numbers of InDown + UpStop and InUp events. Here, N_{low} and N_{high} are the number of events with reconstructed neutrino energies $< 30 \text{ GeV}$ and $> 130 \text{ GeV}$, respectively. InDown and InUp represent events with downward and upward-going tracks starting inside the detector due to neutrino interactions, while UpStop represents entering upward-going tracks which stop in the detector. The best fit is for $\Delta m^2 = 2.3 \times 10^{-3} \text{ eV}^2$.
- ⁵⁵ ASHIE 04 obtained this result from the $L(\text{flight length})/E(\text{estimated neutrino energy})$ distribution of ν_μ disappearance probability, using the Super-Kamiokande-I 1489 live-day atmospheric neutrino data. The best fit is for $\Delta m^2 = 2.4 \times 10^{-3} \text{ eV}^2$.
- ⁵⁶ There are several islands of allowed region from this K2K analysis, extending to high values of Δm^2 . We only include the one that overlaps atmospheric neutrino analyses. The best fit is for $\Delta m^2 = 2.8 \times 10^{-3} \text{ eV}^2$.
- ⁵⁷ AMBROSIO 03 obtained this result on the basis of the ratio $R = N_{low}/N_{high}$, where N_{low} and N_{high} are the number of upward through-going muon events with reconstructed neutrino energy $< 30 \text{ GeV}$ and $> 130 \text{ GeV}$, respectively. The data came from the full detector run started in 1994. The method of FELDMAN 98 is used to obtain the limits. The best fit is for $\Delta m^2 = 2.5 \times 10^{-3} \text{ eV}^2$.
- ⁵⁸ AMBROSIO 03 obtained this result by using the ratio R and the angular distribution of the upward through-going muons. R is given in the previous note and the angular

See key on page 1127

Lepton Particle Listings

Neutrino Mixing

distribution is reported in AMBROSIO 01. The method of FELDMAN 98 is used to obtain the limits. The best fit is for $\Delta m^2 = 2.5 \times 10^{-3} \text{ eV}^2$.

⁵⁹ SANCHEZ 03 is based on an exposure of 5.9 kton yr. The result is obtained using a likelihood analysis of the neutrino L/E distribution for a selection μ flavor sample while the e -flavor sample provides flux normalization. The method of FELDMAN 98 is used to obtain the allowed region. The best fit is for $\Delta m^2 = 5.2 \times 10^{-3} \text{ eV}^2$.

⁶⁰ AMBROSIO 01 result is based on the angular distribution of upward through-going muon tracks with $E_\mu > 1 \text{ GeV}$. The data came from three different detector configurations, but the statistics is largely dominated by the full detector run, from May 1994 to December 2000. The total live time, normalized to the full detector configuration is 6.17 years. The best fit is obtained outside the physical region. The method of FELDMAN 98 is used to obtain the limits.

⁶¹ AMBROSIO 01 result is based on the angular distribution and normalization of upward through-going muon tracks with $E_\mu > 1 \text{ GeV}$. See the previous footnote.

⁶² FUKUDA 99c obtained this result from a total of 537 live days of upward through-going muon data in Super-Kamiokande between April 1996 to January 1998. With a threshold of $E_\mu > 1.6 \text{ GeV}$, the observed flux is $(1.74 \pm 0.07 \pm 0.02) \times 10^{-13} \text{ cm}^{-2}\text{s}^{-1}\text{sr}^{-1}$. The best fit is for $\Delta m^2 = 5.9 \times 10^{-3} \text{ eV}^2$.

⁶³ FUKUDA 99b obtained this result from a simultaneous fitting to zenith angle distributions of upward-stopping and through-going muons. The flux of upward-stopping muons of minimum energy of 1.6 GeV measured between April 1996 and January 1998 is $(0.39 \pm 0.04 \pm 0.02) \times 10^{-13} \text{ cm}^{-2}\text{s}^{-1}\text{sr}^{-1}$. This is compared to the expected flux of $(0.73 \pm 0.16 \text{ (theoretical error)}) \times 10^{-13} \text{ cm}^{-2}\text{s}^{-1}\text{sr}^{-1}$. The best fit is for $\Delta m^2 = 3.9 \times 10^{-3} \text{ eV}^2$.

⁶⁴ FUKUDA 99d obtained this result from the zenith dependence of the upward-stopping/through-going flux ratio. The best fit is for $\Delta m^2 = 3.1 \times 10^{-3} \text{ eV}^2$.

⁶⁵ FUKUDA 98c obtained this result by an analysis of 33.0 kton yr atmospheric neutrino data. The best fit is for $\Delta m^2 = 2.2 \times 10^{-3} \text{ eV}^2$.

⁶⁶ HATAKEYAMA 98 obtained this result from a total of 2456 live days of upward-going muon data in Kamiokande between December 1985 and May 1995. With a threshold of $E_\mu > 1.6 \text{ GeV}$, the observed flux of upward through-going muons is $(1.94 \pm 0.10^{+0.07}_{-0.06}) \times 10^{-13} \text{ cm}^{-2}\text{s}^{-1}\text{sr}^{-1}$. This is compared to the expected flux of $(2.46 \pm 0.54 \text{ (theoretical error)}) \times 10^{-13} \text{ cm}^{-2}\text{s}^{-1}\text{sr}^{-1}$. The best fit is for $\Delta m^2 = 2.2 \times 10^{-3} \text{ eV}^2$.

⁶⁷ HATAKEYAMA 98 obtained this result from a combined analysis of Kamiokande contained events (FUKUDA 94) and upward going muon events. The best fit is for $\Delta m^2 = 13 \times 10^{-3} \text{ eV}^2$.

⁶⁸ FUKUDA 94 obtained the result by a combined analysis of sub- and multi-GeV atmospheric neutrino events in Kamiokande. The best fit is for $\Delta m^2 = 16 \times 10^{-3} \text{ eV}^2$.

$\sin^2(\theta_{13})$

At present time direct measurements of $\sin^2(\theta_{13})$ are derived from the reactor $\bar{\nu}_e$ disappearance at distances corresponding to the Δm_{21}^2 value, i.e. $L \sim 1 \text{ km}$. Alternatively, limits can also be obtained from the analysis of the solar neutrino data and accelerator-based $\nu_\mu \rightarrow \nu_e$ experiments.

If an experiment reports $\sin^2(2\theta_{13})$ we convert the value to $\sin^2(\theta_{13})$.

VALUE (units 10^{-2})	CL%	DOCUMENT ID	TECN	COMMENT
2.20 ± 0.07 OUR AVERAGE				
2.70 ± 0.37		1 DE-KERRET 20	DCHZ	Chooz reactors
2.22 ± 0.21 ± 0.37		2 SHIN 20	RENO	Yonggwang reactors
2.188 ± 0.076		3 ADEY 18A	DAYA	DayaBay, LingAo/Ao II reactors
2.29 ± 0.18		4 BAK 18	RENO	Yonggwang reactors
1.81 ± 0.29		5 AN 16A	DAYA	DayaBay, Ling Ao/Ao II reactors
• • • We do not use the following data for averages, fits, limits, etc. • • •				
2.41 ± 0.45		6 ABRAHAO 21	DCHZ	Chooz reactors
2.200 ⁺ _{-0.062}		7 SALAS 21	FIT	Normal mass ordering, global fit
2.225 ⁺ _{-0.070}		7 SALAS 21	FIT	Inverted mass ordering, global fit
2.219 ⁺ _{-0.063}		8 ESTEBAN 20A	FIT	Normal mass ordering, global fit
2.238 ⁺ _{-0.062}		8 ESTEBAN 20A	FIT	Inverted mass ordering, global fit
< 3.9	68	9 AGAFONOVA 19	OPER	
1.8 ⁺ _{-1.3}		9 ABE 18B	SKAM	3ν osc: normal mass ordering, θ ₁₃ free
0.8 ⁺ _{-0.7}		9 ABE 18B	SKAM	3ν osc: inverted mass ordering, θ ₁₃ free
<12	90	10 AGAFONOVA 18A	OPER	OPERA: ν _e appearance
2.160 ⁺ _{-0.069}		DE-SALAS 18	FIT	Normal mass ordering, global fit
2.220 ⁺ _{-0.076}		DE-SALAS 18	FIT	Inverted mass ordering, global fit
2.09 ± 0.23 ± 0.16		11 SEO 18	RENO	Yonggwang reactors
2.7 ± 0.7		12 ABE 17F	T2K	Normal mass ordering, T2K only
2.149 ± 0.071 ± 0.050		13 AN 17A	DAYA	DayaBay, LingAo/Ao II reactors

2.25 ⁺ _{-0.86}		14 ABE 16B	DCHZ	Chooz reactors
2.09 ± 0.23 ± 0.16		15 CHOI 16	RENO	Yonggwang reactors
2.15 ± 0.13		16 AN 15	DAYA	DayaBay, Ling Ao/Ao II reactors
2.6 ⁺ _{-1.1}		17 ABE 14A	DCHZ	Chooz reactors
3.0 ⁺ _{-1.0}		18 ABE 14C	T2K	Inverted mass ordering
3.6 ⁺ _{-0.9}		18 ABE 14C	T2K	Normal mass ordering
2.3 ⁺ _{-0.8}		19 ABE 14H	DCHZ	Chooz reactors
2.3 ± 0.2		20 AN 14	DAYA	DayaBay, Ling Ao/Ao II reactors
2.12 ± 0.47		21 AN 14B	DAYA	DayaBay, Ling Ao/Ao II reactors
2.34 ± 0.20		22 FORERO 14	FIT	Normal mass ordering
2.40 ± 0.19		22 FORERO 14	FIT	Inverted mass ordering
2.18 ± 0.10		23 GONZALEZ... 14	FIT	Normal mass ordering; global fit
2.19 ⁺ _{-0.11}		23 GONZALEZ... 14	FIT	Inverted mass ordering; global fit
2.5 ± 0.9 ± 0.9		24 ABE 13C	DCHZ	Chooz reactors
2.3 ⁺ _{-1.0}		25 ABE 13E	T2K	Normal mass ordering
2.8 ⁺ _{-1.2}		25 ABE 13E	T2K	Inverted mass ordering
1.6 ⁺ _{-0.9}		26 ADAMSON 13A	MINS	Normal mass ordering
3.0 ⁺ _{-1.6}		26 ADAMSON 13A	MINS	Inverted mass ordering
<13	90	AGAFONOVA 13	OPER	OPERA: 3ν
< 3.6	95	27 AHARMIM 13	FIT	global solar: 3ν
2.3 ± 0.3 ± 0.1		28 AN 13	DAYA	DayaBay, Ling Ao/Ao II reactors
2.2 ± 1.1 ± 0.8		29 ABE 12	DCHZ	Chooz reactors
2.8 ± 0.8 ± 0.7		30 ABE 12B	DCHZ	Chooz reactors
2.9 ± 0.3 ± 0.5		31 AHN 12	RENO	Yonggwang reactors
2.4 ± 0.4 ± 0.1		32 AN 12	DAYA	DayaBay, Ling Ao/Ao II reactors
2.5 ⁺ _{-1.6}		33 ABE 11	FIT	KamLAND + global solar
< 6.1	95	34 ABE 11	FIT	Global solar
1.3 to 5.6	68	35 ABE 11A	T2K	Normal mass ordering
1.5 to 5.6	68	36 ABE 11A	T2K	Inverted mass ordering
0.3 to 2.3	68	37 ADAMSON 11D	MINS	Normal mass ordering
0.8 to 3.9	68	38 ADAMSON 11D	MINS	Inverted mass ordering
8 ± 3		39 FOGLI 11	FIT	Global neutrino data
7.8 ± 6.2		40 GANDO 11	FIT	KamLAND + solar: 3ν
12.4 ± 13.3		41 GANDO 11	FIT	KamLAND: 3ν
3 ⁺ ₋₉	90	42 ADAMSON 10A	MINS	Normal mass ordering
6 ⁺ ₋₆	90	43 ADAMSON 10A	MINS	Inverted mass ordering
8 ⁺ ₋₈		44,45 AHARMIM 10	FIT	KamLAND + global solar: 3ν
< 30	95	44,46 AHARMIM 10	FIT	global solar: 3ν
< 15	90	47 WENDELL 10	SKAM	3ν osc.; normal m ordering
< 33	90	47 WENDELL 10	SKAM	3ν osc.; inverted m ordering
11 ⁺ ₋₈		48 ADAMSON 09	MINS	Normal mass ordering
18 ⁺ ₋₁₁		49 ADAMSON 09	MINS	Inverted mass ordering
6 ± 4		50 FOGLI 08	FIT	Global neutrino data
8 ± 7		51 FOGLI 08	FIT	Solar + KamLAND data
5 ± 5		52 FOGLI 08	FIT	Atmospheric + LBL + CHOOZ
< 36	90	53 YAMAMOTO 06	K2K	Accelerator experiment
< 48	90	54 AHN 04	K2K	Accelerator experiment
< 36	90	55 BOEHM 01		Palo Verde react.
< 45	90	56 BOEHM 00		Palo Verde react.
< 15	90	57 APOLLONIO 99	CHOZ	Reactor Experiment

¹ DE-KERRET 20 uses 481 days of data from single detector operation and also 384 days of data with both near and far detectors operating. A rate and shape analysis is performed on combined neutron captures on H and Gd. Supersedes ABE 16B.

² SHIN 20 uses the RENO detector and 1500 live days of data. The near (far) detector observed 567,690 (90,747) $\bar{\nu}_e$ candidate events with a delayed neutron capture on hydrogen. The extracted value of $\sin^2\theta_{13}$ is consistent with the previous analysis with neutron capture on Gd in BAK 18.

³ ADEY 18A reports results from analysis of 1958 days of data taking with the Daya-Bay experiment, with 3.9×10^6 $\bar{\nu}_e$ candidates. The fit to the data gives $\Delta m_{ee}^2 = (2.522 \pm 0.068) \times 10^{-3} \text{ eV}^2$. Solar oscillation parameters are fixed in the analysis using the global averages, $\sin^2(\theta_{12}) = 0.307^{+0.013}_{-0.012}$, $\Delta m_{21}^2 = (7.53 \pm 0.18) \times 10^{-5} \text{ eV}^2$, from PDG 18. Supersedes AN 17A.

⁴ BAK 18 reports results of the RENO experiment using about 2200 live-days of data taken with detectors placed at 410.6 and 1445.7 m from reactors of the Hanbit Nuclear Power Plant. Supersedes SEO 18.

⁵ AN 16A uses data from the eight antineutrino detectors (404 days) and six antineutrino detectors (217 days) runs to determine the mixing parameter $\sin^2(2\theta_{13})$ using the neutron capture on H only. Supersedes AN 14B.

Lepton Particle Listings

Neutrino Mixing

- ⁶ ABRAHAO 21 uses 865 days of data collected in both near and far detectors with at least one reactor in operation. The analysis is based on a background model independent approach, so called Reactor Rate Modulation, to determine the mixing angle θ_{13} . Adding the background model reduces the uncertainty to 0.0041. Supersedes ABE 16B.
- ⁷ SALAS 21 reports results of a global fit to neutrino oscillation data available at the time of the Neutrino 2020 conference.
- ⁸ ESTEBAN 20A reports results of a global fit to neutrino oscillation data available at the time of the Neutrino2020 conference.
- ⁹ ABE 18B uses 328 kton-years of Super-Kamiokande I-IV atmospheric neutrino data to obtain this result. The fit is performed over the four parameters, Δm_{32}^2 , $\sin^2\theta_{23}$, $\sin^2\theta_{13}$, and δ , while the solar parameters are fixed to $\Delta m_{21}^2 = (7.53 \pm 0.18) \times 10^{-5} \text{ eV}^2$ and $\sin^2\theta_{12} = 0.304 \pm 0.014$.
- ¹⁰ AGAFONOVA 18A reports $\sin^2(2\theta_{13}) < 0.43$ at 90% C.L. The result on the sterile neutrino search in the context of 3+1 model is also reported. A 90% C.L. upper limit on $\sin^2(2\theta_{\mu e}) = 0.021$ for $\Delta m_{41}^2 \geq 0.1 \text{ eV}^2$ is set.
- ¹¹ SEO 18 reports results of the RENO experiment using about 500 days of data, performing a rate and shape analysis. Compared to AHN 12, a significant reduction of the systematic uncertainties is reported. A 3% excess of events near 5 MeV of the prompt energy is observed. SEO 18 is a detailed description of the results published in CHOI 16, which it supersedes. Superseded by BAK 18.
- ¹² Using T2K data only. For inverted mass ordering, all values of θ_{13} are ruled out at 68% CL.
- ¹³ AN 17A reports results from combined rate and spectral shape analysis of 1230 days of data taken with the Daya Bay reactor experiment. The data set contains more than 2.5×10^6 inverse beta-decay events with neutron capture on Gd. A simultaneous fit to θ_{13} and Δm_{ee}^2 is performed. Superseded by ADEY 18A.
- ¹⁴ ABE 16B uses 455.57 live days of data from a detector 1050 m away from two reactor cores of the Chooz nuclear power station, to determine the mixing parameter $\sin^2(2\theta_{13})$. This analysis uses 7.15 reactor-off days for constraining backgrounds. A rate and shape analysis is performed on combined neutron captures on H and Gd. Supersedes ABE 14H and ABE 13C.
- ¹⁵ CHOI 16 reports results of the RENO experiment using about 500 days of data, performing a rate and shape analysis. Compared to AHN 12, a significant reduction of the systematic uncertainties is reported. A 3% excess of events near 5 MeV of the prompt energy is observed. Supersedes AHN 12.
- ¹⁶ AN 15 uses all eight identical detectors, with four placed near the reactor cores and the remaining four at the far hall to determine the mixing angle θ_{13} using the $\overline{\nu}_e$ observed interaction rates with neutron capture on Gd and energy spectra. The result corresponds to the exposure of $6.9 \times 10^5 \text{ GW}_{th}$ -ton-days. Superseded by AN 17A.
- ¹⁷ ABE 14A uses 467.9 live days of one detector, 1050 m away from two reactor cores of the Chooz nuclear power station, to determine the mixing parameter $\sin^2(2\theta_{13})$. The Bugey4 data (DECLAIS 94) is used to constrain the neutrino flux. The data set includes 7.24 reactor-off days. A "rate-modulation" analysis is performed. Supersedes ABE 12B.
- ¹⁸ ABE 14C result is for ν_e appearance and assumes $\Delta m_{32}^2 = 2.4 \times 10^{-3} \text{ eV}^2$, $\sin^2(\theta_{23}) = 0.5$, and $\delta = 0$.
- ¹⁹ ABE 14H uses 467.9 live days of one detector, 1050 m away from two reactor cores of the Chooz nuclear power station, to determine the mixing parameter $\sin^2(2\theta_{13})$. The Bugey4 data (DECLAIS 94) is used to constrain the neutrino flux. The data set includes 7.24 reactor-off days. A rate and shape analysis is performed. Superseded by ABE 16B.
- ²⁰ AN 14 uses six identical detectors, with three placed near the reactor cores (flux-weighted baselines of 512 and 561 m) and the remaining three at the far hall (at the flux averaged distance of 1579 m from all six reactor cores) to determine the mixing angle θ_{13} using the $\overline{\nu}_e$ observed interaction rates with neutron capture on Gd and energy spectra. Supersedes AN 13 and superseded by AN 15.
- ²¹ AN 14B uses six identical anti-neutrino detectors with flux-weighted baselines of $\sim 500 \text{ m}$ and $\sim 1.6 \text{ km}$ to six power reactors. This rate analysis uses a 217-day data set and neutron capture on protons (not Gd) only. $\Delta m_{31}^2 = 2.32 \times 10^{-3} \text{ eV}^2$ is assumed. Superseded by AN 16A.
- ²² FORERO 14 performs a global fit to neutrino oscillations using solar, reactor, long-baseline accelerator, and atmospheric neutrino data.
- ²³ GONZALEZ-GARCIA 14 result comes from a frequentist global fit. The corresponding Bayesian global fit to the same data results are reported in BERGSTROM 15 as $(2.18^{+0.10}_{-0.11}) \times 10^{-2} \text{ eV}^2$ for normal and $(2.19^{+0.12}_{-0.10}) \times 10^{-2} \text{ eV}^2$ for inverted mass ordering.
- ²⁴ ABE 13C uses delayed neutron capture on hydrogen instead of on Gd used previously. The physical volume is thus three times larger. The fit is based on the rate and shape analysis as in ABE 12B. The Bugey4 data (DECLAIS 94) is used to constrain the neutrino flux. Superseded by ABE 16B.
- ²⁵ ABE 13E assumes maximal θ_{23} mixing and CP phase $\delta = 0$.
- ²⁶ ADAMSON 13A results obtained from ν_e appearance, assuming $\delta = 0$, and $\sin^2(2\theta_{23}) = 0.957$.
- ²⁷ AHARMIM 13 obtained this result by a three-neutrino oscillation analysis with the value of Δm_{32}^2 fixed to $2.45 \times 10^{-3} \text{ eV}^2$, using global solar neutrino data. AHARMIM 13 global solar neutrino data include SNO's all-phases-combined analysis results on the total active ^8B neutrino flux and energy-dependent ν_e survival probability parameters, measurements of Cl (CLEVELAND 98), Ga (ABDURASHITOV 09 which contains combined analysis with GNO (ALTMANN 05 and Ph.D. thesis of F. Kaether)), and ^7Be (BELLINI 11A) rates, and ^8B solar-neutrino recoil electron measurements of SK-I (HOSAKA 06) zenith, SK-II (CRAVENS 08) and SK-III (ABE 11) day/night spectra, and Borexino (BELLINI 10A) spectra. AHARMIM 13 also reported a result combining global solar and KamLAND data, which is $\sin^2(2\theta_{13}) = (9.1^{+2.9}_{-3.1}) \times 10^{-2}$.
- ²⁸ AN 13 uses six identical detectors, with three placed near the reactor cores (flux-weighted baselines of 498 and 555 m) and the remaining three at the far hall (at the flux averaged distance of 1628 m from all six reactor cores) to determine the $\overline{\nu}_e$ interaction rate ratios. Superseded by AN 14.
- ²⁹ ABE 12 determines the $\overline{\nu}_e$ interaction rate in a single detector, located 1050 m from the cores of two reactors. A rate and shape analysis is performed. The rate normalization is fixed by the results of the Bugey4 reactor experiment, thus avoiding any dependence on possible very short baseline oscillations. The value of $\Delta m_{31}^2 = 2.4 \times 10^{-3} \text{ eV}^2$ is used in the analysis. Superseded by ABE 12B.
- ³⁰ ABE 12B determines the neutrino mixing angle θ_{13} using a single detector, located 1050 m from the cores of two reactors. This result is based on a spectral shape and rate analysis. The Bugey4 data (DECLAIS 94) is used to constrain the neutrino flux. Superseded by ABE 14A.
- ³¹ AHN 12 uses two identical detectors, placed at flux weighted distances of 408.56 m and 1433.99 m from six reactor cores, to determine the mixing angle θ_{13} . This rate-only analysis excludes the no-oscillation hypothesis at 4.9 standard deviations. The value of $\Delta m_{31}^2 = (2.32^{+0.12}_{-0.08}) \times 10^{-3} \text{ eV}^2$ was assumed in the analysis. Superseded by CHOI 16.
- ³² AN 12 uses six identical detectors with three placed near the reactor cores (flux-weighted baselines of 470 m and 576 m) and the remaining three at the far hall (at the flux averaged distance of 1648 m from all six reactor cores) to determine the mixing angle θ_{13} using the $\overline{\nu}_e$ observed interaction rate ratios. This rate-only analysis excludes the no-oscillation hypothesis at 5.2 standard deviations. The value of $\Delta m_{31}^2 = (2.32^{+0.12}_{-0.08}) \times 10^{-3} \text{ eV}^2$ was assumed in the analysis. Superseded by AN 13.
- ³³ ABE 11 obtained this result by a three-neutrino oscillation analysis with the value of Δm_{32}^2 fixed to $2.4 \times 10^{-3} \text{ eV}^2$, using solar neutrino data including Super-Kamiokande, SNO, Borexino (ARPESELLA 08A), Homestake, GALLEX/GNO, SAGE, and KamLAND data. This result implies an upper bound of $\sin^2\theta_{13} < 0.059$ (95% CL) or $\sin^2 2\theta_{13} < 0.22$ (95% CL). The normal neutrino mass ordering and CPT invariance are assumed.
- ³⁴ ABE 11 obtained this result by a three-neutrino oscillation analysis with the value of Δm_{32}^2 fixed to $2.4 \times 10^{-3} \text{ eV}^2$, using solar neutrino data including Super-Kamiokande, SNO, Borexino (ARPESELLA 08A), Homestake, and GALLEX/GNO data. The normal neutrino mass ordering is assumed.
- ³⁵ The quoted limit is for $\Delta m_{32}^2 = 2.4 \times 10^{-3} \text{ eV}^2$, $\theta_{23} = \pi/2$, $\delta = 0$, and the normal mass ordering. For other values of δ , the 68% region spans from 0.03 to 0.25, and the 90% region from 0.02 to 0.32.
- ³⁶ The quoted limit is for $\Delta m_{32}^2 = 2.4 \times 10^{-3} \text{ eV}^2$, $\theta_{23} = \pi/2$, $\delta = 0$, and the inverted mass ordering. For other values of δ , the 68% region spans from 0.04 to 0.30, and the 90% region from 0.02 to 0.39.
- ³⁷ The quoted limit is for $\Delta m_{32}^2 = 2.32 \times 10^{-3} \text{ eV}^2$, $\theta_{23} = \pi/2$, $\delta = 0$, and the normal mass ordering. For other values of δ , the 68% region spans from 0.02 to 0.12, and the 90% region from 0 to 0.16.
- ³⁸ The quoted limit is for $\Delta m_{32}^2 = 2.32 \times 10^{-3} \text{ eV}^2$, $\theta_{23} = \pi/2$, $\delta = 0$, and the inverted mass ordering. For other values of δ , the 68% region spans from 0.02 to 0.16, and the 90% region from 0 to 0.21.
- ³⁹ FOGLI 11 obtained this result from an analysis using the atmospheric, accelerator long baseline, CHOOZ, solar, and KamLAND data. Recently, MUELLER 11 suggested an average increase of about 3.5% in normalization of the reactor $\overline{\nu}_e$ fluxes, and using these fluxes, the fitted result becomes 0.10 ± 0.03 .
- ⁴⁰ GANDO 11 report $\sin^2\theta_{13} = 0.020 \pm 0.016$. This result was obtained with three-neutrino fit using the KamLAND + solar data.
- ⁴¹ GANDO 11 report $\sin^2\theta_{13} = 0.032 \pm 0.037$. This result was obtained with three-neutrino fit using the KamLAND data only.
- ⁴² This result corresponds to the limit of < 0.12 at 90% CL for $\Delta m_{32}^2 = 2.43 \times 10^{-3} \text{ eV}^2$, $\theta_{23} = \pi/2$, and $\delta = 0$. For other values of δ , the 90% CL region spans from 0 to 0.16.
- ⁴³ This result corresponds to the limit of < 0.20 at 90% CL for $\Delta m_{32}^2 = 2.43 \times 10^{-3} \text{ eV}^2$, $\theta_{23} = \pi/2$, and $\delta = 0$. For other values of δ , the 90% CL region spans from 0 to 0.21.
- ⁴⁴ AHARMIM 10 global solar neutrino data include SNO's low-energy-threshold analysis survival probability day/night curves, SNO Phase III integral rates (AHARMIM 08), Cl (CLEVELAND 98), SAGE (ABDURASHITOV 09), Gallex/GNO (HAMPEL 99, ALTMANN 05), Borexino (ARPESELLA 08A), SK-I zenith (HOSAKA 06), and SK-II day/night spectra (CRAVENS 08).
- ⁴⁵ AHARMIM 10 obtained this result by a three-neutrino oscillation analysis with the value of Δm_{31}^2 fixed to $2.3 \times 10^{-3} \text{ eV}^2$, using global solar neutrino data and KamLAND data (ABE 08A). CPT invariance is assumed. This result implies an upper bound of $\sin^2\theta_{13} < 0.057$ (95% CL) or $\sin^2 2\theta_{13} < 0.22$ (95% CL).
- ⁴⁶ AHARMIM 10 obtained this result by a three-neutrino oscillation analysis with the value of Δm_{31}^2 fixed to $2.3 \times 10^{-3} \text{ eV}^2$, using global solar neutrino data.
- ⁴⁷ WENDELL 10 obtained this result by a three-neutrino oscillation analysis with one mass scale dominance ($\Delta m_{21}^2 = 0$) using the Super-Kamiokande-I+II+III atmospheric neutrino data, and updates the HOSAKA 06A result.
- ⁴⁸ The quoted limit is for $\Delta m_{32}^2 = 2.43 \times 10^{-3} \text{ eV}^2$, $\theta_{23} = \pi/2$, and $\delta = 0$. For other values of δ , the 68% CL region spans from 0.02 to 0.26.
- ⁴⁹ The quoted limit is for $\Delta m_{32}^2 = 2.43 \times 10^{-3} \text{ eV}^2$, $\theta_{23} = \pi/2$, and $\delta = 0$. For other values of δ , the 68% CL region spans from 0.04 to 0.34.
- ⁵⁰ FOGLI 08 obtained this result from a global analysis of all neutrino oscillation data, that is, solar + KamLAND + atmospheric + accelerator long baseline + CHOOZ.
- ⁵¹ FOGLI 08 obtained this result from an analysis using the solar and KamLAND neutrino oscillation data.
- ⁵² FOGLI 08 obtained this result from an analysis using the atmospheric, accelerator long baseline, and CHOOZ neutrino oscillation data.
- ⁵³ YAMAMOTO 06 searched for $\nu_\mu \rightarrow \nu_e$ appearance. Assumes $2 \sin^2(2\theta_{\mu e}) = \sin^2(2\theta_{13})$. The quoted limit is for $\Delta m_{32}^2 = 1.9 \times 10^{-3} \text{ eV}^2$. That value of Δm_{32}^2 is the one- σ low value for AHN 06A. For the AHN 06A best fit value of $2.8 \times 10^{-3} \text{ eV}^2$, the $\sin^2(2\theta_{13})$ limit is < 0.26 . Supersedes AHN 04.

See key on page 1127

Lepton Particle Listings

Neutrino Mixing

- 54 AHN 04 searched for $\nu_\mu \rightarrow \nu_e$ appearance. Assuming $2 \sin^2(2\theta_{\mu e}) = \sin^2(2\theta_{13})$, a limit on $\sin^2(2\theta_{\mu e})$ is converted to a limit on $\sin^2(2\theta_{13})$. The quoted limit is for $\Delta m_{32}^2 = 1.9 \times 10^{-3} \text{ eV}^2$. That value of Δm_{32}^2 is the one- σ low value for ALIU 05. For the ALIU 05 best fit value of $2.8 \times 10^{-3} \text{ eV}^2$, the $\sin^2(2\theta_{13})$ limit is < 0.30 .
- 55 The quoted limit is for $\Delta m_{32}^2 = 1.9 \times 10^{-3} \text{ eV}^2$. That value of Δm_{32}^2 is the 1- σ low value for ALIU 05. For the ALIU 05 best fit value of $2.8 \times 10^{-3} \text{ eV}^2$, the $\sin^2 2\theta_{13}$ limit is < 0.19 . In this range, the θ_{13} limit is larger for lower values of Δm_{32}^2 , and smaller for higher values of Δm_{32}^2 .
- 56 The quoted limit is for $\Delta m_{32}^2 = 1.9 \times 10^{-3} \text{ eV}^2$. That value of Δm_{32}^2 is the 1- σ low value for ALIU 05. For the ALIU 05 best fit value of $2.8 \times 10^{-3} \text{ eV}^2$, the $\sin^2 2\theta_{13}$ limit is < 0.23 .
- 57 The quoted limit is for $\Delta m_{32}^2 = 2.43 \times 10^{-3} \text{ eV}^2$. That value of Δm_{32}^2 is the central value for ADAMSON 08. For the ADAMSON 08 1- σ low value of $2.30 \times 10^{-3} \text{ eV}^2$, the $\sin^2 2\theta_{13}$ limit is < 0.16 . See also APOLLONIO 03 for a detailed description of the experiment.

CP violating phase

δ , CP violating phase

Measurements of δ come from atmospheric and accelerator experiments looking at ν_e appearance. We encode values between 0 and 2π , though it is equivalent to use $-\pi$ to π .

VALUE (π rad)	CL%	DOCUMENT ID	TECN	COMMENT
1.36^{+0.20}_{-0.16}		OUR AVERAGE		
1.40 ^{+0.22} _{-0.18}		1 ABE	20F T2K	Normal mass ordering
0.0 ^{+1.3} _{-0.4}		2 ACERO	19 NOVA	Normal mass ordering, octant II for θ_{23}
1.33 ^{+0.45} _{-0.51}		3 ABE	18B SKAM	Normal mass ordering, θ_{13} constrained
• • • We do not use the following data for averages, fits, limits, etc. • • •				
1.08 ^{+0.13} _{-0.12}		4 SALAS	21 FIT	Normal mass ordering, global fit
1.58 ^{+0.15} _{-0.16}		4 SALAS	21 FIT	Inverted mass ordering, global fit
1.09 ^{+0.15} _{-0.13}		5 ESTEBAN	20A FIT	Normal mass ordering, global fit
1.57 ^{+0.14} _{-0.17}		5 ESTEBAN	20A FIT	Inverted mass ordering, global fit
1.33 ^{+0.46} _{-0.53}		6 ABE	18B SKAM	3 ν osc: normal mass ordering, θ_{13} free
1.22 ^{+0.76} _{-0.67}		6 ABE	18B SKAM	3 ν osc: inverted mass ordering, θ_{13} free
1.33 ^{+0.48} _{-0.53}		3 ABE	18B SKAM	3 ν osc: inverted mass ordering, θ_{13} constrained
1.40 \pm 0.20		7 ABE	18G T2K	Normal mass ordering, θ_{13} constrained
1.54 ^{+0.14} _{-0.12}	95	7 ABE	18G T2K	Inverted mass ordering, θ_{13} constrained
1.21 ^{+0.91} _{-0.30}		8 ACERO	18 NOVA	Normal mass ordering, octant II for θ_{23}
1.46 ^{+0.56} _{-0.42}		8 ACERO	18 NOVA	Normal mass order; octant I for θ_{23}
1.32 ^{+0.21} _{-0.15}		DE-SALAS	18 FIT	Normal mass ordering, global fit
1.56 ^{+0.13} _{-0.15}		DE-SALAS	18 FIT	Inverted mass ordering, global fit
1.45 ^{+0.27} _{-0.26}		9 ABE	17F T2K	Normal mass ordering
1.54 ^{+0.22} _{-0.23}		9 ABE	17F T2K	Inverted mass ordering
1.50 ^{+0.53} _{-0.57}		10 ADAMSON	17B NOVA	Inverted mass ordering; θ_{23} in octant II
0.74 ^{+0.57} _{-0.93}		10 ADAMSON	17B NOVA	Normal mass ordering; θ_{23} in octant II
1.48 ^{+0.69} _{-0.58}		10 ADAMSON	17B NOVA	Normal mass ordering; θ_{23} in octant I
0.0 to 0.1, 0.5 to 2.0	90	10,11 ADAMSON	16 NOVA	Inverted mass ordering
0.0 to 2.0	90	11 ADAMSON	16 NOVA	Normal mass ordering
0 to 0.15, 0.83 to 2	90	ABE	15D T2K	Normal mass ordering
1.09 to 1.92	90	ABE	15D T2K	Inverted mass ordering
0.05 to 1.2	90	12 ADAMSON	14 MINS	Normal mass ordering
1.34 ^{+0.64} _{-0.38}		FORERO	14 FIT	Normal mass ordering
1.48 ^{+0.34} _{-0.32}		FORERO	14 FIT	Inverted mass ordering
1.70 ^{+0.22} _{-0.39}		13 GONZALEZ...	14 FIT	Normal mass ordering; global fit
1.41 ^{+0.35} _{-0.34}		13 GONZALEZ...	14 FIT	Inverted mass ordering; global fit
0 to 1.5 or 1.9 to 2	90	14 ADAMSON	13A MINS	Normal mass ordering

- 1 ABE 20F results are based on data collected between 2009 and 2018 in (anti)neutrino mode and include a neutrino beam exposure of 1.49×10^{21} (1.64×10^{21}) protons on target. For inverted mass ordering, the quoted result is $1.56^{+0.15}_{-0.17} \pi$ rad. Supersedes ABE 18g.
- 2 ACERO 19 is based on a sample size of 1.33×10^{20} protons on target with combined antineutrino and neutrino data. Supersedes ACERO 18.
- 3 ABE 18b uses 328 kton-years of Super-Kamiokande I-IV atmospheric neutrino data to obtain this result. The fit is performed over the three parameters, Δm_{32}^2 , $\sin^2 \theta_{23}$, and δ , while the solar parameters and $\sin^2 \theta_{13}$ are fixed to $\Delta m_{21}^2 = (7.53 \pm 0.18) \times 10^{-5} \text{ eV}^2$, $\sin^2 \theta_{12} = 0.304 \pm 0.014$, and $\sin^2 \theta_{13} = 0.0219 \pm 0.0012$.
- 4 SALAS 21 reports results of a global fit to neutrino oscillation data available at the time of the Neutrino 2020 conference.
- 5 ESTEBAN 20A reports results of a global fit to neutrino oscillation data available at the time of the Neutrino 2020 conference.
- 6 ABE 18b uses 328 kton-years of Super-Kamiokande I-IV atmospheric neutrino data to obtain this result. The fit is performed over the four parameters, Δm_{32}^2 , $\sin^2 \theta_{23}$, $\sin^2 \theta_{13}$, and δ , while the solar parameters are fixed to $\Delta m_{21}^2 = (7.53 \pm 0.18) \times 10^{-5} \text{ eV}^2$ and $\sin^2 \theta_{12} = 0.304 \pm 0.014$.
- 7 ABE 18g confidence intervals are marginalized over both mass orderings. Normal order preferred with a posterior probability of 87%. The 1-sigma result for normal mass ordering in the average was provided by the experiment via private communications. Supersedes ABE 17f.
- 8 ACERO 18 performs a joint fit to the data for ν_μ disappearance and ν_e appearance. The overall best fit favors normal mass ordering and θ_{23} in octant II. No 1 σ confidence intervals are presented for the inverted mass ordering scenarios. Superseded by ACERO 19.
- 9 ABE 17f confidence intervals are obtained using a frequentist analysis including θ_{13} constraint from reactor experiments. Bayesian intervals based on Markov Chain Monte Carlo method are also provided by the authors. Superseded by ABE 18g.
- 10 Errors are projections of 68% C.L. curve of δ_{CP} vs. $\sin^2 \theta_{23}$.
- 11 ADAMSON 16 result is based on a data sample with 2.74×10^{20} protons on target. The likelihood-based analysis observed 6 ν_e events with an expected background of 0.99 ± 0.11 events.
- 12 ADAMSON 14 result is based on three-flavor formalism and $\theta_{23} > \pi/4$. Likelihood as a function of δ is also shown for the other three combinations of hierarchy and θ_{23} octants; all values of δ are allowed at 90% C.L.
- 13 GONZALEZ-GARCIA 14 result comes from a frequentist global fit. The corresponding Bayesian global fit to the same data results are reported in BERGSTROM 15 as 68% CL intervals of 1.24–1.94 for normal and 1.15–1.77 for inverted mass ordering.
- 14 ADAMSON 13A result is based on ν_e appearance in MINOS and the calculated $\sin^2(2\theta_{23}) = 0.957$, $\theta_{23} > \pi/4$, and normal mass hierarchy. Likelihood as a function of δ is also shown for the other three combinations of hierarchy and θ_{23} octants; all values of δ are allowed at 90% C.L.

(C) Other neutrino mixing results

The LSND collaboration reported in AGUILAR 01 a signal which is consistent with $\bar{\nu}_\mu \rightarrow \bar{\nu}_e$ oscillations. In a three neutrino framework, this would be a measurement of θ_{12} and Δm_{21}^2 . This does not appear to be consistent with most of the other neutrino data. The following listings include results from $\nu_\mu \rightarrow \nu_e$, $\bar{\nu}_\mu \rightarrow \bar{\nu}_e$ appearance and ν_μ , $\bar{\nu}_\mu$, ν_e , and $\bar{\nu}_e$ disappearance experiments, and searches for CPT violation.

$\Delta(m^2)$ for $\sin^2(2\theta) = 1$ ($\nu_\mu \rightarrow \nu_e$)

VALUE (eV ²)	CL%	DOCUMENT ID	TECN	COMMENT
• • • We do not use the following data for averages, fits, limits, etc. • • •				
0.03 to 0.55	90	1 AGUILAR-AR...21	MBNE	MiniBooNE $\nu, \bar{\nu}$ combined
0.03 to 0.05	90	2 AGUILAR-AR...18c	MBNE	MiniBooNE $\nu, \bar{\nu}$ combined
0.015 to 0.050	90	3 AGUILAR-AR...13A	MBNE	MiniBooNE
<0.34	90	4 MAHN 12	MBNE	MiniBooNE/SciBooNE
<0.034	90	AGUILAR-AR...07	MBNE	MiniBooNE
<0.0008	90	AHN 04	K2K	Water Cherenkov
<0.4	90	ASTVIER 03	NOMD	CERN SPS
<2.4	90	AVVAKUMOV 02	NTEV	NUTEV FNAL
0.03 to 0.3	95	5 AGUILAR 01	LSND	$\nu_\mu \rightarrow \nu_e$ osc. prob.
<2.3	90	6 ATHANASSO...98	LSND	$\nu_\mu \rightarrow \nu_e$
<0.9	90	7 LOVERRE 96	CHARM/CDHS	
<0.09	90	VILAIN 94c	CHM2	CERN SPS
	90	ANGELINI 86	HLBC	BEBC CERN PS
1 AGUILAR-AREVALO 21 result is based on a total of 18.75×10^{20} POT in neutrino mode, and 11.27×10^{20} POT in anti-neutrino mode. Best fit at 0.043 eV^2 . The allowed region does not extend to large Δm^2 . The quoted value is the entire allowed region of Δm^2 at 90% C.L. for all values of $\sin^2(2\theta)$. Supersedes AGUILAR-AREVALO 18c.				
2 AGUILAR-AREVALO 18c result is based on $\nu_\mu \rightarrow \nu_e$ appearance of 460.5 ± 99.0 events; The best fit value is $\Delta m^2 = 0.041 \text{ eV}^2$. Superseded by AGUILAR-AREVALO 21.				
3 AGUILAR-AREVALO 13A result is based on $\nu_\mu \rightarrow \nu_e$ appearance of 162.0 ± 47.8 events; marginally compatible with twoneutrino oscillations. The best fit value is $\Delta m^2 = 3.14 \text{ eV}^2$.				
4 MAHN 12 is a combined spectral fit of MiniBooNE and SciBooNE neutrino data with the range of Δm^2 up to 25 eV^2 . The best limit is 0.04 at 7 eV^2 .				

Lepton Particle Listings

Neutrino Mixing

⁵ AGUILAR 01 is the final analysis of the LSND full data set. Search is made for the $\nu_\mu \rightarrow \nu_e$ oscillations using ν_μ from π^+ decay in flight by observing beam-on electron events from $\nu_e C \rightarrow e^- X$. Present analysis results in $8.1 \pm 12.2 \pm 1.7$ excess events in the $60 < E_e < 200$ MeV energy range, corresponding to oscillation probability of $0.10 \pm 0.16 \pm 0.04\%$. This is consistent, though less significant, with the previous result of ATHANASSOPOULOS 98, which it supersedes. The present analysis uses selection criteria developed for the decay at rest region, and is less effective in removing the background above 60 MeV than ATHANASSOPOULOS 98.

⁶ ATHANASSOPOULOS 98 is a search for the $\nu_\mu \rightarrow \nu_e$ oscillations using ν_μ from π^+ decay in flight. The 40 observed beam-on electron events are consistent with $\nu_e C \rightarrow e^- X$; the expected background is 21.9 ± 2.1 . Authors interpret this excess as evidence for an oscillation signal corresponding to oscillations with probability $(0.26 \pm 0.10 \pm 0.05)\%$. Although the significance is only 2.3σ , this measurement is an important and consistent cross check of ATHANASSOPOULOS 96 who reported evidence for $\bar{\nu}_\mu \rightarrow \bar{\nu}_e$ oscillations from μ^+ decay at rest. See also ATHANASSOPOULOS 98b.

⁷ LOVERRE 96 uses the charged-current to neutral-current ratio from the combined CHARM (ALLABY 86) and CDHS (ABRAMOWICZ 86) data from 1986.

$\sin^2(2\theta)$ for "Large" $\Delta(m^2)$ ($\nu_\mu \rightarrow \nu_e$)

VALUE (units 10^{-3})	CL%	DOCUMENT ID	TECN	COMMENT
• • • We do not use the following data for averages, fits, limits, etc. • • •				
6 to 1000	90	¹ AGUILAR-AR...21	MBNE	MiniBooNE; $\nu + \bar{\nu}$
< 5	90	² AGUILAR-AR...18c	MBNE	MiniBooNE; $\nu + \bar{\nu}$
< 7.2	90	AGAFONOVA 13	OPER	$\Delta(m^2) > 0.1$ eV ²
0.8 to 3	90	³ AGUILAR-AR...13A	MBNE	MiniBooNE
< 11	90	⁴ ANTONELLO 13	ICAR	$\nu_\mu \rightarrow \nu_e$
< 6.8	90	⁵ ANTONELLO 13A	ICAR	$\nu_\mu \rightarrow \nu_e$
< 100	90	⁶ MAHN 12	MBNE	MiniBooNE/SciBooNE
< 1.8	90	⁷ AGUILAR-AR...07	MBNE	MiniBooNE
< 110	90	⁸ AHN 04	K2K	Water Cherenkov
< 1.4	90	ASTIER 03	NOMD	CERN SPS
< 1.6	90	AVVAKUMOV 02	NTEV	NUTEV FNAL
		⁹ AGUILAR 01	LSND	$\nu_\mu \rightarrow \nu_e$ osc. prob.
0.5 to 30	95	¹⁰ ATHANASSO...98	LSND	$\nu_\mu \rightarrow \nu_e$
< 3.0	90	¹¹ LOVERRE 96		CHARM/CDHS
< 9.4	90	VILAIN 94c	CHM2	CERN SPS
< 5.6	90	VILAIN 94c	CHM2	CERN SPS

¹ AGUILAR-AREVALO 21 result is based on a total of 18.75×10^{20} POT in neutrino mode, and 11.27×10^{20} POT in anti-neutrino mode. The best fit value is $\sin^2(2\theta) = 0.807$. The allowed region does not extend to large Δm^2 . The quoted value is the entire allowed region of $\sin^2(2\theta)$ at 90% C.L. for all values of Δm^2 . Supersedes AGUILAR-AREVALO 18c.

² AGUILAR-AREVALO 18c result is based on $\nu_\mu \rightarrow \nu_e$ appearance of 460.5 ± 99.0 events; The best fit value is $\sin^2(2\theta) = 0.92$. The quoted limit for the two-neutrino mixing angle θ is valid above $\Delta m^2 = 0.59$ eV². Superseded by AGUILAR-AREVALO 21.

³ AGUILAR-AREVALO 13A result is based on $\nu_\mu \rightarrow \nu_e$ appearance of 162.0 ± 47.8 events; marginally compatible with two neutrino oscillations. The best fit value is $\sin^2(2\theta) = 0.002$.

⁴ ANTONELLO 13 use the ICARUS T600 detector at LNGS and ~ 20 GeV beam of ν_μ from CERN 730 km away to search for an excess of ν_e events. Two events are found with 3.7 ± 0.6 expected from conventional sources. This result excludes some parts of the parameter space expected by LSND. Superseded by ANTONELLO 13A.

⁵ Based on four events with a background of 6.4 ± 0.9 from conventional sources with an average energy of 20 GeV and 730 km from the source of ν_μ .

⁶ MAHN 12 is a combined fit of MiniBooNE and SciBooNE neutrino data.

⁷ The limit is $\sin^2 2\theta < 0.9 \times 10^{-3}$ at $\Delta m^2 = 2$ eV². That value of Δm^2 corresponds to the smallest mixing angle consistent with the reported signal from LSND in AGUILAR 01.

⁸ The limit becomes $\sin^2 2\theta < 0.15$ at $\Delta m^2 = 2.8 \times 10^{-3}$ eV², the best-fit value of the ν_μ disappearance analysis in K2K.

⁹ AGUILAR 01 is the final analysis of the LSND full data set of the search for the $\nu_\mu \rightarrow \nu_e$ oscillations. See footnote in preceding table for further details.

¹⁰ ATHANASSOPOULOS 98 report $(0.26 \pm 0.10 \pm 0.05)\%$ for the oscillation probability; the value of $\sin^2 2\theta$ for large Δm^2 is deduced from this probability. See footnote in preceding table for further details, and see the paper for a plot showing allowed regions. If effect is due to oscillation, it is most likely to be intermediate $\sin^2 2\theta$ and Δm^2 . See also ATHANASSOPOULOS 98b.

¹¹ LOVERRE 96 uses the charged-current to neutral-current ratio from the combined CHARM (ALLABY 86) and CDHS (ABRAMOWICZ 86) data from 1986.

¹² VILAIN 94c limit derived by combining the ν_μ and $\bar{\nu}_\mu$ data assuming CP conservation.

$\Delta(m^2)$ for $\sin^2(2\theta) = 1$ ($\bar{\nu}_\mu \rightarrow \bar{\nu}_e$)

VALUE (eV ²)	CL%	DOCUMENT ID	TECN	COMMENT
• • • We do not use the following data for averages, fits, limits, etc. • • •				
0.023 to 0.060	90	¹ AGUILAR-AR...13A	MBNE	MiniBooNE
< 0.16	90	² CHENG 12	MBNE	MiniBooNE/SciBooNE
0.03-0.09	90	³ AGUILAR-AR...10	MBNE	$E_\nu > 475$ MeV
0.03-0.07	90	⁴ AGUILAR-AR...10	MBNE	$E_\nu > 200$ MeV
< 0.06	90	AGUILAR-AR...09B	MBNE	MiniBooNE
< 0.055	90	⁵ ARMBRUSTER02	KAR2	Liquid Sci. calor.
< 2.6	90	AVVAKUMOV 02	NTEV	NUTEV FNAL

0.03-0.05		⁶ AGUILAR 01	LSND	LAMPF
0.05-0.08	90	⁷ ATHANASSO...96	LSND	LAMPF
0.048-0.090	80	⁸ ATHANASSO...95		
< 0.07	90	⁹ HILL 95		
< 0.9	90	VILAIN 94c	CHM2	CERN SPS
< 0.14	90	¹⁰ FREEDMAN 93	CNTR	LAMPF

¹ Based on $\bar{\nu}_\mu \rightarrow \bar{\nu}_e$ appearance of 78.4 ± 28.5 events. The best fit values are $\Delta m^2 = 0.043$ eV² and $\sin^2 2\theta = 0.88$.

² CHENG 12 is a combined fit of MiniBooNE and SciBooNE antineutrino data.

³ This value is for a two neutrino oscillation analysis for excess antineutrino events with $E_\nu > 475$ MeV. The best fit is at 0.07. The allowed region is consistent with LSND reported by AGUILAR 01. Supersedes AGUILAR-AREVALO 09B.

⁴ This value is for a two neutrino oscillation analysis for excess antineutrino events with $E_\nu > 200$ MeV with subtraction of the expected 12 events low energy excess seen in the neutrino component of the beam. The best fit value is 0.007 for $\Delta(m^2) = 4.4$ eV².

⁵ ARMBRUSTER 02 is the final analysis of the KARMEN 2 data for 17.7 m distance from the ISIS stopped pion and muon neutrino source. It is a search for $\bar{\nu}_e$, detected by the inverse β -decay reaction on protons and ¹²C. 15 candidate events are observed, and 15.8 ± 0.5 background events are expected, hence no oscillation signal is detected. The results exclude large regions of the parameter area favored by the LSND experiment.

⁶ AGUILAR 01 is the final analysis of the LSND full data set. It is a search for $\bar{\nu}_e$ 30 m from LAMPF beam stop. Neutrinos originate mainly from π^+ decay at rest. $\bar{\nu}_e$ are detected through $\bar{\nu}_e p \rightarrow e^+ n$ ($20 < E_{e^+} < 60$ MeV) in delayed coincidence with $np \rightarrow d\gamma$. Authors observe $87.9 \pm 22.4 \pm 6.0$ total excess events. The observation is attributed to $\bar{\nu}_\mu \rightarrow \bar{\nu}_e$ oscillations with the oscillation probability of $0.264 \pm 0.067 \pm 0.045\%$, consistent with the previously published result. Taking into account all constraints, the most favored allowed region of oscillation parameters is a band of $\Delta(m^2)$ from $0.2-2.0$ eV². Supersedes ATHANASSOPOULOS 95, ATHANASSOPOULOS 96, and ATHANASSOPOULOS 98.

⁷ ATHANASSOPOULOS 96 is a search for $\bar{\nu}_e$ 30 m from LAMPF beam stop. Neutrinos originate mainly from π^+ decay at rest. $\bar{\nu}_e$ could come from either $\bar{\nu}_\mu \rightarrow \bar{\nu}_e$ or $\nu_e \rightarrow \bar{\nu}_e$; our entry assumes the first interpretation. They are detected through $\bar{\nu}_e p \rightarrow e^+ n$ (20 MeV $< E_{e^+} < 60$ MeV) in delayed coincidence with $np \rightarrow d\gamma$. Authors observe $51 \pm 20 \pm 8$ total excess events over an estimated background 12.5 ± 2.9 . ATHANASSOPOULOS 96B is a shorter version of this paper.

⁸ ATHANASSOPOULOS 95 error corresponds to the 1.6σ band in the plot. The expected background is 2.7 ± 0.4 events. Corresponds to an oscillation probability of $(0.34 \pm 0.20 \pm 0.07)\%$. For a different interpretation, see HILL 95. Replaced by ATHANASSOPOULOS 96.

⁹ HILL 95 is a report by one member of the LSND Collaboration, reporting a different conclusion from the analysis of the data of this experiment (see ATHANASSOPOULOS 95). Contrary to the rest of the LSND Collaboration, Hill finds no evidence for the neutrino oscillation $\bar{\nu}_\mu \rightarrow \bar{\nu}_e$ and obtains only upper limits.

¹⁰ FREEDMAN 93 is a search at LAMPF for $\bar{\nu}_e$ generated from any of the three neutrino types $\nu_\mu, \bar{\nu}_\mu$, and ν_e which come from the beam stop. The $\bar{\nu}_e$'s would be detected by the reaction $\bar{\nu}_e p \rightarrow e^+ n$. FREEDMAN 93 replaces DURKIN 88.

$\sin^2(2\theta)$ for "Large" $\Delta(m^2)$ ($\bar{\nu}_\mu \rightarrow \bar{\nu}_e$)

VALUE (units 10^{-3})	CL%	DOCUMENT ID	TECN	COMMENT
• • • We do not use the following data for averages, fits, limits, etc. • • •				
< 640	90	¹ ANTONELLO 13A	ICAR	$\bar{\nu}_e$ appearance
< 150	90	² CHENG 12	MBNE	MiniBooNE/SciBooNE
0.4-9.0	90	³ AGUILAR-AR...10	MBNE	$E_\nu > 475$ MeV
0.4-9.0	99	⁴ AGUILAR-AR...10	MBNE	$E_\nu > 200$ MeV
< 3.3	90	⁵ AGUILAR-AR...09B	MBNE	MiniBooNE
< 1.7	90	⁶ ARMBRUSTER02	KAR2	Liquid Sci. calor.
< 1.1	90	AVVAKUMOV 02	NTEV	NUTEV FNAL
5.3±1.3±9.0		⁷ AGUILAR 01	LSND	LAMPF
6.2±2.4±1.0		⁸ ATHANASSO...96	LSND	LAMPF
3-12	80	⁹ ATHANASSO...95		
< 6	90	¹⁰ HILL 95		

¹ ANTONELLO 13A obtained the limit by assuming $\bar{\nu}_\mu \rightarrow \bar{\nu}_e$ oscillation from the $\sim 2\%$ of $\bar{\nu}_\mu$ events contamination in the CNGS beam.

² CHENG 12 is a combined fit of MiniBooNE and SciBooNE antineutrino data.

³ This value is for a two neutrino oscillation analysis for excess antineutrino events with $E_\nu > 475$ MeV. At 90% CL there is no solution at high $\Delta(m^2)$. The best fit is at maximal mixing. The allowed region is consistent with LSND reported by AGUILAR 01. Supersedes AGUILAR-AREVALO 09B.

⁴ This value is for a two neutrino oscillation analysis for excess antineutrino events with $E_\nu > 200$ MeV with subtraction of the expected 12 events low energy excess seen in the neutrino component of the beam. At 90% CL there is no solution at high $\Delta(m^2)$. The best fit value is 0.007 for $\Delta(m^2) = 4.4$ eV².

⁵ This result is inconclusive with respect to small amplitude mixing suggested by LSND.

⁶ ARMBRUSTER 02 is the final analysis of the KARMEN 2 data. See footnote in the preceding table for further details, and the paper for the exclusion plot.

⁷ AGUILAR 01 is the final analysis of the LSND full data set. The deduced oscillation probability is $0.264 \pm 0.067 \pm 0.045\%$; the value of $\sin^2 2\theta$ for large $\Delta(m^2)$ is twice this probability (although these values are excluded by other constraints). See footnote in preceding table for further details, and the paper for a plot showing allowed regions. Supersedes ATHANASSOPOULOS 95, ATHANASSOPOULOS 96, and ATHANASSOPOULOS 98.

See key on page 1127

Lepton Particle Listings

Neutrino Mixing

- ⁸ATHANASSOPOULOS 96 reports $(0.31 \pm 0.12 \pm 0.05)\%$ for the oscillation probability; the value of $\sin^2 2\theta$ for large $\Delta(m^2)$ should be twice this probability. See footnote in preceding table for further details, and see the paper for a plot showing allowed regions.
- ⁹ATHANASSOPOULOS 95 error corresponds to the 1.6σ band in the plot. The expected background is 2.7 ± 0.4 events. Corresponds to an oscillation probability of $(0.34 \pm 0.20 \pm 0.07)\%$. For a different interpretation, see HILL 95. Replaced by ATHANASSOPOULOS 96.
- ¹⁰HILL 95 is a report by one member of the LSND Collaboration, reporting a different conclusion from the analysis of the data of this experiment (see ATHANASSOPOULOS 95). Contrary to the rest of the LSND Collaboration, Hill finds no evidence for the neutrino oscillation $\bar{\nu}_\mu \rightarrow \bar{\nu}_e$ and obtains only upper limits.

$\Delta(m^2)$ for $\sin^2(2\theta) = 1$ ($\nu_\mu(\bar{\nu}_\mu) \rightarrow \nu_e(\bar{\nu}_e)$)

VALUE (eV ²)	CL%	DOCUMENT ID	TECN	COMMENT
<0.075	90	BORODOV... 92	CNTR	BNL E776

• • • We do not use the following data for averages, fits, limits, etc. • • •

<1.6	90	¹ ROMOSAN 97	CCFR	FNAL
------	----	-------------------------	------	------

¹ROMOSAN 97 uses wideband beam with a 0.5 km decay region.

$\sin^2(2\theta)$ for "Large" $\Delta(m^2)$ ($\nu_\mu(\bar{\nu}_\mu) \rightarrow \nu_e(\bar{\nu}_e)$)

VALUE (units 10^{-3})	CL%	DOCUMENT ID	TECN	COMMENT
<1.8	90	¹ ROMOSAN 97	CCFR	FNAL

• • • We do not use the following data for averages, fits, limits, etc. • • •

<3.8	90	² MCFARLAND 95	CCFR	FNAL
<3	90	BORODOV... 92	CNTR	BNL E776

¹ROMOSAN 97 uses wideband beam with a 0.5 km decay region.

²MCFARLAND 95 state that "This result is the most stringent to date for 250-$\Delta(m^2)$ <math><450 \text{ eV}^2</math> and also excludes at 90%CL much of the high $\Delta(m^2)$ region favored by the recent LSND observation." See ATHANASSOPOULOS 95 and ATHANASSOPOULOS 96.

$\Delta(m^2)$ for $\sin^2(2\theta) = 1$ ($\bar{\nu}_e \nrightarrow \bar{\nu}_e$)

VALUE (eV ²)	CL%	DOCUMENT ID	TECN	COMMENT
<0.01	90	¹ ACHKAR 95	CNTR	Bugey reactor

• • • We do not use the following data for averages, fits, limits, etc. • • •

¹ACHKAR 95 bound is for $L=15, 40, \text{ and } 95 \text{ m}$.

$\sin^2(2\theta)$ for "Large" $\Delta(m^2)$ ($\bar{\nu}_e \nrightarrow \bar{\nu}_e$)

VALUE	CL%	DOCUMENT ID	TECN	COMMENT
<0.02	90	¹ ACHKAR 95	CNTR	For $\Delta(m^2) = 0.6 \text{ eV}^2$

• • • We do not use the following data for averages, fits, limits, etc. • • •

¹ACHKAR 95 bound is from data for $L=15, 40, \text{ and } 95 \text{ m}$ distance from the Bugey reactor.

———— Sterile neutrino limits ————

$\Delta(m^2)$ for $\sin^2(2\theta) = 1$ ($\nu_\mu \rightarrow \nu_s$)

ν_s means ν_τ or any sterile (noninteracting) ν .

VALUE (10^{-5} eV^2)	CL%	DOCUMENT ID	TECN	COMMENT
<3000 (or <550)	90	¹ OYAMA 89	KAMI	Water Cherenkov
< 4.2 or > 54.	90	BIONTA 88	IMB	Flux has $\nu_\mu, \bar{\nu}_\mu, \nu_e, \text{ and } \bar{\nu}_e$

• • • We do not use the following data for averages, fits, limits, etc. • • •

¹OYAMA 89 gives a range of limits, depending on assumptions in their analysis. They argue that the region $\Delta(m^2) = (100\text{--}1000) \times 10^{-5} \text{ eV}^2$ is not ruled out by any data for large mixing.

Search for ν_μ or $\nu_e \rightarrow \nu_s$

VALUE	CL%	DOCUMENT ID	TECN	COMMENT
<0.05	95	¹ ANDRIAMIR... 21		PROSPECT
<0.005	95	² SEREBROV 21		Neutrino-4
<0.008	95	³ SKROBOVA 20		DANSS
<0.01	90	⁴ ALEKSEEV 18		DANSS
<0.06	90	⁵ ALMAZAN 18		STEREO
<0.1	95	⁶ ASHENFELT... 18		PROSPECT
<0.4	90	⁷ AARTSEN 17b	ICCB	IceCube-DeepCore
<8	$\times 10^{-3}$	⁸ ABDURASHI... 17		T β decay
<1	$\times 10^{-2}$	⁹ KO 17		NEOS
<2	$\times 10^{-2}$	¹⁰ AARTSEN 16	ICCB	IceCube
<4.5	$\times 10^{-4}$	¹¹ ADAMSON 16b		MINOS, DayaBay
<8.6	$\times 10^{-2}$	¹² ADAMSON 16c		MINS
<1.1	$\times 10^{-2}$	¹³ AN 16b		DAYA
		¹⁴ AMBROSIO 01	MCRO	matter effects
		¹⁵ FUKUDA 00	SKAM	neutral currents + matter effects

• • • We do not use the following data for averages, fits, limits, etc. • • •

- ¹ANDRIAMIRADO 21 reports a search for $\bar{\nu}_e \rightarrow \bar{\nu}_s$ oscillations at the HFIR research reactor, at baselines from 6.7 to 9.2 m. The reactor has a ²³⁵U core. 4 tons of ⁶Li-doped liquid scintillator are used in a segmented detector. Oscillations into sterile neutrinos are disfavored. The stated limit for $\sin^2(2\theta_{14})$ is for $\Delta m_{41}^2 \sim 2 \text{ eV}^2$ where the sensitivity is maximal.
- ²SEREBROV 21 searches for $\bar{\nu}_e \rightarrow \bar{\nu}_s$ oscillations with a moveable detector with baseline 6–12 m from the SM-3 research reactor with highly enriched ²³⁵U fuel. Analyzing the L/E dependence a χ^2 minimum is found at $\Delta m_{41}^2 = 7.3 \pm 0.13 \pm 1.16 \text{ eV}^2$ and $\sin^2(2\theta_{14}) = 0.36 \pm 0.12$. The quoted limit of 0.005 for $\sin^2(2\theta_{14})$ corresponds to $\Delta m_{41}^2 \sim 2 \text{ eV}^2$. This is the result from 720 days of reactor ON and 860 days of reactor OFF measurements. The significance of the χ^2 minimum is 2.9 σ . Supersedes SEREBROV 20, SEREBROV 19 and SEREBROV 18a.
- ³SKROBOVA 20 searches for $\bar{\nu}_e \rightarrow \bar{\nu}_s$ oscillations using the DANSS detector at 10.7, 11.2, and 12.7 m from the 3.1 GW_{th} power reactor. The DANSS detector is highly segmented and moveable; the positions are changed usually 3 times a week. The analysis is based on the ratio of the events at top and bottom position; the middle position is used for checks of consistency. No evidence for sterile neutrinos is found. The quoted limit 0.008, the smallest excluded $\sin^2(2\theta_{14})$, corresponds to $\Delta m_{41}^2 \sim 1.0 \text{ eV}^2$. Supersedes ALEKSEEV 18.
- ⁴ALEKSEEV 18 searches for $\bar{\nu}_e \rightarrow \bar{\nu}_s$ oscillations using the DANSS detector at 10.7, 11.2, and 12.7 m from the 3.1 GW_{th} power reactor. The DANSS detector is highly segmented and moveable; the positions are changed usually 3 times a week. The analysis is based on the ratio of the events at top and bottom position; the middle position is used for checks of consistency. The best fit point is at $\Delta m_{41}^2 = 1.4 \text{ eV}^2$ and $\sin^2(2\theta_{14}) = 0.05$ with $\Delta\chi^2 = 13.1$ (statistical errors only) compared to the fit with 3 active neutrinos only. The quoted limit of 0.01 for $\sin^2(2\theta_{14})$ corresponds to $\Delta m_{41}^2 \sim 1.0 \text{ eV}^2$. Superseded by SKROBOVA 20.
- ⁵ALMAZAN 18 searches for the $\bar{\nu}_e \rightarrow \bar{\nu}_s$ oscillations with baseline from 9.4 to 11.1 m from the ILL research reactor with highly enriched ²³⁵U fuel. The STEREO detector consists of six separated cells with Gd loaded scintillator, with 15 m water equivalent overburden. The detected rate is $396.3 \pm 4.7 \bar{\nu}_e/\text{day}$ with signal to background ratio of about 0.9. The reported results corresponds to 66 days of reactor-on. The analysis uses the relative rates normalized to the cell number 1_i . No indication of the oscillation to the sterile neutrinos is found, the stated limit on $\sin^2(2\theta_{14})$ correspond to $\Delta m_{41}^2 \sim 3.5 \text{ eV}^2$ where the exclusion is maximal.
- ⁶ASHENFELTER 18 searches for the $\bar{\nu}_e \rightarrow \bar{\nu}_s$ oscillations at baseline from 6.7 to 9.2 m from the 85 MW research reactor with pure ²³⁵U core. The segmented 4 ton ⁶Li-doped liquid scintillator is operated with about 1 m water equivalent overburden and recorded $25461 \pm 283 \text{ IBD}$ events. No indication of oscillations into sterile neutrinos was observed. The stated limit for $\sin^2(2\theta_{14})$ is for $\Delta m_{41}^2 \sim 2 \text{ eV}^2$ where the sensitivity is maximal.
- ⁷AARTSEN 17b uses three years of upward-going atmospheric neutrino data in the energy range of 10–60 GeV to constrain their disappearance into light sterile neutrinos. The reported limit $\sin^2\theta_{24} < 0.11$ at 90% C.L. is for $\Delta m_{41}^2 = 1.0 \text{ eV}^2$. We convert the result to $\sin^2 2\theta_{24}$ for the listing. AARTSEN 17b also reports $\cos^2\theta_{24} \cdot \sin^2\theta_{34} < 0.15$ at 90% C.L. for $\Delta m_{41}^2 = 1.0 \text{ eV}^2$.
- ⁸ABDURASHITOV 17 use the Troitsk nu-mass experiment to search for sterile neutrinos with mass 0.1 - 2 keV. We convert the reported limit from $U_{e4}^2 < 0.002$ to $\sin^2 2\theta_{14} < 0.008$ assume $U_{e4} \sim \sin\theta_{14}$. The stated limit corresponds to the smallest U_{e4}^2 . The exclusion curve begins at U_{e4}^2 of 0.02 for $m_4 = 0.1 \text{ keV}$.
- ⁹KO 17 reports on short baseline reactor oscillation search ($\bar{\nu}_e \rightarrow \bar{\nu}_s$), motivated by the so-called "reactor antineutrino anomaly". The experiment is conducted at 23.7 m from the core of unit 5 of the Hanbit Nuclear Power Complex in Korea. The reported limited on $\sin^2(2\theta_{41})$ for sterile neutrinos was determined using the reactor antineutrino spectrum determined by the Daya Bay experiment for Δm_{41}^2 around 0.55 eV^2 where the sensitivity is maximal. A fraction of the parameter space derived from the "reactor antineutrino anomaly" is excluded by this work. Compared to reactor models an event excess is observed at about 5 MeV, in agreement with other experiments.
- ¹⁰AARTSEN 16 use one year of upward-going atmospheric muon neutrino data in the energy range of 320 GeV to 20 TeV to constrain their disappearance into light sterile neutrinos. Sterile neutrinos are expected to produce distinctive zenith distribution for these energies for $0.01 \leq \Delta m^2 \leq 10 \text{ eV}^2$. The stated limit is for $\sin^2 2\theta_{24}$ at Δm^2 around 0.3 eV^2 .
- ¹¹ADAMSON 16b combine the results of AN 16b, ADAMSON 16c, and Bugey-3 reactor experiments to constrain ν_μ to ν_e mixing through oscillations into light sterile neutrinos. The stated limit for $\sin^2 2\theta_{\mu e}$ is at $|\Delta m_{41}^2| = 1.2 \text{ eV}^2$.
- ¹²ADAMSON 16c use the NuMI beam and exposure of 10.56×10^{20} protons on target to search for the oscillation of ν_μ dominated beam into light sterile neutrinos with detectors at 1.04 and 735 km. The reported limit $\sin^2(\theta_{24}) < 0.022$ at 95% C.L. is for $|\Delta m_{41}^2| = 0.5 \text{ eV}^2$. We convert the result to $\sin^2(2\theta_{24})$ for the listing.
- ¹³AN 16b utilize 621 days of data to place limits on the $\bar{\nu}_e$ disappearance into a light sterile neutrino. The stated limit corresponds to the smallest $\sin^2(2\theta_{14})$ at $|\Delta m_{41}^2| \sim 3 \times 10^{-2} \text{ eV}^2$ (obtained from Figure 3 in AN 16b). The exclusion curve begins at $|\Delta m_{41}^2| \sim 1.5 \times 10^{-4} \text{ eV}^2$ and extends to $\sim 0.25 \text{ eV}^2$. The analysis assumes $\sin^2(2\theta_{12}) = 0.846 \pm 0.021$, $\Delta m_{21}^2 = (7.53 \pm 0.18) \times 10^{-5} \text{ eV}^2$, and $|\Delta m_{32}^2| = (2.44 \pm 0.06) \times 10^{-3} \text{ eV}^2$.
- ¹⁴AMBROSIO 01 tested the pure 2-flavor $\nu_\mu \rightarrow \nu_s$ hypothesis using matter effects which change the shape of the zenith-angle distribution of upward through-going muons. With maximum mixing and Δm^2 around 0.0024 eV^2 , the $\nu_\mu \rightarrow \nu_s$ oscillation is disfavored with 99% confidence level with respect to the $\nu_\mu \rightarrow \nu_\tau$ hypothesis.
- ¹⁵FUKUDA 00 tested the pure 2-flavor $\nu_\mu \rightarrow \nu_s$ hypothesis using three complementary atmospheric-neutrino data samples. With this hypothesis, zenith-angle distributions are expected to show characteristic behavior due to neutral currents and matter effects. In the

Lepton Particle Listings

Neutrino Mixing

Δm^2 and $\sin^2 2\theta$ region preferred by the Super-Kamiokande data, the $\nu_\mu \rightarrow \nu_s$ hypothesis is rejected at the 99% confidence level, while the $\nu_\mu \rightarrow \nu_\tau$ hypothesis consistently fits all of the data sample.

CPT tests

$\langle \Delta m_{21}^2 - \Delta \bar{m}_{21}^2 \rangle$	CL%	DOCUMENT ID	TECN	COMMENT
< 1.1	99.7	¹ DEGOUVEA 05	FIT	solar vs. reactor

¹ DEGOUVEA 05 obtained this bound at the 3σ CL from the KamLAND (ARAKI 05) and solar neutrino data.

$\langle \Delta m_{32}^2 - \Delta \bar{m}_{32}^2 \rangle$	CL%	DOCUMENT ID	TECN	COMMENT
$-0.12 \pm_{-0.24}^{+0.26}$		¹ ADAMSON 13B	MINS	beam and atmospheric

• • • We do not use the following data for averages, fits, limits, etc. • • •

$0.6 \pm_{-0.8}^{+2.4}$	90	² ADAMSON 12B	MINS	MINOS atmospheric

¹ ADAMSON 13B quotes this difference as a negative of our convention.
² The quoted result is the single-parameter 90% C.L. interval determined from the 90% C.L. contour in the $(\Delta m^2, \Delta \bar{m}^2)$ plane, which is obtained by minimizing the four parameter log-likelihood function with respect to the other oscillation parameters.

REFERENCES FOR Neutrino Mixing

ABE	21A	PR D103 L011101	K. Abe et al.	(T2K Collab.)
ABRAHAO	21	JHEP 2101 190	T. Abrahao et al.	(Double Chooz Collab.)
AGOSTINI	21	ASP 125 102509	M. Agostini et al.	(Borexino Collab.)
AGUILAR-AR...	21	PR D103 052002	A.A. Aguilar-Arevalo et al.	(MiniBoONE Collab.)
ANDRIAMIR...	21	PR D103 032001	M. Andriamirado et al.	(PROSPECT Collab.)
SALAS	21	JHEP 2102 071	P.F. de Salas et al.	(STOH, VALE, INFN+)
SEREBROV	21	PR D104 032003	A.P. Serebrov et al.	(Neutrino-4 Collab.)
AARTSEN	20	EPJ C80 9	M.G. Aartsen et al.	(IceCube Collab.)
ABE	20F	NAT 580 339	K. Abe et al.	(T2K Collab.)
Also		PR D103 112008	M.A. Acero et al.	(T2K Collab.)
ADAMSON	20A	PR D125 131802	P. Adamson et al.	(MINOS+ Collab.)
AGOSTINI	20A	PR D101 062001	M. Agostini et al.	(Borexino Collab.)
AHARMIM	20	PR D102 062006	B. Aharmim et al.	(SNO Collab.)
ALMAZAN	20	PRL 125 201801	H. Almazan et al.	(STEREO Collab.)
DE-KERRET	20	NATP 16 558	H. de Kerret et al.	(Double Chooz Collab.)
ESTEBAN	20A	JHEP 2009 178	I. Esteban et al.	(NuFIT Collab.)
PDG	20	PTEP 2020 083C01	P.A. Zyla et al.	(PDG Collab.)
SEREBROV	20	JETPL 112 199	A.P. Serebrov, R.M. Samoilo	(PNPI)
SHIN	20	JHEP 2004 029	C.D. Shin et al.	(RENO Collab.)
SKROBOVA	20	IJMP A35 2044015	N. Skrobova et al.	(DANSS Collab.)
AARTSEN	19C	PR D99 032007	M.G. Aartsen et al.	(IceCube Collab.)
ACERO	19	PRL 123 151803	M.A. Acero et al.	(NOvA Collab.)
ADEY	19	PR D100 052004	P. Adey et al.	(Daya Bay Collab.)
AGAFONOVA	19	PR D100 051301	N. Agafonova et al.	(OPERA Collab.)
ALBERT	19	JHEP 1906 113	A. Albert et al.	(ANTARES Collab.)
ANDERSON	19	PR D99 012012	M. Anderson et al.	(SNO+ Collab.)
SEREBROV	19	JETPL 109 213	A.P. Serebrov et al.	(Neutrino-4 Collab.)
AARTSEN	18A	PRL 120 071801	M.G. Aartsen et al.	(IceCube Collab.)
ABE	18B	PR D97 072001	K. Abe et al.	(Super-Kamiokande Collab.)
ABE	18G	PRL 121 171802	K. Abe et al.	(T2K Collab.)
ACERO	18	PR D98 032012	M.A. Acero et al.	(NOvA Collab.)
ADEY	18A	PRL 121 241805	D. Adey et al.	(Daya Bay Collab.)
AGAFONOVA	18	PRL 120 211801	N. Agafonova et al.	(OPERA Collab.)
AGAFONOVA	18A	JHEP 1806 151	N. Agafonova et al.	(OPERA Collab.)
AGOSTINI	18B	NAT 582 505	M. Agostini et al.	(Borexino Collab.)
AGUILAR-AR...	18C	PRL 121 221801	A.A. Aguilar-Arevalo et al.	(MiniBoONE Collab.)
ALEKSEEV	18	PR B78 56	I. Alekseev et al.	(DANSS Collab.)
ALMAZAN	18	PRL 121 161801	H. Almazan et al.	(STEREO Collab.)
ASHENFELT...	18	PRL 121 251802	J. Ashenfelter et al.	(PROSPECT Collab.)
BAK	18	PRL 121 201801	G. Bak et al.	(RENO Collab.)
DE-SALAS	18	PR B782 633	P.F. de Salas et al.	(PDG Collab.)
PDG	18	PR D98 030001	M. Tanabashi et al.	(PDG Collab.)
SEO	18	PR D98 012002	S.H. Seo et al.	(RENO Collab.)
SEREBROV	18A	PPN 49 701	A.P. Serebrov et al.	(Neutrino-4 Collab.)
AARTSEN	17B	PR D95 112002	M.G. Aartsen et al.	(IceCube Collab.)
ABDURASHLI...	17	JETPL 105 753	J.N. Abdurashitov et al.	(Troitsk n-u-mass Collab.)
ABE	17A	PRL 118 151801	K. Abe et al.	(T2K Collab.)
ABE	17C	PR D96 011102	K. Abe et al.	(T2K Collab.)
ABE	17F	PR D96 092006	K. Abe et al.	(T2K Collab.)
Also		PR D98 019902 (errata)	K. Abe et al.	(T2K Collab.)
ADAMSON	17A	PRL 118 151802	P. Adamson et al.	(NOvA Collab.)
ADAMSON	17B	PRL 118 231801	P. Adamson et al.	(NOvA Collab.)
AN	17A	PR D95 072006	F.P. An et al.	(Daya Bay Collab.)
ESTEBAN	17	JHEP 1701 087	I. Esteban et al.	(NEOS Collab.)
KO	17	PRL 118 121802	Y.J. Ko et al.	(NEOS Collab.)
VINYOLEAS	17	APJ 835 201001	N. Vinyoles et al.	(IceCube Collab.)
AARTSEN	16	PRL 117 071801	M.G. Aartsen et al.	(IceCube Collab.)
ABE	16B	JHEP 1601 163	Y. Abe et al.	(Double Chooz Collab.)
ABE	16C	PR D94 052010	K. Abe et al.	(Super-Kamiokande Collab.)
ABE	16D	PRL 116 181801	K. Abe et al.	(T2K Collab.)
ADAMSON	16	PRL 116 151806	P. Adamson et al.	(NOvA Collab.)
ADAMSON	16A	PR D93 051104	P. Adamson et al.	(NOvA Collab.)
ADAMSON	16B	PRL 117 151801	P. Adamson et al.	(Daya Bay and MINOS Collab.)
ADAMSON	16C	PRL 117 151803	P. Adamson et al.	(MINOS Collab.)
AN	16	PRL 116 061801	F.P. An et al.	(Daya Bay Collab.)
AN	16A	PR D93 072011	F.P. An et al.	(Daya Bay Collab.)
AN	16B	PRL 117 151802	F.P. An et al.	(Daya Bay Collab.)
CHOI	16	PRL 116 211801	J.H. Choi et al.	(RENO Collab.)
PDG	16	CP C40 100001	C. Patrignani et al.	(PDG Collab.)
AARTSEN	15A	PR D91 072004	M.G. Aartsen et al.	(IceCube Collab.)
ABE	15D	PR D91 072010	K. Abe et al.	(T2K Collab.)
AGAFONOVA	15A	PRL 115 121802	N. Agafonova et al.	(OPERA Collab.)
AN	15	PRL 115 111802	F.P. An et al.	(Daya Bay Collab.)
BERGSTROM	15	JHEP 1509 200	J. Bergstrom et al.	(BARC, STON, MADU+)
GANDO	15	PR C92 055808	A. Gando et al.	(KamLAND Collab.)
ABE	14	PRL 112 181801	K. Abe et al.	(T2K Collab.)
Also		PR D91 072010	K. Abe et al.	(T2K Collab.)
ABE	14A	PL B735 51	Y. Abe et al.	(Double Chooz Collab.)
ABE	14B	PR D89 092003	K. Abe et al.	(T2K Collab.)
ABE	14C	PRL 112 061802	K. Abe et al.	(T2K Collab.)

ABE	14H	JHEP 1410 086	Y. Abe et al.	(Double Chooz Collab.)
Also		JHEP 1502 074 (errata)	Y. Abe et al.	(Double Chooz Collab.)
ADAMSON	14	PRL 112 191801	P. Adamson et al.	(MINOS Collab.)
AN	14	PRL 112 061801	F.P. An et al.	(Daya Bay Collab.)
AN	14B	PR D90 071101	F.P. An et al.	(Daya Bay Collab.)
BELLINI	14A	NAT 512 383	G. Bellini et al.	(Borexino Collab.)
FORERO	14	PR D90 093006	D.V. Forero, M. Tortola, J.W.F. Valle	(PDG Collab.)
GONZALEZ...	14	JHEP 1411 0052	M.C. Gonzalez-Garcia, M. Maltoni, T. Schwetz	(PDG Collab.)
PDG	14	CP C38 070001	K. Olive et al.	(PDG Collab.)
RENSHAW	14	PRL 112 091805	A. Renshaw et al.	(Super-Kamiokande Collab.)
AARTSEN	13B	PRL 111 081801	M.G. Aartsen et al.	(IceCube Collab.)
ABE	13C	PL B723 66	Y. Abe et al.	(Double Chooz Collab.)
ABE	13E	PR D88 032002	K. Abe et al.	(T2K Collab.)
ABE	13G	PRL 111 211803	K. Abe et al.	(T2K Collab.)
ADAMSON	13A	PRL 110 171801	P. Adamson et al.	(MINOS Collab.)
ADAMSON	13B	PRL 110 251801	P. Adamson et al.	(MINOS Collab.)
AGAFONOVA	13	JHEP 1307 004	N. Agafonova et al.	(OPERA Collab.)
AGUILAR-AR...	13A	PRL 110 161801	A.A. Aguilar-Arevalo et al.	(MiniBoONE Collab.)
AHARMIM	13	PR C88 025501	B. Aharmim et al.	(SNO Collab.)
AN	13	CP C37 011001	F.P. An et al.	(Daya Bay Collab.)
ANTONELLO	13	EPJ C73 2345	M. Antonello et al.	(ICARUS Collab.)
ANTONELLO	13A	EPJ C73 2599	M. Antonello et al.	(ICARUS Collab.)
GANDO	13	PR D88 033001	A. Gando et al.	(KamLAND Collab.)
ABE	12	PRL 108 131801	Y. Abe et al.	(Double Chooz Collab.)
ABE	12A	PR D85 031103	K. Abe et al.	(T2K Collab.)
ABE	12B	PR D86 052008	Y. Abe et al.	(Double Chooz Collab.)
ADAMSON	12	PRL 108 191801	P. Adamson et al.	(MINOS Collab.)
ADAMSON	12B	PR D86 052007	P. Adamson et al.	(MINOS Collab.)
ADRIAN-MAR...	12	PL B714 224	S. Adrian-Martinez et al.	(ANTARES Collab.)
AHN	12	PRL 108 171802	J.K. Ahn et al.	(RENO Collab.)
ADAMSON	11C	PRL 107 191802	F.P. An et al.	(Daya Bay Collab.)
BELLINI	12A	PRL 108 051302	G. Bellini et al.	(Borexino Collab.)
CHENG	12	PR D86 052009	G. Cheng et al.	(MiniBoONE/SciBoONE Collab.)
MAHN	12	PR D85 032007	K.B.M. Mahn et al.	(MiniBoONE/SciBoONE Collab.)
ABE	11	PR D83 052010	K. Abe et al.	(Super-Kamiokande Collab.)
ABE	11A	PRL 107 041801	K. Abe et al.	(T2K Collab.)
ABE	11B	PR C84 035804	S. Abe et al.	(KamLAND Collab.)
ABE	11C	PRL 107 241801	K. Abe et al.	(Super-Kamiokande Collab.)
ADAMSON	11	PRL 106 181801	P. Adamson et al.	(MINOS Collab.)
ADAMSON	11B	PRL 107 021801	P. Adamson et al.	(MINOS Collab.)
ADAMSON	11C	PR D84 071103	P. Adamson et al.	(MINOS Collab.)
ADAMSON	11D	PRL 107 191802	P. Adamson et al.	(MINOS Collab.)
BELLINI	11	PL B696 191	G. Bellini et al.	(Borexino Collab.)
BELLINI	11A	PRL 107 141302	G. Bellini et al.	(Borexino Collab.)
FOGLI	11	PR D84 053007	G.L. Fogli et al.	(KamLAND Collab.)
GANDO	11	PR D83 052002	A. Gando et al.	(KamLAND Collab.)
HUBER	11	PR C84 024617	P. Huber	(VPI)
Also		PR C85 029901 (errata)	P. Huber	(VPI)
MUELLER	11	PR C83 054615	Th.A. Mueller et al.	(VPI)
SERENELLI	11	APJ 743 24	A.M. Serenelli, W.C. Haxton, C. Pena-Garay	(ANTARES Collab.)
ADAMSON	10A	PR D82 051102	P. Adamson et al.	(MINOS Collab.)
AGUILAR-AR...	10	PRL 105 181801	A.A. Aguilar-Arevalo et al.	(MiniBoONE Collab.)
AHARMIM	10	PR C81 055504	B. Aharmim et al.	(SNO Collab.)
BELLINI	10A	PR D82 033006	G. Bellini et al.	(Borexino Collab.)
DENIZ	10	PR D81 072001	M. Deniz et al.	(TEXONO Collab.)
KAETHER	10	PL B685 47	F. Kaether et al.	(TEXONO Collab.)
WENDELL	10	PR D81 092004	R. Wendell et al.	(Super-Kamiokande Collab.)
ABDURASHLI...	09	PR C80 015807	J.N. Abdurashitov et al.	(SAGE Collab.)
ADAMSON	09	PRL 103 261802	P. Adamson et al.	(MINOS Collab.)
AGUILAR-AR...	09B	PRL 103 111801	A.A. Aguilar-Arevalo et al.	(MiniBoONE Collab.)
ABE	08A	PRL 100 221803	S. Abe et al.	(KamLAND Collab.)
Also		PRL 101 119904E	S. Abe et al.	(KamLAND Collab.)
ADAMSON	08	PR D77 072002	P. Adamson et al.	(MINOS Collab.)
ADAMSON	08A	PRL 101 131802	P. Adamson et al.	(MINOS Collab.)
AHARMIM	08	PRL 101 111301	B. Aharmim et al.	(SNO Collab.)
Also		PR C87 015502	B. Aharmim et al.	(SNO Collab.)
ARPESELLA	08A	PRL 101 091302	C. Arpesella et al.	(Borexino Collab.)
CRAVENS	08	PR D78 032002	J.P. Cravens et al.	(Super-Kamiokande Collab.)
FOGLI	08	PRL 101 141801	G.L. Fogli et al.	(KamLAND Collab.)
ADAMSON	07	PR D75 092003	P. Adamson et al.	(MINOS Collab.)
AGUILAR-AR...	07	PRL 98 231801	A.A. Aguilar-Arevalo et al.	(MiniBoONE Collab.)
AHARMIM	07	PR C75 045502	B. Aharmim et al.	(SNO Collab.)
ADAMSON	06	PR D73 072002	P. Adamson et al.	(MINOS Collab.)
AHN	06A	PR D74 072003	M.H. Ahn et al.	(K2K Collab.)
BALATA	06	EPJ C47 21	M. Balata et al.	(Borexino Collab.)
HOSAKA	06	PR D73 112001	J. Hosaka et al.	(Super-Kamiokande Collab.)
HOSAKA	06A	PR D74 032002	J. Hosaka et al.	(Super-Kamiokande Collab.)
MICHAEL	06	PRL 97 191801	D. Michael et al.	(MINOS Collab.)
WINTER	06A	PR C73 025503	W.T. Winter et al.	(SNO Collab.)
YAMAMOTO	06	PRL 96 181801	S. Yamamoto et al.	(K2K Collab.)
AHARMIM	05A	PR C72 055502	B. Aharmim et al.	(SNO Collab.)
ALIU	05	PRL 94 081802	E. Aliu et al.	(K2K Collab.)
ALLISON	05	PR D72 052005	W.W.M. Allison et al.	(SOUDAN-2 Collab.)
ALTMANN	05	PL B616 174	M. Altmann et al.	(GNO Collab.)
ARAKI	05	PRL 94 081801	T. Araki et al.	(KamLAND Collab.)
ASHIE	05	PR D71 112005	Y. Ashie et al.	(Super-Kamiokande Collab.)
BARCHALL	05	APJ 621 185	J.N. Barchall, A.M. Serenelli, S. Basu	(IAS+)
DEGOUVEA	05	PR D71 093002	A. de Gouvea, C. Pena-Garay	(IAS+)
AHARMIM	04	PR D70 093014	B. Aharmim et al.	(SNO Collab.)
AHMED	04A	PRL 92 181301	S.N. Ahmed et al.	(SNO Collab.)
AHN	04	PRL 93 051801	M.H. Ahn et al.	(K2K Collab.)
AMBROSIO	04	EPJ C36 323	M. Ambrosio et al.	(MACRO Collab.)
ASHIE	04	PRL 93 101801	Y. Ashie et al.	(Super-Kamiokande Collab.)
EGUCHI	04	PRL 92 071301	K. Eguchi et al.	(KamLAND Collab.)
SMY	04	PR D69 011104	M.B. Smy et al.	(Super-Kamiokande Collab.)
AHN	03	PRL 90 041801	M.H. Ahn et al.	(K2K Collab.)
AMBROSIO	03	PR B556 35	M. Ambrosio et al.	(MACRO Collab.)
APOLLONIO	03	EPJ C27 331	M. Apollonio et al.	(LSND Collab.)
ASTIER	03	PL B570 19	P. Astier et al.	(NOMAD Collab.)
EGUCHI	03	PRL 90 021802	K. Eguchi et al.	(KamLAND Collab.)
GANDO	03	PRL 90 171302	Y. Gando et al.	(Super-Kamiokande Collab.)
IANNI	03	JP J29 2107	A. Ianni	(INFN Gran Sasso)
SANCHEZ	03	PR D68 113004	M. Sanchez et al.	(Soudan 2 Collab.)
ABDURASHLI...	02	JETP 95 181	J.N. Abdurashitov et al.	(SAGE Collab.)
Translating from ZETF 122 211.				
AHMAD	02	PRL 89 011301	Q.R. Ahmad et al.	(SNO Collab.)
ARMSTRONG	02B	PRL 89 011302	Q.R. Ahmad et al.	(SNO Collab.)
ARMBRUSTER	02	PR D65 112001	B. Armbruster et al.	(KARMEN 2 Collab.)
AVVAKUMOV	02	PRL 89 011804	S. Avvakumov et al.	(NuTeV Collab.)
FUKUDA	02	PRL B539 179	S. Fukuda et al.	(Super-Kamiokande Collab.)
AGUILAR	01</			

See key on page 1127

Lepton Particle Listings

Neutrino Mixing, Heavy Neutral Leptons, Searches for

FUKUDA	99C	PRL 82 2644	Y. Fukuda et al.	(Super-Kamiokande Collab.)
FUKUDA	99D	PL B467 185	Y. Fukuda et al.	(Super-Kamiokande Collab.)
HAMPEL	99	PL B447 127	W. Hampel et al.	(GALLEX Collab.)
AMBROSIO	98	PL B434 451	M. Ambrosio et al.	(MACRO Collab.)
APOLLONIO	98	PL B420 397	M. Apollonio et al.	(CHOOZ Collab.)
ATHANASSO...	98	PRL 81 1774	C. Athanassopoulos et al.	(LSND Collab.)
ATHANASSO...	98B	PR C58 2489	C. Athanassopoulos et al.	(LSND Collab.)
CLEVELAND	98	APJ 496 505	B.T. Cleveland et al.	(Homestake Collab.)
FELDMAN	98	PR D57 3873	G.J. Feldman, R.D. Cousins	(Homestake Collab.)
FUKUDA	98C	PRL 81 1562	Y. Fukuda et al.	(Super-Kamiokande Collab.)
HATAKEYAMA	98	PRL 81 2016	S. Hatakeyama et al.	(Kamiokande Collab.)
CLARK	97	PRL 79 345	R. Clark et al.	(IMB Collab.)
ROMOSAN	97	PRL 78 2912	A. Romosan et al.	(CCFR Collab.)
AGLIETTA	96	JETPL 63 791	M. Aglietta et al.	(LSD Collab.)
Translated from ZETFP 63 753				
ATHANASSO...	96	PR C54 2685	C. Athanassopoulos et al.	(LSND Collab.)
ATHANASSO...	96B	PRL 77 3082	C. Athanassopoulos et al.	(LSND Collab.)
FUKUDA	96	PRL 77 1683	Y. Fukuda et al.	(Kamiokande Collab.)
FUKUDA	96B	PL B388 397	Y. Fukuda et al.	(Kamiokande Collab.)
GREENWOOD	96	PR D53 6054	Z.D. Greenwood et al.	(UCI, SVR, SUCU)
HAMPEL	96	PL B398 384	W. Hampel et al.	(GALLEX Collab.)
LOVERRE	96	PR B370 1566	P.F. Loverre	(GALLEX Collab.)
ACHKAR	95	NP B434 503	B. Achkar et al.	(SING, SAACL, CPPM, CDEF+)
AHLEN	95	PL B357 481	S.P. Ahlen et al.	(MACRO Collab.)
ATHANASSO...	95	PRL 75 2650	C. Athanassopoulos et al.	(LSND Collab.)
DAUM	95	ZPHY C66 417	K. Daum et al.	(FREJUS Collab.)
HILL	95	PRL 75 2654	J.E. Hill	(PENN Collab.)
MCFARLAND	95	PRL 75 3993	K.S. McFarland et al.	(CCFR Collab.)
DECLAIS	94	PL B338 383	Y. Declais et al.	(LSD Collab.)
FUKUDA	94	PL B335 237	Y. Fukuda et al.	(Kamiokande Collab.)
VILAIN	94C	ZPHY C64 539	P. Vilain et al.	(CHARM II Collab.)
FREEDMAN	93	PR D47 811	S.J. Freedman et al.	(LAMPF E645 Collab.)
BECKER-SZ.	92B	PR D46 3720	R.A. Becker-Szendy et al.	(IMB Collab.)
BEIER	92	PL B283 446	E.W. Beier et al.	(KAM2 Collab.)
Also				
BORODOV...	92	PRL 68 274	E.W. Beier, E.D. Frank	(PENN Collab.)
HIRATA	92	PL B280 146	L. Borodovsky et al.	(COLU, JHU, ILL)
CASPER	91	PRL 66 2561	K.S. Hirata et al.	(Kamiokande II Collab.)
HIRATA	91	PRL 66 9	D. Casper et al.	(IMB Collab.)
KUVSHIN...	91	JETPL 54 253	K.S. Hirata et al.	(Kamiokande II Collab.)
BERGER	90B	PL B245 305	A.A. Kuvshinnikov et al.	(KIAE Collab.)
HIRATA	90	PRL 65 1297	C. Berger et al.	(FREJUS Collab.)
AGLIETTA	89	EPL 8 611	K.S. Hirata et al.	(Kamiokande II Collab.)
DAVIS	89	ARJPS 39 467	M. Aglietta et al.	(FREJUS Collab.)
OYAMA	89	PR D39 1481	R. Davis, A.K. Mann, L. Wolfenstein	(BNL, PENW+)
BIONTA	88	PR D38 768	Y. Oyama et al.	(Kamiokande II Collab.)
DURKIN	88	PRL 61 1811	R.M. Bionta et al.	(IMB Collab.)
ABRAMOWICZ	86	PRL 57 298	L.S. Durkin et al.	(OSU, ANL, CIT+)
ALLABY	86	PL B177 446	H. Abramowicz et al.	(CDHS Collab.)
ANGELINI	86	PL B179 307	J.V. Allaby et al.	(CHARM Collab.)
VUILLEUMIER	82	PL 114B 298	C. Angelini et al.	(PISA, ATHU, PADO+)
BOLIEV	81	SJNP 34 787	J.L. Vuilleumier et al.	(CIT, SIN, MUNI)
Translated from YAF 34 1418				
KWON	81	PR D24 1097	H. Kwon et al.	(CIT, ISNG, MUNI)
BOEHM	80	PL 97B 310	F. Boehm et al.	(ILLG, CIT, ISNG, MUNI)
CROUCH	78	PR D18 2239	M.F. Crouch et al.	(CASE, UCI, WITW)

<3 × 10 ⁻⁷	90	⁷ CORTINA-GIL 18	NA62	m _{ν_x} ~ 200–400 MeV
<1 × 10 ⁻⁶	90	⁸ PARK	16 BELL	m _{ν_x} ~ 1.4 GeV
<3 × 10 ⁻⁵	90	⁹ LIVENTSEV	13 BELL	Near m _{ν_x} ~ 2–2.5 GeV
<3 × 10 ⁻⁵	95	¹⁰ ABREU	97I DLPH	m _{ν_x} ~ 6–50 GeV
<2 × 10 ⁻⁵	95	¹¹ ABREU	97I DLPH	Near m _{ν_x} ~ 3.5 GeV
<1 × 10 ⁻⁵	90	¹² BARANOV	93I	Near m _π –m _e kin. thres.
<2 × 10 ⁻⁷	90	¹² BARANOV	93	Near m _K –m _e kin. thres.
<1 × 10 ⁻⁷	13,14	^{13,14} BERNARDI	88 CNTR	Near m _π –m _e kin. thres.
<2 × 10 ⁻⁹	14,15	^{14,15} BERNARDI	88 CNTR	Near m _K –m _e kin. thres.
<1 × 10 ⁻⁷	90	¹⁶ DORENBOS...	86 CHR	Near m _D –m _e kin. thres.
<1 × 10 ⁻⁷	90	¹⁷ COOPER...	85 BEBC	Near m _D –m _e kin. thres.
1 Search in electron capture decay ⁷ Be → ⁷ Li ν _x . Kinematic threshold is ~ 850 keV.				
2 Search for K ⁺ → e ⁺ ν _x . Assumes lifetime of ν _x > 50 ns.				
3 Limit from prompt lepton number violating trilepton search.				
4 K ⁺ → e ⁺ ν _x , with ν _x decay through U _{eX} . ABE 19B also considers bounds on U _{eX} U _{e'X} for combinations of lepton flavors in the ν _x decay final state.				
5 Searches for a Majorana Heavy Neutral Lepton producing a π ⁻ e ⁺ resonance in the same sign dilepton decay D → K π ⁻ e ⁺ e ⁺ .				
6 Search for π ⁺ → e ⁺ ν _x .				
7 Search for K ⁺ → e ⁺ ν _x .				
8 PARK 16 quotes an approximate limit B(B ⁺ → e ⁺ ν _x) < 3 × 10 ⁻⁶ in the mass range m _{ν_x} ~ 0.2–1.4 GeV.				
9 Search for B ⁺ → e ⁺ ν _x .				
10 Search for prompt ν _x decay signatures.				
11 Search for displaced ν _x decay signatures.				
12 Searches for K or π → e ⁺ ν _x , ν _x → e ⁺ e ⁻ ν _e using a beam dump experiment at the 70 GeV Serpukhov proton synchrotron. BARANOV 93 also considers limits for U _{eX} U _{μX} from K or π → μ ⁺ ν _x , ν _x → e ⁺ e ⁻ ν _e .				
13 π ⁺ → e ⁺ ν _x , with ν _x decay through U _{eX} .				
14 BERNARDI 88 also considers bounds on U _{eX} U _{μX} .				
15 K ⁺ → e ⁺ ν _x , with ν _x decay through U _{eX} .				
16 D ⁺ → e ⁺ ν _x , with ν _x → e ⁻ ℓ ⁺ ν _ℓ .				
17 D ⁺ → e ⁺ ν _x , with ν _x → e ⁻ ℓ ⁺ ν _ℓ or ν _x → e ⁻ π ⁺ .				

Heavy Neutral Leptons, Searches for

OMITTED FROM SUMMARY TABLE

We define searches for Heavy Neutral Leptons (HNLs) as searches for Dirac or Majorana fermions with sterile neutrino quantum numbers, that are heavy enough to not disrupt the simplest Big Bang Nucleosynthesis bounds and/or unstable on cosmological timescales: Typically HNLs have mass ~ MeV or higher.

Searches for these particles generically set bounds on the mixing between the HNL and the active neutrinos, as parametrized by the extended 3×4 PMNS matrix elements U_{ℓX} (see the "Neutrino mass, mixing and oscillations" review) where ℓ = e, μ or τ, and we denote the HNL as ν_x. While many measurements may be interpreted to place bounds on various combinations of these matrix elements, we quote below limits only for those cases in which one matrix element is assumed to be much larger than the other two, i.e. |U_{ℓX}| ≫ |U_{ℓ'X}| for ℓ' ≠ ℓ.

Experimental searches make use of various different strategies, including e.g. resonance searches in missing mass decay distributions or specific final states, searches for lepton number violating decays, and trilepton signatures. The resulting bounds on U_{ℓX} are typically dependent on the HNL mass. The quoted limits below are either the best limit near an experimental kinematic threshold, or a characteristic value in the mass range of the experimental sensitivity.

Limits on heavy neutral lepton mixing parameters

Limits on |U_{eX}|²

Quoted limits are either the best limit near the kinematic threshold of the experiment, or a characteristic value in the mass range of the experimental sensitivity

VALUE	CL%	DOCUMENT ID	TECN	COMMENT
<2 × 10 ⁻⁴	95	1 FRIEDRICH 21		Near m ₇ Be ⁻ –m ₇ Li kin. thres.
<1 × 10 ⁻⁹	90	2 CORTINA-GIL 20 NA62		m _{ν_x} ~ 150–400 MeV
<2 × 10 ⁻⁵	95	3 AAD 19F ATLS		m _{ν_x} ~ 15–40 GeV
<1 × 10 ⁻⁹	90	4 ABE 19B T2K		Near m _K –m _e kin. thres.
<1 × 10 ⁻⁴	90	5 ABLIKIM 19AL BES3		m _{ν_x} ~ 0.3–0.7 GeV
<1 × 10 ⁻⁸	90	6 AGUILAR-AR...18A PIEN		m _{ν_x} ~ 60–120 MeV ; b̄r̄

Limits on |U_{μX}|²

Quoted limits are either the best limit near the kinematic threshold of the experiment, or a characteristic value in the mass range of the experimental sensitivity

VALUE	CL%	DOCUMENT ID	TECN	COMMENT
<1 × 10 ⁻³	95	1 AAIJ 21AA LHCB		m _{ν_x} ~ 5–50 GeV, pp at 7, 8 TeV
<2 × 10 ⁻⁴	95	2 AAIJ 21AA LHCB		m _{ν_x} ~ 5–50 GeV, pp at 7, 8 TeV
<5 × 10 ⁻⁹	90	3,4 CORTINA-GIL 21 NA62		Near m _K –m _μ kin. thres.
<1 × 10 ⁻⁷	90	5 ABRATENKO 20 MBNE		Near m _K –m _μ kin. thres.
<2 × 10 ⁻²	90	6 PRIM 20 BELL		m _{ν_x} ~ 1 GeV
<2 × 10 ⁻⁵	95	7 AAD 19F ATLS		m _{ν_x} ~ 10–50 GeV
<2 × 10 ⁻⁶	95	8 AAD 19F ATLS		m _{ν_x} ~ 10 GeV
<1 × 10 ⁻⁹	90	9 ABE 19B T2K		Near m _K –m _μ kin. thres.
<5 × 10 ⁻⁶	90	10,11 AGUILAR-AR...19B PIEN		m _{ν_x} ~ 16–30 MeV
<1 × 10 ⁻⁵	90	11 AGUILAR-AR...19B PIEN		Near m _π –m _μ kin. thres.
<3 × 10 ⁻⁷	90	3 CORTINA-GIL 18 NA62		m _{ν_x} ~ 250–350 MeV
<3 × 10 ⁻⁶	90	3 LAZZERONI 17A NA62		Near m _K –m _μ kin. thres.
<5 × 10 ⁻²	90	12 PARK 16 BELL		m _{ν_x} ~ 1.4 GeV
<1 × 10 ⁻⁸	90	3 ARTAMONOV 15A B949		m _{ν_x} ~ 200–300 MeV
<3 × 10 ⁻⁵	90	13 LIVENTSEV 13 BELL		Near m _{ν_x} ~ 2–2.5 GeV
<2.0 × 10 ⁻⁸	95	14 DAUM 00 KARM		m _{ν_x} = 33.905 MeV
<8 × 10 ⁻⁸	90	15 VAITAITIS 99 CCFR		Near m _K –m _μ kin. thres.
<6 × 10 ⁻⁸	90	16 VAITAITIS 99 CCFR		Near m _{D_s} –m _μ kin. thres.
<3 × 10 ⁻⁵	95	17 ABREU 97I DLPH		m _{ν_x} ~ 6–50 GeV
<2 × 10 ⁻⁵	95	18 ABREU 97I DLPH		Near m _{ν_x} ~ 3.5 GeV
<3 × 10 ⁻⁵	90	19 VILAIN 95c CHM2		Near m _K –m _μ kin. thres.
<3 × 10 ⁻⁸		20,21 BERNARDI 88 CNTR		Near m _μ ⁺ –m _π kin. thres.
<2 × 10 ⁻⁹		21,22 BERNARDI 88 CNTR		Near m _K –m _μ kin. thres.
<1 × 10 ⁻⁷	90	23 DORENBOS... 86 CHR		Near m _D –m _μ kin. thres.
<1 × 10 ⁻⁷	90	24 COOPER... 85 BEBC		Near m _D –m _μ kin. thres.

1 Limit from prompt lepton number conserving W → μμj search.
 2 Limit from prompt lepton number violating W → μμj search.
 3 Search for K⁺ → μ⁺ ν_x.
 4 Assumes a lifetime exceeding 50 ns, and searches over m_{ν_x} range 200–384 MeV.

Lepton Particle Listings

Heavy Neutral Leptons, Searches for

- ⁵ $K^+ \rightarrow \mu^+ \nu_X$, with $\nu_X \rightarrow \mu^- \pi^+$, in the mass range $m_{\nu_X} \sim 260\text{--}385$ MeV. ABRATENKO 20 also considers $\nu_X \rightarrow \mu^+ \pi^-$ for the case of Majorana HNL.
- ⁶ Search for $B^+ \rightarrow \mu^+ \nu_X$ in the mass range $m_{\nu_X} \sim 0\text{--}1.5$ GeV.
- ⁷ Limit from prompt lepton number violating trilepton search.
- ⁸ Limit from displaced lepton violating or conserving trilepton searches.
- ⁹ $K^+ \rightarrow \mu^+ \nu_X$, with ν_X decay through $U_{\mu X}$. ABE 19B also considers bounds on $|U_{\ell X} U_{\ell' X}|$ for combinations of lepton flavors in the ν_X decay final state.
- ¹⁰ Limit requires muon kinetic energy > 1.2 MeV.
- ¹¹ Search for $\pi^+ \rightarrow \mu^+ \nu_X$.
- ¹² PARK 16 quotes an approximate limit $B(B^+ \rightarrow \mu^+ \nu_X) < 3 \times 10^{-6}$ in the mass range $m_{\nu_X} \sim 0.2\text{--}1.4$ GeV.
- ¹³ Search for $B^+ \rightarrow \mu^+ \nu_X$.
- ¹⁴ DAUM 00 quotes a branching ratio bound $B(\pi^+ \rightarrow \mu^+ \nu_X) < 6.0 \times 10^{-10}$ at 95% CL.
- ¹⁵ $K^+ \rightarrow \mu^+ \nu_X$, with $\nu_X \rightarrow \mu X$.
- ¹⁶ $D_s \rightarrow \mu^+ \nu_X$, with $\nu_X \rightarrow \mu X$.
- ¹⁷ Search for prompt ν_X decay signatures.
- ¹⁸ Search for displaced ν_X decay signatures.
- ¹⁹ Search for Heavy Neutral Leptons produced by neutral current muon neutrino interactions, with $\nu_X \rightarrow \mu^+ \mu^- \nu_\mu$.
- ²⁰ $K^+ \rightarrow \mu^+ \nu_X$, with ν_X decay through $U_{\mu X}$ and $m_{\nu_X} < m_\mu + m_\pi$.
- ²¹ BERNARDI 88 also considers bounds on $|U_{eX} U_{\mu X}|$.
- ²² $K^+ \rightarrow \mu^+ \nu_X$, with $\nu_X \rightarrow \mu^- \pi^+$.
- ²³ $D^+ \rightarrow \mu^+ \nu_X$, with $\nu_X \rightarrow \mu^- \ell^+ \nu_\ell$.
- ²⁴ $D^+ \rightarrow \mu^+ \nu_X$, with $\nu_X \rightarrow \mu^- \ell^+ \nu_\ell$ or $\nu_X \rightarrow \mu^- \pi^+$.

Limits on $|U_{\tau X}|^2$

Quoted limits are either the best limit near the kinematic threshold of the experiment, or a characteristic value in the mass range of the experimental sensitivity

VALUE	CL%	DOCUMENT ID	TECN	COMMENT
$< 3 \times 10^{-4}$	90	¹ ACCIARRI 21	ARNT	Near $m_{\nu_X} \lesssim 970$ MeV
$< 3 \times 10^{-6}$	90	² BOIARSKA 21	RVUE	Near $m_{\nu_X} \sim 0.8\text{--}1.6$ GeV

$< 2 \times 10^{-4}$	90	³ ORLOFF 02	CHRM	Near $m_D - m_\pi$ kin. thres.
$< 1 \times 10^{-4}$	90	⁴ ORLOFF 02	CHRM	$m_{\nu_X} \sim 200\text{--}250$ MeV
$< 3 \times 10^{-5}$	95	⁵ ABREU 97I	DLPH	$m_{\nu_X} \sim 6\text{--}50$ GeV
$< 2 \times 10^{-5}$	95	⁶ ABREU 97I	DLPH	Near $m_{\nu_X} \sim 3.5$ GeV

- ¹ Search for $\nu_X \rightarrow \mu^+ \mu^- \nu$.
- ² Reanalysis of CHARM results (cf. ORLOFF 02) to include searches for $\nu_X \rightarrow \nu \ell^+ \ell^-$ decays, and including the production of HNLs from τ decays.
- ³ $D_s \rightarrow \tau^+ \nu_X$, with ν_X decay via $U_{\tau X}$.
- ⁴ $D_s \rightarrow \nu_\tau \tau^+$, $\tau^+ \rightarrow \nu_X X$, with ν_X decay via $U_{\tau X}$.
- ⁵ Search for prompt ν_X decay signatures.
- ⁶ Search for displaced ν_X decay signatures. Kinematical suppression of $\nu_X \rightarrow \tau X$ at lower masses leads to rapid loosening of the $|U_{\tau X}|$ bound compared to that for $|U_{eX}|$ and $|U_{\mu X}|$.

REFERENCES FOR Heavy Neutral Leptons, Searches for

AJJ	21AA	EPJ C81 248	R. Aaij <i>et al.</i>	(LHCb Collab.)
ACCIARRI	21	PRL 127 121801	R. Acciarri <i>et al.</i>	(ArgoNeUT Collab.)
BOIARSKA	21	PR D104 095019	I. Boiarska <i>et al.</i>	(BOHR, LEID)
CORTINA-GIL	21	PL B816 136259	E. Cortina Gil <i>et al.</i>	(NA62 Collab.)
FRIEDRICH	21	PRL 126 021803	S. Friedrich <i>et al.</i>	(BeEST Collab.)
ABRATENKO	20	PR D101 052001	P. Abratenko <i>et al.</i>	(MiniBoONE Collab.)
CORTINA-GIL	20	PL B807 135599	E. Cortina Gil <i>et al.</i>	(NA62 Collab.)
PRIM	20	PR D101 032007	M.T. Prim <i>et al.</i>	(BELLE Collab.)
AAD	19F	JHEP 1910 265	G. Aad <i>et al.</i>	(ATLAS Collab.)
ABE	19B	PR D100 052006	K. Abe <i>et al.</i>	(T2K Collab.)
ABLIKIM	19AL	PR D99 112002	M. Ablikim <i>et al.</i>	(BESIII Collab.)
AGUILAR-AR...	19B	PL B798 134980	A. Aguilar-Arevalo <i>et al.</i>	(PIENU Collab.)
AGUILAR-AR...	18A	PR D97 072012	A. Aguilar-Arevalo <i>et al.</i>	(PIENU Collab.)
CORTINA-GIL	18	PL B778 137	E. Cortina Gil <i>et al.</i>	(NA62 Collab.)
LAZZERONI	17A	PL B772 712	C. Lazzeroni <i>et al.</i>	(NA62 Collab.)
PARK	16	PR D94 012003	C.-S. Park <i>et al.</i>	(BELLE Collab.)
ARTAMONOV	15A	PR D91 052001	A.V. Artamonov <i>et al.</i>	(E949 Collab.)
LIVENTSEV	13	PR D87 071102	D. Liventsev <i>et al.</i>	(BELLE Collab.)
Also		PR D95 099903 (errat.)	D. Liventsev <i>et al.</i>	(BELLE Collab.)
ORLOFF	02	PL B550 8	J. Orloff <i>et al.</i>	(CHARM Collab.)
DAUM	00	PRL 85 1815	M. Daum <i>et al.</i>	(KARMEN Collab.)
VAITAITIS	99	PRL 83 4943	A. Vaitaitis <i>et al.</i>	(CCFR Collab.)
ABREU	97I	ZPHY C74 57	P. Abreu <i>et al.</i>	(DELPHI Collab.)
Also		ZPHY C75 580 (errat.)	P. Abreu <i>et al.</i>	(DELPHI Collab.)
VILAIN	95C	PL B351 387	P. Vilain <i>et al.</i>	(CHARM II Collab.)
Also		PL B343 453	P. Vilain <i>et al.</i>	(CHARM II Collab.)
BARANOV	93	PL B302 336	S.A. Baranov <i>et al.</i>	(JINR, SERP, BUDA)
BERNARDI	88	PL B203 332	G. Bernardi <i>et al.</i>	(PARIS, CERN, INFN+)
DORENBOS...	86	PL 166B 473	J. Dorenbosch <i>et al.</i>	(CHARM Collab.)
COOPER-...	85	PL 160B 207	A.M. Cooper-Sarkar <i>et al.</i>	(CERN, LOIC+)

<i>u</i>	1311
<i>d</i>	1311
<i>s</i>	1311
<i>c</i>	1315
<i>b</i>	1317
<i>t</i>	1319
<i>b'</i> (Fourth Generation) Quark	1337
<i>t'</i> (Fourth Generation) Quark	1339
Free Quark Searches	1341

Related Reviews in Volume 1

60. Quark masses (rev.)	808
61. Top quark (rev.)	817

See key on page 1127

Quark Particle Listings

Quarks, *u*, *d*, *s*, Light Quarks (*u*, *d*, *s*)

QUARKS

See the related review(s):

Quark Masses

u $I(J^P) = \frac{1}{2}(\frac{1}{2}^+)$

Mass $m = 2.16^{+0.49}_{-0.26}$ MeV Charge = $\frac{2}{3} e$ $I_z = +\frac{1}{2}$

$m_u/m_d = 0.474^{+0.056}_{-0.074}$

d $I(J^P) = \frac{1}{2}(\frac{1}{2}^+)$

Mass $m = 4.67^{+0.48}_{-0.17}$ MeV Charge = $-\frac{1}{3} e$ $I_z = -\frac{1}{2}$

$m_s/m_d = 17-22$

$\bar{m} = (m_u + m_d)/2 = 3.45^{+0.35}_{-0.15}$ MeV

s $I(J^P) = 0(\frac{1}{2}^+)$

Mass $m = 93.4^{+8.6}_{-3.4}$ MeV Charge = $-\frac{1}{3} e$ Strangeness = -1

$(m_s - (m_u + m_d)/2)/(m_d - m_u) = 27.33^{+0.67}_{-0.77}$

Light Quarks (*u*, *d*, *s*)

OMITTED FROM SUMMARY TABLE

u-QUARK MASS

The *u*-, *d*-, and *s*-quark masses are estimates of so-called “current-quark masses,” in a mass-independent subtraction scheme such as \overline{MS} . The ratios m_u/m_d and m_s/m_d are extracted from pion and kaon masses using chiral symmetry. The estimates of *d* and *u* masses are not without controversy and remain under active investigation. Within the literature there are even suggestions that the *u* quark could be essentially massless. The *s*-quark mass is estimated from SU(3) splittings in hadron masses.

We have normalized the \overline{MS} masses at a renormalization scale of $\mu = 2$ GeV. Results quoted in the literature at $\mu = 1$ GeV have been rescaled by dividing by 1.35. The values of “Our Evaluation” were determined in part via Figures 1 and 2.

\overline{MS} MASS (MeV)	DOCUMENT ID	TECN
2.16 $^{+0.49}_{-0.26}$ OUR EVALUATION	See the ideogram below.	
2.6 ± 0.4	1 DOMINGUEZ 19	THEO
2.130 ± 0.041	2 BAZAVOV 18	LATT
2.27 $\pm 0.06 \pm 0.06$	3 FODOR 16	LATT
2.36 ± 0.24	4 CARRASCO 14	LATT
2.57 $\pm 0.26 \pm 0.07$	5 AOKI 12	LATT
2.24 $\pm 0.10 \pm 0.34$	6 BLUM 10	LATT
2.01 ± 0.14	7 MCNEILE 10	LATT
• • • We do not use the following data for averages, fits, limits, etc. • • •		
2.15 $\pm 0.03 \pm 0.10$	8 DURR 11	LATT
1.9 ± 0.2	9 BAZAVOV 10	LATT
2.01 ± 0.14	7 DAVIES 10	LATT
2.9 ± 0.2	10 DOMINGUEZ 09	THEO
2.9 ± 0.8	11 DEANDREA 08	THEO
3.02 ± 0.33	12 BLUM 07	LATT
2.7 ± 0.4	13 JAMIN 06	THEO
1.9 ± 0.2	14 MASON 06	LATT
2.8 ± 0.2	15 NARISON 06	THEO
1.7 ± 0.3	16 AUBIN 04A	LATT

¹ DOMINGUEZ 19 determine the quark mass from a QCD finite energy sum rule for the divergence of the axial current.

² BAZAVOV 18 determine the quark masses using a lattice computation with staggered fermions and four active quark flavors.

³ FODOR 16 is a lattice simulation with $n_f = 2 + 1$ dynamical flavors and includes partially quenched QED effects.

⁴ CARRASCO 14 is a lattice QCD computation of light quark masses using $2 + 1 + 1$ dynamical quarks, with $m_u = m_d \neq m_s \neq m_c$. The *u* and *d* quark masses are obtained separately by using the *K* meson mass splittings and lattice results for the electromagnetic contributions.

⁵ AOKI 12 is a lattice computation using $1 + 1 + 1$ dynamical quark flavors.

⁶ BLUM 10 determines light quark masses using a QCD plus QED lattice computation of the electromagnetic mass splittings of the low-lying hadrons. The lattice simulations use $2+1$ dynamical quark flavors.

⁷ DAVIES 10 and MCNEILE 10 determine $\overline{m}_c(\mu)/\overline{m}_s(\mu) = 11.85 \pm 0.16$ using a lattice computation with $n_f = 2 + 1$ dynamical fermions of the pseudoscalar meson masses.

Mass m_u is obtained from this using the value of m_c from ALLISON 08 or MCNEILE 10 and the BAZAVOV 10 values for the light quark mass ratios, m_s/\overline{m} and m_u/m_d .

⁸ DURR 11 determine quark mass from a lattice computation of the meson spectrum using $n_f = 2 + 1$ dynamical flavors. The lattice simulations were done at the physical quark mass, so that extrapolation in the quark mass was not needed. The individual m_u, m_d values are obtained using the lattice determination of the average mass m_{ud} and of the ratio m_s/m_{ud} and the value of $Q = (m_s^2 - m_{ud}^2) / (m_d^2 - m_u^2)$ as determined from $\eta \rightarrow 3\pi$ decays.

⁹ BAZAVOV 10 is a lattice computation using $2+1$ dynamical quark flavors.

¹⁰ DOMINGUEZ 09 use QCD finite energy sum rules for the two-point function of the divergence of the axial vector current computed to order α_s^4 .

¹¹ DEANDREA 08 determine $m_u - m_d$ from $\eta \rightarrow 3\pi^0$, and combine with the PDG 06 lattice average value of $m_u + m_d = 7.6 \pm 1.6$ to determine m_u and m_d .

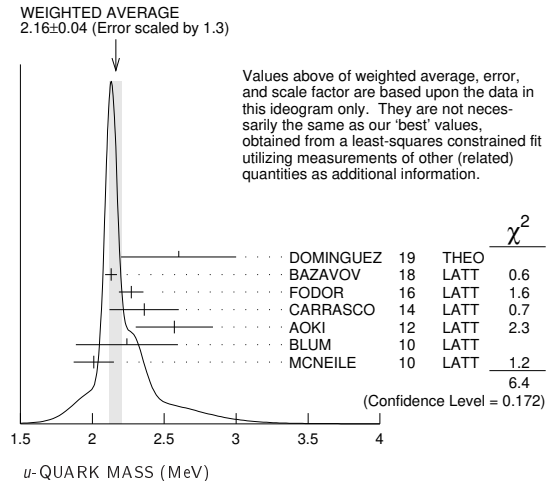
¹² BLUM 07 determine quark masses from the pseudoscalar meson masses using a QED plus QCD lattice computation with two dynamical quark flavors.

¹³ JAMIN 06 determine $m_u(2 \text{ GeV})$ by combining the value of m_s obtained from the spectral function for the scalar *K* π form factor with other determinations of the quark mass ratios.

¹⁴ MASON 06 extract light quark masses from a lattice simulation using staggered fermions with an improved action, and three dynamical light quark flavors with degenerate *u* and *d* quarks. Perturbative corrections were included at NNLO order. The quark masses m_u and m_d were determined from their $(m_u + m_d)/2$ measurement and AUBIN 04A m_u/m_d value.

¹⁵ NARISON 06 uses sum rules for $e^+ e^- \rightarrow$ hadrons to order α_s^3 to determine m_s combined with other determinations of the quark mass ratios.

¹⁶ AUBIN 04A employ a partially quenched lattice calculation of the pseudoscalar meson masses.



d-QUARK MASS

See the comment for the *u* quark above.

We have normalized the \overline{MS} masses at a renormalization scale of $\mu = 2$ GeV. Results quoted in the literature at $\mu = 1$ GeV have been rescaled by dividing by 1.35. The values of “Our Evaluation” were determined in part via Figures 1 and 2.

\overline{MS} MASS (MeV)	DOCUMENT ID	TECN
4.67 $^{+0.48}_{-0.17}$ OUR EVALUATION	See the ideogram below.	
5.3 ± 0.4	1 DOMINGUEZ 19	THEO
4.675 ± 0.056	2 BAZAVOV 18	LATT
4.67 $\pm 0.06 \pm 0.06$	3 FODOR 16	LATT
5.03 ± 0.26	4 CARRASCO 14	LATT
3.68 $\pm 0.29 \pm 0.10$	5 AOKI 12	LATT
4.65 $\pm 0.15 \pm 0.32$	6 BLUM 10	LATT
4.77 ± 0.15	7 MCNEILE 10	LATT
• • • We do not use the following data for averages, fits, limits, etc. • • •		
4.79 $\pm 0.07 \pm 0.12$	8 DURR 11	LATT
4.6 ± 0.3	9 BAZAVOV 10	LATT
4.79 ± 0.16	7 DAVIES 10	LATT
5.3 ± 0.4	10 DOMINGUEZ 09	THEO
4.7 ± 0.8	11 DEANDREA 08	THEO
5.49 ± 0.39	12 BLUM 07	LATT
4.8 ± 0.5	13 JAMIN 06	THEO
4.4 ± 0.3	14 MASON 06	LATT
5.1 ± 0.4	15 NARISON 06	THEO
3.9 ± 0.5	16 AUBIN 04A	LATT

¹ DOMINGUEZ 19 determine the quark mass from a QCD finite energy sum rule for the divergence of the axial current.

² BAZAVOV 18 determine the quark masses using a lattice computation with staggered fermions and four active quark flavors.

³ FODOR 16 is a lattice simulation with $n_f = 2 + 1$ dynamical flavors and includes partially quenched QED effects.

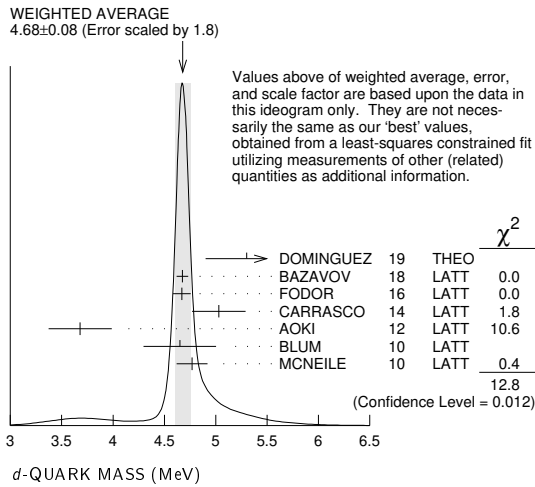
Quark Particle Listings

Light Quarks (*u, d, s*)

- ⁴ CARRASCO 14 is a lattice QCD computation of light quark masses using 2 + 1 + 1 dynamical quarks, with $m_u = m_d \neq m_s \neq m_c$. The *u* and *d* quark masses are obtained separately by using the *K* meson mass splittings and lattice results for the electromagnetic contributions.
- ⁵ AOKI 12 is a lattice computation using 1 + 1 + 1 dynamical quark flavors.
- ⁶ BLUM 10 determines light quark masses using a QCD plus QED lattice computation of the electromagnetic mass splittings of the low-lying hadrons. The lattice simulations use 2+1 dynamical quark flavors.
- ⁷ DAVIES 10 and MCNEILE 10 determine $\overline{m}_C(\mu)/\overline{m}_S(\mu) = 11.85 \pm 0.16$ using a lattice computation with $n_f = 2 + 1$ dynamical fermions of the pseudoscalar meson masses. Mass m_d is obtained from this using the value of m_c from ALLISON 08 or MCNEILE 10 and the BAZAVOV 10 values for the light quark mass ratios, m_s/\overline{m} and m_u/m_d .
- ⁸ DURR 11 determine quark mass from a lattice computation of the meson spectrum using $n_f = 2 + 1$ dynamical flavors. The lattice simulations were done at the physical quark mass, so that extrapolation in the quark mass was not needed. The individual m_u, m_d values are obtained using the lattice determination of the average mass m_{ud} and of the ratio m_s/m_{ud} and the value of $Q = (m_s^2 - m_{ud}^2) / (m_d^2 - m_u^2)$ as determined from $\eta \rightarrow 3\pi$ decays.
- ⁹ BAZAVOV 10 is a lattice computation using 2+1 dynamical quark flavors.
- ¹⁰ DOMINGUEZ 09 use QCD finite energy sum rules for the two-point function of the divergence of the axial vector current computed to order α_s^4 .
- ¹¹ DEANDREA 08 determine $m_u - m_d$ from $\eta \rightarrow 3\pi^0$, and combine with the PDG 06 lattice average value of $m_u + m_d = 7.6 \pm 1.6$ to determine m_u and m_d .
- ¹² BLUM 07 determine quark masses from the pseudoscalar meson masses using a QED plus QCD lattice computation with two dynamical quark flavors.
- ¹³ JAMIN 06 determine m_d (2 GeV) by combining the value of m_s obtained from the spectral function for the scalar $K\pi$ form factor with other determinations of the quark mass ratios.
- ¹⁴ MASON 06 extract light quark masses from a lattice simulation using staggered fermions with an improved action, and three dynamical light quark flavors with degenerate *u* and *d* quarks. Perturbative corrections were included at NNLO order. The quark masses m_u and m_d were determined from their $(m_u + m_d)/2$ measurement and AUBIN 04A m_u/m_d value.
- ¹⁵ NARISON 06 uses sum rules for $e^+e^- \rightarrow$ hadrons to order α_s^3 to determine m_s combined with other determinations of the quark mass ratios.
- ¹⁶ AUBIN 04A perform three flavor dynamical lattice calculation of pseudoscalar meson masses, with continuum estimate of electromagnetic effects in the kaon masses, and one-loop perturbative renormalization constant.

• • • We do not use the following data for averages, fits, limits, etc. • • •

3.59 ± 0.21	¹⁰ AOKI	11A	LATT
3.40 ± 0.07	⁹ DAVIES	10	LATT
4.1 ± 0.2	¹¹ DOMINGUEZ	09	THEO
3.72 ± 0.41	¹² ALLTON	08	LATT
3.85 ± 0.12 ± 0.4	¹³ BLOSSIER	08	LATT
≥ 4.85 ± 0.20	¹⁴ DOMINGUEZ..08B	THEO	
3.55 +0.65 -0.28	¹⁵ ISHIKAWA	08	LATT
4.026 ± 0.048	¹⁶ NAKAMURA	08	LATT
4.25 ± 0.35	¹⁷ BLUM	07	LATT
4.08 ± 0.25 ± 0.42	¹⁸ GOCKELER	06	LATT
4.7 ± 0.2 ± 0.3	¹⁹ GOCKELER	06A	LATT
3.2 ± 0.3	²⁰ MASON	06	LATT
3.95 ± 0.3	²¹ NARISON	06	THEO
2.8 ± 0.3	²² AUBIN	04	LATT
4.29 ± 0.14 ± 0.65	²³ AOKI	03	LATT
3.223 ± 0.3	²⁴ AOKI	03B	LATT
4.4 ± 0.1 ± 0.4	²⁵ BECIREVIC	03	LATT
4.1 ± 0.3 ± 1.0	²⁶ CHIU	03	LATT

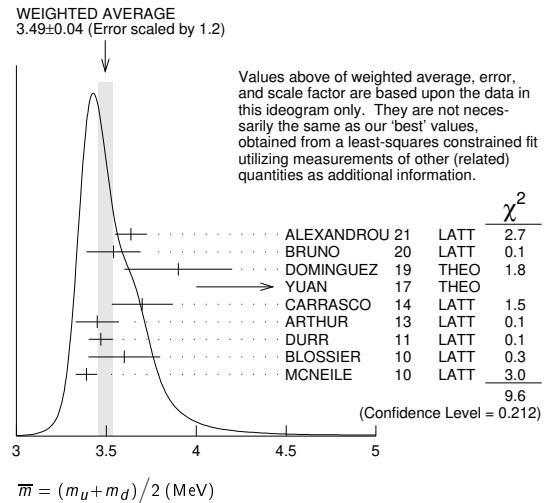


$$\overline{m} = (m_u + m_d)/2$$

See the comments for the *u* quark above.

We have normalized the \overline{m}_S masses at a renormalization scale of $\mu = 2$ GeV. Results quoted in the literature at $\mu = 1$ GeV have been rescaled by dividing by 1.35. The values of "Our Evaluation" were determined in part via Figures 1 and 2.

\overline{m}_S MASS (MeV)	DOCUMENT ID	TECN
3.45 +0.35 -0.15 OUR EVALUATION	See the ideogram below.	
3.636 ± 0.066 ± 0.057	¹ ALEXANDROU 21	LATT
3.54 ± 0.12 ± 0.09	² BRUNO 20	LATT
3.9 ± 0.3	³ DOMINGUEZ 19	THEO
4.7 +0.8 -0.7	⁴ YUAN 17	THEO
3.70 ± 0.17	⁵ CARRASCO 14	LATT
3.45 ± 0.12	⁶ ARTHUR 13	LATT
3.469 ± 0.047 ± 0.048	⁷ DURR 11	LATT
3.6 ± 0.2	⁸ BLOSSIER 10	LATT
3.39 ± 0.06	⁹ MCNEILE 10	LATT



- ¹ ALEXANDROU 21 determines the quark mass using a lattice calculation of the meson and baryon masses with a twisted mass fermion action. The simulations are carried out using 2+1+1 dynamical quarks with $m_u = m_d \neq m_s \neq m_c$, including gauge ensembles close to the physical pion point.
- ² BRUNO 20 determines the light quark mass using a lattice calculation with $n_f = 2+1$ flavors of Wilson fermions. The scale has been set from f_π and f_K . The tuning was done using the masses of the lightest (π) and strange (*K*) pseudoscalar mesons.
- ³ DOMINGUEZ 19 determine the quark mass from a QCD finite energy sum rule for the divergence of the axial current.
- ⁴ YUAN 17 determine \overline{m} using QCD sum rules in the isospin $I=0$ scalar channel. At the end of the "Numerical Results" section of YUAN 17 the authors discuss the significance of their larger value of the light quark mass compared to previous determinations.
- ⁵ CARRASCO 14 is a lattice QCD computation of light quark masses using 2 + 1 + 1 dynamical quarks, with $m_u = m_d \neq m_s \neq m_c$. The *u* and *d* quark masses are obtained separately by using the *K* meson mass splittings and lattice results for the electromagnetic contributions.
- ⁶ ARTHUR 13 is a lattice computation using 2+1 dynamical domain wall fermions. Masses at $\mu = 3$ GeV have been converted to $\mu = 2$ GeV using conversion factors given in their paper.
- ⁷ DURR 11 determine quark mass from a lattice computation of the meson spectrum using $n_f = 2 + 1$ dynamical flavors. The lattice simulations were done at the physical quark mass, so that extrapolation in the quark mass was not needed.
- ⁸ BLOSSIER 10 determines quark masses from a computation of the hadron spectrum using $n_f=2$ dynamical twisted-mass Wilson fermions.
- ⁹ DAVIES 10 and MCNEILE 10 determine $\overline{m}_C(\mu)/\overline{m}_S(\mu) = 11.85 \pm 0.16$ using a lattice computation with $n_f = 2 + 1$ dynamical fermions of the pseudoscalar meson masses. Mass \overline{m} is obtained from this using the value of m_c from ALLISON 08 or MCNEILE 10 and the BAZAVOV 10 values for the light quark mass ratio, m_s/\overline{m} .
- ¹⁰ AOKI 11A determine quark masses from a lattice computation of the hadron spectrum using $n_f = 2 + 1$ dynamical flavors of domain wall fermions.
- ¹¹ DOMINGUEZ 09 use QCD finite energy sum rules for the two-point function of the divergence of the axial vector current computed to order α_s^4 .
- ¹² ALLTON 08 use a lattice computation of the $\pi, K,$ and Ω masses with 2+1 dynamical flavors of domain wall quarks, and non-perturbative renormalization.
- ¹³ BLOSSIER 08 use a lattice computation of pseudoscalar meson masses and decay constants with 2 dynamical flavors and non-perturbative renormalization.
- ¹⁴ DOMINGUEZ-CLARIMON 08B obtain an inequality from sum rules for the scalar two-point correlator.

See key on page 1127

Quark Particle Listings

Light Quarks (*u, d, s*)

- ¹⁵ ISHIKAWA 08 use a lattice computation of the light meson spectrum with 2+1 dynamical flavors of $\mathcal{O}(a)$ improved Wilson quarks, and one-loop perturbative renormalization.
- ¹⁶ NAKAMURA 08 do a lattice computation using quenched domain wall fermions and non-perturbative renormalization.
- ¹⁷ BLUM 07 determine quark masses from the pseudoscalar meson masses using a QED plus QCD lattice computation with two dynamical quark flavors.
- ¹⁸ GOCKELER 06 use an unquenched lattice computation of the axial Ward Identity with $n_f = 2$ dynamical light quark flavors, and non-perturbative renormalization, to obtain $\overline{m}(2 \text{ GeV}) = 4.08 \pm 0.25 \pm 0.19 \pm 0.23 \text{ MeV}$, where the first error is statistical, the second and third are systematic due to the fit range and force scale uncertainties, respectively. We have combined the systematic errors linearly.
- ¹⁹ GOCKELER 06A use an unquenched lattice computation of the pseudoscalar meson masses with $n_f = 2$ dynamical light quark flavors, and non-perturbative renormalization.
- ²⁰ MASON 06 extract light quark masses from a lattice simulation using staggered fermions with an improved action, and three dynamical light quark flavors with degenerate *u* and *d* quarks. Perturbative corrections were included at NNLO order.
- ²¹ NARISON 06 uses sum rules for $e^+ e^- \rightarrow \text{hadrons}$ to order α_s^3 to determine m_s combined with other determinations of the quark mass ratios.
- ²² AUBIN 04 perform three flavor dynamical lattice calculation of pseudoscalar meson masses, with one-loop perturbative renormalization constant.
- ²³ AOKI 03 uses quenched lattice simulation of the meson and baryon masses with degenerate light quarks. The extrapolations are done using quenched chiral perturbation theory.
- ²⁴ The errors given in AOKI 03B were ± 0.046 to ± 0.069 . We changed them to ± 0.3 for calculating the overall best values. AOKI 03B uses lattice simulation of the meson and baryon masses with two dynamical light quarks. Simulations are performed using the $\mathcal{O}(a)$ improved Wilson action.
- ²⁵ BECIREVIC 03 perform quenched lattice computation using the vector and axial Ward identities. Uses $\mathcal{O}(a)$ improved Wilson action and nonperturbative renormalization.
- ²⁶ CHIU 03 determines quark masses from the pion and kaon masses using a lattice simulation with a chiral fermion action in quenched approximation.

- ⁵ BAZAVOV 10 is a lattice computation using 2+1 dynamical quark flavors.
- ⁶ BLUM 10 is a lattice computation using 2+1 dynamical quark flavors.
- ⁷ BLUM 07 determine quark masses from the pseudoscalar meson masses using a QED plus QCD lattice computation with two dynamical quark flavors.
- ⁸ AUBIN 04A perform three flavor dynamical lattice calculation of pseudoscalar meson masses, with continuum estimate of electromagnetic effects in the kaon masses.
- ⁹ NELSON 03 computes coefficients in the order p^4 chiral Lagrangian using a lattice calculation with three dynamical flavors. The ratio m_u/m_d is obtained by combining this with the chiral perturbation theory computation of the meson masses to order p^4 .
- ¹⁰ LEUTWYLER 96 uses a combined fit to $\eta \rightarrow 3\pi$ and $\psi' \rightarrow J/\psi(\pi, \eta)$ decay rates, and the electromagnetic mass differences of the π and K .

s-QUARK MASS

See the comment for the *u* quark above.

We have normalized the \overline{MS} masses at a renormalization scale of $\mu = 2 \text{ GeV}$. Results quoted in the literature at $\mu = 1 \text{ GeV}$ have been rescaled by dividing by 1.35.

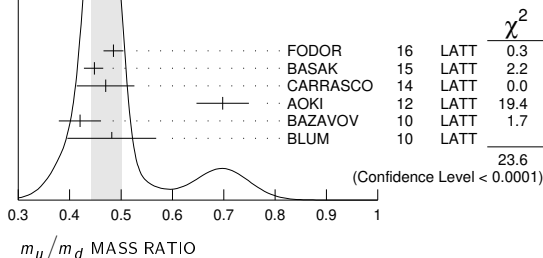
\overline{MS} MASS (MeV)	DOCUMENT ID	TECN
93.4 \pm 8.6 \pm 3.4 OUR EVALUATION	See the ideogram below.	
98.7 \pm 2.4 \pm 4.0	1 ALEXANDROU 21	LATT
95.7 \pm 2.5 \pm 2.4	2 BRUNO 20	LATT
92.47 \pm 0.69	3 BAZAVOV 18	LATT
93.85 \pm 0.75	4 LYTLE 18	LATT
87.6 \pm 6.0	5 ANANTHANA..16	THEO
99.6 \pm 4.3	6 CARRASCO 14	LATT
94.4 \pm 2.3	7 ARTHUR 13	LATT
94 \pm 9	8 BODENSTEIN 13	THEO
102 \pm 3 \pm 1	9 FRITZSCH 12	LATT
95.5 \pm 1.1 \pm 1.5	10 DURR 11	LATT
••• We do not use the following data for averages, fits, limits, etc. •••		
93.6 \pm 0.8	11 CHAKRABOR..15	LATT
96.2 \pm 2.7	12 AOKI 11A	LATT
95 \pm 6	13 BLOSSIER 10	LATT
97.6 \pm 2.9 \pm 5.5	14 BLUM 10	LATT
92.4 \pm 1.5	15 DAVIES 10	LATT
92.2 \pm 1.3	15 MCNEILE 10	LATT
107.3 \pm 11.7	16 ALLTON 08	LATT
105 \pm 3 \pm 9	17 BLOSSIER 08	LATT
102 \pm 8	18 DOMINGUEZ 08A	THEO
90.1 \pm 17.2 \pm 6.1	19 ISHIKAWA 08	LATT
105.6 \pm 1.2	20 NAKAMURA 08	LATT
119.5 \pm 9.3	21 BLUM 07	LATT
105 \pm 6 \pm 7	22 CHETYRKIN 06	THEO
111 \pm 6 \pm 10	23 GOCKELER 06	LATT
119 \pm 5 \pm 8	24 GOCKELER 06A	LATT
92 \pm 9	25 JAMIN 06	THEO
87 \pm 6	26 MASON 06	LATT
104 \pm 15	27 NARISON 06	THEO
$\geq 71 \pm 4, \leq 151 \pm 14$	28 NARISON 06	THEO
96 \pm 5 \pm 18	29 BAIKOV 05	THEO
81 \pm 22	30 GAMIZ 05	THEO
125 \pm 28	31 GORBUNOV 05	THEO
93 \pm 32	32 NARISON 05	THEO
76 \pm 8	33 AUBIN 04	LATT
116 \pm 6 \pm 0.65	34 AOKI 03	LATT
84.5 \pm 12 \pm 1.7	35 AOKI 03B	LATT
106 \pm 2 \pm 8	36 BECIREVIC 03	LATT
92 \pm 9 \pm 16	37 CHIU 03	LATT
117 \pm 17	38 GAMIZ 03	THEO
103 \pm 17	39 GAMIZ 03	THEO

m_u/m_d MASS RATIO

VALUE	DOCUMENT ID	TECN	COMMENT
0.474 \pm 0.056 \pm 0.074 OUR EVALUATION	See the ideogram below.		
0.485 \pm 0.011 \pm 0.016	1 FODOR 16	LATT	
0.4482 \pm 0.0173 \pm 0.0206	2 BASAK 15	LATT	
0.470 \pm 0.056	3 CARRASCO 14	LATT	
0.698 \pm 0.051	4 AOKI 12	LATT	
0.42 \pm 0.01 \pm 0.04	5 BAZAVOV 10	LATT	
0.4818 \pm 0.0096 \pm 0.0860	6 BLUM 10	LATT	
••• We do not use the following data for averages, fits, limits, etc. •••			
0.550 \pm 0.031	7 BLUM 07	LATT	
0.43 \pm 0.08	8 AUBIN 04A	LATT	
0.410 \pm 0.036	9 NELSON 03	LATT	
0.553 \pm 0.043	10 LEUTWYLER 96	THEO	Compilation

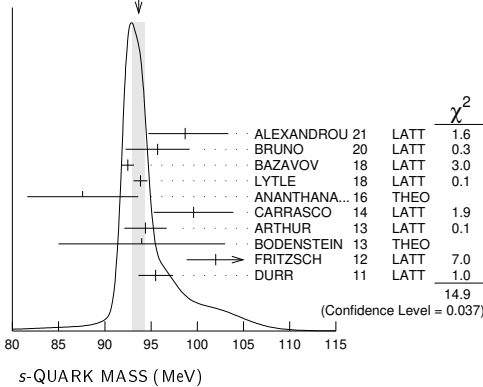
WEIGHTED AVERAGE
0.474 \pm 0.029 (Error scaled by 2.4)

Values above of weighted average, error, and scale factor are based upon the data in this ideogram only. They are not necessarily the same as our 'best' values, obtained from a least-squares constrained fit utilizing measurements of other (related) quantities as additional information.



- ¹ FODOR 16 is a lattice simulation with $n_f = 2 + 1$ dynamical flavors and includes partially quenched QED effects.
- ² BASAK 15 is a lattice computation using 2+1 dynamical quark flavors.
- ³ CARRASCO 14 is a lattice QCD computation of light quark masses using 2 + 1 + 1 dynamical quarks, with $m_u = m_d \neq m_s \neq m_c$. The *u* and *d* quark masses are obtained separately by using the *K* meson mass splittings and lattice results for the electromagnetic contributions.
- ⁴ AOKI 12 is a lattice computation using 1 + 1 + 1 dynamical quark flavors.

WEIGHTED AVERAGE
93.7 \pm 0.7 (Error scaled by 1.5)



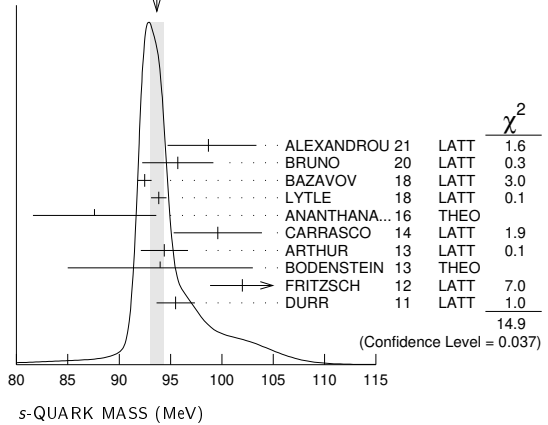
Quark Particle Listings

Light Quarks (u, d, s)

- 1 ALEXANDROU 21 determines the quark mass using a lattice calculation of the meson and baryon masses with a twisted mass fermion action. The simulations are carried out using 2+1+1 dynamical quarks with $m_u = m_d \neq m_s \neq m_c$, including gauge ensembles close to the physical pion point.
- 2 BRUNO 20 determines the light quark mass using a lattice calculation with $n_f = 2+1$ flavors of Wilson fermions. The scale has been set from f_π and f_K . The tuning was done using the masses of the lightest (π) and strange (K) pseudoscalar mesons.
- 3 BAZAVOV 18 determine the quark masses using a lattice computation with staggered fermions and four active quark flavors.
- 4 LYTLE 18 combined with CHAKRABORTY 2015 determine $\overline{m}_s(3 \text{ GeV}) = 84.78 \pm 0.65$ MeV from a lattice simulation with $n_f = 2+1+1$ flavors. They also determine the quoted value $\overline{m}_s(2 \text{ GeV})$ for $n_f = 4$ dynamical flavors.
- 5 ANANTHANARAYAN 16 determine $\overline{m}_s(2 \text{ GeV}) = 106.70 \pm 9.36$ MeV and 74.47 ± 7.77 MeV from fits to ALEPH and OPAL τ decay data, respectively. We have used the weighted average of the two.
- 6 CARRASCO 14 is a lattice QCD computation of light quark masses using 2 + 1 + 1 dynamical quarks, with $m_u = m_d \neq m_s \neq m_c$. The u and d quark masses are obtained separately by using the K meson mass splittings and lattice results for the electromagnetic contributions.
- 7 ARTHUR 13 is a lattice computation using 2+1 dynamical domain wall fermions. Masses at $\mu = 3$ GeV have been converted to $\mu = 2$ GeV using conversion factors given in their paper.
- 8 BODENSTEIN 13 determines m_s from QCD finite energy sum rules, and the perturbative computation of the pseudoscalar correlator to five-loop order.
- 9 FRITZSCH 12 determine m_s using a lattice computation with $n_f = 2$ dynamical flavors.
- 10 DURR 11 determine quark mass from a lattice computation of the meson spectrum using $n_f = 2 + 1$ dynamical flavors. The lattice simulations were done at the physical quark mass, so that extrapolation in the quark mass was not needed.
- 11 CHAKRABORTY 15 is a lattice QCD computation that determines m_c and m_c/m_s using pseudoscalar meson masses tuned on gluon field configurations with 2+1+1 dynamical flavors of HISQ quarks with u/d masses down to the physical value.
- 12 AOKI 11A determine quark masses from a lattice computation of the hadron spectrum using $n_f = 2 + 1$ dynamical flavors of domain wall fermions.
- 13 BLOSSIER 10 determines quark masses from a computation of the hadron spectrum using $n_f=2$ dynamical twisted-mass Wilson fermions.
- 14 BLUM 10 determines light quark masses using a QCD plus QED lattice computation of the electromagnetic mass splittings of the low-lying hadrons. The lattice simulations use 2+1 dynamical quark flavors.
- 15 DAVIES 10 and MCNEILE 10 determine $\overline{m}_c(\mu)/\overline{m}_s(\mu) = 11.85 \pm 0.16$ using a lattice computation with $n_f = 2 + 1$ dynamical fermions of the pseudoscalar meson masses. Mass m_s is obtained from this using the value of m_c from ALLISON 08 or MCNEILE 10.
- 16 ALLTON 08 use a lattice computation of the π, K , and Ω masses with 2+1 dynamical flavors of domain wall quarks, and non-perturbative renormalization.
- 17 BLOSSIER 08 use a lattice computation of pseudoscalar meson masses and decay constants with 2 dynamical flavors and non-perturbative renormalization.
- 18 DOMINGUEZ 08A make determination from QCD finite energy sum rules for the pseudoscalar two-point function computed to order α_s^4 .
- 19 ISHIKAWA 08 use a lattice computation of the light meson spectrum with 2+1 dynamical flavors of $\mathcal{O}(a)$ improved Wilson quarks, and one-loop perturbative renormalization.
- 20 NAKAMURA 08 do a lattice computation using quenched domain wall fermions and non-perturbative renormalization.
- 21 BLUM 07 determine quark masses from the pseudoscalar meson masses using a QED plus QCD lattice computation with two dynamical quark flavors.
- 22 CHETRYKIN 06 use QCD sum rules in the pseudoscalar channel to order α_s^4 .
- 23 GOCKELER 06 use an unquenched lattice computation of the axial Ward Identity with $n_f = 2$ dynamical light quark flavors, and non-perturbative renormalization, to obtain $\overline{m}_s(2 \text{ GeV}) = 111 \pm 6 \pm 4 \pm 6$ MeV, where the first error is statistical, the second and third are systematic due to the fit range and force scale uncertainties, respectively. We have combined the systematic errors linearly.
- 24 GOCKELER 06A use an unquenched lattice computation of the pseudoscalar meson masses with $n_f = 2$ dynamical light quark flavors, and non-perturbative renormalization.
- 25 JAMIN 06 determine $\overline{m}_s(2 \text{ GeV})$ from the spectral function for the scalar $K\pi$ form factor.
- 26 MASON 06 extract light quark masses from a lattice simulation using staggered fermions with an improved action, and three dynamical light quark flavors with degenerate u and d quarks. Perturbative corrections were included at NNLO order.
- 27 NARISON 06 uses sum rules for $e^+e^- \rightarrow$ hadrons to order α_s^3 .
- 28 NARISON 06 obtains the quoted range from positivity of the spectral functions.
- 29 BAIKOV 05 determines $\overline{m}_s(M_\tau) = 100^{+5}_{-3} \pm 17$ from sum rules using the strange spectral function in τ decay. The computations were done to order α_s^3 , with an estimate of the α_s^5 terms. We have converted the result to $\mu = 2$ GeV.
- 30 GAMIZ 05 determines $\overline{m}_s(2 \text{ GeV})$ from sum rules using the strange spectral function in τ decay. The computations were done to order α_s^2 , with an estimate of the α_s^3 terms.
- 31 GORBUNOV 05 use hadronic tau decays to N3LO, including power corrections.
- 32 NARISON 05 determines $\overline{m}_s(2 \text{ GeV})$ from sum rules using the strange spectral function in τ decay. The computations were done to order α_s^3 .
- 33 AUBIN 04 perform three flavor dynamical lattice calculation of pseudoscalar meson masses, with one-loop perturbative renormalization constant.
- 34 AOKI 03 uses quenched lattice simulation of the meson and baryon masses with degenerate light quarks. The extrapolations are done using quenched chiral perturbation theory. Determines $m_s = 113.8 \pm 2.3 \pm 5.8$ using K mass as input and $m_s = 142.3 \pm 5.8 \pm 2.2$ using ϕ mass as input. We have performed a weighted average of these values.
- 35 AOKI 03B uses lattice simulation of the meson and baryon masses with two dynamical light quarks. Simulations are performed using the $\mathcal{O}(a)$ improved Wilson action.
- 36 BECIREVIC 03 perform quenched lattice computation using the vector and axial Ward identities. Uses $\mathcal{O}(a)$ improved Wilson action and nonperturbative renormalization. They also quote $\overline{m}/m_s = 24.3 \pm 0.2 \pm 0.6$.
- 37 CHIU 03 determines quark masses from the pion and kaon masses using a lattice simulation with a chiral fermion action in quenched approximation.
- 38 GAMIZ 03 determines m_s from SU(3) breaking in the τ hadronic width. The value of V_{us} is chosen to satisfy CKM unitarity.

- 39 GAMIZ 03 determines m_s from SU(3) breaking in the τ hadronic width. The value of V_{us} is taken from the PDG.

WEIGHTED AVERAGE
93.7±0.7 (Error scaled by 1.5)



OTHER LIGHT QUARK MASS RATIOS

m_s/m_d MASS RATIO

VALUE	DOCUMENT ID	TECN.	COMMENT
17-22 OUR EVALUATION			
20.0	1 GAO 97	97	THEO
18.9 ± 0.8	2 LEUTWYLER 96	96	THEO Compilation
21	3 DONOGHUE 92	92	THEO
18	4 GERARD 90	90	THEO
18 to 23	5 LEUTWYLER 90B	90B	THEO

1 GAO 97 uses electromagnetic mass splittings of light mesons.
 2 LEUTWYLER 96 uses a combined fit to $\eta \rightarrow 3\pi$ and $\psi' \rightarrow J/\psi(\pi, \eta)$ decay rates, and the electromagnetic mass differences of the π and K .
 3 DONOGHUE 92 result is from a combined analysis of meson masses, $\eta \rightarrow 3\pi$ using second-order chiral perturbation theory including nonanalytic terms, and $(\psi(2S) \rightarrow J/\psi(1S)\pi)/(\psi(2S) \rightarrow J/\psi(1S)\eta)$.
 4 GERARD 90 uses large N and η - η' mixing.
 5 LEUTWYLER 90B determines quark mass ratios using second-order chiral perturbation theory for the meson and baryon masses, including nonanalytic corrections. Also uses Weinberg sum rules to determine L_7 .

m_s/\overline{m} MASS RATIO

VALUE	DOCUMENT ID	TECN.
$\overline{m} \equiv (m_u + m_d)/2$		
27.33^{+0.67}_{-0.77} OUR EVALUATION	See the ideogram below.	
$27.17 \pm 0.32^{+0.56}_{-0.38}$	1 ALEXANDROU 21	LATT
$27.0 \pm 1.0 \pm 0.4$	2 BRUNO 20	LATT
$27.35 \pm 0.05^{+0.10}_{-0.07}$	3 BAZAVOV 14A	LATT
26.66 ± 0.32	4 CARRASCO 14	LATT
27.36 ± 0.54	5 ARTHUR 13	LATT
$27.53 \pm 0.20 \pm 0.08$	6 DURR 11	LATT
• • • We do not use the following data for averages, fits, limits, etc. • • •		
26.8 ± 1.4	7 AOKI 11A	LATT
27.3 ± 0.9	8 BLOSSIER 10	LATT
28.8 ± 1.65	9 ALLTON 08	LATT
$27.3 \pm 0.3 \pm 1.2$	10 BLOSSIER 08	LATT
23.5 ± 1.5	11 OLLER 07A	THEO
27.4 ± 0.4	12 AUBIN 04	LATT

- 1 ALEXANDROU 21 determines the quark mass using a lattice calculation of the meson and baryon masses with a twisted mass fermion action. The simulations are carried out using 2+1+1 dynamical quarks with $m_u = m_d \neq m_s \neq m_c$, including gauge ensembles close to the physical pion point.
- 2 BRUNO 20 determines the light quark mass using a lattice calculation with $n_f = 2+1$ flavors of Wilson fermions. The scale has been set from f_π and f_K . The tuning was done using the masses of the lightest (π) and strange (K) pseudoscalar mesons.
- 3 BAZAVOV 14A is a lattice computation using 4 dynamical flavors of HISQ fermions.
- 4 CARRASCO 14 is a lattice QCD computation of light quark masses using 2 + 1 + 1 dynamical quarks, with $m_u = m_d \neq m_s \neq m_c$. The u and d quark masses are obtained separately by using the K meson mass splittings and lattice results for the electromagnetic contributions.
- 5 ARTHUR 13 is a lattice computation using 2+1 dynamical domain wall fermions.
- 6 DURR 11 determine quark mass from a lattice computation of the meson spectrum using $n_f = 2 + 1$ dynamical flavors. The lattice simulations were done at the physical quark mass, so that extrapolation in the quark mass was not needed.
- 7 AOKI 11A determine quark masses from a lattice computation of the hadron spectrum using $n_f = 2 + 1$ dynamical flavors of domain wall fermions.
- 8 BLOSSIER 10 determines quark masses from a computation of the hadron spectrum using $n_f=2$ dynamical twisted-mass Wilson fermions.

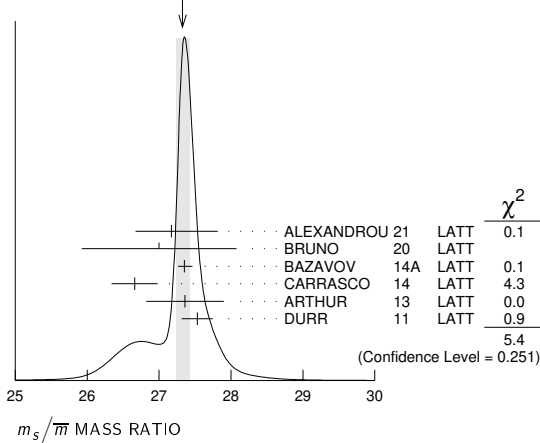
See key on page 1127

Quark Particle Listings

Light Quarks (*u, d, s, c*)

- ⁹ ALLTON 08 use a lattice computation of the π , K , and Ω masses with 2+1 dynamical flavors of domain wall quarks, and non-perturbative renormalization.
- ¹⁰ BLOSSIER 08 use a lattice computation of pseudoscalar meson masses and decay constants with 2 dynamical flavors and non-perturbative renormalization.
- ¹¹ OLLER 07A use unitarized chiral perturbation theory to order p^4 .
- ¹² Three flavor dynamical lattice calculation of pseudoscalar meson masses.

WEIGHTED AVERAGE
27.33±0.11-0.09 (Error scaled by 1.2)



Q MASS RATIO

$$Q \equiv \sqrt{(m^2_s - \bar{m}^2)/(m^2_d - \bar{m}^2)}; \quad \bar{m} \equiv (m_u + m_d)/2$$

VALUE DOCUMENT ID TECN

••• We do not use the following data for averages, fits, limits, etc. •••

22.1±0.7	1 COLANGELO 18	THEO
22.0±0.7	2 COLANGELO 17	THEO
21.6±1.1	3 GUO 17	THEO
23.4±0.4±0.5	4 FODOR 16	LATT
21.4±0.4	5 GUO 15F	THEO
22.8±0.4	6 MARTEMYANOV 05	THEO
22.7±0.8	7 ANISOVICH 96	THEO

¹ COLANGELO 18 obtain Q from a dispersive analysis of $\eta \rightarrow 3\pi$ decay.
² COLANGELO 17 obtain Q from a dispersive analysis of KLOE collaboration data on $\eta \rightarrow \pi^+\pi^-\pi^0$ decays and chiral perturbation theory input.
³ GUO 17 determine Q from a dispersive model fit to KLOE and WA SA-at-COSY data on $\eta \rightarrow \pi^+\pi^-\pi^0$ decay and matching to chiral perturbation theory.
⁴ FODOR 16 is a lattice simulation with $n_f = 2 + 1$ dynamical flavors and includes partially quenched QED effects.
⁵ GUO 15F determine Q from a Khuri-Treiman analysis of $\eta \rightarrow 3\pi$ decays.
⁶ MARTEMYANOV 05 determine Q from $\eta \rightarrow 3\pi$ decay.
⁷ ANISOVICH 96 find Q from $\eta \rightarrow \pi^+\pi^-\pi^0$ decay using dispersion relations and chiral perturbation theory.

LIGHT QUARKS (*u, d, s*) REFERENCES

ALEXANDROU 21	PR D104 074515	C. Alexandrou et al. (ETM Collab.)
BRUNO 20	EPJ C80 169	M. Bruno et al. (ALPHA Collab.)
DOMINGUEZ 19	JHEP 1902 057	C.A. Dominguez, A. Mes, K. Schilcher (CAPE, MAINZ)
BAZAVOV 18	PR D98 054517	A. Bazavov et al. (Fermilab Lattice, MILC, TUMQCD)
COLANGELO 18	EPJ C78 947	G. Colangelo et al. (HPQCD Collab.)
LYTLE 18	PR D98 014513	A.T. Lytle et al. (MILC Collab.)
COLANGELO 17	PRL 118 022001	G. Colangelo et al. (BERN, IND, JLAB)
GUO 17	PL B771 497	P. Guo et al.
YUAN 17	PR D96 014034	J.-M. Yuan et al.
ANANTHANA... 16	PR D94 116014	B. Ananthanarayan, D. Das (BANG, AHMED)
FODOR 16	PRL 117 082001	Z. Fodor et al. (BMW Collab.)
BASAK 15	JPCS 640 012052	S. Basak et al. (MILC Collab.)
CHAKRABOR... 15	PR D91 054508	B. Chakraborty et al. (HPQCD Collab.)
GUO 15F	PR D92 054016	P. Guo et al.
BAZAVOV 14A	PR D90 074509	A. Bazavov et al. (Fermi-LAT and MILC Collabs.)
CARRASCO 14	NP B887 19	N. Carrasco et al. (European Twisted Mass Collab.)
ARTHUR 13	PR D87 094514	R. Arthur et al. (RBC and UKQCD Collabs.)
BODENSTEIN 13	JHEP 1307 138	S. Bodenstein, C.A. Dominguez, K. Schilcher (PACS-CS Collab.)
AOKI 12	PR D86 034507	S. Aoki et al. (ALPHA Collab.)
FRITZSCH 12	NP B865 397	P. Fritzsche et al. (ALPHA Collab.)
AOKI 11A	PR D83 074508	Y. Aoki et al. (RBC-UKQCD Collab.)
DURR 11	PL B701 265	S. Durr et al. (BMW Collab.)
BAZAVOV 10	RMP D82 1349	A. Bazavov et al. (MILC Collab.)
BLOSSIER 10	PR D82 114513	B. Blossier et al. (ETM Collab.)
BLUM 10	PR D82 094508	T. Blum et al.
DAVIES 10	PRL 104 132003	C.T.H. Davies et al. (HPQCD Collab.)
MCNEILE 10	PR D82 034512	C. McNeile et al. (HPQCD Collab.)
DOMINGUEZ 09	PR D79 014009	C.A. Dominguez et al. (HPQCD Collab.)
ALLISON 08	PR D78 054513	I. Allison et al. (HPQCD Collab.)
ALLTON 08	PR D78 114509	C. Allton et al. (RBC and UKQCD Collabs.)
BLOSSIER 08	JHEP 0804 020	B. Blossier et al. (ETM Collab.)
DEANDREA 08	PR D78 034032	A. Deandrea, A. Nehme, P. Talavera
DOMINGUEZ 08A	JHEP 0805 020	C.A. Dominguez et al.
DOMINGUEZ... 08B	PL B660 49	A. Dominguez-Clarimon, E. de Rafael, J. Taron
ISHIKAWA 08	PR D78 011502	T. Ishikawa et al. (CP-PACS and JLQCD Collabs.)
NAKAMURA 08	PR D78 034502	Y. Nakamura et al. (CP-PACS Collab.)
BLUM 07	PR D76 114508	T. Blum et al. (RBC Collab.)
OLLER 07A	EPJ A34 371	J.G. Oller, L. Roca
CHETYRKIN 06	EPJ C46 721	K.G. Chetyrkin, A. Khodjamirian
GOCKELER 06	PR D73 054508	M. Gockeler et al. (QCDSF and UKQCD Collabs.)

GOCKELER 06A	PL B639 307	M. Gockeler et al. (QCDSF and UKQCD Collabs.)
JAMIN 06	PR D74 074009	M. Jamin, J.A. Oller, A. Pich
MASON 06	PR D73 114501	Q. Mason et al. (HPQCD Collab.)
NARISON 06	PR D74 034013	S. Narison
PDG 06	JP G33 1	W.-M. Yao et al. (PDG Collab.)
BAIKOV 05	PRL 95 012003	P.A. Baikov, K.G. Chetyrkin, J.H. Kuhn
GAMIZ 05	PRL 94 011803	E. Gamiz et al.
GORBUNOV 05	PR D71 013002	D.S. Gorbunov, A.A. Pivovarov
MARTEMYA... 05	PR D71 017501	B.V. Martemyanov, V.S. Sopoov
NARISON 05	PL B626 101	S. Narison
AUBIN 04	PR D70 031504	C. Aubin et al. (HPQCD, MILC, UKQCD Collabs.)
AUBIN 04A	PR D70 114501	C. Aubin et al. (MILC Collab.)
AOKI 03	PR D67 034503	S. Aoki et al. (CP-PACS Collab.)
AOKI 03B	PR D68 054502	S. Aoki et al. (CP-PACS Collab.)
BECEVIC 03	PL B558 69	D. Becirevic, V. Lubicz, C. Tarantino
CHIU 03	NP B673 217	T.-W. Chiu, T.-H. Hsieh
GAMIZ 03	JHEP 0301 060	E. Gamiz et al.
NELSON 03	PRL 90 021601	D. Nelson, G.T. Fleming, G.W. Kilcup
GAO 97	PR D56 4115	D.-N. Gao, B.A. Li, M.-L. Yan
ANISOVICH 96	PL B375 335	A.V. Anisovich, H. Leutwyler
LEUTWYLER 96	PL B378 313	H. Leutwyler
DONOGHUE 92	PRL 69 3444	J.F. Donoghue, B.R. Holstein, D. Wyler (MASA+)
GERARD 90	MPL A5 391	J.M. Gerard (MPIM)
LEUTWYLER 90B	NP B337 108	H. Leutwyler (BERN)



$$I(J^P) = 0(\frac{1}{2}^+)$$

Charge = $\frac{2}{3} e$ Charm = +1

c-QUARK MASS

The c -quark mass corresponds to the "running" mass $m_c(\mu = m_c)$ in the \overline{MS} scheme. We have converted masses in other schemes to the \overline{MS} scheme using two-loop QCD perturbation theory with $\alpha_s(\mu=m_c) = 0.38 \pm 0.03$. The value 1.27 ± 0.02 GeV for the \overline{MS} mass corresponds to 1.67 ± 0.07 GeV for the pole mass (see the "Note on Quark Masses").

\overline{MS} MASS (GeV)	OUR EVALUATION	DOCUMENT ID	TECN
----------------------------	----------------	-------------	------

1.27 ± 0.02	+0.019 -0.010	1 ALEXANDROU 21	LATT
1.296 ± 0.019		2 HEITGER 21	LATT
1.2723 ± 0.0078		3 HATTON 20	LATT
1.266 ± 0.006		4 NARISON 20	THEO
1.290 ± 0.077 -0.053		5 ABRAMOWICZ18	HERA
1.273 ± 0.010		6 BAZAVOV 18	LATT
1.2737 ± 0.0077		7 LYTLE 18	LATT
1.223 ± 0.033		8 PESET 18	THEO
1.279 ± 0.008		9 CHETYRKIN 17	THEO
1.272 ± 0.008		10 ERLER 17	THEO
1.246 ± 0.023		11 KIYO 16	THEO
1.288 ± 0.020		12 DEHNADI 15	THEO
1.348 ± 0.046		13 CARRASCO 14	LATT
1.24 ± 0.03 +0.03 -0.07		14 ALEKHIN 13	THEO
1.159 ± 0.075		15 SAMOYLOV 13	NOMD
1.278 ± 0.009		16 BODENSTEIN 11	THEO
1.28 ± 0.07 -0.06		17 LASCHKA 11	THEO
1.196 ± 0.059 ± 0.050		18 AUBERT 10A	BABR
1.25 ± 0.04		19 SIGNER 09	THEO
••• We do not use the following data for averages, fits, limits, etc. •••			
1.263 ± 0.014		20 NARISON 18A	THEO
1.264 ± 0.006		21 NARISON 18B	THEO
1.335 ± 0.043 +0.040 -0.011		22 BERTONE 16	THEO
1.2715 ± 0.0095		23 CHAKRABOR...15	LATT
1.26 ± 0.05 ± 0.04		24 ABRAMOWICZ13C	COMB
1.282 ± 0.011 ± 0.022		25 DEHNADI 13	THEO
1.286 ± 0.066		26 NARISON 13	THEO
1.36 ± 0.04 ± 0.10		27 ALEKHIN 12	THEO
1.261 ± 0.016		28 NARISON 12A	THEO
1.01 ± 0.09 ± 0.03		29 ALEKHIN 11	THEO
1.28 ± 0.04		30 BLOSSIER 10	LATT
1.299 ± 0.026		31 BODENSTEIN 10	THEO
1.273 ± 0.006		32 MCNEILE 10	LATT
1.261 ± 0.018		33 NARISON 10	THEO
1.279 ± 0.013		34 CHETYRKIN 09	THEO
1.268 ± 0.009		35 ALLISON 08	LATT
1.286 ± 0.013		36 KUHN 07	THEO
1.295 ± 0.015		37 BOUGHEZAL 06	THEO
1.24 ± 0.09		38 BUCHMUELL... 06	THEO
1.224 ± 0.017 ± 0.054		39 HOANG 06	THEO
1.33 ± 0.10		40 AUBERT 04X	THEO
1.29 ± 0.07		41 HOANG 04	THEO
1.319 ± 0.028		42 DEDIVITIS 03	LATT
1.19 ± 0.11		43 EIDEMULLER 03	THEO
1.289 ± 0.043		44 ERLER 03	THEO
1.26 ± 0.02		45 ZYABLYUK 03	THEO

¹ ALEXANDROU 21 determines the quark mass using a lattice calculation of the meson and baryon masses with a twisted mass fermion action. We have converted $\overline{m}_c(3 \text{ GeV}) = 1.036 \pm 0.017 \pm 0.015$ to $\overline{m}_c(\overline{m}_c)$. The simulations are carried out using 2+1+1 dynamical quarks with $m_u = m_d \neq m_s \neq m_c$, including gauge ensembles close to the physical pion point.

Quark Particle Listings

C

2 HEITGER 21 determines the charm quark mass using a $n_f = 2+1$ flavor lattice QCD simulation with non-perturbatively O(a) improved Wilson fermions. They also determine $\overline{m}_c(3 \text{ GeV}) = 1.007 \pm 0.016 \text{ GeV}$.

3 HATTON 20 determine the charm quark mass using a $n_f = 2+1+1$ flavor lattice simulation with the HISQ action of ground state charmonium mesons. They also determine $\overline{m}_c(3 \text{ GeV}) = 0.9841 \pm 0.0051 \text{ GeV}$.

4 NARISON 20 determines the quark mass using QCD Laplace sum rules from the B_c mass, combined with previous determinations of the QCD condensates and c and b masses.

5 ABRAMOWICZ 18 determine $\overline{m}_c(\overline{m}_c) = 1.290^{+0.046+0.062+0.003}_{-0.041-0.014-0.031}$ from the production of c quarks in $e p$ collisions at HERA using combined H1 and ZEUS data. The experimental/fitting errors, and those from modeling and parameterization have been combined in quadrature.

6 BAZAVOV 18 determine the quark masses using a lattice computation with staggered fermions and four active quark flavors.

7 LYTLE 18 combined with CHAKRABORTY 15 determine $\overline{m}_c(3 \text{ GeV}) = 0.9874(48) \text{ GeV}$ from a lattice simulation with $n_f = 2+1+1$ flavors. They also determine the quoted value $\overline{m}_c(\overline{m}_c)$ for $n_f = 4$ dynamical flavors.

8 PESET 18 determine $\overline{m}_c(\overline{m}_c)$ and $\overline{m}_b(\overline{m}_b)$ using an N3LO calculation of the η_c, η_b and B_c masses.

9 CHETYRKIN 17 determine $\overline{m}_c(\mu = 3 \text{ GeV}) = 0.993 \pm 0.008 \text{ GeV}$ and $\overline{m}_c(\overline{m}_c)$ from a four-loop sum-rule computation of the cross-section for $e^+ e^- \rightarrow$ hadrons in the charm threshold region.

10 ERLER 17 determine $\overline{m}_c(\overline{m}_c) = 1.272 \pm 0.008 \text{ GeV}$ from a three-loop QCD sum-rule computation of the vector current correlator. This result is for fixed $\alpha_s(M_Z) = 0.1182$. Including an α_s uncertainty of ± 0.0016 , the charm mass error increases from 8 to 9 MeV.

11 KIYO 16 determine $\overline{m}_c(\overline{m}_c)$ from the $J/\psi(1S)$ mass at order α_s^3 (N3LO).

12 DEHNADI 15 determine $\overline{m}_c(\overline{m}_c)$ using sum rules for $e^+ e^- \rightarrow$ hadrons at order α_s^3 (N3LO), and fitting to both experimental data and lattice results.

13 CARRASCO 14 is a lattice QCD computation of light quark masses using $2 + 1 + 1$ dynamical quarks, with $m_u = m_d \neq m_s \neq m_c$. The u and d quark masses are obtained separately by using the K meson mass splittings and lattice results for the electromagnetic contributions.

14 ALEKHIN 13 determines m_c from charm production in deep inelastic scattering at HERA using approximate NNLO QCD.

15 SAMOYLOV 13 determines m_c from a study of charm dimuon production in neutrino-iron scattering using the NLO QCD result for the charm quark production cross section.

16 BODENSTEIN 11 determine $\overline{m}_c(3 \text{ GeV}) = 0.987 \pm 0.009 \text{ GeV}$ and $\overline{m}_c(\overline{m}_c) = 1.278 \pm 0.009 \text{ GeV}$ using QCD sum rules for the charm quark vector current correlator.

17 LASCHKA 11 determine the c mass from the charmonium spectrum. The theoretical computation uses the heavy $Q\overline{Q}$ potential to order $1/m_Q$ obtained by matching the short-distance perturbative result onto lattice QCD result at larger scales.

18 AUBERT 10A determine the b - and c -quark masses from a fit to the inclusive decay spectra in semileptonic B decays in the kinetic scheme (and convert it to the \overline{MS} scheme).

19 SIGNER 09 determines the c -quark mass using non-relativistic sum rules to analyze the $e^+ e^- \rightarrow c\overline{c}$ cross-section near threshold. Also determine the PS mass $m_{PS}(M_F = 0.7 \text{ GeV}) = 1.50 \pm 0.04 \text{ GeV}$.

20 NARISON 18A determines simultaneously $\overline{m}_c(\overline{m}_c)$ and the 4-dimension gluon condensate using QCD exponential sum rules and their ratios evaluated at the optimal scale $\mu = 2.85 \text{ GeV}$ at N2LO-N3LO of perturbative QCD and including condensates up to dimension 6-8 in the (axial-)vector and (pseudo-)scalar charmonium channels.

21 NARISON 18B determines $\overline{m}_c(\overline{m}_c)$ using QCD vector moment sum rules and their ratios at N2LO-N3LO of perturbative QCD and including condensates up to dimension 8.

22 BERTONE 16 determine $\overline{m}_c(\overline{m}_c)$ from HERA deep inelastic scattering data using the FONLL scheme. Also determine $\overline{m}_c(\overline{m}_c) = 1.318 \pm 0.054^{+0.490}_{-0.022}$ using the fixed flavor number scheme.

23 CHAKRABORTY 15 is a lattice QCD computation using $2+1+1$ dynamical flavors. Moments of pseudoscalar current-current correlators are matched to α_s^3 -accurate QCD perturbation theory with the η_c meson mass tuned to experiment.

24 ABRAMOWICZ 13c determines m_c from charm production in deep inelastic $e p$ scattering, using the QCD prediction at NLO order. The uncertainties from model and parameterization assumptions, and the value of α_s , of ± 0.03 , ± 0.02 , and ± 0.02 respectively, have been combined in quadrature.

25 DEHNADI 13 determines m_c using QCD sum rules for the charmonium spectrum and charm continuum to order α_s^3 (N3LO). The statistical and systematic experimental errors of ± 0.006 and ± 0.009 have been combined in quadrature. The theoretical uncertainties ± 0.019 from truncation of the perturbation series, ± 0.010 from α_s , and ± 0.002 from the gluon condensate have been combined in quadrature.

26 NARISON 13 determines m_c using QCD spectral sum rules to order α_s^2 (NNLO) and including condensates up to dimension 6.

27 ALEKHIN 12 determines m_c from heavy quark production in deep inelastic scattering at HERA using approximate NNLO QCD.

28 NARISON 12A determines m_c using sum rules for the vector current correlator to order α_s^3 , including the effect of gluon condensates up to dimension eight.

29 ALEKHIN 11 determines m_c from heavy quark production in deep inelastic scattering using fixed target and HERA data, and approximate NNLO QCD.

30 BLOSSIER 10 determines quark masses from a computation of the hadron spectrum using $n_f=2$ dynamical twisted-mass Wilson fermions.

31 BODENSTEIN 10 determines $\overline{m}_c(3 \text{ GeV}) = 1.008 \pm 0.026 \text{ GeV}$ using finite energy sum rules for the vector current correlator. The authors have converted this to $\overline{m}_c(\overline{m}_c)$ using $\alpha_s(M_Z) = 0.1189 \pm 0.0020$.

32 MCNEILE 10 determines m_c by comparing the order α_s^3 perturbative results for the pseudo-scalar current to lattice simulations with $n_f = 2+1$ sea-quarks by the HPQCD collaboration.

33 NARISON 10 determines m_c from ratios of moments of vector current correlators computed to order α_s^3 and including the dimension-six gluon condensate.

34 CHETYRKIN 09 determine m_c and m_b from the $e^+ e^- \rightarrow Q\overline{Q}$ cross-section and sum rules, using an order α_s^3 computation of the heavy quark vacuum polarization. They also determine $m_c(3 \text{ GeV}) = 0.986 \pm 0.013 \text{ GeV}$.

35 ALLISON 08 determine m_c by comparing four-loop perturbative results for the pseudo-scalar current correlator to lattice simulations by the HPQCD collaboration. The result has been updated in MCNEILE 10.

36 KUHN 07 determine $\overline{m}_c(\mu = 3 \text{ GeV}) = 0.986 \pm 0.013 \text{ GeV}$ and $\overline{m}_c(\overline{m}_c)$ from a four-loop sum-rule computation of the cross-section for $e^+ e^- \rightarrow$ hadrons in the charm threshold region.

37 BOUGHEZAL 06 result comes from the first moment of the hadronic production cross-section to order α_s^3 .

38 BUCHMUELLER 06 determine m_b and m_c by a global fit to inclusive B decay spectra.

39 HOANG 06 determines $\overline{m}_c(\overline{m}_c)$ from a global fit to inclusive B decay data. The B decay distributions were computed to order $\alpha_s^2 g_0$, and the conversion between different m_c mass schemes to order α_s^3 .

40 AUBERT 04x obtain m_c from a fit to the hadron mass and lepton energy distributions in semileptonic B decay. The paper quotes values in the kinetic scheme. The \overline{MS} value has been provided by the BABAR collaboration.

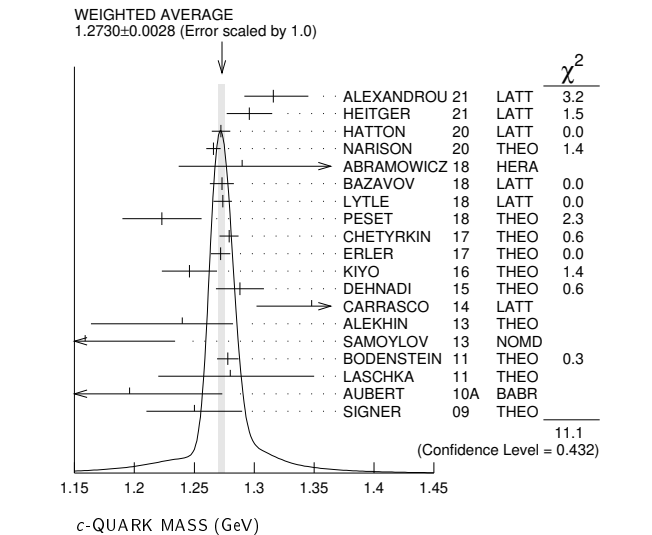
41 HOANG 04 determines $\overline{m}_c(\overline{m}_c)$ from moments at order α_s^2 of the charm production cross-section in $e^+ e^-$ annihilation.

42 DEDIVITHIS 03 use a quenched lattice computation of heavy-heavy and heavy-light meson masses.

43 EIDEMULLER 03 determines m_b and m_c using QCD sum rules.

44 ERLER 03 determines m_b and m_c using QCD sum rules. Includes recent BES data.

45 ZYABLYUK 03 determines m_c by using QCD sum rules in the pseudoscalar channel and comparing with the η_c mass.



m_c/m_s MASS RATIO

The ratio is that of the \overline{MS} masses at a common scale, for four dynamical quark flavors.

VALUE	DOCUMENT ID	TECN
11.76 $^{+0.05}_{-0.10}$	OUR EVALUATION	See the ideogram below.
11.48 ± 0.12	1 ALEXANDROU 21	LATT
11.783 ± 0.025	2 BAZAVOV 18	LATT
11.652 ± 0.065	3 CHAKRABOR. 15	LATT
11.62 ± 0.16	4 CARRASCO 14	LATT
11.27 $\pm 0.30 \pm 0.26$	5 DURR 12	LATT
11.85 ± 0.16	6 DAVIES 10	LATT
11.747 ± 0.019	7 BAZAVOV 14A	LATT
12.0 ± 0.3	8 BLOSSIER 10	LATT

• • • We do not use the following data for averages, fits, limits, etc. • • •

1 ALEXANDROU 21 determines the quark mass using a lattice calculation of the meson and baryon masses with a twisted mass fermion action. The simulations are carried out using $2+1+1$ dynamical quarks with $m_u = m_d \neq m_s \neq m_c$, including gauge ensembles close to the physical pion point.

2 BAZAVOV 18 determine the quark masses using a lattice computation with staggered fermions and four active quark flavors.

3 CHAKRABORTY 15 is a lattice QCD computation on gluon field configurations with $2+1+1$ dynamical flavors of HISQ quarks with u/d masses down to the physical value. m_c and m_s are tuned from pseudoscalar meson masses.

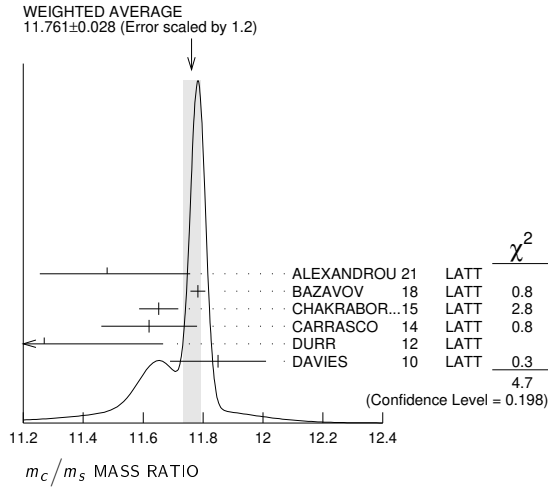
4 CARRASCO 14 is a lattice QCD computation of light quark masses using $2 + 1 + 1$ dynamical quarks, with $m_u = m_d \neq m_s \neq m_c$. The u and d quark masses are obtained separately by using the K meson mass splittings and lattice results for the electromagnetic contributions.

5 DURR 12 determine m_c/m_s using a lattice computation with $n_f = 2$ dynamical fermions. The result is combined with other determinations of m_c to obtain $m_c(2 \text{ GeV}) = 97.0 \pm 2.6 \pm 2.5 \text{ MeV}$.

6 DAVIES 10 determine m_c/m_s from meson masses calculated on gluon fields including u, d , and s sea quarks with lattice spacing down to 0.045 fm. The Highly Improved Staggered quark formalism is used for the valence quarks.

7 BAZAVOV 14A is a lattice computation using 4 dynamical flavors of HISQ fermions.

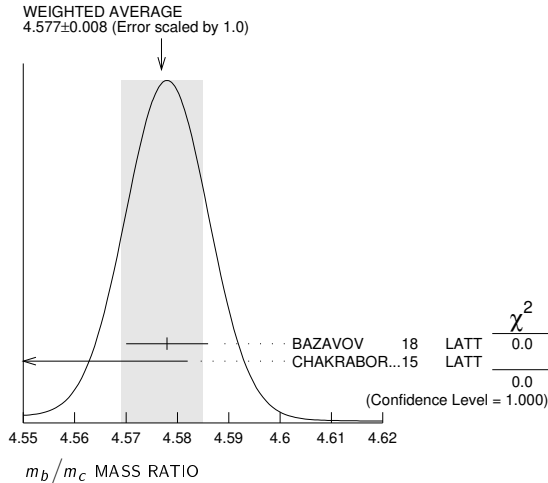
⁸ BLOSSIER 10 determine m_c/m_s from a computation of the hadron spectrum using $n_f = 2$ dynamical twisted-mass Wilson fermions.



m_b/m_c MASS RATIO

The ratio is that of the \overline{MS} masses at a common scale, for four dynamical quark flavors.

VALUE	DOCUMENT ID	TECN
4.58 ± 0.01	OUR EVALUATION	
4.577 ± 0.008	OUR AVERAGE	See the ideogram below.
4.578 ± 0.008	¹ BAZAVOV 18	LATT
4.528 ± 0.054	² CHAKRABOR..15	LATT



- ¹ BAZAVOV 18 determine the quark masses using a lattice computation with staggered fermions and four active quark flavors for the u, d, s, c quarks and five active flavors for the b quark.
- ² CHAKRABORTY 15 is a lattice computation using 4 dynamical quark flavors.

$m_b - m_c$ QUARK MASS DIFFERENCE

VALUE (GeV)	DOCUMENT ID	TECN
3.45 ± 0.05	OUR EVALUATION	
3.472 ± 0.032	¹ AUBERT 10A	BABR
3.42 ± 0.06	² ABDALLAH 06B	DLPH
3.44 ± 0.03	³ AUBERT 04X	BABR
3.41 ± 0.01	³ BAUER 04	THEO

- • • We do not use the following data for averages, fits, limits, etc. • • •
- ¹ AUBERT 10A determine the b - and c -quark masses from a fit to the inclusive decay spectra in semileptonic B decays in the kinetic scheme.
- ² ABDALLAH 06B determine $m_b - m_c$ from moments of the hadron invariant mass and lepton energy spectra in semileptonic inclusive B decays.
- ³ Determine $m_b - m_c$ from a global fit to inclusive B decay spectra.

c-QUARK REFERENCES

ALEXANDROU 21	PR D104 074515	C. Alexandrou et al.	(ETM Collab.)
HEITGER 21	JHEP 2105 288	J. Heitger, F. Joswig, S. Kuberski	(ALPHA Collab.)
HATTON 20	PR D102 054511	D. Hatton et al.	(HPQCD Collab.)
NARISON 20	PL B802 135221	S. Narison	(MONP)
ABRAMOWICZ 18	EPJ C78 473	H. Abramowicz et al.	(HI and ZEUS Collabs.)
BAZAVOV 18	PR D98 054517	A. Bazavov et al.	(Fermilab Lattice, MILC, TUMQCD)
LYTLE 18	PR D98 014513	A.T. Lytle et al.	(HPQCD Collab.)
NARISON 18A	IJMP A33 1850045	S. Narison	(MONP)
NARISON 18B	PL B784 261	S. Narison	(MONP)

PESET 18	JHEP 1809 167	C. Peset, A. Pineda, J. Segovia	(BARC, TUM)
CHETYRKIN 17	PR D96 116007	K.G. Chetyrkin et al.	
ERLER 17	EPJ C77 99	J. Erler, P. Masjuan, H. Spiesberger	
BERTONE 16	JHEP 1608 050	V. Bertone et al.	(xFitter Developers)
KIYO 16	PL B752 122	Y. Kiyo, G. Mishima, Y. Sumino	
CHAKRABOR...15	PR D91 054508	B. Chakraborty et al.	(HPQCD Collab.)
DEHNADI 15	JHEP 1508 155	B. Dehnadi, A.H. Hoang, V. Mateu	
BAZAVOV 14A	PR D90 074509	A. Bazavov et al.	(Fermi-LAT and MILC Collabs.)
CARRASCO 14	NP B887 19	N. Carrasco et al.	(European Twisted Mass Collab.)
ABRAMOWICZ 13C	EPJ C73 2311	H. Abramowicz et al.	(HI and ZEUS Collabs.)
ALEKHIN 13	PL B720 172	S. Alekhin et al.	(SERP, DESYZ, WUPP+)
DEHNADI 13	JHEP 1309 103	B. Dehnadi et al.	(SHRZ, VIEN, MPIMP+)
NARISON 13	PL B718 1321	S. Narison	(MONP)
SAMOYLOV 13	NP B876 339	O. Samoylov et al.	(NOMAD Collab.)
ALEKHIN 12	PL B718 550	S. Alekhin et al.	(SERP, WUPP, DESYZ+)
DURR 12	PRL 108 122003	S. Durr, G. Koutsou	(WUPP, JULI, CYPR)
NARISON 12A	PL B706 412	S. Narison	(MONP)
ALEKHIN 11	PL B699 345	S. Alekhin, S. Moch	
BODENSTEIN 11	PR D83 074014	S. Bodenstein et al.	(HPQCD Collab.)
LASCHKA 11	PR D83 094002	A. Laschka, N. Kaiser, W. Weise	
AUBERT 10A	PR D81 032003	B. Aubert et al.	(BABAR Collab.)
BLOSSIER 10	PR D82 114513	B. Blossier et al.	(ETM Collab.)
BODENSTEIN 10	PR D82 114013	S. Bodenstein et al.	
DAVIES 10	PRL 104 132003	C.T.H. Davies et al.	(HPQCD Collab.)
MCNEILE 10	PR D82 034512	C. McNeile et al.	(HPQCD Collab.)
NARISON 10	PL B693 559	S. Narison	(MONP)
Also	PL B705 544 (errata.)	S. Narison	(MONP)
CHETYRKIN 09	PR D80 074010	K.G. Chetyrkin et al.	(KARL, BNL)
SIGNER 09	PL B672 333	A. Signer	(DURH)
ALLISON 08	PR D78 054513	I. Allison et al.	(HPQCD Collab.)
KUHN 07	NP B778 192	J.H. Kuhn, M. Steinhauser, C. Sturm	
ABDALLAH 06B	EPJ C45 35	J. Abdallah et al.	(DELPHI Collab.)
BOUGHEZAL 06	PR D74 074006	R. Boughezal, M. Czakon, T. Schutzmeier	
BUCHMUELL...06	PR D73 073008	O.L. Buchmueller, H.U. Flacher	(RHBL)
HOANG 06	PL B633 526	A.H. Hoang, A.V. Manohar	
AUBERT 04X	PRL 93 011803	B. Aubert et al.	(BABAR Collab.)
BAUER 04	PR D70 094017	C. Bauer et al.	
HOANG 04	PL B594 127	A.H. Hoang, M. Jamin	
DEDIVITHIS 03	NP B675 309	G.M. de Divitis et al.	
EIDEMULLER 03	PR D67 113002	M. Eidemuller	
ERLER 03	PL B558 125	J. Erler, M. Luo	
ZYABLYUK 03	JHEP 0301 081	K.N. Zybalyuk	(ITEP)



$I(J^P) = 0(\frac{1}{2}^+)$

Charge = $-\frac{1}{3} e$ Bottom = -1

b-QUARK MASS

b -quark mass corresponds to the "running mass" $\overline{m}_b(\mu = \overline{m}_b)$ in the \overline{MS} scheme. We have converted masses in other schemes to the \overline{MS} mass using two-loop QCD perturbation theory with $\alpha_s(\mu = \overline{m}_b) = 0.223 \pm 0.008$. The value $4.18^{+0.04}_{-0.03}$ GeV for the \overline{MS} mass corresponds to 4.78 ± 0.06 GeV for the pole mass, using the two-loop conversion formula. A discussion of masses in different schemes can be found in the "Note on Quark Masses."

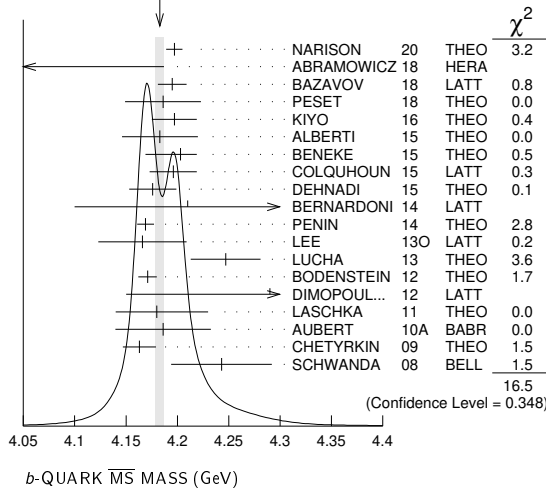
\overline{MS} MASS (GeV)	DOCUMENT ID	TECN
4.18 ± 0.03	OUR EVALUATION	of \overline{MS} Mass. See the ideogram below.
-0.02		
4.197 ± 0.008	¹ NARISON 20	THEO
4.049 + 0.138	² ABRAMOWICZ18	HERA
-0.118		
4.195 ± 0.014	³ BAZAVOV 18	LATT
4.186 ± 0.037	⁴ PESET 18	THEO
4.197 ± 0.022	⁵ KIYO 16	THEO
4.183 ± 0.037	⁶ ALBERTI 15	THEO
4.203 + 0.016	⁷ BENEKE 15	THEO
-0.034		
4.196 ± 0.023	⁸ COLQUHOUN 15	LATT
4.176 ± 0.023	⁹ DEHNADI 15	THEO
4.21 ± 0.11	¹⁰ BERNARDONI 14	LATT
4.169 ± 0.002 ± 0.008	¹¹ PENIN 14	THEO
4.166 ± 0.043	¹² LEE 130	LATT
4.247 ± 0.034	¹³ LUCHA 13	THEO
4.171 ± 0.009	¹⁴ BODENSTEIN 12	THEO
4.29 ± 0.14	¹⁵ DIMOP OUL... 12	LATT
4.18 + 0.05	¹⁶ LASCHKA 11	THEO
-0.04		
4.186 ± 0.044 ± 0.015	¹⁷ AUBERT 10A	BABR
4.163 ± 0.016	¹⁸ CHETYRKIN 09	THEO
4.243 ± 0.049	¹⁹ SCHWANDA 08	BELL
• • • We do not use the following data for averages, fits, limits, etc. • • •		
4.184 ± 0.011	²⁰ NARISON 18A	THEO
4.188 ± 0.008	²¹ NARISON 18B	THEO
4.07 ± 0.17	²² ABRAMOWICZ14A	ZEUS
4.201 ± 0.043	²³ AYALA 14A	THEO
4.236 ± 0.069	²⁴ NARISON 13	THEO
4.213 ± 0.059	²⁵ NARISON 13A	THEO
4.235 ± 0.003 ± 0.055	²⁶ HOANG 12	THEO
4.212 ± 0.032	²⁷ NARISON 12	THEO
4.177 ± 0.011	²⁸ NARISON 12	THEO
4.171 ± 0.014	²⁹ NARISON 12A	THEO
4.164 ± 0.023	³⁰ MCNEILE 10	LATT
4.173 ± 0.010	³¹ NARISON 10	THEO
5.26 ± 1.2	³² ABDALLAH 08D	DLPH
4.42 ± 0.06 ± 0.08	³³ GUAZZINI 08	LATT
4.347 ± 0.048 ± 0.08	³⁴ DELLA-MOR... 07	LATT
4.164 ± 0.025	³⁵ KUHN 07	THEO

Quark Particle Listings

b

4.19 ± 0.40	36	ABDALLAH	06D	DLPH
4.205 ± 0.058	37	BOUGHEZAL	06	THEO
4.20 ± 0.04	38	BUCHMUEL...	06	THEO
4.19 ± 0.06	39	PINEDA	06	THEO
4.4 ± 0.3	40	GRAY	05	LATT
4.22 ± 0.06	41	AUBERT	04X	THEO
4.17 ± 0.03	42	BAUER	04	THEO
4.22 ± 0.11	43	HOANG	04	THEO
4.25 ± 0.11	44	MCNEILE	04	LATT
4.22 ± 0.09	45	BAUER	03	THEO
4.19 ± 0.05	46	BORDES	03	THEO
4.20 ± 0.09	47	CORCELLA	03	THEO
4.33 ± 0.10	48	DEDIVITIS	03	LATT
4.24 ± 0.10	49	EIDEMULLER	03	THEO
4.207 ± 0.03	50	ERLER	03	THEO
4.33 ± 0.06 ± 0.10	51	MAHMOOD	03	CLEO
4.190 ± 0.032	52	BRAMBILLA	02	THEO
4.346 ± 0.070	53	PENIN	02	THEO

WEIGHTED AVERAGE
4.183 ± 0.004 (Error scaled by 1.0)



- 1 NARISON 20 determines the quark mass using QCD Laplace sum rules from the B_c mass, combined with previous determinations of the QCD condensates and c and b masses.
- 2 ABRAMOWICZ 18 determine $\overline{m}_b(\overline{m}_b) = 4.049^{+0.104+0.090+0.001}_{-0.109-0.032-0.031}$ from the production of b quarks in ep collisions at HERA using combined H1 and ZEUS data. The experimental/fitting errors, and those from modeling and parameterization have been combined in quadrature.
- 3 BAZAVOV 18 determine the b mass using a lattice computation with staggered fermions and five active quark flavors.
- 4 PESET 18 determine $\overline{m}_c(\overline{m}_c)$ and $\overline{m}_b(\overline{m}_b)$ using an N3LO calculation of the η_c , η_b and B_c masses.
- 5 KIYO 16 determine $\overline{m}_b(\overline{m}_b)$ from the $\Upsilon(1S)$ mass at order α_s^3 (N3LO).
- 6 ALBERTI 15 determine $\overline{m}_b(\overline{m}_b)$ from fits to inclusive $B \rightarrow X_c e \overline{\nu}$ decay. They also find $m_b^{\text{kin}}(1 \text{ GeV}) = 4.553 \pm 0.020 \text{ GeV}$.
- 7 BENEKE 15 determine $\overline{m}_b(\overline{m}_b)$ using sum rules for $e^+e^- \rightarrow$ hadrons at order N3LO including finite m_c effects. They find $m_b^{\text{PS}}(2 \text{ GeV}) = 4.532^{+0.013}_{-0.039} \text{ GeV}$, and $\overline{m}_b(\overline{m}_b) = 4.193^{+0.022}_{-0.035} \text{ GeV}$. The value quoted is obtained using the four-loop conversion given in BENEKE 16.
- 8 COLQUHOUN 15 determine $\overline{m}_b(\overline{m}_b)$ from moments of the vector current correlator computed with a lattice simulation using the NRQCD action.
- 9 DEHNADI 15 determine $\overline{m}_b(\overline{m}_b)$ using sum rules for $e^+e^- \rightarrow$ hadrons at order α_s^3 (N3LO), and fitting to both experimental data and lattice results.
- 10 BERNARDONI 14 determine m_b from $n_f = 2$ lattice calculations using heavy quark effective theory non-perturbatively renormalized and matched to QCD at $1/m$ order.
- 11 PENIN 14 determine $\overline{m}_b(\overline{m}_b) = 4.169 \pm 0.008 \pm 0.002 \pm 0.002$ using an estimate of the order α_s^3 b -quark vacuum polarization function in the threshold region, including finite m_c effects. The errors of ± 0.008 from theoretical uncertainties, and ± 0.002 from α_s have been combined in quadrature.
- 12 LEE 130 determines m_b using lattice calculations of the Υ and B_S binding energies in NRQCD, including three light dynamical quark flavors. The quark mass shift in NRQCD is determined to order α_s^2 , with partial α_s^3 contributions.
- 13 LUCHA 13 determines m_b from QCD sum rules for heavy-light currents using the lattice value for f_B of $191.5 \pm 7.3 \text{ GeV}$.
- 14 BODENSTEIN 12 determine m_b using sum rules for the vector current correlator and the $e^+e^- \rightarrow Q\overline{Q}$ total cross-section.
- 15 DIMOPOULOS 12 determine quark masses from a lattice computation using $n_f = 2$ dynamical flavors of twisted mass fermions.
- 16 LASCHKA 11 determine the b mass from the charmonium spectrum. The theoretical computation uses the heavy $Q\overline{Q}$ potential to order $1/m_Q$ obtained by matching the short-distance perturbative result onto lattice QCD result at larger scales.
- 17 AUBERT 10A determine the b - and c -quark masses from a fit to the inclusive decay spectra in semileptonic B decays in the kinetic scheme (and convert it to the \overline{MS} scheme).

- 18 CHETYRKIN 09 determine m_c and m_b from the $e^+e^- \rightarrow Q\overline{Q}$ cross-section and sum rules, using an order α_s^3 (N3LO) computation of the heavy quark vacuum polarization.
- 19 SCHWANDA 08 measure moments of the inclusive photon spectrum in $B \rightarrow X_S \gamma$ decay to determine m_b^{1S} . We have converted this to \overline{MS} scheme.
- 20 NARISON 18A determines $\overline{m}_b(\overline{m}_b)$ as a function of α_s using QCD exponential sum rules and their ratios evaluated at the optimal scale $\mu = 9.5 \text{ GeV}$ at N2LO-N3LO of perturbative QCD and including condensates up to dimension 6–8 in the (axial-)vector and (pseudo-)scalar bottomonium channels.
- 21 NARISON 18B determines $\overline{m}_b(\overline{m}_b)$ using QCD vector moment sum rules and their ratios at N2LO-N3LO of perturbative QCD and including condensates up to dimension 8.
- 22 ABRAMOWICZ 14A determine $\overline{m}_b(\overline{m}_b) = 4.07 \pm 0.14^{+0.01+0.05+0.08}_{-0.07-0.00-0.05}$ from the production of b quarks in ep collisions at HERA. The errors due to fitting, modeling, PDF parameterization, and theoretical QCD uncertainties due to the values of α_s , m_c , and the renormalization scale μ have been combined in quadrature.
- 23 AYALA 14A determine $\overline{m}_b(\overline{m}_b)$ from the $\Upsilon(1S)$ mass computed to N3LO order in perturbation theory using a renormalon subtracted scheme.
- 24 NARISON 13 determines m_b using QCD spectral sum rules to order α_s^2 (NNLO) and including condensates up to dimension 6.
- 25 NARISON 13A determines m_b using HQET sum rules to order α_s^2 (NNLO) and the B meson mass and decay constant.
- 26 HOANG 12 determine m_b using non-relativistic sum rules for the Υ system at order α_s^2 (NNLO) with renormalization group improvement.
- 27 NARISON 12 determine m_b using exponential sum rules for the vector current correlator to order α_s^3 , including the effect of gluon condensates up to dimension eight.
- 28 Determines m_b to order α_s^3 (N3LO), including the effect of gluon condensates up to dimension eight combining the methods of NARISON 12 and NARISON 12A.
- 29 NARISON 12A determine m_b using sum rules for the vector current correlator to order α_s^3 , including the effect of gluon condensates up to dimension eight.
- 30 MCNEILE 10 determines m_b by comparing order α_s^3 (N3LO) perturbative results for the pseudo-scalar current to lattice simulations with $n_f = 2+1$ sea-quarks by the HPQCD collaboration.
- 31 NARISON 10 determines m_b from ratios of moments of vector current correlators computed to order α_s^3 and including the dimension-six gluon condensate. These values are taken from the erratum to that reference.
- 32 ABDALLAH 08D determine $\overline{m}_b(M_Z) = 3.76 \pm 1.0 \text{ GeV}$ from a leading order study of four-jet rates at LEP.
- 33 GUAZZINI 08 determine $\overline{m}_b(\overline{m}_b)$ from a quenched lattice simulation of heavy meson masses. The ± 0.08 is an estimate of the quenching error.
- 34 DELLA-MORTE 07 determine $\overline{m}_b(\overline{m}_b)$ from a computation of the spin-averaged B meson mass using quenched lattice HQET at order $1/m$. The ± 0.08 is an estimate of the quenching error.
- 35 KUHNO 07 determine $\overline{m}_b(\mu = 10 \text{ GeV}) = 3.609 \pm 0.025 \text{ GeV}$ and $\overline{m}_b(\overline{m}_b)$ from a four-loop sum-rule computation of the cross-section for $e^+e^- \rightarrow$ hadrons in the bottom threshold region.
- 36 ABDALLAH 06D determine $m_b(M_Z) = 2.85 \pm 0.32 \text{ GeV}$ from Z -decay three-jet events containing a b -quark.
- 37 BOUGHEZAL 06 \overline{MS} scheme result comes from the first moment of the hadronic production cross-section to order α_s^3 .
- 38 BUCHMUELLER 06 determine m_b and m_c by a global fit to inclusive B decay spectra.
- 39 PINEDA 06 \overline{MS} scheme result comes from a partial NNLL evaluation (complete at order α_s^2 (NNLO)) of sum rules of the bottom production cross-section in e^+e^- annihilation.
- 40 GRAY 05 determines $\overline{m}_b(\overline{m}_b)$ from a lattice computation of the Υ spectrum. The simulations have $2+1$ dynamical light flavors. The b quark is implemented using NRQCD.
- 41 AUBERT 04x obtain m_b from a fit to the hadron mass and lepton energy distributions in semileptonic B decay. The paper quotes values in the kinetic scheme. The \overline{MS} value has been provided by the BABAR collaboration.
- 42 BAUER 04 determine m_b , m_c and $m_b - m_c$ by a global fit to inclusive B decay spectra.
- 43 HOANG 04 determines $\overline{m}_b(\overline{m}_b)$ from moments at order α_s^2 of the bottom production cross-section in e^+e^- annihilation.
- 44 MCNEILE 04 use lattice QCD with dynamical light quarks and a static heavy quark to compute the masses of heavy-light mesons.
- 45 BAUER 03 determine the b quark mass by a global fit to B decay observables. The experimental data includes lepton energy and hadron invariant mass moments in semileptonic $B \rightarrow X_c \ell \nu_\ell$ decay, and the inclusive photon spectrum in $B \rightarrow X_S \gamma$ decay. The theoretical expressions used are of order $1/m^3$, and $\alpha_s^2 \beta_0$.
- 46 BORDES 03 determines m_b using QCD finite energy sum rules to order α_s^2 .
- 47 CORCELLA 03 determines \overline{m}_b using sum rules computed to order α_s^2 . Includes charm quark mass effects.
- 48 DEDIVITIS 03 use a quenched lattice computation of heavy-heavy and heavy-light meson masses.
- 49 EIDEMULLER 03 determines \overline{m}_b and \overline{m}_c using QCD sum rules.
- 50 ERLER 03 determines \overline{m}_b and \overline{m}_c using QCD sum rules. Includes recent BES data.
- 51 MAHMOOD 03 determines m_b^{1S} by a fit to the lepton energy moments in $B \rightarrow X_c \ell \nu_\ell$ decay. The theoretical expressions used are of order $1/m^3$ and $\alpha_s^2 \beta_0$. We have converted their result to the \overline{MS} scheme.
- 52 BRAMBILLA 02 determine $\overline{m}_b(\overline{m}_b)$ from a computation of the $\Upsilon(1S)$ mass to order α_s^4 , including finite m_c corrections.
- 53 PENIN 02 determines \overline{m}_b from the spectrum of the Υ system.

 m_b/m_s MASS RATIO

VALUE	DOCUMENT ID	TECN
53.94 ± 0.12	¹ BAZAVOV	18 LATT

- ¹ BAZAVOV 18 determine the quark masses using a lattice computation with staggered fermions and four active quark flavors for the u , d , s , c quarks and five active flavors for the b quark.

b-QUARK REFERENCES

NARISON	20	PL B802 135221	S. Narison (MONP)
ABRAMOWICZ	18	EPJ C78 473	H. Abramowicz et al. (HI and ZEUS Collabs.)
BAZOV	18	PR D98 054517	A. Bazov et al. (Fermilab Lattice, MILC, TUMQCD)
NARISON	18A	UJP A33 1850045	S. Narison (MONP)
NARISON	18B	PL B784 261	S. Narison (MONP)
PESET	18	JHEP 1809 167	C. Peset, A. Pineda, J. Segovia (BARC, TUM)
BENEKE	16	PoS RADCOR2015 035	M. Beneke et al.
KIYO	16	PL B752 122	Y. Kiyo, G. Mishima, Y. Sumino
ALBERTI	15	PRL 114 061802	A. Alberti et al.
BENEKE	15	NP B991 42	M. Beneke et al.
COLQUHOUN	15	PR D91 074514	B. Colquhoun et al. (HPQCD Collab.)
DEHNADI	15	JHEP 1508 155	B. Dehnadi, A.H. Hoang, V. Mateu
ABRAMOWICZ	14A	JHEP 1409 127	H. Abramowicz et al. (ZEUS Collab.)
AYALA	14A	JHEP 1409 045	C. Ayala, G. Cvetcic, A. Pineda
BERNARDONI	14	PL B730 171	F. Bernardoni et al. (ALPHA Collab.)
PENIN	14	JHEP 1404 120	A.A. Penin, N. Zerf
LEE	13O	PR D87 074018	A.J. Lee et al. (HPQCD Collab.)
LUCHA	13	PR D88 056011	W. Lucha, D. Melnikov, S. Simula
NARISON	13	PL B718 1321	S. Narison (MONP)
NARISON	13A	PL B721 269	S. Narison (MONP)
BODENSTEIN	12	PR D85 034003	S. Bodenstein et al. (CAPE, VALE, MAINZ+)
DIMOPOULOS	12	JHEP 1201 046	P. Dimopoulos et al. (ETM Collab.)
HOANG	12	JHEP 1210 188	A.H. Hoang, P. Ruiz-Femenia, M. Stahlfhofen (WIEN+)
NARISON	12	PL B707 259	S. Narison (MONP)
NARISON	12A	PL B706 412	S. Narison (MONP)
LASCHKA	11	PR D83 094002	A. Laschka, N. Kaiser, W. Weise
AUBERT	10A	PR D81 032003	B. Aubert et al. (BABAR Collab.)
MCNEILE	10	PR D82 034512	C. McNeile et al. (HPQCD Collab.)
NARISON	10	PL B693 559	S. Narison (MONP)
Also		PL B705 544 (errata.)	S. Narison (MONP)
CHETRYKIN	09	PR D80 074010	K.C. Cheykin et al. (KARL, BNL)
ABDALLAH	08D	EPJ C55 525	J. Abdallah et al. (DELPHI Collab.)
GUZZINI	08	JHEP 0801 076	D. Guzzini, R. Sommer, N. Tantalo
SCHWANDA	08	PR D78 032016	C. Schwanda et al. (BELLE Collab.)
DELLA-MOR	07	JHEP 0701 007	M. Della Morte et al.
KUHN	07	NP B778 192	J.H. Kuhn, M. Steinhauser, C. Sturm
ABDALLAH	06D	EPJ C46 569	J. Abdallah et al. (DELPHI Collab.)
BOUGHEZAL	06	PR D74 074006	R. Boughezal, M. Czakon, T. Schutzmeier
BUCHMUELLER	06	PR D73 073008	O.L. Buchmueller, H.U. Flacher (RHBL)
PINEDA	06	PR D73 111501	A. Pineda, A. Signer
GRAY	05	PR D72 094507	A. Gray et al. (HPQCD and UKQCD Collab.)
AUBERT	04X	PRL 93 011803	B. Aubert et al. (BABAR Collab.)
BAUER	04	PR D70 094017	C. Bauer et al.
HOANG	04	PL B594 127	A.H. Hoang, M. Jamin
MCNEILE	04	PL B600 77	C. McNeile, C. Michael, G. Thompson (UKQCD Collab.)
BAUER	03	PR D67 054012	C.W. Bauer et al.
BORDES	03	PL B562 81	J. Bordes, J. Penarrocha, K. Schilcher
CORCELLA	03	PL B554 133	G. Corcella, A.H. Hoang
DEDIVITIIS	03	NP B675 309	G.M. de Divitiis et al.
EIDEMULLER	03	PR D67 113002	M. Eidemuller
ERLER	03	PL B558 125	J. Erler, M. Luo
MAHMOOD	03	PR D67 072001	A.H. Mahmood et al. (CLEO Collab.)
BRAMBILLA	02	PR D65 034001	N. Brambilla, Y. Sumino, A. Vairo
PENIN	02	PL B538 335	A. Penin, M. Steinhauser

$I(J^P) = 0(\frac{1}{2}^+)$
 Charge = $\frac{2}{3} e$ Top = +1

See the related review(s):
 Top Quark

t-QUARK MASS

We first list the direct measurements of the top quark mass which employ the event kinematics and then list the measurements which extract a top quark mass from the measured $t\bar{t}$ cross-section using theory calculations. A discussion of the definition of the top quark mass in these measurements can be found in the review "The Top Quark."

For earlier search limits see PDG 96, Physical Review **D54** 1 (1996). We no longer include a compilation of indirect top mass determinations from Standard Model Electroweak fits in the Listings (our last compilation can be found in the Listings of the 2007 partial update). For a discussion of current results see the reviews "The Top Quark" and "Electroweak Model and Constraints on New Physics."

t-Quark Mass (Direct Measurements)

The following measurements extract a t -quark mass from the kinematics of $t\bar{t}$ events. They are sensitive to the top quark mass used in the MC generator that is usually interpreted as the pole mass, but the theoretical uncertainty in this interpretation is hard to quantify. See the review "The Top Quark" and references therein for more information.

OUR AVERAGE of 172.69 ± 0.30 GeV is an average of top mass measurements from LHC and Tevatron Runs. The latest Tevatron average, $174.30 \pm 0.35 \pm 0.54$ GeV, was provided by the Tevatron Electroweak Working Group (TEVEWWG).

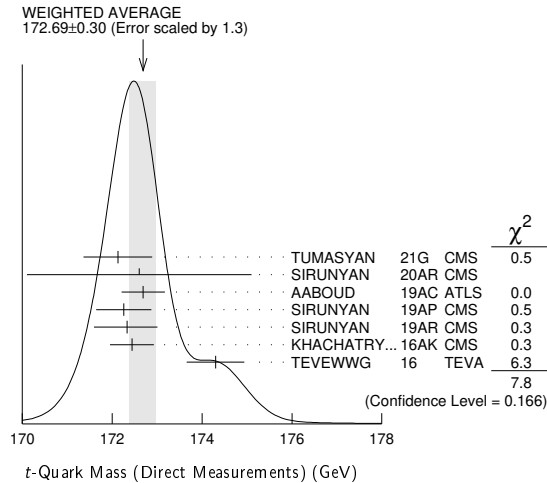
VALUE (GeV)	DOCUMENT ID	TECN	COMMENT
172.69± 0.30 OUR AVERAGE			Error includes scale factor of 1.3. See the ideogram below.
172.13 ^{+0.76} _{-0.77}	1	TUMASYAN 21G CMS	t -channel single top production
172.6 ± 2.5	2	SIRUNYAN 20AR CMS	jet mass from boosted top
172.69 ± 0.25 ± 0.41	3	AABOUD 19AC ATLS	7, 8 TeV ATLAS combination
172.26 ± 0.07 ± 0.61	4	SIRUNYAN 19AP CMS	lepton+jets, all-jets channels
172.33 ± 0.14 ^{+0.66} _{-0.72}	5	SIRUNYAN 19AR CMS	dilepton channel ($e\mu$, $2e$, 2μ)
172.44 ± 0.13 ± 0.47	6	KHACHATRY...16AK CMS	7, 8 TeV CMS combination
174.30 ± 0.35 ± 0.54	7	TEVEWWG 16 TEVA	Tevatron combination
• • • We do not use the following data for averages, fits, limits, etc. • • •			
172.08 ± 0.39 ± 0.82	8	AABOUD 19AC ATLS	$\ell + \geq 4j$ ($2b$)
172.34 ± 0.20 ± 0.70	9	SIRUNYAN 19AP CMS	≥ 6 jets ($\geq 2b$)
172.25 ± 0.08 ± 0.62	10	SIRUNYAN 18DE CMS	$\ell + \geq 4j$ ($2b$)

173.72 ± 0.55 ± 1.01	11	AABOUD 17AH ATLS	≥ 5 jets ($2b$)
174.95 ± 0.40 ± 0.64	12	ABAZOV 17B D0	$\ell +$ jets and dilepton channels
172.95 ± 0.77 ⁺ _{-0.93}	13	SIRUNYAN 17L CMS	t -channel single top production
170.8 ± 9.0	14	SIRUNYAN 17N CMS	jet mass in highly-boosted $t\bar{t}$ events
172.22 ± 0.18 ⁺ _{-0.93}	15	SIRUNYAN 17O CMS	Dilepton channel
172.99 ± 0.41 ± 0.74	16	AABOUD 16T ATLS	dilepton channel
172.84 ± 0.34 ± 0.61	17	AABOUD 16T ATLS	combination of ATLAS
173.32 ± 1.36 ± 0.85	18	ABAZOV 16 D0	$\ell\ell + \cancel{E}_T + \geq 2j$ ($\geq 2b$)
173.93 ± 1.61 ± 0.88	19	ABAZOV 16D D0	$\ell\ell + \cancel{E}_T + \geq 2j$ ($\geq 2b$)
172.35 ± 0.16 ± 0.48	20,21	KHACHATRY...16AK CMS	$\ell + \geq 4j$ ($2b$)
172.32 ± 0.25 ± 0.59	20,21	KHACHATRY...16AK CMS	≥ 6 jets ($2b$)
172.82 ± 0.19 ± 1.22	20,22	KHACHATRY...16AK CMS	$(ee/\mu\mu) + \cancel{E}_T + \geq 2b, e\mu + \geq 2b$
173.68 ± 0.20 ⁺ _{-0.97}	23	KHACHATRY...16CB CMS	semi- + di-lepton channels
173.5 ± 3.0 ± 0.9	24	KHACHATRY...16CB CMS	$t \rightarrow (W \rightarrow \ell\nu)(b \rightarrow J/\psi X \rightarrow \mu^+\mu^-X)$ small \cancel{E}_T , ≥ 6 jets ($2b$ -tag)
175.1 ± 1.4 ± 1.2	25	AAD 15AW ATLS	$\ell +$ jets and dilepton
172.99 ± 0.48 ± 0.78	26	AAD 15BF ATLS	$\ell\ell + \cancel{E}_T + \geq 2j$
171.5 ± 1.9 ± 2.5	27	AALTONEN 15D CDF	small \cancel{E}_T , 6–8 jets ($\geq 1b$ -tag)
175.07 ± 1.19 ⁻ _{-1.58}	28	AALTONEN 14N CDF	$\ell + \cancel{E}_T + 4$ jets ($\geq 1 b$ -tag)
174.98 ± 0.58 ± 0.49	29	ABAZOV 14C D0	≥ 6 jets ($\geq 2 b$ -tag)
173.49 ± 0.69 ± 1.21	30	CHATRCHYAN 14C CMS	$\cancel{E}_T + \geq 4$ jets ($\geq 1 b$)
173.93 ± 1.64 ± 0.87	31	AALTONEN 13H CDF	$\ell\ell + \cancel{E}_T + \geq 2b$ -tag (MT2(T))
173.9 ± 0.9 ± 1.7	32	CHATRCHYAN 13S CMS	$\ell + \cancel{E}_T + \geq 4j$ ($\geq 1 b$), MT
174.5 ± 0.6 ± 2.3	33	AAD 12I ATLS	$\cancel{E}_T + \cancel{E}_T + \geq 4j$ (0,1,2b) template
172.85 ± 0.71 ± 0.85	34	AALTONEN 12AI CDF	$\tau_h + \cancel{E}_T + 4j$ ($\geq 1b$)
172.7 ± 9.3 ± 3.7	35	AALTONEN 12AL CDF	CD, D0 combination
173.18 ± 0.56 ± 0.75	36	AALTONEN 12AP TEVA	6–8 jets with $\geq 1 b$
172.5 ± 1.4 ± 1.5	37	AALTONEN 12G CDF	$\ell\ell + \cancel{E}_T + \geq 2j$ (ν WT+MWT)
173.7 ± 2.8 ± 1.5	38	ABAZOV 12AB D0	$\ell\ell + \cancel{E}_T + \geq 2j$ ($\geq 1b$), AMWT
173.9 ± 1.9 ± 1.6	39	ABAZOV 12AB D0	$\ell + \cancel{E}_T + \geq 4j$ ($\geq 2b$)
172.5 ± 0.4 ± 1.5	40	CHATRCHYAN 12BA CMS	$\ell + \cancel{E}_T + 4$ jets ($\geq 1 b$ -tag)
173.49 ± 0.43 ± 0.98	41	CHATRCHYAN 12BP CMS	Repl. by AALTONEN 13H
172.4 ± 1.4 ± 1.3	42	AALTONEN 11AC CDF	$\ell +$ jets and dilepton
172.3 ± 2.4 ± 1.0	43	AALTONEN 11AK CDF	$\ell + \cancel{E}_T + 4$ jets ($\geq 1 b$ -tag), $\rho_{T}(\ell)$ shape
172.1 ± 1.1 ± 0.9	44	AALTONEN 11E CDF	$\ell + \cancel{E}_T + 4$ jets ($\geq 1 b$ -tag)
176.9 ± 8.0 ± 2.7	45	AALTONEN 11T CDF	$\ell + \cancel{E}_T + 4$ jets ($\geq 1 b$ -tag)
174.94 ± 0.83 ± 1.24	46	ABAZOV 11P D0	dilepton + $\cancel{E}_T + \geq 2$ jets
174.0 ± 1.8 ± 2.4	47	ABAZOV 11R D0	dilepton + $\cancel{E}_T +$ jets
175.5 ± 4.6 ± 4.6	48	CHATRCHYAN 11AF CMS	$\ell + \cancel{E}_T + 4$ jets ($\geq 1 b$ -tag), ME method
173.0 ± 0.9 ± 0.9	49	AALTONEN 10AE CDF	dilepton + b -tag (MT2+NWA)
169.3 ± 2.7 ± 3.2	50	AALTONEN 10C CDF	$\ell + \cancel{E}_T + 4$ jets (b -tag)
170.7 ± 6.3 ± 2.6	51	AALTONEN 10D CDF	≥ 6 jets, vtx b -tag
174.8 ± 2.4 ⁺ _{-1.0}	52	AALTONEN 10E CDF	$\ell + \cancel{E}_T +$ jets (soft μ b -tag)
180.5 ± 12.0 ± 3.6	53	AALTONEN 09AK CDF	$\ell + \cancel{E}_T + 4$ jets (b -tag)
172.7 ± 1.8 ± 1.2	54	AALTONEN 09J CDF	6 jets, vtx b -tag
171.1 ± 3.7 ± 2.1	55	AALTONEN 09K CDF	$\ell +$ jets, $\ell\ell +$ jets
171.9 ± 1.7 ± 1.1	56	AALTONEN 09L CDF	dilepton
171.2 ± 2.7 ± 2.9	57	AALTONEN 09O CDF	$\ell\ell + \cancel{E}_T$ ($\nu\phi$ weighting)
165.5 ^{+3.4} _{-3.3}	58	AALTONEN 09X CDF	dilepton + b -tag (ν WT+MWT)
174.7 ± 4.4 ± 2.0	59	ABAZOV 09AH D0	dilepton, $\sigma_{T\bar{T}}$ constrained
170.7 ⁺ _{-3.9} ± 3.5	60,61	AALTONEN 08C CDF	$\ell + \cancel{E}_T + 4$ jets
171.5 ± 1.8 ± 1.1	62	ABAZOV 08AH D0	6 jets with $\geq 1 b$ vtx
177.1 ± 4.9 ± 4.7	63,64	AALTONEN 07 CDF	≥ 4 jets (b -tag)
172.3 ^{-10.8} _{-9.6} ± 10.8	65	AALTONEN 07B CDF	≥ 6 jets, vtx b -tag
174.0 ± 2.2 ± 4.8	66	AALTONEN 07D CDF	lepton + jets (b -tag)
170.8 ± 2.2 ± 1.4	67,68	AALTONEN 07I CDF	lepton + jets
173.7 ± 4.4 ⁺ _{-2.0} ± 3.9	64,69	ABAZOV 07F D0	dilepton (MWT)
176.2 ± 9.2 ± 3.9	70	ABAZOV 07W D0	dilepton (ν WT)
179.5 ± 7.4 ± 5.6	70	ABAZOV 07W D0	dilepton
164.5 ± 3.9 ± 3.9	68,71	ABULENCIA 07D CDF	lepton + jets
180.7 ^{+15.5} _{-13.4} ± 8.6	72	ABULENCIA 07J CDF	lepton + jets (b -tag)
170.3 ± 4.1 ⁺ _{-4.5} ± 1.2 ⁻ _{-1.8}	68,73	ABAZOV 06U D0	lepton + jets
173.2 ± 2.6 ⁺ _{-2.4} ± 3.2	74,75	ABULENCIA 06D CDF	lepton + jets
173.5 ± 3.7 ⁻ _{-3.6} ± 1.3	61,74	ABULENCIA 06D CDF	dilepton
165.2 ± 6.1 ± 3.4	68,76	ABULENCIA 06G CDF	dilepton
170.1 ± 6.0 ± 4.1	61,77	ABULENCIA 06V CDF	6 or more jets
178.5 ± 13.7 ± 7.7	78,79	ABAZOV 05 D0	lepton + jets
180.1 ± 3.6 ± 3.9	80,81	ABAZOV 04G D0	lepton + jets
176.1 ± 5.1 ± 5.3	82	AFFOLDER 01 CDF	dilepton, lepton+jets, all-jets
176.1 ± 6.6	83	AFFOLDER 01 CDF	di-lepton, lepton+jets
172.1 ± 5.2 ± 4.9	84	ABBOTT 99G D0	dilepton, lepton+jets, all-jets
176.0 ± 6.5	85,86	ABE 99B CDF	dilepton
167.4 ± 10.3 ± 4.8	86,87	ABE 99B CDF	dilepton
168.4 ± 12.3 ± 3.6	81	ABBOTT 98D D0	lepton + jets
173.3 ± 5.6 ± 5.5	81,88	ABBOTT 98F D0	lepton + jets
175.9 ± 4.8 ± 5.3	87,89	ABE 98E CDF	lepton + jets

Quark Particle Listings

t

161	± 17	± 10	87	ABE	98F	CDF	dilepton
172.1	± 5.2	± 4.9	90	BHAT	98B	RVUE	dilepton and lepton+jets
173.8	± 5.0		91	BHAT	98B	RVUE	dilepton, lepton+jets, all-jets
173.3	± 5.6	± 6.2	81	ABACHI	97E	D0	lepton + jets
186	± 10	± 5.7	87,92	ABE	97R	CDF	6 or more jets
199	± 19	± 22		ABACHI	95	D0	lepton + jets
176	± 8	± 10		ABE	95F	CDF	lepton + b-jet
174	± 10	± 13		ABE	94E	CDF	lepton + b-jet



- 1 TUMASYAN 21G based on 35.9 fb⁻¹ of pp data at $\sqrt{s} = 13$ TeV. Events are selected by requiring 1 ℓ + 2jets(1b jet) final state.
- 2 SIRUNYAN 20AR based on 35.9 fb⁻¹ of pp data at $\sqrt{s} = 13$ TeV. The products of the hadronic decay of a top quark with $p_T > 400$ GeV, in the ℓ + jets channel of $t\bar{t}$ are reconstructed as a single jet. The top quark mass is determined from the normalized differential cross section measurement in the m_{jet} distribution.
- 3 AABOUD 19AC is an ATLAS combination of 7 and 8 TeV top-quark mass determination in the dilepton, lepton + jets, and all jets channels.
- 4 SIRUNYAN 19AP based on 35.9 fb⁻¹ of pp data at $\sqrt{s} = 13$ TeV. A combined measurement using the lepton+jets and all-jets channels through a single likelihood function. See SIRUNYAN 18DE and SIRUNYAN 19AP below.
- 5 SIRUNYAN 19AR based on 35.9 fb⁻¹ of pp data at $\sqrt{s} = 13$ TeV. Obtained from a simultaneous fit of the cross section and the top quark mass in the POWHEG simulation. The cross section is used also to extract the M_S mass and the strong coupling constant for different PDF sets.
- 6 KHACHATRYAN 16AK based on 19.7 fb⁻¹ of pp data at $\sqrt{s} = 8$ TeV. Combination of the three top mass measurements in KHACHATRYAN 16AK and with the CMS results at $\sqrt{s} = 7$ TeV.
- 7 TEVEWWG 16 is the latest Tevatron average (July 2016) provided by the Tevatron Electroweak Working Group. It takes correlated uncertainties into account and has a χ^2 of 10.8 for 11 degrees of freedom.
- 8 AABOUD 19AC based on 20.2 fb⁻¹ in pp collisions at $\sqrt{s} = 8$ TeV. Uses optimized event selection to suppress less-well-reconstructed events and template fits to determine m_t together with a global jet energy scale factor and a relative b-to-light-jet energy scale factor.
- 9 SIRUNYAN 19AP based on 35.9 fb⁻¹ of pp data at $\sqrt{s} = 13$ TeV. A kinematical fit is applied to each event assuming the signal event topology. m_t is determined simultaneously with a jet energy scale factor (JES). The second error represents stat.+JES. Modeling uncertainties are larger than in the measurements at $\sqrt{s} = 7$ and 8 TeV because of the use of new alternative color reconnection models.
- 10 SIRUNYAN 18DE based on 35.9 fb⁻¹ of pp data at $\sqrt{s} = 13$ TeV. m_t is determined simultaneously with an overall jet energy scale factor constrained by the mass of the hadronically decayed W. Compared to the Run 1 analysis a more advanced treatment of modeling uncertainties are employed, in particular concerning color-reconnection models.
- 11 AABOUD 17AH based on 20.2 fb⁻¹ of pp data at $\sqrt{s} = 8$ TeV. Uses template fits to the ratio of the masses of three-jets (from t candidate) and dijets (from W candidate), to suppress jet energy scale uncertainty. Large QCD background is modelled using a data-driven method.
- 12 ABAZOV 17B is a combination of measurements of the top quark mass by D0 in the lepton+jets and dilepton channels, using all data collected in Run I (1992-1996) at $\sqrt{s} = 1.8$ TeV and Run II (2001-2011) at $\sqrt{s} = 1.96$ TeV of the Tevatron, corresponding to integrated luminosities of 0.1 fb⁻¹ and 9.7 fb⁻¹, respectively.
- 13 SIRUNYAN 17L based on 19.7 fb⁻¹ of pp data at $\sqrt{s} = 8$ TeV. m_t is reconstructed from a fit to the invariant mass distribution of $\mu\nu b$, where p_T^{miss} and W mass constraint are used to reconstruct ν momentum. The number of events for various contributions, except for the t-channel single top one, are fixed to the values extracted from simulation. Superseded by TUMASYAN 21G.
- 14 SIRUNYAN 17N based on 19.7 fb⁻¹ of pp data at $\sqrt{s} = 8$ TeV. The fully hadronic decay of a highly-boosted t is reconstructed in the ℓ +jets channel and unfolded at the particle level. The sensitivity of the peak position of the m_{jet} distribution is used to test quality of the modelling by the simulation.
- 15 SIRUNYAN 17O based on 19.7 fb⁻¹ of pp data at $\sqrt{s} = 8$ TeV. Analysis is based on the kinematical observables $M(b\ell)$, M_{T2} and $M(b\ell\nu)$. A fit is performed to determine m_t and an overall jet energy scale factor simultaneously.
- 16 AABOUD 16T based on 20.2 fb⁻¹ of pp data at $\sqrt{s} = 8$ TeV. The analysis is refined using the p_T and invariant mass distributions of ℓ +b-jet system. A combination with measurements from $\sqrt{s} = 7$ TeV data in the dilepton and lepton+jets channels gives $172.84 \pm 0.34 \pm 0.61$ GeV.

- 17 AABOUD 16T is an ATLAS combination of 8 TeV top-quark mass in the dilepton channel with previous measurements from $\sqrt{s} = 7$ TeV data in the dilepton and lepton + jets channels.
- 18 ABAZOV 16 based on 9.7 fb⁻¹ of data in p \bar{p} collisions at $\sqrt{s} = 1.96$ TeV. Employs improved fit to minimize statistical errors and improved jet energy calibration, using lepton + jets mode, which reduces error of jet energy scale. Based on previous determination in ABAZOV 12AB with increased integrated luminosity and improved fit and calibrations.
- 19 ABAZOV 16D based on 9.7 fb⁻¹ of data in p \bar{p} collisions at $\sqrt{s} = 1.96$ TeV, using the matrix element technique. Based on previous determination in ABAZOV 11R with increased integrated luminosity. There is a strong correlation with the determination in ABAZOV 16. (See ABAZOV 17B.)
- 20 KHACHATRYAN 16AK based on 19.7 fb⁻¹ of pp data at $\sqrt{s} = 8$ TeV. Combination of the three top mass measurements in KHACHATRYAN 16AK and with the CMS results at $\sqrt{s} = 7$ TeV gives $172.44 \pm 0.13 \pm 0.47$ GeV.
- 21 The top mass and jet energy scale factor are determined by a fit.
- 22 Uses the analytical matrix weighting technique method.
- 23 KHACHATRYAN 16AL based on 19.7 fb⁻¹ in pp collisions at $\sqrt{s} = 8$ TeV. Determined from the invariant mass distribution of leptons and reconstructed secondary vertices from b decays using only charged particles. The uncertainty is dominated by modeling of b fragmentation and top p_T distribution.
- 24 KHACHATRYAN 16CB based on 666 candidate reconstructed events corresponding to 19.7 fb⁻¹ of pp data at $\sqrt{s} = 8$ TeV. The measurement exploits correlation of m_t with $M(J/\psi\ell)$ in the same top quark decay, using a high-purity event sample. A study on modeling of b-quark fragmentation is given in Sec.3.3.
- 25 AAD 15AW based on 4.6 fb⁻¹ of pp data at $\sqrt{s} = 7$ TeV. Uses template fits to the ratio of the masses of three-jets (from t candidate) and dijets (from W candidate). Large background from multijet production is modeled with data-driven methods.
- 26 AAD 15BF based on 4.6 fb⁻¹ in pp collisions at $\sqrt{s} = 7$ TeV. Using a three-dimensional template likelihood technique the lepton plus jets ($\geq 1b$ -tagged) channel gives $172.33 \pm 0.75 \pm 1.02$ GeV, while exploiting a one dimensional template method using $m_{\ell\ell}$ the dilepton channel (1 or 2b-tags) gives $173.79 \pm 0.54 \pm 1.30$ GeV. The results are combined.
- 27 AALTONEN 15D based on 9.1 fb⁻¹ of p \bar{p} data at $\sqrt{s} = 1.96$ TeV. Uses a template technique to fit a distribution of a variable defined by a linear combination of variables sensitive and insensitive to jet energy scale to optimize reduction of systematic errors. b-tagged and non-b-tagged events are separately analyzed and combined.
- 28 Based on 9.3 fb⁻¹ of p \bar{p} data at $\sqrt{s} = 1.96$ TeV. Multivariate algorithm is used to discriminate signal from backgrounds, and templates are used to measure m_t .
- 29 Based on 9.7 fb⁻¹ of p \bar{p} data at $\sqrt{s} = 1.96$ TeV. A matrix element method is used to calculate the probability of an event to be signal or background, and the overall jet energy scale is constrained *in situ* by m_W . See ABAZOV 15G for further details.
- 30 Based on 3.54 fb⁻¹ of pp data at $\sqrt{s} = 7$ TeV. The mass is reconstructed for each event employing a kinematical fit of the jets to a ttbar hypothesis. The combination with the previous CMS measurements in the dilepton and the lepton+jets channels gives $173.54 \pm 0.33 \pm 0.96$ GeV.
- 31 Based on 8.7 fb⁻¹ in p \bar{p} collisions at $\sqrt{s} = 1.96$ TeV. Events with an identified charged lepton or small E_T are rejected from the event sample, so that the measurement is statistically independent from those in the ℓ + jets and all hadronic channels while being sensitive to those events with a τ lepton in the final state.
- 32 Based on 5.0 fb⁻¹ of pp data at $\sqrt{s} = 7$ TeV. CHATRCHYAN 13s studied events with di-lepton + $E_T > 2$ b-jets, and looked for kinematical endpoints of MT2, MT2_T, and subsystem variables.
- 33 AAD 12t based on 1.04 fb⁻¹ of pp data at $\sqrt{s} = 7$ TeV. Uses 2d-template analysis (MT) with m_t and jet energy scale factor (JES) from m_W mass fit.
- 34 Based on 8.7 fb⁻¹ of data in p \bar{p} collisions at 1.96 TeV. The JES is calibrated by using the dijet mass from the W boson decay.
- 35 Use the ME method based on 2.2 fb⁻¹ of data in p \bar{p} collisions at 1.96 TeV.
- 36 Combination based on up to 5.8 fb⁻¹ of data in p \bar{p} collisions at 1.96 TeV.
- 37 Based on 5.8 fb⁻¹ of data in p \bar{p} collisions at 1.96 TeV the quoted value is $m_t = 172.5 \pm 1.4(\text{stat}) \pm 1.0(\text{JES}) \pm 1.1(\text{syst})$ GeV. The measurement is performed with a likelihood fit technique which simultaneously determines m_t and JES (Jet Energy Scale).
- 38 Based on 4.3 fb⁻¹ of data in p-pbar collisions at 1.96 TeV. The measurement reduces the JES uncertainty by using the single lepton channel study of ABAZOV 11P.
- 39 Combination with the result in 1 fb⁻¹ of preceding data reported in ABAZOV 09AH as well as the MWT result of ABAZOV 11R with a statistical correlation of 60%.
- 40 Based on 5.0 fb⁻¹ of pp data at $\sqrt{s} = 7$ TeV. Uses an analytical matrix weighting technique (AMWT) and full kinematic analysis (KIN).
- 41 Based on 5.0 fb⁻¹ of pp data at $\sqrt{s} = 7$ TeV. The first error is statistical and JES combined, and the second is systematic. Ideogram method is used to obtain 2D likelihood for the kinematical fit with two parameters mtop and JES.
- 42 Based on 3.2 fb⁻¹ in p \bar{p} collisions at $\sqrt{s} = 1.96$ TeV. The first error is from statistics and JES combined, and the latter is from the other systematic uncertainties. The result is obtained using an unbinned maximum likelihood method where the top quark mass and the JES are measured simultaneously, with $\Delta_{JES} = 0.3 \pm 0.3(\text{stat})$.
- 43 Based on 5.7 fb⁻¹ in p \bar{p} collisions at $\sqrt{s} = 1.96$ TeV. Events with an identified charged lepton or small E_T are rejected from the event sample, so that the measurement is statistically independent from those in the ℓ + jets and all hadronic channels while being sensitive to those events with a τ lepton in the final state. Supersedes AALTONEN 07B.
- 44 AALTONEN 11E based on 5.6 fb⁻¹ in p \bar{p} collisions at $\sqrt{s} = 1.96$ TeV. Employs a multi-dimensional template likelihood technique where the lepton plus jets (one or two b-tags) channel gives $172.2 \pm 1.2 \pm 0.9$ GeV while the dilepton channel yields $170.3 \pm 2.0 \pm 3.1$ GeV. The results are combined. OUR EVALUATION includes the measurement in the dilepton channel only.
- 45 Uses a likelihood fit of the lepton p_T distribution based on 2.7 fb⁻¹ in p \bar{p} collisions at $\sqrt{s} = 1.96$ TeV.
- 46 Based on 3.6 fb⁻¹ in p \bar{p} collisions at $\sqrt{s} = 1.96$ TeV. ABAZOV 11P reports $174.94 \pm 0.83 \pm 0.78 \pm 0.96$ GeV, where the first uncertainty is from statistics, the second from JES, and the last from other systematic uncertainties. We combine the JES and systematic uncertainties. A matrix-element method is used where the JES uncertainty is constrained by the W mass. ABAZOV 11P describes a measurement based on 2.6 fb⁻¹ that is combined with ABAZOV 08AH, which employs an independent 1 fb⁻¹ of data.
- 47 Based on a matrix-element method which employs 5.4 fb⁻¹ in p \bar{p} collisions at $\sqrt{s} = 1.96$ TeV. Superseded by ABAZOV 12AB.
- 48 Based on 36 pb⁻¹ of pp collisions at $\sqrt{s} = 7$ TeV. A Kinematic Method using b-tagging and an analytical Matrix Weighting Technique give consistent results and are combined. Superseded by CHATRCHYAN 12BA.

- 49 Based on 5.6 fb^{-1} in $p\bar{p}$ collisions at $\sqrt{s} = 1.96 \text{ TeV}$. The likelihood calculated using a matrix element method gives $m_t = 173.0 \pm 0.7(\text{stat}) \pm 0.6(\text{JES}) \pm 0.9(\text{syst}) \text{ GeV}$, for a total uncertainty of 1.2 GeV.
- 50 Based on 3.4 fb^{-1} of $p\bar{p}$ collisions at $\sqrt{s} = 1.96 \text{ TeV}$. The result is obtained by combining the MT2 variable method and the NWA (Neutrino Weighting Algorithm). The MT2 method alone gives $m_t = 168.0^{+4.8}_{-4.0}(\text{stat}) \pm 2.9(\text{syst}) \text{ GeV}$ with smaller systematic error due to small JES uncertainty.
- 51 Based on 1.9 fb^{-1} in $p\bar{p}$ collisions at $\sqrt{s} = 1.96 \text{ TeV}$. The result is from the measurement using the transverse decay length of b -hadrons and that using the transverse momentum of the W decay muons, which are both insensitive to the JES (jet energy scale) uncertainty. OUR EVALUATION uses only the measurement exploiting the decay length significance which yields $166.9^{+9.5}_{-8.5}(\text{stat}) \pm 2.9(\text{syst}) \text{ GeV}$. The measurement that uses the lepton transverse momentum is excluded from the average because of a statistical correlation with other samples.
- 52 Based on 2.9 fb^{-1} of $p\bar{p}$ collisions at $\sqrt{s} = 1.96 \text{ TeV}$. The first error is from statistics and JES uncertainty, and the latter is from the other systematics. Neural-network-based kinematical selection of 6 highest E_{Tj} jets with a vtx b -tag is used to distinguish signal from background. Superseded by AALTONEN 12G.
- 53 Based on 2 fb^{-1} of data at $\sqrt{s} = 1.96 \text{ TeV}$. The top mass is obtained from the measurement of the invariant mass of the lepton (e or μ) from W decays and the soft μ in b -jet. The result is insensitive to jet energy scaling.
- 54 Based on 1.9 fb^{-1} of data at $\sqrt{s} = 1.96 \text{ TeV}$. The first error is from statistics and jet energy scale uncertainty, and the latter is from the other systematics. Matrix element method with effective propagators.
- 55 Based on 943 pb^{-1} of data at $\sqrt{s} = 1.96 \text{ TeV}$. The first error is from statistical and jet-energy-scale uncertainties, and the latter is from other systematics. AALTONEN 09K selected 6 jet events with one or more vertex b -tags and used the tree-level matrix element to construct template models of signal and background.
- 56 Based on 1.9 fb^{-1} of data at $\sqrt{s} = 1.96 \text{ TeV}$. The first error is from statistical and jet-energy-scale (JES) uncertainties, and the second is from other systematics. Events with lepton + jets and those with dilepton + jets were simultaneously fit to constrain m_t and JES. Lepton + jets data only give $m_t = 171.8 \pm 2.2 \text{ GeV}$, and dilepton data only give $m_t = 171.2^{+5.3}_{-5.1} \text{ GeV}$.
- 57 Based on 2 fb^{-1} of data at $\sqrt{s} = 1.96 \text{ TeV}$. Matrix Element method. Optimal selection criteria for candidate events with two high p_{Tj} leptons, high E_{Tj} , and two or more jets with and without b -tag are obtained by neural network with neuroevolution technique to minimize the statistical error of m_t .
- 58 Based on 2.9 fb^{-1} of data at $\sqrt{s} = 1.96 \text{ TeV}$. Mass m_t is estimated from the likelihood for the eight-fold kinematical solutions in the plane of the azimuthal angles of the two neutrino momenta.
- 59 Based on 1 fb^{-1} of data at $\sqrt{s} = 1.96 \text{ TeV}$. Events with two identified leptons, and those with one lepton plus one isolated track and a b -tag were used to constrain m_t . The result is a combination of the μ WT (μ Weighting Technique) result of $176.2 \pm 4.8 \pm 2.1 \text{ GeV}$ and the MWT (Matrix-element Weighting Technique) result of $173.2 \pm 4.9 \pm 2.0 \text{ GeV}$.
- 60 Reports measurement of $170.7^{+4.2}_{-3.9} \pm 2.6 \pm 2.4 \text{ GeV}$ based on 1.2 fb^{-1} of data at $\sqrt{s} = 1.96 \text{ TeV}$. The last error is due to the theoretical uncertainty on $\sigma_{t\bar{t}}$. Without the cross-section constraint a top mass of $169.7^{+5.2}_{-4.9} \pm 3.1 \text{ GeV}$ is obtained.
- 61 Template method.
- 62 Result is based on 1 fb^{-1} of data at $\sqrt{s} = 1.96 \text{ TeV}$. The first error is from statistics and jet energy scale uncertainty, and the latter is from the other systematics.
- 63 Based on 310 pb^{-1} of data at $\sqrt{s} = 1.96 \text{ TeV}$.
- 64 Ideogram method.
- 65 Based on 311 pb^{-1} of data at $\sqrt{s} = 1.96 \text{ TeV}$. Events with 4 or more jets with $E_{Tj} > 15 \text{ GeV}$, significant missing E_{Tj} , and secondary vertex b -tag are used in the fit. About 44% of the signal acceptance is from $\tau\nu + 4$ jets. Events with identified e or μ are vetoed to provide a statistically independent measurement.
- 66 Based on 1.02 fb^{-1} of data at $\sqrt{s} = 1.96 \text{ TeV}$. Superseded by AALTONEN 12G.
- 67 Based on 955 pb^{-1} of data at $\sqrt{s} = 1.96 \text{ TeV}$. m_t and JES (Jet Energy Scale) are fitted simultaneously, and the first error contains the JES contribution of 1.5 GeV.
- 68 Matrix element method.
- 69 Based on 425 pb^{-1} of data at $\sqrt{s} = 1.96 \text{ TeV}$. The first error is a combination of statistics and JES (Jet Energy Scale) uncertainty, which has been measured simultaneously to give $\text{JES} = 0.989 \pm 0.029(\text{stat})$.
- 70 Based on 370 pb^{-1} of data at $\sqrt{s} = 1.96 \text{ TeV}$. Combined result of MWT (Matrix-element Weighting Technique) and μ WT (μ Weighting Technique) analyses is $178.1 \pm 6.7 \pm 4.8 \text{ GeV}$.
- 71 Based on 1.0 fb^{-1} of data at $\sqrt{s} = 1.96 \text{ TeV}$. ABULENCIA 07D improves the matrix element description by including the effects of initial-state radiation.
- 72 Based on 695 pb^{-1} of data at $\sqrt{s} = 1.96 \text{ TeV}$. The transverse decay length of the b hadron is used to determine m_t , and the result is free from the JES (jet energy scale) uncertainty.
- 73 Based on $\sim 400 \text{ pb}^{-1}$ of data at $\sqrt{s} = 1.96 \text{ TeV}$. The first error includes statistical and systematic jet energy scale uncertainties, the second error is from the other systematics. The result is obtained with the b -tagging information. The result without b -tagging is $169.2^{+5.0+1.5}_{-7.4-1.4} \text{ GeV}$. Superseded by ABAZOV 08AH.
- 74 Based on 318 pb^{-1} of data at $\sqrt{s} = 1.96 \text{ TeV}$.
- 75 Dynamical likelihood method.
- 76 Based on 340 pb^{-1} of data at $\sqrt{s} = 1.96 \text{ TeV}$.
- 77 Based on 360 pb^{-1} of data at $\sqrt{s} = 1.96 \text{ TeV}$.
- 78 Based on $110.2 \pm 5.8 \text{ pb}^{-1}$ at $\sqrt{s} = 1.8 \text{ TeV}$.
- 79 Based on the all hadronic decays of $t\bar{t}$ pairs. Single b -quark tagging via the decay chain $b \rightarrow c \rightarrow \mu$ was used to select signal enriched multijet events. The result was obtained by the maximum likelihood method after bias correction.
- 80 Obtained by re-analysis of the lepton + jets candidate events that led to ABBOTT 98F. It is based upon the maximum likelihood method which makes use of the leading order matrix elements.
- 81 Based on $125 \pm 7 \text{ pb}^{-1}$ of data at $\sqrt{s} = 1.8 \text{ TeV}$.
- 82 Based on $\sim 106 \text{ pb}^{-1}$ of data at $\sqrt{s} = 1.8 \text{ TeV}$.
- 83 Obtained by combining the measurements in the lepton + jets [AFFOLDER 01], all-jets [ABE 97R, ABE 99B], and dilepton [ABE 99B] decay topologies.

- 84 Obtained by combining the D0 result $m_t (\text{GeV}) = 168.4 \pm 12.3 \pm 3.6$ from 6 di-lepton events (see also ABBOTT 98D) and $m_t (\text{GeV}) = 173.3 \pm 5.6 \pm 5.5$ from lepton+jet events (ABBOTT 98F).
- 85 Obtained by combining the CDF results of $m_t (\text{GeV}) = 167.4 \pm 10.3 \pm 4.8$ from 8 dilepton events, $m_t (\text{GeV}) = 175.9 \pm 4.8 \pm 5.3$ from lepton+jet events (ABE 98E), and $m_t (\text{GeV}) = 186.0 \pm 10.0 \pm 5.7$ from all-jet events (ABE 97R). The systematic errors in the latter two measurements are changed in this paper.
- 86 See AFFOLDER 01 for details of systematic error re-evaluation.
- 87 Based on $109 \pm 7 \text{ pb}^{-1}$ of data at $\sqrt{s} = 1.8 \text{ TeV}$.
- 88 See ABZOV 04G.
- 89 The updated systematic error is listed. See AFFOLDER 01, appendix C.
- 90 Obtained by combining the D0 results of $m_t (\text{GeV}) = 168.4 \pm 12.3 \pm 3.6$ from 6 dilepton events and $m_t (\text{GeV}) = 173.3 \pm 5.6 \pm 5.5$ from 77 lepton+jet events.
- 91 Obtained by combining the D0 results from dilepton and lepton+jet events, and the CDF results (ABE 99B) from dilepton, lepton+jet events, and all-jet events.
- 92 Based on the first observation of all hadronic decays of $t\bar{t}$ pairs. Single b -quark tagging with jet-shape variable constraints was used to select signal enriched multi-jet events. The updated systematic error is listed. See AFFOLDER 01, appendix C.

t-Quark Mass from Cross-Section Measurements

The top quark $\overline{\text{MS}}$ pole mass can be extracted from a measurement of $\sigma(t\bar{t})$ by using theory calculations. We quote below the $\overline{\text{MS}}$ mass. See the review "The Top Quark" and references therein for more information.

VALUE (GeV)	DOCUMENT ID	TECN	COMMENT
$162.5^{+2.1}_{-1.5}$ OUR AVERAGE			
$162.9 \pm 0.5 \pm 1.0^{+2.1}_{-1.2}$	1 AAD	19G ATLS	$\ell + \cancel{E}_{Tj} + \geq 5 j (2b-j)$
$160.0^{+4.8}_{-4.3}$	2 ABZOV	11s D0	$\sigma(t\bar{t}) + \text{theory}$
• • • We do not use the following data for averages, fits, limits, etc. • • •			
	3 ABZOV	09AG D0	cross sects, theory + exp
	4 ABZOV	09R D0	cross sects, theory + exp

- 1 AAD 19G based on 20.2 fb^{-1} of data in pp collisions at $\sqrt{s} = 8 \text{ TeV}$. Normalized $t\bar{t} + 1$ -jet differential cross section as a function of $t\bar{t}j$ invariant mass is measured in the $\ell + \text{jets}$ mode. The unfolded parton-level distribution is compared with the NLO QCD prediction. The three errors are from statistics, systematics, and theory.
- 2 Based on 5.3 fb^{-1} in $p\bar{p}$ collisions at $\sqrt{s} = 1.96 \text{ TeV}$. ABZOV 11s uses the measured $t\bar{t}$ production cross section of $8.13^{+1.02}_{-0.90} \text{ pb}$ [ABZOV 11E] in the lepton plus jets channel to obtain the top quark $\overline{\text{MS}}$ mass by using an approximate NNLO computation (MOCH 08, LANGENFELD 09). The corresponding top quark pole mass is $167.5^{+5.4}_{-4.9} \text{ GeV}$. A different theory calculation (AHRENS 10, AHRENS 10A) is also used and yields $m_t^{\overline{\text{MS}}} = 154.5^{+5.0}_{-4.3} \text{ GeV}$.
- 3 Based on 1 fb^{-1} of data at $\sqrt{s} = 1.96 \text{ TeV}$. Uses the $\ell + \text{jets}$, $\ell\ell$, and $\ell\tau + \text{jets}$ channels. ABZOV 09AG extract the pole mass of the top quark using two different calculations that yield $169.1^{+5.9}_{-5.2} \text{ GeV}$ (MOCH 08, LANGENFELD 09) and $168.2^{+5.9}_{-5.4} \text{ GeV}$ (KIDONAKIS 08).
- 4 Based on 1 fb^{-1} of data at $\sqrt{s} = 1.96 \text{ TeV}$. Uses the $\ell\ell$ and $\ell\tau + \text{jets}$ channels. ABZOV 09R extract the pole mass of the top quark using two different calculations that yield $173.3^{+9.8}_{-8.6} \text{ GeV}$ (MOCH 08, LANGENFELD 09) and $171.5^{+9.9}_{-8.8} \text{ GeV}$ (CACCIARI 08).

t-Quark Pole Mass from Cross-Section Measurements

VALUE (GeV)	DOCUMENT ID	TECN	COMMENT
172.5 ± 0.7 OUR AVERAGE			
$173.1^{+2.0}_{-2.1}$	1 AAD	20Q ATLS	$e + \mu + 1$ or 2 b -jets
$171.1 \pm 0.4 \pm 0.9^{+0.7}_{-0.3}$	2 AAD	19G ATLS	$\ell + \cancel{E}_{Tj} + \geq 5 j (2b-j)$
$173.2 \pm 0.9 \pm 0.8 \pm 1.2$	3 AABOUD	17BC ATLS	$e + \mu + \geq 1b$ jets
170.6 ± 2.7	4 SIRUNYAN	17W CMS	$\ell + \geq 1j$
$172.8 \pm 1.1^{+3.3}_{-3.1}$	5 ABZOV	16F D0	$\ell\ell, \ell + \text{jets}$ channels
$173.8^{+1.7}_{-1.8}$	6 KHACHATRY...16AW	CMS	$e + \mu + \cancel{E}_{Tj} + \geq 0j$
$173.7^{+2.3}_{-2.1}$	7 AAD	15BWATLS	$\ell + \cancel{E}_{Tj} + \geq 5j (2b\text{-tag})$
$172.9^{+2.5}_{-2.6}$	8 AAD	14AY ATLS	pp at $\sqrt{s} = 7, 8 \text{ TeV}$
• • • We do not use the following data for averages, fits, limits, etc. • • •			
170.5 ± 0.8	9 SIRUNYAN	20BV CMS	$t\bar{t}$ normalized cross-differential cross sections
$176.7^{+3.0}_{-2.8}$	10 CHATRCHYAN14	CMS	pp at $\sqrt{s} = 7 \text{ TeV}$

- 1 AAD 20Q based on 36.1 fb^{-1} of pp data at $\sqrt{s} = 13 \text{ TeV}$. The result is obtained from the inclusive cross section measurement and the NNLO+NNLL prediction.
- 2 AAD 19G based on 20.2 fb^{-1} of data in pp collisions at $\sqrt{s} = 8 \text{ TeV}$. Normalized $t\bar{t} + 1$ -jet differential cross section as a function of $t\bar{t}j$ invariant mass is measured in the $\ell + \text{jets}$ mode. The unfolded parton-level distribution is compared with the NLO QCD prediction. The three errors are from statistics, systematics, and theory.
- 3 AABOUD 17BC based on 20.2 fb^{-1} of pp data at $\sqrt{s} = 8 \text{ TeV}$. The pole mass is extracted from a fit of NLO predictions to eight single lepton and dilepton differential distributions, while simultaneously constraining uncertainties due to PDFs and QCD scales. The three reported uncertainties come from statistics, experimental systematics, and theoretical sources.
- 4 SIRUNYAN 17W based on 2.2 fb^{-1} of pp data at $\sqrt{s} = 13 \text{ TeV}$. Events are categorized according to the jet multiplicity and the number of b -tagged jets. The pole mass is obtained from the inclusive cross section measurement and the NNLO prediction.
- 5 ABZOV 16F based on 9.7 fb^{-1} of data in $p\bar{p}$ collisions at $\sqrt{s} = 1.96 \text{ TeV}$. The result is obtained from the inclusive cross section measurement and the NNLO+NNLL prediction.

Quark Particle Listings

t

- ⁶ KHACHATRYAN 16AW based on 5.0 fb⁻¹ of *pp* collisions at 7 TeV and 19.7 fb⁻¹ at 8 TeV. The 7 TeV data include those used in CHATRCHYAN 14. The result is obtained from the inclusive cross sections.
- ⁷ AAD 15BW based on 4.6 fb⁻¹ of *pp* data at $\sqrt{s} = 7$ TeV. Uses normalized differential cross section for *t* $\bar{t} + 1$ jet as a function of the inverse of the invariant mass of the *t* $\bar{t} + 1$ jet system. The measured cross section is corrected to the parton level. Then a fit to the data using NLO + parton shower prediction is performed.
- ⁸ AAD 14AY used $\sigma(t\bar{t})$ for *eμ* events. The result is a combination of the measurements $m_t = 171.4 \pm 2.6$ GeV based on 4.6 fb⁻¹ of data at 7 TeV and $m_t = 174.1 \pm 2.6$ GeV based on 20.3 fb⁻¹ of data at 8 TeV.
- ⁹ SIRUNYAN 20BV based on 35.9 fb⁻¹ of *pp* data at $\sqrt{s} = 13$ TeV. The error accounts for both experimental and theoretical uncertainties. Events containing two oppositely charged leptons are used. The pole mass is particularly sensitive to the *t* \bar{t} invariant mass distribution close to the threshold. However, the Coulomb and soft gluon resummation effects are not taken into account, hence, an additional theoretical uncertainty of order +1 GeV is assumed.
- ¹⁰ CHATRCHYAN 14 used $\sigma(t\bar{t})$ from *pp* collisions at $\sqrt{s} = 7$ TeV measured in CHATRCHYAN 12AX to obtain $m_t(\text{pole})$ for $\alpha_s(m_Z) = 0.1184 \pm 0.0007$. The errors have been corrected in KHACHATRYAN 14K.

$m_t - m_{\bar{t}}$

Test of *CPT* conservation. OUR AVERAGE assumes that the systematic uncertainties are uncorrelated.

VALUE (GeV)	DOCUMENT ID	TECN	COMMENT
-0.15 ± 0.20 OUR AVERAGE	Error includes scale factor of 1.1.		
0.83 ^{+1.79} _{-1.35}	¹ TUMASYAN 21G	CMS	<i>t</i> -channel single top production
-0.15 ± 0.19 ± 0.09	² CHATRCHYAN17	CMS	$\ell + \cancel{E}_T + \geq 4j$ ($\geq 1b$ j)
0.67 ± 0.61 ± 0.41	³ AAD 14	ATLS	$\ell + \cancel{E}_T + \geq 4j$ (≥ 2 <i>b</i> -tags)
-1.95 ± 1.11 ± 0.59	⁴ AALTONEN 13E	CDF	$\ell + \cancel{E}_T + \geq 4j$ (0,1,2 <i>b</i> -tags)
-0.44 ± 0.46 ± 0.27	⁵ CHATRCHYAN12Y	CMS	$\ell + \cancel{E}_T + \geq 4j$
0.8 ± 1.8 ± 0.5	⁶ ABAZOV 11T	D0	$\ell + \cancel{E}_T + 4$ jets (≥ 1 <i>b</i> -tag)
• • • We do not use the following data for averages, fits, limits, etc. • • •			
-3.3 ± 1.4 ± 1.0	⁷ AALTONEN 11K	CDF	Repl. by AALTONEN 13E
3.8 ± 3.4 ± 1.2	⁸ ABAZOV 09AA	D0	$\ell + \cancel{E}_T + 4$ jets (≥ 1 <i>b</i> -tag)
¹ TUMASYAN 21G based on 35.9 fb ⁻¹ of <i>pp</i> data at $\sqrt{s} = 13$ TeV. Events are selected by requiring $1\ell + 2\text{jets}(1b\text{ jet})$ final state. An average top mass of $172.13^{+0.76}_{-0.77}$ GeV/ <i>c</i> ² is obtained.			
² CHATRCHYAN 17 based on 19.6 fb ⁻¹ of <i>pp</i> data at $\sqrt{s} = 8$ TeV and an average top mass of 172.84 ± 0.10 (stat) GeV is obtained.			
³ Based on 4.7 fb ⁻¹ of <i>pp</i> data at $\sqrt{s} = 7$ TeV and an average top mass of 172.5 GeV/ <i>c</i> ² .			
⁴ Based on 8.7 fb ⁻¹ of <i>pp</i> collisions at $\sqrt{s} = 1.96$ TeV and an average top mass of 172.5 GeV/ <i>c</i> ² .			
⁵ Based on 4.96 fb ⁻¹ of <i>pp</i> data at $\sqrt{s} = 7$ TeV. Based on the fitted m_t for ℓ^+ and ℓ^- events using the Ideogram method.			
⁶ Based on a matrix-element method which employs 3.6 fb ⁻¹ in <i>pp</i> collisions at $\sqrt{s} = 1.96$ TeV.			
⁷ Based on a template likelihood technique which employs 5.6 fb ⁻¹ in <i>pp</i> collisions at $\sqrt{s} = 1.96$ TeV.			
⁸ Based on 1 fb ⁻¹ of data in <i>pp</i> collisions at $\sqrt{s} = 1.96$ TeV.			

t-quark DECAY WIDTH

VALUE (GeV)	CL%	DOCUMENT ID	TECN	COMMENT
1.42^{+0.19}_{-0.15} OUR AVERAGE		Error includes scale factor of 1.4.		
1.76 ± 0.33 ^{+0.79} _{-0.68}		¹ AABOUD 18AZ	ATLS	$\ell + \cancel{E}_T + \geq 4j$ (≥ 1 <i>b</i>)
1.36 ± 0.02 ± 0.14 _{-0.11}		² KHACHATRY...14E	CMS	$\ell\ell + \cancel{E}_T + 2,4\text{jets}$ (0-2 <i>b</i> -tag)
2.00 ^{+0.47} _{-0.43}		³ ABAZOV 12T	D0	$\Gamma(t \rightarrow bW)/\Gamma(t \rightarrow bW)$
• • • We do not use the following data for averages, fits, limits, etc. • • •				
< 6.38	95	⁴ AALTONEN 13Z	CDF	$\ell + \cancel{E}_T + \geq 4j$ (≥ 0 <i>b</i>), direct
1.99 ^{+0.69} _{-0.55}		⁵ ABAZOV 11B	D0	Repl. by ABAZOV 12T
> 1.21	95	⁵ ABAZOV 11B	D0	$\Gamma(t \rightarrow Wb)$
< 7.6	95	⁶ AALTONEN 10AC	CDF	$\ell + \text{jets}$, direct
< 13.1	95	⁷ AALTONEN 09M	CDF	$m_t(\text{rec})$ distribution
¹ Based on 20.2 fb ⁻¹ of <i>pp</i> data at $\sqrt{s} = 8$ TeV. Γ_t is measured using a template fit to the reconstructed invariant mass of the <i>b</i> -jet of the semileptonically decaying top quark and the corresponding lepton, and the angular distance between j_b and j_l in hadronic top decay. Signal templates are generated by reweighting events at parton-level to Breit-Wigner distribution with different Γ_t hypotheses for $m_t = 172.5$ GeV. The result is consistent with the NNLO SM prediction of 1.322 GeV.				
² Based on 19.7 fb ⁻¹ of <i>pp</i> data at $\sqrt{s} = 8$ TeV. The result is obtained by combining the measurement of $R = \Gamma(t \rightarrow Wb)/\Gamma(t \rightarrow Wq(q=b,s,d))$ and a previous CMS measurement of the <i>t</i> -channel single top production cross section of CHATRCHYAN 12BQ, by using the theoretical calculation of $\Gamma(t \rightarrow Wb)$ for $m_t = 172.5$ GeV.				
³ Based on 5.4 fb ⁻¹ of data in <i>pp</i> collisions at 1.96 TeV. $\Gamma(t \rightarrow bW) = 1.87^{+0.44}_{-0.40}$ GeV is obtained from the observed <i>t</i> -channel single top quark production cross section, whereas $B(t \rightarrow bW) = 0.90 \pm 0.04$ is used assuming $\sum_q B(t \rightarrow qW) = 1$. The result is valid for $m_t = 172.5$ GeV. See the paper for the values for $m_t = 170$ or 175 GeV.				
⁴ Based on 8.7 fb ⁻¹ of data. The two sided 68% CL interval is 1.10 GeV < Γ_t < 4.05 GeV for $m_t = 172.5$ GeV.				
⁵ Based on 2.3 fb ⁻¹ in <i>pp</i> collisions at $\sqrt{s} = 1.96$ TeV. ABAZOV 11B extracted Γ_t from the partial width $\Gamma(t \rightarrow Wb) = 1.92^{+0.58}_{-0.51}$ GeV measured using the <i>t</i> -channel single top production cross section, and the branching fraction $\text{br}(t \rightarrow Wb) =$				

$0.962^{+0.068}(\text{stat})^{+0.064}_{-0.052}(\text{syst})$. The $\Gamma(t \rightarrow Wb)$ measurement gives the 95% CL lowerbound of $\Gamma(t \rightarrow Wb)$ and hence that of Γ_t .

⁶ Results are based on 4.3 fb⁻¹ of data in *pp* collisions at $\sqrt{s} = 1.96$ TeV. The top quark mass and the hadronically decaying *W* boson mass are reconstructed for each candidate events and compared with templates of different top quark width. The two sided 68% CL interval is 0.3 GeV < Γ_t < 4.4 GeV for $m_t = 172.5$ GeV.

⁷ Based on 955 pb⁻¹ of *pp* collision data at $\sqrt{s} = 1.96$ TeV. AALTONEN 09M selected *t* \bar{t} candidate events for the $\ell + \cancel{E}_T + \text{jets}$ channel with one or two *b*-tags, and examine the decay width dependence of the reconstructed m_t distribution. The result is for $m_t = 175$ GeV, whereas the upper limit is lower for smaller m_t .

t DECAY MODES

Mode	Fraction (Γ_i/Γ)	Confidence level
Γ_1 $Wq(q = b, s, d)$		
Γ_2 Wb		
Γ_3 $e\nu_e b$	(11.10 ± 0.30) %	
Γ_4 $\mu\nu_\mu b$	(11.40 ± 0.20) %	
Γ_5 $\tau\nu_\tau b$	(10.7 ± 0.5) %	
Γ_6 $q\bar{q}b$	(66.5 ± 1.4) %	
Γ_7 $\gamma q(q = u, c)$	[a] < 1.8	$\times 10^{-4}$ 95%
Γ_8 $H^+ b, H^+ \rightarrow \tau\nu_\tau$		

$\Delta T = 1$ weak neutral current (*T1*) modes

Γ_i	Mode	<i>T1</i>	Confidence level
Γ_9	$Zq(q = u, c)$	[b] < 5	$\times 10^{-4}$ 95%
Γ_{10}	Hu	< 1.2	$\times 10^{-3}$ 95%
Γ_{11}	Hc	< 1.1	$\times 10^{-3}$ 95%
Γ_{12}	$\ell^+ \bar{q} q' (q = d, s, b; q' = u, c)$	< 1.6	$\times 10^{-3}$ 95%

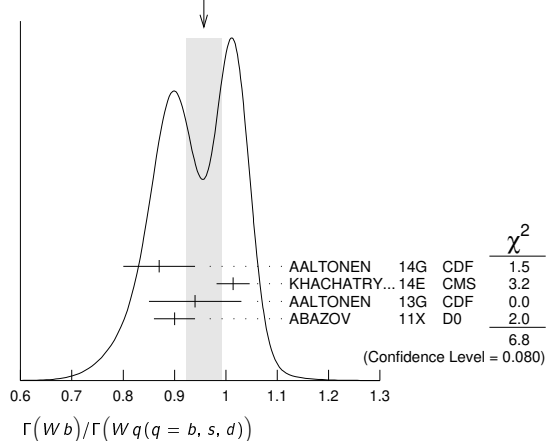
[a] This limit is for $\Gamma(t \rightarrow \gamma q)/\Gamma(t \rightarrow Wb)$.

[b] This limit is for $\Gamma(t \rightarrow Zq)/\Gamma(t \rightarrow Wb)$.

t BRANCHING RATIOS

$\Gamma(Wb)/\Gamma(Wq(q = b, s, d))$	Γ_2/Γ_1
OUR AVERAGE assumes that the systematic uncertainties are uncorrelated.	
0.957 ± 0.034 OUR AVERAGE	Error includes scale factor of 1.5. See the ideogram below.
0.87 ± 0.07	¹ AALTONEN 14G CDF $\ell\ell + \cancel{E}_T + \geq 2j$ (0,1,2 <i>b</i> -tag)
1.014 ± 0.003 ± 0.032	² KHACHATRY...14E CMS $\ell\ell + \cancel{E}_T + 2,3,4j$ (0-2 <i>b</i> -tag)
0.94 ± 0.09	³ AALTONEN 13G CDF $\ell + \cancel{E}_T + \geq 3\text{jets}$ ($\geq 1b$ -tag)
0.90 ± 0.04	⁴ ABAZOV 11X D0
• • • We do not use the following data for averages, fits, limits, etc. • • •	
0.97 ^{+0.09} _{-0.08}	⁵ ABAZOV 08M D0 $\ell + n$ jets with 0,1,2 <i>b</i> -tag
1.03 ^{+0.19} _{-0.17}	⁶ ABAZOV 06K D0
1.12 ^{+0.21} _{-0.19}	⁷ ACOSTA 05A CDF Repl. by AALTONEN 13G
0.94 ^{+0.26} _{-0.21}	⁸ AFFOLDER 01C CDF

WEIGHTED AVERAGE
0.957 ± 0.034 (Error scaled by 1.5)



¹ Based on 8.7 fb⁻¹ of data. This measurement gives $|V_{tb}| = 0.93 \pm 0.04$ and $|V_{cb}| > 0.85$ (95% CL) in the SM.

² Based on 19.7 fb⁻¹ of *pp* data at $\sqrt{s} = 8$ TeV. The result is obtained by counting the number of *b* jets per *t* \bar{t} signal events in the dilepton channel. The *t* \bar{t} production cross section is measured to be $\sigma(t\bar{t}) = 238 \pm 1 \pm 15$ pb, in good agreement with the SM prediction and the latest CMS measurement of CHATRCHYAN 14F. The measurement gives $R > 0.995$ (95% CL), or $|V_{tb}| > 0.975$ (95% CL) in the SM, requiring $R \leq 1$.

³ Based on 8.7 fb⁻¹ of *pp* collisions at $\sqrt{s} = 1.96$ TeV. Measure the fraction of *t* → *Wb* decays simultaneously with the *t* \bar{t} cross section. The correlation coefficient between

those two measurements is -0.434 . Assume unitarity of the 3×3 CKM matrix and set $|V_{tb}| > 0.89$ at 95% CL.

⁴Based on 5.4 fb^{-1} of data. The error is statistical and systematic combined. The result is a combination of 0.95 ± 0.07 from $\ell + \text{jets}$ channel and 0.86 ± 0.05 from $\ell\ell$ channel. $|V_{tb}| = 0.95 \pm 0.02$ follows from the result by assuming unitarity of the 3×3 CKM matrix.

⁵Result is based on 0.9 fb^{-1} of data. The 95% CL lower bound $R > 0.79$ gives $|V_{tb}| > 0.89$ (95% CL).

⁶ABAZOV 06K result is from the analysis of $t\bar{t} \rightarrow \ell\nu + \geq 3$ jets with 230 pb^{-1} of data at $\sqrt{s} = 1.96 \text{ TeV}$. It gives $R > 0.61$ and $|V_{tb}| > 0.78$ at 95% CL. Superseded by ABAZOV 08M.

⁷ACOSTA 05A result is from the analysis of lepton + jets and di-lepton + jets final states of $t\bar{t}$ candidate events with $\sim 162 \text{ pb}^{-1}$ of data at $\sqrt{s} = 1.96 \text{ TeV}$. The first error is statistical and the second systematic. It gives $R > 0.61$, or $|V_{tb}| > 0.78$ at 95% CL.

⁸AFFOLDER 01C measures the top-quark decay width ratio $R = \Gamma(Wb)/\Gamma(Wq)$, where q is a d , s , or b quark, by using the number of events with multiple b tags. The first error is statistical and the second systematic. A numerical integration of the likelihood function gives $R > 0.61$ (0.56) at 90% (95%) CL. By assuming three generation unitarity, $|V_{tb}| = 0.97 \pm 0.16$ or $|V_{tb}| > 0.78$ (0.75) at 90% (95%) CL is obtained. The result is based on 109 pb^{-1} of data at $\sqrt{s} = 1.8 \text{ TeV}$.

$\Gamma(e\nu_e b)/\Gamma_{\text{total}}$		Γ_3/Γ		
VALUE	DOCUMENT ID	TECN	COMMENT	

0.111 \pm 0.003
¹AAD 15cc based on 4.6 fb^{-1} of pp data at $\sqrt{s} = 7 \text{ TeV}$. The original value is given by $13.3 \pm 0.4 \pm 0.5\%$, which includes electrons from the decay of τ leptons. It is assumed that the top branching ratios to leptons and jets add up to one and that only SM processes contribute to the background. The event selection criteria are optimized for the $\ell\tau_h + \text{jets}$ channel. We have converted the original value to eliminate contributions of electrons from τ 's, by using the AAD 15cc measurements of the branching ratios to μ and τ channels, as well as the PDG values of τ branching ratios into e and μ channels.

$\Gamma(\mu\nu_\mu b)/\Gamma_{\text{total}}$		Γ_4/Γ		
VALUE	DOCUMENT ID	TECN	COMMENT	

0.114 \pm 0.002
¹AAD 15cc based on 4.6 fb^{-1} of pp data at $\sqrt{s} = 7 \text{ TeV}$. The original value is given by $13.4 \pm 0.3 \pm 0.5\%$, which includes muons from the decay of τ leptons. It is assumed that the top branching ratios to leptons and jets add up to one and that only SM processes contribute to the background. The event selection criteria are optimized for the $\ell\tau_h + \text{jets}$ channel. We have converted the original value to eliminate contributions of muons from τ 's, by using the AAD 15cc measurements of the branching ratios to μ and τ channels, as well as the PDG values of τ branching ratios into e and τ channels.

$\Gamma(\tau\nu_\tau b)/\Gamma_{\text{total}}$		Γ_5/Γ		
VALUE	DOCUMENT ID	TECN	COMMENT	

0.107 \pm 0.005 OUR AVERAGE
 0.1050 \pm 0.0009 \pm 0.0071
¹SIRUNYAN 20v CMS $\ell\tau_h + \geq 3$ jets ($\geq 1b$ -tag)
 0.112 \pm 0.009
²AAD 15cc ATLS $\ell + \text{jets}, \ell\ell + \text{jets}, \ell\tau_h + \text{jets}$
 0.096 \pm 0.028
³AALTONEN 14A CDF $\ell + \tau_h + \geq 2$ jets ($\geq 1b$ -tag)
 • • • We do not use the following data for averages, fits, limits, etc. • • •
⁴ABULENCIA 06R CDF $\ell\tau + \text{jets}$
⁵ABE 97v CDF $\ell\tau + \text{jets}$

¹SIRUNYAN 20v based on 35.9 fb^{-1} of pp data at $\sqrt{s} = 13 \text{ TeV}$. $t\bar{t}$ events are selected in the $t\bar{t} \rightarrow (\ell\nu_\ell)(\tau\nu_\tau)b\bar{b}$ mode, where τ_h refers to the hadronic decays of τ . The branching ratio is determined with respect to the $t\bar{t}$ inclusive cross section extrapolated from the light dilepton mode. The ratio of the $t\bar{t}$ production cross sections in the $\ell\tau_h$ and $\ell\ell$ channels yields $0.973 \pm 0.009 \pm 0.066$, consistent with lepton universality.

²AAD 15cc based on 4.6 fb^{-1} of pp data at $\sqrt{s} = 7 \text{ TeV}$. The original value is given by $7.0 \pm 0.3 \pm 0.5\%$, which includes only the hadronic decay of τ leptons. It is assumed that the top branching ratios to leptons and jets add up to one and that only SM processes contribute to the background. The event selection criteria are optimized for the $\ell\tau_h + \text{jets}$ channel. We have converted the original value to include leptonic decays of τ 's, by using the AAD 15cc measurements of the branching ratios to e and μ channels, as well as the PDG values of τ branching ratios into e and μ channels.

³Based on 9 fb^{-1} of data. The measurement is in the channel $t\bar{t} \rightarrow (b\ell\nu)(b\tau\nu)$, where τ decays into hadrons (τ_h), and ℓ (e or μ) include ℓ from τ decays (τ_ℓ). The result is consistent with lepton universality.

⁴ABULENCIA 06R looked for $t\bar{t} \rightarrow (\ell\nu_\ell)(\tau\nu_\tau)b\bar{b}$ events in 194 pb^{-1} of $p\bar{p}$ collisions at $\sqrt{s} = 1.96 \text{ TeV}$. 2 events are found where 1.00 ± 0.17 signal and 1.29 ± 0.25 background events are expected, giving a 95% CL upper bound for the partial width ratio $\Gamma(t \rightarrow \tau\nu q) / \Gamma_{SM}(t \rightarrow \tau\nu q) < 5.2$.

⁵ABE 97v searched for $t\bar{t} \rightarrow (\ell\nu_\ell)(\tau\nu_\tau)b\bar{b}$ events in 109 pb^{-1} of $p\bar{p}$ collisions at $\sqrt{s} = 1.8 \text{ TeV}$. They observed 4 candidate events where one expects ~ 1 signal and ~ 2 background events. Three of the four observed events have jets identified as b candidates.

$\Gamma(q\bar{q}b)/\Gamma_{\text{total}}$		Γ_6/Γ		
VALUE	DOCUMENT ID	TECN	COMMENT	

0.665 \pm 0.004 \pm 0.013
¹AAD 15cc based on 4.6 fb^{-1} of pp data at $\sqrt{s} = 7 \text{ TeV}$. Branching ratio of top quark into b and jets. It is assumed that the top branching ratios to leptons and jets add up to one and that only SM processes contribute to the background. The event selection criteria are optimized for the $\ell\tau_h + \text{jets}$ channel.

$\Gamma(\gamma q(q=u,c))/\Gamma_{\text{total}}$		Γ_7/Γ		
VALUE	CL%	DOCUMENT ID	TECN	COMMENT

<2.8 $\times 10^{-5}$ 95 ¹AAD 20b ATLS $B(t \rightarrow \gamma u)$, left-handed $t\bar{t}\gamma$ coupling
<6.1 $\times 10^{-5}$ 95 ¹AAD 20b ATLS $B(t \rightarrow \gamma u)$, right-handed $t\bar{t}\gamma$ coupling
<2.2 $\times 10^{-4}$ 95 ¹AAD 20b ATLS $B(t \rightarrow \gamma c)$, left-handed $t\bar{t}\gamma$ coupling

VALUE	CL%	DOCUMENT ID	TECN	COMMENT
<1.8 $\times 10^{-4}$	95	¹ AAD	20b ATLS	$B(t \rightarrow \gamma c)$, right-handed $t\bar{t}\gamma$ coupling
<1.3 $\times 10^{-4}$	95	² KHACHATRYAN.16As	CMS	$B(t \rightarrow \gamma u)$
<1.7 $\times 10^{-3}$	95	² KHACHATRYAN.16As	CMS	$B(t \rightarrow \gamma c)$
<5.9 $\times 10^{-3}$	95	³ CHEKANOV 03 ZEUS		$B(t \rightarrow \gamma u)$
• • •		We do not use the following data for averages, fits, limits, etc. • • •		
<0.0064	95	⁴ AARON 09A	H1	$t \rightarrow \gamma u$
<0.0465	95	⁵ ABDALLAH 04c	DLPH	$B(\gamma c \text{ or } \gamma u)$
<0.0132	95	⁶ AKTAS 04	H1	$B(t \rightarrow \gamma u)$
<0.041	95	⁷ ACHARD 02j	L3	$B(t \rightarrow \gamma c \text{ or } \gamma u)$
<0.032	95	⁸ ABE 98G	CDF	$t\bar{t} \rightarrow (Wb)(\gamma c \text{ or } \gamma u)$

¹AAD 20b based on 81 fb^{-1} of data in pp collisions at $\sqrt{s} = 13 \text{ TeV}$. FCNC through single top production in association with a photon is searched for in the mode $\ell\gamma + \cancel{E}_T + 1j$ (b -tag). Anomalous FCNC left-handed and right-handed couplings are searched for, which result in different kinematical properties of top decay such as the lepton distribution. Limits are set on the $tq\gamma$ couplings in an effective field theory.

²KHACHATRYAN 16As based on 19.8 fb^{-1} of data in pp collisions at $\sqrt{s} = 8 \text{ TeV}$. FCNC through single top production in association with a photon is searched for in the mode $\mu + \gamma + \cancel{E}_T + \geq 1j$ (0,1b). Bounds on the anomalous FCNC couplings are given by $\kappa_{t\mu\gamma} < 0.025$ and $\kappa_{tc\gamma} < 0.091$.

³CHEKANOV 03 looked for single top production via FCNC in the reaction $e^\pm p \rightarrow e^\pm (t \text{ or } \bar{t}) X$ in 130.1 pb^{-1} of data at $\sqrt{s} = 300\text{--}318 \text{ GeV}$. No evidence for top production and its decay into bW was found. The result is obtained for $m_t = 175 \text{ GeV}$ when $B(\gamma c) = B(Zq) = 0$, where q is a u or c quark. Bounds on the effective $t\text{-}u\text{-}\gamma$ and $t\text{-}u\text{-}Z$ couplings are found in their Fig. 4. The conversion to the constraint listed is from private communication, E. Gallo, January 2004.

⁴AARON 09A looked for single top production via FCNC in $e^\pm p$ collisions at HERA with 474 pb^{-1} . The upper bound of the cross section gives the bound on the FCNC coupling $\kappa_{t\mu\gamma}/\Lambda < 1.03 \text{ TeV}^{-1}$, which corresponds to the result for $m_t = 175 \text{ GeV}$.

⁵ABDALLAH 04c looked for single top production via FCNC in the reaction $e^\pm e^- \rightarrow \bar{c}c$ or $\bar{u}u$ in 541 pb^{-1} of data at $\sqrt{s} = 189\text{--}208 \text{ GeV}$. No deviation from the SM is found, which leads to the bound on $B(t \rightarrow \gamma q)$, where q is a u or c quark, for $m_t = 175 \text{ GeV}$ when $B(t \rightarrow Zq) = 0$ is assumed. The conversion to the listed bound is from private communication, O. Yushchenko, April 2005. The bounds on the effective $t\text{-}q\text{-}\gamma$ and $t\text{-}q\text{-}Z$ couplings are given in their Fig. 7 and Table 4, for $m_t = 170\text{--}180 \text{ GeV}$, where most conservative bounds are found by choosing the chiral couplings to maximize the negative interference between the virtual γ and Z exchange amplitudes.

⁶AKTAS 04 looked for single top production via FCNC in e^\pm collisions at HERA with 118.3 pb^{-1} , and found 5 events in the e or μ channels. By assuming that they are due to statistical fluctuation, the upper bound on the $t\bar{t}\gamma$ coupling $\kappa_{t\mu\gamma} < 0.27$ (95% CL) is obtained. The conversion to the partial width limit, when $B(\gamma c) = B(Zu) = B(Zc) = 0$, is from private communication, E. Perez, May 2005.

⁷ACHARD 02j looked for single top production via FCNC in the reaction $e^\pm e^- \rightarrow \bar{c}c$ or $\bar{u}u$ in 634 pb^{-1} of data at $\sqrt{s} = 189\text{--}209 \text{ GeV}$. No deviation from the SM is found, which leads to a bound on the top-quark decay branching fraction $B(\gamma q)$, where q is a u or c quark. The bound assumes $B(Zq) = 0$ and is for $m_t = 175 \text{ GeV}$; bounds for $m_t = 170 \text{ GeV}$ and 180 GeV and $B(Zq) \neq 0$ are given in Fig. 5 and Table 7.

⁸ABE 98g looked for $t\bar{t}$ events where one t decays into $q\gamma$ while the other decays into bW . The quoted bound is for $\Gamma(\gamma q)/\Gamma(Wb)$.

$\Gamma(H^+ b, H^+ \rightarrow \tau\nu_\tau)/\Gamma_{\text{total}}$		Γ_8/Γ		
VALUE (%)	CL%	DOCUMENT ID	TECN	

<0.25 95 ¹AABOUD 18Bw ATLS
¹AABOUD 18Bw based on 36.1 fb^{-1} of pp data at $\sqrt{s} = 13 \text{ TeV}$. In the mass range of $m_{H^+} = 90\text{--}160 \text{ GeV}$, assuming the SM cross section for the $t\bar{t}$ production, the upper limit for the branching fraction $B(t \rightarrow bH^+) \times B(H^+ \rightarrow \tau\nu_\tau)$ ranges between 0.25% and 0.031%.

$\Gamma(Z q(q=u,c))/\Gamma_{\text{total}}$		Γ_9/Γ		
Test for $\Delta T=1$ weak neutral current. Allowed by higher-order electroweak interaction.				
VALUE (units 10^{-3})	CL%	DOCUMENT ID	TECN	COMMENT

< 0.17 95 ¹AABOUD 18At ATLS $t \rightarrow Z u$
 < 0.24 95 ¹AABOUD 18At ATLS $t \rightarrow Z c$
 < 0.22 95 ²SIRUNYAN 17E CMS $t \rightarrow Z u$
 < 0.49 95 ²SIRUNYAN 17E CMS $t \rightarrow Z c$
 < 0.7 95 ³AAD 16d ATLS $t \rightarrow Z q (q = u, c)$
< 0.5 95 ⁴CHATRCHYAN14S CMS $t \rightarrow Z q (q = u, c)$

• • • We do not use the following data for averages, fits, limits, etc. • • •
 < 0.6 95 ⁵CHATRCHYAN14S CMS $t \rightarrow Z q (q = u, c)$
 < 2.1 95 ⁶CHATRCHYAN13F CMS $t \rightarrow Z q (q = u, c)$
 < 7.3 95 ⁷AAD 12Bt ATLS $t\bar{t} \rightarrow \ell^+ \ell^- \ell'^{\pm} + \cancel{E}_T + \text{jets}$
 < 32 95 ⁸ABAZOV 11M D0 $t \rightarrow Z q (q = u, c)$
 < 83 95 ⁹AALTONEN 09AL CDF $t \rightarrow Z q (q = c)$
 < 37 95 ¹⁰AALTONEN 08Ad CDF $t \rightarrow Z q (q = u, c)$
 < 1.59×10^2 95 ¹¹ABDALLAH 04c DLPH $e^+ e^- \rightarrow \bar{c}c$ or $\bar{u}u$
 < 1.37×10^2 95 ¹²ACHARD 02j L3 $e^+ e^- \rightarrow \bar{c}c$ or $\bar{u}u$
 < 1.4×10^2 95 ¹³HEISTER 02Q ALEP $e^+ e^- \rightarrow \bar{c}c$ or $\bar{u}u$
 < 1.37×10^2 95 ¹⁴ABBIENDI 01T OPAL $e^+ e^- \rightarrow \bar{c}c$ or $\bar{u}u$
 < 1.7×10^2 95 ¹⁵BARATE 00S ALEP $e^+ e^- \rightarrow \bar{c}c$ or $\bar{u}u$
 < 3.3×10^2 95 ¹⁶ABE 98G CDF $t\bar{t} \rightarrow (Wb)(Zc \text{ or } Zu)$

¹Based on 36.1 fb^{-1} of pp data at $\sqrt{s} = 13 \text{ TeV}$. The final states $t\bar{t} \rightarrow \ell^+ \ell^- \ell'^{\pm} \nu$ + jets ($\ell, \ell' = e, \mu$) are investigated and no significant excess over the SM background contributions is observed.

²SIRUNYAN 17E based on 19.7 fb^{-1} of pp data at $\sqrt{s} = 8 \text{ TeV}$. The final states $t\bar{t} \rightarrow \ell^+ \ell^- \ell'^{\pm} \nu$ + jets ($\ell, \ell' = e, \mu$) are investigated and the cross section $\sigma(pp \rightarrow tZq \rightarrow \ell\nu b\ell^+ \ell^- q) = 10^{+8}_{-7} \text{ fb}$ is measured, giving no sign of FCNC decays of the top quark.

Quark Particle Listings

t

- ³ AAD 16D based on 20.3 fb⁻¹ of *pp* data at $\sqrt{s} = 8$ TeV. The FCNC decay is searched for in $t\bar{t}$ events in the final state (bW)(qZ) when both W and Z decay leptonically, giving 3 charged leptons.
- ⁴ CHATRCHYAN 14s combined search limit from this and CHATRCHYAN 13F data.
- ⁵ Based on 19.7 fb⁻¹ of *pp* data at $\sqrt{s} = 8$ TeV. The flavor changing decay is searched for in $t\bar{t}$ events in the final state (bW)(qZ) when both W and Z decay leptonically, giving 3 charged leptons.
- ⁶ Based on 5.0 fb⁻¹ of *pp* data at $\sqrt{s} = 7$ TeV. Search for FCNC decays of the top quark in $t\bar{t} \rightarrow \ell^+ \ell^- \ell'^{\pm} \nu + \text{jets}$ ($\ell, \ell' = e, \mu$) final states found no excess of signal events.
- ⁷ Based on 2.1 fb⁻¹ of *pp* data at $\sqrt{s} = 7$ TeV.
- ⁸ Based on 4.1 fb⁻¹ of data. ABAZOV 11M searched for FCNC decays of the top quark in $t\bar{t} \rightarrow \ell^+ \ell^- \ell'^{\pm} \nu + \text{jets}$ ($\ell, \ell' = e, \mu$) final states, and absence of the signal gives the bound.
- ⁹ Based on *pp* data of 1.52 fb⁻¹. AALTONEN 09AL compared $t\bar{t} \rightarrow WbWb \rightarrow \ell\nu bjjb$ and $t\bar{t} \rightarrow ZcWb \rightarrow \ell\ell cjjb$ decay chains, and absence of the latter signal gives the bound. The result is for 100% longitudinally polarized Z boson and the theoretical $t\bar{t}$ production cross section. The results for different Z polarizations and those without the cross section assumption are given in their Table XII.
- ¹⁰ Result is based on 1.9 fb⁻¹ of data at $\sqrt{s} = 1.96$ TeV. $t\bar{t} \rightarrow WbZq$ or $ZqZq$ processes have been looked for in $Z + \geq 4$ jet events with and without b -tag. No signal leads to the bound $B(t \rightarrow Zq) < 0.037$ (0.041) for $m_t = 175$ (170) GeV.
- ¹¹ ABDALLAH 04C looked for single top production via FCNC in the reaction $e^+e^- \rightarrow \bar{t}c$ or $\bar{t}u$ in 541 pb⁻¹ of data at $\sqrt{s} = 189\text{--}208$ GeV. No deviation from the SM is found, which leads to the bound on $B(t \rightarrow Zq)$, where q is a u or a c quark, for $m_t = 175$ GeV when $B(t \rightarrow \gamma q) = 0$ is assumed. The conversion to the listed bound is from private communication, O. Yuschenko, April 2005. The bounds on the effective t - q - γ and t - q - Z couplings are given in their Fig. 7 and Table 4, for $m_t = 170\text{--}180$ GeV, where most conservative bounds are found by choosing the chiral couplings to maximize the negative interference between the virtual γ and Z exchange amplitudes.
- ¹² ACHARD 02I looked for single top production via FCNC in the reaction $e^+e^- \rightarrow \bar{t}c$ or $\bar{t}u$ in 634 pb⁻¹ of data at $\sqrt{s} = 189\text{--}209$ GeV. No deviation from the SM is found, which leads to a bound on the top-quark decay branching fraction $B(Zq)$, where q is a u or c quark. The bound assumes $B(\gamma q) = 0$ and is for $m_t = 175$ GeV; bounds for $m_t = 170$ GeV and 180 GeV and $B(\gamma q) \neq 0$ are given in Fig. 5 and Table 7. Table 6 gives constraints on t - c - e - e four-fermi contact interactions.
- ¹³ HEISTER 02Q looked for single top production via FCNC in the reaction $e^+e^- \rightarrow \bar{t}c$ or $\bar{t}u$ in 214 pb⁻¹ of data at $\sqrt{s} = 204\text{--}209$ GeV. No deviation from the SM is found, which leads to a bound on the branching fraction $B(Zq)$, where q is a u or c quark. The bound assumes $B(\gamma q) = 0$ and is for $m_t = 174$ GeV. Bounds on the effective t -(c or u)- γ and t -(c or u)- Z couplings are given in their Fig. 2.
- ¹⁴ ABBIENDI 01T looked for single top production via FCNC in the reaction $e^+e^- \rightarrow \bar{t}c$ or $\bar{t}u$ in 600 pb⁻¹ of data at $\sqrt{s} = 189\text{--}209$ GeV. No deviation from the SM is found, which leads to bounds on the branching fractions $B(Zq)$ and $B(\gamma q)$, where q is a u or c quark. The result is obtained for $m_t = 174$ GeV. The upper bound becomes 9.7% (20.6%) for $m_t = 169$ (179) GeV. Bounds on the effective t -(c or u)- γ and t -(c or u)- Z couplings are given in their Fig. 4.
- ¹⁵ BARATE 00s looked for single top production via FCNC in the reaction $e^+e^- \rightarrow \bar{t}c$ or $\bar{t}u$ in 411 pb⁻¹ of data at c.m. energies between 189 and 202 GeV. No deviation from the SM is found, which leads to a bound on the branching fraction. The bound assumes $B(\gamma q) = 0$. Bounds on the effective t -(c or u)- γ and t -(c or u)- Z couplings are given in their Fig. 4.
- ¹⁶ ABE 98G looked for $t\bar{t}$ events where one t decays into three jets and the other decays into qZ with $Z \rightarrow \ell\ell$. The quoted bound is for $\Gamma(Zq)/\Gamma(Wb)$.

$\Gamma(Hu)/\Gamma_{\text{total}}$		Γ_{10}/Γ		
VALUE (units 10^{-3})	CL%	DOCUMENT ID	TECN	COMMENT

<1.2	95	1 AABOUD	19s ATLS	combination of $t \rightarrow Hu$ ($H \rightarrow WW, ZZ, \tau\tau, \gamma\gamma, b\bar{b}$)
••• We do not use the following data for averages, fits, limits, etc. •••				
<5.2	95	2 AABOUD	19s ATLS	$t \rightarrow Hu$ ($H \rightarrow bb$)
<1.7	95	3 AABOUD	19s ATLS	$t \rightarrow Hu$ ($H \rightarrow \tau\tau$)
<1.9	95	4 AABOUD	18x ATLS	$t \rightarrow Hu$ ($H \rightarrow WW, ZZ, \tau\tau$)
<4.7	95	5 SIRUNYAN	18bc CMS	$t \rightarrow Hu$ ($H \rightarrow bb$)
<2.4	95	6 AABOUD	17av ATLS	$t \rightarrow Hu$ ($H \rightarrow \gamma\gamma$)
<5.5	95	7 KHACHATRYAN..17I	CMS	$t \rightarrow Hu$ ($H \rightarrow WW, ZZ, \tau\tau, \gamma\gamma, b\bar{b}$)
<6.1	95	8 AAD	15c0 ATLS	$t \rightarrow Hu$ ($H \rightarrow bb$)
<7.9	95	9 AAD	14aa ATLS	$t \rightarrow Hq$ ($q=u,c; H \rightarrow \gamma\gamma$)

- ¹ AABOUD 19s based on 36.1 fb⁻¹ at $\sqrt{s} = 13$ TeV of *pp* data. The searches using $H \rightarrow bb$ and $H \rightarrow \tau_h\tau_h$ are combined with searches in diphoton and multilepton final states. The upper limit on the Yukawa coupling $|Y_{tH}| < 0.066$ (95% CL) is obtained.
- ² AABOUD 19s based on 36.1 fb⁻¹ at $\sqrt{s} = 13$ TeV of *pp* data. Uses events with one isolated lepton and multiple jets (several of them b -tagged with high purity). A multivariate analysis is performed to distinguish the signal from backgrounds.
- ³ AABOUD 19s based on 36.1 fb⁻¹ at $\sqrt{s} = 13$ TeV of *pp* data. Uses events with one or two hadronically decaying τ and multiple jets. A multivariate analysis is performed to distinguish the signal from backgrounds.
- ⁴ AABOUD 18x based on 36.1 fb⁻¹ at $\sqrt{s} = 13$ TeV of *pp* data. $\ell\ell$ (same sign) + $\geq 4j$ mode and $\ell\ell\ell + \geq 2j$ mode are targeted and specialized boosted decision trees are used to distinguish signals from backgrounds.
- ⁵ SIRUNYAN 18bc based on 35.9 fb⁻¹ at $\sqrt{s} = 13$ TeV of *pp* data. Two channels $pp \rightarrow tH$ and $pp \rightarrow t\bar{t}$ in final states with one isolated lepton and ≥ 3 jets with ≥ 2 b jets are considered assuming a single tHu FCNC coupling. Reconstructed kinematical variables are fed into a multivariate analysis and no significant deviation is observed from the predicted background.
- ⁶ AABOUD 17av based on 36.1 fb⁻¹ at $\sqrt{s} = 13$ TeV of *pp* data. Search for $t\bar{t}$ events, where the other top quark decays hadronically or semi-leptonically.
- ⁷ KHACHATRYAN 17I based on 19.7 fb⁻¹ of *pp* data at $\sqrt{s} = 8$ TeV, using the topologies $t\bar{t} \rightarrow Hq+Wb$, where $q=u, c$.
- ⁸ AAD 15c0 based on 20.3 fb⁻¹ at $\sqrt{s} = 8$ TeV of *pp* data. Searches for $t\bar{t}$ events, where the other top quark decays semi-leptonically. Exploits high multiplicity of b -jets

and uses a likelihood discriminant. Combining with other ATLAS searches for different Higgs decay modes, $B(t \rightarrow Hc) < 0.46\%$ and $B(t \rightarrow Hu) < 0.45\%$ are obtained.

- ⁹ AAD 14AA based on 4.7 fb⁻¹ at $\sqrt{s} = 7$ TeV and 20.3 fb⁻¹ at $\sqrt{s} = 8$ TeV of *pp* data. The upper-bound is for the sum of $B(t \rightarrow Hc)$ and $B(t \rightarrow Hu)$. Search for $t\bar{t}$ events, where the other top quark decays hadronically or semi-leptonically. The upper bound constrains the H - t - c Yukawa couplings $\sqrt{|Y_{tCL}^H|^2 + |Y_{tCR}^H|^2} < 0.17$ (95% CL).

$\Gamma(Hc)/\Gamma_{\text{total}}$		Γ_{11}/Γ		
VALUE (units 10^{-3})	CL%	DOCUMENT ID	TECN	COMMENT

- | | | | | |
|---|----|---------------------|-----------|--|
| < 1.1 | 95 | 1 AABOUD | 19s ATLS | combination of $t \rightarrow Hc$ ($H \rightarrow WW, ZZ, \tau\tau, \gamma\gamma, b\bar{b}$) |
| ••• We do not use the following data for averages, fits, limits, etc. ••• | | | | |
| < 4.2 | 95 | 2 AABOUD | 19s ATLS | $t \rightarrow Hc$ ($H \rightarrow bb$) |
| < 1.9 | 95 | 3 AABOUD | 19s ATLS | $t \rightarrow Hc$ ($H \rightarrow \tau\tau$) |
| < 1.6 | 95 | 4 AABOUD | 18x ATLS | $t \rightarrow Hc$ ($H \rightarrow WW, ZZ, \tau\tau$) |
| < 4.7 | 95 | 5 SIRUNYAN | 18bc CMS | $t \rightarrow Hc$ ($H \rightarrow bb$) |
| < 2.2 | 95 | 6 AABOUD | 17av ATLS | $t \rightarrow Hc$ ($H \rightarrow \gamma\gamma$) |
| < 4 | 95 | 7 KHACHATRYAN..17I | CMS | $t \rightarrow Hc$ ($H \rightarrow WW, ZZ, \tau\tau, \gamma\gamma, b\bar{b}$) |
| < 5.6 | 95 | 8 AAD | 15c0 ATLS | $t \rightarrow Hc$ ($H \rightarrow bb$) |
| < 7.9 | 95 | 9 AAD | 14aa ATLS | $t \rightarrow Hq$ ($q=u,c; H \rightarrow \gamma\gamma$) |
| <13 | 95 | 10 CHATRCHYAN14R | CMS | $t \rightarrow Hc$ ($H \rightarrow \geq 2\ell$) |
| < 5.6 | 95 | 11 KHACHATRYAN..14Q | CMS | $t \rightarrow Hc$ ($H \rightarrow \gamma\gamma$ or leptons) |
- ¹ AABOUD 19s based on 36.1 fb⁻¹ at $\sqrt{s} = 13$ TeV of *pp* data. The searches using $H \rightarrow bb$ and $H \rightarrow \tau_h\tau_h$ are combined with searches in diphoton and multilepton final states. The upper limit on the Yukawa coupling $|Y_{tH}| < 0.064$ (95% CL) is obtained.
- ² AABOUD 19s based on 36.1 fb⁻¹ at $\sqrt{s} = 13$ TeV of *pp* data. Uses events with one isolated lepton and multiple jets (several of them b -tagged with high purity). A multivariate analysis is performed to distinguish the signal from backgrounds.
- ³ AABOUD 19s based on 36.1 fb⁻¹ at $\sqrt{s} = 13$ TeV of *pp* data. Uses events with one or two hadronically decaying τ and multiple jets. A multivariate analysis is performed to distinguish the signal from backgrounds.
- ⁴ AABOUD 18x based on 36.1 fb⁻¹ at $\sqrt{s} = 13$ TeV of *pp* data. $\ell\ell$ (same sign) + $\geq 4j$ mode and $\ell\ell\ell + \geq 2j$ mode are targeted and specialized boosted decision trees are used to distinguish signals from backgrounds.
- ⁵ SIRUNYAN 18bc based on 35.9 fb⁻¹ at $\sqrt{s} = 13$ TeV of *pp* data. Two channels $pp \rightarrow tH$ and $pp \rightarrow t\bar{t}$ in final states with one isolated lepton and ≥ 3 jets with ≥ 2 b jets are considered assuming a single tHc FCNC coupling. Reconstructed kinematical variables are fed into a multivariate analysis and no significant deviation is observed from the predicted background.
- ⁶ AABOUD 17av based on 36.1 fb⁻¹ at $\sqrt{s} = 13$ TeV of *pp* data. Search for $t\bar{t}$ events, where the other top quark decays hadronically or semi-leptonically. The upper bound on the H - t - c Yukawa couplings is 0.090 (95% CL).
- ⁷ KHACHATRYAN 17I based on 19.7 fb⁻¹ of *pp* data at $\sqrt{s} = 8$ TeV, using the topologies $t\bar{t} \rightarrow Hq+Wb$, where $q=u, c$.
- ⁸ AAD 15c0 based on 20.3 fb⁻¹ at $\sqrt{s} = 8$ TeV of *pp* data. Searches for $t\bar{t}$ events, where the other top quark decays semi-leptonically. Exploits high multiplicity of b -jets and uses a likelihood discriminant. Combining with other ATLAS searches for different Higgs decay modes, $B(t \rightarrow Hc) < 0.46\%$ and $B(t \rightarrow Hu) < 0.45\%$ are obtained.
- ⁹ AAD 14AA based on 4.7 fb⁻¹ at $\sqrt{s} = 7$ TeV and 20.3 fb⁻¹ at $\sqrt{s} = 8$ TeV of *pp* data. The upper-bound is for the sum of $B(t \rightarrow Hc)$ and $B(t \rightarrow Hu)$. Search for $t\bar{t}$ events, where the other top quark decays hadronically or semi-leptonically. The upper bound constrains the H - t - c Yukawa couplings $\sqrt{|Y_{tCL}^H|^2 + |Y_{tCR}^H|^2} < 0.17$ (95% CL).
- ¹⁰ Based on 19.5 fb⁻¹ of *pp* data at $\sqrt{s} = 8$ TeV. Search for final states with 3 or more isolated high E_T charged leptons ($\ell = e, \mu$) bounds the $t \rightarrow Hc$ decay in $t\bar{t}$ events when H decays contain a pair of leptons. The upper bound constrains the H - t - c Yukawa couplings $\sqrt{|Y_{tCL}^H|^2 + |Y_{tCR}^H|^2} < 0.21$ (95% CL).
- ¹¹ KHACHATRYAN 14Q based on 19.5 fb⁻¹ at $\sqrt{s} = 8$ TeV of *pp* data. Search for final states with ≥ 3 isolated charged leptons or with a photon pair accompanied by ≥ 1 lepton(s).

$\Gamma(\ell^+ \bar{q} q' (q=d,s,b; q'=u,c))/\Gamma_{\text{total}}$		Γ_{12}/Γ		
VALUE	CL%	DOCUMENT ID	TECN	COMMENT

- | | | | | |
|---|----|-----------------|-----|-----------------------|
| < 1.6×10^{-3} | 95 | 1 CHATRCHYAN14O | CMS | $\mu + \text{dijets}$ |
| ••• We do not use the following data for averages, fits, limits, etc. ••• | | | | |
| < 1.7×10^{-3} | 95 | 1 CHATRCHYAN14O | CMS | $e + \text{dijets}$ |
- ¹ Based on 19.5 fb⁻¹ of *pp* data at $\sqrt{s} = 8$ TeV. Baryon number violating decays of the top quark are searched for in $t\bar{t}$ production events where one of the pair decays into hadronic three jets.

t-quark EW Couplings

W helicity fractions in top decays. F_0 is the fraction of longitudinal and F_{\pm} the fraction of right-handed W bosons. F_{V+A} is the fraction of $V+A$ current in top decays. The effective Lagrangian (cited by ABAZOV 08AI) has terms f_L^i and f_R^i for $V-A$ and $V+A$ couplings, f_T^i and $f_{T'}^i$ for tensor couplings with b_R and b_L respectively.

F_0		$F_{0.693 \pm 0.013}$ OUR AVERAGE		
VALUE	CL%	DOCUMENT ID	TECN	COMMENT

- | | | | | |
|-----------------------------|--|------------------|-----------|--------------------------------|
| $0.693 \pm 0.009 \pm 0.011$ | | 1 AAD | 20Y LHC | ATLAS+CMS combined |
| $0.726 \pm 0.066 \pm 0.067$ | | 2 AALTONEN | 13D CDF | $F_0 = B(t \rightarrow W_0 b)$ |
| $0.682 \pm 0.030 \pm 0.033$ | | 3 CHATRCHYAN13BH | CMS | $F_0 = B(t \rightarrow W_0 b)$ |
| 0.67 ± 0.07 | | 4 AAD | 12BG ATLS | $F_0 = B(t \rightarrow W_0 b)$ |

0.722±0.062±0.052	5	AALTONEN	12z	TEVA	$F_0 = B(t \rightarrow W_0 b)$
0.669±0.078±0.065	6	ABAZOV	11c	D0	$F_0 = B(t \rightarrow W_0 b)$
0.91 ± 0.37 ± 0.13	7	AFFOLDER	00b	CDF	$F_0 = B(t \rightarrow W_0 b)$
• • • We do not use the following data for averages, fits, limits, etc. • • •					
0.70 ± 0.05	8	AABOUD	17bb	ATLS	$F_0 = 1 - f_1$, Repl by AAD 20Y
0.681±0.012±0.023	9	KHACHATRYAN	16bu	CMS	$F_0 = B(t \rightarrow W_0 b)$, Repl by AAD 20Y
0.70 ± 0.07 ± 0.04	10	AALTONEN	10q	CDF	Repl. by AALTONEN 12z
0.62 ± 0.10 ± 0.05	11	AALTONEN	09q	CDF	Repl. by AALTONEN 10q
0.425±0.166±0.102	12	ABAZOV	08b	D0	Repl. by ABAZOV 11c
0.85 $\begin{smallmatrix} +0.15 \\ -0.22 \end{smallmatrix}$ ± 0.06	13	ABULENCIA	07i	CDF	$F_0 = B(t \rightarrow W_0 b)$
0.74 $\begin{smallmatrix} +0.22 \\ -0.34 \end{smallmatrix}$	14	ABULENCIA	06u	CDF	$F_0 = B(t \rightarrow W_0 b)$
0.56 ± 0.31	15	ABAZOV	05g	D0	$F_0 = B(t \rightarrow W_0 b)$

1 AAD 20Y based on about 20 fb⁻¹ of pp data at $\sqrt{s} = 8$ TeV for each experiment. The first error stands for the sum of the statistical and background uncertainties, and the second error for the remaining systematic uncertainties. The measurements used events with one lepton and different jet multiplicities in the final state. The result is consistent with the NNLO SM prediction of 0.687 ± 0.005 for $m_t = 172.8 \pm 1.3$ GeV.

2 Based on 8.7 fb⁻¹ of data in p \bar{p} collisions at $\sqrt{s} = 1.96$ TeV using t \bar{t} events with $\ell + \cancel{E}_T + \geq 4$ jets ($\geq 1 b$), and under the constraint $F_0 + F_+ + F_- = 1$. The statistical errors of F_0 and F_+ are correlated with correlation coefficient $\rho(F_0, F_+) = -0.69$.

3 Based on 5.0 fb⁻¹ of pp data at $\sqrt{s} = 7$ TeV. CHATRCHYAN 13BH studied tt events with large \cancel{E}_T and $\ell + \geq 4$ jets using a constrained kinematic fit.

4 Based on 1.04 fb⁻¹ of pp data at $\sqrt{s} = 7$ TeV. AAD 12Bg studied tt events with large \cancel{E}_T and either $\ell + \geq 4j$ or $\ell\ell + \geq 2j$. The uncertainties are not independent, $\rho(F_0, F_-) = -0.96$.

5 Based on 2.7 and 5.1 fb⁻¹ of CDF data in $\ell +$ jets and dilepton channels, and 5.4 fb⁻¹ of D0 data in $\ell +$ jets and dilepton channels. $F_0 = 0.682 \pm 0.035 \pm 0.046$ if $F_+ = 0.0017(1)$, while $F_+ = -0.015 \pm 0.018 \pm 0.030$ if $F_0 = 0.688(4)$, where the assumed fixed values are the SM prediction for $m_t = 173.3 \pm 1.1$ GeV and $m_W = 80.399 \pm 0.023$ GeV.

6 Results are based on 5.4 fb⁻¹ of data in p \bar{p} collisions at 1.96 TeV, including those of ABAZOV 08b. Under the SM constraint of $f_0 = 0.698$ (for $m_t = 173.3$ GeV, $m_W = 80.399$ GeV), $f_+ = 0.010 \pm 0.022 \pm 0.030$ is obtained.

7 AFFOLDER 00b studied the angular distribution of leptonic decays of W bosons in $t \rightarrow Wb$ events. The ratio F_0 is the fraction of the helicity zero (longitudinal) W bosons in the decaying top quark rest frame. $B(t \rightarrow W_+ b)$ is the fraction of positive helicity (right-handed) positive charge W bosons in the top quark decays. It is obtained by assuming the Standard Model value of F_0 .

8 AABOUD 17bb based on 20.2 fb⁻¹ of pp data at $\sqrt{s} = 8$ TeV. Triple-differential decay rate of top quark in the t-channel single-top production is used to simultaneously determine five generalized Wtb couplings as well as the top polarization. No assumption is made for the other couplings. See this paper for constraints on other couplings not included here. The paper reported f_1 and we converted it to F_0 .

9 KHACHATRYAN 16bu based on 19.8 fb⁻¹ of pp data at $\sqrt{s} = 8$ TeV using t \bar{t} events with $\ell + \cancel{E}_T + \geq 4$ jets ($\geq 2 b$). The errors of F_0 and F_- are correlated with a correlation coefficient $\rho(F_0, F_-) = -0.87$. The result is consistent with the NNLO SM prediction of 0.687 ± 0.005 for $m_t = 172.8 \pm 1.3$ GeV.

10 Results are based on 2.07 fb⁻¹ of data in p \bar{p} collisions at $\sqrt{s} = 1.96$ TeV. F_0 result is obtained by assuming $F_+ = 0$, while F_+ result is obtained for $F_0 = 0.70$, the SM value. Model independent fits for the two fractions give $F_0 = 0.88 \pm 0.11 \pm 0.06$ and $F_+ = -0.15 \pm 0.07 \pm 0.06$ with correlation coefficient of -0.59 . The results are for $m_t = 175$ GeV.

11 Results are based on 1.9 fb⁻¹ of data in p \bar{p} collisions at $\sqrt{s} = 1.96$ TeV. F_0 result is obtained assuming $F_+ = 0$, while F_+ result is obtained for $F_0 = 0.70$, the SM values. Model independent fits for the two fractions give $F_0 = 0.66 \pm 0.16 \pm 0.05$ and $F_+ = -0.03 \pm 0.06 \pm 0.03$.

12 Based on 1 fb⁻¹ at $\sqrt{s} = 1.96$ TeV.

13 Based on 318 pb⁻¹ of data at $\sqrt{s} = 1.96$ TeV.

14 Based on 200 pb⁻¹ of data at $\sqrt{s} = 1.96$ TeV. $t \rightarrow Wb \rightarrow \ell\nu b$ ($\ell = e$ or μ). The errors are stat + syst.

15 ABAZOV 05g studied the angular distribution of leptonic decays of W bosons in t \bar{t} candidate events with lepton + jets final states, and obtained the fraction of longitudinally polarized W under the constraint of no right-handed current, $F_+ = 0$. Based on 125 pb⁻¹ of data at $\sqrt{s} = 1.8$ TeV.

F_-					
0.315±0.010 OUR AVERAGE					
0.315±0.006±0.009	1	AAD	20Y	LHC	ATLAS+CMS combined
0.310±0.022±0.022	2	CHATRCHYAN	13BH	CMS	$F_- = B(t \rightarrow W_- b)$
0.32 ± 0.04	3	AAD	12Bg	ATLS	$F_- = B(t \rightarrow W_- b)$
• • • We do not use the following data for averages, fits, limits, etc. • • •					
> 0.264 ± 0.044	95	4	AABOUD	17BB	ATLS $F_- = f_1(1 - f_1^+)$, Repl. by AAD 20Y
0.323±0.008±0.014	5	KHACHATRYAN	16bu	CMS	$F_- = B(t \rightarrow W_- b)$, Repl. by AAD 20Y

1 AAD 20Y based on about 20 fb⁻¹ of pp data at $\sqrt{s} = 8$ TeV for each experiment. The first error stands for the sum of the statistical and background uncertainties, and the second error for the remaining systematic uncertainties. The measurements used events with one lepton and different jet multiplicities in the final state. The result is consistent with the NNLO SM prediction of 0.311 ± 0.005 for $m_t = 172.8 \pm 1.3$ GeV.

2 Based on 5.0 fb⁻¹ of pp data at $\sqrt{s} = 7$ TeV. CHATRCHYAN 13BH studied tt events with large \cancel{E}_T and $\ell + \geq 4$ jets using a constrained kinematic fit.

3 Based on 1.04 fb⁻¹ of pp data at $\sqrt{s} = 7$ TeV. AAD 12Bg studied tt events with large \cancel{E}_T and either $\ell + \geq 4j$ or $\ell\ell + \geq 2j$. The uncertainties are not independent, $\rho(F_0, F_-) = -0.96$.

4 AABOUD 17BB based on 20.2 fb⁻¹ of pp data at $\sqrt{s} = 8$ TeV. Triple-differential decay rate of top quark in the t-channel single-top production is used to simultaneously determine five generalized Wtb couplings as well as the top polarization. No assumption is made for the other couplings. The authors reported $f_1 = 0.30 \pm 0.05$ and $f_1^+ < 0.120$ which we converted to $F_- = f_1(1 - f_1^+)$. See this paper for constraints on other couplings not included here.

5 KHACHATRYAN 16BU based on 19.8 fb⁻¹ of pp data at $\sqrt{s} = 8$ TeV using t \bar{t} events with $\ell + \cancel{E}_T + \geq 4$ jets ($\geq 2 b$). The errors of F_0 and F_- are correlated with a correlation coefficient $\rho(F_0, F_-) = -0.87$. The result is consistent with the NNLO SM prediction of 0.311 ± 0.005 for $m_t = 172.8 \pm 1.3$ GeV.

F_+					
-0.005±0.007 OUR AVERAGE					
-0.008±0.005±0.006	1	AAD	20Y	LHC	ATLAS+CMS combined
-0.045±0.044±0.058	2	AALTONEN	13D	CDF	$F_+ = B(t \rightarrow W_+ b)$
0.008±0.012±0.014	3	CHATRCHYAN	13BH	CMS	$F_+ = B(t \rightarrow W_+ b)$
0.01 ± 0.05	4	AAD	12Bg	ATLS	$F_+ = B(t \rightarrow W_+ b)$
0.023±0.041±0.034	5	ABAZOV	11c	D0	$F_+ = B(t \rightarrow W_+ b)$
0.11 ± 0.15	6	AFFOLDER	00b	CDF	$F_+ = B(t \rightarrow W_+ b)$
• • • We do not use the following data for averages, fits, limits, etc. • • •					
< 0.036 ± 0.006	95	7	AABOUD	17BB	ATLS $F_+ = f_1 f_1^+$, Repl. by AAD 20Y
-0.004±0.005±0.014	8	KHACHATRYAN	16BU	CMS	$F_+ = B(t \rightarrow W_+ b)$, Repl. by AAD 20Y
-0.033±0.034±0.031	9	AALTONEN	12z	TEVA	$F_+ = B(t \rightarrow W_+ b)$
-0.01 ± 0.02 ± 0.05	10	AALTONEN	10q	CDF	Repl. by AALTONEN 13D
-0.04 ± 0.04 ± 0.03	11	AALTONEN	09q	CDF	Repl. by AALTONEN 10q
0.119±0.090±0.053	12	ABAZOV	08b	D0	Repl. by ABAZOV 11c
0.056±0.080±0.057	13	ABAZOV	07d	D0	$F_+ = B(t \rightarrow W_+ b)$
0.05 $\begin{smallmatrix} +0.11 \\ -0.05 \end{smallmatrix}$ ± 0.03	14	ABULENCIA	07i	CDF	$F_+ = B(t \rightarrow W_+ b)$
< 0.26	95	14	ABULENCIA	07i	CDF $F_+ = B(t \rightarrow W_+ b)$
< 0.27	95	15	ABULENCIA	06u	CDF $F_+ = B(t \rightarrow W_+ b)$
0.00 ± 0.13 ± 0.07	16	ABAZOV	05L	D0	$F_+ = B(t \rightarrow W_+ b)$
< 0.25	95	16	ABAZOV	05L	D0 $F_+ = B(t \rightarrow W_+ b)$
< 0.24	95	17	ACOSTA	05D	CDF $F_+ = B(t \rightarrow W_+ b)$

1 AAD 20Y based on about 20 fb⁻¹ of pp data at $\sqrt{s} = 8$ TeV for each experiment. The first error stands for the sum of the statistical and background uncertainties, and the second error for the remaining systematic uncertainties. The measurements used events with one lepton and different jet multiplicities in the final state. The result is estimated from the measurements of F_0 and F_- assuming unitarity. The value is consistent with the NNLO SM prediction of 0.0017 ± 0.0001 for $m_t = 172.8 \pm 1.3$ GeV.

2 Based on 8.7 fb⁻¹ of data in p \bar{p} collisions at $\sqrt{s} = 1.96$ TeV using t \bar{t} events with $\ell + \cancel{E}_T + \geq 4$ jets ($\geq 1 b$), and under the constraint $F_0 + F_+ + F_- = 1$. The statistical errors of F_0 and F_+ are correlated with correlation coefficient $\rho(F_0, F_+) = -0.69$.

3 Based on 5.0 fb⁻¹ of pp data at $\sqrt{s} = 7$ TeV. CHATRCHYAN 13BH studied tt events with large \cancel{E}_T and $\ell + \geq 4$ jets using a constrained kinematic fit.

4 Based on 1.04 fb⁻¹ of pp data at $\sqrt{s} = 7$ TeV. AAD 12Bg studied tt events with large \cancel{E}_T and either $\ell + \geq 4j$ or $\ell\ell + \geq 2j$.

5 Results are based on 5.4 fb⁻¹ of data in p \bar{p} collisions at 1.96 TeV, including those of ABAZOV 08b. Under the SM constraint of $f_0 = 0.698$ (for $m_t = 173.3$ GeV, $m_W = 80.399$ GeV), $f_+ = 0.010 \pm 0.022 \pm 0.030$ is obtained.

6 AFFOLDER 00b studied the angular distribution of leptonic decays of W bosons in $t \rightarrow Wb$ events. The ratio F_0 is the fraction of the helicity zero (longitudinal) W bosons in the decaying top quark rest frame. $B(t \rightarrow W_+ b)$ is the fraction of positive helicity (right-handed) positive charge W bosons in the top quark decays. It is obtained by assuming the Standard Model value of F_0 .

7 AABOUD 17BB based on 20.2 fb⁻¹ of pp data at $\sqrt{s} = 8$ TeV. Triple-differential decay rate of top quark in the t-channel single-top production is used to simultaneously determine five generalized Wtb couplings as well as the top polarization. No assumption is made for the other couplings. The authors reported $f_1 = 0.30 \pm 0.05$ and $f_1^+ < 0.120$ which we converted to $F_+ = f_1 f_1^+$. See this paper for constraints on other couplings not included here.

8 KHACHATRYAN 16BU based on 19.8 fb⁻¹ of pp data at $\sqrt{s} = 8$ TeV using t \bar{t} events with $\ell + \cancel{E}_T + \geq 4$ jets ($\geq 2 b$). The result is consistent with the NNLO SM prediction of 0.0017 ± 0.0001 for $m_t = 172.8 \pm 1.3$ GeV.

9 Based on 2.7 and 5.1 fb⁻¹ of CDF data in $\ell +$ jets and dilepton channels, and 5.4 fb⁻¹ of D0 data in $\ell +$ jets and dilepton channels. $F_0 = 0.682 \pm 0.035 \pm 0.046$ if $F_+ = 0.0017(1)$, while $F_+ = -0.015 \pm 0.018 \pm 0.030$ if $F_0 = 0.688(4)$, where the assumed fixed values are the SM prediction for $m_t = 173.3 \pm 1.1$ GeV and $m_W = 80.399 \pm 0.023$ GeV.

10 Results are based on 2.7 fb⁻¹ of data in p \bar{p} collisions at $\sqrt{s} = 1.96$ TeV. F_0 result is obtained by assuming $F_+ = 0$, while F_+ result is obtained for $F_0 = 0.70$, the SM value. Model independent fits for the two fractions give $F_0 = 0.88 \pm 0.11 \pm 0.06$ and $F_+ = -0.15 \pm 0.07 \pm 0.06$ with correlation coefficient of -0.59 . The results are for $m_t = 175$ GeV.

11 Results are based on 1.9 fb⁻¹ of data in p \bar{p} collisions at $\sqrt{s} = 1.96$ TeV. F_0 result is obtained assuming $F_+ = 0$, while F_+ result is obtained for $F_0 = 0.70$, the SM values. Model independent fits for the two fractions give $F_0 = 0.66 \pm 0.16 \pm 0.05$ and $F_+ = -0.03 \pm 0.06 \pm 0.03$.

12 Based on 1 fb⁻¹ at $\sqrt{s} = 1.96$ TeV.

13 Based on 370 pb⁻¹ of data at $\sqrt{s} = 1.96$ TeV, using the $\ell +$ jets and dilepton decay channels. The result assumes $F_0 = 0.70$, and it gives $F_+ < 0.23$ at 95% CL.

14 Based on 318 pb⁻¹ of data at $\sqrt{s} = 1.96$ TeV.

15 Based on 200 pb⁻¹ of data at $\sqrt{s} = 1.96$ TeV. $t \rightarrow Wb \rightarrow \ell\nu b$ ($\ell = e$ or μ). The errors are stat + syst.

Quark Particle Listings

 t

- ¹⁶ ABAZOV 05L studied the angular distribution of leptonic decays of W bosons in $t\bar{t}$ events, where one of the W 's from t or \bar{t} decays into e or μ and the other decays hadronically. The fraction of the “+” helicity W boson is obtained by assuming $F_0 = 0.7$, which is the generic prediction for any linear combination of V and A currents. Based on $230 \pm 15 \text{ pb}^{-1}$ of data at $\sqrt{s} = 1.96 \text{ TeV}$.
- ¹⁷ ACOSTA 05D measures the $m_{\ell^+b}^2$ distribution in $t\bar{t}$ production events where one or both W 's decay leptonically to $\ell = e$ or μ , and finds a bound on the V+A coupling of the tbW vertex. By assuming the SM value of the longitudinal W fraction $F_0 = B(t \rightarrow W_0 b) = 0.70$, the bound on F_+ is obtained. If the results are combined with those of AFFOLDER 00B, the bounds become $F_{V+A} < 0.61$ (95% CL) and $F_+ < 0.18$ (95% CL), respectively. Based on $109 \pm 7 \text{ pb}^{-1}$ of data at $\sqrt{s} = 1.8 \text{ TeV}$ (run I).

 F_{V+A}

VALUE	CL%	DOCUMENT ID	TECN	COMMENT
< 0.29	95	¹ ABULENCIA 07G	CDF	$F_{V+A} = B(t \rightarrow Wb_R)$
• • • We do not use the following data for averages, fits, limits, etc. • • •				
$-0.06 \pm 0.22 \pm 0.12$		¹ ABULENCIA 07G	CDF	$F_{V+A} = B(t \rightarrow Wb_R)$
< 0.80	95	² ACOSTA 05D	CDF	$F_{V+A} = B(t \rightarrow Wb_R)$

¹ Based on 700 pb^{-1} of data at $\sqrt{s} = 1.96 \text{ TeV}$.

² ACOSTA 05D measures the $m_{\ell^+b}^2$ distribution in $t\bar{t}$ production events where one or both W 's decay leptonically to $\ell = e$ or μ , and finds a bound on the V+A coupling of the tbW vertex. By assuming the SM value of the longitudinal W fraction $F_0 = B(t \rightarrow W_0 b) = 0.70$, the bound on F_+ is obtained. If the results are combined with those of AFFOLDER 00B, the bounds become $F_{V+A} < 0.61$ (95% CL) and $F_+ < 0.18$ (95% CL), respectively. Based on $109 \pm 7 \text{ pb}^{-1}$ of data at $\sqrt{s} = 1.8 \text{ TeV}$ (run I).

 f_1^R

VALUE	CL%	DOCUMENT ID	TECN	COMMENT
• • • We do not use the following data for averages, fits, limits, etc. • • •				
$-0.11 < f_1^R < 0.16$	95	¹ AAD	20Y LHC	ATLAS+CMS combined
$ f_1^R/f_2^R < 0.37$	95	² AABOUD	17BB ATLS	t -channel single top
$ f_1^R < 0.16$	95	³ KHACHATRYAN..17G	CMS	t -channel single-t prod.
$-0.20 < \text{Re}(V_{tb} f_1^R) < 0.23$	95	⁴ AAD	12BG ATLS	Constr. on Wtb vtx
$(V_{tb} f_1^R)^2 < 0.93$	95	⁵ ABAZOV	12E D0	Single-top
$ f_1^R ^2 < 0.30$	95	⁶ ABAZOV	12I D0	single- t + W helicity
$ f_1^R ^2 < 1.01$	95	⁷ ABAZOV	09J D0	$ f_1^L = 1, f_2^R = f_2^L = 0$
$ f_1^R ^2 < 2.5$	95	⁸ ABAZOV	08AI D0	$ f_1^L ^2 = 1.8_{-1.3}^{+1.0}$

¹ AAD 20Y based on about 20 fb^{-1} of pp data at $\sqrt{s} = 8 \text{ TeV}$ for each experiment. The measurements used events with one lepton and different jet multiplicities in the final state. The measurements of F_0 and F_- are used to set the limit. The limit is obtained by assuming the other couplings to have their SM values.

² AABOUD 17BB based on 20.2 fb^{-1} of pp data at $\sqrt{s} = 8 \text{ TeV}$. Triple-differential decay rate of top quark is used to simultaneously determine five generalized Wtb couplings as well as the top polarization. No assumption is made for the other couplings. See this paper for constraints on other couplings not included here.

³ KHACHATRYAN 17G based on 5.0 and 19.7 fb^{-1} of pp data at $\sqrt{s} = 7$ and 8 TeV , respectively. A Bayesian neural network technique is used to discriminate between signal and backgrounds. This is a 95% CL exclusion limit obtained by a three-dimensional fit with simultaneous variation of (f_1^L, f_1^R, f_2^R) .

⁴ Based on 1.04 fb^{-1} of pp data at $\sqrt{s} = 7 \text{ TeV}$. AAD 12BG studied tt events with large E_T and either $\ell + \geq 4j$ or $\ell\ell + \geq 2j$.

⁵ Based on 5.4 fb^{-1} of data. For each value of the form factor quoted the other two are assumed to have their SM value. Their Fig. 4 shows two-dimensional posterior probability density distributions for the anomalous couplings.

⁶ Based on 5.4 fb^{-1} of data in $p\bar{p}$ collisions at 1.96 TeV . Results are obtained by combining the limits from the W helicity measurements and those from the single top quark production.

⁷ Based on 1 fb^{-1} of data at $p\bar{p}$ collisions $\sqrt{s} = 1.96 \text{ TeV}$. Combined result of the W helicity measurement in $t\bar{t}$ events (ABAZOV 08B) and the search for anomalous tbW couplings in the single top production (ABAZOV 08AI). Constraints when f_1^L and one of the anomalous couplings are simultaneously allowed to vary are given in their Fig. 1 and Table 1.

⁸ Result is based on 0.9 fb^{-1} of data at $\sqrt{s} = 1.96 \text{ TeV}$. Single top quark production events are used to measure the Lorentz structure of the tbW coupling. The upper bounds on the non-standard couplings are obtained when only one non-standard coupling is allowed to be present together with the SM one, $f_1^L = V_{tb}^*$.

 f_2^L

VALUE	CL%	DOCUMENT ID	TECN	COMMENT
• • • We do not use the following data for averages, fits, limits, etc. • • •				
$-0.08 < f_2^L < 0.05$	95	¹ AAD	20Y LHC	ATLAS+CMS combined
$ f_2^L/f_1^L < 0.29$	95	² AABOUD	17BB ATLS	t -channel single top
$ f_2^L < 0.057$	95	³ KHACHATRYAN..17G	CMS	t -channel single-t prod.
$-0.14 < \text{Re}(f_2^L) < 0.11$	95	⁴ AAD	12BG ATLS	Constr. on Wtb vtx
$(V_{tb} f_2^L)^2 < 0.13$	95	⁵ ABAZOV	12E D0	Single-top
$ f_2^L ^2 < 0.05$	95	⁶ ABAZOV	12I D0	single- t + W helicity
$ f_2^L ^2 < 0.28$	95	⁷ ABAZOV	09J D0	$ f_1^L = 1, f_1^R = f_2^R = 0$
$ f_2^L ^2 < 0.5$	95	⁸ ABAZOV	08AI D0	$ f_1^L ^2 = 1.4_{-0.5}^{+0.6}$

¹ AAD 20Y based on about 20 fb^{-1} of pp data at $\sqrt{s} = 8 \text{ TeV}$ for each experiment. The measurements used events with one lepton and different jet multiplicities in the final state. The measurements of F_0 and F_- are used to set the limit. The limit is obtained by assuming the other couplings to have their SM values.

² AABOUD 17BB based on 20.2 fb^{-1} of pp data at $\sqrt{s} = 8 \text{ TeV}$. Triple-differential decay rate of top quark is used to simultaneously determine five generalized Wtb couplings as well as the top polarization. No assumption is made for the other couplings. See this paper for constraints on other couplings not included here.

³ KHACHATRYAN 17G based on 5.0 and 19.7 fb^{-1} of pp data at $\sqrt{s} = 7$ and 8 TeV , respectively. A Bayesian neural network technique is used to discriminate between signal and backgrounds. This is a 95% CL exclusion limit obtained by a three-dimensional fit with simultaneous variation of (f_1^L, f_2^L, f_2^R) .

⁴ Based on 1.04 fb^{-1} of pp data at $\sqrt{s} = 7 \text{ TeV}$. AAD 12BG studied tt events with large E_T and either $\ell + \geq 4j$ or $\ell\ell + \geq 2j$.

⁵ Based on 5.4 fb^{-1} of data. For each value of the form factor quoted the other two are assumed to have their SM value. Their Fig. 4 shows two-dimensional posterior probability density distributions for the anomalous couplings.

⁶ Based on 5.4 fb^{-1} of data in $p\bar{p}$ collisions at 1.96 TeV . Results are obtained by combining the limits from the W helicity measurements and those from the single top quark production.

⁷ Based on 1 fb^{-1} of data at $p\bar{p}$ collisions $\sqrt{s} = 1.96 \text{ TeV}$. Combined result of the W helicity measurement in $t\bar{t}$ events (ABAZOV 08B) and the search for anomalous tbW couplings in the single top production (ABAZOV 08AI). Constraints when f_1^L and one of the anomalous couplings are simultaneously allowed to vary are given in their Fig. 1 and Table 1.

⁸ Result is based on 0.9 fb^{-1} of data at $\sqrt{s} = 1.96 \text{ TeV}$. Single top quark production events are used to measure the Lorentz structure of the tbW coupling. The upper bounds on the non-standard couplings are obtained when only one non-standard coupling is allowed to be present together with the SM one, $f_1^L = V_{tb}^*$.

 f_2^R

VALUE	CL%	DOCUMENT ID	TECN	COMMENT
• • • We do not use the following data for averages, fits, limits, etc. • • •				
$-0.04 < f_2^R < 0.02$	95	¹ AAD	20Y LHC	ATLAS+CMS combined
$-0.12 < \text{Re}(f_2^R/f_1^L) < 0.17$	95	² AABOUD	17BB ATLS	t -channel single top
$-0.07 < \text{Im}(f_2^R/f_1^L) < 0.06$	95	² AABOUD	17BB ATLS	t -channel single top
$-0.18 < \text{Im}(f_2^R) < 0.06$	95	³ AABOUD	17I ATLS	t -channel single top
$-0.049 < f_2^R < 0.048$	95	⁴ KHACHATRYAN..17G	CMS	t -channel single top
$-0.36 < \text{Re}(f_2^R/f_1^L) < 0.10$	95	⁵ AAD	16AK ATLS	Single-top
$-0.17 < \text{Im}(f_2^R/f_1^L) < 0.23$	95	⁵ AAD	16AK ATLS	Single-top
$-0.08 < \text{Re}(f_2^R) < 0.04$	95	⁶ AAD	12BG ATLS	Constr. on Wtb vtx
$(V_{tb} f_2^R)^2 < 0.06$	95	⁷ ABAZOV	12E D0	Single-top
$ f_2^R ^2 < 0.12$	95	⁸ ABAZOV	12I D0	single- t + W helicity
$ f_2^R ^2 < 0.23$	95	⁹ ABAZOV	09J D0	$ f_1^L = 1, f_1^R = f_2^L = 0$
$ f_2^R ^2 < 0.3$	95	¹⁰ ABAZOV	08AI D0	$ f_1^L ^2 = 1.4_{-0.8}^{+0.9}$

¹ AAD 20Y based on about 20 fb^{-1} of pp data at $\sqrt{s} = 8 \text{ TeV}$ for each experiment. The measurements used events with one lepton and different jet multiplicities in the final state. The measurements of F_0 and F_- are used to set the limit. The limit is obtained by assuming the other couplings to have their SM values.

² AABOUD 17BB based on 20.2 fb^{-1} of pp data at $\sqrt{s} = 8 \text{ TeV}$. Triple-differential decay rate of top quark is used to simultaneously determine five generalized Wtb couplings as well as the top polarization. No assumption is made for the other couplings. See this paper for constraints on other couplings not included here.

³ AABOUD 17I based on 20.2 fb^{-1} of pp data at $\sqrt{s} = 8 \text{ TeV}$. A cut-based analysis is used to discriminate between signal and backgrounds. All anomalous couplings other than $\text{Im}(f_2^R)$ are assumed to be zero. See this paper for a number of other asymmetries and measurements that are not included here.

⁴ KHACHATRYAN 17G based on 5.0 and 19.7 fb^{-1} of pp data at $\sqrt{s} = 7$ and 8 TeV , respectively. A Bayesian neural network technique is used to discriminate between signal and backgrounds. This is a 95% CL exclusion limit obtained by a three-dimensional fit with simultaneous variation of (f_1^L, f_2^L, f_2^R) .

⁵ AAD 16AK based on 4.6 fb^{-1} of pp data at $\sqrt{s} = 7 \text{ TeV}$. The results are obtained from an analysis of angular distributions of the decay products of single top quarks, assuming $f_1^L = f_2^L = 0$. The fraction of decays containing transversely polarized W is measured to be $F_+ + F_- = 0.37 \pm 0.07$.

⁶ Based on 1.04 fb^{-1} of pp data at $\sqrt{s} = 7 \text{ TeV}$. AAD 12BG studied tt events with large E_T and either $\ell + \geq 4j$ or $\ell\ell + \geq 2j$.

⁷ Based on 5.4 fb^{-1} of data. For each value of the form factor quoted the other two are assumed to have their SM value. Their Fig. 4 shows two-dimensional posterior probability density distributions for the anomalous couplings.

⁸ Based on 5.4 fb^{-1} of data in $p\bar{p}$ collisions at 1.96 TeV . Results are obtained by combining the limits from the W helicity measurements and those from the single top quark production.

⁹ Based on 1 fb^{-1} of data at $p\bar{p}$ collisions $\sqrt{s} = 1.96 \text{ TeV}$. Combined result of the W helicity measurement in $t\bar{t}$ events (ABAZOV 08B) and the search for anomalous tbW couplings in the single top production (ABAZOV 08AI). Constraints when f_1^L and one of the anomalous couplings are simultaneously allowed to vary are given in their Fig. 1 and Table 1.

¹⁰ Result is based on 0.9 fb^{-1} of data at $\sqrt{s} = 1.96 \text{ TeV}$. Single top quark production events are used to measure the Lorentz structure of the tbW coupling. The upper bounds on the non-standard couplings are obtained when only one non-standard coupling is allowed to be present together with the SM one, $f_1^L = V_{tb}^*$.

 $|f_{LV}V_{tb}|$

Assumed that the top-quark-related CKM matrix elements obey the relation $|V_{td}|, |V_{ts}| \ll |V_{tb}|$ and a form factor f_{LV} is determined for each production mode and centre-of-mass energy.

VALUE	DOCUMENT ID	TECN	COMMENT
0.995 ± 0.021 OUR AVERAGE			
0.988 ± 0.024	¹ SIRUNYAN	20AZ CMS	13 TeV, t -channel single top
$1.02 \pm 0.04 \pm 0.02$	² AABOUD	19R LHC	ATLAS + CMS at 7, 8 TeV

¹ SIRUNYAN 20AZ based on 35.9 fb⁻¹ of *pp* data at $\sqrt{s} = 13$ TeV. Final states enriched in single top quark *t*-channel events are used. Several theories beyond the standard model are considered, and by releasing all constraints among the involved parameters. Under the standard model assumption of CKM unitarity, the values are found to be $|V_{tb}| > 0.970$ and $|V_{td}|^2 + |V_{ts}|^2 < 0.057$, both at 95% CL.

² The combination of single-top production cross-section measurements in the *t*-channel, *tW*, and *s*-channel production modes from ATLAS and CMS at $\sqrt{s} = 7$ and 8 TeV.

$$|f_{LV} \sqrt{|V_{td}|^2 + |V_{ts}|^2}|$$

Assumed that the top-quark-related CKM matrix elements obey the relation $|V_{td}|, |V_{ts}| \ll |V_{tb}|$ and a form factor f_{LV} is determined for each production mode and centre-of-mass energy.

VALUE	DOCUMENT ID	TECN	COMMENT
0.24 ± 0.12	¹ SIRUNYAN 20AZ CMS	t-channel single top	

¹ We report the square root of SIRUNYAN 20AZ result based on 35.9 fb⁻¹ of *pp* data at $\sqrt{s} = 13$ TeV measured $|V_{td}|^2 + |V_{ts}|^2 = 0.06 \pm 0.06$ using final states enriched in single top quark *t*-channel events by releasing all constraints from unitarity of the CKM matrix within the SM. Under the standard model assumption of CKM unitarity, the values are found to be $|V_{tb}| > 0.970$ and $|V_{td}|^2 + |V_{ts}|^2 < 0.057$, both at 95% CL.

Chromo-magnetic dipole moment $\mu_t = g_s \hat{\mu}_t / m_t$

VALUE	CL%	DOCUMENT ID	TECN	COMMENT
-0.024 ^{+0.013+0.016} _{-0.009-0.011}	95	¹ SIRUNYAN 20AM CMS	$\ell + \text{jets}$	
-0.014 < $\hat{\mu}_t$ < 0.004	95	² SIRUNYAN 19BX CMS	$\ell\ell + \geq 2j$ ($\geq 1b$)	
-0.053 < $\text{Re}(\hat{\mu}_t)$ < 0.026	95	³ KHACHATRYAN...16AI CMS	$\ell\ell + \geq 2j$ ($\geq 1b$)	

¹ SIRUNYAN 20AM based on 35.9 fb⁻¹ of *pp* data at $\sqrt{s} = 13$ TeV. $t\bar{t}$ with low and high boosts are reconstructed through a fit of the kinematic distributions. The $q\bar{q}$ initial subprocess is separated using different dependencies of the distributions on the initial states, and the linearized forward-backward asymmetry is measured to be $A_{FB}^{(1)} = 0.048 \pm 0.095 \pm 0.020$ -0.087 - 0.029.

² SIRUNYAN 19BX based on 35.9 fb⁻¹ of *pp* data at $\sqrt{s} = 13$ TeV. A set of parton-level normalized differential cross sections is measured to extract coefficients of the spin-dependent $t\bar{t}$ production density matrix. The coefficients are compared with the NLO MC simulations and with the NLO QCD calculation including EW corrections.

³ KHACHATRYAN 16AI based on 19.5 fb⁻¹ of *pp* data at $\sqrt{s} = 8$ TeV, using lepton angular distributions as a function of the $t\bar{t}$ -system kinematical variables.

Chromo-electric dipole moment $d_t = g_s \hat{d}_t / m_t$

VALUE	CL%	DOCUMENT ID	TECN	COMMENT
$ \hat{d}_t < 0.03$	95	¹ SIRUNYAN 20AM CMS	$\ell + \text{jets}$	
-0.020 < \hat{d}_t < 0.012	95	² SIRUNYAN 19BX CMS	$\ell\ell + \geq 2j$ ($\geq 1b$)	
-0.068 < $\text{Im}(\hat{d}_t)$ < 0.067	95	³ KHACHATRYAN...16AI CMS	$\ell\ell + \geq 2j$ ($\geq 1b$)	

¹ SIRUNYAN 20AM based on 35.9 fb⁻¹ of *pp* data at $\sqrt{s} = 13$ TeV. $t\bar{t}$ with low and high boosts are reconstructed through a fit of the kinematic distributions. The $q\bar{q}$ initial subprocess is separated using different dependencies of the distributions on the initial states, and the linearized forward-backward asymmetry is measured to be $A_{FB}^{(1)} = 0.048 \pm 0.095 \pm 0.020$ -0.087 - 0.029.

² SIRUNYAN 19BX based on 35.9 fb⁻¹ of *pp* data at $\sqrt{s} = 13$ TeV. A set of parton-level normalized differential cross sections is measured to extract coefficients of the spin-dependent $t\bar{t}$ production density matrix and constrain the anomalous chromomagnetic and chromoelectric dipole moments of the top quark. The coefficients are compared with the NLO MC simulations and with the NLO QCD calculation including EW corrections.

³ KHACHATRYAN 16AI based on 19.5 fb⁻¹ of *pp* data at $\sqrt{s} = 8$ TeV, using lepton angular distributions as a function of the $t\bar{t}$ -system kinematical variables.

Spin Correlation in $t\bar{t}$ Production in $p\bar{p}$ Collisions

C is the correlation strength parameter, f is the ratio of events with correlated t and \bar{t} spins (SM prediction: $f = 1$), and κ is the spin correlation coefficient. See "The Top Quark" review for more information.

VALUE	DOCUMENT ID	TECN	COMMENT
0.89 ± 0.22	¹ ABAZOV 16A D0	f ($\ell\ell + \geq 2$ jets, $\ell + \geq 4$ jets)	
0.85 ± 0.29	² ABAZOV 12B D0	f ($\ell\ell + \geq 2$ jets, $\ell + \geq 4$ jets)	
1.15 ^{+0.42} _{-0.43}	³ ABAZOV 12B D0	f ($\ell + \cancel{E}_T + \geq 4$ jets)	
0.60 ^{+0.50} _{-0.16}	⁴ AALTONEN 11AR CDF	κ ($\ell + \cancel{E}_T + \geq 4$ jets)	
0.74 ^{+0.40} _{-0.41}	⁵ ABAZOV 11AE D0	f ($\ell\ell + \cancel{E}_T + \geq 2$ jets)	
0.10 ± 0.45	⁶ ABAZOV 11AF D0	C ($\ell\ell + \cancel{E}_T + \geq 2$ jets)	

¹ ABAZOV 16A based on 9.7 fb⁻¹ of data. A matrix element method is used. It corresponds to evidence of spin correlation at 4.2 σ and is in agreement with the NLO SM prediction 0.80^{+0.01}_{-0.02}.

² This is a combination of the lepton + jets analysis presented in ABAZOV 12B and the dilepton measurement of ABAZOV 11AE. It provides a 3.1 σ evidence for the $t\bar{t}$ spin correlation.

³ Based on 5.3 fb⁻¹ of data. The error is statistical and systematic combined. A matrix element method is used.

⁴ Based on 4.3 fb⁻¹ of data. The measurement is based on the angular study of the top quark decay products in the helicity basis. The theory prediction is $\kappa \approx 0.40$.

⁵ Based on 5.4 fb⁻¹ of data using a matrix element method. The error is statistical and systematic combined. The no-correlation hypothesis is excluded at the 97.7% CL.

⁶ Based on 5.4 fb⁻¹ of data. The error is statistical and systematic combined. The NLO QCD prediction is $C = 0.78 \pm 0.03$. The neutrino weighting method is used for reconstruction of kinematics.

Spin Correlation in $t\bar{t}$ Production in pp Collisions

Spin correlation, f_{SM} , measures the strength of the correlation between the spins of the pair produced $t\bar{t}$. $f_{SM} = 1$ for the SM, while $f_{SM} = 0$ for no spin correlation.

VALUE	DOCUMENT ID	TECN	COMMENT
0.90 ± 0.07 ± 0.09 ± 0.01	¹ SIRUNYAN 19BX CMS	C_{kk} in $\ell\ell + \geq 2j$ ($\geq 1b$)	
1.13 ± 0.32 ± 0.32 ^{+0.10} _{-0.13}	¹ SIRUNYAN 19BX CMS	C_{rr} in $\ell\ell + \geq 2j$ ($\geq 1b$)	
1.01 ± 0.04 ± 0.05 ± 0.01	¹ SIRUNYAN 19BX CMS	C_{nn} in $\ell\ell + \geq 2j$ ($\geq 1b$)	
0.94 ± 0.17 ± 0.26 ± 0.01	¹ SIRUNYAN 19BX CMS	$C_{rk} + C_{kr}$ in $\ell\ell + \geq 2j$ ($\geq 1b$)	
0.98 ± 0.03 ± 0.04 ± 0.01	¹ SIRUNYAN 19BX CMS	$(C_{kk} + C_{rr} + C_{nn})/3$ in $\ell\ell + \geq 2j$ ($\geq 1b$)	
0.74 ± 0.07 ± 0.19 ^{+0.06} _{-0.08}	¹ SIRUNYAN 19BX CMS	$A_{\cos\phi}^{lab}$ in $\ell\ell + \geq 2j$ ($\geq 1b$)	
1.05 ± 0.03 ± 0.08 ^{+0.09} _{-0.12}	¹ SIRUNYAN 19BX CMS	$A_{ \Delta\phi(\ell\ell) }$ in $\ell\ell + \geq 2j$ ($\geq 1b$)	
1.12 ^{+0.12} _{-0.15}	² KHACHATRYAN...16AI CMS	$\ell\ell + \geq 2j$ ($\geq 1b$)	
0.72 ± 0.08 ± 0.15 ^{+0.13} _{-0.13}	³ KHACHATRYAN...16X CMS	$\mu + 4,5j$	
1.20 ± 0.05 ± 0.13	⁴ AAD 15J ATLAS	$\Delta\phi(\ell\ell)$ in $\ell\ell + \geq 2j$ ($\geq 1b$)	
1.19 ± 0.09 ± 0.18	⁵ AAD 14BB ATLAS	$\Delta\phi(\ell\ell)$ in $\ell\ell + \geq 2j$ events	
1.12 ± 0.11 ± 0.22	⁵ AAD 14BB ATLAS	$\Delta\phi(\ell j)$ in $\ell + \geq 4j$ events	
0.87 ± 0.11 ± 0.14	^{5,6} AAD 14BB ATLAS	S-ratio in $\ell\ell + \geq 2j$ events	
0.75 ± 0.19 ± 0.23	^{5,7} AAD 14BB ATLAS	$\cos\theta(\ell^+) \cos\theta(\ell^-)$ in $\ell\ell + \geq 2j$ events	
0.83 ± 0.14 ± 0.18	^{5,8} AAD 14BB ATLAS	$\cos\theta(\ell^+) \cos\theta(\ell^-)$ in $\ell\ell + \geq 2j$ events	

¹ SIRUNYAN 19BX based on 35.9 fb⁻¹ of *pp* data at $\sqrt{s} = 13$ TeV. A set of parton-level normalized differential cross sections sensitive to coefficients of the spin-dependent $t\bar{t}$ production density matrix is measured. The distributions and coefficients are compared with the NLO MC simulations and with the NLO QCD calculation including EW corrections. Three errors are from statistics, experimental systematics, and theory.

² KHACHATRYAN 16AI based on 19.5 fb⁻¹ of *pp* data at $\sqrt{s} = 8$ TeV, using lepton angular distributions as a function of the $t\bar{t}$ -system kinematical variables.

³ KHACHATRYAN 16X based on 19.7 fb⁻¹ of *pp* data at $\sqrt{s} = 8$ TeV. Uses a template fit method. Spin correlation strength in the helicity basis is given by $A_{hel} = 0.23 \pm 0.03 \pm 0.05$ -0.04.

⁴ AAD 15J based on 20.3 fb⁻¹ of *pp* data at $\sqrt{s} = 8$ TeV. Uses a fit including a linear superposition of $\Delta\phi$ distribution from the SM NLO simulation with coefficient f_{SM} and from $t\bar{t}$ simulation without spin correlation with coefficient $(1 - f_{SM})$.

⁵ Based on 4.6 fb⁻¹ of *pp* data at $\sqrt{s} = 7$ TeV. The results are for $m_t = 172.5$ GeV.

⁶ The S-ratio is defined as the SM spin correlation in the like-helicity gluon-gluon collisions normalized to the no spin correlation case; see eq. (6) for the LO expression.

⁷ The polar angle correlation along the helicity axis.

⁸ The polar angle correlation along the direction which maximizes the correlation.

t-quark FCNC Couplings κ^{uqg}/Λ and κ^{dqg}/Λ

VALUE (TeV ⁻¹)	CL%	DOCUMENT ID	TECN	COMMENT
< 0.0041	95	¹ KHACHATRYAN...17G CMS	$ \kappa^{tug} /\Lambda$	
< 0.018	95	¹ KHACHATRYAN...17G CMS	$ \kappa^{tcg} /\Lambda$	
< 0.0058	95	² AAD 16As ATLAS	κ^{tug}/Λ	
< 0.013	95	² AAD 16As ATLAS	κ^{tcg}/Λ	
< 0.0069	95	³ AAD 12BP ATLAS	t^{tug}/Λ ($t^{tug} = 0$)	
< 0.016	95	³ AAD 12BP ATLAS	t^{tcg}/Λ ($t^{tug} = 0$)	
< 0.013	95	⁴ ABAZOV 10K D0	κ^{tug}/Λ	
< 0.057	95	⁴ ABAZOV 10K D0	κ^{tcg}/Λ	
< 0.018	95	⁵ AALTONEN 09N CDF	κ^{tug}/Λ ($\kappa^{tcg} = 0$)	
< 0.069	95	⁵ AALTONEN 09N CDF	κ^{tcg}/Λ ($\kappa^{tug} = 0$)	
< 0.037	95	⁶ ABAZOV 07v D0	κ^{utg}/Λ	
< 0.15	95	⁶ ABAZOV 07v D0	κ^{ctg}/Λ	

¹ KHACHATRYAN 17G based on 5.0 and 19.7 fb⁻¹ of *pp* data at $\sqrt{s} = 7$ and 8 TeV, respectively. *t*-channel single top production is used. The result corresponds to $B(t \rightarrow ug) < 2.0 \times 10^{-5}$ or $B(t \rightarrow cg) < 4.1 \times 10^{-4}$.

² AAD 16As based on 20.3 fb⁻¹ of *pp* data at $\sqrt{s} = 8$ TeV. The results are obtained from the 95% CL upper limit on the single top-quark production $\sigma(qg \rightarrow t) \cdot B(t \rightarrow bW) < 3.4$ pb, $B(t \rightarrow ug) < 4.0 \times 10^{-5}$ and $B(t \rightarrow cg) < 20 \times 10^{-5}$.

³ Based on 2.05 fb⁻¹ of *pp* data at $\sqrt{s} = 7$ TeV. The results are obtained from the 95% CL upper limit on the single top-quark production $\sigma(qg \rightarrow t) \cdot B(t \rightarrow bW) < 3.9$ pb, for $q = u$ or $q = c$, $B(t \rightarrow ug) < 5.7 \times 10^{-5}$ and $B(t \rightarrow cg) < 2.7 \times 10^{-4}$.

⁴ Based on 2.3 fb⁻¹ of data in $p\bar{p}$ collisions at $\sqrt{s} = 1.96$ TeV. Upper limit of single top quark production cross section 0.20 pb and 0.27 pb via FCNC *t*-*u*-*g* and *t*-*c*-*g* couplings, respectively, lead to the bounds without assuming the absence of the other coupling. $B(t \rightarrow ug) < 2.0 \times 10^{-4}$ and $B(t \rightarrow cg) < 3.9 \times 10^{-3}$ follow.

⁵ Based on 2.2 fb⁻¹ of data in $p\bar{p}$ collisions at $\sqrt{s} = 1.96$ TeV. Upper limit of single top quark production cross section $\sigma(u(c) + g \rightarrow t) < 1.8$ pb (95% CL) via FCNC *t*-*u*-*g* and *t*-*c*-*g* couplings lead to the bounds. $B(t \rightarrow ug) < 3.9 \times 10^{-4}$ and $B(t \rightarrow cg) < 5.7 \times 10^{-3}$ follow.

⁶ Result is based on 230 pb⁻¹ of data at $\sqrt{s} = 1.96$ TeV. Absence of single top quark production events via FCNC *t*-*u*-*g* and *t*-*c*-*g* couplings lead to the upper bounds on the dimensioned couplings, κ^{utg}/Λ and κ^{ctg}/Λ , respectively.

Quark Particle Listings

 t **t -Quark Yukawa Coupling from $t\bar{t}$ Kinematic Distributions in pp Collisions**The ratio of t -quark Yukawa coupling to its standard model predicted value.

VALUE	CL%	DOCUMENT ID	TECN	COMMENT
•••				We do not use the following data for averages, fits, limits, etc. •••
$1.16^{+0.24}_{-0.35}$	1	SIRUNYAN	20BH CMS	$\ell\ell$ ($\ell=e,\mu$) + jets ($\geq 2b_j$) + \cancel{E}_T
$1.07^{+0.34}_{-0.43}$	2	SIRUNYAN	19BY CMS	ℓ +jets, $t\bar{t}$ threshold

¹ SIRUNYAN 20BH based on 137 fb^{-1} of data at $\sqrt{s} = 13\text{ TeV}$. Kinematic distributions of $t\bar{t}$ are compared with predictions by different values of the top Yukawa coupling in loop corrections, where the scaling of the SM coupling is used within the κ -framework. The \cancel{E}_T cut applies only to the same-flavor dilepton, not $e\mu$ events.

² SIRUNYAN 19BY based on 35.8 fb^{-1} of data at $\sqrt{s} = 13\text{ TeV}$. Experimental sensitivity is enhanced in the low $M_{t\bar{t}}$ region. The distributions of $M_{t\bar{t}}$, $|y_t - y_{\bar{t}}|$, and the number of reconstructed jets are compared with predictions by different Yukawa couplings which include NNLO QCD and NLO EW corrections.

 $\sigma(Ht\bar{t})/\sigma(Ht\bar{t})_{SM}$

VALUE	CL%	DOCUMENT ID	TECN	COMMENT
•••				We do not use the following data for averages, fits, limits, etc. •••
$1.43^{+0.33+0.21}_{-0.31-0.15}$	1	AAD	20z ATLS	$Ht\bar{t}$ ($H \rightarrow \gamma\gamma$)
$1.38^{+0.29+0.21}_{-0.27-0.11}$	2	SIRUNYAN	20As CMS	$Ht\bar{t}$ ($H \rightarrow \gamma\gamma$)
$0.72 \pm 0.24 \pm 0.38$	3	SIRUNYAN	19R CMS	$Ht\bar{t}$ ($H \rightarrow b\bar{b}$, $t\bar{t} \rightarrow \ell$ +jets or dilepton)
$0.9 \pm 0.7 \pm 1.3$	4	SIRUNYAN	18BD CMS	$Ht\bar{t}$ ($H \rightarrow b\bar{b}$, $t\bar{t} \rightarrow$ all jets)
$1.26^{+0.31}_{-0.26}$	5	SIRUNYAN	18L CMS	combination of CMS
<6.7	95	6 AAD	15 ATLS	$Ht\bar{t}$; $H \rightarrow \gamma\gamma$
2.8 ± 1.0	7	KHACHATRY..14H	CMS	$H \rightarrow b\bar{b}$, $\tau_h\tau_h$, $\gamma\gamma$, WW/ZZ (leptons)

¹ AAD 20z based on 139 fb^{-1} of pp data at 13 TeV . Assuming a CP -even coupling the $t\bar{t}H$ process is observed with a significance of 5.2σ , and the measured $\sigma_{t\bar{t}H} \cdot B_{\gamma\gamma} = 1.64^{+0.38+0.17}_{-0.36-0.14}\text{ fb}$. A CP -mixing angle $|\alpha| > 43^\circ$ is excluded at 95% CL.

² SIRUNYAN 20As based on 137 fb^{-1} of pp data at 13 TeV . The $t\bar{t}H$ process is observed with a significance of 6.6σ , and the measured $\sigma_{t\bar{t}H} \cdot B_{\gamma\gamma} = 1.56^{+0.33+0.09}_{-0.30-0.08}\text{ fb}$. The fractional contribution of the CP -odd component is measured to be $f_{CP}^{t\bar{t}H} = 0.00 \pm 0.33$.

³ SIRUNYAN 19R based on 35.9 fb^{-1} of pp data at 13 TeV . Multivariate techniques are employed to separate the signal from the dominant $t\bar{t}$ +jets background. The result is for $m_H = 125\text{ GeV}$. The measured ratio corresponds to a signal significance of 1.6σ above the background-only hypothesis.

⁴ SIRUNYAN 18BD based on 35.9 fb^{-1} of pp data at 13 TeV . A combined fit of signal and background templates to data is performed in six event categories separated by jet and b -jet multiplicities. An upper limit of 3.8 is obtained for the cross section ratio.

⁵ SIRUNYAN 18L based on up to 5.1 , 19.7 , and 35.9 fb^{-1} of pp data at 7 , 8 , and 13 TeV , respectively. An excess of events is observed, with a significance of 5.2 standard deviations, over the expectation from the background-only hypothesis. The result is for the Higgs boson mass of 125.09 GeV .

⁶ Based on 4.5 fb^{-1} of data at 7 TeV and 20.3 fb^{-1} at 8 TeV . The result is for $m_H = 125.4\text{ GeV}$. The measurement constrains the top quark Yukawa coupling strength parameter $\kappa_t = Y_t/Y_t^{SM}$ to be $-1.3 < \kappa_t < 8.0$ (95% CL).

⁷ Based on 5.1 fb^{-1} of pp data at 7 TeV and 19.7 fb^{-1} at 8 TeV . The results are obtained by assuming the SM decay branching fractions for the Higgs boson of mass 125.6 GeV . The signal strength for individual Higgs decay channels are given in Fig. 13, and the preferred region in the (κ_V, κ_f) space is given in Fig. 14.

Single t -Quark Production Cross Section in $p\bar{p}$ Collisions at $\sqrt{s} = 1.8\text{ TeV}$ Direct probe of the $t\bar{b}W$ coupling and possible new physics at $\sqrt{s} = 1.8\text{ TeV}$.

VALUE (pb)	CL%	DOCUMENT ID	TECN	COMMENT
•••				We do not use the following data for averages, fits, limits, etc. •••
<24	95	1 ACOSTA	04H CDF	$p\bar{p} \rightarrow tb + X$, $tqb + X$
<18	95	2 ACOSTA	02 CDF	$p\bar{p} \rightarrow tb + X$
<13	95	3 ACOSTA	02 CDF	$p\bar{p} \rightarrow tqb + X$

¹ ACOSTA 04H bounds single top-quark production from the s -channel W -exchange process, $q'\bar{q} \rightarrow t\bar{b}$, and the t -channel W -exchange process, $q'\bar{q} \rightarrow qt\bar{b}$. Based on $\sim 106\text{ pb}^{-1}$ of data.

² ACOSTA 02 bounds the cross section for single top-quark production via the s -channel W -exchange process, $q'\bar{q} \rightarrow t\bar{b}$. Based on $\sim 106\text{ pb}^{-1}$ of data.

³ ACOSTA 02 bounds the cross section for single top-quark production via the t -channel W -exchange process, $q'\bar{q} \rightarrow qt\bar{b}$. Based on $\sim 106\text{ pb}^{-1}$ of data.

Single t -Quark Production Cross Section in $p\bar{p}$ Collisions at $\sqrt{s} = 1.96\text{ TeV}$ Direct probes of the $t\bar{b}W$ coupling and possible new physics at $\sqrt{s} = 1.96\text{ TeV}$.

OUR AVERAGE assumes that the systematic uncertainties are uncorrelated.

VALUE (pb)	CL%	DOCUMENT ID	TECN	COMMENT
•••				We do not use the following data for averages, fits, limits, etc. •••
$3.53^{+1.25}_{-1.16}$	1	AALTONEN	16 CDF	s - + t -channels ($0\ell + \cancel{E}_T + 2, 3j$ ($\geq 1b$ -tag))
$2.25^{+0.29}_{-0.31}$	2	AALTONEN	15H TEVA	t -channel
$3.30^{+0.52}_{-0.40}$	2,3	AALTONEN	15H TEVA	s - + t -channels
$1.12^{+0.61}_{-0.57}$	4	AALTONEN	14K CDF	s -channel ($0\ell + \cancel{E}_T + 2, 3j$ ($\geq 1b$ -tag))
$1.41^{+0.44}_{-0.42}$	5	AALTONEN	14L CDF	s -channel ($\ell + \cancel{E}_T + 2j$ ($\geq 1b$ -tag))

$1.29^{+0.26}_{-0.24}$	6	AALTONEN	14M TEVA	s -channel (CDF + D0)	
$3.04^{+0.57}_{-0.53}$	7	AALTONEN	14o CDF	s + t + Wt ($\ell + \cancel{E}_T + 2$ or 3 jets ($\geq 1b$ -tag))	
$1.10^{+0.33}_{-0.31}$	8	ABAZOV	13o D0	s -channel	
$3.07^{+0.54}_{-0.49}$	8	ABAZOV	13o D0	t -channel	
$4.11^{+0.60}_{-0.55}$	8	ABAZOV	13o D0	s - + t -channels	
0.98 ± 0.63	9	ABAZOV	11AA D0	s -channel	
2.90 ± 0.59	9	ABAZOV	11AA D0	t -channel	
$3.43^{+0.73}_{-0.74}$	10	ABAZOV	11AD D0	s - + t -channels	
$1.8^{+0.7}_{-0.5}$	11	AALTONEN	10AB CDF	s -channel	
0.8 ± 0.4	11	AALTONEN	10AB CDF	t -channel	
$4.9^{+2.5}_{-2.2}$	12	AALTONEN	10U CDF	\cancel{E}_T + jets decay	
$3.14^{+0.94}_{-0.80}$	13	ABAZOV	10 D0	t -channel	
1.05 ± 0.81	13	ABAZOV	10 D0	s -channel	
< 7.3	95	14	ABAZOV	10J D0	τ + jets decay
$2.3^{+0.6}_{-0.5}$	15	AALTONEN	09AT CDF	s - + t -channel	
3.94 ± 0.88	16	ABAZOV	09Z D0	s - + t -channel	
$2.2^{+0.7}_{-0.6}$	17	AALTONEN	08AH CDF	s - + t -channel	
4.7 ± 1.3	18	ABAZOV	08I D0	s - + t -channel	
4.9 ± 1.4	19	ABAZOV	07H D0	s - + t -channel	
< 6.4	95	20	ABAZOV	05P D0	$p\bar{p} \rightarrow tb + X$
< 5.0	95	20	ABAZOV	05P D0	$p\bar{p} \rightarrow tqb + X$
< 10.1	95	21	ACOSTA	05N CDF	$p\bar{p} \rightarrow tqb + X$
< 13.6	95	21	ACOSTA	05N CDF	$p\bar{p} \rightarrow tb + X$
< 17.8	95	21	ACOSTA	05N CDF	$p\bar{p} \rightarrow tb + X$, $tqb + X$

¹ AALTONEN 16 based on 9.5 fb^{-1} of data. This includes, as a part, the result of AALTONEN 14K. Combination of this result with that of AALTONEN 14o gives a s + t cross section of $3.02^{+0.49}_{-0.48}\text{ pb}$ and $|V_{tb}| > 0.84$ (95% CL).

² AALTONEN 15H based on 9.7 fb^{-1} of data per experiment. The result is for $m_t = 172.5\text{ GeV}$, and is a combination of the CDF measurements (AALTONEN 16) and the D0 measurements (ABAZOV 13o) on the t -channel single t -quark production cross section. The result is consistent with the NLO+NNLL SM prediction and gives $|V_{tb}| = 1.02^{+0.06}_{-0.05}$ and $|V_{tb}| > 0.92$ (95% CL).

³ AALTONEN 15H is a combined measurement of s -channel single top cross section by CDF + D0. AALTONEN 14M is not included.

⁴ Based on 9.45 fb^{-1} of data, using neural networks to separate signal from backgrounds. The result is for $m_t = 172.5\text{ GeV}$. Combination of this result with the CDF measurement in the 1 lepton channel AALTONEN 14L gives $1.36^{+0.37}_{-0.32}\text{ pb}$, consistent with the SM prediction, and is 4.2 sigma away from the background only hypothesis.

⁵ Based on 9.4 fb^{-1} of data, using neural networks to separate signal from backgrounds. The result is for $m_t = 172.5\text{ GeV}$. The result is 3.8 sigma away from the background only hypothesis.

⁶ Based on 9.7 fb^{-1} of data per experiment. The result is for $m_t = 172.5\text{ GeV}$, and is a combination of the CDF measurements AALTONEN 14L, AALTONEN 14K and the D0 measurement ABAZOV 13o on the s -channel single t -quark production cross section. The result is consistent with the SM prediction of $1.05 \pm 0.06\text{ pb}$ and the significance of the observation is of 6.3 standard deviations.

⁷ Based on 7.5 fb^{-1} of data. Neural network is used to discriminate signals (s -, t - and Wt -channel single top production) from backgrounds. The result is consistent with the SM prediction, and gives $|V_{tb}| = 0.95 \pm 0.09(\text{stat} + \text{syst}) \pm 0.05(\text{theory})$ and $|V_{tb}| > 0.78$ (95% CL). The result is for $m_t = 172.5\text{ GeV}$.

⁸ Based on 9.7 fb^{-1} of data. Events with $\ell + \cancel{E}_T + 2$ or 3 jets (1 or 2 b -tag) are analysed, assuming $m_t = 172.5\text{ GeV}$. The combined s - + t -channel cross section gives $|V_{tb}| f_1^L = 1.12^{+0.09}_{-0.08}$, or $|V_{tb}| > 0.92$ at 95% CL for $f_1^L = 1$ and a flat prior within $0 \leq |V_{tb}|^2 \leq 1$.

⁹ Based on 5.4 fb^{-1} of data. The error is statistical + systematic combined. The results are for $m_t = 172.5\text{ GeV}$. Results for other m_t values are given in Table 2 of ABAZOV 11AA.

¹⁰ Based on 5.4 fb^{-1} of data and for $m_t = 172.5\text{ GeV}$. The error is statistical + systematic combined. Results for other m_t values are given in Table III of ABAZOV 11AD. The result is obtained by assuming the SM ratio between $t\bar{b}$ (s -channel) and tqb (t -channel) productions, and gives $|V_{tb}| f_1^L = 1.02^{+0.10}_{-0.11}$, or $|V_{tb}| > 0.79$ at 95% CL for a flat prior within $0 < |V_{tb}|^2 < 1$.

¹¹ Based on 3.2 fb^{-1} of data. For combined s - + t -channel result see AALTONEN 09AT.

¹² Result is based on 2.1 fb^{-1} of data. Events with large missing E_T and jets with at least one b -jet without identified electron or muon are selected. Result is obtained when observed 2.1σ excess over the background originates from the signal for $m_t = 175\text{ GeV}$, giving $|V_{tb}| = 1.24^{+0.34}_{-0.29} \pm 0.07(\text{theory})$.

¹³ Result is based on 2.3 fb^{-1} of data. Events with isolated $\ell + \cancel{E}_T + 2, 3, 4$ jets with one or two b -tags are selected. The analysis assumes $m_t = 170\text{ GeV}$.

¹⁴ Result is based on 4.8 fb^{-1} of data. Events with an isolated reconstructed tau lepton, missing $E_T + 2, 3$ jets with one or two b -tags are selected. When combined with ABAZOV 09Z result for $e + \mu$ channels, the s - and t -channels combined cross section is $3.84^{+0.89}_{-0.83}\text{ pb}$.

¹⁵ Based on 3.2 fb^{-1} of data. Events with isolated $\ell + \cancel{E}_T$ + jets with at least one b -tag are analyzed and s - and t -channel single top events are selected by using the likelihood function, matrix element, neural-network, boosted decision tree, likelihood function optimized for s -channel process, and neural-network based analysis of events with \cancel{E}_T that has sensitivity for $W \rightarrow \tau\nu$ decays. The result is for $m_t = 175\text{ GeV}$, and the mean value decreases by 0.02 pb/GeV for smaller m_t . The signal has 5.0

sigma significance. The result gives $|V_{tb}| = 0.91 \pm 0.11$ (stat+syst) ± 0.07 (theory), or $|V_{tb}| > 0.71$ at 95% CL.

- 16 Based on 2.3 fb⁻¹ of data. Events with isolated $\ell + \cancel{E}_T + \geq 2$ jets with 1 or 2 *b*-tags are analyzed and *s*- and *t*-channel single top events are selected by using boosted decision tree, Bayesian neural networks and the matrix element method. The signal has 5.0 sigma significance. The result gives $|V_{tb}| = 1.07 \pm 0.12$, or $|V_{tb}| > 0.78$ at 95% CL. The analysis assumes $m_t = 170$ GeV.
- 17 Result is based on 2.2 fb⁻¹ of data. Events with isolated $\ell + \cancel{E}_T + 2, 3$ jets with at least one *b*-tag are selected, and *s*- and *t*-channel single top events are selected by using likelihood, matrix element, and neural network discriminants. The result can be interpreted as $|V_{tb}| = 0.88_{-0.12}^{+0.13}$ (stat + syst) ± 0.07 (theory), and $|V_{tb}| > 0.66$ (95% CL) under the $|V_{tb}| < 1$ constraint.
- 18 Result is based on 0.9 fb⁻¹ of data. Events with isolated $\ell + \cancel{E}_T + 2, 3, 4$ jets with one or two *b*-vertex-tag are selected, and contributions from *W* + jets, *tT*, *sT*, *s*- and *t*-channel single top events are identified by using boosted decision trees, Bayesian neural networks, and matrix element analysis. The result can be interpreted as the measurement of the CKM matrix element $|V_{tb}| = 1.31_{-0.21}^{+0.25}$, or $|V_{tb}| > 0.68$ (95% CL) under the $|V_{tb}| < 1$ constraint.
- 19 Result is based on 0.9 fb⁻¹ of data. This result constrains V_{tb} to $0.68 < |V_{tb}| \leq 1$ at 95% CL.
- 20 ABAZOV 05p bounds single top-quark production from either the *s*-channel *W*-exchange process, $q'\bar{q} \rightarrow t\bar{b}$, or the *t*-channel *W*-exchange process, $q'g \rightarrow q t\bar{b}$, based on ~ 230 pb⁻¹ of data.
- 21 ACOSTA 05n bounds single top-quark production from the *t*-channel *W*-exchange process ($q'g \rightarrow q t\bar{b}$), the *s*-channel *W*-exchange process ($q'\bar{q} \rightarrow t\bar{b}$), and from the combined cross section of *t*- and *s*-channel. Based on ~ 162 pb⁻¹ of data.

t-channel Single t Production Cross Section in pp Collisions at $\sqrt{s} = 7$ TeV

Direct probe of the *tbW* coupling and possible new physics at $\sqrt{s} = 7$ TeV.

VALUE (pb)	DOCUMENT ID	TECN	COMMENT
• • • We do not use the following data for averages, fits, limits, etc. • • •			
67.5 ± 5.7	1 AABOUD	19R LHC	combination of ATLAS+CMS
68 ± 2 ± 8	2 AAD	14BI ATLS	$\ell + \cancel{E}_T + 2j$ or 3j
83 ± 4 ± 20 -19	3 AAD	12CH ATLS	<i>t</i> -channel $\ell + \cancel{E}_T + (2,3)j$ (1b)
67.2 ± 6.1	4 CHATRCHYAN12BQ	CMS	<i>t</i> -channel $\ell + \cancel{E}_T + \geq 2j$ (1b)
83.6 ± 29.8 ± 3.3	5 CHATRCHYAN11R	CMS	<i>t</i> -channel

- 1 AABOUD 19R based on 1.17 to 5.1 fb⁻¹ of data from ATLAS and CMS at 7 TeV.
- 2 Based on 4.59 fb⁻¹ of data, using neural networks for signal and background separation. $\sigma(tq) = 46 \pm 1 \pm 6$ pb and $\sigma(\bar{t}q) = 23 \pm 1 \pm 3$ pb are separately measured, as well as their ratio $R = \sigma(tq)/\sigma(\bar{t}q) = 2.04 \pm 0.13 \pm 0.12$. The results are for $m_t = 172.5$ GeV, and those for other m_t values are given by eq.(4) and Table IV. The measurements give $|V_{tb}| = 1.02 \pm 0.07$ or $|V_{tb}| > 0.88$ (95% CL).
- 3 Based on 1.04 fb⁻¹ of data. The result gives $|V_{tb}| = 1.13_{-0.13}^{+0.14}$ from the ratio $\sigma(\text{exp})/\sigma(\text{th})$, where $\sigma(\text{th})$ is the SM prediction for $|V_{tb}| = 1$. The 95% CL lower bound of $|V_{tb}| > 0.75$ is found if $|V_{tb}| < 1$ is assumed. $\sigma(t) = 59_{-16}^{+18}$ pb and $\sigma(\bar{t}) = 33_{-12}^{+13}$ pb are found for the separate single *t* and \bar{t} production cross sections, respectively. The results assume $m_t = 172.5$ GeV for the acceptance.
- 4 Based on 1.17 fb⁻¹ of data for $\ell = \mu, 1.56$ fb⁻¹ of data for $\ell = e$ at 7 TeV collected during 2011. The result gives $|V_{tb}| = 1.020 \pm 0.046(\text{meas}) \pm 0.017(\text{th})$. The 95% CL lower bound of $|V_{tb}| > 0.92$ is found if $|V_{tb}| < 1$ is assumed. The results assume $m_t = 172.5$ GeV for the acceptance.
- 5 Based on 36 pb⁻¹ of data. The first error is statistical + systematic combined, the second is luminosity. The result gives $|V_{tb}| = 1.114 \pm 0.22(\text{exp}) \pm 0.02(\text{th})$ from the ratio $\sigma(\text{exp})/\sigma(\text{th})$, where $\sigma(\text{th})$ is the SM prediction for $|V_{tb}| = 1$. The 95% CL lower bound of $|V_{tb}| > 0.62$ (0.68) is found from the 2D (BDT) analysis under the constraint $0 < |V_{tb}|^2 < 1$.

t-channel Single t Production Cross Section in pp Collisions at $\sqrt{s} = 8$ TeV

VALUE (pb)	DOCUMENT ID	TECN	COMMENT
• • • We do not use the following data for averages, fits, limits, etc. • • •			
87.7 ± 5.8	1 AABOUD	19R LHC	combination of ATLAS+CMS
89.6 ± 7.1 6.3	2 AABOUD	17T ATLS	$\ell + \cancel{E}_T + 2j$ (1b j)
83.6 ± 2.3 ± 7.4	3 KHACHATRYAN...14F	CMS	$\ell + \cancel{E}_T + \geq 2j$ (1,2 b, 1 forward j)

- 1 AABOUD 19R based on 12.2 to 20.3 fb⁻¹ of data from ATLAS and CMS at 8 TeV.
- 2 AABOUD 17T based on 20.2 fb⁻¹ of data. A maximum-likelihood fit to neural-network discriminant distributions is used to separate signal and background events. Individual cross sections are measured as $\sigma(tq) = 56.7_{-3.8}^{+4.3}$ pb and $\sigma(\bar{t}q) = 32.9_{-2.7}^{+3.0}$ pb, while their ratio is given by $\sigma(tq)/\sigma(\bar{t}q) = 1.72 \pm 0.09$. A lower limit $|V_{tb}| > 0.92$ (95% CL) is obtained. Measured total and differential cross sections are described well by the SM.
- 3 Based on 19.7 fb⁻¹ of data. The *t* and \bar{t} production cross sections are measured separately as $\sigma_{t\text{-ch.}}(t) = 53.8 \pm 1.5 \pm 4.4$ pb and $\sigma_{t\text{-ch.}}(\bar{t}) = 27.6 \pm 1.3 \pm 3.7$ pb, respectively, as well as their ratio $R_{t\text{-ch.}} = \sigma_{t\text{-ch.}}(t)/\sigma_{t\text{-ch.}}(\bar{t}) = 1.95 \pm 0.10 \pm 0.19$, in agreement with the SM predictions. Combination with a previous CMS result at $\sqrt{s} = 7$ TeV [CHATRCHYAN 12BQ] gives $|V_{tb}| = 0.998 \pm 0.038 \pm 0.016$. Also obtained is the ratio $R_{8/7} = \sigma_{t\text{-ch.}}(8\text{TeV})/\sigma_{t\text{-ch.}}(7\text{TeV}) = 1.24 \pm 0.08 \pm 0.12$.

s-channel Single t Production Cross Section in pp Collisions at $\sqrt{s} = 8$ TeV

VALUE (pb)	DOCUMENT ID	TECN	COMMENT
• • • We do not use the following data for averages, fits, limits, etc. • • •			
4.9 ± 1.4	1 AABOUD	19R LHC	ATLAS + CMS
4.8 ± 0.8 ± 1.6 -1.3	2 AAD	16U ATLS	$\ell + \cancel{E}_T + 2b$
13.4 ± 7.3	3 KHACHATRYAN...16AZ	CMS	$\ell + \cancel{E}_T + 2b$
5.0 ± 4.3	4 AAD	15A ATLS	$\ell + \cancel{E}_T + 2b$

- 1 AABOUD 19R based on 12.2 to 20.3 fb⁻¹ of data from ATLAS and CMS at 8 TeV.
- 2 AAD 16U based on 20.3 fb⁻¹ of data, using a maximum-likelihood fit of a matrix element method discriminant. The same data set as in AAD 15A is used. The result corresponds to an observed significance of 3.2 σ .
- 3 KHACHATRYAN 16AZ based on 19.7 fb⁻¹ of data, using a multivariate analysis to separate signal and backgrounds. The same method is applied to 5.1 fb⁻¹ of data at $\sqrt{s} = 7$ TeV, giving 7.1 ± 8.1 pb. Combining both measurements, the observed significance is 2.5 σ . A best fit value of 2.0 ± 0.9 is obtained for the combined ratio of the measured values and SM expectations.
- 4 AAD 15A based on 20.3 fb⁻¹ of data, using a multivariate analysis to separate signal and backgrounds. The 95% CL upper bound of the cross section is 14.6 pb. The results are consistent with the SM prediction of 5.61 ± 0.22 pb at approximate NNLO.

t-channel Single t Production Cross Section in pp Collisions at $\sqrt{s} = 13$ TeV

VALUE (pb)	DOCUMENT ID	TECN	COMMENT
• • • We do not use the following data for averages, fits, limits, etc. • • •			
130 ± 1 ± 19	1 SIRUNYAN	20D CMS	$\sigma(tq, \ell + \cancel{E}_T + \geq 2j$
77 ± 1 ± 12	1 SIRUNYAN	20D CMS	$\sigma(\bar{t}q, \ell + \cancel{E}_T + \geq 2j$
156 ± 5 ± 27 ± 3	2 AABOUD	17H ATLS	$\sigma(tq, \ell + \cancel{E}_T + 2j$ (1b, 1 forward j)
91 ± 4 ± 18 ± 2	2 AABOUD	17H ATLS	$\sigma(\bar{t}q, \ell + \cancel{E}_T + 2j$ (1b, 1 forward j)
154 ± 8 ± 9 ± 19 ± 4	3 SIRUNYAN	17AA CMS	$\sigma(tq, \mu^+ \geq 2j$ (1b)
85 ± 10 ± 4 ± 11 ± 2	3 SIRUNYAN	17AA CMS	$\sigma(\bar{t}q, \mu^+ \geq 2j$ (1b)

- 1 SIRUNYAN 20D based on 35.9 fb⁻¹ of data. Different categories of jet and b jet multiplicity and multivariate discriminators are used to separate signal and background events. The cross section ratio is measured to be $\sigma(tq)/\sigma(\bar{t}q) = 1.68 \pm 0.02 \pm 0.05$. CKM matrix element is obtained as $|f_{LV} V_{tb}| = 0.98 \pm 0.07(\text{exp}) \pm 0.02(\text{theo})$ where f_{LV} is an anomalous form factor. All results are in agreement with the SM.
- 2 AABOUD 17H based on 3.2 fb⁻¹ of data. A maximum-likelihood fit to neural-network discriminant distributions is used to separate signal and background events. The third error is for luminosity. The cross section ratio is measured to be $\sigma(tq)/\sigma(\bar{t}q) = 1.72 \pm 0.09 \pm 0.18$. A lower limit $|V_{tb}| > 0.84$ (95% CL) is obtained. All results are in agreement with the SM.
- 3 SIRUNYAN 17AA based on 2.2 fb⁻¹ of data. A multivariate discriminator is used to separate signal and background events. The four errors are from statistics, experimental systematics, theory, and luminosity. The cross section ratio is measured to be $\sigma(tq)/\sigma(\bar{t}q) = 1.81 \pm 0.18 \pm 0.15$. CKM matrix element is obtained as $|V_{tb}| = 1.05 \pm 0.07(\text{exp}) \pm 0.02(\text{theo})$. All results are in agreement with the SM.

tT Production Cross Section in pp Collisions at $\sqrt{s} = 13$ TeV

VALUE (fb)	DOCUMENT ID	TECN	COMMENT
• • • We do not use the following data for averages, fits, limits, etc. • • •			
670 ± 90 ± 110 -100	1 AABOUD	18BK ATLS	$H \rightarrow b\bar{b}, WW^* \tau\tau, \gamma\gamma, ZZ^*$

- 1 AABOUD 18BK based on 79.8 fb⁻¹ of data. The observed significance is 5.8 σ relative to the background-only hypothesis. The measurement is consistent with the NLO SM prediction of 507_{-50}^{+35} fb. See Table 3 and Fig. 5 for measurements of individual modes. Combined with the measurements at 7 and 8 TeV, the observed significance is 6.3 σ .

Wt Production Cross Section in pp Collisions at $\sqrt{s} = 7$ TeV

VALUE (pb)	DOCUMENT ID	TECN	COMMENT
• • • We do not use the following data for averages, fits, limits, etc. • • •			
16.3 ± 4.1	1 AABOUD	19R LHC	ATLAS + CMS combined
16 ± 5 -4	2 CHATRCHYAN13C	CMS	<i>t</i> + <i>W</i> channel, $2\ell + \cancel{E}_T + 1b$

- 1 AABOUD 19R based on 1.17 to 5.1 fb⁻¹ of data from ATLAS and CMS at 7 TeV.
- 2 Based on 4.9 fb⁻¹ of data. The result gives $|V_{tb}| = 1.01_{-0.13}^{+0.16}(\text{exp})_{-0.04}^{+0.03}(\text{th})$. $V_{tb} > 0.79$ (95% CL) if $V_{tb} < 1$ is assumed. The results assume $m_t = 172.5$ GeV for the acceptance.

Wt Production Cross Section in pp Collisions at $\sqrt{s} = 8$ TeV

VALUE (pb)	DOCUMENT ID	TECN	COMMENT
• • • We do not use the following data for averages, fits, limits, etc. • • •			
26 ± 7	1 AAD	21AT ATLS	$\ell + \geq 3j$
23.1 ± 3.6	2 AABOUD	19R LHC	ATLAS + CMS combined
23.0 ± 1.3 ± 3.2 -3.5 ± 1.1	3 AAD	16B ATLS	$2\ell + \cancel{E}_T + 1b$
23.4 ± 5.4	4 CHATRCHYAN14AC	CMS	<i>t</i> + <i>W</i> channel, $2\ell + \cancel{E}_T + 1b$

- 1 AAD 21AT based on 20.2 fb⁻¹ of data. In this single lepton channel, only single neutrino is emitted, so that both *W* and *t* can be reconstructed. A neural network is trained to separate signal from background. The measured cross section agrees with the NLO+NNLL SM prediction of $22.4 \pm 0.6(\text{scale}) \pm 1.4(\text{PDF})$ pb.
- 2 AABOUD 19R based on 12.2 to 20.3 fb⁻¹ of data from ATLAS and CMS at 8 TeV.
- 3 AAD 16B based on 20.3 fb⁻¹ of data. The result gives $|V_{tb}| = 1.01 \pm 0.10$ and $|V_{tb}| > 0.80$ (95% CL) without assuming unitarity of the CKM matrix. The results assume $m_t = 172.5$ GeV for the acceptance.
- 4 Based on 12.2 fb⁻¹ of data. Events with two oppositely charged leptons, large \cancel{E}_T and a *b*-tagged jet are selected, and a multivariate analysis is used to separate the signal from the backgrounds. The result is consistent with the SM prediction of $22.2 \pm 0.6(\text{scale}) \pm 1.4(\text{PDF})$ pb at approximate NNLO.

Wt Production Cross Section in pp Collisions at $\sqrt{s} = 13$ TeV

VALUE (pb)	DOCUMENT ID	TECN	COMMENT
• • • We do not use the following data for averages, fits, limits, etc. • • •			
89 ± 4 ± 12	1 TUMASYAN	21E CMS	$1\ell + \text{jets}$
94 ± 10 ± 28 -22 ± 2	2 AABOUD	18H ATLS	$\ell^+ \ell^- + \geq 1j$
63.1 ± 1.8 ± 6.4 ± 2.1	3 SIRUNYAN	18DL CMS	$e^\pm \mu^\mp + \geq 1j(b\text{-tag})$

Quark Particle Listings

t

- 1 TUMASYAN 21E based on 36 fb^{-1} of data. A boosted decision tree is used to separate the signal from the dominant $t\bar{t}$ backgrounds. The result corresponds to an observation with a significance exceeding 5σ and is consistent with the NNLO QCD prediction of $71.7 \pm 1.8(\text{scale}) \pm 3.4(\text{PDF}) \text{ pb}$ or with the approximate NNNLO SM prediction of $79.5^{+1.9}_{-1.8}(\text{scale}) \pm 2.0(\text{PDF}) \text{ pb}$.
- 2 AABOUD 18H based on 3.2 fb^{-1} of data. The last error is from luminosity. A multivariate analysis is used to separate the signal from the backgrounds. The result is consistent with the NLO+NNLL SM prediction of $71.7 \pm 1.8(\text{scale}) \pm 3.4(\text{PDF}) \text{ pb}$.
- 3 SIRUNYAN 18DL based on 35.9 fb^{-1} of data. The last error is from luminosity. A multivariate analysis is used to separate the signal from the backgrounds. The result is consistent with the NLO+NNLL SM prediction of $71.7 \pm 1.8(\text{scale}) \pm 3.4(\text{PDF}) \text{ pb}$.

Zt Production Cross Section in pp Collisions at $\sqrt{s} = 13 \text{ TeV}$

VALUE (fb)	DOCUMENT ID	TECN	COMMENT
• • • We do not use the following data for averages, fits, limits, etc. • • •			
$97 \pm 13 \pm 7$	1 AAD	20AB ATLS	$3\ell + 1,2j + 1b_j$
$111 \pm 13 \pm \frac{11}{9}$	2 SIRUNYAN	19BF CMS	$3\ell + \geq 2j (\geq 1b_j)$
$600 \pm 170 \pm 140$	3 AABOUD	18AE ATLS	$3\ell + 1j + 1b_j$
$123 \pm \frac{33}{31} \pm \frac{29}{23}$	4 SIRUNYAN	18Z CMS	$3\ell + 1j + 1b_j$

- 1 AAD 20AB based on 139 fb^{-1} of data at 13 TeV. Neural networks are used to discriminate tZq signal from backgrounds. The result is for the cross section $\sigma(pp \rightarrow t\ell^+\ell^-q)$, including non-resonant dilepton pairs, for dilepton invariant masses above 30 GeV and is consistent with the NLO SM prediction of 102^{+5}_{-2} fb .
- 2 SIRUNYAN 19BF based on 77.4 fb^{-1} of data. Two BDTs are used in the analysis: one to discriminate prompt leptons from non-prompt ones; and one to discriminate tZq signal from backgrounds. The result is for the cross section $\sigma(pp \rightarrow tZq \rightarrow t\ell^+\ell^-q)$ for dilepton invariant masses above 30 GeV and is consistent with the NLO SM prediction of $94.2 \pm 3.1 \text{ fb}$.
- 3 AABOUD 18AE based on 36.1 fb^{-1} of data. A multivariate analysis is used to separate the signal from the backgrounds. The result is consistent with the NLO SM prediction of 800 fb with a scale uncertainty of $\pm 6.1\%$.
- 4 SIRUNYAN 18Z based on 35.9 fb^{-1} of data. A multivariate analysis is used to separate the signal from the backgrounds. The result is for the cross section $\sigma(pp \rightarrow tZq \rightarrow Wb\ell^+\ell^-q)$ and is consistent with the NLO SM prediction of $94.2^{+1.9}_{-1.8}(\text{scale}) \pm 2.5(\text{PDF}) \text{ fb}$. Superseded by SIRUNYAN 19BF.

Single t-Quark Production Cross Section in ep Collisions

VALUE (pb)	CL%	DOCUMENT ID	TECN	COMMENT
• • • We do not use the following data for averages, fits, limits, etc. • • •				
<0.25	95	1 AARON	09A H1	$e^{\pm}p \rightarrow e^{\pm}tX$
<0.55	95	2 AKTAS	04 H1	$e^{\pm}p \rightarrow e^{\pm}tX$
<0.225	95	3 CHEKANOV	03 ZEUS	$e^{\pm}p \rightarrow e^{\pm}tX$

- 1 AARON 09A looked for single top production via FCNC in $e^{\pm}p$ collisions at HERA with 474 pb^{-1} of data at $\sqrt{s} = 301\text{--}319 \text{ GeV}$. The result supersedes that of AKTAS 04.
- 2 AKTAS 04 looked for single top production via FCNC in e^{\pm} collisions at HERA with 118.3 pb^{-1} , and found 5 events in the e or μ channels while 1.31 ± 0.22 events are expected from the Standard Model background. No excess was found for the hadronic channel. The observed cross section of $\sigma(ep \rightarrow e tX) = 0.29^{+0.15}_{-0.14} \text{ pb}$ at $\sqrt{s} = 319 \text{ GeV}$ gives the quoted upper bound if the observed events are due to statistical fluctuation.
- 3 CHEKANOV 03 looked in 130.1 pb^{-1} of data at $\sqrt{s} = 301$ and 318 GeV . The limit is for $\sqrt{s} = 318 \text{ GeV}$ and assumes $m_t = 175 \text{ GeV}$.

 $t\bar{t}$ Production Cross Section in $p\bar{p}$ Collisions at $\sqrt{s} = 1.8 \text{ TeV}$

Only the final combined $t\bar{t}$ production cross sections obtained from Tevatron Run I by the CDF and D0 experiments are quoted below.

VALUE (pb)	DOCUMENT ID	TECN	COMMENT
• • • We do not use the following data for averages, fits, limits, etc. • • •			
$5.69 \pm 1.21 \pm 1.04$	1 ABAZOV	03A D0	Combined Run I data
$6.5 \pm \frac{1.7}{1.4}$	2 AFFOLDER	01A CDF	Combined Run I data

- 1 Combined result from 110 pb^{-1} of Tevatron Run I data. Assume $m_t = 172.1 \text{ GeV}$.
- 2 Combined result from 105 pb^{-1} of Tevatron Run I data. Assume $m_t = 175 \text{ GeV}$.

 $t\bar{t}$ Production Cross Section in $p\bar{p}$ Collisions at $\sqrt{s} = 1.96 \text{ TeV}$

Unless otherwise noted the first quoted error is from statistics, the second from systematic uncertainties, and the third from luminosity. If only two errors are quoted the luminosity is included in the systematic uncertainties.

VALUE (pb)	DOCUMENT ID	TECN	COMMENT
• • • We do not use the following data for averages, fits, limits, etc. • • •			
$7.26 \pm 0.13 \pm \frac{0.57}{0.50}$	1 ABAZOV	16F D0	$\ell\ell, \ell + \text{jets channels}$
8.1 ± 2.1	2 AALTONEN	14A CDF	$\ell + \tau_h + \geq 2\text{jets } (\geq 1b\text{-tag})$
$7.60 \pm 0.20 \pm 0.29 \pm 0.21$	3 AALTONEN	14H TEVA	$\ell\ell, \ell + \text{jets, all-jets channels}$
$8.0 \pm 0.7 \pm 0.6 \pm 0.5$	4 ABAZOV	14K D0	$\ell + \cancel{E}_T + \geq 4 \text{ jets } (\geq 1b\text{-tag})$
7.09 ± 0.84	5 AALTONEN	13AB CDF	$\ell\ell + \cancel{E}_T + \geq 2 \text{ jets}$
7.5 ± 1.0	6 AALTONEN	13G CDF	$\ell + \cancel{E}_T + \geq 3\text{jets } (\geq 1b\text{-tag})$
$8.8 \pm 3.3 \pm 2.2$	7 AALTONEN	12AL CDF	$\tau_h + \cancel{E}_T + 4j (\geq 1b)$
$8.5 \pm 0.6 \pm 0.7$	8 AALTONEN	11D CDF	$\ell + \cancel{E}_T + \text{jets } (\geq 1b\text{-tag})$
$7.64 \pm 0.57 \pm 0.45$	9 AALTONEN	11W CDF	$\ell + \cancel{E}_T + \text{jets } (\geq 1b\text{-tag})$
$7.99 \pm 0.55 \pm 0.76 \pm 0.46$	10 AALTONEN	11Y CDF	$\cancel{E}_T + \geq 4\text{jets } (0,1,2 b\text{-tag})$
$7.78 \pm \frac{0.77}{0.64}$	11 ABAZOV	11E D0	$\ell + \cancel{E}_T + \geq 2\text{jets}$
$7.56 \pm \frac{0.63}{0.56}$	12 ABAZOV	11Z D0	Combination
$6.27 \pm 0.73 \pm 0.63 \pm 0.39$	13 AALTONEN	10AA CDF	Repl. by AALTONEN 13AB
$7.2 \pm 0.5 \pm 1.0 \pm 0.4$	14 AALTONEN	10E CDF	$\geq 6 \text{ jets, vtx } b\text{-tag}$

$7.8 \pm 2.4 \pm 1.6 \pm 0.5$	15 AALTONEN	10V CDF	$\ell + \geq 3 \text{ jets, soft-}e \text{ } b\text{-tag}$
7.70 ± 0.52	16 AALTONEN	10W CDF	$\ell + \cancel{E}_T + \geq 3 \text{ jets } + b\text{-tag, norm. to } \sigma(Z \rightarrow \ell\ell)_{TH}$
6.9 ± 2.0	17 ABAZOV	10I D0	$\geq 6 \text{ jets with } 2 b\text{-tags}$
$6.9 \pm 1.2 \pm \frac{0.8}{0.7} \pm 0.4$	18 ABAZOV	10Q D0	$\tau_h + \text{jets}$
$9.6 \pm 1.2 \pm \frac{0.6}{0.5} \pm 0.6$	19 AALTONEN	09AD CDF	$\ell\ell + \cancel{E}_T / \text{vtx } b\text{-tag}$
$9.1 \pm 1.1 \pm \frac{1.0}{0.9} \pm 0.6$	20 AALTONEN	09H CDF	$\ell + \geq 3 \text{ jets } + \cancel{E}_T / \text{soft } \mu \text{ } b\text{-tag}$
$8.18 \pm \frac{0.98}{0.87}$	21 ABAZOV	09AG D0	$\ell + \text{jets, } \ell\ell \text{ and } \ell\tau + \text{jets}$
$7.5 \pm 1.0 \pm \frac{0.7}{0.6} \pm \frac{0.6}{0.5}$	22 ABAZOV	09R D0	$\ell\ell \text{ and } \ell\tau + \text{jets}$
$8.18 \pm \frac{0.90}{0.84} \pm 0.50$	23 ABAZOV	08M D0	$\ell + n \text{ jets with } 0,1,2 b\text{-tag}$
7.62 ± 0.85	24 ABAZOV	08N D0	$\ell + n \text{ jets } + b\text{-tag or kinematics}$
$8.5 \pm \frac{2.7}{2.2}$	25 ABULENCIA	08 CDF	$\ell^+\ell^- (\ell = e, \mu)$
$8.3 \pm 1.0 \pm \frac{2.0}{1.5} \pm 0.5$	26 AALTONEN	07D CDF	$\geq 6 \text{ jets, vtx } b\text{-tag}$
$7.4 \pm 1.4 \pm 1.0$	27 ABAZOV	07O D0	$\ell\ell + \text{jets, vtx } b\text{-tag}$
$4.5 \pm \frac{2.0}{1.9} \pm \frac{1.4}{1.1} \pm 0.3$	28 ABAZOV	07P D0	$\geq 6 \text{ jets, vtx } b\text{-tag}$
$6.4 \pm \frac{1.3}{1.2} \pm 0.7 \pm 0.4$	29 ABAZOV	07R D0	$\ell + \geq 4 \text{ jets}$
$6.6 \pm 0.9 \pm 0.4$	30 ABAZOV	06X D0	$\ell + \text{jets, vtx } b\text{-tag}$
$8.7 \pm 0.9 \pm \frac{1.1}{0.9}$	31 ABULENCIA	06Z CDF	$\ell + \text{jets, vtx } b\text{-tag}$
$5.8 \pm 1.2 \pm \frac{0.9}{0.7}$	32 ABULENCIA, A 06C	CDF	missing $E_T + \text{jets, vtx } b\text{-tag}$
$7.5 \pm 2.1 \pm \frac{3.3}{2.2} \pm \frac{0.5}{0.4}$	33 ABULENCIA, A 06E	CDF	6–8 jets, $b\text{-tag}$
$8.9 \pm 1.0 \pm \frac{1.1}{1.0}$	34 ABULENCIA, A 06F	CDF	$\ell + \geq 3 \text{ jets, } b\text{-tag}$
$8.6 \pm \frac{1.6}{1.5} \pm 0.6$	35 ABAZOV	05Q D0	$\ell + n \text{ jets}$
$8.6 \pm \frac{3.2}{2.7} \pm 1.1 \pm 0.6$	36 ABAZOV	05R D0	di-lepton + n jets
$6.7 \pm \frac{1.4}{1.3} \pm \frac{1.6}{1.1} \pm 0.4$	37 ABAZOV	05X D0	$\ell + \text{jets } / \text{kinematics}$
$5.3 \pm 3.3 \pm \frac{1.3}{1.0}$	38 ACOSTA	05S CDF	$\ell + \text{jets } / \text{soft } \mu \text{ } b\text{-tag}$
$6.6 \pm 1.1 \pm 1.5$	39 ACOSTA	05T CDF	$\ell + \text{jets } / \text{kinematics}$
$6.0 \pm \frac{1.5}{1.6} \pm \frac{1.2}{1.3}$	40 ACOSTA	05U CDF	$\ell + \text{jets/kinematics } + \text{vtx } b\text{-tag}$
$5.6 \pm \frac{1.2}{1.1} \pm \frac{0.9}{0.6}$	41 ACOSTA	05V CDF	$\ell + n \text{ jets}$
$7.0 \pm \frac{2.4}{2.1} \pm \frac{1.6}{1.1} \pm 0.4$	42 ACOSTA	04I CDF	di-lepton + jets + missing E_T

- 1 ABAZOV 16F based on 9.7 fb^{-1} of data. The result is for $m_t = 172.5 \text{ GeV}$, and the m_t dependence is shown in Table V and Fig. 9. The result agrees with the NNLO+NNLL SM prediction of $7.35^{+0.23}_{-0.27} \text{ pb}$.
- 2 Based on 9 fb^{-1} of data. The measurement is in the channel $t\bar{t} \rightarrow (b\ell\nu)(b\tau\nu)$, where τ decays into hadrons (τ_h), and ℓ (e or μ) include ℓ from τ decays (τ_ℓ). The result is for $m_t = 173 \text{ GeV}$.
- 3 Based on 8.8 fb^{-1} of data. Combination of CDF and D0 measurements given, respectively, by $\sigma(t\bar{t}; \text{CDF}) = 7.63 \pm 0.31 \pm 0.36 \pm 0.16 \text{ pb}$, $\sigma(t\bar{t}; \text{D0}) = 7.56 \pm 0.20 \pm 0.32 \pm 0.46 \text{ pb}$. All the results are for $m_t = 172.5 \text{ GeV}$. The m_t dependence of the mean value is parametrized in eq. (1) and shown in Fig. 2.
- 4 Based on 9.7 fb^{-1} of data. Differential cross sections with respect to $m_{t\bar{t}}, |y(\text{top})|, E_T(\text{top})$ are shown in Figs. 9, 10, 11, respectively, and are compared to the predictions of MC models.
- 5 Based on 8.8 fb^{-1} of $p\bar{p}$ collisions at $\sqrt{s} = 1.96 \text{ TeV}$.
- 6 Based on 8.7 fb^{-1} of $p\bar{p}$ collisions at $\sqrt{s} = 1.96 \text{ TeV}$. Measure the $t\bar{t}$ cross section simultaneously with the fraction of $t \rightarrow Wb$ decays. The correlation coefficient between those two measurements is -0.434 . Assume unitarity of the 3×3 CKM matrix and set $|V_{tb}| > 0.89$ at 95% CL.
- 7 Based on 2.2 fb^{-1} of data in $p\bar{p}$ collisions at 1.96 TeV. The result assumes the acceptance for $m_t = 172.5 \text{ GeV}$.
- 8 Based on 1.12 fb^{-1} and assumes $m_t = 175 \text{ GeV}$, where the cross section changes by $\pm 0.1 \text{ pb}$ for every $\pm 1 \text{ GeV}$ shift in m_t . AALTONEN 11D fits simultaneously the $t\bar{t}$ production cross section and the b -tagging efficiency and find improvements in both measurements.
- 9 Based on 2.7 fb^{-1} . The first error is from statistics and systematics, the second is from luminosity. The result is for $m_t = 175 \text{ GeV}$. AALTONEN 11W fits simultaneously a jet flavor discriminator between b -, c -, and light-quarks, and find significant reduction in the systematic error.
- 10 Based on 2.2 fb^{-1} . The result is for $m_t = 172.5 \text{ GeV}$. AALTONEN 11Y selects multi-jet events with large \cancel{E}_T , and vetoes identified electrons and muons.
- 11 Based on 5.3 fb^{-1} . The error is statistical + systematic + luminosity combined. The result is for $m_t = 172.5 \text{ GeV}$. The results for other m_t values are given in Table XII and eq.(10) of ABAZOV 11E.
- 12 Combination of a dilepton measurement presented in ABAZOV 11Z (based on 5.4 fb^{-1}), which yields $7.36^{+0.90}_{-0.79} (\text{stat+syst}) \text{ pb}$, and the lepton + jets measurement of ABAZOV 11E. The result is for $m_t = 172.5 \text{ GeV}$. The results for other m_t values is given by eq.(5) of ABAZOV 11A.
- 13 Based on 2.8 fb^{-1} . The result is for $m_t = 175 \text{ GeV}$.
- 14 Based on 2.9 fb^{-1} . Result is obtained from the fraction of signal events in the top quark mass measurement in the all hadronic decay channel.
- 15 Based on 1.7 fb^{-1} . The result is for $m_t = 175 \text{ GeV}$. AALTONEN 10V uses soft electrons from b -hadron decays to suppress W +jets background events.
- 16 Based on 4.6 fb^{-1} . The result is for $m_t = 172.5 \text{ GeV}$. The ratio $\sigma(t\bar{t} \rightarrow \ell + \text{jets}) / \sigma(Z/\gamma^* \rightarrow \ell\ell)$ is measured and then multiplied by the theoretical $Z/\gamma^* \rightarrow \ell\ell$ cross section of $\sigma(Z/\gamma^* \rightarrow \ell\ell) = 251.3 \pm 5.0 \text{ pb}$, which is free from the luminosity error.

17 Based on 1 fb^{-1} . The result is for $m_t = 175 \text{ GeV}$. $7.9 \pm 2.3 \text{ pb}$ is found for $m_t = 170 \text{ GeV}$. ABAZOV 10i uses a likelihood discriminant to separate signal from background, where the background model was created from lower jet-multiplicity data.

18 Based on 1 fb^{-1} . The result is for $m_t = 170 \text{ GeV}$. For $m_t = 175 \text{ GeV}$, the result is $6.3^{+1.2}_{-1.1}(\text{stat}) \pm 0.7(\text{syst}) \pm 0.4(\text{lumi}) \text{ pb}$. Cross section of $t\bar{t}$ production has been measured in the $t\bar{t} \rightarrow \tau_h + \text{jets}$ topology, where τ_h denotes hadronically decaying τ leptons. The result for the cross section times the branching ratio is $\sigma(t\bar{t}) \cdot \text{B}(t\bar{t} \rightarrow \tau_h + \text{jets}) = 0.60^{+0.23+0.15}_{-0.22-0.14} \pm 0.04 \text{ pb}$ for $m_t = 170 \text{ GeV}$.

19 Based on 1.1 fb^{-1} . The result is for $\text{B}(W \rightarrow \ell\nu) = 10.8\%$ and $m_t = 175 \text{ GeV}$; the mean value is 9.8 for $m_t = 172.5 \text{ GeV}$ and 10.1 for $m_t = 170 \text{ GeV}$. AALTONEN 09AD used high p_T e or μ with an isolated track to select $t\bar{t}$ decays into dileptons including $\ell = \tau$. The result is based on the candidate event samples with and without vertex b -tag.

20 Based on 2 fb^{-1} . The result is for $m_t = 175 \text{ GeV}$; the mean value is 3% higher for $m_t = 170 \text{ GeV}$ and 4% lower for $m_t = 180 \text{ GeV}$.

21 Result is based on 1 fb^{-1} of data. The result is for $m_t = 170 \text{ GeV}$, and the mean value decreases with increasing m_t ; see their Fig. 2. The result is obtained after combining $\ell + \text{jets}$, $\ell\ell$, and $\ell\tau$ final states, and the ratios of the extracted cross sections are $R^{\ell\ell/\ell j} = 0.86^{+0.19}_{-0.17}$ and $R^{\ell\tau/\ell\ell-\ell j} = 0.97^{+0.32}_{-0.29}$, consistent with the SM expectation of $R = 1$. This leads to the upper bound of $\text{B}(t \rightarrow bH^+)$ as a function of m_{H^+} . Results are shown in their Fig. 1 for $\text{B}(H^+ \rightarrow \tau\nu) = 1$ and $\text{B}(H^+ \rightarrow c\bar{s}) = 1$ cases. Comparison of the m_t dependence of the extracted cross section and a partial NNLO prediction gives $m_t = 169.1^{+5.9}_{-5.2} \text{ GeV}$.

22 Result is based on 1 fb^{-1} of data. The result is for $m_t = 170 \text{ GeV}$, and the mean value changes by $-0.07 [m_t(\text{GeV}) - 170] \text{ pb}$ near the reference m_t value. Comparison of the m_t dependence of the extracted cross section and a partial NNLO QCD prediction gives $m_t = 171.5^{+9.9}_{-8.8} \text{ GeV}$. The $\ell\tau$ channel alone gives $7.6^{+4.9+3.5+1.4}_{-4.3-3.4-0.9} \text{ pb}$ and the $\ell\ell$ channel gives $7.5^{+1.2+0.7+0.7}_{-1.1-0.6-0.5} \text{ pb}$.

23 Result is based on 0.9 fb^{-1} of data. The first error is from stat + syst, while the latter error is from luminosity. The result is for $m_t = 175 \text{ GeV}$, and the mean value changes by $-0.09 \text{ pb} [m_t(\text{GeV}) - 175]$.

24 Result is based on 0.9 fb^{-1} of data. The cross section is obtained from the $\ell + \geq 3$ jet event rates with 1 or 2 b -tag, and also from the kinematical likelihood analysis of the $\ell + 3, 4$ jet events. The result is for $m_t = 172.6 \text{ GeV}$, and its m_t dependence shown in Fig. 3 leads to the constraint $m_t = 170 \pm 7 \text{ GeV}$ when compared to the SM prediction.

25 Result is based on 360 pb^{-1} of data. Events with high p_T oppositely charged dileptons $\ell^+\ell^-$ ($\ell = e, \mu$) are used to obtain cross sections for $t\bar{t}$, W^+W^- , and $Z \rightarrow \tau^+\tau^-$ production processes simultaneously. The other cross sections are given in Table IV.

26 Based on 1.02 fb^{-1} of data. Result is for $m_t = 175 \text{ GeV}$. Secondary vertex b -tag and neural network selections are used to achieve a signal-to-background ratio of about 1/2.

27 Based on 425 pb^{-1} of data. Result is for $m_t = 175 \text{ GeV}$. For $m_t = 170.9 \text{ GeV}$, $7.8 \pm 1.8(\text{stat} + \text{syst}) \text{ pb}$ is obtained.

28 Based on $405 \pm 25 \text{ pb}^{-1}$ of data. Result is for $m_t = 175 \text{ GeV}$. The last error is for luminosity. Secondary vertex b -tag and neural network are used to separate the signal events from the background.

29 Based on 425 pb^{-1} of data. Assumes $m_t = 175 \text{ GeV}$.

30 Based on $\sim 425 \text{ pb}^{-1}$. Assuming $m_t = 175 \text{ GeV}$. The first error is combined statistical and systematic, the second one is luminosity.

31 Based on $\sim 318 \text{ pb}^{-1}$. Assuming $m_t = 178 \text{ GeV}$. The cross section changes by $\pm 0.08 \text{ pb}$ for each $\mp \text{ GeV}$ change in the assumed m_t . Result is for at least one b -tag. For at least two b -tagged jets, $t\bar{t}$ signal of significance greater than 5σ is found, and the cross section is $10.1^{+1.6+2.0}_{-1.4-1.3} \text{ pb}$ for $m_t = 178 \text{ GeV}$.

32 Based on $\sim 311 \text{ pb}^{-1}$. Assuming $m_t = 178 \text{ GeV}$. For $m_t = 175 \text{ GeV}$, the result is $6.0 \pm 1.2^{+0.9}_{-0.7}$. This is the first CDF measurement without lepton identification, and hence it has sensitivity to the $W \rightarrow \tau\nu$ mode.

33 ABULENCIA 06E measures the $t\bar{t}$ production cross section in the all hadronic decay mode by selecting events with 6 to 8 jets and at least one b -jet. $S/B = 1/5$ has been achieved. Based on 311 pb^{-1} . Assuming $m_t = 178 \text{ GeV}$.

34 Based on $\sim 318 \text{ pb}^{-1}$. Assuming $m_t = 178 \text{ GeV}$. Result is for at least one b -tag. For at least two b -tagged jets, the cross section is $11.1^{+2.3+2.5}_{-1.9-1.9} \text{ pb}$.

35 ABAZOV 05q measures the top-quark pair production cross section with $\sim 230 \text{ pb}^{-1}$ of data, based on the analysis of W plus n -jet events where W decays into e or μ plus neutrino, and at least one of the jets is b -jet like. The first error is statistical and systematic, and the second accounts for the luminosity uncertainty. The result assumes $m_t = 175 \text{ GeV}$; the mean value changes by $(175 - m_t(\text{GeV})) \times 0.06 \text{ pb}$ in the mass range 160 to 190 GeV .

36 ABAZOV 05r measures the top-quark pair production cross section with $224\text{--}243 \text{ pb}^{-1}$ of data, based on the analysis of events with two charged leptons in the final state. The result assumes $m_t = 175 \text{ GeV}$; the mean value changes by $(175 - m_t(\text{GeV})) \times 0.08 \text{ pb}$ in the mass range 160 to 190 GeV .

37 Based on 230 pb^{-1} . Assuming $m_t = 175 \text{ GeV}$.

38 Based on 194 pb^{-1} . Assuming $m_t = 175 \text{ GeV}$.

39 Based on $194 \pm 11 \text{ pb}^{-1}$. Assuming $m_t = 175 \text{ GeV}$.

40 Based on $162 \pm 10 \text{ pb}^{-1}$. Assuming $m_t = 175 \text{ GeV}$.

41 ACOSTA 05v measures the top-quark pair production cross section with $\sim 162 \text{ pb}^{-1}$ data, based on the analysis of W plus n -jet events where W decays into e or μ plus neutrino, and at least one of the jets is b -jet like. Assumes $m_t = 175 \text{ GeV}$.

42 ACOSTA 04i measures the top-quark pair production cross section with $197 \pm 12 \text{ pb}^{-1}$ data, based on the analysis of events with two charged leptons in the final state. Assumes $m_t = 175 \text{ GeV}$.

Ratio of the Production Cross Sections of $t\bar{t}\gamma$ to $t\bar{t}$ at $\sqrt{s} = 1.96 \text{ TeV}$

VALUE	DOCUMENT ID	TECN	COMMENT
-------	-------------	------	---------

• • • We do not use the following data for averages, fits, limits, etc. • • •

0.024 ± 0.009 ¹AALTONEN 11z CDF $E_{T(\gamma)} > 10 \text{ GeV}$, $|\eta(\gamma)| < 1.0$

¹Based on 6.0 fb^{-1} of data. The error is statistical and systematic combined. Events with lepton + $E_{T(\gamma)} \geq 3$ jets ($\geq 1b$) with and without central, high $E_{T(\gamma)}$ photon are measured. The result is consistent with the SM prediction of 0.024 ± 0.005 . The absolute production cross section is measured to be $0.18 \pm 0.08 \text{ fb}$. The statistical significance is 3.0 standard deviations.

$t\bar{t}$ Production Cross Section in pp Collisions at $\sqrt{s} = 7 \text{ TeV}$

VALUE (pb)	CL%	DOCUMENT ID	TECN	COMMENT
------------	-----	-------------	------	---------

• • • We do not use the following data for averages, fits, limits, etc. • • •

< 1.7 ¹AAD ^{12BE} ATLAS $\ell^+\ell^+ + E_{T(\gamma)} \geq 2j + \text{HT}$

¹Based on 1.04 fb^{-1} of pp data at $\sqrt{s} = 7 \text{ TeV}$. The upper bounds are the same for LL, LR and RR chiral components of the two top quarks.

$t\bar{t}$ Production Cross Section in pp Collisions at $\sqrt{s} = 5.02 \text{ TeV}$

Unless otherwise noted the first quoted error is from statistics, the second from systematic uncertainties, and the third from luminosity. If only two errors are quoted the luminosity is included in the systematic uncertainties.

VALUE (pb)	DOCUMENT ID	TECN	COMMENT
------------	-------------	------	---------

• • • We do not use the following data for averages, fits, limits, etc. • • •

$69.5 \pm 6.1 \pm 5.6 \pm 1.6$ ¹SIRUNYAN 18AQ CMS $\ell + \text{jets}, \ell\ell + \text{jets}$

¹SIRUNYAN 18AQ based on 27.4 pb^{-1} of data from pp collisions at $\sqrt{s} = 5.02 \text{ TeV}$. The result is in agreement with the NNLO SM prediction $68.9^{+1.9}_{-2.3}(\text{scale}) \pm 2.3(\text{PDF}) \pm 1.4(\alpha_S) \text{ pb}$.

$t\bar{t}$ Production Cross Section in pp Collisions at $\sqrt{s} = 7 \text{ TeV}$

Unless otherwise noted the first quoted error is from statistics, the second from systematic uncertainties, and the third from luminosity. If only two errors are quoted the luminosity is included in the systematic uncertainties.

VALUE (pb)	DOCUMENT ID	TECN	COMMENT
------------	-------------	------	---------

• • • We do not use the following data for averages, fits, limits, etc. • • •

$161.7 \pm 6.0 \pm 12.0 \pm 3.6$ ¹ KHACHATRYAN 17B CMS $\ell + E_{T(\gamma)} \geq 4j (\geq 1b)$

$173.6 \pm 2.1^{+4.5}_{-4.0} \pm 3.8$ ² KHACHATRYAN 16AW CMS $e + \mu + E_{T(\gamma)} \geq 0j$

$181.2 \pm 2.8^{+10.8}_{-10.6}$ ³ AAD ^{15B0} ATLAS $e + \mu + E_{T(\gamma)} \geq 0j$

$178 \pm 3 \pm 16 \pm 3$ ⁴ AAD ^{15CC} ATLAS $\ell + \text{jets}, \ell\ell + \text{jets}, \ell\tau_h + \text{jets}$

⁵ AAIJ ^{15R} LHCB $\mu + \geq 1j(b\text{-tag})$ forward region

$182.9 \pm 3.1 \pm 6.4$ ⁶ AAD ^{14AY} ATLAS $e + \mu + 1$ or $2b$ jets

$194 \pm 18 \pm 46$ ⁷ AAD ^{13X} ATLAS $\tau_h + E_{T(\gamma)} \geq 5j (\geq 2b)$

$139 \pm 10 \pm 26$ ⁸ CHATRCHYAN 13AY CMS ≥ 6 jets with 2 b -tags

$158.1 \pm 2.1 \pm 10.8$ ⁹ CHATRCHYAN 13BB CMS $\ell + E_{T(\gamma)} + \text{jets} (\geq 1 b\text{-tag})$

$152 \pm 12 \pm 32$ ¹⁰ CHATRCHYAN 13BE CMS $\tau_h + E_{T(\gamma)} \geq 4$ jets ($\geq 1 b$)

$177 \pm 20 \pm 14 \pm 7$ ¹¹ AAD ^{12B} ATLAS Repl. by AAD 12BF

$176 \pm 5 \pm 14 \pm 8$ ¹² AAD ^{12BF} ATLAS $\ell\ell + E_{T(\gamma)} \geq 2j$

$187 \pm 11 \pm 18 \pm 6$ ¹³ AAD ^{12B0} ATLAS $\ell + E_{T(\gamma)} \geq 3j$ with b -tag

$186 \pm 13 \pm 20 \pm 7$ ¹⁴ AAD ^{12CG} ATLAS $\ell + \tau_h + E_{T(\gamma)} \geq 2j (\geq 1b)$

$143 \pm 14 \pm 22 \pm 3$ ¹⁵ CHATRCHYAN 12AC CMS $\ell + \tau_h + E_{T(\gamma)} \geq 2j (\geq 1b)$

$161.9 \pm 2.5^{+5.1}_{-5.0} \pm 3.6$ ¹⁶ CHATRCHYAN 12AX CMS $\ell\ell + E_{T(\gamma)} \geq 2b$

$145 \pm 31 \pm 42 \pm 27$ ¹⁷ AAD ^{11A} ATLAS $\ell + E_{T(\gamma)} \geq 4j, \ell\ell + E_{T(\gamma)} \geq 2j$

$173 \pm 39 \pm 7$ ¹⁸ CHATRCHYAN 11AA CMS $\ell + E_{T(\gamma)} \geq 3$ jets

$168 \pm 18 \pm 14 \pm 7$ ¹⁹ CHATRCHYAN 11F CMS $\ell\ell + E_{T(\gamma)} + \text{jets}$

$154 \pm 17 \pm 6$ ²⁰ CHATRCHYAN 11Z CMS Combination

$194 \pm 72 \pm 24 \pm 21$ ²¹ KHACHATRYAN 11A CMS $\ell\ell + E_{T(\gamma)} \geq 2$ jets

¹ KHACHATRYAN 17B based on 5.0 fb^{-1} of data, using a binned likelihood fit of templates to the data. Also the ratio $\sigma(t\bar{t}; 8 \text{ TeV})/\sigma(t\bar{t}; 7 \text{ TeV}) = 1.43 \pm 0.04 \pm 0.07 \pm 0.05$ is reported. The results are in agreement with NNLO SM predictions.

² KHACHATRYAN 16AW based on 5.0 fb^{-1} of data, using a binned likelihood fit to differential distributions of b -tagged and non- b -tagged jets. The result is in good agreement with NNLO SM predictions.

³ Based on 4.6 fb^{-1} of data. Uses a template fit to distributions of $E_{T(\gamma)}$ and jet multiplicities to measure simultaneously $t\bar{t}$, WW , and $Z/\gamma^* \rightarrow \tau\tau$ cross sections, assuming $m_t = 172.5 \text{ GeV}$.

⁴ AAD 15CC based on 4.6 fb^{-1} of data. The event selection criteria are optimized for the $\ell\tau_h + \text{jets}$ channel. Using only this channel $183 \pm 9 \pm 23 \pm 3 \text{ pb}$ is derived for the cross section.

⁵ AAIJ 15R, based on 1.0 fb^{-1} of data, reports $0.239 \pm 0.053 \pm 0.033 \pm 0.024 \text{ pb}$ cross section for the forward fiducial region $p_T(\mu) > 25 \text{ GeV}$, $2.0 < \eta(\mu) < 4.5$, $50 \text{ GeV} < p_T(b) < 100 \text{ GeV}$, $2.2 < \eta(b) < 4.2$, $\Delta R(\mu, b) > 0.5$, and $p_T(\mu + b) > 20 \text{ GeV}$. The three errors are from statistics, systematics, and theory. The result agrees with the SM NNLO prediction.

⁶ AAD 14AY reports $182.9 \pm 3.1 \pm 4.2 \pm 3.6 \pm 3.3 \text{ pb}$ value based on 4.6 fb^{-1} of data. The four errors are from statistics, systematic, luminosity, and the 0.66% beam energy uncertainty. We have combined the systematic uncertainties in quadrature. The result is for $m_t = 172.5 \text{ GeV}$; for other m_t , $\sigma(m_t) = \sigma(172.5 \text{ GeV}) \times [1 - 0.0028 \times (m_t - 172.5 \text{ GeV})]$. The result is consistent with the SM prediction at NNLO.

⁷ Based on 1.67 fb^{-1} of data. The result uses the acceptance for $m_t = 172.5 \text{ GeV}$.

⁸ Based on 3.54 fb^{-1} of data.

⁹ Based on 2.3 fb^{-1} of data.

¹⁰ Based on 3.9 fb^{-1} of data.

¹¹ Based on 35 pb^{-1} of data for an assumed top quark mass of $m_t = 172.5 \text{ GeV}$.

¹² Based on 0.70 fb^{-1} of data. The 3 errors are from statistics, systematics, and luminosity. The result uses the acceptance for $m_t = 172.5 \text{ GeV}$.

¹³ Based on 35 pb^{-1} of data. The 3 errors are from statistics, systematics, and luminosity. The result uses the acceptance for $m_t = 172.5 \text{ GeV}$ and $173 \pm 17 \pm 18 \pm 6 \text{ pb}$ is found without the b -tag.

¹⁴ Based on 2.05 fb^{-1} of data. The hadronic τ candidates are selected using a BDT technique. The 3 errors are from statistics, systematics, and luminosity. The result uses the acceptance for $m_t = 172.5 \text{ GeV}$.

¹⁵ Based on 2.0 fb^{-1} and 2.2 fb^{-1} of data for $\ell = e$ and $\ell = \mu$, respectively. The 3 errors are from statistics, systematics, and luminosity. The result uses the acceptance for $m_t = 172.5 \text{ GeV}$.

Quark Particle Listings

t

- ¹⁶Based on 2.3 fb⁻¹ of data. The 3 errors are from statistics, systematics, and luminosity. The result uses the profile likelihood-ratio (PLB) method and an assumed $m_t = 172.5$ GeV.
- ¹⁷Based on 2.9 pb⁻¹ of data. The result for single lepton channels is $142 \pm 34^{+50}_{-31}$ pb, while for the dilepton channels is 151^{+78+37}_{-62-24} pb.
- ¹⁸Result is based on 36 pb⁻¹ of data. The first uncertainty corresponds to the statistical and systematic uncertainties, and the second corresponds to the luminosity.
- ¹⁹Based on 36 pb⁻¹ of data. The ratio of $t\bar{t}$ and Z/γ^* cross sections is measured as $\sigma(pp \rightarrow t\bar{t})/\sigma(pp \rightarrow Z/\gamma^* \rightarrow e^+e^-/\mu^+\mu^-) = 0.175 \pm 0.018(\text{stat}) \pm 0.015(\text{syst})$ for $60 < m_{\ell\ell} < 120$ GeV, for which they use an NNLO prediction for the denominator cross section of 972 ± 42 pb.
- ²⁰Result is based on 36 pb⁻¹ of data. The first error is from statistical and systematic uncertainties, and the second from luminosity. This is a combination of a measurement in the dilepton channel (CHATRCHYAN 11F) and the measurement in the $\ell + \text{jets}$ channel (CHATRCHYAN 11Z) which yields $150 \pm 9 \pm 17 \pm 6$ pb.
- ²¹Result is based on 3.1 ± 0.3 pb⁻¹ of data.

 $t\bar{t}$ Production Cross Section in pp Collisions at $\sqrt{s} = 8$ TeV

Unless otherwise noted the first quoted error is from statistics, the second from systematic uncertainties, and the third from luminosity. If only two errors are quoted the luminosity is included in the systematic uncertainties.

VALUE (pb)	DOCUMENT ID	TECN	COMMENT
•••	We do not use the following data for averages, fits, limits, etc. •••		
248.3 ± 0.7 ± 13.4 ± 4.7	¹ AABOUD	18BH ATLS	$\ell + \cancel{E}_T + \geq 4j$ ($\geq 1b$)
239 ± 4 ± 28 ± 5	² AABOUD	17Z ATLS	$\tau_h + \cancel{E}_T + \geq 2j$ ($\geq 2b$)
228.5 ± 3.8 ± 13.7 ± 6.0	³ KHACHATRYAN...17B	CMS	$\ell + \cancel{E}_T + \geq 4j$ ($\geq 1b$)
242.9 ± 1.7 ± 8.6	⁴ AAD	16BK ATLS	$e + \mu + 1$ or $2b$ jets
244.9 ± 1.4 ± 6.3 ± 5.5 ± 6.4	⁵ KHACHATRYAN...16AW	CMS	$e + \mu + \cancel{E}_T + \geq 0j$
275.6 ± 6.1 ± 37.8 ± 7.2	⁶ KHACHATRYAN...16BC	CMS	$\geq 6j$ ($\geq 2b$)
260 ± 1 ± 24 ± 25	⁷ AAD	15BP ATLS	$\ell + \cancel{E}_T + \geq 3j$ ($\geq 1b$)
242.4 ± 1.7 ± 10.2	⁸ AAIJ	15R LHCB	$\mu + \geq 1j(b\text{-tag})$ forward region
239 ± 2 ± 11 ± 6	⁹ AAD	14AY ATLS	$e + \mu + 1$ or $2b$ jets
257 ± 3 ± 24 ± 7	¹⁰ CHATRCHYAN 14F	CMS	$\ell\ell + \cancel{E}_T + \geq 2j$ (≥ 1 b -tag)
	¹¹ KHACHATRYAN...14S	CMS	$\ell + \tau_h + \cancel{E}_T + \geq 2j$ ($\geq 1b$)

- ¹AABOUD 18BH based on 20.2 fb⁻¹ of data. The result is for $m_t = 172.5$ GeV. To reduce effects of uncertainties in the jet energy scale and b -tagging efficiency, they are included as nuisance parameters in the fit of discriminant distributions, after separating selected events into three regions. Furthermore the $W + \text{jets}$ background distribution is modelled using $Z + \text{jets}$ event data.
- ²AABOUD 17Z based on 20.2 fb⁻¹ of data, using the mode $t\bar{t} \rightarrow \tau\nu q'\bar{q}b\bar{b}$ with τ decaying hadronically. Single prong and 3 prong decays of τ are separately analyzed. The result is consistent with the SM. The third quoted uncertainty is due to luminosity.
- ³KHACHATRYAN 17B based on 19.6 fb⁻¹ of data, using a binned likelihood fit of templates to the data. Also the ratio $\sigma(t\bar{t}; 8 \text{ TeV})/\sigma(t\bar{t}; 7 \text{ TeV}) = 1.43 \pm 0.04 \pm 0.07 \pm 0.05$ is reported. The results are in agreement with NNLO SM predictions.
- ⁴AAD 16BK is an update of the value from AAD 14AY using the improved luminosity calibration. The value $242.9 \pm 1.7 \pm 5.5 \pm 5.1 \pm 4.2$ pb is reported, where we have combined the systematic uncertainties in quadrature. Also the ratio $\sigma(t\bar{t}; 8 \text{ TeV})/\sigma(t\bar{t}; 7 \text{ TeV}) = 1.328 \pm 0.024 \pm 0.015 \pm 0.038 \pm 0.001$ has been updated. The former result is consistent with the SM predictions at NNLO, while the latter result is 2.1 σ below the expectation.
- ⁵KHACHATRYAN 16AW based on 19.7 fb⁻¹ of data, using a binned likelihood fit to differential distributions of b -tagged and non- b -tagged jets. The result is in good agreement with NNLO SM predictions.
- ⁶KHACHATRYAN 16BC based on 18.4 fb⁻¹ of data. The last uncertainty is due to luminosity. Cuts on kinematical fit probability and $\Delta R(b,b)$ are imposed. The major QCD background is determined from the data. The result is for $m_t = 172.5$ GeV and in agreement with the SM prediction. The top quark p_T spectra, also measured, are significantly softer than theoretical predictions.
- ⁷AAD 15BP based on 20.3 fb⁻¹ of data. The result is for $m_t = 172.5$ GeV and in agreement with the SM prediction 253^{+13}_{-15} pb at NNLO+NNLL. Superseded by AABOUD 18BH.
- ⁸AAIJ 15R, based on 2.0 fb⁻¹ of data, reports $0.289 \pm 0.043 \pm 0.040 \pm 0.029$ pb cross section for the forward fiducial region $p_T(\mu) > 25$ GeV, $2.0 < \eta(\mu) < 4.5$, $50 \text{ GeV} < p_T(b) < 100 \text{ GeV}$, $2.2 < \eta(b) < 4.2$, $\Delta R(\mu,b) > 0.5$, and $p_T(\mu+b) > 20$ GeV. The three errors are from statistics, systematics, and theory. The result agrees with the SM NNLO prediction.
- ⁹AAD 14AY reports $242.4 \pm 1.7 \pm 5.5 \pm 7.5 \pm 4.2$ pb value based on 20.3 fb⁻¹ of data. The four errors are from statistics, systematic, luminosity, and the 0.66% beam energy uncertainty. We have combined the systematic uncertainties in quadrature. The result is for $m_t = 172.5$ GeV; for other m_t , $\sigma(m_t) = \sigma(172.5 \text{ GeV}) \times [1 - 0.0028 \times (m_t - 172.5 \text{ GeV})]$. Also measured is the ratio $\sigma(t\bar{t}; 8 \text{ TeV})/\sigma(t\bar{t}; 7 \text{ TeV}) = 1.326 \pm 0.024 \pm 0.015 \pm 0.049 \pm 0.001$. The results are consistent with the SM predictions at NNLO.
- ¹⁰Based on 5.3 fb⁻¹ of data. The result is for $m_t = 172.5$ GeV, and a parametrization is given in eq.(6.1) for the mean value at other m_t values. The result is in agreement with the SM prediction $252.9^{+6.4}_{-8.6}$ pb at NNLO.
- ¹¹Based on 19.6 fb⁻¹ of data. The measurement is in the channel $t\bar{t} \rightarrow (b\ell\nu)(b\tau\nu)$, where τ decays into hadrons (τ_h). The result is for $m_t = 172.5$ GeV. For $m_t = 173.3$ GeV, the cross section is lower by 3.1 pb.

 $t\bar{t}$ Production Cross Section in pp Collisions at $\sqrt{s} = 13$ TeV

VALUE (pb)	DOCUMENT ID	TECN	COMMENT
•••	We do not use the following data for averages, fits, limits, etc. •••		
791 ± 1 ± 21 ± 14	¹ TUMASYAN	21J CMS	$1\ell + \text{jets}$
830 ± 0.4 ± 36 ± 14	² AAD	20AH ATLS	$\ell + \geq 4$ jets ($\geq 1b$ -tag)
826.4 ± 3.6 ± 11.5 ± 15.8	³ AAD	20Q ATLS	$e\mu + 1$ or 2 b -jets

781 ± 7 ± 62 ± 20	⁴ SIRUNYAN	20V CMS	$\ell\tau_h + \geq 3$ jets ($\geq 1b$ -tag)
803 ± 2 ± 25 ± 20	⁵ SIRUNYAN	19AR CMS	dilepton channel ($e\mu, 2e, 2\mu$)
	⁶ SIRUNYAN	19P CMS	dilepton channel
815 ± 9 ± 38 ± 19	⁷ KHACHATRYAN...17N	CMS	$e\mu + \geq 2j$ ($\geq 1b$ j)
888 ± 2 ± 26 ± 20	⁸ SIRUNYAN	17W CMS	$\ell + \geq 1j$
818 ± 8 ± 35	⁹ AABOUD	16R ATLS	$e + \mu + 1$ or 2 b jets
746 ± 5.8 ± 5.3 ± 36	¹⁰ KHACHATRYAN...16J	CMS	$e + \mu + \geq 2j$

- ¹TUMASYAN 21J result is based on 137 fb⁻¹ of data. The last uncertainty is due to the beam luminosity. The result is in agreement with the SM prediction of 832^{+40}_{-46} pb at NNLO+NNLL. Measurements of differential and double-differential cross sections are also presented.
- ²AAD 20AH based on 139 fb⁻¹ of data. The last quoted uncertainty is due to the beam luminosity. The result is for $m_t = 172.5$ GeV and in agreement with the SM prediction of $832^{+20}_{-29}(\text{scale}) \pm 35(\text{PDF} + \alpha(s))$ pb at NNLO+NNLL.
- ³AAD 20Q reports $826.4 \pm 3.6 \pm 11.5 \pm 15.7 \pm 1.9$ pb based on 36.1 fb⁻¹ of data at 13 TeV. The four errors stem from statistics, systematic effects, luminosity, and beam energy, respectively. We have combined luminosity and beam energy uncertainties in quadrature. The result is in agreement with the SM prediction $832^{+20}_{-29}(\text{scale}) \pm 35(\text{PDF} + \alpha(s))$ pb at NNLO+NNLL for $m_t = 172.5$ GeV.
- ⁴SIRUNYAN 20V based on 35.9 fb⁻¹ of pp data at $\sqrt{s} = 13$ TeV. The last uncertainty is due to beam luminosity. The $t\bar{t}$ production cross section is measured in the $t\bar{t} \rightarrow (\ell\nu_\ell)(\tau_h\nu_\tau)b\bar{b}$ final state, where τ_h refers to the hadronic decays of τ . The result is for $m_t = 172.5$ GeV and in agreement with the SM prediction at NNLO+NNLL.
- ⁵SIRUNYAN 19AR based on 35.9 fb⁻¹ of data. Obtained from the visible cross section measured using a template fit to multidifferential distributions categorized according to the b -tagged jet multiplicity. The result is for $m_t = 172.5$ GeV and in agreement with the SM prediction at NNLO+NNLL.
- ⁶SIRUNYAN 19P reports differential $t\bar{t}$ cross sections measured using dilepton events at 13 TeV with 35.9 fb⁻¹ and compared to NLO predictions.
- ⁷KHACHATRYAN 17N based on 2.2 fb⁻¹ of data. The last quoted uncertainty is due to the beam luminosity. This measurement supersedes that of KHACHATRYAN 16J.
- ⁸SIRUNYAN 17W based on 2.2 fb⁻¹ of pp data at $\sqrt{s} = 13$ TeV. Events are categorized according to the jet multiplicity and the number of b -tagged jets. A likelihood fit is performed to the event distributions to compare to the NNLO+NNLL prediction.
- ⁹AABOUD 16R reported value $818 \pm 8 \pm 27 \pm 19 \pm 12$ pb based on 3.2 fb⁻¹ of data. The four errors are from statistics, systematic, luminosity, and beam energy. We have combined the systematic uncertainties in quadrature. The result is in agreement with the SM prediction $832^{+20}_{-29}(\text{scale}) \pm 35(\text{PDF} + \alpha(s))$ pb at NNLO+NNLL for $m_t = 172.5$ GeV.
- ¹⁰KHACHATRYAN 16J based on 43 pb⁻¹ of data. The last uncertainty is due to luminosity. The result is for $m_t = 172.5$ GeV and in agreement with the SM prediction $832^{+20}_{-29}(\text{scale}) \pm 35(\text{PDF} + \alpha(s))$ pb at NNLO+NNLL.

 $t\bar{t}$ Production Cross Section in Nucleus-Nucleus Collisions

VALUE (μbarn)	DOCUMENT ID	TECN	COMMENT
•••	We do not use the following data for averages, fits, limits, etc. •••		
$2.03^{+0.71}_{-0.64}$	¹ SIRUNYAN	20Bc CMS	Pb-Pb collisions, dilepton + b -jets
$2.54^{+0.84}_{-0.74}$	² SIRUNYAN	20Bc CMS	Pb-Pb collisions, dilepton only

- ¹SIRUNYAN 20Bc based on (1.7 ± 0.1) nb⁻¹ of lead-lead collision data at a nucleon-nucleon c.m. energy of 5.02 TeV. It makes use of the final-state dilepton kinematic properties together with requirements on the number of b -jets. The measured value is compatible with QCD predictions.
- ²SIRUNYAN 20Bc based on (1.7 ± 0.1) nb⁻¹ of lead-lead collision data at a nucleon-nucleon c.m. energy of 5.02 TeV. It makes use of the final-state dilepton kinematic properties alone. The measured value is compatible with QCD predictions.

 $t\bar{t} t\bar{t}$ Production Cross Section in pp Collisions at $\sqrt{s} = 8$ TeV

VALUE (fb)	CL%	DOCUMENT ID	TECN	COMMENT
•••	We do not use the following data for averages, fits, limits, etc. •••			
<23	95	¹ AAD	15AR ATLS	$\ell + \cancel{E}_T + \geq 5j$ (≥ 2 b)
<70	95	² AAD	15BY ATLS	$\geq 2\ell + \cancel{E}_T + \geq 2j$ (≥ 1 b)
<32	95	³ KHACHATRYAN...14R	CMS	$\ell + \cancel{E}_T + \geq 6j$ (≥ 2 b)

- ¹AAD 15AR based on 20.3 fb⁻¹ of data. A fit to H_T distributions in multi-channels classified by the number of jets and of b -tagged jets is performed.
- ²AAD 15BY based on 20.3 fb⁻¹ of data. A same-sign lepton pair is required. An excess over the SM prediction reaches 2.5 σ for hypotheses involving heavy resonances decaying into $t\bar{t}t\bar{t}$.
- ³Based on 19.6 fb⁻¹ of data, using a multivariate analysis to separate signal from backgrounds. About $\sigma(t\bar{t}t\bar{t}) = 1$ fb is expected in the SM.

 $t\bar{t} t\bar{t}$ Production Cross Section in pp Collisions at $\sqrt{s} = 13$ TeV

VALUE (fb)	CL%	DOCUMENT ID	TECN	COMMENT
•••	We do not use the following data for averages, fits, limits, etc. •••			
26^{+17}_{-15}		¹ AAD	21Bc ATLS	ℓ or $\ell^+\ell^- + \text{jets}$
24^{+7}_{-6}		² AAD	21Bc ATLS	combination of $1\ell/2\ell(\text{OS})$ and $2\ell(\text{SS})/3\ell$
24^{+7}_{-6}		³ AAD	20AR ATLS	(same-sign 2ℓ) or $\geq 3\ell + \text{jets}$
$12.6^{+5.8}_{-5.2}$		⁴ SIRUNYAN	20c CMS	(same-sign 2ℓ) or $3\ell + \text{jets}$
<47	95	⁵ AABOUD	19AP ATLS	$\ell + \ell^+\ell^-$ channels
<49	95	⁶ AABOUD	19AP ATLS	combination of ATLAS

VALUE (fb)	DOCUMENT ID	TECN	COMMENT
13^{+11}_{-9}	7 SIRUNYAN	19CN CMS	combination of CMS
<48	95	8 SIRUNYAN	19CN CMS $\ell^+\ell^- + \text{jets}$ channels
<69	95	9 AABOUD	18CE ATLS $\geq 2\ell$ (same sign) + $\cancel{E}_T + \geq 1b_j$
$16.9^{+13.8}_{-11.4}$	10	SIRUNYAN	18BU CMS $t\bar{t}t\bar{t} \rightarrow$ (same sign 2ℓ or $\geq 3\ell$) + $\geq 4j$ ($\geq 2b$)
<94	95	11 SIRUNYAN	17AB CMS $\ell^+\ell^- + \text{jets}$ channels
<42	95	12 SIRUNYAN	17S CMS (same sign 2ℓ) + $\cancel{E}_T + \geq 2j$

- AAD 21BC result is based on 139 fb^{-1} of data. The events are categorized according to the number of jets and how likely to contain b -hadrons and a multivariate analysis is used to discriminate the signal from backgrounds. The result corresponds to observed significance of 1.9σ .
- AAD 21BC combines the results of the four-top-quark production cross section measured from the 1ℓ /opposite-sign 2ℓ channel with that from the same-sign $2\ell/3\ell$ channel (AAD 20AR). The result corresponds to observed significance of 4.7σ and is consistent within 2.0σ with the NLO (QCD+EW) SM prediction of $12.0 \pm 2.4 \text{ fb}$.
- AAD 20AR based on 139 fb^{-1} of data. Jet multiplicity, jet flavor and event kinematics are used in a multivariate analysis to discriminate the signal from backgrounds. The result corresponds to observed significance of 4.3σ and is consistent within 1.7σ with the NLO (QCD+EW) SM prediction of $12.0 \pm 2.4 \text{ fb}$.
- SIRUNYAN 20C based on 137 fb^{-1} of data. Both cut-based and multivariate approaches are taken to discriminate the signal from backgrounds. The result is in agreement with the NLO (QCD+EW) SM prediction of $12.0^{+2.2}_{-2.5} \text{ fb}$. The measurement constrains the top quark Yukawa coupling strength parameter to be $|Y_t/Y_t^{SM}| < 1.7$ (95% CL). It is also used to constrain an oblique parameter of the Higgs boson.
- AABOUD 19AP based on 36.1 fb^{-1} of data. The upper limit corresponds to 5.1 times the NLO SM cross section.
- AABOUD 19AP limit from data combined with AABOUD 18CE. The upper limit corresponds to 5.3 times the NLO SM cross section. Also a limit on the four-top-quark contact interaction $|C_{4t}|/\Lambda^2 < 1.9 \text{ TeV}^{-2}$ (95% CL) is obtained in an EFT model.
- SIRUNYAN 19CN based on 35.8 fb^{-1} of data, combined with SIRUNYAN 18BU. The results are also interpreted in the effective field theory framework.
- SIRUNYAN 19CN based on 35.8 fb^{-1} of data. A multivariate analysis using global event and jet properties is performed to discriminate from $t\bar{t}$ background.
- AABOUD 18CE based on 36.1 fb^{-1} of proton-proton data taken at $\sqrt{s} = 13 \text{ TeV}$. Events including a same-sign lepton pair are used. The result is consistent with the NLO SM cross section of 9.2 fb .
- SIRUNYAN 18BU based on 35.9 fb^{-1} of proton-proton data taken at $\sqrt{s} = 13 \text{ TeV}$. Yields from signal regions and control regions defined based on N_{jets} , N_b and N_l are combined in a maximum-likelihood fit. The result is in agreement with the NLO SM prediction $9.2^{+2.9}_{-2.4} \text{ fb}$. The measurement constrains the top quark Yukawa coupling strength parameter to be $|Y_t/Y_t^{SM}| < 2.1$ (95% CL).
- SIRUNYAN 17AB based on 2.6 fb^{-1} of data. A multivariate analysis is used to discriminate between $t\bar{t}t\bar{t}$ signal and $t\bar{t}$ background. A combination with a previous search (CMS, KHACHATRYAN 16Bj) in the same-sign dilepton channel gives an upper limit of 69 fb (95% CL), corresponding to $7.4 \cdot \text{SM}$ prediction).
- SIRUNYAN 17S based on 35.9 fb^{-1} . The limit is in agreement with the NLO SM prediction $9.2^{+2.9}_{-2.4} \text{ fb}$. Superseded by SIRUNYAN 18BU. The signal events are also used to constrain various new physics models.

$t\bar{t}W$ Production Cross Section in pp Collisions at $\sqrt{s} = 8 \text{ TeV}$

VALUE (fb)	DOCUMENT ID	TECN	COMMENT
$170^{+90}_{-80} \pm 70$	1 KHACHATRYAN	14N CMS	$t\bar{t}W \rightarrow$ same sign dilepton + $\cancel{E}_T + \text{jets}$

1 Based on 19.5 fb^{-1} of data. The result is consistent with the SM prediction of $\sigma(t\bar{t}W) = 206^{+21}_{-23} \text{ fb}$.

$t\bar{t}W$ Production Cross Section in pp Collisions at $\sqrt{s} = 13 \text{ TeV}$

VALUE (pb)	DOCUMENT ID	TECN	COMMENT
$0.87 \pm 0.13 \pm 0.14$	1 AABOUD	19AR ATLS	$2,3,4\ell + \cancel{E}_T + \text{jets}$
$0.77^{+0.12}_{-0.11} \pm 0.13$	2 SIRUNYAN	18Bs CMS	$t\bar{t}W \rightarrow$ same sign dilepton + $\cancel{E}_T + \text{jets}$

- AABOUD 19AR based on 35.9 fb^{-1} of data. $t\bar{t}W$ and $t\bar{t}Z$ cross sections are simultaneously measured using a combined fit to the events divided into multiple regions. The result is consistent with the SM prediction at NLO $0.60^{+0.08}_{-0.07} \text{ pb}$. It is also used to constrain the Wilson coefficients for dimension-six operators which modify the $t\bar{t}Z$ vertex.
- Based on 35.9 fb^{-1} of proton-proton data taken at $\sqrt{s} = 13 \text{ TeV}$. The result is consistent with the SM prediction and is used to constrain the Wilson coefficients for dimension-six operators describing new interactions. The result is consistent with the SM prediction at NLO $0.628 \pm 0.082 \text{ pb}$.

$t\bar{t}W$ Production Cross Section in pp Collisions at $\sqrt{s} = 8 \text{ TeV}$

VALUE (fb)	DOCUMENT ID	TECN	COMMENT
$200^{+80}_{-70} + 40 - 30$	1 KHACHATRYAN	14N CMS	$t\bar{t}Z \rightarrow 3,4 \ell + \cancel{E}_T + \text{jets}$

1 Based on 19.5 fb^{-1} of data. The result is consistent with the SM prediction of $\sigma(t\bar{t}Z) = 197^{+22}_{-25} \text{ fb}$.

$t\bar{t}Z$ Production Cross Section in pp Collisions at $\sqrt{s} = 13 \text{ TeV}$

VALUE (pb)	DOCUMENT ID	TECN	COMMENT
$0.99 \pm 0.05 \pm 0.08$	1 AAD	21As ATLS	$3,4\ell + \text{jets}$

$0.95 \pm 0.05 \pm 0.06$	2 SIRUNYAN	20AB CMS	$3,4\ell + \text{jets}$
$0.95 \pm 0.08 \pm 0.10$	3 AABOUD	19AR ATLS	$2,3,4\ell + \cancel{E}_T + \text{jets}$
$0.99^{+0.09}_{-0.08} \pm 0.12$	4 SIRUNYAN	18Bs CMS	$t\bar{t}Z \rightarrow 3,4 \ell + \cancel{E}_T + \text{jets}$

- AAD 21As based on 139 fb^{-1} of data. The result is consistent with the SM prediction of $0.88^{+0.09}_{-0.10} \text{ pb}$ which includes NLO QCD+EW corrections. Also overall the differential cross sections are in good agreement with the SM predictions.
- SIRUNYAN 20AB based on 77.5 fb^{-1} of data at 13 TeV . The result is consistent with the NLO SM prediction of $0.84 \pm 0.10 \text{ pb}$. Differential cross sections are measured and used to constrain the anomalous couplings and Wilson coefficients for the $t\bar{t}Z$ interaction.
- AABOUD 19AR based on 35.9 fb^{-1} of data. $t\bar{t}W$ and $t\bar{t}Z$ cross sections are simultaneously measured using a combined fit to the events divided into multiple regions. The result is consistent with the SM prediction at NLO $0.88^{+0.09}_{-0.11} \text{ pb}$. It is also used to constrain the Wilson coefficients for dimension-six operators which modify the $t\bar{t}Z$ vertex.
- Based on 35.9 fb^{-1} of proton-proton data taken at $\sqrt{s} = 13 \text{ TeV}$. The result is consistent with the SM prediction and is used to constrain the Wilson coefficients for dimension-six operators describing new interactions. The result is consistent with the SM prediction at NLO $0.839 \pm 0.101 \text{ pb}$.

$t\bar{t}\gamma$ Production Cross Section in pp Collisions at $\sqrt{s} = 13 \text{ TeV}$

VALUE (pb)	DOCUMENT ID	TECN	COMMENT
$0.95 \pm 0.05 \pm 0.06$	1 TUMASYAN	21H CMS	$pp \rightarrow t\bar{t}\gamma$
$0.95 \pm 0.08 \pm 0.10$	2 AABOUD	19AD ATLS	$pp \rightarrow t\bar{t}\gamma$

- We do not use the following data for averages, fits, limits, etc.
 - TUMASYAN 21H measured fiducial inclusive and differential cross-sections for $pp \rightarrow t\bar{t}\gamma$ at 13 TeV with 137 fb^{-1} of data. The results are in agreement with the SM predictions. The results are used to constrain anomalous couplings of the top quark in the SMEFT framework.
 - AABOUD 19AD measured fiducial inclusive and differential cross-sections for $pp \rightarrow t\bar{t}\gamma$ at 13 TeV with 36.1 fb^{-1} of data. The results are in agreement with the theoretical predictions.

$f(Q_0)$: $t\bar{t}$ Fraction of Events with a Veto on Additional Central Jet Activity in pp Collisions at $\sqrt{s} = 7 \text{ TeV}$

VALUE (%)	DOCUMENT ID	TECN	COMMENT
$80.0 \pm 1.1 \pm 1.6$	1 CHATRCHYAN	14AE CMS	$Q_0 = 75 \text{ GeV}$ ($ \eta < 2.4$)
$92.0 \pm 0.7 \pm 0.8$	1 CHATRCHYAN	14AE CMS	$Q_0 = 150 \text{ GeV}$ ($ \eta < 2.4$)
$98.0 \pm 0.3 \pm 0.3$	1 CHATRCHYAN	14AE CMS	$Q_0 = 300 \text{ GeV}$ ($ \eta < 2.4$)
$56.4 \pm 1.3^{+2.6}_{-2.8}$	2 AAD	12BL ATLS	$Q_0 = 25 \text{ GeV}$ ($ \eta < 2.1$)
$84.7 \pm 0.9 \pm 1.0$	2 AAD	12BL ATLS	$Q_0 = 75 \text{ GeV}$ ($ \eta < 2.1$)
$95.2^{+0.5}_{-0.6} \pm 0.4$	2 AAD	12BL ATLS	$Q_0 = 150 \text{ GeV}$ ($ \eta < 2.1$)

- CHATRCHYAN 15 based on 5.0 fb^{-1} of data. The $t\bar{t}$ events are selected in the dilepton and lepton + jets decay channels. For other values of Q_0 see Table 5.
- Based on 2.05 fb^{-1} of data. The $t\bar{t}$ events are selected in the dilepton decay channel with two identified b -jets.

Fraction of $t\bar{t} +$ multi-jet Events in pp Collisions at $\sqrt{s} = 7 \text{ TeV}$

VALUE	DOCUMENT ID	TECN	COMMENT
0.332 ± 0.090	1 AAD	15D ATLS	$\ell + \cancel{E}_T + n_j$ ($n=3$ to 8)
0.436 ± 0.098	2 CHATRCHYAN	14AE CMS	$t\bar{t}(\ell\ell) + 0 \text{ jet}$ ($E_T > 30\text{GeV}$)
0.232 ± 0.125	2 CHATRCHYAN	14AE CMS	$t\bar{t}(\ell\ell) + 1 \text{ jet}$ ($E_T > 30\text{GeV}$)
	2 CHATRCHYAN	14AE CMS	$t\bar{t}(\ell\ell) + \geq 2 \text{ jet}$ ($E_T > 30\text{GeV}$)

- Based on 4.6 fb^{-1} of data. Fiducial $t\bar{t}$ production cross section is presented as a function of the jet multiplicity for up to eight jets with the jet p_T threshold of 25, 40, 60, and 80 GeV, and as a function of jet p_T up to the 5th jet. MC models can be discriminated by using data for high jet multiplicity and by p_T distributions of the leading and 5th jet.
- Based on 5.0 fb^{-1} of data. Events with two oppositely charged leptons, large \cancel{E}_T and jets with at least 1 b -tag are used to measure the fraction of $t\bar{t}$ plus additional jets. The gap fraction ($n=0$ jet rate) as a function of the jet p_T and that of H_T , the scalar sum of the p_T 's of additional jets, is shown in Fig. 8.

$t\bar{t}$ Charge Asymmetry (A_C) in pp Collisions at $\sqrt{s} = 7 \text{ TeV}$

$A_C = (N(\Delta y) > 0) - N(\Delta y) < 0) / (N(\Delta y) > 0) + N(\Delta y) < 0)$ where $|\Delta y| = |y_t| - |y_{\bar{t}}|$ is the difference between the absolute values of the top and antitop rapidities and N is the number of events with $|\Delta y|$ positive or negative.

VALUE (%)	DOCUMENT ID	TECN	COMMENT
$0.5 \pm 0.7 \pm 0.6$	1 AABOUD	18AMLHC	ATLAS+CMS combination (lepton + jets)
$2.1 \pm 2.5 \pm 1.7$	2 AAD	15AJ ATLS	$\ell\ell + \cancel{E}_T + \geq 2j$
0.6 ± 1.0	3 AAD	14I ATLS	$\ell + \cancel{E}_T + \geq 4j$ ($\geq 1b$)
$-1.0 \pm 1.7 \pm 0.8$	4 CHATRCHYAN	14D CMS	$\ell\ell + \cancel{E}_T + \geq 2j$ ($\geq 1b$)
$-1.9 \pm 2.8 \pm 2.4$	5 AAD	12BK ATLS	$\ell + \cancel{E}_T + \geq 4j$ ($\geq 1b$)
$0.4 \pm 1.0 \pm 1.1$	6 CHATRCHYAN	12BB CMS	$\ell + \cancel{E}_T + \geq 4j$ ($\geq 1b$)
$-1.3 \pm 2.8^{+2.9}_{-3.1}$	7 CHATRCHYAN	12Bs CMS	$\ell + \cancel{E}_T + \geq 4j$ ($\geq 1b$)

- ATLAS and CMS combination based on the data of AAD 14I and CHATRCHYAN 12BB. It takes into account the correlations of the measurements and systematic errors. The result is in agreement with the SM prediction (NLO QCD + NLO EW).
- AAD 15AJ based on 4.6 fb^{-1} of data. After kinematic reconstruction the top quark momenta are corrected for detector resolution and acceptance effects by unfolding, using parton level information of the MC generators. The lepton charge asymmetry is measured

Quark Particle Listings

 t

as $A_{CP}^{\ell} = 0.024 \pm 0.015 \pm 0.009$. All the measurements are consistent with the SM predictions.

³Based on 4.7 fb^{-1} of data. The result is consistent with the SM prediction of $A_C = 0.0123 \pm 0.0005$. The asymmetry is 0.011 ± 0.018 if restricted to those events where $\beta_Z(t\bar{t}) > 0.6$, which is also consistent with the SM prediction of $0.020^{+0.006}_{-0.007}$.

⁴Based on 5.0 fb^{-1} of data. The lepton charge asymmetry is measured as $A_C^{\ell} = 0.009 \pm 0.0010 \pm 0.006$. A_C^{ℓ} dependences on $m_{t\bar{t}}$, $|y(t\bar{t})|$, and $p_T(t\bar{t})$ are given in Fig. 5. All measurements are consistent with the SM predictions.

⁵Based on 1.04 fb^{-1} of data. The result is consistent with $A_C = 0.006 \pm 0.002$ (MC at NLO). No significant dependence of A_C on $m_{t\bar{t}}$ is observed.

⁶Based on 5.0 fb^{-1} of data at 7 TeV .

⁷Based on 1.09 fb^{-1} of data. The result is consistent with the SM predictions.

 $t\bar{t}$ Charge Asymmetry (A_C) in pp Collisions at $\sqrt{s} = 8 \text{ TeV}$

VALUE (%)	DOCUMENT ID	TECN	COMMENT
• • • We do not use the following data for averages, fits, limits, etc. • • •			
$0.55 \pm 0.23 \pm 0.25$	¹ AABOUD	18AMLHC	ATLAS+CMS combination (lepton + jets)
2.1 ± 1.6	² AAD	16AE ATLS	$\ell\ell + \cancel{E}_T + \geq 2j$
0.9 ± 0.5	³ AAD	16AZ ATLS	$\ell + \cancel{E}_T + \geq 4j$
4.2 ± 3.2	⁴ AAD	16T ATLS	$m_{t\bar{t}} > 0.75 \text{ TeV}$, $\ y_{t\bar{t}}\ < 2$, $\ell + \cancel{E}_T + \text{jets}$
$1.1 \pm 1.1 \pm 0.7$	⁵ KHACHATRYAN..16AD	CMS	$\ell\ell + \cancel{E}_T + \geq 2j$ ($\geq 1b$)
$0.33 \pm 0.26 \pm 0.33$	⁶ KHACHATRYAN..16AH	CMS	$\ell + \cancel{E}_T + \geq 4j$ ($\geq 1b$)
$0.10 \pm 0.68 \pm 0.37$	⁷ KHACHATRYAN..16T	CMS	$\ell + \cancel{E}_T + \geq 4j$ ($\geq 1b$)

¹ATLAS and CMS combination based on the data of AAD 16AZ and KHACHATRYAN 16AH. It takes into account the correlations of the measurements and systematic errors. A combination of the differential measurements of the charge asymmetry is also presented. The results are in agreement with the SM prediction (NNLO QCD + NLO EW).

²AAD 16AE is based on 20.3 fb^{-1} of data. After kinematic reconstruction, the top quark momenta are corrected for detector resolution and acceptance effects by unfolding, using parton level information of the MC generators. The lepton charge asymmetry is measured as $A_C^{\ell} = 0.008 \pm 0.006$. All the measurements are consistent with the SM predictions.

³AAD 16AZ based on 20.3 fb^{-1} of data. All the differential and inclusive measurements are statistically limited and consistent with the SM predictions.

⁴AAD 16T based on 20.3 fb^{-1} of data. Uses reconstruction techniques for the decay topology of highly boosted top quarks. The observed asymmetry is transformed by unfolding to a parton-level result in the shown fiducial region. The result is consistent with the NLO SM prediction.

⁵KHACHATRYAN 16AD based on 19.5 fb^{-1} of data. The lepton charge asymmetry is measured as $A_C^{\ell} = 0.003 \pm 0.006 \pm 0.003$. All the measurements are consistent with the SM predictions.

⁶KHACHATRYAN 16AH based on 19.6 fb^{-1} of data. The same data set as in KHACHATRYAN 16T is used. A template technique is used, which is sensitive to the charge anti-symmetric component of the $t\bar{t}$ rapidity distributions and statistically advantageous. The result is consistent with the SM predictions.

⁷KHACHATRYAN 16T based on 19.7 fb^{-1} of data. The same data set as in KHACHATRYAN 16AH is used. After kinematic reconstruction the top quark momenta are corrected for detector resolution and acceptance effects by unfolding, using parton level information of the MC generators. All the measurements are consistent with the SM predictions.

 t -quark Polarization in $t\bar{t}$ Events in $p\bar{p}$ Collisions at $\sqrt{s} = 1.96 \text{ TeV}$

VALUE	DOCUMENT ID	TECN	COMMENT
• • • We do not use the following data for averages, fits, limits, etc. • • •			
0.070 ± 0.055	¹ ABAZOV	17 D0	$\ell + \cancel{E}_T + \geq 3j$ ($\geq 1b$)
-0.102 ± 0.061	² ABAZOV	17 D0	$\ell + \cancel{E}_T + \geq 3j$ ($\geq 1b$)
0.040 ± 0.035	³ ABAZOV	17 D0	$\ell + \cancel{E}_T + \geq 3j$ ($\geq 1b$)
$0.113 \pm 0.091 \pm 0.019$	⁴ ABAZOV	15K D0	A_{FB}^{ℓ} in $\ell\ell + \cancel{E}_T + \geq 2j$ ($\geq 1b$)

¹ABAZOV 17 based on 9.7 fb^{-1} of data. The value is top quark polarization times spin analyzing power in the beam basis. Combination with the result of ABAZOV 15K yields 0.081 ± 0.048 . This result together with the helicity polarization is shown in a 2-dimensional plot in Fig. 4. These results are consistent with the SM prediction.

²ABAZOV 17 based on 9.7 fb^{-1} of data. The value is top quark polarization times spin analyzing power in the helicity basis. The result is consistent with the SM prediction. This result together with the beam polarization is shown in a 2-dimensional plot in Fig. 4.

³ABAZOV 17 based on 9.7 fb^{-1} of data. The value is top quark polarization times spin analyzing power in the transverse basis. The result is consistent with the SM prediction.

⁴ABAZOV 15K based on 9.7 fb^{-1} of data. The value is top quark polarization times spin analyzing power in the beam basis. The result is consistent with the SM prediction of -0.0019 ± 0.0005 .

 t -quark Polarization in $t\bar{t}$ Events in pp Collisions at $\sqrt{s} = 7 \text{ TeV}$

The double differential distribution in polar angles, θ_1 (θ_2) of the decay particle of the top (anti-top) decay products, is parameterized as $(1/\sigma)d\sigma/(d\cos\theta_1 d\cos\theta_2) = (1/4)(1 + A_t \cos\theta_1 + A_{\bar{t}} \cos\theta_2 - C \cos\theta_1 \cos\theta_2)$. The charged lepton is used to tag t or \bar{t} . The coefficient A_t and $A_{\bar{t}}$ measure the average helicity of t and \bar{t} , respectively. $A_{CP}^{CP} = A_t = A_{\bar{t}}$ assumes CP conservation, whereas $A_{CP}^{CP} = A_t = -A_{\bar{t}}$ corresponds to maximal CP violation.

VALUE	DOCUMENT ID	TECN	COMMENT
• • • We do not use the following data for averages, fits, limits, etc. • • •			
$-0.035 \pm 0.014 \pm 0.037$	¹ AAD	13BE ATLS	A_{CP}^{CP}
$0.020 \pm 0.016^{+0.013}_{-0.017}$	¹ AAD	13BE ATLS	A_{CP}^{CP}

¹Based on 4.7 fb^{-1} of data using the final states containing one or two isolated electrons or muons and jets with at least one b -tag.

 t -quark Polarization in $t\bar{t}$ Events in pp Collisions at $\sqrt{s} = 8 \text{ TeV}$

A_t , $A_{\bar{t}}$, A_{CP}^{CP} , A_{CP}^{PV} , and A_C are defined in header texts in the subsections, just above.

VALUE	DOCUMENT ID	TECN	COMMENT
• • • We do not use the following data for averages, fits, limits, etc. • • •			
$-0.044 \pm 0.038 \pm 0.027$	¹ AABOUD	17G ATLS	A_t
$-0.064 \pm 0.040 \pm 0.027$	¹ AABOUD	17G ATLS	$A_{\bar{t}}$
$0.296 \pm 0.093 \pm 0.037$	¹ AABOUD	17G ATLS	A_C
-0.022 ± 0.058	² KHACHATRYAN..16AI	CMS	A_{CP}^{CP}
0.000 ± 0.016	² KHACHATRYAN..16AI	CMS	A_{CP}^{PV}

¹AABOUD 17G based on 20.2 fb^{-1} of pp data, using events with two leptons and two or more jets with at least one b -tag. Determined from measurements of 15 top quark spin observables. The second error corresponds to a variation of m_t about 172.5 GeV by 0.7 GeV . The values are consistent with the NLO SM predictions.

²KHACHATRYAN 16AI based on 19.5 fb^{-1} of pp data at $\sqrt{s} = 8 \text{ TeV}$, using events with two leptons and two or more jets with at least one b -tag. Determined from the lepton angular distributions as a function of the $t\bar{t}$ -system kinematical variables.

 t -quark Polarization in Single Top Events in pp Collisions at $\sqrt{s} = 8 \text{ TeV}$

VALUE	CL%	DOCUMENT ID	TECN	COMMENT
• • • We do not use the following data for averages, fits, limits, etc. • • •				
>0.72	95	¹ AABOUD	17BB ATLS	$\alpha_{\ell} P$; t-channel
$0.97 \pm 0.05 \pm 0.11$		² AABOUD	17I ATLS	$\alpha_{\ell} P$; t-channel
$0.25 \pm 0.08 \pm 0.14$		³ AABOUD	17I ATLS	$(F_{\pm} + F_{\mp})P$; t-channel
$0.26 \pm 0.03 \pm 0.10$		⁴ KHACHATRYAN..16B0	CMS	$(\alpha_{\mu} P)/2$; t-channel

¹AABOUD 17BB based on 20.2 fb^{-1} of pp data. Triple-differential decay rate of top quark is used to simultaneously determine five generalized Wtb couplings as well as the top polarization. α_{ℓ} denotes the spin analyzing power of charged lepton, and the spin axis of the top polarization P is taken along the spectator-quark momentum in the top rest frame. The value is compatible with the SM prediction of about 0.9.

²AABOUD 17I based on 20.2 fb^{-1} of pp data. A cut-based analysis is used to discriminate between signal and backgrounds. α_{ℓ} denotes the spin analyzing power of charged lepton, and the spin axis of the top polarization P is taken along the spectator-quark momentum in the top rest frame. See this paper for a number of other asymmetries and measurements that are not included here.

³AABOUD 17I based on 20.2 fb^{-1} of pp data. A cut-based analysis is used to discriminate between signal and backgrounds. F_{\pm} denotes W helicity fraction, and the spin axis of the top polarization P is taken along the spectator-quark momentum in the top rest frame. See this paper for a number of other asymmetries and measurements that are not included here.

⁴KHACHATRYAN 16B0 based on 19.7 fb^{-1} of data. A high-purity sample with a muon is selected by a multivariate analysis. The value is the top spin asymmetry, given by one half of the spin analyzing power $\alpha_{\mu} (=1 \text{ at LO of SM})$ times the top polarization P , where the spin axis is defined as the direction of the untagged jet in the top rest frame. The value is compatible with the SM prediction of 0.44 with a 2.0σ deviation.

 t -quark Polarization in Single Top Events in pp Collisions at $\sqrt{s} = 13 \text{ TeV}$

VALUE	DOCUMENT ID	TECN	COMMENT
• • • We do not use the following data for averages, fits, limits, etc. • • •			
0.440 ± 0.070	¹ SIRUNYAN	20R CMS	$(\alpha_{\ell} P)/2$; t-channel

¹SIRUNYAN 20R based on 36.1 fb^{-1} of data. Differential cross sections for t -channel single top production are measured using $1\ell + 2,3$ -jet mode and found to be in good agreement with SM predictions. The value is the top spin asymmetry, given by $1/2$ of the spin analyzing power $\alpha_{\ell} (=1 \text{ at LO of SM})$ times the top polarization P , where the spin axis is defined as the direction of the spectator quark in the top rest frame at the parton level. It is in good agreement with the NLO SM prediction of 0.436.

 $gg \rightarrow t\bar{t}$ Fraction in $p\bar{p}$ Collisions at $\sqrt{s} = 1.96 \text{ TeV}$

VALUE	CL%	DOCUMENT ID	TECN	COMMENT
• • • We do not use the following data for averages, fits, limits, etc. • • •				
<0.33	68	¹ AALTONEN	09F CDF	$t\bar{t}$ correlations
$0.07 \pm 0.14 \pm 0.07$		² AALTONEN	08AG CDF	low p_T number of tracks

¹Based on 955 pb^{-1} . AALTONEN 09F used differences in the $t\bar{t}$ production angular distribution and polarization correlation to discriminate between $gg \rightarrow t\bar{t}$ and $q\bar{q} \rightarrow t\bar{t}$ subprocesses. The combination with the result of AALTONEN 08AG gives $0.07^{+0.15}_{-0.07}$.

²Result is based on 0.96 fb^{-1} of data. The contribution of the subprocesses $gg \rightarrow t\bar{t}$ and $q\bar{q} \rightarrow t\bar{t}$ is distinguished by using the difference between quark and gluon initiated jets in the number of small p_T ($0.3 \text{ GeV} < p_T < 3 \text{ GeV}$) charged particles in the central region ($|\eta| < 1.1$).

 A_{FB} of $t\bar{t}$ in $p\bar{p}$ Collisions at $\sqrt{s} = 1.96 \text{ TeV}$

A_{FB} = Forward-backward asymmetry.

VALUE (%)	DOCUMENT ID	TECN	COMMENT
• • • We do not use the following data for averages, fits, limits, etc. • • •			
$12.8 \pm 2.1 \pm 1.4$	¹ AALTONEN	18 TEVA	CDF, D0 combination
$17.5 \pm 5.6 \pm 3.1$	² ABAZOV	15K D0	A_{FB}^{ℓ} in $\ell\ell + \cancel{E}_T + \geq 2j$ ($\geq 1b$)
7.2 ± 6.0	³ AALTONEN	14F CDF	A_{FB}^{ℓ} in dilepton channel ($\ell\ell + \cancel{E}_T + \geq 2j$)
7.6 ± 8.2	³ AALTONEN	14F CDF	A_{FB}^{ℓ} in dilepton channel ($\ell\ell + \cancel{E}_T + \geq 2j$)
$4.2 \pm 2.3^{+1.7}_{-2.0}$	⁴ ABAZOV	14G D0	A_{FB}^{ℓ} ($\ell + \cancel{E}_T + \geq 3j$ ($0.1 \geq 2b$))
10.6 ± 3.0	⁵ ABAZOV	14H D0	A_{FB} ($\ell + \cancel{E}_T + \geq 3j$ ($\geq 1b$))
20.1 ± 6.7	⁶ AALTONEN	13AD CDF	a_1/a_0 in $\ell + \cancel{E}_T + \geq 4j$ ($\geq 1b$)
-0.2 ± 3.1	⁶ AALTONEN	13AD CDF	a_3, a_5, a_7 in $\ell + \cancel{E}_T + \geq 4j$ ($\geq 1b$)
16.4 ± 4.7	⁷ AALTONEN	13S CDF	$\ell + \cancel{E}_T + \geq 4$ jets ($\geq 1b$ -tag)

$9.4^{+3.2}_{-2.9}$	⁸ AALTONEN	13x CDF	$\ell + \cancel{E}_T + \geq 4$ jets (≥ 1 b-tag)
11.8 ± 3.2	⁹ ABAZOV	13A D0	$\ell\ell$ & $\ell +$ jets comb.
-11.6 ± 15.3	¹⁰ AALTONEN	11F CDF	$m_{t\bar{t}} < 450$ GeV
47.5 ± 11.4	¹⁰ AALTONEN	11F CDF	$m_{t\bar{t}} > 450$ GeV
19.6 ± 6.5	¹¹ ABAZOV	11AH D0	$\ell + \cancel{E}_T + \geq 4$ jets (≥ 1 b-tag)
17 ± 8	¹² AALTONEN	08AB CDF	$p\bar{p}$ frame
24 ± 14	¹² AALTONEN	08AB CDF	$t\bar{t}$ frame
$12 \pm 8 \pm 1$	¹³ ABAZOV	08L D0	$\ell + \cancel{E}_T + \geq 4$ jets

- ¹ AALTONEN 18 based on $9\text{--}10 \text{ fb}^{-1}$ of $p\bar{p}$ data at $\sqrt{s} = 1.96 \text{ TeV}$. The value is the asymmetry in the number of reconstructed $t\bar{t}$ events with rapidity $y_t > y_{\bar{t}}$ and those with $y_t < y_{\bar{t}}$. The combined fits to CDF and D0 single lepton and $\ell\ell$ asymmetries give $A_{FB}^{\ell} = 0.073 \pm 0.016 \pm 0.012$ and $A_{FB}^{\ell\ell} = 0.108 \pm 0.043 \pm 0.016$, respectively. The results are consistent with the SM predictions.
- ² ABAZOV 15k based on 9.7 fb^{-1} of data. The result is consistent with the SM predictions. By combining with the previous D0 measurement in the $\ell +$ jet channel ABAZOV 14H, $A_{FB}^{\ell} = 0.118 \pm 0.025 \pm 0.013$ is obtained.
- ³ AALTONEN 14F based on 9.1 fb^{-1} of data. A_{FB}^{ℓ} and $A_{FB}^{\ell\ell}$ denote, respectively, the asymmetries $(N(x>0) - N(x<0))/N_{tot}$ for $x = q\eta/q$ (q is the charge of ℓ) and $x = \eta_{\ell^+} - \eta_{\ell^-}$. Both results are consistent with the SM predictions. By combining with the previous CDF measurement in the $\ell +$ jet channel AALTONEN 13x, $A_{FB}^{\ell} = 0.098^{+0.028}_{-0.026}$ is obtained. The combined result is about two sigma larger than the SM prediction of $A_{FB}^{\ell} = 0.038 \pm 0.003$.
- ⁴ Based on 9.7 fb^{-1} of $p\bar{p}$ data at $\sqrt{s} = 1.96 \text{ TeV}$. The asymmetry is corrected for the production level for events with $|y_t| < 1.5$. Asymmetry as functions of $E_{T,(\ell)}$ and $|y_t|$ are given in Figs. 7 and 8, respectively. Combination with the asymmetry measured in the dilepton channel [ABAZOV 13P] gives $A_{FB}^{\ell} = 4.2 \pm 2.0 \pm 1.4$ %, in agreement with the SM prediction of 2.0%.
- ⁵ Based on 9.7 fb^{-1} of data of $p\bar{p}$ data at $\sqrt{s} = 1.96 \text{ TeV}$. The measured asymmetry is in agreement with the SM predictions of 8.8 ± 0.9 % [BERNREUTHER 12], which includes the EW effects. The dependences of the asymmetry on $|y(t) - y(\bar{t})|$ and $m_{t\bar{t}}$ are shown in Figs. 9 and 10, respectively.
- ⁶ Based on 9.4 fb^{-1} of data. Reported A_{FB} values come from the determination of a_j coefficients of $d\sigma/d(\cos\theta_j) = \sum_i a_i P_i(\cos\theta_j)$ measurement. The result of $a_1/a_0 = (40 \pm 12)\%$ seems higher than the NLO SM prediction of $(15^{+7}_{-3})\%$.
- ⁷ Based on 9.4 fb^{-1} of data. The quoted result is the asymmetry at the parton level.
- ⁸ Based on 9.4 fb^{-1} of data. The observed asymmetry is to be compared with the SM prediction of $A_{FB}^{\ell} = 0.038 \pm 0.003$.
- ⁹ Based on 5.4 fb^{-1} of data. ABAZOV 13A studied the dilepton channel of the $t\bar{t}$ events and measured the leptonic forward-backward asymmetry to be $A_{FB}^{\ell} = 5.8 \pm 5.1 \pm 1.3\%$, which is consistent with the SM (QCD+EW) prediction of $4.7 \pm 0.1\%$, which is obtained after combining the measurement $(15.2 \pm 4.0\%)$ in the $\ell +$ jets channel ABAZOV 11AH. The top quark helicity is measured by using the neutrino weighting method to be consistent with zero in both dilepton and $\ell +$ jets channels.
- ¹⁰ Based on 5.3 fb^{-1} of data. The error is statistical and systematic combined. Events with lepton + $\cancel{E}_T + \geq 4$ jets (≥ 1 b) are used. AALTONEN 11F also measures the asymmetry as a function of the rapidity difference $|y_t - y_{\bar{t}}|$. The NLO QCD predictions [MCFM] are $(4.0 \pm 0.6)\%$ and $(8.8 \pm 1.3)\%$ for $m_{t\bar{t}} < 450$ and > 450 GeV, respectively.
- ¹¹ Based on 5.4 fb^{-1} of data. The error is statistical and systematic combined. The quoted asymmetry is obtained after unfolding to be compared with the MC@NLO prediction of $(5.0 \pm 0.1)\%$. No significant difference between the $m_{t\bar{t}} < 450$ and > 450 GeV data samples is found. A corrected asymmetry based on the lepton from a top quark decay of $(15.2 \pm 4.0)\%$ is measured to be compared to the MC@NLO prediction of $(2.1 \pm 0.1)\%$.
- ¹² Result is based on 1.9 fb^{-1} of data. The FB asymmetry in the $t\bar{t}$ events has been measured in the $\ell +$ jets mode, where the lepton charge is used as the flavor tag. The asymmetry in the $p\bar{p}$ frame is defined in terms of $\cos(\theta)$ of hadronically decaying t -quark momentum, whereas that in the $t\bar{t}$ frame is defined in terms of the t and \bar{t} rapidity difference. The results are consistent ($\leq 2\sigma$) with the SM predictions.
- ¹³ Result is based on 0.9 fb^{-1} of data. The asymmetry in the number of $t\bar{t}$ events with $y_t > y_{\bar{t}}$ and those with $y_t < y_{\bar{t}}$ has been measured in the lepton + jets final state. The observed value is consistent with the SM prediction of 0.8% by MC@NLO, and an upper bound on the $Z' \rightarrow t\bar{t}$ contribution for the SM Z-like couplings is given in Fig. 2 for $350 \text{ GeV} < m_{Z'} < 1 \text{ TeV}$.

- ⁴ AALTONEN 10s excludes the charge $-4/3$ assignment for the top quark [CHANG 99] at 95% CL, using 2.7 fb^{-1} of data in $p\bar{p}$ collisions at $\sqrt{s} = 1.96 \text{ TeV}$. Result is obtained by reconstructing $t\bar{t}$ events in the lepton + jets final state, where b -jet charges are tagged by the SLT (soft lepton tag) algorithm.
- ⁵ ABAZOV 07c reports an upper limit $\rho < 0.80$ (90% CL) on the fraction ρ of exotic quark pairs $Q\bar{Q}$ with electric charge $|q| = 4e/3$ in $t\bar{t}$ candidate events with high p_T lepton, missing E_T and ≥ 4 jets. The result is obtained by measuring the fraction of events in which the quark pair decays into $W^- + b$ and $W^+ + \bar{b}$, where b and \bar{b} jets are discriminated by using the charge and momenta of tracks within the jet cones. The maximum CL at which the model of CHANG 99 can be excluded is 92%. Based on 370 pb^{-1} of data at $\sqrt{s} = 1.96 \text{ TeV}$.

t-Quark REFERENCES

AAD	21AS	EPJ C81 737	G. Aad et al.	(ATLAS Collab.)
AAD	21AT	EPJ C81 720	G. Aad et al.	(ATLAS Collab.)
AAD	21BC	JHEP 2111 118	G. Aad et al.	(ATLAS Collab.)
TUMASYAN	21E	JHEP 2111 111	A. Tumasyan et al.	(CMS Collab.)
TUMASYAN	21H	JHEP 2112 161	A. Tumasyan et al.	(CMS Collab.)
TUMASYAN	21G	JHEP 2112 180	A. Tumasyan et al.	(CMS Collab.)
TUMASYAN	21J	PR D104 092013	A. Tumasyan et al.	(CMS Collab.)
AAD	20AB	JHEP 2007 124	G. Aad et al.	(ATLAS Collab.)
AAD	20AH	PL B810 135797	G. Aad et al.	(ATLAS Collab.)
AAD	20AR	EPJ C80 1085	G. Aad et al.	(ATLAS Collab.)
AAD	20B	PL B800 135082	G. Aad et al.	(ATLAS Collab.)
AAD	20Q	EPJ C80 528	G. Aad et al.	(ATLAS Collab.)
AAD	20Y	JHEP 2008 051	G. Aad et al.	(ATLAS and CMS Collab.)
AAD	20Z	PRL 125 061802	G. Aad et al.	(ATLAS Collab.)
SIRUNYAN	20AB	JHEP 2003 056	A.M. Sirunyan et al.	(CMS Collab.)
SIRUNYAN	20AM	JHEP 2006 146	A.M. Sirunyan et al.	(CMS Collab.)
SIRUNYAN	20AR	PRL 124 202001	A.M. Sirunyan et al.	(CMS Collab.)
SIRUNYAN	20AS	PRL 125 061801	A.M. Sirunyan et al.	(CMS Collab.)
SIRUNYAN	20AZ	PL B808 135609	A.M. Sirunyan et al.	(CMS Collab.)
SIRUNYAN	20BC	PRL 125 222001	A.M. Sirunyan et al.	(CMS Collab.)
SIRUNYAN	20BH	PR D102 092013	A.M. Sirunyan et al.	(CMS Collab.)
SIRUNYAN	20BV	EPJ C80 658	A.M. Sirunyan et al.	(CMS Collab.)
SIRUNYAN	20C	EPJ C80 75	A.M. Sirunyan et al.	(CMS Collab.)
SIRUNYAN	20D	PL B800 135042	A.M. Sirunyan et al.	(CMS Collab.)
SIRUNYAN	20R	EPJ C80 370	A.M. Sirunyan et al.	(CMS Collab.)
SIRUNYAN	20V	JHEP 2002 191	A.M. Sirunyan et al.	(CMS Collab.)
AABOUD	19AC	EPJ C79 290	M. Aaboud et al.	(ATLAS Collab.)
AABOUD	19AD	EPJ C79 382	M. Aaboud et al.	(ATLAS Collab.)
AABOUD	19AP	PR D99 052009	M. Aaboud et al.	(ATLAS Collab.)
AABOUD	19AR	PR D99 072009	M. Aaboud et al.	(ATLAS Collab.)
AABOUD	19R	JHEP 1905 088	M. Aaboud et al.	(ATLAS and CMS Collab.)
AABOUD	19S	JHEP 1905 123	M. Aaboud et al.	(ATLAS Collab.)
AAD	19G	JHEP 1911 150	G. Aad et al.	(ATLAS Collab.)
SIRUNYAN	19AP	EPJ C79 313	A.M. Sirunyan et al.	(CMS Collab.)
SIRUNYAN	19AR	EPJ C79 368	A.M. Sirunyan et al.	(CMS Collab.)
SIRUNYAN	19BF	PRL 122 132003	A.M. Sirunyan et al.	(CMS Collab.)
SIRUNYAN	19BX	PR D100 072002	A.M. Sirunyan et al.	(CMS Collab.)
SIRUNYAN	19BY	PR D100 072007	A.M. Sirunyan et al.	(CMS Collab.)
SIRUNYAN	19CN	JHEP 1911 082	A.M. Sirunyan et al.	(CMS Collab.)
SIRUNYAN	19P	JHEP 1902 149	A.M. Sirunyan et al.	(CMS Collab.)
SIRUNYAN	19R	JHEP 1903 026	A.M. Sirunyan et al.	(CMS Collab.)
AABOUD	18AE	PL B780 557	M. Aaboud et al.	(ATLAS Collab.)
AABOUD	18AM	JHEP 1804 033	M. Aaboud et al.	(ATLAS and CMS Collab.)
AABOUD	18AT	JHEP 1807 176	M. Aaboud et al.	(ATLAS Collab.)
AABOUD	18AZ	EPJ C78 129	M. Aaboud et al.	(ATLAS Collab.)
AABOUD	18BH	EPJ C78 487	M. Aaboud et al.	(ATLAS Collab.)
AABOUD	18BK	PL B784 173	M. Aaboud et al.	(ATLAS Collab.)
AABOUD	18BW	JHEP 1809 139	M. Aaboud et al.	(ATLAS Collab.)
AABOUD	18CE	JHEP 1812 039	M. Aaboud et al.	(ATLAS Collab.)
AABOUD	18H	JHEP 1801 063	M. Aaboud et al.	(ATLAS Collab.)
AABOUD	18X	PR D96 032002	M. Aaboud et al.	(ATLAS Collab.)
AALTONEN	18	PRL 120 042001	T. Aaltonen et al.	(CDF and D0 Collab.)
SIRUNYAN	18AQ	JHEP 1803 115	A.M. Sirunyan et al.	(CMS Collab.)
SIRUNYAN	18BC	JHEP 1806 102	A.M. Sirunyan et al.	(CMS Collab.)
SIRUNYAN	18BD	JHEP 1806 101	A.M. Sirunyan et al.	(CMS Collab.)
SIRUNYAN	18BS	JHEP 1808 011	A.M. Sirunyan et al.	(CMS Collab.)
SIRUNYAN	18BU	EPJ C78 140	A.M. Sirunyan et al.	(CMS Collab.)
SIRUNYAN	18DE	EPJ C78 891	A.M. Sirunyan et al.	(CMS Collab.)
SIRUNYAN	18DL	JHEP 1810 117	A.M. Sirunyan et al.	(CMS Collab.)
SIRUNYAN	18L	PRL 120 231801	A.M. Sirunyan et al.	(CMS Collab.)
SIRUNYAN	18Z	PL B779 358	A.M. Sirunyan et al.	(CMS Collab.)
AABOUD	17AH	JHEP 1709 118	M. Aaboud et al.	(ATLAS Collab.)
AABOUD	17B	JHEP 1710 129	M. Aaboud et al.	(ATLAS Collab.)
AABOUD	17BE	JHEP 1712 017	M. Aaboud et al.	(ATLAS Collab.)
AABOUD	17BC	EPJ C77 804	M. Aaboud et al.	(ATLAS Collab.)
AABOUD	17G	JHEP 1703 113	M. Aaboud et al.	(ATLAS Collab.)
AABOUD	17H	JHEP 1704 086	M. Aaboud et al.	(ATLAS Collab.)
AABOUD	17I	JHEP 1704 124	M. Aaboud et al.	(ATLAS Collab.)
AABOUD	17T	EPJ C77 531	M. Aaboud et al.	(ATLAS Collab.)
AABOUD	17Z	PR D95 072003	M. Aaboud et al.	(ATLAS Collab.)
ABAZOV	17	PR D95 011101	V.M. Abazov et al.	(D0 Collab.)
ABAZOV	17B	PR D95 112004	V.M. Abazov et al.	(D0 Collab.)
CHATRCHYAN	17	PL B770 50	S. Chatrchyan et al.	(CMS Collab.)
KHACHATRYAN	17B	EPJ C77 15	V. Khachatryan et al.	(CMS Collab.)
KHACHATRYAN	17G	JHEP 1702 028	V. Khachatryan et al.	(CMS Collab.)
KHACHATRYAN	17I	JHEP 1702 079	V. Khachatryan et al.	(CMS Collab.)
KHACHATRYAN	17N	EPJ C77 172	V. Khachatryan et al.	(CMS Collab.)
SIRUNYAN	17AA	PL B772 752	A.M. Sirunyan et al.	(CMS Collab.)
SIRUNYAN	17AB	PL B772 336	A.M. Sirunyan et al.	(CMS Collab.)
SIRUNYAN	17E	JHEP 1707 003	A.M. Sirunyan et al.	(CMS Collab.)
SIRUNYAN	17L	EPJ C77 354	A.M. Sirunyan et al.	(CMS Collab.)
SIRUNYAN	17N	EPJ C77 467	A.M. Sirunyan et al.	(CMS Collab.)
SIRUNYAN	17O	PR D96 032002	A.M. Sirunyan et al.	(CMS Collab.)
SIRUNYAN	17S	EPJ C77 578	A.M. Sirunyan et al.	(CMS Collab.)
SIRUNYAN	17W	JHEP 1709 051	A.M. Sirunyan et al.	(CMS Collab.)
AABOUD	16R	PL B761 136	M. Aaboud et al.	(ATLAS Collab.)
AABOUD	16T	PL B761 350	M. Aaboud et al.	(ATLAS Collab.)
AAD	16AE	PR D94 032006	G. Aad et al.	(ATLAS Collab.)
AAD	16AK	JHEP 1604 023	G. Aad et al.	(ATLAS Collab.)
AAD	16AS	EPJ C76 55	G. Aad et al.	(ATLAS Collab.)
AAD	16AZ	EPJ C76 87	G. Aad et al.	(ATLAS Collab.)
AAD	16B	JHEP 1601 064	G. Aad et al.	(ATLAS Collab.)
AAD	16BK	EPJ C76 642	G. Aad et al.	(ATLAS Collab.)
AAD	16D	EPJ C76 12	G. Aad et al.	(ATLAS Collab.)
AAD	16U	PL B756 52	G. Aad et al.	(ATLAS Collab.)
AAD	16V	PL B756 228	G. Aad et al.	(ATLAS Collab.)
AALTONEN	16	PR D93 032011	T. Aaltonen et al.	(CDF Collab.)
ABAZOV	16	PL B752 18	V.M. Abazov et al.	(D0 Collab.)
ABAZOV	16A	PL B757 199	V.M. Abazov et al.	(D0 Collab.)
ABAZOV	16D	PR D94 032004	V.M. Abazov et al.	(D0 Collab.)
ABAZOV	16F	PR D94 092004	V.M. Abazov et al.	(D0 Collab.)
KHACHATRYAN	16AD	PL B760 365	V. Khachatryan et al.	(CMS Collab.)
KHACHATRYAN	16AH	PR D93 034014	V. Khachatryan et al.	(CMS Collab.)

t-Quark Electric Charge

VALUE	DOCUMENT ID	TECN	COMMENT
0.64 ± 0.02 ± 0.08	¹ AAD	13AY ATLS	$\ell + \cancel{E}_T + \geq 4$ jets (≥ 1 b)
• • • We do not use the following data for averages, fits, limits, etc. • • •			
	² ABAZOV	14D D0	$\ell + \cancel{E}_T + \geq 4$ jets (≥ 2 b)
	³ AALTONEN	13J CDF	$p\bar{p}$ at 1.96 TeV
	⁴ AALTONEN	10s CDF	Repl. by AALTONEN 13J
	⁵ ABAZOV	07c D0	fraction of $ q =4e/3$ pair

- ¹ AAD 13AY result is based on 2.05 fb^{-1} of pp data at $\sqrt{s} = 7 \text{ TeV}$, the result is obtained by reconstructing $t\bar{t}$ events in the lepton + jets final state, where b -jet charges are tagged by the jet-charge algorithm. This measurement excludes the charge $-4/3$ assignment to the top quark at more than 8 standard deviations.
- ² ABAZOV 14D result is based on 5.3 fb^{-1} of $p\bar{p}$ data at $\sqrt{s} = 1.96 \text{ TeV}$. The electric charge of $b + W$ system in $t\bar{t}$ candidate events is measured from the charges of the leptons from W decay and in b jets. Under the assumption that the $b + W$ system consists of the sum of the top quark and the charge $-4/3$ quark $b'(-4/3)$ of the same mass, the top quark fraction is found to be $f = 0.88 \pm 0.13$ (stat) ± 0.11 (syst), or the upper bound for the $b'(-4/3)$ contamination of $1 - f < 0.46$ (95% CL).
- ³ AALTONEN 13J excludes the charge $-4/3$ assignment to the top quark at 99% CL, using 5.6 fb^{-1} of data in $p\bar{p}$ collisions at $\sqrt{s} = 1.96 \text{ TeV}$. Result is obtained by reconstructing $t\bar{t}$ events in the lepton + jets final state, where b -jet charges are tagged by the jet-charge algorithm.

Quark Particle Listings

t

KHACHATRYAN...16A1	PR D93 052007	V. Khachatryan et al.	(CMS Collab.)	CHATRCHYAN 12AC	PR D85 112007	S. Chatrchyan et al.	(CMS Collab.)
KHACHATRYAN...16AK	PR D93 072004	V. Khachatryan et al.	(CMS Collab.)	CHATRCHYAN 12AB	JHEP 1211 067	S. Chatrchyan et al.	(CMS Collab.)
KHACHATRYAN...16AL	PR D93 092006	V. Khachatryan et al.	(CMS Collab.)	CHATRCHYAN 12XA	EPJ C72 2202	S. Chatrchyan et al.	(CMS Collab.)
KHACHATRYAN...16AS	JHEP 1604 035	V. Khachatryan et al.	(CMS Collab.)	CHATRCHYAN 12BB	PL B717 129	S. Chatrchyan et al.	(CMS Collab.)
KHACHATRYAN...16AW	JHEP 1608 029	V. Khachatryan et al.	(CMS Collab.)	CHATRCHYAN 12BP	JHEP 1212 105	S. Chatrchyan et al.	(CMS Collab.)
KHACHATRYAN...16AZ	JHEP 1609 027	V. Khachatryan et al.	(CMS Collab.)	CHATRCHYAN 12BQ	JHEP 1212 035	S. Chatrchyan et al.	(CMS Collab.)
KHACHATRYAN...16BC	EPJ C76 128	V. Khachatryan et al.	(CMS Collab.)	CHATRCHYAN 12BS	PL B709 28	S. Chatrchyan et al.	(CMS Collab.)
KHACHATRYAN...16BJ	EPJ C76 439	V. Khachatryan et al.	(CMS Collab.)	CHATRCHYAN 12Y	JHEP 1206 109	S. Chatrchyan et al.	(CMS Collab.)
KHACHATRYAN...16BO	JHEP 1604 073	V. Khachatryan et al.	(CMS Collab.)	AAD	11A EPJ C71 1577	G. Aad et al.	(ATLAS Collab.)
KHACHATRYAN...16BU	PL B762 512	V. Khachatryan et al.	(CMS Collab.)	AALTONEN 11AC	PR D84 071105	T. Aaltonen et al.	(CDF Collab.)
KHACHATRYAN...16CB	JHEP 1612 123	V. Khachatryan et al.	(CMS Collab.)	AALTONEN 11AK	PRL 107 232002	T. Aaltonen et al.	(CDF Collab.)
KHACHATRYAN...16J	PRL 116 052002	V. Khachatryan et al.	(CMS Collab.)	AALTONEN 11AR	PR D83 031104	T. Aaltonen et al.	(CDF Collab.)
KHACHATRYAN...16T	PL B757 154	V. Khachatryan et al.	(CMS Collab.)	AALTONEN 11D	PR D83 071102	T. Aaltonen et al.	(CDF Collab.)
KHACHATRYAN...16X	PL B758 321	V. Khachatryan et al.	(CMS Collab.)	AALTONEN 11E	PR D83 111101	T. Aaltonen et al.	(CDF Collab.)
TEVEWVG	16 arXiv:1608.01881	Tevatron Electroweak Working Group		AALTONEN 11F	PR D83 112003	T. Aaltonen et al.	(CDF Collab.)
AAD	15 PL B740 222	G. Aad et al.	(ATLAS Collab.)	AALTONEN 11K	PRL 106 152001	T. Aaltonen et al.	(CDF Collab.)
AAD	15A PL B740 118	G. Aad et al.	(ATLAS Collab.)	AALTONEN 11T	PL B698 371	T. Aaltonen et al.	(CDF Collab.)
AAD	15AJ JHEP 1505 061	G. Aad et al.	(ATLAS Collab.)	AALTONEN 11W	PR D84 031101	T. Aaltonen et al.	(CDF Collab.)
AAD	15AR JHEP 1508 105	G. Aad et al.	(ATLAS Collab.)	ABAZOV 11M	PL B701 313	T. Aaltonen et al.	(CDF Collab.)
AAD	15AW EPJ C75 158	G. Aad et al.	(ATLAS Collab.)	AALTONEN 11Y	PR D84 032003	T. Aaltonen et al.	(CDF Collab.)
AAD	15BF EPJ C75 330	G. Aad et al.	(ATLAS Collab.)	AALTONEN 11Z	PR D84 031104	T. Aaltonen et al.	(CDF Collab.)
AAD	15BO PR D91 052005	G. Aad et al.	(ATLAS Collab.)	ABAZOV 11A	PL B695 88	V.M. Abazov et al.	(DO Collab.)
AAD	15BP PR D91 112013	G. Aad et al.	(ATLAS Collab.)	ABAZOV 11AA	PL B705 313	V.M. Abazov et al.	(DO Collab.)
AAD	15BW JHEP 1510 121	G. Aad et al.	(ATLAS Collab.)	ABAZOV 11AD	PR D84 112001	V.M. Abazov et al.	(DO Collab.)
AAD	15BY JHEP 1510 150	G. Aad et al.	(ATLAS Collab.)	ABAZOV 11AE	PRL 107 032001	V.M. Abazov et al.	(DO Collab.)
AAD	15CC PR D92 072005	G. Aad et al.	(ATLAS Collab.)	ABAZOV 11AF	PL B702 16	V.M. Abazov et al.	(DO Collab.)
AAD	15CO JHEP 1512 061	G. Aad et al.	(ATLAS Collab.)	ABAZOV 11AH	PR D84 112005	V.M. Abazov et al.	(DO Collab.)
AAD	15D JHEP 1501 020	G. Aad et al.	(ATLAS Collab.)	ABAZOV 11B	PRL 106 022001	V.M. Abazov et al.	(DO Collab.)
AAD	15J PRL 114 142001	G. Aad et al.	(ATLAS Collab.)	ABAZOV 11C	PR D83 032009	V.M. Abazov et al.	(DO Collab.)
AALI	15R PRL 115 112001	R. Aaij et al.	(LHCb Collab.)	ABAZOV 11E	PR D84 022008	V.M. Abazov et al.	(DO Collab.)
AALTONEN 15D	PR D92 032003	T. Aaltonen et al.	(CDF Collab.)	ABAZOV 11G	PR D83 032003	T. Aaltonen et al.	(DO Collab.)
AALTONEN 15H	PRL 115 152003	T. Aaltonen et al.	(CDF, DO Collab.)	ABAZOV 11H	PR D83 032004	V.M. Abazov et al.	(DO Collab.)
ABAZOV 15G	PR D91 112003	V.M. Abazov et al.	(DO Collab.)	ABAZOV 11I	PL B703 422	V.M. Abazov et al.	(DO Collab.)
ABAZOV 15K	PR D92 052007	V.M. Abazov et al.	(DO Collab.)	ABAZOV 11S	PR D84 052005	V.M. Abazov et al.	(DO Collab.)
CHATRCHYAN 15	EPJ C75 216 (errata.)	S. Chatrchyan et al.	(CMS Collab.)	ABAZOV 11T	PRL 107 121802	V.M. Abazov et al.	(DO Collab.)
AAD 14	PL B728 363	G. Aad et al.	(ATLAS Collab.)	ABAZOV 11X	PL B704 403	V.M. Abazov et al.	(DO Collab.)
AAD 14AA	JHEP 1406 008	G. Aad et al.	(ATLAS Collab.)	CHATRCHYAN 11AA	EPJ C71 1721	S. Chatrchyan et al.	(CMS Collab.)
AAD 14AY	EPJ C74 3109	G. Aad et al.	(ATLAS Collab.)	CHATRCHYAN 11F	JHEP 1107 049	S. Chatrchyan et al.	(CMS Collab.)
AAD 14BB	PR D90 112016	G. Aad et al.	(ATLAS Collab.)	CHATRCHYAN 11R	PRL 107 091802	S. Chatrchyan et al.	(CMS Collab.)
AAD 14BI	PR D90 112006	G. Aad et al.	(ATLAS Collab.)	CHATRCHYAN 11Z	PR D84 022004	S. Chatrchyan et al.	(CMS Collab.)
AAD 14I	JHEP 1402 107	G. Aad et al.	(ATLAS Collab.)	KHACHATRYAN...	11A PL B695 424	V. Khachatryan et al.	(CMS Collab.)
AALTONEN 14A	PR D89 091101	T. Aaltonen et al.	(CDF Collab.)	AALTONEN 10AA	PR D82 052002	T. Aaltonen et al.	(CDF Collab.)
AALTONEN 14F	PRL 113 042001	T. Aaltonen et al.	(CDF Collab.)	AALTONEN 10AB	PR D82 112005	T. Aaltonen et al.	(CDF Collab.)
Also PRL 117 199901 (errata.)				AALTONEN 10AC	PRL 105 232003	T. Aaltonen et al.	(CDF Collab.)
AALTONEN 14G	PRL 112 221801	T. Aaltonen et al.	(CDF Collab.)	AALTONEN 10AE	PRL 105 252001	T. Aaltonen et al.	(CDF Collab.)
AALTONEN 14H	PR D89 072001	T. Aaltonen et al.	(CDF and DO Collab.)	AALTONEN 10C	PR D81 031102	T. Aaltonen et al.	(CDF Collab.)
AALTONEN 14K	PRL 112 231805	T. Aaltonen et al.	(CDF Collab.)	AALTONEN 10D	PR D81 032002	T. Aaltonen et al.	(CDF Collab.)
AALTONEN 14L	PRL 112 231804	T. Aaltonen et al.	(CDF Collab.)	AALTONEN 10E	PR D81 052011	T. Aaltonen et al.	(CDF Collab.)
AALTONEN 14M	PRL 112 231803	T. Aaltonen et al.	(CDF and DO Collab.)	AALTONEN 10F	PRL 105 042002	T. Aaltonen et al.	(CDF Collab.)
AALTONEN 14N	PR D90 091101	T. Aaltonen et al.	(CDF Collab.)	AALTONEN 10S	PRL 105 101801	T. Aaltonen et al.	(CDF Collab.)
AALTONEN 14O	PRL 113 261804	T. Aaltonen et al.	(CDF Collab.)	AALTONEN 10U	PR D81 072003	T. Aaltonen et al.	(CDF Collab.)
ABAZOV 14C	PRL 113 032002	V.M. Abazov et al.	(DO Collab.)	AALTONEN 10V	PR D81 092002	T. Aaltonen et al.	(CDF Collab.)
Also V.M. Abazov et al.				AALTONEN 10W	PRL 105 02001	T. Aaltonen et al.	(DO Collab.)
ABAZOV 14D	PR D90 051101	V.M. Abazov et al.	(DO Collab.)	ABAZOV 10	PL B682 363	V.M. Abazov et al.	(DO Collab.)
ABAZOV 14G	PR D90 072001	V.M. Abazov et al.	(DO Collab.)	ABAZOV 10J	PR D82 032002	V.M. Abazov et al.	(DO Collab.)
ABAZOV 14H	PR D90 072011	V.M. Abazov et al.	(DO Collab.)	ABAZOV 10I	PL B690 5	V.M. Abazov et al.	(DO Collab.)
ABAZOV 14K	PR D90 092006	V.M. Abazov et al.	(DO Collab.)	ABAZOV 10K	PL B693 81	V.M. Abazov et al.	(DO Collab.)
CHATRCHYAN 14	PL B728 496	S. Chatrchyan et al.	(CMS Collab.)	ABAZOV 10L	PR D82 071102	V.M. Abazov et al.	(DO Collab.)
CHATRCHYAN 14AC	PRL 112 231802	S. Chatrchyan et al.	(CMS Collab.)	AHRENS 10	JHEP 1009 097	V. Ahrens et al.	(MAINZ, HEIDH)
CHATRCHYAN 14AE	EPJ C74 3014	S. Chatrchyan et al.	(CMS Collab.)	AHRENS 10A	NPBPS 205-206 48	V. Ahrens et al.	(MAINZ, HEIDH)
Also EPJ C75 216 (errata.)				AALTONEN 09AD	PR D79 112007	T. Aaltonen et al.	(CDF Collab.)
CHATRCHYAN 14C	EPJ C74 2758	S. Chatrchyan et al.	(CMS Collab.)	AALTONEN 09AK	PR D80 051104	T. Aaltonen et al.	(CDF Collab.)
CHATRCHYAN 14D	JHEP 1404 191	S. Chatrchyan et al.	(CMS Collab.)	AALTONEN 09AL	PR D80 052001	T. Aaltonen et al.	(CDF Collab.)
CHATRCHYAN 14E	JHEP 1402 024	S. Chatrchyan et al.	(CMS Collab.)	AALTONEN 09B	PR D79 1032002	T. Aaltonen et al.	(CDF Collab.)
CHATRCHYAN 14O	PL B731 173	S. Chatrchyan et al.	(CMS Collab.)	AALTONEN 09F	PR D79 031101	T. Aaltonen et al.	(CDF Collab.)
CHATRCHYAN 14R	PR D90 032006	S. Chatrchyan et al.	(CMS Collab.)	AALTONEN 09H	PR D79 052007	T. Aaltonen et al.	(CDF Collab.)
CHATRCHYAN 14S	PRL 112 171802	S. Chatrchyan et al.	(CMS Collab.)	AALTONEN 09J	PR D79 072001	T. Aaltonen et al.	(CDF Collab.)
KHACHATRYAN...14E	PL B736 33	V. Khachatryan et al.	(CMS Collab.)	AALTONEN 09K	PR D79 072010	T. Aaltonen et al.	(CDF Collab.)
KHACHATRYAN...14F	JHEP 1406 090	V. Khachatryan et al.	(CMS Collab.)	AALTONEN 09L	PR D79 092005	T. Aaltonen et al.	(CDF Collab.)
KHACHATRYAN...14H	JHEP 1409 087	V. Khachatryan et al.	(CMS Collab.)	AALTONEN 09M	PRL 102 042001	T. Aaltonen et al.	(CDF Collab.)
KHACHATRYAN...14K	PL B738 526 (errata.)	S. Chatrchyan et al.	(CMS Collab.)	AALTONEN 09N	PRL 102 151801	T. Aaltonen et al.	(CDF Collab.)
KHACHATRYAN...14N	EPJ C74 3060	V. Khachatryan et al.	(CMS Collab.)	AALTONEN 09O	PRL 102 152001	T. Aaltonen et al.	(CDF Collab.)
KHACHATRYAN...14Q	PR D90 112013	V. Khachatryan et al.	(CMS Collab.)	AALTONEN 09P	PL B674 160	T. Aaltonen et al.	(CDF Collab.)
KHACHATRYAN...14R	JHEP 1411 154	V. Khachatryan et al.	(CMS Collab.)	AALTONEN 09X	PR D79 072005	T. Aaltonen et al.	(CDF Collab.)
KHACHATRYAN...14S	PL B739 283	V. Khachatryan et al.	(CMS Collab.)	ABAZOV 09A	PL B676 450	F.M. Abazov et al.	(DO Collab.)
AAD 13AY	JHEP 1311 031	G. Aad et al.	(ATLAS Collab.)	ABAZOV 09AA	PRL 103 132001	V.M. Abazov et al.	(DO Collab.)
AAD 13BE	PRL 111 232002	G. Aad et al.	(ATLAS Collab.)	ABAZOV 09AG	PR D80 071102	V.M. Abazov et al.	(DO Collab.)
AAD 13X	EPJ C73 2328	G. Aad et al.	(ATLAS Collab.)	ABAZOV 09AH	PR D80 092006	V.M. Abazov et al.	(DO Collab.)
AALTONEN 13AB	PR D88 091103	T. Aaltonen et al.	(CDF Collab.)	ABAZOV 09J	PRL 102 092002	V.M. Abazov et al.	(DO Collab.)
AALTONEN 13AD	PRL 111 182002	T. Aaltonen et al.	(CDF Collab.)	ABAZOV 09K	PR B679 177	V.M. Abazov et al.	(DO Collab.)
AALTONEN 13D	PR D87 031104	T. Aaltonen et al.	(CDF Collab.)	ABAZOV 09Z	PRL 103 092001	V.M. Abazov et al.	(DO Collab.)
AALTONEN 13E	PR D87 052013	T. Aaltonen et al.	(CDF Collab.)	LANGENFELD 09	PR D80 054009	U. Langenfeld, S. Moch, P. Uwer	(DO Collab.)
AALTONEN 13G	PR D87 111101	T. Aaltonen et al.	(CDF Collab.)	AALTONEN 08AB	PRL 101 202001	T. Aaltonen et al.	(CDF Collab.)
AALTONEN 13H	PR D88 011101	T. Aaltonen et al.	(CDF Collab.)	AALTONEN 08AD	PRL 101 192002	T. Aaltonen et al.	(CDF Collab.)
AALTONEN 13J	PR D88 032003	T. Aaltonen et al.	(CDF Collab.)	AALTONEN 08AG	PR D78 111101	T. Aaltonen et al.	(CDF Collab.)
AALTONEN 13S	PR D87 092002	T. Aaltonen et al.	(CDF Collab.)	AALTONEN 08AH	PRL 101 252001	T. Aaltonen et al.	(CDF Collab.)
AALTONEN 13X	PR D88 072003	T. Aaltonen et al.	(CDF Collab.)	AALTONEN 08C	PRL 100 062005	T. Aaltonen et al.	(CDF Collab.)
AALTONEN 13Z	PRL 111 202001	T. Aaltonen et al.	(CDF Collab.)	ABAZOV 08AH	PRL 101 182001	V.M. Abazov et al.	(DO Collab.)
ABAZOV 13A	PR D87 011103	V.M. Abazov et al.	(DO Collab.)	ABAZOV 08AI	PRL 101 221801	V.M. Abazov et al.	(DO Collab.)
ABAZOV 13O	PL B726 656	V.M. Abazov et al.	(DO Collab.)	ABAZOV 08B	PRL 100 062004	V.M. Abazov et al.	(DO Collab.)
ABAZOV 13P	PR D88 112002	V.M. Abazov et al.	(DO Collab.)	ABAZOV 08I	PR D78 012005	V.M. Abazov et al.	(DO Collab.)
CHATRCHYAN 13AY	JHEP 1305 065	S. Chatrchyan et al.	(CMS Collab.)	ABAZOV 08L	PRL 100 142002	V.M. Abazov et al.	(DO Collab.)
CHATRCHYAN 13BB	PL B720 83	S. Chatrchyan et al.	(CMS Collab.)	ABAZOV 08M	PRL 100 192003	V.M. Abazov et al.	(DO Collab.)
CHATRCHYAN 13BE	EPJ C73 2386	S. Chatrchyan et al.	(CMS Collab.)	ABAZOV 08N	PRL 100 192004	V.M. Abazov et al.	(DO Collab.)
CHATRCHYAN 13BH	JHEP 1310 167	S. Chatrchyan et al.	(CMS Collab.)	ABULENCIA 08	PR D78 012003	A. Abulencia et al.	(CDF Collab.)
CHATRCHYAN 13C	PRL 110 022003	S. Chatrchyan et al.	(CMS Collab.)	CACCIARI 08	JHEP 0809 127	M. Cacciari et al.	(CDF Collab.)
CHATRCHYAN 13F	PL B718 1252	S. Chatrchyan et al.	(CMS Collab.)	KIDONAKIS 08	PR D78 074005	N. Kidonakis, R. Vogt	(CDF Collab.)
CHATRCHYAN 13S	EPJ C73 2494	S. Chatrchyan et al.	(CMS Collab.)	MOCH 08	PR D78 034003	S. Moch, P. Uwer	(BEHL, KARLE)
AAD 12B	PL B707 459	G. Aad et al.	(ATLAS Collab.)	AALTONEN 07	PRL 98 142001	T. Aaltonen et al.	(CDF Collab.)
AAD 12BE	JHEP 1204 069	G. Aad et al.	(ATLAS Collab.)	AALTONEN 07B	PR D75 111103	T. Aaltonen et al.	(CDF Collab.)
AAD 12BF	JHEP 1205 059	G. Aad et al.	(ATLAS Collab.)	AALTONEN 07C	PR D76 072009	T. Aaltonen et al.	(CDF Collab.)
AAD 12BG	JHEP 1206 088	G. Aad et al.	(ATLAS Collab.)	AALTONEN 07D	PRL 99 182002	T. Aaltonen et al.	(CDF Collab.)
AAD 12BK	EPJ C72 2039	G. Aad et al.	(ATLAS Collab.)	ABAZOV 07C	PRL 98 041801	V.M. Abazov et al.	(DO Collab.)
AAD 12BL	EPJ C72 2043	G. Aad et al.	(ATLAS Collab.)	ABAZOV 07D	PR D75 031102	V.M. Abazov et al.	(DO Collab.)
AAD 12BO	PL B711 244	G. Aad et al.	(ATLAS Collab.)	ABAZOV 07E	PR D75 092001	V.M. Abazov et al.	(DO Collab.)
AAD 12BP	PL B712 351	G. Aad et al.	(ATLAS Collab.)	ABAZOV 07F	PRL 98 181802	V.M. Abazov et al.	(DO Collab.)
AAD 12BT	JHEP 1209 139	G. Aad et al.	(ATLAS Collab.)	ABAZOV 07G	PR D76 052006	V.M. Abazov et al.	(DO Collab.)
AAD 12CG	PL B717 89	G. Aad et al.	(ATLAS Collab.)	ABAZOV 07P	PR D76 072007	V.M. Abazov et al.	(DO Collab.)
AAD 12CH	PL B717 330	G. Aad et al.	(ATLAS Collab.)	ABAZOV 07R	PR D76 092007	V.M. Abazov et al.	(DO Collab.)
AAD 12I	EPJ C72 2046	G. Aad et al.	(ATLAS Collab.)	ABAZOV 07V	PRL 99 191802	V.M. Abazov et al.	(DO Collab.)
AALTONEN 12AI	PRL 109 152003	T. Aaltonen et al.	(CDF Collab.)	ABAZOV 07W	PL B655 7	V.M. Abazov et al.	(DO Collab.)
AALTONEN 12AL	PRL 109 192001	T. Aaltonen et al.	(CDF Collab.)	ABULENCIA 07D	PR D75 031105	A. Abulencia et al.	(CDF Collab.)
AALTONEN 12AP	PR D86 092003	T. Aaltonen et al.	(CDF, DO Collab.)	ABULENCIA 07G	PRL 98 072001	A. Abulencia et al.	(CDF Collab.)
AALTONEN 12G	PL B714 24	T. Aaltonen et al.	(CDF Collab.)	ABULENCIA 07I	PR D75 052001	A. Abulencia et al.	(CDF Collab.)
AALTONEN 12Z	PR D85 071106	T. Aaltonen et al.	(CDF, DO Collab.)	ABULENCIA 07J	PR D75 071102	A. Abulencia et al.	(CDF Collab.)
ABAZOV 12AB	PR D86 051103	V.M. Abazov et al.	(DO Collab.)	ABAZOV 06K	PL B639 616	V.M. Abazov et al.	(DO Collab.)
ABAZOV 12B	PRL 108 032004	V.M. Abazov et al.	(DO Collab.)	ABAZOV 06L	PR D74 092005	V.M. Abazov et al.	(DO Collab.)
ABAZOV 12E	PL B708 21	V.M. Abazov et al.	(DO Collab.)	ABAZOV 06D	PR D74 112004	V.M. Abazov et al.	(DO Collab.)
ABAZOV 12F	PL B713 165	V.M. Abazov et al.	(DO Collab.)	ABULENCIA 06X	PRL 96 022004	A. Abulencia et al.	(CDF Collab.)
ABAZOV 12T	PR D85 091104	V.M. Abazov et al.	(DO Collab.)	Also PR D73 032003		A. Abulencia et al.	(CDF Collab.)
BERNREUTH...12	PR D86 034026	W. Bernreuther, Z.-G. Si	(AACH, SHDN)	Also PR D73 092002		A. Abulencia et al.	(CDF

See key on page 1127

Quark Particle Listings

t, b' (Fourth Generation) Quark

ABULENCIA	06G	PRL 96 152002	A. Abulencia et al.	(CDF Collab.)	> 372
Also	PR D74 032009	A. Abulencia et al.	(CDF Collab.)	> 361	
ABULENCIA	06R	PL B639 172	A. Abulencia et al.	(CDF Collab.)	> 338
ABULENCIA	06U	PR D73 111103	A. Abulencia et al.	(CDF Collab.)	> 380-430
ABULENCIA	06V	PR D73 112006	A. Abulencia et al.	(CDF Collab.)	> 268
ABULENCIA	06Z	PRL 97 082004	A. Abulencia et al.	(CDF Collab.)	> 199
ABULENCIA,A	06C	PRL 96 202002	A. Abulencia et al.	(CDF Collab.)	> 148
ABULENCIA,A	06E	PR D74 072005	A. Abulencia et al.	(CDF Collab.)	> 96
ABULENCIA,A	06F	PR D74 072006	A. Abulencia et al.	(CDF Collab.)	> 128
ABAZOV	05	PL B606 25	V.M. Abazov et al.	(DO Collab.)	> 75
ABAZOV	05L	PL B617 1	V.M. Abazov et al.	(DO Collab.)	> 85
ABAZOV	05L	PR D72 011104	V.M. Abazov et al.	(DO Collab.)	> 72
ABAZOV	05P	PL B622 265	V.M. Abazov et al.	(DO Collab.)	> 54
Also	PL B517 282	V.M. Abazov et al.	(DO Collab.)	> 43	
Also	PR D63 031101	B. Abbott et al.	(DO Collab.)	> 34	
Also	PR D75 092007	V.M. Abazov et al.	(DO Collab.)		
ABAZOV	05Q	PL B626 35	V.M. Abazov et al.	(DO Collab.)	
ABAZOV	05R	PL B626 55	V.M. Abazov et al.	(DO Collab.)	
ABAZOV	05X	PL B626 45	V.M. Abazov et al.	(DO Collab.)	
ACOSTA	05A	PRL 95 102002	D. Acosta et al.	(CDF Collab.)	
ACOSTA	05D	PR D71 031101	D. Acosta et al.	(CDF Collab.)	
ACOSTA	05N	PR D71 012005	D. Acosta et al.	(CDF Collab.)	
ACOSTA	05S	PR D72 032002	D. Acosta et al.	(CDF Collab.)	
ACOSTA	05T	PR D72 052003	D. Acosta et al.	(CDF Collab.)	
ACOSTA	05U	PR D71 072005	D. Acosta et al.	(CDF Collab.)	
ACOSTA	05V	PR D71 052003	D. Acosta et al.	(CDF Collab.)	
ABAZOV	04G	NAT 429 638	V.M. Abazov et al.	(DO Collab.)	
ABDALLAH	04C	PL B590 21	J. Abdallah et al.	(DELPHI Collab.)	
ACOSTA	04H	PR D69 052003	D. Acosta et al.	(CDF Collab.)	
ACOSTA	04I	PRL 93 142001	D. Acosta et al.	(CDF Collab.)	
AKTAS	04	EPJ C33 9	A. Aktas et al.	(H1 Collab.)	
ABAZOV	03A	PR D67 012004	V.M. Abazov et al.	(DO Collab.)	
CHEKANOV	03	PL B559 153	S. Chekanov et al.	(ZEUS Collab.)	
ACHARD	02J	PL B549 290	P. Achard et al.	(L3 Collab.)	
ACOSTA	02	PR D65 091102	D. Acosta et al.	(CDF Collab.)	
HEISTER	02Q	PL B543 173	A. Heister et al.	(ALEPH Collab.)	
ABBIENDI	01T	PL B521 181	G. Abbiendi et al.	(OPAL Collab.)	
AFFOLDER	01	PR D63 032003	T. Affolder et al.	(CDF Collab.)	
AFFOLDER	01A	PR D64 032002	T. Affolder et al.	(CDF Collab.)	
AFFOLDER	01C	PR D63 3233	T. Affolder et al.	(CDF Collab.)	
AFFOLDER	00B	PRL 84 216	T. Affolder et al.	(CDF Collab.)	
BARATE	00S	PL B494 33	S. Barate et al.	(ALEPH Collab.)	
ABBOTT	99G	PR D60 052001	F. Abe et al.	(CDF Collab.)	
ABE	99B	PR D62 271	F. Abe et al.	(CDF Collab.)	
Also	PR 82 2808 (erratum)	F. Abe et al.	(CDF Collab.)		
CHANG	99	PR D59 091503	D. Chang, W. Chang, E. Ma	(CDF Collab.)	
ABBOTT	98D	PRL 80 2063	B. Abbott et al.	(DO Collab.)	
ABBOTT	98F	PR D58 052001	B. Abbott et al.	(DO Collab.)	
ABE	98E	PRL 80 2767	F. Abe et al.	(CDF Collab.)	
ABE	98F	PRL 80 2779	F. Abe et al.	(CDF Collab.)	
ABE	98G	PRL 80 2525	F. Abe et al.	(CDF Collab.)	
BHAT	98B	JUMP A13 5113	P.C. Bhat, H.B. Prosper, S.S. Snyder	(CDF Collab.)	
ABACHI	97E	PRL 79 1197	S. Abachi et al.	(DO Collab.)	
ABE	97R	PRL 79 1902	F. Abe et al.	(CDF Collab.)	
ABE	97V	PRL 79 3585	F. Abe et al.	(CDF Collab.)	
PDG	96	PR D54 1	R. M. Barnett et al.	(PDG Collab.)	
ABACHI	95	PRL 74 2632	S. Abachi et al.	(DO Collab.)	
ABE	95F	PRL 74 2626	F. Abe et al.	(CDF Collab.)	
ABE	94E	PR D50 2966	F. Abe et al.	(CDF Collab.)	
Also	PRL 73 225	F. Abe et al.	(CDF Collab.)		

b' (4^{th} Generation) Quark, Searches for

$b'(-1/3)$ -quark/hadron mass limits in $p\bar{p}$ and pp collisions

VALUE (GeV)	CL%	DOCUMENT ID	TECN	COMMENT
>1570	95	1 SIRUNYAN	20b1 CMS	$B(b' \rightarrow Hb) = 1$
>1390	95	1 SIRUNYAN	20b1 CMS	$B(b' \rightarrow Zb) = 1$
>1130	95	2 SIRUNYAN	19AQ CMS	$B(b' \rightarrow Zb) = 1$
>1230	95	3 SIRUNYAN	19BWCMS	$B(b' \rightarrow Wt) = 1$
>1350	95	4 AABOUD	18AW ATLS	$B(b' \rightarrow Wt) = 1$
>1000	95	5 AABOUD	18CE ATLS	$\geq 2\ell + \cancel{E}_T + \geq 1b_j$
> 950	95	6 AABOUD	18CL ATLS	Wt, Zb, hb modes
>1010	95	7,8 AABOUD	18CP ATLS	2,3 ℓ , singlet model
>1140	95	6,9 AABOUD	18CP ATLS	2,3 ℓ , doublet model
>1220	95	10,11 AABOUD	18CR ATLS	singlet b' . ATLAS Combination
>1370	95	10,12 AABOUD	18CR ATLS	b' in a weak isospin doublet (t', b'). ATLAS combination.
> 910	95	13 SIRUNYAN	18BM CMS	Wt, Zb, hb modes
> 845	95	14 SIRUNYAN	18Q CMS	$B(b' \rightarrow Wu) = 1$
> 730	95	15 SIRUNYAN	17AU CMS	
> 880	95	16 KHACHATRYAN	16AN CMS	$B(b' \rightarrow Wt) = 1$
> 620	95	17 AAD	15BY ATLS	Wt, Zb, hb modes
> 730	95	18 AAD	15BY ATLS	$B(b' \rightarrow Wt) = 1$
> 810	95	19 AAD	15Z ATLS	
> 755	95	20 AAD	14AZ ATLS	$B(b' \rightarrow Wt) = 1$
> 675	95	21 CHATRCHYAN	13I CMS	$B(b' \rightarrow Wt) = 1$
> 190	95	22 ABAZOV	08X D0	$c\tau = 200\text{m}$
> 190	95	23 ACOSTA	03 CDF	quasi-stable b'
< 350, 580-635, >700	95	24 AAD	15AR ATLS	$B(b' \rightarrow Hb) = 1$
> 690	95	25 AAD	15CN ATLS	$B(b' \rightarrow Wq) = 1 (q=u)$
> 480	95	26 AAD	12AT ATLS	$B(b' \rightarrow Wt) = 1$
> 400	95	27 AAD	12AU ATLS	$B(b' \rightarrow Zb) = 1$
> 350	95	28 AAD	12BC ATLS	$B(b' \rightarrow Wq) = 1 (q=u,c)$
> 450	95	29 AAD	12BE ATLS	$B(b' \rightarrow Wt) = 1$
> 685	95	30 CHATRCHYAN	12BH CMS	$m_{b'} = m_{b'}$
> 611	95	31 CHATRCHYAN	12X CMS	$B(b' \rightarrow Wt) = 1$

••• We do not use the following data for averages, fits, limits, etc. •••

32 AALTONEN	11I	CDF	$b' \rightarrow Wt$
33 CHATRCHYAN	11L	CMS	Repl. by CHATRCHYAN 12x
34 AALTONEN	10H	CDF	$b' \rightarrow Wt$
35 FLACCO	10	RVUE	$m_{b'} > m_{b'}$
36,37 AALTONEN	07C	CDF	$B(b' \rightarrow Zb) = 1$
38 AFFOLDER	00	CDF	NC: $b' \rightarrow Zb$
39 ABE	98F	D0	NC: $b' \rightarrow Zb + \text{vertex}$
40 ABACHI	97D	D0	NC: $b' \rightarrow b\gamma$
41 ABACHI	95F	D0	$\ell\ell + \text{jets}, \ell + \text{jets}$
42 MUKHOPAD...	93	RVUE	NC: $b' \rightarrow b\ell\ell$
43 ABE	92	CDF	CC: $\ell\ell$
44 ABE	90B	CDF	CC: $e + \mu$
45 AKESSON	90	UA2	CC: $e + \text{jets} + \cancel{E}_T$
46 ALBAJAR	90B	UA1	CC: $\mu + \text{jets}$
47 ALBAJAR	88	UA1	CC: e or $\mu + \text{jets}$

- SIRUNYAN 20b1 based on 137 fb^{-1} of pp data at $\sqrt{s} = 13 \text{ TeV}$. Pair production of vector-like b' is searched for with each b' decaying into Zb or hb . Analysis focuses on final states consisting of jets from six quarks. Mass limits are obtained for a variety of branching ratios of b' decays.
- SIRUNYAN 19AQ based on 35.9 fb^{-1} of pp data at $\sqrt{s} = 13 \text{ TeV}$. Pair production of vector-like b' is searched for with one b' decaying into Zb and the other b' decaying into Wt, Zb, hb . Events with an opposite-sign lepton pair consistent with coming from Z and jets are used. Mass limits are obtained for a variety of branching ratios of b' .
- SIRUNYAN 19BW based on 35.9 fb^{-1} of pp data at $\sqrt{s} = 13 \text{ TeV}$. The limit is for the pair-produced vector-like b' using all-hadronic final state. The analysis is made for the Zb, Wt, hb modes and mass limits are obtained for a variety of branching ratios.
- AABOUD 18AW based on 36.1 fb^{-1} of pp data at $\sqrt{s} = 13 \text{ TeV}$. The limit is for the pair-produced vector-like b' using lepton-plus-jets final state. The search is also sensitive to the decays into Zb and Hb final states.
- AABOUD 18CE based on 36.1 fb^{-1} of proton-proton data taken at $\sqrt{s} = 13 \text{ TeV}$. Events including a same-sign lepton pair are used. The limit is for a singlet model, assuming the branching ratios of b' into Zb, Wt and Hb as predicted by the model.
- AABOUD 18CL, AABOUD 18CP based on 36.1 fb^{-1} of pp data at $\sqrt{s} = 13 \text{ TeV}$. The limit is for the pair-produced vector-like b' using all-hadronic final state. The analysis is particularly powerful for the $b' \rightarrow hb$ mode. Assuming the pure decay only in this mode sets a limit $m_{b'} > 1010 \text{ GeV}$.
- AABOUD 18CP based on 36.1 fb^{-1} of pp data at $\sqrt{s} = 13 \text{ TeV}$. Pair and single production of vector-like b' are searched for with at least one b' decaying into Zb . In the case of $B(b' \rightarrow Zb) = 1$, the limit is $m_{b'} > 1220 \text{ GeV}$.
- The limit is for the singlet model, assuming that the branching ratios into Wt, Zb, hb add up to one.
- The limit is for the doublet model, assuming that the branching ratios into Wt, Zb, hb add up to one.
- AABOUD 18CR based on 36.1 fb^{-1} of pp data at $\sqrt{s} = 13 \text{ TeV}$. A combination of searches for the pair-produced vector-like b' in various decay channels ($b' \rightarrow Wt, Zb, hb$). Also a model-independent limit is obtained as $m_{b'} > 1.03 \text{ TeV}$, assuming that the branching ratios into Zb, Wt , and hb add up to one.
- The limit is for the singlet b' .
- The limit is for b' in a weak isospin doublet (t', b') and $|V_{tb'}| \ll |V_{cb'}|$. For a b' in a doublet with a charge $-4/3$ vector-like quark, the limit $m_{b'} > 1.14 \text{ TeV}$ is obtained.
- SIRUNYAN 18BM based on 35.9 fb^{-1} of pp data at $\sqrt{s} = 13 \text{ TeV}$. The limit is for the pair-produced vector-like b' . Three channels (single lepton, same-charge 2 leptons, or at least 3 leptons) are considered for various branching fraction combinations. Assuming $B(tW) = 1$, the limit is 1240 GeV and for $B(bZ) = 1$ it is 960 GeV .
- SIRUNYAN 18g based on 19.7 fb^{-1} of pp data at $\sqrt{s} = 8 \text{ TeV}$. The limit is for the pair-produced vector-like b' that couple only to light quarks. Upper cross section limits on the single production of a b' and constraints for other decay channels (Zq and Hq) are also given in the paper.
- SIRUNYAN 17AU based on $2.3\text{-}2.6 \text{ fb}^{-1}$ of pp data at $\sqrt{s} = 13 \text{ TeV}$. Limit on pair-produced singlet vector-like b' using one lepton and several jets. The mass bound is given for a b' transforming as a singlet under the electroweak symmetry group, assumed to decay through W, Z or Higgs boson (which decays to jets) and to a third generation quark.
- KHACHATRYAN 16AN based on 19.7 fb^{-1} of pp data at $\sqrt{s} = 8 \text{ TeV}$. Limit on pair-produced vector-like b' using 1, 2, and >2 leptons as well as fully hadronic final states. Other limits depending on the branching fractions to tW, bZ , and bH are given in Table IX.
- AAD 15BY based on 20.3 fb^{-1} of pp data at $\sqrt{s} = 8 \text{ TeV}$. Limit on pair-produced vector-like b' assuming the branching fractions to W, Z , and h modes of the singlet model. Used events containing $\geq 2\ell + \cancel{E}_T + \geq 2j (\geq 1b)$ and including a same-sign lepton pair.
- AAD 15BZ based on 20.3 fb^{-1} of pp data at $\sqrt{s} = 8 \text{ TeV}$. Limit on pair-produced chiral b' -quark. Used events containing $\geq 2\ell + \cancel{E}_T + \geq 2j (\geq 1b)$ and including a same-sign lepton pair.
- AAD 15Z based on 20.3 fb^{-1} of pp data at $\sqrt{s} = 8 \text{ TeV}$. Used events with $\ell + \cancel{E}_T + \geq 6j (\geq 1b)$ and at least one pair of jets from weak boson decay, primarily designed to select the signature $b'\bar{b}' \rightarrow WWt\bar{t} \rightarrow WWWWb\bar{b}$. This is a limit on pair-produced vector-like b' . The lower mass limit is 640 GeV for a vector-like singlet b' .
- Based on 20.3 fb^{-1} of pp data at $\sqrt{s} = 8 \text{ TeV}$. No significant excess over SM expectation is found in the search for pair production or single production of b' in the events with dilepton from a high $p_{T,Z}$ and additional jets ($\geq 1b$ -tag). If instead of $B(b' \rightarrow Wt) = 1$ an electroweak singlet with $B(b' \rightarrow Wt) \sim 0.45$ is assumed, the limit reduces to 685 GeV .
- Based on 5.0 fb^{-1} of pp data at $\sqrt{s} = 7 \text{ TeV}$. CHATRCHYAN 13I looked for events with one isolated electron or muon, large \cancel{E}_T , and at least four jets with large transverse momenta, where one jet is likely to originate from the decay of a bottom quark.

Quark Particle Listings

b' (Fourth Generation) Quark

- ²² Result is based on 1.1 fb^{-1} of data. No signal is found for the search of long-lived particles which decay into final states with two electrons or photons, and upper bound on the cross section times branching fraction is obtained for $2 < c\tau < 7000 \text{ nm}$; see Fig. 3. 95% CL excluded region of b' lifetime and mass is shown in Fig. 4.
- ²³ ACOSTA 03 looked for long-lived fourth generation quarks in the data sample of 90 pb^{-1} of $\sqrt{s}=1.8 \text{ TeV}$ $p\bar{p}$ collisions by using the muon-like penetration and anomalously high ionization energy loss signature. The corresponding lower mass bound for the charge $(2/3)e$ quark (t') is 220 GeV . The t' bound is higher than the b' bound because t' is more likely to produce charged hadrons than b' . The 95% CL upper bounds for the production cross sections are given in their Fig. 3.
- ²⁴ AAD 15AR based on 20.3 fb^{-1} of pp data at $\sqrt{s} = 8 \text{ TeV}$. Used lepton-plus-jets final state. See Fig. 24 for mass limits in the plane of $B(b' \rightarrow Wt)$ vs. $B(b' \rightarrow Hb)$ from $b'\bar{b}' \rightarrow Hb + X$ searches.
- ²⁵ AAD 15CN based on 20.3 fb^{-1} of pp data at $\sqrt{s} = 8 \text{ TeV}$. Limit on pair-production of chiral b' -quark. Used events with $\ell + \cancel{E}_T + \geq 4j$ (non- b -tagged). Limits on a heavy vector-like quark, which decays into Wq, Zq, hq , are presented in the plane $B(Q \rightarrow Wq)$ vs. $B(Q \rightarrow hq)$ in Fig. 12.
- ²⁶ Based on 1.04 fb^{-1} of pp data at $\sqrt{s} = 7 \text{ TeV}$. No signal is found for the search of heavy quark pair production that decay into W and a t quark in the events with a high p_T isolated lepton, large \cancel{E}_T , and at least 6 jets in which one, two or more dijets are from W .
- ²⁷ Based on 2.0 fb^{-1} of pp data at $\sqrt{s} = 7 \text{ TeV}$. No $b' \rightarrow Zb$ invariant mass peak is found in the search of heavy quark pair production that decay into Z and a b quark in events with $Z \rightarrow e^+e^-$ and at least one b -jet. The lower mass limit is 358 GeV for a vector-like singlet b' mixing solely with the third SM generation.
- ²⁸ Based on 1.04 fb^{-1} of pp data at $\sqrt{s} = 7 \text{ TeV}$. No signal is found for the search of heavy quark pair production that decay into W and a quark in the events with dileptons, large \cancel{E}_T , and ≥ 2 jets.
- ²⁹ Based on 1.04 fb^{-1} of pp data at $\sqrt{s} = 7 \text{ TeV}$. AAD 12BE looked for events with two isolated like-sign leptons and at least 2 jets, large \cancel{E}_T and $H_T > 350 \text{ GeV}$.
- ³⁰ Based on 5 fb^{-1} of pp data at $\sqrt{s} = 7 \text{ TeV}$. CHATRCHYAN 12BH searched for QCD and EW production of single and pair of degenerate 4th generation quarks that decay to bW or tW . Absence of signal in events with one lepton, same-sign dileptons or tripletons gives the bound. With a mass difference of $25 \text{ GeV}/c^2$ between $m_{b'}$ and $m_{b''}$, the corresponding limit shifts by about $\pm 20 \text{ GeV}/c^2$.
- ³¹ Based on 4.9 fb^{-1} of pp data at $\sqrt{s} = 7 \text{ TeV}$. CHATRCHYAN 12X looked for events with tripletons or same-sign dileptons and at least one b -jet.
- ³² Based on 4.8 fb^{-1} of data in $p\bar{p}$ collisions at 1.96 TeV . AALTONEN 11J looked for events with $\ell + \cancel{E}_T + \geq 5j$ ($\geq 1 b$ or c). No signal is observed and the bound $\sigma(b'\bar{b}') < 30 \text{ fb}$ for $m_{b'} > 375 \text{ GeV}$ is found for $B(b' \rightarrow Wt) = 1$.
- ³³ Based on 34 pb^{-1} of data in pp collisions at 7 TeV . CHATRCHYAN 11L looked for multi-jet events with tripletons or same-sign dileptons. No excess above the SM background excludes $m_{b'}$ between 255 and 361 GeV at 95% CL for $B(b' \rightarrow Wt) = 1$.
- ³⁴ Based on 2.7 fb^{-1} of data in $p\bar{p}$ collisions at $\sqrt{s} = 1.96 \text{ TeV}$. AALTONEN 10H looked for pair production of heavy quarks which decay into tW^- or tW^+ , in events with same sign dileptons (e or μ), several jets and large missing E_T . The result is obtained for b' which decays into tW^- . For the charge $5/3$ quark ($T_{5/3}$) which decays into tW^+ , $m_{T_{5/3}} > 365 \text{ GeV}$ (95% CL) is found when it has the charge $-1/3$ partner B of the same mass.
- ³⁵ FLACCO 10 result is obtained from AALTONEN 10H result of $m_{b'} > 338 \text{ GeV}$, by relaxing the condition $B(b' \rightarrow Wt) = 100\%$ when $m_{b'} > m_{b''}$.
- ³⁶ Result is based on 1.06 fb^{-1} of data. No excess from the SM Z -jet events is found when Z decays into e^+e^- or $\mu^+\mu^-$. The $m_{b'}$ bound is found by comparing the resulting upper bound on $\sigma(b'\bar{b}') [1 - (1 - B(b' \rightarrow Zb))^2]$ and the LO estimate of the b' pair production cross section shown in Fig. 38 of the article.
- ³⁷ HUANG 08 reexamined the b' mass lower bound of 268 GeV obtained in AALTONEN 07c that assumes $B(b' \rightarrow Zb) = 1$, which does not hold for $m_{b'} > 255 \text{ GeV}$. The lower mass bound is given in the plane of $\sin^2(\theta_{tb'})$ and $m_{b'}$.
- ³⁸ AFFOLDER 00 looked for b' that decays in to $b+Z$. The signal searched for is $bbZZ$ events where one Z decays into e^+e^- or $\mu^+\mu^-$ and the other Z decays hadronically. The bound assumes $B(b' \rightarrow Zb) = 100\%$. Between 100 GeV and 199 GeV , the 95%CL upper bound on $\sigma(b' \rightarrow \bar{b}') \times B^2(b' \rightarrow Zb)$ is also given (see their Fig. 2).
- ³⁹ ABE 98n looked for $Z \rightarrow e^+e^-$ decays with displaced vertices. Quoted limit assumes $B(b' \rightarrow Zb) = 1$ and $c\tau_{b'} = 1 \text{ cm}$. The limit is lower than m_{Z+m_b} ($\sim 96 \text{ GeV}$) if $c\tau > 22 \text{ cm}$ or $c\tau < 0.009 \text{ cm}$. See their Fig. 4.
- ⁴⁰ ABACHI 97D searched for b' that decays mainly via FCNC. They obtained 95%CL upper bounds on $B(b'\bar{b}' \rightarrow \gamma + 3 \text{ jets})$ and $B(b'\bar{b}' \rightarrow 2\gamma + 2 \text{ jets})$, which can be interpreted as the lower mass bound $m_{b'} > m_{Z+m_b}$.
- ⁴¹ ABACHI 95F bound on the top-quark also applies to b' and t' quarks that decay predominantly into W . See FROGGATT 97.
- ⁴² MUKHOPADHYAYA 93 analyze CDF dilepton data of ABE 92g in terms of a new quark decaying via flavor-changing neutral current. The above limit assumes $B(b' \rightarrow b\ell^+\ell^-) = 1$. For an exotic quark decaying only via virtual Z [$B(b\ell^+\ell^-) = 3\%$], the limit is 85 GeV .
- ⁴³ ABE 92 dilepton analysis limit of $>85 \text{ GeV}$ at $\text{CL}=95\%$ also applies to b' quarks, as discussed in ABE 90b.
- ⁴⁴ ABE 90b exclude the region $28-72 \text{ GeV}$.
- ⁴⁵ AKESSON 90 searched for events having an electron with $p_T > 12 \text{ GeV}$, missing momentum $> 15 \text{ GeV}$, and a jet with $E_T > 10 \text{ GeV}$, $|\eta| < 2.2$, and excluded $m_{b'}$ between 30 and 69 GeV .
- ⁴⁶ For the reduction of the limit due to non-charged-current decay modes, see Fig. 19 of ALBAJAR 90b.
- ⁴⁷ ALBAJAR 88 study events at $E_{\text{cm}} = 546$ and 630 GeV with a muon or isolated electron, accompanied by one or more jets and find agreement with Monte Carlo predictions for the production of charm and bottom, without the need for a new quark. The lower mass limit is obtained by using a conservative estimate for the $b'\bar{b}'$ production cross section and by assuming that it cannot be produced in W decays. The value quoted here is revised using the full $Q(\alpha_s^3)$ cross section of ALTARELLI 88.

$b'(-1/3)$ mass limits from single production in $p\bar{p}$ and pp collisions

VALUE (GeV)	CL%	DOCUMENT ID	TECN	COMMENT
>1500	95	¹ AAD	16AH ATLS	$g b \rightarrow b' \rightarrow tW, B(b' \rightarrow tW)=1$
>1390	95	² KHACHATRY...16i	CMS	$g b \rightarrow b' \rightarrow tW, B(b' \rightarrow tW)=1$
>1430	95	³ KHACHATRY...16i	CMS	$g b \rightarrow b' \rightarrow tW, B(b' \rightarrow tW)=1$
>1530	95	⁴ KHACHATRY...16i	CMS	$g b \rightarrow b' \rightarrow tW, B(b' \rightarrow tW)=1$
> 693	95	⁵ ABAZOV	11F D0	$qu \rightarrow q'b' \rightarrow q'(Wu)$ $\tilde{\kappa}_{ub'}=1, B(b' \rightarrow Wu)=1$
> 430	95	⁵ ABAZOV	11F D0	$qd \rightarrow qb' \rightarrow q(Zd)$ $\tilde{\kappa}_{db'}=\sqrt{2}, B(b' \rightarrow Zd)=1$
		⁶ SIRUNYAN	19AI CMS	$bZ/tW \rightarrow b' \rightarrow tW$

• • • We do not use the following data for averages, fits, limits, etc. • • •

- ¹ AAD 16AH based on 20.3 fb^{-1} of data in pp collisions at 8 TeV . No significant excess over SM expectation is found in the search for a vector-like b' in the single-lepton and dilepton channels (ℓ or $\ell\ell$) + $1,2,3 j$ ($\geq 1b$). The model assumes that the b' has the excited quark couplings.
- ² Based on 19.7 fb^{-1} of data in pp collisions at 8 TeV . Limit on left-handed b' assuming 100% decay to tW and using all-hadronic, lepton + jets, and dilepton final states.
- ³ Based on 19.7 fb^{-1} of data in pp collisions at 8 TeV . Limit on right-handed b' assuming 100% decay to tW and using all-hadronic, lepton + jets, and dilepton final states.
- ⁴ Based on 19.7 fb^{-1} of data in pp collisions at 8 TeV . Limit on vector-like b' assuming 100% decay to tW and using all-hadronic, lepton+jets, and dilepton final states.
- ⁵ Based on 5.4 fb^{-1} of data in $p\bar{p}$ collisions at 1.96 TeV . ABAZOV 11F looked for single production of b' via the W or Z coupling to the first generation up or down quarks, respectively. Model independent cross section limits for the single production processes $p\bar{p} \rightarrow b'q \rightarrow Wuq$, and $p\bar{p} \rightarrow b'q \rightarrow Zdq$ are given in Figs. 3 and 4, respectively, and the mass limits are obtained for the model of ATRE 09 with degenerate bi-doublets of vector-like quarks.
- ⁶ SIRUNYAN 19AI based on 35.9 fb^{-1} of pp data at $\sqrt{s} = 13 \text{ TeV}$. Exclusion limits are set on the product of the production cross section and branching fraction for the $b'(-1/3) + b$ and $b'(-1/3) + t$ modes as a function of the vector-like quark mass in Figs. 7 and 8 and in Tab. 2 for relative vector-like quark widths between 1 and 30% for left- and right-handed vector-like quark couplings. No significant deviation from the SM prediction is observed.

MASS LIMITS for b' (4th Generation) Quark or Hadron in e^+e^- Collisions

Search for hadrons containing a fourth-generation $-1/3$ quark denoted b' .

The last column specifies the assumption for the decay mode (CC denotes the conventional charged-current decay) and the event signature which is looked for.

VALUE (GeV)	CL%	DOCUMENT ID	TECN	COMMENT
>46.0	95	¹ DECAMP	90F ALEP	any decay
		• • • We do not use the following data for averages, fits, limits, etc. • • •		
none 96-103	95	² ABDALLAH	07 DLPH	$b' \rightarrow bZ, cW$
		³ ADRIANI	93G L3	Quarkonium
>44.7	95	ADRIANI	93M L3	$\Gamma(Z)$
>45	95	ABREU	91F DLPH	$\Gamma(Z)$
none 19.4-28.2	95	ABE	90D VNS	Any decay; event shape
>45.0	95	ABREU	90D DLPH	$B(C C) = 1$; event shape
>44.5	95	⁴ ABREU	90D DLPH	$b' \rightarrow cH^-, H^- \rightarrow \bar{c}s, \tau^- \nu$
>40.5	95	⁵ ABREU	90D DLPH	$\Gamma(Z \rightarrow \text{hadrons})$
>28.3	95	ADACHI	90 TOPZ	$B(\text{FCNC})=100\%$; isol. γ or 4 jets
>41.4	95	⁶ AKRAWY	90B OPAL	Any decay; acoplanarity
>45.2	95	⁶ AKRAWY	90B OPAL	$B(C C) = 1$; acoplanarity
>46	95	⁷ AKRAWY	90J OPAL	$b' \rightarrow \gamma + \text{any}$
>27.5	95	⁸ ABE	89E VNS	$B(C C) = 1; \mu, e$
none 11.4-27.3	95	⁹ ABE	89G VNS	$B(b' \rightarrow b\gamma) > 10\%$; isolated γ
>44.7	95	¹⁰ ABRAMS	89C MRK2	$B(C C) = 100\%$; isol. track
>42.7	95	¹⁰ ABRAMS	89C MRK2	$B(b'g) = 100\%$; event shape
>42.0	95	¹⁰ ABRAMS	89C MRK2	Any decay; event shape
>28.4	95	^{11,12} ADACHI	89C TOPZ	$B(C C) = 1; \mu$
>28.8	95	¹³ ENO	89 AMY	$B(C C) \geq 90\%; \mu, e$
>27.2	95	^{13,14} ENO	89 AMY	any decay; event shape
>29.0	95	¹³ ENO	89 AMY	$B(b' \rightarrow b\gamma) \geq 85\%$; event shape
>24.4	95	¹⁵ IGARASHI	88 AMY	μ, e
>23.8	95	¹⁶ SAGAWA	88 AMY	event shape
>22.7	95	¹⁷ ADEVA	86 MRKJ	μ
>21		¹⁸ ALTHOFF	84C TASS	R , event shape
>19		¹⁹ ALTHOFF	84I TASS	Aplanarity

- ¹ DECAMP 90F looked for isolated charged particles, for isolated photons, and for four-jet final states. The modes $b' \rightarrow bg$ for $B(b' \rightarrow bg) > 65\%$ or $b' \rightarrow b\gamma$ for $B(b' \rightarrow b\gamma) > 5\%$ are excluded. Charged Higgs decay were not discussed.
- ² ABDALLAH 07 searched for b' pair production at $E_{\text{cm}}=196-209 \text{ GeV}$, with 420 pb^{-1} . No signal leads to the 95% CL upper limits on $B(b' \rightarrow bZ)$ and $B(b' \rightarrow cW)$ for $m_{b'} = 96$ to 103 GeV .
- ³ ADRIANI 93g search for vector quarkonium states near Z and give limit on quarkonium- Z mixing parameter $\delta m^2 < (10-30) \text{ GeV}^2$ (95%CL) for the mass $88-94.5 \text{ GeV}$. Using

See key on page 1127

Quark Particle Listings

b' (Fourth Generation) Quark, t' (Fourth Generation) Quark

Richardson potential, a 1S (b'b') state is excluded for the mass range 87.7-94.7 GeV.

This range depends on the potential choice.

4 ABREU 90d assumed m_{H^-} < m_{b'} - 3 GeV.

5 Superseded by ABREU 91F.

6 AKRAWY 90B search was restricted to data near the Z peak at E_{cm} = 91.26 GeV at LEP.

The excluded region is between 23.6 and 41.4 GeV if no H^+ decays exist. For charged Higgs decays the excluded regions are between (m_{H^+} + 1.5 GeV) and 45.5 GeV.

7 AKRAWY 90J search for isolated photons in hadronic Z decay and derive B(Z -> b'b')/B(b' -> gamma)/B(Z -> hadrons) < 2.2 x 10^-3. Mass limit assumes B(b' -> gamma) > 10%.

8 ABE 89E search at E_{cm} = 56-57 GeV at TRISTAN for multihadron events with a spherical shape (using thrust and acoplanarity) or containing isolated leptons.

9 ABE 89G search was at E_{cm} = 55-60.8 GeV at TRISTAN.

10 If the photonic decay mode is large (B(b' -> b gamma) > 25%), the ABRAMS 89c limit is 45.4 GeV. The limit for Higgs decay (b' -> c H^-, H^- -> tau s) is 45.2 GeV.

11 ADACHI 89c search was at E_{cm} = 56.5-60.8 GeV at TRISTAN using multi-hadron events accompanying muons.

12 ADACHI 89c also gives limits for any mixture of CC and bg decays.

13 ENO 89 search at E_{cm} = 50-60.8 at TRISTAN.

14 ENO 89 considers arbitrary mixture of the charged current, bg, and b gamma decays.

15 IGARASHI 88 searches for leptons in low-thrust events and gives Delta R(b') < 0.26 (95% CL) assuming charged current decay, which translates to m_{b'} > 24.4 GeV.

16 SAGAWA 88 set limit sigma(top) < 6.1 pb at CL=95% for top-flavored hadron production from event shape analyses at E_{cm} = 52 GeV. By using the quark parton model cross-section formula near threshold, the above limit leads to lower mass bounds of 23.8 GeV for charge -1/3 quarks.

17 ADEVA 86 give 95%CL upper bound on an excess of the normalized cross section, Delta R, as a function of the minimum c.m. energy (see their figure 3). Production of a pair of 1/3 charge quarks is excluded up to E_{cm} = 45.4 GeV.

18 ALTHOFF 84c narrow state search sets limit Gamma(e+ e-) B(hadrons) < 2.4 keV CL = 95% and heavy charge 1/3 quark pair production m > 21 GeV, CL = 95%.

19 ALTHOFF 84i exclude heavy quark pair production for 7 < m < 19 GeV (1/3 charge) using aplanarity distributions (CL = 95%).

REFERENCES FOR Searches for (Fourth Generation) b' Quark

SIRUNYAN 20BI PR D102 112004
SIRUNYAN 19AI EPJ C79 90
SIRUNYAN 19AQ EPJ C79 364
SIRUNYAN 19BW PR D100 072001
AABOUD 18AW JHEP 1808 048
AABOUD 18CE JHEP 1812 039
AABOUD 18CL PR D98 092005
AABOUD 18CP PR D98 112010
AABOUD 18CR PRL 121 211871
SIRUNYAN 18BM JHEP 1808 177
SIRUNYAN 18Q PR D97 072008
SIRUNYAN 17AU JHEP 1711 085
AAD 16AH JHEP 1602 1110
KHACHATRYAN...16AN PR D93 112009
KHACHATRYAN...16I JHEP 1601 166
AAD 15AR JHEP 1508 105
AAD 15BY JHEP 1510 150
AAD 15CN PR D92 112007
AAD 15Z PR D91 112011
AAD 14AZ JHEP 1411 104
CHATRCHYAN 13I JHEP 1301 154
AAD 12AT PRL 109 032001
AAD 12AU PRL 109 071801
AAD 12BC PR D96 012007
AAD 12BE JHEP 1204 069
CHATRCHYAN 12BH PR D86 112003
CHATRCHYAN 12X JHEP 1205 123
AALTONEN 11J PRL 106 141803
ABAZOV 11F PRL 106 081801
CHATRCHYAN 11L PL B701 204
AALTONEN 10H PRL 104 091801
FLACCO 10 PRL 105 111801
ATRE 09 PR D79 054018
ABAZOV 08X PRL 101 111802
HUANG 08 PR D77 037302
AALTONEN 07C PR D76 072006
ABDALLAH 07 EPJ C50 507
ACOSTA 03 PRL 90 131801
AFFOLDER 00 PRL 84 835
ABE 98N PR D58 051102
ABACHI 97D PRL 78 3818
FROGGATT 97 ZPHY C73 333
ABACHI 95F PR D52 4877
ADRIANI 93G PL B313 326
ADRIANI 93M PRPL 236 1
MUKHOPAD...92 PR D48 2105
ABE 92 PR 68 447
Also
ABE 92G PR D45 3921
ABREU 91F NP B367 511
ABE 90B PRL 64 147
ABE 90D PL B234 382
ABREU 90D PL B242 536
ADACHI 90 PL B234 197
AKESSON 90 ZPHY C46 179
AKRAWY 90B PL B236 364
AKRAWY 90J PL B246 285
ALBAJAR 90B ZPHY C48 1
DECAMP 90F PL B236 511
ABE 89E PR D39 3524
ABE 89G PRL 63 1776
ABRAMS 89C PRL 63 2447
ADACHI 89C PL B229 427
ENO 89 PRL 63 1910
ALBAJAR 88 ZPHY C37 505
ALTARELLI 88 NP B308 724
IGARASHI 88 PRL 60 2359
SAGAWA 88 PRL 60 93
ADEVA 86 PR D34 681
ALTHOFF 84C PL B38B 441
ALTHOFF 84I ZPHY C22 307
A.M. Sirunyan et al. (CMS Collab.)
A.M. Sirunyan et al. (CMS Collab.)
A.M. Sirunyan et al. (CMS Collab.)
A.M. Sirunyan et al. (CMS Collab.)
M. Aaboud et al. (ATLAS Collab.)
M. Aaboud et al. (ATLAS Collab.)
M. Aaboud et al. (ATLAS Collab.)
M. Aaboud et al. (ATLAS Collab.)
M. Aaboud et al. (ATLAS Collab.)
M. Aaboud et al. (ATLAS Collab.)
A.M. Sirunyan et al. (CMS Collab.)
A.M. Sirunyan et al. (CMS Collab.)
G. Aad et al. (ATLAS Collab.)
V. Khachatryan et al. (CMS Collab.)
V. Khachatryan et al. (CMS Collab.)
G. Aad et al. (ATLAS Collab.)
G. Aad et al. (ATLAS Collab.)
G. Aad et al. (ATLAS Collab.)
G. Aad et al. (ATLAS Collab.)
G. Aad et al. (ATLAS Collab.)
S. Chatrchyan et al. (CMS Collab.)
G. Aad et al. (ATLAS Collab.)
G. Aad et al. (ATLAS Collab.)
G. Aad et al. (ATLAS Collab.)
G. Aad et al. (ATLAS Collab.)
G. Aad et al. (ATLAS Collab.)
S. Chatrchyan et al. (CMS Collab.)
S. Chatrchyan et al. (CMS Collab.)
T. Aaltonen et al. (CDF Collab.)
V.M. Abazov et al. (D0 Collab.)
S. Chatrchyan et al. (CMS Collab.)
C.J. Flacco et al. (UCI, HAIF)
A. Atre et al. (D0 Collab.)
V.M. Abazov et al. (D0 Collab.)
E.Q. Hung, M. Sher (UVA, WLL)
T. Aaltonen et al. (CDF Collab.)
F. Abdallah et al. (DELPHI Collab.)
D. Acosta et al. (CDF Collab.)
A. Afolder et al. (CDF Collab.)
F. Abe et al. (CDF Collab.)
S. Abachi et al. (D0 Collab.)
C.D. Froggatt, D.J. Smith, H.B. Nielsen (GLAS+)
S. Abachi et al. (D0 Collab.)
O. Adriani et al. (L3 Collab.)
O. Adriani et al. (L3 Collab.)
B. Mukhopadhyaya, D.P. Roy (TATA)
F. Abe et al. (CDF Collab.)
F. Abe et al. (CDF Collab.)
F. Abe et al. (CDF Collab.)
P. Abreu et al. (DELPHI Collab.)
F. Abe et al. (CDF Collab.)
K. Abe et al. (VENUS Collab.)
P. Abreu et al. (DELPHI Collab.)
I. Adachi et al. (TOPAZ Collab.)
T. Akesson et al. (UA2 Collab.)
M.Z. Akrawy et al. (OPAL Collab.)
M.Z. Akrawy et al. (OPAL Collab.)
M. Z. Akrawy et al. (UA1 Collab.)
C. Albajar et al. (ALEPH Collab.)
D. Decamp et al. (VENUS Collab.)
K. Abe et al. (VENUS Collab.)
K. Abe et al. (VENUS Collab.)
G.S. Abrams et al. (Mark II Collab.)
I. Adachi et al. (TOPAZ Collab.)
S. Eno et al. (AMY Collab.)
C. Albajar et al. (UA1 Collab.)
G. Altarelli et al. (CERN, ROMA, ETH)
S. Igarashi et al. (AMY Collab.)
H. Sägawa et al. (AMY Collab.)
B. Adeva et al. (Mark-J Collab.)
M. Althoff et al. (TASSO Collab.)
M. Althoff et al. (TASSO Collab.)

t' (4th Generation) Quark, Searches for

t'(2/3)-quark/hadron mass limits in pp and pp collisions

Table with columns: VALUE (GeV), CL%, DOCUMENT ID, TECN, COMMENT. Rows list various experiments and their mass limits for t' quarks.

••• We do not use the following data for averages, fits, limits, etc. •••

Table listing excluded data points for averages, fits, limits, etc. Includes experiments like AAD, CHATRCHYAN, AALTONEN, ABAZOV.

1 SIRUNYAN 19AQ based on 35.9 fb^-1 of pp data at sqrt(s) = 13 TeV. Pair production of vector-like t' is searched for with one t' decaying into Z t and the other t' decaying into Wb, Zt, ht. Events with an opposite-sign lepton pair consistent with coming from Z and jets are used. Mass limits are obtained for a variety of branching ratios of t'.

2 SIRUNYAN 19BW based on 35.9 fb^-1 of pp data at sqrt(s) = 13 TeV. The limit is for the pair-produced vector-like t' using all-hadronic final state. The analysis is made for the Wb, Zt, ht modes and mass limits are obtained for a variety of branching ratios.

3 AABOUD 18CE based on 36.1 fb^-1 of proton-proton data taken at sqrt(s) = 13 TeV. Events including a same-sign lepton pair are used. The limit is for a singlet model, assuming the branching ratios of t' into Zt, Wb and ht as predicted by the model.

4 AABOUD 18CL based on 36.1 fb^-1 of pp data at sqrt(s) = 13 TeV. The limit is for the pair-produced vector-like t' using all-hadronic final state. The analysis is also made for the Wb, Zt, ht modes and mass limits are obtained for a variety of branching ratios.

5 AABOUD 18CP based on 36.1 fb^-1 of pp data at sqrt(s) = 13 TeV. Pair and single production of vector-like t' are searched for with at least one t' decaying into Zt. In the case of B(t' -> Zt) = 1, the limit is m_{t'} > 1340 GeV.

6 The limit is for the singlet model, assuming that the branching ratios into Zt, Wb, and ht add up to one.

7 The limit is for the doublet model, assuming that the branching ratios into Zt, Wb, and ht add up to one.

8 AABOUD 18CR based on 36.1 fb^-1 of pp data at sqrt(s) = 13 TeV. A combination of searches for the pair-produced vector-like t' in various decay channels (t' -> Wb, Zt, ht). Also a model-independent limit is obtained as m_{t'} > 1.31 TeV, assuming that the branching ratios into Zt, Wb and ht add up to one.

9 The limit is for the singlet t'.

10 The limit is for t' in a weak isospin doublet (t', b') and |V_{tb}| << |V_{t'b'}|.

11 SIRUNYAN 18BM based on 35.9 fb^-1 of pp data at sqrt(s) = 13 TeV. The limit is for the pair-produced vector-like t'. Three channels (single lepton, same-charge 2 leptons, or at least 3 leptons) are considered for various branching fraction combinations. Assuming B(t'H) = 1, the limit is 1270 GeV and for B(t'Z) = 1 it is 1300 GeV.

12 SIRUNYAN 18Q based on 19.7 fb^-1 of pp data at sqrt(s) = 8 TeV. The limit is for the pair-produced vector-like t' that couple only to light quarks. Constraints for other decay channels (Zq and Hq) are also given in the paper.

13 SIRUNYAN 18W based on 35.8 fb^-1 of pp data at sqrt(s) = 13 TeV. The limit is for the vector-like t' pair-produced by strong interaction using lepton-plus-jets mode and assuming that B(t' -> Wb) is 100% product of the production cross section and branching fraction to Wb for any new pair-produced heavy quark decaying to this channel as a narrow resonance.

14 AABOUD 17L based on 36.1 fb^-1 of pp data at sqrt(s) = 13 TeV. No signal is found in the search for heavy quark pair production that decay into Zt followed by Z -> nu nu

Downloaded from https://academic.oup.com/ptep/article/2022/8/083C01/6651666 by CERIN Library user on 11 October 2022

Quark Particle Listings

t' (Fourth Generation) Quark

- the events with one lepton, large E_T , and ≥ 4 jets. The lower mass limit 0.87 (1.05) TeV is obtained for the singlet (doublet) model with other possible decay modes.
- SIRUNYAN 17AU based on 2.3-2.6 fb⁻¹ of pp data at $\sqrt{s} = 13$ TeV. Limit on pair-produced singlet vector-like t' using one lepton and several jets. The mass bound is given for a t' transforming as a singlet under the electroweak symmetry group, assumed to decay through W , Z or Higgs boson (which decays to jets) and to a third generation quark. For a doublet, the limit is >830 GeV. Other limits are also given in the paper.
 - AAD 15AR based on 20.3 fb⁻¹ of pp data at $\sqrt{s} = 8$ TeV. Used lepton-plus-jets final state. See Fig. 20 for mass limits in the plane of $B(t' \rightarrow Ht)$ vs. $B(t' \rightarrow Wb)$ from a combination of $t't' \rightarrow Wb + X$ and $t't' \rightarrow Ht + X$ searches. Any branching ratio scenario is excluded for mass below 715 GeV.
 - AAD 15BY based on 20.3 fb⁻¹ of pp data at $\sqrt{s} = 8$ TeV. Limit on pair-produced vector-like t' assuming the branching fractions to W , Z , and h modes of the singlet model. Used events containing $\geq 2\ell + E_T + \geq 2j$ ($\geq 1b$) and including a same-sign lepton pair.
 - KHACHATRYAN 15AI based on 19.7 fb⁻¹ of pp data at $\sqrt{s} = 8$ TeV. The search exploits all-hadronic final states by tagging boosted Higgs boson using jet substructure and b -tagging.
 - Based on 20.3 fb⁻¹ of pp data at $\sqrt{s} = 8$ TeV. No significant excess over SM expectation is found in the search for pair production or single production of t' in the events with dilepton from a high p_T Z and additional jets ($\geq 1b$ -tag). If instead of $B(b' \rightarrow Wt) = 1$ an electroweak singlet with $B(b' \rightarrow Wt) \sim 0.45$ is assumed, the limit reduces to 685 GeV.
 - Based on 19.5 fb⁻¹ of pp data at $\sqrt{s} = 8$ TeV. The t' quark is pair produced and is assumed to decay into three different final states of bW , tZ , and th . The search is carried out using events with at least one isolated lepton.
 - Based on 1.04 fb⁻¹ of pp data at $\sqrt{s} = 7$ TeV. No signal is found for the search of heavy quark pair production that decay into W and a quark in the events with dileptons, large E_T , and ≥ 2 jets.
 - Based on 1.04 fb⁻¹ of data in pp collisions at 7 TeV. AAD 12c looked for $t't'$ production followed by t' decaying into a top quark and X , an invisible particle, in a final state with an isolated high- p_T lepton, four or more jets, and a large missing transverse energy. No excess over the SM $t\bar{t}$ production gives the upper limit on $t't'$ production cross section as a function of $m_{t'}$ and m_X . The result is obtained for $B(t' \rightarrow Wt) = 1$.
 - Based on 5 fb⁻¹ of pp data at $\sqrt{s} = 7$ TeV. CHATRCHYAN 12BH searched for QCD and EW production of single and pair of degenerate 4th generation quarks that decay to Wb or Wt . Absence of signal in events with one lepton, same-sign dileptons or tripletons gives the bound. With a mass difference of 25 GeV/ c^2 between $m_{t'}$ and $m_{b'}$, the corresponding limit shifts by about ± 20 GeV/ c^2 .
 - Based on 5.0 fb⁻¹ of pp data at $\sqrt{s} = 7$ TeV. CHATRCHYAN 12P looked for $t't'$ production events with two isolated high p_T leptons, large E_T , and 2 high p_T jets with b -tag. The absence of signal above the SM background gives the limit for $B(t' \rightarrow Wb) = 1$.
 - Based on 4.7 fb⁻¹ of pp data at $\sqrt{s} = 7$ TeV. No signal is found for the search of heavy quark pair production that decay into W and a b quark in the events with a high p_T isolated lepton, large E_T and at least 3 jets ($\geq 1b$ -tag). Vector-like quark of charge $2/3$ with $400 < m_{t'} < 550$ GeV and $B(t' \rightarrow Wb) > 0.63$ is excluded at 95% CL.
 - Based on 5.0 fb⁻¹ of pp data at $\sqrt{s} = 7$ TeV. CHATRCHYAN 13I looked for events with one isolated electron or muon, large E_T , and at least four jets with large transverse momenta, where one jet is likely to originate from the decay of a bottom quark.
 - Based on 1.04 fb⁻¹ of pp data at $\sqrt{s} = 7$ TeV. No signal is found in the search for pair produced heavy quarks that decay into W boson and a b quark in the events with a high p_T isolated lepton, large E_T and at least 3 jets ($\geq 1b$ -tag).
 - Based on 5.0 fb⁻¹ of pp data at $\sqrt{s} = 7$ TeV. CHATRCHYAN 12Bc looked for $t't'$ production events with a single isolated high p_T lepton, large E_T and at least 4 high p_T jets with a b -tag. The absence of signal above the SM background gives the limit for $B(t' \rightarrow Wb) = 1$.
 - Based on 5.7 fb⁻¹ of data in $p\bar{p}$ collisions at 1.96 TeV. AALTONEN 11AH looked for $t't'$ production followed by t' decaying into a top quark and X , an invisible particle, in the all hadronic decay mode of $t\bar{t}$. No excess over the SM $t\bar{t}$ production gives the upper limit on $t't'$ production cross section as a function of $m_{t'}$ and m_X . The result is obtained for $B(t' \rightarrow Xt) = 1$.
 - Based on 5.6 fb⁻¹ of data in $p\bar{p}$ collisions at 1.96 TeV. AALTONEN 11AL looked for $\ell + \geq 4j$ events and set upper limits on $\sigma(t't')$ as functions of $m_{t'}$.
 - Based on 4.8 fb⁻¹ of data in $p\bar{p}$ collisions at 1.96 TeV. AALTONEN 11I looked for $t't'$ production signal when t' decays into a top quark and X , an invisible particle, in $\ell + E_T +$ jets channel. No excess over the SM $t\bar{t}$ production gives the upper limit on $t't'$ production cross section as a function of $m_{t'}$ and m_X . The result is obtained for $B(t' \rightarrow Xt) = 1$.
 - Based on 5.3 fb⁻¹ of data in $p\bar{p}$ collisions at 1.96 TeV. ABAZOV 11Q looked for $\ell + E_T + \geq 4j$ events and set upper limits on $\sigma(t't')$ as functions of $m_{t'}$.
 - Searches for pair production of a new heavy top-like quark t' decaying to a W boson and another quark by fitting the observed spectrum of total transverse energy and reconstructed t' mass in the lepton + jets events.
 - HUANG 08 reexamined the t' mass lower bound of 256 GeV obtained in AALTONEN 08H that assumes $B(b' \rightarrow qZ) = 1$ for $q = u, c$ which does not hold when $m_{b'} < m_{t'} - m_W$ or the mixing $\sin^2(\theta_{b't'})$ is so tiny that the decay occurs outside of the vertex detector. Fig. 1 gives that lower bound on $m_{t'}$ in the plane of $\sin^2(\theta_{b't'})$ and $m_{b'}$.

$t'(5/3)$ -quark/hadron mass limits in $p\bar{p}$ and pp collisions

VALUE (GeV)	CL%	DOCUMENT ID	TECN	COMMENT
>1330	95	1 SIRUNYAN 19T	CMS	$t'_R(5/3) \rightarrow tW^+$
>1300	95	1 SIRUNYAN 19T	CMS	$t'_L(5/3) \rightarrow tW^+$
>1350	95	2 AABOUD 18AW	ATLS	$t'(5/3) \rightarrow tW^+$
>1190	95	3 AABOUD 18CE	ATLS	$\geq 2\ell + E_T + \geq 1bj$
>1020	95	4 SIRUNYAN 17J	CMS	$t'_R(5/3) \rightarrow tW^+$

> 990	95	4 SIRUNYAN 17J	CMS	$t'_L(5/3) \rightarrow tW^+$
> 750	95	5 AAD 15BY	ATLS	$t'(5/3) \rightarrow tW^+$
> 840	95	6 AAD 15Z	ATLS	$t'(5/3) \rightarrow tW^+$
> 800	95	7 CHATRCHYAN 14T	CMS	$t'(5/3) \rightarrow tW^+$

- SIRUNYAN 19T based on 35.9 fb⁻¹ of pp data at $\sqrt{s} = 13$ TeV. Signals are searched in the final states of $t't'$ pair production, with same-sign leptons (which come from a t' decay) or a single lepton (which comes from a W out of 4Ws), along with jets, and no excess over the SM expectation is found.
- AABOUD 18AW based on 36.1 fb⁻¹ of pp data at $\sqrt{s} = 13$ TeV. Limit on $t'(5/3)$ in pair production assuming its coupling to Wt is equal to one. Lepton-plus-jets final state is used, characterized by $\ell + E_T +$ jets ($\geq 1b$ -tagged).
- AABOUD 18CE based on 36.1 fb⁻¹ of proton-proton data taken at $\sqrt{s} = 13$ TeV. Events including a same-sign lepton pair are used. The limit is for the pair-produced vector-like t' . With single t' production included, assuming $t't'W$ coupling of one, the limit is $m_{t'} > 1.6$ TeV.
- SIRUNYAN 17J based on 2.3 fb⁻¹ of pp data at $\sqrt{s} = 13$ TeV. Signals are searched in the final states of $t't'$ pair production, with same-sign leptons (which come from a t' decay) or a single lepton (which comes from a W out of 4Ws), along with jets, and no excess over the SM expectation is found.
- AAD 15BY based on 20.3 fb⁻¹ of pp data at $\sqrt{s} = 8$ TeV. Limit on $t'(5/3)$ in pair and single production assuming its coupling to Wt is equal to one. Used events containing $\geq 2\ell + E_T + \geq 2j$ ($\geq 1b$) and including a same-sign lepton pair.
- AAD 15Z based on 20.3 fb⁻¹ of pp data at $\sqrt{s} = 8$ TeV. Used events with $\ell + E_T + \geq 6j$ ($\geq 1b$) and at least one pair of jets from weak boson decay, sensitive to the final state $b\bar{b}W^+W^-W^+W^-$.
- CHATRCHYAN 14T based on 19.5 fb⁻¹ of pp data at $\sqrt{s} = 8$ TeV. Non-observation of anomaly in H_T distribution in the same-sign dilepton events leads to the limit when pair produced $t'(5/3)$ quark decays exclusively into t and W^+ , resulting in the final state with $b\bar{b}W^+W^-W^+W^-$.

$t'(2/3)$ mass limits from single production in $p\bar{p}$ and pp collisions

VALUE (GeV)	CL%	DOCUMENT ID	TECN	COMMENT
>950	95	1 AAD 16AV	ATLS	$qg \rightarrow q't'b, B(t' \rightarrow Wb)=0.5$
>403	95	2 ABAZOV 11F	D0	$q\bar{d} \rightarrow q't' \rightarrow q'(Wd)$ $\bar{\kappa}_{d't'}=1, B(t' \rightarrow Wd)=1$
>551	95	2 ABAZOV 11F	D0	$qu \rightarrow q't' \rightarrow q(Zu)$ $\bar{\kappa}_{u't'}=\sqrt{2}, B(t' \rightarrow Zu)=1$

- AAD 16AV based on 20.3 fb⁻¹ of pp data at $\sqrt{s} = 8$ TeV. No significant excess over SM expectation is found in the search for a fully reconstructed vector-like t' in the mode $\ell + E_T + \geq 2j$ ($\geq 1b$). A veto on massive large-radius jets is used to reject the $t\bar{t}$ background.
- Based on 5.4 fb⁻¹ of data in $p\bar{p}$ collisions at 1.96 TeV. ABAZOV 11F looked for single production of t' via the Z or E coupling to the first generation up or down quarks, respectively. Model independent cross section limits for the single production processes $p\bar{p} \rightarrow t'q \rightarrow (Wd)q$, and $p\bar{p} \rightarrow t'q \rightarrow (Zd)q$ are given in Figs. 3 and 4, respectively, and the mass limits are obtained for the model of ATRE 09 with degenerate bi-doublets of vector-like quarks.

$t'(5/3)$ mass limits from single production in $p\bar{p}$ and pp collisions

VALUE (GeV)	DOCUMENT ID	TECN	COMMENT
•••	1 SIRUNYAN 19AI	CMS	$tW \rightarrow t'(5/3) \rightarrow tW$

1 SIRUNYAN 19AI based on 35.9 fb⁻¹ of pp data at $\sqrt{s} = 13$ TeV. Exclusion limits are set on the product of the production cross section and branching fraction for the $b'(-1/3) + t$ and $t'(5/3) + t$ modes as a function of the vector-like quark mass in Fig. 8 and Tab. 2 for relative vector-like quark widths between 1 and 30% for left- and right-handed vector-like quark couplings. No significant deviation from the SM prediction is observed.

REFERENCES FOR Searches for (Fourth Generation) t' Quark

SIRUNYAN 19AI	EPJ C79 90	A.M. Sirunyan et al.	(CMS Collab.)
SIRUNYAN 19AQ	EPJ C79 364	A.M. Sirunyan et al.	(CMS Collab.)
SIRUNYAN 19BW	PR D100 072001	A.M. Sirunyan et al.	(CMS Collab.)
SIRUNYAN 19T	JHEP 1903 082	A.M. Sirunyan et al.	(CMS Collab.)
AABOUD 18AW	JHEP 1808 048	M. Aaboud et al.	(ATLAS Collab.)
AABOUD 18CE	JHEP 1812 039	M. Aaboud et al.	(ATLAS Collab.)
AABOUD 18CL	PR D98 092005	M. Aaboud et al.	(ATLAS Collab.)
AABOUD 18CP	PR D98 112010	M. Aaboud et al.	(ATLAS Collab.)
AABOUD 18CR	PRL 121 211801	M. Aaboud et al.	(ATLAS Collab.)
SIRUNYAN 18BM	JHEP 1808 177	A.M. Sirunyan et al.	(CMS Collab.)
SIRUNYAN 18BQ	PR D97 072008	A.M. Sirunyan et al.	(CMS Collab.)
SIRUNYAN 18W	PL B779 82	A.M. Sirunyan et al.	(CMS Collab.)
AABOUD 17L	JHEP 1708 052	M. Aaboud et al.	(ATLAS Collab.)
SIRUNYAN 17AU	JHEP 1711 085	A.M. Sirunyan et al.	(CMS Collab.)
SIRUNYAN 17J	JHEP 1708 073	A.M. Sirunyan et al.	(CMS Collab.)
AAD 16AV	EPJ C76 442	G. Aad et al.	(ATLAS Collab.)
AAD 15AR	JHEP 1508 105	G. Aad et al.	(ATLAS Collab.)
AAD 15BY	JHEP 1510 150	G. Aad et al.	(ATLAS Collab.)
AAD 15Z	PR D91 112011	G. Aad et al.	(ATLAS Collab.)
KHACHATRYAN... 15AI	JHEP 1506 080	V. Khachatryan et al.	(CMS Collab.)
AAD 14AZ	JHEP 1411 104	G. Aad et al.	(ATLAS Collab.)
CHATRCHYAN 14A	PL B729 149	S. Chatrchyan et al.	(CMS Collab.)
CHATRCHYAN 14T	PRL 112 171801	S. Chatrchyan et al.	(CMS Collab.)
AAD 13F	PL B718 1284	G. Aad et al.	(ATLAS Collab.)
CHATRCHYAN 13I	JHEP 1301 154	S. Chatrchyan et al.	(CMS Collab.)
AAD 12AR	PRL 108 261802	G. Aad et al.	(ATLAS Collab.)
AAD 12BC	PR D86 012007	G. Aad et al.	(ATLAS Collab.)
AAD 12C	PRL 108 041805	G. Aad et al.	(ATLAS Collab.)
CHATRCHYAN 12BC	PL B718 307	S. Chatrchyan et al.	(CMS Collab.)
CHATRCHYAN 12BH	PR D86 112003	S. Chatrchyan et al.	(CMS Collab.)
CHATRCHYAN 12P	PL B716 103	S. Chatrchyan et al.	(CMS Collab.)
AALTONEN 11AH	PRL 107 191803	T. Aaltonen et al.	(CDF Collab.)
AALTONEN 11AL	PRL 107 261801	T. Aaltonen et al.	(CDF Collab.)
AALTONEN 11I	PRL 106 191801	T. Aaltonen et al.	(CDF Collab.)
ABAZOV 11F	PRL 106 081801	V.M. Abazov et al.	(DO Collab.)
ABAZOV 11Q	PRL 107 082001	V.M. Abazov et al.	(DO Collab.)

ATRE	09	PR D79 054018	A. Atre <i>et al.</i>	
AALTONEN	08H	PRL 100 161803	T. Aaltonen <i>et al.</i>	(CDF Collab.)
HUANG	08	PR D77 037302	P.Q. Hung, M. Sher	(UVA, WILL)

Free Quark Searches

FREE QUARK SEARCHES

The basis for much of the theory of particle scattering and hadron spectroscopy is the construction of the hadrons from a set of fractionally charged constituents (quarks). A central element of Quantum Chromodynamics is that quarks cannot be observed as free particles but are confined to mesons and baryons. Experiments have produced no evidence for free quarks.

This compilation is only a guide to the literature, since the quoted experimental limits are often only indicative. Reviews can be found in Refs. 1-4.

References

- M.L. Perl, E.R. Lee, and D. Lomha, *Mod. Phys. Lett.* **A19**, 2595 (2004).
- P.F. Smith, *Ann. Rev. Nucl. and Part. Sci.* **39**, 73 (1989).
- L. Lyons, *Phys. Reports* **129**, 225 (1985).
- M. Marinelli and G. Morpurgo, *Phys. Reports* **85**, 161 (1982).

Quark Production Cross Section — Accelerator Searches

X-SECT (cm ²)	CHG (e/3)	MASS (GeV)	ENERGY (GeV)	BEAM	EVTS	DOCUMENT ID	TECN
<1.7-2.3E-39	±2	100-600	7000	p p	0	1 CHATRCHYAN13AR	CMS
<14.5.4E-39	±1	100-600	7000	p p	0	1 CHATRCHYAN13AR	CMS
<1.3E-36	±2	45-84	130-172	e ⁺ e ⁻	0	ABREU 97D	DLPH
<2.E-35	+2	250	1800	p p	0	2 ABE 92J	CDF
<1.E-35	+4	250	1800	p p	0	2 ABE 92J	CDF
<3.8E-28		14.5A	28	Si-Pb	0	3 HE 91	PLAS
<3.2E-28		14.5A	28	Si-Cu	0	3 HE 91	PLAS
<1.E-40	±1,2	<10		ρ, ν, τ	0	BERGSMA 84B	CHRM
<1.E-36	±1,2	<9	200	μ	0	AUBERT 83C	SPEC
<2.E-10	±2,4	1-3	200	p	0	4 BUSSIÈRE 80	CNTR
<5.E-38	+1,2	>5	300	p	0	5,6 STEVENSON 79	CNTR
<1.E-33	±1	<20	52	p p	0	BASILE 78	SPEC
<9.E-39	±1,2	<6	400	p	0	5 ANTREASYAN 77	SPEC
<8.E-35	+1,2	<20	52	p p	0	7 FABJAN 75	CNTR
<5.E-38	-1,2	4-9	200	p	0	NASH 74	CNTR
<1.E-32	+2,4	4-24	52	p p	0	ALPER 73	SPEC
<5.E-31	+1,2,4	<12	300	p	0	LEIPUNER 73	CNTR
<6.E-34	±1,2	<13	52	p p	0	BOTT 72	CNTR
<1.E-36	-4	4	70	p	0	ANTIPOV 71	CNTR
<1.E-35	±1,2	2	28	p	0	8 ALLABY 69B	CNTR
<4.E-37	-2	<5	70	p	0	4 ANTIPOV 69	CNTR
<3.E-37	-1,2	2-5	70	p	0	8 ANTIPOV 69B	CNTR
<1.E-35	+1,2	<7	30	p	0	DORFAN 65	CNTR
<2.E-35	-2	<2.5-5	30	p	0	9 FRANZINI 65B	CNTR
<5.E-35	+1,2	<2.2	21	p	0	BINGHAM 64	HLBC
<1.E-32	+1,2	<4.0	28	p	0	BLUM 64	HBC
<1.E-35	+1,2	<2.5	31	p	0	9 HAGOPIAN 64	HBC
<1.E-34	+1	<2	28	p	0	LEIPUNER 64	CNTR
<1.E-33	+1,2	<2.4	24	p	0	MORRISON 64	HBC

1 CHATRCHYAN 13AR limits assume pair-produced long-lived spin-1/2 particles neutral under SU(3)_C and SU(2)_L.
2 ABE 92J flux limits decrease as the mass increases from 50 to 500 GeV.
3 HE 91 limits are for charges of the form N±1/3 from 23/3 to 38/3.
4 Hadronic or leptonic quarks.
5 Cross section cm²/GeV².
6 3 × 10⁻⁵ < lifetime < 1 × 10⁻³ s.
7 Includes BOTT 72 results.
8 Assumes isotropic cm production.
9 Cross section inferred from flux.

Quark Differential Production Cross Section — Accelerator Searches

X-SECT (cm ² sr ⁻¹ GeV ⁻¹)	CHG (e/3)	MASS (GeV)	ENERGY (GeV)	BEAM	EVTS	DOCUMENT ID	TECN
<4.E-36	-2,4	1.5-6	70	p	0	BALDIN 76	CNTR
<2.E-33	±4	5-20	52	p p	0	ALBROW 75	SPEC
<5.E-34	<7	7-15	44	p p	0	JOVANOVIĆ 75	CNTR
<5.E-35			20	γ	0	1 GALIK 74	CNTR

<9.E-35	-1,2		200	p	0	NASH 74	CNTR
<4.E-36	-4	2.3-2.7	70	p	0	ANTIPOV 71	CNTR
<3.E-35	±1,2	<2.7	27	p	0	ALLABY 69B	CNTR
<7.E-38	-1,2	<2.5	70	p	0	ANTIPOV 69B	CNTR

¹ Cross section in cm²/sr/equivalent quanta.

Quark Flux — Accelerator Searches

The definition of FLUX depends on the experiment

- (a) is the ratio of measured free quarks to predicted free quarks if there is no "confinement."
- (b) is the probability of fractional charge on nuclear fragments. Energy is in GeV/nucleon.
- (c) is the 90%CL upper limit on fractionally-charged particles produced per interaction.
- (d) is quarks per collision.
- (e) is inclusive quark-production cross-section ratio to σ(e⁺e⁻ → μ⁺μ⁻).
- (f) is quark flux per charged particle.
- (g) is the flux per ν-event.
- (h) is quark yield per π⁻ yield.
- (i) is 2-body exclusive quark-production cross-section ratio to σ(e⁺e⁻ → μ⁺μ⁻).

FLUX	CHG (e/3)	MASS (GeV)	ENERGY (GeV)	BEAM	EVTS	DOCUMENT ID	TECN	
<1.6E-3	b	see note	200	32S-Pb	0	1 HUENTRUP 96	PLAS	
<6.2E-4	b	see note	10.6	32S-Pb	0	1 HUENTRUP 96	PLAS	
<0.94E-4	e	±2	2-30	88-94	e ⁺ e ⁻	0	AKERS 95R	OPAL
<1.7E-4	e	±2	30-40	88-94	e ⁺ e ⁻	0	AKERS 95R	OPAL
<3.6E-4	e	±4	5-30	88-94	e ⁺ e ⁻	0	AKERS 95R	OPAL
<1.9E-4	e	±4	30-45	88-94	e ⁺ e ⁻	0	AKERS 95R	OPAL
<2.E-3	e	+1	5-40	88-94	e ⁺ e ⁻	0	2 BUSKULIC 93C	ALEP
<6.E-4	e	+2	5-30	88-94	e ⁺ e ⁻	0	2 BUSKULIC 93C	ALEP
<1.2E-3	e	+4	15-40	88-94	e ⁺ e ⁻	0	2 BUSKULIC 93C	ALEP
<3.6E-4	i	+4	5.0-10.2	88-94	e ⁺ e ⁻	0	BUSKULIC 93C	ALEP
<3.6E-4	i	+4	16.5-26.0	88-94	e ⁺ e ⁻	0	BUSKULIC 93C	ALEP
<6.9E-4	i	+4	26.0-33.3	88-94	e ⁺ e ⁻	0	BUSKULIC 93C	ALEP
<9.1E-4	i	+4	33.3-38.6	88-94	e ⁺ e ⁻	0	BUSKULIC 93C	ALEP
<1.1E-3	i	+4	38.6-44.9	88-94	e ⁺ e ⁻	0	BUSKULIC 93C	ALEP
<1.6E-4	b	see note	see note			3 CECCHINI 93	PLAS	
	b	4,5,7,8	2.1A	16O	0,2,0,6	4 GHOSH 92	EMUL	
<6.4E-5	g	1		ν, τ	1	5 BASILE 91	CNTR	
<3.7E-5	g	2		ν, τ	1	5 BASILE 91	CNTR	
<3.9E-5	g	1		ν, τ	1	6 BASILE 91	CNTR	
<2.8E-5	g	2		ν, τ	0	6 BASILE 91	CNTR	
<1.9E-4	c		14.5A	28	Si-Pb	0	7 HE 91	PLAS
<3.9E-4	c		14.5A	28	Si-Cu	0	7 HE 91	PLAS
<1.E-9	c	±1,2,4	14.5A	16O-Ar	0	MATIS 91	MDRP	
<5.1E-10	c	±1,2,4	14.5A	16O-Hg	0	MATIS 91	MDRP	
<8.1E-9	c	±1,2,4	14.5A	Si-Hg	0	MATIS 91	MDRP	
<1.7E-6	c	±1,2,4	60A	16O-Hg	0	MATIS 91	MDRP	
<3.5E-7	c	±1,2,4	200A	16O-Hg	0	MATIS 91	MDRP	
<1.3E-6	c	±1,2,4	200A	S-Hg	0	MATIS 91	MDRP	
<5E-2	e	2	19-27	52-60	e ⁺ e ⁻	0	ADACHI 90C	TOPZ
<5E-2	e	4	<24	52-60	e ⁺ e ⁻	0	ADACHI 90C	TOPZ
<1.E-4	e	+2	<3.5	10	e ⁺ e ⁻	0	BOWCOCK 89B	CLEO
<1.E-6	d	±1,2	60	16O-Hg	0	CALLOWAY 89	MDRP	
<3.5E-7	d	±1,2	200	16O-Hg	0	CALLOWAY 89	MDRP	
<1.3E-6	d	±1,2	200	S-Hg	0	CALLOWAY 89	MDRP	
<1.2E-10	d	±1	1	800	p-Hg	0	MATIS 89	MDRP
<1.1E-10	d	±2	1	800	p-Hg	0	MATIS 89	MDRP
<1.2E-10	d	±1	1	800	p-N ₂	0	MATIS 89	MDRP
<7.7E-11	d	±2	1	800	p-N ₂	0	MATIS 89	MDRP
<6.E-9	h	-5	0.9-2.3	12	p	0	NAKAMURA 89	SPEC
<5.E-5	g	1,2	<0.5		ν, τ, d	0	ALLASIA 88	BECB
<3.E-4	b	See note	14.5	16O-Pb	0	8 HOFFMANN 88	PLAS	
<2.E-4	b	See note	200	16O-Pb	0	9 HOFFMANN 88	PLAS	
<8E-5	b	19,20,22,23	200A			GERBIER 87	PLAS	
<2.E-4	a	±1,2	<300	320	p p	0	LYONS 87	MLEV
<1.E-9	c	±1,2,4,5	14.5	16O-Hg	0	SHAW 87	MDRP	
<3.E-3	d	-1,2,3,4,6	<5	2	Si-Si	0	10 ABACHI 86C	CNTR
<1.E-4	e	±1,2,4	<4	10	e ⁺ e ⁻	0	ALBRECHT 85G	ARG
<6.E-5	b	±1,2	1	540	p p	0	BANNER 85	UA2
<5.E-3	e	-4	1-8	29	e ⁺ e ⁻	0	AIHARA 84	TPC
<1.E-2	e	±1,2	1-13	29	e ⁺ e ⁻	0	AIHARA 84B	TPC
<2.E-4	b	±1	72	40Ar	0	11 BARWICK 84	CNTR	
<1.E-4	e	±2	<0.4	1.4	e ⁺ e ⁻	0	BONDAR 84	OLYA
<5E-1	e	±1,2	<13	29	e ⁺ e ⁻	0	GURYN 84	CNTR
<3.E-3	b	±1,2	<2	540	p p	0	BANNER 83	CNTR
<1.E-4	b	±1,2	106	56Fe	0	LINDGREN 83	CNTR	
<3.E-3	b	> ± 0.1	74	40Ar	0	11 PRICE 83	PLAS	
<1.E-2	e	±1,2	<14	29	e ⁺ e ⁻	0	MARINI 82B	CNTR
<8.E-2	e	±1,2	<12	29	e ⁺ e ⁻	0	ROSS 82	CNTR
<3.E-4	e	±2	1.8-2	7	e ⁺ e ⁻	0	WEISS 81	MRK2
<5.E-2	e	+1,2,4,5	2-12	27	e ⁺ e ⁻	0	BARTEL 80	JADE

Quark Particle Listings

Free Quark Searches

<2.E-5	g	1,2		ν	0	^{5,6} BASILE	80	CNTR	
<3.E-10	f	$\pm 2,4$	1-3	200	p	0	¹² BOZZOLI	79	CNTR
<6.E-11	f	± 1	<21	52	pp	0	BASILE	78	SPEC
<5.E-3	g				ν_{μ}	0	BASILE	78B	CNTR
<2.E-9	f	± 1	<26	62	pp	0	BASILE	77	SPEC
<7.E-10	f	+1,2	<20	52	p	0	¹³ FABJAN	75	CNTR
		+1,2	>4.5		γ	0	^{5,6} GALIK	74	CNTR
		+1,2	>1.5	12	e^{-}	0	^{5,6} BELLAMY	68	CNTR
		+1,2	>0.9		γ	0	⁶ BATHOW	67	CNTR
		+1,2	>0.9	6	γ	0	⁶ FOSS	67	CNTR

<4.E-10		+1,2						GOMEZ	67	CNTR
<2.E-9		+2						KASHA	67	CNTR
<2.E-10		+2						BARTON	66	CNTR
<2.E-9		+1,2					220	BUHLER	66	CNTR
<3.E-9		+1,2						KASHA	66	CNTR
<2.E-9		+1,2						LAMB	66	CNTR
<2.E-8		+1,2	>7				2.8 *	DELISE	65	CNTR
<5.E-8		+2	>2.5				0.5 *	MASSAM	65	CNTR
<2.E-8		+1					2.5 *	BOWEN	64	CNTR
<2.E-7		+1					0.8	SUNYAR	64	CNTR

¹ HUENTRUP 96 quote 95% CL limits for production of fragments with charge differing by as much as $\pm 1/3$ (in units of e) for charge $6 \leq Z \leq 10$.
² BUSKULIC 93c limits for inclusive quark production are more conservative if the ALEPH hadronic fragmentation function is assumed.
³ CECCHINI 93 limit at 90%CL for $23/3 \leq Z \leq 40/3$, for 16A GeV O, 14.5A Si, and 200A S incident on Cu target. Other limits are 2.3×10^{-4} for $17/3 \leq Z \leq 20/3$ and 1.2×10^{-4} for $20/3 \leq Z \leq 23/3$.
⁴ GHOSH 92 reports measurement of spallation fragment charge based on ionization in emulsion. Out of 650 measured tracks, 2 were consistent with charge $5e/3$, and 4 with $7e/3$.
⁵ Hadronic quark.
⁶ Leptonic quark.
⁷ HE 91 limits are for charges of the form $N \pm 1/3$ from $23/3$ to $38/3$, and correspond to cross-section limits of $380\mu\text{b}$ (Pb) and $320\mu\text{b}$ (Cu).
⁸ The limits apply to projectile fragment charges of 17, 19, 20, 22, 23 in units of $e/3$.
⁹ The limits apply to projectile fragment charges of 16, 17, 19, 20, 22, 23 in units of $e/3$.
¹⁰ Flux limits and mass range depend on charge.
¹¹ Bound to nuclei.
¹² Quark lifetimes $> 1 \times 10^{-8}$ s.
¹³ One candidate $m < 0.17$ GeV.

¹ See AGNESE 15 Fig.6 for limits on vertical density as function of charge extending to $|q|/e < 1/10$.
² AMBROSIO 00c limit is below 11×10^{-15} for $0.25 < q/e < 0.5$, and is changing rapidly near $q/e=2/3$, where it is 2×10^{-14} .
³ Distribution in celestial sphere was described as anisotropic.
⁴ With telescope axis at zenith angle 40° to the south.
⁵ Leptonic quarks.
⁶ Lifetime $> 10^{-8}$ s; charge $\pm 0.70, 0.68, 0.42$; and mass $> 4.4, 4.8$, and 20 GeV, respectively.
⁷ Time delayed air shower search.
⁸ Prompt air shower search.
⁹ Also $e/4$ and $e/6$ charges.
¹⁰ No events in subsequent experiments.

Quark Flux — Cosmic Ray Searches

Shielding values followed with an asterisk indicate altitude in km. Shielding values not followed with an asterisk indicate sea level in kg/cm^2 .

FLUX ($\text{cm}^{-2}\text{sr}^{-1}\text{s}^{-1}$)	CHG ($e/3$)	MASS (GeV)	SHIELDING	DOCUMENT ID	TECN	
< 1.E-8	$\pm 1/6-1/10$			¹ AGNESE 15	CDMS	
< 9.2E-15	± 1		3800	² AMBROSIO 00c	MCR0	
< 2.1E-15	± 1			MORI 91	KAM2	
< 2.3E-15	± 2			MORI 91	KAM2	
< 2.E-10	$\pm 1,2$		0.3	WADA 88	CNTR	
	± 4		0.3	³ WADA 88	CNTR	
	± 4		0.3	⁴ WADA 86	CNTR	
< 1.E-12	$\pm 2,3/2$		-70.	⁵ KAWAGOE 84b	PLAS	
< 9.E-10	$\pm 1,2$		0.3	WADA 84b	CNTR	
< 4.E-9	± 4		0.3	WADA 84b	CNTR	
< 2.E-12	$\pm 1,2,3$		-0.3 *	MASHIMO 83	CNTR	
< 3.E-10	$\pm 1,2$		0.3	MARINI 82	CNTR	
< 2.E-11	$\pm 1,2$		0.3	MASHIMO 82	CNTR	
< 8.E-10	$\pm 1,2$		0.3	⁵ NAPOLITANO 82	CNTR	
				⁶ YOCK 78	CNTR	
				⁷ BRIATORE 76	ELEC	
				⁸ HAZEN 75	CC	
				KRISOR 75	CNTR	
				^{8,9} CLARK 74b	CC	
				KIFUNE 74	CNTR	
				⁸ ASHTON 73	CNTR	
				HICKS 73b	CNTR	
			2.8 *	BEAUCHAMP 72	CNTR	
				⁸ BOHM 72b	CNTR	
				COX 72	ELEC	
			2.8 *	CROUCH 72	CNTR	
				⁷ DARDO 72	CNTR	
				⁷ EVANS 72	CC	
				⁷ TONWAR 72	CNTR	
			2.8 *	CHIN 71	CNTR	
				⁸ CLARK 71b	CC	
				⁸ HAZEN 71	CC	
			3.5 *	BOSIA 70	CNTR	
			<6.5	⁸ CHU 70	HLBC	
				FAISSNER 70b	CNTR	
				KRIDER 70	CNTR	
			0.8 *	CAIRNS 69	CC	
				FUKUSHIMA 69	CNTR	
				^{8,10} MCCUSKER 69	CC	
			>5	⁷ BJORNBOE 68	CNTR	
			1.7,3.6	⁵ BRIATORE 68	CNTR	
			6.3,2 *	FRANZINI 68	CNTR	
			>2	GARMIRE 68	CNTR	
				HANAYAMA 68	CNTR	
				KASHA 68	OSPK	
			>15	KASHA 68b	CNTR	
				KASHA 68c	CNTR	
				BARTON 68	CNTR	
			6	BUHLER 67	CNTR	
			0.008,0.5 *	BUHLER 67	CNTR	
			1,2	0.008,0.5 *	BUHLER 67b	CNTR

Quark Density — Matter Searches

QUARKS/ NUCLEON	CHG ($e/3$)	MASS (GeV)	MATERIAL/METHOD	EVTS	DOCUMENT ID
< 1.17E-22			silicone oil drops	0	¹ LEE 02
< 4.71E-22			silicone oil drops	1	² HALYO 00
< 4.7E-21	$\pm 1,2$		silicone oil drops	0	MAR 96
< 8.E-22	+2		Si/infrared photoionization	0	PERERA 93
< 5.E-27	$\pm 1,2$		sea water/levitation	0	HOMER 92
< 4.E-20	$\pm 1,2$		meteorites/mag. levitation	0	JONES 89
< 1.E-19	$\pm 1,2$		various/spectrometer	0	MLNER 87
< 5.E-22	$\pm 1,2$		W/levitation	0	SMITH 87
< 3.E-20	+1,2		org liq/droplet tower	0	VAN POLEN 87
< 6.E-20	-1,2		org liq/droplet tower	0	VAN POLEN 87
< 3.E-21	± 1		Hg drops-untreated	0	SAVAGE 86
< 3.E-22	$\pm 1,2$		levitated niobium	0	SMITH 86
< 2.E-26	$\pm 1,2$		⁴ He/levitation	0	SMITH 86b
< 2.E-20	> ± 1	0.2-250	niobium+tungs/ion	0	MLNER 85
< 1.E-21	± 1		levitated niobium	0	SMITH 85
	+1,2	<100	niobium/mass spec	0	KUTSCHERA 84
< 5.E-22			levitated steel	0	MARINELLI 84
< 9.E-20	$\pm < 1.3$		water/oil drop	0	JOYCE 83
< 2.E-21	> $ \pm 1/2 $		levitated steel	0	LIEBOWITZ 83
< 1.E-19	$\pm 1,2$		photo ion spec	0	VANDESTEEG 83
< 2.E-20			mercury/oil drop	0	³ HODGES 81
1.E-20	+1		levitated niobium	4	⁴ LARUE 81
1.E-20	-1		levitated niobium	4	⁴ LARUE 81
< 1.E-21			levitated steel	0	MARINELLI 80b
< 6.E-16			helium/mass spec	0	BOYD 79
1.E-20	+1		levitated niobium	2	⁴ LARUE 79
< 4.E-28			earth+/ion beam	0	OGOROD... 79
< 5.E-15	+1		tungs./mass spec	0	BOYD 78
< 5.E-16	+3	<1.7	hydrogen/mass spec	0	BOYD 78b
< 1.E-21	$\pm 2,4$		water/ion beam	0	LUND 78
< 6.E-15	>1/2		levitated tungsten	0	PUTT 78
< 1.E-22			metals/mass spec	0	SCHIFFER 78
< 5.E-15			levitated tungsten ox	0	BLAND 77
< 3.E-21			levitated iron	0	GALLINARO 77
2.E-21	-1		levitated niobium	1	⁴ LARUE 77
4.E-21	+1		levitated niobium	2	⁴ LARUE 77
< 1.E-13	+3	<7.7	hydrogen/mass spec	0	MULLER 77
< 5.E-27			water+/ion beam	0	OGOROD... 77
< 1.E-21			lunar+/ion spec	0	STEVENS 76
< 1.E-15	+1	<60	oxygen+/ion spec	0	ELBERT 70
< 5.E-19			levitated graphite	0	MORPURGO 70
< 5.E-23			water+/atom beam	0	COOK 69
< 1.E-17	$\pm 1,2$		levitated graphite	0	BRAGINSK 68
< 1.E-17			water+/uv spec	0	RANK 68
< 3.E-19	± 1		levitated iron	0	STOVER 67
< 1.E-10			sun/uv spec	0	⁵ BENNETT 66
< 1.E-17	+1,2		meteorites+/ion beam	0	CHUPKA 66
< 1.E-16	± 1		levitated graphite	0	GALLINARO 66
< 1.E-22			argon/electrometer	0	HILLAS 59
	-2		levitated oil	0	MILLIKAN 10

¹ 95% CL limit for fractional charge particles with $0.18e \leq |Q_{residual}| \leq 0.82e$ in total of 70.1 mg of silicone oil.
² 95% CL limit for particles with fractional charge $|Q_{residual}| > 0.16e$ in total of 17.4 mg of silicone oil.
³ Also set limits for $Q = \pm e/6$.
⁴ Note that in PHILLIPS 88 these authors report a subtle magnetic effect which could account for the apparent fractional charges.
⁵ Limit inferred by JONES 77b.

Quark Particle Listings
Free Quark Searches

REFERENCES FOR Free Quark Searches

AGNESE 15 PRL 114 111302 R. Agnese et al. (CDMS Collab.)
 CHATRCHYAN 13AR PR D87 092008 S. Chattrchyan et al. (CMS Collab.)
 LEE 02 PR D66 012002 I.T. Lee et al. (CMS Collab.)
 AMBROSIO 00C PR D62 052003 M. Ambrosio et al. (MACRO Collab.)
 HALYO 00 PRL 84 2576 V. Halyo et al.
 ABREU 97D PL B396 315 P. Abreu et al. (DELPHI Collab.)
 HUENRUP 96 PR C53 358 G. Huenrup et al. (SIEG)
 MAR 96 PR D53 6017 N.M. Mar et al. (SLAC, SCHA, LANL, UCI)
 AKERS 95R ZPHY C67 203 R. Akers et al. (OPAL Collab.)
 BUSKULIC 93C PL B303 198 D. Buskulic et al. (ALEPH Collab.)
 CECCHINI 93 ASP 1 369 S. Cecchini et al.
 PERERA 93 PRL 70 1053 A.G.U. Perera et al. (PITT)
 ABE 92J PR D46 1889 F. Abe et al. (CDF Collab.)
 GHOSH 92 NC 105A 99 D. Ghosh et al. (JADA, BANGB)
 HOMER 92 ZPHY C55 549 G.J. Homer et al. (RAL, SHMP, LOQM)
 BASILE 91 NC 104A 405 M. Basile et al. (BGNA, INFN, CERN, PLRMB)
 HE 91 PR C44 1672 Y.B. He, P.B. Price
 MATIS 91 NP A525 513 H.S. Matis et al. (LBL, SFSU, UCI+)
 MORI 91 PR D43 2843 M. Mori et al. (Kamokande II Collab.)
 ADACHI 90C PL B244 352 I. Adachi et al. (TOPAZ Collab.)
 BOWCOCK 89B PR D40 263 T.J.V. Bowcock et al. (CLEO Collab.)
 CALLOWAY 89 PL B232 549 D. Calloway et al. (SFSU, UCI, LBL+)
 JONES 89 ZPHY C43 349 W.G. Jones et al. (LOIC, RAL)
 MATIS 89 PR D39 1851 H.S. Matis et al. (LBL, SFSU, UCI+)
 NAKAMURA 89 PR D39 1261 T.T. Nakamura et al. (KYOT, TMT C)
 ALLASIA 88 PR D37 219 D. Allasia et al. (WA25 Collab.)
 HOFFMANN 88 PL B200 583 A. Hofmann et al. (SIEG, USF)
 PHILLIPS 88 NIM A264 125 J.D. Phillips, W.M. Fairbank, J. Navarro
 WADA 88 NC 11C 229 T. Wada, Y. Yamashita, I. Yamamoto
 GERBIER 87 PRL 59 2535 G. Gerbier et al. (UCB, CERN)
 LYONS 87 ZPHY C36 363 K. Lyons et al. (OXF, RAL, LOIC)
 MILNER 87 PR D36 37 R.E. Milner et al. (CIT)
 SHAW 87 PR D36 3533 P.L. Shaw et al. (UCI, LBL, LANL, SFSU)
 SMITH 87 PL B197 447 G.F. Smith et al. (RAL, LOIC)
 VANPOLEN 87 PR D36 1983 J. van Polen, R.T. Hagstrom, G. Hirsch
 ABACHI 86C PR D33 2733 S. Abachi et al. (UCLA, LBL, UCD)
 SAVAGE 86 PL 167B 481 M.L. Savage et al. (SFSU)
 SMITH 86 PL B171 129 P.F. Smith et al. (RAL, LOIC)
 SMITH 86B PL B181 407 P.F. Smith et al. (RAL, LOIC)
 WADA 86 NC 9C 358 T. Wada
 ALBRECHT 85G PL 156B 134 H. Albrecht et al. (ARGUS Collab.)
 BANMER 85 PL 156B 129 M. Benmer et al. (UA2 Collab.)
 MILNER 85 PRL 54 1472 R.E. Milner et al. (CIT)
 SMITH 85 PL 153B 188 P.F. Smith et al. (RAL, LOIC)
 AIHARA 84 PRL 52 168 H. Aihara et al. (TPC Collab.)
 AIHARA 84B PRL 52 2332 H. Aihara et al. (TPC Collab.)
 BARWICK 84 PR D30 691 S.W. Barwick, J.A. Musser, J.D. Stevenson
 BERGSMÄ 84B ZPHY C24 217 F. Bergsmä et al. (CHARM Collab.)
 BONDAR 84 JETPL 40 1265 A.E. Bondar et al. (NOVO)
 GURYN 84 PL 139B 313 W. Guryin et al. (FRAS, LBL, NWES, STAN+)
 KAWAGOE 84B LNC 41 604 K. Kawagoe et al. (TOKY)
 KUTSCHERA 84 PR D29 791 W. Kutschera et al. (ANL, FNAL)
 MARINELLI 84 PL 137B 439 M. Marinelli, G. Morpurgo (GENO)
 WADA 84B LNC 40 329 T. Wada, Y. Yamashita, I. Yamamoto (OKAY)
 AUBERT 83C PL 133B 461 J.J. Aubert et al. (EMC Collab.)
 BANNER 83 PL 121B 187 M. Banner et al. (UA2 Collab.)
 JOYCE 83 PRL 51 731 D.C. Joyce et al. (SFSU)
 LIEBOWITZ 83 PRL 50 1640 D. Liebowitz, M. Binder, K.O.H. Ziock (UVA)
 LINDGREN 83 PRL 51 1621 M.A. Lindgren et al. (SFSU, UCR, UCI+)
 MASHIMO 83 PL 128B 327 T. Mashimo et al. (ICEPP)
 PRICE 83 PRL 50 566 P.B. Price et al. (UCB)
 VANDESTEEG 83 NC 123A M.J.H. van de Steeg, H.W.H.M. Jongbloets, P. Wyder
 MARINI 82 PR D26 1777 A. Marini et al. (FRAS, LBL, NWES, STAN+)
 MARINI 82B PR D26 1777 A. Marini et al. (FRAS, LBL, NWES, STAN+)
 MASHIMO 82 JPSJ 51 3067 T. Mashimo, K. Kawagoe, M. Koshiba (INUS)
 NAPOLITANO 82 PR D25 2837 J. Napolitano et al. (STAN, FRAS, LBL+)
 ROSS 82 PL 118B 199 M.C. Ross et al. (FRAS, LBL, NWES, STAN+)
 HODGES 81 PRL 47 1651 C.L. Hodges et al. (UCR, SFSU)
 LARUE 81 PRL 46 967 G.S. Larue, J.D. Phillips, W.M. Fairbank (STAN)
 WEISS 81 PL 101B 439 J.M. Weiss et al. (SLAC, LBL, UCB)
 BARTEL 80 ZPHY C6 295 W. Bartel et al. (JADE Collab.)
 BASILE 80 LNC 29 251 M. Basile et al. (BGNA, CERN, FRAS, ROMA+)
 BUSIERE 80 NP B174 1 A. Busiere et al. (BGNA, SAFL, LAPP)
 MARINELLI 80B PL 94B 433 M. Marinelli, G. Morpurgo (GENO)
 Also PL 94B 427 M. Marinelli, G. Morpurgo (GENO)
 BOYD 79 PRL 43 1288 R.N. Boyd et al. (OSU)
 BOZZOLI 79 NP B159 363 W. Bozzoli et al. (BGNA, LAPP, SAFL+)
 LARUE 79 PRL 42 142 G.S. Larue, W.M. Fairbank, J.D. Phillips (STAN)
 Also PRL 42 1019 G.S. Larue, W.M. Fairbank, J.D. Phillips
 OGOROD... 79 JETP 49 953 D.D. Ogorodnikov, I.M. Samoilov, A.M. Soltsev
 STEVENSON 79 PR D20 82 M.L. Stevenson (LBL)
 BASILE 78 NC 45A 171 M. Basile et al. (CERN, BGNA)
 BASILE 78B NC 45A 281 M. Basile et al. (CERN, BGNA)
 BOYD 78 PRL 40 216 R.N. Boyd et al. (ROCH)
 BOYD 78B PL 72B 484 R.N. Boyd et al. (ROCH)
 LUND 78 RA 25 75 T. Lund, R. Brandt, Y. Fares (MARB)
 PUTT 78 PR D17 1466 G.D. Putt, P.C.M. Yock (AUCK)
 SCHIFFER 78 PR D17 2241 P.J. Schiffer et al. (CHIC, ANL)
 YOCK 78 PR D18 641 P.C.M. Yock (AUCK)
 ANTREASAYN 77 PRL 39 513 D. Antreasayan et al. (EFI, PRIN)
 BASILE 77 NC 40A 41 M. Basile et al. (CERN, BGNA)
 BLAND 77 PRL 39 369 R.W. Bland et al. (SFSU)
 GALLINARO 77 PRL 38 1255 G. Gallinaro, M. Marinelli, G. Morpurgo (GENO)
 JONES 77B RMP 49 717 L.W. Jones

LARUE 77 PRL 38 1011 G.S. Larue, W.M. Fairbank, A.F. Hebard (STAN)
 MULLER 77 SCI 196 521 R.A. Muller et al. (LBL)
 OGOROD... 77 JETP 45 857 D.D. Ogorodnikov, I.M. Samoilov, A.M. Soltsev
 BALDIN 76 S JNP 22 264 B.Y. Baldin et al. (JINR)
 Translated from YAF 22 512
 BRIATORE 76 NC 31A 553 L. Briatore et al. (LCGT, FRAS, FREIB)
 STEVENS 76 PR D14 716 C.M. Stevens, J.P. Schiffer, W. Chupka (ANL)
 ALBROW 75 NP B97 189 M.G. Albrow et al. (CERN, DARE, FOM+)
 FABJAN 75 NP B101 349 C.W. Fabjan et al. (CERN, MPIM)
 HAZEN 75 NP B95 189 W.E. Hazen et al. (MICH, LEED)
 JOVANOV... 75 PL 56B 105 J.V. Jovanovich et al. (MANI, AACH, CERN+)
 KRISOR 75 NC 27A 132 K. Krisor (AACH3)
 CLARK 74B PR D10 2721 A.F. Clark et al. (LLL)
 GALIK 74 PR D9 1856 R.S. Galik et al. (SLAC, FNAL)
 KIFUNE 74 JPSJ 36 629 T. Kifune et al. (TOKY, KEK)
 NASH 74 PRL 32 858 T. Nash et al. (FNAL, CORN, NYU)
 ALPER 73 PL 46B 265 B. Alper et al. (CERN, LVP, LUND, BOHR+)
 ASHTON 73 JP A6 577 F. Ashton et al. (DURH)
 HICKS 73B NC 14A 65 R.B. Hicks, R.W. Flint, S. Standil (MANI)
 LEIPUNER 73 PRL 31 1226 L.B. Leipuner et al. (BNL, YALE)
 BEAUCHAMP 72 PR D6 1211 W.T. Beauchamp et al. (ARIZ)
 BOHM 72B PRL 28 326 A. Bohm et al. (AACH)
 BOTT 72 PL 40B 693 M. Bott-Bodenhausen et al. (CERN, MPIM)
 COX 72 PR D6 1203 A.J. Cox et al. (ARIZ)
 CROUCH 72 PR D5 2667 M.F. Crouch, K. Mori, G.R. Smith (CASE)
 DARDO 72 NC 9A 319 M. Dardo et al. (TORI)
 EVANS 72 PRSE A70 143 G.R. Evans et al. (EDIN, LEED)
 TONVAVR 72 JP 5A 569 S.C. Tonvavr, S. Naranan, B.V. Sreekantan (TATA)
 ANTIPOV 71 NP B29 374 Y.M. Antipov et al. (SERP)
 CHIN 71 NC 2A 419 S. Chin et al. (OSAK)
 CLARK 71B PRL 27 51 A.F. Clark et al. (LLL, LBL)
 HAZEN 71 PRL 26 582 W.E. Hazen (MICH)
 BOSIA 70 NC 66A 167 G.F. Bosia, L. Briatore (TORI)
 CHU 70 PRL 24 917 W.T. Chu et al. (OSU, ROSE, KANS)
 Also PRL 25 550
 ELBERT 70 NP B20 217 J.W. Elbert et al. (ANL)
 FAISSNER 70B PRL 24 1357 H. Faissner et al. (AACH3)
 KRIDER 70 PR D1 835 E.P. Krider, T. Bowen, R.M. Kalbach (ARIZ)
 MORPURGO 70 NIM 79 95 G. Morpurgo, G. Gallinaro, G. Palmieri (GENO)
 ALLABY 69B NC 64A 75 J.V. Allaby et al. (CERN)
 ANTIPOV 69 PL 29B 245 Y.M. Antipov et al. (SERP)
 ANTIPOV 69B PL 30B 576 Y.M. Antipov et al. (SERP)
 CAIRNS 69 PR 186 1394 I. Cairns et al. (SYDN)
 COOK 69 PR 188 2092 D.D. Cook et al. (ILL)
 FUKUSHIMA 69 PR 178 2058 Y. Fukushima et al. (TOKY)
 MCCUSKER 69 PRL 23 658 C.B.A. McCusker, I. Cairns (SYDN)
 BELLAMY 68 PR 166 1391 E.H. Bellamy et al. (STAN, SLAC)
 BJORNBOE 68 NC B53 241 J. Bjornboe et al. (BOHR, TATA, BERN+)
 BRAGINSK 68 JETP 27 51 V.B. Braginsky et al. (MOSU)
 Translated from ZETF 54 91
 BRIATORE 68 NC 57A 850 L. Briatore et al. (TORI, CERN, BGNA)
 FRANZINI 68 PRL 21 1013 P. Franzini, S. Shulman (COLU)
 GARMIRE 68 PR 166 1280 G. Garmire, C. Leong, V. Sreekantan (MIT)
 HANAYAMA 68 CJP 46 5734 Y. Hanayama et al. (OSAK)
 KASHA 68 PR 172 1297 H. Kasha, R.J. Stefanski (BNL, YALE)
 KASHA 68B PRL 20 217 H. Kasha et al. (BNL, YALE)
 KASHA 68C CJP 46 5730 H. Kasha et al. (BNL, YALE)
 RANK 68 PR 176 1635 D. Rank (MICH)
 BARTON 67 PRSL 90 87 J.C. Barton (NPOL)
 BATHOW 67 PL 25B 163 G. Bathow et al. (DESY)
 BUHLER 67 NC 49A 209 A. Buhler-Broglin et al. (CERN, BGNA)
 BUHLER 67B NC 51A 837 A. Buhler-Broglin et al. (CERN, BGNA+)
 FOSS 67 PL 25B 166 R. Foss et al. (MIT)
 GOMEZ 67 PRL 18 1022 R. Gomez et al. (CIT)
 KASHA 67 PR 154 1263 H. Kasha et al. (BNL, YALE)
 STOVER 67 PR 164 1599 R.W. Stover, T.J. Moran, J.W. Trischka (SYRA)
 BARTON 66 PL 21 360 J.C. Barton, C.T. Stockel (NPOL)
 BENNETT 66 PR 17 1196 W.R. Bennett (YALE)
 BUEHLER 66 NC 45A 520 A. Buhler-Broglin et al. (CERN, BGNA+)
 CHUPKA 66 PRL 17 60 W.A. Chupka, J.P. Schiffer, C.M. Stevens (ANL)
 GALLINARO 66 PL 23 609 G. Gallinaro, G. Morpurgo (GENO)
 KASHA 66 PR 150 1140 H. Kasha, L.B. Leipuner, R.K. Adair (BNL, YALE)
 LAMB 66 PRL 17 1068 R.C. Lamb et al. (BNL, YALE)
 DELISE 65 PR 140 B458 D.A. de Lise, T. Bowen (ARIZ)
 DORFAN 65 PRL 14 999 D.E. Dorfman et al. (COLU)
 FRANZINI 65B PR 14 196 P. Franzini et al. (BNL, COLU)
 MASSAM 65 NC 40A 589 T. Massam, T. Muller, A. Zichichi (CERN)
 BINGHAM 64 PL 9 201 H.H. Bingham et al. (CERN, EPOL)
 BLUM 64 PRL 13 353A W. Blum et al. (CERN)
 BOWEN 64 PRL 13 728 T. Bowen et al. (ARIZ)
 HAGOPIAN 64 PRL 13 280 V. Hagopian et al. (PENN, BNL)
 LEIPUNER 64 PRL 12 423 L.B. Leipuner et al. (BNL, YALE)
 MORRISON 64 PL 9 199 D.R.O. Morrison (CERN)
 SUNYAR 64 PR 136 B1157 A.W. Sunyar, A.Z. Schwarzschild, P.I. Connors (BNL)
 HILLAS 59 NAT 184 B92 A.M. Hillas, T.E. Cranshaw (AERE)
 MILLIKAN 10 Phil Mag 19 209 R.A. Millikan (CHIC)

OTHER RELATED PAPERS

LYONS 85 PRPL C129 225 L. Lyons (OXF)
 Review
 MARINELLI 82 PRPL 85 161 M. Marinelli, G. Morpurgo (GENO)
 Review

• π^\pm	1349	• $f_2(2010)$	1459
• π^0	1352	• $f_0(2020)$	1459
• η	1354	• $f_4(2050)$	1460
• $f_0(500)$ aka σ ; was $f_0(600)$	1359	• $\pi_2(2100)$	1461
• $\rho(770)$	1361	• $f_0(2100)$	1462
• $\omega(782)$	1367	• $f_2(2150)$	1462
• $\eta'(958)$	1373	• $\rho(2150)$	1464
• $f_0(980)$	1379	• $\phi(2170)$	1465
• $a_0(980)$	1382	• $f_0(2200)$	1466
• $\phi(1020)$	1383	• $f_J(2220)$	1467
• $h_1(1170)$	1391	• $\eta(2225)$	1468
• $b_1(1235)$	1391	• $\rho_3(2250)$	1468
• $a_1(1260)$	1392	• $f_2(2300)$	1469
• $f_2(1270)$	1395	• $f_4(2300)$	1469
• $f_1(1285)$	1398	• $f_0(2330)$	1470
• $\eta(1295)$	1401	• $f_2(2340)$	1470
• $\pi(1300)$	1402	• $\rho_5(2350)$	1471
• $a_2(1320)$	1402	• $X(2370)$	1471
• $f_0(1370)$	1406	• $f_6(2510)$	1472
• $\pi_1(1400)$	1409		
• $\eta(1405)$	1410	• K^\pm	1473
• $h_1(1415)$	1412	• K^0	1488
• $h_1(1415)$ was $h_1(1380)$	1412	• K_S^0	1489
• $f_1(1420)$	1413	• K_L^0	1493
• $\omega(1420)$	1414	• $K_0^*(700)$ aka κ ; was $K_0^*(800)$	1508
• $f_2(1430)$	1416	• $K^*(892)$	1509
• $a_0(1450)$	1416	• $K_1(1270)$	1512
• $\rho(1450)$	1417	• $K_1(1400)$	1513
• $\eta(1475)$	1420	• $K^*(1410)$	1514
• $f_0(1500)$	1421	• $K_0^*(1430)$	1515
• $f_1(1510)$	1424	• $K_2^*(1430)$	1516
• $f_2'(1525)$	1425	• $K(1460)$	1518
• $f_2(1565)$	1429	• $K_2(1580)$	1519
• $\rho(1570)$	1430	• $K(1630)$	1519
• $h_1(1595)$	1430	• $K_1(1650)$	1519
• $\pi_1(1600)$	1430	• $K^*(1680)$	1519
• $a_1(1640)$	1431	• $K_2(1770)$	1520
• $f_2(1640)$	1432	• $K_3^*(1780)$	1521
• $\eta_2(1645)$	1432	• $K_2(1820)$	1522
• $\omega(1650)$	1433	• $K(1830)$	1523
• $\omega_3(1670)$	1434	• $K_0^*(1950)$	1523
• $\pi_2(1670)$	1435	• $K_2^*(1980)$	1523
• $\phi(1680)$	1437	• $K_4^*(2045)$	1524
• $\rho_3(1690)$	1438	• $K_2(2250)$	1525
• $\rho(1700)$	1441	• $K_3(2320)$	1525
• $a_2(1700)$	1445	• $K_5^*(2380)$	1525
• $f_0(1710)$	1446	• $K_4(2500)$	1525
• $X(1750)$	1449	• $K(3100)$	1526
• $\eta(1760)$	1449		
• $\pi(1800)$	1450	• D^\pm	1527
• $f_2(1810)$	1451	• D^0	1543
• $X(1835)$	1452	• $D^*(2007)^0$	1578
• $\phi_3(1850)$	1453	• $D^*(2010)^\pm$	1578
• $\eta_2(1870)$	1453	• $D_0^*(2300)$ was $D_0^*(2400)$	1580
• $\pi_2(1880)$	1454	• $D_1(2420)$	1580
• $\rho(1900)$	1455	• $D_1(2430)^0$	1582
• $f_2(1910)$	1455	• $D_2^*(2460)$	1582
• $a_0(1950)$	1456		
• $f_2(1950)$	1456		
• $a_4(1970)$ was $a_4(2040)$	1458		
• $\rho_3(1990)$	1458		
• $\pi_2(2005)$	1459		

• Indicates the particle is in the Meson Summary Table

(Continued on the next page)

$D_0(2550)^0$	1584	• $\chi_{c2}(3930)$	1917
$D_1^*(2600)^0$ was $D(2600)$	1584	$X(3940)$	1918
$D^*(2640)^\pm$	1585	• $X(4020)^\pm$	1918
$D_2(2740)^0$ was $D(2740)^0$	1585	• $\psi(4040)$	1919
• $D_3^*(2750)$	1586	$X(4050)^\pm$	1921
$D_1^*(2760)^0$	1586	$X(4055)^\pm$	1922
$D(3000)^0$	1587	$X(4100)^\pm$	1922
		• $\chi_{c1}(4140)$ was $X(4140)$	1922
• D_s^\pm	1588	• $\psi(4160)$	1923
• $D_s^{*\pm}$	1601	$X(4160)$	1926
• $D_{s0}^*(2317)^\pm$	1601	$Z_c(4200)$ was $X(4200)^\pm$	1926
• $D_{s1}(2460)^\pm$	1602	$R_{c0}(4240)$ was $X(4240)^\pm$	1931
• $D_{s1}(2536)^\pm$	1604	$X(4250)^\pm$	1932
• $D_{s2}^*(2573)$	1605	• $\psi(4230)$ aka $Y(4260)$; was $X(4260)$	1927
$D_{s0}(2590)^+$	1605	• $\chi_{c1}(4274)$ was $X(4274)$	1932
• $D_{s1}^*(2700)^\pm$	1606	$X(4350)$	1932
$D_{s1}^*(2860)^\pm$	1606	• $\psi(4360)$ aka $Y(4360)$; was $X(4360)$	1933
• $D_{s3}^*(2860)^\pm$	1607	was $X(4390)$	
$X_0(2900)$	1607	• $\psi(4415)$	1934
$X_1(2900)$	1607	• $Z_c(4430)$ was $X(4430)^\pm$	1936
$D_{sJ}(3040)^\pm$	1608	$\chi_{c0}(4500)$ was $X(4500)$	1936
		$X(4630)$	1937
• B^\pm	1610	• $\psi(4660)$ aka $Y(4660)$; was $X(4660)$	1937
• B^0	1675	$\chi_{c1}(4685)$	1939
• B^\pm/B^0 ADMIXTURE	1750	$\chi_{c0}(4700)$ was $X(4700)$	1939
• $B^\pm/B^0/B_s^0/b$ -baryon ADMIXTURE	1772		
V_{cb} and V_{ub} CKM Matrix Elements	1780	• $\eta_b(1S)$	1940
• B^*	1781	• $\Upsilon(1S)$	1942
• $B_1(5721)$	1782	• $\chi_{b0}(1P)$	1948
$B_J^*(5732)$ aka B^{**}	1782	• $\chi_{b1}(1P)$	1950
• $B_2^*(5747)$	1783	• $h_b(1P)$	1952
$B_J(5840)$	1783	• $\chi_{b2}(1P)$	1952
• $B_J(5970)$	1784	$\eta_b(2S)$	1954
		• $\Upsilon(2S)$	1954
• B_s^0	1786	• $\Upsilon_2(1D)$ was $\Upsilon(1D)$	1959
• B_s^*	1810	• $\chi_{b0}(2P)$	1960
$X(5568)^\pm$	1810	• $\chi_{b1}(2P)$	1961
• $B_{s1}(5830)^0$	1811	• $h_b(2P)$	1964
• $B_{s2}^*(5840)^0$	1811	• $\chi_{b2}(2P)$	1964
$B_{sJ}^*(5850)$	1811	• $\Upsilon(3S)$	1966
		• $\chi_{b1}(3P)$	1969
• B_c^+	1813	• $\chi_{b2}(3P)$	1970
$B_c(2S)^\pm$	1817	• $\Upsilon(4S)$ aka $\Upsilon(10580)$	1970
		• $Z_b(10610)$ was $X(10610)$	1972
• $\eta_c(1S)$	1818	• $Z_b(10650)$ was $X(10650)^\pm$	1973
• $J/\psi(1S)$	1826	$\Upsilon(10753)$	1974
• $\chi_{c0}(1P)$	1851	• $\Upsilon(10860)$	1975
• $\chi_{c1}(1P)$	1861	• $\Upsilon(11020)$	1978
• $h_c(1P)$	1870		
• $\chi_{c2}(1P)$	1872	Further States	1980
• $\eta_c(2S)$	1883		
• $\psi(2S)$	1886		
• $\psi(3770)$	1903		
• $\psi_2(3823)$ was $\psi(3823)$, $X(3823)$	1910		
• $\psi_3(3842)$	1911		
$\chi_{c0}(3860)$	1911		
• $\chi_{c1}(3872)$ aka $X(3872)$	1911		
• $Z_c(3900)$ was $X(3900)$	1915		
• $\chi_{c0}(3915)$ was $X(3915)$	1916		
• Indicates the particle is in the Meson Summary Table			

Notes in the Listings

Charged kaon mass	1473
Dalitz plot parameters for $K \rightarrow 3\pi$ decays	1482
CP -violation in $K_S \rightarrow 3\pi$	1492
Heavy Flavor Averaging Group (rev.)	1609
Charmonium system (rev.)	1818
Branching ratios of $\psi(2S)$ and $\chi_{c0,1,2}$ (rev.)	1850
Bottomonium system (rev.)	1940
Width determination of the Υ states	1940

(Continued on next page.)

Related Reviews in Volume 1

62. Form factors for semileptonic kaon ($K_{\ell 3}$), radiative pion ($\pi_{\ell 2\gamma}$) & kaon ($K_{\ell 2\gamma}$) decays (rev.)	842
63. Spectroscopy of light meson resonances (new)	845
64. Scalar mesons below 1 GeV (rev.)	858
65. Rare kaon decays (rev.)	865
66. CPT invariance tests in neutral kaon decay (rev.)	871
67. V_{ud} , V_{us} , Cabibbo angle, and CKM unitarity (rev.)	873
68. CP -violation in K_L decays (rev.)	877
69. Review of multibody charm analyses (rev.)	880
70. $D^0-\bar{D}^0$ mixing (rev.)	885
71. D_s^+ branching fractions (rev.)	895
72. Leptonic decays of charged pseudoscalar mesons (rev.)	897
73. Production and decay of b -flavored hadrons (rev.)	908
74. Polarization in B decays (rev.)	919
75. $B^0-\bar{B}^0$ mixing (rev.)	923
76. Semileptonic B decays, V_{cb} and V_{ub} (rev.)	930
77. CKM angles from B hadrons, determination of (rev.)	946
78. Spectroscopy of mesons containing two heavy quarks (rev.)	951
79. Heavy non- $q\bar{q}$ mesons (rev.)	959

See key on page 1127

Meson Particle Listings

π^\pm

LIGHT UNFLAVORED MESONS
(S = C = B = 0)

For $I = 1$ (π, b, ρ, a): $u\bar{d}, (u\bar{u}-d\bar{d})/\sqrt{2}, d\bar{u}$;
for $I = 0$ ($\eta, \eta', h, h', \omega, \phi, f, f'$): $c_1(u\bar{u} + d\bar{d}) + c_2(s\bar{s})$

π^\pm

$I^G(J^P) = 1^-(0^-)$

We have omitted some results that have been superseded by later experiments. The omitted results may be found in our 1988 edition Physics Letters **B204** 1 (1988).

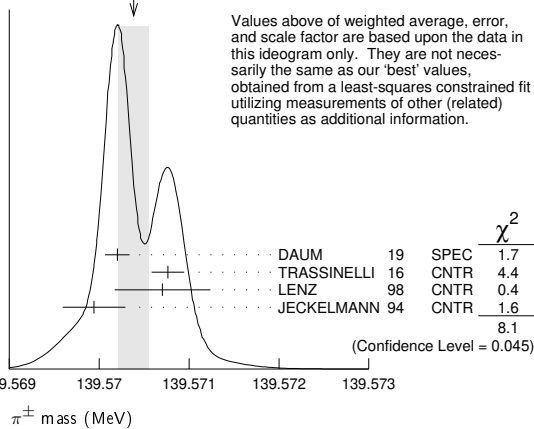
π^\pm MASS

The most accurate charged pion mass measurements are based upon x-ray wavelength measurements for transitions in π^- -mesonic atoms. The observed line is the blend of three components, corresponding to different K-shell occupancies. JECKELMANN 94 revisits the occupancy question, with the conclusion that two sets of occupancy ratios, resulting in two different pion masses (Solutions A and B), are equally probable. We choose the higher Solution B since only this solution is consistent with a positive mass-squared for the muon neutrino, given the precise muon momentum measurements now available (DAUM 91, ASSAMAGAN 94, and ASSAMAGAN 96) for the decay of pions at rest. Earlier mass determinations with p-mesonic atoms may have used incorrect K-shell screening corrections.

Measurements with an error of > 0.005 MeV have been omitted from this Listing.

VALUE (MeV)	DOCUMENT ID	TECN	CHG	COMMENT
139.57039 ± 0.00018 OUR FIT	Error includes scale factor of 1.8.			
139.57039 ± 0.00017 OUR AVERAGE	Error includes scale factor of 1.6. See the ideogram below.			
139.57021 ± 0.00014	¹ DAUM	19	SPEC	$\pi^+ \rightarrow \mu^+ \nu_\mu$
139.57077 ± 0.00018	² TRASSINELLI	16	CNTR	X-ray transitions in pionic N2
139.57071 ± 0.00053	³ LENZ	98	CNTR	pionic N2-atoms gas target
139.56995 ± 0.00035	⁴ JECKELMANN 94	CNTR	-	π^- atom, Soln. B
• • • We do not use the following data for averages, fits, limits, etc. • • •				
139.57022 ± 0.00014	⁵ ASSAMAGAN 96	SPEC	+	$\pi^+ \rightarrow \mu^+ \nu_\mu$
139.56782 ± 0.00037	⁶ JECKELMANN 94	CNTR	-	π^- atom, Soln. A
139.56996 ± 0.00067	⁷ DAUM	91	SPEC	$\pi^+ \rightarrow \mu^+ \nu$
139.56752 ± 0.00037	⁸ JECKELMANN 86b	CNTR	-	Mesonic atoms
139.5704 ± 0.0011	⁷ ABELA	84	SPEC	See DAUM 91
139.5664 ± 0.0009	⁹ LU	80	CNTR	Mesonic atoms
139.5686 ± 0.0020	⁹ CARTER	76	CNTR	Mesonic atoms
139.5660 ± 0.0024	^{9,10} MARUSHEN...	76	CNTR	Mesonic atoms

WEIGHTED AVERAGE
139.57039 ± 0.00017 (Error scaled by 1.6)



Values above of weighted average, error, and scale factor are based upon the data in this ideogram only. They are not necessarily the same as our 'best' values, obtained from a least-squares constrained fit utilizing measurements of other (related) quantities as additional information.

¹ DAUM 19 value is based on their previous (1991+1996) measurements of the μ^+ momentum of 29.79200 ± 0.00011 MeV for π^+ decay at rest. It also uses $m_\mu = 105.6583745 \pm 0.0000024$ MeV, and assumes conservatively $m_{\nu_\mu} = 2.0 \pm 2.0$ MeV. It is the most precise charged pion mass determination.
² TRASSINELLI 16 use the muonic oxygen line for online energy calibration of the pionic line.
³ LENZ 98 result does not suffer K-electron configuration uncertainties as does JECKELMANN 94.
⁴ JECKELMANN 94 Solution B (dominant 2-electron K-shell occupancy), chosen for consistency with positive $m_{\nu_\mu}^2$.

⁵ ASSAMAGAN 96 measures the μ^+ momentum p_μ in $\pi^+ \rightarrow \mu^+ \nu_\mu$ decay at rest to be 29.79200 ± 0.00011 MeV/c. Combined with the μ^+ mass and the assumption $m_{\nu_\mu} = 0$, this gives the π^+ mass above; if $m_{\nu_\mu} > 0$, m_{π^+} given above is a lower limit.

Combined instead with m_μ and (assuming CPT) the π^- mass of JECKELMANN 94, p_μ gives an upper limit on m_{ν_μ} (see the ν_μ).

⁶ JECKELMANN 94 Solution A (small 2-electron K-shell occupancy) in combination with either the DAUM 91 or ASSAMAGAN 94 pion decay muon momentum measurement yields a significantly negative $m_{\nu_\mu}^2$. It is accordingly not used in our fits.

⁷ The DAUM 91 value includes the ABELA 84 result. The value is based on a measurement of the μ^+ momentum for π^+ decay at rest, $p_\mu = 29.79179 \pm 0.00053$ MeV, uses $m_\mu = 105.658389 \pm 0.000034$ MeV, and assumes that $m_{\nu_\mu} = 0$. The last assumption means that in fact the value is a lower limit.

⁸ JECKELMANN 86b gives $m_\pi/m_e = 273.12677(71)$. We use $m_e = 0.51099906(15)$ MeV from COHEN 87. The authors note that two solutions for the probability distribution of K-shell occupancy fit equally well, and use other data to choose the lower of the two possible π^\pm masses.

⁹ These values are scaled with a new wavelength-energy conversion factor $V\lambda = 1.23984244(37) \times 10^{-6}$ eV m from COHEN 87. The LU 80 screening correction relies upon a theoretical calculation of inner-shell refilling rates.

¹⁰ This MARUSHENKO 76 value used at the authors' request to use the accepted set of calibration γ energies. Error increased from 0.0017 MeV to include QED calculation error of 0.0017 MeV (12 ppm).

$m_{\pi^+} - m_{\mu^+}$

Measurements with an error > 0.05 MeV have been omitted from this Listing.

VALUE (MeV)	EVTS	DOCUMENT ID	TECN	CHG	COMMENT	
• • • We do not use the following data for averages, fits, limits, etc. • • •						
33.91157 ± 0.00067		¹ DAUM	91	SPEC	+	$\pi^+ \rightarrow \mu^+ \nu$
33.9111 ± 0.0011		ABELA	84	SPEC		See DAUM 91
33.925 ± 0.025		BOOTH	70	CNTR	+	Magnetic spect.
33.881 ± 0.035	145	HYMAN	67	HEBC	+	K^- He

¹ The DAUM 91 value assumes that $m_{\nu_\mu} = 0$ and uses our $m_\mu = 105.658389 \pm 0.000034$ MeV.

$(m_{\pi^+} - m_{\pi^-}) / m_{\text{average}}$

A test of CPT invariance.

VALUE (units 10^{-4})	DOCUMENT ID	TECN
2 ± 5	AYRES	71

π^\pm MEAN LIFE

Measurements with an error $> 0.02 \times 10^{-8}$ s have been omitted.

VALUE (10^{-8} s)	DOCUMENT ID	TECN	CHG	COMMENT	
2.6033 ± 0.0005 OUR AVERAGE	Error includes scale factor of 1.2.				
2.60361 ± 0.00052	¹ KOPTEV	95	SPEC	+	Surface μ^+ 's
2.60231 ± 0.00050 ± 0.00084	NUMAO	95	SPEC	+	Surface μ^+ 's
2.609 ± 0.008	DUNAITSEV	73	CNTR	+	
2.602 ± 0.004	AYRES	71	CNTR	±	
2.604 ± 0.005	NORDBERG	67	CNTR	+	
2.602 ± 0.004	ECKHAUSE	65	CNTR	+	
• • • We do not use the following data for averages, fits, limits, etc. • • •					
2.640 ± 0.008	² KINSEY	66	CNTR	+	

¹ KOPTEV 95 combines the statistical and systematic errors; the statistical error dominates.
² Systematic errors in the calibration of this experiment are discussed by NORDBERG 67.

$(\tau_{\pi^+} - \tau_{\pi^-}) / \tau_{\text{average}}$

A test of CPT invariance.

VALUE (units 10^{-4})	DOCUMENT ID	TECN
5.5 ± 7.1	AYRES	71
• • • We do not use the following data for averages, fits, limits, etc. • • •		
-14 ± 29	PETRUKHIN	68
40 ± 70	BARDON	66
23 ± 40	¹ LOBKOWICZ	66

¹ This is the most conservative value given by LOBKOWICZ 66.

π ELECTRIC POLARIZABILITY α_π

See HOLSTEIN 14 for a general review on hadron polarizability.

VALUE (10^{-4} fm ³)	EVTS	DOCUMENT ID	TECN	COMMENT	
2.0 ± 0.6 ± 0.7	63k	¹ ADOLPH	15A	SPEC	$\pi^- \gamma \rightarrow \pi^- \gamma$ Compton scatt.

¹ Value is derived assuming $\alpha_\pi = -\beta_\pi$.

Meson Particle Listings

 π^\pm π^+ DECAY MODES π^- modes are charge conjugates of the modes below.

For decay limits to particles which are not established, see the section on Searches for Axions and Other Very Light Bosons.

Mode	Fraction (Γ_i/Γ)	Confidence level
Γ_1 $\mu^+ \nu_\mu$	[a] (99.98770 ± 0.00004) %	
Γ_2 $\mu^+ \nu_\mu \gamma$	[b] (2.00 ± 0.25) × 10 ⁻⁴	
Γ_3 $e^+ \nu_e$	[a] (1.230 ± 0.004) × 10 ⁻⁴	
Γ_4 $e^+ \nu_e \gamma$	[b] (7.39 ± 0.05) × 10 ⁻⁷	
Γ_5 $e^+ \nu_e \pi^0$	(1.036 ± 0.006) × 10 ⁻⁸	
Γ_6 $e^+ \nu_e e^+ e^-$	(3.2 ± 0.5) × 10 ⁻⁹	
Γ_7 $\mu^+ \nu_\mu \nu \bar{\nu}$	< 9 × 10 ⁻⁶	90%
Γ_8 $e^+ \nu_e \nu \bar{\nu}$	< 1.6 × 10 ⁻⁷	90%

Lepton Family number (LF) or Lepton number (L) violating modes

Γ_9 $\mu^+ \bar{\nu}_e$	L	[c] < 1.5	× 10 ⁻³	90%
Γ_{10} $\mu^+ \nu_e$	LF	[c] < 8.0	× 10 ⁻³	90%
Γ_{11} $\mu^- e^+ e^+ \nu$	LF	< 1.6	× 10 ⁻⁶	90%

[a] Measurements of $\Gamma(e^+ \nu_e)/\Gamma(\mu^+ \nu_\mu)$ always include decays with γ 's, and measurements of $\Gamma(e^+ \nu_e \gamma)$ and $\Gamma(\mu^+ \nu_\mu \gamma)$ never include low-energy γ 's. Therefore, since no clean separation is possible, we consider the modes with γ 's to be subreactions of the modes without them, and let $[\Gamma(e^+ \nu_e) + \Gamma(\mu^+ \nu_\mu)]/\Gamma_{\text{total}} = 100\%$.

[b] See the Particle Listings below for the energy limits used in this measurement; low-energy γ 's are not included.

[c] Derived from an analysis of neutrino-oscillation experiments.

 π^+ BRANCHING RATIOS

$\Gamma(e^+ \nu_e)/\Gamma_{\text{total}}$	Γ_3/Γ
See note [a] in the list of π^+ decay modes just above, and see also the next block of data. See also the note on "Decay Constants of Charged Pseudoscalar Mesons" in the D_s^+ Listings.	

VALUE (units 10 ⁻⁴)	DOCUMENT ID
1.230 ± 0.004 OUR EVALUATION	

$$\frac{\Gamma(e^+ \nu_e) + \Gamma(e^+ \nu_e \gamma)}{\Gamma(\mu^+ \nu_\mu) + \Gamma(\mu^+ \nu_\mu \gamma)} \quad (\Gamma_3 + \Gamma_4)/(\Gamma_1 + \Gamma_2)$$

See note [a] in the list of π^+ decay modes above. See NUMAO 92 for a discussion of $e-\mu$ universality. See also the note on "Decay Constants of Charged Pseudoscalar Mesons" in the D_s^+ Listings.

VALUE (units 10 ⁻⁴)	EVTS	DOCUMENT ID	TECN	CHG	COMMENT
1.2327 ± 0.0023 OUR AVERAGE					
1.2344 ± 0.0023 ± 0.0019	400k	AGUILAR-AR...15	CNTR	+	Stopping π^+
1.2346 ± 0.0035 ± 0.0036	120k	CZAPEK 93	CALO		Stopping π^+
1.2265 ± 0.0034 ± 0.0044	190k	BRITTON 92	CNTR		Stopping π^+
1.218 ± 0.014	32k	BRYMAN 86	CNTR		Stopping π^+
••• We do not use the following data for averages, fits, limits, etc. •••					
1.273 ± 0.028	11k	¹ DICAPUA 64	CNTR		
1.21 ± 0.07		ANDERSON 60	SPEC		
¹ DICAPUA 64 has been updated using the current mean life.					

$\Gamma(\mu^+ \nu_\mu \gamma)/\Gamma_{\text{total}}$	Γ_2/Γ
Note that measurements here do not cover the full kinematic range.	

VALUE (units 10 ⁻⁴)	EVTS	DOCUMENT ID	TECN	CHG	COMMENT
2.0 ± 0.24 ± 0.08		¹ BRESSI 98	CALO	+	Stopping π^+
••• We do not use the following data for averages, fits, limits, etc. •••					
1.24 ± 0.25	26	CASTAGNOLI 58	EMUL		KE $_{\mu} < 3.38$ MeV

¹BRESSI 98 result is given for $E_\gamma > 1$ MeV only. Result agrees with QED expectation, 2.283×10^{-4} and does not confirm discrepancy of earlier experiment CASTAGNOLI 58.

$\Gamma(e^+ \nu_e \gamma)/\Gamma_{\text{total}}$	Γ_4/Γ
The very different values reflect the very different kinematic ranges covered (bigger range, bigger value). And none of them covers the whole kinematic range.	

VALUE (units 10 ⁻⁸)	EVTS	DOCUMENT ID	TECN	COMMENT
73.86 ± 0.54	65k	¹ BYCHKOV 09	PIBE	$e^+ \nu_\mu \gamma$ at rest
••• We do not use the following data for averages, fits, limits, etc. •••				
16.1 ± 2.3		² BOLOTOV 90B	SPEC	17 GeV $\pi^- \rightarrow e^- \bar{\nu}_e \gamma$
5.6 ± 0.7	226	³ STETZ 78	SPEC	$P_e > 56$ MeV/c
3.0	143	DEPOMMIER 63B	CNTR	(KE) $_{e^+ \gamma} > 48$ MeV

¹This BYCHKOV 09 value is for $E_\gamma > 10$ MeV and $\Theta_{e^+ \gamma} > 40^\circ$.

²BOLOTOV 90B is for $E_\gamma > 21$ MeV, $E_e > 70 - 0.8 E_\gamma$.

³STETZ 78 is for an $e^- \gamma$ opening angle $> 132^\circ$. Obtains 3.7 when using same cutoffs as DEPOMMIER 63B.

 $\Gamma(e^+ \nu_e \pi^0)/\Gamma_{\text{total}}$ Γ_5/Γ

VALUE (units 10 ⁻⁸)	EVTS	DOCUMENT ID	TECN	CHG	COMMENT
1.036 ± 0.006 OUR AVERAGE					
1.036 ± 0.006	64k	^{1,2} POCANIC 04	PIBE	+	π decay at rest
1.026 ± 0.039	1224	³ MCFARLANE 85	CNTR	+	Decay in flight
1.00 ^{+0.08} _{-0.10}	332	DEPOMMIER 68	CNTR	+	
1.07 ± 0.21	38	⁴ BACASTOW 65	OSPK	+	
1.10 ± 0.26		⁴ BERTRAM 65	OSPK	+	
1.1 ± 0.2	43	⁴ DUNAITSEV 65	CNTR	+	
0.97 ± 0.20	36	⁴ BARTLETT 64	OSPK	+	

••• We do not use the following data for averages, fits, limits, etc. •••

1.15 ± 0.22 52 ⁴DEPOMMIER 63 CNTR + See DEPOMMIER 68

¹POCANIC 04 normalizes to $e^+ \nu_e$ decays, using the PDG 2004 value $B(\pi^+ \rightarrow e^+ \nu_e) = (1.230 \pm 0.004) \times 10^{-4}$. We add their statistical (0.004×10^{-8}) , systematic (0.004×10^{-8}) and systematic error due to the uncertainty of $B(\pi^+ \rightarrow e^+ \nu_e)$ (0.003×10^{-8}) in quadrature.

²This result can be used to calculate V_{ud} from pion beta decay: $V_{ud}^{PIBETA} = 0.9728 \pm 0.0030$.

³MCFARLANE 85 combines a measured rate $(0.394 \pm 0.015)/s$ with 1982 PDG mean life.

⁴DEPOMMIER 68 says the result of DEPOMMIER 63 is at least 10% too large because of a systematic error in the π^0 detection efficiency, and that this may be true of all the previous measurements (also V. Soergel, private communication, 1972).

 $\Gamma(e^+ \nu_e e^+ e^-)/\Gamma(\mu^+ \nu_\mu)$ Γ_6/Γ_1

VALUE (units 10 ⁻⁹)	CL%	EVTS	DOCUMENT ID	TECN	COMMENT
3.2 ± 0.5 ± 0.2		98	EGLI 89	SPEC	Uses $R_{PAC} = 0.068 \pm 0.004$

••• We do not use the following data for averages, fits, limits, etc. •••

0.46 ± 0.16 ± 0.07 7 ¹BARANOV 92 SPEC Stopped π^+

< 4.8 90 KORENCHE... 76B SPEC

< 34 90 KORENCHE... 71 OSPK

¹This measurement by BARANOV 92 is of the structure-dependent part of the decay. The value depends on values assumed for ratios of form factors.

 $\Gamma(\mu^+ \nu_\mu \nu \bar{\nu})/\Gamma(\mu^+ \nu_\mu)$ Γ_7/Γ_1

VALUE	CL%	EVTS	DOCUMENT ID	TECN	COMMENT
< 8.6 × 10⁻⁶	90	9.1M	AGUILAR-AR...20A	SPEC	fit E_μ spectrum

 $\Gamma(e^+ \nu_e \nu \bar{\nu})/\Gamma_{\text{total}}$ Γ_8/Γ

VALUE	CL%	EVTS	DOCUMENT ID	TECN	COMMENT
< 1.6 × 10⁻⁷	90	1.3M	AGUILAR-AR...20A	SPEC	fit E_e spectrum
••• We do not use the following data for averages, fits, limits, etc. •••					
< 5 × 10 ⁻⁶	90		PICCIOTTO 88	SPEC	

••• We do not use the following data for averages, fits, limits, etc. •••

 $\Gamma(\mu^+ \bar{\nu}_e)/\Gamma_{\text{total}}$ Γ_9/Γ

Forbidden by total lepton number conservation. See the note on "Decay Constants of Charged Pseudoscalar Mesons" in the D_s^+ Listings.

VALUE (units 10 ⁻³)	CL%	DOCUMENT ID	TECN	COMMENT
< 1.5	90	¹ COOPER 82	HLBC	Wideband ν beam

¹COOPER 82 limit on $\bar{\nu}_e$ observation is here interpreted as a limit on lepton number violation.

 $\Gamma(\mu^+ \nu_e)/\Gamma_{\text{total}}$ Γ_{10}/Γ

VALUE (units 10 ⁻³)	CL%	DOCUMENT ID	TECN	COMMENT
< 8.0	90	¹ COOPER 82	HLBC	Wideband ν beam

¹COOPER 82 limit on ν_e observation is here interpreted as a limit on lepton family number violation.

 $\Gamma(\mu^- e^+ e^+ \nu)/\Gamma_{\text{total}}$ Γ_{11}/Γ

VALUE (units 10 ⁻⁶)	CL%	DOCUMENT ID	TECN	CHG
< 1.6	90	BARANOV 91B	SPEC	+
••• We do not use the following data for averages, fits, limits, etc. •••				
< 7.7	90	KORENCHE... 87	SPEC	+

••• We do not use the following data for averages, fits, limits, etc. •••

 π^+ — POLARIZATION OF EMITTED μ^+ $\pi^+ \rightarrow \mu^+ \nu$

Tests the Lorentz structure of leptonic charged weak interactions.

VALUE	CL%	DOCUMENT ID	TECN	CHG	COMMENT
••• We do not use the following data for averages, fits, limits, etc. •••					
< (-0.9959)	90	¹ FETSCHER 84	RVUE	+	
-0.99 ± 0.16		² ABELA 83	SPEC	-	μ X-rays

¹FETSCHER 84 uses only the measurement of CARR 83.

²Sign of measurement reversed in ABELA 83 to compare with μ^+ measurements.

See the related review(s):

Form Factors for Semileptonic Kaon ($K_{\ell 3}$), Radiative Pion ($\pi_{\ell 2\gamma}$) and Kaon ($K_{\ell 2\gamma}$) Decays

See key on page 1127

Meson Particle Listings

π^\pm

π^\pm FORM FACTORS

F_V , VECTOR FORM FACTOR

VALUE	EVTS	DOCUMENT ID	TECN	COMMENT
0.0254 ± 0.0017 OUR AVERAGE				
0.0258 ± 0.0017	65k	1 BYCHKOV	09 PIBE	$e^+ \nu_\gamma$ at rest
0.014 ± 0.009		2 BOLOTOV	90B SPEC	17 GeV $\pi^- \rightarrow e^- \bar{\nu}_e \gamma$
0.023 ^{+0.015} / _{-0.013}	98	EGLI	89 SPEC	$\pi^+ \rightarrow e^+ \nu_e e^+ e^-$

¹ The BYCHKOV 09 F_A and F_V results are highly (anti-)correlated: $F_A + 1.0286 F_V = 0.03853 \pm 0.00014$.
² BOLOTOV 90B only determines the absolute value.

F_A , AXIAL-VECTOR FORM FACTOR

VALUE	EVTS	DOCUMENT ID	TECN	COMMENT
0.0119 ± 0.0001				
• • • We do not use the following data for averages, fits, limits, etc. • • •				
0.0115 ± 0.0004	41k	1,3 FRLEZ	04 PIBE	$\pi^+ \rightarrow e^+ \nu_\gamma$ at rest
0.0106 ± 0.0060		1,4 BOLOTOV	90B SPEC	17 GeV $\pi^- \rightarrow e^- \bar{\nu}_e \gamma$
0.021 ^{+0.011} / _{-0.013}	98	EGLI	89 SPEC	$\pi^+ \rightarrow e^+ \nu_e e^+ e^-$
0.0135 ± 0.0016		1,4 BAY	86 SPEC	$\pi^+ \rightarrow e^+ \nu_\gamma$
0.006 ± 0.003		1,4 PIILONEN	86 SPEC	$\pi^+ \rightarrow e^+ \nu_\gamma$
0.011 ± 0.003		1,4,5 STETZ	78 SPEC	$\pi^+ \rightarrow e^+ \nu_\gamma$

¹ These values come from fixing the vector form factor at the CVC prediction, $F_V = 0.0259 \pm 0.0005$.
² When F_V is released, the BYCHKOV 09 F_A is 0.0117 ± 0.0017 , and F_A and F_V results are highly (anti-)correlated: $F_A + 1.0286 F_V = 0.03853 \pm 0.00014$.
³ The sign of $\gamma = F_A / F_V$ is determined to be positive.
⁴ Only the absolute value of F_A is determined.
⁵ The result of STETZ 78 has a two-fold ambiguity. We take the solution compatible with later determinations.

VECTOR FORM FACTOR SLOPE PARAMETER a

This is a in $F_V(q^2) = F_V(0) (1 + a q^2)$

VALUE	EVTS	DOCUMENT ID	TECN	COMMENT
0.10 ± 0.06				
0.10 ± 0.06	65k	BYCHKOV	09 PIBE	$e^+ \nu_\gamma$ at rest

R, SECOND AXIAL-VECTOR FORM FACTOR

VALUE	EVTS	DOCUMENT ID	TECN	COMMENT
0.059 ^{+0.009}/_{-0.008}				
0.059 ^{+0.009} / _{-0.008}	98	EGLI	89 SPEC	$\pi^+ \rightarrow e^+ \nu_e e^+ e^-$

π^\pm CHARGE RADIUS

The charge radius of the pion $\sqrt{\langle r_\pi^2 \rangle}$ is defined in relation to the form factor of the pion electromagnetic vertex, called vector form factor VFF, F_V . The VFF is a function of the squared four-momentum transfer t , or of the squared c.m. energy s , depending on the channel in which the photon exchange takes place. In both cases, it is related to the slope of the VFF at zero, namely

$$\langle r_\pi^2 \rangle = 6 \frac{dF_V(q^2)}{dq^2} (q=0) \text{ where } q = t, s.$$

The quantity cannot be measured directly. It can be extracted from the cross sections of three processes: pion electroproduction, $eN \rightarrow eN\pi$, and pion electron scattering $e\pi \rightarrow e\pi$, for the t channel, and positron electron annihilation into two charged pions, $e^+e^- \rightarrow \pi^+\pi^-$, for the s channel. We encode all measurements, but we do not use electroproduction data in averaging because the extraction of the pion radius involves, in this case, theoretical uncertainties that cannot be controlled at the needed level of accuracy. In case of analyses based on the same data set, as ANANTHANARAYAN 17 and COLANGELO 19, which cannot be averaged, we combine the results into a common value, with the uncertainty range chosen to cover both analyses. Note that for consistency the form factor needs to be defined in both channels with the vacuum polarisation removed. For details see COLANGELO 19 or Appendix B of ANANTHANARAYAN 16A.

VALUE (fm)	DOCUMENT ID	TECN	COMMENT
0.659 ± 0.004 OUR AVERAGE			
0.656 ± 0.005	1 PDG	19 FIT	Fit existing data
0.65 ± 0.05 ± 0.06	ESCHRICH	01 CNTR	$\pi e \rightarrow \pi e$
0.663 ± 0.006	AMENDOLIA	86 CNTR	$\pi e \rightarrow \pi e$
0.663 ± 0.023	DALLY	82 CNTR	$\pi e \rightarrow \pi e$
• • • We do not use the following data for averages, fits, limits, etc. • • •			
0.640 ± 0.007	2 CUI	21A FIT	Fit existing data
0.655 ± 0.004	3 COLANGELO	19 FIT	Fit existing data
0.657 ± 0.003	4 ANANTHANARAYAN..17	FIT	Fit existing data
0.6603 ± 0.0005 ± 0.0004	5 HANHART	17 FIT	Fit existing data
0.740 ± 0.031	6 LIESENFELD	99 CNTR	$e p \rightarrow e \pi^+ n$
0.661 ± 0.012	7 BIJNENS	98 CNTR	χ PT extraction
0.660 ± 0.024	AMENDOLIA	84 CNTR	$\pi e \rightarrow \pi e$
0.711 ± 0.009 ± 0.016	6 BEBEK	78 CNTR	$e N \rightarrow e \pi N$
0.678 ± 0.004 ± 0.008	8 QUENZER	78 CNTR	$e^+ e^- \rightarrow \pi^+ \pi^-$
0.78 ^{+0.09} / _{-0.10}	ADYLOV	77 CNTR	$\pi e \rightarrow \pi e$
0.74 ^{+0.11} / _{-0.13}	BARDIN	77 CNTR	$e p \rightarrow e \pi^+ n$
0.56 ± 0.04	DALLY	77 CNTR	$\pi e \rightarrow \pi e$

- ¹ This value combines the measurements of ANANTHANARAYAN 17 and COLANGELO 19 which are based on the same data set. The uncertainty range is chosen to cover both results.
- ² CUI 21A perform a fit including spacelike data only. Employ a new mathematical procedure based on interpolation via continued fractions augmented by statistical sampling. Also do not impose the charge conserving normalization condition $F(0) = 1$.
- ³ COLANGELO 19 fit existing F_V data, using an extended Omnes dispersive representation. This analysis is based on the same data set of ANANTHANARAYAN 17. Accordingly, they cannot be averaged. We combine the results into a common value, with the uncertainty range chosen to cover the uncertainty ranges of both analyses.
- ⁴ ANANTHANARAYAN 17 fit existing F_V data, using a mixed phase-modulus dispersive representation. This analysis is based on the same data set of COLANGELO 19. Accordingly, they cannot be averaged. We combine the results into a common value, with the uncertainty range chosen to cover the uncertainty ranges of both analyses.
- ⁵ According to the authors the uncertainty could be underestimated. The value quoted omits the BaBar data AUBERT 09.
- ⁶ The extractions could contain an additional theoretical uncertainty which cannot be sufficiently quantified.
- ⁷ BIJNENS 98 fits existing data.
- ⁸ The extraction is based on a parametrization that does not have correct analytic properties.

π^\pm REFERENCES

We have omitted some papers that have been superseded by later experiments. The omitted papers may be found in our 1988 edition Physics Letters **B204** 1 (1988).

CUI	21A	PL B822 136631	Z.-F. Cui <i>et al.</i>	(NJU, ECT, HZDR)
AGUILAR-AR...	20A	PR D102 012001	A. Aguilar-Arevalo <i>et al.</i>	(PIENU Collab.)
COLANGELO	19	JHEP 1902 006	G. Colangelo, M. Hoferichter, P. Stoffer	(BERN+)
DAUM	19	PL B796 11	M. Daum, R. Frosch, P.-R. Kettle	(PSI)
PDG	19	RPP 2019 at pdg.lbl.gov	M. Tanabashi <i>et al.</i>	(PDG Collab.)
ANANTHANARAYAN..17	PRL 119 132002		B. Ananthanarayan, I. Caprini, D. Das	
HANHART	17	EPJ C77 98	C. Hanhart <i>et al.</i>	
ANANTHANARAYAN..16A	PR D93 116007		B. Ananthanarayan <i>et al.</i>	
TRASSINELLI	16	PL B759 583	M. Trassinelli <i>et al.</i>	
ADOLPH	15A	PRL 114 062002	C. Adolph <i>et al.</i>	(COMPASS Collab.)
AGUILAR-AR...	15	PRL 115 071801	A. Aguilar-Arevalo <i>et al.</i>	(PIENU Collab.)
HOLSTEIN	14	ARNPS 64 51	B. Holstein, S. Scherer	(MASA, MAINZ)
AUBERT	09	PR D79 011102	B. Aubert <i>et al.</i>	(BABAR Collab.)
BYCHKOV	09	PRL 103 051802	M. Bychkov <i>et al.</i>	(PSI PIBETA Collab.)
FRLEZ	04	PRL 93 181804	E. Frlez <i>et al.</i>	(PSI PIBETA Collab.)
POCANIC	04	PRL 93 181803	D. Pocanic <i>et al.</i>	(PSI PIBETA Collab.)
ESCHRICH	01	PL B522 233	I. Eschrich <i>et al.</i>	(FNAL SELEX Collab.)
LIESENFELD	99	PL B468 20	A. Liesenfeld <i>et al.</i>	
BIJNENS	98	JHEP 9805 014	J. Bijmens <i>et al.</i>	
BRESSI	98	NP B513 555	G. Bressi <i>et al.</i>	
LENZ	98	PL B416 50	S. Lenz <i>et al.</i>	
ASSAMAGAN	96	PR D53 6065	K.A. Assamagan <i>et al.</i>	(PSI, ZURI, VILL+)
KOPTEV	95	JETPL 61 877	V.P. Koptev <i>et al.</i>	(PNPI)
		Translated from ZETFP 61 865		
NUMAO	95	PR D52 4855	T. Numao <i>et al.</i>	(TRIU, BROO)
ASSAMAGAN	94	PL B335 231	K.A. Assamagan <i>et al.</i>	(PSI, ZURI, VILL+)
JECKELMANN	94	PL B335 326	B. Jeckelmann, P.F.A. Goudsmit, H.J. Leisi	(WABRN+)
CZAPEK	93	PRL 70 17	G. Czapek <i>et al.</i>	(BERN, VILL)
BARANOV	92	SJNP 55 1644	V.A. Baranov <i>et al.</i>	(JINR)
		Translated from YAF 55 2940.		
BRITTON	92	PRL 68 3000	D.I. Britton <i>et al.</i>	(TRIU, CARL)
		Also PR D49 26	D.I. Britton <i>et al.</i>	(TRIU, CARL)
NUMAO	92	MPL A7 3357	T. Numao	(TRIU)
BARANOV	91B	SJNP 54 790	V.A. Baranov <i>et al.</i>	(JINR)
		Translated from YAF 54 1298.		
DAUM	91	PL B265 425	M. Daum <i>et al.</i>	(VILL)
BOLOTOV	90B	PL B243 308	V.N. Bolotov <i>et al.</i>	(INRM)
EGLI	89	PL B222 533	S. Egli <i>et al.</i>	(SINDRUM Collab.)
		Also PL B175 97	S. Egli <i>et al.</i>	(AACH3, ETH, SIN, ZURI)
PDG	88	PL B204 1	G.P. Yost <i>et al.</i>	(LBL+)
PICCIOTTO	88	PR D37 1131	C.E. Picciotto <i>et al.</i>	(TRIU, CNRC)
COHEN	87	RMP 59 1121	E.R. Cohen, B.M. Taylor	(RISC, NBS)
KORENCHENCO...	87	SJNP 46 192	S.M. Korenchenko <i>et al.</i>	(JINR)
		Translated from YAF 46 313.		
AMENDOLIA	86	NP B277 168	S.R. Amendolia <i>et al.</i>	(CERN NA7 Collab.)
BAY	86	PL B174 445	A. Bay <i>et al.</i>	(LAUS, ZURI)
BRYMAN	86	PR D33 1211	D.A. Bryman <i>et al.</i>	(TRIU, CNRC)
		Also PRL 50 7	D.A. Bryman <i>et al.</i>	(TRIU, CNRC)
JECKELMANN	86B	NP A457 709	B. Jeckelmann <i>et al.</i>	(ETH, FRIB)
		Also PRL 56 1445	B. Jeckelmann <i>et al.</i>	(ETH, FRIB)
PIILONEN	86	PRL 57 1402	L.E. Piilonen <i>et al.</i>	(LANL, TEMP, LANL)
MCFARLANE	85	PR D32 547	W.K. McFarlane <i>et al.</i>	(TEMP, LANL)
ABELA	84	PL 146B 431	R. Abela <i>et al.</i>	(SIN)
		Also PL 74B 126	M. Daum <i>et al.</i>	(SIN)
		Also PR D20 2692	M. Daum <i>et al.</i>	(SIN)
AMENDOLIA	84	PL 146B 116	S.R. Amendolia <i>et al.</i>	(CERN NA7 Collab.)
FETSCHER	84	PL 140B 117	W. Fetscher	(ETH)
ABELA	83	NP A395 413	R. Abela <i>et al.</i>	(BASL, KARLK, KARLE)
CARR	83	PRL 51 627	J. Carr <i>et al.</i>	(LBL, NWES, TRIU)
COOPER	82	PL 112B 97	A.M. Cooper <i>et al.</i>	(RL)
DALLY	82	PR 48 375	E.B. Dally <i>et al.</i>	
LU	80	PR 45 1066	D.C. Lu <i>et al.</i>	
BEBEK	78	PR D17 1693	C.J. Bebek <i>et al.</i>	(YALE, COLU, JHU)
QUENZER	78	PL 76B 512	A. Quenzer <i>et al.</i>	(LALO)
STETZ	78	NP B138 285	A.W. Stetz <i>et al.</i>	(LBL, UCLA)
ADYLOV	77	NP B128 461	G.T. Adylov <i>et al.</i>	
BARDIN	77	NP B120 45	G. Bardin <i>et al.</i>	
DALLY	77	PRL 39 1176	E.B. Dally <i>et al.</i>	
CARTER	76	PRL 37 1380	A.L. Carter <i>et al.</i>	(CARL, CNRC, CHIC+)
KORENCHENCO...	76B	JETP 44 35	S.M. Korenchenko <i>et al.</i>	(JINR)
		Translated from ZETFP 71 69.		
MARUSHENCO...	76	JETPL 23 72	V.I. Marushenko <i>et al.</i>	(PNPI)
		Translated from ZETFP 23 80.		
		Also Private Comm.	R.E. Shafer	(FNAL)
		Also Private Comm.	A. Smirnov	(PNPI)
DUNAITSEV	73	SJNP 16 292	A.F. Dunaitsev <i>et al.</i>	(SERP)
		Translated from YAF 16 524.		
AYRES	71	PR D3 1051	D.S. Ayres <i>et al.</i>	(LRL, UCSB)
		Also PR 157 1288	D.S. Ayres <i>et al.</i>	(LRL)
		Also PRL 21 261	D.S. Ayres <i>et al.</i>	(LRL, UCSB)
		Also Thesis UCLR 18369	D.S. Ayres	(LRL)
		Also PRL 23 1267	A.J. Greenberg <i>et al.</i>	(LRL, UCSB)
KORENCHENCO...	71	SJNP 13 189	S.M. Korenchenko <i>et al.</i>	(JINR)
		Translated from YAF 13 339.		
BOOTH	70	PL 32B 723	P.S.L. Booth <i>et al.</i>	(LVP)
DEPOMMIER	68	NP B4 189	P. Depommier <i>et al.</i>	(CERN)
PETURKHIN	68	JINR P1 3862	V.I. Peturkhin <i>et al.</i>	(JINR)
HYMAN	67	PL 25B 376	L.G. Hyman <i>et al.</i>	(ANL, CMU, NWES)

Meson Particle Listings

π^\pm, π^0

NORDBERG	67	PL 24B 594	M.E. Nordberg, F. Lobkowicz, R.L. Burman	(ROCH)
BARDON	66	PRL 16 775	M. Bardon <i>et al.</i>	(COLU)
KINSEY	66	PR 144 1132	K.F. Kinsey, F. Lobkowicz, M.E. Nordberg	(ROCH)
LOBKOWICZ	66	PRL 17 548	F. Lobkowicz <i>et al.</i>	(ROCH, BNL)
BACASTOW	65	PR 139 B407	R.B. Bacastow <i>et al.</i>	(LRL, SLAC)
BERTRAM	65	PR 139 B617	W.K. Bertram <i>et al.</i>	(MICH, CMU)
DUNAITSSEV	65	JETP 20 58	A.F. Dunaitsev <i>et al.</i>	(JINR)
		Translated from ZETF 47 84.		
ECKHAUSE	65	PL 19 348	M. Eckhause <i>et al.</i>	(WILL)
BARTLETT	64	PR 136 B1452	D. Bartlett <i>et al.</i>	(COLU)
DICAPUA	64	PR 133 B1333	M. di Capua <i>et al.</i>	(COLU)
		Also Private Comm.	L. Pondrom	(WISC)
DEPOMMIER	63	PL 5 61	P. Depommier <i>et al.</i>	(CERN)
DEPOMMIER	63B	PL 7 285	P. Depommier <i>et al.</i>	(CERN)
ANDERSON	60	PR 119 2050	H.L. Anderson <i>et al.</i>	(EFI)
CASTAGNOLI	58	PR 112 1779	C. Castagnoli, M. Muchnik	(ROMA)

π^0

$$I^G(JPC) = 1^-(0^-+)$$

We have omitted some results that have been superseded by later experiments. The omitted results may be found in our 1988 edition Physics Letters **B204** 1 (1988).

π^0 MASS

The value is calculated from m_{π^\pm} and $(m_{\pi^\pm} - m_{\pi^0})$. See also the notes under the π^\pm Mass Listings.

VALUE (MeV)	DOCUMENT ID
134.9768 ± 0.0005 OUR FIT	Error includes scale factor of 1.1.

$$m_{\pi^\pm} - m_{\pi^0}$$

Measurements with an error > 0.01 MeV have been omitted.

VALUE (MeV)	DOCUMENT ID	TECN	COMMENT
4.5936 ± 0.0005 OUR FIT			
4.5936 ± 0.0005 OUR AVERAGE			
4.59364 ± 0.00048	CRAWFORD 91	CNTR	$\pi^- p \rightarrow \pi^0 n, n$ TOF
4.5930 ± 0.0013	CRAWFORD 86	CNTR	$\pi^- p \rightarrow \pi^0 n, n$ TOF
• • • We do not use the following data for averages, fits, limits, etc. • • •			
4.59366 ± 0.00048	CRAWFORD 88B	CNTR	See CRAWFORD 91
4.6034 ± 0.0052	VASILEVSKY 66	CNTR	
4.6056 ± 0.0055	CZIRR 63	CNTR	

π^0 MEAN LIFE

Most experiments measure the π^0 width which we convert to a lifetime. ATHERTON 85 is the only direct measurement of the π^0 lifetime. The two Primakoff measurements from 1970 have been excluded from our average because they suffered model-related systematics unknown at the time. More information on the π^0 lifetime can be found in BERNSTEIN 13.

VALUE (10^{-17} s)	EVTS	DOCUMENT ID	TECN	COMMENT
8.43 ± 0.13 OUR AVERAGE				Error includes scale factor of 1.2.
8.337 ± 0.056 ± 0.112		¹ LARIN 20	PRMX	Primakoff effect
8.5 ± 1.1		² BYCHKOV 09	PIBE	$\pi^+ \rightarrow e^+ \nu \gamma$ at rest
8.4 ± 0.5 ± 0.5	1182	³ WILLIAMS 88	CBAL	$e^+ e^- \rightarrow e^+ e^- \pi^0$
8.97 ± 0.22 ± 0.17		⁴ ATHERTON 85	CNTR	Direct measurement
8.2 ± 0.4		⁵ BROWMAN 74	CNTR	Primakoff effect
• • • We do not use the following data for averages, fits, limits, etc. • • •				
8.32 ± 0.15 ± 0.18		¹ LARIN 11	PRMX	Primakoff effect
5.6 ± 0.6		BELLETTINI 70	CNTR	Primakoff effect
9 ± 0.68		KRYSHKIN 70	CNTR	Primakoff effect
7.3 ± 1.1		BELLETTINI 65B	CNTR	Primakoff effect

- LARIN 20 reported this lifetime value from a measurement of $\Gamma(\pi^0 \rightarrow \gamma\gamma) = 7.802 \pm 0.052 \pm 0.105$ eV, combining data from PrimEX-II on 12C and 28Si targets with previous PrimEX-I LARIN 11 measurements. This result supersedes LARIN 11.
- BYCHKOV 09 obtains this using the conserved-vector-current relation between the vector form factor F_V and the π^0 lifetime.
- WILLIAMS 88 gives $\Gamma(\gamma\gamma) = 7.7 \pm 0.5 \pm 0.5$ eV. We give here $\tau = \hbar/\Gamma(\text{total})$.
- BROWMAN 74 gives a π^0 width $\Gamma = 8.02 \pm 0.42$ eV. The mean life is \hbar/Γ .
- LARIN 11 reported $\Gamma(\pi^0 \rightarrow \gamma\gamma) = 7.82 \pm 0.14 \pm 0.17$ eV which we converted to mean life $\tau = \hbar/\Gamma(\text{total})$.

π^0 DECAY MODES

For decay limits to particles which are not established, see the appropriate Search sections (A^0 (axion) and Other Light Boson (X^0) Searches, etc.).

Mode	Fraction (Γ_i/Γ)	Scale factor/Confidence level
Γ_1 2γ	(98.823 ± 0.034) %	S=1.5
Γ_2 $e^+ e^- \gamma$	(1.174 ± 0.035) %	S=1.5
Γ_3 γ positronium	(1.82 ± 0.29) × 10 ⁻⁹	
Γ_4 $e^+ e^+ e^- e^-$	(3.34 ± 0.16) × 10 ⁻⁵	
Γ_5 $e^+ e^-$	(6.46 ± 0.33) × 10 ⁻⁸	

Γ_6 4γ	< 2	× 10 ⁻⁸	CL=90%
Γ_7 $\nu\bar{\nu}$	[a] < 4.4	× 10 ⁻⁹	CL=90%
Γ_8 $\nu_e \bar{\nu}_e$	< 1.7	× 10 ⁻⁶	CL=90%
Γ_9 $\nu_\mu \bar{\nu}_\mu$	< 1.6	× 10 ⁻⁶	CL=90%
Γ_{10} $\nu_\tau \bar{\nu}_\tau$	< 2.1	× 10 ⁻⁶	CL=90%
Γ_{11} $\gamma\nu\bar{\nu}$	< 1.9	× 10 ⁻⁷	CL=90%

Charge conjugation (C) or Lepton Family number (LF) violating modes

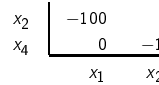
Γ_{12} 3γ	C	< 3.1	× 10 ⁻⁸	CL=90%
Γ_{13} $\mu^+ e^-$	LF	< 3.8	× 10 ⁻¹⁰	CL=90%
Γ_{14} $\mu^- e^+$	LF	< 3.2	× 10 ⁻¹⁰	CL=90%
Γ_{15} $\mu^+ e^- + \mu^- e^+$	LF	< 3.6	× 10 ⁻¹⁰	CL=90%

[a] Astrophysical and cosmological arguments give limits of order 10⁻¹³, but they are model dependent and for the summary value we use the best laboratory limit, which includes any final state of invisible particles.

CONSTRAINED FIT INFORMATION

An overall fit to 2 branching ratios uses 6 measurements and one constraint to determine 3 parameters. The overall fit has a $\chi^2 = 4.6$ for 4 degrees of freedom.

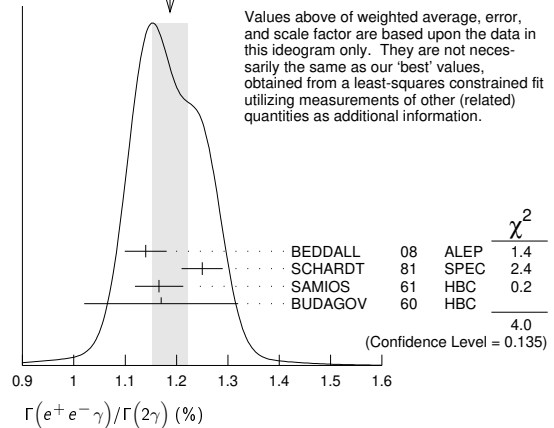
The following *off-diagonal* array elements are the correlation coefficients $\langle \delta x_i \delta x_j \rangle / (\delta x_i \delta x_j)$, in percent, from the fit to the branching fractions, $x_i \equiv \Gamma_i/\Gamma_{\text{total}}$. The fit constrains the x_i whose labels appear in this array to sum to one.



π^0 BRANCHING RATIOS

$\Gamma(e^+ e^- \gamma)/\Gamma(2\gamma)$	VALUE (%)	EVTS	DOCUMENT ID	TECN	COMMENT	Γ_2/Γ_1
1.188 ± 0.035 OUR FIT					Error includes scale factor of 1.5.	
1.188 ± 0.034 OUR AVERAGE					Error includes scale factor of 1.4. See the ideogram below.	
1.140 ± 0.024 ± 0.033	12.5k	¹ BEDDALL 08	ALEP		$e^+ e^- \rightarrow Z \rightarrow \text{hadrons}$	
1.25 ± 0.04		SCHARDT 81	SPEC		$\pi^- p \rightarrow n\pi^0$	
1.166 ± 0.047	3k	² SAMIOS 61	HBC		$\pi^- p \rightarrow n\pi^0$	
1.17 ± 0.15	27	BUDAGOV 60	HBC			
• • • We do not use the following data for averages, fits, limits, etc. • • •						
1.1559 ± 0.0047 ± 0.0106	60k	³ ABOUZAID 19	KTEV		$K_L \rightarrow 3\pi^0$ in flight	
1.196		JOSEPH 60	THEO		QED calculation	

WEIGHTED AVERAGE
1.188 ± 0.034 (Error scaled by 1.4)



- BEDDALL 08 value is obtained from ALEPH archived data.
- SAMIOS 61 value uses a Panofsky ratio = 1.62.
- ABOUZAID 19 measured a value of (0.3920 ± 0.0016 ± 0.0036)% from 1999 KTEV data in $K_L \rightarrow 3\pi^0 \rightarrow 5\gamma e^+ e^-$ decays, normalised to $K_L \rightarrow 3\pi^0$, for $m(ee) > 15$ MeV and then extrapolated it to the full $m(ee)$ range using the Mikaelian and Smith predictions for the mass spectrum.

$\Gamma(\gamma$ positronium) $\Gamma(2\gamma)$

VALUE (units 10 ⁻⁹)	EVTS	DOCUMENT ID	TECN	COMMENT	Γ_3/Γ_1
1.84 ± 0.29	277	AFANASYEV 90	CNTR	pC 70 GeV	

See key on page 1127

Meson Particle Listings

π^0

$\Gamma(e^+e^-e^-)/\Gamma(2\gamma)$ Γ_4/Γ_1

VALUE (units 10^{-5})	EVTS	DOCUMENT ID	TECN	COMMENT
3.38 ± 0.16 OUR FIT				
3.38 ± 0.16 OUR AVERAGE				
3.46 ± 0.19	30.5k	¹ ABOUZAID	08D KTEV	$K_L^0 \rightarrow \pi^0 \pi^0 \pi_{DD}^0$
3.18 ± 0.30	146	² SAMIOS	62B HBC	

¹ This ABOUZAID 08D value includes all radiative final states. The error includes both statistical and systematic errors. The correlation between the Dalitz-pair planes gives a direct measurement of the π^0 parity. The $\pi^0 2\gamma^*$ form factor is measured and limits are placed on a scalar contribution to the decay.
² SAMIOS 62B value uses a Panofsky ratio = 1.62.

$\Gamma(e^+e^-)/\Gamma_{total}$ Γ_5/Γ

Experimental results are listed; branching ratios corrected for radiative effects are given in the footnotes. BERMAN 60 found $B(\pi^0 \rightarrow e^+e^-) \geq 4.69 \times 10^{-8}$ via an exact QED calculation.

VALUE (units 10^{-8})	EVTS	DOCUMENT ID	TECN	CHG	COMMENT
6.46 ± 0.33 OUR AVERAGE					
6.44 ± 0.25 ± 0.22	794	¹ ABOUZAID	07 KTEV		$K_L^0 \rightarrow 3\pi^0$ in flight
6.9 ± 2.3 ± 0.6	21	² DESHPANDE	93 SPEC		$K^+ \rightarrow \pi^+ \pi^0$
7.6 $\begin{smallmatrix} +2.9 \\ -2.8 \end{smallmatrix}$ ± 0.5	8	³ MCFARLAND	93 SPEC		$K_L^0 \rightarrow 3\pi^0$ in flight

••• We do not use the following data for averages, fits, limits, etc. •••
 6.09 ± 0.40 ± 0.24 275 ⁴ ALAVI-HARATI 99c SPEC 0 Repl. by ABOUZAID 07
¹ ABOUZAID 07 result is for $m_{e^+e^-}/m_{\pi^0} > 0.95$. With radiative corrections the result becomes $(7.48 \pm 0.29 \pm 0.25) \times 10^{-8}$.
² The DESHPANDE 93 result with bremsstrahlung radiative corrections is $(8.0 \pm 2.6 \pm 0.6) \times 10^{-8}$.
³ The MCFARLAND 93 result is for $B[\pi^0 \rightarrow e^+e^-, (m_{e^+e^-}/m_{\pi^0})^2 > 0.95]$. With radiative corrections it becomes $(8.8 \begin{smallmatrix} +4.5 \\ -3.2 \end{smallmatrix} \pm 0.6) \times 10^{-8}$.
⁴ ALAVI-HARATI 99c quote result for $B[\pi^0 \rightarrow e^+e^-, (m_{e^+e^-}/m_{\pi^0})^2 > 0.95]$ to minimize radiative contributions from $\pi^0 \rightarrow e^+e^-\gamma$. After radiative corrections they obtain $(7.04 \pm 0.46 \pm 0.28) \times 10^{-8}$.

$\Gamma(e^+e^-)/\Gamma(2\gamma)$ Γ_5/Γ_1

VALUE (units 10^{-7})	CL%	EVTS	DOCUMENT ID	TECN	COMMENT
•••					We do not use the following data for averages, fits, limits, etc. •••
<1.3	90		NIEBUHR	89 SPEC	$\pi^- p \rightarrow \pi^0 n$ at rest
<5.3	90		ZEPHAT	87 SPEC	$\pi^- p \rightarrow \pi^0 n$ 0.3 GeV/c
1.7 ± 0.6 ± 0.3	59		FRANK	83 SPEC	$\pi^- p \rightarrow n \pi^0$
1.8 ± 0.6	58		MISCHKE	82 SPEC	See FRANK 83
2.23 $\begin{smallmatrix} +2.40 \\ -1.10 \end{smallmatrix}$	90	8	FISCHER	78B SPRK	$K^+ \rightarrow \pi^+ \pi^0$

$\Gamma(4\gamma)/\Gamma_{total}$ Γ_6/Γ

VALUE (units 10^{-8})	CL%	EVTS	DOCUMENT ID	TECN	COMMENT
< 2	90		MCDONOUGH	88 CBOX	$\pi^- p$ at rest
•••					We do not use the following data for averages, fits, limits, etc. •••
<160	90		BOLOTOV	86c CALO	
<440	90	0	AUERBACH	80 CNTR	

$\Gamma(\nu\bar{\nu})/\Gamma_{total}$ Γ_7/Γ

The astrophysical and cosmological limits are many orders of magnitude lower, but they are model dependent and for the summary value we use the best laboratory limit, which includes any final state of invisible particles.

VALUE (units 10^{-6})	CL%	DOCUMENT ID	TECN	COMMENT
< 4.4 × 10⁻³	90	¹ CORTINA-GIL 21c	SPEC	$K^+ \rightarrow \pi^+ \pi^0(\gamma)$
•••				We do not use the following data for averages, fits, limits, etc. •••
< 0.27	90	¹ ARTAMONOV 05A	B949	$K^+ \rightarrow \pi^+ \pi^0$
< 0.83	90	¹ ATIYA	91 B787	$K^+ \rightarrow \pi^+ \nu\bar{\nu}$
< 2.9 × 10 ⁻⁷		² LAM	91	Cosmological limit
< 3.2 × 10 ⁻⁷		³ NATALE	91	SN 1987A
< 6.5	90	DORENBOS...	88 CHRMB	Beam dump, prompt ν
<24	90	¹ HERCZEG	81 RVUE	$K^+ \rightarrow \pi^+ \nu\bar{\nu}$

¹ This limit applies to all possible "invisible" channels.
² LAM 91 considers the production of right-handed neutrinos produced from the cosmic thermal background at the temperature of about the pion mass through the reaction $\gamma\gamma \rightarrow \pi^0 \rightarrow \nu\bar{\nu}$.
³ NATALE 91 considers the excess energy-loss rate from SN1987A if the process $\gamma\gamma \rightarrow \pi^0 \rightarrow \nu\bar{\nu}$ occurs, permitted if the neutrinos have a right-handed component. As pointed out in LAM 91 (and confirmed by Natale), there is a factor 4 error in the NATALE 91 published result (0.8×10^{-7}) .

$\Gamma(\nu_e\bar{\nu}_e)/\Gamma_{total}$ Γ_8/Γ

VALUE (units 10^{-6})	CL%	DOCUMENT ID	TECN	COMMENT
<1.7	90	DORENBOS...	88 CHRMB	Beam dump, prompt ν
•••				We do not use the following data for averages, fits, limits, etc. •••
<3.1	90	¹ HOFFMAN	88 RVUE	Beam dump, prompt ν

¹ HOFFMAN 88 analyzes data from a 400-GeV BEBC beam-dump experiment.

$\Gamma(\nu_\mu\bar{\nu}_\mu)/\Gamma_{total}$ Γ_9/Γ

VALUE (units 10^{-6})	CL%	EVTS	DOCUMENT ID	TECN	COMMENT
<1.6	90	8.7	AUERBACH	04 LSND	800 MeV p on Cu
<3.1	90		¹ HOFFMAN	88 RVUE	Beam dump, prompt ν
•••					We do not use the following data for averages, fits, limits, etc. •••
<7.8	90		DORENBOS...	88 CHRMB	Beam dump, prompt ν

¹ HOFFMAN 88 analyzes data from a 400-GeV BEBC beam-dump experiment.

$\Gamma(\nu_\tau\bar{\nu}_\tau)/\Gamma_{total}$ Γ_{10}/Γ

VALUE (units 10^{-6})	CL%	DOCUMENT ID	TECN	COMMENT
<2.1	90	¹ HOFFMAN	88 RVUE	Beam dump, prompt ν
•••				We do not use the following data for averages, fits, limits, etc. •••
<4.1	90	DORENBOS...	88 CHRMB	Beam dump, prompt ν

¹ HOFFMAN 88 analyzes data from a 400-GeV BEBC beam-dump experiment.

$\Gamma(\gamma\nu\bar{\nu})/\Gamma_{total}$ Γ_{11}/Γ

VALUE (units 10^{-6})	CL%	DOCUMENT ID	TECN	COMMENT
<1.9 × 10⁻⁷	90	CORTINA-GIL 19	SPEC	$K^+ \rightarrow \pi^+ \gamma\nu\bar{\nu}$
•••				We do not use the following data for averages, fits, limits, etc. •••
<6 × 10 ⁻⁴	90	ATIYA	92 CNTR	$K^+ \rightarrow \gamma\nu\bar{\nu}\pi^+$

Standard Model prediction is 6×10^{-18} .

$\Gamma(3\gamma)/\Gamma_{total}$ Γ_{12}/Γ

VALUE (units 10^{-8})	CL%	EVTS	DOCUMENT ID	TECN	COMMENT
< 3.1	90		MCDONOUGH	88 CBOX	$\pi^- p$ at rest
•••					We do not use the following data for averages, fits, limits, etc. •••
< 38	90	0	HIGHLAND	80 CNTR	
<150	90	0	AUERBACH	78 CNTR	
<490	90	0	¹ DUCLOS	65 CNTR	
<490	90	0	¹ KUTIN	65 CNTR	

¹ These experiments give $B(3\gamma/2\gamma) < 5.0 \times 10^{-6}$.

$\Gamma(\mu^+e^-)/\Gamma_{total}$ Γ_{13}/Γ

VALUE (units 10^{-3})	CL%	EVTS	DOCUMENT ID	TECN	COMMENT
< 0.38	90	0	APPEL	00 SPEC	$K^+ \rightarrow \pi^+ \mu^+ e^-$
•••					We do not use the following data for averages, fits, limits, etc. •••
<16	90		LEE	90 SPEC	$K^+ \rightarrow \pi^+ \mu^+ e^-$
<78	90		CAMPAGNARI	88 SPEC	See LEE 90

$\Gamma(\mu^-e^+)/\Gamma_{total}$ Γ_{14}/Γ

VALUE	CL%	DOCUMENT ID	TECN	COMMENT
<3.2 × 10⁻¹⁰	90	ALIBERTI 21	NA62	$K^+ \rightarrow \pi^+ e^+ \mu^-$
•••				We do not use the following data for averages, fits, limits, etc. •••
<3.4 × 10 ⁻⁹	90	APPEL	00B B865	$K^+ \rightarrow \pi^+ e^+ \mu^-$

$[\Gamma(\mu^+e^-) + \Gamma(\mu^-e^+)]/\Gamma_{total}$ Γ_{15}/Γ

VALUE (units 10^{-3})	CL%	DOCUMENT ID	TECN	COMMENT
< 0.36	90	ABOUZAID 08c	KTEV	$K_L^0 \rightarrow 2\pi^0 \mu^\pm e^\mp$
•••				We do not use the following data for averages, fits, limits, etc. •••
< 17.2	90	KROLAK	94 E799	$\ln K_L^0 \rightarrow 3\pi^0$
<140		HERCZEG	84 RVUE	$K^+ \rightarrow \pi^+ \mu e$
< 2 × 10 ⁻⁶		HERCZEG	84 THEO	$\mu^- \rightarrow e^-$ conversion
< 70	90	BRYMAN	82 RVUE	$K^+ \rightarrow \pi^+ \mu e$

π^0 ELECTROMAGNETIC FORM FACTOR

The amplitude for the process $\pi^0 \rightarrow e^+e^-\gamma$ contains a form factor $F(x)$ at the $\pi^0\gamma\gamma$ vertex, where $x = [m_{e^+e^-}/m_{\pi^0}]^2$. The parameter a in the linear expansion $F(x) = 1 + ax$ is listed below.

All the measurements except that of BEHREND 91 are in the time-like region of momentum transfer.

LINEAR COEFFICIENT OF π^0 ELECTROMAGNETIC FORM FACTOR

VALUE (units 10^{-2})	EVTS	DOCUMENT ID	TECN	COMMENT
3.35 ± 0.31 OUR AVERAGE				
3.68 ± 0.51 ± 0.25	1.1M	LAZZERONI	17 SPEC	$K^\pm \rightarrow \pi^0 \pi^\pm; \pi^0 \rightarrow e^+e^-\gamma$
2.6 ± 2.4 ± 4.8	7.5k	FARZANPAY	92 SPEC	$\pi^- p \rightarrow \pi^0 n$ at rest
2.5 ± 1.4 ± 2.6	54k	MEIJERDREES 92B	SPEC	$\pi^- p \rightarrow \pi^0 n$ at rest
3.26 ± 0.26 ± 0.26	127	¹ BEHREND	91 CELL	$e^+e^- \rightarrow e^+e^-\pi^0$
-11 ± 3 ± 8	32k	FONVIEILLE	89 SPEC	Radiation corr.
•••				We do not use the following data for averages, fits, limits, etc. •••
12 $\begin{smallmatrix} +5 \\ -4 \end{smallmatrix}$		² TUPPER	83 THEO	FISCHER 78 data
10 ± 3	31k	³ FISCHER	78 SPEC	Radiation corr.
1 ± 11	2.2k	DEVONS	69 OSPK	No radiation corr.
-15 ± 10	7.6k	KOBRACK	61 HBC	No radiation corr.
-24 ± 16	3.0k	SAMIOS	61 HBC	No radiation corr.

Meson Particle Listings

π^0, η

¹ BEHREND 91 estimates that their systematic error is of the same order of magnitude as their statistical error, and so we have included a systematic error of this magnitude. The value of λ is obtained by extrapolation from the region of large space-like momentum transfer assuming vector dominance.

² TUPPER 83 is a theoretical analysis of FISCHER 78 including 2-photon exchange in the corrections.

³ The FISCHER 78 error is statistical only. The result without radiation corrections is $+0.05 \pm 0.03$.

π^0 REFERENCES

We have omitted some papers that have been superseded by later experiments. The omitted papers may be found in our 1988 edition Physics Letters **B204** 1 (1988).

ALIBERTI 21 PRL 127 131802 R. Aliberti <i>et al.</i> (NA62 Collab.)	CORTINA-GIL 21C JHEP 2102 201 E. Cortina Gil <i>et al.</i> (NA62 Collab.)	LARIN 20 SCI 368 506 I. Larin <i>et al.</i> (PrimEx II Collab.)	ABOUZAID 19 PR D100 032003 E. Abouzaïd <i>et al.</i> (KTeV Collab.)	CORTINA-GIL 19 JHEP 1905 182 E. Cortina Gil <i>et al.</i> (NA62 Collab.)	LAZZERONI 17 PL 87 68 38 C. Lazzeroni <i>et al.</i> (NA62 Collab.)	BERNSTEIN 13 RMP 85 49 A.M. Bernstein, B. R. Holstein (AMHT, MIT)	LARIN 11 PRL 106 162303 I. Larin <i>et al.</i> (PrimEx Collab.)	BYCHKOV 09 PRL 103 051802 M. Bychkov <i>et al.</i> (PSI PIBETA Collab.)	ABOUZAID 08C PRL 100 131803 E. Abouzaïd <i>et al.</i> (FNAL KTeV Collab.)	ABOUZAID 08D PRL 100 182001 E. Abouzaïd <i>et al.</i> (FNAL KTeV Collab.)	BEDDALL 08 EPJ C54 365 A. Beddall, A. Beddall (UGAZ)	ABOUZAID 07 PR D75 012004 E. Abouzaïd <i>et al.</i> (KTeV Collab.)	ARTAMONOV 05A PR D72 091102 A.V. Artamonov <i>et al.</i> (BNL E949 Collab.)	AUERBACH 04 PRL 92 091801 L.B. Auerbach <i>et al.</i> (LNSD Collab.)	APPEL 00 PRL 85 2450 R. Appel <i>et al.</i> (BNL 865 Collab.)	Also Thesis, Yale Univ. D.R. Bergman	Also Thesis, Univ. Zurich S. Pislak	APPEL 00B PRL 85 2877 R. Appel <i>et al.</i> (BNL 865 Collab.)	ALAVI-HARATI 99C PRL 83 922 A. Alavi-Harati <i>et al.</i> (FNAL KTeV Collab.)	KROLAK 94 PL B320 407 P. Krolak <i>et al.</i> (EFI, UCLA, COLO, ELMT+) (BNL E851 Collab.)	DESHPANDE 93 PRL 71 27 A. Deshpande <i>et al.</i> (BNL, LANL, PRIN+) (EFI, UCLA, COLO+)	MCFARLAND 93 PRL 71 31 K.S. McFarland <i>et al.</i> (BNL, LANL, PRIN+) (ORST, TRIU, BRCO+)	ATIYA 92 PRL 69 733 M.S. Atiya <i>et al.</i> (PSI SINDRUM-I Collab.)	FARZANPAY 92 PL B278 413 F. Farzanpay <i>et al.</i> (BNL, LANL, PRIN+) (CELLO Collab.)	MEIJERDREES 92B PR D45 1439 R. Meijer Drees <i>et al.</i> (VILL, UVA)	ATIYA 91 PRL 66 2189 M.S. Atiya <i>et al.</i> (AST)	BEHREND 91 ZPHY C49 401 H.J. Behrend <i>et al.</i> (SPIFT)	CRAWFORD 91 PR D43 46 J.F. Crawford <i>et al.</i> (JINR, MOSU, SERP)	LAM 91 PR D44 3345 W.P. Lam, K.W. Ng (JINR)	NATALE 91 PL B258 227 A.A. Natale	AFANASYEV 90 PL B236 116 L.G. Afanasyev <i>et al.</i> (JINR)	Also SJNP 51 664 L.G. Afanasyev <i>et al.</i>	LEE 90 PRL 64 165 A.M. Lee <i>et al.</i> (BNL, FNAL, VILL, WASH+)	FONVIEILLE 89 PL B233 65 H. Fonvieille <i>et al.</i> (CLER, LYON, SACL)	NIEBUHR 89 PR D40 2796 C. Niebuhr <i>et al.</i> (SINDRUM Collab.)	CAMPAGNARI 88 PRL 61 2062 C. Campagnari <i>et al.</i> (BNL, FNAL, PSI+)	CRAWFORD 88B PL B213 391 J.F. Crawford <i>et al.</i> (PSI, UVA)	DORENBOSCH... 88 ZPHY C40 4 497 J. Dorenbosch <i>et al.</i> (CHARM Collab.)	HOFFMAN 88 PL B208 149 C.M. Hoffman (LANL)	MCDONOUGH 88 PR D38 2121 J.M. McDonough <i>et al.</i> (TEMP, LANL, CHIC)	PDG 88 PL B204 1 G.P. Yost <i>et al.</i> (LBL+)	WILLIAMS 88 PR D38 1365 D.A. Williams <i>et al.</i> (Crystal Ball Collab.)	ZEPHAT 87 JP G13 1375 A.G. Zephat <i>et al.</i> (OMICRON Collab.)	BOLOTOV 86C JETPL 43 520 V.N. Bolotov <i>et al.</i> (INRM)	CRAWFORD 86 PRL 56 1043 J.F. Crawford <i>et al.</i> (SIN, UVA)	ATHERTON 85 PL 158B 81 H.W. Atherton <i>et al.</i> (CERN, ISU, LUND+)	HERCZEG 84 PR D29 1954 P. Herczeg, C.M. Hoffman (LANL)	FRANK 83 PR D28 423 J.S. Frank <i>et al.</i> (LANL, ARZS)	TUPPER 83 PR D28 2905 G.B. Tupper, T.R. Grose, M.A. Samuel (OKSU)	BRYMAN 82 PR D26 2538 D.A. Bryman (TRIU)	MISCHKE 82 PRL 48 1153 R.E. Mischke <i>et al.</i> (LANL, ARZS)	HERCZEG 81 PL 100B 347 P. Herczeg, C.M. Hoffman (LANL)	SCHARDT 81 PR D23 639 M.A. Schardt <i>et al.</i> (ARZS, LANL)	AUERBACH 80 PL 90B 317 L.B. Auerbach <i>et al.</i> (TEMP, LASL)	HIGHLAND 80 PRL 44 628 V.L. Highland <i>et al.</i> (TEMP, LASL)	AUERBACH 78 PRL 41 2275 L.B. Auerbach <i>et al.</i> (TEMP, LASL)	FISCHER 78 PL 73B 359 J. Fischer <i>et al.</i> (GEVA, SACL)	FISCHER 78B PL 73B 364 J. Fischer <i>et al.</i> (GEVA, SACL)	BROWMAN 74 PRL 33 1400 A. Browman <i>et al.</i> (CORN, BING)	BELLETTINI 70 NC 66A 243 G. Bellentini <i>et al.</i> (PISA, BONN)	KRYSHKIN 70 JETP 30 1037 V.I. Kryshkin, A.G. Sterligov, Y.P. Usov (TMSK)	Translated from ZETFP 57 1917	DEVONS 69 PR 184 1356 S. Devons <i>et al.</i> (COLU, ROMA)	VASILEVSKY 66 PL 23 281 I.M. Vasilevsky <i>et al.</i> (JINR)	BELLETTINI 65B NC 40A 1139 G. Bellentini <i>et al.</i> (PISA, FIRZ)	DUCLOS 65 PL 19 253 G. Duclos <i>et al.</i> (CERN, HEID)	KUTIN 65 JETPL 2 243 V.M. Kutjin, V.I. Petrukhin, Y.D. Prokoshkin (JINR)	Translated from ZETFP 2 387	CZIRR 63 PR 130 341 J.B. Czirr (LRL)	SAMIOS 62B PR 126 1844 N.P. Samios <i>et al.</i> (COLU, BNL)	KOBRAK 61 NC 20 1115 H. Kobrak (EFI)	SAMIOS 61 PR 121 275 N.P. Samios (COLU, BNL)	BERMAN 60 NC 18 1192 S. Berman, D. Geffen	BUDAGOV 60 JETP 11 765 Y.A. Budagov <i>et al.</i> (JINR)	Translated from ZETFP 38 1047	JOSEPH 60 NC 16 997 D.W. Joseph (EFI)
---	---	---	---	--	--	---	---	---	---	---	--	--	---	--	---	--------------------------------------	-------------------------------------	--	---	---	---	--	--	--	---	---	--	--	---	-----------------------------------	--	---	---	---	---	---	---	---	--	--	---	--	---	--	--	---	--	---	---	--	--	--	---	---	---	--	---	--	--	---	--	-------------------------------	--	--	---	--	--	-----------------------------	--------------------------------------	--	--------------------------------------	--	---	--	-------------------------------	---------------------------------------

η

$$J^G(J^{PC}) = 0^+(0^-)$$

We have omitted some results that have been superseded by later experiments. The omitted results may be found in our 1988 edition Physics Letters **B204** (1988).

η MASS

Recent measurements resolve the obvious inconsistency in previous η mass measurements in favor of the higher value first reported by NA48 (LAI 02). We use only precise measurements consistent with this higher mass value for our η mass average.

VALUE (MeV)	EVTS	DOCUMENT ID	TECN	COMMENT
547.862 ± 0.017 OUR AVERAGE				
547.865 ± 0.031 ± 0.062		NIKOLAEV	14	CRYB $\gamma p \rightarrow p \eta$
547.873 ± 0.005 ± 0.027	1 M	GOSLAWSKI	12	SPEC $d p \rightarrow {}^3\text{He} \eta$
547.874 ± 0.007 ± 0.029		AMBROSINO	07B	KLOE $e^+ e^- \rightarrow \phi \rightarrow \eta \gamma$
547.785 ± 0.017 ± 0.057	1.6k	MILLER	07	CLEO $\psi(2S) \rightarrow J/\psi \eta$
547.843 ± 0.030 ± 0.041	1134	LAI	02	NA48 $\eta \rightarrow 3\pi^0$
• • • We do not use the following data for averages, fits, limits, etc. • • •				
547.311 ± 0.028 ± 0.032		¹ ABDEL-BARY	05	SPEC $d p \rightarrow {}^3\text{He} \eta$
547.12 ± 0.06 ± 0.25		KRUSCHE	95D	SPEC $\gamma p \rightarrow \eta p$, threshold
547.30 ± 0.15		PLOUIN	92	SPEC $d p \rightarrow {}^3\text{He} \eta$
547.45 ± 0.25		DUANE	74	SPEC $\pi^- p \rightarrow n$ neutrals
548.2 ± 0.65		FOSTER	65c	HBC
549.0 ± 0.7	148	FOELSCHKE	64	HBC
548.0 ± 1.0	91	ALFF-...	62	HBC
549.0 ± 1.2	53	BASTIEN	62	HBC

¹ ABDEL-BARY 05 disagrees significantly with recent measurements of similar or better precision. See comment in the header.

η WIDTH

This is the partial decay rate $\Gamma(\eta \rightarrow \gamma\gamma)$ divided by the fitted branching fraction for that mode. See the note at the start of the $\Gamma(2\gamma)$ data block, next below.

VALUE (keV)	DOCUMENT ID
1.31 ± 0.05 OUR FIT	

η DECAY MODES

Mode	Fraction (Γ_i/Γ)	Scale factor/ Confidence level
Neutral modes		
Γ_1 neutral modes	(71.96 ± 0.30) %	S=1.3
Γ_2 2γ	(39.36 ± 0.18) %	S=1.1
Γ_3 $3\pi^0$	(32.57 ± 0.21) %	S=1.2
Γ_4 $\pi^0 2\gamma$	(2.55 ± 0.22) × 10 ⁻⁴	
Γ_5 $2\pi^0 2\gamma$	< 1.2 × 10 ⁻³	CL=90%
Γ_6 $4\pi^0$	< 2.8 × 10 ⁻⁴	CL=90%
Γ_7 invisible	< 1.0 × 10 ⁻⁴	CL=90%
Charged modes		
Γ_8 charged modes	(28.04 ± 0.30) %	S=1.3
Γ_9 $\pi^+ \pi^- \pi^0$	(23.02 ± 0.25) %	S=1.2
Γ_{10} $\pi^+ \pi^- \gamma$	(4.28 ± 0.07) %	S=1.1
Γ_{11} $e^+ e^- \gamma$	(6.9 ± 0.4) × 10 ⁻³	S=1.2
Γ_{12} $\mu^+ \mu^- \gamma$	(3.1 ± 0.4) × 10 ⁻⁴	
Γ_{13} $e^+ e^-$	< 7 × 10 ⁻⁷	CL=90%
Γ_{14} $\mu^+ \mu^-$	(5.8 ± 0.8) × 10 ⁻⁶	
Γ_{15} $2e^+ 2e^-$	(2.40 ± 0.22) × 10 ⁻⁵	
Γ_{16} $\pi^+ \pi^- e^+ e^- (\gamma)$	(2.68 ± 0.11) × 10 ⁻⁴	
Γ_{17} $e^+ e^- \mu^+ \mu^-$	< 1.6 × 10 ⁻⁴	CL=90%
Γ_{18} $2\mu^+ 2\mu^-$	< 3.6 × 10 ⁻⁴	CL=90%
Γ_{19} $\mu^+ \mu^- \pi^+ \pi^-$	< 3.6 × 10 ⁻⁴	CL=90%
Γ_{20} $\pi^+ e^- \bar{\nu}_e + c.c.$	< 1.7 × 10 ⁻⁴	CL=90%
Γ_{21} $\pi^+ \pi^- 2\gamma$	< 2.1 × 10 ⁻³	
Γ_{22} $\pi^+ \pi^- \pi^0 \gamma$	< 6 × 10 ⁻⁴	CL=90%
Γ_{23} $\pi^0 \mu^+ \mu^- \gamma$	< 3 × 10 ⁻⁶	CL=90%

Charge conjugation (C), Parity (P), Charge conjugation × Parity (CP), or Lepton Family number (LF) violating modes

Γ_{24} $\pi^0 \gamma$	C	[a] < 9	× 10 ⁻⁵	CL=90%
Γ_{25} $\pi^+ \pi^-$	P, CP	< 4.4	× 10 ⁻⁶	CL=90%
Γ_{26} $2\pi^0$	P, CP	< 3.5	× 10 ⁻⁴	CL=90%
Γ_{27} $2\pi^0 \gamma$	C	< 5	× 10 ⁻⁴	CL=90%
Γ_{28} $3\pi^0 \gamma$	C	< 6	× 10 ⁻⁵	CL=90%
Γ_{29} 3γ	C	< 1.6	× 10 ⁻⁵	CL=90%
Γ_{30} $4\pi^0$	P, CP	< 6.9	× 10 ⁻⁷	CL=90%
Γ_{31} $\pi^0 e^+ e^-$	C	[b] < 8	× 10 ⁻⁶	CL=90%
Γ_{32} $\pi^0 \mu^+ \mu^-$	C	[b] < 5	× 10 ⁻⁶	CL=90%
Γ_{33} $\mu^+ e^- + \mu^- e^+$	LF	< 6	× 10 ⁻⁶	CL=90%

[a] Forbidden by angular momentum conservation.

[b] C parity forbids this to occur as a single-photon process.

Meson Particle Listings

 η

• • • We do not use the following data for averages, fits, limits, etc. • • •

2.5 ± 0.6 70 BINON 82 GAM2 See ALDE 84

$\Gamma(\pi^0 2\gamma)/\Gamma(3\pi^0)$ Γ_4/Γ_3

VALUE (units 10⁻⁴) DOCUMENT ID TECN COMMENT

7.8 ± 0.7 OUR FIT

• • • We do not use the following data for averages, fits, limits, etc. • • •

8.3 ± 2.8 ± 1.4 1 KNECHT 04 CRYB $\pi^- p \rightarrow n\eta$

¹Independent analysis of same data as PRAKHOV 05.

$\Gamma(2\pi^0 2\gamma)/\Gamma_{\text{total}}$ Γ_5/Γ

VALUE CL% DOCUMENT ID TECN COMMENT

<1.2 × 10⁻³

90 1 NEFKENS 05A CRYB $\rho(720 \text{ MeV}/c) \pi^- \rightarrow n\eta$

• • • We do not use the following data for averages, fits, limits, etc. • • •

<4.0 × 10⁻³ 90 BLIK 07 GAM4 $\pi^- p \rightarrow \eta\eta$

¹Measurement is done in limited $\gamma\gamma$ energy range.

$\Gamma(4\gamma)/\Gamma_{\text{total}}$ Γ_6/Γ

VALUE CL% DOCUMENT ID TECN COMMENT

<2.8 × 10⁻⁴

90 BLIK 07 GAM4 $\pi^- p \rightarrow \eta\eta$

$\Gamma(\text{invisible})/\Gamma(2\gamma)$ Γ_7/Γ_2

VALUE CL% DOCUMENT ID TECN COMMENT

<2.6 × 10⁻⁴

90 1 ABLIKIM 13 BES3 $J/\psi \rightarrow \phi\eta$

• • • We do not use the following data for averages, fits, limits, etc. • • •

<1.65 × 10⁻³ 90 2 ABLIKIM 06Q BES2 $J/\psi \rightarrow \phi\eta$

¹Based on 225M J/ψ decays.

²Based on 58M J/ψ decays.

Charged modes

$\Gamma(\text{charged modes})/\Gamma_{\text{total}}$ $\Gamma_8/\Gamma = (\Gamma_9 + \Gamma_{10} + \Gamma_{11} + \Gamma_{12} + \Gamma_{16})/\Gamma$

VALUE DOCUMENT ID TECN COMMENT

0.2804 ± 0.0030 OUR FIT Error includes scale factor of 1.3.

$\Gamma(\pi^+ \pi^- \pi^0)/\Gamma_{\text{total}}$ Γ_9/Γ

VALUE (units 10⁻²) EVTS DOCUMENT ID TECN COMMENT

23.02 ± 0.25 OUR FIT Error includes scale factor of 1.2.

23.04 ± 0.03 ± 0.54 60k 1 ABLIKIM 21AMBES3 $J/\psi \rightarrow \gamma\eta$

• • • We do not use the following data for averages, fits, limits, etc. • • •

22.60 ± 0.35 ± 0.29 3915 2 LOPEZ 07 CLEO $\psi(2S) \rightarrow J/\psi\eta$

¹ABLIKIM 21AM normalize the branching ratio ($\eta \rightarrow \pi^+ \pi^- \pi^0$) to $B(J/\psi \rightarrow \gamma\eta)$, which they measured absolutely.

²Not independent of other results listed for LOPEZ 07. Assuming decays of $\eta \rightarrow \gamma\gamma$, $3\pi^0$, $\pi^+ \pi^- \pi^0$, $\pi^+ \pi^- \gamma$, and $e^+ e^- \gamma$ account for all η decays within a contribution of 0.3% to the systematic error.

$\Gamma(\text{neutral modes})/\Gamma(\pi^+ \pi^- \pi^0)$ $\Gamma_1/\Gamma_9 = (\Gamma_2 + \Gamma_3 + \Gamma_4)/\Gamma_9$

VALUE EVTS DOCUMENT ID TECN COMMENT

3.13 ± 0.05 OUR FIT Error includes scale factor of 1.3.

3.26 ± 0.30 OUR AVERAGE

2.54 ± 1.89 74 KENDALL 74 OSPK

3.4 ± 1.1 29 AGUILAR... 72B HBC

2.83 ± 0.80 70 1 BLOODW... 72B HBC

3.6 ± 0.6 244 FLATTE... 67B HBC

2.89 ± 0.56 ALFF... 66 HBC

3.6 ± 0.8 50 KRAEMER 64 DBC

3.8 ± 1.1 PAULI 64 DBC

¹Error increased from published value 0.5 by Bloodworth (private communication).

$\Gamma(2\gamma)/\Gamma(\pi^+ \pi^- \pi^0)$ Γ_2/Γ_9

VALUE EVTS DOCUMENT ID TECN COMMENT

1.710 ± 0.025 OUR FIT Error includes scale factor of 1.2.

1.70 ± 0.04 OUR AVERAGE

1.704 ± 0.032 ± 0.026 3915 1 LOPEZ 07 CLEO $\psi(2S) \rightarrow J/\psi\eta$

1.61 ± 0.14 ABLIKIM 06E BES2 $e^+ e^- \rightarrow J/\psi \rightarrow \eta\gamma$

1.78 ± 0.10 ± 0.13 1077 AMSLER 95 CBAR $\bar{p}p \rightarrow \pi^+ \pi^- \eta$ at rest

1.72 ± 0.25 401 BAGLIN 69 HLBC

1.61 ± 0.39 FOSTER 65 HBC

¹LOPEZ 07 reports $\Gamma(\eta \rightarrow \pi^+ \pi^- \pi^0) / \Gamma(\eta \rightarrow 2\gamma) = \Gamma_9/\Gamma_2 = 0.587 \pm 0.011 \pm 0.009$.

$\Gamma(3\pi^0)/\Gamma(\pi^+ \pi^- \pi^0)$ Γ_3/Γ_9

VALUE EVTS DOCUMENT ID TECN COMMENT

1.415 ± 0.023 OUR FIT Error includes scale factor of 1.2.

1.48 ± 0.05 OUR AVERAGE

1.46 ± 0.03 ± 0.09 ACHASOV 06A SND $e^+ e^- \rightarrow \eta\gamma$

1.52 ± 0.04 ± 0.08 23k 1 AKHMETSHIN 01B CMD2 $e^+ e^- \rightarrow \phi \rightarrow \eta\gamma$

1.44 ± 0.09 ± 0.10 1627 AMSLER 95 CBAR $\bar{p}p \rightarrow \pi^+ \pi^- \eta$ at rest

1.50 ± 0.15 -0.29 199 BAGLIN 69 HLBC

1.47 ± 0.20 -0.17 BULLOCK 68 HLBC

• • • We do not use the following data for averages, fits, limits, etc. • • •

1.3 ± 0.4 BAGLIN 67B HLBC

0.90 ± 0.24 FOSTER 65 HBC

2.0 ± 1.0 FOELSCH 64 HBC

0.83 ± 0.32 CRAWFORD 63 HBC

¹AKHMETSHIN 01B uses results from AKHMETSHIN 99F.

$\Gamma(\pi^+ \pi^- \pi^0)/[\Gamma(2\gamma) + \Gamma(3\pi^0)]$ $\Gamma_9/(\Gamma_2 + \Gamma_3)$

VALUE DOCUMENT ID TECN COMMENT

0.320 ± 0.005 OUR FIT Error includes scale factor of 1.2.

0.304 ± 0.012 ACHASOV 00B SND $e^+ e^- \rightarrow \phi \rightarrow \eta\gamma$

• • • We do not use the following data for averages, fits, limits, etc. • • •

0.3141 ± 0.0081 ± 0.0058 ACHASOV 00B SND See ACHASOV 00B

$\Gamma(\pi^+ \pi^- \gamma)/\Gamma_{\text{total}}$ Γ_{10}/Γ

VALUE (units 10⁻²) EVTS DOCUMENT ID TECN COMMENT

4.28 ± 0.07 OUR FIT Error includes scale factor of 1.1.

4.38 ± 0.02 ± 0.10 200k 1 ABLIKIM 21AMBES3 $J/\psi \rightarrow \gamma\eta$

• • • We do not use the following data for averages, fits, limits, etc. • • •

3.96 ± 0.14 ± 0.14 859 2 LOPEZ 07 CLEO $\psi(2S) \rightarrow J/\psi\eta$

¹ABLIKIM 21AM normalize the branching ratio ($\eta \rightarrow \pi^+ \pi^- \gamma$) to $B(J/\psi \rightarrow \gamma\eta)$, which they measured absolutely.

²Not independent of other results listed for LOPEZ 07. Assuming decays of $\eta \rightarrow \gamma\gamma$, $3\pi^0$, $\pi^+ \pi^- \pi^0$, $\pi^+ \pi^- \gamma$, and $e^+ e^- \gamma$ account for all η decays within a contribution of 0.3% to the systematic error.

$\Gamma(\pi^+ \pi^- \gamma)/\Gamma(\pi^+ \pi^- \pi^0)$ Γ_{10}/Γ_9

VALUE EVTS DOCUMENT ID TECN COMMENT

0.1858 ± 0.0025 OUR FIT

0.1847 ± 0.0030 OUR AVERAGE Error includes scale factor of 1.1.

0.1856 ± 0.0005 ± 0.0028 200k BABUSCI 13 KLOE $e^+ e^- \rightarrow \phi \rightarrow \eta\gamma$

0.175 ± 0.007 ± 0.006 859 LOPEZ 07 CLEO $\psi(2S) \rightarrow J/\psi\eta$

• • • We do not use the following data for averages, fits, limits, etc. • • •

0.209 ± 0.004 18k THALER 73 ASPK

0.201 ± 0.006 7250 GORMLEY 70 ASPK

0.28 ± 0.04 BALTAY 67B DBC

0.25 ± 0.035 LITCHFIELD 67 DBC

0.30 ± 0.06 CRAWFORD 66 HBC

0.196 ± 0.041 FOSTER 65C HBC

$\Gamma(e^+ e^- \gamma)/\Gamma_{\text{total}}$ Γ_{11}/Γ

VALUE (units 10⁻³) EVTS DOCUMENT ID TECN COMMENT

6.9 ± 0.4 OUR FIT Error includes scale factor of 1.2.

6.7 ± 0.5 OUR AVERAGE Error includes scale factor of 1.2.

6.6 ± 0.4 ± 0.4 1345 BERGHAUSER 11 SPEC $\gamma p \rightarrow p\eta$

7.8 ± 0.5 ± 0.8 435 ± 31 BERLOWSKI 08 WASA $p d \rightarrow {}^3\text{He} \eta$

5.15 ± 0.62 ± 0.74 283 ACHASOV 01B SND $e^+ e^- \rightarrow \phi \rightarrow \eta\gamma$

7.10 ± 0.64 ± 0.46 323 AKHMETSHIN 01 CMD2 $e^+ e^- \rightarrow \phi \rightarrow \eta\gamma$

• • • We do not use the following data for averages, fits, limits, etc. • • •

9.4 ± 0.7 ± 0.5 172 1 LOPEZ 07 CLEO $\psi(2S) \rightarrow J/\psi\eta$

¹Not independent of other results listed for LOPEZ 07. Assuming decays of $\eta \rightarrow \gamma\gamma$, $3\pi^0$, $\pi^+ \pi^- \pi^0$, $\pi^+ \pi^- \gamma$, and $e^+ e^- \gamma$ account for all η decays within a contribution of 0.3% to the systematic error.

$\Gamma(e^+ e^- \gamma)/\Gamma(\pi^+ \pi^- \gamma)$ Γ_{11}/Γ_{10}

VALUE EVTS DOCUMENT ID TECN COMMENT

0.161 ± 0.010 OUR FIT Error includes scale factor of 1.2.

0.237 ± 0.021 ± 0.015 172 LOPEZ 07 CLEO $\psi(2S) \rightarrow J/\psi\eta$

$\Gamma(e^+ e^- \gamma)/\Gamma(\pi^+ \pi^- \pi^0)$ Γ_{11}/Γ_9

VALUE (units 10⁻²) EVTS DOCUMENT ID TECN COMMENT

2.98 ± 0.19 OUR FIT Error includes scale factor of 1.3.

2.1 ± 0.5 80 JANE 75B OSPK See the erratum

$\Gamma(\text{neutral modes})/[\Gamma(\pi^+ \pi^- \pi^0) + \Gamma(\pi^+ \pi^- \gamma) + \Gamma(e^+ e^- \gamma)]$
 $\Gamma_1/(\Gamma_9 + \Gamma_{10} + \Gamma_{11}) = (\Gamma_2 + \Gamma_3 + \Gamma_4)/(\Gamma_9 + \Gamma_{10} + \Gamma_{11})$

VALUE EVTS DOCUMENT ID TECN COMMENT

2.57 ± 0.04 OUR FIT Error includes scale factor of 1.3.

2.64 ± 0.23 BALTAY 67B DBC

• • • We do not use the following data for averages, fits, limits, etc. • • •

4.5 ± 1.0 280 1 JAMES 66 HBC

3.20 ± 1.26 53 1 BASTIEN 62 HBC

2.5 ± 1.0 10 1 PICKUP 62 HBC

¹These experiments are not used in the averages as they do not separate clearly $\eta \rightarrow \pi^+ \pi^- \pi^0$ and $\eta \rightarrow \pi^+ \pi^- \gamma$ from each other. The reported values thus probably contain some unknown fraction of $\eta \rightarrow \pi^+ \pi^- \gamma$.

$\Gamma(2\gamma)/[\Gamma(\pi^+ \pi^- \pi^0) + \Gamma(\pi^+ \pi^- \gamma) + \Gamma(e^+ e^- \gamma)]$ $\Gamma_2/(\Gamma_9 + \Gamma_{10} + \Gamma_{11})$

VALUE EVTS DOCUMENT ID TECN COMMENT

1.407 ± 0.020 OUR FIT Error includes scale factor of 1.2.

1.1 ± 0.4 OUR AVERAGE

1.51 ± 0.93 75 KENDALL 74 OSPK

0.99 ± 0.48 CRAWFORD 63 HBC

$\Gamma(\mu^+ \mu^- \gamma)/\Gamma_{\text{total}}$ Γ_{12}/Γ

VALUE (units 10⁻⁴) EVTS DOCUMENT ID TECN COMMENT

3.1 ± 0.4 OUR FIT

3.1 ± 0.4 600 DZHELADIN 80 SPEC $\pi^- p \rightarrow \eta n$

• • • We do not use the following data for averages, fits, limits, etc. • • •

1.5 ± 0.75 100 BUSHNIN 78 SPEC See DZHELADIN 80

$\Gamma(e^+e^-)/\Gamma_{\text{total}}$ Γ_{13}/Γ

VALUE	CL%	DOCUMENT ID	TECN	COMMENT
$<7 \times 10^{-7}$	90	ACHASOV 18B	CNTR	Inverse reaction $e^+e^- \rightarrow \eta$
• • • We do not use the following data for averages, fits, limits, etc. • • •				
$<2.3 \times 10^{-6}$	90	AGAKISHIEV 14		$pp \rightarrow \eta + X$
$<5.6 \times 10^{-6}$	90	¹ AGAKISHIEV 12A	SPEC	$pp \rightarrow \eta + X$
$<2.7 \times 10^{-5}$	90	BERLOWSKI 08	WASA	$pd \rightarrow {}^3\text{He } \eta$
$<0.77 \times 10^{-4}$	90	BROWDER 97B	CLE2	$e^+e^- \simeq 10.5 \text{ GeV}$
$<2 \times 10^{-4}$	90	WHITE 96	SPEC	$pd \rightarrow \eta {}^3\text{He}$
$<3 \times 10^{-4}$	90	DAVIES 74	RVUE	Uses ESTEN 67

¹AGAKISHIEV 12A uses a data sample of 3.5 GeV proton beam collisions on liquid hydrogen target collected by the HADES detector.

 $\Gamma(\mu^+\mu^-)/\Gamma_{\text{total}}$ Γ_{14}/Γ

VALUE (units 10^{-6})	CL%	EVTS	DOCUMENT ID	TECN	COMMENT
5.8 ± 0.8 OUR AVERAGE					
$5.7 \pm 0.7 \pm 0.5$	114		ABEGG 94	SPEC	$pd \rightarrow \eta {}^3\text{He}$
6.5 ± 2.1	27		DZHELJADIN 80B	SPEC	$\pi^- p \rightarrow \eta n$
• • • We do not use the following data for averages, fits, limits, etc. • • •					
$5.6^{+0.6}_{-0.7} \pm 0.5$	100		KESSLER 93	SPEC	See ABEGG 94
<20	95	0	WEHMANN 68	OSPK	

 $\Gamma(\mu^+\mu^-)/\Gamma(2\gamma)$ Γ_{14}/Γ_2

VALUE (units 10^{-5})	DOCUMENT ID	TECN
• • • We do not use the following data for averages, fits, limits, etc. • • •		
5.9 ± 2.2	HYAMS 69	OSPK

 $\Gamma(2e^+2e^-)/\Gamma_{\text{total}}$ Γ_{15}/Γ

VALUE (units 10^{-5})	CL%	EVTS	DOCUMENT ID	TECN	COMMENT
$2.4 \pm 0.2 \pm 0.1$	362		¹ AMBROSINO 11B	KLOE	$e^+e^- \rightarrow \phi \rightarrow \eta\gamma$
• • • We do not use the following data for averages, fits, limits, etc. • • •					
<9.7	90		BERLOWSKI 08	WASA	$pd \rightarrow {}^3\text{He } \eta$
<6.9	90		AKHMETSHIN 01	CMD2	$e^+e^- \rightarrow \phi \rightarrow \eta\gamma$

¹This measurement is fully inclusive (includes " $2e^+2e^- \gamma$ " channel).

 $\Gamma(\pi^+\pi^-e^+e^-(\gamma))/\Gamma_{\text{total}}$ Γ_{16}/Γ

VALUE (units 10^{-4})	EVTS	DOCUMENT ID	TECN	COMMENT
2.68 ± 0.11 OUR FIT	1555 \pm 52	¹ AMBROSINO 09B	KLOE	$e^+e^- \rightarrow \phi \rightarrow \eta\gamma$
• • • We do not use the following data for averages, fits, limits, etc. • • •				
$4.3^{+2.0}_{-1.6} \pm 0.4$	16	BERLOWSKI 08	WASA	$pd \rightarrow {}^3\text{He } \eta$
$4.3 \pm 1.3 \pm 0.4$	16	BARGHOLTZ 07	CNTR	See BERLOWSKI 08
$3.7^{+2.5}_{-1.8} \pm 0.3$	4	AKHMETSHIN 01	CMD2	$e^+e^- \rightarrow \phi \rightarrow \eta\gamma$

¹This AMBROSINO 09B value includes radiative events.

 $\Gamma(e^+e^-\mu^+\mu^-)/\Gamma_{\text{total}}$ Γ_{17}/Γ

VALUE	CL%	DOCUMENT ID	TECN	COMMENT
$<1.6 \times 10^{-4}$	90	BERLOWSKI 08	WASA	$pd \rightarrow {}^3\text{He } \eta$

 $\Gamma(2\mu^+2\mu^-)/\Gamma_{\text{total}}$ Γ_{18}/Γ

VALUE	CL%	DOCUMENT ID	TECN	COMMENT
$<3.6 \times 10^{-4}$	90	BERLOWSKI 08	WASA	$pd \rightarrow {}^3\text{He } \eta$

 $\Gamma(\mu^+\mu^-\pi^+\pi^-)/\Gamma_{\text{total}}$ Γ_{19}/Γ

VALUE	CL%	DOCUMENT ID	TECN	COMMENT
$<3.6 \times 10^{-4}$	90	BERLOWSKI 08	WASA	$pd \rightarrow {}^3\text{He } \eta$

 $\Gamma(\pi^+e^-\nu_e + \text{c.c.})/\Gamma(\pi^+\pi^-\pi^0)$ Γ_{20}/Γ_9

VALUE	CL%	DOCUMENT ID	TECN	COMMENT
$<7.3 \times 10^{-4}$	90	ABLIKIM 13G	BES3	$J/\psi \rightarrow \phi \eta$

 $\Gamma(\pi^+\pi^-2\gamma)/\Gamma(\pi^+\pi^-\pi^0)$ Γ_{21}/Γ_9

VALUE	CL%	DOCUMENT ID	TECN
$<9 \times 10^{-3}$		PRICE 67	HBC
• • • We do not use the following data for averages, fits, limits, etc. • • •			
$<16 \times 10^{-3}$	95	BALTAY 67B	DBC

 $\Gamma(\pi^+\pi^-\pi^0\gamma)/\Gamma(\pi^+\pi^-\pi^0)$ Γ_{22}/Γ_9

VALUE	CL%	EVTS	DOCUMENT ID	TECN
$<0.24 \times 10^{-2}$	90	0	THALER 73	ASPK
• • • We do not use the following data for averages, fits, limits, etc. • • •				
$<1.7 \times 10^{-2}$	90		ARNOLD 68	HLBC
$<1.6 \times 10^{-2}$	95		BALTAY 67B	DBC
$<7.0 \times 10^{-2}$			FLATTE 67	HBC
$<0.9 \times 10^{-2}$			PRICE 67	HBC

 $\Gamma(\pi^0\mu^+\mu^-)/\Gamma_{\text{total}}$ Γ_{23}/Γ

VALUE	CL%	DOCUMENT ID	TECN	COMMENT
$<3 \times 10^{-6}$	90	DZHELJADIN 81	SPEC	$\pi^- p \rightarrow \eta n$

Forbidden modes

 $\Gamma(\pi^0\gamma)/\Gamma_{\text{total}}$ Γ_{24}/Γ

VALUE	CL%	DOCUMENT ID	TECN	COMMENT
Forbidden by angular momentum conservation.				
$<9 \times 10^{-5}$	90	NEFKENS 05A	CRYB	$p(720 \text{ MeV}/c) \pi^- \rightarrow n\eta$

 $\Gamma(\pi^+\pi^-)/\Gamma_{\text{total}}$ Γ_{25}/Γ

VALUE	CL%	EVTS	DOCUMENT ID	TECN	COMMENT
Forbidden by P and CP invariance.					
$<4.4 \times 10^{-6}$	90	83M	¹ BABUSCI	20A	KLOE $e^+e^- \rightarrow \phi \rightarrow \eta\gamma$
• • • We do not use the following data for averages, fits, limits, etc. • • •					
$<5.3 \times 10^{-17}$			² ZHEVLAKOV 19	THEO	from nEDM limits
$<1.6 \times 10^{-5}$	90	25M	AAIJ 17D	LHCB	in $D \rightarrow \pi\pi\pi$ decays
$<3.9 \times 10^{-4}$	90	225M	ABLIKIM 11G	BES3	$e^+e^- \rightarrow J/\psi \rightarrow \eta\gamma$
$<1.3 \times 10^{-5}$	90	16M	AMBROSINO 05A	KLOE	$e^+e^- \rightarrow \phi \rightarrow \eta\gamma$
$<3.3 \times 10^{-4}$	90		AKHMETSHIN 99B	CMD2	$e^+e^- \rightarrow \phi \rightarrow \eta\gamma$
$<9 \times 10^{-4}$	90		AKHMETSHIN 97C	CMD2	See AKHMETSHIN 99B
$<15 \times 10^{-4}$	0		THALER 73	ASPK	

¹BABUSCI 20A combines new data with the previous AMBROSINO 05A data, and thus supersedes AMBROSINO 05A.

²ZHEVLAKOV 19 derives the value from the experimental limits of nEDM by a calculation using an effective Lagrangian.

 $\Gamma(2\pi^0)/\Gamma_{\text{total}}$ Γ_{26}/Γ

VALUE	CL%	EVTS	DOCUMENT ID	TECN	COMMENT
Forbidden by P and CP invariance.					
$<3.5 \times 10^{-4}$	90		BLIK 07	GAM4	$\pi^- p \rightarrow \eta n$
• • • We do not use the following data for averages, fits, limits, etc. • • •					
$<2.7 \times 10^{-17}$			¹ ZHEVLAKOV 19	THEO	from nEDM limits
$<6.9 \times 10^{-4}$	90	225M	ABLIKIM 11G	BES3	$e^+e^- \rightarrow J/\psi \rightarrow \eta\gamma$
$<4.3 \times 10^{-4}$	90		AKHMETSHIN 99C	CMD2	$e^+e^- \rightarrow \phi \rightarrow \eta\gamma$
$<6 \times 10^{-4}$	90		² ACHASOV 98	SND	$e^+e^- \rightarrow \phi \rightarrow \eta\gamma$

¹ZHEVLAKOV 19 derives the value from the experimental limits of nEDM by a calculation using an effective Lagrangian.

²ACHASOV 98 observes one event in a $\pm 3\sigma$ region around the η mass, while a Monte Carlo calculation gives 10 ± 5 events. The limit here is the Poisson upper limit for one observed event and no background.

 $\Gamma(2\pi^0\gamma)/\Gamma_{\text{total}}$ Γ_{27}/Γ

VALUE	CL%	DOCUMENT ID	TECN	CHG	COMMENT
Forbidden by C invariance.					
$<5 \times 10^{-4}$	90	NEFKENS 05	CRYB 0		$p(720 \text{ MeV}/c) \pi^- \rightarrow n\eta$
• • • We do not use the following data for averages, fits, limits, etc. • • •					
$<17 \times 10^{-4}$	90	BLIK 07	GAM4		$\pi^- p \rightarrow \eta n$

 $\Gamma(3\pi^0\gamma)/\Gamma_{\text{total}}$ Γ_{28}/Γ

VALUE	CL%	DOCUMENT ID	TECN	CHG	COMMENT
Forbidden by C invariance.					
$<6 \times 10^{-5}$	90	NEFKENS 05	CRYB 0		$p(720 \text{ MeV}/c) \pi^- \rightarrow n\eta$
• • • We do not use the following data for averages, fits, limits, etc. • • •					
$<24 \times 10^{-5}$	90	BLIK 07	GAM4		$\pi^- p \rightarrow \eta n$

 $\Gamma(3\gamma)/\Gamma_{\text{total}}$ Γ_{29}/Γ

VALUE	CL%	DOCUMENT ID	TECN	COMMENT
Forbidden by C invariance.				
• • • We do not use the following data for averages, fits, limits, etc. • • •				
$<16 \times 10^{-5}$	90	BLIK 07	GAM4	$\pi^- p \rightarrow \eta n$
$<4 \times 10^{-5}$	90	NEFKENS 05A	CRYB	$p(720 \text{ MeV}/c) \pi^- \rightarrow n\eta$

 $\Gamma(3\gamma)/\Gamma(2\gamma)$ Γ_{29}/Γ_2

VALUE	CL%	DOCUMENT ID	TECN	CHG
$<1.2 \times 10^{-3}$	95	ALDE 84	GAM2	0

 $\Gamma(3\gamma)/\Gamma(3\pi^0)$ Γ_{29}/Γ_3

VALUE	CL%	DOCUMENT ID	TECN	COMMENT
$<4.9 \times 10^{-5}$	90	ALOISIO 04	KLOE	$\phi \rightarrow \eta\gamma$

 $\Gamma(4\pi^0)/\Gamma_{\text{total}}$ Γ_{30}/Γ

VALUE	CL%	DOCUMENT ID	TECN	COMMENT
Forbidden by P and CP invariance.				
$<6.9 \times 10^{-7}$	90	PRAKHOV 00	CRYB	$\pi^- p \rightarrow n\eta$, 720 MeV/c
• • • We do not use the following data for averages, fits, limits, etc. • • •				
$<200 \times 10^{-7}$	90	BLIK 07	GAM4	$\pi^- p \rightarrow \eta n$

 $\Gamma(\pi^0e^+e^-)/\Gamma_{\text{total}}$ Γ_{31}/Γ

VALUE	CL%	DOCUMENT ID	TECN	COMMENT
C parity forbids this to occur as a single-photon process.				
• • • We do not use the following data for averages, fits, limits, etc. • • •				
$<7.5 \times 10^{-6}$	90	ADLARSON 18C	WASA	$pd \rightarrow \eta {}^3\text{He}$
$<1.6 \times 10^{-4}$	90	MARTYNOV 76	HLBC	
$<8.4 \times 10^{-4}$	90	BAZIN 68	DBC	
$<70 \times 10^{-4}$		RIITENBERG 65	HBC	

Meson Particle Listings

 η $\Gamma(\pi^0 e^+ e^-)/\Gamma(\pi^+ \pi^- \pi^0)$ Γ_{31}/Γ_9

C parity forbids this to occur as a single-photon process.

VALUE	CL%	DOCUMENT ID	TECN	COMMENT
$< 3.28 \times 10^{-5}$	90	ADLARSON 18c	WASA	$p d \rightarrow \eta^3 \text{He}$
••• We do not use the following data for averages, fits, limits, etc. •••				
$< 1.9 \times 10^{-4}$	90	JANE	75	OSPK
$< 42 \times 10^{-4}$	90	BAGLIN	67	HLBC
$< 16 \times 10^{-4}$	90	BILLING	67	HLBC
$< 77 \times 10^{-4}$		FOSTER	65B	HBC
$< 110 \times 10^{-4}$		PRICE	65	HBC

 $\Gamma(\pi^0 \mu^+ \mu^-)/\Gamma_{\text{total}}$ Γ_{32}/Γ

C parity forbids this to occur as a single-photon process.

VALUE	CL%	DOCUMENT ID	TECN	COMMENT
$< 5 \times 10^{-6}$	90	DZHELYADIN 81	SPEC	$\pi^- p \rightarrow \eta n$
••• We do not use the following data for averages, fits, limits, etc. •••				
$< 500 \times 10^{-6}$		WEHMANN 68	OSPK	

 $[\Gamma(\mu^+ e^-) + \Gamma(\mu^- e^+)]/\Gamma_{\text{total}}$ Γ_{33}/Γ

Forbidden by lepton family number conservation.

VALUE	CL%	DOCUMENT ID	TECN	COMMENT
$< 6 \times 10^{-6}$	90	WHITE 96	SPEC	$p d \rightarrow \eta^3 \text{He}$

 η C-NONCONSERVING DECAY PARAMETERS $\pi^+ \pi^- \pi^0$ LEFT-RIGHT ASYMMETRY PARAMETERMeasurements with an error $> 1.0 \times 10^{-2}$ have been omitted.

VALUE (units 10^{-2})	EVTS	DOCUMENT ID	TECN
$0.09^{+0.11}_{-0.12}$ OUR AVERAGE			
$+0.09 \pm 0.10^{+0.09}_{-0.14}$	1.34M	AMBROSINO 08D	KLOE
0.28 ± 0.26	165k	JANE 74	OSPK
-0.05 ± 0.22	220k	LAYTER 72	ASPK
••• We do not use the following data for averages, fits, limits, etc. •••			
1.5 ± 0.5	37k	¹ GORMLEY 68c	ASPK

¹The GORMLEY 68c asymmetry is probably due to unmeasured ($\mathbf{E} \times \mathbf{B}$) spark chamber effects. New experiments with ($\mathbf{E} \times \mathbf{B}$) controls don't observe an asymmetry. $\pi^+ \pi^- \pi^0$ SEXTANT ASYMMETRY PARAMETERMeasurements with an error $> 2.0 \times 10^{-2}$ have been omitted.

VALUE (units 10^{-2})	EVTS	DOCUMENT ID	TECN
$0.12^{+0.10}_{-0.11}$ OUR AVERAGE			
$+0.08 \pm 0.10^{+0.08}_{-0.13}$	1.34M	AMBROSINO 08D	KLOE
0.20 ± 0.25	165k	JANE 74	OSPK
0.10 ± 0.22	220k	LAYTER 72	ASPK
0.5 ± 0.5	37k	GORMLEY 68c	WIRE

 $\pi^+ \pi^- \pi^0$ QUADRANT ASYMMETRY PARAMETER

VALUE (units 10^{-2})	EVTS	DOCUMENT ID	TECN
-0.09 ± 0.09 OUR AVERAGE			
$-0.05 \pm 0.10^{+0.03}_{-0.05}$	1.34M	AMBROSINO 08D	KLOE
-0.30 ± 0.25	165k	JANE 74	OSPK
-0.07 ± 0.22	220k	LAYTER 72	ASPK

 $\pi^+ \pi^- \gamma$ LEFT-RIGHT ASYMMETRY PARAMETERMeasurements with an error $> 2.0 \times 10^{-2}$ have been omitted.

VALUE (units 10^{-2})	EVTS	DOCUMENT ID	TECN
0.9 ± 0.4 OUR AVERAGE			
1.2 ± 0.6	35k	JANE 74B	OSPK
0.5 ± 0.6	36k	THALER 72	ASPK
1.22 ± 1.56	7257	GORMLEY 70	ASPK

 $\pi^+ \pi^- \gamma$ PARAMETER β (D -wave)Sensitive to a D -wave contribution: $dN/d\cos\theta = \sin^2\theta (1 + \beta \cos^2\theta)$.

VALUE	EVTS	DOCUMENT ID	TECN
-0.02 ± 0.07 OUR AVERAGE			
0.11 ± 0.11	35k	JANE 74B	OSPK
-0.060 ± 0.065	7250	GORMLEY 70	WIRE
••• We do not use the following data for averages, fits, limits, etc. •••			
0.12 ± 0.06		¹ THALER 72	ASPK

¹The authors don't believe this indicates D -wave because the dependence of β on the γ energy is inconsistent with the theoretical prediction. A $\cos^2\theta$ dependence can also come from P - and F -wave interference. η CP-NONCONSERVING DECAY PARAMETER $\pi^+ \pi^- e^+ e^-$ DECAY-PLANE ASYMMETRY PARAMETER A_ϕ In the η rest frame, the total momentum of the $e^+ e^-$ pair is equal and opposite to that of the $\pi^+ \pi^-$ pair. Let \hat{z} be the unit vector along the momentum of the $e^+ e^-$ pair; let \hat{n}_{ee} and $\hat{n}_{\pi\pi}$ be the unit vectors normal to the $e^+ e^-$ and $\pi^+ \pi^-$ planes; and let ϕ be the angle between the two normals. Then

$$\sin\phi \cos\phi = [(\hat{n}_{ee} \times \hat{n}_{\pi\pi}) \cdot \hat{z}] (\hat{n}_{ee} \cdot \hat{n}_{\pi\pi}),$$

and

$$A_\phi \equiv \frac{N_{\sin\phi \cos\phi > 0} - N_{\sin\phi \cos\phi < 0}}{N_{\sin\phi \cos\phi > 0} + N_{\sin\phi \cos\phi < 0}}.$$

VALUE (units 10^{-2})	EVTS	DOCUMENT ID	TECN	COMMENT
$-0.6 \pm 2.5 \pm 1.8$	1555 \pm 52	AMBROSINO 09B	KLOE	$e^+ e^- \rightarrow \phi \rightarrow \eta \gamma$

ENERGY DEPENDENCE OF $\eta \rightarrow 3\pi$ DALITZ PLOTSPARAMETERS FOR $\eta \rightarrow \pi^+ \pi^- \pi^0$ See the "Note on η Decay Parameters," page 1454, in our 1994 edition (Physical Review **D50** 1173 (1994)). The following experiments fit to one or more of the coefficients a, b, c, d, e, f for g for $|\text{matrix element}|^2 = 1 + ay + by^2 + cx + dx^2 + exy + fy^3 + gx^2y$.

VALUE	EVTS	DOCUMENT ID	TECN	COMMENT
••• We do not use the following data for averages, fits, limits, etc. •••				
4.7M		¹ ANASTASI 16A	16A	KLOE $e^+ e^- \rightarrow \phi \rightarrow \eta \gamma$
79k		ABLIKIM 15G	BES3	$e^+ e^- \rightarrow J/\psi \rightarrow \eta \gamma$
174k		ADLARSON 14A	WASA	$p d \rightarrow \eta^3 \text{He}$
1.34M		AMBROSINO 08D	KLOE	
3230		² ABELE 98D	CBAR	$\bar{p} p \rightarrow \pi^0 \pi^0 \eta$ at rest
1077		³ AMSLER 95	CBAR	$\bar{p} p \rightarrow \pi^+ \pi^- \eta$ at rest
81k		LAYTER 73	ASPK	
220k		LAYTER 72	ASPK	
1138		CARPENTER 70	HBC	
349		DANBURG 70	DBC	
7250		GORMLEY 70	WIRE	
5.26		BAGLIN 69	HLBC	
7170		CNOPS 68	OSPK	
37k		GORMLEY 68c	WIRE	
1300		CLPWY 66	HBC	
705		LARRIBE 66	HBC	

¹ANASTASI 16A measure the Dalitz parameters a, b, d, f , and g . This is the first measurement of g .²ABELE 98D obtains $a = -1.22 \pm 0.07$ and $b = 0.22 \pm 0.11$ when c (or d) is fixed at 0.06.³AMSLER 95 fits to $(1+ay+by^2)$ and obtains $a = -0.94 \pm 0.15$ and $b = 0.11 \pm 0.27$. α PARAMETER FOR $\eta \rightarrow 3\pi^0$ See the "Note on η Decay Parameters" in our 1994 edition, Phys. Rev. **D50**, 1 August 1994, Part I, p. 1454. The value here is of α in $|\text{matrix element}|^2 = 1 + 2\alpha z$.

VALUE	EVTS	DOCUMENT ID	TECN	COMMENT
-0.288 ± 0.0012 OUR AVERAGE				Error includes scale factor of 1.1.
$-0.0265 \pm 0.0010 \pm 0.0009$	7M	PRAKHOV 18	CRYB	$\gamma p \rightarrow p \eta$
$-0.055 \pm 0.014 \pm 0.004$	33k	ABLIKIM 15G	BES3	$e^+ e^- \rightarrow J/\psi \rightarrow \eta \gamma$
$-0.0301 \pm 0.0035^{+0.0022}_{-0.0035}$	512k	AMBROSINO 10A	KLOE	$e^+ e^- \rightarrow \phi \rightarrow \eta \gamma$
$-0.027 \pm 0.008 \pm 0.005$	120k	¹ ADOLPH 09	WASA	$p p \rightarrow p p \eta$
$-0.0322 \pm 0.0012 \pm 0.0022$	3M	² PRAKHOV 09	CRYB	$\gamma p \rightarrow p \eta$
$-0.032 \pm 0.002 \pm 0.002$	1.8M	² UNVERZAGT 09	CRYB	$\gamma p \rightarrow p \eta$
$-0.026 \pm 0.010 \pm 0.010$	75k	BASHKANOV 07	WASA	$p p \rightarrow p p \eta$
$-0.010 \pm 0.021 \pm 0.010$	12k	ACHASOV 01c	SND	$e^+ e^- \rightarrow \phi \rightarrow \eta \gamma$
-0.031 ± 0.004	1M	TIPPENS 01	CRYB	$\pi^- p \rightarrow n \eta$, 720 MeV
$-0.052 \pm 0.017 \pm 0.010$	98k	ABELE 98c	CBAR	$\bar{p} p \rightarrow 5\pi^0$
-0.022 ± 0.023	50k	ALDE 84	GAM2	
••• We do not use the following data for averages, fits, limits, etc. •••				
$-0.038 \pm 0.003^{+0.012}_{-0.008}$	1.34M	³ AMBROSINO 08D	KLOE	
-0.32 ± 0.37	192	BAGLIN 70	HLBC	

¹This ADOLPH 09 result is independent of the BASHKANOV 07 result.²The PRAKHOV 09 and UNVERZAGT 09 results are independent.³This AMBROSINO 08D value is an indirect result using $\eta \rightarrow \pi^+ \pi^0 \pi^-$ events and a rescattering matrix that mixes isospin decay amplitudes.PARAMETER Λ IN $\eta \rightarrow \ell^+ \ell^- \gamma$ DECAYIn the pole approximation the electromagnetic transition form factor for a resonance of mass M is given by the expression:

$$|F|^2 = (1 - M_\ell^2/\Lambda^2)^{-2},$$

where for the parameter Λ vector dominance predicts $\Lambda \approx 0.770$ GeV.

VALUE (GeV/ c^2)	EVTS	DOCUMENT ID	TECN	COMMENT
0.716 ± 0.011 OUR AVERAGE				
0.712 ± 0.020		¹ ADLARSON 17B	A2MM	$\gamma p \rightarrow \eta p$
$0.7191 \pm 0.0125 \pm 0.0093$		² ARNALDI 16	NA60	400 GeV p - A collisions
$0.716 \pm 0.031 \pm 0.009$		³ ARNALDI 09	NA60	158A In-In collisions
0.72 ± 0.09	600	DZHELYADIN 80	SPEC	$\pi^- p \rightarrow \eta n, \eta \rightarrow \gamma \mu^+ \mu^-$

¹ADLARSON 17B reports $\Lambda^{-2}(\eta \rightarrow \gamma e^+ e^-) = 1.97 \pm 0.11$ (GeV/ c^2) $^{-2}$ which we converted to the quoted Λ value and uncertainty (total=statistical plus systematic).²ARNALDI 16 reports $\Lambda^{-2}(\eta \rightarrow \gamma \mu^+ \mu^-) = 1.934 \pm 0.067 \pm 0.050$ (GeV/ c^2) $^{-2}$ which we converted to the quoted Λ value.³ARNALDI 09 reports $\Lambda^{-2}(\eta \rightarrow \gamma \mu^+ \mu^-) = 1.95 \pm 0.17 \pm 0.05$ (GeV/ c^2) $^{-2}$ which we converted to the quoted Λ value.

See key on page 1127

Meson Particle Listings

$\eta, f_0(500)$

η REFERENCES

ABLIKIM 21AM PR D104 092004
 BABUSCI 20A JHEP 2010 047
 ZHEVLAKOV 19 PR D99 031703
 ACHASOV 18B PR D98 052007
 ADLARSON 18C PL B784 378
 PRAKHOV 18B PR C97 065203
 AAU 17D PL B764 233
 ADLARSON 17B PR C95 035208
 ANASTASI 16A JHEP 1605 019
 ARNALDI 16 PL B757 437
 ABLIKIM 15G PR D92 012014
 ADLARSON 14A PR D91 052070
 AGAKISHIEV 14 PL B731 265
 NEFKENS 14 PR C90 025206
 NIKOLAEV 14 EPJ A50 58
 ABLIKIM 13 PR D87 012009
 ABLIKIM 13G PR D87 032006
 BABUSCI 13 PL B718 910
 BABUSCI 13A JHEP 1301 119
 AGAKISHIEV 12A EPJ A48 64
 GOSLAWSKI 12 PR D85 112011
 ABLIKIM 11G PR D84 032006
 AMBROSINO 11B PR D84 032006
 BERGHAUSER 11 PL B701 562
 AMBROSINO 10A PL B694 16
 ADOLPH 09 PL B677 24
 AMBROSINO 09B PL B675 283
 ARNALDI 09 PL B677 260
 PRAKHOV 09 PR C79 035204
 UNVERZAGT 09 EPJ A39 169
 AMBROSINO 08D JHEP 0805 006
 BERLOWSKI 08 PR D77 032004
 PRAKHOV 08 PR C78 015206
 RODRIGUES 08 PR L101 012301
 AMBROSINO 07B JHEP 0712 073
 BARGHOLTZ 07 PL B644 299
 BASHKANOV 07 PR C76 048201
 BLIK 07 PAN 70 693
 Translated from YAF 70 724.
 LOPEZ 07 PRL 99 122001
 MILLER 07 PRL 99 122002
 ABLIKIM 06E PR D73 052008
 ABLIKIM 06Q PRL 97 202002
 ACHASOV 06A PR D74 014016
 ABDEL-BARY 05 PL B619 281
 AKHMETSHPIN 05 PL B605 26
 AMBROSINO 05A PL B606 276
 NEFKENS 05 PRL 94 041601
 NEFKENS 05A PR C72 035212
 PRAKHOV 05 PR C72 025201
 ALOISIO 04 PL B591 49
 KNECHT 04 PL B589 14
 LAI 02 PL B533 196
 NEFKENS 02 PS T99 114
 ACHASOV 01B PL B504 075
 ACHASOV 01C JETPL 73 451
 Translated from ZETFP 73 511.
 ACHASOV 01D NP B600 3
 AKHMETSHPIN 01 PL B501 191
 AKHMETSHPIN 01B PL B509 217
 TIPPENS 01 PRL 87 192001
 ACHASOV 00 EPJ C12 25
 ACHASOV 00B JETP 90 17
 Translated from ZETF 117 22.
 ACHASOV 00D JETPL 72 282
 Translated from ZETFP 72 411.
 PRAKHOV 00 PRL 84 4802
 AKHMETSHPIN 99B PL B462 371
 AKHMETSHPIN 99C PL B462 380
 AKHMETSHPIN 99F PL B460 242
 ABLE 98 PL B417 193
 ABLE 98D PL B417 197
 ACHASOV 98 PL B425 388
 AKHMETSHPIN 97C PL B415 452
 BROWDER 97B PR D56 5359
 ABEGG 96 PR D53 11
 WHITE 96 PR D53 6658
 AMSLER 95 PL B346 203
 KRUSCHE 95D ZPHY A351 237
 ABEGG 94 PR D50 92
 PDG 94 PR D50 1173
 AMSLER 93 ZPHY C58 175
 KESSLER 93 PRL 70 992
 PLOUIN 92 PL B276 526
 BARU 90 ZPHY C48 581
 ROE 90 PR D41 17
 WILLIAMS 88 PR D38 1365
 AIHARA 86 PR D33 844
 BARTEL 85E PL 160B 421
 LANDSBERG 85 PRPL 128 301
 ALDE 84 ZPHY C25 225
 Also SJNP 40 918
 WEINSTEIN 83 PR D28 2896
 BINON 82 SJNP 36 391
 Translated from YAF 36 670.
 Also NC 71A 497
 DAVYDOV 81 LNC 32 45
 Also SJNP 33 825
 DZHELJADIN 81 PL 105B 239
 Also SJNP 33 822
 Translated from YAF 33 1529.
 ABROSIMOV 80 SJNP 31 195
 Translated from YAF 31 371.
 DZHELJADIN 80 PL 94B 548
 Also SJNP 32 516
 Translated from YAF 32 998.
 DZHELJADIN 80B PL 97B 471
 Also SJNP 32 518
 Translated from YAF 32 1002.
 BUSHNIN 78 PL 79B 147
 Also SJNP 28 775
 Translated from YAF 28 1507.
 MARTYNOV 76 SJNP 23 48
 Translated from YAF 23 93.
 JANE 75 PL 59B 99
 JANE 75B PL 59B 103
 Also PL 73B 503
 Erratum in private communication.
 BROWMAN 74B PRL 32 1067
 M. Ablikim et al. (BESIII Collab.)
 D. Babusci et al. (KLOE-2 Collab.)
 A.S. Zhevlakov et al. (TMSK, MAINZ, TUBIN+) (SND Collab.)
 M.N. Achasov et al. (WASA-at-COSY Collab.)
 P. Adlarson et al. (A2 Collab. at MAMI) (LHCb Collab.)
 S. Prakhov et al. (A2 Collab. at MAMI) (KLOE-2 Collab.)
 A. Anastasi et al. (KLOE-2 Collab.)
 R. Arnaldi et al. (NA60 Collab.)
 M. Ablikim et al. (BESIII Collab.)
 P. Adlarson et al. (WASA-at-COSY Collab.)
 G. Agakishiev et al. (HADES Collab.)
 B.M.K. Nefkens et al. (A2 Collab. at MAMI) (MAMI-B, MAINZ, BONN) (BESIII Collab.)
 M. Ablikim et al. (BESIII Collab.)
 M. Ablikim et al. (BESIII Collab.)
 D. Babusci et al. (KLOE-2 Collab.)
 D. Babusci et al. (KLOE-2 Collab.)
 G. Agakishiev et al. (HADES Collab.)
 P. Goslawski et al. (COSY-ANKE Collab.)
 M. Ablikim et al. (BESIII Collab.)
 F. Ambrosino et al. (KLOE Collab.)
 H. Berghauser et al. (GIES, UCLA, GUTE) (KLOE Collab.)
 F. Ambrosino et al. (WASA-at-COSY Collab.)
 F. Ambrosino et al. (KLOE Collab.)
 C. Adolph et al. (KLOE Collab.)
 F. Ambrosino et al. (KLOE Collab.)
 R. Arnaldi et al. (NA60 Collab.)
 S. Prakhov et al. (MAMI-C Crystal Ball Collab.)
 M. Unverzagt et al. (MAMI-B Crystal Ball Collab.)
 F. Ambrosino et al. (DAPHNE KLOE Collab.)
 M. Berlofski et al. (CELSIUS/WASA Collab.)
 S. Prakhov et al. (BNL Crystal Ball Collab.)
 T.E. Browder et al. (USP, FESP, UNESP+) (KLOE Collab.)
 F. Ambrosino et al. (CELSIUS/WASA Collab.)
 M. Bashkanov et al. (CELSIUS/WASA Collab.)
 A.M. Blik et al. (GAMS Collab.)
 A. Lopez et al. (CLEO Collab.)
 D.H. Miller et al. (CLEO Collab.)
 M. Ablikim et al. (BES Collab.)
 M. Ablikim et al. (BES Collab.)
 M.N. Achasov et al. (SND Collab.)
 M. Abdel-Bary et al. (GEM Collab.)
 R.R. Akhmetshin et al. (Novosibirsk CMD-2 Collab.)
 F. Ambrosino et al. (KLOE Collab.)
 B.M.K. Nefkens et al. (BNL Crystal Ball Collab.)
 B.M.K. Nefkens et al. (BNL Crystal Ball Collab.)
 S. Prakhov et al. (BNL Crystal Ball Collab.)
 A. Aloisio et al. (KLOE Collab.)
 N. Knecht et al. (CERN NA48 Collab.)
 A. Lai et al. (UCLA Collab.)
 M.B.M.K. Nefkens, J.W. Price (Novosibirsk SND Collab.)
 M.N. Achasov et al. (Novosibirsk SND Collab.)
 M.N. Achasov et al. (Novosibirsk SND Collab.)
 R.R. Akhmetshin et al. (Novosibirsk CMD-2 Collab.)
 R.R. Akhmetshin et al. (Novosibirsk CMD-2 Collab.)
 W.B. Tippens et al. (BNL Crystal Ball Collab.)
 M.N. Achasov et al. (Novosibirsk SND Collab.)
 M.N. Achasov et al. (Novosibirsk SND Collab.)
 M.N. Achasov et al. (Novosibirsk SND Collab.)
 S. Prakhov et al. (BNL Crystal Ball Collab.)
 R.R. Akhmetshin et al. (Novosibirsk CMD-2 Collab.)
 R.R. Akhmetshin et al. (Novosibirsk CMD-2 Collab.)
 R.R. Akhmetshin et al. (Novosibirsk CMD-2 Collab.)
 A. Abele et al. (Crystal Barrel Collab.)
 A. Abele et al. (Crystal Barrel Collab.)
 M.N. Achasov et al. (Novosibirsk SND Collab.)
 R.R. Akhmetshin et al. (Novosibirsk CMD-2 Collab.)
 T.E. Browder et al. (CLEO Collab.)
 R. Abegg et al. (Saturne SPES2 Collab.)
 D.B. White et al. (Saturne SPES2 Collab.)
 C. Amisler et al. (Crystal Barrel Collab.)
 B. Krusche et al. (TAPS + A2 Collab.)
 R. Abegg et al. (Saturne SPES2 Collab.)
 L. Montanet et al. (CERN, LBL, BOST+) (Crystal Barrel Collab.)
 C. Amisler et al. (Crystal Barrel Collab.)
 R.S. Kessler et al. (Saturne SPES2 Collab.)
 F. Plouin et al. (Saturne SPES4 Collab.)
 S.E. Baru et al. (MD-1 Collab.)
 N.A. Roe et al. (ASP Collab.)
 D.A. Williams et al. (Crystal Ball Collab.)
 A. Aihara et al. (TPC-2 Collab.)
 W. Bartel et al. (JADE Collab.)
 L.G. Landsberg (SERP) (SERP)
 D.M. Alde et al. (SERP, BELG, LAPP) (SERP, BELG, LAPP)
 D.M. Alde et al. (Crystal Ball Collab.)
 A.J. Weinstein et al. (SERP, BELG, LAPP+) (SERP, BELG, LAPP+) (SERP, BELG, LAPP+) (SERP, BELG, LAPP+)
 V.A. Davydov et al. (SERP, BELG, LAPP+) (SERP, BELG, LAPP+) (SERP, BELG, LAPP+)
 V.A. Davydov et al. (SERP) (SERP)
 R.I. Dzheilyadin et al. (SERP) (SERP)
 R.I. Dzheilyadin et al. (SERP) (SERP)
 A.T. Abrosimov et al. (JINR)
 R.I. Dzheilyadin et al. (SERP) (SERP)
 R.I. Dzheilyadin et al. (SERP) (SERP)
 R.I. Dzheilyadin et al. (SERP) (SERP)
 Y.B. Bushnin et al. (SERP) (SERP)
 Y.B. Bushnin et al. (SERP) (SERP)
 A.S. Martynov et al. (JINR)
 M.R. Jane et al. (RHEL, LOWC) (RHEL, LOWC)
 M.R. Jane et al. (RHEL, LOWC)
 M.R. Jane (CORN, BING)

DAVIES 74 NC 24A 324
 DUANE 74 PRL 32 425
 JANE 74 PL 48B 260
 JANE 74B PL 48B 265
 KENDALL 74 NC 21A 387
 LAYER 73 PR D7 2565
 THALER 73 PR D7 2569
 AGUILAR... 72B PR D6 29
 BLOODWORTH 72B NP B39 525
 LAYTER 72 PRL 29 316
 THALER 72 PRL 29 313
 BASILE 71D NC 3A 796
 STRUGALSKI 71 NP B27 429
 BAGLIN 70 NP B22 66
 BUTTRAM 70 PRL 25 1358
 CARPENTER 70 PR D1 1303
 COX 70B PRL 24 534
 DANBURG 70 PR D2 2564
 DEVONS 70 PR D1 1936
 GORMLEY 70 PR D2 501
 Also Thesis Nova 181
 BAGLIN 69 PL 29B 445
 Also NP B22 66
 HYAMS 69 PL 29B 128
 ARNOLD 68 PL 27B 466
 BAZIN 68 PRL 20 895
 BULLOCK 68 PL 27B 402
 CNOPS 68 PRL 21 1609
 GORMLEY 68C PRL 21 402
 WEHMANN 68 PRL 20 748
 BAGLIN 67 PL 24B 637
 BAGLIN 67B BAPS 12 567
 BALTAY 67B PRL 19 1498
 BALTAY 67D PRL 19 1495
 BEMPORAD 67 PL 25B 380
 Also Private Comm.
 BILLING 67 PL 25B 435
 BUNIATOV 67 PL 25B 560
 CENCE 67 PRL 19 1393
 ESTEN 67 PL 24B 115
 FELDMAN 67 PRL 18 868
 FLATTE 67B PRL 18 976
 FLATTE 67B PRL 163 1441
 LITCHFIELD 67 PL 24B 84
 PRICE 67 PRL 18 1207
 ALFF... 66 PR 145 1072
 CLPWY 66 PR 149 1044
 CRAWFORD 66 PRL 16 333
 DIGUONO 66 PRL 16 767
 GRUNHAUS 66 Thesis
 JAMES 66 PR 142 896
 JONES 66 PL 23 597
 LARRIBE 66 PL 23 600
 FOSTER 65 PR 138 B652
 FOSTER 65B Athens Conf.
 FOSTER 65 Thesis
 PRICE 65 PRL 15 123
 RITTENBERG 65 PRL 15 556
 FOELSCHER 64 PR 134 B1138
 KRAEMER 64 PR 136 B496
 PAULI 64 PL 13 351
 BACCI 63 PRL 11 37
 CRAWFORD 63 PRL 10 546
 Also PRL 16 907
 ALFF... 62 PRL 9 322
 BASTIEN 62 PRL 8 114
 PICKUP 62 PRL 8 329
 J.D. Davies, J.G. Guy, R.K.P. Zia (BIRM, RHEL+) (LOIC, SHMP)
 A. Duane et al. (RHEL, LOWC, SUSS)
 M.R. Jane et al. (RHEL, LOWC, SUSS)
 B.N. Kendall et al. (BROW, BARI, MIT)
 J.G. Layter et al. (COLU)
 J.J. Thaler et al. (COLU)
 M. Aguilar-Benitez et al. (BNL)
 I.J. Bloodworth et al. (TNTO)
 J.G. Layter et al. (COLU)
 J.J. Thaler et al. (COLU)
 M. Basile et al. (CERN, BGNA, STRB)
 Z.S. Strugalski et al. (JINR)
 C. Baglin et al. (EPOL, MADR, STRB)
 M.T. Buttram, M.N. Kreisler, R.E. Mischke (PRIN)
 D.W. Carpenter et al. (DUKE)
 B. Cox, L. Fortney, J.P. Golson (DUKE)
 J.S. Danburg et al. (COLU, SYRA)
 S. Devons et al. (COLU, BNL)
 M. Gormley (COLU)
 C. Baglin et al. (EPOL, UCB, MADR, STRB)
 C. Baglin et al. (EPOL, MADR, STRB)
 B.D. Hyams et al. (CERN, MPIM)
 R.G. Arnold et al. (STRB, MADR, EPOL+)
 M.J. Bazin et al. (PRIN, QUKI)
 F.W. Bullock et al. (LOUC)
 A.M. Cnops et al. (BNL, ORNL, UCND+)
 M. Gormley et al. (COLU, BNL)
 A.W. Wehmann et al. (HARV, CASE, SLAC+)
 C. Baglin et al. (EPOL, UCB)
 C. Baglin et al. (EPOL, UCB)
 C. Baltay et al. (COLU, STON)
 C. Baltay et al. (COLU, BROWN)
 C. Bemporad et al. (PISA, BONN)
 I. Ion (LOUC, XAF)
 K.D. Billing et al. (CERN, KARL)
 S.A. Bunyatov et al. (HAWA, LRL)
 R.J. Cence et al. (LOUC, OXF)
 M.J. Esten et al. (PENN)
 M. Feldman et al. (LRL)
 S.M. Flatte, C.G. Wohl (LRL)
 S.M. Flatte, C.G. Wohl (RHEL, SACL)
 L.R. Price, F.S. Crawford (COLU, RUTG)
 C. Alf-Steinberger et al. (SCUC, LRL, PURD, WISC, YALE)
 F.S. Crawford, L.R. Price (NAPL, TRST, FRAS)
 G. di Giugno et al. (COLU)
 F.E. James, H.L. Kraybill (YALE, BNL)
 W.G. Jones et al. (LOIC, RHEL)
 A. Larribe et al. (SACL, RHEL)
 M. Foster, M. Good, M. Meer (WISC, PURD)
 M. Foster (WISC)
 M. Foster (WISC)
 L.R. Price, F.S. Crawford (LRL, BNL)
 A. Rittenberg, G.R. Kalbfleisch (JHU, NWES, WOOD)
 H.W.J. Foelsche, H.L. Kraybill (YALE)
 R.W. Kraemer et al. (ROMA, FRAS)
 E. Pauli, A. Muller (LRL+)
 C. Bacci et al. (ROMA, FRAS)
 F.S. Crawford, L.J. Lloyd, E.C. Fowler (LRL+)
 F.S. Crawford, L.J. Lloyd, E.C. Fowler (COLU, RUTG)
 P.L. Bastien et al. (LRL)
 E. Pickup, D.K. Robinson, E.O. Salant (CNR+)

$f_0(500)$ $I(G^{JPC}) = 0^+(0^{++})$

also known as σ ; was $f_0(600)$
 See the related review(s):
 Scalar Mesons below 1 GeV

$f_0(500)$ T-MATRIX POLE \sqrt{s}

Note that $\Gamma \approx 2 \text{Im}(\sqrt{s_{\text{pole}}})$.

VALUE (MeV)	DOCUMENT ID	TECN	COMMENT
(400-550)-i(200-350) OUR ESTIMATE (see Fig. 64.3 in the review)			
• • • We do not use the following data for averages, fits, limits, etc. • • •			
$(410 \pm 20) - i(240 \pm 15)$	SARANTSEV 21	RVUE	$J/\psi(1S) \rightarrow \gamma(\pi\pi, K\bar{K}, \eta\eta, \omega\phi)$
$(512 \pm 15) - i(188 \pm 12)$	1 ABLIKIM 17	BES3	$J/\psi \rightarrow \gamma 3\pi$
$(440 \pm 10) - i(238 \pm 10)$	2 ALBALADEJO 12	RVUE	Compilation
$(445 \pm 25) - i(278 \pm 18)$	3.4 GARCIA-MAR..11	RVUE	Compilation
$(457 \pm 14) - i(279 \pm 11)$	3.5 GARCIA-MAR..11	RVUE	Compilation
$(442 \pm 8) - i(274 \pm 6)$	6 MOUSSALLAM11	RVUE	Compilation
$(452 \pm 13) - i(259 \pm 16)$	7 MENNESSIER 10	RVUE	Compilation
$(448 \pm 43) - i(266 \pm 43)$	8 MENNESSIER 10	RVUE	Compilation
$(455 \pm 6 \pm 31) - i(278 \pm 6 \pm 34)$	9 CAPRINI 08	RVUE	Compilation
$(463 \pm 6 \pm 17) - i(259 \pm 6 \pm 34)$	10 CAPRINI 08	RVUE	Compilation
$(552 \pm 84) - i(232 \pm 81)$	11 ABLIKIM 07A	BES2	$\psi(2S) \rightarrow \pi^+\pi^- J/\psi$
$(466 \pm 18) - i(223 \pm 28)$	12 BONVICINI 07	CLEO	$D^+ \rightarrow \pi^-\pi^+\pi^+$
$(472 \pm 30) - i(271 \pm 30)$	13 BUGG 07A	RVUE	Compilation
$(484 \pm 17) - i(255 \pm 10)$	14 GARCIA-MAR..07	RVUE	Compilation
$(430) - i(325)$	14 ANISOVICH 06	RVUE	Compilation
$(441 \pm 16) - i(272 \pm 9)$	15 CAPRINI 06	RVUE	$\pi\pi \rightarrow \pi\pi$
$(470 \pm 50) - i(285 \pm 25)$	16 ZHOU 05	RVUE	
$(541 \pm 39) - i(252 \pm 42)$	17 ABLIKIM 04A	BES2	$J/\psi \rightarrow \omega\pi^+\pi^-$
$(528 \pm 32) - i(207 \pm 23)$	18 GALLEGOS 04	RVUE	Compilation
$(533 \pm 25) - i(249 \pm 25)$	19 BUGG 03	RVUE	

Meson Particle Listings

$f_0(500)$

517 - i240 (470 ± 30) - i(295 ± 20) (535 ± 48) - i(155 ± 75) 610 ± 14 - i(310 ± 13) (540 ± 36) - i(193 ± 32) -29 - i(193 ± 40)	BLACK 01 15 COLANGELO 01 20 ISHIDA 01 21 SUROVTSEV 01 ISHIDA 00B	RVUE $\pi\pi \rightarrow \pi\pi$ RVUE $\pi\pi \rightarrow \pi\pi$ $\Upsilon(3S) \rightarrow \Upsilon\pi\pi$ RVUE $\pi\pi \rightarrow \pi\pi, K\bar{K}$ $p\bar{p} \rightarrow \pi^0\pi^0\pi^0$
445 - i235 (523 ± 12) - i(259 ± 7) 442 - i 227 469 - i203 445 - i221 420 - i 212 440 - i245 (602 ± 26) - i(196 ± 27) (537 ± 20) - i(250 ± 17) 470 - i250	HANNAH 99 KA MINSKI 99 OLLER 99 OLLER 99B OLLER 99C LOCHER 98 22 DOBADO 97 23 ISHIDA 97 24 KA MINSKI 97B 25,26 TORNQVIST 96	RVUE π scalar form factor RVUE $\pi\pi \rightarrow \pi\pi, K\bar{K}, \sigma\sigma$ RVUE $\pi\pi \rightarrow \pi\pi, K\bar{K}$ RVUE $\pi\pi \rightarrow \pi\pi, K\bar{K}$ RVUE $\pi\pi \rightarrow \pi\pi, K\bar{K}, \eta\eta$ RVUE $\pi\pi \rightarrow \pi\pi, K\bar{K}$ RVUE Compilation RVUE $\pi\pi \rightarrow \pi\pi$ RVUE $\pi\pi \rightarrow \pi\pi, K\bar{K}, 4\pi$ RVUE $\pi\pi \rightarrow \pi\pi, K\bar{K}, K\pi,$ $\eta\pi$
387 - i305 420 - i370 (506 ± 10) - i(247 ± 3) 370 - i356 408 - i342 470 - i208	26,27 JANSSEN 95 28 ACHASOV 94 KA MINSKI 94 29 ZOU 94B 26,29 ZOU 93 30 VANBEVEREN 86	RVUE $\pi\pi \rightarrow \pi\pi, K\bar{K}$ RVUE $\pi\pi \rightarrow \pi\pi, K\bar{K}$ RVUE $\pi\pi \rightarrow \pi\pi, K\bar{K}$ RVUE $\pi\pi \rightarrow \pi\pi, K\bar{K}$ RVUE $\pi\pi \rightarrow \pi\pi, K\bar{K}, \eta\eta,$ \dots
(750 ± 50) - i(450 ± 50) (660 ± 100) - i(320 ± 70) 650 - i370	31 ESTABROOKS 79 PROTOP... 73 32 BASDEVANT 72	RVUE $\pi\pi \rightarrow \pi\pi, K\bar{K}$ HBC $\pi\pi \rightarrow \pi\pi, K\bar{K}$ RVUE $\pi\pi \rightarrow \pi\pi$

- S-matrix pole; 8595 events.
- Applying the chiral unitary approach at NLO to the K_{e4} data of BATLEY 10 and $\pi N \rightarrow \pi\pi N$ data of HYAMS 73, GRAYER 74, and PROTOPOESCU 73.
- Uses the K_{e4} data of BATLEY 10c and the $\pi N \rightarrow \pi\pi N$ data of HYAMS 73, GRAYER 74, and PROTOPOESCU 73.
- Analytic continuation using Roy equations.
- Analytic continuation using GKP equations.
- Using Roy equations.
- Average of three variants of the analytic K-matrix model. Uses the K_{e4} data of BATLEY 08a and the $\pi N \rightarrow \pi\pi N$ data of HYAMS 73 and GRAYER 74.
- Average of the analyses of three data sets in the K-matrix model. Uses the data of BATLEY 08a, HYAMS 73, and GRAYER 74, partially of COHEN 80 or ETKIN 82b.
- From the K_{e4} data of BATLEY 08a and $\pi N \rightarrow \pi\pi N$ data of HYAMS 73.
- From the K_{e4} data of BATLEY 08a and $\pi N \rightarrow \pi\pi N$ data of PROTOPOESCU 73, GRAYER 74, and ESTABROOKS 74.
- From a mean of three different $f_0(500)$ parametrizations. Uses 40k events.
- From an isobar model using 2.6k events.
- Reanalysis of ABLIKIM 04a, PISLAK 01, and HYAMS 73 data.
- Using the N/D method.
- From the solution of the Roy equation (ROY 71) for the isoscalar S-wave and using a phase-shift analysis of HYAMS 73 and PROTOPOESCU 73 data.
- Reanalysis of the data from PROTOPOESCU 73, ESTABROOKS 74, GRAYER 74, ROSSELET 77, PISLAK 03, and AKHMETSHIN 04.
- From a mean of six different analyses and $f_0(500)$ parameterizations.
- Using data on $\psi(2S) \rightarrow J/\psi\pi\pi$ from BAI 00E and on $\Upsilon(3S) \rightarrow \Upsilon(mS)\pi\pi$ from BUTLER 94b and ALEXANDER 98.
- From a combined analysis of HYAMS 73, AUGUSTIN 89, AITALA 01b, and PISLAK 01.
- A similar analysis (KOMADA 01) finds $(580^{+79}_{-30}) - i(190^{+107}_{-49})$ MeV.
- Coupled channel reanalysis of BATON 70, BENSINGER 71, BAILLON 72, HYAMS 73, HYAMS 75, ROSSELET 77, COHEN 80, and ETKIN 82b using the uniformizing variable.
- Using the inverse amplitude method and data of ESTABROOKS 73, GRAYER 74, and PROTOPOESCU 73.
- Reanalysis of data from HYAMS 73, GRAYER 74, SRINIVASAN 75, and ROSSELET 77 using the interfering amplitude method.
- Average and spread of 4 variants ("up" and "down") of KAMINSKI 97b 3-channel model.
- Uses data from BEIER 72b, OCHS 73, HYAMS 73, GRAYER 74, ROSSELET 77, CASON 83, ASTON 88, and ARMSTRONG 91b. Coupled channel analysis with flavor symmetry and all light two-pseudoscalars systems.
- Demonstrates explicitly that $f_0(500)$ and $f_0(1370)$ are two different poles.
- Analysis of data from FALVARD 88.
- Analysis of data from OCHS 73, ESTABROOKS 75, ROSSELET 77, and MUKHIN 80.
- Analysis of data from OCHS 73, GRAYER 74, and ROSSELET 77.
- Coupled-channel analysis using data from PROTOPOESCU 73, HYAMS 73, HYAMS 75, GRAYER 74, ESTABROOKS 74, ESTABROOKS 75, FROGGATT 77, CORDEN 79, BISWAS 81.
- Analysis of data from APEL 72c, GRAYER 74, CASON 76, PAWLICKI 77. Includes spread and errors of 4 solutions.
- Analysis of data from BATON 70, BENSINGER 71, COLTON 71, BAILLON 72, PROTOPOESCU 73, and WALKER 67.

$f_0(500)$ BREIT-WIGNER MASS

VALUE (MeV)	DOCUMENT ID	TECN	COMMENT
400 to 800 OUR ESTIMATE			
• • • We do not use the following data for averages, fits, limits, etc. • • •			
513 ± 32	33 MURAMATSU 02	CLEO	$e^+e^- \approx 10$ GeV
478 ± 24 -23 ± 17	AITALA 01B	E791	$D^+ \rightarrow \pi^-\pi^+\pi^+$
563 ± 58 -29	34 ISHIDA 01		$\Upsilon(3S) \rightarrow \Upsilon\pi\pi$
555	35 ASNER 00	CLE2	$\tau^- \rightarrow \pi^-\pi^0\pi^0\nu_\tau$
540 ± 36	ISHIDA 00B		$p\bar{p} \rightarrow \pi^0\pi^0\pi^0$
750 ± 4	ALEKSEEV 99	SPEC	$1.78 \pi^-\rho_{\text{polar}} \rightarrow \pi^-\pi^+n$
744 ± 5	ALEKSEEV 98	SPEC	$1.78 \pi^-\rho_{\text{polar}} \rightarrow \pi^-\pi^+n$

759 ± 5 780 ± 30 585 ± 20 761 ± 12 ~ 860 1165 ± 50	36 TROYAN 98 ALDE 97 37 ISHIDA 97 38 SVEC 96 39,40 TORNQVIST 96 41,42 ANISOVICH 95	5.2 $np \rightarrow np\pi^+\pi^-$ 450 $pp \rightarrow pp\pi^0\pi^0$ $\pi\pi \rightarrow \pi\pi$ 6-17 $\pi N_{\text{polar}} \rightarrow \pi^+\pi^-N$ $\pi\pi \rightarrow \pi\pi, K\bar{K}, K\pi, \eta\pi$ $\pi^-p \rightarrow \pi^0\pi^0n,$ $\bar{p}p \rightarrow \pi^0\pi^0\pi^0, \pi^0\pi^0\eta,$ $\pi^0\eta\eta$
414 ± 20	38 AUGUSTIN 89	DM2

$f_0(500)$ BREIT-WIGNER WIDTH

VALUE (MeV)	DOCUMENT ID	TECN	COMMENT
100 to 800 OUR ESTIMATE			
• • • We do not use the following data for averages, fits, limits, etc. • • •			
335 ± 67	43 MURAMATSU 02	CLEO	$e^+e^- \approx 10$ GeV
324 ± 42 -40 ± 21	AITALA 01B	E791	$D^+ \rightarrow \pi^-\pi^+\pi^+$
372 ± 229 -95	44 ISHIDA 01		$\Upsilon(3S) \rightarrow \Upsilon\pi\pi$
540	45 ASNER 00	CLE2	$\tau^- \rightarrow \pi^-\pi^0\pi^0\nu_\tau$
372 ± 80	ISHIDA 00B		$p\bar{p} \rightarrow \pi^0\pi^0\pi^0$
119 ± 13	ALEKSEEV 99	SPEC	$1.78 \pi^-\rho_{\text{polar}} \rightarrow \pi^-\pi^+n$
77 ± 22	ALEKSEEV 98	SPEC	$1.78 \pi^-\rho_{\text{polar}} \rightarrow \pi^-\pi^+n$
35 ± 12	46 TROYAN 98		$5.2 np \rightarrow np\pi^+\pi^-$
780 ± 60	ALDE 97	GAM2	$450 pp \rightarrow pp\pi^0\pi^0$
385 ± 70	47 ISHIDA 97		$\pi\pi \rightarrow \pi\pi$
290 ± 54	48 SVEC 96	RVUE	6-17 $\pi N_{\text{polar}} \rightarrow \pi^+\pi^-N$
~ 880	49,50 TORNQVIST 96	RVUE	$\pi\pi \rightarrow \pi\pi, K\bar{K}, K\pi, \eta\pi$
460 ± 40	51,52 ANISOVICH 95	RVUE	$\pi^-p \rightarrow \pi^0\pi^0n,$ $\bar{p}p \rightarrow \pi^0\pi^0\pi^0, \pi^0\pi^0\eta,$ $\pi^0\eta\eta$
494 ± 58	48 AUGUSTIN 89	DM2	

$f_0(500)$ DECAY MODES

Mode	Fraction (Γ_i/Γ)
Γ_1 $\pi\pi$	seen
Γ_2 $\gamma\gamma$	seen

$f_0(500)$ PARTIAL WIDTHS

VALUE (keV)	DOCUMENT ID	TECN	COMMENT
• • • We do not use the following data for averages, fits, limits, etc. • • •			
2.05 ± 0.21	53 DAI 14A	RVUE	Compilation
1.7 ± 0.4	54 HOFERICH... 11	RVUE	Compilation
3.08 ± 0.82	55 MENNESSIER 11	RVUE	Compilation
2.08 ± 0.2 ± 0.07 -0.04	56 MOUSSALLAMI 11	RVUE	Compilation
2.08	57 MAO 09	RVUE	Compilation
1.2 ± 0.4	58 BERNABEU 08	RVUE	
3.9 ± 0.6	55 MENNESSIER 08	RVUE	$\gamma\gamma \rightarrow \pi^+\pi^-, \pi^0\pi^0$

See key on page 1127

Meson Particle Listings

f_0(500), rho(770)

Table of references for f_0(500) and rho(770) mesons, listing authors, years, and methods.

Table of references for rho(770) meson, listing authors, years, and methods.

f_0(500) REFERENCES

Table of references for f_0(500) meson, listing authors, years, and methods.

rho(770)

I^G(J^PC) = 1^+(1^-)

rho(770) T-MATRIX POLE sqrt(s)

Table of rho(770) T-matrix pole values, document IDs, and comments.

rho(770) MASS

We no longer list S-wave Breit-Wigner fits, or data with high combinatorial background.

NEUTRAL ONLY, e+e-

Table of neutral rho(770) mass measurements from e+e- collisions.

- Footnotes explaining the data selection criteria and fit methods.

Downloaded from https://academic.oup.com/ptep/article/2022/8/083C01/6651666 by CERN Library user on 11 October 2022

Meson Particle Listings

$\rho(770)$

- ⁴ Supersedes ACHASOV 05A.
- ⁵ A fit of the SND data from 400 to 1000 MeV using parameters of the $\rho(1450)$ and $\rho(1700)$ from a fit of the data of BARKOV 85, BISELLO 89 and ANDERSON 00A.
- ⁶ Using the GOUNARIS 68 parametrization with the complex phase of the ρ - ω interference.
- ⁷ Update of AKHMETSHIN 02.
- ⁸ Assuming $m_{\rho^+} = m_{\rho^-}, \Gamma_{\rho^+} = \Gamma_{\rho^-}$.
- ⁹ From the GOUNARIS 68 parametrization of the pion form factor.
- ¹⁰ Applies the Unitary & Analytic Model of the pion electromagnetic form factor of DUBNICKA 10 to analyze the data of LEES 12G and ABLIKIM 16C.
- ¹¹ Applies the Unitary & Analytic Model of the pion electromagnetic form factor of DUBNICKA 10 to analyze the data of ACHASOV 06, AKHMETSHIN 07, AUBERT 09As, and AMBROSINO 11A.
- ¹² Assuming $m_{\rho^+} = m_{\rho^-} = m_{\rho^0}, \Gamma_{\rho^+} = \Gamma_{\rho^-} = \Gamma_{\rho^0}$.
- ¹³ Without limitations on masses and widths.
- ¹⁴ Assuming $m_{\rho^0} = m_{\rho^\pm}, g_{\rho^0\pi\pi} = g_{\rho^\pm\pi\pi}$.
- ¹⁵ Using the data of BARKOV 85 in the hidden local symmetry model.
- ¹⁶ From the fit to $e^+e^- \rightarrow \pi^+\pi^-$ data from the compilations of HEYN 81 and BARKOV 85, including the GOUNARIS 68 parametrization of the pion form factor.
- ¹⁷ A fit of BARKOV 85 data assuming the direct $\omega\pi\pi$ coupling.
- ¹⁸ Applying the S-matrix formalism to the BARKOV 85 data.
- ¹⁹ Includes BARKOV 85 data. Model-dependent width definition.

CHARGED ONLY, τ DECAYS and e^+e^-

VALUE (MeV)	EVTS	DOCUMENT ID	TECN	CHG	COMMENT
775.11 ± 0.34 OUR AVERAGE					
774.6 ± 0.2 ± 0.5	5.4M	^{1,2} FUJIKAWA 08	BELL	±	$\tau^- \rightarrow \pi^- \pi^0 \nu_\tau$
775.5 ± 0.7		^{2,3} SCHAELE 05C	ALEP		$\tau^- \rightarrow \pi^- \pi^0 \nu_\tau$
775.5 ± 0.5 ± 0.4	1.98M	⁴ ALOISIO 03	KLOE		$1.02 e^+e^- \rightarrow \pi^+\pi^-\pi^0$
775.1 ± 1.1 ± 0.5	87k	^{5,6} ANDERSON 00A	CLE2		$\tau^- \rightarrow \pi^- \pi^0 \nu_\tau$

- • • We do not use the following data for averages, fits, limits, etc. • • •
- ⁷ BARTOS 17A RVUE $\tau^- \rightarrow \pi^- \pi^0 \nu_\tau$
- ⁸ ALOISIO 03 KLOE - $1.02 e^+e^- \rightarrow \pi^+\pi^-\pi^0$
- ⁸ ALOISIO 03 KLOE + $1.02 e^+e^- \rightarrow \pi^+\pi^-\pi^0$
- ⁹ SANZ-CILLERO03 RVUE $\tau^- \rightarrow \pi^- \pi^0 \nu_\tau$
- ⁴ ACHASOV 02 SND ± $1.02 e^+e^- \rightarrow \pi^+\pi^-\pi^0$
- ¹⁰ PICH 01 RVUE $\tau^- \rightarrow \pi^- \pi^0 \nu_\tau$
- ¹ $|F_\pi(0)|^2$ fixed to 1.
- ² From the GOUNARIS 68 parametrization of the pion form factor.
- ³ The error combines statistical and systematic uncertainties. Supersedes BARATE 97M.
- ⁴ Assuming $m_{\rho^+} = m_{\rho^-}, \Gamma_{\rho^+} = \Gamma_{\rho^-}$.
- ⁵ $\rho(1700)$ mass and width fixed at 1700 MeV and 235 MeV respectively.
- ⁶ From the GOUNARIS 68 parametrization of the pion form factor. The second error is a model error taking into account different parametrizations of the pion form factor.
- ⁷ Applies the Unitary & Analytic Model of the pion electromagnetic form factor of DUBNICKA 10 to analyze the data of FUJIKAWA 08.
- ⁸ Without limitations on masses and widths.
- ⁹ Using the data of BARATE 97M and the effective chiral Lagrangian.
- ¹⁰ From a fit of the model-independent parameterization of the pion form factor to the data of BARATE 97M.

MIXED CHARGES, OTHER REACTIONS

VALUE (MeV)	EVTS	DOCUMENT ID	TECN	CHG	COMMENT
763.0 ± 0.3 ± 1.2	600k	¹ ABELE 99E	CBAR	0±	$0.0 \bar{p}p \rightarrow \pi^+\pi^-\pi^0$

- ¹ Assuming the equality of ρ^+ and ρ^- masses and widths.

CHARGED ONLY, HADROPRODUCED

VALUE (MeV)	EVTS	DOCUMENT ID	TECN	CHG	COMMENT
766.5 ± 1.1 OUR AVERAGE					
763.7 ± 3.2		ABELE 97	CBAR		$\bar{p}n \rightarrow \pi^- \pi^0 \pi^0$
768 ± 9		AGUILAR... 91	EHS		400 pp
767 ± 3	2935	¹ CAPRARO 87	SPEC	-	$200 \pi^- \text{Cu} \rightarrow \pi^- \pi^0 \text{Cu}$
761 ± 5	967	¹ CAPRARO 87	SPEC	-	$200 \pi^- \text{Pb} \rightarrow \pi^- \pi^0 \text{Pb}$
771 ± 4		HUSTON 86	SPEC	+	$202 \pi^+ \text{A} \rightarrow \pi^+ \pi^0 \text{A}$
766 ± 7	6500	² BYERLY 73	OSPK		$5 \pi^- p$
766.8 ± 1.5	9650	³ PISUT 68	RVUE	-	$1.7-3.2 \pi^- p, t < 10$
767 ± 6	900	¹ EISNER 67	HBC	-	$4.2 \pi^- p, t < 10$

- ¹ Mass errors enlarged by us to Γ/\sqrt{N} ; see the note with the $K^*(892)$ mass.
- ² Phase shift analysis. Systematic errors added corresponding to spread of different fits.
- ³ From fit of 3-parameter relativistic P-wave Breit-Wigner to total mass distribution. Includes BATON 68, MILLER 67B, ALFF-STEINBERGER 66, HAGOPIAN 66, HAGOPIAN 66B, JACOBS 66B, JAMES 66, WEST 66, BLIEDEN 65 and CARMONY 64.

NEUTRAL ONLY, PHOTOPRODUCED

VALUE (MeV)	EVTS	DOCUMENT ID	TECN	COMMENT
769.2 ± 0.9 OUR AVERAGE				
770.8 ± 1.3 ± 2.3 ± 2.4	900k	ANDREEV 20	H1	$ep \rightarrow e\pi^+\pi^-p$
771 ± 2 ± 2 ± 1	63.5k	¹ ABRA MOWICZ12	ZEUS	$ep \rightarrow e\pi^+\pi^-p$
770 ± 2 ± 1	79k	² BREITWEG 98B	ZEUS	50-100 γp
767.6 ± 2.7		BARTALUCCI 78	CNTR	$\gamma p \rightarrow e^+e^-p$
775 ± 5		GLADDING 73	CNTR	2.9-4.7 γp

767 ± 4	1930	BALLAM 72	HBC	2.8 γp
770 ± 4	2430	BALLAM 72	HBC	4.7 γp
765 ± 10		ALVENSLEB... 70	CNTR	$\gamma A, t < 0.01$
767.7 ± 1.9	140k	BIGGS 70	CNTR	$< 4.1 \gamma C \rightarrow \pi^+\pi^-C$
765 ± 5	4000	ASBURY 67B	CNTR	$\gamma + \text{Pb}$

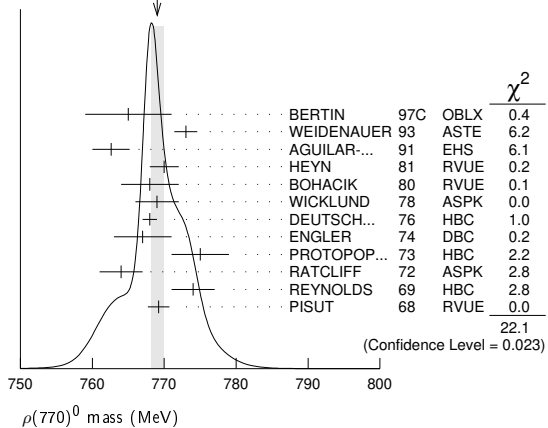
- • • We do not use the following data for averages, fits, limits, etc. • • •
- ¹ Using the KUHN 90 parametrization of the pion form factor, neglecting ρ - ω interference.
- ² From the parametrization according to SOEDING 66.
- ³ From the parametrization according to ROSS 66.

NEUTRAL ONLY, OTHER REACTIONS

VALUE (MeV)	EVTS	DOCUMENT ID	TECN	COMMENT
769.0 ± 0.9 OUR AVERAGE				Error includes scale factor of 1.4. See the ideogram below.
765 ± 6		BERTIN 97C	OBLX	$0.0 \bar{p}p \rightarrow \pi^+\pi^-\pi^0$
773 ± 1.6		WEIDENAUER 93	ASTE	$\bar{p}p \rightarrow \pi^+\pi^-\omega$
762.6 ± 2.6		AGUILAR... 91	EHS	400 pp
770 ± 2		¹ HEYN 81	RVUE	Pion form factor
768 ± 4		^{2,3} BOHACIK 80	RVUE	
769 ± 3		⁴ WICKLUND 78	ASPK	3,4,6 $\pi^\pm N$
768 ± 1	76k	DEUTSCH... 76	HBC	16 $\pi^+ p$
767 ± 4	4100	ENGLER 74	DBC	$6 \pi^+ n \rightarrow \pi^+\pi^-\pi^0$
775 ± 4	32k	² PROTOPO... 73	HBC	$7.1 \pi^+ p, t < 0.4$
764 ± 3	6.8k	⁵ RATCLIFF 72	ASPK	15 $\pi^- p, t < 0.3$
774 ± 3	1.7k	REYNOLDS 69	HBC	2.26 $\pi^- p$
769.2 ± 1.5	13.3k	⁶ PISUT 68	RVUE	$1.7-3.2 \pi^- p, t < 10$

- • • We do not use the following data for averages, fits, limits, etc. • • •
- ⁷ ABLIKIM 18C BES3 $\eta'(958) \rightarrow \gamma\pi^+\pi^-$
- ⁸ ABLIKIM 18C BES3 $\eta'(958) \rightarrow \gamma\pi^+\pi^-$
- ⁹ COLANGELO 01 RVUE $\pi\pi \rightarrow \pi\pi$
- ¹⁰ ABELE 99E CBAR $0.0 \bar{p}p \rightarrow \pi^+\pi^-\pi^0$
- ¹¹ ADAMS 97 E665 $470 \mu p \rightarrow \mu X B$
- ¹² BOGOLYUB... 97 MIRA $32 \bar{p}p \rightarrow \pi^+\pi^-X$
- ¹² BOGOLYUB... 97 MIRA $32 pp \rightarrow \pi^+\pi^-X$
- DUBNICKA 89 RVUE π form factor
- ¹³ CHABAUD 83 ASPK $17 \pi^- p$ polarized
- ^{2,3} LANG 79 RVUE
- ³ ESTABROOKS 74 RVUE $17 \pi^- p \rightarrow \pi^+\pi^-n$
- ¹⁴ JACOBS 72 HBC $2.8 \pi^- p$
- ¹⁵ HYAMS 68 OSPK $11.2 \pi^- p$

WEIGHTED AVERAGE
769.0 ± 0.9 (Error scaled by 1.4)



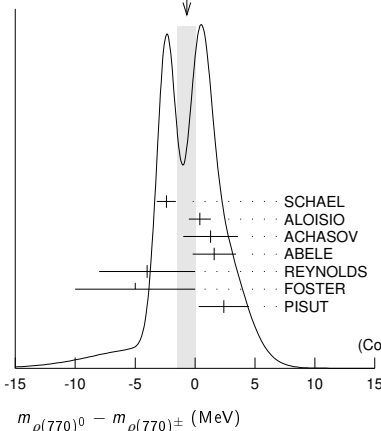
- ¹ HEYN 81 includes all spacelike and timelike F_π values until 1978.
- ² From pole extrapolation.
- ³ From phase shift analysis of GRAYER 74 data.
- ⁴ Phase shift analysis. Systematic errors added corresponding to spread of different fits.
- ⁵ Published values contain misprints. Corrected by private communication RATCLIFF 74.
- ⁶ Includes MALAMUD 69, ARMENSE 68, BACON 67, HUVE 67, MILLER 67B, ALFF-STEINBERGER 66, HAGOPIAN 66, HAGOPIAN 66B, JACOBS 66B, JAMES 66, WEST 66, GOLDBERGER 64, ABOLINS 63.
- ⁷ From a fit to $\pi^+\pi^-$ mass using $\rho(770)$ (parametrized with the Gounaris-Sakurai approach), $\omega(782)$, and box anomaly components.
- ⁸ From a fit to $\pi^+\pi^-$ mass using $\rho(770)$ (parametrized with the Gounaris-Sakurai approach), $\omega(782)$, and $\rho(1450)$ components.
- ⁹ Breit-Wigner mass from a phase-shift analysis of HYAMS 73 and PROTOPESCU 73 data.
- ¹⁰ Using relativistic Breit-Wigner and taking into account ρ - ω interference.
- ¹¹ Systematic errors not evaluated.
- ¹² Systematic effects not studied.
- ¹³ From fit of 3-parameter relativistic Breit-Wigner to helicity-zero part of P-wave intensity. CHABAUD 83 includes data of GRAYER 74.
- ¹⁴ Mass errors enlarged by us to Γ/\sqrt{N} ; see the note with the $K^*(892)$ mass.
- ¹⁵ Of HYAMS 68 six parametrizations, this is theoretically soundest. MR

$m_{\rho(770)^0} - m_{\rho(770)^\pm}$

VALUE (MeV)	EVTs	DOCUMENT ID	TECN	CHG	COMMENT
-0.7 ± 0.8 OUR AVERAGE					Error includes scale factor of 1.5. See the ideogram below.
-2.4 ± 0.8		1 SCHAEL	05c	ALEP	$\tau^- \rightarrow \pi^- \pi^0 \nu_\tau$
0.4 ± 0.7 ± 0.6 1.98M		2 ALOISIO	03	KLOE	$1.02 e^+ e^- \rightarrow \pi^+ \pi^- \pi^0$
1.3 ± 1.1 ± 2.0 500k		2 ACHASOV	02	SND	$1.02 e^+ e^- \rightarrow \pi^+ \pi^- \pi^0$
1.6 ± 0.6 ± 1.7 600k		ABELE	99E	CBAR ± 0	$0.0 \bar{p} p \rightarrow \pi^+ \pi^- \pi^0$
-4 ± 4 3000		3 REYNOLDS	69	HBC - 0	$2.26 \pi^- p$
-5 ± 5 3600		3 FOSTER	68	HBC ± 0	$0.0 \bar{p} p$
2.4 ± 2.1 22950		4 PISUT	68	RVUE	$\pi N \rightarrow \rho N$
-3.37 ± 1.06		5 BARTOS	17A	RVUE	$e^+ e^- \rightarrow \pi^+ \pi^-$, $\tau^- \rightarrow \pi^- \pi^0 \nu_\tau$

• • • We do not use the following data for averages, fits, limits, etc. • • •

WEIGHTED AVERAGE
-0.7±0.8 (Error scaled by 1.5)



1 From the combined fit of the τ^- data from ANDERSON 00A and SCHAEL 05c and $e^+ e^-$ data from the compilation of BARKOV 85, AKHMETSHIN 04, and ALOISIO 05. Supersedes BARATE 97M.

2 Assuming $m_{\rho^+} = m_{\rho^-}$, $\Gamma_{\rho^+} = \Gamma_{\rho^-}$.

3 From quoted masses of charged and neutral modes.

4 Includes MALAMUD 69, ARMENISE 68, BATON 68, BACON 67, HUWE 67, MILLER 67B, ALFF-STEINBERGER 66, HAGOPIAN 66, HAGOPIAN 66B, JACOBS 66B, JAMES 66, WEST 66, BLIEDEN 65, CARMONY 64, GOLDBABER 64, ABOLINS 63.

5 Applies the Unitary & Analytic Model of the pion electromagnetic form factor of DUBNICKA 10 to analyze the data of ACHASOV 06, AKHMETSHIN 07, AUBERT 09As, AMBROSINO 11A, and FUJIKAWA 08.

$m_{\rho(770)^+} - m_{\rho(770)^-}$

VALUE (MeV)	EVTs	DOCUMENT ID	TECN	CHG	COMMENT
1.5 ± 0.8 ± 0.7	1.98M	1 ALOISIO	03	KLOE	$1.02 e^+ e^- \rightarrow \pi^+ \pi^- \pi^0$

1 Without limitations on masses and widths.

$\rho(770)$ RANGE PARAMETER

The range parameter R enters an energy-dependent correction to the width, of the form $(1 + q^2 R^2) / (1 + q^2 R^2)$, where q is the momentum of one of the pions in the $\pi\pi$ rest system. At resonance, $q = q_r$.

VALUE (GeV ⁻¹)	DOCUMENT ID	TECN	CHG	COMMENT
5.3 ± 0.9	1 CHABAUD	83	ASPK	0 17 $\pi^- p$ polarized

1 The old PISUT 68 value, properly corrected, was 3.2 ± 0.6 .

$\rho(770)$ WIDTH

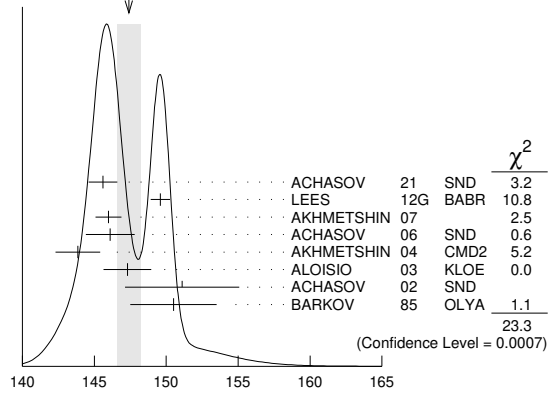
We no longer list S-wave Breit-Wigner fits, or data with high combinatorial background.

NEUTRAL ONLY, $e^+ e^-$

VALUE (MeV)	EVTs	DOCUMENT ID	TECN	CHG	COMMENT
147.4 ± 0.8 OUR AVERAGE					Error includes scale factor of 2.0. See the ideogram below.
145.6 ± 0.6 ± 0.8		1 ACHASOV	21	SND	$e^+ e^- \rightarrow \pi^+ \pi^-$
149.59 ± 0.67		2 LEES	12G	BABR	$e^+ e^- \rightarrow \pi^+ \pi^- \gamma$
145.98 ± 0.75 ± 0.50	900k	3 AKHMETSHIN	07		$e^+ e^- \rightarrow \pi^+ \pi^-$
146.1 ± 0.8 ± 1.5	800k	4.5 ACHASOV	06	SND	$e^+ e^- \rightarrow \pi^+ \pi^-$

143.85 ± 1.33 ± 0.80	114k	6,7 AKHMETSHIN	04	CMD2	$e^+ e^- \rightarrow \pi^+ \pi^-$
147.3 ± 1.5 ± 0.7	1.98M	8 ALOISIO	03	KLOE	$1.02 e^+ e^- \rightarrow \pi^+ \pi^- \pi^0$
151.1 ± 2.6 ± 3.0	500k	8 ACHASOV	02	SND	$1.02 e^+ e^- \rightarrow \pi^+ \pi^- \pi^0$
150.5 ± 3.0		9 BARKOV	85	OLYA	$e^+ e^- \rightarrow \pi^+ \pi^-$
• • • We do not use the following data for averages, fits, limits, etc. • • •					
144.06 ± 0.85		10 BARTOS	17	RVUE	$e^+ e^- \rightarrow \pi^+ \pi^-$
144.56 ± 0.80		11 BARTOS	17A	RVUE	$e^+ e^- \rightarrow \pi^+ \pi^-$
143.9 ± 1.3 ± 1.1	1.98M	12 ALOISIO	03	KLOE	$1.02 e^+ e^- \rightarrow \pi^+ \pi^- \pi^0$
147.4 ± 1.5 ± 0.7	1.98M	13 ALOISIO	03	KLOE	$1.02 e^+ e^- \rightarrow \pi^+ \pi^- \pi^0$
149.8 ± 2.2 ± 2.0	500k	14 ACHASOV	02	SND	$1.02 e^+ e^- \rightarrow \pi^+ \pi^- \pi^0$
147.9 ± 1.5 ± 7.5		15 BENAYOUN	98	RVUE	$e^+ e^- \rightarrow \pi^+ \pi^-$, $\mu^+ \mu^-$
153.5 ± 1.3 ± 4.6		16 GARDNER	98	RVUE	$0.28-0.92 e^+ e^- \rightarrow \pi^+ \pi^-$
145.0 ± 1.7		17 O'CONNELL	97	RVUE	$e^+ e^- \rightarrow \pi^+ \pi^-$
142.5 ± 3.5		18 BERNICHA	94	RVUE	$e^+ e^- \rightarrow \pi^+ \pi^-$
138 ± 1		19 GESHKEN...	89	RVUE	$e^+ e^- \rightarrow \pi^+ \pi^-$

WEIGHTED AVERAGE
147.4±0.8 (Error scaled by 2.0)



1 From a fit of the cross section in the energy range $0.525 < \sqrt{s} < 0.883$ GeV parameterized by the sum of the Breit-Wigner amplitudes for the $\rho(770)$, ω and $\rho(1450)$ resonances.

2 Using the GOUNARIS 68 parametrization with the complex phase of the ρ - ω interference and leaving the masses and widths of the $\rho(1450)$, $\rho(1700)$, and $\rho(2150)$ resonances as free parameters of the fit.

3 A combined fit of AKHMETSHIN 07, AULCHENKO 06, and AULCHENKO 05.

4 Supersedes ACHASOV 05A.

5 A fit of the SND data from 400 to 1000 MeV using parameters of the $\rho(1450)$ and $\rho(1700)$ from a fit of the data of BARKOV 85, BISELLO 89 and ANDERSON 00A.

6 Using the GOUNARIS 68 parametrization with the complex phase of the ρ - ω interference.

7 From a fit in the energy range 0.61 to 0.96 GeV. Update of AKHMETSHIN 02.

8 Assuming $m_{\rho^+} = m_{\rho^-}$, $\Gamma_{\rho^+} = \Gamma_{\rho^-}$.

9 From the GOUNARIS 68 parametrization of the pion form factor.

10 Applies the Unitary & Analytic Model of the pion electromagnetic form factor of DUBNICKA 10 to analyze the data of LEES 12G and ABLIKIM 16c.

11 Applies the Unitary & Analytic Model of the pion electromagnetic form factor of DUBNICKA 10 to analyze the data of ACHASOV 06, AKHMETSHIN 07, AUBERT 09As, and AMBROSINO 11A.

12 Assuming $m_{\rho^+} = m_{\rho^-} = m_{\rho^0}$, $\Gamma_{\rho^+} = \Gamma_{\rho^-} = \Gamma_{\rho^0}$.

13 Without limitations on masses and widths.

14 Assuming $m_{\rho^0} = m_{\rho^\pm}$, $g_{\rho^0 \pi \pi} = g_{\rho^\pm \pi \pi}$.

15 Using the data of BARKOV 85 in the hidden local symmetry model.

16 From the fit to $e^+ e^- \rightarrow \pi^+ \pi^-$ data from the compilations of HEYN 81 and BARKOV 85, including the GOUNARIS 68 parametrization of the pion form factor.

17 A fit of BARKOV 85 data assuming the direct $\omega \pi \pi$ coupling.

18 Applying the S-matrix formalism to the BARKOV 85 data.

19 Includes BARKOV 85 data. Model-dependent width definition.

CHARGED ONLY, τ DECAYS and $e^+ e^-$

VALUE (MeV)	EVTs	DOCUMENT ID	TECN	CHG	COMMENT
149.1 ± 0.8 OUR FIT					
149.1 ± 0.8 OUR AVERAGE					
148.1 ± 0.4 ± 1.7 5.4M		1,2 FUJIKAWA	08	BELL ±	$\tau^- \rightarrow \pi^- \pi^0 \nu_\tau$
149.0 ± 1.2		2,3 SCHAEL	05c	ALEP	$\tau^- \rightarrow \pi^- \pi^0 \nu_\tau$
149.9 ± 2.3 ± 2.0 500k		4 ACHASOV	02	SND ±	$1.02 e^+ e^- \rightarrow \pi^+ \pi^- \pi^0$
150.4 ± 1.4 ± 1.4 87k		5,6 ANDERSON	00A	CLE2	$\tau^- \rightarrow \pi^- \pi^0 \nu_\tau$
• • • We do not use the following data for averages, fits, limits, etc. • • •					
139.90 ± 0.46		7 BARTOS	17A	RVUE	$\tau^- \rightarrow \pi^- \pi^0 \nu_\tau$
143.7 ± 1.3 ± 1.2 1.98M		4 ALOISIO	03	KLOE ±	$1.02 e^+ e^- \rightarrow \pi^+ \pi^- \pi^0$

Meson Particle Listings

$\rho(770)$

142.9 ± 1.3 ± 1.4	1.98M	⁸ ALOISIO	03	KLOE	-	1.02 $e^+e^- \rightarrow \pi^+\pi^-\pi^0$
144.7 ± 1.4 ± 1.2	1.98M	⁸ ALOISIO	03	KLOE	+	1.02 $e^+e^- \rightarrow \pi^+\pi^-\pi^0$
150.2 ± 2.0	$\begin{smallmatrix} +0.7 \\ -1.6 \end{smallmatrix}$	⁹ SANZ-CILLERO	003	RVUE		$\tau^- \rightarrow \pi^-\pi^0\nu_\tau$
150.9 ± 2.2 ± 2.0	500k	¹⁰ ACHASOV	02	SND		1.02 $e^+e^- \rightarrow \pi^+\pi^-\pi^0$

148.0 ± 1.3		^{1,2} LANG	79	RVUE		
146 ± 14		ENGLER	74	DBC		$6\pi^+n \rightarrow \pi^+\pi^-p$
143 ± 13		² ESTABROOKS	74	RVUE		$17\pi^-p \rightarrow \pi^+\pi^-n$
160 ± 10		¹ PROTOPOP...	73	HBC		$7.1\pi^+p, t < 0.4$
145 ± 12		^{3,11} HYAMS	68	OSPK		$11.2\pi^-p$
163 ± 15		¹² PISUT	68	RVUE		$1.7-3.2\pi^-p, t < 10$

- $|F_\pi(0)|^2$ fixed to 1.
- From the GOUNARIS 68 parametrization of the pion form factor.
- The error combines statistical and systematic uncertainties. Supersedes BARATE 97M.
- Assuming $m_{\rho^+} = m_{\rho^-}, \Gamma_{\rho^+} = \Gamma_{\rho^-}$.
- $\rho(1700)$ mass and width fixed at 1700 MeV and 235 MeV respectively.
- From the GOUNARIS 68 parametrization of the pion form factor. The second error is a model error taking into account different parametrizations of the pion form factor.
- Applies the Unitary & Analytic Model of the pion electromagnetic form factor of DUBNICKA 10 to analyze the data of FUJIKAWA 08.
- Without limitations on masses and widths.
- Using the data of BARATE 97M and the effective chiral Lagrangian.
- Assuming $m_{\rho^0} = m_{\rho^\pm}, g_{\rho^0\pi\pi} = g_{\rho^\pm\pi\pi}$.

- From pole extrapolation.
- From phase shift analysis of GRAYER 74 data.
- Width errors enlarged by us to $4\Gamma/\sqrt{N}$; see the note with the $K^*(892)$ mass.
- Published values contain misprints. Corrected by private communication RATCLIFF 74.
- From a fit to $\pi^+\pi^-$ mass using $\rho(770)$ (parametrized with the Gounaris-Sakurai approach), $\omega(782)$, and box anomaly components.
- From a fit to $\pi^+\pi^-$ mass using $\rho(770)$ (parametrized with the Gounaris-Sakurai approach), $\omega(782)$, and $\rho(1450)$ components.
- Using relativistic Breit-Wigner and taking into account $\rho-\omega$ interference.
- Systematic errors not evaluated.
- From fit of 3-parameter relativistic Breit-Wigner to helicity-zero part of P -wave intensity. CHABAUD 83 includes data of GRAYER 74.
- HEYNI 81 includes all spacelike and timelike F_π values until 1978.
- Of HYAMS 68 six parametrizations this is theoretically soundest. MR
- Includes MALAMUD 69, ARMENISE 68, BACON 67, HUWE 67, MILLER 67B, ALFF-STEINBERGER 66, HAGOPIAN 66, HAGOPIAN 66B, JACOBS 66B, JAMES 66, WEST 66, GOLDBERGER 64, ABOLINS 63.

MIXED CHARGES, OTHER REACTIONS

VALUE (MeV)	EVTS	DOCUMENT ID	TECN	CHG	COMMENT
149.5 ± 1.3	600k	¹ ABELE	99E	CBAR	$0 \pm 0.0 \bar{p}p \rightarrow \pi^+\pi^-\pi^0$

¹ Assuming the equality of ρ^+ and ρ^- masses and widths.

CHARGED ONLY, HADROPRODUCED

VALUE (MeV)	EVTS	DOCUMENT ID	TECN	CHG	COMMENT
150.2 ± 2.4 OUR FIT					
150.2 ± 2.4 OUR AVERAGE					
152.8 ± 4.3		ABELE	97	CBAR	$\bar{p}n \rightarrow \pi^-\pi^0\pi^0$
155 ± 11	2.9k	¹ CAPRARO	87	SPEC	$- 200\pi^-Cu \rightarrow \pi^-\pi^0Cu$
154 ± 20	967	¹ CAPRARO	87	SPEC	$- 200\pi^-Pb \rightarrow \pi^-\pi^0Pb$
150 ± 5		HUSTON	86	SPEC	$+ 202\pi^+A \rightarrow \pi^+\pi^0A$
146 ± 12	6.5k	² BYERLY	73	OSPK	$- 5\pi^-p$
148.2 ± 4.1	9.6k	³ PISUT	68	RVUE	$- 1.7-3.2\pi^-p, t < 10$
146 ± 13	900	EISNER	67	HBC	$- 4.2\pi^-p, t < 10$
• • •					We do not use the following data for averages, fits, limits, etc. • • •
137.0 ± 0.4		⁴ ABLIKIM	17	BES3	$J/\psi \rightarrow \gamma 3\pi$

- Width errors enlarged by us to $4\Gamma/\sqrt{N}$; see the note with the $K^*(892)$ mass.
- Phase shift analysis. Systematic errors added corresponding to spread of different fits.
- From fit of 3-parameter relativistic P -wave Breit-Wigner to total mass distribution. Includes BATON 68, MILLER 67B, ALFF-STEINBERGER 66, HAGOPIAN 66, HAGOPIAN 66B, JACOBS 66B, JAMES 66, WEST 66, BLIEDEN 65 and CARMONY 64.
- S-matrix pole at a fixed ρ meson mass of 775.49 MeV.

NEUTRAL ONLY, PHOTOPRODUCED

VALUE (MeV)	EVTS	DOCUMENT ID	TECN	COMMENT	
151.5 ± 1.9 OUR AVERAGE					
151.3 ± 2.2 ± $\begin{smallmatrix} 1.6 \\ 2.8 \end{smallmatrix}$	900k	ANDREEV	20	H1	$ep \rightarrow e\pi^+\pi^-p$
155 ± 5 ± 2	63.5k	¹ ABRA MOWICZ	12	ZEUS	$ep \rightarrow e\pi^+\pi^-p$
146 ± 3 ± 13	79k	² BREITWEG	98B	ZEUS	$50-100\gamma p$
150.9 ± 3.0		BARTALUCCI	78	CNTR	$\gamma p \rightarrow e^+e^-p$
• • •					We do not use the following data for averages, fits, limits, etc. • • •
138 ± 3	79k	³ BREITWEG	98B	ZEUS	$50-100\gamma p$
147 ± 11		GLADDING	73	CNTR	$2.9-4.7\gamma p$
155 ± 12	2430	BALLAM	72	HBC	$4.7\gamma p$
145 ± 13	1930	BALLAM	72	HBC	$2.8\gamma p$
140 ± 5		ALVENSLEB...	70	CNTR	$\gamma A, t < 0.01$
146.1 ± 2.9	140k	BIGGS	70	CNTR	$< 4.1\gamma C \rightarrow \pi^+\pi^-C$
160 ± 10		LANZEROTTI	68	CNTR	γp
130 ± 5	4000	ASBURY	67B	CNTR	$\gamma + Pb$

- Using the KUHN 90 parametrization of the pion form factor, neglecting $\rho-\omega$ interference.
- From the parametrization according to SOEDING 66.
- From the parametrization according to ROSS 66.

NEUTRAL ONLY, OTHER REACTIONS

VALUE (MeV)	EVTS	DOCUMENT ID	TECN	COMMENT	
150.9 ± 1.7 OUR AVERAGE				Error includes scale factor of 1.1.	
122 ± 20		BERTIN	97c	OBLX	$0.0\bar{p}p \rightarrow \pi^+\pi^-\pi^0$
145.7 ± 5.3		WEIDENAUER	93	ASTE	$\bar{p}p \rightarrow \pi^+\pi^-\omega$
144.9 ± 3.7		DUBNICKA	89	RVUE	π form factor
148 ± 6		^{1,2} BOHACIK	80	RVUE	
152 ± 9		³ WICKLUND	78	ASPK	$3,4,6\pi^\pm pN$
154 ± 2	76k	DEUTSCH...	76	HBC	$16\pi^+p$
157 ± 8	6.8k	RATCLIFF	72	ASPK	$15\pi^-p, t < 0.3$
143 ± 8	1.7k	REYNOLDS	69	HBC	$2.26\pi^-p$
• • •					We do not use the following data for averages, fits, limits, etc. • • •
150.85 ± 0.55 ± 0.67	970k	⁵ ABLIKIM	18c	BES3	$\eta'(958) \rightarrow \gamma\pi^+\pi^-$
150.18 ± 0.55 ± 0.65	970k	⁶ ABLIKIM	18c	BES3	$\eta'(958) \rightarrow \gamma\pi^+\pi^-$
147.0 ± 2.5	600k	⁷ ABELE	99E	CBAR	$0.0\bar{p}p \rightarrow \pi^+\pi^-\pi^0$
146 ± 3	4.9k	⁸ ADAMS	97	E665	$470\mu p \rightarrow \mu XB$
160.0 ± 4.1		⁹ CHABAUD	83	ASPK	$17\pi^-p$ polarized
155 ± 1		¹⁰ HEYNI	81	RVUE	π form factor

$\Gamma_{\rho(770)^0} - \Gamma_{\rho(770)^\pm}$

VALUE (MeV)	EVTS	DOCUMENT ID	TECN	COMMENT	
0.3 ± 1.3 OUR AVERAGE				Error includes scale factor of 1.4.	
-0.2 ± 1.0		¹ SCHAEEL	05c	ALEP	$\tau^- \rightarrow \pi^-\pi^0\nu_\tau$
3.6 ± 1.8 ± 1.7	1.98M	² ALOISIO	03	KLOE	$1.02e^+e^- \rightarrow \pi^+\pi^-\pi^0$
• • •					We do not use the following data for averages, fits, limits, etc. • • •
4.66 ± 0.85		³ BARTOS	17A	RVUE	$e^+e^- \rightarrow \pi^+\pi^-, \tau^- \rightarrow \pi^-\pi^0\nu_\tau$

- From the combined fit of the τ^- data from ANDERSON 00A and SCHAEEL 05c and e^+e^- data from the compilation of BARKOV 85, A KHMETSIN 04, and ALOISIO 05. Supersedes BARATE 97M.
- Assuming $m_{\rho^+} = m_{\rho^-}, \Gamma_{\rho^+} = \Gamma_{\rho^-}$.
- Applies the Unitary & Analytic Model of the pion electromagnetic form factor of DUBNICKA 10 to analyze the data of ACHASOV 06, AKHMETSIN 07, AUBERT 09as, AMBROSINO 11A, and FUJIKAWA 08.

$\Gamma_{\rho(770)^+} - \Gamma_{\rho(770)^-}$

VALUE	EVTS	DOCUMENT ID	TECN	COMMENT	
1.8 ± 2.0 ± 0.5	1.98M	¹ ALOISIO	03	KLOE	$1.02e^+e^- \rightarrow \pi^+\pi^-\pi^0$

¹ Without limitations on masses and widths.

$\rho(770)$ DECAY MODES

Mode	Fraction (Γ_i/Γ)	Scale factor/Confidence level
Γ_1 $\pi\pi$	~ 100	%
Γ_2 $K\bar{K}$		
$\rho(770)^\pm$ decays		
Γ_3 $\pi^\pm\pi^0$	~ 100	%
Γ_4 $\pi^\pm\gamma$	(4.5 ± 0.5)	$\times 10^{-4}$ S=2.2
Γ_5 $\pi^\pm\eta$	< 6	$\times 10^{-3}$ CL=84%
Γ_6 $\pi^\pm\pi^+\pi^-\pi^0$	< 2.0	$\times 10^{-3}$ CL=84%
$\rho(770)^0$ decays		
Γ_7 $\pi^+\pi^-$	~ 100	%
Γ_8 $\pi^+\pi^-\gamma$	(9.9 ± 1.6)	$\times 10^{-3}$
Γ_9 $\pi^0\gamma$	(4.7 ± 0.8)	$\times 10^{-4}$ S=1.7
Γ_{10} $\eta\gamma$	(3.00 ± 0.21)	$\times 10^{-4}$
Γ_{11} $\pi^0\pi^0\gamma$	(4.5 ± 0.8)	$\times 10^{-5}$
Γ_{12} $\mu^+\mu^-$	[a] (4.55 ± 0.28)	$\times 10^{-5}$
Γ_{13} e^+e^-	[a] (4.72 ± 0.05)	$\times 10^{-5}$
Γ_{14} $\pi^+\pi^-\pi^0$	(1.01 $\begin{smallmatrix} +0.54 \\ -0.36 \end{smallmatrix}$ ± 0.34)	$\times 10^{-4}$
Γ_{15} $\pi^+\pi^-\pi^+\pi^-$	(1.8 ± 0.9)	$\times 10^{-5}$
Γ_{16} $\pi^+\pi^-\pi^0\pi^0$	(1.6 ± 0.8)	$\times 10^{-5}$
Γ_{17} $\pi^0e^+e^-$	< 1.2	$\times 10^{-5}$ CL=90%
Γ_{18} ηe^+e^-		

[a] The $\omega\rho$ interference is then due to $\omega\rho$ mixing only, and is expected to be small. If $e\mu$ universality holds, $\Gamma(\rho^0 \rightarrow \mu^+\mu^-) = \Gamma(\rho^0 \rightarrow e^+e^-) \times 0.99785$.

CONSTRAINED FIT INFORMATION

An overall fit to the total width and a partial width uses 10 measurements and one constraint to determine 3 parameters. The overall fit has a $\chi^2 = 10.7$ for 8 degrees of freedom.

See key on page 1127

Meson Particle Listings

$\rho(770)$

The following *off-diagonal* array elements are the correlation coefficients $\langle \delta p_i \delta p_j \rangle / (\delta p_i \delta p_j)$, in percent, from the fit to parameters p_i , including the branching fractions, $x_i \equiv \Gamma_i / \Gamma_{\text{total}}$. The fit constrains the x_i whose labels appear in this array to sum to one.

x_4	-100	
Γ	15	-15
	x_3	x_4

Mode	Rate (MeV)	Scale factor
Γ_3 $\pi^+ \pi^0$	150.2 ± 2.4	
Γ_4 $\pi^+ \gamma$	0.068 ± 0.007	2.3

CONSTRAINED FIT INFORMATION

An overall fit to the total width, a partial width, and 7 branching ratios uses 21 measurements and one constraint to determine 9 parameters. The overall fit has a $\chi^2 = 9.5$ for 13 degrees of freedom.

The following *off-diagonal* array elements are the correlation coefficients $\langle \delta p_i \delta p_j \rangle / (\delta p_i \delta p_j)$, in percent, from the fit to parameters p_i , including the branching fractions, $x_i \equiv \Gamma_i / \Gamma_{\text{total}}$. The fit constrains the x_i whose labels appear in this array to sum to one.

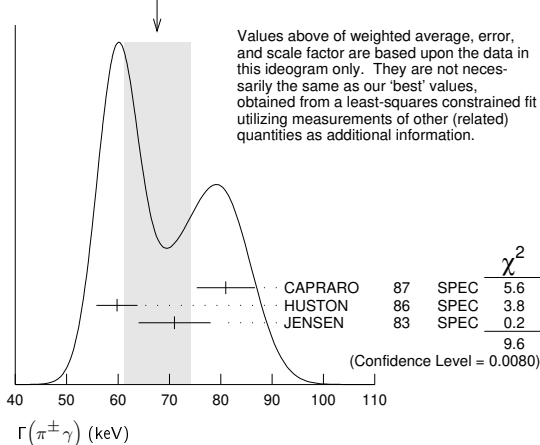
x_8	-100							
x_9	-5	0						
x_{10}	-1	0	1					
x_{11}	-1	0	0	0				
x_{12}	2	-3	0	0	0			
x_{13}	0	0	-6	-9	0	0		
x_{15}	-1	0	0	0	0	0	0	
Γ	0	0	3	5	0	0	-54	
	x_7	x_8	x_9	x_{10}	x_{11}	x_{12}	x_{13}	x_{15}

Mode	Rate (MeV)	Scale factor
Γ_7 $\pi^+ \pi^-$	147.5 ± 0.9	
Γ_8 $\pi^+ \pi^- \gamma$	1.48 ± 0.24	
Γ_9 $\pi^0 \gamma$	0.070 ± 0.012	1.7
Γ_{10} $\eta \gamma$	0.0447 ± 0.0032	
Γ_{11} $\pi^0 \pi^0 \gamma$	0.0066 ± 0.0012	
Γ_{12} $\mu^+ \mu^-$	[a] 0.0068 ± 0.0004	
Γ_{13} $e^+ e^-$	[a] 0.00704 ± 0.00006	
Γ_{15} $\pi^+ \pi^- \pi^+ \pi^-$	0.0027 ± 0.0014	

$\rho(770)$ PARTIAL WIDTHS

$\Gamma(\pi^\pm \gamma)$	VALUE (keV)	DOCUMENT ID	TECN	CHG	COMMENT
68 ± 7 OUR FIT		Error includes scale factor of 2.3.			
68 ± 7 OUR AVERAGE		Error includes scale factor of 2.2. See the ideogram below.			
81 ± 4 ± 4	CAPRARO	87	SPEC	-	200 $\pi^- A \rightarrow \pi^- \pi^0 A$
59.8 ± 4.0	HUSTON	86	SPEC	+	202 $\pi^+ A \rightarrow \pi^+ \pi^0 A$
71 ± 7	JENSEN	83	SPEC	-	156-260 $\pi^- A \rightarrow \pi^- \pi^0 A$

WEIGHTED AVERAGE
68±7 (Error scaled by 2.2)



$\Gamma(\pi^0 \gamma)$	VALUE (keV)	EVTS	DOCUMENT ID	TECN	COMMENT
77 ± 17 ± 11	36500		¹ ACHASOV	03	SND 0.60-0.97 $e^+ e^- \rightarrow \pi^0 \gamma$
121 ± 31			DOLINSKY	89	ND $e^+ e^- \rightarrow \pi^0 \gamma$

¹ Using $\Gamma_{\text{total}} = 147.9 \pm 1.3$ MeV and $B(\rho \rightarrow \pi^0 \gamma)$ from ACHASOV 03.

$\Gamma(\eta \gamma)$	VALUE (keV)	DOCUMENT ID	TECN	COMMENT
62 ± 17		¹ DOLINSKY	89	ND $e^+ e^- \rightarrow \eta \gamma$

¹ Solution corresponding to constructive ω - ρ interference.

$\Gamma(e^+ e^-)$	VALUE (keV)	EVTS	DOCUMENT ID	TECN	COMMENT
7.04 ± 0.06 OUR FIT					
7.04 ± 0.06 OUR AVERAGE					

7.048 ± 0.057 ± 0.050	900k		¹ AKHMETSHIN	07	$e^+ e^- \rightarrow \pi^+ \pi^-$
7.06 ± 0.11 ± 0.05	114k		^{2,3} AKHMETSHIN	04	CMD2 $e^+ e^- \rightarrow \pi^+ \pi^-$
6.77 ± 0.10 ± 0.30			BARKOV	85	OLYA $e^+ e^- \rightarrow \pi^+ \pi^-$
7.12 ± 0.02 ± 0.11	800k		⁴ ACHASOV	06	SND $e^+ e^- \rightarrow \pi^+ \pi^-$
6.3 ± 0.1			⁵ BENAYOUN	98	RVUE $e^+ e^- \rightarrow \pi^+ \pi^-, \mu^+ \mu^-$

¹ A combined fit of AKHMETSHIN 07, AULCHENKO 06, and AULCHENKO 05.
² Using the GOUNARIS 68 parametrization with the complex phase of the ρ - ω interference.
³ From a fit in the energy range 0.61 to 0.96 GeV. Update of AKHMETSHIN 02.
⁴ Supersedes ACHASOV 05A.
⁵ Using the data of BARKOV 85 in the hidden local symmetry model.

$\Gamma(\pi^+ \pi^- \pi^+ \pi^-)$	VALUE (keV)	EVTS	DOCUMENT ID	TECN	COMMENT
2.8 ± 1.4 ± 0.5	153		AKHMETSHIN	00	CMD2 0.6-0.97 $e^+ e^- \rightarrow \pi^+ \pi^- \pi^+ \pi^-$

$\rho(770) \Gamma(e^+ e^-) \Gamma(i) / \Gamma^2(\text{total})$

$\Gamma(e^+ e^-) / \Gamma_{\text{total}} \times \Gamma(\pi^+ \pi^-) / \Gamma_{\text{total}}$	VALUE (units 10^{-5})	EVTS	DOCUMENT ID	TECN	COMMENT
4.89 ± 0.04 OUR AVERAGE					

4.889 ± 0.015 ± 0.039			¹ ACHASOV	21	SND $e^+ e^- \rightarrow \pi^+ \pi^-$
4.876 ± 0.023 ± 0.064	800k		^{2,3} ACHASOV	06	SND $e^+ e^- \rightarrow \pi^+ \pi^-$
4.72 ± 0.02			⁴ BENAYOUN	10	RVUE 0.4-1.05 $e^+ e^-$

¹ From a fit of the cross section in the energy range $0.525 < \sqrt{s} < 0.883$ GeV parameterized by the sum of the Breit-Wigner amplitudes for the $\rho(770)$, ω and $\rho(1450)$ resonances.
² Supersedes ACHASOV 05A.
³ A fit of the SND data from 400 to 1000 MeV using parameters of the $\rho(1450)$ and $\rho(1700)$ from a fit of the data of BARKOV 85, BISELLO 89 and ANDERSON 00A.
⁴ A simultaneous fit of $e^+ e^- \rightarrow \pi^+ \pi^-, \pi^+ \pi^- \pi^0, \pi^0 \gamma, \eta \gamma$ data.

$\Gamma(e^+ e^-) / \Gamma_{\text{total}} \times \Gamma(\eta \gamma) / \Gamma_{\text{total}}$	VALUE (units 10^{-8})	EVTS	DOCUMENT ID	TECN	COMMENT
1.42 ± 0.10 OUR FIT					
1.45 ± 0.12 OUR AVERAGE					

1.32 ± 0.14 ± 0.08	33k		¹ ACHASOV	07B	SND 0.6-1.38 $e^+ e^- \rightarrow \eta \gamma$
1.50 ± 0.65 ± 0.09	17.4k		² AKHMETSHIN	05	CMD2 0.60-1.38 $e^+ e^- \rightarrow \eta \gamma$
1.61 ± 0.20 ± 0.11	23k		^{3,4} AKHMETSHIN	01B	CMD2 $e^+ e^- \rightarrow \eta \gamma$
1.85 ± 0.49			⁵ DOLINSKY	89	ND $e^+ e^- \rightarrow \eta \gamma$
1.05 ± 0.02			⁶ BENAYOUN	10	RVUE 0.4-1.05 $e^+ e^-$

¹ From a combined fit of $\sigma(e^+ e^- \rightarrow \eta \gamma)$ with $\eta \rightarrow 3\pi^0$ and $\eta \rightarrow \pi^+ \pi^- \pi^0$, and fixing $B(\eta \rightarrow 3\pi^0) / B(\eta \rightarrow \pi^+ \pi^- \pi^0) = 1.44 \pm 0.04$. Recalculated by us from the cross section at the peak. Supersedes ACHASOV 00D and ACHASOV 06A.
² From the $\eta \rightarrow 2\gamma$ decay and using $B(\eta \rightarrow \gamma \gamma) = 39.43 \pm 0.26\%$.
³ From the $\eta \rightarrow 3\pi^0$ decay and using $B(\eta \rightarrow 3\pi^0) = (32.24 \pm 0.29) \times 10^{-2}$.
⁴ The combined fit from 600 to 1380 MeV taking into account $\rho(770)$, $\omega(782)$, $\phi(1020)$, and $\rho(1450)$ (mass and width fixed at 1450 MeV and 310 MeV respectively).
⁵ Recalculated by us from the cross section in the peak.
⁶ A simultaneous fit of $e^+ e^- \rightarrow \pi^+ \pi^-, \pi^+ \pi^- \pi^0, \pi^0 \gamma, \eta \gamma$ data.

$\Gamma(e^+ e^-) / \Gamma_{\text{total}} \times \Gamma(\pi^0 \gamma) / \Gamma_{\text{total}}$	VALUE (units 10^{-8})	EVTS	DOCUMENT ID	TECN	COMMENT
2.2 ± 0.4 OUR FIT					Error includes scale factor of 1.7.
2.21 ± 0.34 OUR AVERAGE					Error includes scale factor of 1.6. See the ideogram below.

1.98 ± 0.22 ± 0.10			¹ ACHASOV	16A	SND 0.60-1.38 $e^+ e^- \rightarrow \pi^0 \gamma$
2.90 ± 0.60 ± 0.18	18k		AKHMETSHIN	05	CMD2 0.60-1.38 $e^+ e^- \rightarrow \pi^0 \gamma$
3.61 ± 0.74 ± 0.49	10k		² DOLINSKY	89	ND $e^+ e^- \rightarrow \pi^0 \gamma$
1.875 ± 0.026			³ BENAYOUN	10	RVUE 0.4-1.05 $e^+ e^-$
2.37 ± 0.53 ± 0.33	36k		⁴ ACHASOV	03	SND 0.60-0.97 $e^+ e^- \rightarrow \pi^0 \gamma$

Meson Particle Listings

$\rho(770)$

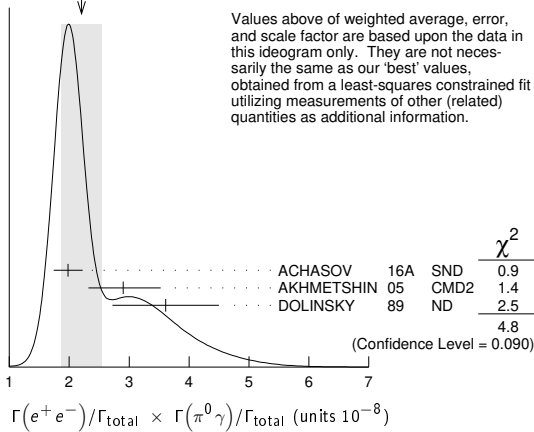
¹ From the VMD model with the $\rho(770)$, $\omega(782)$, $\phi(1020)$ resonances, and an additional resonance describing the total contribution of the $\rho(1450)$ and $\omega(1420)$ states. Supersedes ACHASOV 03.

² Recalculated by us from the cross section in the peak.

³ A simultaneous fit of $e^+e^- \rightarrow \pi^+\pi^-, \pi^+\pi^-\pi^0, \pi^0\gamma, \eta\gamma$ data.

⁴ Using $\sigma_{\phi \rightarrow \pi^0\gamma}$ from ACHASOV 00 and $m_\rho = 775.97$ MeV in the model with the energy-independent phase of ρ - ω interference equal to $(-10.2 \pm 7.0)^\circ$.

WEIGHTED AVERAGE
2.21±0.34 (Error scaled by 1.6)



Values above of weighted average, error, and scale factor are based upon the data in this ideogram only. They are not necessarily the same as our 'best' values, obtained from a least-squares constrained fit utilizing measurements of other (related) quantities as additional information.

$\Gamma(e^+e^-)/\Gamma_{total} \times \Gamma(\pi^+\pi^-\pi^0)/\Gamma_{total}$ $\Gamma_{13}/\Gamma \times \Gamma_{14}/\Gamma$

VALUE (units 10^{-9})	EVTS	DOCUMENT ID	TECN	COMMENT
0.903±0.076		¹ BENAYOUN 10	RVUE	0.4-1.05 e^+e^-
4.58 ^{+2.46} _{-1.64} ±1.56	1.2M	² ACHASOV 03D	RVUE	0.44-2.00 $e^+e^- \rightarrow \pi^+\pi^-\pi^0$

¹ A simultaneous fit of $e^+e^- \rightarrow \pi^+\pi^-, \pi^+\pi^-\pi^0, \pi^0\gamma, \eta\gamma$ data.
² Statistical significance is less than 3 σ .

$\rho(770)$ BRANCHING RATIOS

$\Gamma(\pi^\pm\eta)/\Gamma(\pi\pi)$	CL%	DOCUMENT ID	TECN	CHG	COMMENT
<60	84	FERBEL 66	HBC	±	$\pi^\pm\rho$ above 2.5

$\Gamma(\pi^\pm\pi^+\pi^-\pi^0)/\Gamma(\pi\pi)$	CL%	DOCUMENT ID	TECN	CHG	COMMENT
<20	84	FERBEL 66	HBC	±	$\pi^\pm\rho$ above 2.5
35±40		JAMES 66	HBC	+	2.1 $\pi^+\rho$

••• We do not use the following data for averages, fits, limits, etc. •••

$\Gamma(\pi^+\pi^-\gamma)/\Gamma_{total}$	CL%	DOCUMENT ID	TECN	COMMENT
0.0099±0.0016 OUR FIT				
0.0111±0.0014		¹ DOLINSKY 91	ND	$e^+e^- \rightarrow \pi^+\pi^-\gamma$
<0.005	90	² VASSERMAN 88	ND	$e^+e^- \rightarrow \pi^+\pi^-\gamma$
		³ VASSERMAN 88	ND	$e^+e^- \rightarrow \pi^+\pi^-\gamma$

¹ Bremsstrahlung from a decay pion and for photon energy above 50 MeV.
² Superseded by DOLINSKY 91.
³ Structure radiation due to quark rearrangement in the decay.

$\Gamma(\pi^0\gamma)/\Gamma_{total}$	EVTS	DOCUMENT ID	TECN	COMMENT
4.20±0.52		¹ ACHASOV 16A	SND	0.60-1.38 $e^+e^- \rightarrow \pi^0\gamma$
6.21 ^{+1.28} _{-1.18} ±0.39	18k	^{2,3} AKHMETSHIN 05	CMD2	0.60-1.38 $e^+e^- \rightarrow \pi^0\gamma$
5.22±1.17±0.75	36k	^{3,4} ACHASOV 03	SND	0.60-0.97 $e^+e^- \rightarrow \pi^0\gamma$
6.8 ±1.7		⁵ BENAYOUN 96	RVUE	0.54-1.04 $e^+e^- \rightarrow \pi^0\gamma$
7.9 ±2.0		³ DOLINSKY 89	ND	$e^+e^- \rightarrow \pi^0\gamma$

¹ Using $B(\rho \rightarrow e^+e^-)$ from PDG 15. Supersedes ACHASOV 03.
² Using $B(\rho \rightarrow e^+e^-) = (4.67 \pm 0.09) \times 10^{-5}$.
³ Not independent of the corresponding $\Gamma(e^+e^-) \times \Gamma(\pi^0\gamma)/\Gamma_{total}^2$.
⁴ Using $B(\rho \rightarrow e^+e^-) = (4.54 \pm 0.10) \times 10^{-5}$.
⁵ Reanalysis of DRUZHININ 84, DOLINSKY 89, and DOLINSKY 91 taking into account a triangle anomaly contribution.

$\Gamma(\eta\gamma)/\Gamma_{total}$ Γ_{10}/Γ

VALUE (units 10^{-4})	EVTS	DOCUMENT ID	TECN	CHG	COMMENT
3.00±0.21 OUR FIT					
2.90±0.32 OUR AVERAGE					
2.79±0.34±0.03	33k	¹ ACHASOV 07B	SND		0.6-1.38 $e^+e^- \rightarrow \eta\gamma$
3.6 ±0.9		² ANDREWS 77	CNTR	0	6.7-10 γ Cu
3.21±1.39±0.20	17.4k	^{3,4} AKHMETSHIN 05	CMD2		0.60-1.38 $e^+e^- \rightarrow \eta\gamma$
3.39±0.42±0.23	25,6	⁶ AKHMETSHIN 01B	CMD2		$e^+e^- \rightarrow \eta\gamma$
1.9 ^{+0.6} _{-0.8}		⁷ BENAYOUN 96	RVUE		0.54-1.04 $e^+e^- \rightarrow \eta\gamma$
4.0 ±1.1		^{2,4} DOLINSKY 89	ND		$e^+e^- \rightarrow \eta\gamma$

••• We do not use the following data for averages, fits, limits, etc. •••

¹ ACHASOV 07B reports $[\Gamma(\rho(770) \rightarrow \eta\gamma)/\Gamma_{total}] \times [B(\rho(770) \rightarrow e^+e^-)] = (1.32 \pm 0.14 \pm 0.08) \times 10^{-8}$ which we divide by our best value $B(\rho(770) \rightarrow e^+e^-) = (4.72 \pm 0.05) \times 10^{-5}$. Our first error is their experiment's error and our second error is the systematic error from using our best value. Supersedes ACHASOV 00D and ACHASOV 06A.
² Solution corresponding to constructive ω - ρ interference.
³ Using $B(\rho \rightarrow e^+e^-) = (4.67 \pm 0.09) \times 10^{-5}$ and $B(\eta \rightarrow \gamma\gamma) = 39.43 \pm 0.26\%$.
⁴ Not independent of the corresponding $\Gamma(e^+e^-) \times \Gamma(\eta\gamma)/\Gamma_{total}^2$.
⁵ The combined fit from 600 to 1380 MeV taking into account $\rho(770)$, $\omega(782)$, $\phi(1020)$, and $\rho(1450)$ (mass and width fixed at 1450 MeV and 310 MeV respectively).
⁶ Using $B(\rho \rightarrow e^+e^-) = (4.75 \pm 0.10) \times 10^{-5}$ from AKHMETSHIN 02 and $B(\eta \rightarrow 3\pi^0) = (32.24 \pm 0.29) \times 10^{-2}$.
⁷ Reanalysis of DRUZHININ 84, DOLINSKY 89, and DOLINSKY 91 taking into account a triangle anomaly contribution. Constructive ρ - ω interference solution.

$\Gamma(\pi^0\pi^0\gamma)/\Gamma_{total}$ Γ_{11}/Γ

VALUE (units 10^{-5})	EVTS	DOCUMENT ID	TECN	COMMENT
4.5±0.8 OUR FIT				
4.5^{+0.9}_{-0.8} OUR AVERAGE				
5.2 ^{+1.5} _{-1.3} ±0.6	190	¹ AKHMETSHIN 04B	CMD2	0.6-0.97 $e^+e^- \rightarrow \pi^0\pi^0\gamma$
4.1 ^{+1.0} _{-0.9} ±0.3	295	² ACHASOV 02F	SND	0.36-0.97 $e^+e^- \rightarrow \pi^0\pi^0\gamma$
4.8 ^{+3.4} _{-1.8} ±0.5	63	³ ACHASOV 00G	SND	$e^+e^- \rightarrow \pi^0\pi^0\gamma$

••• We do not use the following data for averages, fits, limits, etc. •••

¹ This branching ratio includes the conventional VMD mechanism $\rho \rightarrow \omega\pi^0, \omega \rightarrow \pi^0\gamma$, and the new decay mode $\rho \rightarrow f_0(500)\gamma, f_0(500) \rightarrow \pi^0\pi^0$ with a branching ratio $(2.0^{+1.1}_{-0.9} ± 0.3) \times 10^{-5}$ differing from zero by 2.0 standard deviations.
² This branching ratio includes the conventional VMD mechanism $\rho \rightarrow \omega\pi^0, \omega \rightarrow \pi^0\gamma$ and the new decay mode $\rho \rightarrow f_0(500)\gamma, f_0(500) \rightarrow \pi^0\pi^0$ with a branching ratio $(1.9^{+0.9}_{-0.8} ± 0.4) \times 10^{-5}$ differing from zero by 2.4 standard deviations. Supersedes ACHASOV 00G.
³ Superseded by ACHASOV 02F.

$\Gamma(\mu^+\mu^-)/\Gamma(\pi^+\pi^-)$ Γ_{12}/Γ_7

VALUE (units 10^{-5})	DOCUMENT ID	TECN	COMMENT
4.60±0.28 OUR FIT			
4.6 ±0.2 ±0.2	ANTIPOV 89	SIGM	π^- Cu $\rightarrow \mu^+\mu^-\pi^-$ Cu
8.2 ^{+1.6} _{-3.6}	¹ ROTHWELL 69	CNTR	Photoproduction
5.6 ±1.5	² WEHMANN 69	OSPK	12 π^- C, Fe
9.7 ^{+3.1} _{-3.3}	^{3,4} HYAMS 67	OSPK	11 π^- Li, H

¹ Possibly large ρ - ω interference leads us to increase the minus error.
² Result contains 11 ± 11% correction using SU(3) for central value. The error on the correction takes account of possible ρ - ω interference and the upper limit agrees with the upper limit of $\omega \rightarrow \mu^+\mu^-$ from this experiment.
³ But he even enlarges his error to take residual ω contamination into account. Since his value is high, seems the other experiments also can't have too many ω 's. But maybe Hyams has additional μ 's from $\rho \rightarrow \pi\pi$, decaying π 's.
⁴ HYAMS 67's mass resolution is 20 MeV. The ω region was excluded.

$\Gamma(e^+e^-)/\Gamma(\pi\pi)$ Γ_{13}/Γ_1

VALUE (units 10^{-4})	DOCUMENT ID	TECN	COMMENT
0.40±0.05	^{1,2} BENAKSAS 72	OSPK	$e^+e^- \rightarrow \pi^+\pi^-$

••• We do not use the following data for averages, fits, limits, etc. •••

¹ The ρ' contribution is not taken into account.
² Barkov excludes Auslender and Benaksas for large statistical and systematic errors.

$\Gamma(\pi^+\pi^-\pi^0)/\Gamma_{total}$ Γ_{14}/Γ

VALUE (units 10^{-4})	CL%	EVTS	DOCUMENT ID	TECN	COMMENT
0.88±0.23±0.30					
1.01 ^{+0.54} _{-0.36} ±0.34	1.2M	² ACHASOV 03D	RVUE	0.44-2.00 $e^+e^- \rightarrow \pi^+\pi^-\pi^0$	
<1.2	90	VASSERMAN 88B	ND	$e^+e^- \rightarrow \pi^+\pi^-\pi^0$	

••• We do not use the following data for averages, fits, limits, etc. •••

¹ From the cross section for $e^+e^- \rightarrow \pi^+\pi^-\pi^0$ with contributions from $\rho(770)$, $\omega(782)$, $\phi(1020)$, $\omega(1420)$, and $\omega(1650)$. Statistical evidence is more than 6 σ .
² Statistical significance is less than 3 σ .

See key on page 1127

Meson Particle Listings

$\rho(770), \omega(782)$

$\Gamma(\pi^+\pi^-\pi^0)/\Gamma(\pi\pi)$ Γ_{14}/Γ_1

Table with columns: VALUE, CL%, DOCUMENT ID, TECN, CHG, COMMENT. Includes entries for BRAMON, ABRA MS, etc.

$\Gamma(\pi^+\pi^-\pi^+\pi^-)/\Gamma_{total}$ Γ_{15}/Γ

Table with columns: VALUE (units 10^-5), CL%, EVTS, DOCUMENT ID, TECN, COMMENT. Includes entry for AKHMETSHIN 00.

$\Gamma(\pi^+\pi^-\pi^+\pi^-)/\Gamma(\pi\pi)$ Γ_{15}/Γ_1

Table with columns: VALUE (units 10^-4), CL%, DOCUMENT ID, TECN, CHG, COMMENT. Includes entries for ERBE, CHUNG, HUSON, JAMES.

$\Gamma(\pi^+\pi^-\pi^0\pi^0)/\Gamma_{total}$ Γ_{16}/Γ

Table with columns: VALUE (units 10^-5), CL%, DOCUMENT ID, TECN, COMMENT. Includes entry for ACHASOV 09A.

$\Gamma(\pi^0 e^+ e^-)/\Gamma_{total}$ Γ_{17}/Γ

Table with columns: VALUE (units 10^-5), CL%, DOCUMENT ID, TECN, COMMENT. Includes entry for ACHASOV 08.

$\Gamma(\eta e^+ e^-)/\Gamma_{total}$ Γ_{18}/Γ

Table with columns: VALUE (units 10^-5), DOCUMENT ID, TECN, COMMENT. Includes entry for AKHMETSHIN 05A.

$\rho(770)$ REFERENCES

Large table of references for rho(770) with columns: Author, Year, Journal, Page, Comment.

Main table of meson listings with columns: Author, Year, Journal, Page, Comment. Includes entries for ACHASOV, AKHMETSHIN, ANDERSON, etc.

$\omega(782)$

$I^G(J^{PC}) = 0^-(1^{--})$

$\omega(782)$ MASS

Table of omega(782) mass measurements with columns: VALUE (MeV), EVTS, DOCUMENT ID, TECN, COMMENT.

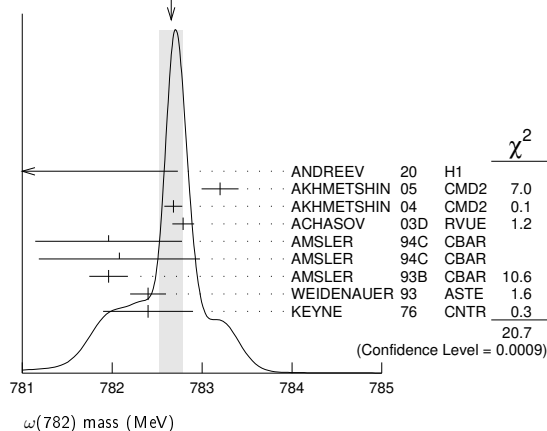
Meson Particle Listings

$\omega(782)$

782.08 ± 0.36 ± 0.82	3463	4	AMSLER	94C	CBAR	0.0 $\bar{p}p \rightarrow \omega \eta \pi^0$
781.96 ± 0.13 ± 0.17	15k		AMSLER	93B	CBAR	0.0 $\bar{p}p \rightarrow \omega \pi^0 \pi^0$
782.4 ± 0.2	270k		WEIDENAUER	93	ASTE	$\bar{p}p \rightarrow 2\pi^+ 2\pi^- \pi^0$
782.4 ± 0.5	7000	5	KEYNE	76	CNTR	$\pi^- p \rightarrow \omega n$
••• We do not use the following data for averages, fits, limits, etc. •••						
782.58 ± 0.03 ± 0.01		6	HOID	20	RVUE	$e^+ e^- \rightarrow \pi^0 \gamma$
781.68 ± 0.09 ± 0.03		7	COLANGELO	19	RVUE	$e^+ e^- \rightarrow \pi^+ \pi^-$
782.63 ± 0.03 ± 0.01		8	HOFERICHT...	19	RVUE	$e^+ e^- \rightarrow \pi^+ \pi^- \pi^0$
781.91 ± 0.24		9	LEES	12G	BABR	$e^+ e^- \rightarrow \pi^+ \pi^- \gamma$
782.7 ± 0.1 ± 1.5	19500	10	WURZINGER	95	SPEC	1.33 $\rho d \rightarrow {}^3\text{He} \omega$
781.78 ± 0.10		10	BARKOV	87	CMD	$e^+ e^- \rightarrow \pi^+ \pi^- \pi^0$
782.2 ± 0.4	1488	11	KURDADZE	83B	OLYA	$e^+ e^- \rightarrow \pi^+ \pi^- \pi^0$
783.3 ± 0.4	433		CORDIER	80	DM1	$e^+ e^- \rightarrow \pi^+ \pi^- \pi^0$
782.5 ± 0.8	33260		ROOS	80	RVUE	0.0-3.6 $\bar{p}p$
782.6 ± 0.8	3000		BENKHEIRI	79	OMEG	9-12 $\pi^\pm p$
781.8 ± 0.6	1430		COOPER	78B	HBC	0.7-0.8 $\bar{p}p \rightarrow 5\pi$
782.7 ± 0.9	535		VANAPEL...	78	HBC	7.2 $\bar{p}p \rightarrow \bar{p}p \omega$
783.5 ± 0.8	2100		GESSAROLI	77	HBC	11 $\pi^- p \rightarrow \omega n$
782.5 ± 0.8	418		AGUILAR...	72B	HBC	3.9, 4.6 $K^- p$
783.4 ± 1.0	248		BIZZARRI	71	HBC	0.0 $\rho \bar{p} \rightarrow K^+ K^- \omega$
781.0 ± 0.6	510		BIZZARRI	71	HBC	0.0 $\rho \bar{p} \rightarrow K_1^+ K_1^- \omega$
783.7 ± 1.0	3583	12	COYNE	71	HBC	3.7 $\pi^+ p \rightarrow p \pi^+ \pi^+ \pi^- \pi^0$
784.1 ± 1.2	750		ABRA MOVI...	70	HBC	3.9 $\pi^- p$
783.2 ± 1.6		13	BIGGS	70B	CNTR	< 4.1 $\gamma C \rightarrow \pi^+ \pi^- C$
782.4 ± 0.5	2400		BIZZARRI	69	HBC	0.0 $\bar{p}p$

- Update of AKHMETSIN 00c.
- From the combined fit of ANTONELLI 92, ACHASOV 01E, ACHASOV 02E, and ACHASOV 03D data on the $\pi^+ \pi^- \pi^0$ and ANTONELLI 92 on the $\omega \pi^+ \pi^-$ final states. Supersedes ACHASOV 99E and ACHASOV 02E.
- From the $\eta \rightarrow \gamma \gamma$ decay.
- From the $\eta \rightarrow 3\pi^0$ decay.
- Observed by threshold-crossing technique. Mass resolution = 4.8 MeV FWHM.
- The values were extracted from a dispersively improved Breit-Wigner parameterization and do not include vacuum polarization. Inclusion of vacuum polarization gives 782.736 ± 0.024 MeV.
- The ω mass was extracted from a dispersively improved Breit-Wigner parameterization, the ω width fixed at 8.49 ± 0.08 MeV. The value does not include vacuum polarization which would shift the mass to 781.81 ± 0.09 ± 0.03 MeV. The mixing parameter is assumed real valued.
- The values were extracted from a dispersively improved Breit-Wigner parameterization and do not include vacuum polarization.
- From the $\rho-\omega$ interference in the $\pi^+ \pi^-$ mass spectrum using the Breit-Wigner for the ω and leaving its mass and width as free parameters of the fit.
- Systematic uncertainties underestimated.
- Systematic uncertainties not estimated.
- From best-resolution sample of COYNE 71.
- From $\omega-\rho$ interference in the $\pi^+ \pi^-$ mass spectrum assuming ω width 12.6 MeV.

WEIGHTED AVERAGE
782.66 ± 0.13 (Error scaled by 2.0)



$\omega(782)$ WIDTH

VALUE (MeV)	EVTS	DOCUMENT ID	TECN	COMMENT
8.68 ± 0.13 OUR AVERAGE				
8.68 ± 0.23 ± 0.10	11200	1	AKHMETSIN 04	CMD2 $e^+ e^- \rightarrow \pi^+ \pi^- \pi^0$
8.68 ± 0.04 ± 0.15	1.2M	2	ACHASOV 03D	RVUE 0.44-2.00 $e^+ e^- \rightarrow \pi^+ \pi^- \pi^0$
••• We do not use the following data for averages, fits, limits, etc. •••				
8.65 ± 0.06 ± 0.01		3	HOID	20 RVUE $e^+ e^- \rightarrow \pi^0 \gamma$
8.71 ± 0.04 ± 0.04		4	HOFERICHT...	19 RVUE $e^+ e^- \rightarrow \pi^+ \pi^- \pi^0$
8.13 ± 0.45		5	LEES	12G BABR $e^+ e^- \rightarrow \pi^+ \pi^- \gamma$
8.2 ± 0.3	19500	6	WURZINGER	95 SPEC 1.33 $\rho d \rightarrow {}^3\text{He} \omega$
8.4 ± 0.1		7	AULCHENKO	87 ND $e^+ e^- \rightarrow \pi^+ \pi^- \pi^0$

8.30 ± 0.40		6	BARKOV	87	CMD	$e^+ e^- \rightarrow \pi^+ \pi^- \pi^0$
9.8 ± 0.9	1488	8	KURDADZE	83B	OLYA	$e^+ e^- \rightarrow \pi^+ \pi^- \pi^0$
9.0 ± 0.8	433	6	CORDIER	80	DM1	$e^+ e^- \rightarrow \pi^+ \pi^- \pi^0$
12 ± 2	1430		COOPER	78B	HBC	0.7-0.8 $\bar{p}p \rightarrow 5\pi$
9.4 ± 2.5	2100		GESSAROLI	77	HBC	11 $\pi^- p \rightarrow \omega n$
10.22 ± 0.43	20000	9	KEYNE	76	CNTR	$\pi^- p \rightarrow \omega n$
13.3 ± 2	418		AGUILAR...	72B	HBC	3.9, 4.6 $K^- p$
9.1 ± 0.8	451	6	BENAKSAS	72B	OSPK	$e^+ e^- \rightarrow \pi^+ \pi^- \pi^0$
10.5 ± 1.5			BORENSTEIN	72	HBC	2.18 $K^- p$
7.70 ± 0.9 ± 1.15	940		BROWN	72	MMS	2.5 $\pi^- p \rightarrow n \text{MM}$
10.3 ± 1.4	510		BIZZARRI	71	HBC	0.0 $\rho \bar{p} \rightarrow K_1^+ K_1^- \omega$
12.8 ± 3.0	248		BIZZARRI	71	HBC	0.0 $\rho \bar{p} \rightarrow K^+ K^- \omega$
9.5 ± 1.0	3583		COYNE	71	HBC	3.7 $\pi^+ p \rightarrow p \pi^+ \pi^+ \pi^- \pi^0$

- Update of AKHMETSIN 00c.
- From the combined fit of ANTONELLI 92, ACHASOV 01E, ACHASOV 02E, and ACHASOV 03D data on the $\pi^+ \pi^- \pi^0$ and ANTONELLI 92 on the $\omega \pi^+ \pi^-$ final states. Supersedes ACHASOV 99E and ACHASOV 02E.
- The values were extracted from a dispersively improved Breit-Wigner parameterization and do not include vacuum polarization. Inclusion of vacuum polarization gives 8.63 ± 0.05 MeV.
- The values were extracted from a dispersively improved Breit-Wigner parameterization and do not include vacuum polarization.
- From the $\rho-\omega$ interference in the $\pi^+ \pi^-$ mass spectrum using the Breit-Wigner for the ω and leaving its mass and width as free parameters of the fit.
- Systematic uncertainties underestimated.
- Relativistic Breit-Wigner includes radiative corrections. Systematic uncertainties not estimated.
- Systematic uncertainties not estimated.
- Observed by threshold-crossing technique. Mass resolution = 4.8 MeV FWHM.

$\omega(782)$ DECAY MODES

Mode	Fraction (Γ_i/Γ)	Scale factor/ Confidence level
Γ_1 $\pi^+ \pi^- \pi^0$	(89.2 ± 0.7) %	
Γ_2 $\pi^0 \gamma$	(8.35 ± 0.27) %	S=2.2
Γ_3 $\pi^+ \pi^-$	(1.53 ± 0.11) %	S=1.2
Γ_4 neutrals (excluding $\pi^0 \gamma$)	(7 +8 / -4) × 10 ⁻³	S=1.1
Γ_5 $\eta \gamma$	(4.5 ± 0.4) × 10 ⁻⁴	S=1.1
Γ_6 $\pi^0 e^+ e^-$	(7.7 ± 0.6) × 10 ⁻⁴	
Γ_7 $\pi^0 \mu^+ \mu^-$	(1.34 ± 0.18) × 10 ⁻⁴	S=1.5
Γ_8 $\eta e^+ e^-$		
Γ_9 $e^+ e^-$	(7.38 ± 0.22) × 10 ⁻⁵	S=1.9
Γ_{10} $\pi^+ \pi^- \pi^0 \pi^0$	< 2 × 10 ⁻⁴	CL=90%
Γ_{11} $\pi^+ \pi^- \gamma$	< 3.6 × 10 ⁻³	CL=95%
Γ_{12} $\pi^+ \pi^- \pi^+ \pi^-$	< 1 × 10 ⁻³	CL=90%
Γ_{13} $\pi^0 \pi^0 \gamma$	(6.7 ± 1.1) × 10 ⁻⁵	
Γ_{14} $\eta \pi^0 \gamma$	< 3.3 × 10 ⁻⁵	CL=90%
Γ_{15} $\mu^+ \mu^-$	(7.4 ± 1.8) × 10 ⁻⁵	
Γ_{16} 3γ	< 1.9 × 10 ⁻⁴	CL=95%

Charge conjugation (C) violating modes

Γ_{17} $\eta \pi^0$	C	< 2.1 × 10 ⁻⁴	CL=90%
Γ_{18} $2\pi^0$	C	< 2.2 × 10 ⁻⁴	CL=90%
Γ_{19} $3\pi^0$	C	< 2.3 × 10 ⁻⁴	CL=90%
Γ_{20} invisible		< 7 × 10 ⁻⁵	CL=90%

CONSTRAINED FIT INFORMATION

An overall fit to 15 branching ratios uses 48 measurements and one constraint to determine 10 parameters. The overall fit has a $\chi^2 = 48.0$ for 39 degrees of freedom.

The following off-diagonal array elements are the correlation coefficients $\langle \delta x_i \delta x_j \rangle / (\delta x_i \delta x_j)$, in percent, from the fit to the branching fractions, $x_i \equiv \Gamma_i/\Gamma_{\text{total}}$. The fit constrains the x_i whose labels appear in this array to sum to one.

x_2	23								
x_3	-18	-4							
x_4	-92	-55	1						
x_5	7	23	-1	-15					
x_6	-1	0	0	0	0				
x_7	0	0	0	0	0	0			
x_9	-24	-73	4	47	-31	0	0		
x_{13}	1	4	0	-2	1	0	0	-3	
x_{15}	0	0	0	0	0	0	0	0	0
	x_1	x_2	x_3	x_4	x_5	x_6	x_7	x_9	x_{13}

$\omega(782)$ PARTIAL WIDTHS

$\Gamma(\pi^0\gamma)$ Γ_2

VALUE (keV)	EVTS	DOCUMENT ID	TECN	COMMENT
880±5.0	7815	¹ ACHASOV	13 SND	1.05–2.00 $e^+e^- \rightarrow \pi^0\pi^0\gamma$
788±12±27	36500	² ACHASOV	03 SND	0.60–0.97 $e^+e^- \rightarrow \pi^0\gamma$
764±5.1	10625	DOLINSKY	89 ND	$e^+e^- \rightarrow \pi^0\gamma$

¹ Systematic uncertainty not estimated.
² Using $\Gamma_\omega = 8.44 \pm 0.09$ MeV and $B(\omega \rightarrow \pi^0\gamma)$ from ACHASOV 03.

$\Gamma(\eta\gamma)$ Γ_5

VALUE (keV)	DOCUMENT ID	TECN	COMMENT
6.1±2.5	¹ DOLINSKY 89 ND		$e^+e^- \rightarrow \eta\gamma$

¹ Using $\Gamma_\omega = 8.4 \pm 0.1$ MeV and $B(\omega \rightarrow \eta\gamma)$ from DOLINSKY 89.

$\Gamma(e^+e^-)$ Γ_9

VALUE (keV)	EVTS	DOCUMENT ID	TECN	COMMENT
0.60 ± 0.02 OUR EVALUATION				
0.591 ± 0.015	11200	^{1,2} AKHMETSHIN 04 CMD2		$e^+e^- \rightarrow \pi^+\pi^-\pi^0$
0.653 ± 0.003 ± 0.021	1.2M	³ ACHASOV 03D RVUE		0.44–2.00 $e^+e^- \rightarrow \pi^+\pi^-\pi^0$
0.600 ± 0.031	10625	DOLINSKY 89 ND		$e^+e^- \rightarrow \pi^0\gamma$

¹ Using $B(\omega \rightarrow \pi^+\pi^-\pi^0) = 0.891 \pm 0.007$ and $\Gamma_{total} = 8.44 \pm 0.09$ MeV.
² Update of AKHMETSHIN 00c.
³ Using ACHASOV 03, ACHASOV 03D and $B(\omega \rightarrow \pi^+\pi^-) = (1.70 \pm 0.28)\%$.

$\omega(782) \Gamma(i)\Gamma(e^+e^-)/\Gamma(total)$

$\Gamma(\pi^+\pi^-\pi^0) \times \Gamma(e^+e^-)/\Gamma_{total}$ $\Gamma_1\Gamma_9/\Gamma$

VALUE (eV)	DOCUMENT ID	TECN	COMMENT
569.8 ± 3.1 ± 8.2	¹ LEES 21B BABR		10.5 $e^+e^- \rightarrow \pi^+\pi^-\pi^0\gamma$

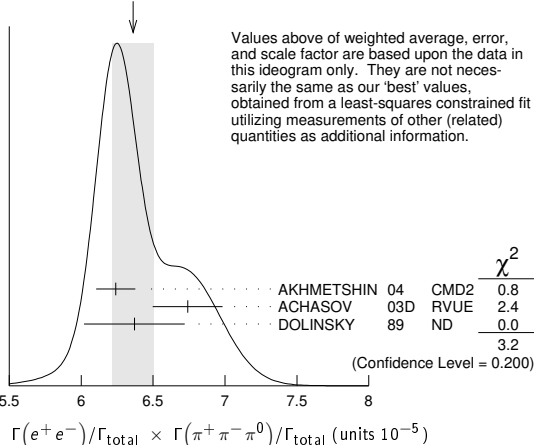
¹ From the cross section for $e^+e^- \rightarrow \pi^+\pi^-\pi^0$ with contributions from $\rho(770)$, $\omega(782)$, $\phi(1020)$, $\omega(1420)$, and $\omega(1650)$.

$\omega(782) \Gamma(e^+e^-)\Gamma(i)/\Gamma^2(total)$

$\Gamma(e^+e^-)/\Gamma_{total} \times \Gamma(\pi^+\pi^-\pi^0)/\Gamma_{total}$ $\Gamma_9/\Gamma \times \Gamma_1/\Gamma$

VALUE (units 10 ⁻⁵)	EVTS	DOCUMENT ID	TECN	COMMENT
6.59 ± 0.19 OUR FIT				Error includes scale factor of 2.1.
6.36 ± 0.14 OUR AVERAGE				Error includes scale factor of 1.3. See the ideogram below.
6.24 ± 0.11 ± 0.08	11.2k	¹ AKHMETSHIN 04 CMD2		$e^+e^- \rightarrow \pi^+\pi^-\pi^0$
6.74 ± 0.04 ± 0.24	1.2M	^{2,3} ACHASOV 03D RVUE		0.44–2.00 $e^+e^- \rightarrow \pi^+\pi^-\pi^0$
6.37 ± 0.35		² DOLINSKY 89 ND		$e^+e^- \rightarrow \pi^+\pi^-\pi^0$
6.20 ± 0.13		⁴ BENAYOUN 10 RVUE		0.4–1.05 e^+e^-
6.70 ± 0.06 ± 0.27		⁵ AUBERT,B 04N BABR		10.6 $e^+e^- \rightarrow \pi^+\pi^-\pi^0\gamma$
6.45 ± 0.24		⁶ BARKOV 87 CMD		$e^+e^- \rightarrow \pi^+\pi^-\pi^0$
5.79 ± 0.42	1488	⁷ KURDADZE 83B OLYA		$e^+e^- \rightarrow \pi^+\pi^-\pi^0$
5.89 ± 0.54	433	⁶ CORDIER 80 DM1		$e^+e^- \rightarrow \pi^+\pi^-\pi^0$
7.54 ± 0.84	451	⁶ BENAKSAS 72B OSPK		$e^+e^- \rightarrow \pi^+\pi^-\pi^0$

WEIGHTED AVERAGE
 6.36±0.14 (Error scaled by 1.3)



Values above of weighted average, error, and scale factor are based upon the data in this ideogram only. They are not necessarily the same as our 'best' values, obtained from a least-squares constrained fit utilizing measurements of other (related) quantities as additional information.

¹ Update of AKHMETSHIN 00c.
² Recalculated by us from the cross section in the peak.

³ From the combined fit of ANTONELLI 92, ACHASOV 01E, ACHASOV 02E, and ACHASOV 03D data on the $\pi^+\pi^-\pi^0$ and ANTONELLI 92 on the $\omega\pi^+\pi^-$ final states. Supersedes ACHASOV 99E and ACHASOV 02E.

⁴ A simultaneous fit of $e^+e^- \rightarrow \pi^+\pi^-, \pi^+\pi^-\pi^0, \pi^0\gamma, \eta\gamma$ data.

⁵ Superseded by LEES 21B.

⁶ Recalculated by us from the cross section in the peak. Systematic uncertainties underestimated.

⁷ Recalculated by us from the cross section in the peak. Systematic uncertainties not estimated.

$\Gamma(e^+e^-)/\Gamma_{total} \times \Gamma(\pi^0\gamma)/\Gamma_{total}$ $\Gamma_9/\Gamma \times \Gamma_2/\Gamma$

VALUE (units 10 ⁻⁶)	EVTS	DOCUMENT ID	TECN	COMMENT
6.16 ± 0.14 OUR FIT				Error includes scale factor of 1.8.
6.34 ± 0.10 OUR AVERAGE				
6.336 ± 0.056 ± 0.089		¹ ACHASOV 16A SND		0.60–1.38 $e^+e^- \rightarrow \pi^0\gamma$
6.47 ± 0.14 ± 0.39	18k	² AKHMETSHIN 05 CMD2		0.60–1.38 $e^+e^- \rightarrow \pi^0\gamma$
6.34 ± 0.21 ± 0.21	10k	² DOLINSKY 89 ND		$e^+e^- \rightarrow \pi^0\gamma$
6.80 ± 0.13		³ BENAYOUN 10 RVUE		0.4–1.05 e^+e^-
6.50 ± 0.11 ± 0.20	36k	⁴ ACHASOV 03 SND		0.60–0.97 $e^+e^- \rightarrow \pi^0\gamma$

¹ From the VMD model with the interfering $\rho(770)$, $\omega(782)$, $\phi(1020)$, and an additional resonance describing the total contribution of the $\rho(1450)$ and $\omega(1420)$ states. Supersedes ACHASOV 03.

² Recalculated by us from the cross section in the peak.

³ A simultaneous fit of $e^+e^- \rightarrow \pi^+\pi^-, \pi^+\pi^-\pi^0, \pi^0\gamma, \eta\gamma$ data.

⁴ Using $\sigma(\phi \rightarrow \pi^0\gamma)$ from ACHASOV 00 and $m_\omega = 782.57$ MeV in the model with the energy-independent phase of ρ - ω interference equal to $(-10.2 \pm 7.0)^\circ$.

$\Gamma(e^+e^-)/\Gamma_{total} \times \Gamma(\pi^+\pi^-)/\Gamma_{total}$ $\Gamma_9/\Gamma \times \Gamma_3/\Gamma$

VALUE (units 10 ⁻⁶)	EVTS	DOCUMENT ID	TECN	COMMENT
1.28 ± 0.05 OUR AVERAGE				
1.318 ± 0.051 ± 0.021		¹ ACHASOV 21 SND		$e^+e^- \rightarrow \pi^+\pi^-$
1.225 ± 0.058 ± 0.041	800k	² ACHASOV 06 SND		$e^+e^- \rightarrow \pi^+\pi^-$
1.166 ± 0.036		³ BENAYOUN 13 RVUE		0.4–1.05 e^+e^-
1.05 ± 0.08		⁴ DAVIER 13 RVUE		$e^+e^- \rightarrow \pi^+\pi^-(\gamma)$

¹ From a fit of the cross section in the energy range $0.525 < \sqrt{s} < 0.883$ GeV parameterized by the sum of the Breit-Wigner amplitudes for the $\rho(770)$, ω and $\rho(1450)$ resonances. The measured phase of the $\rho(770)$ - ω interference is $(110.7 \pm 1.5 \pm 1.0)^\circ$.

² Supersedes ACHASOV 05A.

³ A simultaneous fit to $e^+e^- \rightarrow \pi^+\pi^-, \pi^+\pi^-\pi^0, \pi^0\gamma, \eta\gamma, K\bar{K}$, and $\tau^- \rightarrow \pi^-\pi^0\nu_\tau$ data. Supersedes BENAYOUN 10.

⁴ From $e^+e^- \rightarrow \pi^+\pi^-(\gamma)$ data of LEES 12c.

$\Gamma(e^+e^-)/\Gamma_{total} \times \Gamma(\eta\gamma)/\Gamma_{total}$ $\Gamma_9/\Gamma \times \Gamma_5/\Gamma$

VALUE (units 10 ⁻⁸)	EVTS	DOCUMENT ID	TECN	COMMENT
3.32 ± 0.28 OUR FIT				Error includes scale factor of 1.1.
3.18 ± 0.28 OUR AVERAGE				
3.10 ± 0.31 ± 0.11	33k	¹ ACHASOV 07B SND		0.6–1.38 $e^+e^- \rightarrow \eta\gamma$
3.17 ± 1.85 ± 0.21	17.4k	² AKHMETSHIN 05 CMD2		0.60–1.38 $e^+e^- \rightarrow \eta\gamma$
3.41 ± 0.52 ± 0.21	23k	^{3,4} AKHMETSHIN 01B CMD2		$e^+e^- \rightarrow \eta\gamma$
4.50 ± 0.10		⁵ BENAYOUN 10 RVUE		0.4–1.05 e^+e^-

¹ From a combined fit of $\sigma(e^+e^- \rightarrow \eta\gamma)$ with $\eta \rightarrow 3\pi^0$ and $\eta \rightarrow \pi^+\pi^-\pi^0$, and fixing $B(\eta \rightarrow 3\pi^0) / B(\eta \rightarrow \pi^+\pi^-\pi^0) = 1.44 \pm 0.04$. Recalculated by us from the cross section at the peak. Supersedes ACHASOV 00D and ACHASOV 06A.

² From the $\eta \rightarrow 2\gamma$ decay and using $B(\eta \rightarrow \gamma\gamma) = 39.43 \pm 0.26\%$.

³ From the $\eta \rightarrow 3\pi^0$ decay and using $B(\eta \rightarrow 3\pi^0) = (32.24 \pm 0.29) \times 10^{-2}$.

⁴ The combined fit from 600 to 1380 MeV taking into account $\rho(770)$, $\omega(782)$, $\phi(1020)$, and $\rho(1450)$ (mass and width fixed at 1450 MeV and 310 MeV respectively).

⁵ A simultaneous fit of $e^+e^- \rightarrow \pi^+\pi^-, \pi^+\pi^-\pi^0, \pi^0\gamma, \eta\gamma$ data.

$\Gamma(e^+e^-)/\Gamma_{total} \times \Gamma(\mu^+\mu^-)/\Gamma_{total}$ $\Gamma_9/\Gamma \times \Gamma_{15}/\Gamma$

VALUE (units 10 ⁻³)	EVTS	DOCUMENT ID	TECN	COMMENT
4.3 ± 1.8 ± 2.2	4.5M	¹ ANASTASI 17 KLOE		$e^+e^- \rightarrow \mu^+\mu^-\gamma$

¹ From a fit of the real part of the vacuum polarization by a sum of the leptonic and hadronic contributions, where the hadronic contribution is parametrized as a sum of Breit-Wigner resonances $\omega(782)$, $\phi(1020)$ and using a GOUNARIS 68 parametrization for the $\rho(770)$, and a non-resonant term.

$\omega(782)$ BRANCHING RATIOS

$\Gamma(\pi^+\pi^-\pi^0)/\Gamma_{total}$ Γ_1/Γ

NIECKING 12 describes final-state interactions between the three pions in a dispersive framework using data on the $\pi\pi P$ -wave scattering phase shift.

VALUE	EVTS	DOCUMENT ID	TECN	COMMENT
0.9024 ± 0.0019		¹ AMBROSINO 08G KLOE		1.0–1.03 $e^+e^- \rightarrow \pi^+\pi^-\pi^0, 2\pi^0\gamma$
0.8965 ± 0.0016 ± 0.0048	1.2M	^{2,3} ACHASOV 03D RVUE		0.44–2.00 $e^+e^- \rightarrow \pi^+\pi^-\pi^0$
0.880 ± 0.020 ± 0.032	11200	^{3,4} AKHMETSHIN 00c CMD2		$e^+e^- \rightarrow \pi^+\pi^-\pi^0$
0.8942 ± 0.0062		³ DOLINSKY 89 ND		$e^+e^- \rightarrow \pi^+\pi^-\pi^0$

¹ Not independent of $\Gamma(\pi^0\gamma) / \Gamma(\pi^+\pi^-\pi^0)$ from AMBROSINO 08G.

² Using ACHASOV 03, ACHASOV 03D and $B(\omega \rightarrow \pi^+\pi^-) = (1.70 \pm 0.28)\%$.

³ Not independent of the corresponding $\Gamma(e^+e^-) \times \Gamma(\pi^+\pi^-\pi^0)/\Gamma_{total}$.

⁴ Using $\Gamma(e^+e^-) = 0.60 \pm 0.02$ keV.

Meson Particle Listings

$\omega(782)$

$\Gamma(\pi^0\gamma)/\Gamma_{\text{total}}$	Γ_2/Γ
VALUE (units 10^{-2})	EVTS

DOCUMENT ID	TECN	COMMENT
1 ACHASOV 16A	SND	0.60-1.38 $e^+e^- \rightarrow \pi^0\gamma$
2 AMBROSINO 08G	KLOE	$e^+e^- \rightarrow \pi^+\pi^-2\pi^0, 2\pi^0\gamma$
3,4 AKHMETSHIN 05	CMD2	0.60-1.38 $e^+e^- \rightarrow \pi^0\gamma$
4 ACHASOV 03	SND	0.60-0.97 $e^+e^- \rightarrow \pi^0\gamma$
5,6 ACHASOV 03D	RVUE	0.44-2.00 $e^+e^- \rightarrow \pi^0\gamma$
7 BENAYOUN 9K	RVUE	$e^+\pi^+\pi^-\pi^0$
8 DOLINSKY 86	ND	$e^+e^- \rightarrow \pi^0\gamma$

- • • We do not use the following data for averages, fits, limits, etc. • • •
- 1 Using $B(\omega \rightarrow e^+e^-)$ from PDG 15. Supersedes ACHASOV 03.
- 2 Not independent of $\Gamma(\pi^0\gamma) / \Gamma(\pi^+\pi^-\pi^0)$ from AMBROSINO 08G.
- 3 Using $B(\omega \rightarrow e^+e^-) = (7.14 \pm 0.13) \times 10^{-5}$.
- 4 Not independent of the corresponding $\Gamma(e^+e^-) \times \Gamma(\pi^0\gamma)/\Gamma_{\text{total}}^2$.
- 5 Using ACHASOV 03, ACHASOV 03D and $B(\omega \rightarrow \pi^+\pi^-) = (1.70 \pm 0.28)\%$.
- 6 Not independent of the corresponding $\Gamma(e^+e^-) \times \Gamma(\pi^+\pi^-\pi^0)/\Gamma_{\text{total}}^2$.
- 7 Reanalysis of DRUZHININ 84, DOLINSKY 89, DOLINSKY 91 taking into account the triangle anomaly contributions.

$\Gamma(\pi^0\gamma)/\Gamma(\pi^+\pi^-\pi^0)$	Γ_2/Γ_1
VALUE (units 10^{-2})	DOCUMENT ID

TECN	COMMENT
9.35 ± 0.30 OUR FIT	Error includes scale factor of 2.4.
9.05 ± 0.27 OUR AVERAGE	Error includes scale factor of 1.8.
8.97 ± 0.16	1 AMBROSINO 08G KLOE $e^+e^- \rightarrow \pi^+\pi^-2\pi^0, 2\pi^0\gamma$
9.94 ± 0.36 ± 0.38	1 AULCHENKO 00A SND $e^+e^- \rightarrow \pi^+\pi^-2\pi^0, 2\pi^0\gamma$
8.4 ± 1.3	KEYNE 76 CNTR $\pi^-p \rightarrow \omega n$
10.9 ± 2.5	BENAKSAS 72C OSPK $e^+e^- \rightarrow \pi^0\gamma$
8.1 ± 2.0	BALDIN 71 HLBC $2.9 \pi^+\pi^-$
13 ± 4	JACQUET 69B HLBC $2.05 \pi^+\pi^- \rightarrow \pi^+\pi^0$
9.7 ± 0.2 ± 0.5	2,3 ACHASOV 03D RVUE $0.44-2.00 e^+e^- \rightarrow \pi^+\pi^-\pi^0$
9.9 ± 0.7	2 DOLINSKY 89 ND $e^+e^- \rightarrow \pi^0\gamma$

- • • We do not use the following data for averages, fits, limits, etc. • • •
- 1 From $\omega \pi^0 \rightarrow \pi^0 \pi^0 \gamma (m_\phi) / \sigma_0^{\omega \pi^0} \rightarrow \pi^+\pi^-\pi^0 \pi^0 (m_\phi)$ with a phase-space correction factor of 1/1.023.
- 2 Not independent of the corresponding $\Gamma(e^+e^-) \times \Gamma(\pi^0\gamma)/\Gamma_{\text{total}}^2$.
- 3 Using ACHASOV 03. Based on 1.2M events.

$\Gamma(\pi^+\pi^-)/\Gamma_{\text{total}}$	Γ_3/Γ
VALUE (units 10^{-2})	EVTS

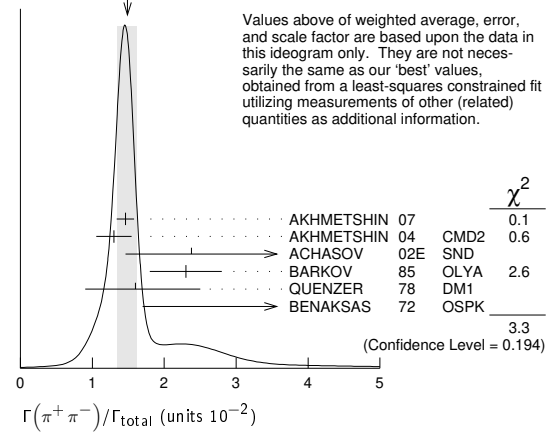
DOCUMENT ID	TECN	COMMENT
1.53 ± 0.11 OUR FIT	Error includes scale factor of 1.2.	
1.49 ± 0.13 OUR AVERAGE	Error includes scale factor of 1.3. See the ideogram below.	
1.46 ± 0.12 ± 0.02	900k	1 AKHMETSHIN 07 $e^+e^- \rightarrow \pi^+\pi^-$
1.30 ± 0.24 ± 0.05	11.2k	2 AKHMETSHIN 04 CMD2 $e^+e^- \rightarrow \pi^+\pi^-$
2.36 ± 1.77 ± 0.90 ± 0.18	5.4k	3 ACHASOV 02E SND $1.1-1.38 e^+e^- \rightarrow \pi^+\pi^-$
2.3 ± 0.5		BARKOV 85 OLYA $e^+e^- \rightarrow \pi^+\pi^-$
1.6 ± 0.9 ± 0.7		QUENZER 78 DM1 $e^+e^- \rightarrow \pi^+\pi^-$
3.6 ± 1.9		BENAKSAS 72 OSPK $e^+e^- \rightarrow \pi^+\pi^-$

DOCUMENT ID	TECN	COMMENT
• • • We do not use the following data for averages, fits, limits, etc. • • •		
1.29 ± 0.22 ± 0.03	970k	4,5 ABLIKIM 18C BES3 $\eta'(958) \rightarrow \gamma\pi^+\pi^-$
1.28 ± 0.22 ± 0.03	970k	6,7 ABLIKIM 18C BES3 $\eta'(958) \rightarrow \gamma\pi^+\pi^-$
1.52 ± 0.08		8 HANHART 18 RVUE $e^+e^- \rightarrow \pi^+\pi^-$
1.75 ± 0.11	4.5M	9 ACHASOV 05A SND $e^+e^- \rightarrow \pi^+\pi^-$
2.01 ± 0.29		10 BENAYOUN 03 RVUE $e^+e^- \rightarrow \pi^+\pi^-$
1.9 ± 0.3		11 GARDNER 99 RVUE $e^+e^- \rightarrow \pi^+\pi^-$
2.3 ± 0.4		12 BENAYOUN 98 RVUE $e^+e^- \rightarrow \pi^+\pi^-, \mu^+\mu^-$
1.0 ± 0.11		13 WICKLUND 78 ASPK $3,4,6 \pi^\pm N$
1.22 ± 0.30		ALVENSLEB... 71C CNTR Photoproduction
1.3 ± 1.2 ± 0.9		MOFFEIT 71 HBC $2.8,4,7 \gamma p$
0.80 ± 0.28 ± 0.20		14 BIGGS 70B CNTR $4,2,7 C \rightarrow \pi^+\pi^- C$

- 1 A combined fit of AKHMETSHIN 07, AULCHENKO 06, and AULCHENKO 05.
- 2 Update of AKHMETSHIN 02.
- 3 From the $m_{\pi^+\pi^-}$ spectrum taking into account the interference of the $\rho\pi$ and $\omega\pi$ amplitudes.
- 4 From a fit to $\pi^+\pi^-$ mass using $\rho(770)$ (parametrized with the Gounaris-Sakurai approach), $\omega(782)$, and box anomaly components.
- 5 ABLIKIM 18C reports $[\Gamma(\omega(782) \rightarrow \pi^+\pi^-)/\Gamma_{\text{total}}] \times [B(\eta'(958) \rightarrow \omega\gamma)] = (3.25 \pm 0.21 \pm 0.52) \times 10^{-4}$ which we divide by our best value $B(\eta'(958) \rightarrow \omega\gamma) = (2.52 \pm 0.07) \times 10^{-2}$. Our first error is their experiment's error and our second error is the systematic error from using our best value.
- 6 From a fit to $\pi^+\pi^-$ mass using $\rho(770)$ (parametrized with the Gounaris-Sakurai approach), $\omega(782)$, and $\rho(1450)$ components.
- 7 ABLIKIM 18C reports $[\Gamma(\omega(782) \rightarrow \pi^+\pi^-)/\Gamma_{\text{total}}] \times [B(\eta'(958) \rightarrow \omega\gamma)] = (3.22 \pm 0.21 \pm 0.52) \times 10^{-4}$ which we divide by our best value $B(\eta'(958) \rightarrow \omega\gamma) = (2.52 \pm 0.07) \times 10^{-2}$. Our first error is their experiment's error and our second error is the systematic error from using our best value.

- 8 Dispersive analysis. Value extracted from average of data from AUBERT 09As, AKHMETSHIN 07, ACHASOV 06, AMBROSINO 11A, BABUSCI 13D, ABLIKIM 16B normalised by PDG 16 evaluation for $\Gamma(\omega \rightarrow e^+e^-)$.
- 9 Using $\Gamma(\omega \rightarrow e^+e^-)$ from the 2004 Edition of this Review (PDG 04).
- 10 Using the data of AKHMETSHIN 02 in the hidden local symmetry model.
- 11 Using the data of BARKOV 85.
- 12 Using the data of BARKOV 85 in the hidden local symmetry model.
- 13 From a model-dependent analysis assuming complete coherence.
- 14 Re-evaluated under $\Gamma(\pi^+\pi^-)/\Gamma(\pi^+\pi^-\pi^0)$ by BEHREND 71 using more accurate $\omega \rightarrow \rho$ photoproduction cross-section ratio.

WEIGHTED AVERAGE
1.49 ± 0.13 (Error scaled by 1.3)



$\Gamma(\pi^+\pi^-)/\Gamma(\pi^+\pi^-\pi^0)$	Γ_3/Γ_1
VALUE	DOCUMENT ID

TECN	COMMENT
0.0172 ± 0.0014 OUR FIT	Error includes scale factor of 1.2.
0.026 ± 0.005 OUR AVERAGE	
0.021 ± 0.028 ± 0.009	1,2 RATCLIFF 72 ASPK $15 \pi^-p \rightarrow n2\pi$
0.028 ± 0.006	1 BEHREND 71 ASPK Photoproduction
0.022 ± 0.009 ± 0.01	3 ROOS 70 RVUE

- 1 The fitted width of these data is 160 MeV in agreement with present average, thus the ω contribution is overestimated. Assuming ρ width 145 MeV.
- 2 Significant interference effect observed. NB of $\omega \rightarrow 3\pi$ comes from an extrapolation.
- 3 ROOS 70 combines ABRAOVICH 70 and BIZZARRI 70.

$\Gamma(\pi^+\pi^-)/\Gamma(\pi^0\gamma)$	Γ_3/Γ_2
VALUE	EVTS

DOCUMENT ID	TECN	COMMENT
0.20 ± 0.04	1.98M	1 ALOISIO 03 KLOE $1.02 e^+e^- \rightarrow \pi^+\pi^-\pi^0$

- 1 Using the data of ALOISIO 02D.

$\Gamma(\text{neutrals})/\Gamma_{\text{total}}$	$(\Gamma_2+\Gamma_4)/\Gamma$
VALUE	EVTS

DOCUMENT ID	TECN	COMMENT
0.091 ± 0.006 OUR FIT		
0.081 ± 0.011 OUR AVERAGE		
0.075 ± 0.025		BIZZARRI 71 HBC $0.0 \rho\bar{p}$
0.079 ± 0.019		DEINET 69B OSPK $1.5 \pi^-p$
0.084 ± 0.015		BOLLINI 68C CNTR $1.4 \pi^-p$
• • • We do not use the following data for averages, fits, limits, etc. • • •		
0.073 ± 0.018	42	BASILE 72B CNTR $1.67 \pi^-p$

$\Gamma(\text{neutrals})/\Gamma(\pi^+\pi^-\pi^0)$	$(\Gamma_2+\Gamma_4)/\Gamma_1$
VALUE	EVTS

DOCUMENT ID	TECN	COMMENT
0.102 ± 0.008 OUR FIT		
0.103 ± 0.011 ± 0.010 OUR AVERAGE		
0.15 ± 0.04	46	AGUILAR... 72B HBC $3,9,4,6 K^-p$
0.10 ± 0.03	19	BARASH 67B HBC $0.0 \bar{p}p$
0.134 ± 0.026	850	DIGIUGNO 66B CNTR $1.4 \pi^-p$
0.097 ± 0.016	348	FLATTE 66 HBC $1.4 - 1.7 K^-p \rightarrow \Lambda MM$
0.06 ± 0.05 ± 0.02		JAMES 66 HBC $2.1 \pi^+p$
0.08 ± 0.03	35	KRAEMER 64 DBC $1.2 \pi^+d$
• • • We do not use the following data for averages, fits, limits, etc. • • •		
0.11 ± 0.02	20	BUSCHBECK 63 HBC $1.5 K^-p$

$\Gamma(\pi^0\gamma)/\Gamma(\text{neutrals})$	$\Gamma_2/(\Gamma_2+\Gamma_4)$
VALUE	CL%

DOCUMENT ID	TECN	COMMENT
• • • We do not use the following data for averages, fits, limits, etc. • • •		
0.78 ± 0.07		1 DAKIN 72 OSPK $1.4 \pi^-p \rightarrow nMM$
> 0.81	90	DEINET 69B OSPK

- 1 Error statistical only. Authors obtain good fit also assuming $\pi^0\gamma$ as the only neutral decay.

$\Gamma(\text{neutrals})/\Gamma(\text{charged particles})$		$(\Gamma_2+\Gamma_4)/(\Gamma_1+\Gamma_3)$	
VALUE	DOCUMENT ID	TECN	COMMENT
0.100 ± 0.008 OUR FIT			
0.124 ± 0.021	FELDMAN	67c	OSPK 1.2 $\pi^- p$

$\Gamma(\eta\gamma)/\Gamma_{\text{total}}$		Γ_5/Γ		
VALUE (units 10^{-4})	EVTS	DOCUMENT ID	TECN	COMMENT
4.5 ± 0.4 OUR FIT				Error includes scale factor of 1.1.
6.3 ± 1.3 OUR AVERAGE				Error includes scale factor of 1.2.
6.6 ± 1.7		¹ ABELE	97E	CBAR 0.0 $\bar{p}p \rightarrow 5\gamma$
8.3 ± 2.1		ALDE	93	GAM2 38 $\pi^- p \rightarrow \omega n$
3.0 $^{+2.5}_{-1.8}$		² ANDREWS	77	CNTR 6.7-10 γCu

• • • We do not use the following data for averages, fits, limits, etc. • • •

4.2 ± 0.4 ± 0.1	33k	³ ACHASOV	07B	SND 0.6-1.38 $e^+e^- \rightarrow \eta\gamma$
4.44 $^{+2.59}_{-1.83}$ ± 0.28	17.4k	^{4,5} AKHMETSHIN	05	CMD2 0.60-1.38 $e^+e^- \rightarrow \eta\gamma$
5.10 ± 0.72 ± 0.34	23k	⁶ AKHMETSHIN	01B	CMD2 $e^+e^- \rightarrow \eta\gamma$
0.7 to 5.5		⁷ CASE	00	CBAR 0.0 $p\bar{p} \rightarrow \eta\eta\gamma$
6.56 $^{+2.41}_{-2.55}$	3525	^{2,8} BENAYOUN	96	RVUE $e^+e^- \rightarrow \eta\gamma$
7.3 ± 2.9		^{2,4} DOLINSKY	89	ND $e^+e^- \rightarrow \eta\gamma$

¹ No flat $\eta\eta\gamma$ background assumed.
² Solution corresponding to constructive $\omega\rho$ interference.
³ ACHASOV 07B reports $[\Gamma(\omega(782) \rightarrow \eta\gamma)/\Gamma_{\text{total}}] \times [B(\omega(782) \rightarrow e^+e^-)] = (3.10 \pm 0.31 \pm 0.11) \times 10^{-8}$ which we divide by our best value $B(\omega(782) \rightarrow e^+e^-) = (7.38 \pm 0.22) \times 10^{-5}$. Our first error is their experiment's error and our second error is the systematic error from using our best value. Supersedes ACHASOV 00D and ACHASOV 06A.
⁴ Not independent of the corresponding $\Gamma(e^+e^-) \times \Gamma(\eta\gamma)/\Gamma_{\text{total}}^2$.
⁵ Using $B(\omega \rightarrow e^+e^-) = (7.14 \pm 0.13) \times 10^{-5}$ and $B(\eta \rightarrow \gamma\gamma) = 39.43 \pm 0.26\%$.
⁶ Using $B(\omega \rightarrow e^+e^-) = (7.07 \pm 0.19) \times 10^{-5}$ and using $B(\eta \rightarrow 3\pi^0) = (32.24 \pm 0.29) \times 10^{-2}$. Solution corresponding to constructive $\omega\rho$ interference. The combined fit from 600 to 1380 MeV taking into account $\rho(770)$, $\omega(782)$, $\phi(1020)$, and $\rho(1450)$ (mass and width fixed at 1450 MeV and 310 MeV respectively). Not independent of the corresponding $\Gamma(e^+e^-) \times \Gamma(\eta\gamma)/\Gamma_{\text{total}}^2$.
⁷ Depending on the degree of coherence with the flat $\eta\eta\gamma$ background and using $B(\omega \rightarrow \pi^0\gamma) = (8.5 \pm 0.5) \times 10^{-2}$.
⁸ Reanalysis of DRUZHININ 84, DOLINSKY 89, DOLINSKY 91 taking into account the triangle anomaly contributions.

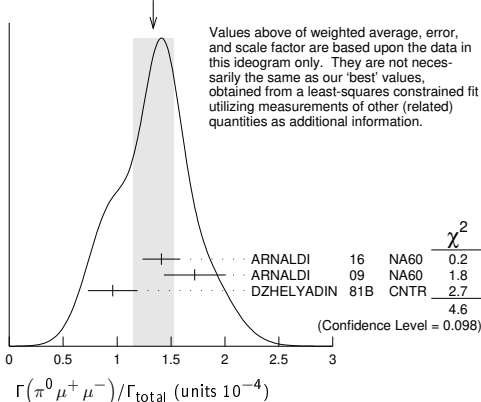
$\Gamma(\eta\gamma)/\Gamma(\pi^0\gamma)$		Γ_5/Γ_2	
VALUE	DOCUMENT ID	TECN	COMMENT
• • • We do not use the following data for averages, fits, limits, etc. • • •			
0.0098 ± 0.0024	¹ ALDE	93	GAM2 38 $\pi^- p \rightarrow \omega n$
0.0082 ± 0.0033	² DOLINSKY	89	ND $e^+e^- \rightarrow \eta\gamma$
0.010 ± 0.045	APEL	72B	OSPK 4-8 $\pi^- p \rightarrow n3\gamma$

¹ Model independent determination.
² Solution corresponding to constructive $\omega\rho$ interference.

$\Gamma(\pi^0 e^+ e^-)/\Gamma_{\text{total}}$		Γ_6/Γ		
VALUE (units 10^{-4})	EVTS	DOCUMENT ID	TECN	COMMENT
7.7 ± 0.6 OUR FIT				
7.7 ± 0.6 OUR AVERAGE				
7.61 ± 0.53 ± 0.64		ACHASOV	08	SND 0.36-0.97 $e^+e^- \rightarrow \pi^0 e^+ e^-$
8.19 ± 0.71 ± 0.62		AKHMETSHIN	05A	CMD2 0.72-0.84 e^+e^-
5.9 ± 1.9	43	DOLINSKY	88	ND $e^+e^- \rightarrow \pi^0 e^+ e^-$

$\Gamma(\pi^0 \mu^+ \mu^-)/\Gamma_{\text{total}}$		Γ_7/Γ		
VALUE (units 10^{-4})	EVTS	DOCUMENT ID	TECN	COMMENT
1.34 ± 0.18 OUR FIT				Error includes scale factor of 1.5.
1.34 ± 0.19 OUR AVERAGE				Error includes scale factor of 1.5. See the ideogram below.
1.41 ± 0.09 ± 0.15		ARNALDI	16	NA60 400 GeV (p -A) collisions
1.72 ± 0.25 ± 0.14	3k	ARNALDI	09	NA60 158A In-In collisions
0.96 ± 0.23		DZHELJADIN	81B	CNTR 25-33 $\pi^- p \rightarrow \omega n$

WEIGHTED AVERAGE
 1.34 ± 0.19 (Error scaled by 1.5)



Values above of weighted average, error, and scale factor are based upon the data in this ideogram only. They are not necessarily the same as our 'best' values, obtained from a least-squares constrained fit utilizing measurements of other (related) quantities as additional information.

$\Gamma(\eta e^+ e^-)/\Gamma_{\text{total}}$		Γ_8/Γ	
VALUE (units 10^{-5})	DOCUMENT ID	TECN	COMMENT
• • • We do not use the following data for averages, fits, limits, etc. • • •			
< 1.1	AKHMETSHIN	05A	CMD2 0.72-0.84 e^+e^-

$\Gamma(e^+e^-)/\Gamma_{\text{total}}$		Γ_9/Γ		
VALUE (units 10^{-4})	EVTS	DOCUMENT ID	TECN	COMMENT
0.738 ± 0.022 OUR FIT				Error includes scale factor of 1.9.
• • • We do not use the following data for averages, fits, limits, etc. • • •				
0.700 ± 0.016	11200	^{1,2} AKHMETSHIN	04	CMD2 $e^+e^- \rightarrow \pi^+ \pi^- \pi^0$
0.752 ± 0.004 ± 0.024	1.2M	^{2,3} ACHASOV	03D	RVUE 0.44-2.00 $e^+e^- \rightarrow \pi^+ \pi^- \pi^0$
0.714 ± 0.036		² DOLINSKY	89	ND $e^+e^- \rightarrow \pi^+ \pi^- \pi^0$
0.72 ± 0.03		² BARKOV	87	CMD $e^+e^- \rightarrow \pi^+ \pi^- \pi^0$
0.64 ± 0.04	1488	² KURDADZE	83B	OLYA $e^+e^- \rightarrow \pi^+ \pi^- \pi^0$
0.675 ± 0.069	433	² CORDIER	80	DM1 $e^+e^- \rightarrow \pi^+ \pi^- \pi^0$
0.83 ± 0.10	451	² BENAKSAS	72B	OSPK $e^+e^- \rightarrow \pi^+ \pi^- \pi^0$
0.77 ± 0.06		⁴ AUGUSTIN	69D	OSPK $e^+e^- \rightarrow \pi^+ \pi^- \pi^0$
0.65 ± 0.13	33	⁵ ASTVACAT...	68	OSPK Assume SU(3)+mixing

¹ Using $B(\omega \rightarrow \pi^+ \pi^- \pi^0) = 0.891 \pm 0.007$. Update of AKHMETSHIN 00c.
² Not independent of the corresponding $\Gamma(e^+e^-) \times \Gamma(\pi^+ \pi^- \pi^0)/\Gamma_{\text{total}}^2$.
³ Using ACHASOV 03, ACHASOV 03D and $B(\omega \rightarrow \pi^+ \pi^-) = (1.70 \pm 0.28)\%$.
⁴ Rescaled by us to correspond to ω width 8.4 MeV. Systematic errors underestimated.
⁵ Not resolved from ρ decay. Error statistical only.

$\Gamma(\pi^+ \pi^- \pi^0 \pi^0)/\Gamma_{\text{total}}$		Γ_{10}/Γ		
VALUE (units 10^{-4})	CL%	DOCUMENT ID	TECN	COMMENT
< 2	90	ACHASOV	09A	SND $e^+e^- \rightarrow \pi^+ \pi^- \pi^0 \pi^0$
• • • We do not use the following data for averages, fits, limits, etc. • • •				
< 200	90	KURDADZE	86	OLYA $e^+e^- \rightarrow \pi^+ \pi^- \pi^0 \pi^0$

$\Gamma(\pi^+ \pi^- \gamma)/\Gamma_{\text{total}}$		Γ_{11}/Γ		
VALUE	CL%	DOCUMENT ID	TECN	COMMENT
< 0.0036	95	WEIDENAUER	90	ASTE $p\bar{p} \rightarrow \pi^+ \pi^- \pi^+ \pi^- \gamma$
• • • We do not use the following data for averages, fits, limits, etc. • • •				
< 0.004	95	BITYUKOV	88B	SPEC 32 $\pi^- p \rightarrow \pi^+ \pi^- \gamma X$

$\Gamma(\pi^+ \pi^- \gamma)/\Gamma(\pi^+ \pi^- \pi^0)$		Γ_{11}/Γ_1		
VALUE	CL%	DOCUMENT ID	TECN	COMMENT
• • • We do not use the following data for averages, fits, limits, etc. • • •				
< 0.066	90	KALBFLEISCH	75	HBC 2.18 $K^- p \rightarrow \Lambda \pi^+ \pi^- \gamma$
< 0.05	90	FLATTE	66	HBC 1.2-1.7 $K^- p \rightarrow \Lambda \pi^+ \pi^- \gamma$

$\Gamma(\pi^+ \pi^- \pi^+ \pi^-)/\Gamma_{\text{total}}$		Γ_{12}/Γ		
VALUE	CL%	DOCUMENT ID	TECN	COMMENT
< 1 × 10 ⁻³	90	KURDADZE	88	OLYA $e^+e^- \rightarrow \pi^+ \pi^- \pi^+ \pi^-$

$\Gamma(\pi^0 \pi^0 \gamma)/\Gamma_{\text{total}}$		Γ_{13}/Γ		
VALUE (units 10^{-5})	EVTS	DOCUMENT ID	TECN	COMMENT
6.7 ± 1.1 OUR FIT				
6.5 ± 1.2 OUR AVERAGE				
6.4 $^{+2.4}_{-2.0}$ ± 0.8	190	¹ AKHMETSHIN	04B	CMD2 0.6-0.97 $e^+e^- \rightarrow \pi^0 \pi^0 \gamma$
6.6 $^{+1.4}_{-1.3}$ ± 0.6	295	ACHASOV	02F	SND 0.36-0.97 $e^+e^- \rightarrow \pi^0 \pi^0 \gamma$

• • • We do not use the following data for averages, fits, limits, etc. • • •

11.8 $^{+2.1}_{-1.9}$ ± 1.4	190	² AKHMETSHIN	04B	CMD2 0.6-0.97 $e^+e^- \rightarrow \pi^0 \pi^0 \gamma$
7.8 ± 2.7 ± 2.0	63	^{1,3} ACHASOV	00G	SND $e^+e^- \rightarrow \pi^0 \pi^0 \gamma$
12.7 ± 2.3 ± 2.5	63	^{2,3} ACHASOV	00G	SND $e^+e^- \rightarrow \pi^0 \pi^0 \gamma$

¹ In the model assuming the $\rho \rightarrow \pi^0 \pi^0 \gamma$ decay via the $\omega\pi$ and $f_0(500)\gamma$ mechanisms.
² In the model assuming the $\rho \rightarrow \pi^0 \pi^0 \gamma$ decay via the $\omega\pi$ mechanism only.
³ Superseded by ACHASOV 02F.

$\Gamma(\pi^0 \pi^0 \gamma)/\Gamma(\pi^+ \pi^- \pi^0)$		Γ_{13}/Γ_1		
VALUE	CL%	DOCUMENT ID	TECN	COMMENT
< 0.00045	90	DOLINSKY	89	ND $e^+e^- \rightarrow \pi^0 \pi^0 \gamma$
• • • We do not use the following data for averages, fits, limits, etc. • • •				
< 0.08	95	JACQUET	69B	HLBC 2.05 $\pi^+ p \rightarrow \pi^+ \rho\omega$

$\Gamma(\pi^0 \pi^0 \gamma)/\Gamma(\pi^0 \gamma)$		Γ_{13}/Γ_2			
VALUE (units 10^{-4})	CL%	EVTS	DOCUMENT ID	TECN	COMMENT
8.0 ± 1.3 OUR FIT					
8.5 ± 2.9		40 ± 14	ALDE	94B	GAM2 38 $\pi^- p \rightarrow \pi^0 \pi^0 \gamma n$
• • • We do not use the following data for averages, fits, limits, etc. • • •					
< 50	90		DOLINSKY	89	ND $e^+e^- \rightarrow \pi^0 \pi^0 \gamma$
< 1800	95		KEYNE	76	CNTR $\pi^- p \rightarrow \omega n$
< 1500	90		BENAKSAS	72C	OSPK e^+e^-
< 1400			BALDIN	71	HLBC 2.9 $\pi^+ p$
< 1000	90		BARMIN	64	HLBC 1.3-2.8 $\pi^- p$

Meson Particle Listings

 $\omega(782)$ $\Gamma(\pi^0\pi^0\gamma)/\Gamma(\text{neutrals})$ $\Gamma_{13}/(\Gamma_2+\Gamma_4)$

VALUE	CL%	DOCUMENT ID	TECN	COMMENT
0.22±0.07		¹ DAKIN	72	OSPK 1.4 $\pi^- p \rightarrow nMM$
<0.19	90	DEINET	69B	OSPK

¹ See $\Gamma(\pi^0\gamma)/\Gamma(\text{neutrals})$.

 $\Gamma(\eta\pi^0\gamma)/\Gamma_{\text{total}}$ Γ_{14}/Γ

VALUE (units 10 ⁻⁵)	CL%	DOCUMENT ID	TECN	COMMENT
<3.3	90	AKHMETSHIN 04B	CMD2	0.6-0.97 $e^+e^- \rightarrow \eta\pi^0\gamma$

 $\Gamma(\mu^+\mu^-)/\Gamma_{\text{total}}$ Γ_{15}/Γ

VALUE (units 10 ⁻⁵)	EVTS	DOCUMENT ID	TECN	COMMENT
7.4±1.8 OUR FIT				
7.4±1.8 OUR AVERAGE				
6.6±1.4±1.7	4.5M	¹ ANASTASI	17	KLOE $e^+e^- \rightarrow \mu^+\mu^-\gamma$
9.0±2.9±1.1	18	HEISTER	02C	ALEP $Z \rightarrow \mu^+\mu^- + X$

¹ Assuming lepton universality in the decay $\omega \rightarrow \ell^+\ell^-$ and correcting for different phase space between electron and muon final states.

 $\Gamma(\mu^+\mu^-)/\Gamma(\pi^+\pi^-\pi^0)$ Γ_{15}/Γ_1

VALUE (units 10 ⁻³)	CL%	DOCUMENT ID	TECN	COMMENT
<0.2	90	WILSON	69	OSPK 12 $\pi^- C \rightarrow Fe$
<1.7	74	FLATTE	66	HBC 1.2-1.7 $K^- p \rightarrow \Lambda\mu^+\mu^-$
<1.2		BARBARO...	65	HBC 2.7 $K^- p$

 $\Gamma(\pi^0\mu^+\mu^-)/\Gamma(\mu^+\mu^-)$ Γ_7/Γ_{15}

VALUE	EVTS	DOCUMENT ID	TECN	COMMENT
1.2±0.6	30	¹ DZHELADIN 79	CNTR	25-33 $\pi^- p$

¹ Superseded by DZHELADIN 81B result above.

 $\Gamma(3\gamma)/\Gamma_{\text{total}}$ Γ_{16}/Γ

VALUE (units 10 ⁻⁴)	CL%	DOCUMENT ID	TECN	COMMENT
<1.9	95	¹ ABELE	97E	CBAR 0.0 $\bar{p}p \rightarrow 5\gamma$
<2	90	¹ PROKOSHKIN 95	GAM2	38 $\pi^- p \rightarrow 3\gamma n$

¹ From direct 3γ decay search.

 $\Gamma(\eta\pi^0)/\Gamma_{\text{total}}$ Γ_{17}/Γ

VALUE	CL%	DOCUMENT ID	TECN	COMMENT
<0.001	90	ALDE	94B	GAM2 38 $\pi^- p \rightarrow \eta\pi^0 n$

 $[\Gamma(\eta\gamma) + \Gamma(\eta\pi^0)]/\Gamma(\pi^+\pi^-\pi^0)$ $(\Gamma_5 + \Gamma_{17})/\Gamma_1$

VALUE	CL%	DOCUMENT ID	TECN	COMMENT
<0.016	90	¹ FLATTE	66	HBC 1.2-1.7 $K^- p \rightarrow \Lambda\pi^+\pi^-MM$
<0.045	95	JACQUET	69B	HLBC 2.05 $\pi^+ p \rightarrow \pi^+ p\omega$

¹ Restated by us using $B(\eta \rightarrow \text{charged modes}) = 29.2\%$.

 $\Gamma(\eta\pi^0)/\Gamma(\pi^0\gamma)$ Γ_{17}/Γ_2

VALUE (units 10 ⁻³)	CL%	DOCUMENT ID	TECN	COMMENT
<2.6	90	¹ STAROSTIN 09	CRYM	$\gamma p \rightarrow \eta\pi^0 p$

¹ STAROSTIN 09 reports $[\Gamma(\omega(782) \rightarrow \eta\pi^0)/\Gamma(\omega(782) \rightarrow \pi^0\gamma)] \times [B(\eta \rightarrow 2\gamma)] < 1.01 \times 10^{-3}$ which we divide by our best value $B(\eta \rightarrow 2\gamma) = 39.36 \times 10^{-2}$.

 $\Gamma(2\pi^0)/\Gamma(\pi^0\gamma)$ Γ_{18}/Γ_2

VALUE (units 10 ⁻³)	CL%	DOCUMENT ID	TECN	COMMENT
<2.59	90	STAROSTIN 09	CRYM	$\gamma p \rightarrow 2\pi^0 p$

 $\Gamma(3\pi^0)/\Gamma_{\text{total}}$ Γ_{19}/Γ

VALUE	CL%	DOCUMENT ID	TECN	COMMENT
<3 × 10 ⁻⁴	90	PROKOSHKIN 95	GAM2	38 $\pi^- p \rightarrow 3\pi^0 n$

 $\Gamma(3\pi^0)/\Gamma(\pi^0\gamma)$ Γ_{19}/Γ_2

VALUE (units 10 ⁻³)	CL%	DOCUMENT ID	TECN	COMMENT
<2.72	90	STAROSTIN 09	CRYM	$\gamma p \rightarrow 3\pi^0 p$

 $\Gamma(3\pi^0)/\Gamma(\pi^+\pi^-\pi^0)$ Γ_{19}/Γ_1

VALUE	CL%	DOCUMENT ID	COMMENT
<0.009	90	BARBERIS 01	450 $pp \rightarrow p_f 3\pi^0 p_s$

 $\Gamma(\text{invisible})/\Gamma(\pi^+\pi^-\pi^0)$ Γ_{20}/Γ_1

VALUE	CL%	DOCUMENT ID	TECN	COMMENT
<8.1 × 10 ⁻⁵	90	ABLIKIM	18s	BES3 $J/\psi \rightarrow \omega\eta \rightarrow \omega\pi^+\pi^-\pi^0$

PARAMETER Λ IN $\omega \rightarrow \pi^0\ell^+\ell^-$ DECAY

In the pole approximation the electromagnetic transition form factor for a resonance of mass M is given by the expression:

$$|F|^2 = (1 - M^2/\Lambda^2)^{-2},$$

where for the parameter Λ vector dominance predicts $\Lambda = M_p \approx 0.770$ GeV. The ARNALDI 09 measurement is in obvious conflict with this expectation. Note that for $\eta \rightarrow \gamma\mu^+\mu^-$ decay ARNALDI 09 and DZHELADIN 80 obtain the value of Λ consistent with vector dominance.

PARAMETER Λ IN $\omega \rightarrow \pi^0\mu^+\mu^-$ DECAY

VALUE (GeV)	EVTS	DOCUMENT ID	TECN	COMMENT
0.670 ± 0.006 OUR AVERAGE				
0.6707 ± 0.0039 ± 0.0056		¹ ARNALDI	16	NA60 400 GeV (p -A) collisions
0.668 ± 0.009 ± 0.003	3k	² ARNALDI	09	NA60 158A In-In collisions

• • • We do not use the following data for averages, fits, limits, etc. • • •

0.65 ± 0.03 DZHELADIN 81B CNTR 25-33 $\pi^- p \rightarrow \omega n$

¹ ARNALDI 16 reports $\Lambda^{-2}(\omega) = 2.223 \pm 0.026 \pm 0.037$ GeV⁻² which we converted to the quoted Λ value.

² ARNALDI 09 reports $\Lambda^{-2}(\omega) = 2.24 \pm 0.06 \pm 0.02$ GeV⁻² which we converted to the quoted Λ value.

PARAMETER Λ IN $\omega \rightarrow \pi^0 e^+e^-$ DECAY

VALUE (GeV)	EVTS	DOCUMENT ID	TECN	COMMENT
0.709 ± 0.037	1.1k	¹ ADLARSON	17B	A2MM $\gamma p \rightarrow \omega p$

¹ ADLARSON 17B reports $\Lambda^{-2}(\omega\pi^0) = 1.99 \pm 0.21$ GeV⁻² that we converted to the quoted Λ value.

ENERGY DEPENDENCE OF $\omega \rightarrow \pi^+\pi^-\pi^0$ DALITZ PLOT

The following experiments fit to one or more of the coefficients α, β, γ for $|matrix element|^2 \propto P(1 + 2\alpha Z + 2\beta Z^2 \sin(3\phi) + 2\gamma Z^2 + O(Z^5/2))$ where P is the P -wave phase-space factor and Z, ϕ are kinematical variables as defined in ADLARSON 17.

VALUE	EVTS	DOCUMENT ID	TECN	COMMENT
0.133 ± 0.008 OUR AVERAGE				
0.1321 ± 0.0067 ± 0.0046	260k	¹ ABLIKIM	18AD	BES3 $J/\psi \rightarrow \omega\eta$
0.147 ± 0.036	44k	ADLARSON	17	WASA α in $pd \rightarrow {}^3\text{He}, \omega, pp \rightarrow pp\omega$

¹ Keeping a term linear in Z only. A fit with the terms proportional to Z and $Z^3/2$ gives $\alpha = 0.133 \pm 0.041$ and $\beta = 0.037 \pm 0.054$.

 $\omega(782)$ REFERENCES

ACHASOV	21	JHEP 2101 113	M.N. Achasov et al.	(SND Collab.)
LEES	21B	PR D104 112003	J.P. Lees et al.	(BABAR Collab.)
ANDREEV	20	EPJ C80 1189	V. Andreev et al.	(HI Collab.)
HOID	20	EPJ C80 988	B.-L. Hoid, M. Hoferichter, B. Kubis	(BONN, BERN)
COLANGELO	19	JHEP 1902 006	G. Colangelo, M. Hoferichter, P. Stoffer	(BERN+)
HOEFERICHTER...	19	JHEP 1908 137	M. Hoferichter, B.-L. Hoid, B. Kubis	(WASH, BONN)
ABLIKIM	18AD	PR D98 112007	M. Ablikim et al.	(BESIII Collab.)
ABLIKIM	18C	PRL 120 242003	M. Ablikim et al.	(BESIII Collab.)
ABLIKIM	18S	PR D98 032001	M. Ablikim et al.	(BESIII Collab.)
HANHART	18	EPJ C78 450	C. Hanhart et al.	(BESIII Collab.)
ADLARSON	17B	PL B770 418	P. Adlarson et al.	(WASA-at-COSY Collab.)
ADLARSON	17B	PR C95 035208	P. Adlarson et al.	(A2 Collab. at MAMI)
ANASTASI	17	PL B767 485	A. Anastasi et al.	(KLOE-2 Collab.)
ABLIKIM	16B	PL B753 103	M. Ablikim et al.	(BESIII Collab.)
ACHASOV	16A	PR D93 092001	M.N. Achasov et al.	(SND Collab.)
ARNALDI	16A	PL B757 437	R. Arnaldi et al.	(NA60 Collab.)
PDG	16	CP C40 100001	C. Patrignani et al.	(PDG Collab.)
PDG	15	RPP 2015 at pdg.lbl.gov		(PDG Collab.)
ACHASOV	13D	PR D88 054013	M.N. Achasov et al.	(SND Collab.)
BABUSCI	13D	PL B720 336	D. Babusci et al.	(CATA, CALB, BARI)
BENAYOUN	13	EPJ C73 2453	M. Benayoun, P. David, L. DelBuono	(PARIN, BERLIN+)
DAVIER	13	EPJ C73 2597	M. Davier et al.	(BABAR Collab.)
LEES	12G	PR D86 032013	J.P. Lees et al.	(BONN)
NIECKNIG	12	EPJ C72 2014	F. Niecknig, B. Kubis, S.P. Schneider	(KLOE Collab.)
AMBROSINO	11A	PL B700 102	F. Ambrosino et al.	(KLOE Collab.)
BENAYOUN	10	EPJ C65 211	M. Benayoun et al.	(SND Collab.)
ACHASOV	09A	JETP 109 379	M.N. Achasov et al.	(SND Collab.)
ARNALDI	09	PL B677 2650	R. Arnaldi et al.	(NA60 Collab.)
AUBERT	09AS	PL 103 231801	B. Aubert et al.	(BABAR Collab.)
STAROSTIN	09	PR C79 045201	A. Starostin et al.	(Crystal Ball Collab. at MAMI)
ACHASOV	08B	JETP 107 61	M.N. Achasov et al.	(SND Collab.)
AMBROSINO	08G	PL B669 223	F. Ambrosino et al.	(KLOE Collab.)
ACHASOV	07B	PR D76 077101	M.N. Achasov et al.	(SND Collab.)
AKHMETSHIN	07	PL B648 28	R.R. Akhmetshin et al.	(Novosibirsk CMD-2 Collab.)
ACHASOV	06	JETP 103 380	M.N. Achasov et al.	(Novosibirsk SND Collab.)
ACHASOV	06A	PR D74 014016	M.N. Achasov et al.	(SND Collab.)
AULCHENKO	06	JETPL 84 413	V.M. Aulchenko et al.	(Novosibirsk CMD-2 Collab.)
ACHASOV	05A	JETP 101 1053	M.N. Achasov et al.	(Novosibirsk SND Collab.)
AKHMETSHIN	05	PL B605 26	R.R. Akhmetshin et al.	(Novosibirsk CMD-2 Collab.)
AKHMETSHIN	05A	PL B613 29	R.R. Akhmetshin et al.	(Novosibirsk CMD-2 Collab.)
AULCHENKO	05	JETPL 82 743	V.M. Aulchenko et al.	(Novosibirsk CMD-2 Collab.)
AKHMETSHIN	04	PL B578 285	R.R. Akhmetshin et al.	(Novosibirsk CMD-2 Collab.)
AKHMETSHIN	04B	PL B580 119	R.R. Akhmetshin et al.	(Novosibirsk CMD-2 Collab.)
AUBERT,B	04N	PR D70 072004	B. Aubert et al.	(BABAR Collab.)
PDG	04	PL B592 1	S. Eidelman et al.	(PDG Collab.)
ACHASOV	03	PL B559 171	M.N. Achasov et al.	(Novosibirsk SND Collab.)
ACHASOV	03D	PR D68 052006	M.N. Achasov et al.	(Novosibirsk SND Collab.)

See key on page 1127

Meson Particle Listings

$\omega(782), \eta'(958)$

ALOISIO	03	PL B561 55	A. Aloisio et al.	(KLOE Collab.)
BENAYOUN	03	EPJ C29 397	M. Benayoun et al.	
ACHASOV	02E	PR D66 032001	M.N. Achasov et al.	(Novosibirsk SND Collab.)
ACHASOV	02F	PL B537 201	M.N. Achasov et al.	(Novosibirsk SND Collab.)
AKHMETSHIN	02	PL B527 161	R.R. Akhmetshin et al.	(Novosibirsk CMD-2 Collab.)
ALOISIO	02D	PL B537 21	A. Aloisio et al.	(KLOE Collab.)
HEISTER	02C	PL B528 19	A. Heister et al.	(ALEPH Collab.)
ACHASOV	01E	PR D63 072002	M.N. Achasov et al.	(Novosibirsk SND Collab.)
AKHMETSHIN	01B	PL B509 217	R.R. Akhmetshin et al.	(Novosibirsk CMD-2 Collab.)
BARBERIS	01	PL B507 14	D. Barberis et al.	
ACHASOV	00	EPJ C12 25	M.N. Achasov et al.	(Novosibirsk SND Collab.)
ACHASOV	00D	JETPL 72 282	M.N. Achasov et al.	(Novosibirsk SND Collab.)
ACHASOV	00G	Translated from ZETFP 72 411. JETPL 71 355	M.N. Achasov et al.	(Novosibirsk SND Collab.)
AKHMETSHIN	00C	PL B476 33	R.R. Akhmetshin et al.	(Novosibirsk CMD-2 Collab.)
AULCHENKO	00A	JETP 90 927	V.M. Aulchenko et al.	(Novosibirsk SND Collab.)
CASE	00	PR D61 032002	T. Case et al.	(Crystal Barrel Collab.)
ACHASOV	99E	PL B462 365	M.N. Achasov et al.	(Novosibirsk SND Collab.)
GARDNER	99	PR D59 076002	S. Gardner, H.B. O'Connell	
BENAYOUN	98	EPJ C2 269	M. Benayoun et al.	(IPNP, NOVO, ADLD+)
ABELE	97E	PL B411 361	A. Abele et al.	(Crystal Barrel Collab.)
BENAYOUN	96	ZPHY C72 221	M. Benayoun et al.	(IPNP, NOVO)
PROKOSHKIN	95	PD 40 273	Y.D. Prokoshkin, V.D. Samoilenko	(SERP)
WURZINGER	95	PR C51 443	R. Wurzinger et al.	(BONN, ORSAY, SACL+)
ALDE	94B	PL B340 122	D.M. Alde et al.	(SERP, BELG, LANL, LAPP+)
AMSLER	94C	PL B327 425	C. Amstler et al.	(Crystal Barrel Collab.)
ALDE	93	PAN 56 1229	D.M. Alde et al.	(SERP, LAPP, LANL, BELG+)
Also		Translated from YAF 56 137.		
AMSLER	93B	ZPHY C61 35	D.M. Alde et al.	(SERP, LAPP, LANL, BELG+)
WEIDENAUER	93	NP B311 362	C. Amstler et al.	(Crystal Barrel Collab.)
ANTONELLI	92	ZPHY C56 15	P. Antonelli et al.	(ASTERIX Collab.)
DOLINSKY	91	PRPL 202 99	S.I. Dolinsky et al.	(NOVO)
WEIDENAUER	90	ZPHY C47 353	P. Weidenauer et al.	(ASTERIX Collab.)
DOLINSKY	89	ZPHY C42 511	S.I. Dolinsky et al.	(NOVO)
BITUKOV	88B	SJNP 47 800	S.I. Bitukov et al.	(SERP)
DOLINSKY	88	SJNP 48 277	S.I. Dolinsky et al.	(NOVO)
KURDADZE	88	Translated from YAF 48 412. JETPL 47 512	L.M. Kurdadze et al.	(NOVO)
AULCHENKO	87	PL B186 432	V.M. Aulchenko et al.	(NOVO)
BARKOV	87	JETPL 46 164	L.M. Barkov et al.	(NOVO)
KURDADZE	86	Translated from ZETFP 46 132. JETPL 43 643	L.M. Kurdadze et al.	(NOVO)
BARKOV	85	NP B256 365	L.M. Barkov et al.	(NOVO)
DRUZHININ	84	PL 144B 136	V.P. Druzhinin et al.	(NOVO)
KURDADZE	83B	JETPL 36 274	A.M. Kurdadze et al.	(NOVO)
DZHELYADIN	81B	PL 102B 296	R.I. Dzheilyadin et al.	(SERP)
CORDIER	80	NP B171 13	A. Cordier et al.	(LALO)
DZHELYADIN	80	PL 94B 548	R.I. Dzheilyadin et al.	(SERP)
ROOS	80	LNC 27 321	M. Roos, A. Pellinen	(HEL5)
BENKHEIRI	79	NP B150 268	P. Benkheiri et al.	(EPOL, CERN, CDEF+)
DZHELYADIN	79	PL 84B 143	R.I. Dzheilyadin et al.	(SERP)
COOPER	78B	NP B146 1	A.M. Cooper et al.	(TATA, CERN, CDEF+)
QUENZER	78	PL 76B 512	A. Quenzer et al.	(LALO)
VANAPEL...	78	NP B133 245	G.W. van Apeldoorn et al.	(ZEEM)
WICKLUND	78	PR D17 1197	A.B. Wicklund et al.	(ANL)
ANDREWS	77	PRL 38 198	D.E. Andrews et al.	(ROCH)
GESSAROLI	77	NP B126 382	R. Gessaroli et al.	(BGNA, FIRZ, GENO+)
KEYNE	76	PR D14 28	J. Keyne et al.	(LOIC, SHMP)
Also		PR D5 2789	D.M. Binnie et al.	(LOIC, SHMP)
KALBFLEISCH	75	PR D11 987	G.R. Kalbfleisch, R.C. Strand, J.W. Chapman	(BNL+)
AUGULAR...	72B	PR D6 29	M. Aguilar-Benitez et al.	(BNL)
APEL	72B	PL 41B 234	W.D. Apel et al.	(KARLK, KARLE, PISA)
BASILE	72B	Phil. Conf. 153	M. Basile et al.	(CERN)
BENAKSAS	72	PL 39B 289	D. Benaksas et al.	(ORSAY)
BENAKSAS	72B	PL 42B 507	D. Benaksas et al.	(ORSAY)
BENAKSAS	72C	PL 42B 511	D. Benaksas et al.	(ORSAY)
BORENSTEIN	72	PR D5 1559	S.R. Borenstein et al.	(BNL, MICH)
BROWN	72	PL 42B 117	R.M. Brown et al.	(ILL, ILLC)
DAKIN	72	PR D6 2321	J.T. Dakin et al.	(PRIN)
RATCLIFF	72	PL 38B 345	B.M. Ratcliff et al.	(SLAC)
ALVENSLEB...	71C	PRL 27 888	H. Alvensleben et al.	(DESY)
BALDIN	71	SJNP 13 758	A.B. Baldin et al.	(ITEP)
BEHREND	71	PRL 27 61	H.J. Behrend et al.	(ROCH, CORN, FNAL)
BIZZARRI	71	NP B27 140	R. Bizzarri et al.	(CERN, CDEF)
COYNE	71	NP B32 333	D.G. Coyne et al.	(LRL)
MOFFEIT	71	NP B29 349	K.C. Moffeit et al.	(LRL, UCB, SLAC+)
ABRAMOVICH...	70	NP B20 209	M. Abramovich et al.	(CERN)
BIGGS	70B	PRL 24 1201	P.J. Biggs et al.	(DARE)
BIZZARRI	70	PRL 25 1385	R. Bizzarri et al.	(ROMA, SYRA)
ROOS	70	DNPL/R7 173	M. Roos	(CERN)
Proc. Daresbury Study Weekend No. 1.				
AUGUSTIN	69D	PL 28B 513	J.E. Augustin et al.	(ORSAY)
BIZZARRI	69	NP B14 169	R. Bizzarri et al.	(CERN, CDEF)
DEINET	69B	PL 30B 426	W. Deinet et al.	(KARL, CERN)
JACQUET	69B	NC 63A 743	F. Jacquet et al.	(EPOL, BERG)
WILSON	69	Private Comm.	R. Wilson	(HARV)
Also		PR 178 2095	A.A. Wehmman et al.	(HARV, CASE, SLAC+)
ASTVACAT...	68	PL 27B 45	R.G. Astvatsaturov et al.	(JINR, MOSU)
BOLLINI	68C	NC 56B 531	D. Bollini et al.	(CERN, BGNA, STRB)
GOUNARIS	68	PRL 21 244	G.J. Gounaris, J.J. Sakurai	
BARASH	67B	PR 156 1399	N. Barash et al.	(COLU)
FELDMAN	67C	PR 159 1219	M. Feldman et al.	(PENN)
DIGIUGNO	66B	NC 44A 1272	G. Di Giugno et al.	(NAPL, FRAS, TRST)
FLATTE	66	PR 145 1050	S.M. Flatte et al.	(LRL)
JAMES	66	PR 142 896	F.E. James, H.L. Kraybill	(YALE, BNL)
BARBARO...	65	PRL 14 279	A. Barbaro-Galtieri, R.D. Tripp	(LRL)
BARMIN	64	JETP 18 1289	V.V. Barmin et al.	(ITEP)
KRAEMER	64	PR 136 849	R.W. Kraemer et al.	(JHU, NWES, WOOD)
BUSCHBECK	63	Sienna Conf. 1 166	B. Buschbeck et al.	(VIEN, CERN, ANIK)

$\eta'(958)$

$$J^G(J^{PC}) = 0^+(0^{-+})$$

$\eta'(958)$ MASS

VALUE (MeV)	EVTS	DOCUMENT ID	TECN	COMMENT
957.78 ± 0.06	OUR AVERAGE			
957.793 ± 0.054 ± 0.036	3.9k	LIBBY	08	CLEO $J/\psi \rightarrow \gamma \eta'$

957.9 ± 0.2 ± 0.6	4800	WURZINGER	96	SPEC	1.68 $p d \rightarrow {}^3\text{He} n'$
957.46 ± 0.33		DUANE	74	MMS	$\pi^- p \rightarrow n \text{MM}$
958.2 ± 0.5	1414	DANBURG	73	HBC	$2.2 K^- p \rightarrow \Lambda \eta'$
958 ± 1	400	JACOBS	73	HBC	$2.9 K^- p \rightarrow \Lambda \eta'$
956.1 ± 1.1	3415	¹ BASILE	71	CNTR	$1.6 \pi^- p \rightarrow n \eta'$
• • • We do not use the following data for averages, fits, limits, etc. • • •					
957.5 ± 0.2		BAI	04J	BES2	$J/\psi \rightarrow \gamma \gamma \pi^+ \pi^-$
959 ± 1	630	² BELADIDZE	92C	VES	$36 \pi^- \text{Be} \rightarrow \pi^- \eta' \eta \text{Be}$
958 ± 1	340	² ARMSTRONG	91B	OMEG	$300 pp \rightarrow pp \eta \pi^+ \pi^-$
958.2 ± 0.4	622	² AUGUSTIN	90	DM2	$J/\psi \rightarrow \gamma \eta \pi^+ \pi^-$
957.8 ± 0.2	2420	² AUGUSTIN	90	DM2	$J/\psi \rightarrow \gamma \gamma \pi^+ \pi^-$
956.3 ± 1.0	143	² GIDAL	87	MRK2	$e^+ e^- \rightarrow e^+ e^- \eta \pi^+ \pi^-$
957.4 ± 1.4	535	³ BASILE	71	CNTR	$1.6 \pi^- p \rightarrow n \eta'$
957 ± 1		RITTENBERG	69	HBC	$1.7\text{-}2.7 K^- p$

¹Using all η' decays.
²Systematic uncertainty not estimated.
³Using η' decays into neutrals. Not independent of the other listed BASILE 71 η' mass measurement.

$\eta'(958)$ WIDTH

VALUE (MeV)	EVTS	DOCUMENT ID	TECN	CHG	COMMENT
0.188 ± 0.006	OUR FIT				
0.230 ± 0.021	OUR AVERAGE				
0.226 ± 0.017 ± 0.014	2300	CZERWINSKI	10	MMS	$pp \rightarrow pp \eta'$
0.40 ± 0.22	4800	WURZINGER	96	SPEC	$1.68 p d \rightarrow {}^3\text{He} n'$
0.28 ± 0.10	1000	BINNIE	79	MMS	$\pi^- p \rightarrow n \text{MM}$
• • • We do not use the following data for averages, fits, limits, etc. • • •					
0.20 ± 0.04		BAI	04J	BES2	$J/\psi \rightarrow \gamma \gamma \pi^+ \pi^-$

$\eta'(958)$ DECAY MODES

Mode	Fraction (Γ_i/Γ)	Confidence level
$\Gamma_1 \pi^+ \pi^- \eta$	(42.5 ± 0.5) %	
$\Gamma_2 \rho^0 \gamma$ (including non-resonant)	(29.5 ± 0.4) %	
$\pi^+ \pi^- \pi^- \gamma$		
$\Gamma_3 \rho^0 \gamma$		
$\Gamma_4 \pi^0 \pi^0 \eta$	(22.4 ± 0.5) %	
$\Gamma_5 \omega \gamma$	(2.52 ± 0.07) %	
$\Gamma_6 \omega e^+ e^-$	(2.0 ± 0.4) × 10 ⁻⁴	
$\Gamma_7 \gamma \gamma$	(2.307 ± 0.033) %	
$\Gamma_8 3\pi^0$	(2.50 ± 0.17) × 10 ⁻³	
$\Gamma_9 \mu^+ \mu^- \gamma$	(1.13 ± 0.28) × 10 ⁻⁴	
$\Gamma_{10} \pi^+ \pi^- \mu^+ \mu^-$	(2.0 ± 0.4) × 10 ⁻⁵	
$\Gamma_{11} \pi^+ \pi^- \pi^0$	(3.61 ± 0.17) × 10 ⁻³	
$\Gamma_{12} (\pi^+ \pi^- \pi^0) \text{ S-wave}$	(3.8 ± 0.5) × 10 ⁻³	
$\Gamma_{13} \pi^\mp \rho^\pm$	(7.4 ± 2.3) × 10 ⁻⁴	
$\Gamma_{14} \pi^0 \rho^0$	< 4 %	90%
$\Gamma_{15} 2(\pi^+ \pi^-)$	(8.4 ± 0.9) × 10 ⁻⁵	
$\Gamma_{16} \pi^+ \pi^- 2\pi^0$	(1.8 ± 0.4) × 10 ⁻⁴	
$\Gamma_{17} 2(\pi^+ \pi^-) \text{ neutrals}$	< 1 %	95%
$\Gamma_{18} 2(\pi^+ \pi^-) \pi^0$	< 1.8 × 10 ⁻³	90%
$\Gamma_{19} 2(\pi^+ \pi^-) 2\pi^0$	< 1 %	95%
$\Gamma_{20} 3(\pi^+ \pi^-)$	< 3.1 × 10 ⁻⁵	90%
$\Gamma_{21} K^\pm \pi^\mp$	< 4 × 10 ⁻⁵	90%
$\Gamma_{22} \pi^+ \pi^- e^+ e^-$	(2.42 ± 0.10) × 10 ⁻³	
$\Gamma_{23} \pi^+ e^- \nu_e + \text{c.c.}$	< 2.1 × 10 ⁻⁴	90%
$\Gamma_{24} \gamma e^+ e^-$	(4.91 ± 0.27) × 10 ⁻⁴	
$\Gamma_{25} \pi^0 \gamma \gamma$	(3.20 ± 0.24) × 10 ⁻³	
$\Gamma_{26} \pi^0 \gamma \gamma$ (non resonant)	(6.2 ± 0.9) × 10 ⁻⁴	
$\Gamma_{27} \eta \gamma \gamma$	< 1.33 × 10 ⁻⁴	90%
$\Gamma_{28} 4\pi^0$	< 4.94 × 10 ⁻⁵	90%
$\Gamma_{29} e^+ e^-$	< 5.6 × 10 ⁻⁹	90%
$\Gamma_{30} \text{invisible}$	< 6 × 10 ⁻⁴	90%

Charge conjugation (C), Parity (P), Lepton family number (LF) violating modes

$\Gamma_{31} \pi^+ \pi^-$	P, CP	< 1.8 × 10 ⁻⁵	90%
$\Gamma_{32} \pi^0 \pi^0$	P, CP	< 4 × 10 ⁻⁴	90%
$\Gamma_{33} \pi^0 e^+ e^-$	C	[a] < 1.4 × 10 ⁻³	90%
$\Gamma_{34} \eta e^+ e^-$	C	[a] < 2.4 × 10 ⁻³	90%
$\Gamma_{35} 3\gamma$	C	< 1.0 × 10 ⁻⁴	90%
$\Gamma_{36} \mu^+ \mu^- \pi^0$	C	[a] < 6.0 × 10 ⁻⁵	90%
$\Gamma_{37} \mu^+ \mu^- \eta$	C	[a] < 1.5 × 10 ⁻⁵	90%
$\Gamma_{38} e \mu$	LF	< 4.7 × 10 ⁻⁴	90%

[a] C parity forbids this to occur as a single-photon process.

Meson Particle Listings

$\eta'(958)$

CONSTRAINED FIT INFORMATION

An overall fit to the total width, a partial width, 2 combinations of partial widths obtained from integrated cross section, and 20 branching ratios uses 52 measurements and one constraint to determine 9 parameters. The overall fit has a $\chi^2 = 69.5$ for 44 degrees of freedom.

The following *off-diagonal* array elements are the correlation coefficients $\langle \delta p_i \delta p_j \rangle / (\delta p_i \delta p_j)$, in percent, from the fit to parameters p_i , including the branching fractions, $x_i \equiv \Gamma_i / \Gamma_{\text{total}}$. The fit constrains the x_i whose labels appear in this array to sum to one.

x_2	-25																				
x_4	-75	-43																			
x_5	-7	-6	-2																		
x_7	-11	-7	9	-1																	
x_8	-17	-10	19	0	2																
x_{11}	-1	-1	-1	0	0	0															
x_{22}	-8	30	-14	-2	-2	-3	0														
Γ	11	-10	-1	1	-40	0	0	-3													
	x_1	x_2	x_4	x_5	x_7	x_8	x_{11}	x_{22}													

Mode	Rate (MeV)
Γ_1 $\pi^+ \pi^- \eta$	0.0799 ± 0.0029
Γ_2 $\rho^0 \gamma$ (including non-resonant $\pi^+ \pi^- \gamma$)	0.0554 ± 0.0019
Γ_4 $\pi^0 \pi^0 \eta$	0.0421 ± 0.0017
Γ_5 $\omega \gamma$	0.00474 ± 0.00020
Γ_7 $\gamma \gamma$	0.00434 ± 0.00013
Γ_8 $3\pi^0$	(4.7 ± 0.4) × 10 ⁻⁴
Γ_{11} $\pi^+ \pi^- \pi^0$	(6.8 ± 0.4) × 10 ⁻⁴
Γ_{22} $\pi^+ \pi^- e^+ e^-$	(4.54 ± 0.23) × 10 ⁻⁴

$\eta'(958)$ PARTIAL WIDTHS

$\Gamma(\gamma\gamma)$	Γ_7			
VALUE (keV)	EVTS	DOCUMENT ID	TECN	COMMENT
4.34 ± 0.14 OUR FIT				
4.28 ± 0.19 OUR AVERAGE				
4.17 ± 0.10 ± 0.27	2000	¹ ACCIARRI	98Q L3	$e^+ e^- \rightarrow e^+ e^- \pi^+ \pi^- \gamma$
4.53 ± 0.29 ± 0.51	266	KARCH	92 CBAL	$e^+ e^- \rightarrow e^+ e^- \eta \pi^0 \pi^0$
3.61 ± 0.13 ± 0.48		² BEHREND	91 CELL	$e^+ e^- \rightarrow e^+ e^- \eta'(958)$
4.6 ± 1.1 ± 0.6	23	BARU	90 MD1	$e^+ e^- \rightarrow e^+ e^- \pi^+ \pi^- \gamma$
4.57 ± 0.25 ± 0.44		BUTLER	90 MRK2	$e^+ e^- \rightarrow e^+ e^- \eta'(958)$
5.08 ± 0.24 ± 0.71	547	³ ROE	90 ASP	$e^+ e^- \rightarrow e^+ e^- 2\gamma$
3.8 ± 0.7 ± 0.6	34	AIHARA	88c TPC	$e^+ e^- \rightarrow e^+ e^- \eta \pi^+ \pi^-$
4.9 ± 0.5 ± 0.5	136	⁴ WILLIAMS	88 CBAL	$e^+ e^- \rightarrow e^+ e^- 2\gamma$
••• We do not use the following data for averages, fits, limits, etc. •••				
4.7 ± 0.6 ± 0.9	143	⁵ GIDAL	87 MRK2	$e^+ e^- \rightarrow e^+ e^- \eta \pi^+ \pi^-$
4.0 ± 0.9		⁶ BARTEL	85E JADE	$e^+ e^- \rightarrow e^+ e^- 2\gamma$

¹ No non-resonant $\pi^+ \pi^-$ contribution found.
² Reevaluated by us using $B(\eta' \rightarrow \rho(770)\gamma) = (30.2 \pm 1.3)\%$.
³ Reevaluated by us using $B(\eta' \rightarrow \gamma\gamma) = (2.11 \pm 0.13)\%$.
⁴ Reevaluated by us using $B(\eta' \rightarrow \gamma\gamma) = (2.11 \pm 0.13)\%$.
⁵ Superseded by BUTLER 90.
⁶ Systematic error not evaluated.

$\Gamma(e^+ e^-)$	Γ_{29}			
VALUE (eV)	CL%	DOCUMENT ID	TECN	COMMENT
<1.1 × 10⁻³	90	^{1,2} ACHASOV	15 SND	0.958 $e^+ e^- \rightarrow \pi^+ \pi^- \eta$
••• We do not use the following data for averages, fits, limits, etc. •••				
<2.0 × 10 ⁻³	90	² ACHASOV	15 SND	0.958 $e^+ e^- \rightarrow \pi^+ \pi^- \eta$
<2.4 × 10 ⁻³	90	² AKHMETSHIN	15 CMD3	0.958 $e^+ e^- \rightarrow \pi^+ \pi^- \eta$

¹ Combining data of ACHASOV 15 and AKHMETSHIN 15.
² Using η and η' branching fractions from PDG 14.

$\eta'(958) \Gamma(i)\Gamma(\gamma\gamma)/\Gamma(\text{total})$

This combination of a partial width with the partial width into $\gamma\gamma$ and with the total width is obtained from the integrated cross section into channel(i) in the $\gamma\gamma$ annihilation.

$\Gamma(\gamma\gamma) \times \Gamma(\rho^0 \gamma \text{ (including non-resonant } \pi^+ \pi^- \gamma)) / \Gamma_{\text{total}}$	$\Gamma_7 \Gamma_2 / \Gamma$			
VALUE (keV)	EVTS	DOCUMENT ID	TECN	COMMENT
1.28 ± 0.04 OUR FIT				
1.26 ± 0.07 OUR AVERAGE				Error includes scale factor of 1.2.
1.09 ± 0.04 ± 0.13		BEHREND	91 CELL	$e^+ e^- \rightarrow e^+ e^- \rho(770)^0 \gamma$
1.35 ± 0.09 ± 0.21		AIHARA	87 TPC	$e^+ e^- \rightarrow e^+ e^- \rho \gamma$
1.13 ± 0.04 ± 0.13	867	ALBRECHT	87B ARG	$e^+ e^- \rightarrow e^+ e^- \rho \gamma$

1.53 ± 0.09 ± 0.21		ALTHOFF	84E TASS	$e^+ e^- \rightarrow e^+ e^- \rho \gamma$
1.14 ± 0.08 ± 0.11	243	BERGER	84B PLUT	$e^+ e^- \rightarrow e^+ e^- \rho \gamma$
1.73 ± 0.34 ± 0.35	95	JENNI	83 MRK2	$e^+ e^- \rightarrow e^+ e^- \rho \gamma$
1.49 ± 0.13 ± 0.027	213	BARTEL	82B JADE	$e^+ e^- \rightarrow e^+ e^- \rho \gamma$
••• We do not use the following data for averages, fits, limits, etc. •••				
1.85 ± 0.31 ± 0.24	43	BEHREND	82c CELL	$e^+ e^- \rightarrow e^+ e^- \rho \gamma$

$\Gamma(\gamma\gamma) \times \Gamma(\pi^0 \pi^0 \eta) / \Gamma_{\text{total}}$ $\Gamma_7 \Gamma_4 / \Gamma$

VALUE (keV)	DOCUMENT ID	TECN	COMMENT
0.97 ± 0.04 OUR FIT			Error includes scale factor of 1.1.
0.92 ± 0.06 ± 0.11	¹ KARCH	92 CBAL	$e^+ e^- \rightarrow e^+ e^- \eta \pi^0 \pi^0$
••• We do not use the following data for averages, fits, limits, etc. •••			
0.95 ± 0.05 ± 0.08	² KARCH	90 CBAL	$e^+ e^- \rightarrow e^+ e^- \eta \pi^0 \pi^0$
1.00 ± 0.08 ± 0.10	^{2,3} ANTREASNYAN	87 CBAL	$e^+ e^- \rightarrow e^+ e^- \eta \pi^0 \pi^0$
¹ Reevaluated by us using $B(\eta \rightarrow \gamma\gamma) = (39.21 \pm 0.34)\%$. Supersedes ANTREASNYAN 87 and KARCH 90.			
² Superseded by KARCH 92.			
³ Using $BR(\eta \rightarrow 2\gamma) = (38.9 \pm 0.5)\%$.			

$\eta'(958) \Gamma(i)\Gamma(e^+ e^-) / \Gamma(\text{total})$

$\Gamma(\pi^+ \pi^- \eta) \times \Gamma(e^+ e^-) / \Gamma_{\text{total}}$ $\Gamma_1 \Gamma_{29} / \Gamma$

VALUE (10 ⁻³ eV)	CL%	DOCUMENT ID	TECN	COMMENT
<1.0	90	¹ AKHMETSHIN	15 CMD3	0.958 $e^+ e^- \rightarrow \pi^+ \pi^- \eta$
¹ AKHMETSHIN 15 reports $[\Gamma(\eta'(958) \rightarrow \pi^+ \pi^- \eta) \times \Gamma(\eta'(958) \rightarrow e^+ e^-) / \Gamma_{\text{total}}] \times [B(\eta \rightarrow 2\gamma)] < 4.1 \times 10^{-4}$ eV which we divide by our best value $B(\eta \rightarrow 2\gamma) = 39.36 \times 10^{-2}$.				

$\eta'(958)$ BRANCHING RATIOS

$\Gamma(\pi^+ \pi^- \eta) / \Gamma_{\text{total}}$ Γ_1 / Γ

VALUE (units 10 ⁻²)	EVTS	DOCUMENT ID	TECN	COMMENT
42.5 ± 0.5 OUR FIT				Error includes scale factor of 1.1.
41.24 ± 0.08 ± 1.24	312k	ABLIKIM	19T BES	$J/\psi \rightarrow \gamma \eta'$
••• We do not use the following data for averages, fits, limits, etc. •••				
42.4 ± 1.1 ± 0.4	1.2k	¹ PEDLAR	09 CLEO	$J/\psi \rightarrow \gamma \eta'$
¹ Not independent of other η' branching fractions and ratios in PEDLAR 09.				

$\Gamma(\pi^+ \pi^- \eta \text{ (charged decay)}) / \Gamma_{\text{total}}$ $0.2804 \Gamma_1 / \Gamma$

VALUE	EVTS	DOCUMENT ID	TECN	COMMENT
0.1191 ± 0.0015 OUR FIT				Error includes scale factor of 1.1.
••• We do not use the following data for averages, fits, limits, etc. •••				
0.123 ± 0.014	107	RITTENBERG	69 HBC	1.7-2.7 $K^- p$
0.10 ± 0.04	10	LONDON	66 HBC	2.24 $K^- p \rightarrow \Lambda 2\pi^+ 2\pi^- \pi^0$
0.07 ± 0.04	7	BADIER	65B HBC	3 $K^- p$

$\Gamma(\pi^+ \pi^- \eta \text{ (neutral decay)}) / \Gamma_{\text{total}}$ $0.7196 \Gamma_1 / \Gamma$

VALUE	EVTS	DOCUMENT ID	TECN	COMMENT
0.306 ± 0.004 OUR FIT				Error includes scale factor of 1.1.
••• We do not use the following data for averages, fits, limits, etc. •••				
0.314 ± 0.026	281	RITTENBERG	69 HBC	1.7-2.7 $K^- p$

$\Gamma(\rho^0 \gamma \text{ (including non-resonant } \pi^+ \pi^- \gamma)) / \Gamma_{\text{total}}$ Γ_2 / Γ

VALUE (units 10 ⁻²)	EVTS	DOCUMENT ID	TECN	COMMENT
29.5 ± 0.4 OUR FIT				Error includes scale factor of 1.1.
29.90 ± 0.03 ± 0.55	913k	ABLIKIM	19T BES	$J/\psi \rightarrow \gamma \eta'$
••• We do not use the following data for averages, fits, limits, etc. •••				
28.7 ± 0.7 ± 0.4	0.2k	¹ PEDLAR	09 CLEO	$J/\psi \rightarrow \gamma \eta'$
32.9 ± 3.3	298	RITTENBERG	69 HBC	1.7-2.7 $K^- p$
20 ± 10	20	LONDON	66 HBC	2.24 $K^- p \rightarrow \Lambda \pi^+ \pi^- \gamma$
34 ± 9	35	BADIER	65B HBC	3 $K^- p$
¹ Not independent of other η' branching fractions and ratios in PEDLAR 09.				

$\Gamma(\rho^0 \gamma) / \Gamma_{\text{total}}$ Γ_3 / Γ

VALUE (%)	EVTS	DOCUMENT ID	TECN	COMMENT
••• We do not use the following data for averages, fits, limits, etc. •••				
33.34 ± 0.06 ± 1.60	970k	¹ ABLIKIM	18c BES3	$\eta'(958) \rightarrow \gamma \pi^+ \pi^-$
34.43 ± 0.52 ± 1.97	970k	² ABLIKIM	18c BES3	$\eta'(958) \rightarrow \gamma \pi^+ \pi^-$
¹ From a fit to $\pi^+ \pi^-$ mass using $\rho(770)$, $\omega(782)$, and box anomaly components. ² From a fit to $\pi^+ \pi^-$ mass using $\rho(770)$, $\omega(782)$, and $\rho(1450)$ components.				

$\Gamma(\rho^0 \gamma \text{ (including non-resonant } \pi^+ \pi^- \gamma)) / \Gamma(\pi^+ \pi^- \eta)$ Γ_2 / Γ_1

VALUE	DOCUMENT ID	TECN	COMMENT
0.694 ± 0.014 OUR FIT			Error includes scale factor of 1.1.
0.683 ± 0.020 OUR AVERAGE			
0.677 ± 0.024 ± 0.011	PEDLAR	09 CLE3	$J/\psi \rightarrow \eta' \gamma$
0.69 ± 0.03	ABLIKIM	06E BES2	$J/\psi \rightarrow \eta' \gamma$

$\Gamma(\rho^0 \gamma \text{ (including non-resonant } \pi^+ \pi^- \gamma)) / \Gamma(\pi^+ \pi^- \eta \text{ (neutral decay)})$ $\Gamma_2 / 0.714 \Gamma_1$

VALUE	EVTS	DOCUMENT ID	TECN	COMMENT
0.972 ± 0.020 OUR FIT				Error includes scale factor of 1.1.
0.97 ± 0.09 OUR AVERAGE				
0.70 ± 0.22		AMSLER	04B CBAR	$0 \bar{p} p \rightarrow \pi^+ \pi^- \eta$

See key on page 1127

Meson Particle Listings

$\eta'(958)$

1.07 ± 0.17		BELADIDZE	92c	VES	36 $\pi^- \text{Be} \rightarrow \pi^- \eta' \eta \text{Be}$
0.92 ± 0.14	473	DANBURG	73	HBC	2.2 $K^- p \rightarrow \Lambda X^0$
1.11 ± 0.18	192	JACOBS	73	HBC	2.9 $K^- p \rightarrow \Lambda X^0$

$\Gamma(\pi^0 \pi^0 \eta)/\Gamma_{\text{total}}$ Γ_4/Γ

VALUE (units 10^{-2})	EVTS	DOCUMENT ID	TECN	COMMENT
22.4 ± 0.6 OUR FIT				Error includes scale factor of 1.1.
21.36 ± 0.10 ± 0.92	52k	ABLIKIM	19T	BES $J/\psi \rightarrow \gamma \eta'$
• • • We do not use the following data for averages, fits, limits, etc. • • •				
23.5 ± 1.3 ± 0.4	3.2k	¹ PEDLAR	09	CLEO $J/\psi \rightarrow \gamma \eta'$
¹ Not independent of other η' branching fractions and ratios in PEDLAR 09.				

$\Gamma(\pi^0 \pi^0 \eta(3\pi^0 \text{ decay}))/\Gamma_{\text{total}}$ $0.321\Gamma_4/\Gamma$

VALUE	EVTS	DOCUMENT ID	TECN	COMMENT
0.0718 ± 0.0018 OUR FIT				Error includes scale factor of 1.1.
• • • We do not use the following data for averages, fits, limits, etc. • • •				
0.11 ± 0.06	4	BENSINGER	70	DBC 2.2 $\pi^+ d$

$\Gamma(\pi^0 \pi^0 \eta)/\Gamma(\pi^+ \pi^- \eta)$ Γ_4/Γ_1

VALUE	DOCUMENT ID	TECN	COMMENT
0.527 ± 0.019 OUR FIT			Error includes scale factor of 1.1.
0.555 ± 0.043 ± 0.013	PEDLAR	09	CLE3 $J/\psi \rightarrow \eta' \gamma$

$\Gamma(\rho^0 \gamma(\text{including non-resonant } \pi^+ \pi^- \gamma))/\Gamma(\pi \pi \eta)$ $\Gamma_2/(\Gamma_1 + \Gamma_4)$

VALUE	DOCUMENT ID	TECN	COMMENT
0.454 ± 0.009 OUR FIT			Error includes scale factor of 1.1.
0.43 ± 0.02 ± 0.02	BARBERIS	98c	OMEG 450 $p p \rightarrow \rho_f \eta' \rho_s$
• • • We do not use the following data for averages, fits, limits, etc. • • •			
0.31 ± 0.15	DAVIS	68	HBC 5.5 $K^- p$

$\Gamma(\omega \gamma)/\Gamma_{\text{total}}$ Γ_5/Γ

VALUE (units 10^{-2})	EVTS	DOCUMENT ID	TECN	COMMENT
2.52 ± 0.07 OUR FIT				Error includes scale factor of 1.1.
2.50 ± 0.07 OUR AVERAGE				
2.489 ± 0.018 ± 0.074	23k	ABLIKIM	19T	BES $J/\psi \rightarrow \gamma \eta'$
2.55 ± 0.03 ± 0.16	33.2k	¹ ABLIKIM	15AD	BES3 $J/\psi \rightarrow \eta' \gamma$
• • • We do not use the following data for averages, fits, limits, etc. • • •				
2.34 ± 0.30 ± 0.04	70	² PEDLAR	09	CLEO $J/\psi \rightarrow \gamma \eta'$
¹ Using $B(J/\psi \rightarrow \eta' \gamma) = (5.15 \pm 0.16) \times 10^{-3}$ and $B(\omega \rightarrow \pi^+ \pi^- \pi^0) = (89.2 \pm 0.7)\%$.				
² Not independent of other η' branching fractions and ratios in PEDLAR 09.				

$\Gamma(\omega \gamma)/\Gamma(\pi^+ \pi^- \eta)$ Γ_5/Γ_1

VALUE	EVTS	DOCUMENT ID	TECN	COMMENT
0.0593 ± 0.0018 OUR FIT				Error includes scale factor of 1.1.
0.055 ± 0.007 ± 0.001		PEDLAR	09	CLE3 $J/\psi \rightarrow \eta' \gamma$
• • • We do not use the following data for averages, fits, limits, etc. • • •				
0.068 ± 0.013	68	ZANFINO	77	ASPK 8.4 $\pi^- p$

$\Gamma(\omega \gamma)/\Gamma(\pi^0 \pi^0 \eta)$ Γ_5/Γ_4

VALUE	DOCUMENT ID	TECN	COMMENT
0.113 ± 0.004 OUR FIT			
0.147 ± 0.016	ALDE	87B	GAM2 38 $\pi^- p \rightarrow n4\gamma$

$\Gamma(\omega e^+ e^-)/\Gamma(\omega \gamma)$ Γ_6/Γ_5

VALUE (units 10^{-3})	DOCUMENT ID	TECN	COMMENT
• • • We do not use the following data for averages, fits, limits, etc. • • •			
7.71 ± 1.34 ± 0.54	¹ ABLIKIM	15AD	BES3 $J/\psi \rightarrow \eta' \gamma$
¹ Obtained from other ABLIKIM 15AD measurements with common systematics taken into account.			

$\Gamma(\omega e^+ e^-)/\Gamma_{\text{total}}$ Γ_6/Γ

VALUE (units 10^{-4})	EVTS	DOCUMENT ID	TECN	COMMENT
1.97 ± 0.34 ± 0.17	66	¹ ABLIKIM	15AD	BES3 $J/\psi \rightarrow \eta' \gamma$
¹ Using $B(J/\psi \rightarrow \eta' \gamma) = (5.15 \pm 0.16) \times 10^{-3}$ and $B(\omega \rightarrow \pi^+ \pi^- \pi^0) = (89.2 \pm 0.7)\%$.				

$\Gamma(\rho^0 \gamma(\text{including non-resonant } \pi^+ \pi^- \gamma))/[\Gamma(\pi^+ \pi^- \eta) + \Gamma(\pi^0 \pi^0 \eta) + \Gamma(\omega \gamma)]$ $\Gamma_2/(\Gamma_1 + \Gamma_4 + \Gamma_5)$

VALUE	DOCUMENT ID	TECN	COMMENT
0.437 ± 0.008 OUR FIT			Error includes scale factor of 1.1.
• • • We do not use the following data for averages, fits, limits, etc. • • •			
0.25 ± 0.14	DAUBER	64	HBC 1.95 $K^- p$

$[\Gamma(\pi^0 \pi^0 \eta(\text{charged decay})) + \Gamma(\omega(\text{charged decay})\gamma)]/\Gamma_{\text{total}}$ $(0.286\Gamma_4 + 0.89\Gamma_5)/\Gamma$

VALUE	EVTS	DOCUMENT ID	TECN	COMMENT
0.0864 ± 0.0017 OUR FIT				Error includes scale factor of 1.1.
• • • We do not use the following data for averages, fits, limits, etc. • • •				
0.045 ± 0.029	42	RITTENBERG	69	HBC 1.7-2.7 $K^- p$

$\Gamma(\pi^+ \pi^- \text{ neutrals})/\Gamma_{\text{total}}$ $(0.714\Gamma_1 + 0.286\Gamma_4 + 0.89\Gamma_5)/\Gamma$

VALUE	EVTS	DOCUMENT ID	TECN	COMMENT
0.3897 ± 0.0028 OUR FIT				Error includes scale factor of 1.1.
• • • We do not use the following data for averages, fits, limits, etc. • • •				
0.4 ± 0.1	39	LONDON	66	HBC 2.24 $K^- p \rightarrow \Lambda \pi^+ \pi^- \text{ neutrals}$
0.35 ± 0.06	33	BADIER	65B	HBC 3 $K^- p$

$\Gamma(\gamma \gamma)/\Gamma_{\text{total}}$ Γ_7/Γ

VALUE (units 10^{-2})	EVTS	DOCUMENT ID	TECN	COMMENT
2.307 ± 0.035 OUR FIT				Error includes scale factor of 1.1.
2.31 ± 0.06 OUR AVERAGE				Error includes scale factor of 1.8.
2.331 ± 0.012 ± 0.035	71k	ABLIKIM	19T	BES $J/\psi \rightarrow \gamma \eta'$
1.99 ^{+0.31} _{-0.27} ± 0.07	114	¹ WICHT	08	BELL $B^{\pm} \rightarrow K^{\pm} \gamma \gamma$
2.00 ± 0.18		² STANTON	80	SPEC 8.45 $\pi^- p \rightarrow n \pi^+ \pi^- 2\gamma$
• • • We do not use the following data for averages, fits, limits, etc. • • •				
2.25 ± 0.16 ± 0.03	0.3k	³ PEDLAR	09	CLEO $J/\psi \rightarrow \gamma \eta'$
1.8 ± 0.2	6000	⁴ APEL	79	NICE 15-40 $\pi^- p \rightarrow n 2\gamma$
2.5 ± 0.7		DUANE	74	MMS $\pi^- p \rightarrow n M M$
1.71 ± 0.33	68	DALPIAZ	72	CNTR 1.6 $\pi^- p \rightarrow n X^0$
2.0 ^{+0.8} _{-0.6}	31	HARVEY	71	OSPK 3.65 $\pi^- p \rightarrow n X^0$

¹ WICHT 08 reports $[\Gamma(\eta'(958) \rightarrow \gamma \gamma)/\Gamma_{\text{total}}] \times [B(B^+ \rightarrow \eta' K^+)] = (1.40^{+0.16+0.15}_{-0.15-0.12}) \times 10^{-6}$ which we divide by our best value $B(B^+ \rightarrow \eta' K^+) = (7.04 \pm 0.25) \times 10^{-5}$. Our first error is their experiment's error and our second error is the systematic error from using our best value.

² Includes APEL 79 result.

³ Not independent of other η' branching fractions and ratios in PEDLAR 09.

⁴ Data is included in STANTON 80 evaluation.

$\Gamma(\gamma \gamma)/\Gamma(\pi^+ \pi^- \eta)$ Γ_7/Γ_1

VALUE	DOCUMENT ID	TECN	COMMENT
0.0543 ± 0.0012 OUR FIT			Error includes scale factor of 1.1.
0.053 ± 0.004 ± 0.001	PEDLAR	09	CLE3 $J/\psi \rightarrow \eta' \gamma$

$\Gamma(\gamma \gamma)/\Gamma(\rho^0 \gamma(\text{including non-resonant } \pi^+ \pi^- \gamma))$ Γ_7/Γ_2

VALUE	DOCUMENT ID	TECN	COMMENT
0.0783 ± 0.0016 OUR FIT			Error includes scale factor of 1.1.
0.080 ± 0.008	ABLIKIM	06E	BES2 $J/\psi \rightarrow \eta' \gamma$

$\Gamma(\gamma \gamma)/\Gamma(\pi^0 \pi^0 \eta)$ Γ_7/Γ_4

VALUE	DOCUMENT ID	TECN	COMMENT
0.1031 ± 0.0028 OUR FIT			Error includes scale factor of 1.9.
0.105 ± 0.010 OUR AVERAGE			
0.091 ± 0.009	AMSLER	93	CBAR 0.0 $\bar{p} p$
0.112 ± 0.002 ± 0.006	ALDE	87B	GAM2 38 $\pi^- p \rightarrow n 2\gamma$

$\Gamma(\gamma \gamma)/\Gamma(\pi^0 \pi^0 \eta(\text{neutral decay}))$ $\Gamma_7/0.714\Gamma_4$

VALUE	EVTS	DOCUMENT ID	TECN	COMMENT
0.144 ± 0.004 OUR FIT				
• • • We do not use the following data for averages, fits, limits, etc. • • •				
0.188 ± 0.058	16	APEL	72	OSPK 3.8 $\pi^- p \rightarrow n X^0$

$\Gamma(\text{neutrals})/\Gamma_{\text{total}}$ $(0.714\Gamma_4 + 0.09\Gamma_5 + \Gamma_7)/\Gamma$

VALUE	EVTS	DOCUMENT ID	TECN	COMMENT
0.185 ± 0.004 OUR FIT				Error includes scale factor of 1.1.
• • • We do not use the following data for averages, fits, limits, etc. • • •				
0.185 ± 0.022	535	BASILE	71	CNTR 1.6 $\pi^- p \rightarrow n X^0$
0.189 ± 0.026	123	RITTENBERG	69	HBC 1.7-2.7 $K^- p$

$\Gamma(3\pi^0)/\Gamma_{\text{total}}$ Γ_8/Γ

VALUE (units 10^{-3})	EVTS	DOCUMENT ID	TECN	COMMENT
2.50 ± 0.17 OUR FIT				
3.57 ± 0.26 OUR AVERAGE				
3.522 ± 0.082 ± 0.254	2015	ABLIKIM	17	BES3 $J/\psi \rightarrow \gamma(3\pi^0)$
4.79 ± 0.59 ± 1.14	183	¹ ABLIKIM	15P	BES3 $J/\psi \rightarrow K^+ K^- 3\pi$
• • • We do not use the following data for averages, fits, limits, etc. • • •				
3.56 ± 0.22 ± 0.34	309	² ABLIKIM	12E	BES3 $J/\psi \rightarrow \gamma(3\pi^0)$
¹ We have added all systematic uncertainties in quadrature to a single value.				
² Superseded by ABLIKIM 17.				

$\Gamma(3\pi^0)/\Gamma(\pi^0 \pi^0 \eta)$ Γ_8/Γ_4

VALUE (units 10^{-4})	EVTS	DOCUMENT ID	TECN	COMMENT
112 ± 8 OUR FIT				
78 ± 10 OUR AVERAGE				
86 ± 19	235	BLIK	08	GAMS 32 $\pi^- p \rightarrow \eta' n$
74 ± 15		ALDE	87B	GAM2 38 $\pi^- p \rightarrow n 6\gamma$
75 ± 18		BINON	84	GAM2 30-40 $\pi^- p \rightarrow n 6\gamma$

$\Gamma(\mu^+ \mu^- \gamma)/\Gamma(\gamma \gamma)$ Γ_9/Γ_7

VALUE (units 10^{-3})	EVTS	DOCUMENT ID	TECN	COMMENT
4.9 ± 1.2	33	VIKTOROV	80	CNTR 25,33 $\pi^- p \rightarrow 2\mu \gamma$

Meson Particle Listings

 $\eta'(958)$ $\Gamma(\pi^+\pi^-\mu^+\mu^-)/\Gamma_{\text{total}}$ Γ_{10}/Γ

VALUE (units 10^{-5})	CL%	EVTS	DOCUMENT ID	TECN	COMMENT
1.95 ± 0.37 ± 0.03		53	¹ ABLIKIM	21i BES3	$J/\psi \rightarrow \gamma\eta'(958)$

• • • We do not use the following data for averages, fits, limits, etc. • • •

< 2.9	90		² ABLIKIM	130 BES3	$J/\psi \rightarrow \gamma\eta'$
< 24	90		³ NAIK	09 CLEO	$J/\psi \rightarrow \gamma\eta'$

¹ ABLIKIM 21i reports $(1.97 \pm 0.33 \pm 0.19) \times 10^{-5}$ from a measurement of $[\Gamma(\eta'(958) \rightarrow \pi^+\pi^-\mu^+\mu^-)/\Gamma_{\text{total}}] \times [B(J/\psi(1S) \rightarrow \gamma\eta'(958))]$ assuming $B(J/\psi(1S) \rightarrow \gamma\eta'(958)) = (5.21 \pm 0.17) \times 10^{-3}$, which we rescale to our best value $B(J/\psi(1S) \rightarrow \gamma\eta'(958)) = (5.25 \pm 0.07) \times 10^{-3}$. Our first error is their experiment's error and our second error is the systematic error from using our best value.

² Using $\Gamma_2/\Gamma = (29.3 \pm 0.6)\%$ from PDG 12.

³ Not independent of measured value of Γ_{10}/Γ_1 from NAIK 09.

 $\Gamma(\pi^+\pi^-\mu^+\mu^-)/\Gamma(\pi^+\pi^-)$ Γ_{10}/Γ_1

VALUE (units 10^{-3})	CL%	DOCUMENT ID	TECN	COMMENT
< 0.5	90	¹ NAIK	09 CLEO	$J/\psi \rightarrow \gamma\eta'$

¹ NAIK 09 reports $[\Gamma(\eta'(958) \rightarrow \pi^+\pi^-\mu^+\mu^-)/\Gamma(\eta'(958) \rightarrow \pi^+\pi^-)] / [B(\eta \rightarrow 2\gamma)] < 1.3 \times 10^{-3}$ which we multiply by our best value $B(\eta \rightarrow 2\gamma) = 39.36 \times 10^{-2}$.

 $\Gamma(\pi^+\pi^-\mu^+\mu^-)/\Gamma(\rho^0 \gamma (\text{including non-resonant } \pi^+\pi^-))$ Γ_{10}/Γ_2

VALUE (units 10^{-4})	CL%	DOCUMENT ID	TECN	COMMENT
< 1.0	90	ABLIKIM	130 BES3	$J/\psi \rightarrow \gamma\eta'$

 $\Gamma(\pi^+\pi^-\pi^0)/\Gamma_{\text{total}}$ Γ_{11}/Γ

VALUE (units 10^{-3})	EVTS	DOCUMENT ID	TECN	COMMENT
3.61 ± 0.18 OUR FIT				
3.61 ± 0.18 OUR AVERAGE				

3.591 ± 0.054 ± 0.174 6067 ABLIKIM 17 BES3 $J/\psi \rightarrow \gamma(\pi^+\pi^-\pi^0)$

4.28 ± 0.49 ± 1.11 78 ¹ ABLIKIM 15P BES3 $J/\psi \rightarrow K^+K^-\pi$

3.7 $^{+1.1}_{-0.9} \pm 0.4$ ² NAIK 09 CLEO $J/\psi \rightarrow \gamma\eta'$

• • • We do not use the following data for averages, fits, limits, etc. • • •

3.83 ± 0.15 ± 0.39 1014 ³ ABLIKIM 12E BES3 $J/\psi \rightarrow \gamma(\pi^+\pi^-\pi^0)$

¹ We have added all systematic uncertainties in quadrature to a single value.

² Not independent of measured value of Γ_{11}/Γ_1 from NAIK 09.

³ Superseded by ABLIKIM 17.

 $\Gamma((\pi^+\pi^-\pi^0) \text{ S-wave})/\Gamma_{\text{total}}$ Γ_{12}/Γ

VALUE (units 10^{-4})	EVTS	DOCUMENT ID	TECN	COMMENT
37.63 ± 0.77 ± 5.00	6580	¹ ABLIKIM	17 BES3	$J/\psi \rightarrow \gamma(\pi^+\pi^-\pi^0)$

¹ We have added all systematic uncertainties in quadrature.

 $\Gamma(\pi^-\pi^{\pm})/\Gamma_{\text{total}}$ Γ_{13}/Γ

VALUE (units 10^{-4})	EVTS	DOCUMENT ID	TECN	COMMENT
7.44 ± 0.60 ± 2.23	1231	¹ ABLIKIM	17 BES3	$J/\psi \rightarrow \gamma(\pi^-\pi^{\pm})$

¹ We have added all systematic uncertainties in quadrature.

 $\Gamma(\pi^+\pi^-\pi^0)/\Gamma(\pi^+\pi^-)$ Γ_{11}/Γ_1

VALUE (units 10^{-3})	EVTS	DOCUMENT ID	TECN	COMMENT
8.5 ± 0.4 OUR FIT				Error includes scale factor of 1.1.
8.27 $^{+2.49}_{-2.12} \pm 0.04$	20	¹ NAIK	09 CLEO	$J/\psi \rightarrow \gamma\eta'$

¹ NAIK 09 reports $[\Gamma(\eta'(958) \rightarrow \pi^+\pi^-\pi^0)/\Gamma(\eta'(958) \rightarrow \pi^+\pi^-)] / [B(\eta \rightarrow 2\gamma)] = (21 $^{+5}_{-5} \pm 2) \times 10^{-3}$ which we multiply by our best value $B(\eta \rightarrow 2\gamma) = (39.36 \pm 0.18) \times 10^{-2}$. Our first error is their experiment's error and our second error is the systematic error from using our best value.$

 $\Gamma(\pi^0\rho^0)/\Gamma_{\text{total}}$ Γ_{14}/Γ

VALUE	CL%	DOCUMENT ID	TECN	COMMENT
< 0.04	90	RITTENBERG	65 HBC	2.7 $K^-\pi$

 $\Gamma(2(\pi^+\pi^-))/\Gamma_{\text{total}}$ Γ_{15}/Γ

VALUE (units 10^{-5})	CL%	EVTS	DOCUMENT ID	TECN	COMMENT
8.4 ± 0.9 ± 0.1		199	¹ ABLIKIM	14M BES3	$J/\psi \rightarrow \gamma\eta'$

• • • We do not use the following data for averages, fits, limits, etc. • • •

< 24	90		² NAIK	09 CLEO	$J/\psi \rightarrow \gamma\eta'$
< 1000	90		RITTENBERG	69 HBC	1.7-2.7 $K^-\pi$

¹ ABLIKIM 14M reports $[\Gamma(\eta'(958) \rightarrow 2(\pi^+\pi^-))/\Gamma_{\text{total}}] \times [B(J/\psi(1S) \rightarrow \gamma\eta'(958))] = (4.40 \pm 0.35 \pm 0.30) \times 10^{-7}$ which we divide by our best value $B(J/\psi(1S) \rightarrow \gamma\eta'(958)) = (5.25 \pm 0.07) \times 10^{-3}$. Our first error is their experiment's error and our second error is the systematic error from using our best value.

² Not independent of measured value of Γ_{15}/Γ_1 from NAIK 09.

 $\Gamma(2(\pi^+\pi^-))/\Gamma(\pi^+\pi^-)$ Γ_{15}/Γ_1

VALUE (units 10^{-3})	CL%	DOCUMENT ID	TECN	COMMENT
< 0.6	90	¹ NAIK	09 CLEO	$J/\psi \rightarrow \gamma\eta'$

¹ NAIK 09 reports $[\Gamma(\eta'(958) \rightarrow 2(\pi^+\pi^-))/\Gamma(\eta'(958) \rightarrow \pi^+\pi^-)] / [B(\eta \rightarrow 2\gamma)] < 1.4 \times 10^{-3}$ which we multiply by our best value $B(\eta \rightarrow 2\gamma) = 39.36 \times 10^{-2}$.

 $\Gamma(\pi^+\pi^-2\pi^0)/\Gamma_{\text{total}}$ Γ_{16}/Γ

VALUE (units 10^{-4})	CL%	EVTS	DOCUMENT ID	TECN	COMMENT
1.79 ± 0.38 ± 0.02		84	¹ ABLIKIM	14M BES3	$J/\psi \rightarrow \gamma\eta'$

• • • We do not use the following data for averages, fits, limits, etc. • • •

< 27	90		² NAIK	09 CLEO	$J/\psi \rightarrow \gamma\eta'$
------	----	--	-------------------	---------	----------------------------------

¹ ABLIKIM 14M reports $[\Gamma(\eta'(958) \rightarrow \pi^+\pi^-2\pi^0)/\Gamma_{\text{total}}] \times [B(J/\psi(1S) \rightarrow \gamma\eta'(958))] = (9.38 \pm 1.79 \pm 0.89) \times 10^{-7}$ which we divide by our best value $B(J/\psi(1S) \rightarrow \gamma\eta'(958)) = (5.25 \pm 0.07) \times 10^{-3}$. Our first error is their experiment's error and our second error is the systematic error from using our best value.

² Not independent of measured value of Γ_{16}/Γ_1 from NAIK 09.

 $\Gamma(\pi^+\pi^-2\pi^0)/\Gamma(\pi^+\pi^-)$ Γ_{16}/Γ_1

VALUE (units 10^{-3})	CL%	DOCUMENT ID	TECN	COMMENT
< 6	90	¹ NAIK	09 CLEO	$J/\psi \rightarrow \gamma\eta'$

¹ NAIK 09 reports $[\Gamma(\eta'(958) \rightarrow \pi^+\pi^-2\pi^0)/\Gamma(\eta'(958) \rightarrow \pi^+\pi^-)] / [B(\eta \rightarrow 2\gamma)] < 15 \times 10^{-3}$ which we multiply by our best value $B(\eta \rightarrow 2\gamma) = 39.36 \times 10^{-2}$.

 $\Gamma(2(\pi^+\pi^-) \text{ neutrals})/\Gamma_{\text{total}}$ Γ_{17}/Γ

VALUE	CL%	DOCUMENT ID	TECN	COMMENT
< 0.01	95	DANBURG	73 HBC	2.2 $K^-\pi \rightarrow \Lambda X^0$

• • • We do not use the following data for averages, fits, limits, etc. • • •

< 0.01	90	RITTENBERG	69 HBC	1.7-2.7 $K^-\pi$
--------	----	------------	--------	------------------

 $\Gamma(2(\pi^+\pi^-)\pi^0)/\Gamma_{\text{total}}$ Γ_{18}/Γ

VALUE	CL%	DOCUMENT ID	TECN	COMMENT
< 0.002	90	¹ NAIK	09 CLEO	$J/\psi \rightarrow \gamma\eta'$
< 0.01	90	RITTENBERG	69 HBC	1.7-2.7 $K^-\pi$

¹ Not independent of measured value of Γ_{18}/Γ_1 from NAIK 09.

 $\Gamma(2(\pi^+\pi^-)\pi^0)/\Gamma(\pi^+\pi^-)$ Γ_{18}/Γ_1

VALUE (units 10^{-3})	CL%	DOCUMENT ID	TECN	COMMENT
< 4	90	¹ NAIK	09 CLEO	$J/\psi \rightarrow \gamma\eta'$

¹ NAIK 09 reports $[\Gamma(\eta'(958) \rightarrow 2(\pi^+\pi^-)\pi^0)/\Gamma(\eta'(958) \rightarrow \pi^+\pi^-)] / [B(\eta \rightarrow 2\gamma)] < 11 \times 10^{-3}$ which we multiply by our best value $B(\eta \rightarrow 2\gamma) = 39.36 \times 10^{-2}$.

 $\Gamma(2(\pi^+\pi^-)2\pi^0)/\Gamma_{\text{total}}$ Γ_{19}/Γ

VALUE	CL%	DOCUMENT ID	TECN	COMMENT
< 0.01	95	KALBFLEISCH	64B HBC	$K^-\pi \rightarrow \Lambda 2(\pi^+\pi^-) + \text{MM}$

• • • We do not use the following data for averages, fits, limits, etc. • • •

< 0.01	90	LONDON	66 HBC	Compilation
--------	----	--------	--------	-------------

 $\Gamma(3(\pi^+\pi^-))/\Gamma_{\text{total}}$ Γ_{20}/Γ

VALUE (units 10^{-5})	CL%	DOCUMENT ID	TECN	COMMENT
< 3.1	90	¹ ABLIKIM	13U BES3	$J/\psi \rightarrow \gamma 3(\pi^+\pi^-)$

• • • We do not use the following data for averages, fits, limits, etc. • • •

< 53	90		² NAIK	09 CLEO	$J/\psi \rightarrow \gamma\eta'$
< 500	95	KALBFLEISCH	64B HBC	$K^-\pi \rightarrow \Lambda 2(\pi^+\pi^-)$	

¹ Using $B(J/\psi \rightarrow \gamma\eta'(958)) = (5.16 \pm 0.15) \times 10^{-3}$.

² Not independent of measured value of Γ_{20}/Γ_1 from NAIK 09.

 $\Gamma(3(\pi^+\pi^-))/\Gamma(\pi^+\pi^-)$ Γ_{20}/Γ_1

VALUE (units 10^{-3})	CL%	DOCUMENT ID	TECN	COMMENT
< 1.2	90	¹ NAIK	09 CLEO	$J/\psi \rightarrow \gamma\eta'$

¹ NAIK 09 reports $[\Gamma(\eta'(958) \rightarrow 3(\pi^+\pi^-))/\Gamma(\eta'(958) \rightarrow \pi^+\pi^-)] / [B(\eta \rightarrow 2\gamma)] < 3.0 \times 10^{-3}$ which we multiply by our best value $B(\eta \rightarrow 2\gamma) = 39.36 \times 10^{-2}$.

 $\Gamma(K^{\pm}\pi^{\mp})/\Gamma(\rho^0 \gamma (\text{including non-resonant } \pi^+\pi^-))$ Γ_{21}/Γ_2

VALUE	CL%	DOCUMENT ID	TECN	COMMENT
< 1.3 × 10⁻⁴	90	ABLIKIM	16M BES3	$e^+e^- \rightarrow J/\psi \rightarrow \text{hadrons}$

 $\Gamma(\pi^+\pi^-e^+e^-)/\Gamma_{\text{total}}$ Γ_{22}/Γ

VALUE (units 10^{-3})	CL%	EVTS	DOCUMENT ID	TECN	COMMENT
2.42 ± 0.10 OUR FIT					

• • • We do not use the following data for averages, fits, limits, etc. • • •

2.11 ± 0.12 ± 0.14	429		¹ ABLIKIM	130 BES3	$J/\psi \rightarrow \gamma\eta'$
2.5 $^{+1.2}_{-0.9} \pm 0.5$			² NAIK	09 CLEO	$J/\psi \rightarrow \gamma\eta'$

¹ Using $\Gamma_2/\Gamma = (29.3 \pm 0.6)\%$ from PDG 12.

² Not independent of measured value of Γ_{22}/Γ_1 from NAIK 09.

 $\Gamma(\pi^+\pi^-e^+e^-)/\Gamma(\pi^+\pi^-)$ Γ_{22}/Γ_1

VALUE (units 10^{-3})	EVTS	DOCUMENT ID	TECN	COMMENT
5.69 ± 0.25 OUR FIT				
5.51 $^{+3.00}_{-2.30} \pm 0.03$	8	¹ NAIK	09 CLEO	$J/\psi \rightarrow \gamma\eta'$

¹ NAIK 09 reports $[\Gamma(\eta'(958) \rightarrow \pi^+\pi^-e^+e^-)/\Gamma(\eta'(958) \rightarrow \pi^+\pi^-)] / [B(\eta \rightarrow 2\gamma)] = (14 $^{+7}_{-5} \pm 3) \times 10^{-3}$ which we multiply by our best value $B(\eta \rightarrow 2\gamma) = (39.36 \pm 0.18) \times 10^{-2}$. Our first error is their experiment's error and our second error is the systematic error from using our best value.$

$\Gamma(\pi^+\pi^-\rho^0\gamma(\text{including non-resonant } \pi^+\pi^-\gamma)) / \Gamma_{22}/\Gamma_{22}$

VALUE (units 10^{-3})	EVTS	DOCUMENT ID	TECN	COMMENT
8.20±0.31 OUR FIT				
8.20±0.16±0.27	2584	ABLIKIM 21J	BES3	$J/\psi \rightarrow \gamma\eta'$
••• We do not use the following data for averages, fits, limits, etc. •••				
7.2 ±0.4 ±0.5	429	¹ ABLIKIM 130	BES3	$J/\psi \rightarrow \gamma\eta'$
¹ Superseded by ABLIKIM 21J.				

$\Gamma(\pi^+e^-\nu_e + c.c.) / \Gamma(\pi^+\pi^-\eta)$

VALUE (units 10^{-4})	CL%	DOCUMENT ID	TECN	COMMENT
<5.0	90	ABLIKIM 13G	BES3	$J/\psi \rightarrow \phi\eta'$

$\Gamma(\gamma e^+e^-) / \Gamma_{total}$

VALUE (units 10^{-3})	CL%	DOCUMENT ID	TECN	COMMENT
••• We do not use the following data for averages, fits, limits, etc. •••				
<0.9	90	BRIERE 00	CLEO	10.6 e^+e^-

$\Gamma(\gamma e^+e^-) / \Gamma(\gamma\gamma)$

VALUE (units 10^{-3})	EVTS	DOCUMENT ID	TECN	COMMENT
2.13±0.09±0.07	864	ABLIKIM 150	BES3	$J/\psi \rightarrow \gamma e^+e^-$

$\Gamma(\pi^0\gamma\gamma) / \Gamma_{total}$

VALUE (units 10^{-3})	EVTS	DOCUMENT ID	TECN	COMMENT
3.20±0.07±0.23	3.4k	ABLIKIM 17T	BES3	$J/\psi \rightarrow \gamma\eta'$

$\Gamma(\pi^0\gamma\gamma(\text{non resonant})) / \Gamma_{total}$

VALUE (units 10^{-4})	EVTS	DOCUMENT ID	TECN	COMMENT
6.16±0.64±0.67	655	ABLIKIM 17T	BES3	$J/\psi \rightarrow \gamma\eta'$

$\Gamma(\pi^0\gamma\gamma) / \Gamma(\pi^0\pi^0\eta)$

VALUE (units 10^{-4})	CL%	DOCUMENT ID	TECN	COMMENT
<37	90	ALDE 87B	GAM2	38 $\pi^-\rho \rightarrow n4\gamma$

$\Gamma(\eta\gamma\gamma) / \Gamma_{total}$

VALUE	CL%	DOCUMENT ID	TECN	COMMENT
<1.33 × 10⁻⁴	90	ABLIKIM 19AW	BES3	$J/\psi \rightarrow \eta\eta' \rightarrow \gamma\gamma\gamma 2\gamma$

$\Gamma(4\pi^0) / \Gamma_{total}$

VALUE	CL%	DOCUMENT ID	TECN	COMMENT
<4.94 × 10⁻⁵	90	ABLIKIM 20E	BES3	$J/\psi \rightarrow \eta'\gamma$
••• We do not use the following data for averages, fits, limits, etc. •••				
<3.2 × 10 ⁻⁴	90	DONSKOV 14	GAM4	32.5 $\pi^-\rho \rightarrow \eta'n$

$\Gamma(4\pi^0) / \Gamma(\pi^0\pi^0\eta)$

VALUE (units 10^{-4})	CL%	DOCUMENT ID	TECN	COMMENT
••• We do not use the following data for averages, fits, limits, etc. •••				
<23	90	ALDE 87B	GAM2	38 $\pi^-\rho \rightarrow n8\gamma$

$\Gamma(e^+e^-) / \Gamma_{total}$

VALUE	CL%	DOCUMENT ID	TECN	COMMENT
< 5.6 × 10⁻⁹	90	¹ ACHASOV 15	SND	0.958 $e^+e^- \rightarrow \pi\pi\eta$
••• We do not use the following data for averages, fits, limits, etc. •••				
<12 × 10 ⁻⁹	90	² AKHMETSHIN 15	CMD3	0.958 $e^+e^- \rightarrow \pi^+\pi^-\eta$
< 2.1 × 10 ⁻⁷	90	VOROBYEV 88	ND	$e^+e^- \rightarrow \pi^+\pi^-\eta$

¹ Combining data of ACHASOV 15 and AKHMETSHIN 15 and using $\Gamma(\eta') = 0.198 \pm 0.009$ MeV.
² Using $\Gamma_{\eta'(958)} = 198 \pm 9$ keV, $B(\eta'(958) \rightarrow \pi^+\pi^-\eta) = (42.9 \pm 0.7)\%$, and $B(\eta \rightarrow \gamma\gamma) = (39.41 \pm 0.20)\%$.

$\Gamma(\text{invisible}) / \Gamma_{total}$

VALUE (units 10^{-4})	CL%	DOCUMENT ID	TECN	COMMENT
••• We do not use the following data for averages, fits, limits, etc. •••				
<9.5	90	¹ NAIK 09	CLEO	$J/\psi \rightarrow \gamma\eta'$
¹ Not independent of measured value of Γ_{30}/Γ_1 from NAIK 09.				

$\Gamma(\text{invisible}) / \Gamma(\gamma\gamma)$

VALUE (units 10^{-2})	CL%	DOCUMENT ID	TECN	COMMENT
<2.4	90	ABLIKIM 13	BES3	$J/\psi \rightarrow \phi\eta'$
••• We do not use the following data for averages, fits, limits, etc. •••				
<6.69	90	ABLIKIM 06Q	BES	$J/\psi \rightarrow \phi\eta'$

$\Gamma(\text{invisible}) / \Gamma(\pi^+\pi^-\eta)$

VALUE (units 10^{-3})	CL%	DOCUMENT ID	TECN	COMMENT
••• We do not use the following data for averages, fits, limits, etc. •••				
<2.1	90	¹ NAIK 09	CLEO	$J/\psi \rightarrow \gamma\eta'$
¹ NAIK 09 reports $[\Gamma(\eta'(958) \rightarrow \text{invisible}) / \Gamma(\eta'(958) \rightarrow \pi^+\pi^-\eta)] / [B(\eta \rightarrow 2\gamma)] < 5.4 \times 10^{-3}$ which we multiply by our best value $B(\eta \rightarrow 2\gamma) = 39.36 \times 10^{-2}$.				

$\Gamma(\pi^+\pi^-) / \Gamma_{total}$

VALUE (units 10^{-4})	CL%	DOCUMENT ID	TECN	COMMENT
< 0.18	90	¹ AAIJ 17D	LHCb	$D_{(s)}^+ \rightarrow \pi^+\pi^-\pi^+$
••• We do not use the following data for averages, fits, limits, etc. •••				
< 0.5	90	² ABLIKIM 11G	BES3	$J/\psi \rightarrow \gamma\pi^+\pi^-$
< 29	90	³ MORI 07A	BELL	$\gamma\gamma \rightarrow \pi^+\pi^-$
< 3.3	90	⁴ MORI 07A	BELL	$\gamma\gamma \rightarrow \pi^+\pi^-$
<800	95	DANBURG 73	HBC	2.2 $K^-\rho \rightarrow \Lambda\chi^0$
<200	90	RITTENBERG 69	HBC	1.7-2.7 $K^-\rho$

¹ Using branching fractions of $D_{(s)}^+$ decays from PDG 15.
² ABLIKIM 11G reports $[\Gamma(\eta'(958) \rightarrow \pi^+\pi^-) / \Gamma_{total}] \times [B(J/\psi(1S) \rightarrow \gamma\eta'(958))] < 2.84 \times 10^{-7}$ which we divide by our best value $B(J/\psi(1S) \rightarrow \gamma\eta'(958)) = 5.25 \times 10^{-3}$.
³ Taking into account interference with the $\gamma\gamma \rightarrow \pi^+\pi^-$ continuum.
⁴ Without interference with the $\gamma\gamma \rightarrow \pi^+\pi^-$ continuum.

$\Gamma(\pi^0\pi^0) / \Gamma_{total}$

VALUE	CL%	DOCUMENT ID	TECN	COMMENT
<4 × 10⁻⁴	90	¹ ABLIKIM 11G	BES3	$J/\psi \rightarrow \gamma\pi^0\pi^0$
¹ ABLIKIM 11G reports $[\Gamma(\eta'(958) \rightarrow \pi^+\pi^-) / \Gamma_{total}] \times [B(J/\psi(1S) \rightarrow \gamma\eta'(958))] < 2.84 \times 10^{-7}$ which we divide by our best value $B(J/\psi(1S) \rightarrow \gamma\eta'(958)) = 5.25 \times 10^{-3}$.				

$\Gamma(\pi^0\pi^0) / \Gamma(\pi^0\pi^0\eta)$

VALUE (units 10^{-4})	CL%	DOCUMENT ID	TECN	COMMENT
<45	90	ALDE 87B	GAM2	38 $\pi^-\rho \rightarrow n4\gamma$

$\Gamma(\pi^0e^+e^-) / \Gamma_{total}$

VALUE (units 10^{-3})	CL%	DOCUMENT ID	TECN	COMMENT
< 1.4	90	BRIERE 00	CLEO	10.6 e^+e^-
••• We do not use the following data for averages, fits, limits, etc. •••				
<13	90	RITTENBERG 65	HBC	2.7 $K^-\rho$

$\Gamma(\eta e^+e^-) / \Gamma_{total}$

VALUE (units 10^{-3})	CL%	DOCUMENT ID	TECN	COMMENT
< 2.4	90	BRIERE 00	CLEO	10.6 e^+e^-
••• We do not use the following data for averages, fits, limits, etc. •••				
<11	90	RITTENBERG 65	HBC	2.7 $K^-\rho$

$\Gamma(3\gamma) / \Gamma(\pi^0\pi^0\eta)$

VALUE (units 10^{-4})	CL%	DOCUMENT ID	TECN	COMMENT
<4.6	90	ALDE 87B	GAM2	38 $\pi^-\rho \rightarrow n3\gamma$

$\Gamma(\mu^+\mu^-\pi^0) / \Gamma_{total}$

VALUE (units 10^{-5})	CL%	DOCUMENT ID	TECN	COMMENT
<6.0	90	DZHELADIN 81	CNTR	30 $\pi^-\rho \rightarrow \eta'n$

$\Gamma(\mu^+\mu^-\eta) / \Gamma_{total}$

VALUE (units 10^{-5})	CL%	DOCUMENT ID	TECN	COMMENT
<1.5	90	DZHELADIN 81	CNTR	30 $\pi^-\rho \rightarrow \eta'n$

$\Gamma(e\mu) / \Gamma_{total}$

VALUE (units 10^{-4})	CL%	DOCUMENT ID	TECN	COMMENT
<4.7	90	BRIERE 00	CLEO	10.6 e^+e^-

$\eta'(958) \rightarrow \eta\pi\pi$ DECAY PARAMETERS

$|\text{MATRIX ELEMENT}|^2 = |1 + \alpha Y|^2 + CX + DX^2$

X and Y are Dalitz variables; α is complex and C, and D are real-valued. Parameters C and D are not necessarily equal to c and d, respectively, in the generalized parameterization following this one. May be different for $\eta'(958) \rightarrow \eta\pi^+\pi^-$ and $\eta'(958) \rightarrow \eta\pi^0\pi^0$ decays. Because of different initial assumptions and strong correlations of the parameters we do not average the parameters in the section below.

Re(α) decay parameter

VALUE	EVTS	DOCUMENT ID	TECN	COMMENT
••• We do not use the following data for averages, fits, limits, etc. •••				
-0.034±0.002±0.002	351k	ABLIKIM 18	BES3	$\eta' \rightarrow \eta\pi^+\pi^-$
-0.054±0.004±0.001	56k	ABLIKIM 18	BES3	$\eta' \rightarrow \eta\pi^0\pi^0$
-0.033±0.005±0.003	44k	¹ ABLIKIM 11	BES3	$J/\psi \rightarrow \gamma\eta\pi^+\pi^-$
-0.072±0.012±0.006	7k	² AMELIN 05A	VES	28 $\pi^-A \rightarrow \eta\pi^+\pi^-\pi^-A^*$
-0.021±0.018±0.017	6.7k	³ BRIERE 00	CLEO	10.6 $e^+e^- \rightarrow \eta\pi^+\pi^-X$
-0.058±0.013±0.003	5.4k	⁴ ALDE 86	GAM2	38 $\pi^-\rho \rightarrow n\eta\pi^0\pi^0$
-0.08 ±0.03		^{4.5} KALBFLEISCH 74	RVUE	$\eta' \rightarrow \eta\pi^+\pi^-$

¹ See ABLIKIM 11 for the full correlation matrix.
² Superseded by DOROFEEV 07, which found this parameterization unacceptable. See below.
³ Assuming $\text{Im}(\alpha) = 0$, $C = 0$, and $D = 0$.
⁴ Assuming $C = 0$.
⁵ From the data of DAUBER 64, RITTENBERG 69, AGUILAR-BENITEZ 72B, JACOBS 73, and DANBURG 73.

Meson Particle Listings

 $\eta'(958)$ **$Im(\alpha)$ decay parameter**

VALUE	EVTS	DOCUMENT ID	TECN	COMMENT
••• We do not use the following data for averages, fits, limits, etc. •••				
$0.000 \pm 0.019 \pm 0.001$	351k	ABLIKIM	18 BES3	$\eta' \rightarrow \eta\pi^+\pi^-$
$0.000 \pm 0.038 \pm 0.002$	56k	ABLIKIM	18 BES3	$\eta' \rightarrow \eta\pi^0\pi^0$
$0.000 \pm 0.049 \pm 0.001$	44k	¹ ABLIKIM	11 BES3	$J/\psi \rightarrow \gamma\eta\pi^+\pi^-$
$0.0 \pm 0.1 \pm 0.0$	7k	² AMELIN	05A VES	$28\pi^-A \rightarrow \eta\pi^+\pi^-\pi^-A^*$
$-0.00 \pm 0.13 \pm 0.00$	5.4k	³ ALDE	86 GAM2	$38\pi^-\rho \rightarrow n\eta\pi^0\pi^0$
0.0 ± 0.3		^{3,4} KALBFLEISCH	74 RVUE	$\eta' \rightarrow \eta\pi^+\pi^-$

¹ See ABLIKIM 11 for the full correlation matrix.
² Superseded by DOROFEEV 07, which found this parameterization unacceptable. See below.
³ Assuming $C = 0$.
⁴ From the data of DAUBER 64, RITTENBERG 69, AGUILAR-BENITEZ 72B, JACOBS 73, and DANBURG 73.

C decay parameter

VALUE	EVTS	DOCUMENT ID	TECN	COMMENT
••• We do not use the following data for averages, fits, limits, etc. •••				
$0.0027 \pm 0.0024 \pm 0.0015$	351k	ABLIKIM	18 BES3	$\eta' \rightarrow \eta\pi^+\pi^-$
$0.018 \pm 0.009 \pm 0.003$	44k	¹ ABLIKIM	11 BES3	$J/\psi \rightarrow \gamma\eta\pi^+\pi^-$
$0.020 \pm 0.018 \pm 0.004$	7k	² AMELIN	05A VES	$28\pi^-A \rightarrow \eta\pi^+\pi^-\pi^-A^*$

¹ See ABLIKIM 11 for the full correlation matrix.
² Superseded by DOROFEEV 07, which found this parameterization unacceptable. See below.
³ Assuming $C = 0$.
⁴ From the data of DAUBER 64, RITTENBERG 69, AGUILAR-BENITEZ 72B, JACOBS 73, and DANBURG 73.

D decay parameter

VALUE	EVTS	DOCUMENT ID	TECN	COMMENT
••• We do not use the following data for averages, fits, limits, etc. •••				
$-0.053 \pm 0.004 \pm 0.004$	351k	ABLIKIM	18 BES3	$\eta' \rightarrow \eta\pi^+\pi^-$
$-0.061 \pm 0.009 \pm 0.005$	56k	ABLIKIM	18 BES3	$\eta' \rightarrow \eta\pi^0\pi^0$
$-0.059 \pm 0.012 \pm 0.004$	44k	¹ ABLIKIM	11 BES3	$J/\psi \rightarrow \gamma\eta\pi^+\pi^-$
$-0.066 \pm 0.030 \pm 0.015$	7k	² AMELIN	05A VES	$28\pi^-A \rightarrow \eta\pi^+\pi^-\pi^-A^*$
$0.00 \pm 0.03 \pm 0.00$	5.4k	³ ALDE	86 GAM2	$38\pi^-\rho \rightarrow n\eta\pi^0\pi^0$
0		^{3,4} KALBFLEISCH	74 RVUE	$\eta' \rightarrow \eta\pi^+\pi^-$

¹ See ABLIKIM 11 for the full correlation matrix.
² Superseded by DOROFEEV 07, which found this parameterization unacceptable. See below.
³ Assuming $C = 0$.
⁴ From the data of DAUBER 64, RITTENBERG 69, AGUILAR-BENITEZ 72B, JACOBS 73, and DANBURG 73.

 $\eta'(958) \rightarrow \eta\pi\pi$ DECAY PARAMETERS

$$|\text{MATRIX ELEMENT}|^2 \propto 1 + aY + bY^2 + cX + dX^2$$

X and Y are Dalitz variables and a, b, c, and d are real-valued parameters. May be different for $\eta'(958) \rightarrow \eta\pi^+\pi^-$ and $\eta'(958) \rightarrow \eta\pi^0\pi^0$ decays. We do not average measurements in the section below because parameter values from each experiment are strongly correlated.

a decay parameter

VALUE	EVTS	DOCUMENT ID	TECN	COMMENT
••• We do not use the following data for averages, fits, limits, etc. •••				
$-0.056 \pm 0.004 \pm 0.002$	351k	ABLIKIM	18 BES3	$\eta' \rightarrow \eta\pi^+\pi^-$
$-0.087 \pm 0.009 \pm 0.006$	56k	ABLIKIM	18 BES3	$\eta' \rightarrow \eta\pi^0\pi^0$
$-0.074 \pm 0.008 \pm 0.006$	124k	ADLARSON	18A A2MM	$\eta' \rightarrow \eta\pi^0\pi^0$
$-0.072 \pm 0.007 \pm 0.008$		¹ GONZALEZ-S.	1.18A RVUE	$\eta' \rightarrow \eta\pi^0\pi^0$
$-0.047 \pm 0.011 \pm 0.003$	44k	² ABLIKIM	11 BES3	$J/\psi \rightarrow \gamma\eta\pi^+\pi^-$
$-0.066 \pm 0.016 \pm 0.003$	15k	³ BLIK	09 GAM4	$32.5\pi^-\rho \rightarrow \eta' n$
$-0.127 \pm 0.016 \pm 0.008$	20k	⁴ DOROFEEV	07 VES	$27\pi^-\rho \rightarrow \eta' n, \pi^-A \rightarrow \eta'\pi^-A^*$

¹ Theoretical analysis of ADLARSON 18A using resonance chiral perturbation theory to one loop.
² See ABLIKIM 11 for the full correlation matrix.
³ From $\eta' \rightarrow \eta\pi^0\pi^0$ decay.
⁴ From $\eta' \rightarrow \eta\pi^+\pi^-$ decay.

b decay parameter

VALUE	EVTS	DOCUMENT ID	TECN	COMMENT
••• We do not use the following data for averages, fits, limits, etc. •••				
$-0.049 \pm 0.006 \pm 0.006$	351k	ABLIKIM	18 BES3	$\eta' \rightarrow \eta\pi^+\pi^-$
$-0.073 \pm 0.014 \pm 0.005$	56k	ABLIKIM	18 BES3	$\eta' \rightarrow \eta\pi^0\pi^0$
$-0.063 \pm 0.014 \pm 0.005$	124k	ADLARSON	18A A2MM	$\eta' \rightarrow \eta\pi^0\pi^0$
$-0.052 \pm 0.001 \pm 0.002$		¹ GONZALEZ-S.	1.18A RVUE	$\eta' \rightarrow \eta\pi^0\pi^0$
$-0.069 \pm 0.019 \pm 0.009$	44k	² ABLIKIM	11 BES3	$J/\psi \rightarrow \gamma\eta\pi^+\pi^-$
$-0.063 \pm 0.028 \pm 0.004$	15k	³ BLIK	09 GAM4	$32.5\pi^-\rho \rightarrow \eta' n$
$-0.106 \pm 0.028 \pm 0.014$	20k	⁴ DOROFEEV	07 VES	$27\pi^-\rho \rightarrow \eta' n, \pi^-A \rightarrow \eta'\pi^-A^*$

¹ Theoretical analysis of ADLARSON 18A using resonance chiral perturbation theory to one loop.
² See ABLIKIM 11 for the full correlation matrix.
³ From $\eta' \rightarrow \eta\pi^0\pi^0$ decay.
⁴ From $\eta' \rightarrow \eta\pi^+\pi^-$ decay.

c decay parameter

VALUE	EVTS	DOCUMENT ID	TECN	COMMENT
••• We do not use the following data for averages, fits, limits, etc. •••				
$0.0027 \pm 0.0024 \pm 0.0018$	351k	ABLIKIM	18 BES3	$\eta' \rightarrow \eta\pi^+\pi^-$
$0.019 \pm 0.011 \pm 0.003$	44k	¹ ABLIKIM	11 BES3	$J/\psi \rightarrow \gamma\eta\pi^+\pi^-$
$-0.107 \pm 0.096 \pm 0.003$	15k	² BLIK	09 GAM4	$32.5\pi^-\rho \rightarrow \eta' n$
$0.015 \pm 0.011 \pm 0.014$	20k	³ DOROFEEV	07 VES	$27\pi^-\rho \rightarrow \eta' n, \pi^-A \rightarrow \eta'\pi^-A^*$

¹ See ABLIKIM 11 for the full correlation matrix.
² From $\eta' \rightarrow \eta\pi^0\pi^0$ decay.
³ From $\eta' \rightarrow \eta\pi^+\pi^-$ decay.

d decay parameter

VALUE	EVTS	DOCUMENT ID	TECN	COMMENT
••• We do not use the following data for averages, fits, limits, etc. •••				
$-0.063 \pm 0.004 \pm 0.003$	351k	ABLIKIM	18 BES3	$\eta' \rightarrow \eta\pi^+\pi^-$
$-0.074 \pm 0.009 \pm 0.004$	56k	ABLIKIM	18 BES3	$\eta' \rightarrow \eta\pi^0\pi^0$
$-0.050 \pm 0.009 \pm 0.005$	124k	ADLARSON	18A A2MM	$\eta' \rightarrow \eta\pi^0\pi^0$
$-0.051 \pm 0.008 \pm 0.006$		¹ GONZALEZ-S.	1.18A RVUE	$\eta' \rightarrow \eta\pi^0\pi^0$
$-0.073 \pm 0.012 \pm 0.003$	44k	² ABLIKIM	11 BES3	$J/\psi \rightarrow \gamma\eta\pi^+\pi^-$
$0.018 \pm 0.078 \pm 0.006$	15k	³ BLIK	09 GAM4	$32.5\pi^-\rho \rightarrow \eta' n$
$-0.082 \pm 0.017 \pm 0.008$	20k	⁴ DOROFEEV	07 VES	$27\pi^-\rho \rightarrow \eta' n, \pi^-A \rightarrow \eta'\pi^-A^*$

¹ Theoretical analysis of ADLARSON 18A using resonance chiral perturbation theory to one loop.
² See ABLIKIM 11 for the full correlation matrix.
³ From $\eta' \rightarrow \eta\pi^0\pi^0$ decay. If $c \equiv 0$ from Bose-Einstein symmetry, $d = -0.067 \pm 0.020 \pm 0.003$.
⁴ From $\eta' \rightarrow \eta\pi^+\pi^-$ decay.

 $\eta'(958) \beta$ PARAMETER
 $|\text{MATRIX ELEMENT}|^2 = (1 + 2\beta Z)$

See the "Note on η Decay Parameters" in our 1994 edition Physical Review D50 1173 (1994), p. 1454.

 β decay parameter

VALUE	EVTS	DOCUMENT ID	TECN	COMMENT
-0.61 ± 0.08 OUR AVERAGE				Error includes scale factor of 1.2.
$-0.640 \pm 0.046 \pm 0.047$	1.8k	ABLIKIM	15G BES3	$J/\psi \rightarrow \gamma(\pi^0\pi^0\pi^0)$
-0.59 ± 0.18	235	BLIK	08 GAMS	$32\pi^-\rho \rightarrow \eta' n$
-0.1 ± 0.3		ALDE	87B GAM2	$38\pi^-\rho \rightarrow n3\pi^0$

 $\eta'(958)$ C-NONCONSERVING DECAY PARAMETER

See the note on η decay parameters in the Stable Particle Particle Listings for definition of this parameter.

DECAY ASYMMETRY PARAMETER FOR $\pi^+\pi^-\gamma$

VALUE	EVTS	DOCUMENT ID	TECN	COMMENT
-0.03 ± 0.04 OUR AVERAGE				
-0.019 ± 0.056		AIHARA	87 TPC	$2\gamma \rightarrow \pi^+\pi^-\gamma$
-0.069 ± 0.078	295	GRIGORIAN	75 STRC	$2.1\pi^-\rho$
0.00 ± 0.10	103	KALBFLEISCH	75 HBC	$2.18K^-\rho \rightarrow \Lambda\pi^+\pi^-\gamma$

••• We do not use the following data for averages, fits, limits, etc. •••

0.07 ± 0.08	152	RITTENBERG	65 HBC	$2.1-2.7K^-\rho$
-----------------	-----	------------	--------	------------------

 $\eta'(958) \rightarrow \gamma\ell^+\ell^-$ TRANSITION FORM FACTOR SLOPE

Related to the effective virtual meson mass Λ , via slope $\approx \Lambda^{-2}$. See e.g. LANDSBERG 85, eq. (3.8), for a detailed definition.

VALUE (GeV ⁻²)	EVTS	DOCUMENT ID	TECN	COMMENT
1.62 ± 0.17 OUR AVERAGE				
$1.60 \pm 0.17 \pm 0.08$	864	¹ ABLIKIM	15G BES3	$J/\psi \rightarrow \gamma e^+e^-$
1.7 ± 0.4	33	¹ VIKTOROV	80	$25,33\pi^-\rho \rightarrow 2\mu\gamma$

¹ In the single-pole Ansatz where slope = $1/(\Lambda^2 + \gamma^2)$ with Λ, γ being a Breit-Wigner mass, width for the effective contributing vector meson.

 $\eta'(958)$ REFERENCES

ABLIKIM	21I	PR D103 072006	M. Ablikim et al.	(BESIII Collab.)
ABLIKIM	21J	PR D103 092005	M. Ablikim et al.	(BESIII Collab.)
ABLIKIM	20E	PR D101 032001	M. Ablikim et al.	(BESIII Collab.)
ABLIKIM	19AW	PR D100 052015	M. Ablikim et al.	(BESIII Collab.)
ABLIKIM	19T	PRL 122 142002	M. Ablikim et al.	(BESIII Collab.)
ABLIKIM	18	PR D97 012003	M. Ablikim et al.	(BESIII Collab.)
ABLIKIM	18C	PRL 120 242003	M. Ablikim et al.	(BESIII Collab.)
ADLARSON	18A	PR D98 012001	P. Adlarson et al.	(A2 Collab. at MAMI)
GONZALEZ-S.	1.18A	EPJ C78 758	S. Gonzalez-Solis, E. Passemar	(BEJ, INO+)
AAJ	17D	PL B764 233	R. Aaij et al.	(LHC Collab.)
ABLIKIM	17	PRL 118 012001	M. Ablikim et al.	(BESIII Collab.)
ABLIKIM	17T	PR D96 012005	M. Ablikim et al.	(BESIII Collab.)
ABLIKIM	16M	PR D93 072008	M. Ablikim et al.	(BESIII Collab.)
ABLIKIM	15AD	PR D92 051101	M. Ablikim et al.	(BESIII Collab.)
ABLIKIM	15G	PR D92 012014	M. Ablikim et al.	(BESIII Collab.)
ABLIKIM	15O	PR D92 012001	M. Ablikim et al.	(BESIII Collab.)
ABLIKIM	15P	PR D92 012007	M. Ablikim et al.	(BESIII Collab.)
ACHASOV	15	PR D91 092010	M.N. Achasov et al.	(SND Collab.)
AKHMETSHIN	15	PL B740 273	R.R. Akhmetshin et al.	(CMD-3 Collab.)
PDG	15	RPP 2015 at pdg.lbl.gov		(PDG Collab.)
ABLIKIM	14M	PRL 112 251801	M. Ablikim et al.	(BESIII Collab.)

See key on page 1127

Meson Particle Listings

$\eta'(958), f_0(980)$

Table listing meson particles with columns for name, mass, width, and references. Includes entries like DONSKOV, ABLIKIM, LIBBY, etc.

1 5 poles, 5 channels, including scattering data from HYAMS 75 (pi pi), LONGACRE 86 (K K-bar), BINON 83 (eta eta), and BINON 84c (eta eta'). Based on 18.5k events. Second solution 977.8 +/- 1.7 MeV.

f_0(980) MASS

Table of f_0(980) mass measurements. Columns: VALUE (MeV), EVTS, DOCUMENT ID, TECN, COMMENT. Includes entries like AAIJ, ABLIKIM, ECKLUND, etc.

f_0(980)

J^G(JPC) = 0+(0++)

See the related review(s): Scalar Mesons below 1 GeV

f_0(980) T-MATRIX POLE sqrt(s)

Table of f_0(980) T-matrix pole data. Columns: VALUE (MeV), DOCUMENT ID, TECN, COMMENT. Includes entries like SARANTSEV, ALBRECHT, etc.

Meson Particle Listings

$f_0(980)$

Mass	Source	Decay	Width	Source	Decay	Width	
988	34 ZOU	94B RVUE	$66.9 \pm 2.2^{+17.6}_{-12.5}$	2 UEHARA	08A BELL	$10.6 e^+e^- \rightarrow e^+e^- \pi^0 \pi^0$	
988 ± 10	35 MORGAN	93 RVUE $\pi\pi(K\bar{K}) \rightarrow \pi\pi(K\bar{K}), J/\psi \rightarrow \phi\pi\pi(K\bar{K}), D_S \rightarrow \pi(\pi\pi)$	65 ± 13	262 ± 30	3 AUBERT	07AK BABR $10.6 e^+e^- \rightarrow \phi\pi^+\pi^-\gamma$	
971.1 ± 4.0	24 AGUILAR...	91 EHS 400 pp	81 ± 21	54 ± 9	3 AUBERT	07AK BABR $10.6 e^+e^- \rightarrow \phi\pi^0\pi^0\gamma$	
979 ± 4	36 ARMSTRONG	91 OMEG 300 $pp \rightarrow pp\pi\pi, ppK\bar{K}$	$51.3^{+20.8+13.2}_{-17.7-3.8}$		4 MORI	07 BELL $10.6 e^+e^- \rightarrow e^+e^- \pi^+\pi^-$	
956 ± 12	BREAKSTONE	90 SFM $pp \rightarrow pp\pi^+\pi^-$	61 ± 9	$^{+14}_{-8}$	2584	5 GARMASH	05 BELL $B^+ \rightarrow K^+\pi^+\pi^-$
959.4 ± 6.5	24 AUGUSTIN	89 DM2 $J/\psi \rightarrow \omega\pi^+\pi^-$	64 ± 16		6 ANISOVICH	03 RVUE	
978 ± 9	24 ABACHI	86B HRS $e^+e^- \rightarrow \pi^+\pi^-X$	121 ± 23		TIKHOMIROV	03 SPEC $40.0 \frac{C}{K_S^0 K_S^0 K_L^0 X}$	
$985.0^{+9.0}_{-39.0}$	ETKIN	82B MPS 23 $\pi^-p \rightarrow n2K_S^0$	~ 70		7 BRAMON	02 RVUE $1.02 e^+e^- \rightarrow \pi^0\pi^0\gamma$	
974 ± 4	36 GIDAL	81 MRK2 $J/\psi \rightarrow \pi^+\pi^-X$	$44 \pm 2 \pm 2$	848	8 AITALA	01A E791 $D_S^+ \rightarrow \pi^-\pi^+\pi^+$	
975	37 ACHASOV	80 RVUE	201 ± 28	419	9 ACHASOV	00H SND $e^+e^- \rightarrow \pi^0\pi^0\gamma$	
986 ± 10	36 AGUILAR...	78 HBC $0.7 \bar{p}p \rightarrow K_S^0 K_S^0$	122 ± 13	419	10,11 ACHASOV	00H SND $e^+e^- \rightarrow \pi^0\pi^0\gamma$	
969 ± 5	36 LEEPER	77 ASPK $2-2.4 \pi^-p \rightarrow \pi^+\pi^-n, K^+K^-n$	56 ± 20		12 AKHMETSHIN	99C CMD2 $e^+e^- \rightarrow \pi^0\pi^0\gamma$	
987 ± 7	36 BINNIE	73 CNTR $\pi^-p \rightarrow nMM$	65 ± 20		BARBERIS	99 OMEG 450 $pp \rightarrow p_S p_f K^+ K^-$	
1012 ± 6	38 GRAYR	73 ASPK $17 \pi^-p \rightarrow \pi^+\pi^-n$	80 ± 10		BARBERIS	99B OMEG 450 $pp \rightarrow p_S p_f \pi^+\pi^-$	
1007 ± 20	38 HYAMS	73 ASPK $17 \pi^-p \rightarrow \pi^+\pi^-n$	80 ± 10		BARBERIS	99C OMEG 450 $pp \rightarrow p_S p_f \pi^0\pi^0$	
997 ± 6	38 PROTOPOP...	73 HBC $7 \pi^+p \rightarrow \pi^+p\pi^+\pi^-$	$48 \pm 12 \pm 8$		13 BARBERIS	99D OMEG 450 $pp \rightarrow K^+K^-, \pi^+\pi^-$	

1 From the $D_S^\pm \rightarrow K^\pm K^+ K^-$ Dalitz plot fit with the Triple-M amplitude in the multi-meson model of AOUDE 18.
 2 Using a relativistic Breit-Wigner function and taking into account the finite D_S mass.
 3 Breit-Wigner mass. Using finite width corrections according to FLATTE 76 and ACHASOV 05, and the ratio $g_{f_0} K K / g_{f_0} \pi\pi = 0$.
 4 In the kaon-loop fit.
 5 In the no-structure fit.
 6 Systematic errors not estimated.
 7 FLATTE 76 parameterization. $g_{f_0} \pi\pi = 329 \pm 96$ MeV/ c^2 assuming $g_{f_0} K \bar{K} / g_{f_0} \pi\pi = 2$.
 8 Breit-Wigner mass. Using finite width corrections according to FLATTE 76 and ACHASOV 05, and the ratio $g_{f_0} K K / g_{f_0} \pi\pi = 4.21 \pm 0.25 \pm 0.21$ from ABLIKIM 05.
 9 In the kaon-loop fit following formalism of ACHASOV 89.
 10 In the no-structure fit assuming a direct coupling of ϕ to $f_0\gamma$.
 11 FLATTE 76 parameterization. Supersedes GARMASH 05.
 12 FLATTE 76 parameterization. $g_{f_0} K \bar{K} / g_{f_0} \pi\pi = 4.21 \pm 0.25 \pm 0.21$.
 13 K-matrix pole from combined analysis of $\pi^-p \rightarrow \pi^0\pi^0 n, \pi^-p \rightarrow K \bar{K} n, \pi^+\pi^- \rightarrow \pi^+\pi^-, \bar{p}p \rightarrow \pi^0\pi^0\pi^0, \pi^0\eta\eta, \pi^0\pi^0\eta, \pi^+\pi^-\pi^0, K^+K^-\pi^0, K_S^0 K_S^0 \pi^0, K^+K_S^0 \pi^-$ at rest, $\bar{p}n \rightarrow \pi^-\pi^-\pi^+, K_S^0 K^-\pi^0, K_S^0 K_S^0 \pi^-$ at rest.
 14 From the negative interference with the $f_0(500)$ meson of AITALA 01B using the ACHASOV 89 parameterization for the $f_0(980)$, a Breit-Wigner for the $f_0(500)$, and ACHASOV 01F for the $\rho\pi$ contribution.
 15 Coupled-channel Breit-Wigner, couplings $g_\pi = 0.09 \pm 0.01 \pm 0.01, g_K = 0.02 \pm 0.04 \pm 0.03$.
 16 Supersedes ACHASOV 98i. Using the model of ACHASOV 89.
 17 Supersedes ACHASOV 98i.
 18 In the "narrow resonance" approximation.
 19 Assuming $\Gamma(f_0) = 40$ MeV.
 20 From a narrow pole fit taking into account $f_0(980)$ and $f_0(1200)$ intermediate mechanisms.
 21 From the combined fit of the photon spectra in the reactions $e^+e^- \rightarrow \pi^+\pi^-\gamma, \pi^0\pi^0\gamma$.
 22 Supersedes BARBERIS 99 and BARBERIS 99B
 23 T-matrix pole.
 24 From invariant mass fit.
 25 On sheet II in a 2 pole solution. The other pole is found on sheet III at (1039–93i) MeV.
 26 On sheet II in a 2 pole solution. The other pole is found on sheet III at (963–29i) MeV.
 27 Reanalysis of data from HYAMS 73, GRAYR 74, SRINIVASAN 75, and ROSSELET 77 using the interfering amplitude method.
 28 At high $|t|$.
 29 At low $|t|$.
 30 On sheet II in a 4-pole solution, the other poles are found on sheet III at (953–55i) MeV and on sheet IV at (938–35i) MeV.
 31 Combined fit of ALDE 95B, ANISOVICH 94, AMSLER 94D.
 32 On sheet II in a 2 pole solution. The other pole is found on sheet III at (996–103i) MeV.
 33 From sheet II pole position.
 34 On sheet II in a 2 pole solution. The other pole is found on sheet III at (797–185i) MeV and can be interpreted as a shadow pole.
 35 On sheet II in a 2 pole solution. The other pole is found on sheet III at (978–28i) MeV.
 36 From coupled channel analysis.
 37 Coupled channel analysis with finite width corrections.
 38 Included in AGUILAR-BENITEZ 78 fit.

$f_0(980)$ WIDTH

Width determination very model dependent. Peak width in $\pi\pi$ is about 50 MeV, but decay width can be much larger.

VALUE (MeV)	EVTs	DOCUMENT ID	TECN	COMMENT
10 to 100 OUR ESTIMATE				
• • • We do not use the following data for averages, fits, limits, etc. • • •				
15.3 ± 4.7	424	ABLIKIM	15P BES3	$J/\psi \rightarrow K^+K^-3\pi$
9.5 ± 1.1	706	ABLIKIM	12E BES3	$J/\psi \rightarrow \gamma 3\pi$
$91^{+30}_{-22} \pm 3$	44	1 ECKLUND	09 CLEO	$4.17 e^+e^- \rightarrow D_S^- D_S^{*+} + c.c.$

1 Using a relativistic Breit-Wigner function and taking into account the finite D_S mass.
 2 Breit-Wigner $\pi\pi$ width. Using finite width corrections according to FLATTE 76 and ACHASOV 05, and the ratio $g_{f_0} K K / g_{f_0} \pi\pi = 0$.
 3 Systematic errors not estimated.
 4 Breit-Wigner $\pi\pi$ width. Using finite width corrections according to FLATTE 76 and ACHASOV 05, and the ratio $g_{f_0} K K / g_{f_0} \pi\pi = 4.21 \pm 0.25 \pm 0.21$ from ABLIKIM 05.
 5 Breit-Wigner, solution 1, PWA ambiguous.
 6 K-matrix pole from combined analysis of $\pi^-p \rightarrow \pi^0\pi^0 n, \pi^-p \rightarrow K \bar{K} n, \pi^+\pi^- \rightarrow \pi^+\pi^-, \bar{p}p \rightarrow \pi^0\pi^0\pi^0, \pi^0\eta\eta, \pi^0\pi^0\eta, \pi^+\pi^-\pi^0, K^+K^-\pi^0, K_S^0 K_S^0 \pi^0, K^+K_S^0 \pi^-$ at rest, $\bar{p}n \rightarrow \pi^-\pi^-\pi^+, K_S^0 K^-\pi^0, K_S^0 K_S^0 \pi^-$ at rest.
 7 Using the data of AKHMETSHIN 99C, ACHASOV 00H, and ALOISIO 02D.
 8 Breit-Wigner width.
 9 Supersedes ACHASOV 98i. Using the model of ACHASOV 89.
 10 Supersedes ACHASOV 98i.
 11 In the "narrow resonance" approximation.
 12 From the combined fit of the photon spectra in the reactions $e^+e^- \rightarrow \pi^+\pi^-\gamma, \pi^0\pi^0\gamma$.

- ¹³Supersedes BARBERIS 99 and BARBERIS 99b
- ¹⁴T-matrix pole.
- ¹⁵On sheet II in a 2 pole solution. The other pole is found on sheet III at (1039–93i) MeV.
- ¹⁶From invariant mass fit.
- ¹⁷On sheet II in a 2 pole solution. The other pole is found on sheet III at (963–29i) MeV.
- ¹⁸Reanalysis of data from HYAMS 73, GRAYER 74, SRINIVASAN 75, and ROSSELET 77 using the interfering amplitude method.
- ¹⁹At high |t|.
- ²⁰At low |t|.
- ²¹On sheet II in a 4-pole solution, the other poles are found on sheet III at (953–55i) MeV and on sheet IV at (938–35i) MeV.
- ²²Combined fit of ALDE 95b, ANISOVICH 94,
- ²³On sheet II in a 2 pole solution. The other pole is found on sheet III at (996–103i) MeV.
- ²⁴From sheet II pole position.
- ²⁵On sheet II in a 2 pole solution. The other pole is found on sheet III at (797–185i) MeV and can be interpreted as a shadow pole.
- ²⁶On sheet II in a 2 pole solution. The other pole is found on sheet III at (978–28i) MeV.
- ²⁷From coupled channel analysis.
- ²⁸Coupled channel analysis with finite width corrections.
- ²⁹From coupled channel fit to the HYAMS 73 and PROTOPOESCU 73 data. With a simultaneous fit to the ππ phase-shifts, inelasticity and to the K_S⁰ K_S⁰ invariant mass.
- ³⁰Included in AGUILAR-BENITEZ 78 fit.

f₀(980) DECAY MODES

Mode	Fraction (Γ _i /Γ)
Γ ₁ ππ	seen
Γ ₂ K \bar{K}	seen
Γ ₃ γγ	seen
Γ ₄ e ⁺ e ⁻	

f₀(980) PARTIAL WIDTHS

Γ(γ)	VALUE (keV)	DOCUMENT ID	TECN	COMMENT	Γ ₃	
	0.29 -0.06	OUR AVERAGE				
	0.286 ± 0.017 ± 0.211 -0.070	1 UEHARA	08A	BELL	10.6 e ⁺ e ⁻ → e ⁺ e ⁻ π ⁰ π ⁰	
	0.205 ± 0.095 ± 0.147 -0.083 -0.117	2 MORI	07	BELL	10.6 e ⁺ e ⁻ → e ⁺ e ⁻ π ⁺ π ⁻	
	0.42 ± 0.06 ± 0.18	3 OEST	90	JADE	e ⁺ e ⁻ → e ⁺ e ⁻ π ⁰ π ⁰	
	0.32 ± 0.05	4 DAI	14A	RVUE	Compilation	
	0.16 ± 0.01	5 MENNESSIER	11	RVUE		
	0.29 ± 0.21 ± 0.02 -0.07	6 MOUSSALLAM	11	RVUE	Compilation	
	0.42	7,8 PENNINGTON	08	RVUE	Compilation	
	0.10	8,9 PENNINGTON	08	RVUE	Compilation	
	0.28 ± 0.09 -0.13	10 BOGLIONE	99	RVUE	γγ → π ⁺ π ⁻ , π ⁰ π ⁰	
	0.29 ± 0.07 ± 0.12	11,12 BOYER	90	MRK2	e ⁺ e ⁻ → e ⁺ e ⁻ π ⁺ π ⁻	
	0.31 ± 0.14 ± 0.09	11,12 MARSISKE	90	CBAL	e ⁺ e ⁻ → e ⁺ e ⁻ π ⁰ π ⁰	
	0.63 ± 0.14	13 MORGAN	90	RVUE	γγ → π ⁺ π ⁻ , π ⁰ π ⁰	

- ¹Using finite width corrections according to FLATTE 76 and ACHASOV 05, and the ratio g_{f₀} K K / g_{f₀} π π = 0.
- ²Using finite width corrections according to FLATTE 76 and ACHASOV 05, and the ratio g_{f₀} K K / g_{f₀} π π = 4.21 ± 0.25 ± 0.21 from ABLIKIM 05.
- ³OEST 90 quote systematic errors ± 0.08, ± 0.18. We use ± 0.18. Observed 60 events.
- ⁴Using dispersive analysis with phases from GARCIA-MARTIN 11A and BUETTIKER 04 as input.
- ⁵Uses an analytic K-matrix model. Compilation.
- ⁶Using dispersion integral with phase input from Roy equations and data from MARSISKE 90, BOYER 90, BEHREND 92, UEHARA 08A, and MORI 07.
- ⁷Solution A (preferred solution based on χ²-analysis).
- ⁸Dispersion theory based amplitude analysis of BOYER 90, MARSISKE 90, BEHREND 92, and MORI 07.
- ⁹Solution B (worse than solution A; still acceptable when systematic uncertainties are included).
- ¹⁰Supersedes MORGAN 90.
- ¹¹From analysis allowing arbitrary background unconstrained by unitarity.
- ¹²Data included in MORGAN 90, BOGLIONE 99 analyses.
- ¹³From amplitude analysis of BOYER 90 and MARSISKE 90, data corresponds to resonance parameters m = 989 MeV, Γ = 61 MeV.

Γ(e ⁺ e ⁻)	VALUE (eV)	CL%	DOCUMENT ID	TECN	COMMENT	Γ ₄
	<8.4	90	VOROBYEV	88	ND	e ⁺ e ⁻ → π ⁰ π ⁰

f₀(980) BRANCHING RATIOS

Γ(ππ) / [Γ(ππ) + Γ(K \bar{K})]	VALUE	EVTS	DOCUMENT ID	TECN	COMMENT	Γ ₁ / (Γ ₁ + Γ ₂)
	0.52 ± 0.12	9.9k	1 AUBERT	06o	BABR	B [±] → K [±] π [±] π [∓]
	0.75 ± 0.11 -0.13		2 ABLIKIM	05q	BES2	χ _{C0} → 2π ⁺ 2π ⁻ , π ⁺ π ⁻ K ⁺ K ⁻

- 0.84 ± 0.02
- ~ 0.68
- 0.67 ± 0.09
- 0.81 ± 0.09
-0.04
- 0.78 ± 0.03

- ³ANISOVICH 02b SPEC Combined fit
- OLLER 99b RVUE ππ → ππ, K \bar{K}
- ⁴LOVERRE 80 HBC 4 π⁻p → n2K_S⁰
- ⁴CASON 78 STRC 7 π⁻p → n2K_S⁰
- ⁴WETZEL 76 OSPK 8.9 π⁻p → n2K_S⁰

f₀(980) REFERENCES

SARANTSEV 21 PL B816 136227 A.V. Sarantsev et al. (BONN, PNPI)

ALBRECHT 20 EPJ C80 453 M. Albrecht et al. (Crystal Barrel Collab.)

AAJ 19H JHEP 1904 063 R. Aaij et al. (LHCb Collab.)

AOUDE 18 PR D98 056021 R.T. Aoude et al.

ABLIKIM 15P PR D92 012007 M. Ablikim et al. (BESIII Collab.)

DAI 14A PR D90 036004 L.-Y. Dai, M.R. Pennington (CEBAF)

ABLIKIM 12E PRL 108 182001 M. Ablikim et al. (BESIII Collab.)

GARCIA-MAR. 11A PRL 107 072001 R. Garcia-Martin et al. (MADR, CRAC)

GARCIA-MAR. 11A PR D83 074004 R. Garcia-Martin et al. (MADR, CRAC)

MENNESSIER 11 PL B696 40 G. Mennessier, S. Narison, X.-G. Wang

MOUSSALLAM 11 EPJ C71 1814 B. Moussallam

BATLEY 10C EPJ C70 635 J.R. Batley et al. (CERN NA48/2 Collab.)

MENNESSIER 10 PL B688 59 G. Mennessier, S. Narison, X.-G. Wang

ANISOVICH 09 IJMP A24 2481 V.V. Anisovich, A.V. Sarantsev

ECKLUND 09 PR D80 052009 K.M. Ecklund et al. (CLEO Collab.)

BATLEY 08A EPJ C54 411 J.R. Batley et al. (CERN NA48/2 Collab.)

PENNINGTON 08 EPJ C56 1 M.R. Pennington et al.

UEHARA 08A PR D78 052004 S. Uehara et al. (BELLE Collab.)

AMBROSINO 07 EPJ C19 473 F. Ambrosino et al. (KLOE Collab.)

AUBERT 07AK PR D76 012008 B. Aubert et al. (BABAR Collab.)

BONVICINI 07 PR D76 012001 G. Bonvicini et al. (CLEO Collab.)

MORI 07 PR D75 051101 T. Mori et al. (BELLE Collab.)

AMBROSINO 06B PL B634 148 F. Ambrosino et al. (KLOE Collab.)

AUBERT 06O PR D74 032003 B. Aubert et al. (BABAR Collab.)

GARMASH 06 PRL 96 251803 A. Garmash et al. (BELLE Collab.)

ABLIKIM 05 PL B607 243 M. Ablikim et al. (BES Collab.)

ABLIKIM 05Q PR D72 092002 M. Ablikim et al. (BES Collab.)

ACHASOV 05 PR D72 013006 N.N. Achasov, G.N. Shestakov

GARMASH 05 PR D71 092003 A. Garmash et al. (BELLE Collab.)

ABLIKIM 04G PR D70 022002 M. Ablikim et al. (BES Collab.)

BUETTIKER 04 EPJ C33 409 P. Buettiker, S. Descotes-Genon, B. Moussallam

PELAEZ 04A MPL A19 2879 J.R. Pelaez

ANISOVICH 03 EPJ A16 229 V.V. Anisovich et al. (MADU)

TIKHOMIROV 03 PAN 66 828 G.D. Tikhomirov et al.

Translated from YAF 66 860.

ALOISIO 02D PL B537 21 A. Aloisio et al. (KLOE Collab.)

ANISOVICH 02D PAN 65 1545 V.V. Anisovich et al.

Translated from YAF 65 1583.

BRAMON 02 EPJ C26 253 A. Bramon et al.

ACHASOV 01F PR D63 094007 N.N. Achasov, V.V. Gubin (Novosibirsk SND Collab.)

AITALA 01A PRL 86 765 E.M. Aitala et al. (FNAL E791 Collab.)

AITALA 01B PRL 86 770 E.M. Aitala et al. (FNAL E791 Collab.)

ACHASOV 00B PL B485 349 M.N. Achasov et al. (Novosibirsk SND Collab.)

AKHMETSHIN 99H PL B462 371 R.R. Akhmetshin et al. (Novosibirsk CMD-2 Collab.)

AKHMETSHIN 99C PL B462 380 R.R. Akhmetshin et al. (Novosibirsk CMD-2 Collab.)

BARBERIS 99 PL B453 305 D. Barberis et al. (Omega Expt.)

BARBERIS 99B PL B453 316 D. Barberis et al. (Omega Expt.)

BARBERIS 99C PL B453 325 D. Barberis et al. (Omega Expt.)

BARBERIS 99D PL B462 462 D. Barberis et al. (Omega Expt.)

BELLAZZINI 99 PL B467 296 R. Bellazzini et al.

BOGLIONE 99 EPJ C9 11 M. Boglione, M.R. Pennington

KAMINSKI 99 EPJ C9 141 R. Kaminski, L. Lesniak, B. Loiseau (CRAC, PARIN)

OLLER 99 PR D60 099906 (erratum) J.A. Oller et al.

OLLER 99B NP A652 407 (erratum) J.A. Oller, E. Oset

OLLER 99C PR D60 074023 J.A. Oller, E. Oset

ACHASOV 98Q PL B440 442 M.N. Achasov et al.

ACKERSTAFF 98 EPJ C4 19 K. Ackerstaff et al. (OPAL Collab.)

ALDE 98 EPJ A3 361 D. Alde et al. (GAM4 Collab.)

Also PAN 62 405 D. Alde et al. (GAMS Collab.)

Translated from YAF 62 446.

ANISOVICH 98B SPU 41 419 V.V. Anisovich et al.

Translated from UFN 168 481.

LOCHER 98 EPJ C4 317 M.P. Locher et al. (PSI)

ALDE 97 PL B397 350 D.M. Alde et al. (GAMS Collab.)

BERTIN 97C PL B408 476 A. Bertin et al. (OBELIX Collab.)

ISHIDA 96 PTP 95 745 S. Ishida et al. (TOKY, MIYA, KEK)

TORNQVIST 96 PRL 76 1575 N.A. Tornqvist, M. Roos (HEL)

ALDE 95B ZPHY C66 375 D.M. Alde et al. (GAMS Collab.)

AMSLER 95B PL B342 433 C. Amstler et al. (Crystal Barrel Collab.)

AMSLER 95D PL B355 425 C. Amstler et al. (Crystal Barrel Collab.)

ANISOVICH 95 PL B355 363 V.V. Anisovich et al. (PNPI, SERP)

JANSEN 95 PR D52 2690 G. Janssen et al. (STON, ADDL, JULI)

AMSLER 94D PL B333 277 C. Amstler et al. (Crystal Barrel Collab.)

ANISOVICH 94 PL B323 233 V.V. Anisovich et al. (Crystal Barrel Collab.)

BUGG 94 PR D50 4412 D.V. Bugg et al. (LOQM)

KAMINSKI 94 PR D50 3145 R. Kaminski, L. Lesniak, J.P. Maillet (CRAC+)

ZOU 94B PR D50 591 B.S. Zou, D.V. Bugg (LOQM)

MORGAN 93 PR D48 1185 D. Morgan, M.R. Pennington (RAL, DURH)

BEHREND 92 ZPHY C56 381 H.J. Behrend et al. (CELLC Collab.)

AGUILAR... 91 ZPHY C50 405 M. Aguilar-Benitez et al. (LEBC-EHS Collab.)

ARMSTRONG 91 ZPHY C51 351 T.A. Armstrong et al. (ATHU, BARI, BIRM+)

BOYER 90 PR D42 1350 J. Boyer et al. (Mark II Collab.)

BREAKSTONE 90 ZPHY C48 569 A.M. Breakstone et al. (ISU, BGNA, CERN+)

MARSISKE 90 PR D41 3324 H. Marsiske et al. (Crystal Ball Collab.)

MORGAN 90 ZPHY C48 623 D. Morgan, M.R. Pennington (RAL, DURH)

OEST 90 ZPHY C47 343 T. Oest et al. (JADE Collab.)

ACHASOV 89 NP B315 465 N.N. Achasov, V.N. Ivanchenko

AUGUSTIN 89 NP B320 1 J.E. Augustin, G. Cosme (DM2 Collab.)

VOROBYEV 88 SJP 48 273 P.V. Vorobyev et al. (NOVO)

Translated from YAF 48 436.

ABACHI 86B PRL 57 1990 S. Abachi et al. (PURD, ANL, IND, MICH+)

LONGACRE 86 PL B177 223 R.S. Longacre et al. (BNL, BRAN, CUNY+)

BINON 84C NC 80A 363 F.G. Binon et al. (BELG, LAPP, SERP+)

BINON 83 NC 78A 313 F.G. Binon et al. (BELG, LAPP, SERP+)

ETKIN 82B PR D25 1786 A. Etkin et al. (BNL, CUNY, TUFTS, VAND)

GIDAL 81 PL 107B 153 G. Gidal et al. (SLAC, LBL)

ACHASOV 80 SJP 32 566 N.N. Achasov, S.A. Devyanin, G.N. Shestakov (NOVM)

Translated from YAF 32 109B.

Meson Particle Listings

$f_0(980)$, $a_0(980)$

COHEN	80	PR D22 2595	D. Cohen <i>et al.</i>	(ANL)JUP
LOVERRE	80	ZPHY C6 187	P.F. Loverre <i>et al.</i>	(CERN, CDEF, MADR+)JUP
AGUILAR...	78	NP B140 73	M. Aguilar-Benitez <i>et al.</i>	(MADR, BOMB+)
CASON	78	PRL 41 271	N.M. Cason <i>et al.</i>	(NDAM, ANL)
LEEPER	77	PR D16 2054	R.J. Leeper <i>et al.</i>	(ISU)
ROSSELET	77	PR D15 574	L. Rosselet <i>et al.</i>	(GEVA, SAEL)
FLATTE	76	PL 63B 224	S.M. Flatte	(CERN)
WETZEL	76	NP B115 208	W. Wetzel <i>et al.</i>	(ETH, CERN, LOIC)
HYAMS	75	NP B100 205	B.D. Hyams <i>et al.</i>	(CERN, MPIM)
SRINIVASAN	75	PR D12 681	V. Srinivasan <i>et al.</i>	(NDAM, ANL)
ESTABROOKS	74	NP B79 301	P.G. Estabrooks, A.D. Martin	(DURH)
GRAYER	74	NP B75 189	G. Grayer <i>et al.</i>	(CERN, MPIM)
BINNIE	73	PRL 31 1534	D.M. Binnie <i>et al.</i>	(LOIC, SHMP)
GRAYER	73	Tallahassee	G. Grayer <i>et al.</i>	(CERN, MPIM)
HYAMS	73	NP B64 134	B.D. Hyams <i>et al.</i>	(CERN, MPIM)
PROTOPOP...	73	PR D7 1279	S.D. Protopopescu <i>et al.</i>	(LBL)

$a_0(980)$

$$I^G(JPC) = 1^-(0^{++})$$

See the related review(s):
[Scalar Mesons below 1 GeV](#)

$a_0(980)$ T-MATRIX POLE \sqrt{s}

VALUE (MeV)	DOCUMENT ID	TECN	COMMENT
(960-1030) - i (20-70) OUR ESTIMATE (see Fig. 64.2 in the review)			
• • • We do not use the following data for averages, fits, limits, etc. • • •			
$(989 \pm 5) - i(40 \pm 5)$	¹ BUGG	08A	RVUE $\bar{p}p$ annihilation data
$(1117 \pm 24) - i(12 \pm 43)$	² PELAEZ	04A	RVUE $\pi\pi \rightarrow \pi\pi, \pi K \rightarrow \pi K$
$(982 \pm 3) - i(46 \pm 4)$	³ ABELE	98	CBAR $0.0 \bar{p}p \rightarrow K_L^0 K_S^0 \pi^\mp$
¹ T-matrix pole on sheet II. Parameterizes couplings to $\bar{K}K$, $\pi\eta$, and $\pi\eta'$. Uses AMSLER 94D and ABELE 98.			
² Reanalysis of data from LINGLIN 73, ESTABROOKS 78, and ASTON 88 in the unitarized ChPT model.			
³ T-matrix pole on sheet II; the pole on sheet III is at (1006 - i 49) MeV.			

$a_0(980)$ MASS

VALUE (MeV)	DOCUMENT ID	TECN	COMMENT
980 \pm 20 OUR ESTIMATE Mass determination very model dependent			
• • • We do not use the following data for averages, fits, limits, etc. • • •			
$1000.7 \pm 12.9 - 0.7$	¹ LU	20	RVUE $\gamma\gamma \rightarrow \pi^0\eta, K_S^0 K_S^0$
¹ T-matrix pole on sheet II.			

$\eta\pi$ FINAL STATE ONLY

VALUE (MeV)	EVTS	DOCUMENT ID	TECN	CHG	COMMENT
• • • We do not use the following data for averages, fits, limits, etc. • • •					
$1004.1 \pm 1.5 \pm 6.5$		¹ ALBRECHT	20	CBAR	$0.9 \bar{p}p \rightarrow \pi^0\pi^0\eta, \pi^0\eta\eta, \pi^0 K^+ K^-$
$982.5 \pm 1.6 \pm 1.1$	16.9k	² AMBROSINO	09F	KLOE	$1.02 e^+e^- \rightarrow \eta\pi^0\gamma$
986 ± 4		³ ANISOVICH	09	RVUE	$0.0 \bar{p}p, \pi N$
$982.3 \pm 0.6 \pm 3.1 - 0.7 - 4.7$		³ UEHARA	09A	BELL	$\gamma\gamma \rightarrow \pi^0\eta$
$985 \pm 4 \pm 6$	318	ACHARD	02B	L3	$183-209 e^+e^- \rightarrow e^+e^-\eta\pi^+\pi^-$
$995 \pm 52 - 10$	36	⁴ ACHASOV	00F	SND	$e^+e^- \rightarrow \eta\pi^0\gamma$
$994 \pm 33 - 8$	36	⁵ ACHASOV	00F	SND	$e^+e^- \rightarrow \eta\pi^0\gamma$
975 ± 7		BARBERIS	00H		$450 pp \rightarrow p_f\eta\pi^0 p_S$
988 ± 8		BARBERIS	00H		$450 pp \rightarrow \Delta_f^{++}\eta\pi^- p_S$
~ 1055		⁶ OLLER	99	RVUE	$\eta\pi, K\bar{K}$
~ 1009.2		⁶ OLLER	99B	RVUE	$\pi\pi \rightarrow \pi\pi, K\bar{K}$
993.1 ± 2.1		⁷ TEIGE	99	B852	$18.3 \pi^- p \rightarrow \eta\pi^+\pi^- n$
988 ± 6		⁶ ANISOVICH	98B	RVUE	Compilation
987		TORNQVIST	96	RVUE	$\pi\pi \rightarrow \pi\pi, K\bar{K}, K\pi,$
991		JANSSSEN	95	RVUE	$\eta\pi \rightarrow \eta\pi, K\bar{K}, K\pi,$
$984.45 \pm 1.23 \pm 0.34$		AMSLER	94C	CBAR	$0.0 \bar{p}p \rightarrow \omega\eta\pi^0$
982 ± 2		⁸ AMSLER	92	CBAR	$0.0 \bar{p}p \rightarrow \eta\eta\pi^0$
984 ± 4	1040	⁸ ARMSTRONG	91B	OMEG \pm	$300 pp \rightarrow pp\eta\pi^+\pi^-$
976 ± 6		ATKINSON	84E	OMEG \pm	$25-55 \gamma p \rightarrow \eta\pi n$
986 ± 3	500	⁹ EVANGELIS...	81	OMEG \pm	$12 \pi^- p \rightarrow \eta\pi^+\pi^-\pi^- p$
990 ± 7	145	⁹ GURTU	79	HBC \pm	$4.2 K^- p \rightarrow \Lambda\eta 2\pi$
980 ± 11	47	CONFORTO	78	OSPK -	$4.5 \pi^- p \rightarrow pX^-$
978 ± 16	50	CORDEN	78	OMEG \pm	$12-15 \pi^- p \rightarrow n\eta 2\pi$
977 ± 7		GRASSLER	77	HBC -	$16 \pi^\mp p \rightarrow p\eta 3\pi$
989 ± 4	70	WELLS	75	HBC -	$3.1-6 K^- p \rightarrow \Lambda\eta 2\pi$
972 ± 10	150	DEFOIX	72	HBC \pm	$0.7 \bar{p}p \rightarrow 7\pi$
970 ± 15	20	BARNES	69C	HBC -	$4-5 K^- p \rightarrow \Lambda\eta 2\pi$
980 ± 10		CAMPBELL	69	DBC \pm	$2.7 \pi^+ d$
980 ± 10	15	MILLER	69B	HBC -	$4.5 K^- N \rightarrow \eta\pi\Lambda$
980 ± 10	30	AMMAR	68	HBC \pm	$5.5 K^- p \rightarrow \Lambda\eta 2\pi$
¹ T-matrix pole with 2 poles, 2 channels, pole mass on adjacent sheet $1002.4 \pm 1.4 \pm 6.6$ MeV.					

- ²Using the model of ACHASOV 89 and ACHASOV 03B.
- ³From a fit with the S-wave amplitude including two interfering Breit-Wigners plus a background term.
- ⁴Using the model of ACHASOV 89. Supersedes ACHASOV 98B.
- ⁵Using the model of JAFFE 77. Supersedes ACHASOV 98B.
- ⁶T-matrix pole.
- ⁷Breit-Wigner fit, average between a_0^\pm and a_0^0 . The fit favors a slightly heavier a_0^\pm .
- ⁸From a single Breit-Wigner fit.
- ⁹From $f_1(1285)$ decay.

$K\bar{K}$ ONLY

VALUE (MeV)	EVTS	DOCUMENT ID	TECN	COMMENT
• • • We do not use the following data for averages, fits, limits, etc. • • •				
$947.7 \pm 5.5 - 5.0 \pm 6.6$		¹ AAIJ	19H	LHCB $p\bar{p} \rightarrow D^\pm X$
$925 \pm 5 \pm 8$	190k	² AAIJ	16N	LHCB $D^0 \rightarrow K_S^0 K^\pm \pi^\mp$
~ 1053		³ OLLER	99C	RVUE $\pi\pi \rightarrow \pi\pi, K\bar{K}$
975 ± 15		BERTIN	98B	OBLX $0.0 \bar{p}p \rightarrow K^\pm K_S^0 \pi^\mp$
970 ± 10	316	DEBILLY	80	HBC $1.2-2 \bar{p}p \rightarrow f_1(1285)\omega$
1016 ± 10	100	⁴ ASTIER	67	HBC $0.0 \bar{p}p$
1003.3 ± 7.0	143	^{5,6} ROSENFELD	65	RVUE

- ¹From the $D^\pm \rightarrow K^\pm K^+ K^-$ Dalitz plot fit with the Triple-M amplitude in the multi-meson model of AOUDE 18.
- ²Using a two-channel resonance parametrization with couplings fixed to ABELE 98.
- ³T-matrix pole.
- ⁴ASTIER 67 includes data of BARLOW 67, CONFORTO 67, ARMENTEROS 65.
- ⁵Note on J^P . Main argument for 0^+ is small Q value. Isotropy of decay distribution in $(\bar{p}p)$ at rest proves nothing. See discussion by Rosenfeld (Oxford) and Butterworth (Heidelberg).
- ⁶Plus systematic errors.

$a_0(980)$ WIDTH

VALUE (MeV)	EVTS	DOCUMENT ID	TECN	CHG	COMMENT
50 to 100 OUR ESTIMATE Width determination very model dependent. Peak width in $\eta\pi$ is about 60 MeV, but decay width can be much larger.					
• • • We do not use the following data for averages, fits, limits, etc. • • •					
$97.2 \pm 1.9 \pm 5.7$		¹ ALBRECHT	20	CBAR	$0.9 \bar{p}p \rightarrow \pi^0\pi^0\eta, \pi^0\eta\eta, \pi^0 K^+ K^-$
$73.2 \pm 25.4 - 5.2$		² LU	20	RVUE	$\gamma\gamma \rightarrow \pi^0\eta, K_S^0 K_S^0$
$75.6 \pm 1.6 \pm 17.4 - 10.0$		³ UEHARA	09A	BELL	$\gamma\gamma \rightarrow \pi^0\eta$
$50 \pm 13 \pm 4$	318	ACHARD	02B	L3	$183-209 e^+e^- \rightarrow e^+e^-\eta\pi^+\pi^-$
72 ± 16		BARBERIS	00H		$450 pp \rightarrow p_f\eta\pi^0 p_S$
61 ± 19		BARBERIS	00H		$450 pp \rightarrow \Delta_f^{++}\eta\pi^- p_S$
~ 42		⁴ OLLER	99	RVUE	$\eta\pi, K\bar{K}$
~ 112		⁴ OLLER	99B	RVUE	$\pi\pi \rightarrow \pi\pi, K\bar{K}$
71 ± 7		TEIGE	99	B852	$18.3 \pi^- p \rightarrow \eta\pi^+\pi^- n$
92 ± 20		⁴ ANISOVICH	98B	RVUE	Compilation
65 ± 10		⁵ BERTIN	98B	OBLX \pm	$0.0 \bar{p}p \rightarrow K^\pm K_S^0 \pi^\mp$
~ 100		TORNQVIST	96	RVUE	$\pi\pi \rightarrow \pi\pi, K\bar{K}, K\pi,$
202		JANSSSEN	95	RVUE	$\eta\pi \rightarrow \eta\pi, K\bar{K}, K\pi,$
$54.12 \pm 0.34 \pm 0.12$		AMSLER	94C	CBAR	$0.0 \bar{p}p \rightarrow \omega\eta\pi^0$
54 ± 10		⁶ AMSLER	92	CBAR	$0.0 \bar{p}p \rightarrow \eta\eta\pi^0$
95 ± 14	1040	⁶ ARMSTRONG	91B	OMEG \pm	$300 pp \rightarrow pp\eta\pi^+\pi^-$
62 ± 15	500	⁷ EVANGELIS...	81	OMEG \pm	$12 \pi^- p \rightarrow \eta\pi^+\pi^-\pi^- p$
60 ± 20	145	⁷ GURTU	79	HBC \pm	$4.2 K^- p \rightarrow \Lambda\eta 2\pi$
$60 \pm 50 - 30$	47	CONFORTO	78	OSPK -	$4.5 \pi^- p \rightarrow pX^-$
$86.0 \pm 60.0 - 50.0$	50	CORDEN	78	OMEG \pm	$12-15 \pi^- p \rightarrow n\eta 2\pi$
44 ± 22		GRASSLER	77	HBC -	$16 \pi^\mp p \rightarrow p\eta 3\pi$
80 ± 300		⁸ FLATTE	76	RVUE -	$4.2 K^- p \rightarrow \Lambda\eta 2\pi$
$16.0 \pm 25.0 - 16.0$	70	⁹ WELLS	75	HBC -	$3.1-6 K^- p \rightarrow \Lambda\eta 2\pi$
30 ± 5	150	¹⁰ DEFOIX	72	HBC \pm	$0.7 \bar{p}p \rightarrow 7\pi$
40 ± 15		CAMPBELL	69	DBC \pm	$2.7 \pi^+ d$
60 ± 30	15	MILLER	69B	HBC -	$4.5 K^- N \rightarrow \eta\pi\Lambda$
80 ± 30	30	AMMAR	68	HBC \pm	$5.5 K^- p \rightarrow \Lambda\eta 2\pi$

- ¹T-matrix pole with 2 poles, 2 channels, pole width on adjacent sheet $127.0 \pm 2.3 \pm 6.7$ MeV.
- ²T-matrix pole on sheet II.
- ³From a fit with the S-wave amplitude including two interfering Breit-Wigners plus a background term.
- ⁴T-matrix pole.
- ⁵The $\eta\pi$ width.
- ⁶From a single Breit-Wigner fit.
- ⁷From $f_1(1285)$ decay.
- ⁸Using a two-channel resonance parametrization of GAY 76B data.
- ⁹Weak evidence only for $a_0(980)^+$ production.
- ¹⁰This number has very little meaning. Error is much too small. Vlada

See key on page 1127

Meson Particle Listings

a₀(980), ϕ(1020)

K \bar{K} ONLY

Table with columns: VALUE (MeV), EVTS, DOCUMENT ID, TECN, CHG, COMMENT. Contains data for K \bar{K} decays and a list of references.

a₀(980) DECAY MODES

Table with columns: Mode, Fraction (Γ_i/Γ). Lists decay modes like ηπ, K \bar{K} , η'π, ρπ, γγ, e⁺e⁻ and their fractions.

a₀(980) PARTIAL WIDTHS

Table with columns: Γ(γγ), VALUE (keV), DOCUMENT ID, TECN, COMMENT. Includes Γ₅ and Γ₆ labels. Lists partial widths for γγ decays.

a₀(980) Γ(i)Γ(γγ)/Γ(total)

Table with columns: Γ(ηπ) × Γ(γγ)/Γtotal, VALUE (keV), EVTS, DOCUMENT ID, TECN, COMMENT, Γ₁Γ₅/Γ. Lists ratios of partial widths.

Table with columns: Γ(ηπ) × Γ(e⁺e⁻)/Γtotal, VALUE (eV), CL%, DOCUMENT ID, TECN, COMMENT, Γ₁Γ₆/Γ. Lists ratios of partial widths.

a₀(980) BRANCHING RATIOS

Table with columns: Γ(K \bar{K})/Γ(ηπ), VALUE, DOCUMENT ID, TECN, CHG, COMMENT, Γ₂/Γ₁. Lists branching ratios for K \bar{K} decays.

Table with columns: Γ(η'π)/Γtotal, VALUE, EVTS, DOCUMENT ID, TECN, COMMENT, Γ₃/Γ. Lists ratios of partial widths.

Table with columns: Γ(ρπ)/Γ(ηπ), VALUE, CL%, DOCUMENT ID, TECN, CHG, COMMENT, Γ₄/Γ₁. Lists ratios of partial widths.

a₀(980) REFERENCES

Large table of references for a₀(980) and ϕ(1020) decays, listing authors, document IDs, and techniques.

ϕ(1020)

I^{G(J^{PC})} = 0⁻(1⁻-)

ϕ(1020) MASS

Table with columns: VALUE (MeV), EVTS, DOCUMENT ID, TECN, COMMENT. Lists mass measurements for ϕ(1020) with various decay channels.

Meson Particle Listings

$\phi(1020)$

1019.21 ± 0.04 ± 0.03	10	HOID	20	RVUE	$e^+e^- \rightarrow \pi^0\gamma$
1019.54 ± 0.10 ± 0.51	11	AAIJ	19H	LHCB	$pp \rightarrow D^\pm X$
1019.20 ± 0.02 ± 0.01	12	HOFERICH...	19	RVUE	$e^+e^- \rightarrow \pi^+\pi^-\pi^0$
1019.469 ± 0.061	1.7M	KOZYREV	18	CMD3	$e^+e^- \rightarrow K^+K^-$
1019.457 ± 0.061	610k	KOZYREV	16	CMD3	$e^+e^- \rightarrow K_S^0 K_L^0$
1019.48 ± 0.01		LEES	13F	BABR	$D^+ \rightarrow K^+K^-\pi^+$
1019.441 ± 0.008 ± 0.080	542k	AKHMETS...	08	CMD2	$1.02 e^+e^- \rightarrow K^+K^-$
1019.63 ± 0.07	12540	AUBERT,B	05J	BABR	$D^0 \rightarrow \bar{K}^0 K^+ K^-$
1019.8 ± 0.7		ARMSTRONG	86	OMEG	$85 \pi^+ / pp \rightarrow \pi^+ / p 4 K p$
1020.1 ± 0.11	5526	ATKINSON	86	OMEG	20-70 γp
1019.7 ± 1.0		BEBEK	86	CLEO	$e^+e^- \rightarrow \Upsilon(4S)$
1019.411 ± 0.008	642k	DIJKSTRA	86	SPEC	100-200 $\pi^\pm, \bar{p}, p, K^\pm$, on Be
1020.9 ± 0.2		FRAME	86	OMEG	13 $K^+p \rightarrow \phi K^+p$
1021.0 ± 0.2		ARMSTRONG	83b	OMEG	18.5 $K^-p \rightarrow K^-K^+\Lambda$
1020.0 ± 0.5		ARMSTRONG	83b	OMEG	18.5 $K^-p \rightarrow K^-K^+\Lambda$
1019.7 ± 0.3		BARATE	83	GOLI	190 $\pi^-Be \rightarrow 2\mu X$
1019.8 ± 0.2 ± 0.5	766	IVANOV	81	OLYA	1-1.4 $e^+e^- \rightarrow K^+K^-$
1019.4 ± 0.5	337	COOPER	78b	HBC	0.7-0.8 $\bar{p}p \rightarrow K_S^0 K_L^0 \pi^+\pi^-$
1020 ± 1	383	BALDI	77	CNTR	10 $\pi^-p \rightarrow \pi^- \phi p$
1018.9 ± 0.6	800	COHEN	77	ASPK	6 $\pi^\pm N \rightarrow K^+K^-N$
1019.7 ± 0.5	454	KALBFLEISCH	76	HBC	2.18 $K^-p \rightarrow \Lambda K \bar{K}$
1019.4 ± 0.8	984	BESCH	74	CNTR	2 $\gamma p \rightarrow p K^+ K^-$
1020.3 ± 0.4	100	BALLAM	73	HBC	2.8-9.3 γp
1019.4 ± 0.7		BINNIE	73b	CNTR	$\pi^-p \rightarrow \phi n$
1019.6 ± 0.5	120	AGUILAR...	72b	HBC	3.9, 4.6 $K^-p \rightarrow \Lambda K^+K^-$
1019.9 ± 0.5	100	AGUILAR...	72b	HBC	3.9, 4.6 $K^-p \rightarrow K^-p K^+K^-$
1020.4 ± 0.5	131	COLLEY	72	HBC	10 $K^+p \rightarrow K^+p \phi$
1019.9 ± 0.3	410	STOTTLE...	71	HBC	2.9 $K^-p \rightarrow \Sigma/\Lambda K \bar{K}$

1 Average of KOZYREV 16 and KOZYREV 18 values taking into account the correlated uncertainties. Supersedes individual KOZYREV 16 and KOZYREV 18 results.
 2 Using a vector meson dominance model with contribution from $\phi(1020)$ and higher mass excitations of $\rho(770)$, $\omega(782)$, and $\phi(1020)$.
 3 Using a phenomenological model based on KUHN 90 with a sum of Breit-Wigner resonances for $\rho(770)$, $\omega(782)$, $\phi(1020)$ and their higher mass excitations.
 4 Update of AKHMETS... 99d
 5 From the combined fit assuming that the total $\phi(1020)$ production cross section is saturated by those of K^+K^- , $K_S K_L$, $\pi^+\pi^-\pi^0$, and $\eta\gamma$ decays modes and using ACHASOV 00b for the $\eta\gamma$ decay mode.
 6 Using a total width of 4.43 ± 0.05 MeV. Systematic uncertainty included.
 7 Using a total width of 4.43 ± 0.05 MeV.
 8 PELLINEN 82 review includes AKERLOF 77, DAUM 81, BALDI 77, AYRES 74, DE-GROOT 74.
 9 Width fixed at 4.2 MeV.
 10 The values were extracted from a dispersively improved Breit-Wigner parameterization and do not include vacuum polarization. Inclusion of vacuum polarization gives 1019.457 ± 0.020 MeV.
 11 From the $D^\pm \rightarrow K^\pm K^+ K^-$ Dalitz plot fit with the Triple-M amplitude in the multi-meson model of AOUDE 18.
 12 The values were extracted from a dispersively improved Breit-Wigner parameterization and do not include vacuum polarization.
 13 Strongly correlated with AKHMETS... 04.
 14 Systematic errors not evaluated.
 15 Weighted and scaled average of 12 measurements of DIJKSTRA 86.
 16 Mass errors enlarged by us to Γ/\sqrt{N} ; see the note with the $K^*(892)$ mass.

$\phi(1020)$ WIDTH

VALUE (MeV)	EVTS	DOCUMENT ID	TECN	COMMENT
4.249 ± 0.013 OUR AVERAGE		Error includes scale factor of 1.1.		
4.245 ± 0.013	2.3M	1 KOZYREV	18	CMD3 $e^+e^- \rightarrow K^+K^-$, $K_S^0 K_L^0$
4.205 ± 0.103 ± 0.067	28k	2 LEES	14H	BABR $e^+e^- \rightarrow K_S^0 K_L^0 \gamma$
4.29 ± 0.04 ± 0.07		3 LEES	13Q	BABR $e^+e^- \rightarrow K^+K^-\gamma$
4.30 ± 0.06 ± 0.17	105k	4 AKHMETS...	06	CMD2 0.98-1.06 $e^+e^- \rightarrow \pi^+\pi^-\pi^0$
4.280 ± 0.033 ± 0.025	272k	4 AKHMETS...	04	CMD2 $e^+e^- \rightarrow K_S^0 K_L^0$
4.21 ± 0.04	1900k	5 ACHASOV	01E	SND $e^+e^- \rightarrow K^+K^-$, $K_S K_L, \pi^+\pi^-\pi^0$
4.44 ± 0.09	55600	AKHMETS...	95	CMD2 $e^+e^- \rightarrow$ hadrons
4.5 ± 0.7	1500	ARENTON	82	AEMS 11.8 polar. $pp \rightarrow K K$
4.2 ± 0.6	766	6 IVANOV	81	OLYA 1-1.4 $e^+e^- \rightarrow K^+K^-$
4.3 ± 0.6		6 CORDIER	80	DMI $e^+e^- \rightarrow \pi^+\pi^-\pi^0$
4.36 ± 0.29	3681	6 BUKIN	78c	OLYA $e^+e^- \rightarrow$ hadrons
4.4 ± 0.6	984	6 BESCH	74	CNTR 2 $\gamma p \rightarrow p K^+ K^-$
4.67 ± 0.72	681	6 BALAKIN	71	OSPK $e^+e^- \rightarrow$ hadrons
4.09 ± 0.29		6 BIZOT	70	OSPK $e^+e^- \rightarrow$ hadrons

••• We do not use the following data for averages, fits, limits, etc. •••

4.07 ± 0.13 ± 0.01	7	HOID	20	RVUE	$e^+e^- \rightarrow \pi^0\gamma$
4.23 ± 0.04 ± 0.02	8	HOFERICH...	19	RVUE	$e^+e^- \rightarrow \pi^+\pi^-\pi^0$
4.249 ± 0.015	1.7M	KOZYREV	18	CMD3	$e^+e^- \rightarrow K^+K^-$
4.240 ± 0.017	610k	KOZYREV	16	CMD3	$e^+e^- \rightarrow K_S^0 K_L^0$
4.37 ± 0.02		LEES	13F	BABR	$D^+ \rightarrow K^+K^-\pi^+$
4.24 ± 0.02 ± 0.03	542k	AKHMETS...	08	CMD2	$1.02 e^+e^- \rightarrow K^+K^-$
4.28 ± 0.13	12540	AUBERT,B	05J	BABR	$D^0 \rightarrow \bar{K}^0 K^+ K^-$
4.45 ± 0.06	271k	DIJKSTRA	86	SPEC	100 π^-Be
3.6 ± 0.8	337	6 COOPER	78b	HBC	0.7-0.8 $\bar{p}p \rightarrow K_S^0 K_L^0 \pi^+\pi^-$
4.5 ± 0.50	1300	6,10 AKERLOF	77	SPEC	400 $pA \rightarrow K^+K^-X$
4.5 ± 0.8	500	6,10 AYRES	74	ASPK	3-6 $\pi^-p \rightarrow K^+K^-\pi^-$, $K^+K^-\pi^-$, $K^+K^-\Lambda/\Sigma^0$
3.81 ± 0.37		COSME	74B	OSPK	$e^+e^- \rightarrow K_S^0 K_L^0$
3.8 ± 0.7	454	6 BORENSTEIN	72	HBC	2.18 $K^-p \rightarrow K \bar{K} n$

1 Average of KOZYREV 16 and KOZYREV 18 values taking into account the correlated uncertainties. Supersedes individual KOZYREV 16 and KOZYREV 18 results.
 2 Using a vector meson dominance model with contribution from $\phi(1020)$ and higher mass excitations of $\rho(770)$, $\omega(782)$, and $\phi(1020)$.
 3 Using a phenomenological model based on KUHN 90 with a sum of Breit-Wigner resonances for $\rho(770)$, $\omega(782)$, $\phi(1020)$ and their higher mass excitations.
 4 Update of AKHMETS... 99d
 5 From the combined fit assuming that the total $\phi(1020)$ production cross section is saturated by those of K^+K^- , $K_S K_L$, $\pi^+\pi^-\pi^0$, and $\eta\gamma$ decays modes and using ACHASOV 00b for the $\eta\gamma$ decay mode.
 6 Width errors enlarged by us to $4\Gamma/\sqrt{N}$; see the note with the $K^*(892)$ mass.
 7 The values were extracted from a dispersively improved Breit-Wigner parameterization.
 8 The values were extracted from a dispersively improved Breit-Wigner parameterization and do not include vacuum polarization.
 9 Strongly correlated with AKHMETS... 04.
 10 Systematic errors not evaluated.

$\phi(1020)$ DECAY MODES

Mode	Fraction (Γ_i/Γ)	Scale factor/ Confidence level
Γ_1 K^+K^-	(49.1 ± 0.5) %	S=1.3
Γ_2 $K_S^0 K_L^0$	(33.9 ± 0.4) %	S=1.2
Γ_3 $\rho\pi + \pi^+\pi^-\pi^0$	(15.4 ± 0.4) %	S=1.2
Γ_4 $\rho\pi$		
Γ_5 $\pi^+\pi^-\pi^0$		
Γ_6 $\eta\gamma$	(1.301 ± 0.025) %	S=1.2
Γ_7 $\pi^0\gamma$	(1.32 ± 0.05) × 10 ⁻³	
Γ_8 $\ell^+\ell^-$	—	
Γ_9 e^+e^-	(2.979 ± 0.033) × 10 ⁻⁴	S=1.3
Γ_{10} $\mu^+\mu^-$	(2.85 ± 0.19) × 10 ⁻⁴	
Γ_{11} ηe^+e^-	(1.08 ± 0.04) × 10 ⁻⁴	
Γ_{12} $\pi^+\pi^-$	(7.3 ± 1.3) × 10 ⁻⁵	
Γ_{13} $\omega\pi^0$	(4.7 ± 0.5) × 10 ⁻⁵	
Γ_{14} $\omega\gamma$	< 5 %	CL=84%
Γ_{15} $\rho\gamma$	< 1.2 × 10 ⁻⁵	CL=90%
Γ_{16} $\pi^+\pi^-\gamma$	(4.1 ± 1.3) × 10 ⁻⁵	
Γ_{17} $f_0(980)\gamma$	(3.22 ± 0.19) × 10 ⁻⁴	S=1.1
Γ_{18} $\pi^0\pi^0\gamma$	(1.12 ± 0.06) × 10 ⁻⁴	
Γ_{19} $\pi^+\pi^-\pi^+\pi^-$	(3.9 ± 2.8) × 10 ⁻⁶	
Γ_{20} $\pi^+\pi^+\pi^-\pi^-\pi^0$	< 4.6 × 10 ⁻⁶	CL=90%
Γ_{21} $\pi^0 e^+e^-$	(1.33 ± 0.07) × 10 ⁻⁵	
Γ_{22} $\pi^0\eta\gamma$	(7.27 ± 0.30) × 10 ⁻⁵	S=1.5
Γ_{23} $a_0(980)\gamma$	(7.6 ± 0.6) × 10 ⁻⁵	
Γ_{24} $K^0 \bar{K}^0 \gamma$	< 1.9 × 10 ⁻⁸	CL=90%
Γ_{25} $\eta'(958)\gamma$	(6.21 ± 0.21) × 10 ⁻⁵	
Γ_{26} $\eta\pi^0\pi^0\gamma$	< 2 × 10 ⁻⁵	CL=90%
Γ_{27} $\mu^+\mu^-\gamma$	(1.4 ± 0.5) × 10 ⁻⁵	
Γ_{28} $\rho\gamma\gamma$	< 1.2 × 10 ⁻⁴	CL=90%
Γ_{29} $\eta\pi^+\pi^-$	< 1.8 × 10 ⁻⁵	CL=90%
Γ_{30} $\eta\mu^+\mu^-$	< 9.4 × 10 ⁻⁶	CL=90%
Γ_{31} $\eta U \rightarrow \eta e^+e^-$	< 1 × 10 ⁻⁶	CL=90%
Γ_{32} invisible	< 1.7 × 10 ⁻⁴	CL=90%

Lepton Family number (LF) violating modes

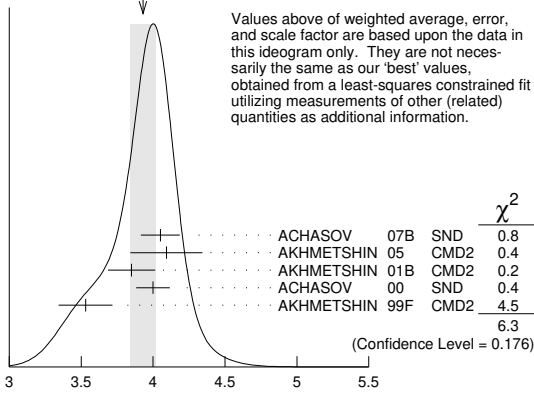
Γ_{33} $e^\pm\mu^\mp$	LF	< 2 × 10 ⁻⁶	CL=90%
------------------------------	----	------------------------	--------

Meson Particle Listings

$\phi(1020)$

$\Gamma(\eta\gamma)/\Gamma_{total} \times \Gamma(e^+e^-)/\Gamma_{total}$		$\Gamma_6/\Gamma \times \Gamma_9/\Gamma$	
VALUE (units 10^{-6})	EVTS	DOCUMENT ID	TECN COMMENT
3.88 ± 0.07 OUR FIT	Error	includes scale factor of 1.2.	
3.93 ± 0.09 OUR AVERAGE	Error	includes scale factor of 1.3. See the ideogram below.	
4.050 ± 0.067 ± 0.118	33k	1 ACHASOV 07B	SND 0.6-1.38 $e^+e^- \rightarrow \eta\gamma$
4.093 ^{+0.040} _{-0.043} ± 0.247	17.4k	2 AKHMETSHIN 05	CMD2 0.60-1.38 $e^+e^- \rightarrow \eta\gamma$
3.850 ± 0.041 ± 0.159	23k	3,4 AKH METSHIN 01B	CMD2 $e^+e^- \rightarrow \eta\gamma$
4.00 ± 0.04 ± 0.11		5 ACHASOV 00	SND $e^+e^- \rightarrow \eta\gamma$
3.53 ± 0.08 ± 0.17	2200	6,7 AKHMETSHIN 99F	CMD2 $e^+e^- \rightarrow \eta\gamma$
• • • We do not use the following data for averages, fits, limits, etc. • • •			
4.19 ± 0.06		8 BENAYOUN 10	RVUE 0.4-1.05 e^+e^-

WEIGHTED AVERAGE
3.93±0.09 (Error scaled by 1.3)



$\Gamma(\eta\gamma)/\Gamma_{total} \times \Gamma(e^+e^-)/\Gamma_{total}$ $\Gamma_6/\Gamma \times \Gamma_9/\Gamma$

- From a combined fit of $\sigma(e^+e^- \rightarrow \eta\gamma)$ with $\eta \rightarrow 3\pi^0$ and $\eta \rightarrow \pi^+\pi^-\pi^0$, and fixing $B(\eta \rightarrow 3\pi^0) / B(\eta \rightarrow \pi^+\pi^-\pi^0) = 1.44 \pm 0.04$. Recalculated by us from the cross section at the peak. Supersedes ACHASOV 00D and ACHASOV 06A.
- From the $\eta \rightarrow 2\gamma$ decay and using $B(\eta \rightarrow \gamma\gamma) = 39.43 \pm 0.26\%$.
- From the $\eta \rightarrow 3\pi^0$ decay and using $B(\eta \rightarrow 3\pi^0) = (32.24 \pm 0.29) \times 10^{-2}$.
- The combined fit from 600 to 1380 MeV taking into account $\rho(770)$, $\omega(782)$, $\phi(1020)$, and $\rho(1450)$ (mass and width fixed at 1450 MeV and 310 MeV respectively).
- From the $\eta \rightarrow 2\gamma$ decay and using $B(\eta \rightarrow 2\gamma) = (39.21 \pm 0.34) \times 10^{-2}$.
- Recalculated by the authors from the cross section in the peak.
- From the $\eta \rightarrow \pi^+\pi^-\pi^0$ decay and using $B(\eta \rightarrow \pi^+\pi^-\pi^0) = (23.1 \pm 0.5) \times 10^{-2}$.
- A simultaneous fit of $e^+e^- \rightarrow \pi^+\pi^-$, $\pi^+\pi^-\pi^0$, $\pi^0\gamma$, $\eta\gamma$ data.

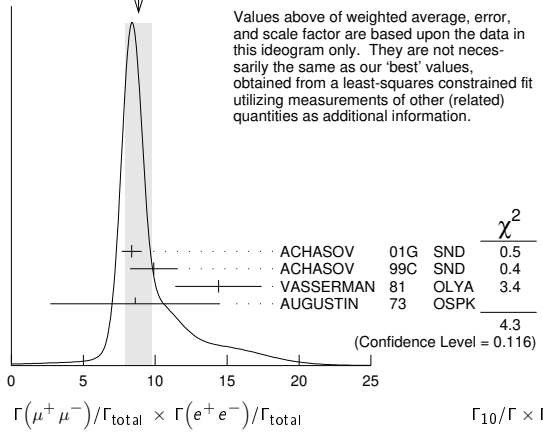
$\Gamma(\pi^0\gamma)/\Gamma_{total} \times \Gamma(e^+e^-)/\Gamma_{total}$		$\Gamma_7/\Gamma \times \Gamma_9/\Gamma$	
VALUE (units 10^{-7})	EVTS	DOCUMENT ID	TECN COMMENT
3.94 ± 0.16 OUR FIT			
3.95 ± 0.17 OUR AVERAGE			
4.04 ± 0.09 ± 0.19		1 ACHASOV 16A	SND 0.60-1.38 $e^+e^- \rightarrow \pi^0\gamma$
3.75 ± 0.11 ± 0.29	18k	AKHMETSHIN 05	CMD2 0.60-1.38 $e^+e^- \rightarrow \pi^0\gamma$
• • • We do not use the following data for averages, fits, limits, etc. • • •			
4.29 ± 0.11		2 BENAYOUN 10	RVUE 0.4-1.05 e^+e^-
3.67 ± 0.10 ^{+0.27} _{-0.25}		3 ACHASOV 00	SND $e^+e^- \rightarrow \pi^0\gamma$

- From the VMD model with the interfering $\rho(770)$, $\omega(782)$, $\phi(1020)$ resonances, and an additional resonance describing the total contribution of the $\rho(1450)$ and $\omega(1420)$ states. Supersedes ACHASOV 00.
- A simultaneous fit of $e^+e^- \rightarrow \pi^+\pi^-$, $\pi^+\pi^-\pi^0$, $\pi^0\gamma$, $\eta\gamma$ data.
- From the $\pi^0 \rightarrow 2\gamma$ decay and using $B(\pi^0 \rightarrow 2\gamma) = (98.798 \pm 0.032) \times 10^{-2}$.

$\Gamma(\mu^+\mu^-)/\Gamma_{total} \times \Gamma(e^+e^-)/\Gamma_{total}$		$\Gamma_{10}/\Gamma \times \Gamma_9/\Gamma$	
VALUE (units 10^{-8})	EVTS	DOCUMENT ID	TECN COMMENT
8.5 ± 0.6 OUR FIT			
8.8 ± 0.9 OUR AVERAGE	Error	includes scale factor of 1.5. See the ideogram below.	
8.36 ± 0.59 ± 0.37		ACHASOV 01G	SND $e^+e^- \rightarrow \mu^+\mu^-$
9.9 ± 1.4 ± 0.9		1 ACHASOV 99C	SND $e^+e^- \rightarrow \mu^+\mu^-$
14.4 ± 3.0		2 VASSERMAN 81	OLYA $e^+e^- \rightarrow \mu^+\mu^-$
8.6 ± 5.9		2 AUGUSTIN 73	OSPK $e^+e^- \rightarrow \mu^+\mu^-$

- Recalculated by the authors from the cross section in the peak.
- Recalculated by us from the cross section in the peak.

WEIGHTED AVERAGE
8.8±0.9 (Error scaled by 1.5)



$\Gamma(\mu^+\mu^-)/\Gamma_{total} \times \Gamma(e^+e^-)/\Gamma_{total}$ $\Gamma_{10}/\Gamma \times \Gamma_9/\Gamma$

$\Gamma(\pi^+\pi^-)/\Gamma_{total} \times \Gamma(e^+e^-)/\Gamma_{total}$		$\Gamma_{12}/\Gamma \times \Gamma_9/\Gamma$	
VALUE (units 10^{-8})	DOCUMENT ID	TECN	COMMENT
2.2 ± 0.4 OUR FIT			
2.2 ± 0.4 OUR AVERAGE			
2.1 ± 0.3 ± 0.3	1 ACHASOV 00C	SND	$e^+e^- \rightarrow \pi^+\pi^-$
1.95 ^{+1.15} _{-0.87}	2 GOLUBEV 86	ND	$e^+e^- \rightarrow \pi^+\pi^-$
6.01 ^{+3.19} _{-2.51}	2 VASSERMAN 81	OLYA	$e^+e^- \rightarrow \pi^+\pi^-$
• • • We do not use the following data for averages, fits, limits, etc. • • •			
3.31 ± 0.99	3 BENAYOUN 13	RVUE	0.4-1.05 e^+e^-

- Recalculated by the authors from the cross section in the peak.
- Recalculated by us from the cross section in the peak.
- A simultaneous fit to $e^+e^- \rightarrow \pi^+\pi^-$, $\pi^+\pi^-\pi^0$, $\pi^0\gamma$, $\eta\gamma$, $K\bar{K}$, and $\tau^- \rightarrow \pi^-\pi^0\nu_\tau$ data.

$\Gamma(\omega\pi^0)/\Gamma_{total} \times \Gamma(e^+e^-)/\Gamma_{total}$		$\Gamma_{13}/\Gamma \times \Gamma_9/\Gamma$	
VALUE (units 10^{-8})	DOCUMENT ID	TECN	COMMENT
1.40 ± 0.15 OUR FIT			
1.37 ± 0.17 ± 0.01	1,2 AMBROSINO 08G	KLOE	$e^+e^- \rightarrow \pi^+\pi^-\pi^0, 2\pi^0\gamma$
• • • We do not use the following data for averages, fits, limits, etc. • • •			

$\Gamma(\pi^0\pi^0\gamma)/\Gamma_{total} \times \Gamma(e^+e^-)/\Gamma_{total}$		$\Gamma_{18}/\Gamma \times \Gamma_9/\Gamma$	
VALUE (units 10^{-8})	DOCUMENT ID	TECN	COMMENT
3.34 ± 0.17 OUR FIT			
3.33 ± 0.04 ± 0.19 3.33 ± 0.09 ± 0.20	1 AMBROSINO 07	KLOE	$e^+e^- \rightarrow \pi^0\pi^0\gamma$

- Calculated by the authors from the cross section at the peak.

$\Gamma(\pi^+\pi^-\pi^+\pi^-)/\Gamma_{total} \times \Gamma(e^+e^-)/\Gamma_{total}$		$\Gamma_{19}/\Gamma \times \Gamma_9/\Gamma$	
VALUE (units 10^{-9})	EVTS	DOCUMENT ID	TECN COMMENT
1.2 ± 0.8 OUR FIT			
1.17 ± 0.52 ± 0.64	3285	1 AKHMETSHIN 00E	CMD2 $e^+e^- \rightarrow \pi^+\pi^-\pi^+\pi^-$
• • • We do not use the following data for averages, fits, limits, etc. • • •			

- Recalculated by the authors from the cross section in the peak.

$\phi(1020)$ BRANCHING RATIOS

$\Gamma(K^+K^-)/\Gamma_{total}$		Γ_1/Γ	
VALUE	EVTS	DOCUMENT ID	TECN COMMENT
0.491 ± 0.005 OUR FIT	Error	includes scale factor of 1.3.	
0.493 ± 0.010 OUR AVERAGE			
0.492 ± 0.012	2913	AKHMETSHIN 95	CMD2 $e^+e^- \rightarrow K^+K^-$
0.44 ± 0.05	321	KALBFLEISCH 76	HBC 2.18 $K^-p \rightarrow \Lambda K^+K^-$
0.49 ± 0.06	270	DEGROOT 74	HBC 4.2 $K^-p \rightarrow \Lambda\phi$
0.540 ± 0.034	565	BALAKIN 71	OSPK $e^+e^- \rightarrow K^+K^-$
0.48 ± 0.04	252	LINDSEY 66	HBC 2.1-2.7 $K^-p \rightarrow \Lambda K^+K^-$
• • • We do not use the following data for averages, fits, limits, etc. • • •			
0.493 ± 0.003 ± 0.007		1 AKHMETSHIN 11	CMD2 1.02 $e^+e^- \rightarrow K^+K^-$
0.476 ± 0.017	1000k	2 ACHASOV 01E	SND $e^+e^- \rightarrow K^+K^-, K_S^0 K_L^0, \pi^+\pi^-\pi^0$

- Combined analysis of the CMD-2 data on $\phi \rightarrow K^+K^-, K_S^0 K_L^0, \pi^+\pi^-\pi^0, \eta\gamma$ assuming that the sum of their branching fractions is 0.99741 ± 0.000007 .
- Using $B(\phi \rightarrow e^+e^-) = (2.93 \pm 0.14) \times 10^{-4}$.

$\Gamma(K_L^0 K_S^0)/\Gamma_{\text{total}}$

VALUE	EVTS	DOCUMENT ID	TECN	COMMENT	Γ_2/Γ
0.339±0.004 OUR FIT				Error includes scale factor of 1.2.	
0.331±0.009 OUR AVERAGE					
0.335±0.010	40644	AKHMETSHIN 95	CMD2	$e^+e^- \rightarrow K_L^0 K_S^0$	
0.326±0.035		DOLINSKY 91	ND	$e^+e^- \rightarrow K_L^0 K_S^0$	
0.310±0.024		DRUZHININ 84	ND	$e^+e^- \rightarrow K_L^0 K_S^0$	

• • • We do not use the following data for averages, fits, limits, etc. • • •

0.336±0.002±0.006		1 AKHMETSHIN 11	CMD2	$1.02 e^+e^- \rightarrow K_S^0 K_L^0$	
0.351±0.013	500k	2 ACHASOV	01E	SND $e^+e^- \rightarrow K^+K^-$ $K_S^0 K_L^0, \pi^+\pi^-\pi^0$	

0.27 ±0.03	133	KALBFLEISCH 76	HBC	$2.18 K^-p \rightarrow \Lambda K_L^0 K_S^0$	
0.257±0.030	95	3 BALAKIN	71	OSPK $e^+e^- \rightarrow K_L^0 K_S^0$	
0.40 ±0.04	167	LINDSEY	66	HBC $2.1-2.7 K^-p \rightarrow \Lambda K_L^0 K_S^0$	

1 Combined analysis of the CMD-2 data on $\phi \rightarrow K^+K^-, K_S^0 K_L^0, \pi^+\pi^-\pi^0, \eta\gamma$ assuming that the sum of their branching fractions is 0.99741 ± 0.00007 .

2 Using $B(\phi \rightarrow e^+e^-) = (2.93 \pm 0.14) \times 10^{-4}$.

3 Balakin error increased by Paul.

• • • We do not use the following data for averages, fits, limits, etc. • • •

VALUE	EVTS	DOCUMENT ID	TECN	COMMENT	Γ_2/Γ_1
0.690±0.015 OUR FIT				Error includes scale factor of 1.3.	
0.740±0.031 OUR AVERAGE					
0.70 ±0.06	2732	BUKIN	78c	OLYA $e^+e^- \rightarrow K_L^0 K_S^0$	
0.82 ±0.08		LOSTY	78	HBC $4.2 K^-p \rightarrow \phi$ hyperon	
0.71 ±0.05		LAVEN	77	HBC $10 K^-p \rightarrow \Lambda K^+K^-$	
0.71 ±0.08		LYONS	77	HBC $3-4 K^-p \rightarrow \Lambda \phi$	
0.89 ±0.10	144	AGUILAR...	72B	HBC $3.9, 4.6 K^-p$	

• • • We do not use the following data for averages, fits, limits, etc. • • •

0.638±0.022	2.3M	1 KOZYREV	18	CMD3 $e^+e^- \rightarrow K_L^0 K_S^0$	
0.68 ±0.03		2 AKHMETSHIN 95	CMD2	$e^+e^- \rightarrow K_L^0 K_S^0, K^+K^-$	

1 The prediction taking into account phase-space difference, radiative corrections, isospin breaking, and the Sommerfeld-Gamow-Sakharov factor gives 0.630.

2 Theoretical analysis of BRAMON 00 taking into account phase-space difference, electromagnetic radiative corrections, as well as isospin breaking, predicts 0.62. FLOREZ-BAEZ 08 predicts 0.63 considering also structure-dependent radiative corrections. FISCHBACH 02 calculates additional corrections caused by the close threshold and predicts 0.68. See also BENAYOUN 01 and DUBYNYSKIY 07. BENAYOUN 12 obtains 0.71 ± 0.01 in the HLS model.

• • • We do not use the following data for averages, fits, limits, etc. • • •

VALUE	EVTS	DOCUMENT ID	TECN	COMMENT	$\Gamma_2/(\Gamma_1+\Gamma_2)$
0.408±0.005 OUR FIT				Error includes scale factor of 1.3.	
0.45 ±0.04 OUR AVERAGE					
0.44 ±0.07		1 LONDON	66	HBC $2.24 K^-p \rightarrow \Lambda K \bar{K}$	
0.48 ±0.07	52	BADIER	65B	HBC $3 K^-p$	
0.40 ±0.10	34	SCHLEIN	63	HBC $1.95 K^-p \rightarrow \Lambda K \bar{K}$	

1 This is probably not affected by their controversial background subtraction; the value is from their numbers of $K_1 K_2$ vs K^+K^- events.

• • • We do not use the following data for averages, fits, limits, etc. • • •

VALUE	EVTS	DOCUMENT ID	TECN	COMMENT	Γ_3/Γ
0.154±0.004 OUR FIT				Error includes scale factor of 1.2.	
0.151±0.009 OUR AVERAGE					
0.161±0.008	11761	AKHMETSHIN 95	CMD2	$e^+e^- \rightarrow \pi^+\pi^-\pi^0$	
0.143±0.007		DOLINSKY 91	ND	$e^+e^- \rightarrow \pi^+\pi^-\pi^0$	

• • • We do not use the following data for averages, fits, limits, etc. • • •

0.155±0.002±0.005		1 AKHMETSHIN 11	CMD2	$1.02 e^+e^- \rightarrow \pi^+\pi^-\pi^0$	
0.159±0.008	400k	2 ACHASOV	01E	SND $e^+e^- \rightarrow K^+K^-$ $K_S^0 K_L^0, \pi^+\pi^-\pi^0$	

0.145±0.009±0.003	11169	3 AKHMETSHIN 98	CMD2	$e^+e^- \rightarrow \pi^+\pi^-\pi^0$	
0.139±0.007		4 PARROUR	76B	OSPK e^+e^-	

1 Combined analysis of the CMD-2 data on $\phi \rightarrow K^+K^-, K_S^0 K_L^0, \pi^+\pi^-\pi^0, \eta\gamma$ assuming that the sum of their branching fractions is 0.99741 ± 0.00007 .

2 Using $B(\phi \rightarrow e^+e^-) = (2.93 \pm 0.14) \times 10^{-4}$.

3 Using $B(\phi \rightarrow e^+e^-) = (2.99 \pm 0.08) \times 10^{-4}$.

4 Using $\Gamma(\phi) = 4.1$ MeV. If interference between the $\rho\pi$ and 3π modes is neglected, the fraction of the $\rho\pi$ is more than 80% at the 90% confidence level.

• • • We do not use the following data for averages, fits, limits, etc. • • •

VALUE	EVTS	DOCUMENT ID	TECN	COMMENT	Γ_3/Γ_1
0.313±0.010 OUR FIT				Error includes scale factor of 1.2.	
0.28 ±0.09					
	34	AGUILAR...	72B	HBC $3.9, 4.6 K^-p$	

• • • We do not use the following data for averages, fits, limits, etc. • • •

VALUE	EVTS	DOCUMENT ID	TECN	COMMENT	$\Gamma_3/(\Gamma_1+\Gamma_2)$
0.185±0.005 OUR FIT				Error includes scale factor of 1.2.	
0.24 ±0.04 OUR AVERAGE					
0.237±0.039		CERRADA	77B	HBC $4.2 K^-p \rightarrow \Lambda 3\pi$	
0.30 ±0.15		LONDON	66	HBC $2.24 K^-p \rightarrow \Lambda \pi^+\pi^-\pi^0$	

 $[\Gamma(\rho\pi) + \Gamma(\pi^+\pi^-\pi^0)]/\Gamma(K_L^0 K_S^0)$

VALUE	EVTS	DOCUMENT ID	TECN	COMMENT	Γ_3/Γ_2
0.453±0.012 OUR FIT				Error includes scale factor of 1.1.	
0.51 ±0.05 OUR AVERAGE					
0.56 ±0.07	3681	BUKIN	78c	OLYA $e^+e^- \rightarrow K_L^0 K_S^0, \pi^+\pi^-\pi^0$	
0.47 ±0.06	516	COSME	74	OSPK $e^+e^- \rightarrow \pi^+\pi^-\pi^0$	

• • • We do not use the following data for averages, fits, limits, etc. • • •

VALUE	CL%	EVTS	DOCUMENT ID	TECN	COMMENT	Γ_5/Γ
0.51 ±0.05 OUR AVERAGE						
≈ 0.0087		1.98M	1,2 ALOISIO	03	KLOE $1.02 e^+e^- \rightarrow \pi^+\pi^-\pi^0$	
<0.0006	90		3 ACHASOV	02	SND $1.02 e^+e^- \rightarrow \pi^+\pi^-\pi^0$	
<0.23	90		3 CORDIER	80	DM1 $e^+e^- \rightarrow \pi^+\pi^-\pi^0$	
<0.20	90		3 PARROUR	76B	OSPK $e^+e^- \rightarrow \pi^+\pi^-\pi^0$	

1 From a fit without limitations on charged and neutral ρ masses and widths.

2 Adding the direct and $\omega\pi$ contributions and considering the interference between the $\rho\pi$ and $\pi^+\pi^-\pi^0$.

3 Neglecting the interference between the $\rho\pi$ and $\pi^+\pi^-\pi^0$.

• • • We do not use the following data for averages, fits, limits, etc. • • •

VALUE (units 10^{-2})	EVTS	DOCUMENT ID	TECN	COMMENT	Γ_6/Γ
1.301±0.025 OUR FIT				Error includes scale factor of 1.2.	
1.26 ±0.04 OUR AVERAGE					
1.246±0.025±0.057	10k	1 ACHASOV	98F	SND $e^+e^- \rightarrow 7\gamma$	
1.18 ±0.11	279	2 AKHMETSHIN 95	CMD2	$e^+e^- \rightarrow \pi^+\pi^-\pi^0$	
1.30 ±0.06		3 DRUZHININ 84	ND	$e^+e^- \rightarrow 3\gamma$	
1.4 ±0.2		4 DRUZHININ 84	ND	$e^+e^- \rightarrow 6\gamma$	
0.88 ±0.20	290	KURDADZE	83c	OLYA $e^+e^- \rightarrow 3\gamma$	
1.35 ±0.29		ANDREWS	77	CNTR $6.7-10 \gamma$	
1.5 ±0.4	54	3 COSME	76	OSPK e^+e^-	

• • • We do not use the following data for averages, fits, limits, etc. • • •

1.38 ±0.02 ±0.02		5 AKHMETSHIN 11	CMD2	$1.02 e^+e^- \rightarrow \eta\gamma$	
1.36 ±0.05 ±0.02	33k	6 ACHASOV	07B	SND $0.6-1.38 e^+e^- \rightarrow \eta\gamma$	
1.373±0.014±0.085	17.4k	7,8 AKHMETSHIN 05	CMD2	$0.60-1.38 e^+e^- \rightarrow \eta\gamma$	
1.287±0.013±0.063		9,10 AKHMETSHIN 01B	CMD2	$e^+e^- \rightarrow \eta\gamma$	
1.338±0.012±0.052		11 ACHASOV	00	SND $e^+e^- \rightarrow \eta\gamma$	
1.18 ±0.03 ±0.06	2200	12 AKHMETSHIN 99F	CMD2	$e^+e^- \rightarrow \eta\gamma$	
1.21 ±0.07		13 BENAYOUN 96	RVUE	$0.54-1.04 e^+e^- \rightarrow \eta\gamma$	

1 Using $B(\phi \rightarrow e^+e^-) = (2.99 \pm 0.08) \times 10^{-4}$ and $B(\eta \rightarrow 3\pi^0) = (32.2 \pm 0.4) \times 10^{-2}$.

2 From $\pi^+\pi^-\pi^0$ decay mode of η .

3 From 2γ decay mode of η .

4 From $3\pi^0$ decay mode of η .

5 Combined analysis of the CMD-2 data on $\phi \rightarrow K^+K^-, K_L^0 K_S^0, \pi^+\pi^-\pi^0, \eta\gamma$ assuming that the sum of their branching fractions is 0.99741 ± 0.00007 .

6 ACHASOV 07b reports $[\Gamma(\phi(1020) \rightarrow \eta\gamma)/\Gamma_{\text{total}}] \times [B(\phi(1020) \rightarrow e^+e^-)] = (4.050 \pm 0.067 \pm 0.118) \times 10^{-6}$ which we divide by our best value $B(\phi(1020) \rightarrow e^+e^-) = (2.979 \pm 0.033) \times 10^{-4}$. Our first error is their experiment's error and our second error is the systematic error from using our best value. Supersedes ACHASOV 00b and ACHASOV 06a.

7 Using $B(\phi \rightarrow e^+e^-) = (2.98 \pm 0.04) \times 10^{-4}$ and $B(\eta \rightarrow \gamma\gamma) = 39.43 \pm 0.26\%$.

8 Not independent of the corresponding $\Gamma(e^+e^-) \times \Gamma(\eta\gamma)/\Gamma_{\text{total}}^2$.

9 Using $B(\phi \rightarrow e^+e^-) = (2.99 \pm 0.08) \times 10^{-4}$ and $B(\eta \rightarrow 3\pi^0) = (32.24 \pm 0.29) \times 10^{-2}$.

10 The combined fit from 600 to 1380 MeV taking into account $\rho(770), \omega(782), \phi(1020)$, and $\rho(1450)$ (mass and width fixed at 1450 MeV and 310 MeV respectively).

11 From the $\eta \rightarrow 2\gamma$ decay and using $B(\phi \rightarrow e^+e^-) = (2.99 \pm 0.08) \times 10^{-4}$.

12 From $\pi^+\pi^-\pi^0$ decay mode of η and using $B(\phi \rightarrow e^+e^-) = (2.99 \pm 0.08) \times 10^{-4}$.

13 Reanalysis of DRUZHININ 84, DOLINSKY 89, and DOLINSKY 91 taking into account a triangle anomaly contribution.

• • • We do not use the following data for averages, fits, limits, etc. • • •

VALUE (units 10^{-3})	EVTS	DOCUMENT ID	TECN	COMMENT	Γ_7/Γ
1.32 ±0.05 OUR FIT					
1.31 ±0.13 OUR AVERAGE					
1.30 ±0.13		DRUZHININ 84	ND	$e^+e^- \rightarrow 3\gamma$	
1.4 ±0.5	32	COSME	76	OSPK e^+e^-	

• • • We do not use the following data for averages, fits, limits, etc. • • •

1.367±0.072		1 ACHASOV	16A	SND $0.60-1.38 e^+e^- \rightarrow \pi^0\gamma$	
1.258±0.037±0.077	18k	2,3 AKHMETSHIN 05	CMD2	$0.60-1.38 e^+e^- \rightarrow \pi^0\gamma$	
1.226±0.036 $^{+0.096}_{-0.089}$		4 ACHASOV	00	SND $e^+e^- \rightarrow \pi^0\gamma$	
1.26 ±0.17		5 BENAYOUN 96	RVUE	$0.54-1.04 e^+e^- \rightarrow \pi^0\gamma$	

1 Using $B(\phi \rightarrow e^+e^-)$ from PDG 15. Supersedes ACHASOV 00.

2 Using $B(\phi \rightarrow e^+e^-) = (2.98 \pm 0.04) \times 10^{-4}$.

3 Not independent of the corresponding $\Gamma(e^+e^-) \times \Gamma(\pi^0\gamma)/\Gamma_{\text{total}}^2$.

4 From the $\pi^0 \rightarrow 2\gamma$ decay and using $B(\phi \rightarrow e^+e^-) = (2.99 \pm 0.08) \times 10^{-4}$.

5 Reanalysis of DRUZHININ 84, DOLINSKY 89, and DOLINSKY 91 taking into account a triangle anomaly contribution.

• • • We do not use the following data for averages, fits, limits, etc. • • •

VALUE	EVTS	DOCUMENT ID	TECN	COMMENT	Γ_6/Γ_7
1.301±0.025 OUR FIT				Error includes scale factor of 1.2.	
1.26 ±0.04 OUR AVERAGE					
1.246±0.025±0.057	10k	1 ACHASOV	98F	SND $e^+e^- \rightarrow 7\gamma$	
1.18 ±0.11	279	2 AKHMETSHIN 95	CMD2	$e^+e^- \rightarrow \pi^+\pi^-\pi^0$	
1.30 ±0.06		3 DRUZHININ 84	ND	$e^+e^- \rightarrow 3\gamma$	
1.4 ±0.2		4 DRUZHININ 84	ND	$e^+e^- \rightarrow 6\gamma$	
0.88 ±0.20	290	KURDADZE	83c	OLYA $e^+e^- \rightarrow 3\gamma$	
1.35 ±0.29		ANDREWS	77	CNTR $6.7-10 \gamma$	
1.5 ±0.4	54	3 COSME	76	OSPK e^+e^-	

• • • We do not use the following data for averages, fits, limits, etc. • • •

1.38 ±0.02 ±0.02		5 AKHMETSHIN 11	CMD2	$1.02 e^+e^- \rightarrow \eta\gamma$	
1.36 ±0.05 ±0.02	33k	6 ACHASOV	07B	SND $0.6-1.38 e^+e^- \rightarrow \eta\gamma$	
1.373±0.014±0.085	17.4k	7,8 AKHMETSHIN 05	CMD2	$0.60-1.38 e^+e^- \rightarrow \eta\gamma$	
1.287±0.013±0.063		9,10 AKHMETSHIN 01B	CMD2	$e^+e^- \rightarrow \eta\gamma$	
1.338±0.012±0.052		11 ACHASOV	00	SND $e^+e^- \rightarrow \eta\gamma$	
1.18 ±0.03 ±0.06	2200	12 AKHMETSHIN 99F	CMD2	$e^+e^- \rightarrow \eta\gamma$	

Meson Particle Listings

 $\phi(1020)$ $\Gamma(e^+e^-)/\Gamma_{\text{total}}$ Γ_9/Γ

VALUE (units 10^{-4})	EVTS	DOCUMENT ID	TECN	COMMENT
2.979 ± 0.033 OUR FIT	Error	includes scale factor of 1.1.		
2.98 ± 0.07 OUR AVERAGE	1900k	1 ACHASOV	01E SND	$e^+e^- \rightarrow K^+K^-, K_S^0 K_L^0, \pi^+\pi^-\pi^0$
2.88 ± 0.09	55600	AKHMETSHIN 95	CMD2	$e^+e^- \rightarrow$ hadrons
3.00 ± 0.21	3681	BUKIN	78c OLYA	$e^+e^- \rightarrow$ hadrons
3.10 ± 0.14		2 PARROUR	76 OSPK	$e^+e^- \rightarrow$ hadrons
3.3 ± 0.3		COSME	74 OSPK	$e^+e^- \rightarrow$ hadrons
2.81 ± 0.25	681	BALAKIN	71 OSPK	$e^+e^- \rightarrow$ hadrons
3.50 ± 0.27		CHATELUS	71 OSPK	$e^+e^- \rightarrow$ hadrons

¹ From the combined fit assuming that the total $\phi(1020)$ production cross section is saturated by those of K^+K^- , $K_S^0 K_L^0$, $\pi^+\pi^-\pi^0$, and $\eta\gamma$ decays modes and using ACHASOV 00B for the $\eta\gamma$ decay mode.

² Using total width 4.2 MeV. They detect 3π mode and observe significant interference with ω tail. This is accounted for in the result quoted above.

 $\Gamma(\mu^+\mu^-)/\Gamma_{\text{total}}$ Γ_{10}/Γ

VALUE (units 10^{-4})	DOCUMENT ID	TECN	COMMENT
2.85 ± 0.19 OUR FIT			
2.5 ± 0.4 OUR AVERAGE			
2.69 ± 0.46	1 HAYES	71 CNTR	8.3, 9.8 $\gamma C \rightarrow \mu^+\mu^- X$
2.17 ± 0.60	1 EARLES	70 CNTR	6.0 $\gamma C \rightarrow \mu^+\mu^- X$
• • • We do not use the following data for averages, fits, limits, etc. • • •			
2.87 ± 0.20 ± 0.14	2 ACHASOV	01G SND	$e^+e^- \rightarrow \mu^+\mu^-$
3.30 ± 0.45 ± 0.32	3 ACHASOV	99c SND	$e^+e^- \rightarrow \mu^+\mu^-$
4.83 ± 1.02	4 VASSERMAN	81 OLYA	$e^+e^- \rightarrow \mu^+\mu^-$
2.87 ± 1.98	4 AUGUSTIN	73 OSPK	$e^+e^- \rightarrow \mu^+\mu^-$

¹ Neglecting interference between resonance and continuum.

² Using $B(\phi \rightarrow e^+e^-) = (2.91 \pm 0.07) \times 10^{-4}$.

³ Using $B(\phi \rightarrow e^+e^-) = (2.99 \pm 0.08) \times 10^{-4}$.

⁴ Recalculated by us using $B(\phi \rightarrow e^+e^-) = (2.99 \pm 0.08) \times 10^{-4}$.

 $\Gamma(\eta e^+e^-)/\Gamma_{\text{total}}$ Γ_{11}/Γ

VALUE (units 10^{-4})	EVTS	DOCUMENT ID	TECN	COMMENT
1.08 ± 0.04 OUR AVERAGE				
1.075 ± 0.007 ± 0.038	30k	1 BABUSCI	15 KLOE	1.02 $e^+e^- \rightarrow \eta e^+e^-$
1.19 ± 0.19 ± 0.12	213	2 ACHASOV	01B SND	$e^+e^- \rightarrow \eta e^+e^-$
1.14 ± 0.10 ± 0.06	355	3 AKHMETSHIN 01	CMD2	$e^+e^- \rightarrow \eta e^+e^-$
• • • We do not use the following data for averages, fits, limits, etc. • • •				
1.13 ± 0.14 ± 0.07	183	4 AKHMETSHIN 01	CMD2	$e^+e^- \rightarrow \eta e^+e^-$
1.21 ± 0.14 ± 0.09	130	5 AKHMETSHIN 01	CMD2	$e^+e^- \rightarrow \eta e^+e^-$
1.04 ± 0.20 ± 0.08	42	6 AKHMETSHIN 01	CMD2	$e^+e^- \rightarrow \eta e^+e^-$
1.3 $\begin{smallmatrix} +0.8 \\ -0.6 \end{smallmatrix}$	7	GOLUBEV	85 ND	$e^+e^- \rightarrow \eta e^+e^-$

¹ Using $B(\eta \rightarrow 3\pi^0) = (32.57 \pm 0.23)\%$ from PDG 12.

² Using $B(\eta \rightarrow \gamma\gamma) = (39.25 \pm 0.32)\%$, $B(\phi \rightarrow \eta\gamma) = (1.26 \pm 0.06)\%$, and $B(\phi \rightarrow e^+e^-) = (3.00 \pm 0.06) \times 10^{-4}$.

³ The average of the branching ratios separately obtained from the $\eta \rightarrow \gamma\gamma$, $3\pi^0$, $\pi^+\pi^-\pi^0$ decays.

⁴ From $\eta \rightarrow \gamma\gamma$ decays and using $B(\eta \rightarrow \gamma\gamma) = (39.33 \pm 0.25) \times 10^{-2}$, $B(\eta \rightarrow \pi^+\pi^-\gamma) = (4.75 \pm 11) \times 10^{-2}$, and $B(\phi \rightarrow \eta\gamma) = (1.297 \pm 0.033) \times 10^{-2}$.

⁵ From $\eta \rightarrow 3\pi^0$ decays and using $B(\pi^0 \rightarrow \gamma\gamma) = (98.798 \pm 0.033) \times 10^{-2}$, $B(\eta \rightarrow 3\pi^0) = (32.24 \pm 0.29) \times 10^{-2}$, $B(\eta \rightarrow \pi^+\pi^-\gamma) = (4.75 \pm 0.11) \times 10^{-2}$, and $B(\phi \rightarrow \eta\gamma) = (1.297 \pm 0.033) \times 10^{-2}$.

⁶ From $\eta \rightarrow \pi^+\pi^-\pi^0$ decays and using $B(\pi^0 \rightarrow \gamma\gamma) = (98.798 \pm 0.033) \times 10^{-2}$, $B(\pi^0 \rightarrow e^+e^-\gamma) = (1.198 \pm 0.032) \times 10^{-2}$, $B(\eta \rightarrow \pi^+\pi^-\pi^0) = (23.0 \pm 0.4) \times 10^{-2}$, $B(\phi \rightarrow \pi^+\pi^-\pi^0) = (15.5 \pm 0.6) \times 10^{-2}$, and $B(\phi \rightarrow \eta\gamma) = (1.297 \pm 0.033) \times 10^{-2}$.

 $\Gamma(\pi^+\pi^-)/\Gamma_{\text{total}}$ Γ_{12}/Γ

VALUE (units 10^{-4})	CL%	DOCUMENT ID	TECN	COMMENT
• • • We do not use the following data for averages, fits, limits, etc. • • •				
0.71 ± 0.11 ± 0.09		1 ACHASOV	00c SND	$e^+e^- \rightarrow \pi^+\pi^-$
0.65 $\begin{smallmatrix} +0.38 \\ -0.29 \end{smallmatrix}$		1 GOLUBEV	86 ND	$e^+e^- \rightarrow \pi^+\pi^-$
2.01 $\begin{smallmatrix} +1.07 \\ -0.84 \end{smallmatrix}$		1 VASSERMAN	81 OLYA	$e^+e^- \rightarrow \pi^+\pi^-$
< 6.6	95	BUKIN	78B OLYA	$e^+e^- \rightarrow \pi^+\pi^-$
< 2.7	95	ALVENSLEB...	72 CNTR	6.7 $\gamma C \rightarrow C\pi^+\pi^-$

¹ Using $B(\phi \rightarrow e^+e^-) = (2.99 \pm 0.08) \times 10^{-4}$.

 $\Gamma(\omega\pi^0)/\Gamma_{\text{total}}$ Γ_{13}/Γ

VALUE (units 10^{-5})	DOCUMENT ID	TECN	COMMENT
4.7 ± 0.5 OUR FIT			
5.2 $\begin{smallmatrix} +1.3 \\ -1.1 \end{smallmatrix}$	1,2 AULCHENKO	00A SND	$e^+e^- \rightarrow \pi^+\pi^-\pi^0\pi^0$
• • • We do not use the following data for averages, fits, limits, etc. • • •			
4.4 ± 0.6	3 AMBROSINO	08G KLOE	$e^+e^- \rightarrow \pi^+\pi^-\pi^0\pi^0, 2\pi^0\pi^0$
~ 5.4	4 ACHASOV	00E SND	$e^+e^- \rightarrow \pi^0\pi^0\pi^0$
5.5 $\begin{smallmatrix} +1.6 \\ -1.4 \end{smallmatrix}$ ± 0.3	2,5 AULCHENKO	00A SND	$e^+e^- \rightarrow \pi^+\pi^-\pi^0\pi^0$
4.8 $\begin{smallmatrix} +1.9 \\ -1.7 \end{smallmatrix}$ ± 0.8	4 ACHASOV	99 SND	$e^+e^- \rightarrow \pi^+\pi^-\pi^0\pi^0$

¹ Using the 1996 and 1998 data.

² $(2.3 \pm 0.3)\%$ correction for other decay modes of the $\omega(782)$ applied.

³ Not independent of the corresponding $\Gamma(\omega\pi^0) \times \Gamma(e^+e^-) / \Gamma^2(\text{total})$.

⁴ Using the 1996 data.

⁵ Using the 1998 data.

 $\Gamma(\omega\gamma)/\Gamma_{\text{total}}$ Γ_{14}/Γ

VALUE	CL%	DOCUMENT ID	TECN	COMMENT
< 0.05	84	LINDSEY	66 HBC	2.1–2.7 $K^-p \rightarrow \Lambda\pi^+\pi^-$ neutrals

 $\Gamma(\rho\gamma)/\Gamma_{\text{total}}$ Γ_{15}/Γ

VALUE (units 10^{-4})	CL%	DOCUMENT ID	TECN	COMMENT
< 0.12	90	1 AKHMETSHIN 99B	CMD2	$e^+e^- \rightarrow \pi^+\pi^-\gamma$
• • • We do not use the following data for averages, fits, limits, etc. • • •				
< 7	90	AKHMETSHIN 97C	CMD2	$e^+e^- \rightarrow \pi^+\pi^-\gamma$
< 200	84	LINDSEY	66 HBC	2.1–2.7 $K^-p \rightarrow \Lambda\pi^+\pi^-$ neutrals

¹ Supersedes AKHMETSHIN 97C.

 $\Gamma(\pi^+\pi^-\gamma)/\Gamma_{\text{total}}$ Γ_{16}/Γ

VALUE (units 10^{-4})	CL%	EVTS	DOCUMENT ID	TECN	COMMENT
0.41 ± 0.12 ± 0.04		30175	1 AKHMETSHIN 99B	CMD2	$e^+e^- \rightarrow \pi^+\pi^-\gamma$
• • • We do not use the following data for averages, fits, limits, etc. • • •					
< 0.3	90		2 AKHMETSHIN 97C	CMD2	$e^+e^- \rightarrow \pi^+\pi^-\gamma$
< 600	90		KALBFLEISCH 75	HBC	2.18 $K^-p \rightarrow \Lambda\pi^+\pi^-\gamma$
< 70	90		COSME	74 OSPK	$e^+e^- \rightarrow \pi^+\pi^-\gamma$
< 400	90		LINDSEY	65 HBC	2.1–2.7 $K^-p \rightarrow \Lambda\pi^+\pi^-$ neutrals

¹ For $E_\gamma > 20$ MeV and assuming that $B(\phi(1020) \rightarrow f_0(980)\gamma)$ is negligible. Supersedes AKHMETSHIN 97C.

² For $E_\gamma > 20$ MeV and assuming that $B(\phi(1020) \rightarrow f_0(980)\gamma)$ is negligible.

 $\Gamma(f_0(980)\gamma)/\Gamma_{\text{total}}$ Γ_{17}/Γ

VALUE (units 10^{-4})	CL%	EVTS	DOCUMENT ID	TECN	COMMENT
3.22 ± 0.19 OUR FIT					Error includes scale factor of 1.1.
3.21 ± 0.03 ± 0.18					
3.21 ± 0.09 ± 0.18					
3.21 ± 0.21 ± 1.54					
• • • We do not use the following data for averages, fits, limits, etc. • • •					
3.21 ± 0.03 ± 1.3 $\begin{smallmatrix} +1.3 \\ -0.5 \end{smallmatrix}$			4,5 ACHASOV	00H SND	$e^+e^- \rightarrow \pi^0\pi^0\gamma$
4.47 ± 0.21	2438		3 ALOISIO	02D KLOE	$e^+e^- \rightarrow \pi^0\pi^0\gamma$
3.5 ± 0.3 ± 0.5	419		6 AKHMETSHIN 99B	CMD2	$e^+e^- \rightarrow \pi^+\pi^-\gamma$
1.93 ± 0.46 ± 0.50	27188		7 AKHMETSHIN 99C	CMD2	$e^+e^- \rightarrow \pi^0\pi^0\gamma$
3.05 ± 0.25 ± 0.72	268		8 AKHMETSHIN 99C	CMD2	$e^+e^- \rightarrow \pi^0\pi^0\gamma$
1.5 ± 0.5	268		9 AKHMETSHIN 97C	CMD2	$e^+e^- \rightarrow \pi^+\pi^-\gamma$
3.42 ± 0.30 ± 0.36	164		4 ACHASOV	98I SND	$e^+e^- \rightarrow 5\gamma$
< 1	90		10 AKHMETSHIN 97C	CMD2	$e^+e^- \rightarrow \pi^+\pi^-\gamma$
< 7	90		11 AKHMETSHIN 97C	CMD2	$e^+e^- \rightarrow \pi^+\pi^-\gamma$
< 20	90		12 DRUZHININ	87 ND	$e^+e^- \rightarrow \pi^0\pi^0\gamma$

¹ Obtained by the authors taking into account the $\pi^+\pi^-$ decay mode. Includes a component due to $\pi\pi$ production via the $f_0(500)$ meson. Supersedes ALOISIO 02D.

² From the combined fit of the photon spectra in the reactions $e^+e^- \rightarrow \pi^+\pi^-\gamma$, $\pi^0\pi^0\gamma$.

³ From the negative interference with the $f_0(500)$ meson of AITALA 01B using the ACHASOV 89 parameterization for the $f_0(980)$, a Breit-Wigner for the $f_0(500)$, and ACHASOV 01F for the $\rho\pi$ contribution. Superseded by AMBROSINO 07.

⁴ Assuming that the $\pi^0\pi^0\gamma$ final state is completely determined by the $f_0\gamma$ mechanism, neglecting the decay $B(\phi \rightarrow K\bar{K}\gamma)$ and using $B(f_0 \rightarrow \pi^+\pi^-) = 2B(f_0 \rightarrow \pi^0\pi^0)$.

⁵ Using the value $B(\phi \rightarrow \eta\gamma) = (1.338 \pm 0.053) \times 10^{-2}$.

⁶ For $E_\gamma > 20$ MeV. Supersedes AKHMETSHIN 97C.

⁷ Neglecting other intermediate mechanisms ($\rho\pi, \sigma\gamma$).

⁸ A narrow pole fit taking into account $f_0(980)$ and $f_0(1200)$ intermediate mechanisms.

⁹ For destructive interference with the Bremsstrahlung process

¹⁰ For constructive interference with the Bremsstrahlung process

 $\Gamma(f_0(980)\gamma)/\Gamma(\eta\gamma)$ Γ_{17}/Γ_6

VALUE (units 10^{-2})	EVTS	DOCUMENT ID	TECN	COMMENT
2.48 ± 0.15 OUR FIT				Error includes scale factor of 1.1.
2.6 ± 0.2 $\begin{smallmatrix} +0.8 \\ -0.3 \end{smallmatrix}$	419	1 ACHASOV	00H SND	$e^+e^- \rightarrow \pi^0\pi^0\gamma$

¹ Assuming that the $\pi^0\pi^0\gamma$ final state is completely determined by the $f_0\gamma$ mechanism, neglecting the decay $B(\phi \rightarrow K\bar{K}\gamma)$ and using $B(f_0 \rightarrow \pi^+\pi^-) = 2B(f_0 \rightarrow \pi^0\pi^0)$.

 $\Gamma(\pi^0\pi^0\gamma)/\Gamma_{\text{total}}$ Γ_{18}/Γ

VALUE (units 10^{-4})	CL%	EVTS	DOCUMENT ID	TECN	COMMENT
1.07 ± 0.06 OUR AVERAGE					
1.07 $\begin{smallmatrix} +0.01 \\ -0.03 \end{smallmatrix}$ ± 0.06			1 AMBROSINO	07 KLOE	$e^+e^- \rightarrow \pi^0\pi^0\gamma$
1.08 ± 0.17 ± 0.09		268	AKHMETSHIN 99C	CMD2	$e^+e^- \rightarrow \pi^0\pi^0\gamma$

••• We do not use the following data for averages, fits, limits, etc. •••

1.09 ± 0.03 ± 0.05	2438	ALOISIO	02D	KLOE	$e^+e^- \rightarrow \pi^0\pi^0\gamma$
1.158 ± 0.093 ± 0.052	419	^{2,3} ACHASOV	00H	SND	$e^+e^- \rightarrow \pi^0\pi^0\gamma$
<10	90	DRUZHNIN	87	ND	$e^+e^- \rightarrow 5\gamma$

- ¹Supersedes ALOISIO 02D.
- ²Using the value $B(\phi \rightarrow \eta\gamma) = (1.338 \pm 0.053) \times 10^{-2}$.
- ³Supersedes ACHASOV 98i. Excluding $\omega\pi^0$.

$\Gamma(\pi^0\pi^0\gamma)/\Gamma(\eta\gamma)$ Γ_{18}/Γ_6

VALUE (units 10^{-2})	CL%	EVTS	DOCUMENT ID	TECN	COMMENT
0.86 ± 0.04 OUR FIT					
0.865 ± 0.070 ± 0.017		419	¹ ACHASOV	00H	SND $e^+e^- \rightarrow \pi^0\pi^0\gamma$
0.90 ± 0.08 ± 0.07		164	ACHASOV	98i	SND $e^+e^- \rightarrow 5\gamma$

- ¹Supersedes ACHASOV 98i. Excluding $\omega\pi^0$.

$\Gamma(\pi^+\pi^-\pi^+\pi^-)/\Gamma_{total}$ Γ_{19}/Γ

VALUE (units 10^{-6})	CL%	EVTS	DOCUMENT ID	TECN	COMMENT
6.5 ± 2.7 ± 1.6		6.8k	¹ AKHMETSHIN	17	CMD3 $e^+e^- \rightarrow \pi^+\pi^-\pi^+\pi^-$
3.93 ± 1.74 ± 2.14		3.3k	AKHMETSHIN	00E	CMD2 $e^+e^- \rightarrow \pi^+\pi^-\pi^+\pi^-$
< 870		90	CORDIER	79	WIRE $e^+e^- \rightarrow \pi^+\pi^-\pi^+\pi^-$

- ¹Using the cross section at the ϕ meson peak $\sigma(\phi) = 4172 \pm 42$ nb, the nonresonant cross section $\sigma(0) = 1.263 \pm 0.027$ nb and $\text{Re}(Z) = 0.146 \pm 0.030$, $\text{Im}(Z) = -0.002 \pm 0.024$ for the complex amplitude of the $\phi \rightarrow \pi^+\pi^-\pi^+\pi^-$ transition.

$\Gamma(\pi^+\pi^-\pi^-\pi^0)/\Gamma_{total}$ Γ_{20}/Γ

VALUE (units 10^{-6})	CL%	DOCUMENT ID	TECN	COMMENT	
< 4.6		90	AKHMETSHIN	00E	CMD2 $e^+e^- \rightarrow \pi^+\pi^-\pi^-\pi^0$
< 15.0		95	BARKOV	88	CMD $e^+e^- \rightarrow \pi^+\pi^-\pi^-\pi^0$

$\Gamma(\pi^0 e^+ e^-)/\Gamma_{total}$ Γ_{21}/Γ

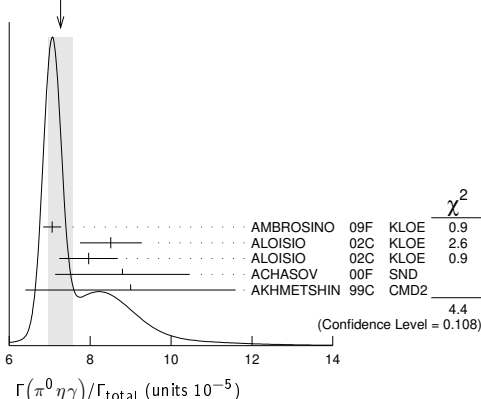
VALUE (units 10^{-5})	CL%	EVTS	DOCUMENT ID	TECN	COMMENT
1.33 ± 0.07 OUR AVERAGE					
1.35 ± 0.05 ± 0.05		9.5k	¹ ANASTASI	16B	KLOE $e^+e^- \rightarrow \pi^0 e^+ e^-$
1.01 ± 0.28 ± 0.29		52	² ACHASOV	02D	SND $e^+e^- \rightarrow \pi^0 e^+ e^-$
1.22 ± 0.34 ± 0.21		46	³ AKHMETSHIN	01c	CMD2 $e^+e^- \rightarrow \pi^0 e^+ e^-$

- ¹Using $B(\pi^0 \rightarrow \gamma\gamma)$ from the 2014 Edition of this Review (PDG 14).
- ²Using various branching ratios from the 2000 Edition of this Review (PDG 00).
- ³Using $B(\pi^0 \rightarrow \gamma\gamma) = 0.98798 \pm 0.00032$, $B(\phi \rightarrow \eta\gamma) = (1.297 \pm 0.033) \times 10^{-2}$, and $B(\eta \rightarrow \pi^+\pi^-\gamma) = (4.75 \pm 0.11) \times 10^{-2}$.

$\Gamma(\pi^0\eta\gamma)/\Gamma_{total}$ Γ_{22}/Γ

VALUE (units 10^{-5})	CL%	EVTS	DOCUMENT ID	TECN	COMMENT
7.27 ± 0.30 OUR AVERAGE					Error includes scale factor of 1.5. See the ideogram below.
7.06 ± 0.22		16.9k	¹ AMBROSINO	09F	KLOE $1.02 e^+e^- \rightarrow \eta\pi^0\gamma$
8.51 ± 0.51 ± 0.57		607	² ALOISIO	02c	KLOE $e^+e^- \rightarrow \eta\pi^0\gamma$
7.96 ± 0.60 ± 0.40		197	³ ALOISIO	02c	KLOE $e^+e^- \rightarrow \eta\pi^0\gamma$
8.8 ± 1.4 ± 0.9		36	⁴ ACHASOV	00F	SND $e^+e^- \rightarrow \eta\pi^0\gamma$
9.0 ± 2.4 ± 1.0		80	AKHMETSHIN	99c	CMD2 $e^+e^- \rightarrow \eta\pi^0\gamma$
7.01 ± 0.10 ± 0.20		13.3k	^{2,5} AMBROSINO	09F	KLOE $1.02 e^+e^- \rightarrow \eta\pi^0\gamma$
7.12 ± 0.13 ± 0.22		3.6k	^{3,6} AMBROSINO	09F	KLOE $1.02 e^+e^- \rightarrow \eta\pi^0\gamma$
8.3 ± 2.3 ± 1.2		20	ACHASOV	98B	SND $e^+e^- \rightarrow 5\gamma$
<250		90	DOLINSKY	91	ND $e^+e^- \rightarrow \pi^0\eta\gamma$

WEIGHTED AVERAGE
7.27 ± 0.30 (Error scaled by 1.5)



- ¹Combined results of $\eta \rightarrow \gamma\gamma$ and $\eta \rightarrow \pi^+\pi^-\pi^0$ decay modes measurements.

²From the decay mode $\eta \rightarrow \gamma\gamma$.

³From the decay mode $\eta \rightarrow \pi^+\pi^-\pi^0$.

⁴Supersedes ACHASOV 98B.

⁵Using $B(\phi \rightarrow \eta\gamma) = (1.304 \pm 0.025)\%$, $B(\eta \rightarrow 3\pi^0) = (32.56 \pm 0.23)\%$, and $B(\eta \rightarrow \gamma\gamma) = (39.31 \pm 0.20)\%$.

⁶Using $B(\phi \rightarrow \eta\gamma) = (1.304 \pm 0.025)\%$, $B(\eta \rightarrow 3\pi^0) = (32.56 \pm 0.23)\%$, and $B(\eta \rightarrow \pi^+\pi^-\pi^0) = (22.73 \pm 0.28)\%$.

$\Gamma(a_0(980)\gamma)/\Gamma_{total}$ Γ_{23}/Γ

VALUE (units 10^{-5})	CL%	EVTS	DOCUMENT ID	TECN	COMMENT
7.6 ± 0.6 OUR FIT					
7.6 ± 0.6 OUR AVERAGE					
7.4 ± 0.7			¹ ALOISIO	02c	KLOE $e^+e^- \rightarrow \eta\pi^0\gamma$
8.8 ± 1.7		36	² ACHASOV	00F	SND $e^+e^- \rightarrow \eta\pi^0\gamma$
11 ± 2			³ GOKALP	02	RVUE $e^+e^- \rightarrow \eta\pi^0\gamma$
<500		90	DOLINSKY	91	ND $e^+e^- \rightarrow \pi^0\eta\gamma$

- ¹Using $M_{a_0(980)} = 984.8$ MeV and assuming $a_0(980)\gamma$ dominance.
- ²Assuming $a_0(980)\gamma$ dominance in the $\eta\pi^0\gamma$ final state.
- ³Using data of ACHASOV 00F.

$\Gamma(f_0(980)\gamma)/\Gamma(a_0(980)\gamma)$ Γ_{17}/Γ_{23}

VALUE	DOCUMENT ID	TECN	COMMENT
6.1 ± 0.6	¹ ALOISIO	02c	KLOE $e^+e^- \rightarrow \eta\pi^0\gamma$

- ¹Using results of ALOISIO 02D and assuming that $f_0(980)$ decays into $\pi\pi$ only and $a_0(980)$ into $\eta\pi$ only.

$\Gamma(K^0\bar{K}^0\gamma)/\Gamma_{total}$ Γ_{24}/Γ

VALUE	CL%	DOCUMENT ID	TECN	COMMENT	
< 1.9 × 10⁻⁸		90	AMBROSINO	09c	KLOE $e^+e^- \rightarrow K_S^0\bar{K}_S^0\gamma$

$\Gamma(\eta'(958)\gamma)/\Gamma_{total}$ Γ_{25}/Γ

VALUE (units 10^{-5})	CL%	EVTS	DOCUMENT ID	TECN	COMMENT
6.21 ± 0.21 OUR FIT					
6.21 ± 0.30 OUR AVERAGE					
6.21 ± 0.27 ± 0.12		3407	¹ AMBROSINO	07A	KLOE $1.02 e^+e^- \rightarrow \pi^+\pi^-\pi^-\gamma$
6.7 ± 2.8 ± 0.8		12	² AULCHENKO	03B	SND $e^+e^- \rightarrow \eta'\gamma$
6.7 ± 5.0 ± 1.5		7	AULCHENKO	03B	SND $e^+e^- \rightarrow 7\gamma$
6.10 ± 0.61 ± 0.43		120	³ ALOISIO	02E	KLOE $1.02 e^+e^- \rightarrow \pi^+\pi^-\pi^-\gamma$
8.2 ± 2.1 ± 1.1		21	⁴ AKHMETSHIN	00B	CMD2 $e^+e^- \rightarrow \pi^+\pi^-\pi^-\gamma$
4.9 ± 2.2 ± 1.6		9	⁵ AKHMETSHIN	00F	CMD2 $e^+e^- \rightarrow \pi^+\pi^-\pi^-\pi^-\gamma$
6.4 ± 1.6		30	⁶ AKHMETSHIN	00F	CMD2 $e^+e^- \rightarrow \eta'(958)\gamma$
6.7 ± 3.4 ± 2.9		5	⁷ AULCHENKO	99	SND $e^+e^- \rightarrow \pi^+\pi^-\pi^-\gamma$
<11		90	AULCHENKO	98	SND $e^+e^- \rightarrow 7\gamma$
12 ± 7 ± 5		±2	⁴ AKHMETSHIN	97B	CMD2 $e^+e^- \rightarrow \pi^+\pi^-\pi^-\gamma$
<41		90	DRUZHNIN	87	ND $e^+e^- \rightarrow \gamma\eta\pi^+\pi^-$

- ¹AMBROSINO 07A reports $[\Gamma(\phi(1020) \rightarrow \eta'(958)\gamma)/\Gamma_{total}] / [B(\phi(1020) \rightarrow \eta\gamma)] = (4.77 \pm 0.09 \pm 0.19) \times 10^{-3}$ which we multiply by our best value $B(\phi(1020) \rightarrow \eta\gamma) = (1.301 \pm 0.025) \times 10^{-2}$. Our first error is their experiment's error and our second error is the systematic error from using our best value.
- ²Averaging AULCHENKO 03B with AULCHENKO 99.
- ³Using $B(\phi \rightarrow \eta\gamma) = (1.297 \pm 0.033)\%$.
- ⁴Using the value $B(\phi \rightarrow \eta\gamma) = (1.26 \pm 0.06) \times 10^{-2}$.
- ⁵Using $B(\phi \rightarrow K_L^0\bar{K}_S^0) = (33.8 \pm 0.6)\%$.
- ⁶Averaging AKHMETSHIN 00B with AKHMETSHIN 00F.
- ⁷Using the value $B(\eta' \rightarrow \eta\pi^+\pi^-) = (43.7 \pm 1.5) \times 10^{-2}$ and $B(\eta \rightarrow \gamma\gamma) = (39.25 \pm 0.31) \times 10^{-2}$.

$\Gamma(\eta'(958)\gamma)/\Gamma(K_L^0\bar{K}_S^0)$ Γ_{25}/Γ_2

VALUE (units 10^{-4})	CL%	EVTS	DOCUMENT ID	TECN	COMMENT
1.83 ± 0.06 OUR FIT					
1.46 ± 0.64 ± 0.18		9	¹ AKHMETSHIN	00F	CMD2 $e^+e^- \rightarrow \pi^+\pi^-\pi^+\pi^- \geq 2\gamma$

- ¹Using various branching ratios of K_S^0 , K_L^0 , η , η' from the 2000 edition (The European Physical Journal **C15** 1 (2000)) of this Review.

$\Gamma(\eta'(958)\gamma)/\Gamma(\eta\gamma)$ Γ_{25}/Γ_6

VALUE (units 10^{-3})	CL%	EVTS	DOCUMENT ID	TECN	COMMENT
4.77 ± 0.15 OUR FIT					
4.78 ± 0.20 OUR AVERAGE					
4.77 ± 0.09 ± 0.19		3407	AMBROSINO	07A	KLOE $1.02 e^+e^- \rightarrow \pi^+\pi^-\pi^-\gamma$
4.70 ± 0.47 ± 0.31		120	¹ ALOISIO	02E	KLOE $1.02 e^+e^- \rightarrow \pi^+\pi^-\pi^-\gamma$
6.5 ± 1.7 ± 1.5		±0.8	AKHMETSHIN	00B	CMD2 $e^+e^- \rightarrow \pi^+\pi^-\pi^-\gamma$
9.5 ± 5.2 ± 4.0		±1.4	² AKHMETSHIN	97B	CMD2 $e^+e^- \rightarrow \pi^+\pi^-\pi^-\gamma$

- ¹From the decay mode $\eta' \rightarrow \eta\pi^+\pi^-$, $\eta \rightarrow \gamma\gamma$.
- ²Superseded by AKHMETSHIN 00B.

Meson Particle Listings

$\phi(1020)$

$\Gamma(\eta\pi^0\pi^0\gamma)/\Gamma_{total}$		Γ_{26}/Γ	
VALUE (units 10^{-5})	CL%	DOCUMENT ID	TECN COMMENT
<2	90	AULCHENKO 98	SND $e^+e^- \rightarrow 7\gamma$

$\Gamma(\mu^+\mu^-\gamma)/\Gamma_{total}$		Γ_{27}/Γ	
VALUE (units 10^{-5})	EVTS	DOCUMENT ID	TECN COMMENT
$1.43 \pm 0.45 \pm 0.14$	27188	1 AKHMETSHIN 99B	CMD2 $e^+e^- \rightarrow \mu^+\mu^-\gamma$
••• We do not use the following data for averages, fits, limits, etc. •••			
2.3 ± 1.0	824 ± 33	2 AKHMETSHIN 97C	CMD2 $e^+e^- \rightarrow \mu^+\mu^-\gamma$

¹ For $E_\gamma > 20$ MeV. Supersedes AKHMETSHIN 97C.
² For $E_\gamma > 20$ MeV.

$\Gamma(\rho\gamma\gamma)/\Gamma_{total}$		Γ_{28}/Γ	
VALUE (units 10^{-4})	CL%	DOCUMENT ID	TECN COMMENT
<1.2	90	AULCHENKO 08	CMD2 $\phi \rightarrow \pi^+\pi^-\gamma\gamma$
••• We do not use the following data for averages, fits, limits, etc. •••			
<5	90	AKHMETSHIN 98	CMD2 $e^+e^- \rightarrow \pi^+\pi^-\gamma\gamma$

$\Gamma(\eta\pi^+\pi^-)/\Gamma_{total}$		Γ_{29}/Γ	
VALUE (units 10^{-5})	CL%	DOCUMENT ID	TECN COMMENT
<1.8	90	AKHMETSHIN 00E	CMD2 $e^+e^- \rightarrow \pi^+\pi^-\pi^+\pi^-\pi^0$
••• We do not use the following data for averages, fits, limits, etc. •••			
<6.1	90	AULCHENKO 08	CMD2 $\phi \rightarrow \eta\pi^+\pi^-$
<30	90	AKHMETSHIN 98	CMD2 $e^+e^- \rightarrow \pi^+\pi^-\gamma\gamma$

$\Gamma(\eta\mu^+\mu^-)/\Gamma_{total}$		Γ_{30}/Γ	
VALUE (units 10^{-6})	CL%	DOCUMENT ID	TECN COMMENT
<9.4	90	AKHMETSHIN 01	CMD2 $e^+e^- \rightarrow \eta e^+e^-$

$\Gamma(\eta U \rightarrow \eta e^+e^-)/\Gamma_{total}$		Γ_{31}/Γ	
VALUE	CL%	DOCUMENT ID	TECN COMMENT
$<1 \times 10^{-6}$	90	1 BABUSCI 13B	KLOE $1.02 e^+e^- \rightarrow \eta e^+e^-$

¹ For a narrow vector U with mass between 5 and 470 MeV, from the combined analysis of $\eta \rightarrow \pi^+\pi^-\pi^0$ and $\eta \rightarrow \pi^0\pi^0\pi^0$ from ARCHILLI 12. Measured 90% CL limits as a function of m_U range from 2.2×10^{-8} to 10^{-6} .

$\Gamma(\text{invisible})/\Gamma(K^+K^-)$		Γ_{32}/Γ_1	
VALUE	CL%	DOCUMENT ID	TECN COMMENT
$<3.4 \times 10^{-4}$	90	ABLIKIM 18S	BES3 $J/\psi \rightarrow \phi\eta \rightarrow \phi\pi^+\pi^-\pi^0$

Lepton Family number (LF) violating modes

$\Gamma(e^\pm\mu^\mp)/\Gamma_{total}$		Γ_{33}/Γ	
VALUE	CL%	DOCUMENT ID	TECN COMMENT
$<2 \times 10^{-6}$	90	ACHASOV 10A	SND $e^+e^- \rightarrow e^\pm\mu^\mp$

$\pi^+\pi^-\pi^0 / \rho\pi$ AMPLITUDE RATIO a_1 IN DECAY OF $\phi \rightarrow \pi^+\pi^-\pi^0$

NIECKNIG 12 describes final-state interactions between the three pions in a dispersive framework using data on the $\pi\pi$ P-wave scattering phase shift.

VALUE (units 10^{-2})	CL%	EVTS	DOCUMENT ID	TECN COMMENT
9.1 ± 1.2 OUR AVERAGE				
$10.1 \pm 4.4 \pm 1.7$		80k	1 AKHMETSHIN 06	CMD2 $1.017-1.021 e^+e^- \rightarrow \pi^+\pi^-\pi^0$
$9.0 \pm 1.1 \pm 0.6$		1.98M	2,3 ALOISIO 03	KLOE $1.02 e^+e^- \rightarrow \pi^+\pi^-\pi^0$

••• We do not use the following data for averages, fits, limits, etc. •••
 $-6 < a_1 < 6$ 500k ³ACHASOV 02 SND $e^+e^- \rightarrow \pi^+\pi^-\pi^0$
 $-16 < a_1 < 11$ 90 9.8k ^{1,4}AKHMETSHIN 98 CMD2 $e^+e^- \rightarrow \pi^+\pi^-\gamma\gamma$

¹ Dalitz plot analysis taking into account interference between the contact and $\rho\pi$ amplitudes.
² From a fit without limitations on charged and neutral ρ masses and widths.
³ Recalculated by us to match the notations of AKHMETSHIN 98.
⁴ Assuming zero phase for the contact term.

PARAMETER β IN $\phi \rightarrow P e^+e^-$ DECAYS

In the one-pole approximation the electromagnetic transition form factor for $\phi \rightarrow P e^+e^-$ ($P = \pi, \eta$) is given as a function of the e^+e^- invariant mass squared, q^2 , by the expression:

$$|F(q^2)|^2 = (1 - q^2/\Lambda^2)^{-2},$$

where vector meson dominance predicts parameter $\Lambda \approx 0.770$ GeV ($\Lambda^{-2} \approx 1.687$ GeV $^{-2}$). The slope of this form factor, $\beta = dF/dq^2(q^2=0)$, equals Λ^{-2} in this approximation.

The measurements below obtain β in the one-pole approximation.

PARAMETER β IN $\phi \rightarrow \pi^0 e^+e^-$ DECAY

VALUE (GeV $^{-2}$)	EVTS	DOCUMENT ID	TECN COMMENT
2.02 ± 0.11	9.5k	1 ANASTASI 16B	KLOE $1.02 e^+e^- \rightarrow \pi^0 e^+e^-$

¹ The error combines statistical and systematic uncertainties.

PARAMETER β IN $\phi \rightarrow \eta e^+e^-$ DECAY

VALUE (GeV $^{-2}$)	EVTS	DOCUMENT ID	TECN COMMENT
1.29 ± 0.13 OUR AVERAGE			
$1.28 \pm 0.10 \pm 0.09$	30k	BABUSCI 15	KLOE $1.02 e^+e^- \rightarrow \eta e^+e^-$
3.8 ± 1.8	213	1 ACHASOV 01B	SND $1.02 e^+e^- \rightarrow \eta e^+e^-$

¹ The uncertainty is statistical only. The systematic one is negligible, in comparison.

$\phi(1020)$ REFERENCES

LEES 21B	PR D104 112003	J.P. Lees et al.	(BABAR Collab.)
ALBRECHT 20	EPJ C80 453	M. Albrecht et al.	(Crystal Barrel Collab.)
HOID 20	EPJ C80 988	B.-L. Hoid, M. Hoferichter, B. Kubis	(BONN, BERN)
AAJ 19H	JHEP 1904 063	R. Aaij et al.	(LHCb Collab.)
HOEFERICHT... 19	JHEP 1908 137	M. Hoferichter, B.-L. Hoid, B. Kubis	(WASH, BONN)
ABLIKIM 18S	PR D98 032001	M. Ablikim et al.	(BESIII Collab.)
AOUDE 18	PR D98 056021	R.T. Aoude et al.	(CMD-3 Collab.)
KOZYREV 18	PL B779 64	E.A. Kozyrev et al.	(CMD-3 Collab.)
AKHMETSHIN 17	PL B768 345	R.R. Akhmetshin et al.	(CMD-3 Collab.)
ACHASOV 16A	PR D93 092001	M.N. Achasov et al.	(SND Collab.)
ANASTASI 16B	PL B757 362	A. Anastasi et al.	(KLOE-2 Collab.)
KOZYREV 16	PL B760 314	E.A. Kozyrev et al.	(CMD-3 Collab.)
BABUSCI 15	PL B742 1	D. Babusci et al.	(KLOE-2 Collab.)
PDG 15	RPP 2015 at pdg.lbl.gov		(PDG Collab.)
LEES 14H	PR D89 092002	J.P. Lees et al.	(BABAR Collab.)
PDG 14B	CP C38 070001	K. Olive et al.	(PDG Collab.)
BABUSCI 13B	PL B720 111	D. Babusci et al.	(KLOE-2 Collab.)
BENAYOUN 13F	EPJ C73 2453	M. Benayoun, P. David, L. DeBuono	(PARIN, BERLIN+)
LEES 13F	PR D87 052010	J.P. Lees et al.	(BABAR Collab.)
LEES 13Q	PR D88 032013	J.P. Lees et al.	(BABAR Collab.)
ARCHILLI 12	PL B706 251	F. Archilli et al.	(KLOE-2 Collab.)
BENAYOUN 12	EPJ C72 1848	M. Benayoun et al.	(KLOE Collab.)
NIECKNIG 12	EPJ C72 2014	F. Niecknig, B. Kubis, S.P. Schneider	(BONN)
PDG 12	PR D86 010001	J. Beringer et al.	(PDG Collab.)
AKHMETSHIN 11	PL B695 412	R.R. Akhmetshin et al.	(CMD-2 Collab.)
ACHASOV 10A	PR D81 057102	M.N. Achasov et al.	(Novosibirsk SND Collab.)
BENAYOUN 10	EPJ C65 211	M. Benayoun et al.	(KLOE Collab.)
AMBROSINO 09C	PL B679 10	F. Ambrosino et al.	(KLOE Collab.)
AMBROSINO 09F	PL B681 5	F. Ambrosino et al.	(KLOE Collab.)
AKHMETSHIN 08	PL B669 217	R.R. Akhmetshin et al.	(CMD-2 Collab.)
AMBROSINO 08G	PL B669 223	F. Ambrosino et al.	(KLOE Collab.)
AULCHENKO 08	JETPL 88 85	V. Aulchenko et al.	(CMD-2 Collab.)
FLOREZ-BAEZ 08	PR D78 077301	F.V. Florez-Baez, G. Lopez Castro	(SND Collab.)
ACHASOV 07B	PR D76 077101	M.N. Achasov et al.	(SND Collab.)
AMBROSINO 07	EPJ C49 473	F. Ambrosino et al.	(KLOE Collab.)
AMBROSINO 07A	PL B648 267	F. Ambrosino et al.	(KLOE Collab.)
DUBYSNKIY 07	PR D75 113001	S. Dubynskiy et al.	(SND Collab.)
ACHASOV 06A	PR D74 014016	M.N. Achasov et al.	(SND Collab.)
AKHMETSHIN 06	PL B642 203	R.R. Akhmetshin et al.	(CMD-2 Collab.)
AKHMETSHIN 05	PL B605 26	R.R. Akhmetshin et al.	(Novosibirsk CMD-2 Collab.)
AMBROSINO 05	PL B608 139	F. Ambrosino et al.	(KLOE Collab.)
AUBERT B 05J	PR D73 052008	B. Aubert et al.	(BABAR Collab.)
AKHMETSHIN 04	PL B578 285	R.R. Akhmetshin et al.	(Novosibirsk CMD-2 Collab.)
AUBERT B 04N	PR D70 072004	B. Aubert et al.	(BABAR Collab.)
ALOISIO 03	PL B561 55	A. Aloisio et al.	(KLOE Collab.)
AULCHENKO 03B	JETP 97 24	V.M. Aulchenko et al.	(Novosibirsk SND Collab.)
ACHASOV 02D	PR D65 032002	M.N. Achasov et al.	(Novosibirsk SND Collab.)
ACHASOV 02D	JETPL 75 449	M.N. Achasov et al.	(Novosibirsk SND Collab.)
ALOISIO 02C	PL B536 209	A. Aloisio et al.	(KLOE Collab.)
ALOISIO 02D	PL B537 21	A. Aloisio et al.	(KLOE Collab.)
ALOISIO 02E	PL B541 45	A. Aloisio et al.	(KLOE Collab.)
FISCHBACH 02	PL B526 355	E. Fischbach, A.W. Overhauser, B. Woodahl	(KLOE Collab.)
GOKALP 02	JP G28 2783	A. Gokalp et al.	(Novosibirsk SND Collab.)
ACHASOV 01B	PL B504 275	M.N. Achasov et al.	(Novosibirsk SND Collab.)
ACHASOV 01F	PR D63 072002	M.N. Achasov et al.	(Novosibirsk SND Collab.)
ACHASOV 01E	PR D63 094007	M.N. Achasov, V.V. Gubin	(Novosibirsk SND Collab.)
ACHASOV 01G	PRL 86 1638	M.N. Achasov et al.	(Novosibirsk SND Collab.)
AITALA 01B	PL B501 191	R.R. Akhmetshin et al.	(FIAL ET91 Collab.)
AKHMETSHIN 01	PL B501 191	R.R. Akhmetshin et al.	(Novosibirsk CMD-2 Collab.)
AKHMETSHIN 01B	PL B509 217	R.R. Akhmetshin et al.	(Novosibirsk CMD-2 Collab.)
AKHMETSHIN 01C	PL B503 237	R.R. Akhmetshin et al.	(Novosibirsk CMD-2 Collab.)
BENAYOUN 01	EPJ C22 503	M. Benayoun, H.B. O'Connell	(Novosibirsk SND Collab.)
ACHASOV 00	EPJ C12 25	M.N. Achasov et al.	(Novosibirsk SND Collab.)
ACHASOV 00B	JETP 90 17	M.N. Achasov et al.	(Novosibirsk SND Collab.)
ACHASOV 00C	PL B474 188	M.N. Achasov et al.	(Novosibirsk SND Collab.)
ACHASOV 00D	JETPL 72 282	M.N. Achasov et al.	(Novosibirsk SND Collab.)
ACHASOV 00E	NP B569 158	M.N. Achasov et al.	(Novosibirsk SND Collab.)
ACHASOV 00F	PL B479 53	M.N. Achasov et al.	(Novosibirsk SND Collab.)
ACHASOV 00H	PL B485 349	M.N. Achasov et al.	(Novosibirsk SND Collab.)
AKHMETSHIN 00B	PL B473 337	R.R. Akhmetshin et al.	(Novosibirsk CMD-2 Collab.)
AKHMETSHIN 00E	PL B491 81	R.R. Akhmetshin et al.	(Novosibirsk CMD-2 Collab.)
AKHMETSHIN 00F	PL B494 26	R.R. Akhmetshin et al.	(Novosibirsk CMD-2 Collab.)
AULCHENKO 00A	JETP 90 927	V.M. Aulchenko et al.	(Novosibirsk SND Collab.)
BRAMON 00	PL B486 406	A. Bramon et al.	(Novosibirsk SND Collab.)
PDG 00	EPJ C15 1	D.E. Groom et al.	(PDG Collab.)
ACHASOV 99	PL B449 122	M.N. Achasov et al.	(Novosibirsk CMD-2 Collab.)
ACHASOV 99C	PL B456 304	M.N. Achasov et al.	(Novosibirsk CMD-2 Collab.)
AKHMETSHIN 99B	PL B462 371	R.R. Akhmetshin et al.	(Novosibirsk CMD-2 Collab.)
AKHMETSHIN 99C	PL B462 380	R.R. Akhmetshin et al.	(Novosibirsk CMD-2 Collab.)
AKHMETSHIN 99D	PL B466 385	R.R. Akhmetshin et al.	(Novosibirsk CMD-2 Collab.)
AKHMETSHIN 99F	PL B508 217 (err.)	R.R. Akhmetshin et al.	(Novosibirsk CMD-2 Collab.)
AKHMETSHIN 99G	PL B500 242	R.R. Akhmetshin et al.	(Novosibirsk CMD-2 Collab.)
AULCHENKO 99	JETPL 69 97	V.M. Aulchenko et al.	(Novosibirsk CMD-2 Collab.)
ACHASOV 98B	PL B438 441	M.N. Achasov et al.	(Novosibirsk SND Collab.)
ACHASOV 98F	JETPL 68 573	M.N. Achasov et al.	(Novosibirsk SND Collab.)
ACHASOV 98I	PL B440 442	M.N. Achasov et al.	(Novosibirsk SND Collab.)
AKHMETSHIN 98	PL B434 426	R.R. Akhmetshin et al.	(CMD-2 Collab.)
AULCHENKO 98	PL B436 199	V.M. Aulchenko et al.	(Novosibirsk SND Collab.)
BARBERIS 98	PL B432 436	D. Barberis et al.	(Omega Expt.)
AKHMETSHIN 97B	PL B415 445	R.R. Akhmetshin et al.	(NOVO, BOST, PITT+)
AKHMETSHIN 97C	PL B415 452	R.R. Akhmetshin et al.	(Novosibirsk CMD-2 Collab.)
BENAYOUN 96	ZPHY C72 221	M. Benayoun et al.	(IPNP, NOVO)
AKHMETSHIN 95	PL B364 199	R.R. Akhmetshin et al.	(Novosibirsk CMD-2 Collab.)
DOLINSKY 91	PRPL 202 99	S.I. Dolinsky et al.	(NOVO)
KUHN 90	ZPHY C48 445	J.H. Kuhn et al.	(MPIM)
ACHASOV 89	NP B315 465	M.N. Achasov, V.N. Ivanchenko	(NOVO)
DOLINSKY 89	ZPHY C42 511	S.I. Dolinsky et al.	(NOVO)
BARKOV 88	SJNP 47 248	L.M. Barkov et al.	(NOVO)
DOLINSKY 88	SJNP 48 277	S.I. Dolinsky et al.	(NOVO)

See key on page 1127

Meson Particle Listings

$\phi(1020)$, $h_1(1170)$, $b_1(1235)$

NAME	PDG	REF	TECN	CHG	COMMENT
DRUZHININ	87	ZPHY C37 1			V.P. Druzhinin et al. (NOVO)
ARMSTRONG	86	PL 166B 245			T.A. Armstrong et al. (ATHU, BARI, BIRM+) (NOVO)
ATKINSON	86	ZPHY C30 521			M. Atkinson et al. (BONN, CERN, GLAS+) (NOVO)
BEBEK	86	PRL 56 1893			C. Bebek et al. (CLEO Collab.) (NOVO)
DAVENPORT	86	PR D33 2519			T.F. Davenport (TUFTS, ARIZ, FNAL, FSU, NDAM+) (NOVO)
DIJKSTRA	86	ZPHY C31 375			H. Dijkstra et al. (ANIK, BRIS, CERN+) (NOVO)
FRAME	86	NP B276 667			D. Frame et al. (GLAS) (NOVO)
GOLUBEV	86	SJNP 44 400			V.B. Golubev et al. (NOVO)
ALBRECHT	85D	PL 153B 343			H. Albrecht et al. (ARGUS Collab.) (NOVO)
GOLUBEV	85	SJNP 41 756			V.B. Golubev et al. (NOVO)
DRUZHININ	84	PL 144B 136			V.P. Druzhinin et al. (NOVO)
ARMSTRONG	83B	NP B224 193			T.A. Armstrong et al. (BARI, BIRM, CERN+) (NOVO)
BARATE	83	PL 121B 449			R. Barate et al. (SACL, LOIC, SHMP, IND) (NOVO)
KURDADZE	83C	JETPL 38 366			L.M. Kurdadze et al. (NOVO)
ARENTO	82	PR D25 2241			M.W. Arenton et al. (ANL, ILL) (NOVO)
PELLINEN	82	PS 25 599			A. Pellinen, M. Roos (HEL5) (NOVO)
DAUM	81	PL 100B 439			C. Daum et al. (AMST, BRIS, CERN, CRAC+) (NOVO)
IVANOV	81	PL 107B 297			P.M. Ivanov et al. (NOVO)
VASSERMAN	81	PL 99B 62			S.I. Eidelman (NOVO)
CORDIER	80	NP B172 13			A. Cordier et al. (LALO) (NOVO)
CORDIER	79	PL 81B 389			A. Cordier et al. (LALO) (NOVO)
BUKIN	78B	SJNP 27 521			A.D. Bukin et al. (NOVO)
BUKIN	78C	SJNP 27 516			A.D. Bukin et al. (NOVO)
COOPER	78B	NP 146 1			A.M. Cooper et al. (TATA, CERN, CDEF+) (NOVO)
LOSTY	78	NP B133 38			M.J. Losty et al. (CERN, AMST, NIJM+) (NOVO)
AKERLOF	77	PRL 39 861			C.W. Akerlof et al. (FNAL, MICH, PURD) (NOVO)
ANDREWS	77	PRL 38 198			D.E. Andrews et al. (ROCH) (NOVO)
BALDI	77	PL 68B 381			R. Baldi et al. (GEVA) (NOVO)
CERRADA	77B	NP B126 241			M. Cerrada et al. (AMST, CERN, NIJM+) (NOVO)
COHEN	77	PRL 38 269			D. Cohen et al. (ANL) (NOVO)
LAVEN	77	NP B127 43			H. Laven et al. (AACH3, BERL, CERN, LOIC+) (NOVO)
LYONS	77	NP B125 207			L. Lyons, A.M. Cooper, A.G. Clark (OXF) (NOVO)
COSME	76	PL 63B 352			G. Cosme et al. (ORSAY) (NOVO)
KALBFLEISCH	76	PR D13 22			G.R. Kalbfleisch, R.C. Strand, J.W. Chapman (BNL+) (NOVO)
PARROUR	76	PL 63B 357			G. Parrou et al. (ORSAY) (NOVO)
PARROUR	76B	PL 63B 342			G. Parrou et al. (ORSAY) (NOVO)
KALBFLEISCH	75	PR D11 987			G.R. Kalbfleisch, R.C. Strand, J.W. Chapman (BNL+) (NOVO)
AYRES	74	PRL 32 1463			D.S. Ayres et al. (ANL) (NOVO)
BESCH	74	NP B70 257			H.J. Besch et al. (BONN) (NOVO)
COSME	74	PL 48B 155			G. Cosme et al. (ORSAY) (NOVO)
COSME	74B	PL 48B 159			G. Cosme et al. (ORSAY) (NOVO)
DEGROOT	74	NP B74 77			A.J. de Groot et al. (AMST, NIJM) (NOVO)
AUGUSTIN	73	PRL 30 462			J.E. Augustin et al. (ORSAY) (NOVO)
BALLAM	73	PR D7 3150			J. Ballam et al. (SLAC, LBL) (NOVO)
BINNIE	73B	PR D8 2789			D.M. Binnie et al. (LOIC, SHMP) (NOVO)
AGUILAR	72B	PR D6 29			M. Aguilar-Benitez et al. (BNL) (NOVO)
ALVENSELEB	72	PRL 28 666			H. Alvensleben et al. (MIT, DESY) (NOVO)
BORENSTEIN	72	PR D5 1559			S.R. Borenstein et al. (BNL, MICH) (NOVO)
COLLEY	72	NP B50 1			D.C. Colley et al. (BIRM, GLAS) (NOVO)
BALAKIN	71	PL 34B 328			V.E. Balakin et al. (NOVO)
CHATELUS	71	Thesis LAL 1247			Y. Chatelus (STRB) (NOVO)
HAYES	71	PR D4 899			S. Hayes et al. (CORN) (NOVO)
STOTTLEMYER	71	Thesis ORO 2504 170			A.R. Stottlemeyer (UMD) (NOVO)
BIZOT	70	PL 32B 416			J.C. Bizot et al. (ORSAY) (NOVO)
EARLES	70	PRL 25 1312			D.R. Earles et al. (NEAS) (NOVO)
LINDSEY	66	PR 147 913			J.S. Lindsey, G. Smith (LRL) (NOVO)
LONDON	66	PR 143 1034			G.W. London et al. (BNL, SYR) IGJPC (NOVO)
BADIER	65B	PL 17 337			J. Badier et al. (EPOL, SACL, AMST) (NOVO)
LINDSEY	65	PRL 15 221			J.S. Lindsey, G.A. Smith (LRL) (NOVO)
SCHLEIN	63	PRL 10 368			P.E. Schlein et al. (UCLA) IGJPC (NOVO)

$h_1(1170)$ BRANCHING RATIOS

$\Gamma(\rho\pi)/\Gamma_{total}$	DOCUMENT ID	TECN	COMMENT	Γ_1/Γ
••• We do not use the following data for averages, fits, limits, etc. •••				
seen	ANDO	92	SPEC	$8\pi^-p \rightarrow \pi^+\pi^-\pi^0 n$
seen	ATKINSON	84	OMEG	$20-70 \gamma p \rightarrow \pi^+\pi^-\pi^0 p$
seen	DANKOWY...	81	SPEC	$8\pi p \rightarrow 3\pi n$

$h_1(1170)$ REFERENCES

NAME	PDG	REF	TECN	CHG	COMMENT
ANDO	92	PL B291 496			A. Ando et al. (KEK, KYOT, NIRS, SAGA+) (NOVO)
ATKINSON	84	NP B231 15			M. Atkinson et al. (BONN, CERN, GLAS+) (NOVO)
DANKOWY...	81	PRL 46 580			J.A. Dankowych et al. (TNT0, BNL, CARL+) (NOVO)
BOWLER	75	NP B97 227			M.G. Bowler et al. (OXFT, DARE) (NOVO)

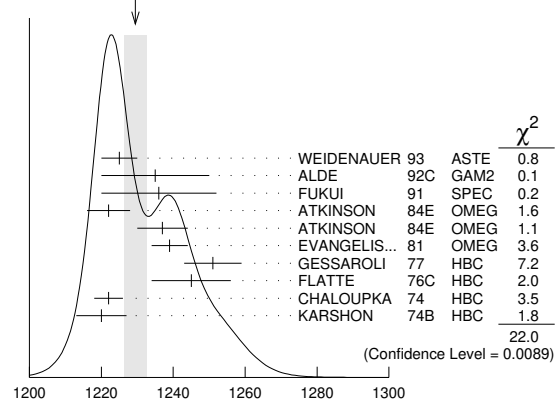
$b_1(1235)$

$$I^G(J^{PC}) = 1^+(1^{+-})$$

$b_1(1235)$ MASS

VALUE (MeV)	EVTS	DOCUMENT ID	TECN	CHG	COMMENT
1229.5 ± 3.2 OUR AVERAGE		Error includes scale factor of 1.6.			See the ideogram below.
1225 ± 5		WEIDENAUER	93	ASTE	$\bar{p}p \rightarrow 2\pi^+2\pi^-\pi^0$
1235 ± 15		ALDE	92C	GAM2	$38,100 \pi^-p \rightarrow \omega\pi^0 n$
1236 ± 16		FUKUI	91	SPEC	$8.95 \pi^-p \rightarrow \omega\pi^0 n$
1222 ± 6		ATKINSON	84E	OMEG ±	$25-55 \gamma p \rightarrow \omega\pi X$
1237 ± 7		ATKINSON	84E	OMEG 0	$25-55 \gamma p \rightarrow \omega\pi X$
1239 ± 5		EVANGELIS...	81	OMEG -	$12 \pi^-p \rightarrow \omega\pi p$
1251 ± 8	450	GESSAROLI	77	HBC -	$11 \pi^-p \rightarrow \pi^-\omega p$
1245 ± 11	890	FLATTE	76C	HBC -	$4.2 K^-p \rightarrow \pi^-\omega\Sigma^+$
1222 ± 4	1400	CHALLOUPKA	74	HBC -	$3.9 \pi^-p$
1220 ± 7	600	KARSHON	74B	HBC +	$4.9 \pi^+p$
••• We do not use the following data for averages, fits, limits, etc. •••					
1190 ± 10		AUGUSTIN	89	DM2 ±	$e^+e^- \rightarrow 5\pi$
1213 ± 5		ATKINSON	84C	OMEG 0	$20-70 \gamma p$
1271 ± 11		COLLICK	84	SPEC +	$200 \pi^+Z \rightarrow Z\pi\omega$

WEIGHTED AVERAGE
1229.5±3.2 (Error scaled by 1.6)



NAME	PDG	TECN	CHG	χ^2
WEIDENAUER	93	ASTE		0.8
ALDE	92C	GAM2		0.1
FUKUI	91	SPEC		0.2
ATKINSON	84E	OMEG		1.6
ATKINSON	84E	OMEG		1.1
EVANGELIS...	81	OMEG		3.6
GESSAROLI	77	HBC		7.2
FLATTE	76C	HBC		2.0
CHALLOUPKA	74	HBC		3.5
KARSHON	74B	HBC		1.8
				22.0

$h_1(1170)$

$$I^G(J^{PC}) = 0^-(1^{+-})$$

$h_1(1170)$ MASS

VALUE (MeV)	DOCUMENT ID	TECN	CHG	COMMENT
1166 ± 5 ± 3	1 ANDO	92	SPEC	$8\pi^-p \rightarrow \pi^+\pi^-\pi^0 n$
••• We do not use the following data for averages, fits, limits, etc. •••				
1168 ± 4	ANDO	92	SPEC	$8\pi^-p \rightarrow \pi^+\pi^-\pi^0 n$
1190 ± 60	2 DANKOWY...	81	SPEC 0	$8\pi p \rightarrow 3\pi n$
1 Average and spread of values using 2 variants of the model of BOWLER 75.				
2 Uses the model of BOWLER 75.				

$h_1(1170)$ WIDTH

VALUE (MeV)	DOCUMENT ID	TECN	CHG	COMMENT
375 ± 6 ± 34	3 ANDO	92	SPEC	$8\pi^-p \rightarrow \pi^+\pi^-\pi^0 n$
••• We do not use the following data for averages, fits, limits, etc. •••				
345 ± 6	ANDO	92	SPEC	$8\pi^-p \rightarrow \pi^+\pi^-\pi^0 n$
320 ± 50	4 DANKOWY...	81	SPEC 0	$8\pi p \rightarrow 3\pi n$
3 Average and spread of values using 2 variants of the model of BOWLER 75.				
4 Uses the model of BOWLER 75.				

$h_1(1170)$ DECAY MODES

Mode	Fraction (Γ_i/Γ)
$\rho\pi$	seen

$b_1(1235)$ WIDTH

VALUE (MeV)	EVTS	DOCUMENT ID	TECN	CHG	COMMENT
142 ± 9 OUR AVERAGE		Error includes scale factor of 1.2.			
113 ± 12		WEIDENAUER	93	ASTE	$\bar{p}p \rightarrow 2\pi^+2\pi^-\pi^0$
160 ± 30		ALDE	92C	GAM2	$38,100 \pi^-p \rightarrow \omega\pi^0 n$
151 ± 31		FUKUI	91	SPEC	$8.95 \pi^-p \rightarrow \omega\pi^0 n$
170 ± 15		EVANGELIS...	81	OMEG -	$12 \pi^-p \rightarrow \omega\pi p$
170 ± 50	225	BALTAY	78B	HBC +	$15 \pi^+p \rightarrow p4\pi$
155 ± 32	450	GESSAROLI	77	HBC -	$11 \pi^-p \rightarrow \pi^-\omega p$
182 ± 45	890	FLATTE	76C	HBC -	$4.2 K^-p \rightarrow \pi^-\omega\Sigma^+$
135 ± 20	1400	CHALLOUPKA	74	HBC -	$3.9 \pi^-p$
156 ± 22	600	KARSHON	74B	HBC +	$4.9 \pi^+p$
••• We do not use the following data for averages, fits, limits, etc. •••					
210 ± 19		AUGUSTIN	89	DM2 ±	$e^+e^- \rightarrow 5\pi$
231 ± 14		ATKINSON	84C	OMEG 0	$20-70 \gamma p$
232 ± 29		COLLICK	84	SPEC +	$200 \pi^+Z \rightarrow Z\pi\omega$

Meson Particle Listings

$b_1(1235), a_1(1260)$

$b_1(1235)$ DECAY MODES

Mode	Fraction (Γ_i/Γ)	Confidence level
Γ_1 $\omega\pi$ [D/S amplitude ratio = 0.277 ± 0.027]	seen	
Γ_2 $\pi^\pm\gamma$	$(1.6 \pm 0.4) \times 10^{-3}$	
Γ_3 $\eta\rho$	seen	
Γ_4 $\pi^+\pi^+\pi^-\pi^0$	< 50 %	84%
Γ_5 $K^*(892)^\pm K^\mp$	seen	
Γ_6 $(K\bar{K})^\pm\pi^0$	< 8 %	90%
Γ_7 $K_S^0 K_S^0 \pi^\pm$	< 6 %	90%
Γ_8 $K_S^0 K_S^0 \pi^\pm$	< 2 %	90%
Γ_9 $\phi\pi$	< 1.5 %	84%

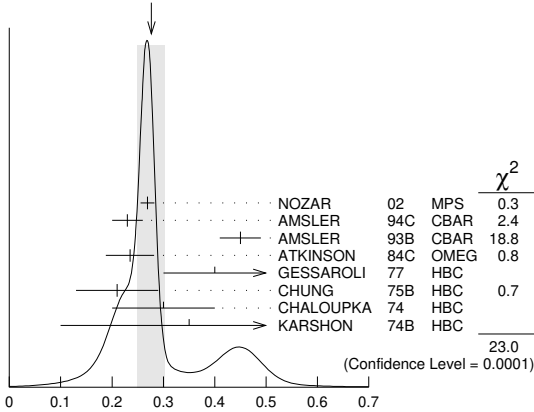
$b_1(1235)$ PARTIAL WIDTHS

$\Gamma(\pi^\pm\gamma)$	VALUE (keV)	DOCUMENT ID	TECN	CHG	COMMENT
Γ_2	230 ± 60	COLLICK	84	SPEC	+ 200 $\pi^+ Z \rightarrow Z\pi\omega$

$b_1(1235)$ D-wave/S-wave AMPLITUDE RATIO IN DECAY OF $b_1(1235) \rightarrow \omega\pi$

VALUE	EVTS	DOCUMENT ID	TECN	CHG	COMMENT
0.277 ± 0.027 OUR AVERAGE		Error includes scale factor of 2.4. See the ideogram below.			
$0.269 \pm 0.009 \pm 0.010$		NOZAR	02	MPS	- 18 $\pi^- p \rightarrow \omega\pi^- p$
0.23 ± 0.03		AMSLER	94c	CBAR	$0.0 \bar{p} p \rightarrow \omega\eta\pi^0$
0.45 ± 0.04		AMSLER	93b	CBAR	$0.0 \bar{p} p \rightarrow \omega\pi^0\pi^0$
0.235 ± 0.047		ATKINSON	84c	OMEG	20-70 γp
0.4 -0.1		GESSAROLI	77	HBC	- 11 $\pi^- p \rightarrow \pi^- \omega p$
0.21 ± 0.08		CHUNG	75b	HBC	+ 7.1 $\pi^+ p$
0.3 ± 0.1		CHALOUPKA	74	HBC	- 3.9-7.5 $\pi^- p$
0.35 ± 0.25	600	KARSHON	74b	HBC	+ 4.9 $\pi^+ p$

WEIGHTED AVERAGE
 0.277 ± 0.027 (Error scaled by 2.4)



$b_1(1235)$ D-wave/S-wave amplitude ratio in decay of $b_1(1235) \rightarrow \omega\pi$

$b_1(1235)$ D-wave/S-wave AMPLITUDE PHASE DIFFERENCE IN DECAY OF $b_1(1235) \rightarrow \omega\pi$

VALUE ($^\circ$)	DOCUMENT ID	TECN	CHG	COMMENT
$10.5 \pm 2.4 \pm 3.9$	NOZAR	02	MPS	- 18 $\pi^- p \rightarrow \omega\pi^- p$

$b_1(1235)$ BRANCHING RATIOS

$\Gamma(\eta\rho)/\Gamma(\omega\pi)$	VALUE	DOCUMENT ID	TECN	COMMENT
Γ_3/Γ_1	<0.10	ATKINSON	84d	OMEG 20-70 γp

$\Gamma(\pi^+\pi^+\pi^-\pi^0)/\Gamma(\omega\pi)$	VALUE	DOCUMENT ID	TECN	CHG	COMMENT
Γ_4/Γ_1	<0.5	ABOLINS	63	HBC	+ 3.5 $\pi^+ p$

$\Gamma(K^*(892)^\pm K^\mp)/\Gamma_{total}$	VALUE	DOCUMENT ID	TECN	COMMENT
Γ_5/Γ	seen	1 ABLIKIM	10E	BES2 $J/\psi \rightarrow K^\pm K_S^0 \pi^\mp \pi^0$

¹ From a fit including ten additional resonances and energy-independent Breit-Wigner width.

$\Gamma((K\bar{K})^\pm\pi^0)/\Gamma(\omega\pi)$	VALUE	CL%	DOCUMENT ID	TECN	CHG	COMMENT	Γ_6/Γ_1
Γ_6/Γ_1	<0.08	90	BALTAY	67	HBC	\pm 0.0 $\bar{p} p$	

$\Gamma(K_S^0 K_S^0 \pi^\pm)/\Gamma(\omega\pi)$	VALUE	CL%	DOCUMENT ID	TECN	CHG	COMMENT	Γ_7/Γ_1
Γ_7/Γ_1	<0.06	90	BALTAY	67	HBC	\pm 0.0 $\bar{p} p$	

$\Gamma(K_S^0 K_S^0 \pi^\pm)/\Gamma(\omega\pi)$	VALUE	CL%	DOCUMENT ID	TECN	CHG	COMMENT	Γ_8/Γ_1
Γ_8/Γ_1	<0.02	90	BALTAY	67	HBC	\pm 0.0 $\bar{p} p$	

$\Gamma(\phi\pi)/\Gamma(\omega\pi)$	VALUE	CL%	DOCUMENT ID	TECN	CHG	COMMENT	Γ_9/Γ_1
Γ_9/Γ_1	<0.004	95	VIKTOROV	96	SPEC	0 32.5 $\pi^- p \rightarrow K^+ K^- \pi^0 n$	
	<0.04	95	BIZZARRI	69	HBC	\pm 0.0 $\bar{p} p$	
	<0.015		DAHL	67	HBC	1.6-4.2 $\pi^- p$	

$b_1(1235)$ REFERENCES

ABLIKIM 10E	PL B693 88	M. Ablikim et al.	(BES II Collab.)
NOZAR 02	PL B541 35	M. Nozar et al.	(SERP)
VIKTOROV 96	PAN 59 1184	V.A. Viktorov et al.	(SERP)
	Translated from YAF 59 1239.		
AMSLER 94C	PL B327 425	C. Amstler et al.	(Crystal Barrel Collab.)
AMSLER 93B	PL B311 362	C. Amstler et al.	(Crystal Barrel Collab.)
WEIDENAUER 93	ZPHY C59 387	P. Weidenauer et al.	(ASTERIX Collab.)
ALDE 92C	ZPHY C54 553	D.M. Alde et al.	(BELG, SERP, KEK, LANL+)
FUKUI 91	PL B257 241	S. Fukui et al.	(SUGI, NAGO, KEK, KYOT+)
AUGUSTIN 89	NP B320 1	J.E. Augustin, G. Cosme	(DM2 Collab.)
ATKINSON 84C	NP B243 1	M. Atkinson et al.	(BONN, CERN, GLAS+)
ATKINSON 84D	NP B242 269	M. Atkinson et al.	(BONN, CERN, GLAS+)
ATKINSON 84E	PL 138B 459	M. Atkinson et al.	(BONN, CERN, GLAS+)
COLLICK 84	PRL 53 2374	B. Collick et al.	(MINN, ROCH, FNAL)
EVANGELISTA... 81	NP B178 197	C. Evangelista et al.	(BARI, BONN, CERN+)
BALTAY 78B	PR D17 62	C. Baltay et al.	(COLU, BING)
GESSAROLI 77	NP B126 382	R. Gessaroli et al.	(BGN, FIRZ, GENO+)
FLATTE 76C	PL 64B 225	S.M. Flatte et al.	(CERN, AMST, NIJ+)
CHUNG 75B	PR D11 2426	S.U. Chung et al.	(BNL, LBL, UCSC)
CHALOUPKA 74	PL 51B 407	V. Chaloupka et al.	(CERN) JP
KARSHON 74B	PR D10 3608	U. Karshon et al.	(REHO) JP
BIZZARRI 69	NP B14 169	R. Bizzarri et al.	(CERN, CDEF)
BALTAY 67	PRL 18 93	C. Baltay et al.	(COLU)
DAHL 67	PR 163 1377	O.I. Dahl et al.	(LRL)
ABOLINS 63	PRL 11 381	M.A. Abolins et al.	(UCSD)

$a_1(1260)$

$$J^{PC} = 1^-(1^{++})$$

See also our review under the $a_1(1260)$ in PDG 06, Journal of Physics **G33** 1 (2006).

$a_1(1260)$ MASS

VALUE (MeV)	EVTS	DOCUMENT ID	TECN	COMMENT
1230 ± 40 OUR ESTIMATE				
1299 ± 12	46M	1 AGHASYAN	18B	COMP $190 \pi^- p \rightarrow \pi^- \pi^+ \pi^- p$
-28				

• • • We do not use the following data for averages, fits, limits, etc. • • •				
$1195.05 \pm 1.05 \pm 6.33$	894k	AAIJ	18A1	LHCB $D^0 \rightarrow K^\mp \pi^\pm \pi^\pm \pi^\mp$
1209 ± 4	$+12$ -9	2 MIKHASENKO	18	RVUE $\tau^- \rightarrow \pi^- \pi^+ \pi^- \nu_\tau$
1225 ± 9	± 20	3 DARGENT	17	RVUE $D^0 \rightarrow \pi^- \pi^+ \pi^- \pi^+$
1255 ± 6	$+7$ -17	4 ALEKSEEV	10	COMP $190 \pi^- p \rightarrow \pi^- \pi^+ \pi^- p$
1243 ± 12	± 20	5 AUBERT	07AU	BABR $10.6 e^+ e^- \rightarrow \pi^0 \rho^\pm \pi^\mp \gamma$
1230-1270	6360	6 LINK	07A	FOCS $D^0 \rightarrow \pi^- \pi^+ \pi^- \pi^+$
1203 ± 3		7 GOMEZ-DUM...	04	RVUE $\tau^+ \rightarrow \pi^+ \pi^+ \pi^- \nu_\tau$
1330 ± 24	90k	SALVINI	04	OBLX $\bar{p} p \rightarrow 2\pi^+ 2\pi^-$
1331 ± 10	± 3	8 ASNER	00	CLE2 $10.6 e^+ e^- \rightarrow \pi^+ \pi^- \nu_\tau$
1255 ± 7	± 6	9 ABREU	98G	DLPH $e^+ e^-$
1207 ± 5	± 8	10 ABREU	98G	DLPH $e^+ e^-$
1196 ± 4	± 5	11,12 ABREU	98G	DLPH $e^+ e^-$
1240 ± 10		BARBERIS	98B	$450 \bar{p} p \rightarrow \rho_\tau \pi^+ \pi^- \pi^0 p_S$
1262 ± 9	± 7	9,13 ACKERSTAFF	97R	OPAL $E_{cm}^{e^+e^-} = 88-94, \tau \rightarrow$
1210 ± 7	± 2	10,13 ACKERSTAFF	97R	OPAL $E_{cm}^{3\pi\nu} = 88-94, \tau \rightarrow$
1211 ± 7	$+50$ -0	10 ALBRECHT	93C	ARG $\tau^+ \rightarrow \pi^+ \pi^+ \pi^- \nu$
1121 ± 8		14 ANDO	92	SPEC $8 \pi^- p \rightarrow \pi^+ \pi^- \pi^0 n$
1242 ± 37		15 IVANOV	91	RVUE $\tau \rightarrow \pi^+ \pi^+ \pi^- \nu$
1260 ± 14		16 IVANOV	91	RVUE $\tau \rightarrow \pi^+ \pi^+ \pi^- \nu$
1250 ± 9		17 IVANOV	91	RVUE $\tau \rightarrow \pi^+ \pi^+ \pi^- \nu$
1208 ± 15		ARMSTRONG	90	OMEG $300.0 \bar{p} p \rightarrow \bar{p} p \pi^+ \pi^- \pi^0$

See key on page 1127

Meson Particle Listings

$a_1(1260)$

1220	±15	18	ISGUR	89	RVUE	$\tau^+ \rightarrow \pi^+ \pi^+ \pi^- \nu$
1260	±25	19	BOWLER	88	RVUE	
1166	±18		BAND	87	MAC	$\tau^+ \rightarrow \pi^+ \pi^+ \pi^- \nu$
1164	±41	±23	BAND	87	MAC	$\tau^+ \rightarrow \pi^+ \pi^0 \pi^0 \nu$
1250	±40	18	TORNQVIST	87	RVUE	
1046	±11		ALBRECHT	86B	ARG	$\tau^+ \rightarrow \pi^+ \pi^+ \pi^- \nu$
1056	±20	±15	RUCKSTUHL	86	DLCO	$\tau^+ \rightarrow \pi^+ \pi^+ \pi^- \nu$
1194	±14	±10	SCHMIDKE	86	MRK2	$\tau^+ \rightarrow \pi^+ \pi^+ \pi^- \nu$
1255	±23		BELLINI	85	SPEC	$40 \pi^- A \rightarrow \pi^- \pi^+ \pi^- A$
1240	±80		DANKOWY...	81	SPEC	$8.45 \pi^- \rho \rightarrow n3\pi$
1280	±30		DAUM	81B	CNTR	$63,94 \pi^- \rho \rightarrow p3\pi$
1041	±13		GAVILLET	77	HBC	$4.2 K^- \rho \rightarrow \Sigma 3\pi$

405	±75	±25	BAND	87	MAC	$\tau^+ \rightarrow \pi^+ \pi^+ \pi^- \nu$
419	±108	±57	BAND	87	MAC	$\tau^+ \rightarrow \pi^+ \pi^0 \pi^0 \nu$
521	±27		ALBRECHT	86B	ARG	$\tau^+ \rightarrow \pi^+ \pi^+ \pi^- \nu$
476	+132	±54	RUCKSTUHL	86	DLCO	$\tau^+ \rightarrow \pi^+ \pi^+ \pi^- \nu$
462	±56	±30	SCHMIDKE	86	MRK2	$\tau^+ \rightarrow \pi^+ \pi^+ \pi^- \nu$
292	±40		BELLINI	85	SPEC	$40 \pi^- A \rightarrow \pi^- \pi^+ \pi^- A$
380	±100		DANKOWY...	81	SPEC	$8.45 \pi^- \rho \rightarrow n3\pi$
300	±50		DAUM	81B	CNTR	$63,94 \pi^- \rho \rightarrow p3\pi$
230	±50		GAVILLET	77	HBC	$4.2 K^- \rho \rightarrow \Sigma 3\pi$

- Statistical error negligible.
- From the pole position. Using an amplitude analysis based on approximate three-body unitarity of τ data from SCHAEEL 05c.
- Superseded by AGHASYAN 2018B.
- The $\rho^\pm \pi^\mp$ state can be also due to the $\pi(1300)$.
- Using the Breit-Wigner parameterization; strong correlation between mass and width.
- Using the data of BARATE 98R.
- From a fit to the 3π mass spectrum including the $K\bar{K}^*(892)$ threshold.
- Uses the model of KUHN 90.
- Uses the model of ISGUR 89.
- Includes the effect of a possible a_1' state.
- Uses the model of FEINDT 90.
- Supersedes AKERS 95P.
- Average and spread of values using 2 variants of the model of BOWLER 75.
- Reanalysis of RUCKSTUHL 86.
- Reanalysis of SCHMIDKE 86.
- Reanalysis of ALBRECHT 86B.
- From a combined reanalysis of ALBRECHT 86B, SCHMIDKE 86, and RUCKSTUHL 86.
- From a combined reanalysis of ALBRECHT 86B and DAUM 81B.
- Uses the model of BOWLER 75.
- Produced in K^- backward scattering.

- Statistical error negligible.
- From the pole position. Using an amplitude analysis based on approximate three-body unitarity of τ data from SCHAEEL 05c.
- Superseded by AGHASYAN 2018B.
- The $\rho^\pm \pi^\mp$ state can be also due to the $\pi(1300)$.
- Using the Breit-Wigner parameterization; strong correlation between mass and width.
- Using the data of BARATE 98R.
- From a fit of the $K^- K^{*0}$ distribution assuming $m_{a_1} = 1230$ MeV and purely resonant production of the $K^- K^{*0}$ system.
- From a fit to the 3π mass spectrum including the $K\bar{K}^*(892)$ threshold.
- Using the $a_1(1260)$ mass of 1230 MeV.
- From AKHMETSHIN 99E and ASNER 00 data using the $a_1(1260)$ mass of 1230 MeV.
- Uses the model of KUHN 90.
- Uses the model of ISGUR 89.
- Includes the effect of a possible a_1' state.
- Uses the model of FEINDT 90.
- Supersedes AKERS 95P.
- Average and spread of values using 2 variants of the model of BOWLER 75.
- Reanalysis of RUCKSTUHL 86.
- Reanalysis of SCHMIDKE 86.
- Reanalysis of ALBRECHT 86B.
- From a combined reanalysis of ALBRECHT 86B, SCHMIDKE 86, and RUCKSTUHL 86.
- From a combined reanalysis of ALBRECHT 86B and DAUM 81B.
- Uses the model of BOWLER 75.
- Produced in K^- backward scattering.

$a_1(1260)$ WIDTH

VALUE (MeV)	EVTs	DOCUMENT ID	TECN	COMMENT
250 to 600 OUR ESTIMATE				
420 ± 35 OUR AVERAGE				
380 ± 80	46M	1 AGHASYAN	18B	COMP 190 $\pi^- \rho \rightarrow \pi^- \pi^+ \pi^- \rho$
430 ± 24 ± 31		DARGENT	17	RVUE $D^0 \rightarrow \pi^- \pi^+ \pi^- \pi^+$
422.01 ± 2.10 ± 12.72	894k	AAIJ	18AI	LHCB $D^0 \rightarrow K^\mp \pi^\pm \pi^\pm \pi^\mp \pi^\mp$
576 ± 11 ± 89		2 MIKHASENKO	18	RVUE $\tau^- \rightarrow \pi^- \pi^+ \pi^- \nu_\tau$
367 ± 9 ± 28	420k	3 ALEKSEEV	10	COMP 190 $\pi^- Pb \rightarrow \pi^- \pi^+ \pi^- Pb'$
410 ± 31 ± 30		4 AUBERT	07AU	BABR $10.6 e^+ e^- \rightarrow \rho^0 \rho^\pm \pi^\mp \pi^\mp$
520-680	6360	5 LINK	07A	FOCS $D^0 \rightarrow \pi^- \pi^+ \pi^- \pi^+$
480 ± 20		6 GOMEZ-DUM.	04	RVUE $\tau^+ \rightarrow \pi^+ \pi^+ \pi^- \nu_\tau$
580 ± 41	90k	SALVINI	04	OBLX $\bar{p}p \rightarrow 2\pi^+ 2\pi^-$
460 ± 85	205	7 DRUTSKOY	02	BELL $B \rightarrow D^{(*)} K^- K^{*0}$
814 ± 36 ± 13	37k	8 ASNER	00	CLE2 $10.6 e^+ e^- \rightarrow \tau^+ \tau^-, \tau^- \tau^+ \rightarrow \pi^- \pi^0 \pi^0 \nu_\tau$
450 ± 50	22k	9 AKHMETSHIN	99E	CMD2 $1.05-1.38 e^+ e^- \rightarrow \pi^+ \pi^- \pi^0 \pi^0$
570 ± 10		10 BONDAR	99	RVUE $e^+ e^- \rightarrow 4\pi, \tau \rightarrow 3\pi \nu_\tau$
587 ± 27 ± 21	5904	11 ABREU	98G	DLPH $e^+ e^-$
478 ± 3 ± 15	5904	12 ABREU	98G	DLPH $e^+ e^-$
425 ± 14 ± 8	5904	13,14 ABREU	98G	DLPH $e^+ e^-$
400 ± 35		BARBERIS	98B	$450 pp \rightarrow p_f \pi^+ \pi^- \pi^0 p_s$
621 ± 32 ± 58		11,15 ACKERSTAFF	97R	OPAL $E_{cm}^{ee} = 88-94, \tau \rightarrow 3\pi \nu$
457 ± 15 ± 17		12,15 ACKERSTAFF	97R	OPAL $E_{cm}^{ee} = 88-94, \tau \rightarrow 3\pi \nu$
446 ± 21 ± 140	0	12 ALBRECHT	93C	ARG $\tau^+ \rightarrow \pi^+ \pi^+ \pi^- \nu$
239 ± 11		ANDO	92	SPEC $8 \pi^- \rho \rightarrow \pi^+ \pi^- \pi^0 n$
266 ± 13 ± 4		16 ANDO	92	SPEC $8 \pi^- \rho \rightarrow \pi^+ \pi^- \pi^0 n$
465 + 228 - 143		17 IVANOV	91	RVUE $\tau \rightarrow \pi^+ \pi^+ \pi^- \nu$
298 + 40 - 34		18 IVANOV	91	RVUE $\tau \rightarrow \pi^+ \pi^+ \pi^- \nu$
488 ± 32		19 IVANOV	91	RVUE $\tau \rightarrow \pi^+ \pi^+ \pi^- \nu$
430 ± 50		ARMSTRONG	90	OMEG $300.0 pp \rightarrow p p \pi^+ \pi^- \pi^0$
420 ± 40		20 ISGUR	89	RVUE $\tau^+ \rightarrow \pi^+ \pi^+ \pi^- \nu$
396 ± 43		21 BOWLER	88	RVUE

$a_1(1260)$ DECAY MODES

Mode	Fraction (Γ_i/Γ)
Γ_1 3π	seen
Γ_2 $(\rho\pi)S$ -wave, $\rho \rightarrow \pi\pi$	seen
Γ_3 $(\rho\pi)D$ -wave, $\rho \rightarrow \pi\pi$	seen
Γ_4 $(\rho(1450)\pi)S$ -wave, $\rho \rightarrow \pi\pi$	seen
Γ_5 $(\rho(1450)\pi)D$ -wave, $\rho \rightarrow \pi\pi$	seen
Γ_6 $f_0(500)\pi, f_0 \rightarrow \pi\pi$	seen
Γ_7 $f_0(980)\pi, f_0 \rightarrow \pi\pi$	not seen
Γ_8 $f_0(1370)\pi, f_0 \rightarrow \pi\pi$	seen
Γ_9 $f_2(1270)\pi, f_2 \rightarrow \pi\pi$	seen
Γ_{10} $\pi^+ \pi^- \pi^0$	seen
Γ_{11} $\pi^0 \pi^0 \pi^0$	not seen
Γ_{12} $K K \pi$	seen
Γ_{13} $K^*(892) K$	seen
Γ_{14} $\pi \gamma$	seen

$a_1(1260)$ PARTIAL WIDTHS

$\Gamma(\pi\gamma)$	VALUE (keV)	DOCUMENT ID	TECN	COMMENT
	640 ± 246	ZIELINSKI	84C	SPEC 200 $\pi^+ Z \rightarrow Z 3\pi$

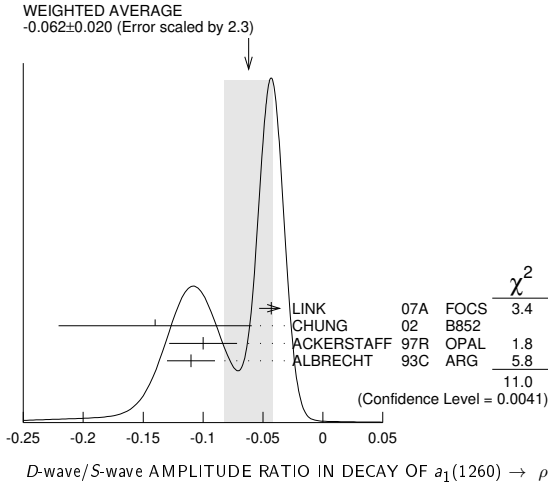
D-wave/S-wave AMPLITUDE RATIO IN DECAY OF $a_1(1260) \rightarrow \rho\pi$

VALUE	DOCUMENT ID	TECN	COMMENT
-0.062 ± 0.020 OUR AVERAGE			Error includes scale factor of 2.3. See the ideogram below.
-0.043 ± 0.009 ± 0.005	LINK	07A	FOCS $D^0 \rightarrow \pi^- \pi^+ \pi^- \pi^+$
-0.14 ± 0.04 ± 0.07	1 CHUNG	02	B852 $18.3 \pi^- \rho \rightarrow \pi^+ \pi^- \pi^- \rho$
-0.10 ± 0.02 ± 0.02	2,3 ACKERSTAFF	97R	OPAL $E_{cm}^{ee} = 88-94, \tau \rightarrow 3\pi \nu$
-0.11 ± 0.02	2 ALBRECHT	93C	ARG $\tau^+ \rightarrow \pi^+ \pi^+ \pi^- \nu$

- Deck-type background not subtracted.
- Uses the model of ISGUR 89.
- Supersedes AKERS 95P.

Meson Particle Listings

$a_1(1260)$



$a_1(1260)$ BRANCHING RATIOS

$\Gamma((\rho\pi)S\text{-wave}, \rho \rightarrow \pi\pi)/\Gamma_{\text{total}}$					Γ_2/Γ
VALUE (units 10^{-2})	EVTS	DOCUMENT ID	TECN	COMMENT	
• • • We do not use the following data for averages, fits, limits, etc. • • •					
60.19	37k	¹ ASNER	00	CLE2	$10.6 e^+ e^- \rightarrow \tau^+ \tau^-$, $\tau^- \rightarrow \pi^- \pi^0 \pi^0 \nu_\tau$

$\Gamma((\rho\pi)D\text{-wave}, \rho \rightarrow \pi\pi)/\Gamma_{\text{total}}$					Γ_3/Γ
VALUE (units 10^{-2})	EVTS	DOCUMENT ID	TECN	COMMENT	
• • • We do not use the following data for averages, fits, limits, etc. • • •					
$1.30 \pm 0.60 \pm 0.22$	37k	¹ ASNER	00	CLE2	$10.6 e^+ e^- \rightarrow \tau^+ \tau^-$, $\tau^- \rightarrow \pi^- \pi^0 \pi^0 \nu_\tau$

$\Gamma((\rho(1450)\pi)S\text{-wave}, \rho \rightarrow \pi\pi)/\Gamma_{\text{total}}$					Γ_4/Γ
VALUE (units 10^{-2})	EVTS	DOCUMENT ID	TECN	COMMENT	
• • • We do not use the following data for averages, fits, limits, etc. • • •					
$0.56 \pm 0.84 \pm 0.32$	37k	^{1,2} ASNER	00	CLE2	$10.6 e^+ e^- \rightarrow \tau^+ \tau^-$, $\tau^- \rightarrow \pi^- \pi^0 \pi^0 \nu_\tau$

$\Gamma((\rho(1450)\pi)D\text{-wave}, \rho \rightarrow \pi\pi)/\Gamma_{\text{total}}$					Γ_5/Γ
VALUE (units 10^{-2})	EVTS	DOCUMENT ID	TECN	COMMENT	
• • • We do not use the following data for averages, fits, limits, etc. • • •					
$2.04 \pm 1.20 \pm 0.28$	37k	^{1,2} ASNER	00	CLE2	$10.6 e^+ e^- \rightarrow \tau^+ \tau^-$, $\tau^- \rightarrow \pi^- \pi^0 \pi^0 \nu_\tau$

$\Gamma(f_0(500)\pi, f_0 \rightarrow \pi\pi)/\Gamma_{\text{total}}$					Γ_6/Γ
VALUE (units 10^{-2})	EVTS	DOCUMENT ID	TECN	COMMENT	
• • • We do not use the following data for averages, fits, limits, etc. • • •					
seen		CHUNG	02	B852	$18.3 \pi^- \rho \rightarrow$ $\pi^+ \pi^- \pi^- \rho$
$18.76 \pm 4.29 \pm 1.48$	37k	^{1,3} ASNER	00	CLE2	$10.6 e^+ e^- \rightarrow \tau^+ \tau^-$, $\tau^- \rightarrow \pi^- \pi^0 \pi^0 \nu_\tau$

$\Gamma(f_0(500)\pi, f_0 \rightarrow \pi\pi)/\Gamma((\rho\pi)S\text{-wave}, \rho \rightarrow \pi\pi)$					Γ_6/Γ_2
VALUE	EVTS	DOCUMENT ID	TECN	COMMENT	
• • • We do not use the following data for averages, fits, limits, etc. • • •					
0.06 ± 0.05	90k	SALVINI	04	OBLX	$\bar{p} p \rightarrow 2\pi^+ 2\pi^-$
~ 0.3	28k	AKHMETSHIN	99E	CMD2	$1.05-1.38 e^+ e^- \rightarrow$ $\pi^+ \pi^- \pi^+ \pi^-$
0.003 ± 0.003		⁴ LONGACRE	82	RVUE	

$\Gamma(f_0(980)\pi, f_0 \rightarrow \pi\pi)/\Gamma_{\text{total}}$					Γ_7/Γ
VALUE (units 10^{-2})	EVTS	DOCUMENT ID	TECN	COMMENT	
• • • We do not use the following data for averages, fits, limits, etc. • • •					
not seen	37k	ASNER	00	CLE2	$10.6 e^+ e^- \rightarrow \tau^+ \tau^-$, $\tau^- \rightarrow \pi^- \pi^0 \pi^0 \nu_\tau$

$\Gamma(f_0(1370)\pi, f_0 \rightarrow \pi\pi)/\Gamma_{\text{total}}$					Γ_8/Γ
VALUE (units 10^{-2})	EVTS	DOCUMENT ID	TECN	COMMENT	
• • • We do not use the following data for averages, fits, limits, etc. • • •					
$7.40 \pm 2.71 \pm 1.26$	37k	^{1,5} ASNER	00	CLE2	$10.6 e^+ e^- \rightarrow \tau^+ \tau^-$, $\tau^- \rightarrow \pi^- \pi^0 \pi^0 \nu_\tau$

$\Gamma(f_2(1270)\pi, f_2 \rightarrow \pi\pi)/\Gamma_{\text{total}}$

VALUE (units 10^{-2})	EVTS	DOCUMENT ID	TECN	COMMENT	Γ_9/Γ
• • • We do not use the following data for averages, fits, limits, etc. • • •					
$1.19 \pm 0.49 \pm 0.17$	37k	^{1,6} ASNER	00	CLE2	$10.6 e^+ e^- \rightarrow \tau^+ \tau^-$, $\tau^- \rightarrow \pi^- \pi^0 \pi^0 \nu_\tau$

$\Gamma(\pi^+ \pi^- \pi^0)/\Gamma_{\text{total}}$					Γ_{10}/Γ
VALUE	DOCUMENT ID	TECN	COMMENT		
seen	BARBERIS	98B	450 $p p \rightarrow p_f \pi^+ \pi^- \pi^0 p_s$		

$\Gamma(\pi^0 \pi^0 \pi^0)/\Gamma(\pi^+ \pi^- \pi^0)$					Γ_{11}/Γ_{10}
VALUE	CL%	DOCUMENT ID	TECN	COMMENT	
• • • We do not use the following data for averages, fits, limits, etc. • • •					
< 0.008	90	⁷ BARBERIS	01	450 $p p \rightarrow p_f 3\pi^0 p_s$	

$\Gamma(K^*(892)K)/\Gamma_{\text{total}}$

VALUE (units 10^{-2})	EVTS	DOCUMENT ID	TECN	COMMENT	Γ_{13}/Γ
• • • We do not use the following data for averages, fits, limits, etc. • • •					
2.2 ± 0.5	2255	⁸ COAN	04	CLEO	$\tau^- \rightarrow K^- \pi^- K^+ \nu_\tau$
8 to 15	205	⁹ DRUTSKOY	02	BELL	$B \rightarrow D^{(*)} K^- K^* 0$
$3.3 \pm 0.5 \pm 0.1$	37k	¹⁰ ASNER	00	CLE2	$10.6 e^+ e^- \rightarrow \tau^+ \tau^-$, $\tau^- \rightarrow \pi^- \pi^0 \pi^0 \nu_\tau$
2.6 ± 0.3		¹¹ BARATE	99R	ALEP	$\tau \rightarrow K \bar{K} \pi \nu_\tau$

- From a fit to the Dalitz plot.
- Assuming for $\rho(1450)$ mass and width of 1370 and 386 MeV respectively.
- Assuming for $f_0(500)$ (σ) mass and width of 860 and 880 MeV respectively.
- Uses multichannel Aitchison-Bowler model (BOWLER 75). Uses data from GAVILLET 77, DAUM 80, and DANKOWYCH 81.
- Assuming for $f_0(1370)$ mass and width of 1186 and 350 MeV respectively.
- Assuming for $f_2(1270)$ mass and width of 1275 and 185 MeV respectively.
- Inconsistent with observations of $\sigma\pi$, $f_0(1370)\pi$, and $f_2(1270)\pi$ decay modes.
- Using structure functions from KUHN 92 and DECKER 93A and B ($\tau^- \rightarrow K^- \pi^- K^+ \nu_\tau$) = $(0.155 \pm 0.006 \pm 0.009)\%$ from BRIERE 03.
- From a comparison to ALAM 94 assuming purely resonant production of the $K^- K^* 0$ system.
- From a fit to the 3π mass spectrum including the $K \bar{K}^*(892)$ threshold.
- Assuming $a_1(1260)$ dominance and taking $B(\tau \rightarrow a_1(1260)\nu_\tau)$ from BUSKULIC 96.

$a_1(1260)$ REFERENCES

AALI	18A1	EPJ C78 443	R. Aaij <i>et al.</i>	(LHCb Collab.)
AGHASYAN	18B	PR D98 092003	M. Aghasyan <i>et al.</i>	(COMPASS Collab.)
MIKHASENKO	18	PR D98 096021	M. Mikhasenko <i>et al.</i>	(JPACE Collab.)
DARGENT	17	JHEP 1705 143	P. Dargent <i>et al.</i>	(HELD, BRIS)
ALEKSEEV	10	PRL 104 241803	M.G. Alekseev <i>et al.</i>	(COMPASS Collab.)
AUBERT	07AU	PR D76 092005	B. Aubert <i>et al.</i>	(BABAR Collab.)
LINK	07A	PR D75 052003	J.M. Link <i>et al.</i>	(FNAL FOCUS Collab.)
PDG	06	JP G33 1	W.-M. Yao <i>et al.</i>	(PDG Collab.)
SCHAEEL	05C	PRPL 421 191	S. Schaeel <i>et al.</i>	(ALEPH Collab.)
COAN	04	PRL 92 232001	T.E. Coan <i>et al.</i>	(CLEO Collab.)
GOMEZ-DUMM...	04	PR D69 073002	D. Gomez Dumm, A. Pich, J. Portoles	
SALVINI	04	EPJ C35 21	P. Salvini <i>et al.</i>	(OBELIX Collab.)
BRIERE	03	PRL 90 181802	R. A. Briere <i>et al.</i>	(CLEO Collab.)
CHUNG	02	PR D65 072001	S.U. Chung <i>et al.</i>	(BNL E852 Collab.)
DRUTSKOY	02	PL B542 171	A. Drutskoy <i>et al.</i>	(BELLE Collab.)
BARBERIS	01	PL B507 14	D. Barberis <i>et al.</i>	
ASNER	00	PR D61 012002	D.M. Asner <i>et al.</i>	
AKHMETSHIN	99E	PL B466 392	R.R. Akhmetshin <i>et al.</i>	(Novosibirsk CMD-2 Collab.)
BARATE	99R	EPJ C11 599	R. Barate <i>et al.</i>	(ALEPH Collab.)
BONDAR	99	PL B466 403	A.E. Bondar <i>et al.</i>	(Novosibirsk CMD-2 Collab.)
ABREU	98G	PL B426 411	P. Abreu <i>et al.</i>	(DELPHI Collab.)
BARATE	98B	EPJ C4 409	R. Barate <i>et al.</i>	(ALEPH Collab.)
BARBERIS	98B	PL B422 399	D. Barberis <i>et al.</i>	(WA 102 Collab.)
ACKERSTAFF	97R	ZPHY C75 593	K. Ackerstaff <i>et al.</i>	(OPAL Collab.)
BUSKULIC	96	ZPHY C70 579	D. Buskulic <i>et al.</i>	(ALEPH Collab.)
AKERS	95P	ZPHY C67 45	R. Akers <i>et al.</i>	(OPAL Collab.)
ALAM	94	PR D50 43	M.S. Alam <i>et al.</i>	(CLEO Collab.)
ALBRECHT	93C	ZPHY C58 61	H. Albrecht <i>et al.</i>	(ARGUS Collab.)
DECKER	93A	ZPHY C58 445	R. Decker <i>et al.</i>	
ANDO	92	PL B291 496	A. Ando <i>et al.</i>	(KEK, KYOT, NIRS, SAGA+)
KUHN	92	ZPHY C56 661	J.H. Kuhn, E. Mirkes	
IVANOV	91	ZPHY C49 563	Y.P. Ivanov, A.A. Osipov, M.K. Volkov	(JINR)
ARMSTRONG	90	ZPHY C48 213	T.A. Armstrong, M. Benayoun, W. Beusch	(WA76 Coll.)
FEINDT	90	ZPHY C48 681	M. Feindt	(HAMB)
KUHN	90	ZPHY C48 445	J.H. Kuhn <i>et al.</i>	(MPIM)
ISGUR	89	PR D39 1357	N. Isgur, C. Morningstar, C. Reader	(TNTO)
BOWLER	88	PL B209 99	M.G. Bowler	(OXF)
BAND	87	PL B198 297	H.R. Band <i>et al.</i>	(MAC Collab.)
TORNQVIST	87	ZPHY C36 695	N.A. Tornqvist	(HELS)
ALBRECHT	86B	ZPHY C33 7	H. Albrecht <i>et al.</i>	(ARGUS Collab.)
RUCKSTUHL	86	PRL 56 2132	W. Ruckstuhl <i>et al.</i>	(DELCO Collab.)
SCHMIDKE	86	PRL 57 527	W.B. Schmidke <i>et al.</i>	(Mark II Collab.)
BELLINI	85	SJNP 41 781	D. Bellini <i>et al.</i>	
ZIELINSKI	84C	PRL 52 1195	M. Zielinski <i>et al.</i>	(ROCH, MINN, FNAL)
LONGACRE	82	PR D26 82	R.S. Longacre	(BNL)
DANKOWYCH...	81	PRL 46 580	J.A. Dankowych <i>et al.</i>	(TNTO, BNL, CARL+)
DAUM	81B	NP B182 269	C. Daum <i>et al.</i>	(AMST, CERN, CRAC, MPIM+)
DAUM	80	PL B93 281	C. Daum <i>et al.</i>	(AMST, CERN, CRAC, MPIM+)
GAVILLET	77	PL 69B 119	P. Gavillet <i>et al.</i>	(AMST, CERN, NUM+)
BOWLER	75	NP B97 227	M.G. Bowler <i>et al.</i>	(OXFT, DARE)

See key on page 1127

Meson Particle Listings

f₂(1270)

f₂(1270)

I^G(J^{PC}) = 0⁺(2⁺⁺)

f₂(1270) MASS

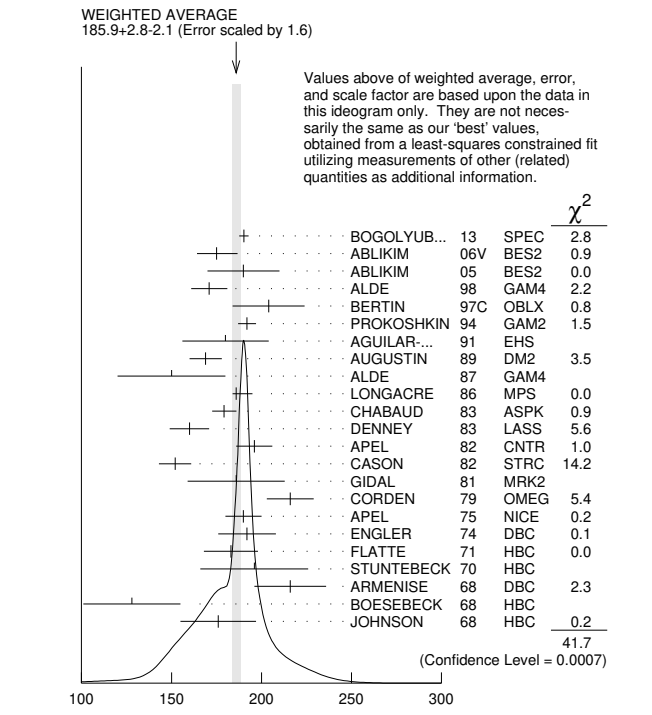
Table with columns: VALUE (MeV), EVTS, DOCUMENT ID, TECN, COMMENT. Lists various experimental data points for the mass of f2(1270).

1 Averaged over six nuclear targets, no statistically significant dependence on target nucleus observed. 2 Breit-Wigner mass. 3 T-matrix pole. 4 Mass errors enlarged by us to Γ/√N; see the note with the K*(892) mass. 5 From a partial-wave analysis of data using a K-matrix formalism with 5 poles. 6 From an energy-independent partial-wave analysis. 7 From an amplitude analysis of the reaction π+π- → 2π0. 8 From an amplitude analysis of π+π- → π+π- scattering data. 9 T-matrix pole from coupled channel K-matrix fit to data on J/ψ → γπ0π0 (ABLIKIM 15AE) and J/ψ → γK0S K0S (ABLIKIM 18AA). 10 T-matrix pole, 5 poles, 5 channels, including scattering data from HYAMS 75 (ππ), LONGACRE 86 (K K-bar), BINON 83 (ηη). 11 Using CLEO-c data but not authored by the CLEO Collaboration. 12 From a fit to a Breit-Wigner line shape with fixed Γ = 185 MeV. 13 4-poles, 5-channel K matrix fit. 14 From analysis of L3 data at 91 and 183-209 GeV. 15 Systematic uncertainties not estimated. 16 JOHNSON 68 includes BONDAR 63, LEE 64, DERADO 65, EISNER 67.

f₂(1270) WIDTH

Table with columns: VALUE (MeV), EVTS, DOCUMENT ID, TECN, COMMENT. Lists various experimental data points for the width of f2(1270).

Continuation of the f2(1270) MASS table, listing data from various experiments like ALDE, BERTIN, PROKOSHKIN, etc.



f₂(1270) width (MeV) 1 Averaged over six nuclear targets, no statistically significant dependence on target nucleus observed. 2 Breit-Wigner width 3 T-matrix pole. 4 Width errors enlarged by us to 4Γ/√N; see the note with the K*(892) mass. 5 From a partial-wave analysis of data using a K-matrix formalism with 5 poles. 6 From an energy-independent partial-wave analysis. 7 From an amplitude analysis of the reaction π+π- → 2π0. 8 From an amplitude analysis of π+π- → π+π- scattering data. 9 JOHNSON 68 includes BONDAR 63, LEE 64, DERADO 65, EISNER 67.

Meson Particle Listings

$f_2(1270)$

- ¹⁰T-matrix pole from coupled channel K-matrix fit to data on $J/\psi \rightarrow \gamma\pi^0\pi^0$ (ABLIKIM 15AE) and $J/\psi \rightarrow \gamma K_S^0 K_S^0$ (ABLIKIM 18AA).
- ¹¹T-matrix pole, 4 poles, 4 channels, including scattering data from HYAMS 75 ($\pi\pi$), LONGACRE 86 ($K\bar{K}$), BINON 83 ($\eta\eta$).
- ¹²4-poles, 5-channel K matrix fit.
- ¹³From analysis of L3 data at 91 and 183–209 GeV.
- ¹⁴Systematic uncertainties not estimated.

$f_2(1270)$ DECAY MODES

Mode	Fraction (Γ_i/Γ)	Scale factor/ Confidence level
$\Gamma_1 \pi\pi$	(84.2 \pm 2.9 \pm 0.9) %	S=1.1
$\Gamma_2 \pi^+\pi^-2\pi^0$	(7.7 \pm 1.1 \pm 3.2) %	S=1.2
$\Gamma_3 K\bar{K}$	(4.6 \pm 0.5 \pm 0.4) %	S=2.7
$\Gamma_4 2\pi^+2\pi^-$	(2.8 \pm 0.4) %	S=1.2
$\Gamma_5 \eta\eta$	(4.0 \pm 0.8) $\times 10^{-3}$	S=2.1
$\Gamma_6 4\pi^0$	(3.0 \pm 1.0) $\times 10^{-3}$	
$\Gamma_7 \gamma\gamma$	(1.42 \pm 0.24) $\times 10^{-5}$	S=1.4
$\Gamma_8 \eta\pi\pi$	< 8 $\times 10^{-3}$	CL=95%
$\Gamma_9 K^0 K^- \pi^+ + c.c.$	< 3.4 $\times 10^{-3}$	CL=95%
$\Gamma_{10} e^+e^-$	< 6 $\times 10^{-10}$	CL=90%

CONSTRAINED FIT INFORMATION

An overall fit to the total width, 4 partial widths, a combination of partial widths obtained from integrated cross sections, and 6 branching ratios uses 45 measurements and one constraint to determine 8 parameters. The overall fit has a $\chi^2 = 83.0$ for 38 degrees of freedom.

The following *off-diagonal* array elements are the correlation coefficients $\langle \delta p_i \delta p_j \rangle / (\delta p_i \delta p_j)$, in percent, from the fit to parameters p_i , including the branching fractions, $x_i \equiv \Gamma_i/\Gamma_{\text{total}}$. The fit constrains the x_i whose labels appear in this array to sum to one.

x_2	-90						
x_3	10	-39					
x_4	10	-38	1				
x_5	1	-6	0	0			
x_6	0	-7	0	0	0		
x_7	3	1	-15	0	0	0	
Γ	-71	65	-10	-7	-1	0	-6
	x_1	x_2	x_3	x_4	x_5	x_6	x_7

Mode	Rate (MeV)	Scale factor
$\Gamma_1 \pi\pi$	157.2 \pm 4.0 \pm 1.1	
$\Gamma_2 \pi^+\pi^-2\pi^0$	14.4 \pm 2.1 \pm 6.0	1.2
$\Gamma_3 K\bar{K}$	8.5 \pm 0.8	2.8
$\Gamma_4 2\pi^+2\pi^-$	5.2 \pm 0.7	1.2
$\Gamma_5 \eta\eta$	0.75 \pm 0.14	2.1
$\Gamma_6 4\pi^0$	0.56 \pm 0.19	
$\Gamma_7 \gamma\gamma$	0.0026 \pm 0.0005	1.4

$f_2(1270)$ PARTIAL WIDTHS

$\Gamma(\pi\pi)$	VALUE (MeV)	EVTS	DOCUMENT ID	TECN	COMMENT	Γ_1
157.2 \pm 4.0 \pm 1.1	OUR FIT					
157.0 \pm 6.0 \pm 1.0			¹ LONGACRE 86	MPS	$22\pi^-\rho \rightarrow n2K_S^0$	

- • • We do not use the following data for averages, fits, limits, etc. • • •
- 152 \pm 8 870 ² SCHEGELSKY 06A RVUE $\gamma\gamma \rightarrow K_S^0 K_S^0$
- ¹ From a partial-wave analysis of data using a K-matrix formalism with 5 poles.
- ² From analysis of L3 data at 91 and 183–209 GeV and using SU(3) relations.

$\Gamma(K\bar{K})$	VALUE (MeV)	EVTS	DOCUMENT ID	TECN	COMMENT	Γ_3
8.5 \pm 0.8	OUR FIT					
9.0 \pm 0.7 \pm 0.3			¹ LONGACRE 86	MPS	$22\pi^-\rho \rightarrow n2K_S^0$	
7.5 \pm 2.0		870	² SCHEGELSKY 06A	RVUE	$\gamma\gamma \rightarrow K_S^0 K_S^0$	

- • • We do not use the following data for averages, fits, limits, etc. • • •
- ¹ From a partial-wave analysis of data using a K-matrix formalism with 5 poles.
- ² From analysis of L3 data at 91 and 183–209 GeV and using SU(3) relations.

$\Gamma(\eta\eta)$ Γ_5

VALUE (MeV)	EVTS	DOCUMENT ID	TECN	COMMENT
0.75 \pm 0.14	OUR FIT			Error includes scale factor of 2.1.
1.0 \pm 0.1		¹ LONGACRE 86	MPS	$22\pi^-\rho \rightarrow n2K_S^0$
• • •				We do not use the following data for averages, fits, limits, etc. • • •
1.8 \pm 0.4	870	² SCHEGELSKY 06A	RVUE	$\gamma\gamma \rightarrow K_S^0 K_S^0$

- ¹ From a partial-wave analysis of data using a K-matrix formalism with 5 poles.
- ² From analysis of L3 data at 91 and 183–209 GeV and using SU(3) relations.

$\Gamma(\gamma\gamma)$ Γ_7

The value of this width depends on the theoretical model used. Unitary approaches with scalars typically (with exception of PENNINGTON 08) give values clustering around 2.6 keV; without an S-wave contribution, values are systematically higher (typically around 3 keV).

VALUE (keV)	EVTS	DOCUMENT ID	TECN	COMMENT
2.6 \pm 0.5	OUR FIT			Error includes scale factor of 1.4.
2.93 \pm 0.40		¹ DAI 14A	RVUE	Compilation
• • •				We do not use the following data for averages, fits, limits, etc. • • •
3.14 \pm 0.20		^{2,3} PENNINGTON 08	RVUE	Compilation
3.82 \pm 0.30		^{3,4} PENNINGTON 08	RVUE	Compilation
2.55 \pm 0.15	870	⁵ SCHEGELSKY 06A	RVUE	$\gamma\gamma \rightarrow K_S^0 K_S^0$
2.84 \pm 0.35		BOGLIONE 99	RVUE	$\gamma\gamma \rightarrow \pi^+\pi^-, \pi^0\pi^0$
2.93 \pm 0.23 \pm 0.32		⁶ YABUKI 95	VNS	
2.58 \pm 0.13 \pm 0.36 \pm 0.27		⁷ BEHREND 92	CELL	$e^+e^- \rightarrow e^+e^-\pi^+\pi^-$
3.10 \pm 0.35 \pm 0.35		⁸ BLINOV 92	MD1	$e^+e^- \rightarrow e^+e^-\pi^+\pi^-$
2.27 \pm 0.47 \pm 0.11		ADACHI 90D	TOPZ	$e^+e^- \rightarrow e^+e^-\pi^+\pi^-$
3.15 \pm 0.04 \pm 0.39		BOYER 90	MRK2	$e^+e^- \rightarrow e^+e^-\pi^+\pi^-$
3.19 \pm 0.16 \pm 0.29 \pm 0.28		MARSISKE 90	CBAL	$e^+e^- \rightarrow e^+e^-\pi^0\pi^0$
2.35 \pm 0.65		⁹ MORGAN 90	RVUE	$\gamma\gamma \rightarrow \pi^+\pi^-, \pi^0\pi^0$
3.19 \pm 0.09 \pm 0.22 \pm 0.38	2177	OEST 90	JADE	$e^+e^- \rightarrow e^+e^-\pi^0\pi^0$
3.2 \pm 0.1 \pm 0.4		¹⁰ AIHARA 86B	TPC	$e^+e^- \rightarrow e^+e^-\pi^+\pi^-$
2.5 \pm 0.1 \pm 0.5		BEHREND 84B	CELL	$e^+e^- \rightarrow e^+e^-\pi^+\pi^-$
2.85 \pm 0.25 \pm 0.5		¹¹ BERGER 84	PLUT	$e^+e^- \rightarrow e^+e^-2\pi$
2.70 \pm 0.05 \pm 0.20		COURAU 84	DLCO	$e^+e^- \rightarrow e^+e^-\pi^+\pi^-$
2.52 \pm 0.13 \pm 0.38		¹² SMITH 84C	MRK2	$e^+e^- \rightarrow e^+e^-\pi^+\pi^-$
2.7 \pm 0.2 \pm 0.6		EDWARDS 82F	CBAL	$e^+e^- \rightarrow e^+e^-2\pi^0$
2.9 \pm 0.6 \pm 0.6 \pm 0.4		¹³ EDWARDS 82F	CBAL	$e^+e^- \rightarrow e^+e^-2\pi^0$
3.2 \pm 0.2 \pm 0.6		BRANDELIK 81B	TASS	$e^+e^- \rightarrow e^+e^-\pi^+\pi^-$
3.6 \pm 0.3 \pm 0.5		ROUSSARIE 81	MRK2	$e^+e^- \rightarrow e^+e^-\pi^+\pi^-$
2.3 \pm 0.8		¹⁴ BERGER 80B	PLUT	e^+e^-

- ¹ Based on a K-matrix analysis of BELLE data from MORI 07, UEHARA 08a, UEHARA 09 and UEHARA 13. The width is derived from the pole on the third sheet which is closest to the physical axis. Supersedes PENNINGTON 08.
- ² Solution A (preferred solution based on χ^2 -analysis).
- ³ Dispersion theory based amplitude analysis of BOYER 90, MARSISKE 90, BEHREND 92, and MORI 07.
- ⁴ Solution B (worse than solution A; still acceptable when systematic uncertainties are included).
- ⁵ From analysis of L3 data at 91 and 183–209 GeV and using SU(3) relations.
- ⁶ With a narrow scalar state around 1220 MeV.
- ⁷ Using a unitarized model with a 300–500 keV wide scalar at 1100 MeV.
- ⁸ Using the unitarized model of LYTH 85.
- ⁹ Error includes spread of different solutions. Data of MARK2 and CRYSTAL BALL used in the analysis. Authors report strong correlations with $\gamma\gamma$ width of $f_0(1370)$: $\Gamma(f_2) + 1/4 \Gamma(f^0) = 3.6 \pm 0.3$ KeV.
- ¹⁰ Radiative corrections modify the partial widths; for instance the COURAU 84 value becomes 2.66 ± 0.21 in the calculation of LANDRO 86.
- ¹¹ Using the MENNESSIER 83 model.
- ¹² Superseded by BOYER 90.
- ¹³ If helicity = 2 assumption is not made.
- ¹⁴ Using mass, width and $B(f_2(1270) \rightarrow 2\pi)$ from PDG 78.

$\Gamma(e^+e^-)$ Γ_{10}

VALUE (eV)	CL%	DOCUMENT ID	TECN	COMMENT
<0.11	90	ACHASOV 00k	SND	$e^+e^- \rightarrow \pi^0\pi^0$
• • •				We do not use the following data for averages, fits, limits, etc. • • •
<1.7	90	VOROBYEV 88	ND	$e^+e^- \rightarrow \pi^0\pi^0$

$f_2(1270) \Gamma(i)\Gamma(\gamma\gamma)/\Gamma(\text{total})$

$\Gamma(K\bar{K}) \times \Gamma(\gamma\gamma)/\Gamma(\text{total})$ $\Gamma_3\Gamma_7/\Gamma$

VALUE (keV)	DOCUMENT ID	TECN	COMMENT
0.121 \pm 0.020	OUR FIT		Error includes scale factor of 1.3.
0.091 \pm 0.007 \pm 0.027		¹ ALBRECHT 90c	ARG $e^+e^- \rightarrow e^+e^-K^+K^-$
• • •			We do not use the following data for averages, fits, limits, etc. • • •
0.104 \pm 0.007 \pm 0.072		² ALBRECHT 90c	ARG $e^+e^- \rightarrow e^+e^-K^+K^-$

- ¹ Using an incoherent background.
- ² Using a coherent background.

$\Gamma(\eta\eta) \times \Gamma(\gamma\gamma)/\Gamma_{total}$	$\Gamma_5\Gamma_7/\Gamma$		
VALUE (eV)	DOCUMENT ID	TECN	COMMENT
$11.5^{+1.8+4.5}_{-2.0-3.7}$	1 UEHARA	10A BELL	$10.6 e^+e^- \rightarrow e^+e^-\eta\eta$

¹Including interference with the $f_2'(1525)$ (parameters fixed to the values from the 2008 edition of this review, PDG 08) and $f_0(Y)$.

Helicity-0/Helicity-2 RATIO IN $\gamma\gamma \rightarrow f_2(1270) \rightarrow \pi\pi$			
VALUE (units 10^{-2})	DOCUMENT ID	TECN	COMMENT
$3.7 \pm 0.3^{+15.9}_{-2.9}$	UEHARA	08A BELL	$10.6 e^+e^- \rightarrow e^+e^-\pi^0\pi^0$

• • • We do not use the following data for averages, fits, limits, etc. • • •
 9.5 ± 1.8 ¹DAI 14A RVUE Compilation
 13 2,3 PENNINGTON 08 RVUE Compilation
 26 3,4 PENNINGTON 08 RVUE Compilation
¹Based on a K-matrix analysis of BELLE data from MORI 07, UEHARA 08A, UEHARA 09 and UEHARA 13. The width is derived for the pole on the third sheet which is closest to the physical axis.
²Solution A (preferred solution based on χ^2 -analysis).
³Dispersion theory based amplitude analysis of BOYER 90, MARSISKE 90, BEHREND 92, and MORI 07.
⁴Solution B (worse than solution A; still acceptable when systematic uncertainties are included).

$f_2(1270)$ BRANCHING RATIOS

$\Gamma(\pi\pi)/\Gamma_{total}$	Γ_1/Γ		
VALUE	EVTS	DOCUMENT ID	TECN COMMENT
$0.842^{+0.029}_{-0.009}$ OUR FIT			Error includes scale factor of 1.1.
0.837 ± 0.020 OUR AVERAGE			
0.849 ± 0.025		CHABAUD 83 ASPK	$17 \pi^-p$ polarized
0.85 ± 0.05	250	BEAUPRE 71 HBC	$8 \pi^+p \rightarrow \Delta^{++} f_2$
0.8 ± 0.04	600	OH 70 HBC	$1.26 \pi^-p \rightarrow \pi^+\pi^-n$

• • • We do not use the following data for averages, fits, limits, etc. • • •
 0.856 ± 0.001 ± 0.05 ¹ALBRECHT 20 RVUE $0.9 \bar{p}p \rightarrow \pi^0\pi^0\eta, \pi^0\eta\eta, \pi^0K^+K^-$

¹Residue from T-matrix pole, 4 poles, 4 channels, including scattering data from HYAMS 75 ($\pi\pi$), LONGACRE 86 ($K\bar{K}$), BINON 83 ($\eta\eta$).

$\Gamma(\pi^+\pi^-2\pi^0)/\Gamma(\pi\pi)$	Γ_2/Γ_1		
VALUE	EVTS	DOCUMENT ID	TECN COMMENT
$0.091^{+0.014}_{-0.040}$ OUR FIT			Error includes scale factor of 1.2.
0.15 ± 0.06	600	EISENBERG 74 HBC	$4.9 \pi^+p \rightarrow \Delta^{++} f_2$
0.07		EMMS 75D DBC	$4 \pi^+n \rightarrow p f_2$

$\Gamma(K\bar{K})/\Gamma_{total}$	Γ_3/Γ		
VALUE	DOCUMENT ID	TECN	COMMENT
$0.033 \pm 0.001 \pm 0.005$	1 ALBRECHT 20 RVUE		$0.9 \bar{p}p \rightarrow \pi^0\pi^0\eta, \pi^0\eta\eta, \pi^0K^+K^-$

¹Residue from T-matrix pole, 4 poles, 4 channels, including scattering data from HYAMS 75 ($\pi\pi$), LONGACRE 86 ($K\bar{K}$), BINON 83 ($\eta\eta$).

$\Gamma(K\bar{K})/\Gamma(\pi\pi)$	Γ_3/Γ_1		
VALUE	EVTS	DOCUMENT ID	TECN COMMENT
$0.054^{+0.005}_{-0.006}$ OUR FIT			Error includes scale factor of 2.7.
0.041 ± 0.004 OUR AVERAGE			
0.045 ± 0.01	1 BARGIOTTI 03 OBLX		$\bar{p}p$
$0.037^{+0.008}_{-0.021}$	ETKIN 82B	MPS	$23 \pi^-p \rightarrow n2K_S^0$
0.045 ± 0.009	CHABAUD 81	ASPK	$17 \pi^-p$ polarized
0.039 ± 0.008	LOVERRE 80	HBC	$4 \pi^-p \rightarrow K\bar{K}N$

• • • We do not use the following data for averages, fits, limits, etc. • • •
 0.052 ± 0.025 ABLIKIM 04E BES2 $J/\psi \rightarrow \omega K^+K^-$
 0.036 ± 0.005 2 COSTA 80 OMEG 1-2.2 $\pi^-p \rightarrow K^+K^-n$
 0.030 ± 0.005 3 MARTIN 79 RVUE
 0.027 ± 0.009 4 POLYCHRO... 79 STRC $7 \pi^-p \rightarrow n2K_S^0$
 0.025 ± 0.015 EMMS 75D DBC $4 \pi^+n \rightarrow p f_2$
 0.031 ± 0.012 20 ADERHOLZ 69 HBC $8 \pi^+p \rightarrow K^+K^- \pi^+p$

¹ Coupled channel analysis of $\pi^+\pi^-\pi^0, K^+K^-\pi^0$, and $K^\pm K_S^0 \pi^\mp$.
² Re-evaluated by CHABAUD 83.
³ Includes PAWLICKI 77 data.
⁴ Takes into account the $f_2(1270)$ - $f_2'(1525)$ interference.

$\Gamma(2\pi^+2\pi^-)/\Gamma(\pi\pi)$	Γ_4/Γ_1		
VALUE	EVTS	DOCUMENT ID	TECN COMMENT
0.033 ± 0.005 OUR FIT			Error includes scale factor of 1.2.
0.033 ± 0.004 OUR AVERAGE			Error includes scale factor of 1.1.
0.024 ± 0.006	160	EMMS 75D DBC	$4 \pi^+n \rightarrow p f_2$
0.051 ± 0.025	70	EISENBERG 74 HBC	$4.9 \pi^+p \rightarrow \Delta^{++} f_2$
$0.043^{+0.007}_{-0.011}$	285	1 LOUIE 74 HBC	$3.9 \pi^-p \rightarrow n f_2$
0.037 ± 0.007	154	ANDERSON 73 DBC	$6 \pi^+n \rightarrow p f_2$
0.047 ± 0.013		OH 70 HBC	$1.26 \pi^-p \rightarrow \pi^+\pi^-n$

¹ LOUIE 74 was quoted as 0.065 in PDG 74. Factor 2/3 to go from $\pi^+\pi^- \rightarrow \pi\pi$ forgotten. Mike L.

$\Gamma(\eta\eta)/\Gamma_{total}$	Γ_5/Γ		
VALUE (units 10^{-3})	DOCUMENT ID	TECN	COMMENT
4.0 ± 0.8 OUR FIT			Error includes scale factor of 2.1.
2.9 ± 0.5 OUR AVERAGE			
2.7 ± 0.7	BINON 05	GAMS	$33 \pi^-p \rightarrow \eta\eta n$
2.8 ± 0.7	ALDE 86D	GAM4	$100 \pi^-p \rightarrow 2\eta n$
5.2 ± 1.7	BINON 83	GAM2	$38 \pi^-p \rightarrow 2\eta n$

• • • We do not use the following data for averages, fits, limits, etc. • • •
 4.0 ± 1.0 ± 2.0 ¹ALBRECHT 20 RVUE $0.9 \bar{p}p \rightarrow \pi^0\pi^0\eta, \pi^0\eta\eta, \pi^0K^+K^-$

$\Gamma(\eta\eta)/\Gamma(\pi\pi)$	Γ_5/Γ_1		
VALUE	CL%	DOCUMENT ID	TECN COMMENT
0.003 ± 0.001		BARBERIS 00E	$450 p\bar{p} \rightarrow p_f \eta\eta p_S$
< 0.05	95	EDWARDS 82F CBAL	$e^+e^- \rightarrow e^+e^-2\eta$
< 0.016	95	EMMS 75D DBC	$4 \pi^+n \rightarrow p f_2$
< 0.09	95	EISENBERG 74 HBC	$4.9 \pi^+p \rightarrow \Delta^{++} f_2$

$\Gamma(4\pi^0)/\Gamma_{total}$	Γ_6/Γ		
VALUE	EVTS	DOCUMENT ID	TECN COMMENT
0.0030 ± 0.0010 OUR FIT			
0.003 ± 0.001	400 ± 50	ALDE 87	GAM4 $100 \pi^-p \rightarrow 4\pi^0 n$

$\Gamma(\gamma\gamma)/\Gamma_{total}$	Γ_7/Γ		
VALUE (units 10^{-5})	DOCUMENT ID	TECN	COMMENT
$1.57 \pm 0.01^{+1.39}_{-0.14}$	UEHARA 08A BELL		$10.6 e^+e^- \rightarrow e^+e^-\pi^0\pi^0$

$\Gamma(\eta\pi\pi)/\Gamma(\pi\pi)$	Γ_8/Γ_1		
VALUE	CL%	DOCUMENT ID	TECN COMMENT
< 0.010	95	EMMS 75D DBC	$4 \pi^+n \rightarrow p f_2$

$\Gamma(K^0K^- \pi^+ + c.c.)/\Gamma(\pi\pi)$	Γ_9/Γ_1		
VALUE	CL%	DOCUMENT ID	TECN COMMENT
< 0.004	95	EMMS 75D DBC	$4 \pi^+n \rightarrow p f_2$

$\Gamma(e^+e^-)/\Gamma_{total}$	Γ_{10}/Γ		
VALUE (units 10^{-10})	CL%	DOCUMENT ID	TECN COMMENT
< 6	90	ACHASOV 00K SND	$e^+e^- \rightarrow \pi^0\pi^0$

$f_2(1270)$ REFERENCES

RODAS 22	EPJ C82 80	A. Rodas et al.	(JPAC Collab.)
CARVER 21	PRL 126 082002	M. Carver et al.	(CLAS Collab.)
ALBRECHT 20	EPJ C80 453	M. Albrecht et al.	(Crystal Barrel Collab.)
ABLIKIM 18AA	PR D98 072003	M. Ablikim et al.	(BESIII Collab.)
ABLIKIM 15AE	PR D92 052003	M. Ablikim et al.	(BESIII Collab.)
DOBBS 15	PR D91 052006	S. Dobbs et al.	(NWES)
DAI 14A	PR D90 036004	L.-Y. Dai, M.R. Pennington	(CEBAF)
BOGOLYUB... 13	PAN 76 1324	M.Yu. Bogolyubsky et al.	(HYPERON-M Collab.)
	Translated from YAF 76 1389.		
UEHARA 13	PTEP 2013 123C01	S. Uehara et al.	(BELLE Collab.)
UEHARA 10A	PR D82 114031	S. Uehara et al.	(BELLE Collab.)
ANISOVICH 09	IJMP A24 2481	V.V. Anisovich, A.V. Sarantsev	
UEHARA 09	PR D79 052009	S. Uehara et al.	(BELLE Collab.)
PDG 08	PL B667 1	C. Amsler et al.	(PDG Collab.)
PENNINGTON 08	EPJ C56 1	M.R. Pennington et al.	
UEHARA 08A	PR D78 052004	S. Uehara et al.	(BELLE Collab.)
MORI 07	PR D75 051101	T. Mori et al.	(BELLE Collab.)
ABLIKIM 06V	PL B642 441	M. Ablikim et al.	(BES Collab.)
SCHEGELSKY 06A	EPJ A27 207	V.A. Schegelsky et al.	
ABLIKIM 05	PL B607 243	M. Ablikim et al.	(BES Collab.)
BINON 05	PAN 68 960	F. Binon et al.	
	Translated from YAF 68 998.		
ABLIKIM 04E	PL B503 138	M. Ablikim et al.	(BES Collab.)
BARGIOTTI 03	EPJ C26 371	M. Bargiotti et al.	(OBELIX Collab.)
TIKHOMIROV 03	PAN 66 828	G.D. Tikhomirov et al.	
	Translated from YAF 66 860.		
ACHASOV 00K	PL B492 8	M.N. Achasov et al.	(Novosibirsk SND Collab.)
BARBERIS 00E	PL B479 59	D. Barberis et al.	(WA 102 Collab.)
BOGLIONE 99	EPJ C9 11	M. Boglione, M.R. Pennington	
ALDE 98	EPJ A3 361	D. Alde et al.	(GAMMA Collab.)
	Also	D. Alde et al.	(GAMS Collab.)
	Translated from YAF 62 446.		
ALDE 97	PL B397 350	D.M. Alde et al.	(GAMS Collab.)
BERTIN 97C	PL B408 476	A. Bertin et al.	(OBELIX Collab.)
GRYGOREV 96	PAN 59 2105	V.K. Grigoriev, O.N. Baloshin, B.P. Barkov	(ITEP)
	Translated from YAF 59 2187.		

Meson Particle Listings

$f_2(1270)$, $f_1(1285)$

YABUKI 95	JPSJ 64 435	F. Yabuki et al.	(VENUS Collab.)	1278 ± 2		ARMSTRONG 89G	OMEG	85 $\pi^+ p \rightarrow 4\pi\pi p, pp \rightarrow 4\pi pp$
PROKOSHKIN 94	PD 39 420	Y.D. Prokoshkin, A.A. Kondashov	(SERP)			RATH 89	MPS	21.4 $\pi^- p \rightarrow K_S^0 K_S^0 \pi^0 n$
BEHREND 92	ZPHY C56 381	H.J. Behrend	(CELLO Collab.)	1280.1 ± 2.1	60	4 BIRMAN 88	MPS	8 $\pi^- p \rightarrow K^+ \bar{K}^0 \pi^- n$
BLINOV 92	ZPHY C53 33	A.E. Blinov et al.	(NOVO)	1285 ± 1	4750	BITYUKOV 88	SPEC	32.5 $\pi^- p \rightarrow K^+ K^- \pi^0 n$
AGUILAR... 91	ZPHY C50 405	M. Aguilar-Benitez et al.	(LEBC-EHS Collab.)	1280 ± 1	504	ANDO 86	SPEC	8 $\pi^- p \rightarrow \eta\pi^+ \pi^- n$
AKER 91	PL B260 249	E. Aker et al.	(Crystal Barrel Collab.)	1277 ± 2	420	REEVES 86	SPEC	6.6 $p\bar{p} \rightarrow K K \pi X$
ADACHI 90D	PL B234 185	I. Adachi et al.	(TOPAZ-2 Collab.)	1285 ± 2		CHUNG 85	SPEC	8 $\pi^- p \rightarrow N K \bar{K} \pi$
ALBRECHT 90G	ZPHY C48 183	H. Albrecht et al.	(ARGUS Collab.)	1279 ± 2	604	ARMSTRONG 84	OMEG	85 $\pi^+ p \rightarrow K \bar{K} \pi \pi p, p p \rightarrow K \bar{K} \pi p p$
BOYER 90	PR D42 1350	J. Boyer et al.	(Mark II Collab.)	1286 ± 1		CHAUVAT 84	SPEC	ISR 31.5 $p p$
BREAKSTONE 90	ZPHY C48 569	A.M. Breakstone et al.	(ISU, BGNA, CERN+)	1278 ± 4		EVANGELIS... 81	OMEG	12 $\pi^- p \rightarrow \eta\pi^+ \pi^- \pi^- p$
MARSISKE 90	PR D41 3324	H. Marsiske et al.	(Crystal Ball Collab.)	1283 ± 3	103	DIONISI 80	HBC	4 $\pi^- p \rightarrow K \bar{K} \pi n$
MORGAN 90	ZPHY C48 623	D. Morgan, M.R. Pennington	(RAL, DURH)	1282 ± 2	320	NACASCH 78	HBC	0.7, 0.76 $p\bar{p} \rightarrow K \bar{K} 3\pi$
OEST 90	ZPHY C47 343	T. Oest et al.	(JADE Collab.)	1279 ± 5	210	GRASSLER 77	HBC	16 $\pi^+ p$
AUGUSTIN 89	NP B320 1	J.E. Augustin, G. Cosme	(DM2 Collab.)	1286 ± 3	180	DUBOC 72	HBC	1.2 $p\bar{p} \rightarrow 2K4\pi$
VOROBYEV 88	SJNP 48 273	P.V. Vorobiev et al.	(NOVO)	1283 ± 5		DAHL 67	HBC	1.6-4.2 $\pi^- p$
ALDE 87	PL B198 286	D.M. Alde et al.	(LANL, BRUX, SERP, LAPP)	1289.3 ± 2.8	234	5 ABLIKIM 19BA	BES3	$e^+ e^- \rightarrow \psi(2S)$
AUGUSTIN 87	ZPHY C36 369	J.E. Augustin et al.	(LALO, CLER, FRAS+)	1284.2 ± 2.2		5 AAJ 14Y	LHCB	$\bar{B}_0(s) \rightarrow J/\psi 2(\pi^+ \pi^-)$
ABACHI 86B	PRL 57 1990	S. Abachi et al.	(PURD, ANL, IND, MICH+)	1281.9 ± 0.5		5 SOSA 99	SPEC	$p p \rightarrow p_{\text{slow}} (K_S^0 K^+ \pi^-) p_{\text{fast}}$
AIHARA 86B	PRL 57 404	H. Aihara et al.	(TPC-Z Collab.)	1282.8 ± 0.6		5 SOSA 99	SPEC	$p p \rightarrow p_{\text{slow}} (K_S^0 K^+ \pi^+) p_{\text{fast}}$
ALDE 86D	NP B269 485	D.M. Alde et al.	(BELG, LAPP, SERP, CERN+)	1270 ± 10		AMELIN 95	VES	37 $\pi^- N \rightarrow \pi^- \pi^+ \pi^- \gamma N$
LANDRO 86	PL B172 445	M. Landro, K.J. Mork, H.A. Olsen	(UTRO)	1280 ± 2		ABATZIS 94	OMEG	450 $p p \rightarrow p p 2(\pi^+ \pi^-)$
LONGACRE 86	PL B177 223	R.S. Longacre et al.	(BNL, BRAN, CUNY+)	1282 ± 4		ARMSTRONG 93C	E760	$p\bar{p} \rightarrow \pi^0 \eta \eta \rightarrow 6\gamma$
LYTH 85	JP G11 459	D.H. Lyth	(CELLO Collab.)	1270 ± 6 ± 10		ARMSTRONG 92C	OMEG	300 $p p \rightarrow p p \pi^+ \pi^- \gamma$
BEHREND 84B	ZPHY C23 223	H.J. Behrend et al.	(PLUTO Collab.)	1281 ± 1		ARMSTRONG 89E	OMEG	300 $p p \rightarrow p p 2(\pi^+ \pi^-)$
BERGER 84	ZPHY C26 199	C. Berger et al.	(PLUTO Collab.)	1279 ± 6 ± 10	16	BECKER 87	MRK3	$e^+ e^- \rightarrow \phi K \bar{K} \pi$
COURAU 84	PL 1478 227	A. Courau et al.	(CIT, SLAC)	1286 ± 9		GIDAL 87	MRK2	$e^+ e^- \rightarrow e^+ e^- \eta \pi^+ \pi^-$
SMITH 84C	PR D30 851	J.R. Smith et al.	(SLAC, LBL, HARV)	1287 ± 5	353	BITYUKOV 84B	SPEC	32 $\pi^- p \rightarrow K^+ K^- \pi^0 n$
BINON 83	NC 78A 313	F.G. Binon et al.	(BELG, LAPP, SERP+)	~ 1279		6 TORNQVIST 82B	RVUE	100 $\pi^- p \rightarrow K \bar{K} \pi X$
Also	SJNP 38 561	F.G. Binon et al.	(BELG, LAPP, SERP+)	1275 ± 6	31	BROMBERG 80	SPEC	100 $\pi^- p \rightarrow K \bar{K} \pi X$
Translated from YAF 38 934.				1288 ± 9	200	7 GURTU 79	HBC	4.2 $K^- p \rightarrow n \eta 2\pi$
CHABAUD 83	NP B223 1	V. Chabaud et al.	(CERN, CRAC, MPIM)	~ 1275.0	46	7 STANTON 79	CNTR	8.5 $\pi^- p \rightarrow n 2\gamma 2\pi$
DENNEY 83	PR D28 2726	D.L. Denney et al.	(IOWA, MICH)	1271 ± 10	34	CORDEN 78	OMEG	12-15 $\pi^- p \rightarrow K^+ K^- \pi n$
MENNESSIER 83	ZPHY C16 241	G. Mennessier	(MONP)	1295 ± 12	85	CORDEN 78	OMEG	12-15 $\pi^- p \rightarrow n 5\pi$
APEL 82	NP B201 197	W.D. Apel et al.	(KARLK, KARLE, PISA, SERP+)	1292 ± 10	150	DEFOIX 72	HBC	0.7 $p\bar{p} \rightarrow 7\pi$
CASON 82	PLR 49 1316	N.M. Cason et al.	(NDAM, ANL)	1280 ± 3	500	8 THUN 72	MMS	13.4 $\pi^- p$
EDWARDS 82F	PL 1478 227	A. Edwards et al.	(CIT, HARV, PRIN+)	1303 ± 8		BARDADIN... 71	HBC	8 $\pi^+ p \rightarrow p 6\pi$
ETKIN 82B	PR D25 1796	A. Etkin et al.	(BNL, CUNY, TUFTS, VAND)	1283 ± 6		BOESEBECK 71	HBC	16.0 $\pi p \rightarrow p 5\pi$
BRANDELK 81B	ZPHY C10 117	R. Brandelik et al.	(TASSO Collab.)	1270 ± 10		CAMPBELL 69	DBC	2.7 $\pi^+ d$
CHABAUD 81	APP B12 575	V. Chabaud et al.	(CERN, CRAC, MPIM)	1290 ± 7		LORSTAD 69	HBC	0.7 $p\bar{p}, 4,5\text{-body}$
GIDAL 81	PL 107B 153	G. Gidal et al.	(SLAC, LBL)	1290 ± 7		D'ANDLAU 68	HBC	1.2 $p\bar{p}, 5\text{-body}$
ROUSSARIE 81	PL 105B 304	A. Roussarie et al.	(SLAC, LBL)					
BERGER 80B	PL 94B 254	C. Berger et al.	(PLUTO Collab.)					
COSTA 80	NP B175 402	G. Costa et al.	(BARI, BONN, CERN, GLAS+)					
LOVERRE 80	ZPHY C6 187	P.F. Løverre et al.	(CERN, CDEF, MADR+)					
CORDEN 79	NP B157 250	M.J. Corden et al.	(BIRM, RHEL, TELA+)					
MARTIN 79	NP B158 520	A.D. Martin, E.N. Ozmutlu	(DURH)					
POLYCHRO... 79	PR D19 1317	V.K. Polychromakos et al.	(NDAM, ANL)					
PDG 78	PL 75B 1	C. Brifman et al.	(SERP, GEVA)					
ANTIPOV 77	NP B119 45	Y.M. Antipov et al.	(ANL)					
PAWLICKI 77	PR D15 3196	A.J. Pawlicki et al.	(AACH3, BERL, BONN+)					
DEUTSCH... 76	NP B103 426	M. Deuschmann et al.	(KARLK, KARLE, PISA, SERP+)					
APEL 75	PL 57B 398	W.D. Apel et al.	(BIRM, DURH, RHEL)					
EMMS 75D	NP B96 155	M.J. Emms et al.	(CERN, MPIM)					
HYAMS 75	NP B100 205	B.D. Hyams et al.	(REHO)					
EISENBERG 74	PL 52B 239	Y. Eisenberg et al.	(CMU, CASE)					
ENGLER 74	PR D10 2070	A. Engler et al.	(SACL, CERN)					
LOUIE 74	PL 48B 385	J. Louie et al.	(CMU, CASE)					
PDG 74	PL 50B 1	V. Chaloupka et al.	(TOHOK, PENN, NDAM+)					
ANDERSON 73	PRL 31 562	J.C. Anderson et al.	(AACH, BERL, CERN)					
TAKAHASHI 72	PR D6 1266	K. Takahashi et al.	(LBL)					
BEAUPRE 71	NP B28 77	J.V. Beaupre et al.	(BARI, BGNA, FIRZ)					
FLATTE 71	PL 34B 551	S.M. Flatte et al.	(WISC, TINTO) JP					
ARMENISE 70	LNC 4 199	N. Armenise et al.	(NDAM)					
OH 70	PR D1 2494	B.Y. Oh et al.	(AACH3, BERL, CERN+)					
STUNTEBECK 70	PL 32B 391	P.H. Stuntebeck et al.	(BARI, BGNA, FIRZ+)					
ADERHOLZ 69	NP B11 259	M. Aderholz et al.	(AACH, BERL, ILL)					
ARMENISE 68	NC 54A 999	N. Armenise et al.	(BARI, BGNA, FIRZ+)					
ASCOLI 68D	PRL 21 1712	G. Ascoli et al.	(AACH, BERL, SLAC)					
BOESEBECK 68	NP B4 501	K. Boesebeck et al.	(PURD)					
JOHNSON 68	PR 176 1651	P.B. Johnson et al.	(NDAM, PURD, SLAC)					
EISNER 67	PR 164 1699	R.L. Eisner et al.	(NDAM)					
DERADO 65	PRL 14 872	I. Derado et al.	(MICH)					
LEE 64	PRL 12 342	Y.Y. Lee et al.	(MICH)					
BONDAR 63	PL 5 153	L.Y. Bondar et al.	(AACH, BIRM, BONN, DESY+)					

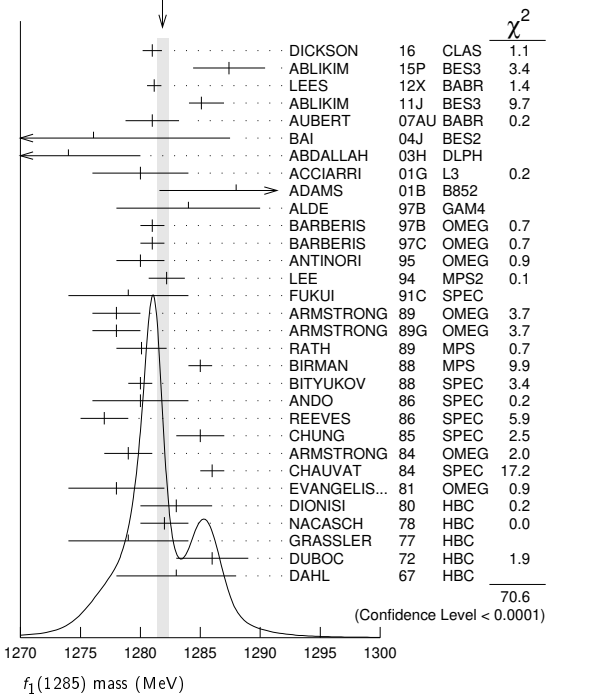
$f_1(1285)$

$$I^G(J^{PC}) = 0^+(1^{++})$$

$f_1(1285)$ MASS

VALUE (MeV)	EVTS	DOCUMENT ID	TECN	COMMENT
1281.9 ± 0.5	OUR AVERAGE	Error includes scale factor of 1.8. See the ideogram below.		
1281.0 ± 0.8		DICKSON 16	CLAS	2.55 $\gamma p \rightarrow \eta\pi^+ \pi^- p$
1287.4 ± 3.0	87	ABLIKIM 15P	BES3	$J/\psi \rightarrow K^+ K^- 3\pi$
1281.16 ± 0.39 ± 0.45		1 LEES 12X	BABR	$\tau^- \rightarrow \pi^- f_1(1285) \nu_\tau$
1285.1 ± 1.0 ± 1.6	0.3	2 ABLIKIM 11J	BES3	$J/\psi \rightarrow \omega(\eta\pi^+ \pi^-)$
1281 ± 2 ± 1		AUBERT 07AU	BABR	10.6 $e^+ e^- \rightarrow f_1(1285) \pi^+ \pi^- \gamma$
1276.1 ± 8.1 ± 8.0	203	BAI 04J	BES2	$J/\psi \rightarrow \gamma\gamma\pi^+ \pi^-$
1274 ± 6	237	ABDALLAH 03H	DLPH	91.2 $e^+ e^- \rightarrow K_S^0 K^\pm \pi^\mp + X$
1280 ± 4		ACCIARRI 01G	L3	
1288 ± 4 ± 5	20k	ADAMS 01B	B852	18 GeV $\pi^- p \rightarrow K^+ K^- \pi^0 n$
1284 ± 6	1400	ALDE 97B	GAM4	100 $\pi^- p \rightarrow \eta\pi^0 \pi^0 n$
1281 ± 1		BARBERIS 97B	OMEG	450 $p p \rightarrow p p 2(\pi^+ \pi^-)$
1281 ± 1		BARBERIS 97C	OMEG	450 $p p \rightarrow p p K_S^0 K^\pm \pi^\mp$
1280 ± 2		3 AN TINORI 95	OMEG	300,450 $p p \rightarrow p p 2(\pi^+ \pi^-)$
1282.2 ± 1.5		LEE 94	MPS2	18 $\pi^- p \rightarrow K^+ \bar{K}^0 2\pi^- p$
1279 ± 5		FUKUI 91C	SPEC	8.95 $\pi^- p \rightarrow \eta\pi^+ \pi^- n$
1278 ± 2	140	ARMSTRONG 89	OMEG	300 $p p \rightarrow K \bar{K} \pi p p$

WEIGHTED AVERAGE
1281.9±0.5 (Error scaled by 1.8)



¹Using the $2\pi^+ 2\pi^-$ and $\pi^+ \pi^- \eta$ modes of $f_1(1285)$ decay.

- ²The selected process is $J/\psi \rightarrow \omega a_0(980)\pi$.
- ³Supersedes ABATZIS 94, ARMSTRONG 89E.
- ⁴From partial wave analysis of $K^+K^0\pi^-$ system.
- ⁵No systematic error given.
- ⁶From a unitarized quark-model calculation.
- ⁷From phase shift analysis of $\eta\pi^+\pi^-$ system.
- ⁸Seen in the missing mass spectrum.

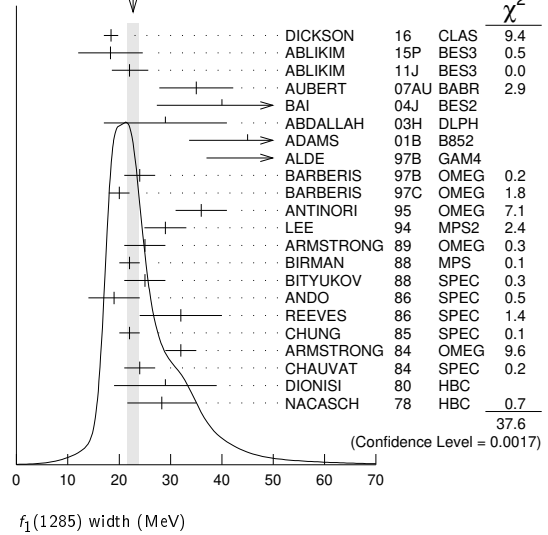
$f_1(1285)$ WIDTH

Only experiments giving width error less than 20 MeV are kept for averaging.

VALUE (MeV)	EVTS	DOCUMENT ID	TECN	COMMENT
22.7 ± 1.1 OUR AVERAGE				Error includes scale factor of 1.5. See the ideogram below.
18.4 ± 1.4		DICKSON 16	CLAS	2.55 $\gamma p \rightarrow \eta\pi^+\pi^-p$
18.3 ± 6.3	87	ABLIKIM 15P	BES3	$J/\psi \rightarrow K^+K^-3\pi$
22.0 ± 3.1 ± 2.0 ± 1.5		¹ ABLIKIM 11J	BES3	$J/\psi \rightarrow \omega(\eta\pi^+\pi^-)$
35 ± 6 ± 4		AUBERT 07AU	BABR	10.6 $e^+e^- \rightarrow f_1(1285)\pi^+\pi^-\gamma$
40.0 ± 8.6 ± 9.3	203	BAI 04J	BES2	$J/\psi \rightarrow \gamma\gamma\pi^+\pi^-$
29 ± 12	237	ABDALLAH 03H	DLPH	91.2 $e^+e^- \rightarrow K_S^0 K^\pm \pi^\mp + X$
45 ± 9 ± 7	20k	ADAMS 01B	B852	18 GeV $\pi^-p \rightarrow K^+K^-\pi^0 n$
55 ± 18	1400	ALDE 97B	GAM4	100 $\pi^-p \rightarrow \eta\pi^0\pi^0 n$
24 ± 3		BARBERIS 97B	OMEG	450 $pp \rightarrow pp2(\pi^+\pi^-)$
20 ± 2		BARBERIS 97C	OMEG	450 $pp \rightarrow ppK_S^0 K^\pm \pi^\mp$
36 ± 5		² ANTINORI 95	OMEG	300,450 $pp \rightarrow pp2(\pi^+\pi^-)$
29.0 ± 4.1		LEE 94	MPS2	18 $\pi^-p \rightarrow K^+\bar{K}^0 2\pi^-p$
25 ± 4	140	ARMSTRONG 89	OMEG	300 $pp \rightarrow K\bar{K}pp$
22 ± 2	4750	³ BIRMAN 88	MPS	8 $\pi^-p \rightarrow K^+\bar{K}^0\pi^-n$
25 ± 4	504	BITYUKOV 88	SPEC	32.5 $\pi^-p \rightarrow K^+K^-\pi^0 n$
19 ± 5		ANDO 86	SPEC	8 $\pi^-p \rightarrow \eta\pi^+\pi^-n$
32 ± 8	420	REEVES 86	SPEC	6.6 $p\bar{p} \rightarrow K K\pi X$
22 ± 2		CHUNG 85	SPEC	8 $\pi^-p \rightarrow N K\bar{K}\pi$
32 ± 3	604	ARMSTRONG 84	OMEG	85 $\pi^+p \rightarrow K\bar{K}\pi p,$ $pp \rightarrow K\bar{K}\pi pp$
24 ± 3		CHAUVAT 84	SPEC	ISR 31.5 pp
29 ± 10	103	DIONISI 80	HBC	4 $\pi^-p \rightarrow K\bar{K}\pi n$
28.3 ± 6.7	320	NACASCH 78	HBC	0.7, 0.76 $p\bar{p} \rightarrow K\bar{K}3\pi$
• • • We do not use the following data for averages, fits, limits, etc. • • •				
17.1 ± 3.4	234	ABLIKIM 19BA	BES3	$e^+e^- \rightarrow \psi(2S)$
32.4 ± 5.8		⁴ AAIJ 14Y	LHCB	$\bar{B}_{(s)}^0 \rightarrow J/\psi 2(\pi^+\pi^-)$
18.2 ± 1.2		⁴ SOSA 99	SPEC	$pp \rightarrow p_{slow} (K_S^0 K^+\pi^-)$
19.4 ± 1.5		⁴ SOSA 99	SPEC	$pp \rightarrow p_{slow} (K_S^0 K^-\pi^+)$
40 ± 5		ABATZIS 94	OMEG	450 $pp \rightarrow pp2(\pi^+\pi^-)$
31 ± 5		ARMSTRONG 89E	OMEG	300 $pp \rightarrow pp2(\pi^+\pi^-)$
41 ± 12		ARMSTRONG 89G	OMEG	85 $\pi^+p \rightarrow 4\pi\pi p, pp \rightarrow 4\pi pp$
17.9 ± 10.9	60	RATH 89	MPS	21.4 $\pi^-p \rightarrow K_S^0 K_S^0 \pi^0 n$
14 ± 20 ± 14 ± 10	16	BECKER 87	MRK3	$e^+e^- \rightarrow \phi K\bar{K}\pi$
26 ± 12		EVANGELIS... 81	OMEG	12 $\pi^-p \rightarrow \eta\pi^+\pi^-\pi^-p$
25 ± 15	200	GURTU 79	HBC	4.2 $K^-p \rightarrow n\eta 2\pi$
~10		⁵ STANTON 79	CNTR	8.5 $\pi^-p \rightarrow n2\gamma 2\pi$
24 ± 18	210	GRASSLER 77	HBC	16 $\pi^{\mp}p$
28 ± 5	150	⁶ DEFOIX 72	HBC	0.7 $p\bar{p} \rightarrow 7\pi$
46 ± 9	180	⁶ DUBOC 72	HBC	1.2 $p\bar{p} \rightarrow 2K4\pi$
37 ± 5	500	⁷ THUN 72	MMS	13.4 π^-p
10 ± 10		BOESEBECK 71	HBC	16.0 $\pi p \rightarrow p5\pi$
30 ± 15		CAMPBELL 69	DBC	2.7 π^+d
60 ± 15		⁶ LORSTAD 69	HBC	0.7 $p\bar{p}, 4,5$ -body
35 ± 10		⁶ DAHL 67	HBC	1.6-4.2 π^-p

- ¹The selected process is $J/\psi \rightarrow \omega a_0(980)\pi$.
- ²Supersedes ABATZIS 94, ARMSTRONG 89E.
- ³From partial wave analysis of $K^+K^0\pi^-$ system.
- ⁴No systematic error given.
- ⁵From phase shift analysis of $\eta\pi^+\pi^-$ system.
- ⁶Resolution is not unfolded.
- ⁷Seen in the missing mass spectrum.

WEIGHTED AVERAGE
22.7±1.1 (Error scaled by 1.5)



$f_1(1285)$ DECAY MODES

Mode	Fraction (Γ_i/Γ)	Scale factor/ Confidence level
Γ_1 4π	(32.7 ± 1.9) %	S=1.2
Γ_2 $\pi^0\pi^0\pi^+\pi^-$	(21.8 ± 1.3) %	S=1.2
Γ_3 $2\pi^+2\pi^-$	(10.9 ± 0.6) %	S=1.2
Γ_4 $\rho^0\pi^+\pi^-$	(10.9 ± 0.6) %	S=1.2
Γ_5 $\rho^0\rho^0$	seen	
Γ_6 $4\pi^0$	< 7 × 10 ⁻⁴	CL=90%
Γ_7 $\eta\pi^+\pi^-$	(35 ± 15) %	
Γ_8 $\eta\pi\pi$	(52.2 ± 2.0) %	S=1.2
Γ_9 $a_0(980)\pi$ [ignoring $a_0(980) \rightarrow K\bar{K}$]	(38 ± 4) %	
Γ_{10} $\eta\pi\pi$ [excluding $a_0(980)\pi$]	(14 ± 4) %	
Γ_{11} $K\bar{K}\pi$	(9.0 ± 0.4) %	S=1.1
Γ_{12} $K\bar{K}^*(892)$	not seen	
Γ_{13} $\pi^+\pi^-\pi^0$	(3.0 ± 0.9) × 10 ⁻³	
Γ_{14} $\rho^\pm\pi^\mp$	< 3.1 × 10 ⁻³	CL=95%
Γ_{15} $\gamma\rho^0$	(6.1 ± 1.0) %	S=1.7
Γ_{16} $\phi\gamma$	(7.4 ± 2.6) × 10 ⁻⁴	
Γ_{17} e^+e^-	< 9.4 × 10 ⁻⁹	CL=90%
Γ_{18} $\gamma\gamma^*$		
Γ_{19} $\gamma\gamma$		

CONSTRAINED FIT INFORMATION

An overall fit to 6 branching ratios uses 18 measurements and one constraint to determine 5 parameters. The overall fit has a $\chi^2 = 24.0$ for 14 degrees of freedom.

The following *off-diagonal* array elements are the correlation coefficients $\langle \delta x_i \delta x_j \rangle / (\delta x_i \delta x_j)$, in percent, from the fit to the branching fractions, $x_i \equiv \Gamma_i/\Gamma_{total}$. The fit constrains the x_i whose labels appear in this array to sum to one.

x_9	-30			
x_{10}	-12	-88		
x_{11}	22	-10	-4	
x_{15}	-25	-7	-3	-27
	x_1	x_9	x_{10}	x_{11}

$f_1(1285)$ $\Gamma(i)\Gamma(\gamma\gamma)/\Gamma(total)$

$\Gamma(\eta\pi\pi) \times \Gamma(\gamma\gamma)/\Gamma_{total}$	$\Gamma_8\Gamma_{19}/\Gamma = (\Gamma_9+\Gamma_{10})\Gamma_{19}/\Gamma$			
VALUE (keV)	CL%	DOCUMENT ID	TECN	COMMENT
<0.62	95	GIDAL	87	MRK2 $e^+e^- \rightarrow e^+e^-\eta\pi^+\pi^-$

Meson Particle Listings

$f_1(1285)$

$\Gamma(\eta\pi\pi) \times \Gamma(\gamma\gamma^*)/\Gamma_{\text{total}}$		$\Gamma_8\Gamma_{18}/\Gamma = (\Gamma_9+\Gamma_{10})\Gamma_{18}/\Gamma$		
VALUE (keV)	EVTS	DOCUMENT ID	TECN	COMMENT
1.4 ± 0.4 OUR AVERAGE		Error includes scale factor of 1.4.		
1.18 ± 0.25 ± 0.20	26	^{1,2} AIHARA	88B TPC	$e^+e^- \rightarrow e^+e^-\eta\pi^+\pi^-$
2.30 ± 0.61 ± 0.42		^{1,3} GIDAL	87 MRK2	$e^+e^- \rightarrow e^+e^-\eta\pi^+\pi^-$
• • • We do not use the following data for averages, fits, limits, etc. • • •				
1.8 ± 0.3 ± 0.3	420	⁴ ACHARD	02B L3	183–209 $e^+e^- \rightarrow e^+e^-\eta\pi^+\pi^-$

¹ Assuming a ρ -pole form factor.
² Published value multiplied by $\eta\pi\pi$ branching ratio 0.49.
³ Published value divided by 2 and multiplied by the $\eta\pi\pi$ branching ratio 0.49.
⁴ Published value multiplied by the $\eta\pi\pi$ branching ratio 0.52.

$f_1(1285)$ BRANCHING RATIOS

$\Gamma(K\bar{K}\pi)/\Gamma(4\pi)$		Γ_{11}/Γ_1		
VALUE	DOCUMENT ID	TECN	COMMENT	
0.274 ± 0.017 OUR FIT		Error includes scale factor of 1.4.		
0.271 ± 0.016 OUR AVERAGE		Error includes scale factor of 1.2.		
0.265 ± 0.014	¹ BARBERIS	97C OMEG	450 $pp \rightarrow ppK_S^0 K^\pm \pi^\mp$	
0.28 ± 0.05	² ARMSTRONG	89E OMEG	300 $pp \rightarrow pp f_1(1285)$	
0.37 ± 0.03 ± 0.05	³ ARMSTRONG	89G OMEG	85 $\pi p \rightarrow 4\pi X$	
• • • We do not use the following data for averages, fits, limits, etc. • • •				
1.8 ± 0.3 ± 0.3	420	⁴ ACHARD	02B L3	183–209 $e^+e^- \rightarrow e^+e^-\eta\pi^+\pi^-$

¹ Using $2(\pi^+\pi^-)$ data from BARBERIS 97B.
² Assuming $\rho\pi\pi$ and $a_0(980)\pi$ intermediate states.
³ 4π consistent with being entirely $\rho\pi\pi$.

$\Gamma(\rho^0\pi^+\pi^-)/\Gamma_{\text{total}}$		$\Gamma_2/\Gamma = \frac{2}{3}\Gamma_1/\Gamma$		
VALUE	DOCUMENT ID	TECN	COMMENT	
0.218 ± 0.013 OUR FIT		Error includes scale factor of 1.2.		

$\Gamma(2\pi^+2\pi^-)/\Gamma_{\text{total}}$		$\Gamma_3/\Gamma = \frac{1}{3}\Gamma_1/\Gamma$		
VALUE	DOCUMENT ID	TECN	COMMENT	
0.109 ± 0.006 OUR FIT		Error includes scale factor of 1.2.		

$\Gamma(\rho^0\pi^+\pi^-)/\Gamma_{\text{total}}$		$\Gamma_4/\Gamma = \frac{1}{3}\Gamma_1/\Gamma$		
VALUE	DOCUMENT ID	TECN	COMMENT	
0.109 ± 0.006 OUR FIT		Error includes scale factor of 1.2.		

$\Gamma(\rho^0\pi^+\pi^-)/\Gamma(2\pi^+2\pi^-)$		Γ_4/Γ_3		
VALUE	DOCUMENT ID	TECN	COMMENT	
1.0 ± 0.4	GRASSLER	77 HBC	16 GeV $\pi^\pm p$	

• • • We do not use the following data for averages, fits, limits, etc. • • •

$\Gamma(\rho^0\rho^0)/\Gamma_{\text{total}}$		Γ_5/Γ		
VALUE	DOCUMENT ID	TECN	COMMENT	
seen	BARBERIS	00C	450 $pp \rightarrow p f_4 \pi p_S$	

$\Gamma(4\pi^0)/\Gamma_{\text{total}}$		Γ_6/Γ		
VALUE (units 10^{-4})	CL%	DOCUMENT ID	TECN	COMMENT
<7	90	ALDE	87 GAM4	100 $\pi^- p \rightarrow 4\pi^0 n$

$\Gamma(\pi^+\pi^-\pi^0)/\Gamma(\eta\pi^+\pi^-)$		Γ_{13}/Γ_7		
VALUE (%)	EVTS	DOCUMENT ID	TECN	COMMENT
0.86 ± 0.16 ± 0.20	2.3k	¹ DOROFEEV	11 VES	$\pi^- N \rightarrow \pi^- f_1(1285) N$

¹ Value obtained selecting the region corresponding to $f_0(980)$ in the $\pi^+\pi^-$ mass spectrum.

$\Gamma(\eta\pi\pi)/\Gamma_{\text{total}}$		$\Gamma_8/\Gamma = (\Gamma_9+\Gamma_{10})/\Gamma$		
VALUE	DOCUMENT ID	TECN	COMMENT	
0.522 ± 0.020 OUR FIT		Error includes scale factor of 1.2.		

$\Gamma(4\pi)/\Gamma(\eta\pi\pi)$		$\Gamma_1/\Gamma_8 = \Gamma_1/(\Gamma_9+\Gamma_{10})$		
VALUE	DOCUMENT ID	TECN	COMMENT	
0.63 ± 0.06 OUR FIT		Error includes scale factor of 1.3.		
0.41 ± 0.14 OUR AVERAGE				
0.37 ± 0.11 ± 0.11	BOLTON	92 MRK3	$J/\psi \rightarrow \gamma f_1(1285)$	
0.64 ± 0.40	GURTU	79 HBC	4.2 $K^- p$	
• • • We do not use the following data for averages, fits, limits, etc. • • •				
0.93 ± 0.30	¹ GRASSLER	77 HBC	16 $\pi^\mp p$	

¹ Assuming $\rho\pi\pi$ and $a_0(980)\pi$ intermediate states.

$\Gamma(2\pi^+2\pi^-)/\Gamma(\eta\pi\pi)$		Γ_3/Γ_8		
VALUE	DOCUMENT ID	TECN	COMMENT	
0.28 ± 0.02 ± 0.02		Error includes scale factor of 1.2.		
	¹ LEES	12X BABR	$\tau^- \rightarrow \pi^- f_1(1285) \nu_\tau$	

¹ Assuming $B(f_1(1285) \rightarrow \pi\pi\eta) = 3/2 B(f_1(1285) \rightarrow \pi^+\pi^-\eta)$.

$\Gamma(a_0(980)\pi [\text{ignoring } a_0(980) \rightarrow K\bar{K}])/(\eta\pi\pi)$		$\Gamma_9/\Gamma_8 = \Gamma_9/(\Gamma_9+\Gamma_{10})$		
VALUE	CL%	DOCUMENT ID	TECN	COMMENT
0.72 ± 0.08 OUR FIT		Error includes scale factor of 1.5.		
0.72 ± 0.07 OUR AVERAGE				
0.74 ± 0.02 ± 0.09		DICKSON	16 CLAS	$\gamma p \rightarrow f_1(1285) p$
0.72 ± 0.15		GURTU	79 HBC	4.2 $K^- p$
0.6 ± 0.3		CORDEN	78 OMEG	12–15 $\pi^- p$
–0.2				

• • • We do not use the following data for averages, fits, limits, etc. • • •

>0.69	95	ACHARD	02B L3	183–209 $e^+e^- \rightarrow e^+e^-\eta\pi^+\pi^-$
0.28 ± 0.07		ALDE	97B GAM4	100 $\pi^- p \rightarrow \eta\pi^0\pi^0 n$
1.0 ± 0.3		GRASSLER	77 HBC	16 $\pi^\mp p$

$\Gamma(K\bar{K}\pi)/\Gamma(\eta\pi\pi)$		$\Gamma_{11}/\Gamma_8 = \Gamma_{11}/(\Gamma_9+\Gamma_{10})$		
VALUE	DOCUMENT ID	TECN	COMMENT	
0.172 ± 0.012 OUR FIT		Error includes scale factor of 1.1.		
0.176 ± 0.012 OUR AVERAGE				
0.216 ± 0.010 ± 0.031	DICKSON	16 CLAS	$\gamma p \rightarrow f_1(1285) p$	
0.166 ± 0.01 ± 0.008	BARBERIS	98C OMEG	450 $pp \rightarrow p f_1(1285) p_S$	
0.42 ± 0.15	GURTU	79 HBC	4.2 $K^- p$	
0.5 ± 0.2	¹ CORDEN	78 OMEG	12–15 $\pi^- p$	
0.20 ± 0.08	² DEFOIX	72 HBC	0.7 $\bar{p} p \rightarrow 7\pi$	
0.16 ± 0.08	CAMPBELL	69 DBC	2.7 $\pi^+ d$	

¹ CORDEN 78 assumes low-mass $\eta\pi\pi$ region is dominantly 1^{++} . See BARBERIS 98c and MANAK 00a for discussion.
² $K\bar{K}$ system characterized by the $l = 1$ threshold enhancement. (See under $a_0(980)$).

$\Gamma(K\bar{K}^*(892))/\Gamma_{\text{total}}$		Γ_{12}/Γ		
VALUE	DOCUMENT ID	TECN	COMMENT	
not seen	NACASCH	78 HBC	0.7, 0.76 $\bar{p} p \rightarrow K\bar{K}3\pi$	
• • • We do not use the following data for averages, fits, limits, etc. • • •				
seen	¹ ACHARD	07 L3	183–209 $e^+e^- \rightarrow e^+e^-K_S^0 K^\pm \pi^\mp$	

¹ A clear signal of 19.8 ± 4.4 events observed at high Q^2 .

$\Gamma(\pi^+\pi^-\pi^0)/\Gamma_{\text{total}}$		Γ_{13}/Γ		
VALUE (%)	EVTS	DOCUMENT ID	TECN	COMMENT
0.30 ± 0.055 ± 0.074	2.3k	¹ DOROFEEV	11 VES	$\pi^- N \rightarrow \pi^- f_1(1285) N$

¹ Value obtained selecting the region corresponding to $f_0(980)$ in the $\pi^+\pi^-$ mass spectrum. The systematic error includes the uncertainty on the partial width $f_1 \rightarrow \eta\pi\pi$ obtained from PDG 10 data.

$\Gamma(\rho^\pm\pi^\mp)/\Gamma_{\text{total}}$		Γ_{14}/Γ		
VALUE (%)	CL%	DOCUMENT ID	TECN	COMMENT
<0.31	95	DOROFEEV	11 VES	$\pi^- N \rightarrow \pi^- f_1(1285) N$

$\Gamma(\gamma\rho^0)/\Gamma_{\text{total}}$		Γ_{15}/Γ		
VALUE (units 10^{-2})	CL%	DOCUMENT ID	TECN	COMMENT
6.1 ± 1.0 OUR FIT		Error includes scale factor of 1.7.		
• • • We do not use the following data for averages, fits, limits, etc. • • •				
2.8 ± 0.7 ± 0.6		¹ AMELIN	95 VES	37 $\pi^- N \rightarrow \pi^- \pi^+ \pi^- \gamma N$
<5	95	BITYUKOV	91B SPEC	32 $\pi^- p \rightarrow \pi^+ \pi^- \gamma n$

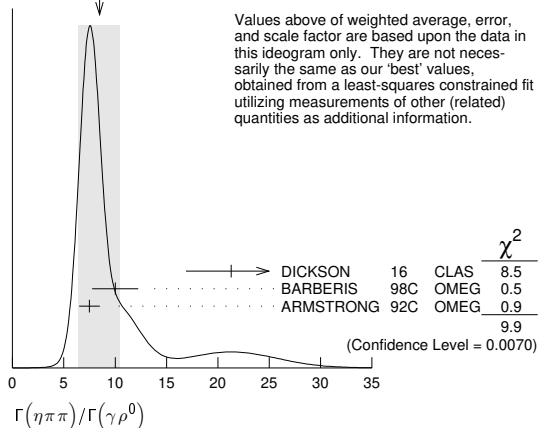
¹ Not an independent measurement.

$\Gamma(\gamma\rho^0)/\Gamma(2\pi^+2\pi^-)$		$\Gamma_{15}/\Gamma_3 = \Gamma_{15}/\frac{1}{3}\Gamma_1$		
VALUE	DOCUMENT ID	TECN	COMMENT	
0.55 ± 0.10 OUR FIT		Error includes scale factor of 1.5.		
0.45 ± 0.18				
	¹ COFFMAN	90 MRK3	$J/\psi \rightarrow \gamma\gamma\pi^+\pi^-$	

¹ Using $B(J/\psi \rightarrow \gamma f_1(1285) \rightarrow \gamma\gamma\rho^0) = 0.25 \times 10^{-4}$ and $B(J/\psi \rightarrow \gamma f_1(1285) \rightarrow \gamma 2\pi^+ 2\pi^-) = 0.55 \times 10^{-4}$ given by MIR 88.

$\Gamma(\eta\pi\pi)/\Gamma(\gamma\rho^0)$		$\Gamma_8/\Gamma_{15} = (\Gamma_9+\Gamma_{10})/\Gamma_{15}$		
VALUE	DOCUMENT ID	TECN	COMMENT	
8.6 ± 1.6 OUR FIT		Error includes scale factor of 1.9.		
8.5 ± 2.0 OUR AVERAGE		Error includes scale factor of 2.2. See the ideogram below.		
21.3 ± 4.4	DICKSON	16 CLAS	$\gamma p \rightarrow f_1(1285) p$	
10.0 ± 1.0 ± 2.0	BARBERIS	98C OMEG	450 $pp \rightarrow p f_1(1285) p_S$	
7.5 ± 1.0	¹ ARMSTRONG	92C OMEG	300 $pp \rightarrow \rho p \pi^+ \pi^- \gamma, \rho p \eta \pi^+ \pi^-$	

WEIGHTED AVERAGE
8.5 ± 2.0 (Error scaled by 2.2)



¹ Published value multiplied by 1.5.

See key on page 1127

Meson Particle Listings

$f_1(1285), \eta(1295)$

$\Gamma(\gamma\rho^0)/\Gamma(K\bar{K}\pi)$ Γ_{15}/Γ_{11}

VALUE	CL%	DOCUMENT ID	TECN	COMMENT
• • • We do not use the following data for averages, fits, limits, etc. • • •				
>0.035	90	¹ COFFMAN 90	MRK3	$J/\psi \rightarrow \gamma\gamma\pi^+\pi^-$
¹ Using $B(J/\psi \rightarrow \gamma f_1(1285)) \rightarrow \gamma\gamma\rho^0 = 0.25 \times 10^{-4}$ and $B(J/\psi \rightarrow \gamma f_1(1285)) \rightarrow \gamma K\bar{K}\pi < 0.72 \times 10^{-3}$.				

$\Gamma(\phi\gamma)/\Gamma(K\bar{K}\pi)$ Γ_{16}/Γ_{11}

VALUE (units 10^{-2})	CL%	EVTS	DOCUMENT ID	TECN	COMMENT
0.82 ± 0.21 ± 0.20		19	BITYUKOV	88	SPEC 32.5 $\pi^-p \rightarrow K^+K^-\pi^0n$
• • • We do not use the following data for averages, fits, limits, etc. • • •					
<0.50	95		BARBERIS	98c	OMEG 450 $pp \rightarrow p_f f_1(1285) p_s$
<0.93	95		AMELIN	95	VES 37 $\pi^-N \rightarrow \pi^-\pi^+\pi^-\gamma N$

$\Gamma(e^+e^-)/\Gamma_{total}$ Γ_{17}/Γ

VALUE	CL%	DOCUMENT ID	TECN	COMMENT
<9.4 × 10⁻⁹	90	¹ ACHASOV 20	SND	$e^+e^- \rightarrow \eta\pi^0\pi^0$
¹ ACHASOV 20 reports two candidate events corresponding to a significance of 2.5 σ and the branching fraction of $(5.1^{+3.7}_{-2.7}) \times 10^{-9}$.				

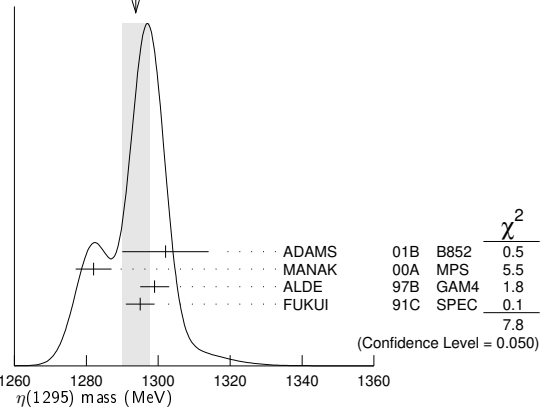
$f_1(1285)$ REFERENCES

ACHASOV	20	PL B800 135074	M.N. Achasov et al.	(SND Collab.)
ABLIKIM	19BA	PR D100 092003	M. Ablikim et al.	(BESIII Collab.)
DICKSON	16	PR C93 065202	R. Dickson et al.	(JLab CLAS Collab.)
ABLIKIM	15P	PR D92 012007	M. Ablikim et al.	(BESIII Collab.)
AALI	14Y	PRL 112 091802	R. Aaij et al.	(LHCb Collab.)
LEES	12X	PR D86 092010	J.P. Lees et al.	(BABAR Collab.)
ABLIKIM	11J	PRL 107 182001	M. Ablikim et al.	(BESIII Collab.)
DOROFEEV	11	EPJ A47 68	V. Dorofeev et al.	(SERP, MIPT)
PDG	10	JP G37 075021	K. Nakamura et al.	(PDG Collab.)
ACHARD	07	JHEP 0703 018	P. Achard et al.	(L3 Collab.)
AUBERT	07AU	PR D76 092005	B. Aubert et al.	(BABAR Collab.)
BAI	04J	PL B594 47	J.Z. Bai et al.	(BES Collab.)
ABDALLAH	03H	PL B569 129	J. Abdallah et al.	(DELPHI Collab.)
ACHARD	02B	PL B526 269	P. Achard et al.	(L3 Collab.)
ACCIARRI	01G	PL B501 1	M. Acciarrri et al.	(L3 Collab.)
ADAMS	01B	PL B516 264	G.S. Adams et al.	(BNL E852 Collab.)
BARBERIS	00C	PL B471 440	D. Barberis et al.	(WA 102 Collab.)
MANAK	00A	PR D62 012003	J.J. Manak et al.	(BNL E852 Collab.)
SOSA	99	PRL 83 913	M. Sosa et al.	
BARBERIS	98C	PL B440 225	D. Barberis et al.	(WA 102 Collab.)
ALDE	97B	PAN 60 386	D. Alde et al.	(GAMS Collab.)
Translated from YAF 60 458.				
BARBERIS	97B	PL B413 217	D. Barberis et al.	(WA 102 Collab.)
BARBERIS	97C	PL B413 225	D. Barberis et al.	(WA 102 Collab.)
AMELIN	95	ZPHY C66 71	V. Amelin et al.	(VES Collab.)
ANTINORI	95	PL B353 589	F. Antinori et al.	(ATHU, BARI, BIRM+)
ABATZIS	94	PL B324 509	S. Abatzis et al.	(ATHU, BARI, BIRM+)
LEE	94	PL B323 227	J.H. Lee et al.	(BNL, IND, KYUN, MASD+)
ARMSTRONG	93C	PL B307 394	T.A. Armstrong et al.	(FNAL, FERR, GENO+)
ARMSTRONG	92C	ZPHY C54 371	T.A. Armstrong et al.	(ATHU, BARI, BIRM+)
BOLTON	92	PL B278 495	T. Bolton et al.	(Mark III Collab.)
BITYUKOV	91B	SJNP 54 318	S.I. Bityukov et al.	(SERP)
Translated from YAF 54 529.				
FUKUI	91C	PL B267 293	S. Fukui et al.	(SUGI, NAGO, KEK, KYOT+)
COFFMAN	90	PR D41 1410	D.M. Coffman et al.	(Mark III Collab.)
ARMSTRONG	89	PL B221 216	T.A. Armstrong et al.	(CERN, CDEF, BIRM+ JPC)
ARMSTRONG	89E	PL B228 536	T.A. Armstrong, M. Benayoun	(ATHU, BARI, BIRM+)
ARMSTRONG	89G	ZPHY C43 55	T.A. Armstrong et al.	(CERN, BIRM, BARI+)
RATH	89	PR D40 693	M.G. Rath et al.	(NDAM, BRAN, BNL, CUNY+)
AIHARA	88B	PL B209 107	H. Aihara et al.	(TPC-2 γ Collab.)
BIRMAN	88	PRL 61 1557	A. Birman et al.	(BNL, FSU, IND, MASD) JP
BITYUKOV	88	PL B203 327	S.I. Bityukov et al.	(SERP)
MIR	88	Photon-Photon 88, 126	R. Mir	(Mark III Collab.)
Conference				
ALDE	87	PL B198 286	D.M. Alde et al.	(LANL, BRUX, SERP, LAPP)
BECKER	87	PRL 59 186	J.J. Becker et al.	(Mark III Collab.)
GIDAL	87	PRL 59 2012	G. Gidal et al.	(LBL, SLAC, HARV)
ANDO	86	PRL 57 1296	A. Ando et al.	(KEK, KYOT, NIRS, SAGA+) IJP
REEVES	86	PR D34 1960	D.F. Reeves et al.	(FLOR, BNL, IND+ JP)
CHUNG	85	PRL 55 779	S.U. Chung et al.	(BNL, FLOR, IND+ JP)
ARMSTRONG	84	PL 146B 273	T.A. Armstrong et al.	(ATHU, BARI, BIRM+ JP)
BITYUKOV	84B	PL 144B 133	S.I. Bityukov et al.	(SERP)
CHAUVAUT	84	PL 148B 382	P. Chauvaud et al.	(CERN, CLER, UCLA+)
TORNGVIST	82B	NP B203 268	N.A. Torngvist	(HELS)
EVANGELISTA	81	NP B178 197	C. Evangelista et al.	(BARI, BONN, CERN+)
BROMBERG	80	PR D22 1513	C.M. Bromberg et al.	(GIT, FNAL, ILLC+)
DIONISI	80	NP B169 1	C. Dionisi et al.	(CERN, MADR, CDEF+)
GURTU	79	NP B151 181	A. Gurtu et al.	(CERN, ZEEM, NIJM, OXF)
STANTON	79	PRL 42 346	N.R. Stanton et al.	(OSU, CARL, MCGI+ JP)
CORDEN	78	NP B144 253	M.J. Corden et al.	(BIRM, RHEL, TELA+ JP)
NACASCH	78	NP B135 203	R. Nacasch et al.	(PARIS, MADR, CERN)
GRASSLER	77	NP B121 189	H. Grassler et al.	(AACH3, BERL, BONN+)
DEFOIX	72	NP B44 125	C. Defoix et al.	(CDEF, CERN)
DUBOC	72	NP B46 429	J. Duboc et al.	(PARIS, LIVP)
THUN	72	PRL 28 1733	R. Thun et al.	(STON, NEAS)
BARDAJIN...	71	NP D4 2711	M. Bardajin-Ostrowska et al.	(WARS)
BOESEBECK	71	PL 34B 659	K. Boesebeck et al.	(AACH, BERL, BONN, CERN, CAC+)
CAMPBELL	69	PRL 22 1204	J.H. Campbell et al.	(PURD)
LORSTAD	69	NP B14 63	B. Lorstad et al.	(CDEF, CERN) JP
D'ANDLAU	68	NP B5 693	C. d'Andlau et al.	(CDEF, CERN, IRAD+ IJP)
DAHL	67	PR 163 1377	O.I. Dahl et al.	(LRL) IJP

$\eta(1295)$ MASS

VALUE (MeV)	EVTS	DOCUMENT ID	TECN	COMMENT
1294 ± 4 OUR AVERAGE	Error	includes scale factor of 1.6. See the ideogram below.		
1302 ± 9 ± 8	20k	ADAMS	01B B852	18 GeV $\pi^-p \rightarrow K^+K^-\pi^0n$
1282 ± 5	9082	MANAK	00A MPS	18 $\pi^-p \rightarrow \eta\pi^+\pi^-n$
1299 ± 4	2100	ALDE	97B GAM4	100 $\pi^-p \rightarrow \eta\pi^0\pi^0n$
1295 ± 4		FUKUI	91c SPEC	8.95 $\pi^-p \rightarrow \eta\pi^+\pi^-n$
• • • We do not use the following data for averages, fits, limits, etc. • • •				
1264 ± 8		¹ AUGUSTIN	90 DM2	$J/\psi \rightarrow \gamma\eta\pi^+\pi^-$
~ 1275		STANTON	79 CNTR	8.4 $\pi^-p \rightarrow n\eta 2\pi$

WEIGHTED AVERAGE
1294 ± 4 (Error scaled by 1.6)



¹ PWA analysis of AUGUSTIN 92 assigns 0^{++} quantum numbers to this state rather than 1^{++} as before.

$\eta(1295)$ WIDTH

VALUE (MeV)	EVTS	DOCUMENT ID	TECN	COMMENT
55 ± 5 OUR AVERAGE				
57 ± 23 ± 21	20k	ADAMS	01B B852	18 GeV $\pi^-p \rightarrow K^+K^-\pi^0n$
66 ± 13	9082	MANAK	00A MPS	18 $\pi^-p \rightarrow \eta\pi^+\pi^-n$
53 ± 6		FUKUI	91c SPEC	8.95 $\pi^-p \rightarrow \eta\pi^+\pi^-n$
• • • We do not use the following data for averages, fits, limits, etc. • • •				
<40	2100	ALDE	97B GAM4	100 $\pi^-p \rightarrow \eta\pi^0\pi^0n$
44 ± 20		² AUGUSTIN	90 DM2	$J/\psi \rightarrow \gamma\eta\pi^+\pi^-$
~ 70		STANTON	79 CNTR	8.4 $\pi^-p \rightarrow n\eta 2\pi$
² PWA analysis of AUGUSTIN 92 assigns 0^{++} quantum numbers to this state rather than 1^{++} as before.				

$\eta(1295)$ DECAY MODES

Mode	Fraction (Γ_i/Γ)
Γ_1 $\eta\pi^+\pi^-$	seen
Γ_2 $a_0(980)\pi$	seen
Γ_3 $\gamma\gamma$	
Γ_4 $\eta\pi^0\pi^0$	seen
Γ_5 $\eta(\pi\pi)S$ -wave	seen
Γ_6 $\sigma\eta$	
Γ_7 $K\bar{K}\pi$	

$\eta(1295)$ $\Gamma(\eta\pi\pi)/\Gamma(\text{total})$

VALUE (keV)	CL%	DOCUMENT ID	TECN	COMMENT
<0.066	95	ACCIARRI	01G L3	183-202 $e^+e^- \rightarrow e^+e^-\eta\pi^+\pi^-$
• • • We do not use the following data for averages, fits, limits, etc. • • •				
<0.6	90	AIHARA	88c TPC	$e^+e^- \rightarrow e^+e^-\eta\pi^+\pi^-$
<0.3		ANTREASIAN	87 CBAL	$e^+e^- \rightarrow e^+e^-\eta\pi\pi$

$\Gamma(K\bar{K}\pi) \times \Gamma(\gamma\gamma)/\Gamma_{total}$ $\Gamma_7\Gamma_3/\Gamma$

VALUE (keV)	CL%	DOCUMENT ID	TECN	COMMENT
<0.014	90	^{3,4} AHOHE	05 CLE2	10.6 $e^+e^- \rightarrow e^+e^-K_S^0K^\pm\pi^\mp$

³ Using $\eta(1295)$ mass and width 1294 MeV and 55 MeV, respectively.

⁴ Assuming three-body phase-space decay to $K_S^0K^\pm\pi^\mp$.

$\eta(1295)$

$$I^G(J^{PC}) = 0^+(0^{-+})$$

See the review on "Spectroscopy of Light Meson Resonances."

Meson Particle Listings

$\eta(1295)$, $\pi(1300)$, $a_2(1320)$

$\eta(1295)$ BRANCHING RATIOS

$\Gamma(a_0(980)\pi)/\Gamma_{total}$	DOCUMENT ID	TECN	COMMENT	Γ_2/Γ
VALUE				
••• We do not use the following data for averages, fits, limits, etc. •••				
not seen	BERTIN 97	OBLX	$0.0 \bar{p}p \rightarrow K^\pm(K^0)\pi^\mp\pi^+\pi^-$	
seen	BIRMAN 88	MPS	$8 \pi^-p \rightarrow K^+\bar{K}^0\pi^-n$	
large	ANDO 86	SPEC	$8 \pi^-p \rightarrow \eta\pi^+\pi^-n$	
large	STANTON 79	CNTR	$8.4 \pi^-p \rightarrow n\eta 2\pi$	

$\Gamma(a_0(980)\pi)/\Gamma(\eta\pi^0\pi^0)$	DOCUMENT ID	TECN	COMMENT	Γ_2/Γ_4
VALUE				
0.65 ± 0.10	5 ALDE 97B	GAM4	$100 \pi^-p \rightarrow \eta\pi^0\pi^0n$	

⁵ Assuming that $a_0(980)$ decays only to $\eta\pi$.

$\Gamma(\eta(\pi\pi)_{s-wave})/\Gamma(\eta\pi^0\pi^0)$	DOCUMENT ID	TECN	COMMENT	Γ_5/Γ_4
VALUE				
0.35 ± 0.10	ALDE 97B	GAM4	$100 \pi^-p \rightarrow \eta\pi^0\pi^0n$	

$\Gamma(a_0(980)\pi)/\Gamma(\sigma\eta)$	EVTS	DOCUMENT ID	TECN	COMMENT	Γ_2/Γ_6
VALUE					
0.48 ± 0.22	9082	MANAK	00A	MPS	$18 \pi^-p \rightarrow \eta\pi^+\pi^-n$

$\eta(1295)$ REFERENCES

AHOHE 05	PR D71 072001	R. Ahohe et al.	(CLEO Collab.)
ACCIARRI 01G	PL B501 1	M. Acciari et al.	(L3 Collab.)
ADAMS 01B	PL B516 264	G.S. Adams et al.	(BNL E852 Collab.)
MANAK 00A	PR D62 012003	J.J. Manak et al.	(BNL E852 Collab.)
ALDE 97B	PAN 60 386	D. Alde et al.	(GAMS Collab.)
	Translated from YAF 60 458		
BERTIN 97	PL B400 226	A. Bertin et al.	(OBELIX Collab.)
AUGUSTIN 92	PR D46 1951	J.E. Augustin, G. Cosme	(DM2 Collab.)
FUKUI 91C	PL B267 293	S. Fukui et al.	(SUGI, NAGO, KEK, KYOT+)
AUGUSTIN 90	PR D42 10	J.E. Augustin et al.	(DM2 Collab.)
AIHARA 88C	PR D38 1	H. Aihara et al.	(TPC-2 γ Collab.)
BIRMAN 88	PRL 61 1557	A. Birman et al.	(BNL FSU, IND, MASD) JP
ANTREASAYAN 87	PR D36 2633	D. Antreasyan et al.	(Crystal Ball Collab.)
ANDO 86	PRL 57 1296	A. Ando et al.	(KEK, KYOT, NIRS, SAGA+)JP
STANTON 79	PRL 42 346	N.R. Stanton et al.	(OSU, CARL, MCGI+)JP

$\pi(1300)$

$$I^G(J^{PC}) = 1^-(0^{-+})$$

$\pi(1300)$ MASS

VALUE (MeV)	EVTS	DOCUMENT ID	TECN	COMMENT
1300 ± 100 OUR ESTIMATE				
••• We do not use the following data for averages, fits, limits, etc. •••				
$1128 \pm 26 \pm 70$		DARGENT 17	RVUE	$D^0 \rightarrow \pi^-\pi^+\pi^-\pi^+$
$1345 \pm 8 \pm 10$	18k	1 SCHEGELSKY 06	RVUE	$\gamma\gamma \rightarrow \pi^+\pi^-\pi^0$
1200 ± 40	90k	SALVINI 04	OBLX	$\bar{p}p \rightarrow 2\pi^+ 2\pi^-$
$1343 \pm 15 \pm 24$		CHUNG 02	B852	$18.3 \pi^-p \rightarrow \pi^+\pi^-\pi^-p$
1375 ± 40		ABELE 01	CBAR	$0.0 \bar{p}d \rightarrow \pi^- 4\pi^0 p$
1275 ± 15		BERTIN 97D	OBLX	$0.05 \bar{p}p \rightarrow 2\pi^+ 2\pi^-$
~ 1114		ABELE 96	CBAR	$0.0 \bar{p}p \rightarrow 5\pi^0$
1190 ± 30		ZIELINSKI 84	SPEC	$200 \pi^+ Z \rightarrow Z 3\pi$
1240 ± 30		BELLINI 82	SPEC	$40 \pi^- A \rightarrow A 3\pi$
1273 ± 50		2 AARON 81	RVUE	
1342 ± 20		BONESINI 81	OMEG	$12 \pi^-p \rightarrow p 3\pi$
~ 1400		DAUM 81B	SPEC	$63,94 \pi^-p$

¹ From analysis of L3 data at 183–209 GeV.
² Uses multichannel Aitchison-Bowler model (BOWLER 75). Uses data from DAUM 80 and DANKOWYCH 81.

$\pi(1300)$ WIDTH

VALUE (MeV)	EVTS	DOCUMENT ID	TECN	COMMENT
200 to 600 OUR ESTIMATE				
••• We do not use the following data for averages, fits, limits, etc. •••				
$314 \pm 39 \pm 66$		DARGENT 17	RVUE	$D^0 \rightarrow \pi^-\pi^+\pi^-\pi^+$
$260 \pm 20 \pm 30$		3 SCHEGELSKY 06	RVUE	$\gamma\gamma \rightarrow \pi^+\pi^-\pi^0$
470 ± 120	90k	SALVINI 04	OBLX	$\bar{p}p \rightarrow 2\pi^+ 2\pi^-$
$449 \pm 39 \pm 47$		CHUNG 02	B852	$18.3 \pi^-p \rightarrow \pi^+\pi^-\pi^-p$
268 ± 50		ABELE 01	CBAR	$0.0 \bar{p}d \rightarrow \pi^- 4\pi^0 p$
218 ± 100		BERTIN 97D	OBLX	$0.05 \bar{p}p \rightarrow 2\pi^+ 2\pi^-$
~ 340		ABELE 96	CBAR	$0.0 \bar{p}p \rightarrow 5\pi^0$
440 ± 80		ZIELINSKI 84	SPEC	$200 \pi^+ Z \rightarrow Z 3\pi$
360 ± 120		BELLINI 82	SPEC	$40 \pi^- A \rightarrow A 3\pi$
580 ± 100		4 AARON 81	RVUE	
220 ± 70		BONESINI 81	OMEG	$12 \pi^-p \rightarrow p 3\pi$
~ 600		DAUM 81B	SPEC	$63,94 \pi^-p$

³ From analysis of L3 data at 183–209 GeV.
⁴ Uses multichannel Aitchison-Bowler model (BOWLER 75). Uses data from DAUM 80 and DANKOWYCH 81.

$\pi(1300)$ DECAY MODES

Mode	Fraction (Γ_i/Γ)
Γ_1 $\rho\pi$	seen
Γ_2 $\pi(\pi\pi)_{s-wave}$	seen
Γ_3 $\gamma\gamma$	

$\pi(1300)$ $\Gamma(i)\Gamma(\gamma\gamma)/\Gamma(total)$

$\Gamma(\rho\pi) \times \Gamma(\gamma\gamma)/\Gamma_{total}$	DOCUMENT ID	TECN	COMMENT	$\Gamma_1\Gamma_3/\Gamma$
VALUE (keV)				
<0.085	90	ACCIARRI 97T	L3	$e^+e^- \rightarrow e^+e^-\pi^+\pi^-\pi^0$
••• We do not use the following data for averages, fits, limits, etc. •••				
<0.8	95	5 SCHEGELSKY 06	RVUE	$\gamma\gamma \rightarrow \pi^+\pi^-\pi^0$
<0.54	90	ALBRECHT 97B	ARG	$e^+e^- \rightarrow e^+e^-\pi^+\pi^-\pi^0$

⁵ From analysis of L3 data at 183–209 GeV.

$\pi(1300)$ BRANCHING RATIOS

$\Gamma(\pi(\pi\pi)_{s-wave})/\Gamma(\rho\pi)$	DOCUMENT ID	TECN	COMMENT	Γ_2/Γ_1
VALUE				
••• We do not use the following data for averages, fits, limits, etc. •••				
2.2 ± 0.4	90k	SALVINI 04	OBLX	$\bar{p}p \rightarrow 2\pi^+ 2\pi^-$
seen		CHUNG 02	B852	$18.3 \pi^-p \rightarrow \pi^+ 2\pi^-p$
<0.15	90	ABELE 01	CBAR	$0.0 \bar{p}d \rightarrow \pi^- 4\pi^0 p$
2.12		6 AARON 81	RVUE	

⁶ Uses multichannel Aitchison-Bowler model (BOWLER 75). Uses data from DAUM 80 and DANKOWYCH 81.

$\pi(1300)$ REFERENCES

DARGENT 17	JHEP 1705 143	P. d'Argent et al.	(HEID, BRIS)
SCHEGELSKY 06	EPJ A27 199	V.A. Schegelsky et al.	
SALVINI 04	EPJ C35 21	P. Salvini et al.	(OBELIX Collab.)
CHUNG 02	PR D65 072001	S.U. Chung et al.	(BNL E852 Collab.)
ABELE 01	EPJ C19 667	A. Abele et al.	(Crystal Barrel Collab.)
ACCIARRI 97T	PL B413 147	M. Acciari et al.	(L3 Collab.)
ALBRECHT 97B	ZPHY C74 469	H. Albrecht et al.	(ARGUS Collab.)
BERTIN 97D	PL B414 220	A. Bertin et al.	(OBELIX Collab.)
ABELE 96	PL B380 453	A. Abele et al.	(Crystal Barrel Collab.)
ZIELINSKI 84	PR D30 1855	M. Zielinski et al.	(ROCH, MINN, FNAL)
BELLINI 82	PRL 48 1697	G. Bellini et al.	(MILA, BGNA, JINR)
AARON 81	PR D24 1207	R.A. Aaron, R.S. Longacre	(NEAS, BNL)
BONESINI 81	PL 103B 75	M. Bonesini et al.	(MILA, LIVP, DARE+)
DANKOWYCH... 81	PRL 46 580	J.A. Dankowych et al.	(TNT0, BNL, CARL+)
DAUM 81B	NP B182 269	C. Daum et al.	(AMST, CERN, CRAC, MPIM+)
DAUM 80	PL 89B 281	C. Daum et al.	(AMST, CERN, CRAC, MPIM+)
BOWLER 75	NP B97 227	M.G. Bowler et al.	(OXFT, DARE)

$a_2(1320)$

$$I^G(J^{PC}) = 1^-(2^{++})$$

$a_2(1320)$ MASS

VALUE (MeV)	DOCUMENT ID				
1318.2 ± 0.6 OUR AVERAGE	Includes data from the 4 datablocks that follow this one. Error includes scale factor of 1.2.				
3 π MODE					
VALUE (MeV)	EVTS	DOCUMENT ID	TECN	CHG	COMMENT

The data in this block is included in the average printed for a previous datablock.

1318.6 ± 1.3 OUR AVERAGE	Error includes scale factor of 1.4. See the ideogram below.				
$1314.5^{+4.0}_{-3.3}$	46M	1 AGHASYAN 18B	COMP		$190 \pi^-p \rightarrow \pi^-\pi^+\pi^-p$
$1326 \pm 2 \pm 2$		CHUNG 02	B852		$18.3 \pi^-p \rightarrow \pi^+\pi^-\pi^-p$
1317 ± 3		BARBERIS 98B			$450 p\rho \rightarrow \rho_f \pi^+\pi^-\pi^0 \rho_s$
$1323 \pm 4 \pm 3$		ACCIARRI 97T	L3		$e^+e^- \rightarrow e^+e^-\pi^+\pi^-\pi^0$
1320 ± 7		ALBRECHT 97B	ARG		$e^+e^- \rightarrow e^+e^-\pi^+\pi^-\pi^0$
$1311.3 \pm 1.6 \pm 3.0$	72.4k	AMELIN 96	VES		$36 \pi^-p \rightarrow \pi^+\pi^-\pi^0 n$
1310 ± 5		ARMSTRONG 90	OMEG 0		$300.0 p\rho \rightarrow \rho\rho\pi^+\pi^-\pi^0$
1323.8 ± 2.3	4022	AUGUSTIN 89	DM2 \pm		$J/\psi \rightarrow \rho^\pm a_2^\mp$
1320.6 ± 3.1	3562	AUGUSTIN 89	DM2 0		$J/\psi \rightarrow \rho^0 a_2^0$
1317 ± 2	25k	2 DAUM 80c	SPEC -		$63,94 \pi^-p \rightarrow 3p\pi$
1320 ± 10	1097	2 BALTAY 78B	HBC +0		$15 \pi^+p \rightarrow p 4\pi$
1306 ± 8		FERRERSORIA 78	OMEG -		$9 \pi^-p \rightarrow p 3\pi$
1318 ± 7	1.6k	2 EMMS 75	DBC 0		$4 \pi^+n \rightarrow p(3\pi)^0$
1315 ± 5		2 ANTIPOV 73c	CNTR -		$25,40 \pi^-p \rightarrow p\eta\pi^-$
1306 ± 9	1580	CHALOUPKA 73	HBC -		$3.9 \pi^-p$

See key on page 1127

Meson Particle Listings

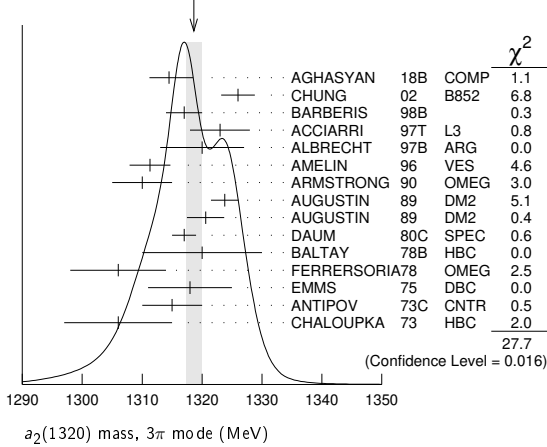
$a_2(1320)$

••• We do not use the following data for averages, fits, limits, etc. •••

1321 ± 1 $^{+0}_{-7}$	420k	³ ALEKSEEV	10	COMP	190 $\pi^- P_b \rightarrow \pi^- \pi^+ \pi^+ P_b'$
1300 ± 2 ± 4	18k	⁴ SCHEGELSKY	06	RVUE	0 $\gamma\gamma \rightarrow \pi^+ \pi^+ \pi^- \pi^-$
1305 ± 14		CONDO	93	SHF	$\gamma p \rightarrow n \pi^+ \pi^+ \pi^-$
1310 ± 2		² EVANGELIS...	81	OMEG	- 12 $\pi^- p \rightarrow 3\pi p$
1343 ± 11	490	BALTAY	78B	HBC	0 15 $\pi^+ p \rightarrow \Delta 3\pi$
1309 ± 5	5k	BINNIE	71	MMS	- $\pi^- p$ near a_2 thresh-old
1299 ± 6	28k	BOWEN	71	MMS	- 5 $\pi^- p$
1300 ± 6	24k	BOWEN	71	MMS	+ 5 $\pi^+ p$
1309 ± 4	17k	BOWEN	71	MMS	- 7 $\pi^- p$
1306 ± 4	941	ALSTON...	70	HBC	+ 7.0 $\pi^+ p \rightarrow 3\pi p$

- 1 Statistical error negligible.
- 2 From a fit to $J^P = 2^+ \rho\pi$ partial wave.
- 3 Superseded by AGHASYAN 2018B.
- 4 From analysis of L3 data at 183–209 GeV.

WEIGHTED AVERAGE
1318.6±1.3 (Error scaled by 1.4)



$K\bar{K}$ MODE

VALUE (MeV)	EVTS	DOCUMENT ID	TECN	CHG	COMMENT
-------------	------	-------------	------	-----	---------

The data in this block is included in the average printed for a previous datablock.

1318.1 ± 0.7 OUR AVERAGE

1319 ± 5	4700	^{1,2} CLELAND	82B	SPEC	+ 50 $\pi^+ p \rightarrow K_S^0 K^+ p$
1324 ± 6	5200	^{1,2} CLELAND	82B	SPEC	- 50 $\pi^- p \rightarrow K_S^0 K^- p$
1320 ± 2	4000	CHABAUD	80	SPEC	- 17 $\pi^- A \rightarrow K_S^0 K^- A$
1312 ± 4	11000	CHABAUD	78	SPEC	- 9.8 $\pi^- p \rightarrow K^- K_S^0 p$
1316 ± 2	4730	CHABAUD	78	SPEC	- 18.8 $\pi^- p \rightarrow K^- K_S^0 p$
1318 ± 1		^{1,3} MARTIN	78D	SPEC	- 10 $\pi^- p \rightarrow K_S^0 K^- p$
1320 ± 2	2724	MARGULIE	76	SPEC	- 23 $\pi^- p \rightarrow K^- K_S^0 p$
1313 ± 4	730	FOLEY	72	CNTR	- 20.3 $\pi^- p \rightarrow K^- K_S^0 p$
1319 ± 3	1500	³ GRAYER	71	ASPK	- 17.2 $\pi^- p \rightarrow K^- K_S^0 p$

••• We do not use the following data for averages, fits, limits, etc. •••

1304 ± 10	870	⁴ SCHEGELSKY	06A	RVUE	0 $\gamma\gamma \rightarrow K_S^0 K_S^0$
1330 ± 11	1000	^{1,2} CLELAND	82B	SPEC	+ 30 $\pi^+ p \rightarrow K_S^0 K^+ p$
1324 ± 5	350	HYAMS	78	ASPK	+ 12.7 $\pi^+ p \rightarrow K^+ K_S^0 p$

- 1 From a fit to $J^P = 2^+$ partial wave.
- 2 Number of events evaluated by us.
- 3 Systematic error in mass scale subtracted.
- 4 From analysis of L3 data at 91 and 183–209 GeV.

$\eta\pi$ MODE

VALUE (MeV)	EVTS	DOCUMENT ID	TECN	CHG	COMMENT
-------------	------	-------------	------	-----	---------

The data in this block is included in the average printed for a previous datablock.

1317.7 ± 1.4 OUR AVERAGE

1308 ± 9		BARBERIS	00H		450 $pp \rightarrow \rho_f \eta \pi^0 p_S$
1316 ± 9		BARBERIS	00H		450 $pp \rightarrow \Delta^{++} \eta \pi^- p_S$
1317 ± 1 ± 2		THOMPSON	97	MPS	18 $\pi^- p \rightarrow \eta \pi^- p$
1315 ± 5 ± 2		¹ AMSLER	94D	CBAR	0.0 $\bar{p} p \rightarrow \pi^0 \pi^0 \eta$
1325.1 ± 5.1		AOYAGI	93	BKEI	$\pi^- p \rightarrow \eta \pi^- p$
1317.7 ± 1.4 ± 2.0		BELADIDZE	93	VES	37 $\pi^- N \rightarrow \eta \pi^- N$
1323 ± 8	1000	² KEY	73	OSPK	- 6 $\pi^- p \rightarrow \rho \pi^- \eta$

••• We do not use the following data for averages, fits, limits, etc. •••

1318.7 ± 1.9 $^{+1.3}_{-1.3}$		³ KOPF	21	RVUE	0.9 $\bar{p} p \rightarrow \pi^0 \pi^0 \eta, \pi^0 \eta \eta, \pi^0 K^+ K^-$ and 191 $\pi^- p \rightarrow \pi^- \pi^- \pi^+ p$
-------------------------------	--	-------------------	----	------	--

1312.5 ± 0.7 ± 2.6		⁴ ALBRECHT	20	RVUE	0.9 $\bar{p} p \rightarrow \pi^0 \pi^0 \eta, \pi^0 \eta \eta, \pi^0 K^+ K^-$
1306.0 ± 0.8 ± 1.3		⁵ RODAS	19	JPAC	191 $\pi^- p \rightarrow \eta^{(\prime)} \pi^- p$
1307 ± 1 ± 6		⁶ JACKURA	18	JPAC	$\pi^- p \rightarrow \eta \pi^- p$
1315 ± 12		⁷ ADOLPH	15	COMP	191 $\pi^- p \rightarrow \eta^{(\prime)} \pi^- p$
1309 ± 4		ANISOVICH	09	RVUE	$\bar{p} p, \pi N$
1324 ± 5		ARMSTRONG	93C	E760	0 $\bar{p} p \rightarrow \pi^0 \eta \eta \rightarrow 6\gamma$
1336.2 ± 1.7	2561	DELFOSE	81	SPEC	+ $\pi^\pm p \rightarrow \rho \pi^\pm \eta$
1330.7 ± 2.4	1653	DELFOSE	81	SPEC	- $\pi^\pm p \rightarrow \rho \pi^\pm \eta$
1324 ± 8	6200	^{2,8} CONFORTO	73	OSPK	- 6 $\pi^- p \rightarrow \rho MM^-$

- 1 The systematic error of 2 MeV corresponds to the spread of solutions.
- 2 Error includes 5 MeV systematic mass-scale error.
- 3 From T-matrix pole based on combined fit of Crystal Barrel and $\pi\pi$ scattering data (ALBRECHT 20), and COMPASS data (ADOLPH 15), using a coupled-channel model of $\eta\pi, \eta'\pi$ and $K\bar{K}$ systems.
- 4 T-matrix pole with 2 poles, 2 channels ($\pi^0\eta$ and $K\bar{K}$).
- 5 The coupled-channel analysis of both the $\eta\pi$ and $\eta'\pi$ systems using ADOLPH 15 data. The mass is extracted from the T-matrix pole.
- 6 Superseded by RODAS 19.
- 7 ADOLPH 15 value is derived from a Breit-Wigner fit with mass-dependent width taking the $\eta\pi$ and $\rho\pi$ channels into account.
- 8 Missing mass with enriched MMS = $\eta\pi^-, \eta = 2\gamma$.

$\eta'\pi$ MODE

VALUE (MeV)	EVTS	DOCUMENT ID	TECN	CHG	COMMENT
-------------	------	-------------	------	-----	---------

The data in this block is included in the average printed for a previous datablock.

1322 ± 7 OUR AVERAGE

1318 ± 8 $^{+3}_{-5}$		IVANOV	01	B852	18 $\pi^- p \rightarrow \eta' \pi^- p$
1327.0 ± 10.7		BELADIDZE	93	VES	37 $\pi^- N \rightarrow \eta' \pi^- N$

$a_2(1320)$ WIDTH

3π MODE

VALUE (MeV)	EVTS	DOCUMENT ID	TECN	CHG	COMMENT
-------------	------	-------------	------	-----	---------

105.0 $^{+1.7}_{-1.9}$ OUR AVERAGE

106.6 $^{+3.4}_{-7.0}$	46M	¹ AGHASYAN	18B	COMP	190 $\pi^- p \rightarrow \pi^- \pi^+ \pi^- p$
108 ± 3 ± 15		CHUNG	02	B852	18.3 $\pi^- p \rightarrow \pi^+ \pi^- \pi^- p$
120 ± 10		BARBERIS	98B		450 $pp \rightarrow \rho_f \pi^+ \pi^- \pi^0 p_S$
105 ± 10 ± 11		ACCIARRI	97T	L3	$e^+ e^- \rightarrow \pi^+ \pi^- \pi^0$
120 ± 10		ALBRECHT	97B	ARG	$e^+ e^- \rightarrow \pi^+ \pi^- \pi^0$
103.0 ± 6.0 ± 3.3	72.4k	AMELIN	96	VES	36 $\pi^- p \rightarrow \pi^+ \pi^- \pi^0 n$
120 ± 10		ARMSTRONG	90	OMEG	0 300.0 $pp \rightarrow \rho p \pi^+ \pi^- \pi^0$
107.0 ± 9.7	4022	AUGUSTIN	89	DM2	± $J/\psi \rightarrow \rho^\pm a_2^\mp$
118.5 ± 12.5	3562	AUGUSTIN	89	DM2	0 $J/\psi \rightarrow \rho^0 a_2^0$
97 ± 5		² EVANGELIS...	81	OMEG	- 12 $\pi^- p \rightarrow 3\pi p$
96 ± 9	25k	² DAUM	80C	SPEC	- 63,94 $\pi^- p \rightarrow 3\pi p$
110 ± 15	1097	² BALTAY	78B	HBC	+0 15 $\pi^+ p \rightarrow \rho 4\pi$
112 ± 18	1.6k	² EMMS	75	DBC	0 4 $\pi^+ n \rightarrow \rho(3\pi)^0$
122 ± 14	1.2k	^{2,3} WAGNER	75	HBC	0 7 $\pi^+ p \rightarrow \Delta^{++}(3\pi)^0$
115 ± 15		² ANTIPOV	73C	CNTR	- 25,40 $\pi^- p \rightarrow \rho \eta \pi^-$
99 ± 15	1580	CHALOU PKA	73	HBC	- 3.9 $\pi^- p$
105 ± 5	28k	BOWEN	71	MMS	- 5 $\pi^- p$
99 ± 5	24k	BOWEN	71	MMS	+ 5 $\pi^+ p$
103 ± 5	17k	BOWEN	71	MMS	- 7 $\pi^- p$

••• We do not use the following data for averages, fits, limits, etc. •••

110 ± 2 $^{+2}_{-15}$	420k	⁴ ALEKSEEV	10	COMP	190 $\pi^- P_b \rightarrow \pi^- \pi^+ \pi^+ P_b'$
117 ± 6 ± 20	18k	⁵ SCHEGELSKY	06	RVUE	0 $\gamma\gamma \rightarrow \pi^+ \pi^+ \pi^- \pi^-$
120 ± 40		CONDO	93	SHF	$\gamma p \rightarrow n \pi^+ \pi^+ \pi^-$
115 ± 14	490	BALTAY	78B	HBC	0 15 $\pi^+ p \rightarrow \Delta 3\pi$
72 ± 16	5k	BINNIE	71	MMS	- $\pi^- p$ near a_2 thresh-old
79 ± 12	941	ALSTON...	70	HBC	+ 7.0 $\pi^+ p \rightarrow 3\pi p$

- 1 Statistical error negligible.
- 2 From a fit to $J^P = 2^+ \rho\pi$ partial wave.
- 3 Width errors enlarged by us to $4\Gamma/\sqrt{N}$; see the note with the $K^*(892)$ mass.
- 4 Superseded by AGHASYAN 2018B.
- 5 From analysis of L3 data at 183–209 GeV.

$K\bar{K}$ AND $\eta\pi$ MODES

VALUE (MeV)	EVTS	DOCUMENT ID	TECN	CHG	COMMENT
-------------	------	-------------	------	-----	---------

107 ± 5 OUR ESTIMATE
110.4 ± 1.7 OUR AVERAGE Includes data from the 2 datablocks that follow this one.

Meson Particle Listings

 $a_2(1320)$ $K\bar{K}$ MODE

VALUE (MeV)	EVTS	DOCUMENT ID	TECN	CHG	COMMENT
-------------	------	-------------	------	-----	---------

The data in this block is included in the average printed for a previous datablock.

109.8 ± 2.4 OUR AVERAGE

112 ± 20	4700	^{1,2} CLELAND	82B	SPEC +	50 $\pi^+ p \rightarrow K_S^0 K^+ p$
120 ± 25	5200	^{1,2} CLELAND	82B	SPEC -	50 $\pi^- p \rightarrow K_S^0 K^- p$
106 ± 4	4000	CHABAUD	80	SPEC -	17 $\pi^- A \rightarrow K_S^0 K^- A$
126 ± 11	11000	CHABAUD	78	SPEC -	9.8 $\pi^- p \rightarrow K^- K_S^0 p$
101 ± 8	4730	CHABAUD	78	SPEC -	18.8 $\pi^- p \rightarrow K^- K_S^0 p$
113 ± 4		^{1,3} MARTIN	78D	SPEC -	10 $\pi^- p \rightarrow K_S^0 K^- p$
105 ± 8	2724	³ MARGULIE	76	SPEC -	23 $\pi^- p \rightarrow K^- K_S^0 p$
113 ± 19	730	FOLEY	72	CNTR -	20.3 $\pi^- p \rightarrow K^- K_S^0 p$
123 ± 13	1500	³ GRAYR	71	ASPK -	17.2 $\pi^- p \rightarrow K^- K_S^0 p$

• • • We do not use the following data for averages, fits, limits, etc. • • •

120 ± 15	870	⁴ SCHEGELSKY	06A	RVUE 0	$\gamma\gamma \rightarrow K_S^0 K_S^0$
121 ± 51	1000	^{1,2} CLELAND	82B	SPEC +	30 $\pi^+ p \rightarrow K_S^0 K^+ p$
110 ± 18	350	HYAMS	78	ASPK +	12.7 $\pi^+ p \rightarrow K^+ K_S^0 p$

¹ From a fit to $J^P = 2^+$ partial wave.

² Number of events evaluated by us.

³ Width errors enlarged by us to $4\Gamma/\sqrt{N}$; see the note with the $K^*(892)$ mass.

⁴ From analysis of L3 data at 91 and 183–209 GeV.

 $\eta\pi$ MODE

VALUE (MeV)	EVTS	DOCUMENT ID	TECN	CHG	COMMENT
-------------	------	-------------	------	-----	---------

The data in this block is included in the average printed for a previous datablock.

111.1 ± 2.4 OUR AVERAGE

115 ± 20		BARBERIS	00H		450 $p\bar{p} \rightarrow \rho_f \eta \pi^0 p_S$
112 ± 14		BARBERIS	00H		450 $p\bar{p} \rightarrow \Delta_f^+ \eta \pi^- p_S$

112 ± 3 ± 2		¹ AMSLER	94D	CBAR	0.0 $\bar{p}p \rightarrow \pi^0 \pi^0 \eta$
103 ± 6 ± 3		BELADIDZE	93	VES	37 $\pi^- N \rightarrow \eta \pi^- N$
112.2 ± 5.7	2561	DELFOSE	81	SPEC +	$\pi^\pm p \rightarrow \rho \pi^\pm \eta$
116.6 ± 7.7	1653	DELFOSE	81	SPEC -	$\pi^\pm p \rightarrow \rho \pi^\pm \eta$
108 ± 9	1000	KEY	73	OSPK -	6 $\pi^- p \rightarrow \rho \pi^- \eta$

• • • We do not use the following data for averages, fits, limits, etc. • • •

107.5 ± 4.6 +3.3 -1.8		² KOPF	21	RVUE	0.9 $\bar{p}p \rightarrow \pi^0 \pi^0 \eta$, $\pi^0 \eta \eta$, $\pi^0 K^+ K^-$ and 191 $\pi^- p \rightarrow$ $\pi^- \pi^- \pi^+ p$
-----------------------	--	-------------------	----	------	--

106.9 ± 1.2 ± 3.7		³ ALBRECHT	20	RVUE	0.9 $\bar{p}p \rightarrow \pi^0 \pi^0 \eta$, $\pi^0 \eta \eta$, $\pi^0 K^+ K^-$
-------------------	--	-----------------------	----	------	--

114.4 ± 1.6 ± 0.0		⁴ RODAS	19	JPAC	191 $\pi^- p \rightarrow$ $\eta^{(\prime)} \pi^- p$
-------------------	--	--------------------	----	------	--

112 ± 1 ± 8		⁵ JACKURA	18	JPAC	$\pi^- p \rightarrow \eta \pi^- p$
119 ± 14		⁶ ADOLPH	15	COMP	191 $\pi^- p \rightarrow$ $\eta^{(\prime)} \pi^- p$

110 ± 4		ANISOVICH	09	RVUE	$\bar{p}p, \pi N$
127 ± 2 ± 2		⁷ THOMPSON	97	MPS	18 $\pi^- p \rightarrow \eta \pi^- p$
118 ± 10		ARMSTRONG	93C	E760 0	$\bar{p}p \rightarrow \pi^0 \eta \eta \rightarrow 6\gamma$
104 ± 9	6200	⁸ CONFORTO	73	OSPK -	6 $\pi^- p \rightarrow \rho MM^-$

¹ The systematic error of 2 MeV corresponds to the spread of solutions.

² From T-matrix pole based on combined fit of Crystal Barrel and $\pi\pi$ scattering data (ALBRECHT 20), and COMPASS data (ADOLPH 15), using a coupled-channel model of $\eta\pi$, $\eta'\pi$ and $K\bar{K}$ systems.

³ T-matrix pole with 2 poles, 2 channels ($\pi^0 \eta$ and $K\bar{K}$).

⁴ The coupled-channel analysis of both the $\eta\pi$ and $\eta'\pi$ systems using ADOLPH 15 data. The width is extracted from the T-matrix pole.

⁵ Superseded by RODAS 19.

⁶ ADOLPH 15 value is derived from a Breit-Wigner fit with mass-dependent width taking the $\eta\pi$ and $\rho\pi$ channels into account.

⁷ Resolution is not unfolded.

⁸ Missing mass with enriched MMS = $\eta\pi^-$, $\eta = 2\gamma$.

 $\eta'\pi$ MODE

VALUE (MeV)	DOCUMENT ID	TECN	COMMENT
-------------	-------------	------	---------

119 ± 25 OUR AVERAGE

140 ± 35 ± 20	IVANOV	01	B852 18 $\pi^- p \rightarrow \eta' \pi^- p$
106 ± 32	BELADIDZE	93	VES 37 $\pi^- N \rightarrow \eta' \pi^- N$

 $a_2(1320)$ DECAY MODES

Mode	Fraction (Γ_i/Γ)	Scale factor/ Confidence level
Γ_1 3 π	(70.1 ± 2.7) %	S=1.2
Γ_2 $\rho(770)\pi$		
Γ_3 $f_2(1270)\pi$		
Γ_4 $\rho(1450)\pi$		
Γ_5 $\eta\pi$	(14.5 ± 1.2) %	

Γ_6 $\omega\pi\pi$	(10.6 ± 3.2) %	S=1.3
Γ_7 $K\bar{K}$	(4.9 ± 0.8) %	
Γ_8 $\eta'(958)\pi$	(5.5 ± 0.9) × 10 ⁻³	
Γ_9 $\pi^\pm\gamma$	(2.91 ± 0.27) × 10 ⁻³	
Γ_{10} $\gamma\gamma$	(9.4 ± 0.7) × 10 ⁻⁶	
Γ_{11} e^+e^-	< 5 × 10 ⁻⁹	CL=90%

CONSTRAINED FIT INFORMATION

An overall fit to 5 branching ratios uses 18 measurements and one constraint to determine 4 parameters. The overall fit has a $\chi^2 = 9.3$ for 15 degrees of freedom.

The following *off-diagonal* array elements are the correlation coefficients $\langle \delta x_i \delta x_j \rangle / (\delta x_i \delta x_j)$, in percent, from the fit to the branching fractions, $x_i \equiv \Gamma_i/\Gamma_{\text{total}}$. The fit constrains the x_i whose labels appear in this array to sum to one.

x_5	10		
x_6	-89	-46	
x_7	-1	-2	-24
	x_1	x_5	x_6

 $a_2(1320)$ PARTIAL WIDTHS

VALUE (MeV)	EVTS	DOCUMENT ID	TECN	CHG	COMMENT
-------------	------	-------------	------	-----	---------

• • • We do not use the following data for averages, fits, limits, etc. • • •

18.5 ± 3.0	870	¹ SCHEGELSKY	06A	RVUE 0	$\gamma\gamma \rightarrow K_S^0 K_S^0$
------------	-----	-------------------------	-----	--------	--

¹ From analysis of L3 data at 91 and 183–209 GeV, using $\Gamma(a_2(1320) \rightarrow \gamma\gamma) = 0.91$ keV and SU(3) relations.

 $\Gamma(K\bar{K})$

VALUE (MeV)	EVTS	DOCUMENT ID	TECN	CHG	COMMENT
-------------	------	-------------	------	-----	---------

• • • We do not use the following data for averages, fits, limits, etc. • • •

7.0 ± 2.0 -1.5	870	¹ SCHEGELSKY	06A	RVUE 0	$\gamma\gamma \rightarrow K_S^0 K_S^0$
----------------	-----	-------------------------	-----	--------	--

¹ From analysis of L3 data at 91 and 183–209 GeV, using $\Gamma(a_2(1320) \rightarrow \gamma\gamma) = 0.91$ keV and SU(3) relations.

 $\Gamma(\pi^\pm\gamma)$

VALUE (keV)	EVTS	DOCUMENT ID	TECN	CHG	COMMENT
-------------	------	-------------	------	-----	---------

311 ± 25 OUR AVERAGE

358 ± 6 ± 42		¹ ADOLPH	14	COMP -	190 $\pi^- p \rightarrow$ $\pi^+ \pi^- \pi^- p$
284 ± 25 ± 25	7.1k	MOLCHANOV	01	SELX	600 $\pi^- A \rightarrow \pi^+ \pi^- \pi^- A$
295 ± 60		CHANGIR	82	SPEC +	200 $\pi^+ A$

• • • We do not use the following data for averages, fits, limits, etc. • • •

461 ± 110		² MAY	77	SPEC ±	9.7 γA
-----------	--	------------------	----	--------	----------------

¹ Primakoff reaction using $a_2(1320) \rightarrow 3\pi$ branching ratio of 70.1%.

² Assuming one-pion exchange.

 $\Gamma(\gamma\gamma)$

VALUE (keV)	EVTS	DOCUMENT ID	TECN	CHG	COMMENT
-------------	------	-------------	------	-----	---------

1.00 ± 0.06 OUR AVERAGE

0.98 ± 0.05 ± 0.09		ACCIARRI	97T	L3	$e^+e^- \rightarrow e^+e^- \pi^+ \pi^- \pi^0$
0.96 ± 0.03 ± 0.13		ALBRECHT	97B	ARG	$e^+e^- \rightarrow e^+e^- \pi^+ \pi^- \pi^0$
1.26 ± 0.26 ± 0.18	36	BARU	90	MD1	$e^+e^- \rightarrow e^+e^- \pi^+ \pi^- \pi^0$
1.00 ± 0.07 ± 0.15	415	BEHREND	90C	CELL 0	$e^+e^- \rightarrow e^+e^- \pi^+ \pi^- \pi^0$
1.03 ± 0.13 ± 0.21		BUTLER	90	MRK2	$e^+e^- \rightarrow e^+e^- \pi^+ \pi^- \pi^0$
1.01 ± 0.14 ± 0.22	85	OEST	90	JADE	$e^+e^- \rightarrow e^+e^- \pi^0 \eta$
0.90 ± 0.27 ± 0.15	56	¹ ALTHOFF	86	TASS 0	$e^+e^- \rightarrow e^+e^- 3\pi$
1.14 ± 0.20 ± 0.26		² ANTREASYSAN	86	CBAL 0	$e^+e^- \rightarrow e^+e^- \pi^0 \eta$
1.06 ± 0.18 ± 0.19		BERGER	84C	PLUT 0	$e^+e^- \rightarrow e^+e^- 3\pi$

• • • We do not use the following data for averages, fits, limits, etc. • • •

0.81 ± 0.19 +0.42 -0.11	35	¹ BEHREND	82C	CELL 0	$e^+e^- \rightarrow e^+e^- 3\pi$
0.77 ± 0.18 ± 0.27	22	² EDWARDS	82F	CBAL 0	$e^+e^- \rightarrow e^+e^- \pi^0 \eta$

¹ From $\rho\pi$ decay mode.

² From $\eta\pi^0$ decay mode.

 $\Gamma(e^+e^-)$

VALUE (eV)	CL%	DOCUMENT ID	TECN	COMMENT
------------	-----	-------------	------	---------

< 0.56 90 ACHASOV 00K SND $e^+e^- \rightarrow \pi^0 \pi^0$

• • • We do not use the following data for averages, fits, limits, etc. • • •

< 25	90	VOROBYEV	88	ND $e^+e^- \rightarrow \pi^0 \eta$
------	----	----------	----	------------------------------------

$a_2(1320) \Gamma(i)\Gamma(\gamma\gamma)/\Gamma(\text{total})$

$\Gamma(3\pi) \times \Gamma(\gamma\gamma)/\Gamma_{\text{total}}$		$\Gamma_1\Gamma_{10}/\Gamma$	
VALUE (keV)	EVTS	DOCUMENT ID	TECN COMMENT
••• We do not use the following data for averages, fits, limits, etc. •••			
$0.65 \pm 0.02 \pm 0.02$	18k	¹ SCHEGELSKY 06	RVUE $\gamma\gamma \rightarrow \pi^+\pi^-\pi^0$
¹ From analysis of L3 data at 183–209 GeV.			

$\Gamma(\eta\pi) \times \Gamma(\gamma\gamma)/\Gamma_{\text{total}}$		$\Gamma_5\Gamma_{10}/\Gamma$	
VALUE (keV)	DOCUMENT ID	TECN	COMMENT
••• We do not use the following data for averages, fits, limits, etc. •••			
$0.145^{+0.097}_{-0.034}$	¹ UEHARA 09A	BELL	$e^+e^- \rightarrow e^+e^-\eta\pi^0$
¹ From the D_2 -wave. The fraction of the D_0 -wave is $3.4^{+2.3}_{-1.1}\%$.			

$\Gamma(K\bar{K}) \times \Gamma(\gamma\gamma)/\Gamma_{\text{total}}$		$\Gamma_7\Gamma_{10}/\Gamma$	
VALUE (keV)	DOCUMENT ID	TECN	COMMENT
••• We do not use the following data for averages, fits, limits, etc. •••			
$0.126 \pm 0.007 \pm 0.028$	¹ ALBRECHT 90G	ARG	$e^+e^- \rightarrow e^+e^-K^+K^-$
••• We do not use the following data for averages, fits, limits, etc. •••			
$0.081 \pm 0.006 \pm 0.027$	² ALBRECHT 90G	ARG	$e^+e^- \rightarrow e^+e^-K^+K^-$
¹ Using an incoherent background.			
² Using a coherent background.			

$a_2(1320)$ BRANCHING RATIOS

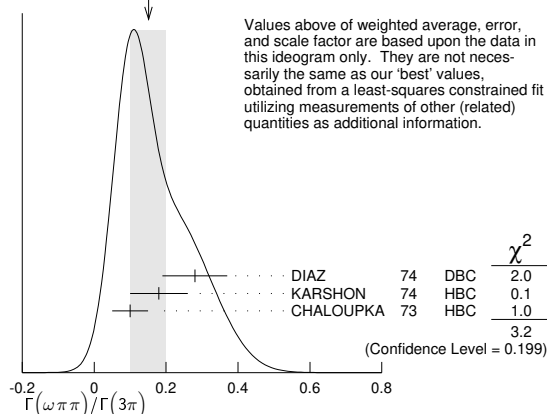
$[\Gamma(f_2(1270)\pi) + \Gamma(\rho(1450)\pi)]/\Gamma(\rho(770)\pi)$		$(\Gamma_3 + \Gamma_4)/\Gamma_2$	
VALUE	CL%	DOCUMENT ID	TECN CHG COMMENT
<0.12	90	ABRA MOVI...	70B HBC - 3.93 π^-p

$\Gamma(\rho(770)\pi)/\Gamma(f_2(1270)\pi)$		Γ_2/Γ_3	
VALUE	EVTS	DOCUMENT ID	TECN COMMENT
$16.5^{+1.2}_{-2.4}$	46M	¹ AGHASYAN 18B	COMP 190 $\pi^-p \rightarrow \pi^-\pi^+\pi^-p$
¹ Statistical error negligible.			

$\Gamma(\eta\pi)/\Gamma(3\pi)$		Γ_5/Γ_1	
VALUE	EVTS	DOCUMENT ID	TECN CHG COMMENT
0.207 ± 0.018 OUR FIT			
0.213 ± 0.020 OUR AVERAGE			
0.18 ± 0.05		FORINO 76	HBC 11 π^-p
0.22 ± 0.05	52	ANTIPOV 73	CNTR - 40 π^-p
0.211 ± 0.044	149	CHALOUKKA 73	HBC - 3.9 π^-p
0.246 ± 0.042	167	ALSTON-... 71	HBC + 7.0 π^+p
0.25 ± 0.09	15	BOECKMANN 70	HBC + 5.0 π^+p
0.23 ± 0.08	22	ASCOLI 68	HBC - 5 π^-p
0.12 ± 0.08		CHUNG 68	HBC - 3.2 π^-p
0.22 ± 0.09		CONTE 67	HBC - 11.0 π^-p

$\Gamma(\omega\pi\pi)/\Gamma(3\pi)$		Γ_6/Γ_1	
VALUE	EVTS	DOCUMENT ID	TECN CHG COMMENT
0.15 ± 0.05 OUR FIT Error includes scale factor of 1.3.			
0.15 ± 0.05 OUR AVERAGE Error includes scale factor of 1.3. See the ideogram below.			
0.28 ± 0.09	60	DIAZ 74	DBC 0 $6\pi^+n$
0.18 ± 0.08		¹ KARSHON 74	HBC Avg. of above two
0.10 ± 0.05	279	² CHALOUKKA 73	HBC - 3.9 π^-p
••• We do not use the following data for averages, fits, limits, etc. •••			
0.29 ± 0.08	140	¹ KARSHON 74	HBC 0 $4.9\pi^+p$
0.10 ± 0.04	60	¹ KARSHON 74	HBC + $4.9\pi^+p$
0.19 ± 0.08		DEFOIX 73	HBC 0 $0.7\bar{p}p$

WEIGHTED AVERAGE
0.15 ± 0.05 (Error scaled by 1.3)



¹ KARSHON 74 suggest an additional $l = 0$ state strongly coupled to $\omega\pi\pi$ which could explain discrepancies in branching ratios and masses. We use a central value and a systematic spread.

² Decays to $b_1(1040)\pi$, $b_1 \rightarrow \omega\pi$. Error increased to account for possible systematic errors of complicated analysis.

$\Gamma(K\bar{K})/\Gamma(3\pi)$		Γ_7/Γ_1	
VALUE	EVTS	DOCUMENT ID	TECN CHG COMMENT
0.070 ± 0.012 OUR FIT			
0.078 ± 0.017			
0.011 ± 0.003		CHABAUD 78	RVUE
••• We do not use the following data for averages, fits, limits, etc. •••			
0.056 ± 0.014	50	¹ BERTIN 98B	OBLX $0.0\bar{p}p \rightarrow K^\pm K_S^\mp \pi^\mp$
0.097 ± 0.018	113	² CHALOUKKA 73	HBC - 3.9 π^-p
0.06 ± 0.03		² ALSTON-... 71	HBC + 7.0 π^+p
0.054 ± 0.022		² ABRAMOVI... 70B	HBC - 3.93 π^-p
		² CHUNG 68	HBC - 3.2 π^-p
¹ Using 4 π data from BERTIN 97D.			
² Included in CHABAUD 78 review.			

$\Gamma(K\bar{K})/\Gamma(\eta\pi)$		Γ_7/Γ_5	
VALUE	DOCUMENT ID	TECN	COMMENT
••• We do not use the following data for averages, fits, limits, etc. •••			
$0.31 \pm 0.22^{+0.09}_{-0.11}$	¹ KOPF 21	RVUE	$0.9\bar{p}p \rightarrow \pi^0\pi^0\eta, \pi^0\eta\eta, \pi^0K^+K^-$ and 191 $\pi^-p \rightarrow \pi^-\pi^-\pi^+p$
$0.352 \pm 0.011 \pm 0.175$	² ALBRECHT 20	RVUE	$0.9\bar{p}p \rightarrow \pi^0\pi^0\eta, \pi^0\eta\eta, \pi^0K^+K^-$
0.08 ± 0.02	³ BERTIN 98B	OBLX	$0.0\bar{p}p \rightarrow K^\pm K_S^\mp \pi^\mp$
¹ From T-matrix pole based on combined fit of Crystal Barrel and $\pi\pi$ scattering data (ALBRECHT 20), and COMPASS data (ADOLPH 15), using a coupled-channel model of $\eta\pi, \eta'\pi$ and $K\bar{K}$ systems.			
² Residues from T-matrix pole with 2 poles, 2 channels ($\pi^0\eta$ and $K\bar{K}$).			
³ Using $\eta\pi\pi$ data from AMSLER 94D.			

$\Gamma(\eta\pi)/[\Gamma(3\pi) + \Gamma(\eta\pi) + \Gamma(K\bar{K})]$		$\Gamma_5/(\Gamma_1 + \Gamma_5 + \Gamma_7)$	
VALUE	EVTS	DOCUMENT ID	TECN CHG COMMENT
0.162 ± 0.012 OUR FIT			
0.140 ± 0.028 OUR AVERAGE			
0.13 ± 0.04		ESPIGAT 72	HBC ± 0.0 $\bar{p}p$
0.15 ± 0.04	34	BARNHAM 71	HBC + 3.7 π^+p

$\Gamma(K\bar{K})/[\Gamma(3\pi) + \Gamma(\eta\pi) + \Gamma(K\bar{K})]$		$\Gamma_7/(\Gamma_1 + \Gamma_5 + \Gamma_7)$	
VALUE	EVTS	DOCUMENT ID	TECN CHG COMMENT
0.054 ± 0.009 OUR FIT			
0.048 ± 0.012 OUR AVERAGE			
0.05 ± 0.02		TOET 73	HBC + 5 π^+p
0.09 ± 0.04		TOET 73	HBC 0 5 π^+p
0.03 ± 0.02	8	¹ DAMERI 72	HBC - 11 π^-p
0.06 ± 0.03	17	BARNHAM 71	HBC + 3.7 π^+p
••• We do not use the following data for averages, fits, limits, etc. •••			
0.020 ± 0.004		² ESPIGAT 72	HBC ± 0.0 $\bar{p}p$
¹ Montanet agrees. Vlada.			
² Not averaged because of discrepancy between masses from $K\bar{K}$ and $\rho\pi$ modes.			

$\Gamma(\eta'(958)\pi)/\Gamma_{\text{total}}$		Γ_8/Γ	
VALUE	CL%	DOCUMENT ID	TECN CHG COMMENT
••• We do not use the following data for averages, fits, limits, etc. •••			
<0.006	95	ALDE 92B	GAM2 38,100 $\pi^-p \rightarrow \eta'\pi^0n$
<0.02	97	BARNHAM 71	HBC + 3.7 π^+p
0.004 ± 0.004		¹ BOESEBECK 68	HBC + 8 π^+p
¹ No longer valid since $\Gamma(K\bar{K})/\Gamma(3\pi)$ value has changed (MORRISON 71).			

$\Gamma(\eta'(958)\pi)/\Gamma(3\pi)$		Γ_8/Γ_1	
VALUE	CL%	DOCUMENT ID	TECN CHG COMMENT
••• We do not use the following data for averages, fits, limits, etc. •••			
<0.011	90	EISENSTEIN 73	HBC - 5 π^-p
<0.04		ALSTON-... 71	HBC + 7.0 π^+p
$0.04^{+0.03}_{-0.04}$		BOECKMANN 70	HBC 0 5.0 π^+p

$\Gamma(\eta'(958)\pi)/\Gamma(\eta\pi)$		Γ_8/Γ_5	
VALUE	DOCUMENT ID	TECN	COMMENT
0.038 ± 0.005 OUR AVERAGE			
0.05 ± 0.02	ADOLPH 15	COMP	191 $\pi^-p \rightarrow \eta^{(\prime)}\pi^-p$
0.032 ± 0.009	ABELE 97C	CBAR	$0.0\bar{p}p \rightarrow \pi^0\pi^0\eta'$
$0.047 \pm 0.010 \pm 0.004$	¹ BELADIDZE 93	VES	$37\pi^-N \rightarrow a_2^-N$
$0.034 \pm 0.008 \pm 0.005$	BELADIDZE 92	VES	$36\pi^-C \rightarrow a_2^-C$
••• We do not use the following data for averages, fits, limits, etc. •••			
$0.046 \pm 0.015^{+0.007}_{-0.006}$	² KOPF 21	RVUE	$0.9\bar{p}p \rightarrow \pi^0\pi^0\eta, \pi^0\eta\eta, \pi^0K^+K^-$ and 191 $\pi^-p \rightarrow \pi^-\pi^-\pi^+p$

¹ Using $B(\eta' \rightarrow \pi^+\pi^-\eta) = 0.441$, $B(\eta \rightarrow \gamma\gamma) = 0.389$ and $B(\eta \rightarrow \pi^+\pi^-\pi^0) = 0.236$.

² From T-matrix pole based on combined fit of Crystal Barrel and $\pi\pi$ scattering data (ALBRECHT 20), and COMPASS data (ADOLPH 15), using a coupled-channel model of $\eta\pi, \eta'\pi$ and $K\bar{K}$ systems.

Meson Particle Listings

$a_2(1320), f_0(1370)$

$\Gamma(\pi^\pm\gamma)/\Gamma_{total}$	DOCUMENT ID	TECN	COMMENT	Γ_9/Γ
--	-------------	------	---------	-------------------

••• We do not use the following data for averages, fits, limits, etc. •••
 $0.005^{+0.005}_{-0.003}$ ¹EISENBERG 72 HBC 4.3,5,25,7,5 γp
¹Pion-exchange model used in this estimation.

$\Gamma(e^+e^-)/\Gamma_{total}$	CL%	DOCUMENT ID	TECN	COMMENT	Γ_{11}/Γ
---------------------------------	-----	-------------	------	---------	----------------------

••• We do not use the following data for averages, fits, limits, etc. •••
 <6 90 ACHASOV 00k SND $e^+e^- \rightarrow \pi^0\pi^0$

$a_2(1320)$ REFERENCES

KOPF	21	EPJ C81 1056	B. Kopf et al.	(BOCH)
ALBRECHT	20	EPJ C80 453	M. Albrecht et al.	(Crystal Barrel Collab.)
RODAS	19	PR L22 042002	A. Rodas et al.	(JPAC Collab.)
AGHASYAN	18B	PR D98 092003	M. Aghasyan et al.	(COMPASS Collab.)
JACKURA	18	PL B779 464	A. Jackura et al.	(JPAC and COMPASS Collab.)
ADOLPH	15	PL B740 303	M. Adolph et al.	(COMPASS Collab.)
ADOLPH	14	EPJ A50 79	C. Adolph et al.	(COMPASS Collab.)
ALEKSEEV	10	PRL 104 214803	M.G. Alekseev et al.	(COMPASS Collab.)
ANISOVICH	09	IJMP A24 2481	V.V. Anisovich, A.V. Sarantsev	
UEHARA	09A	PR D60 032001	S. Uehara et al.	(BELLE Collab.)
SCHEGELSKY	06	EPJ A27 199	V.A. Schegelsky et al.	
SCHEGELSKY	06A	EPJ A27 207	V.A. Schegelsky et al.	
CHUNG	02	PR D65 072001	S.U. Chung et al.	
IVANOV	01	PRL 86 3977	E.I. Ivanov et al.	(BNL E852 Collab.)
MOLCHANOV	01	PL B521 171	V.V. Molchanov et al.	(FNAL SELEX Collab.)
ACHASOV	00K	PL B492 8	M.N. Achasov et al.	(Novosibirsk SND Collab.)
BARBERIS	00H	PL B488 225	D. Barberis et al.	(WA 102 Collab.)
BARBERIS	98B	PL B422 399	D. Barberis et al.	(WA 102 Collab.)
BERTIN	98B	PL B434 180	A. Bertin et al.	(OBELIX Collab.)
ABELE	97C	PL B404 179	A. Abele et al.	(Crystal Barrel Collab.)
ACCIARRI	97T	PL B413 147	M. Acciari et al.	(L3 Collab.)
ALBRECHT	97B	ZPHY C74 4649	H. Albrecht et al.	(ARGUS Collab.)
THOMPSON	97	PRL 79 1630	D.R. Thompson et al.	(BNL E852 Collab.)
AMELIN	96	ZPHY C70 71	D.V. Amelin et al.	(SERP, TBL)
AMSLER	94D	PL B333 277	C. Amstler et al.	(Crystal Barrel Collab.)
AOYAGI	93	PL B314 246	H. Aoyagi et al.	(BKEI Collab.)
ARMSTRONG	93C	PL B307 394	T.A. Armstrong et al.	(FNAL, FERR, GENO+)
BELADIDZE	93	PL B313 276	G.M. Beladidze et al.	(YES Collab.)
CONDO	93	PR D48 3045	G.T. Condo et al.	(SLAC Hybrid Collab.)
ALDE	92B	ZPHY C54 544	D.M. Alde et al.	(SERP, BELG, LANL, LAPP+)
BELADIDZE	92	ZPHY C54 239	G.M. Beladidze et al.	(VES Collab.)
ALBRECHT	90G	ZPHY C48 183	H. Albrecht et al.	(ARGUS Collab.)
ARMSTRONG	90	ZPHY C48 213	T.A. Armstrong, M. Benayoun, W. Beusch	(WA76 Coll.)
BARU	90	ZPHY C48 581	S.E. Baru et al.	(MD-1 Collab.)
BEHREND	90C	ZPHY C46 583	H.J. Behrend et al.	(CELLO Collab.)
BUTLER	90	PR D42 1368	F. Butler et al.	(Mark II Collab.)
OEST	90	ZPHY C47 343	T. Oest et al.	(JADE Collab.)
AUGUSTIN	89	NP B320 1	J.E. Augustin, G. Cosme	(DM2 Collab.)
VOROBYEV	88	SJNP 48 273	P.V. Vorobyev et al.	(NOVO)
ALTHOFF	86	ZPHY C31 537	M. Althoff et al.	(TASSO Collab.)
ANTREASYAN	86	PR D33 3947	D. Antreasyan et al.	(Crystal Ball Collab.)
BERGER	84C	PL 149B 427	C. Berger et al.	(PLUTO Collab.)
BEHREND	82C	PL 114B 378	H.J. Behrend et al.	(CELLO Collab.)
Also		PL 125B 518 (erratum)	H.J. Behrend et al.	(CELLO Collab.)
CHANGIR	82	PL 117B 123	S. Changir et al.	(FNAL, MINN, ROCH)
CLELAND	82B	NP B208 228	W.E. Cleland, LAUS+	(DURH, GEVA, LAUS+)
EDWARDS	82F	PL 110B 82	C. Edwards et al.	(CIT, HEAV, PRIN+)
DELFOSE	81	NP B183 349	A. Delfosse et al.	(GEVA, LAUS)
EVANGELIS...	81	NP B178 197	C. Evangelista et al.	(BARI, BONN, CERN+)
CHABAUD	80	NP B175 189	V. Chabaud et al.	(CERN, MPIM, AMST)
DAUM	80C	PL 89B 276	C. Daum et al.	(AMST, CERN, CRAC, MPIM+ JP)
BALTAY	78B	PR D17 62	C. Baltay et al.	(COLU, BING)
CHABAUD	78	NP B145 349	V. Chabaud et al.	(CERN, MPIM)
FERRERSORIA	78	PL 74B 287	A. Ferrer Soria et al.	(ORSAY, CERN, CDEF+)
HYAMS	78	NP B146 303	B.D. Hyams et al.	(CERN, MPIM, ATEN)
MARTIN	78D	PL 74B 417	A.D. Martin et al.	(DURH, GEVA) JP
MAY	77	PR D16 1983	E.N. May et al.	(ROCH, CORN)
FORINO	76	NC 35A 465	A. Forino et al.	(BGNA, FIRZ, GENO, MILA+)
MARGULIE	76	PR D14 667	M. Margulies et al.	(BNL, CUNY)
EMMS	75	PL 58B 117	M.J. Emms et al.	(BIRM, DURH, RHEL) JP
WAGNER	75	PL 58B 201	F. Wagner, M. Tabak, D.M. Chew	(LBL) JP
DIAZ	74	PRL 32 260	J. Diaz et al.	(CASE, CMU)
KARSHON	74	PRL 32 252	U. Karshon et al.	(REHO, SLAC, TELA)
ANTIPOV	73	NP B63 175	Y.M. Antipov et al.	(CERN, SERP) JP
ANTIPOV	73C	NP B63 153	Y.M. Antipov et al.	(CERN, SERP) JP
CHALOUKPA	73	PL 44B 211	V. Chaloukpa et al.	(CERN)
CONFORTO	73	PL 45B 154	G. Conforto et al.	(EFL, FNAL, TINTO+)
DEFOIX	73	PL 43B 141	C. Defoix et al.	(CDEF)
EISENSTEIN	73	PR D7 278	L. Eisenstein et al.	(ILL)
KEY	73	PRL 30 503	A.W. Key et al.	(TNT0, EFL, FNAL, WISC)
TOET	73	NP B63 248	D.Z. Toet et al.	(NUM, BONN, DURH, TORI)
DAMERI	72	NC 9A 1	M. Dameri et al.	(GENO, MILA, SACL)
EISENBERG	72	PR D5 15	Y. Eisenberg et al.	(REHO, SLAC, TELA)
ESPIGAT	72	NP B36 93	P. Espigat et al.	(CERN, CDEF)
FOLEY	72	PR D6 747	K.J. Foley et al.	(BNL, CUNY)
ALSTON...	71	PL 34B 156	M. Alston-Garnjost et al.	(LRL)
BARNHAM	71	PRL 26 1494	K.W.J. Barnham et al.	(LBL)
BINNIE	71	PL 36B 257	D.M. Binnie et al.	(LOIC, SHMP)
BOWEN	71	PRL 26 1663	D.R. Bowen et al.	(NEAS, STON)
GRAYER	71	PL 34B 333	G. Grayer et al.	(CERN, MPIM)
ABRAMOVICH...	70B	NP B23 466	M. Abramovich et al.	(CERN) JP
ALSTON...	70	PL 33B 607	M. Alston-Garnjost et al.	(LRL)
BOECKMANN	70	NP B16 221	K. Boeckmann et al.	(BONN, DURH, NIJM+)
ASCOLI	68	PRL 20 1321	G. Ascoli et al.	(ILL) JP
BOESEBECK	68	NP B4 501	K. Boesebeck et al.	(AACH, BERL, CERN)
CHUNG	68	PR 165 1491	S.U. Chung et al.	(LRL)
CONTE	67	NC 51A 175	F. Conte et al.	(GENO, HAMB, MILA, SACL)

$f_0(1370)$

$$J^{PC} = 0^+(0^+ +)$$

See the review on "Spectroscopy of Light Meson Resonances" and a note on "Non- $q\bar{q}$ Candidates" in PDG 06, Journal of Physics **G33** 1 (2006).

$f_0(1370)$ T-MATRIX POLE POSITION

Note that $\Gamma \approx 2 \text{Im}(\sqrt{s_{\text{pole}}})$.

VALUE (MeV)	DOCUMENT ID	TECN	COMMENT
-------------	-------------	------	---------

(1200-1500)- i (150-250) OUR ESTIMATE
 ••• We do not use the following data for averages, fits, limits, etc. •••

$(1370 \pm 40) - i(195 \pm 20)$	SARANTSEV 21	RVUE	$J/\psi(1S) \rightarrow \gamma(\pi\pi, K\bar{K}, \eta\eta, \omega\phi)$
$(1280.6 \pm 1.6 \pm 47.4) - i(205.2 \pm 1.7 \pm 20.7)$	¹ ALBRECHT 20	RVUE	$0.9 \bar{p}p \rightarrow \pi^0\pi^0\eta, \pi^0\eta\eta, \pi^0K^+K^-$
$(1290 \pm 50) - i(170 \pm 20)$	² ANISOVICH 09	RVUE	$0.0 \bar{p}p, \pi N$
$(1373 \pm 15) - i(137 \pm 10)$	³ BARGIOTTI 03	OBLX	$\bar{p}p$
$(1302 \pm 17) - i(166 \pm 18)$	⁴ BARBERIS 00C		$450 \bar{p}p \rightarrow p_f 4\pi p_S$
$(1312 \pm 25 \pm 10) - i(109 \pm 22 \pm 15)$	BARBERIS 99D	OMEG	$450 \bar{p}p \rightarrow K^+K^-, \pi^+\pi^-$
$(1406 \pm 19) - i(80 \pm 6)$	⁵ KAMINSKI 99	RVUE	$\pi\pi \rightarrow \pi\pi, K\bar{K}, \sigma\sigma$
$(1330 \pm 50) - i(120 \pm 20)$	ANISOVICH 98B	RVUE	Compilation
$(1290 \pm 15) - i(145 \pm 15)$	BARBERIS 97B	OMEG	$450 \bar{p}p \rightarrow p_f 2(\pi^+\pi^-)$
$(1548 \pm 40) - i(560 \pm 40)$	BERTIN 97C	OBLX	$0.0 \bar{p}p \rightarrow \pi^+\pi^-\pi^0$
$(1380 \pm 40) - i(180 \pm 25)$	ABELE 96B	CBAR	$0.0 \bar{p}p \rightarrow \pi^0 K_L^0 K_L^0$
$(1300 \pm 15) - i(115 \pm 8)$	BUGG 96	RVUE	
$(1330 \pm 50) - i(150 \pm 40)$	⁶ AMSLER 95B	CBAR	$\bar{p}p \rightarrow 3\pi^0$
$(1360 \pm 35) - i(150-300)$	⁶ AMSLER 95C	CBAR	$\bar{p}p \rightarrow \pi^0\eta\eta$
$(1390 \pm 30) - i(190 \pm 40)$	⁷ AMSLER 95D	CBAR	$\bar{p}p \rightarrow 3\pi^0, \pi^0\eta\eta, \pi^0\pi^0\eta$
$1346 - i249$	^{8,9} JANSSSEN 95	RVUE	$\pi\pi \rightarrow \pi\pi, K\bar{K}$
$1214 - i168$	^{9,10} TORNQVIST 95	RVUE	$\pi\pi \rightarrow \pi\pi, K\bar{K}, K\pi, \eta\pi$
$1364 - i139$	AMSLER 94D	CBAR	$\bar{p}p \rightarrow \pi^0\pi^0\eta$
$(1365 \pm 20) - i(134 \pm 35)$	ANISOVICH 94	CBAR	$\bar{p}p \rightarrow 3\pi^0, \pi^0\eta\eta$
$(1340 \pm 40) - i(127 \pm 30)$	¹¹ BUGG 94	RVUE	$\bar{p}p \rightarrow 3\pi^0, \eta\eta\pi^0, \eta\pi^0\pi^0$
$(1430 \pm 5) - i(73 \pm 13)$	¹² KAMINSKI 94	RVUE	$\pi\pi \rightarrow \pi\pi, K\bar{K}$
$1420 - i220$	¹³ AU 87	RVUE	$\pi\pi \rightarrow \pi\pi, K\bar{K}$

- T-matrix pole, 5 poles, 5 channels, including scattering data from HYAMS 75 ($\pi\pi$), LONGACRE 86 ($K\bar{K}$), BINON 83 ($\eta\eta$), and BINON 84C ($\eta\eta'$).
- Another pole is found at $(1510 \pm 130) - i(800 \pm 100)$ MeV.
- Coupled channel analysis of $\pi^+\pi^-\pi^0, K^+K^-\pi^0$, and $K^+K_S^0\pi^+$.
- Average between $\pi^+\pi^-\pi^0$ and $2(\pi^+\pi^-)$.
- T-matrix pole on sheet ---.
- Supersedes ANISOVICH 94.
- Coupled-channel analysis of $\bar{p}p \rightarrow 3\pi^0, \pi^0\eta\eta$, and $\pi^0\pi^0\eta$ on sheet IV. Demonstrates explicitly that $f_0(500)$ and $f_0(1370)$ are two different poles.
- Analysis of data from FALVARD 88.
- The pole is on Sheet III. Demonstrates explicitly that $f_0(500)$ and $f_0(1370)$ are two different poles.
- Uses data from BEIER 72b, OCHS 73, HYAMS 73, GRAYER 74, ROSSELET 77, CASON 83, ASTON 88, and ARMSTRONG 91b. Coupled channel analysis with flavor symmetry and all light two-pseudoscalars systems.
- Reanalysis of ANISOVICH 94 data.
- T-matrix pole on sheet III.
- Analysis of data from OCHS 73, GRAYER 74, BECKER 79, and CASON 83.

$f_0(1370)$ BREIT-WIGNER MASS

VALUE (MeV)	DOCUMENT ID
-------------	-------------

1200 to 1500 OUR ESTIMATE

$\pi\pi$ MODE	VALUE (MeV)	EVTS	DOCUMENT ID	TECN	COMMENT
---------------	-------------	------	-------------	------	---------

••• We do not use the following data for averages, fits, limits, etc. •••

1400 ± 40	¹ AUBERT 09L	BABR	$B^\pm \rightarrow \pi^\pm \pi^\pm \pi^\mp$
$1470 \pm \sqrt[6]{7-25}$	² UEHARA 08A	BELL	$10.6 e^+e^- \rightarrow e^+e^-\pi^0\pi^0$
1259 ± 55	2.6k	BONVICINI 07	$CLEO D^+ \rightarrow \pi^-\pi^+\pi^+$
$1309 \pm 1 \pm 15$	³ BUGG 07A	RVUE	$0.0 \bar{p}p \rightarrow 3\pi^0$
1449 ± 13	4.3k	⁴ GARMA SH 06	BELL $B^+ \rightarrow K^+\pi^+\pi^-$
1350 ± 50		ABLIIKIM 05	BES2 $J/\psi \rightarrow \phi\pi^+\pi^-$
$1265 \pm 30 \pm \sqrt[20]{35}$		ABLIIKIM 05Q	BES2 $\psi(2S) \rightarrow \gamma\pi^+\pi^-K^+K^-$
$1434 \pm 18 \pm 3$	848	AITALA 01A	E791 $D_s^+ \rightarrow \pi^-\pi^+\pi^+$
1308 ± 10		BARBERIS 99B	OMEG $450 \bar{p}p \rightarrow p_S p_f \pi^+\pi^-$

Table with columns: VALUE (MeV), EVTS, DOCUMENT ID, TECN, COMMENT. Rows include BELLAZZINI 99, ALDE 98, BERTIN 98, TORNQVIST 95, ARMSTRONG 91, BREAKSTONE 90, AKESSON 86, FROGGATT 77.

Table with columns: VALUE (MeV), EVTS, DOCUMENT ID, TECN, COMMENT. Rows include BELLAZZINI 99, ALDE 98, BERTIN 98, TORNQVIST 95, ARMSTRONG 91, BREAKSTONE 90, AKESSON 86, FROGGATT 77.

- 1 Breit-Wigner mass.
2 Breit-Wigner mass. May also be the f0(1500).
3 Reanalysis of ABELE 96c data.
4 Also observed by GARMASH 07 in B0 -> KS0 pi+ pi- decays. Supersedes GARMASH 05.
5 Uses data from BEIER 72b, OCHS 73, HYAMS 73, GRAYER 74, ROSSELET 77, CA-SON 83, ASTON 88, and ARMSTRONG 91b. Coupled channel analysis with flavor symmetry and all light two-pseudoscalars systems.
6 Also observed by ASNER 00 in tau- -> pi- pi0 pi0 nu_tau decays

- 1 The systematic errors are not reported.
2 Breit-Wigner width. May also be the f0(1500).
3 Also observed by GARMASH 07 in B0 -> KS0 pi+ pi- decays. Supersedes GARMASH 05.
4 Uses data from BEIER 72b, OCHS 73, HYAMS 73, GRAYER 74, ROSSELET 77, CA-SON 83, ASTON 88, and ARMSTRONG 91b. Coupled channel analysis with flavor symmetry and all light two-pseudoscalars systems.
5 Also observed by ASNER 00 in tau- -> pi- pi0 pi0 nu_tau decays
6 Width defined as distance between 45 and 135 degrees phase shift.

KK MODE

Table with columns: VALUE (MeV), EVTS, DOCUMENT ID, TECN, COMMENT. Rows include AAIJ 19H, DOBBS 2,3, DOBBS 2,3, VLADIMIRSK...06, TIKHOMIROV 03, BOLONKIN 88, ETKIN 82B, WICKLUND 80, POLYCHRO... 79.

- 1 From the D+ -> K+ K+ K- Dalitz plot fit with the isobar model A.
2 Using CLEO-c data but not authored by the CLEO Collaboration.
3 From a fit to a Breit-Wigner line shape with fixed Gamma = 346 MeV.

KK MODE

Table with columns: VALUE (MeV), EVTS, DOCUMENT ID, TECN, COMMENT. Rows include AAIJ 19H, VLADIMIRSK...06, TIKHOMIROV 03, BOLONKIN 88, ETKIN 82B, WICKLUND 80, POLYCHRO... 79.

- 1 From the D+ -> K+ K+ K- Dalitz plot fit with the isobar model A.

4pi MODE 2(pi pi)S+pp

Table with columns: VALUE (MeV), EVTS, DOCUMENT ID, TECN, COMMENT. Rows include ABELE 01, AMSLER 94, ADAMO 93, GASPERO 93, BETTINI 66.

- 1 rho rho dominant.

4pi MODE 2(pi pi)S+pp

Table with columns: VALUE (MeV), EVTS, DOCUMENT ID, TECN, COMMENT. Rows include ABELE 01, AMSLER 94, ADAMO 93, GASPERO 93, BETTINI 66.

- 1 rho rho dominant.

eta eta MODE

Table with columns: VALUE (MeV), DOCUMENT ID, TECN, COMMENT. Rows include UEHARA 10A, AMSLER 92, ALDE 86D.

- 1 Breit-Wigner mass. May also be the f0(1500).

eta eta MODE

Table with columns: VALUE (MeV), DOCUMENT ID, TECN, COMMENT. Rows include UEHARA 10A, AMSLER 92, ALDE 86D.

- 1 Breit-Wigner width. May also be the f0(1500).

COUPLED CHANNEL MODE

Table with columns: VALUE (MeV), DOCUMENT ID, TECN, COMMENT. Rows include AAIJ 19H, ANISOVICH 03.

- 1 From the D+ -> K+ K+ K- Dalitz plot fit with the Triple-M amplitude in the multi-meson model of AOUDE 18.
2 K-matrix pole from combined analysis of pi- p -> pi0 pi0 n, pi- p -> K K n, pi+ pi- -> pi+ pi-, p p -> pi0 pi0 pi0, pi0 eta, pi0 pi0 eta, pi+ pi- pi0, K+ K- pi0, KS0 KS0 pi0, K+ KS0 pi- at rest, p n -> pi- pi- pi+, KS0 K- pi0, KS0 KS0 pi- at rest.

COUPLED CHANNEL MODE

Table with columns: VALUE (MeV), DOCUMENT ID, TECN, COMMENT. Rows include ANISOVICH 03.

- 1 K-matrix pole from combined analysis of pi- p -> pi0 pi0 n, pi- p -> K K n, pi+ pi- -> pi+ pi-, p p -> pi0 pi0 pi0, pi0 eta, pi0 pi0 eta, pi+ pi- pi0, K+ K- pi0, KS0 KS0 pi0, K+ KS0 pi- at rest, p n -> pi- pi- pi+, KS0 K- pi0, KS0 KS0 pi- at rest.

f0(1370) BREIT-WIGNER WIDTH

Table with columns: VALUE (MeV), DOCUMENT ID. Row: 200 to 500 OUR ESTIMATE.

pi pi MODE

Table with columns: VALUE (MeV), EVTS, DOCUMENT ID, TECN, COMMENT. Rows include AUBERT 09L, UEHARA 08A, BONVICINI 07, GARMASH 06, ABLIKIM 05, ABLIKIM 05Q, AITALA 01A, BARBERIS 99B.

f0(1370) DECAY MODES

Table with columns: Mode, Fraction (Gamma_i/Gamma). Rows include pi pi, 4 pi, 4 pi^0, 2 pi+ 2 pi-, pi+ pi- 2 pi^0, rho rho, 2(pi pi)S-wave, pi(1300) pi, a1(1260) pi, eta eta, K K, K K n pi, 6 pi, omega omega, gamma gamma, e+ e-.

f0(1370) PARTIAL WIDTHS

Table with columns: Gamma(gamma), Gamma(gamma) values. Row: Gamma(gamma) See gamma gamma widths under f0(500) and MORGAN 90.

Meson Particle Listings

 $f_0(1370)$

$\Gamma(e^+e^-)$					Γ_{16}
VALUE (eV)	CL%	DOCUMENT ID	TECN	COMMENT	
<20	90	VOROBYEV	88	ND	$e^+e^- \rightarrow \pi^0\pi^0$

 $f_0(1370) \Gamma(i)\Gamma(\gamma\gamma)/\Gamma(\text{total})$

$\Gamma(\eta\eta) \times \Gamma(\gamma\gamma)/\Gamma_{\text{total}}$					$\Gamma_{10}\Gamma_{15}/\Gamma$
VALUE (eV)	DOCUMENT ID	TECN	COMMENT		
121 ⁺¹³³⁺¹⁶⁹ ₋₅₃₋₁₀₆	1 UEHARA	10A	BELL	10.6	$e^+e^- \rightarrow e^+e^-\eta\eta$

¹Including interference with the $f_2'(1525)$ (parameters fixed to the values from the 2008 edition of this review, PDG 08) and $f_2(1270)$. May also be the $f_0(1500)$.

 $f_0(1370)$ BRANCHING RATIOS

$\Gamma(\pi\pi)/\Gamma_{\text{total}}$					Γ_1/Γ
VALUE	CL%	DOCUMENT ID	TECN	COMMENT	
<0.10	95	OCHS	13	RVUE	
0.26 ± 0.09		BUGG	96	RVUE	
<0.15		1 AMSLER	94	CBAR	$\bar{p}p \rightarrow \pi^+\pi^-\pi^0$
<0.06		GASPERO	93	DBC	$0.0 \bar{p}n \rightarrow \text{hadrons}$

¹Using AMSLER 95B ($3\pi^0$).

$\Gamma(4\pi)/\Gamma_{\text{total}}$					$\Gamma_2/\Gamma = (\Gamma_3+\Gamma_4+\Gamma_5)/\Gamma$
VALUE	DOCUMENT ID	TECN	COMMENT		
>0.72	GASPERO	93	DBC	0.0	$\bar{p}n \rightarrow \text{hadrons}$

$\Gamma(4\pi^0)/\Gamma(4\pi)$					Γ_3/Γ_2
VALUE	DOCUMENT ID	TECN	COMMENT		
seen	ABELE	96	CBAR	0.0	$\bar{p}p \rightarrow 5\pi^0$
0.068 ± 0.005	1 GASPERO	93	DBC	0.0	$\bar{p}n \rightarrow \text{hadrons}$

¹Model-dependent evaluation.

$\Gamma(2\pi^+2\pi^-)/\Gamma(4\pi)$					$\Gamma_4/\Gamma_2 = \Gamma_4/(\Gamma_3+\Gamma_4+\Gamma_5)$
VALUE	DOCUMENT ID	TECN	COMMENT		
0.420 ± 0.014	1 GASPERO	93	DBC	0.0	$\bar{p}n \rightarrow 2\pi^+3\pi^-$

¹Model-dependent evaluation.

$\Gamma(\pi^+\pi^-\pi^0)/\Gamma(4\pi)$					$\Gamma_5/\Gamma_2 = \Gamma_5/(\Gamma_3+\Gamma_4+\Gamma_5)$
VALUE	DOCUMENT ID	TECN	COMMENT		
0.512 ± 0.019	1 GASPERO	93	DBC	0.0	$\bar{p}n \rightarrow \text{hadrons}$

¹Model-dependent evaluation.

$\Gamma(\rho\rho)/\Gamma(4\pi)$					Γ_6/Γ_2
VALUE	DOCUMENT ID	TECN	COMMENT		
0.26 ± 0.07	ABELE	01B	CBAR	0.0	$\bar{p}d \rightarrow 5\pi\rho$

$\Gamma(2(\pi\pi)s\text{-wave})/\Gamma(\pi\pi)$					Γ_7/Γ_1
VALUE	DOCUMENT ID	TECN	COMMENT		
5.6 ± 2.6	1 ABELE	01	CBAR	0.0	$\bar{p}d \rightarrow \pi^-4\pi^0\rho$

¹From the combined data of ABELE 96 and ABELE 96c.

$\Gamma(2(\pi\pi)s\text{-wave})/\Gamma(4\pi)$					Γ_7/Γ_2
VALUE	DOCUMENT ID	TECN	COMMENT		
0.51 ± 0.09	ABELE	01B	CBAR	0.0	$\bar{p}d \rightarrow 5\pi\rho$

$\Gamma(\rho\rho)/\Gamma(2(\pi\pi)s\text{-wave})$					Γ_6/Γ_7
VALUE	DOCUMENT ID	TECN	COMMENT		
large	BARBERIS	00C		450	$\bar{p}p \rightarrow \rho_f 4\pi\rho_s$
1.6 ± 0.2	AMSLER	94	CBAR		$\bar{p}p \rightarrow \pi^+\pi^-\pi^0$
~0.65	GASPERO	93	DBC	0.0	$\bar{p}n \rightarrow \text{hadrons}$

$\Gamma(\pi(1300)\pi)/\Gamma(4\pi)$					Γ_8/Γ_2
VALUE	DOCUMENT ID	TECN	COMMENT		
0.17 ± 0.06	ABELE	01B	CBAR	0.0	$\bar{p}d \rightarrow 5\pi\rho$

$\Gamma(a_1(1260)\pi)/\Gamma(4\pi)$					Γ_9/Γ_2
VALUE	DOCUMENT ID	TECN	COMMENT		
0.06 ± 0.02	ABELE	01B	CBAR	0.0	$\bar{p}d \rightarrow 5\pi\rho$

$\Gamma(\eta\eta)/\Gamma(4\pi)$					$\Gamma_{10}/\Gamma_2 = \Gamma_{10}/(\Gamma_3+\Gamma_4+\Gamma_5)$
VALUE	DOCUMENT ID	TECN	COMMENT		
(28 ± 11) × 10 ⁻³	1 ANISOVICH	02D	SPEC		Combined fit
(4.7 ± 2.0) × 10 ⁻³	BARBERIS	00E		450	$\bar{p}p \rightarrow \rho_f\eta\eta\rho_s$

¹From a combined K-matrix analysis of Crystal Barrel ($0. \rho\bar{p} \rightarrow \pi^0\pi^0\pi^0, \pi^0\eta\eta, \pi^0\pi^0\eta$), GAMS ($\pi\rho \rightarrow \pi^0\pi^0n, \eta\eta n, \eta\eta'n$), and BNL ($\pi\rho \rightarrow K\bar{K}n$) data.

$\Gamma(K\bar{K})/\Gamma_{\text{total}}$					Γ_{11}/Γ
VALUE	DOCUMENT ID	TECN	COMMENT		
0.35 ± 0.13	BUGG	96	RVUE		

$\Gamma(K\bar{K})/\Gamma(\pi\pi)$					Γ_{11}/Γ_1
VALUE	DOCUMENT ID	TECN	COMMENT		
0.08 ± 0.08	ABLIKIM	05	BES2		$J/\psi \rightarrow \phi\pi^+\pi^-, \phi K^+K^-$
0.91 ± 0.20	1 BARGIOTTI	03	OBLX		$\bar{p}p$
0.12 ± 0.06	2 ANISOVICH	02D	SPEC		Combined fit
0.46 ± 0.15 ± 0.11	BARBERIS	99D	OMEG	450	$\bar{p}p \rightarrow K^+K^-, \pi^+\pi^-$

¹Coupled channel analysis of $\pi^+\pi^-\pi^0, K^+K^-\pi^0$, and $K^{\pm}K_S^0\pi^{\mp}$.

²From a combined K-matrix analysis of Crystal Barrel ($0. \rho\bar{p} \rightarrow \pi^0\pi^0\pi^0, \pi^0\eta\eta, \pi^0\pi^0\eta$), GAMS ($\pi\rho \rightarrow \pi^0\pi^0n, \eta\eta n, \eta\eta'n$), and BNL ($\pi\rho \rightarrow K\bar{K}n$) data.

$\Gamma(K\bar{K}n\pi)/\Gamma_{\text{total}}$					Γ_{12}/Γ
VALUE	DOCUMENT ID	TECN	COMMENT		
<0.03	GASPERO	93	DBC	0.0	$\bar{p}n \rightarrow \text{hadrons}$

$\Gamma(6\pi)/\Gamma_{\text{total}}$					Γ_{13}/Γ
VALUE	DOCUMENT ID	TECN	COMMENT		
<0.22	GASPERO	93	DBC	0.0	$\bar{p}n \rightarrow \text{hadrons}$

$\Gamma(\omega\omega)/\Gamma_{\text{total}}$					Γ_{14}/Γ
VALUE	DOCUMENT ID	TECN	COMMENT		
<0.13	GASPERO	93	DBC	0.0	$\bar{p}n \rightarrow \text{hadrons}$

 $f_0(1370)$ REFERENCES

SARANTSEV	21	PL B816	136227	A.V. Sarantsev et al.	(BONN, PNPI)
ALBRECHT	20	EPJ C80	453	M. Albrecht et al.	(Crystal Barrel Collab.)
AALI	19H	JHEP	1904 063	R. Aali et al.	(LHCb Collab.)
AOUDE	18	PR D98	056021	R.T. Aoude et al.	(LHCb Collab.)
DOBBS	15	PR D91	052006	S. Dobbs et al.	(NWES)
OCHS	13	JP G40	043001	W. Ochs	
UEHARA	10A	PR D82	114031	S. Uehara et al.	(BELLE Collab.)
ANISOVICH	09	IJMP	A24 2481	V.V. Anisovich, A.V. Sarantsev	
AUBERT	09L	PR D79	072006	B. Aubert et al.	(BABAR Collab.)
PDG	08	PL B667	1	C. Amisler et al.	(PDG Collab.)
UEHARA	08A	PR D78	052004	S. Uehara et al.	(BELLE Collab.)
BONVICINI	07	PR D76	012001	G. Bonvicini et al.	(CLEO Collab.)
BUGG	07A	JP G34	151	D.V. Bugg et al.	
GARMASH	07	PR D75	012006	A. Garmash et al.	(BELLE Collab.)
GARMASH	06	PRL 96	251803	A. Garmash et al.	(BELLE Collab.)
PDG	06	JP G33	1	W.-M. Yao et al.	(PDG Collab.)
VLADIMIRSKY...	06	PAN 69	493	V.V. Vladimirov et al.	(ITEP, Moscow)
				Translated from YAF 69 515.	
ABLIKIM	05	PL B607	243	M. Ablikim et al.	(BES Collab.)
ABLIKIM	05Q	PR D72	092002	M. Ablikim et al.	(BES Collab.)
GARMASH	05	PR D71	092003	A. Garmash et al.	(BELLE Collab.)
ANISOVICH	03	EPJ A16	229	V.V. Anisovich et al.	
BARGIOTTI	03	EPJ C26	371	M. Bargiotti et al.	(OBELIX Collab.)
TIKHOMIROV	03	PAN 66	828	G.D. Tikhomirov et al.	
				Translated from YAF 66 860.	
ANISOVICH	02D	PAN 65	1545	V.V. Anisovich et al.	
				Translated from YAF 65 1583.	
ABELE	01	EPJ C19	667	A. Abele et al.	(Crystal Barrel Collab.)
ABELE	01B	EPJ C21	261	A. Abele et al.	(Crystal Barrel Collab.)
AITALA	01A	PRL 86	765	E.M. Aitala et al.	(FNAL E791 Collab.)
ASNER	00	PR D61	012002	D.M. Asner et al.	(CLEO Collab.)
BARBERIS	00C	PL B471	440	D. Barberis et al.	(WA 102 Collab.)
BARBERIS	00E	PL B479	59	D. Barberis et al.	(WA 102 Collab.)
BARBERIS	99D	PL B453	316	D. Barberis et al.	(Omega Expt.)
BARBERIS	99B	PL B462	462	D. Barberis et al.	(Omega Expt.)
BELLAZZINI	99	PL B467	296	R. Bellazzini et al.	
KAMINSKI	99	EPJ C9	141	R. Kaminski, L. Lesniak, B. Loiseau	(CRAC, PARIN)
ALDE	98	EPJ A3	361	D. Alde et al.	(GAMMA Collab.)
				Also PAN 62 405	
				Translated from YAF 62 446.	
ANISOVICH	98B	SPI 411	419	V.V. Anisovich et al.	(GAMS Collab.)
				Translated from UFN 168 481.	
BERTIN	98	PR D57	55	A. Bertin et al.	(OBELIX Collab.)
BARBERIS	97B	PL B413	217	D. Barberis et al.	(WA 102 Collab.)
BERTIN	97C	PL B408	476	A. Bertin et al.	(OBELIX Collab.)
ABELE	96	PL B380	453	A. Abele et al.	(Crystal Barrel Collab.)
ABELE	96B	PL B385	425	A. Abele et al.	(Crystal Barrel Collab.)
ABELE	96C	NP A409	562	A. Abele et al.	(Crystal Barrel Collab.)
BUGG	96	NP B471	59	D.V. Bugg, A.V. Sarantsev, B.S. Zou	(LOQM, PNPI)
AMSLER	95B	PL B342	433	C. Amisler et al.	(Crystal Barrel Collab.)
AMSLER	95C	PL B353	571	C. Amisler et al.	(Crystal Barrel Collab.)
AMSLER	95D	PL B355	425	C. Amisler et al.	(Crystal Barrel Collab.)
JANSEN	95	PR D52	2690	G. Janssen et al.	(STON, ADDL, JULI)
TORNQVIST	95	ZPHY	C68 647	N.A. Tornqvist	(HELS)
AMSLER	94	PL B322	431	C. Amisler et al.	(Crystal Barrel Collab.)
AMSLER	94D	PL B333	277	C. Amisler et al.	(Crystal Barrel Collab.)
ANISOVICH	94	PL B323	233	V.V. Anisovich et al.	(Crystal Barrel Collab.)
BUGG	94	PR D50	4412	D.V. Bugg et al.	(LOQM)

Meson Particle Listings

$f_0(1370), \pi_1(1400)$

NAME	PR	NO	PAGE	EVTS	DOCUMENT ID	TECN	CHG	COMMENT
KAMINSKI	94	PR D50	3145		R. Kaminski, L. Lesniak, J.P. Maillet (CRAC+)			
ADAMO	93	NP A558	13C		A. Adamo et al. (OBELIX Collab.) JPC			
GASPERO	93	NP A562	407		M. Gaspero (ROMAI) JPC			
AMSLER	92	PL B291	347		C. Amisler et al. (Crystal Barrel Collab.)			
ARMSTRONG	91	ZPHY C51	351		T.A. Armstrong et al. (ATHU, BARI, BIRM+)			
ARMSTRONG	91B	ZPHY C52	389		T.A. Armstrong et al. (ATHU, BARI, BIRM+)			
BREAKSTONE	90	ZPHY C48	569		A.M. Breakstone et al. (ISU, BGNA, CERN+)			
MORGAN	90	ZPHY C48	623		D. Morgan, M.R. Pennington (RAL, DURH)			
ASTON	88	NP B296	493		D. Aston et al. (SLAC, NAGO, CINC, INUS)			
BOLONKIN	88	NP B309	426		B.V. Bolonkin et al. (ITEP, SERP)			
FALVARD	88	PR D38	2706		A. Falvard et al. (CLER, FRAS, LALO+)			
VOROBYEV	88	SJNP 48	273		P.V. Vorobiev et al. (NOVO)			
Transferred from	YAF	48	436					
AU	87	PR D35	1633		K.L. Au, D. Morgan, M.R. Pennington (DURH, RAL)			
AKESSON	86	NP B264	154		T. Akesson et al. (Axial Field Spec. Collab.)			
ALDE	86D	NP B269	485		D.M. Alde et al. (BELG, LAPP, SERP, CERN+)			
LONGACRE	86	PL B177	223		R.S. Longacre et al. (BNL, BRAN, CUNY+)			
BINON	84C	NC 80A	363		F.G. Binon et al. (BELG, LAPP, SERP+)			
BINON	83	NC 78A	313		F.G. Binon et al. (BELG, LAPP, SERP+)			
CASON	83	PR D28	1586		N.M. Cason et al. (NDAM, ANL)			
ETKIN	82B	PR D25	1786		A. Etkin et al. (BNL, CUNY, TUFTS, VAND)			
WICKLUND	80	PRL 45	1469		A.B. Wicklund et al. (ANL)			
BECKER	79	NP B151	46		H. Becker et al. (MPIM, CERN, ZEEM, CRAC)			
POLYCHRO...	79	PR D19	1317		V.A. Polychronakos et al. (NDAM, ANL)			
FROGGATT	77	NP B129	89		C.D. Froggatt, J.L. Petersen (GLAS, NORD)			
ROSSELET	77	PR D15	574		L. Rosselet et al. (GEVA, SAACL)			
HYAMS	75	NP B100	205		B.D. Hyams et al. (CERN, MPIM)			
GRAYER	74	NP B75	189		G. Grayer et al. (CERN, MPIM)			
HYAMS	73	NP B64	134		B.D. Hyams et al. (CERN, MPIM)			
OCHS	73	Thesis			W. Ochs (MPIM, MUNI)			
BEIER	72B	PRL 29	511		E.W. Beier et al. (PENN)			
BETTINI	66	NC 42A	695		A. Bettini et al. (PADO, PISA)			

$\pi_1(1400)$

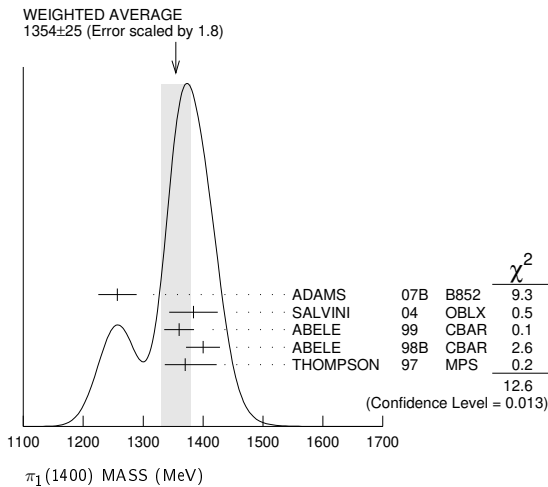
$$J^{PC} = 1^-(1^--)$$

Coupled channel analyses favor the existence of only one broad 1^-- isovector state consistent with $\pi_1(1600)$ in the 1400–1600 MeV region. See the review on "Spectroscopy of Light Meson Resonances." See also $\pi_1(1600)$.

$\pi_1(1400)$ MASS

VALUE (MeV)	EVTS	DOCUMENT ID	TECN	CHG	COMMENT
1354 ± 25	OUR AVERAGE	Error includes scale factor of 1.8. See the ideogram below.			
1257 ± 20	± 25	23.5k	ADAMS	07B B852	18 $\pi^- p \rightarrow \eta \pi^0 n$
1384 ± 20	± 35	90k	SALVINI	04 OBLX	$\bar{p} p \rightarrow 2\pi^+ 2\pi^-$
1360 ± 25			ABELE	99 CBAR	0.0 $\bar{p} p \rightarrow \pi^0 \pi^0 \eta$
1400 ± 20	± 20		ABELE	98B CBAR	0.0 $\bar{p} n \rightarrow \pi^- \pi^0 \eta$
1370 ± 16	+50 -30		¹ THOMPSON	97 MPS	18 $\pi^- p \rightarrow \eta \pi^- p$
•••	We do not use the following data for averages, fits, limits, etc. •••				
1404.7 ± 3.5	+15.1 -17.7		² ALBRECHT	20 RVUE	0.9 $\bar{p} p \rightarrow \pi^0 \pi^0 \eta$
1323.1 ± 4.6			³ AOYAGI	93 BKEI	$\pi^- p \rightarrow \eta \pi^- p$
1406 ± 20			⁴ ALDE	88B GAM4 0	100 $\pi^- p \rightarrow \eta \pi^0 n$

- ¹ Natural parity exchange, questioned by DZIERBA 03.
- ² T-matrix pole, 1 pole, 2 channels ($\pi\eta, \pi\eta'$ for unitarity).
- ³ Unnatural parity exchange.
- ⁴ Seen in the P_0 -wave intensity of the $\eta\pi^0$ system, unnatural parity exchange.



$\pi_1(1400)$ WIDTH

VALUE (MeV)	EVTS	DOCUMENT ID	TECN	CHG	COMMENT
330 ± 35	OUR AVERAGE				
354 ± 64	± 58	23.5k	ADAMS	07B B852	18 $\pi^- p \rightarrow \eta \pi^0 n$
378 ± 50	± 50	90k	SALVINI	04 OBLX	$\bar{p} p \rightarrow 2\pi^+ 2\pi^-$
220 ± 90			ABELE	99 CBAR	0.0 $\bar{p} p \rightarrow \pi^0 \pi^0 \eta$
310 ± 50	+50 -30		ABELE	98B CBAR	0.0 $\bar{p} n \rightarrow \pi^- \pi^0 \eta$
385 ± 40	+65 -105		¹ THOMPSON	97 MPS	18 $\pi^- p \rightarrow \eta \pi^- p$
•••	We do not use the following data for averages, fits, limits, etc. •••				
628.3 ± 27.1	+35.8 -138.2		² ALBRECHT	20 RVUE	0.9 $\bar{p} p \rightarrow \pi^0 \pi^0 \eta$
143.2 ± 12.5			³ AOYAGI	93 BKEI	$\pi^- p \rightarrow \eta \pi^- p$
180 ± 20			⁴ ALDE	88B GAM4 0	100 $\pi^- p \rightarrow \eta \pi^0 n$

- ¹ Resolution is not unfolded, natural parity exchange, questioned by DZIERBA 03.
- ² T-matrix pole, 1 pole, 2 channels ($\pi\eta, \pi\eta'$ for unitarity).
- ³ Unnatural parity exchange.
- ⁴ Seen in the P_0 -wave intensity of the $\eta\pi^0$ system, unnatural parity exchange.

$\pi_1(1400)$ DECAY MODES

Mode	Fraction (Γ_i/Γ)
$\Gamma_1 \eta\pi^0$	seen
$\Gamma_2 \eta\pi^-$	seen
$\Gamma_3 \eta' \pi$	
$\Gamma_4 \rho(770)\pi$	not seen

$\pi_1(1400)$ BRANCHING RATIOS

$\Gamma(\eta\pi^0)/\Gamma_{total}$	Γ_1/Γ			
VALUE	DOCUMENT ID	TECN	CHG	COMMENT
•••	We do not use the following data for averages, fits, limits, etc. •••			
not seen	PROKOSHKIN	95B	GAM4	100 $\pi^- p \rightarrow \eta \pi^0 n$
not seen	¹ BUGG	94	RVUE	$\bar{p} p \rightarrow \eta 2\pi^0$
not seen	² APEL	81	NICE 0	40 $\pi^- p \rightarrow \eta \pi^0 n$

- ¹ Using Crystal Barrel data.
- ² A general fit allowing S, D, and P waves (including $m=0$) is not done because of limited statistics.

$\Gamma(\eta\pi^-)/\Gamma_{total}$	Γ_2/Γ		
VALUE	DOCUMENT ID	TECN	COMMENT
•••	We do not use the following data for averages, fits, limits, etc. •••		
possibly seen	BELADIDZE	93	VES 37 $\pi^- N \rightarrow \eta \pi^- N$

$\Gamma(\eta' \pi)/\Gamma(\eta\pi^0)$	Γ_3/Γ_1			
VALUE	CL%	DOCUMENT ID	TECN	COMMENT
•••	We do not use the following data for averages, fits, limits, etc. •••			
<0.80	95	BOUTEMEUR	90	GAM4 100 $\pi^- p \rightarrow 4\gamma n$

$\Gamma(\rho(770)\pi)/\Gamma_{total}$	Γ_4/Γ		
VALUE	DOCUMENT ID	TECN	COMMENT
not seen	AGHASYAN	18B	COMP 190 $\pi^- p \rightarrow \pi^- \pi^+ \pi^- p$

$\pi_1(1400)$ REFERENCES

ALBRECHT 20	EPJ C80 453	M. Albrecht et al.	(Crystal Barrel Collab.)
AGHASYAN 18B	PR D38 092003	M. Aghasyan et al.	(COMPASS Collab.)
ADAMS 07B	PL B657 27	G.S. Adams et al.	(BNL E852 Collab.)
SALVINI 04	EPJ C35 21	P. Salvini et al.	(OBELIX Collab.)
DZIERBA 03	PR D67 094015	A.R. Dzierba et al.	
ABELE 99	PL B446 349	A. Abele et al.	(Crystal Barrel Collab.)
ABELE 98B	PL B423 175	A. Abele et al.	(Crystal Barrel Collab.)
THOMPSON 97	PRL 79 1630	D.R. Thompson et al.	(BNL E852 Collab.)
PROKOSHKIN 95B	PAN 58 606	Y.D. Prokoshkin, S.A. Sadovsky	(SERP)
Translated from YAF 58 662.			
BUGG 94	PR D50 4412	D.V. Bugg et al.	(LOQM)
AOYAGI 93	PL B314 246	H. Aoyagi et al.	(BKEI Collab.)
BELADIDZE 93	PL B313 276	G.M. Beladidze et al.	(VES Collab.)
BOUTEMEUR 90	Hadron 89 Conf. p 119	M. Boutemeur, M. Poulet	(SERP, BELG, LANL+)
ALDE 88B	PL B205 397	D.M. Alde et al.	(SERP, BELG, LANL, LAPP)IGJPC
APEL 81	NP B193 269	W.D. Apel et al.	(SERP, CERN)

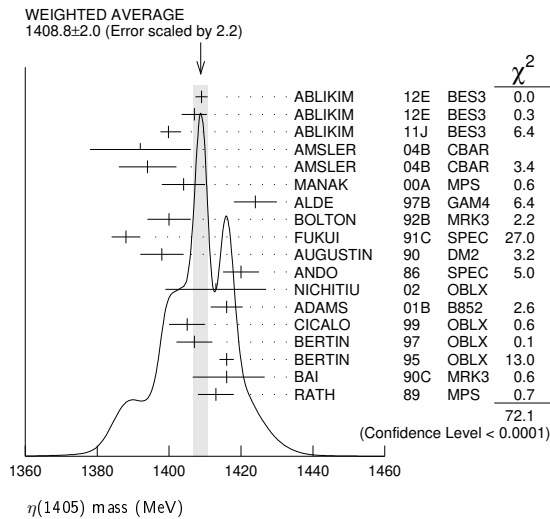
Meson Particle Listings

 $\eta(1405)$ $\eta(1405)$ See also the $\eta(1475)$.

$$I^G(J^{PC}) = 0^+(0^{-+})$$

 $\eta(1405)$ MASS

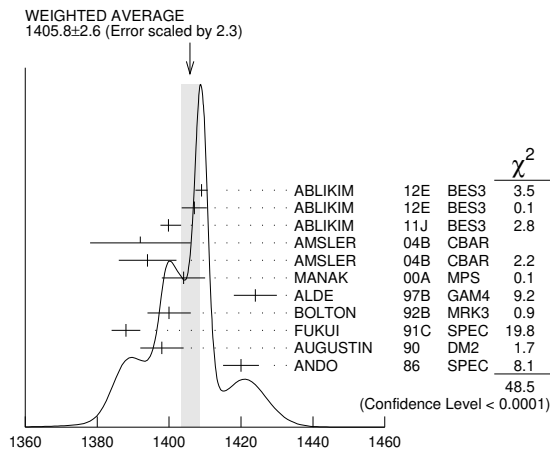
VALUE (MeV) DOCUMENT ID
1408.8 ± 2.0 OUR AVERAGE Includes data from the 2 datablocks that follow this one. Error includes scale factor of 2.2. See the ideogram below.

 $\eta\pi\pi$ MODE

VALUE (MeV) EVTS DOCUMENT ID TECN COMMENT
 The data in this block is included in the average printed for a previous datablock.

1405.8 ± 2.6 OUR AVERAGE Error includes scale factor of 2.3. See the ideogram below.

1409.0 ± 1.7	743	ABLIKIM 12E BES3		$J/\psi \rightarrow \gamma(\pi^+\pi^-\pi^0)$
1407.0 ± 3.5	198	ABLIKIM 12E BES3		$J/\psi \rightarrow \gamma(\pi^0\pi^0\pi^0)$
1399.8 ± 2.2 ^{+2.8} _{-0.1}		¹ ABLIKIM 11J BES3		$J/\psi \rightarrow \omega(\eta\pi^+\pi^-)$
1392 ± 14	900 ± 375	AMSLER 04B CBAR		$0\bar{p}p \rightarrow \pi^+\pi^-\pi^+\pi^-$
1394 ± 8	6.6 ± 2.0k	AMSLER 04B CBAR		$0\bar{p}p \rightarrow \pi^+\pi^-\pi^0\pi^0\eta$
1404 ± 6	9082	MANAK 00A MPS		$18\pi^-p \rightarrow \eta\pi^+\pi^-n$
1424 ± 6	2200	ALDE 97B GAM4		$100\pi^-p \rightarrow \eta\pi^0\pi^0n$
1400 ± 6		² BOLTON 92B MRK3		$J/\psi \rightarrow \gamma\eta\pi^+\pi^-$
1388 ± 4		FUKUI 91C SPEC		$8.95\pi^-p \rightarrow \eta\pi^+\pi^-n$
1398 ± 6	261	³ AUGUSTIN 90 DM2		$J/\psi \rightarrow \gamma\eta\pi^+\pi^-$
1420 ± 5		ANDO 86 SPEC		$8\pi^-p \rightarrow \eta\pi^+\pi^-n$
••• We do not use the following data for averages, fits, limits, etc. •••				
1404.0 ± 11.0	195	ABLIKIM 19B ^A BES3		$e^+e^- \rightarrow \psi(2S)$
1385 ± 7		BAI 99 BES		$J/\psi \rightarrow \gamma\eta\pi^+\pi^-$
1409 ± 3		⁴ AMSLER 95F CBAR		$0\bar{p}p \rightarrow \pi^+\pi^-\pi^0\pi^0\eta$



¹ The selected process is $J/\psi \rightarrow \omega a_0(980)\pi$.

² From fit to the $a_0(980)\pi 0^{-+}$ partial wave.

³ Best fit with a single Breit Wigner.

⁴ Superseded by AMSLER 04B.

 $K\bar{K}\pi$ MODE ($a_0(980)\pi$ or direct $K\bar{K}\pi$)

VALUE (MeV) EVTS DOCUMENT ID TECN COMMENT
 The data in this block is included in the average printed for a previous datablock.

1413.9 ± 1.7 OUR AVERAGE Error includes scale factor of 1.1.

1413 ± 14	3651	¹ NICHITIU 02 OBLX		$0\bar{p}p \rightarrow K^+K^-\pi^+\pi^-\pi^0$
1416 ± 4 ± 2	20k	ADAMS 01B B852		$18\text{ GeV } \pi^-p \rightarrow K^+K^-\pi^0n$
1405 ± 5		² CICALO 99 OBLX		$0\bar{p}p \rightarrow K^\pm K_S^0 \pi^\mp \pi^+\pi^-$
1407 ± 5		² BERTIN 97 OBLX		$0\bar{p}p \rightarrow K^\pm(K^0)\pi^\mp \pi^+\pi^-$
1416 ± 2		² BERTIN 95 OBLX		$0\bar{p}p \rightarrow K\bar{K}\pi\pi\pi$
1416 ± 8 ⁺⁷ ₋₅	700	³ BAI 90C MRK3		$J/\psi \rightarrow \gamma K_S^0 K^\pm \pi^\mp$
1413 ± 5		³ RATH 89 MPS		$21.4\pi^-p \rightarrow n K_S^0 K_S^0 \pi^0$
••• We do not use the following data for averages, fits, limits, etc. •••				
1459 ± 5		⁴ AUGUSTIN 92 DM2		$J/\psi \rightarrow \gamma K\bar{K}\pi$

¹ Decaying dominantly directly to $K^+K^-\pi^0$.

² Decaying into $(K\bar{K})_S\pi$, $(K\pi)_S\bar{K}$, and $a_0(980)\pi$.

³ From fit to the $a_0(980)\pi 0^{-+}$ partial wave. Cannot rule out a $a_0(980)\pi 1^{++}$ partial wave.

⁴ Excluded from averaging because averaging would be meaningless.

 $\pi\pi\gamma$ MODE

VALUE (MeV) EVTS DOCUMENT ID TECN COMMENT
1403 ± 17 OUR AVERAGE Error includes scale factor of 1.8.

1390 ± 12	235 ± 91	AMSLER 04B CBAR		$0\bar{p}p \rightarrow \pi^+\pi^-\pi^+\pi^-$
1424 ± 10 ± 11	547	BAI 04J BES2		$J/\psi \rightarrow \gamma\gamma\pi^+\pi^-$
••• We do not use the following data for averages, fits, limits, etc. •••				
1401 ± 18		^{1,2} AUGUSTIN 90 DM2		$J/\psi \rightarrow \pi^+\pi^-\gamma\gamma$
1432 ± 8		² COFFMAN 90 MRK3		$J/\psi \rightarrow \pi^+\pi^-\gamma\gamma$

¹ Best fit with a single Breit Wigner.

² This peak in the $\gamma\rho$ channel may not be related to the $\eta(1405)$.

4 π MODE

VALUE (MeV) EVTS DOCUMENT ID TECN COMMENT
 ••• We do not use the following data for averages, fits, limits, etc. •••

1420 ± 20		BUGG 95 MRK3		$J/\psi \rightarrow \gamma\pi^+\pi^-\pi^+\pi^-$
1489 ± 12	3270	¹ BISELLO 89B DM2		$J/\psi \rightarrow 4\pi\gamma$

¹ Estimated by us from various fits.

 $K\bar{K}\pi$ MODE (unresolved)

VALUE (MeV) EVTS DOCUMENT ID TECN COMMENT
 ••• We do not use the following data for averages, fits, limits, etc. •••

1452.7 ± 3.3	191	^{1,2} ABLIKIM 13M BES3		$\psi(2S) \rightarrow \omega K K \pi$
1437.6 ± 3.2	249 ± 35	^{1,2} ABLIKIM 08E BES2		$J/\psi \rightarrow \omega K_S^0 K^+\pi^- + c.c.$
1445.9 ± 5.7	62 ± 18	^{1,2} ABLIKIM 08E BES2		$J/\psi \rightarrow \omega K^+K^-\pi^0$
1442 ± 10	410	¹ BAI 98C BES		$J/\psi \rightarrow \gamma K^+K^-\pi^0$
1445 ± 8	693	¹ AUGUSTIN 90 DM2		$J/\psi \rightarrow \gamma K_S^0 K^\pm \pi^\mp$
1433 ± 8	296	¹ AUGUSTIN 90 DM2		$J/\psi \rightarrow \gamma K^+K^-\pi^0$
1413 ± 8	500	¹ DUCH 89 ASTE		$\bar{p}p \rightarrow \pi^+\pi^-K^\pm\pi^\mp K^0$
1453 ± 7	170	¹ RATH 89 MPS		$21.4\pi^-p \rightarrow K_S^0 K_S^0 \pi^0 n$
1419 ± 1	8800	¹ BIRMAN 88 MPS		$8\pi^-p \rightarrow K^+\bar{K}^0\pi^-n$
1424 ± 3	620	¹ REEVES 86 SPEC		$6.6\text{ p}\bar{p} \rightarrow K\bar{K}\pi X$
1421 ± 2		¹ CHUNG 85 SPEC		$8\pi^-p \rightarrow K\bar{K}\pi n$
1440 ⁺²⁰ ₋₁₅	174	¹ EDWARDS 82E CBAL		$J/\psi \rightarrow \gamma K^+K^-\pi^0$
1440 ⁺¹⁰ ₋₁₅		¹ SCHARRE 80 MRK2		$J/\psi \rightarrow \gamma K_S^0 K^\pm \pi^\mp$
1425 ± 7	800	^{1,3} BAILLON 67 HBC		$0\bar{p}p \rightarrow K\bar{K}\pi\pi\pi$

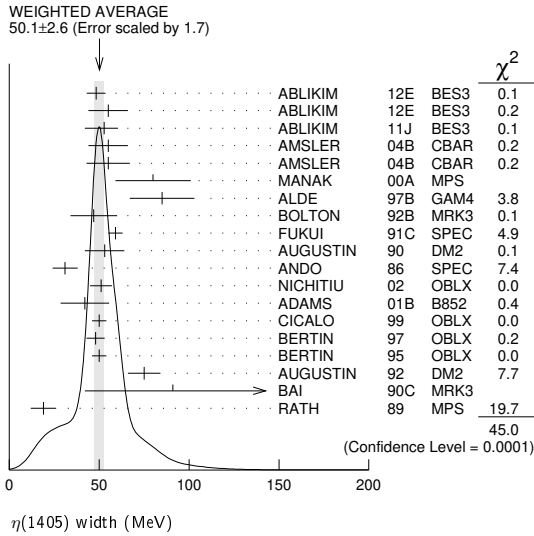
¹ These experiments identify only one pseudoscalar in the 1400–1500 range. Data could also refer to $\eta(1475)$.

² Systematic uncertainty not evaluated.

³ From best fit of 0^{-+} partial wave, 50% $K^*(892)K$, 50% $a_0(980)\pi$.

 $\eta(1405)$ WIDTH

VALUE (MeV) DOCUMENT ID
50.1 ± 2.6 OUR AVERAGE Includes data from the 2 datablocks that follow this one. Error includes scale factor of 1.7. See the ideogram below.

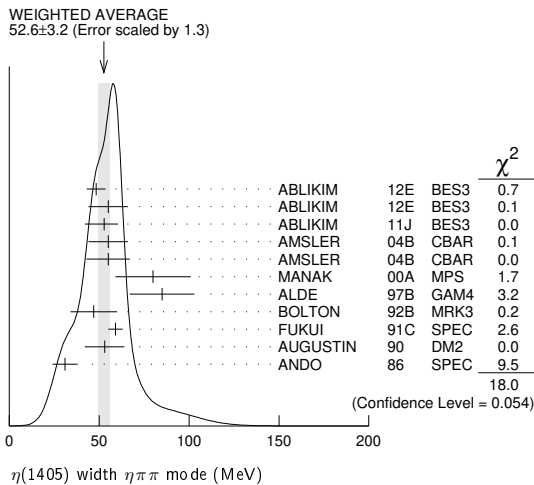


$\eta\pi\pi$ MODE

VALUE (MeV) EVTS DOCUMENT ID TECN COMMENT
The data in this block is included in the average printed for a previous datablock.

VALUE (MeV)	EVTS	DOCUMENT ID	TECN	COMMENT
52.6 ± 3.2 OUR AVERAGE				Error includes scale factor of 1.3. See the ideogram below.
48.3 ± 5.2	743	ABLIKIM 12E BES3		$J/\psi \rightarrow \gamma(\pi^+\pi^-\pi^0)$
55.0 ± 11.0	198	ABLIKIM 12E BES3		$J/\psi \rightarrow \gamma(\pi^0\pi^0\pi^0)$
52.8 ± 7.6 ^{+0.1} _{-7.6}		¹ ABLIKIM 11J BES3		$J/\psi \rightarrow \omega(\eta\pi^+\pi^-)$
55 ± 11	900	AMSLER 04B CBAR		$0\bar{p}p \rightarrow \pi^+\pi^-\pi^+\pi^-$
55 ± 12	6.6k	AMSLER 04B CBAR		$0\bar{p}p \rightarrow \pi^+\pi^-\pi^0\pi^0\gamma$
80 ± 21	9.0k	MANAK 00A MPS		$18\pi^-\rho \rightarrow \eta\pi^+\pi^-n$
85 ± 18	2.2k	ALDE 97B GAM4		$100\pi^-\rho \rightarrow \eta\pi^0\pi^0n$
47 ± 13		² BOLTON 92B MRK3		$J/\psi \rightarrow \gamma\eta\pi^+\pi^-$
59 ± 4		FUKUI 91C SPEC		$8.95\pi^-\rho \rightarrow \eta\pi^+\pi^-n$
53 ± 11		³ AUGUSTIN 90 DM2		$J/\psi \rightarrow \gamma\eta\pi^+\pi^-$
31 ± 7		ANDO 86 SPEC		$8\pi^-\rho \rightarrow \eta\pi^+\pi^-n$
79.0 ± 16.0	195	ABLIKIM 19BA BES3		$e^+e^- \rightarrow \psi(2S)$
86 ± 10		⁴ AMSLER 95F CBAR		$0\bar{p}p \rightarrow \pi^+\pi^-\pi^0\pi^0\eta$

• • • We do not use the following data for averages, fits, limits, etc. • • •
¹ The selected process is $J/\psi \rightarrow \omega a_0(980)\pi$.
² From fit to the $a_0(980)\pi 0^-+$ partial wave.
³ From $\eta\pi^+\pi^-$ mass distribution - mainly $a_0(980)\pi$ - no spin-parity determination available.
⁴ Superseded by AMSLER 04B.



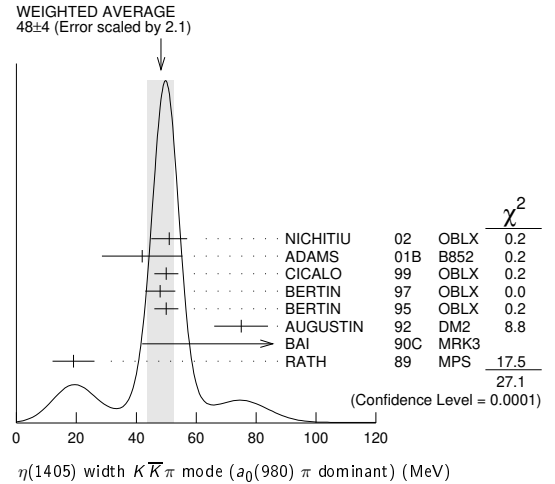
$K\bar{K}\pi$ MODE ($a_0(980)\pi$ or direct $K\bar{K}\pi$)

VALUE (MeV) EVTS DOCUMENT ID TECN COMMENT
The data in this block is included in the average printed for a previous datablock.

VALUE (MeV)	EVTS	DOCUMENT ID	TECN	COMMENT
48 ± 4 OUR AVERAGE				Error includes scale factor of 2.1. See the ideogram below.
51 ± 6	3651	¹ NICHITIU 02 OBLX		$0\bar{p}p \rightarrow K^+K^-\pi^+\pi^-\pi^0$
42 ± 10 ± 9	20k	ADAMS 01B B852		$18\text{ GeV } \pi^-\rho \rightarrow K^+K^-\pi^0n$
50 ± 4		CICALO 99 OBLX		$0\bar{p}p \rightarrow K^\pm K_S^0 \pi^\mp \pi^+\pi^-$
48 ± 5		² BERTIN 97 OBLX		$0.0\bar{p}p \rightarrow K^\pm(K^0)\pi^\mp \pi^+\pi^-$

50 ± 4	² BERTIN 95 OBLX		$0\bar{p}p \rightarrow K\bar{K}\pi\pi\pi$
75 ± 9	AUGUSTIN 92 DM2		$J/\psi \rightarrow \gamma K\bar{K}\pi$
91 ± 67 ± 15 -31 -38	³ BAI 90C MRK3		$J/\psi \rightarrow \gamma K_S^0 K^\pm \pi^\mp$
19 ± 7	³ RATH 89 MPS		$21.4\pi^-\rho \rightarrow n K_S^0 K_S^0 \pi^0$

¹ Decaying dominantly directly to $K^+K^-\pi^0$.
² Decaying into $(K\bar{K})_S\pi$, $(K\pi)_S\bar{K}$, and $a_0(980)\pi$.
³ From fit to the $a_0(980)\pi 0^-+$ partial wave, but $a_0(980)\pi 1^++$ cannot be excluded.



$\pi\pi\gamma$ MODE

VALUE (MeV)	EVTS	DOCUMENT ID	TECN	COMMENT
89 ± 17 OUR AVERAGE				Error includes scale factor of 1.7.
64 ± 18	235 ± 91	AMSLER 04B CBAR		$0\bar{p}p \rightarrow \pi^+\pi^-\pi^+\pi^-$
101.0 ± 8.8 ± 8.8	547	BAI 04J BES2		$J/\psi \rightarrow \gamma\gamma\pi^+\pi^-$
174 ± 44		AUGUSTIN 90 DM2		$J/\psi \rightarrow \pi^+\pi^-\gamma\gamma$
90 ± 26		¹ COFFMAN 90 MRK3		$J/\psi \rightarrow \pi^+\pi^-\gamma$

• • • We do not use the following data for averages, fits, limits, etc. • • •
¹ This peak in the $\gamma\rho$ channel may not be related to the $\eta(1405)$.

4 π MODE

VALUE (MeV)	EVTS	DOCUMENT ID	TECN	COMMENT
160 ± 30		BUGG 95 MRK3		$J/\psi \rightarrow \gamma\pi^+\pi^-\pi^+\pi^-$
144 ± 13	3270	¹ BISELLO 89B DM2		$J/\psi \rightarrow 4\pi\gamma$

¹ Estimated by us from various fits.

$K\bar{K}\pi$ MODE (unresolved)

VALUE (MeV)	EVTS	DOCUMENT ID	TECN	COMMENT
45.9 ± 8.2	191	^{1,2} ABLIKIM 13M BES3		$\psi(2S) \rightarrow \omega K K \pi$
48.9 ± 9.0	249 ± 35	^{1,2} ABLIKIM 08E BES2		$J/\psi \rightarrow \omega K_S^0 K^+\pi^- + c.c.$
34.2 ± 18.5	62 ± 18	^{1,2} ABLIKIM 08E BES2		$J/\psi \rightarrow \omega K^+K^-\pi^0$
93 ± 14	296	¹ AUGUSTIN 90 DM2		$J/\psi \rightarrow \gamma K^+K^-\pi^0$
105 ± 10	693	¹ AUGUSTIN 90 DM2		$J/\psi \rightarrow \gamma K_S^0 K^\pm \pi^\mp$
62 ± 16	500	¹ DUCH 89 ASTE		$\bar{p}p \rightarrow K\bar{K}\pi\pi\pi$
100 ± 11	170	¹ RATH 89 MPS		$21.4\pi^-\rho \rightarrow K_S^0 K_S^0 \pi^0 n$
66 ± 2	8800	¹ BIRMAN 88 MPS		$8\pi^-\rho \rightarrow K^+\bar{K}^0\pi^-n$
60 ± 10	620	¹ REEVES 86 SPEC		$6.6\bar{p}p \rightarrow K K \pi X$
60 ± 10		¹ CHUNG 85 SPEC		$8\pi^-\rho \rightarrow K\bar{K}\pi n$
55 ± 20 -30	174	¹ EDWARDS 82E CBAL		$J/\psi \rightarrow \gamma K^+K^-\pi^0$
50 ± 30 -20		¹ SCHARRE 80 MRK2		$J/\psi \rightarrow \gamma K_S^0 K^\pm \pi^\mp$
80 ± 10	800	^{1,3} BAILLON 67 HBC		$0.0\bar{p}p \rightarrow K\bar{K}\pi\pi\pi$

¹ These experiments identify only one pseudoscalar in the 1400–1500 range. Data could also refer to $\eta(1475)$.
² Systematic uncertainty not evaluated.
³ From best fit to 0^-+ partial wave, 50% $K^*(892)K$, 50% $a_0(980)\pi$.

$\eta(1405)$ DECAY MODES

Mode	Fraction (Γ_i/Γ)	Confidence level
Γ_1 $K\bar{K}\pi$	seen	
Γ_2 $\eta\pi\pi$	seen	
Γ_3 $a_0(980)\pi$	seen	
Γ_4 $\eta(\pi\pi)_S$ -wave	seen	
Γ_5 $f_0(980)\pi^0 \rightarrow \pi^+\pi^-\pi^0$	not seen	
Γ_6 $f_0(980)\eta$	seen	

Meson Particle Listings

$\eta(1405)$, $h_1(1415)$

Γ_7	4π	seen	
Γ_8	$\rho\rho$	<58 %	99.85%
Γ_9	$\gamma\gamma$		
Γ_{10}	$\rho^0\gamma$	seen	
Γ_{11}	$\phi\gamma$		
Γ_{12}	$K^*(892)K$	seen	

$\eta(1405) \Gamma(i)\Gamma(\gamma\gamma)/\Gamma(\text{total})$

$\Gamma(K\bar{K}\pi) \times \Gamma(\gamma\gamma)/\Gamma(\text{total})$		$\Gamma_1\Gamma_9/\Gamma$	
VALUE (keV)	CL%	DOCUMENT ID	TECN COMMENT

• • • We do not use the following data for averages, fits, limits, etc. • • •
 <0.035 90 1,2 AHOHE 05 CLE2 10.6 $e^+e^- \rightarrow e^+e^-K_S^0 K^\pm\pi^\mp$
 1 Using $\eta(1405)$ mass and width 1410 MeV and 51 MeV, respectively.
 2 Assuming three-body phase-space decay to $K_S^0 K^\pm\pi^\mp$.

$\Gamma(\eta\pi\pi) \times \Gamma(\gamma\gamma)/\Gamma(\text{total})$		$\Gamma_2\Gamma_9/\Gamma$	
VALUE (keV)	CL%	DOCUMENT ID	TECN COMMENT

<0.095 95 ACCIARRI 01G L3 183-202 $e^+e^- \rightarrow e^+e^-\eta\pi^+\pi^-$

$\Gamma(\rho^0\gamma) \times \Gamma(\gamma\gamma)/\Gamma(\text{total})$		$\Gamma_{10}\Gamma_9/\Gamma$	
VALUE (keV)	CL%	DOCUMENT ID	TECN COMMENT

• • • We do not use the following data for averages, fits, limits, etc. • • •
 <1.5 95 ALTHOFF 84E TASS $e^+e^- \rightarrow e^+e^-\pi^+\pi^-\gamma$

$\eta(1405)$ BRANCHING RATIOS

$\Gamma(\eta\pi\pi)/\Gamma(K\bar{K}\pi)$		Γ_2/Γ_1	
VALUE	CL%	DOCUMENT ID	TECN COMMENT

1.09 ± 0.48 1 AMSLER 04B CBAR 0 $\bar{p}p \rightarrow \pi^+\pi^-\pi^+\pi^-\eta$
 • • • We do not use the following data for averages, fits, limits, etc. • • •
 <0.5 90 EDWARDS 83B CBAL $J/\psi \rightarrow \eta\pi\pi\gamma$
 <1.1 90 SCHARRE 80 MRK2 $J/\psi \rightarrow \eta\pi\pi\gamma$
 <1.5 95 FOSTER 68B HBC 0.0 $\bar{p}p$
 1 Using the data of BAILLON 67 on $\bar{p}p \rightarrow K\bar{K}\pi$.

$\Gamma(\rho^0\gamma)/\Gamma(\eta\pi\pi)$		Γ_{10}/Γ_2	
VALUE	CL%	DOCUMENT ID	TECN COMMENT

0.111 ± 0.064 AMSLER 04B CBAR 0 $\bar{p}p$

$\Gamma(a_0(980)\pi)/\Gamma(K\bar{K}\pi)$		Γ_3/Γ_1	
VALUE	EVTS	DOCUMENT ID	TECN COMMENT

• • • We do not use the following data for averages, fits, limits, etc. • • •
 ~0.15 1 BERTIN 95 OBLX 0 $\bar{p}p \rightarrow K\bar{K}\pi\pi\pi$
 ~0.8 500 1 DUCH 89 ASTE $\bar{p}p \rightarrow \pi^+\pi^-K^\pm\pi^\mp K^0$
 ~0.75 1 REEVES 86 SPEC 6.6 $p\bar{p} \rightarrow K K\pi X$
 1 Assuming that the $a_0(980)$ decays only into $K\bar{K}$.

$\Gamma(a_0(980)\pi)/\Gamma(\eta\pi\pi)$		Γ_3/Γ_2	
VALUE	EVTS	DOCUMENT ID	TECN COMMENT

• • • We do not use the following data for averages, fits, limits, etc. • • •
 0.29 ± 0.10 ABELE 98E CBAR 0 $p\bar{p} \rightarrow \eta\pi^0\pi^0\pi^0$
 0.19 ± 0.04 2200 1 ALDE 97B GAM4 100 $\pi^-\pi^+ \rightarrow \eta\pi^0\pi^0\eta$
 0.56 ± 0.04 ± 0.03 1 AMSLER 95F CBAR 0 $\bar{p}p \rightarrow \pi^+\pi^-\pi^0\pi^0\eta$
 1 Assuming that the $a_0(980)$ decays only into $\eta\pi$.

$\Gamma(a_0(980)\pi)/\Gamma(\eta(\pi\pi)s\text{-wave})$		Γ_3/Γ_4	
VALUE	EVTS	DOCUMENT ID	TECN COMMENT

• • • We do not use the following data for averages, fits, limits, etc. • • •
 0.91 ± 0.12 ANISOVICH 01 SPEC 0.0 $\bar{p}p \rightarrow \eta\pi^+\pi^-\pi^+\pi^-$
 0.15 ± 0.04 9082 1 MANAK 00A MPS 18 $\pi^-\pi^+ \rightarrow \eta\pi^+\pi^-\eta$
 0.70 ± 0.12 ± 0.20 2 BAI 99 BES $J/\psi \rightarrow \gamma\eta\pi^+\pi^-$
 1 Statistical error only.
 2 Assuming that the $a_0(980)$ decays only into $\eta\pi$.

$\Gamma(\rho^0\gamma)/\Gamma(K\bar{K}\pi)$		Γ_{10}/Γ_1	
VALUE	CL%	DOCUMENT ID	TECN COMMENT

0.0152 ± 0.0038 1 COFFMAN 90 MRK3 $J/\psi \rightarrow \gamma\gamma\pi^+\pi^-$
 1 Using $B(J/\psi \rightarrow \gamma\eta(1405) \rightarrow \gamma K\bar{K}\pi) = 4.2 \times 10^{-3}$ and $B(J/\psi \rightarrow \gamma\eta(1405) \rightarrow \gamma\gamma\rho^0) = 6.4 \times 10^{-5}$.

$\Gamma(\gamma\gamma)/\Gamma(K\bar{K}\pi)$		Γ_9/Γ_1	
VALUE	CL%	DOCUMENT ID	TECN COMMENT

<1.78 × 10⁻³ 90 1 ABLIKIM 180 BES3 $\psi(2S) \rightarrow \pi^+\pi^-\gamma\gamma\gamma$
 1 Using results from BAI 00b.

$\Gamma(\eta(\pi\pi)s\text{-wave})/\Gamma(\eta\pi\pi)$		Γ_4/Γ_2	
VALUE	EVTS	DOCUMENT ID	TECN COMMENT

• • • We do not use the following data for averages, fits, limits, etc. • • •
 0.81 ± 0.04 2200 ALDE 97B GAM4 100 $\pi^-\pi^+ \rightarrow \eta\pi^0\pi^0 n$

$\Gamma(f_0(980)\eta)/\Gamma(\eta\pi\pi)$ Γ_6/Γ_2

VALUE DOCUMENT ID TECN COMMENT
 • • • We do not use the following data for averages, fits, limits, etc. • • •
 0.32 ± 0.07 1 ANISOVICH 00 SPEC 0.9-1.2 $\bar{p}p \rightarrow \eta 3\pi^0$
 1 Using preliminary Crystal Barrel data.

$\Gamma(f_0(980)\pi^0 \rightarrow \pi^+\pi^-\pi^0)/\Gamma(\text{total})$		Γ_5/Γ	
VALUE	CL%	DOCUMENT ID	TECN COMMENT

not seen 1 ABLIKIM 17AJ BES3 $\psi(2S) \rightarrow \gamma\pi^+\pi^-\pi^0$
 1 ABLIKIM 17AJ reports $B(\psi(2S) \rightarrow \gamma\eta(1405) \rightarrow \gamma f_0(980)\pi^0 \rightarrow \gamma\pi^+\pi^-\pi^0) < 5.0 \times 10^{-7}$.

$\Gamma(\rho\rho)/\Gamma(\text{total})$		Γ_8/Γ	
VALUE	CL%	DOCUMENT ID	TECN COMMENT

<0.58 99.85 1,2 AMSLER 04B CBAR 0 $\bar{p}p$
 1 Assuming that the $\eta(1405)$ decays are saturated by the $\pi\pi\eta$, $K\bar{K}\pi$ and $\rho\rho$ modes.
 2 Using the data of BAILLON 67 on $\bar{p}p \rightarrow K\bar{K}\pi$.

$\Gamma(K^*(892)K)/\Gamma(a_0(980)\pi)$		Γ_{12}/Γ_3	
VALUE	CL%	DOCUMENT ID	TECN COMMENT

• • • We do not use the following data for averages, fits, limits, etc. • • •
 0.084 ± 0.024 1 ADAMS 01B B852 18 GeV $\pi^-\pi^+ \rightarrow K^+K^-\pi^0 n$
 1 Statistical error only.

$\Gamma(\phi\gamma)/\Gamma(\rho^0\gamma)$		Γ_{11}/Γ_{10}	
VALUE	CL%	DOCUMENT ID	TECN COMMENT

• • • We do not use the following data for averages, fits, limits, etc. • • •
 0.09 ± 0.03 1 ABLIKIM 18I BES3 $J/\psi \rightarrow \gamma\gamma\phi(1020)$
 0.13 ± 0.04 2 ABLIKIM 18I BES3 $J/\psi \rightarrow \gamma\gamma\phi(1020)$
 <0.77 95 3 BAI 04J BES2 $J/\psi \rightarrow \gamma\gamma K^+K^-$
 1 Constructive interference between $X(1835)$ and $\eta(1405)/\eta(1475)$ decays to $\gamma\phi$ is assumed. Also see $\eta(1475)$. ABLIKIM 18I reports the inverse as 11.10 ± 3.5 .
 2 Destructive interference between $X(1835)$ and $\eta(1405)/\eta(1475)$ decays to $\gamma\phi$ is assumed. Also see $\eta(1475)$. ABLIKIM 18I reports the inverse as 7.53 ± 2.49 .
 3 Calculated by us from $B(J/\psi \rightarrow \eta(1405)\gamma \rightarrow \phi\gamma\gamma) < 0.82 \times 10^{-4}$ and $B(J/\psi \rightarrow \eta(1405)\gamma \rightarrow \rho^0\gamma\gamma) = (1.07 \pm 0.17 \pm 0.11) \times 10^{-4}$.

$\eta(1405)$ REFERENCES

ABLIKIM 198A PR D100 092003	M. Ablikim <i>et al.</i>	(BESIII Collab.)
ABLIKIM 18I PR D37 051101	M. Ablikim <i>et al.</i>	(BESIII Collab.)
ABLIKIM 18O PR D37 072014	M. Ablikim <i>et al.</i>	(BESIII Collab.)
ABLIKIM 17AJ PR D36 112008	M. Ablikim <i>et al.</i>	(BESIII Collab.)
ABLIKIM 13M PR D87 092006	M. Ablikim <i>et al.</i>	(BESIII Collab.)
ABLIKIM 11J PRL 108 182001	M. Ablikim <i>et al.</i>	(BESIII Collab.)
ABLIKIM 12E PRL 107 182001	M. Ablikim <i>et al.</i>	(BESIII Collab.)
ABLIKIM 08E PR D77 032005	M. Ablikim <i>et al.</i>	(BES Collab.)
AHOHE 05 PR D71 072001	R. Ahohe <i>et al.</i>	(CLEO Collab.)
AMSLER 04B EPJ C33 23	C. Amisler <i>et al.</i>	(Crystal Barrel Collab.)
BAI 04J PL B594 47	J.Z. Bai <i>et al.</i>	(BES Collab.)
NICHTIUI 02 PL B545 261	F. Nichtiui <i>et al.</i>	(OBELIX Collab.)
ACCIARRI 01G PL B501 1	M. Acciarrri <i>et al.</i>	(L3 Collab.)
ADAMS 01B PL B516 264	G.S. Adams <i>et al.</i>	(BNL E852 Collab.)
ANISOVICH 01 NP A690 567	A.V. Anisovich <i>et al.</i>	
ANISOVICH 00 PL B472 168	A.V. Anisovich <i>et al.</i>	
BAI 00D PL B476 25	J.Z. Bai <i>et al.</i>	(BES Collab.)
MANAK 00A PR D62 012003	J.J. Manak <i>et al.</i>	(BNL E852 Collab.)
BAI 99 PL B446 356	J.Z. Bai <i>et al.</i>	(BES Collab.)
CICALO 99 PL B462 453	C. Cicalo <i>et al.</i>	(OBELIX Collab.)
ABELE 98E NP B514 45	A. Abele <i>et al.</i>	(Crystal Barrel Collab.)
BAI 98C PL B440 217	J.Z. Bai <i>et al.</i>	(BES Collab.)
ALDE 97B PAN 60 386	D. Alde <i>et al.</i>	(GAMS Collab.)
BERTIN 97 PL B400 226	Bertin <i>et al.</i>	(OBELIX Collab.)
AMSLER 95F PL B358 389	C. Amisler <i>et al.</i>	(Crystal Barrel Collab.)
BERTIN 95 PL B361 187	A. Bertin <i>et al.</i>	(OBELIX Collab.)
BUGG 95 PL B353 378	D.V. Bugg <i>et al.</i>	(LOQM, PNPI, WASH)
AUGUSTIN 92 PR D46 1951	J.E. Augustin, G. Cosme	(DM2 Collab.)
BOLTON 92B PRL 69 1328	T. Bolton <i>et al.</i>	(Mark III Collab.)
FUKUI 91C PL B267 293	S. Fukui <i>et al.</i>	(SUGI, NAGO, KEK, KYOT+)
AUGUSTIN 90 PR D42 10	J.E. Augustin <i>et al.</i>	(DM2 Collab.)
BAI 90C PRL 65 2507	Z. Bai <i>et al.</i>	(Mark III Collab.)
COFFMAN 90 PR D41 1410	D.M. Coffman <i>et al.</i>	(Mark III Collab.)
BISELLO 89B PR D39 701	G. Bisetto <i>et al.</i>	(DM2 Collab.)
DUCH 89 ZPHY C45 223	K.D. Duch <i>et al.</i>	(ASTERIX Collab.) JP
RATH 89 PR D40 693	M.G. Rath <i>et al.</i>	(NDAM, BRAN, BNL, CUNY+)
BIRMAN 88 PRL 61 1557	A. Birman <i>et al.</i>	(BNL, FSU, IND, MASD) JP
ANDO 86 PRL 57 1296	A. Ando <i>et al.</i>	(KEK, KYOT, NIRS, SAGA+) JP
REEVES 86 PR D34 1960	D.F. Reeves <i>et al.</i>	(FLOR, BNL, IND+) JP
CHUNG 85 PRL 55 779	S.U. Chung <i>et al.</i>	(BNL, FLOR, IND+) JP
ALTHOFF 84E PL 147B 487	M. Althoff <i>et al.</i>	(TASSO Collab.)
EDWARDS 83B PRL 51 859	C. Edwards <i>et al.</i>	(CIT, HARV, PRIN+)
EDWARDS 82E PRL 49 253	C. Edwards <i>et al.</i>	(CIT, HARV, PRIN+)
Also PR 50 219	C. Edwards <i>et al.</i>	(CIT, HARV, PRIN+)
SCHARRE 80 PL 97B 329	D.L. Scharre <i>et al.</i>	(SLAC, LBL)
FOSTER 68B NP B8 174	M. Foster <i>et al.</i>	(CERN, CDEF)
BAILLON 67 NC 50A 393	P.H. Baillon <i>et al.</i>	(CERN, CDEF, IRAD)

$h_1(1415)$

$$I^G(J^{PC}) = 0^-(1^{+-})$$

was $h_1(1380)$

$h_1(1415)$ MASS

VALUE (MeV)	EVTS	DOCUMENT ID	TECN COMMENT
-------------	------	-------------	--------------

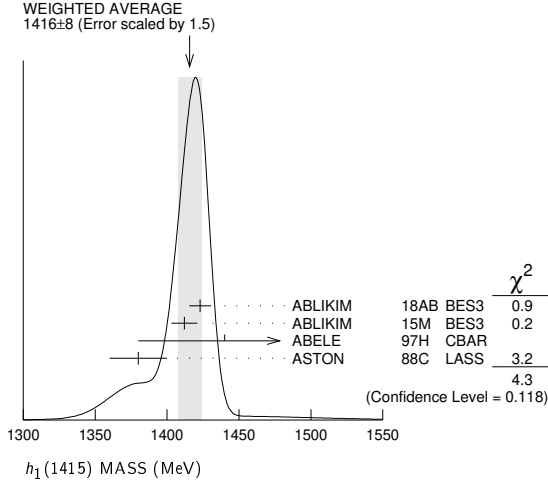
1416 ± 8 OUR AVERAGE Error includes scale factor of 1.5. See the ideogram below.
 1423 ± 2.1 ± 7.3 2.2k 1 ABLIKIM 18AB BES3 $J/\psi \rightarrow \eta' h_1 \rightarrow \eta' K^* \bar{K}$

See key on page 1127

Meson Particle Listings

$h_1(1415), f_1(1420)$

1412 ± 4 ± 8	¹ ABLIKIM	15M BES3	$\psi(2S) \rightarrow \gamma \chi_{c1,2} \rightarrow \gamma \phi(h_1 \rightarrow K^* \bar{K})$
1440 ± 60	ABELE	97H CBAR	$\bar{p}p \rightarrow K_L^0 K_S^0 \pi^0 \pi^0$
1380 ± 20	ASTON	88C LASS	11 $K^- p \rightarrow K_S^0 K^\pm \pi^\mp \Lambda$



¹ Final states $K^+ K^- \pi^0$ and $K_S^0 K^\pm \pi^\mp$.

$h_1(1415)$ WIDTH

VALUE (MeV)	EVTS	DOCUMENT ID	TECN	COMMENT
90 ± 15 OUR AVERAGE				
90.3 ± 9.8 ± 17.5	2.2k	¹ ABLIKIM	18AB BES3	$J/\psi \rightarrow \eta' h_1 \rightarrow \eta' K^* \bar{K}$
84 ± 12 ± 40		¹ ABLIKIM	15M BES3	$\psi(2S) \rightarrow \gamma \chi_{c1,2} \rightarrow \gamma \phi(h_1 \rightarrow K^* \bar{K})$
170 ± 80		ABELE	97H CBAR	$\bar{p}p \rightarrow K_L^0 K_S^0 \pi^0 \pi^0$
80 ± 30		ASTON	88C LASS	11 $K^- p \rightarrow K_S^0 K^\pm \pi^\mp \Lambda$

¹ Final states $K^+ K^- \pi^0$ and $K_S^0 K^\pm \pi^\mp$.

$h_1(1415)$ DECAY MODES

Mode	Γ_1
$K \bar{K}^*(892) + c.c.$	

$h_1(1415)$ REFERENCES

ABLIKIM	18AB PR D98 072005	M. Ablikim et al.	(BESIII Collab.)
ABLIKIM	15M PR D91 112008	M. Ablikim et al.	(BESIII Collab.)
ABELE	97H PL B415 280	A. Abele et al.	(Crystal Barrel Collab.)
ASTON	88C PL B201 573	D. Aston et al.	(SLAC, NAGO, CINC, INUS)

$f_1(1420)$

$$J^{PC} = 0^+(1^{++})$$

See the review on "Spectroscopy of Light Meson Resonances."

$f_1(1420)$ MASS

VALUE (MeV)	EVTS	DOCUMENT ID	TECN	COMMENT
1426.3 ± 0.9 OUR AVERAGE				Error includes scale factor of 1.1.
1434 ± 5 ± 5	133	¹ ACHARD	07 L3	183-209 $e^+ e^- \rightarrow e^+ e^- K_S^0 K^\pm \pi^\mp$
1426 ± 6	711	ABDALLAH	03H DLPH	91.2 $e^+ e^- \rightarrow K_S^0 K^\pm \pi^\mp + X$
1420 ± 14	3651	NICHITIU	02 OBLX	0 $\bar{p}p \rightarrow K^+ K^- \pi^+ \pi^- \pi^0$
1428 ± 4 ± 2	20k	ADAMS	01B B852	18 GeV $\pi^- p \rightarrow K^+ K^- \pi^0 n$
1426 ± 1		BARBERIS	97C OMEG	450 $pp \rightarrow pp K_S^0 K^\pm \pi^\mp$
1425 ± 8		BERTIN	97 OBLX	0.0 $\bar{p}p \rightarrow K^\pm (K^0) \pi^\mp \pi^+ \pi^-$
1430 ± 4		² ARMSTRONG	92E OMEG	85,300 $\pi^+ p, pp \rightarrow \pi^+ p, pp(K \bar{K} \pi)$
1462 ± 20		³ AUGUSTIN	92 DM2	$J/\psi \rightarrow \gamma K \bar{K} \pi$
1443 ± 7 ± 3	1100	BAI	90C MRK3	$J/\psi \rightarrow \gamma K_S^0 K^\pm \pi^\mp$
1425 ± 10	17	BEHREND	89 CELL	$\gamma \gamma \rightarrow K_S^0 K^\pm \pi^\mp$

1442 ± 5 ± 10	111	BECKER	87 MRK3	$e^+ e^- \rightarrow \omega K \bar{K} \pi$
1423 ± 4		GIDAL	87B MRK2	$e^+ e^- \rightarrow e^+ e^- K \bar{K} \pi$
1417 ± 13	13	AIHARA	86C TPC	$e^+ e^- \rightarrow e^+ e^- K \bar{K} \pi$
1422 ± 3		CHAUVAT	84 SPEC	ISR 31.5 pp
1440 ± 10		⁴ BROMBERG	80 SPEC	100 $\pi^- p \rightarrow K \bar{K} \pi X$
1426 ± 6	221	DIONISI	80 HBC	4 $\pi^- p \rightarrow K \bar{K} \pi n$
1420 ± 20		DAHL	67 HBC	1.6-4.2 $\pi^- p$
1430.8 ± 0.9		⁵ SOSA	99 SPEC	$pp \rightarrow p_{slow} (K_S^0 K^\pm \pi^-) p_{fast}$
1433.4 ± 0.8		⁵ SOSA	99 SPEC	$pp \rightarrow p_{slow} (K_S^0 K^- \pi^+) p_{fast}$
1435 ± 9		PROKOSHKIN	97B GAM4	100 $\pi^- p \rightarrow \eta \pi^0 \pi^0 n$
1429 ± 3	389	ARMSTRONG	89 OMEG	300 $pp \rightarrow K \bar{K} \pi pp$
1425 ± 2	1520	ARMSTRONG	84 OMEG	85 $\pi^+ p, pp \rightarrow (\pi^+, p)(K \bar{K} \pi) p$
~ 1420		BITYUKOV	84 SPEC	32 $K^- p \rightarrow K^+ K^- \pi^0 \gamma$

¹ From a fit with a width fixed at 55 MeV.
² This result supersedes ARMSTRONG 84, ARMSTRONG 89.
³ From fit to the $K^*(892) K 1^{++}$ partial wave.
⁴ Mass error increased to account for $a_0(980)$ mass cut uncertainties.
⁵ No systematic error given.

$f_1(1420)$ WIDTH

VALUE (MeV)	EVTS	DOCUMENT ID	TECN	COMMENT
54.5 ± 2.6 OUR AVERAGE				
51 ± 14	711	ABDALLAH	03H DLPH	91.2 $e^+ e^- \rightarrow K_S^0 K^\pm \pi^\mp + X$
61 ± 8	3651	NICHITIU	02 OBLX	0 $\bar{p}p \rightarrow K^+ K^- \pi^+ \pi^- \pi^0$
38 ± 9 ± 6	20k	ADAMS	01B B852	18 GeV $\pi^- p \rightarrow K^+ K^- \pi^0 n$
58 ± 4		BARBERIS	97C OMEG	450 $pp \rightarrow pp K_S^0 K^\pm \pi^\mp$
45 ± 10		BERTIN	97 OBLX	0.0 $\bar{p}p \rightarrow K^\pm (K^0) \pi^\mp \pi^+ \pi^-$
58 ± 10		⁶ ARMSTRONG	92E OMEG	85,300 $\pi^+ p, pp \rightarrow \pi^+ p, pp(K \bar{K} \pi)$
129 ± 41		⁷ AUGUSTIN	92 DM2	$J/\psi \rightarrow \gamma K \bar{K} \pi$
68 ± 29 ± 8	1100	BAI	90C MRK3	$J/\psi \rightarrow \gamma K_S^0 K^\pm \pi^\mp$
42 ± 22	17	BEHREND	89 CELL	$\gamma \gamma \rightarrow K_S^0 K^\pm \pi^\mp$
40 ± 17 ± 13 ± 5	111	BECKER	87 MRK3	$e^+ e^- \rightarrow \omega K \bar{K} \pi$
35 ± 47 ± 20	13	AIHARA	86C TPC	$e^+ e^- \rightarrow e^+ e^- K \bar{K} \pi$
47 ± 10		CHAUVAT	84 SPEC	ISR 31.5 pp
62 ± 14		BROMBERG	80 SPEC	100 $\pi^- p \rightarrow K \bar{K} \pi X$
40 ± 15	221	DIONISI	80 HBC	4 $\pi^- p \rightarrow K \bar{K} \pi n$
60 ± 20		DAHL	67 HBC	1.6-4.2 $\pi^- p$
68.7 ± 2.9		⁸ SOSA	99 SPEC	$pp \rightarrow p_{slow} (K_S^0 K^\pm \pi^-) p_{fast}$
58.8 ± 3.3		⁸ SOSA	99 SPEC	$pp \rightarrow p_{slow} (K_S^0 K^- \pi^+) p_{fast}$
90 ± 25		PROKOSHKIN	97B GAM4	100 $\pi^- p \rightarrow \eta \pi^0 \pi^0 n$
58 ± 8	389	ARMSTRONG	89 OMEG	300 $pp \rightarrow K \bar{K} \pi pp$
62 ± 5	1520	ARMSTRONG	84 OMEG	85 $\pi^+ p, pp \rightarrow (\pi^+, p)(K \bar{K} \pi) p$
~ 50		BITYUKOV	84 SPEC	32 $K^- p \rightarrow K^+ K^- \pi^0 \gamma$

⁶ This result supersedes ARMSTRONG 84, ARMSTRONG 89.
⁷ From fit to the $K^*(892) K 1^{++}$ partial wave.
⁸ No systematic error given.

$f_1(1420)$ DECAY MODES

Mode	Fraction (Γ_i/Γ)
Γ_1 $K \bar{K} \pi$	seen
Γ_2 $K \bar{K}^*(892) + c.c.$	seen
Γ_3 $\eta \pi \pi$	possibly seen
Γ_4 $a_0(980) \pi$	
Γ_5 $\pi \pi \rho$	
Γ_6 4π	
Γ_7 $\rho^0 \gamma$	
Γ_8 $\phi \gamma$	seen

Meson Particle Listings

$f_1(1420), \omega(1420)$

$f_1(1420) \Gamma(i)\Gamma(\gamma\gamma)/\Gamma(\text{total})$					
VALUE (keV)	CL%	DOCUMENT ID	TECN	COMMENT	
$\Gamma(K\bar{K}\pi) \times \Gamma(\gamma\gamma^*)/\Gamma_{\text{total}}$					
1.9±0.4 OUR AVERAGE					
3.2±0.6±0.7	133	9,10 ACHARD	07 L3	183-209 $e^+e^- \rightarrow e^+e^- K_S^0 K_{\pm}^{\pm}\pi^{\mp}$	
3.0±0.9±0.7		11,12 BEHREND	89 CELL	$e^+e^- \rightarrow e^+e^- K_S^0 K_{\pm}^{\pm}\pi^{\mp}$	
2.3 $^{+1.0}_{-0.9}$ ±0.8		HILL	89 JADE	$e^+e^- \rightarrow e^+e^- K_{\pm}^{\pm} K_S^0 \pi^{\mp}$	
1.3±0.5±0.3		AIHARA	88B TPC	$e^+e^- \rightarrow e^+e^- K_{\pm}^{\pm} K_S^0 \pi^{\mp}$	
1.6±0.7±0.3		11,13 GIDAL	87B MRK2	$e^+e^- \rightarrow e^+e^- K\bar{K}\pi$	
••• We do not use the following data for averages, fits, limits, etc. •••					
<8.0	95	JENNI	83 MRK2	$e^+e^- \rightarrow e^+e^- K\bar{K}\pi$	

⁹From a fit with a width fixed at 55 MeV.
¹⁰The form factor parameter from the fit is 926 ± 78 MeV.
¹¹Assume a ρ -pole form factor.
¹²A ϕ -pole form factor gives considerably smaller widths.
¹³Published value divided by 2.

$f_1(1420)$ BRANCHING RATIOS

$\Gamma(K\bar{K}^*(892) + c.c.)/\Gamma(K\bar{K}\pi)$					
VALUE	CL%	DOCUMENT ID	TECN	COMMENT	Γ_2/Γ_1
••• We do not use the following data for averages, fits, limits, etc. •••					
0.76±0.06		BROMBERG	80 SPEC	$100 \pi^- p \rightarrow K\bar{K}\pi X$	
0.86±0.12		DIONIISI	80 HBC	$4 \pi^- p \rightarrow K\bar{K}\pi n$	

$\Gamma(\pi\pi\rho)/\Gamma(K\bar{K}\pi)$					
VALUE	CL%	DOCUMENT ID	TECN	COMMENT	Γ_5/Γ_1
••• We do not use the following data for averages, fits, limits, etc. •••					
<0.3	95	CORDEN	78 OMEG	$12-15 \pi^- p$	
<2.0		DAHL	67 HBC	$1.6-4.2 \pi^- p$	

$\Gamma(\eta\pi\pi)/\Gamma(K\bar{K}\pi)$					
VALUE	CL%	DOCUMENT ID	TECN	COMMENT	Γ_3/Γ_1
••• We do not use the following data for averages, fits, limits, etc. •••					
1.35±0.75		KOPKE	89 MRK3	$J/\psi \rightarrow \omega\eta\pi\pi(K\bar{K}\pi)$	
<0.6	90	GIDAL	87 MRK2	$e^+e^- \rightarrow e^+\eta\pi^+\pi^-$	
<0.5	95	CORDEN	78 OMEG	$12-15 \pi^- p$	
1.5 ± 0.8		DEFOIX	72 HBC	$0.7 \bar{p}p$	

$\Gamma(a_0(980)\pi)/\Gamma(\eta\pi\pi)$					
VALUE	CL%	DOCUMENT ID	TECN	COMMENT	Γ_4/Γ_3
••• We do not use the following data for averages, fits, limits, etc. •••					
>0.1	90	PROKOSHKIN	97B GAM4	$100 \pi^- p \rightarrow \eta\pi^0\pi^0 n$	
not seen in either mode		ANDO	86 SPEC	$8 \pi^- p$	
not seen in either mode		CORDEN	78 OMEG	$12-15 \pi^- p$	
0.4±0.2		DEFOIX	72 HBC	$0.7 \bar{p}p \rightarrow \tau\pi$	

$\Gamma(4\pi)/\Gamma(K\bar{K}^*(892) + c.c.)$					
VALUE	CL%	DOCUMENT ID	TECN	COMMENT	Γ_6/Γ_2
••• We do not use the following data for averages, fits, limits, etc. •••					
<0.90	95	DIONIISI	80 HBC	$4 \pi^- p$	

$\Gamma(K\bar{K}\pi)/[\Gamma(K\bar{K}^*(892) + c.c.) + \Gamma(a_0(980)\pi)]$					
VALUE	CL%	DOCUMENT ID	TECN	COMMENT	$\Gamma_1/(\Gamma_2+\Gamma_4)$
••• We do not use the following data for averages, fits, limits, etc. •••					
0.65±0.27		¹⁴ DIONIISI	80 HBC	$4 \pi^- p$	
¹⁴ Calculated using $\Gamma(K\bar{K})/\Gamma(\eta\pi) = 0.24 \pm 0.07$ for $a_0(980)$ fractions.					

$\Gamma(a_0(980)\pi)/\Gamma(K\bar{K}^*(892) + c.c.)$					
VALUE	CL%	DOCUMENT ID	TECN	COMMENT	Γ_4/Γ_2
0.042±0.014 OUR AVERAGE					
0.44 ± 0.19		ABLIKIM	21U BES3	$D_s^+ \rightarrow f_1(1420)\pi^+$	
0.04 ± 0.01 ± 0.01		BARBERIS	98C OMEG	$450 pp \rightarrow p_f f_1(1420) p_S$	
••• We do not use the following data for averages, fits, limits, etc. •••					
<0.04	68	ARMSTRONG	84 OMEG	$85 \pi^+ p$	

$\Gamma(4\pi)/\Gamma(K\bar{K}\pi)$					
VALUE	CL%	DOCUMENT ID	TECN	COMMENT	Γ_6/Γ_1
<0.62	95	ARMSTRONG	89G OMEG	$85 \pi p \rightarrow 4\pi X$	

$\Gamma(\rho^0\gamma)/\Gamma_{\text{total}}$					
VALUE	CL%	DOCUMENT ID	TECN	COMMENT	Γ_7/Γ
<0.08	95	¹⁵ ARMSTRONG	92C SPEC	$300 pp \rightarrow pp\pi^+\pi^-\gamma$	
¹⁵ Using the data on the $\bar{K}K\pi$ mode from ARMSTRONG 89.					

$\Gamma(\rho^0\gamma)/\Gamma(K\bar{K}\pi)$					
VALUE	CL%	DOCUMENT ID	TECN	COMMENT	Γ_7/Γ_1
<0.02	95	BARBERIS	98C OMEG	$450 pp \rightarrow p_f f_1(1420) p_S$	

$\Gamma(\phi\gamma)/\Gamma(K\bar{K}\pi)$					
VALUE	CL%	DOCUMENT ID	TECN	COMMENT	Γ_8/Γ_1
0.003±0.001±0.001		BARBERIS	98C OMEG	$450 pp \rightarrow p_f f_1(1420) p_S$	

$f_1(1420)$ REFERENCES

ABLIKIM 21U PR D104 032011 M. Ablikim <i>et al.</i> (BESIII Collab.)	
ACHARD 07 JHEP 0703 018 P. Achard <i>et al.</i> (L3 Collab.)	
ABDALLAH 03H PL B569 129 J. Abdallah <i>et al.</i> (DELPHI Collab.)	
NICHITIU 02 PL B545 261 F. Nichitiu <i>et al.</i> (OBELIX Collab.)	
ADAMS 01B PL B516 264 G.S. Adams <i>et al.</i> (BNL E852 Collab.)	
SOSA 99 PRL 83 913 M. Sosa <i>et al.</i> (WA 102 Collab.)	
BARBERIS 98C PL B440 225 D. Barberis <i>et al.</i> (WA 102 Collab.)	
BARBERIS 97C PL B413 225 D. Barberis <i>et al.</i> (WA 102 Collab.)	
BERTIN 97 PL B400 226 A. Bertin <i>et al.</i> (OBELIX Collab.)	
PROKOSHKIN 97B PD 42 298 Yu.D. Prokoshkin, S.A. Sadovskiy (DANS 354 751)	
ARMSTRONG 92C ZPHY C54 371 T.A. Armstrong <i>et al.</i> (ATHU, BARI, BIRM+)	
ARMSTRONG 92E ZPHY C56 29 T.A. Armstrong <i>et al.</i> (ATHU, BARI, BIRM+) JPC	
AUGUSTIN 92 PR D46 1951 J.E. Augustin, G. Cosme (DM2 Collab.)	
ARMSTRONG 91B ZPHY C52 389 T.A. Armstrong <i>et al.</i> (ATHU, BARI, BIRM+)	
BAI 90C PRL 65 2507 Z. Bai <i>et al.</i> (Mark III Collab.)	
ARMSTRONG 89C PL B221 216 T.A. Armstrong <i>et al.</i> (CERN, BIRM, BARI+) JPC	
ARMSTRONG 89G ZPHY C43 55 T.A. Armstrong <i>et al.</i> (CERN, BIRM, BARI+)	
BEHREND 89 ZPHY C42 367 H.J. Behrend <i>et al.</i> (CELLO Collab.)	
HILL 89 ZPHY C42 355 P. Hill <i>et al.</i> (JADE Collab.) JP	
KOPKE 89 PRPL 174 67 L. Kopke <i>et al.</i> (CERN)	
AIHARA 88B PL B209 107 H. Aihara <i>et al.</i> (TPC-2γ Collab.)	
BECKER 87 PRL 59 186 J.J. Becker <i>et al.</i> (Mark III Collab.) JP	
GIDAL 87 PRL 59 2012 G. Gidal <i>et al.</i> (LBL, SLAC, HARV)	
GIDAL 87B PRL 59 2016 G. Gidal <i>et al.</i> (LBL, SLAC, HARV)	
AIHARA 86C PRL 57 2500 H. Aihara <i>et al.</i> (TPC-2γ Collab.) JP	
ANDO 86 PRL 57 1296 A. Ando <i>et al.</i> (KEK, KYOT, NIRS, SAGA+) JPC	
ARMSTRONG 84 PL 146B 273 T.A. Armstrong <i>et al.</i> (ATHU, BARI, BIRM+) JP	
BITYUKOV 84 SJNP 39 735 S. Bitiyukov <i>et al.</i> (SERP)	
CHAUVAUT 84 PL 148B 382 P. Chauvat <i>et al.</i> (CERN, CLER, UCLA+) JPC	
JENNI 83 PR D27 1031 P. Jenni <i>et al.</i> (SLAC, LBL)	
BROMBERG 80 PR D22 1513 C.M. Bromberg <i>et al.</i> (CIT, FNAL, ILLC+) JPC	
DIONIISI 80 NP B169 1 C. Dioniisi <i>et al.</i> (CERN, MADR, CDF+) JJP	
CORDEN 78 NP B144 253 M.J. Corden <i>et al.</i> (BIRM, RHEL, TEL+) JPC	
DEFOIX 72 NP B44 125 C. Defoix <i>et al.</i> (CDFE, CERN)	
DAHL 67 PRL 163 1377 O.I. Dahl <i>et al.</i> (LRL) IJP	
Also PRL 14 1074 D.H. Miller <i>et al.</i> (LRL, UCB)	

$\omega(1420)$

$$J^{PC} = 0^-(1^--)$$

See also the $\omega(1650)$ particle listing.

$\omega(1420)$ MASS

VALUE (MeV)	EVTS	DOCUMENT ID	TECN	COMMENT
1410±60 OUR ESTIMATE				
••• We do not use the following data for averages, fits, limits, etc. •••				
1418±30±10	824	¹ AKHMETSHIN 17A	CMD3	$1.4-2.0 e^+e^- \rightarrow \omega\eta$
1470±50	13.1k	² AULCHENKO 15A	SND	$1.05-1.80 e^+e^- \rightarrow \pi^+\pi^-\pi^0\gamma$
1382±23±70		AUBERT 07AU	BABR	$10.6 e^+e^- \rightarrow \omega\pi^+\pi^-\gamma$
1350±20±20		AUBERT,B 04N	BABR	$10.6 e^+e^- \rightarrow \pi^+\pi^-\pi^0\gamma$
1400±50±130	1.2M	³ ACHASOV 03D	RVUE	$0.44-2.00 e^+e^- \rightarrow \pi^+\pi^-\pi^0$
1450±10		⁴ HENNER 02	RVUE	$1.2-2.0 e^+e^- \rightarrow \rho\pi, \omega\pi\pi$
1373±70	177	⁵ AKHMETSHIN 00D	CMD2	$1.2-1.38 e^+e^- \rightarrow \pi^+\pi^-\pi^0$
1370±25	5095	ANISOVICH 00H	SPEC	$0.0 \rho\bar{p} \rightarrow \omega\pi^0\pi^0\pi^0$
1400 $^{+100}_{-200}$		⁶ ACHASOV 98H	RVUE	$e^+e^- \rightarrow \pi^+\pi^-\pi^0$
~1400		⁷ ACHASOV 98H	RVUE	$e^+e^- \rightarrow \omega\pi^+\pi^-$
~1460		⁸ ACHASOV 98H	RVUE	$e^+e^- \rightarrow K^+K^-$
1440±70		⁹ CLEGG 94	RVUE	
1419±31	315	¹⁰ ANTONELLI 92	DM2	$1.34-2.4e^+e^- \rightarrow \rho\pi$
¹ From a fit of the interfering $\omega(1420)$ and $\omega(1650)$ with a relative phase of π and other parameters floating.				
² From a fit with contributions from $\omega(782)$, $\phi(1020)$, $\omega(1420)$, and $\omega(1650)$. See ACHASOV 20A for a further analysis of the $\pi^+\pi^-\pi^0$ data.				
³ From the combined fit of ANTONELLI 92, ACHASOV 01E, ACHASOV 02E, and ACHASOV 03D data on the $\pi^+\pi^-\pi^0$ and ANTONELLI 92 on the $\omega\pi^+\pi^-$ final states. Supersedes ACHASOV 99E and ACHASOV 02E.				
⁴ Using results of CORDIER 81 and preliminary data of DOLINSKY 91 and ANTONELLI 92.				
⁵ Using the data of AKHMETSHIN 00D and ANTONELLI 92. The $\rho\pi$ dominance for the energy dependence of the $\omega(1420)$ and $\omega(1650)$ width assumed.				
⁶ Using data from BARKOV 87, DOLINSKY 91, and ANTONELLI 92.				
⁷ Using the data from ANTONELLI 92.				
⁸ Using the data from IVANOV 81 and BISELLO 88b.				
⁹ From a fit to two Breit-Wigner functions and using the data of DOLINSKY 91 and ANTONELLI 92.				
¹⁰ From a fit to two Breit-Wigner functions interfering between them and with the ω, ϕ tails with fixed (+,-,+,-) phases.				

$\omega(1420)$ WIDTH

Table with columns: VALUE (MeV), EVTS, DOCUMENT ID, TECN, COMMENT. Includes data for various decays like $\rho\pi$, $\omega\pi\pi$, $\omega\eta$, $\pi^+\pi^-\pi^0$, $\rho\pi\pi$, $\omega\pi^0\gamma$, $\omega\pi^+\pi^-\gamma$, $\omega\pi^+\pi^-\pi^0\gamma$, $\rho\pi$, $\omega\pi^0\pi^0$, $\rho\pi$.

1 From a fit with contributions from $\omega(1420)$, $\omega(1650)$, and $\phi(1680)$. The mass of $\omega(1420)$ is fixed to the PDG 18 value of 1420 MeV.
2 From a fit of the interfering $\omega(1420)$ and $\omega(1650)$ with a relative phase of π and other parameters floating.
3 From a fit with contributions from $\omega(782)$, $\phi(1020)$, $\omega(1420)$, and $\omega(1650)$. See ACHASOV 20A for a further analysis of the $\pi^+\pi^-\pi^0$ data.
4 From a fit of a VMD model with two effective resonances with masses of 1450 MeV and 1700 MeV to describe the excited vector states $\omega(1420)$, $\rho(1450)$, $\omega(1650)$, and $\rho(1700)$. Systematic errors not evaluated.
5 From the combined fit of ANTONELLI 92, ACHASOV 01E, ACHASOV 02E, and ACHASOV 03D data on the $\pi^+\pi^-\pi^0$ and ANTONELLI 92 on the $\omega\pi^+\pi^-$ final states. Supersedes ACHASOV 99E and ACHASOV 02E.
6 Using results of CORDIER 81 and preliminary data of DOLINSKY 91 and ANTONELLI 92.
7 Using the data of AKHMETSHIN 00D and ANTONELLI 92. The $\rho\pi$ dominance for the energy dependence of the $\omega(1420)$ and $\omega(1650)$ width assumed.
8 From a fit to two Breit-Wigner functions and using the data of DOLINSKY 91 and ANTONELLI 92.
9 From a fit to two Breit-Wigner functions interfering between them and with the ω,ϕ tails with fixed (+,-,+) phases.

$\omega(1420)$ DECAY MODES

Table with columns: Mode, Fraction (Γ_i/Γ). Rows include $\rho\pi$, $\omega\pi\pi$, $\omega\eta$, $b_1(1235)\pi$, e^+e^- , $\pi^0\gamma$.

$\omega(1420)$ $\Gamma(\rho\pi)\Gamma(e^+e^-)/\Gamma^2(\text{total})$

Table with columns: VALUE (units 10^{-6}), EVTS, DOCUMENT ID, TECN, COMMENT. Includes data for $\Gamma(\rho\pi)/\Gamma_{\text{total}} \times \Gamma(e^+e^-)/\Gamma_{\text{total}}$ and $\Gamma_1/\Gamma \times \Gamma_5/\Gamma$.

1 From a fit with contributions from $\omega(782)$, $\phi(1020)$, $\omega(1420)$, and $\omega(1650)$. See ACHASOV 20A for a further analysis of the $\pi^+\pi^-\pi^0$ data.
2 Calculated by us from the cross section at the peak.
3 From the combined fit of ANTONELLI 92, ACHASOV 01E, ACHASOV 02E, and ACHASOV 03D data on the $\pi^+\pi^-\pi^0$ and ANTONELLI 92 on the $\omega\pi^+\pi^-$ final states. Supersedes ACHASOV 99E and ACHASOV 02E.
4 From a fit to two Breit-Wigner functions and using the data of DOLINSKY 91 and ANTONELLI 92.
5 From the partial and leptonic width given by the authors.
6 From a fit to two Breit-Wigner functions interfering between them and with the ω,ϕ tails with fixed (+,-,+) phases.
7 From the product of the leptonic width and partial branching ratio given by the authors.

Table with columns: VALUE (units 10^{-8}), DOCUMENT ID, TECN, COMMENT. Includes data for $\Gamma(\omega\pi\pi)/\Gamma_{\text{total}} \times \Gamma(e^+e^-)/\Gamma_{\text{total}}$ and $\Gamma_2/\Gamma \times \Gamma_5/\Gamma$.

1 Using the data of AKHMETSHIN 00D and ANTONELLI 92. The $\rho\pi$ dominance for the energy dependence of the $\omega(1420)$ and $\omega(1650)$ width assumed.

$\Gamma(\omega\eta)/\Gamma_{\text{total}} \times \Gamma(e^+e^-)/\Gamma_{\text{total}}$ $\Gamma_3/\Gamma \times \Gamma_5/\Gamma$

Table with columns: VALUE (units 10^{-8}), EVTS, DOCUMENT ID, TECN, COMMENT. Includes data for $\Gamma(\omega\eta)/\Gamma_{\text{total}} \times \Gamma(e^+e^-)/\Gamma_{\text{total}}$ and $\Gamma_3/\Gamma \times \Gamma_5/\Gamma$.

1 From a fit with contributions from $\omega(1420)$, $\omega(1650)$, and $\phi(1680)$. The mass of $\omega(1420)$ is fixed to the PDG 18 value of 1420 MeV. Fixing also the width of $\omega(1420)$ to the PDG 18 value of 220 MeV results in $(3.0 \pm 1.6) \times 10^{-8}$ measurement.
2 From a fit of the interfering $\omega(1420)$ and $\omega(1650)$ with a relative phase of π and other parameters floating. From an alternative fit $\Gamma(\omega(1420) \rightarrow \omega\eta)/\Gamma_{\text{total}} \times \Gamma(\omega(1420) \rightarrow e^+e^-) = 5.3 \pm 1.6$ eV.
3 From a fit with contributions from $\omega(1420)$, $\omega(1650)$, and $\phi(1680)$. The mass and the width of $\omega(1420)$ are fixed to the 2014 edition (PDG 14) of this review.

$\Gamma(\pi^0\gamma)/\Gamma_{\text{total}} \times \Gamma(e^+e^-)/\Gamma_{\text{total}}$ $\Gamma_6/\Gamma \times \Gamma_5/\Gamma$

Table with columns: VALUE (units 10^{-8}), DOCUMENT ID, TECN, COMMENT. Includes data for $\Gamma(\pi^0\gamma)/\Gamma_{\text{total}} \times \Gamma(e^+e^-)/\Gamma_{\text{total}}$ and $\Gamma_6/\Gamma \times \Gamma_5/\Gamma$.

1 From a fit of a VMD model with two effective resonances with masses of 1450 MeV and 1700 MeV to describe the excited vector states $\omega(1420)$, $\rho(1450)$, $\omega(1650)$, and $\rho(1700)$. Systematic errors not evaluated.
2 Using 1420 MeV and 220 MeV for the $\omega(1420)$ mass and width.

$\omega(1420)$ BRANCHING RATIOS

$\Gamma(\omega\pi\pi)/\Gamma_{\text{total}}$ Γ_2/Γ

Table with columns: VALUE, DOCUMENT ID, TECN, COMMENT. Includes data for $\Gamma(\omega\pi\pi)/\Gamma_{\text{total}}$ and Γ_2/Γ .

$\Gamma(\omega\pi\pi)/\Gamma(b_1(1235)\pi)$ Γ_2/Γ_4

Table with columns: VALUE, EVTS, DOCUMENT ID, TECN, COMMENT. Includes data for $\Gamma(\omega\pi\pi)/\Gamma(b_1(1235)\pi)$ and Γ_2/Γ_4 .

$\Gamma(\rho\pi)/\Gamma_{\text{total}}$ Γ_1/Γ

Table with columns: VALUE, DOCUMENT ID, TECN, COMMENT. Includes data for $\Gamma(\rho\pi)/\Gamma_{\text{total}}$ and Γ_1/Γ .

$\Gamma(e^+e^-)/\Gamma_{\text{total}}$ Γ_5/Γ

Table with columns: VALUE (units 10^{-7}), EVTS, DOCUMENT ID, TECN, COMMENT. Includes data for $\Gamma(e^+e^-)/\Gamma_{\text{total}}$ and Γ_5/Γ .

$\omega(1420)$ REFERENCES

ACHASOV 20A EPJ C80 993 M.N. Achasov et al. (SND Collab.)
ACHASOV 20B EPJ C80 1008 M.N. Achasov et al. (SND Collab.)
ACHASOV 19 PR D99 112004 M.N. Achasov et al. (SND Collab.)
PDG 18 PR D98 030001 M. Tanabashi et al. (PDG Collab.)
AKHMETSHIN 17A PL B773 150 R.R. Akhmetshin et al. (CMD-3 Collab.)
ACHASOV 16B PR D94 092002 M.N. Achasov et al. (SND Collab.)
AULCHENKO 15A JETP 121 27 V.M. Aulchenko et al. (SND Collab.)
PDG 14 CP C38 070001 K. Olive et al. (PDG Collab.)
ACHASOV 10D PR D98 112001 M.N. Achasov et al. (SND Collab.)
AUBERT 07AU PR D76 092005 B. Aubert et al. (BABAR Collab.)
AKHMETSHIN 05 PL B605 26 R.R. Akhmetshin et al. (Novosibirsk CMD-2 Collab.)
AUBERT.B 04N PR D70 072004 B. Aubert et al. (BABAR Collab.)
ACHASOV 03D PR D68 052006 M.N. Achasov et al. (Novosibirsk SND Collab.)
ACHASOV 02E PR D66 032001 M.N. Achasov et al. (Novosibirsk SND Collab.)
HENNER 02 EPJ C26 3 V.K. Henner et al.
ACHASOV 01E PR D63 072002 M.N. Achasov et al. (Novosibirsk SND Collab.)
AKHMETSHIN 00D PL B489 125 R.R. Akhmetshin et al. (Novosibirsk CMD-2 Collab.)
ANISOVICH 00H PL B485 341 A.V. Anisovich et al.
ACHASOV 99E PL B462 365 M.N. Achasov et al. (BABAR Collab.)
ACHASOV 98B PR D57 4334 N.N. Achasov, A.A. Kozhevnikov (Novosibirsk SND Collab.)
CLEGG 94 ZPHY C62 455 A.B. Clegg, A. Donnachie (LANC, MCHS)
ANTONELLI 92 ZPHY C56 15 A. Antonelli et al. (DM2 Collab.)
DOLINSKY 91 PRPL 202 99 S.I. Dolinsky et al. (NOVO)
BISELLO 88B ZPHY C39 13 D. Bisello et al. (PADO, CLER, FRAS+)
BARKOV 87 JETPL 46 164 L.M. Barkov et al. (NOVO)
CORDIER 81 PL 106B 155 A. Cordier et al. (ORSAY)
IVANOV 81 PL 107B 297 P.M. Ivanov et al. (NOVO)

Meson Particle Listings

$f_2(1430)$, $a_0(1450)$

$f_2(1430)$

$$I^G(J^{PC}) = 0^+(2^{++})$$

OMITTED FROM SUMMARY TABLE

This entry lists nearby peaks observed in the D wave of the $K\bar{K}$ and $\pi^+\pi^-$ systems. Needs confirmation.

$f_2(1430)$ MASS

VALUE (MeV)	DOCUMENT ID	TECN	COMMENT
≈ 1430 OUR ESTIMATE			
• • • We do not use the following data for averages, fits, limits, etc. • • •			
1440 ± 11 ± 3	LEES	21A	BABR $\gamma\gamma \rightarrow \eta_c(1S) \rightarrow \eta' \pi^+ \pi^-$
1453 ± 4	¹ VLADIMIRSK...	01	SPEC $40 \pi^- p \rightarrow K_S^0 K_S^0 n$
1421 ± 5	AUGUSTIN	87	DM2 $J/\psi \rightarrow \gamma \pi^+ \pi^-$
1480 ± 5.0	AKESSON	86	SPEC $pp \rightarrow pp \pi^+ \pi^-$
1436 $^{+26}_{-16}$	DAUM	84	CNTR $17-18 \pi^- p \rightarrow K^+ K^- n$
1412 ± 3	DAUM	84	CNTR $63 \pi^- p \rightarrow K_S^0 K_S^0 n, K^+ K^- n$
1439 $^{+5}_{-6}$	² BEUSCH	67	OSPK $5,7,12 \pi^- p \rightarrow K_S^0 K_S^0 n$

¹ $J^{PC} = 0^{++}$ or 2^{++} .
² Not seen by WETZEL 76.

$f_2(1430)$ WIDTH

VALUE (MeV)	DOCUMENT ID	TECN	COMMENT
• • • We do not use the following data for averages, fits, limits, etc. • • •			
46 ± 15 ± 5	LEES	21A	BABR $\gamma\gamma \rightarrow \eta_c(1S) \rightarrow \eta' \pi^+ \pi^-$
13 ± 5	³ VLADIMIRSK..	01	SPEC $40 \pi^- p \rightarrow K_S^0 K_S^0 n$
30 ± 9	AUGUSTIN	87	DM2 $J/\psi \rightarrow \gamma \pi^+ \pi^-$
150 ± 5.0	AKESSON	86	SPEC $pp \rightarrow pp \pi^+ \pi^-$
81 $^{+5.6}_{-2.9}$	DAUM	84	CNTR $17-18 \pi^- p \rightarrow K^+ K^- n$
14 ± 6	DAUM	84	CNTR $63 \pi^- p \rightarrow K_S^0 K_S^0 n, K^+ K^- n$
43 $^{+17}_{-18}$	⁴ BEUSCH	67	OSPK $5,7,12 \pi^- p \rightarrow K_S^0 K_S^0 n$

³ $J^{PC} = 0^{++}$ or 2^{++} .
⁴ Not seen by WETZEL 76.

$f_2(1430)$ DECAY MODES

Mode	Fraction (Γ_i/Γ)
Γ_1 $K\bar{K}$	
Γ_2 $\pi\pi$	

$f_2(1430)$ REFERENCES

LEES	21A	PR D104 072002	J.P. Lees et al.	(BABAR Collab.)
VLADIMIRSK...	01	PAN 64 1895	V.V. Vladimisky et al.	
AUGUSTIN	87	ZPHY C36 369	J.E. Augustin et al.	(LALO, CLER, FRAS+)
AKESSON	86	NP B264 154	T. Akesson et al.	(Axial Field Spec. Collab.)
DAUM	84	ZPHY C23 339	C. Daum et al.	(AMST, CERN, CRA, MPIM+)
WETZEL	76	NP B115 208	W. Wetzel et al.	(ETH, CERN, LOIC)
BEUSCH	67	PL 25B 357	W. Beusch et al.	(ETH, CERN)

$a_0(1450)$

$$I^G(J^{PC}) = 1^-(0^{++})$$

See the review on "Spectroscopy of Light Meson Resonances."

$a_0(1450)$ MASS

VALUE (MeV)	EVTS	DOCUMENT ID	TECN	COMMENT
1474 ± 19 OUR AVERAGE				
1480 ± 30		ABELE	98	CBAR $0.0 \bar{p}p \rightarrow K^0 K^\pm \pi^\mp$
1470 ± 25		¹ AMSLER	95D	CBAR $0.0 \bar{p}p \rightarrow \pi^0 \pi^0 \pi^0, \pi^0 \eta, \pi^0 \pi^0 \eta$
• • • We do not use the following data for averages, fits, limits, etc. • • •				
1302.1 ± 1.1 ± 3.9		² ALBRECHT	20	RVUE $0.9 \bar{p}p \rightarrow \pi^0 \pi^0 \eta, \pi^0 \eta \eta, \pi^0 K^+ K^-$
1458 ± 14 ± 15	190k	³ AAIJ	16N	LHCB $D^0 \rightarrow K_S^0 K^\pm \pi^\mp$
1515 ± 30		⁴ ANISOVICH	09	RVUE $0.0 \bar{p}p, \pi N$
1316.8 $^{+0.7+24.7}_{-1.0-4.6}$		⁵ UEHARA	09A	BELL $\gamma\gamma \rightarrow \pi^0 \eta$
1432 ± 13 ± 25		⁶ BUGG	08A	RVUE $\bar{p}p$
1477 ± 10	80k	⁷ UMAN	06	E835 $5.2 \bar{p}p \rightarrow \eta \eta \pi^0$
1441 $^{+40}_{-15}$	35k	⁴ BAKER	03	SPEC $\bar{p}p \rightarrow \omega \pi^+ \pi^- \pi^0$
1303 ± 16		⁸ BARGIOTTI	03	OBLX $\bar{p}p$

1296 ± 10	⁹ AMSLER	02	CBAR $0.9 \bar{p}p \rightarrow \pi^0 \pi^0 \eta$
1565 ± 30	⁹ ANISOVICH	98B	RVUE Compilation
1290 ± 10	¹⁰ BERTIN	98B	OBLX $0.0 \bar{p}p \rightarrow K^\pm K_S \pi^\mp$
1450 ± 40	AMSLER	94D	CBAR $0.0 \bar{p}p \rightarrow \pi^0 \pi^0 \eta$
1410 ± 25	ETKIN	82C	MPS $23 \pi^- p \rightarrow n 2 K_S^0$
~ 1300	MARTIN	78	SPEC $10 K^\pm p \rightarrow K_S^0 \pi p$
1255 ± 5	¹¹ CASON	76	

¹ Coupled-channel analysis of AMSLER 95B, AMSLER 95c, and AMSLER 94D.
² T-matrix pole, 2 poles, 2 channels ($\pi\eta, K\bar{K}$).
³ Using a model with Gaussian constraints to the PDG averaged values.
⁴ From the pole position.
⁵ May be a different state.
⁶ Using data from AMSLER 94D, ABELE 98, and BAKER 03. Supersedes BUGG 94.
⁷ Statistical error only.
⁸ Coupled channel analysis of $\pi^+\pi^-\pi^0, K^+K^-\pi^0$, and $K^\pm K_S^0 \pi^\mp$.
⁹ T-matrix pole.
¹⁰ Not confirmed by BUGG 08A.
¹¹ Isospin 0 not excluded.

$a_0(1450)$ WIDTH

VALUE (MeV)	EVTS	DOCUMENT ID	TECN	COMMENT
265 ± 13 OUR AVERAGE				
265 ± 15		ABELE	98	CBAR $0.0 \bar{p}p \rightarrow K^0 K^\pm \pi^\mp$
265 ± 30		¹ AMSLER	95D	CBAR $0.0 \bar{p}p \rightarrow \pi^0 \pi^0 \pi^0, \pi^0 \eta, \pi^0 \pi^0 \eta$

• • • We do not use the following data for averages, fits, limits, etc. • • •				
112.4 ± 1.4 ± 3.4		² ALBRECHT	20	RVUE $0.9 \bar{p}p \rightarrow \pi^0 \pi^0 \eta, \pi^0 \eta \eta, \pi^0 K^+ K^-$
282 ± 12 ± 13	190k	³ AAIJ	16N	LHCB $D^0 \rightarrow K_S^0 K^\pm \pi^\mp$
230 ± 36		⁴ ANISOVICH	09	RVUE $0.0 \bar{p}p, \pi N$
65.0 $^{+2.1+99.1}_{-5.4-32.6}$		⁵ UEHARA	09A	BELL $\gamma\gamma \rightarrow \pi^0 \eta$
196 ± 10 ± 10		⁶ BUGG	08A	RVUE $\bar{p}p$
267 ± 11	80k	⁷ UMAN	06	E835 $5.2 \bar{p}p \rightarrow \eta \eta \pi^0$
110 ± 14	35k	⁴ BAKER	03	SPEC $\bar{p}p \rightarrow \omega \pi^+ \pi^- \pi^0$
92 ± 16		⁸ BARGIOTTI	03	OBLX $\bar{p}p$
81 ± 21		⁹ AMSLER	02	CBAR $0.9 \bar{p}p \rightarrow \pi^0 \pi^0 \eta$
292 ± 40		⁹ ANISOVICH	98B	RVUE Compilation
80 ± 5		¹⁰ BERTIN	98B	OBLX $0.0 \bar{p}p \rightarrow K^\pm K_S \pi^\mp$
270 ± 40		AMSLER	94D	CBAR $0.0 \bar{p}p \rightarrow \pi^0 \pi^0 \eta$
230 ± 30		ETKIN	82C	MPS $23 \pi^- p \rightarrow n 2 K_S^0$
~ 250		MARTIN	78	SPEC $10 K^\pm p \rightarrow K_S^0 \pi p$
79 ± 10		¹¹ CASON	76	

¹ Coupled-channel analysis of AMSLER 95B, AMSLER 95c, and AMSLER 94D.
² T-matrix pole, 2 poles, 2 channels ($\pi\eta, K\bar{K}$).
³ Using a model with Gaussian constraints to the PDG averaged values.
⁴ From the pole position.
⁵ May be a different state.
⁶ Using data from AMSLER 94D, ABELE 98, and BAKER 03. Supersedes BUGG 94.
⁷ Statistical error only.
⁸ Coupled channel analysis of $\pi^+\pi^-\pi^0, K^+K^-\pi^0$, and $K^\pm K_S^0 \pi^\mp$.
⁹ T-matrix pole.
¹⁰ Not confirmed by BUGG 08A.
¹¹ Isospin 0 not excluded.

$a_0(1450)$ DECAY MODES

Branching fractions are given relative to the one **DEFINED AS 1**.

Mode	Fraction (Γ_i/Γ)
Γ_1 $\pi\eta$	0.093 ± 0.020
Γ_2 $\pi\eta'(958)$	0.033 ± 0.017
Γ_3 $K\bar{K}$	0.082 ± 0.028
Γ_4 $\omega\pi\pi$	DEFINED AS 1
Γ_5 $a_0(980)\pi\pi$	seen
Γ_6 $\gamma\gamma$	seen

$a_0(1450)$ $\Gamma(\pi\eta)\Gamma(\gamma\gamma)/\Gamma(\text{total})$

VALUE (eV)	DOCUMENT ID	TECN	COMMENT
• • • We do not use the following data for averages, fits, limits, etc. • • •			
432 ± 6 $^{+1073}_{-256}$	¹ UEHARA	09A	BELL $\gamma\gamma \rightarrow \pi^0 \eta$

¹ May be a different state.

See key on page 1127

Meson Particle Listings

$a_0(1450)$, $\rho(1450)$

$a_0(1450)$ BRANCHING RATIOS

$\Gamma(\pi\eta'(958))/\Gamma(\pi\eta)$ Γ_2/Γ_1

VALUE	DOCUMENT ID	TECN	COMMENT
0.35 ± 0.16	¹ ABELE 98	CBAR	0.0 $\bar{p}p \rightarrow K_L^0 K^\pm \pi^\mp$

• • • We do not use the following data for averages, fits, limits, etc. • • •

0.43 ± 0.19 ABELE 97c CBAR 0.0 $\bar{p}p \rightarrow \pi^0 \pi^0 \eta'$
¹ Using $\pi^0 \eta$ from AMSLER 94d.

$\Gamma(K\bar{K})/\Gamma(\pi\eta)$ Γ_3/Γ_1

VALUE	DOCUMENT ID	TECN	COMMENT
0.88 ± 0.23	¹ ABELE 98	CBAR	0.0 $\bar{p}p \rightarrow K_L^0 K^\pm \pi^\mp$

• • • We do not use the following data for averages, fits, limits, etc. • • •

1.887 ± 0.041 ± 0.97 ² ALBRECHT 20 RVUE 0.9 $\bar{p}p \rightarrow \pi^0 \pi^0 \eta$, $\pi^0 \eta \eta$, $\pi^0 K^+ K^-$

¹ Using $\pi^0 \eta$ from AMSLER 94d.
² Residues from T-matrix pole, 2 poles, 2 channels ($\pi\eta$, $K\bar{K}$).

$\Gamma(\omega\pi\pi)/\Gamma(\pi\eta)$ Γ_4/Γ_1

VALUE	EVTS	DOCUMENT ID	TECN	COMMENT
10.7 ± 2.3	35280	¹ BAKER 03	SPEC	$\bar{p}p \rightarrow \omega\pi^+\pi^-\pi^0$

• • • We do not use the following data for averages, fits, limits, etc. • • •

¹ Using results on $\bar{p}p \rightarrow a_0(1450)\pi^0$, $a_0(1450) \rightarrow \eta\pi^0$ from ABELE 96c and assuming the $\omega\rho$ mechanism for the $\omega\pi\pi$ state.

$\Gamma(a_0(980)\pi\pi)/\Gamma_{total}$ Γ_5/Γ

VALUE	DOCUMENT ID	TECN	COMMENT
seen	BUGG 08a	RVUE	$\bar{p}p$

$\Gamma(a_0(980)\pi\pi)/\Gamma(\pi\eta)$ Γ_5/Γ_1

VALUE	DOCUMENT ID	TECN	CHG	COMMENT
≤ 4.3	ANISOVICH 01	RVUE	0	$\bar{p}p \rightarrow \eta 2\pi^+ 2\pi^-$

$\Gamma(\gamma\gamma)/\Gamma_{total}$ Γ_6/Γ

VALUE	DOCUMENT ID	TECN	COMMENT
seen	¹ UEHARA 09a	BELL	$\gamma\gamma \rightarrow \pi^0 \eta$

¹ May be a different state.

$a_0(1450)$ REFERENCES

ALBRECHT 20	EPJ C80 453	M. Albrecht et al.	(Crystal Barrel Collab.)
AUU 16N	PR D93 052018	R. Aaij et al.	(LHCb Collab.)
ANISOVICH 09	JUMP A24 2481	V. V. Anisovich, A. V. Sarantsev	
UEHARA 09a	PR D80 032001	S. Uehara et al.	(BELLE Collab.)
BUGG 08a	PR D78 074023	D. V. Bugg	(LOQM)
UMAN 06	PR D73 052009	I. Uman et al.	(FNAL E835)
BAKER 03	PL B563 140	C. A. Baker et al.	
BARGIOTTI 03	EPJ C26 371	M. Bargiotti et al.	(OBELIX Collab.)
AMSLER 02	EPJ C23 29	C. Amisler et al.	
ANISOVICH 01	NP A690 567	A. V. Anisovich et al.	
ABELE 98	PR D57 3860	A. Abele et al.	(Crystal Barrel Collab.)
ANISOVICH 98b	SPIU 41 419	V. V. Anisovich et al.	
	Translated from UFN 168 481.		
BERTIN 98b	PL B434 180	A. Bertin et al.	(OBELIX Collab.)
ABELE 97c	PL B404 179	A. Abele et al.	(Crystal Barrel Collab.)
ABELE 96c	NP A609 562	A. Abele et al.	(Crystal Barrel Collab.)
AMSLER 95b	PL B342 433	C. Amisler et al.	(Crystal Barrel Collab.)
AMSLER 95c	PL B353 571	C. Amisler et al.	(Crystal Barrel Collab.)
AMSLER 95d	PL B355 425	C. Amisler et al.	(Crystal Barrel Collab.)
AMSLER 94d	PL B333 277	C. Amisler et al.	(Crystal Barrel Collab.)
BUGG 94	PR D50 4412	D. V. Bugg et al.	(LOQM)
ETKIN 82c	PR D25 2446	A. Etkin et al.	(BNL, CUNY, TUFTS, VAND)
MARTIN 78	NP B134 392	A. D. Martin et al.	(DURH, GEVA)
CASON 76	PRL 36 1485	N. M. Cason et al.	(NDAM, ANL)

$\rho(1450)$ $I^G(J^{PC}) = 1^+(1^{--})$

$\rho(1450)$ MASS

$\rho(1450)$ MASS

VALUE (MeV)	DOCUMENT ID
1465 ± 25 OUR ESTIMATE	This is only an educated guess; the error given is larger than the error on the average of the published values.

$\eta\rho^0$ MODE

VALUE (MeV)	EVTS	DOCUMENT ID	TECN	COMMENT
• • • We do not use the following data for averages, fits, limits, etc. • • •				

1506 ± 11	13.4k	¹ GRIBANOV 20	CMD3	1.1–2.0 $e^+e^- \rightarrow \eta\pi^+\pi^-$
1500 ± 10	7.4k	² ACHASOV 18	SND	1.22–2.00 $e^+e^- \rightarrow \eta\pi^+\pi^-$
1497 ± 14		³ AKHMETSHIN 01b	CMD2	$e^+e^- \rightarrow \eta\gamma$
1421 ± 15		⁴ AKHMETSHIN 00d	CMD2	$e^+e^- \rightarrow \eta\pi^+\pi^-$
1470 ± 20		ANTONELLI 88	DM2	$e^+e^- \rightarrow \eta\pi^+\pi^-$
1446 ± 10		FUKUI 88	SPEC	8.95 $\pi^-\rho \rightarrow \eta\pi^+\pi^-n$

¹ Mass and width of the $\rho(770)$ fixed at 775 and 149 MeV, respectively; solution 2 of model 2, $\eta \rightarrow \gamma\gamma$ decays used.
² From the combined fit of AULCHENKO 15 and ACHASOV 18 in the model with the interfering $\rho(1450)$, $\rho(1700)$ and $\rho(2150)$ with the parameters of the $\rho(1450)$ and $\rho(1700)$

floating and the mass and width of the $\rho(2150)$ fixed at 2155 MeV and 320 MeV, respectively. The phases of the resonances are π , 0 and π , respectively.

³ Using the data of AKHMETSHIN 01b on $e^+e^- \rightarrow \eta\gamma$, AKHMETSHIN 00d and ANTONELLI 88 on $e^+e^- \rightarrow \eta\pi^+\pi^-$.

⁴ Using the data of ANTONELLI 88, DOLINSKY 91, and AKHMETSHIN 00d. The energy-independent width of the $\rho(1450)$ and $\rho(1700)$ mesons assumed.

$\omega\pi$ MODE

VALUE (MeV)	EVTS	DOCUMENT ID	TECN	COMMENT
• • • We do not use the following data for averages, fits, limits, etc. • • •				

1510 ± 7	10.2k	¹ ACHASOV 16d	SND	1.05–2.00 $e^+e^- \rightarrow \pi^0\pi^0\gamma$
1544 ± 22 ⁺¹¹ ₋₄₆	821	² MATVIENKO 15	BELL	$\bar{B}^0 \rightarrow D^{*+}\omega\pi^-$
1491 ± 19	7815	³ ACHASOV 13	SND	1.05–2.00 $e^+e^- \rightarrow \pi^0\pi^0\gamma$
1582 ± 17 ± 25	2382	⁴ AKHMETSHIN 03b	CMD2	$e^+e^- \rightarrow \pi^0\pi^0\gamma$
1349 ± 25 ⁺¹⁰ ₋₅	341	⁵ ALEXANDER 01b	CLE2	$B \rightarrow D^{(*)}\omega\pi^-$
1523 ± 10		⁶ EDWARDS 00a	CLE2	$\tau^- \rightarrow \omega\pi^- \nu_\tau$
1463 ± 25		⁷ CLEGG 94	RVUE	
1250		⁸ ASTON 80c	OMEG	20–70 $\gamma\rho \rightarrow \omega\pi^0\rho$
1290 ± 40		⁸ BARBER 80c	SPEC	3–5 $\gamma\rho \rightarrow \omega\pi^0\rho$

¹ From a phenomenological model based on vector meson dominance with interfering $\rho(770)$, $\rho(1450)$, and $\rho(1700)$. The $\rho(1700)$ mass and width are fixed at 1720 MeV and 250 MeV, respectively. Systematic uncertainties not estimated. Supersedes ACHASOV 13.

² Using Breit-Wigner parameterization of the $\rho(1450)$ and assuming equal probabilities of the $\rho(1450) \rightarrow \pi\pi$ and $\rho(1450) \rightarrow \omega\pi$ decays.

³ From a phenomenological model based on vector meson dominance with the interfering $\rho(1450)$ and $\rho(1700)$ and their widths fixed at 400 and 250 MeV, respectively. Systematic uncertainty not estimated.

⁴ Using the data of AKHMETSHIN 03b and BISELLO 91b assuming the $\omega\pi^0$ and $\pi^+\pi^-$ mass dependence of the total width. $\rho(1700)$ mass and width fixed at 1700 MeV and 240 MeV, respectively.

⁵ Using Breit-Wigner parameterization of the $\rho(1450)$ and assuming the $\omega\pi^-$ mass dependence for the total width.

⁶ Mass-independent width parameterization. $\rho(1700)$ mass and width fixed at 1700 MeV and 235 MeV respectively.

⁷ Using data from BISELLO 91b, DOLINSKY 86 and ALBRECHT 87L.

⁸ Not separated from $b_1(1235)$, not pure $J^P = 1^-$ effect.

4π MODE

VALUE (MeV)	DOCUMENT ID	TECN	COMMENT
• • • We do not use the following data for averages, fits, limits, etc. • • •			

1435 ± 40	ABELE 01b	CBAR	0.0 $\bar{p}n \rightarrow 2\pi^- 2\pi^0 \pi^+$
1350 ± 50	ACHASOV 97	RVUE	$e^+e^- \rightarrow 2(\pi^+\pi^-)$
1449 ± 4	¹ ARMSTRONG 89e	OMEG	300 $pp \rightarrow pp 2(\pi^+\pi^-)$

¹ Not clear whether this observation has $l=1$ or 0.

$\pi\pi$ MODE

VALUE (MeV)	EVTS	DOCUMENT ID	TECN	COMMENT
• • • We do not use the following data for averages, fits, limits, etc. • • •				

1326.35 ± 3.46		¹ BARTOS 17	RVUE	$e^+e^- \rightarrow \pi^+\pi^-$
1342.31 ± 46.62		² BARTOS 17a	RVUE	$e^+e^- \rightarrow \pi^+\pi^-$
1373.83 ± 11.37		³ BARTOS 17a	RVUE	$\tau^- \rightarrow \pi^-\pi^0 \nu_\tau$
1429 ± 41	20k	⁴ LEES 17c	BABR	$J/\psi \rightarrow \pi^+\pi^-\pi^0$
1350 ± 20 ⁺²⁰ ₋₃₀	63.5k	⁵ ABRAMOWICZ12	ZEUS	$ep \rightarrow e\pi^+\pi^-p$
1493 ± 15		⁶ LEES 12g	BABR	$e^+e^- \rightarrow \pi^+\pi^-\gamma$
1446 ± 7 ± 28	5.4 M	^{7,8} FUJIKAWA 08	BELL	$\tau^- \rightarrow \pi^-\pi^0 \nu_\tau$
1328 ± 15		⁹ SCHAE 05c	ALEP	$\tau^- \rightarrow \pi^-\pi^0 \nu_\tau$
1406 ± 15	87k	^{7,10} ANDERSON 00a	CLE2	$\tau^- \rightarrow \pi^-\pi^0 \nu_\tau$
~ 1368		¹¹ ABELE 99c	CBAR	0.0 $\bar{p}d \rightarrow \pi^+\pi^-\pi^-\rho$
1348 ± 33		BERTIN 98	OBLX	0.05–0.405 $\bar{p}p \rightarrow$
1411 ± 14		¹² ABELE 97	CBAR	$2\pi^+\pi^-\pi^0\pi^0$
1370 ⁺⁹⁰ ₋₇₀		ACHASOV 97	RVUE	$e^+e^- \rightarrow \pi^+\pi^-$
1359 ± 40		¹⁰ BERTIN 97c	OBLX	0.0 $\bar{p}p \rightarrow \pi^+\pi^-\pi^0$
1282 ± 37		BERTIN 97d	OBLX	0.05 $\bar{p}p \rightarrow 2\pi^+ 2\pi^-$
1424 ± 25		BISELLO 89	DM2	$e^+e^- \rightarrow \pi^+\pi^-$
1265.5 ± 75.3		DUBNICKA 89	RVUE	$e^+e^- \rightarrow \pi^+\pi^-$
1292 ± 17		¹³ KURDADZE 83	OLYA	0.64–1.4 $e^+e^- \rightarrow \pi^+\pi^-$

¹ Applies the Unitary & Analytic Model of the pion electromagnetic form factor of DUBNICKA 10 to analyze the data of LEES 12c and ABLIKIM 16c.

² Applies the Unitary & Analytic Model of the pion electromagnetic form factor of DUBNICKA 10 to analyze the data of ACHASOV 06, AKHMETSHIN 07, AUBERT 09as, and AMBROSINO 11a.

³ Applies the Unitary & Analytic Model of the pion electromagnetic form factor of DUBNICKA 10 to analyze the data of FUJIKAWA 08.

⁴ From a Dalitz plot analysis in an isobar model with $\rho(1450)$ and $\rho(1700)$ masses and widths floating.

⁵ Using the KUHN 90 parametrization of the pion form factor, neglecting $\rho-\omega$ interference.

⁶ Using the GOUNARIS 68 parametrization of the pion form factor leaving the masses and widths of the $\rho(1450)$, $\rho(1700)$, and $\rho(2150)$ resonances as free parameters of the fit.

⁷ From the GOUNARIS 68 parametrization of the pion form factor.

⁸ $|F_\pi(0)|^2$ fixed to 1.

⁹ From the combined fit of the τ^- data from ANDERSON 00a and SCHAE 05c and e^+e^- data from the compilation of BARKOV 85, A KHMETSHIN 04, and ALOISIO 05.

Meson Particle Listings

$\rho(1450)$

$\rho(1700)$ mass and width fixed at 1713 MeV and 235 MeV, respectively. Supersedes BARATE 97M.
¹⁰ $\rho(1700)$ mass and width fixed at 1700 MeV and 235 MeV, respectively.
¹¹ $\rho(1700)$ mass and width fixed at 1780 MeV and 275 MeV respectively.
¹² T-matrix pole.
¹³ Using for $\rho(1700)$ mass and width 1600 ± 20 and 300 ± 10 MeV respectively.

$K\bar{K}$ MODE

VALUE (MeV)	EVTS	DOCUMENT ID	TECN	CHG	COMMENT
••• We do not use the following data for averages, fits, limits, etc. •••					
$1208 \pm 8 \pm 9$	190k	¹ AAIJ	16N	LHCB	$D^0 \rightarrow K_S^0 K^\pm \pi^\mp$
1422.8 ± 6.5	27k	² ABELE	99D	CBAR	$\pm 0.0 \bar{p}p \rightarrow K^+ K^- \pi^0$

¹ Using the GOUNARIS 68 parameterization with fixed width.
² K-matrix pole. Isospin not determined, could be $\omega(1420)$.

$K\bar{K}^*(892) + c.c.$ MODE

VALUE (MeV)	DOCUMENT ID	TECN	COMMENT
••• We do not use the following data for averages, fits, limits, etc. •••			
$1505 \pm 19 \pm 7$	AUBERT	08s	BABR $10.6 e^+ e^- \rightarrow K\bar{K}^*(892)\gamma$

$m_{\rho(1450)^0} - m_{\rho(1450)^\pm}$

VALUE (MeV)	DOCUMENT ID	TECN	COMMENT
••• We do not use the following data for averages, fits, limits, etc. •••			
-31.53 ± 47.99	¹ BARTOS	17A	RVUE $e^+ e^- \rightarrow \pi^+ \pi^-$, $\tau^- \rightarrow \pi^- \pi^0 \nu_\tau$

¹ Applies the Unitary & Analytic Model of the pion electromagnetic form factor of DUBNICKA 10 to analyze the data of ACHASOV 06, AKHMETSHIN 07, AUBERT 09As, AMBROSINO 11A, and FUJIKAWA 08.

$\rho(1450)$ WIDTH

$\rho(1450)$ WIDTH

VALUE (MeV)	DOCUMENT ID	TECN	COMMENT
400 ± 60 OUR ESTIMATE This is only an educated guess; the error given is larger than the error on the average of the published values.			
••• We do not use the following data for averages, fits, limits, etc. •••			
480 ± 180	¹ ACHASOV	10D	SND $1.075-2.0 e^+ e^- \rightarrow \pi^0 \gamma$

¹ From a fit of a VMD model with two effective resonances with masses of 1450 MeV and 1700 MeV to describe the excited vector states $\omega(1420)$, $\rho(1450)$, $\omega(1650)$, and $\rho(1700)$. Systematic errors not evaluated.

$\eta\rho^0$ MODE

VALUE (MeV)	EVTS	DOCUMENT ID	TECN	COMMENT
••• We do not use the following data for averages, fits, limits, etc. •••				
321 ± 27	13.4k	¹ GRIBANOV	20	CMD3 $1.1-2.0 e^+ e^- \rightarrow \eta\pi^+ \pi^-$
280 ± 20	7.4k	² ACHASOV	18	SND $1.22-2.00 e^+ e^- \rightarrow \eta\pi^+ \pi^-$
226 ± 44		³ AKHMETSHIN	01B	CMD2 $e^+ e^- \rightarrow \eta\gamma$
211 ± 31		⁴ AKHMETSHIN	00D	CMD2 $e^+ e^- \rightarrow \eta\pi^+ \pi^-$
230 ± 30		ANTONELLI	88	DM2 $e^+ e^- \rightarrow \eta\pi^+ \pi^-$
60 ± 15		FUKUI	88	SPEC $8.95 \pi^- p \rightarrow \eta\pi^+ \pi^- n$

¹ Mass and width of the $\rho(770)$ fixed at 775 and 149 MeV, respectively; solution 2 of model 2, $\eta \rightarrow \gamma\gamma$ decays used.
² From the combined fit of AULCHENKO 15 and ACHASOV 18 in the model with the interfering $\rho(1450)$, $\rho(1700)$ and $\rho(2150)$ with the parameters of the $\rho(1450)$ and $\rho(1700)$ floating and the mass and width of the $\rho(2150)$ fixed at 2155 MeV and 320 MeV, respectively. The phases of the resonances are π , 0 and π , respectively.
³ Using the data of AKHMETSHIN 01B on $e^+ e^- \rightarrow \eta\gamma$, AKHMETSHIN 00D and ANTONELLI 88 on $e^+ e^- \rightarrow \eta\pi^+ \pi^-$.
⁴ Using the data of ANTONELLI 88, DOLINSKY 91, and AKHMETSHIN 00D. The energy-independent width of the $\rho(1450)$ and $\rho(1700)$ mesons assumed.

$\omega\pi$ MODE

VALUE (MeV)	EVTS	DOCUMENT ID	TECN	COMMENT
••• We do not use the following data for averages, fits, limits, etc. •••				
440 ± 40	10.2k	¹ ACHASOV	16D	SND $1.05-2.00 e^+ e^- \rightarrow \pi^0 \pi^0 \gamma$
$303 \pm \frac{31}{52} \pm \frac{69}{7}$	821	² MATVIENKO	15	BELL $\bar{B}^0 \rightarrow D^{*+} \omega\pi^-$
$429 \pm 42 \pm 10$	2382	³ AKHMETSHIN	03B	CMD2 $e^+ e^- \rightarrow \pi^0 \pi^0 \gamma$
$547 \pm \frac{86}{45} \pm \frac{46}{45}$	341	⁴ ALEXANDER	01B	CLE2 $B \rightarrow D^{(*)} \omega\pi^-$
400 ± 35		⁵ EDWARDS	00A	CLE2 $\tau^- \rightarrow \omega\pi^- \nu_\tau$
311 ± 62		⁶ CLEGG	94	RVUE
300		⁷ ASTON	80c	OMEG 20-70 $\gamma p \rightarrow \omega\pi^0 p$
320 ± 100		⁷ BARBER	80c	SPEC 3-5 $\gamma p \rightarrow \omega\pi^0 p$

¹ From a phenomenological model based on vector meson dominance with interfering $\rho(770)$, $\rho(1450)$, and $\rho(1700)$. The $\rho(1700)$ mass and width are fixed at 1720 MeV and 250 MeV, respectively. Systematic uncertainties not estimated. Supersedes ACHASOV 13.
² Using Breit-Wigner parameterization of the $\rho(1450)$ and assuming equal probabilities of the $\rho(1450) \rightarrow \pi\pi$ and $\rho(1450) \rightarrow \omega\pi$ decays.
³ Using the data of AKHMETSHIN 03B and BISELLO 91B assuming the $\omega\pi^0$ and $\pi^+ \pi^-$ mass dependence of the total width. $\rho(1700)$ mass and width fixed at 1700 MeV and 240 MeV, respectively.
⁴ Using Breit-Wigner parameterization of the $\rho(1450)$ and assuming the $\omega\pi^-$ mass dependence for the total width.
⁵ Mass-independent width parameterization. $\rho(1700)$ mass and width fixed at 1700 MeV and 235 MeV respectively.
⁶ Using data from BISELLO 91B, DOLINSKY 86 and ALBRECHT 87L.
⁷ Not separated from $b_1(1235)$, not pure $J^P = 1^-$ effect.

4 π MODE

VALUE (MeV)	DOCUMENT ID	TECN	COMMENT
••• We do not use the following data for averages, fits, limits, etc. •••			
325 ± 100	ABELE	01B	CBAR $0.0 \bar{p}n \rightarrow 2\pi^- 2\pi^0 \pi^+$

$\pi\pi$ MODE

VALUE (MeV)	EVTS	DOCUMENT ID	TECN	COMMENT
••• We do not use the following data for averages, fits, limits, etc. •••				
324.13 ± 12.01		¹ BARTOS	17	RVUE $e^+ e^- \rightarrow \pi^+ \pi^-$
492.17 ± 138.38		² BARTOS	17A	RVUE $e^+ e^- \rightarrow \pi^+ \pi^-$
340.87 ± 23.84		³ BARTOS	17A	RVUE $\tau^- \rightarrow \pi^- \pi^0 \nu_\tau$
576 ± 29	20k	⁴ LEES	17C	BABR $J/\psi \rightarrow \pi^+ \pi^- \pi^0$
460 ± 30	$\frac{+40}{-45}$ 63.5k	⁵ ABRAMOWICZ	12	ZEUS $e p \rightarrow e\pi^+ \pi^- p$
427 ± 31		⁶ LEES	12G	BABR $e^+ e^- \rightarrow \pi^+ \pi^- \gamma$
434 ± 16	± 60 5.4M	^{7,8} FUJIKAWA	08	BELL $\tau^- \rightarrow \pi^- \pi^0 \nu_\tau$
468 ± 41		⁹ SCHAEEL	05c	ALEP $\tau^- \rightarrow \pi^- \pi^0 \nu_\tau$
455 ± 41	87k	^{9,10} ANDERSON	00A	CLE2 $\tau^- \rightarrow \pi^- \pi^0 \nu_\tau$
~ 374		¹¹ ABELE	99C	CBAR $0.0 \bar{p}d \rightarrow \pi^+ \pi^- \pi^+ \pi^- p$
275 ± 10		BERTIN	98	OBLX $0.05-0.405 \bar{p}p \rightarrow \pi^+ \pi^+ \pi^-$
343 ± 20		¹² ABELE	97	CBAR $\bar{p}n \rightarrow \pi^- \pi^0 \pi^0$
310 ± 40		¹⁰ BERTIN	97c	OBLX $0.0 \bar{p}p \rightarrow \pi^+ \pi^- \pi^0$
236 ± 36		BERTIN	97D	OBLX $0.05 \bar{p}p \rightarrow 2\pi^+ 2\pi^-$
269 ± 31		BISELLO	89	DM2 $e^+ e^- \rightarrow \pi^+ \pi^-$
391 ± 70		DUBNICKA	89	RVUE $e^+ e^- \rightarrow \pi^+ \pi^-$
218 ± 46		¹³ KURDADZE	83	OLYA $0.64-1.4 e^+ e^- \rightarrow \pi^+ \pi^-$

¹ Applies the Unitary & Analytic Model of the pion electromagnetic form factor of DUBNICKA 10 to analyze the data of LEES 12G and ABLIKIM 16c.
² Applies the Unitary & Analytic Model of the pion electromagnetic form factor of DUBNICKA 10 to analyze the data of ACHASOV 06, AKHMETSHIN 07, AUBERT 09As, and AMBROSINO 11A.
³ Applies the Unitary & Analytic Model of the pion electromagnetic form factor of DUBNICKA 10 to analyze the data of FUJIKAWA 08.
⁴ From a Dalitz plot analysis in an isobar model with $\rho(1450)$ and $\rho(1700)$ masses and widths floating.
⁵ Using the KUHN 90 parametrization of the pion form factor, neglecting $\rho-\omega$ interference.
⁶ Using the GOUNARIS 68 parametrization of the pion form factor leaving the masses and widths of the $\rho(1450)$, $\rho(1700)$, and $\rho(2150)$ resonances as free parameters of the fit.
⁷ From the GOUNARIS 68 parametrization of the pion form factor.
⁸ $|F_\pi(0)|^2$ fixed to 1.
⁹ From the combined fit of the τ^- data from ANDERSON 00A and SCHAEEL 05c and $e^+ e^-$ data from the compilation of BARKOV 85, AKHMETSHIN 04, and ALOISIO 05. $\rho(1700)$ mass and width fixed at 1713 MeV and 235 MeV, respectively. Supersedes BARATE 97M.
¹⁰ $\rho(1700)$ mass and width fixed at 1700 MeV and 235 MeV, respectively.
¹¹ $\rho(1700)$ mass and width fixed at 1780 MeV and 275 MeV respectively.
¹² T-matrix pole.
¹³ Using for $\rho(1700)$ mass and width 1600 ± 20 and 300 ± 10 MeV respectively.

$K\bar{K}$ MODE

VALUE (MeV)	EVTS	DOCUMENT ID	TECN	CHG	COMMENT
••• We do not use the following data for averages, fits, limits, etc. •••					
$410 \pm 19 \pm 35$	190k	¹ AAIJ	16N	LHCB	$D^0 \rightarrow K_S^0 K^\pm \pi^\mp$
146.5 ± 10.5	27k	² ABELE	99D	CBAR	$\pm 0.0 \bar{p}p \rightarrow K^+ K^- \pi^0$

¹ Using the GOUNARIS 68 parameterization with fixed mass.
² K-matrix pole. Isospin not determined, could be $\omega(1420)$.

$K\bar{K}^*(892) + c.c.$ MODE

VALUE (MeV)	DOCUMENT ID	TECN	COMMENT
••• We do not use the following data for averages, fits, limits, etc. •••			
$418 \pm 25 \pm 4$	AUBERT	08s	BABR $10.6 e^+ e^- \rightarrow K\bar{K}^*(892)\gamma$

$\Gamma_{\rho(1450)^0} - \Gamma_{\rho(1450)^\pm}$

VALUE (MeV)	DOCUMENT ID	TECN	COMMENT
••• We do not use the following data for averages, fits, limits, etc. •••			
151.30 ± 140.42	¹ BARTOS	17A	RVUE $e^+ e^- \rightarrow \pi^+ \pi^-$, $\tau^- \rightarrow \pi^- \pi^0 \nu_\tau$

¹ Applies the Unitary & Analytic Model of the pion electromagnetic form factor of DUBNICKA 10 to analyze the data of ACHASOV 06, AKHMETSHIN 07, AUBERT 09As, AMBROSINO 11A, and FUJIKAWA 08.

$\rho(1450)$ DECAY MODES

Mode	Fraction (Γ_i/Γ)
Γ_1 $\pi\pi$	seen
Γ_2 $\pi^+ \pi^-$	seen
Γ_3 4π	seen
Γ_4 $\omega\pi$	
Γ_5 $a_1(1260)\pi$	
Γ_6 $h_1(1170)\pi$	
Γ_7 $\pi(1300)\pi$	
Γ_8 $\rho\rho$	

$\rho(1450)$

Γ_9	$\rho(\pi\pi)$ s-wave			
Γ_{10}	e^+e^-	seen		
Γ_{11}	$\eta\rho$	seen		
Γ_{12}	$a_2(1320)\pi$	not seen		
Γ_{13}	$K\bar{K}$	seen		
Γ_{14}	K^+K^-	seen		
Γ_{15}	$K\bar{K}^*(892) + c.c.$	possibly seen		
Γ_{16}	$\pi^0\gamma$			
Γ_{17}	$\eta\gamma$	seen		
Γ_{18}	$f_0(500)\gamma$	not seen		
Γ_{19}	$f_0(980)\gamma$	not seen		
Γ_{20}	$f_0(1370)\gamma$	not seen		
Γ_{21}	$f_2(1270)\gamma$	not seen		

$\rho(1450) \Gamma(i)\Gamma(e^+e^-)/\Gamma(\text{total})$

$\Gamma(\pi\pi) \times \Gamma(e^+e^-)/\Gamma(\text{total})$	$\Gamma_1\Gamma_{10}/\Gamma$
VALUE (keV)	DOCUMENT ID TECN COMMENT

••• We do not use the following data for averages, fits, limits, etc. •••
 0.12 ¹ DIEKMANN 88 RVUE $e^+e^- \rightarrow \pi^+\pi^-$
 0.027^{+0.015}_{-0.010} ² KURDADZE 83 OLYA 0.64-1.4 $e^+e^- \rightarrow \pi^+\pi^-$
¹ Using total width = 235 MeV.
² Using for $\rho(1700)$ mass and width 1600 ± 20 and 300 ± 10 MeV respectively.

$\Gamma(\eta\rho) \times \Gamma(e^+e^-)/\Gamma(\text{total})$	$\Gamma_{11}\Gamma_{10}/\Gamma$
VALUE (eV)	EVTS DOCUMENT ID TECN COMMENT

••• We do not use the following data for averages, fits, limits, etc. •••
 335 ± 27 ± 20 13.4k ¹ GRIBANOV 20 CMD3 1.1-2.0 $e^+e^- \rightarrow \eta\pi^+\pi^-$
 210 ± 24 ± 10 ² LEES 18 BABR $e^+e^- \rightarrow \eta\pi^+\pi^-$
 74 ± 20 ³ AKHMETSHIN 00D CMD2 $e^+e^- \rightarrow \eta\pi^+\pi^-$
 91 ± 19 ANTONELLI 88 DM2 $e^+e^- \rightarrow \eta\pi^+\pi^-$
¹ Mass and width of the $\rho(770)$ fixed at 775 and 149 MeV, respectively; solution 2 of model 2, $\eta \rightarrow \gamma\gamma$ decays used.
² Includes non-resonant contribution. The selected fit model includes three ρ excited states. Model uncertainty is 20%.
³ Using the data of ANTONELLI 88, DOLINSKY 91, and AKHMETSHIN 00D. The energy-independent width of the $\rho(1450)$ and $\rho(1700)$ mesons assumed.

$\Gamma(\eta\gamma) \times \Gamma(e^+e^-)/\Gamma(\text{total})$	$\Gamma_{17}\Gamma_{10}/\Gamma$
VALUE (eV)	DOCUMENT ID TECN COMMENT

••• We do not use the following data for averages, fits, limits, etc. •••
 <16.4 ¹ AKHMETSHIN 05 CMD2 0.60-1.38 $e^+e^- \rightarrow \eta\gamma$
 2.2 ± 0.5 ± 0.3 ² AKHMETSHIN 01B CMD2 $e^+e^- \rightarrow \eta\gamma$
¹ From 2 γ decay mode of η using 1465 MeV and 310 MeV for the $\rho(1450)$ mass and width. Recalculated by us.
² Using the data of AKHMETSHIN 01B on $e^+e^- \rightarrow \eta\gamma$, AKHMETSHIN 00D and ANTONELLI 88 on $e^+e^- \rightarrow \eta\pi^+\pi^-$. Recalculated by us using width of 226 MeV.

$\Gamma(K\bar{K}^*(892) + c.c.) \times \Gamma(e^+e^-)/\Gamma(\text{total})$	$\Gamma_{15}\Gamma_{10}/\Gamma$
VALUE (eV)	DOCUMENT ID TECN COMMENT

••• We do not use the following data for averages, fits, limits, etc. •••
 127 ± 15 ± 6 AUBERT 08s BABR 10.6 $e^+e^- \rightarrow K\bar{K}^*(892)\gamma$

$\rho(1450) \Gamma(i)\Gamma(\text{total}) \times \Gamma(e^+e^-)/\Gamma(\text{total})$

$\Gamma(\omega\pi)/\Gamma(\text{total}) \times \Gamma(e^+e^-)/\Gamma(\text{total})$	$\Gamma_4/\Gamma \times \Gamma_{10}/\Gamma$
VALUE (units 10 ⁻⁶)	EVTS DOCUMENT ID TECN COMMENT

••• We do not use the following data for averages, fits, limits, etc. •••
 2.1 ± 0.4 10.2k ¹ ACHASOV 16D SND 1.05-2.00 $e^+e^- \rightarrow \pi^0\pi^0\gamma$
 5.3 ± 0.4 7815 ² ACHASOV 13 SND 1.05-2.00 $e^+e^- \rightarrow \pi^0\pi^0\gamma$
¹ From a phenomenological model based on vector meson dominance with interfering $\rho(770)$, $\rho(1450)$, and $\rho(1700)$. The $\rho(1700)$ mass and width are fixed at 1720 MeV and 250 MeV, respectively. Systematic uncertainties not estimated. Supersedes ACHASOV 13.
² From a phenomenological model based on vector meson dominance with the interfering $\rho(1450)$ and $\rho(1700)$ and their widths fixed at 400 and 250 MeV, respectively. Systematic uncertainty not estimated.

$\Gamma(\eta\rho)/\Gamma(\text{total}) \times \Gamma(e^+e^-)/\Gamma(\text{total})$	$\Gamma_{11}/\Gamma \times \Gamma_{10}/\Gamma$
VALUE (units 10 ⁻⁷)	EVTS DOCUMENT ID TECN COMMENT

••• We do not use the following data for averages, fits, limits, etc. •••
 7.3 ± 0.3 7.4k ¹ ACHASOV 18 SND 1.22-2.00 $e^+e^- \rightarrow \eta\pi^+\pi^-$
 4.3^{+1.1}_{-0.9} ± 0.2 4.9k ² AULCHENKO 15 SND 1.22-2.00 $e^+e^- \rightarrow \eta\pi^+\pi^-$

¹ From the combined fit of AULCHENKO 15 and ACHASOV 18 in the model with the interfering $\rho(1450)$, $\rho(1700)$ and $\rho(2150)$ with the parameters of the $\rho(1450)$ and $\rho(1700)$ floating and the mass and width of the $\rho(2150)$ fixed at 2155 MeV and 320 MeV, respectively. The phases of the resonances are π , 0 and π , respectively.
² From a fit to the $e^+e^- \rightarrow \eta\pi^+\pi^-$ cross section with vector meson dominance model including $\rho(770)$, $\rho(1450)$, and $\rho(1700)$ decaying exclusively via $\eta\rho(770)$. Masses and widths of vector states are fixed to PDG 14. Coupling constants are assumed to be real.

$\Gamma(f_0(500)\gamma)/\Gamma(\text{total}) \times \Gamma(e^+e^-)/\Gamma(\text{total})$	$\Gamma_{18}/\Gamma \times \Gamma_{10}/\Gamma$
VALUE (units 10 ⁻⁹)	CL% DOCUMENT ID TECN COMMENT

<4.0 90 ACHASOV 11 SND $e^+e^- \rightarrow \pi^0\pi^0\gamma$

$\Gamma(\pi^0\gamma)/\Gamma(\text{total}) \times \Gamma(e^+e^-)/\Gamma(\text{total})$	$\Gamma_{16}/\Gamma \times \Gamma_{10}/\Gamma$
VALUE (units 10 ⁻⁹)	DOCUMENT ID TECN COMMENT

••• We do not use the following data for averages, fits, limits, etc. •••
 2.3 ± 1.4 ¹ ACHASOV 10D SND 1.075-2.0 $e^+e^- \rightarrow \pi^0\gamma$
¹ From a fit of a VMD model with two effective resonances with masses of 1450 MeV and 1700 MeV to describe the excited vector states $\omega(1420)$, $\rho(1450)$, $\omega(1650)$, and $\rho(1700)$. Systematic errors not evaluated.

$\Gamma(f_0(980)\gamma)/\Gamma(\text{total}) \times \Gamma(e^+e^-)/\Gamma(\text{total})$	$\Gamma_{19}/\Gamma \times \Gamma_{10}/\Gamma$
VALUE (units 10 ⁻⁹)	CL% DOCUMENT ID TECN COMMENT

<2.6 90 ACHASOV 11 SND $e^+e^- \rightarrow \pi^0\pi^0\gamma$

$\Gamma(f_0(1370)\gamma)/\Gamma(\text{total}) \times \Gamma(e^+e^-)/\Gamma(\text{total})$	$\Gamma_{20}/\Gamma \times \Gamma_{10}/\Gamma$
VALUE (units 10 ⁻⁹)	CL% DOCUMENT ID TECN COMMENT

<3.5 90 ACHASOV 11 SND $e^+e^- \rightarrow \pi^0\pi^0\gamma$

$\Gamma(f_2(1270)\gamma)/\Gamma(\text{total}) \times \Gamma(e^+e^-)/\Gamma(\text{total})$	$\Gamma_{21}/\Gamma \times \Gamma_{10}/\Gamma$
VALUE (units 10 ⁻⁹)	CL% DOCUMENT ID TECN COMMENT

<0.8 90 ¹ ACHASOV 11 SND $e^+e^- \rightarrow \pi^0\pi^0\gamma$
¹ Using Breit-Wigner parameterization of the $\rho(1450)$ with mass and width of 1465 MeV and 400 MeV, respectively.

$\rho(1450)$ BRANCHING RATIOS

$\Gamma(\pi\pi)/\Gamma(4\pi)$	Γ_1/Γ_3
VALUE	DOCUMENT ID TECN COMMENT

••• We do not use the following data for averages, fits, limits, etc. •••
 0.37 ± 0.10 ^{1,2} ABELE 01B CBAR 0.0 $\bar{p}n \rightarrow 5\pi$
¹ $\omega\pi$ not included.
² Using ABELE 97.

$\Gamma(K^+K^-)/\Gamma(\pi^+\pi^-)$	Γ_{14}/Γ_2
VALUE (%)	EVTS DOCUMENT ID TECN COMMENT

30.7 ± 8.4 ± 8.2 20k ¹ LEES 17C BABR $J/\psi \rightarrow h^+h^-\pi^0$
¹ From Dalitz plot analyses in isobar models.

$\Gamma(\omega\pi)/\Gamma(\text{total})$	Γ_4/Γ
VALUE	EVTS DOCUMENT ID TECN COMMENT

••• We do not use the following data for averages, fits, limits, etc. •••
 seen 821 ¹ MATVIENKO 15 BELL $\bar{B}^0 \rightarrow D^{*+}\omega\pi^-$
 seen 1.6k ACHASOV 12 SND $e^+e^- \rightarrow \pi^0\pi^0\gamma$
 ~ 0.21 CLEGG 94 RVUE
¹ Using Breit-Wigner parameterization of the $\rho(1450)$ and assuming equal probabilities of the $\rho(1450) \rightarrow \pi\pi$ and $\rho(1450) \rightarrow \omega\pi$ decays.

$\Gamma(\pi\pi)/\Gamma(\omega\pi)$	Γ_1/Γ_4
VALUE	DOCUMENT ID TECN COMMENT

••• We do not use the following data for averages, fits, limits, etc. •••
 ~ 0.32 CLEGG 94 RVUE

$\Gamma(\omega\pi)/\Gamma(4\pi)$	Γ_4/Γ_3
VALUE	DOCUMENT ID TECN COMMENT

••• We do not use the following data for averages, fits, limits, etc. •••
 <0.14 CLEGG 88 RVUE

$\Gamma(a_1(1260)\pi)/\Gamma(4\pi)$	Γ_5/Γ_3
VALUE	DOCUMENT ID TECN COMMENT

••• We do not use the following data for averages, fits, limits, etc. •••
 0.27 ± 0.08 ¹ ABELE 01B CBAR 0.0 $\bar{p}n \rightarrow 5\pi$
¹ $\omega\pi$ not included.

$\Gamma(h_1(1170)\pi)/\Gamma(4\pi)$	Γ_6/Γ_3
VALUE	DOCUMENT ID TECN COMMENT

••• We do not use the following data for averages, fits, limits, etc. •••
 0.08 ± 0.04 ¹ ABELE 01B CBAR 0.0 $\bar{p}n \rightarrow 5\pi$
¹ $\omega\pi$ not included.

$\Gamma(\pi(1300)\pi)/\Gamma(4\pi)$	Γ_7/Γ_3
VALUE	DOCUMENT ID TECN COMMENT

••• We do not use the following data for averages, fits, limits, etc. •••
 0.37 ± 0.13 ¹ ABELE 01B CBAR 0.0 $\bar{p}n \rightarrow 5\pi$
¹ $\omega\pi$ not included.

$\Gamma(\rho\rho)/\Gamma(4\pi)$	Γ_8/Γ_3
VALUE	DOCUMENT ID TECN COMMENT

••• We do not use the following data for averages, fits, limits, etc. •••
 0.11 ± 0.05 ¹ ABELE 01B CBAR 0.0 $\bar{p}n \rightarrow 5\pi$
¹ $\omega\pi$ not included.

Meson Particle Listings

$\rho(1450), \eta(1475)$

$\Gamma(\rho(\pi\pi)\text{-s-wave})/\Gamma(4\pi)$	DOCUMENT ID	TECN	COMMENT	Γ_9/Γ_3
---	-------------	------	---------	---------------------

• • • We do not use the following data for averages, fits, limits, etc. • • •

0.17±0.09 ¹ ABELE 01B CBAR 0.0 $\bar{p}n \rightarrow 5\pi$
¹ $\omega\pi$ not included.

$\Gamma(\eta\rho)/\Gamma_{\text{total}}$	EVTs	DOCUMENT ID	TECN	COMMENT	Γ_{11}/Γ
--	------	-------------	------	---------	----------------------

• • • We do not use the following data for averages, fits, limits, etc. • • •

<0.04 DONNACHIE 87B RVUE

¹ From a phenomenological model based on vector meson dominance with $\rho(1450)$ and $\phi(1680)$ masses and widths from the PDG 12.

$\Gamma(\eta\rho)/\Gamma(\omega\pi)$	DOCUMENT ID	TECN	COMMENT	Γ_{11}/Γ_4
--------------------------------------	-------------	------	---------	------------------------

• • • We do not use the following data for averages, fits, limits, etc. • • •

0.081±0.020 ^{1,2} AULCHENKO 15 SND 1.22-2.00 $e^+e^- \rightarrow \eta\pi^+\pi^-$
 ~ 0.24 ³ DONNACHIE 91 RVUE
 >2 FUKUI 91 SPEC 8.95 $\pi^-p \rightarrow \omega\pi^0 n$

¹ From a fit to the $e^+e^- \rightarrow \eta\pi^+\pi^-$ cross section with vector meson dominance model including $\rho(770)$, $\rho(1450)$, and $\rho(1700)$ decaying exclusively via $\eta\rho(770)$. Masses and widths of vector states are fixed to PDG 14. Coupling constants are assumed to be real.
² Reports the inverse of the quoted value as 12.3 ± 3.1 .
³ Using data from BISELLO 91B, DOLINSKY 86 and ALBRECHT 87L.

$\Gamma(\pi\pi)/\Gamma(\eta\rho)$	DOCUMENT ID	TECN	COMMENT	Γ_1/Γ_{11}
-----------------------------------	-------------	------	---------	------------------------

• • • We do not use the following data for averages, fits, limits, etc. • • •

1.3±0.4 ¹ AULCHENKO 15 SND 1.22-2.00 $e^+e^- \rightarrow \eta\pi^+\pi^-$
¹ From a fit to the $e^+e^- \rightarrow \eta\pi^+\pi^-$ cross section with vector meson dominance model including $\rho(770)$, $\rho(1450)$, and $\rho(1700)$ decaying exclusively via $\eta\rho(770)$. Masses and widths of vector states are fixed to PDG 14. Coupling constants are assumed to be real.

$\Gamma(a_2(1320)\pi)/\Gamma_{\text{total}}$	DOCUMENT ID	TECN	COMMENT	Γ_{12}/Γ
--	-------------	------	---------	----------------------

• • • We do not use the following data for averages, fits, limits, etc. • • •

not seen AMELIN 00 VES 37 $\pi^-p \rightarrow \eta\pi^+\pi^-n$

$\Gamma(K\bar{K})/\Gamma(\omega\pi)$	DOCUMENT ID	TECN	COMMENT	Γ_{13}/Γ_4
--------------------------------------	-------------	------	---------	------------------------

• • • We do not use the following data for averages, fits, limits, etc. • • •

<0.08 ¹ DONNACHIE 91 RVUE
¹ Using data from BISELLO 91B, DOLINSKY 86 and ALBRECHT 87L.

$\Gamma(K\bar{K}^*(892) + \text{c.c.})/\Gamma_{\text{total}}$	DOCUMENT ID	TECN	COMMENT	Γ_{15}/Γ
---	-------------	------	---------	----------------------

• • • We do not use the following data for averages, fits, limits, etc. • • •

possibly seen COAN 04 CLEO $\tau^- \rightarrow K^-\pi^-K^+\nu_\tau$

$\Gamma(\eta\rho)/\Gamma_{\text{total}}$	EVTs	DOCUMENT ID	TECN	COMMENT	Γ_{17}/Γ
--	------	-------------	------	---------	----------------------

• • • We do not use the following data for averages, fits, limits, etc. • • •

seen 35 ¹ ACHASOV 14 SND 1.15-2.00 $e^+e^- \rightarrow \eta\rho$
¹ From a phenomenological model based on vector meson dominance with $\rho(1450)$ and $\phi(1680)$ masses and widths from the PDG 12.

$\rho(1450)$ REFERENCES

GRIBANOV 20 JHEP 2001 112 S.S. Gribov et al. (CMD-3 Collab.)	ACHASOV 18 PR D97 012008 M.N. Achasov et al. (SND Collab.)	LEES 18 PR D97 052007 J.P. Lees et al. (BABAR Collab.)
BARTOS 17 PR D96 113004 E. Bartos et al.	BARTOS 17A JUMP A32 1750154 E. Bartos et al.	LEES 17C PR D95 072007 J.P. Lees et al. (BABAR Collab.)
AALI 16N PR D93 052018 R. Aaij et al. (LHCb Collab.)	ABLIKIM 16C PL B753 629 M. Ablikim et al. (BESIII Collab.)	ACHASOV 16D PR D94 112001 M.N. Achasov et al. (SND Collab.)
AULCHENKO 15 PR D91 052013 V.M. Aulchenko et al. (SND Collab.)	MATVIENKO 15 PR D92 012013 D. Matvienko et al. (BELLE Collab.)	ACHASOV 14 PR D90 032002 M.N. Achasov et al. (SND Collab.)
PDG 14 CP C38 070001 K. Olive et al. (PDG Collab.)	ACHASOV 13 PR D88 054013 M.N. Achasov et al. (SND Collab.)	ABRAMOWICZ 12 EPJ C72 1869 H. Abramowicz et al. (ZEUS Collab.)
ACHASOV 12 JETPL 94 734 M.N. Achasov et al. Translated from ZETFP 94 796.	LEES 12G PR D86 032013 J.P. Lees et al. (BABAR Collab.)	PDG 12 PR D86 010001 J. Beringer et al. (PDG Collab.)
ACHASOV 11 JETPL 113 75 M.N. Achasov et al. Translated from ZETFP 140 87.	AMBROSINO 11A PL B700 102 F. Ambrosino et al. (KLOE Collab.)	ACHASOV 10D PR D98 112001 M.N. Achasov et al. (SND Collab.)
DUBNICKA 10 APS 60 1 M.N. Dubnicka, A.Z. Dubnickova	AUBERT 09AS PRL 103 231801 B. Aubert et al. (BABAR Collab.)	AUBERT 08S PR D77 092002 B. Aubert et al. (BABAR Collab.)
FUJIKAWA 08 PR D78 072006 M. Fujikawa et al. (BELLE Collab.)	AKHMETSHIN 07 PL B648 28 R.R. Akhmetshin et al. (Novosibirsk CMD-2 Collab.)	ACHASOV 06 JETPL 103 380 M.N. Achasov et al. (Novosibirsk SND Collab.)
ACHASOV 06 Translated from ZETFP 130 437.	AKHMETSHIN 05 PL B605 26 R.R. Akhmetshin et al. (Novosibirsk CMD-2 Collab.)	ALOISIO 05 PL B606 12 A. Aloisio et al. (KLOE Collab.)
SCHAEEL 05C PRPL 421 191 S. Schaeel et al. (ALEPH Collab.)		

AKHMETSHIN 04 PL B578 285 R.R. Akhmetshin et al. (Novosibirsk CMD-2 Collab.)	COAN 04 PRL 92 232001 T.E. Coan et al. (CLEO Collab.)
AKHMETSHIN 03B PL B562 173 R.R. Akhmetshin et al. (Novosibirsk CMD-2 Collab.)	ABELE 01B EPJ C21 261 A. Abele et al. (Crystal Barrel Collab.)
AKHMETSHIN 01B PL B509 217 R.R. Akhmetshin et al. (Novosibirsk CMD-2 Collab.)	ALEXANDER 01B PR D64 092001 J.P. Alexander et al. (CLEO Collab.)
AKHMETSHIN 00B PL B489 125 R.R. Akhmetshin et al. (Novosibirsk CMD-2 Collab.)	AMELIN 00 NP A668 83 D. Amelin et al. (VES Collab.)
ANDERSON 00A PR D61 112002 S. Anderson et al. (CLEO Collab.)	EDWARDS 00A PR D61 072003 K.W. Edwards et al. (CLEO Collab.)
ABELE 99C PL B450 275 A. Abele et al. (Crystal Barrel Collab.)	ABELE 99D PL B468 178 A. Abele et al. (Crystal Barrel Collab.)
BERTIN 98 PR D57 55 A. Bertin et al. (OBELIX Collab.)	ABELE 97 PL B391 191 A. Abele et al. (Crystal Barrel Collab.)
ACHASOV 97 PR D55 2663 N.N. Achasov et al. (NOVM)	BARATE 97M ZPHY C76 15 R. Barate et al. (ALEPH Collab.)
BERTIN 97C PL B408 476 A. Bertin et al. (OBELIX Collab.)	BERTIN 97D PL B414 220 A. Bertin et al. (OBELIX Collab.)
CLEGG 94 ZPHY C62 455 A.B. Clegg, A. Donnachie (LANC, MCHS)	BISELLO 91B NPBP5 B21 111 D. Bisello (DM2 Collab.)
DOLINSKY 91 PRPL 202 99 S.I. Dolinsky et al. (NOVO)	DONNACHIE 91 ZPHY C51 689 A. Donnachie, A.B. Clegg (MCHS, LANC)
FUKUI 91 PL B257 241 S. Fukui et al. (SUGI, NAGO, KEK, KYOT+)	KUHN 90 ZPHY C48 445 J.H. Kuhn et al. (MFIM)
ARMSTRONG 89E PL B228 536 T.A. Armstrong, M. Benayoun (ATHU, BARI, BIRN+)	BISELLO 89 PL B220 321 D. Bisello et al. (DM2 Collab.)
DUBNICKA 89 JP J15 1349 S. Dubnicka et al. (JINR, SLOV)	ANTONELLI 88 PL B212 133 A. Antonelli et al. (DM2 Collab.)
CLEGG 88 ZPHY C40 313 A.B. Clegg, A. Donnachie (MCHS, LANC)	DIEKMANN 88 PRPL 159 99 B. Diekmann (BONN)
FUKUI 88 PL B202 441 S. Fukui et al. (SUGI, NAGO, KEK, KYOT+)	ALBRECHT 87L PL B185 223 H. Albrecht et al. (ARGUS Collab.)
DONNACHIE 87B ZPHY C34 257 A. Donnachie, A.B. Clegg (MCHS, LANC)	DOLINSKY 86 PL B174 453 S.I. Dolinsky et al. (NOVO)
BARKOV 85 NP B256 365 L.M. Barkov et al. (NOVO)	KURDADZE 83 JETPL 37 733 L.M. Kurdadze et al. (NOVO)
ASTON 80C PL 92B 211 D. Aston (BONN, CERN, EPOL, GLAS, LANC+)	BARBER 80C ZPHY C4 169 D.P. Barber et al. (DARE, LANC, SHEP)
GOUNARIS 68 PRL 21 244 G.J. Gounaris, J.J. Sakurai	

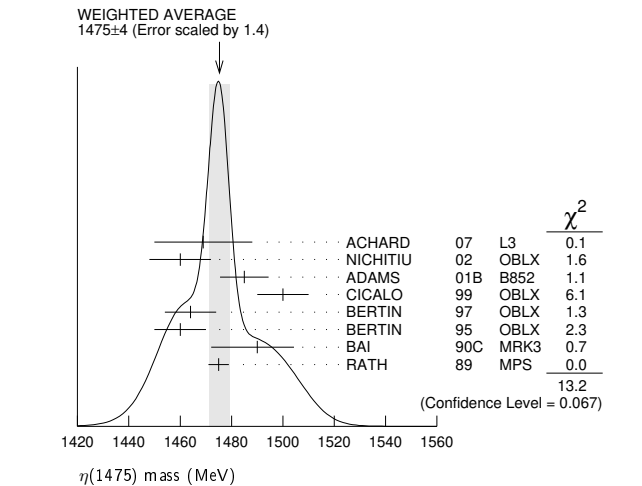
$\eta(1475)$

$I^G(J^{PC}) = 0^+(0^-+)$

See the $\eta(1405)$ and the related review on "Spectroscopy of Light Meson Resonances."

$\eta(1475)$ MASS

VALUE (MeV)	EVTs	DOCUMENT ID	TECN	COMMENT
1475 ± 4 OUR AVERAGE		Error includes scale factor of 1.4. See the ideogram below.		
1469 ± 14 ± 13	74	ACHARD 07 L3		183-209 $e^+e^- \rightarrow e^+e^-K_S^0 K_{\pm}^{\pm}\pi^{\mp}$
1460 ± 12	3651	NICHITIU 02 OBLX		0 $\bar{p}p \rightarrow K^+K^-\pi^+\pi^-\pi^0$
1485 ± 8 ± 5	20k	ADAMS 01B B852		18 GeV $\pi^-p \rightarrow K^+K^-\pi^0 n$
1500 ± 10		CICALO 99 OBLX		0 $\bar{p}p \rightarrow K_{\pm}^{\pm}K_S^0\pi^{\mp}\pi^{\pm}\pi^{\mp}$
1464 ± 10		BERTIN 97 OBLX		0 $\bar{p}p \rightarrow K^{\pm}(K^0)\pi^{\mp}\pi^{\pm}\pi^{\mp}$
1460 ± 10		BERTIN 95 OBLX		0 $\bar{p}p \rightarrow K\bar{K}\pi\pi\pi$
1490 ⁺¹⁴ / ₋₈ ⁺³ / ₋₁₆	1100	BAI 90C MRK3		0 $J/\psi \rightarrow \gamma K_S^0 K_{\pm}^{\pm}\pi^{\mp}$
1475 ± 4		RATH 89 MPS		21.4 $\pi^-p \rightarrow n K_S^0 K_S^0 \pi^0$
• • • We do not use the following data for averages, fits, limits, etc. • • •				
1477 ± 7 ± 13		¹ ABLIKIM 18i BES3		0 $J/\psi \rightarrow \gamma\gamma\phi(1020)$
1565 ± 8 ⁺⁰ / ₋₆₃		² ABLIKIM 15T BES3		0 $J/\psi \rightarrow \gamma K_S^0 K_S^0 \eta$
1421 ± 14		AUGUSTIN 92 DM2		0 $J/\psi \rightarrow \gamma K\bar{K}\pi$



¹ From a fit to $\gamma\phi$ invariant mass. Angular analysis consistent with $J^{PC} = 0^-+$. Other J^{PC} not excluded.
² Could also be the $\eta(1405)$.

See key on page 1127

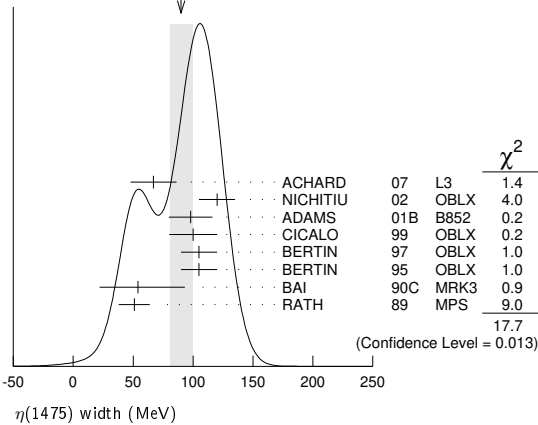
Meson Particle Listings

$\eta(1475), f_0(1500)$

$\eta(1475)$ WIDTH

VALUE (MeV)	EVTs	DOCUMENT ID	TECN	COMMENT
90 ± 9 OUR AVERAGE		Error includes scale factor of 1.6. See the ideogram below.		
67 ± 18 ± 7	74	ACHARD	07 L3	183-209 $e^+e^- \rightarrow K_S^0 K^\pm \pi^\mp$
120 ± 15	3651	NICHITIU	02 OBLX	$0 \bar{p}p \rightarrow K^+ K^- \pi^+ \pi^- \pi^0$
98 ± 18 ± 3	20k	ADAMS	01B B852	18 GeV $\pi^- p \rightarrow K^+ K^- \pi^0 n$
100 ± 20		CICALO	99 OBLX	$0 \bar{p}p \rightarrow K^\pm K_S^0 \pi^\mp \pi^+ \pi^-$
105 ± 15		BERTIN	97 OBLX	$0.0 \bar{p}p \rightarrow K^\pm (K^0) \pi^\mp \pi^+ \pi^-$
105 ± 15		BERTIN	95 OBLX	$0 \bar{p}p \rightarrow K \bar{K} \pi \pi$
54 + 37 + 13 - 21 - 24		BAI	90c MRK3	$J/\psi \rightarrow \gamma K_S^0 K^\pm \pi^\mp$
51 ± 13		RATH	89 MPS	$21.4 \pi^- p \rightarrow n K_S^0 K_S^0 \pi^0$
• • • We do not use the following data for averages, fits, limits, etc. • • •				
118 ± 22 ± 17		¹ ABLIKIM	18i BES3	$J/\psi \rightarrow \gamma \gamma \phi(1020)$
45 + 14 + 21 - 13 - 28		² ABLIKIM	15t BES3	$J/\psi \rightarrow \gamma K_S^0 K_S^0 \eta$
63 ± 18		AUGUSTIN	92 DM2	$J/\psi \rightarrow \gamma K \bar{K} \pi$

WEIGHTED AVERAGE
90 ± 9 (Error scaled by 1.6)



¹ From a fit to $\gamma\phi$ invariant mass. Angular analysis consistent with $J^{PC} = 0^{-+}$. Other J^{PC} not excluded.
² Could also be the $\eta(1405)$.

$\eta(1475)$ DECAY MODES

Mode	Fraction (Γ_i/Γ)
$\Gamma_1 K \bar{K} \pi$	seen
$\Gamma_2 K \bar{K}^*(892) + c.c.$	seen
$\Gamma_3 a_0(980) \pi$	seen
$\Gamma_4 \gamma \gamma$	seen
$\Gamma_5 K_S^0 K_S^0 \eta$	possibly seen
$\Gamma_6 \gamma \phi(1020)$	possibly seen

$\eta(1475)$ $\Gamma(i)\Gamma(\gamma\gamma)/\Gamma(\text{total})$

VALUE (keV)	CL%	EVTs	DOCUMENT ID	TECN	COMMENT	$\Gamma_1 \Gamma_4 / \Gamma$
0.23 ± 0.05 ± 0.05		74	¹ ACHARD	07 L3	183-209 $e^+e^- \rightarrow K_S^0 K^\pm \pi^\mp$	

• • • We do not use the following data for averages, fits, limits, etc. • • •
 < 0.089 90 ^{2,3} AHOHE 05 CLE2 $10.6 e^+e^- \rightarrow K_S^0 K^\pm \pi^\mp$
¹ Supersedes ACCIARRI 01g. Using $B(K_S^0 \rightarrow \pi^+ \pi^-) = 0.6895$.
² Using $\eta(1475)$ mass of 1481 MeV and width of 48 MeV. The upper limit increases to 0.140 keV if the world average value, 87 MeV, of the width is used.
³ Assuming three-body phase-space decay to $K_S^0 K^\pm \pi^\mp$.

$\eta(1475)$ BRANCHING RATIOS

$\Gamma(K \bar{K}^*(892) + c.c.) / \Gamma(K \bar{K} \pi)$	Γ_2 / Γ_1		
VALUE	DOCUMENT ID	TECN	COMMENT
• • • We do not use the following data for averages, fits, limits, etc. • • •			
0.50 ± 0.10	¹ BAILLON	67 HBC	$0.0 \bar{p}p \rightarrow K \bar{K} \pi \pi$
¹ Data could also refer to $\eta(1405)$.			

$\Gamma(K \bar{K}^*(892) + c.c.) / [\Gamma(K \bar{K}^*(892) + c.c.) + \Gamma(a_0(980) \pi)]$	$\Gamma_2 / (\Gamma_2 + \Gamma_3)$			
VALUE	CL%	DOCUMENT ID	TECN	COMMENT
• • • We do not use the following data for averages, fits, limits, etc. • • •				
< 0.25	90	EDWARDS	82E CBAL	$J/\psi \rightarrow K^+ K^- \pi^0 \gamma$

$\Gamma(\gamma\gamma)/\Gamma(K \bar{K} \pi)$

VALUE	CL%	DOCUMENT ID	TECN	COMMENT	Γ_4 / Γ_1
< 1.27 × 10⁻³	90	¹ ABLIKIM	18o BES3	$\psi(2S) \rightarrow \pi^+ \pi^- \gamma \gamma$	
¹ Using results from BAI 00d.					

$\Gamma(\gamma\phi(1020))/\Gamma_{\text{total}}$

VALUE	CL%	DOCUMENT ID	TECN	COMMENT	Γ_6 / Γ
possibly seen		¹ ABLIKIM	18i BES3	$J/\psi \rightarrow \gamma \gamma \phi(1020)$	
¹ Seen as a peak in $\gamma\phi$ invariant mass. Angular analysis consistent with $J^{PC} = 0^{-+}$. Other J^{PC} not excluded. Also see $\eta(1405)$.					

$\eta(1475)$ REFERENCES

ABLIKIM 18i PR D97 051101	M. Ablikim et al.	(BESIII Collab.)
ABLIKIM 18o PR D97 072014	M. Ablikim et al.	(BESIII Collab.)
ABLIKIM 15T PRL 115 091803	M. Ablikim et al.	(BESIII Collab.)
ACHARD 07 JHEP 0703 018	P. Achard et al.	(L3 Collab.)
AHOHE 05 PR D71 072001	R. Ahohe et al.	(CLEO Collab.)
NICHITIU 02 PL B545 261	F. Nichitiu et al.	(OBELIX Collab.)
ACCIARRI 01G PL B501 1	M. Acciari et al.	(L3 Collab.)
ADAMS 01B PL B516 264	G.S. Adams et al.	(BNL E852 Collab.)
BAI 00D PL B476 25	J.Z. Bai et al.	(BES Collab.)
CICALO 99 PL B462 453	C. Cicalo et al.	(OBELIX Collab.)
BERTIN 97 PL B400 226	A. Bertin et al.	(OBELIX Collab.)
BERTIN 95 PL B361 187	A. Bertin et al.	(OBELIX Collab.)
AUGUSTIN 92 PR D46 1951	J.E. Augustin, G. Cosme	(DM2 Collab.)
BAI 90C PRL 65 2507	Z. Bai et al.	(Mark III Collab.)
RATH 89 PR D40 693	M.G. Rath et al.	(NDAM, BRAN, BNL, CUNY+)
EDWARDS 82E PRL 49 259	C. Edwards et al.	(CIT, HARV, PRIN+)
BAILLON 67 NC 50A 393	P.H. Baillon et al.	(CERN, CDEF, IRAD)

$f_0(1500)$

$$J^G(J^{PC}) = 0^+(0^{++})$$

See the review on "Spectroscopy of Light Meson Resonances."

$f_0(1500)$ MASS

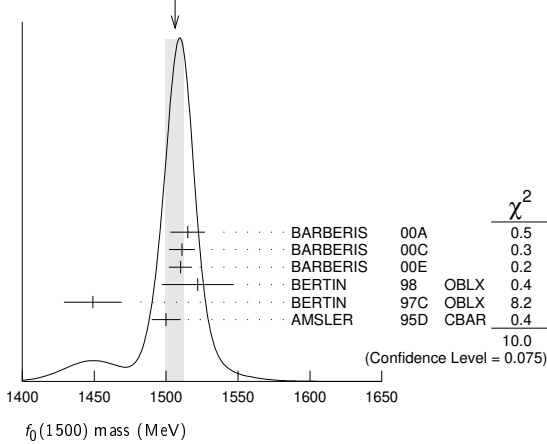
VALUE (MeV)	EVTs	DOCUMENT ID	TECN	COMMENT
1506 ± 6 OUR AVERAGE		Error includes scale factor of 1.4. See the ideogram below.		
1515 ± 12		¹ BARBERIS	00A	$450 pp \rightarrow p_f \eta \eta p_S$
1511 ± 9		^{1,2} BARBERIS	00c	$450 pp \rightarrow p_f 4 \pi p_S$
1510 ± 8		¹ BARBERIS	00E	$450 pp \rightarrow p_f \eta \eta p_S$
1522 ± 25		¹ BERTIN	98 OBLX	$0.05-0.405 \bar{p}p \rightarrow \pi^+ \pi^+ \pi^- \pi^-$
1449 ± 20		¹ BERTIN	97c OBLX	$0.0 \bar{p}p \rightarrow \pi^+ \pi^- \pi^0$
1500 ± 10		³ AMSLER	95D CBAR	$0.0 \bar{p}p \rightarrow \pi^0 \pi^0 \pi^0, \pi^0 \eta \eta, \pi^0 \pi^0 \eta$
• • • We do not use the following data for averages, fits, limits, etc. • • •				
1450 ± 10		⁴ RODAS	22 RVUE	$J/\psi(1S) \rightarrow \gamma(\pi \pi, K \bar{K})$
1483 ± 15		¹ SARANTSEV	21 RVUE	$J/\psi(1S) \rightarrow \gamma(\pi \pi, K \bar{K}, \eta \eta, \omega \phi)$
1496 ± 1.2 ± 4.4 - 15 - 26.4		⁵ ALBRECHT	20 RVUE	$0.9 \bar{p}p \rightarrow \pi^0 \pi^0 \eta, \pi^0 \eta \eta, \pi^0 K^+ K^-$
1465 ± 18		⁶ ROPERTZ	18 RVUE	$\bar{B}_S^0 \rightarrow J/\psi(\pi^+ \pi^- / K^+ K^-)$
1447 ± 16 ± 13	163	^{7,8} DOBBS	15	$J/\psi \rightarrow \gamma \pi^+ \pi^-$
1442 ± 9 ± 4	261	^{7,8} DOBBS	15	$\psi(2S) \rightarrow \gamma \pi^+ \pi^-$
1460.9 ± 2.9		⁹ AAIJ	14BR LHCB	$\bar{B}_S^0 \rightarrow J/\psi \pi^+ \pi^-$
1468 + 14 + 23 - 15 - 74	5.5k	¹⁰ ABLIKIM	13N BES3	$e^+e^- \rightarrow J/\psi \rightarrow \gamma \eta \eta$
1486 ± 10		¹ ANISOVICH	09 RVUE	$0.0 \bar{p}p, \pi N$
1470 ± 60	5.68	¹¹ KLEMPAT	08 E791	$D_S^+ \rightarrow \pi^- \pi^+ \pi^+$
1470 + 6 + 72 - 7 - 255		¹² UEHARA	08A BELL	$10.6 e^+e^- \rightarrow e^+e^- \pi^0 \pi^0$
1466 ± 6 ± 20		¹³ ABLIKIM	06V BES2	$e^+e^- \rightarrow J/\psi \rightarrow \gamma \pi^+ \pi^-$
1495 ± 4		AMSLER	06 CBAR	$0.9 \bar{p}p \rightarrow K^+ K^- \pi^0$
1539 ± 20	9.9k	AUBERT	06O BABR	$B^+ \rightarrow K^+ K^+ K^-$
1473 ± 5	80k	^{13,14} UMAN	06 E835	$5.2 \bar{p}p \rightarrow \eta \eta \pi^0$
1478 ± 6		VLADIMIRSK..	06 SPEC	$40 \pi^- p \rightarrow K_S^0 K_S^0 \eta$
1493 ± 7		¹³ BINON	05 GAMS	$33 \pi^- p \rightarrow \eta \eta \eta$
1524 ± 14	1400	¹⁵ GARMASH	05 BELL	$B^+ \rightarrow K^+ K^+ K^-$
1489 ± 8 - 4		¹⁶ ANISOVICH	03 RVUE	
1490 ± 30		¹³ ABELE	01 CBAR	$0.0 \bar{p}d \rightarrow \pi^- 4 \pi^0 p$
1497 ± 10		¹³ BARBERIS	99 OMEG	$450 pp \rightarrow p_S p_f K^+ K^-$
1502 ± 10		¹³ BARBERIS	99B OMEG	$450 pp \rightarrow p_S p_f \pi^+ \pi^-$
1502 ± 12 ± 10		¹⁷ BARBERIS	99D OMEG	$450 pp \rightarrow K^+ K^-, \pi^+ \pi^-$
1530 ± 45		¹³ BELLAZZINI	99 GAM4	$450 pp \rightarrow pp \pi^0 \pi^0$
1505 ± 18		¹³ FRENCH	99	$300 pp \rightarrow p_f(K^+ K^-) p_S$
1447 ± 27		¹⁸ KAMINSKI	99 RVUE	$\pi \pi \rightarrow \pi \pi, K \bar{K}, \sigma \sigma$
1580 ± 80		¹³ ALDE	98 GAM4	$100 \pi^- p \rightarrow \pi^0 \pi^0 \eta$
1499 ± 8		¹ ANISOVICH	98B RVUE	Compilation
~ 1520		REYES	98 SPEC	$800 pp \rightarrow p_S p_f K_S^0 K_S^0$

Meson Particle Listings

$f_0(1500)$

1510 ± 20		¹ BARBERIS	97B	OMEG	450 $pp \rightarrow pp2(\pi^+ \pi^-)$
~ 1475		FRABETTI	97D	E687	$D_S^\pm \rightarrow \pi^\mp \pi^\pm \pi^\pm$
~ 1505		ABELE	96	CBAR	$0.0 \bar{p}p \rightarrow 5\pi^0$
1515 ± 20		ABELE	96B	CBAR	$0.0 \bar{p}p \rightarrow \pi^0 K_L^0 K_L^0$
1500 ± 8		¹ ABELE	96C	RVUE	Compilation
1460 ± 20	120	¹³ AMELIN	96B	VES	$37 \pi^- A \rightarrow \eta\eta\pi^- A$
1500 ± 8		BUGG	96	RVUE	
1500 ± 15		¹⁹ AMSLER	95B	CBAR	$0.0 \bar{p}p \rightarrow 3\pi^0$
1505 ± 15		²⁰ AMSLER	95C	CBAR	$0.0 \bar{p}p \rightarrow \eta\eta\pi^0$
1445 ± 5		²¹ ANTINORI	95	OMEG	300,450 $pp \rightarrow pp2(\pi^+ \pi^-)$
1497 ± 30		¹³ ANTINORI	95	OMEG	300,450 $pp \rightarrow pp\pi^+ \pi^-$
~ 1505		BUGG	95	MRK3	$J/\psi \rightarrow \gamma\pi^+ \pi^- \pi^+ \pi^-$
1446 ± 5		¹³ ABATZIS	94	OMEG	450 $pp \rightarrow pp2(\pi^+ \pi^-)$
1545 ± 25		¹³ AMSLER	94E	CBAR	$0.0 \bar{p}p \rightarrow \pi^0 \eta\eta'$
1520 ± 25		^{1,22} ANISOVICH	94	CBAR	$0.0 \bar{p}p \rightarrow 3\pi^0, \pi^0 \eta\eta$
1505 ± 20		^{1,23} BUGG	94	RVUE	$\bar{p}p \rightarrow 3\pi^0, \eta\eta\pi^0, \eta\pi^0 \pi^0$
1560 ± 25		¹³ AMSLER	92	CBAR	$0.0 \bar{p}p \rightarrow \pi^0 \eta\eta$
1550 ± 45 ± 30		¹³ BELADIDZE	92C	VES	$36 \pi^- Be \rightarrow \pi^- \eta' \eta Be$
1449 ± 4		¹³ ARMSTRONG	89E	OMEG	300 $pp \rightarrow pp2(\pi^+ \pi^-)$
1610 ± 20		¹³ ALDE	88	GAM4	$300 \pi^- N \rightarrow \pi^- N2\eta$
~ 1525		ASTON	88D	LASS	$11 K^- p \rightarrow K_S^0 K_S^0 \Lambda$
1570 ± 20	600	¹³ ALDE	87	GAM4	$100 \pi^- p \rightarrow 4\pi^0 n$
1575 ± 45		²⁴ ALDE	86D	GAM4	$100 \pi^- p \rightarrow 2\eta n$
1568 ± 33		¹³ BINON	84C	GAM2	$38 \pi^- p \rightarrow \eta\eta' n$
1592 ± 25		¹³ BINON	83	GAM2	$38 \pi^- p \rightarrow 2\eta n$
1525 ± 5		¹³ GRAY	83	DBC	$0.0 \bar{p}N \rightarrow 3\pi$

WEIGHTED AVERAGE
1506±6 (Error scaled by 1.4)



¹ T-matrix pole.
² Average between $\pi^+ \pi^- 2\pi^0$ and $2(\pi^+ \pi^-)$.
³ T-matrix pole. Coupled-channel analysis of AMSLER 95B, AMSLER 95C, and AMSLER 94D.
⁴ T-matrix pole from coupled channel K-matrix fit to data on $J/\psi \rightarrow \gamma\pi^0 \pi^0$ (ABLIKIM 15AE) and $J/\psi \rightarrow \gamma K_S^0 K_S^0$ (ABLIKIM 18AA).
⁵ T-matrix pole, 5 poles, 5 channels, including scattering data from HYAMS 75 ($\pi\pi$), LONGACRE 86 ($K\bar{K}$), BINON 83 ($\eta\eta$), and BINON 84C ($\eta\eta'$).
⁶ T-matrix pole of 3 channel unitary model fit to data from AAIJ 14BR and AAIJ 17V extracted using Pade approximants.
⁷ Using CLEO-c data but not authored by the CLEO Collaboration.
⁸ From a fit to a Breit-Wigner line shape with fixed $\Gamma = 109$ MeV.
⁹ Solution 1, statistical error only.
¹⁰ From partial wave analysis including all possible combinations of 0^{++} , 2^{++} , and 4^{++} resonances.
¹¹ Reanalysis of AITALA 01A data. This state could also be $f_0(1370)$.
¹² Breit-Wigner mass. May also be the $f_0(1370)$.
¹³ Breit-Wigner mass.
¹⁴ Statistical error only.
¹⁵ Breit-Wigner, solution 1, PWA ambiguous.
¹⁶ K-matrix pole from combined analysis of $\pi^- p \rightarrow \pi^0 \pi^0 n$, $\pi^- p \rightarrow K\bar{K} n$, $\pi^+ \pi^- \rightarrow \pi^+ \pi^-$, $\bar{p}p \rightarrow \pi^0 \pi^0 \pi^0$, $\pi^0 \eta\eta$, $\pi^0 \pi^0 \eta$, $\pi^+ \pi^- \pi^0$, $K^+ K^- \pi^0$, $K_S^0 K_S^0 \pi^0$, $K^+ K_S^0 \pi^-$ at rest, $\bar{p}n \rightarrow \pi^- \pi^- \pi^+$, $K_S^0 K^- \pi^0$, $K_S^0 K_S^0 \pi^-$ at rest.
¹⁷ Supersedes BARBERIS 99 and BARBERIS 99B.
¹⁸ T-matrix pole on sheet $-\ - +$.
¹⁹ T-matrix pole, supersedes ANISOVICH 94.
²⁰ T-matrix pole, supersedes ANISOVICH 94 and AMSLER 92.
²¹ Supersedes ABATZIS 94, ARMSTRONG 89E. Breit-Wigner mass.
²² From a simultaneous analysis of the annihilations $\bar{p}p \rightarrow 3\pi^0, \pi^0 \eta\eta$.
²³ Reanalysis of ANISOVICH 94 data.
²⁴ From central value and spread of two solutions. Breit-Wigner mass.

$f_0(1500)$ WIDTH

VALUE (MeV)	EVTS	DOCUMENT ID	TECN	COMMENT
112 ± 9 OUR AVERAGE				
110 ± 24		¹ BARBERIS	00A	450 $pp \rightarrow p_f \eta \eta p_s$
102 ± 18		^{1,2} BARBERIS	00C	450 $pp \rightarrow p_f 4\pi p_s$
110 ± 16		¹ BARBERIS	00E	450 $pp \rightarrow p_f \eta \eta p_s$
108 ± 33		¹ BERTIN	98 OBLX	$0.05-0.405 \bar{p}p \rightarrow \pi^+ \pi^+ \pi^-$
114 ± 30		¹ BERTIN	97C OBLX	$0.0 \bar{p}p \rightarrow \pi^+ \pi^- \pi^0$
154 ± 30		³ AMSLER	95D CBAR	$0.0 \bar{p}p \rightarrow \pi^0 \pi^0 \pi^0, \pi^0 \eta\eta, \pi^0 \pi^0 \eta$
••• We do not use the following data for averages, fits, limits, etc. •••				
106 ± 16		⁴ RODAS	22 RVUE	$J/\psi(1S) \rightarrow \gamma(\pi\pi, K\bar{K})$
116 ± 12		¹ SARANTSEV	21 RVUE	$J/\psi(1S) \rightarrow \gamma(\pi\pi, K\bar{K}, \eta\eta, \omega\phi)$
80.8 ± 0.6 ± 20.0	20.0	⁵ ALBRECHT	20 RVUE	$0.9 \bar{p}p \rightarrow \pi^0 \pi^0 \eta, \pi^0 \eta\eta, \pi^0 K^+ K^-$
100 ± 18		⁶ ROPERTZ	18 RVUE	$\bar{B}_S^0 \rightarrow J/\psi(\pi^+ \pi^- / K^+ K^-)$
124 ± 7		⁷ AAIJ	14BR LHCB	$\bar{B}_S^0 \rightarrow J/\psi \pi^+ \pi^-$
136 ± 41 ± 28	5.5k	⁸ ABLIKIM	13N BES3	$e^+ e^- \rightarrow J/\psi \rightarrow \gamma \eta \eta$
114 ± 10		¹ ANISOVICH	09 RVUE	$0.0 \bar{p}p, \pi N$
90 ± 2 ± 50	1	⁹ UEHARA	08A BELL	$10.6 e^+ e^- \rightarrow e^+ e^- \pi^0 \pi^0$
108 ± 11 ± 25		¹⁰ ABLIKIM	06V BES2	$e^+ e^- \rightarrow J/\psi \rightarrow \gamma \pi^+ \pi^-$
121 ± 8		AMSLER	06 CBAR	$0.9 \bar{p}p \rightarrow K^+ K^- \pi^0$
257 ± 33	9.9k	AUBERT	06O BABR	$B^+ \rightarrow K^+ K^+ K^-$
108 ± 9	80k	^{10,11} UMAN	06 E835	$5.2 \bar{p}p \rightarrow \eta \eta \pi^0$
119 ± 10		VLADIMIRSK...	06 SPEC	$40 \pi^- p \rightarrow K_S^0 K_S^0 \eta$
90 ± 15		¹⁰ BINON	05 GAMS	$33 \pi^- p \rightarrow \eta \eta n$
136 ± 23	1400	¹² GARMASH	05 BELL	$B^+ \rightarrow K^+ K^+ K^-$
102 ± 10		¹³ ANISOVICH	03 RVUE	
140 ± 40		¹⁰ ABELE	01 CBAR	$0.0 \bar{p}d \rightarrow \pi^- 4\pi^0 p$
104 ± 25		¹⁰ BARBERIS	99B OMEG	450 $pp \rightarrow p_s p_f K^+ K^-$
131 ± 15		¹⁰ BARBERIS	99B OMEG	450 $pp \rightarrow p_s p_f \pi^+ \pi^-$
98 ± 18 ± 16		¹⁴ BARBERIS	99D OMEG	450 $pp \rightarrow K^+ K^-, \pi^+ \pi^-$
160 ± 50		¹⁰ BELLAZZINI	99 GAM4	450 $pp \rightarrow pp\pi^0 \pi^0$
100 ± 33		¹⁰ FRENCH	99	300 $pp \rightarrow p_f(K^+ K^-) p_s$
108 ± 46		¹⁵ KAMINSKI	99 RVUE	$\pi\pi \rightarrow \pi\pi, K\bar{K}, \sigma\sigma$
280 ± 100		¹⁰ ALDE	98 GAM4	$100 \pi^- p \rightarrow \pi^0 \pi^0 n$
130 ± 20		¹ ANISOVICH	98B RVUE	Compilation
120 ± 35		¹ BARBERIS	97B OMEG	450 $pp \rightarrow pp2(\pi^+ \pi^-)$
~ 100		FRABETTI	97D E687	$D_S^\pm \rightarrow \pi^\mp \pi^\pm \pi^\pm$
~ 169		ABELE	96B CBAR	$0.0 \bar{p}p \rightarrow 5\pi^0$
105 ± 15		ABELE	96C CBAR	$0.0 \bar{p}p \rightarrow \pi^0 K_L^0 K_L^0$
100 ± 30	120	¹⁰ AMELIN	96B VES	$37 \pi^- A \rightarrow \eta\eta\pi^- A$
132 ± 15		BUGG	96 RVUE	
120 ± 25		¹⁶ AMSLER	95B CBAR	$0.0 \bar{p}p \rightarrow 3\pi^0$
120 ± 30		¹⁷ AMSLER	95C CBAR	$0.0 \bar{p}p \rightarrow \eta\eta\pi^0$
65 ± 10		¹⁸ ANTINORI	95 OMEG	300,450 $pp \rightarrow pp2(\pi^+ \pi^-)$
199 ± 30		¹⁰ ANTINORI	95 OMEG	300,450 $pp \rightarrow pp\pi^+ \pi^-$
56 ± 12		¹⁰ ABATZIS	94 OMEG	450 $pp \rightarrow pp2(\pi^+ \pi^-)$
100 ± 40		¹⁰ AMSLER	94E CBAR	$0.0 \bar{p}p \rightarrow \pi^0 \eta\eta'$
148 ± 20		^{1,19} ANISOVICH	94 CBAR	$0.0 \bar{p}p \rightarrow 3\pi^0, \pi^0 \eta\eta$
150 ± 20		^{1,20} BUGG	94 RVUE	$\bar{p}p \rightarrow 3\pi^0, \eta\eta\pi^0, \eta\pi^0 \pi^0$
245 ± 50		¹⁰ AMSLER	92 CBAR	$0.0 \bar{p}p \rightarrow \pi^0 \eta\eta$
153 ± 67 ± 50		¹⁰ BELADIDZE	92C VES	$36 \pi^- Be \rightarrow \pi^- \eta' \eta Be$
78 ± 18		¹⁰ ARMSTRONG	89E OMEG	300 $pp \rightarrow pp2(\pi^+ \pi^-)$
170 ± 40		¹⁰ ALDE	88 GAM4	$300 \pi^- N \rightarrow \pi^- N2\eta$
150 ± 20	600	¹⁰ ALDE	87 GAM4	$100 \pi^- p \rightarrow 4\pi^0 n$
265 ± 65		²¹ ALDE	86D GAM4	$100 \pi^- p \rightarrow 2\eta n$
260 ± 60		¹⁰ BINON	84C GAM2	$38 \pi^- p \rightarrow \eta\eta' n$
210 ± 40		¹⁰ BINON	83 GAM2	$38 \pi^- p \rightarrow 2\eta n$
101 ± 13		¹⁰ GRAY	83 DBC	$0.0 \bar{p}N \rightarrow 3\pi$

¹ T-matrix pole.
² Average between $\pi^+ \pi^- 2\pi^0$ and $2(\pi^+ \pi^-)$.
³ T-matrix pole. Coupled-channel analysis of AMSLER 95B, AMSLER 95C, and AMSLER 94D.
⁴ T-matrix pole from coupled channel K-matrix fit to data on $J/\psi \rightarrow \gamma\pi^0 \pi^0$ (ABLIKIM 15AE) and $J/\psi \rightarrow \gamma K_S^0 K_S^0$ (ABLIKIM 18AA).
⁵ T-matrix pole, 5 poles, 5 channels, including scattering data from HYAMS 75 ($\pi\pi$), LONGACRE 86 ($K\bar{K}$), BINON 83 ($\eta\eta$), and BINON 84C ($\eta\eta'$).
⁶ T-matrix pole of 3 channel unitary model fit to data from AAIJ 14BR and AAIJ 17V extracted using Pade approximants.
⁷ Solution 1, statistical error only.

- ⁸ From partial wave analysis including all possible combinations of 0⁺⁺, 2⁺⁺, and 4⁺⁺ resonances.
- ⁹ Breit-Wigner width. May also be the f₀(1370).
- ¹⁰ Breit-Wigner width.
- ¹¹ Statistical error only.
- ¹² Breit-Wigner, solution 1, PWA ambiguous.
- ¹³ K-matrix pole from combined analysis of $\pi^- p \rightarrow \pi^0 \pi^0 n$, $\pi^- p \rightarrow K \bar{K} n$, $\pi^+ \pi^- \rightarrow \pi^+ \pi^-$, $\bar{p} p \rightarrow \pi^0 \pi^0 \pi^0$, $\pi^0 \eta \eta$, $\pi^0 \pi^0 \eta$, $\pi^+ \pi^- \pi^0$, $K^+ K^- \pi^0$, $K_S^0 K_S^0 \pi^0$, $K^+ K_S^0 \pi^-$ at rest, $\bar{p} n \rightarrow \pi^- \pi^- \pi^+$, $K_S^0 K^- \pi^0$, $K_S^0 K_S^0 \pi^-$ at rest.
- ¹⁴ Supersedes BARBERIS 99 and BARBERIS 99B.
- ¹⁵ T-matrix pole on sheet --+.
- ¹⁶ T-matrix pole, supersedes ANISOVICH 94.
- ¹⁷ T-matrix pole, supersedes ANISOVICH 94 and AMSLER 92.
- ¹⁸ Supersedes ABATZIS 94, ARMSTRONG 89E. Breit-Wigner mass.
- ¹⁹ From a simultaneous analysis of the annihilations $\bar{p} p \rightarrow 3\pi^0, \pi^0 \eta \eta$.
- ²⁰ Reanalysis of ANISOVICH 94 data.
- ²¹ From central value and spread of two solutions. Breit-Wigner mass.

f₀(1500) DECAY MODES

Mode	Fraction (Γ _i /Γ)	Scale factor
Γ ₁ π π	(34.5 ± 2.2) %	1.2
Γ ₂ π ⁺ π ⁻	seen	
Γ ₃ 2π ⁰	seen	
Γ ₄ 4π	(48.9 ± 3.3) %	1.2
Γ ₅ 4π ⁰	seen	
Γ ₆ 2π ⁺ 2π ⁻	seen	
Γ ₇ 2(ππ) _{s-wave}	seen	
Γ ₈ ρρ	seen	
Γ ₉ π(1300)π	seen	
Γ ₁₀ a ₁ (1260)π	seen	
Γ ₁₁ ηη	(6.0 ± 0.9) %	1.1
Γ ₁₂ ηη'(958)	(2.2 ± 0.8) %	1.4
Γ ₁₃ K \bar{K}	(8.5 ± 1.0) %	1.1
Γ ₁₄ γγ	not seen	

CONSTRAINED FIT INFORMATION

An overall fit to 6 branching ratios uses 10 measurements and one constraint to determine 5 parameters. The overall fit has a χ² = 5.6 for 6 degrees of freedom.

The following off-diagonal array elements are the correlation coefficients <δx_iδx_j>/(δx_iδx_j), in percent, from the fit to the branching fractions, x_i ≡ Γ_i/Γ_{total}. The fit constrains the x_i whose labels appear in this array to sum to one.

x ₄	-88			
x ₁₁	27	-56		
x ₁₂	3	-32	26	
x ₁₃	43	-64	20	2
	x ₁	x ₄	x ₁₁	x ₁₂

f₀(1500) Γ(i)Γ(γγ)/Γ(total)

Γ(ππ) × Γ(γγ)/Γ _{total}	CL%	DOCUMENT ID	TECN	COMMENT	Γ ₁₄ /Γ
33 ⁺¹² ₋₆ + 1809 ⁺²¹		¹ UEHARA	08A	BELL	10.6 e ⁺ e ⁻ → e ⁺ e ⁻ π ⁰ π ⁰
not seen		ACCIARRI	01H	L3	γγ → K _S ⁰ K _S ⁰ , E _{cm} ^{ee} = 91, 183-209 GeV
<460	95	BARATE	00E	ALEP	γγ → π ⁺ π ⁻

¹ May also be the f₀(1370). Multiplied by us by 3 to obtain the ππ value.

f₀(1500) BRANCHING RATIOS

Γ(ππ)/Γ _{total}	DOCUMENT ID	TECN	COMMENT	Γ ₁ /Γ
0.454 ± 0.104	BUGG	96	RVUE	

Γ(π ⁺ π ⁻)/Γ _{total}	DOCUMENT ID	TECN	COMMENT	Γ ₂ /Γ
seen	BERTIN	98	OBLX	0.05-0.405 $\bar{p} p \rightarrow \pi^+ \pi^+ \pi^-$
possibly seen	FRABETTI	97D	E687	D _S [±] → π [∓] π [±] π [±]

Γ(4π)/Γ(ππ)	DOCUMENT ID	TECN	COMMENT	Γ ₄ /Γ ₁
1.42 ± 0.18 OUR FIT	Error includes scale factor of 1.2.			
1.42 ± 0.18 OUR AVERAGE	Error includes scale factor of 1.2.			
1.37 ± 0.16	BARBERIS	00D	450 pp → p _f 4πp _s	
2.1 ± 0.6	¹ AMSLER	98	RVUE	
••• We do not use the following data for averages, fits, limits, etc. •••				
2.1 ± 0.2	² ANISOVICH	02D	SPEC	Combined fit
3.4 ± 0.8	¹ ABELE	96	CBAR	0.0 $\bar{p} p \rightarrow 5\pi^0$

¹ Excluding ρρ contribution to 4π.
² From a combined K-matrix analysis of Crystal Barrel (0. $p\bar{p} \rightarrow \pi^0 \pi^0 \pi^0, \pi^0 \eta \eta, \pi^0 \pi^0 \eta$), GAMS (πρ → π⁰π⁰n, ηηη, ηη'η), and BNL (πρ → K \bar{K} n) data.

Γ(2(ππ) _{s-wave})/Γ(ππ)	DOCUMENT ID	TECN	COMMENT	Γ ₇ /Γ ₁
0.42 ± 0.26	¹ ABELE	01	CBAR	0.0 $\bar{p} d \rightarrow \pi^- 4\pi^0 p$

¹ From the combined data of ABELE 96 and ABELE 96C.

Γ(2(ππ) _{s-wave})/Γ(4π)	DOCUMENT ID	TECN	COMMENT	Γ ₇ /Γ ₄
0.26 ± 0.07	ABELE	01B	CBAR	0.0 $\bar{p} d \rightarrow 5\pi p$

••• We do not use the following data for averages, fits, limits, etc. •••

Γ(ρρ)/Γ(4π)	DOCUMENT ID	TECN	COMMENT	Γ ₈ /Γ ₄
0.13 ± 0.08	ABELE	01B	CBAR	0.0 $\bar{p} d \rightarrow 5\pi p$

••• We do not use the following data for averages, fits, limits, etc. •••

Γ(ρρ)/Γ(2(ππ) _{s-wave})	DOCUMENT ID	COMMENT	Γ ₈ /Γ ₇
2.87 ± 0.34 OUR AVERAGE	Error includes scale factor of 1.1.		
3.3 ± 0.5	BARBERIS	00c 450 pp → p _f π ⁺ π ⁻ 2π ⁰ p _s	
2.6 ± 0.4	BARBERIS	00c 450 pp → p _f 2(π ⁺ π ⁻)p _s	

Γ(π(1300)π)/Γ(4π)	DOCUMENT ID	TECN	COMMENT	Γ ₉ /Γ ₄
0.50 ± 0.25	ABELE	01B	CBAR	0.0 $\bar{p} d \rightarrow 5\pi p$

••• We do not use the following data for averages, fits, limits, etc. •••

Γ(a ₁ (1260)π)/Γ(4π)	DOCUMENT ID	TECN	COMMENT	Γ ₁₀ /Γ ₄
0.12 ± 0.05	ABELE	01B	CBAR	0.0 $\bar{p} d \rightarrow 5\pi p$

••• We do not use the following data for averages, fits, limits, etc. •••

Γ(ηη)/Γ _{total}	DOCUMENT ID	TECN	COMMENT	Γ ₁₁ /Γ
large	ALDE	88	GAM4	300 π ⁻ N → ηηπ ⁻ N
large	BINON	83	GAM2	38 π ⁻ p → 2η n

••• We do not use the following data for averages, fits, limits, etc. •••

Γ(ηη)/Γ(ππ)	DOCUMENT ID	TECN	COMMENT	Γ ₁₁ /Γ ₁
0.175 ± 0.024 OUR FIT	Error includes scale factor of 1.1.			
0.175 ± 0.027 OUR AVERAGE				
0.18 ± 0.03	BARBERIS	00E	450 pp → p _f ηηp _s	
0.157 ± 0.060	¹ AMSLER	95D	CBAR	0.0 $\bar{p} p \rightarrow \pi^0 \pi^0 \pi^0, \pi^0 \eta \eta, \pi^0 \pi^0 \eta$
••• We do not use the following data for averages, fits, limits, etc. •••				
0.080 ± 0.033	AMSLER	02	CBAR	0.9 $\bar{p} p \rightarrow \pi^0 \eta \eta, \pi^0 \pi^0 \pi^0$
0.11 ± 0.03	² ANISOVICH	02D	SPEC	Combined fit
0.078 ± 0.013	³ ABELE	96c	RVUE	Compilation
0.230 ± 0.097	⁴ AMSLER	95c	CBAR	0.0 $\bar{p} p \rightarrow \eta \eta \pi^0$

- ¹ Coupled-channel analysis of AMSLER 95B, AMSLER 95C, and AMSLER 94D.
- ² From a combined K-matrix analysis of Crystal Barrel (0. $p\bar{p} \rightarrow \pi^0 \pi^0 \pi^0, \pi^0 \eta \eta, \pi^0 \pi^0 \eta$), GAMS (πρ → π⁰π⁰n, ηηη, ηη'η), and BNL (πρ → K \bar{K} n) data.
- ³ 2π width determined to be 60 ± 12 MeV.
- ⁴ Using AMSLER 95B (3π⁰).

Γ(4π ⁰)/Γ(ηη)	DOCUMENT ID	TECN	COMMENT	Γ ₅ /Γ ₁₁
0.8 ± 0.3	ALDE	87	GAM4	100 π ⁻ p → 4π ⁰ n

••• We do not use the following data for averages, fits, limits, etc. •••

Γ(ηη'(958))/Γ(ππ)	DOCUMENT ID	TECN	COMMENT	Γ ₁₂ /Γ ₁
0.064 ± 0.022 OUR FIT	Error includes scale factor of 1.4.			
0.095 ± 0.026	BARBERIS	00A	450 pp → p _f ηηp _s	
••• We do not use the following data for averages, fits, limits, etc. •••				
0.005 ± 0.003	¹ ANISOVICH	02D	SPEC	Combined fit

¹ From a combined K-matrix analysis of Crystal Barrel (0. $p\bar{p} \rightarrow \pi^0 \pi^0 \pi^0, \pi^0 \eta \eta, \pi^0 \pi^0 \eta$), GAMS (πρ → π⁰π⁰n, ηηη, ηη'η), and BNL (πρ → K \bar{K} n) data.

Meson Particle Listings

$f_0(1500)$, $f_1(1510)$

$\Gamma(\eta'(\eta))/\Gamma(\eta)$

VALUE	DOCUMENT ID	TECN	COMMENT
0.37±0.13 OUR FIT	Error includes scale factor of 1.5.		
0.29±0.10	¹ AMSLER 95c	CBAR	0.0 $\bar{p}p \rightarrow \eta\eta\pi^0$
• • • We do not use the following data for averages, fits, limits, etc. • • •			
0.05±0.03	² ANISOVICH 02d	SPEC	Combined fit
0.84±0.23	ABELE 96c	RVUE	Compilation
2.7 ± 0.8	BINON 84c	GAM2	38 $\pi^- p \rightarrow \eta\eta' n$

¹ Using AMSLER 94E ($\eta\eta'\pi^0$).
² From a combined K-matrix analysis of Crystal Barrel (0. $p\bar{p} \rightarrow \pi^0\pi^0\pi^0$, $\pi^0\eta\eta$, $\pi^0\pi^0\eta$), GAMS ($\pi p \rightarrow \pi^0\pi^0 n$, $\eta\eta n$, $\eta\eta' n$), and BNL ($\pi p \rightarrow K\bar{K}n$) data.

$\Gamma(K\bar{K})/\Gamma_{total}$

VALUE	DOCUMENT ID	TECN	COMMENT
• • • We do not use the following data for averages, fits, limits, etc. • • •			
0.044±0.021	BUGG 96	RVUE	

$\Gamma(K\bar{K})/\Gamma(\pi\pi)$

VALUE	DOCUMENT ID	TECN	COMMENT
0.246±0.025 OUR FIT			
0.236±0.026 OUR AVERAGE			
0.25 ± 0.03	¹ BARGIOTTI 03	OBLX	$\bar{p}p$
0.19 ± 0.07	² ABELE 98	CBAR	0.0 $\bar{p}p \rightarrow K^0 K^\pm \pi^\mp$
0.20 ± 0.08	³ ABELE 96b	CBAR	0.0 $\bar{p}p \rightarrow \pi^0 K_L^0 K_L^0$
• • • We do not use the following data for averages, fits, limits, etc. • • •			
0.16 ± 0.05	⁴ ANISOVICH 02d	SPEC	Combined fit
0.33 ± 0.03 ± 0.07	BARBERIS 99d	OMEG	450 $pp \rightarrow K^+ K^- \pi^+ \pi^-$

¹ Coupled channel analysis of $\pi^+\pi^-\pi^0$, $K^+K^-\pi^0$, and $K^\pm K_S^0 \pi^\mp$.
² Using $\pi^0\pi^0$ from AMSLER 95b.
³ Using AMSLER 95b ($3\pi^0$), AMSLER 94c ($2\pi^0\eta$) and SU(3).
⁴ From a combined K-matrix analysis of Crystal Barrel (0. $p\bar{p} \rightarrow \pi^0\pi^0\pi^0$, $\pi^0\eta\eta$, $\pi^0\pi^0\eta$), GAMS ($\pi p \rightarrow \pi^0\pi^0 n$, $\eta\eta n$, $\eta\eta' n$), and BNL ($\pi p \rightarrow K\bar{K}n$) data.

$\Gamma(K\bar{K})/\Gamma(\eta\eta)$

VALUE	CL%	DOCUMENT ID	TECN	COMMENT
1.43±0.24 OUR FIT	Error includes scale factor of 1.1.			
1.85±0.41		BARBERIS 00e	450	$pp \rightarrow p\eta\eta\eta_S$
• • • We do not use the following data for averages, fits, limits, etc. • • •				
1.5 ± 0.6		¹ ANISOVICH 02d	SPEC	Combined fit
<0.4	90	² PROKOSHKIN 91	GAM4	300 $\pi^- p \rightarrow \pi^- \rho\eta\eta$
<0.6		³ BINON 83	GAM2	38 $\pi^- p \rightarrow 2\eta n$

¹ From a combined K-matrix analysis of Crystal Barrel (0. $p\bar{p} \rightarrow \pi^0\pi^0\pi^0$, $\pi^0\eta\eta$, $\pi^0\pi^0\eta$), GAMS ($\pi p \rightarrow \pi^0\pi^0 n$, $\eta\eta n$, $\eta\eta' n$), and BNL ($\pi p \rightarrow K\bar{K}n$) data.
² Combining results of GAM4 with those of WA76 on $K\bar{K}$ central production.
³ Using ETKIN 82b and COHEN 80.

$f_0(1500)$ REFERENCES

RODAS 22	EPJ C82 80	A. Rodas et al.	(JPAK Collab.)
SARANTSEV 21	PL B816 136227	A.V. Sarantsev et al.	(BONN, PNPI)
ALBRECHT 20	EPJ C80 453	M. Albrecht et al.	(Crystal Barrel Collab.)
ABLIKIM 18AA	PR D98 072003	M. Ablikim et al.	(BESIII Collab.)
ROPERTZ 18	EPJ C78 1000	S. Roperitz, C. Hanhart, B. Kubis	(BONN, JULI)
AALJ 17V	JHEP 1708 037	R. Aaij et al.	(LHCb Collab.)
ABLIKIM 15AE	PR D92 052003	M. Ablikim et al.	(BESIII Collab.)
DOBBS 15	PR D91 052006	S. Dobbs et al.	(NWES)
AALJ 14BR	PR D89 092006	R. Aaij et al.	(LHCb Collab.)
ABLIKIM 13N	PR D87 092009	M. Ablikim et al.	(BESIII Collab.)
ANISOVICH 09	JUMP A24 2481	V.V. Anisovich, A.V. Sarantsev	(BONN+)
KLEMP 08	EPJ C55 39	E. Klempt, M. Matveev, A.V. Sarantsev	(BONN+)
UEHARA 08A	PR D78 052004	S. Uehara et al.	(BELLE Collab.)
ABLIKIM 06V	PL B642 441	M. Ablikim et al.	(BES Collab.)
AMSLER 06	PL B639 165	C. Amstler et al.	(Crystal Barrel Collab.)
AUBERT 06O	PR D74 032003	B. Aubert et al.	(BABAR Collab.)
UMAN 06	PR D73 052009	I. Uman et al.	(FNAL E835)
VLADIMIRSK... 06	PAN 69 493	V.V. Vladimirov et al.	(ITEP, Moscow)
	Translated from YAF 69 515.		
BINON 05	PAN 68 960	F. Binon et al.	(ALEPH Collab.)
	Translated from YAF 68 998.		
GARMASH 05	PR D71 092003	A. Garmash et al.	(BELLE Collab.)
ANISOVICH 03	EPJ A16 229	V.V. Anisovich et al.	(BONN)
BARGIOTTI 03	EPJ C26 371	M. Bargiotti et al.	(OBELIX Collab.)
AMSLER 02	EPJ C23 29	C. Amstler et al.	(WA 102 Collab.)
ANISOVICH 02D	PAN 65 1545	V.V. Anisovich et al.	(ALEPH Collab.)
	Translated from YAF 65 1583.		
ABELE 01	EPJ C19 667	A. Abele et al.	(Crystal Barrel Collab.)
ABELE 01B	EPJ C21 261	A. Abele et al.	(Crystal Barrel Collab.)
ACCIARRI 01H	PL B501 173	M. Acciari et al.	(L3 Collab.)
AITALA 01A	PRL 86 765	E.M. Aitala et al.	(FNAL E791 Collab.)
BARATE 00E	PL B472 189	R. Barate et al.	(ALEPH Collab.)
BARBERIS 00A	PL B471 429	D. Barberis et al.	(WA 102 Collab.)
BARBERIS 00C	PL B471 440	D. Barberis et al.	(WA 102 Collab.)
BARBERIS 00D	PL B474 423	D. Barberis et al.	(WA 102 Collab.)
BARBERIS 00E	PL B479 59	D. Barberis et al.	(WA 102 Collab.)
BARBERIS 99	PL B453 305	D. Barberis et al.	(Omega Expt.)
BARBERIS 99B	PL B453 316	D. Barberis et al.	(Omega Expt.)
BARBERIS 99D	PL B462 462	D. Barberis et al.	(Omega Expt.)
BELLAZZINI 99	PL B467 296	R. Bellazzini et al.	(WA 102 Collab.)
FRENCH 99	PL B460 213	B. French et al.	(WA76 Collab.)
KAMINSKI 99	EPJ C9 141	R. Kaminski, L. Lesniak, B. Loiseau	(CRAC, PARIN)
ABELE 98	PR D57 3860	A. Abele et al.	(Crystal Barrel Collab.)
ALDE 98	EPJ A3 361	D. Alde et al.	(GAMMA Collab.)
	PAN 62 405	D. Alde et al.	(GAMS Collab.)
	Translated from YAF 62 446.		
AMSLER 98	RMP 70 1293	C. Amstler	
ANISOVICH 98B	SPU 41 419	V.V. Anisovich et al.	
	Translated from UFN 168 481.		

BERTIN 98	PR D57 55	A. Bertin et al.	(OBELIX Collab.)
REYES 98	PRL 81 4079	M.A. Reyes et al.	(WA 102 Collab.)
BARBERIS 97B	PL B413 217	D. Barberis et al.	(OBELIX Collab.)
BERTIN 97C	PL B408 476	A. Bertin et al.	(OBELIX Collab.)
FRABETTI 97D	PL B407 79	P.L. Frabetti et al.	(FNAL E687 Collab.)
ABELE 96	PL B380 453	A. Abele et al.	(Crystal Barrel Collab.)
ABELE 96B	PL B385 425	A. Abele et al.	(Crystal Barrel Collab.)
ABELE 96C	NP A609 562	A. Abele et al.	(Crystal Barrel Collab.)
AMELIN 96B	PAN 59 976	D.V. Amelin et al.	(SERP, TBLI)
	Translated from YAF 59 1021.		
BUGG 96	NP B471 59	D.V. Bugg, A.V. Sarantsev, B.S. Zou	(LOQM, PNPI)
AMSLER 95B	PL B342 433	C. Amstler et al.	(Crystal Barrel Collab.)
AMSLER 95C	PL B353 571	C. Amstler et al.	(Crystal Barrel Collab.)
AMSLER 95D	PL B355 425	C. Amstler et al.	(Crystal Barrel Collab.)
ANTINORI 95	PL B353 589	F. Antinori et al.	(ATHU, BARI, BIRM+)
BUGG 95	PL B353 378	D.V. Bugg et al.	(ATHU, BARI, BIRM+)
ABATZIS 94	PL B324 509	S. Abatzis et al.	(ATHU, BARI, BIRM+)
AMSLER 94C	PL B327 425	C. Amstler et al.	(Crystal Barrel Collab.)
AMSLER 94D	PL B333 277	C. Amstler et al.	(Crystal Barrel Collab.)
AMSLER 94E	PL B340 259	C. Amstler et al.	(Crystal Barrel Collab.)
ANISOVICH 94	PL B323 233	V.V. Anisovich et al.	(Crystal Barrel Collab.)
BUGG 94	PR D50 4412	D.V. Bugg et al.	(LOQM)
AMSLER 92	PL B291 347	C. Amstler et al.	(Crystal Barrel Collab.)
BELADIDZE 92C	SJNP 55 1535	G.M. Beladidze, S.I. Bityukov, G.V. Borisov	(SERP+)
	Translated from YAF 55 2748.		
PROKOSHKIN 91	SPD 36 155	Y.D. Prokoshkin	(GAM2 and GAM4 Collab.)
	Translated from DANS 316 900.		
ARMSTRONG 89E	PL B228 536	T.A. Armstrong, M. Benayoun	(ATHU, BARI, BIRM+)
ALDE 88	PL B201 160	D.M. Alde et al.	(SERP, BELG, LANL, LAPP+)
ASTON 88D	NP B301 525	D. Aston et al.	(SLAC, NAGO, CIN, INUS)
ALDE 87	PL B198 286	D.M. Alde et al.	(LANL, BRUX, SERP, LAPP)
ALDE 86D	NP B269 485	D.M. Alde et al.	(BELG, LAPP, SERP, CERN+)
LON GACRE 86	PL B177 223	R.S. Longacre et al.	(BNL, BRAN, CUNY+)
BINON 84C	NC 80A 363	F.G. Binon et al.	(BELG, LAPP, SERP+)
BINON 83	NC 78A 313	F.G. Binon et al.	(BELG, LAPP, SERP+)
	Also SJNP 38 561	F.G. Binon et al.	(BELG, LAPP, SERP+)
	Translated from YAF 38 934.		
GRAY 83	PR D27 307	L. Gray et al.	(SYRA)
ETKIN 82B	PR D25 1786	A. Etkin et al.	(BNL, CUNY, TUFTS, VAND)
COHEN 80	PR D22 2595	D. Cohen et al.	(ANL)
HYAMS 75	NP B100 205	B.D. Hyams et al.	(CERN, MPIM)

$f_1(1510)$

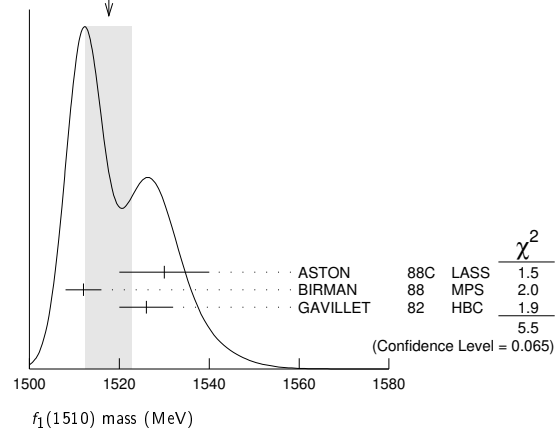
$$I^G(J^{PC}) = 0^+(1^+)$$

OMITTED FROM SUMMARY TABLE
 See the review on "Spectroscopy of Light Meson Resonances."

$f_1(1510)$ MASS

VALUE (MeV)	EVTS	DOCUMENT ID	TECN	COMMENT
1518±5 OUR AVERAGE	Error includes scale factor of 1.7. See the ideogram below.			
1530±10		ASTON 88C	LASS	11 $K^- p \rightarrow K_S^0 K^\pm \pi^\mp \Lambda$
1512±4	600	¹ BIRMAN 88	MPS	8 $\pi^- p \rightarrow K^+ K^0 \pi^- n$
1526±6	271	GAVILLET 82	HBC	4.2 $K^- p \rightarrow \Lambda K K \pi$
• • • We do not use the following data for averages, fits, limits, etc. • • •				
~ 1525		² BAUER 93b		$\gamma\gamma^* \rightarrow \pi^+ \pi^- \pi^0 \pi^0$

WEIGHTED AVERAGE
 1518±5 (Error scaled by 1.7)



¹ From partial wave analysis of $K^+ K^0 \pi^-$ state.
² Not seen by AIHARA 88c in the $K_S^0 K^\pm \pi^\mp$ final state.

$f_1(1510)$ WIDTH

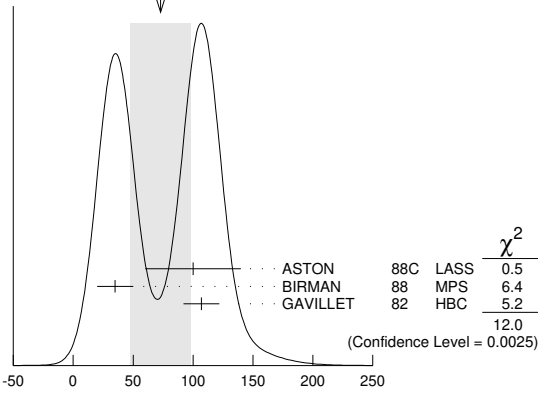
VALUE (MeV)	EVTS	DOCUMENT ID	TECN	COMMENT
73±25 OUR AVERAGE	Error includes scale factor of 2.5. See the ideogram below.			
100±40		ASTON 88C	LASS	11 $K^- p \rightarrow K_S^0 K^\pm \pi^\mp \Lambda$
35±15	600	³ BIRMAN 88	MPS	8 $\pi^- p \rightarrow K^+ K^0 \pi^- n$
107±15	271	GAVILLET 82	HBC	4.2 $K^- p \rightarrow \Lambda K K \pi$

See key on page 1127

Meson Particle Listings

$f_1(1510), f'_2(1525)$

WEIGHTED AVERAGE
73±25 (Error scaled by 2.5)



³From partial wave analysis of $K^+\bar{K}^0\pi^-$ state.

$f_1(1510)$ DECAY MODES

Mode	Fraction (Γ_i/Γ)
Γ_1 $K\bar{K}^*(892) + c.c.$	seen
Γ_2 $\pi^+\pi^-\eta'$	seen

$f_1(1510)$ BRANCHING RATIOS

$\Gamma(\pi^+\pi^-\eta')/\Gamma_{total}$	VALUE	EVTS	DOCUMENT ID	TECN	COMMENT	Γ_2/Γ
seen	230		ABLIKIM	11c	BES3	$J/\psi \rightarrow \gamma\pi^+\pi^-\eta'$

$f_1(1510)$ REFERENCES

ABLIKIM	11C	PRL 106 072002	M. Ablikim et al.	(BESIII Collab.)
BAUER	93B	PR D48 3976	D.A. Bauer et al.	(SLAC)
AIHARA	88C	PR D38 1	H. Aihara et al.	(TPC-2 γ Collab.)
ASTON	88C	PL B201 573	D. Aston et al.	(SLAC, NAGO, CINC, INUS) JP
BIRMAN	88	PRL 61 1557	A. Birman et al.	(BNL, FSU, IND, MASD) JP
GAVILLET	82	ZPHY C16 119	P. Gavillet et al.	(CERN, CDEF, PADO+)

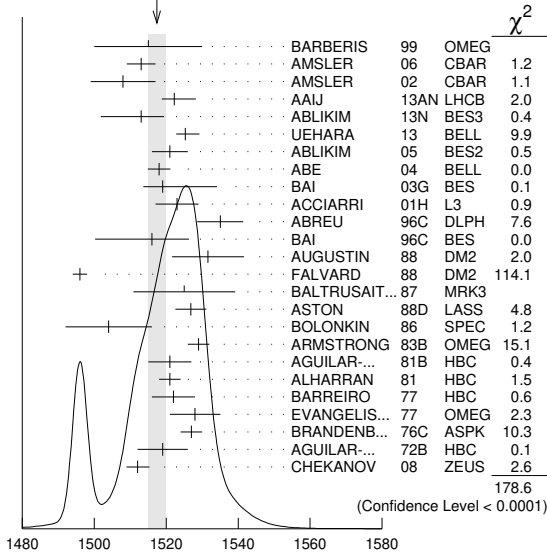
$f'_2(1525)$

$I^G(J^{PC}) = 0^+(2^{++})$

$f'_2(1525)$ MASS

VALUE (MeV) DOCUMENT ID
1517.4±2.5 OUR AVERAGE Includes data from the 6 datablocks that follow this one. Error includes scale factor of 2.8. See the ideogram below.

WEIGHTED AVERAGE
1517.4±2.5 (Error scaled by 2.8)



$f'_2(1525)$ MASS (MeV)

PRODUCED BY PION BEAM

VALUE (MeV) EVTS DOCUMENT ID TECN COMMENT
The data in this block is included in the average printed for a previous datablock.

1521±13		TIKHOMIROV 03	SPEC	40.0	$\pi^-C \rightarrow K_S^0 K_S^0 K_L^0 X$
1547 ⁺¹⁰ ₋₂	1	LONGACRE 86	MPS	22	$\pi^-p \rightarrow K_S^0 K_S^0 n$
1496 ⁺⁹ ₋₈	2	CHABAUD 81	ASPK	6	$\pi^-p \rightarrow K^+ K^- n$
1497 ⁺⁸ ₋₉		CHABAUD 81	ASPK	18.4	$\pi^-p \rightarrow K^+ K^- n$
1492±29		GORLICH 80	ASPK	17	π^-p polarized $\rightarrow K^+ K^- n$
1502±25	3	CORDEN 79	OMEG	12-15	$\pi^-p \rightarrow \pi^+\pi^- n$
1480	14	CRENNELL 66	HBC	6.0	$\pi^-p \rightarrow K_S^0 K_S^0 n$

¹From a partial-wave analysis of data using a K-matrix formalism with 5 poles.
²CHABAUD 81 is a reanalysis of PAWLICKI 77 data.
³From an amplitude analysis where the $f'_2(1525)$ width and elasticity are in complete disagreement with the values obtained from $K\bar{K}$ channel, making the solution dubious.

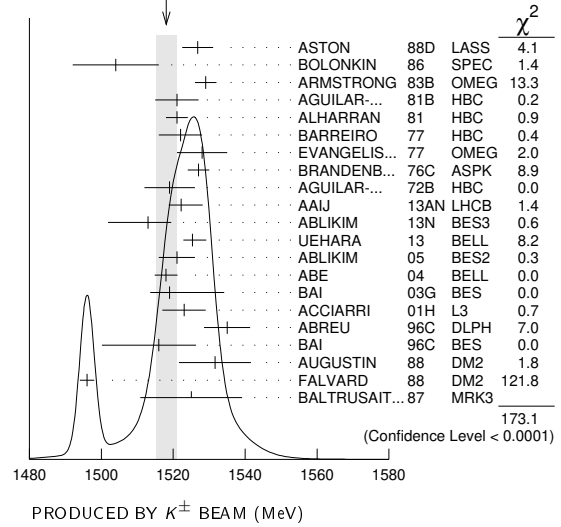
PRODUCED BY K^\pm BEAM

VALUE (MeV) EVTS DOCUMENT ID TECN COMMENT
The data in this block is included in the average printed for a previous datablock.

1518.1± 2.8 OUR AVERAGE Includes data from the datablock that follows this one. Error includes scale factor of 3.0. See the ideogram below.

1526.8± 4.3		ASTON 88D	LASS	11	$K^-p \rightarrow K_S^0 K_S^0 \Lambda$	
1504 ± 12		BOLONKIN 86	SPEC	40	$K^-p \rightarrow K_S^0 K_S^0 Y$	
1529 ± 3		ARMSTRONG 83B	OMEG	18.5	$K^-p \rightarrow K^- K^+ \Lambda$	
1521 ± 6	650	AGUILAR...	81B	HBC	4.2	$K^-p \rightarrow \Lambda K^+ K^-$
1521 ± 3	572	ALHARRAN 81	HBC	8.25	$K^-p \rightarrow \Lambda K\bar{K}$	
1522 ± 6	123	BARREIRO 77	HBC	4.15	$K^-p \rightarrow \Lambda K_S^0 K_S^0$	
1528 ± 7	166	EVA NGELIS... 77	OMEG	10	$K^-p \rightarrow K^+ K^- (\Lambda, \Sigma)$	
1527 ± 3	120	BRANDENB... 76C	ASPK	13	$K^-p \rightarrow K^+ K^- (\Lambda, \Sigma)$	
1519 ± 7	100	AGUILAR... 72B	HBC	3.9,4.6	$K^-p \rightarrow K\bar{K}(\Lambda, \Sigma)$	
1514 ± 8	61	BINON 07	GAMS	32.5	$K^-p \rightarrow \eta\eta(\Lambda/\Sigma^0)$	
1513 ± 10		BARKOV 99	SPEC	40	$K^-p \rightarrow K_S^0 K_S^0 Y$	

WEIGHTED AVERAGE
1518.1±2.8 (Error scaled by 3.0)



¹Systematic errors not estimated.

PRODUCED IN e^+e^- ANNIHILATION AND PARTICLE DECAYS

VALUE (MeV) EVTS DOCUMENT ID TECN COMMENT
The data in this block is included in the average printed for a previous datablock.

1514⁺⁵₋₄ OUR AVERAGE Error includes scale factor of 3.8. See the ideogram below.

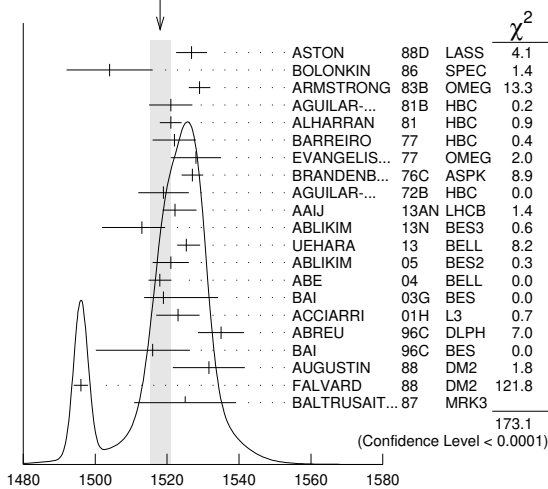
1522.2± 2.8 ^{+5.3} _{-2.0}		AAIJ	13AN	LHCB	$\bar{B}_s^0 \rightarrow J/\psi K^+ K^-$
1513 ± 5 ⁺⁴ ₋₁₀	5.5k	¹ ABLIKIM	13N	BES3	$e^+e^- \rightarrow J/\psi \rightarrow \gamma\eta\eta$
1525.3 ^{+1.2+3.7} _{-1.4-2.1}		UEHARA	13	BELL	$\gamma\gamma \rightarrow K_S^0 K_S^0$
1521 ± 5		ABLIKIM	05	BES2	$J/\psi \rightarrow \phi K^+ K^-$
1518 ± 1 ± 3		ABE	04	BELL	$10.6 e^+e^- \rightarrow e^+e^- K^+ K^-$
1519 ± 2 ⁺¹⁵ ₋₅		BAI	03G	BES	$J/\psi \rightarrow \gamma K\bar{K}$

Meson Particle Listings

$f'_2(1525)$

VALUE (MeV)	DOCUMENT ID	TECN	COMMENT
1523 ± 6	331	2	ACCIARRI 01H L3 91, 183-209 $e^+e^- \rightarrow e^+e^-K_S^0K_S^0$
1535 ± 5 ± 4			ABREU 96C DLPH $Z^0 \rightarrow K^+K^- + X$
1516 ± 5 ± $\frac{9}{15}$			BAI 96C BES $J/\psi \rightarrow \gamma K^+K^-$
1531.6 ± 10.0			AUGUSTIN 88 DM2 $J/\psi \rightarrow \gamma K^+K^-$
1496 ± 2			FALVARD 88 DM2 $J/\psi \rightarrow \phi K^+K^-$
1525 ± 10 ± 10			BALTRUSAIT...87 MRK3 $J/\psi \rightarrow \gamma K^+K^-$
1503 ± 11			4 RODAS 22 RVUE $J/\psi(1S) \rightarrow \gamma(\pi\pi, K\bar{K})$
1532 ± 3 ± 6	644	5,6	DOBBS 15 $J/\psi \rightarrow \gamma K^+K^-$
1557 ± 9 ± 3	113	5,6	DOBBS 15 $\psi(2S) \rightarrow \gamma K^+K^-$
1526 ± 7			7 LEES 29 14H BABR $e^+e^- \rightarrow K_S^0K_S^0K^+K^-\gamma$
1523 ± 5			8 SCHEGELSKY 06A RVUE $\gamma\gamma \rightarrow K_S^0K_S^0$
1515 ± 5			9 FALVARD 88 DM2 $J/\psi \rightarrow \phi K^+K^-$

WEIGHTED AVERAGE
1518.1±2.8 (Error scaled by 3.0)



PRODUCED BY K^\pm BEAM (MeV)

- From partial wave analysis including all possible combinations of 0^{++} , 2^{++} , and 4^{++} resonances.
- Supersedes ACCIARRI 95J.
- From an analysis including interference with $f_0(1710)$.
- T-matrix pole from coupled channel K-matrix fit to data on $J/\psi \rightarrow \gamma \pi^0 \pi^0$ (ABLIKIM 15AE) and $J/\psi \rightarrow \gamma K_S^0 K_S^0$ (ABLIKIM 18AA).
- Using CLEO-c data but not authored by the CLEO Collaboration.
- From a fit to a Breit-Wigner line shape with fixed $\Gamma = 73$ MeV.
- From a fit to a Breit-Wigner line shape plus a second-order polynomial function. Systematic errors not evaluated.
- From analysis of L3 data at 91 and 183-209 GeV.
- From an analysis ignoring interference with $f_0(1710)$.

PRODUCED IN $\bar{p}p$ ANNIHILATION

VALUE (MeV)	DOCUMENT ID	TECN	COMMENT
The data in this block is included in the average printed for a previous datablock.			

1512 ± 4 OUR AVERAGE

VALUE (MeV)	DOCUMENT ID	TECN	COMMENT
1513 ± 4			AMSLER 06 CBAR 0.9 $\bar{p}p \rightarrow K^+K^-\pi^0$
1508 ± 9	1		AMSLER 02 CBAR 0.9 $\bar{p}p \rightarrow \pi^0\eta\eta, \pi^0\pi^0\pi^0$
1495.0 ± 1.1 ± 8.1	2		ALBRECHT 20 RVUE 0.9 $\bar{p}p \rightarrow \pi^0\pi^0\eta, \pi^0\eta\eta$
1530 ± 12	3		ANISOVICH 09 RVUE 0.0 $\bar{p}p, \pi N$

- T-matrix pole.
- T-matrix pole, 4 poles, 4 channels, including scattering data from HYAMS 75 ($\pi\pi$), LONGACRE 86 ($K\bar{K}$), BINON 83 ($\eta\eta$).
- 4-poles, 5-channel K matrix fit.

CENTRAL PRODUCTION

VALUE (MeV)	DOCUMENT ID	TECN	COMMENT
The data in this block is included in the average printed for a previous datablock.			

VALUE (MeV)	DOCUMENT ID	TECN	COMMENT
1515 ± 15	BARBERIS 99	OMEG	450 $pp \rightarrow p_S p_f K^+ K^-$

PRODUCED IN $e\bar{p}$ COLLISIONS

VALUE (MeV)	EVTS	DOCUMENT ID	TECN	COMMENT
The data in this block is included in the average printed for a previous datablock.				

VALUE (MeV)	EVTS	DOCUMENT ID	TECN	COMMENT
1512 ± 3 ± $\frac{1.4}{0.5}$				1 CHEKANOV 08 ZEUS $e\bar{p} \rightarrow K_S^0 K_S^0 X$

VALUE (MeV)	EVTS	DOCUMENT ID	TECN	COMMENT
1537 ± $\frac{9}{8}$				2 CHEKANOV 04 ZEUS $e\bar{p} \rightarrow K_S^0 K_S^0 X$

- In the SU(3) based model with a specific interference pattern of the $f_2(1270)$, $a_2^0(1320)$, and $f'_2(1525)$ mesons incoherently added to the $f_0(1710)$ and non-resonant background.
- Systematic errors not estimated.

$f'_2(1525)$ WIDTH

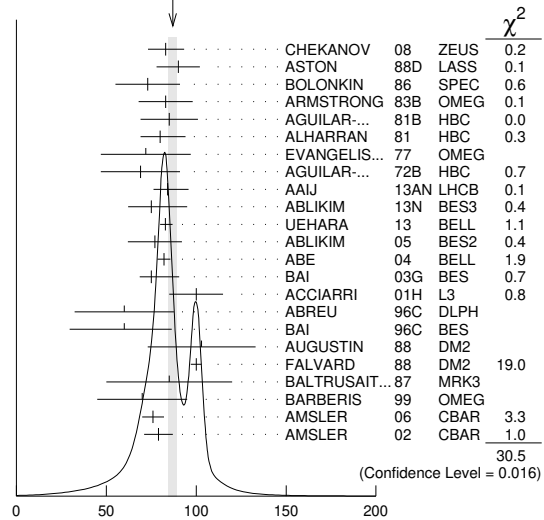
VALUE (MeV)	DOCUMENT ID	TECN	COMMENT
86 ± 5	OUR FIT		Error includes scale factor of 2.2.
86.9 ± $\frac{2.3}{2.1}$	PDG	18	Average of width measurements

PRODUCED BY PION BEAM

VALUE (MeV)	DOCUMENT ID	TECN	COMMENT
86.9 ± $\frac{2.3}{2.1}$	OUR AVERAGE		Includes data from the 5 datablocks that follow this one. Error includes scale factor of 1.4. See the ideogram below.

- We do not use the following data for averages, fits, limits, etc.
- TIKHOMIROV 03 SPEC 40.0 $\pi^- C \rightarrow K_S^0 K_S^0 K_L^0 X$
- LONGACRE 86 MPS 22 $\pi^- p \rightarrow K_S^0 K_S^0 n$
- CHABAUD 81 ASPK 6 $\pi^- p \rightarrow K^+ K^- n$
- CHABAUD 81 ASPK 18.4 $\pi^- p \rightarrow K^+ K^- n$
- GORLICH 80 ASPK 17 $\pi^- p$ polarized $\rightarrow K^+ K^- n$
- CORDEN 79 OMEG 12-15 $\pi^- p \rightarrow \pi^+ \pi^- n$
- POLYCHRO... 79 STRC 7 $\pi^- p \rightarrow n K_S^0 K_S^0$

WEIGHTED AVERAGE
86.9-2.3-2.1 (Error scaled by 1.4)



$f'_2(1525)$ WIDTH (MeV)

- From a partial-wave analysis of data using a K-matrix formalism with 5 poles.
- CHABAUD 81 is a reanalysis of PAWLICKI 77 data.
- From an amplitude analysis where the $f'_2(1525)$ width and elasticity are in complete disagreement with the values obtained from $K\bar{K}$ channel, making the solution dubious.
- From a fit to the D with $f_2(1270)$ - $f'_2(1525)$ interference. Mass fixed at 1516 MeV.

PRODUCED BY K^\pm BEAM

VALUE (MeV)	EVTS	DOCUMENT ID	TECN	COMMENT
The data in this block is included in the average printed for a previous datablock.				

82 ± 6 OUR AVERAGE

VALUE (MeV)	EVTS	DOCUMENT ID	TECN	COMMENT
90 ± 12				ASTON 88D LASS 11 $K^- p \rightarrow K_S^0 K_S^0 \Lambda$
73 ± 18				BOLONKIN 86 SPEC 40 $K^- p \rightarrow K_S^0 K_S^0 Y$
83 ± 15				ARMSTRONG 83B OMEG 18.5 $K^- p \rightarrow K^- K^+ \Lambda$
85 ± 16	650			AGUILAR... 81B HBC 4.2 $K^- p \rightarrow \Lambda K^+ K^-$
80 ± $\frac{14}{11}$	572			ALHARRAN 81 HBC 8.25 $K^- p \rightarrow \Lambda K\bar{K}$
72 ± 25	166			EVANGELIS... 77 OMEG 10 $K^- p \rightarrow K^+ K^- (\Lambda, \Sigma)$
69 ± 22	100			AGUILAR... 72B HBC 3.9, 4.6 $K^- p \rightarrow K\bar{K} (\Lambda, \Sigma)$

- We do not use the following data for averages, fits, limits, etc.
- BINON 07 GAMS 32.5 $K^- p \rightarrow \eta\eta (\Lambda/\Sigma^0)$
- BARKOV 99 SPEC 40 $K^- p \rightarrow K_S^0 K_S^0 y$
- BARREIRO 77 HBC 4.15 $K^- p \rightarrow \Lambda K_S^0 K_S^0$
- BRANDENB... 76C ASPK 13 $K^- p \rightarrow K^+ K^- (\Lambda, \Sigma)$
- Systematic errors not estimated.

See key on page 1127

Meson Particle Listings

$f_2'(1525)$

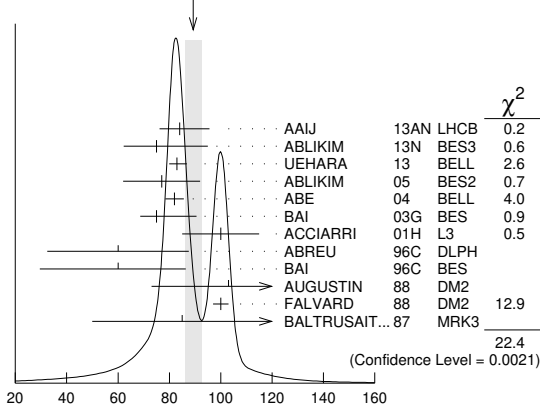
PRODUCED IN e^+e^- ANNIHILATION AND PARTICLE DECAYS

VALUE (MeV) EVTS DOCUMENT ID TECN COMMENT

The data in this block is included in the average printed for a previous datablock.

89.2^{+3.4}_{-3.0} OUR AVERAGE	Error includes scale factor of 1.8. See the ideogram below.
84 ± 6 ⁺¹⁰ ₋₅	AAIJ 13AN LHCb $\bar{B}_S^0 \rightarrow J/\psi K^+ K^-$
75 ⁺¹² ₋₁₀ ⁺¹⁶ ₋₈	5.5k 1 ABLIKIM 13N BES3 $e^+e^- \rightarrow J/\psi \rightarrow \gamma\eta\eta$
82.9 ^{+2.1} _{-2.2} ^{+3.3} _{-2.0}	UEHARA 13 BELL $\gamma\gamma \rightarrow K_S^0 K_S^0$
77 ± 15	ABLIKIM 05 BES2 $J/\psi \rightarrow \phi K^+ K^-$
82 ± 2 ± 3	ABE 04 BELL 10.6 $e^+e^- \rightarrow e^+e^- K^+ K^-$
75 ± 4 ⁺¹⁵ ₋₅	BAI 03G BES $J/\psi \rightarrow \gamma K\bar{K}$
100 ± 15	331 2 ACCIARRI 01H L3 91, 183-209 $e^+e^- \rightarrow e^+e^- K_S^0 K_S^0$
60 ± 20 ± 19	ABREU 96c DLPH $Z^0 \rightarrow K^+ K^- + X$
60 ± 23 ⁺¹³ ₋₂₀	BAI 96c BES $J/\psi \rightarrow \gamma K^+ K^-$
103 ± 30	AUGUSTIN 88 DM2 $J/\psi \rightarrow \gamma K^+ K^-$
100 ± 3	3 FALVARD 88 DM2 $J/\psi \rightarrow \phi K^+ K^-$
85 ± 35	BALTRUSAIT...87 MRK3 $J/\psi \rightarrow \gamma K^+ K^-$
• • • We do not use the following data for averages, fits, limits, etc. • • •	
84 ± 15	4 RODAS 22 RVUE $J/\psi(1S) \rightarrow \gamma(\pi\pi, K\bar{K})$
37 ± 12	29 5 LEES 14H BABR $e^+e^- \rightarrow K_S^0 K_S^0 K^+ K^- \gamma$
104 ± 10	870 6 SCHEGELSKY 06A RVUE $\gamma\gamma \rightarrow K_S^0 K_S^0$
62 ± 10	7 FALVARD 88 DM2 $J/\psi \rightarrow \phi K^+ K^-$

WEIGHTED AVERAGE
89.2±3.4-3.0 (Error scaled by 1.8)



$f_2'(1525)$ width, e^+e^- annihilation and particle decays (MeV)

- From partial wave analysis including all possible combinations of 0^{++} , 2^{++} , and 4^{++} resonances.
- Supersedes ACCIARRI 95J.
- From an analysis including interference with $f_0(1710)$.
- T-matrix pole from coupled channel K-matrix fit to data on $J/\psi \rightarrow \gamma\pi^0\pi^0$ (ABLIKIM 15AE) and $J/\psi \rightarrow \gamma K_S^0 K_S^0$ (ABLIKIM 18AA).
- From a fit to a Breit-Wigner line shape plus a second-order polynomial function. Systematic errors not evaluated.
- From analysis of L3 data at 91 and 183-209 GeV.
- From an analysis ignoring interference with $f_0(1710)$.

PRODUCED IN $p\bar{p}$ ANNIHILATION

VALUE (MeV) DOCUMENT ID TECN COMMENT

The data in this block is included in the average printed for a previous datablock.

77 ± 5 OUR AVERAGE	
76 ± 6	AMSLER 06 CBAR 0.9 $\bar{p}p \rightarrow K^+ K^- \pi^0$
79 ± 8	1 AMSLER 02 CBAR 0.9 $\bar{p}p \rightarrow \pi^0 \eta\eta, \pi^0 \pi^0 \pi^0$
• • • We do not use the following data for averages, fits, limits, etc. • • •	
104.8 ± 0.9 ± 9.8	2 ALBRECHT 20 RVUE 0.9 $\bar{p}p \rightarrow \pi^0 \pi^0 \eta, \pi^0 \eta\eta,$
128 ± 20	3 ANISOVICH 09 RVUE 0.0 $\bar{p}p, \pi N$
1 T-matrix pole.	
2 T-matrix pole, 4 poles, 4 channels, including scattering data from HYAMS 75 ($\pi\pi$), LONGACRE 86 ($K\bar{K}$), BINON 83 ($\eta\eta$).	
3 K-matrix, 4-poles, 5-channel fit.	

CENTRAL PRODUCTION

VALUE (MeV) DOCUMENT ID TECN COMMENT

The data in this block is included in the average printed for a previous datablock.

70 ± 25	BARBERIS 99 OMEG 450 $p\bar{p} \rightarrow p_S p_F K^+ K^-$
----------------	---

PRODUCED IN ep COLLISIONS

VALUE (MeV) EVTS DOCUMENT ID TECN COMMENT

The data in this block is included in the average printed for a previous datablock.

83 ± 9⁺⁵₋₄	1 CHEKANOV 08 ZEUS $ep \rightarrow K_S^0 K_S^0 X$
• • • We do not use the following data for averages, fits, limits, etc. • • •	
50 ⁺³⁴ ₋₂₂	84 2 CHEKANOV 04 ZEUS $ep \rightarrow K_S^0 K_S^0 X$
1 In the SU(3) based model with a specific interference pattern of the $f_2(1270)$, $a_2^0(1320)$, and $f_2'(1525)$ mesons incoherently added to the $f_0(1710)$ and non-resonant background.	
2 Systematic errors not estimated.	

$f_2'(1525)$ DECAY MODES

Mode	Fraction (Γ_i/Γ)	Scale factor
Γ_1 $K\bar{K}$	(87.6 ± 2.2) %	1.1
Γ_2 $\eta\eta$	(11.6 ± 2.2) %	1.1
Γ_3 $\pi\pi$	(8.3 ± 1.6) × 10 ⁻³	
Γ_4 $K\bar{K}^*(892) + c.c.$		
Γ_5 $\pi K\bar{K}$		
Γ_6 $\pi\pi\eta$		
Γ_7 $\pi^+\pi^+\pi^-\pi^-$		
Γ_8 $\gamma\gamma$	(9.5 ± 1.1) × 10 ⁻⁷	1.1

CONSTRAINED FIT INFORMATION

An overall fit to the total width, 2 partial widths, a combination of partial widths obtained from integrated cross sections, and 3 branching ratios uses 17 measurements and one constraint to determine 5 parameters. The overall fit has a $\chi^2 = 18.2$ for 13 degrees of freedom.

The following off-diagonal array elements are the correlation coefficients $\langle \delta p_i \delta p_j \rangle / (\delta p_i \delta p_j)$, in percent, from the fit to parameters p_i , including the branching fractions, $x_i \equiv \Gamma_i/\Gamma_{total}$. The fit constrains the x_i whose labels appear in this array to sum to one.

x_2	-100			
x_3	-6	-1		
x_8	-19	19	1	
Γ	-4	4	0	-44
	x_1	x_2	x_3	x_8

Mode	Rate (MeV)	Scale factor
Γ_1 $K\bar{K}$	75 ± 4	1.8
Γ_2 $\eta\eta$	9.9 ± 1.9	1.1
Γ_3 $\pi\pi$	0.71 ± 0.14	1.1
Γ_8 $\gamma\gamma$	(8.2 ± 0.9) × 10 ⁻⁵	

$f_2'(1525)$ PARTIAL WIDTHS

VALUE (MeV)	DOCUMENT ID	TECN	COMMENT
75 ± 4 OUR FIT	Error includes scale factor of 1.8.		

63 ± 6₋₅	1 LONGACRE 86 MPS 22 $\pi^- p \rightarrow K_S^0 K_S^0 n$
1 From a partial-wave analysis of data using a K-matrix formalism with 5 poles.	

VALUE (MeV)	EVTS	DOCUMENT ID	TECN	COMMENT
9.9 ± 1.9 OUR FIT	Error includes scale factor of 1.1.			

5.0 ± 0.8	870 1 SCHEGELSKY 06A RVUE $\gamma\gamma \rightarrow K_S^0 K_S^0$
24 ⁺³ ₋₁	2 LONGACRE 86 MPS 22 $\pi^- p \rightarrow K_S^0 K_S^0 n$

- From analysis of L3 data at 91 and 183-209 GeV, using $\Gamma(f_2'(1525) \rightarrow K\bar{K}) = 68$ MeV and SU(3) relations.
- From a partial-wave analysis of data using a K-matrix formalism with 5 poles.

VALUE (MeV)	EVTS	DOCUMENT ID	TECN	COMMENT
0.71 ± 0.14 OUR FIT	Error includes scale factor of 1.1.			

1.4 ^{+1.0}_{-0.5}	1 LONGACRE 86 MPS 22 $\pi^- p \rightarrow K_S^0 K_S^0 n$
• • • We do not use the following data for averages, fits, limits, etc. • • •	

0.2 ^{+1.0} _{-0.2}	870 2 SCHEGELSKY 06A RVUE $\gamma\gamma \rightarrow K_S^0 K_S^0$
1 From a partial-wave analysis of data using a K-matrix formalism with 5 poles.	
2 From analysis of L3 data at 91 and 183-209 GeV, using $\Gamma(f_2'(1525) \rightarrow K\bar{K}) = 68$ MeV and SU(3) relations.	

Meson Particle Listings

$f_2'(1525)$

$\Gamma(\gamma\gamma)$ Γ_8

VALUE (keV)	EVTS	DOCUMENT ID	TECN	COMMENT
-------------	------	-------------	------	---------

0.082 ± 0.009 OUR FIT

• • • We do not use the following data for averages, fits, limits, etc. • • •

0.13 ± 0.03 870 ¹ SCHEGELSKY 06A RVUE $\gamma\gamma \rightarrow K_S^0 K_S^0$

¹ From analysis of L3 data at 91 and 183–209 GeV, using $\Gamma(f_2'(1525) \rightarrow K\bar{K}) = 68$ MeV and SU(3) relations.

$\Gamma(K\bar{K})/\Gamma_{total}$ Γ_1/Γ

VALUE	DOCUMENT ID	TECN	COMMENT
-------	-------------	------	---------

• • • We do not use the following data for averages, fits, limits, etc. • • •

0.746 ± 0.002^{+0.166}_{-0.162} ¹ ALBRECHT 20 RVUE $\bar{p}p \rightarrow \pi^0 \pi^0 \eta, \pi^0 \eta \eta, \pi^0 K^+ K^-$

¹ Residue from T-matrix pole, 4 poles, 4 channels, including scattering data from HYAMS 75 ($\pi\pi$), LONGACRE 86 ($K\bar{K}$), BINON 83 ($\eta\eta$).

$f_2'(1525) \Gamma(i)\Gamma(\gamma\gamma)/\Gamma_{total}$

$\Gamma(K\bar{K}) \times \Gamma(\gamma\gamma)/\Gamma_{total}$ $\Gamma_1\Gamma_8/\Gamma$

VALUE (keV)	EVTS	DOCUMENT ID	TECN	COMMENT
-------------	------	-------------	------	---------

0.072 ± 0.007 OUR FIT

0.072 ± 0.007 OUR AVERAGE

0.048^{+0.067}_{-0.008} ± ^{+0.108}_{-0.012} UEHARA 13 BELL $\gamma\gamma \rightarrow K_S^0 K_S^0$

0.0564 ± 0.0048 ± 0.0116 ABE 04 BELL $10.6 e^+ e^- \rightarrow e^+ e^- K^+ K^-$

0.076 ± 0.006 ± 0.011 331 ¹ ACCIARRI 01H L3 $e^+ e^- \rightarrow e^+ e^- K_S^0 K_S^0$

0.067 ± 0.008 ± 0.015 ² ALBRECHT 90G ARG $e^+ e^- \rightarrow e^+ e^- K^+ K^-$

0.11^{+0.03}_{-0.02} ± 0.02 BEHREND 89c CELL $e^+ e^- \rightarrow e^+ e^- K_S^0 K_S^0$

0.10^{+0.04}_{-0.03} ± ^{+0.03}_{-0.02} BERGER 88 PLUT $e^+ e^- \rightarrow e^+ e^- K_S^0 K_S^0$

0.12 ± 0.07 ± 0.04 ² AIHARA 86B TPC $e^+ e^- \rightarrow e^+ e^- K^+ K^-$

0.11 ± 0.02 ± 0.04 ² ALTHOFF 83 TASS $e^+ e^- \rightarrow e^+ e^- K\bar{K}$

• • • We do not use the following data for averages, fits, limits, etc. • • •

0.0314 ± 0.0050 ± 0.0077 ³ ALBRECHT 90G ARG $e^+ e^- \rightarrow e^+ e^- K^+ K^-$

¹ Supersedes ACCIARRI 95J. From analysis of L3 data at 91 and 183–209 GeV,

² Using an incoherent background.

³ Using a coherent background.

$f_2'(1525)$ BRANCHING RATIOS

$\Gamma(\eta\eta)/\Gamma_{total}$ Γ_2/Γ

VALUE	DOCUMENT ID	TECN	COMMENT
-------	-------------	------	---------

• • • We do not use the following data for averages, fits, limits, etc. • • •

0.059 ± 0.003 ± 0.026 ¹ ALBRECHT 20 RVUE $0.9 \bar{p}p \rightarrow \pi^0 \pi^0 \eta, \pi^0 \eta \eta, \pi^0 K^+ K^-$

seen UEHARA 10A BELL $10.6 e^+ e^- \rightarrow e^+ e^- \eta \eta$

0.10 ± 0.03 ² PROKOSHKIN 91 GAM4 $300 \pi^- p \rightarrow \pi^- p \eta \eta$

¹ Residue from T-matrix pole, 4 poles, 4 channels, including scattering data from HYAMS 75 ($\pi\pi$), LONGACRE 86 ($K\bar{K}$), BINON 83 ($\eta\eta$).

² Combining results of GAM4 with those of WA76 on $K\bar{K}$ central production and results of CBAL, MRK3 and DM2 on $J/\psi \rightarrow \gamma\eta\eta$.

$\Gamma(\eta\eta)/\Gamma(K\bar{K})$ Γ_2/Γ_1

VALUE	CL%	EVTS	DOCUMENT ID	TECN	COMMENT
-------	-----	------	-------------	------	---------

0.132 ± 0.028 OUR FIT

0.115 ± 0.028 OUR AVERAGE

0.119 ± 0.015 ± 0.036 61 ¹ BINON 07 GAMS $32.5 K^- p \rightarrow \eta \eta (\Lambda/\Sigma^0)$

0.11 ± 0.04 ² PROKOSHKIN 91 GAM4 $300 \pi^- p \rightarrow \pi^- p \eta \eta$

• • • We do not use the following data for averages, fits, limits, etc. • • •

< 0.14 90 BARBERIS 00E $450 \bar{p}p \rightarrow p f \eta \eta p_S$

< 0.50 BARNES 67 HBC $4.6, 5.0 K^- p$

¹ Using the compilation of the cross sections for $f_2'(1525)$ production in $K^- p$ collisions from ASTON 88D.

² Combining results of GAM4 with those of WA76 on $K\bar{K}$ central production and results of CBAL, MRK3 and DM2 on $J/\psi \rightarrow \gamma\eta\eta$.

$\Gamma(\pi\pi)/\Gamma_{total}$ Γ_3/Γ

VALUE (units 10 ⁻²)	CL%	DOCUMENT ID	TECN	COMMENT
---------------------------------	-----	-------------	------	---------

0.83 ± 0.16 OUR FIT

0.75 ± 0.16 OUR AVERAGE

0.7 ± 0.2 COSTA 80 OMEG $10 \pi^- p \rightarrow K^+ K^- n$

2.7^{+7.1}_{-1.3} ¹ GORLICH 80 ASPK $17.18 \pi^- p$

0.75 ± 0.25 ^{1,2} MARTIN 79 RVUE

• • • We do not use the following data for averages, fits, limits, etc. • • •

3.4 ± 1.5 ± 1.0 ³ ALBRECHT 20 RVUE $0.9 \bar{p}p \rightarrow \pi^0 \pi^0 \eta, \pi^0 \eta \eta, \pi^0 K^+ K^-$

< 6 95 AGUILAR... 81B HBC $4.2 K^- p \rightarrow \Lambda K^+ K^-$

19 ± 3 CORDEN 79 OMEG $12-15 \pi^- p \rightarrow \pi^+ \pi^- n$

< 4.5 95 BARREIRO 77 HBC $4.15 K^- p \rightarrow \Lambda K_S^0 K_S^0$

1.2 ± 0.4 ¹ PAWLICKI 77 SPEC $6 \pi N \rightarrow K^+ K^- N$

< 6.3 90 BRANDENB... 76C ASPK $13 K^- p \rightarrow K^+ K^- (\Lambda, \Sigma)$

< 0.86 ¹ BEUSCH 75B OSPK $8.9 \pi^- p \rightarrow K^0 \bar{K}^0 n$

¹ Assuming that the $f_2'(1525)$ is produced by a one-pion exchange production mechanism.

² MARTIN 79 uses the PAWLICKI 77 data with different input value of the $f_2'(1525) \rightarrow K\bar{K}$ branching ratio.

³ Residue from T-matrix pole, 4 poles, 4 channels, including scattering data from HYAMS 75 ($\pi\pi$), LONGACRE 86 ($K\bar{K}$), BINON 83 ($\eta\eta$).

$\Gamma(\pi\pi)/\Gamma(K\bar{K})$ Γ_3/Γ_1

VALUE	DOCUMENT ID	TECN	COMMENT
-------	-------------	------	---------

0.0094 ± 0.0018 OUR FIT

0.075 ± 0.035 AUGUSTIN 87 DM2 $J/\psi \rightarrow \gamma \pi^+ \pi^-$

$[\Gamma(K\bar{K}^*(892) + c.c.) + \Gamma(\pi K\bar{K})]/\Gamma(K\bar{K})$ $(\Gamma_4 + \Gamma_5)/\Gamma_1$

VALUE	CL%	DOCUMENT ID	TECN	COMMENT
-------	-----	-------------	------	---------

• • • We do not use the following data for averages, fits, limits, etc. • • •

< 0.35 95 AGUILAR... 72B HBC $3.9, 4.6 K^- p$

< 0.4 67 AMMAR 67 HBC

$\Gamma(\pi\pi\eta)/\Gamma(K\bar{K})$ Γ_6/Γ_1

VALUE	CL%	DOCUMENT ID	TECN	COMMENT
-------	-----	-------------	------	---------

• • • We do not use the following data for averages, fits, limits, etc. • • •

< 0.41 95 AGUILAR... 72B HBC $3.9, 4.6 K^- p$

< 0.3 67 AMMAR 67 HBC

$\Gamma(\pi^+ \pi^+ \pi^- \pi^-)/\Gamma(K\bar{K})$ Γ_7/Γ_1

VALUE	CL%	DOCUMENT ID	TECN	COMMENT
-------	-----	-------------	------	---------

• • • We do not use the following data for averages, fits, limits, etc. • • •

< 0.32 95 AGUILAR... 72B HBC $3.9, 4.6 K^- p$

$f_2'(1525)$ REFERENCES

RODAS 22	EPJ C82 80	A. Rodas et al.	(JPAC Collab.)
ALBRECHT 20	EPJ C80 453	M. Albrecht et al.	(Crystal Barrel Collab.)
ABLIKIM 18A	PR D38 072003	M. Ablikim et al.	(BESII Collab.)
PDG 18	PR D98 030001	M. Tanabashi et al.	(PDG Collab.)
ABLIKIM 15AE	PR D92 052003	M. Ablikim et al.	(BESIII Collab.)
DOBBS 15	PR D91 052006	S. Dobbs et al.	(NWES)
LEES 14H	PR D89 092002	J.P. Lees et al.	(BABAR Collab.)
AAU 13AN	PR D87 072004	R. Aaij et al.	(LHCb Collab.)
ABLIKIM 13N	PR D87 092009	M. Ablikim et al.	(BESIII Collab.)
UEHARA 13	PTEP 2013 123C01	S. Uehara et al.	(BELLE Collab.)
UEHARA 10A	PR D82 114031	S. Uehara et al.	(BELLE Collab.)
ANISOVICH 09	IJMP A24 2481	V.V. Anisovich, A.V. Sarantsev	
CHEKANOV 08	PRL 101 112003	S. Chekanov et al.	(ZEUS Collab.)
BINON 07	PAN 70 1713	F. Binon et al.	(GAMS Collab.)
Translated from YAF 70 1788.			
AMSLER 06	PL B639 165	C. Amshar et al.	(Crystal Barrel Collab.)
SCHEGELSKY 06A	EPJ A27 207	V.A. Schegelsky et al.	
ABLIKIM 05	PL B607 243	M. Ablikim et al.	(BES Collab.)
ABE 04	EPJ C32 323	K. Abe et al.	(BELLE Collab.)
CHEKANOV 04	PL B578 33	S. Chekanov et al.	(ZEUS Collab.)
BAI 03G	PR D68 052003	J.Z. Bai et al.	(BES Collab.)
TIKHOMIROV 03	PAN 66 828	G.D. Tikhomirov et al.	
Translated from YAF 66 860.			
AMSLER 02	EPJ C23 29	C. Amshar et al.	
ACCIARRI 01H	PL B501 173	M. Acciarri et al.	(L3 Collab.)
BARBERIS 00E	PL B479 59	D. Barberis et al.	(WA 102 Collab.)
BARBERIS 99	PL B453 305	D. Barberis et al.	(Omega Expt.)
BARKOV 99	JETPL 70 248	B.P. Barkov et al.	
Translated from ZETFP 70 242.			
ABREU 96C	PL B379 309	F. Abreu et al.	(DELPHI Collab.)
BAI 96C	PRL 77 3959	J.Z. Bai et al.	(BES Collab.)
ACCIARRI 95J	PL B363 118	M. Acciarri et al.	(L3 Collab.)
PROKOSHKIN 91	SPD 36 155	Y.D. Prokoshkin	(GAM2 and GAM4 Collab.)
Translated from DANS 316 900.			
ALBRECHT 90G	ZPHY C48 183	H. Albrecht et al.	(ARGUS Collab.)
BEHREND 89C	ZPHY C43 91	H.J. Behrend et al.	(CELLO Collab.)
ASTON 88D	NP B301 525	D. Aston et al.	(SLAC, NAGO, CINC, INUS)
AUGUSTIN 88	PRL 60 2238	J.E. Augustin et al.	(DM2 Collab.)
BERGER 88	ZPHY C37 329	C. Berger et al.	(PLUTO Collab.)
FALVARD 88	PR D38 2706	A. Falvard et al.	(CLER, FRAS, LALO+)
AUGUSTIN 87	ZPHY C36 369	J.E. Augustin et al.	(LALO, CLER, FRAS+)
BALTRUSAIT... 87	PR D35 2077	R.M. Baltrusaitis et al.	(Mark III Collab.)
AIHARA 86B	PRL 57 404	H. Aihara et al.	(TPC-2γ Collab.)
BOLONKIN 86	SJNP 43 776	B.V. Bolonkin et al.	(ITEP)JP
Translated from YAF 43 1211.			
LONGACRE 86	PL B177 223	R.S. Longacre et al.	(BNL, BRAN, CUNY+)
ALTHOFF 83B	PL 121B 216	M. Althoff et al.	(TASSO Collab.)
ARMSTRONG 83	NP B224 193	T.A. Armstrong et al.	(BARI, BIRM, CERN+)
BINON 83	NC 78A 313	F.G. Binon et al.	(BELG, LAPP, SERP+)
AGUILAR... 81B	ZPHY C8 313	M. Aguilar-Benitez et al.	(CERN, CDEF+)
ALHARRAN 81	NP B191 26	S. Al-Harran et al.	(BIRM, CERN, GLAS+)
CHABAUD 81	APP B12 575	V. Chabaud et al.	(CERN, CRAC, MPIM)
COSTA 80	NP B175 402	G. Costa et al.	(BARI, BONN, CERN, GLAS+)
GORLICH 80	NP B174 16	L. Gorlich et al.	(CRAC, MPIM, CERN+)
CORDEN 79	NP B157 250	M.J. Corden et al.	(BIRM, HELV, TELA+JP)
MARTIN 79	NP B158 520	A.D. Martin, E.N. Ozmutlu	(DURH)
POLYCHRO... 79	PR D19 1317	V.A. Polychronakos et al.	(NDAM, ANL)
BARREIRO 77	NP B121 237	F. Barreiro et al.	(CERN, AMST, NIJH+)
EVANGELIS... 77	NP B127 384	C. Evangelista et al.	(BARI, BONN, CERN+)
PAWLICKI 77	PR D15 3196	A.J. Pawlicki et al.	(ANL)
BRANDENB... 76C	NP B104 413	G.W. Brandenburg et al.	(SLAC)
BEUSCH 75B	PL 60B 101	W. Beusch et al.	(CERN, ETH)
HYAMS 75	NP B100 205	B.D. Hyams et al.	(CERN, MPIM)
AGUILAR... 72B	PR D6 29	M. Aguilar-Benitez et al.	(BNL)
AMMAR 67	PRL 19 1071	R. Ammar et al.	(NWES, ANL)JP
BARNES 67	PRL 19 964	V.E. Barnes et al.	(BNL, SYRAC)
CRENNELL 66	PRL 16 1025	D.J. Crennell et al.	(BNL)I

f₂(1565)

I^G(J^{PC}) = 0⁺(2⁺⁺)

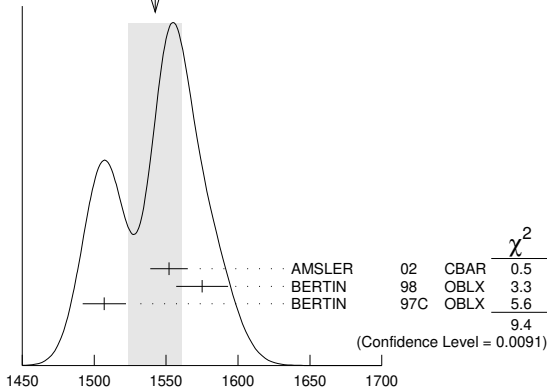
OMITTED FROM SUMMARY TABLE

Seen mostly in antinucleon-nucleon annihilation. Needs confirmation in other channels. See the review on "Spectroscopy of Light Meson Resonances."

f₂(1565) MASS

Table with columns: VALUE (MeV), DOCUMENT ID, TECN, COMMENT. Includes 'OUR AVERAGE' and various experimental data points with error bars.

WEIGHTED AVERAGE 1542±19 (Error scaled by 2.2)



- 1 T-matrix pole.
2 On sheet II in a two-pole solution.
3 Supersedes the omega state of BELADIDZE 92b earlier assigned to the f2(1640).
4 Breit-Wigner width.
5 T-matrix pole, large coupling to rho rho and omega omega, could be f2(1640).
6 Coupled-channel analysis of AMSLER 95b, AMSLER 95c, and AMSLER 94d.
7 From a simultaneous analysis of the annihilations p-bar p -> 3pi^0, pi^0 eta eta including AKER 91 data.
8 J^P not determined, could be partly f_0(1500).
9 J^P not determined.
10 Superseded by AMSLER 95b.

f₂(1565) WIDTH

Table with columns: VALUE (MeV), DOCUMENT ID, TECN, COMMENT. Lists various width measurements and the 'OUR AVERAGE'.

Table with columns: ~ 142, 16 AMSLER 95D CBAR, 95D CBAR, 95 SPEC, 17 ANISOVICH 94 CBAR, 18 ADAMO 93 OBLX, 19 ARMSTRONG 93c E760, 19 ARMSTRONG 93D E760, 19 ARMSTRONG 93D E760, ~ 206, 20 WEIDENAUER 93 ASTE, 19 ADAMO 92 OBLX, 21 AKER 91 CBAR, MAY 90 ASTE, BRIDGES 86c DBC. Includes decay channels like pi^0 pi^0 pi^0, pi^0 eta eta, pi^- C -> K_S^0 K_S^0 X, etc.

- 11 T-matrix pole.
12 On sheet II in a two-pole solution.
13 Supersedes the omega state of BELADIDZE 92b earlier assigned to the f2(1640).
14 Breit-Wigner width.
15 T-matrix pole, large coupling to rho rho and omega omega, could be f2(1640).
16 Coupled-channel analysis of AMSLER 95b, AMSLER 95c, and AMSLER 94d.
17 From a simultaneous analysis of the annihilations p-bar p -> 3pi^0, pi^0 eta eta including AKER 91 data.
18 Supersedes ADAMO 92.
19 J^P not determined, could be partly f_0(1500).
20 J^P not determined.
21 Superseded by AMSLER 95b.

f₂(1565) DECAY MODES

Table with columns: Mode, Fraction (Gamma_i/Gamma). Lists decay modes like pi pi, pi^+ pi^-, pi^0 pi^0, rho^0 rho^0, 2pi^+ 2pi^-, eta eta, omega omega, K K-bar, gamma gamma.

f₂(1565) PARTIAL WIDTHS

Table with columns: Gamma (eta eta), Gamma (K K-bar), Gamma (gamma gamma). Includes values and references like SCHEGELSKY 06A, RVUE, etc.

f₂(1565) BRANCHING RATIOS

Table with columns: Gamma(pi pi)/Gamma total, Gamma(pi^+ pi^-)/Gamma total, Gamma(pi^0 pi^0)/Gamma total. Includes values and references like BAKER 99B, BERTIN 98, ANISOVICH 94B, etc.

Meson Particle Listings

$f_2(1565), \rho(1570), h_1(1595), \pi_1(1600)$

$\Gamma(\pi^+\pi^-)/\Gamma(\rho^0\rho^0)$ Γ_2/Γ_4

VALUE	DOCUMENT ID	TECN	COMMENT
0.042±0.013	BRIDGES 86B	DBC	$\bar{p}N \rightarrow 3\pi^- 2\pi^+$

$\Gamma(\eta\eta)/\Gamma(\pi^0\pi^0)$ Γ_6/Γ_3

VALUE	DOCUMENT ID	TECN	COMMENT
0.024±0.005±0.012	24 ARMSTRONG 93C	E760	$\bar{p}p \rightarrow \pi^0 \eta \eta \rightarrow 6\gamma$
24 J^P not determined, could be partly $f_0(1500)$.			

$\Gamma(\omega\pi)/\Gamma_{total}$ Γ_7/Γ

VALUE	DOCUMENT ID	TECN	COMMENT
seen	BAKER 99B	SPEC	$0 \bar{p}p \rightarrow \omega \pi^0$

$f_2(1565)$ REFERENCES

Author	Year	Document ID	TECN	COMMENT
ANISOVICH	09	JUMP A24 2481		V.V. Anisovich, A.V. Sarantsev
AMELIN	06	PAN 69 690		D.V. Amelin et al. (VES Collab.)
SCHEGELSKY	06A	EPJ A27 207		V.A. Schegelsky et al.
AMSLER	02	EPL C23 29		C. Amisler et al.
AMELIN	00	NP A668 83		D. Amelin et al. (VES Collab.)
BAKER	99B	PL B467 147		C.A. Baker et al.
BERTIN	98	PR D57 55		A. Bertin et al. (OBELIX Collab.)
BERTIN	97C	PL B408 476		A. Bertin et al. (OBELIX Collab.)
ABELE	96C	NP A609 562		A. Abele et al. (Crystal Barrel Collab.)
AMSLER	95B	PL B342 433		C. Amisler et al. (Crystal Barrel Collab.)
AMSLER	95C	PL B353 571		C. Amisler et al. (Crystal Barrel Collab.)
AMSLER	95D	PL B355 425		C. Amisler et al. (Crystal Barrel Collab.)
BALOSHIN	95	PAN 58 46		O.N. Baboshin et al. (ITEP)
AMSLER	94D	PL B333 277		C. Amisler et al. (Crystal Barrel Collab.)
ANISOVICH	94	PL B323 233		V.V. Anisovich et al. (Crystal Barrel Collab.)
ANISOVICH	94B	PR D50 1972		V.V. Anisovich et al. (LOQM)
ADAMO	93	NP A558 13C		A. Adamo et al. (OBELIX Collab.)
ARMSTRONG	93C	PL B307 394		T.A. Armstrong et al. (FNAL, FERR, GENO+)
ARMSTRONG	93D	PL B307 399		T.A. Armstrong et al. (FNAL, FERR, GENO+)
WEIDENAUER	93	ZPHY C59 387		P. Weidenauer et al. (ASTERIX Collab.)
ADAMO	92	PL B287 368		A. Adamo et al. (OBELIX Collab.)
BELADIDZE	92B	ZPHY C54 367		G.M. Beladidze et al. (VES Collab.)
AKER	91	PL B260 249		E. Aker et al. (Crystal Barrel Collab.)
MAY	90	ZPHY C46 203		B. May et al. (ASTERIX Collab.)
MAY	89	PL B225 450		B. May et al. (ASTERIX Collab.)
BRIDGES	86B	PRL 56 215		D.L. Bridges et al. (SYRA, CASE)
BRIDGES	86C	PRL 57 1534		D.L. Bridges et al. (SYRA)

$\rho(1570)$ $I^G(J^{PC}) = 1^+(1^{--})$

OMITTED FROM SUMMARY TABLE
 May be an OZI-violating decay mode of $\rho(1700)$. See the review on "Spectroscopy of Light Meson Resonances."

$\rho(1570)$ MASS

VALUE (MeV)	EVTS	DOCUMENT ID	TECN	COMMENT
1570±36±62	54	1 AUBERT 08s	BABR	10.6 $e^+e^- \rightarrow \phi\pi^0\gamma$
1585±15		2 ACHASOV 20c	SND	1.3-2.0 $e^+e^- \rightarrow K^+K^-\pi^0$
1480±40		3 BITYUKOV 87	SPEC	32.5 $\pi^-p \rightarrow \phi\pi^0n$

1 From the fit with two resonances.
 2 From a fit using a two resonance model in which the mass and width of the other resonance are fixed at the $\rho(1700)$ values from PDG 20.
 3 Systematic errors not estimated.

$\rho(1570)$ WIDTH

VALUE (MeV)	EVTS	DOCUMENT ID	TECN	COMMENT
144±75±43	54	4 AUBERT 08s	BABR	10.6 $e^+e^- \rightarrow \phi\pi^0\gamma$
75±30		5 ACHASOV 20c	SND	1.3-2.0 $e^+e^- \rightarrow K^+K^-\pi^0$
130±60		6 BITYUKOV 87	SPEC	32.5 $\pi^-p \rightarrow \phi\pi^0n$

4 From the fit with two resonances.
 5 From a fit using a two resonance model in which the mass and width of the other resonance are fixed at the $\rho(1700)$ values from PDG 20.
 6 Systematic errors not estimated.

$\rho(1570)$ DECAY MODES

Mode	Fraction (Γ_i/Γ)
Γ_1 e^+e^-	
Γ_2 $\phi\pi$	not seen
Γ_3 $\omega\pi$	

$\rho(1570)$ $\Gamma(i)\Gamma(e^+e^-)/\Gamma_{total}$

$\Gamma(\phi\pi) \times \Gamma(e^+e^-)/\Gamma_{total}$ $\Gamma_2\Gamma_1/\Gamma$

VALUE (eV)	CL%	EVTS	DOCUMENT ID	TECN	COMMENT
3.5±0.9±0.3		54	7 AUBERT 08s	BABR	10.6 $e^+e^- \rightarrow \phi\pi^0\gamma$
<70		90	8 AULCHENKO 87B	ND	$e^+e^- \rightarrow K_S^0 K_L^0 \pi^0$

7 From the fit with two resonances.
 8 Using mass and width of BITYUKOV 87.

$\rho(1570)$ BRANCHING RATIOS

$\Gamma(\phi\pi)/\Gamma_{total}$ Γ_2/Γ

VALUE	DOCUMENT ID	TECN	COMMENT
not seen	ABELE 97H	CBAR	$\bar{p}p \rightarrow K_L^0 K_S^0 \pi^0 \pi^0$
<0.01	9 DONNACHIE 91	RVUE	

9 Using data from BISELLO 91B, DOLINSKY 86, and ALBRECHT 87L.

$\Gamma(\phi\pi)/\Gamma(\omega\pi)$ Γ_2/Γ_3

VALUE	CL%	DOCUMENT ID	TECN	COMMENT
>0.5	95	BITYUKOV 87	SPEC	32.5 $\pi^-p \rightarrow \phi\pi^0n$

$\rho(1570)$ REFERENCES

Author	Year	Document ID	TECN	COMMENT
ACHASOV	20C	EPJ C80 1139		M.N. Achasov et al. (SND Collab.)
PDG	20	PTEP 2020 083C01		P.A. Zyla et al. (PDG Collab.)
AUBERT	08s	PL B415 280		B. Aubert et al. (BABAR Collab.)
ABELE	97H	PL B415 280		A. Abele et al. (Crystal Barrel Collab.)
BISELLO	91B	NPBS B21 111		D. Bisello (DM2 Collab.)
DONNACHIE	91	ZPHY C51 689		A. Donnachie, A.B. Clegg (MCHS, LANU)
ALBRECHT	87L	PL B185 223		H. Albrecht et al. (ARGUS Collab.)
AULCHENKO	87B	JETPL 45 145		V.M. Aulchenko et al. (NOVO)
		Translated from ZETFP 45 118.		
BITYUKOV	87	PL B188 383		S.I. Bitiyukov et al. (SERP)
DOLINSKY	86	PL B174 453		S.I. Dolinsky et al. (NOVO)

$h_1(1595)$ $I^G(J^{PC}) = 0^-(1^{+-})$

OMITTED FROM SUMMARY TABLE
 Seen in a partial-wave analysis of the $\omega\eta$ system produced in the reaction $\pi^-p \rightarrow \omega\eta n$ at 1.8 GeV/c.

$h_1(1595)$ MASS

VALUE (MeV)	DOCUMENT ID	TECN	COMMENT
1594±15±10-60	EUGENIO 01	SPEC	18 $\pi^-p \rightarrow \omega\eta n$

$h_1(1595)$ WIDTH

VALUE (MeV)	DOCUMENT ID	TECN	COMMENT
384±60±100	EUGENIO 01	SPEC	18 $\pi^-p \rightarrow \omega\eta n$

$h_1(1595)$ DECAY MODES

Mode	Fraction (Γ_i/Γ)
Γ_1 $\omega\eta$	seen

$h_1(1595)$ REFERENCES

Author	Year	Document ID	TECN	COMMENT
EUGENIO	01	PL B497 190		P. Eugenio et al.

$\pi_1(1600)$ $I^G(J^{PC}) = 1^-(1^{-+})$

See the review on "Spectroscopy of Light Meson Resonances" and a note in PDG 06, Journal of Physics **G33** 1 (2006).

$\pi_1(1600)$ T-Matrix Pole \sqrt{s}

VALUE (MeV)	DOCUMENT ID	TECN	COMMENT
(1623 ± 47 ± 24) - i(228 ± 44 ± 88)	1 KOPF 21	RVUE	0.9 $p\bar{p} \rightarrow \pi^0\pi^0\eta$, $\pi^0\eta\eta$, $\pi^0K^+K^-$ and 191 $\pi^-p \rightarrow \pi^- \pi^- \pi^+ p$

(1564 ± 24 ± 86) - i(246 ± 27 ± 51) ² RODAS 19 JPAC 191 $\pi^- p \rightarrow \eta^{(\prime)} \pi^- p$

¹ From T-matrix pole based on combined fit of Crystal Barrel and $\pi\pi$ scattering data (ALBRECHT 20), and COMPASS data (ADOLPH 15), using a coupled-channel model of $\eta\pi, \eta'\pi$ and $K\bar{K}$ systems.
² The coupled-channel analysis of both the $\eta\pi$ and $\eta'\pi$ systems using ADOLPH 15 data.

$\pi_1(1600)$ MASS

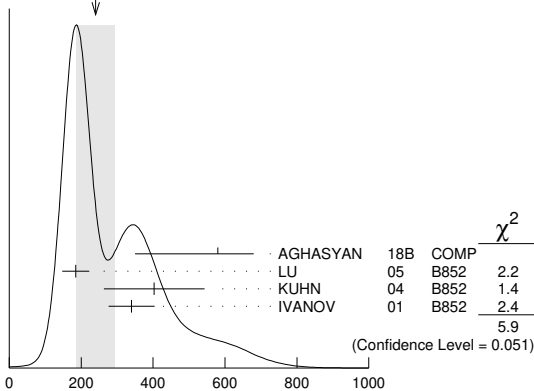
VALUE (MeV)	EVTS	DOCUMENT ID	TECN	COMMENT
1661 ± ¹⁵/₁₁ OUR AVERAGE		Error includes scale factor of 1.2.		
1600 ⁺¹¹⁰ / ₋₆₀	46M	¹ AGHASYAN	18B COMP	190 $\pi^- p \rightarrow \pi^- \pi^+ \pi^- p$
1664 ± 8 ± 10	145k	² LU	05 B852	18 $\pi^- p \rightarrow \omega \pi^- \pi^0 p$
1709 ± 24 ± 41	69k	³ KUHN	04 B852	18 $\pi^- p \rightarrow \eta \pi^+ \pi^- \pi^- p$
1597 ± 10 ⁺⁴⁵ / ₋₁₀		³ IVANOV	01 B852	18 $\pi^- p \rightarrow \eta' \pi^- p$
• • • We do not use the following data for averages, fits, limits, etc. • • •				
1660 ± 10 ⁺⁰ / ₋₆₄	420k	⁴ ALEKSEEV	10 COMP	190 $\pi^- Pb \rightarrow \pi^- \pi^- \pi^+ Pb$
1593 ± 8 ⁺²⁹ / ₋₄₇		^{3,5} ADAMS	98B B852	18.3 $\pi^- p \rightarrow \pi^+ \pi^- \pi^- p$

¹ Statistical error negligible. See also the review ALEXEEV 22.
² May be a different state: natural and unnatural parity exchanges.
³ Natural parity exchange.
⁴ Superseded by AGHASYAN 2018B.
⁵ Superseded by DZIERBA 06 excluding this state in a more refined PWA analysis, with 2.6 M events of $\pi^- p \rightarrow \pi^- \pi^- \pi^+ p$ and 3 M events of $\pi^- p \rightarrow \pi^- \pi^0 \pi^0 p$ of E852 data.

$\pi_1(1600)$ WIDTH

VALUE (MeV)	EVTS	DOCUMENT ID	TECN	COMMENT
240 ± 50 OUR AVERAGE		Error includes scale factor of 1.7. See the ideogram below.		
580 ⁺¹⁰⁰ / ₋₂₃₀	46M	¹ AGHASYAN	18B COMP	190 $\pi^- p \rightarrow \pi^- \pi^+ \pi^- p$
185 ± 25 ± 28	145k	² LU	05 B852	18 $\pi^- p \rightarrow \omega \pi^- \pi^0 p$
403 ± 80 ± 115	69k	³ KUHN	04 B852	18 $\pi^- p \rightarrow \eta \pi^+ \pi^- \pi^- p$
340 ± 40 ± 50		³ IVANOV	01 B852	18 $\pi^- p \rightarrow \eta' \pi^- p$
• • • We do not use the following data for averages, fits, limits, etc. • • •				
269 ± 21 ⁺⁴² / ₋₆₄	420k	⁴ ALEKSEEV	10 COMP	190 $\pi^- Pb \rightarrow \pi^- \pi^- \pi^+ Pb$
168 ± 20 ⁺¹⁵⁰ / ₋₁₂		^{3,5} ADAMS	98B B852	18.3 $\pi^- p \rightarrow \pi^+ \pi^- \pi^- p$

WEIGHTED AVERAGE
240±50 (Error scaled by 1.7)



¹ Statistical error negligible. See also the review ALEXEEV 22.
² May be a different state: natural and unnatural parity exchanges.
³ Natural parity exchange.
⁴ Superseded by AGHASYAN 2018B.
⁵ Superseded by DZIERBA 06 excluding this state in a more refined PWA analysis, with 2.6 M events of $\pi^- p \rightarrow \pi^- \pi^- \pi^+ p$ and 3 M events of $\pi^- p \rightarrow \pi^- \pi^0 \pi^0 p$ of E852 data.

$\pi_1(1600)$ DECAY MODES

Mode	Fraction (Γ_i/Γ)
Γ_1 $\pi\pi\pi$	seen
Γ_2 $\rho^0 \pi^-$	seen
Γ_3 $f_2(1270) \pi^-$	not seen

Γ_4 $b_1(1235) \pi$	seen
Γ_5 $\eta'(958) \pi^-$	seen
Γ_6 $\eta \pi$	
Γ_7 $f_1(1285) \pi$	seen

$\pi_1(1600)$ BRANCHING RATIOS

$\Gamma(\rho^0 \pi^-)/\Gamma_{total}$	Γ_2/Γ
VALUE	DOCUMENT ID TECN COMMENT
seen	ALEKSEEV 10 COMP 190 $\pi^- Pb \rightarrow \pi^- \pi^- \pi^+ Pb$
• • • We do not use the following data for averages, fits, limits, etc. • • •	
not seen	NOZAR 09 CLAS $\gamma p \rightarrow 2\pi^+ \pi^- n$
not seen	¹ DZIERBA 06 B852 18 $\pi^- p$
¹ From the PWA analysis of 2.6 M $\pi^- p \rightarrow \pi^- \pi^- \pi^+ p$ and 3 M events of $\pi^- p \rightarrow \pi^- \pi^0 \pi^0 p$ of E852 data. Supersedes ADAMS 98B.	

$\Gamma(f_2(1270) \pi^-)/\Gamma_{total}$	Γ_3/Γ
VALUE	DOCUMENT ID TECN COMMENT
not seen	¹ DZIERBA 06 B852 18 $\pi^- p$
¹ From the PWA analysis of 2.6 M $\pi^- p \rightarrow \pi^- \pi^- \pi^+ p$ and 3 M events of $\pi^- p \rightarrow \pi^- \pi^0 \pi^0 p$ of E852 data. Supersedes CHUNG 02.	

$\Gamma(b_1(1235) \pi)/\Gamma_{total}$	Γ_4/Γ
VALUE	EVTS DOCUMENT ID TECN COMMENT
seen	35280 ¹ BAKER 03 SPEC $\bar{p} p \rightarrow \omega \pi^+ \pi^- \pi^0$
• • • We do not use the following data for averages, fits, limits, etc. • • •	
seen	145k LU 05 B852 18 $\pi^- p \rightarrow \omega \pi^- \pi^0 p$
¹ $B((b_1 \pi)_{D-wave})/B((b_1 \pi)_{S-wave}) = 0.3 \pm 0.1$.	

$\Gamma(\eta'(958) \pi^-)/\Gamma_{total}$	Γ_5/Γ
VALUE	DOCUMENT ID TECN COMMENT
seen	IVANOV 01 B852 18 $\pi^- p \rightarrow \eta' \pi^- p$

$\Gamma(\eta'(958) \pi^-)/\Gamma(\eta \pi)$	Γ_5/Γ_6
VALUE	DOCUMENT ID TECN COMMENT
5.54 ± 1.1 ^{+1.8} / _{-0.27}	¹ KOPF 21 RVUE 0.9 $\rho \bar{p} \rightarrow \pi^0 \pi^0 \eta, \pi^0 \eta \eta, \pi^0 K^+ K^-$ and 191 $\pi^- p \rightarrow \pi^- \pi^- \pi^+ p$
¹ From T-matrix pole based on combined fit of Crystal Barrel and $\pi\pi$ scattering data (ALBRECHT 20), and COMPASS data (ADOLPH 15), using a coupled-channel model of $\eta\pi, \eta'\pi$ and $K\bar{K}$ systems.	

$\Gamma(f_1(1285) \pi)/\Gamma(\eta'(958) \pi^-)$	Γ_7/Γ_5
VALUE	EVTS DOCUMENT ID TECN COMMENT
3.80 ± 0.78	69k ¹ KUHN 04 B852 18 $\pi^- p \rightarrow \eta \pi^+ \pi^- \pi^- p$
¹ Using $\eta'(958) \pi$ data from IVANOV 01.	

$\pi_1(1600)$ REFERENCES

ALEXEEV 22	PR D105 012005	G.D. Alexeev et al.	(COMPASS Collab.)
KOPF 21	EPJ C81 1056	B. Kopf et al.	(BOCH)
ALBRECHT 20	EPJ C80 453	M. Albrecht et al.	(Crystal Barrel Collab.)
RODAS 19	PRL 122 042002	A. Rodas et al.	(JPAC Collab.)
AGHASYAN 18B	PR D98 092003	M. Aghasyan et al.	(COMPASS Collab.)
ADOLPH 15	PL B740 303	M. Adolph et al.	(COMPASS Collab.)
ALEKSEEV 10	PRL 104 241803	M.G. Alekseev et al.	(COMPASS Collab.)
NOZAR 09	PRL 102 102002	M. Nozar et al.	(JLab CLAS Collab.)
DZIERBA 06	PR D73 072001	A.R. Dzierba et al.	(BNL E852 Collab.)
PDG 06	JP G33 1	W.-M. Yao et al.	(PDG Collab.)
LU 05	PRL 94 032002	M. Lu et al.	(BNL E852 Collab.)
KUHN 04	PL B595 109	J. Kuhn et al.	(BNL E852 Collab.)
BAKER 03	PL B563 140	C.A. Baker et al.	(BNL E852 Collab.)
CHUNG 02	PR D65 072001	S.U. Chung et al.	(BNL E852 Collab.)
IVANOV 01	PRL 86 3977	E.I. Ivanov et al.	(BNL E852 Collab.)
ADAMS 98B	PRL 81 5760	G.S. Adams et al.	(BNL E852 Collab.)

$a_1(1640)$

$I^G(J^{PC}) = 1^-(1^{++})$

Possibly seen in the study of the hadronic structure in decay $\tau \rightarrow 3\pi \nu_\tau$ (ABREU 98G and ASNER 00).

$a_1(1640)$ MASS

VALUE (MeV)	EVTS	DOCUMENT ID	TECN	COMMENT
1655 ± 16 OUR AVERAGE		Error includes scale factor of 1.2.		
1700 ⁺³⁵ / ₋₁₃₀	46M	¹ AGHASYAN	18B COMP	190 $\pi^- p \rightarrow \pi^- \pi^+ \pi^- p$
1691 ± 18 ± 30		DARGENT	17 RVUE	$D^0 \rightarrow \pi^- \pi^+ \pi^- \pi^+$
1630 ± 20	35k	² BAKER	03 SPEC	$\bar{p} p \rightarrow \omega \pi^+ \pi^- \pi^0$
1714 ± 9 ± 36		CHUNG	02 B852	18.3 $\pi^- p \rightarrow \pi^+ \pi^- \pi^- p$
1640 ± 12 ± 30		BAKER	99 SPEC	1.94 $\bar{p} p \rightarrow 4\pi^0$

Meson Particle Listings

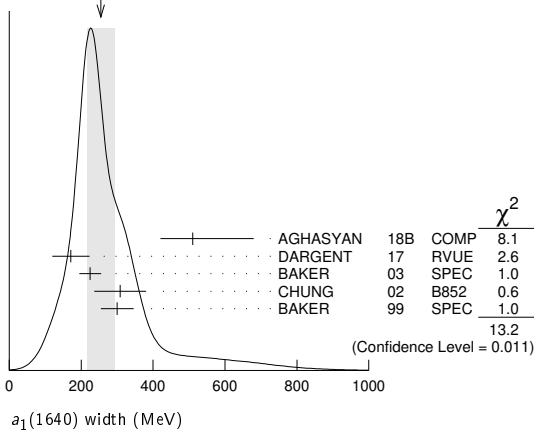
$a_1(1640)$, $f_2(1640)$, $\eta_2(1645)$

• • • We do not use the following data for averages, fits, limits, etc. • • •
 1670 ± 90 BELLINI 85 SPEC 40 $\pi^- A \rightarrow \pi^- \pi^+ \pi^- A$
¹ Statistical error negligible.
² Using the $a_1(1260)$ mass and width results of BOWLER 88.

$a_1(1640)$ WIDTH

VALUE (MeV)	EVTS	DOCUMENT ID	TECN	COMMENT
254 ± 40 OUR AVERAGE		Error includes scale factor of 1.8. See the ideogram below.		
510 ⁺¹⁷⁰ ₋₉₀	46M	¹ AGHASYAN	18B	COMP 190 $\pi^- p \rightarrow \pi^- \pi^+ \pi^- p$
171 ± 33 ± 40		DARGENT	17	RVUE $D^0 \rightarrow \pi^- \pi^+ \pi^- \pi^+$
225 ± 30	35k	² BAKER	03	SPEC $\bar{p} p \rightarrow \omega \pi^+ \pi^- \pi^0$
308 ± 37 ± 62		CHUNG	02	B852 18.3 $\pi^- p \rightarrow \pi^+ \pi^- \pi^- p$
300 ± 22 ± 40		BAKER	99	SPEC 1.94 $\bar{p} p \rightarrow 4\pi^0$
• • • We do not use the following data for averages, fits, limits, etc. • • •				
300 ± 100		BELLINI	85	SPEC 40 $\pi^- A \rightarrow \pi^- \pi^+ \pi^- A$
¹ Statistical error negligible.				
² Using the $a_1(1260)$ mass and width results of BOWLER 88.				

WEIGHTED AVERAGE
254 ± 40 (Error scaled by 1.8)



$a_1(1640)$ DECAY MODES

Mode	Fraction (Γ_i/Γ)
Γ_1 $\pi \pi \pi$	seen
Γ_2 $f_2(1270) \pi$	seen
Γ_3 $\sigma \pi$	seen
Γ_4 $\rho \pi S$ -wave	seen
Γ_5 $\rho \pi D$ -wave	seen
Γ_6 $\omega \pi \pi$	seen
Γ_7 $f_1(1285) \pi$	seen
Γ_8 $a_1(1260) \eta$	not seen

$a_1(1640)$ BRANCHING RATIOS

$\Gamma(f_2(1270)\pi)/\Gamma(\sigma\pi)$	Γ_2/Γ_3	
0.24 ± 0.07		
DOCUMENT ID	TECN	COMMENT
BAKER 99	SPEC	1.94 $\bar{p} p \rightarrow 4\pi^0$

$\Gamma(\rho\pi D\text{-wave})/\Gamma_{\text{total}}$	Γ_5/Γ	
• • • We do not use the following data for averages, fits, limits, etc. • • •		
CHUNG 02	B852	18.3 $\pi^- p \rightarrow \pi^+ \pi^- \pi^- p$
seen	AMELIN 95B	VES 36 $\pi^- A \rightarrow \pi^+ \pi^- \pi^- A$

$\Gamma(\omega\pi\pi)/\Gamma_{\text{total}}$	Γ_6/Γ	
• • • We do not use the following data for averages, fits, limits, etc. • • •		
seen	35280	¹ BAKER 03 SPEC $\bar{p} p \rightarrow \omega \pi^+ \pi^- \pi^0$
¹ Assuming the $\omega\rho$ mechanism for the $\omega\pi\pi$ state.		

$\Gamma(f_1(1285)\pi)/\Gamma_{\text{total}}$	Γ_7/Γ
• • • We do not use the following data for averages, fits, limits, etc. • • •	
not seen	KUHN 04 B852 18 $\pi^- p \rightarrow \eta \pi^+ \pi^- \pi^- p$
seen	LEE 94 MPS2 18 $\pi^- p \rightarrow K^+ \bar{K}^0 \pi^- \pi^- p$

$\Gamma(a_1(1260)\eta)/\Gamma_{\text{total}}$	Γ_8/Γ	
not seen		
DOCUMENT ID	TECN	COMMENT
KUHN 04	B852	18 $\pi^- p \rightarrow \eta \pi^+ \pi^- \pi^- p$

$a_1(1640)$ REFERENCES

AGHASYAN 18B	PR D98 092003	M. Aghasyan et al.	(COMPASS Collab.)
DARGENT 17	JHEP 1705 143	P. Dargent et al.	(HEID, BRIS)
KUHN 04	PL B595 109	J. Kuhn et al.	(BNL E852 Collab.)
BAKER 03	PL B563 140	C.A. Baker et al.	(BNL E852 Collab.)
CHUNG 02	PR D65 072001	S.U. Chung et al.	(CLEO Collab.)
ASNER 00	PR D61 012002	D.M. Asner et al.	(CLEO Collab.)
BAKER 99	PL B449 114	C.A. Baker et al.	(DELPHI Collab.)
ABREU 98G	PL B426 411	P. Abreu et al.	(SERP, TBL)
AMELIN 95B	PL B356 595	D.V. Amelin et al.	(BNL, IND, KYUN, MASD+)
LEE 94	PL B323 227	J.H. Lee et al.	(OXF)
BOWLER 88	PL B209 99	M.G. Bowler	
BELLINI 85	SJNP 41 781	D. Bellini et al.	
Translated from YAF 41 1223.			

$f_2(1640)$

 $I^G(J^{PC}) = 0^+(2^+ +)$

OMITTED FROM SUMMARY TABLE

$f_2(1640)$ MASS

VALUE (MeV)	DOCUMENT ID	TECN	COMMENT
1639 ± 6 OUR AVERAGE	Error includes scale factor of 1.2.		
1620 ± 16	BUGG 95	MRK3	$J/\psi \rightarrow \gamma \pi^+ \pi^- \pi^+ \pi^-$
1647 ± 7	ADAMO 92	OBLX	$\bar{p} p \rightarrow 3\pi^+ 2\pi^-$
1635 ± 7	ALDE 90	GAM2	38 $\pi^- p \rightarrow \omega \omega n$
• • • We do not use the following data for averages, fits, limits, etc. • • •			
1640 ± 5	AMSLER 06	CBAR	0.9 $\bar{p} p \rightarrow K^+ K^- \pi^0$
1659 ± 6	VLADIMIRSK...06	SPEC	40 $\pi^- p \rightarrow K_S^0 K_S^0 n$
1643 ± 7	¹ ALDE 89B	GAM2	38 $\pi^- p \rightarrow \omega \omega n$
¹ Superseded by ALDE 90.			

$f_2(1640)$ WIDTH

VALUE (MeV)	CL%	DOCUMENT ID	TECN	COMMENT
99⁺⁶⁰₋₄₀ OUR AVERAGE		Error includes scale factor of 2.9.		
140 ⁺⁶⁰ ₋₂₀		BUGG 95	MRK3	$J/\psi \rightarrow \gamma \pi^+ \pi^- \pi^+ \pi^-$
58 ± 20		ADAMO 92	OBLX	$\bar{p} p \rightarrow 3\pi^+ 2\pi^-$
• • • We do not use the following data for averages, fits, limits, etc. • • •				
44 ± 9		AMSLER 06	CBAR	0.9 $\bar{p} p \rightarrow K^+ K^- \pi^0$
152 ± 18		VLADIMIRSK...06	SPEC	40 $\pi^- p \rightarrow K_S^0 K_S^0 n$
< 70	90	ALDE 90	GAM2	38 $\pi^- p \rightarrow \omega \omega n$

$f_2(1640)$ DECAY MODES

Mode	Fraction (Γ_i/Γ)
Γ_1 $\omega \omega$	seen
Γ_2 4π	seen
Γ_3 $K \bar{K}$	seen

$f_2(1640)$ BRANCHING RATIOS

$\Gamma(K\bar{K})/\Gamma_{\text{total}}$	Γ_3/Γ	
seen		
DOCUMENT ID	TECN	COMMENT
AMSLER 06	CBAR	0.9 $\bar{p} p \rightarrow K^+ K^- \pi^0$

$f_2(1640)$ REFERENCES

AMSLER 06	PL B639 165	C. Amisler et al.	(Crystal Barrel Collab.)
VLADIMIRSK...06	PAN 69 493	V.V. Vladimirov et al.	(ITEP, Moscow)
Translated from YAF 69 515.			
BUGG 95	PL B353 378	D.V. Bugg et al.	(LOQM, PNPI, WASH)JP
ADAMO 92	PL B287 368	A. Adamo et al.	(OBELIX Collab.)
ALDE 90	PL B241 600	D.M. Alde et al.	(SERP, BELG, LANL, LAPP+)
ALDE 89B	PL B216 451	D.M. Alde et al.	(SERP, BELG, LANL, LAPP+)IGJPC

$\eta_2(1645)$

 $I^G(J^{PC}) = 0^+(2^- +)$

$\eta_2(1645)$ MASS

VALUE (MeV)	DOCUMENT ID	TECN	CHG	COMMENT
1617 ± 5 OUR AVERAGE				
1613 ± 8	BARBERIS 00B			450 $pp \rightarrow p_f \eta \pi^+ \pi^- p_S$
1617 ± 8	BARBERIS 00C			450 $pp \rightarrow p_f 4\pi p_S$
1620 ± 20	BARBERIS 97B	OMEG		450 $pp \rightarrow pp 2(\pi^+ \pi^-)$
1645 ± 14 ± 15	ADOMEIT 96	CBAR	0	1.94 $\bar{p} p \rightarrow \eta 3\pi^0$

See key on page 1127

Meson Particle Listings

 $\eta_2(1645), \omega(1650)$

••• We do not use the following data for averages, fits, limits, etc. •••
1645 ± 6 ± 20 ANISOVICH 00E SPEC 0.9–1.94 $\bar{p}p \rightarrow \eta 3\pi^0$

 $\eta_2(1645)$ WIDTH

VALUE (MeV)	DOCUMENT ID	TECN	CHG	COMMENT
181 ± 11 OUR AVERAGE				
185 ± 17	BARBERIS	00B		450 $pp \rightarrow \rho_f \eta \pi^+ \pi^- \rho_S$
177 ± 18	BARBERIS	00C		450 $pp \rightarrow \rho_f 4\pi \rho_S$
180 ± 25	BARBERIS	97B OMEG		450 $pp \rightarrow \rho p 2(\pi^+ \pi^-)$
180 +40 -21 ± 25	ADOMEIT	96 CBAR 0		1.94 $\bar{p}p \rightarrow \eta 3\pi^0$
••• We do not use the following data for averages, fits, limits, etc. •••				
200 ± 25	ANISOVICH	00E SPEC		0.9–1.94 $\bar{p}p \rightarrow \eta 3\pi^0$

 $\eta_2(1645)$ DECAY MODES

Mode	Fraction (Γ_i/Γ)
Γ_1 $a_2(1320)\pi$	seen
Γ_2 $K\bar{K}\pi$	seen
Γ_3 $K^*\bar{K}$	seen
Γ_4 $\eta\pi^+\pi^-$	seen
Γ_5 $a_0(980)\pi$	seen
Γ_6 $f_2(1270)\eta$	not seen

 $\eta_2(1645)$ BRANCHING RATIOS

$\Gamma(K\bar{K}\pi)/\Gamma(a_2(1320)\pi)$	DOCUMENT ID	TECN	COMMENT	Γ_2/Γ_1
0.07 ± 0.03	¹ BARBERIS	97C OMEG	450 $pp \rightarrow \rho p K\bar{K}\pi$	
¹ Using $2(\pi^+\pi^-)$ data from BARBERIS 97B.				

$\Gamma(a_2(1320)\pi)/\Gamma(a_0(980)\pi)$	DOCUMENT ID	TECN	COMMENT	Γ_1/Γ_5
13.1 ± 2.3 OUR AVERAGE				
13.5 ± 4.6	² ANISOVICH	11 SPEC	0.9–1.94 $\rho\bar{p}$	
13.0 ± 2.7	BARBERIS	00B	450 $pp \rightarrow \rho_f \eta \pi^+ \pi^- \rho_S$	
² Reanalysis of ADOMEIT 96 and ANISOVICH 00E.				

$\Gamma(f_2(1270)\eta)/\Gamma_{total}$	DOCUMENT ID	COMMENT	Γ_6/Γ
not seen	BARBERIS	00B 450 $pp \rightarrow \rho_f \eta \pi^+ \pi^- \rho_S$	

 $\eta_2(1645)$ REFERENCES

ANISOVICH	11	EPJ C71 1511	A.V. Anisovich et al.	(LOQM, RAL, PNPI)
ANISOVICH	00E	PL B477 19	A.V. Anisovich et al.	
BARBERIS	00B	PL B471 435	D. Barberis et al.	(WA 102 Collab.)
BARBERIS	00C	PL B471 440	D. Barberis et al.	(WA 102 Collab.)
BARBERIS	97B	PL B413 217	D. Barberis et al.	(WA 102 Collab.)
BARBERIS	97C	PL B413 225	D. Barberis et al.	(WA 102 Collab.)
ADOMEIT	96	ZPHY C71 227	J. Adomeit et al.	(Crystal Barrel Collab.)

 $\omega(1650)$

$$J^G(J^{PC}) = 0^-(1^{--})$$

See also the $\omega(1420)$ particle listing. $\omega(1650)$ MASS

VALUE (MeV)	EVTS	DOCUMENT ID	TECN	COMMENT
1670 ± 30 OUR ESTIMATE				
1698 ± 10	267	¹ ACHASOV	20B SND	$e^+e^- \rightarrow \omega\eta \rightarrow \eta\pi^0\gamma$
1651 ± 3 +16 -6	183k	² ABLIKIM	19AQ BES	$J/\psi \rightarrow K^+K^-\pi^0$
1673 + -7		ACHASOV	19 SND	$e^+e^- \rightarrow \pi^+\pi^-\pi^0\eta$
1671 ± 6 ± 10	824	³ AKHMETSIN	17A CMD3	1.4–2.0 $e^+e^- \rightarrow \omega\eta$
1660 ± 10	898	⁴ ACHASOV	16B SND	1.34–2.00 $e^+e^- \rightarrow \omega\eta$
1680 ± 10	13.1k	⁵ AULCHENKO	15A SND	1.05–1.80 $e^+e^- \rightarrow$ $\pi^+\pi^-\pi^0$
1667 ± 13 ± 6		AUBERT	07AU BABR	10.6 $e^+e^- \rightarrow \omega\pi^+\pi^-\gamma$
1645 ± 8	13	AUBERT	06D BABR	10.6 $e^+e^- \rightarrow \omega\eta\gamma$
1660 ± 10 ± 2		AUBERT,B	04N BABR	10.6 $e^+e^- \rightarrow \pi^+\pi^-\pi^0\gamma$
1770 ± 50 ± 60	1.2M	⁶ ACHASOV	03D RVUE	0.44–2.00 $e^+e^- \rightarrow$ $\pi^+\pi^-\pi^0$
1619 ± 5		⁷ HENNER	02 RVUE	1.2–2.0 $e^+e^- \rightarrow \rho\pi,$ $\omega\pi\pi$
1700 ± 20		EUGENIO	01 SPEC	18 $\pi^-\pi^0 \rightarrow \omega\eta\eta$
1705 ± 26	612	⁸ AKHMETSIN	00D CMD2	$e^+e^- \rightarrow \omega\pi^+\pi^-$

1820 +190 -150		⁹ ACHASOV	98H RVUE	$e^+e^- \rightarrow \pi^+\pi^-\pi^0$
1840 +100 -70		¹⁰ ACHASOV	98H RVUE	$e^+e^- \rightarrow \omega\pi^+\pi^-$
1780 +170 -300		¹¹ ACHASOV	98H RVUE	$e^+e^- \rightarrow K^+K^-$
~2100		¹² ACHASOV	98H RVUE	$e^+e^- \rightarrow K_S^0 K^\pm \pi^\mp$
1606 ± 9		¹³ CLEGG	94 RVUE	
1662 ± 13	750	¹⁴ ANTONELLI	92 DM2	1.34–2.4 $e^+e^- \rightarrow \rho\pi,$ $\omega\pi\pi$
1670 ± 20		ATKINSON	83B OMEG	20–70 $\gamma\rho \rightarrow 3\pi X$
1657 ± 13		CORDIER	81 DM1	$e^+e^- \rightarrow \omega 2\pi$
1679 ± 34	21	ESPOSITO	80 FRAM	$e^+e^- \rightarrow 3\pi$
1652 ± 17		COSME	79 OSPK	$e^+e^- \rightarrow 3\pi$

¹ From a fit with contributions from $\omega(1420), \omega(1650),$ and $\phi(1680)$. The mass of $\omega(1420)$ is fixed to the PDG 18 value of 1420 MeV. Fixing also the width of $\omega(1420)$ to the PDG 18 value of 220 MeV results in 1694 ± 9 MeV measurement.

² Could also be $\rho(1700)$. Branching ratio $J/\psi \rightarrow X\pi^0 \rightarrow K^+K^-\pi^0 = (5.3 \pm 0.3 \pm_{-0.5}^{+0.6}) \times 10^{-5}$.

³ From a fit of the interfering $\omega(1420)$ and $\omega(1650)$ with a relative phase of π and other parameters floating.

⁴ From a fit with contributions from $\omega(1420), \omega(1650),$ and $\phi(1680)$.

⁵ From a fit with contributions from $\omega(782), \phi(1020), \omega(1420),$ and $\omega(1650)$. See ACHASOV 20A for a further analysis of the $\pi^+\pi^-\pi^0$ data.

⁶ From the combined fit of ANTONELLI 92, ACHASOV 01E, ACHASOV 02E, and ACHASOV 03D data on the $\pi^+\pi^-\pi^0$ and ANTONELLI 92 on the $\omega\pi^+\pi^-$ final states. Supersedes ACHASOV 99E and ACHASOV 02E.

⁷ Using results of CORDIER 81 and preliminary data of DOLINSKY 91 and ANTONELLI 92.

⁸ Using the data of AKHMETSIN 00D and ANTONELLI 92. The $\rho\pi$ dominance for the energy dependence of the $\omega(1420)$ and $\omega(1650)$ width assumed.

⁹ Using data from BARKOV 87, DOLINSKY 91, and ANTONELLI 92.

¹⁰ Using the data from ANTONELLI 92.

¹¹ Using the data from IVANOV 81 and BISELLO 88B.

¹² Using the data from BISELLO 91C.

¹³ From a fit to two Breit-Wigner functions and using the data of DOLINSKY 91 and ANTONELLI 92.

¹⁴ From the combined fit of the $\rho\pi$ and $\omega\pi\pi$ final states.

 $\omega(1650)$ WIDTH

VALUE (MeV)	EVTS	DOCUMENT ID	TECN	COMMENT
315 ± 35 OUR ESTIMATE				
110 ± 16	267	¹ ACHASOV	20B SND	$e^+e^- \rightarrow \omega\eta \rightarrow \eta\pi^0\gamma$
194 ± 8 +15 -7	183k	² ABLIKIM	19AQ BES	$J/\psi \rightarrow K^+K^-\pi^0$
95 ± 11		ACHASOV	19 SND	$e^+e^- \rightarrow \pi^+\pi^-\pi^0\eta$
113 ± 9 ± 10	824	³ AKHMETSIN	17A CMD3	1.4–2.0 $e^+e^- \rightarrow \omega\eta$
110 ± 20	898	⁴ ACHASOV	16B SND	1.34–2.00 $e^+e^- \rightarrow \omega\eta$
310 ± 30	13.1k	⁵ AULCHENKO	15A SND	1.05–1.80 $e^+e^- \rightarrow$ $\pi^+\pi^-\pi^0$
222 ± 25 ± 20		AUBERT	07AU BABR	10.6 $e^+e^- \rightarrow \omega\pi^+\pi^-\gamma$
114 ± 14	13	AUBERT	06D BABR	10.6 $e^+e^- \rightarrow \omega\eta\gamma$
230 ± 30 ± 20		AUBERT,B	04N BABR	10.6 $e^+e^- \rightarrow \pi^+\pi^-\pi^0\gamma$
490 +200 -150 ± 130	1.2M	⁶ ACHASOV	03D RVUE	0.44–2.00 $e^+e^- \rightarrow$ $\pi^+\pi^-\pi^0$
250 ± 14		⁷ HENNER	02 RVUE	1.2–2.0 $e^+e^- \rightarrow \rho\pi, \omega\pi\pi$
250 ± 50		EUGENIO	01 SPEC	18 $\pi^-\pi^0 \rightarrow \omega\eta\eta$
370 ± 25	612	⁸ AKHMETSIN	00D CMD2	$e^+e^- \rightarrow \omega\pi^+\pi^-$
113 ± 20		⁹ CLEGG	94 RVUE	
280 ± 24	750	¹⁰ ANTONELLI	92 DM2	1.34–2.4 $e^+e^- \rightarrow \rho\pi, \omega\pi\pi$
160 ± 20		ATKINSON	83B OMEG	20–70 $\gamma\rho \rightarrow 3\pi X$
136 ± 46		CORDIER	81 DM1	$e^+e^- \rightarrow \omega 2\pi$
99 ± 49	21	ESPOSITO	80 FRAM	$e^+e^- \rightarrow 3\pi$
42 ± 17		COSME	79 OSPK	$e^+e^- \rightarrow 3\pi$

¹ From a fit with contributions from $\omega(1420), \omega(1650),$ and $\phi(1680)$. The mass of $\omega(1420)$ is fixed to the PDG 18 value of 1420 MeV. Fixing also the width of $\omega(1420)$ to the PDG 18 value of 220 MeV results in 94 ± 13 MeV measurement.

² Could also be $\rho(1700)$. Branching ratio $J/\psi \rightarrow X\pi^0 \rightarrow K^+K^-\pi^0 = (5.3 \pm 0.3 \pm_{-0.5}^{+0.6}) \times 10^{-5}$.

³ From a fit of the interfering $\omega(1420)$ and $\omega(1650)$ with a relative phase of π and other parameters floating.

⁴ From a fit with contributions from $\omega(1420), \omega(1650),$ and $\phi(1680)$.

⁵ From a fit with contributions from $\omega(782), \phi(1020), \omega(1420),$ and $\omega(1650)$. See ACHASOV 20A for a further analysis of the $\pi^+\pi^-\pi^0$ data.

⁶ From the combined fit of ANTONELLI 92, ACHASOV 01E, ACHASOV 02E, and ACHASOV 03D data on the $\pi^+\pi^-\pi^0$ and ANTONELLI 92 on the $\omega\pi^+\pi^-$ final states. Supersedes ACHASOV 99E and ACHASOV 02E.

⁷ Using results of CORDIER 81 and preliminary data of DOLINSKY 91 and ANTONELLI 92.

⁸ Using the data of AKHMETSIN 00D and ANTONELLI 92. The $\rho\pi$ dominance for the energy dependence of the $\omega(1420)$ and $\omega(1650)$ width assumed.

⁹ From a fit to two Breit-Wigner functions and using the data of DOLINSKY 91 and ANTONELLI 92.

¹⁰ From the combined fit of the $\rho\pi$ and $\omega\pi\pi$ final states.

Meson Particle Listings

$\omega(1650)$, $\omega_3(1670)$

$\omega(1650)$ DECAY MODES

Mode	Fraction (Γ_i/Γ)
Γ_1 $\rho\pi$	seen
Γ_2 $\rho(1450)\pi$	seen
Γ_3 $\omega\pi\pi$	seen
Γ_4 $\omega\eta$	seen
Γ_5 e^+e^-	seen
Γ_6 $\pi^0\gamma$	not seen

$\omega(1650)$ $\Gamma(\pi)\Gamma(e^+e^-)/\Gamma^2(\text{total})$

$\Gamma(\rho\pi)/\Gamma_{\text{total}} \times \Gamma(e^+e^-)/\Gamma_{\text{total}}$	$\Gamma_1/\Gamma \times \Gamma_5/\Gamma$			
VALUE (units 10^{-6})	EVTs	DOCUMENT ID	TECN	COMMENT
●●● We do not use the following data for averages, fits, limits, etc. ●●●				
1.56 ± 0.23	13.1k	¹ AULCHENKO	15A	SND 1.05-1.80 $e^+e^- \rightarrow \pi^+\pi^-\pi^0$
$1.3 \pm 0.1 \pm 0.1$		AUBERT,B	04N	BABR 10.6 $e^+e^- \rightarrow \pi^+\pi^-\pi^0\gamma$
1.2 ± 0.4 -0.1	± 0.8	^{2,3} ACHASOV	03D	RVUE 0.44-2.00 $e^+e^- \rightarrow \pi^+\pi^-\pi^0$
0.921 ± 0.230		^{4,5} CLEGG	94	RVUE $\pi^+\pi^-\pi^0$
0.479 ± 0.050	750	^{6,7} ANTONELLI	92	DM2 1.34-2.4 $e^+e^- \rightarrow \rho\pi, \omega\pi\pi$

¹ From a fit with contributions from $\omega(782)$, $\phi(1020)$, $\omega(1420)$, and $\omega(1650)$. See ACHASOV 20A for a further analysis of the $\pi^+\pi^-\pi^0$ data.
² Calculated by us from the cross section at the peak.
³ From the combined fit of ANTONELLI 92, ACHASOV 01E, ACHASOV 02E, and ACHASOV 03D data on the $\pi^+\pi^-\pi^0$ and ANTONELLI 92 on the $\omega\pi^+\pi^-$ final states. Supersedes ACHASOV 99E and ACHASOV 02E.
⁴ From a fit to two Breit-Wigner functions and using the data of DOLINSKY 91 and ANTONELLI 92.
⁵ From the partial and leptonic width given by the authors.
⁶ From the combined fit of the $\rho\pi$ and $\omega\pi\pi$ final states.
⁷ From the product of the leptonic width and partial branching ratio given by the authors.

$\Gamma(\omega\pi\pi)/\Gamma_{\text{total}} \times \Gamma(e^+e^-)/\Gamma_{\text{total}}$	$\Gamma_3/\Gamma \times \Gamma_5/\Gamma$			
VALUE (units 10^{-7})	EVTs	DOCUMENT ID	TECN	COMMENT
●●● We do not use the following data for averages, fits, limits, etc. ●●●				
7.0 ± 0.5		AUBERT	07AU	BABR 10.6 $e^+e^- \rightarrow \omega\pi^+\pi^-\gamma$
$4.1 \pm 0.9 \pm 1.3$	$1.2M$	^{1,2} ACHASOV	03D	RVUE 0.44-2.00 $e^+e^- \rightarrow \pi^+\pi^-\pi^0$
5.40 ± 0.95		³ AKHMETSHIN	00D	CMD2 1.2-1.38 $e^+e^- \rightarrow \omega\pi^+\pi^-$
3.18 ± 0.80		^{4,5} CLEGG	94	RVUE $\pi^+\pi^-\pi^0$
6.07 ± 0.61	750	^{6,7} ANTONELLI	92	DM2 1.34-2.4 $e^+e^- \rightarrow \rho\pi, \omega\pi\pi$

¹ Calculated by us from the cross section at the peak.
² From the combined fit of ANTONELLI 92, ACHASOV 01E, ACHASOV 02E, and ACHASOV 03D data on the $\pi^+\pi^-\pi^0$ and ANTONELLI 92 on the $\omega\pi^+\pi^-$ final states. Supersedes ACHASOV 99E and ACHASOV 02E.
³ Using the data of AKHMETSHIN 00D and ANTONELLI 92. The $\rho\pi$ dominance for the energy dependence of the $\omega(1420)$ and $\omega(1650)$ width assumed.
⁴ From a fit to two Breit-Wigner functions and using the data of DOLINSKY 91 and ANTONELLI 92.
⁵ From the partial and leptonic width given by the authors.
⁶ From the combined fit of the $\rho\pi$ and $\omega\pi\pi$ final states.
⁷ From the product of the leptonic width and partial branching ratio given by the authors.

$\Gamma(\omega\eta)/\Gamma_{\text{total}} \times \Gamma(e^+e^-)/\Gamma_{\text{total}}$	$\Gamma_4/\Gamma \times \Gamma_5/\Gamma$			
VALUE (units 10^{-7})	EVTs	DOCUMENT ID	TECN	COMMENT
●●● We do not use the following data for averages, fits, limits, etc. ●●●				
6.4 ± 0.9	267	¹ ACHASOV	20B	SND $e^+e^- \rightarrow \omega\eta \rightarrow \eta\pi^0\gamma$
5.62 ± 0.45 -0.42		ACHASOV	19	SND $e^+e^- \rightarrow \pi^+\pi^-\pi^0\eta$
$4.5 \pm 0.3 \pm 0.3$	824	² AKHMETSHIN	17A	CMD3 1.4-2.0 $e^+e^- \rightarrow \omega\eta$
4.4 ± 0.5	898	³ ACHASOV	16B	SND 1.34-2.00 $e^+e^- \rightarrow \omega\eta$
5.7 ± 0.6	13	AUBERT	06D	BABR 10.6 $e^+e^- \rightarrow \omega\eta\gamma$
< 60 at 90% CL		⁴ AKHMETSHIN	03B	CMD2 $e^+e^- \rightarrow \eta\pi^0\gamma$

¹ From a fit with contributions from $\omega(1420)$, $\omega(1650)$, and $\phi(1680)$. The mass of $\omega(1420)$ is fixed to the PDG 18 value of 1420 MeV. Fixing also the width of $\omega(1420)$ to the PDG 18 value of 220 MeV results in $(5.4 \pm 0.6) \times 10^{-7}$ measurement.
² From a fit of the interfering $\omega(1420)$ and $\omega(1650)$ with a relative phase of π and other parameters floating. From an alternative fit $\Gamma(\omega(1650) \rightarrow \omega\eta)/\Gamma_{\text{total}} \times \Gamma(\omega(1650) \rightarrow e^+e^-) = 51 \pm 3$ eV.
³ From a fit with contributions from $\omega(1420)$, $\omega(1650)$, and $\phi(1680)$.
⁴ $\omega(1650)$ mass and width fixed at 1700 MeV and 250 MeV, respectively.

$\omega(1650)$ BRANCHING RATIOS

$\Gamma(\rho\pi)/\Gamma_{\text{total}}$	Γ_1/Γ			
VALUE	EVTs	DOCUMENT ID	TECN	COMMENT
●●● We do not use the following data for averages, fits, limits, etc. ●●●				
~ 0.65	$1.2M$	¹ ACHASOV	03D	RVUE 0.44-2.00 $e^+e^- \rightarrow \pi^+\pi^-\pi^0$
0.380 ± 0.014		² HENNER	02	RVUE 1.2-2.0 $e^+e^- \rightarrow \rho\pi, \omega\pi\pi$

¹ From the combined fit of ANTONELLI 92, ACHASOV 01E, ACHASOV 02E, and ACHASOV 03D data on the $\pi^+\pi^-\pi^0$ and ANTONELLI 92 on the $\omega\pi^+\pi^-$ final states. Supersedes ACHASOV 99E and ACHASOV 02E.
² Assuming that the $\omega(1650)$ decays into $\rho\pi$ and $\omega\pi\pi$ only.

$\Gamma(\rho(1450)\pi)/\Gamma_{\text{total}}$

VALUE	DOCUMENT ID	TECN	COMMENT
seen	ACHASOV	20A	SND 1.15-2.00 $e^+e^- \rightarrow \pi^+\pi^-\pi^0$

$\Gamma(\omega\pi\pi)/\Gamma_{\text{total}}$

VALUE	EVTs	DOCUMENT ID	TECN	COMMENT
●●● We do not use the following data for averages, fits, limits, etc. ●●●				
~ 0.35	$1.2M$	¹ ACHASOV	03D	RVUE 0.44-2.00 $e^+e^- \rightarrow \pi^+\pi^-\pi^0$
0.620 ± 0.014		² HENNER	02	RVUE 1.2-2.0 $e^+e^- \rightarrow \rho\pi, \omega\pi\pi$

¹ From the combined fit of ANTONELLI 92, ACHASOV 01E, ACHASOV 02E, and ACHASOV 03D data on the $\pi^+\pi^-\pi^0$ and ANTONELLI 92 on the $\omega\pi^+\pi^-$ final states. Supersedes ACHASOV 99E and ACHASOV 02E.
² Assuming that the $\omega(1650)$ decays into $\rho\pi$ and $\omega\pi\pi$ only.

$\Gamma(e^+e^-)/\Gamma_{\text{total}}$

VALUE (units 10^{-7})	EVTs	DOCUMENT ID	TECN	COMMENT
●●● We do not use the following data for averages, fits, limits, etc. ●●●				
~ 18	$1.2M$	^{1,2} ACHASOV	03D	RVUE 0.44-2.00 $e^+e^- \rightarrow \pi^+\pi^-\pi^0$
32 ± 1		² HENNER	02	RVUE 1.2-2.0 $e^+e^- \rightarrow \rho\pi, \omega\pi\pi$

¹ Calculated by us from the cross section at the peak.
² Assuming that the $\omega(1650)$ decays into $\rho\pi$ and $\omega\pi\pi$ only.

$\Gamma(\pi^0\gamma)/\Gamma_{\text{total}}$

VALUE	DOCUMENT ID	TECN	COMMENT
not seen	¹ ACHASOV	10D	SND 1.075-2.0 $e^+e^- \rightarrow \pi^0\gamma$

¹ From a fit of a VMD model with two effective resonances with masses of 1450 MeV and 1700 MeV to describe the excited vector states $\omega(1420)$, $\rho(1450)$, $\omega(1650)$, and $\rho(1700)$. The width of the highest mass effective resonance is fixed at 315 MeV.

$\omega(1650)$ REFERENCES

ACHASOV	20A	EPJ C80 993	M.N. Achasov et al.	(SND Collab.)
ACHASOV	20B	EPJ C80 1008	M.N. Achasov et al.	(SND Collab.)
ABLIKIM	19AQ	PR D100 032004	M. Ablikim et al.	(BESIII Collab.)
ACHASOV	19	PR D99 112004	M.N. Achasov et al.	(SND Collab.)
PDG	18	PR D98 030001	M. Tanabashi et al.	(PDG Collab.)
AKHMETSHIN	17A	PL B773 150	R.R. Akhmetshin et al.	(CMD-3 Collab.)
ACHASOV	16B	PR D94 092002	M.N. Achasov et al.	(SND Collab.)
AULCHENKO	15A	JETP 121 27	V.M. Aulchenko et al.	(SND Collab.)
Translated from ZETF 148 34.				
ACHASOV	10D	PR D98 112001	M.N. Achasov et al.	(SND Collab.)
AUBERT	07AU	PR D76 092005	B. Aubert et al.	(BABAR Collab.)
AUBERT	06D	PR D73 052003	B. Aubert et al.	(BABAR Collab.)
AUBERT,B	04N	PR D70 072004	B. Aubert et al.	(BABAR Collab.)
ACHASOV	03D	PR D68 052006	M.N. Achasov et al.	(Novosibirsk SND Collab.)
AKHMETSHIN	03B	PL B562 173	R.R. Akhmetshin et al.	(Novosibirsk CMD-2 Collab.)
ACHASOV	02E	PR D66 032001	M.N. Achasov et al.	(Novosibirsk SND Collab.)
HENNER	02	EPJ C26 3	V.K. Henner et al.	(Novosibirsk SND Collab.)
ACHASOV	01E	PR D63 072002	M.N. Achasov et al.	(Novosibirsk SND Collab.)
EUGENIO	01	PL B497 190	P. Eugenio et al.	(Novosibirsk SND Collab.)
AKHMETSHIN	00D	PL B489 125	R.R. Akhmetshin et al.	(Novosibirsk CMD-2 Collab.)
ACHASOV	99E	PL B462 365	M.N. Achasov et al.	(Novosibirsk SND Collab.)
ACHASOV	98H	PR D57 4334	N.N. Achasov, A.A. Kozhevnikov	(Novosibirsk SND Collab.)
CLEGG	94	ZPHY C62 455	A.B. Clegg, A. Donnachie	(LANC, MCHS)
ANTONELLI	92	ZPHY C56 15	A. Antonelli et al.	(DM2 Collab.)
BISELLO	91C	ZPHY C52 227	D. Bisello et al.	(DM2 Collab.)
DOLINSKY	91	PRPL 202 99	S.I. Dolinsky et al.	(NOVO)
BISELLO	88B	ZPHY C39 13	D. Bisello et al.	(PADO, CLER, FRAS+)
BARKOV	87	JETPL 46 164	L.M. Barkov et al.	(NOVO)
Translated from ZETFP 46 132.				
ATKINSON	83B	PL D27B 132	M. Atkinson et al.	(BONN, CERN, GLAS+)
CORDIER	81	PL D06B 155	A. Cordier et al.	(ORSAY)
IVANOV	81	PL D07B 297	P.M. Ivanov et al.	(NOVO)
ESPOSITO	80	LNCD 28 195	B. Esposito et al.	(FRAS, NAPL, PADO+)
COSME	79	NP B152 215	G. Cosme et al.	(IPN)

$\omega_3(1670)$

$$I^G(J^{PC}) = 0^-(3^{-})$$

$\omega_3(1670)$ MASS

VALUE (MeV)	EVTs	DOCUMENT ID	TECN	COMMENT
1667 ± 4 OUR AVERAGE				
$1665.3 \pm 5.2 \pm 4.5$	23400	AMELIN	96	VES 36 $\pi^-p \rightarrow \pi^+\pi^-\pi^0n$
1685 ± 20	60	BAUBILLIER	79	HBC 8.2 K^-p backward
1673 ± 12	430	^{1,2} BALTAY	78E	HBC 15 $\pi^+p \rightarrow \Delta 3\pi$
1650 ± 12		CORDEN	78B	OMEG 8-12 $\pi^-p \rightarrow N3\pi$
1669 ± 11	600	² WAGNER	75	HBC 7 $\pi^+p \rightarrow \Delta^{++} 3\pi$
1678 ± 14	500	DIAZ	74	DBC 6 $\pi^+n \rightarrow p3\pi^0$
1660 ± 13	200	DIAZ	74	DBC 6 $\pi^+n \rightarrow \rho\omega^0\pi^0$
1679 ± 17	200	MATTHEWS	71D	DBC 7.0 $\pi^+n \rightarrow p3\pi^0$
1670 ± 20		KENYON	69	DBC 8 $\pi^+n \rightarrow p3\pi^0$
●●● We do not use the following data for averages, fits, limits, etc. ●●●				
~ 1700	110	¹ CERRADA	77B	HBC 4.2 $K^-p \rightarrow \Lambda 3\pi$
1695 ± 20		BARNES	69B	HBC 4.6 $K^-p \rightarrow \omega 2\pi X$
1636 ± 20		ARMENISE	68B	DBC 5.1 $\pi^+n \rightarrow p3\pi^0$

¹ Phase rotation seen for $J^P = 3^- \rho\pi$ wave.
² From a fit to $I(J^P) = 0(3^-) \rho\pi$ partial wave.

See key on page 1127

Meson Particle Listings

ω₃(1670), π₂(1670)

ω₃(1670) WIDTH

Table with columns: VALUE (MeV), EVTS, DOCUMENT ID, TECN, COMMENT. Includes 'OUR AVERAGE' and various experimental data points with comments.

ω₃(1670) DECAY MODES

Table with columns: Mode, Fraction (Γ_i/Γ). Lists decay modes like ρπ, ωππ, and b₁(1235)π.

ω₃(1670) BRANCHING RATIOS

Table with columns: Γ(ωππ)/Γ(ρπ), Γ(b₁(1235)π)/Γ(ρπ), Γ(b₁(1235)π)/Γ(ωππ). Includes values and document references.

ω₃(1670) REFERENCES

Table listing references for ω₃(1670) with columns: AUTHOR, DOCUMENT ID, TECN, COMMENT.

π₂(1670)

J^G(J^{PC}) = 1⁻(2⁻⁺)

π₂(1670) MASS

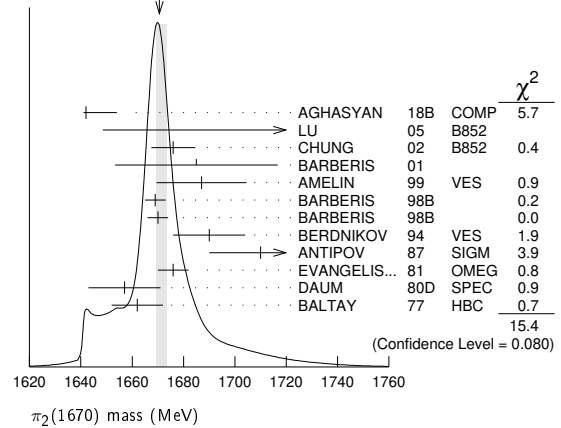
Table with columns: VALUE (MeV), EVTS, DOCUMENT ID, TECN, CHG, COMMENT. Includes 'OUR AVERAGE' and various experimental data points.

••• We do not use the following data for averages, fits, limits, etc. •••

Table listing excluded data points for π₂(1670) with columns: VALUE, EVTS, DOCUMENT ID, TECN, COMMENT.

- 1 Statistical error negligible.
2 From f₂(1270)π decay.
3 From a fit to J^P = 2⁻S-wave f₂(1270)π partial wave.
4 Clear phase rotation seen in 2⁻S, 2⁻P, 2⁻D waves.
5 Superseded by AGHASYAN 2018B.
6 J^{PC} ambiguous.
7 From ρπ decay.
8 From σπ decay.
9 From a two-resonance fit to four 2⁻0⁺ waves.

WEIGHTED AVERAGE 1670.6±2.9-1.2 (Error scaled by 1.3)



π₂(1670) WIDTH

Table with columns: VALUE (MeV), EVTS, DOCUMENT ID, TECN, CHG, COMMENT. Includes 'OUR AVERAGE' and various experimental data points.

Meson Particle Listings

$\pi_2(1670)$

¹¹ From $f_2(1270)\pi$ decay.
¹² From a fit to $J^P = 2^- f_2(1270)\pi$ partial wave.
¹³ Clear phase rotation seen in $2^-S, 2^-P, 2^-D$ waves. We quote central value and spread of single-resonance fits to three channels.
¹⁴ Superseded by AGHASYAN 2018B.
¹⁵ J^{PC} ambiguous.
¹⁶ From $\rho\pi$ decay.
¹⁷ From $\sigma\pi$ decay.
¹⁸ From a two-resonance fit to four 2^-0^+ waves. This should not be averaged with all the single resonance fits.

$\pi_2(1670)$ DECAY MODES

Mode	Fraction (Γ_i/Γ)	Confidence level
Γ_1 3π	(95.8 \pm 1.4) %	
Γ_2 $\pi^+\pi^-\pi^0$		
Γ_3 $\pi^0\pi^0\pi^0$		
Γ_4 $f_2(1270)\pi$	(56.3 \pm 3.2) %	
Γ_5 $\rho\pi$	(31 \pm 4) %	
Γ_6 $\sigma\pi$	(10 \pm 4) %	
Γ_7 $\pi(\pi\pi)S$ -wave	(8.7 \pm 3.4) %	
Γ_8 $\pi^\pm\pi^+\pi^-$	(53 \pm 4) %	
Γ_9 $K\bar{K}^*(892) + c.c.$	(4.2 \pm 1.4) %	
Γ_{10} $\omega\rho$	(2.7 \pm 1.1) %	
Γ_{11} $\pi^\pm\gamma$	(7.0 \pm 1.2) $\times 10^{-4}$	
Γ_{12} $\gamma\gamma$	< 2.8 $\times 10^{-7}$	90%
Γ_{13} $\eta\pi$	< 5 %	
Γ_{14} $\pi^\pm 2\pi^+ 2\pi^-$	< 5 %	
Γ_{15} $\rho(1450)\pi$	< 3.6 $\times 10^{-3}$	97.7%
Γ_{16} $b_1(1235)\pi$	< 1.9 $\times 10^{-3}$	97.7%
Γ_{17} $\eta 3\pi$		
Γ_{18} $f_1(1285)\pi$	possibly seen	
Γ_{19} $a_2(1320)\pi$	not seen	

CONSTRAINED FIT INFORMATION

An overall fit to 4 branching ratios uses 6 measurements and one constraint to determine 4 parameters. The overall fit has a $\chi^2 = 1.9$ for 3 degrees of freedom.

The following *off-diagonal* array elements are the correlation coefficients $\langle \delta x_i \delta x_j \rangle / (\delta x_i \delta x_j)$, in percent, from the fit to the branching fractions, $x_i \equiv \Gamma_i/\Gamma_{\text{total}}$. The fit constrains the x_i whose labels appear in this array to sum to one.

x_5	-53		
x_7	-29	-59	
x_9	-8	-21	-9
	x_4	x_5	x_7

$\pi_2(1670)$ PARTIAL WIDTHS

$\Gamma(\pi^\pm\gamma)$	Γ_{11}			
VALUE (keV)	DOCUMENT ID	TECN	CHG	COMMENT
181 \pm 11 \pm 27	¹⁹ ADOLPH	14	COMP	190 $\pi^-\text{Pb}$ \rightarrow $\pi^+\pi^-\pi^-\text{Pb}$?

¹⁹Primakoff reaction. Assumes incoherent $f_2(1270)\pi$ contribution to 3π final state and uses $B(\pi_2(1670) \rightarrow f_2\pi) = 56\%$.

$\Gamma(\gamma\gamma)$	Γ_{12}				
VALUE (keV)	CL%	DOCUMENT ID	TECN	CHG	COMMENT
<0.072	90	20 ACCIARRI	97T	L3	$e^+e^- \rightarrow e^+e^-\pi^+\pi^-\pi^0$
••• We do not use the following data for averages, fits, limits, etc. •••					
<0.19	90	20 ALBRECHT	97B	ARG	$e^+e^- \rightarrow e^+e^-\pi^+\pi^-\pi^0$
1.41 \pm 0.23 \pm 0.28		ANTREASNYAN	90	CBAL	0
0.8 \pm 0.3 \pm 0.12		21 BEHREND	90C	CELL	0
1.3 \pm 0.3 \pm 0.2		22 BEHREND	90C	CELL	0

²⁰Decaying into $f_2(1270)\pi$ and $\rho\pi$.
²¹ Constructive interference between $f_2(1270)\pi, \rho\pi$ and background.
²² Incoherent Ansatz.

$\pi_2(1670)$ $\Gamma(i)\Gamma(\gamma\gamma)/\Gamma(\text{total})$

$\Gamma(\pi^+\pi^-\pi^0) \times \Gamma(\gamma\gamma)/\Gamma_{\text{total}}$	Γ_{12}/Γ			
VALUE (keV)	CL%	DOCUMENT ID	TECN	COMMENT
<0.1	95	23 SCHEGELSKY	06	RVUE $\gamma\gamma \rightarrow \pi^+\pi^-\pi^0$

²³From analysis of L3 data at 183–209 GeV.

$\pi_2(1670)$ BRANCHING RATIOS

$\Gamma(3\pi)/\Gamma_{\text{total}}$	$\Gamma_1/\Gamma = (\Gamma_4+\Gamma_5+\Gamma_7)/\Gamma$	
VALUE	DOCUMENT ID	
0.958 \pm 0.014 OUR FIT		
$\Gamma(\pi^0\pi^0\pi^0)/\Gamma(\pi^+\pi^-\pi^0)$	Γ_3/Γ_2	
VALUE	DOCUMENT ID	COMMENT
0.29 \pm 0.03 \pm 0.05	BARBERIS 01	450 $\rho\rho \rightarrow \rho_f 3\pi^0 \rho_s$

$\Gamma(\rho\pi)/0.565\Gamma(f_2(1270)\pi)$	$\Gamma_5/0.565\Gamma_4$		
(With $f_2(1270) \rightarrow \pi^+\pi^-$.)			
VALUE	DOCUMENT ID	TECN	COMMENT
0.97 \pm 0.09 OUR AVERAGE	Error includes scale factor of 1.9.		
0.76 \pm 0.07 \pm 0.10	CHUNG 02	B852	18.3 $\pi^-\rho \rightarrow \pi^+\pi^-\pi^-\rho$
1.01 \pm 0.05	BARBERIS 98B		450 $\rho\rho \rightarrow \rho_f \pi^+\pi^-\pi^0 \rho_s$

$\Gamma(\sigma\pi)/\Gamma(f_2(1270)\pi)$	Γ_6/Γ_4		
VALUE	DOCUMENT ID	TECN	COMMENT
0.17 \pm 0.02 \pm 0.07	CHUNG 02	B852	18.3 $\pi^-\rho \rightarrow \pi^+\pi^-\pi^-\rho$
••• We do not use the following data for averages, fits, limits, etc. •••			
0.24 \pm 0.10	24,25 BAKER	99	SPEC 1.94 $\bar{p}p \rightarrow 4\pi^0$

$\frac{1}{2}\Gamma(\rho\pi)/\Gamma(\pi^\pm\pi^+\pi^-)$	$\frac{1}{2}\Gamma_5/\Gamma_8 = \frac{1}{2}\Gamma_5/(0.565\Gamma_4 + \frac{1}{2}\Gamma_5 + 0.624\Gamma_7)$			
VALUE	DOCUMENT ID	TECN	CHG	COMMENT
0.29 \pm 0.04 OUR FIT	26 DAUM	81B	SPEC	63,94 $\pi^-\rho$
0.29 \pm 0.05	••• We do not use the following data for averages, fits, limits, etc. •••			
<0.3	BARTSCH 68	HBC	+	8 $\pi^+\rho \rightarrow 3\pi\rho$

$0.565\Gamma(f_2(1270)\pi)/\Gamma(\pi^\pm\pi^+\pi^-)$	$0.565\Gamma_4/\Gamma_8 = 0.565\Gamma_4/(0.565\Gamma_4 + \frac{1}{2}\Gamma_5 + 0.624\Gamma_7)$			
(With $f_2(1270) \rightarrow \pi^+\pi^-$.)				
VALUE	DOCUMENT ID	TECN	CHG	COMMENT
0.604 \pm 0.035 OUR FIT	Error includes scale factor of 1.3.			
0.61 \pm 0.04	26 DAUM	81B	SPEC	63,94 $\pi^-\rho$
0.76 \pm 0.24 -0.34	ARMENISE 69	DBC	+	5.1 $\pi^+\rho \rightarrow d 3\pi$
0.35 \pm 0.20	BALTAY 68	HBC	+	7-8.5 $\pi^+\rho$
••• We do not use the following data for averages, fits, limits, etc. •••				
0.59	BARTSCH 68	HBC	+	8 $\pi^+\rho \rightarrow 3\pi\rho$

$0.624\Gamma(\pi(\pi\pi)S\text{-wave})/\Gamma(\pi^\pm\pi^+\pi^-)$	$0.624\Gamma_7/\Gamma_8 = 0.624\Gamma_7/(0.565\Gamma_4 + \frac{1}{2}\Gamma_5 + 0.624\Gamma_7)$		
(With $(\pi\pi)S$ -wave $\rightarrow \pi^+\pi^-$.)			
VALUE	DOCUMENT ID	TECN	COMMENT
0.10 \pm 0.04 OUR FIT			
0.10 \pm 0.05	26 DAUM	81B	SPEC 63,94 $\pi^-\rho$

$\Gamma(K\bar{K}^*(892) + c.c.)/\Gamma(f_2(1270)\pi)$	Γ_9/Γ_4			
VALUE	DOCUMENT ID	TECN	CHG	COMMENT
0.075 \pm 0.025 OUR FIT				
0.075 \pm 0.025	27 ARMSTRONG	82B	OMEG	16 $\pi^-\rho \rightarrow K^+K^-\pi^-\rho$

$\Gamma(\omega\rho)/\Gamma_{\text{total}}$	Γ_{10}/Γ		
VALUE	DOCUMENT ID	TECN	COMMENT
0.027 \pm 0.004 \pm 0.010	28 AMELIN	99	VES 37 $\pi^-A \rightarrow \omega\pi^-\pi^0A^*$

$\Gamma(\eta\pi)/\Gamma(\pi^\pm\pi^+\pi^-)$	$\Gamma_{13}/\Gamma_8 = \Gamma_{13}/(0.565\Gamma_4 + \frac{1}{2}\Gamma_5 + 0.624\Gamma_7)$			
(All η decays.)				
VALUE	DOCUMENT ID	TECN	CHG	COMMENT
<0.09	BALTAY 68	HBC	+	7-8.5 $\pi^+\rho$
••• We do not use the following data for averages, fits, limits, etc. •••				
<0.10	CRENNELL 70	HBC	-	6 $\pi^-\rho \rightarrow f_2\pi^-N$

$\Gamma(\pi^\pm 2\pi^+ 2\pi^-)/\Gamma(\pi^\pm\pi^+\pi^-)$	$\Gamma_{14}/\Gamma_8 = \Gamma_{14}/(0.565\Gamma_4 + \frac{1}{2}\Gamma_5 + 0.624\Gamma_7)$			
VALUE	DOCUMENT ID	TECN	CHG	COMMENT
<0.10	CRENNELL 70	HBC	-	6 $\pi^-\rho \rightarrow f_2\pi^-N$
••• We do not use the following data for averages, fits, limits, etc. •••				
<0.1	BALTAY 68	HBC	+	7,8.5 $\pi^+\rho$

$\Gamma(\rho(1450)\pi)/\Gamma_{\text{total}}$	Γ_{15}/Γ			
VALUE	CL%	DOCUMENT ID	TECN	COMMENT
<0.0036	97.7	AMELIN 99	VES	37 $\pi^-A \rightarrow \omega\pi^-\pi^0A^*$

$\Gamma(b_1(1235)\pi)/\Gamma_{\text{total}}$	Γ_{16}/Γ			
VALUE	CL%	DOCUMENT ID	TECN	COMMENT
<0.0019	97.7	AMELIN 99	VES	37 $\pi^-A \rightarrow \omega\pi^-\pi^0A^*$

$\Gamma(f_1(1285)\pi)/\Gamma_{\text{total}}$	Γ_{18}/Γ			
VALUE	EVTS	DOCUMENT ID	TECN	COMMENT
possibly seen	69k	KUHN 04	B852	18 $\pi^-\rho \rightarrow \eta\pi^+\pi^-\pi^-\rho$

See key on page 1127

Meson Particle Listings

$\pi_2(1670), \phi(1680)$

Table with 5 columns: VALUE, EVTS, DOCUMENT ID, TECN, COMMENT. Row for $\Gamma(\pi_2(1320)\pi)/\Gamma_{total}$ with value 'not seen' and 69k events.

D-wave/S-wave RATIO FOR $\pi_2(1670) \rightarrow f_2(1270)\pi$. Table with 4 columns: VALUE, DOCUMENT ID, TECN, COMMENT. Value: -0.18 ± 0.06 .

F-wave/P-wave RATIO FOR $\pi_2(1670) \rightarrow \rho\pi$. Table with 4 columns: VALUE, DOCUMENT ID, TECN, COMMENT. Value: $-0.72 \pm 0.07 \pm 0.14$.

$\pi_2(1670)$ REFERENCES

Large table of references for $\pi_2(1670)$ with columns: AUTHOR, YEAR, DOCUMENT ID, TECN, COMMENT. Includes entries like AGHASYAN 1988, ADOLPH 14, etc.

$\phi(1680)$

$J^G(J^{PC}) = 0^-(1^{--})$

$\phi(1680)$ MASS

e+e- PRODUCTION table for $\phi(1680)$. Columns: VALUE (MeV), EVTS, DOCUMENT ID, TECN, COMMENT. Includes 'OUR ESTIMATE' and various experimental data points.

1 Seen in $\psi(2S)$ decay with branching ratio $\psi(2S) \rightarrow X\eta \rightarrow K^+K^-\eta = (12.0 \pm 1.3^{+6.5}_{-6.9}) \times 10^{-6}$.

6 Using events with $\pi\pi$ invariant mass less than 0.85 GeV. 7 From a fit with two incoherent Breit-Wigners. 8 From the simultaneous fit to the $K\bar{K}^*(892) + c.c.$ and $\phi\eta$ data from AUBERT 08s...

pP ANNIHILATION table for $\phi(1680)$. Columns: VALUE (MeV), DOCUMENT ID, TECN, COMMENT. Value: 1700 ± 8 .

$\phi(1680)$ WIDTH

e+e- PRODUCTION table for $\phi(1680)$ with various decay channels. Columns: VALUE (MeV), EVTS, DOCUMENT ID, TECN, COMMENT. Includes 'OUR ESTIMATE' and various experimental data points.

1 Seen in $\psi(2S)$ decay with branching ratio $\psi(2S) \rightarrow X\eta \rightarrow K^+K^-\eta = (12.0 \pm 1.3^{+6.5}_{-6.9}) \times 10^{-6}$. 2 From a fit using a vector meson dominance model with contribution from $\rho(770), \omega(782), \phi(1020), \omega(1420), \rho(1450)$.

pP ANNIHILATION table for $\phi(1680)$. Columns: VALUE (MeV), DOCUMENT ID, TECN, COMMENT. Value: 143 ± 24 .

$\phi(1680)$ DECAY MODES

Table with 2 columns: Mode, Fraction (Γ_i/Γ). Rows include $K\bar{K}^*(892) + c.c.$, $K_S^0 K\pi$, $K\bar{K}$, $K_L^0 K_S^0$, e^+e^- , $\omega\pi\pi$.

Downloaded from https://academic.oup.com/ptep/article/2022/8/083C01/6651666 by CERN Library user on 11 October 2022

Meson Particle Listings

$\phi(1680), \rho_3(1690)$

Γ	ϕ	
Γ_7	$\phi\pi\pi$	
Γ_8	$K^+K^-\pi^+\pi^-$	seen
Γ_9	$\eta\phi$	seen
Γ_{10}	$K^+K^-\eta$	
Γ_{11}	$\eta\gamma$	seen
Γ_{12}	$K^+K^-\pi^0$	

$\phi(1680) \Gamma(i)\Gamma(e^+e^-)/\Gamma(\text{total})$

This combination of a partial width with the partial width into e^+e^- and with the total width is obtained from the integrated cross section into channel (i) in e^+e^- annihilation. We list only data that have not been used to determine the partial width $\Gamma(i)$ or the branching ratio $\Gamma(i)/\text{total}$.

$\Gamma(K_L^0 K_S^0) \times \Gamma(e^+e^-)/\Gamma_{\text{total}}$				
VALUE (eV)	EVTS	DOCUMENT ID	TECN	COMMENT
$14.3 \pm 2.4 \pm 6.2$	6.2k	¹ LEES	14H	BABR $e^+e^- \rightarrow K_S^0 K_L^0 \gamma$

¹ Using a vector meson dominance model with contribution from $\phi(1020)$, $\phi(1680)$, and higher mass excitations of $\rho(770)$ and $\omega(782)$.

$\Gamma(\phi\pi\pi) \times \Gamma(e^+e^-)/\Gamma_{\text{total}}$				
VALUE (10^{-2} keV)	DOCUMENT ID	TECN	COMMENT	
$4.2 \pm 0.2 \pm 0.3$	LEES	12F	BABR	$10.6 e^+e^- \rightarrow \phi\pi^+\pi^-\gamma$

$\Gamma(\eta\phi) \times \Gamma(e^+e^-)/\Gamma_{\text{total}}$				
VALUE (eV)	EVTS	DOCUMENT ID	TECN	COMMENT
$94 \pm 13 \pm 15$	3k	¹ IVANOV	19A	CMD3 $1.59\text{--}2.007 e^+e^- \rightarrow K^+K^-\eta$

¹ From a fit with coherent interference of the $\phi(1680)$ with a non-resonant contribution.

$\phi(1680) \Gamma(i)\Gamma(e^+e^-)/\Gamma^2(\text{total})$

This combination of a branching ratio into channel (i) and branching ratio into e^+e^- is directly measured and obtained from the cross section at the peak. We list only data that have not been used to determine the branching ratio into (i) or e^+e^- .

$\Gamma(K_L^0 K_S^0)/\Gamma_{\text{total}} \times \Gamma(e^+e^-)/\Gamma_{\text{total}}$				
VALUE (units 10^{-6})	EVTS	DOCUMENT ID	TECN	COMMENT
0.131 ± 0.059	948	¹ AKHMETSHIN	03	CMD2 $1.05\text{--}1.38 e^+e^- \rightarrow K_L^0 K_S^0$

¹ From the combined fit of AKHMETSHIN 03 and MANE 81 also including ρ, ω , and ϕ . Neither isospin nor flavor structure known. Recalculated by us.

$\Gamma(K\bar{K}^*(892) + \text{c.c.})/\Gamma_{\text{total}} \times \Gamma(e^+e^-)/\Gamma_{\text{total}}$				
VALUE (units 10^{-6})	EVTS	DOCUMENT ID	TECN	COMMENT
$1.15 \pm 0.16 \pm 0.01$		¹ AUBERT	08s	BABR $10.6 e^+e^- \rightarrow K\bar{K}^*(892)\gamma + \text{c.c.}$
3.29 ± 1.57	367	² BISELLO	91c	DM2 $1.35\text{--}2.40 e^+e^- \rightarrow K_S^0 K^\pm \pi^\mp$

¹ From the simultaneous fit to the $K\bar{K}^*(892) + \text{c.c.}$ and $\phi\eta$ data from AUBERT 08s using the results of AUBERT 07AK.
² Recalculated by us with the published value of $B(K\bar{K}^*(892) + \text{c.c.}) \times \Gamma(e^+e^-)$.

$\Gamma(\phi\pi\pi)/\Gamma_{\text{total}} \times \Gamma(e^+e^-)/\Gamma_{\text{total}}$				
VALUE (units 10^{-7})	EVTS	DOCUMENT ID	TECN	COMMENT
$1.86 \pm 0.14 \pm 0.21$	4.8k	¹ SHEN	09	BELL $10.6 e^+e^- \rightarrow K^+K^-\pi^+\pi^-\eta$

¹ Multiplied by 3/2 to take into account the $\phi\pi^0\pi^0$ mode. Using $B(\phi \rightarrow K^+K^-) = (49.2 \pm 0.6)\%$.

$\Gamma(\eta\phi)/\Gamma_{\text{total}} \times \Gamma(e^+e^-)/\Gamma_{\text{total}}$				
VALUE (units 10^{-7})	EVTS	DOCUMENT ID	TECN	COMMENT
$5.64_{-1.80}^{+1.74}$		ACHASOV	19	SND $e^+e^- \rightarrow \pi^+\pi^-\pi^0\eta$
$5.3 \pm 0.6 \pm 0.9$	3k	¹ IVANOV	19A	CMD3 $1.59\text{--}2.007 e^+e^- \rightarrow K^+K^-\eta$
$4.3 \pm 1.0 \pm 0.9$		² AUBERT	08s	BABR $10.6 e^+e^- \rightarrow \phi\eta\gamma$

¹ From a fit with coherent interference of the $\phi(1680)$ with a non-resonant contribution.
² From the simultaneous fit to the $K\bar{K}^*(892) + \text{c.c.}$ and $\phi\eta$ data from AUBERT 08s using the results of AUBERT 07AK.

$\phi(1680) \text{ BRANCHING RATIOS}$

$\Gamma(K\bar{K}^*(892) + \text{c.c.})/\Gamma(K_S^0 K_\pi)$				
VALUE	DOCUMENT ID	TECN	COMMENT	
dominant	MANE	82	DM1	$e^+e^- \rightarrow K_S^0 K^\pm \pi^\mp$

$\Gamma(K\bar{K})/\Gamma(K\bar{K}^*(892) + \text{c.c.})$				
VALUE	DOCUMENT ID	TECN	COMMENT	
0.07 ± 0.01	BUON	82	DM1	e^+e^-

$\Gamma(\omega\pi\pi)/\Gamma(K\bar{K}^*(892) + \text{c.c.})$				
VALUE	DOCUMENT ID	TECN	COMMENT	
< 0.10	BUON	82	DM1	e^+e^-

$\Gamma(\eta\phi)/\Gamma_{\text{total}}$				
VALUE	EVTS	DOCUMENT ID	TECN	COMMENT
seen	35	¹ ACHASOV	14	SND $1.15\text{--}2.00 e^+e^- \rightarrow \eta\gamma$

¹ From a phenomenological model based on vector meson dominance with $\rho(1450)$ and $\phi(1680)$ masses and widths from the PDG 12.

$\Gamma(\eta\phi)/\Gamma(K\bar{K}^*(892) + \text{c.c.})$				
VALUE	DOCUMENT ID	TECN	COMMENT	
≈ 0.37	¹ AUBERT	08s	BABR	$10.6 e^+e^- \rightarrow \text{hadrons}$

¹ From the fit including data from AUBERT 07AK.

$\Gamma(\eta\gamma)/\Gamma_{\text{total}}$				
VALUE	EVTS	DOCUMENT ID	TECN	COMMENT
seen	35	¹ ACHASOV	14	SND $1.15\text{--}2.00 e^+e^- \rightarrow \eta\gamma$

¹ From a phenomenological model based on vector meson dominance with $\rho(1450)$ and $\phi(1680)$ masses and widths from the PDG 12.

$\phi(1680) \text{ REFERENCES}$

ABLIKIM	20F	PR D101 032008	M. Ablikim <i>et al.</i>	(BESIII Collab.)
ACHASOV	20C	EPJ C80 1139	M.N. Achasov <i>et al.</i>	(SND Collab.)
ACHASOV	19	PR D99 112004	M.N. Achasov <i>et al.</i>	(SND Collab.)
IVANOV	19A	PL B798 134946	V.L. Ivanov <i>et al.</i>	(CMD-3 Collab.)
ACHASOV	18A	PR D97 032011	M.N. Achasov <i>et al.</i>	(SND Collab.)
ACHASOV	14	PR D90 032002	M.N. Achasov <i>et al.</i>	(SND Collab.)
LEES	14H	PR D89 022002	J.P. Lees <i>et al.</i>	(BABAR Collab.)
LEES	12F	PR D86 012008	J.P. Lees <i>et al.</i>	(BABAR Collab.)
PDG	12	PR D86 010001	J. Beringer <i>et al.</i>	(PDG Collab.)
SHEN	09	PR D80 031101	C.P. Shen <i>et al.</i>	(BELLE Collab.)
AUBERT	08S	PR D77 092002	B. Aubert <i>et al.</i>	(BABAR Collab.)
AUBERT	07AK	PR D76 012008	B. Aubert <i>et al.</i>	(BABAR Collab.)
AMSLE	06	PL B639 165	C. Amstler <i>et al.</i>	(Crystal Barrel Collab.)
AKHMETSHIN	03	PL B551 27	R.R. Akhmetshin <i>et al.</i>	(Novosibirsk CMD-2 Collab.)
Also		PAN 65 1222	E.V. Anashkin, V.M. Aulchenko, R.R. Akhmetshin	
ACHASOV	90H	PR D57 4334	M.N. Achasov, A.A. Kozhevnikov	
CLEGG	94	ZPHY C62 455	A.B. Clegg, A. Donnachie	(LANC, MCHS)
ANTONELLI	92	ZPHY C56 15	A. Antonelli <i>et al.</i>	(DM2 Collab.)
BISELLO	91C	ZPHY C52 227	D. Bisello <i>et al.</i>	(DM2 Collab.)
DOLINSKY	91C	PRPL 202 99	S.I. Dolinsky <i>et al.</i>	(NOVO)
BISELLO	88B	ZPHY C39 13	D. Bisello <i>et al.</i>	(PADO, CLER, FRAS+)
BARKOV	87	JETPL 46 164	L.M. Barkov <i>et al.</i>	(NOVO)
		Translated from ZETFP 46 132.		
BUON	82	PL 118B 221	J. Buon <i>et al.</i>	(LALO, MONP)
MANE	82	PL 112B 378	F. Mane <i>et al.</i>	(LALO)
IVANOV	81	PL 107B 297	P.M. Ivanov <i>et al.</i>	(NOVO)
MANE	81	PL 99B 261	F. Mane <i>et al.</i>	(ORSAY)

$\rho_3(1690)$

$$J^{PC} = 1^+(3^{--})$$

$\rho_3(1690) \text{ MASS}$

VALUE (MeV)	DOCUMENT ID
1688.8 ± 2.1 OUR AVERAGE	Includes data from the 5 datablocks that follow this one.

2 π MODE

VALUE (MeV)	EVTS	DOCUMENT ID	TECN	CHG	COMMENT
The data in this block is included in the average printed for a previous datablock.					

1686 ± 4 OUR AVERAGE

1677 ± 14		EVA NGELIS...	81	OMEG -	$12 \pi^- p \rightarrow 2\pi p$
1679 ± 11	476	BALTAY	78B	HBC 0	$15 \pi^+ p \rightarrow \pi^+ \pi^- n$
1678 ± 12	175	¹ ANTIPOV	77	CIBS 0	$25 \pi^- p \rightarrow p3\pi$
1690 ± 7	600	¹ ENGLER	74	DBC 0	$6 \pi^+ n \rightarrow \pi^+ \pi^- p$
1693 ± 8		² GRAYER	74	ASPK 0	$17 \pi^- p \rightarrow \pi^+ \pi^- n$
1678 ± 12		MATTHEWS	71c	DBC 0	$7 \pi^+ n$
••• We do not use the following data for averages, fits, limits, etc. •••					
1734 ± 10		³ CORDEN	79	OMEG	$12\text{--}15 \pi^- p \rightarrow n2\pi$
1692 ± 12		^{2,4} ESTABROOKS	75	RVUE	$17 \pi^- p \rightarrow \pi^+ \pi^- n$
1737 ± 23		ARMENISE	70	DBC 0	$9 \pi^+ n$
1650 ± 35	122	BARTSCH	70B	HBC +	$8 \pi^+ p \rightarrow N2\pi$
1687 ± 21		STUNTEBECK	70	HDDB	$8 \pi^- p, 5.4 \pi^+ d$
1683 ± 13		ARMENISE	68	DBC 0	$5.1 \pi^+ d$
1670 ± 30		GOLDBERG	65	HBC 0	$6 \pi^+ d, 8 \pi^- p$

¹ Mass errors enlarged by us to Γ/\sqrt{N} ; see the note with the $K^*(892)$ mass.

² Uses same data as HYAMS 75.

³ From a phase shift solution containing a $f_2'(1525)$ width two times larger than the $K\bar{K}$ result.

⁴ From phase-shift analysis. Error takes account of spread of different phase-shift solutions.

See key on page 1127

Meson Particle Listings

$\rho_3(1690)$

$K\bar{K}$ AND $K\bar{K}\pi$ MODES

VALUE (MeV) EVTS DOCUMENT ID TECN CHG COMMENT
The data in this block is included in the average printed for a previous datablock.

1696 ± 4 OUR AVERAGE

1699 ± 5		ALPER	80	CNTR	0	$62 \pi^- p \rightarrow K^+ K^- n$
1698 ± 12	6k	5,6 MARTIN	78D	SPEC		$10 \pi p \rightarrow K_S^0 K^- p$
1692 ± 6		BLUM	75	ASPK	0	$18.4 \pi^- p \rightarrow n K^+ K^-$
1690 ± 16		ADERHOLZ	69	HBC	+	$8 \pi^+ p \rightarrow K \bar{K} \pi$

• • • We do not use the following data for averages, fits, limits, etc. • • •

1694 ± 8		7 COSTA	80	OMEG		$10 \pi^- p \rightarrow K^+ K^- n$
----------	--	---------	----	------	--	------------------------------------

⁵ From a fit to $J^P = 3^-$ partial wave.
⁶ Systematic error on mass scale subtracted.
⁷ They cannot distinguish between $\rho_3(1690)$ and $\omega_3(1670)$.

$(4\pi)^\pm$ MODE

VALUE (MeV) EVTS DOCUMENT ID TECN CHG COMMENT
The data in this block is included in the average printed for a previous datablock.

1686 ± 5 OUR AVERAGE

Error includes scale factor of 1.1.

1694 ± 6		8 EVANGELIS...	81	OMEG	-	$12 \pi^- p \rightarrow p 4\pi$
1665 ± 15	177	BALTAY	78B	HBC	+	$15 \pi^+ p \rightarrow p 4\pi$
1670 ± 10		THOMPSON	74	HBC	+	$13 \pi^+ p$
1687 ± 20		CASON	73	HBC	-	$8,18.5 \pi^- p$
1685 ± 14		9 CASON	73	HBC	-	$8,18.5 \pi^- p$
1680 ± 40	144	BARTSCH	70B	HBC	+	$8 \pi^+ p \rightarrow N 4\pi$
1689 ± 20	102	9 BARTSCH	70B	HBC	+	$8 \pi^+ p \rightarrow N 2\rho$
1705 ± 21		CASO	70	HBC	-	$11.2 \pi^- p \rightarrow n \rho 2\pi$

• • • We do not use the following data for averages, fits, limits, etc. • • •

1718 ± 10		10 EVANGELIS...	81	OMEG	-	$12 \pi^- p \rightarrow p 4\pi$
1673 ± 9		11 EVANGELIS...	81	OMEG	-	$12 \pi^- p \rightarrow p 4\pi$
1733 ± 9	66	9 KLIGER	74	HBC	-	$4.5 \pi^- p \rightarrow p 4\pi$
1630 ± 15		HOLMES	72	HBC	+	$10-12 K^+ p$
1720 ± 15		BALTAY	68	HBC	+	$7, 8.5 \pi^+ p$

⁸ From $\rho^-\rho^0$ mode, not independent of the other two EVANGELISTA 81 entries.
⁹ From $\rho^+\rho^0$ mode.
¹⁰ From $a_2(1320)\pi^0\pi^0$ mode, not independent of the other two EVANGELISTA 81 entries.
¹¹ From $a_2(1320)\pi^0\pi^0$ mode, not independent of the other two EVANGELISTA 81 entries.

$\omega\pi$ MODE

VALUE (MeV) DOCUMENT ID TECN CHG COMMENT
The data in this block is included in the average printed for a previous datablock.

1681 ± 7 OUR AVERAGE

1670 ± 25		12 ALDE	95	GAM2		$38 \pi^- p \rightarrow \omega\pi^0 n$
1690 ± 15		EVANGELIS...	81	OMEG	-	$12 \pi^- p \rightarrow \omega\pi p$
1666 ± 14		GESSAROLI	77	HBC		$11 \pi^- p \rightarrow \omega\pi p$
1686 ± 9		THOMPSON	74	HBC	+	$13 \pi^+ p$

• • • We do not use the following data for averages, fits, limits, etc. • • •

1654 ± 24		BARNHAM	70	HBC	+	$10 K^+ p \rightarrow \omega\pi X$
-----------	--	---------	----	-----	---	------------------------------------

¹² Supersedes ALDE 92c.

$\eta\pi^+\pi^-$ MODE

(For difficulties with MMS experiments, see the $a_2(1320)$ mini-review in the 1973 edition.)

VALUE (MeV) DOCUMENT ID TECN CHG COMMENT
The data in this block is included in the average printed for a previous datablock.

1682 ± 12 OUR AVERAGE

1685 ± 10 ± 20		AMELIN	00	VES		$37 \pi^- p \rightarrow \eta\pi^+\pi^- n$
1680 ± 15		FUKUI	88	SPEC	0	$8.95 \pi^- p \rightarrow \eta\pi^+\pi^- n$

• • • We do not use the following data for averages, fits, limits, etc. • • •

1700 ± 47		13 ANDERSON	69	MMS	-	$16 \pi^- p$ backward
1632 ± 15		13,14 FOACCI	66	MMS	-	$7-12 \pi^- p \rightarrow p MM$
1700 ± 15		13,14 FOACCI	66	MMS	-	$7-12 \pi^- p \rightarrow p MM$
1748 ± 15		13,14 FOACCI	66	MMS	-	$7-12 \pi^- p \rightarrow p MM$

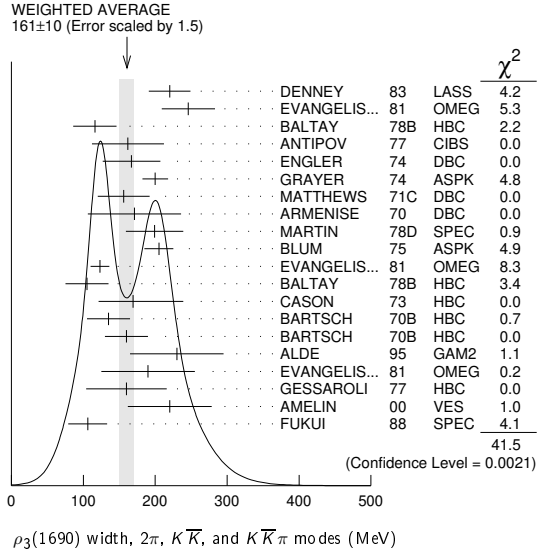
¹³ Seen in 2.5-3 GeV/c $\bar{p}p$. $2\pi^+2\pi^-$, with 0, 1, 2 $\pi^+\pi^-$ pairs in ρ band not seen by OREN 74 (2.3 GeV/c $\bar{p}p$) with more statistics. (Jan. 1976)

¹⁴ Not seen by BOWEN 72.

$\rho_3(1690)$ WIDTH

$2\pi, K\bar{K},$ AND $K\bar{K}\pi$ MODES

VALUE (MeV) DOCUMENT ID TECN CHG COMMENT
161 ± 10 OUR AVERAGE Includes data from the 5 datablocks that follow this one. Error includes scale factor of 1.5. See the ideogram below.



2π MODE

VALUE (MeV) EVTS DOCUMENT ID TECN CHG COMMENT
The data in this block is included in the average printed for a previous datablock.

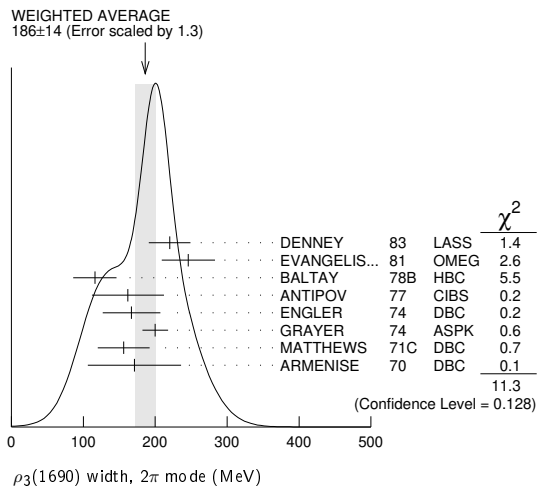
186 ± 14 OUR AVERAGE

Error includes scale factor of 1.3. See the ideogram below.

220 ± 29		DENNEY	83	LASS		$10 \pi^+ N$
246 ± 37		EVANGELIS...	81	OMEG	-	$12 \pi^- p \rightarrow 2\pi p$
116 ± 30	476	BALTAY	78B	HBC	0	$15 \pi^+ p \rightarrow \pi^+\pi^- n$
162 ± 50	175	15 ANTIPOV	77	CIBS	0	$25 \pi^- p \rightarrow p 3\pi$
167 ± 40	600	ENGLER	74	DBC	0	$6 \pi^+ n \rightarrow \pi^+\pi^- p$
200 ± 18		16 GRAYER	74	ASPK	0	$17 \pi^- p \rightarrow \pi^+\pi^- n$
156 ± 36		MATTHEWS	71C	DBC	0	$7 \pi^+ n$
171 ± 65		ARMENISE	70	DBC	0	$9 \pi^+ d$

• • • We do not use the following data for averages, fits, limits, etc. • • •

322 ± 35		17 CORDEN	79	OMEG		$12-15 \pi^- p \rightarrow n 2\pi$
240 ± 30		16,18 ESTABROOKS	75	RVUE		$17 \pi^- p \rightarrow \pi^+\pi^- n$
180 ± 30	122	BARTSCH	70B	HBC	+	$8 \pi^+ p \rightarrow N 2\pi$
267 ± 72		STUNTEBECK	70	HDBC	0	$8 \pi^- p, 5.4 \pi^+ d$
188 ± 49		ARMENISE	68	DBC	0	$5.1 \pi^+ d$
180 ± 40		GOLDBERG	65	HBC	0	$6 \pi^+ d, 8 \pi^- p$



¹⁵ Width errors enlarged by us to $4\Gamma/\sqrt{N}$; see the note with the $K^*(892)$ mass.

¹⁶ Uses same data as HYAMS 75 and BECKER 79.

¹⁷ From a phase shift solution containing a $f_2'(1225)$ width two times larger than the $K\bar{K}$ result.

¹⁸ From phase-shift analysis. Error takes account of spread of different phase-shift solutions.

$K\bar{K}$ AND $K\bar{K}\pi$ MODES

VALUE (MeV) EVTS DOCUMENT ID TECN CHG COMMENT
The data in this block is included in the average printed for a previous datablock.

204 ± 18 OUR AVERAGE

199 ± 40	6000	19 MARTIN	78D	SPEC		$10 \pi p \rightarrow K_S^0 K^- p$
205 ± 20		BLUM	75	ASPK	0	$18.4 \pi^- p \rightarrow n K^+ K^-$

Meson Particle Listings

ρ₃(1690)

• • • We do not use the following data for averages, fits, limits, etc. • • •

219± 4	ALPER	80	CNTR	0	62 π ⁻ ρ → K ⁺ K ⁻ n
186±11	²⁰ COSTA	80	OMEG		10 π ⁻ ρ → K ⁺ K ⁻ n
112±60	ADERHOLZ	69	HBC	+	8 π ⁺ ρ → K ⁺ K ⁻ π

¹⁹ From a fit to J^P = 3⁻ partial wave.
²⁰ They cannot distinguish between ρ₃(1690) and ω₃(1670).

(4π)[±] MODE

VALUE (MeV)	EVTs	DOCUMENT ID	TECN	CHG	COMMENT
The data in this block is included in the average printed for a previous datablock.					

123±10 OUR AVERAGE

123±13		²¹ EVANGELIS...	81	OMEG	-	12 π ⁻ ρ → p4π
105±30	177	BALTAY	78B	HBC	+	15 π ⁺ ρ → p4π
169 ⁺⁷⁰ ₋₄₈		CASON	73	HBC	-	8,18.5 π ⁻ ρ
135±30	144	BARTSCH	70B	HBC	+	8 π ⁺ ρ → N4π
160±30	102	BARTSCH	70B	HBC	+	8 π ⁺ ρ → N2ρ

• • • We do not use the following data for averages, fits, limits, etc. • • •

230±28		²² EVANGELIS...	81	OMEG	-	12 π ⁻ ρ → p4π
184±33		²³ EVANGELIS...	81	OMEG	-	12 π ⁻ ρ → p4π
150	66	²⁴ KLIGER	74	HBC	-	4.5 π ⁻ ρ → p4π
106±25		THOMPSON	74	HBC	+	13 π ⁺ ρ
125 ⁺⁸³ ₋₃₅		²⁴ CASON	73	HBC	-	8,18.5 π ⁻ ρ
130±30		HOLMES	72	HBC	+	10-12 K ⁺ ρ
180±30	90	²⁴ BARTSCH	70B	HBC	+	8 π ⁺ ρ → Na ₂ π
100±35		BALTAY	68	HBC	+	7, 8.5 π ⁺ ρ

²¹ From ρ⁻ρ⁰ mode, not independent of the other two EVANGELISTA 81 entries.
²² From a₂(1320)⁻π⁰ mode, not independent of the other two EVANGELISTA 81 entries.
²³ From a₂(1320)⁰π⁻ mode, not independent of the other two EVANGELISTA 81 entries.
²⁴ From ρ[±]ρ⁰ mode.

ωπ MODE

VALUE (MeV)	DOCUMENT ID	TECN	CHG	COMMENT
The data in this block is included in the average printed for a previous datablock.				

190±40 OUR AVERAGE

230±65		²⁵ ALDE	95	GAM2		38 π ⁻ ρ → ωπ ⁰ n
190±65		EVANGELIS...	81	OMEG	-	12 π ⁻ ρ → ωπρ
160±56		GESSERTAL	77	HBC		11 π ⁻ ρ → ωπρ
89±25		THOMPSON	74	HBC	+	13 π ⁺ ρ
130 ⁺⁷³ ₋₄₃		BARNHAM	70	HBC	+	10 K ⁺ ρ → ωπX

²⁵ Supersedes ALDE 92c.

ηπ⁺π⁻ MODE

(For difficulties with MMS experiments, see the a₂(1320) mini-review in the 1973 edition.)

VALUE (MeV)	DOCUMENT ID	TECN	CHG	COMMENT
The data in this block is included in the average printed for a previous datablock.				

126±40 OUR AVERAGE Error includes scale factor of 1.8.					
220±30±50	AMELIN	00	VES		37 π ⁻ ρ → ηπ ⁺ π ⁻ n
106±27	FUKUI	88	SPEC	0	8.95 π ⁻ ρ → ηπ ⁺ π ⁻ n

• • • We do not use the following data for averages, fits, limits, etc. • • •					
195	²⁶ ANDERSON	69	MMS	-	16 π ⁻ ρ backward
< 21	^{26,27} FOCACCI	66	MMS	-	7-12 π ⁻ ρ → pMM
< 30	^{26,27} FOCACCI	66	MMS	-	7-12 π ⁻ ρ → pMM
< 38	^{26,27} FOCACCI	66	MMS	-	7-12 π ⁻ ρ → pMM

²⁶ Seen in 2.5-3 GeV/c $\bar{p}p$. 2π⁺2π⁻, with 0, 1, 2 π⁺π⁻ pairs in ρ⁰ band not seen by OREN 74 (2.3 GeV/c $\bar{p}p$) with more statistics. (Jan. 1979)
²⁷ Not seen by BOWEN 72.

ρ₃(1690) DECAY MODES

Mode	Fraction (Γ _i /Γ)	Scale factor
Γ ₁ 4π	(71.1 ± 1.9) %	
Γ ₂ π [±] π ⁺ π ⁻ π ⁰	(67 ± 22) %	
Γ ₃ ωπ	(16 ± 6) %	
Γ ₄ ππ	(23.6 ± 1.3) %	
Γ ₅ K ⁺ K ⁻ π	(3.8 ± 1.2) %	
Γ ₆ K ⁺ K ⁻	(1.58 ± 0.26) %	1.2
Γ ₇ ηπ ⁺ π ⁻	seen	
Γ ₈ ρ(770)η	seen	
Γ ₉ ππρ	seen	
Γ ₁₀ a ₂ (1320)π	seen	
Γ ₁₁ ρρ	seen	
Γ ₁₂ φπ		
Γ ₁₃ ηπ		
Γ ₁₄ π [±] 2π ⁺ 2π ⁻ π ⁰		

CONSTRAINED FIT INFORMATION

An overall fit to 5 branching ratios uses 10 measurements and one constraint to determine 4 parameters. The overall fit has a χ² = 14.7 for 7 degrees of freedom.

The following *off-diagonal* array elements are the correlation coefficients ⟨δx_iδx_j⟩/(δx_iδx_j), in percent, from the fit to the branching fractions, x_i ≡ Γ_i/Γ_{total}. The fit constrains the x_i whose labels appear in this array to sum to one.

x ₄	-77		
x ₅	-74	17	
x ₆	-15	2	0
	x ₁	x ₄	x ₅

ρ₃(1690) BRANCHING RATIOS

Γ(ππ)/Γ _{total}	DOCUMENT ID	TECN	CHG	COMMENT	Γ ₄ /Γ
0.236±0.013 OUR FIT					
0.243±0.013 OUR AVERAGE					

0.259 ^{+0.018} _{-0.019}		BECKER	79	ASPK	0	17 π ⁻ ρ polarized
0.23 ± 0.02		CORDEN	79	OMEG		12-15 π ⁻ ρ → n2π
0.22 ± 0.04		²⁸ MATTHEWS	71c	HDBC	0	7 π ⁺ n → π ⁻ ρ

• • • We do not use the following data for averages, fits, limits, etc. • • •

0.245 ± 0.006	²⁹ ESTABROOKS	75	RVUE			17 π ⁻ ρ → π ⁺ π ⁻ n
---------------	--------------------------	----	------	--	--	---

²⁸ One-pion-exchange model used in this estimation.
²⁹ From phase-shift analysis of HYAMS 75 data.

Γ(ππ)/Γ(π [±] π ⁺ π ⁻ π ⁰)	DOCUMENT ID	TECN	CHG	COMMENT	Γ ₄ /Γ ₂
0.35 ± 0.11					

< 0.2		HOLMES	72	HBC	+	10-12 K ⁺ ρ
< 0.12		BALLAM	71B	HBC	-	16 π ⁻ ρ

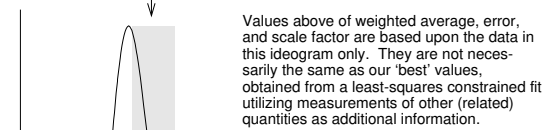
Γ(ππ)/Γ(4π)	DOCUMENT ID	TECN	CHG	COMMENT	Γ ₄ /Γ ₁
0.332±0.026 OUR FIT Error includes scale factor of 1.1.					
0.30 ± 0.10					

		BALTAY	78B	HBC	0	15 π ⁺ ρ → p4π
--	--	--------	-----	-----	---	---------------------------

Γ(K ⁺ K ⁻)/Γ(ππ)	DOCUMENT ID	TECN	CHG	COMMENT	Γ ₆ /Γ ₄
0.067 ± 0.011 OUR FIT Error includes scale factor of 1.2.					

0.118^{+0.040}_{-0.032} OUR AVERAGE Error includes scale factor of 1.7. See the ideogram below.						
0.191 ^{+0.040} _{-0.037}		GORLICH	80	ASPK	0	17,18 π ⁻ ρ polarized
0.08 ± 0.03		BARTSCH	70B	HBC	+	8 π ⁺ ρ
0.08 ^{+0.08} _{-0.03}		CRENNELL	68B	HBC		6.0 π ⁻ ρ

WEIGHTED AVERAGE
 0.118+0.040-0.032 (Error scaled by 1.7)



	DOCUMENT ID	TECN	CHG	COMMENT	χ ²
	GORLICH	80	ASPK		3.8
	BARTSCH	70B	HBC		1.6
	CRENNELL	68B	HBC		0.4
					5.9
					(Confidence Level = 0.053)

Γ(K ⁺ K ⁻ π)/Γ(ππ)	DOCUMENT ID	TECN	CHG	COMMENT	Γ ₅ /Γ ₄
0.16 ± 0.05 OUR FIT					
0.16 ± 0.05					

³⁰ BARTSCH 70B HBC + 8 π⁺ρ
³⁰ Increased by us to correspond to B(ρ₃(1690) → ππ)=0.24.

$[\Gamma(\pi\pi\rho) + \Gamma(a_2(1320)\pi) + \Gamma(\rho\rho)] / \Gamma(\pi^\pm\pi^+\pi^-\pi^0)$ ($\Gamma_9 + \Gamma_{10} + \Gamma_{11}$) / Γ_2

Table with columns: VALUE, DOCUMENT ID, TECN, CHG, COMMENT. Row 1: 0.94 ± 0.09 OUR AVERAGE. Rows 2-5: BALTAY 78B HBC + 15 π+ p → p4π, BALLAM 71B HBC - 16 π- p, BARTSCH 70B HBC + 8 π+ p, CASO 68 HBC - 11 π- p.

$\Gamma(\rho\rho) / \Gamma(\pi^\pm\pi^+\pi^-\pi^0)$ Γ_{11} / Γ_2

Table with columns: VALUE, EVTS, DOCUMENT ID, TECN, CHG, COMMENT. Row 1: 0.12 ± 0.11. Row 2: 0.56. Row 3: 0.13 ± 0.09. Row 4: 0.7 ± 0.15. Row 5: 31 ρρ and a2(1320)π modes are indistinguishable.

$\Gamma(\rho\rho) / [\Gamma(\pi\pi\rho) + \Gamma(a_2(1320)\pi) + \Gamma(\rho\rho)]$ $\Gamma_{11} / (\Gamma_9 + \Gamma_{10} + \Gamma_{11})$

Table with columns: VALUE, DOCUMENT ID, TECN, CHG, COMMENT. Row 1: 0.48 ± 0.16.

$\Gamma(a_2(1320)\pi) / \Gamma(\pi^\pm\pi^+\pi^-\pi^0)$ Γ_{10} / Γ_2

Table with columns: VALUE, DOCUMENT ID, TECN, CHG, COMMENT. Row 1: 0.66 ± 0.08. Row 2: 0.36 ± 0.14. Row 3: not seen. Row 4: 0.6 ± 0.15. Row 5: 0.6. Row 6: 32 ρρ and a2(1320)π modes are indistinguishable.

$\Gamma(\omega\pi) / \Gamma(\pi^\pm\pi^+\pi^-\pi^0)$ Γ_3 / Γ_2

Table with columns: VALUE, CL%, DOCUMENT ID, TECN, CHG, COMMENT. Row 1: 0.23 ± 0.05 OUR AVERAGE. Row 2: 0.33 ± 0.07. Row 3: 0.12 ± 0.07. Row 4: 0.25 ± 0.10. Row 5: 0.25 ± 0.10. Row 6: <0.11. Row 7: <0.09.

$\Gamma(\phi\pi) / \Gamma(\pi^\pm\pi^+\pi^-\pi^0)$ Γ_{12} / Γ_2

Table with columns: VALUE, DOCUMENT ID, TECN, CHG, COMMENT. Row 1: <0.11.

$\Gamma(\pi^\pm 2\pi^+ 2\pi^-\pi^0) / \Gamma(\pi^\pm\pi^+\pi^-\pi^0)$ Γ_{14} / Γ_2

Table with columns: VALUE, DOCUMENT ID, TECN, CHG, COMMENT. Row 1: <0.15.

$\Gamma(\eta\pi) / \Gamma(\pi^\pm\pi^+\pi^-\pi^0)$ Γ_{13} / Γ_2

Table with columns: VALUE, DOCUMENT ID, TECN, CHG, COMMENT. Row 1: <0.02.

$\Gamma(K\bar{K}) / \Gamma_{total}$ Γ_6 / Γ

Table with columns: VALUE, DOCUMENT ID, TECN, CHG, COMMENT. Row 1: 0.0158 ± 0.0026 OUR FIT. Row 2: 0.0130 ± 0.0024 OUR AVERAGE. Row 3: 0.013 ± 0.003. Row 4: 0.013 ± 0.004. Row 5: 33 From $(\Gamma_4\Gamma_6)^{1/2} = 0.056 \pm 0.034$ assuming $B(\rho_3(1690) \rightarrow \pi\pi) = 0.24$.

$\Gamma(\omega\pi) / [\Gamma(\omega\pi) + \Gamma(\rho\rho)]$ $\Gamma_3 / (\Gamma_3 + \Gamma_{11})$

Table with columns: VALUE, DOCUMENT ID, TECN, CHG, COMMENT. Row 1: 0.22 ± 0.08.

$\Gamma(\eta\pi^+\pi^-) / \Gamma_{total}$ Γ_7 / Γ

Table with columns: VALUE, DOCUMENT ID, TECN, COMMENT. Row 1: seen. Row 2: FUKUI 88 SPEC 8.95 π- p → ηπ+ π- n.

$\Gamma(a_2(1320)\pi) / \Gamma(\rho(770)\eta)$ Γ_{10} / Γ_8

Table with columns: VALUE, DOCUMENT ID, TECN, COMMENT. Row 1: 5.5 ± 2.0. Row 2: AMELIN 00 VES 37 π- p → ηπ+ π- n.

$\rho_3(1690)$ REFERENCES

Table with columns: NAME, YEAR, REF, AUTHOR, COMMENT. Lists references for ρ3(1690) from 1968 to 2002.

$\rho(1700)$

$G(J^{PC}) = 1^+(1^--)$

$\rho(1700)$ MASS

$\eta\rho^0$ AND $\pi^+\pi^-$ MODES

Table with columns: VALUE (MeV), DOCUMENT ID. Row 1: 1720 ± 20 OUR ESTIMATE.

$\eta\rho^0$ MODE

Table with columns: VALUE (MeV), EVTS, DOCUMENT ID, TECN, COMMENT. Row 1: 1740 ± 20. Row 2: 1701 ± 15.

- • • We do not use the following data for averages, fits, limits, etc. • • •
1834 ± 12 13.4k 1 GRIBANOV 20 CMD3 1.1-2.0 e+ e- → ηπ+ π-
1840 ± 10 7.4k 2 ACHASOV 18 SND 1.22-2.00 e+ e- → ηπ+ π-
1740 ± 20 ANTONELLI 88 DM2 e+ e- → ηπ+ π-
1701 ± 15 3 FUKUI 88 SPEC 8.95 π- p → ηπ+ π- n
1 Mass and width of the ρ(770) fixed at 775 and 149 MeV, respectively; solution 2 of model 2, η → γγ decays used.
2 From the combined fit of AULCHENKO 15 and ACHASOV 18 in the model with the interfering ρ(1450), ρ(1700) and ρ(2150) with the parameters of the ρ(1450) and ρ(1700) floating and the mass and width of the ρ(2150) fixed at 2155 MeV and 320 MeV, respectively. The phases of the resonances are π, 0 and π, respectively.
3 Assuming ρ+ f0(1370) decay mode interferes with a1(1260)+ π background. From a two Breit-Wigner fit.

$\pi\pi$ MODE

Table with columns: VALUE (MeV), EVTS, DOCUMENT ID, TECN, COMMENT. Row 1: 1770.54 ± 5.49. Row 2: 1718.50 ± 65.44. Row 3: 1766.80 ± 52.36. Row 4: 1644 ± 36. Row 5: 1780 ± 20. Row 6: 1861 ± 17. Row 7: 1728 ± 17. Row 8: 1780 ± 37. Row 9: 1719 ± 15. Row 10: 1730 ± 30. Row 11: 1768 ± 21. Row 12: 1745.7 ± 91.9. Row 13: 1546 ± 26. Row 14: 1650.

- • • We do not use the following data for averages, fits, limits, etc. • • •
1770.54 ± 5.49 1 BARTOS 17 RVUE e+ e- → π+ π-
1718.50 ± 65.44 2 BARTOS 17A RVUE e+ e- → π+ π-
1766.80 ± 52.36 3 BARTOS 17A RVUE τ- → π- π0 ντ
1644 ± 36 20k 4 LEES 17c BABR J/ψ → π+ π- π0
1780 ± 20 +15 -20 63.5k 5 ABRAMOWICZ12 ZEUS e p → e π+ π- p
1861 ± 17 6 LEES 12G BABR e+ e- → π+ π- γ
1728 ± 17 ± 89 5.4M 7,8 FUJIKAWA 08 BELL τ- → π- π0 ντ
1780 ± 37 -29 9 ABELE 97 CBAR p n → π- π0 π0
1719 ± 15 9 BERTIN 97C OBLX 0.0 p p → π+ π- π0
1730 ± 30 CLEGG 94 RVUE e+ e- → π+ π-
1768 ± 21 BISELLO 89 DM2 e+ e- → π+ π-
1745.7 ± 91.9 DUBNICKA 89 RVUE e+ e- → π+ π-
1546 ± 26 GESHKEN... 89 RVUE
1650 10 ERKAL 85 RVUE 20-70 γ p → γ π

Meson Particle Listings

 $\rho(1700)$

VALUE (MeV)	EVTS	DOCUMENT ID	TECN	COMMENT
1550 \pm 70		ABE	84B	HYBR 20 $\gamma\rho \rightarrow \pi^+\pi^-p$
1590 \pm 20		11 ASTON	80	OMEG 20-70 $\gamma\rho \rightarrow p2\pi$
1600 \pm 10		12 ATIYA	79B	SPEC 50 $\gamma C \rightarrow C2\pi$
1598 \pm 24 -22		BECKER	79	ASPK 17 π^-p polarized
1659 \pm 25		10 LANG	79	RVUE
1575		10 MARTIN	78C	RVUE 17 $\pi^-p \rightarrow \pi^+\pi^-n$
1610 \pm 30		10 FROGGATT	77	RVUE 17 $\pi^-p \rightarrow \pi^+\pi^-n$
1590 \pm 20		13 HYAMS	73	ASPK 17 $\pi^-p \rightarrow \pi^+\pi^-n$

- Applies the Unitary & Analytic Model of the pion electromagnetic form factor of DUBNICKA 10 to analyze the data of LEES 12c and ABLIKIM 16c.
- Applies the Unitary & Analytic Model of the pion electromagnetic form factor of DUBNICKA 10 to analyze the data of ACHASOV 06, AKHMETSHIN 07, AUBERT 09AS, and AMBROSINO 11A.
- Applies the Unitary & Analytic Model of the pion electromagnetic form factor of DUBNICKA 10 to analyze the data of FUJIKAWA 08.
- From a Dalitz plot analysis in an isobar model with $\rho(1450)$ and $\rho(1700)$ masses and widths floating.
- Using the KUHN 90 parametrization of the pion form factor, neglecting $\rho-\omega$ interference.
- Using the GOUNARIS 68 parametrization of the pion form factor leaving the masses and widths of the $\rho(1450)$, $\rho(1700)$, and $\rho(2150)$ resonances as free parameters of the fit.
- $|F_{\pi}(0)|^2$ fixed to 1.
- From the GOUNARIS 68 parametrization of the pion form factor.
- T-matrix pole.
- From phase shift analysis of HYAMS 73 data.
- Simple relativistic Breit-Wigner fit with constant width.
- An additional 40 MeV uncertainty in both the mass and width is present due to the choice of the background shape.
- Included in BECKER 79 analysis.

 $\pi\omega$ MODE

VALUE (MeV)	EVTS	DOCUMENT ID	TECN	COMMENT
1708 \pm 41	7815	1 ACHASOV	13	SND 1.05-2.00 $e^+e^- \rightarrow \pi^0\pi^0\gamma$
1550 to 1620		2 ACHASOV	00i	SND $e^+e^- \rightarrow \pi^0\pi^0\gamma$
1580 to 1710		3 ACHASOV	00i	SND $e^+e^- \rightarrow \pi^0\pi^0\gamma$
1710 \pm 90		ACHASOV	97	RVUE $e^+e^- \rightarrow \omega\pi^0$

- From a phenomenological model based on vector meson dominance with the interfering $\rho(1450)$ and $\rho(1700)$ and their widths fixed at 400 and 250 MeV, respectively. Systematic uncertainty not estimated.
- Taking into account both $\rho(1450)$ and $\rho(1700)$ contributions. Using the data of ACHASOV 00i on $e^+e^- \rightarrow \omega\pi^0$ and of EDWARDS 00A on $\tau^- \rightarrow \omega\pi^- \nu_{\tau}$. $\rho(1450)$ mass and width fixed at 1400 MeV and 500 MeV respectively.
- Taking into account the $\rho(1700)$ contribution only. Using the data of ACHASOV 00i on $e^+e^- \rightarrow \omega\pi^0$ and of EDWARDS 00A on $\tau^- \rightarrow \omega\pi^- \nu_{\tau}$.

 $K\bar{K}$ MODE

VALUE (MeV)	EVTS	DOCUMENT ID	TECN	CHG	COMMENT
1688.7 \pm 3.1 \pm 141.1 1.3		1 ALBRECHT	20	RVUE	0.9 $\bar{p}p \rightarrow K^+K^-\pi^0$
1541 \pm 12 \pm 33	190k	2 AAJ	16N	LHCB	$D^0 \rightarrow K_S^0 K^{\pm}\pi^{\mp}$
1740.8 \pm 22.2	27k	3 ABELE	99D	CBAR \pm	0.0 $\bar{p}p \rightarrow K^+K^-\pi^0$
1582 \pm 36	1600	CLELAND	82B	SPEC \pm	50 $\pi\rho \rightarrow K_S^0 K^{\pm}\rho$

- T-matrix pole, 2 poles, 3 channels, including $\pi\pi$ scattering data from HYAMS 75.
- Using the GOUNARIS 68 parameterization with a fixed width. Value is average using different $K\pi$ S-wave parameterizations in fit.
- K-matrix pole. Isospin not determined, could be $\omega(1650)$ or $\phi(1680)$.

 $2(\pi^+\pi^-)$ MODE

VALUE (MeV)	EVTS	DOCUMENT ID	TECN	COMMENT
1851 \pm 27 -24		ACHASOV	97	RVUE $e^+e^- \rightarrow 2(\pi^+\pi^-)$
1570 \pm 20		1 CORDIER	82	DM1 $e^+e^- \rightarrow 2(\pi^+\pi^-)$
1520 \pm 30		2 ASTON	81E	OMEG 20-70 $\gamma\rho \rightarrow p4\pi$
1654 \pm 25		3 DIBIANCA	81	DBC $\pi^+d \rightarrow pp2(\pi^+\pi^-)$
1666 \pm 39		1 BACCI	80	FRAG $e^+e^- \rightarrow 2(\pi^+\pi^-)$
1780	34	KILLIAN	80	SPEC 11 $e^-p \rightarrow 2(\pi^+\pi^-)$
1500		4 ATIYA	79B	SPEC 50 $\gamma C \rightarrow C4\pi^{\pm}$
1570 \pm 60	65	5 ALEXANDER	75	HBC 7.5 $\gamma\rho \rightarrow p4\pi$
1550 \pm 60		2 CONVERSI	74	OSPK $e^+e^- \rightarrow 2(\pi^+\pi^-)$
1550 \pm 50	160	SCHACHT	74	STRC 5.5-9 $\gamma\rho \rightarrow p4\pi$
1450 \pm 100	340	SCHACHT	74	STRC 9-18 $\gamma\rho \rightarrow p4\pi$
1430 \pm 50	400	BINGHAM	72B	HBC 9.3 $\gamma\rho \rightarrow p4\pi$

- Simple relativistic Breit-Wigner fit with model dependent width.
- Simple relativistic Breit-Wigner fit with constant width.
- One peak fit result.
- Parameters roughly estimated, not from a fit.
- Skew mass distribution compensated by Ross-Stodolsky factor.

 $\pi^+\pi^-\pi^0\pi^0$ MODE

VALUE (MeV)	DOCUMENT ID	TECN	COMMENT
1660 \pm 30	ATKINSON	85B	OMEG 20-70 $\gamma\rho$

- • • We do not use the following data for averages, fits, limits, etc. • • •

 $3(\pi^+\pi^-)$ AND $2(\pi^+\pi^-\pi^0)$ MODES

VALUE (MeV)	DOCUMENT ID	TECN	COMMENT
1730 \pm 34	1 FRABETTI	04	E687 $\gamma\rho \rightarrow 3\pi^+3\pi^-p$
1783 \pm 15	CLEGG	90	RVUE $e^+e^- \rightarrow 3(\pi^+\pi^-)\pi^0$

- • • We do not use the following data for averages, fits, limits, etc. • • •

¹From a fit with two resonances with the JACOB 72 continuum.

 $m_{\rho(1700)^0} - m_{\rho(1700)^{\pm}}$

VALUE (MeV)	DOCUMENT ID	TECN	COMMENT
-48.30 \pm 83.81	1 BARTOS	17A	RVUE $e^+e^- \rightarrow \pi^+\pi^-$, $\tau^- \rightarrow \pi^-\pi^0\nu_{\tau}$

- Applies the Unitary & Analytic Model of the pion electromagnetic form factor of DUBNICKA 10 to analyze the data of ACHASOV 06, AKHMETSHIN 07, AUBERT 09AS, AMBROSINO 11A, and FUJIKAWA 08.

 $\rho(1700)$ WIDTH $\eta\rho^0$ AND $\pi^+\pi^-$ MODES

VALUE (MeV)	DOCUMENT ID
250 \pm 100 OUR ESTIMATE	

 $\eta\rho^0$ MODE

VALUE (MeV)	EVTS	DOCUMENT ID	TECN	COMMENT
47 \pm 19	13.4k	1 GRIBANOV	20	CMD3 1.1-2.0 $e^+e^- \rightarrow \eta\pi^+\pi^-$
132 \pm 40	7.4k	2 ACHASOV	18	SND 1.22-2.00 $e^+e^- \rightarrow \eta\pi^+\pi^-$
150 \pm 30		ANTONELLI	88	DM2 $e^+e^- \rightarrow \eta\pi^+\pi^-$
282 \pm 44		3 FUKUI	88	SPEC 8.95 $\pi^-p \rightarrow \eta\pi^+\pi^-n$

The data in this block is included in the average printed for a previous datablock.

- • • We do not use the following data for averages, fits, limits, etc. • • •

47 \pm 19	13.4k	1 GRIBANOV	20	CMD3 1.1-2.0 $e^+e^- \rightarrow \eta\pi^+\pi^-$
132 \pm 40	7.4k	2 ACHASOV	18	SND 1.22-2.00 $e^+e^- \rightarrow \eta\pi^+\pi^-$
150 \pm 30		ANTONELLI	88	DM2 $e^+e^- \rightarrow \eta\pi^+\pi^-$
282 \pm 44		3 FUKUI	88	SPEC 8.95 $\pi^-p \rightarrow \eta\pi^+\pi^-n$

- Mass and width of the $\rho(770)$ fixed at 775 and 149 MeV, respectively; solution 2 of model 2, $\eta \rightarrow \gamma\gamma$ decays used.
- From the combined fit of AULCHENKO 15 and ACHASOV 18 in the model with the interfering $\rho(1450)$, $\rho(1700)$ and $\rho(2150)$ with the parameters of the $\rho(1450)$ and $\rho(1700)$ floating and the mass and width of the $\rho(2150)$ fixed at 2155 MeV and 320 MeV, respectively. The phases of the resonances are π , 0 and π , respectively.
- Assuming $\rho^+ f_0(1370)$ decay mode interferes with $a_1(1260)^+\pi$ background. From a two Breit-Wigner fit.

 $\pi\pi$ MODE

VALUE (MeV)	EVTS	DOCUMENT ID	TECN	COMMENT
268.98 \pm 11.40		1 BARTOS	17	RVUE $e^+e^- \rightarrow \pi^+\pi^-$
489.58 \pm 16.95		2 BARTOS	17A	RVUE $e^+e^- \rightarrow \pi^+\pi^-$
414.71 \pm 119.48		3 BARTOS	17A	RVUE $\tau^- \rightarrow \pi^-\pi^0\nu_{\tau}$
109 \pm 19	20k	4 LEES	17C	BABR $J/\psi \rightarrow \pi^+\pi^-\pi^0$
310 \pm 30	\pm 25 -35	65.5k	5	ABRAMOWICZ12 ZEUS $e p \rightarrow e\pi^+\pi^-p$
316 \pm 26		6	LEES	12G BABR $e^+e^- \rightarrow \pi^+\pi^-\gamma$
164 \pm 21	\pm 89 -26	5.4M	7.8	FUJIKAWA 08 BELL $\tau^- \rightarrow \pi^-\pi^0\nu_{\tau}$
275 \pm 45		9	ABELE	97 CBAR $\bar{p}n \rightarrow \pi^-\pi^0\nu_{\tau}$
310 \pm 40		9	BERTIN	97C OBLX 0.0 $\bar{p}p \rightarrow \pi^+\pi^-\pi^0$
400 \pm 100			CLEGG	94 RVUE $e^+e^- \rightarrow \pi^+\pi^-$
224 \pm 22			BISELLO	89 DM2 $e^+e^- \rightarrow \pi^+\pi^-$
242.5 \pm 163.0			DUBNICKA	89 RVUE $e^+e^- \rightarrow \pi^+\pi^-$
620 \pm 60			GESHKEN...	89 RVUE
<315			10 ERKAL	85 RVUE 20-70 $\gamma\rho \rightarrow \gamma\pi$
280 \pm 80			ABE	84B HYBR 20 $\gamma\rho \rightarrow \pi^+\pi^-p$
230 \pm 80			11 ASTON	80 OMEG 20-70 $\gamma\rho \rightarrow p2\pi$
283 \pm 14			12 ATIYA	79B SPEC 50 $\gamma C \rightarrow C2\pi$
175 \pm 98			BECKER	79 ASPK 17 π^-p polarized
232 \pm 34			10 LANG	79 RVUE
340			10 MARTIN	78C RVUE 17 $\pi^-p \rightarrow \pi^+\pi^-n$
300 \pm 100			10 FROGGATT	77 RVUE 17 $\pi^-p \rightarrow \pi^+\pi^-n$
180 \pm 50			13 HYAMS	73 ASPK 17 $\pi^-p \rightarrow \pi^+\pi^-n$

- • • We do not use the following data for averages, fits, limits, etc. • • •

268.98 \pm 11.40		1 BARTOS	17	RVUE $e^+e^- \rightarrow \pi^+\pi^-$
489.58 \pm 16.95		2 BARTOS	17A	RVUE $e^+e^- \rightarrow \pi^+\pi^-$
414.71 \pm 119.48		3 BARTOS	17A	RVUE $\tau^- \rightarrow \pi^-\pi^0\nu_{\tau}$
109 \pm 19	20k	4 LEES	17C	BABR $J/\psi \rightarrow \pi^+\pi^-\pi^0$
310 \pm 30	\pm 25 -35	65.5k	5	ABRAMOWICZ12 ZEUS $e p \rightarrow e\pi^+\pi^-p$
316 \pm 26		6	LEES	12G BABR $e^+e^- \rightarrow \pi^+\pi^-\gamma$
164 \pm 21	\pm 89 -26	5.4M	7.8	FUJIKAWA 08 BELL $\tau^- \rightarrow \pi^-\pi^0\nu_{\tau}$
275 \pm 45		9	ABELE	97 CBAR $\bar{p}n \rightarrow \pi^-\pi^0\nu_{\tau}$
310 \pm 40		9	BERTIN	97C OBLX 0.0 $\bar{p}p \rightarrow \pi^+\pi^-\pi^0$
400 \pm 100			CLEGG	94 RVUE $e^+e^- \rightarrow \pi^+\pi^-$
224 \pm 22			BISELLO	89 DM2 $e^+e^- \rightarrow \pi^+\pi^-$
242.5 \pm 163.0			DUBNICKA	89 RVUE $e^+e^- \rightarrow \pi^+\pi^-$
620 \pm 60			GESHKEN...	89 RVUE
<315			10 ERKAL	85 RVUE 20-70 $\gamma\rho \rightarrow \gamma\pi$
280 \pm 80			ABE	84B HYBR 20 $\gamma\rho \rightarrow \pi^+\pi^-p$
230 \pm 80			11 ASTON	80 OMEG 20-70 $\gamma\rho \rightarrow p2\pi$
283 \pm 14			12 ATIYA	79B SPEC 50 $\gamma C \rightarrow C2\pi$
175 \pm 98			BECKER	79 ASPK 17 π^-p polarized
232 \pm 34			10 LANG	79 RVUE
340			10 MARTIN	78C RVUE 17 $\pi^-p \rightarrow \pi^+\pi^-n$
300 \pm 100			10 FROGGATT	77 RVUE 17 $\pi^-p \rightarrow \pi^+\pi^-n$
180 \pm 50			13 HYAMS	73 ASPK 17 $\pi^-p \rightarrow \pi^+\pi^-n$

- Applies the Unitary & Analytic Model of the pion electromagnetic form factor of DUBNICKA 10 to analyze the data of LEES 12c and ABLIKIM 16c.
- Applies the Unitary & Analytic Model of the pion electromagnetic form factor of DUBNICKA 10 to analyze the data of ACHASOV 06, AKHMETSHIN 07, AUBERT 09AS, and AMBROSINO 11A.
- Applies the Unitary & Analytic Model of the pion electromagnetic form factor of DUBNICKA 10 to analyze the data of FUJIKAWA 08.
- From a Dalitz plot analysis in an isobar model with $\rho(1450)$ and $\rho(1700)$ masses and widths floating.
- Using the KUHN 90 parametrization of the pion form factor, neglecting $\rho-\omega$ interference.
- Using the GOUNARIS 68 parametrization of the pion form factor leaving the masses and widths of the $\rho(1450)$, $\rho(1700)$, and $\rho(2150)$ resonances as free parameters of the fit.
- $|F_{\pi}(0)|^2$ fixed to 1.
- From the GOUNARIS 68 parametrization of the pion form factor.
- T-matrix pole.
- From phase shift analysis of HYAMS 73 data.
- Simple relativistic Breit-Wigner fit with constant width.
- An additional 40 MeV uncertainty in both the mass and width is present due to the choice of the background shape.
- Included in BECKER 79 analysis.

$K\bar{K}$ MODE

Table with columns: VALUE (MeV), EVTS, DOCUMENT ID, TECN, CHG, COMMENT

••• We do not use the following data for averages, fits, limits, etc. •••

Table with columns: VALUE (MeV), EVTS, DOCUMENT ID, TECN, CHG, COMMENT

¹T-matrix pole, 2 poles, 3 channels, including $\pi\pi$ scattering data from HYAMS 75.
²K-matrix pole. Isospin not determined, could be $\omega(1650)$ or $\phi(1680)$.

$2(\pi^+\pi^-)$ MODE

Table with columns: VALUE (MeV), EVTS, DOCUMENT ID, TECN, COMMENT

••• We do not use the following data for averages, fits, limits, etc. •••

Table with columns: VALUE (MeV), EVTS, DOCUMENT ID, TECN, COMMENT

¹ Simple relativistic Breit-Wigner fit with model-dependent width.
² Simple relativistic Breit-Wigner fit with constant width.
³ One peak fit result.
⁴ Parameters roughly estimated, not from a fit.
⁵ Skew mass distribution compensated by Ross-Stodolsky factor.
⁶ Width errors enlarged by us to $4\Gamma\sqrt{N}$; see the note with the $K^*(892)$ mass.

$\pi^+\pi^-\pi^0\pi^0$ MODE

Table with columns: VALUE (MeV), DOCUMENT ID, TECN, COMMENT

••• We do not use the following data for averages, fits, limits, etc. •••

Table with columns: VALUE (MeV), DOCUMENT ID, TECN, COMMENT

$\omega\pi^0$ MODE

Table with columns: VALUE (MeV), DOCUMENT ID, TECN, COMMENT

••• We do not use the following data for averages, fits, limits, etc. •••

Table with columns: VALUE (MeV), DOCUMENT ID, TECN, COMMENT

¹ Taking into account both $\rho(1450)$ and $\rho(1700)$ contributions. Using the data of ACHASOV 00i on $e^+e^- \rightarrow \omega\pi^0$ and of EDWARDS 00a on $\tau^- \rightarrow \omega\pi^-\nu_\tau$. $\rho(1450)$ mass and width fixed at 1400 MeV and 500 MeV respectively.
² Taking into account the $\rho(1700)$ contribution only. Using the data of ACHASOV 00i on $e^+e^- \rightarrow \omega\pi^0$ and of EDWARDS 00a on $\tau^- \rightarrow \omega\pi^-\nu_\tau$.

$3(\pi^+\pi^-)$ AND $2(\pi^+\pi^-\pi^0)$ MODES

Table with columns: VALUE (MeV), DOCUMENT ID, TECN, COMMENT

••• We do not use the following data for averages, fits, limits, etc. •••

Table with columns: VALUE (MeV), DOCUMENT ID, TECN, COMMENT

¹ From a fit with two resonances with the JACOB 72 continuum.

$\Gamma_{\rho(1700)^0} - \Gamma_{\rho(1700)^\pm}$

Table with columns: VALUE (MeV), DOCUMENT ID, TECN, COMMENT

••• We do not use the following data for averages, fits, limits, etc. •••

Table with columns: VALUE (MeV), DOCUMENT ID, TECN, COMMENT

¹ Applies the Unitary & Analytic Model of the pion electromagnetic form factor of DUBNICKA 10 to analyze the data of ACHASOV 06, AKHMETSHIN 07, AUBERT 09as, AMBROSINO 11a, and FUJIKAWA 08.

$\rho(1700)$ DECAY MODES

Table with columns: Mode, Fraction (Γ_i/Γ)

Table with columns: Γ_{15} , Γ_{16} , Γ_{17} , Γ_{18} , Γ_{19} , decay channel, status

$\rho(1700) \Gamma(i)\Gamma(e^+e^-)/\Gamma(\text{total})$

This combination of a partial width with the partial width into e^+e^- and with the total width is obtained from the cross-section into channel i in e^+e^- annihilation.

$\Gamma(2(\pi^+\pi^-)) \times \Gamma(e^+e^-)/\Gamma_{\text{total}}$ Γ_{217}/Γ

Table with columns: VALUE (keV), DOCUMENT ID, TECN, COMMENT

••• We do not use the following data for averages, fits, limits, etc. •••

Table with columns: VALUE (keV), DOCUMENT ID, TECN, COMMENT

$\Gamma(\pi^+\pi^-) \times \Gamma(e^+e^-)/\Gamma_{\text{total}}$ Γ_{1117}/Γ

Table with columns: VALUE (keV), DOCUMENT ID, TECN, COMMENT

••• We do not use the following data for averages, fits, limits, etc. •••

Table with columns: VALUE (keV), DOCUMENT ID, TECN, COMMENT

¹ Using total width = 220 MeV.

$\Gamma(K\bar{K}^*(892) + \text{c.c.}) \times \Gamma(e^+e^-)/\Gamma_{\text{total}}$ Γ_{1317}/Γ

Table with columns: VALUE (keV), DOCUMENT ID, TECN, COMMENT

••• We do not use the following data for averages, fits, limits, etc. •••

Table with columns: VALUE (keV), DOCUMENT ID, TECN, COMMENT

¹ Model dependent.

$\Gamma(\eta\rho) \times \Gamma(e^+e^-)/\Gamma_{\text{total}}$ Γ_{1417}/Γ

Table with columns: VALUE (eV), EVTS, DOCUMENT ID, TECN, COMMENT

••• We do not use the following data for averages, fits, limits, etc. •••

Table with columns: VALUE (eV), EVTS, DOCUMENT ID, TECN, COMMENT

¹ Mass and width of the $\rho(770)$ fixed at 775 and 149 MeV, respectively; solution 2 of model 2, $\eta \rightarrow \gamma\gamma$ decays used.
² Includes non-resonant contribution. The selected fit model includes three ρ excited states. Model uncertainty is 80%.

$\Gamma(K\bar{K}) \times \Gamma(e^+e^-)/\Gamma_{\text{total}}$ Γ_{1617}/Γ

Table with columns: VALUE (keV), DOCUMENT ID, TECN, COMMENT

••• We do not use the following data for averages, fits, limits, etc. •••

Table with columns: VALUE (keV), DOCUMENT ID, TECN, COMMENT

¹ Model dependent.

$\Gamma(\rho\pi\pi) \times \Gamma(e^+e^-)/\Gamma_{\text{total}}$ Γ_{317}/Γ

Table with columns: VALUE (keV), DOCUMENT ID, TECN, COMMENT

••• We do not use the following data for averages, fits, limits, etc. •••

Table with columns: VALUE (keV), DOCUMENT ID, TECN, COMMENT

¹ Model dependent.

$\rho(1700) \Gamma(i)/\Gamma(\text{total}) \times \Gamma(e^+e^-)/\Gamma(\text{total})$

$\Gamma(\pi^0\omega)/\Gamma_{\text{total}} \times \Gamma(e^+e^-)/\Gamma_{\text{total}}$ $\Gamma_{18}/\Gamma \times \Gamma_{17}/\Gamma$

Table with columns: VALUE (units 10^{-8}), EVTS, DOCUMENT ID, TECN, COMMENT

••• We do not use the following data for averages, fits, limits, etc. •••

Table with columns: VALUE (units 10^{-8}), EVTS, DOCUMENT ID, TECN, COMMENT

¹ From a phenomenological model based on vector meson dominance with interfering $\rho(700)$, $\rho(1450)$, and $\rho(1700)$. The $\rho(1700)$ mass and width are fixed at 1720 MeV and 250 MeV, respectively. Systematic uncertainty not estimated. Supersedes ACHASOV 13.
² From a phenomenological model based on vector meson dominance with the interfering $\rho(1450)$ and $\rho(1700)$ and their widths fixed at 400 and 250 MeV, respectively. Systematic uncertainty not estimated.

$\Gamma(\eta\rho)/\Gamma_{\text{total}} \times \Gamma(e^+e^-)/\Gamma_{\text{total}}$ $\Gamma_{14}/\Gamma \times \Gamma_{17}/\Gamma$

Table with columns: VALUE (units 10^{-8}), EVTS, DOCUMENT ID, TECN, COMMENT

••• We do not use the following data for averages, fits, limits, etc. •••

Table with columns: VALUE (units 10^{-8}), EVTS, DOCUMENT ID, TECN, COMMENT

¹ From the combined fit of AULCHENKO 15 and ACHASOV 18 in the model with the interfering $\rho(1450)$, $\rho(1700)$ and $\rho(2150)$ with the parameters of the $\rho(1450)$ and $\rho(1700)$ floating and the mass and width of the $\rho(2150)$ fixed at 2155 MeV and 320 MeV, respectively. The phases of the resonances are π , 0 and π , respectively.

Meson Particle Listings

 $\rho(1700)$ $\rho(1700)$ BRANCHING RATIOS $\Gamma(\rho\pi\pi)/\Gamma(4\pi)$ Γ_3/Γ_1

VALUE	DOCUMENT ID	TECN	COMMENT
••• We do not use the following data for averages, fits, limits, etc. •••			
0.28 ± 0.06	¹ ABELE	01B	CBAR $0.0 \bar{p}n \rightarrow 5\pi$
¹ $\omega\pi$ not included.			

 $\Gamma(\rho^0\pi^+\pi^-)/\Gamma(2(\pi^+\pi^-))$ Γ_4/Γ_2

VALUE	EVTS	DOCUMENT ID	TECN	COMMENT
••• We do not use the following data for averages, fits, limits, etc. •••				
~ 1.0		DEL COURT	81B	DM1 $e^+e^- \rightarrow 2(\pi^+\pi^-)$
0.7 ± 0.1	500	SCHACHT	74	STRC $5.5-18 \gamma p \rightarrow p4\pi$
0.80		¹ BINGHAM	72B	HBC $9.3 \gamma p \rightarrow p4\pi$
¹ The $\pi\pi$ system is in S-wave.				

 $\Gamma(\rho^0\pi^0\pi^0)/\Gamma(\rho^\pm\pi^\mp\pi^0)$ Γ_5/Γ_6

VALUE	DOCUMENT ID	TECN	CHG	COMMENT
••• We do not use the following data for averages, fits, limits, etc. •••				
<0.10	ATKINSON	85B	OMEG	20-70 γp
<0.15	ATKINSON	82	OMEG	0 20-70 $\gamma p \rightarrow p4\pi$

 $\Gamma(a_1(1260)\pi)/\Gamma(4\pi)$ Γ_7/Γ_1

VALUE	DOCUMENT ID	TECN	COMMENT
••• We do not use the following data for averages, fits, limits, etc. •••			
0.16 ± 0.05	¹ ABELE	01B	CBAR $0.0 \bar{p}n \rightarrow 5\pi$
¹ $\omega\pi$ not included.			

 $\Gamma(h_1(1170)\pi)/\Gamma(4\pi)$ Γ_8/Γ_1

VALUE	DOCUMENT ID	TECN	COMMENT
••• We do not use the following data for averages, fits, limits, etc. •••			
0.17 ± 0.06	¹ ABELE	01B	CBAR $0.0 \bar{p}n \rightarrow 5\pi$
¹ $\omega\pi$ not included.			

 $\Gamma(\pi(1300)\pi)/\Gamma(4\pi)$ Γ_9/Γ_1

VALUE	DOCUMENT ID	TECN	COMMENT
••• We do not use the following data for averages, fits, limits, etc. •••			
0.30 ± 0.10	¹ ABELE	01B	CBAR $0.0 \bar{p}n \rightarrow 5\pi$
¹ $\omega\pi$ not included.			

 $\Gamma(\rho\rho)/\Gamma(4\pi)$ Γ_{10}/Γ_1

VALUE	DOCUMENT ID	TECN	COMMENT
••• We do not use the following data for averages, fits, limits, etc. •••			
0.09 ± 0.03	¹ ABELE	01B	CBAR $0.0 \bar{p}n \rightarrow 5\pi$
¹ $\omega\pi$ not included.			

 $\Gamma(\pi^+\pi^-)/\Gamma_{total}$ Γ_{11}/Γ

VALUE	DOCUMENT ID	TECN	COMMENT
••• We do not use the following data for averages, fits, limits, etc. •••			
$0.108 \pm 0.017^{+0.162}_{-0.004}$	¹ ALBRECHT	20	RVUE $0.9 \bar{p}p \rightarrow K^+K^-\pi^0$
$0.287^{+0.043}_{-0.042}$	BECKER	79	ASPK $17 \pi^- p$ polarized
0.15 to 0.30	² MARTIN	78C	RVUE $17 \pi^- p \rightarrow \pi^+\pi^-n$
<0.20	³ COSTA...	77B	RVUE $e^+e^- \rightarrow 2\pi, 4\pi$
0.30 \pm 0.05	⁴ FROGGATT	77	RVUE $17 \pi^- p \rightarrow \pi^+\pi^-n$
<0.15	⁴ EISENBERG	73	HBC $5 \pi^+ p \rightarrow \Delta^+\pi$
0.25 \pm 0.05	⁵ HYAMS	73	ASPK $17 \pi^- p \rightarrow \pi^+\pi^-n$

¹ Residue from T-matrix pole, 2 poles, 3 channels, Chew-Mandelstam functions and simplified analytic continuation for the 4π channel. Includes scattering data from HYAMS 75 and model-independent calculation of GARCIA-MARTIN 11A.

² From phase shift analysis of HYAMS 73 data.

³ Estimate using unitarity, time reversal invariance, Breit-Wigner.

⁴ Estimated using one-pion-exchange model.

⁵ Included in BECKER 79 analysis.

 $\Gamma(K\bar{K})/\Gamma_{total}$ Γ_{16}/Γ

VALUE	DOCUMENT ID	TECN	COMMENT
••• We do not use the following data for averages, fits, limits, etc. •••			
$0.007 \pm 0.006^{+0.041}_{-0.002}$	¹ ALBRECHT	20	RVUE $0.9 \bar{p}p \rightarrow K^+K^-\pi^0$

¹ Residue from T-matrix pole, 2 poles, 3 channels, Chew-Mandelstam functions and simplified analytic continuation for the 4π channel. Includes scattering data from HYAMS 75 and model-independent calculation of GARCIA-MARTIN 11A.

 $\Gamma(\pi^+\pi^-)/\Gamma(2(\pi^+\pi^-))$ Γ_{11}/Γ_2

VALUE	DOCUMENT ID	TECN	COMMENT
••• We do not use the following data for averages, fits, limits, etc. •••			
0.13 \pm 0.05	ASTON	80	OMEG 20-70 $\gamma p \rightarrow p2\pi$
<0.14	¹ DAVIER	73	STRC $6-18 \gamma p \rightarrow p4\pi$
<0.2	² BINGHAM	72B	HBC $9.3 \gamma p \rightarrow p2\pi$
¹ Upper limit is estimate.			
² 2σ upper limit.			

 $\Gamma(\pi\pi)/\Gamma(4\pi)$ Γ_{12}/Γ_1

VALUE	DOCUMENT ID	TECN	COMMENT
••• We do not use the following data for averages, fits, limits, etc. •••			
0.16 ± 0.04	^{1,2} ABELE	01B	CBAR $0.0 \bar{p}n \rightarrow 5\pi$
¹ Using ABELE 97.			
² $\omega\pi$ not included.			

 $\Gamma(K\bar{K}^*(892) + c.c.)/\Gamma_{total}$ Γ_{13}/Γ

VALUE	DOCUMENT ID	TECN	COMMENT
••• We do not use the following data for averages, fits, limits, etc. •••			
possibly seen	COAN	04	CLEO $\tau^- \rightarrow K^-\pi^-K^+\nu_\tau$

 $\Gamma(K\bar{K}^*(892) + c.c.)/\Gamma(2(\pi^+\pi^-))$ Γ_{13}/Γ_2

VALUE	DOCUMENT ID	TECN	COMMENT
••• We do not use the following data for averages, fits, limits, etc. •••			
0.15 ± 0.03	¹ DELCOURT	81B	DM1 $e^+e^- \rightarrow \bar{K}K\pi$
¹ Assuming $\rho(1700)$ and ω radial excitations to be degenerate in mass.			

 $\Gamma(\eta\rho)/\Gamma_{total}$ Γ_{14}/Γ

VALUE	CL%	DOCUMENT ID	TECN	COMMENT
••• We do not use the following data for averages, fits, limits, etc. •••				
possibly seen		AKHMETSHIN	00D	CMD2 $e^+e^- \rightarrow \eta\pi^+\pi^-$
<0.04		DONNACHIE	87B	RVUE
<0.02	58	ATKINSON	86B	OMEG 20-70 γp

 $\Gamma(\eta\rho)/\Gamma(2(\pi^+\pi^-))$ Γ_{14}/Γ_2

VALUE	DOCUMENT ID	TECN	COMMENT
••• We do not use the following data for averages, fits, limits, etc. •••			
0.123 ± 0.027	DEL COURT	82	DM1 $e^+e^- \rightarrow \pi^+\pi^-MM$
~ 0.1	ASTON	80	OMEG 20-70 γp

 $\Gamma(\pi^+\pi^- \text{ neutrals})/\Gamma(2(\pi^+\pi^-))$ $(\Gamma_5 + \Gamma_6 + 0.714\Gamma_{14})/\Gamma_2$

VALUE	DOCUMENT ID	TECN	COMMENT
••• We do not use the following data for averages, fits, limits, etc. •••			
2.6 ± 0.4	¹ BALLAM	74	HBC $9.3 \gamma p$
¹ Upper limit. Background not subtracted.			

 $\Gamma(a_2(1320)\pi)/\Gamma_{total}$ Γ_{15}/Γ

VALUE	DOCUMENT ID	TECN	COMMENT
••• We do not use the following data for averages, fits, limits, etc. •••			
not seen	AMELIN	00	VES $37 \pi^- p \rightarrow \eta\pi^+\pi^-n$

 $\Gamma(K\bar{K})/\Gamma(2(\pi^+\pi^-))$ Γ_{16}/Γ_2

VALUE	CL%	DOCUMENT ID	TECN	CHG	COMMENT
••• We do not use the following data for averages, fits, limits, etc. •••					
0.015 ± 0.010		¹ DELCOURT	81B	DM1	$e^+e^- \rightarrow \bar{K}K$
<0.04	95	BINGHAM	72B	HBC	0 $9.3 \gamma p$
¹ Assuming $\rho(1700)$ and ω radial excitations to be degenerate in mass.					

 $\Gamma(K\bar{K})/\Gamma(K\bar{K}^*(892) + c.c.)$ Γ_{16}/Γ_{13}

VALUE	DOCUMENT ID	TECN	COMMENT
••• We do not use the following data for averages, fits, limits, etc. •••			
0.052 ± 0.026	BUON	82	DM1 $e^+e^- \rightarrow$ hadrons

 $\Gamma(\pi^0\omega)/\Gamma_{total}$ Γ_{18}/Γ

VALUE	EVTS	DOCUMENT ID	TECN	COMMENT
••• We do not use the following data for averages, fits, limits, etc. •••				
not seen		MATVIENKO	15	BELL $\bar{B}^0 \rightarrow D^{*+}\omega\pi^-$
seen	1.6k	ACHASOV	12	SND $e^+e^- \rightarrow \pi^0\pi^0\gamma$
not seen	2382	AKHMETSHIN	03B	CMD2 $e^+e^- \rightarrow \pi^0\pi^0\gamma$
seen		ACHASOV	97	RVUE $e^+e^- \rightarrow \omega\pi^0$

 $\Gamma(\pi^0\gamma)/\Gamma_{total}$ Γ_{19}/Γ

VALUE	DOCUMENT ID	TECN	COMMENT
not seen	¹ ACHASOV	10D	SND $1.075-2.0 e^+e^- \rightarrow \pi^0\gamma$
¹ From a fit of a VMD model with two effective resonances with masses of 1450 MeV and 1700 MeV to describe the excited vector states $\omega(1420)$, $\rho(1450)$, $\omega(1650)$, and $\rho(1700)$. The width of the highest mass effective resonance is fixed at 315 MeV.			

 $\rho(1700)$ REFERENCES

ALBRECHT	20	EPJ C80 453	M. Albrecht <i>et al.</i>	(Crystal Barrel Collab.)
GRIBANOV	20	JHEP 2001 112	S.S. Gribov <i>et al.</i>	(CMD-3 Collab.)
ACHASOV	18	PR D97 012008	M.N. Achasov <i>et al.</i>	(SND Collab.)
LEES	18	PR D97 052007	J.P. Lees <i>et al.</i>	(BABAR Collab.)
BARTOS	17	PR D96 113004	E. Bartos <i>et al.</i>	
BARTOS	17A	IJMP A32 1750154	E. Bartos <i>et al.</i>	
LEES	17C	PR D95 072007	J.P. Lees <i>et al.</i>	(BABAR Collab.)
AALI	16N	PR D93 052018	R. Aaij <i>et al.</i>	(LHCb Collab.)
ABLIKIM	16C	PL B753 629	M. Ablikim <i>et al.</i>	(BESIII Collab.)
ACHASOV	16D	PR D94 112001	M.N. Achasov <i>et al.</i>	(SND Collab.)
AULCHENKO	15D	PR D91 052013	V.M. Aulchenko <i>et al.</i>	(SND Collab.)
MATVIENKO	15	PR D92 012013	D. Matvienko <i>et al.</i>	(BELLE Collab.)
ACHASOV	13	PR D88 054013	M.N. Achasov <i>et al.</i>	(SND Collab.)
ABRAMOWICZ	12	EPJ C72 1869	H. Abramowicz <i>et al.</i>	(ZEUS Collab.)
ACHASOV	12	JETPL 94 734	M.N. Achasov <i>et al.</i>	
Translated from ZETFP 94 796.				

See key on page 1127

Meson Particle Listings

$\rho(1700)$, $a_2(1700)$

Table listing meson particles with columns: NAME, JPC, MASS, WIDTH, DOCUMENT ID, TECN, COMMENT. Includes entries for LEES, AMBROSINO, GARCIA-MAR., etc.

- 3 T-matrix pole, 2 poles, 2 channels (pi eta, K K-bar).
4 The coupled-channel analysis of both the eta pi and eta' pi systems using ADOLPH 15 data.
5 Statistical error negligible.
6 Breit-Wigner mass.
7 Superseded by RODAS 19.
8 From analysis of L3 data at 183-209 GeV.
9 Statistical error only.
10 Spin 2 dominant, isospin not determined, could also be l=1.
11 Possibly two J^P = 2^+ resonances with isospins 0 and 1.

a2(1700) WIDTH

Table for a2(1700) WIDTH with columns: VALUE (MeV), EVTS, DOCUMENT ID, TECN, COMMENT. Includes entries for AMSLER, KOPF, ALBRECHT, RODAS, AGHASYAN, JACKURA, ABLIKIM, ANISOVICH, SCHEGELSKY, UMAN, LU, ABE, ACCIARRI, ABELE.

- 1 T-matrix pole.
2 From T-matrix pole based on combined fit of Crystal Barrel and pi pi scattering data (ALBRECHT 20), and COMPASS data (ADOLPH 15), using a coupled-channel model of eta pi, eta' pi and K K-bar systems.
3 T-matrix pole, 2 poles, 2 channels (pi eta, K K-bar).
4 The coupled-channel analysis of both the eta pi and eta' pi systems using ADOLPH 15 data. The width is extracted from the T-matrix pole.
5 Statistical error negligible.
6 Breit-Wigner width.
7 Superseded by RODAS 19.
8 From analysis of L3 data at 183-209 GeV.
9 Statistical error only.
10 Spin 2 dominant, isospin not determined, could also be l=1.

a2(1700) G(JPC) = 1-(2++)

a2(1700) MASS

Table for a2(1700) MASS with columns: VALUE (MeV), EVTS, DOCUMENT ID, TECN, COMMENT. Includes entries for AMSLER, KOPF, ALBRECHT, RODAS, AGHASYAN, JACKURA, ABLIKIM, ANISOVICH, UMAN, LU, ABE, ACCIARRI, ABELE, GRYGOREV.

- 1 T-matrix pole.
2 From T-matrix pole based on combined fit of Crystal Barrel and pi pi scattering data (ALBRECHT 20), and COMPASS data (ADOLPH 15), using a coupled-channel model of eta pi, eta' pi and K K-bar systems.

a2(1700) DECAY MODES

Table for a2(1700) DECAY MODES with columns: Mode, Fraction (Gamma_i/Gamma). Includes entries for eta pi, eta' pi, gamma gamma, rho pi, f2(1270) pi, K K-bar, omega pi pi, omega rho.

a2(1700) PARTIAL WIDTHS

Table for a2(1700) PARTIAL WIDTHS with columns: Gamma(eta pi), Gamma(eta' pi), Gamma(gamma gamma), Gamma(K K-bar), Gamma(omega pi pi). Includes entries for SCHEGELSKY 06A, RVUE.

- 1 From analysis of L3 data at 91 and 183-209 GeV, using a2(1700) mass of 1730 MeV and width of 340 MeV, and SU(3) relations.

Meson Particle Listings

 $a_2(1700)$, $f_0(1710)$

$a_2(1700) \Gamma(i)\Gamma(\gamma\gamma)/\Gamma(\text{total})$				
$[\Gamma(\rho\pi) + \Gamma(f_2(1270)\pi)] \times \Gamma(\gamma\gamma)/\Gamma(\text{total}) \quad (\Gamma_4 + \Gamma_5)\Gamma_3/\Gamma$				
VALUE (keV)	EVTS	DOCUMENT ID	TECN	COMMENT
$0.29 \pm 0.04 \pm 0.02$		ACCIARRI 97T	L3	$\gamma\gamma \rightarrow \pi^+ \pi^- \pi^0$
••• We do not use the following data for averages, fits, limits, etc. •••				
$0.37^{+0.12}_{-0.08} \pm 0.10$	18k	1 SCHEGELSKY 06	RVUE	$\gamma\gamma \rightarrow \pi^+ \pi^- \pi^0$
1 From analysis of L3 data at 183–209 GeV.				
$\Gamma(K\bar{K}) \times \Gamma(\gamma\gamma)/\Gamma(\text{total}) \quad \Gamma_6/\Gamma_3/\Gamma$				
VALUE (eV)	DOCUMENT ID	TECN	COMMENT	
••• We do not use the following data for averages, fits, limits, etc. •••				
$20.6 \pm 4.2 \pm 4.6$	1 ABE 04	BELL	$10.6 e^+ e^- \rightarrow e^+ e^- K^+ K^-$	
$49 \pm 11 \pm 13$	2 ACCIARRI 01H	L3	$\gamma\gamma \rightarrow K_S^0 K_S^0, E_{\text{cm}}^{E_{\text{cm}}=91, 183-209 \text{ GeV}}$	
1 Assuming spin 2.				
2 Spin 2 dominant, isospin not determined, could also be $l=1$.				

$a_2(1700)$ BRANCHING RATIOS				
$\Gamma(\rho\pi)/\Gamma(f_2(1270)\pi) \quad \Gamma_4/\Gamma_5$				
VALUE	EVTS	DOCUMENT ID	TECN	COMMENT
••• We do not use the following data for averages, fits, limits, etc. •••				
$3.4 \pm 0.4 \pm 0.1$	18k	1 SCHEGELSKY 06	RVUE	$\gamma\gamma \rightarrow \pi^+ \pi^- \pi^0$
1 From analysis of L3 data at 183–209 GeV.				
$\Gamma(K\bar{K})/\Gamma(\eta\pi) \quad \Gamma_6/\Gamma_1$				
VALUE	DOCUMENT ID	TECN	COMMENT	
••• We do not use the following data for averages, fits, limits, etc. •••				
0.029 ± 0.04	$+0.011$ -0.012	1 KOPF 21	RVUE	$0.9 p\bar{p} \rightarrow \pi^0 \pi^0 \eta, \pi^0 \eta\eta,$ $\pi^0 K^+ K^- \text{ and } 191 \pi^- p \rightarrow$ $\pi^- \pi^- \pi^+ p$
4.134 ± 0.106	$+4.909$ -2.988	2 ALBRECHT 20	RVUE	$0.9 p\bar{p} \rightarrow \pi^0 \pi^0 \eta, \pi^0 \eta\eta,$ $\pi^0 K^+ K^-$
1 From T-matrix pole based on combined fit of Crystal Barrel and $\pi\pi$ scattering data (ALBRECHT 20), and COMPASS data (ADOLPH 15), using a coupled-channel model of $\eta\pi, \eta'\pi$ and $K\bar{K}$ systems.				
2 Residues from T-matrix pole, 2 poles, 2 channels ($\pi\eta, K\bar{K}$).				

$\Gamma(\eta'\pi)/\Gamma(\eta\pi) \quad \Gamma_2/\Gamma_1$				
VALUE	DOCUMENT ID	TECN	COMMENT	
••• We do not use the following data for averages, fits, limits, etc. •••				
0.035 ± 0.044	$+0.069$ -0.012	1 KOPF 21	RVUE	$0.9 p\bar{p} \rightarrow \pi^0 \pi^0 \eta, \pi^0 \eta\eta,$ $\pi^0 K^+ K^- \text{ and } 191 \pi^- p \rightarrow$ $\pi^- \pi^- \pi^+ p$
1 From T-matrix pole based on combined fit of Crystal Barrel and $\pi\pi$ scattering data (ALBRECHT 20), and COMPASS data (ADOLPH 15), using a coupled-channel model of $\eta\pi, \eta'\pi$ and $K\bar{K}$ systems.				

$a_2(1700)$ REFERENCES				
KOPF 21	EPJ C81 1056	B. Kopf et al.	(BOCH)	
ALBRECHT 20	EPJ C80 453	M. Albrecht et al.	(Crystal Barrel Collab.)	
RODAS 19	PRL 122 042002	A. Rodas et al.	(JPAC Collab.)	
AGHASYAN 18B	PR D98 092003	M. Aghasyan et al.	(COMPASS Collab.)	
JACKURA 18	PL B779 464	A. Jackura et al.	(JPAC and COMPASS Collab.)	
ABLIKIM 17K	PR D95 032002	M. Ablikim et al.	(BESIII Collab.)	
ADOLPH 15	PL B740 303	M. Adolph et al.	(COMPASS Collab.)	
ANISOVICH 09	IJMP A24 2481	V.V. Anisovich, A.V. Sarantsev		
SCHEGELSKY 06	EPJ A27 199	V.A. Schegelsky et al.		
SCHEGELSKY 06A	EPJ A27 207	V.A. Schegelsky et al.		
UMAN 06	PR D73 052009	I. Uman et al.	(FNAL E835)	
LU 05	PRL 94 032002	M. Lu et al.	(BNL E852 Collab.)	
ABE 04	EPJ C32 323	K. Abe et al.	(BELLE Collab.)	
AMSLER 02	EPJ C23 29	C. Amisler et al.		
ACCIARRI 01H	PL B501 173	M. Acciarri et al.	(L3 Collab.)	
ABELE 99B	EPJ C8 67	A. Abele et al.	(Crystal Barrel Collab.)	
GRYGOREV 99	PAN 62 470	V.K. Grygorev et al.		
ACCIARRI 97T	PL B413 147	M. Acciarri et al.	(L3 Collab.)	

 $f_0(1710)$

$$I^G(J^{PC}) = 0^+(0^{++})$$

See the review on "Spectroscopy of Light Meson Resonances."

$f_0(1710)$ MASS				
OUR EVALUATION below is based on T-matrix poles from BARBERIS 00E and BARBERIS 99D.				
VALUE (MeV)	EVTS	DOCUMENT ID	TECN	COMMENT
1704 ± 12 OUR EVALUATION				
1733 ± 8 OUR AVERAGE Error includes scale factor of 1.5. See the ideogram below.				
$1757 \pm 24 \pm 9$		1 LEES 21A	BABR	$\eta_C(1S) \rightarrow \eta' K^+ K^-$
1759 ± 6	$+14$ -25	5.5k	2 ABLIKIM 13N	BES3 $e^+ e^- \rightarrow J/\psi \rightarrow \gamma\eta\eta$
1750 ± 6	$+29$ -18		3 UEHARA 13	BELL $\gamma\gamma \rightarrow K_S^0 K_S^0$

1701 ± 5	$+9$ -2	4k	4 CHEKANOV 08	ZEUS $e p \rightarrow K_S^0 K_S^0 X$
1765 ± 4	$+13$		1 ABLIKIM 06v	BES2 $e^+ e^- \rightarrow J/\psi \rightarrow \gamma\pi^+ \pi^-$
1738 ± 30			ABLIKIM 04E	BES2 $J/\psi \rightarrow \omega K^+ K^-$
1740 ± 4	$+10$ -25		BAI 03G	BES $J/\psi \rightarrow \gamma K\bar{K}$
1740 ± 30	$+30$ -25		BAI 00A	BES $J/\psi \rightarrow \gamma(\pi^+ \pi^- \pi^+ \pi^-)$
1710 ± 25			5 FRENCH 99	300 $pp \rightarrow p f(K^+ K^-) p_S$
••• We do not use the following data for averages, fits, limits, etc. •••				
1769 ± 8			6 RODAS 22	RVUE $J/\psi(1S) \rightarrow \gamma(\pi\pi, K\bar{K})$
1814 ± 31		7.2k	7 KHOLODENK.21	VES $29 \pi^- p \rightarrow n\omega\phi$
1700 ± 18			8,9 SARANTSEV 21	RVUE $J/\psi(1S) \rightarrow \gamma(\pi\pi, K\bar{K}, \eta\eta, \omega\phi)$
1803 ± 3.5	$+45.5$ -10.4		10 ALBRECHT 20	RVUE $0.9 p\bar{p} \rightarrow \pi^0 \pi^0 \eta, \pi^0 \eta\eta,$ $\pi^0 K^+ K^-$
1744 ± 7	± 5	381	11,12 DOBBS 15	$J/\psi \rightarrow \gamma\pi^+ \pi^-$
1705 ± 11	± 5	237	11,12 DOBBS 15	$\psi(2S) \rightarrow \gamma\pi^+ \pi^-$
1706 ± 4	± 5	1.0k	11,12 DOBBS 15	$J/\psi \rightarrow \gamma K^+ K^-$
1690 ± 8	± 3	349	11,12 DOBBS 15	$\psi(2S) \rightarrow \gamma K^+ K^-$
1795 ± 7	$+23$ -20		ABLIKIM 13J	BES3 $J/\psi \rightarrow \gamma\omega\phi$
1812 ± 19	$+26$		13 ABLIKIM 06J	BES2 $J/\psi \rightarrow \gamma\omega\phi$
1750 ± 13			AMSLER 06	CBAR $1.64 p\bar{p} \rightarrow K^+ K^- \pi^0$
1747 ± 5		80k	1.14 UMAN 06	E835 $5.2 p\bar{p} \rightarrow \eta\eta\pi^0$
1776 ± 15			VLADIMIRSK.06	SPEC $40 \pi^- p \rightarrow K_S^0 K_S^0 n$
1790 ± 40	-30		15 ABLIKIM 05	BES2 $J/\psi \rightarrow \phi\pi^+ \pi^-$
1760 ± 15	$+15$ -10		15 ABLIKIM 05Q	BES2 $\psi(2S) \rightarrow \gamma\pi^+ \pi^- K^+ K^-$
1670 ± 20			1 BINON 05	GAMS $33 \pi^- p \rightarrow \eta\eta n$
1732 ± 15			16 ANISOVICH 03	RVUE
1682 ± 16			TIKHOMIROV 03	SPEC $40.0 \pi^- C \rightarrow K_S^0 K_S^0 K_L^0 X$
1670 ± 26		3.6k	17 NICHITIU 02	OBLX $0 p\bar{p} \rightarrow K^+ K^- \pi^+ \pi^- \pi^0$
1698 ± 18			8 BARBERIS 00E	$450 p\bar{p} \rightarrow p f \eta\eta p_S$
1770 ± 12			18 ANISOVICH 99B	SPEC $0.6-1.2 p\bar{p} \rightarrow \eta\eta\pi^0$
1730 ± 15			BARBERIS 99	OMEG $450 p\bar{p} \rightarrow p_S p f K^+ K^-$
1750 ± 20			BARBERIS 99B	OMEG $450 p\bar{p} \rightarrow p_S p f \pi^+ \pi^-$
1710 ± 12	± 11		19 BARBERIS 99D	OMEG $450 p\bar{p} \rightarrow K^+ K^-, \pi^+ \pi^-$
1750 ± 30			20 ANISOVICH 98B	RVUE Compilation
1720 ± 39			BAI 98H	BES $J/\psi \rightarrow \gamma\pi^0 \pi^0$
1775 ± 1.5		57	21 BARKOV 98	$\pi^- p \rightarrow K_S^0 K_S^0 n$
1690 ± 11			22 ABREU 96C	DLPH $Z^0 \rightarrow K^+ K^- + X$
1696 ± 5	$+9$ -34		23 BAI 96C	BES $J/\psi \rightarrow \gamma K^+ K^-$
1781 ± 8	$+10$ -31		BAI 96C	BES $J/\psi \rightarrow \gamma K^+ K^-$
1768 ± 14			BALOSHIN 95	SPEC $40 \pi^- C \rightarrow K_S^0 K_S^0 X$
1750 ± 15			24 BUGG 95	MRK3 $J/\psi \rightarrow \gamma\pi^+ \pi^- \pi^+ \pi^-$
1620 ± 16			23 BUGG 95	MRK3 $J/\psi \rightarrow \gamma\pi^+ \pi^- \pi^+ \pi^-$
1748 ± 10			25 ARMSTRONG 93C	E760 $p\bar{p} \rightarrow \pi^0 \eta\eta \rightarrow 6\gamma$
~ 1750			BREAKSTONE 93	SFM $pp \rightarrow pp\pi^+ \pi^- \pi^+ \pi^-$
1744 ± 15			26 ALDE 92D	GAM2 $38 \pi^- p \rightarrow \eta\eta n$
1713 ± 10			27 ARMSTRONG 89D	OMEG $300 p\bar{p} \rightarrow pp K^+ K^-$
1706 ± 10			27 ARMSTRONG 89D	OMEG $300 p\bar{p} \rightarrow pp K_S^0 K_S^0$
1707 ± 10			25 AUGUSTIN 88	DM2 $J/\psi \rightarrow \gamma K^+ K^-, K_S^0 K_S^0$
1700 ± 15			23 BOLONKIN 88	SPEC $40 \pi^- p \rightarrow K_S^0 K_S^0 n$
1720 ± 60			BOLONKIN 88	SPEC $40 \pi^- p \rightarrow K_S^0 K_S^0 n$
1638 ± 10			28 FALVARD 88	DM2 $J/\psi \rightarrow \phi K^+ K^-, K_S^0 K_S^0$
1690 ± 4			29 FALVARD 88	DM2 $J/\psi \rightarrow \phi K^+ K^-, K_S^0 K_S^0$
1698 ± 15			25 AUGUSTIN 87	DM2 $J/\psi \rightarrow \gamma\pi^+ \pi^-$
1720 ± 10	± 10		23 BALTRUSAIT.87	MRK3 $J/\psi \rightarrow \gamma K^+ K^-$
1755 ± 8			30 ALDE 86C	GAM2 $38 \pi^- p \rightarrow n2\eta$
1730 ± 2	-10		31 LONGACRE 86	RVUE $22 \pi^- p \rightarrow n2K_S^0$
1742 ± 15			25 WILLIAMS 84	MP SF $200 \pi^- N \rightarrow 2K_S^0 X$
1670 ± 50			BLOOM 83	CBAL $J/\psi \rightarrow \gamma2\eta$
1650 ± 50			BURKE 82	MRK2 $J/\psi \rightarrow \gamma2p$
1640 ± 50			32,33 EDWARDS 82D	CBAL $J/\psi \rightarrow \gamma2\eta$
1730 ± 10	± 20		34 ETKIN 82C	MPS $23 \pi^- p \rightarrow n2K_S^0$

1 Breit-Wigner mass.

2 From partial wave analysis including all possible combinations of $0^{++}, 2^{++}$, and 4^{++} resonances.

3 Spin 0 favored over spin 2.

4 In the SU(3) based model with a specific interference pattern of the $f_2(1270)$, $a_2^0(1320)$, and $f_2'(1525)$ mesons incoherently added to the $f_0(1710)$ and non-resonant background.

5 $J^P = 0^+$, superseded by ARMSTRONG 89D.

6 T-matrix pole from coupled channel K-matrix fit to data on $J/\psi \rightarrow \gamma\pi^0 \pi^0$ (ABLIKIM 15AE) and $J/\psi \rightarrow \gamma K_S^0 K_S^0$ (ABLIKIM 18AA).

7 From partial wave analysis of $\omega\phi$ invariant mass including $0^{++}, 2^{++}$, and 0^{-+} resonances.

8 T-matrix pole.

9 Close-by state with mass 1765 ± 15 MeV and width 180 ± 20 MeV.

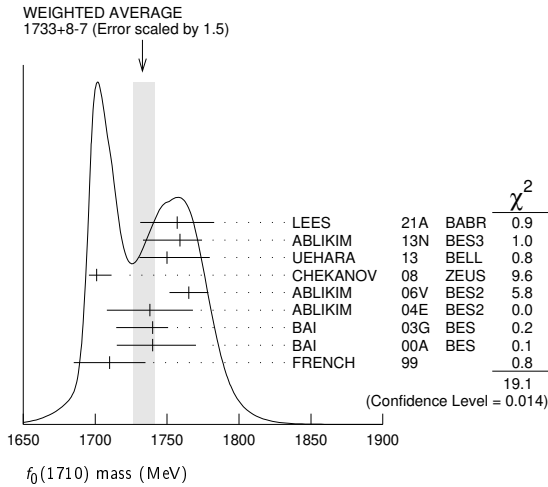
10 T-matrix pole, 5 poles, 5 channels, including scattering data from HYAMS 75 ($\pi\pi$), LONGACRE 86 ($K\bar{K}$), BINON 83 ($\eta\eta$), and BINON 84C ($\eta\eta'$).

See key on page 1127

Meson Particle Listings

$f_0(1710)$

- 11 Using CLEO-c data but not authored by the CLEO Collaboration.
- 12 From a fit to a Breit-Wigner line shape with fixed $\Gamma = 135$ MeV.
- 13 Not seen by LIU 09 in $B^\pm \rightarrow K^\pm \omega \phi$.
- 14 Systematic errors not estimated.
- 15 This state may be different from $f_0(1710)$, see CLOSE 05.
- 16 K-matrix pole, assuming $J^P = 0^+$, from combined analysis of $\pi^- p \rightarrow \pi^0 \pi^0 n, \pi^- p \rightarrow K \bar{K} n, \pi^+ \pi^- \rightarrow \pi^+ \pi^-, \bar{p} p \rightarrow \pi^0 \pi^0 \pi^0, \pi^0 \eta \eta, \pi^0 \pi^0 \eta, \pi^+ \pi^- \pi^0, K^+ K^- \pi^0, K_S^0 K_S^0 \pi^0, K^+ K_S^0 \pi^-$ at rest, $\bar{p} n \rightarrow \pi^- \pi^- \pi^+, K_S^0 K^- \pi^0, K_S^0 K_S^0 \pi^-$ at rest.
- 17 Decaying to $f_0(1370) \pi \pi$.
- 18 Not seen by AMSLER 02.
- 19 Supersedes BARBERIS 99 and BARBERIS 99b.
- 20 T-matrix pole, assuming $J^P = 0^+$
- 21 No J^{PC} determination.
- 22 No J^{PC} determination, width not determined.
- 23 $J^P = 2^+$.
- 24 From a fit to the 0^+ partial wave.
- 25 No J^{PC} determination.
- 26 ALDE 92d combines all the GAMS-2000 data.
- 27 $J^P = 2^+$, superseded by FRENCH 99.
- 28 From an analysis ignoring interference with $f_2'(1525)$.
- 29 From an analysis including interference with $f_2'(1525)$.
- 30 Superseded by ALDE 92d.
- 31 Uses MRK3 data. From a partial-wave analysis of data using a K-matrix formalism with 5 poles, but assuming spin 2. Fit with constrained inelasticity.
- 32 $J^P = 2^+$ preferred.
- 33 From fit neglecting nearby $f_2'(1525)$. Replaced by BLOOM 83.
- 34 Superseded by LONGACRE 86.



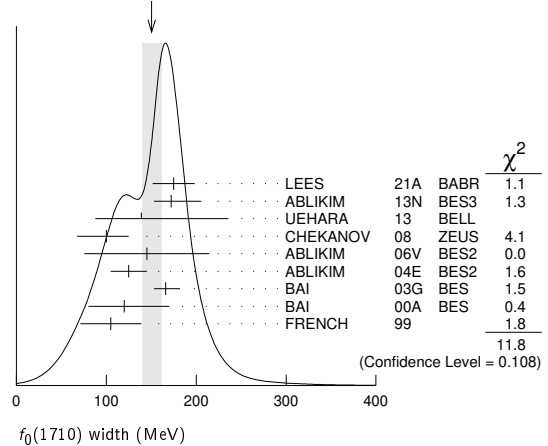
$f_0(1710)$ WIDTH

OUR EVALUATION below is based on T-matrix poles from BARBERIS 00E and BARBERIS 99d.

VALUE (MeV)	EVTS	DOCUMENT ID	TECN	COMMENT
123 ± 18				OUR EVALUATION
150 ± 12				OUR AVERAGE Error includes scale factor of 1.3. See the ideogram below.
175 ± 23 ± 4		1 LEES	21A BABR	$\eta_c(1S) \rightarrow \eta' K^+ K^-$
172 ± 10 $^{+32}_{-16}$	5.5k	2 ABLIKIM	13N BES3	$e^+ e^- \rightarrow J/\psi \rightarrow \gamma \eta \eta$
139 ± 11 $^{+96}_{-50}$		3 UEHARA	13 BELL	$\gamma \gamma \rightarrow K_S^0 K_S^0$
100 ± 24 $^{+7}_{-22}$	4k	4 CHEKANOV	08 ZEUS	$e p \rightarrow K_S^0 K_S^0 X$
145 ± 8 ± 69		1 ABLIKIM	06V BES2	$e^+ e^- \rightarrow J/\psi \rightarrow \gamma \pi^+ \pi^-$
125 ± 20		ABLIKIM	04E BES2	$J/\psi \rightarrow \omega K^+ K^-$
166 ± 5 $^{+15}_{-10}$		BAI	03G BES	$J/\psi \rightarrow \gamma K \bar{K}$
120 ± 50 $^{+40}_{-40}$		BAI	00A BES	$J/\psi \rightarrow \gamma(\pi^+ \pi^- \pi^+ \pi^-)$
105 ± 34		5 FRENCH	99	$300 p p \rightarrow p_f(K^+ K^-) p_S$
••• We do not use the following data for averages, fits, limits, etc. •••				
156 ± 12		6 RODAS	22 RVUE	$J/\psi(1S) \rightarrow \gamma(\pi \pi, K \bar{K})$
182 ± 19	7.2k	7 KHOLODENK.	21 VES	$29 \pi^- p \rightarrow n \omega \phi$
255 ± 25		8.9 SARANTSEV	21 RVUE	$J/\psi(1S) \rightarrow \gamma(\pi \pi, K \bar{K}, \eta \eta, \omega \phi)$
289.7 ± 5.0 $^{+32.6}_{-19.3}$		10 ALBRECHT	20 RVUE	$0.9 \bar{p} p \rightarrow \pi^0 \pi^0 \eta, \pi^0 \eta \eta, \pi^0 K^+ K^-$
95 ± 10 $^{+78}_{-82}$		ABLIKIM	13J BES3	$J/\psi \rightarrow \gamma \omega \phi$

105 ± 20 ± 28	11 ABLIKIM	06J BES2	$J/\psi \rightarrow \gamma \omega \phi$
148 ± 40 $^{+40}_{-30}$	AMSLER	06 CBAR	$1.64 \bar{p} p \rightarrow K^+ K^- \pi^0$
188 ± 13	80k 1,12 UMAN	06 E835	$5.2 \bar{p} p \rightarrow \eta \eta \pi^0$
250 ± 30	VLADIMIRSK...	06 SPEC	$40 \pi^- p \rightarrow K_S^0 K_S^0 n$
270 ± 60 $^{+60}_{-30}$	13 ABLIKIM	05 BES2	$J/\psi \rightarrow \phi \pi^+ \pi^-$
125 ± 25 $^{+10}_{-15}$	1 ABLIKIM	05Q BES2	$\psi(2S) \rightarrow \gamma \pi^+ \pi^- K^+ K^-$
260 ± 50	1 BINON	05 GAMS	$33 \pi^- p \rightarrow \eta \eta n$
144 ± 30	14,15 ANISOVICH	03 RVUE	
320 ± 50 $^{+50}_{-20}$	15,16 ANISOVICH	03 RVUE	
102 ± 26	TIKHOMIROV	03 SPEC	$40.0 \pi^- C \rightarrow K_S^0 K_S^0 K_L^0 X$
267 ± 44	3651 17 NICHITIU	02 OBLX	$0 \bar{p} p \rightarrow K^+ K^- \pi^+ \pi^- \pi^0$
120 ± 26	9 BARBERIS	00E SPEC	$450 p p \rightarrow p_f \eta \eta p_S$
220 ± 40	18,19 ANISOVICH	99B SPEC	$0.6-1.2 p \bar{p} \rightarrow \eta \eta \pi^0$
100 ± 25	BARBERIS	99 OMEG	$450 p p \rightarrow p_S p_f K^+ K^-$
160 ± 30	BARBERIS	99B OMEG	$450 p p \rightarrow p_S p_f \pi^+ \pi^-$
126 ± 16 ± 18	9,20 BARBERIS	99D OMEG	$450 p p \rightarrow K^+ K^-$
250 ± 140	21 ANISOVICH	98B RVUE	$\pi^+ \pi^-$ Compilation
30 ± 7	57 22 BARKOV	98	$\pi^- p \rightarrow K_S^0 K_S^0 n$
103 ± 18 $^{+30}_{-11}$	23 BAI	96C BES	$J/\psi \rightarrow \gamma K^+ K^-$
85 ± 24 $^{+22}_{-19}$	BAI	96C BES	$J/\psi \rightarrow \gamma K^+ K^-$
56 ± 19	BALOSHIN	95 SPEC	$40 \pi^- C \rightarrow K_S^0 K_S^0 X$
160 ± 40	24 BUGG	95 MRK3	$J/\psi \rightarrow \gamma \pi^+ \pi^- \pi^+ \pi^-$
160 ± 60 $^{+60}_{-20}$	23 BUGG	95 MRK3	$J/\psi \rightarrow \gamma \pi^+ \pi^- \pi^+ \pi^-$
264 ± 25	25 ARMSTRONG	93C E760	$\bar{p} p \rightarrow \pi^0 \eta \eta \rightarrow 6 \gamma$
200 to 300	BREAKSTONE	93 SFM	$p p \rightarrow p p \pi^+ \pi^- \pi^+ \pi^-$
< 80 90% CL	26 ALDE	92D GAM2	$38 \pi^- p \rightarrow \eta \eta N^*$
181 ± 30	27 ARMSTRONG	89D OMEG	$300 p p \rightarrow p p K^+ K^-$
104 ± 30	27 ARMSTRONG	89D OMEG	$300 p p \rightarrow p p K_S^0 K_S^0$
166.4 ± 33.2	25 AUGUSTIN	88 DM2	$J/\psi \rightarrow \gamma K^+ K^-, K_S^0 K_S^0$
30 ± 20	23 BOLONKIN	88 SPEC	$40 \pi^- p \rightarrow K_S^0 K_S^0 n$
350 ± 150	BOLONKIN	88 SPEC	$40 \pi^- p \rightarrow K_S^0 K_S^0 n$
148 ± 17	28 FALVARD	88 DM2	$J/\psi \rightarrow \phi K^+ K^-, K_S^0 K_S^0$
184 ± 6	29 FALVARD	88 DM2	$J/\psi \rightarrow \phi K^+ K^-, K_S^0 K_S^0$
136 ± 28	25 AUGUSTIN	87 DM2	$J/\psi \rightarrow \gamma \pi^+ \pi^-$
130 ± 20	23 BALTRUSAIT..	87 MRK3	$J/\psi \rightarrow \gamma K^+ K^-$
122 ± 74 $^{+74}_{-15}$	30 LONGACRE	86 RVUE	$22 \pi^- p \rightarrow n 2 K_S^0$
57 ± 38	31 WILLIAMS	84 MPFS	$200 \pi^- N \rightarrow 2 K_S^0 X$
160 ± 80	BLOOM	83 CBAL	$J/\psi \rightarrow \gamma 2 \eta$
200 ± 100	BURKE	82 MRK2	$J/\psi \rightarrow \gamma 2 p$
220 ± 100 $^{+100}_{-70}$	32,33 EDWARDS	82D CBAL	$J/\psi \rightarrow \gamma 2 \eta$
200 ± 156 $^{+156}_{-9}$	34 ETKIN	82B MPS	$23 \pi^- p \rightarrow n 2 K_S^0$

WEIGHTED AVERAGE



- 1 Breit-Wigner width.
- 2 From partial wave analysis including all possible combinations of $0^{++}, 2^{++}$, and 4^{++} resonances.
- 3 Spin 0 favored over spin 2.
- 4 In the SU(3) based model with a specific interference pattern of the $f_2(1270)$, $a_2(1320)$, and $f_2'(1525)$ mesons incoherently added to the $f_0(1710)$ and non-resonant background.
- 5 $J^P = 0^+$, superseded by ARMSTRONG 89D.

Meson Particle Listings

 $f_0(1710)$

- ⁶T-matrix pole from coupled channel K-matrix fit to data on $J/\psi \rightarrow \gamma \pi^0 \pi^0$ (ABLIKIM 15AE) and $J/\psi \rightarrow \gamma K_S^0 K_S^0$ (ABLIKIM 18AA).
- ⁷From partial wave analysis of $\omega \phi$ invariant mass including 0^{++} , 2^{++} , and 0^{-+} resonances.
- ⁸Close-by state with mass 1765 ± 15 MeV and width 180 ± 20 MeV.
- ⁹T-matrix pole.
- ¹⁰T-matrix pole, 5 poles, 5 channels, including scattering data from HYAMS 75 ($\pi\pi$), LONGACRE 86 ($K\bar{K}$), BINON 83 ($\eta\eta$), and BINON 84C ($\eta\eta'$).
- ¹¹Not seen by LIU 09 in $B^\pm \rightarrow K^\pm \omega \phi$.
- ¹²Systematic errors not estimated.
- ¹³This state may be different from $f_0(1710)$, see CLOSE 05.
- ¹⁴(Solution I)
- ¹⁵K-matrix pole, assuming $J^P = 0^+$, from combined analysis of $\pi^- p \rightarrow \pi^0 \pi^0 n$, $\pi^- p \rightarrow K\bar{K}n$, $\pi^+ \pi^- \rightarrow \pi^+ \pi^-$, $\bar{p} p \rightarrow \pi^0 \pi^0 \pi^0$, $\pi^0 \eta\eta$, $\pi^0 \pi^0 \eta$, $\pi^+ \pi^- \pi^0$, $K^+ K^- \pi^0$, $K_S^0 K_S^0 \pi^0$, $K^+ K_S^0 \pi^-$ at rest, $\bar{p} n \rightarrow \pi^- \pi^- \pi^+$, $K_S^0 K^- \pi^0$, $K_S^0 K_S^0 \pi^-$ at rest.
- ¹⁶Solution I.
- ¹⁷Decaying to $f_0(1370) \pi \pi$.
- ¹⁸ $J^P = 0^+$.
- ¹⁹Not seen by AMSLER 02.
- ²⁰Supersedes BARBERIS 99 and BARBERIS 99b.
- ²¹T-matrix pole, assuming $J^P = 0^+$
- ²²No J^{PC} determination.
- ²³ $J^P = 2^+$.
- ²⁴From a fit to the 0^+ partial wave.
- ²⁵No J^{PC} determination.
- ²⁶ALDE 92d combines all the GAMS-2000 data.
- ²⁷ $J^P = 2^+$, (0^+ excluded).
- ²⁸From an analysis ignoring interference with $f_2'(1525)$.
- ²⁹From an analysis including interference with $f_2'(1525)$.
- ³⁰Uses MRK3 data. From a partial-wave analysis of data using a K-matrix formalism with 5 poles, but assuming spin 2. Fit with constrained inelasticity.
- ³¹No J^{PC} determination.
- ³² $J^P = 2^+$ preferred.
- ³³From fit neglecting nearby $f_2'(1525)$. Replaced by BLOOM 83.
- ³⁴From an amplitude analysis of the $K_S^0 K_S^0$ system, superseded by LONGACRE 86.

 $f_0(1710)$ DECAY MODES

Mode	Fraction (Γ_i/Γ)
Γ_1 $K\bar{K}$	seen
Γ_2 $\eta\eta$	seen
Γ_3 $\pi\pi$	seen
Γ_4 $\gamma\gamma$	seen
Γ_5 $\omega\omega$	seen

 $f_0(1710)$ $\Gamma(i)\Gamma(\gamma\gamma)/\Gamma(\text{total})$

$\Gamma(K\bar{K}) \times \Gamma(\gamma\gamma)/\Gamma_{\text{total}}$	CL%	DOCUMENT ID	TECN	COMMENT	Γ_1/Γ
$12 \pm \frac{3+227}{8}$		UEHARA	13	BELL	$\gamma\gamma \rightarrow K_S^0 K_S^0$

• • • We do not use the following data for averages, fits, limits, etc. • • •

<480	95	ALBRECHT	90G	ARG	$\gamma\gamma \rightarrow K^+ K^-$
<110	95	1 BEHREND	89C	CELL	$\gamma\gamma \rightarrow K_S^0 K_S^0$
<280	95	1 ALTHOFF	85B	TASS	$\gamma\gamma \rightarrow K\bar{K}\pi$

¹ Assuming helicity 2.

$\Gamma(\pi\pi) \times \Gamma(\gamma\gamma)/\Gamma_{\text{total}}$	CL%	DOCUMENT ID	TECN	COMMENT	Γ_3/Γ
<0.82	95	1 BARATE	00E	ALEP	$\gamma\gamma \rightarrow \pi^+ \pi^-$

¹ Assuming spin 0.

 $f_0(1710)$ BRANCHING RATIOS

$\Gamma(K\bar{K})/\Gamma_{\text{total}}$	EVTS	DOCUMENT ID	TECN	COMMENT	Γ_1/Γ
• • • We do not use the following data for averages, fits, limits, etc. • • •					
seen	1004	1 DOBBS	15	$J/\psi \rightarrow \gamma K^+ K^-$	
seen	349	1 DOBBS	15	$\psi(2S) \rightarrow \gamma K^+ K^-$	
0.36 ± 0.12		ALBALADEJO	08	RVUE	
$0.36 \pm \frac{0.09}{-0.19}$		2 LONGACRE	86	MPS	$22 \pi^- p \rightarrow n 2K_S^0$

¹ Using CLEO-c data but not authored by the CLEO Collaboration.

² From a partial-wave analysis of data using a K-matrix formalism with 5 poles, but assuming spin 2. Fit with constrained inelasticity.

$\Gamma(\eta\eta)/\Gamma_{\text{total}}$	DOCUMENT ID	TECN	COMMENT	Γ_2/Γ
• • • We do not use the following data for averages, fits, limits, etc. • • •				
0.22 ± 0.12	ALBALADEJO	08	RVUE	
$0.18 \pm \frac{0.03}{-0.13}$	1 LONGACRE	86	RVUE	

¹ From a partial-wave analysis of data using a K-matrix formalism with 5 poles, but assuming spin 2. Fit with constrained inelasticity.

$\Gamma(\pi\pi)/\Gamma_{\text{total}}$	EVTS	DOCUMENT ID	TECN	COMMENT	Γ_3/Γ
• • • We do not use the following data for averages, fits, limits, etc. • • •					
seen	381	1 DOBBS	15	$J/\psi \rightarrow \gamma \pi^+ \pi^-$	
seen	237	1 DOBBS	15	$\psi(2S) \rightarrow \gamma \pi^+ \pi^-$	
not seen		AMSLER	02	CBAR	$0.9 \bar{p} p \rightarrow \pi^0 \eta\eta, \pi^0 \pi^0 \pi^0$
$0.039 \pm \frac{0.002}{-0.024}$		2 LONGACRE	86	RVUE	

¹ Using CLEO-c data but not authored by the CLEO Collaboration.

² From a partial-wave analysis of data using a K-matrix formalism with 5 poles, but assuming spin 2. Fit with constrained inelasticity.

$\Gamma(\pi\pi)/\Gamma(K\bar{K})$	CL%	DOCUMENT ID	TECN	COMMENT	Γ_3/Γ_1
0.23 ± 0.05	OUR AVERAGE	Error includes scale factor of 1.2.			
$0.64 \pm 0.27 \pm 0.18$		LEES	18A	BABR	$\Upsilon(1S) \rightarrow \gamma \pi^+ \pi^-, \gamma K^+ K^-$
$0.41 \pm \frac{0.11}{-0.17}$		ABLIKIM	06v	BES2	$e^+ e^- \rightarrow J/\psi \rightarrow \gamma \pi^+ \pi^-$
$0.2 \pm 0.024 \pm 0.036$		BARBERIS	99d	OMEG	$450 \rho\rho \rightarrow K^+ K^-, \pi^+ \pi^-$
0.39 ± 0.14		ARMSTRONG	91	OMEG	$300 \rho\rho \rightarrow \rho\rho\pi\pi, \rho\rho K\bar{K}$
• • • We do not use the following data for averages, fits, limits, etc. • • •					
0.32 ± 0.14		ALBALADEJO	08	RVUE	
< 0.11	95	1 ABLIKIM	04E	BES2	$J/\psi \rightarrow \omega K^+ K^-$
$5.8 \pm \frac{9.1}{-5.5}$		2 ANISOVICH	02d	SPEC	Combined fit

¹ Using data from ABLIKIM 04A.

² From a combined K-matrix analysis of Crystal Barrel ($0^- \rho\bar{p} \rightarrow \pi^0 \pi^0 \pi^0, \pi^0 \eta\eta, \pi^0 \pi^0 \eta$), GAMS ($\pi\rho \rightarrow \pi^0 \pi^0 n, \eta\eta n, \eta\eta' n$), and BNL ($\pi\rho \rightarrow K\bar{K}n$) data.

$\Gamma(\eta\eta)/\Gamma(K\bar{K})$	CL%	DOCUMENT ID	TECN	COMMENT	Γ_2/Γ_1
0.48 ± 0.15		BARBERIS	00E	450 $\rho\rho \rightarrow \rho_f \eta\eta \rho_s$	

• • • We do not use the following data for averages, fits, limits, etc. • • •

$0.46 \pm \frac{0.70}{-0.38}$		1 ANISOVICH	02d	SPEC	Combined fit
<0.02	90	2 PROKOSHKIN	91	GA24	$300 \pi^- p \rightarrow \pi^- \rho \eta\eta$
					$\pi^0 \pi^0 \eta$, GAMS ($\pi\rho \rightarrow \pi^0 \pi^0 n, \eta\eta n, \eta\eta' n$), and BNL ($\pi\rho \rightarrow K\bar{K}n$) data.
					² Combining results of GAM4 with those of ARMSTRONG 89d.

$\Gamma(\omega\omega)/\Gamma_{\text{total}}$	EVTS	DOCUMENT ID	TECN	COMMENT	Γ_5/Γ
seen	180	ABLIKIM	06H	BES	$J/\psi \rightarrow \gamma \omega\omega$

 $f_0(1710)$ REFERENCES

RODAS	22	EPJ C82 80	A. Rodas et al.	(JPAC Collab.)
KHOLODENK...	21	PAN 83 1602	M.S. Kholodenko	(VES Collab.)
LEES	21A	PR D104 072002	J.P. Lees et al.	(BABAR Collab.)
SARANTSEV	21	PL B816 136227	A.V. Sarantsev et al.	(BONN, PNPI)
ALBRECHT	20	EPJ C80 453	M. Albrecht et al.	(Crystal Barrel Collab.)
ABLIKIM	18AA	PR D98 072003	M. Ablikim et al.	(BESIII Collab.)
LEES	18A	D37 112006	J.P. Lees et al.	(BABAR Collab.)
ABLIKIM	15AE	PR D92 052003	M. Ablikim et al.	(BESIII Collab.)
DOBBS	15	PR D91 052006	S. Dobbs et al.	(NWES)
ABLIKIM	13J	PR D87 032008	M. Ablikim et al.	(BESIII Collab.)
ABLIKIM	13N	PR D87 032009	M. Ablikim et al.	(BESIII Collab.)
UEHARA	13	PTEP 2013 123C01	S. Uehara et al.	(BELLE Collab.)
LIU	09	PR D79 071102	C. Liu et al.	(BELLE Collab.)
ALBALADEJO	08	PRL 101 252002	M. Albaladejo, J.A. Oller	
CHEKANOV	08	PRL 101 112003	S. Chekanov et al.	(ZEUS Collab.)
ABLIKIM	06H	PR D73 112007	M. Ablikim et al.	(BES Collab.)
ABLIKIM	06J	PRL 96 162002	M. Ablikim et al.	(BES Collab.)
ABLIKIM	06V	PL B642 441	M. Ablikim et al.	(BES Collab.)
AMSLER	06	PL B639 165	C. Amshler et al.	(Crystal Barrel Collab.)
UMAN	06	PR D73 052009	I. Uman et al.	(FNAL E835)
VLADIMIRSK...	06	PAN 69 493	V.V. Vladimirov et al.	(ITEP, Moscow)
		Translated from YAF 69 515.		
ABLIKIM	05	PL B607 243	M. Ablikim et al.	(BES Collab.)
ABLIKIM	05Q	PR D72 092002	M. Ablikim et al.	(BES Collab.)
BINON	05	PAN 68 960	F. Binon et al.	
		Translated from YAF 68 998.		
CLOSE	05	PR D71 094022	F.E. Close, Q. Zhao	
ABLIKIM	04A	PL B598 149	M. Ablikim et al.	(BES Collab.)
ABLIKIM	04E	PL B603 138	M. Ablikim et al.	(BES Collab.)
ANISOVICH	03	EPJ A16 229	V.V. Anisovich et al.	
BAI	03G	PR D68 052003	J.Z. Bai et al.	(BES Collab.)
TIKHOMIROV	03	PAN 66 828	G.D. Tikhomirov et al.	
		Translated from YAF 66 860.		
AMSLER	02	EPJ C23 29	C. Amshler et al.	
ANISOVICH	02D	PAN 65 1545	V.V. Anisovich et al.	
		Translated from YAF 65 1583.		
NICHTIU	02	PL B545 261	F. Nichtiu et al.	(OBELIX Collab.)
BAI	00A	PL B472 207	J.Z. Bai et al.	(BES Collab.)
BARATE	00E	PL B472 189	R. Barate et al.	(ALEPH Collab.)
BARBERIS	00E	PL B479 59	D. Barberis et al.	(WA 102 Collab.)
ANISOVICH	99B	PL B449 154	A.V. Anisovich et al.	
BARBERIS	99	PL B453 305	D. Barberis et al.	(Omega Expt.)
BARBERIS	99B	PL B453 316	D. Barberis et al.	(Omega Expt.)
BARBERIS	99D	PL B462 462	D. Barberis et al.	(Omega Expt.)
FRENCH	99	PL B460 213	B. French et al.	(WAT6 Collab.)
ANISOVICH	98B	SFU 41 419	V.V. Anisovich et al.	
		Translated from UFN 168 481.		
BAI	98H	PRL 81 1179	J.Z. Bai et al.	(BES Collab.)
BARKOV	98	JETPL 68 764	B.P. Barkov et al.	
ABREU	96C	PL B379 309	P. Abreu et al.	(DELPHI Collab.)
BAI	96C	PRL 77 3959	J.Z. Bai et al.	(BES Collab.)
BALOSHIN	95	PAN 58 46	O.N. Baloshin et al.	(ITEP)
		Translated from YAF 58 50.		

See key on page 1127

Meson Particle Listings
 $f_0(1710)$, $X(1750)$, $\eta(1760)$

BUGG 95	PL B353 378	D.V. Bugg <i>et al.</i>	(LOQM, PNPI, WASH)
ARMSTRONG 93C	PL B307 394	T.A. Armstrong <i>et al.</i>	(FNAL, FERR, GENO+)
BREAKSTONE 93	ZPHY C58 251	A.M. Breakstone <i>et al.</i>	(IOWA, CERN, DORT+)
ALDE 92D	PL B284 457	D.M. Alde <i>et al.</i>	(GAM2 Collab.)
Also	SJNP 54 451	D.M. Alde <i>et al.</i>	(GAM2 Collab.)
ARMSTRONG 91	ZPHY C51 351	T.A. Armstrong <i>et al.</i>	(ATHU, BARI, BIRM+)
PROKOSHKIN 91	SPD 36 155	Y.D. Prokoshkin	(GAM2 and GAM4 Collab.)
ALBRECHT 90G	ZPHY C48 183	H. Albrecht <i>et al.</i>	(ARGUS Collab.)
ARMSTRONG 89D	PL B227 186	T.A. Armstrong, M. Benayoun	(ATHU, BARI, BIRM+)
BEHREND 89C	ZPHY C43 91	H.J. Behrend <i>et al.</i>	(CELLO Collab.)
AUGUSTIN 88	PRL 60 2238	J.E. Augustin <i>et al.</i>	(DM2 Collab.)
BOLONKIN 88	NP B309 426	B.V. Bolonkin <i>et al.</i>	(ITEP, SERP)
FALVARD 88	PR D38 2706	A. Falvard <i>et al.</i>	(CLER, FRAS, LALO+)
AUGUSTIN 87	ZPHY C36 369	J.E. Augustin <i>et al.</i>	(LALO, CLER, FRAS+)
BALTRUSAITIS 87	PR D35 2077	R.M. Baltrusaitis <i>et al.</i>	(Mark III Collab.)
ALDE 86C	PL B182 105	D.M. Alde <i>et al.</i>	(SERP, BELG, LAML, LAPP)
LONGACRE 86	PL B177 223	R.S. Longacre <i>et al.</i>	(BNL, BRAN, CUNY+)
ALTHOFF 85B	ZPHY C29 189	M. Althoff <i>et al.</i>	(TASSO Collab.)
BINON 84C	NC 80A 363	F.G. Binon <i>et al.</i>	(BELG, LAPP, SERP+)
WILLIAMS 84	PR D30 877	E.G.H. Williams <i>et al.</i>	(VAND, NDAM, TUFTS+)
BINON 83	NC 78A 313	F.G. Binon <i>et al.</i>	(BELG, LAPP, SERP+)
BLOOM 83	ARNS 33 143	E.D. Bloom, C. Peck	(SLAC, CIT)
BURKE 82	PRL 49 632	D.L. Burke <i>et al.</i>	(LBL, SLAC)
EDWARDS 82D	PRL 48 458	C. Edwards <i>et al.</i>	(CIT, HARV, PRIN+)
ETKIN 82B	PR D25 1786	A. Etkin <i>et al.</i>	(BNL, CUNY, TUFTS, VAND)
ETKIN 82C	PR D25 2446	A. Etkin <i>et al.</i>	(BNL, CUNY, TUFTS, VAND)
HYAMS 75	NP B100 205	B.D. Hyams <i>et al.</i>	(CERN, MPIM)

$X(1750)$

$I^G(J^{PC}) = ?^-(1^{--})$

OMITTED FROM SUMMARY TABLE

The $X(1750)$ was separated from the $\phi(1680)$ in the 2022 listings due to its incompatible mass and incompatible pattern of $\bar{K}K$ and $\bar{K}^*(892)K$ branching fractions.

$X(1750)$ MASS

VALUE (MeV)	DOCUMENT ID	TECN	COMMENT
1753.8 ± 2.7 OUR AVERAGE			
1784 ± 12 ± 0	ABLIKIM	20F BES3	$\psi(2S) \rightarrow K^+ K^- \eta$
1753.5 ± 1.5 ± 2.3	LINK	02K FOCUS	20-160 $\gamma p \rightarrow K^+ K^- p$
• • • We do not use the following data for averages, fits, limits, etc. • • •			
1726 ± 22	BUSENITZ	89 TPS	$\gamma p \rightarrow K^+ K^- X$
1760 ± 20	ATKINSON	85c OMEG	20-70 $\gamma p \rightarrow K \bar{K} X$
1690 ± 10	ASTON	81F OMEG	25-70 $\gamma p \rightarrow K^+ K^- X$

$X(1750)$ WIDTH

VALUE (MeV)	DOCUMENT ID	TECN	COMMENT
120 ± 10 OUR AVERAGE			
106 +22 +8	ABLIKIM	20F BES3	$\psi(2S) \rightarrow K^+ K^- \eta$
-19 -36			
122.2 ± 6.2 ± 8.0	LINK	02K FOCUS	20-160 $\gamma p \rightarrow K^+ K^- p$
• • • We do not use the following data for averages, fits, limits, etc. • • •			
121 ± 47	BUSENITZ	89 TPS	$\gamma p \rightarrow K^+ K^- X$
80 ± 40	ATKINSON	85c OMEG	20-70 $\gamma p \rightarrow K \bar{K} X$
100 ± 40	ASTON	81F OMEG	25-70 $\gamma p \rightarrow K^+ K^- X$

$X(1750)$ DECAY MODES

Mode	Fraction (Γ_i/Γ)
Γ_1 $K^+ K^-$	seen
Γ_2 $\bar{K}^*(892)^0 K_S^0$	not seen
Γ_3 $K^*(892)^\pm K^\mp$	not seen

$\Gamma(\bar{K}^*(892)^0 K_S^0)/\Gamma(K^+ K^-)$		Γ_2/Γ_1
VALUE	CL%	DOCUMENT ID
<0.065	90	LINK 02K FOCUS
		$\gamma p \rightarrow K^+ K^- p$

$\Gamma(K^*(892)^\pm K^\mp)/\Gamma(K^+ K^-)$		Γ_3/Γ_1
VALUE	CL%	DOCUMENT ID
<0.183	90	LINK 02K FOCUS
		$\gamma p \rightarrow K^+ K^- p$

$X(1750)$ REFERENCES

ABLIKIM 20F	PR D101 032008	M. Ablikim <i>et al.</i>	(BESIII Collab.)
LINK 02K	PL B545 50	J.M. Link <i>et al.</i>	(FNAL FOCUS Collab.)
BUSENITZ 89	PR D40 1	J.K. Busewitz <i>et al.</i>	(ILL, FNAL)
ATKINSON 85C	ZPHY C27 233	M. Atkinson <i>et al.</i>	(BONN, CERN, GLAS+)
ASTON 81F	PL 104B 231	D. Aston	(BONN, CERN, EPOL, GLAS, LAN-C+)

$\eta(1760)$

$I^G(J^{PC}) = 0^+(0^{-+})$

OMITTED FROM SUMMARY TABLE

Seen by DM2 in the $\rho\rho$ system (BISELLO 89B). Structure in this region has been reported before in the same system (BALTRUSAITIS 86B) and in the $\omega\omega$ system (BALTRUSAITIS 85C, BISELLO 87).

$\eta(1760)$ MASS

VALUE (MeV)	EVTS	DOCUMENT ID	TECN	COMMENT
1751 ± 15 OUR AVERAGE				
1768 +24 +10	465	¹ ZHANG	12A BELL	$e^+ e^- \rightarrow e^+ e^- \eta' \pi^+ \pi^-$
-25				
1744 ± 10 ± 15	1045	² ABLIKIM	06H BES	$J/\psi \rightarrow \gamma \omega \omega$
• • • We do not use the following data for averages, fits, limits, etc. • • •				
1703 +12 +11	2	³ ZHANG	12A BELL	$e^+ e^- \rightarrow e^+ e^- \eta' \pi^+ \pi^-$
-11				
1760 ± 11	320	⁴ BISELLO	89B DM2	$J/\psi \rightarrow 4\pi \gamma$
¹ From a single-resonance fit.				
² From a partial wave analysis including $\eta(1760)$, $f_0(1710)$, $f_2(1640)$, and $f_2(1910)$.				
³ From a two-resonance fit.				
⁴ Estimated by us from various fits. Systematic uncertainties not estimated.				

$\eta(1760)$ WIDTH

VALUE (MeV)	EVTS	DOCUMENT ID	TECN	COMMENT
240 ± 30 OUR AVERAGE				
224 +62 +25	465	⁵ ZHANG	12A BELL	$e^+ e^- \rightarrow e^+ e^- \eta' \pi^+ \pi^-$
-56				
244 +24 +25	1045	⁶ ABLIKIM	06H BES	$J/\psi \rightarrow \gamma \omega \omega$
-21				
• • • We do not use the following data for averages, fits, limits, etc. • • •				
42 +36 +15		⁷ ZHANG	12A BELL	$e^+ e^- \rightarrow e^+ e^- \eta' \pi^+ \pi^-$
-22				
60 ± 16	320	⁸ BISELLO	89B DM2	$J/\psi \rightarrow 4\pi \gamma$
⁵ From a single-resonance fit.				
⁶ From a partial wave analysis including $\eta(1760)$, $f_0(1710)$, $f_2(1640)$, and $f_2(1910)$.				
⁷ From a two-resonance fit.				
⁸ Estimated by us from various fits. Systematic uncertainties not estimated.				

$\eta(1760)$ DECAY MODES

Mode	Fraction (Γ_i/Γ)
Γ_1 4π	
Γ_2 $2\pi^+ 2\pi^-$	seen
Γ_3 $\pi^+ \pi^- 2\pi^0$	seen
Γ_4 $\rho^0 \rho^0$	seen
Γ_5 $\rho^+ \rho^-$	seen
Γ_6 $\omega\omega$	seen
Γ_7 $\eta' \pi^+ \pi^-$	seen
Γ_8 $\gamma\gamma$	seen

$\eta(1760)$ $\Gamma(i)\Gamma(\gamma\gamma)/\Gamma(\text{total})$

$\Gamma(\eta' \pi^+ \pi^-) \times \Gamma(\gamma\gamma)/\Gamma_{\text{total}}$		$\Gamma_7 \Gamma_8/\Gamma$
VALUE (eV)	EVTS	DOCUMENT ID
28.2 ± 7.9 ± 3.7	465	⁹ ZHANG
		12A BELL
		$e^+ e^- \rightarrow e^+ e^- \eta' \pi^+ \pi^-$
• • • We do not use the following data for averages, fits, limits, etc. • • •		
3.0 ± 2.0 ± 0.8	52	¹⁰ ZHANG
		12A BELL
		$e^+ e^- \rightarrow e^+ e^- \eta' \pi^+ \pi^-$
18 +13 +5	315	¹¹ ZHANG
-10		12A BELL
		$e^+ e^- \rightarrow e^+ e^- \eta' \pi^+ \pi^-$
⁹ From a single-resonance fit.		
¹⁰ From a two-resonance fit. For constructive interference with the $X(1835)$.		
¹¹ From a two-resonance fit. For destructive interference with the $X(1835)$.		

$\eta(1760)$ BRANCHING RATIOS

$\Gamma(2\pi^+ 2\pi^-)/\Gamma_{\text{total}}$		Γ_2/Γ
VALUE	DOCUMENT ID	TECN
seen	BISELLO	89B DM2
		$J/\psi \rightarrow \gamma 2\pi^+ 2\pi^-$

$\Gamma(\pi^+ \pi^- 2\pi^0)/\Gamma_{\text{total}}$		Γ_3/Γ
VALUE	DOCUMENT ID	TECN
seen	BISELLO	89B DM2
		$J/\psi \rightarrow \gamma \pi^+ \pi^- 2\pi^0$

Meson Particle Listings

$\eta(1760), \pi(1800)$

$\Gamma(\rho^0\rho^0)/\Gamma_{\text{total}}$			Γ_4/Γ				
VALUE	DOCUMENT ID	TECN	COMMENT	VALUE	DOCUMENT ID	TECN	COMMENT
seen	BISELLO	89B	DM2	$J/\psi \rightarrow \gamma\rho^0\rho^0$			
seen	BALTRUSAIT...86	MRK3		$J/\psi \rightarrow \gamma\rho^0\rho^0$			

$\Gamma(\rho^+\rho^-)/\Gamma_{\text{total}}$			Γ_5/Γ				
VALUE	DOCUMENT ID	TECN	COMMENT	VALUE	DOCUMENT ID	TECN	COMMENT
seen	BISELLO	89B	DM2	$J/\psi \rightarrow \gamma\rho^+\rho^-$			
seen	BALTRUSAIT...86	MRK3		$J/\psi \rightarrow \gamma\rho^+\rho^-$			

$\Gamma(\omega\omega)/\Gamma_{\text{total}}$			Γ_6/Γ				
VALUE	DOCUMENT ID	TECN	COMMENT	VALUE	DOCUMENT ID	TECN	COMMENT
seen	BISELLO	87	DM2	$J/\psi \rightarrow \omega\omega$			
seen	BALTRUSAIT...85C	MRK3		$J/\psi \rightarrow \gamma\omega\omega$			

$\Gamma(\gamma\gamma)/\Gamma(\omega\omega)$			Γ_8/Γ_6					
VALUE	CL%	DOCUMENT ID	TECN	COMMENT	VALUE	DOCUMENT ID	TECN	COMMENT
$<2.48 \times 10^{-3}$	90	12 ABLIKIM	180	BES3	$\psi(2S) \rightarrow \pi^+\pi^-\gamma\gamma\gamma$			

¹²Using results from ABLIKIM 06H.

$\eta(1760)$ REFERENCES

ABLIKIM	180	PR D97 072014	M. Ablikim et al.	(BESIII Collab.)
ZHANG	12A	PR D86 052002	C.C. Zhang et al.	(BELLE Collab.)
ABLIKIM	06H	PR D73 112007	M. Ablikim et al.	(BES Collab.)
BISELLO	89B	PR D39 701	G. Busetto et al.	(DM2 Collab.)
BISELLO	87	PL B192 239	D. Bisello et al.	(PADO, CLER, FRAS+)
BALTRUSAIT...86	PR D33 629	R.M. Baltrusaitis et al.	(Mark III Collab.)	
BALTRUSAIT...86B	PR D33 1222	R.M. Baltrusaitis et al.	(Mark III Collab.)	
BALTRUSAIT...85C	PRL 55 1723	R.M. Baltrusaitis et al.	(CIT, UCSC+)	

$\pi(1800)$

$$J^{PC} = 1^-(0^-+)$$

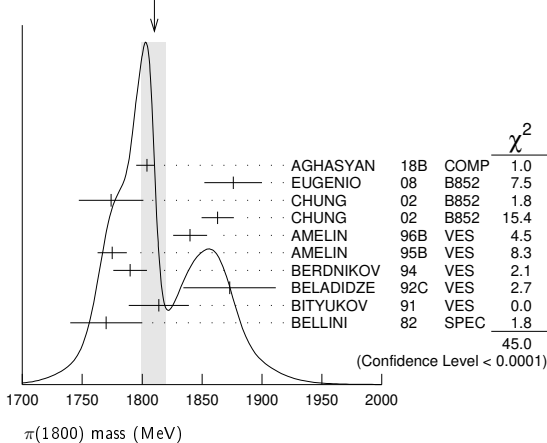
See the review on "Non- $q\bar{q}$ Mesons."

$\pi(1800)$ MASS

VALUE (MeV)	EVTS	DOCUMENT ID	TECN	CHG	COMMENT
1810^{+9}_{-11}	OUR AVERAGE	Error includes scale factor of 2.2. See the ideogram below.			
1804^{+6}_{-9}	46M	1 AGHASYAN	18B	COMP	$190 \pi^- p \rightarrow \pi^- \pi^+ \pi^- p$
$1876 \pm 18 \pm 16$	4k	2 EUGENIO	08	B852	$18 \pi^- p \rightarrow \eta\eta\pi^- p$
$1774 \pm 18 \pm 20$		3 CHUNG	02	B852	$18.3 \pi^- p \rightarrow \pi^+ \pi^- \pi^- p$
$1863 \pm 9 \pm 10$		4 CHUNG	02	B852	$18.3 \pi^- p \rightarrow \pi^+ \pi^- \pi^- p$
$1840 \pm 10 \pm 10$	1.2k	AMELIN	96B	VES	$37 \pi^- A \rightarrow \eta\eta\pi^- A$
$1775 \pm 7 \pm 10$		5 AMELIN	95B	VES	$36 \pi^- A \rightarrow \pi^+ \pi^- \pi^- A$
1790 ± 14		6 BERDNIKOV	94	VES	$37 \pi^- A \rightarrow K^+ K^- \pi^- A$
$1873 \pm 33 \pm 20$		BELADIDZE	92C	VES	$36 \pi^- \text{Be} \rightarrow \pi^- \eta' \eta \text{Be}$
$1814 \pm 10 \pm 23$	426	BITYUKOV	91	VES	$36 \pi^- C \rightarrow \pi^- \eta\eta C$
1770 ± 30	1.1k	BELLINI	82	SPEC	$40 \pi^- A \rightarrow 3\pi A$
$1785 \pm 9^{+12}_{-6}$	420k	7 ALEKSEEV	10	COMP	$190 \pi^- Pb \rightarrow \pi^- \pi^- \pi^+ Pb'$
$1737 \pm 5 \pm 15$		AMELIN	99	VES	$37 \pi^- A \rightarrow \omega \pi^- \pi^0 A^*$

• • • We do not use the following data for averages, fits, limits, etc. • • •

WEIGHTED AVERAGE
1810+9-11 (Error scaled by 2.2)



- Statistical error negligible.
- From a single-pole fit.
- In the $f_0(980)$ π wave.
- In the $f_0(500)$ π wave.
- From a fit to $J^{PC} = 0^- + f_0(980)\pi, f_0(1370)\pi$ waves.
- From a fit to $J^{PC} = 0^- + K_0^*(1430)K^-$ and $f_0(980)\pi^-$ waves.
- Superseded by AGHASYAN 2018B.

$\pi(1800)$ WIDTH

VALUE (MeV)	EVTS	DOCUMENT ID	TECN	CHG	COMMENT
215^{+8}_{-11}	OUR AVERAGE				
220^{+8}_{-11}	46M	8 AGHASYAN	18B	COMP	$190 \pi^- p \rightarrow \pi^- \pi^+ \pi^- p$
$221 \pm 26 \pm 38$	4k	9 EUGENIO	08	B852	$18 \pi^- p \rightarrow \eta\eta\pi^- p$
$223 \pm 48 \pm 50$		10 CHUNG	02	B852	$18.3 \pi^- p \rightarrow \pi^+ \pi^- \pi^- p$
$191 \pm 21 \pm 20$		11 CHUNG	02	B852	$18.3 \pi^- p \rightarrow \pi^+ \pi^- \pi^- p$
$210 \pm 30 \pm 30$	1.2k	AMELIN	96B	VES	$37 \pi^- A \rightarrow \eta\eta\pi^- A$
$190 \pm 15 \pm 15$		12 AMELIN	95B	VES	$36 \pi^- A \rightarrow \pi^+ \pi^- \pi^- A$
210 ± 70		13 BERDNIKOV	94	VES	$37 \pi^- A \rightarrow K^+ K^- \pi^- A$
$225 \pm 35 \pm 20$		BELADIDZE	92C	VES	$36 \pi^- \text{Be} \rightarrow \pi^- \eta' \eta \text{Be}$
$205 \pm 18 \pm 32$	426	BITYUKOV	91	VES	$36 \pi^- C \rightarrow \pi^- \eta\eta C$
310 ± 50	1.1k	BELLINI	82	SPEC	$40 \pi^- A \rightarrow 3\pi A$
$208 \pm 22^{+21}_{-37}$	420k	14 ALEKSEEV	10	COMP	$190 \pi^- Pb \rightarrow \pi^- \pi^- \pi^+ Pb'$
$259 \pm 19 \pm 6$		AMELIN	99	VES	$37 \pi^- A \rightarrow \omega \pi^- \pi^0 A^*$

• • • We do not use the following data for averages, fits, limits, etc. • • •

- Statistical error negligible.
- From a single-pole fit.
- In the $f_0(980)$ π wave.
- In the $f_0(500)$ π wave.
- From a fit to $J^{PC} = 0^- + f_0(980)\pi, f_0(1370)\pi$ waves.
- From a fit to $J^{PC} = 0^- + K_0^*(1430)K^-$ and $f_0(980)\pi^-$ waves.
- Superseded by AGHASYAN 2018B.

$\pi(1800)$ DECAY MODES

Mode	Fraction (Γ_i/Γ)
Γ_1 $\pi^+\pi^-\pi^-$	seen
Γ_2 $f_0(500)\pi^-$	seen
Γ_3 $f_0(980)\pi^-$	seen
Γ_4 $f_0(1370)\pi^-$	seen
Γ_5 $f_0(1500)\pi^-$	not seen
Γ_6 $\rho\pi^-$	not seen
Γ_7 $\eta\eta\pi^-$	seen
Γ_8 $a_0(980)\eta$	seen
Γ_9 $a_2(1320)\eta$	not seen
Γ_{10} $f_2(1270)\pi$	not seen
Γ_{11} $f_0(1370)\pi^-$	not seen
Γ_{12} $f_0(1500)\pi^-$	seen
Γ_{13} $\eta\eta'(958)\pi^-$	seen
Γ_{14} $K_0^*(1430)K^-$	seen
Γ_{15} $K^*(892)K^-$	not seen

$\pi(1800)$ BRANCHING RATIOS

$\Gamma(f_0(980)\pi^-)/\Gamma(f_0(500)\pi^-)$			Γ_3/Γ_2				
VALUE	DOCUMENT ID	TECN	COMMENT	VALUE	DOCUMENT ID	TECN	COMMENT
$0.44 \pm 0.08 \pm 0.38$	15 CHUNG	02	B852	$18.3 \pi^- p \rightarrow \pi^+ \pi^- \pi^- p$			

$\Gamma(f_0(980)\pi^-)/\Gamma(f_0(1370)\pi^-)$			Γ_3/Γ_4					
VALUE	DOCUMENT ID	TECN	CHG	COMMENT	VALUE	DOCUMENT ID	TECN	COMMENT
1.7 ± 1.3	16 AMELIN	95B	VES	$36 \pi^- A \rightarrow \pi^+ \pi^- \pi^- A$				

• • • We do not use the following data for averages, fits, limits, etc. • • •

$\Gamma(f_0(1370)\pi^-)/\Gamma_{\text{total}}$			Γ_4/Γ					
VALUE	DOCUMENT ID	TECN	CHG	COMMENT	VALUE	DOCUMENT ID	TECN	COMMENT
seen	BELLINI	82	SPEC	$40 \pi^- A \rightarrow 3\pi A$				

$\Gamma(f_0(1500)\pi^-)/\Gamma_{\text{total}}$			Γ_5/Γ				
VALUE	DOCUMENT ID	TECN	COMMENT	VALUE	DOCUMENT ID	TECN	COMMENT
not seen	CHUNG	02	B852	$18.3 \pi^- p \rightarrow \pi^+ \pi^- \pi^- p$			

$\Gamma(\rho\pi^-)/\Gamma_{\text{total}}$			Γ_6/Γ					
VALUE	DOCUMENT ID	TECN	CHG	COMMENT	VALUE	DOCUMENT ID	TECN	COMMENT
not seen	BELLINI	82	SPEC	$40 \pi^- A \rightarrow 3\pi A$				

See key on page 1127

Meson Particle Listings

$\pi(1800)$, $f_2(1810)$

$\Gamma(\rho\pi^-)/\Gamma(f_0(980)\pi^-)$ Γ_6/Γ_3

VALUE	CL%	DOCUMENT ID	TECN	CHG	COMMENT
••• We do not use the following data for averages, fits, limits, etc. •••					
<0.25		CHUNG 02	B852		18.3 $\pi^- p \rightarrow \pi^+ \pi^- \pi^- p$
<0.14	90	AMELIN 95B	VES	-	36 $\pi^- A \rightarrow \pi^+ \pi^- \pi^- A$

$\Gamma(\eta\eta\pi^-)/\Gamma(\pi^+ \pi^- \pi^-)$ Γ_7/Γ_1

VALUE	EVTS	DOCUMENT ID	TECN	CHG	COMMENT
••• We do not use the following data for averages, fits, limits, etc. •••					
0.5 ± 0.1	1200	16 AMELIN	96B	VES	- 37 $\pi^- A \rightarrow \eta\eta\pi^- A$

$\Gamma(a_2(1320)\eta)/\Gamma_{total}$ Γ_9/Γ

VALUE	DOCUMENT ID	TECN	COMMENT
not seen	EUGENIO 08	B852	18 $\pi^- p \rightarrow \eta\eta\pi^- p$

$\Gamma(f_2(1270)\pi)/\Gamma_{total}$ Γ_{10}/Γ

VALUE	DOCUMENT ID	TECN	COMMENT
not seen	EUGENIO 08	B852	18 $\pi^- p \rightarrow \eta\eta\pi^- p$

$\Gamma(f_0(1370)\pi^-)/\Gamma_{total}$ Γ_{11}/Γ

VALUE	DOCUMENT ID	TECN	COMMENT
not seen	EUGENIO 08	B852	18 $\pi^- p \rightarrow \eta\eta\pi^- p$

$\Gamma(f_0(1500)\pi^-)/\Gamma(a_0(980)\eta)$ Γ_{12}/Γ_8

VALUE	EVTS	DOCUMENT ID	TECN	CHG	COMMENT
••• We do not use the following data for averages, fits, limits, etc. •••					
0.48 ± 0.17	4k	16,17 EUGENIO 08	B852	-	18 $\pi^- p \rightarrow \eta\eta\pi^- p$
0.030 ± 0.014		16 ANISOVICH 01B	SPEC	0	0.6-1.94 $p\bar{p} \rightarrow \eta\eta\pi^0\pi^0$
-0.011					
0.08 ± 0.03	1200	16,18 AMELIN	96B	VES	- 37 $\pi^- A \rightarrow \eta\eta\pi^- A$

$\Gamma(\eta\eta(958)\pi^-)/\Gamma(\eta\eta\pi^-)$ Γ_{13}/Γ_7

VALUE	EVTS	DOCUMENT ID	TECN	CHG	COMMENT
••• We do not use the following data for averages, fits, limits, etc. •••					
0.29 ± 0.07		16 BELADIDZE 92C	VES	-	36 $\pi^- Be \rightarrow \pi^- \eta' Be$
0.3 ± 0.1	426 ± 57	16 BITYUKOV 91	VES	-	36 $\pi^- C \rightarrow \pi^- \eta\eta C$

$\Gamma(K_0^*(1430)K^-)/\Gamma_{total}$ Γ_{14}/Γ

VALUE	DOCUMENT ID	TECN	CHG	COMMENT
seen	BERDNIKOV 94	VES	-	37 $\pi^- A \rightarrow K^+ K^- \pi^- A$

$\Gamma(K^*(892)K^-)/\Gamma_{total}$ Γ_{15}/Γ

VALUE	DOCUMENT ID	TECN	CHG	COMMENT
not seen	BERDNIKOV 94	VES	-	37 $\pi^- A \rightarrow K^+ K^- \pi^- A$

15 Assuming that $f_0(980)$ decays only to $\pi\pi$.
 16 Systematic errors not estimated.
 17 From a single-pole fit.
 18 Assuming that $f_0(1500)$ decays only to $\eta\eta$ and $a_0(980)$ decays only to $\eta\pi$.

$\pi(1800)$ REFERENCES

Author	Year	PR	Doc ID	TECN	CHG	COMMENT
AGHASYAN	18B	PR D98 092003	M. Aghasyan et al.	(COMPASS Collab.)		
ALEKSEEV	10	PRL 104 241803	M. G. Alekseev et al.	(COMPASS Collab.)		
EUGENIO	08	PL B660 466	P. Eugenio et al.	(BNL E852 Collab.)		
CHUNG	02	PR D55 072001	S.U. Chung et al.	(BNL E852 Collab.)		
ANISOVICH	01B	PL B500 222	A.V. Anisovich et al.	(BNL E852 Collab.)		
AMELIN	99	PAN 62 445	D.V. Amelin et al.	(VES Collab.)		
AMELIN	96B	PAN 59 976	D.V. Amelin et al.	(SERP, TBIL)IGJPC		
AMELIN	95B	PL B356 595	D.V. Amelin et al.	(SERP, TBIL)		
BERDNIKOV	94	PL B337 219	E.B. Berdnikov et al.	(SERP, TBIL)		
BELADIDZE	92C	SJNP 55 1535	G.M. Beladidze, S.I. Bityukov, G.V. Borisov	(SERP+)		
BITYUKOV	91	PL B268 137	S.I. Bityukov et al.	(SERP, TBIL)		
BELLINI	82	PRL 48 1697	G. Bellini et al.	(MILA, BGNA, JINR)		

$f_2(1810)$

$$J^{PC} = 0^+(2^{++})$$

OMITTED FROM SUMMARY TABLE
Needs confirmation.

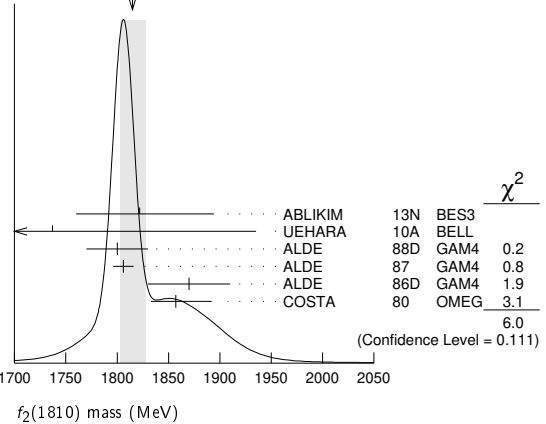
$f_2(1810)$ MASS

VALUE (MeV)	EVTS	DOCUMENT ID	TECN	COMMENT
1815 ± 12	OUR AVERAGE	Error includes scale factor of 1.4. See the ideogram below.		
1822 +29 -24	+66 -57	5.5k	1 ABLIKIM	13N BES3 $e^+e^- \rightarrow J/\psi \rightarrow \gamma\eta\eta$
1737 ± 9	+198 -65		2 UEHARA	10A BELL $10.6 e^+e^- \rightarrow e^+e^- \eta\eta$
1800 ± 30	40		ALDE	88D GAM4 $300 \pi^- p \rightarrow \pi^- p 4\pi^0$
1806 ± 10	1600		ALDE	87 GAM4 $100 \pi^- p \rightarrow 4\pi^0 n$
1870 ± 40			3 ALDE	86D GAM4 $100 \pi^- p \rightarrow \eta\eta n$
1857 +35 -24			4 COSTA	80 OMEG $10 \pi^- p \rightarrow K^+ K^- n$

••• We do not use the following data for averages, fits, limits, etc. •••

1845.0 ± 2.2 ± 1.6 - 7.2			5 ALBRECHT	20 RVUE	0.9 $\bar{p}p \rightarrow \pi^0 \pi^0 \eta, \pi^0 \eta\eta, \pi^0 K^+ K^-$
1858 +18 -71			6 LONGACRE	86 RVUE	Compilation
1799 ± 15			7 CASON	82 STRC	$8 \pi^+ p \rightarrow \Delta^{++} \pi^0 \pi^0$

WEIGHTED AVERAGE
1815±12 (Error scaled by 1.4)

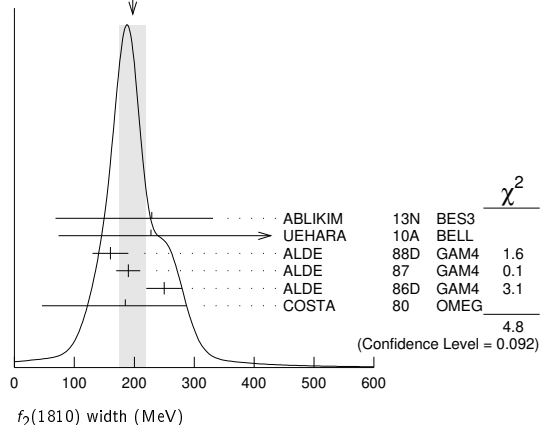


- From partial wave analysis including all possible combinations of 0^{++} , 2^{++} , and 4^{++} resonances.
- Breit-Wigner mass. Could also be the $f_2(1910)$.
- Seen in only one solution.
- Error increased by spread of two solutions. Included in LONGACRE 86 global analysis.
- T-matrix pole, 4 poles, 4 channels, including scattering data from HYAMS 75 ($\pi\pi$), LONGACRE 86 ($K\bar{K}$), BINON 83 ($\eta\eta$).
- From a partial-wave analysis of data using a K-matrix formalism with 5 poles. Includes compilation of several other experiments.
- From an amplitude analysis of the reaction $\pi^+ \pi^- \rightarrow 2\pi^0$. The resonance in the $2\pi^0$ final state is not confirmed by PROKOSHIN 97.

$f_2(1810)$ WIDTH

VALUE (MeV)	EVTS	DOCUMENT ID	TECN	COMMENT	
197 ± 22	OUR AVERAGE	Error includes scale factor of 1.5. See the ideogram below.			
229 + 52 - 42	+ 88 - 155	5.5k	1 ABLIKIM	13N BES3 $e^+e^- \rightarrow J/\psi \rightarrow \gamma\eta\eta$	
228 + 21 - 20	+ 234 - 153		2 UEHARA	10A BELL $10.6 e^+e^- \rightarrow e^+e^- \eta\eta$	
160 ± 30	40		ALDE	88D GAM4 $300 \pi^- p \rightarrow \pi^- p 4\pi^0$	
190 ± 20	1600		ALDE	87 GAM4 $100 \pi^- p \rightarrow 4\pi^0 n$	
250 ± 30			3 ALDE	86D GAM4 $100 \pi^- p \rightarrow \eta\eta n$	
185 + 102 - 139			4 COSTA	80 OMEG $10 \pi^- p \rightarrow K^+ K^- n$	
••• We do not use the following data for averages, fits, limits, etc. •••					
260.9 ± 3.9 ± 199.9 - 38.2			5 ALBRECHT	20 RVUE $0.9 \bar{p}p \rightarrow \pi^0 \pi^0 \eta, \pi^0 \eta\eta, \pi^0 K^+ K^-$	
388 + 15 - 21			6 LONGACRE	86 RVUE	Compilation
280 + 42 - 35			7 CASON	82 STRC	$8 \pi^+ p \rightarrow \Delta^{++} \pi^0 \pi^0$

WEIGHTED AVERAGE
197±22 (Error scaled by 1.5)



Meson Particle Listings

$f_2(1810)$, $X(1835)$

- From partial wave analysis including all possible combinations of 0^{++} , 2^{++} , and 4^{++} resonances.
- Breit-Wigner width. Could also be the $f_2(1910)$.
- Seen in only one solution.
- Error increased by spread of two solutions. Included in LONGACRE 86 global analysis.
- T-matrix pole, 4 poles, 4 channels, including scattering data from HYAMS 75 ($\pi\pi$), LONGACRE 86 ($K\bar{K}$), BINON 83 ($\eta\eta$).
- From a partial-wave analysis of data using a K-matrix formalism with 5 poles. Includes compilation of several other experiments.
- From an amplitude analysis of the reaction $\pi^+\pi^-\rightarrow 2\pi^0$. The resonance in the $2\pi^0$ final state is not confirmed by PROKOSHKIN 97.

$f_2(1810)$ DECAY MODES

Mode	Fraction (Γ_i/Γ)
Γ_1 $\pi\pi$	
Γ_2 $\eta\eta$	seen
Γ_3 $4\pi^0$	seen
Γ_4 K^+K^-	
Γ_5 $\gamma\gamma$	seen

$f_2(1810)$ $\Gamma(i)\Gamma(\gamma\gamma)/\Gamma(\text{total})$

$\Gamma(\eta\eta) \times \Gamma(\gamma\gamma)/\Gamma(\text{total})$	DOCUMENT ID	TECN	COMMENT	$\Gamma_2\Gamma_5/\Gamma$
$5.2^{+0.9}_{-0.8} - 4.5^{+3.3}_{-4.5}$	1 UEHARA	10A	BELL	$10.6 e^+e^- \rightarrow e^+e^-\eta\eta$

- Including interference with the $f_2'(1525)$ (parameters fixed to the values from the 2008 edition of this review, PDG 08) and $f_2(1270)$. May also be the $f_0(1500)$.

$f_2(1810)$ BRANCHING RATIOS

$\Gamma(\pi\pi)/\Gamma(\text{total})$	DOCUMENT ID	TECN	COMMENT	Γ_1/Γ
not seen	AMSLER 02	CBAR	$0.9 \bar{p}p \rightarrow \pi^0\eta\eta, \pi^0\pi^0\pi^0$	
not seen	PROKOSHKIN 97	GAM2	$38 \pi^-\pi^+ \rightarrow \pi^0\pi^0n$	
$0.21^{+0.02}_{-0.03}$	1 LONGACRE 86	RVUE	Compilation	
0.44 ± 0.03	2 CASON 82	STRC	$8 \pi^+\pi^- \rightarrow \Delta^+\pi^0\pi^0$	

- From a partial-wave analysis of data using a K-matrix formalism with 5 poles. Includes compilation of several other experiments.
- Included in LONGACRE 86 global analysis.

$\Gamma(\eta\eta)/\Gamma(\text{total})$	DOCUMENT ID	TECN	COMMENT	Γ_2/Γ
seen	ABLIKIM 13N	BES3	PWA of $J/\psi \rightarrow \gamma\eta\eta$	
$0.008^{+0.028}_{-0.003}$	1 LONGACRE 86	RVUE	Compilation	

- From a partial-wave analysis of data using a K-matrix formalism with 5 poles. Includes compilation of several other experiments.

$\Gamma(\pi\pi)/\Gamma(4\pi^0)$	DOCUMENT ID	TECN	COMMENT	Γ_1/Γ_3
<0.75	ALDE 87	GAM4	$100 \pi^-\pi^+ \rightarrow 4\pi^0n$	

- From a partial-wave analysis of data using a K-matrix formalism with 5 poles. Includes compilation of several other experiments.

$\Gamma(4\pi^0)/\Gamma(\eta\eta)$	DOCUMENT ID	TECN	COMMENT	Γ_3/Γ_2
0.8 ± 0.3	ALDE 87	GAM4	$100 \pi^-\pi^+ \rightarrow 4\pi^0n$	

- From a partial-wave analysis of data using a K-matrix formalism with 5 poles. Includes compilation of several other experiments.

$\Gamma(K^+K^-)/\Gamma(\text{total})$	DOCUMENT ID	TECN	COMMENT	Γ_4/Γ
$0.003^{+0.019}_{-0.002}$	1 LONGACRE 86	RVUE	Compilation	
seen	COSTA 80	OMEG	$10 \pi^-\pi^+ \rightarrow K^+K^-n$	

- From a partial-wave analysis of data using a K-matrix formalism with 5 poles. Includes compilation of several other experiments.

$f_2(1810)$ REFERENCES

ALBRECHT 20	EPJ C80 453	M. Albrecht et al.	(Crystal Barrel Collab.)
ABLIKIM 13N	PR D87 092009	M. Ablikim et al.	(BESIII Collab.)
UEHARA 10A	PR D82 114031	S. Uehara et al.	(BELLE Collab.)
PDG 08	PL B667 1	C. Amstler et al.	(PDG Collab.)
AMSLER 02	EPJ C23 29	C. Amstler et al.	
PROKOSHKIN 97	PD 42 117	Y.D. Prokoshkin et al.	(SERP)
	Translated from DANS 353 323		
ALDE 88D	SJNP 47 810	D.M. Alde et al.	(SERP, BELG, LANL, LAPP+)
	Translated from YAF 47 1273		
ALDE 87	PL B198 286	D.M. Alde et al.	(LANL, BRUX, SERP, LAPP)
ALDE 86D	NP B269 485	D.M. Alde et al.	(BELG, LAPP, SERP, CERN+)
LONGACRE 86	PL B177 223	R.S. Longacre et al.	(BNL, BRAN, CUNY+)
BINON 83	NC 78A 313	F.G. Binon et al.	(BELG, LAPP, SERP+)
CASON 82	PRL 48 1316	N.M. Cason et al.	(NDAM, ANL)
COSTA 80	NP B175 402	G. Costa et al.	(BARI, BONN, CERN, GLAS+)
HYAMS 75	NP B100 205	B.D. Hyams et al.	(CERN, MPIM)

$X(1835)$

$$I^G(J^{PC}) = ?(0^{-+})$$

OMITTED FROM SUMMARY TABLE

Could be a superposition of two states, one with small width appearing as threshold enhancement in $p\bar{p}$, the other one with a larger width. For the former ABLIKIM 12D determine $J^{PC} = 0^{-+}$.

$X(1835)$ MASS

VALUE (MeV)	EVTS	DOCUMENT ID	TECN	COMMENT
$1826.5^{+13.0}_{-3.4}$		OUR AVERAGE		
$1825.3 \pm 2.4^{+17.3}_{-2.4}$		1 ABLIKIM	16J	BES3 $J/\psi \rightarrow \gamma\pi^+\pi^-\eta'$
$1844 \pm 9^{+16}_{-25}$		ABLIKIM	15T	BES3 $J/\psi \rightarrow \gamma K_S^0 K_S^0 \eta$
• • • We do not use the following data for averages, fits, limits, etc. • • •				
$1839 \pm 26 \pm 26$		2 ABLIKIM	18I	BES3 $J/\psi \rightarrow \gamma\gamma\phi(1020)$
$1909.5 \pm 15.9^{+9.4}_{-27.5}$		3 ABLIKIM	16J	BES3 $J/\psi \rightarrow \gamma\pi^+\pi^-\eta'$
$1842.2 \pm 4.2^{+7.1}_{-2.6}$	0.6k	ABLIKIM	13U	BES3 $J/\psi \rightarrow \gamma 3(\pi^+\pi^-)$
$1832^{+19}_{-5} \pm 26$		4 ABLIKIM	12D	BES3 $J/\psi \rightarrow \gamma\rho\bar{p}$
$1836.5 \pm 3.0^{+5.6}_{-2.1}$	4265	5 ABLIKIM	11C	BES3 $J/\psi \rightarrow \gamma\pi^+\pi^-\eta'$
$1877.3 \pm 6.3^{+3.4}_{-7.4}$		6 ABLIKIM	11J	BES3 $J/\psi \rightarrow \omega(\eta\pi^+\pi^-)$
$1837^{+10}_{-12} \pm 9$	231	7,8 ALEXANDER	10	CLEO $J/\psi \rightarrow \gamma\rho\bar{p}$
$1833.7 \pm 6.1 \pm 2.7$	264	ABLIKIM	05R	BES2 $J/\psi \rightarrow \gamma\pi^+\pi^-\eta'$
1831 ± 7		8,9 ABLIKIM	05R	BES2 $J/\psi \rightarrow \gamma\rho\bar{p}$
$1859^{+3}_{-10} \pm 5$		8 BAI	03F	BES2 $J/\psi \rightarrow \gamma\rho\bar{p}$

- From a fit of the measured $\pi^+\pi^-\eta'$ lineshape that accounts for the abrupt distortion observed at the $p\bar{p}$ threshold through interference with a second previously unseen narrow resonance near 1870 MeV. The fit uses Breit-Wigner functions for the signal shapes and includes known backgrounds and contributors.
- From a fit to $\gamma\phi$ invariant mass. Angular analysis consistent with $J^{PC} = 0^{-+}$. Other J^{PC} not excluded.
- Pole mass from a fit of the measured $\pi^+\pi^-\eta'$ lineshape to a Flatte formula that accounts for the abrupt distortion observed at the $p\bar{p}$ threshold; the fit also includes known backgrounds and contributors, as well as an *ad hoc* Breit-Wigner function ($M \approx 1919$ MeV; $\Gamma \approx 51$ MeV) that is required for a good fit.
- From the fit including final state interaction effects in isospin 0 S-wave according to SIBIRTEV 05A. Supersedes ABLIKIM 10G.
- From a fit of the $\pi^+\pi^-\eta'$ mass distribution to a combination of $\gamma f_1(1510)$, $\gamma X(1835)$, and two states $\gamma X(2120)$ and $\gamma X(2370)$, for $M(\pi^+\pi^-\eta') < 2.8$ GeV, and accounting for backgrounds from non- η' events and $J/\psi \rightarrow \pi^0\pi^+\pi^-\eta'$.
- The selected process is $J/\psi \rightarrow \omega a_0(980)\pi$. This state may be due also to $\eta_2(1870)$ or to a combination of $X(1835)$ and $\eta_2(1870)$.
- From a fit of the $p\bar{p}$ mass distribution to a combination of $\gamma X(1835)$, γR with $M(R) = 2100$ MeV and $\Gamma(R) = 160$ MeV, and $\gamma\rho\bar{p}$ phase space, for $M(p\bar{p}) < 2.85$ GeV.
- Evidence for a threshold enhancement in the $p\bar{p}$ mass spectrum was also reported by ABE 02K, AUBERT, B 05L, and WANG 05A in $B^+ \rightarrow p\bar{p}K^+$, WANG 05A in $B^0 \rightarrow p\bar{p}K_S^0$, ABE 02w in $\bar{B}^0 \rightarrow p\bar{p}D^0$, DEL-AMO-SANCHEZ 12 in $B \rightarrow D(D^*)p\bar{p}(\pi)$, and WEI 08 in $B^+ \rightarrow p\bar{p}\pi^+$ decays. Not seen by ATHAR 06 in $\Upsilon(1S) \rightarrow p\bar{p}\pi$.
- From the fit including final state interaction effects in isospin 0 S-wave according to SIBIRTEV 05A. Systematic errors not estimated.

$X(1835)$ WIDTH

VALUE (MeV)	CL%	EVTS	DOCUMENT ID	TECN	COMMENT
242^{+14}_{-15}			OUR AVERAGE		
$245.2^{+13.1}_{-9.6}$			1 ABLIKIM	16J	BES3 $J/\psi \rightarrow \gamma\pi^+\pi^-\eta'$
$192^{+20}_{-17} \pm 62$			ABLIKIM	15T	BES3 $J/\psi \rightarrow \gamma K_S^0 K_S^0 \eta$
• • • We do not use the following data for averages, fits, limits, etc. • • •					
$175 \pm 57 \pm 25$			2 ABLIKIM	18I	BES3 $J/\psi \rightarrow \gamma\gamma\phi(1020)$
$273.5 \pm 21.4^{+6.1}_{-64.0}$			3 ABLIKIM	16J	BES3 $J/\psi \rightarrow \gamma\pi^+\pi^-\eta'$
$83 \pm 14 \pm 11$	0.6k		ABLIKIM	13U	BES3 $J/\psi \rightarrow \gamma 3(\pi^+\pi^-)$
< 76	90		4 ABLIKIM	12D	BES3 $J/\psi \rightarrow \gamma\rho\bar{p}$
$190 \pm 9^{+38}_{-36}$		4265	5 ABLIKIM	11C	BES3 $J/\psi \rightarrow \gamma\pi^+\pi^-\eta'$
$57 \pm 12^{+19}_{-4}$			6 ABLIKIM	11J	BES3 $J/\psi \rightarrow \omega(\eta\pi^+\pi^-)$
0^{+44}_{-0}	231	7,8	ALEXANDER	10	CLEO $J/\psi \rightarrow \gamma\rho\bar{p}$
$67.7 \pm 20.3 \pm 7.7$		264	ABLIKIM	05R	BES2 $J/\psi \rightarrow \gamma\pi^+\pi^-\eta'$
< 153	90		8,9 ABLIKIM	05R	BES2 $J/\psi \rightarrow \gamma\rho\bar{p}$
< 30			8 BAI	03F	BES2 $J/\psi \rightarrow \gamma\rho\bar{p}$

- From a fit of the measured $\pi^+\pi^-\eta'$ lineshape that accounts for the abrupt distortion observed at the $p\bar{p}$ threshold through interference with a second previously unseen narrow resonance near 1870 MeV. The fit uses Breit-Wigner functions for the signal shapes and includes known backgrounds and contributors.
- From a fit to $\gamma\phi$ invariant mass. Angular analysis consistent with $J^{PC} = 0^{-+}$. Other J^{PC} not excluded.

Meson Particle Listings

X(1835), $\phi_3(1850)$, $\eta_2(1870)$

³ Pole width from a fit of the measured $\pi^+\pi^-\eta'$ lineshape to a Flatté formula that accounts for the abrupt distortion observed at the $p\bar{p}$ threshold; the fit also includes known backgrounds and contributors, as well as an *ad hoc* Breit-Wigner function ($M \approx 1919$ MeV; $\Gamma \approx 51$ MeV) that is required for a good fit.

⁴ From the fit including final state interaction effects in isospin 0 S-wave according to SIBIRTSSEV 05A. Supersedes ABLIKIM 10G.

⁵ From a fit of the $\pi^+\pi^-\eta'$ mass distribution to a combination of $\gamma f_1(1510)$, $\gamma X(1835)$, and two states $\gamma X(2120)$ and $\gamma X(2370)$, for $M(\pi^+\pi^-\eta') < 2.8$ GeV, and accounting for backgrounds from non- η' events and $J/\psi \rightarrow \pi^0\pi^+\pi^-\eta'$.

⁶ The selected process is $J/\psi \rightarrow \omega a_0(980)\pi$. This state may be due also to $\eta_2(1870)$ or to a combination of X(1835) and $\eta_2(1870)$.

⁷ From a fit of the $p\bar{p}$ mass distribution to a combination of $\gamma X(1835)$, γR with $M(R) = 2100$ MeV and $\Gamma(R) = 160$ MeV, and $\gamma p\bar{p}$ phase space, for $M(p\bar{p}) < 2.85$ GeV.

⁸ Evidence for a threshold enhancement in the $p\bar{p}$ mass spectrum was also reported by ABE 02K, AUBERT,B 05L, and WANG 05A in $B^+ \rightarrow p\bar{p}K^+$, WANG 05A in $B^0 \rightarrow p\bar{p}K_S^0$, ABE 02W in $\bar{B}^0 \rightarrow p\bar{p}D^0$, DEL-AMO-SANCHEZ 12 in $B \rightarrow D(D^*)p\bar{p}(\pi)$, and WEI 08 in $B^+ \rightarrow p\bar{p}\pi^+$ decays. Not seen by ATHAR 06 in $\Upsilon(1S) \rightarrow p\bar{p}\gamma$.

⁹ From the fit including final state interaction effects in isospin 0 S-wave according to SIBIRTSSEV 05A. Systematic errors not estimated.

X(1835) DECAY MODES

Mode	Fraction (Γ_i/Γ)
Γ_1 $p\bar{p}$	seen
Γ_2 $\eta'\pi^+\pi^-$	seen
Γ_3 $\gamma\gamma$	
Γ_4 $K_S^0 K_S^0 \eta$	seen
Γ_5 $\gamma\phi(1020)$	possibly seen
Γ_6 $3(\pi^+\pi^-)$	seen

X(1835) $\Gamma(i)\Gamma(\gamma\gamma)/\Gamma(\text{total})$

$\Gamma(\eta'\pi^+\pi^-) \times \Gamma(\gamma\gamma)/\Gamma_{\text{total}}$	$\Gamma_2\Gamma_3/\Gamma$			
VALUE (eV)	CL%	DOCUMENT ID	TECN	COMMENT
<35.6	90	¹ ZHANG	12A	BELL $e^+e^- \rightarrow e^+e^-\eta'\pi^+\pi^-$
<83	90	² ZHANG	12A	BELL $e^+e^- \rightarrow e^+e^-\eta'\pi^+\pi^-$

¹ From a two-resonance fit and constructive interference of the $\eta(1760)$ and X(1835), a significance of 2.8 σ .

² From a two-resonance fit and destructive interference of the $\eta(1760)$ and X(1835), a significance of 2.8 σ .

X(1835) BRANCHING RATIOS

$\Gamma(p\bar{p})/\Gamma(\eta'\pi^+\pi^-)$	Γ_1/Γ_2		
VALUE	DOCUMENT ID	TECN	COMMENT
0.333	ABLIKIM	05R	BES2 $J/\psi \rightarrow \gamma\pi^+\pi^-\eta'$

$\Gamma(\eta'\pi^+\pi^-)/\Gamma(K_S^0 K_S^0 \eta)$	Γ_2/Γ_4		
VALUE	DOCUMENT ID	TECN	COMMENT
6.7 ± 1.8	¹ ABLIKIM	15T	BES3 $J/\psi \rightarrow \gamma K_S^0 K_S^0 \eta$

¹ Using results from ABLIKIM 05R.

$\Gamma(\eta'\pi^+\pi^-)/\Gamma_{\text{total}}$	Γ_2/Γ		
VALUE	DOCUMENT ID	TECN	COMMENT
seen	¹ ABLIKIM	16J	BES3 $J/\psi \rightarrow \gamma\pi^+\pi^-\eta'$

¹ ABLIKIM 16J quotes $B(J/\psi \rightarrow \gamma X(1835)) \times B(X(1835) \rightarrow \pi^+\pi^-\eta') = (3.93 \pm 0.38^{+0.31}_{-0.84}) \times 10^{-4}$ from a fit of the measured $\pi^+\pi^-\eta'$ lineshape that accounts for the abrupt distortion observed at the $p\bar{p}$ threshold with a Flatté formula in addition to known backgrounds and contributors, as well as an *ad hoc* Breit-Wigner ($M \approx 1919$ MeV; $\Gamma \approx 51$ MeV) that is required for a good fit. Another explanation for the distortion provided by ABLIKIM 16J is that a second resonance near 1870 MeV interferes with the X(1835); fits to this possibility yield product branching fraction values compatible with that shown within the respective systematic uncertainties.

$\Gamma(\gamma\phi(1020))/\Gamma_{\text{total}}$	Γ_5/Γ		
VALUE	DOCUMENT ID	TECN	COMMENT
possibly seen	¹ ABLIKIM	18i	BES3 $J/\psi \rightarrow \gamma\gamma\phi(1020)$

¹ Seen as a peak in $\gamma\phi$ invariant mass. Angular analysis consistent with $J^{PC} = 0^{-+}$. Other J^{PC} not excluded.

$\Gamma(\gamma\gamma)/\Gamma(\eta'\pi^+\pi^-)$	Γ_3/Γ_2			
VALUE	CL%	DOCUMENT ID	TECN	COMMENT
$<9.80 \times 10^{-3}$	90	¹ ABLIKIM	18o	BES3 $\psi(2S) \rightarrow \pi^+\pi^-\gamma\gamma\gamma$

¹ Using results from ABLIKIM 16J.

$\Gamma(3(\pi^+\pi^-))/\Gamma_{\text{total}}$	Γ_6/Γ			
VALUE	EVTS	DOCUMENT ID	TECN	COMMENT
seen	0.6k	ABLIKIM	13u	BES3 $J/\psi \rightarrow \gamma 3(\pi^+\pi^-)$

X(1835) REFERENCES

ABLIKIM	18i	PR D97 051101	M. Ablikim et al.	(BESIII Collab.)
ABLIKIM	18o	PR D97 072014	M. Ablikim et al.	(BESIII Collab.)
ABLIKIM	16J	PRL 117 042002	M. Ablikim et al.	(BESIII Collab.)
ABLIKIM	15T	PRL 115 091803	M. Ablikim et al.	(BESIII Collab.)
ABLIKIM	13U	PR D88 091502	M. Ablikim et al.	(BESIII Collab.)
ABLIKIM	12D	PRL 108 112003	M. Ablikim et al.	(BESIII Collab.) JPC
DEL-AMO-SA...	12	PR D85 092017	P. del Amo Sanchez et al.	(BABAR Collab.)
ZHANG	12A	PR D86 052002	C. C. Zhang et al.	(BELLE Collab.)
ABLIKIM	11C	PRL 106 072002	M. Ablikim et al.	(BESIII Collab.)
ABLIKIM	11J	PRL 107 182001	M. Ablikim et al.	(BESIII Collab.)
ABLIKIM	10G	CP C34 421	M. Ablikim et al.	(BESIII Collab.)
ALEXANDER	10	PR D82 092002	J.P. Alexander et al.	(CLEO Collab.)
WEI	08	PL B659 80	J.-T. Wei et al.	(BELLE Collab.)
ATHAR	06	PR D73 032001	S.B. Athar et al.	(CLEO Collab.)
ABLIKIM	05R	PRL 95 262001	M. Ablikim et al.	(BES Collab.)
AUBERT,B	05L	PR D72 051101	B. Aubert et al.	(BABAR Collab.)
SIBIRTSSEV	05A	PR D71 054010	A. Sibirtsev, J. Haidenbauer	
WANG	05A	PL B617 141	M.-Z. Wang et al.	(BELLE Collab.)
BAI	03F	PRL 91 022001	J.Z. Bai et al.	(BES II Collab.)
ABE	02K	PRL 88 181803	K. Abe et al.	(BELLE Collab.)
ABE	02W	PRL 89 151802	K. Abe et al.	(BELLE Collab.)

$\phi_3(1850)$

$$I^G(J^{PC}) = 0^-(3^{- -})$$

$\phi_3(1850)$ MASS

VALUE (MeV)	EVTS	DOCUMENT ID	TECN	COMMENT
1854 ± 7	OUR AVERAGE			
1855 ± 10		ASTON	88E	LASS $11 K^-p \rightarrow K^-K^+\Lambda, K_S^0 K^\pm \pi^\mp \Lambda$
1870^{+30}_{-20}	430	ARMSTRONG	82	OMEG $18.5 K^-p \rightarrow K^-K^+\Lambda$
1850 ± 10	123	ALHARRAN	81B	HBC $8.25 K^-p \rightarrow K^-\bar{K}\Lambda$

$\phi_3(1850)$ WIDTH

VALUE (MeV)	EVTS	DOCUMENT ID	TECN	COMMENT
87^{+28}_{-23}	OUR AVERAGE			Error includes scale factor of 1.2.
64 ± 31		ASTON	88E	LASS $11 K^-p \rightarrow K^-K^+\Lambda, K_S^0 K^\pm \pi^\mp \Lambda$
160^{+90}_{-50}	430	ARMSTRONG	82	OMEG $18.5 K^-p \rightarrow K^-K^+\Lambda$
80^{+40}_{-30}	123	ALHARRAN	81B	HBC $8.25 K^-p \rightarrow K^-\bar{K}\Lambda$

$\phi_3(1850)$ DECAY MODES

Mode	Fraction (Γ_i/Γ)
Γ_1 $K^-\bar{K}$	seen
Γ_2 $K^-\bar{K}^*(892) + \text{c.c.}$	seen

$\phi_3(1850)$ BRANCHING RATIOS

$\Gamma(K^-\bar{K}^*(892) + \text{c.c.})/\Gamma(K^-\bar{K})$	Γ_2/Γ_1		
VALUE	DOCUMENT ID	TECN	COMMENT
$0.55^{+0.85}_{-0.45}$	ASTON	88E	LASS $11 K^-p \rightarrow K^-K^+\Lambda, K_S^0 K^\pm \pi^\mp \Lambda$
0.8 ± 0.4	ALHARRAN	81B	HBC $8.25 K^-p \rightarrow K^-\bar{K}\pi\Lambda$

••• We do not use the following data for averages, fits, limits, etc. •••

$\phi_3(1850)$ REFERENCES

ASTON	88E	PL B208 324	D. Aston et al.	(SLAC, NAGO, CINC, INUS)IGJPC
ARMSTRONG	82	PL 110B 77	T.A. Armstrong et al.	(BARI, BIRM, CERN+)JP
ALHARRAN	81B	PL 101B 357	S. Al-Harran et al.	(BIRM, CERN, GLAS+)

$\eta_2(1870)$

$$I^G(J^{PC}) = 0^+(2^{- +})$$

$\eta_2(1870)$ MASS

VALUE (MeV)	EVTS	DOCUMENT ID	TECN	COMMENT
1842 ± 8	OUR AVERAGE			
1835 ± 12		BARBERIS	00B	450 $pp \rightarrow p_f \eta \pi^+ \pi^- p_s$
1844 ± 13		BARBERIS	00C	450 $pp \rightarrow p_f 4\pi p_s$
1840 ± 25		BARBERIS	97B	OMEG $450 pp \rightarrow pp 2(\pi^+\pi^-)$
$1875 \pm 20 \pm 35$		ADOMEIT	96	CBAR $1.94 \bar{p}p \rightarrow \eta 3\pi^0$
$1881 \pm 32 \pm 40$	26	KARCH	92	CBAL $e^+e^- \rightarrow e^+e^-\eta^0\pi^0$
$1860 \pm 5 \pm 15$		ANISOVICH	00E	SPEC $0.9-1.94 \bar{p}p \rightarrow \eta 3\pi^0$
1840 ± 15		BAI	99	BES $J/\psi \rightarrow \gamma \eta \pi^+ \pi^-$

••• We do not use the following data for averages, fits, limits, etc. •••

Meson Particle Listings

$\eta_2(1870)$, $\pi_2(1880)$

$\eta_2(1870)$ WIDTH

VALUE (MeV)	EVTS	DOCUMENT ID	TECN	COMMENT
225 ± 14 OUR AVERAGE				
235 ± 22		BARBERIS	00B	450 $p\bar{p} \rightarrow \rho_f \eta \pi^+ \pi^- \rho_S$
228 ± 23		BARBERIS	00c	450 $p\bar{p} \rightarrow \rho_f 4\pi \rho_S$
200 ± 40		BARBERIS	97B	OMEG 450 $p\bar{p} \rightarrow \rho \rho 2(\pi^+ \pi^-)$
200 ± 25 ± 45		ADOMEIT	96	CBAR 1.94 $\bar{p}p \rightarrow \eta 3\pi^0$
221 ± 92 ± 44	26	KARCH	92	CBAL $e^+ e^- \rightarrow e^+ e^- \eta \pi^0 \pi^0$
• • • We do not use the following data for averages, fits, limits, etc. • • •				
250 ± 25 ± $\frac{50}{35}$		ANISOVICH	00E	SPEC 0.9-1.94 $\bar{p}p \rightarrow \eta 3\pi^0$
170 ± 40		BAI	99	BES $J/\psi \rightarrow \gamma \eta \pi^+ \pi^-$

$\eta_2(1870)$ DECAY MODES

Mode	Fraction (Γ_i/Γ)
Γ_1 $\eta \pi \pi$	seen
Γ_2 $a_2(1320) \pi$	seen
Γ_3 $f_2(1270) \eta$	seen
Γ_4 $a_0(980) \pi$	seen
Γ_5 $\gamma \gamma$	seen

$\eta_2(1870)$ BRANCHING RATIOS

$\Gamma(a_2(1320) \pi) / \Gamma(f_2(1270) \eta)$		Γ_2/Γ_3	
VALUE	DOCUMENT ID	TECN	COMMENT
1.7 ± 0.4 OUR AVERAGE			
1.60 ± 0.40	¹ ANISOVICH	11	SPEC 0.9-1.94 $p\bar{p}$
20.4 ± 6.6	BARBERIS	00B	450 $p\bar{p} \rightarrow \rho_f \eta \pi^+ \pi^- \rho_S$
4.1 ± 2.3	ADOMEIT	96	CBAR 1.94 $\bar{p}p \rightarrow \eta 3\pi^0$
¹ Reanalysis of ADOMEIT 96 and ANISOVICH 00E.			

$\Gamma(a_2(1320) \pi) / \Gamma(a_0(980) \pi)$		Γ_2/Γ_4	
VALUE	DOCUMENT ID	TECN	COMMENT
32.6 ± 12.6			
	BARBERIS	00B	450 $p\bar{p} \rightarrow \rho_f \eta \pi^+ \pi^- \rho_S$

$\Gamma(a_0(980) \pi) / \Gamma(f_2(1270) \eta)$		Γ_4/Γ_3	
VALUE	DOCUMENT ID	TECN	COMMENT
0.48 ± 0.45			
	¹ ANISOVICH	11	SPEC 0.9-1.94 $p\bar{p}$
¹ Reanalysis of ADOMEIT 96 and ANISOVICH 00E.			

$\Gamma(\gamma \gamma) / \Gamma_{total}$		Γ_5/Γ	
VALUE	DOCUMENT ID	TECN	COMMENT
seen			
	KARCH	92	CBAL $e^+ e^- \rightarrow e^+ e^- \eta \pi^0 \pi^0$

$\eta_2(1870)$ REFERENCES

ANISOVICH	11	EPJ C71 1511	A.V. Anisovich et al.	(LOQM, RAL, PNPI)
ANISOVICH	00E	PL B477 19	A.V. Anisovich et al.	
BARBERIS	00B	PL B471 435	D. Barberis et al.	(WA 102 Collab.)
BARBERIS	00C	PL B471 440	D. Barberis et al.	(WA 102 Collab.)
BAI	99	PL B446 356	J.Z. Bai et al.	(BES Collab.)
BARBERIS	97B	PL B413 217	D. Barberis et al.	(WA 102 Collab.)
ADOMEIT	96	ZPHY C71 227	J. Adomeit et al.	(Crystal Barrel Collab.)
KARCH	92	ZPHY C54 33	K. Karch et al.	(Crystal Ball Collab.)

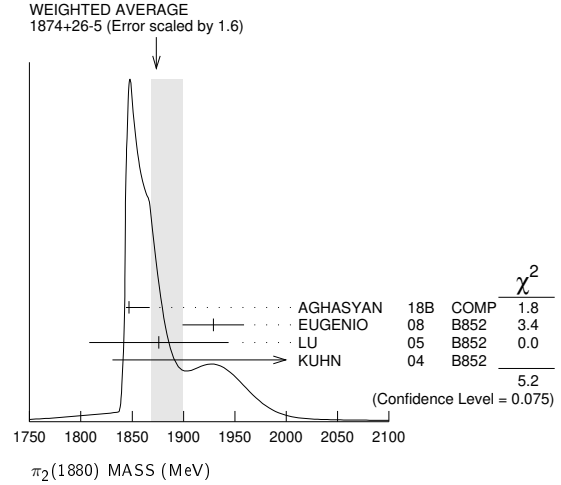
$\pi_2(1880)$

$$J^{PC} = 1^-(2^{-+})$$

$\pi_2(1880)$ MASS

VALUE (MeV)	EVTS	DOCUMENT ID	TECN	CHG	COMMENT
1874 ± $\frac{26}{5}$ OUR AVERAGE Error includes scale factor of 1.6. See the ideogram below.					
1847 ± $\frac{20}{3}$	46M	¹ AGHASYAN	18B	COMP	190 $\pi^- p \rightarrow \pi^- \pi^+ \pi^- p$
1929 ± 24 ± 18	4k	EUGENIO	08	B852	- 18 $\pi^- p \rightarrow \eta \eta \pi^- p$
1876 ± 11 ± 67	145k	LU	05	B852	- 18 $\pi^- p \rightarrow \omega \pi^- \pi^0 p$
2003 ± 88 ± 148	69k	KUHN	04	B852	- 18 $\pi^- p \rightarrow \eta \pi^+ \pi^- \pi^- p$
• • • We do not use the following data for averages, fits, limits, etc. • • •					
1880 ± 20		ANISOVICH	01B	SPEC	0 0.6-1.94 $\bar{p}p \rightarrow \eta \eta \pi^0 \pi^0$

¹ Statistical error negligible.



$\pi_2(1880)$ WIDTH

VALUE (MeV)	EVTS	DOCUMENT ID	TECN	CHG	COMMENT
237 ± $\frac{33}{30}$ OUR AVERAGE Error includes scale factor of 1.2.					
246 ± $\frac{33}{28}$	46M	² AGHASYAN	18B	COMP	190 $\pi^- p \rightarrow \pi^- \pi^+ \pi^- p$
323 ± 87 ± 43	4k	EUGENIO	08	B852	- 18 $\pi^- p \rightarrow \eta \eta \pi^- p$
146 ± 17 ± 62	145k	LU	05	B852	- 18 $\pi^- p \rightarrow \omega \pi^- \pi^0 p$
306 ± 132 ± 121	69k	KUHN	04	B852	- 18 $\pi^- p \rightarrow \eta \pi^+ \pi^- \pi^- p$
• • • We do not use the following data for averages, fits, limits, etc. • • •					
255 ± 45		ANISOVICH	01B	SPEC	0 0.6-1.94 $\bar{p}p \rightarrow \eta \eta \pi^0 \pi^0$
² Statistical error negligible.					

$\pi_2(1880)$ DECAY MODES

Mode	Fraction (Γ_i/Γ)
Γ_1 $\eta \eta \pi^-$	seen
Γ_2 $a_0(980) \eta$	seen
Γ_3 $a_2(1320) \eta$	seen
Γ_4 $f_0(1500) \pi$	seen
Γ_5 $f_1(1285) \pi$	seen
Γ_6 $\omega \pi^- \pi^0$	seen

$\Gamma(a_2(1320) \eta) / \Gamma(f_1(1285) \pi)$		Γ_3/Γ_5			
VALUE	EVTS	DOCUMENT ID	TECN	CHG	COMMENT
• • • We do not use the following data for averages, fits, limits, etc. • • •					
22.7 ± 7.3	69k	KUHN	04	B852	- 18 $\pi^- p \rightarrow \eta \pi^+ \pi^- \pi^- p$

$\Gamma(f_0(1500) \pi) / \Gamma(a_0(980) \eta)$		Γ_4/Γ_2		
VALUE	DOCUMENT ID	TECN	CHG	COMMENT
• • • We do not use the following data for averages, fits, limits, etc. • • •				
0.28 ± $\frac{0.20}{0.15}$	³ ANISOVICH	01B	SPEC	0 0.6-1.94 $\bar{p}p \rightarrow \eta \eta \pi^0 \pi^0$
³ Systematic errors not estimated.				

$\pi_2(1880)$ REFERENCES

AGHASYAN	18B	PR D98 092003	M. Aghasyan et al.	(COMPASS Collab.)
EUGENIO	08	PL B660 466	P. Eugenio et al.	(BNL E852 Collab.)
LU	05	PRL 94 032002	M. Lu et al.	(BNL E852 Collab.)
KUHN	04	PL B595 109	J. Kuhn et al.	(BNL E852 Collab.)
ANISOVICH	01B	PL B500 222	A.V. Anisovich et al.	

See key on page 1127

Meson Particle Listings

$\rho(1900)$, $f_2(1910)$

$\rho(1900)$

$I^G(J^{PC}) = 1^+(1^{--})$

OMITTED FROM SUMMARY TABLE
See the review on "Spectroscopy of Light Meson Resonances."

$\rho(1900)$ MASS

VALUE (MeV)	EVTS	DOCUMENT ID	TECN	COMMENT
• • • We do not use the following data for averages, fits, limits, etc. • • •				
1909 ± 17 ± 25	54	¹ AUBERT 08s	BABR	10.6 e ⁺ e ⁻ → φπ ⁰ γ
1880 ± 30		AUBERT 06d	BABR	10.6 e ⁺ e ⁻ → 3π ⁺ 3π ⁻ γ
1860 ± 20		AUBERT 06d	BABR	10.6 e ⁺ e ⁻ → 2(π ⁺ π ⁻ π ⁰)γ
1910 ± 10	2,3	FRABETTI 04	E687	γγp → 3π ⁺ 3π ⁻ p
1870 ± 10		ANTONELLI 96	SPEC	e ⁺ e ⁻ → hadrons

¹ From the fit with two resonances.
² From a fit with two resonances with the JACOB 72 continuum.
³ Supersedes FRABETTI 01.

$\rho(1900)$ WIDTH

VALUE (MeV)	EVTS	DOCUMENT ID	TECN	COMMENT
• • • We do not use the following data for averages, fits, limits, etc. • • •				
48 ± 17 ± 2	54	⁴ AUBERT 08s	BABR	10.6 e ⁺ e ⁻ → φπ ⁰ γ
130 ± 30		AUBERT 06d	BABR	10.6 e ⁺ e ⁻ → 3π ⁺ 3π ⁻ γ
160 ± 20		AUBERT 06d	BABR	10.6 e ⁺ e ⁻ → 2(π ⁺ π ⁻ π ⁰)γ
37 ± 13	5,6	FRABETTI 04	E687	γγp → 3π ⁺ 3π ⁻ p
10 ± 5		ANTONELLI 96	SPEC	e ⁺ e ⁻ → hadrons

⁴ From the fit with two resonances.
⁵ From a fit with two resonances with the JACOB 72 continuum.
⁶ Supersedes FRABETTI 01.

$\rho(1900)$ Γ(i)Γ(e⁺e⁻)/Γ²(total)

Γ(φπ)/Γ _{total} × Γ(e ⁺ e ⁻)/Γ _{total}	EVTS	DOCUMENT ID	TECN	COMMENT
• • • We do not use the following data for averages, fits, limits, etc. • • •				
4.2 ± 1.2 ± 0.8	54	⁷ AUBERT 08s	BABR	10.6 e ⁺ e ⁻ → φπ ⁰ γ

⁷ From the fit with two resonances.

$\rho(1900)$ DECAY MODES

Mode	Fraction (Γ _i /Γ)
Γ ₁ 6π	seen
Γ ₂ 3π ⁺ 3π ⁻	seen
Γ ₃ 2π ⁺ 2π ⁻ 2π ⁰	
Γ ₄ φπ	
Γ ₅ hadrons	seen
Γ ₆ e ⁺ e ⁻	seen
Γ ₇ $\bar{N}N$	not seen

$\rho(1900)$ BRANCHING RATIOS

Γ(6π)/Γ _{total}	EVTS	DOCUMENT ID	TECN	COMMENT
seen	8k	AKHMETSHIN 13	CMD3	e ⁺ e ⁻ → 3π ⁺ 3π ⁻
not seen		AGNELLO 02	OBLX	πp → 3π ⁺ 2π ⁻ π ⁰
seen		FRABETTI 01	E687	γγp → 3π ⁺ 3π ⁻ p
seen		ANTONELLI 96	SPEC	e ⁺ e ⁻ → hadrons

$\rho(1900)$ REFERENCES

AKHMETSHIN 13	PL B723 82	R.R. Akhmetshin <i>et al.</i>	(CMD-3 Collab.)
AUBERT 08s	PR D77 092002	B. Aubert <i>et al.</i>	(BABAR Collab.)
AUBERT 06d	PR D73 052003	B. Aubert <i>et al.</i>	(BABAR Collab.)
FRABETTI 04	PL B578 290	P.L. Frabetti <i>et al.</i>	(FNAL E687 Collab.)
AGNELLO 02	PL B527 39	M. Agnello <i>et al.</i>	(OBLIX Collab.)
FRABETTI 01	PL B514 240	P.L. Frabetti <i>et al.</i>	(FNAL E687 Collab.)
ANTONELLI 96	PL B365 427	A. Antonelli <i>et al.</i>	(FENICE Collab.)
JACOB 72	PR D5 1847	M. Jacob, R. Slansky	

$f_2(1910)$

$I^G(J^{PC}) = 0^+(2^{++})$

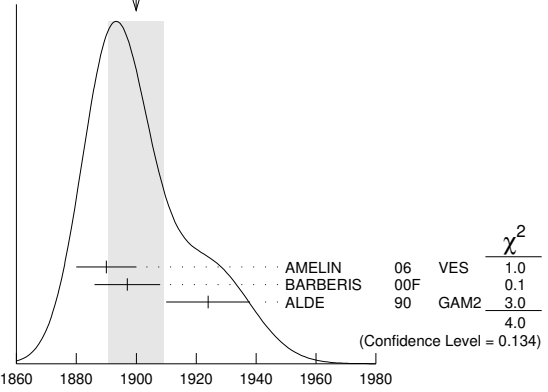
OMITTED FROM SUMMARY TABLE
We list here three different peaks with close masses and widths seen in the mass distributions of ωω, ηη', and K⁺K⁻ final states. ALDE 91B argues that they are of different nature.

$f_2(1910)$ MASS

$f_2(1910)$ ωω MODE

VALUE (MeV)	DOCUMENT ID	TECN	COMMENT
1900 ± 9 OUR AVERAGE Error includes scale factor of 1.4. See the ideogram below.			
1890 ± 10	¹ AMELIN 06	VES	36 π ⁻ p → ωωn
1897 ± 11	BARBERIS 00F		450 pp → p _f ωωp _s
1924 ± 14	ALDE 90	GAM2	38 π ⁻ p → ωωn

WEIGHTED AVERAGE
1900 ± 9 (Error scaled by 1.4)



$f_2(1910)$ ωω MODE MASS (MeV)

¹ Supersedes BELADIDZE 92b.

$f_2(1910)$ ηη' MODE

VALUE (MeV)	DOCUMENT ID	TECN	COMMENT
1934 ± 16 We do not use the following data for averages, fits, limits, etc. • • •			
1934 ± 20	² ANISOVICH 00j	SPEC	
1911 ± 10	ALDE 91B	GAM2	38 π ⁻ p → ηη'n

¹ Also compatible with J^{PC} = 1⁻ +.
² Combined fit with ηη, ππ, and ηππ.

$f_2(1910)$ K⁺K⁻ MODE

VALUE (MeV)	DOCUMENT ID	TECN	COMMENT
• • • We do not use the following data for averages, fits, limits, etc. • • •			
1941 ± 18	¹ AMSLER 06	CBAR	1.64 p̄p → K ⁺ K ⁻ π ⁰

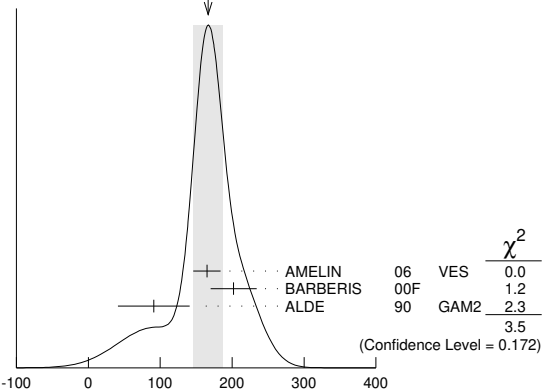
¹ Tentative, could be f₂(1950).

$f_2(1910)$ WIDTH

$f_2(1910)$ ωω MODE

VALUE (MeV)	DOCUMENT ID	TECN	COMMENT
167 ± 21 OUR AVERAGE Error includes scale factor of 1.3. See the ideogram below.			
165 ± 19	¹ AMELIN 06	VES	36 π ⁻ p → ωωn
202 ± 32	BARBERIS 00F		450 pp → p _f ωωp _s
91 ± 50	ALDE 90	GAM2	38 π ⁻ p → ωωn

WEIGHTED AVERAGE
167 ± 21 (Error scaled by 1.3)



$f_2(1910)$ ωω mode width (MeV)

¹ Supersedes BELADIDZE 92b.

Meson Particle Listings

$f_2(1910)$, $a_0(1950)$, $f_2(1950)$

$f_2(1910) \eta\eta'$ MODE

VALUE (MeV)	DOCUMENT ID	TECN	COMMENT
141 ± 41	¹ BARBERIS 00A	00A	450 $pp \rightarrow p_f \eta \eta' p_S$
• • • We do not use the following data for averages, fits, limits, etc. • • •			
271 ± 25	² ANISOVICH 00J	SPEC	
90 ± 35	ALDE 91B	GAM2	38 $\pi^- p \rightarrow \eta \eta' n$
¹ Also compatible with $J^{PC}=1^-+$.			
² Combined fit with $\eta\eta$, $\pi\pi$, and $\eta\pi\pi$.			

$f_2(1910) K^+ K^-$ MODE

VALUE (MeV)	DOCUMENT ID	TECN	COMMENT
• • • We do not use the following data for averages, fits, limits, etc. • • •			
120 ± 40	AMSLER 06	CBAR	1.64 $\bar{p}p \rightarrow K^+ K^- \pi^0$

$f_2(1910)$ DECAY MODES

Mode	Fraction (Γ_i/Γ)
Γ_1 $\pi^0 \pi^0$	
Γ_2 $K^+ K^-$	seen
Γ_3 $K_S^0 K_S^0$	
Γ_4 $\eta\eta$	seen
Γ_5 $\omega\omega$	seen
Γ_6 $\eta\eta'$	seen
Γ_7 $\eta'\eta'$	
Γ_8 $\rho\rho$	seen
Γ_9 $a_2(1320)\pi$	seen
Γ_{10} $f_2(1270)\eta$	seen

$f_2(1910)$ BRANCHING RATIOS

$\Gamma(K^+ K^-)/\Gamma_{\text{total}}$	VALUE	DOCUMENT ID	TECN	COMMENT
seen		¹ AMSLER 06	CBAR	1.64 $\bar{p}p \rightarrow K^+ K^- \pi^0$
				¹ Tentative, could be $f_2(1950)$.

$\Gamma(\pi^0 \pi^0)/\Gamma(\eta\eta')$	VALUE	DOCUMENT ID	TECN	COMMENT
• • • We do not use the following data for averages, fits, limits, etc. • • •				
<0.1		ALDE 89	GAM2	38 $\pi^- p \rightarrow \eta \eta' n$

$\Gamma(K_S^0 K_S^0)/\Gamma(\eta\eta')$	VALUE	CL%	DOCUMENT ID	TECN	COMMENT
• • • We do not use the following data for averages, fits, limits, etc. • • •					
<0.066	90		BALOSHIN 86	SPEC	40 $\pi p \rightarrow K_S^0 K_S^0 n$

$\Gamma(\eta\eta)/\Gamma(\eta\eta')$	VALUE	CL%	DOCUMENT ID	TECN	COMMENT
• • • We do not use the following data for averages, fits, limits, etc. • • •					
<0.05	90		ALDE 91B	GAM2	38 $\pi^- p \rightarrow \eta \eta' n$

$\Gamma(\omega\omega)/\Gamma(\eta\eta')$	VALUE	DOCUMENT ID	COMMENT
• • • We do not use the following data for averages, fits, limits, etc. • • •			
2.6 ± 0.6		BARBERIS 00F	450 $pp \rightarrow p_f \omega \omega p_S$

$\Gamma(\eta'\eta')/\Gamma_{\text{total}}$	VALUE	DOCUMENT ID	TECN	COMMENT
• • • We do not use the following data for averages, fits, limits, etc. • • •				
probably not seen		BARBERIS 00A	00A	450 $pp \rightarrow p_f \eta' \eta' p_S$
possibly seen		BELADIDZE 92D	VES	37 $\pi^- p \rightarrow \eta' \eta' n$

$\Gamma(\rho\rho)/\Gamma(\omega\omega)$	VALUE	DOCUMENT ID	COMMENT
• • • We do not use the following data for averages, fits, limits, etc. • • •			
2.6 ± 0.4		BARBERIS 00F	450 $pp \rightarrow p_f \omega \omega p_S$

$\Gamma(f_2(1270)\eta)/\Gamma(a_2(1320)\pi)$	VALUE	DOCUMENT ID	TECN	COMMENT
0.09 ± 0.05		¹ ANISOVICH 11	SPEC	0.9–1.94 $p\bar{p}$
				¹ Reanalysis of ADOMEIT 96 and ANISOVICH 00E.

$f_2(1910)$ REFERENCES

ANISOVICH 11	EPJ C71 1511	A.V. Anisovich et al.	(LOQM, RAL, PNPI)
AMELIN 06	PAN 69 690	D.V. Amelin et al.	(VES Collab.)
	Translated from YAF 69 715.		

AMSLER 06	PL B639 165	C. Amshler et al.	(Crystal Barrel Collab.)
ANISOVICH 00E	PL B477 19	A.V. Anisovich et al.	
ANISOVICH 00J	PL B491 47	A.V. Anisovich et al.	(RAL, LOQM, PNPI+)
BARBERIS 00A	PL B471 429	D. Barberis et al.	(WA 102 Collab.)
BARBERIS 00F	PL B484 198	D. Barberis et al.	(WA 102 Collab.)
ADOMEIT 96	ZPHY C71 227	J. Adomeit et al.	(Crystal Barrel Collab.)
BELADIDZE 92B	ZPHY C54 367	G.M. Beladidze et al.	(VES Collab.)
BELADIDZE 92D	ZPHY C57 13	G.M. Beladidze et al.	(VES Collab.)
ALDE 91B	SJNP 54 455	D.M. Alde et al.	(SERP, BELG, LANL, LAPP+)
	Translated from YAF 54 751.		
	PL B276 375	D.M. Alde et al.	(BELG, SERP, KEK, LANL+)
ALDE 90	PL B241 600	D.M. Alde et al.	(SERP, BELG, LANL, LAPP+)
ALDE 89	PL B216 447	D.M. Alde et al.	(SERP, BELG, LANL, LAPP)
	Also		
	SJNP 48 1035	D.M. Alde et al.	(BELG, SERP, LANL, LAPP)
	Translated from YAF 48 1724.		
BALOSHIN 86	SJNP 43 959	G.N. Baloshin et al.	(ITEP)
	Translated from YAF 43 1467.		

$a_0(1950)$

$$I^G(J^{PC}) = 1^-(0^{++})$$

OMITTED FROM SUMMARY TABLE

Needs confirmation. Seen in $\gamma\gamma \rightarrow \eta_c(1S) \rightarrow K\bar{K}\pi$ by LEES 16A with significance 2.5 σ in $K_S^0 K^\pm \pi^\mp$ and 4.2 σ in $K^+ K^- \pi^0$.

$a_0(1950)$ MASS

VALUE (MeV)	EVTS	DOCUMENT ID	TECN	COMMENT
1931 ± 14 ± 22	12k	^{1,2} LEES	16A	BABR $\gamma\gamma \rightarrow \eta_c(1S) \rightarrow K\bar{K}\pi$
• • • We do not use the following data for averages, fits, limits, etc. • • •				
1949 ± 32 ± 76	8k	¹ LEES	16A	BABR $\gamma\gamma \rightarrow \eta_c(1S) \rightarrow K_S^0 K^\pm \pi^\mp$
1927 ± 15 ± 23	4k	¹ LEES	16A	BABR $\gamma\gamma \rightarrow \eta_c(1S) \rightarrow K^+ K^- \pi^0$
				¹ From a model-independent partial wave analysis fit to a relativistic Breit-Wigner function with a floating width.
				² Weighted average of the $K_S^0 K^\pm$ and $K^+ K^-$ decay modes.

$a_0(1950)$ WIDTH

VALUE (MeV)	EVTS	DOCUMENT ID	TECN	COMMENT
271 ± 22 ± 29	12k	^{1,2} LEES	16A	BABR $\gamma\gamma \rightarrow \eta_c(1S) \rightarrow K\bar{K}\pi$
• • • We do not use the following data for averages, fits, limits, etc. • • •				
265 ± 36 ± 110	8k	¹ LEES	16A	BABR $\gamma\gamma \rightarrow \eta_c(1S) \rightarrow K_S^0 K^\pm \pi^\mp$
274 ± 28 ± 30	4k	¹ LEES	16A	BABR $\gamma\gamma \rightarrow \eta_c(1S) \rightarrow K^+ K^- \pi^0$
				¹ From a model-independent partial wave analysis fit to a relativistic Breit-Wigner function with a floating mass.
				² Weighted average of the $K_S^0 K^\pm$ and $K^+ K^-$ decay modes.

$a_0(1950)$ DECAY MODES

Mode	Fraction (Γ_i/Γ)
Γ_1 $K\bar{K}$	seen

$a_0(1950)$ BRANCHING RATIOS

$\Gamma(K\bar{K})/\Gamma_{\text{total}}$	VALUE	EVTS	DOCUMENT ID	TECN	COMMENT
seen		12k	¹ LEES	16A	BABR $\gamma\gamma \rightarrow \eta_c(1S) \rightarrow K\bar{K}\pi$
					¹ From a model-independent partial wave analysis.

$a_0(1950)$ REFERENCES

LEES 16A	PR D93 012005	J.P. Lees et al.	(BABAR Collab.)
----------	---------------	------------------	-----------------

$f_2(1950)$

$$I^G(J^{PC}) = 0^+(2^{++})$$

$f_2(1950)$ MASS

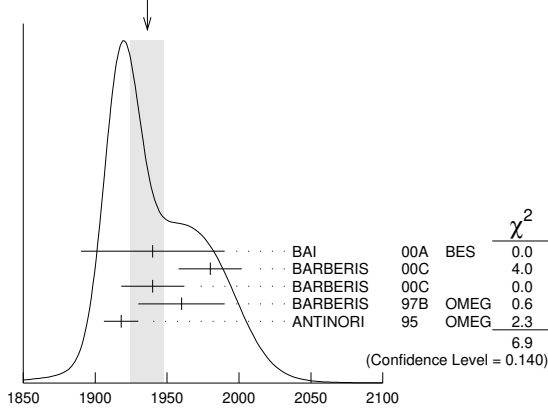
VALUE (MeV)	DOCUMENT ID	TECN	COMMENT
1936 ± 12	OUR AVERAGE		Error includes scale factor of 1.3. See the ideogram below.
1940 ± 50	BAI 00A	BES	$J/\psi \rightarrow \gamma(\pi^+ \pi^- \pi^+ \pi^-)$
1980 ± 22	¹ BARBERIS 00C	00C	450 $pp \rightarrow pp4\pi$
1940 ± 22	² BARBERIS 00C	00C	450 $pp \rightarrow pp2\pi2\pi^0$
1960 ± 30	BARBERIS 97B	OMEG	450 $pp \rightarrow pp2(\pi^+ \pi^-)$
1918 ± 12	ANTINORI 95	OMEG	300,450 $pp \rightarrow pp2(\pi^+ \pi^-)$

$f_2(1950)$

• • • We do not use the following data for averages, fits, limits, etc. • • •

1955 ± 75	³ RODAS	22	RVUE	$J/\psi(1S) \rightarrow \gamma(\pi\pi, K\bar{K})$
1978.2 $\pm 1.8^{+28.4}_{-16.9}$	⁴ ALBRECHT	20	RVUE	$0.9 \bar{p}p \rightarrow \pi^0 \pi^0 \eta, \pi^0 \eta\eta, \pi^0 K^+ K^-$
2038 $\pm 13^{+12}_{-73}$	⁵ UEHARA	09	BELL	$10.6 e^+ e^- \rightarrow e^+ e^- \pi^0 \pi^0$
1930 ± 25	⁶ BINON	05	GAMS	$33 \pi^- p \rightarrow \eta\eta n$
1980 $\pm 2 \pm 14$	ABE	04	BELL	$10.6 e^+ e^- \rightarrow e^+ e^- K^+ K^-$
1867 ± 46	⁷ AMSLER	02	CBAR	$0.9 \bar{p}p \rightarrow \pi^0 \eta\eta, \pi^0 \pi^0 \pi^0$
2010 ± 25	ANISOVICH	00J	SPEC	
1980 ± 50	ANISOVICH	99B	SPEC	$1.35-1.94 \rho \bar{p} \rightarrow \eta\eta \pi^0$
~ 1990	⁸ OAKDEN	94	RVUE	$0.36-1.55 \bar{p}p \rightarrow \pi\pi$
1950 ± 15	⁹ ASTON	91	LASS	$11 K^- p \rightarrow \Lambda K \bar{K} \pi\pi$

WEIGHTED AVERAGE
1936±12 (Error scaled by 1.3)



$f_2(1950)$ mass (MeV)

- Decaying into $\pi^+ \pi^- 2\pi^0$.
- Decaying into $2(\pi^+ \pi^-)$.
- T-matrix pole from coupled channel K-matrix fit to data on $J/\psi \rightarrow \gamma \pi^0 \pi^0$ (ABLKIM 15AE) and $J/\psi \rightarrow \gamma K_S^0 K_S^0$ (ABLKIM 18AA).
- T-matrix pole, 4 poles, 4 channels, including scattering data from HYAMS 75 ($\pi\pi$), LONGACRE 86 ($K\bar{K}$), BINON 83 ($\eta\eta$).
- Taking into account $f_4(2050)$.
- First solution, PWA is ambiguous.
- T-matrix pole.
- From solution B of amplitude analysis of data on $\bar{p}p \rightarrow \pi\pi$. See however KLOET 96 who fit $\pi^+ \pi^-$ only and find waves only up to $J = 3$ to be important but not significantly resonant.

$f_2(1950)$ WIDTH

VALUE (MeV)	DOCUMENT ID	TECN	COMMENT
464 ± 24	OUR AVERAGE		
380 $\pm 120^{+120}_{-90}$	BAI	00A	BES $J/\psi \rightarrow \gamma(\pi^+ \pi^- \pi^+ \pi^-)$
520 ± 50	¹ BARBERIS	00C	450 $pp \rightarrow pp4\pi$
485 ± 55	² BARBERIS	00C	450 $pp \rightarrow pp4\pi$
460 ± 40	BARBERIS	97B	OMEG 450 $pp \rightarrow pp2(\pi^+ \pi^-)$
390 ± 60	ANTINORI	95	OMEG 300,450 $pp \rightarrow pp2(\pi^+ \pi^-)$
• • • We do not use the following data for averages, fits, limits, etc. • • •			
350 ± 113	³ RODAS	22	RVUE $J/\psi(1S) \rightarrow \gamma(\pi\pi, K\bar{K})$
237.6 $\pm 1.6^{+41.6}_{-15.5}$	⁴ ALBRECHT	20	RVUE $0.9 \bar{p}p \rightarrow \pi^0 \pi^0 \eta, \pi^0 \eta\eta, \pi^0 K^+ K^-$
441 $\pm 27^{+28}_{-192}$	⁵ UEHARA	09	BELL $10.6 e^+ e^- \rightarrow e^+ e^- \pi^0 \pi^0$
450 ± 50	⁶ BINON	05	GAMS $33 \pi^- p \rightarrow \eta\eta n$
297 $\pm 12 \pm 6$	ABE	04	BELL $10.6 e^+ e^- \rightarrow e^+ e^- K^+ K^-$
385 ± 58	⁷ AMSLER	02	CBAR $0.9 \bar{p}p \rightarrow \pi^0 \eta\eta, \pi^0 \pi^0 \pi^0$
495 ± 35	ANISOVICH	00J	SPEC
500 ± 100	ANISOVICH	99B	SPEC $1.35-1.94 \rho \bar{p} \rightarrow \eta\eta \pi^0$
~ 100	⁸ OAKDEN	94	RVUE $0.36-1.55 \bar{p}p \rightarrow \pi\pi$
250 ± 50	⁹ ASTON	91	LASS $11 K^- p \rightarrow \Lambda K \bar{K} \pi\pi$

- Decaying into $\pi^+ \pi^- 2\pi^0$.
- Decaying into $2(\pi^+ \pi^-)$.
- T-matrix pole from coupled channel K-matrix fit to data on $J/\psi \rightarrow \gamma \pi^0 \pi^0$ (ABLKIM 15AE) and $J/\psi \rightarrow \gamma K_S^0 K_S^0$ (ABLKIM 18AA).
- T-matrix pole, 4 poles, 4 channels, including scattering data from HYAMS 75 ($\pi\pi$), LONGACRE 86 ($K\bar{K}$), BINON 83 ($\eta\eta$).
- Taking into account $f_4(2050)$.
- First solution, PWA is ambiguous.
- T-matrix pole.
- From solution B of amplitude analysis of data on $\bar{p}p \rightarrow \pi\pi$. See however KLOET 96 who fit $\pi^+ \pi^-$ only and find waves only up to $J = 3$ to be important but not significantly resonant.
- Cannot determine spin to be 2.

$f_2(1950)$ DECAY MODES

Mode	Fraction (Γ_i/Γ)
Γ_1	$K^*(892)\bar{K}^*(892)$ seen
Γ_2	$\pi\pi$
Γ_3	$\pi^+ \pi^-$ seen
Γ_4	$\pi^0 \pi^0$ seen
Γ_5	4π seen
Γ_6	$\pi^+ \pi^- \pi^+ \pi^-$
Γ_7	$a_2(1320)\pi$
Γ_8	$f_2(1270)\pi\pi$
Γ_9	$\eta\eta$ seen
Γ_{10}	$K\bar{K}$ seen
Γ_{11}	$\gamma\gamma$ seen
Γ_{12}	$\rho\bar{\rho}$ seen

$f_2(1950)$ $\Gamma(i)\Gamma(\gamma\gamma)/\Gamma(\text{total})$

$\Gamma(K\bar{K}) \times \Gamma(\gamma\gamma)/\Gamma_{\text{total}}$	VALUE (eV)	DOCUMENT ID	TECN	COMMENT	$\Gamma_{10}\Gamma_{11}/\Gamma$
--	------------	-------------	------	---------	---------------------------------

• • • We do not use the following data for averages, fits, limits, etc. • • •

122 $\pm 4 \pm 26$	¹ ABE	04	BELL	$10.6 e^+ e^- \rightarrow e^+ e^- K^+ K^-$	
--------------------	------------------	----	------	--	--

¹ Assuming spin 2.

$\Gamma(\pi\pi) \times \Gamma(\gamma\gamma)/\Gamma_{\text{total}}$	VALUE	DOCUMENT ID	TECN	COMMENT	$\Gamma_2\Gamma_{11}/\Gamma$
--	-------	-------------	------	---------	------------------------------

• • • We do not use the following data for averages, fits, limits, etc. • • •

162 $\pm 69^{+1137}_{-42-204}$	¹ UEHARA	09	BELL	$10.6 e^+ e^- \rightarrow e^+ e^- \pi^0 \pi^0$	
--------------------------------	---------------------	----	------	--	--

¹ Taking into account $f_4(2050)$.

$f_2(1950)$ BRANCHING RATIOS

$\Gamma(K^*(892)\bar{K}^*(892))/\Gamma_{\text{total}}$	VALUE	DOCUMENT ID	TECN	CHG	COMMENT	Γ_1/Γ
--	-------	-------------	------	-----	---------	-------------------

seen ASTON 91 LASS 0 11 $K^- p \rightarrow \Lambda K \bar{K} \pi\pi$

$\Gamma(a_2(1320)\pi)/\Gamma_{\text{total}}$	VALUE	DOCUMENT ID	TECN	COMMENT	Γ_7/Γ
--	-------	-------------	------	---------	-------------------

• • • We do not use the following data for averages, fits, limits, etc. • • •

not seen	BARBERIS	00B	450 $pp \rightarrow p_f \eta \pi^+ \pi^- p_s$	
not seen	BARBERIS	00C	450 $pp \rightarrow p_f 4\pi p_s$	
possibly seen	BARBERIS	97B	OMEG 450 $pp \rightarrow pp2(\pi^+ \pi^-)$	

$\Gamma(\eta\eta)/\Gamma(4\pi)$	VALUE	CL%	DOCUMENT ID	COMMENT	Γ_9/Γ_5
---------------------------------	-------	-----	-------------	---------	---------------------

• • • We do not use the following data for averages, fits, limits, etc. • • •

< 5.0×10^{-3}	90	BARBERIS	00E	450 $pp \rightarrow p_f \eta\eta p_s$	
------------------------	----	----------	-----	---------------------------------------	--

$\Gamma(\eta\eta)/\Gamma(\pi^+ \pi^-)$	VALUE	DOCUMENT ID	TECN	COMMENT	Γ_9/Γ_3
--	-------	-------------	------	---------	---------------------

0.14 ± 0.05 AMSLER 02 CBAR 0.9 $\bar{p}p \rightarrow \pi^0 \eta\eta, \pi^0 \pi^0 \pi^0$

$\Gamma(\rho\bar{\rho})/\Gamma_{\text{total}}$	VALUE	EVTS	DOCUMENT ID	TECN	COMMENT	Γ_{12}/Γ
--	-------	------	-------------	------	---------	----------------------

seen 111 ALEXANDER 10 CLEO $\psi(2S) \rightarrow \gamma\rho\bar{\rho}$

$f_2(1950)$ REFERENCES

RODAS 22 EPJ C82 80	A. Rodas et al.	(JPAC Collab.)
ALBRECHT 20 EPJ C80 453	M. Albrecht et al.	(Crystal Barrel Collab.)
ABLKIM 18AA PR D98 072003	M. Ablkikim et al.	(BESIII Collab.)
ABLKIM 15AE PR D92 052003	M. Ablkikim et al.	(BESIII Collab.)
ALEXANDER 10 PR D82 092002	J.P. Alexander et al.	(CLEO Collab.)
UEHARA 09 PR D79 052009	S. Uehara et al.	(BELLE Collab.)
BINON 05 PAN 68 960	F. Binon et al.	(BELLE Collab.)
	Translated from YAF 68 998.	
ABE 04 EPJ C32 323	K. Abe et al.	(BELLE Collab.)
AMSLER 02 EPJ C23 29	C. Amshler et al.	
ANISOVICH 00J PL B491 47	A.V. Anisovich et al.	(RAL, LOQM, PNPI+)
BAI 00A PL B472 207	J.Z. Bai et al.	(BES Collab.)
BARBERIS 00B PL B471 435	D. Barberis et al.	(WA 102 Collab.)
BARBERIS 00C PL B471 440	D. Barberis et al.	(WA 102 Collab.)
BARBERIS 00E PL B479 59	D. Barberis et al.	(WA 102 Collab.)
ANISOVICH 99B PL B449 154	A.V. Anisovich et al.	(WA 102 Collab.)
BARBERIS 97B PL B413 217	D. Barberis et al.	(WA 102 Collab.)
KLOET 96 PR D53 6120	W.M. Kloet, F. Myhrer	(RUTG, NORD)
ANTINORI 95 PL B353 589	F. Antinori et al.	(ATHU, BARI, BIRM+)
OAKDEN 94 NP A574 731	M.N. Oakden, M.R. Pennington	(LASS Collab.)
ASTON 81 NP BPS B21 5	D. Aston et al.	(LASS Collab.)
LONGACRE 86 PL B177 223	R.S. Longacre et al.	(BNL, BRAN, CUINY+)
BINON 83 NC 78A 313	F.G. Binon et al.	(BELG, LAPP, SERP+)
HYAMS 75 NP B100 205	B.D. Hyams et al.	(CERN, MPIM)

Meson Particle Listings

$a_4(1970), \rho_3(1990)$

$a_4(1970)$

was $a_4(2040)$

$$I^G(J^{PC}) = 1^-(4^{++})$$

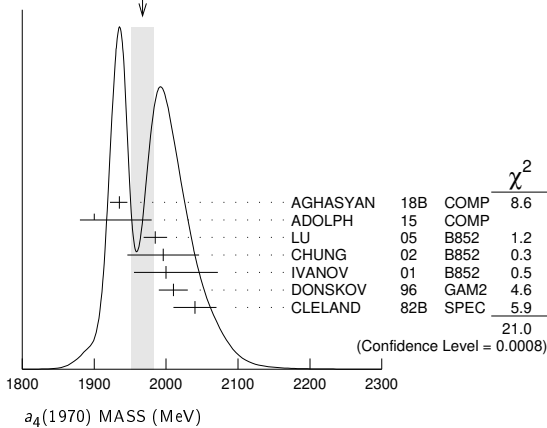
- 1 Statistical error negligible.
- 2 From a simultaneous fit to the G_\perp and G_0 wave intensities.
- 3 From an amplitude analysis.
- 4 Superseded by AGHASYAN 2018B.
- 5 Statistical error only.
- 6 From the combined analysis of ANISOVICH 99C, ANISOVICH 99E, and ANISOVICH 01F.
- 7 May be a different state.
- 8 From a fit to the Y_8^0 moment. Limited by phase space.
- 9 $J^P = 4^+$ is favored, though $J^P = 2^+$ cannot be excluded.

$a_4(1970)$ MASS

VALUE (MeV)	EVTS	DOCUMENT ID	TECN	CHG	COMMENT
1967 ± 16	OUR AVERAGE Error includes scale factor of 2.1. See the ideogram below.				
1935 ⁺¹¹ / ₋₁₃	46M	¹ AGHASYAN	18B	COMP	190 $\pi^- p \rightarrow \pi^- \pi^+ \pi^- p$
1900 ⁺⁸⁰ / ₋₂₀		ADOLPH	15	COMP	191 $\pi^- p \rightarrow \eta^{(\prime)} \pi^- p$
1985 ± 10 ± 13	145k	LU	05	B852	18 $\pi^- p \rightarrow \omega \pi^- \pi^0 p$
1996 ± 25 ± 43		CHUNG	02	B852	18.3 $\pi^- p \rightarrow 3\pi p$
2000 ± 40 ⁺⁵⁰ / ₋₂₀		IVANOV	01	B852	18 $\pi^- p \rightarrow \eta' \pi^- p$
2010 ± 20		² DONSKOV	96	GAM2 0	38 $\pi^- p \rightarrow \eta \pi^0 n$
2040 ± 30		³ CLELAND	82B	SPEC ±	50 $\pi p \rightarrow K_S^0 K^\pm p$
• • • We do not use the following data for averages, fits, limits, etc. • • •					
1885 ± 13 ⁺⁵⁰ / ₋₂	420k	⁴ ALEKSEEV	10	COMP	190 $\pi^- Pb \rightarrow \pi^- \pi^- \pi^+ Pb'$
2004 ± 6	80k	⁵ UMAN	06	E835	5.2 $\bar{p} p \rightarrow \eta \eta \pi^0$
2005 ⁺²⁵ / ₋₄₅		⁶ ANISOVICH	01F	SPEC	2.0 $\bar{p} p \rightarrow 3\pi^0, \pi^0 \eta, \pi^0 \eta'$
1944 ± 8 ± 50		⁷ AMELIN	99	VES	37 $\pi^- A \rightarrow \omega \pi^- \pi^0 A^*$
1903 ± 10		⁸ BALDI	78	SPEC -	10 $\pi^- p \rightarrow \rho K_S^0 K^-$
2030 ± 50		⁹ CORDEN	78C	OMEG 0	15 $\pi^- p \rightarrow 3\pi n$

- 1 Statistical error negligible.
- 2 From a simultaneous fit to the G_\perp and G_0 wave intensities.
- 3 From an amplitude analysis.
- 4 Superseded by AGHASYAN 2018B.
- 5 Statistical error only.
- 6 From the combined analysis of ANISOVICH 99C, ANISOVICH 99E, and ANISOVICH 01F.
- 7 May be a different state.
- 8 From a fit to the Y_8^0 moment. Limited by phase space.
- 9 $J^P = 4^+$ is favored, though $J^P = 2^+$ cannot be excluded.

WEIGHTED AVERAGE
1967±16 (Error scaled by 2.1)



$a_4(1970)$ WIDTH

VALUE (MeV)	EVTS	DOCUMENT ID	TECN	CHG	COMMENT
324 ⁺¹⁵/₋₁₈	OUR AVERAGE				
333 ⁺¹⁶ / ₋₂₁	46M	¹ AGHASYAN	18B	COMP	190 $\pi^- p \rightarrow \pi^- \pi^+ \pi^- p$
300 ⁺⁸⁰ / ₋₁₀₀		ADOLPH	15	COMP	191 $\pi^- p \rightarrow \eta^{(\prime)} \pi^- p$
231 ± 30 ± 46	145k	LU	05	B852	18 $\pi^- p \rightarrow \omega \pi^- \pi^0 p$
298 ± 81 ± 85		CHUNG	02	B852	18.3 $\pi^- p \rightarrow 3\pi p$
350 ± 100 ⁺⁷⁰ / ₋₅₀		IVANOV	01	B852	18 $\pi^- p \rightarrow \eta' \pi^- p$
370 ± 80		² DONSKOV	96	GAM2 0	38 $\pi^- p \rightarrow \eta \pi^0 n$
380 ± 150		³ CLELAND	82B	SPEC ±	50 $\pi p \rightarrow K_S^0 K^\pm p$
• • • We do not use the following data for averages, fits, limits, etc. • • •					
294 ± 25 ⁺⁴⁶ / ₋₁₉	420k	⁴ ALEKSEEV	10	COMP	190 $\pi^- Pb \rightarrow \pi^- \pi^- \pi^+ Pb'$
401 ± 16	80k	⁵ UMAN	06	E835	5.2 $\bar{p} p \rightarrow \eta \eta \pi^0$
180 ± 30		⁶ ANISOVICH	01F	SPEC	2.0 $\bar{p} p \rightarrow 3\pi^0, \pi^0 \eta, \pi^0 \eta'$
324 ± 26 ± 75		⁷ AMELIN	99	VES	37 $\pi^- A \rightarrow \omega \pi^- \pi^0 A^*$
166 ± 43		⁸ BALDI	78	SPEC -	10 $\pi^- p \rightarrow \rho K_S^0 K^-$
510 ± 200		⁹ CORDEN	78C	OMEG 0	15 $\pi^- p \rightarrow 3\pi n$

$a_4(1970)$ DECAY MODES

Mode	Fraction (Γ_i/Γ)
Γ_1 $K \bar{K}$	seen
Γ_2 $\pi^+ \pi^- \pi^0$	seen
Γ_3 $\rho \pi$	seen
Γ_4 $f_2(1270) \pi$	seen
Γ_5 $\omega \pi^- \pi^0$	seen
Γ_6 $\omega \rho$	seen
Γ_7 $\eta \pi$	seen
Γ_8 $\eta'(958) \pi$	seen

$a_4(1970)$ BRANCHING RATIOS

$\Gamma(K \bar{K})/\Gamma_{total}$					Γ_1/Γ
VALUE	DOCUMENT ID	TECN	CHG	COMMENT	
seen	BALDI	78	SPEC ±	10 $\pi^- p \rightarrow K_S^0 K^- p$	

$\Gamma(\pi^+ \pi^- \pi^0)/\Gamma_{total}$					Γ_2/Γ
VALUE	DOCUMENT ID	TECN	CHG	COMMENT	
seen	CORDEN	78C	OMEG 0	15 $\pi^- p \rightarrow 3\pi n$	

$\Gamma(\rho \pi)/\Gamma(f_2(1270) \pi)$					Γ_3/Γ_4
VALUE	EVTS	DOCUMENT ID	TECN	COMMENT	
1.7 ^{+0.9}/_{-0.8}	OUR AVERAGE Error includes scale factor of 3.7.				

2.9 ^{+0.6} / _{-0.4}	46M	¹ AGHASYAN	18B	COMP	190 $\pi^- p \rightarrow \pi^- \pi^+ \pi^- p$
1.1 ± 0.2 ± 0.2		CHUNG	02	B852	18.3 $\pi^- p \rightarrow 3\pi p$

$\Gamma(\eta \pi)/\Gamma_{total}$					Γ_7/Γ
VALUE	DOCUMENT ID	TECN	CHG	COMMENT	
seen	DONSKOV	96	GAM2 0	38 $\pi^- p \rightarrow \eta \pi^0 n$	

$\Gamma(\eta'(958) \pi)/\Gamma(\eta \pi)$					Γ_8/Γ_7
VALUE	DOCUMENT ID	TECN	COMMENT		
0.23 ± 0.07	ADOLPH	15	COMP	191 $\pi^- p \rightarrow \eta^{(\prime)} \pi^- p$	

$\Gamma(\omega \rho)/\Gamma_{total}$					Γ_6/Γ
VALUE	EVTS	DOCUMENT ID	TECN	COMMENT	
seen	145k	LU	05	B852	18 $\pi^- p \rightarrow \omega \pi^- \pi^0 p$

$a_4(1970)$ REFERENCES

AGHASYAN 18B	PR D98 092003	M. Aghasyan <i>et al.</i>	(COMPASS Collab.)
ADOLPH 15	PL B740 303	M. Adolph <i>et al.</i>	(COMPASS Collab.)
ALEKSEEV 10	PRL 104 241803	M.G. Alekseev <i>et al.</i>	(COMPASS Collab.)
UMAN 06	PR D73 052009	I. Uman <i>et al.</i>	(FNAL E835)
LU 05	PRL 94 032002	M. Lu <i>et al.</i>	(BNL E852 Collab.)
CHUNG 02	PR D65 072001	S.U. Chung <i>et al.</i>	(BNL E852 Collab.)
ANISOVICH 01F	PL B517 261	A.V. Anisovich <i>et al.</i>	
IVANOV 01	PRL 86 3977	E.I. Ivanov <i>et al.</i>	(BNL E852 Collab.)
AMELIN 99	PAN 62 445	D.V. Amelin <i>et al.</i>	(VES Collab.)
	Translated from YAF 62 487.		
ANISOVICH 99C	PL B452 173	A.V. Anisovich <i>et al.</i>	
ANISOVICH 99E	PL B452 187	A.V. Anisovich <i>et al.</i>	
DONSKOV 96	PAN 59 982	S.V. Donskov <i>et al.</i>	(GAMS Collab.) IGJPC
	Translated from YAF 59 1027.		
CLELAND 82B	NP B208 228	W.E. Cleland <i>et al.</i>	(DURH, GEVA, LAUS+)
BALDI 78	PL 74B 413	R. Baldi <i>et al.</i>	(GEVA) JP
CORDEN 78C	NP B136 77	M.J. Corden <i>et al.</i>	(BIRM, RHEL, TELA+) JP

$\rho_3(1990)$

$$I^G(J^{PC}) = 1^+(3^{--})$$

OMITTED FROM SUMMARY TABLE

$\rho_3(1990)$ MASS

VALUE (MeV)	DOCUMENT ID	TECN	COMMENT
• • • We do not use the following data for averages, fits, limits, etc. • • •			
1982 ± 14	¹ ANISOVICH	02	SPEC 0.6-1.9 $p \bar{p} \rightarrow \omega \pi^0, \omega \eta \pi^0, \pi^+ \pi^-$
~ 2007	HASAN	94	RVUE $\bar{p} p \rightarrow \pi \pi$
¹ From the combined analysis of ANISOVICH 00J, ANISOVICH 01D, ANISOVICH 01E, and ANISOVICH 02.			

See key on page 1127

Meson Particle Listings

$\rho_3(1990)$, $\pi_2(2005)$, $f_2(2010)$, $f_0(2020)$

$\rho_3(1990)$ WIDTH

VALUE (MeV)	DOCUMENT ID	TECN	COMMENT
188 ± 24	² ANISOVICH 02	SPEC	$0.6-1.9 \rho \bar{p} \rightarrow \omega \pi^0, \omega \eta \pi^0, \pi^+ \pi^-$
~ 287	HASAN 94	RVUE	$\bar{p} p \rightarrow \pi \pi$
² From the combined analysis of ANISOVICH 00J, ANISOVICH 01D, ANISOVICH 01E, and ANISOVICH 02.			

$\rho_3(1990)$ REFERENCES

ANISOVICH 02	PL B542 8	A.V. Anisovich et al.	
ANISOVICH 01D	PL B508 6	A.V. Anisovich et al.	
ANISOVICH 01E	PL B513 281	A.V. Anisovich et al.	
ANISOVICH 00J	PL B491 47	A.V. Anisovich et al.	(RAL, LOQM, PNPI+)
HASAN 94	PL B334 215	A. Hasan, D.V. Bugg	(LOQM)

$\pi_2(2005)$ $I^G(J^{PC}) = 1^-(2^{-+})$
 OMITTED FROM SUMMARY TABLE

$\pi_2(2005)$ MASS

VALUE (MeV)	EVTs	DOCUMENT ID	TECN	COMMENT
1963^{+17}_{-27}	OUR AVERAGE			
1962^{+17}_{-29}	46M	¹ AGHASYAN 18B	COMP	$190 \pi^- p \rightarrow \pi^- \pi^+ \pi^- p$
$1974 \pm 14 \pm 83$	145k	LU 05	B852	$18 \pi^- p \rightarrow \omega \pi^- \pi^0 p$
••• We do not use the following data for averages, fits, limits, etc. •••				
2005 ± 15		ANISOVICH 01F	SPEC	$2.0 \bar{p} p \rightarrow 3\pi^0, \pi^0 \eta, \pi^0 \eta'$
¹ Statistical uncertainty negligible.				

$\pi_2(2005)$ WIDTH

VALUE (MeV)	EVTs	DOCUMENT ID	TECN	COMMENT
$370^{+}_{-} 16_{90}$	OUR AVERAGE			
371^{+16}_{-120}	46M	¹ AGHASYAN 18B	COMP	$190 \pi^- p \rightarrow \pi^- \pi^+ \pi^- p$
$341 \pm 61 \pm 139$	145k	LU 05	B852	$18 \pi^- p \rightarrow \omega \pi^- \pi^0 p$
••• We do not use the following data for averages, fits, limits, etc. •••				
200 ± 40		ANISOVICH 01F	SPEC	$2.0 \bar{p} p \rightarrow 3\pi^0, \pi^0 \eta, \pi^0 \eta'$
¹ Statistical uncertainty negligible.				

$\pi_2(2005)$ DECAY MODES

Mode	Fraction (Γ_i/Γ)
$\Gamma_1 \pi^- \pi^+ \pi^-$	seen
$\Gamma_2 \omega \pi^0 \pi^-$	seen

$\pi_2(2005)$ BRANCHING RATIOS

$\Gamma(\pi^- \pi^+ \pi^-)/\Gamma_{\text{total}}$	DOCUMENT ID	TECN	COMMENT	Γ_1/Γ
seen	AGHASYAN 18B	COMP	$190 \pi^- p \rightarrow \pi^- \pi^+ \pi^- p$	
$\Gamma(\omega \pi^0 \pi^-)/\Gamma_{\text{total}}$	DOCUMENT ID	TECN	COMMENT	Γ_2/Γ
seen	LU 05	B852	$18 \pi^- p \rightarrow \omega \pi^- \pi^0 p$	

$\pi_2(2005)$ REFERENCES

AGHASYAN 18B	PR D98 092003	M. Aghasyan et al.	(COMPASS Collab.)
LU 05	PRL 94 032002	M. Lu et al.	(BNL E852 Collab.)
ANISOVICH 01F	PL B517 261	A.V. Anisovich et al.	

$f_2(2010)$ $I^G(J^{PC}) = 0^+(2^{++})$

$f_2(2010)$ MASS

VALUE (MeV)	DOCUMENT ID	TECN	COMMENT
$2011^{+}_{-} 62_{76}$	OUR AVERAGE		
2005 ± 12	VLADIMIRSK...06	SPEC	$40 \pi^- p \rightarrow K_S^0 K_S^0 \eta$
1980 ± 20	BOLONKIN 88	SPEC	$40 \pi^- p \rightarrow K_S^0 K_S^0 \eta$

$f_2(2010)$ MASS

VALUE (MeV)	DOCUMENT ID	TECN	COMMENT
2050^{+90}_{-50}	ETKIN 85	MPS	$22 \pi^- p \rightarrow 2\phi n$
2120^{+20}_{-120}	LINDENBAUM 84	RVUE	
2160 ± 50	ETKIN 82	MPS	$22 \pi^- p \rightarrow 2\phi n$
¹ Includes data of ETKIN 85. The percentage of the resonance going into $\phi \phi 2^{++} S_2, D_2,$ and D_0 is $98^{+1}_{-3}, 0^{+1}_{-0}$, and 2^{+2}_{-1} , respectively.			
² Statistically very weak, only 1.4 s.d.			

$f_2(2010)$ WIDTH

VALUE (MeV)	DOCUMENT ID	TECN	COMMENT
$202^{+}_{-} 67_{62}$	OUR AVERAGE		
209 ± 32	VLADIMIRSK...06	SPEC	$40 \pi^- p \rightarrow K_S^0 K_S^0 \eta$
145 ± 50	BOLONKIN 88	SPEC	$40 \pi^- p \rightarrow K_S^0 K_S^0 \eta$
200^{+160}_{-50}	ETKIN 85	MPS	$22 \pi^- p \rightarrow 2\phi n$
300^{+150}_{-50}	LINDENBAUM 84	RVUE	
310 ± 70	ETKIN 82	MPS	$22 \pi^- p \rightarrow 2\phi n$
³ Includes data of ETKIN 85.			
⁴ Statistically very weak, only 1.4 s.d.			

$f_2(2010)$ DECAY MODES

Mode	Fraction (Γ_i/Γ)
$\Gamma_1 \phi \phi$	seen
$\Gamma_2 K \bar{K}$	seen

$f_2(2010)$ BRANCHING RATIOS

$\Gamma(K \bar{K})/\Gamma_{\text{total}}$	DOCUMENT ID	TECN	COMMENT	Γ_2/Γ
seen	VLADIMIRSK...06	SPEC	$40 \pi^- p \rightarrow K_S^0 K_S^0 \eta$	

$f_2(2010)$ REFERENCES

VLADIMIRSK...06	PAN 69 493	V.V. Vladimirsky et al.	(ITEP, Moscow)
	Translated from YAF 69 515.		
BOLONKIN 88	NP B309 426	B.V. Bolonkin et al.	(ITEP, SERP)
ETKIN 88	PL B201 568	A. Etkin et al.	(BNL, CUNY)
ETKIN 85	PL B65B 217	A. Etkin et al.	(BNL, CUNY)
LINDENBAUM 84	CNPP 13 285	S.J. Lindenbaum	(CUNY)
ETKIN 82	PRL 49 1620	A. Etkin et al.	(BNL, CUNY)
Also	Brighton Conf. 351	S.J. Lindenbaum	(BNL, CUNY)

$f_0(2020)$ $I^G(J^{PC}) = 0^+(0^{++})$
 OMITTED FROM SUMMARY TABLE
 Needs confirmation.

$f_0(2020)$ MASS

VALUE (MeV)	EVTs	DOCUMENT ID	TECN	COMMENT
1992 ± 16	OUR AVERAGE			
2038 ± 48	^{1,2}	BARBERIS 00c		$450 pp \rightarrow p_f 4\pi p_S$
1925 ± 25		³ RODAS 22	RVUE	$J/\psi(1S) \rightarrow \gamma(\pi\pi, K\bar{K})$
		SARANTSEV 21	RVUE	$J/\psi(1S) \rightarrow \gamma(\pi\pi, K\bar{K}, \eta\eta, \omega\phi)$
1910 ± 50		⁴ ROPERTZ 18	RVUE	$\bar{B}_S^0 \rightarrow J/\psi(\pi^+ \pi^- / K^+ K^-)$
2037 ± 8	80k	⁵ UMAN 06	E835	$5.2 \bar{p} p \rightarrow \eta\eta \pi^0$
2040 ± 38		ANISOVICH 00J	SPEC	
2010 ± 60		ALDE 98	GAM4	$100 \pi^- p \rightarrow \pi^0 \pi^0 n$
2020 ± 35		BARBERIS 97b	OMEG	$450 pp \rightarrow p p 2(\pi^+ \pi^-)$

¹ Average between $\pi^+ \pi^- 2\pi^0$ and $2(\pi^+ \pi^-)$.
² T-matrix pole.
³ T-matrix pole from coupled channel K-matrix fit to data on $J/\psi \rightarrow \gamma \pi^0 \pi^0$ (ABLIKIM 15AE) and $J/\psi \rightarrow \gamma K_S^0 K_S^0$ (ABLIKIM 18AA).
⁴ T-matrix pole of 3 channel unitary model fit to data from AAIJ 14BR and AAIJ 17V extracted using Pade approximants.
⁵ Statistical error only.

$f_0(2020)$ WIDTH

VALUE (MeV)	EVTs	DOCUMENT ID	TECN	COMMENT
442 ± 60	OUR AVERAGE			
312 ± 82	^{1,2}	BARBERIS 00c		$450 pp \rightarrow p_f 4\pi p_S$
320 ± 35		³ RODAS 22	RVUE	$J/\psi(1S) \rightarrow \gamma(\pi\pi, K\bar{K})$
		SARANTSEV 21	RVUE	$J/\psi(1S) \rightarrow \gamma(\pi\pi, K\bar{K}, \eta\eta, \omega\phi)$
400 ± 80		⁴ ROPERTZ 18	RVUE	$\bar{B}_S^0 \rightarrow J/\psi(\pi^+ \pi^- / K^+ K^-)$

Meson Particle Listings

f₀(2020), f₄(2050)

Table with 5 columns: Mass, Count, Document ID, TECN, Comment. Row 1: 296 ± 17, 80k, 5 UMAN, 06 E835, 5.2 p-bar p → ηηπ⁰

- 1 Average between π⁺π⁻2π⁰ and 2(π⁺π⁻).
2 T-matrix pole.
3 T-matrix pole from coupled channel K-matrix fit to data on J/ψ → γπ⁰π⁰ (ABLIKIM 15AE) and J/ψ → γK_S⁰K_S⁰ (ABLIKIM 18AA).

f₀(2020) DECAY MODES

Table with 2 columns: Mode, Fraction (Γ_i/Γ). Row 1: Γ₁ ρππ, seen

f₀(2020) BRANCHING RATIOS

Table with 4 columns: Γ(ρρ)/Γ(ωω), DOCUMENT ID, COMMENT, Γ₃/Γ₄. Row 1: ~ 3, BARBERIS 00F, 450 p-p → p_fωωρ_s

f₀(2020) REFERENCES

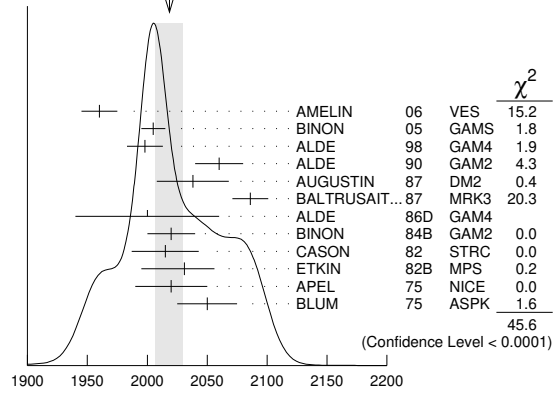
Table with 4 columns: AUTHOR, DOCUMENT ID, TECN, COMMENT. Row 1: RODAS 22, EPJ C82 80, A. Rodas et al. (JPAC Collab.)

f₄(2050) J^G(JPC) = 0⁺(4⁺⁺)

f₄(2050) MASS

Table with 5 columns: VALUE (MeV), EVTS, DOCUMENT ID, TECN, COMMENT. Row 1: 237 ± 18 OUR AVERAGE, Error includes scale factor of 2.1. See the ideogram below.

WEIGHTED AVERAGE 2018±11 (Error scaled by 2.1)



f₄(2050) mass (MeV)

- 1 From the first PWA solution.
2 From a partial-wave analysis of the data.
3 From an amplitude analysis of the reaction π⁺π⁻ → 2π⁰.
4 K matrix pole.
5 Taking into account the f₂(1950). Helicity-2 production favored.

f₄(2050) WIDTH

Table with 5 columns: VALUE (MeV), EVTS, DOCUMENT ID, TECN, COMMENT. Row 1: 237 ± 18 OUR AVERAGE, Error includes scale factor of 1.9. See the ideogram below.

- 12 From the first PWA solution.
13 From a partial-wave analysis of the data.
14 From an amplitude analysis of the reaction π⁺π⁻ → 2π⁰.
15 K matrix pole.
16 Taking into account the f₂(1950). Helicity-2 production favored.

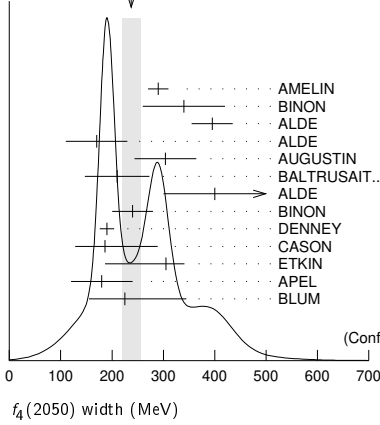
See key on page 1127

Meson Particle Listings

$f_4(2050)$, $\pi_2(2100)$

²²Width errors enlarged by us to $4\Gamma/\sqrt{N}$; see the note with the $K^*(892)$ mass.

WEIGHTED AVERAGE
237±18 (Error scaled by 1.9)



(Confidence Level < 0.0001)

$f_4(2050)$ DECAY MODES

Mode	Fraction (Γ_i/Γ)
Γ_1	$\omega\omega$ seen
Γ_2	$\pi\pi$ (17.0±1.5) %
Γ_3	$K\bar{K}$ (6.8±3.4) × 10 ⁻³
Γ_4	$\eta\eta$ (2.1±0.8) × 10 ⁻³
Γ_5	$4\pi^0$ < 1.2 %
Γ_6	$\gamma\gamma$ seen
Γ_7	$a_2(1320)\pi$ seen

$f_4(2050)$ $\Gamma(i)\Gamma(\gamma\gamma)/\Gamma(\text{total})$

$\Gamma(K\bar{K}) \times \Gamma(\gamma\gamma)/\Gamma_{\text{total}}$ $\Gamma_3\Gamma_6/\Gamma$					
VALUE (keV)	CL%	DOCUMENT ID	TECN	COMMENT	
••• We do not use the following data for averages, fits, limits, etc. •••					
<0.29	95	ALTHOFF	85B	TASS $\gamma\gamma \rightarrow K\bar{K}\pi$	
$\Gamma(\pi\pi) \times \Gamma(\gamma\gamma)/\Gamma_{\text{total}}$ $\Gamma_2\Gamma_6/\Gamma$					
VALUE (eV)	CL%	EVTS	DOCUMENT ID	TECN	COMMENT
••• We do not use the following data for averages, fits, limits, etc. •••					
23.1 ^{+3.6} +70.5 -3.3-15.6		23	UEHARA	09	BELL $10.6 e^+e^- \rightarrow \pi^0\pi^0$
<1100	95	13 ± 4	OEST	90	JADE $e^+e^- \rightarrow \pi^0\pi^0$

²³Taking into account the $f_2(1950)$. Helicity-2 production favored.

$f_4(2050)$ BRANCHING RATIOS

$\Gamma(\omega\omega)/\Gamma_{\text{total}}$ Γ_1/Γ				
VALUE	DOCUMENT ID	TECN	COMMENT	
seen	AMELIN	06	VES	$36 \pi^- p \rightarrow \omega\omega n$
not seen	BARBERIS	00F		$450 pp \rightarrow p_f \omega p_s$
$\Gamma(\omega\omega)/\Gamma(\pi\pi)$ Γ_1/Γ_2				
VALUE	DOCUMENT ID	TECN	COMMENT	
1.5 ± 0.3	ALDE	90	GAM2	$38 \pi^- p \rightarrow \omega\omega n$
$\Gamma(\pi\pi)/\Gamma_{\text{total}}$ Γ_2/Γ				
VALUE	DOCUMENT ID	TECN	COMMENT	
0.170 ± 0.015 OUR AVERAGE				
0.18 ± 0.03	24	BINON	83C	GAM2 $38 \pi^- p \rightarrow n4\gamma$
0.16 ± 0.03	24	CASON	82	STRC $8 \pi^+ p \rightarrow \Delta^{++}\pi^0\pi^0$
0.17 ± 0.02	24	CORDEN	79	OMEG $12-15 \pi^- p \rightarrow n2\pi$

²⁴Assuming one pion exchange.

$\Gamma(K\bar{K})/\Gamma(\pi\pi)$ Γ_3/Γ_2				
VALUE	DOCUMENT ID	TECN	COMMENT	
0.04 ± 0.02 -0.01	ETKIN	82B	MPS	$23 \pi^- p \rightarrow n2K_S^0$
$\Gamma(\eta\eta)/\Gamma_{\text{total}}$ Γ_4/Γ				
VALUE (units 10 ⁻³)	DOCUMENT ID	TECN	COMMENT	
2.1 ± 0.8	ALDE	86D	GAM4	$100 \pi^- p \rightarrow n4\gamma$

$\Gamma(4\pi^0)/\Gamma_{\text{total}}$ Γ_5/Γ			
VALUE	DOCUMENT ID	TECN	COMMENT
<0.012	ALDE	87	GAM4 $100 \pi^- p \rightarrow 4\pi^0 n$
$\Gamma(a_2(1320)\pi)/\Gamma_{\text{total}}$ Γ_7/Γ			
VALUE	DOCUMENT ID	TECN	COMMENT
seen	AMELIN	00	VES $37 \pi^- p \rightarrow \eta\pi^+\pi^- n$

$f_4(2050)$ REFERENCES

ANISOVICH	09	IJMP	A24 2481	V.V. Anisovich, A.V. Sarantsev	
UEHARA	09	PR	D79 052009	S. Uehara et al.	(BELLE Collab.)
AMELIN	06	PAN	69 590	D.V. Amelin et al.	(VES Collab.)
			Translated from YAF 69 715		
BINON	05	PAN	68 960	F. Binon et al.	
			Translated from YAF 68 998		
AMELIN	00	NP	A668 83	D. Amelin et al.	(VES Collab.)
ANISOVICH	00J	PL	B491 47	A.V. Anisovich et al.	(RAL, LOQM, PNP1+)
BARBERIS	00F	PL	B484 198	D. Barberis et al.	(WA 102 Collab.)
ALDE	98	EPJ	A3 361	D. Alde et al.	(GAM4 Collab.)
			Also PAN 62 405	D. Alde et al.	(GAMS Collab.)
			Translated from YAF 62 446		
MARTIN	98	PR	C57 3492	B.R. Martin et al.	
MARTIN	97	PR	C56 1114	B.R. Martin, G.C. Oades	(LOUC, AARH)
KLOET	96	PR	D53 6120	W.M. Kloet, F. Myhrer	(RUTG, NORH)
OAKDEN	94	NP	A574 731	M.N. Oakden, M.R. Pennington	(DURH)
ALDE	90	PL	B241 600	D.M. Alde et al.	(SERP, BELG, LANL, LAPP+)
OEST	90	ZPHY	C47 343	T. Oest et al.	(JADE Collab.)
ALDE	87	PL	B198 286	D.M. Alde et al.	(LANL, BRUX, SERP, LAPP)
AUGUSTIN	87	ZPHY	C36 369	J.E. Augustin et al.	(LALO, CLER, FRAS+)
BALTRUSAIT...	87	PR	D35 2077	R.M. Baltrusaitis et al.	(Mark III Collab.)
ALDE	86D	NP	B269 485	D.M. Alde et al.	(BELG, LAPP, SERP, CERN+)
ALTHOFF	85B	ZPHY	C29 189	M. Althoff et al.	(TASSO Collab.)
BINON	84B	LNC	39 41	F.G. Binon et al.	(SERP, BELG, LAPP)
BINON	83C	SJNP	38 723	F.G. Binon et al.	(SERP, BRUX+)
			Translated from YAF 38 1199		
DENNEY	83	PR	D28 2726	D.L. Denney et al.	(IOWA, MICH)
CASON	82	PRL	48 1316	N.M. Cason et al.	(NDAM, ANL)
ETKIN	82B	PR	D25 1786	A. Etkin et al.	(BNL, CUNY, TUFTS, VAND)
ALPER	80	PL	94B 422	B. Alper et al.	(AMST, CERN, CRAC, MPIM+)
ROZANSKA	80	NP	B162 505	M. Rozanska et al.	(MPIM, CERN)
CORDEN	79	NP	B157 250	M.J. Corden et al.	(BIRM, RHEL, TEHA+ JP)
EVANGELIS...	79B	NP	B154 381	C. Evangelista et al.	(BARI, BONN, CERN+)
ANTIPOV	77	NP	B119 45	Y.M. Antipov et al.	(SERP, GEVA)
APEL	75	PL	57B 398	W.D. Apel et al.	(KARLK, KARLE, PISA, SERP+ JP)
BLUM	75	PL	57B 403	W. Blum et al.	(CERN, MPIM) JP

$\pi_2(2100)$

$$J^{PC} = 1^-(2^-+)$$

OMITTED FROM SUMMARY TABLE

Needs confirmation.

$\pi_2(2100)$ MASS

VALUE (MeV)	DOCUMENT ID	TECN	COMMENT
2090 ± 29 OUR AVERAGE			
2090 ± 30	1	AMELIN	95B VES $36 \pi^- A \rightarrow \pi^+\pi^-\pi^- A$
2100 ± 150	2	DAUM	81B CNTR $63,94 \pi^- p \rightarrow 3\pi X$
			1 From a fit to $J^{PC} = 2^-+$ $f_2(1270)\pi$, $(\pi\pi)\pi$ waves.
			2 From a two-resonance fit to four 2^-0^+ waves.

$\pi_2(2100)$ WIDTH

VALUE (MeV)	DOCUMENT ID	TECN	COMMENT
625 ± 50 OUR AVERAGE			Error includes scale factor of 1.2.
520 ± 100	3	AMELIN	95B VES $36 \pi^- A \rightarrow \pi^+\pi^-\pi^- A$
651 ± 50	4	DAUM	81B CNTR $63,94 \pi^- p \rightarrow 3\pi X$
			3 From a fit to $J^{PC} = 2^-+$ $f_2(1270)\pi$, $(\pi\pi)\pi$ waves.
			4 From a two-resonance fit to four 2^-0^+ waves.

$\pi_2(2100)$ DECAY MODES

Mode	Fraction (Γ_i/Γ)
Γ_1	3π seen
Γ_2	$\rho\pi$ seen
Γ_3	$f_2(1270)\pi$ seen
Γ_4	$(\pi\pi)_S\pi$ seen

$\pi_2(2100)$ BRANCHING RATIOS

$\Gamma(\rho\pi)/\Gamma(3\pi)$ Γ_2/Γ_1			
VALUE	DOCUMENT ID	TECN	COMMENT
0.19 ± 0.05	5	DAUM	81B CNTR $63,94 \pi^- p$
$\Gamma(f_2(1270)\pi)/\Gamma(3\pi)$ Γ_3/Γ_1			
VALUE	DOCUMENT ID	TECN	COMMENT
0.36 ± 0.09	5	DAUM	81B CNTR $63,94 \pi^- p$
$\Gamma((\pi\pi)_S\pi)/\Gamma(3\pi)$ Γ_4/Γ_1			
VALUE	DOCUMENT ID	TECN	COMMENT
0.45 ± 0.07	5	DAUM	81B CNTR $63,94 \pi^- p$

Meson Particle Listings

$\pi_2(2100)$, $f_0(2100)$, $f_2(2150)$

D-wave/S-wave RATIO FOR $\pi_2(2100) \rightarrow f_2(1270)\pi$

VALUE	DOCUMENT ID	TECN	COMMENT
0.39±0.23	⁵ DAUM	81B	CNTR 63.94 π^-p

⁵ From a two-resonance fit to four 2^{-0+} waves.

$\pi_2(2100)$ REFERENCES

AMELIN DAUM	95B 81B	PL B356 595 NP B182 269	D.V. Amelin et al. C. Daum et al.	(SERP, TBIL) (AMST, CERN, CRAC, MPIM+)
----------------	------------	----------------------------	--------------------------------------	---

$f_0(2100)$

$$I^G(J^{PC}) = 0^+(0^{++})$$

OMITTED FROM SUMMARY TABLE
Needs confirmation.

$f_0(2100)$ MASS

VALUE (MeV)	EVTS	DOCUMENT ID	TECN	COMMENT
2095⁺¹⁷₋₁₉ OUR AVERAGE				
2116±27±17		LEES	21A	BABR $\gamma\gamma \rightarrow \eta_c(1S) \rightarrow \eta' \pi^+ \pi^-$
2081±13±24 ₋₃₆	5.5k	¹ ABLIKIM	13N	BES3 $e^+e^- \rightarrow J/\psi \rightarrow \gamma\eta\eta$
2090±30		BAI	00A	BES $J/\psi \rightarrow \gamma(\pi^+\pi^-\pi^+\pi^-)$
2075±20		SARANTSEV	21	RVUE $J/\psi(1S) \rightarrow \gamma(\pi\pi, K\bar{K}, \eta\eta, \omega\phi)$
2090±10±6	529	^{2,3} DOBBS	15	$J/\psi \rightarrow \gamma\pi^+\pi^-$
2099±17±8	283	^{2,3} DOBBS	15	$\psi(2S) \rightarrow \gamma\pi^+\pi^-$
2105±8	80k	⁴ UMAN	06	E835 $5.2 \bar{p}p \rightarrow \eta\eta\pi^0$
2102±13		⁵ ANISOVICH	00J	SPEC $2.0 \bar{p}p \rightarrow \eta\pi^0\pi^0, \pi^0\pi^0, \eta\eta, \eta\eta', \pi^+\pi^-$
2105±10		ANISOVICH	99K	SPEC $0.6\text{-}1.94 \bar{p}p \rightarrow \eta\eta, \eta\eta'$
~2104		BUGG	95	$J/\psi \rightarrow \gamma\pi^+\pi^-\pi^+\pi^-$
~2122		HASAN	94	RVUE $\bar{p}p \rightarrow \pi\pi$

¹ From partial wave analysis including all possible combinations of 0^{++} , 2^{++} , and 4^{++} resonances.
² Using CLEO-c data but not authored by the CLEO Collaboration.
³ From a fit to a Breit-Wigner line shape with fixed $\Gamma = 209$ MeV.
⁴ Statistical error only.
⁵ Includes the data of ANISOVICH 00B indicating to exotic decay pattern.

$f_0(2100)$ WIDTH

VALUE (MeV)	EVTS	DOCUMENT ID	TECN	COMMENT
287⁺³²₋₂₄ OUR AVERAGE				
289±34±15		LEES	21A	BABR $\gamma\gamma \rightarrow \eta_c(1S) \rightarrow \eta' \pi^+ \pi^-$
273±27±70 ₋₂₄₋₂₃	5.5k	¹ ABLIKIM	13N	BES3 $e^+e^- \rightarrow J/\psi \rightarrow \gamma\eta\eta$
330±100		BAI	00A	BES $J/\psi \rightarrow \gamma(\pi^+\pi^-\pi^+\pi^-)$
260±25		SARANTSEV	21	RVUE $J/\psi(1S) \rightarrow \gamma(\pi\pi, K\bar{K}, \eta\eta, \omega\phi)$
236±14	80k	² UMAN	06	E835 $5.2 \bar{p}p \rightarrow \eta\eta\pi^0$
211±29		³ ANISOVICH	00J	SPEC $2.0 \bar{p}p \rightarrow \eta\pi^0\pi^0, \pi^0\pi^0, \eta\eta, \eta\eta', \pi^+\pi^-$
200±25		ANISOVICH	99K	SPEC $0.6\text{-}1.94 \bar{p}p \rightarrow \eta\eta, \eta\eta'$
~203		BUGG	95	$J/\psi \rightarrow \gamma\pi^+\pi^-\pi^+\pi^-$
~273		HASAN	94	RVUE $\bar{p}p \rightarrow \pi\pi$

¹ From partial wave analysis including all possible combinations of 0^{++} , 2^{++} , and 4^{++} resonances.
² Statistical error only.
³ Includes the data of ANISOVICH 00B indicating to exotic decay pattern.

$f_0(2100)$ REFERENCES

LEES	21A	PR D104 072002	J.P. Lees et al.	(BABAR Collab.)
SARANTSEV	21	PL B816 136227	A.V. Sarantsev et al.	(BONN, PNPI)
DOBBS	15	PR D91 052006	S. Dobbs et al.	(NWES)
ABLIKIM	13N	PR D87 092009	M. Ablikim et al.	(BESIII Collab.)
UMAN	06	PR D73 052009	I. Uman et al.	(FNAL E835)
ANISOVICH	00B	NP A662 319	A.V. Anisovich et al.	
ANISOVICH	00J	PL B491 47	A.V. Anisovich et al.	(RAL, LOQM, PNPI+)
BAI	00A	PL B472 207	J.Z. Bai et al.	(BES Collab.)
ANISOVICH	99K	PL B468 309	A.V. Anisovich et al.	
BUGG	95	PL B353 378	D.V. Bugg et al.	(LOQM, PNPI, WASH)
HASAN	94	PL B334 215	A. Hasan, D.V. Bugg	(LOQM)

$f_2(2150)$

$$I^G(J^{PC}) = 0^+(2^{++})$$

OMITTED FROM SUMMARY TABLE
This entry was previously called T_0 .

$f_2(2150)$ MASS

$f_2(2150)$ MASS, COMBINED MODES (MeV)

VALUE (MeV)	EVTS	DOCUMENT ID	TECN	COMMENT
2157±12 OUR AVERAGE	Includes data from the datablock that follows this one.			
2170±6	80k	¹ UMAN	06	E835 $5.2 \bar{p}p \rightarrow \eta\eta\pi^0$

• • • We do not use the following data for averages, fits, limits, etc. • • •

¹ Statistical error only.

$\eta\eta$ MODE

VALUE (MeV)	DOCUMENT ID	TECN	COMMENT
2151±16	BARBERIS 00E		$450 pp \rightarrow p_f \eta \eta p_S$
2175±20	PROKOSHKIN 95D	GAM4	$300 \pi^- N \rightarrow \pi^- N 2\eta$ $450 pp \rightarrow pp 2\eta$
2130±35	SINGOVSKI 94	GAM4	$450 pp \rightarrow pp 2\eta$

2157±12 OUR AVERAGE

2140±30	² ABELE	99B	CBAR	$1.94 \bar{p}p \rightarrow \pi^0 \eta\eta$
2104±20	³ ARMSTRONG	93C	E760	$\bar{p}p \rightarrow \pi^0 \eta\eta \rightarrow 6\gamma$

• • • We do not use the following data for averages, fits, limits, etc. • • •

² Spin not determined
³ No J^{PC} determination.

$\eta\eta\pi$ MODE

VALUE (MeV)	DOCUMENT ID	TECN	CHG	COMMENT
2135±20±45	⁴ ADOMEIT	96	CBAR	0 $1.94 \bar{p}p \rightarrow \eta 3\pi^0$

• • • We do not use the following data for averages, fits, limits, etc. • • •

⁴ ANISOVICH 00E recommends to withdraw ADOMEIT 96 that assumed a single $J^P = 2^+$ resonance.

$\bar{p}p \rightarrow \pi\pi$

VALUE (MeV)	DOCUMENT ID	TECN	COMMENT
~2090	⁵ OAKDEN	94	RVUE $0.36\text{-}1.55 \bar{p}p \rightarrow \pi\pi$
~2120	⁶ OAKDEN	94	RVUE $0.36\text{-}1.55 \bar{p}p \rightarrow \pi\pi$
~2170	⁷ MARTIN	80B	RVUE
~2150	⁷ MARTIN	80C	RVUE
~2150	⁸ DULUDE	78B	OSPK $1\text{-}2 \bar{p}p \rightarrow \pi^0\pi^0$

• • • We do not use the following data for averages, fits, limits, etc. • • •

⁵ OAKDEN 94 makes an amplitude analysis of LEAR data on $\bar{p}p \rightarrow \pi\pi$ using a method based on Barrelet zeros. This is solution A. The amplitude analysis of HASAN 94 includes earlier data as well, and assume that the data can be parametrized in terms of towers of nearly degenerate resonances on the leading Regge trajectory. See also KLOET 96 and MARTIN 97 who make related analyses.
⁶ From solution B of amplitude analysis of data on $\bar{p}p \rightarrow \pi\pi$.
⁷ $I(J^P) = 0(2^+)$ from simultaneous analysis of $p\bar{p} \rightarrow \pi^-\pi^+$ and $\pi^0\pi^0$.
⁸ $I^G(J^P) = 0^+(2^+)$ from partial-wave amplitude analysis.

S-CHANNEL $\bar{p}p$, $\bar{N}N$ or $K\bar{K}$

VALUE (MeV)	DOCUMENT ID	TECN	CHG	COMMENT
2139 ⁺⁸ ₋₉	⁹ EVANGELIS...	97	SPEC	$0.6\text{-}2.4 \bar{p}p \rightarrow K_S^0 K_S^0$
~2190	⁹ CUTTS	78B	CNTR	$0.97\text{-}3 \bar{p}p \rightarrow \bar{N}N$
2155±15	^{9,10} COUPLAND	77	CNTR	0 $0.7\text{-}2.4 \bar{p}p \rightarrow \bar{p}p$
2193±2	^{9,11} ALSPECTOR	73	CNTR	$\bar{p}p$ S channel

• • • We do not use the following data for averages, fits, limits, etc. • • •

⁹ Isospins 0 and 1 not separated.
¹⁰ From a fit to the total elastic cross section.
¹¹ Referred to as T or T region by ALSPECTOR 73.

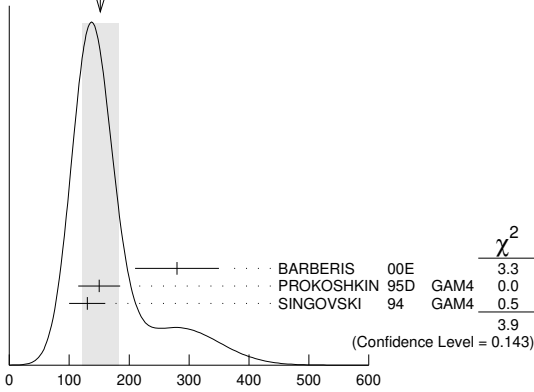
$K\bar{K}$ MODE

VALUE (MeV)	DOCUMENT ID	TECN	COMMENT
2200±13	VLADIMIRSK...06	SPEC	$40 \pi^-p \rightarrow K_S^0 K_S^0 n$
2150±20	ABLIKIM	04E	BES2 $J/\psi \rightarrow \omega K^+ K^-$
2130±35	BARBERIS	99	OMEG $450 pp \rightarrow p_S p_f K^+ K^-$

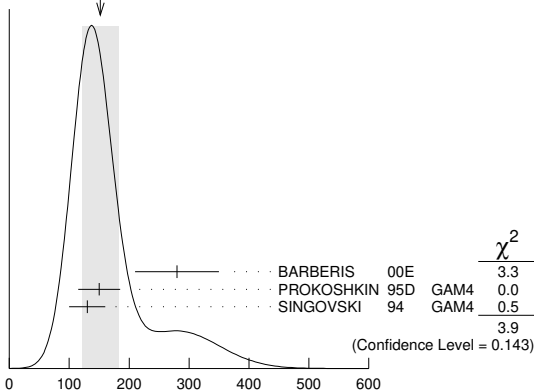
• • • We do not use the following data for averages, fits, limits, etc. • • •

$f_2(2150)$ WIDTH $f_2(2150)$ WIDTH, COMBINED MODES (MeV)

VALUE (MeV)	EVTS	DOCUMENT ID	TECN	COMMENT
152±30 OUR AVERAGE				Includes data from the datablock that follows this one. Error includes scale factor of 1.4. See the ideogram below.
•••				We do not use the following data for averages, fits, limits, etc. •••
182±11	80k	12 UMAN	06	E835 5.2 $\bar{p}p \rightarrow \eta\eta\pi^0$
12 Statistical error only.				

WEIGHTED AVERAGE
152±30 (Error scaled by 1.4) $f_2(2150)$ width, combined modes (MeV) $\eta\eta$ MODE

VALUE (MeV)	DOCUMENT ID	TECN	COMMENT
The data in this block is included in the average printed for a previous datablock.			
152±30 OUR AVERAGE			Error includes scale factor of 1.4. See the ideogram below.
280±70	BARBERIS 00E		450 $pp \rightarrow p_f \eta \eta \rho_S$
150±35	PROKOSHKIN 95D	GAM4	300 $\pi^- N \rightarrow \pi^- N 2\eta$, 450 $pp \rightarrow pp 2\eta$
130±30	SINGOVSKI 94	GAM4	450 $pp \rightarrow pp 2\eta$
•••			We do not use the following data for averages, fits, limits, etc. •••
310±50	13 ABELE 99B	CBAR	1.94 $\bar{p}p \rightarrow \pi^0 \eta \eta$
203±10	14 ARMSTRONG 93C	E760	$\bar{p}p \rightarrow \pi^0 \eta \eta \rightarrow 6\gamma$

WEIGHTED AVERAGE
152±30 (Error scaled by 1.4) $f_2(2150)$ width, $\eta\eta$ mode (MeV)

13 Spin not determined.

14 No J^{PC} determination. $\eta\pi\pi$ MODE

VALUE (MeV)	DOCUMENT ID	TECN	CHG	COMMENT
•••				We do not use the following data for averages, fits, limits, etc. •••
250±25±45	15 ADOMEIT 96	CBAR	0	1.94 $\bar{p}p \rightarrow \eta 3\pi^0$
15 ANISOVICH 00E recommends to withdraw ADOMEIT 96 that assumed a single $J^P = 2^+$ resonance.				

 $\bar{p}p \rightarrow \pi\pi$

VALUE (MeV)	DOCUMENT ID	TECN	COMMENT
250 OUR ESTIMATE			
•••			We do not use the following data for averages, fits, limits, etc. •••
~ 70	16 OAKDEN 94	RVUE	0.36-1.55 $\bar{p}p \rightarrow \pi\pi$
~ 250	17 MARTIN 80B	RVUE	
~ 250	17 MARTIN 80C	RVUE	
~ 250	18 DULUDE 78B	OSPCK	1-2 $\bar{p}p \rightarrow \pi^0 \pi^0$
16 See however KLOET 96 who fit $\pi^+ \pi^-$ only and find waves only up to $J = 3$ to be important but not significantly resonant.			
17 $I(J^P) = 0(2^+)$ from simultaneous analysis of $p\bar{p} \rightarrow \pi^- \pi^+$ and $\pi^0 \pi^0$.			
18 $I^G(J^P) = 0^+(2^+)$ from partial-wave amplitude analysis.			

S-CHANNEL $\bar{p}p, \bar{N}N$ or $\bar{K}K$

VALUE (MeV)	DOCUMENT ID	TECN	CHG	COMMENT
•••				We do not use the following data for averages, fits, limits, etc. •••
56^{+31}_{-16}	19 EVANGELIS... 97	SPEC		0.6-2.4 $\bar{p}p \rightarrow K_S^0 K_S^0$
135±75	20,21 COUPLAND 77	CNTR	0	0.7-2.4 $\bar{p}p \rightarrow \bar{p}p$
98±8	21 ALSPECTOR 73	CNTR		$\bar{p}p$ S channel
19 Isospin 0 and 2 not separated.				
20 From a fit to the total elastic cross section.				
21 Isospins 0 and 1 not separated.				

 $K\bar{K}$ MODE

VALUE (MeV)	DOCUMENT ID	TECN	COMMENT
•••			We do not use the following data for averages, fits, limits, etc. •••
91±62	VLADIMIRSK...06	SPEC	40 $\pi^- p \rightarrow K_S^0 K_S^0 n$
150±30	ABLIKIM 04E	BES2	$J/\psi \rightarrow \omega K^+ K^-$
270±50	BARBERIS 99	OMEGA	450 $pp \rightarrow p_S p_f K^+ K^-$

 $f_2(2150)$ DECAY MODES

Mode	Fraction (Γ_i/Γ)
Γ_1	$\pi\pi$
Γ_2	$\eta\eta$
Γ_3	$K\bar{K}$
Γ_4	$f_2(1270)\eta$
Γ_5	$a_2(1320)\pi$
Γ_6	$p\bar{p}$
	seen
	seen
	seen
	seen
	seen

 $f_2(2150)$ BRANCHING RATIOS

$\Gamma(K\bar{K})/\Gamma(\eta\eta)$	CL%	DOCUMENT ID	TECN	COMMENT	Γ_3/Γ_2
1.28±0.23		BARBERIS 00E		450 $pp \rightarrow p_f \eta \eta \rho_S$	
•••				We do not use the following data for averages, fits, limits, etc. •••	
<0.1	95	22 PROKOSHKIN 95D	GAM4	300 $\pi^- N \rightarrow \pi^- N 2\eta$, 450 $pp \rightarrow pp 2\eta$	
22 Using data from ARMSTRONG 89D.					

 $\Gamma(\pi\pi)/\Gamma(\eta\eta)$

VALUE	CL%	DOCUMENT ID	TECN	COMMENT	Γ_1/Γ_2
<0.33	95	23 PROKOSHKIN 95D	GAM4	300 $\pi^- N \rightarrow \pi^- N 2\eta$, 450 $pp \rightarrow pp 2\eta$	
23 Derived from a $\pi^0 \pi^0/\eta\eta$ limit.					

 $\Gamma(f_2(1270)\eta)/\Gamma(a_2(1320)\pi)$

VALUE	DOCUMENT ID	TECN	COMMENT	Γ_4/Γ_5
0.79±0.11	24 ADOMEIT 96	CBAR	1.94 $\bar{p}p \rightarrow \eta 3\pi^0$	
24 Using $B(a_2(1320) \rightarrow \eta\pi) = 0.145$				

 $\Gamma(p\bar{p})/\Gamma_{total}$

VALUE	EVTS	DOCUMENT ID	TECN	COMMENT	Γ_6/Γ
seen	73	ALEXANDER 10	CLEO	$\psi(2S) \rightarrow \gamma p\bar{p}$	

 $f_2(2150)$ REFERENCES

ALEXANDER 10	PR D82 092002	J.P. Alexander <i>et al.</i>	(CLEO Collab.)
UMAN 06	PR D73 052009	I. Uman <i>et al.</i>	(FNAL E835)
VLADIMIRSK... 06	PAN 69 493	V.V. Vladimirovsky <i>et al.</i>	(ITEP, Moscow)
	Translated from YAF 69 515.		
ABLIKIM 04E	PL B603 138	M. Ablikim <i>et al.</i>	(BES Collab.)
ANISOVICH 00E	PL B477 19	A.V. Anisovich <i>et al.</i>	
BARBERIS 00E	PL B479 59	D. Barberis <i>et al.</i>	(WA 102 Collab.)
ABELE 99B	EPJ C8 67	A. Abele <i>et al.</i>	(Crystal Barrel Collab.)
BARBERIS 99	PL B453 305	D. Barberis <i>et al.</i>	(Omega Expt.)
EVANGELIS... 97	PR D56 3803	C. Evangelista <i>et al.</i>	(LEAR Collab.)
MARTIN 97	PR C56 1114	B.R. Martin, G.C. Oades	(LOUC, AARH)
ADOMEIT 96	ZPHY C71 227	J. Adomeit <i>et al.</i>	(Crystal Barrel Collab.)
KLOET 96	PR D53 6120	W.M. Kloet, F. Myhrer	(RUTG, NJORD)
PROKOSHKIN 95D	PD 40 495	Y.D. Prokoshkin	(SERP) IJGPC
	Translated from DANS 344 469.		

Meson Particle Listings

 $f_2(2150), \rho(2150)$

HASAN	94	PL B334 215	A. Hasan, D.V. Bugg	(LOQM)
OAKDEN	94	NC A574 731	M.N. Oakden, M.R. Pennington	(DURH)
SINGOVSKI	94	NC A107 1911	A.V. Singovsky	(SERP)
ARMSTRONG	93C	PL B307 394	T.A. Armstrong <i>et al.</i>	(FNAL, FERR, GENO+)
ARMSTRONG	89D	PL B227 186	T.A. Armstrong, M. Benayoun	(ATHU, BARI, BIRM+)
MARTIN	80B	NP B176 355	B.R. Martin, D. Morgan	(LOUC, RHEL) JP
MARTIN	80C	NP B169 216	A.D. Martin, M.R. Pennington	(DURH) JP
CUTTS	78B	PR D17 16	D. Cutts <i>et al.</i>	(STON, WIS C)
DULUDE	78B	PL 79B 335	R.S. Dulude <i>et al.</i>	(BROW, MIT, BARI) JP
COUPLAND	77	PL 71B 460	M. Coupland <i>et al.</i>	(LOQM, RHEL)
ALSPECTOR	73	PRL 30 511	J. Alspector <i>et al.</i>	(RUTG, UPNJ)

 $\rho(2150)$

$$I^G(J^{PC}) = 1^+(1^{--})$$

OMITTED FROM SUMMARY TABLE

This entry was previously called $T_1(2190)$. See the review on "Spectroscopy of Light Meson Resonances."

 $\rho(2150)$ MASS e^+e^- PRODUCED

VALUE (MeV)	EVTS	DOCUMENT ID	TECN	COMMENT
2034 ± 13 ± 9		1 ABLIKIM	21A BES3	$e^+e^- \rightarrow \omega\pi^0$
2111 ± 43 ± 25		2 ABLIKIM	21X BES3	$e^+e^- \rightarrow \eta'\pi^+\pi^-$
2255 +17 -18 +50 -41	1.8k	3 ABLIKIM	20F BES3	$\psi(2S) \rightarrow K^+K^-\eta$
2201 ± 19		4 LEES	20 BABR	$e^+e^- \rightarrow K^+K^-\eta$
2227 ± 9 ± 9		5 LEES	20 RVUE	$e^+e^- \rightarrow K^+K^-$
2039 ± 8 +36 -18		6 ABLIKIM	19AQ BES	$J/\psi \rightarrow K^+K^-\pi^0$
2239.2 ± 7.1 ± 11.3		7 ABLIKIM	19L BES3	$e^+e^- \rightarrow K^+K^-$
2254 ± 22		8 LEES	12G BABR	$e^+e^- \rightarrow \pi^+\pi^-\gamma$
2150 ± 40 ± 50		AUBERT	07AU BABR	10.6 $e^+e^- \rightarrow f_1(1285)\pi^+\pi^-\gamma$
1990 ± 80		AUBERT	07AU BABR	10.6 $e^+e^- \rightarrow \eta'\pi^+\pi^-\gamma$
2153 ± 37		BIAGINI	91 RVUE	$e^+e^- \rightarrow \pi^+\pi^-, K^+K^-$
2110 ± 50		9 CLEGG	90 RVUE	$e^+e^- \rightarrow 3(\pi^+\pi^-), 2(\pi^+\pi^-\pi^0)$

- 1 From a fit to the cross section between 2.00 and 3.08 GeV with a coherent sum of Breit-Wigner amplitudes, including contributions from $\rho(770)$, $\rho(1450)$ and $\rho(1700)$. Could be another state.
- 2 From a Breit-Wigner fit to the Born cross section, including an s -dependent continuum amplitude.
- 3 Seen in $\psi(2S)$ decay with branching ratio $\psi(2S) \rightarrow X\eta \rightarrow K^+K^-\eta = (21.7 \pm 1.9^{+7.7}_{-8.3}) \times 10^{-6}$.
- 4 From the fit to the BABAR data of LEES 13Q assuming a coherent sum of a single Breit-Wigner resonance and a nonresonant contribution. The resonance significance is 3.5 σ .
- 5 From the fit to the BABAR data of LEES 13Q and BESIII data of ABLIKIM 19L assuming a coherent sum of a single Breit-Wigner resonance and a nonresonant contribution.
- 6 Could also be another state. Seen in J/ψ decay with branching ratio $J/\psi \rightarrow X\pi^0 \rightarrow K^+K^-\pi^0 = (6.7 \pm 1.1^{+2.2}_{-1.8}) \times 10^{-6}$.
- 7 The observed structure can be due to both the $\phi(2170)$ and $\rho(2150)$.
- 8 Using the GOUNARIS 68 parametrization of the pion form factor leaving the masses and widths of the $\rho(1450)$, $\rho(1700)$, and $\rho(2150)$ resonances as free parameters of the fit.
- 9 Includes ATKINSON 85.

 $\bar{p}p \rightarrow \pi\pi$

VALUE (MeV)	DOCUMENT ID	TECN	COMMENT
~ 2191	HASAN	94 RVUE	$\bar{p}p \rightarrow \pi\pi$
~ 2070	1 OAKDEN	94 RVUE	0.36–1.55 $\bar{p}p \rightarrow \pi\pi$
~ 2170	2 MARTIN	80B RVUE	
~ 2100	2 MARTIN	80C RVUE	

- 1 See however KLOET 96 who fit $\pi^+\pi^-$ only and find waves only up to $J = 3$ to be important but not significantly resonant.
- 2 $I(J^P) = 1(1^-)$ from simultaneous analysis of $\rho\bar{p} \rightarrow \pi^-\pi^+$ and $\pi^0\pi^0$.

S-CHANNEL $\bar{N}N$

VALUE (MeV)	DOCUMENT ID	TECN	COMMENT
2110 ± 35	1 ANISOVICH	02 SPEC	0.6–1.9 $\rho\bar{p} \rightarrow \omega\pi^0, \omega\eta\pi^0, \pi^+\pi^-$
~ 2190	2 CUTTS	78B CNTR	0.97–3 $\bar{p}p \rightarrow \bar{N}N$
2155 ± 15	2,3 COUPLAND	77 CNTR	0.7–2.4 $\bar{p}p \rightarrow \bar{p}p$
2193 ± 2	2,4 ALSPECTOR	73 CNTR	$\bar{p}p$ S channel
2190 ± 10	5 ABRAMS	70 CNTR	S channel $\bar{p}N$

- 1 From the combined analysis of ANISOVICH 00I, ANISOVICH 01D, ANISOVICH 01E, and ANISOVICH 02.
- 2 Isospins 0 and 1 not separated.
- 3 From a fit to the total elastic cross section.
- 4 Referred to as T or T' region by ALSPECTOR 73.
- 5 Seen as bump in $l = 1$ state. See also COOPER 68. PEASLEE 75 confirm $\bar{p}p$ results of ABRAMS 70, no narrow structure.

 $\pi^-p \rightarrow \omega\pi^0 n$

VALUE (MeV)	DOCUMENT ID	TECN	COMMENT
2140 ± 30	ALDE	95 GAM2	38 $\pi^-p \rightarrow \omega\pi^0 n$
2170 ± 30	ALDE	92C GAM4	100 $\pi^-p \rightarrow \omega\pi^0 n$

- • • We do not use the following data for averages, fits, limits, etc. • • •

 $\rho(2150)$ WIDTH e^+e^- PRODUCED

VALUE (MeV)	EVTS	DOCUMENT ID	TECN	COMMENT
234 ± 30 ± 25		1 ABLIKIM	21A BES3	$e^+e^- \rightarrow \omega\pi^0$
135 ± 34 ± 30		2 ABLIKIM	21X BES3	$e^+e^- \rightarrow \eta'\pi^+\pi^-$
460 +54 -48 +160 -90	1.8k	3 ABLIKIM	20F BES3	$\psi(2S) \rightarrow K^+K^-\eta$
70 ± 38		4 LEES	20 BABR	$e^+e^- \rightarrow K^+K^-\eta$
127 ± 14 ± 4		5 LEES	20 RVUE	$e^+e^- \rightarrow K^+K^-$
196 ± 23 +25 -27		6 ABLIKIM	19AQ BES	$J/\psi \rightarrow K^+K^-\pi^0$
139.8 ± 12.3 ± 20.6		7 ABLIKIM	19L BES3	$e^+e^- \rightarrow K^+K^-$
109 ± 76		8 LEES	12G BABR	$e^+e^- \rightarrow \pi^+\pi^-\gamma$
350 ± 40 ± 50		AUBERT	07AU BABR	10.6 $e^+e^- \rightarrow f_1(1285)\pi^+\pi^-\gamma$
310 ± 140		AUBERT	07AU BABR	10.6 $e^+e^- \rightarrow \eta'\pi^+\pi^-\gamma$
389 ± 79		BIAGINI	91 RVUE	$e^+e^- \rightarrow \pi^+\pi^-, K^+K^-$
410 ± 100		9 CLEGG	90 RVUE	$e^+e^- \rightarrow 3(\pi^+\pi^-), 2(\pi^+\pi^-\pi^0)$

- 1 From a fit to the cross section between 2.00 and 3.08 GeV with a coherent sum of Breit-Wigner amplitudes, including contributions from $\rho(770)$, $\rho(1450)$ and $\rho(1700)$. Could be another state.
- 2 From a Breit-Wigner fit to the Born cross section, including an s -dependent continuum amplitude.
- 3 Seen in $\psi(2S)$ decay with branching ratio $\psi(2S) \rightarrow X\eta \rightarrow K^+K^-\eta = (21.7 \pm 1.9^{+7.7}_{-8.3}) \times 10^{-6}$.
- 4 From the fit to the BABAR data of LEES 13Q assuming a coherent sum of a single Breit-Wigner resonance and a nonresonant contribution. The resonance significance is 3.5 σ .
- 5 From the fit to the BABAR data of LEES 13Q and BESIII data of ABLIKIM 19L assuming a coherent sum of a single Breit-Wigner resonance and a nonresonant contribution.
- 6 Could also be another state. Seen in J/ψ decay with branching ratio $J/\psi \rightarrow X\pi^0 \rightarrow K^+K^-\pi^0 = (6.7 \pm 1.1^{+2.2}_{-1.8}) \times 10^{-6}$.
- 7 The observed structure can be due to both the $\phi(2170)$ and $\rho(2150)$.
- 8 Using the GOUNARIS 68 parametrization of the pion form factor leaving the masses and widths of the $\rho(1450)$, $\rho(1700)$, and $\rho(2150)$ resonances as free parameters of the fit.
- 9 Includes ATKINSON 85.

 $\bar{p}p \rightarrow \pi\pi$

VALUE (MeV)	DOCUMENT ID	TECN	COMMENT
~ 296	HASAN	94 RVUE	$\bar{p}p \rightarrow \pi\pi$
~ 40	1 OAKDEN	94 RVUE	0.36–1.55 $\bar{p}p \rightarrow \pi\pi$
~ 250	2 MARTIN	80B RVUE	
~ 200	2 MARTIN	80C RVUE	

- • • We do not use the following data for averages, fits, limits, etc. • • •

- 1 See however KLOET 96 who fit $\pi^+\pi^-$ only and find waves only up to $J = 3$ to be important but not significantly resonant.
- 2 $I(J^P) = 1(1^-)$ from simultaneous analysis of $\rho\bar{p} \rightarrow \pi^-\pi^+$ and $\pi^0\pi^0$.

S-CHANNEL $\bar{N}N$

VALUE (MeV)	DOCUMENT ID	TECN	COMMENT
230 ± 50	1 ANISOVICH	02 SPEC	0.6–1.9 $\rho\bar{p} \rightarrow \omega\pi^0, \omega\eta\pi^0, \pi^+\pi^-$
135 ± 75	2,3 COUPLAND	77 CNTR	0.7–2.4 $\bar{p}p \rightarrow \bar{p}p$
98 ± 8	3 ALSPECTOR	73 CNTR	$\bar{p}p$ S channel
~ 85	4 ABRAMS	70 CNTR	S channel $\bar{p}N$

- 1 From the combined analysis of ANISOVICH 00I, ANISOVICH 01D, ANISOVICH 01E, and ANISOVICH 02.
- 2 From a fit to the total elastic cross section.
- 3 Isospins 0 and 1 not separated.
- 4 Seen as bump in $l = 1$ state. See also COOPER 68. PEASLEE 75 confirm $\bar{p}p$ results of ABRAMS 70, no narrow structure.

 $\pi^-p \rightarrow \omega\pi^0 n$

VALUE (MeV)	DOCUMENT ID	TECN	COMMENT
320 ± 70	ALDE	95 GAM2	38 $\pi^-p \rightarrow \omega\pi^0 n$
~ 300	ALDE	92C GAM4	100 $\pi^-p \rightarrow \omega\pi^0 n$

- • • We do not use the following data for averages, fits, limits, etc. • • •

 $\rho(2150)$ DECAY MODES

Mode	Fraction (Γ_i/Γ)
Γ_1 e^+e^-	
Γ_2 $\pi^+\pi^-$	seen
Γ_3 K^+K^-	seen

See key on page 1127

Meson Particle Listings

$\rho(2150)$, $\phi(2170)$

Γ_4	$3(\pi^+\pi^-)$	seen
Γ_5	$2(\pi^+\pi^-\pi^0)$	seen
Γ_6	$\eta'\pi^+\pi^-$	seen
Γ_7	$f_1(1285)\pi^+\pi^-$	seen
Γ_8	$\omega\pi^0$	seen
Γ_9	$\omega\pi^0\eta$	seen
Γ_{10}	$\rho\bar{\rho}$	

$\rho(2150) \Gamma(i)\Gamma(e^+e^-)/\Gamma(\text{total})$

$\Gamma(\omega\pi^0) \times \Gamma(e^+e^-)/\Gamma_{\text{total}}$	DOCUMENT ID	TECN	COMMENT	$\Gamma_8\Gamma_1/\Gamma$
34 ± 11 ± 16	ABLIKIM	21A	BES3 $e^+e^- \rightarrow \omega\pi^0$	

$\Gamma(\eta'\pi^+\pi^-) \times \Gamma(e^+e^-)/\Gamma_{\text{total}}$	DOCUMENT ID	TECN	COMMENT	$\Gamma_6\Gamma_1/\Gamma$
23.3 ± 5.3 ± 3.3	1 ABLIKIM	21X	BES3 $e^+e^- \rightarrow \eta'\pi^+\pi^-$	

¹ From a Breit-Wigner fit to the Born cross section interfering constructively with the continuum. For destructive interference the value is 0.64 ± 0.49 ± 0.42 eV.

$\rho(2150) \Gamma(i)\Gamma(e^+e^-)/\Gamma^2(\text{total})$

$\Gamma(f_1(1285)\pi^+\pi^-)/\Gamma_{\text{total}} \times \Gamma(e^+e^-)/\Gamma_{\text{total}}$	DOCUMENT ID	TECN	COMMENT	$\Gamma_7/\Gamma \times \Gamma_1/\Gamma$
3.1 ± 0.6 ± 0.5	1 AUBERT	07AU	BABR 10.6 $e^+e^- \rightarrow f_1(1285)\pi^+\pi^-$	

¹ Calculated by us from the reported value of cross section at the peak.

$\Gamma(\eta'\pi^+\pi^-)/\Gamma_{\text{total}} \times \Gamma(e^+e^-)/\Gamma_{\text{total}}$	DOCUMENT ID	TECN	COMMENT	$\Gamma_6/\Gamma \times \Gamma_1/\Gamma$
4.9 ± 1.9	1 AUBERT	07AU	BABR 10.6 $e^+e^- \rightarrow \eta'\pi^+\pi^-$	

¹ Calculated by us from the reported value of cross section at the peak.

$\rho(2150)$ REFERENCES

ABLIKIM	21A	PL B813 136059	M. Ablikim et al.	(BESIII Collab.)
ABLIKIM	21X	PR D103 072007	M. Ablikim et al.	(BESIII Collab.)
ABLIKIM	20F	PR D101 032008	M. Ablikim et al.	(BESIII Collab.)
LEES	20	PR D101 012011	J.P. Lees et al.	(BESIII Collab.)
ABLIKIM	19AQ	PR D100 032004	M. Ablikim et al.	(BESIII Collab.)
ABLIKIM	19L	PR D99 032001	M. Ablikim et al.	(BESIII Collab.)
LEES	13Q	PR D88 032013	J.P. Lees et al.	(BABAR Collab.)
LEES	12G	PR D86 032013	J.P. Lees et al.	(BABAR Collab.)
AUBERT	07AU	PR D76 092005	B. Aubert et al.	(BABAR Collab.)
ANISOVICH	02	PL B542 8	A.V. Anisovich et al.	
ANISOVICH	01D	PL B508 6	A.V. Anisovich et al.	
ANISOVICH	01E	PL B513 281	A.V. Anisovich et al.	
ANISOVICH	00J	PL B491 47	A.V. Anisovich et al.	(RAL, LOQM, PNPI+)
KLOET	96	PR D53 6120	W.M. Kloet, F. Myhrer	(RUTG, NORD)
ALDE	95	ZPHY C66 379	D.M. Alde et al.	(GAMS Collab.) JP
HASAN	94	PL B334 215	A. Hasan, D.V. Bugg	(LOQM)
OKARDEN	94	NP A574 731	M.N. Okaiden, M.R. Pennington	(DURH)
ALDE	92C	ZPHY C54 553	D.M. Alde et al.	(BELG, SERP, KEK, LANL+)
BIAGINI	91	NC 104A 363	M.E. Biagini et al.	(FRAS, PRAG)
CLEGG	90	ZPHY C45 677	A.B. Clegg, A. Donnachie	(LANC, MCHS)
ATKINSON	85	ZPHY C29 333	M. Atkinson et al.	(BONN, CERN, GLAS+)
MARTIN	80B	NP B176 355	B.R. Martin, D. Morgan	(LOUC, RHEL) JP
MARTIN	80C	NP B169 216	A.D. Martin, M.R. Pennington	(DURH) JP
CUTTS	78B	PR D17 16	D. Cutts et al.	(STON, WIS C)
COUPLAND	77	PL 71B 460	M. Coupland et al.	(LOQM, RHEL)
PEASLEE	75	PL 57B 189	D.C. Peaslee et al.	(CANB, BARI, BROW+)
ALSPECTOR	73	PRL 30 511	J. Alspector et al.	(RUTG, UPNJ)
ABRAMS	70	PR D1 1917	R.J. Abrams et al.	(BNL)
COOPER	68	PRL 20 1059	W.A. Cooper et al.	(ANL)
GOUNARIS	68	PRL 21 244	G.J. Gounaris, J.J. Sakurai	

$\phi(2170)$

$$I^G(J^{PC}) = 0^-(1^{--})$$

See the review on "Spectroscopy of Light Meson Resonances."

$\phi(2170)$ MASS

VALUE (MeV)	EVTS	DOCUMENT ID	TECN	COMMENT
2162 ± 7	OUR AVERAGE	Error includes scale factor of 1.1.		
2176 ± 24 ± 3		1 ABLIKIM	21A	BES3 $e^+e^- \rightarrow \omega\eta$
2163.5 ± 6.2 ± 3.0		2 ABLIKIM	21T	BES3 $e^+e^- \rightarrow \phi\eta$
2177.5 ± 4.8 ± 19.5		3 ABLIKIM	20M	BES3 $e^+e^- \rightarrow \eta'\phi$
2126.5 ± 16.8 ± 12.4		4 ABLIKIM	20S	BES3 $e^+e^- \rightarrow K^+K^-\pi^0\pi^0$
2273.7 ± 5.7 ± 19.3		5 ABLIKIM	21AP	BES3 $e^+e^- \rightarrow K_S^0 K_L^0$
2135 ± 8 ± 9	95	6 ABLIKIM	19I	BES3 $e^+e^- \rightarrow \eta\phi f_0(980)$
2239.2 ± 7.1 ± 11.3		6 ABLIKIM	19L	BES3 $e^+e^- \rightarrow K^+K^-$
2200 ± 6 ± 5	471	ABLIKIM	15H	BES3 $J/\psi \rightarrow \eta\phi\pi^+\pi^-$
2180 ± 8 ± 8	7,8	LEES	12F	BABR 10.6 $e^+e^- \rightarrow \phi\pi^+\pi^-$

• • • We do not use the following data for averages, fits, limits, etc. • • •

2079 ± 13	⁺⁷⁹ ₋₂₈	4.8k	9 SHEN	09	BELL	10.6 $e^+e^- \rightarrow K^+K^-\pi^+\pi^-$
2186 ± 10	± 6	52	ABLIKIM	08F	BES	$J/\psi \rightarrow \eta\phi f_0(980)$
2125 ± 22	± 10	483	AUBERT	08S	BABR	10.6 $e^+e^- \rightarrow \phi\eta\eta$
2192 ± 14		116	¹⁰ AUBERT	07AK	BABR	10.6 $e^+e^- \rightarrow K^+K^-\pi^+\pi^-$
2169 ± 20		149	¹⁰ AUBERT	07AK	BABR	10.6 $e^+e^- \rightarrow K^+K^-\pi^0\pi^0$
2175 ± 10	± 15	201	^{8,11} AUBERT, BE	06D	BABR	10.6 $e^+e^- \rightarrow K^+K^-\pi\pi\eta$

¹ From a fit to the cross section between 2.00 and 3.08 GeV with a coherent sum of Breit-Wigner amplitudes, including contributions from $\omega(1420)$ and $\omega(1650)/\phi(1680)$.

² From a fit to the cross section below 3.5 GeV measured by BaBar and BESIII with a coherent sum of two modified Breit-Wigner amplitudes ($\phi(1680)$ and $\phi(2170)$) and a nonresonant term.

³ From a fit using a coherent sum of a phase-space modified Breit-Wigner function and a phase-space term.

⁴ By a simultaneous fit of the intermediate channels in a partial-wave analysis, assuming the same structure, modelled with a coherent sum of a nonresonant component and a resonant component by a Breit-Wigner function.

⁵ From a fit to the cross section between 2.00 and 3.08 GeV with a sum of Breit-Wigner amplitude and a nonresonant contribution. The observed structure can be also due to $\rho(2150)$.

⁶ The observed structure can be due to both the $\phi(2170)$ and $\rho(2150)$.

⁷ Fit includes interference with the $\phi(1680)$.

⁸ From the $\phi f_0(980)$ component.

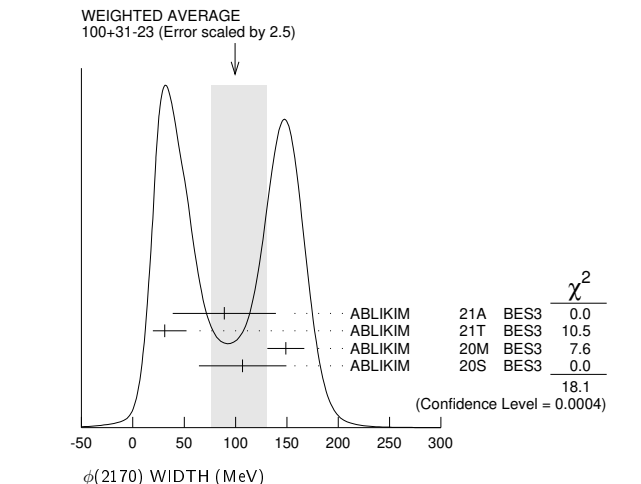
⁹ From a fit with two incoherent Breit-Wigners.

¹⁰ From the $K^+K^- f_0(980)$ component.

¹¹ Superseded by LEES 12F.

$\phi(2170)$ WIDTH

VALUE (MeV)	EVTS	DOCUMENT ID	TECN	COMMENT	
100 ⁺³¹₋₂₃	OUR AVERAGE	Error includes scale factor of 2.5. See the ideogram below.			
89 ± 50 ± 5		1 ABLIKIM	21A	BES3 $e^+e^- \rightarrow \omega\eta$	
31.1 ^{+21.1} _{-11.6} ± 1.1		2 ABLIKIM	21T	BES3 $e^+e^- \rightarrow \phi\eta$	
149.0 ± 15.6 ± 8.9		3 ABLIKIM	20M	BES3 $e^+e^- \rightarrow \eta'\phi$	
106.9 ± 32.1 ± 28.1		4 ABLIKIM	20S	BES3 $e^+e^- \rightarrow K^+K^-\pi^0\pi^0$	
86 ± 44 ± 51		5 ABLIKIM	21AP	BES3 $e^+e^- \rightarrow K_S^0 K_L^0$	
104 ± 24 ± 12	95	6 ABLIKIM	19I	BES3 $e^+e^- \rightarrow \eta\phi f_0(980)$	
139.8 ± 12.3 ± 20.6		6 ABLIKIM	19L	BES3 $e^+e^- \rightarrow K^+K^-$	
104 ± 15 ± 15	471	ABLIKIM	15H	BES3 $J/\psi \rightarrow \eta\phi\pi^+\pi^-$	
77 ± 15 ± 10		7,8	LEES	12F	BABR 10.6 $e^+e^- \rightarrow \phi\pi^+\pi^-$
192 ± 23 ⁺²⁵ ₋₆₁	4.8k	9 SHEN	09	BELL	10.6 $e^+e^- \rightarrow K^+K^-\pi^+\pi^-$
65 ± 23 ± 17	52	ABLIKIM	08F	BES	$J/\psi \rightarrow \eta\phi f_0(980)$
61 ± 50 ± 13	483	AUBERT	08S	BABR	10.6 $e^+e^- \rightarrow \phi\eta\eta$
71 ± 21	116	¹⁰ AUBERT	07AK	BABR	10.6 $e^+e^- \rightarrow K^+K^-\pi^+\pi^-$
102 ± 27	149	¹⁰ AUBERT	07AK	BABR	10.6 $e^+e^- \rightarrow K^+K^-\pi^0\pi^0$
58 ± 16 ± 20	201	^{8,11} AUBERT, BE	06D	BABR	10.6 $e^+e^- \rightarrow K^+K^-\pi\pi\eta$



¹ From a fit to the cross section between 2.00 and 3.08 GeV with a coherent sum of Breit-Wigner amplitudes, including contributions from $\omega(1420)$ and $\omega(1650)/\phi(1680)$.

² From a fit to the cross section below 3.5 GeV measured by BaBar and BESIII with a coherent sum of two modified Breit-Wigner amplitudes ($\phi(1680)$ and $\phi(2170)$) and a nonresonant term.

³ From a fit using a coherent sum of a phase-space modified Breit-Wigner function and a phase-space term.

Meson Particle Listings

$\phi(2170)$, $f_0(2200)$

- ⁴ By a simultaneous fit of the intermediate channels in a partial-wave analysis, assuming the same structure, modelled with a coherent sum of a nonresonant component and a resonant component by a Breit-Wigner function.
⁵ From a fit to the cross section between 2.00 and 3.08 GeV with a sum of Breit-Wigner amplitude and a nonresonant contribution. The observed structure can be also due to $\rho(2150)$.
⁶ The observed structure can be due to both the $\phi(2170)$ and $\rho(2150)$.
⁷ Fit includes interference with the $\phi(1680)$.
⁸ From the $\phi f_0(980)$ component.
⁹ From a fit with two incoherent Breit-Wigners.
¹⁰ From the $K^+ K^- f_0(980)$ component.
¹¹ Superseded by LEES 12f.

$\phi(2170)$ DECAY MODES

Mode	Fraction (Γ_i/Γ)
Γ_1 $e^+ e^-$	seen
Γ_2 $\phi\eta$	
Γ_3 $\omega\eta$	
Γ_4 $\phi\eta'$	
Γ_5 $\phi\pi\pi$	
Γ_6 $\phi f_0(980)$	seen
Γ_7 $K_S^0 K_L^0$	
Γ_8 $K^+ K^- \pi^+ \pi^-$	
Γ_9 $K^+ K^- f_0(980) \rightarrow K^+ K^- \pi^+ \pi^-$	seen
Γ_{10} $K^+ K^- \pi^0 \pi^0$	
Γ_{11} $K^+ K^- f_0(980) \rightarrow K^+ K^- \pi^0 \pi^0$	seen
Γ_{12} $K^{*0} K^\pm \pi^\mp$	not seen
Γ_{13} $K^*(892)^0 \bar{K}^*(892)^0$	not seen
Γ_{14} $K^*(892)^+ K^*(892)^-$	
Γ_{15} $K(1460)^+ K^- + c.c.$	
Γ_{16} $K_1(1270)^+ K^- + c.c.$	
Γ_{17} $K_1(1400)^+ K^- + c.c.$	

$\phi(2170)$ $\Gamma(i)\Gamma(e^+e^-)/\Gamma(\text{total})$

$\Gamma(\phi\eta) \times \Gamma(e^+e^-)/\Gamma_{\text{total}}$	$\Gamma_2\Gamma_1/\Gamma$
VALUE (eV) EVTS DOCUMENT ID TECN COMMENT	
••• We do not use the following data for averages, fits, limits, etc. •••	
$0.24^{+0.12}_{-0.07}$	¹ ABLIKIM 21T BES3 $e^+e^- \rightarrow \phi\eta$
$1.7 \pm 0.7 \pm 1.3$	483 AUBERT 08s BABR $10.6 e^+e^- \rightarrow \phi\eta\gamma$
¹ From a solution of the fit to the cross section below 3.5 GeV measured by BaBar and BESIII with a coherent sum of two modified Breit-Wigner amplitudes ($\phi(1680)$ and $\phi(2170)$) and a nonresonant term. The other solution gives $10.11^{+3.87}_{-3.13}$ eV.	
$\Gamma(\omega\eta) \times \Gamma(e^+e^-)/\Gamma_{\text{total}}$	$\Gamma_3\Gamma_1/\Gamma$
VALUE (eV) DOCUMENT ID TECN COMMENT	
$0.43 \pm 0.15 \pm 0.04$	¹ ABLIKIM 21A BES3 $e^+e^- \rightarrow \omega\eta$
¹ For constructive interference with $\omega(1420)$ and $\omega(1650)/\phi(1680)$. For destructive interference: $1.25 \pm 0.48 \pm 0.18$ eV.	
$\Gamma(\phi\eta') \times \Gamma(e^+e^-)/\Gamma_{\text{total}}$	$\Gamma_4\Gamma_1/\Gamma$
VALUE (eV) DOCUMENT ID TECN COMMENT	
$7.1 \pm 0.7 \pm 0.7$	¹ ABLIKIM 20M BES3 $e^+e^- \rightarrow \eta'\phi$
¹ From a fit using a coherent sum of a phase-space modified Breit-Wigner function and a phase-space term.	
$\Gamma(\phi f_0(980)) \times \Gamma(e^+e^-)/\Gamma_{\text{total}}$	$\Gamma_6\Gamma_1/\Gamma$
VALUE (eV) EVTS DOCUMENT ID TECN COMMENT	
$2.3 \pm 0.3 \pm 0.3$	^{1,2} LEES 12F BABR $10.6 e^+e^- \rightarrow \phi\pi^+\pi^-\gamma$
••• We do not use the following data for averages, fits, limits, etc. •••	
$2.5 \pm 0.8 \pm 0.4$	201 ^{2,3} AUBERT,BE 06D BABR $10.6 e^+e^- \rightarrow K^+K^-\pi\pi\gamma$
¹ From a fit with constructive interference with the $\phi(1680)$. In a fit with destructive interference, the value is larger by a factor of 12.	
² From the $\phi f_0(980)$ component.	
³ Superseded by LEES 12f.	
$\Gamma(K_S^0 K_L^0) \times \Gamma(e^+e^-)/\Gamma_{\text{total}}$	$\Gamma_7\Gamma_1/\Gamma$
VALUE (eV) DOCUMENT ID TECN COMMENT	
••• We do not use the following data for averages, fits, limits, etc. •••	
$0.9 \pm 0.6 \pm 0.7$	¹ ABLIKIM 21AP BES3 $e^+e^- \rightarrow K_S^0 K_L^0$
¹ From a fit to the cross section between 2.00 and 3.08 GeV with a sum of Breit-Wigner amplitude and a nonresonant contribution. The observed structure can be also due to $\rho(2150)$.	
$\Gamma(K^*(892)^+ K^*(892)^-) \times \Gamma(e^+e^-)/\Gamma_{\text{total}}$	$\Gamma_{14}\Gamma_1/\Gamma$
VALUE (eV) CL% DOCUMENT ID TECN COMMENT	
<1.9	90 ¹ ABLIKIM 20s BES3 $e^+e^- \rightarrow K^+K^-\pi^0\pi^0$
¹ By a simultaneous fit of the intermediate channels in a partial-wave analysis, assuming the same structure, modelled with a coherent sum of a nonresonant component and a resonant component by a Breit-Wigner function.	

$\Gamma(K(1460)^+ K^- + c.c.) \times \Gamma(e^+e^-)/\Gamma_{\text{total}}$	$\Gamma_{15}\Gamma_1/\Gamma$
VALUE (eV) DOCUMENT ID TECN COMMENT	
••• We do not use the following data for averages, fits, limits, etc. •••	
3.0 ± 3.8	¹ ABLIKIM 20s BES3 $e^+e^- \rightarrow K^+K^-\pi^0\pi^0$
¹ By a simultaneous fit of the intermediate channels in a partial-wave analysis, assuming the same structure, modelled with a coherent sum of a nonresonant component and a resonant component by a Breit-Wigner function.	

$\Gamma(K_1(1270)^+ K^- + c.c.) \times \Gamma(e^+e^-)/\Gamma_{\text{total}}$	$\Gamma_{16}\Gamma_1/\Gamma$
VALUE (eV) CL% DOCUMENT ID TECN COMMENT	
<12.5	90 ¹ ABLIKIM 20s BES3 $e^+e^- \rightarrow K^+K^-\pi^0\pi^0$
¹ By a simultaneous fit of the intermediate channels in a partial-wave analysis, assuming the same structure, modelled with a coherent sum of a nonresonant component and a resonant component by a Breit-Wigner function. A second solution of the fit with equal fit quality gives an upper limit value of 297.6 eV.	

$\Gamma(K_1(1400)^+ K^- + c.c.) \times \Gamma(e^+e^-)/\Gamma_{\text{total}}$	$\Gamma_{17}\Gamma_1/\Gamma$
VALUE (eV) DOCUMENT ID TECN COMMENT	
••• We do not use the following data for averages, fits, limits, etc. •••	
4.7 ± 3.3	¹ ABLIKIM 20s BES3 $e^+e^- \rightarrow K^+K^-\pi^0\pi^0$
¹ By a simultaneous fit of the intermediate channels in a partial-wave analysis, assuming the same structure, modelled with a coherent sum of a nonresonant component and a resonant component by a Breit-Wigner function. A second solution of the fit with equal fit quality gives a value of 98.8 ± 7.8 eV.	

$\phi(2170)$ $\Gamma(i)\Gamma(e^+e^-)/\Gamma^2(\text{total})$

$\Gamma(\phi\pi\pi)/\Gamma_{\text{total}} \times \Gamma(e^+e^-)/\Gamma_{\text{total}}$	$\Gamma_5/\Gamma \times \Gamma_1/\Gamma$
VALUE (units 10^{-7}) EVTS DOCUMENT ID TECN COMMENT	
••• We do not use the following data for averages, fits, limits, etc. •••	
$1.65 \pm 0.15 \pm 0.18$	4.8k ¹ SHEN 09 BELL $10.6 e^+e^- \rightarrow K^+K^-\pi^+\pi^-\gamma$
¹ Multiplied by 3/2 to take into account the $\phi\pi^0\pi^0$ mode. Using $B(\phi \rightarrow K^+K^-) = (49.2 \pm 0.6)\%$.	

$\phi(2170)$ BRANCHING RATIOS

$\Gamma(K^+K^- f_0(980) \rightarrow K^+K^-\pi^+\pi^-)/\Gamma_{\text{total}}$	Γ_9/Γ
VALUE DOCUMENT ID TECN COMMENT	
seen	AUBERT 07AK BABR $10.6 e^+e^- \rightarrow K^+K^-\pi^+\pi^-\gamma$
$\Gamma(K^+K^- f_0(980) \rightarrow K^+K^-\pi^0\pi^0)/\Gamma_{\text{total}}$	Γ_{11}/Γ
VALUE DOCUMENT ID TECN COMMENT	
seen	AUBERT 07AK BABR $10.6 e^+e^- \rightarrow K^+K^-\pi^0\pi^0\gamma$
$\Gamma(K^{*0} K^\pm \pi^\mp)/\Gamma_{\text{total}}$	Γ_{12}/Γ
VALUE DOCUMENT ID TECN COMMENT	
not seen	AUBERT 07AK BABR $10.6 \text{ GeV } e^+e^-$
$\Gamma(K^*(892)^0 \bar{K}^*(892)^0)/\Gamma_{\text{total}}$	Γ_{13}/Γ
VALUE DOCUMENT ID TECN COMMENT	
not seen	ABLIKIM 10c BES2 $J/\psi \rightarrow \eta K^+ \pi^- K^- \pi^+$

$\phi(2170)$ REFERENCES

ABLIKIM 21A	PL B813 136059	M. Ablikim et al.	(BESIII Collab.)
ABLIKIM 21AP	PR D104 092014	M. Ablikim et al.	(BESIII Collab.)
ABLIKIM 21T	PR D104 032007	M. Ablikim et al.	(BESIII Collab.)
ABLIKIM 20M	PR D102 012008	M. Ablikim et al.	(BESIII Collab.)
ABLIKIM 20S	PRL 124 112001	M. Ablikim et al.	(BESIII Collab.)
ABLIKIM 19I	PR D99 012014	M. Ablikim et al.	(BESIII Collab.)
ABLIKIM 19L	PR D99 032001	M. Ablikim et al.	(BESIII Collab.)
ABLIKIM 15H	PR D91 052017	M. Ablikim et al.	(BESIII Collab.)
LEES 12F	PR D86 012008	J.P. Lees et al.	(BABAR Collab.)
ABLIKIM 10C	PL B685 27	M. Ablikim et al.	(BES II Collab.)
SHEN 09	PR D80 031101	C.P. Shen et al.	(BELLE Collab.)
ABLIKIM 08F	PRL 100 102003	M. Ablikim et al.	(BES Collab.)
AUBERT 08S	PR D77 092002	B. Aubert et al.	(BABAR Collab.)
AUBERT 07AK	PR D76 012008	B. Aubert et al.	(BABAR Collab.)
AUBERT_BE 06D	PR D74 091103	B. Aubert et al.	(BABAR Collab.)

$f_0(2200)$

$$I^G(J^{PC}) = 0^+(0^+ +)$$

OMITTED FROM SUMMARY TABLE

Seen in $K_S^0 K_S^0$ (AUGUSTIN 88), $K^+ K^-$ (ABLIKIM 05Q) and $\eta\eta$ (BINON 05) system. Not seen in $\Upsilon(1S)$ radiative decays (BARU 89).

$f_0(2200)$ MASS

VALUE (MeV) EVTS DOCUMENT ID TECN COMMENT	
2187 ± 14 OUR AVERAGE	
$2170 \pm 20^{+10}_{-15}$	ABLIKIM 05Q BES2 $\psi(2S) \rightarrow \gamma\pi^+\pi^-K^+K^-$
2197 ± 17	¹ AUGUSTIN 88 DM2 $J/\psi \rightarrow \gamma K_S^0 K_S^0$

See key on page 1127

Meson Particle Listings

$f_0(2200)$, $f_J(2220)$

••• We do not use the following data for averages, fits, limits, etc. •••

2200 ± 25		SARANTSEV	21	RVUE	$J/\psi(1S) \rightarrow \gamma(\pi\pi, K\bar{K}, \eta\eta, \omega\phi)$
2206 ± 12 ± 8	381	^{2,3} DOBBS	15		$J/\psi \rightarrow \gamma K^+ K^-$
2188 ± 17 ± 16	203	^{2,3} DOBBS	15		$\psi(2S) \rightarrow \gamma K^+ K^-$
2210 ± 5.0		⁴ BINON	05	GAMS	$33 \pi^- p \rightarrow \eta\eta n$
~ 2122		HASAN	94	RVUE	$\bar{p}p \rightarrow \pi\pi$
~ 2321		HASAN	94	RVUE	$\bar{p}p \rightarrow \pi\pi$

¹ Cannot determine spin to be 0.
² Using CLEO-c data but not authored by the CLEO Collaboration.
³ From a fit to a Breit-Wigner line shape with fixed $\Gamma = 238$ MeV.
⁴ First solution, PWA is ambiguous.

$f_0(2200)$ WIDTH

VALUE (MeV)	DOCUMENT ID	TECN	COMMENT
207 ± 40 OUR AVERAGE			
220 ± 60 ⁺⁴⁰ ₋₄₅	ABLIKIM	05Q	BES2 $\psi(2S) \rightarrow \gamma\pi^+\pi^-K^+K^-$
201 ± 51	⁵ AUGUSTIN	88	DM2 $J/\psi \rightarrow \gamma K_S^0 K_S^0$
••• We do not use the following data for averages, fits, limits, etc. •••			
150 ± 30	SARANTSEV	21	RVUE $J/\psi(1S) \rightarrow \gamma(\pi\pi, K\bar{K}, \eta\eta, \omega\phi)$
380 ± 90	⁶ BINON	05	GAMS $33 \pi^- p \rightarrow \eta\eta n$
~ 273	HASAN	94	RVUE $\bar{p}p \rightarrow \pi\pi$
~ 223	HASAN	94	RVUE $\bar{p}p \rightarrow \pi\pi$

⁵ Cannot determine spin to be 0.
⁶ First solution, PWA is ambiguous.

$f_0(2200)$ REFERENCES

SARANTSEV	21	PL B816 136227	A.V. Sarantsev et al.	(BONN, PNPI)
DOBBS	15	PR D91 052006	S. Dobbs et al.	(NWES)
ABLIKIM	05Q	PR D72 092002	M. Ablikim et al.	(BES Collab.)
BINON	05	PAN 68 960	F. Binon et al.	
HASAN	94	Translated from YAF 68 998.		
BARU	89	PL B334 215	A. Hasan, D.V. Bugg	(LOQM)
AUGUSTIN	88	ZPHY C42 505	S.E. Baru et al.	(NOVO)
		PRL 60 2238	J.E. Augustin et al.	(DM2 Collab.)

$f_J(2220)$

 $I^G(J^{PC}) = 0^+(2^{++} \text{ or } 4^{++})$

OMITTED FROM SUMMARY TABLE
 Needs confirmation. See our mini-review in the 2004 edition of this Review, PDG 04.

$f_J(2220)$ MASS

VALUE (MeV)	CL%	EVTs	DOCUMENT ID	TECN	COMMENT
2231.1 ± 3.5 OUR AVERAGE					
2235 ± 4 ± 6	74		BAI	96B	BES $e^+e^- \rightarrow J/\psi \rightarrow \gamma\pi^+\pi^-$
2230 ± 6 ⁺⁷ ₋₇	±16	46	BAI	96B	BES $e^+e^- \rightarrow J/\psi \rightarrow \gamma K^+ K^-$
2232 ± 8 ⁺⁷ ₋₇	±15	23	BAI	96B	BES $e^+e^- \rightarrow J/\psi \rightarrow \gamma K_S^0 K_S^0$
2235 ± 4 ± 5	32		BAI	96B	BES $e^+e^- \rightarrow J/\psi \rightarrow \gamma\rho\bar{\rho}$
2209 ± 17 ⁺¹⁵ ₋₁₅	±10		ASTON	88F	LASS $11 K^- p \rightarrow K^+ K^- \Lambda$
2230 ± 20			BOLONKIN	88	SPEC $40 \pi^- p \rightarrow K_S^0 K_S^0 n$
2220 ± 10	41		¹ ALDE	86B	GA24 $38-100 \pi p \rightarrow n\eta\eta'$
2230 ± 6 ± 14	93		BALTRUSAIT..86D	MRK3	$e^+e^- \rightarrow \gamma K^+ K^-$
2232 ± 7 ± 7	23		BALTRUSAIT..86D	MRK3	$e^+e^- \rightarrow \gamma K_S^0 K_S^0$

••• We do not use the following data for averages, fits, limits, etc. •••

2223.9 ± 2.5 ² VLADIMIRSK..08 SPEC $40 \pi^- p \rightarrow K_S^0 K_S^0 n + m\pi^0$

2246 ± 36 BAI 98H BES $J/\psi \rightarrow \gamma\pi^0\pi^0$

¹ ALDE 86B uses data from both the GAMS-2000 and GAMS-4000 detectors.
² $J^{PC} = 2^{++}$. Systematic uncertainties not evaluated

$f_J(2220)$ WIDTH

VALUE (MeV)	CL%	EVTs	DOCUMENT ID	TECN	COMMENT
23 ± 8 OUR AVERAGE					
19 ± 13 ⁺¹¹ ₋₁₁	±12	74	BAI	96B	BES $e^+e^- \rightarrow J/\psi \rightarrow \gamma\pi^+\pi^-$
20 ± 20 ⁺¹⁵ ₋₁₅	±17	46	BAI	96B	BES $e^+e^- \rightarrow J/\psi \rightarrow \gamma K^+ K^-$
20 ± 25 ⁺¹⁶ ₋₁₆	±14	23	BAI	96B	BES $e^+e^- \rightarrow J/\psi \rightarrow \gamma K_S^0 K_S^0$
15 ± 12 ⁺⁹ ₋₉	±9	32	BAI	96B	BES $e^+e^- \rightarrow J/\psi \rightarrow \gamma\rho\bar{\rho}$

60 ⁺¹⁰⁷ ₋₅₇		ASTON	88F	LASS	$11 K^- p \rightarrow K^+ K^- \Lambda$
80 ± 30		BOLONKIN	88	SPEC	$40 \pi^- p \rightarrow K_S^0 K_S^0 n$
26 ± 20 ⁺¹⁶ ₋₁₆	±17	93	BALTRUSAIT..86D	MRK3	$e^+e^- \rightarrow \gamma K^+ K^-$
18 ± 23 ⁺¹⁵ ₋₁₅	±10	23	BALTRUSAIT..86D	MRK3	$e^+e^- \rightarrow \gamma K_S^0 K_S^0$

••• We do not use the following data for averages, fits, limits, etc. •••

8.6 ± 2.5 ¹ VLADIMIRSK..08 SPEC $40 \pi^- p \rightarrow K_S^0 K_S^0 n + m\pi^0$

< 80 90 ALDE 87c GAM2 $38 \pi^- p \rightarrow \eta' n$

¹ $J^{PC} = 2^{++}$. Systematic uncertainties not evaluated

$f_J(2220)$ DECAY MODES

Mode	Fraction (Γ_i/Γ)
Γ_1 $\pi\pi$	not seen
Γ_2 $\pi^+\pi^-$	not seen
Γ_3 $K\bar{K}$	not seen
Γ_4 $\rho\bar{\rho}$	not seen
Γ_5 $\gamma\gamma$	not seen
Γ_6 $\eta\eta'(958)$	seen
Γ_7 $\phi\phi$	not seen
Γ_8 $\eta\eta$	not seen

$f_J(2220)$ $\Gamma(i)\Gamma(\gamma\gamma)/\Gamma(\text{total})$

VALUE (eV)	CL%	DOCUMENT ID	TECN	COMMENT	$\Gamma_3\Gamma_5/\Gamma$	
< 1.4	95	¹ ACCIARRI	01H	L3	$\gamma\gamma \rightarrow K_S^0 K_S^0, E_{CM}^{ee} = 91, 183-209$ GeV	
••• We do not use the following data for averages, fits, limits, etc. •••						
< 5.6	95	¹ GODANG	97	CLE2	$\gamma\gamma \rightarrow K_S^0 K_S^0$	
< 86	95	¹ ALBRECHT	90G	ARG	$\gamma\gamma \rightarrow K^+ K^-$	
< 1000	95	² ALTHOFF	85B	TASS	$\gamma\gamma, K\bar{K}\pi$	

$f_J(2220)$ $\Gamma(\pi\pi) \times \Gamma(\gamma\gamma)/\Gamma(\text{total})$

VALUE (eV)	CL%	DOCUMENT ID	TECN	COMMENT	$\Gamma_1\Gamma_5/\Gamma$	
< 2.5	95	ALAM	98c	CLE2	$\gamma\gamma \rightarrow \pi^+\pi^-$	
¹ Assuming $J^P = 2^+$.						
² True for $J^P = 0^+$ and $J^P = 2^+$.						

$f_J(2220)$ $\Gamma(i)\Gamma(\rho\bar{\rho})/\Gamma^2(\text{total})$

VALUE (units 10^{-5})	CL%	DOCUMENT ID	TECN	COMMENT	$\Gamma_4/\Gamma \times \Gamma_1/\Gamma$	
< 18	95	¹ AMSLER	01	CBAR	$1.4-1.5 \rho\bar{\rho} \rightarrow \pi^0\pi^0$	
••• We do not use the following data for averages, fits, limits, etc. •••						
< (11-42)	99	² HASAN	96	SPEC	$1.35-1.55 \rho\bar{\rho} \rightarrow \pi^+\pi^-$	

$f_J(2220)$ $\Gamma(\rho\bar{\rho})/\Gamma(\text{total}) \times \Gamma(\phi\phi)/\Gamma(\text{total})$

VALUE (units 10^{-5})	CL%	DOCUMENT ID	TECN	COMMENT	$\Gamma_4/\Gamma \times \Gamma_7/\Gamma$	
< 6	95	³ EVANGELIS...	98	SPEC	$1.1-2.0 \rho\bar{\rho} \rightarrow \phi\phi$	

$f_J(2220)$ $\Gamma(\rho\bar{\rho})/\Gamma(\text{total}) \times \Gamma(\eta\eta)/\Gamma(\text{total})$

VALUE (units 10^{-5})	CL%	DOCUMENT ID	TECN	COMMENT	$\Gamma_4/\Gamma \times \Gamma_8/\Gamma$	
< 4	95	¹ AMSLER	01	CBAR	$1.4-1.5 \rho\bar{\rho} \rightarrow \eta\eta$	
¹ For $J^P = 2^+$ in the mass range 2222-2240 MeV and the total width between 10 and 20 MeV.						
² For $J^P = 2^+$ and $J^P = 4^+$ in the mass range 2220-2245 MeV and the total width of 15 MeV.						
³ For $J^P = 2^+$, the mass of 2235 MeV and the total width of 15 MeV.						

$f_J(2220)$ BRANCHING RATIOS

$\Gamma(\pi\pi)/\Gamma(\text{total})$	VALUE	DOCUMENT ID	TECN	COMMENT	Γ_1/Γ
not seen		¹ DOBBS	15	$J/\psi \rightarrow \gamma\pi\pi$	
not seen		¹ DOBBS	15	$\psi(2S) \rightarrow \gamma\pi\pi$	
¹ Using CLEO-c data but not authored by the CLEO Collaboration.					

$\Gamma(K\bar{K})/\Gamma(\text{total})$	VALUE	DOCUMENT ID	TECN	COMMENT	Γ_3/Γ
not seen		¹ DOBBS	15	$J/\psi \rightarrow \gamma K\bar{K}$	
not seen		¹ DOBBS	15	$\psi(2S) \rightarrow \gamma K\bar{K}$	
¹ Using CLEO-c data but not authored by the CLEO Collaboration.					

$\Gamma(\pi\pi)/\Gamma(K\bar{K})$	VALUE	DOCUMENT ID	TECN	COMMENT	Γ_1/Γ_3
1.0 ± 0.5		BAI	96B	BES	$e^+e^- \rightarrow J/\psi \rightarrow \gamma 2\pi, K\bar{K}$

Meson Particle Listings

$f_J(2220)$, $\eta(2225)$, $\rho_3(2250)$

$\Gamma(p\bar{p})/\Gamma_{total}$ Γ_4/Γ

VALUE (units 10^{-4})	CL%	DOCUMENT ID	TECN	COMMENT
•••		We do not use the following data for averages, fits, limits, etc. •••		
not seen		1 AUBERT 07AV	BABR	$B \rightarrow p\bar{p}K^{(*)}$
not seen		WANG 05A	BELL	$B^+ \rightarrow \bar{p}pK^+$
<3.0	95	2 EVANGELIS... 97	SPEC	$1.96-2.40 \bar{p}p \rightarrow K_S^0 K_S^0$
<1.1	99.7	3 BARNES 93	SPEC	$1.3-1.57 \bar{p}p \rightarrow K_S^0 K_S^0$
<2.6	99.7	3 BARDIN 87	CNTR	$1.3-1.5 \bar{p}p \rightarrow K^+ K^-$
<3.6	99.7	3 SCULLI 87	CNTR	$1.29-1.55 \bar{p}p \rightarrow K^+ K^-$
1 Assuming $\Gamma < 30$ MeV. 2 Assuming $\Gamma \sim 20$ MeV, $J^P = 2^+$ and $B(f_J(2220) \rightarrow K\bar{K}) = 100\%$. 3 Assuming $\Gamma = 30-35$ MeV, $J^P = 2^+$ and $B(f_J(2220) \rightarrow K\bar{K}) = 100\%$.				

$\Gamma(p\bar{p})/\Gamma(K\bar{K})$ Γ_4/Γ_3

VALUE	DOCUMENT ID	TECN	COMMENT
0.17 ± 0.09	BAI 96B	BES	$e^+e^- \rightarrow J/\psi \rightarrow \gamma p\bar{p}, K\bar{K}$

$f_J(2220)$ REFERENCES

DOBS	PR D91 052006	S. Dobbs et al.	(NWES)
VLADIMIRSK...	PAN 71 2129	V.V. Vladimirov et al.	(ITEP)
Translated from YAF 71 2166.			
AUBERT	07AV	B. Aubert et al.	(BABAR Collab.)
WANG	05A	M.-Z. Wang et al.	(BELLE Collab.)
PDG	PL B592 1	S. Eidelman et al.	(PDG Collab.)
ACCIARRI	01H	M. Acciarri et al.	(L3 Collab.)
AMSLER	01	C. Amisler et al.	(Crystal Barrel Collab.)
ALAM	95C	M.S. Alam et al.	(CLEO Collab.)
BAI	98H	J.Z. Bai et al.	(BES Collab.)
EVANGELIS...	98	PR D57 5370	(JETSET Collab.)
EVANGELIS...	97	PR D56 3803	(LEAR Collab.)
GODANG	97	PRL 79 3829	(CLEO Collab.)
BAI	96B	PRL 76 3502	(BES Collab.)
HASAN	96	PL B388 376	(BRUN, LOQM)
BARNES	93	PL B309 469	(PS185 Collab.)
ALBRECHT	90G	ZPHY C48 183	(ARGUS Collab.)
ASTON	88F	PL B215 199	(SLAC, NAGO, CINC, INUS, JP)
BOLONKIN	88	NP B309 426	(B.V. Bolonkin et al.)
ALDE	87C	SJNP 45 255	(D. Alde et al.)
Translated from YAF 45 405.			
BARDIN	87	PL B195 292	(SACL, FERR, CERN, PADO+)
SCULLI	87	PRL 58 1715	(NYU, BNL)
ALDE	86B	PL B177 120	(SERP, BELG, LANL, LAPP)
BALTRUSAIT...	86D	PRL 56 107	(R.M. Baltrusaitis)
ALTHOFF	85B	ZPHY C29 189	(M. Althoff et al.)

OTHER RELATED PAPERS

DEL-AMO-SA...	100	PRL 105 172001	P. del Amo Sanchez et al.	(BABAR Collab.)
---------------	-----	----------------	---------------------------	-----------------

$\eta(2225)$

$$I^G(J^{PC}) = 0^+(0^{-+})$$

OMITTED FROM SUMMARY TABLE

Seen in $J/\psi \rightarrow \gamma\phi\phi$. Possibly seen in $B \rightarrow \phi\phi K$ by LEES 11A.

$\eta(2225)$ MASS

VALUE (MeV)	EVTS	DOCUMENT ID	TECN	COMMENT
2221 ± 13	OUR AVERAGE			
2216 ± 4	5-11	1 ABLIKIM 16N	BES3	$J/\psi \rightarrow \gamma K^+ K^- K^+ K^-$
2240 ± 30	196 ± 19	ABLIKIM 08I	BES	$J/\psi \rightarrow \gamma K^+ K^- K_S^0 K_L^0$
2230 ± 25 ± 15		BAI 90B	MRK3	$J/\psi \rightarrow \gamma K^+ K^- K^+ K^-$
2214 ± 20 ± 13		BAI 90B	MRK3	$J/\psi \rightarrow \gamma K^+ K^- K_S^0 K_L^0$

••• We do not use the following data for averages, fits, limits, etc. •••
 ~ 2220 BISELLO 86B DM2 $J/\psi \rightarrow \gamma K^+ K^- K^+ K^-$
 1 From a partial wave analysis of $J/\psi \rightarrow \gamma\phi\phi$ that also finds significant signals for $\eta(2100)$, 0^{-+} phase space, $f_0(2100)$, $f_2(2010)$, $f_2(2300)$, $f_2(2340)$, and a previously unseen 0^{-+} state $X(2500)$ ($M = 2470^{+15+101}_{-19-23}$ MeV, $\Gamma = 230^{+64+56}_{-35-33}$ MeV).

$\eta(2225)$ WIDTH

VALUE (MeV)	EVTS	DOCUMENT ID	TECN	COMMENT
185 ± 40	OUR AVERAGE			
185 ± 12	14-17	1 ABLIKIM 16N	BES3	$J/\psi \rightarrow \gamma K^+ K^- K^+ K^-$
190 ± 30	196 ± 19	ABLIKIM 08I	BES	$J/\psi \rightarrow \gamma K^+ K^- K_S^0 K_L^0$
150 ± 300	60 ± 60	BAI 90B	MRK3	$J/\psi \rightarrow \gamma K^+ K^- K^+ K^-$

••• We do not use the following data for averages, fits, limits, etc. •••
 ~ 80 BISELLO 86B DM2 $J/\psi \rightarrow \gamma K^+ K^- K^+ K^-$
 1 From a partial wave analysis of $J/\psi \rightarrow \gamma\phi\phi$ that also finds significant signals for $\eta(2100)$, 0^{-+} phase space, $f_0(2100)$, $f_2(2010)$, $f_2(2300)$, $f_2(2340)$, and a previously unseen 0^{-+} state $X(2500)$ ($M = 2470^{+15+101}_{-19-23}$ MeV, $\Gamma = 230^{+64+56}_{-35-33}$ MeV).

$\eta(2225)$ REFERENCES

ABLIKIM 16N	PR D93 112001	M. Ablikim et al.	(BESIII Collab.)
LEES 11A	PR D84 012001	J.P. Lees et al.	(BABAR Collab.)
ABLIKIM 08I	PL B662 330	M. Ablikim et al.	(BES Collab.)
BAI 90B	PRL 65 1309	Z. Bai et al.	(Mark III Collab.)
BISELLO 86B	PL B179 294	D. Bisello et al.	(DM2 Collab.)

$\rho_3(2250)$

$$I^G(J^{PC}) = 1^+(3^{-})$$

OMITTED FROM SUMMARY TABLE

Contains results mostly from formation experiments. For further production experiments see the Further States entry. See also $\rho(2150)$, $f_2(2150)$, $f_4(2300)$, $\rho_5(2350)$.

$\rho_3(2250)$ MASS

$\bar{p}p \rightarrow \pi\pi$ or $K\bar{K}$

VALUE (MeV)	EVTS	DOCUMENT ID	TECN	CHG	COMMENT
•••		We do not use the following data for averages, fits, limits, etc. •••			
2248 ± 17	5-9	1.8k	1 ABLIKIM 20F	BES3	$\psi(2S) \rightarrow K^+ K^- \eta$
~ 2232		HASAN 94	RVUE		$\bar{p}p \rightarrow \pi\pi$
~ 2090		2 OAKDEN 94	RVUE		0.36-1.55 $\bar{p}p \rightarrow \pi\pi$
~ 2250		3 MARTIN 80B	RVUE		
~ 2300		3 MARTIN 80C	RVUE		
~ 2140		4 CARTER 78B	CNTR	0	0.7-2.4 $\bar{p}p \rightarrow K^- K^+$
~ 2150		5 CARTER 77	CNTR	0	0.7-2.4 $\bar{p}p \rightarrow \pi\pi$

1 Seen in $\psi(2S)$ decay with branching ratio $\psi(2S) \rightarrow X\eta \rightarrow K^+ K^- \eta = (1.9 \pm 0.4^{+0.5}_{-1.3}) \times 10^{-6}$.
 2 See however KLOET 96 who fit $\pi^+ \pi^-$ only and find waves only up to $J = 3$ to be important but not significantly resonant.
 3 $I(J^P) = 1(3^-)$ from simultaneous analysis of $\bar{p}p \rightarrow \pi^- \pi^+$ and $\pi^0 \pi^0$.
 4 $I = 0, 1$. $J^P = 3^-$ from Barrelet-zero analysis.
 5 $I(J^P) = 1(3^-)$ from amplitude analysis.

S-CHANNEL $\bar{N}N$

VALUE (MeV)	DOCUMENT ID	TECN	CHG	COMMENT
•••	We do not use the following data for averages, fits, limits, etc. •••			
2260 ± 20	6 ANISOVICH 02	SPEC		0.6-1.9 $p\bar{p} \rightarrow \omega\pi^0$, $\omega\eta\pi^0$, $\pi^+\pi^-$
~ 2190	7 CUTTS 78B	CNTR		0.97-3 $\bar{p}p \rightarrow \bar{N}N$
2155 ± 15	7,8 COUPLAND 77	CNTR	0	0.7-2.4 $\bar{p}p \rightarrow \bar{p}p$
2193 ± 2	7,9 ALSPECTOR 73	CNTR		$\bar{p}p$ S channel
2190 ± 10	10 ABRAMS 70	CNTR		S channel $\bar{p}N$

6 From the combined analysis of ANISOVICH 00I, ANISOVICH 01D, ANISOVICH 01E, and ANISOVICH 02.
 7 Isospins 0 and 1 not separated.
 8 From a fit to the total elastic cross section.
 9 Referred to as T or T region by ALSPECTOR 73.
 10 Seen as bump in $I = 1$ state. See also COOPER 68. PEASLEE 75 confirm $\bar{p}p$ results of ABRAMS 70, no narrow structure.

Other processes

VALUE (MeV)	DOCUMENT ID	TECN	COMMENT
•••	We do not use the following data for averages, fits, limits, etc. •••		
2290 ± 20 ± 30	AMELIN 00	VES	37 $\pi^- p \rightarrow \eta\pi^+\pi^- n$

$\rho_3(2250)$ WIDTH

$\bar{p}p \rightarrow \pi\pi$ or $K\bar{K}$

VALUE (MeV)	EVTS	DOCUMENT ID	TECN	CHG	COMMENT
•••		We do not use the following data for averages, fits, limits, etc. •••			
185 ± 31	17	1.8k	11 ABLIKIM 20F	BES3	$\psi(2S) \rightarrow K^+ K^- \eta$
~ 220		HASAN 94	RVUE		$\bar{p}p \rightarrow \pi\pi$
~ 60		12 OAKDEN 94	RVUE		0.36-1.55 $\bar{p}p \rightarrow \pi\pi$
~ 250		13 MARTIN 80B	RVUE		
~ 200		13 MARTIN 80C	RVUE		
~ 150		14 CARTER 78B	CNTR	0	0.7-2.4 $\bar{p}p \rightarrow K^- K^+$
~ 200		15 CARTER 77	CNTR	0	0.7-2.4 $\bar{p}p \rightarrow \pi\pi$

11 Seen in $\psi(2S)$ decay with branching ratio $\psi(2S) \rightarrow X\eta \rightarrow K^+ K^- \eta = (1.9 \pm 0.4^{+0.5}_{-1.3}) \times 10^{-6}$.
 12 See however KLOET 96 who fit $\pi^+ \pi^-$ only and find waves only up to $J = 3$ to be important but not significantly resonant.
 13 $I(J^P) = 1(3^-)$ from simultaneous analysis of $\bar{p}p \rightarrow \pi^- \pi^+$ and $\pi^0 \pi^0$.
 14 $I = 0, 1$. $J^P = 3^-$ from Barrelet-zero analysis.
 15 $I(J^P) = 1(3^-)$ from amplitude analysis.

S-CHANNEL $\bar{N}N$

VALUE (MeV)	DOCUMENT ID	TECN	CHG	COMMENT
•••	We do not use the following data for averages, fits, limits, etc. •••			
160 ± 25	16 ANISOVICH 02	SPEC		0.6-1.9 $p\bar{p} \rightarrow \omega\pi^0$, $\omega\eta\pi^0$, $\pi^+\pi^-$
135 ± 75	17,18 COUPLAND 77	CNTR	0	0.7-2.4 $\bar{p}p \rightarrow \bar{p}p$

See key on page 1127

Meson Particle Listings

$\rho_3(2250)$, $f_2(2300)$, $f_4(2300)$

98 ± 8	¹⁸ ALSPECTOR	73	CNTR	$\bar{p}p$ S channel
~ 85	¹⁹ ABRAMS	70	CNTR	S channel $\bar{p}N$

¹⁶ From the combined analysis of ANISOVICH 00i, ANISOVICH 01d, ANISOVICH 01e, and ANISOVICH 02.
¹⁷ From a fit to the total elastic cross section.
¹⁸ Isospins 0 and 1 not separated.
¹⁹ Seen as bump in $I = 1$ state. See also COOPER 68. PEASLEE 75 confirm $\bar{p}p$ results of ABRAMS 70, no narrow structure.

Other processes

VALUE (MeV)	DOCUMENT ID	TECN	COMMENT
$230 \pm 5.0 \pm 8.0$	AMELIN	00	VES 37 $\pi^- p \rightarrow \eta \pi^+ \pi^- n$

• • • We do not use the following data for averages, fits, limits, etc. • • •

$\rho_3(2250)$ REFERENCES

ABLIKIM	20F	PR D101 032008	M. Ablikim et al.	(BESIII Collab.)
ANISOVICH	02	PL B542 8	A.V. Anisovich et al.	
ANISOVICH	01D	PL B508 6	A.V. Anisovich et al.	
ANISOVICH	01E	PL B513 201	A.V. Anisovich et al.	
AMELIN	00	NP A668 83	D. Amelin et al.	(VES Collab.)
ANISOVICH	00J	PL B491 47	A.V. Anisovich et al.	(RAL, LOQM, PNP+)
KLOET	95	PR D53 6120	W.M. Kloet, F. Myhrer	(RUTG, W0RD)
HASAN	94	PL B334 215	A. Hasan, D.V. Bugg	(LOQM)
OAKDEN	94	NP A574 731	M.N. Oakden, M.R. Pennington	(DURH)
MARTIN	80B	NP B176 355	B.R. Martin, D. Morgan	(LOUC, RHEL) JP
MARTIN	80C	NP B169 216	A.D. Martin, M.R. Pennington	(DURH) JP
CARTER	78B	NP B141 467	A.A. Carter	(LOQM)
CUTTS	78B	PR D17 16	D. Cutts et al.	(STON, WISC)
CARTER	77	PL 67B 117	A.A. Carter et al.	(LOQM, RHEL) JP
COUPLAND	77	PL 71B 460	M. Coupland et al.	(LOQM, RHEL)
PEASLEE	75	PL 57B 189	D.C. Peaslee et al.	(CANB, BARI, BROW+)
ALSPECTOR	73	PR L30 511	J. Alspector et al.	(RUTG, UPNJ)
ABRAMS	70	PR D1 1917	R.J. Abrams et al.	(BNL)
COOPER	68	PRL 20 1059	W.A. Cooper et al.	(ANL)

$f_2(2300)$

$$I^G(J^{PC}) = 0^+(2^{++})$$

$f_2(2300)$ MASS

VALUE (MeV)	DOCUMENT ID	TECN	COMMENT
2297 ± 28	¹ ETKIN	88	MPS 22 $\pi^- p \rightarrow \phi \phi n$
• • • We do not use the following data for averages, fits, limits, etc. • • •			
2262 ± 4 ± 28	² ABLIKIM	21A1	BES3 3.51-4.60 $e^+ e^- \rightarrow \phi \Lambda \bar{\Lambda}$
2243 ± 7 ± 29	³ UEHARA	13	BELL $\gamma\gamma \rightarrow K_S^0 K_S^0$
2270 ± 12	VLADIMIRSK...06	SPEC	40 $\pi^- p \rightarrow K_S^0 K_S^0 n$
2327 ± 9 ± 6	ABE	04	BELL 10.6 $e^+ e^- \rightarrow e^+ e^- K^+ K^-$
2231 ± 10	BOOTH	86	OMEG 85 $\pi^- \text{Be} \rightarrow 2\phi \text{Be}$
2220 ± 90 -20	LINDENBAUM	84	RVUE
2320 ± 40	ETKIN	82	MPS 22 $\pi^- p \rightarrow 2\phi n$

¹ Includes data of ETKIN 85. The percentage of the resonance going into $\phi\phi$ 2^{++} S_2 , D_2 , and D_0 is 6^{+15}_{-5} , 25^{+18}_{-14} , and 69^{+16}_{-27} , respectively.

² Threshold enhancement in $\Lambda\bar{\Lambda}$, preferred J^{PC} are 2^{++} , 2^{-+} , or 1^{++} . Could be another state.

³ Spin 2 preferred, tentatively assigned to $f_2(2300)$.

$f_2(2300)$ WIDTH

VALUE (MeV)	DOCUMENT ID	TECN	COMMENT
149 ± 41	¹ ETKIN	88	MPS 22 $\pi^- p \rightarrow \phi \phi n$
• • • We do not use the following data for averages, fits, limits, etc. • • •			
72 ± 5 ± 43	² ABLIKIM	21A1	BES3 3.51-4.60 $e^+ e^- \rightarrow \phi \Lambda \bar{\Lambda}$
145 ± 12 ± 27 -34	³ UEHARA	13	BELL $\gamma\gamma \rightarrow K_S^0 K_S^0$
90 ± 29	VLADIMIRSK...06	SPEC	40 $\pi^- p \rightarrow K_S^0 K_S^0 n$
275 ± 36 ± 20	ABE	04	BELL 10.6 $e^+ e^- \rightarrow e^+ e^- K^+ K^-$
133 ± 5.0	BOOTH	86	OMEG 85 $\pi^- \text{Be} \rightarrow 2\phi \text{Be}$
200 ± 5.0	LINDENBAUM	84	RVUE
220 ± 7.0	ETKIN	82	MPS 22 $\pi^- p \rightarrow 2\phi n$

¹ Includes data of ETKIN 85.

² Threshold enhancement in $\Lambda\bar{\Lambda}$, preferred J^{PC} are 2^{++} , 2^{-+} , or 1^{++} . Could be another state.

³ Spin 2 preferred, tentatively assigned to $f_2(2300)$.

$f_2(2300)$ DECAY MODES

Mode	Fraction (Γ_i/Γ)
Γ_1 $\phi\phi$	seen
Γ_2 $K\bar{K}$	seen
Γ_3 $\gamma\gamma$	seen
Γ_4 $\Lambda\bar{\Lambda}$	seen

$f_2(2300)$ $\Gamma(I)\Gamma(\gamma\gamma)/\Gamma(\text{total})$

VALUE (eV)	DOCUMENT ID	TECN	COMMENT	$\Gamma_2\Gamma_3/\Gamma$
$3.2^{+0.5+1.3}_{-0.4-2.2}$	UEHARA	13	BELL $\gamma\gamma \rightarrow K_S^0 K_S^0$	
$44 \pm 6 \pm 12$	¹ ABE	04	BELL 10.6 $e^+ e^- \rightarrow e^+ e^- K^+ K^-$	

¹ Assuming spin 2.

$f_2(2340)$ BRANCHING RATIOS

$\Gamma(\phi\phi)/\Gamma_{\text{total}}$	DOCUMENT ID	TECN	COMMENT	Γ_1/Γ
seen	BOOTH	86	OMEG 85 $\pi^- \text{Be} \rightarrow 2\phi \text{Be}$	
seen	ETKIN	82	MPS 22 $\pi^- p \rightarrow 2\phi n$	

$\Gamma(K\bar{K})/\Gamma_{\text{total}}$	DOCUMENT ID	TECN	COMMENT	Γ_2/Γ
seen	VLADIMIRSK...06	SPEC	40 $\pi^- p \rightarrow K_S^0 K_S^0 n$	
seen	ABE	04	BELL 10.6 $e^+ e^- \rightarrow e^+ e^- K^+ K^-$	

$\Gamma(\gamma\gamma)/\Gamma_{\text{total}}$	DOCUMENT ID	TECN	COMMENT	Γ_3/Γ
seen	UEHARA	13	BELL $\gamma\gamma \rightarrow K_S^0 K_S^0$	

$\Gamma(\Lambda\bar{\Lambda})/\Gamma_{\text{total}}$	DOCUMENT ID	TECN	COMMENT	Γ_4/Γ
seen	¹ ABLIKIM	21A1	BES3 3.51-4.60 $e^+ e^- \rightarrow \phi \Lambda \bar{\Lambda}$	

¹ Threshold enhancement in $\Lambda\bar{\Lambda}$, preferred J^{PC} are 2^{++} , 2^{-+} , or 1^{++} . Could be another state.

$f_2(2300)$ REFERENCES

ABLIKIM	21A1	PR D104 052006	M. Ablikim et al.	(BESIII Collab.)
UEHARA	13	PTEP 2013 123C01	S. Uehara et al.	(BELLE Collab.)
VLADIMIRSK...06	06	PAN 69 493	V.V. Vladimirov et al.	(ITEP, Moscow)
ABE	04	Translated from YAF 69 515.	K. Abe et al.	(BELLE Collab.)
ETKIN	88	FJPI C32 323	A. Etkin et al.	(BNL, CUNY)
BOOTH	86	NP B273 677	P.S.L. Booth et al.	(LIVP, GLAS, CERN)
ETKIN	85	PL 165B 217	A. Etkin et al.	(BNL, CUNY)
LINDENBAUM	84	CNPP 13 285	S.J. Lindenbaum	(CUNY)
ETKIN	82	PRL 49 1620	A. Etkin et al.	(BNL, CUNY)

$f_4(2300)$

$$I^G(J^{PC}) = 0^+(4^{++})$$

OMITTED FROM SUMMARY TABLE

This entry was previously called $U_0(2350)$. Contains results mostly from formation experiments. For further production experiments see the Further States entry. See also $\rho(2150)$, $f_2(2150)$, $\rho_3(2250)$, $\rho_5(2350)$.

$f_4(2300)$ MASS

$\bar{p}p \rightarrow \pi\pi$ or $K\bar{K}$

VALUE (MeV)	DOCUMENT ID	TECN	COMMENT
• • • We do not use the following data for averages, fits, limits, etc. • • •			
~ 2314	HASAN	94	RVUE $\bar{p}p \rightarrow \pi\pi$
~ 2300	¹ MARTIN	80B	RVUE
~ 2300	¹ MARTIN	80C	RVUE
~ 2340	² CARTER	78B	CNTR 0.7-2.4 $\bar{p}p \rightarrow K^- K^+$
~ 2330	DULUDE	78B	OSPK 1-2 $\bar{p}p \rightarrow \pi^0 \pi^0$
~ 2310	³ CARTER	77	CNTR 0.7-2.4 $\bar{p}p \rightarrow \pi\pi$

¹ $I(J^P) = 0(4^+)$ from simultaneous analysis of $p\bar{p} \rightarrow \pi^- \pi^+$ and $\pi^0 \pi^0$.
² $I(J^P) = 0(4^+)$ from Barrelet-zero analysis.
³ $I(J^P) = 0(4^+)$ from amplitude analysis.

S-CHANNEL $\bar{p}p$ or $\bar{N}N$

VALUE (MeV)	DOCUMENT ID	TECN	COMMENT
• • • We do not use the following data for averages, fits, limits, etc. • • •			
2283 ± 17	⁴ ANISOVICH	00J	SPEC
~ 2380	⁵ CUTTS	78B	CNTR 0.97-3 $\bar{p}p \rightarrow \bar{N}N$
2345 ± 15	^{5,6} COUPLAND	77	CNTR 0.7-2.4 $\bar{p}p \rightarrow \bar{p}p$
2359 ± 2	^{5,7} ALSPECTOR	73	CNTR $\bar{p}p$ S channel
2375 ± 10	ABRAMS	70	CNTR S channel $\bar{N}N$

⁴ From the combined analysis of ANISOVICH 99c and ANISOVICH 99f on $\bar{p}p \rightarrow \eta \pi^0 \pi^0$, $\pi^0 \pi^0$, $\eta\eta$, $\eta\eta'$, $\pi^+ \pi^-$.

⁵ Isospins 0 and 1 not separated.

⁶ From a fit to the total elastic cross section.

⁷ Referred to as U or U region by ALSPECTOR 73.

Meson Particle Listings

 $f_4(2300)$, $f_0(2330)$, $f_2(2340)$ $\pi^- \rho \rightarrow \eta \pi \pi$

VALUE (MeV)	DOCUMENT ID	TECN	COMMENT
••• We do not use the following data for averages, fits, limits, etc. •••			
2330 ± 20 ± 40	AMELIN	00	VES 37 $\pi^- \rho \rightarrow \eta \pi^+ \pi^- n$

 $\rho\rho$ CENTRAL PRODUCTION

VALUE (MeV)	DOCUMENT ID	COMMENT
2320 ± 60 OUR ESTIMATE		
••• We do not use the following data for averages, fits, limits, etc. •••		
2332 ± 15	BARBERIS	00F 450 $\rho\rho \rightarrow \rho_f \omega \rho_S$

 $f_4(2300)$ WIDTH $\bar{p} p \rightarrow \pi\pi$ or $\bar{K}K$

VALUE (MeV)	DOCUMENT ID	TECN	COMMENT
••• We do not use the following data for averages, fits, limits, etc. •••			
~ 278	HASAN	94	RVUE $\bar{p} p \rightarrow \pi\pi$
~ 200	8 MARTIN	80C	RVUE
~ 150	9 CARTER	78B	CNTR 0.7-2.4 $\bar{p} p \rightarrow K^- K^+$
~ 210	10 CARTER	77	CNTR 0.7-2.4 $\bar{p} p \rightarrow \pi\pi$
⁸ $I(J^P) = 0(4^+)$ from simultaneous analysis of $\rho\bar{p} \rightarrow \pi^- \pi^+$ and $\pi^0 \pi^0$.			
⁹ $I(J^P) = 0(4^+)$ from Barrelet-zero analysis.			
¹⁰ $I(J^P) = 0(4^+)$ from amplitude analysis.			

S-CHANNEL $\bar{p} p$ or $\bar{N}N$

VALUE (MeV)	DOCUMENT ID	TECN	COMMENT
••• We do not use the following data for averages, fits, limits, etc. •••			
310 ± 25	11 ANISOVICH	00J	SPEC
135 \pm 150 65	12,13 COUPLAND	77	CNTR 0.7-2.4 $\bar{p} p \rightarrow \bar{p} p$
165 \pm 18 8	13 ALSPECTOR	73	CNTR $\bar{p} p$ S channel
~ 190	ABRAMS	70	CNTR S channel $\bar{N}N$

¹¹ From the combined analysis of ANISOVICH 99c and ANISOVICH 99f on $\bar{p} p \rightarrow \eta \pi^0 \pi^0$, $\pi^0 \pi^0$, $\eta \eta$, $\eta \eta'$, $\pi^+ \pi^-$.
¹² From a fit to the total elastic cross section.
¹³ Isospins 0 and 1 not separated.

 $\pi^- \rho \rightarrow \eta \pi \pi$

VALUE (MeV)	DOCUMENT ID	TECN	COMMENT
••• We do not use the following data for averages, fits, limits, etc. •••			
235 ± 5.0 ± 4.0	AMELIN	00	VES 37 $\pi^- \rho \rightarrow \eta \pi^+ \pi^- n$

 $\rho\rho$ CENTRAL PRODUCTION

VALUE (MeV)	DOCUMENT ID	COMMENT
250 ± 80 OUR ESTIMATE		
••• We do not use the following data for averages, fits, limits, etc. •••		
260 ± 5.7	BARBERIS	00F 450 $\rho\rho \rightarrow \rho_f \omega \rho_S$

 $f_4(2300)$ DECAY MODES

Mode	Fraction (Γ_i/Γ)
Γ_1 $\rho\rho$	seen
Γ_2 $\omega\omega$	seen
Γ_3 $\eta\pi\pi$	seen
Γ_4 $\pi\pi$	seen
Γ_5 $K\bar{K}$	seen
Γ_6 $\bar{N}\bar{N}$	seen

 $f_4(2300)$ BRANCHING RATIOS

$\Gamma(\rho\rho)/\Gamma(\omega\omega)$	Γ_1/Γ_2
••• We do not use the following data for averages, fits, limits, etc. •••	
2.8 ± 0.5	BARBERIS

 $f_4(2300)$ REFERENCES

AMELIN	00	NP A668 83	D. Amelin et al.	(VES Collab.)
ANISOVICH	00J	PL B491 47	A.V. Anisovich et al.	(RAL, LOQM, PNPI+)
BARBERIS	00F	PL B484 198	D. Barberis et al.	(WA 102 Collab.)
ANISOVICH	99C	PL B452 173	A.V. Anisovich et al.	
ANISOVICH	99F	NP A651 253	A.V. Anisovich et al.	
HASAN	94	PL B334 215	A. Hasan, D.V. Bugg	(LOQM)
MARTIN	80B	NP B176 355	B.R. Martin, D. Morgan	(LOU, RHEL) JP
MARTIN	80C	NP B169 216	A.D. Martin, M.R. Pennington	(DURH) JP
CARTER	78B	NP B141 467	A.A. Carter	(LOQM)
CUTTS	78B	PR D17 16	D. Cutts et al.	(STON, WISC)
DULUDE	78B	PL 79B 335	R.S. Dulude et al.	(BROW, MIT, BARI) JP
CARTER	77	PL 67B 117	A.A. Carter et al.	(LOQM, RHEL) JP
COUPLAND	77	PL 71B 460	M. Coupland et al.	(LOQM, RHEL)
ALSPECTOR	73	PRL 30 511	J. Alspector et al.	(RUTG, UPNJ)
ABRAMS	70	PR D1 1917	R.J. Abrams et al.	(BNL)

 $f_0(2330)$

$$I^G(J^{PC}) = 0^+(0^{++})$$

OMITTED FROM SUMMARY TABLE

 $f_0(2330)$ MASS

VALUE (MeV)	DOCUMENT ID	TECN	COMMENT
••• We do not use the following data for averages, fits, limits, etc. •••			
2419 ± 64	¹ RODAS	22	RVUE $J/\psi(1S) \rightarrow \gamma(\pi\pi, K\bar{K})$
2340 ± 20	SARANTSEV	21	RVUE $J/\psi(1S) \rightarrow \gamma(\pi\pi, K\bar{K}, \eta\eta, \omega\phi)$
2314 ± 25	² BUGG	04A	RVUE
2337 ± 14	ANISOVICH	00J	SPEC 2.0 $\bar{p} p \rightarrow \pi\pi, \eta\eta$
~ 2321	HASAN	94	RVUE $\bar{p} p \rightarrow \pi\pi$
¹ T-matrix pole from coupled channel K-matrix fit to data on $J/\psi \rightarrow \gamma \pi^0 \pi^0$ (ABLIKIM 15AE) and $J/\psi \rightarrow \gamma K_S^0 K_S^0$ (ABLIKIM 18AA).			
² Partial wave analysis of the data on $\rho\bar{p} \rightarrow \bar{\Lambda}\Lambda$ from BARNES 00.			

 $f_0(2330)$ WIDTH

VALUE (MeV)	DOCUMENT ID	TECN	COMMENT
••• We do not use the following data for averages, fits, limits, etc. •••			
274 ± 94	¹ RODAS	22	RVUE $J/\psi(1S) \rightarrow \gamma(\pi\pi, K\bar{K})$
165 ± 25	SARANTSEV	21	RVUE $J/\psi(1S) \rightarrow \gamma(\pi\pi, K\bar{K}, \eta\eta, \omega\phi)$
144 ± 20	² BUGG	04A	RVUE
217 ± 33	ANISOVICH	00J	SPEC 2.0 $\bar{p} p \rightarrow \pi\pi, \eta\eta$
~ 223	HASAN	94	RVUE $\bar{p} p \rightarrow \pi\pi$
¹ T-matrix pole from coupled channel K-matrix fit to data on $J/\psi \rightarrow \gamma \pi^0 \pi^0$ (ABLIKIM 15AE) and $J/\psi \rightarrow \gamma K_S^0 K_S^0$ (ABLIKIM 18AA).			
² Partial wave analysis of the data on $\rho\bar{p} \rightarrow \bar{\Lambda}\Lambda$ from BARNES 00.			

 $f_0(2330)$ REFERENCES

RODAS	22	EPJ C82 80	A. Rodas et al.	(JPAC Collab.)
SARANTSEV	21	PL B816 136227	A.V. Sarantsev et al.	(BONN, PNPI)
ABLIKIM	18AA	PR D98 072003	M. Ablikim et al.	(BESIII Collab.)
ABLIKIM	15AE	PR D92 052003	M. Ablikim et al.	(BESIII Collab.)
BUGG	04A	EPJ C36 161	D.V. Bugg	
ANISOVICH	00J	PL B491 47	A.V. Anisovich et al.	(RAL, LOQM, PNPI+)
BARNES	00	PR C62 055203	P.D. Barnes et al.	
HASAN	94	PL B334 215	A. Hasan, D.V. Bugg	(LOQM)

 $f_2(2340)$

$$I^G(J^{PC}) = 0^+(2^{++})$$

 $f_2(2340)$ MASS

VALUE (MeV)	EVTS	DOCUMENT ID	TECN	COMMENT
2345 \pm 50 - 40 OUR AVERAGE				
2362 \pm 31 \pm 140 - 30 - 63	5.5k	¹ ABLIKIM	13N BES3	$e^+e^- \rightarrow J/\psi \rightarrow \gamma\eta\eta$
2339 ± 55		² ETKIN	88 MPS	22 $\pi^- \rho \rightarrow \phi\phi n$
••• We do not use the following data for averages, fits, limits, etc. •••				
2350 ± 7	80k	³ UMAN	06 E835	5.2 $\bar{p} p \rightarrow \eta\eta\pi^0$
2392 ± 10		BOOTH	86 OMEG	85 $\pi^- \text{Be} \rightarrow 2\phi\text{Be}$
2360 ± 20		LINDENBAUM	84 RVUE	
¹ From partial wave analysis including all possible combinations of 0^{++} , 2^{++} , and 4^{++} resonances.				
² Includes data of ETKIN 85. The percentage of the resonance going into $\phi\phi 2^{++} S_2$, D_2 , and D_0 is 37 ± 19, 4 \pm 12, and 59 \pm 21, respectively.				
³ Statistical error only.				

 $f_2(2340)$ WIDTH

VALUE (MeV)	EVTS	DOCUMENT ID	TECN	COMMENT
322 \pm 70 - 60 OUR AVERAGE				
334 \pm 62 \pm 165 - 54 - 100	5.5k	¹ ABLIKIM	13N BES3	$e^+e^- \rightarrow J/\psi \rightarrow \gamma\eta\eta$
319 \pm 81 - 69		² ETKIN	88 MPS	22 $\pi^- \rho \rightarrow \phi\phi n$
••• We do not use the following data for averages, fits, limits, etc. •••				
218 ± 16	80k	³ UMAN	06 E835	5.2 $\bar{p} p \rightarrow \eta\eta\pi^0$
198 ± 50		BOOTH	86 OMEG	85 $\pi^- \text{Be} \rightarrow 2\phi\text{Be}$
150 \pm 150 - 50		LINDENBAUM	84 RVUE	
¹ From partial wave analysis including all possible combinations of 0^{++} , 2^{++} , and 4^{++} resonances.				
² Includes data of ETKIN 85.				
³ Statistical error only.				

See key on page 1127

Meson Particle Listings

$f_2(2340)$, $\rho_5(2350)$, $X(2370)$

$f_2(2340)$ DECAY MODES

Mode	Fraction (Γ_i/Γ)
$\Gamma_1 \phi\phi$	seen
$\Gamma_2 \eta\eta$	seen

$f_2(2340)$ BRANCHING RATIOS

$\Gamma(\eta\eta)/\Gamma_{total}$	Γ_2/Γ		
VALUE	DOCUMENT ID	TECN	COMMENT
seen	UMAN	06	E835 $5.2 \bar{p}p \rightarrow \eta\eta\pi^0$

$f_2(2340)$ REFERENCES

ABLIKIM	13N	PR D87 092009	M. Ablikim et al.	(BESIII Collab.)
UMAN	06	PR D73 052009	I. Uman et al.	(FNAL E835)
ETKIN	88	PL B201 568	A. Etkin et al.	(BNL, CUNY)
BOOTH	86	NP B273 677	P.S.L. Booth et al.	(LIVP, GLAS, CERN)
ETKIN	85	PL 165B 217	A. Etkin et al.	(BNL, CUNY)
LINDENBAUM	84	CNPP 13 285	S.J. Lindenbaum	(CUNY)

$\rho_5(2350)$ $I^G(J^{PC}) = 1^+(5^{--})$

OMITTED FROM SUMMARY TABLE
 This entry was previously called $U_1(2400)$. See also $\rho(2150)$, $f_2(2150)$, $\rho_3(2250)$, $f_4(2300)$.

$\rho_5(2350)$ MASS

$\pi^- p \rightarrow \omega\pi^0 n$	VALUE (MeV)	DOCUMENT ID	TECN	COMMENT
	2330 ± 35	ALDE	95	GAM2 $38 \pi^- p \rightarrow \omega\pi^0 n$

$\bar{p}p \rightarrow \pi\pi$ or $\bar{K}K$	VALUE (MeV)	DOCUMENT ID	TECN	CHG	COMMENT
••• We do not use the following data for averages, fits, limits, etc. •••					
~ 2303	HASAN	94	RVUE		$\bar{p}p \rightarrow \pi\pi$
~ 2300	¹ MARTIN	80B	RVUE		
~ 2250	¹ MARTIN	80C	RVUE		
~ 2500	² CARTER	78B	CNTR 0		$0.7\text{--}2.4 \bar{p}p \rightarrow K^- K^+$
~ 2480	³ CARTER	77	CNTR 0		$0.7\text{--}2.4 \bar{p}p \rightarrow \pi\pi$

S-CHANNEL $\bar{N}N$	VALUE (MeV)	DOCUMENT ID	TECN	CHG	COMMENT
••• We do not use the following data for averages, fits, limits, etc. •••					
	2300 ± 45	⁴ ANISOVICH	02	SPEC	$0.6\text{--}1.9 p\bar{p} \rightarrow \omega\pi^0, \omega\eta\pi^0, \pi^+\pi^-$
	2295 ± 30	ANISOVICH	00J	SPEC	
~ 2380	^{5,6} CUTTS	78B	CNTR		$0.97\text{--}3 \bar{p}p \rightarrow \bar{N}N$
2345 ± 15	^{5,6} COUPLAND	77	CNTR 0		$0.7\text{--}2.4 \bar{p}p \rightarrow \bar{p}p$
2359 ± 2	^{5,7} ALSPECTOR	73	CNTR		$\bar{p}p$ S channel
2350 ± 10	⁸ ABRAMS	70	CNTR		S channel $\bar{N}N$
2360 ± 25	⁹ OH	70B	HDHC -0		$\bar{p}(pn), K^* K 2\pi$

$\pi^- p \rightarrow K^+ K^- n$	VALUE (MeV)	DOCUMENT ID	TECN	CHG	COMMENT
••• We do not use the following data for averages, fits, limits, etc. •••					
	2307 ± 6	ALPER	80	CNTR 0	$62 \pi^- p \rightarrow K^+ K^- n$
¹ $I(J^P) = 1(5^-)$ from simultaneous analysis of $p\bar{p} \rightarrow \pi^- \pi^+$ and $\pi^0 \pi^0$.					
² $I = 0(1); J^P = 5^-$ from Barrelet-zero analysis.					
³ $I(J^P) = 1(5^-)$ from amplitude analysis.					
⁴ From the combined analysis of ANISOVICH 00J, ANISOVICH 01D, ANISOVICH 01E, and ANISOVICH 02.					
⁵ Isospins 0 and 1 not separated.					
⁶ From a fit to the total elastic cross section.					
⁷ Referred to as U or U region by ALSPECTOR 73.					
⁸ For $I = 1 \bar{N}N$.					
⁹ No evidence for this bump seen in the $\bar{p}p$ data of CHAPMAN 71B. Narrow state not confirmed by OH 73 with more data.					

$\rho_5(2350)$ WIDTH

$\pi^- p \rightarrow \omega\pi^0 n$	VALUE (MeV)	DOCUMENT ID	TECN	COMMENT
	400 ± 100	ALDE	95	GAM2 $38 \pi^- p \rightarrow \omega\pi^0 n$

$\bar{p}p \rightarrow \pi\pi$ or $\bar{K}K$	VALUE (MeV)	DOCUMENT ID	TECN	CHG	COMMENT
••• We do not use the following data for averages, fits, limits, etc. •••					
~ 169	HASAN	94	RVUE		$\bar{p}p \rightarrow \pi\pi$
~ 250	¹⁰ MARTIN	80B	RVUE		

~ 300	¹⁰ MARTIN	80C	RVUE		
~ 150	¹¹ CARTER	78B	CNTR 0		$0.7\text{--}2.4 \bar{p}p \rightarrow K^- K^+$
~ 210	¹² CARTER	77	CNTR 0		$0.7\text{--}2.4 \bar{p}p \rightarrow \pi\pi$

S-CHANNEL $\bar{N}N$	VALUE (MeV)	DOCUMENT ID	TECN	CHG	COMMENT
••• We do not use the following data for averages, fits, limits, etc. •••					
	260 ± 75	¹³ ANISOVICH	02	SPEC	$0.6\text{--}1.9 p\bar{p} \rightarrow \omega\pi^0, \omega\eta\pi^0, \pi^+\pi^-$
	235 ± ⁶⁵/₄₀	ANISOVICH	00J	SPEC	
	135 ± ¹⁵⁰/₆₅	^{14,15} COUPLAND	77	CNTR 0	$0.7\text{--}2.4 \bar{p}p \rightarrow \bar{p}p$
	165 ± ¹⁸/₈	¹⁵ ALSPECTOR	73	CNTR	$\bar{p}p$ S channel
< 60	¹⁶ OH	70B	HDHC -0		$\bar{p}(pn), K^* K 2\pi$
~ 140	ABRAMS	67C	CNTR		S channel $\bar{N}N$

$\pi^- p \rightarrow K^+ K^- n$	VALUE (MeV)	DOCUMENT ID	TECN	CHG	COMMENT
••• We do not use the following data for averages, fits, limits, etc. •••					
	245 ± 20	ALPER	80	CNTR 0	$62 \pi^- p \rightarrow K^+ K^- n$
¹⁰ $I(J^P) = 1(5^-)$ from simultaneous analysis of $p\bar{p} \rightarrow \pi^- \pi^+$ and $\pi^0 \pi^0$.					
¹¹ $I = 0(1); J^P = 5^-$ from Barrelet-zero analysis.					
¹² $I(J^P) = 1(5^-)$ from amplitude analysis.					
¹³ From the combined analysis of ANISOVICH 00J, ANISOVICH 01D, ANISOVICH 01E, and ANISOVICH 02.					
¹⁴ From a fit to the total elastic cross section.					
¹⁵ Isospins 0 and 1 not separated.					
¹⁶ No evidence for this bump seen in the $\bar{p}p$ data of CHAPMAN 71B. Narrow state not confirmed by OH 73 with more data.					

$\rho_5(2350)$ REFERENCES

ANISOVICH	02	PL B542 8	A.V. Anisovich et al.	
ANISOVICH	01D	PL B508 6	A.V. Anisovich et al.	
ANISOVICH	01E	PL B513 281	A.V. Anisovich et al.	
ANISOVICH	00J	PL B491 47	A.V. Anisovich et al.	(RAL, LOQM, PNPI+)
ALDE	95	ZPHY C66 379	D.M. Alde et al.	(GAMS Collab.) JP
HASAN	94	PL B334 215	A. Hasan, D.V. Bugg	(LOQM)
ALPER	80	PL 94B 422	B. Alper et al.	(AMST, CERN, CRAC, MPIM+)
MARTIN	80B	NP B176 355	B.R. Martin, D. Morgan	(LOUC, RHEL) JP
MARTIN	80C	NP B169 216	A.D. Martin, M.R. Pennington	(DURH) JP
CARTER	78B	NP B141 467	A.A. Carter	(LOQM)
CUTTS	78B	PR D17 16	D. Cutts et al.	(STON, WISC)
CARTER	77	PL 67B 117	A.A. Carter et al.	(LOQM, RHEL) JP
COUPLAND	77	PL 71B 460	M. Coupland et al.	(LOQM, RHEL)
ALSPECTOR	73	PRL 30 511	J. Alspector et al.	(RUTG, UPNJ)
OH	73	NP B51 57	B.Y. Oh et al.	(MSU)
CHAPMAN	71B	PR D4 1275	J.W. Chapman et al.	(MICH)
ABRAMS	70	PR D1 1917	R.J. Abrams et al.	(BNL)
OH	70B	PRL 24 1257	B.Y. Oh et al.	(MSU)
ABRAMS	67C	PRL 18 1209	R.J. Abrams et al.	(BNL)

$X(2370)$ $I^G(J^{PC}) = ?(???)$

OMITTED FROM SUMMARY TABLE

$X(2370)$ MASS

VALUE (MeV)	EVTS	DOCUMENT ID	TECN	COMMENT
2341.6 ± 6.5 ± 5.7		¹ ABLIKIM	20Q	BES3 $J/\psi \rightarrow \gamma K \bar{K} \eta'$
••• We do not use the following data for averages, fits, limits, etc. •••				
2376.3 ± 8.7 ± ^{3.2}/_{4.3}	565	ABLIKIM	11c	BES3 $J/\psi \rightarrow \gamma\pi^+\pi^-\eta'$
¹ The state observed by ABLIKIM 11c at 2120 MeV is not observed with 90% CL upper limit of 1.49×10^{-5} for $J/\psi \rightarrow \gamma X(2120) \rightarrow \gamma K^+ K^- \eta'$ and 6.38×10^{-6} for $K_S^0 K_S^0 \eta'$.				

$X(2370)$ WIDTH

VALUE (MeV)	DOCUMENT ID	TECN	COMMENT
117 ± 10 ± 8	¹ ABLIKIM	20Q	BES3 $J/\psi \rightarrow \gamma K \bar{K} \eta'$
••• We do not use the following data for averages, fits, limits, etc. •••			
83 ± 17 ± ⁴⁴/₆	ABLIKIM	11c	BES3 $J/\psi \rightarrow \gamma\pi^+\pi^-\eta'$
¹ The state observed by ABLIKIM 11c at 2120 MeV is not observed with 90% CL upper limit of 1.49×10^{-5} for $J/\psi \rightarrow \gamma X(2120) \rightarrow \gamma K^+ K^- \eta'$ and 6.38×10^{-6} for $K_S^0 K_S^0 \eta'$.			

$X(2370)$ DECAY MODES

Mode	Fraction (Γ_i/Γ)
$\Gamma_1 K^+ K^- \eta'$	seen
$\Gamma_2 K_S^0 K_S^0 \eta'$	seen
$\Gamma_3 \pi^+\pi^-\eta'$	seen

Meson Particle Listings

 $X(2370)$, $f_6(2510)$ $X(2370)$ BRANCHING RATIOS

$\Gamma(K^+ K^- \eta')/\Gamma_{\text{total}}$				Γ_1/Γ
VALUE	DOCUMENT ID	TECN	COMMENT	
seen	ABLIKIM	20Q	BES3 $J/\psi \rightarrow \gamma K^+ K^- \eta'$	

$\Gamma(K_S^0 K_S^0 \eta')/\Gamma_{\text{total}}$				Γ_2/Γ
VALUE	DOCUMENT ID	TECN	COMMENT	
seen	ABLIKIM	20Q	BES3 $J/\psi \rightarrow \gamma K_S^0 K_S^0 \eta'$	

$\Gamma(\pi^+ \pi^- \eta')/\Gamma_{\text{total}}$				Γ_3/Γ
VALUE	DOCUMENT ID	TECN	COMMENT	
seen	ABLIKIM	11c	BES3 $J/\psi \rightarrow \gamma \pi^+ \pi^- \eta'$	

 $X(2370)$ REFERENCES

ABLIKIM	20Q	EPJ C80 746	M. Ablikim <i>et al.</i>	(BESIII Collab.)
ABLIKIM	11C	PRL 106 072002	M. Ablikim <i>et al.</i>	(BESIII Collab.)

 $f_6(2510)$

$$J^G(J^{PC}) = 0^+(6^{++})$$

OMITTED FROM SUMMARY TABLE
Needs confirmation.

 $f_6(2510)$ MASS

VALUE (MeV)	DOCUMENT ID	TECN	COMMENT
2465 ± 50 OUR AVERAGE	Error includes scale factor of 2.1.		
2420 ± 30	ALDE	98	GAM4 $100 \pi^- p \rightarrow \pi^0 \pi^0 n$
2510 ± 30	BINON	84B	GAM2 $38 \pi^- p \rightarrow n 2\pi^0$
• • • We do not use the following data for averages, fits, limits, etc. • • •			
2485 ± 40	¹ ANISOVICH	00J	SPEC 1.92–2.41 $p\bar{p}$
¹ From the combined analysis of ANISOVICH 99c, ANISOVICH 99f, ANISOVICH 99j, ANISOVICH 99k, and ANISOVICH 00b.			

 $f_6(2510)$ WIDTH

VALUE (MeV)	DOCUMENT ID	TECN	COMMENT
255 ± 40 OUR AVERAGE			
270 ± 60	ALDE	98	GAM4 $100 \pi^- p \rightarrow \pi^0 \pi^0 n$
240 ± 60	BINON	84B	GAM2 $38 \pi^- p \rightarrow n 2\pi^0$
• • • We do not use the following data for averages, fits, limits, etc. • • •			
410 ± 90	² ANISOVICH	00J	SPEC 1.92–2.41 $p\bar{p}$
² From the combined analysis of ANISOVICH 99c, ANISOVICH 99f, ANISOVICH 99j, ANISOVICH 99k, and ANISOVICH 00b.			

 $f_6(2510)$ DECAY MODES

Mode	Fraction (Γ_i/Γ)
$\Gamma_1 \pi \pi$	(6.0 ± 1.0) %

 $f_6(2510)$ BRANCHING RATIOS

$\Gamma(\pi \pi)/\Gamma_{\text{total}}$				Γ_1/Γ
VALUE	DOCUMENT ID	TECN	COMMENT	
0.06 ± 0.01	³ BINON	83c	GAM2 $38 \pi^- p \rightarrow n 4\gamma$	
³ Assuming one pion exchange and using data of BOLOTOV 74.				

 $f_6(2510)$ REFERENCES

ANISOVICH	00B	NP A662 319	A.V. Anisovich <i>et al.</i>	
ANISOVICH	00J	PL B491 47	A.V. Anisovich <i>et al.</i>	(RAL, LOQM, PNPI+)
ANISOVICH	99C	PL B452 173	A.V. Anisovich <i>et al.</i>	
ANISOVICH	99F	NP A651 253	A.V. Anisovich <i>et al.</i>	
ANISOVICH	99J	PL B471 271	A.V. Anisovich <i>et al.</i>	
ANISOVICH	99K	PL B468 309	A.V. Anisovich <i>et al.</i>	
ALDE	98	EPJ A3 361	D. Alde <i>et al.</i>	(GAM4 Collab.)
Also		PAN 62 405	D. Alde <i>et al.</i>	(GAMS Collab.)
		Translated from YAF 62 446.		
BINON	84B	LNC 39 41	F.G. Binon <i>et al.</i>	(SERP, BELG, LAPP)JP
BINON	83C	SJNP 38 723	F.G. Binon <i>et al.</i>	(SERP, BRUX+)
		Translated from YAF 38 1199.		
BOLOTOV	74	PL 52B 489	V.N. Bolotov <i>et al.</i>	(SERP)

STRANGE MESONS
($S = \pm 1, C = B = 0$)
 $K^+ = u\bar{s}, K^0 = d\bar{s}, \bar{K}^0 = \bar{d}s, K^- = \bar{u}s,$ similarly for K^{*} 's

K^\pm

$I(J^P) = \frac{1}{2}(0^-)$

CHARGED KAON MASS

Revised 1994 by T.G. Trippe (LBNL).

The average of the six charged kaon mass measurements which we use in the Particle Listings is

$$m_{K^\pm} = 493.677 \pm 0.013 \text{ MeV } (S = 2.4), \quad (1)$$

where the error has been increased by the scale factor S . The large scale factor indicates a serious disagreement between different input data. The average before scaling the error is

$$m_{K^\pm} = 493.677 \pm 0.005 \text{ MeV }, \quad (2)$$

$$\chi^2 = 22.9 \text{ for } 5 \text{ D.F.}, \text{ Prob. } = 0.04\%,$$

where the high χ^2 and correspondingly low χ^2 probability further quantify the disagreement.

The main disagreement is between the two most recent and precise results,

$$m_{K^\pm} = 493.696 \pm 0.007 \text{ MeV} \quad \text{DENISOV 91}$$

$$m_{K^\pm} = 493.636 \pm 0.011 \text{ MeV } (S = 1.5) \quad \text{GALL 88}$$

$$\text{Average} = 493.679 \pm 0.006 \text{ MeV}$$

$$\chi^2 = 21.2 \text{ for } 1 \text{ D.F.}, \text{ Prob. } = 0.0004\%, \quad (3)$$

both of which are measurements of x-ray energies from kaonic atoms. Comparing the average in Eq. (3) with the overall average in Eq. (2), it is clear that DENISOV 91 [1] and GALL 88 [2] dominate the overall average, and that their disagreement is responsible for most of the high χ^2 .

The GALL 88 measurement was made using four different kaonic atom transitions, $K^- \text{Pb } (9 \rightarrow 8)$, $K^- \text{Pb } (11 \rightarrow 10)$, $K^- \text{W } (9 \rightarrow 8)$, and $K^- \text{W } (11 \rightarrow 10)$. The m_{K^\pm} values they obtain from each of these transitions is shown in the Particle Listings and in Fig. 1. Their $K^- \text{Pb } (9 \rightarrow 8)$ m_{K^\pm} is below and somewhat inconsistent with their other three transitions. The average of their four measurements is

$$m_{K^\pm} = 493.636 \pm 0.007,$$

$$\chi^2 = 7.0 \text{ for } 3 \text{ D.F.}, \text{ Prob. } = 7.2\%. \quad (4)$$

This is a low but acceptable χ^2 probability so, to be conservative, GALL 88 scaled up the error on their average by $S=1.5$ to obtain their published error ± 0.011 shown in Eq. (3) above and used in the Particle Listings average.

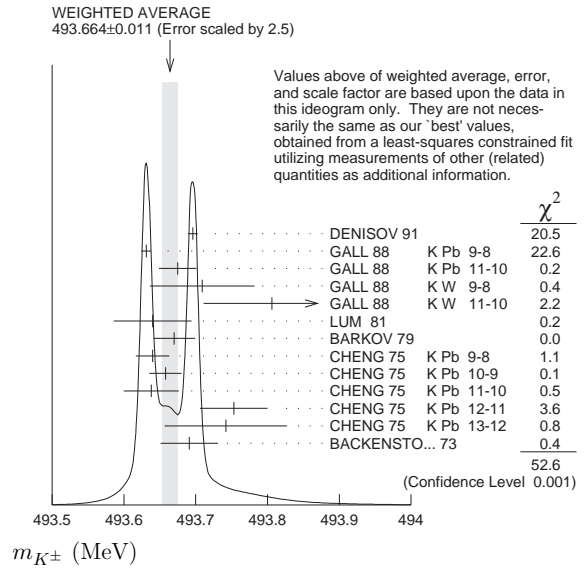


Figure 1: Ideogram of m_{K^\pm} mass measurements. GALL 88 and CHENG 75 measurements are shown separately for each transition they measured.

The ideogram in Fig. 1 shows that the DENISOV 91 measurement and the GALL 88 $K^- \text{Pb } (9 \rightarrow 8)$ measurement yield two well-separated peaks. One might suspect the GALL 88 $K^- \text{Pb } (9 \rightarrow 8)$ measurement since it is responsible both for the internal inconsistency in the GALL 88 measurements and the disagreement with DENISOV 91.

To see if the disagreement could result from a systematic problem with the $K^- \text{Pb } (9 \rightarrow 8)$ transition, we have separated the CHENG 75 [3] data, which also used $K^- \text{Pb}$, into its separate transitions. Figure 1 shows that the CHENG 75 and GALL 88 $K^- \text{Pb } (9 \rightarrow 8)$ values are consistent, suggesting the possibility of a common effect such as contaminant nuclear γ rays near the $K^- \text{Pb } (9 \rightarrow 8)$ transition energy, although the CHENG 75 errors are too large to make a strong conclusion. The average of all 13 measurements has a χ^2 of 52.6 as shown in Fig. 1 and the first line of Table 1, yielding an unacceptable χ^2 probability of 0.00005%. The second line of Table 1 excludes both the GALL 88 and CHENG 75 measurements of the $K^- \text{Pb } (9 \rightarrow 8)$ transition and yields a χ^2 probability of 43%. The third [fourth] line of Table 1 excludes only the GALL 88 $K^- \text{Pb } (9 \rightarrow 8)$ [DENISOV 91] measurement and yields a χ^2 probability of 20% [8.6%]. Table 1 shows that removing both measurements of the $K^- \text{Pb } (9 \rightarrow 8)$ transition produces the most consistent set of data, but that excluding only the GALL 88 $K^- \text{Pb } (9 \rightarrow 8)$ transition or DENISOV 91 also produces acceptable probabilities.

Meson Particle Listings

 K^\pm **Table 1:** m_{K^\pm} averages for some combinations of Fig. 1 data.

m_{K^\pm} (MeV)	χ^2	D.F.	Prob. (%)	Measurements used
493.664 ± 0.004	52.6	12	0.00005	all 13 measurements
493.690 ± 0.006	10.1	10	43	no K^- Pb(9→8)
493.687 ± 0.006	14.6	11	20	no GALL 88 K^- Pb(9→8)
493.642 ± 0.006	17.8	11	8.6	no DENISOV 91

Yu.M. Ivanov, representing DENISOV 91, has estimated corrections needed for the older experiments because of improved ^{192}Ir and ^{198}Au calibration γ -ray energies. He estimates that CHENG 75 and BACKENSTOSS 73 [4] m_{K^\pm} values could be raised by about 15 keV and 22 keV, respectively. With these estimated corrections, Table 1 becomes Table 2. The last line of Table 2 shows that if such corrections are assumed, then GALL 88 K^- Pb (9 → 8) is inconsistent with the rest of the data even when DENISOV 91 is excluded. Yu.M. Ivanov warns that these are rough estimates. Accordingly, we do not use Table 2 to reject the GALL 88 K^- Pb (9 → 8) transition, but we note that a future reanalysis of the CHENG 75 data could be useful because it might provide supporting evidence for such a rejection.

Table 2: m_{K^\pm} averages for some combinations of Fig. 1 data after raising CHENG 75 and BACKENSTOSS 73 values by 0.015 and 0.022 MeV respectively.

m_{K^\pm} (MeV)	χ^2	D.F.	Prob. (%)	Measurements used
493.666 ± 0.004	53.9	12	0.00003	all 13 measurements
493.693 ± 0.006	9.0	10	53	no K^- Pb(9→8)
493.690 ± 0.006	11.5	11	40	no GALL 88 K^- Pb(9→8)
493.645 ± 0.006	23.0	11	1.8	no DENISOV 91

The GALL 88 measurement uses a Ge semiconductor spectrometer which has a resolution of about 1 keV, so they run the risk of some contaminant nuclear γ rays. Studies of γ rays following stopped π^- and Σ^- absorption in nuclei (unpublished) do not show any evidence for contaminants according to GALL 88 spokesperson, B.L. Roberts. The DENISOV 91 measurement uses a crystal diffraction spectrometer with a resolution of 6.3 eV for radiation at 22.1 keV to measure the 4f-3d transition in K^- ^{12}C . The high resolution and the light nucleus reduce the probability for overlap by contaminant γ rays, compared with the measurement of GALL 88. The DENISOV 91 measurement is supported by their high-precision measurement of the 4d-2p transition energy in π^- ^{12}C , which is good agreement with the calculated energy.

While we suspect that the GALL 88 K^- Pb (9 → 8) measurements could be the problem, we are unable to find clear grounds for rejecting it. Therefore, we retain their measurement in the average and accept the large scale factor until further information can be obtained from new measurements and/or from reanalysis of GALL 88 and CHENG 75 data.

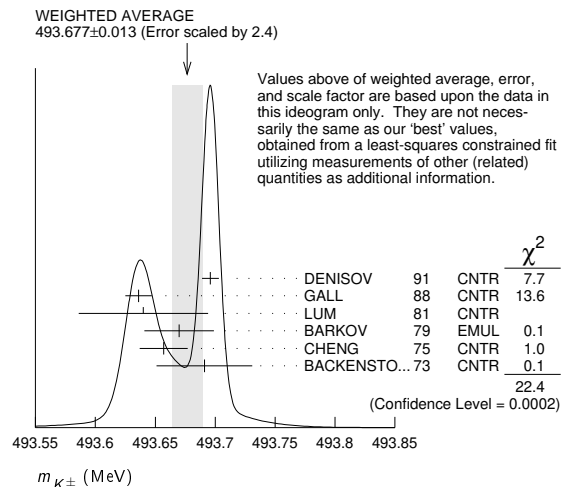
We thank B.L. Roberts (Boston Univ.) and Yu.M. Ivanov (Petersburg Nuclear Physics Inst.) for their extensive help in understanding this problem.

References

- A.S. Denisov, *et al.* [DENISOV 91], Sov. Phys. JETP Lett. **54**, 558 (1991).
- K.P. Gall, *et al.* [GALL 88], Phys. Rev. Lett. **60**, 186 (1988).
- S.C. Cheng, *et al.* [CHENG 75], Nucl. Phys. **A254**, 381 (1975).
- G. Backenstoss, *et al.* [BACKENSTOSS 73], Phys. Lett. **43B**, 431 (1973).

 K^\pm MASS

VALUE (MeV)	DOCUMENT ID	TECN	CHG	COMMENT
493.677 ± 0.016 OUR FIT	Error includes scale factor of 2.8.			
493.677 ± 0.013 OUR AVERAGE	Error includes scale factor of 2.4. See the ideogram below.			
493.696 ± 0.007	1 DENISOV	91	CNTR	— Kaonic atoms
493.636 ± 0.011	2 GALL	88	CNTR	— Kaonic atoms
493.640 ± 0.054	LUM	81	CNTR	— Kaonic atoms
493.670 ± 0.029	BARKOV	79	EMUL	± $e^+ e^- \rightarrow K^+ K^-$
493.657 ± 0.020	2 CHENG	75	CNTR	— Kaonic atoms
493.691 ± 0.040	BACKENSTO...73	CNTR	—	Kaonic atoms
● ● ● We do not use the following data for averages, fits, limits, etc. ● ● ●				
493.631 ± 0.007	GALL	88	CNTR	— K^- Pb (9 → 8)
493.675 ± 0.026	GALL	88	CNTR	— K^- Pb (11 → 10)
493.709 ± 0.073	GALL	88	CNTR	— K^- W (9 → 8)
493.806 ± 0.095	GALL	88	CNTR	— K^- W (11 → 10)
$493.640 \pm 0.022 \pm 0.008$	3 CHENG	75	CNTR	— K^- Pb (9 → 8)
$493.658 \pm 0.019 \pm 0.012$	3 CHENG	75	CNTR	— K^- Pb (10 → 9)
$493.638 \pm 0.035 \pm 0.016$	3 CHENG	75	CNTR	— K^- Pb (11 → 10)
$493.753 \pm 0.042 \pm 0.021$	3 CHENG	75	CNTR	— K^- Pb (12 → 11)
$493.742 \pm 0.081 \pm 0.027$	3 CHENG	75	CNTR	— K^- Pb (13 → 12)



- Error increased from 0.0059 based on the error analysis in IVANOV 92.
- This value is the authors' combination of all of the separate transitions listed for this paper.
- The CHENG 75 values for separate transitions were calculated from their Table 7 transition energies. The first error includes a 20% systematic error in the noncircular contaminant shift. The second error is due to a ± 5 eV uncertainty in the theoretical transition energies.

 $m_{K^+} - m_{K^-}$

Test of CPT.

VALUE (MeV)	EVTS	DOCUMENT ID	TECN	CHG
-0.032 ± 0.090	1.5M	1 FORD	72	ASPK ±

- FORD 72 uses $m_{\pi^+} - m_{\pi^-} = +28 \pm 70$ keV.

See key on page 1127

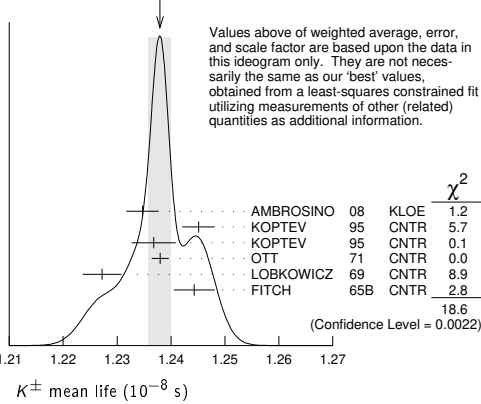
Meson Particle Listings

K^\pm

K^\pm MEAN LIFE

VALUE (10^{-8} s)	EVTS	DOCUMENT ID	TECN	CHG	COMMENT
1.2380 ± 0.0020 OUR FIT		Error includes scale factor of 1.8.			
1.2379 ± 0.0021 OUR AVERAGE		Error includes scale factor of 1.9. See the ideogram below.			
1.2347 ± 0.0030	15M	1 AMBROSINO 08	KLOE	±	$\phi \rightarrow K^+ K^-$
1.2451 ± 0.0030	250k	KOPTEV 95	CNTR		K at rest, U target
1.2368 ± 0.0041	150k	KOPTEV 95	CNTR		K at rest, Cu target
1.2380 ± 0.0016	3M	OTT 71	CNTR	+	K at rest
1.2272 ± 0.0036		LOBKOWICZ 69	CNTR	+	K in flight
1.2443 ± 0.0038		FITCH 65B	CNTR	+	K at rest
• • • We do not use the following data for averages, fits, limits, etc. • • •					
1.2415 ± 0.0024	400k	2 KOPTEV 95	CNTR		K at rest
1.221 ± 0.011		FORD 67	CNTR	±	
1.231 ± 0.011		BOYARSKI 62	CNTR	+	

WEIGHTED AVERAGE
1.2379 ± 0.0021 (Error scaled by 1.9)



Values above of weighted average, error, and scale factor are based upon the data in this ideogram only. They are not necessarily the same as our 'best' values, obtained from a least-squares constrained fit utilizing measurements of other (related) quantities as additional information.

¹ Result obtained by averaging the decay length and decay time analyses taking correlations into account.
² KOPTEV 95 report this weighted average of their U-target and Cu-target results, where they have weighted by $1/\sigma$ rather than $1/\sigma^2$.

$$(\tau_{K^+} - \tau_{K^-}) / \tau_{\text{average}}$$

This quantity is a measure of CPT invariance in weak interactions.

VALUE (%)	DOCUMENT ID	TECN
0.10 ± 0.09 OUR AVERAGE	Error includes scale factor of 1.2.	
-0.4 ± 0.4	AMBROSINO 08	KLOE
0.090 ± 0.078	LOBKOWICZ 69	CNTR
0.47 ± 0.30	FORD 67	CNTR

See the related review(s):
Rare Kaon Decays

K^+ DECAY MODES

K^- modes are charge conjugates of the modes below.

Mode	Fraction (Γ_i/Γ)	Scale factor/ Confidence level
Leptonic and semileptonic modes		
Γ_1 $e^+ \nu_e$	(1.582 ± 0.007) × 10 ⁻⁵	
Γ_2 $\mu^+ \nu_\mu$	(63.56 ± 0.11) %	S=1.2
Γ_3 $\pi^0 e^+ \nu_e$	(5.07 ± 0.04) %	S=2.1
Called K_{e3}^+ .		
Γ_4 $\pi^0 \mu^+ \nu_\mu$	(3.352 ± 0.033) %	S=1.9
Called $K_{\mu 3}^+$.		
Γ_5 $\pi^0 \pi^0 e^+ \nu_e$	(2.55 ± 0.04) × 10 ⁻⁵	S=1.1
Γ_6 $\pi^+ \pi^- e^+ \nu_e$	(4.247 ± 0.024) × 10 ⁻⁵	
Γ_7 $\pi^+ \pi^- \mu^+ \nu_\mu$	(1.4 ± 0.9) × 10 ⁻⁵	
Γ_8 $\pi^0 \pi^0 \pi^0 e^+ \nu_e$	< 3.5 × 10 ⁻⁶	CL=90%
Hadronic modes		
Γ_9 $\pi^+ \pi^0$	(20.67 ± 0.08) %	S=1.2
Γ_{10} $\pi^+ \pi^0 \pi^0$	(1.760 ± 0.023) %	S=1.1
Γ_{11} $\pi^+ \pi^+ \pi^-$	(5.583 ± 0.024) %	
Leptonic and semileptonic modes with photons		
Γ_{12} $\mu^+ \nu_\mu \gamma$	[a,b] (6.2 ± 0.8) × 10 ⁻³	
Γ_{13} $\mu^+ \nu_\mu \gamma (SD^+)$	[c,d] (1.33 ± 0.22) × 10 ⁻⁵	
Γ_{14} $\mu^+ \nu_\mu \gamma (SD^+ INT)$	[c,d] < 2.7 × 10 ⁻⁵	CL=90%
Γ_{15} $\mu^+ \nu_\mu \gamma (SD^- + SD^- INT)$	[c,d] < 2.6 × 10 ⁻⁴	CL=90%

Γ_{16} $e^+ \nu_e \gamma$	(9.4 ± 0.4) × 10 ⁻⁶	
Γ_{17} $\pi^0 e^+ \nu_e \gamma$	[a,b] (2.66 ± 0.09) × 10 ⁻⁴	
Γ_{18} $\pi^0 e^+ \nu_e \gamma (SD)$	[c,d] < 5.3 × 10 ⁻⁵	CL=90%
Γ_{19} $\pi^0 \mu^+ \nu_\mu \gamma$	[a,b] (1.25 ± 0.25) × 10 ⁻⁵	
Γ_{20} $\pi^0 \pi^0 e^+ \nu_e \gamma$	< 5 × 10 ⁻⁶	CL=90%

Hadronic modes with photons or $\ell\bar{\ell}$ pairs

Γ_{21} $\pi^+ \pi^0 \gamma (INT)$	(- 4.2 ± 0.9) × 10 ⁻⁶	
Γ_{22} $\pi^+ \pi^0 \gamma (DE)$	[a,e] (6.0 ± 0.4) × 10 ⁻⁶	
Γ_{23} $\pi^+ \pi^0 e^+ e^-$	(4.24 ± 0.14) × 10 ⁻⁶	
Γ_{24} $\pi^+ \pi^0 \pi^0 \gamma$	[a,b] (7.6 ± 3.0) × 10 ⁻⁶	
Γ_{25} $\pi^+ \pi^+ \pi^- \gamma$	[a,b] (7.1 ± 0.5) × 10 ⁻⁶	
Γ_{26} $\pi^+ \gamma \gamma$	[a] (1.01 ± 0.06) × 10 ⁻⁶	
Γ_{27} $\pi^+ 3\gamma$	[a] < 1.0 × 10 ⁻⁴	CL=90%
Γ_{28} $\pi^+ e^+ e^- \gamma$	(1.19 ± 0.13) × 10 ⁻⁸	

Leptonic modes with $\ell\bar{\ell}$ pairs

Γ_{29} $e^+ \nu_e \nu\bar{\nu}$	< 6 × 10 ⁻⁵	CL=90%
Γ_{30} $\mu^+ \nu_\mu \nu\bar{\nu}$	< 1.0 × 10 ⁻⁶	CL=90%
Γ_{31} $e^+ \nu_e e^+ e^-$	(2.48 ± 0.20) × 10 ⁻⁸	
Γ_{32} $\mu^+ \nu_\mu e^+ e^-$	(7.06 ± 0.31) × 10 ⁻⁸	
Γ_{33} $e^+ \nu_e \mu^+ \mu^-$	(1.7 ± 0.5) × 10 ⁻⁸	
Γ_{34} $\mu^+ \nu_\mu \mu^+ \mu^-$	< 4.1 × 10 ⁻⁷	CL=90%

Lepton family number (LF), Lepton number (L), $\Delta S = \Delta Q$ (SQ) violating modes, or $\Delta S = 1$ weak neutral current (S1) modes

Γ_{35} $\pi^+ \pi^+ e^- \bar{\nu}_e$	SQ	< 1.3 × 10 ⁻⁸	CL=90%
Γ_{36} $\pi^+ \pi^+ \mu^- \bar{\nu}_\mu$	SQ	< 3.0 × 10 ⁻⁶	CL=95%
Γ_{37} $\pi^+ e^+ e^-$	S1	(3.00 ± 0.09) × 10 ⁻⁷	
Γ_{38} $\pi^+ \mu^+ \mu^-$	S1	(9.4 ± 0.6) × 10 ⁻⁸	S=2.6
Γ_{39} $\pi^+ \nu\bar{\nu}$	S1	(1.14 ± 0.40 - 0.33) × 10 ⁻¹⁰	
Γ_{40} $\pi^+ \pi^0 \nu\bar{\nu}$	S1	< 4.3 × 10 ⁻⁵	CL=90%
Γ_{41} $\mu^- \nu e^+ e^+$	LF	< 2.1 × 10 ⁻⁸	CL=90%
Γ_{42} $\mu^+ \nu e$	LF [f]	< 4 × 10 ⁻³	CL=90%
Γ_{43} $\pi^+ \mu^+ e^-$	LF	< 1.3 × 10 ⁻¹¹	CL=90%
Γ_{44} $\pi^+ \mu^- e^+$	LF	< 6.6 × 10 ⁻¹¹	CL=90%
Γ_{45} $\pi^- \mu^+ e^+$	L	< 4.2 × 10 ⁻¹¹	CL=90%
Γ_{46} $\pi^- e^+ e^+$	L	< 2.2 × 10 ⁻¹⁰	CL=90%
Γ_{47} $\pi^- \mu^+ \mu^+$	L	< 4.2 × 10 ⁻¹¹	CL=90%
Γ_{48} $\mu^+ \bar{\nu}_e$	L [f]	< 3.3 × 10 ⁻³	CL=90%
Γ_{49} $\pi^0 e^+ \bar{\nu}_e$	L	< 3 × 10 ⁻³	CL=90%
Γ_{50} $\pi^+ \gamma$	[g]	< 2.3 × 10 ⁻⁹	CL=90%

[a] See the Particle Listings below for the energy limits used in this measurement.

[b] Most of this radiative mode, the low-momentum γ part, is also included in the parent mode listed without γ 's.

[c] Structure-dependent part.

[d] See the review on "Form Factors for Radiative Pion and Kaon Decays" for definitions and details.

[e] Direct-emission branching fraction.

[f] Derived from an analysis of neutrino-oscillation experiments.

[g] Violates angular-momentum conservation.

CONSTRAINED FIT INFORMATION

An overall fit to the mean life, a decay rate, and 15 branching ratios uses 35 measurements and one constraint to determine 8 parameters. The overall fit has a $\chi^2 = 53.4$ for 28 degrees of freedom.

The following off-diagonal array elements are the correlation coefficients $\langle \delta p_i \delta p_j \rangle / (\delta p_i \delta p_j)$, in percent, from the fit to parameters p_i , including the branching fractions, $x_i \equiv \Gamma_i / \Gamma_{\text{total}}$. The fit constrains the x_i whose labels appear in this array to sum to one.

x_3	-66						
x_4	-64	90					
x_5	-12	-5	-5				
x_9	-67	0	-1	-6			
x_{10}	-13	-6	-5	91	-6		
x_{11}	-14	-6	-6	2	-7	2	
Γ	3	1	1	0	2	0	-24
	x_2	x_3	x_4	x_5	x_9	x_{10}	x_{11}

Meson Particle Listings

 K^\pm

Mode	Rate (10^8 s^{-1})	Scale factor
Γ_2 $\mu^+ \nu_\mu$	0.5134 ± 0.0012	1.5
Γ_3 $\pi^0 e^+ \nu_e$ Called K_{e3}^+ .	0.0410 ± 0.0004	2.1
Γ_4 $\pi^0 \mu^+ \nu_\mu$ Called $K_{\mu 3}^+$.	0.02707 ± 0.00027	1.9
Γ_5 $\pi^0 \pi^0 e^+ \nu_e$	$(2.059 \pm 0.029) \times 10^{-5}$	1.1
Γ_9 $\pi^+ \pi^0$	0.1670 ± 0.0007	1.3
Γ_{10} $\pi^+ \pi^0 \pi^0$	0.01421 ± 0.00018	1.1
Γ_{11} $\pi^+ \pi^+ \pi^-$	0.04510 ± 0.00019	

 K^\pm DECAY RATES

$\Gamma(\mu^+ \nu_\mu)$ Γ_2			
VALUE (10^6 s^{-1})	EVTS	DOCUMENT ID	TECN CHG
51.34 ± 0.12 OUR FIT			Error includes scale factor of 1.5.
• • • We do not use the following data for averages, fits, limits, etc. • • •			
51.2 ± 0.8		FORD 67 CNTR ±	
$\Gamma(\pi^+ \pi^+ \pi^-)$ Γ_{11}			
VALUE (10^6 s^{-1})	EVTS	DOCUMENT ID	TECN CHG
4.510 ± 0.019 OUR FIT			
4.511 ± 0.024		¹ FORD 70 ASPK	
• • • We do not use the following data for averages, fits, limits, etc. • • •			
4.529 ± 0.032	3.2M	¹ FORD 70 ASPK	
4.496 ± 0.030		¹ FORD 67 CNTR ±	
¹ First FORD 70 value is second FORD 70 combined with FORD 67.			

 K^+ BRANCHING RATIOS

Leptonic and semileptonic modes

$\Gamma(e^+ \nu_e)/\Gamma(\mu^+ \nu_\mu)$ Γ_1/Γ_2			
VALUE (units 10^{-5})	EVTS	DOCUMENT ID	TECN CHG
2.488 ± 0.009 OUR AVERAGE			
$2.488 \pm 0.007 \pm 0.007$	150k	¹ LAZZERONI 13 NA62 ±	
$2.493 \pm 0.025 \pm 0.019$	13.8k	² AMBROSINO 09E KLOE ±	
• • • We do not use the following data for averages, fits, limits, etc. • • •			
$2.487 \pm 0.011 \pm 0.007$	60k	³ LAZZERONI 11 NA62 +	
2.51 ± 0.15	404	HEINTZE 76 SPEC +	
2.37 ± 0.17	534	HEARD 75B SPEC +	
2.42 ± 0.42	112	CLARK 72 OSPK +	
¹ LAZZERONI 13 uses full data sample collected from 2007 to 2008. This ratio is defined to be fully inclusive, including internal-bremsstrahlung.			
² The ratio is defined to include internal-bremsstrahlung, ignoring direct-emission contributions. AMBROSINO 09E determined the ratio from the measurement of $\Gamma(K \rightarrow e \nu(\gamma))$, $E_\gamma < 10 \text{ MeV}$ / $\Gamma(K \rightarrow \mu \nu(\gamma))$. 89.8% of $K \rightarrow e \nu(\gamma)$ events had $E_\gamma < 10 \text{ MeV}$.			
³ This ratio is defined to be fully inclusive, including internal-bremsstrahlung.			

$\Gamma(\mu^+ \nu_\mu)/\Gamma_{\text{total}}$ Γ_2/Γ			
VALUE (units 10^{-2})	EVTS	DOCUMENT ID	TECN CHG COMMENT
63.56 ± 0.11 OUR FIT			Error includes scale factor of 1.2.
63.60 ± 0.16 OUR AVERAGE			
$63.66 \pm 0.09 \pm 0.15$	865k	¹ AMBROSINO 06A KLOE +	
63.24 ± 0.44	62k	CHIANG 72 OSPK + 1.84 GeV/c K^+	
¹ Fully inclusive. Used tagged kaons from ϕ decays.			
$\Gamma(\pi^0 e^+ \nu_e)/\Gamma_{\text{total}}$ Γ_3/Γ			
VALUE (units 10^{-2})	EVTS	DOCUMENT ID	TECN CHG COMMENT
5.07 ± 0.04 OUR FIT			Error includes scale factor of 2.1.
4.94 ± 0.05 OUR AVERAGE			
$4.965 \pm 0.038 \pm 0.037$		¹ AMBROSINO 08A KLOE ±	
4.86 ± 0.10	3516	CHIANG 72 OSPK + 1.84 GeV/c K^+	
• • • We do not use the following data for averages, fits, limits, etc. • • •			
4.7 ± 0.3	429	SHAKLEE 64 HLBC +	
5.0 ± 0.5		ROE 61 HLBC +	
¹ Depends on K^+ lifetime τ . AMBROSINO 08A uses PDG 06 value of $\tau = (1.2385 \pm 0.0024) \times 10^{-8}$ sec. The correlation between K_{e3}^+ and $K_{\mu 3}^+$ branching fraction measurements is 62.7%.			

$\Gamma(\pi^0 e^+ \nu_e)/\Gamma(\mu^+ \nu_\mu)$ Γ_3/Γ_2			
VALUE	EVTS	DOCUMENT ID	TECN CHG
0.0798 ± 0.0008 OUR FIT			Error includes scale factor of 1.9.
• • • We do not use the following data for averages, fits, limits, etc. • • •			
0.069 ± 0.006	350	ZELLER 69 ASPK +	
0.0775 ± 0.0033	960	BOTTERILL 68c ASPK +	
0.069 ± 0.006	561	GARLAND 68 OSPK +	
0.0791 ± 0.0054	295	¹ AUERBACH 67 OSPK +	
¹ AUERBACH 67 changed from 0.0797 ± 0.0054 . See comment with ratio $\Gamma(\pi^0 \mu^+ \nu_\mu)/\Gamma(\mu^+ \nu_\mu)$. The value 0.0785 ± 0.0025 given in AUERBACH 67 is an average of AUERBACH 67 $\Gamma(\pi^0 e^+ \nu_e)/\Gamma(\mu^+ \nu_\mu)$ and CESTER 66 $\Gamma(\pi^0 e^+ \nu_e)/[\Gamma(\mu^+ \nu_\mu) + \Gamma(\pi^+ \pi^0)]$.			

$\Gamma(\pi^0 e^+ \nu_e)/[\Gamma(\mu^+ \nu_\mu) + \Gamma(\pi^+ \pi^0)]$ $\Gamma_3/(\Gamma_2 + \Gamma_9)$			
VALUE (units 10^{-2})	EVTS	DOCUMENT ID	TECN CHG
6.02 ± 0.06 OUR FIT			Error includes scale factor of 2.1.
6.02 ± 0.15 OUR AVERAGE			
6.16 ± 0.22	5110	ESCHSTRUTH 68 OSPK +	
5.89 ± 0.21	1679	CESTER 66 OSPK +	
• • • We do not use the following data for averages, fits, limits, etc. • • •			
5.92 ± 0.65		¹ WEISSENBERG... 76 SPEC +	
¹ Value calculated from WEISSENBERG 76 ($\pi^0 e \nu$), ($\mu \nu$), and ($\pi \pi^0$) values to eliminate dependence on our 1974 ($\pi 2\pi^0$) and ($\pi \pi^+ \pi^-$) fractions.			

$\Gamma(\pi^0 e^+ \nu_e)/[\Gamma(\pi^0 \mu^+ \nu_\mu) + \Gamma(\pi^+ \pi^0) + \Gamma(\pi^+ \pi^0 \pi^0)]$ $\Gamma_3/(\Gamma_4 + \Gamma_9 + \Gamma_{10})$			
VALUE	EVTS	DOCUMENT ID	TECN CHG
0.1967 ± 0.0016 OUR FIT			Error includes scale factor of 2.5.
$0.1962 \pm 0.0008 \pm 0.0035$	71k	SHER 03 B865 +	

$\Gamma(\pi^0 e^+ \nu_e)/\Gamma(\pi^+ \pi^0)$ Γ_3/Γ_9			
VALUE	EVTS	DOCUMENT ID	TECN CHG COMMENT
0.2454 ± 0.0023 OUR FIT			Error includes scale factor of 2.6.
0.2467 ± 0.0011 OUR AVERAGE			Error includes scale factor of 1.1.
$0.2423 \pm 0.0015 \pm 0.0037$	31k	UVAROV 14 ISTR - ISTR+	
$0.2470 \pm 0.0009 \pm 0.0004$	87k	BATLEY 07A NA48 ±	
• • • We do not use the following data for averages, fits, limits, etc. • • •			
0.221 ± 0.012	786	¹ LUCAS 73B HBC - Dalitz pairs only	
¹ LUCAS 73B gives $N(K_{e3}) = 786 \pm 3.1\%$, $N(2\pi) = 3564 \pm 3.1\%$. We use these values to obtain quoted result.			

$\Gamma(\pi^0 e^+ \nu_e)/\Gamma(\pi^+ \pi^+ \pi^-)$ Γ_3/Γ_{11}			
VALUE	EVTS	DOCUMENT ID	TECN CHG
0.908 ± 0.009 OUR FIT			Error includes scale factor of 1.6.
• • • We do not use the following data for averages, fits, limits, etc. • • •			
0.867 ± 0.027	2768	BARMIN 87 XEBC +	
0.856 ± 0.040	2827	BRAUN 75 HLBC +	
0.850 ± 0.019	4385	¹ HAIDT 71 HLBC +	
0.846 ± 0.021	4385	¹ EICHTEN 68 HLBC +	
0.94 ± 0.09	854	BELLOTTI 67B HLBC	
0.90 ± 0.06	230	BORREANI 64 HBC +	
¹ HAIDT 71 is a reanalysis of EICHTEN 68. Not included in average because of large discrepancy in $\Gamma(\pi^0 \mu^+ \nu)/\Gamma(\pi^0 e^+ \nu)$ with more precise results.			

$\Gamma(\pi^0 \mu^+ \nu_\mu)/\Gamma_{\text{total}}$ Γ_4/Γ			
VALUE (units 10^{-2})	EVTS	DOCUMENT ID	TECN CHG COMMENT
3.352 ± 0.033 OUR FIT			Error includes scale factor of 1.9.
3.24 ± 0.04 OUR AVERAGE			
$3.233 \pm 0.029 \pm 0.026$		¹ AMBROSINO 08A KLOE ±	
3.33 ± 0.16	2345	CHIANG 72 OSPK + 1.84 GeV/c K^+	
• • • We do not use the following data for averages, fits, limits, etc. • • •			
2.8 ± 0.4		² TAYLOR 59 EMUL +	
¹ Depends on K^+ lifetime τ . AMBROSINO 08A uses PDG 06 value of $\tau = (1.2385 \pm 0.0024) \times 10^{-8}$ sec. The correlation between K_{e3}^+ and $K_{\mu 3}^+$ branching fraction measurements is 62.7%.			
² Earlier experiments not averaged.			

$\Gamma(\pi^0 \mu^+ \nu_\mu)/\Gamma(\mu^+ \nu_\mu)$ Γ_4/Γ_2			
VALUE	EVTS	DOCUMENT ID	TECN CHG
0.0527 ± 0.0006 OUR FIT			Error includes scale factor of 1.8.
• • • We do not use the following data for averages, fits, limits, etc. • • •			
0.054 ± 0.009	240	ZELLER 69 ASPK +	
0.0480 ± 0.0037	424	¹ GARLAND 68 OSPK +	
0.0486 ± 0.0040	307	² AUERBACH 67 OSPK +	
¹ GARLAND 68 changed from 0.055 ± 0.004 in agreement with μ -spectrum calculation of GAILLARD 70 appendix B. L.G.Pondrom, (private communication 73).			
² AUERBACH 67 changed from 0.0602 ± 0.0046 by erratum which brings the μ -spectrum calculation into agreement with GAILLARD 70 appendix B.			

$\Gamma(\pi^0 \mu^+ \nu_\mu) / \Gamma(\pi^0 e^+ \nu_e)$ Γ_4 / Γ_3

VALUE	EVTS	DOCUMENT ID	TECN	CHG	COMMENT
0.6608 ± 0.0029 OUR FIT					Error includes scale factor of 1.1.
0.6618 ± 0.0027 OUR AVERAGE					
0.663 ± 0.003 ± 0.001	77k	BATLEY	07A	NA48	±
0.671 ± 0.007 ± 0.008	24k	HORIE	01	SPEC	
0.670 ± 0.014		¹ HEINTZE	77	SPEC	+
0.667 ± 0.017	5601	BOTTERILL	68B	ASPK	+
••• We use the following data for averages but not for fits. •••					
0.6511 ± 0.0064		² AMBROSINO	08A	KLOE	±
••• We do not use the following data for averages, fits, limits, etc. •••					
0.608 ± 0.014	1585	³ BRAUN	75	HLBC	+
0.705 ± 0.063	554	⁴ LUCAS	73B	HBC	- Dalitz pairs only
0.698 ± 0.025	3480	⁵ CHIANG	72	OSPK	+ 1.84 GeV/c K^+
0.596 ± 0.025		⁶ HAIDT	71	HLBC	+
0.604 ± 0.022	1398	⁶ EICHTEN	68	HLBC	
0.703 ± 0.056	1509	CALLAHAN	66B	HLBC	

¹ HEINTZE 77 value from fit to λ_0 . Assumes μ -e universality.
² Not used in the fit. This result enters the fit via correlation of K_{e3}^+ and $K_{\mu 3}^+$ branching fraction measurements of AMBROSINO 08A.
³ BRAUN 75 value is from form factor fit. Assumes μ -e universality.
⁴ LUCAS 73B gives $N(K_{\mu 3}) = 554 \pm 7.6\%$, $N(K_{e3}) = 786 \pm 3.1\%$. We divide.
⁵ CHIANG 72 $\Gamma(\pi^0 \mu^+ \nu_\mu) / \Gamma(\pi^0 e^+ \nu_e)$ is statistically independent of CHIANG 72 $\Gamma(\pi^0 \mu^+ \nu_\mu) / \Gamma_{total}$ and $\Gamma(\pi^0 e^+ \nu_e) / \Gamma_{total}$.
⁶ HAIDT 71 is a reanalysis of EICHTEN 68. Not included in average because of large discrepancy with more precise results.

$[\Gamma(\pi^0 \mu^+ \nu_\mu) + \Gamma(\pi^+ \pi^0)] / \Gamma_{total}$ $(\Gamma_4 + \Gamma_9) / \Gamma$

We combine these two modes for experiments measuring them in xenon bubble chamber because of difficulties of separating them there.

VALUE (units 10^{-2})	EVTS	DOCUMENT ID	TECN	CHG
24.02 ± 0.08 OUR FIT				Error includes scale factor of 1.2.
••• We do not use the following data for averages, fits, limits, etc. •••				
25.4 ± 0.9	886	SHAKLEE	64	HLBC +
23.4 ± 1.1		ROE	61	HLBC +

$\Gamma(\pi^0 \mu^+ \nu_\mu) / \Gamma(\pi^+ \pi^0)$ Γ_4 / Γ_9

VALUE	EVTS	DOCUMENT ID	TECN	CHG
0.1637 ± 0.0006 ± 0.0003	77k	BATLEY	07A	NA48 ±

$\Gamma(\pi^0 \mu^+ \nu_\mu) / \Gamma(\pi^+ \pi^+ \pi^-)$ Γ_4 / Γ_{11}

VALUE	EVTS	DOCUMENT ID	TECN	CHG	COMMENT
0.600 ± 0.007 OUR FIT					Error includes scale factor of 1.6.
••• We do not use the following data for averages, fits, limits, etc. •••					
0.503 ± 0.019	1505	¹ HAIDT	71	HLBC	+
0.510 ± 0.017	1505	¹ EICHTEN	68	HLBC	+
0.63 ± 0.07	2845	² BISI	65B	BC	+ HBC+HLBC

¹ HAIDT 71 is a reanalysis of EICHTEN 68. Not included in average because of large discrepancy in $\Gamma(\pi^0 \mu^+ \nu) / \Gamma(\pi^0 e^+ \nu)$ with more precise results.
² Error enlarged for background problems. See GAILLARD 70.

$\Gamma(\pi^0 \pi^0 e^+ \nu_e) / \Gamma_{total}$ Γ_5 / Γ

VALUE (units 10^{-5})	EVTS	DOCUMENT ID	TECN	CHG
2.55 ± 0.04 OUR FIT				Error includes scale factor of 1.1.
2.54 ± 0.89	10	BARMIN	88B	HLBC +

$\Gamma(\pi^0 \pi^0 e^+ \nu_e) / \Gamma(\pi^+ \pi^0 \pi^0)$ Γ_5 / Γ_{10}

VALUE (units 10^{-3})	EVTS	DOCUMENT ID	TECN	CHG
1.449 ± 0.008 OUR FIT				
1.449 ± 0.006 ± 0.006	65.2k	¹ BATLEY	14A	NA48 ±

¹ Data collected in 2003–2004. This leads to the scalar form factor $(1 + \delta_{PM}) f_5 = 6.079 \pm 0.012 \pm 0.027 \pm 0.046$ where the last error is due to the normalizing decay mode uncertainty.

$\Gamma(\pi^0 \pi^0 e^+ \nu_e) / \Gamma(\pi^0 e^+ \nu_e)$ Γ_5 / Γ_3

VALUE (units 10^{-4})	EVTS	DOCUMENT ID	TECN	CHG
5.03 ± 0.09 OUR FIT				Error includes scale factor of 1.2.
••• We do not use the following data for averages, fits, limits, etc. •••				
4.1 ^{+1.0} _{-0.7} OUR AVERAGE				
4.2 ^{+1.0} _{-0.9}	25	BOLOTOV	86B	CALO -
3.8 ^{+5.0} _{-1.2}	2	LJUNG	73	HLBC +

$\Gamma(\pi^+ \pi^- e^+ \nu_e) / \Gamma(\pi^+ \pi^+ \pi^-)$ Γ_6 / Γ_{11}

VALUE (units 10^{-4})	EVTS	DOCUMENT ID	TECN	CHG
7.606 ± 0.029 OUR AVERAGE				
7.615 ± 0.008 ± 0.028	1.1M	¹ BATLEY	12	NA48 ±
7.35 ± 0.01 ± 0.19	388k	² PISLAK	01	B865
7.21 ± 0.32	30k	ROSSELET	77	SPEC +

••• We do not use the following data for averages, fits, limits, etc. •••

7.36 ± 0.68	500	BOURQUIN	71	ASPK
7.0 ± 0.9	106	SCHWEIN...	71	HLBC +
5.83 ± 0.63	269	ELY	69	HLBC +

¹ BATLEY 12 uses data collected in 2003–2004. The result is inclusive of $K^\pm \rightarrow \pi^+ \pi^- e^\pm \nu \gamma$ decays. Using PDG 12 value for $\Gamma(\pi^+ \pi^- \pi^+) / \Gamma = (5.59 \pm 0.04) \times 10^{-2}$.
 BATLEY 12 obtains $B(\pi^+ \pi^- e \nu) = (4.257 \pm 0.004 \pm 0.035) \times 10^{-5}$ where the syst. error is dominated by the error on the normalization mode.
² PISLAK 01 reports $\Gamma(\pi^+ \pi^- e^+ \nu_e) / \Gamma_{total} = (4.109 \pm 0.008 \pm 0.110) \times 10^{-5}$ using the PDG 00 value $\Gamma(\pi^+ \pi^+ \pi^-) / \Gamma_{total} = (5.59 \pm 0.05) \times 10^{-2}$. We divide by the PDG value and unfold its error from the systematic error. PISLAK 03 and PISLAK 10A give additional details on the branching ratio measurement and give improved errors on the S-wave π - π scattering length: $a_0^0 = 0.235 \pm 0.013$ and $a_0^2 = -0.0410 \pm 0.0027$.

$\Gamma(\pi^+ \pi^- \mu^+ \nu_\mu) / \Gamma_{total}$ Γ_7 / Γ

VALUE (units 10^{-5})	EVTS	DOCUMENT ID	TECN	CHG
••• We do not use the following data for averages, fits, limits, etc. •••				
0.77 ^{+0.54} _{-0.50}	1	CLINE	65	FBC +

$\Gamma(\pi^+ \pi^- \mu^+ \nu_\mu) / \Gamma(\pi^+ \pi^+ \pi^-)$ Γ_7 / Γ_{11}

VALUE (units 10^{-4})	EVTS	DOCUMENT ID	TECN	CHG
2.57 ± 1.55	7	BISI	67	DBC +
••• We do not use the following data for averages, fits, limits, etc. •••				
~ 2.5	1	GREINER	64	EMUL +

$\Gamma(\pi^0 \pi^0 \pi^0 e^+ \nu_e) / \Gamma_{total}$ Γ_8 / Γ

VALUE (units 10^{-6})	CL%	EVTS	DOCUMENT ID	TECN	CHG
<3.5	90	0	BOLOTOV	88	SPEC -
••• We do not use the following data for averages, fits, limits, etc. •••					
<9	90	0	BARMIN	92	XEBC +

Hadronic modes

$\Gamma(\pi^+ \pi^0) / \Gamma_{total}$ Γ_9 / Γ

VALUE (units 10^{-2})	EVTS	DOCUMENT ID	TECN	CHG	COMMENT
20.67 ± 0.08 OUR FIT					Error includes scale factor of 1.2.
20.70 ± 0.16 OUR AVERAGE					Error includes scale factor of 1.8.
20.65 ± 0.05 ± 0.08	1.4M	¹ AMBROSINO	08E	KLOE +	$\phi \rightarrow K^+ K^-$
21.18 ± 0.28	16k	CHIANG	72	OSPK +	1.84 GeV/c K^+
••• We do not use the following data for averages, fits, limits, etc. •••					
21.0 ± 0.6		CALLAHAN	65	HLBC	See Γ_9 / Γ_{11}

¹ Fully inclusive of final-state radiation. The branching ratio is evaluated using K^+ lifetime, $\tau = 12.385$ ns.

$\Gamma(\pi^+ \pi^0) / \Gamma(\mu^+ \nu_\mu)$ Γ_9 / Γ_2

VALUE	EVTS	DOCUMENT ID	TECN	CHG	COMMENT
0.3252 ± 0.0016 OUR FIT					Error includes scale factor of 1.2.
0.3325 ± 0.0032 OUR AVERAGE					
0.3329 ± 0.0047 ± 0.0010	45k	USHER	92	SPEC +	$p\bar{p}$ at rest
0.3355 ± 0.0057		¹ WEISSENBE...	76	SPEC +	
0.3277 ± 0.0065	4517	² AUERBACH	67	OSPK +	
••• We do not use the following data for averages, fits, limits, etc. •••					
0.328 ± 0.005	25k	¹ WEISSENBE...	74	STRC +	
0.305 ± 0.018	1600	ZELLER	69	ASPK +	

¹ WEISSENBERG 76 revises WEISSENBERG 74.
² AUERBACH 67 changed from 0.3253 ± 0.0065. See comment with ratio $\Gamma(\pi^0 \mu^+ \nu_\mu) / \Gamma(\mu^+ \nu_\mu)$.

$\Gamma(\pi^+ \pi^0) / \Gamma(\pi^+ \pi^+ \pi^-)$ Γ_9 / Γ_{11}

VALUE	EVTS	DOCUMENT ID	TECN	CHG
3.702 ± 0.022 OUR FIT				Error includes scale factor of 1.1.
••• We do not use the following data for averages, fits, limits, etc. •••				
3.96 ± 0.15	1045	CALLAHAN	66	FBC +

$\Gamma(\pi^+ \pi^0 \pi^0) / \Gamma_{total}$ Γ_{10} / Γ

VALUE (units 10^{-2})	EVTS	DOCUMENT ID	TECN	CHG	COMMENT
1.760 ± 0.023 OUR FIT					Error includes scale factor of 1.1.
1.775 ± 0.028 OUR AVERAGE					Error includes scale factor of 1.2.
1.763 ± 0.013 ± 0.022		ALOISIO	04A	KLOE ±	
1.84 ± 0.06	1307	CHIANG	72	OSPK +	1.84 GeV/c K^+
••• We do not use the following data for averages, fits, limits, etc. •••					
1.53 ± 0.11	198	¹ PANDOULAS	70	EMUL +	
1.8 ± 0.2	108	SHAKLEE	64	HLBC +	
1.7 ± 0.2		ROE	61	HLBC +	
1.5 ± 0.2		² TAYLOR	59	EMUL +	

¹ Includes events of TAYLOR 59.
² Earlier experiments not averaged.

Meson Particle Listings

K^\pm

$\Gamma(\pi^+\pi^0\pi^0)/\Gamma(\pi^+\pi^0)$ Γ_{10}/Γ_9

VALUE	EVTS	DOCUMENT ID	TECN	CHG	COMMENT
0.0851 ± 0.0012 OUR FIT					Error includes scale factor of 1.1.
•••					We do not use the following data for averages, fits, limits, etc. •••
0.081 ± 0.005	574	¹ LUCAS	73B	HBC	— Dalitz pairs only
					¹ LUCAS 73B gives $N(\pi^2\pi^0) = 574 \pm 5.9\%$, $N(2\pi) = 3564 \pm 3.1\%$. We quote $0.5N(\pi^2\pi^0)/N(2\pi)$ where 0.5 is because only Dalitz pair π^0 's were used.

$\Gamma(\pi^+\pi^0\pi^0)/\Gamma(\pi^+\pi^+\pi^-)$ Γ_{10}/Γ_{11}

VALUE	EVTS	DOCUMENT ID	TECN	CHG	COMMENT
0.315 ± 0.004 OUR FIT					Error includes scale factor of 1.1.
0.303 ± 0.009	2027	BISI	65	BC	+ HBC+HLBC
•••					We do not use the following data for averages, fits, limits, etc. •••
0.393 ± 0.099	17	YOUNG	65	EMUL	+

$\Gamma(\pi^+\pi^+\pi^-)/\Gamma_{total}$ Γ_{11}/Γ

VALUE (units 10^{-2})	EVTS	DOCUMENT ID	TECN	CHG	COMMENT
5.583 ± 0.024 OUR FIT					
5.565 ± 0.031 ± 0.025	68k	¹ BABUSCI	14B	KLOE	+
•••					We do not use the following data for averages, fits, limits, etc. •••
5.56 ± 0.20	2330	² CHIANG	72	OSPK	+ 1.84 GeV/c K^\pm
5.34 ± 0.21	693	³ PANDOULAS	70	EMUL	+
5.71 ± 0.15		DEMARCO	65	HBC	
6.0 ± 0.4	44	YOUNG	65	EMUL	+
5.54 ± 0.12	2332	CALLAHAN	64	HLBC	+
5.1 ± 0.2	540	SHALLEE	64	HLBC	+
5.7 ± 0.3		ROE	61	HLBC	+

¹Inclusive of final-state radiation. Result obtained from averaging two branching ratios: one from a sample with $K^- \rightarrow \mu\nu(\gamma)$ tagging and another with $K^- \rightarrow \pi^-\pi^0(\gamma)$ tagging.
²Value is not independent of CHIANG 72 $\Gamma(\mu^+\nu_\mu)/\Gamma_{total}$, $\Gamma(\pi^+\pi^0)/\Gamma_{total}$, $\Gamma(\pi^+\pi^0\pi^0)/\Gamma_{total}$, $\Gamma(\pi^0\mu^+\nu_\mu)/\Gamma_{total}$, and $\Gamma(\pi^0e^+\nu_e)/\Gamma_{total}$.
³Includes events of TAYLOR 59.

Leptonic and semileptonic modes with photons

$\Gamma(\mu^+\nu_\mu\gamma)/\Gamma_{total}$ Γ_{12}/Γ

VALUE (units 10^{-3})	EVTS	DOCUMENT ID	TECN	CHG	COMMENT
6.2 ± 0.8 OUR AVERAGE					
6.6 ± 1.5		^{1,2} DEMIDOV	90	XEBC	$P(\mu) < 231.5$ MeV/c
6.0 ± 0.9		BARMIN	88	HLBC	+ $P(\mu) < 231.5$ MeV/c
•••					We do not use the following data for averages, fits, limits, etc. •••
3.5 ± 0.8		^{2,3} DEMIDOV	90	XEBC	$E(\gamma) > 20$ MeV
3.2 ± 0.5	57	⁴ BARMIN	88	HLBC	+ $E(\gamma) > 20$ MeV
5.4 ± 0.3		⁵ AKIBA	85	SPEC	$P(\mu) < 231.5$ MeV/c

¹ $P(\mu)$ cut given in DEMIDOV 90 paper, 235.1 MeV/c, is a misprint according to authors (private communication).
²DEMIDOV 90 quotes only inner bremsstrahlung (IB) part.
³Not independent of above DEMIDOV 90 value. Cuts differ.
⁴Not independent of above BARMIN 88 value. Cuts differ.
⁵Assumes μ - e universality and uses constraints from $K \rightarrow e\nu\gamma$.

$\Gamma(\mu^+\nu_\mu\gamma(SD^+))/\Gamma_{total}$ Γ_{13}/Γ

Structure-dependent part with $+\gamma$ helicity (SD^+ term). See the "Note on $\pi^\pm \rightarrow \ell^\pm\nu\gamma$ and $K^\pm \rightarrow \ell^\pm\nu\gamma$ Form Factors" in the π^\pm section of the Particle Data Listings above.

VALUE (units 10^{-5})	CL%	EVTS	DOCUMENT ID	TECN	
1.33 ± 0.12 ± 0.18		2588	¹ ADLER	00B B787	
•••					We do not use the following data for averages, fits, limits, etc. •••
<3.0	90		AKIBA	85 SPEC	

¹ADLER 00B obtains the branching ratio by extrapolating the measurement in the kinematic region $E_\mu > 137$ MeV, $E_\gamma > 90$ MeV to the full SD^+ phase-space. Also reports $|F_V + F_A| = 0.165 \pm 0.007 \pm 0.011$ and $-0.04 < F_V - F_A < 0.24$ at 90% CL.

$\Gamma(\mu^+\nu_\mu\gamma(SD^+INT))/\Gamma_{total}$ Γ_{14}/Γ

Interference term between internal Bremsstrahlung and SD^+ term. See the "Note on $\pi^\pm \rightarrow \ell^\pm\nu\gamma$ and $K^\pm \rightarrow \ell^\pm\nu\gamma$ Form Factors" in the π^\pm section of the Particle Data Listings above.

VALUE (units 10^{-5})	CL%	DOCUMENT ID	TECN
<2.7	90	AKIBA	85 SPEC

$\Gamma(\mu^+\nu_\mu\gamma(SD^- + SD^-INT))/\Gamma_{total}$ Γ_{15}/Γ

Sum of structure-dependent part with $-\gamma$ helicity (SD^- term) and interference term between internal Bremsstrahlung and SD^- term. See the "Note on $\pi^\pm \rightarrow \ell^\pm\nu\gamma$ and $K^\pm \rightarrow \ell^\pm\nu\gamma$ Form Factors" in the π^\pm section of the Particle Data Listings above.

VALUE (units 10^{-4})	CL%	DOCUMENT ID	TECN
<2.6	90	¹ AKIBA	85 SPEC

¹Assumes μ - e universality and uses constraints from $K \rightarrow e\nu\gamma$.

$\Gamma(e^+\nu_e\gamma)/\Gamma(\mu^+\nu_\mu)$ Γ_{16}/Γ_2

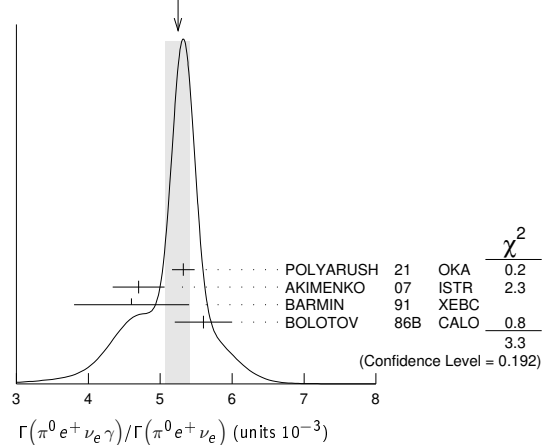
VALUE (units 10^{-5})	EVTS	DOCUMENT ID	TECN	CHG	COMMENT
1.483 ± 0.066 ± 0.013	1.4k	¹ AMBROSINO 09E	KLOE	±	E_γ in 10–250 MeV, $p_e > 200$ MeV/c

¹AMBROSINO 09E measured the differential width $dR_\gamma/dE_\gamma = (1/\Gamma(K \rightarrow \mu\nu)) (d\Gamma(K \rightarrow e\nu\gamma)/dE_\gamma)$. Result obtained by integrating the differential width over E_γ from 10 to 250 MeV.

$\Gamma(\pi^0e^+\nu_e\gamma)/\Gamma(\pi^0e^+\nu_e)$ Γ_{17}/Γ_3

VALUE (units 10^{-3})	EVTS	DOCUMENT ID	TECN	CHG	COMMENT
5.25 ± 0.17 OUR AVERAGE					Error includes scale factor of 1.3. See the ideogram below.
5.32 ± 0.10 ± 0.12	7248	¹ POLYARUSH 21	OKA	+	$E_\gamma > 10$ MeV, $0.6 < \cos(\theta_{e\gamma}) < 0.9$
4.7 ± 0.2 ± 0.3	1456	² AKIMENKO 07	ISTR	—	$E_\gamma > 10$ MeV, $0.6 < \cos(\theta_{e\gamma}) < 0.9$
4.6 ± 0.8	82	³ BARMIN 91	XEBC		$E_\gamma > 10$ MeV, $0.6 < \cos(\theta_{e\gamma}) < 0.9$
5.6 ± 0.4	192	⁴ BOLOTOV 86B	CALO	—	$E_\gamma > 10$ MeV
•••					We do not use the following data for averages, fits, limits, etc. •••
18.1 ± 0.3 ± 0.7	4476	² AKIMENKO 07	ISTR	—	$E_\gamma > 10$ MeV, $\theta_{e\gamma} > 10^\circ$
6.3 ± 0.2 ± 0.3		² AKIMENKO 07	ISTR	—	$E_\gamma > 30$ MeV, $\theta_{e\gamma} > 20^\circ$
15.1 ± 2.5	82	³ BARMIN 91	XEBC		$E_\gamma > 10$ MeV, $\cos(\theta_{e\gamma}) < 0.98$
4.8 ± 2.0	16	⁵ LJUNG 73	HLBC	+	$E_\gamma > 30$ MeV
2.2 +1.5 -1.0		⁵ LJUNG 73	HLBC	+	$E_\gamma > 30$ MeV
7.6 ± 2.8	13	⁶ ROMANO 71	HLBC	+	$E_\gamma > 10$ MeV
5.3 ± 2.2		⁶ ROMANO 71	HLBC	+	$E_\gamma > 30$ MeV
12 ± 8		BELLOTTI 67	HLBC		$E_\gamma > 30$ MeV

WEIGHTED AVERAGE
5.25±0.17 (Error scaled by 1.3)



¹POLYARUSH 21 provides values for three kinematic regions. For averaging, we use value with $E_\gamma > 10$ MeV and $0.6 < \cos(\theta_{e\gamma}) < 0.9$.
²AKIMENKO 07 provides values for three kinematic regions. For averaging, we use value with $E_\gamma > 10$ MeV and $0.6 < \cos(\theta_{e\gamma}) < 0.9$.
³BARMIN 91 quotes branching ratio $\Gamma(K \rightarrow e\pi^0\nu_\gamma)/\Gamma_{all}$. The measured normalization is $[\Gamma(K \rightarrow e\pi^0\nu) + \Gamma(K \rightarrow \pi^+\pi^-\pi^0)]$. For comparison with other experiments we used $\Gamma(K \rightarrow e\pi^0\nu)/\Gamma_{all} = 0.0482$ to calculate the values quoted here.
⁴ $\cos(\theta_{e\gamma})$ between 0.6 and 0.9.
⁵First LJUNG 73 value is for $\cos(\theta_{e\gamma}) < 0.9$, second value is for $\cos(\theta_{e\gamma})$ between 0.6 and 0.9 for comparison with ROMANO 71.
⁶Both ROMANO 71 values are for $\cos(\theta_{e\gamma})$ between 0.6 and 0.9. Second value is for comparison with second LJUNG 73 value. We use lowest E_γ cut for Summary Table value. See ROMANO 71 for E_γ dependence.

$\Gamma(\pi^0e^+\nu_e\gamma(SD))/\Gamma_{total}$ Γ_{18}/Γ

Structure-dependent part.

VALUE (units 10^{-5})	CL%	DOCUMENT ID	TECN	CHG
<5.3	90	BOLOTOV	86B	CALO

$\Gamma(\pi^0\mu^+\nu_\mu\gamma)/\Gamma_{total}$ Γ_{19}/Γ

VALUE (units 10^{-5})	CL%	EVTS	DOCUMENT ID	TECN	CHG	COMMENT
1.25 ± 0.25 OUR AVERAGE						
1.10 ± 0.32 ± 0.05		23	¹ ADLER	10	B787	$30 < E_\gamma < 60$ MeV
1.46 ± 0.22 ± 0.32		153	² TCHIKILEV	07	ISTR	— $30 < E_\gamma < 60$ MeV

••• We do not use the following data for averages, fits, limits, etc. •••
 2.4 ± 0.5 ± 0.6 125 SHIMIZU 06 K470 + $E_\gamma > 30$ MeV;
 $\theta_{\mu\gamma} > 20^\circ$

<6.1 90 0 LJUNG 73 HLBC + $E(\gamma) > 30$ MeV
¹ Value obtained from $B(K^+ \rightarrow \pi^0 \mu^+ \nu_\mu \gamma) = (2.51 \pm 0.74 \pm 0.12) \times 10^{-5}$ obtained in the kinematic region $E_\gamma > 20$ MeV, and then theoretical $K_{\mu 3\gamma}$ spectrum has been used. Also $B(K^+ \rightarrow \pi^0 \mu^+ \nu_\mu \gamma) = (1.58 \pm 0.46 \pm 0.08) \times 10^{-5}$, for $E_\gamma > 30$ MeV and $\theta_{\mu\gamma} > 20^\circ$, was determined.

² Obtained from measuring $B(K_{\mu 3\gamma}) / B(K_{\mu 3})$ and using PDG 02 value $B(K_{\mu 3}) = 3.27\%$. $B(K_{\mu 3\gamma}) = (8.82 \pm 0.94 \pm 0.86) \times 10^{-5}$ is obtained for $5 \text{ MeV} < E_\gamma < 30 \text{ MeV}$.

$\Gamma(\pi^0 \pi^0 e^+ \nu_e \gamma) / \Gamma_{\text{total}}$		Γ_{20} / Γ			
VALUE (units 10^{-6})	CL% EVTS	DOCUMENT ID	TECN	CHG	COMMENT
<5	90 0	BARMIN	92	XEBC	+ $E_\gamma > 10$ MeV

Hadronic modes with photons

$\Gamma(\pi^+ \pi^0 \gamma (\text{INT})) / \Gamma_{\text{total}}$ Γ_{21} / Γ
 The $K^+ \rightarrow \pi^+ \pi^0 \gamma$ differential decay rate can be described in terms of T_{π^+} , the charged pion kinetic energy, and $W^2 = (P_{K^+} \cdot P_\gamma) (P_{\pi^+} \cdot P_\gamma) / (m_K m_\pi)^2$; then we can write $d^2\Gamma(K^+ \rightarrow \pi^+ \pi^0 \gamma) / (dT_{\pi^+} dW^2) = d^2\Gamma(K^+ \rightarrow \pi^+ \pi^0 \gamma)_{IB} / (dT_{\pi^+} dW^2) [1 + 2 \cos(\pm\phi + \delta_1^+ - \delta_2^+) m_\pi^2 m_K^2 W^2 X_E + m_\pi^4 m_K^4 (X_E^2 + X_M^2) W^4]$. The IB differential and total branching ratios are expressed in terms of the non-radiative experimental width $\Gamma(K^+ \rightarrow \pi^+ \pi^0)$ by Low's theorem. Using PDG 10 $B(K^+ \rightarrow \pi^+ \pi^0) = 0.2066 \pm 0.0008$, one obtains respectively $B(K^+ \rightarrow \pi^+ \pi^0 \gamma)_{IB} (55 < T_{\pi^+} < 90 \text{ MeV}) = 2.55 \times 10^{-4}$ and $B(K^+ \rightarrow \pi^+ \pi^0 \gamma)_{IB} (0 < T_{\pi^+} < 80 \text{ MeV}) = 1.80 \times 10^{-4}$. Fitting respectively the piece proportional to W^2 and the piece proportional to W^4 , the interference contribution (INT), proportional to X_E , and the direct contribution (DE) proportional to $X_E^2 + X_M^2$ are extracted.

VALUE (units 10^{-6})	EVTS	DOCUMENT ID	TECN	CHG	COMMENT
-4.24 ± 0.63 ± 0.70	600k	¹ BATLEY	10A	NA48 ±	T_{π^+} 0-80 MeV

¹ The cut on the photon energy implies $W^2 > 0.2$. BATLEY 10A obtains the INT and DE fractional branchings with respect to IB from a simultaneous kinematical fit of INT and DE and then we use the PDG 10 value for $B(K^+ \rightarrow \pi^+ \pi^0) = 20.66 \pm 0.08$ to determine the IB. The INT and DE correlation coefficients -0.83. Assuming a constant electric amplitude, X_E , this INT value implies $X_E = -24 \pm 6 \text{ GeV}^{-4}$.

$\Gamma(\pi^+ \pi^0 \gamma (\text{DE})) / \Gamma_{\text{total}}$ Γ_{22} / Γ
 Direct emission (DE) part of $\Gamma(\pi^+ \pi^0 \gamma) / \Gamma_{\text{total}}$, assuming that interference (INT) component is zero.

VALUE (units 10^{-6})	EVTS	DOCUMENT ID	TECN	CHG	COMMENT
5.99 ± 0.27 ± 0.25	600k	¹ BATLEY	10A	NA48 ±	T_{π^+} 0-80 MeV

••• We do not use the following data for averages, fits, limits, etc. •••
 3.8 ± 0.8 ± 0.7 10k ALIEV 06 K470 + T_{π^+} 55-90 MeV
 3.7 ± 3.9 ± 1.0 930 UVAROV 06 ISTR - T_{π^+} 55-90 MeV
 3.2 ± 1.3 ± 1.0 4k ALIEV 03 K470 + T_{π^+} 55-90 MeV
 6.1 ± 2.5 ± 1.9 4k ALIEV 03 K470 + T_{π^+} full range
 4.7 ± 0.8 ± 0.3 20k ² ADLER 00c B787 + T_{π^+} 55-90 MeV
 20.5 ± 4.6 ± 3.9 BOLOTOV 87 WIRE - T_{π^+} 55-90 MeV
 -2.3
 15.6 ± 3.5 ± 5.0 ABRAMS 72 ASPK ± T_{π^\pm} 55-90 MeV

¹ The cut on the photon energy implies $W^2 > 0.2$. BATLEY 10A obtains the INT and DE fractional branchings with respect to IB from a simultaneous kinematical fit of INT and DE and then we use the PDG 10 value for $B(K^+ \rightarrow \pi^+ \pi^0) = 20.66 \pm 0.08$ to determine the IB. The INT and DE correlation coefficients -0.93. Assuming constant electric and magnetic amplitudes, X_E and X_M , these INT and DE values imply $X_E = -24 \pm 6 \text{ GeV}^{-4}$ and $X_M = -254 \pm 9 \text{ GeV}^{-4}$.

² ADLER 00c measures the INT component to be $(-0.4 \pm 1.6)\%$ of the inner bremsstrahlung (IB) component.

$\Gamma(\pi^+ \pi^0 e^+ e^-) / \Gamma_{\text{total}}$		Γ_{23} / Γ			
VALUE (units 10^{-6})	EVTS	DOCUMENT ID	TECN	CHG	COMMENT
4.24 ± 0.14	4.9k	¹ BATLEY	19	NA48	

¹ BATLEY 19 result is obtained from an exposure of 1.7×10^{11} charged kaon decays recorded in 2003-2004. The study of the kinematic space shows evidence for a structure dependent contribution consistent with predictions from chiral perturbation theory.

$\Gamma(\pi^+ \pi^0 \pi^0 \gamma) / \Gamma(\pi^+ \pi^0 \pi^0)$		$\Gamma_{24} / \Gamma_{10}$			
VALUE (units 10^{-4})	EVTS	DOCUMENT ID	TECN	CHG	COMMENT
4.3 - 1.7		BOLOTOV	85	SPEC	- $E(\gamma) > 10$ MeV

$\Gamma(\pi^+ \pi^+ \pi^- \gamma) / \Gamma_{\text{total}}$		Γ_{25} / Γ			
VALUE (units 10^{-4})	EVTS	DOCUMENT ID	TECN	CHG	COMMENT
0.071 ± 0.005	450	SHAPKIN	19	OKA	+ $E(\gamma) > 30$ MeV
1.10 ± 0.48	7	BARMIN	89	XEBC	$E(\gamma) > 5$ MeV
1.0 ± 0.4		STAMER	65	EMUL	+ $E(\gamma) > 11$ MeV

$\Gamma(\pi^+ \gamma \gamma) / \Gamma_{\text{total}}$		Γ_{26} / Γ			
VALUE (units 10^{-7})	CL% EVTS	DOCUMENT ID	TECN	CHG	COMMENT
10.1 ± 0.6	OUR AVERAGE				
10.03 ± 0.51 ± 0.24	215	¹ LAZZERONI	14	NA62 ±	
11 ± 3 ± 1	31	² KITCHING	97	B787 +	

••• We do not use the following data for averages, fits, limits, etc. •••
 9.10 ± 0.72 ± 0.22 149 ³ BATLEY 14 NA48 ±
 < 0.083 90 ⁴ ARTAMONOV 05 B949 + $P_\pi > 213 \text{ MeV}/c$
 < 10 90 0 ATIYA 90b B787 + T_π 117-127 MeV
 < 84 90 0 ASANO 82 CNTR + T_π 117-127 MeV
 -420 ± 520 0 ABRAMS 77 SPEC + $T_\pi < 92 \text{ MeV}$
 < 350 90 0 LJUNG 73 HLBC + 6-102, 114-127 MeV
 < 500 90 0 KLEMS 71 OSPK + $T_\pi < 117 \text{ MeV}$
 -100 ± 600 CHEN 68 OSPK + T_π 60-90 MeV

¹ LAZZERONI 14 combines NA62 and NA48/2 results. The result for the full kinematic range is extrapolated from the model-independent branching fraction $(9.65 \pm 0.61 \pm 0.14) \times 10^{-7}$ for $(m_{\gamma\gamma}/m_K)^2 > 0.2$. The measured ChPT parameter $\hat{c} = 1.86 \pm 0.25$.

² KITCHING 97 is extrapolated from their model-independent branching fraction $(6.0 \pm 1.5 \pm 0.7) \times 10^{-7}$ for $100 \text{ MeV}/c < P_{\pi^+} < 180 \text{ MeV}/c$ using Chiral Perturbation Theory.

³ BATLEY 14 uses data collected in 2003 and 2004. Branching ratio is obtained by determining the parameter $\hat{c} = 1.41 \pm 0.38 \pm 0.11$ and integrating the $O(p^6)$ chiral spectrum. A model independent value for the branching ratio is also obtained $(8.77 \pm 0.87 \pm 0.17) \times 10^{-7}$ for kinematic range $(m_{\gamma\gamma}/m_K)^2 > 0.2$.

⁴ ARTAMONOV 05 limit assumes ChPT with $\hat{c} = 1.8$ with unitarity corrections. With $\hat{c} = 1.6$ and no unitarity corrections they obtain $< 2.3 \times 10^{-8}$ at 90% CL. This partial branching ratio is predicted to be 6.10×10^{-9} and 0.49×10^{-9} for the cases with and without unitarity correction.

$\Gamma(\pi^+ 3\gamma) / \Gamma_{\text{total}}$ Γ_{27} / Γ
 Values given here assume a phase space pion energy spectrum.

VALUE (units 10^{-4})	CL%	DOCUMENT ID	TECN	CHG	COMMENT
<1.0	90	ASANO	82	CNTR +	$T(\pi)$ 117-127 MeV

••• We do not use the following data for averages, fits, limits, etc. •••
 <3.0 90 KLEMS 71 OSPK + $T(\pi) > 117 \text{ MeV}$

$\Gamma(\pi^+ e^+ e^- \gamma) / \Gamma_{\text{total}}$		Γ_{28} / Γ			
VALUE (units 10^{-8})	EVTS	DOCUMENT ID	TECN	CHG	COMMENT
1.19 ± 0.12 ± 0.04	113	¹ BATLEY	08	NA48	$m_{e\bar{e}\gamma} > 260 \text{ MeV}$

¹ BATLEY 08 also reports the Chiral Perturbation Theory parameter $\hat{c} = 0.9 \pm 0.45$ obtained by the shape of the $e^+ e^- \gamma$ invariant mass spectrum. By extrapolating the theoretical amplitude to $m_{e\bar{e}\gamma} < 260 \text{ MeV}$, it obtains the inclusive $B(K^+ \rightarrow \pi^+ e^+ e^- \gamma) = (1.29 \pm 0.13 \pm 0.03) \times 10^{-8}$, where the first error is the combined statistical and systematic errors and the second error is from the uncertainty in \hat{c} .

Leptonic modes with $e\bar{e}$ pairs

$\Gamma(e^+ \nu_e \nu \bar{\nu}) / \Gamma(e^+ \nu_e)$		Γ_{29} / Γ_1			
VALUE	CL% EVTS	DOCUMENT ID	TECN	CHG	COMMENT
<3.8	90 0	HEINTZE	79	SPEC	+

$\Gamma(\mu^+ \nu_\mu \nu \bar{\nu}) / \Gamma_{\text{total}}$		Γ_{30} / Γ			
VALUE	CL%	DOCUMENT ID	TECN	CHG	COMMENT
<1.0 × 10 ⁻⁶	90	¹ CORTINA-GIL	21	NA62	+

••• We do not use the following data for averages, fits, limits, etc. •••
 <2.4 × 10⁻⁶ 90 ² ARTAMONOV 16 B949 +
 <6.0 × 10⁻⁶ 90 ³ PANG 73 CNTR +

¹ CORTINA-GIL 21 assumes Standard Model μ spectrum. The search is performed in the reconstructed missing mass interval $m_{\text{miss}} > 316 \text{ MeV}/c^2$.

² ARTAMONOV 16 assumes Standard model μ spectrum. The search is performed in the muon momentum region between 130 and 175 MeV/c.

³ PANG 73 assumes μ spectrum from ν - ν interaction of BARDIN 70.

$\Gamma(e^+ \nu_e e^+ e^-) / \Gamma_{\text{total}}$		Γ_{31} / Γ			
VALUE (units 10^{-8})	EVTS	DOCUMENT ID	TECN	CHG	COMMENT
2.48 ± 0.14 ± 0.14	410	POBLAGUEV	02	B865 +	$m_{e\bar{e}} > 150 \text{ MeV}$

••• We do not use the following data for averages, fits, limits, etc. •••
 20 ± 20 4 DIAMANT-... 76 SPEC + $m_{e^+ e^-} > 140 \text{ MeV}$

$\Gamma(\mu^+ \nu_\mu e^+ e^-) / \Gamma_{\text{total}}$		Γ_{32} / Γ			
VALUE (units 10^{-8})	EVTS	DOCUMENT ID	TECN	CHG	COMMENT
7.06 ± 0.16 ± 0.26	2.7k	POBLAGUEV	02	B865 +	$m_{e\bar{e}} > 145 \text{ MeV}$

••• We do not use the following data for averages, fits, limits, etc. •••
 100 ± 30 14 DIAMANT-... 76 SPEC + $m_{e^+ e^-} > 140 \text{ MeV}$

$\Gamma(e^+ \nu_e \mu^+ \mu^-) / \Gamma_{\text{total}}$		Γ_{33} / Γ			
VALUE (units 10^{-8})	CL%	DOCUMENT ID	TECN	CHG	COMMENT
1.72 ± 0.45		MA	06	B865	

••• We do not use the following data for averages, fits, limits, etc. •••
 <50 90 ADLER 98 B787

Meson Particle Listings

K^\pm

$\Gamma(\mu^+ \nu_\mu \mu^+ \mu^-)/\Gamma_{\text{total}}$		Γ_{34}/Γ		
VALUE (units 10^{-7})	CL%	DOCUMENT ID	TECN	CHG
<4.1	90	ATIYA	89 B787	+

Lepton Family number (LF), Lepton number (L), $\Delta S = \Delta Q$ (SQ) violating modes, or $\Delta S = 1$ weak neutral current (SI) modes

$\Gamma(\pi^+ \pi^+ e^- \bar{\nu}_e)/\Gamma_{\text{total}}$		Γ_{35}/Γ			
VALUE (units 10^{-7})	CL%	EVTS	DOCUMENT ID	TECN	CHG
< 9.0	95	0	SCHWEINB...	71 HLBC	+
< 6.9	95	0	ELY	69 HLBC	+
<20.	95		BIRGE	65 FBC	+

$\Gamma(\pi^+ \pi^+ e^- \bar{\nu}_e)/\Gamma(\pi^+ \pi^- e^+ \nu_e)$		Γ_{35}/Γ_6		
VALUE (units 10^{-4})	CL%	EVTS	DOCUMENT ID	TECN
< 3	90	3	BLOCH	76 SPEC
<130.	95	0	BOURQUIN	71 ASPK

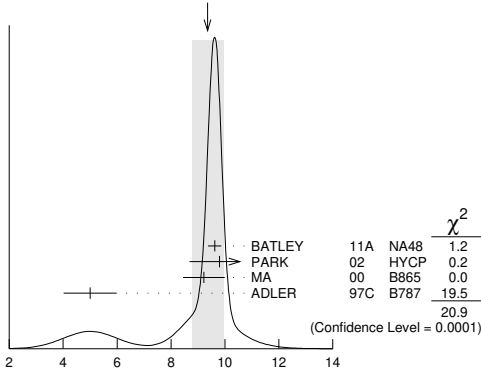
$\Gamma(\pi^+ \pi^+ \mu^- \bar{\nu}_\mu)/\Gamma_{\text{total}}$		Γ_{36}/Γ			
VALUE (units 10^{-6})	CL%	EVTS	DOCUMENT ID	TECN	CHG
<3.0	95	0	BIRGE	65 FBC	+

$\Gamma(\pi^+ e^+ e^-)/\Gamma_{\text{total}}$		Γ_{37}/Γ		
VALUE (units 10^{-7})	EVTS	DOCUMENT ID	TECN	CHG
3.00 ± 0.09 OUR AVERAGE				
3.11 ± 0.04 ± 0.12	7253	1 BATLEY	09 NA48	±
2.94 ± 0.05 ± 0.14	10300	2 APPEL	99 SPEC	+
2.75 ± 0.23 ± 0.13	500	3 ALLIEGRO	92 SPEC	+
2.7 ± 0.5	41	4 BLOCH	75 SPEC	+

¹ Value extrapolated from a measurement in the region $z = (m_{ee}/m_K)^2 > 0.08$. BATLEY 09 also evaluated the shape of the form factor using four different theoretical models.
² APPEL 99 establishes vector nature of this decay and determines form factor $f(z) = f_0(1 + \delta z)$, $Z = M_{ee}^2/m_K^2$, $\delta = 2.14 \pm 0.13 \pm 0.15$. Also reports constraints on scalar and tensor interactions: $|f_S| < 6.6 \times 10^{-5}$, $|f_T| < 3.7 \times 10^{-4}$ at 90% C.L.
³ ALLIEGRO 92 assumes a vector interaction with a form factor given by $\lambda = 0.105 \pm 0.035 \pm 0.015$ and a correlation coefficient of -0.82 .
⁴ BLOCH 75 assumes a vector interaction.

$\Gamma(\pi^+ \mu^+ \mu^-)/\Gamma_{\text{total}}$		Γ_{38}/Γ				
VALUE (units 10^{-8})	CL%	EVTS	DOCUMENT ID	TECN	CHG	COMMENT
9.4 ± 0.6 OUR AVERAGE						Error includes scale factor of 2.6. See the ideogram below.
9.62 ± 0.21 ± 0.13	3120		1 BATLEY	11A NA48	±	2003-04 data
9.8 ± 1.0 ± 0.5	110		2 PARK	02 HYCP	±	
9.22 ± 0.60 ± 0.49	402		3 MA	00 B865	+	
5.0 ± 0.4 ± 0.9	207		4 ADLER	97C B787	+	
9.7 ± 1.2 ± 0.4	65		PARK	02 HYCP	+	
10.0 ± 1.9 ± 0.7	35		PARK	02 HYCP	-	
<23	90		ATIYA	89 B787	+	

WEIGHTED AVERAGE
9.4 ± 0.6 (Error scaled by 2.6)



¹ BATLEY 11A also studies the form factor $f(z)$ dependence of the decay, described via single photon exchange: i) assuming a linear form factor, $f(z) = f_0(1 + \delta z)$, $z = (M_{\mu\mu}/m_K)^2$, finding $f_0 = 0.470 \pm 0.040$ and $\delta = 3.11 \pm 0.57$ and ii) assuming a linear

form factor including π - π rescattering, $W_{\pi\pi}$, as in DAMBROSIO 98A, finding $f(z) = G_F m_K^2 (a_+ + b_+ z) + W_{\pi\pi}(z)$, $a_+ = -0.575 \pm 0.039$, $b_+ = -0.813 \pm 0.145$.
² PARK 02 “±” result comes from combining $K^+ \rightarrow \pi^+ \mu^+ \mu^-$ and $K^- \rightarrow \pi^- \mu^+ \mu^-$, assuming CP is conserved.
³ MA 00 establishes vector nature of this decay and determines form factor $f(z) = f_0(1 + \delta z)$, $z = (M_{\mu\mu}/m_K)^2$, $\delta = 2.45^{+1.30}_{-0.95}$.
⁴ ADLER 97c gives systematic error 0.7×10^{-8} and theoretical uncertainty 0.6×10^{-8} , which we combine in quadrature to obtain our second error.

$\Gamma(\pi^+ \nu \bar{\nu})/\Gamma_{\text{total}}$		Γ_{39}/Γ				
VALUE (units 10^{-10})	CL%	EVTS	DOCUMENT ID	TECN	CHG	COMMENT
1.14 ± 0.40 OUR AVERAGE						
1.06 ± 0.41 - 0.35	20		1 CORTINA-GIL	21B NA62	+	
1.73 ± 1.15 - 1.05	7		2 ARTAMONOV	08 B949	+	140 < P _π < 199 MeV, 211 < P _π < 229 MeV
0.48 ± 0.72 - 0.48			3 CORTINA-GIL	20c NA62	+	
< 11	90	1	4 CORTINA-GIL	19B NA62	+	decay-in-flight
7.89 ± 9.26 - 5.10	3		5 ARTAMONOV	08 B949	+	140 < P _π < 199 MeV
< 22	90	1	6 ADLER	04 B787	+	211 < P _π < 229 MeV
< 27	90		ADLER	04 B787	+	Scalar
< 18	90		ADLER	04 B787	+	Tensor
1.47 ± 1.30 - 0.89	3		7 ANISIMOVSK..	04 B949	+	211 < P _π < 229 MeV
1.57 ± 1.75 - 0.82	2		ADLER	02 B787	+	P _π > 211 MeV/c
< 42	90	1	ADLER	02c B787	+	140 < P _π < 195 MeV
< 47	90		8 ADLER	02c B787	+	Scalar
< 25	90		8 ADLER	02c B787	+	Tensor
1.5 ± 3.4 - 1.2	1		ADLER	00 B787		In ADLER 02
4.2 ± 9.7 - 3.5	1		ADLER	97 B787		
< 24	90		ADLER	96 B787		
< 75	90		ATIYA	93 B787	+	T(π) 115–127 MeV
< 52	90		9 ATIYA	93 B787	+	
< 170	90	0	ATIYA	93B B787	+	T(π) 60–100 MeV
< 340	90		ATIYA	90 B787	+	
<1400	90		ASANO	81B CNTR	+	T(π) 116–127 MeV

¹ CORTINA-GIL 21B analysis of the NA62 data taken in 2016–2018 observed 20 candidate events with an expected background of 7 events. The achieved single event sensitivity is $(0.839 \pm 0.054) \times 10^{-11}$. The quoted branching ratio includes result from CORTINA-GIL 20c which observed two candidate events. This provides evidence for the very rare $K^+ \rightarrow \pi^+ \nu \bar{\nu}$ decay, observed with a significance of 3.4σ . Search for a feebly interacting scalar or pseudo-scalar particle X in the decay $K^+ \rightarrow \pi^+ X$ was performed and an upper limit from $< 3 \times 10^{-11}$ to $< 6 \times 10^{-11}$ at the 90% C.L. was set for an invisible particle with a mass of 0–110 MeV/c² and $< 1 \times 10^{-11}$ for mass of 160–260 MeV/c².
² Value obtained combining ANISIMOVSKY 04, ADLER 04, and the present ARTAMONOV 08 results.
³ CORTINA-GIL 20c analysis of the NA62 data taken in 2017 observed two candidate events with an expected background of 1.5 events. The achieved single event sensitivity is $(0.389 \pm 0.024) \times 10^{-10}$. The quoted branching ratio includes result from CORTINA-GIL 19B which observed one candidate event. The corresponding upper limit $B(K^+ \rightarrow \pi^+ \nu \bar{\nu}) < 1.78 \times 10^{-10}$ at 90% C.L. Superseded by CORTINA-GIL 21B.
⁴ Based on a sample of 1.21×10^{11} K^+ decays collected in 2016. One signal candidate is observed while the expected background is 0.152 events. The single-event-sensitivity is estimated to be 3.15×10^{-10} .
⁵ Observed 3 events with an estimated background of $0.93 \pm 0.17^{+0.32}_{-0.24}$. Signal-to-background ratio for each of these 3 events is 0.20, 0.42, and 0.47.
⁶ Value obtained combining the previous result ADLER 02c with 1 event and the present result with 0 events to obtain an expected background 1.22 ± 0.24 events and 1 event observed.
⁷ Value obtained combining the previous E787 result ADLER 02 with 2 events and the present E949 with 1 event. The additional event has a signal-to-background ratio 0.9. Superseded by ARTAMONOV 08.
⁸ Superseded by ADLER 04.
⁹ Combining ATIYA 93 and ATIYA 93B results. Superseded by ADLER 96.

$\Gamma(\pi^+ \pi^0 \nu \bar{\nu})/\Gamma_{\text{total}}$		Γ_{40}/Γ		
VALUE (units 10^{-5})	CL%	DOCUMENT ID	TECN	CHG
<4.3	90	1 ADLER	01 SPEC	

¹ Search region defined by $90 \text{ MeV} < P_{\pi^+} < 188 \text{ MeV}/c$ and $135 \text{ MeV} < E_{\pi^0} < 180 \text{ MeV}$.

$\Gamma(\mu^- \nu_e e^+)/\Gamma(\pi^+ \pi^- e^+ \nu_e)$		Γ_{41}/Γ_6			
VALUE (units 10^{-3})	CL%	EVTS	DOCUMENT ID	TECN	CHG
<0.5	90	0	1 DIAMANT-...	76 SPEC	+

¹ DIAMANT-BERGER 76 quotes this result times our 1975 $\pi^+ \pi^- e \nu$ BR ratio.

$\Gamma(\mu^+ \nu_e)/\Gamma_{\text{total}}$ Γ_{42}/Γ

Forbidden by lepton family number conservation.

VALUE	CL%	EVTS	DOCUMENT ID	TECN	CHG	COMMENT
<0.004	90	0	¹ LYONS	81	HLBC	200 GeV K^+ narrow band ν beam

• • • We do not use the following data for averages, fits, limits, etc. • • •

<0.012 90 ¹ COOPER 82 HLBC Wideband ν beam¹ COOPER 82 and LYONS 81 limits on ν_e observation are here interpreted as limits on lepton family number violation in the absence of mixing. $\Gamma(\pi^+ \mu^+ e^-)/\Gamma_{\text{total}}$ Γ_{43}/Γ

Test of lepton family number conservation.

VALUE (units 10^{-10})	CL%	DOCUMENT ID	TECN	CHG
<0.13	90	¹ SHER	05	RVUE +

• • • We do not use the following data for averages, fits, limits, etc. • • •

<0.21 90 SHER 05 B865 +

<0.39 90 APPEL 00 B865 +

<2.1 90 LEE 90 SPEC +

¹ This result combines SHER 05 1998 data, APPEL 00 1996 data, and data from BERGMAN 97 and PISLAK 97 theses, all from BNL-E865, with LEE 90 BNL-E777 data. $\Gamma(\pi^+ \mu^- e^+)/\Gamma_{\text{total}}$ Γ_{44}/Γ

Test of lepton family number conservation.

VALUE	CL%	DOCUMENT ID	TECN	CHG
< 6.6×10^{-11}	90	ALIBERTI	21	NA62 +

• • • We do not use the following data for averages, fits, limits, etc. • • •

< 5.2×10^{-10} 90 APPEL 00B B865 +< 70×10^{-10} 90 ¹ DIAMANT-... 76 SPEC +¹ Measurement actually applies to the sum of the $\pi^+ \mu^- e^+$ and $\pi^- \mu^+ e^+$ modes. $\Gamma(\pi^- \mu^+ e^+)/\Gamma_{\text{total}}$ Γ_{45}/Γ

Test of total lepton number conservation.

VALUE	CL%	DOCUMENT ID	TECN	CHG
< 4.2×10^{-11}	90	ALIBERTI	21	NA62 +

• • • We do not use the following data for averages, fits, limits, etc. • • •

< 5.0×10^{-10} 90 APPEL 00B B865 +< 70×10^{-10} 90 ¹ DIAMANT-... 76 SPEC +¹ Measurement actually applies to the sum of the $\pi^+ \mu^- e^+$ and $\pi^- \mu^+ e^+$ modes. $\Gamma(\pi^- e^+ e^+)/\Gamma_{\text{total}}$ Γ_{46}/Γ

Test of total lepton number conservation.

VALUE	CL%	DOCUMENT ID	TECN	CHG	COMMENT
< 2.2×10^{-10}	90	¹ CORTINA-GIL	19A	NA62 +	decay-in-flight

• • • We do not use the following data for averages, fits, limits, etc. • • •

< 6.4×10^{-10} 90 APPEL 00B B865 +< 9.2×10^{-9} 90 DIAMANT-... 76 SPEC +< 1.5×10^{-5} CHANG 68 HBC -¹ CORTINA-GIL 19A results are obtained with 2017 data. $\Gamma(\pi^- \mu^+ \mu^+)/\Gamma_{\text{total}}$ Γ_{47}/Γ

Forbidden by total lepton number conservation.

VALUE	CL%	DOCUMENT ID	TECN	CHG	COMMENT
< 4.2×10^{-11}	90	¹ CORTINA-GIL	19A	NA62 +	decay-in-flight

• • • We do not use the following data for averages, fits, limits, etc. • • •

< 8.6×10^{-11} 90 ² BATLEY 17 NA48 ±< 1.1×10^{-9} 90 BATLEY 11A NA48 ±< 3.0×10^{-9} 90 APPEL 00B B865 +< 1.5×10^{-4} 90 ³ LITTENBERG 92 HBC¹ CORTINA-GIL 19A results are obtained with 2017 data.² BATLEY 17 result is based on data taken in 2003 to 2004. Limits for two-body resonance X in $K^\pm \rightarrow \pi \mu \mu$ decays are also reported.³ LITTENBERG 92 is from retroactive data analysis of CHANG 68 bubble chamber data. $\Gamma(\mu^+ \bar{\nu}_e)/\Gamma_{\text{total}}$ Γ_{48}/Γ

Forbidden by total lepton number conservation.

VALUE (units 10^{-3})	CL%	DOCUMENT ID	TECN	COMMENT
<3.3	90	¹ COOPER	82	HLBC Wideband ν beam

¹ COOPER 82 limit on $\bar{\nu}_e$ observation is here interpreted as a limit on lepton number violation in the absence of mixing. $\Gamma(\pi^0 e^+ \bar{\nu}_e)/\Gamma_{\text{total}}$ Γ_{49}/Γ

Forbidden by total lepton number conservation.

VALUE	CL%	DOCUMENT ID	TECN	COMMENT
<0.003	90	¹ COOPER	82	HLBC Wideband ν beam

¹ COOPER 82 limit on $\bar{\nu}_e$ observation is here interpreted as a limit on lepton number violation in the absence of mixing. $\Gamma(\pi^+ \gamma)/\Gamma_{\text{total}}$ Γ_{50}/Γ

Violates angular momentum conservation and gauge invariance. Current interest in this decay is as a search for non-commutative space-time effects as discussed in ARTAMONOV 05 and for exotic physics such as a vacuum expectation value of a new vector field, non-local Superstring effects, or departures from Lorentz invariance, as discussed in ADLER 02b.

VALUE (units 10^{-9})	CL%	DOCUMENT ID	TECN	CHG
< 2.3	90	ARTAMONOV 05	B949	+

• • • We do not use the following data for averages, fits, limits, etc. • • •

< 360 90 ADLER 02B B787 +

<1400 90 ASANO 82 CNTR +

<4000 90 ¹ KLEMS 71 OSPK +¹ Test of model of Selleri, Nuovo Cimento **60A** 291 (1969).CPT VIOLATION TESTS IN K^\pm DECAYS

$$\Delta = (\Gamma(K^+) - \Gamma(K^-)) / (\Gamma(K^+) + \Gamma(K^-))$$

 $\Delta(K^\pm \rightarrow \mu^\pm \nu_\mu)$ RATE DIFFERENCE/SUM

VALUE (%)	DOCUMENT ID	TECN
-0.27 ± 0.21	FORD	67 CNTR

 $\Delta(K^\pm \rightarrow \pi^\pm \pi^0)$ RATE DIFFERENCE/SUM

VALUE (%)	DOCUMENT ID	TECN
0.4 ± 0.6	HERZO	69 OSPK

CP VIOLATION TESTS IN K^\pm DECAYS

$$\Delta = (\Gamma(K^+) - \Gamma(K^-)) / (\Gamma(K^+) + \Gamma(K^-))$$

 $\Delta(K^\pm \rightarrow \pi^\pm e^+ e^-)$ RATE DIFFERENCE/SUM

VALUE (units 10^{-2})	DOCUMENT ID	TECN
-2.2 ± 1.5 ± 0.6	¹ BATLEY	09 NA48

¹ This implies an upper limit of 2.1×10^{-2} at 90% CL. $\Delta(K^\pm \rightarrow \pi^\pm \mu^+ \mu^-)$ RATE DIFFERENCE/SUM

VALUE	DOCUMENT ID	TECN
0.010 ± 0.023 OUR AVERAGE		
0.011 ± 0.023	¹ BATLEY	11A NA48
-0.02 ± 0.11 ± 0.04	PARK	02 HYP

¹ This corresponds to the asymmetry upper limit of $< 2.9 \times 10^{-2}$ at 90% CL. $\Delta(K^\pm \rightarrow \pi^\pm \pi^0 \gamma)$ RATE DIFFERENCE/SUM

VALUE (units 10^{-3})	EVTS	DOCUMENT ID	TECN	CHG	COMMENT
0.0 ± 1.2 OUR AVERAGE					
0.0 ± 1.0 ± 0.6	1M	¹ BATLEY	10A	NA48	
4 ± 29	2461	SMITH	76	WIRE ±	E_π 55-90 MeV
5 ± 20	4000	ABRAMS	73B	ASPK ±	E_π 51-100 MeV

¹ This value implies the upper bound for this asymmetry 1.5×10^{-3} at 90% CL. $\Delta(K^\pm \rightarrow \pi^\pm \pi^+ \pi^-)$ RATE DIFFERENCE/SUM

VALUE (%)	EVTS	DOCUMENT ID	TECN	CHG
0.04 ± 0.06		¹ FORD	70	ASPK

• • • We do not use the following data for averages, fits, limits, etc. • • •

-0.01 ± 0.08

0.05 ± 0.07 3.2M ² SMITH 73 ASPK ±-0.25 ± 0.45 ¹ FORD 70 ASPK-0.02 ± 0.11 ¹ FLETCHER 67 OSPK ±-0.02 ± 0.11 ¹ FORD 67 CNTR¹ First FORD 70 value is second FORD 70 combined with FORD 67.² SMITH 73 value of $K^\pm \rightarrow \pi^\pm \pi^+ \pi^-$ rate difference is derived from SMITH 73 value of $K^\pm \rightarrow \pi^\pm 2\pi^0$ rate difference. $\Delta(K^\pm \rightarrow \pi^\pm \pi^0 \pi^0)$ RATE DIFFERENCE/SUM

VALUE (%)	EVTS	DOCUMENT ID	TECN	CHG
-0.02 ± 0.28 OUR AVERAGE				
0.04 ± 0.29		SMITH	73	ASPK ±
-0.6 ± 0.9	1802	HERZO	69	OSPK

T VIOLATION TESTS IN K^+ AND K^- DECAYS P_T in $K^+ \rightarrow \pi^0 \mu^+ \nu_\mu$

T-violating muon polarization. Sensitive to new sources of CP violation beyond the Standard Model.

VALUE (units 10^{-3})	EVTS	DOCUMENT ID	TECN	CHG
< -1.7 ± 2.3 ± 1.1		¹ ABE	04F	K246 +

• • • We do not use the following data for averages, fits, limits, etc. • • •

< -4.2 ± 4.9 ± 0.9 3.9M ABE 99S K246 +

¹ Includes three sets of data: 96-97 (ABE 99S), 98, and 99-00 totaling about three times the ABE 99S data sample. Corresponds to $P_T < 5.0 \times 10^{-3}$ at 90% CL.

Meson Particle Listings

 K^\pm P_T in $K^+ \rightarrow \mu^+ \nu_\mu \gamma$

T-violating muon polarization. Sensitive to new sources of CP violation beyond the Standard Model.

VALUE (units 10^{-2})	EVTS	DOCUMENT ID	TECN	CHG
$-0.64 \pm 1.85 \pm 0.10$	114k	¹ ANISIMOVSK...03	K246	+

¹ Muons stopped and polarization measured from decay to positrons.

 $\text{Im}(\xi)$ in $K^+ \rightarrow \pi^0 \mu^+ \nu_\mu$ DECAY (from transverse μ pol.)

Test of T reversal invariance.

VALUE	EVTS	DOCUMENT ID	TECN	CHG	COMMENT
-0.006 ± 0.008 OUR AVERAGE					
$-0.0053 \pm 0.0071 \pm 0.0036$		¹ ABE	04F K246	+	
-0.016 ± 0.025	20M	CAMPBELL	81 CNTR	+	Pol.

• • • We do not use the following data for averages, fits, limits, etc. • • •

$-0.013 \pm 0.016 \pm 0.003$ 3.9M ABE 99s CNTR + p_T K^+ at rest

¹ Includes three sets of data: 96-97 (ABE 99s), 98, and 99-00 totaling about three times the ABE 99s data sample. Corresponds to $\text{Im}(\xi) < 0.016$ at 90% CL.

DALITZ PLOT PARAMETERS FOR $K \rightarrow 3\pi$ DECAYS

Revised 1999 by T.G. Trippe (LBNL).

The Dalitz plot distribution for $K^\pm \rightarrow \pi^\pm \pi^\pm \pi^\mp$, $K^\pm \rightarrow \pi^0 \pi^0 \pi^\pm$, and $K_L^0 \rightarrow \pi^+ \pi^- \pi^0$ can be parameterized by a series expansion such as that introduced by Weinberg [1]. We use the form

$$\begin{aligned} |M|^2 &\propto 1 + g \frac{(s_3 - s_0)}{m_{\pi^+}^2} + h \left[\frac{s_3 - s_0}{m_{\pi^+}^2} \right]^2 \\ &+ j \frac{(s_2 - s_1)}{m_{\pi^+}^2} + k \left[\frac{s_2 - s_1}{m_{\pi^+}^2} \right]^2 \\ &+ f \frac{(s_2 - s_1)(s_3 - s_0)}{m_{\pi^+}^2 m_{\pi^+}^2} + \dots, \end{aligned} \quad (1)$$

where $m_{\pi^+}^2$ has been introduced to make the coefficients g , h , j , and k dimensionless, and

$$s_i = (P_K - P_i)^2 = (m_K - m_i)^2 - 2m_K T_i, \quad i = 1, 2, 3,$$

$$s_0 = \frac{1}{3} \sum_i s_i = \frac{1}{3} (m_K^2 + m_1^2 + m_2^2 + m_3^2).$$

Here the P_i are four-vectors, m_i and T_i are the mass and kinetic energy of the i^{th} pion, and the index 3 is used for the odd pion.

The coefficient g is a measure of the slope in the variable s_3 (or T_3) of the Dalitz plot, while h and k measure the quadratic dependence on s_3 and $(s_2 - s_1)$, respectively. The coefficient j is related to the asymmetry of the plot and must be zero if CP invariance holds. Note also that if CP is good, g , h , and k must be the same for $K^+ \rightarrow \pi^+ \pi^+ \pi^-$ as for $K^- \rightarrow \pi^- \pi^- \pi^+$.

Since different experiments use different forms for $|M|^2$, in order to compare the experiments we have converted to g , h , j , and k whatever coefficients have been measured. Where such conversions have been done, the measured coefficient a_y , a_t , a_u , or a_v is given in the comment at the right. For definitions of these coefficients, details of this conversion, and discussion of the data, see the April 1982 version of this note [2].

References

1. S. Weinberg, Phys. Rev. Lett. **4**, 87 (1960).
2. Particle Data Group, Phys. Lett. **111B**, 69 (1982).

ENERGY DEPENDENCE OF K^\pm DALITZ PLOT

$$|\text{matrix element}|^2 = 1 + gu + hu^2 + kv^2$$

where $u = (s_3 - s_0) / m_{\pi^+}^2$ and $v = (s_2 - s_1) / m_{\pi^+}^2$

LINEAR COEFFICIENT g FOR $K^\pm \rightarrow \pi^\pm \pi^+ \pi^-$

Some experiments use Dalitz variables x and y . In the comments we give a_y = coefficient of y term. See note above on "Dalitz Plot Parameters for $K \rightarrow 3\pi$ Decays." For discussion of the conversion of a_y to g , see the earlier version of the same note in the Review published in Physics Letters **111B** 70 (1982).

VALUE	EVTS	DOCUMENT ID	TECN	CHG	COMMENT
-0.21134 ± 0.00017	471M	¹ BATLEY	07B NA48	±	
• • • We do not use the following data for averages, fits, limits, etc. • • •					
-0.2221 ± 0.0065	225k	DEVAUX	77 SPEC	+	$a_y = .2814 \pm .0082$
-0.199 ± 0.008	81k	² LUCAS	73 HBC	-	$a_y = 0.252 \pm 0.011$
-0.2157 ± 0.0028	750k	FORD	72 ASPK	+	$a_y = .2734 \pm .0035$
-0.2186 ± 0.0028	750k	FORD	72 ASPK	-	$a_y = .2770 \pm .0035$
-0.200 ± 0.009	39819	³ HOFFMASTER	72 HLBC	+	
-0.196 ± 0.012	17898	⁴ GRAUMAN	70 HLBC	+	$a_y = 0.228 \pm 0.030$
-0.193 ± 0.010	50919	MAST	69 HBC	-	$a_y = 0.244 \pm 0.013$
-0.218 ± 0.016	9994	⁵ BUTLER	68 HBC	+	$a_y = 0.277 \pm 0.020$
-0.190 ± 0.023	5778	^{5,6} MOSCOSO	68 HBC	-	$a_y = 0.242 \pm 0.029$
-0.22 ± 0.024	5428	^{5,6} ZINCHENKO	67 HBC	+	$a_y = 0.28 \pm 0.03$
-0.220 ± 0.035	1347	⁷ FERRO-LUZZI	61 HBC	-	$a_y = 0.28 \pm 0.045$

¹ Final state strong interaction and radiative corrections not included in the fit.

² Quadratic dependence is required by K_L^0 experiments.

³ HOFFMASTER 72 includes GRAUMAN 70 data.

⁴ Emulsion data added — all events included by HOFFMASTER 72.

⁵ Experiments with large errors not included in average.

⁶ Also includes DBC events.

⁷ No radiative corrections included.

QUADRATIC COEFFICIENT h FOR $K^\pm \rightarrow \pi^\pm \pi^+ \pi^-$

VALUE (units 10^{-2})	EVTS	DOCUMENT ID	TECN	CHG
1.848 ± 0.040	471M	¹ BATLEY	07B NA48	±
• • • We do not use the following data for averages, fits, limits, etc. • • •				
-0.06 ± 1.43	225k	DEVAUX	77 SPEC	+
1.87 ± 0.62	750k	FORD	72 ASPK	+
1.25 ± 0.62	750k	FORD	72 ASPK	-
-0.9 ± 1.4	39819	HOFFMASTER	72 HLBC	+
-0.1 ± 1.2	50919	MAST	69 HBC	-

¹ Final state strong interaction and radiative corrections not included in the fit.

QUADRATIC COEFFICIENT k FOR $K^\pm \rightarrow \pi^\pm \pi^+ \pi^-$

VALUE (units 10^{-3})	EVTS	DOCUMENT ID	TECN	CHG
-4.63 ± 0.14	471M	¹ BATLEY	07B NA48	±
• • • We do not use the following data for averages, fits, limits, etc. • • •				
-20.5 ± 3.9	225k	DEVAUX	77 SPEC	+
-7.5 ± 1.9	750k	FORD	72 ASPK	+
-8.3 ± 1.9	750k	FORD	72 ASPK	-
-10.5 ± 4.5	39819	HOFFMASTER	72 HLBC	+
-14 ± 12	50919	MAST	69 HBC	-

¹ Final state strong interaction and radiative corrections not included in the fit.

 $(g_+ - g_-) / (g_+ + g_-)$ FOR $K^\pm \rightarrow \pi^\pm \pi^+ \pi^-$

This is a CP violating asymmetry between linear coefficients g_\pm for $K^+ \rightarrow \pi^+ \pi^+ \pi^-$ decay and g_- for $K^- \rightarrow \pi^- \pi^+ \pi^-$ decay.

VALUE (units 10^{-4})	EVTS	DOCUMENT ID	TECN
$-1.5 \pm 1.5 \pm 1.6$	3.1G	¹ BATLEY	07E NA48
• • • We do not use the following data for averages, fits, limits, etc. • • •			
$1.7 \pm 2.1 \pm 2.0$	1.7G	² BATLEY	06 NA48
-70.0 ± 53	3.2M	FORD	70 ASPK

¹ BATLEY 07E includes data from BATLEY 06. Uses quadratic parametrization and value $g_+ + g_- = 2g$ from BATLEY 07B. This measurement neglects any possible charge asymmetries in higher order slope parameters h or k .

² This measurement neglects any possible charge asymmetries in higher order slope parameters h or k .

LINEAR COEFFICIENT g FOR $K^\pm \rightarrow \pi^\pm \pi^0 \pi^0$

Unless otherwise stated, all experiments include terms quadratic in $(s_3 - s_0) / m_{\pi^+}^2$. See note above on "Dalitz Plot Parameters for $K \rightarrow 3\pi$ Decays."

See BATUSOV 98 for a discussion of the discrepancy between their result and others, especially BOLOTOV 86. At this time we have no way to resolve the discrepancy so we depend on the large scale factor as a warning.

VALUE	EVTS	DOCUMENT ID	TECN	CHG	COMMENT
0.626 ± 0.007 OUR AVERAGE					
$0.6259 \pm 0.0043 \pm 0.0093$	493k	AKOPDZHAN..05B	TNF	±	
$0.627 \pm 0.004 \pm 0.010$	252k	^{1,2} AJINENKO	03B ISTR	-	

• • • We do not use the following data for averages, fits, limits, etc. • • •

VALUE	EVTS	DOCUMENT ID	TECN	CHG
0.736 ± 0.014 ± 0.012	33k	BATUSOV 98	SPEC	+
0.582 ± 0.021	43k	BOLOTOV 86	CALO	-
0.670 ± 0.054	3263	BRAUN 76b	HLBC	+
0.630 ± 0.038	5635	SHEAFF 75	HLBC	+
0.510 ± 0.060	27k	SMITH 75	WIRE	+
0.67 ± 0.06	1365	AUBERT 72	HLBC	+
0.544 ± 0.048	4048	DAVISON 69	HLBC	+

¹ Measured using in-flight decays of the 25 GeV negative secondary beam.

² They form new world averages $g_- = (0.617 \pm 0.018)$ and $g_+ = (0.684 \pm 0.033)$ which give $\Delta g_{\pi^+} = 0.051 \pm 0.028$.

QUADRATIC COEFFICIENT h FOR $K^\pm \rightarrow \pi^\pm \pi^0 \pi^0$

VALUE	EVTS	DOCUMENT ID	TECN	CHG	COMMENT
0.052 ± 0.008 OUR AVERAGE					
0.0551 ± 0.0044 ± 0.0086	493k	AKOPDZHAN.05b	TNF	±	
0.046 ± 0.004 ± 0.012	252k	¹ AJINENKO 03b	ISTR	-	

• • • We do not use the following data for averages, fits, limits, etc. • • •

VALUE	EVTS	DOCUMENT ID	TECN	CHG
0.128 ± 0.015 ± 0.024	33k	BATUSOV 98	SPEC	+
0.037 ± 0.024	43k	BOLOTOV 86	CALO	-
0.152 ± 0.082	3263	BRAUN 76b	HLBC	+
0.041 ± 0.030	5635	SHEAFF 75	HLBC	+
0.009 ± 0.040	27k	SMITH 75	WIRE	+
-0.01 ± 0.08	1365	AUBERT 72	HLBC	+
0.026 ± 0.050	4048	DAVISON 69	HLBC	+

¹ Measured using in-flight decays of the 25 GeV negative secondary beam.

QUADRATIC COEFFICIENT k FOR $K^\pm \rightarrow \pi^\pm \pi^0 \pi^0$

VALUE	EVTS	DOCUMENT ID	TECN	CHG
0.0054 ± 0.0035 OUR AVERAGE				
0.0082 ± 0.0011 ± 0.0014	493k	AKOPDZHAN.05b	TNF	±
0.001 ± 0.001 ± 0.002	252k	¹ AJINENKO 03b	ISTR	-

• • • We do not use the following data for averages, fits, limits, etc. • • •

VALUE	EVTS	DOCUMENT ID	TECN	CHG
0.0197 ± 0.0045 ± 0.0029	33k	BATUSOV 98	SPEC	+

¹ Measured using in-flight decays of the 25 GeV negative secondary beam.

$(g_+ - g_-) / (g_+ + g_-)$ FOR $K^\pm \rightarrow \pi^\pm \pi^0 \pi^0$

A nonzero value for this quantity indicates CP violation.

VALUE (units 10^{-4})	EVTS	DOCUMENT ID	TECN
1.8 ± 1.8 OUR AVERAGE			
1.8 ± 1.7 ± 0.6	91.3M	¹ BATLEY 07E	NA48
2 ± 18 ± 5	619k	² AKOPDZHAN.05	TNF

• • • We do not use the following data for averages, fits, limits, etc. • • •

VALUE	EVTS	DOCUMENT ID	TECN
1.8 ± 2.2 ± 1.3	47M	³ BATLEY 06A	NA48

¹ BATLEY 07E includes data from BATLEY 06A. Uses quadratic parametrization and PDG 06 value $g = 0.626 \pm 0.007$ to obtain $g_+ - g_- = (2.2 \pm 2.1 \pm 0.7) \times 10^{-4}$. Neglects any possible charge asymmetries in higher order slope parameters h or k .

² Asymmetry obtained assuming that $g_+ + g_- = 2 \times 0.652$ (PDG 02) and that asymmetries in h and k are zero.

³ Linear and quadratic slopes from PDG 04 are used. Any possible charge asymmetries in higher order slope parameters h or k are neglected.

ALTERNATIVE PARAMETRIZATIONS OF $K^\pm \rightarrow \pi^\pm \pi^0 \pi^0$ DALITZ PLOT

The following functional form for the matrix element suggested by $\pi\pi$ rescattering in $K^+ \rightarrow \pi^+ \pi^+ \pi^- \pi^0 \rightarrow \pi^+ \pi^0 \pi^0$ is used for this fit (CABIBBO 04A, CABIBBO 05): Matrix element = $M_0 + M_1$ where $M_0 = 1 + (1/2)g_0 u + (1/2)h' u^2 + (1/2)k_0 v^2$ with $u = (s_3 - s_0)/(m_{\pi^+})^2$, $v = (s_2 - s_1)/(m_{\pi^+})^2$ and where M_1 takes into account the non-analytic piece due to $\pi\pi$ rescattering amplitudes a_0 and a_2 ; The parameters g_0 and h' are related to the parameters g and h of the matrix element squared given in the previous section by the approximations $g_0 \sim g^{PDG}$ and $h' \sim h^{PDG} - (g/2)^2$ and $k_0 \sim k^{PDG}$.

In addition, we also consider the effective field theory framework of COLANGELO 06A and BISSEGGGER 09 to extract g_{BB} and h'_{BB} .

LINEAR COEFFICIENT g_0 FOR $K^\pm \rightarrow \pi^\pm \pi^0 \pi^0$

VALUE	EVTS	DOCUMENT ID	TECN	CHG
0.6525 ± 0.0009 ± 0.0033	60M	¹ BATLEY 09A	NA48	±
0.645 ± 0.004 ± 0.009	23M	² BATLEY 06b	NA48	±

¹ This fit is obtained with the CABIBBO 05 matrix element in the $2\pi^0$ invariant mass squared range $0.074094 < m_{2\pi^0}^2 < 0.104244 \text{ GeV}^2$. Electromagnetic corrections and CHPT constraints for $\pi\pi$ phase shifts (a_0 and a_2) have been used. Also measured ($a_0 - a_2$) $m_{\pi^+} = 0.2646 \pm 0.0021 \pm 0.0023$, where k_0 was kept fixed in the fit at -0.0099 .

² Superseded by BATLEY 09A. This fit is obtained with the CABIBBO 05 matrix element in the $2\pi^0$ invariant mass squared range $0.074 \text{ GeV}^2 < m_{2\pi^0}^2 < 0.097 \text{ GeV}^2$, assuming $k = 0$ (no term proportional to $(s_2 - s_1)^2$) and excluding the kinematic region around the cusp ($m_{2\pi^0}^2 = (2m_{\pi^+})^2 \pm 0.000525 \text{ GeV}^2$). Also $\pi\pi$ phase shifts a_0 and a_2 are measured: ($a_0 - a_2$) $m_{\pi^+} = 0.268 \pm 0.010 \pm 0.004 \pm 0.013$ (external) and $a_2 m_{\pi^+} = -0.041 \pm 0.022 \pm 0.014$.

QUADRATIC COEFFICIENT h' FOR $K^\pm \rightarrow \pi^\pm \pi^0 \pi^0$

VALUE	EVTS	DOCUMENT ID	TECN	CHG
-0.0433 ± 0.0008 ± 0.0026	60M	¹ BATLEY 09A	NA48	±
-0.047 ± 0.012 ± 0.011	23M	² BATLEY 06b	NA48	±

• • • We do not use the following data for averages, fits, limits, etc. • • •

¹ This fit is obtained with the CABIBBO 05 matrix element in the $2\pi^0$ invariant mass squared range $0.074094 < m_{2\pi^0}^2 < 0.104244 \text{ GeV}^2$. Electromagnetic corrections and CHPT constraints for $\pi\pi$ phase shifts (a_0 and a_2) have been used. Also measured ($a_0 - a_2$) $m_{\pi^+} = 0.2646 \pm 0.0021 \pm 0.0023$, where k_0 was kept fixed in the fit at -0.0099 .

² Superseded by BATLEY 09A. This fit is obtained with the CABIBBO 05 matrix element in the $2\pi^0$ invariant mass squared range $0.074 \text{ GeV}^2 < m_{2\pi^0}^2 < 0.097 \text{ GeV}^2$, assuming $k = 0$ (no term proportional to $(s_2 - s_1)^2$) and excluding the kinematic region around the cusp ($m_{2\pi^0}^2 = (2m_{\pi^+})^2 \pm 0.000525 \text{ GeV}^2$). Also $\pi\pi$ phase shifts a_0 and a_2 are measured: ($a_0 - a_2$) $m_{\pi^+} = 0.268 \pm 0.010 \pm 0.004 \pm 0.013$ (external) and $a_2 m_{\pi^+} = -0.041 \pm 0.022 \pm 0.014$.

QUADRATIC COEFFICIENT k_0 FOR $K^\pm \rightarrow \pi^\pm \pi^0 \pi^0$

VALUE	EVTS	DOCUMENT ID	TECN	CHG
0.0095 ± 0.00017 ± 0.00048	60M	¹ BATLEY 09A	NA48	±

¹ Assumed $a_2 m_{\pi^+} = -0.0044$ in the fit.

LINEAR COEFFICIENT g_{BB} FOR $K^\pm \rightarrow \pi^\pm \pi^0 \pi^0$

VALUE	EVTS	DOCUMENT ID	TECN	CHG
0.6219 ± 0.0009 ± 0.0033	60M	¹ BATLEY 09A	NA48	±

¹ This fit is obtained using parametrizations of COLANGELO 06A and BISSEGGGER 09 in the $2\pi^0$ invariant mass squared range $0.074094 < m_{2\pi^0}^2 < 0.104244 \text{ GeV}^2$. Electromagnetic corrections and CHPT constraints for $\pi\pi$ phase shifts (a_0 and a_2) have been used. Also measured ($a_0 - a_2$) $m_{\pi^+} = 0.2633 \pm 0.0024 \pm 0.0024$, where k_0 was kept fixed in the fit at 0.0085.

QUADRATIC COEFFICIENT h'_{BB} FOR $K^\pm \rightarrow \pi^\pm \pi^0 \pi^0$

VALUE	EVTS	DOCUMENT ID	TECN	CHG
-0.0520 ± 0.0009 ± 0.0026	60M	¹ BATLEY 09A	NA48	±

¹ This fit is obtained using parametrizations of COLANGELO 06A and BISSEGGGER 09 in the $2\pi^0$ invariant mass squared range $0.074094 < m_{2\pi^0}^2 < 0.104244 \text{ GeV}^2$. Electromagnetic corrections and CHPT constraints for $\pi\pi$ phase shifts (a_0 and a_2) have been used. Also measured ($a_0 - a_2$) $m_{\pi^+} = 0.2633 \pm 0.0024 \pm 0.0024$, where k_0 was kept fixed in the fit at 0.0085.

$K_{\frac{1}{3}}^\pm$ FORM FACTORS

In the form factor comments, the following symbols are used.

f_+ and f_- are form factors for the vector matrix element.

f_S and f_T refer to the scalar and tensor term.

$f_0 = f_+ + f_- t / (m_{K^\pm}^2 - m_{\pi^0}^2)$.

t = momentum transfer to the π .

λ_+ and λ_0 are the linear expansion coefficients of f_+ and f_0 :

$f_+(t) = f_+(0) (1 + \lambda_+ t / m_{\pi^+}^2)$

For quadratic expansion

$f_+(t) = f_+(0) (1 + \lambda_+ t / m_{\pi^+}^2 + \frac{\lambda_+''}{2} t^2 / m_{\pi^+}^4)$

as used by KTeV. If there is a non-vanishing quadratic term, then λ_+ represents an average slope, which is then different from λ_+' .

NA48/2 and OKA quadratic expansion coefficients are converted with

$\lambda_+'^{PDG} = \lambda_+'^{NA48/2}$ and $\lambda_+''^{PDG} = 2 \lambda_+''^{NA48/2}$

$\lambda_+'^{PDG} = (\frac{m_{\pi^+}}{m_{\pi^0}})^2 \lambda_+'^{OKA}$ and

$\lambda_+''^{PDG} = 2 (\frac{m_{\pi^+}}{m_{\pi^0}})^4 \lambda_+''^{OKA}$

OKA linear expansion coefficients are converted with

$\lambda_+'^{PDG} = (\frac{m_{\pi^+}}{m_{\pi^0}})^2 \lambda_+'^{OKA}$ and $\lambda_0^{PDG} = (\frac{m_{\pi^+}}{m_{\pi^0}})^2 \lambda_0^{OKA}$

The pole parametrization is

$f_+(t) = f_+(0) (\frac{M_V^2}{M_V^2 - t})$

$f_0(t) = f_0(0) (\frac{M_S^2}{M_S^2 - t})$

where M_V and M_S are the vector and scalar pole masses.

The following abbreviations are used:

DP = Dalitz plot analysis.

PI = π spectrum analysis.

MU = μ spectrum analysis.

POL = μ polarization analysis.

BR = $K_{\frac{1}{3}}^\pm / K_{\frac{2}{3}}^\pm$ branching ratio analysis.

E = positron or electron spectrum analysis.

RC = radiative corrections.

For previous λ_+' and λ_+'' parametrizations used by NA48 (e.g. LAI 07A) and ISTRA (e.g. YUSHCHENKO 04b) see PDG 18.

Meson Particle Listings

 K^\pm λ_+ (LINEAR ENERGY DEPENDENCE OF f_+ IN K_{e3}^\pm DECAY)

These results are for a linear expansion only. See the next section for fits including a quadratic term. For radiative correction of the K_{e3}^\pm Dalitz plot, see GINSBERG 67, BECHERRAWY 70, CIRIGLIANO 02, CIRIGLIANO 04, and ANDRE 07. Results labeled OUR FIT are discussed in the review “ K_{e3}^\pm and $K_{\mu 3}^0$ Form Factors” above. For earlier, lower statistics results, see the 2004 edition of this review, Physics Letters **B592** 1 (2004).

VALUE (units 10^{-2})	EVTS	DOCUMENT ID	TECN	CHG	COMMENT
2.959 ± 0.025 OUR FIT	Assuming $\mu-e$ universality				
2.956 ± 0.025 OUR AVERAGE					
2.95 ± 0.022 ± 0.018	5.25M	YUSHCHENKO 18	OKA	+	
3.044 ± 0.083 ± 0.074	1.1M	AKOPDZANOV 09	TNF	±	
2.966 ± 0.050 ± 0.034	919k	¹ YUSHCHENKO 04B	ISTR	-	DP
2.78 ± 0.26 ± 0.30	41k	SHIMIZU 00	SPEC	+	DP
2.84 ± 0.27 ± 0.20	32k	² AKIMENKO 91	SPEC	PI, no RC	
2.9 ± 0.4	62k	³ BOLOTOV 88	SPEC	PI, no RC	
••• We do not use the following data for averages, fits, limits, etc. •••					
3.06 ± 0.09 ± 0.06	550k	^{1,4} AJINENKO 03c	ISTR	-	DP
2.93 ± 0.15 ± 0.2	130k	⁴ AJINENKO 02	SPEC	DP	

¹ Rescaled to agree with our conventions as noted above.

² AKIMENKO 91 state that radiative corrections would raise λ_+ by 0.0013.

³ BOLOTOV 88 state radiative corrections of GINSBERG 67 would raise λ_+ by 0.002.

⁴ Superseded by YUSHCHENKO 04b.

 λ_+ (LINEAR ENERGY DEPENDENCE OF f_+ IN $K_{\mu 3}^\pm$ DECAY)

Results labeled OUR FIT are discussed in the review “ K_{e3}^\pm and $K_{\mu 3}^0$ Form Factors” above. For earlier, lower statistics results, see the 2004 edition of this review, Physics Letters **B592** 1 (2004).

VALUE (units 10^{-2})	EVTS	DOCUMENT ID	TECN	CHG	COMMENT
2.959 ± 0.025 OUR FIT	Assuming $\mu-e$ universality				
3.09 ± 0.25 OUR FIT	Error includes scale factor of 1.5. Not assuming $\mu-e$ universality				
2.96 ± 0.14 ± 0.10	540k	¹ YUSHCHENKO04	ISTR	-	DP
••• We do not use the following data for averages, fits, limits, etc. •••					
3.21 ± 0.45	112k	² AJINENKO 03	ISTR	-	DP
¹ Rescaled to agree with our conventions as noted above.					
² Superseded by YUSHCHENKO 04.					

 λ_0 (LINEAR ENERGY DEPENDENCE OF f_0 IN $K_{\mu 3}^\pm$ DECAY)

Results labeled OUR FIT are discussed in the review “ K_{e3}^\pm and $K_{\mu 3}^0$ Form Factors” above. For earlier, lower statistics results, see the 2004 edition of this review, Physics Letters **B592** 1 (2004).

VALUE (units 10^{-2})	$d\lambda_0/d\lambda_+$	EVTS	DOCUMENT ID	TECN	CHG	COMMENT
1.76 ± 0.25 OUR FIT	Error includes scale factor of 2.7. Assuming $\mu-e$ universality					
1.73 ± 0.27 OUR FIT	Error includes scale factor of 2.6. Not assuming $\mu-e$ universality					
1.420 ± 0.114 ± 0.107		2.3M	¹ BATLEY 18	NA48	±	
1.96 ± 0.12 ± 0.06	-0.348	540k	² YUSHCHENKO04	ISTR	-	DP
••• We do not use the following data for averages, fits, limits, etc. •••						
2.09 ± 0.45	-0.46	112k	³ AJINENKO 03	ISTR	-	DP
1.9 ± 0.64		24k	⁴ HORIE 01	SPEC	+	BR
1.9 ± 1.0	+0.03	55k	⁵ HEINTZE 77	SPEC	+	BR

¹ Data collected in 2004 by NA48/2. Obtained from a fit with a quadratic vector form factor. Correlation coefficient with linear slope is 0.511, with quadratic slope is -0.513. $\chi^2/NDF = 409.9/381$. BATLEY 18 also performed a combined K_{e3}^\pm and $K_{\mu 3}^\pm$ fit assuming $\mu-e$ universality and obtained $(14.47 \pm 0.63 \pm 1.17) \times 10^{-3}$.

² Rescaled to agree with our conventions as noted above.

³ Superseded by YUSHCHENKO 04.

⁴ HORIE 01 assumes $\mu-e$ universality in K_{e3}^\pm decay and uses SHIMIZU 00 value $\lambda=0.0278 \pm 0.0040$ from K_{e3}^\pm decay.

⁵ HEINTZE 77 uses $\lambda_+ = 0.029 \pm 0.003$. $d\lambda_0/d\lambda_+$ estimated by us.

 λ'_+ (LINEAR K_{e3}^\pm FORM FACTOR FROM QUADRATIC FIT)

VALUE (units 10^{-2})	EVTS	DOCUMENT ID	TECN	CHG	COMMENT
2.59 ± 0.04 OUR AVERAGE					
2.426 ± 0.078 ± 0.130	4.4M	¹ BATLEY 18	NA48	±	
2.611 ± 0.035 ± 0.028	5.25M	YUSHCHENKO18	OKA	+	
2.485 ± 0.163 ± 0.034	919k	^{2,3} YUSHCHENKO04B	ISTR	-	DP
••• We do not use the following data for averages, fits, limits, etc. •••					
3.07 ± 0.21	550k	^{2,4} AJINENKO 03c	ISTR	-	DP

¹ Data collected in 2004 by NA48/2. Correlation coefficient with quadratic slope is -0.929. $\chi^2/NDF = 569.1/687$. BATLEY 18 also performed a combined K_{e3}^\pm and $K_{\mu 3}^\pm$ fit assuming $\mu-e$ universality and obtained $(24.24 \pm 0.75 \pm 1.3) \times 10^{-3}$.

² Rescaled to agree with our conventions as noted above.

³ YUSHCHENKO 04B λ'_+ and λ''_+ are strongly correlated with coefficient $\rho(\lambda'_+, \lambda''_+) = -0.95$.

⁴ Superseded by YUSHCHENKO 04b.

 λ''_+ (QUADRATIC K_{e3}^\pm FORM FACTOR)

VALUE (units 10^{-2})	EVTS	DOCUMENT ID	TECN	CHG	COMMENT
0.186 ± 0.021 OUR AVERAGE					
0.164 ± 0.030 ± 0.039	4.4M	¹ BATLEY 18	NA48	±	
0.191 ± 0.019 ± 0.014	5.25M	YUSHCHENKO18	OKA	+	
0.192 ± 0.062 ± 0.071	919k	^{2,3} YUSHCHENKO04B	ISTR	-	DP
••• We do not use the following data for averages, fits, limits, etc. •••					
-0.5 ± 0.7 ± 1.5	550k	^{2,4} AJINENKO 03c	ISTR	-	DP

¹ Data collected in 2004 by NA48/2. Correlation coefficient with quadratic slope is -0.929. $\chi^2/NDF = 569.1/687$. BATLEY 18 also performed a combined K_{e3}^\pm and $K_{\mu 3}^\pm$ fit assuming $\mu-e$ universality and obtained $(1.67 \pm 0.29 \pm 0.41) \times 10^{-3}$.

² Rescaled to agree with our conventions as noted above.

³ YUSHCHENKO 04B λ'_+ and λ''_+ are strongly correlated with coefficient $\rho(\lambda'_+, \lambda''_+) = -0.95$.

⁴ Superseded by YUSHCHENKO 04b.

 λ'_+ (LINEAR $K_{\mu 3}^\pm$ FORM FACTOR FROM QUADRATIC FIT)

VALUE (units 10^{-3})	EVTS	DOCUMENT ID	TECN	CHG
24.27 ± 2.88 ± 2.89	2.3M	¹ BATLEY 18	NA48	±

¹ Data collected in 2004 by NA48/2. Correlation coefficient with quadratic slope is -0.974, with scalar slope is 0.513. $\chi^2/NDF = 409.9/381$. BATLEY 18 also performed a combined K_{e3}^\pm and $K_{\mu 3}^\pm$ fit assuming $\mu-e$ universality and obtained $(24.24 \pm 0.75 \pm 1.3) \times 10^{-3}$.

 λ''_+ (QUADRATIC $K_{\mu 3}^\pm$ FORM FACTOR)

VALUE (units 10^{-3})	EVTS	DOCUMENT ID	TECN	CHG
1.83 ± 1.05 ± 1.09	2.3M	¹ BATLEY 18	NA48	±

¹ Data collected in 2004 by NA48/2. Correlation coefficient with linear slope is -0.974, with scalar slope is 0.513. $\chi^2/NDF = 409.9/381$. BATLEY 18 also performed a combined K_{e3}^\pm and $K_{\mu 3}^\pm$ fit assuming $\mu-e$ universality and obtained $(1.67 \pm 0.29 \pm 0.41) \times 10^{-3}$.

 M_V (VECTOR POLE MASS FOR K_{e3}^\pm DECAY)

See the review on K_{e3}^\pm and $K_{\mu 3}^0$ Form Factors for details.

VALUE (MeV)	EVTS	DOCUMENT ID	TECN	CHG
890.3 ± 2.8 OUR AVERAGE				
885.2 ± 3.3 ± 7.2	4.4M	¹ BATLEY 18	NA48	±
891 ± 3	5.25M	² YUSHCHENKO18	OKA	+

¹ Data collected in 2004 by NA48/2. $\chi^2/NDF = 568.9/688$. BATLEY 18 also performed a combined K_{e3}^\pm and $K_{\mu 3}^\pm$ fit assuming $\mu-e$ universality and obtained $884.4 \pm 3.1 \pm 6.7$ MeV.

² Assumed no scalar or tensor contributions to the form factor.

 M_V (VECTOR POLE MASS FOR $K_{\mu 3}^\pm$ DECAY)

VALUE (MeV)	EVTS	DOCUMENT ID	TECN	CHG
878.4 ± 8.8 ± 8.3	2.3M	¹ BATLEY 18	NA48	±

¹ Data collected in 2004 by NA48/2. $\chi^2/NDF = 409.9/382$. BATLEY 18 also performed a combined K_{e3}^\pm and $K_{\mu 3}^\pm$ fit assuming $\mu-e$ universality and obtained $884.4 \pm 3.1 \pm 6.7$ MeV.

 M_S (SCALAR POLE MASS FOR $K_{\mu 3}^\pm$ DECAY)

VALUE (MeV)	EVTS	DOCUMENT ID	TECN	CHG
1214.8 ± 23.5 ± 49.2	2.3M	¹ BATLEY 18	NA48	±

¹ Data collected in 2004 by NA48/2. $\chi^2/NDF = 409.9/382$. BATLEY 18 also performed a combined K_{e3}^\pm and $K_{\mu 3}^\pm$ fit assuming $\mu-e$ universality and obtained $1208.3 \pm 21.2 \pm 47.5$ MeV.

 A_+ (DISPERSIVE VECTOR FORM FACTOR IN K_{e3}^\pm DECAY)

See the review on K_{e3}^\pm and $K_{\mu 3}^0$ Form Factors for details.

VALUE (units 10^{-2})	EVTS	DOCUMENT ID	TECN	CHG
2.460 ± 0.017 OUR AVERAGE				
2.494 ± 0.021 ± 0.064	4.4M	¹ BATLEY 18	NA48	±
2.458 ± 0.018	5.25M	² YUSHCHENKO18	OKA	+

¹ Data collected in 2004 by NA48/2. $\chi^2/NDF = 569.0/688$. BATLEY 18 also performed a combined K_{e3}^\pm and $K_{\mu 3}^\pm$ fit assuming $\mu-e$ universality and obtained $(24.99 \pm 0.20 \pm 0.62) \times 10^{-3}$.

² Assumed no scalar or tensor contributions to the form factor.

 A_+ (DISPERSIVE VECTOR FORM FACTOR IN $K_{\mu 3}^\pm$ DECAY)

VALUE (units 10^{-3})	EVTS	DOCUMENT ID	TECN	CHG
25.36 ± 0.58 ± 0.72	2.3M	¹ BATLEY 18	NA48	±

¹ Data collected in 2004 by NA48/2. $\chi^2/NDF = 410.3/382$. BATLEY 18 also performed a combined K_{e3}^\pm and $K_{\mu 3}^\pm$ fit assuming $\mu-e$ universality and obtained $(24.99 \pm 0.20 \pm 0.62) \times 10^{-3}$.

$\ln(C)$ (DISPERSIVE SCALAR FORM FACTOR IN $K_{\mu 3}^\pm$ DECAYS)

VALUE (units 10^{-3})	EVTS	DOCUMENT ID	TECN	CHG
$182.17 \pm 6.31 \pm 14.45$	2.3M	¹ BATLEY	18	NA48 ±

¹Data collected in 2004 by NA48/2. Combined fit with dispersive vector form factor $\Lambda_+ = 25.36 \pm 0.58 \pm 0.72$. Correlation coefficient is 0.104. $\chi^2/NDF = 410.3/382$. BATLEY 18 also performed a combined K_{e3}^\pm and $K_{\mu 3}^\pm$ fit assuming $\mu - e$ universality and obtained $(183.65 \pm 5.92 \pm 14.25) \times 10^{-3}$.

 $|f_S/f_+|$ FOR K_{e3}^\pm DECAYRatio of scalar to f_+ couplings.

VALUE (units 10^{-2})	CL%	EVTS	DOCUMENT ID	TECN	CHG	COMMENT	
-0.08 ± 0.34						OUR AVERAGE	
0.01 ± 0.38		5.25M	YUSHCHENKO18	OKA	+	$\lambda'_+, \lambda''_+, f_S$ fit	
$-0.37 \pm 0.66 \pm 0.41$		919k	YUSHCHENKO04B	ISTR	-	$\lambda'_+, \lambda''_+, f_S$ fit	
$0.2 \pm 2.6 \pm 1.4$		41k	SHIMIZU	00	SPEC	λ_+, f_S, f_T fit	
••• We do not use the following data for averages, fits, limits, etc. •••							
0.2 ± 2.0		550k	¹ AJINENKO	03c	ISTR	λ_+, f_S, f_T fit	
-1.9 ± 1.6		130k	¹ AJINENKO	02	SPEC	λ_+, f_S fit	
$7.0 \pm 1.6 \pm 1.6$		32k	AKIMENKO	91	SPEC	$\lambda_+, f_S, f_T, \phi$ fit	
0 ± 10		2827	² BRAUN	75	HLBC	+	
< 13		90	4017	CHIANG	72	OSPK	+
14 ± 3		2707	² STEINER	71	HLBC	$\lambda_+, f_S, f_T, \phi$ fit	
< 23		90	BOTTERILL	68c	ASPK		
< 18		90	BELLOTTI	67B	HLBC		
< 30		95	KALMUS	67	HLBC	+	

¹Superseded by YUSHCHENKO 04b.
²Statistical errors only.

 $|f_T/f_+|$ FOR K_{e3}^\pm DECAYRatio of tensor to f_+ couplings.

VALUE (units 10^{-2})	EVTS	DOCUMENT ID	TECN	CHG	COMMENT	
-1.2 ± 1.3					OUR AVERAGE	
-1.24 ± 1.6		5.25M	YUSHCHENKO18	OKA	+	$\lambda'_+, \lambda''_+, f_T$ fit
$-1.2 \pm 2.1 \pm 1.1$		919k	YUSHCHENKO04B	ISTR	-	$\lambda'_+, \lambda''_+, f_T$ fit
$1 \pm 14 \pm 9$		41k	SHIMIZU	00	SPEC	λ_+, f_S, f_T fit
••• We do not use the following data for averages, fits, limits, etc. •••						
2.1 ± 6.4		550k	¹ AJINENKO	03c	ISTR	λ_+, f_S, f_T fit
-4.5 ± 6.0		130k	¹ AJINENKO	02	SPEC	λ_+, f_T fit
53 ± 9		32k	AKIMENKO	91	SPEC	$\lambda_+, f_S, f_T, \phi$ fit

¹Superseded by YUSHCHENKO 04b.

 f_S/f_+ FOR $K_{\mu 3}^\pm$ DECAYRatio of scalar to f_+ couplings.

VALUE (units 10^{-2})	EVTS	DOCUMENT ID	TECN	CHG	COMMENT	
$0.17 \pm 0.14 \pm 0.54$	540k	¹ YUSHCHENKO04	ISTR	-	DP	
••• We do not use the following data for averages, fits, limits, etc. •••						
$0.4 \pm 0.5 \pm 0.5$	112k	² AJINENKO	03	ISTR	-	DP

¹The second error is the theoretical error from the uncertainty in the chiral perturbation theory prediction for λ_0 , ± 0.0053 , combined in quadrature with the systematic error ± 0.0009 .

²The second error is the theoretical error from the uncertainty in the chiral perturbation theory prediction for λ_0 . Superseded by YUSHCHENKO 04.

 f_T/f_+ FOR $K_{\mu 3}^\pm$ DECAYRatio of tensor to f_+ couplings.

VALUE (units 10^{-2})	EVTS	DOCUMENT ID	TECN	CHG	COMMENT	
$-0.07 \pm 0.71 \pm 0.20$	540k	YUSHCHENKO04	ISTR	-	DP	
••• We do not use the following data for averages, fits, limits, etc. •••						
$-2.1 \pm 2.8 \pm 1.4$	112k	¹ AJINENKO	03	ISTR	-	DP
2 ± 12	1585	BRAUN	75	HLBC		

¹The second error is the theoretical error from the uncertainty in the chiral perturbation theory prediction for λ_0 . Superseded by YUSHCHENKO 04.

 $K_{\mu 4}^\pm$ FORM FACTORS

Based on the parametrizations of AMOROS 99, the $K_{\mu 4}^\pm$ form factors can be expressed as

$$F_S = f_S + f'_S q^2 + f''_S q^4 + f'_e S_e / 4m_\pi^2$$

$$F_P = f_P$$

$$G_P = g_P + g'_P q^2$$

$$H_P = h_P$$

where $q^2 = (S_\pi / 4m_\pi^2) - 1$, S_π is the invariant mass squared of the dipion, and S_e is the invariant mass squared of the dilepton.

 f_S FOR $K^\pm \rightarrow \pi^+ \pi^- e^\pm \nu$ DECAY

VALUE	EVTS	DOCUMENT ID	TECN	CHG
5.712 ± 0.032				OUR AVERAGE
$5.705 \pm 0.003 \pm 0.035$	1.1M	¹ BATLEY	12	NA48 ±
$5.75 \pm 0.02 \pm 0.08$	400k	² PISLAK	03	B865 ±

¹BATLEY 12 uses data collected in 2003–2004. The result is obtained from a measurement of $\Gamma(\pi^+ \pi^- e \nu) / \Gamma(\pi^+ \pi^- \pi^+)$ and assumed PDG 12 value of $\Gamma(\pi^+ \pi^- \pi^+) / \Gamma = (5.59 \pm 0.04) \times 10^{-2}$.

²Radiative corrections included. Using Roy equations and not including isospin breaking, PISLAK 03 obtains the following $\pi\pi$ scattering lengths $a_0^0 = 0.228 \pm 0.012 \pm 0.004 \pm 0.012$ (theor.) and $a_0^2 = -0.0365 \pm 0.0023 \pm 0.0008 \pm 0.0031$ (theor.).

 f'_S/f_S FOR $K^\pm \rightarrow \pi^+ \pi^- e^\pm \nu$ DECAY

VALUE (units 10^{-2})	EVTS	DOCUMENT ID	TECN	CHG
$15.2 \pm 0.7 \pm 0.5$	1.13M	¹ BATLEY	10c	NA48 ±
••• We do not use the following data for averages, fits, limits, etc. •••				
$17.2 \pm 0.9 \pm 0.6$	670k	² BATLEY	08A	NA48 ±

¹Radiative corrections included. Using Roy equations and including isospin breaking, BATLEY 10c obtains the following scattering lengths $a_0^0 = 0.2220 \pm 0.0128 \pm 0.0050 \pm 0.0037$ (theor.), $a_0^2 = -0.0432 \pm 0.0086 \pm 0.0034 \pm 0.0028$ (theor.). The correlation with $f''_S/f_S = -0.954$ and with $f'_e/f_S = 0.080$. Supersedes BATLEY 08A.

²Radiative corrections included. Using Roy equations and not including isospin breaking, BATLEY 08A obtains the following $\pi\pi$ scattering length $a_0^0 = 0.233 \pm 0.016 \pm 0.007$ and $a_0^2 = -0.0471 \pm 0.011 \pm 0.004$.

 f''_S/f_S FOR $K^\pm \rightarrow \pi^+ \pi^- e^\pm \nu$ DECAY

VALUE (units 10^{-2})	EVTS	DOCUMENT ID	TECN	CHG
$-7.3 \pm 0.7 \pm 0.6$	1.13M	¹ BATLEY	10c	NA48 ±
••• We do not use the following data for averages, fits, limits, etc. •••				
$-9.0 \pm 0.9 \pm 0.7$	670k	² BATLEY	08A	NA48 ±

¹Radiative corrections included. Using Roy equations and including isospin breaking, BATLEY 10c obtains the following scattering lengths $a_0^0 = 0.2220 \pm 0.0128 \pm 0.0050 \pm 0.0037$ (theor.), $a_0^2 = -0.0432 \pm 0.0086 \pm 0.0034 \pm 0.0028$ (theor.). The correlation with $f'_S/f_S = -0.954$ and with $f'_e/f_S = 0.019$. Supersedes BATLEY 08A.

²Radiative corrections included. Using Roy equations and not including isospin breaking, BATLEY 08A obtains the following $\pi\pi$ scattering length $a_0^0 = 0.233 \pm 0.016 \pm 0.007$ and $a_0^2 = -0.0471 \pm 0.011 \pm 0.004$.

 f'_e/f_S FOR $K^\pm \rightarrow \pi^+ \pi^- e^\pm \nu$ DECAY

VALUE (units 10^{-2})	EVTS	DOCUMENT ID	TECN	CHG
$6.8 \pm 0.6 \pm 0.7$	1.13M	¹ BATLEY	10c	NA48 ±
••• We do not use the following data for averages, fits, limits, etc. •••				
$8.1 \pm 0.8 \pm 0.9$	670k	² BATLEY	08A	NA48 ±

¹Radiative corrections included. Using Roy equations and including isospin breaking, BATLEY 10c obtains the following scattering lengths $a_0^0 = 0.2220 \pm 0.0128 \pm 0.0050 \pm 0.0037$ (theor.), $a_0^2 = -0.0432 \pm 0.0086 \pm 0.0034 \pm 0.0028$ (theor.). The correlation with $f'_S/f_S = 0.080$ and with $f''_S/f_S = 0.019$. Supersedes BATLEY 08A.

²Radiative corrections included. Using Roy equations and not including isospin breaking, BATLEY 08A obtains the following $\pi\pi$ scattering length $a_0^0 = 0.233 \pm 0.016 \pm 0.007$ and $a_0^2 = -0.0471 \pm 0.011 \pm 0.004$.

 f_P/f_S FOR $K^\pm \rightarrow \pi^+ \pi^- e^\pm \nu$ DECAY

VALUE (units 10^{-2})	EVTS	DOCUMENT ID	TECN	CHG
$-4.8 \pm 0.3 \pm 0.4$	1.13M	¹ BATLEY	10c	NA48 ±
••• We do not use the following data for averages, fits, limits, etc. •••				
$-4.8 \pm 0.4 \pm 0.4$	670k	² BATLEY	08A	NA48 ±

¹Radiative corrections included. Using Roy equations and including isospin breaking, BATLEY 10c obtains the following scattering lengths $a_0^0 = 0.2220 \pm 0.0128 \pm 0.0050 \pm 0.0037$ (theor.), $a_0^2 = -0.0432 \pm 0.0086 \pm 0.0034 \pm 0.0028$ (theor.). Supersedes BATLEY 08A.

²Radiative corrections included. Using Roy equations and not including isospin breaking, BATLEY 08A obtains the following $\pi\pi$ scattering length $a_0^0 = 0.233 \pm 0.016 \pm 0.007$ and $a_0^2 = -0.0471 \pm 0.011 \pm 0.004$.

 g_P/f_S FOR $K^\pm \rightarrow \pi^+ \pi^- e^\pm \nu$ DECAY

VALUE (units 10^{-2})	EVTS	DOCUMENT ID	TECN	CHG
$86.8 \pm 1.0 \pm 1.0$	1.13M	¹ BATLEY	10c	NA48 ±
••• We do not use the following data for averages, fits, limits, etc. •••				
$87.3 \pm 1.3 \pm 1.2$	670k	² BATLEY	08A	NA48 ±
$80.9 \pm 0.9 \pm 1.2$	400k	³ PISLAK	03	B865 ±

¹Radiative corrections included. Using Roy equations and including isospin breaking, BATLEY 10c obtains the following scattering lengths $a_0^0 = 0.2220 \pm 0.0128 \pm 0.0050 \pm 0.0037$ (theor.), $a_0^2 = -0.0432 \pm 0.0086 \pm 0.0034 \pm 0.0028$ (theor.). Supersedes BATLEY 08A. The correlation with $g'_P/f_S = -0.914$. Supersedes BATLEY 08A.

²Radiative corrections included. Using Roy equations and not including isospin breaking, BATLEY 08A obtains the following $\pi\pi$ scattering length $a_0^0 = 0.233 \pm 0.016 \pm 0.007$ and $a_0^2 = -0.0471 \pm 0.011 \pm 0.004$.

³Radiative corrections included. Using Roy equations PISLAK 03 obtains the following scattering lengths $a_0^0 = 0.203 \pm 0.033 \pm 0.004$, $a_0^2 = -0.055 \pm 0.023 \pm 0.003$.

Meson Particle Listings

K^\pm

g'_p/f_s FOR $K^\pm \rightarrow \pi^\pm \pi^- e^\pm \nu$ DECAY

VALUE (units 10^{-2})	EVTS	DOCUMENT ID	TECN	CHG
$8.9 \pm 1.7 \pm 1.3$	1.13M	¹ BATLEY	10c	NA48 ±
$8.1 \pm 2.2 \pm 1.5$	670k	² BATLEY	08A	NA48 ±
$12.0 \pm 1.9 \pm 0.7$	400k	³ PISLAK	03	B865 ±

¹ Radiative corrections included. Using Roy equations and including isospin breaking, BATLEY 10c obtains the following scattering lengths $a_0^0 = 0.2220 \pm 0.0128 \pm 0.0050 \pm 0.0037$ (theor.), $a_0^2 = -0.0432 \pm 0.0086 \pm 0.0034 \pm 0.0028$ (theor.). The correlation with $g_p/f_s = -0.914$. Supersedes BATLEY 08A.

² Radiative corrections included. Using Roy equations and not including isospin breaking, BATLEY 08A obtains the following $\pi\pi$ scattering length $a_0^0 = 0.233 \pm 0.016 \pm 0.007$, $a_0^2 = -0.0471 \pm 0.011 \pm 0.004$.

³ Radiative corrections included. Using Roy equations PISLAK 03 obtains the following scattering lengths $a_0^0 = 0.203 \pm 0.033 \pm 0.004$, $a_0^2 = -0.055 \pm 0.023 \pm 0.003$.

h_p/f_s FOR $K^\pm \rightarrow \pi^\pm \pi^- e^\pm \nu$ DECAY

VALUE (units 10^{-2})	EVTS	DOCUMENT ID	TECN	CHG
$-39.8 \pm 1.5 \pm 0.8$	1.13M	¹ BATLEY	10c	NA48 ±
$-41.1 \pm 1.9 \pm 0.8$	670k	² BATLEY	08A	NA48 ±
$-51.3 \pm 3.3 \pm 3.5$	400k	³ PISLAK	03	B865 ±

¹ Radiative corrections included. Using Roy equations and including isospin breaking, BATLEY 10c obtains the following scattering lengths $a_0^0 = 0.2220 \pm 0.0128 \pm 0.0050 \pm 0.0037$ (theor.), $a_0^2 = -0.0432 \pm 0.0086 \pm 0.0034 \pm 0.0028$ (theor.). Supersedes BATLEY 08A.

² Radiative corrections included. Using Roy equations and not including isospin breaking, BATLEY 08A obtains the following $\pi\pi$ scattering length $a_0^0 = 0.233 \pm 0.016 \pm 0.007$, $a_0^2 = -0.0471 \pm 0.011 \pm 0.004$.

³ Radiative corrections included. Using Roy equations PISLAK 03 obtains the following scattering lengths $a_0^0 = 0.203 \pm 0.033 \pm 0.004$, $a_0^2 = -0.055 \pm 0.023 \pm 0.003$.

DECAY FORM FACTOR FOR $K^\pm \rightarrow \pi^0 \pi^0 e^\pm \nu$

Given in BOLOTOV 86B, BARMIN 88B, and SHIMIZU 04.

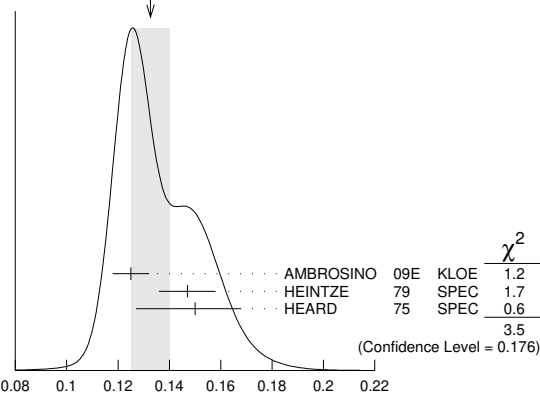
$K^\pm \rightarrow \ell^\pm \nu \gamma$ FORM FACTORS

For definitions of the axial-vector F_A and vector F_V form factor, see the "Note on $\pi^\pm \rightarrow \ell^\pm \nu \gamma$ and $K^\pm \rightarrow \ell^\pm \nu \gamma$ Form Factors" in the π^\pm section. In the kaon literature, often different definitions $a_K = F_A/m_K$ and $v_K = F_V/m_K$ are used.

$F_A + F_V$, SUM OF AXIAL-VECTOR AND VECTOR FORM FACTOR FOR $K \rightarrow e \nu \gamma$

VALUE	EVTS	DOCUMENT ID	TECN	COMMENT
0.133 ± 0.008 OUR AVERAGE				Error includes scale factor of 1.3. See the ideogram below.
$0.125 \pm 0.007 \pm 0.001$	1.4k	¹ AMBROSINO	09E	KLOE E_γ in 10–250 MeV, $p_e > 200$ MeV/c
0.147 ± 0.011	51	² HEINTZE	79	SPEC
0.150 ± 0.018 -0.023	56	³ HEARD	75	SPEC

WEIGHTED AVERAGE
 0.133 ± 0.008 (Error scaled by 1.3)



$F_A + F_V$, SUM OF AXIAL-VECTOR AND VECTOR FORM FACTOR FOR $K \rightarrow e \nu \gamma$

- ¹ AMBROSINO 09E measures the absolute value $|F_A + F_V|$ which is parametrized as $|F_A + F_V| = F_V (1 + \lambda(1-x)) + F_A$, $x = 2E_\gamma/m_K$. ($F_A + F_V$) and λ are fit parameters. The fitted value of $\lambda = 0.38 \pm 0.20 \pm 0.02$ with a correlation of -0.93 between ($F_A + F_V$) and λ .
- ² HEINTZE 79 quotes absolute value of $|F_A + F_V| \sin \theta_C$. We use $\sin \theta_C = V_{us} = 0.2205$.
- ³ HEARD 75 quotes absolute value of $|F_A + F_V| \sin \theta_C$. We use $\sin \theta_C = V_{us} = 0.2205$.

$F_A + F_V$, SUM OF AXIAL-VECTOR AND VECTOR FORM FACTOR FOR $K \rightarrow \mu \nu \gamma$

VALUE	CL%	EVTS	DOCUMENT ID	TECN	CHG
$0.165 \pm 0.007 \pm 0.011$		2588	¹ ADLER	00B	B787 +
-1.2 to 1.1	90		DEMIDOV	90	XEBC
< 0.23	90		¹ AKIBA	85	SPEC

¹ Quotes absolute value. Sign not determined.

$F_A - F_V$, DIFFERENCE OF AXIAL-VECTOR AND VECTOR FORM FACTOR FOR $K \rightarrow e \nu \gamma$

VALUE	CL%	DOCUMENT ID	TECN	
< 0.49	90	¹ HEINTZE	79	SPEC

¹ HEINTZE 79 quotes $|F_A - F_V| < \sqrt{11} |F_A + F_V|$.

$F_A - F_V$, DIFFERENCE OF AXIAL-VECTOR AND VECTOR FORM FACTOR FOR $K \rightarrow \mu \nu \gamma$

VALUE	CL%	EVTS	DOCUMENT ID	TECN	CHG
-0.153 ± 0.033 OUR AVERAGE					Error includes scale factor of 1.1.
$-0.134 \pm 0.021 \pm 0.027$	95k		KRAVTSOV	19	OKA +
-0.21 ± 0.06	22k		DUK	11	ISTR -
-0.24 to 0.04	90	2588	ADLER	00B	B787 +
-2.2 to 0.6	90		DEMIDOV	90	XEBC
-2.5 to 0.3	90		AKIBA	85	SPEC

K^\pm CHARGE RADIUS

VALUE (fm)	DOCUMENT ID	COMMENT
0.560 ± 0.031 OUR AVERAGE		
0.580 ± 0.040	AMENDOLIA 86B	$K_e \rightarrow K_e$
0.530 ± 0.050	DALLY 80	$K_e \rightarrow K_e$
0.620 ± 0.037	BLATNIK 79	VMD + dispersion relations

K^\pm LONGITUDINAL POLARIZATION OF EMITTED μ^\pm

VALUE	CL%	DOCUMENT ID	TECN	CHG	COMMENT
< -0.990	90	¹ AOKI	94	SPEC	+
< -0.990	90	IMAZATO 92	SPEC	+	Repl. by AOKI 94
-0.970 ± 0.047		² YAMANAKA	86	SPEC	+
-1.0 ± 0.1		² CUTTS	69	SPRK	+
-0.96 ± 0.12		² COOMBES	57	CNTR	+

¹ AOKI 94 measures $\xi P_\mu = -0.9996 \pm 0.0030 \pm 0.0048$. The above limit is obtained by summing the statistical and systematic errors in quadrature, normalizing to the physically significant region ($|\xi P_\mu| < 1$) and assuming that $\xi=1$, its maximum value.

² Assumes $\xi=1$.

FORWARD-BACKWARD ASYMMETRY IN K^\pm DECAYS

$$A_{FB}(K^\pm_{\pi\mu\mu}) = \frac{\Gamma(\cos(\theta_{K\mu}) > 0) - \Gamma(\cos(\theta_{K\mu}) < 0)}{\Gamma(\cos(\theta_{K\mu}) > 0) + \Gamma(\cos(\theta_{K\mu}) < 0)}$$

VALUE	CL%	DOCUMENT ID	TECN	
$< 2.3 \times 10^{-2}$	90	¹ BATLEY	11A	NA48

¹ BATLEY 11A gives a corresponding value of the asymmetry $A_{FB} = (-2.4 \pm 1.8) \times 10^{-2}$.

K^\pm REFERENCES

ALIBERTI 21	PRL 127 131802	R. Aliberti et al.	(NA62 Collab.)
CORTINA-GIL 21	PL B816 136259	E. Cortina Gil et al.	(NA62 Collab.)
CORTINA-GIL 21B	JHEP 2106 093	E. Cortina Gil et al.	(NA62 Collab.)
POLYARUSH 21	EPJ C81 161	A.Yu. Polyarush et al.	(OKA Collab.)
CORTINA-GIL 20C	JHEP 2011 042	E. Cortina Gil et al.	(NA62 Collab.)
BATLEY 19	PL B788 552	J.R. Batley et al.	(NA48/2 Collab.)
CORTINA-GIL 19A	PL B797 134794	E. Cortina Gil et al.	(NA62 Collab.)
CORTINA-GIL 19B	PL B791 156	E. Cortina Gil et al.	(NA62 Collab.)
KRAVTSOV 19	EPJ C79 635	V.I. Kravitsov et al.	(OKA Collab.)
SHAPKIN 19	EPJ C79 296	M.M. Shapkin et al.	(OKA Collab.)
BATLEY 18	JHEP 1810 1500	J.R. Batley et al.	(NA48/2 Collab.)
PDG	PR D98 030001	M. Tanabashi et al.	(PDG Collab.)
YUSHCHENKO 18	JETPL 107 139	O.P. Yushchenko et al.	(OKA Collab.)
BATLEY 17	PL B769 67	J.R. Batley et al.	(NA48/2 Collab.)
ARTAMONOV 16	PR D94 032012	A.V. Artamonov et al.	(BNL E949 Collab.)
BABUSCI 14B	PL B738 128	D. Babusci et al.	(KLOE and KLOE-2 Collab.)
BATLEY 14	PL B730 141	J.R. Batley et al.	(CERN NA48/2 Collab.)
BATLEY 14A	JHEP 1408 159	J.R. Batley et al.	(CERN NA48/2 Collab.)
LAZZERONI 14	PL B732 65	C. Lazzeroni et al.	(CERN NA62 Collab.)
UVAROV 14	PAN 77 725	V.A. Uvarov et al.	(ISTRA+ Collab.)
LAZZERONI 13	PL B719 326	C. Lazzeroni et al.	(CERN NA62 Collab.)
BATLEY 12	PL B715 105	J.R. Batley et al.	(CERN NA48/2 Collab.)
PDG	PR D86 010001	J. Beringer et al.	(PDG Collab.)
BATLEY 11A	PL B697 107	J.R. Batley et al.	(CERN NA48/2 Collab.)
DUK 11	PL B695 59	V.A. Duk et al.	(ISTRA+ Collab.)
LAZZERONI 11	PL B698 105	C. Lazzeroni et al.	(CERN NA62 Collab.)
ADLER 10	PR D81 092001	S. Adler et al.	(BNL E787 Collab.)
BATLEY 10A	EPJ C68 75	J.R. Batley et al.	(CERN NA48/2 Collab.)
BATLEY 10C	EPJ C70 635	J.R. Batley et al.	(CERN NA48/2 Collab.)
PDG	JP G37 075021	K. Nakamura et al.	(PDG Collab.)
PISLAK 10A	PRL 105 01901E	S. Pislak et al.	(BNL E865 Collab.)
AKOPDZANOV 09	PAN 71 2074	G.A. Akopdzanov et al.	(IHEP)
	Translated from YAF 71 2108.		

Meson Particle Listings

K^\pm, K^0

CALLAHAN	65	PRL 15 129	A. Callahan, D. Cline	(WIS C)
CLINE	65	PL 15 293	D. Cline, W.F. Fry	(WIS C)
DEMARCO	65	PR 140 B1430	A. de Marco, C. Grosso, G. Rinaudo	(TORI, CERN)
FITCH	65B	PR 140 B1088	V.L. Fitch, C.A. Quarles, H.C. Wilkins	(PRIN+)
STAMER	65	PR 138 B440	P. Stamer <i>et al.</i>	(STEV)
YOUNG	65	Thesis UCRL 16362	P.S. Young	(LRL)
Also		PR 156 1464	P.S. Young, W.Z. Osborne, W.H. Barkas	(LRL)
BORREANI	64	PL 12 123	G. Borreani, G. Rinaudo, A.E. Werbroeck	(TORI)
CALLAHAN	64	PR 136 B1463	A. Callahan, R. March, R. Stark	(WIS C)
GREINER	64	PRL 13 284	D.E. Greiner, W.Z. Osborne, W.H. Barkas	(LRL)
SHAKLEE	64	PR 136 B1423	F.S. Shaklee <i>et al.</i>	(MICH)
BOYARSKI	62	PR 128 2398	A.M. Boyarski <i>et al.</i>	(MIT)
FERRI-LUZZI	61	NC 22 1087	M. Ferro-Luzzi <i>et al.</i>	(LRL)
ROE	61	PRL 7 346	B.P. Roe <i>et al.</i>	(MICH, LRL)
TAYLOR	59	PR 114 359	S. Taylor <i>et al.</i>	(COLU)
COOMBES	57	PR 108 1348	C.A. Coombes <i>et al.</i>	(LBL)

OTHER RELATED PAPERS

LITTENBERG	93	ARNPS 43 729	L.S. Littenberg, G. Valencia	(BNL, FNAL)
Rare and Radiative Kaon Decays				
RITCHIE	93	RMP 65 1149	J.L. Ritchie, S.G. Wojcicki	
"Rare K Decays"				
BATTISTON	92	PRPL 214 293	R. Battiston <i>et al.</i>	(PGIA, CERN, TRSTT)
Status and Perspectives of K Decay Physics				
BRYMAN	89	JMP A4 79	D.A. Bryman	(TRIU)
"Rare Kaon Decays"				
CHOUNET	72	PRPL 4C 199	L.M. Chounet, J.M. Gaillard, M.K. Gaillard	(ORSAY+)
FEARING	70	PR D2 542	H.W. Fearing, E. Fischbach, J. Smith	(STON, BOHR)
HAIDT	69B	PL 29B 696	D. Haidt <i>et al.</i>	(AACH, BARI, CERN, EPOL+)
CRONIN	68B	Vienna Conf. 241	J.W. Cronin	(PRIN)
Rapporteur talk.				
WILLIS	67	Heidelberg Conf. 273	W.J. Willis	(YALE)
Rapporteur talk.				
CABIBBO	66	Berkeley Conf. 33	N. Cabibbo	(CERN)
ADAIR	64	PL 12 67	R.K. Adair, L.B. Leipuner	(YALE, BNL)
CABIBBO	64	PL 9 352	N. Cabibbo, A. Maksymowicz	(CERN)
Also		PL 11 360	N. Cabibbo, A. Maksymowicz	(CERN)
Also		PL 14 72	N. Cabibbo, A. Maksymowicz	(CERN)
BIRGE	63	PRL 11 35	R.W. Birge <i>et al.</i>	(LRL, WIS C, BARI)
BLOCK	62B	CERN Conf. 371	M.M. Block, L. Lendinara, L. Monari	(NWES, BGNA)
BRENE	61	NP 22 553	N. Brene, L. Egardt, B. Qvist	(NORD)



$$J(J^P) = \frac{1}{2}(0^-)$$

K^0 MASS

VALUE (MeV)	EVTS	DOCUMENT ID	TECN	COMMENT
497.611 ± 0.013 OUR FIT				Error includes scale factor of 1.2.
497.611 ± 0.013 OUR AVERAGE				Error includes scale factor of 1.2.
497.607 ± 0.007 ± 0.015	261k	¹ TOMARADZE 14		$\psi(2S) \rightarrow K_S^0 X$
497.583 ± 0.005 ± 0.020	35k	AMBROSINO 07B	KLOE	$e^+e^- \rightarrow K_L^0 K_S^0$
497.625 ± 0.001 ± 0.031	655k	LAI 02	NA48	K_L^0 beam
497.661 ± 0.033	3713	BARKOV 87B	CMD	$e^+e^- \rightarrow K_L^0 K_S^0$
497.742 ± 0.085	780	BARKOV 85B	CMD	$e^+e^- \rightarrow K_L^0 K_S^0$
• • • We do not use the following data for averages, fits, limits, etc. • • •				
497.44 ± 0.50		FITCH 67	OSPK	
498.9 ± 0.5	4500	BALTAY 66	HBC	K^0 from $\bar{p}p$
497.44 ± 0.33	2223	KIM 65B	HBC	K^0 from $\bar{p}p$
498.1 ± 0.4		CHRISTENS... 64	OSPK	

¹ Obtained by analyzing CLEO-c data but not authored by the CLEO Collaboration.

$m_{K^0} - m_{K^\pm}$

VALUE (MeV)	EVTS	DOCUMENT ID	TECN	CHG	COMMENT
3.934 ± 0.020 OUR FIT					Error includes scale factor of 1.6.
• • • We do not use the following data for averages, fits, limits, etc. • • •					
3.95 ± 0.21	417	HILL 68B	DBC	+	$K^+d \rightarrow K^0 pp$
3.90 ± 0.25	9	BURNSTEIN 65	HBC	+	
3.71 ± 0.35	7	KIM 65B	HBC	-	$K^-p \rightarrow n\bar{K}^0$
5.4 ± 1.1		CRAWFORD 59	HBC	+	
3.9 ± 0.6		ROSENFELD 59	HBC	-	

K^0 MEAN SQUARE CHARGE RADIUS

VALUE (m^2)	EVTS	DOCUMENT ID	TECN	COMMENT
-0.077 ± 0.010 OUR AVERAGE				
-0.077 ± 0.007 ± 0.011	5037	ABOUZAID 06	KTEV	$K_L^0 \rightarrow \pi^+\pi^-e^+e^-$
-0.090 ± 0.021		LAI 03C	NA48	$K_L^0 \rightarrow \pi^+\pi^-e^+e^-$
-0.054 ± 0.026		MOLZON 78		K_S^0 regen. by electrons
• • • We do not use the following data for averages, fits, limits, etc. • • •				
-0.087 ± 0.046		BLATNIK 79		VMD + dispersion relations
-0.050 ± 0.130		FOETH 69B		K_S^0 regen. by electrons

T-VIOLATION PARAMETER IN $K^0-\bar{K}^0$ MIXING

The asymmetry $A_T = \frac{\Gamma(\bar{K}^0 \rightarrow K^0) - \Gamma(K^0 \rightarrow \bar{K}^0)}{\Gamma(\bar{K}^0 \rightarrow K^0) + \Gamma(K^0 \rightarrow \bar{K}^0)}$ must vanish if T invariance holds.

ASYMMETRY A_T IN $K^0-\bar{K}^0$ MIXING

VALUE (units 10^{-3})	EVTS	DOCUMENT ID	TECN
6.6 ± 1.3 ± 1.0	640k	¹ ANGELOPO... 98E	CPLR

¹ANGELOPOULOS 98E measures the asymmetry $A_T = [\Gamma(\bar{K}^0_{t=0} \rightarrow e^+\pi^-\nu_{t=\tau}) - \Gamma(K^0_{t=0} \rightarrow e^-\pi^+\bar{\nu}_{t=\tau})]/[\Gamma(\bar{K}^0_{t=0} \rightarrow e^+\pi^-\nu_{t=\tau}) + \Gamma(K^0_{t=0} \rightarrow e^-\pi^+\bar{\nu}_{t=\tau})]$ as a function of the neutral-kaon eigentime τ . The initial strangeness of the neutral kaon is tagged by the charge of the accompanying charged kaon in the reactions $p\bar{p} \rightarrow K^-\pi^+K^0$ and $p\bar{p} \rightarrow K^+\pi^-K^0$. The strangeness at the time of the decay is tagged by the lepton charge. The reported result is the average value of A_T over the interval $1\tau_S < \tau < 20\tau_S$. From this value of A_T ANGELOPOULOS 01B, assuming CP invariance in the $e\nu$ decay amplitude, determine the T -violating as $\Delta S = \Delta S$ conserving parameter (for its definition, see Review below) $4\text{Re}(\epsilon) = (6.2 \pm 1.4 \pm 1.0) \times 10^{-3}$.

See the related review(s):
[CPT Invariance Tests in Neutral Kaon Decay](#)

CP-VIOLATION PARAMETERS

Re(ϵ)	VALUE (units 10^{-3})	DOCUMENT ID	TECN
1.596 ± 0.013		¹ AMBROSINO 06H	KLOE
• • • We do not use the following data for averages, fits, limits, etc. • • •			
1.664 ± 0.010		² LAI 05A	NA48

¹AMBROSINO 06H uses Bell-Steinberger relations with the following measurements: $B(K_L^0 \rightarrow \pi^+\pi^-)$ in AMBROSINO 06F, $B(K_S^0 \rightarrow \pi^0\pi^0\pi^0)$ in AMBROSINO 05B, the K_S^0 -semileptonic charge asymmetry in AMBROSINO 06E, and K^0 -semileptonic results in ANGELOPOULOS 98F.

²LAI 05A values are obtained through unitarity (Bell-Steinberger relations), improving determination of η_{000} and combining other data from PDG 04 and APOSTOLAKIS 99B.

CPT-VIOLATION PARAMETERS

In $K^0-\bar{K}^0$ mixing, if CP -violating interactions include a T conserving part then

$$|K_S\rangle = [|K_1\rangle + (\epsilon + \delta)|K_2\rangle]/\sqrt{|1 + |\epsilon + \delta|^2|}$$

$$|K_L\rangle = [|K_2\rangle + (\epsilon - \delta)|K_1\rangle]/\sqrt{|1 + |\epsilon - \delta|^2|}$$

where

$$|K_1\rangle = [|K^0\rangle + |\bar{K}^0\rangle]/\sqrt{2}$$

$$|K_2\rangle = [|K^0\rangle - |\bar{K}^0\rangle]/\sqrt{2}$$

and

$$|\bar{K}^0\rangle = CP|K^0\rangle.$$

The parameter δ specifies the CP -violating part.

Estimates of δ are given below assuming the validity of the $\Delta S = \Delta Q$ rule. See also THOMSON 95 for a test of CP -symmetry conservation in K^0 decays using the Bell-Steinberger relation.

REAL PART OF δ

A nonzero value violates CP invariance.

VALUE (units 10^{-4})	EVTS	DOCUMENT ID	TECN	COMMENT
2.51 ± 2.25		¹ ABOUZAID 11	KTEV	
• • • We do not use the following data for averages, fits, limits, etc. • • •				
2.3 ± 2.7		² AMBROSINO 06H	KLOE	
2.4 ± 2.8		³ APOSTOLA... 99B	RVUE	
2.9 ± 2.6 ± 0.6	1.3M	⁴ ANGELOPO... 98F	CPLR	
180 ± 200	6481	⁵ DEMIDOV 95		$K_{\ell 3}$ reanalysis

¹ABOUZAID 11 uses Bell-Steinberger relations.

²AMBROSINO 06H uses Bell-Steinberger relations with the following measurements: $B(K_L^0 \rightarrow \pi^+\pi^-)$ in AMBROSINO 06F, $B(K_S^0 \rightarrow \pi^0\pi^0\pi^0)$ in AMBROSINO 05B, the K_S^0 -semileptonic charge asymmetry in AMBROSINO 06E, and K^0 -semileptonic results in ANGELOPOULOS 98F.

³APOSTOLAKIS 99B assumes only unitarity and combines CPLEAR and other results.

⁴ANGELOPOULOS 98F use $\Delta S = \Delta Q$. If $\Delta S = \Delta Q$ is not assumed, they find $\text{Re}\delta = (3.0 \pm 3.3 \pm 0.6) \times 10^{-4}$.

⁵DEMIDOV 95 reanalyzes data from HART 73 and NIEBERGALL 74.

IMAGINARY PART OF δ

A nonzero value violates CP invariance.

VALUE (units 10^{-3})	EVTS	DOCUMENT ID	TECN	COMMENT
-1.5 ± 1.6		¹ ABOUZAID 11	KTEV	
• • • We do not use the following data for averages, fits, limits, etc. • • •				
0.4 ± 2.1		² AMBROSINO 06H	KLOE	
0.2 ± 2.0		³ LAI 05A	NA48	
2.4 ± 5.0		⁴ APOSTOLA... 99B	RVUE	
-90 ± 290 ± 100	1.3M	⁵ ANGELOPO... 98F	CPLR	
2100 ± 3700	6481	⁶ DEMIDOV 95		$K_{\ell 3}$ reanalysis

¹ABOUZAID 11 uses Bell-Steinberger relations.

²AMBROSINO 06H uses Bell-Steinberger relations with the following measurements: $B(K_L^0 \rightarrow \pi^+\pi^-)$ in AMBROSINO 06F, $B(K_S^0 \rightarrow \pi^0\pi^0\pi^0)$ in AMBROSINO 05B, the K_S^0 -semileptonic charge asymmetry in AMBROSINO 06E, and K^0 -semileptonic results in ANGELOPOULOS 98F.

³LAI 05A values are obtained through unitarity (Bell-Steinberger relations), improving determination of η_{000} and combining other data from PDG 04 and APOSTOLAKIS 99B.

⁴APOSTOLAKIS 99B assumes only unitarity and combines CPLEAR and other results.

⁵If $\Delta S = \Delta Q$ is not assumed, ANGELOPOULOS 98F finds $\text{Im}\delta = (-15 \pm 23 \pm 3) \times 10^{-3}$.

⁶DEMIDOV 95 reanalyzes data from HART 73 and NIEBERGALL 74.

See key on page 1127

Meson Particle Listings

K^0, K_S^0

Re(y)

A non-zero value would violate CPT invariance in $\Delta S = \Delta Q$ amplitude. Re(y) is the following combination of K_{e3} decay amplitudes:

$$\text{Re}(y) = \text{Re} \left(\frac{A(K^0 \rightarrow e^- \pi^+ \bar{\nu}_e) - A(K^0 \rightarrow e^+ \pi^- \nu_e)}{A(K^0 \rightarrow e^- \pi^+ \bar{\nu}_e) + A(K^0 \rightarrow e^+ \pi^- \nu_e)} \right)$$

VALUE (units 10^{-3})	EVTS	DOCUMENT ID	TECN
0.4 ± 2.5	13k	1 AMBROSINO 06E	KLOE
0.3 ± 3.1		2 APOSTOLA... 99B	CPLR

- We do not use the following data for averages, fits, limits, etc. •••
- 1 They use the PDG 04 for the K_L^0 semileptonic charge asymmetry and PDG 04 (CP review, CPT NOT ASSUMED) for Re(ϵ).
- 2 Constrained by Bell-Steinberger (or unitarity) relation.

Re(x₋)

A non-zero value would violate CPT invariance in decay amplitudes with $\Delta S \neq \Delta Q$. x_{-} , used here to define Re(x₋), and x_{+} , used below in the $\Delta S = \Delta Q$ section are the following combinations of K_{e3} decay amplitudes:

$$x_{\pm} = \frac{1}{2} \left(\frac{A(K^0 \rightarrow \pi^+ e^- \nu_e)}{A(K^0 \rightarrow \pi^- e^+ \bar{\nu}_e)} \pm \frac{A(K^0 \rightarrow \pi^+ e^- \bar{\nu}_e)}{A(K^0 \rightarrow \pi^- e^+ \nu_e)} \right)$$

VALUE (units 10^{-3})	EVTS	DOCUMENT ID	TECN	COMMENT
-2.9 ± 2.0		1 AMBROSINO 06H	KLOE	
-0.8 ± 2.5	13k	2 AMBROSINO 06E	KLOE	
-0.5 ± 3.0		3 APOSTOLA... 99B	CPLR	Strangeness tagged
$2 \pm 13 \pm 3$	650k	ANGELOPO... 98F	CPLR	Strangeness tagged

- We do not use the following data for averages, fits, limits, etc. •••
- 1 AMBROSINO 06H uses Bell-Steinberger relations with the following measurements: $B(K_L^0 \rightarrow \pi^+ \pi^-)$ in AMBROSINO 06F, $B(K_S^0 \rightarrow \pi^0 \pi^0 \pi^0)$ in AMBROSINO 05B, the K_S^0 -semileptonic charge asymmetry in AMBROSINO 06E, and K^0 -semileptonic results in ANGELOPOULOS 98F.
- 2 Uses PDG 04 for the K_L^0 semileptonic charge asymmetry and Re(δ) from CPLEAR, ANGELOPOULOS 98F.
- 3 Constrained by Bell-Steinberger (or unitarity) relation.

$$|m_{K^0} - m_{\bar{K}^0}| / m_{\text{average}}$$

A test of CPT invariance. "Our Evaluation" is described in the "Tests of Conservation Laws" section. It assumes CPT invariance in the decay and neglects some contributions from decay channels other than $\pi\pi$.

VALUE	CL%	DOCUMENT ID	TECN
$<6 \times 10^{-19}$	90	PDG	12
$(-3 \pm 4) \times 10^{-18}$		1 ANGELOPO... 99B	RVUE

- We do not use the following data for averages, fits, limits, etc. •••
- 1 ANGELOPOULOS 99B assumes only unitarity and combines CPLEAR and other results.

$$(\Gamma_{K^0} - \Gamma_{\bar{K}^0}) / m_{\text{average}}$$

A test of CPT invariance.

VALUE	DOCUMENT ID	TECN
$(7.8 \pm 8.4) \times 10^{-18}$	1 ANGELOPO... 99B	RVUE

- We do not use the following data for averages, fits, limits, etc. •••
- 1 ANGELOPOULOS 99B assumes only unitarity and combines CPLEAR with other results. Correlated with $(m_{K^0} - m_{\bar{K}^0}) / m_{\text{average}}$ with a correlation coefficient of -0.95 .

TESTS OF $\Delta S = \Delta Q$ RULE

Re(x₊)

A non-zero value would violate the $\Delta S = \Delta Q$ rule in CPT conserving transitions. x_{+} is defined above in the Re(x₋) section.

VALUE (units 10^{-3})	EVTS	DOCUMENT ID	TECN
-0.9 ± 3.0 OUR AVERAGE			
-2 ± 10		1 BATLEY 07D	NA48
-0.5 ± 3.6	13k	2 AMBROSINO 06E	KLOE
-1.8 ± 6.1		3 ANGELOPO... 98D	CPLR

- We do not use the following data for averages, fits, limits, etc. •••
- 1 Result obtained from the measurement $\Gamma(K_S^0 \rightarrow \pi e \nu) / \Gamma(K_L^0 \rightarrow \pi e \nu) = 0.993 \pm 0.34$, neglecting possible CPT non-invariance and using PDG 06 values of $B(K_L^0 \rightarrow \pi e \nu) = 0.4053 \pm 0.0015$, $\tau_L = (5.114 \pm 0.021) \times 10^{-8}$ s and $\tau_S = (0.8958 \pm 0.0005) \times 10^{-10}$ s.
- 2 Re(x₊) can be shown to be equal to the following combination of rates:

$$\text{Re}(x_{+}) = \frac{1}{2} \frac{\Gamma(K_S^0 \rightarrow \pi e \nu) - \Gamma(K_L^0 \rightarrow \pi e \nu)}{\Gamma(K_S^0 \rightarrow \pi e \nu) + \Gamma(K_L^0 \rightarrow \pi e \nu)}$$

which is valid up to first order in terms violating CPT and/or the $\Delta S = \Delta Q$ rule.

- We do not use the following data for averages, fits, limits, etc. •••
- 3 Obtained neglecting CPT violating amplitudes.

K^0 REFERENCES

TOMARADZE 14	PR D89 031501	A. Tomaradze et al.	(NWES, WAYN)
PDG 12	PR D86 010001	J. Beringer et al.	(PDG Collab.)
ABOUZAIID 11	PR D83 092001	E. Abouzaid et al.	(FNAL KTeV Collab.)
AMBROSINO 07B	JHEP 0712 073	F. Ambrosino et al.	(KLOE Collab.)
BATLEY 07D	PL B653 145	J.R. Batley et al.	(CERN NA48 Collab.)
ABOUZAIID 06	PRL 96 101801	E. Abouzaid et al.	(KTeV Collab.)
AMBROSINO 06E	PL B636 173	F. Ambrosino et al.	(KLOE Collab.)
AMBROSINO 06F	PL B638 140	F. Ambrosino et al.	(KLOE Collab.)
AMBROSINO 06H	JHEP 0612 011	F. Ambrosino et al.	(KLOE Collab.)
PDG 06	JP G33 1	W.-M. Yao et al.	(PDG Collab.)

AMBROSINO 05B	PL B619 61	F. Ambrosino et al.	(KLOE Collab.)
LAI 05A	PL B610 165	A. Lai et al.	(CERN NA48 Collab.)
PDG 04	PL B592 1	S. Eidelman et al.	(PDG Collab.)
LAI 03C	EPJ C30 33	A. Lai et al.	(CERN NA48 Collab.)
LAI 02	PL B533 196	A. Lai et al.	(CERN NA48 Collab.)
ANGELOPO... 01B	EPJ C22 55	A. Angelopoulos et al.	(CLEAR Collab.)
ANGELOPO... 99B	PL B471 332	A. Angelopoulos et al.	(CLEAR Collab.)
APOSTOLA... 98F	PL B456 297	A. Apostolakis et al.	(CLEAR Collab.)
ANGELOPO... 98D	PL B444 38	A. Angelopoulos et al.	(CLEAR Collab.)
Also	EPJ C22 55	A. Angelopoulos et al.	(CLEAR Collab.)
ANGELOPO... 98E	PL B444 43	A. Angelopoulos et al.	(CLEAR Collab.)
ANGELOPO... 98F	PL B444 52	A. Angelopoulos et al.	(CLEAR Collab.)
Also	EPJ C22 55	A. Angelopoulos et al.	(CLEAR Collab.)
DEMIDOV 95	PAN 58 968	V. Demidov, K. Gusev, E. Shabalov	(ITEP)
From YAF 58	1041.		
THOMSON 95	PR D51 1412	G.B. Thomson, Y. Zou	(RUTG)
BARKOV 87B	SJNP 46 630	L.M. Barkov et al.	(NOVO)
Also	Translated from YAF 46		
BARKOV 85B	JETPL 42 138	L.M. Barkov et al.	(NOVO)
Also	Translated from ZETFP 42		
BLATNIK 79	LNC 24 39	S. Blatnik, J. Stahov, C.B. Lang	(TUZL, GRAZ)
MOLZON 78	PRL 41 1213	W.R. Molzon et al.	(EFI+)
NIEBERGALL 74	PL 49B 103	F. Niebergall et al.	(CERN, ORSAY, VIEN)
HART 73	NP B66 317	J.C. Hart et al.	(CAVE, RHEL)
FOETH 69B	PL 30B 276	H. Foeth et al.	(AACH, CERN, TORI)
HILL 68B	PR 168 1534	D.G. Hill et al.	(BNL, CHU)
FITCH 67	PR 164 1711	V.L. Fitch et al.	(PRIN)
BALTAJ 66	PR 142 932	C. Baltaj et al.	(YALE, BNL)
BURNSTEIN 65	PR 138 B895	R.A. Burnstein, H.A. Rubin	(UMD)
KIM 65B	PR 140 B1334	J.K. Kim, L. Kirsch, D. Miller	(COLU)
CHRISTENS... 64	PRL 13 138	J.H. Christenson et al.	(PRIN)
CRAWFORD 59	PRL 2 112	F.S. Crawford et al.	(LRL)
ROSENFELD 59	PRL 2 110	A.H. Rosenfeld, F.T. Solmitz, R.D. Tripp	(LRL)

K_S^0

$$I(J^P) = \frac{1}{2}(0^-)$$

K_S^0 MEAN LIFE

For earlier measurements, beginning with BOLDT 58B, see our 1986 edition, Physics Letters **170B** 130 (1986).

OUR FIT is described in the note on "CP violation in K_L decays" in the K_L^0 Particle Listings. The result labeled "OUR FIT Assuming CP^T " ["OUR FIT Not assuming CP^T "] includes all measurements except those with the comment "Not assuming CP^T " ["Assuming CP^T "]. Measurements with neither comment do not assume CPT and enter both fits.

VALUE (10^{-10} s)	EVTS	DOCUMENT ID	TECN	COMMENT
0.8954 ± 0.0004 OUR FIT				Error includes scale factor of 1.1. Assuming CPT
0.89564 ± 0.00033 OUR FIT				Not assuming CP^T
0.89589 ± 0.00070		1,2 ABOUZAIID 11	KTEV	Not assuming CPT
0.89623 ± 0.00047		1,3 ABOUZAIID 11	KTEV	Assuming CPT
$0.89562 \pm 0.00029 \pm 0.00043$	20M	4 AMBROSINO 11	KLOE	Not assuming CPT
$0.89598 \pm 0.00048 \pm 0.00051$	16M	LAI 02C	NA48	
0.8971 ± 0.0021		BERTANZA 97	NA31	
$0.8941 \pm 0.0014 \pm 0.0009$		SCHWINGEN... 95	E773	Assuming CPT
0.8929 ± 0.0016		GIBBONS 93	E731	Assuming CPT
0.8965 ± 0.0007		5 ALAVI-HARATI 03	KTEV	Assuming CPT
0.8958 ± 0.0013		6 ALAVI-HARATI 03	KTEV	Not assuming CPT
0.8920 ± 0.0044	214k	GROSSMAN 87	SPEC	
0.905 ± 0.007		7 ARONSON 82B	SPEC	
0.881 ± 0.009	26k	ARONSON 76	SPEC	
$0.8926 \pm 0.0032 \pm 0.0002$		8 CARITHERS 75	SPEC	
0.8937 ± 0.0048	6M	GEWENGER 74B	ASPK	
0.8958 ± 0.0045	50k	9 SK JEGGEST... 72	HBC	
0.856 ± 0.008	19994	10 DONALD 68B	X	
0.872 ± 0.009	20000	9,10 HILL 68	DBC	

- We do not use the following data for averages, fits, limits, etc. •••
- 1 The two ABOUZAIID 11 values use the same full KTeV dataset from 1996, 1997, and 1999. The first enters the "assuming CP^T " fit and the second enters the "not assuming CP^T " fit.
- 2 ABOUZAIID 11 fit has Δm , τ_S , ϕ_e , Re(e'/ϵ), and Im(e'/ϵ) as free parameters. See Im(e'/ϵ) in the " K_L^0 CP violation" section for correlation information.
- 3 ABOUZAIID 11 fit has Δm and τ_S free but constrains ϕ_e to the Superweak value, i.e. assumes CP^T . This τ_S value is correlated with their $\Delta m = m_{K_L^0} - m_{K_S^0}$ measurement in the K_L^0 listings. The correlation coefficient $\rho(\tau_S, \Delta m) = -0.670$.
- 4 Fit to the proper time distribution.
- 5 This ALAVI-HARATI 03 fit has Δm and τ_S free but constrains ϕ_{+-} to the Superweak value, i.e. assumes CPT . This τ_S value is correlated with their $\Delta m = m_{K_L^0} - m_{K_S^0}$ measurement in the K_L^0 listings. The correlation coefficient $\rho(\tau_S, \Delta m) = -0.396$. Superseded by ABOUZAIID 11.
- 6 This ALAVI-HARATI 03 fit has Δm , ϕ_{+-} , and τ_{KS} free. See ϕ_{+-} in the " K_L CP violation" section for correlation information. Superseded by ABOUZAIID 11.
- 7 ARONSON 82 find that K_S^0 mean life may depend on the kaon energy.
- 8 CARITHERS 75 measures the Δm dependence of the total decay rate (inverse mean life) to be $\Gamma(K_S^0) = [(1.122 \pm 0.004) + 0.16(\Delta m - 0.5348)/\Delta m] 10^{10} / \text{s}$, or, in terms of mean life, CARITHERS 75 measures $\tau_S = (0.8913 \pm 0.0032) - 0.238 [\Delta m - 0.5348] (10^{-10} \text{ s})$. We have adjusted the measurement to use our best values of ($\Delta m = 0.5293 \pm 0.0009$) (10^{10} h s^{-1}). Our first error is their experiment's error and our second error is the systematic error from using our best values.

Meson Particle Listings

 K_S^0

⁹HILL 68 has been changed by the authors from the published value (0.865 ± 0.009) because of a correction in the shift due to η_{+-} . SKJEGGESTAD 72 and HILL 68 give detailed discussions of systematics encountered in this type of experiment.
¹⁰Pre-1971 experiments are excluded from the average because of disagreement with later more precise experiments.

 K_S^0 DECAY MODES

Mode	Fraction (Γ_i/Γ)	Scale factor/ Confidence level
------	--------------------------------	-----------------------------------

Hadronic modes

Γ_1	$\pi^0 \pi^0$	$(30.69 \pm 0.05) \%$
Γ_2	$\pi^+ \pi^-$	$(69.20 \pm 0.05) \%$
Γ_3	$\pi^+ \pi^- \pi^0$	$(3.5 \pm_{-0.9}^{+1.1}) \times 10^{-7}$

Modes with photons or $\ell\bar{\ell}$ pairs

Γ_4	$\pi^+ \pi^- \gamma$	[a,b] $(1.79 \pm 0.05) \times 10^{-3}$	S=3.1
Γ_5	$\pi^+ \pi^- e^+ e^-$	$(4.79 \pm 0.15) \times 10^{-5}$	
Γ_6	$\pi^0 \gamma \gamma$	[a] $(4.9 \pm 1.8) \times 10^{-8}$	
Γ_7	$\gamma \gamma$	$(2.63 \pm 0.17) \times 10^{-6}$	

Semileptonic modes

Γ_8	$\pi^\pm e^\mp \nu_e$	[c] $(7.04 \pm 0.08) \times 10^{-4}$
Γ_9	$\pi^\pm \mu^\mp \nu_\mu$	[c,d] $(4.56 \pm 0.20) \times 10^{-4}$

CP violating (CP) and $\Delta S = 1$ weak neutral current (S1) modes

Γ_{10}	$3\pi^0$	CP	< 2.6	$\times 10^{-8}$	CL=90%
Γ_{11}	$\mu^+ \mu^-$	S1	< 2.1	$\times 10^{-10}$	CL=90%
Γ_{12}	$e^+ e^-$	S1	< 9	$\times 10^{-9}$	CL=90%
Γ_{13}	$\pi^0 e^+ e^-$	S1	[a] $(3.0 \pm_{-1.2}^{+1.5})$	$\times 10^{-9}$	
Γ_{14}	$\pi^0 \mu^+ \mu^-$	S1	$(2.9 \pm_{-1.2}^{+1.5})$	$\times 10^{-9}$	

[a] See the Particle Listings below for the energy limits used in this measurement.

[b] Most of this radiative mode, the low-momentum γ part, is also included in the parent mode listed without γ 's.

[c] The value is for the sum of the charge states or particle/antiparticle states indicated.

[d] Not a measurement. Calculated as $0.666 \cdot B(\pi^\pm e^\mp \nu_e)$.

CONSTRAINED FIT INFORMATION

An overall fit to 4 branching ratios uses 5 measurements and one constraint to determine 4 parameters. The overall fit has a $\chi^2 = 0.1$ for 2 degrees of freedom.

The following *off-diagonal* array elements are the correlation coefficients $\langle \delta x_i \delta x_j \rangle / (\delta x_i \delta x_j)$, in percent, from the fit to the branching fractions, $x_i \equiv \Gamma_i / \Gamma_{\text{total}}$. The fit constrains the x_i whose labels appear in this array to sum to one.

x_2	-100		
x_8	-6	4	
x_9	-1	-3	0
	x_1	x_2	x_8

 K_S^0 DECAY RATES

$\Gamma(\pi^\pm e^\mp \nu_e)$	Γ_8			
VALUE (10^6 s^{-1})	EVTS	DOCUMENT ID	TECN	COMMENT

••• We do not use the following data for averages, fits, limits, etc. •••				
8.1 \pm 1.6	75	1 AKHMETSHIN 99	CMD2	Tagged K_S^0 using $\phi \rightarrow K_L^0 K_S^0$
7.50 \pm 0.08		2 PDG	98	
seen		BURGUN	72	HBC $K^+ p \rightarrow K^0 p \pi^+$
9.3 \pm 2.5		AUBERT	65	HLBC $\Delta S = \Delta Q$, CP cons. not assumed

¹AKHMETSHIN 99 is from a measured branching ratio $B(K_S^0 \rightarrow \pi e \nu_e) = (7.2 \pm 1.4) \times 10^{-4}$ and $\tau_{K_S^0} = (0.8934 \pm 0.0008) \times 10^{-10}$ s. Not independent of measured branching ratio.

²PDG 98 from K_L^0 measurements, assuming that $\Delta S = \Delta Q$ in K^0 decay so that $\Gamma(K_S^0 \rightarrow \pi^\pm e^\mp \nu_e) = \Gamma(K_L^0 \rightarrow \pi^\pm e^\mp \nu_e)$.

$\Gamma(\pi^\pm \mu^\mp \nu_\mu)$	Γ_9		
VALUE (10^6 s^{-1})	DOCUMENT ID	TECN	COMMENT

••• We do not use the following data for averages, fits, limits, etc. •••			
5.25 \pm 0.07	1 PDG	98	
¹ PDG 98 from K_L^0 measurements, assuming that $\Delta S = \Delta Q$ in K^0 decay so that $\Gamma(K_S^0 \rightarrow \pi^\pm \mu^\mp \nu_\mu) = \Gamma(K_L^0 \rightarrow \pi^\pm \mu^\mp \nu_\mu)$.			

 K_S^0 BRANCHING RATIOS

Hadronic modes

$\Gamma(\pi^0 \pi^0) / \Gamma_{\text{total}}$	Γ_1 / Γ		
VALUE	EVTS	DOCUMENT ID	TECN
0.3069 \pm 0.0005 OUR FIT			
••• We do not use the following data for averages, fits, limits, etc. •••			
0.335 \pm 0.014	1066	BROWN	63 HLBC
0.288 \pm 0.021	198	CHRETIEN	63 HLBC
0.30 \pm 0.035		BROWN	61 HLBC

$\Gamma(\pi^+ \pi^-) / \Gamma_{\text{total}}$	Γ_2 / Γ			
VALUE	EVTS	DOCUMENT ID	TECN	COMMENT
0.6920 \pm 0.0005 OUR FIT				
••• We do not use the following data for averages, fits, limits, etc. •••				
0.670 \pm 0.010	3447	DOYLE	69 HBC	$\pi^- p \rightarrow \Lambda K^0$

$\Gamma(\pi^+ \pi^-) / \Gamma(\pi^0 \pi^0)$	Γ_2 / Γ_1			
VALUE	EVTS	DOCUMENT ID	TECN	COMMENT
2.255 \pm 0.005 OUR FIT				
••• We do not use the following data for averages, fits, limits, etc. •••				
2.2555 \pm 0.0012 \pm 0.0054		1 AMBROSINO	06c	KLOE
2.236 \pm 0.003 \pm 0.015	766k	2 ALOISIO	02b	KLOE

2.11 \pm 0.09	1315	EVERHART	76	WIRE $\pi^- p \rightarrow \Lambda K^0$
2.169 \pm 0.094	16k	COWELL	74	OSPK $\pi^- p \rightarrow \Lambda K^0$
2.16 \pm 0.08	4799	HILL	73	DBC $K^+ d \rightarrow K^0 p p$
2.22 \pm 0.10	3068	3 ALITTI	72	HBC $K^+ p \rightarrow \pi^+ p K^0$
2.22 \pm 0.08	6380	MORSE	72b	DBC $K^+ n \rightarrow K^0 p$
2.10 \pm 0.11	701	4 NAGY	72	HLBC $K^+ n \rightarrow K^0 p$
2.22 \pm 0.095	6150	5 BALTAY	71	HBC $K p \rightarrow K^0 \text{ neutrals}$
2.282 \pm 0.043	7944	6 MOFFETT	70	OSPK $K^+ n \rightarrow K^0 p$
2.12 \pm 0.17	267	4 BOZOKI	69	HLBC $K^+ n \rightarrow K^0 p$
2.285 \pm 0.055	3016	6 GOBBI	69	OSPK $K^+ n \rightarrow K^0 p$
2.10 \pm 0.06	3700	MORFIN	69	HLBC $K^+ n \rightarrow K^0 p$

¹This result combines AMBROSINO 06c KLOE 2001-02 data with ALOISIO 02b KLOE 2000 data. $K_S^0 \rightarrow \pi^+ \pi^-$ fully inclusive.

²Includes radiative decays $\pi^+ \pi^- \gamma$.

³The directly measured quantity is $K_S^0 \rightarrow \pi^+ \pi^- / \text{all } K^0 = 0.345 \pm 0.005$.

⁴NAGY 72 is a final result which includes BOZOKI 69.

⁵The directly measured quantity is $K_S^0 \rightarrow \pi^+ \pi^- / \text{all } \bar{K}^0 = 0.345 \pm 0.005$.

⁶MOFFETT 70 is a final result which includes GOBBI 69.

$\Gamma(\pi^+ \pi^- \pi^0) / \Gamma_{\text{total}}$	Γ_3 / Γ			
VALUE (units 10^{-7})	EVTS	DOCUMENT ID	TECN	COMMENT

3.5 \pm 1.1 \pm 0.9 OUR AVERAGE				
4.7 \pm 2.2 \pm 1.7		1 BATLEY	05	NA48
-1.7 \pm 1.5		2 ADLER	97b	CPLR
2.5 \pm 1.3 \pm 0.5	500k	3 ZOU	96	E621
-1.0 \pm 0.6		4 ADLER	96E	CPLR Sup. by ADLER 97b
4.8 \pm 2.2 \pm 1.1		5 THOMSON	94	E621 Sup. by ZOU 96
-1.6 \pm 0.7				

••• We do not use the following data for averages, fits, limits, etc. •••

¹BATLEY 05 is obtained by measuring the interference parameters in $K_S, K_L \rightarrow \pi^+ \pi^- \pi^0$. $\text{Re}(\lambda) = 0.038 \pm 0.008 \pm 0.006$ and $\text{Im}(\lambda) = -0.013 \pm 0.005 \pm 0.004$; the correlation coeff. between $\text{Re}(\lambda)$ and $\text{Im}(\lambda)$ is 0.66 (statistical only).

²ADLER 97b find the CP-conserving parameters $\text{Re}(\lambda) = (28 \pm 7 \pm 3) \times 10^{-3}$, $\text{Im}(\lambda) = (-10 \pm 8 \pm 2) \times 10^{-3}$. They estimate $B(K_S^0 \rightarrow \pi^+ \pi^- \pi^0)$ from $\text{Re}(\lambda)$ and the K_L^0 decay parameters. See also ANGELOPOULOS 98c.

³ZOU 96 is from the the measured quantities $|\rho_{+-0}| = 0.039 \pm_{-0.006}^{+0.009} \pm 0.005$ and $\phi_\rho = (-9 \pm 18)^\circ$.

⁴ADLER 96E is from the measured quantities $\text{Re}(\lambda) = 0.036 \pm 0.010 \pm_{-0.003}^{+0.002}$ and $\text{Im}(\lambda)$ consistent with zero. Note that the quantity λ is the same as ρ_{+-0} used in other footnotes.

⁵THOMSON 94 calculates this branching ratio from their measurements $|\rho_{+-0}| = 0.035 \pm_{-0.011}^{+0.019} \pm 0.004$ and $\phi_\rho = (-59 \pm 48)^\circ$ where $|\rho_{+-0}| e^{i\phi_\rho} = A(K_S^0 \rightarrow \pi^+ \pi^- \pi^0, I = 2) / A(K_L^0 \rightarrow \pi^+ \pi^- \pi^0)$.

Modes with photons or $\ell\bar{\ell}$ pairs

$\Gamma(\pi^+ \pi^- \gamma) / \Gamma(\pi^+ \pi^-)$	Γ_4 / Γ_2			
VALUE (units 10^{-3})	EVTS	DOCUMENT ID	TECN	COMMENT

2.59 \pm 0.08 OUR AVERAGE				
2.56 \pm 0.09	1286	RAMBERG	93	E731 $p_\gamma > 50$ MeV/c
2.68 \pm 0.15		1 TAUREG	76	SPEC $p_\gamma > 50$ MeV/c

See key on page 1127

Meson Particle Listings

K_S^0

• • • We do not use the following data for averages, fits, limits, etc. • • •

7.10 ± 0.22	3723	RAMBERG	93	E731	$p_\gamma > 20$ MeV/c
3.0 ± 0.6	29	² BOBISUT	74	HLBC	$p_\gamma > 40$ MeV/c
2.8 ± 0.6		³ BURGUN	73	HBC	$p_\gamma > 50$ MeV/c

- ¹ TAUREG 76 find direct emission contribution < 0.06, CL = 90%.
² BOBISUT 74 not included in average because p_γ cut differs. Estimates direct emission contribution to be 0.5 or less, CL = 95%.
³ BURGUN 73 estimates that direct emission contribution is 0.3 ± 0.6 .

$\Gamma(\pi^+ \pi^- e^+ e^-) / \Gamma_{total}$ Γ_5 / Γ

VALUE (units 10^{-5})	CL%	EVTS	DOCUMENT ID	TECN	COMMENT
4.79 ± 0.15 OUR AVERAGE					
4.83 ± 0.11 ± 0.14	23k	¹ BATLEY	11	NA48	2002 data
4.69 ± 0.30	676	² LAI	03c	NA48	1998+1999 data

• • • We do not use the following data for averages, fits, limits, etc. • • •

4.71 ± 0.23 ± 0.22	620	^{2,3} LAI	03c	NA48	1999 data
4.5 ± 0.7 ± 0.4	56	LAI	00b	NA48	1998 data

- ¹ BATLEY 11 reports $[\Gamma(K_S^0 \rightarrow \pi^+ \pi^- e^+ e^-) / \Gamma_{total}] / [B(K_L^0 \rightarrow \pi^+ \pi^- \pi^0)] / [B(\pi^0 \rightarrow e^+ e^- \gamma)] = (3.28 \pm 0.06 \pm 0.04) \times 10^{-2}$ which we multiply by our best values $B(K_L^0 \rightarrow \pi^+ \pi^- \pi^0) = (12.54 \pm 0.05) \times 10^{-2}$, $B(\pi^0 \rightarrow e^+ e^- \gamma) = (1.174 \pm 0.035) \times 10^{-2}$. Our first error is their experiment's error and our second error is the systematic error from using our best values. Also a limit on the absolute value of the interference between bremsstrahlung and E1 transition is given : $< 4 \times 10^{-7}$ at 90% CL.
² Uses normalization $BR(K_L \rightarrow \pi^+ \pi^- \pi^0) * BR(\pi^0 \rightarrow e^+ e^-) = (1.505 \pm 0.047) \times 10^{-3}$ from our 2000 Edition.
³ Second error is $0.16(\text{syst}) \pm 0.15(\text{norm})$ combined in quadrature.

$\Gamma(\pi^0 \gamma \gamma) / \Gamma_{total}$ Γ_6 / Γ

VALUE (units 10^{-3})	CL%	EVTS	DOCUMENT ID	TECN	COMMENT
4.9 ± 1.6 ± 0.9	17	¹ LAI	04	NA48	$m_{\gamma\gamma}^2 / m_K^2 > 0.2$

- • • We do not use the following data for averages, fits, limits, etc. • • •
- | | | | | | |
|------|----|-----|-----|------|------------------------------------|
| < 33 | 90 | LAI | 03b | NA48 | $m_{\gamma\gamma}^2 / m_K^2 > 0.2$ |
|------|----|-----|-----|------|------------------------------------|
- ¹ Spectrum also measured and found consistent with the one generated by a constant matrix element.

$\Gamma(\gamma \gamma) / \Gamma_{total}$ Γ_7 / Γ

VALUE (units 10^{-6})	CL%	EVTS	DOCUMENT ID	TECN	COMMENT
2.63 ± 0.17 OUR AVERAGE					Error includes scale factor of 3.1.
2.26 ± 0.12 ± 0.06	711	¹ AMBROSINO	08c	KLOE	$\phi \rightarrow K_S^0 K_L^0$
2.713 ± 0.063 ± 0.005	7.5k	² LAI	03	NA48	

• • • We do not use the following data for averages, fits, limits, etc. • • •

2.58 ± 0.36 ± 0.22	149	LAI	00	NA48	
2.2 ± 1.1	16	³ BARR	95b	NA31	
2.4 ± 0.9	35	⁴ BARR	95b	NA31	
< 13	90	BALATS	89	SPEC	
2.4 ± 1.2	19	BURKHARDT	87	NA31	
< 133	90	BARMIN	86b	XEBC	

- ¹ AMBROSINO 08c reports $(2.26 \pm 0.12 \pm 0.06) \times 10^{-6}$ from a measurement of $[\Gamma(K_S^0 \rightarrow \gamma \gamma) / \Gamma_{total}] \times [B(K_S^0 \rightarrow \pi^0 \pi^0)]$ assuming $B(K_S^0 \rightarrow \pi^0 \pi^0) = (30.69 \pm 0.05) \times 10^{-2}$.
² LAI 03 reports $[\Gamma(K_S^0 \rightarrow \gamma \gamma) / \Gamma_{total}] / [B(K_S^0 \rightarrow \pi^0 \pi^0)] = (8.84 \pm 0.18 \pm 0.10) \times 10^{-6}$ which we multiply by our best value $B(K_S^0 \rightarrow \pi^0 \pi^0) = (30.69 \pm 0.05) \times 10^{-2}$. Our first error is their experiment's error and our second error is the systematic error from using our best value.
³ BARR 95b result is calculated using $B(K_L \rightarrow \gamma \gamma) = (5.86 \pm 0.17) \times 10^{-4}$.
⁴ BARR 95b quotes this as the combined BARR 95b + BURKHARDT 87 result after rescaling BURKHARDT 87 to use same branching ratios and lifetimes as BARR 95b.

———— Semileptonic modes ————

$\Gamma(\pi^\pm e^\mp \nu_e) / \Gamma_{total}$ Γ_8 / Γ

VALUE (units 10^{-4})	CL%	EVTS	DOCUMENT ID	TECN	COMMENT
7.04 ± 0.08 OUR FIT					
7.04 ± 0.08 OUR AVERAGE					
7.046 ± 0.18 ± 0.16			¹ BATLEY	07d	NA48 $K^0(\bar{K}^0)(t) \rightarrow \pi e \nu$
6.91 ± 0.34 ± 0.15	624	² ALOISIO	02	KLOE	Tagged K_S^0 using $\phi \rightarrow K_L^0 K_S^0$

- • • We use the following data for averages but not for fits. • • •
 7.05 ± 0.09 13k ³ AMBROSINO 06E Not fitted
 • • • We do not use the following data for averages, fits, limits, etc. • • •
 7.2 ± 1.4 75 AKHMETSHIN 99 CMD2 Tagged K_S^0 using $\phi \rightarrow K_L^0 K_S^0$
- ¹ Reconstructed from $K^0(\bar{K}^0)(t) \rightarrow \pi e \nu$ distributions using PDG values of $B(K_L^0 \rightarrow \pi e \nu) = 0.4053 \pm 0.0015$, $\tau_L = (5.114 \pm 0.021) \times 10^{-8}$ s and $\tau_S = (0.8958 \pm 0.0005) \times 10^{-10}$ s.
² Uses the PDG 00 value for $B(K_S^0 \rightarrow \pi^+ \pi^-)$.
³ Obtained by imposing $\sum_i B(K_S^0 \rightarrow i) = 1$, where i runs over all the four branching ratios $\pi^+ \pi^-$, $\pi^0 \pi^0$, $\pi e \nu$, and $\pi \mu \nu$. Input value of $B(K_S^0 \rightarrow \pi^+ \pi^-) / B(K_S^0 \rightarrow \pi^0 \pi^0)$ from AMBROSINO 06c is used. To derive $\Gamma(K_S^0 \rightarrow \pi^+ \mu \nu) / \Gamma(K_S^0 \rightarrow \pi^+ e \nu)$, lepton universality is assumed, radiative corrections from ANDRE 07 are used, and phase space integrals are taken from KTeV, ALEXOPOULOS 04A. This branching fraction enters our fit via their $\Gamma(\pi^\pm e^\mp \nu_e) / \Gamma(\pi^+ \pi^-)$ branching ratio measurement.

$\Gamma(\pi^\pm \mu^\mp \nu_\mu) / \Gamma_{total}$ Γ_9 / Γ

VALUE (units 10^{-4})	CL%	EVTS	DOCUMENT ID	TECN	COMMENT
4.56 ± 0.20 OUR FIT					
4.56 ± 0.11 ± 0.17		7223	¹ BABUSCI	20	KLOE direct measurement

- ¹ Value obtained by normalizing to the KLOE measurement $B(K_S^0 \rightarrow \pi^+ \pi^-) = (69.196 \pm 0.051)\%$. Also comparison with the PDG 18 based derived value leads to a lepton flavor universality test $|V_{us} \bar{f}_+(0)|_{K_S^0 \rightarrow \pi \mu \nu}^2 / |V_{us} \bar{f}_+(0)|_{K_S^0 \rightarrow \pi e \nu}^2 = 0.975 \pm 0.044$.

$\Gamma(\pi^\pm e^\mp \nu_e) / \Gamma(\pi^+ \pi^-)$ Γ_8 / Γ_2

VALUE (units 10^{-4})	CL%	EVTS	DOCUMENT ID	TECN	COMMENT
10.18 ± 0.12 OUR FIT					
10.19 ± 0.11 ± 0.07		13k	AMBROSINO	06E	KLOE

———— CP violating (CP) and $\Delta S = 1$ weak neutral current (S1) modes ————

$\Gamma(3\pi^0) / \Gamma_{total}$ Γ_{10} / Γ

VALUE (units 10^{-4})	CL%	EVTS	DOCUMENT ID	TECN	COMMENT
< 0.26	90	590M	¹ BABUSCI	13c	KLOE $\phi \rightarrow K_L^0 K_S^0$

- Violates CP conservation.
 • • • We do not use the following data for averages, fits, limits, etc. • • •
- | | | | | | |
|-------|----|-------|--------------------------|-----|------|
| < 1.2 | 90 | 37.8M | AMBROSINO | 05b | KLOE |
| < 7.4 | 90 | 4.9M | LAI | 05A | NA48 |
| < 140 | 90 | 7M | ACHASOV | 99b | SND |
| < 190 | 90 | 17300 | ³ ANGELOPO... | 98b | CPLR |
| < 370 | 90 | | BARMIN | 83 | HLBC |
- ¹ BABUSCI 13c uses 1.7 fb^{-1} of data of $\phi \rightarrow K_L^0 K_S^0$ decays with K_L^0 interaction in the calorimeter, collected from 2004 to 2005. No candidate events were found in the data with an expected background of $0.04^{+0.15}_{-0.03}$ events. Upper limit is obtained by normalizing to $K_S^0 \rightarrow 2\pi^0$ decays.
² LAI 05A value is obtained from their bound on $|\eta_{000}|$ (not assuming CP T) and $B(K_L^0 \rightarrow 3\pi^0) = 0.211 \pm 0.003$, and PDG 04 values for K_L^0 and K_S^0 lifetimes. If CPT is assumed then $B(K_S^0 \rightarrow 3\pi^0)_{CPT} < 2.3 \times 10^{-7}$ at 90% CL
³ ANGELOPOULOS 98b is from $\text{Im}(\eta_{000}) = -0.05 \pm 0.12 \pm 0.05$, assuming $\text{Re}(\eta_{000}) = \text{Re}(\epsilon) = 1.635 \times 10^{-3}$ and using the value $B(K_L^0 \rightarrow \pi^0 \pi^0 \pi^0) = 0.2112 \pm 0.0027$.

$\Gamma(\mu^+ \mu^-) / \Gamma_{total}$ Γ_{11} / Γ

VALUE	CL%	DOCUMENT ID	TECN	COMMENT
< 2.1 × 10⁻¹⁰	90	¹ AAIJ	20AE	LHCB

- Test for $\Delta S = 1$ weak neutral current. Allowed by first-order weak interaction combined with electromagnetic interaction.
 • • • We do not use the following data for averages, fits, limits, etc. • • •
- | | | | | |
|--------------------------|----|-------------------|------|------|
| < 8 × 10 ⁻¹⁰ | 90 | ² AAIJ | 17BQ | LHCB |
| < 9 × 10 ⁻⁹ | 90 | ³ AAIJ | 13G | LHCB |
| < 3.2 × 10 ⁻⁷ | 90 | GJESDAL | 73 | ASPK |
| < 7 × 10 ⁻⁶ | 90 | HYAMS | 69b | OSPK |
- ¹ AAIJ 20AE uses 8.6 fb^{-1} of LHCb data from 2011 to 2012 and 2016 to 2018. The result utilizes the normalization mode branching fraction $B(K_S^0 \rightarrow \pi^+ \pi^-) = (69.20 \pm 0.05) \times 10^{-2}$ from PDG 18. Supersedes AAIJ 17BQ.
² AAIJ 17BQ uses 3.0 fb^{-1} of pp collisions at $\sqrt{s} = 7$ and 8 TeV. The result utilizes the normalization mode branching fraction $B(K_S^0 \rightarrow \pi^+ \pi^-) = (69.20 \pm 0.05) \times 10^{-2}$ from PDG 16. Supersedes AAIJ 13G.
³ AAIJ 13G uses 1.0 fb^{-1} of pp collisions at $\sqrt{s} = 7$ TeV. They obtained $B(K_S^0 \rightarrow \mu^+ \mu^-) < 11 \times 10^{-9}$ at 95% CL.

$\Gamma(e^+ e^-) / \Gamma_{total}$ Γ_{12} / Γ

VALUE (units 10^{-7})	CL%	DOCUMENT ID	TECN	COMMENT
< 0.09	90	¹ AMBROSINO	09A	KLOE $e^+ e^- \rightarrow \phi \rightarrow K_S^0 K_L^0$

- Test for $\Delta S = 1$ weak neutral current. Allowed by first-order weak interaction combined with electromagnetic interaction.
 • • • We do not use the following data for averages, fits, limits, etc. • • •
- | | | | | |
|-------|----|-------------|----|-----------------------|
| < 1.4 | 90 | ANGELOPO... | 97 | CPLR |
| < 28 | 90 | BLICK | 94 | CNTR Hyperon facility |
| < 100 | 90 | BARMIN | 86 | XEBC |
- ¹ AMBROSINO 09A reports $< 0.09 \times 10^{-7}$ from a measurement of $[\Gamma(K_S^0 \rightarrow e^+ e^-) / \Gamma_{total}] / [B(K_S^0 \rightarrow \pi^+ \pi^-)]$ assuming $B(K_S^0 \rightarrow \pi^+ \pi^-) = (69.20 \pm 0.05) \times 10^{-2}$.

$\Gamma(\pi^0 e^+ e^-) / \Gamma_{total}$ Γ_{13} / Γ

VALUE (units 10^{-3})	CL%	EVTS	DOCUMENT ID	TECN	COMMENT
3.0 + 1.5 ± 0.2		7	¹ BATLEY	03	NA48 $m_{ee} > 0.165$ GeV

- • • We do not use the following data for averages, fits, limits, etc. • • •
- | | | | | | |
|---------|----|-----|---------|------|------|
| < 140 | 90 | LAI | 01 | NA48 | |
| < 1100 | 90 | 0 | BARR | 93b | NA31 |
| < 45000 | 90 | 0 | GIBBONS | 88 | E731 |
- ¹ BATLEY 03 extrapolate also to the full kinematical region using a constant form factor and a vector matrix element. The resulting branching ratio is $(5.8^{+2.9}_{-2.4}) \times 10^{-9}$.

Meson Particle Listings

 K_S^0

$\Gamma(\pi^0 \mu^+ \mu^-) / \Gamma_{\text{total}}$ Γ_{14} / Γ
 Test for $\Delta S = 1$ weak neutral current. Allowed by first-order weak interaction combined with electromagnetic interaction.

VALUE (units 10^{-3})	EVTS	DOCUMENT ID	TECN	COMMENT
$2.9 \pm 1.5 \pm 0.2$	6	¹ BATLEY	04A NA48	NA48/1 K_S^0 beam

¹ Background estimate is 0.22 ± 0.18 events. Branching ratio assumes a vector matrix element and unit form factor.

 K_S^0 FORM FACTORS

For discussion, see note on $K_{\ell 3}$ form factors in the K^\pm section of the Particle Listings above. Because the semileptonic branching fraction is smaller in K_S^0 than K_L^0 by the ratio of the mean lives, the K_S^0 semileptonic form factor has so far been measured only in the K_{e3} mode using the linear expansion $f_+(t) = f_+(0) (1 + \lambda_+ t / m_{\pi^+}^2)$, which gives the vector form factor $f_+(t)$ relative to its value at $t = 0$.

 λ_+ (LINEAR ENERGY DEPENDENCE OF f_+ IN K_{e3}^0 DECAY)

VALUE (units 10^{-2})	EVTS	DOCUMENT ID	TECN
3.39 ± 0.41	15k	AMBROSINO 06E	KLOE

CP VIOLATION IN $K_S \rightarrow 3\pi$

Written 1996 by T. Nakada (Paul Scherrer Institute) and L. Wolfenstein (Carnegie-Mellon University).

The possible final states for the decay $K^0 \rightarrow \pi^+ \pi^- \pi^0$ have isospin $I = 0, 1, 2$, and 3 . The $I = 0$ and $I = 2$ states have $CP = +1$ and K_S can decay into them without violating CP symmetry, but they are expected to be strongly suppressed by centrifugal barrier effects. The $I = 1$ and $I = 3$ states, which have no centrifugal barrier, have $CP = -1$ so that the K_S decay to these requires CP violation.

In order to see CP violation in $K_S \rightarrow \pi^+ \pi^- \pi^0$, it is necessary to observe the interference between K_S and K_L decay, which determines the amplitude ratio

$$\eta_{+-0} = \frac{A(K_S \rightarrow \pi^+ \pi^- \pi^0)}{A(K_L \rightarrow \pi^+ \pi^- \pi^0)}. \quad (1)$$

If η_{+-0} is obtained from an integration over the whole Dalitz plot, there is no contribution from the $I = 0$ and $I = 2$ final states and a nonzero value of η_{+-0} is entirely due to CP violation.

Only $I = 1$ and $I = 3$ states, which are $CP = -1$, are allowed for $K^0 \rightarrow \pi^0 \pi^0 \pi^0$ decays and the decay of K_S into $3\pi^0$ is an unambiguous sign of CP violation. Similarly to η_{+-0} , η_{000} is defined as

$$\eta_{000} = \frac{A(K_S \rightarrow \pi^0 \pi^0 \pi^0)}{A(K_L \rightarrow \pi^0 \pi^0 \pi^0)}. \quad (2)$$

If one assumes that CPT invariance holds and that there are no transitions to $I = 3$ (or to nonsymmetric $I = 1$ states), it can be shown that

$$\eta_{+-0} = \eta_{000} = \epsilon + i \frac{\text{Im } a_1}{\text{Re } a_1}. \quad (3)$$

With the Wu-Yang phase convention, a_1 is the weak decay amplitude for K^0 into $I = 1$ final states; ϵ is determined from CP violation in $K_L \rightarrow 2\pi$ decays. The real parts of η_{+-0} and η_{000} are equal to $\text{Re}(\epsilon)$. Since currently-known upper limits on $|\eta_{+-0}|$ and $|\eta_{000}|$ are much larger than $|\epsilon|$, they can be interpreted as upper limits on $\text{Im}(\eta_{+-0})$ and $\text{Im}(\eta_{000})$ and so as limits on the CP -violating phase of the decay amplitude a_1 .

CP-VIOLATION PARAMETERS IN K_S^0 DECAY

$$A_S = [\Gamma(K_S^0 \rightarrow \pi^- e^+ \nu_e) - \Gamma(K_S^0 \rightarrow \pi^+ e^- \bar{\nu}_e)] / \text{SUM}$$

Such asymmetry violates CP . If CPT is assumed then $A_S = 2 \text{Re}(\epsilon)$.

VALUE (units 10^{-3})	EVTS	DOCUMENT ID	TECN
$-3.8 \pm 5.0 \pm 2.6$	83k	¹ ANASTASI 18A	KLOE
$1.5 \pm 9.6 \pm 2.9$	13k	AMBROSINO 06E	KLOE

¹ ANASTASI 18A result is a combination of the new measurement and AMBROSINO 06E. The new ANASTASI 18A measurement using data collected from 2004–2005, which corresponds to an integrated luminosity of 1.63 fb^{-1} is $A_S = (-4.9 \pm 5.7 \pm 2.6) \times 10^{-3}$.

PARAMETERS FOR $K_S^0 \rightarrow 3\pi$ DECAY

$$\text{Im}(\eta_{+-0})^2 = \Gamma(K_S^0 \rightarrow \pi^+ \pi^- \pi^0, CP\text{-violating}) / \Gamma(K_L^0 \rightarrow \pi^+ \pi^- \pi^0)$$

CPT assumed valid (i.e. $\text{Re}(\eta_{+-0}) \simeq 0$).

VALUE	CL%	EVTS	DOCUMENT ID	TECN
< 0.23	90	601	¹ BARMIN 85	HLBC
< 0.12	90	384	METCALF 72	ASPK

¹ BARMIN 85 find $\text{Re}(\eta_{+-0}) = (0.05 \pm 0.17)$ and $\text{Im}(\eta_{+-0}) = (0.15 \pm 0.33)$. Includes events of BALDO-CEOLIN 75.

$$\text{Im}(\eta_{+-0}) = \text{Im}(A(K_S^0 \rightarrow \pi^+ \pi^- \pi^0, CP\text{-violating}) / A(K_L^0 \rightarrow \pi^+ \pi^- \pi^0))$$

VALUE	EVTS	DOCUMENT ID	TECN	COMMENT
$-0.002 \pm 0.009 \pm 0.002$	500k	¹ ADLER 97B	97B	CPLR
$-0.002 \pm 0.018 \pm 0.003$	137k	² ADLER 96D	96D	CPLR Sup. by ADLER 97B
$-0.015 \pm 0.017 \pm 0.025$	272k	³ ZOU 94	94	SPEC

¹ ADLER 97B also find $\text{Re}(\eta_{+-0}) = -0.002 \pm 0.007 \pm 0.004$. See also ANGELOPOULOS 98C.

² The ADLER 96D fit also yields $\text{Re}(\eta_{+-0}) = 0.006 \pm 0.013 \pm 0.001$ with a correlation of 0.66 between real and imaginary parts. Their results correspond to $|\eta_{+-0}| < 0.037$ with 90% CL.

³ ZOU 94 use theoretical constraint $\text{Re}(\eta_{+-0}) = \text{Re}(\epsilon) = 0.0016$. Without this constraint they find $\text{Im}(\eta_{+-0}) = 0.019 \pm 0.061$ and $\text{Re}(\eta_{+-0}) = 0.019 \pm 0.027$.

$$\text{Im}(\eta_{000})^2 = \Gamma(K_S^0 \rightarrow 3\pi^0) / \Gamma(K_L^0 \rightarrow 3\pi^0)$$

CPT assumed valid (i.e. $\text{Re}(\eta_{000}) \simeq 0$). This limit determines branching ratio $\Gamma(3\pi^0) / \Gamma_{\text{total}}$ above.

VALUE	CL%	EVTS	DOCUMENT ID	TECN	COMMENT
< 0.1	90	632	¹ BARMIN 83	HLBC	
< 0.28	90		² GJESDAL 74B	SPEC	Indirect meas.

¹ BARMIN 83 find $\text{Re}(\eta_{000}) = (-0.08 \pm 0.18)$ and $\text{Im}(\eta_{000}) = (-0.05 \pm 0.27)$. Assuming CPT invariance they obtain the limit quoted above.

² GJESDAL 74B uses $K_{2\pi}$, $K_{\mu 3}$, and K_{e3} decay results, unitarity, and CPT . Calculates $|\langle \eta_{000} \rangle| = 0.26 \pm 0.20$. We convert to upper limit.

$$\text{Im}(\eta_{000}) = \text{Im}(A(K_S^0 \rightarrow \pi^0 \pi^0 \pi^0) / A(K_L^0 \rightarrow \pi^0 \pi^0 \pi^0))$$

$K_S^0 \rightarrow \pi^0 \pi^0 \pi^0$ violates CP conservation, in contrast to $K_S^0 \rightarrow \pi^+ \pi^- \pi^0$ which has a CP -conserving part.

VALUE	EVTS	DOCUMENT ID	TECN	COMMENT
-0.001 ± 0.016 OUR AVERAGE				
$0.000 \pm 0.009 \pm 0.013$	4.9M	¹ LAI	05A NA48	Assumes CPT
$-0.05 \pm 0.12 \pm 0.05$	17300	² ANGELOPOULOS...	98B	CPLR Assumes CPT

¹ LAI 05A assumes $\text{Re}(\eta_{000}) = \text{Re}(\epsilon) = 1.66 \times 10^{-3}$. The equivalent limit is $|\eta_{000}|_{CPT} < 0.025$ at 90% CL. Without assuming CPT invariance, they obtain $\text{Re}(\eta_{000}) = -0.002 \pm 0.011 \pm 0.015$ and $\text{Im}(\eta_{000}) = -0.003 \pm 0.013 \pm 0.017$ with a statistical correlation coefficient of 0.77 and an overall correlation coefficient of 0.57 between imaginary and real part. The equivalent limit is $|\eta_{000}| < 0.045$ at 90% CL.

² ANGELOPOULOS 98B assumes $\text{Re}(\eta_{000}) = \text{Re}(\epsilon) = 1.635 \times 10^{-3}$. Without assuming CPT invariance, they obtain $\text{Re}(\eta_{000}) = 0.18 \pm 0.14 \pm 0.06$ and $\text{Im}(\eta_{000}) = 0.15 \pm 0.20 \pm 0.03$.

$$|\eta_{000}| = |A(K_S^0 \rightarrow 3\pi^0) / A(K_L^0 \rightarrow 3\pi^0)|$$

A non-zero value violates CP invariance.

VALUE	CL%	EVTS	DOCUMENT ID	TECN
< 0.0088	90	590M	BABUSCI 13C	KLOE
< 0.018	90	37.8M	AMBROSINO 05B	KLOE
< 0.045	90	4.9M	LAI	05A NA48

$\bullet \bullet \bullet$ We do not use the following data for averages, fits, limits, etc. $\bullet \bullet \bullet$

DECAY-PLANE ASYMMETRY IN $\pi^+\pi^-e^+e^-$ DECAYS

This is the CP-violating asymmetry

$$A = \frac{N_{\sin\phi\cos\phi>0.0} - N_{\sin\phi\cos\phi<0.0}}{N_{\sin\phi\cos\phi>0.0} + N_{\sin\phi\cos\phi<0.0}}$$

where ϕ is the angle between the e^+e^- and $\pi^+\pi^-$ planes in the K_S^0 rest frame.

CP asymmetry A in $K_S^0 \to \pi^+\pi^-e^+e^-$

Table with columns: VALUE (%), DOCUMENT ID, TECN, COMMENT. Includes entries for BATLEY, LAI, and LAI with various NA48 and 1999 data points.

K_S^0 REFERENCES

Extensive list of references for K_S^0 decays, including authors like AAIJ, BABUSCI, ANASTASI, PDG, etc., and their respective publications.

Continuation of references for K_S^0 decays, including authors like MORSE, NAGY, SKJEGGESTAD, BALTY, etc., and their respective publications.

OTHER RELATED PAPERS

List of other related papers including LITTENBERG, BATTISTON, TRILLING, CRAWFORD, FITCH, GOOD, BIRGE, MULLER, etc.



$$I(J^P) = \frac{1}{2}(0^-)$$

$$m_{K_L^0} - m_{K_S^0}$$

For earlier measurements, beginning with GOOD 61 and FITCH 61, see our 1986 edition, Physics Letters 170B 132 (1986).

OUR FIT is described in the note on "CP violation in K_L decays" in the K_L^0 Particle Listings. The result labeled "OUR FIT Assuming CP T" ["OUR FIT Not assuming CP T"] includes all measurements except those with the comment "Not assuming CP T" ["Assuming CP T"]. Measurements with neither comment do not assume CP T and enter both fits.

Table with columns: VALUE (10^10 h s^-1), DOCUMENT ID, TECN, COMMENT. Lists various measurements for the mass difference m_{K_L^0} - m_{K_S^0} with associated document IDs and technical details.

Footnote 1: The two ABOUZAID 11 values use the same data. The first enters the "assuming CP T" fit and the second enters the "not assuming CP T" fit.
Footnote 2: ABOUZAID 11 fit has Delta m, tau_S, phi_e, Re(epsilon'/epsilon), and Im(epsilon'/epsilon) as free parameters.
Footnote 3: ABOUZAID 11 fit has Delta m and tau_S free but constrains phi_e to the Superweak value, i.e. assumes CP T.
Footnote 4: Fits Delta m and phi_+- simultaneously. GIBBONS 93s systematic error is from B. Winstein via private communication.
Footnote 5: GIBBONS 93 value assume phi_+- = phi_0 = phi_SW = (43.7 +/- 0.2) degrees, i.e. assumes CP T.
Footnote 6: These two experiments have a common systematic error due to the uncertainty in the momentum scale, as pointed out in WAHL 89.
Footnote 7: GJESDAL 74 uses charge asymmetry in K_2^0 decays.
Footnote 8: ALAVI-HARATI 03 fit Delta m and tau_{K_S^0} simultaneously. phi_+- is constrained to the Superweak value, i.e. CP T is assumed.
Footnote 9: ALAVI-HARATI 03 fit Delta m, phi_+-, and tau_{K_S^0} simultaneously. See phi_+- in the "K_L CP violation" section for correlation information. Superseded by ABOUZAID 11.
Footnote 10: ANGELOPOULOS 01 uses strong interactions strangeness tagging at two different times.
Footnote 11: Uses K_2^0 and K_3^0 strangeness tagging at production and decay. Assumes CP T conservation on Delta S = -Delta Q transitions.

Meson Particle Listings

K_L^0

¹²ADLER 96c is the result of a fit which includes nearly the same data as entered into the "OUR FIT" value above.
¹³ARONSON 82 find that Δm may depend on the kaon energy.
¹⁴ARONSON 70 and CARNEGIE 71 use K_S^0 mean life = $(0.862 \pm 0.006) \times 10^{-10}$ s. We have not attempted to adjust these values for the subsequent change in the K_S^0 mean life or in η_{+-} .

K_L^0 MEAN LIFE

VALUE (10^{-8} s)	EVTS	DOCUMENT ID	TECN	COMMENT
5.116 ± 0.021 OUR FIT		Error includes scale factor of 1.1.		
5.099 ± 0.021 OUR AVERAGE				
5.072 ± 0.011 ± 0.035	13M	¹ AMBROSINO 06	KLOE	$\sum_i B_i = 1$
5.092 ± 0.017 ± 0.025	15M	AMBROSINO 05c	KLOE	
5.154 ± 0.044	0.4M	VOSBURGH 72	CNTR	

• • • We do not use the following data for averages, fits, limits, etc. • • •

5.15 ± 0.14		DEVLIN 67	CNTR	
-------------	--	-----------	------	--

¹AMBROSINO 06 uses $\phi \rightarrow K_L K_S$ with K_L tagged by $K_S \rightarrow \pi^+ \pi^-$. The four major K_L BR's are measured, the small remainder ($\pi^+ \pi^-, \pi^0 \pi^0, \gamma \gamma$) is taken from PDG 04. This KLOE K_L lifetime is obtained by imposing $\sum_i B_i = 1$. The correlation matrix among the four measured K_L BR's and this K_L lifetime is

	K_{e3}	$K_{\mu 3}$	$3\pi^0$	$\pi^+ \pi^- \pi^0$	τ_{K_L}
K_{e3}	1	-0.25	-0.56	-0.07	0.25
$K_{\mu 3}$		1	-0.43	-0.20	0.33
$3\pi^0$			1	-0.39	-0.21
$\pi^+ \pi^- \pi^0$				1	-0.39
τ_{K_L}					1

These correlations are taken into account in our fit. The average of this KLOE mean life measurement and the independent KLOE measurement in AMBROSINO 05c is $(5.084 \pm 0.023) \times 10^{-8}$ s.

K_L^0 DECAY MODES

Mode	Fraction (Γ_i/Γ)	Scale factor/ Confidence level
Semileptonic modes		
Γ_1 $\pi^\pm e^\mp \nu_e$ Called K_{e3}^0 .	[a] $(40.55 \pm 0.11) \%$	S=1.7
Γ_2 $\pi^\pm \mu^\mp \nu_\mu$ Called $K_{\mu 3}^0$.	[a] $(27.04 \pm 0.07) \%$	S=1.1
Γ_3 $(\pi \mu \text{atom}) \nu$	$(1.05 \pm 0.11) \times 10^{-7}$	
Γ_4 $\pi^0 \pi^\pm e^\mp \nu$	[a] $(5.20 \pm 0.11) \times 10^{-5}$	
Γ_5 $\pi^\pm e^\mp \nu e^+ e^-$	[a] $(1.26 \pm 0.04) \times 10^{-5}$	

Hadronic modes, including Charge conjugation × Parity Violating (CPV) modes

Γ_6 $3\pi^0$	$(19.52 \pm 0.12) \%$	S=1.6
Γ_7 $\pi^+ \pi^- \pi^0$	$(12.54 \pm 0.05) \%$	
Γ_8 $\pi^+ \pi^-$	CPV [b] $(1.967 \pm 0.010) \times 10^{-3}$	S=1.5
Γ_9 $\pi^0 \pi^0$	CPV $(8.64 \pm 0.06) \times 10^{-4}$	S=1.8

Semileptonic modes with photons

Γ_{10} $\pi^\pm e^\mp \nu_e \gamma$	[a,c,d] $(3.79 \pm 0.06) \times 10^{-3}$	
Γ_{11} $\pi^\pm \mu^\mp \nu_\mu \gamma$	$(5.65 \pm 0.23) \times 10^{-4}$	

Hadronic modes with photons or $\ell\bar{\ell}$ pairs

Γ_{12} $\pi^0 \pi^0 \gamma$	< 2.43	$\times 10^{-7}$	CL=90%
Γ_{13} $\pi^+ \pi^- \gamma$	[c,d] $(4.15 \pm 0.15) \times 10^{-5}$		S=2.8
Γ_{14} $\pi^+ \pi^- \gamma$ (DE)	$(2.84 \pm 0.11) \times 10^{-5}$		S=2.0
Γ_{15} $\pi^0 2\gamma$	[c] $(1.273 \pm 0.033) \times 10^{-6}$		
Γ_{16} $\pi^0 \gamma e^+ e^-$	$(1.62 \pm 0.17) \times 10^{-8}$		

Other modes with photons or $\ell\bar{\ell}$ pairs

Γ_{17} 2γ	$(5.47 \pm 0.04) \times 10^{-4}$	S=1.1	
Γ_{18} 3γ	< 7.4	$\times 10^{-8}$	CL=90%
Γ_{19} $e^+ e^- \gamma$	$(9.4 \pm 0.4) \times 10^{-6}$	S=2.0	
Γ_{20} $\mu^+ \mu^- \gamma$	$(3.59 \pm 0.11) \times 10^{-7}$	S=1.3	
Γ_{21} $e^+ e^- \gamma \gamma$	[c] $(5.95 \pm 0.33) \times 10^{-7}$		
Γ_{22} $\mu^+ \mu^- \gamma \gamma$	[c] $(1.0 \pm_{-0.6}^{+0.8}) \times 10^{-8}$		

Charge conjugation × Parity (CP) or Lepton Family number (LF) violating modes, or $\Delta S = 1$ weak neutral current (S1) modes

Γ_{23} $\mu^+ \mu^-$	S1 $(6.84 \pm 0.11) \times 10^{-9}$		
Γ_{24} $e^+ e^-$	S1 $(9 \pm_{-4}^{+6}) \times 10^{-12}$		
Γ_{25} $\pi^+ \pi^- e^+ e^-$	S1 [c] $(3.11 \pm 0.19) \times 10^{-7}$		
Γ_{26} $\pi^0 \pi^0 e^+ e^-$	S1 < 6.6	$\times 10^{-9}$	CL=90%
Γ_{27} $\pi^0 \pi^0 \mu^+ \mu^-$	S1 < 9.2	$\times 10^{-11}$	CL=90%
Γ_{28} $\mu^+ \mu^- e^+ e^-$	S1 $(2.69 \pm 0.27) \times 10^{-9}$		
Γ_{29} $e^+ e^- e^+ e^-$	S1 $(3.56 \pm 0.21) \times 10^{-8}$		

Γ_{30} $\pi^0 \mu^+ \mu^-$	CP,S1 [e] < 3.8	$\times 10^{-10}$	CL=90%
Γ_{31} $\pi^0 e^+ e^-$	CP,S1 [e] < 2.8	$\times 10^{-10}$	CL=90%
Γ_{32} $\pi^0 \nu \bar{\nu}$	CP,S1 [f] < 3.0	$\times 10^{-9}$	CL=90%
Γ_{33} $\pi^0 \pi^0 \nu \bar{\nu}$	S1 < 8.1	$\times 10^{-7}$	CL=90%
Γ_{34} $e^\pm \mu^\mp$	LF [a] < 4.7	$\times 10^{-12}$	CL=90%
Γ_{35} $e^\pm e^\pm \mu^\mp \mu^\mp$	LF [a] < 4.12	$\times 10^{-11}$	CL=90%
Γ_{36} $\pi^0 \mu^\pm e^\mp$	LF [a] < 7.6	$\times 10^{-11}$	CL=90%
Γ_{37} $\pi^0 \pi^0 \mu^\pm e^\mp$	LF < 1.7	$\times 10^{-10}$	CL=90%

Lorentz invariance violating modes

Γ_{38} $\pi^0 \gamma$	< 1.7	$\times 10^{-7}$	CL=90%
------------------------------	-------	------------------	--------

[a] The value is for the sum of the charge states or particle/antiparticle states indicated.

[b] This mode includes gammas from inner bremsstrahlung but not the direct emission mode $K_L^0 \rightarrow \pi^+ \pi^- \gamma$ (DE).

[c] See the Particle Listings below for the energy limits used in this measurement.

[d] Most of this radiative mode, the low-momentum γ part, is also included in the parent mode listed without γ 's.

[e] Allowed by higher-order electroweak interactions.

[f] Violates CP in leading order. Test of direct CP violation since the indirect CP-violating and CP-conserving contributions are expected to be suppressed.

CONSTRAINED FIT INFORMATION

An overall fit to the mean life and 15 branching ratios uses 27 measurements and one constraint to determine 11 parameters. The overall fit has a $\chi^2 = 37.4$ for 17 degrees of freedom.

The following off-diagonal array elements are the correlation coefficients $\langle \delta p_i \delta p_j \rangle / (\delta p_i \delta p_j)$, in percent, from the fit to parameters p_i , including the branching fractions, $x_i \equiv \Gamma_i / \Gamma_{\text{total}}$. The fit constrains the x_i whose labels appear in this array to sum to one.

x_2	-21									
x_6	-77	-29								
x_7	-15	-20	-18							
x_8	53	-11	-47	4						
x_9	30	-23	-11	-12	64					
x_{13}	6	-1	-6	0	12	8				
x_{14}	6	-1	-6	0	11	7	93			
x_{17}	-46	-22	64	-14	-21	8	-3	-3		
x_{19}	-5	-2	7	-1	-3	-1	0	0	4	
Γ	-27	-9	24	15	-13	-6	-2	-2	15	2
	x_1	x_2	x_6	x_7	x_8	x_9	x_{13}	x_{14}	x_{17}	x_{19}

Mode	Rate (10^8 s^{-1})	Scale factor
Γ_1 $\pi^\pm e^\mp \nu_e$ Called K_{e3}^0 .	[a] 0.07927 ± 0.00034	1.1
Γ_2 $\pi^\pm \mu^\mp \nu_\mu$ Called $K_{\mu 3}^0$.	[a] 0.05286 ± 0.00025	1.1
Γ_6 $3\pi^0$	0.03815 ± 0.00030	1.5
Γ_7 $\pi^+ \pi^- \pi^0$	0.02451 ± 0.00015	
Γ_8 $\pi^+ \pi^-$	[b] $(3.844 \pm 0.023) \times 10^{-4}$	1.2
Γ_9 $\pi^0 \pi^0$	$(1.690 \pm 0.013) \times 10^{-4}$	1.4
Γ_{13} $\pi^+ \pi^- \gamma$	[c,d] $(8.11 \pm 0.29) \times 10^{-6}$	2.7
Γ_{14} $\pi^+ \pi^- \gamma$ (DE)	$(5.55 \pm 0.21) \times 10^{-6}$	2.0
Γ_{17} 2γ	$(1.069 \pm 0.010) \times 10^{-4}$	1.2
Γ_{19} $e^+ e^- \gamma$	$(1.84 \pm 0.08) \times 10^{-6}$	1.9

K_L^0 DECAY RATES

$\Gamma(\pi^+ \pi^- \pi^0)$	VALUE (10^6 s^{-1})	EVTS	DOCUMENT ID	TECN	COMMENT
2.451 ± 0.015 OUR FIT					
• • • We do not use the following data for averages, fits, limits, etc. • • •					
	2.32 $\pm_{-0.15}^{+0.13}$	192	BALDO-...	75	HLBC Assumes CP
	2.35 ± 0.20	180	¹ JAMES	72	HBC Assumes CP
	2.71 ± 0.28	99	CHO	71	DBC Assumes CP
	2.5 ± 0.3	98	¹ JAMES	71	HBC Assumes CP
	2.12 ± 0.33	50	MEISNER	71	HBC Assumes CP
	2.20 ± 0.35	53	WEBBER	70	HBC Assumes CP
	2.62 $\pm_{-0.27}^{+0.28}$	136	BEHR	66	HLBC Assumes CP

3.26 ± 0.77	18	ANDERSON	65	HBC
1.4 ± 0.4	14	FRANZINI	65	HBC

¹ JAMES 72 is a final measurement and includes JAMES 71.

$\Gamma(\pi^\pm e^\mp \nu_e)$ Γ_1

VALUE ($10^6 s^{-1}$)	EVTS	DOCUMENT ID	TECN	COMMENT
7.927 ± 0.034 OUR FIT	Error includes scale factor of 1.1.			
• • • We do not use the following data for averages, fits, limits, etc. • • •				
7.81 ± 0.56	620	CHAN	71	HBC
7.52 ± 0.85		AUBERT	65	HLBC $\Delta S = \Delta Q, CP$ assumed
-0.72				

$\Gamma(\pi^\pm e^\mp \nu_e) + \Gamma(\pi^\pm \mu^\mp \nu_\mu)$ $(\Gamma_1 + \Gamma_2)$

VALUE ($10^6 s^{-1}$)	EVTS	DOCUMENT ID	TECN	COMMENT
13.21 ± 0.05 OUR FIT	• • • We do not use the following data for averages, fits, limits, etc. • • •			
12.4 ± 0.7	410	¹ BURGUN	72	HBC $K^+ p \rightarrow K^0 p \pi^+$
8.47 ± 1.69	126	¹ MANN	72	HBC $K^- p \rightarrow n \bar{K}^0$
13.1 ± 1.3	252	¹ WEBBER	71	HBC $K^- p \rightarrow n \bar{K}^0$
11.6 ± 0.9	393	^{1,2} CHO	70	DBC $K^+ n \rightarrow K^0 p$
10.3 ± 0.8	335	² HILL	67	DBC $K^+ n \rightarrow K^0 p$
9.85 ^{+1.15} _{-1.05}	109	¹ FRANZINI	65	HBC

¹ Assumes $\Delta S = \Delta Q$ rule.
² CHO 70 includes events of HILL 67.

K_L^0 BRANCHING RATIOS

Semileptonic modes

$\Gamma(\pi^\pm e^\mp \nu_e)/\Gamma_{total}$ Γ_1/Γ

VALUE	EVTS	DOCUMENT ID	TECN	COMMENT
0.4055 ± 0.0011 OUR FIT	Error includes scale factor of 1.7.			
0.4047 ± 0.0028 OUR AVERAGE	Error includes scale factor of 3.1.			
0.4007 ± 0.0005 ± 0.0015	13M	¹ AMBROSINO	06	KLOE
0.4067 ± 0.0011		² ALEXOPOU...	04	KTEV

¹ There are correlations between these five KLOE measurements: $B(K_L \rightarrow \pi e \nu)$, $B(K_L \rightarrow \pi \mu \nu)$, $B(K_L \rightarrow 3\pi^0)$, $B(K_L \rightarrow \pi^+ \pi^- \pi^0)$, and τ_{K_L} measured in AMBROSINO 06. See the footnote for the τ_{K_L} measurement for the correlation matrix.

² ALEXOPOULOS 04 constrains $\sum_i B_i = 0.9993$ for the six major K_L branching fractions. The correlations, among these branching fractions are taken into account in our fit. The correlation matrix is

	K_{e3}	$K_{\mu 3}$	$3\pi^0$	$\pi^+ \pi^- \pi^0$	$\pi^+ \pi^-$	$\pi^0 \pi^0$
K_{e3}	1					
$K_{\mu 3}$	0.15	1				
$3\pi^0$	-0.77	-0.62	1			
$\pi^+ \pi^- \pi^0$	0.18	0.08	-0.54	1		
$\pi^+ \pi^-$	0.28	0.22	-0.48	0.49	1	
$\pi^0 \pi^0$	-0.72	-0.54	0.89	-0.46	-0.39	1

$\Gamma(\pi^\pm \mu^\mp \nu_\mu)/\Gamma_{total}$ Γ_2/Γ

VALUE	EVTS	DOCUMENT ID	TECN	COMMENT
0.2704 ± 0.0007 OUR FIT	Error includes scale factor of 1.1.			
0.2700 ± 0.0008 OUR AVERAGE				
0.2698 ± 0.0005 ± 0.0015	13M	¹ AMBROSINO	06	KLOE
0.2701 ± 0.0009		² ALEXOPOU...	04	KTEV

¹ There are correlations between these five KLOE measurements: $B(K_L \rightarrow \pi e \nu)$, $B(K_L \rightarrow \pi \mu \nu)$, $B(K_L \rightarrow 3\pi^0)$, $B(K_L \rightarrow \pi^+ \pi^- \pi^0)$, and τ_{K_L} measured in AMBROSINO 06. See the footnote for the τ_{K_L} measurement for the correlation matrix.

² For correlations with other ALEXOPOULOS 04 measurements, see the footnote with their $B(K_L \rightarrow \pi e \nu)$ measurement.

$[\Gamma(\pi^\pm e^\mp \nu_e) + \Gamma(\pi^\pm \mu^\mp \nu_\mu)]/\Gamma_{total}$ $(\Gamma_1 + \Gamma_2)/\Gamma$

VALUE	DOCUMENT ID
0.6760 ± 0.0012 OUR FIT	Error includes scale factor of 1.6.

$\Gamma(\pi^\pm \mu^\mp \nu_\mu)/\Gamma(\pi^\pm e^\mp \nu_e)$ Γ_2/Γ_1

VALUE	EVTS	DOCUMENT ID	TECN	COMMENT
0.6669 ± 0.0027 OUR FIT	Error includes scale factor of 1.2.			
0.666 ± 0.004 OUR AVERAGE	Error includes scale factor of 1.6.			
• • • We use the following data for averages but not for fits. • • •				
0.6740 ± 0.0059	13M	¹ AMBROSINO	06	KLOE Not in fit
0.6640 ± 0.0014 ± 0.0022	394k	² ALEXOPOU...	04	KTEV Not in fit
• • • We do not use the following data for averages, fits, limits, etc. • • •				
0.702 ± 0.011	33k	CHO	80	HBC
0.662 ± 0.037	10k	WILLIAMS	74	ASPK
0.741 ± 0.044	6700	BRANDENB...	73	HBC
0.662 ± 0.030	1309	EVANS	73	HLBC
0.68 ± 0.08	3548	BASILE	70	OSPK
0.71 ± 0.05	770	BUDAGOV	68	HLBC

¹ AMBROSINO 06 enters the fit via their separate measurements of these two modes.
² ALEXOPOULOS 04 enters the fit via their separate measurements of these two modes.

$\Gamma((\pi \mu \text{atom}) \nu)/\Gamma(\pi^\pm \mu^\mp \nu_\mu)$ Γ_3/Γ_2

VALUE (units 10^{-7})	EVTS	DOCUMENT ID	TECN	COMMENT
3.90 ± 0.39	155	¹ ARONSON	86	SPEC
• • • We do not use the following data for averages, fits, limits, etc. • • •				
seen	18	COOMBES	76	WIRE
¹ ARONSON 86 quote theoretical value of $(4.31 \pm 0.08) \times 10^{-7}$.				

$\Gamma(\pi^0 \pi^\pm e^\mp \nu)/\Gamma_{total}$ Γ_4/Γ

VALUE (units 10^{-5})	CL%	EVTS	DOCUMENT ID	TECN
5.20 ± 0.11 OUR AVERAGE				
5.21 ± 0.07 ± 0.09		5402	BATLEY	04 NA48
5.16 ± 0.20 ± 0.22		729	MAKOFF	93 E731
• • • We do not use the following data for averages, fits, limits, etc. • • •				
6.2 ± 2.0	16		CARROLL	80c SPEC
< 220	90		¹ DONALDSON	74 SPEC
¹ DONALDSON 74 uses $K_L^0 \rightarrow \pi^+ \pi^- \pi^0$ / (all K_L^0 decays) = 0.126.				

$\Gamma(\pi^\pm e^\mp \nu e^+ e^-)/\Gamma(\pi^+ \pi^- \pi^0)$ Γ_5/Γ_7

VALUE (units 10^{-5})	EVTS	DOCUMENT ID	TECN	COMMENT
10.02 ± 0.17 ± 0.29	19k	¹ ABOUZAID	07c	KTEV $M_{ee} > 5$ MeV, $E_{ee}^* > 30$ MeV
¹ E_{ee}^* is the energy of the $e^+ e^-$ pair in the kaon rest frame. ABOUZAID 07c reports $[\Gamma(K_L^0 \rightarrow \pi^\pm e^\mp \nu e^+ e^-)/\Gamma(K_L^0 \rightarrow \pi^+ \pi^- \pi^0)] / [B(\pi^0 \rightarrow e^+ e^- \gamma)] = (8.54 \pm 0.07 \pm 0.13) \times 10^{-3}$ which we multiply by our best value $B(\pi^0 \rightarrow e^+ e^- \gamma) = (1.174 \pm 0.035) \times 10^{-2}$. Our first error is their experiment's error and our second error is the systematic error from using our best value.				

Hadronic modes,

including Charge conjugation × Parity Violating (CPV) modes

$\Gamma(3\pi^0)/\Gamma_{total}$ Γ_6/Γ

VALUE	EVTS	DOCUMENT ID	TECN	COMMENT
0.1952 ± 0.0012 OUR FIT	Error includes scale factor of 1.6.			
0.1969 ± 0.0026 OUR AVERAGE	Error includes scale factor of 2.0.			
• • • We use the following data for averages but not for fits. • • •				
0.1997 ± 0.0003 ± 0.0019	13M	¹ AMBROSINO	06	KLOE Not fitted
0.1945 ± 0.0018		¹ ALEXOPOU...	04	KTEV Not fitted

¹ We exclude these $B(K_L \rightarrow 3\pi^0)$ measurements from our fit because the authors have constrained K_L branching fractions to sum to one. It enters our fit via the other measurements from the experiment and their correlations, along with our constraint that the fitted branching fractions sum to one.

$\Gamma(3\pi^0)/\Gamma(\pi^\pm e^\mp \nu_e)$ Γ_6/Γ_1

VALUE	EVTS	DOCUMENT ID	TECN	COMMENT
0.481 ± 0.004 OUR FIT	Error includes scale factor of 1.8.			
• • • We use the following data for averages but not for fits. • • •				
0.4782 ± 0.0014 ± 0.0053	209k	¹ ALEXOPOU...	04	KTEV Not in fit
• • • We do not use the following data for averages, fits, limits, etc. • • •				
0.545 ± 0.004 ± 0.009	38k	KREUTZ	95	NA31

¹ This measurement enters the fit via their separate measurements of these two modes.

$\Gamma(3\pi^0)/[\Gamma(\pi^\pm e^\mp \nu_e) + \Gamma(\pi^\pm \mu^\mp \nu_\mu) + \Gamma(\pi^+ \pi^- \pi^0)]$ $\Gamma_6/(\Gamma_1 + \Gamma_2 + \Gamma_7)$

VALUE	EVTS	DOCUMENT ID	TECN	COMMENT
0.2436 ± 0.0018 OUR FIT	Error includes scale factor of 1.6.			
• • • We do not use the following data for averages, fits, limits, etc. • • •				
0.251 ± 0.014	549	BUDAGOV	68	HLBC ORSAY measur.
0.277 ± 0.021	444	BUDAGOV	68	HLBC Ecole polytec.meas
0.31 ^{+0.07} _{-0.06}	29	KULYUKINA	68	CC
0.24 ± 0.08	24	ANIKINA	64	CC

$\Gamma(3\pi^0)/\Gamma(\pi^+ \pi^- \pi^0)$ Γ_6/Γ_7

VALUE	EVTS	DOCUMENT ID	TECN	COMMENT
1.557 ± 0.012 OUR FIT	Error includes scale factor of 1.3.			
• • • We use the following data for averages but not for fits. • • •				
1.582 ± 0.027	13M	¹ AMBROSINO	06	KLOE Not in fit
• • • We do not use the following data for averages, fits, limits, etc. • • •				
1.611 ± 0.014 ± 0.034	28k	KREUTZ	95	NA31
1.65 ± 0.07	883	BARMIN	72b	HLBC Error statistical only
1.80 ± 0.13	1010	BUDAGOV	68	HLBC
2.0 ± 0.6	188	ALEKSANYAN	64b	FBC

¹ AMBROSINO 06 enters the fit via their separate measurements of these two modes.

$\Gamma(\pi^+ \pi^- \pi^0)/\Gamma_{total}$ Γ_7/Γ

VALUE	EVTS	DOCUMENT ID	TECN	COMMENT
0.1254 ± 0.0005 OUR FIT				
0.1255 ± 0.0006 OUR AVERAGE				
0.1263 ± 0.0004 ± 0.0011	13M	¹ AMBROSINO	06	KLOE
0.1252 ± 0.0007		² ALEXOPOU...	04	KTEV

¹ There are correlations between these five KLOE measurements: $B(K_L \rightarrow \pi e \nu)$, $B(K_L \rightarrow \pi \mu \nu)$, $B(K_L \rightarrow 3\pi^0)$, $B(K_L \rightarrow \pi^+ \pi^- \pi^0)$, and τ_{K_L} measured in AMBROSINO 06. See the footnote for the τ_{K_L} measurement for the correlation matrix.

² For correlations with other ALEXOPOULOS 04 measurements, see the footnote with their $B(K_L \rightarrow \pi e \nu)$ measurement.

Meson Particle Listings

K_L^0

$\Gamma(\pi^+\pi^-\pi^0)/\Gamma(\pi^\pm e^\mp \nu_e)$ Γ_7/Γ_1

VALUE	EVTS	DOCUMENT ID	TECN	COMMENT
0.3092±0.0016 OUR FIT				Error includes scale factor of 1.1.
•••				We use the following data for averages but not for fits. •••
0.3078±0.0005±0.0017	799k	¹ ALEXOPOU...	04 KTEV	Not in fit
•••				We do not use the following data for averages, fits, limits, etc. •••
0.336 ± 0.003 ± 0.007	28k	KREUTZ	95 NA31	

¹This measurement enters the fit via their separate measurements for the two modes.

$\Gamma(\pi^+\pi^-\pi^0)/[\Gamma(\pi^\pm e^\mp \nu_e) + \Gamma(\pi^\pm \mu^\mp \nu_\mu) + \Gamma(\pi^+\pi^-\pi^0)]$ $\Gamma_7/(\Gamma_1+\Gamma_2+\Gamma_7)$

VALUE	EVTS	DOCUMENT ID	TECN	COMMENT
0.1565±0.0006 OUR FIT				Error includes scale factor of 1.1.
•••				We do not use the following data for averages, fits, limits, etc. •••
0.163 ± 0.003	6499	CHO	77 HBC	
0.1605 ± 0.0038	1590	ALEXANDER	73B HBC	
0.146 ± 0.004	3200	BRANDENB...	73 HBC	
0.159 ± 0.010	558	EVANS	73 HLBC	
0.167 ± 0.016	1402	KULYUKINA	68 CC	
0.161 ± 0.005		HOPKINS	67 HBC	
0.162 ± 0.015	126	HAWKINS	66 HBC	
0.159 ± 0.015	326	ASTBURY	65B CC	
0.178 ± 0.017	566	GUIDONI	65 HBC	
0.144 ± 0.004	1729	HOPKINS	65 HBC	See HOPKINS 67

$\Gamma(\pi^+\pi^-)/\Gamma_{total}$ Γ_8/Γ

Violates CP conservation.

VALUE (units 10 ⁻³)	DOCUMENT ID	TECN
1.967±0.010 OUR FIT		
•••		
1.975±0.012	¹ ALEXOPOU...	04 KTEV

¹For correlations with other ALEXOPOULOS 04 measurements, see the footnote with their $B(K_L \rightarrow \pi e \nu)$ measurement.

$\Gamma(\pi^+\pi^-)/\Gamma(\pi^\pm e^\mp \nu_e)$ Γ_8/Γ_1

VALUE (units 10 ⁻³)	EVTS	DOCUMENT ID	TECN	COMMENT
4.849±0.020 OUR FIT				Error includes scale factor of 1.1.
4.840±0.020 OUR AVERAGE				
4.826±0.022±0.016	47k	¹ LAI	07 NA48	
•••				We use the following data for averages but not for fits. •••
4.856±0.017±0.023	84k	² ALEXOPOU...	04 KTEV	Not in fit

¹The LAI 07 central value of 4.835×10^{-3} has been reduced by 0.19% to 4.826×10^{-3} to subtract the contribution from the direct emission mode $K_L^0 \rightarrow \pi^+\pi^-\gamma(DE)$.

²This measurement enters the fit via their separate measurements for the two modes.

$[\Gamma(\pi^+\pi^-) + \Gamma(\pi^+\pi^-\gamma(DE))]/\Gamma(\pi^\pm e^\mp \nu_e)$ $(\Gamma_8+\Gamma_{14})/\Gamma_2$

VALUE (units 10 ⁻³)	EVTS	DOCUMENT ID	TECN	COMMENT
7.38 ± 0.04 OUR FIT				Error includes scale factor of 1.4.
7.275 ± 0.042 ± 0.054	45k	¹ AMBROSINO	06F KLOE	

¹Fully inclusive. Taking $B(K_L^0 \rightarrow \pi \mu \nu)$ from KLOE, AMBROSINO 06, $B(K_L^0 \rightarrow \pi^+\pi^- + \pi^+\pi^-\gamma(DE)) = (1.963 \pm 0.012 \pm 0.017) \times 10^{-3}$ is obtained.

$\Gamma(\pi^+\pi^-)/[\Gamma(\pi^\pm e^\mp \nu_e) + \Gamma(\pi^\pm \mu^\mp \nu_\mu)]$ $\Gamma_8/(\Gamma_1+\Gamma_2)$

Violates CP conservation.

VALUE (units 10 ⁻³)	EVTS	DOCUMENT ID	TECN	COMMENT
2.909±0.013 OUR FIT				Error includes scale factor of 1.3.
•••				We do not use the following data for averages, fits, limits, etc. •••
3.13 ± 0.14	1687	COUPAL	85 SPEC	$\eta_{+-} = 2.28 \pm 0.06$
3.04 ± 0.14	2703	DEVOE	77 SPEC	$\eta_{+-} = 2.25 \pm 0.05$
2.51 ± 0.23	309	¹ DEBOUARD	67 OSPK	$\eta_{+-} = 2.00 \pm 0.09$
2.35 ± 0.19	525	¹ FITCH	67 OSPK	$\eta_{+-} = 1.94 \pm 0.08$

¹Old experiments excluded from fit. See subsection on η_{+-} in section on "PARAMETERS FOR $K_L^0 \rightarrow 2\pi$ DECAY" below for average η_{+-} of these experiments and for note on discrepancy.

$\Gamma(\pi^\pm e^\mp \nu_e)/\Gamma(2 \text{ tracks})$ $\Gamma_1/(\Gamma_1+\Gamma_2+0.03508\Gamma_6+\Gamma_7+\Gamma_8)$

$\Gamma(2 \text{ tracks}) = \Gamma(\pi^\pm e^\mp \nu_e) + \Gamma(\pi^\pm \mu^\mp \nu_\mu) + 0.03508 \Gamma(3\pi^0) + \Gamma(\pi^+\pi^-\pi^0) + \Gamma(\pi^+\pi^-)$ where 0.03508 is the fraction of $3\pi^0$ events with one Dalitz decay ($\pi^0 \rightarrow \gamma e^+e^-$).

VALUE	EVTS	DOCUMENT ID	TECN
0.5006±0.0009 OUR FIT			
0.4978±0.0035	6.8M	LAI	04B NA48

$\Gamma(\pi^+\pi^-)/[\Gamma(\pi^\pm e^\mp \nu_e) + \Gamma(\pi^\pm \mu^\mp \nu_\mu) + \Gamma(\pi^+\pi^-\pi^0)]$ $\Gamma_8/(\Gamma_1+\Gamma_2+\Gamma_7)$

Violates CP conservation.

VALUE (units 10 ⁻³)	EVTS	DOCUMENT ID	TECN	COMMENT
2.454±0.011 OUR FIT				Error includes scale factor of 1.3.
•••				We do not use the following data for averages, fits, limits, etc. •••
2.60 ± 0.07	4200	¹ MESSNER	73 ASPK	$\eta_{+-} = 2.23 \pm 0.05$

¹From same data as $\Gamma(\pi^+\pi^-)/\Gamma(\pi^+\pi^-\pi^0)$ MESSNER 73, but with different normalization.

$\Gamma(\pi^+\pi^-)/\Gamma(\pi^+\pi^-\pi^0)$ Γ_8/Γ_7

Violates CP conservation.

VALUE (units 10 ⁻²)	EVTS	DOCUMENT ID	TECN	COMMENT
1.568±0.010 OUR FIT				Error includes scale factor of 1.3.
•••				We do not use the following data for averages, fits, limits, etc. •••
1.64 ± 0.04	4200	MESSNER	73 ASPK	$\eta_{+-} = 2.23$

$\Gamma(\pi^0\pi^0)/\Gamma_{total}$ Γ_9/Γ

Violates CP conservation.

VALUE (units 10 ⁻³)	DOCUMENT ID	TECN
0.864±0.006 OUR FIT		
0.865±0.012	¹ ALEXOPOU...	04 KTEV

¹For correlations with other ALEXOPOULOS 04 measurements, see the footnote with their $B(K_L \rightarrow \pi e \nu)$ measurement.

$\Gamma(\pi^0\pi^0)/\Gamma(\pi^+\pi^-)$ Γ_9/Γ_8

Violates CP conservation.

VALUE	DOCUMENT ID	TECN
0.4395±0.0023 OUR FIT		
0.4390±0.0012	ETAFIT	16

$\Gamma(\pi^0\pi^0)/\Gamma(3\pi^0)$ Γ_9/Γ_6

Violates CP conservation.

VALUE (units 10 ⁻²)	EVTS	DOCUMENT ID	TECN	COMMENT
0.443 ± 0.004 OUR FIT				Error includes scale factor of 2.1.
•••				We use the following data for averages but not for fits. •••
0.4446±0.0016±0.0019	100k	¹ ALEXOPOU...	04 KTEV	Not in fit
•••				We do not use the following data for averages, fits, limits, etc. •••
0.37 ± 0.08	29	BARMIN	70 HLBC	$\eta_{00} = 2.02 \pm 0.23$
0.32 ± 0.15	30	BUDAGOV	70 HLBC	$\eta_{00} = 1.9 \pm 0.5$
0.46 ± 0.11	57	BANNER	69 OSPK	$\eta_{00} = 2.2 \pm 0.3$

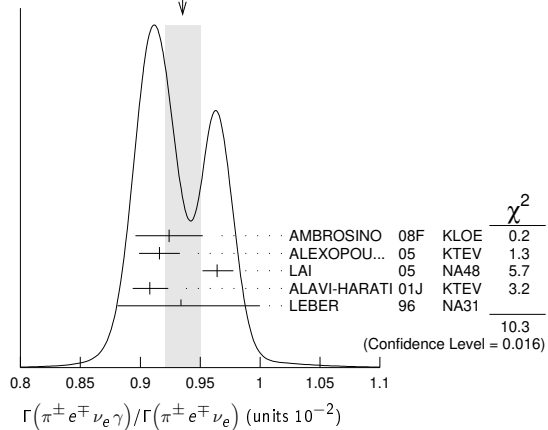
¹This measurement enters the fit via their separate measurements for the two modes.

Semileptonic modes with photons

$\Gamma(\pi^\pm e^\mp \nu_e \gamma)/\Gamma(\pi^\pm e^\mp \nu_e)$ Γ_{10}/Γ_1

VALUE (units 10 ⁻²)	EVTS	DOCUMENT ID	TECN	COMMENT
0.935±0.015 OUR AVERAGE				Error includes scale factor of 1.9. See the ideogram below.
0.924±0.023±0.016	9k	¹ AMBROSINO	08F KLOE	$E_\gamma^* > 30 \text{ MeV}, \theta_{e\gamma}^* > 20^\circ$
0.916±0.017	4309	² ALEXOPOU...	05 KTEV	$E_\gamma^* > 30 \text{ MeV}, \theta_{e\gamma}^* > 20^\circ$
0.964±0.008 ^{+0.011} _{-0.009}	19k	LAI	05 NA48	$E_\gamma^* > 30 \text{ MeV}, \theta_{e\gamma}^* > 20^\circ$
0.908±0.008 ^{+0.013} _{-0.012}	15k	ALAVI-HARATI	01J KTEV	$E_\gamma^* \geq 30 \text{ MeV}, \theta_{e\gamma}^* \geq 20^\circ$
0.934±0.036 ^{+0.055} _{-0.039}	1384	LEBER	96 NA31	$E_\gamma^* \geq 30 \text{ MeV}, \theta_{e\gamma}^* \geq 20^\circ$

WEIGHTED AVERAGE
0.935±0.015 (Error scaled by 1.9)



¹Direct emission contribution measured (χ) = $-2.3 \pm 1.3 \pm 1.4$.

²Also measured cut $E_\gamma^* > 10 \text{ MeV}, \theta_{e\gamma}^* > 0^\circ$ 14221 evts: $\Gamma(\pi^\pm e^\mp \nu_e \gamma) / \Gamma(\pi^\pm e^\mp \nu_e) = (4.942 \pm 0.062)\%$.

$\Gamma(\pi^\pm \mu^\mp \nu_\mu \gamma)/\Gamma(\pi^\pm \mu^\mp \nu_\mu)$ Γ_{11}/Γ_2

VALUE (units 10 ⁻³)	EVTS	DOCUMENT ID	TECN	COMMENT
2.09±0.08 OUR AVERAGE				
2.09±0.09		¹ ALEXOPOU...	05 KTEV	$E_\gamma^* > 30 \text{ MeV}$
2.08±0.17 ^{+0.16} _{-0.21}	252	BENDER	98 NA48	$E_\gamma^* \geq 30 \text{ MeV}$

¹Also measured cut $E_\gamma^* > 10 \text{ MeV}$, 1385 evts: $\Gamma(\pi^\pm \mu^\mp \nu_\mu \gamma) / \Gamma(\pi^\pm \mu^\mp \nu_\mu) = (0.530 \pm 0.014 \pm 0.012)\%$.

Hadronic modes with photons or $\ell\bar{\ell}$ pairs

$\Gamma(\pi^0\pi^0\gamma)/\Gamma_{total}$ Γ_{12}/Γ

VALUE (units 10^{-6})	CL%	DOCUMENT ID	TECN	COMMENT
< 0.243	90	ABOUZAID	08B KTEV	$K_L^0 \rightarrow \pi^0\pi^0\gamma, \pi_D^0 \rightarrow e\bar{e}\gamma$
••• We do not use the following data for averages, fits, limits, etc. •••				
< 5.6	90	BARR	94 NA31	
<230	90	ROBERTS	94 E799	

$\Gamma(\pi^+\pi^-\gamma)/\Gamma(\pi^+\pi^-\pi^0)$ Γ_{13}/Γ_7

For earlier limits see our 1992 edition Physical Review **D45** S1 (1992).

VALUE (units 10^{-4})	EVTS	DOCUMENT ID	TECN	COMMENT
••• We do not use the following data for averages, fits, limits, etc. •••				
1.23±0.13	516	1,2 CARROLL	80B SPEC	$E_\gamma^* > 20$ MeV
2.33±0.23	546	1,3 CARROLL	80B SPEC	
3.56±0.26	1062	1,4 CARROLL	80B SPEC	$E_\gamma^* > 20$ MeV

¹ CARROLL 80B quotes $B(\pi^+\pi^-\gamma)$ using normalization $B(\pi^+\pi^-\pi^0) = 0.1239$. We divide by this value to obtain their measured $\Gamma(\pi^+\pi^-\gamma) / \Gamma(\pi^+\pi^-\pi^0)$.
² Internal Bremsstrahlung component only.
³ Direct γ emission component only.
⁴ Both IB and DE components.

$\Gamma(\pi^+\pi^-\gamma)/\Gamma(\pi^+\pi^-)$ Γ_{13}/Γ_8

VALUE (units 10^{-2})	EVTS	DOCUMENT ID	TECN	COMMENT
2.11±0.08 OUR FIT				Error includes scale factor of 2.9.
2.11±0.08 OUR AVERAGE				Error includes scale factor of 2.9.
2.08±0.02±0.02	8669	1 ALAVI-HARATI 01B	KTEV	$E_\gamma^* > 20$ MeV
2.30±0.07	3136	RAMBERG	93 E731	$E_\gamma^* > 20$ MeV

¹ ALAVI-HARATI 01B includes both Direct Emission (DE) and Inner Bremsstrahlung (IB) processes.

$\Gamma(\pi^+\pi^-\gamma(DE))/\Gamma(\pi^+\pi^-)$ Γ_{14}/Γ_{13}

These values assume that $\Gamma(K_L^0 \rightarrow \pi^+\pi^-\gamma) = \Gamma(K_L^0 \rightarrow \pi^+\pi^-\gamma(DE)) + \Gamma(K_L^0 \rightarrow \pi^+\pi^-\gamma(IB))$, the sum of widths for the direct emission (DE) and inner bremsstrahlung (IB) processes, with no IB-DE interference. DE assumes a form factor as described in RAMBERG 93.

VALUE	EVTS	DOCUMENT ID	TECN	COMMENT
0.684±0.009 OUR FIT				
0.684±0.009 OUR AVERAGE				
0.689±0.021	111k	ABOUZAID	06A KTEV	$E_\gamma^* > 20$ MeV
0.683±0.011	8669	ALAVI-HARATI 01B	KTEV	$E_\gamma^* > 20$ MeV
0.685±0.041	3136	RAMBERG	93 E731	$E_\gamma^* > 20$ MeV

$\Gamma(\pi^0 2\gamma)/\Gamma_{total}$ Γ_{15}/Γ

VALUE (units 10^{-6})	CL%	EVTS	DOCUMENT ID	TECN	COMMENT
1.273±0.033 OUR AVERAGE					
1.28 ± 0.06 ± 0.01	1.4k	1 ABOUZAID	08 KTEV		
1.27 ± 0.04 ± 0.01	2.5k	2 LAI	02b NA48		
••• We do not use the following data for averages, fits, limits, etc. •••					
1.68 ± 0.07 ± 0.08	884	3 ALAVI-HARATI 99b	KTEV		
1.7 ± 0.2 ± 0.2	63	4 BARR	92 NA31		
1.86 ± 0.60 ± 0.60	60	PAPADIMITR...91	E731	$m_{\gamma\gamma} > 280$ MeV	
<5.1	90	PAPADIMITR...91	E731	$m_{\gamma\gamma} < 264$ MeV	
2.1 ± 0.6	14	5 BARR	90c NA31	$m_{\gamma\gamma} > 280$ MeV	

¹ ABOUZAID 08 reports $(1.29 \pm 0.03 \pm 0.05) \times 10^{-6}$ from a measurement of $[\Gamma(K_L^0 \rightarrow \pi^0 2\gamma)/\Gamma_{total}] / [B(K_L^0 \rightarrow \pi^0\pi^0)]$ assuming $B(K_L^0 \rightarrow \pi^0\pi^0) = (8.69 \pm 0.04) \times 10^{-4}$, which we rescale to our best value $B(K_L^0 \rightarrow \pi^0\pi^0) = (8.64 \pm 0.06) \times 10^{-4}$. Our first error is their experiment's error and our second error is the systematic error from using our best value.
² LAI 02b reports $[\Gamma(K_L^0 \rightarrow \pi^0 2\gamma)/\Gamma_{total}] / [B(K_L^0 \rightarrow \pi^0\pi^0)] = (1.467 \pm 0.032 \pm 0.032) \times 10^{-3}$ which we multiply by our best value $B(K_L^0 \rightarrow \pi^0\pi^0) = (8.64 \pm 0.06) \times 10^{-4}$. Our first error is their experiment's error and our second error is the systematic error from using our best value. They also find that $B(\pi^0 2\gamma, m_{\gamma\gamma} < 110$ MeV) $< 0.6 \times 10^{-8}$ (90% CL).
³ ALAVI-HARATI 99b finds that $\Gamma(\pi^0 2\gamma, m_{\gamma\gamma} < 240$ MeV) / $\Gamma(\pi^0 2\gamma) = (17.3 \pm 1.3 \pm 1.5)\%$. Superseded by ABOUZAID 08.
⁴ BARR 92 find that $\Gamma(\pi^0 2\gamma, m_{\gamma\gamma} < 240$ MeV) / $\Gamma(\pi^0 2\gamma) < 0.09$ (90% CL).
⁵ BARR 90c superseded by BARR 92.

$\Gamma(\pi^0\gamma e^+e^-)/\Gamma_{total}$ Γ_{16}/Γ

VALUE (units 10^{-8})	CL%	EVTS	DOCUMENT ID	TECN
1.62±0.14±0.09		125	1 ABOUZAID	07D KTEV
••• We do not use the following data for averages, fits, limits, etc. •••				
2.34±0.35±0.13	44		ALAVI-HARATI 01E	KTEV
<71	90	0	MURAKAMI	99 SPEC

¹ ABOUZAID 07D includes 1997 (ALAVI-HARATI 01E) and 1999 data. It measures the ratio of $B(K_L^0 \rightarrow \pi^0\gamma e^+e^-) / B(K_L^0 \rightarrow \pi^0\pi_D^0)$, where π_D^0 is the Dalitz decaying π^0 , and uses PDG 06 values $B(K_L^0 \rightarrow \pi^0\pi^0) = (8.69 \pm 0.04) \times 10^{-4}$, and $B(\pi_D^0 \rightarrow e^+e^-) = (1.198 \pm 0.032) \times 10^{-2}$. Supersedes ALAVI-HARATI 01E result.

Other modes with photons or $\ell\bar{\ell}$ pairs

$\Gamma(2\gamma)/\Gamma_{total}$ Γ_{17}/Γ

VALUE (units 10^{-4})	EVTS	DOCUMENT ID	TECN	COMMENT
5.47±0.04 OUR FIT				Error includes scale factor of 1.1.
••• We do not use the following data for averages, fits, limits, etc. •••				
4.54±0.84		1 BANNER	72B OSPK	
4.5 ± 1.0	23	ENSTROM	71 OSPK	K_L^0 1.5–9 GeV/c
5.0 ± 1.0		2 REPELLIN	71 OSPK	
5.5 ± 1.1	90	KUNZ	68 OSPK	Norm. to $3\pi(C+N)$

¹ This value uses $(\eta_{00}/\eta_{+-})^2 = 1.05 \pm 0.14$. In general, $\Gamma(2\gamma)/\Gamma_{total} = [(4.32 \pm 0.55) \times 10^{-4}] / [(\eta_{00}/\eta_{+-})^2]$.
² Assumes regeneration amplitude in copper at 2 GeV is 22 mb. To evaluate for a given regeneration amplitude and error, multiply by (regeneration amplitude/22mb)².

$\Gamma(2\gamma)/\Gamma(3\pi^0)$ Γ_{17}/Γ_6

VALUE (units 10^{-3})	EVTS	DOCUMENT ID	TECN	COMMENT
2.802±0.017 OUR FIT				
2.802±0.018 OUR AVERAGE				
2.79 ± 0.02 ± 0.02	27k	ADINOLFI	03 KLOE	
2.81 ± 0.01 ± 0.02		LAI	03 NA48	
••• We do not use the following data for averages, fits, limits, etc. •••				
2.13 ± 0.43	28	BARMIN	71 HLBC	
2.24 ± 0.28	115	BANNER	69 OSPK	
2.5 ± 0.7	16	ARNOLD	68B HLBC	Vacuum decay

$\Gamma(2\gamma)/\Gamma(\pi^0\pi^0)$ Γ_{17}/Γ_9

VALUE	EVTS	DOCUMENT ID	TECN
0.633±0.006 OUR FIT			
Error includes scale factor of 1.4.			
0.632±0.004±0.008	110k	BURKHARDT	87 NA31

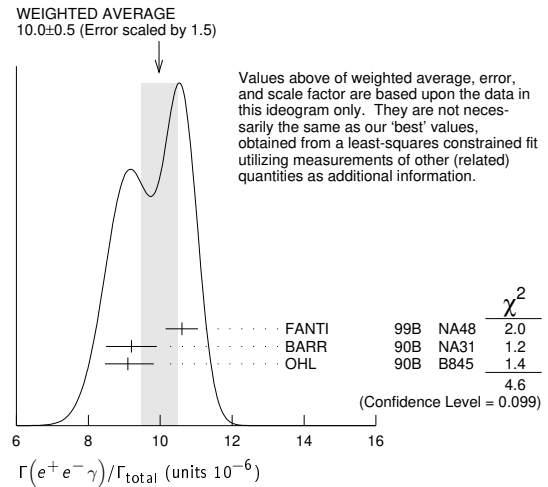
$\Gamma(3\gamma)/\Gamma_{total}$ Γ_{18}/Γ

VALUE	CL%	DOCUMENT ID	TECN
<7.4 × 10 ⁻⁸	90	1 TUNG	11 K391
••• We do not use the following data for averages, fits, limits, etc. •••			
<2.4 × 10 ⁻⁷	90	2 BARR	95c NA31

¹ TUNG 11 reports the result assuming parity violating interaction and using 2005 data (Run-II and III). Assuming parity conserving or phase space interaction, the 90% upper limits obtained are 7.5×10^{-8} and 8.6×10^{-8} , respectively.
² Assumes a phase-space decay distribution.

$\Gamma(e^+e^-)/\Gamma_{total}$ Γ_{19}/Γ

VALUE (units 10^{-6})	EVTS	DOCUMENT ID	TECN
9.4±0.4 OUR FIT			
Error includes scale factor of 2.0.			
10.0±0.5 OUR AVERAGE			
Error includes scale factor of 1.5. See the ideogram below.			
10.6±0.2±0.4	6864	1 FANTI	99B NA48
9.2±0.5±0.5	1053	BARR	90B NA31
9.1±0.4 ^{+0.6} _{-0.5}	919	OHL	90B B845



¹ For FANTI 99b, the ±0.4 systematic error includes for uncertainties in the calculation, primarily uncertainties in the $\pi^0 \rightarrow e^+e^-$ and $K_L^0 \rightarrow \pi^0\pi^0$ branching ratios, evaluated using our 1999 Web edition values.

$\Gamma(e^+e^-)/\Gamma(3\pi^0)$ Γ_{19}/Γ_6

VALUE (units 10^{-5})	EVTS	DOCUMENT ID	TECN
4.82±0.21 OUR FIT			
Error includes scale factor of 2.0.			
4.63±0.04±0.13	83k	1 ABOUZAID	07B KTEV

¹ ABOUZAID 07B reports $[\Gamma(K_L^0 \rightarrow e^+e^-)/\Gamma(K_L^0 \rightarrow 3\pi^0)] / [3\Gamma(\pi^0 \rightarrow 2\gamma)/\Gamma_{total} \times \Gamma(\pi^0 \rightarrow e^+e^-)/\Gamma_{total}] = (1.3302 \pm 0.0046 \pm 0.0103) \times 10^{-3}$ which we multiply by our best value $3\Gamma(\pi^0 \rightarrow 2\gamma)/\Gamma_{total} \times \Gamma(\pi^0 \rightarrow e^+e^-)/\Gamma_{total} = 0.0348 \pm 0.0010$. Our first error is their experiment's error and our second error is the systematic error from using our best value.

Meson Particle Listings

K_L^0

$\Gamma(\mu^+ \mu^- \gamma)/\Gamma_{\text{total}}$ Γ_{20}/Γ

Test for $\Delta S = 1$ weak neutral current. Allowed by higher-order electroweak interaction.

VALUE (units 10^{-7})	EVTS	DOCUMENT ID	TECN
3.59 ± 0.11 OUR AVERAGE	Error	includes scale factor of 1.3.	
3.62 ± 0.04 ± 0.08	9100	ALAVI-HARATI01G	KTEV
3.4 ± 0.6 ± 0.4	45	FANTI	97 NA48
3.23 ± 0.23 ± 0.19	197	SPENCER	95 E799

$\Gamma(e^+ e^- \gamma \gamma)/\Gamma_{\text{total}}$ Γ_{21}/Γ

Test for $\Delta S = 1$ weak neutral current. Allowed by higher-order electroweak interaction.

VALUE (units 10^{-7})	EVTS	DOCUMENT ID	TECN	COMMENT
5.95 ± 0.33 OUR AVERAGE				
5.84 ± 0.15 ± 0.32	1543	ALAVI-HARATI01F	KTEV	$E_\gamma^* > 5$ MeV
8.0 ± 1.5 ± 1.4	40	SETZU	98 NA31	$E_\gamma^* > 5$ MeV
6.5 ± 1.2 ± 0.6	58	NAKAYA	94 E799	$E_\gamma^* > 5$ MeV
6.6 ± 3.2		MORSE	92 B845	$E_\gamma^* > 5$ MeV

$\Gamma(\mu^+ \mu^- \gamma \gamma)/\Gamma_{\text{total}}$ Γ_{22}/Γ

Test for $\Delta S = 1$ weak neutral current. Allowed by higher-order electroweak interaction.

VALUE (units 10^{-3})	EVTS	DOCUMENT ID	TECN	COMMENT
10.4 ± 7.5 ± 0.7	4	ALAVI-HARATI00E	KTEV	$m_{\gamma\gamma} \geq 1$ MeV/ c^2

Charge conjugation × Parity (CP) or Lepton Family number (LF) violating modes, or $\Delta S = 1$ weak neutral current (SI) modes

$\Gamma(\mu^+ \mu^-)/\Gamma(\pi^+ \pi^-)$ Γ_{23}/Γ_8

Test for $\Delta S = 1$ weak neutral current. Allowed by higher-order electroweak interaction.

VALUE (units 10^{-6})	EVTS	DOCUMENT ID	TECN	COMMENT
3.48 ± 0.05 OUR AVERAGE				
3.474 ± 0.057	6210	AMBROSE	00 B871	
3.87 ± 0.30	179	¹ AKAGI	95 SPEC	
3.38 ± 0.17	707	HEINSON	95 B791	
3.9 ± 0.3 ± 0.1	178	² AKAGI	91B SPEC	ln AKAGI 95
3.45 ± 0.18 ± 0.13	368	³ HEINSON	91 SPEC	ln HEINSON 95
4.1 ± 0.5	54	INAGAKI	89 SPEC	ln AKAGI 91B
2.8 ± 0.3 ± 0.2	87	MATHIAZHA...89B	SPEC	ln HEINSON 91

••• We do not use the following data for averages, fits, limits, etc. ••••

¹AKAGI 95 gives this number multiplied by the PDG 1992 average for $\Gamma(K_L^0 \rightarrow \pi^+ \pi^-)/\Gamma(\text{total})$.

²AKAGI 91B give this number multiplied by the 1990 PDG average for $\Gamma(K_L^0 \rightarrow \pi^+ \pi^-)/\Gamma(\text{total})$.

³HEINSON 91 give $\Gamma(K_L^0 \rightarrow \mu\mu)/\Gamma_{\text{total}}$. We divide out the $\Gamma(K_L^0 \rightarrow \pi^+ \pi^-)/\Gamma_{\text{total}}$ PDG average which they used.

$\Gamma(e^+ e^-)/\Gamma_{\text{total}}$ Γ_{24}/Γ

Test for $\Delta S = 1$ weak neutral current. Allowed by higher-order electroweak interaction.

VALUE (units 10^{-10})	CL%	EVTS	DOCUMENT ID	TECN
0.087 ± 0.057 - 0.041		4	AMBROSE	98 B871
<1.6	90	1	AKAGI	95 SPEC
<0.41	90	0	¹ ARISAKA	93B B791

¹ARISAKA 93B includes all events with <6 MeV radiated energy.

$\Gamma(\pi^+ \pi^- e^+ e^-)/\Gamma_{\text{total}}$ Γ_{25}/Γ

Test for $\Delta S = 1$ weak neutral current. Allowed by higher-order electroweak interaction.

VALUE (units 10^{-7})	CL%	EVTS	DOCUMENT ID	TECN	COMMENT
3.11 ± 0.19 OUR AVERAGE					
3.08 ± 0.09 ± 0.18	1125	¹ LAI	03c	NA48	
3.2 ± 0.6 ± 0.4	37	ADAMS	98	KTEV	
4.4 ± 1.3 ± 0.5	13	TAKEUCHI	98	SPEC	
<4.6	90	NOMURA	97	SPEC	$m_{ee} > 4$ MeV

••• We do not use the following data for averages, fits, limits, etc. ••••

¹LAI 03c second error is 0.15(syst) ± 0.10(norm) combined in quadrature. The normalization uses $BR(K_L^0 \rightarrow \pi^+ \pi^- \pi^0) * BR(\pi^0 \rightarrow e^+ e^-) = (1.505 \pm 0.047) \times 10^{-3}$ from our 2000 Edition.

$\Gamma(\pi^0 \pi^0 e^+ e^-)/\Gamma_{\text{total}}$ Γ_{26}/Γ

Test for $\Delta S = 1$ weak neutral current. Allowed by higher-order electroweak interaction.

VALUE (units 10^{-3})	CL%	EVTS	DOCUMENT ID	TECN
<6.6	90	1	ALAVI-HARATI02c	E799

$\Gamma(\pi^0 \pi^0 \mu^+ \mu^-)/\Gamma_{\text{total}}$ Γ_{27}/Γ

Test for $\Delta S = 1$ weak neutral current. Allowed by higher-order electroweak interaction.

VALUE	CL%	DOCUMENT ID	TECN
<9.2 × 10⁻¹¹	90	¹ ABOUZAID	11A E799

¹ABOUZAID 11A also reports $B(K_L^0 \rightarrow \pi^0 \pi^0 X^0 \rightarrow \pi^0 \pi^0 \mu^+ \mu^-) < 1.0 \times 10^{-10}$ at 90% C.L., where the X^0 is a possible new neutral boson that was reported by PARK 05 with a mass of 214.3 ± 0.5 MeV/ c^2 .

$\Gamma(\mu^+ \mu^- e^+ e^-)/\Gamma_{\text{total}}$ Γ_{28}/Γ

Test for $\Delta S = 1$ weak neutral current. Allowed by higher-order electroweak interaction.

VALUE (units 10^{-3})	CL%	EVTS	DOCUMENT ID	TECN	COMMENT
2.69 ± 0.27 OUR AVERAGE					
2.69 ± 0.24 ± 0.12	131	¹ ALAVI-HARATI03B	KTEV		
2.9 ± 6.7 - 2.4	1	GU	96	E799	

••• We do not use the following data for averages, fits, limits, etc. ••••

2.62 ± 0.40 ± 0.17 43 ALAVI-HARATI01H KTEV Sup. by ALAVI-HARATI 03B

<4900 90 BALATS 83 SPEC

¹ALAVI-HARATI 03B also measures the linear slope $\alpha = -1.59 \pm 0.37$.

$\Gamma(e^+ e^- e^+ e^-)/\Gamma_{\text{total}}$ Γ_{29}/Γ

Test for $\Delta S = 1$ weak neutral current. Allowed by higher-order electroweak interaction.

VALUE (units 10^{-8})	EVTS	DOCUMENT ID	TECN	COMMENT
3.56 ± 0.21 OUR AVERAGE				
3.30 ± 0.24 ± 0.25	200	¹ LAI	05B	NA48
3.72 ± 0.18 ± 0.23	441	ALAVI-HARATI01D	KTEV	
3.96 ± 0.78 ± 0.32	27	GU	94	E799
3.07 ± 1.25 ± 0.26	6	VAGINS	93	B845

••• We do not use the following data for averages, fits, limits, etc. ••••

6 ± 2 ± 1 18 ²AKAGI 95 SPEC $m_{ee} > 470$ MeV

7 ± 3 ± 2 6 ²AKAGI 95 SPEC $m_{ee} > 470$ MeV

10.4 ± 3.7 ± 1.1 8 ³BARR 95 NA31

6 ± 2 ± 1 18 AKAGI 93 CNTR Sup. by AKAGI 95

4 ± 3 2 BARR 91 NA31 Sup. by BARR 95

¹LAI 05B uses 1998 and 1999 data. Data are normalized to the observed events of $K_L^0 \rightarrow \pi^+ \pi^- \pi^0$ (π^0 into Dalitz pair) and PDG 04 values are used for $B(K_L^0 \rightarrow \pi^+ \pi^- \pi^0)$ and $B(\pi^0 \rightarrow e^+ e^- \gamma)$. The systematic error includes a normalization error of ±0.10.

²Values are for the total branching fraction, acceptance-corrected for the m_{ee} cuts shown.

³Distribution of angles between two $e^+ e^-$ pair planes favors $CP = -1$ for K_L^0 .

$\Gamma(\pi^0 \mu^+ \mu^-)/\Gamma_{\text{total}}$ Γ_{30}/Γ

Violates CP in leading order. Test for $\Delta S = 1$ weak neutral current. Allowed by higher-order electroweak interaction.

VALUE (units 10^{-3})	CL%	EVTS	DOCUMENT ID	TECN
<0.38	90		ALAVI-HARATI00D	KTEV
<5.1	90	0	HARRIS	93 E799

$\Gamma(\pi^0 e^+ e^-)/\Gamma_{\text{total}}$ Γ_{31}/Γ

Violates CP in leading order. Direct and indirect CP-violating contributions are expected to be comparable and to dominate the CP-conserving part. LAI 02B result suggests that CP-violation effects dominate. Test for $\Delta S = 1$ weak neutral current. Allowed by higher-order electroweak interaction.

VALUE (units 10^{-10})	CL%	EVTS	DOCUMENT ID	TECN	COMMENT
< 2.8	90		¹ ALAVI-HARATI04A	KTEV	combined result
< 3.5	90		ALAVI-HARATI04A	KTEV	
0.0047 ± 0.0022 - 0.0018			² LAI	02B	NA48 CP-conserving part
< 5.1	90	2	ALAVI-HARATI01	KTEV	
0.01 to 0.02			ALAVI-HARATI99B	KTEV	CP-conserving part
< 43	90	0	HARRIS	93B	E799
< 75	90	0	BARKER	90	E731
< 55	90	0	OHL	90	B845
< 400	90		BARR	88	NA31
<3200	90		JASTRZEM...	88	SPEC

¹Combined result of ALAVI-HARATI 04A 1999-2000 data set and ALAVI-HARATI 01 1997 data set.

²LAI 02B uses the absence of a signal in $K_L^0 \rightarrow \pi^0 \gamma \gamma$ with $m(\gamma\gamma) < m(\pi^0)$ and their a_V value to predict this value.

$\Gamma(\pi^0 \nu \bar{\nu})/\Gamma_{\text{total}}$ Γ_{32}/Γ

Violates CP in leading order. Test of direct CP violation since the indirect CP-violating and CP-conserving contributions are expected to be suppressed. Test of $\Delta S = 1$ weak neutral current.

VALUE (units 10^{-8})	CL%	DOCUMENT ID	TECN
< 0.49	90	¹ AHN	21 KOTO
< 0.30	90	² AHN	19 KOTO
< 5.1	90	³ AHN	17 KOTO
< 2.6	90	⁴ AHN	10 K391
< 6.7	90	⁵ AHN	08 K391
<21	90	⁶ AHN	06 K391
<59	90	ALAVI-HARATI00	KTEV

••• We do not use the following data for averages, fits, limits, etc. ••••

¹AHN 21 result is based on data collected in 2016, 2017 and 2018, which corresponds to 3.05×10^{19} protons on target. A single event sensitivity of $(7.20 \pm 0.05 \pm 0.66) \times 10^{-10}$ was achieved with 3 candidate events observed and total 1.22 ± 0.26 background events.

²AHN 19 result is based on data collected in 2015, which corresponds to 2.2×10^{19} protons on target. A single event sensitivity of $(1.30 \pm 0.01 \pm 0.14) \times 10^{-9}$ was achieved with no candidate events observed. An upper limit of $< 2.4 \times 10^{-9}$ at the 90% C.L. for the $K_L^0 \rightarrow \pi^0 X^0$ decay was also set, where X^0 is an invisible particle with a mass of 135 MeV/ c^2 .

See key on page 1127

Meson Particle Listings

K_L^0

³AHN 17 result is based on the first 100 hours of physics running in 2013. One candidate event was observed with an expected background of 0.34 ± 0.16 events. An upper limit of $< 3.7 \times 10^{-8}$ at the 90% C.L. for the $K_L^0 \rightarrow \pi^0 X^0$ decay was also set, where X^0 is an invisible particle with a mass of 135 MeV/c².

⁴Obtained combining Run-2 (AHN 08) and Run-3 data.

⁵Value obtained using data from February to April 2005.

⁶Value obtained analyzing 10% of data of RUN 1 (performed in 2004).

$\Gamma(\pi^0 \pi^0 \nu \bar{\nu})/\Gamma_{total}$ Γ_{33}/Γ

VALUE	CL%	DOCUMENT ID	TECN
<8.1 × 10⁻⁷	90	¹ OGATA	11 K391

• • • We do not use the following data for averages, fits, limits, etc. • • •

<4.7 × 10 ⁻⁵	90	² NIX	07 K391
-------------------------	----	------------------	---------

¹Using 2005 Run-I data. OGATA 11 also sets a limit on the $K_L^0 \rightarrow \pi^0 \pi^0 X^0 \rightarrow$ invisible particles process: the limit on the branching fraction varied from 7.0×10^{-7} to 4.0×10^{-5} for the mass of X ranging from 50 to 200 MeV/c².

²Observed 1 event with expected background of 0.43 ± 0.35 events. NIX 07 also measured $B(K_L^0 \rightarrow \pi^0 \pi^0 P) < 1.2 \times 10^{-6}$ at 90% CL, where P is the pseudoscalar particle and $m_P < 100$ MeV.

$\Gamma(e^\pm \mu^\mp)/\Gamma_{total}$ Γ_{34}/Γ

Test of lepton family number conservation.

VALUE (units 10 ⁻¹¹)	CL%	EVTS	DOCUMENT ID	TECN
<0.47	90		AMBROSE	98B B871

• • • We do not use the following data for averages, fits, limits, etc. • • •

<9.4	90	0	AKAGI	95 SPEC
<3.9	90	0	ARISAKA	93 B791
<3.3	90	0	¹ ARISAKA	93 B791

¹This is the combined result of ARISAKA 93 and MATHIAZHAGAN 89.

$\Gamma(e^\pm e^\pm \mu^\mp \mu^\mp)/\Gamma_{total}$ Γ_{35}/Γ

Test of lepton family number conservation.

VALUE (units 10 ⁻¹¹)	CL%	EVTS	DOCUMENT ID	TECN	COMMENT
< 4.12	90	0	ALAVI-HARATI03B	KTEV	

• • • We do not use the following data for averages, fits, limits, etc. • • •

< 12.3	90	0	¹ ALAVI-HARATI01H	KTEV	Sup. by ALAVI-HARATI 03B
<610	90	0	¹ GU	96 E799	

¹Assuming uniform phase space distribution.

$\Gamma(\pi^0 \mu^\pm e^\mp)/\Gamma_{total}$ Γ_{36}/Γ

Test of lepton family number conservation.

VALUE (units 10 ⁻¹⁰)	CL%	DOCUMENT ID	TECN
< 0.76	90	ABOUZAID	08c KTEV

• • • We do not use the following data for averages, fits, limits, etc. • • •

<62	90	ARISAKA	98 E799
-----	----	---------	---------

$\Gamma(\pi^0 \pi^0 \mu^\pm e^\mp)/\Gamma_{total}$ Γ_{37}/Γ

Test of lepton family number conservation.

VALUE (units 10 ⁻¹⁰)	CL%	DOCUMENT ID	TECN
<1.7	90	ABOUZAID	08c KTEV

Lorentz invariance violating modes

$\Gamma(\pi^0 \gamma)/\Gamma_{total}$ Γ_{38}/Γ

VALUE	CL%	DOCUMENT ID	TECN
<1.7 × 10⁻⁷	90	¹ SHIMIZU	20 KOTO

¹SHIMIZU 20 uses data collected from 2016 to 2018 at the J-PARC KOTO experiment. The single event sensitivity is $(7.1 \pm 0.3 \pm 1.6) \times 10^{-8}$. No candidate event was observed.

See the related review(s):

V_{ud}, V_{us} the Cabibbo Angle, and CKM Unitarity

ENERGY DEPENDENCE OF K_L^0 DALITZ PLOT

For discussion, see note on Dalitz plot parameters in the K^\pm section of the Particle Listings above. For definitions of $a_U, a_T, a_{U'},$ and $a_{U''}$, see the earlier version of the same note in the 1982 edition of this Review published in Physics Letters **111B** 70 (1982).

$$|\text{matrix element}|^2 = 1 + gu + hu^2 + jv + kv^2 + fuv$$

$$\text{where } u = (s_3 - s_0) / m_\pi^2 \text{ and } v = (s_2 - s_1) / m_\pi^2$$

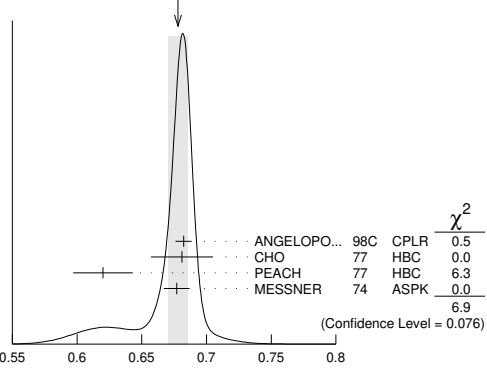
LINEAR COEFFICIENT g FOR $K_L^0 \rightarrow \pi^+ \pi^- \pi^0$

VALUE	EVTS	DOCUMENT ID	TECN	COMMENT
0.678 ± 0.008 OUR AVERAGE				Error includes scale factor of 1.5. See the ideogram below.
0.6823 ± 0.0044 ± 0.0044	500k	ANGELOPO...	98c CPLR	
0.681 ± 0.024	6499	CHO	77 HBC	
0.620 ± 0.023	4709	PEACH	77 HBC	
0.677 ± 0.010	509k	MESSNER	74 ASPK	$a_Y = -0.917 \pm 0.013$

• • • We do not use the following data for averages, fits, limits, etc. • • •

0.69 ± 0.07	192	¹ BALDO...	75 HLBC
0.590 ± 0.022	56k	¹ BUCHANAN	75 SPEC $a_U = -0.277 \pm 0.010$
0.619 ± 0.027	20k	^{1,2} BISI	74 ASPK $a_T = -0.282 \pm 0.011$
0.612 ± 0.032		¹ ALEXANDER	73B HBC
0.73 ± 0.04	3200	¹ BRANDENB...	73 HBC
0.608 ± 0.043	1486	¹ KRENZ	72 HLBC $a_T = -0.277 \pm 0.018$
0.650 ± 0.012	29k	¹ ALBROW	70 ASPK $a_Y = -0.858 \pm 0.015$
0.593 ± 0.022	36k	^{1,3} BUCHANAN	70 SPEC $a_U = -0.278 \pm 0.010$
0.664 ± 0.056	4400	¹ SMITH	70 OSPK $a_T = -0.306 \pm 0.024$
0.400 ± 0.045	2446	¹ BASILE	68B OSPK $a_T = -0.188 \pm 0.020$
0.649 ± 0.044	1350	¹ HOPKINS	67 HBC $a_T = -0.294 \pm 0.018$
0.428 ± 0.055	1198	¹ NEFKENS	67 OSPK $a_U = -0.204 \pm 0.025$

WEIGHTED AVERAGE
0.678±0.008 (Error scaled by 1.5)



Linear coeff. g for $K_L^0 \rightarrow \pi^+ \pi^- \pi^0$ matrix element squared

¹Quadratic dependence required by some experiments. (See sections on "QUADRATIC COEFFICIENT h " and "QUADRATIC COEFFICIENT k " below.) Correlations prevent us from averaging results of fits not including $g, h,$ and k terms.

²BISI 74 value comes from quadratic fit with quad. term consistent with zero. g error is thus larger than if linear fit were used.

³BUCHANAN 70 result revised by BUCHANAN 75 to include radiative correlations and to use more reliable K_L^0 momentum spectrum of second experiment (had same beam).

QUADRATIC COEFFICIENT h FOR $K_L^0 \rightarrow \pi^+ \pi^- \pi^0$

See notes in section "LINEAR COEFFICIENT g FOR $K_L^0 \rightarrow \pi^+ \pi^- \pi^0$ [MATRIX ELEMENT]²" above.

VALUE	EVTS	DOCUMENT ID	TECN
0.076 ± 0.006 OUR AVERAGE			
0.061 ± 0.004 ± 0.015	500k	ANGELOPO...	98c CPLR
0.095 ± 0.032	6499	CHO	77 HBC
0.048 ± 0.036	4709	PEACH	77 HBC
0.079 ± 0.007	509k	MESSNER	74 ASPK

• • • We do not use the following data for averages, fits, limits, etc. • • •

-0.011 ± 0.018	29k	¹ ALBROW	70 ASPK
0.043 ± 0.052	4400	¹ SMITH	70 OSPK

¹Quadratic coefficients h and k required by some experiments. (See section on "QUADRATIC COEFFICIENT k " below.) Correlations prevent us from averaging results of fits not including $g, h,$ and k terms.

QUADRATIC COEFFICIENT k FOR $K_L^0 \rightarrow \pi^+ \pi^- \pi^0$

VALUE	EVTS	DOCUMENT ID	TECN
0.0099 ± 0.0015 OUR AVERAGE			
0.0104 ± 0.0017 ± 0.0024	500k	ANGELOPO...	98c CPLR
0.024 ± 0.010	6499	CHO	77 HBC
-0.008 ± 0.012	4709	PEACH	77 HBC
0.0097 ± 0.0018	509k	MESSNER	74 ASPK

LINEAR COEFFICIENT j FOR $K_L^0 \rightarrow \pi^+ \pi^- \pi^0$ (CP-VIOLATING TERM)

Listed in CP-violation section below.

QUADRATIC COEFFICIENT f FOR $K_L^0 \rightarrow \pi^+ \pi^- \pi^0$ (CP-VIOLATING TERM)

Listed in CP-violation section below.

QUADRATIC COEFFICIENT h FOR $K_L^0 \rightarrow \pi^0 \pi^0 \pi^0$

We do not average measurements that do not account for the effect of final state rescattering.

VALUE (units 10 ⁻³)	EVTS	DOCUMENT ID	TECN
+0.59 ± 0.20 ± 1.16	68M	¹ ABOUZAID	08A KTEV

• • • We do not use the following data for averages, fits, limits, etc. • • •

-6.1 ± 0.9 ± 0.5	14.7M	² LAI	01B NA48
-3.3 ± 1.1 ± 0.7	5M	^{2,3} SOMALWAR	92 E731

¹Result obtained using CI3pl model of CABIBBO 05 to include $\pi\pi$ rescattering effects. The systematic error includes an external error of 1.06×10^{-3} from the parametrization input of $(a_0 - a_2) m_{\pi^+} = 0.268 \pm 0.017$ from BATLEY 06B.

Meson Particle Listings

K_L^0

²LAI 01B and SOMALWAR 92 results do not include $\pi\pi$ final state rescattering effects.
³SOMALWAR 92 chose m_{π^+} as normalization to make it compatible with the Particle Data Group $K_L^0 \rightarrow \pi^+\pi^-\pi^0$ definitions.

K_L^0 FORM FACTORS

For discussion, see note on form factors in the K^\pm section of the Particle Listings above.

In the form factor comments, the following symbols are used.

- f_+ and f_- are form factors for the vector matrix element.
- f_S and f_T refer to the scalar and tensor term.
- $f_0(t) = f_+(t) + f_-(t) t / (m_{K^0}^2 - m_{\pi^+}^2)$.
- $t =$ momentum transfer to the π .
- λ_+ and λ_0 are the linear expansion coefficients of f_+ and f_0 :
- $f_+(t) = f_+(0) (1 + \lambda_+ t / m_{\pi^+}^2)$

For quadratic expansion

$$f_+(t) = f_+(0) (1 + \lambda'_+ t / m_{\pi^+}^2 + \frac{\lambda''_+}{2} t^2 / m_{\pi^+}^4)$$

as used by KTeV. If there is a non-vanishing quadratic term, then λ_+ represents an average slope, which is then different from λ'_+ .

NA48 (K_{e3}) and ISTR A quadratic expansion coefficients are converted with $\lambda'_+ PDG = \lambda_+ NA48$ and $\lambda''_+ PDG = 2 \lambda'_+ NA48$

$$\lambda'_+ PDG = (\frac{m_{\pi^+}}{m_{K^0}})^2 \lambda_+ ISTR A \text{ and}$$

$$\lambda''_+ PDG = 2 (\frac{m_{\pi^+}}{m_{K^0}})^4 \lambda'_+ ISTR A$$

ISTR A linear expansion coefficients are converted with $\lambda_+ PDG = (\frac{m_{\pi^+}}{m_{K^0}})^2 \lambda_+ ISTR A$ and $\lambda_0 PDG = (\frac{m_{\pi^+}}{m_{K^0}})^2 \lambda_0 ISTR A$

The pole parametrization is

$$f_+(t) = f_+(0) (\frac{M_V^2}{M_V^2 - t})$$

$$f_0(t) = f_0(0) (\frac{M_S^2}{M_S^2 - t})$$

where M_V and M_S are the vector and scalar pole masses.

The dispersive parametrization is

$$f_+(t) = f_+(0) \exp[\frac{t}{m_{\pi^+}^2} (\Lambda_+ + H(t))];$$

$$f_0(t) = f_0(0) \exp[\frac{t}{m_K^2 - m_{\pi^+}^2} (\ln[C] - G(t))],$$

where Λ_+ is the slope parameter and $\ln[C] = \ln[f_0(m_K^2 - m_{\pi^+}^2)]$

is the logarithm of the scalar form factor at the Callan-Treiman point.

$H(t)$ and $G(t)$ are dispersive integrals.

The following abbreviations are used:

- DP = Dalitz plot analysis.
- PI = π spectrum analysis.
- MU = μ spectrum analysis.
- POL = μ polarization analysis.
- BR = $K_{\mu 3}^0 / K_{e 3}^0$ branching ratio analysis.
- E = positron or electron spectrum analysis.
- RC = radiative corrections.

λ_+ (LINEAR ENERGY DEPENDENCE OF f_+ IN $K_{e 3}^0$ DECAY)

For radiative correction of $K_{e 3}^0$ DP, see GINSBERG 67, BECHERRAWY 70, CIRIGLIANO 02, CIRIGLIANO 04, and ANDRE 07. Results labeled OUR FIT are discussed in the review " $K_{e 3}^0$ and $K_{\mu 3}^0$ Form Factors" in the K^\pm Listings. For earlier, lower statistics results, see the 2004 edition of this review, Physics Letters **B592** 1 (2004).

VALUE (units 10^{-2})	EVTS	DOCUMENT ID	TECN	COMMENT
2.82 ± 0.04 OUR FIT				Error includes scale factor of 1.1. Assuming μ -e universality
2.85 ± 0.04 OUR AVERAGE				
2.86 ± 0.05 ± 0.04	2M	AMBROSINO 06D	KLOE	
2.832 ± 0.037 ± 0.043	1.9M	ALEXOPOU... 04A	KTEV	PI, no $\mu = e$
2.88 ± 0.04 ± 0.11	5.6M	¹ LAI 04C	NA48	DP
• • • We do not use the following data for averages, fits, limits, etc. • • •				
2.84 ± 0.07 ± 0.13	5.6M	² LAI 04C	NA48	DP
2.45 ± 0.12 ± 0.22	366k	APOSTOLA... 00	CPLR	DP
3.06 ± 0.34	74k	BIRULEV 81	SPEC	DP
3.12 ± 0.25	500k	GJESDAL 76	SPEC	DP
2.70 ± 0.28	25k	BLUMENTHAL 75	SPEC	DP

¹ Results from linear fit and assuming only vector and axial couplings.
² Results from linear fit with $|f_S/f_+|$ and $|f_T/f_+|$ free.

λ_+ (LINEAR ENERGY DEPENDENCE OF f_+ IN $K_{\mu 3}^0$ DECAY)

Results labeled OUR FIT are discussed in the review " $K_{e 3}^0$ and $K_{\mu 3}^0$ Form Factors" in the K^\pm Listings. For earlier, lower statistics results, see the 2004 edition of this review, Physics Letters **B592** 1 (2004).

VALUE (units 10^{-2})	EVTS	DOCUMENT ID	TECN	COMMENT
2.82 ± 0.04 OUR FIT				Error includes scale factor of 1.1. Assuming μ -e universality
2.71 ± 0.10 OUR FIT				Error includes scale factor of 1.4. Not assuming μ -e universality

2.67 ± 0.06 ± 0.08	2.3M	¹ LAI 07A	NA48	DP
2.745 ± 0.088 ± 0.063	1.5M	ALEXOPOU... 04A	KTEV	DP, no $\mu = e$
2.813 ± 0.051	3.4M	ALEXOPOU... 04A	KTEV	PI, DP, $\mu = e$
3.0 ± 0.3	1.6M	DONALDSON 74B	SPEC	DP
• • • We do not use the following data for averages, fits, limits, etc. • • •				
4.27 ± 0.44	150k	BIRULEV 81	SPEC	DP

¹ LAI 07A gives a correlation -0.40 between their λ_0 and λ_+ measurements.

λ_0 (LINEAR ENERGY DEPENDENCE OF f_0 IN $K_{\mu 3}^0$ DECAY)

Wherever possible, we have converted the above values of $\xi(0)$ into values of λ_0 using the associated λ'_+ and $d\xi(0)/d\lambda_+$. Results labeled OUR FIT are discussed in the review " $K_{e 3}^0$ and $K_{\mu 3}^0$ Form Factors" in the K^\pm Listings. For earlier, lower statistics results, see the 2004 edition of this review, Physics Letters **B592** 1 (2004).

VALUE (units 10^{-2})	$d\lambda_0/d\lambda_+$	EVTS	DOCUMENT ID	TECN	COMMENT
1.38 ± 0.18 OUR FIT					Error includes scale factor of 2.2. Assuming μ -e universality
1.42 ± 0.23 OUR FIT					Error includes scale factor of 2.8. Not assuming μ -e universality
1.17 ± 0.07 ± 0.10		2.3M	¹ LAI 07A	NA48	DP
1.657 ± 0.125	-0.44	1.5M	² ALEXOPOU... 04A	KTEV	DP, no $\mu = e$
1.635 ± 0.121	-0.85	3.4M	³ ALEXOPOU... 04A	KTEV	PI, DP, $\mu = e$
+1.9 ± 0.4	-0.47	1.6M	⁴ DONALDSON 74B	SPEC	DP
• • • We do not use the following data for averages, fits, limits, etc. • • •					
3.41 ± 0.67	unknown	150k	⁵ BIRULEV 81	SPEC	DP

¹ LAI 07A gives a correlation -0.40 between their λ_0 and λ_+ measurements.

² ALEXOPOULOS 04A gives a correlation -0.38 between their λ_0 and λ_+ measurements.

³ ALEXOPOULOS 04A gives a correlation -0.36 between their λ_0 and λ_+ measurements.

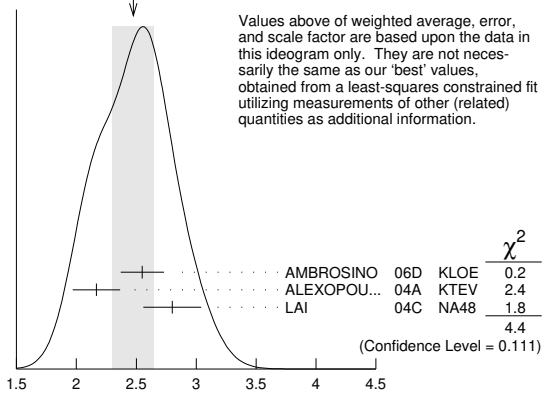
⁴ DONALDSON 74B $d\lambda_0/d\lambda_+$ obtained from figure 18.

⁵ BIRULEV 81 gives $d\lambda_0/d\lambda_+ = -1.5$, giving an unreasonably narrow error ellipse which dominates all other results. We use $d\lambda_0/d\lambda_+ = 0$.

λ'_+ (LINEAR $K_{e 3}^0$ FORM FACTOR FROM QUADRATIC FIT)

VALUE (units 10^{-2})	EVTS	DOCUMENT ID	TECN	COMMENT
2.40 ± 0.12 OUR FIT				Error includes scale factor of 1.2. Assuming μ -e universality
2.49 ± 0.13 OUR FIT				Error includes scale factor of 1.1. Not assuming μ -e universality
2.48 ± 0.17 OUR AVERAGE				Error includes scale factor of 1.5. See the ideogram below.
2.55 ± 0.15 ± 0.10	2M	¹ AMBROSINO 06D	KLOE	
2.167 ± 0.137 ± 0.143	1.9M	² ALEXOPOU... 04A	KTEV	PI, no $\mu = e$
2.80 ± 0.19 ± 0.15	5.6M	³ LAI 04C	NA48	DP

WEIGHTED AVERAGE
 2.48±0.17 (Error scaled by 1.5)



λ'_+ (LINEAR $K_{e 3}^0$ FORM FACTOR FROM QUADRATIC FIT) (units 10^{-2})

¹ We use AMBROSINO 06D result in the fit not assuming μ -e universality. This result enters the fit assuming μ -e universality via AMBROSINO 07C measurement of λ'_+ in $K_{\mu 3}$ decays. AMBROSINO 06D gives a correlation -0.95 between their λ'_+ and λ''_+ .
² ALEXOPOULOS 04A gives a correlation -0.97 between their λ'_+ and λ''_+ .
³ For LAI 04C we calculate a correlation -0.88 between their λ'_+ and λ''_+ . /LINEAR00

λ''_+ (QUADRATIC $K_{e 3}^0$ FORM FACTOR)

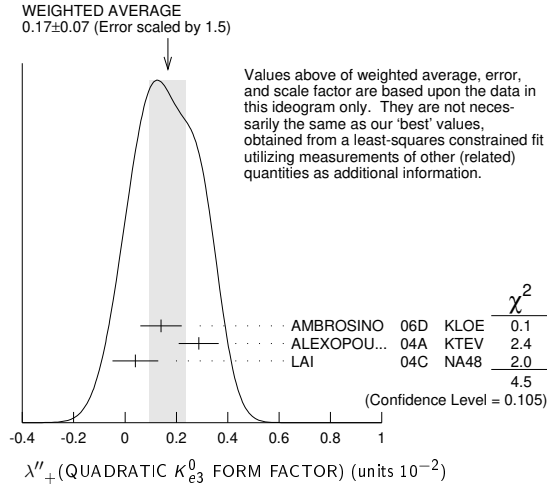
VALUE (units 10^{-2})	EVTS	DOCUMENT ID	TECN	COMMENT
0.20 ± 0.05 OUR FIT				Error includes scale factor of 1.2. Assuming μ -e universality
0.16 ± 0.05 OUR FIT				Error includes scale factor of 1.1. Not assuming μ -e universality
0.17 ± 0.07 OUR AVERAGE				Error includes scale factor of 1.5. See the ideogram below.
0.14 ± 0.07 ± 0.04	2M	¹ AMBROSINO 06D	KLOE	
0.287 ± 0.057 ± 0.053	1.9M	² ALEXOPOU... 04A	KTEV	PI, no $\mu = e$
0.04 ± 0.08 ± 0.04	5.6M	^{3,4} LAI 04C	NA48	DP

¹ We use AMBROSINO 06D result in the fit not assuming μ -e universality. This result enters the fit assuming μ -e universality via AMBROSINO 07C measurement of λ'_+ in $K_{\mu 3}$ decays. AMBROSINO 06D gives a correlation -0.95 between their λ'_+ and λ''_+ .

² ALEXOPOULOS 04A gives a correlation -0.97 between their λ'_+ and λ''_+ .

³ Values doubled to agree with PDG conventions described above.

⁴ LAI 04c gives a correlation -0.88 between their χ'_{+} and χ''_{+} .



χ'_{+} (LINEAR $K_{\mu 3}^0$ FORM FACTOR FROM QUADRATIC FIT)

VALUE (units 10^{-2})	EVTS	DOCUMENT ID	TECN	COMMENT
2.40 ± 0.12 OUR FIT				Error includes scale factor of 1.2. Assuming μ -e universality
1.89 ± 0.24 OUR FIT				Not assuming μ -e universality
2.23 ± 0.98 ± 0.37	1.8M	¹ AMBROSINO 07c	KLOE	no $\mu = e$
2.56 ± 0.15 ± 0.09	3.8M	¹ AMBROSINO 07c	KLOE	$\mu = e$
2.05 ± 0.22 ± 0.24	2.3M	¹ LAI 07A	NA48	DP
1.703 ± 0.319 ± 0.177	1.5M	¹ ALEXOPOULOS 04A	KTEV	DP, no $\mu = e$
2.064 ± 0.175	3.4M	¹ ALEXOPOULOS 04A	KTEV	PI, DP, $\mu = e$

¹ See section λ_0 below for correlations.

χ''_{+} (QUADRATIC $K_{\mu 3}^0$ FORM FACTOR)

VALUE (units 10^{-2})	EVTS	DOCUMENT ID	TECN	COMMENT
0.20 ± 0.05 OUR FIT				Error includes scale factor of 1.2. Assuming μ -e universality
0.37 ± 0.12 OUR FIT				Error includes scale factor of 1.3. Not assuming μ -e universality
0.48 ± 0.49 ± 0.16	1.8M	¹ AMBROSINO 07c	KLOE	no $\mu = e$
0.15 ± 0.07 ± 0.04	3.8M	¹ AMBROSINO 07c	KLOE	$\mu = e$
0.26 ± 0.09 ± 0.10	2.3M	¹ LAI 07A	NA48	DP
0.443 ± 0.131 ± 0.072	1.5M	¹ ALEXOPOULOS 04A	KTEV	DP, no $\mu = e$
0.320 ± 0.069	3.4M	¹ ALEXOPOULOS 04A	KTEV	PI, DP, $\mu = e$

¹ See section λ_0 below for correlations.

λ_0 (LINEAR $f_0 K_{\mu 3}^0$ FORM FACTOR FROM QUADRATIC FIT)

VALUE (units 10^{-2})	EVTS	DOCUMENT ID	TECN	COMMENT
1.16 ± 0.09 OUR FIT				Error includes scale factor of 1.2. Assuming μ -e universality
1.07 ± 0.14 OUR FIT				Error includes scale factor of 1.3. Not assuming μ -e universality
0.91 ± 0.59 ± 0.26	1.8M	¹ AMBROSINO 07c	KLOE	no $\mu = e$
1.54 ± 0.18 ± 0.13	3.8M	² AMBROSINO 07c	KLOE	$\mu = e$
0.95 ± 0.11 ± 0.08	2.3M	³ LAI 07A	NA48	DP
1.281 ± 0.136 ± 0.122	1.5M	⁴ ALEXOPOULOS 04A	KTEV	DP, no $\mu = e$
1.372 ± 0.131	3.4M	⁵ ALEXOPOULOS 04A	KTEV	PI, DP, $\mu = e$

¹ AMBROSINO 07c, not assuming μ -e universality, gives a correlation matrix

$$\begin{matrix} \chi'_{+} & \chi''_{+} \\ \chi''_{+} & -0.97 & 1 \\ \lambda_0 & 0.81 & -0.91 & 1 \end{matrix}$$

² AMBROSINO 07c, assuming μ -e universality, gives a correlation matrix

$$\begin{matrix} \chi'_{+} & \chi''_{+} \\ \chi''_{+} & -0.95 & 1 \\ \lambda_0 & 0.29 & -0.38 & 1 \end{matrix}$$

³ LAI 07A gives a correlation matrix

$$\begin{matrix} \chi'_{+} & \chi''_{+} \\ \chi''_{+} & -0.96 & 1 \\ \lambda_0 & 0.63 & -0.73 & 1 \end{matrix}$$

⁴ ALEXOPOULOS 04A, not assuming μ -e universality, gives a correlation matrix

$$\begin{matrix} \chi'_{+} & \chi''_{+} & \lambda_0 \\ \chi''_{+} & -0.96 & 1 \\ \lambda_0 & 0.65 & -0.75 & 1 \end{matrix}$$

⁵ ALEXOPOULOS 04A, assuming μ -e universality, gives a correlation matrix

$$\begin{matrix} \chi'_{+} & \chi''_{+} & \lambda_0 \\ \chi''_{+} & -0.97 & 1 \\ \lambda_0 & 0.34 & -0.44 & 1 \end{matrix}$$

M_V^e (POLE MASS FOR K_{e3}^0 DECAY)

VALUE (MeV)	EVTS	DOCUMENT ID	TECN	COMMENT
878 ± 6 OUR FIT				Error includes scale factor of 1.1. Assuming μ -e universality
875 ± 5 OUR AVERAGE				
870 ± 6 ± 7	2M	AMBROSINO 06D	KLOE	
881.03 ± 5.12 ± 4.94	1.9M	ALEXOPOULOS 04A	KTEV	PI, no $\mu = e$
859 ± 18	5.6M	LAI 04C	NA48	

M_V^μ (POLE MASS FOR $K_{\mu 3}^0$ DECAY)

VALUE (MeV)	EVTS	DOCUMENT ID	TECN	COMMENT
878 ± 6 OUR FIT				Error includes scale factor of 1.1. Assuming μ -e universality
900 ± 21 OUR FIT				Error includes scale factor of 1.7. Not assuming μ -e universality
905 ± 9 ± 17	2.3M	¹ LAI 07A	NA48	DP
889.19 ± 12.81 ± 9.92	1.5M	¹ ALEXOPOULOS 04A	KTEV	DP, no $\mu = e$
882.32 ± 6.54	3.4M	¹ ALEXOPOULOS 04A	KTEV	PI, DP, $\mu = e$

¹ See section M_S^μ below for correlations.

M_S^μ (POLE MASS FOR $K_{\mu 3}^0$ DECAY)

VALUE (MeV)	EVTS	DOCUMENT ID	TECN	COMMENT
1252 ± 90 OUR FIT				Error includes scale factor of 2.6. Assuming μ -e universality
1222 ± 80 OUR FIT				Error includes scale factor of 2.3. Not assuming μ -e universality
1400 ± 46 ± 53	2.3M	¹ LAI 07A	NA48	DP
1167.14 ± 28.30 ± 31.04	1.5M	² ALEXOPOULOS 04A	KTEV	PI, no $\mu = e$
1173.80 ± 39.47	3.4M	³ ALEXOPOULOS 04A	KTEV	PI, DP, $\mu = e$

¹ LAI 07A gives a correlation -0.47 between their M_S^μ and M_V^μ measurements, not assuming μ -e universality.

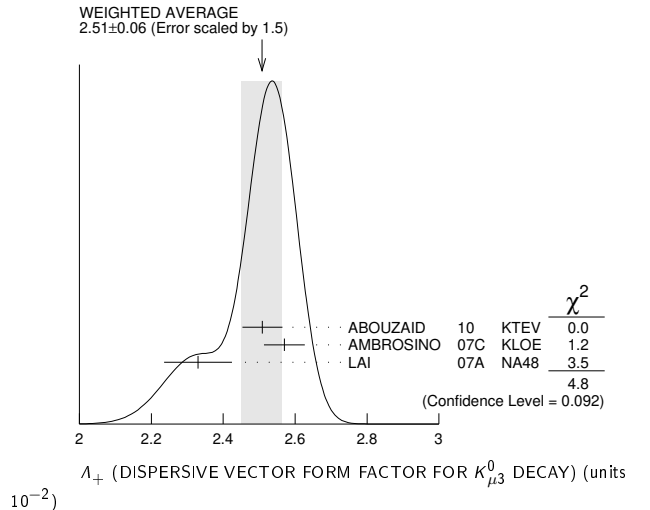
² ALEXOPOULOS 04A gives a correlation -0.46 between their M_S^μ and M_V^μ and measurements, not assuming μ -e universality.

³ ALEXOPOULOS 04A gives a correlation -0.40 between their M_S^μ and M_V^μ and measurements, assuming μ -e universality.

A_{+} (DISPERSIVE VECTOR FORM FACTOR FOR $K_{\mu 3}^0$ DECAY)

See the review on " $K_{\mu 3}^{\pm}$ and $K_{\ell 3}^0$ Form Factors" for details of the dispersive parametrization.

VALUE (units 10^{-2})	EVTS	DOCUMENT ID	TECN	COMMENT
2.51 ± 0.06 OUR AVERAGE				Error includes scale factor of 1.5. See the ideogram below.
2.509 ± 0.035 ± 0.043	3.4M	¹ ABOUZAID 10	KTEV	$\mu = e$
2.57 ± 0.04 ± 0.04	3.8M	² AMBROSINO 07c	KLOE	$\mu = e$
2.33 ± 0.05 ± 0.08	2.3M	³ LAI 07A	NA48	DP



¹ Obtained from a sample of 1.9 M K_{e3} and 1.5 M $K_{\mu 3}$. The correlation between A_{+} and $\ln(C)$ is -0.269 .

² AMBROSINO 07c results include 2M K_{e3} events from AMBROSINO 06d. The correlation between A_{+} and $\ln(C)$ is -0.26 .

³ LAI 07A gives a correlation -0.44 between their A_{+} and $\ln(C)$ measurements.

$\ln(C)$ (DISPERSIVE SCALAR FORM FACTOR FOR $K_{\mu 3}^0$ DECAY)

See the review on " $K_{\mu 3}^{\pm}$ and $K_{\ell 3}^0$ Form Factors" for details of the dispersive parametrization.

VALUE (units 10^{-1})	EVTS	DOCUMENT ID	TECN	COMMENT
1.75 ± 0.18 OUR AVERAGE				Error includes scale factor of 2.0. See the ideogram below.
1.915 ± 0.078 ± 0.094	3.4M	¹ ABOUZAID 10	KTEV	$\mu = e$
2.04 ± 0.19 ± 0.15	3.8M	² AMBROSINO 07c	KLOE	$\mu = e$
1.438 ± 0.080 ± 0.112	2.3M	³ LAI 07A	NA48	DP

¹ Obtained from a sample of 1.9 M K_{e3} and 1.5 M $K_{\mu 3}$. The correlation between A_{+} and $\ln(C)$ is -0.269 .

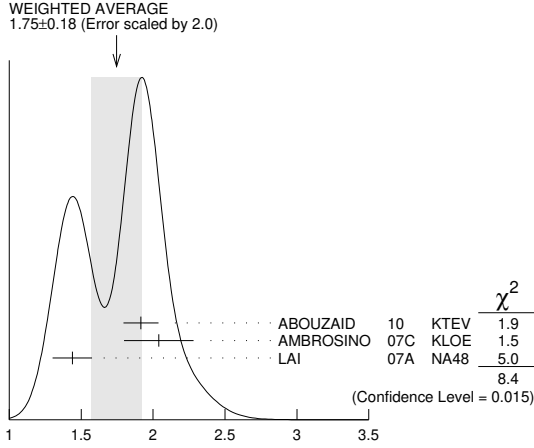
² AMBROSINO 07c results include 2M K_{e3} events from AMBROSINO 06d. We convert (A_{+}, A_0) to $(A_{+}, \ln(C))$ parametrization using $\ln(C) = (A_0 \cdot 11.713 + 0.0398) \pm 0.0041$,

Meson Particle Listings

K_L^0

where the error is due to theory parametrization of the form factor. The correlation between Λ_+ and $\ln(C)$ is -0.26 .

³LAI 07A gives a correlation -0.44 between their Λ_+ and $\ln(C)$ measurements.



$\ln(C)$ (DISPERSIVE SCALAR FORM FACTOR FOR K_L^0 DECAY) (units 10^{-1})

$a_1(t_0, Q^2)$ FORM FACTOR PARAMETER

See HILL 06 for a definition of this parameter.

VALUE	EVTS	DOCUMENT ID	TECN
$1.023 \pm 0.028 \pm 0.029$	2M	¹ ABOUZAID 06c	KTEV

¹ $Q^2 = 2 \text{ GeV}^2$, $t_0 = 0.49 (m_K - m_\pi)^2$. Correlation between a_1 and a_2 : $\rho_{12} = -0.064$.

$a_2(t_0, Q^2)$ FORM FACTOR PARAMETER

See HILL 06 for a definition of this parameter.

VALUE	EVTS	DOCUMENT ID	TECN
$0.75 \pm 1.58 \pm 1.47$	2M	¹ ABOUZAID 06c	KTEV

¹ $Q^2 = 2 \text{ GeV}^2$, $t_0 = 0.49 (m_K - m_\pi)^2$. Correlation between a_1 and a_2 : $\rho_{12} = -0.064$.

$|f_S/f_+|$ FOR K_{e3}^0 DECAY

Ratio of scalar to f_+ couplings.

VALUE (units 10^{-2})	CL%	EVTS	DOCUMENT ID	TECN	COMMENT
1.5 ± 0.7 -1.0 ± 1.2		5.6M	¹ LAI	04c	NA48

• • • We do not use the following data for averages, fits, limits, etc. • • •

<9.5	95	18k	HILL	78	STRC	
<7.	68	48k	BIRULEV	76	SPEC	See also BIRULEV 81
<4.	68	25k	BLUMENTHAL75		SPEC	

¹Results from linear fit with $|f_S/f_+|$ and $|f_T/f_+|$ free.

$|f_T/f_+|$ FOR K_{e3}^0 DECAY

Ratio of tensor to f_+ couplings.

VALUE (units 10^{-2})	CL%	EVTS	DOCUMENT ID	TECN	COMMENT
5 ± 3 -4 ± 3		5.6M	¹ LAI	04c	NA48

• • • We do not use the following data for averages, fits, limits, etc. • • •

<40.	95	18k	HILL	78	STRC	
<34.	68	48k	BIRULEV	76	SPEC	See also BIRULEV 81
<23.	68	25k	BLUMENTHAL75		SPEC	

¹Results from linear fit with $|f_S/f_+|$ and $|f_T/f_+|$ free.

$|f_T/f_+|$ FOR $K_{\mu 3}^0$ DECAY

Ratio of tensor to f_+ couplings.

VALUE (units 10^{-2})	DOCUMENT ID	TECN
12 ± 12	BIRULEV 81	SPEC

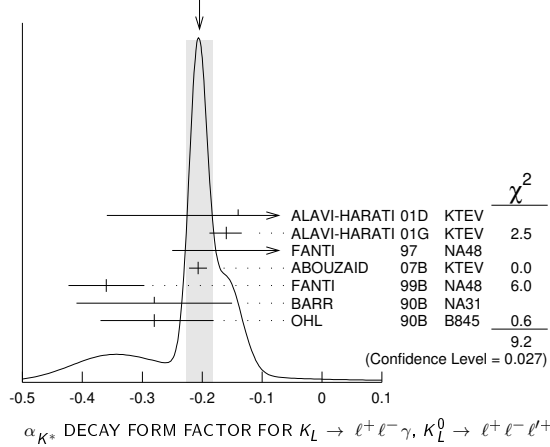
α_{K^*} DECAY FORM FACTOR FOR $K_L \rightarrow \ell^+ \ell^- \gamma$, $K_L^0 \rightarrow \ell^+ \ell^- \ell'^+ \ell'^-$

Average of all α_{K^*} measurements (from each of three datablocks following this one) assuming lepton universality.

VALUE	DOCUMENT ID
-0.205 ± 0.022 OUR AVERAGE	

Includes data from the 3 datablocks that follow this one. Error includes scale factor of 1.8. See the ideogram below.

WEIGHTED AVERAGE
 -0.205 ± 0.022 (Error scaled by 1.8)



α_{K^*} DECAY FORM FACTOR FOR $K_L \rightarrow e^+ e^- \gamma$

α_{K^*} is the constant in the model of BERGSTROM 83 which measures the relative strength of the vector-vector transition $K_L \rightarrow K^* \gamma$ with $K^* \rightarrow \rho, \omega, \phi \rightarrow \gamma^*$ and the pseudoscalar-pseudoscalar transition $K_L \rightarrow \pi, \eta, \eta' \rightarrow \gamma \gamma^*$.

VALUE	EVTS	DOCUMENT ID	TECN
The data in this block is included in the average printed for a previous datablock.			

-0.217 ± 0.034 OUR AVERAGE Error includes scale factor of 2.4.

$-0.207 \pm 0.012 \pm 0.009$	83k	¹ ABOUZAID 07b	KTEV
$-0.36 \pm 0.06 \pm 0.02$	6864	FANTI 99b	NA48
-0.28 ± 0.13		BARR 90b	NA31
-0.280 ± 0.099		OHL 90b	B845
-0.090			

¹ABOUZAID 07b measures $C \cdot \alpha_{K^*} = -0.517 \pm 0.030 \pm 0.022$. We assume $C = 2.5$, as in all other measurements.

α_{K^*} DECAY FORM FACTOR FOR $K_L \rightarrow \mu^+ \mu^- \gamma$

α_{K^*} is the constant in the model of BERGSTROM 83 described in the previous section.

VALUE	EVTS	DOCUMENT ID	TECN
The data in this block is included in the average printed for a previous datablock.			

-0.158 ± 0.027 OUR AVERAGE

-0.160 ± 0.026 -0.028	9100	ALAVI-HARATI 01G	KTEV
-0.04 ± 0.24 -0.21		FANTI 97	NA48

$\alpha_{K^*}^{\text{eff}}$ DECAY FORM FACTOR FOR $K_L \rightarrow e^+ e^- e^+ e^-$

$\alpha_{K^*}^{\text{eff}}$ is the parameter describing the relative strength of an intermediate pseudoscalar decay amplitude and a vector meson decay amplitude in the model of BERGSTROM 83. It takes into account both the radiative effects and the form factor. Since there are two $e^+ e^-$ pairs here compared with one in $e^+ e^- \gamma$ decays, a factorized expression is used for the $e^+ e^- e^+ e^-$ decay form factor.

VALUE	EVTS	DOCUMENT ID	TECN
The data in this block is included in the average printed for a previous datablock.			

$-0.14 \pm 0.16 \pm 0.15$ 441 ALAVI-HARATI 01D KTEV

α_{DIP} DECAY FORM FACTOR FOR $K_L^0 \rightarrow \ell^+ \ell^- \gamma$, $K_L^0 \rightarrow \ell^+ \ell^- \ell'^+ \ell'^-$

Average of all α_{DIP} measurements (from each of three datablocks following this one) assuming lepton universality.

VALUE	DOCUMENT ID
-1.69 ± 0.08 OUR AVERAGE	

Includes data from the 3 datablocks that follow this one. Error includes scale factor of 1.7.

α_{DIP} DECAY FORM FACTOR FOR $K_L^0 \rightarrow e^+ e^- \gamma$

α_{DIP} parameter in $K_L^0 \rightarrow \gamma^* \gamma^*$ form factor by DAMBROSIO 98, motivated by vector meson dominance and a proper short distance behavior.

VALUE	EVTS	DOCUMENT ID	TECN
The data in this block is included in the average printed for a previous datablock.			

$-1.729 \pm 0.043 \pm 0.028$ 83k ABOUZAID 07b KTEV

α_{DIP} DECAY FORM FACTOR FOR $K_L^0 \rightarrow \mu^+ \mu^- \gamma$

α_{DIP} is a constant in the model of DAMBROSIO 98 described in the previous section.

VALUE	EVTS	DOCUMENT ID	TECN
The data in this block is included in the average printed for a previous datablock.			

-1.54 ± 0.10 9100 ALAVI-HARATI 01G KTEV

α_{DIP} DECAY FORM FACTOR FOR $K_L^0 \rightarrow e^+ e^- \mu^+ \mu^-$

α_{DIP} is a constant in the model of DAMBROSIO 98 described in the previous section.

VALUE	EVTS	DOCUMENT ID	TECN
The data in this block is included in the average printed for a previous datablock.			

-1.59 ± 0.37 131 ALAVI-HARATI 03B KTEV

a_1/a_2 FORM FACTOR FOR M_1 DIRECT EMISSION AMPLITUDEForm factor = $\tilde{g}_{M1} \left[1 + \frac{a_1/a_2}{(M_{\tilde{P}}^2 - M_K^2) + 2M_K E_{\tilde{\gamma}}} \right]$ as described in ALAVI-HARATI 00b.

VALUE (GeV ²)	EVTS	DOCUMENT ID	TECN	COMMENT
-0.737 ± 0.014 OUR AVERAGE				
-0.744 ± 0.027 ± 0.032	5241	¹ ABOUZAID 06	KTEV	$\pi^+ \pi^- e^+ e^-$
-0.738 ± 0.007 ± 0.018	111k	² ABOUZAID 06A	KTEV	$\pi^+ \pi^+ \gamma$
-0.81 ± 0.07 ± 0.02		³ LAI 03c	NA48	$\pi^+ \pi^- e^+ e^-$
-0.737 ± 0.026 ± 0.022		⁴ ALAVI-HARATI01B		$\pi^+ \pi^- \gamma$
-0.720 ± 0.028 ± 0.009	1766	⁵ ALAVI-HARATI00B	KTEV	$\pi^+ \pi^- e^+ e^-$

¹ ABOUZAID 06 also measured $|\tilde{g}_{M1}| = 1.11 \pm 0.14$.² ABOUZAID 06A also measured $|\tilde{g}_{M1}| = 1.198 \pm 0.035 \pm 0.086$.³ LAI 03c also measured $\tilde{g}_{M1} = 0.99^{+0.28}_{-0.27} \pm 0.07$.⁴ ALAVI-HARATI 01B fit gives $\chi^2/\text{DOF} = 38.8/27$. Linear and quadratic fits give $\chi^2/\text{DOF} = 43.2/27$ and $37.6/26$ respectively.⁵ ALAVI-HARATI 00B also measured $|\tilde{g}_{M1}| = 1.35^{+0.20}_{-0.17} \pm 0.04$. **$\tilde{\tau}_S$ DECAY FORM FACTOR FOR $K_L^0 \rightarrow \pi^\pm \pi^0 e^\mp \nu_e$**

VALUE	DOCUMENT ID	TECN
0.049 ± 0.011 OUR AVERAGE		
0.052 ± 0.006 ± 0.002	BATLEY 04	NA48
0.010 ± 0.016 ± 0.017	MAKOFF 93	E731

Error includes scale factor of 1.7.

 $\tilde{\tau}_P$ DECAY FORM FACTOR FOR $K_L^0 \rightarrow \pi^\pm \pi^0 e^\mp \nu_e$

VALUE	DOCUMENT ID	TECN
-0.052 ± 0.012 OUR AVERAGE		
-0.051 ± 0.011 ± 0.005	BATLEY 04	NA48
-0.079 ± 0.049 ± 0.022	MAKOFF 93	E731

 λ_g DECAY FORM FACTOR FOR $K_L^0 \rightarrow \pi^\pm \pi^0 e^\mp \nu_e$

VALUE	DOCUMENT ID	TECN
0.085 ± 0.020 OUR AVERAGE		
0.087 ± 0.019 ± 0.006	BATLEY 04	NA48
0.014 ± 0.087 ± 0.070	MAKOFF 93	E731

 $\tilde{\eta}$ DECAY FORM FACTOR FOR $K_L^0 \rightarrow \pi^\pm \pi^0 e^\mp \nu_e$

VALUE	DOCUMENT ID	TECN
-0.30 ± 0.13 OUR AVERAGE		
-0.32 ± 0.12 ± 0.07	BATLEY 04	NA48
-0.07 ± 0.31 ± 0.31	MAKOFF 93	E731

 L_3 CHIRAL PERT. THEO. PARAM. FOR $K_L^0 \rightarrow \pi^\pm \pi^0 e^\mp \nu_e$

VALUE (units 10 ⁻³)	DOCUMENT ID	TECN
-3.96 ± 0.28 OUR AVERAGE		
-4.1 ± 0.2	BATLEY 04	NA48
-3.4 ± 0.4	¹ MAKOFF 93	E731

¹ MAKOFF 93 sign has been changed to negative to agree with the sign convention used in BATLEY 04. **a_V , VECTOR MESON EXCHANGE CONTRIBUTION**

VALUE	EVTS	DOCUMENT ID	TECN	COMMENT
-0.43 ± 0.06 OUR AVERAGE				
-0.31 ± 0.05 ± 0.07	1.4k	¹ ABOUZAID 08	KTEV	
-0.46 ± 0.03 ± 0.04		LAI 02B	NA48	$K_L^0 \rightarrow \pi^0 2\gamma$
-0.67 ± 0.21 ± 0.12		ALAVI-HARATI01E	KTEV	$K_L^0 \rightarrow \pi^0 e^+ e^- \gamma$
• • • We do not use the following data for averages, fits, limits, etc. • • •				
-0.72 ± 0.05 ± 0.06		² ALAVI-HARATI99B	KTEV	$K_L^0 \rightarrow \pi^0 2\gamma$

¹ Using KTeV dataset collected in 1996, 1997, and 1999.² Superseded by ABOUZAID 08.

See the related review(s):

[CP Violation in \$K_L^0\$ Decays](#)**CP-VIOLATION PARAMETERS IN K_L^0 DECAYS****CHARGE ASYMMETRY IN K_{L3}^0 DECAYS**Such asymmetry violates CP. It is related to $\text{Re}(\epsilon)$. **A_L = weighted average of $A_L(\mu)$ and $A_L(e)$** In previous editions and in the literature the symbol used for this asymmetry was δ_L or δ . We use A_L for consistency with B^0 asymmetry notation and with recent K_S^0 notation.

VALUE (%)	EVTS	DOCUMENT ID	TECN	COMMENT
0.332 ± 0.006 OUR AVERAGE				
0.333 ± 0.050	33M	WILLIAMS 73	ASPK	$K_{\mu 3} + K_{e 3}$

Includes data from the 2 datablocks that follow this one.

 $A_L(\mu) = [\Gamma(\pi^- \mu^+ \nu_\mu) - \Gamma(\pi^+ \mu^- \bar{\nu}_\mu)]/\text{SUM}$

Only the combined value below is put into the Meson Summary Table.

VALUE (%)	EVTS	DOCUMENT ID	TECN
0.304 ± 0.025 OUR AVERAGE			
0.313 ± 0.029	15M	GEWENIGER 74	ASPK
0.278 ± 0.051	7.7M	PICCONI 72	ASPK

0.304 ± 0.025 OUR AVERAGE0.313 ± 0.029 15M GEWENIGER 74 ASPK
0.278 ± 0.051 7.7M PICCONI 72 ASPK

• • • We do not use the following data for averages, fits, limits, etc. • • •

0.60 ± 0.14 4.1M MCCARTHY 73 CNTR
0.57 ± 0.17 1M ¹ PACIOTTI 69 OSPK
0.403 ± 0.134 1M ¹ DORFAN 67 OSPK¹ PACIOTTI 69 is a reanalysis of DORFAN 67 and is corrected for $\mu^+ \mu^-$ range difference in MCCARTHY 72. **$A_L(e) = [\Gamma(\pi^- e^+ \nu_e) - \Gamma(\pi^+ e^- \bar{\nu}_e)]/\text{SUM}$**

Only the combined value below is put into the Meson Summary Table.

VALUE (%)	EVTS	DOCUMENT ID	TECN
0.334 ± 0.007 OUR AVERAGE			
0.3322 ± 0.0058 ± 0.0047	298M	ALAVI-HARATI02	
0.341 ± 0.018	34M	GEWENIGER 74	ASPK
0.318 ± 0.038	40M	FITCH 73	ASPK
0.346 ± 0.033	10M	MARX 70	CNTR

0.334 ± 0.007 OUR AVERAGE

0.3322 ± 0.0058 ± 0.0047 298M ALAVI-HARATI02

0.341 ± 0.018 34M GEWENIGER 74 ASPK

0.318 ± 0.038 40M FITCH 73 ASPK

0.346 ± 0.033 10M MARX 70 CNTR

• • • We do not use the following data for averages, fits, limits, etc. • • •

0.36 ± 0.18 600k ASHFORD 72 ASPK

0.246 ± 0.059 10M ¹ SAAL 69 CNTR0.224 ± 0.036 10M ¹ BENNETT 67 CNTR¹ SAAL 69 is a reanalysis of BENNETT 67.**PARAMETERS FOR $K_L^0 \rightarrow 2\pi$ DECAY**

$$\eta_{+-} = A(K_L^0 \rightarrow \pi^+ \pi^-) / A(K_S^0 \rightarrow \pi^+ \pi^-)$$

$$\eta_{00} = A(K_L^0 \rightarrow \pi^0 \pi^0) / A(K_S^0 \rightarrow \pi^0 \pi^0)$$

The fitted values of $|\eta_{+-}|$ and $|\eta_{00}|$ given below are the results of a fit to $|\eta_{+-}|$, $|\eta_{00}|$, $|\eta_{00}/\eta_{+-}|$, and $\text{Re}(\epsilon'/\epsilon)$. Independent information on $|\eta_{+-}|$ and $|\eta_{00}|$ can be obtained from the fitted values of the $K_L^0 \rightarrow \pi\pi$ and $K_S^0 \rightarrow \pi\pi$ branching ratios and the K_L^0 and K_S^0 lifetimes. This information is included as data in the $|\eta_{+-}|$ and $|\eta_{00}|$ sections with a Document ID "BRFIT." See the note "CP violation in K_L decays" above for details. **$|\eta_{00}| = |A(K_L^0 \rightarrow 2\pi^0) / A(K_S^0 \rightarrow 2\pi^0)|$**

VALUE (units 10 ⁻³)	DOCUMENT ID	TECN	COMMENT
2.220 ± 0.011 OUR FIT			
2.243 ± 0.014	BRFIT 16		

• • • We do not use the following data for averages, fits, limits, etc. • • •

2.47 ± 0.31 ± 0.24 ANGELOPO... 98 CPLR

2.49 ± 0.40 ¹ ADLER 96B CPLR Sup. by ANGELOPOULOS 98

2.33 ± 0.18 CHRISTENS... 79 ASPK

2.71 ± 0.37 ² WOLFF 71 OSPK Cu reg., 4 γ 's2.95 ± 0.63 ² CHOLLET 70 OSPK Cu reg., 4 γ 's¹ Error is statistical only.² CHOLLET 70 gives $|\eta_{00}| = (1.23 \pm 0.24) \times (\text{regeneration amplitude, 2 GeV/c Cu})/10000\text{mb}$. WOLFF 71 gives $|\eta_{00}| = (1.13 \pm 0.12) \times (\text{regeneration amplitude, 2 GeV/c Cu})/10000\text{mb}$. We compute both $|\eta_{00}|$ values for (regeneration amplitude, 2 GeV/c Cu) = 24 ± 2mb. This regeneration amplitude results from averaging over FAISSNER 69, extrapolated using optical-model calculations of Bohm et al., Physics Letters **27B** 594 (1968) and the data of BALATS 71. (From H. Faissner, private communication). **$|\eta_{+-}| = |A(K_L^0 \rightarrow \pi^+ \pi^-) / A(K_S^0 \rightarrow \pi^+ \pi^-)|$**

VALUE (units 10 ⁻³)	EVTS	DOCUMENT ID	TECN	COMMENT
2.232 ± 0.011 OUR FIT				
2.226 ± 0.007		BRFIT 16		

• • • We do not use the following data for averages, fits, limits, etc. • • •

2.223 ± 0.012 ¹ LAI 07 NA482.219 ± 0.013 ² AMBROSINO 06F KLOE2.228 ± 0.010 ³ ALEXOPOU... 04 KTEV2.286 ± 0.023 ± 0.026 70M ⁴ APOSTOLA... 99c CPLR $K^0-\bar{K}^0$ asymmetry2.310 ± 0.043 ± 0.031 ⁵ ADLER 95B CPLR $K^0-\bar{K}^0$ asymmetry2.32 ± 0.14 ± 0.03 10⁵ ADLER 92B CPLR $K^0-\bar{K}^0$ asymmetry

2.30 ± 0.035 GEWENIGER 74B ASPK

¹ Value obtained from the NA48 measurements of $\Gamma(K_L^0 \rightarrow \pi^+ \pi^-)/\Gamma(K_L^0 \rightarrow \pi^0 \nu_e)$ and $\tau_{K_S^0}$ and KLOE measurements of $B(K_S^0 \rightarrow \pi^+ \pi^-)$ and $\tau_{K_L^0}$. $\Gamma(K_L^0 \rightarrow \pi^+ \pi^-)$ is defined to include the inner bremsstrahlung component $\Gamma(K_L^0 \rightarrow \pi^+ \pi^- \gamma(\text{IB}))$ but exclude the direct emission component $B(K_S^0 \rightarrow \pi^+ \pi^- (\text{DE}))$. Their $|\eta_{+-}|$ value is not directly used in our fit, but enters the fit via their branching ratio and lifetime measurements.² AMBROSINO 06f uses KLOE branching ratios and τ_L together with τ_S from PDG 04. Their $|\eta_{+-}|$ value is not directly used in our fit, but enters the fit via their branching ratio and lifetime measurements.

Meson Particle Listings

K_L^0

³ALEXOPOULOS 04 $|\eta_{+-}|$ uses their $K_L^0 \rightarrow \pi\pi$ branching fractions, $\tau_S = (0.8963 \pm 0.0005) \times 10^{-10}$ s from the average of KTeV and NA48 τ_S measurements, and assumes that $\Gamma(K_S^0 \rightarrow \pi\ell\nu_\ell) = \Gamma(K_L^0 \rightarrow \pi\ell\nu_\ell)$ giving $B(K_S^0 \rightarrow \pi\ell\nu_\ell) = 0.118\%$. Their η_{+-} is not directly used in our fit, but enters our fit via their branching ratio measurements.
⁴APOSTOLAKIS 99c report $(2.264 \pm 0.023 \pm 0.026 + 9.1[\tau_S - 0.8934]) \times 10^{-3}$. We evaluate for our 2006 best value $\tau_S = (0.8958 \pm 0.0005) \times 10^{-10}$ s.
⁵ADLER 95B report $(2.312 \pm 0.043 \pm 0.030 - 1[\Delta m - 0.5274] + 9.1[\tau_S - 0.8926]) \times 10^{-3}$. We evaluate for our 1996 best values $\Delta m = (0.5304 \pm 0.0014) \times 10^{-10} \text{ h s}^{-1}$ and $\tau_S = (0.8927 \pm 0.0009) \times 10^{-10}$ s. Superseded by APOSTOLAKIS 99c.

$$|\epsilon| = (2|\eta_{+-}| + |\eta_{00}|)/3$$

This expression is a very good approximation, good to about one part in 10^{-4} because of the small measured value of $\phi_{00} - \phi_{+-}$ and small theoretical ambiguities.

VALUE (units 10^{-3})	DOCUMENT ID
2.228 ± 0.011 OUR FIT	Error includes scale factor of 1.8.

$|\eta_{00}/\eta_{+-}|$

VALUE	EVTS	DOCUMENT ID	TECN
0.9950 ± 0.0007 OUR FIT		Error includes scale factor of 1.6.	
0.9930 ± 0.0020 OUR AVERAGE			

0.9931 ± 0.0020	1,2	BARR	93D	NA31
0.9904 ± 0.0084 ± 0.0036	3	WOODS	88	E731
0.9939 ± 0.0013 ± 0.0015	1M	BARR	93D	NA31
0.9899 ± 0.0020 ± 0.0025	1	BURKHARDT	88	NA31

• • • We do not use the following data for averages, fits, limits, etc. • • •
 • • • We do not use the following data for averages, fits, limits, etc. • • •
¹This is the square root of the ratio R given by BURKHARDT 88 and BARR 93D.
²This is the combined results from BARR 93D and BURKHARDT 88, taking into account a common systematic uncertainty of 0.0014.
³We calculate $|\eta_{00}/\eta_{+-}| = 1 - 3(\epsilon'/\epsilon)$ from WOODS 88 (ϵ'/ϵ) value.

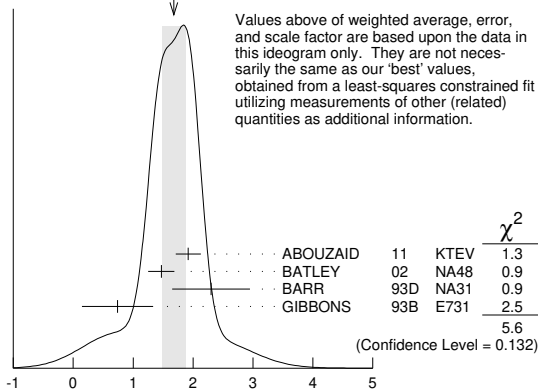
$$\text{Re}(\epsilon'/\epsilon) = (1 - |\eta_{00}/\eta_{+-}|)/3$$

We have neglected terms of order $\omega \cdot \text{Re}(\epsilon'/\epsilon)$, where $\omega = \text{Re}(A_2)/\text{Re}(A_0) \simeq 1/22$. If included, this correction would lower $\text{Re}(\epsilon'/\epsilon)$ by about 0.04×10^{-3} . See SOZZI 04.

VALUE (units 10^{-3})	DOCUMENT ID	TECN	COMMENT
1.66 ± 0.23 OUR FIT		Error includes scale factor of 1.6.	
1.68 ± 0.20 OUR AVERAGE		Error includes scale factor of 1.4. See the ideogram below.	

1.92 ± 0.21	1	ABOUZAID	11	KTEV	Assuming CPT
1.47 ± 0.22		BATLEY	02	NA48	
0.74 ± 0.52 ± 0.29		GIBBONS	93B	E731	
• • • We use the following data for averages but not for fits. • • •					
2.3 ± 0.65	2,3	BARR	93D	NA31	
• • • We do not use the following data for averages, fits, limits, etc. • • •					
2.110 ± 0.343	1,4	ABOUZAID	11	KTEV	Not assuming CPT
2.07 ± 0.28		ALAVI-HARATI	03	KTEV	In ABOUZAID 11
1.53 ± 0.26		LAI	01C	NA48	In BATLEY 02
2.80 ± 0.30 ± 0.28		ALAVI-HARATI	99D	KTEV	In ALAVI-HARATI 03
1.85 ± 0.45 ± 0.58		FANTI	99C	NA48	In LAI 01C
2.0 ± 0.7	5	BARR	93D	NA31	
-0.4 ± 1.4 ± 0.6		PATTERSON	90	E731	In GIBBONS 93B
3.3 ± 1.1	5	BURKHARDT	88	NA31	
3.2 ± 2.8 ± 1.2	2	WOODS	88	E731	

WEIGHTED AVERAGE
 1.68 ± 0.20 (Error scaled by 1.4)



Values above of weighted average, error, and scale factor are based upon the data in this ideogram only. They are not necessarily the same as our 'best' values, obtained from a least-squares constrained fit utilizing measurements of other (related) quantities as additional information.

$$\text{Re}(\epsilon'/\epsilon) = (1 - |\eta_{00}/\eta_{+-}|)/3$$

¹The two ABOUZAID 11 values use the same data. The fits are performed with and without CPT invariance requirement.
²These values are derived from $|\eta_{00}/\eta_{+-}|$ measurements. They enter the average in this section but enter the fit via the $|\eta_{00}/\eta_{+-}|$ only.
³This is the combined results from BARR 93D and BURKHARDT 88, taking into account their common systematic uncertainty.
⁴We use ABOUZAID 11 $\text{Re}(\epsilon'/\epsilon)$ value with CPT assumption in our fits for $|\eta_{+-}|$, $|\eta_{00}|$, and $\text{Re}(\epsilon'/\epsilon)$.

⁵These values are derived from $|\eta_{00}/\eta_{+-}|$ measurements.

ϕ_{+-} , PHASE of η_{+-}

The dependence of the phase on Δm and τ_S is given for each experiment in the comments below, where Δm is the $K_L^0 - K_S^0$ mass difference in units 10^{10} h s^{-1} and τ_S is the K_S mean life in units 10^{-10} s. We also give the regeneration phase ϕ_f in the comments below.

OUR FIT is described in the note on "CP violation in K_L decays" in the K_L^0 Particle Listings. Most experiments in this section are included in both the "Not Assuming CPT" and "Assuming CPT" fits. In the latter fit, they have little direct influence on ϕ_{+-} because their errors are large compared to that assuming CPT, but they influence Δm and τ_S through their dependencies on these parameters, which are given in the footnotes.

VALUE (°)	EVTS	DOCUMENT ID	TECN	COMMENT
43.51 ± 0.05 OUR FIT		Error includes scale factor of 1.2. Assuming CPT		
43.4 ± 0.5 OUR FIT		Error includes scale factor of 1.2. Not assuming CPT		
42.9 ± 0.6 ± 0.3	70M	1 APOSTOLA... 99c	CPLR	K^0, \bar{K}^0 asymmetry
42.9 ± 0.8 ± 0.2		2,3 SCHWINGEN... 95	E773	CH _{1,1} regenerator
41.4 ± 0.9 ± 0.2		3,4 GIBBONS 93	E731	B ₄ C regenerator
44.5 ± 1.6 ± 0.6		5 CAROSI 90	NA31	Vacuum regen.
43.3 ± 1.0 ± 0.5		6 GEWENIGER 74B	ASPK	Vacuum regen.
• • • We do not use the following data for averages, fits, limits, etc. • • •				
43.76 ± 0.64		7 ABOUZAID 11	KTEV	Not assuming CPT
44.12 ± 0.72 ± 1.20		8 ALAVI-HARATI 03	KTEV	Not assuming CPT
42.5 ± 0.4 ± 0.3		9,10 ADLER 96C	RVUE	
43.4 ± 1.1 ± 0.3		11 ADLER 95B	CPLR	K^0, \bar{K}^0 asymmetry
42.3 ± 4.4 ± 1.4	100k	12 ADLER 92B	CPLR	K^0, \bar{K}^0 asymmetry
47.7 ± 2.0 ± 0.9		3,13 KARLSSON 90	E731	
44.3 ± 2.8 ± 0.2		14 CARITHERS 75	SPEC	C regenerator

¹APOSTOLAKIS 99c measures $\phi_{+-} = (43.19 \pm 0.53 \pm 0.28) + 300 [\Delta m - 0.5301] (^\circ)$. We have adjusted the measurement to use our best values of ($\Delta m = 0.5293 \pm 0.0009$) (10^{10} h s^{-1}). Our first error is their experiment's error and our second error is the systematic error from using our best values.
²SCHWINGENHEUER 95 measures $\phi_{+-} = (43.53 \pm 0.76) + 173 [\Delta m - 0.5282] - 275 [\tau_S - 0.8926] (^\circ)$. We have adjusted the measurement to use our best values of ($\Delta m = 0.5293 \pm 0.0009$) (10^{10} h s^{-1}), ($\tau_S = 0.8954 \pm 0.0004$) (10^{-10} s). Our first error is their experiment's error and our second error is the systematic error from using our best values.
³These experiments measure $\phi_{+-} - \phi_f$ and calculate the regeneration phase from the power law momentum dependence of the regeneration amplitude using analyticity and dispersion relations. SCHWINGENHEUER 95 [GIBBONS 93] includes a systematic error of $0.35^\circ [0.5^\circ]$ for uncertainties in their modeling of the regeneration amplitude.
⁴GIBBONS 93 measures $\phi_{+-} = (42.21 \pm 0.9) + 189 [\Delta m - 0.5257] - 460 [\tau_S - 0.8922] (^\circ)$. We have adjusted the measurement to use our best values of ($\Delta m = 0.5293 \pm 0.0009$) (10^{10} h s^{-1}), ($\tau_S = 0.8954 \pm 0.0004$) (10^{-10} s). Our first error is their experiment's error and our second error is the systematic error from using our best values. This is actually reported in SCHWINGENHEUER 95, footnote 8. GIBBONS 93 reports $\phi_{+-} (42.2 \pm 1.4)^\circ$. They measure $\phi_{+-} - \phi_f$ and calculate the regeneration phase ϕ_f from the power law momentum dependence of the regeneration amplitude using analyticity. An error of 0.6° is included for possible uncertainties in the regeneration phase.
⁵CAROSI 90 measures $\phi_{+-} = (46.9 \pm 1.4 \pm 0.7) + 579 [\Delta m - 0.5351] + 303 [\tau_S - 0.8922] (^\circ)$. We have adjusted the measurement to use our best values of ($\Delta m = 0.5293 \pm 0.0009$) (10^{10} h s^{-1}), ($\tau_S = 0.8954 \pm 0.0004$) (10^{-10} s). Our first error is their experiment's error and our second error is the systematic error from using our best values.
⁶GEWENIGER 74B measures $\phi_{+-} = (49.4 \pm 1.0) + 565 [\Delta m - 0.540] (^\circ)$. We have adjusted the measurement to use our best values of ($\Delta m = 0.5293 \pm 0.0009$) (10^{10} h s^{-1}). Our first error is their experiment's error and our second error is the systematic error from using our best values.
⁷Not independent of other phase parameters reported in ABOUZAID 11.
⁸ALAVI-HARATI 03 ϕ_{+-} is correlated with their $\Delta m = m_{K_L^0} - m_{K_S^0}$ and τ_{K_S} measurements in the K_L^0 and K_S^0 sections respectively. The correlation coefficients are $\rho(\phi_{+-}, \Delta m) = +0.955$, $\rho(\phi_{+-}, \tau_S) = -0.871$, and $\rho(\tau_S, \Delta m) = -0.840$. CPT is not assumed. Uses scintillator Pb regenerator. Superseded by ABOUZAID 11.
⁹ADLER 96C measures $\phi_{+-} = (43.82 \pm 0.41) + 339 [\Delta m - 0.5307] - 252 [\tau_S - 0.8922] (^\circ)$. We have adjusted the measurement to use our best values of ($\Delta m = 0.5293 \pm 0.0009$) (10^{10} h s^{-1}), ($\tau_S = 0.8954 \pm 0.0004$) (10^{-10} s). Our first error is their experiment's error and our second error is the systematic error from using our best values.
¹⁰ADLER 96C is the result of a fit which includes nearly the same data as entered into the "OUR FIT" value in the 1996 edition of this Review (Physical Review D54 1 (1996)).
¹¹ADLER 95B measures $\phi_{+-} = (42.7 \pm 0.9 \pm 0.6) + 316 [\Delta m - 0.5274] + 30 [\tau_S - 0.8926] (^\circ)$. We have adjusted the measurement to use our best values of ($\Delta m = 0.5293 \pm 0.0009$) (10^{10} h s^{-1}), ($\tau_S = 0.8954 \pm 0.0004$) (10^{-10} s). Our first error is their experiment's error and our second error is the systematic error from using our best values.
¹²ADLER 92B quote separately two systematic errors: ± 0.4 from their experiment and ± 1.0 degrees due to the uncertainty in the value of Δm .
¹³KARLSSON 90 systematic error does not include regeneration phase uncertainty.
¹⁴CARITHERS 75 measures $\phi_{+-} = (45.5 \pm 2.8) + 224 [\Delta m - 0.5348] (^\circ)$. We have adjusted the measurement to use our best values of ($\Delta m = 0.5293 \pm 0.0009$) (10^{10} h s^{-1}). Our first error is their experiment's error and our second error is the systematic error from using our best values. $\phi_f = -40.9 \pm 2.6^\circ$.

ϕ_{00} , PHASE OF η_{00}

See comment in ϕ_{+-} header above for treatment of Δm and τ_S dependence, as well as for the inclusion of data in both the "Assuming CPT" and "Not Assuming CPT" fits.

OUR FIT is described in the note on "CP violation in K_L decays" in the K_L^0 Particle Listings.

Table with 5 columns: VALUE (°), DOCUMENT ID, TECN, COMMENT. Rows include OUR FIT values and experimental data from CAROSI, ABOUZAID, ANGELOPOULOS, ADLER, and KARLSSON.

- 1 CAROSI 90 measures $\phi_{00} = (47.1 \pm 2.1 \pm 1.0) + 579 [\Delta m - 0.5351] + 252 [\tau_S - 0.8922]$ (°). We have adjusted the measurement to use our best values of ($\Delta m = 0.5293 \pm 0.0009$) (10^{10} h s^{-1}), ($\tau_S = 0.8954 \pm 0.0004$) (10^{-10} s). Our first error is their experiment's error and our second error is the systematic error from using our best values.
2 Not independent of other phase parameters reported in ABOUZAID 11.
3 ANGELOPOULOS 98 measures $\phi_{00} = (42.0 \pm 5.6 \pm 1.9) + 240 [\Delta m - 0.5307]$ (°). We have adjusted the measurement to use our best values of ($\Delta m = 0.5293 \pm 0.0009$) (10^{10} h s^{-1}). Our first error is their experiment's error and our second error is the systematic error from using our best values. The τ_S dependence is negligible.
4 ADLER 96B identified initial neutral kaon individually as being a K^0 or a \bar{K}^0 . The systematic uncertainty is $\pm 1.5^\circ$ combined in quadrature with $\pm 0.8^\circ$ due to Δm .
5 KARLSSON 90 systematic error does not include regeneration phase uncertainty.

$\phi_\epsilon = (2\phi_{+-} + \phi_{00})/3$

This expression is a very good approximation, good to about 10^{-3} degrees because of the small measured values of $\phi_{00} - \phi_{+-}$ and $\text{Re } \epsilon'/\epsilon$, and small theoretical ambiguities.

Table with 5 columns: VALUE (°), DOCUMENT ID, TECN, COMMENT. Rows include OUR FIT values and experimental data from SUPERWEAK and ABOUZAID.

- 1 SUPERWEAK 16 is a fake measurement used to impose the CPT or Superweak constraint $\phi_{+-} = \phi_{SW} = \tan^{-1}[2 \frac{\Delta m}{\hbar} (\frac{\tau_S \tau_L}{\tau_S - \tau_L})]$. This "measurement" is linearized using values near the PDG 04 edition values of Δm , τ_S and τ_L , and then adjusted to our current values as described in the following "measurement". SUPERWEAK 16 measures $\phi_\epsilon = (43.50258 \pm 0.00021) + 54.1 [\Delta m - 0.5289] + 32.0 [\tau_S - 0.89564]$ (°). We have adjusted the measurement to use our best values of ($\Delta m = 0.5293 \pm 0.0009$) (10^{10} h s^{-1}), ($\tau_S = 0.8954 \pm 0.0004$) (10^{-10} s). Our first error is their experiment's error and our second error is the systematic error from using our best values.
2 ABOUZAID 11 uses the full KTeV dataset collected in 1996, 1997, and 1999. See $\text{Im}(\epsilon'/\epsilon)$ section for correlation information.

$\text{Im}(\epsilon'/\epsilon) = -(\phi_{00} - \phi_{+-})/3$

For small $|\epsilon'/\epsilon|$, $\text{Im}(\epsilon'/\epsilon)$ is related to the phases of η_{00} and η_{+-} by the above expression.

Table with 5 columns: VALUE (°), DOCUMENT ID, TECN, COMMENT. Rows include OUR FIT values and experimental data from ABOUZAID.

- 1 ABOUZAID 11 uses the full KTeV dataset collected in 1996, 1997, and 1999. The fit has Δm , τ_S , ϕ_ϵ , $\text{Re}(\epsilon'/\epsilon)$, and $\text{Im}(\epsilon'/\epsilon)$ as free parameters. The reported value of $\text{Im}(\epsilon'/\epsilon) = (-17.20 \pm 20.20) \times 10^{-4}$ rad. The correlation coefficients are $\rho(\phi_\epsilon, \Delta m) = 0.828$, $\rho(\phi_\epsilon, \tau_S) = -0.765$, $\rho(\Delta m, \tau_S) = -0.858$, $\rho(\text{Im}(\epsilon'/\epsilon), \phi_\epsilon) = -0.041$, $\rho(\text{Im}(\epsilon'/\epsilon), \Delta m) = 0.026$, $\rho(\text{Im}(\epsilon'/\epsilon), \tau_S) = -0.010$.

DECAY-PLANE ASYMMETRY IN $\pi^+ \pi^- e^+ e^-$ DECAYS

This is the CP-violating asymmetry

$A = \frac{N_{\sin\phi\cos\phi>0.0} - N_{\sin\phi\cos\phi<0.0}}{N_{\sin\phi\cos\phi>0.0} + N_{\sin\phi\cos\phi<0.0}}$

where ϕ is the angle between the $e^+ e^-$ and $\pi^+ \pi^-$ planes in the K_L^0 rest frame.

CP ASYMMETRY A in $K_L^0 \rightarrow \pi^+ \pi^- e^+ e^-$

Table with 5 columns: VALUE (%), DOCUMENT ID, TECN. Rows include OUR AVERAGE and experimental data from ABOUZAID, LAI, and ALAVI-HARATI.

PARAMETERS FOR $e^+ e^- e^+ e^-$ DECAYS

These are the CP-violating parameters in the ϕ distribution, where ϕ is the angle between the planes of the two $e^+ e^-$ pairs in the kaon rest frame:

$d\Gamma/d\phi \propto 1 + \beta_{CP} \cos(2\phi) + \gamma_{CP} \sin(2\phi)$

where $\beta_{CP} = -0.20$ and $\gamma_{CP} = 0$ values correspond to no CP violation.

β_{CP} from $K_L^0 \rightarrow e^+ e^- e^+ e^-$

Table with 5 columns: VALUE, EVTS, DOCUMENT ID, TECN, COMMENT. Rows include OUR AVERAGE and experimental data from LAI and ALAVI-HARATI.

- 1 LAI 05B obtains $\beta_{CP} = -0.13 \pm 0.10$ (stat) if $\gamma_{CP} = 0$ is assumed.

γ_{CP} from $K_L^0 \rightarrow e^+ e^- e^+ e^-$

Table with 5 columns: VALUE, EVTS, DOCUMENT ID, TECN, COMMENT. Rows include OUR AVERAGE and experimental data from LAI and ALAVI-HARATI.

CHARGE ASYMMETRY IN $\pi^+ \pi^- \pi^0$ DECAYS

These are CP-violating charge-asymmetry parameters, defined at beginning of section "LINEAR COEFFICIENT g FOR $K_L^0 \rightarrow \pi^+ \pi^- \pi^0$ " above.

See also note on Dalitz plot parameters in K^\pm section and note on "CP violation in K_L decays" above.

LINEAR COEFFICIENT j FOR $K_L^0 \rightarrow \pi^+ \pi^- \pi^0$

Table with 5 columns: VALUE, EVTS, DOCUMENT ID, TECN. Rows include OUR AVERAGE and experimental data from ANGELOPOULOS, CHO, PEACH, SCRIBANO, SMITH, and BLANPIED.

QUADRATIC COEFFICIENT f FOR $K_L^0 \rightarrow \pi^+ \pi^- \pi^0$

Table with 5 columns: VALUE, EVTS, DOCUMENT ID, TECN. Rows include OUR AVERAGE and experimental data from ANGELOPOULOS.

PARAMETERS for $K_L^0 \rightarrow \pi^+ \pi^- \gamma$ DECAY

$|\eta_{+-\gamma}| = |A(K_L^0 \rightarrow \pi^+ \pi^- \gamma, CP \text{ violating})/A(K_S^0 \rightarrow \pi^+ \pi^- \gamma)|$

Table with 5 columns: VALUE (units 10^{-3}), EVTS, DOCUMENT ID, TECN. Rows include OUR AVERAGE and experimental data from MATTHEWS and RAMBERG.

$\phi_{+-\gamma} = \text{phase of } \eta_{+-\gamma}$

Table with 5 columns: VALUE (°), EVTS, DOCUMENT ID, TECN. Rows include OUR AVERAGE and experimental data from MATTHEWS and RAMBERG.

$|\epsilon'_{+-\gamma}|/\epsilon$ for $K_L^0 \rightarrow \pi^+ \pi^- \gamma$

Table with 5 columns: VALUE, CL%, EVTS, DOCUMENT ID, TECN. Rows include experimental data from RAMBERG.

- 1 RAMBERG 93B limit on $|\epsilon'_{+-\gamma}|/\epsilon$ assumes that any difference between η_{+-} and $\eta_{+-\gamma}$ is due to direct CP violation.

$|\mathcal{E}|$ for $K_L^0 \rightarrow \pi^+ \pi^- \gamma$

This parameter is the amplitude of the direct emission of a CP violating E1 electric dipole photon.

Table with 5 columns: VALUE, CL%, EVTS, DOCUMENT ID, TECN, COMMENT. Rows include experimental data from ABOUZAID.

T VIOLATION TESTS IN K_L^0 DECAYS

$\text{Im}(\xi)$ in $K_{\mu 3}^0$ DECAY (from transverse μ pol.)

Test of T reversal invariance.

Table with 5 columns: VALUE, EVTS, DOCUMENT ID, TECN, COMMENT. Rows include OUR AVERAGE and experimental data from MORSE, CLARK, SANDWEISS, LONGO, and ABRAMS.

- • • We do not use the following data for averages, fits, limits, etc. • • •
0.012 \pm 0.026 SCHMIDT 79 CNTR Repl. by MORSE 80
1 CLARK 77 value has additional $\xi(0)$ dependence $+0.21\text{Re}\{\xi(0)\}$.
2 SANDWEISS 73 value corrected from value quoted in their paper due to new value of $\text{Re}(\xi)$. See footnote 4 of SCHMIDT 79.

CPT-INVARIANCE TESTS IN K_L^0 DECAYS

PHASE DIFFERENCE $\phi_{00} - \phi_{+-}$

Test of CPT.

OUR FIT is described in the note on "CP violation in K_L decays" in the K_L^0 Particle Listings.

Table with 5 columns: VALUE (°), DOCUMENT ID, TECN, COMMENT. Rows include OUR FIT and experimental data from SUPERWEAK and SCHWINGEN.

Meson Particle Listings

K_L^0

- • • We do not use the following data for averages, fits, limits, etc. • • •
- 0.30 ± 0.35 ³ ABOUZAID 11 KTEV Not assuming *CPT*
- 0.39 ± 0.22 ± 0.45 ⁴ ALAVI-HARATI 03 KTEV
- 0.62 ± 0.71 ± 0.75 SCHWINGEN... 95 E773
- 1.6 ± 1.2 ⁵ GIBBONS 93 E731
- 0.2 ± 2.6 ± 1.2 ⁶ CAROSI 90 NA31
- 0.3 ± 2.4 ± 1.2 KARLSSON 90 E731

¹ SUPERWEAK 16 is a fake experiment to constrain $\phi_{00} - \phi_{+-}$ to a small value as described in the note "CP violation in K_L decays."
² This SCHWINGENHEUER 95 values is the combined result of SCHWINGENHEUER 95 and GIBBONS 93, accounting for correlated systematic errors.
³ Not independent of other phase parameters reported in ABOUZAID 11.
⁴ ALAVI-HARATI 03 fit $\text{Re}(\epsilon'/\epsilon)$, $\text{Im}(\epsilon'/\epsilon)$, Δm , τ_{KS} , and ϕ_{+-} simultaneously, not assuming *CPT*. Phase difference is obtained from $\phi_{00} - \phi_{+-} \approx -3\text{Im}(\epsilon'/\epsilon)$ for small $|\epsilon'/\epsilon|$. Superseded by ABOUZAID 11.
⁵ GIBBONS 93 give detailed dependence of systematic error on lifetime (see the section on the K_S^0 mean life) and mass difference (see the section on $m_{K_L^0} - m_{K_S^0}$).
⁶ CAROSI 90 is excluded from the fit because it is not independent of ϕ_{+-} and ϕ_{00} values.

PHASE DIFFERENCE $\phi_{+-} - \phi_{SW}$

Test of *CPT*. The Superweak phase $\phi_{SW} \equiv \tan^{-1}(2\Delta m/\Delta\Gamma)$ where $\Delta m = m_{K_L^0} - m_{K_S^0}$ and $\Delta\Gamma = \hbar(\tau_L - \tau_S)/(\tau_L\tau_S)$.

VALUE (°)	DOCUMENT ID	TECN	COMMENT
0.61 ± 0.62 ± 1.01	¹ ALAVI-HARATI 03	KTEV	

¹ ALAVI-HARATI 03 fit is the same as their ϕ_{+-} , τ_{KS} , Δm fit, except that the parameter $\phi_{+-} - \phi_{SW}$ is used in place of ϕ .

$\text{Re}(\frac{2}{3}\eta_{+-} + \frac{1}{3}\eta_{00}) - \frac{A_L}{2}$

Test of *CPT*

VALUE (units 10^{-6})	DOCUMENT ID	TECN	COMMENT
-3 ± 35	¹ ALAVI-HARATI 02	E799	Uses A_L from K_{e3} decays

¹ ALAVI-HARATI 02 uses PDG 00 values of η_{+-} and η_{00} .

$\Delta S = \Delta Q$ IN K^0 DECAYS

The relative amount of $\Delta S \neq \Delta Q$ component present is measured by the parameter x , defined as

$$x = A(\bar{K}^0 \rightarrow \pi^- \ell^+ \nu) / A(K^0 \rightarrow \pi^- \ell^+ \nu).$$

We list $\text{Re}\{x\}$ and $\text{Im}\{x\}$ for K_{e3} and $K_{\mu 3}$ combined.

$$x = A(\bar{K}^0 \rightarrow \pi^- \ell^+ \nu) / A(K^0 \rightarrow \pi^- \ell^+ \nu) = A(\Delta S = -\Delta Q) / A(\Delta S = \Delta Q)$$

REAL PART OF x

VALUE	EVTS	DOCUMENT ID	TECN	COMMENT
-0.0018 ± 0.0041 ± 0.0045		ANGELOPO... 98D	CPLR	K_{e3} from K^0
• • • We do not use the following data for averages, fits, limits, etc. • • •				
0.10 ^{+0.18} _{-0.19}	79	SMITH	75B WIRE	$\pi^- p \rightarrow K^0 \Lambda$
0.04 ± 0.03	4724	NIEBERGALL	74 ASPK	$K^+ p \rightarrow K^0 p \pi^+$
-0.008 ± 0.044	1757	FACKLER	73 OSPK	K_{e3} from K^0
-0.03 ± 0.07	1367	HART	73 OSPK	K_{e3} from $K^0 \Lambda$
-0.070 ± 0.036	1079	MALLARY	73 OSPK	K_{e3} from $K^0 \Lambda X$
0.03 ± 0.06	410	¹ BURGUN	72 HBC	$K^+ p \rightarrow K^0 p \pi^+$
0.04 ^{+0.10} _{-0.13}	100	² GRAHAM	72 OSPK	$K_{\mu 3}$ from $K^0 \Lambda$
-0.05 ± 0.09	442	² GRAHAM	72 OSPK	$\pi^- p \rightarrow K^0 \Lambda$
0.26 ^{+0.10} _{-0.14}	126	MANN	72 HBC	$K^- p \rightarrow n \bar{K}^0$
-0.13 ± 0.11	342	² MANTSCH	72 OSPK	K_{e3} from $K^0 \Lambda$
0.04 ^{+0.07} _{-0.08}	222	¹ BURGUN	71 HBC	$K^+ p \rightarrow K^0 p \pi^+$
0.25 ^{+0.07} _{-0.09}	252	WEBBER	71 HBC	$K^- p \rightarrow n \bar{K}^0$
0.12 ± 0.09	215	³ CHO	70 DBC	$K^+ d \rightarrow K^0 p p$
-0.020 ± 0.025		⁴ BENNETT	69 CNTR	Charge asym + Cu regen.
0.09 ^{+0.14} _{-0.16}	686	LITTENBERG	69 OSPK	$K^+ n \rightarrow K^0 p$
0.03 ± 0.03		⁴ BENNETT	68 CNTR	
0.09 ^{+0.07} _{-0.09}	121	JAMES	68 HBC	$\bar{p} p$
0.17 ^{+0.16} _{-0.35}	116	FELDMAN	67B OSPK	$\pi^- p \rightarrow K^0 \Lambda$
0.17 ± 0.10	335	³ HILL	67 DBC	$K^+ d \rightarrow K^0 p p$
0.035 ^{+0.11} _{-0.13}	196	AUBERT	65 HLBC	K^+ charge exch.
0.06 ^{+0.18} _{-0.44}	152	⁵ BALDO-...	65 HLBC	K^+ charge exch.
-0.08 ^{+0.16} _{-0.28}	109	⁶ FRANZINI	65 HBC	$\bar{p} p$

¹ BURGUN 72 is a final result which includes BURGUN 71.

- ² First GRAHAM 72 value is second GRAHAM 72 value combined with MANTSCH 72.
- ³ CHO 70 is analysis of unambiguous events in new data and HILL 67.
- ⁴ BENNETT 69 is a reanalysis of BENNETT 68.
- ⁵ BALDO-CEOLIN 65 gives x and θ converted by us to $\text{Re}(x)$ and $\text{Im}(x)$.
- ⁶ FRANZINI 65 gives x and θ for $\text{Re}(x)$ and $\text{Im}(x)$. See SCHMIDT 67.

IMAGINARY PART OF x

Assumes $m_{K_L^0} - m_{K_S^0}$ positive. See Listings above.

VALUE	EVTS	DOCUMENT ID	TECN	COMMENT
0.0012 ± 0.0019 ± 0.0009	640k	ANGELOPO... 01B	CPLR	K_{e3} from K^0
• • • We do not use the following data for averages, fits, limits, etc. • • •				
0.0012 ± 0.0019	640k	¹ ANGELOPO... 98E	CPLR	K_{e3} from K^0
-0.10 ^{+0.16} _{-0.19}	79	SMITH	75B WIRE	$\pi^- p \rightarrow K^0 \Lambda$
-0.06 ± 0.05	4724	NIEBERGALL	74 ASPK	$K^+ p \rightarrow K^0 p \pi^+$
-0.017 ± 0.060	1757	FACKLER	73 OSPK	K_{e3} from K^0
0.09 ± 0.07	1367	HART	73 OSPK	K_{e3} from $K^0 \Lambda$
0.107 ^{+0.092} _{-0.074}	1079	MALLARY	73 OSPK	K_{e3} from $K^0 \Lambda X$
0.07 ^{+0.06} _{-0.07}	410	² BURGUN	72 HBC	$K^+ p \rightarrow K^0 p \pi^+$
0.12 ^{+0.17} _{-0.16}	100	³ GRAHAM	72 OSPK	$K_{\mu 3}$ from $K^0 \Lambda$
0.05 ± 0.13	442	³ GRAHAM	72 OSPK	$\pi^- p \rightarrow K^0 \Lambda$
0.21 ^{+0.15} _{-0.12}	126	MANN	72 HBC	$K^- p \rightarrow n \bar{K}^0$
-0.04 ± 0.16	342	³ MANTSCH	72 OSPK	K_{e3} from $K^0 \Lambda$
0.12 ^{+0.08} _{-0.09}	222	² BURGUN	71 HBC	$K^+ p \rightarrow K^0 p \pi^+$
0.0 ± 0.08	252	WEBBER	71 HBC	$K^- p \rightarrow n \bar{K}^0$
-0.08 ± 0.07	215	⁴ CHO	70 DBC	$K^+ d \rightarrow K^0 p p$
-0.11 ^{+0.10} _{-0.11}	686	LITTENBERG	69 OSPK	$K^+ n \rightarrow K^0 p$
+0.22 ^{+0.37} _{-0.29}	121	JAMES	68 HBC	$\bar{p} p$
0.0 ± 0.25	116	FELDMAN	67B OSPK	$\pi^- p \rightarrow K^0 \Lambda$
-0.20 ± 0.10	335	⁴ HILL	67 DBC	$K^+ d \rightarrow K^0 p p$
-0.21 ^{+0.11} _{-0.15}	196	AUBERT	65 HLBC	K^+ charge exch.
-0.44 ^{+0.32} _{-0.19}	152	⁵ BALDO-...	65 HLBC	K^+ charge exch.
+0.24 ^{+0.40} _{-0.30}	109	⁶ FRANZINI	65 HBC	$\bar{p} p$

- ¹ Superseded by ANGELOPOULOS 01B.
- ² BURGUN 72 is a final result which includes BURGUN 71.
- ³ First GRAHAM 72 value is second GRAHAM 72 value combined with MANTSCH 72.
- ⁴ Footnote 10 of HILL 67 should read +0.58, not -0.58 (private communication) CHO 70 is analysis of unambiguous events in new data and HILL 67.
- ⁵ BALDO-CEOLIN 65 gives x and θ converted by us to $\text{Re}(x)$ and $\text{Im}(x)$.
- ⁶ FRANZINI 65 gives x and θ for $\text{Re}(x)$ and $\text{Im}(x)$. See SCHMIDT 67.

K_L^0 REFERENCES

AHN 21	PRL 126 121801	J.K. Ahn et al.	(KOTO Collab.)
SHIMIZU 20	PR D102 051103	W. Shimizu et al.	(KOTO Collab.)
AHN 19	PRL 122 021802	J.K. Ahn et al.	(KOTO Collab.)
AHN 17	PTEP 2017 021C01	J.K. Ahn et al.	(KOTO Collab.)
BRFIT 16	RPP 2016 edition	C.-J. Lin	(PDG Collab.)
ETAFIT 16	RPP 2016 edition	C.-J. Lin	(PDG Collab.)
SUPERWEAK 16	RPP 2016 edition	C.-J. Lin	(PDG Collab.)
ABOUZAID 11	PR D83 092001	E. Abouzaid et al.	(FNAL KTeV Collab.)
ABOUZAID 11A	PRL 107 201803	E. Abouzaid et al.	(KTeV Collab.)
OGATA 11	PR D84 052009	R. Ogata et al.	(KEK E391a Collab.)
TUNG 11	PR D83 031101	Y.-C. Tung et al.	(KEK E391a Collab.)
ABOUZAID 10	PR D81 052001	E. Abouzaid et al.	(FNAL KTeV Collab.)
AHN 10	PR D81 072004	J.K. Ahn et al.	(KEK E391a Collab.)
ABOUZAID 08A	PR D77 112004	E. Abouzaid et al.	(FNAL KTeV Collab.)
ABOUZAID 08B	PR D78 032009	E. Abouzaid et al.	(FNAL KTeV Collab.)
ABOUZAID 08B	PR D78 032014	E. Abouzaid et al.	(FNAL KTeV Collab.)
ABOUZAID 08C	PRL 100 131803	E. Abouzaid et al.	(FNAL KTeV Collab.)
AHN 08	PRL 100 201802	J.K. Ahn et al.	(KEK E391a Collab.)
AMBROSINO 08F	EPJ C55 539	F. Ambrosino et al.	(KLOE Collab.)
ABOUZAID 07B	PRL 99 051804	E. Abouzaid et al.	(FNAL KTeV Collab.)
ABOUZAID 07C	PRL 99 081803	E. Abouzaid et al.	(FNAL KTeV Collab.)
ABOUZAID 07D	PR D76 052001	E. Abouzaid et al.	(FNAL KTeV Collab.)
AMBROSINO 07C	JHEP 0712 105	F. Ambrosino et al.	(KLOE Collab.)
ANDRE 07	ANP 222 2518	T. Andre	(FEI)
LAI 07	PL B645 26	A. Lai et al.	(CERN NA48 Collab.)
LAI 07A	PL B647 341	A. Lai et al.	(CERN NA48 Collab.)
NIX 07	PR D76 011101	J. Nix et al.	(KEK E391a Collab.)
ABOUZAID 06	PRL 96 101801	E. Abouzaid et al.	(KTeV Collab.)
ABOUZAID 06A	PR D74 032004	E. Abouzaid et al.	(KTeV Collab.)
Also	PR D74 039905 (err.)	E. Abouzaid et al.	(KTeV Collab.)
ABOUZAID 06C	PR D74 097101	E. Abouzaid et al.	(KTeV Collab.)
AHN 06	PR D74 051105	J.K. Ahn et al.	(KEK E391a Collab.)
Also	PR D74 079901 (err.)	J.K. Ahn et al.	(KEK E391a Collab.)
AMBROSINO 06D	PL B632 43	F. Ambrosino et al.	(KLOE Collab.)
AMBROSINO 06D	PL B636 166	F. Ambrosino et al.	(KLOE Collab.)
AMBROSINO 06F	PL B638 140	F. Ambrosino et al.	(KLOE Collab.)
BATLEY 06B	PL B633 173	J.R. Batley et al.	(CERN NA48/2 Collab.)
HILL 06	PR D74 096006	R.J. Hill	(FNAL)
PDG 06	JP G33 1	W.-M. Yao et al.	(PDG Collab.)
ALEXOPOU... 05	PR D71 012001	T. Alexopoulos et al.	(FNAL KTeV Collab.)
AMBROSINO 05C	PL B626 15	F. Ambrosino et al.	(KLOE Collab.)
CABIBBO 05	JHEP 0503 021	N. Cabibbo, G. Isidori	(CERN, ROMA1, FRAS)
LAI 05	PL B605 247	A. Lai et al.	(CERN NA48 Collab.)
LAI 05B	PL B615 31	A. Lai et al.	(CERN NA48 Collab.)
PARK 05	PRL 94 021801	H.K. Park et al.	(FNAL HyperCP Collab.)
ALAVI-HARATI 04A	PRL 93 021805	A. Alavi-Harati et al.	(FNAL KTeV/E799 Collab.)
ALEXOPOU... 04	PR D70 092006	T. Alexopoulos et al.	(FNAL KTeV Collab.)
ALEXOPOU... 04A	PR D70 092007	T. Alexopoulos et al.	(FNAL KTeV Collab.)
BATLEY 04	PL B595 75	J.R. Batley et al.	(CERN NA48 Collab.)
CIRIGLIANO 04	EPJ C35 53	V. Cirigliano, H. Neufeld, H. Pichl	(CIT, VALE+)

Meson Particle Listings

K^0_L

LAI	04B	PL B602 41	A. Lai et al.	(CERN N448 Collab.)	COUPAL	85	PRL 55 566	D.P. Coupal et al.	(CHIC, SACL)
LAI	04C	PL B604 1	A. Lai et al.	(CERN N448 Collab.)	BALATS	83	JNP 38 556	M.Y. Balats et al.	(ITEP)
PDG	04	PL B592 1	S. Edelman et al.	(PDG)	Translated from YAF 38 927.				
SOZZI	04	EPJ C36 37	M. Sozzi	(PISA)	BERGSTROM	83	PL 131B 229	L. Bergstrom, E. Masso, P. Singer	(CERN)
ADINOLFI	03	PL B566 61	M. Adinolfi et al.	(KLOE Collab.)	ARONSON	82	PRL 48 1078	S.H. Aronson et al.	(BNL, CHIC, STAN+)
ALAVI-HARATI	03	PR D67 012005	A. Alavi-Harati et al.	(FNAL KTeV Collab.)	ARONSON	82B	PRL 48 1306	S.H. Aronson et al.	(BNL, CHIC, PURD)
Also		PR D70 079904 (errata)	A. Alavi-Harati et al.	(FNAL KTeV Collab.)	Also		PL 116B 73	E. Fischbach et al.	(PURD, BNL, CHIC)
ALAVI-HARATI	03B	PRL 90 141801	A. Alavi-Harati et al.	(FNAL KTeV Collab.)	Also		PR D28 476	S.H. Aronson et al.	(BNL, CHIC, PURD)
LAI	03C	EPJ C30 33	A. Lai et al.	(CERN N448 Collab.)	Also		PR D28 476	S.H. Aronson et al.	(BNL, CHIC, PURD)
ALAVI-HARATI	02	PRL 88 181601	A. Alavi-Harati et al.	(FNAL KTeV Collab.)	PDG	82B	PL 111B 70	M. Roos et al.	(HELSE, CIT, CERN)
ALAVI-HARATI	02C	PRL 89 211801	A. Alavi-Harati et al.	(FNAL KTeV Collab.)	BIRULEV	81	NP B182 1	V.K. Birulev et al.	(JINR)
BATLEY	02	PL B544 97	J.R. Batley et al.	(CERN N448 Collab.)	Also		JNP 31 622	V.K. Birulev et al.	(JINR)
CIRIGLIANO	02	EPJ C23 121	V. Cirigliano et al.	(VIEN, VALE, MARS)	CARROLL	80B	PRL 44 529	A.S. Carroll et al.	(BNL, ROCH)
LAI	02B	PL B536 229	A. Lai et al.	(CERN N448 Collab.)	CARROLL	80C	PL 96B 407	A.S. Carroll et al.	(BNL, ROCH)
ALAVI-HARATI	01	PRL 86 397	A. Alavi-Harati et al.	(FNAL KTeV Collab.)	CHO	80	PR D22 2688	Y. Cho et al.	(ANL, CMU)
ALAVI-HARATI	01B	PRL 86 761	A. Alavi-Harati et al.	(FNAL KTeV Collab.)	MORSE	80	PR D21 1750	W.H. Morse et al.	(BNL, YALE)
ALAVI-HARATI	01D	PRL 86 5425	A. Alavi-Harati et al.	(FNAL KTeV Collab.)	CHRISTENS...	79	PRL 43 1209	M.H. Christensen et al.	(NYU)
ALAVI-HARATI	01E	PRL 87 021801	A. Alavi-Harati et al.	(FNAL KTeV Collab.)	HILL	78	PL 73B 483	D.G. Hill et al.	(BNL, SLAC, SBER)
ALAVI-HARATI	01G	PR D64 012003	A. Alavi-Harati et al.	(FNAL KTeV Collab.)	CHO	77	PR D15 587	Y. Cho et al.	(ANL, CMU)
ALAVI-HARATI	01H	PRL 87 111802	A. Alavi-Harati et al.	(FNAL KTeV Collab.)	CLARK	77	PR D15 553	A.R. Clark et al.	(LBL)
ALAVI-HARATI	01J	PR D64 112004	A. Alavi-Harati et al.	(FNAL KTeV Collab.)	Also		Thesis LBL-4275	G. Shen	(YALE, BNL)
ANGELOPO...	01	PL B503 49	A. Angelopoulos et al.	(CLEAR Collab.)	DEVOE	77	PR D16 565	R. Devoe et al.	(EFI, ANL)
ANGELOPO...	01B	EPJ C22 55	A. Angelopoulos et al.	(CLEAR Collab.)	PEACH	77	NP B127 399	K.J. Peach et al.	(BGNA, EDIN, GLAS+)
LAI	01B	PL B515 261	A. Lai et al.	(CERN N448 Collab.)	BIRULEV	76	JNP 24 178	V.K. Birulev et al.	(JINR)
LAI	01C	EPJ C22 231	A. Lai et al.	(CERN N448 Collab.)	Also		Translated from YAF 24 340		
ALAVI-HARATI	00	PR D61 072006	A. Alavi-Harati et al.	(FNAL KTeV Collab.)	COOMBES	76	PRL 37 249	R.W. Coombes et al.	(STAN, NYU)
ALAVI-HARATI	00B	PRL 84 408	A. Alavi-Harati et al.	(FNAL KTeV Collab.)	GJESDAL	76	NP B109 118	G. Gjesdal et al.	(CERN, HEIDH)
ALAVI-HARATI	00D	PRL 84 5279	A. Alavi-Harati et al.	(FNAL KTeV Collab.)	BALDO...	75	NC 25A 688	M. Baldo-Ceolin et al.	(PADO, WISC)
ALAVI-HARATI	00E	PR D62 112001	A. Alavi-Harati et al.	(FNAL KTeV Collab.)	BLUMENTHAL	75	PRL 34 164	R.D. Blumenthal et al.	(PENN, CHIC, TEMP)
AMBROSE	00	PRL 84 1389	D. Ambrose et al.	(BNL E871 Collab.)	BUCHANAN	75	PR D11 457	C.B. Buchanan et al.	(UCLA, SLAC, JHU)
APOSTOLA...	00	PL B473 186	A. Apostolakis et al.	(CLEAR Collab.)	CARITHERS	75	PRL 34 1244	W.C.J. Carithers et al.	(COLU, NYU)
PDG	00	EPJ C15 1	D.E. Groom et al.	(PDG Collab.)	SMITH	75B	Thesis UCSB unpub.	J.G. Smith	(UCSD)
ALAVI-HARATI	99B	PRL 83 917	A. Alavi-Harati et al.	(FNAL KTeV Collab.)	BISI	74	PL 50B 504	V. Bisi, M.I. Ferrero	(TORI)
ALAVI-HARATI	99D	PRL 83 822	A. Alavi-Harati et al.	(FNAL KTeV Collab.)	DONALDSON	74	Thesis SLAC-0184	G. Donaldson	(SLAC)
APOSTOLA...	99C	PL B458 545	A. Apostolakis et al.	(CLEAR Collab.)	Also		PR D14 2839	G. Donaldson et al.	(SLAC)
Also		EPJ C18 41	A. Apostolakis et al.	(CLEAR Collab.)	DONALDSON	74B	PR D9 2360	G. Donaldson et al.	(SLAC, UCS)
FANTI	99B	PL B458 553	V. Fanti et al.	(CERN N448 Collab.)	GEWENIGER	74	PL 48B 483	C. Geweniger et al.	(CERN, HEIDH)
FANTI	99C	PL B465 335	V. Fanti et al.	(CERN N448 Collab.)	Also		Thesis CERN Int. 74-4	V. Luth	(CERN)
MURAKAMI	99	PL B463 333	K. Murakami et al.	(KEK E162 Collab.)	GEWENIGER	74B	PL 48B 487	C. Geweniger et al.	(CERN, HEIDH)
ADAMS	98	PRL 80 4123	J. Adams et al.	(FNAL KTeV Collab.)	Also		PL 52B 119	S. Gjesdal et al.	(CERN, HEIDH)
AMBROSE	98B	PRL 81 4309	D. Ambrose et al.	(BNL E871 Collab.)	GEWENIGER	74C	PL 52B 108	C. Geweniger et al.	(CERN, HEIDH)
ANGELOPO...	98	PL B420 191	A. Angelopoulos et al.	(CLEAR Collab.)	GJESDAL	74	PL 52B 113	S. Gjesdal et al.	(CERN, HEIDH)
ANGELOPO...	98C	EPJ C5 389	A. Angelopoulos et al.	(CLEAR Collab.)	MESSNER	74	PRL 33 1458	R. Messner et al.	(COLO, SLAC, UCS)
ANGELOPO...	98D	PL B444 38	A. Angelopoulos et al.	(CLEAR Collab.)	NIEBERGALL	74	PL 49B 103	F. Niebergall et al.	(CERN, ORSAY, VIEN)
Also		EPJ C22 55	A. Angelopoulos et al.	(CLEAR Collab.)	WILLIAMS	74	PRL 33 240	H.H. Williams et al.	(BNL, YALE)
ANGELOPO...	98E	PL B444 43	A. Angelopoulos et al.	(CLEAR Collab.)	ALEXANDER	73B	NP B45 301	G. Alexander et al.	(TELA, HEID)
ARISAKA	98	PL B432 230	K. Arisaka et al.	(FNAL E799 Collab.)	BRANDENB...	73	PR D8 1978	G.W. Brandenburg et al.	(SLAC)
BENDER	98	PL B418 411	M. Bender et al.	(CERN N448 Collab.)	EVANS	73	PR D7 36	G.R. Evans et al.	(EDIN, CERN)
DAMBROSIO	98	PL B423 385	G. D'Ambrósio, G. Isidori, J. Portoles		Also		PRL 23 427	G.R. Evans et al.	(EDIN, CERN)
SETZU	98	PL B420 205	M. G. Setzu et al.		FACKLER	73	PRL 31 847	O. Fackler et al.	(MIT)
TAKEUCHI	98	PR B443 409	Y. Takeuchi et al.	(KYOT, KEK, HIRO)	FITCH	73	PRL 31 1524	V.L. Fitch et al.	(PRIN)
FANTI	97	ZPHY C76 653	V. Fanti et al.	(CERN N448 Collab.)	Also		Thesis COO-3072-13	R.C. Webb	(RHEN)
NOMURA	97	PL B408 445	T. Nomura et al.	(KYOT, KEK, HIRO)	HART	73	NP B66 317	J.C. Hart et al.	(CAVE, PHEL)
ADLER	96B	ZPHY C70 211	R. Adler et al.	(CLEAR Collab.)	MALLARY	73	PR D7 1953	M.L. Mallary et al.	(CIT)
ADLER	96C	PL B369 367	R. Adler et al.	(CLEAR Collab.)	Also		PRL 25 1214	F.J. Sciulli et al.	(CIT)
GU	96	PRL 76 4312	P. Gu et al.	(RUTG, UCLA, EFI, COLO+)	MCCARTHY	73	PR D7 687	R.L. McCarthy et al.	(LBL)
LEBER	96	PL B369 69	F. Leber et al.	(MAINZ, CERN, EDIN, ORSAY+)	Also		PL 42B 291	R.L. McCarthy et al.	(LBL)
PDG	96	PR D54 1	R. M. Barnett et al.	(PDG Collab.)	Also		Thesis LBL-550	R.L. McCarthy et al.	(LBL)
ADLER	95B	PL B363 237	R. Adler et al.	(CLEAR Collab.)	MESSNER	73	PRL 30 876	R. Messner et al.	(COLO, SLAC, UCS)
ADLER	95B	PR D51 2061	T. Akagi et al.	(TOHOK, TOKY, KYOT, KEK)	SANDWEISS	73	NP 30 1002	J. Sandweiss et al.	(YALE, ANL)
BARR	95	ZPHY C65 361	G.D. Barr et al.	(CERN, EDIN, MAINZ, LALO+)	WILLIAMS	73	PRL 31 1521	H.H. Williams et al.	(BNL, YALE)
BARR	95C	PL B359 399	G.D. Barr et al.	(CERN, EDIN, MAINZ, LALO+)	ASHFORD	72	PL 38B 47	V.A. Ashford et al.	(UCSD)
HEINSON	95	PR D51 985	A.P. Heinson et al.	(BNL E791 Collab.)	BANNER	72B	PRL 29 237	M. Banner et al.	(PRIN)
KREUTZ	95	ZPHY C65 67	A. Kreutz et al.	(SIEG, EDIN, MAINZ, ORSAY+)	BARMIN	72B	SJNP 15 638	V.V. Barmin et al.	(ITEP)
MATTHEWS	95	PRL 75 2803	J.N. Matthews et al.	(RUTG, EFI, ELMT+)	BURGUN	72	NP B50 194	G. Burgun et al.	(SACL, CERN, OSLO)
SCHWINGEN...	95	PRL 74 4376	B. Schwingenheuer et al.	(EFI, CHIC+)	GRAHAM	72	NC 9A 163	G.W. Graham et al.	(ILL, NEAS)
SPENCER	95	PRL 74 3323	M.B. Spencer et al.	(UCLA, EFI, COLO+)	JAMES	72	NP B49 1	F. James et al.	(CERN, SAFL, OSLO)
BARR	94	PL B328 528	G.D. Barr et al.	(CERN, EDIN, MAINZ, LALO+)	KRENZ	72	LNC 4 213	W. Krenz et al.	(AACH, CERN, EDIN)
GU	94	PRL 72 3000	P. Gu et al.	(RUTG, UCLA, EFI, COLO+)	MANN	72	PR D6 137	W.A. Mann et al.	(MASA, BNL, YALE)
NAKAYA	94	PRL 73 2169	T. Nakaya et al.	(OSAK, UCLA, EFI, COLO+)	MANTSCH	72	NC 9A 160	P.M. Mantich et al.	(ILL, NEAS)
ROBERTS	94	PR D50 1874	D. Roberts et al.	(UCLA, EFI, COLO+)	MCCARTHY	72	PL 42B 291	R.L. McCarthy et al.	(LBL)
AKAGI	93	PL B7 2444	T. Akagi et al.	(TOHOK, TOKY, KYOT, KEK)	PICCIONI	72	PRL 29 1412	R. Piccioni et al.	(SLAC)
ARISAKA	93	PRL 70 1049	K. Arisaka et al.	(BNL E791 Collab.)	Also		PR D9 2339	R. Piccioni et al.	(SLAC, UCS, COLO)
ARISAKA	93B	PRL 71 3910	K. Arisaka et al.	(BNL E791 Collab.)	VOSBURGH	72	PR D6 1834	K.G. Vosburgh et al.	(RUTG, MASA)
BARR	93D	PL B317 233	G.D. Barr et al.	(CERN, EDIN, MAINZ, LALO+)	Also		PRL 26 866	K.G. Vosburgh et al.	(RUTG, MASA)
GIBBONS	93	PRL 70 1199	L.K. Gibbons et al.	(FNAL E731 Collab.)	BALATS	71	SJNP 13 53	M.Y. Balats et al.	(ITEP)
Also		PR D55 6625	L.K. Gibbons et al.	(FNAL E731 Collab.)	Also		Translated from YAF 15 93		
GIBBONS	93B	PRL 70 1203	L.K. Gibbons et al.	(FNAL E731 Collab.)	BARMIN	71	PL 35B 604	V.V. Barmin et al.	(ITEP)
GIBBONS	93C	Thesis RX-1487	L.K. Gibbons	(CHIC)	BURGUN	71	LNC 2 1169	G. Burgun et al.	(SACL, CERN, OSLO)
Also		PR D55 6625	L.K. Gibbons et al.	(FNAL E731 Collab.)	CARNEGIE	71	PR D4 1	R.K. Carnegie et al.	(PRIN)
HARRIS	93	PRL 71 3914	D.A. Harris et al.	(EFI, UCLA, COLO+)	CHAN	71	Thesis LBL-350	J.H.S. Chan	(LBL)
HARRIS	93B	PRL 71 3918	D.A. Harris et al.	(EFI, UCLA, COLO+)	CHO	71	PR D3 1557	Y. Cho et al.	(CMU, BNL, CASE)
MAKOFF	93	PRL 70 1591	G. Makoff et al.	(FNAL E731 Collab.)	ENSTRÖM	71	PR D4 2629	J. Enstrom et al.	(SLAC, STAN)
Also		PR D55 2069 (erratum)	G. Makoff et al.	(FNAL E731 Collab.)	Also		Thesis SLAC-0125	J.E. Enstrom	(STAN)
RAMBERG	93	PRL 70 2525	E. Ramberg et al.	(FNAL E731 Collab.)	JAMES	71	PL 52C 265	F. James et al.	(CERN, SAFL, OSLO)
RAMBERG	93B	PRL 70 2529	E.J. Ramberg et al.	(FNAL E731 Collab.)	MEISNER	71	PR D3 59	M.A. Meisner et al.	(MASA, BNL, YALE)
VAGINS	93	PRL 71 35	M.R. Vagins et al.	(BNL E845 Collab.)	REPPELLIN	71	PL 36B 603	J.P. Repellin et al.	(ORSAY, CERN)
ADLER	92B	PL B286 180	R. Adler et al.	(CLEAR Collab.)	WEBBER	71	PR D3 64	B.R. Webber et al.	(LRL)
Also		SJNP 55 840	R. Adler et al.	(CLEAR Collab.)	Also		PRL 21 498	B.R. Webber et al.	(LRL)
BARR	92	PL B284 440	G.D. Barr et al.	(CERN, EDIN, MAINZ, LALO+)	Also		Thesis UCLR 19226	B.R. Webber	(LRL)
MORSE	92	PR D45 36	W.M. Morse et al.	(BNL, YALE, VASS)	WOLFF	71	PL 36B 517	B. Wolff et al.	(ORSAY, CERN)
PDG	92	PR D45 51	K. Hikasa et al.	(KEK, LBL, BOST+)	ALBROW	70	PL 33B 516	M.G. Albrow et al.	(MCHS, DARE)
SOMALWAR	92	PRL 68 2580	S.V. Somalwar et al.	(FNAL E731 Collab.)	ARONSON	70	PRL 25 1057	S.H. Aronson et al.	(EFI, ILLC, SLAC)
AKAGI	91B	PR 67 2618	T. Akagi et al.	(TOHOK, TOKY, KYOT, KEK)	BARMIN	70	PL 33B 377	V.V. Barmin et al.	(ITEP, JINR)
BARR	91	PL B259 389	G.D. Barr et al.	(CERN, EDIN, MAINZ, LALO+)	BASILE	70	PR D2 78	P. Basile et al.	(SACL)
HEINSON	91	PR D44 1	A.P. Heinson et al.	(UCL, UCLA, LANL+)	BECHERRAWY	70	PR D1 1452	T. Bechererawy	(ROCH)
PAPADIMITR...	91	PR D44 573	V. Papadimitriou et al.	(FNAL E731 Collab.)	BUCHANAN	70	PL 33B 623	C.D. Buchanan et al.	(SLAC, JHU, UCLA)
BARKER	90	PR D41 3546	A.R. Barker et al.	(FNAL E731 Collab.)	Also		Private Comm.	A.J. Cox	
Also		PRL 61 2661	L.K. Gibbons et al.	(FNAL E731 Collab.)	BUZAGOV	70	PR D2 815	I.A. Budagov et al.	(CERN, ORSAY, EPOL)
BARR	90B	PL B240 283	G.D. Barr et al.	(CERN, EDIN, MAINZ, LALO+)	Also		PR D2B 215	I.A. Budagov et al.	(CERN, ORSAY, EPOL)
BARR	90C	PL B242 523	G.D. Barr et al.	(CERN, EDIN, MAINZ, LALO+)	CHO	70	PR D1 3031	Y. Cho et al.	(CMU, BNL, CASE)
CAROSI	90	PL B237 303	R. Carosi et al.	(CERN, EDIN, MAINZ, LALO+)	Also		PRL 19 668	D.G. Hill et al.	(BNL, CMU)
KARLSSON	90	PRL 64 2976	M. Karlsson et al.	(FNAL E731 Collab.)	CHOLLET	70	PL 31B 658	J.C. Chollet et al.	(BNL, CMU)
OHL	90	PRL 64 2755	K.E. Ohi et al.	(BNL E845 Collab.)	CULLEN	70	PL 32B 523	M. Cullen et al.	(AACH, CERN, TORI)
OHL	90B	PRL 65 1407	K.E. Ohi et al.	(BNL E845 Collab.)	MARX	70	PL 32B 219		

Meson Particle Listings

$K_L^0, K_0^*(700)$

ABRAMS	68B	PR 176 1603	R. J. Abrams et al.	(ILL)
ARNOLD	68B	PL 28B 56	R. G. Arnold et al.	(CERN, ORSAY)
BASILE	68B	PL 28B 58	P. Basile et al.	(SACL)
BENNETT	68	PL 27B 244	S. Bennett et al.	(COLU, CERN)
BLANPIED	68	PRL 21 1650	W.A. Blanpied et al.	(CASE, HARV, MCGI)
BOHM	68B	PL 27B 594	A. Bohm et al.	
BU DAGOV	68	NC 57A 182	I.A. Budagov et al.	(CERN, ORSAY, IPNP)
Also		PL 28B 215	I.A. Budagov et al.	(CERN, ORSAY, EPOL)
JAMES	68	NP B9 365	F. James, H. Briand	(IPNP, CERN)
Also		PRL 21 257	J.A. Helland, M.J. Longo, K.K. Young	(UCLA, MICH)
KULYUKINA	68	JETP 26 20	L.A. Kulyukina et al.	(JINR)
Also		Translated from ZETF 53 29		
KUNZ	68	Thesis PU-68-46	P.F. Kunz	(PRIN)
BENNETT	67	PRL 19 993	S. Bennett et al.	(COLU)
DEBOUARD	67	NC 52A 662	X. de Bouard et al.	(CERN)
Also		PL 15 58	X. de Bouard et al.	(CERN, ORSAY, MPIM)
DEVLIN	67	PRL 18 54	T.J. Devlin et al.	(PRIN, UMD)
Also		PR 169 1045	G.A. Sayer et al.	(UMD, FPA, PRIN)
DORFAN	67	PRL 19 887	D.E. Dorfman et al.	(SLAC, LRL)
FELDMAN	67B	PR 155 1611	L. Feldman et al.	(PENN)
FITCH	67	PR 164 1711	V.L. Fitch et al.	(PRIN)
GINSBERG	67	PR 162 1570	E.S. Ginsberg	(MASB)
HILL	67	PRL 19 668	D.G. Hill et al.	(BNL, CMU)
HOPKINS	67	PRL 19 185	H.W.K. Hopkins, T.C. Bacon, F.R. Eisler	(BNL)
NEFKENS	67	PR 157 1233	B.M.K. Nefkens et al.	(ILL)
SCHMIDT	67	Thesis Nevis 160	P. Schmidt	(COLU)
BEHR	66	PL 22 540	L. Behr et al.	(EPOL, MILA, PADO, ORSAY)
HAWKINS	66	PL 21 238	C.J.B. Hawkins	(YALE)
Also		PR 156 1444	C.J.B. Hawkins	(YALE)
ANDERSON	65	PRL 14 475	J.A. Anderson et al.	(LRL, WISC)
ASTBURY	65B	PL 18 175	P. Astbury et al.	(CERN, ZURI)
AUBERT	65	PL 17 59	B. Aubert et al.	(EPOL, ORSAY)
Also		PL 24B 75	J.P. Lowys et al.	(EPOL, ORSAY)
BALDO...	65	NC 38 684	M. Baldo-Geolin et al.	(PADO)
FRANZINI	65	PR 140 B127	P. Franzini et al.	(COLU, YUTG)
GUIDONI	65	Argonne Conf. 49	P. Guidoni et al.	(BNL, RAL)
HOPKINS	65	Argonne Conf. 67	H.W.K. Hopkins, T.C. Bacon, F. Eisler	(VAND+)
ALEKSANYAN	64B	Dubna Conf. 2 102	A.S. Aleksanyan et al.	(YERE)
Also		JETP 19 1019	A.S. Aleksanyan et al.	(LEBD, MPEI, YERE)
Also		Translated from ZETF 46 150A		
ANIKINA	64	JETP 19 42	M.K. Anikina et al.	(GEOR, JINR)
Also		Translated from ZETF 46 59		
FITCH	61	NC 22 1160	V.L. Fitch, P.A. Piroué, R.B. Perkins	(PRIN+)
GOOD	61	PR 124 1223	R.H. Good et al.	(LRL)

OTHER RELATED PAPERS

HAYAKAWA	93	PR D48 1150	M. Hayakawa, A.I. Sanda	(NAGO)
Also		"Searching for $T, CP, CPT, \Delta S = \Delta Q$ Rule Violations in the Neutral K Meson System: A Guide"		
LITTENBERG	93	ARNPS 43 729	L.S. Littenberg, G. Valencia	(BNL, FNAL)
Also		Rare and Radiative Kaon Decays		
RITCHIE	93	RMP 65 1149	J.L. Ritchie, S.G. Wojcicki	
Also		"Rare K Decays"		
WINSTEIN	93	RMP 65 1113	B. Winstein, L. Wolfenstein	
Also		"The Search for Direct CP Violation"		
BATTISTON	92	PRPL 214 293	R. Battiston et al.	(PGIA, CERN, TRSTT)
Also		Status and Perspectives of K Decay Physics		
DIB	92	PR D46 2265	C.O. Dib, R.D. Peccei	(UCLA)
Also		Tests of CP conservation in the neutral kaon system.		
KLEINKNECHT	92	CNPP 20 281	K. Kleinknecht	(MAINZ)
Also		New Results on CP Violation in Decays of Neutral K Mesons.		
KLEINKNECHT	90	ZPHY C46 557	K. Kleinknecht	(MAINZ)
PEACH	90	JP G16 131	K.J. Peach	(EDIN)
BRYMAN	89	JMP A4 79	D.A. Bryman	(TRIU)
Also		"Rare Kaon Decays"		
KLEINKNECHT	76	ARNS 26 1	K. Kleinknecht	(DORT)
GINSBERG	73	PR D8 3887	E.S. Ginsberg, J. Smith	(MIT, STON)
GINSBERG	70	PR D1 229	E.S. Ginsberg	(HAIF)
HEUSSE	70	LNC 3 449	P. Heusse et al.	(ORSAY)
CRONIN	68C	Vienna Conf. 281	J.W. Cronin	(PRIN)
RUBBIA	67	PL 24B 531	C. Rubbia, J. Steinberger	(CERN, COLU)
Also		PL 23 167	C. Rubbia, J. Steinberger	(CERN, COLU)
Also		PL 20 207	C. Alfi-Steinberger et al.	(CERN)
Also		PL 21 595	C. Alfi-Steinberger et al.	(CERN)
AUERBACH	66	PR 149 1052	L.B. Auerbach et al.	(PENN)
Also		PRL 14 192	L.B. Auerbach et al.	(PENN)
FIRESTONE	66B	PRL 17 116	A. Firestone et al.	(YALE, BNL)
BEHR	65	Argonne Conf. 59	L. Behr et al.	(EPOL, MILA, PADO)
MESTVIRSHIL	65	JINR P 2449	A.N. Mestvirishvili et al.	(JINR)
TRILLING	65B	UCRL 16473	G.N. Trilling	(LRL)
Also		Updated from 1965 Argonne Conference, page 115.		
JOVANOV...	63	BNL Conf. 42	J.V. Jovanovich et al.	(BNL, UMD)

$K_0^*(700)$

$$J(J^P) = \frac{1}{2}(0^+)$$

also known as κ ; was $K_0^*(800)$
See the related review(s):
Scalar Mesons below 1 GeV

$K_0^*(700)$ T-Matrix Pole \sqrt{s}

VALUE (MeV)	DOCUMENT ID	TECN	COMMENT
(630-730) - i (260-340)	OUR ESTIMATE	(see Fig. 64.1 in the review)	
••• We do not use the following data for averages, fits, limits, etc. •••			
(648 \pm 7) - i (280 \pm 16)	¹ PELAEZ	20 RVUE	$\pi K \rightarrow \pi K$
(670 \pm 18) - i (295 \pm 28)	² PELAEZ	17 RVUE	$\pi K \rightarrow \pi K$
(764 \pm 63 $^{+71}_{-54}$) - i (306 \pm 149 $^{+143}_{-85}$)	³ ABLIKIM	11B BES2	1.3k $J/\psi \rightarrow K_S^0 K_S^0 \pi^+ \pi^-$
(665 \pm 9) - i (268 $^{+21}_{-6}$)	⁴ GUO	11B RVUE	
(849 \pm 77 $^{+18}_{-14}$) - i (256 \pm 40 $^{+46}_{-22}$)	³ ABLIKIM	10E BES2	1.4k $J/\psi \rightarrow K^\pm K_S^0 \pi^\mp \pi^0$
(663 \pm 8 \pm 34) - i (329 \pm 5 \pm 22)	⁵ BUGG	10 RVUE	S-matrix pole
(706.0 \pm 1.8 \pm 22.8) - i (319.4 \pm 2.2 \pm 20.2)	⁶ BONVICINI	08A CLEO	141k $D^+ \rightarrow K^- \pi^+ \pi^+$
(841 \pm 30 $^{+81}_{-73}$) - i (309 \pm 45 $^{+48}_{-72}$)	³ ABLIKIM	06C BES2	25k $J/\psi \rightarrow \bar{K}^*(892)^0 K^+ \pi^-$

(750 $^{+30}_{-55}$) - i (342 \pm 60)	⁷ BUGG	06 RVUE	
(658 \pm 13) - i (279 \pm 12)	⁸ DESCOTES-G.	06 RVUE	$\pi K \rightarrow \pi K$
(757 \pm 33) - i (279 \pm 41)	⁹ GUO	06 RVUE	
(694 \pm 53) - i (303 \pm 30)	¹⁰ ZHOU	06 RVUE	$K p \rightarrow K^- \pi^+ n$
(594 \pm 79) - i (362 \pm 166)	¹⁰ ZHENG	04 RVUE	$K^- p \rightarrow K^- \pi^+ n$
(722 \pm 60) - i (386 \pm 50)	¹⁰ BUGG	03 RVUE	11 $K^- p \rightarrow K^- \pi^+ n$
(875 \pm 75) - i (335 \pm 110)	¹¹ ISHIDA	97B RVUE	11 $K^- p \rightarrow K^- \pi^+ n$
727 - i 263	¹² VANBEVEREN	86 RVUE	

- 1 Extracted employing πK partial wave analysis from ESTABROOKS 78 and ASTON 88, Roy-Steiner equations and once subtracted forward dispersion relations.
- 2 Reanalysis of ESTABROOKS 78 and ASTON 88 satisfying Forward Dispersion Relations and using sequences of Pade approximants.
- 3 Extracted from Breit-Wigner parameters.
- 4 Fit to scattering phase shifts using UChPT amplitudes with explicit resonances.
- 5 Supersedes BUGG 06. Combined analysis of ASTON 88, ABLIKIM 06c, AITALA 06, and LINK 09 using an s -dependent width with couplings to $K\pi$ and $K\eta'$, and the Adler zero near thresholds.
- 6 From a complex pole included in the fit. Using parameters from the model that fits data best.
- 7 Reanalysis of ASTON 88, AITALA 02, and ABLIKIM 06c using for the κ an s -dependent width with an Adler zero near threshold.
- 8 Using Roy-Steiner equations (ROY 71) consistent with unitarity, analyticity and crossing symmetry constraints.
- 9 From UChPT fitted to MERCER 71, BINGHAM 72 and ESTABROOKS 78. Amplitude shown to be consistent with data of ABLIKIM 06c.
- 10 Reanalysis of ASTON 88 data.
- 11 Reanalysis of ASTON 88 using interfering Breit-Wigner amplitudes. Extracted from Breit-Wigner parameters.
- 12 Unitarized Quark Model.

$K_0^*(700)$ Breit-Wigner Mass

VALUE (MeV)	EVTS	DOCUMENT ID	TECN	COMMENT
845 \pm 17	OUR AVERAGE			
826 \pm 49	$^{+49}_{-34}$	1.3k	¹ ABLIKIM	11B BES2 $J/\psi \rightarrow K_S^0 K_S^0 \pi^+ \pi^-$
810 \pm 68	$^{+15}_{-24}$	1.4k	² ABLIKIM	10E BES2 $J/\psi \rightarrow K^\pm K_S^0 \pi^\mp \pi^0$
856 \pm 17	\pm 13	54k	LINK	07B FOCS $D^+ \rightarrow K^- \pi^+ \pi^+$
878 \pm 23	$^{+64}_{-55}$	25k	³ ABLIKIM	06C BES2 $J/\psi \rightarrow \bar{K}^*(892)^0 K^+ \pi^-$
797 \pm 19	\pm 43	15k	^{4,5} AITALA	02 E791 $D^+ \rightarrow K^- \pi^+ \pi^+$
••• We do not use the following data for averages, fits, limits, etc. •••				
888.0 \pm 1.9	141k	⁶ BONVICINI	08A CLEO	$D^+ \rightarrow K^- \pi^+ \pi^+$
855 \pm 15	0.6k	⁷ CAWLFIELD	06A CLEO	$D^0 \rightarrow K^+ K^- \pi^0$
905 $^{+65}_{-30}$		⁸ ISHIDA	97B RVUE	11 $K^- p \rightarrow K^- \pi^+ n$

- 1 The Breit-Wigner parameters from a fit with seven intermediate resonances. The S-matrix pole position is (764 \pm 63 $^{+71}_{-54}$) - i (306 \pm 149 $^{+143}_{-85}$) MeV.
- 2 From a fit including ten additional resonances and energy-independent Breit-Wigner width.
- 3 A fit in the $K_0^*(700) + K^*(892) + K^*(1410)$ model with mass and width of the $K_0^*(700)$ from ABLIKIM 06c well describes the left slope of the $K_S^0 \pi^-$ invariant mass spectrum from $\tau^- \rightarrow K_S^0 \pi^- \nu_\tau$ decay studied by EPIFANOV 07. Averaged value from different parameterizations.
- 4 Not seen by KOPP 01 using 7070 events of $D^0 \rightarrow K^- \pi^+ \pi^0$. LINK 02e and LINK 05i show clear evidence for a constant non-resonant scalar amplitude rather than $K_0^*(700)$ in their high statistics analysis of $D^+ \rightarrow K^- \pi^+ \mu^+ \nu_\mu$.
- 5 AUBERT 07t does not find evidence for the charged $K_0^*(700)$ using 11k events of $D^0 \rightarrow K^- K^+ \pi^0$.
- 6 Using parameters from the model that fits data best.
- 7 Breit-Wigner parameters. A significant S-wave can be also modeled as a non-resonant contribution.
- 8 Reanalysis of ASTON 88 using interfering Breit-Wigner amplitudes.

$K_0^*(700)$ Breit-Wigner Width

VALUE (MeV)	EVTS	DOCUMENT ID	TECN	COMMENT
468 \pm 30	OUR AVERAGE			
449 \pm 156	$^{+144}_{-81}$	1.3k	¹ ABLIKIM	11B BES2 $J/\psi \rightarrow K_S^0 K_S^0 \pi^+ \pi^-$
536 \pm 87	$^{+106}_{-47}$	1.4k	² ABLIKIM	10E BES2 $J/\psi \rightarrow K^\pm K_S^0 \pi^\mp \pi^0$
464 \pm 28	\pm 22	54k	LINK	07B FOCS $D^+ \rightarrow K^- \pi^+ \pi^+$
499 \pm 52	$^{+55}_{-87}$	25k	³ ABLIKIM	06C BES2 $J/\psi \rightarrow \bar{K}^*(892)^0 K^+ \pi^-$
410 \pm 43	\pm 87	15k	^{4,5} AITALA	02 E791 $D^+ \rightarrow K^- \pi^+ \pi^+$
••• We do not use the following data for averages, fits, limits, etc. •••				
550.4 \pm 11.8	141k	⁶ BONVICINI	08A CLEO	$D^+ \rightarrow K^- \pi^+ \pi^+$
251 \pm 48	0.6k	⁷ CAWLFIELD	06A CLEO	$D^0 \rightarrow K^+ K^- \pi^0$
545 $^{+235}_{-110}$		⁸ ISHIDA	97B RVUE	11 $K^- p \rightarrow K^- \pi^+ n$

- 1 The Breit-Wigner parameters from a fit with seven intermediate resonances. The S-matrix pole position is (764 \pm 63 $^{+71}_{-54}$) - i (306 \pm 149 $^{+143}_{-85}$) MeV.
- 2 From a fit including ten additional resonances and energy-independent Breit-Wigner width.
- 3 A fit in the $K_0^*(700) + K^*(892) + K^*(1410)$ model with mass and width of the $K_0^*(700)$ from ABLIKIM 06c well describes the left slope of the $K_S^0 \pi^-$ invariant mass spectrum

See key on page 1127

Meson Particle Listings

$K_0^*(700)$, $K^*(892)$

in $\tau^- \rightarrow K_0^0 \pi^- \nu_\tau$ decay studied by EPIFANOV 07. Averaged value from different parameterizations.

4 Not seen by KOPP 01 using 7070 events of $D^0 \rightarrow K^- \pi^+ \pi^0$. LINK 02E and LINK 051 show clear evidence for a constant non-resonant scalar amplitude rather than $K_0^*(700)$ in their high statistics analysis of $D^+ \rightarrow K^- \pi^+ \mu^+ \nu_\mu$.

5 AUBERT 07T does not find evidence for the charged $K_0^*(700)$ using 11k events of $D^0 \rightarrow K^- K^+ \pi^0$.

6 Using parameters from the model that fits data best.

7 Statistical error only. A fit to the Dalitz plot including the $K_0^*(700)^\pm$, $K^*(892)^\pm$, and ϕ resonances modeled as Breit-Wigners. A significant S-wave can be also modeled as a non-resonant contribution.

8 Reanalysis of ASTON 88 using interfering Breit-Wigner amplitudes.

$K_0^*(700)$ DECAY MODES

Table with 2 columns: Mode, Fraction (Γ_i/Γ)

$K_0^*(700)$ REFERENCES

List of references for K0*(700) including PELA EZ, ABLIKIM, GUO, etc.

Continuation of references for K0*(700) and K*(892) including AGUILAR..., CRENNELL, BARLOW, etc.

- 1 Inclusive reaction. Complicated background and phase-space effects.
2 Mass errors enlarged by us to Γ/\sqrt{N} . See note.
3 Number of events in peak reevaluated by us.
4 From a Dalitz plot analysis in an isobar model with charged and neutral K*(892) masses and widths floating.
5 Average of fit results with different parameterizations for the K pi S-wave.
6 K-matrix pole.
7 From a partial wave amplitude analysis.

CHARGED ONLY, PRODUCED IN τ LEPTON DECAYS

Table with 5 columns: VALUE (MeV), EVTS, DOCUMENT ID, TECN, COMMENT

- 1 From a fit in the $K_0^*(700) + K^*(892) + K^*(1410)$ model.
2 From the pole position of the K pi vector form factor using EPIFANOV 07 and constraints from K_{J3} decays in ANTONELLI 10.
3 From the pole position of the K pi vector form factor in the complex s-plane and using EPIFANOV 07 data.
4 Systematic uncertainties not estimated.
5 Reanalysis of EPIFANOV 07 using resonance chiral theory.
6 Calculated by us from the shift by 4.7 ± 0.9 MeV (statistical uncertainty only) reported in BONVICINI 02 with respect to the world average value from PDG 00.
7 With mass and width of the $K^*(1410)$ fixed at 1412 MeV and 227 MeV, respectively.

$K^*(892)$

$I(J^P) = \frac{1}{2}(1^-)$

$K^*(892)$ T-Matrix Pole \sqrt{s}

Table with 5 columns: VALUE (MeV), DOCUMENT ID, TECN, COMMENT

- 1 Extracted employing πK partial wave analysis from ESTABROOKS 78 and ASTON 88, Roy-Steiner equations and once subtracted forward dispersion relations.
2 Reanalysis of ESTABROOKS 78 and ASTON 88 satisfying Forward Dispersion Relations and using sequences of Padé approximants.
3 Reanalysis of data from ESTABROOKS 78 and ASTON 88 in the unitarized ChPT model.

$K^*(892)$ MASS

CHARGED ONLY, HADROPRODUCED

Table with 5 columns: VALUE (MeV), EVTS, DOCUMENT ID, TECN, CHG, COMMENT

NEUTRAL ONLY

Table with 5 columns: VALUE (MeV), EVTS, DOCUMENT ID, TECN, COMMENT

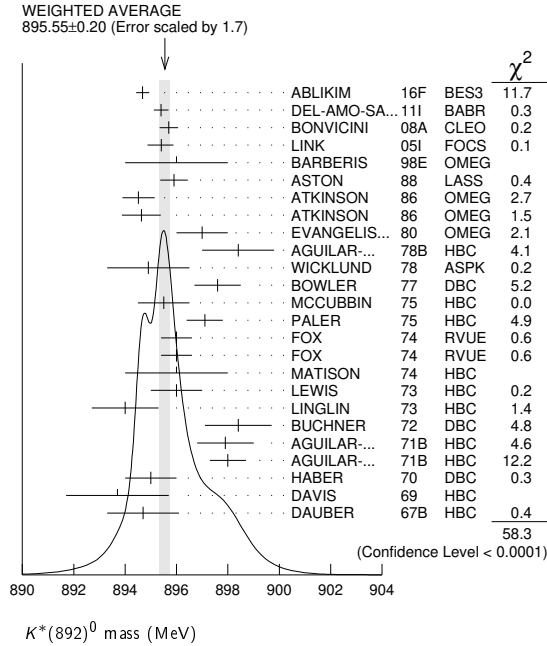
Meson Particle Listings

$K^*(892)$

• • • We do not use the following data for averages, fits, limits, etc. • • •

895.50 ± 0.92 ± 2.6		9 ADUSZKIEW...20A	NA61	158	pp
898.1 ± 1.0	4k	10 LEES	17C	BABR	$J/\psi \rightarrow K_S^0 K^\pm \pi^\mp$
895.53 ± 0.17		LEES	13F	BABR	$D^+ \rightarrow K^+ K^- \pi^+$
894.9 ± 0.5 ± 0.7	14.4k	11 MITCHELL	09A	CLEO	$D_s^+ \rightarrow K^+ K^- \pi^+$
896.2 ± 0.3	20k	12 AUBERT	07AK	BABR	$10.6 e^+ e^- \rightarrow K^* \pi^0 \gamma$
900.7 ± 1.1	5900	BARTH	83	HBC	$70 K^+ p \rightarrow K^+ \pi^- X$

- ¹ Taking also into account the $K_0^*(1430)^0$ and $K_2^*(1430)^0$.
- ² Taking into account the $K^*(892)^0$, S -wave and P -wave ($K^*(1410)^0$).
- ³ From the isobar model with a complex pole for the κ .
- ⁴ Fit to $K\pi$ mass spectrum includes a non-resonant scalar component.
- ⁵ Inclusive reaction. Complicated background and phase-space effects.
- ⁶ From pole extrapolation.
- ⁷ Mass errors enlarged by us to Γ/\sqrt{N} . See note.
- ⁸ Number of events in peak reevaluated by us.
- ⁹ For transverse momenta between 0.6 and 0.8 GeV/c and rapidity $0 < y < 0.5$.
- ¹⁰ From a Dalitz plot analysis in an isobar model with charged and neutral $K^*(892)$ masses and widths floating.
- ¹¹ This value comes from a fit with χ^2 of 178/117.
- ¹² Systematic uncertainties not estimated.



$K^*(892)$ MASSES AND MASS DIFFERENCES

Unrealistically small errors have been reported by some experiments. We use simple “realistic” tests for the minimum errors on the determination of a mass and width from a sample of N events:

$$\delta_{\min}(m) = \frac{\Gamma}{\sqrt{N}}, \quad \delta_{\min}(\Gamma) = 4 \frac{\Gamma}{\sqrt{N}}. \quad (1)$$

We consistently increase unrealistic errors before averaging. For a detailed discussion, see the 1971 edition of this Note.

VALUE (MeV)	EVTS	DOCUMENT ID	TECN	CHG	COMMENT
6.7 ± 1.2 OUR AVERAGE					
7.7 ± 1.7	2980	AGUILAR...	78B	HBC	$\pm 0.76 \bar{p} p \rightarrow K^\mp K_S^0 \pi^\pm$
5.7 ± 1.7	7338	AGUILAR...	71B	HBC	$-0.3, 9.4, 6 K^- p$
6.3 ± 4.1	283	¹ BARASH	67B	HBC	$0.0 \bar{p} p$

¹ Number of events in peak reevaluated by us.

$K^*(892)$ RANGE PARAMETER

All from partial wave amplitude analyses.

VALUE (GeV ⁻¹)	EVTS	DOCUMENT ID	TECN	CHG	COMMENT
2.1 ± 0.5 ± 0.5	243k	¹ DEL-AMO-SA..111	BABR	0	$D^+ \rightarrow K^- \pi^+ e^+ \nu_e$
3.96 ± 0.54 ± 1.31	18k	² LINK	05I	FOCS	$D^+ \rightarrow K^- \pi^+ \mu^+ \nu_\mu$
3.4 ± 0.7		ASTON	88	LASS	0 11 $K^- p \rightarrow K^- \pi^+ n$
12.1 ± 3.2 ± 3.0		BIRD	89	LASS	- 11 $K^- p \rightarrow \bar{K}^0 \pi^- p$

• • • We do not use the following data for averages, fits, limits, etc. • • •

- ¹ Taking into account the $K^*(892)^0$, S -wave and P -wave ($K^*(1410)^0$).
- ² Fit to $K\pi$ mass spectrum includes a non-resonant scalar component.

$K^*(892)$ WIDTH

CHARGED ONLY, HADROPRODUCED

VALUE (MeV)	EVTS	DOCUMENT ID	TECN	CHG	COMMENT
51.4 ± 0.8 OUR FIT					
51.4 ± 0.8 OUR AVERAGE					
54.4 ± 0.9 ± 1.7		ALBRECHT	20	CBAR	$0.9 \bar{p} p \rightarrow K^+ K^- \pi^0$
49 ± 2	5840	BAUBILLIER	84B	HBC	- 8.25 $K^- p \rightarrow \bar{K}^0 \pi^- p$
56 ± 4		NAPIER	84	SPEC	- 200 $\pi^- p \rightarrow 2K_S^0 X$
51 ± 2	4100	TOAFF	81	HBC	- 6.5 $K^- p \rightarrow \bar{K}^0 \pi^- p$
50.5 ± 5.6		AJINENKO	80	HBC	+ 32 $K^+ p \rightarrow K^0 \pi^+ X$
45.8 ± 3.6	1800	AGUILAR...	78B	HBC	$\pm 0.76 \bar{p} p \rightarrow K^\mp K_S^0 \pi^\pm$
52.0 ± 2.5	6706	¹ COOPER	78	HBC	$\pm 0.76 \bar{p} p \rightarrow (K\pi)^\pm X$
52.1 ± 2.2	9000	² PALER	75	HBC	- 14.3 $K^- p \rightarrow (K\pi)^- X$
46.3 ± 6.7	765	¹ CLARK	73	HBC	- 3.13 $K^- p \rightarrow \bar{K}^0 \pi^- p$
48.2 ± 5.7	1150	^{1,3} CLARK	73	HBC	- 3.3 $K^- p \rightarrow \bar{K}^0 \pi^- p$
54.3 ± 3.3	4404	¹ AGUILAR...	71B	HBC	- 3.9, 4.6 $K^- p \rightarrow (K\pi)^- p$
46 ± 5	1700	^{1,3} WOJCICKI	64	HBC	- 1.7 $K^- p \rightarrow \bar{K}^0 \pi^- p$

• • • We do not use the following data for averages, fits, limits, etc. • • •

46.7 ± 0.2 ± 0.1	183k	ABLIKIM	19AQ	BES	$\pm J/\psi \rightarrow K^+ K^- \pi^0$
43.6 ± 1.3	4k	⁴ LEES	17C	BABR	$J/\psi \rightarrow K_S^0 K^\pm \pi^\mp$
47.2 ± 0.3 ± 2.3	190k	⁵ AAIJ	16N	LHCB	$D^0 \rightarrow K_S^0 K^\pm \pi^\mp$
54.8 ± 1.7	27k	⁶ ABELE	99D	CBAR	$\pm 0.0 \bar{p} p \rightarrow K^+ K^- \pi^0$
45.2 ± 1 ± 2	80k	⁷ BIRD	89C	LASS	- 11 $K^- p \rightarrow \bar{K}^0 \pi^- p$
42.8 ± 7.1	3700	BARTH	83	HBC	+ 70 $K^+ p \rightarrow K^0 \pi^+ X$
64.0 ± 9.2	800	^{1,3} CLELAND	82	SPEC	+ 30 $K^+ p \rightarrow K_S^0 \pi^+ p$
62.0 ± 4.4	3200	^{1,3} CLELAND	82	SPEC	+ 50 $K^+ p \rightarrow K_S^0 \pi^+ p$
55 ± 4	3600	^{1,3} CLELAND	82	SPEC	- 50 $K^+ p \rightarrow K_S^0 \pi^- p$
62.6 ± 3.8	380	DELFOSSSE	81	SPEC	+ 50 $K^\pm p \rightarrow K^\pm \pi^0 p$
50.5 ± 3.9	187	DELFOSSSE	81	SPEC	- 50 $K^\pm p \rightarrow K^\pm \pi^0 p$

- ¹ Width errors enlarged by us to $4 \times \Gamma/\sqrt{N}$; see note.
- ² Inclusive reaction. Complicated background and phase-space effects.
- ³ Number of events in peak reevaluated by us.
- ⁴ From a Dalitz plot analysis in an isobar model with charged and neutral $K^*(892)$ masses and widths floating.
- ⁵ Average of fit results with different parametrizations for the $K\pi$ S -wave.
- ⁶ K -matrix pole.
- ⁷ From a partial wave amplitude analysis.

CHARGED ONLY, PRODUCED IN τ LEPTON DECAYS

VALUE (MeV)	EVTS	DOCUMENT ID	TECN	COMMENT
46.2 ± 0.6 ± 1.2	53k	¹ EPIFANOV	07	BELL $\tau^- \rightarrow K_S^0 \pi^- \nu_\tau$
46.5 ± 1.1		² BOITO	10	RVUE $\tau^- \rightarrow K_S^0 \pi^- \nu_\tau$
46.2 ± 0.4		^{3,4} BOITO	09	RVUE $\tau^- \rightarrow K_S^0 \pi^- \nu_\tau$
47.5 ± 0.4		^{4,5} JAMIN	08	RVUE $\tau^- \rightarrow K_S^0 \pi^- \nu_\tau$
55 ± 8		⁶ BARATE	99R	ALEP $\tau^- \rightarrow K^- \pi^0 \nu_\tau$

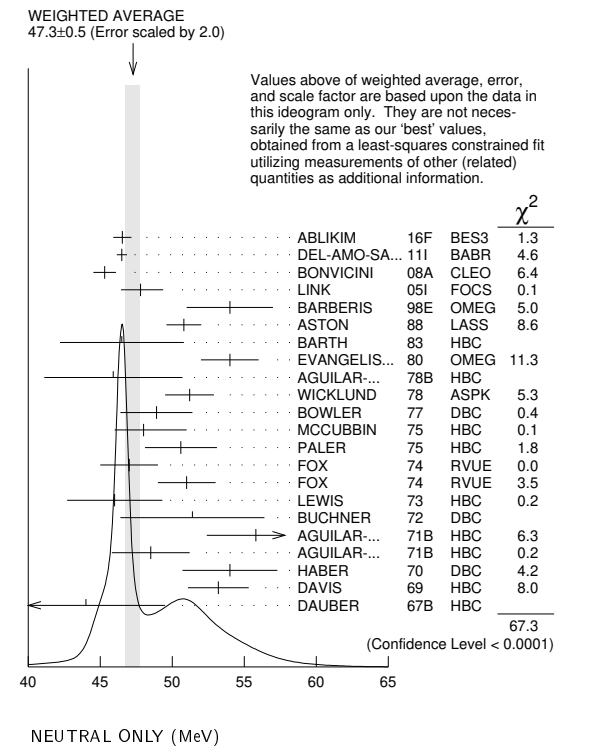
- ¹ From a fit in the $K_0^*(700) + K^*(892) + K^*(1410)$ model.
- ² From the pole position of the $K\pi$ vector form factor using EPIFANOV 07 and constraints from K_{f3} decays in ANTONELLI 10.
- ³ From the pole position of the $K\pi$ vector form factor in the complex s -plane and using EPIFANOV 07 data.
- ⁴ Systematic uncertainties not estimated.
- ⁵ Reanalysis of EPIFANOV 07 using resonance chiral theory.
- ⁶ With mass and width of the $K^*(1410)$ fixed at 1412 MeV and 227 MeV, respectively.

NEUTRAL ONLY

VALUE (MeV)	EVTS	DOCUMENT ID	TECN	COMMENT
47.3 ± 0.5 OUR FIT				Error includes scale factor of 1.9.
47.3 ± 0.5 OUR AVERAGE				Error includes scale factor of 2.0. See the ideogram below.
46.53 ± 0.56 ± 0.31		¹ ABLIKIM	16F	BES3 $D^+ \rightarrow K^- \pi^+ e^+ \nu_e$
46.5 ± 0.3 ± 0.2	243k	² DEL-AMO-SA..111	BABR	$D^+ \rightarrow K^- \pi^+ e^+ \nu_e$
45.3 ± 0.5 ± 0.6	141k	³ BONVICINI	08A	CLEO $D^+ \rightarrow K^- \pi^+ \pi^+$
47.79 ± 0.86 ± 1.32	18k	⁴ LINK	05I	FOCS $D^+ \rightarrow K^- \pi^+ \mu^+ \nu_\mu$
54 ± 3		BARBERIS	98E	OMEG 450 $pp \rightarrow p_f p_S K^* \bar{K}^*$
50.8 ± 0.8 ± 0.9		ASTON	88	LASS 11 $K^- p \rightarrow K^- \pi^+ n$
46.5 ± 4.3	5900	BARTH	83	HBC 70 $K^+ p \rightarrow K^+ \pi^- X$
54 ± 2	28k	EVANGELIS...	80	OMEG 10 $\pi^- p \rightarrow K^+ \pi^- (\Lambda, \Sigma)$

45.9 ± 4.8	1180	AGUILAR...	78B	HBC	0.76 $\bar{p}p \rightarrow K^\mp K_S^0 \pi^\pm$
51.2 ± 1.7		WICKLUND	78	ASP K	3,4,6 $K^\pm N \rightarrow (K\pi)^0 N$
48.9 ± 2.5		BOWLER	77	DBC	5.4 $K^+ d \rightarrow K^+ \pi^- p p$
48 $\begin{smallmatrix} +3 \\ -2 \end{smallmatrix}$	3600	MCCUBBIN	75	HBC	3.6 $K^- p \rightarrow K^- \pi^+ n$
50.6 ± 2.5	22k	⁵ PALER	75	HBC	14.3 $K^- p \rightarrow (K\pi)^0 X$
47 ± 2	10k	FOX	74	RVUE	2 $K^- p \rightarrow K^- \pi^+ n$
51 ± 2		FOX	74	RVUE	2 $K^+ n \rightarrow K^+ \pi^- p$
46.0 ± 3.3	3186	⁶ LEWIS	73	HBC	2.1-2.7 $K^+ p \rightarrow K\pi\pi p$
51.4 ± 5.0	1700	⁶ BUCHNER	72	DBC	4.6 $K^+ n \rightarrow K^+ \pi^- p$
55.8 $\begin{smallmatrix} +4.2 \\ -3.4 \end{smallmatrix}$	2934	⁶ AGUILAR...	71B	HBC	3.9,4.6 $K^- p \rightarrow K^- \pi^+ n$
48.5 ± 2.7	5362	AGUILAR...	71B	HBC	3.9,4.6 $K^- p \rightarrow K^- \pi^+ n$ $K^- \pi^+ \pi^- p$
54.0 ± 3.3	4300	^{6,7} HABER	70	DBC	3 $K^- N \rightarrow K^- \pi^+ X$
53.2 ± 2.1	10k	⁶ DAVIS	69	HBC	12 $K^+ p \rightarrow K^+ \pi^- \pi^+ p$
44 ± 5.5	1040	⁶ DAUBER	67B	HBC	2.0 $K^- p \rightarrow K^- \pi^+ \pi^- p$
•••		We do not use the following data for averages, fits, limits, etc. •••			
48.8 ± 1.8 ± 2.0		⁸ ADUSZKIEW...20A	NA61	158	pp
52.6 ± 1.7	4k	⁹ LEES	17C	BABR	$J/\psi \rightarrow K_S^0 K^\pm \pi^\mp$
44.90 ± 0.30		LEES	13F	BABR	$D^+ \rightarrow K^+ K^- \pi^+$
45.7 ± 1.1 ± 0.5	14.4k	¹⁰ MITCHELL	09A	CLEO	$D^+ \rightarrow K^+ K^- \pi^+$
50.6 ± 0.9	20k	¹¹ AUBERT	07AK	BABR	10.6 $e^+ e^- \rightarrow K^* K^\pm \pi^\mp \gamma$

- 1 Taking also into account the $K_S^0(1430)^0$ and $K_S^*(1430)^0$.
- 2 Taking into account the $K^*(892)^0$, S-wave and P-wave ($K^*(1410)^0$).
- 3 From the isobar model with a complex pole for the κ .
- 4 Fit to $K\pi$ mass spectrum includes a non-resonant scalar component.
- 5 Inclusive reaction. Complicated background and phase-space effects.
- 6 Width errors enlarged by us to $4 \times \Gamma/\sqrt{N}$; see note.
- 7 Number of events in peak reevaluated by us.
- 8 For transverse momenta between 0.6 and 0.8 GeV/c and rapidity $0 < y < 0.5$.
- 9 From a Dalitz plot analysis in an isobar model with charged and neutral $K^*(892)$ masses and widths floating.
- 10 This value comes from a fit with χ^2 of 178/117.
- 11 Systematic uncertainties not estimated.



$K^*(892)$ DECAY MODES

Mode	Fraction (Γ_i/Γ)	Confidence level
Γ_1 $K\pi$	~ 100	%
Γ_2 $(K\pi)^\pm$	(99.902 ± 0.009)	%
Γ_3 $(K\pi)^0$	(99.754 ± 0.021)	%
Γ_4 $K^0 \gamma$	(2.46 ± 0.21)	$\times 10^{-3}$
Γ_5 $K^\pm \gamma$	(9.8 ± 0.9)	$\times 10^{-4}$
Γ_6 $K\pi\pi$	< 7	$\times 10^{-4}$ 95%

CONSTRAINED FIT INFORMATION

An overall fit to the total width and a partial width uses 14 measurements and one constraint to determine 3 parameters. The overall fit has a $\chi^2 = 10.7$ for 12 degrees of freedom.

The following *off-diagonal* array elements are the correlation coefficients $\langle \delta p_i \delta p_j \rangle / (\delta p_i \delta p_j)$, in percent, from the fit to parameters p_i , including the branching fractions, $x_i \equiv \Gamma_i/\Gamma_{total}$. The fit constrains the x_i whose labels appear in this array to sum to one.

$$\Gamma \begin{matrix} & x_5 & \\ & \begin{matrix} -100 & \\ 17 & -17 \end{matrix} & \\ x_2 & & x_5 \end{matrix}$$

Mode	Rate (MeV)
Γ_2 $(K\pi)^\pm$	51.4 ± 0.8
Γ_5 $K^\pm \gamma$	0.050 ± 0.005

CONSTRAINED FIT INFORMATION

An overall fit to the total width and a partial width uses 23 measurements and one constraint to determine 3 parameters. The overall fit has a $\chi^2 = 68.4$ for 21 degrees of freedom.

The following *off-diagonal* array elements are the correlation coefficients $\langle \delta p_i \delta p_j \rangle / (\delta p_i \delta p_j)$, in percent, from the fit to parameters p_i , including the branching fractions, $x_i \equiv \Gamma_i/\Gamma_{total}$. The fit constrains the x_i whose labels appear in this array to sum to one.

$$\Gamma \begin{matrix} & x_4 & \\ & \begin{matrix} -100 & \\ 12 & -12 \end{matrix} & \\ x_3 & & x_4 \end{matrix}$$

Mode	Rate (MeV)	Scale factor
Γ_3 $(K\pi)^0$	47.2 ± 0.5	1.9
Γ_4 $K^0 \gamma$	0.117 ± 0.010	

$K^*(892)$ PARTIAL WIDTHS

$\Gamma(K^0 \gamma)$						Γ_4
VALUE (keV)	EVTS	DOCUMENT ID	TECN	CHG	COMMENT	
116 ± 10 OUR FIT						
116.5 ± 9.9	584	CARLSMITH	86	SPEC	0	$K_L^0 A \rightarrow K_S^0 \pi^0 A$
$\Gamma(K^\pm \gamma)$						Γ_5
VALUE (keV)		DOCUMENT ID	TECN	CHG	COMMENT	
50 ± 5 OUR FIT						
50 ± 5 OUR AVERAGE						
48 ± 11		BERG	83	SPEC	-	156 $K^- A \rightarrow \bar{K} \pi A$
51 ± 5		CHANDLEE	83	SPEC	+	200 $K^+ A \rightarrow K \pi A$

$K^*(892)$ BRANCHING RATIOS

$\Gamma(K^0 \gamma)/\Gamma_{total}$					Γ_4/Γ	
VALUE (units 10^{-3})		DOCUMENT ID	TECN	CHG	COMMENT	
2.46 ± 0.21 OUR FIT						
•••	We do not use the following data for averages, fits, limits, etc. •••					
1.5 ± 0.7		CARITHERS	75B	CNTR	0	8-16 $\bar{K}^0 A$
$\Gamma(K^\pm \gamma)/\Gamma_{total}$					Γ_5/Γ	
VALUE (units 10^{-3})	CL%	DOCUMENT ID	TECN	CHG	COMMENT	
0.98 ± 0.09 OUR FIT						
•••	We do not use the following data for averages, fits, limits, etc. •••					
< 1.6	95	BEMPORAD	73	CNTR	+	10-16 $K^+ A$
$\Gamma(K\pi\pi)/\Gamma((K\pi)^\pm)$					Γ_6/Γ_2	
VALUE	CL%	DOCUMENT ID	TECN	CHG	COMMENT	
< 7 × 10⁻⁴	95	JONGEJANS	78	HBC		4 $K^- p \rightarrow p \bar{K}^0 2\pi$
•••	We do not use the following data for averages, fits, limits, etc. •••					
< 20 × 10 ⁻⁴		WOJCICKI	64	HBC	-	1.7 $K^- p \rightarrow \bar{K}^0 \pi^- p$

$K^*(892)$ REFERENCES

ADUSZKIEW... 20A	EPJ C80 460	A. Aduszkiewicz et al.	(CERN NA61 Collab.)
ALBRECHT 20	EPJ C80 453	M. Albrecht et al.	(Crystal Barrel Collab.)
PELAEZ 20	PRL 124 172001	J.R. Pelaez et al.	
ABLIKIM 19AQ	PR D100 032004	M. Ablikim et al.	(BESIII Collab.)
LEES 17C	PR D95 072007	J.P. Lees et al.	(BABAR Collab.)
PELAEZ 17	EPJ C77 91	J.R. Pelaez, A.Rodas, J.R. de Elvira	
AAIJ 16N	PR D93 052018	R. Aaij et al.	(LHCb Collab.)
ABLIKIM 16F	PR D94 032001	M. Ablikim et al.	(BESIII Collab.)
LEES 13F	PR D87 052010	J.P. Lees et al.	(BABAR Collab.)

Meson Particle Listings

$K^*(892)$, $K_1(1270)$

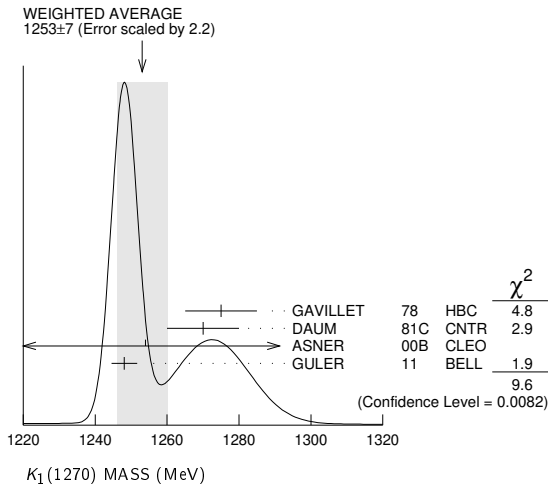
DEL-AMO-SA...	111	PR D83 072001	P. del Amo Sanchez et al.	(BABAR Collab.)
ANTONELLI	10	EPJ C69 399	M. Antonelli et al.	(FlavorNet Working Group)
BOITO	10	JHEP 1009 031	D.R. Boito, R. Escribano, M. Jamin	(BARC)
BOITO	09	EPJ C59 821	D.R. Boito, R. Escribano, M. Jamin	
MITCHELL	09A	PR D79 072008	R.E. Mitchell et al.	(CLEO Collab.)
BONVICINI	08A	PR D78 052001	G. Bonvicini et al.	(CLEO Collab.)
JAMIN	08	PL B664 78	M. Jamin, A. Pich, J. Portoles	
AUBERT	07AK	PR D76 012008	B. Aubert et al.	(BABAR Collab.)
EPIFANOV	07	PL B654 65	D. Epifanov et al.	(BELLE Collab.)
LINK	05I	PL B621 72	J.M. Link et al.	(FNAL FOCUS Collab.)
PELAEZ	04A	MPL A19 2879	J.R. Pelaez	(MADU)
BONVICINI	02	PRL 88 11803	G. Bonvicini et al.	(CLEO Collab.)
PDG	00	EPJ C15 1	D.E. Groom et al.	(PDG Collab.)
ABELE	99D	PL B468 178	A. Abele et al.	(Crystal Barrel Collab.)
BARATE	99R	EPJ C11 599	R. Barate et al.	(ALEPH Collab.)
BARBERIS	98E	PL B436 204	D. Barberis et al.	(Omega Expt.)
BIRD	89	SLAC-332	P.F. Bird	(SLAC)
ASTON	88	NP B296 493	D. Aston et al.	(SLAC, NAGO, CINC, INUS)
ATKINSON	86	ZPHY C30 521	M. Atkinson et al.	(BONN, CERN, GLAS+)
CARLSMITH	86	PRL 56 18	D. Carlsmith et al.	(EFI, SACL)
BAUBILLIER	84B	ZPHY C26 37	M. Baubillier et al.	(BIRM, CERN, GLAS+)
NAPIER	84	PL 149B 514	A. Napier et al.	(TUFTS, ARIZ, FNAL, FLOR+)
BARTH	83	NP B223 296	M. Barth et al.	(BRUX, CERN, GENO, MONS+)
BERG	83	Thesis UMI 83-21652	D.M. Berg	(ROCH)
CHANDLEE	83	PRL 51 168	C. Chandlee et al.	(ROCH, FNAL, MINN)
CLELAND	82	NP B208 189	W.E. Cleland et al.	(DURH, GEVA, LAUS+)
DELFOSE	81	NP B183 349	A. Delfosse et al.	(GEVA, LAUS)
TOAFF	81	PR D23 1500	S. Toaff et al.	(ANL, KANS)
AJINENKO	80	ZPHY C5 177	I.V. Ajinenko et al.	(SERP, BRUX, MONS+)
EVANGELIS...	80	NP B165 383	C. Evangelista et al.	(BARI, BONN, CERN+)
AGUILAR...	78B	NP B141 101	M. Aguilar-Benitez et al.	(MADR, TATA+)
BALAND	78	NP B140 220	J.F. Baland et al.	(MONS, BELG, CERN+)
COOPER	78	NP B136 365	A.M. Cooper et al.	(TATA, CERN, CDEF+)
ESTABROOKS	78	NP B133 490	P.G. Estabrooks et al.	(MCGI, CARL, DURH+)
Also		PR D17 658	P.G. Estabrooks et al.	(MCGI, CARL, DURH+)
JONGEJANS	78	NP B139 383	B. Jongejans et al.	(ZEEM, CERN, NIJM+)
WICKLUND	78	PR D17 1197	A.B. Wicklund et al.	(ANL)
BOWLER	77	NP B126 31	M.G. Bowler et al.	(OXF)
CARITHERS	75B	PRL 35 349	W.C.J. Carithers et al.	(ROCH, MCGI)
MCCUBBIN	75	NP B86 13	N.A. McCubbin, L. Lyons	(OXF)
PALER	75	NP B96 1	K. Paler et al.	(RHEL, SACL, EPOL)
FOX	74	NP B80 403	G.C. Fox, M.L. Griss	(CIT)
MATTISON	74	PR D9 1872	M.J. Mattison et al.	(LBL)
BEMPORAD	73	NP B51 1	C. Bemporad et al.	(CERN, ETH, LOIC)
CLARK	73	NP B54 432	A.G. Clark, L. Lyons, D. Radojicic	(OXF)
LEWIS	73	NP B60 283	P.H. Lewis et al.	(LOWC, LOIC, CDEF)
LINGLIN	73	NP B55 408	D. Linglin	(CERN)
BUCHNER	72	NP B45 333	K. Buchner et al.	(MPIIM, CERN, BRUX)
AGUILAR...	71B	PR D4 2583	M. Aguilar-Benitez, R.L. Eisner, J.B. Kinson	(BNL)
HABER	70	NP B17 289	B. Haber et al.	(REHO, SACL, BGNA, EPOL)
CRENNELL	69D	PRL 22 487	D.J. Crennell et al.	(BNL)
DAVIS	69	PRL 23 1071	P.J. Davis et al.	(LRL)
SCHWEING...	68	PR 166 1317	F. Schweingruber et al.	(ANL, NWES)
BARASH	67B	PR 156 1399	N. Barash et al.	(COLU)
BARLOW	67	NC 50A 701	J. Barlow et al.	(CERN, CDEF, IRAD, LVP)
DAUBER	67B	PR 153 1403	P.M. Dauber et al.	(UCLA)
DEBAERE	67B	NC 51A 401	W. de Baere et al.	(BRUX, CERN)
WOJCICKI	64	PR 135 B484	S.G. Wojcicki	(LRL)

$K_1(1270)$

$$J^{PC} = \frac{1}{2}(1^+)$$

$K_1(1270)$ MASS

1253 ± 7 OUR AVERAGE Includes data from the 4 datablocks that follow this one. Error includes scale factor of 2.2. See the ideogram below.



PRODUCED BY K^- , BACKWARD SCATTERING, HYPERON EXCHANGE

VALUE (MeV)	EVTs	DOCUMENT ID	TECN	CHG	COMMENT
1275 ± 10	700	GAVILLET	78	HBC	+ 4.2 $K^- p \rightarrow \Xi^- (K\pi\pi)^+$

PRODUCED BY K BEAMS

The data in this block is included in the average printed for a previous datablock.

VALUE (MeV)	EVTs	DOCUMENT ID	TECN	CHG	COMMENT
1270 ± 10	1	DAUM	81C	CNTR	- 63 $K^- p \rightarrow K^- 2\pi p$
~ 1276	2	TORNQVIST	82B	RVUE	
~ 1300		VERGEEST	79	HBC	- 4.2 $K^- p \rightarrow (\bar{K}\pi\pi)^- p$
1289 ± 25	3	CARNEGIE	77	ASPK	± 13 $K^\pm p \rightarrow (K\pi\pi)^\pm p$
~ 1300		BRANDENB...	76	ASPK	± 13 $K^\pm p \rightarrow (K\pi\pi)^\pm p$
~ 1270		OTTER	76	HBC	- 10,14,16 $K^- p \rightarrow (\bar{K}\pi\pi)^- p$
1260		DAVIS	72	HBC	+ 12 $K^+ p$
1234 ± 12		FIRESTONE	72B	DBC	+ 12 $K^+ d$

¹ Well described in the chiral unitary approach of GENG 07 with two poles at 1195 and 1284 MeV and widths of 246 and 146 MeV, respectively.
² From a unitarized quark-model calculation.
³ From a model-dependent fit with Gaussian background to BRANDENBURG 76 data.

PRODUCED BY BEAMS OTHER THAN K MESONS

The data in this block is included in the average printed for a previous datablock.

VALUE (MeV)	EVTs	DOCUMENT ID	TECN	CHG	COMMENT
1248.1 ± 3.3 ± 1.4		GULER	11	BELL	$B^+ \rightarrow J/\psi K^+ \pi^+ \pi^-$
1289.81 ± 0.56 ± 1.66	894k	AAIJ	18A	LHCB	$D^0 \rightarrow K^\mp \pi^\pm \pi^\pm \pi^\mp$
1279 ± 10	25k	¹ ABLKIM	06c	BES2	$J/\psi \rightarrow \bar{K}^*(892)^0 K^+ \pi^-$
1294 ± 10	310	RODEBACK	81	HBC	4 $\pi^- p \rightarrow \Lambda K 2\pi$
1300	40	CRENNELL	72	HBC	4.5 $\pi^- p \rightarrow \Lambda K 2\pi$
1242 ± ⁹ / ₋₁₀		² ASTIER	69	HBC	$\bar{p} p$
1300	45	CRENNELL	67	HBC	6 $\pi^- p \rightarrow \Lambda K 2\pi$

¹ Systematic errors not estimated.
² This was called the C meson.

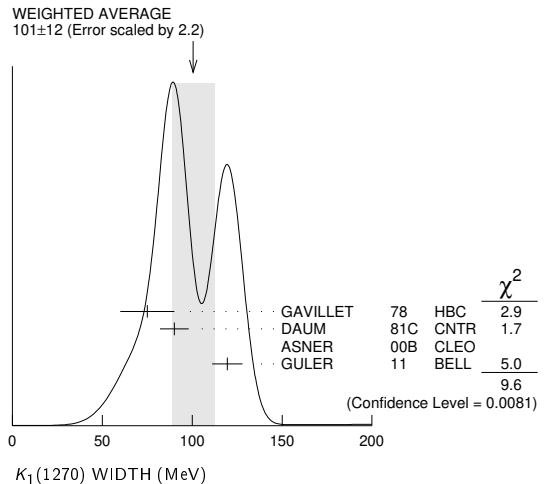
PRODUCED IN τ LEPTON DECAYS

The data in this block is included in the average printed for a previous datablock.

1254 ± 33 ± 34	7k	ASNER	00B	CLEO	± $\tau^- \rightarrow K^- \pi^+ \pi^- \nu_\tau$
-----------------------	----	-------	-----	------	---

$K_1(1270)$ WIDTH

90 ± 20 OUR ESTIMATE This is only an educated guess; the error given is larger than the error on the average of the published values.
101 ± 12 OUR AVERAGE Includes data from the 4 datablocks that follow this one. Error includes scale factor of 2.2. See the ideogram below.



PRODUCED BY K^- , BACKWARD SCATTERING, HYPERON EXCHANGE

VALUE (MeV)	EVTs	DOCUMENT ID	TECN	CHG	COMMENT
75 ± 15	700	GAVILLET	78	HBC	+ 4.2 $K^- p \rightarrow \Xi^- K\pi\pi$

PRODUCED BY K BEAMS

VALUE (MeV)	EVTs	DOCUMENT ID	TECN	CHG	COMMENT
90 ± 8	1	DAUM	81c	CNTR	- 63 $K^- p \rightarrow K^- 2\pi p$

See key on page 1127

Meson Particle Listings

$K_1(1270)$, $K_1(1400)$

••• We do not use the following data for averages, fits, limits, etc. •••

~ 150	VERGEEST	79	HBC	-	4.2	$K^- p \rightarrow (\bar{K}\pi\pi)^- p$
150 ± 71	² CARNEGIE	77	ASPK	±	13	$K^\pm p \rightarrow (K\pi\pi)^\pm p$
~ 200	BRANDENB...	76	ASPK	±	13	$K^\pm p \rightarrow (K\pi\pi)^\pm p$
120	DAVIS	72	HBC	+	12	$K^+ p$
188 ± 21	FIRESTONE	72B	DBC	+	12	$K^+ d$

¹ Well described in the chiral unitary approach of GENG 07 with two poles at 1195 and 1284 MeV and widths of 246 and 146 MeV, respectively.
² From a model-dependent fit with Gaussian background to BRANDENBURG 76 data.

PRODUCED BY BEAMS OTHER THAN K MESONS

VALUE (MeV)	EVTS	DOCUMENT ID	TECN	CHG	COMMENT
-------------	------	-------------	------	-----	---------

The data in this block is included in the average printed for a previous datablock.

119.5 ± 5.2 ± 6.7	GULER	11	BELL	$B^+ \rightarrow J/\psi K^+ \pi^+ \pi^-$
••• We do not use the following data for averages, fits, limits, etc. •••				
116.11 ± 1.65 ± 2.96	894k	AAIJ	18A1	LHCB $D^0 \rightarrow K^\mp \pi^\pm \pi^\pm \pi^\mp$
131 ± 21	25k	¹ ABLIKIM	06c	BES2 $J/\psi \rightarrow \bar{K}^*(892)^0 K^+ \pi^-$
66 ± 15	310	RODEBACK	81	HBC $4 \pi^- p \rightarrow \Lambda K 2\pi$
60	40	CRENNELL	72	HBC $4.5 \pi^- p \rightarrow \Lambda K 2\pi$
127 \pm $\frac{7}{-25}$	ASTIER	69	HBC	$\bar{p} p$
60	45	CRENNELL	67	HBC $6 \pi^- p \rightarrow \Lambda K 2\pi$

¹ Systematic errors not estimated.

PRODUCED IN τ LEPTON DECAYS

VALUE (MeV)	EVTS	DOCUMENT ID	TECN	CHG	COMMENT
-------------	------	-------------	------	-----	---------

The data in this block is included in the average printed for a previous datablock.

260 \pm $\frac{90}{-70}$ ± 80	7k	ASNER	00B	CLEO	$\tau^- \rightarrow K^- \pi^+ \pi^- \nu_\tau$
--	----	-------	-----	------	---

$K_1(1270)$ DECAY MODES

Mode	Fraction (Γ_i/Γ)	Scale factor
Γ_1 $K\rho$	(38 ± 13) %	2.2
Γ_2 $K_0^*(1430)\pi$	(28 ± 4) %	
Γ_3 $K^*(892)\pi$	(21 ± 10) %	2.2
Γ_4 $K\omega$	(11.0 ± 2.0) %	
Γ_5 $Kf_0(1370)$	(3.0 ± 2.0) %	
Γ_6 γK^0	seen	

$K_1(1270)$ PARTIAL WIDTHS

$\Gamma(K\rho)$	VALUE (MeV)	DOCUMENT ID	TECN	CHG	COMMENT
••• We do not use the following data for averages, fits, limits, etc. •••					
57 ± 5	MAZZUCATO	79	HBC	+	4.2 $K^- p \rightarrow \Xi^- (K\pi\pi)^+$
75 ± 6	CARNEGIE	77B	ASPK	±	13 $K^\pm p \rightarrow (K\pi\pi)^\pm p$

$\Gamma(K_0^*(1430)\pi)$	VALUE (MeV)	DOCUMENT ID	TECN	CHG	COMMENT
••• We do not use the following data for averages, fits, limits, etc. •••					
26 ± 6	CARNEGIE	77B	ASPK	±	13 $K^\pm p \rightarrow (K\pi\pi)^\pm p$

$\Gamma(K^*(892)\pi)$	VALUE (MeV)	DOCUMENT ID	TECN	CHG	COMMENT
••• We do not use the following data for averages, fits, limits, etc. •••					
14 ± 11	MAZZUCATO	79	HBC	+	4.2 $K^- p \rightarrow \Xi^- (K\pi\pi)^+$
2 ± 2	CARNEGIE	77B	ASPK	±	13 $K^\pm p \rightarrow (K\pi\pi)^\pm p$

$\Gamma(K\omega)$	VALUE (MeV)	DOCUMENT ID	TECN	CHG	COMMENT
••• We do not use the following data for averages, fits, limits, etc. •••					
4 ± 4	MAZZUCATO	79	HBC	+	4.2 $K^- p \rightarrow \Xi^- (K\pi\pi)^+$
24 ± 3	CARNEGIE	77B	ASPK	±	13 $K^\pm p \rightarrow (K\pi\pi)^\pm p$

$\Gamma(Kf_0(1370))$	VALUE (MeV)	DOCUMENT ID	TECN	CHG	COMMENT
••• We do not use the following data for averages, fits, limits, etc. •••					
22 ± 5	CARNEGIE	77B	ASPK	±	13 $K^\pm p \rightarrow (K\pi\pi)^\pm p$

$\Gamma(\gamma K^0)$	VALUE (keV)	DOCUMENT ID	TECN	COMMENT
73.2 ± 6.1 ± 28.3		ALAVI-HARATI02B	KTEV	$K + A \rightarrow K^* + A$

$K_1(1270)$ BRANCHING RATIOS

$\Gamma(K\rho)/\Gamma_{total}$	VALUE	DOCUMENT ID	TECN	COMMENT
0.38 ± 0.13 OUR FIT				Error includes scale factor of 2.2.
0.42 ± 0.06		¹ DAUM	81c CNTR	63 $K^- p \rightarrow K^- 2\pi p$
••• We do not use the following data for averages, fits, limits, etc. •••				
0.584 ± 0.043		² GULER	11 BELL	$B^+ \rightarrow J/\psi K^+ \pi^+ \pi^-$
dominant		RODEBACK	81 HBC	$4 \pi^- p \rightarrow \Lambda K 2\pi$

$\Gamma(K_0^*(1430)\pi)/\Gamma_{total}$	VALUE	DOCUMENT ID	TECN	COMMENT
0.28 ± 0.04		¹ DAUM	81c CNTR	63 $K^- p \rightarrow K^- 2\pi p$
••• We do not use the following data for averages, fits, limits, etc. •••				
0.0201 ± 0.0064		² GULER	11 BELL	$B^+ \rightarrow J/\psi K^+ \pi^+ \pi^-$

$\Gamma(K^*(892)\pi)/\Gamma_{total}$	VALUE	DOCUMENT ID	TECN	COMMENT
0.21 ± 0.10 OUR FIT				Error includes scale factor of 2.2.
0.16 ± 0.05		¹ DAUM	81c CNTR	63 $K^- p \rightarrow K^- 2\pi p$
••• We do not use the following data for averages, fits, limits, etc. •••				
0.171 ± 0.023		² GULER	11 BELL	$B^+ \rightarrow J/\psi K^+ \pi^+ \pi^-$

$\Gamma(K^*(892)\pi)/\Gamma(K\rho)$	VALUE	DOCUMENT ID	TECN	COMMENT
0.56 ± 0.29 OUR FIT				Error includes scale factor of 2.2.
0.99 ± 0.15 ± 0.18		ABLIKIM	21U BES3	$D_S^+ \rightarrow \bar{K}_1(1270)^0 K^+ \pi^-$

$\Gamma(K\omega)/\Gamma_{total}$	VALUE	DOCUMENT ID	TECN	COMMENT
0.11 ± 0.02		¹ DAUM	81c CNTR	63 $K^- p \rightarrow K^- 2\pi p$
••• We do not use the following data for averages, fits, limits, etc. •••				
0.225 ± 0.052		² GULER	11 BELL	$B^+ \rightarrow J/\psi K^+ \pi^+ \pi^-$

$\Gamma(K\omega)/\Gamma(K\rho)$	VALUE	CL%	DOCUMENT ID	TECN	COMMENT
••• We do not use the following data for averages, fits, limits, etc. •••					
< 0.30		95	RODEBACK	81 HBC	$4 \pi^- p \rightarrow \Lambda K 2\pi$

$\Gamma(Kf_0(1370))/\Gamma_{total}$	VALUE	DOCUMENT ID	TECN	COMMENT
0.03 ± 0.02		¹ DAUM	81c CNTR	63 $K^- p \rightarrow K^- 2\pi p$

D-wave/S-wave RATIO FOR $K_1(1270) \rightarrow K^*(892)\pi$

VALUE	DOCUMENT ID	TECN	COMMENT
1.0 ± 0.7	¹ DAUM	81c CNTR	63 $K^- p \rightarrow K^- 2\pi p$
¹ Average from low and high t data.			
² Assuming that decays are saturated by the $K\rho$, $K_0^*(1430)\pi$, $K^*(892)\pi$, $K\omega$ decay modes and neglecting interference between them. The values $B(\omega \rightarrow \pi^+ \pi^-) = (1.53 \pm 0.11)_{-0.13}^{\pm 0.11}$ % and $B(K_0^*(1430) \rightarrow K\pi) = (93 \pm 10)$ % are used. Systematic uncertainties not estimated.			

$K_1(1270)$ REFERENCES

ABLIKIM	21U	PR D104 032011	M. Ablikim <i>et al.</i>	(BESIII Collab.)
AAIJ	18A1	EPJ C78 443	R. Aaij <i>et al.</i>	(LHCB Collab.)
GULER	11	PR D83 032005	H. Guler <i>et al.</i>	(BELLE Collab.)
GENG	07	PR D75 014017	L.S. Geng <i>et al.</i>	
ABLIKIM	06C	PL B633 681	M. Ablikim <i>et al.</i>	(BES Collab.)
ALAVI-HARATI	02B	PRL 89 072001	A. Alavi-Harati <i>et al.</i>	(FNAL KTeV Collab.)
ASNER	00B	PR D62 072006	D.M. Asner <i>et al.</i>	(CLEO Collab.)
TORNQVIST	82B	NP B203 268	N.A. Tornqvist	(HELS)
DAUM	81C	NP B187 1	C. Daum <i>et al.</i>	(AMST, CERN, CRAC, MPIM+)
RODEBACK	81	ZPHY C9 9	S. Rodeback <i>et al.</i>	(CERN, CDEF, MADR+)
MAZZUCATO	79	NP B156 532	M. Mazzucato <i>et al.</i>	(CERN, ZEEM, NIJM+)
VERGEEST	79	NP B158 265	J.S.M. Vergeest <i>et al.</i>	(NIJM, AMST, CERN+)
GAVILLET	78	PL 76B 517	P. Gavillet <i>et al.</i>	(SLAC)
CARNEGIE	77	NP B127 509	R.K. Carnegie <i>et al.</i>	(AMST, CERN, NIJM+)
CARNEGIE	77B	PL 68B 287	R.K. Carnegie <i>et al.</i>	(SLAC)
BRANDENB...	76	PRL 36 703	G.W. Brandenburg <i>et al.</i>	(SLAC) JP
OTTER	76	NP B106 77	G. Otter <i>et al.</i>	(AACH3, BERL, CERN, LOIC+)
CRENNELL	72	PR D6 1220	D.J. Crennell <i>et al.</i>	(BNL)
DAVIS	72	PR D5 2688	P.J. Davis <i>et al.</i>	(LBL)
FIRESTONE	72B	PR D5 505	A. Firestone <i>et al.</i>	(LBL)
ASTIER	69	NP B10 65	A. Astier <i>et al.</i>	(CDEF, CERN, IPNP, LIPV) JP
CRENNELL	67	PRL 19 44	D.J. Crennell <i>et al.</i>	(BNL) I

$K_1(1400)$

$$I(J^P) = \frac{1}{2}(1^+)$$

$K_1(1400)$ MASS

VALUE (MeV)	EVTS	DOCUMENT ID	TECN	CHG	COMMENT
1403 ± 7 OUR AVERAGE					
1463 ± 64 ± 68	7k	ASNER	00B	CLEO	$\tau^- \rightarrow K^- \pi^+ \pi^- \nu_\tau$
1373 ± 14 ± 18		¹ ASTON	87	LASS	0 11 $K^- p \rightarrow \bar{K}^0 \pi^+ \pi^- n$
1392 ± 18		BAUBILLIER	82B	HBC	0 8.25 $K^- p \rightarrow K_S^0 \pi^+ \pi^- n$
1410 ± 25		DAUM	81c	CNTR	- 63 $K^- p \rightarrow K^- 2\pi p$
1415 ± 15		ETKIN	80	MPS	0 6 $K^- p \rightarrow \bar{K}^0 \pi^+ \pi^- n$
1404 ± 10		² CARNEGIE	77	ASPK	± 13 $K^\pm p \rightarrow (K\pi\pi)^\pm p$
••• We do not use the following data for averages, fits, limits, etc. •••					
1418 ± 8	25k	³ ABLIKIM	06c	BES2	$J/\psi \rightarrow \bar{K}^*(892)^0 K^+ \pi^-$
~ 1350		⁴ TORNQVIST	82B	RVUE	
~ 1400		VERGEEST	79	HBC	- 4.2 $K^- p \rightarrow (\bar{K}\pi\pi)^- p$
~ 1400		BRANDENB...	76	ASPK	± 13 $K^\pm p \rightarrow (K\pi\pi)^\pm p$

Meson Particle Listings

$K_1(1400)$, $K^*(1410)$

1420	DAVIS	72	HBC	+	12	K^+p
1368 ± 18	FIRESTONE	72B	DBC	+	12	K^+d

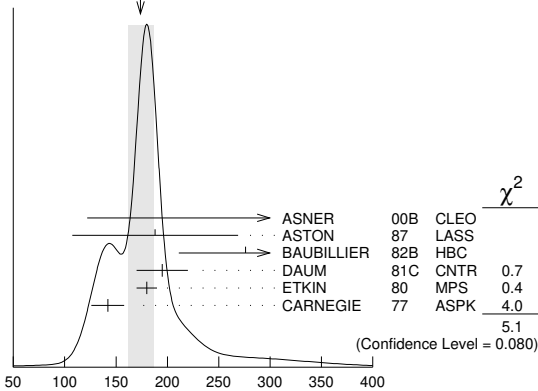
¹ From partial-wave analysis of $K^0\pi^+\pi^-$ system.
² From a model-dependent fit with Gaussian background to BRANDENBURG 76 data.
³ Systematic errors not estimated.
⁴ From a unitarized quark-model calculation.

$K_1(1400)$ WIDTH

VALUE (MeV)	EVTs	DOCUMENT ID	TECN	CHG	COMMENT		
174 ± 13 OUR AVERAGE		Error includes scale factor of 1.6. See the ideogram below.					
$300^{+370}_{-110} \pm 140$	7k	ASNER	00B	CLEO	$\tau^- \rightarrow K^- \pi^+ \pi^- \nu_\tau$		
$188 \pm 54 \pm 60$		¹ ASTON	87	LASS	0 11 $K^-p \rightarrow \bar{K}^0 \pi^+ \pi^- n$		
276 ± 65		BAUBILLIER	82B	HBC	0 8.25 $K^-p \rightarrow K_S^0 \pi^+ \pi^- n$		
195 ± 25		DAUM	81C	CNTR	- 63 $K^-p \rightarrow K^- 2\pi p$		
180 ± 10		ETKIN	80	MPS	0 6 $K^-p \rightarrow \bar{K}^0 \pi^+ \pi^- n$		
142 ± 16		² CARNEGIE	77	ASPK	\pm 13 $K^\pm p \rightarrow (K\pi\pi)^\pm p$		
152 ± 16	25k	³ ABLIKIM	06c	BES2	$J/\psi \rightarrow \bar{K}^*(892)^0 K^+ \pi^-$		
~ 200		VERGEEST	79	HBC	- 4.2 $K^-p \rightarrow (\bar{K}\pi\pi)^- p$		
~ 160		BRANDENB...	76	ASPK	\pm 13 $K^\pm p \rightarrow (K\pi\pi)^\pm p$		
80		DAVIS	72	HBC	+	12	K^+p
241 ± 30		FIRESTONE	72B	DBC	+	12	K^+d

• • • We do not use the following data for averages, fits, limits, etc. • • •
 χ^2
 ASNER 00B CLEO 0.7
 ASTON 87 LASS 0.4
 BAUBILLIER 82B HBC 4.0
 DAUM 81C CNTR 5.1
 ETKIN 80 MPS 5.1
 CARNEGIE 77 ASPK 4.0

WEIGHTED AVERAGE
 174 ± 13 (Error scaled by 1.6)



$K_1(1400)$ width (MeV)

- ¹ From partial-wave analysis of $K^0\pi^+\pi^-$ system.
² From a model-dependent fit with Gaussian background to BRANDENBURG 76 data.
³ Systematic errors not estimated.

$K_1(1400)$ DECAY MODES

Mode	Fraction (Γ_i/Γ)
Γ_1 $K^*(892)\pi$	(94 \pm 6) %
Γ_2 $K\rho$	(3.0 \pm 3.0) %
Γ_3 $Kf_0(1370)$	(2.0 \pm 2.0) %
Γ_4 $K\omega$	(1.0 \pm 1.0) %
Γ_5 $K_S^0(1430)\pi$	not seen
Γ_6 γK^0	seen
Γ_7 $K\phi$	seen

$K_1(1400)$ PARTIAL WIDTHS

$\Gamma(K^*(892)\pi)$ Γ_1					
VALUE (MeV)	DOCUMENT ID	TECN	CHG	COMMENT	
117 ± 10	CARNEGIE	77	ASPK	\pm 13 $K^\pm p \rightarrow (K\pi\pi)^\pm p$	
$\Gamma(K\rho)$ Γ_2					
VALUE (MeV)	DOCUMENT ID	TECN	CHG	COMMENT	
2 ± 1	CARNEGIE	77	ASPK	\pm 13 $K^\pm p \rightarrow (K\pi\pi)^\pm p$	
$\Gamma(K\omega)$ Γ_4					
VALUE (MeV)	DOCUMENT ID	TECN	CHG	COMMENT	
23 ± 12	CARNEGIE	77	ASPK	\pm 13 $K^\pm p \rightarrow (K\pi\pi)^\pm p$	
$\Gamma(\gamma K^0)$ Γ_6					
VALUE (keV)	DOCUMENT ID	TECN	COMMENT		
$280.8 \pm 23.2 \pm 40.4$	ALAVI-HARATI02B	KTEV	$K + A \rightarrow K^* + A$		

$K_1(1400)$ BRANCHING RATIOS

$\Gamma(K^*(892)\pi)/\Gamma_{total}$ Γ_1/Γ				
VALUE	DOCUMENT ID	TECN	COMMENT	
0.94 ± 0.06	¹ DAUM	81c	CNTR	63 $K^-p \rightarrow K^- 2\pi p$

¹ Average from low and high t data.

$\Gamma(K\rho)/\Gamma_{total}$ Γ_2/Γ				
VALUE	DOCUMENT ID	TECN	COMMENT	
0.03 ± 0.03	¹ DAUM	81c	CNTR	63 $K^-p \rightarrow K^- 2\pi p$

¹ Average from low and high t data.

$\Gamma(Kf_0(1370))/\Gamma_{total}$ Γ_3/Γ				
VALUE	DOCUMENT ID	TECN	COMMENT	
0.02 ± 0.02	¹ DAUM	81c	CNTR	63 $K^-p \rightarrow K^- 2\pi p$

¹ Average from low and high t data.

$\Gamma(K\omega)/\Gamma_{total}$ Γ_4/Γ				
VALUE	DOCUMENT ID	TECN	COMMENT	
0.01 ± 0.01	¹ DAUM	81c	CNTR	63 $K^-p \rightarrow K^- 2\pi p$

¹ Average from low and high t data.

$\Gamma(K\phi)/\Gamma_{total}$ Γ_7/Γ				
VALUE	EVTs	DOCUMENT ID	TECN	COMMENT
seen	24k	¹ AAIJ	21E	LHCB $B^+ \rightarrow J/\psi \phi K^+$

¹ From an amplitude analysis of the decay $B^+ \rightarrow J/\psi \phi K^+$ with a significance of 9.2 σ .

$\Gamma(K_S^0(1430)\pi)/\Gamma_{total}$ Γ_5/Γ				
VALUE	DOCUMENT ID	TECN	COMMENT	
not seen	¹ DAUM	81c	CNTR	63 $K^-p \rightarrow K^- 2\pi p$

¹ Average from low and high t data.

D-wave/S-wave RATIO FOR $K_1(1400) \rightarrow K^*(892)\pi$

VALUE	DOCUMENT ID	TECN	COMMENT
0.04 ± 0.01	¹ DAUM	81c	CNTR 63 $K^-p \rightarrow K^- 2\pi p$

¹ Average from low and high t data.

$K_1(1400)$ REFERENCES

AAIJ	21E	PRL 127 082001	R. Aaij et al.	(LHCb Collab.)
ABLIKIM	06c	PL B633 681	M. Ablikim et al.	(BES Collab.)
ALAVI-HARATI	02B	PRL 89 072001	A. Alavi-Harati et al.	(FNAL KTeV Collab.)
ASNER	00B	PR D52 072006	D.M. Asner et al.	(CLEO Collab.)
ASTON	87	NP B292 693	D. Aston et al.	(SLAC, NAGC, CINC, INUS)
BAUBILLIER	82B	NP B202 21	M. Baubillier et al.	(BIRM, CERN, GLAS+)
TORNQVIST	82B	NP B203 268	N.A. Tornqvist	(HELS)
DAUM	81C	NP B187 1	C. Daum et al.	(AMST, CERN, CRAC, MPIM+)
ETKIN	80	PR D22 42	A. Etkin et al.	(BNL, CUNY)JP
VERGEEST	79	NP B158 265	J.S.M. Vergeest et al.	(NUM, AMST, CERN+)
CARNEGIE	77	NP B127 509	R.K. Carnegie et al.	(SLAC)
BRANDENB...	76	PRL 36 703	G.W. Brandenburg et al.	(SLAC)JP
DAVIS	72	PR D5 2688	P.J. Davis et al.	(LBL)
FIRESTONE	72B	PR D5 505	A. Firestone et al.	(LBL)

$K^*(1410)$

$$I(J^P) = \frac{1}{2}(1^-)$$

$K^*(1410)$ T-MATRIX POLE \sqrt{s}

VALUE (MeV)	DOCUMENT ID	TECN	COMMENT
$(1368 \pm 38) - i(106^{+48}_{-59})$	¹ PELAEZ	17	RVUE $\pi K \rightarrow \pi K$

• • • We do not use the following data for averages, fits, limits, etc. • • •
¹ Reanalysis of ESTABROOKS 78 and ASTON 88 satisfying Forward Dispersion Relations and using sequences of Padé approximants.

$K^*(1410)$ MASS

VALUE (MeV)	EVTs	DOCUMENT ID	TECN	CHG	COMMENT
1414 ± 15 OUR AVERAGE		Error includes scale factor of 1.3.			
$1380 \pm 21 \pm 19$		ASTON	88	LASS	0 11 $K^-p \rightarrow K^- \pi^+ n$
$1420 \pm 7 \pm 10$		ASTON	87	LASS	0 11 $K^-p \rightarrow \bar{K}^0 \pi^+ \pi^- n$
$1437 \pm 8 \pm 16$	190k	¹ AAIJ	16N	LHCB	$D^0 \rightarrow (K_S^0 \pi^\mp) K^\pm$
$1426 \pm 8 \pm 24$	190k	² AAIJ	16N	LHCB	$D^0 \rightarrow K_S^0 (K^\pm \pi^\mp)$
1276^{+72}_{-77}		^{3,4} BOITO	09	RVUE	$\tau^- \rightarrow K_S^0 \pi^- \nu_\tau$
1367 ± 54		BIRD	89	LASS	- 11 $K^-p \rightarrow \bar{K}^0 \pi^- p$
1474 ± 25		BAUBILLIER	82B	HBC	0 8.25 $K^-p \rightarrow \bar{K}^0 2\pi n$
1500 ± 30		ETKIN	80	MPS	0 6 $K^-p \rightarrow \bar{K}^0 \pi^+ \pi^- n$

¹ Using a parametrization for the $K\pi$ S-wave similar to ASTON 88 with fixed resonance width.
² Using a $K\pi$ S-wave parametrization with resonant and non-resonant contributions.
³ From the pole position of the $K\pi$ vector form factor in the complex s -plane and using EPIFANOV 07 data.

See key on page 1127

Meson Particle Listings

$K^*(1410)$, $K_0^*(1430)$

⁴ Systematic uncertainties not estimated.

$K^*(1410)$ WIDTH

VALUE (MeV)	EVTS	DOCUMENT ID	TECN	CHG	COMMENT	
232 ± 21 OUR AVERAGE		Error includes scale factor of 1.1.				
176 ± 52 ± 22		ASTON	88	LASS	0	11 $K^-p \rightarrow K^- \pi^+ n$
240 ± 18 ± 12		ASTON	87	LASS	0	11 $K^-p \rightarrow \bar{K}^0 \pi^+ \pi^- n$
• • • We do not use the following data for averages, fits, limits, etc. • • •						
210 ± 20 ± 60	190k	¹ AAIJ	16N	LHCB		$D^0 \rightarrow (K_S^0 \pi^\mp) K^\pm$
270 ± 20 ± 40	190k	¹ AAIJ	16N	LHCB		$D^0 \rightarrow K_S^0 (K^\pm \pi^\mp)$
198 ± $\frac{61}{87}$		^{2,3} BOITO	09	RVUE		$\tau^- \rightarrow K_S^0 \pi^- \nu_\tau$
114 ± 101		BIRD	89	LASS	-	11 $K^-p \rightarrow \bar{K}^0 \pi^- p$
275 ± 65		BAUBILLIER	82B	HBC	0	8.25 $K^-p \rightarrow \bar{K}^0 2\pi n$
500 ± 100		ETKIN	80	MPS	0	6 $K^-p \rightarrow \bar{K}^0 \pi^+ \pi^- n$

¹ Using a $K\pi$ S-wave parameterization with resonant and non-resonant contributions.
² From the pole position of the $K\pi$ vector form factor in the complex s-plane and using EPIFANOV 07 data.
³ Systematic uncertainties not estimated.

$K^*(1410)$ DECAY MODES

Mode	Fraction (Γ_i/Γ)	Confidence level
Γ_1 $K^*(892)\pi$	> 40 %	95%
Γ_2 $K\pi$	(6.6 ± 1.3) %	
Γ_3 $K\rho$	< 7 %	95%
Γ_4 γK^0	< 2.3 × 10 ⁻⁴	90%
Γ_5 $K\phi$	seen	

$K^*(1410)$ PARTIAL WIDTHS

$\Gamma(\gamma K^0)$	CL%	DOCUMENT ID	TECN	COMMENT	Γ_4
< 52.9	90	ALAVI-HARATI02B	KTEV	$K + A \rightarrow K^* + A$	

$K^*(1410)$ BRANCHING RATIOS

$\Gamma(K\rho)/\Gamma(K^*(892)\pi)$	CL%	DOCUMENT ID	TECN	CHG	COMMENT	Γ_3/Γ_1
< 0.17	95	ASTON	84	LASS	0	11 $K^-p \rightarrow \bar{K}^0 2\pi n$

$\Gamma(K\pi)/\Gamma(K^*(892)\pi)$	CL%	DOCUMENT ID	TECN	CHG	COMMENT	Γ_2/Γ_1
< 0.16	95	ASTON	84	LASS	0	11 $K^-p \rightarrow \bar{K}^0 2\pi n$

$\Gamma(K\pi)/\Gamma_{total}$	DOCUMENT ID	TECN	CHG	COMMENT	Γ_2/Γ
0.066 ± 0.010 ± 0.008	ASTON	88	LASS	0	11 $K^-p \rightarrow K^- \pi^+ n$

$\Gamma(K\phi)/\Gamma_{total}$	EVTS	DOCUMENT ID	TECN	COMMENT	Γ_5/Γ
seen	24k	¹ AAIJ	21E	LHCB	$B^+ \rightarrow J/\psi \phi K^+$

¹ From an amplitude analysis of the decay $B^+ \rightarrow J/\psi \phi K^+$ with a significance of 7.7 σ .

$K^*(1410)$ REFERENCES

AAIJ	21E	PRL 127 082001	R. Aaij et al.	(LHCb Collab.)
PELAEZ	17	EPJ C77 91	J.R. Peláez, A.Rodas, J.R. de Elvira	(LHCb Collab.)
AAIJ	16N	PR D93 052018	R. Aaij et al.	(LHCb Collab.)
BOITO	09	EPJ C59 821	D.R. Boito, R. Escribano, M. Jamin	
EPIFANOV	07	PL B654 65	D. Epifanov et al.	(BELLE Collab.)
ALAVI-HARATI	02B	PRL 89 072001	A. Alavi-Harati et al.	(FNAL KTeV Collab.)
BIRD	89	SLAC-332	P.F. Bird	(SLAC)
ASTON	88	NP B296 493	D. Aston et al.	(SLAC, NAGO, CINC, INUS)
ASTON	87	NP B292 693	D. Aston et al.	(SLAC, NAGO, CINC, INUS)
ASTON	84	PL 149B 258	D. Aston et al.	(SLAC, CARL, OTTA)JP
BAUBILLIER	82B	NP B202 21	M. Baubillier et al.	(BIRM, CERN, GLAS-)
ETKIN	80	PR D22 42	A. Etkin et al.	(BNL, CUNY)JP
ESTABROOKS	78	NP B133 490	P.G. Estabrooks et al.	(MCGI, CARL, DURH+)

$K_0^*(1430)$

$$I(J^P) = \frac{1}{2}(0^+)$$

$K_0^*(1430)$ T-MATRIX POLE \sqrt{s}

VALUE (MeV)	DOCUMENT ID	TECN	COMMENT
(1431 ± 6) - i(110 ± 19)	¹ PELAEZ	17	RVUE $\pi K \rightarrow \pi K$

¹ Reanalysis of ESTABROOKS 78 and ASTON 88 satisfying Forward Dispersion Relations and using sequences of Pade approximants.

$K_0^*(1430)$ MASS

VALUE (MeV)	EVTS	DOCUMENT ID	TECN	COMMENT
1425 ± 50 OUR ESTIMATE		• • • We do not use the following data for averages, fits, limits, etc. • • •		
1449 ± 17 ± 2		¹ LEES	21A	BABR $\eta_c(1S) \rightarrow \eta' K^+ K^-$
1438 ± 8 ± 4	5.4k	² LEES	14E	BABR $\eta_c(1S) \rightarrow K^+ K^- \eta/\pi^0$
1427 ± 4 ± 13		³ BUGG	10	RVUE S-matrix pole
1466.6 ± 0.7 ± 3.4	141k	⁴ BONVICINI	08A	CLEO $D^+ \rightarrow K^- \pi^+ \pi^+$
~ 1412		⁵ LINK	07	FOCS $D^+ \rightarrow K^- K^+ \pi^+$
1461.0 ± 4.0 ± 2.1	54k	⁶ LINK	07B	FOCS $D^+ \rightarrow K^- \pi^+ \pi^+$
1406 ± 29		⁷ BUGG	06	RVUE
1435 ± 6		⁸ ZHOU	06	RVUE $K\rho \rightarrow K^- \pi^+ n$
1455 ± 20 ± 15		ABLIKIM	05Q	BES2 $\psi(2S) \rightarrow \gamma \pi^+ \pi^- K^+ K^-$
1456 ± 8		⁹ ZHENG	04	RVUE $K^-p \rightarrow K^- \pi^+ n$
~ 1419		¹⁰ BUGG	03	RVUE $11 K^-p \rightarrow K^- \pi^+ n$
~ 1440		¹¹ LI	03	RVUE $11 K^-p \rightarrow K^- \pi^+ n$
1459 ± 9	15k	¹² AITALA	02	E791 $D^+ \rightarrow K^- \pi^+ \pi^+$
~ 1440		¹³ JAMIN	00	RVUE $K\rho \rightarrow K\rho$
1436 ± 8		¹⁴ BARBERIS	98E	OMEG $450 pp \rightarrow p_f p_s K^+ K^- \pi^+ \pi^-$
1415 ± 25		¹⁰ ANISOVICH	97c	RVUE $11 K^-p \rightarrow K^- \pi^+ n$
~ 1450		¹⁵ TORNQVIST	96	RVUE $\pi\pi \rightarrow \pi\pi, K\bar{K}, K\pi$
1412 ± 6		¹⁶ ASTON	88	LASS $11 K^-p \rightarrow K^- \pi^+ n$
~ 1430		BAUBILLIER	84B	HBC $8.25 K^-p \rightarrow \bar{K}^0 \pi^- p$
~ 1425		¹⁷ ESTABROOKS	78	ASPK $13 K^\pm p \rightarrow K^\pm \pi^\pm (n, \Delta)$
~ 1450.0		MARTIN	78	SPEC $10 K^\pm p \rightarrow K_S^0 \pi p$

¹ Using a $K\pi-K\eta'$ coupled channel Breit-Wigner function.
² Using both $\eta \rightarrow \gamma\gamma$ and $\eta \rightarrow \pi^+ \pi^- \pi^0$. From a likelihood scan in the presence of several interfering scalar-meson resonances with fixed width $\Gamma(K_0^*(1430)) = 210$ MeV.
³ S-Matrix pole. Supersedes BUGG 06. Combined analysis of ASTON 88, ABLIKIM 06c, AITALA 06, and LINK 09 using an s-dependent width with couplings to $K\pi$ and $K\eta'$, and the Adler zero near thresholds.
⁴ From the isobar model with a complex pole for the κ .
⁵ From a non-parametric analysis.
⁶ A Breit-Wigner mass and width.
⁷ S-matrix pole. Reanalysis of ASTON 88, AITALA 02, and ABLIKIM 06c including the κ with an s-dependent width and an Adler zero near threshold.
⁸ S-matrix pole. Using ASTON 88 and assuming $K_0^*(700)$, $K_0^*(1950)$.
⁹ Using ASTON 88 and assuming $K_0^*(700)$.
¹⁰ T-matrix pole. Reanalysis of ASTON 88 data.
¹¹ Breit-Wigner fit. Using ASTON 88.
¹² Assuming a low-mass scalar $K\pi$ resonance, $\kappa(700)$.
¹³ T-matrix pole. Using data from ESTABROOKS 78 and ASTON 88.
¹⁴ J^P not determined, could be $K_2^*(1430)$.
¹⁵ T-matrix pole.
¹⁶ Uses a model for the background, without this background they get a mass 1340 MeV, where the phase shift passes 90°.
¹⁷ Mass defined by pole position. From elastic $K\pi$ partial-wave analysis.

$K_0^*(1430)$ WIDTH

VALUE (MeV)	EVTS	DOCUMENT ID	TECN	COMMENT
270 ± 80 OUR ESTIMATE		• • • We do not use the following data for averages, fits, limits, etc. • • •		
210 ± 20 ± 12	5.4k	¹ LEES	14E	BABR $\eta_c(1S) \rightarrow K^+ K^- \eta/\pi^0$
270 ± 10 ± 40		² BUGG	10	RVUE S-matrix pole
174.2 ± 1.9 ± 3.2	141k	³ BONVICINI	08A	CLEO $D^+ \rightarrow K^- \pi^+ \pi^+$
~ 500		⁴ LINK	07	FOCS $D^+ \rightarrow K^- K^+ \pi^+$
177.0 ± 8.0 ± 3.4	54k	⁵ LINK	07B	FOCS $D^+ \rightarrow K^- \pi^+ \pi^+$
350 ± 40		⁶ BUGG	06	RVUE
288 ± 22		⁷ ZHOU	06	RVUE $K\rho \rightarrow K^- \pi^+ n$
270 ± 45 ± $\frac{+30}{-35}$		ABLIKIM	05Q	BES2 $\psi(2S) \rightarrow \gamma \pi^+ \pi^- K^+ K^-$
217 ± 31		⁸ ZHENG	04	RVUE $K^-p \rightarrow K^- \pi^+ n$
~ 316		⁹ BUGG	03	RVUE $11 K^-p \rightarrow K^- \pi^+ n$
~ 350		¹⁰ LI	03	RVUE $11 K^-p \rightarrow K^- \pi^+ n$
175 ± 17	15k	¹¹ AITALA	02	E791 $D^+ \rightarrow K^- \pi^+ \pi^+$
~ 300		¹² JAMIN	00	RVUE $K\rho \rightarrow K\rho$
196 ± 45		¹³ BARBERIS	98E	OMEG $450 pp \rightarrow p_f p_s K^+ K^- \pi^+ \pi^-$
330 ± 50		⁹ ANISOVICH	97c	RVUE $11 K^-p \rightarrow K^- \pi^+ n$
~ 320		¹⁴ TORNQVIST	96	RVUE $\pi\pi \rightarrow \pi\pi, K\bar{K}, K\pi$
294 ± 23		ASTON	88	LASS $11 K^-p \rightarrow K^- \pi^+ n$
~ 200		BAUBILLIER	84B	HBC $8.25 K^-p \rightarrow \bar{K}^0 \pi^- p$
200 to 300		¹⁵ ESTABROOKS	78	ASPK $13 K^\pm p \rightarrow K^\pm \pi^\pm (n, \Delta)$

¹ Using both $\eta \rightarrow \gamma\gamma$ and $\eta \rightarrow \pi^+ \pi^- \pi^0$. From a likelihood scan in the presence of several interfering scalar-meson resonances with fixed mass $M(K_0^*(1430)) = 1435$ MeV.
² S-Matrix pole. Supersedes BUGG 06. Combined analysis of ASTON 88, ABLIKIM 06c, AITALA 06, and LINK 09 using an s-dependent width with couplings to $K\pi$ and $K\eta'$, and the Adler zero near thresholds.
³ From the isobar model with a complex pole for the κ .
⁴ From a non-parametric analysis.

Meson Particle Listings

$K_0^*(1430)$, $K_2^*(1430)$

- ⁵ A Breit-Wigner mass and width.
- ⁶ S-matrix pole. Reanalysis of ASTON 88, AITALA 02, and ABLIKIM 06c including the κ with an s-dependent width and an Adler zero near threshold.
- ⁷ S-matrix pole. Using ASTON 88 and assuming $K_0^*(700)$, $K_0^*(1950)$.
- ⁸ Using ASTON 88 and assuming $K_0^*(700)$.
- ⁹ T-matrix pole. Reanalysis of ASTON 88 data.
- ¹⁰ Breit-Wigner fit. Using ASTON 88.
- ¹¹ Assuming a low-mass scalar $K\pi$ resonance, $\kappa(700)$.
- ¹² T-matrix pole. Using data from ESTABROOKS 78 and ASTON 88.
- ¹³ J^P not determined, could be $K_2^*(1430)$.
- ¹⁴ T-matrix pole.
- ¹⁵ From elastic $K\pi$ partial-wave analysis.

$K_0^*(1430)$ DECAY MODES

Mode	Fraction (Γ_i/Γ)
Γ_1 $K\pi$	(93 ± 10) %
Γ_2 $K\eta$	(8.6 ± 2.7 / 3.4) %
Γ_3 $K\eta'(958)$	seen

$K_0^*(1430)$ BRANCHING RATIOS

$\Gamma(K\pi)/\Gamma_{total}$	DOCUMENT ID	TECN	CHG	COMMENT	Γ_1/Γ
0.93 ± 0.04 ± 0.09	ASTON	88	LASS	0	11 $K^-p \rightarrow K^- \pi^+ n$

$\Gamma(K\eta)/\Gamma(K\pi)$	EVTS	DOCUMENT ID	TECN	COMMENT	Γ_2/Γ_1
9.2 ± 2.5 ± 1.0 / 2.5	5.4k	¹ LEES	14E	BABR $\eta_c(1S) \rightarrow K^+ K^- \eta/\pi^0$	

¹ Using both $\eta \rightarrow \gamma\gamma$ and $\eta \rightarrow \pi^+ \pi^- \pi^0$. From a Dalitz analysis in the presence of several interfering scalar-meson resonances.

$\Gamma(K\eta'(958))/\Gamma_{total}$	DOCUMENT ID	TECN	COMMENT	Γ_3/Γ
seen	ABLIKIM	14J	BES3 $\psi(2S) \rightarrow \gamma K^+ K^- \eta'(958)$	

$\Gamma(K\eta'(958))/\Gamma(K\pi)$	DOCUMENT ID	TECN	COMMENT	Γ_3/Γ_1
0.397 ± 0.064 ± 0.054	¹ LEES	21A	BABR $\eta_c(1S) \rightarrow \eta' K^+ K^-$	

¹ Using $K\pi$ data from LEES 14E.

$K_0^*(1430)$ REFERENCES

LEES	21A	PR D104 072002	J.P. Lees et al.	(BABAR Collab.)
PELAEZ	17	EPL C77 91	J.R. Pelaez, A.Rodas, J.R. de Elvira	(BESIII Collab.)
ABLIKIM	14J	PR D89 074030	M. Ablikim et al.	(BABAR Collab.)
LEES	14E	PR D89 112004	J.P. Lees et al.	(BABAR Collab.)
BUGG	10	PR D81 014002	D.V. Bugg	(LOQM)
LINK	09	PL B681 14	J.M. Link et al.	(FNAL FOCUS Collab.)
BONVICINI	08A	PR D78 052001	G. Bonvicini et al.	(CLEO Collab.)
LINK	07	PL B648 156	J.M. Link et al.	(FNAL FOCUS Collab.)
LINK	07B	PL B653 1	J.M. Link et al.	(FNAL FOCUS Collab.)
ABLIKIM	06C	PL B633 681	M. Ablikim et al.	(BES Collab.)
AITALA	06	PR D73 032004	E.M. Aitala et al.	(FNAL E791 Collab.)
Also	PR D74 059901 (errata)	E.M. Aitala et al.	(FNAL E791 Collab.)	
BUGG	06	PL B632 471	D.V. Bugg	(LOQM)
ZHOU	06	NP A775 212	Z.Y. Zhou, H.Q. Zheng	(LOQM)
ABLIKIM	05Q	PR D72 092002	M. Ablikim et al.	(BES Collab.)
ZHENG	04	NP A733 235	H.Q. Zheng et al.	(BES Collab.)
BUGG	03	PL B572 1	D.V. Bugg	(LOQM)
LI	03	PR D67 034025	L. Li, B. Zou, G. Li	(FNAL E791 Collab.)
AITALA	02	PRL 89 121801	E.M. Aitala et al.	(FNAL E791 Collab.)
JAMIN	00	NP B587 331	M. Jamin et al.	(Omega Expt.)
BARBERIS	98E	PL B436 204	D. Barberis et al.	(Omega Expt.)
ANISOVICH	97C	PL B413 137	A.V. Anisovich, A.V. Sarantsev	(Omega Expt.)
TORNVIST	96	PRL 76 1575	N.A. Tornqvist, M. Roos	(HELS)
ASTON	88	NP B296 493	D. Aston et al.	(SLAC NAGO, CINC, INUS)
BAUBILLIER	84B	ZPHY C26 37	M. Baubillier et al.	(BIRM, CERN, GLAS-)
ESTABROOKS	78	NP B133 490	P.G. Estabrooks et al.	(MCGI, CARL, DURH-)
MARTIN	78	NP B134 392	A.D. Martin et al.	(DURH, GEVA)

$K_2^*(1430)$

$$I(J^P) = \frac{1}{2}(2^+)$$

We consider that phase-shift analyses provide more reliable determinations of the mass and width.

$K_2^*(1430)$ T-MATRIX POLE \sqrt{s}

VALUE (MeV)	DOCUMENT ID	TECN	COMMENT
(1424 ± 4) - i (66 ± 2)	¹ PELAEZ	17	RVUE $\pi K \rightarrow \pi K$

¹ Reanalysis of ESTABROOKS 78 and ASTON 88 satisfying Forward Dispersion Relations and using sequences of Pade approximants.

$K_2^*(1430)$ MASS

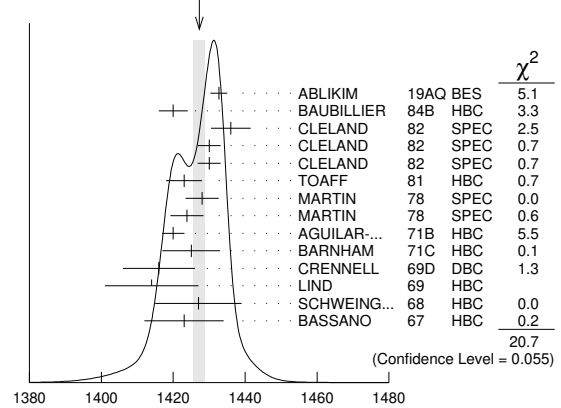
CHARGED ONLY, WITH FINAL STATE $K\pi$

VALUE (MeV)	EVTS	DOCUMENT ID	TECN	CHG	COMMENT
1427.3 ± 1.5 OUR AVERAGE					Error includes scale factor of 1.3. See the ideogram below.
1432.7 ± 0.7 ± 2.2 / 2.3	183k	ABLIKIM	19AQ	BES	$J/\psi \rightarrow K^+ K^- \pi^0$
1420 ± 4	1587	BAUBILLIER	84B	HBC	$8.25 K^- p \rightarrow \bar{K}^0 \pi^- p$
1436 ± 5.5	400	^{2,3} CLELAND	82	SPEC	$30 K^+ p \rightarrow K_S^0 \pi^+ p$
1430 ± 3.2	1500	^{2,3} CLELAND	82	SPEC	$50 K^+ p \rightarrow K_S^0 \pi^+ p$
1430 ± 3.2	1200	^{2,3} CLELAND	82	SPEC	$50 K^+ p \rightarrow K_S^0 \pi^- p$
1423 ± 5	935	TOAFF	81	HBC	$6.5 K^- p \rightarrow \bar{K}^0 \pi^- p$
1428.0 ± 4.6		⁴ MARTIN	78	SPEC	$10 K^\pm p \rightarrow K_S^0 \pi p$
1423.8 ± 4.6		⁴ MARTIN	78	SPEC	$10 K^\pm p \rightarrow K_S^0 \pi p$
1420.0 ± 3.1	1400	AGUILAR...	71B	HBC	$3.9, 4.6 K^- p$
1425 ± 8.0	225	^{2,3} BARNHAM	71c	HBC	$K^+ p \rightarrow K^0 \pi^+ p$
1416 ± 10	220	CRENNELL	69D	DBC	$3.9 K^- N \rightarrow \bar{K}^0 \pi^- N$
1414 ± 13.0	60	² LIND	69	HBC	$9 K^+ p \rightarrow K^0 \pi^+ p$
1427 ± 12	63	² SCHWEING...	68	HBC	$5.5 K^- p \rightarrow \bar{K} \pi N$
1423 ± 11.0	39	² BASSANO	67	HBC	$4.6-5.0 K^- p \rightarrow \bar{K}^0 \pi^- p$

••• We do not use the following data for averages, fits, limits, etc. •••

1423.4 ± 2 ± 3	24809 ± 820	⁵ BIRD	89	LASS	-	11 $K^- p \rightarrow \bar{K}^0 \pi^- p$
----------------	-------------	-------------------	----	------	---	--

WEIGHTED AVERAGE
1427.3 ± 1.5 (Error scaled by 1.3)



NEUTRAL ONLY

VALUE (MeV)	EVTS	DOCUMENT ID	TECN	COMMENT
1432.4 ± 1.3 OUR AVERAGE				
1431.2 ± 1.8 ± 0.7		⁶ ASTON	88	LASS $11 K^- p \rightarrow K^- \pi^+ n$
1434 ± 4 ± 6		⁶ ASTON	87	LASS $11 K^- p \rightarrow \bar{K}^0 \pi^+ \pi^- n$
1433 ± 6 ± 10		⁶ ASTON	84B	LASS $11 K^- p \rightarrow \bar{K}^0 2\pi n$
1471 ± 12		⁶ BAUBILLIER	82B	HBC $8.25 K^- p \rightarrow NK_S^0 \pi$
1428 ± 3		⁶ ASTON	81c	LASS $11 K^- p \rightarrow K^- \pi^+ n$
1434 ± 2		⁶ ESTABROOKS	78	ASPK $13 K^\pm p \rightarrow pK\pi$
1440 ± 10		⁶ BOWLER	77	DBC $5.5 K^+ d \rightarrow K\pi pp$
1428.5 ± 3.9	1786 ± 127	⁷ AUBERT	07AK	BABR $10.6 e^+ e^- \rightarrow K^{*0} K^\pm \pi^\mp \gamma$
1420 ± 7	300	HENDRICK	76	DBC $8.25 K^+ N \rightarrow K^+ \pi N$
1421.6 ± 4.2	800	MCCUBBIN	75	HBC $3.6 K^- p \rightarrow K^- \pi^+ n$
1420.1 ± 4.3		⁸ LINGLIN	73	HBC $2-13 K^+ p \rightarrow K^+ \pi^- X$
1419.1 ± 3.7	1800	AGUILAR...	71B	HBC $3.9, 4.6 K^- p$
1416 ± 6	600	CORDS	71	DBC $9 K^+ n \rightarrow K^+ \pi^- p$
1421.1 ± 2.6	2200	DAVIS	69	HBC $12 K^+ p \rightarrow K^+ \pi^- X$

² Errors enlarged by us to Γ/\sqrt{N} ; see the note with the $K^*(892)$ mass.

³ Number of events in peak re-evaluated by us.

⁴ Systematic error added by us.

⁵ From a partial wave amplitude analysis.

⁶ From phase shift or partial-wave analysis.

⁷ Systematic errors not estimated.

⁸ From pole extrapolation, using world $K^+ p$ data summary tape.

$K_2^*(1430)$ WIDTH

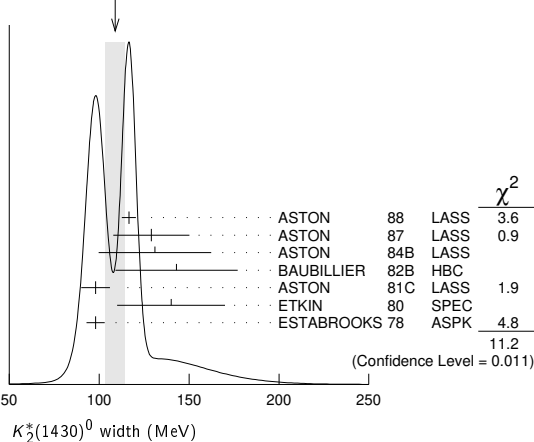
CHARGED ONLY, WITH FINAL STATE $K\pi$

VALUE (MeV)	EVTs	DOCUMENT ID	TECN	CHG	COMMENT
100.0 ± 2.1 OUR FIT					
100.0 ± 2.2 OUR AVERAGE					Error includes scale factor of 1.1.
102.5 ± 1.6 ^{+3.1} _{-2.8}	183k	ABLIKIM	19A Q	BES ±	$J/\psi \rightarrow K^+ K^- \pi^0$
109 ± 22	400	9,10 CLELAND	82	SPEC +	$30 K^+ p \rightarrow K_S^0 \pi^+ p$
124 ± 12.8	1500	9,10 CLELAND	82	SPEC +	$50 K^+ p \rightarrow K_S^0 \pi^+ p$
113 ± 12.8	1200	9,10 CLELAND	82	SPEC +	$50 K^+ p \rightarrow K_S^0 \pi^- p$
85 ± 16	935	TOAFF	81	HBC -	$6.5 K^- p \rightarrow \bar{K}^0 \pi^- p$
96.5 ± 3.8		MARTIN	78	SPEC +	$10 K^\pm p \rightarrow K_S^0 \pi p$
97.7 ± 4.0		MARTIN	78	SPEC -	$10 K^\pm p \rightarrow K_S^0 \pi p$
94.7 ^{+15.1} _{-12.5}	1400	AGUILAR-...	71B	HBC -	$3.9, 4.6 K^- p$
• • • We do not use the following data for averages, fits, limits, etc. • • •					
98 ± 4 ± 4	25k	11 BIRD	89	LASS -	$11 K^- p \rightarrow \bar{K}^0 \pi^- p$

NEUTRAL ONLY

VALUE (MeV)	EVTs	DOCUMENT ID	TECN	COMMENT
109 ± 5 OUR AVERAGE				Error includes scale factor of 1.9. See the ideogram below.
116.5 ± 3.6 ± 1.7	12	ASTON	88	LASS 11 $K^- p \rightarrow K^- \pi^+ n$
129 ± 15 ± 15	12	ASTON	87	LASS 11 $K^- p \rightarrow \bar{K}^0 \pi^+ \pi^- n$
131 ± 24 ± 20	12	ASTON	84B	LASS 11 $K^- p \rightarrow \bar{K}^0 2\pi n$
143 ± 34	12	BAUBILLIER	82B	HBC 8.25 $K^- p \rightarrow N K_S^0 \pi \pi$
98 ± 8	12	ASTON	81C	LASS 11 $K^- p \rightarrow K^- \pi^+ n$
140 ± 30	12	ETKIN	80	SPEC 6 $K^- p \rightarrow \bar{K}^0 \pi^+ \pi^- n$
98 ± 5	12	ESTABROOKS	78	ASPK 13 $K^\pm p \rightarrow p K \pi$
• • • We do not use the following data for averages, fits, limits, etc. • • •				
113.7 ± 9.2	1786 ± 127	13 AUBERT	07AK	BABR 10.6 $e^+ e^- \rightarrow K_S^0 K^\pm \pi^\mp \gamma$
125 ± 29	300	9 HENDRICK	76	DBC 8.25 $K^+ N \rightarrow K^+ \pi N$
116 ± 18	800	MCCUBBIN	75	HBC 3.6 $K^- p \rightarrow K^- \pi^+ n$
61 ± 14		14 LINGLIN	73	HBC 2-13 $K^+ p \rightarrow K^+ \pi^- X$
116.6 ^{+10.3} _{-15.5}	1800	AGUILAR-...	71B	HBC 3.9, 4.6 $K^- p$
144 ± 24.0	600	9 CORDS	71	DBC 9 $K^+ n \rightarrow K^+ \pi^- p$
101 ± 10	2200	DAVIS	69	HBC 12 $K^+ p \rightarrow K^+ \pi^- \pi^+ p$

WEIGHTED AVERAGE
109±5 (Error scaled by 1.9)



9 Errors enlarged by us to $4\Gamma/\sqrt{N}$; see the note with the $K^*(892)$ mass.
 10 Number of events in peak re-evaluated by us.
 11 From a partial wave amplitude analysis.
 12 From phase shift or partial-wave analysis.
 13 Systematic errors not estimated.
 14 From pole extrapolation, using world $K^+ p$ data summary tape.

$K_2^*(1430)$ DECAY MODES

Mode	Fraction (Γ_i/Γ)	Scale factor/ Confidence level
Γ_1 $K\pi$	(49.9 ± 1.2) %	
Γ_2 $K^*(892)\pi$	(24.7 ± 1.5) %	
Γ_3 $K^*(892)\pi\pi$	(13.4 ± 2.2) %	
Γ_4 $K\rho$	(8.7 ± 0.8) %	S=1.2
Γ_5 $K\omega$	(2.9 ± 0.8) %	
Γ_6 $K^+\gamma$	(2.4 ± 0.5) × 10 ⁻³	S=1.1
Γ_7 $K\eta$	(1.5 ^{+3.4} _{-1.0}) × 10 ⁻³	S=1.3
Γ_8 $K\omega\pi$	< 7.2 × 10 ⁻⁴	CL=95%
Γ_9 $K^0\gamma$	< 9 × 10 ⁻⁴	CL=90%

CONSTRAINED FIT INFORMATION

An overall fit to the total width, a partial width, and 10 branching ratios uses 32 measurements and one constraint to determine 8 parameters. The overall fit has a $\chi^2 = 21.1$ for 25 degrees of freedom.

The following off-diagonal array elements are the correlation coefficients $\langle \delta p_i \delta p_j \rangle / (\delta p_i \delta p_j)$, in percent, from the fit to parameters p_i , including the branching fractions, $x_i \equiv \Gamma_i / \Gamma_{\text{total}}$. The fit constrains the x_i whose labels appear in this array to sum to one.

x_2	-9						
x_3	-40	-73					
x_4	-8	36	-52				
x_5	-11	-3	-26	-7			
x_6	-1	-1	-1	-1	0		
x_7	-4	-7	-5	-5	-2	0	
Γ	0	0	0	0	0	-10	0
	x_1	x_2	x_3	x_4	x_5	x_6	x_7

Mode	Rate (MeV)	Scale factor
Γ_1 $K\pi$	49.9 ± 1.6	
Γ_2 $K^*(892)\pi$	24.7 ± 1.6	
Γ_3 $K^*(892)\pi\pi$	13.5 ± 2.3	
Γ_4 $K\rho$	8.7 ± 0.8	1.2
Γ_5 $K\omega$	2.9 ± 0.8	
Γ_6 $K^+\gamma$	0.24 ± 0.05	1.1
Γ_7 $K\eta$	0.15 ^{+0.34} _{-0.10}	1.3

$K_2^*(1430)$ PARTIAL WIDTHS

Mode	VALUE (keV)	DOCUMENT ID	TECN	CHG	COMMENT
$\Gamma(K^+\gamma)$	241 ± 50 OUR FIT				Error includes scale factor of 1.1.
	240 ± 45	CIHANGIR	82	SPEC +	$200 K^+ Z \rightarrow Z K^+ \pi^0, Z K_S^0 \pi^+$

Mode	VALUE (keV)	CL%	DOCUMENT ID	TECN	CHG	COMMENT
$\Gamma(K^0\gamma)$	< 5.4	90	ALAVI-HARATI02B	KTEV		$K^+ A \rightarrow K^+ + A$
	< 84	90	CARLSMITH	87	SPEC 0	$60-200 K_L^0 A \rightarrow K_S^0 \pi^0 A$

$K_2^*(1430)$ BRANCHING RATIOS

Mode	VALUE	DOCUMENT ID	TECN	CHG	COMMENT
$\Gamma(K\pi)/\Gamma_{\text{total}}$	0.499 ± 0.012 OUR FIT				
	0.488 ± 0.014 OUR AVERAGE				
	0.485 ± 0.006 ± 0.020	15 ASTON	88	LASS 0	11 $K^- p \rightarrow K^- \pi^+ n$
	0.49 ± 0.02	15 ESTABROOKS	78	ASPK ±	13 $K^\pm p \rightarrow p K \pi$

Mode	VALUE	DOCUMENT ID	TECN	CHG	COMMENT
$\Gamma(K^*(892)\pi)/\Gamma(K\pi)$	0.496 ± 0.034 OUR FIT				
	0.47 ± 0.04 OUR AVERAGE				
	0.44 ± 0.09	ASTON	84B	LASS 0	11 $K^- p \rightarrow \bar{K}^0 2\pi n$
	0.62 ± 0.19	LAUSCHER	75	HBC 0	10,16 $K^- p \rightarrow K^- \pi^+ n$
	0.54 ± 0.16	DEHM	74	DBC 0	4.6 $K^+ N$
	0.47 ± 0.08	AGUILAR-...	71B	HBC	3.9, 4.6 $K^- p$
	0.47 ± 0.10	BASSANO	67	HBC -0	4.6, 5.0 $K^- p$
	0.45 ± 0.13	BADIER	65c	HBC -	3 $K^- p$

Mode	VALUE	DOCUMENT ID	TECN	CHG	COMMENT
$\Gamma(K\omega)/\Gamma(K\pi)$	0.059 ± 0.017 OUR FIT				
	0.070 ± 0.035 OUR AVERAGE				
	0.05 ± 0.04	AGUILAR-...	71B	HBC	3.9, 4.6 $K^- p$
	0.13 ± 0.07	BASSOMPIE...	69	HBC 0	5 $K^+ p$

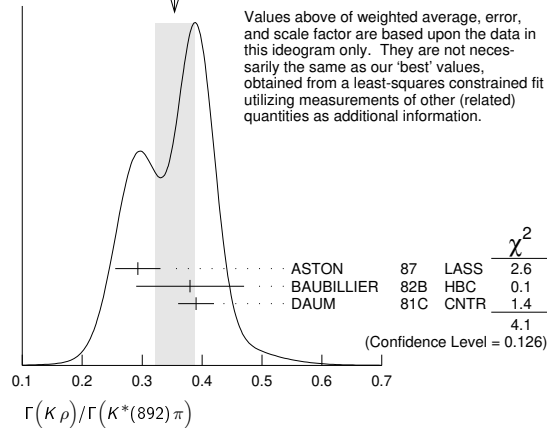
Mode	VALUE	DOCUMENT ID	TECN	CHG	COMMENT
$\Gamma(K\rho)/\Gamma(K\pi)$	0.174 ± 0.017 OUR FIT				Error includes scale factor of 1.2.
	0.150^{+0.029}_{-0.017} OUR AVERAGE				
	0.18 ± 0.05	ASTON	84B	LASS 0	11 $K^- p \rightarrow \bar{K}^0 2\pi n$
	0.02 ^{+0.10} _{-0.02}	DEHM	74	DBC 0	4.6 $K^+ N$
	0.16 ± 0.05	AGUILAR-...	71B	HBC	3.9, 4.6 $K^- p$
	0.14 ± 0.10	BASSANO	67	HBC -0	4.6, 5.0 $K^- p$
	0.14 ± 0.07	BADIER	65c	HBC -	3 $K^- p$

Meson Particle Listings

$K_2^*(1430)$, $K(1460)$

$\Gamma(K\rho)/\Gamma(K^*(892)\pi)$	VALUE	DOCUMENT ID	TECN	CHG	COMMENT
0.350 ± 0.031 OUR FIT					Error includes scale factor of 1.4.
0.354 ± 0.033 OUR AVERAGE					Error includes scale factor of 1.4. See the ideogram below.
0.293 ± 0.032 ± 0.020	ASTON	87	LASS	0	11 $K^-p \rightarrow \bar{K}^0 \pi^+ \pi^- n$
0.38 ± 0.09	BAUBILLIER	82B	HBC	0	8.25 $K^-p \rightarrow N K_S^0 \pi \pi$
0.39 ± 0.03	DAUM	81c	CNTR		63 $K^-p \rightarrow K^- 2\pi$

WEIGHTED AVERAGE
0.354 ± 0.033 (Error scaled by 1.4)



$\Gamma(K\omega)/\Gamma(K^*(892)\pi)$	VALUE	DOCUMENT ID	TECN	CHG	COMMENT
0.118 ± 0.034 OUR FIT					
0.10 ± 0.04	FIELD	67	HBC	-	3.8 K^-p

$\Gamma(K\eta)/\Gamma(K^*(892)\pi)$	VALUE	DOCUMENT ID	TECN	CHG	COMMENT
0.006 ± 0.014 OUR FIT					Error includes scale factor of 1.2.
0.07 ± 0.04	FIELD	67	HBC	-	3.8 K^-p

$\Gamma(K\eta)/\Gamma(K\pi)$	VALUE	CL%	DOCUMENT ID	TECN	CHG	COMMENT	
0.0030 ± 0.0070 OUR FIT						Error includes scale factor of 1.3.	
0 ± 0.0056	16		ASTON	88B	LASS	-	11 $K^-p \rightarrow K^- \eta p$
••• We do not use the following data for averages, fits, limits, etc. •••							
<0.04	95		AGUILAR-...	71B	HBC		3.9, 4.6 K^-p
<0.065			BASSOMPIE...	69	HBC		5.0 K^+p
<0.02			BISHOP	69	HBC		3.5 K^+p

$\Gamma(K^*(892)\pi\pi)/\Gamma_{total}$	VALUE	DOCUMENT ID	TECN	CHG	COMMENT		
0.134 ± 0.022 OUR FIT							
0.12 ± 0.04	18		GOLDBERG	76	HBC	-	3 $K^-p \rightarrow \rho \bar{K}^0 \pi \pi \pi$

$\Gamma(K^*(892)\pi\pi)/\Gamma(K\pi)$	VALUE	DOCUMENT ID	TECN	CHG	COMMENT		
0.27 ± 0.05 OUR FIT							
0.21 ± 0.08	17,18		JONGEJANS	78	HBC	-	4 $K^-p \rightarrow \rho \bar{K}^0 \pi \pi \pi$

$\Gamma(K\omega\pi)/\Gamma_{total}$	VALUE (units 10^{-3})	CL%	EVTS	DOCUMENT ID	TECN	COMMENT	
<0.72							
	95	0		JONGEJANS	78	HBC	4 $K^-p \rightarrow \rho \bar{K}^0 4\pi$

¹⁵ From phase shift analysis.
¹⁶ ASTON 88B quote < 0.0092 at CL=95%. We convert this to a central value and 1 sigma error in order to be able to use it in our constrained fit.
¹⁷ Restated by us.
¹⁸ Assuming $\pi\pi$ system has isospin 1, which is supported by the data.

$K_2^*(1430)$ REFERENCES

ABLIKIM 19A Q PR D100 032004	M. Ablikim et al.	(BESIII Collab.)
PELAEZ 17 EPJ C77 91	J.R. Pelaez, A.Rodas, J.R. de Elvira	
AUBERT 07AK PR D76 012008	B. Aubert et al.	(BABAR Collab.)
ALAVI-HARATI 02B PRL 89 072001	A. Alavi-Harati et al.	(FNAL KTeV Collab.)
BIRD 89 SLAC-332	P.F. Bird	(SLAC)
ASTON 88 NP B296 493	D. Aston et al.	(SLAC, NAGO, CINC, INUS)
ASTON 88B PL B201 169	D. Aston et al.	(SLAC, NAGO, CINC, INUS)
ASTON 87 NP B292 693	D. Aston et al.	(SLAC, NAGO, CINC, INUS)
CARLSMITH 87 PR D36 3502	D. Carlsmith et al.	(EFL, SACL)
ASTON 84B NP B247 261	D. Aston et al.	(SLAC, CARL, OTTA)
BAUBILLIER 84B ZPHY C26 37	M. Baubillier et al.	(BIRM, CERN, GLAS+)
BAUBILLIER 82B NP B202 21	M. Baubillier et al.	(BIRM, CERN, GLAS+)
CHANGIR 82 PL 117B 123	S. Changir et al.	(FNAL, MINN, ROCH)
CLELAND 82 NP B208 189	W.E. Cleland et al.	(DURH, GEVA, LAUS+)
ASTON 81C PL 106B 235	D. Aston et al.	(SLAC, CARL, OTTA) JP
DAUM 81C NP B187 1	C. Daum et al.	(AMST, CERN, CRAC, MPIM+)

TOAFF 81 PR D23 1500	S. Toaff et al.	(ANL, KANS)
ETKIN 80 PR D22 42	A. Etkin et al.	(BNL, CUNY) JP
ESTABROOKS 78 NP B133 490	P.G. Estabrooks et al.	(MCGI, CARL, DURH+)
Also PR D17 658	P.G. Estabrooks et al.	(MCGI, CARL, DURH+)
JONGEJANS 78 NP B139 383	B. Jongejans et al.	(ZEEM, CERN, NIJ+)
MARTIN 78 NP B134 392	A.D. Martin et al.	(DURH, GEVA)
BOWLER 77 NP B126 31	M.G. Bowler et al.	(OXF)
GOLDBERG 76 LNC 17 253	J. Goldberg	(HAIF)
HENDRICK 76 NP B112 189	K. Hendrickx et al.	(MONS, SACL, PARIS+)
LAUSCHER 75 NP B86 189	P. Lauscher et al.	(ABCLV Collab.) JP
MCCUBBIN 75 NP B86 13	N.A. McCubbin, L. Lyons	(OXF)
DEHM 74 NP B75 47	G. Dehm et al.	(MPIM, BRUX, MONS, CERN)
LINGLIN 73 NP B55 408	D. Linglin	(CERN)
AGUILAR-... 71B PR D4 2583	M. Aguilar-Benitez, R.L. Eisner, J.B. Kinson	(BNL)
BARNHAM 71C NP B28 171	K.W.J. Barnham et al.	(BIRM, GLAS)
CORDS 71 PR D4 1974	D. Cords et al.	(PURD, UCD, IUPU)
BASSOMPIE... 69 NP B13 189	G. Bassompierre et al.	(CERN, BRUX) JP
BISHOP 69 NP B9 403	J.M. Bishop et al.	(WISC)
CRENNELL 69D PRL 22 487	D.J. Crennell et al.	(BNL)
DAVIS 69 PRL 23 1071	P.J. Davis et al.	(LRL)
LIND 69 NP B14 1	V.G. Lind et al.	(LRL) JP
SCHWEING... 68 PR 166 1317	F. Schweingruber et al.	(ANL, NWES)
Also Thesis	F.L. Schweingruber	(NWES, INWES)
BASSANO 67 PRL 19 968	D. Bassano et al.	(BNL, SYRA)
FIELD 67 PL 24B 638	J.H. Field et al.	(UCSD)
BADIER 65C PL 19 612	J. Badier et al.	(EPOL, SACL, AMST)

$K(1460)$

$$I(J^P) = \frac{1}{2}(0^-)$$

Observed in $K\pi\pi$ partial-wave analysis.

$K(1460)$ MASS

VALUE (MeV)	EVTS	DOCUMENT ID	TECN	CHG	COMMENT
••• We do not use the following data for averages, fits, limits, etc. •••					
1482.40 ± 3.58 ± 15.22	894k	AAIJ	18A1	LHCB	$D^0 \rightarrow K^{\mp} 2\pi^{\pm} \pi^{\mp}$
~ 1460	63	DAUM	81C	CNTR	- $K^-p \rightarrow K^- 2\pi p$
~ 1400	13	¹ BRANDENB...	76B	ASPK	± $K^{\pm} p \rightarrow K^{\pm} 2\pi p$
					¹ Coupled mainly to $K f_0(1370)$. Decay into $K^*(892)\pi$ seen.

$K(1460)$ WIDTH

VALUE (MeV)	EVTS	DOCUMENT ID	TECN	CHG	COMMENT
••• We do not use the following data for averages, fits, limits, etc. •••					
335.60 ± 6.20 ± 8.65	894k	AAIJ	18A1	LHCB	$D^0 \rightarrow K^{\mp} 2\pi^{\pm} \pi^{\mp}$
~ 260	63	DAUM	81C	CNTR	- $K^-p \rightarrow K^- 2\pi p$
~ 250	15	¹ BRANDENB...	76B	ASPK	± $K^{\pm} p \rightarrow K^{\pm} 2\pi p$
					¹ Coupled mainly to $K f_0(1370)$. Decay into $K^*(892)\pi$ seen.

$K(1460)$ DECAY MODES

Mode	Fraction (Γ_i/Γ)
Γ_1 $K^*(892)\pi$	seen
Γ_2 $K\rho$	seen
Γ_3 $K_0^*(1430)\pi$	seen
Γ_4 $K\phi$	seen

$K(1460)$ PARTIAL WIDTHS

$\Gamma(K^*(892)\pi)$	VALUE (MeV)	DOCUMENT ID	TECN	COMMENT	
••• We do not use the following data for averages, fits, limits, etc. •••					
~ 109		DAUM	81C	CNTR	63 $K^-p \rightarrow K^- 2\pi p$

$\Gamma(K\rho)$	VALUE (MeV)	DOCUMENT ID	TECN	COMMENT	
••• We do not use the following data for averages, fits, limits, etc. •••					
~ 34		DAUM	81C	CNTR	63 $K^-p \rightarrow K^- 2\pi p$

$\Gamma(K_0^*(1430)\pi)$	VALUE (MeV)	DOCUMENT ID	TECN	COMMENT	
••• We do not use the following data for averages, fits, limits, etc. •••					
~ 117		DAUM	81C	CNTR	63 $K^-p \rightarrow K^- 2\pi p$

$\Gamma(K\phi)/\Gamma_{total}$	VALUE	EVTS	DOCUMENT ID	TECN	COMMENT	
seen		24k	¹ AAIJ	21E	LHCB	$B^+ \rightarrow J/\psi \phi K^+$
						¹ From an amplitude analysis of the decay $B^+ \rightarrow J/\psi \phi K^+$ with a significance of 12 σ .

$K(1460)$ REFERENCES

AAIJ 21E PRL 127 082001	R. Aaij et al.	(LHCb Collab.)
AAIJ 18A1 EPJ C78 443	R. Aaij et al.	(LHCb Collab.)
DAUM 81C NP B187 1	C. Daum et al.	(AMST, CERN, CRAC, MPIM+)
BRANDENB... 76B PRL 36 1239	G.W. Brandenburg et al.	(SLAC) JP

See key on page 1127

Meson Particle Listings

$K_2(1580)$, $K(1630)$, $K_1(1650)$, $K^*(1680)$

$K_2(1580)$ $I(J^P) = \frac{1}{2}(2^-)$
 OMITTED FROM SUMMARY TABLE
 Seen in partial-wave analysis of the $K^- \pi^+ \pi^-$ system. Needs confirmation.

$K_2(1580)$ MASS

VALUE (MeV)	DOCUMENT ID	CHG	COMMENT
• • • We do not use the following data for averages, fits, limits, etc. • • •			
~ 1580	OTTER	79	- 10,14,16 $K^- p$

$K_2(1580)$ WIDTH

VALUE (MeV)	DOCUMENT ID	CHG	COMMENT
• • • We do not use the following data for averages, fits, limits, etc. • • •			
~ 110	OTTER	79	- 10,14,16 $K^- p$

$K_2(1580)$ DECAY MODES

Mode	Fraction (Γ_i/Γ)
Γ_1 $K^*(892) \pi$	seen
Γ_2 $K_2^*(1430) \pi$	possibly seen

$K_2(1580)$ BRANCHING RATIOS

$\Gamma(K^*(892)\pi)/\Gamma_{total}$	Γ_1/Γ
seen	
possibly seen	

VALUE	DOCUMENT ID	TECN	CHG	COMMENT
seen	OTTER	79	HBC	- 10,14,16 $K^- p$
possibly seen	GULER	11	BELL	$B^+ \rightarrow J/\psi K^+ \pi^+ \pi^-$

$K_2(1580)$ REFERENCES

GULER	11	PR D83 032005	H. Guler et al.	(Belle Collab.)
OTTER	79	NP B147 1	G. Otter et al.	(AACH3, BERL, CERN, LOIC+)JP

$K(1630)$ $I(J^P) = \frac{1}{2}(?)^?$
 OMITTED FROM SUMMARY TABLE
 Seen as a narrow peak, compatible with the experimental resolution, in the invariant mass of the $K_S^0 \pi^+ \pi^-$ system produced in $\pi^- p$ interactions at high momentum transfers.

$K(1630)$ MASS

VALUE (MeV)	EVTS	DOCUMENT ID	TECN	COMMENT
1629 ± 7	~ 75	KARNAUKHOV98	BC	16.0 $\pi^- p \rightarrow (K_S^0 \pi^+ \pi^-) X^+ \pi^- X^0$

$K(1630)$ WIDTH

VALUE (MeV)	EVTS	DOCUMENT ID	TECN	COMMENT
16⁺¹⁹₋₁₆	~ 75	¹ KARNAUKHOV98	BC	16.0 $\pi^- p \rightarrow (K_S^0 \pi^+ \pi^-) X^+ \pi^- X^0$

¹ Compatible with an experimental resolution of 14 ± 1 MeV.

$K(1630)$ DECAY MODES

Mode
Γ_1 $K_S^0 \pi^+ \pi^-$

$K(1630)$ REFERENCES

KARNAUKHOV 98	PAN 61 203	V.M. Karnaukhov, C. Coca, V.I. Moroz
	Translated from YAF 61 252.	

$K_1(1650)$ $I(J^P) = \frac{1}{2}(1^+)$
 This entry contains various peaks in strange meson systems ($K^+ \phi$, $K \pi \pi$) reported in partial-wave analysis in the 1600–1900 mass region.

$K_1(1650)$ MASS

VALUE (MeV)	EVTS	DOCUMENT ID	TECN	CHG	COMMENT
1650 ± 50		FRAME	86	OMEG +	13 $K^+ p \rightarrow \phi K^+ p$
• • • We do not use the following data for averages, fits, limits, etc. • • •					
1861 ± 10 ⁺¹⁶ ₋₄₆	24k	¹ AAIJ	21E	LHCB	$B^+ \rightarrow J/\psi \phi K^+$
1911 ± 37 ⁺¹²⁴ ₋₄₈	24k	¹ AAIJ	21E	LHCB	$B^+ \rightarrow J/\psi \phi K^+$
1793 ± 59 ⁺¹⁵³ ₋₁₀₁	4289	^{2,3} AAIJ	17c	LHCB	$B^+ \rightarrow J/\psi \phi K^+$
~ 1840		ARMSTRONG	83	OMEG -	18.5 $K^- p \rightarrow 3K p$
~ 1800		DAUM	81c	CNTR -	63 $K^- p \rightarrow K^- 2\pi p$

¹ One of two K_1 states reported by AAIJ 21E. From an amplitude analysis of the decay $B^+ \rightarrow J/\psi \phi K^+$ with a significance of 4.5 σ .
² From an amplitude analysis of the decay $B^+ \rightarrow J/\psi \phi K^+$ with a significance of 7.6 σ .
³ Superseded by AAIJ 21E.

$K_1(1650)$ WIDTH

VALUE (MeV)	EVTS	DOCUMENT ID	TECN	CHG	COMMENT
150 ± 50		FRAME	86	OMEG +	13 $K^+ p \rightarrow \phi K^+ p$
• • • We do not use the following data for averages, fits, limits, etc. • • •					
149 ± 41 ⁺²³¹ ₋₂₃	24k	¹ AAIJ	21E	LHCB	$B^+ \rightarrow J/\psi \phi K^+$
276 ± 50 ⁺³¹⁹ ₋₁₅₉	24k	¹ AAIJ	21E	LHCB	$B^+ \rightarrow J/\psi \phi K^+$
365 ± 157 ⁺¹³⁸ ₋₂₁₅	4289	^{2,3} AAIJ	17c	LHCB	$B^+ \rightarrow J/\psi \phi K^+$
~ 250		DAUM	81c	CNTR -	63 $K^- p \rightarrow K^- 2\pi p$

¹ One of two K_1 states reported by AAIJ 21E. From an amplitude analysis of the decay $B^+ \rightarrow J/\psi \phi K^+$ with a significance of 4.5 σ .
² From an amplitude analysis of the decay $B^+ \rightarrow J/\psi \phi K^+$ with a significance of 7.6 σ .
³ Superseded by AAIJ 21E.

$K_1(1650)$ DECAY MODES

Mode
Γ_1 $K \pi \pi$
Γ_2 $K \phi$

$K_1(1650)$ REFERENCES

AAIJ	21E	PRL 127 082001	R. Aaij et al.	(LHCb Collab.)
AAIJ	17C	PRL 118 022003	R. Aaij et al.	(LHCb Collab.)
Also		PR D95 012002	R. Aaij et al.	(LHCb Collab.)
FRAME	86	NP B276 667	D. Frame et al.	(GLAS)
ARMSTRONG	83	NP B221 1	T.A. Armstrong et al.	(BARI, BIRM, CERN+)
DAUM	81C	NP B187 1	C. Daum et al.	(AMST, CERN, CRAC, MPIM+)

$K^*(1680)$ $I(J^P) = \frac{1}{2}(1^-)$

$K^*(1680)$ MASS

VALUE (MeV)	EVTS	DOCUMENT ID	TECN	CHG	COMMENT
1718 ± 18 OUR AVERAGE					
1722 ± 20 ⁺³³ ₋₁₀₉	4289	¹ AAIJ	17c	LHCB	$B^+ \rightarrow J/\psi \phi K^+$
1677 ± 10 ± 32		ASTON	88	LASS 0	11 $K^- p \rightarrow K^- \pi^+ n$
1735 ± 10 ± 20		ASTON	87	LASS 0	11 $K^- p \rightarrow \bar{K}^0 \pi^+ \pi^- n$
• • • We do not use the following data for averages, fits, limits, etc. • • •					
1678 ± 64		BIRD	89	LASS -	11 $K^- p \rightarrow \bar{K}^0 \pi^- p$
1800 ± 70		ETKIN	80	MPS 0	6 $K^- p \rightarrow \bar{K}^0 \pi^+ \pi^- n$
~ 1650		ESTABROOKS	78	ASPK 0	13 $K^+ p \rightarrow K^+ \pi^+ n$

¹ From an amplitude analysis of the decay $B^+ \rightarrow J/\psi \phi K^+$ with a significance of 8.5 σ .

$K^*(1680)$ WIDTH

VALUE (MeV)	EVTS	DOCUMENT ID	TECN	CHG	COMMENT
322 ± 110 OUR AVERAGE					
Error includes scale factor of 4.2.					
354 ± 75 ⁺¹⁴⁰ ₋₁₈₁	4289	² AAIJ	17c	LHCB	$B^+ \rightarrow J/\psi \phi K^+$
205 ± 16 ± 34		ASTON	88	LASS 0	11 $K^- p \rightarrow K^- \pi^+ n$
423 ± 18 ± 30		ASTON	87	LASS 0	11 $K^- p \rightarrow \bar{K}^0 \pi^+ \pi^- n$

Meson Particle Listings

$K^*(1680)$, $K_2(1770)$

• • • We do not use the following data for averages, fits, limits, etc. • • •

454 ± 270	BIRD	89	LASS	—	11	$K^- p \rightarrow \bar{K}^0 \pi^- p$
170 ± 30	ETKIN	80	MPS	0	6	$K^- p \rightarrow \bar{K}^0 \pi^+ \pi^- n$
250 to 300	ESTABROOKS	78	ASPK	0	13	$K^\pm p \rightarrow K^\pm \pi^\pm n$

² From an amplitude analysis of the decay $B^+ \rightarrow J/\psi \phi K^+$ with a significance of 8.5 σ .

$K^*(1680)$ DECAY MODES

Mode	Fraction (Γ_i/Γ)
Γ_1 $K \pi$	(38.7 ± 2.5) %
Γ_2 $K \rho$	(31.4 $^{+5.0}_{-2.1}$) %
Γ_3 $K^*(892) \pi$	(29.9 $^{+2.2}_{-5.0}$) %
Γ_4 $K \phi$	seen
Γ_5 $K \eta$	(1.4 $^{+1.0}_{-0.8}$) %

CONSTRAINED FIT INFORMATION

An overall fit to 4 branching ratios uses 4 measurements and one constraint to determine 3 parameters. The overall fit has a $\chi^2 = 2.9$ for 2 degrees of freedom.

The following *off-diagonal* array elements are the correlation coefficients $\langle \delta x_i \delta x_j \rangle / (\delta x_i \delta x_j)$, in percent, from the fit to the branching fractions, $x_i \equiv \Gamma_i / \Gamma_{\text{total}}$. The fit constrains the x_i whose labels appear in this array to sum to one.

x_2	−36	
x_3	−39	−72
	x_1	x_2

$K^*(1680)$ BRANCHING RATIOS

$\Gamma(K \pi) / \Gamma_{\text{total}}$	VALUE	DOCUMENT ID	TECN	CHG	COMMENT	Γ_1 / Γ
	0.387 ± 0.026 OUR FIT					
	0.388 ± 0.014 ± 0.022	ASTON	88	LASS	0	11 $K^- p \rightarrow K^- \pi^+ n$

$\Gamma(K \pi) / \Gamma(K^*(892) \pi)$	VALUE	DOCUMENT ID	TECN	CHG	COMMENT	Γ_1 / Γ_3
	1.30 $^{+0.23}_{-0.14}$ OUR FIT					
	2.8 ± 1.1	ASTON	84	LASS	0	11 $K^- p \rightarrow \bar{K}^0 2\pi n$

$\Gamma(K \rho) / \Gamma(K \pi)$	VALUE	DOCUMENT ID	TECN	CHG	COMMENT	Γ_2 / Γ_1
	0.81 $^{+0.14}_{-0.09}$ OUR FIT					
	1.2 ± 0.4	ASTON	84	LASS	0	11 $K^- p \rightarrow \bar{K}^0 2\pi n$

$\Gamma(K \rho) / \Gamma(K^*(892) \pi)$	VALUE	DOCUMENT ID	TECN	CHG	COMMENT	Γ_2 / Γ_3
	1.05 $^{+0.27}_{-0.11}$ OUR FIT					
	0.97 ± 0.09 $^{+0.30}_{-0.10}$	ASTON	87	LASS	0	11 $K^- p \rightarrow \bar{K}^0 \pi^+ \pi^- n$

$\Gamma(K \phi) / \Gamma_{\text{total}}$	VALUE	EVTS	DOCUMENT ID	TECN	COMMENT	Γ_4 / Γ
seen	24k	3	AAIJ	21E	LHCB $B^+ \rightarrow J/\psi \phi K^+$	
• • • We do not use the following data for averages, fits, limits, etc. • • •						
seen	4289	4.5	AAIJ	17c	LHCB $B^+ \rightarrow J/\psi \phi K^+$	

³ From an amplitude analysis of the decay $B^+ \rightarrow J/\psi \phi K^+$ with a significance of 4.7 σ .

⁴ From an amplitude analysis of the decay $B^+ \rightarrow J/\psi \phi K^+$ with a significance of 8.5 σ .

⁵ Superseded by AAIJ 21E.

$\Gamma(K \eta) / \Gamma(K \pi)$	VALUE	EVTS	DOCUMENT ID	TECN	COMMENT	Γ_5 / Γ_1
	0.037 ± 0.007 $^{+0.024}_{-0.018}$	116k	6	CHEN	20A BELL $D^0 \rightarrow K^- \pi^+ \eta$	

⁶ CHEN 20A quotes the ratio $\Gamma(K^*(1680)^- \rightarrow K^- \eta) / \Gamma(K^*(1680)^- \rightarrow K^- \pi^0) = 0.11 \pm 0.02 \pm 0.06 \pm 0.04$ (BPDG) where the last uncertainty comes from $B(\eta \rightarrow \gamma \gamma) = (39.41 \pm 0.20)\%$. We divide it by 3 taking into account that $\Gamma(K^*(1680)^- \rightarrow K^- \pi^0) / \Gamma(K^*(1680)^- \rightarrow (K \pi)^-) = 1/3$.

$\Gamma(K \eta) / \Gamma_{\text{total}}$	VALUE (units 10^{-2})	EVTS	DOCUMENT ID	TECN	COMMENT	Γ_5 / Γ
--	--------------------------	------	-------------	------	---------	---------------------

• • • We do not use the following data for averages, fits, limits, etc. • • •

1.44 ± 0.21 $^{+0.96}_{-0.73}$	116k	7	CHEN	20A BELL	$D^0 \rightarrow K^- \pi^+ \eta$	
--------------------------------	------	---	------	----------	----------------------------------	--

⁷ From an amplitude analysis of the decay $D^0 \rightarrow K^- \pi^+ \eta$ with a significance of 16 σ . Not independent of the CHEN 20A measurement of $\Gamma(K^*(1680) \rightarrow K \eta) / \Gamma(K^*(1680) \rightarrow K \pi)$.

$K^*(1680)$ REFERENCES

AAIJ	21E	PRL 127 082001	R. Aaij et al.	(LHCb Collab.)
CHEN	20A	PR D102 012002	Y.Q. Chen et al.	(BELLE Collab.)
AAIJ	17C	PRL 118 022003	R. Aaij et al.	(LHCb Collab.)
Also		PR D95 012002	R. Aaij et al.	(LHCb Collab.)
BIRD	89	SLA C-322	P.F. Bird	(SLAC)
ASTON	88	NP B296 493	D. Aston et al.	(SLAC, NAGO, CIN, INUS)
ASTON	87	NP B292 693	D. Aston et al.	(SLAC, NAGO, CIN, INUS)
ASTON	84	PL 149B 258	D. Aston et al.	(SLAC, CARL, OTTA)JP
ETKIN	80	PR D22 42	A. Etkin et al.	(BNL, CUNY)JP
ESTABROOKS	78	NP B133 490	P.G. Estabrooks et al.	(MCGI, CARL, DURH+)JP

$K_2(1770)$

$$I(J^P) = \frac{1}{2}(2^-)$$

See our mini-review in the 2004 edition of this Review, PDG 04.

$K_2(1770)$ MASS

VALUE (MeV)	EVTS	DOCUMENT ID	TECN	CHG	COMMENT	
1773 ± 8 OUR AVERAGE						
1777 ± 35 $^{+122}_{-77}$	4289	1	AAIJ	17c	LHCB $B^+ \rightarrow J/\psi \phi K^+$	
1773 ± 8		2	ASTON	93	LASS $11 K^- p \rightarrow K^- \omega p$	
• • • We do not use the following data for averages, fits, limits, etc. • • •						
1743 ± 15			TIKHOMIROV	03	SPEC $40.0 \pi^- C \rightarrow K_S^0 K_S^0 K_L^0 X$	
1810 ± 20			FRAME	86	OMEG + $13 K^+ p \rightarrow \phi K^+ p$	
~ 1730			ARMSTRONG	83	OMEG − $18.5 K^- p \rightarrow 3 K p$	
~ 1780			3	DAUM	81c	CNTR − $63 K^- p \rightarrow K^- 2\pi p$
1710 ± 15	60		CHUNG	74	HBC − $7.3 K^- p \rightarrow K^- \omega p$	
1767 ± 6			BLIEDEN	72	MMS − $11-16 K^- p$	
1730 ± 20	306		4	FIRESTONE	72B	DBC + $12 K^+ d$
1765 ± 40			5	COLLEY	71	HBC + $10 K^+ p \rightarrow K_2 \pi N$
1740			DENEGRI	71	DBC − $12.6 K^- d \rightarrow \bar{K} 2\pi d$	
1745 ± 20			AGUILAR...	70c	HBC − $4.6 K^- p$	
1780 ± 15			BARTSCH	70c	HBC − $10.1 K^- p$	
1760 ± 15			LUDLAM	70	HBC − $12.6 K^- p$	

¹ From an amplitude analysis of the decay $B^+ \rightarrow J/\psi \phi K^+$ with a significance of 5.0 σ .

² From a partial wave analysis of the $K^- \omega$ system.

³ From a partial wave analysis of the $K^- 2\pi$ system.

⁴ Produced in conjunction with excited deuteron.

⁵ Systematic errors added correspond to spread of different fits.

$K_2(1770)$ WIDTH

VALUE (MeV)	EVTS	DOCUMENT ID	TECN	CHG	COMMENT	
186 ± 14 OUR AVERAGE						
217 ± 116 $^{+221}_{-154}$	4289	6	AAIJ	17c	LHCB $B^+ \rightarrow J/\psi \phi K^+$	
186 ± 14			7	ASTON	93	LASS $11 K^- p \rightarrow K^- \omega p$
• • • We do not use the following data for averages, fits, limits, etc. • • •						
147 ± 70			TIKHOMIROV	03	SPEC $40.0 \pi^- C \rightarrow K_S^0 K_S^0 K_L^0 X$	
140 ± 40			FRAME	86	OMEG + $13 K^+ p \rightarrow \phi K^+ p$	
~ 220			ARMSTRONG	83	OMEG − $18.5 K^- p \rightarrow 3 K p$	
~ 210			8	DAUM	81c	CNTR − $63 K^- p \rightarrow K^- 2\pi p$
110 ± 50	60		CHUNG	74	HBC − $7.3 K^- p \rightarrow K^- \omega p$	
100 ± 26			BLIEDEN	72	MMS − $11-16 K^- p$	
210 ± 30	306		9	FIRESTONE	72B	DBC + $12 K^+ d$
90 ± 70			10	COLLEY	71	HBC + $10 K^+ p \rightarrow K_2 \pi N$
130			DENEGRI	71	DBC − $12.6 K^- d \rightarrow \bar{K} 2\pi d$	
100 ± 50			AGUILAR...	70c	HBC − $4.6 K^- p$	
138 ± 40			BARTSCH	70c	HBC − $10.1 K^- p$	
50 $^{+40}_{-20}$			LUDLAM	70	HBC − $12.6 K^- p$	

⁶ From an amplitude analysis of the decay $B^+ \rightarrow J/\psi \phi K^+$ with a significance of 5.0 σ .

⁷ From a partial wave analysis of the $K^- \omega$ system.

⁸ From a partial wave analysis of the $K^- 2\pi$ system.

⁹ Produced in conjunction with excited deuteron.

¹⁰ Systematic errors added correspond to spread of different fits.

See key on page 1127

Meson Particle Listings

K₂(1770), K₃^{*}(1780)

K₂(1770) DECAY MODES

Table with 2 columns: Mode and Fraction (Γ_i/Γ). Rows include Kππ, K₂^{*}(1430)π, K₂^{*}(892)π, Kf₂(1270), Kf₀(980), Kφ, and Kω.

K₂(1770) BRANCHING RATIOS

Table for Γ(K₂^{*}(1430)π)/Γ(Kππ) with columns for VALUE, DOCUMENT ID, TECN, CHG, COMMENT. Includes a note about data not being used for averages.

Table for Γ(K^{*}(892)π)/Γ(Kππ) with columns for VALUE, DOCUMENT ID, TECN, COMMENT. Includes a note about data not being used for averages.

Table for Γ(Kf₂(1270))/Γ(Kππ) with columns for VALUE, DOCUMENT ID, TECN, COMMENT. Includes a note about data not being used for averages.

Table for Γ(Kf₀(980))/Γ_{total} with columns for VALUE, DOCUMENT ID, TECN, COMMENT. Includes a note about data not being used for averages.

Table for Γ(Kφ)/Γ_{total} with columns for VALUE, EVTS, DOCUMENT ID, TECN, CHG, COMMENT. Includes a note about data not being used for averages.

Table for Γ(Kω)/Γ_{total} with columns for VALUE, DOCUMENT ID, TECN, CHG, COMMENT. Includes a note about data not being used for averages.

K₂(1770) REFERENCES

Reference list table with columns: Author, Year, Journal, and other identifiers.

K₃^{*}(1780)

I(J^P) = 1/2(3⁻)

K₃^{*}(1780) T-MATRIX POLE √S

Table for T-matrix pole with columns: VALUE (MeV), DOCUMENT ID, TECN, COMMENT. Includes a note about data not being used for averages.

K₃^{*}(1780) MASS

Table for mass with columns: VALUE (MeV), EVTS, DOCUMENT ID, TECN, CHG, COMMENT. Includes a note about data not being used for averages.

- Footnotes for the mass table: 1 Seen in ψ(2S) decay... 2 From energy-independent partial-wave analysis... 3 From a fit to Y₆² moment... 4 Confirmed by phase shift analysis... 5 From a partial wave amplitude analysis... 6 From a fit to the Y₆⁰ moment.

K₃^{*}(1780) WIDTH

Table for width with columns: VALUE (MeV), EVTS, DOCUMENT ID, TECN, CHG, COMMENT. Includes a note about data not being used for averages.

- Footnotes for the width table: 1 Seen in ψ(2S) decay... 2 From energy-independent partial-wave analysis... 3 From a fit to Y₆² moment... 4 From a partial wave amplitude analysis... 5 From a fit to Y₆⁰ moment... 6 Errors enlarged by us to 4Γ/√N... 7 ESTABROOKS 78 find that BRANDENBURG 76D data are consistent with 175 MeV width. Not averaged.

Meson Particle Listings

K₃^{*}(1780), K₂(1820)

K₃^{*}(1780) DECAY MODES

Mode	Fraction (Γ _i /Γ)	Confidence level
Γ ₁ K ρ	(31 ± 9) %	
Γ ₂ K [*] (892) π	(20 ± 5) %	
Γ ₃ K π	(18.8 ± 1.0) %	
Γ ₄ K η	(30 ± 13) %	
Γ ₅ K ₂ [*] (1430) π	< 16 %	95%

CONSTRAINED FIT INFORMATION

An overall fit to 3 branching ratios uses 4 measurements and one constraint to determine 4 parameters. The overall fit has a χ² = 0.0 for 1 degrees of freedom.

The following *off-diagonal* array elements are the correlation coefficients $\langle \delta x_i \delta x_j \rangle / (\delta x_i \delta x_j)$, in percent, from the fit to the branching fractions, $x_i \equiv \Gamma_i / \Gamma_{total}$. The fit constrains the x_i whose labels appear in this array to sum to one.

x ₂	85		
x ₃	18	21	
x ₄	-98	-94	-27
	x ₁	x ₂	x ₃

K₃^{*}(1780) BRANCHING RATIOS

Γ(K ρ)/Γ(K [*] (892) π)	DOCUMENT ID	TECN	CHG	COMMENT	Γ ₁ /Γ ₂
<u>VALUE</u> 1.52 ± 0.23 OUR FIT 1.52 ± 0.21 ± 0.10	ASTON	87	LASS	0	11 K ⁻ p → $\overline{K}^0 \pi^+ \pi^- n$

Γ(K [*] (892) π)/Γ(K π)	DOCUMENT ID	TECN	CHG	COMMENT	Γ ₂ /Γ ₃
<u>VALUE</u> 1.09 ± 0.26 OUR FIT 1.09 ± 0.26	ASTON	84B	LASS	0	11 K ⁻ p → $\overline{K}^0 2\pi n$

Γ(K η)/Γ _{total}	DOCUMENT ID	TECN	CHG	COMMENT	Γ ₃ /Γ
<u>VALUE</u> 0.188 ± 0.010 OUR FIT 0.188 ± 0.010 OUR AVERAGE	ASTON	88	LASS	0	11 K ⁻ p → K ⁻ π ⁺ n
0.187 ± 0.008 ± 0.008	ESTABROOKS	78	ASPK	0	13 K [±] p → KπN

Γ(K η)/Γ(K π)	DOCUMENT ID	TECN	CHG	COMMENT	Γ ₄ /Γ ₃
<u>VALUE</u> 1.6 ± 0.7 OUR FIT	• • • We do not use the following data for averages, fits, limits, etc. • • •				
0.41 ± 0.050	¹ BIRD	89	LASS	—	11 K ⁻ p → $\overline{K}^0 \pi^- p$
0.50 ± 0.18	ASTON	88B	LASS	—	11 K ⁻ p → K ⁻ ηp
	¹ This result supersedes ASTON 88B.				

Γ(K ₂ [*] (1430) π)/Γ(K [*] (892) π)	DOCUMENT ID	TECN	CHG	COMMENT	Γ ₅ /Γ ₂
<u>VALUE</u> < 0.78	ASTON	87	LASS	0	11 K ⁻ p → $\overline{K}^0 \pi^+ \pi^- n$

K₃^{*}(1780) REFERENCES

ABLIKIM	20F	PR D101 032008	M. Ablikim et al.	(BESIII Collab.)
PELAEZ	17	EPJ C77 91	J.R. Pelaez, A.Rodas, J.R. de Elvira	
BIRD	89	SLAC-332	P.F. Bird	(SLAC)
ASTON	88	NP B296 493	D. Aston et al.	(SLAC, NAGO, CINC, INUS)
ASTON	88B	PL B201 169	D. Aston et al.	(SLAC, NAGO, CINC, INUS) JP
ASTON	87	NP B292 693	D. Aston et al.	(SLAC, NAGO, CINC, INUS)
ASTON	84B	NP B247 261	D. Aston et al.	(SLAC, CARL, OTTA)
BAUBILLIER	84B	ZPHY C26 37	M. Baubillier et al.	(BIRM, CERN, GLAS+)
BAUBILLIER	82B	NP B202 21	M. Baubillier et al.	(BIRM, CERN, GLAS+)
CLELAND	82	NP B308 189	W.E. Cleland et al.	(DURH, GEVA, LAUS+)
ASTON	81D	PL 99B 502	D. Aston et al.	(SLAC, CARL, OTTA) JP
TOAFF	81	PR D23 1500	S. Toaff et al.	(ANL, KANS)
ETKIN	80	PR D22 42	A. Etkin et al.	(BNL, CUNY) JP
BEUSCH	78	PL 74B 282	W. Beusch et al.	(CERN, AACH3, ETH) JP
CHUNG	78	PRL 40 355	S.U. Chung et al.	(BNL, BRAN, CUNY+) JP
ESTABROOKS	78	NP B133 490	P.G. Estabrooks et al.	(MCGI, CARL, DURH+) JP
Also		PR D17 658	P.G. Estabrooks et al.	(MCGI, CARL, DURH+) JP
BALDI	76	PL 63B 344	R. Baldi et al.	(GEVA) JP
BRANDENB...	76D	PL 60B 478	G.W. Brandenburg et al.	(SLAC) JP

K₂(1820)

$$I(J^P) = \frac{1}{2}(2^-)$$

See our mini-review in the 2004 edition of this Review (PDG 04) under K₂(1770).

K₂(1820) MASS

VALUE (MeV)	EVTS	DOCUMENT ID	TECN	COMMENT
1819 ± 12 OUR AVERAGE				
1853 ± 27 ⁺¹⁸ ₋₃₅	4289	¹ AAIJ	17c LHCb	B ⁺ → J/ψ φ K ⁺
1816 ± 13		² ASTON	93 LASS	11 K ⁻ p → K ⁻ ωp
• • • We do not use the following data for averages, fits, limits, etc. • • •				
~ 1840		³ DAUM	81c CNTR	63 K ⁻ p → K ⁻ 2πp
		¹ From an amplitude analysis of the decay B ⁺ → J/ψ φ K ⁺ with a significance of 3.0 σ.		
		² From a partial wave analysis of the K ⁻ ω system.		
		³ From a partial wave analysis of the K ⁻ 2π system.		

K₂(1820) WIDTH

VALUE (MeV)	EVTS	DOCUMENT ID	TECN	COMMENT
264 ± 34 OUR AVERAGE				
167 ± 58 ⁺⁸² ₋₇₂	4289	¹ AAIJ	17c LHCb	B ⁺ → J/ψ φ K ⁺
276 ± 35		² ASTON	93 LASS	11 K ⁻ p → K ⁻ ωp
• • • We do not use the following data for averages, fits, limits, etc. • • •				
~ 230		³ DAUM	81c CNTR	63 K ⁻ p → K ⁻ 2πp
		¹ From an amplitude analysis of the decay B ⁺ → J/ψ φ K ⁺ with a significance of 3.0 σ.		
		² From a partial wave analysis of the K ⁻ ω system.		
		³ From a partial wave analysis of the K ⁻ 2π system.		

K₂(1820) DECAY MODES

Mode	Fraction (Γ _i /Γ)
Γ ₁ K π π	seen
Γ ₂ K ₂ [*] (1430) π	seen
Γ ₃ K [*] (892) π	seen
Γ ₄ K f ₂ (1270)	seen
Γ ₅ K ω	seen
Γ ₆ K φ	seen

K₂(1820) BRANCHING RATIOS

Γ(K ₂ [*] (1430) π)/Γ(K π π)	DOCUMENT ID	TECN	COMMENT	Γ ₂ /Γ ₁
<u>VALUE</u>				
• • • We do not use the following data for averages, fits, limits, etc. • • •				
~ 0.77	DAUM	81c CNTR	63 K ⁻ p → $\overline{K}^0 2\pi p$	

Γ(K [*] (892) π)/Γ(K π π)	DOCUMENT ID	TECN	COMMENT	Γ ₃ /Γ ₁
<u>VALUE</u>				
• • • We do not use the following data for averages, fits, limits, etc. • • •				
~ 0.05	DAUM	81c CNTR	63 K ⁻ p → $\overline{K}^0 2\pi p$	

Γ(K f ₂ (1270))/Γ(K π π)	DOCUMENT ID	TECN	COMMENT	Γ ₄ /Γ ₁
<u>VALUE</u>				
• • • We do not use the following data for averages, fits, limits, etc. • • •				
~ 0.18	DAUM	81c CNTR	63 K ⁻ p → $\overline{K}^0 2\pi p$	

Γ(K φ)/Γ _{total}	DOCUMENT ID	TECN	COMMENT	Γ ₆ /Γ
<u>VALUE</u>				
seen	24k	¹ AAIJ	21E LHCb	B ⁺ → J/ψ φ K ⁺
• • • We do not use the following data for averages, fits, limits, etc. • • •				
seen	4289	^{2,3} AAIJ	17c LHCb	B ⁺ → J/ψ φ K ⁺
		¹ From an amplitude analysis of the decay B ⁺ → J/ψ φ K ⁺ with a significance of 5.8 σ.		
		² From an amplitude analysis of the decay B ⁺ → J/ψ φ K ⁺ with a significance of 3.0 σ.		
		³ Superseded by AAJ 21E.		

K₂(1820) REFERENCES

AAIJ	21E	PRL 127 082001	R. Aaij et al.	(LHCb Collab.)
AAIJ	17C	PRL 118 022003	R. Aaij et al.	(LHCb Collab.)
Also		PR D95 012002	R. Aaij et al.	(LHCb Collab.)
PDG	04	PL B592 1	S. Eidelman et al.	(PDG Collab.)
ASTON	93	PL B308 186	D. Aston et al.	(SLAC, NAGO, CINC, INUS)
DAUM	81C	NP B187 1	C. Daum et al.	(AMST, CERN, CRAC, MPIM+)

$K(1830)$

$$J(P) = \frac{1}{2}(0^-)$$

OMITTED FROM SUMMARY TABLE
Seen in partial-wave analysis of $K\phi$ system. Needs confirmation.

$K(1830)$ MASS

VALUE (MeV)	EVTS	DOCUMENT ID	TECN	CHG	COMMENT
$1874 \pm 43^{+59}_{-115}$	4289	^{1,2} AAIJ	17c	LHCB	$B^+ \rightarrow J/\psi\phi K^+$

- • • We do not use the following data for averages, fits, limits, etc. • • •

~ 1830 ARMSTRONG 83 OMEG - $18.5 K^-p \rightarrow 3Kp$

¹ From an amplitude analysis of the decay $B^+ \rightarrow J/\psi\phi K^+$ with a significance of 3.5σ .
² A subsequent amplitude analysis of $B^+ \rightarrow J/\psi\phi K^+$ by AAIJ 21E did not confirm this measurement.

$K(1830)$ WIDTH

VALUE (MeV)	EVTS	DOCUMENT ID	TECN	CHG	COMMENT
$168 \pm 90^{+280}_{-104}$	4289	^{3,4} AAIJ	17c	LHCB	$B^+ \rightarrow J/\psi\phi K^+$

- • • We do not use the following data for averages, fits, limits, etc. • • •

~ 250 ARMSTRONG 83 OMEG - $18.5 K^-p \rightarrow 3Kp$

³ From an amplitude analysis of the decay $B^+ \rightarrow J/\psi\phi K^+$ with a significance of 3.5σ .
⁴ A subsequent amplitude analysis of $B^+ \rightarrow J/\psi\phi K^+$ by AAIJ 21E did not confirm this measurement.

$K(1830)$ DECAY MODES

Mode	Γ_1
$K\phi$	

$K(1830)$ REFERENCES

AAIJ 21E PRL 127 082001 R. Aaij <i>et al.</i> (LHCB Collab.)
AAIJ 17C PRL 118 022003 R. Aaij <i>et al.</i> (LHCB Collab.)
Also PR D95 012002 R. Aaij <i>et al.</i> (LHCB Collab.)
ARMSTRONG 83 NP B221 1 T.A. Armstrong <i>et al.</i> (BARI, BIRM, CERN+) JP

$K_0^*(1950)$

$$J(P) = \frac{1}{2}(0^+)$$

OMITTED FROM SUMMARY TABLE
Seen in partial-wave analysis of the $K^- \pi^+$ system. Needs confirmation.

$K_0^*(1950)$ MASS

VALUE (MeV)	DOCUMENT ID	TECN	CHG	COMMENT
1944 ± 18 OUR AVERAGE				Error includes scale factor of 1.3.
$1942 \pm 22 \pm 21$	LEES 21A BABR			$\gamma\gamma \rightarrow \eta_c(1S) \rightarrow \eta' K^+ K^-$
$1945 \pm 10 \pm 20$	¹ ASTON 88 LASS 0			$11 K^-p \rightarrow K^- \pi^+ n$

- • • We do not use the following data for averages, fits, limits, etc. • • •

1917 ± 12	² ZHOU 06 RVUE			$Kp \rightarrow K^- \pi^+ n$
1820 ± 40	³ ANISOVICH 97c RVUE			$11 K^-p \rightarrow K^- \pi^+ n$

¹ We take the central value of the two solutions and the larger error given.
² S-matrix pole. Using ASTON 88 and assuming $K_0^*(700)$, $K_0^*(1430)$.
³ T-matrix pole. Reanalysis of ASTON 88 data.

$K_0^*(1950)$ WIDTH

VALUE (MeV)	DOCUMENT ID	TECN	CHG	COMMENT
100 ± 40 OUR AVERAGE				Error includes scale factor of 1.3.
$80 \pm 32 \pm 20$	LEES 21A BABR			$\gamma\gamma \rightarrow \eta_c(1S) \rightarrow \eta' K^+ K^-$
$201 \pm 34 \pm 79$	⁴ ASTON 88 LASS 0			$11 K^-p \rightarrow K^- \pi^+ n$

- • • We do not use the following data for averages, fits, limits, etc. • • •

145 ± 38	⁵ ZHOU 06 RVUE			$Kp \rightarrow K^- \pi^+ n$
250 ± 100	⁶ ANISOVICH 97c RVUE			$11 K^-p \rightarrow K^- \pi^+ n$

⁴ We take the central value of the two solutions and the larger error given.
⁵ S-matrix pole. Using ASTON 88 and assuming $K_0^*(700)$, $K_0^*(1430)$.
⁶ T-matrix pole. Reanalysis of ASTON 88 data.

$K_0^*(1950)$ DECAY MODES

Mode	Fraction (Γ_i/Γ)
$K^- \pi^+$	$(52 \pm 14)\%$

$K_0^*(1950)$ BRANCHING RATIOS

$\Gamma(K^- \pi^+)/\Gamma_{\text{total}}$	Γ_1/Γ
$0.52 \pm 0.08 \pm 0.12$	⁷ ASTON 88 LASS 0

- • • We do not use the following data for averages, fits, limits, etc. • • •

~ 0.60 ⁸ ZHOU 06 RVUE $Kp \rightarrow K^- \pi^+ n$

⁷ We take the central value of the two solutions and the larger error given.
⁸ S-matrix pole. Using ASTON 88 and assuming $K_0^*(700)$, $K_0^*(1430)$.

$K_0^*(1950)$ REFERENCES

LEES 21A PR D104 072002 J.P. Lees <i>et al.</i> (BABAR Collab.)
ZHOU 06 NP A775 212 Z.Y. Zhou, H.Q. Zheng
ANISOVICH 97c PL B413 137 A.V. Anisovich, A.V. Sarantsev
ASTON 88 NP B296 493 D. Aston <i>et al.</i> (SLAC, NAGO, CINC, INUS)

$K_2^*(1980)$

$$J(P) = \frac{1}{2}(2^+)$$

Needs confirmation.

$K_2^*(1980)$ MASS

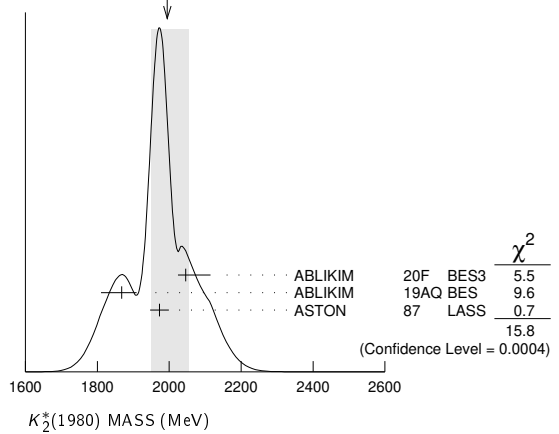
VALUE (MeV)	EVTS	DOCUMENT ID	TECN	CHG	COMMENT
1994 ± 60 OUR AVERAGE					Error includes scale factor of 2.8. See the ideogram below.

$2046 \pm 17^{+67}_{-16}$	¹ 1.8k	ABLIIKIM 20F BES3			$\psi(2S) \rightarrow K^+ K^- \eta$
$1868 \pm 8^{+40}_{-57}$	183k	ABLIIKIM 19AQ BES \pm			$J/\psi \rightarrow K^+ K^- \pi^0$
$1973 \pm 8 \pm 25$		ASTON 87 LASS 0			$11 K^-p \rightarrow \bar{K}^0 \pi^+ \pi^- n$

- • • We do not use the following data for averages, fits, limits, etc. • • •

$2073 \pm 94^{+245}_{-240}$	4289	^{2,3} AAIJ 17c LHCB			$B^+ \rightarrow J/\psi\phi K^+$
2020 ± 20		TIKHOMIROV 03 SPEC			$40.0 \pi^- C \rightarrow K_S^0 K_S^0 K_L^0 X$
1978 ± 40	241	BIRD 89 LASS -			$11 K^-p \rightarrow \bar{K}^0 \pi^- p$

WEIGHTED AVERAGE
1994+60-50 (Error scaled by 2.8)



¹ Seen in $\psi(2S)$ decay with branching ratio $\psi(2S) \rightarrow K^\pm X \rightarrow K^+ K^- \eta = (7.0 \pm 0.5^{+3.7}_{-0.6}) \times 10^{-6}$.
² From an amplitude analysis of the decay $B^+ \rightarrow J/\psi\phi K^+$ with a significance of 5.4σ .
³ A reanalysis by AAIJ 21E using a larger data sample did not confirm this measurement, the new result having a significance of only 1.6σ .

$K_2^*(1980)$ WIDTH

VALUE (MeV)	EVTS	DOCUMENT ID	TECN	CHG	COMMENT
348 ± 30 OUR AVERAGE					Error includes scale factor of 1.3. See the ideogram below.

$408 \pm 38^{+72}_{-34}$	¹ 1.8k	ABLIIKIM 20F BES3			$\psi(2S) \rightarrow K^+ K^- \eta$
$272 \pm 24^{+50}_{-15}$	183k	ABLIIKIM 19AQ BES \pm			$J/\psi \rightarrow K^+ K^- \pi^0$
$373 \pm 33 \pm 60$		ASTON 87 LASS 0			$11 K^-p \rightarrow \bar{K}^0 \pi^+ \pi^- n$

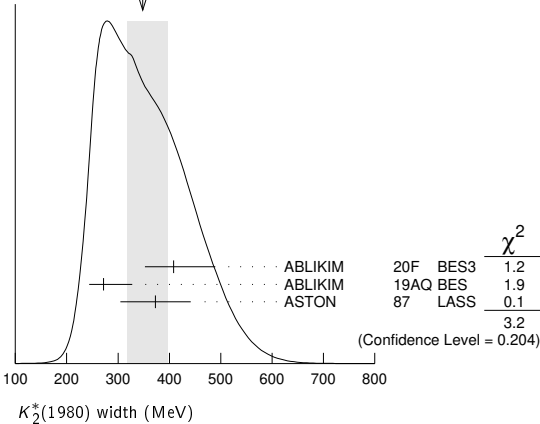
- • • We do not use the following data for averages, fits, limits, etc. • • •

$678 \pm 311^{+1153}_{-559}$	4289	^{2,3} AAIJ 17c LHCB			$B^+ \rightarrow J/\psi\phi K^+$
180 ± 70		TIKHOMIROV 03 SPEC			$40.0 \pi^- C \rightarrow K_S^0 K_S^0 K_L^0 X$
398 ± 47	241	BIRD 89 LASS -			$11 K^-p \rightarrow \bar{K}^0 \pi^- p$

Meson Particle Listings

$K_2^*(1980)$, $K_4^*(2045)$

WEIGHTED AVERAGE
348±50-30 (Error scaled by 1.3)



- Seen in $\psi(2S)$ decay with branching ratio $\psi(2S) \rightarrow K^\pm X \rightarrow K^+ K^- \eta = (7.0 \pm 0.5 - 3.7) \times 10^{-6}$.
- From an amplitude analysis of the decay $B^+ \rightarrow J/\psi \phi K^+$ with a significance of 5.4 σ .
- A reanalysis by AAIJ 21E using a larger data sample did not confirm this measurement, the new result having a significance of only 1.6 σ .

$K_2^*(1980)$ DECAY MODES

Mode	Fraction (Γ_i/Γ)
Γ_1 $K^*(892)\pi$	possibly seen
Γ_2 $K\rho$	possibly seen
Γ_3 $K f_2(1270)$	possibly seen
Γ_4 $K\phi$	seen
Γ_5 $K\eta$	seen

$K_2^*(1980)$ BRANCHING RATIOS

$\Gamma(K^*(892)\pi)/\Gamma_{total}$	VALUE	DOCUMENT ID	TECN	CHG	COMMENT	Γ_1/Γ
possibly seen		GULER	11	BELL	$B^+ \rightarrow J/\psi K^+ \pi^+ \pi^-$	

$\Gamma(K\rho)/\Gamma_{total}$	VALUE	DOCUMENT ID	TECN	CHG	COMMENT	Γ_2/Γ
possibly seen		GULER	11	BELL	$B^+ \rightarrow J/\psi K^+ \pi^+ \pi^-$	

$\Gamma(K\rho)/\Gamma(K^*(892)\pi)$	VALUE	DOCUMENT ID	TECN	CHG	COMMENT	Γ_2/Γ_1
	$1.49 \pm 0.24 \pm 0.09$	ASTON	87	LASS	0	$11 K^- p \rightarrow \bar{K}^0 \pi^+ \pi^- n$

$\Gamma(K f_2(1270))/\Gamma_{total}$	VALUE	DOCUMENT ID	TECN	CHG	COMMENT	Γ_3/Γ
possibly seen		TIKHOMIROV	03	SPEC	$40.0 \pi^- C \rightarrow K_S^0 K_S^0 K_L^0 X$	

$\Gamma(K\phi)/\Gamma_{total}$	VALUE	EVTS	DOCUMENT ID	TECN	CHG	COMMENT	Γ_4/Γ
seen		4289	1,2 AAIJ	17c	LHCB	$B^+ \rightarrow J/\psi \phi K^+$	

- From an amplitude analysis of the decay $B^+ \rightarrow J/\psi \phi K^+$ with a significance of 5.4 σ .
- A reanalysis by AAIJ 21E using a larger data sample did not confirm this measurement, the new result having a significance of only 1.6 σ .

$\Gamma(K\eta)/\Gamma_{total}$	VALUE	EVTS	DOCUMENT ID	TECN	CHG	COMMENT	Γ_5/Γ
seen		1.8k	1 ABLIKIM	20F	BES3	$\psi(2S) \rightarrow K^+ K^- \eta$	
seen		116k	2 CHEN	20a	BELL	$D^0 \rightarrow K^- \pi^+ \eta$	

- Seen decaying to $K\eta$ in an amplitude analysis of $\psi(2S) \rightarrow K^+ K^- \eta$.
- From an amplitude analysis of the decay $D^0 \rightarrow K^- \pi^+ \eta$ with a significance of 17 σ .

$K_2^*(1980)$ REFERENCES

AAIJ	21E	PRL 127 082001	R. Aaij et al.	(LHCb Collab.)
ABLIKIM	20F	PR D101 032008	M. Ablikim et al.	(BESIII Collab.)
CHEN	20A	PR D102 012002	Y.Q. Chen et al.	(BELLE Collab.)
ABLIKIM	19AQ	PR D100 032004	M. Ablikim et al.	(BESIII Collab.)
AAIJ	17C	PRL 118 022003	R. Aaij et al.	(LHCb Collab.)
Also		PR D95 012002	R. Aaij et al.	(LHCb Collab.)
GULER	11	PR D83 032005	H. Guler et al.	(BELLE Collab.)
TIKHOMIROV	03	PAN 66 828	G.D. Tikhomirov et al.	
BIRD	89	SLAC-332	P.F. Bird	(SLAC)
ASTON	87	NP B292 693	D. Aston et al.	(SLAC, NAGO, CINC, INUS)

$K_4^*(2045)$

$I(J^P) = \frac{1}{2}(4^+)$

$K_4^*(2045)$ MASS

VALUE (MeV)	EVTS	DOCUMENT ID	TECN	CHG	COMMENT	
2048 ± 8	OUR AVERAGE	Error includes scale factor of 1.1.				
$2090 \pm 9 \pm 11$	183k	ABLIKIM	19AQ	BES	\pm $J/\psi \rightarrow K^+ K^- \pi^0$	
$2062 \pm 14 \pm 13$		1 ASTON	86	LASS	0	$11 K^- p \rightarrow K^- \pi^+ n$
2039 ± 10	400	2,3 CLELAND	82	SPEC	\pm $50 K^+ p \rightarrow K_S^0 \pi^\pm p$	
2070 ± 100		4 ASTON	81c	LASS	0	$11 K^- p \rightarrow K^- \pi^+ n$
2079 ± 7	431	TORRES	86	MPSF	400	$pA \rightarrow 4KX$
2088 ± 20	650	BAUBILLIER	82	HBC	—	$8.25 K^- p \rightarrow K_S^0 \pi^- p$
2115 ± 46	488	CARMONY	77	HBC	0	$9 K^+ d \rightarrow K^+ \pi^+ X$

- • • We do not use the following data for averages, fits, limits, etc. • • •
- From a fit to all moments.
 - From a fit to 8 moments.
 - Number of events evaluated by us.
 - From energy-independent partial-wave analysis.

$K_4^*(2045)$ WIDTH

VALUE (MeV)	EVTS	DOCUMENT ID	TECN	CHG	COMMENT	
199 ± 27	OUR AVERAGE					
$201 \pm 19 \pm 57$	183k	ABLIKIM	19AQ	BES	\pm $J/\psi \rightarrow K^+ K^- \pi^0$	
$221 \pm 48 \pm 27$		5 ASTON	86	LASS	0	$11 K^- p \rightarrow K^- \pi^+ n$
189 ± 35	400	6,7 CLELAND	82	SPEC	\pm $50 K^+ p \rightarrow K_S^0 \pi^\pm p$	
61 ± 58	431	TORRES	86	MPSF	400	$pA \rightarrow 4KX$
170 ± 100	650	BAUBILLIER	82	HBC	—	$8.25 K^- p \rightarrow K_S^0 \pi^- p$
240 ± 500		8 ASTON	81c	LASS	0	$11 K^- p \rightarrow K^- \pi^+ n$
300 ± 200		CARMONY	77	HBC	0	$9 K^+ d \rightarrow K^+ \pi^+ X$

- From a fit to all moments.
- From a fit to 8 moments.
- Number of events evaluated by us.
- From energy-independent partial-wave analysis.

$K_4^*(2045)$ DECAY MODES

Mode	Fraction (Γ_i/Γ)
Γ_1 $K\pi$	(9.9±1.2) %
Γ_2 $K^*(892)\pi\pi$	(9 ± 5) %
Γ_3 $K^*(892)\pi\pi\pi$	(7 ± 5) %
Γ_4 $\rho K\pi$	(5.7±3.2) %
Γ_5 $\omega K\pi$	(5.0±3.0) %
Γ_6 $\phi K\pi$	(2.8±1.4) %
Γ_7 $\phi K^*(892)$	(1.4±0.7) %

$K_4^*(2045)$ BRANCHING RATIOS

$\Gamma(K\pi)/\Gamma_{total}$	VALUE	DOCUMENT ID	TECN	CHG	COMMENT	Γ_1/Γ
	0.099 ± 0.012	ASTON	88	LASS	0	$11 K^- p \rightarrow K^- \pi^+ n$

$\Gamma(K^*(892)\pi\pi)/\Gamma(K\pi)$	VALUE	DOCUMENT ID	TECN	CHG	COMMENT	Γ_2/Γ_1
	0.89 ± 0.53	BAUBILLIER	82	HBC	—	$8.25 K^- p \rightarrow \rho K_S^0 3\pi$

$\Gamma(K^*(892)\pi\pi\pi)/\Gamma(K\pi)$	VALUE	DOCUMENT ID	TECN	CHG	COMMENT	Γ_3/Γ_1
	0.75 ± 0.49	BAUBILLIER	82	HBC	—	$8.25 K^- p \rightarrow \rho K_S^0 3\pi$

$\Gamma(\rho K\pi)/\Gamma(K\pi)$	VALUE	DOCUMENT ID	TECN	CHG	COMMENT	Γ_4/Γ_1
	0.58 ± 0.32	BAUBILLIER	82	HBC	—	$8.25 K^- p \rightarrow \rho K_S^0 3\pi$

$\Gamma(\omega K\pi)/\Gamma(K\pi)$	VALUE	DOCUMENT ID	TECN	CHG	COMMENT	Γ_5/Γ_1
	0.50 ± 0.30	BAUBILLIER	82	HBC	—	$8.25 K^- p \rightarrow \rho K_S^0 3\pi$

$\Gamma(\phi K\pi)/\Gamma_{total}$	VALUE	DOCUMENT ID	TECN	CHG	COMMENT	Γ_6/Γ
	0.028 ± 0.014	9 TORRES	86	MPSF	400	$pA \rightarrow 4KX$

See key on page 1127

Meson Particle Listings

$K_4^*(2045), K_2(2250), K_3(2320), K_5^*(2380), K_4(2500)$

$\Gamma(\phi K^*(892))/\Gamma_{total}$	Γ_7/Γ		
VALUE	DOCUMENT ID	TECN	COMMENT
0.014 ± 0.007	⁹ TORRES	86	MPSF 400 pA → 4KX

⁹ Error determination is model dependent.

$K_4^*(2045)$ REFERENCES

ABLIKIM 19AQ PR D100 032004	M. Ablkim <i>et al.</i>	(BESIII Collab.)
ASTON 88 NP B296 493	D. Aston <i>et al.</i>	(SLAC, NAGO, CINC, INUS)
ASTON 86 PL B180 308	D. Aston <i>et al.</i>	(SLAC, NAGO, CINC, INUS)
TORRES 86 PR D34 707	S. Torres <i>et al.</i>	(VPI, ARIZ, FNAL, FSU+)
BAUBILLIER 82 PL 118B 447	M. Baubillier <i>et al.</i>	(BIRM, CERN, GLAS+)
CLELAND 82 NP B208 189	W.E. Cleland <i>et al.</i>	(DURH, GEVA, LAUS+)
ASTON 81C PL 106B 235	D. Aston <i>et al.</i>	(SLAC, CARL, OTTA) JP
CARMONY 77 PR D16 1251	D.D. Carmony <i>et al.</i>	(PURD, UCD, IUPU)

$K_2(2250)$

$$I(J^P) = \frac{1}{2}(2^-)$$

OMITTED FROM SUMMARY TABLE

This entry contains various peaks in strange meson systems reported in the 2150–2260 MeV region, as well as enhancements seen in the antihyperon-nucleon system, either in the mass spectra or in the J^P = 2^- wave.

$K_2(2250)$ MASS

VALUE (MeV)	EVTS	DOCUMENT ID	TECN	CHG	COMMENT
2247 ± 17 OUR AVERAGE					
2200 ± 40		¹ ARMSTRONG 83C	OMEG	–	18 $K^- p \rightarrow \Lambda \bar{p} X$
2235 ± 50		¹ BAUBILLIER 81	HBC	–	8 $K^- p \rightarrow \Lambda \bar{p} X$
2260 ± 20		¹ CLELAND 81	SPEC	±	50 $K^+ p \rightarrow \Lambda \bar{p} X$
• • • We do not use the following data for averages, fits, limits, etc. • • •					
2280 ± 20		TIKHOMIROV 03	SPEC		40.0 $\pi^- \bar{C} \rightarrow K_S^0 \bar{K}_S^0 K_L^0 X$
2147 ± 4	37	CHLIAPNIK... 79	HBC	+	32 $K^+ p \rightarrow \bar{\Lambda} p X$
2240 ± 20	20	LISSAUER 70	HBC		9 $K^+ p$

¹ J^P = 2^- from moments analysis.

$K_2(2250)$ WIDTH

VALUE (MeV)	EVTS	DOCUMENT ID	TECN	CHG	COMMENT
180 ± 30 OUR AVERAGE					Error includes scale factor of 1.4.
150 ± 30		² ARMSTRONG 83C	OMEG	–	18 $K^- p \rightarrow \Lambda \bar{p} X$
210 ± 30		² CLELAND 81	SPEC	±	50 $K^+ p \rightarrow \Lambda \bar{p} X$
• • • We do not use the following data for averages, fits, limits, etc. • • •					
180 ± 60		TIKHOMIROV 03	SPEC		40.0 $\pi^- \bar{C} \rightarrow K_S^0 \bar{K}_S^0 K_L^0 X$
~ 200		² BAUBILLIER 81	HBC	–	8 $K^- p \rightarrow \Lambda \bar{p} X$
~ 40	37	CHLIAPNIK... 79	HBC	+	32 $K^+ p \rightarrow \bar{\Lambda} p X$
80 ± 20	20	LISSAUER 70	HBC		9 $K^+ p$

² J^P = 2^- from moments analysis.

$K_2(2250)$ DECAY MODES

Mode
Γ_1 $K \pi \pi$
Γ_2 $K f_2(1270)$
Γ_3 $K^*(892) f_0(980)$
Γ_4 $\rho \bar{\Lambda}$

$K_2(2250)$ REFERENCES

TIKHOMIROV 03 PAN 66 828	G.D. Tikhomirov <i>et al.</i>	
ARMSTRONG 83C NP B227 365	T.A. Armstrong <i>et al.</i>	(BARI, BIRM, CERN+)
BAUBILLIER 81 NP B183 1	M. Baubillier <i>et al.</i>	(BIRM, CERN, GLAS+)
CLELAND 81 NP B184 1	W.E. Cleland <i>et al.</i>	(PITT, GEVA, LAUS+)
CHLIAPNIK... 79 NP B158 253	P.V. Chliapnikov <i>et al.</i>	(CERN, BELG, MONS)
LISSAUER 70 NP B18 491	D. Lissauer <i>et al.</i>	(LBL)

$K_3(2320)$

$$I(J^P) = \frac{1}{2}(3^+)$$

OMITTED FROM SUMMARY TABLE

Seen in the J^P = 3^+ wave of the antihyperon-nucleon system. Needs confirmation.

$K_3(2320)$ MASS

VALUE (MeV)	DOCUMENT ID	TECN	CHG	COMMENT	
2324 ± 24 OUR AVERAGE					
2330 ± 40		¹ ARMSTRONG 83C	OMEG	–	18 $K^- p \rightarrow \Lambda \bar{p} X$
2320 ± 30		¹ CLELAND 81	SPEC	±	50 $K^+ p \rightarrow \Lambda \bar{p} X$

¹ J^P = 3^+ from moments analysis.

$K_3(2320)$ WIDTH

VALUE (MeV)	DOCUMENT ID	TECN	CHG	COMMENT
150 ± 30	² ARMSTRONG 83C	OMEG	–	18 $K^- p \rightarrow \Lambda \bar{p} X$
• • • We do not use the following data for averages, fits, limits, etc. • • •				
~ 250	² CLELAND 81	SPEC	±	50 $K^+ p \rightarrow \Lambda \bar{p} X$

² J^P = 3^+ from moments analysis.

$K_3(2320)$ DECAY MODES

Mode
Γ_1 $\rho \bar{\Lambda}$

$K_3(2320)$ REFERENCES

ARMSTRONG 83C NP B227 365	T.A. Armstrong <i>et al.</i>	(BARI, BIRM, CERN+)
CLELAND 81 NP B184 1	W.E. Cleland <i>et al.</i>	(PITT, GEVA, LAUS+)

$K_5^*(2380)$

$$I(J^P) = \frac{1}{2}(5^-)$$

OMITTED FROM SUMMARY TABLE

Needs confirmation.

$K_5^*(2380)$ MASS

VALUE (MeV)	DOCUMENT ID	TECN	CHG	COMMENT
2382 ± 14 ± 19	¹ ASTON 86	LASS	0	11 $K^- p \rightarrow K^- \pi^+ n$

¹ From a fit to all the moments.

$K_5^*(2380)$ WIDTH

VALUE (MeV)	DOCUMENT ID	TECN	CHG	COMMENT
178 ± 37 ± 32	² ASTON 86	LASS	0	11 $K^- p \rightarrow K^- \pi^+ n$

² From a fit to all the moments.

$K_5^*(2380)$ DECAY MODES

Mode	Fraction (Γ_i/Γ)
Γ_1 $K \pi$	(6.1 ± 1.2) %

$K_5^*(2380)$ BRANCHING RATIOS

$\Gamma(K \pi)/\Gamma_{total}$	Γ_1/Γ			
VALUE	DOCUMENT ID	TECN	CHG	COMMENT
0.061 ± 0.012	ASTON 88	LASS	0	11 $K^- p \rightarrow K^- \pi^+ n$

$K_5^*(2380)$ REFERENCES

ASTON 88 NP B296 493	D. Aston <i>et al.</i>	(SLAC, NAGO, CINC, INUS)
ASTON 86 PL B180 308	D. Aston <i>et al.</i>	(SLAC, NAGO, CINC, INUS)

$K_4(2500)$

$$I(J^P) = \frac{1}{2}(4^-)$$

OMITTED FROM SUMMARY TABLE

Needs confirmation.

$K_4(2500)$ MASS

VALUE (MeV)	DOCUMENT ID	TECN	CHG	COMMENT
2490 ± 20	¹ CLELAND 81	SPEC	±	50 $K^+ p \rightarrow \Lambda \bar{p}$

¹ J^P = 4^- from moments analysis.

$K_4(2500)$ WIDTH

VALUE (MeV)	DOCUMENT ID	TECN	CHG	COMMENT
• • • We do not use the following data for averages, fits, limits, etc. • • •				
~ 250	² CLELAND 81	SPEC	±	50 $K^+ p \rightarrow \Lambda \bar{p}$

² J^P = 4^- from moments analysis.

$K_4(2500)$ DECAY MODES

Mode
Γ_1 $\rho \bar{\Lambda}$

$K_4(2500)$ REFERENCES

CLELAND 81 NP B184 1	W.E. Cleland <i>et al.</i>	(PITT, GEVA, LAUS+)
----------------------	----------------------------	---------------------

Meson Particle Listings

K(3100)

K(3100)

$$J^G(J^{PC}) = ?^{?}(???)$$

OMITTED FROM SUMMARY TABLE

Narrow peak observed in several ($\Lambda\bar{p}$ + pions) and ($\bar{\Lambda}p$ + pions) states in Σ^- Be reactions by BOURQUIN 86 and in np and nA reactions by ALEEVEV 93. Not seen by BOEHNLEIN 91. If due to strong decays, this state has exotic quantum numbers ($B=0, Q=+1, S=-1$ for $\Lambda\bar{p}\pi^+\pi^+$ and $I \geq 3/2$ for $\Lambda\bar{p}\pi^-$). Needs confirmation.

K(3100) MASS

VALUE (MeV)

DOCUMENT ID

 ≈ 3100 OUR ESTIMATE

3-BODY DECAYS

VALUE (MeV)

DOCUMENT ID

TECN

COMMENT

3054 ± 11 OUR AVERAGE

3060 ± 7 ± 20	¹ ALEEVEV	93	BIS2	K(3100) → $\Lambda\bar{p}\pi^+$
3056 ± 7 ± 20	¹ ALEEVEV	93	BIS2	K(3100) → $\bar{\Lambda}p\pi^-$
3055 ± 8 ± 20	¹ ALEEVEV	93	BIS2	K(3100) → $\Lambda\bar{p}\pi^-$
3045 ± 8 ± 20	¹ ALEEVEV	93	BIS2	K(3100) → $\bar{\Lambda}p\pi^+$

4-BODY DECAYS

VALUE (MeV)

DOCUMENT ID

TECN

COMMENT

3059 ± 11 OUR AVERAGE

3067 ± 6 ± 20	¹ ALEEVEV	93	BIS2	K(3100) → $\Lambda\bar{p}\pi^+\pi^+$
3060 ± 8 ± 20	¹ ALEEVEV	93	BIS2	K(3100) → $\Lambda\bar{p}\pi^+\pi^-$
3055 ± 7 ± 20	¹ ALEEVEV	93	BIS2	K(3100) → $\bar{\Lambda}p\pi^-\pi^-$
3052 ± 8 ± 20	¹ ALEEVEV	93	BIS2	K(3100) → $\bar{\Lambda}p\pi^-\pi^+$
• • • We do not use the following data for averages, fits, limits, etc. • • •				
3105 ± 30	BOURQUIN	86	SPEC	K(3100) → $\Lambda\bar{p}\pi^+\pi^+$
3115 ± 30	BOURQUIN	86	SPEC	K(3100) → $\bar{\Lambda}p\pi^+\pi^-$

5-BODY DECAYS

VALUE (MeV)

DOCUMENT ID

TECN

COMMENT

• • • We do not use the following data for averages, fits, limits, etc. • • •

3095 ± 30	BOURQUIN	86	SPEC	K(3100) → $\Lambda\bar{p}\pi^+\pi^+\pi^-$
¹ Supersedes ALEEVEV 90.				

K(3100) WIDTH

3-BODY DECAYS

VALUE (MeV)

DOCUMENT ID

TECN

COMMENT

• • • We do not use the following data for averages, fits, limits, etc. • • •

42 ± 16	² ALEEVEV	93	BIS2	K(3100) → $\Lambda\bar{p}\pi^+$
---------	----------------------	----	------	---------------------------------

36 ± 15	² ALEEVEV	93	BIS2	K(3100) → $\bar{\Lambda}p\pi^-$
50 ± 18	² ALEEVEV	93	BIS2	K(3100) → $\Lambda\bar{p}\pi^-$
30 ± 15	² ALEEVEV	93	BIS2	K(3100) → $\bar{\Lambda}p\pi^+$

4-BODY DECAYS

VALUE (MeV)

CL%

DOCUMENT ID

TECN

COMMENT

• • • We do not use the following data for averages, fits, limits, etc. • • •

22 ± 8	² ALEEVEV	93	BIS2	K(3100) → $\Lambda\bar{p}\pi^+\pi^+$
28 ± 12	² ALEEVEV	93	BIS2	K(3100) → $\Lambda\bar{p}\pi^+\pi^-$
32 ± 15	² ALEEVEV	93	BIS2	K(3100) → $\bar{\Lambda}p\pi^-\pi^-$
30 ± 15	² ALEEVEV	93	BIS2	K(3100) → $\bar{\Lambda}p\pi^-\pi^+$
<30	90	BOURQUIN	86	SPEC K(3100) → $\Lambda\bar{p}\pi^+\pi^+$
<80	90	BOURQUIN	86	SPEC K(3100) → $\Lambda\bar{p}\pi^+\pi^-$

5-BODY DECAYS

VALUE (MeV)

CL%

DOCUMENT ID

TECN

COMMENT

• • • We do not use the following data for averages, fits, limits, etc. • • •

<30	90	BOURQUIN	86	SPEC K(3100) → $\Lambda\bar{p}\pi^+\pi^+\pi^-$
² Supersedes ALEEVEV 90.				

K(3100) DECAY MODES

Mode	
Γ_1	$K(3100)^0 \rightarrow \Lambda\bar{p}\pi^+$
Γ_2	$K(3100)^{-} \rightarrow \Lambda\bar{p}\pi^-$
Γ_3	$K(3100)^{-} \rightarrow \Lambda\bar{p}\pi^+\pi^-$
Γ_4	$K(3100)^+ \rightarrow \bar{\Lambda}p\pi^+\pi^+$
Γ_5	$K(3100)^0 \rightarrow \Lambda\bar{p}\pi^+\pi^+\pi^-$
Γ_6	$K(3100)^0 \rightarrow \Sigma(1385)^+\bar{p}$

 $\Gamma(\Sigma(1385)^+\bar{p})/\Gamma(\Lambda\bar{p}\pi^+)$ Γ_6/Γ_1

VALUE	CL%	DOCUMENT ID	TECN	COMMENT
<0.04	90	ALEEVEV	93	BIS2 K(3100) ⁰ → $\Sigma(1385)^+\bar{p}$

K(3100) REFERENCES

ALEEVEV	93	PAN 56 1358	A.N. Akeev et al.	(BIS-2 Collab.)
		Translated from YAF 56 100.		
BOEHNLEIN	91	NPBPS B21 174	A. Boehnlein et al.	(FLOR, BNL, IND+)
ALEEVEV	90	ZPHY C47 533	A.N. Akeev et al.	(BIS-2 Collab.)
BOURQUIN	86	PL B172 113	M.H. Bourquin et al.	(GEVA, RAL, HEIDP+)

CHARMED MESONS ($C = \pm 1$)

$D^+ = c\bar{d}, D^0 = c\bar{u}, \bar{D}^0 = \bar{c}u, D^- = \bar{c}d,$ similarly for D^{*s}

D^\pm

$$J^{PC} = \frac{1}{2}(0^-)$$

D^\pm MASS

The fit includes $D^\pm, D^0, D_s^\pm, D^{*s}, D^{*0}, D_1(2420)^0, D_2^*(2460)^0,$ and $D_{s1}(2536)^\pm$ mass and mass difference measurements.

VALUE (MeV)	EVTS	DOCUMENT ID	TECN	COMMENT
1869.66 ± 0.05 OUR FIT				
1869.5 ± 0.4 OUR AVERAGE				
1869.53 ± 0.49 ± 0.20	110 ± 15	ANASHIN	10A	KEDR e^+e^- at $\psi(3770)$
1870.0 ± 0.5 ± 1.0	317	BARLAG	90c	ACCM π^- Cu 230 GeV
1869.4 ± 0.6		¹ TRILLING	81	RVUE e^+e^- 3.77 GeV
••• We do not use the following data for averages, fits, limits, etc. •••				
1875 ± 10	9	ADAMOVIČH	87	EMUL Photoproduction
1860 ± 16	6	ADAMOVIČH	84	EMUL Photoproduction
1863 ± 4		DERRICK	84	HRS e^+e^- 29 GeV
1868.4 ± 0.5		¹ SCHINDLER	81	MRK2 e^+e^- 3.77 GeV
1874 ± 5		GOLDHABER	77	MRK1 D^0, D^+ recoil spectra
1868.3 ± 0.9		¹ PERUZZI	77	LGW e^+e^- 3.77 GeV
1874 ± 11		PICCOLO	77	MRK1 e^+e^- 4.03, 4.41 GeV
1876 ± 15	50	PERUZZI	76	MRK1 $K^\mp\pi^\pm\pi^\pm$

¹PERUZZI 77 and SCHINDLER 81 errors do not include the 0.13% uncertainty in the absolute SPEAR energy calibration. TRILLING 81 uses the high precision $J/\psi(1S)$ and $\psi(2S)$ measurements of ZHOLENTZ 80 to determine this uncertainty and combines the PERUZZI 77 and SCHINDLER 81 results to obtain the value quoted.

D^\pm MEAN LIFE

Measurements with an error $> 100 \times 10^{-15}$ s have been omitted from the Listings.

VALUE (10^{-15} s)	EVTS	DOCUMENT ID	TECN	COMMENT
1033 ± 5 OUR AVERAGE				
1030.4 ± 4.7 ± 3.1	171k	¹ ABUDINEN	21A	BEL2 e^+e^- at $\Upsilon(4S)$
1039.4 ± 4.3 ± 7.0	110k	LINK	02F	FOCS γ nucleus, ≈ 180 GeV
••• We do not use the following data for averages, fits, limits, etc. •••				
1033.6 ± 22.1 ^{+9.9} _{-12.7}	3.7k	BONVICINI	99	CLEO $e^+e^- \approx \Upsilon(4S)$
1048 ± 15 ± 11	9k	FRABETTI	94D	E687 $D^+ \rightarrow K^-\pi^+\pi^+$
1075 ± 40 ± 18	2.4k	FRABETTI	E1	E687 γ Be, $D^+ \rightarrow K^-\pi^+\pi^+$
1030 ± 80 ± 60	200	ALVAREZ	90	NA14 $\gamma, D^+ \rightarrow K^-\pi^+\pi^+$
1050 ⁺⁷⁷ ₋₇₂	317	² BARLAG	90c	ACCM π^- Cu 230 GeV
1050 ± 80 ± 70	363	ALBRECHT	88i	ARG e^+e^- 10 GeV
1090 ± 30 ± 25	2.9k	RAAB	88	E691 Photoproduction

¹ABUDINEN 21A determines the lifetime ratio $\tau(D^+)/\tau(D^0) = 2.510 \pm 0.013 \pm 0.007$.
²BARLAG 90c estimates the systematic error to be negligible.

D^+ DECAY MODES

Most decay modes (other than the semileptonic modes) that involve a neutral K meson are now given as K_S^0 modes, not as \bar{K}^0 modes. Nearly always it is a K_S^0 that is measured, and interference between Cabibbo-allowed and doubly Cabibbo-suppressed modes can invalidate the assumption that $2\Gamma(K_S^0) = \Gamma(\bar{K}^0)$.

Mode	Fraction (Γ_i/Γ)	Scale factor/ Confidence level
Inclusive modes		
Γ_1 e^+ semileptonic	(16.07 ± 0.30) %	
Γ_2 μ^+ anything	(17.6 ± 3.2) %	
Γ_3 K^- anything	(25.7 ± 1.4) %	
Γ_4 \bar{K}^0 anything + K^0 anything	(61 ± 5) %	
Γ_5 K^+ anything	(5.9 ± 0.8) %	
Γ_6 $K^*(892)^-$ anything	(6 ± 5) %	
Γ_7 $\bar{K}^*(892)^0$ anything	(23 ± 5) %	
Γ_8 $K^*(892)^0$ anything	< 6.6 %	CL=90%
Γ_9 η anything	(6.3 ± 0.7) %	
Γ_{10} η' anything	(1.04 ± 0.18) %	
Γ_{11} ϕ anything	(1.12 ± 0.04) %	

Leptonic and semileptonic modes

Γ_{12} $e^+ \nu_e$	< 8.8	$\times 10^{-6}$	CL=90%
Γ_{13} $\gamma e^+ \nu_e$	< 3.0	$\times 10^{-5}$	CL=90%
Γ_{14} $\mu^+ \nu_\mu$	(3.74 ± 0.17)	$\times 10^{-4}$	
Γ_{15} $\tau^+ \nu_\tau$	(1.20 ± 0.27)	$\times 10^{-3}$	
Γ_{16} $\bar{K}^0 e^+ \nu_e$	(8.72 ± 0.09) %		
Γ_{17} $\bar{K}^0 \mu^+ \nu_\mu$	(8.76 ± 0.19) %		
Γ_{18} $K^- \pi^+ e^+ \nu_e$	(4.02 ± 0.18) %		S=3.2
Γ_{19} $\bar{K}^*(892)^0 e^+ \nu_e, \bar{K}^*(892)^0 \rightarrow K^- \pi^+$	(3.77 ± 0.17) %		
Γ_{20} $(K^- \pi^+)_{[0.8-1.0]\text{GeV}} e^+ \nu_e$	(3.39 ± 0.09) %		
Γ_{21} $(K^- \pi^+)_{S\text{-wave}} e^+ \nu_e$	(2.28 ± 0.11)	$\times 10^{-3}$	
Γ_{22} $\bar{K}^*(1410)^0 e^+ \nu_e, \bar{K}^*(1410)^0 \rightarrow K^- \pi^+$	< 6	$\times 10^{-3}$	CL=90%
Γ_{23} $\bar{K}_2^*(1430)^0 e^+ \nu_e, \bar{K}_2^*(1430)^0 \rightarrow K^- \pi^+$	< 5	$\times 10^{-4}$	CL=90%
Γ_{24} $K^- \pi^+ e^+ \nu_e$ nonresonant	< 7	$\times 10^{-3}$	CL=90%
Γ_{25} $\bar{K}^*(892)^0 \mu^+ \nu_\mu$	(5.40 ± 0.10) %		S=1.1
Γ_{26} $K^- \pi^+ \mu^+ \nu_\mu$	(3.65 ± 0.34) %		
Γ_{27} $\bar{K}^*(892)^0 \mu^+ \nu_\mu, \bar{K}^*(892)^0 \rightarrow K^- \pi^+$	(3.52 ± 0.10) %		
Γ_{28} $K^- \pi^+ \mu^+ \nu_\mu$ nonresonant	(1.9 ± 0.5)	$\times 10^{-3}$	
Γ_{29} $\bar{K}^*(892)^0 \mu^+ \nu_\mu$	(5.27 ± 0.15) %		
Γ_{30} $K^- \pi^+ \pi^0 \mu^+ \nu_\mu$	< 1.5	$\times 10^{-3}$	CL=90%
Γ_{31} $\bar{K}_1(1270)^0 e^+ \nu_e, \bar{K}_1^0 \rightarrow K^- \pi^+ \pi^0$	(1.06 ± 0.15)	$\times 10^{-3}$	
Γ_{32} $\bar{K}_0^*(1430)^0 \mu^+ \nu_\mu$	< 2.3	$\times 10^{-4}$	CL=90%
Γ_{33} $\bar{K}^*(1680)^0 \mu^+ \nu_\mu$	< 1.5	$\times 10^{-3}$	CL=90%
Γ_{34} $\pi^0 e^+ \nu_e$	(3.72 ± 0.17)	$\times 10^{-3}$	S=2.0
Γ_{35} $\pi^0 \mu^+ \nu_\mu$	(3.50 ± 0.15)	$\times 10^{-3}$	
Γ_{36} $\eta e^+ \nu_e$	(1.11 ± 0.07)	$\times 10^{-3}$	
Γ_{37} $\eta \mu^+ \nu_\mu$	(1.04 ± 0.11)	$\times 10^{-3}$	
Γ_{38} $\pi^- \pi^+ e^+ \nu_e$	(2.45 ± 0.10)	$\times 10^{-3}$	
Γ_{39} $f_0(500)^0 e^+ \nu_e, f_0(500)^0 \rightarrow \pi^+ \pi^-$	(6.3 ± 0.5)	$\times 10^{-4}$	
Γ_{40} $\rho^0 e^+ \nu_e$	(2.18 ± 0.17)	$\times 10^{-3}$	
Γ_{41} $\rho^0 \mu^+ \nu_\mu$	(2.4 ± 0.4)	$\times 10^{-3}$	
Γ_{42} $\omega e^+ \nu_e$	(1.69 ± 0.11)	$\times 10^{-3}$	
Γ_{43} $\omega \mu^+ \nu_\mu$	(1.77 ± 0.21)	$\times 10^{-3}$	
Γ_{44} $\eta'(958) e^+ \nu_e$	(2.0 ± 0.4)	$\times 10^{-4}$	
Γ_{45} $a(980)^0 e^+ \nu_e, a(980)^0 \rightarrow \eta \pi^0$	(1.7 ± 0.8)	$\times 10^{-4}$	
Γ_{46} $b_1(1235)^0 e^+ \nu_e, b_1^0 \rightarrow \omega \pi^0$	< 1.75	$\times 10^{-4}$	CL=90%
Γ_{47} $\phi e^+ \nu_e$	< 1.3	$\times 10^{-5}$	CL=90%
Γ_{48} $D^0 e^+ \nu_e$	< 1.0	$\times 10^{-4}$	CL=90%

Hadronic modes with a \bar{K} or $\bar{K}\bar{K}$

Γ_{49} $K_S^0 \pi^+$	(1.562 ± 0.031) %		S=1.7
Γ_{50} $K_L^0 \pi^+$	(1.46 ± 0.05) %		
Γ_{51} $K^- 2\pi^+$	[a] (9.38 ± 0.16) %		S=1.6
Γ_{52} $(K^- \pi^+)_{S\text{-wave}} \pi^+$	(7.52 ± 0.17) %		
Γ_{53} $\bar{K}_0^*(700)^0 \pi^+, \bar{K}_0^*(700) \rightarrow K^- \pi^+$			
Γ_{54} $\bar{K}_0^*(1430)^0 \pi^+, \bar{K}_0^*(1430)^0 \rightarrow K^- \pi^+$	[b] (1.25 ± 0.06) %		
Γ_{55} $\bar{K}^*(892)^0 \pi^+, \bar{K}^*(892)^0 \rightarrow K^- \pi^+$	(1.04 ± 0.12) %		
Γ_{56} $\bar{K}^*(1410)^0 \pi^+, \bar{K}^{*0} \rightarrow K^- \pi^+$	not seen		
Γ_{57} $\bar{K}_2^*(1430)^0 \pi^+, \bar{K}_2^*(1430)^0 \rightarrow K^- \pi^+$	[b] (2.3 ± 0.7)	$\times 10^{-4}$	
Γ_{58} $\bar{K}^*(1680)^0 \pi^+, \bar{K}^*(1680)^0 \rightarrow K^- \pi^+$	[b] (2.2 ± 1.1)	$\times 10^{-4}$	
Γ_{59} $K^- (2\pi^+)_{I=2}$	(1.45 ± 0.26) %		
Γ_{60} $K^- 2\pi^+$ nonresonant			
Γ_{61} $K_S^0 \pi^+ \pi^0$	[a] (7.36 ± 0.21) %		
Γ_{62} $K_S^0 \rho^+$	(6.14 ± 0.60)	%	
Γ_{63} $K_S^0 \rho(1450)^+, \rho^+ \rightarrow \pi^+ \pi^0$	(1.5 ± 1.2)	$\times 10^{-3}$	
Γ_{64} $\bar{K}^*(892)^0 \pi^+, \bar{K}^*(892)^0 \rightarrow K_S^0 \pi^0$	(2.64 ± 0.32)	$\times 10^{-3}$	
Γ_{65} $\bar{K}_0^*(1430)^0 \pi^+, \bar{K}_0^* \rightarrow K_S^0 \pi^0$	(2.7 ± 0.9)	$\times 10^{-3}$	

Meson Particle Listings

 D^\pm

Γ_{66}	$\bar{K}_0^*(1680)^0 \pi^+, \bar{K}_0^0 \rightarrow K_S^0 \pi^0$	$(10 \pm_{-10}^7) \times 10^{-4}$	Γ_{121}	$K^+ \bar{K}_2^*(1430)^0, \bar{K}_2^* \rightarrow K^- \pi^+$	$(1.6 \pm_{0.8}^{1.2}) \times 10^{-4}$
Γ_{67}	$\bar{K}^0 \pi^+, \bar{K}^0 \rightarrow K_S^0 \pi^0$	$(6 \pm_4^5) \times 10^{-3}$	Γ_{122}	$K^+ \bar{K}_0^*(700), \bar{K}_0^* \rightarrow K^- \pi^+$	$(6.8 \pm_{2.1}^{3.5}) \times 10^{-4}$
Γ_{68}	$K_S^0 \pi^+ \pi^0$ nonresonant	$(3 \pm_4) \times 10^{-3}$	Γ_{123}	$a_0(1450)^0 \pi^+, a_0^0 \rightarrow K^+ K^-$	$(4.5 \pm_{1.8}^{7.0}) \times 10^{-4}$
Γ_{69}	$K_S^0 \pi^+ \pi^0$ nonresonant and $\bar{K}^0 \pi^+$	$(1.37 \pm_{0.40}^{0.21}) \%$	Γ_{124}	$\phi(1680) \pi^+, \phi \rightarrow K^+ K^-$	$(4.9 \pm_{1.9}^{4.0}) \times 10^{-5}$
Γ_{70}	$(K_S^0 \pi^0)_{S\text{-wave}} \pi^+$	$(1.27 \pm_{0.33}^{0.27}) \%$	Γ_{125}	$\phi \pi^+, \phi \rightarrow K^+ K^-$	$(2.69 \pm_{0.08}^{0.07}) \times 10^{-3}$
Γ_{71}	$K_S^0 \pi^+ \eta$	$(1.31 \pm 0.05) \%$	Γ_{126}	$\phi \pi^+$	$(5.70 \pm 0.14) \times 10^{-3}$
Γ_{72}	$K_S^0 \pi^+ \eta'(958)$	$(1.90 \pm 0.21) \times 10^{-3}$	Γ_{127}	$K^+ K^- \pi^+ \pi^0$	$(6.62 \pm 0.32) \times 10^{-3}$
Γ_{73}	$K^- 2\pi^+ \pi^0$	[c] $(6.25 \pm 0.18) \%$	Γ_{128}	$K_S^0 K_S^0 \pi^+$	$(2.70 \pm 0.13) \times 10^{-3}$
Γ_{74}	$K_S^0 2\pi^+ \pi^-$	[c] $(3.10 \pm 0.09) \%$	Γ_{129}	$K_S^0 K_S^0 \pi^+ \pi^0$	$(1.34 \pm 0.21) \times 10^{-3}$
Γ_{75}	$K^- 2\pi^+ \eta$	$(1.35 \pm 0.12) \times 10^{-3}$	Γ_{130}	$K_S^0 K^+ \eta$	$(1.8 \pm 0.5) \times 10^{-4}$
Γ_{76}	$K_S^0 \pi^+ \pi^0 \eta$	$(1.22 \pm 0.25) \times 10^{-3}$	Γ_{131}	$K^+ K_S^0 \pi^+ \pi^-$	$(1.89 \pm 0.13) \times 10^{-3}$
Γ_{77}	$K^- 3\pi^+ \pi^-$	[a] $(5.7 \pm 0.5) \times 10^{-3}$	Γ_{132}	$K_S^0 K^+ \pi^0 \pi^0$	$(5.8 \pm 1.3) \times 10^{-4}$
Γ_{78}	$\bar{K}^*(892)^0 2\pi^+ \pi^-, \bar{K}^*(892)^0 \rightarrow K^- \pi^+$	$(1.2 \pm 0.4) \times 10^{-3}$	Γ_{133}	$K_S^0 K^- 2\pi^+$	$(2.27 \pm 0.13) \times 10^{-3}$
Γ_{79}	$\bar{K}^*(892)^0 \rho^0 \pi^+, \bar{K}^*(892)^0 \rightarrow K^- \pi^+$	$(2.3 \pm 0.4) \times 10^{-3}$	Γ_{134}	$K^+ K^- 2\pi^+ \pi^-$	$(2.3 \pm 1.2) \times 10^{-4}$
Γ_{80}	$\bar{K}^*(892)^0 a_1(1260)^+$	[d] $(9.3 \pm 1.9) \times 10^{-3}$	A few poorly measured branching fractions:		
Γ_{81}	$\bar{K}^*(892)^0 2\pi^+ \pi^- \text{ no-}\rho, \bar{K}^*(892)^0 \rightarrow K^- \pi^+$		Γ_{135}	$\phi \pi^+ \pi^0$	$(2.3 \pm 1.0) \%$
Γ_{82}	$K^- \rho^0 2\pi^+$	$(1.72 \pm 0.28) \times 10^{-3}$	Γ_{136}	$\phi \rho^+$	$< 1.5 \%$ CL=90%
Γ_{83}	$K^- 3\pi^+ \pi^-$ nonresonant	$(4.0 \pm 2.9) \times 10^{-4}$	Γ_{137}	$K^+ K^- \pi^+ \pi^0$ non- ϕ	$(1.5 \pm_{0.6}^{0.7}) \%$
Γ_{84}	$K^+ 2K_S^0$	$(2.54 \pm 0.13) \times 10^{-3}$	Doubly Cabibbo-suppressed modes		
Γ_{85}	$K^+ K^- K_S^0 \pi^+$	$(2.4 \pm 0.5) \times 10^{-4}$	Γ_{138}	$K^+ \pi^0$	$(2.08 \pm 0.21) \times 10^{-4}$ S=1.4
Γ_{86}	$\pi^+ \pi^0$	$(1.247 \pm 0.033) \times 10^{-3}$	Γ_{139}	$K^+ \eta$	$(1.25 \pm 0.16) \times 10^{-4}$ S=1.1
Γ_{87}	$2\pi^+ \pi^-$	$(3.27 \pm 0.18) \times 10^{-3}$	Γ_{140}	$K^+ \eta'(958)$	$(1.85 \pm 0.20) \times 10^{-4}$
Γ_{88}	$\rho^0 \pi^+$	$(8.3 \pm 1.5) \times 10^{-4}$	Γ_{141}	$K^+ \pi^+ \pi^-$	$(4.91 \pm 0.09) \times 10^{-4}$
Γ_{89}	$\pi^+ (\pi^+ \pi^-)_{S\text{-wave}}$	$(1.83 \pm 0.16) \times 10^{-3}$	Γ_{142}	$K^+ \rho^0$	$(1.9 \pm 0.5) \times 10^{-4}$
Γ_{90}	$\sigma \pi^+, \sigma \rightarrow \pi^+ \pi^-$	$(1.38 \pm 0.12) \times 10^{-3}$	Γ_{143}	$K^*(892)^0 \pi^+, K^*(892)^0 \rightarrow K^+ \pi^-$	$(2.3 \pm 0.4) \times 10^{-4}$
Γ_{91}	$f_0(980) \pi^+, f_0(980) \rightarrow \pi^+ \pi^-$	$(1.56 \pm 0.33) \times 10^{-4}$	Γ_{144}	$K^+ f_0(980), f_0(980) \rightarrow K^+ \pi^-$	$(4.4 \pm 2.6) \times 10^{-5}$
Γ_{92}	$f_0(1370) \pi^+, f_0(1370) \rightarrow \pi^+ \pi^-$	$(8 \pm 4) \times 10^{-5}$	Γ_{145}	$K_2^*(1430)^0 \pi^+, K_2^*(1430)^0 \rightarrow K^+ \pi^-$	$(3.9 \pm 2.7) \times 10^{-5}$
Γ_{93}	$f_2(1270) \pi^+, f_2(1270) \rightarrow \pi^+ \pi^-$	$(5.0 \pm 0.9) \times 10^{-4}$	Γ_{146}	$K^+ \pi^+ \pi^-$ nonresonant	not seen
Γ_{94}	$\rho(1450)^0 \pi^+, \rho(1450)^0 \rightarrow \pi^+ \pi^-$	$< 8 \times 10^{-5}$ CL=95%	Γ_{147}	$K^+ \pi^+ \pi^- \pi^0$	$(1.21 \pm 0.09) \times 10^{-3}$
Γ_{95}	$f_0(1500) \pi^+, f_0(1500) \rightarrow \pi^+ \pi^-$	$(1.1 \pm 0.4) \times 10^{-4}$	Γ_{148}	$K^+ \pi^+ \pi^- \pi^0$ nonresonant	$(1.10 \pm 0.07) \times 10^{-3}$
Γ_{96}	$f_0(1710) \pi^+, f_0(1710) \rightarrow \pi^+ \pi^-$	$< 5 \times 10^{-5}$ CL=95%	Γ_{149}	$K^+ \omega$	$(5.7 \pm_{2.1}^{2.5}) \times 10^{-5}$
Γ_{97}	$f_0(1790) \pi^+, f_0(1790) \rightarrow \pi^+ \pi^-$	$< 7 \times 10^{-5}$ CL=95%	Γ_{150}	$2K^+ K^-$	$(6.14 \pm 0.11) \times 10^{-5}$
Γ_{98}	$(\pi^+ \pi^+)_{S\text{-wave}} \pi^-$	$< 1.2 \times 10^{-4}$ CL=95%	Γ_{151}	$\phi(1020)^0 K^+$	$< 2.1 \times 10^{-5}$ CL=90%
Γ_{99}	$2\pi^+ \pi^-$ nonresonant	$< 1.1 \times 10^{-4}$ CL=95%	Γ_{152}	$K^+ \phi(1020), \phi \rightarrow K^+ K^-$	$(4.4 \pm 0.6) \times 10^{-6}$
Γ_{100}	$\pi^+ 2\pi^0$	$(4.7 \pm 0.4) \times 10^{-3}$	Γ_{153}	$K^+ (K^+ K^-)_{S\text{-wave}}$	$(5.77 \pm 0.12) \times 10^{-5}$
Γ_{101}	$2\pi^+ \pi^- \pi^0$	$(1.16 \pm 0.08) \%$	$\Delta C = 1$ weak neutral current (C1) modes, or Lepton Family number (LF), or Lepton number (L), or Baryon number (B) violating modes		
Γ_{102}	$3\pi^+ 2\pi^-$	$(1.66 \pm 0.16) \times 10^{-3}$ S=1.1	Γ_{154}	$\pi^+ e^+ e^-$	CI $< 1.1 \times 10^{-6}$ CL=90%
Γ_{103}	$\eta \pi^+$	$(3.77 \pm 0.09) \times 10^{-3}$	Γ_{155}	$\pi^+ \pi^0 e^+ e^-$	$< 1.4 \times 10^{-5}$ CL=90%
Γ_{104}	$\eta \pi^+ \pi^0$	$(2.05 \pm 0.35) \times 10^{-3}$ S=2.2	Γ_{156}	$\pi^+ \phi, \phi \rightarrow e^+ e^-$	[e] $(1.7 \pm_{0.9}^{1.4}) \times 10^{-6}$
Γ_{105}	$\eta 2\pi^+ \pi^-$	$(3.41 \pm 0.20) \times 10^{-3}$	Γ_{157}	$\pi^+ \mu^+ \mu^-$	CI $< 6.7 \times 10^{-8}$ CL=90%
Γ_{106}	$\eta \pi^+ 2\pi^0$	$(3.20 \pm 0.33) \times 10^{-3}$	Γ_{158}	$\pi^+ \phi, \phi \rightarrow \mu^+ \mu^-$	[e] $(1.8 \pm 0.8) \times 10^{-6}$
Γ_{107}	$\eta \eta \pi^+$	$(2.96 \pm 0.26) \times 10^{-3}$	Γ_{159}	$\rho^+ \mu^+ \mu^-$	CI $< 5.6 \times 10^{-4}$ CL=90%
Γ_{108}	$\omega \pi^+$	$(2.8 \pm 0.6) \times 10^{-4}$	Γ_{160}	$K^+ e^+ e^-$	[f] $< 8.5 \times 10^{-7}$ CL=90%
Γ_{109}	$\omega \pi^+ \pi^0$	$(3.9 \pm 0.9) \times 10^{-3}$	Γ_{161}	$K^+ \pi^0 e^+ e^-$	$< 1.5 \times 10^{-5}$ CL=90%
Γ_{110}	$\eta'(958) \pi^+$	$(4.97 \pm 0.19) \times 10^{-3}$	Γ_{162}	$K_S^0 \pi^+ e^+ e^-$	$< 2.6 \times 10^{-5}$ CL=90%
Γ_{111}	$\eta'(958) \pi^+ \pi^0$	$(1.6 \pm 0.5) \times 10^{-3}$	Γ_{163}	$K_S^0 K^+ e^+ e^-$	$< 1.1 \times 10^{-5}$ CL=90%
Hadronic modes with a $K\bar{K}$ pair			Γ_{164}	$K^+ \mu^+ \mu^-$	[f] $< 5.4 \times 10^{-8}$ CL=90%
Γ_{112}	$K_S^0 K^+$	$(3.04 \pm 0.09) \times 10^{-3}$ S=2.2	Γ_{165}	$\pi^+ e^+ \mu^-$	LF $< 2.1 \times 10^{-7}$ CL=90%
Γ_{113}	$K_S^0 K^+$	$(3.21 \pm 0.16) \times 10^{-3}$	Γ_{166}	$\pi^+ e^- \mu^+$	LF $< 2.2 \times 10^{-7}$ CL=90%
Γ_{114}	$K_S^0 K^+ \pi^0$	$(5.07 \pm 0.30) \times 10^{-3}$	Γ_{167}	$K^+ e^+ \mu^-$	LF $< 7.5 \times 10^{-8}$ CL=90%
Γ_{115}	$K^*(892)^+ K_S^0$	$(2.89 \pm 0.30) \times 10^{-3}$	Γ_{168}	$K^+ e^- \mu^+$	LF $< 1.0 \times 10^{-7}$ CL=90%
Γ_{116}	$\bar{K}^*(892)^0 K^+$	$(5.2 \pm 1.4) \times 10^{-4}$	Γ_{169}	$\pi^- 2e^+$	L $< 5.3 \times 10^{-7}$ CL=90%
Γ_{117}	$K_L^0 K^+ \pi^0$	$(5.24 \pm 0.31) \times 10^{-3}$	Γ_{170}	$\pi^- 2\mu^+$	L $< 1.4 \times 10^{-8}$ CL=90%
Γ_{118}	$K^+ K^- \pi^+$	[a] $(9.68 \pm 0.18) \times 10^{-3}$	Γ_{171}	$\pi^- e^+ \mu^+$	L $< 1.3 \times 10^{-7}$ CL=90%
Γ_{119}	$K^+ \bar{K}^*(892)^0, \bar{K}^*(892)^0 \rightarrow K^- \pi^+$	$(2.49 \pm_{0.13}^{0.08}) \times 10^{-3}$	Γ_{172}	$\rho^- 2\mu^+$	L $< 5.6 \times 10^{-4}$ CL=90%
Γ_{120}	$K^+ \bar{K}_0^*(1430)^0, \bar{K}_0^*(1430)^0 \rightarrow K^- \pi^+$	$(1.82 \pm 0.35) \times 10^{-3}$	Γ_{173}	$K^- 2e^+$	L $< 9 \times 10^{-7}$ CL=90%
			Γ_{174}	$K_S^0 \pi^- 2e^+$	$< 3.3 \times 10^{-6}$ CL=90%
			Γ_{175}	$K^- \pi^0 2e^+$	$< 8.5 \times 10^{-6}$ CL=90%
			Γ_{176}	$K^- 2\mu^+$	L $< 1.0 \times 10^{-5}$ CL=90%
			Γ_{177}	$K^- e^+ \mu^+$	L $< 1.9 \times 10^{-6}$ CL=90%
			Γ_{178}	$K^*(892)^- 2\mu^+$	L $< 8.5 \times 10^{-4}$ CL=90%
			Γ_{179}	$L e^+$	L,B $< 1.1 \times 10^{-6}$ CL=90%

Meson Particle Listings

 D^\pm

$\Gamma(K^*(892)^- \text{ anything})/\Gamma_{\text{total}}$			Γ_6/Γ		
VALUE (%)	EVTs	DOCUMENT ID	TECN	COMMENT	
5.7 ± 5.2 ± 0.7	7.2 ± 6.5	ABLIKIM	06u BES2	e^+e^- at 3773 MeV	

$\Gamma(K^*(892)^0 \text{ anything})/\Gamma_{\text{total}}$			Γ_7/Γ		
VALUE (%)	EVTs	DOCUMENT ID	TECN	COMMENT	
23.2 ± 4.5 ± 3.0	189 ± 36	ABLIKIM	05P BES	$e^+e^- \approx 3773$ MeV	

$\Gamma(K^*(892)^0 \text{ anything})/\Gamma_{\text{total}}$			Γ_8/Γ		
VALUE (%)	CL%	DOCUMENT ID	TECN	COMMENT	
<6.6	90	ABLIKIM	05P BES	$e^+e^- \approx 3773$ MeV	

$\Gamma(\eta \text{ anything})/\Gamma_{\text{total}}$			Γ_9/Γ		
This ratio includes η particles from η' decays.					
VALUE (%)	EVTs	DOCUMENT ID	TECN	COMMENT	
6.3 ± 0.5 ± 0.5	1972 ± 142	HUANG	06b CLEO	e^+e^- at $\psi(3770)$	

$\Gamma(\eta' \text{ anything})/\Gamma_{\text{total}}$			Γ_{10}/Γ		
VALUE (%)	EVTs	DOCUMENT ID	TECN	COMMENT	
1.04 ± 0.16 ± 0.09	82 ± 13	HUANG	06b CLEO	e^+e^- at $\psi(3770)$	

$\Gamma(\phi \text{ anything})/\Gamma_{\text{total}}$			Γ_{11}/Γ		
VALUE (%)	EVTs	DOCUMENT ID	TECN	COMMENT	
1.12 ± 0.04 OUR AVERAGE					
1.135 ± 0.034 ± 0.031	2.7k	ABLIKIM	19AY BES3	e^+e^- at 3773 MeV	
1.03 ± 0.10 ± 0.07	248 ± 21	HUANG	06b CLEO	e^+e^- at $\psi(3770)$	

Leptonic and semileptonic modes

$\Gamma(e^+ \nu_e)/\Gamma_{\text{total}}$			Γ_{12}/Γ		
VALUE	CL%	DOCUMENT ID	TECN	COMMENT	
<8.8 × 10⁻⁶	90	EISENSTEIN	08 CLEO	e^+e^- at $\psi(3770)$	
••• We do not use the following data for averages, fits, limits, etc. •••					
<2.4 × 10 ⁻⁵	90	ARTUSO	05A CLEO	See EISENSTEIN 08	

$\Gamma(\gamma e^+ \nu_e)/\Gamma_{\text{total}}$			Γ_{13}/Γ		
VALUE	CL%	DOCUMENT ID	TECN	COMMENT	
<3.0 × 10⁻⁵	90	1 ABLIKIM	17M BES3	e^+e^- at 3.773 GeV	
1 This ABLIKIM 17M limit is for photons with energies greater than 10 MeV.					

$\Gamma(\mu^+ \nu_\mu)/\Gamma_{\text{total}}$			Γ_{14}/Γ		
See the note on "Decay Constants of Charged Pseudoscalar Mesons" in the D_s^\pm Listings.					
VALUE (units 10 ⁻⁴)	EVTs	DOCUMENT ID	TECN	COMMENT	
3.74 ± 0.17 OUR AVERAGE					
3.71 ± 0.19 ± 0.06	409 ± 21	1 ABLIKIM	14F BES3	e^+e^- at $\psi(3770)$	
3.82 ± 0.32 ± 0.09	150 ± 12	2 EISENSTEIN	08 CLEO	e^+e^- at $\psi(3770)$	
••• We do not use the following data for averages, fits, limits, etc. •••					
12.2 \pm $\frac{+11.1}{-5.3}$ ± 1.0	3	3 ABLIKIM	05D BES	$e^+e^- \approx 3.773$ GeV	
4.40 ± 0.66 \pm $\frac{+0.09}{-0.12}$	47 ± 7	4 ARTUSO	05A CLEO	See EISENSTEIN 08	
3.5 ± 1.4 ± 0.6	7	5 BONVICINI	04A CLEO	Incl. in ARTUSO 05A	
8 \pm $\frac{+16}{-5}$ \pm $\frac{+5}{-2}$	1	6 BAI	98b BES	$e^+e^- \rightarrow D^{*+} D^-$	

1 ABLIKIM 14F obtain $|V_{cd}| \cdot f_{D^+} = (45.75 \pm 1.20 \pm 0.39)$ MeV, and using $|V_{cd}| = 0.22520 \pm 0.00065$ gets $f_{D^+} = (203.2 \pm 5.3 \pm 1.8)$ MeV.

2 EISENSTEIN 08, using the D^+ lifetime and assuming $|V_{cd}| = |V_{us}|$, gets $f_{D^+} = (205.8 \pm 8.5 \pm 2.5)$ MeV from this measurement.

3 ABLIKIM 05D finds a background-subtracted 2.67 ± 1.74 $D^+ \rightarrow \mu^+ \nu_\mu$ events, and from this obtains $f_{D^+} = 371 \pm \frac{+129}{-119} \pm 25$ MeV.

4 ARTUSO 05A obtains $f_{D^+} = 222.6 \pm 16.7 \pm \frac{+2.8}{-3.4}$ MeV from this measurement.

5 BONVICINI 04A finds eight events with an estimated background of one, and from the branching fraction obtains $f_{D^+} = 202 \pm 41 \pm 17$ MeV.

6 BAI 98b obtains $f_{D^+} = (300 \pm \frac{+180}{-150} \pm \frac{+80}{-40})$ MeV from this measurement.

$\Gamma(\tau^+ \nu_\tau)/\Gamma_{\text{total}}$			Γ_{15}/Γ		
VALUE (units 10 ⁻³)	CL%	EVTs	DOCUMENT ID	TECN	COMMENT
1.20 ± 0.24 ± 0.12		137	1 ABLIKIM	19Bg BES3	e^+e^- at 3773 MeV
••• We do not use the following data for averages, fits, limits, etc. •••					
<1.2	90		EISENSTEIN	08 CLEO	e^+e^- at $\psi(3770)$
<2.1	90		RUBIN	06A CLEO	See EISENSTEIN 08

1 ABLIKIM 19Bg observe this mode with a significance of 5.1 σ .

$\Gamma(K^0 e^+ \nu_e)/\Gamma_{\text{total}}$			Γ_{16}/Γ		
VALUE (%)	EVTs	DOCUMENT ID	TECN	COMMENT	
8.72 ± 0.09 OUR AVERAGE					
8.68 ± 0.14 ± 0.16	1172	ABLIKIM	21BA BES3	e^+e^- at 3.773 GeV	
8.60 ± 0.06 ± 0.15	26k	ABLIKIM	17s BES3	Using $\bar{K}^0 \rightarrow \pi^+ \pi^-$	
8.59 ± 0.14 ± 0.21	5013	ABLIKIM	16V BES3	Using $\bar{K}^0 \rightarrow 2\pi^0$	
8.962 ± 0.054 ± 0.206	40k	1 ABLIKIM	15AF BES3	from $D^+ \rightarrow K_L^+ e^+ \nu_e$	
8.83 ± 0.10 ± 0.20	8.5k	2 BESSON	09 CLEO	from $D^+ \rightarrow K_S^+ e^+ \nu_e$	
8.95 ± 1.59 ± 0.67	34	3 ABLIKIM	05A BES	from $D^+ \rightarrow K_S^+ e^+ \nu_e$	

••• We do not use the following data for averages, fits, limits, etc. •••

8.53 ± 0.13 ± 0.23 4 DOBBS 08 CLEO See BESSON 09

8.71 ± 0.38 ± 0.37 545 HUANG 05b CLEO See DOBBS 08

1 ABLIKIM 15AF report $\Gamma(D^+ \rightarrow K_L^+ e^+ \nu_e)/\Gamma_{\text{total}} = (4.481 \pm 0.027 \pm 0.103)\%$. See also the form-factor parameters near the end of this D^+ Listing.

2 See the form-factor parameters near the end of this D^+ Listing.

3 The ABLIKIM 05A result together with the $D^0 \rightarrow K^- e^+ \nu_e$ branching fraction of ABLIKIM 04c and Particle Data Group lifetimes gives $\Gamma(D^0 \rightarrow K^- e^+ \nu_e) / \Gamma(D^+ \rightarrow \bar{K}^0 e^+ \nu_e) = 1.08 \pm 0.22 \pm 0.07$; isospin invariance predicts the ratio is 1.0.

4 DOBBS 08 establishes $|\frac{V_{cd}}{V_{cs}} \cdot \frac{f_+^{\pi(0)}}{f_+^{K(0)}}| = 0.188 \pm 0.008 \pm 0.002$ from the D^+ and D^0 decays to $\bar{K}^0 e^+ \nu_e$ and $\pi^+ e^+ \nu_e$. It also finds $\Gamma(D^0 \rightarrow K^- e^+ \nu_e) / \Gamma(D^+ \rightarrow \bar{K}^0 e^+ \nu_e) = 1.06 \pm 0.02 \pm 0.03$; isospin invariance predicts the ratio is 1.0.

$\Gamma(K^0 \mu^+ \nu_\mu)/\Gamma_{\text{total}}$			Γ_{17}/Γ		
VALUE (units 10 ⁻²)	EVTs	DOCUMENT ID	TECN	COMMENT	
8.76 ± 0.19 OUR FIT					
8.72 ± 0.07 ± 0.18	21k	ABLIKIM	16g BES3	e^+e^- at 3773 MeV	
••• We do not use the following data for averages, fits, limits, etc. •••					
10.3 ± 2.3 ± 0.8	29 ± 6	ABLIKIM	07 BES2	e^+e^- at 3773 MeV	

$\Gamma(\bar{K}^0 \mu^+ \nu_\mu)/\Gamma(K^- 2\pi^+)$			Γ_{17}/Γ_{51}		
VALUE	EVTs	DOCUMENT ID	TECN	COMMENT	
0.934 ± 0.025 OUR FIT					
Error includes scale factor of 1.2.					
1.019 ± 0.076 ± 0.065	555 ± 39	LINK	04E FOCS	γ nucleus, $\bar{E}_\gamma \approx 180$ GeV	

$\Gamma(K^- \pi^+ e^+ \nu_e)/\Gamma_{\text{total}}$			Γ_{18}/Γ		
VALUE (units 10 ⁻²)	EVTs	DOCUMENT ID	TECN	COMMENT	
4.02 ± 0.18 OUR FIT					
Error includes scale factor of 3.2.					
3.77 ± 0.03 ± 0.08	18.3k	ABLIKIM	16F BES3	e^+e^- at $\psi(3770)$	
••• We do not use the following data for averages, fits, limits, etc. •••					
3.50 ± 0.75 ± 0.27	29	ABLIKIM	06o BES2	e^+e^- at 3773 MeV	
3.5 \pm $\frac{+1.2}{-0.7}$ ± 0.4	14	BAI	91 MRK3	$e^+e^- \approx 3.77$ GeV	

$\Gamma(K^- \pi^+ e^+ \nu_e)/\Gamma(K^- 2\pi^+)$			Γ_{18}/Γ_{51}		
VALUE	EVTs	DOCUMENT ID	TECN	COMMENT	
0.428 ± 0.018 OUR FIT					
Error includes scale factor of 3.7.					
0.4380 ± 0.0036 ± 0.0042	70k ± 363	DEL-AMO-SA..11i	BABR	$e^+e^- \approx 10.6$ GeV	

$\Gamma(\bar{K}^*(892)^0 e^+ \nu_e, \bar{K}^*(892)^0 \rightarrow K^- \pi^+)/\Gamma(K^- \pi^+ e^+ \nu_e)$			Γ_{19}/Γ_{18}		
VALUE (%)	EVTs	DOCUMENT ID	TECN	COMMENT	
93.94 ± 0.27 OUR AVERAGE					
93.93 ± 0.22 ± 0.18		ABLIKIM	16F BES3	e^+e^- at $\psi(3770)$	
94.11 ± 0.74 ± 0.75		DEL-AMO-SA..11i	BABR	$e^+e^- \approx 10.6$ GeV	

$\Gamma((K^- \pi^+)_{[0.8-1.0]\text{GeV}} e^+ \nu_e)/\Gamma_{\text{total}}$			Γ_{20}/Γ		
VALUE (units 10 ⁻²)	EVTs	DOCUMENT ID	TECN	COMMENT	
3.39 ± 0.03 ± 0.08	16.2k	ABLIKIM	16F BES3	e^+e^- at $\psi(3770)$	

$\Gamma((K^- \pi^+)_{S\text{-wave}} e^+ \nu_e)/\Gamma_{\text{total}}$			Γ_{21}/Γ		
VALUE (units 10 ⁻³)	EVTs	DOCUMENT ID	TECN	COMMENT	
2.28 ± 0.08 ± 0.08					
6.05 ± 0.22 ± 0.18		ABLIKIM	16F BES3	e^+e^- at $\psi(3770)$	
5.79 ± 0.16 ± 0.15		DEL-AMO-SA..11i	BABR	$e^+e^- \approx 10.6$ GeV	

$\Gamma((K^- \pi^+)_{S\text{-wave}} e^+ \nu_e)/\Gamma(K^- \pi^+ e^+ \nu_e)$			Γ_{21}/Γ_{18}		
VALUE (%)	EVTs	DOCUMENT ID	TECN	COMMENT	
5.89 ± 0.17 OUR AVERAGE					
6.05 ± 0.22 ± 0.18		ABLIKIM	16F BES3	e^+e^- at $\psi(3770)$	
5.79 ± 0.16 ± 0.15		DEL-AMO-SA..11i	BABR	$e^+e^- \approx 10.6$ GeV	

$\Gamma(\bar{K}^*(1410)^0 e^+ \nu_e, \bar{K}^*(1410)^0 \rightarrow K^- \pi^+)/\Gamma_{\text{total}}$			Γ_{22}/Γ		
VALUE	CL%	DOCUMENT ID	TECN	COMMENT	
<6 × 10⁻³	90	DEL-AMO-SA..11i	BABR	$e^+e^- \approx 10.6$ GeV	

$\Gamma(\bar{K}_2^*(1430)^0 e^+ \nu_e, \bar{K}_2^*(1430)^0 \rightarrow K^- \pi^+)/\Gamma_{\text{total}}$			Γ_{23}/Γ		
VALUE	CL%	DOCUMENT ID	TECN	COMMENT	
<5 × 10⁻⁴	90	DEL-AMO-SA..11i	BABR	$e^+e^- \approx 10.6$ GeV	

$\Gamma(K^- \pi^+ e^+ \nu_e \text{ nonresonant})/\Gamma_{\text{total}}$			Γ_{24}/Γ		
VALUE	CL%	DOCUMENT ID	TECN	COMMENT	
<0.007	90	ANJOS	89b E691	Photoproduction	

$\Gamma(\bar{K}^*(892)^0 e^+ \nu_e)/\Gamma_{\text{total}}$			Γ_{25}/Γ		
Unseen decay modes of $\bar{K}^*(892)^0$ are included. See the end of the D^+ Listings for measurements of $D^+ \rightarrow \bar{K}^*(892)^0 e^+ \nu_e$ form-factor ratios.					
VALUE (units 10 ⁻²)	EVTs	DOCUMENT ID	TECN	COMMENT	
5.40 ± 0.10 OUR FIT					
Error includes scale factor of 1.1.					
5.40 ± 0.10 OUR AVERAGE					
Error includes scale factor of 1.1.					
5.31 ± 0.05 ± 0.12	16.2k	ABLIKIM	16F BES3	e^+e^- at $\psi(3770)$	
5.52 ± 0.07 ± 0.13	$\approx 5k$	BRIERE	10 CLEO	e^+e^- at $\psi(3770)$	
••• We do not use the following data for averages, fits, limits, etc. •••					
5.06 ± 1.21 ± 0.40	28 ± 7	ABLIKIM	06o BES2	e^+e^- at 3773 MeV	
5.56 ± 0.27 ± 0.23	422 ± 21	1 HUANG	05b CLEO	e^+e^- at $\psi(3770)$	

1 HUANG 05b finds $\Gamma(D^0 \rightarrow K^{*+} e^+ \nu_e) / \Gamma(D^+ \rightarrow \bar{K}^{*0} e^+ \nu_e) = 0.98 \pm 0.08 \pm 0.04$; isospin invariance predicts the ratio is 1.0.

$\Gamma(\bar{K}^*(892)^0 e^+ \nu_e) / \Gamma(K^- 2\pi^+)$ $\Gamma_{25} / \Gamma_{51}$
 Unseen decay modes of the $\bar{K}^*(892)^0$ are included. See the end of the D^+ Listings for measurements of $D^+ \rightarrow \bar{K}^*(892)^0 e^+ \nu_e$ form-factor ratios.

VALUE	EVTS	DOCUMENT ID	TECN	COMMENT
• • • We do not use the following data for averages, fits, limits, etc. • • •				
$0.74 \pm 0.04 \pm 0.05$		BRANDENB...	02	CLEO $e^+ e^- \approx \gamma(4S)$
$0.62 \pm 0.15 \pm 0.09$	35	ADAMOVICH	91	OMEG π^- 340 GeV
$0.55 \pm 0.08 \pm 0.10$	880	ALBRECHT	91	ARG $e^+ e^- \approx 10.4$ GeV
$0.49 \pm 0.04 \pm 0.05$		ANJOS	89B	E691 Photoproduction

$\Gamma(K^- \pi^+ \mu^+ \nu_\mu) / \Gamma(K^0 \mu^+ \nu_\mu)$ $\Gamma_{26} / \Gamma_{17}$
 Unseen decay modes of the $\bar{K}^*(892)^0$ are included. See the end of the D^+ Listings for measurements of $D^+ \rightarrow \bar{K}^*(892)^0 e^+ \nu_e$ form-factor ratios.

VALUE	EVTS	DOCUMENT ID	TECN	COMMENT
$0.417 \pm 0.030 \pm 0.023$	555 ± 39	LINK	04E	FOCS γ nucleus, $\bar{E}_\gamma \approx 180$ GeV

$\Gamma(K^- \pi^+ \mu^+ \nu_\mu \text{ nonresonant}) / \Gamma(K^- \pi^+ \mu^+ \nu_\mu)$ $\Gamma_{28} / \Gamma_{26}$
 Unseen decay modes of the $\bar{K}^*(892)^0$ are included. See the end of the D^+ Listings for measurements of $D^+ \rightarrow \bar{K}^*(892)^0 e^+ \nu_e$ form-factor ratios.

VALUE	EVTS	DOCUMENT ID	TECN	COMMENT
$0.0530 \pm 0.0074 \pm 0.0099$	14k	LINK	05i	FOCS γ nucleus, $\bar{E}_\gamma \approx 180$ GeV

$\Gamma(\bar{K}^*(892)^0 \mu^+ \nu_\mu) / \Gamma_{\text{total}}$ Γ_{29} / Γ
 Unseen decay modes of the $\bar{K}^*(892)^0$ are included. See the end of the D^+ Listings for measurements of $D^+ \rightarrow \bar{K}^*(892)^0 e^+ \nu_e$ form-factor ratios.

VALUE (units 10^{-2})	EVTS	DOCUMENT ID	TECN	COMMENT
5.27 ± 0.15 OUR FIT				
$5.27 \pm 0.07 \pm 0.14$	$\approx 5k$	BRIERE	10	CLEO $e^+ e^-$ at $\psi(3770)$

$\Gamma(\bar{K}^*(892)^0 \mu^+ \nu_\mu) / \Gamma(K^- 2\pi^+)$ $\Gamma_{29} / \Gamma_{17}$
 Unseen decay modes of the $\bar{K}^*(892)^0$ are included. See the end of the D^+ Listings for measurements of $D^+ \rightarrow \bar{K}^*(892)^0 e^+ \nu_e$ form-factor ratios.

VALUE	EVTS	DOCUMENT ID	TECN	COMMENT
0.562 ± 0.018 OUR FIT				Error includes scale factor of 1.1.
0.57 ± 0.06 OUR AVERAGE				Error includes scale factor of 1.2.
$0.72 \pm 0.10 \pm 0.05$		BRANDENB...	02	CLEO $e^+ e^- \approx \gamma(4S)$
$0.56 \pm 0.04 \pm 0.06$	875	FRABETTI	93E	E687 γ Be $\bar{E}_\gamma \approx 200$ GeV
$0.46 \pm 0.07 \pm 0.08$	224	KODAMA	92C	E653 π^- emulsion 600 GeV
• • • We do not use the following data for averages, fits, limits, etc. • • •				
$0.602 \pm 0.010 \pm 0.021$	12k	LINK	02j	FOCS γ nucleus, ≈ 180 GeV

¹This LINK 02j result includes the effects of an interference of a small S-wave $K^- \pi^+$ amplitude with the dominant \bar{K}^*0 amplitude. (The interference effect is reported in LINK 02E.) This result is redundant with results of LINK 04E elsewhere in these Listings.

$\Gamma(K^- \pi^+ \pi^0 \mu^+ \nu_\mu) / \Gamma(K^- \pi^+ \mu^+ \nu_\mu)$ $\Gamma_{30} / \Gamma_{26}$
 Unseen decay modes of the $\bar{K}^*(892)^0$ are included. See the end of the D^+ Listings for measurements of $D^+ \rightarrow \bar{K}^*(892)^0 e^+ \nu_e$ form-factor ratios.

VALUE	CL%	DOCUMENT ID	TECN	COMMENT
<0.042	90	FRABETTI	93E	E687 γ Be $\bar{E}_\gamma \approx 200$ GeV

$\Gamma(\bar{K}_1(1270)^0 e^+ \nu_e, \bar{K}_1^0 \rightarrow K^- \pi^+ \pi^0) / \Gamma_{\text{total}}$ Γ_{31} / Γ
 Unseen decay modes of the $\bar{K}^*(892)^0$ are included. See the end of the D^+ Listings for measurements of $D^+ \rightarrow \bar{K}^*(892)^0 e^+ \nu_e$ form-factor ratios.

VALUE (units 10^{-3})	EVTS	DOCUMENT ID	TECN	COMMENT
$1.06 \pm 0.12 \pm 0.08$	120	ABLIKIM	19BH	BES3 $e^+ e^-$ at 3773 MeV

¹ABLIKIM 19BH quotes $B(D^+ \rightarrow \bar{K}_1(1270)^0 e^+ \nu_e) = (2.30 \pm 0.26 \pm 0.18 \pm 0.25) \times 10^{-3}$, where the last uncertainty is due to $B(\bar{K}_1(1270)^0 \rightarrow K^- \pi^+ \pi^0) = 0.467 \pm 0.050$.

$\Gamma(\bar{K}_0^*(1430)^0 \mu^+ \nu_\mu) / \Gamma(K^- \pi^+ \mu^+ \nu_\mu)$ $\Gamma_{32} / \Gamma_{26}$
 Unseen decay modes of the $\bar{K}^*(892)^0$ are included. See the end of the D^+ Listings for measurements of $D^+ \rightarrow \bar{K}^*(892)^0 e^+ \nu_e$ form-factor ratios.

VALUE	CL%	DOCUMENT ID	TECN	COMMENT
<0.0064	90	LINK	05i	FOCS γ A, $\bar{E}_\gamma \approx 180$ GeV

$\Gamma(\bar{K}^*(1680)^0 \mu^+ \nu_\mu) / \Gamma(K^- \pi^+ \mu^+ \nu_\mu)$ $\Gamma_{33} / \Gamma_{26}$
 Unseen decay modes of the $\bar{K}^*(1680)^0$ are included. See the end of the D^+ Listings for measurements of $D^+ \rightarrow \bar{K}^*(1680)^0 e^+ \nu_e$ form-factor ratios.

VALUE	CL%	DOCUMENT ID	TECN	COMMENT
<0.04	90	LINK	05i	FOCS γ A, $\bar{E}_\gamma \approx 180$ GeV

¹See the form-factor parameters near the end of this D^+ Listing.

²DOBBS 08 establishes $|\frac{V_{cd}}{V_{cs}} \cdot \frac{f_{\pi^+}(0)}{f_{K^+}(0)}| = 0.188 \pm 0.008 \pm 0.002$ from the D^+ and D^0 decays to $\bar{K} e^+ \nu_e$ and $\pi e^+ \nu_e$. It finds $\Gamma(D^0 \rightarrow \pi^- e^+ \nu_e) / \Gamma(D^+ \rightarrow \pi^0 e^+ \nu_e) = 2.03 \pm 0.14 \pm 0.08$; isospin invariance predicts the ratio is 2.0.

$\Gamma(\pi^0 \mu^+ \nu_\mu) / \Gamma_{\text{total}}$ Γ_{35} / Γ
 Unseen decay modes of the $\bar{K}^*(892)^0$ are included. See the end of the D^+ Listings for measurements of $D^+ \rightarrow \bar{K}^*(892)^0 e^+ \nu_e$ form-factor ratios.

VALUE (%)	EVTS	DOCUMENT ID	TECN	COMMENT
$0.350 \pm 0.011 \pm 0.010$	1.3k	ABLIKIM	18AE	BES3 $e^+ e^-$, 3773 MeV

$\Gamma(\eta e^+ \nu_e) / \Gamma_{\text{total}}$ Γ_{36} / Γ
 Unseen decay modes of the $\bar{K}^*(892)^0$ are included. See the end of the D^+ Listings for measurements of $D^+ \rightarrow \bar{K}^*(892)^0 e^+ \nu_e$ form-factor ratios.

VALUE (units 10^{-4})	EVTS	DOCUMENT ID	TECN	COMMENT
11.1 ± 0.7 OUR AVERAGE				
$10.74 \pm 0.81 \pm 0.51$	373	ABLIKIM	18R	BES3 $e^+ e^-$, 3773 MeV
$11.4 \pm 0.9 \pm 0.4$		YELTON	11	CLEO $e^+ e^-$ at $\psi(3770)$
• • • We do not use the following data for averages, fits, limits, etc. • • •				
$13.3 \pm 2.0 \pm 0.6$	46	MITCHELL	09B	CLEO See YELTON 11

$\Gamma(\eta \mu^+ \nu_\mu) / \Gamma_{\text{total}}$ Γ_{37} / Γ
 Unseen decay modes of the $\bar{K}^*(892)^0$ are included. See the end of the D^+ Listings for measurements of $D^+ \rightarrow \bar{K}^*(892)^0 e^+ \nu_e$ form-factor ratios.

VALUE (units 10^{-4})	EVTS	DOCUMENT ID	TECN	COMMENT
$10.41 \pm 1.12 \pm 0.05$	234	ABLIKIM	20T	BES3 $e^+ e^-$, 3773 MeV

¹ABLIKIM 20T reports $(10.4 \pm 1.0 \pm 0.5) \times 10^{-4}$ from a measurement of $[\Gamma(D^+ \rightarrow \eta \mu^+ \nu_\mu) / \Gamma_{\text{total}}] \times [B(\eta \rightarrow 2\gamma)]$ assuming $B(\eta \rightarrow 2\gamma) = (39.41 \pm 0.20) \times 10^{-2}$, which we rescale to our best value $B(\eta \rightarrow 2\gamma) = (39.36 \pm 0.18) \times 10^{-2}$. Our first error is their experiment's error and our second error is the systematic error from using our best value.

$\Gamma(\pi^- \pi^+ e^+ \nu_e) / \Gamma_{\text{total}}$ Γ_{38} / Γ
 Unseen decay modes of the $\bar{K}^*(892)^0$ are included. See the end of the D^+ Listings for measurements of $D^+ \rightarrow \bar{K}^*(892)^0 e^+ \nu_e$ form-factor ratios.

VALUE (units 10^{-3})	EVTS	DOCUMENT ID	TECN	COMMENT
$2.449 \pm 0.074 \pm 0.073$	1.7k	ABLIKIM	19C	BES3 $e^+ e^-$ at 3773 MeV

$\Gamma(\rho(500)^0 e^+ \nu_e, \rho(500)^0 \rightarrow \pi^+ \pi^-) / \Gamma(\pi^- \pi^+ e^+ \nu_e)$ $\Gamma_{39} / \Gamma_{38}$
 Unseen decay modes of the $\bar{K}^*(892)^0$ are included. See the end of the D^+ Listings for measurements of $D^+ \rightarrow \bar{K}^*(892)^0 e^+ \nu_e$ form-factor ratios.

VALUE (units 10^{-2})	EVTS	DOCUMENT ID	TECN	COMMENT
$25.7 \pm 1.6 \pm 1.1$	1.5k	ABLIKIM	19C	BES3 $\pi^- \pi^+ e^+ \nu_e$ events

$\Gamma(\rho^0 e^+ \nu_e) / \Gamma_{\text{total}}$ Γ_{40} / Γ
 Unseen decay modes of the $\bar{K}^*(892)^0$ are included. See the end of the D^+ Listings for measurements of $D^+ \rightarrow \bar{K}^*(892)^0 e^+ \nu_e$ form-factor ratios.

VALUE (units 10^{-3})	EVTS	DOCUMENT ID	TECN	COMMENT
2.18 ± 0.17 OUR FIT				
$2.17 \pm 0.12 \pm 0.22$	447 ± 25	DOBBS	13	CLEO $e^+ e^-$ at $\psi(3770)$

¹DOBBS 13 finds $\Gamma(D^0 \rightarrow \rho^- e^+ \nu_e) / 2 \Gamma(D^+ \rightarrow \rho^0 e^+ \nu_e) = 1.03 \pm 0.09 \pm 0.08$; isospin invariance predicts the ratio is 1.0.
²HUANG 05B finds $\Gamma(D^0 \rightarrow \rho^- e^+ \nu_e) / 2 \Gamma(D^+ \rightarrow \rho^0 e^+ \nu_e) = 1.2 \pm 0.4 \pm 0.1$; isospin invariance predicts the ratio is 1.0.

$\Gamma(\rho^0 \mu^+ \nu_\mu) / \Gamma(\pi^- \pi^+ e^+ \nu_e)$ $\Gamma_{40} / \Gamma_{38}$
 Unseen decay modes of the $\bar{K}^*(892)^0$ are included. See the end of the D^+ Listings for measurements of $D^+ \rightarrow \bar{K}^*(892)^0 e^+ \nu_e$ form-factor ratios.

VALUE (units 10^{-2})	EVTS	DOCUMENT ID	TECN	COMMENT
$76.0 \pm 1.7 \pm 1.1$	1.5k	ABLIKIM	19C	BES3 $\pi^- \pi^+ e^+ \nu_e$ events

$\Gamma(\rho^0 e^+ \nu_e) / \Gamma(\bar{K}^*(892)^0 e^+ \nu_e)$ $\Gamma_{40} / \Gamma_{25}$
 Unseen decay modes of the $\bar{K}^*(892)^0$ are included. See the end of the D^+ Listings for measurements of $D^+ \rightarrow \bar{K}^*(892)^0 e^+ \nu_e$ form-factor ratios.

VALUE	EVTS	DOCUMENT ID	TECN	COMMENT
0.0404 ± 0.0033 OUR FIT				
$0.045 \pm 0.014 \pm 0.009$	49	AITALA	97	E791 π^- nucleus, 500 GeV

¹AITALA 97 explicitly subtracts $D^+ \rightarrow \eta' e^+ \nu_e$ and other backgrounds to get this result.
²Because the reconstruction efficiency for photons is low, this FRABETTI 97 result also includes any $D^+ \rightarrow \eta' \mu^+ \nu_\mu \rightarrow \gamma \rho^0 \mu^+ \nu_\mu$ events in the numerator.

$\Gamma(\omega e^+ \nu_e) / \Gamma_{\text{total}}$ Γ_{42} / Γ
 Unseen decay modes of the $\bar{K}^*(892)^0$ are included. See the end of the D^+ Listings for measurements of $D^+ \rightarrow \bar{K}^*(892)^0 e^+ \nu_e$ form-factor ratios.

VALUE (units 10^{-3})	EVTS	DOCUMENT ID	TECN	COMMENT
1.69 ± 0.11 OUR AVERAGE				
$1.63 \pm 0.11 \pm 0.08$	491 ± 32	ABLIKIM	15W	BES3 292 fb ⁻¹ , 3773 MeV
$1.82 \pm 0.18 \pm 0.07$	129 ± 13	DOBBS	13	CLEO $e^+ e^-$ at $\psi(3770)$
• • • We do not use the following data for averages, fits, limits, etc. • • •				
$1.6 \pm 0.7 \pm 0.1$	7.6 ± 3.3 -0.6	HUANG	05B	CLEO See DOBBS 13

Meson Particle Listings

D^\pm

$\Gamma(\omega e^+ \nu_e)/\Gamma(\pi^- \pi^+ e^+ \nu_e)$ Γ_{42}/Γ_{38}

VALUE (units 10^{-2})	EVTS	DOCUMENT ID	TECN	COMMENT
1.28 ± 0.41 ± 0.15	1.5k	ABLIKIM	19c	BES3 $\pi^- \pi^+ e^+ \nu_e$ events

$\Gamma(\omega \mu^+ \nu_\mu)/\Gamma_{total}$ Γ_{43}/Γ

VALUE (units 10^{-4})	EVTS	DOCUMENT ID	TECN	COMMENT
17.7 ± 2.1 ± 0.1	194	¹ ABLIKIM	20H	BES3 $e^+ e^-$, 3773 MeV

¹ ABLIKIM 20H reports $(17.7 \pm 1.8 \pm 1.1) \times 10^{-4}$ from a measurement of $[\Gamma(D^+ \rightarrow \omega \mu^+ \nu_\mu)/\Gamma_{total}] \times [B(\omega(782) \rightarrow \pi^+ \pi^- \pi^0)]$ assuming $B(\omega(782) \rightarrow \pi^+ \pi^- \pi^0) = (89.3 \pm 0.6) \times 10^{-2}$, which we rescale to our best value $B(\omega(782) \rightarrow \pi^+ \pi^- \pi^0) = (89.2 \pm 0.7) \times 10^{-2}$. Our first error is their experiment's error and our second error is the systematic error from using our best value.

$\Gamma(\eta(958) e^+ \nu_e)/\Gamma_{total}$ Γ_{44}/Γ

VALUE (units 10^{-4})	CL%	EVTS	DOCUMENT ID	TECN	COMMENT
2.0 ± 0.4 OUR AVERAGE					
1.91 ± 0.51 ± 0.13		32	ABLIKIM	18R	BES3 $e^+ e^-$, 3773 MeV
2.16 ± 0.53 ± 0.07			YELTON	11	CLEO $e^+ e^-$ at $\psi(3770)$

• • • We do not use the following data for averages, fits, limits, etc. • • •

<3.5	90	MITCHELL	09B	CLEO	See YELTON 11
------	----	----------	-----	------	---------------

$\Gamma(a(980)^0 e^+ \nu_e, a(980)^0 \rightarrow \eta \pi^0)/\Gamma_{total}$ Γ_{45}/Γ

VALUE (units 10^{-4})	EVTS	DOCUMENT ID	TECN	COMMENT
1.66 ± 0.81 ± 0.11	10^{+5}_{-4}	¹ ABLIKIM	18F	BES3 $e^+ e^-$ at 3773 MeV

¹ Signal observed at 2.9 σ C.L.

$\Gamma(b_1(1235)^0 e^+ \nu_e, b_1^0 \rightarrow \omega \pi^0)/\Gamma_{total}$ Γ_{46}/Γ

VALUE	CL%	DOCUMENT ID	TECN	COMMENT
<1.75 × 10⁻⁴	90	ABLIKIM	20AF	BES3 $e^+ e^-$, 3773 MeV

$\Gamma(\phi e^+ \nu_e)/\Gamma_{total}$ Γ_{47}/Γ

Unseen decay modes of the ϕ are included.

VALUE	CL%	DOCUMENT ID	TECN	COMMENT
<1.3 × 10⁻⁵	90	ABLIKIM	15W	BES3 292 fb ⁻¹ , 3773 MeV

• • • We do not use the following data for averages, fits, limits, etc. • • •

<0.9 × 10 ⁻⁴	90	YELTON	11	CLEO $e^+ e^-$ at $\psi(3770)$
<1.6 × 10 ⁻⁴	90	MITCHELL	09B	CLEO See YELTON 11
<0.0201	90	ABLIKIM	06P	BES2 $e^+ e^-$ at 3773 MeV
<0.0209	90	BAI	91	MRK3 $e^+ e^- \approx 3.77$ GeV

$\Gamma(D^0 e^+ \nu_e)/\Gamma_{total}$ Γ_{48}/Γ

VALUE	CL%	DOCUMENT ID	TECN	COMMENT
<1.0 × 10⁻⁴	90	ABLIKIM	17AD	BES3 $e^+ e^-$ at 3.773 GeV

Hadronic modes with a \bar{K} or $\bar{K}K\bar{K}$

$\Gamma(K_S^0 \pi^+)/\Gamma_{total}$ Γ_{49}/Γ

VALUE (units 10^{-2})	EVTS	DOCUMENT ID	TECN	COMMENT
1.562 ± 0.031 OUR FIT	Error includes scale factor of 1.7.			
1.591 ± 0.006 ± 0.030	94k	ABLIKIM	18W	BES3 $e^+ e^-$, 3773 MeV

• • • We do not use the following data for averages, fits, limits, etc. • • •

1.526 ± 0.022 ± 0.038		¹ DOBBS	07	CLEO See MENDEZ 10
1.55 ± 0.05 ± 0.06	2.2k	¹ HE	05	CLEO See DOBBS 07
1.6 ± 0.3 ± 0.1	161	ADLER	88c	MRK3 $e^+ e^- \approx 3.77$ GeV

¹ DOBBS 07 and HE 05 use single- and double-tagged events in an overall fit. DOBBS 07 supersedes HE 05.

$\Gamma(K_S^0 \pi^+)/\Gamma(K^- 2\pi^+)$ Γ_{49}/Γ_{51}

VALUE	EVTS	DOCUMENT ID	TECN	COMMENT
0.167 ± 0.004 OUR FIT	Error includes scale factor of 2.4.			
0.162 ± 0.009 OUR AVERAGE	Error includes scale factor of 4.5.			
0.171 ± 0.002 ± 0.002		BONVICINI	14	CLEO All CLEO-c runs
0.1530 ± 0.0023 ± 0.0016	10.6k	LINK	02B	FOCS γ nucleus, $E_\gamma \approx 180$ GeV

• • • We do not use the following data for averages, fits, limits, etc. • • •

0.1682 ± 0.0012 ± 0.0037	30k	MENDEZ	10	CLEO See BONVICINI 14
0.174 ± 0.012 ± 0.011	473	¹ BISHAI	97	CLEO $e^+ e^- \approx \gamma(4S)$
0.137 ± 0.015 ± 0.016	264	ANJOS	90c	E691 Photoproduction

¹ See BISHAI 97 for an isospin analysis of $D^+ \rightarrow \bar{K} \pi$ amplitudes.

$\Gamma(K_L^0 \pi^+)/\Gamma_{total}$ Γ_{50}/Γ

VALUE (units 10^{-2})	EVTS	DOCUMENT ID	TECN	COMMENT
1.460 ± 0.040 ± 0.035	2023 ± 54	¹ HE	08	CLEO $e^+ e^-$ at $\psi(3770)$

¹ The difference of CLEO $D^+ \rightarrow K_S^0 \pi^+$ and $K_L^0 \pi^+$ branching fractions over the sum (DOBBS 07 and HE 08) is $+0.022 \pm 0.016 \pm 0.018$.

$\Gamma(K^- 2\pi^+)/\Gamma_{total}$ Γ_{51}/Γ

VALUE (units 10^{-2})	EVTS	DOCUMENT ID	TECN	COMMENT
9.38 ± 0.16 OUR FIT	Error includes scale factor of 1.6.			
9.224 ± 0.059 ± 0.157		BONVICINI	14	CLEO All CLEO-c runs

• • • We do not use the following data for averages, fits, limits, etc. • • •

9.14 ± 0.10 ± 0.17		¹ DOBBS	07	CLEO See BONVICINI 14
9.5 ± 0.2 ± 0.3	15.1k	¹ HE	05	CLEO See DOBBS 07
9.3 ± 0.6 ± 0.8	1502	² BALEST	94	CLEO $e^+ e^- \approx \gamma(4S)$
6.4 $^{+1.5}_{-1.4}$		³ BARLAG	92c	ACCM π^- Cu 230 GeV
9.1 ± 1.3 ± 0.4	1164	ADLER	88c	MRK3 $e^+ e^-$ 3.77 GeV
9.1 ± 1.9	239	⁴ SCHINDLER	81	MRK2 $e^+ e^-$ 3.771 GeV

¹ DOBBS 07 and HE 05 use single- and double-tagged events in an overall fit. DOBBS 07 supersedes HE 05.

² BALEST 94 measures the ratio of $D^+ \rightarrow K^- \pi^+ \pi^+$ and $D^0 \rightarrow K^- \pi^+$ branching fractions to be $2.35 \pm 0.16 \pm 0.16$ and uses their absolute measurement of the $D^0 \rightarrow K^- \pi^+$ fraction (AKERIB 93).

³ BARLAG 92c computes the branching fraction by topological normalization.

⁴ SCHINDLER 81 (MARK-2) measures $\sigma(e^+ e^- \rightarrow \psi(3770)) \times$ branching fraction to be 0.38 ± 0.05 nb. We use the MARK-3 (ADLER 88c) value of $\sigma = 4.2 \pm 0.6 \pm 0.3$ nb.

See the related review(s): Review of Multibody Charm Analyses

$\Gamma((K^- \pi^+)_{S\text{-wave}} \pi^+)/\Gamma(K^- 2\pi^+)$ Γ_{52}/Γ_{51}

This is the "fit fraction" from the Dalitz-plot analysis. The $K^- \pi^+$ S-wave includes a broad scalar κ ($\bar{K}_0^*(700)$), the $\bar{K}_0^*(1430)$, and non-resonant background.

VALUE	DOCUMENT ID	TECN	COMMENT
0.801 ± 0.012 OUR AVERAGE			
0.8024 ± 0.0138 ± 0.0043	¹ LINK	09	FOCS MIPWA fit, 53k evts
0.838 ± 0.038	² BONVICINI	08A	CLEO QMIPWA fit, 141k evts
0.786 ± 0.014 ± 0.018	AITALA	06	E791 Dalitz fit, 15.1k events

• • • We do not use the following data for averages, fits, limits, etc. • • •

0.8323 ± 0.0150 ± 0.0008	³ LINK	07B	FOCS See LINK 09
--------------------------	-------------------	-----	------------------

¹ This LINK 09 model-independent partial-wave analysis of the $K^- \pi^+$ S-wave slices the $K^- \pi^+$ mass range into 39 bins.

² The BONVICINI 08A QMIPWA (quasi-model-independent partial-wave analysis) of the $K^- \pi^+$ S-wave amplitude slices the $K^- \pi^+$ mass range into 26 bins but keeps the Breit-Wigner $\bar{K}_0^*(1430)$.

³ This LINK 07B fit uses a K matrix. The $K^- \pi^+$ S-wave fit fraction given above breaks down into $(207.3 \pm 25.5 \pm 12.4)\%$ isospin-1/2 and $(40.5 \pm 9.6 \pm 3.2)\%$ isospin-3/2 — with large interference between the two. The isospin-1/2 component includes the κ (or $\bar{K}_0^*(700)$) and $\bar{K}_0^*(1430)$.

$\Gamma(\bar{K}_0^*(700) \pi^+, \bar{K}_0^*(700) \rightarrow K^- \pi^+)/\Gamma(K^- 2\pi^+)$ Γ_{53}/Γ_{51}

This is the "fit fraction" from the Dalitz-plot analysis.

VALUE	DOCUMENT ID	TECN	COMMENT
0.478 ± 0.121 ± 0.053	AITALA	02	E791 See AITALA 06

$\Gamma(\bar{K}_0^*(1430) \pi^+, \bar{K}_0^*(1430) \rightarrow K^- \pi^+)/\Gamma(K^- 2\pi^+)$ Γ_{54}/Γ_{51}

This is the "fit fraction" from the Dalitz-plot analysis.

VALUE	DOCUMENT ID	TECN	COMMENT
0.1330 ± 0.0062	BONVICINI	08A	CLEO QMIPWA fit, 141k evts

• • • We do not use the following data for averages, fits, limits, etc. • • •

0.125 ± 0.014 ± 0.005	AITALA	02	E791 See AITALA 06
0.284 ± 0.022 ± 0.059	FRABETTI	94G	E687 Dalitz fit, 8800 evts
0.248 ± 0.019 ± 0.017	ANJOS	93	E691 γ Be 90–260 GeV

$\Gamma(\bar{K}^*(892) \pi^+, \bar{K}^*(892) \rightarrow K^- \pi^+)/\Gamma(K^- 2\pi^+)$ Γ_{55}/Γ_{51}

This is the "fit fraction" from the Dalitz-plot analysis.

VALUE	DOCUMENT ID	TECN	COMMENT
0.111 ± 0.012 OUR AVERAGE	Error includes scale factor of 3.7.		
0.1236 ± 0.0034 ± 0.0034	LINK	09	FOCS MIPWA fit, 53k evts
0.0988 ± 0.0046	BONVICINI	08A	CLEO QMIPWA fit, 141k evts
0.119 ± 0.002 ± 0.020	AITALA	06	E791 Dalitz fit, 15.1k events

• • • We do not use the following data for averages, fits, limits, etc. • • •

0.1361 ± 0.0041 ± 0.0030	¹ LINK	07B	FOCS See LINK 09
0.123 ± 0.010 ± 0.009	AITALA	02	E791 See AITALA 06
0.137 ± 0.006 ± 0.009	FRABETTI	94G	E687 Dalitz fit, 8800 evts
0.170 ± 0.009 ± 0.034	ANJOS	93	E691 γ Be 90–260 GeV
0.14 ± 0.04 ± 0.04	ALVAREZ	91B	NA14 Photoproduction
0.13 ± 0.01 ± 0.07	ADLER	87	MRK3 $e^+ e^-$ 3.77 GeV

¹ The statistical error on this LINK 07B value is corrected in LINK 09.

$\Gamma(\bar{K}^*(1410) \pi^+, \bar{K}^{*0} \rightarrow K^- \pi^+)/\Gamma(K^- 2\pi^+)$ Γ_{56}/Γ_{51}

VALUE (units 10^{-3})	DOCUMENT ID	TECN	COMMENT
not seen	LINK	09	FOCS MIPWA fit, 53k evts
not seen	BONVICINI	08A	CLEO QMIPWA fit, 141k evts

• • • We do not use the following data for averages, fits, limits, etc. • • •

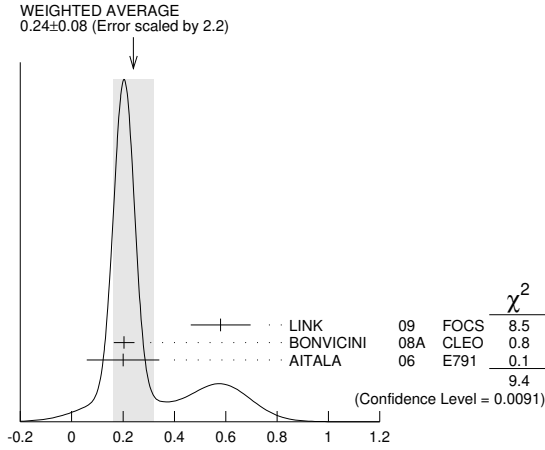
4.8 ± 2.1 ± 1.7	LINK	07B	FOCS See LINK 09
-----------------	------	-----	------------------

$\Gamma(\bar{K}_2^*(1430) \pi^+, \bar{K}_2^*(1430) \rightarrow K^- \pi^+)/\Gamma(K^- 2\pi^+)$ Γ_{57}/Γ_{51}

This is the "fit fraction" from the Dalitz-plot analysis.

VALUE (units 10^{-2})	DOCUMENT ID	TECN	COMMENT
0.24 ± 0.08 OUR AVERAGE	Error includes scale factor of 2.2. See the ideogram below.		
0.58 ± 0.10 ± 0.06	LINK	09	FOCS MIPWA fit, 53k evts
0.204 ± 0.040	BONVICINI	08A	CLEO QMIPWA fit, 141k evts
0.2 ± 0.1 ± 0.1	AITALA	06	E791 Dalitz fit, 15.1k events

• • • We do not use the following data for averages, fits, limits, etc. • • •
 0.39 ± 0.09 ± 0.05 LINK 07b FOCS See LINK 09
 0.5 ± 0.1 ± 0.2 AITALA 02 E791 See AITALA 06



$\Gamma(\bar{K}_2^*(1430)^0 \pi^+, \bar{K}_2^*(1430)^0 \rightarrow K^- \pi^+) / \Gamma(K^- 2\pi^+)$ $\Gamma_{57} / \Gamma_{51}$
 (units 10^{-2})

$\Gamma(\bar{K}^*(1680)^0 \pi^+, \bar{K}^*(1680)^0 \rightarrow K^- \pi^+) / \Gamma(K^- 2\pi^+)$ $\Gamma_{58} / \Gamma_{51}$
 This is the "fit fraction" from the Dalitz-plot analysis.

VALUE (units 10^{-2})	DOCUMENT ID	TECN	COMMENT
0.23 ± 0.12 OUR AVERAGE			
1.75 ± 0.62 ± 0.54	LINK 09	FOCS	MIPWA fit, 53k evts
0.196 ± 0.118	BONVICINI 08A	CLEO	QMIPWA fit, 141k evts
1.2 ± 0.6 ± 1.2	AITALA 06	E791	Dalitz fit, 15.1k events

• • • We do not use the following data for averages, fits, limits, etc. • • •

1.90 ± 0.63 ± 0.43	LINK 07b	FOCS	See LINK 09
2.5 ± 0.7 ± 0.3	AITALA 02	E791	See AITALA 06
4.7 ± 0.6 ± 0.7	FRABETTI 94G	E687	Dalitz fit, 8800 evts
3.0 ± 0.4 ± 1.3	ANJOS 93	E691	γ Be 90–260 GeV

$\Gamma(K^- (2\pi^+)_{I=2}) / \Gamma(K^- 2\pi^+)$ $\Gamma_{59} / \Gamma_{51}$
 VALUE DOCUMENT ID TECN COMMENT
0.155 ± 0.028 BONVICINI 08A CLEO QMIPWA fit, 141k evts

$\Gamma(K^- 2\pi^+ \text{ nonresonant}) / \Gamma(K^- 2\pi^+)$ $\Gamma_{60} / \Gamma_{51}$
 This is the "fit fraction" from the Dalitz-plot analysis. Later analyses find little need for this decay mode.

VALUE	DOCUMENT ID	TECN	COMMENT
• • • We do not use the following data for averages, fits, limits, etc. • • •			
0.130 ± 0.058 ± 0.044	AITALA 02	E791	See AITALA 06
0.998 ± 0.037 ± 0.072	FRABETTI 94G	E687	Dalitz fit, 8800 evts
0.838 ± 0.088 ± 0.275	ANJOS 93	E691	γ Be 90–260 GeV
0.79 ± 0.07 ± 0.15	ADLER 87	MRK3	$e^+ e^-$ 3.77 GeV

$\Gamma(K_S^0 \pi^+ \pi^0) / \Gamma_{\text{total}}$ Γ_{61} / Γ

VALUE (units 10^{-2})	EVTS	DOCUMENT ID	TECN	COMMENT
• • • We do not use the following data for averages, fits, limits, etc. • • •				
6.99 ± 0.09 ± 0.25		¹ DOBBS 07	CLEO	See BONVICINI 14
7.2 ± 0.2 ± 0.4	5.1k	¹ HE 05	CLEO	See DOBBS 07
5.1 ± 1.3 ± 0.8	159	ADLER 88c	MRK3	$e^+ e^-$ 3.77 GeV

¹ DOBBS 07 and HE 05 use single- and double-tagged events in an overall fit. DOBBS 07 supersedes HE 05.

$\Gamma(K_S^0 \pi^+ \pi^0) / \Gamma(K^- 2\pi^+)$ $\Gamma_{61} / \Gamma_{51}$
 VALUE DOCUMENT ID TECN COMMENT
0.785 ± 0.007 ± 0.016 BONVICINI 14 CLEO All CLEO-c runs

$\Gamma(K_S^0 \rho^+) / \Gamma(K_S^0 \pi^+ \pi^0)$ $\Gamma_{62} / \Gamma_{61}$
 This is the "fit fraction" from the Dalitz-plot analysis.

VALUE (units 10^{-2})	DOCUMENT ID	TECN	COMMENT
83.4 ± 2.2 ± 7.1	¹ ABLIKIM 14E	BES3	$e^+ e^-$ at $\psi(3770)$

¹ Fit fraction from Dalitz plot analysis of 142k $D^+ \rightarrow K_S^0 \pi^+ \pi^0$ events.

$\Gamma(K_S^0 \rho(1450)^+, \rho^+ \rightarrow \pi^+ \pi^0) / \Gamma(K_S^0 \pi^+ \pi^0)$ $\Gamma_{63} / \Gamma_{61}$
 This is the "fit fraction" from the Dalitz-plot analysis.

VALUE (%)	DOCUMENT ID	TECN	COMMENT
2.1 ± 0.3 ± 1.6	ABLIKIM 14E	BES3	$e^+ e^-$ at $\psi(3770)$

$\Gamma(\bar{K}^*(892)^0 \pi^+, \bar{K}^*(892)^0 \rightarrow K_S^0 \pi^0) / \Gamma(K_S^0 \pi^+ \pi^0)$ $\Gamma_{64} / \Gamma_{61}$
 This is the "fit fraction" from the Dalitz-plot analysis.

VALUE (units 10^{-2})	DOCUMENT ID	TECN	COMMENT
3.58 ± 0.17 ± 0.39	¹ ABLIKIM 14E	BES3	$e^+ e^-$ at $\psi(3770)$

¹ Fit fraction from Dalitz plot analysis of 142k $D^+ \rightarrow K_S^0 \pi^+ \pi^0$ events.

$\Gamma(\bar{K}_0^*(1430)^0 \pi^+, \bar{K}_0^*(1430)^0 \rightarrow K_S^0 \pi^0) / \Gamma(K_S^0 \pi^+ \pi^0)$ $\Gamma_{65} / \Gamma_{61}$
 This is the "fit fraction" from the Dalitz-plot analysis.

VALUE (%)	DOCUMENT ID	TECN	COMMENT
3.7 ± 0.6 ± 1.1	ABLIKIM 14E	BES3	$e^+ e^-$ at $\psi(3770)$

$\Gamma(\bar{K}_0^*(1680)^0 \pi^+, \bar{K}_0^*(1680)^0 \rightarrow K_S^0 \pi^0) / \Gamma(K_S^0 \pi^+ \pi^0)$ $\Gamma_{66} / \Gamma_{61}$
 This is the "fit fraction" from the Dalitz-plot analysis.

VALUE (%)	DOCUMENT ID	TECN	COMMENT
1.3 ± 0.2 ± 0.9	ABLIKIM 14E	BES3	$e^+ e^-$ at $\psi(3770)$

$\Gamma(\bar{\pi}^0 \pi^+, \bar{\pi}^0 \rightarrow K_S^0 \pi^0) / \Gamma(K_S^0 \pi^+ \pi^0)$ $\Gamma_{67} / \Gamma_{61}$
 This is the "fit fraction" from the Dalitz-plot analysis.

VALUE (%)	DOCUMENT ID	TECN	COMMENT
7.7 ± 1.2 ± 6.5	ABLIKIM 14E	BES3	$e^+ e^-$ at $\psi(3770)$

$\Gamma(K_S^0 \pi^+ \pi^0 \text{ nonresonant}) / \Gamma(K_S^0 \pi^+ \pi^0)$ $\Gamma_{68} / \Gamma_{61}$
 This is the "fit fraction" from the Dalitz-plot analysis.

VALUE (units 10^{-2})	DOCUMENT ID	TECN	COMMENT
4.6 ± 0.7 ± 5.4	¹ ABLIKIM 14E	BES3	$e^+ e^-$ at $\psi(3770)$

¹ Fit fraction from Dalitz plot analysis of 142k $D^+ \rightarrow K_S^0 \pi^+ \pi^0$ events.

$\Gamma(K_S^0 \pi^+ \pi^0 \text{ nonresonant and } \bar{\pi}^0 \pi^+) / \Gamma(K_S^0 \pi^+ \pi^0)$ $\Gamma_{69} / \Gamma_{61}$
 This is the "fit fraction" from the Dalitz-plot analysis.

VALUE (%)	DOCUMENT ID	TECN	COMMENT
18.6 ± 1.7 ± 2.3	ABLIKIM 14E	BES3	$e^+ e^-$ at $\psi(3770)$

$\Gamma((K_S^0 \pi^0)_{S\text{-wave}} \pi^+) / \Gamma(K_S^0 \pi^+ \pi^0)$ $\Gamma_{70} / \Gamma_{61}$
 The numerator here is the coherent sum of the $\bar{K}_0^*(1430)^0 \pi^+$, $\bar{\pi}^0 \pi^+$, and nonresonant contributions.

VALUE (%)	DOCUMENT ID	TECN	COMMENT
17.3 ± 1.4 ± 3.4	ABLIKIM 14E	BES3	$e^+ e^-$ at $\psi(3770)$

$\Gamma(K_S^0 \pi^+ \eta) / \Gamma_{\text{total}}$ Γ_{71} / Γ
 VALUE (units 10^{-3}) EVTS DOCUMENT ID TECN COMMENT
13.09 ± 0.37 ± 0.31 1.3k ABLIKIM 20v BES3 $e^+ e^-$, 3773 MeV

$\Gamma(K_S^0 \pi^+ \eta(958)) / \Gamma_{\text{total}}$ Γ_{72} / Γ
 VALUE (units 10^{-3}) EVTS DOCUMENT ID TECN COMMENT
1.90 ± 0.17 ± 0.13 267 ABLIKIM 18ac BES3 $e^+ e^-$, 3773 MeV

$\Gamma(K^- 2\pi^+ \pi^0) / \Gamma_{\text{total}}$ Γ_{73} / Γ
 See our 2008 Review (Physics Letters **B667** 1 (2008)) for measurements of submodes of this mode. There is nothing new since 1992, and the two papers, ANJOS 92c, with 91 ± 12 events above background, and COFFMAN 92b, with 142 ± 20 such events, could not determine submode fractions with much accuracy.

VALUE (units 10^{-2})	EVTS	DOCUMENT ID	TECN	COMMENT
• • • We do not use the following data for averages, fits, limits, etc. • • •				
5.98 ± 0.08 ± 0.16		¹ DOBBS 07	CLEO	See BONVICINI 14
6.0 ± 0.2 ± 0.2	4.8k	¹ HE 05	CLEO	See DOBBS 07
5.8 ± 1.2 ± 1.2	142	COFFMAN 92b	MRK3	$e^+ e^-$ 3.77 GeV
6.3 ± 1.4 ± 1.3	175	BALTRUSAIT..86E	MRK3	See COFFMAN 92b

¹ DOBBS 07 and HE 05 use single- and double-tagged events in an overall fit. DOBBS 07 supersedes HE 05.

$\Gamma(K^- 2\pi^+ \pi^0) / \Gamma(K^- 2\pi^+)$ $\Gamma_{73} / \Gamma_{51}$
 VALUE DOCUMENT ID TECN COMMENT
0.666 ± 0.006 ± 0.014 BONVICINI 14 CLEO All CLEO-c runs

$\Gamma(K_S^0 2\pi^+ \pi^-) / \Gamma_{\text{total}}$ Γ_{74} / Γ
 See our 2008 Review (Physics Letters **B667** 1 (2008)) for measurements of submodes of this mode. There is nothing new since 1992, and the two papers, ANJOS 92c, with 229 ± 17 events above background, and COFFMAN 92b, with 209 ± 20 such events, could not determine submode fractions with much accuracy.

VALUE (units 10^{-2})	EVTS	DOCUMENT ID	TECN	COMMENT
• • • We do not use the following data for averages, fits, limits, etc. • • •				
3.122 ± 0.046 ± 0.096		¹ DOBBS 07	CLEO	See BONVICINI 14
3.2 ± 0.1 ± 0.2	3.2k	¹ HE 05	CLEO	See DOBBS 07
2.1 ± 1.0 ± 0.9		² BARLAG 92c	ACCM	π^- Cu 230 GeV
3.3 ± 0.8 ± 0.2	168	ADLER 88c	MRK3	$e^+ e^-$ 3.77 GeV

¹ DOBBS 07 and HE 05 use single- and double-tagged events in an overall fit. DOBBS 07 supersedes HE 05.

² BARLAG 92c computes the branching fraction by topological normalization.

Meson Particle Listings

D^\pm

$\Gamma(K^- 2\pi^+ \eta)/\Gamma_{\text{total}}$				Γ_{75}/Γ
VALUE (units 10^{-3})	EVTS	DOCUMENT ID	TECN	COMMENT
$1.35 \pm 0.11 \pm 0.04$	190	ABLIKIM	20v	BES3 $e^+ e^-$, 3773 MeV

$\Gamma(K_S^0 \pi^+ \pi^0 \eta)/\Gamma_{\text{total}}$				Γ_{76}/Γ
VALUE (units 10^{-3})	EVTS	DOCUMENT ID	TECN	COMMENT
$1.22 \pm 0.24 \pm 0.06$	50	ABLIKIM	20v	BES3 $e^+ e^-$, 3773 MeV

$\Gamma(K_S^0 2\pi^+ \pi^-)/\Gamma(K^- 2\pi^+)$				Γ_{74}/Γ_{51}
VALUE	EVTS	DOCUMENT ID	TECN	COMMENT
$0.331 \pm 0.004 \pm 0.006$		BONVICINI	14	CLEO All CLEO-c runs

$\Gamma(K^- 3\pi^+ \pi^-)/\Gamma(K^- 2\pi^+)$				Γ_{77}/Γ_{51}
VALUE	EVTS	DOCUMENT ID	TECN	COMMENT
0.061 ± 0.005 OUR FIT		Error includes scale factor of 1.1.		
0.062 ± 0.008 OUR AVERAGE		Error includes scale factor of 1.3.		
$0.058 \pm 0.002 \pm 0.006$	2923	LINK	03D	FOCS $\gamma A, \bar{E}_\gamma \approx 180$ GeV
$0.077 \pm 0.008 \pm 0.010$	239	FRABETTI	97c	E687 $\gamma Be, \bar{E}_\gamma \approx 200$ GeV
• • • We do not use the following data for averages, fits, limits, etc. • • •				
$0.09 \pm 0.01 \pm 0.01$	113	ANJOS	90D	E691 Photoproduction

$\Gamma(\bar{K}^*(892)^0 2\pi^+ \pi^-, \bar{K}^*(892)^0 \rightarrow K^- \pi^+)/\Gamma(K^- 3\pi^+ \pi^-)$				Γ_{78}/Γ_{77}
VALUE	EVTS	DOCUMENT ID	TECN	COMMENT
$0.21 \pm 0.04 \pm 0.06$		LINK	03D	FOCS $\gamma A, \bar{E}_\gamma \approx 180$ GeV

$\Gamma(\bar{K}^*(892)^0 \rho^0 \pi^+, \bar{K}^*(892)^0 \rightarrow K^- \pi^+)/\Gamma(K^- 2\pi^+)$				Γ_{79}/Γ_{51}
VALUE	EVTS	DOCUMENT ID	TECN	COMMENT
• • • We do not use the following data for averages, fits, limits, etc. • • •				
$0.016 \pm 0.007 \pm 0.004$		FRABETTI	97c	E687 $\gamma Be, \bar{E}_\gamma \approx 200$ GeV

$\Gamma(\bar{K}^*(892)^0 \rho^0 \pi^+, \bar{K}^*(892)^0 \rightarrow K^- \pi^+)/\Gamma(K^- 3\pi^+ \pi^-)$				Γ_{79}/Γ_{77}
VALUE	EVTS	DOCUMENT ID	TECN	COMMENT
$0.40 \pm 0.03 \pm 0.06$		LINK	03D	FOCS $\gamma A, \bar{E}_\gamma \approx 180$ GeV

$\Gamma(\bar{K}^*(892)^0 a_1(1260)^+)/\Gamma(K^- 2\pi^+)$				Γ_{80}/Γ_{51}
Unseen decay modes of the $\bar{K}^*(892)^0$ and $a_1(1260)^+$ are included.				
VALUE	EVTS	DOCUMENT ID	TECN	COMMENT
$0.099 \pm 0.008 \pm 0.018$		LINK	03D	FOCS $\gamma A, \bar{E}_\gamma \approx 180$ GeV

$\Gamma(\bar{K}^*(892)^0 2\pi^+ \pi^- \text{ non-}\rho, \bar{K}^*(892)^0 \rightarrow K^- \pi^+)/\Gamma(K^- 2\pi^+)$				Γ_{81}/Γ_{51}
VALUE	EVTS	DOCUMENT ID	TECN	COMMENT
• • • We do not use the following data for averages, fits, limits, etc. • • •				
$0.032 \pm 0.010 \pm 0.008$		FRABETTI	97c	E687 $\gamma Be, \bar{E}_\gamma \approx 200$ GeV

$\Gamma(K^- \rho^0 2\pi^+)/\Gamma(K^- 2\pi^+)$				Γ_{82}/Γ_{51}
VALUE	EVTS	DOCUMENT ID	TECN	COMMENT
• • • We do not use the following data for averages, fits, limits, etc. • • •				
$0.034 \pm 0.009 \pm 0.005$		FRABETTI	97c	E687 $\gamma Be, \bar{E}_\gamma \approx 200$ GeV

$\Gamma(K^- \rho^0 2\pi^+)/\Gamma(K^- 3\pi^+ \pi^-)$				Γ_{82}/Γ_{77}
VALUE	EVTS	DOCUMENT ID	TECN	COMMENT
$0.30 \pm 0.04 \pm 0.01$		LINK	03D	FOCS $\gamma A, \bar{E}_\gamma \approx 180$ GeV

$\Gamma(K^- 3\pi^+ \pi^- \text{ nonresonant})/\Gamma(K^- 3\pi^+ \pi^-)$				Γ_{83}/Γ_{77}
VALUE	CL%	DOCUMENT ID	TECN	COMMENT
$0.07 \pm 0.05 \pm 0.01$		LINK	03D	FOCS $\gamma A, \bar{E}_\gamma \approx 180$ GeV
• • • We do not use the following data for averages, fits, limits, etc. • • •				
<0.026	90	FRABETTI	97c	E687 $\gamma Be, \bar{E}_\gamma \approx 200$ GeV

$\Gamma(K^+ 2K_S^0)/\Gamma_{\text{total}}$				Γ_{84}/Γ
VALUE (units 10^{-4})	EVTS	DOCUMENT ID	TECN	COMMENT
$25.4 \pm 0.5 \pm 1.2$	3551	ABLIKIM	17A	BES3 $e^+ e^- \rightarrow \psi(3770)$

$\Gamma(K^+ 2K_S^0)/\Gamma(K^- 2\pi^+)$				Γ_{84}/Γ_{51}
VALUE	EVTS	DOCUMENT ID	TECN	COMMENT
• • • We do not use the following data for averages, fits, limits, etc. • • •				
$0.035 \pm 0.010 \pm 0.005$	39 ± 9	ALBRECHT	94i	ARG $e^+ e^- \approx 10$ GeV
0.085 ± 0.018	70 ± 12	AMMAR	91	CLEO $e^+ e^- \approx 10.5$ GeV

$\Gamma(\phi(1020)^0 K^+)/\Gamma_{\text{total}}$				Γ_{151}/Γ
VALUE	CL%	DOCUMENT ID	TECN	COMMENT
< 2.1×10^{-5}	90	ABLIKIM	19B1	BES3 $e^+ e^-$ at 3773 MeV

$\Gamma(K^+ K^- K_S^0 \pi^+)/\Gamma(K_S^0 2\pi^+ \pi^-)$				Γ_{85}/Γ_{74}
VALUE (units 10^{-3})	EVTS	DOCUMENT ID	TECN	COMMENT
$7.7 \pm 1.5 \pm 0.9$	35 ± 7	LINK	01c	FOCS γ nucleus, $\bar{E}_\gamma \approx 180$ GeV

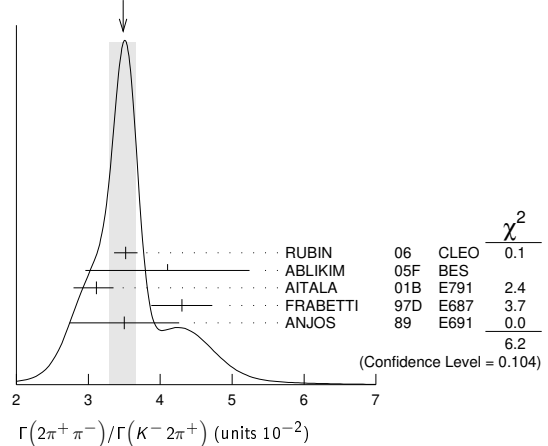
Pionic modes

$\Gamma(\pi^+ \pi^0)/\Gamma_{\text{total}}$				Γ_{86}/Γ
VALUE (units 10^{-3})	EVTS	DOCUMENT ID	TECN	COMMENT
1.247 ± 0.033 OUR FIT				
$1.259 \pm 0.033 \pm 0.023$	10k	ABLIKIM	18w	BES3 $e^+ e^-$, 3773 MeV

$\Gamma(\pi^+ \pi^0)/\Gamma(K^- 2\pi^+)$				Γ_{86}/Γ_{51}
VALUE (units 10^{-2})	EVTS	DOCUMENT ID	TECN	COMMENT
1.33 ± 0.04 OUR FIT		Error includes scale factor of 1.1.		
1.31 ± 0.06 OUR AVERAGE				
$1.29 \pm 0.04 \pm 0.05$	2649 ± 76	MENDEZ	10	CLEO $e^+ e^-$ at 3774 MeV
$1.33 \pm 0.11 \pm 0.09$	1229 ± 99	AUBERT,B	06F	BABR $e^+ e^- \approx \Upsilon(4S)$
$1.44 \pm 0.19 \pm 0.10$	171 ± 22	ARMS	04	CLEO $e^+ e^- \approx 10$ GeV
• • • We do not use the following data for averages, fits, limits, etc. • • •				
$1.33 \pm 0.07 \pm 0.06$	914 ± 46	RUBIN	06	CLEO See MENDEZ 10

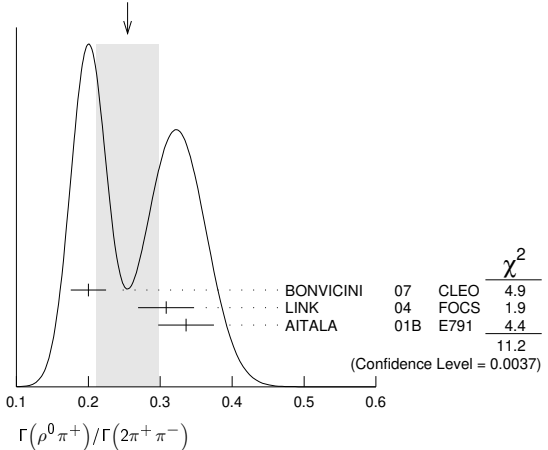
$\Gamma(2\pi^+ \pi^-)/\Gamma(K^- 2\pi^+)$				Γ_{87}/Γ_{51}
VALUE (units 10^{-2})	EVTS	DOCUMENT ID	TECN	COMMENT
3.48 ± 0.19 OUR AVERAGE		Error includes scale factor of 1.4. See the ideogram below.		
$3.52 \pm 0.11 \pm 0.12$	3303 ± 95	RUBIN	06	CLEO $e^+ e^-$ at $\psi(3770)$
$4.1 \pm 1.1 \pm 0.3$	85 ± 22	ABLIKIM	05F	BES $e^+ e^- \approx \psi(3770)$
$3.11 \pm 0.18 \pm 0.16$	1172	AITALA	01B	E791 π^- nucleus, 500 GeV
$4.3 \pm 0.3 \pm 0.3$	236	FRABETTI	97D	E687 $\gamma Be \approx 200$ GeV
$3.5 \pm 0.7 \pm 0.3$	83	ANJOS	89	E691 Photoproduction

WEIGHTED AVERAGE
3.48±0.19 (Error scaled by 1.4)



$\Gamma(\rho^0 \pi^+)/\Gamma(2\pi^+ \pi^-)$				Γ_{88}/Γ_{87}
This is the "fit fraction" from the Dalitz-plot analysis.				
VALUE	EVTS	DOCUMENT ID	TECN	COMMENT
0.25 ± 0.04 OUR AVERAGE		Error includes scale factor of 2.4. See the ideogram below.		
$0.200 \pm 0.023 \pm 0.009$		BONVICINI	07	CLEO Dalitz fit, ≈ 2240 evts
$0.3082 \pm 0.0314 \pm 0.0230$		LINK	04	FOCS Dalitz fit, 1527 ± 51 evts
$0.336 \pm 0.032 \pm 0.022$		AITALA	01B	E791 Dalitz fit, 1172 evts

WEIGHTED AVERAGE
0.25±0.04 (Error scaled by 2.4)



$\Gamma(\pi^+(\pi^+\pi^-)_{S\text{-wave}})/\Gamma(2\pi^+\pi^-)$ Γ_{89}/Γ_{87}
This is the "fit fraction" from the Dalitz-plot analysis. See also the next three data blocks.

VALUE	DOCUMENT ID	TECN	COMMENT
0.5600 ± 0.0324 ± 0.0214	1 LINK	04	FOCS Dalitz fit, 1527 ± 51 evts

¹ LINK 04 borrows a K-matrix parametrization from ANISOVICH 03 of the full $\pi\pi$ S-wave isoscalar scattering amplitude to describe the $\pi^+\pi^-$ S-wave component of the $\pi^+\pi^+\pi^-$ state. The fit fraction given above is a sum over five f_0 mesons, the $f_0(980)$, $f_0(1300)$, $f_0(1200-1600)$, $f_0(1500)$, and $f_0(1750)$. See LINK 04 for details and discussion.

$\Gamma(\sigma\pi^+, \sigma \rightarrow \pi^+\pi^-)/\Gamma(2\pi^+\pi^-)$ Γ_{90}/Γ_{87}
This is the "fit fraction" from the Dalitz-plot analysis.

VALUE	DOCUMENT ID	TECN	COMMENT
0.422 ± 0.027 OUR AVERAGE			
0.418 ± 0.014 ± 0.025	BONVICINI 07	CLEO	Dalitz fit, ≈ 2240 evts
0.463 ± 0.090 ± 0.021	AITALA 01B	E791	Dalitz fit, 1172 evts

$\Gamma(f_0(980)\pi^+, f_0(980) \rightarrow \pi^+\pi^-)/\Gamma(2\pi^+\pi^-)$ Γ_{91}/Γ_{87}
This is the "fit fraction" from the Dalitz-plot analysis.

VALUE	DOCUMENT ID	TECN	COMMENT
0.048 ± 0.010 OUR AVERAGE	Error includes scale factor of 1.3.		
0.041 ± 0.009 ± 0.003	BONVICINI 07	CLEO	Dalitz fit, ≈ 2240 evts
0.062 ± 0.013 ± 0.004	AITALA 01B	E791	Dalitz fit, 1172 evts

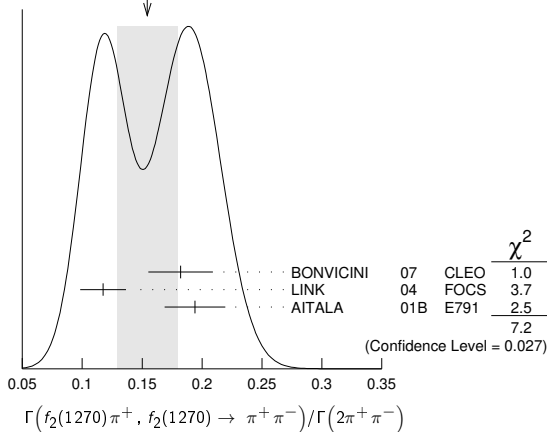
$\Gamma(f_0(1370)\pi^+, f_0(1370) \rightarrow \pi^+\pi^-)/\Gamma(2\pi^+\pi^-)$ Γ_{92}/Γ_{87}
This is the "fit fraction" from the Dalitz-plot analysis.

VALUE	DOCUMENT ID	TECN	COMMENT
0.024 ± 0.013 OUR AVERAGE			
0.026 ± 0.018 ± 0.006	BONVICINI 07	CLEO	Dalitz fit, ≈ 2240 evts
0.023 ± 0.015 ± 0.008	AITALA 01B	E791	Dalitz fit, 1172 evts

$\Gamma(f_2(1270)\pi^+, f_2(1270) \rightarrow \pi^+\pi^-)/\Gamma(2\pi^+\pi^-)$ Γ_{93}/Γ_{87}
This is the "fit fraction" from the Dalitz-plot analysis.

VALUE	DOCUMENT ID	TECN	COMMENT
0.154 ± 0.025 OUR AVERAGE	Error includes scale factor of 1.9. See the ideogram below.		
0.182 ± 0.026 ± 0.007	BONVICINI 07	CLEO	Dalitz fit, ≈ 2240 evts
0.1174 ± 0.0190 ± 0.0029	LINK 04	FOCS	Dalitz fit, 1527 ± 51 evts
0.194 ± 0.025 ± 0.004	AITALA 01B	E791	Dalitz fit, 1172 evts

WEIGHTED AVERAGE
0.154 ± 0.025 (Error scaled by 1.9)



$\Gamma(\rho(1450)^0\pi^+, \rho(1450)^0 \rightarrow \pi^+\pi^-)/\Gamma(2\pi^+\pi^-)$ Γ_{94}/Γ_{87}
This is the "fit fraction" from the Dalitz-plot analysis.

VALUE	CL%	DOCUMENT ID	TECN	COMMENT
<0.024	95	BONVICINI 07	CLEO	Dalitz fit, ≈ 2240 evts
0.007 ± 0.007 ± 0.003		AITALA 01B	E791	Dalitz fit, 1172 evts

$\Gamma(f_0(1500)\pi^+, f_0(1500) \rightarrow \pi^+\pi^-)/\Gamma(2\pi^+\pi^-)$ Γ_{95}/Γ_{87}
This is the "fit fraction" from the Dalitz-plot analysis.

VALUE	DOCUMENT ID	TECN	COMMENT
0.034 ± 0.010 ± 0.008	BONVICINI 07	CLEO	Dalitz fit, ≈ 2240 evts

$\Gamma(f_0(1710)\pi^+, f_0(1710) \rightarrow \pi^+\pi^-)/\Gamma(2\pi^+\pi^-)$ Γ_{96}/Γ_{87}
This is the "fit fraction" from the Dalitz-plot analysis.

VALUE	CL%	DOCUMENT ID	TECN	COMMENT
<0.016	95	BONVICINI 07	CLEO	Dalitz fit, ≈ 2240 evts

$\Gamma(f_0(1790)\pi^+, f_0(1790) \rightarrow \pi^+\pi^-)/\Gamma(2\pi^+\pi^-)$ Γ_{97}/Γ_{87}
This is the "fit fraction" from the Dalitz-plot analysis.

VALUE	CL%	DOCUMENT ID	TECN	COMMENT
<0.02	95	BONVICINI 07	CLEO	Dalitz fit, ≈ 2240 evts

$\Gamma((\pi^+\pi^+)_{S\text{-wave}}\pi^-)/\Gamma(2\pi^+\pi^-)$ Γ_{98}/Γ_{87}
This is the "fit fraction" from the Dalitz-plot analysis.

VALUE	CL%	DOCUMENT ID	TECN	COMMENT
<0.037	95	BONVICINI 07	CLEO	Dalitz fit, ≈ 2240 evts

$\Gamma(2\pi^+\pi^- \text{ nonresonant})/\Gamma(2\pi^+\pi^-)$ Γ_{99}/Γ_{87}
This is the "fit fraction" from the Dalitz-plot analysis.

VALUE	CL%	DOCUMENT ID	TECN	COMMENT
<0.035	95	BONVICINI 07	CLEO	Dalitz fit, ≈ 2240 evts
0.078 ± 0.060 ± 0.027		AITALA 01B	E791	Dalitz fit, 1172 evts

$\Gamma(\pi^+2\pi^0)/\Gamma(K^-2\pi^+)$ Γ_{100}/Γ_{51}
This is the "fit fraction" from the Dalitz-plot analysis.

VALUE (units 10^{-2})	EVTS	DOCUMENT ID	TECN	COMMENT
5.0 ± 0.3 ± 0.3	1535 ± 89	RUBIN 06	CLEO	e^+e^- at $\psi(3770)$

$\Gamma(2\pi^+\pi^-\pi^0)/\Gamma(K^-2\pi^+)$ Γ_{101}/Γ_{51}
This is the "fit fraction" from the Dalitz-plot analysis.

VALUE (units 10^{-2})	EVTS	DOCUMENT ID	TECN	COMMENT
12.4 ± 0.5 ± 0.6	5701 ± 205	RUBIN 06	CLEO	e^+e^- at $\psi(3770)$

$\Gamma(3\pi^+2\pi^-)/\Gamma(K^-2\pi^+)$ Γ_{102}/Γ_{51}
This is the "fit fraction" from the Dalitz-plot analysis.

VALUE (units 10^{-2})	EVTS	DOCUMENT ID	TECN	COMMENT
1.77 ± 0.17 OUR FIT				
1.73 ± 0.20 ± 0.17	732 ± 77	RUBIN 06	CLEO	e^+e^- at $\psi(3770)$
2.3 ± 0.4 ± 0.2	58	FRABETTI 97c	E687	$\gamma\text{Be}, \bar{E}_\gamma \approx 200 \text{ GeV}$

$\Gamma(3\pi^+2\pi^-)/\Gamma(K^-3\pi^+\pi^-)$ Γ_{102}/Γ_{77}
This is the "fit fraction" from the Dalitz-plot analysis.

VALUE	EVTS	DOCUMENT ID	TECN	COMMENT
0.289 ± 0.019 OUR FIT				
0.290 ± 0.017 ± 0.011	835	LINK 03D	FOCS	$\gamma A, \bar{E}_\gamma \approx 180 \text{ GeV}$

$\Gamma(\eta\pi^+)/\Gamma_{\text{total}}$ Γ_{103}/Γ
Unseen decay modes of the η are included.

VALUE (units 10^{-4})	EVTS	DOCUMENT ID	TECN	COMMENT
37.7 ± 0.9 OUR FIT				
37.90 ± 0.70 ± 0.68	12k	ABLIKIM 18w	BES3	e^+e^- , 3773 MeV
30.7 ± 2.2 ± 1.3	258	ABLIKIM 16D	BES3	e^+e^- at 3773 MeV
34.3 ± 1.4 ± 1.7	1033 ± 42	ARTUSO 08	CLEO	See MENDEZ 10

$\Gamma(\eta\pi^+)/\Gamma(K^-2\pi^+)$ Γ_{103}/Γ_{51}
Unseen decay modes of the η are included.

VALUE (units 10^{-2})	EVTS	DOCUMENT ID	TECN	COMMENT
4.02 ± 0.11 OUR FIT	Error includes scale factor of 1.1.			
3.87 ± 0.09 ± 0.19	2940 ± 68	MENDEZ 10	CLEO	e^+e^- at 3774 MeV
3.81 ± 0.26 ± 0.21	377 ± 26	RUBIN 06	CLEO	See ARTUSO 08

$\Gamma(\eta\pi^+\pi^0)/\Gamma_{\text{total}}$ Γ_{104}/Γ
Unseen decay modes of the η are included.

VALUE (units 10^{-4})	EVTS	DOCUMENT ID	TECN	COMMENT
20.5 ± 3.5 OUR AVERAGE	Error includes scale factor of 2.2.			
22.3 ± 1.5 ± 1.0	381	ABLIKIM 20G	BES3	e^+e^- , 3773 MeV
13.8 ± 3.1 ± 1.6	149 ± 34	ARTUSO 08	CLEO	e^+e^- at $\psi(3770)$
24.7 ± 9.3 ± 1.6	42	ABLIKIM 20AA	BES3	e^+e^- , 3773 MeV

$\Gamma(\eta2\pi^+\pi^-)/\Gamma_{\text{total}}$ Γ_{105}/Γ
Unseen decay modes of the η are included.

VALUE (units 10^{-3})	EVTS	DOCUMENT ID	TECN	COMMENT
3.41 ± 0.17 ± 0.10	515	ABLIKIM 20V	BES3	e^+e^- , 3773 MeV

$\Gamma(\eta\pi^+2\pi^0)/\Gamma_{\text{total}}$ Γ_{106}/Γ
Unseen decay modes of the η are included.

VALUE (units 10^{-3})	EVTS	DOCUMENT ID	TECN	COMMENT
3.20 ± 0.28 ± 0.17	190	ABLIKIM 20V	BES3	e^+e^- , 3773 MeV

$\Gamma(\eta\eta\pi^+)/\Gamma_{\text{total}}$ Γ_{107}/Γ
Unseen decay modes of the η are included.

VALUE (units 10^{-4})	EVTS	DOCUMENT ID	TECN	COMMENT
29.6 ± 2.4 ± 1.0	179	ABLIKIM 20G	BES3	e^+e^- , 3773 MeV

$\Gamma(\omega\pi^+)/\Gamma_{\text{total}}$ Γ_{108}/Γ
Unseen decay modes of the ω are included.

VALUE (units 10^{-4})	CL%	EVTS	DOCUMENT ID	TECN	COMMENT
2.79 ± 0.57 ± 0.16		79	ABLIKIM 16D	BES3	e^+e^- at 3773 MeV
<3.4	90		RUBIN 06	CLEO	e^+e^- at $\psi(3770)$

$\Gamma(\omega\pi^+\pi^0)/\Gamma_{\text{total}}$ Γ_{109}/Γ
Unseen decay modes of the ω are included.

VALUE (units 10^{-3})	EVTS	DOCUMENT ID	TECN	COMMENT
3.87 ± 0.83 ± 0.25	233	¹ ABLIKIM 20AA	BES3	e^+e^- , 3773 MeV

¹ ABLIKIM 20AA reports a statistical significance of 7.7 σ for this measurement.

Meson Particle Listings

D^\pm

$\Gamma(\eta'(958)\pi^+)/\Gamma_{total}$ Γ_{110}/Γ
 Unseen decay modes of the $\eta'(958)$ are included.

VALUE (units 10^{-4})	EVTS	DOCUMENT ID	TECN	COMMENT
49.7 ± 1.9 OUR FIT				
51.2 ± 1.4 ± 2.1	3.1k	ABLIKIM	18w BES3	e^+e^- , 3773 MeV
• • • We do not use the following data for averages, fits, limits, etc. • • •				
44.2 ± 2.5 ± 2.9	352 ± 20	ARTUSO	08 CLEO	See MENDEZ 10

$\Gamma(\eta'(958)\pi^+)/\Gamma(K^-2\pi^+)$ Γ_{110}/Γ_{51}
 Unseen decay modes of the $\eta'(958)$ are included.

VALUE (units 10^{-2})	EVTS	DOCUMENT ID	TECN	COMMENT
5.30 ± 0.21 OUR FIT				
5.12 ± 0.17 ± 0.25	1037 ± 35	MENDEZ	10 CLEO	e^+e^- at 3774 MeV

$\Gamma(\eta'(958)\pi^+\pi^0)/\Gamma_{total}$ Γ_{111}/Γ
 Unseen decay modes of the $\eta'(958)$ are included.

VALUE (units 10^{-4})	EVTS	DOCUMENT ID	TECN	COMMENT
15.7 ± 4.3 ± 2.5	33 ± 9	ARTUSO	08 CLEO	e^+e^- at $\psi(3770)$

Hadronic modes with a $K\bar{K}$ pair

$\Gamma(K_S^0 K^+)/\Gamma_{total}$ Γ_{112}/Γ

VALUE (units 10^{-3})	EVTS	DOCUMENT ID	TECN	COMMENT
3.04 ± 0.09 OUR FIT				Error includes scale factor of 2.2.
3.183 ± 0.029 ± 0.060	18k	ABLIKIM	18w BES3	e^+e^- , 3773 MeV
• • • We do not use the following data for averages, fits, limits, etc. • • •				
3.02 ± 0.09 ± 0.08	780	ABLIKIM	19m BES3	See ABLIKIM 18w.
3.14 ± 0.09 ± 0.08	1971 ± 51	BONVICINI	08 CLEO	See MENDEZ 10

$\Gamma(K_S^0 K^+)/\Gamma(K_S^0 \pi^+)$ Γ_{112}/Γ_{49}

VALUE	EVTS	DOCUMENT ID	TECN	COMMENT
0.194 ± 0.006 OUR FIT				Error includes scale factor of 2.8.
0.1901 ± 0.0024 OUR AVERAGE				
0.1899 ± 0.0011 ± 0.0022	101k ± 561	WON	09 BELL	e^+e^- at $\Upsilon(4S)$
0.1892 ± 0.0155 ± 0.0073	278 ± 21	ARMS	04 CLEO	$e^+e^- \approx 10$ GeV
0.1996 ± 0.0119 ± 0.0096	949	LINK	02b FOCS	$\gamma A, \bar{E}_\gamma \approx 180$ GeV
• • • We do not use the following data for averages, fits, limits, etc. • • •				
0.222 ± 0.037 ± 0.013	63 ± 10	ABLIKIM	05f BES	$e^+e^- \approx \psi(3770)$
0.222 ± 0.041 ± 0.019	70	BISHAI	97 CLEO	See ARMS 04
0.25 ± 0.04 ± 0.02	129	FRABETTI	95 E687	$\gamma Be, \bar{E}_\gamma \approx 200$ GeV
0.271 ± 0.065 ± 0.039	69	ANJOS	90c E691	γBe
0.317 ± 0.086 ± 0.048	31	BALTRUSAIT...85E	MRK3	e^+e^- 3.77 GeV
0.25 ± 0.15	6	SCHINDLER	81 MRK2	e^+e^- 3.771 GeV

$\Gamma(K_S^0 K^+)/\Gamma(K^-2\pi^+)$ Γ_{112}/Γ_{51}

VALUE (units 10^{-2})	EVTS	DOCUMENT ID	TECN	COMMENT
3.24 ± 0.09 OUR FIT				Error includes scale factor of 2.3.
3.35 ± 0.06 ± 0.07	5161 ± 86	MENDEZ	10 CLEO	e^+e^- at 3774 MeV
• • • We do not use the following data for averages, fits, limits, etc. • • •				
3.02 ± 0.18 ± 0.15	949	¹ LINK	02b FOCS	γ nucleus, $\bar{E}_\gamma \approx 180$ GeV
¹ This LINK 02b result is redundant with a result in the previous datablock.				

$\Gamma(K_S^0 K^+)/\Gamma_{total}$ Γ_{113}/Γ

VALUE (units 10^{-3})	EVTS	DOCUMENT ID	TECN	COMMENT
3.21 ± 0.11 ± 0.11	650	ABLIKIM	19m BES3	e^+e^- at 3773 MeV

$\Gamma(K_S^0 K^+\pi^0)/\Gamma_{total}$ Γ_{114}/Γ

VALUE (units 10^{-3})	EVTS	DOCUMENT ID	TECN	COMMENT
5.07 ± 0.19 ± 0.23	470	ABLIKIM	19m BES3	e^+e^- at 3773 MeV

$\Gamma(K^*(892)^+ K_S^0)/\Gamma(K_S^0 \pi^+)$ Γ_{115}/Γ_{49}
 Unseen decay modes of the $K^*(892)^+$ are included.

VALUE	EVTS	DOCUMENT ID	TECN	COMMENT
1.1 ± 0.3 ± 0.4	67	FRABETTI	95 E687	$\gamma Be, \bar{E}_\gamma \approx 200$ GeV

$\Gamma(K^*(892)^+ K_S^0)/\Gamma(K_S^0 K^+\pi^0)$ $\Gamma_{115}/\Gamma_{114}$

VALUE	EVTS	DOCUMENT ID	TECN	COMMENT
0.571 ± 0.026 ± 0.042	692	¹ ABLIKIM	21AD BES3	e^+e^- at 3.773 GeV

¹ ABLIKIM 21AD value is a fit fraction from an amplitude analysis of $D^+ \rightarrow K^+ K_S^0 \pi^0$ with four components. Reconstructs the $K^*(892)^+$ from its $K^+\pi^0$ final state.

$\Gamma(\bar{K}^*(892)^0 K^+)/\Gamma(K_S^0 K^+\pi^0)$ $\Gamma_{116}/\Gamma_{114}$

VALUE	EVTS	DOCUMENT ID	TECN	COMMENT
0.102 ± 0.015 ± 0.022	692	¹ ABLIKIM	21AD BES3	e^+e^- at 3.773 GeV

¹ ABLIKIM 21AD value is a fit fraction from an amplitude analysis of $D^+ \rightarrow K^+ K_S^0 \pi^0$ with four components. Reconstructs the $\bar{K}^*(892)^0$ from its $K_S^0 \pi^0$ final state.

$\Gamma(K_S^0 K^+\pi^0)/\Gamma_{total}$ Γ_{117}/Γ

VALUE (units 10^{-3})	EVTS	DOCUMENT ID	TECN	COMMENT
5.24 ± 0.22 ± 0.22	410	ABLIKIM	19m BES3	e^+e^- at 3773 MeV

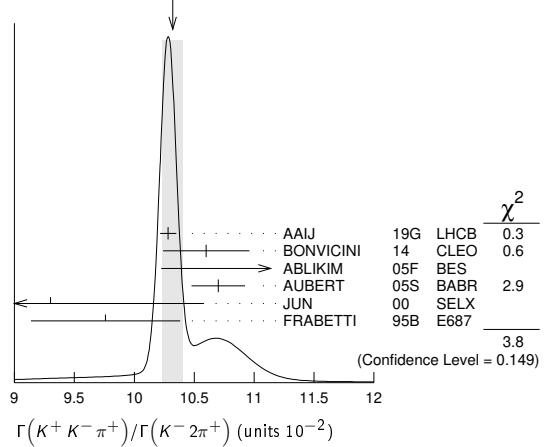
$\Gamma(K^+ K^- \pi^+)/\Gamma_{total}$ Γ_{118}/Γ

VALUE (units 10^{-2})	EVTS	DOCUMENT ID	TECN	COMMENT
• • • We do not use the following data for averages, fits, limits, etc. • • •				
0.935 ± 0.017 ± 0.024		¹ DOBBS	07 CLEO	See BONVICINI 14
0.97 ± 0.04 ± 0.04	1250 ± 40	¹ HE	05 CLEO	See DOBBS 07
¹ DOBBS 07 and HE 05 use single- and double-tagged events in an overall fit. DOBBS 07 supersedes HE 05.				

$\Gamma(K^+ K^- \pi^+)/\Gamma(K^-2\pi^+)$ Γ_{118}/Γ_{51}

VALUE (units 10^{-2})	EVTS	DOCUMENT ID	TECN	COMMENT
10.32 ± 0.09 OUR AVERAGE				Error includes scale factor of 1.4. See the ideogram below.
10.282 ± 0.002 ± 0.068	23M	AAIJ	19g LHCb	pp at 8 TeV
10.6 ± 0.2 ± 0.3		BONVICINI	14 CLEO	All CLEO-c runs
11.7 ± 1.3 ± 0.7	181 ± 20	ABLIKIM	05f BES	$e^+e^- \approx \psi(3770)$
10.7 ± 0.1 ± 0.2	43k	AUBERT	05s BABR	$e^+e^- \approx \Upsilon(4S)$
9.3 ± 1.0 ± 0.8		JUN	00 SELX	Σ^- nucleus, 600 GeV
9.76 ± 0.42 ± 0.46		FRABETTI	95b E687	$\gamma Be, \bar{E}_\gamma \approx 200$ GeV

WEIGHTED AVERAGE
 10.32 ± 0.09 (Error scaled by 1.4)



$\Gamma(K^+ K^- \pi^+\pi^0)/\Gamma_{total}$ Γ_{127}/Γ

VALUE (units 10^{-3})	EVTS	DOCUMENT ID	TECN	COMMENT
6.62 ± 0.20 ± 0.25	1.3k	ABLIKIM	20Ac BES3	e^+e^- at 3.773 GeV

$\Gamma(\phi\pi^+)/\Gamma_{total}$ Γ_{126}/Γ

VALUE (units 10^{-3})	EVTS	DOCUMENT ID	TECN	COMMENT
5.70 ± 0.05 ± 0.13	18k	ABLIKIM	19b1 BES3	e^+e^- at 3773 MeV

$\Gamma(\phi\pi^+, \phi \rightarrow K^+ K^-)/\Gamma(K^+ K^- \pi^+)$ $\Gamma_{125}/\Gamma_{118}$
 This is the "fit fraction" from the Dalitz-plot analysis.

VALUE (%)	DOCUMENT ID	TECN	COMMENT
27.8 ± 0.4 ± 0.2	RUBIN	08 CLEO	Dalitz fit, 19,458 ± 163 evts
• • • We do not use the following data for averages, fits, limits, etc. • • •			
29.2 ± 3.1 ± 3.0	FRABETTI	95b E687	Dalitz fit, 915 evts

$\Gamma(K^+ \bar{K}^*(892)^0, \bar{K}^*(892)^0 \rightarrow K^- \pi^+)/\Gamma(K^+ K^- \pi^+)$ $\Gamma_{119}/\Gamma_{118}$
 This is the "fit fraction" from the Dalitz-plot analysis.

VALUE (%)	DOCUMENT ID	TECN	COMMENT
25.7 ± 0.5 ± 0.4	RUBIN	08 CLEO	Dalitz fit, 19,458 ± 163 evts
• • • We do not use the following data for averages, fits, limits, etc. • • •			
30.1 ± 2.0 ± 2.5	FRABETTI	95b E687	Dalitz fit, 915 evts

$\Gamma(K^+ \bar{K}_0^*(1430)^0, \bar{K}_0^*(1430)^0 \rightarrow K^- \pi^+)/\Gamma(K^+ K^- \pi^+)$ $\Gamma_{120}/\Gamma_{118}$
 This is the "fit fraction" from the Dalitz-plot analysis.

VALUE (%)	DOCUMENT ID	TECN	COMMENT
18.8 ± 1.2 ± 3.3	RUBIN	08 CLEO	Dalitz fit, 19,458 ± 163 evts
• • • We do not use the following data for averages, fits, limits, etc. • • •			
37.0 ± 3.5 ± 1.8	FRABETTI	95b E687	Dalitz fit, 915 evts

$\Gamma(K^+ \bar{K}_2^*(1430)^0, \bar{K}_2^*(1430)^0 \rightarrow K^- \pi^+)/\Gamma(K^+ K^- \pi^+)$ $\Gamma_{121}/\Gamma_{118}$
 This is the "fit fraction" from the Dalitz-plot analysis.

VALUE (%)	DOCUMENT ID	TECN	COMMENT
1.7 ± 0.4 ± 1.2	RUBIN	08 CLEO	Dalitz fit, 19,458 ± 163 evts

$\Gamma(K^+ \bar{K}_S^0(700), \bar{K}_S^0 \rightarrow K^- \pi^+)/\Gamma(K^+ K^- \pi^+)$ $\Gamma_{122}/\Gamma_{118}$
 This is the "fit fraction" from the Dalitz-plot analysis.
 VALUE (%) DOCUMENT ID TECN COMMENT
7.0 ± 0.8^{+3.5}_{-2.0} RUBIN 08 CLEO Dalitz fit, 19,458 ± 163 evts

$\Gamma(a_0(1450)^0 \pi^+, a_0^0 \rightarrow K^+ K^-)/\Gamma(K^+ K^- \pi^+)$ $\Gamma_{123}/\Gamma_{118}$
 This is the "fit fraction" from the Dalitz-plot analysis.
 VALUE (%) DOCUMENT ID TECN COMMENT
4.6 ± 0.6^{+7.2}_{-1.8} RUBIN 08 CLEO Dalitz fit, 19,458 ± 163 evts

$\Gamma(\phi(1680) \pi^+, \phi \rightarrow K^+ K^-)/\Gamma(K^+ K^- \pi^+)$ $\Gamma_{124}/\Gamma_{118}$
 This is the "fit fraction" from the Dalitz-plot analysis.
 VALUE (%) DOCUMENT ID TECN COMMENT
0.51 ± 0.11^{+0.37}_{-0.16} RUBIN 08 CLEO Dalitz fit, 19,458 ± 163 evts

$\Gamma(K_S^0 K_S^0 \pi^+)/\Gamma_{total}$ Γ_{128}/Γ
 VALUE (units 10⁻⁴) EVTS DOCUMENT ID TECN COMMENT
27.0 ± 0.5 ± 1.2 4897 ABLIKIM 17A BES3 e⁺e⁻ → ψ(3770)

$\Gamma(K_S^0 K_S^0 \pi^+ \pi^0)/\Gamma_{total}$ Γ_{129}/Γ
 VALUE (units 10⁻³) EVTS DOCUMENT ID TECN COMMENT
1.34 ± 0.20 ± 0.06 80 ABLIKIM 20Ac BES3 e⁺e⁻ at 3.773 GeV

$\Gamma(K_S^0 K^+ \eta)/\Gamma_{total}$ Γ_{130}/Γ
 VALUE (units 10⁻⁴) EVTS DOCUMENT ID TECN COMMENT
1.85 ± 0.52 ± 0.08 14 ABLIKIM 20V BES3 e⁺e⁻, 3773 MeV

$\Gamma(K^+ K_S^0 \pi^+ \pi^-)/\Gamma(K_S^0 2\pi^+ \pi^-)$ Γ_{131}/Γ_{74}
 VALUE (units 10⁻²) EVTS DOCUMENT ID TECN COMMENT
5.62 ± 0.39 ± 0.40 469 ± 32 LINK 01c FOCS γ nucleus, $\bar{E}_\gamma \approx 180$ GeV

$\Gamma(K^+ K_S^0 \pi^+ \pi^-)/\Gamma_{total}$ Γ_{131}/Γ
 VALUE (units 10⁻³) EVTS DOCUMENT ID TECN COMMENT
1.89 ± 0.12 ± 0.05 277 ABLIKIM 20Ac BES3 e⁺e⁻ at 3.773 GeV

$\Gamma(K_S^0 K^+ \pi^0 \pi^0)/\Gamma_{total}$ Γ_{132}/Γ
 VALUE (units 10⁻⁴) EVTS DOCUMENT ID TECN COMMENT
5.8 ± 1.2 ± 0.4 34 ABLIKIM 20Ac BES3 e⁺e⁻ at 3.773 GeV

$\Gamma(K_S^0 K^- 2\pi^+)/\Gamma_{total}$ Γ_{133}/Γ
 VALUE (units 10⁻³) EVTS DOCUMENT ID TECN COMMENT
2.27 ± 0.12 ± 0.06 467 ABLIKIM 20Ac BES3 e⁺e⁻ at 3.773 GeV

$\Gamma(K_S^0 K^- 2\pi^+)/\Gamma(K_S^0 2\pi^+ \pi^-)$ Γ_{133}/Γ_{74}
 VALUE (units 10⁻²) EVTS DOCUMENT ID TECN COMMENT
7.68 ± 0.41 ± 0.32 670 ± 35 LINK 01c FOCS γ nucleus, $\bar{E}_\gamma \approx 180$ GeV

$\Gamma(K^+ K^- 2\pi^+ \pi^-)/\Gamma(K^- 3\pi^+ \pi^-)$ Γ_{134}/Γ_{77}
 VALUE EVTS DOCUMENT ID TECN COMMENT
0.040 ± 0.009 ± 0.019 38 LINK 03d FOCS γ A, $\bar{E}_\gamma \approx 180$ GeV

$\Gamma(\phi \pi^+ \pi^0)/\Gamma_{total}$ Γ_{135}/Γ
 Unseen decay modes of the φ are included.
 VALUE DOCUMENT ID TECN COMMENT
0.023 ± 0.010 ¹BARLAG 92c ACCM π⁻ Cu 230 GeV
¹BARLAG 92c computes the branching fraction using topological normalization.

$\Gamma(\phi \rho^+)/\Gamma(K^- 2\pi^+)$ Γ_{136}/Γ_{51}
 Unseen decay modes of the φ are included.
 VALUE CL% DOCUMENT ID TECN COMMENT
<0.16 90 DAUDI 92 CLEO e⁺e⁻ ≈ 10.5 GeV

$\Gamma(K^+ K^- \pi^+ \pi^0 \text{ non-}\phi)/\Gamma_{total}$ Γ_{137}/Γ
 VALUE DOCUMENT ID TECN COMMENT
0.015 ± 0.007_{-0.006} ¹BARLAG 92c ACCM π⁻ Cu 230 GeV
¹BARLAG 92c computes the branching fraction using topological normalization.

$\Gamma(K^+ K^- \pi^+ \pi^0 \text{ non-}\phi)/\Gamma(K^- 2\pi^+)$ Γ_{137}/Γ_{51}
 VALUE CL% DOCUMENT ID TECN COMMENT
 • • • We do not use the following data for averages, fits, limits, etc. • • •
<0.25 90 ANJOS 89E E691 Photoproduction

Doubly Cabibbo-suppressed modes

$\Gamma(K^+ \pi^0)/\Gamma_{total}$ Γ_{138}/Γ
 VALUE (units 10⁻⁴) EVTS DOCUMENT ID TECN COMMENT
2.08 ± 0.21 OUR FIT Error includes scale factor of 1.4.
2.35 ± 0.20 OUR AVERAGE
 2.32 ± 0.21 ± 0.06 1.8k ABLIKIM 18w BES3 e⁺e⁻, 3773 MeV
 2.52 ± 0.47 ± 0.26 189 ± 37 AUBERT,B 06F BABR e⁺e⁻ ≈ γ(4S)
 • • • We do not use the following data for averages, fits, limits, etc. • • •
 2.28 ± 0.36 ± 0.17 148 ± 23 DYTMAN 06 CLEO See MENDEZ 10

$\Gamma(K^+ \pi^0)/\Gamma(K^- 2\pi^+)$ Γ_{138}/Γ_{51}
 VALUE (units 10⁻³) EVTS DOCUMENT ID TECN COMMENT
2.21 ± 0.23 OUR FIT Error includes scale factor of 1.5.
1.9 ± 0.2 ± 0.1 343 ± 37 MENDEZ 10 CLEO e⁺e⁻ at 3774 MeV

$\Gamma(K^+ \eta)/\Gamma_{total}$ Γ_{139}/Γ
 VALUE (units 10⁻³) EVTS DOCUMENT ID TECN COMMENT
0.125 ± 0.016 OUR FIT Error includes scale factor of 1.
0.151 ± 0.025 ± 0.014 439 ABLIKIM 18w BES3 e⁺e⁻, 3773 MeV

$\Gamma(K^+ \eta)/\Gamma(\eta \pi^+)$ $\Gamma_{139}/\Gamma_{103}$
 VALUE (%) EVTS DOCUMENT ID TECN COMMENT
3.3 ± 0.4 OUR FIT Error includes scale factor of 1.
3.06 ± 0.43 ± 0.14 166 ± 23 WON 11 BELL e⁺e⁻ ≈ γ(4S)

$\Gamma(K^+ \eta'(958))/\Gamma_{total}$ Γ_{140}/Γ
 VALUE (units 10⁻³) EVTS DOCUMENT ID TECN COMMENT
0.185 ± 0.020 OUR FIT
0.164 ± 0.051 ± 0.024 87 ABLIKIM 18w BES3 e⁺e⁻, 3773 MeV

$\Gamma(K^+ \eta'(958))/\Gamma(\eta'(958) \pi^+)$ $\Gamma_{140}/\Gamma_{110}$
 VALUE (%) EVTS DOCUMENT ID TECN COMMENT
3.7 ± 0.4 OUR FIT
3.77 ± 0.39 ± 0.10 180 ± 19 WON 11 BELL e⁺e⁻ ≈ γ(4S)

$\Gamma(K^+ \pi^+ \pi^-)/\Gamma(K^- 2\pi^+)$ Γ_{141}/Γ_{51}
 VALUE (units 10⁻³) EVTS DOCUMENT ID TECN COMMENT
5.238 ± 0.025 OUR AVERAGE
 5.231 ± 0.009 ± 0.023 795k AAIJ 19G LHCB pp at 8 TeV
 5.69 ± 0.18 ± 0.14 2638 ± 84 KO 09 BELL e⁺e⁻ at γ(4S)
 6.5 ± 0.8 ± 0.4 189 ± 24 LINK 04F FOCS γ A, $\bar{E}_\gamma \approx 180$ GeV
 7.7 ± 1.7 ± 0.8 59 ± 13 AITALA 97c E791 π⁻ A, 500 GeV
 7.2 ± 2.3 ± 1.7 21 FRABETTI 95E E687 γBe, $\bar{E}_\gamma = 220$ GeV

$\Gamma(K^+ \rho^0)/\Gamma(K^+ \pi^+ \pi^-)$ $\Gamma_{142}/\Gamma_{141}$
 This is the "fit fraction" from the Dalitz-plot analysis.
 VALUE DOCUMENT ID TECN COMMENT
0.39 ± 0.09 OUR AVERAGE
 0.3943 ± 0.0787 ± 0.0815 LINK 04F FOCS Dalitz fit, 189 evts
 0.37 ± 0.14 ± 0.07 AITALA 97c E791 Dalitz fit, 59 evts

$\Gamma(K^*(892)^0 \pi^+, K^*(892)^0 \rightarrow K^+ \pi^-)/\Gamma(K^+ \pi^+ \pi^-)$ $\Gamma_{143}/\Gamma_{141}$
 This is the "fit fraction" from the Dalitz-plot analysis.
 VALUE DOCUMENT ID TECN COMMENT
0.47 ± 0.08 OUR AVERAGE
 0.5220 ± 0.0684 ± 0.0638 LINK 04F FOCS Dalitz fit, 189 evts
 0.35 ± 0.14 ± 0.01 AITALA 97c E791 Dalitz fit, 59 evts

$\Gamma(K^+ f_0(980), f_0(980) \rightarrow \pi^+ \pi^-)/\Gamma(K^+ \pi^+ \pi^-)$ $\Gamma_{144}/\Gamma_{141}$
 This is the "fit fraction" from the Dalitz-plot analysis.
 VALUE DOCUMENT ID TECN COMMENT
0.0892 ± 0.0333 ± 0.0412 LINK 04F FOCS Dalitz fit, 189 evts

$\Gamma(K_S^2(1430)^0 \pi^+, K_S^2(1430)^0 \rightarrow K^+ \pi^-)/\Gamma(K^+ \pi^+ \pi^-)$ $\Gamma_{145}/\Gamma_{141}$
 This is the "fit fraction" from the Dalitz-plot analysis.
 VALUE DOCUMENT ID TECN COMMENT
0.0803 ± 0.0372 ± 0.0391 LINK 04F FOCS Dalitz fit, 189 evts

$\Gamma(K^+ \pi^+ \pi^- \text{ nonresonant})/\Gamma(K^+ \pi^+ \pi^-)$ $\Gamma_{146}/\Gamma_{141}$
 This is the "fit fraction" from the Dalitz-plot analysis.
 VALUE DOCUMENT ID TECN COMMENT
 • • • We do not use the following data for averages, fits, limits, etc. • • •
0.36 ± 0.14 ± 0.07 ¹AITALA 97c E791 Dalitz fit, 59 evts
¹LINK 04F, with three times as many events, finds no need for a nonresonant amplitude.

$\Gamma(K^+ \pi^+ \pi^- \pi^0)/\Gamma_{total}$ Γ_{147}/Γ
 VALUE (units 10⁻³) EVTS DOCUMENT ID TECN COMMENT
1.21 ± 0.08 ± 0.03 350 ¹ABLIKIM 20z BES3 e⁺e⁻ at 3773 MeV
¹ABLIKIM 20z subtracted the known branching fractions of $D^+ \rightarrow K^+ \eta, D^+ \rightarrow K^+ \phi$, and $D^+ \rightarrow K^+ \omega$ to obtain an estimate of the non-resonant component (ignoring interference effects and possible additional resonant contributions) $B(D^+ \rightarrow K^+ \pi^+ \pi^- \pi^0 \text{ non-resonant}) = (1.13 \pm 0.08 \pm 0.03) \times 10^{-3}$.

$\Gamma(K^+ \pi^+ \pi^- \pi^0 \text{ nonresonant})/\Gamma_{total}$ Γ_{148}/Γ
 VALUE (units 10⁻³) EVTS DOCUMENT ID TECN COMMENT
1.10 ± 0.07 OUR AVERAGE
 1.03 ± 0.12 ± 0.06 112 ¹ABLIKIM 21Bb BES3 e⁺e⁻ at 3.773 GeV
 1.13 ± 0.08 ± 0.03 350 ²ABLIKIM 20z BES3 e⁺e⁻ at 3.773 GeV
¹ABLIKIM 21Bb result has subtracted the known branching fractions of $D^+ \rightarrow K^+ \eta, D^+ \rightarrow K^+ \phi$, and $D^+ \rightarrow K^+ \omega$ resonances (ignoring interference effects). The result including these components is measured to be $B(D^+ \rightarrow K^+ \pi^+ \pi^- \pi^0) = (1.11 \pm 0.12) \times 10^{-3}$, where the uncertainty is statistical only.
²ABLIKIM 20z result has subtracted the known branching fractions of $D^+ \rightarrow K^+ \eta, D^+ \rightarrow K^+ \phi$, and $D^+ \rightarrow K^+ \omega$, ignoring interference effects. The result including these components is measured to be $(1.21 \pm 0.08 \pm 0.03) \times 10^{-3}$.

Meson Particle Listings

D^\pm

$\Gamma(K^+\omega)/\Gamma_{\text{total}}$		Γ_{149}/Γ		
VALUE (units 10^{-5})	EVTS	DOCUMENT ID	TECN	COMMENT
$5.7^{+2.5}_{-2.1} \pm 0.2$	9	ABLIKIM	20z BES3	e^+e^- , 3773 MeV

$\Gamma(2K^+K^-)/\Gamma(K^-2\pi^+)$		Γ_{150}/Γ_{51}		
VALUE (units 10^{-4})	EVTS	DOCUMENT ID	TECN	COMMENT
6.54 ± 0.05 OUR AVERAGE				
6.541 ± 0.025 ± 0.042	134k	AAIJ	19g LHCb	pp at 8 TeV
9.49 ± 2.17 ± 0.22	65	¹ LINK	02i FOCUS	γ nucleus, ≈ 180 GeV

¹LINK 02i finds little evidence for ϕK^+ or $f_0(980) K^+$ submodes.

$\Gamma(K^+\phi(1020), \phi \rightarrow K^+K^-)/\Gamma(2K^+K^-)$		$\Gamma_{152}/\Gamma_{150}$		
VALUE (%)		DOCUMENT ID	TECN	COMMENT
7.1 ± 0.9		¹ AAIJ	19h LHCb	pp at 8TeV

¹Fit fraction from a Dalitz plot analysis of $D^+ \rightarrow K^+K^+K^-$ decays. The last uncertainty is due to the amplitude model.

$\Gamma(K^+(K^+K^-)_{s\text{-wave}})/\Gamma(2K^+K^-)$		$\Gamma_{153}/\Gamma_{150}$		
VALUE		DOCUMENT ID	TECN	COMMENT
0.94 ± 0.01		¹ AAIJ	19h LHCb	pp at 8TeV

¹Fit fraction from a Dalitz plot analysis of $D^+ \rightarrow K^+K^+K^-$ decays. The last uncertainty is due to the amplitude model.

————— Rare or forbidden modes —————

$\Gamma(\pi^+e^+e^-)/\Gamma_{\text{total}}$		Γ_{154}/Γ		
VALUE	CL%	DOCUMENT ID	TECN	COMMENT
<1.1 × 10⁻⁶	90	LEES	11g BABR	$e^+e^- \approx \Upsilon(4S)$

- • • We do not use the following data for averages, fits, limits, etc. • • •
- <1.6 × 10⁻⁶ 90 AAIJ 21T LHCb 1.6 fb⁻¹ pp
- <5.9 × 10⁻⁶ 90 ¹RUBIN 10 CLEO e^+e^- at $\psi(3770)$
- <7.4 × 10⁻⁶ 90 HE 05A CLEO See RUBIN 10
- <5.2 × 10⁻⁵ 90 AITALA 99G E791 $\pi^- N$ 500 GeV
- <1.1 × 10⁻⁴ 90 FRABETTI 97B E687 γ Be, $\overline{E}_\gamma \approx 220$ GeV
- <6.6 × 10⁻⁵ 90 AITALA 96 E791 $\pi^- N$ 500 GeV
- <2.5 × 10⁻³ 90 WEIR 90B MRK2 e^+e^- 29 GeV
- <2.6 × 10⁻³ 90 HAAS 88 CLEO e^+e^- 10 GeV

¹This RUBIN 10 limit is for the e^+e^- mass in the continuum away from the $\phi(1020)$. See the next data block.

$\Gamma(\pi^+\pi^0e^+e^-)/\Gamma_{\text{total}}$		Γ_{155}/Γ		
VALUE	CL%	DOCUMENT ID	TECN	COMMENT
<1.4 × 10⁻⁵	90	ABLIKIM	18p BES3	e^+e^- , 3773 MeV

$\Gamma(\pi^+\phi, \phi \rightarrow e^+e^-)/\Gamma_{\text{total}}$		Γ_{156}/Γ		
VALUE	EVTS	DOCUMENT ID	TECN	COMMENT
(1.7^{+1.4}_{-0.9} ± 0.1) × 10⁻⁶	4	¹ RUBIN	10 CLEO	e^+e^- at $\psi(3770)$

- • • We do not use the following data for averages, fits, limits, etc. • • •
- (2.7^{+3.6}_{-1.8} ± 0.2) × 10⁻⁶ 2 HE 05A CLEO See RUBIN 10

¹This RUBIN 10 result is consistent with the known $D^+ \rightarrow \phi\pi^+$ and $\phi \rightarrow e^+e^-$ fractions.

$\Gamma(\pi^+\mu^+\mu^-)/\Gamma_{\text{total}}$		Γ_{157}/Γ		
VALUE	CL%	DOCUMENT ID	TECN	COMMENT
<6.7 × 10⁻⁸	90	AAIJ	21T LHCb	1.6 fb ⁻¹ pp

- • • We do not use the following data for averages, fits, limits, etc. • • •
- <7.3 × 10⁻⁸ 90 AAIJ 13Af LHCb pp at 7 TeV
- <6.5 × 10⁻⁶ 90 LEES 11g BABR $e^+e^- \approx \Upsilon(4S)$
- <3.9 × 10⁻⁶ 90 ¹ABAZOV 08D D0 $p\overline{p}$, $E_{\text{cm}} = 1.96$ TeV
- <8.8 × 10⁻⁶ 90 LINK 03F FOCUS γ A, $\overline{E}_\gamma \approx 180$ GeV
- <1.5 × 10⁻⁵ 90 AITALA 99G E791 $\pi^- N$ 500 GeV
- <8.9 × 10⁻⁵ 90 FRABETTI 97B E687 γ Be, $\overline{E}_\gamma \approx 220$ GeV
- <1.8 × 10⁻⁵ 90 AITALA 96 E791 $\pi^- N$ 500 GeV
- <2.2 × 10⁻⁴ 90 KODAMA 95 E653 π^- emulsion 600 GeV
- <5.9 × 10⁻³ 90 WEIR 90B MRK2 e^+e^- 29 GeV
- <2.9 × 10⁻³ 90 HAAS 88 CLEO e^+e^- 10 GeV

¹This ABAZOV 08D limit is for the $\mu^+\mu^-$ mass in the continuum away from the $\phi(1020)$. See the next data block.

$\Gamma(\pi^+\phi, \phi \rightarrow \mu^+\mu^-)/\Gamma_{\text{total}}$		Γ_{158}/Γ		
VALUE		DOCUMENT ID	TECN	COMMENT
(1.8 ± 0.5 ± 0.6) × 10⁻⁶		¹ ABAZOV	08D D0	$p\overline{p}$, $E_{\text{cm}} = 1.96$ TeV

¹This ABAZOV 08D value is consistent with the known $D^+ \rightarrow \phi\pi^+$ and $\phi \rightarrow \mu^+\mu^-$ fractions.

$\Gamma(\rho^+\mu^+\mu^-)/\Gamma_{\text{total}}$		Γ_{159}/Γ		
VALUE	CL%	DOCUMENT ID	TECN	COMMENT
<5.6 × 10⁻⁴	90	KODA MA	95 E653	π^- emulsion 600 GeV

A test for the $\Delta C = 1$ weak neutral current. Allowed by higher-order electroweak interactions.

$\Gamma(K^+e^+e^-)/\Gamma_{\text{total}}$		Γ_{160}/Γ		
VALUE	CL%	DOCUMENT ID	TECN	COMMENT
<8.5 × 10⁻⁷	90	AAIJ	21T LHCb	1.6 fb ⁻¹ pp

Both quarks would have to change flavor for this decay to occur.

- • • We do not use the following data for averages, fits, limits, etc. • • •
- <1.0 × 10⁻⁶ 90 LEES 11g BABR $e^+e^- \approx \Upsilon(4S)$
- <3.0 × 10⁻⁶ 90 RUBIN 10 CLEO e^+e^- at $\psi(3770)$
- <6.2 × 10⁻⁶ 90 HE 05A CLEO See RUBIN 10
- <2.0 × 10⁻⁴ 90 AITALA 99G E791 $\pi^- N$ 500 GeV
- <2.0 × 10⁻⁴ 90 FRABETTI 97B E687 γ Be, $\overline{E}_\gamma \approx 220$ GeV
- <4.8 × 10⁻³ 90 WEIR 90B MRK2 e^+e^- 29 GeV

$\Gamma(K^+\pi^0e^+e^-)/\Gamma_{\text{total}}$		Γ_{161}/Γ		
VALUE	CL%	DOCUMENT ID	TECN	COMMENT
<1.5 × 10⁻⁵	90	ABLIKIM	18p BES3	e^+e^- , 3773 MeV

$\Gamma(K_S^0\pi^+e^+e^-)/\Gamma_{\text{total}}$		Γ_{162}/Γ		
VALUE	CL%	DOCUMENT ID	TECN	COMMENT
<2.6 × 10⁻⁵	90	ABLIKIM	18p BES3	e^+e^- , 3773 MeV

$\Gamma(K_S^0K^+e^+e^-)/\Gamma_{\text{total}}$		Γ_{163}/Γ		
VALUE	CL%	DOCUMENT ID	TECN	COMMENT
<1.1 × 10⁻⁵	90	ABLIKIM	18p BES3	e^+e^- , 3773 MeV

$\Gamma(K^+\mu^+\mu^-)/\Gamma_{\text{total}}$		Γ_{164}/Γ		
VALUE	CL%	DOCUMENT ID	TECN	COMMENT
<5.4 × 10⁻⁸	90	AAIJ	21T LHCb	1.6 fb ⁻¹ pp

- • • We do not use the following data for averages, fits, limits, etc. • • •
- <4.3 × 10⁻⁶ 90 LEES 11g BABR $e^+e^- \approx \Upsilon(4S)$
- <9.2 × 10⁻⁶ 90 LINK 03F FOCUS γ A, $\overline{E}_\gamma \approx 180$ GeV
- <4.4 × 10⁻⁵ 90 AITALA 99G E791 $\pi^- N$ 500 GeV
- <9.7 × 10⁻⁵ 90 FRABETTI 97B E687 γ Be, $\overline{E}_\gamma \approx 220$ GeV
- <3.2 × 10⁻⁴ 90 KODA MA 95 E653 π^- emulsion 600 GeV
- <9.2 × 10⁻³ 90 WEIR 90B MRK2 e^+e^- 29 GeV

$\Gamma(\pi^+e^+\mu^-)/\Gamma_{\text{total}}$		Γ_{165}/Γ		
VALUE	CL%	DOCUMENT ID	TECN	COMMENT
<2.1 × 10⁻⁷	90	AAIJ	21T LHCb	1.6 fb ⁻¹ pp

- • • We do not use the following data for averages, fits, limits, etc. • • •
- <2.9 × 10⁻⁶ 90 LEES 11g BABR $e^+e^- \approx \Upsilon(4S)$
- <1.1 × 10⁻⁴ 90 FRABETTI 97B E687 γ Be, $\overline{E}_\gamma \approx 220$ GeV
- <3.3 × 10⁻³ 90 WEIR 90B MRK2 e^+e^- 29 GeV

$\Gamma(\pi^+e^-\mu^+)/\Gamma_{\text{total}}$		Γ_{166}/Γ		
VALUE	CL%	DOCUMENT ID	TECN	COMMENT
<2.2 × 10⁻⁷	90	AAIJ	21T LHCb	1.6 fb ⁻¹ pp

- • • We do not use the following data for averages, fits, limits, etc. • • •
- <3.6 × 10⁻⁶ 90 LEES 11g BABR $e^+e^- \approx \Upsilon(4S)$
- <1.3 × 10⁻⁴ 90 FRABETTI 97B E687 γ Be, $\overline{E}_\gamma \approx 220$ GeV
- <3.3 × 10⁻³ 90 WEIR 90B MRK2 e^+e^- 29 GeV

$\Gamma(K^+e^+\mu^-)/\Gamma_{\text{total}}$		Γ_{167}/Γ		
VALUE	CL%	DOCUMENT ID	TECN	COMMENT
<7.5 × 10⁻⁸	90	AAIJ	21T LHCb	1.6 fb ⁻¹ pp

- • • We do not use the following data for averages, fits, limits, etc. • • •
- <1.2 × 10⁻⁶ 90 LEES 11g BABR $e^+e^- \approx \Upsilon(4S)$
- <1.3 × 10⁻⁴ 90 FRABETTI 97B E687 γ Be, $\overline{E}_\gamma \approx 220$ GeV
- <3.4 × 10⁻³ 90 WEIR 90B MRK2 e^+e^- 29 GeV

$\Gamma(K^+e^-\mu^+)/\Gamma_{\text{total}}$		Γ_{168}/Γ		
VALUE	CL%	DOCUMENT ID	TECN	COMMENT
<1.0 × 10⁻⁷	90	AAIJ	21T LHCb	1.6 fb ⁻¹ pp

- • • We do not use the following data for averages, fits, limits, etc. • • •
- <2.8 × 10⁻⁶ 90 LEES 11g BABR $e^+e^- \approx \Upsilon(4S)$
- <1.2 × 10⁻⁴ 90 FRABETTI 97B E687 γ Be, $\overline{E}_\gamma \approx 220$ GeV
- <3.4 × 10⁻³ 90 WEIR 90B MRK2 e^+e^- 29 GeV

$\Gamma(\pi^-2e^+)/\Gamma_{\text{total}}$		Γ_{169}/Γ		
VALUE	CL%	DOCUMENT ID	TECN	COMMENT
<5.3 × 10⁻⁷	90	AAIJ	21T LHCb	1.6 fb ⁻¹ pp

A test of lepton-number conservation.

••• We do not use the following data for averages, fits, limits, etc. •••

Table with columns: VALUE, CL%, DOCUMENT ID, TECN, COMMENT. Rows include data for LEES, RUBIN, HE, AITALA, FRABETTI, WEIR.

Γ(π⁻ 2μ⁺)/Γtotal Γ170/Γ

Table with columns: VALUE, CL%, DOCUMENT ID, TECN, COMMENT. Row: <1.4 x 10⁻⁸, 90, AAIJ, 21T, LHCB, 1.6 fb⁻¹ pp

••• We do not use the following data for averages, fits, limits, etc. •••

Table with columns: VALUE, CL%, DOCUMENT ID, TECN, COMMENT. Rows include data for AAIJ, LEES, LINK, AITALA, FRABETTI, KODAMA, WEIR.

Γ(π⁻ e⁺ μ⁺)/Γtotal Γ171/Γ

Table with columns: VALUE, CL%, DOCUMENT ID, TECN, COMMENT. Row: <1.3 x 10⁻⁷, 90, AAIJ, 21T, LHCB, 1.6 fb⁻¹ pp

••• We do not use the following data for averages, fits, limits, etc. •••

Table with columns: VALUE, CL%, DOCUMENT ID, TECN, COMMENT. Rows include data for LEES, AITALA, FRABETTI, WEIR.

Γ(ρ⁻ 2μ⁺)/Γtotal Γ172/Γ

Table with columns: VALUE, CL%, DOCUMENT ID, TECN, COMMENT. Row: <5.6 x 10⁻⁴, 90, KODAMA, 95, E653, π⁻ emulsion 600 GeV

Γ(K⁻ 2e⁺)/Γtotal Γ173/Γ

Table with columns: VALUE, CL%, DOCUMENT ID, TECN, COMMENT. Row: <0.9 x 10⁻⁶, 90, LEES, 11G, BABR, e⁺ e⁻ ≈ 7(45)

••• We do not use the following data for averages, fits, limits, etc. •••

Table with columns: VALUE, CL%, DOCUMENT ID, TECN, COMMENT. Rows include data for RUBIN, HE, FRABETTI, WEIR.

Γ(K_S⁰ π⁻ 2e⁺)/Γtotal Γ174/Γ

Table with columns: VALUE, CL%, DOCUMENT ID, TECN, COMMENT. Row: <3.3 x 10⁻⁶, 90, ABLIKIM, 19AL, BES3, e⁺ e⁻ at 3773 MeV

Γ(K⁻ π⁰ 2e⁺)/Γtotal Γ175/Γ

Table with columns: VALUE, CL%, DOCUMENT ID, TECN, COMMENT. Row: <8.5 x 10⁻⁶, 90, ABLIKIM, 19AL, BES3, e⁺ e⁻ at 3773 MeV

Γ(K⁻ 2μ⁺)/Γtotal Γ176/Γ

Table with columns: VALUE, CL%, DOCUMENT ID, TECN, COMMENT. Row: <10 x 10⁻⁶, 90, LEES, 11G, BABR, e⁺ e⁻ ≈ 7(45)

••• We do not use the following data for averages, fits, limits, etc. •••

Table with columns: VALUE, CL%, DOCUMENT ID, TECN, COMMENT. Rows include data for LINK, FRABETTI, KODAMA, WEIR.

Γ(K⁻ e⁺ μ⁺)/Γtotal Γ177/Γ

Table with columns: VALUE, CL%, DOCUMENT ID, TECN, COMMENT. Row: <1.9 x 10⁻⁶, 90, LEES, 11G, BABR, e⁺ e⁻ ≈ 7(45)

••• We do not use the following data for averages, fits, limits, etc. •••

Table with columns: VALUE, CL%, DOCUMENT ID, TECN, COMMENT. Rows include data for FRABETTI, WEIR.

Γ(K*(892)⁻ 2μ⁺)/Γtotal Γ178/Γ

Table with columns: VALUE, CL%, DOCUMENT ID, TECN, COMMENT. Row: <8.5 x 10⁻⁴, 90, KODAMA, 95, E653, π⁻ emulsion 600 GeV

Γ(Λe⁺)/Γtotal Γ179/Γ

Table with columns: VALUE, CL%, DOCUMENT ID, TECN, COMMENT. Row: <1.1 x 10⁻⁶, 90, ABLIKIM, 20D, BES3, e⁺ e⁻, 3773 MeV

Table with columns: VALUE, CL%, DOCUMENT ID, TECN, COMMENT. Row: <6.5 x 10⁻⁷, 90, ABLIKIM, 20D, BES3, e⁺ e⁻, 3773 MeV

Table with columns: VALUE, CL%, DOCUMENT ID, TECN, COMMENT. Row: <1.7 x 10⁻⁶, 90, ABLIKIM, 20D, BES3, e⁺ e⁻, 3773 MeV

Table with columns: VALUE, CL%, DOCUMENT ID, TECN, COMMENT. Row: <1.3 x 10⁻⁶, 90, ABLIKIM, 20D, BES3, e⁺ e⁻, 3773 MeV

D± CP-VIOLATING DECAY-RATE ASYMMETRIES

This is the difference between D⁺ and D⁻ partial widths for the decay to state f, divided by the sum of the widths:

A_CP(f) = [Γ(D⁺ → f) - Γ(D⁻ → f̄)] / [Γ(D⁺ → f) + Γ(D⁻ → f̄)]

Table with columns: VALUE (%), DOCUMENT ID, TECN, COMMENT. Row: +8±8, EISENSTEIN, 08, CLEO, e⁺ e⁻ at ψ(3770)

Table with columns: VALUE (%), DOCUMENT ID, TECN, COMMENT. Row: -0.59 ± 0.60 ± 1.48, ABLIKIM, 15AF, BES3, e⁺ e⁻ 3773 MeV

A_CP(K_S⁰ π±) in D± → K_S⁰ π±

Table with columns: VALUE (%), EVTS, DOCUMENT ID, TECN, COMMENT. Rows include data for BONVICINI, KO, DEL-AMO-SA., LINK.

••• We do not use the following data for averages, fits, limits, etc. •••

Table with columns: VALUE (%), EVTS, DOCUMENT ID, TECN, COMMENT. Rows include data for KO, MENDEZ, DOBBS.

1 KO 12A finds that after subtracting the contribution due to K⁰ - π⁰ mixing, the CP asymmetry due to the change of charm is (-0.024 ± 0.094 ± 0.067)%, consistent with zero.

2 LINK 02B measures N(D⁺ → K_S⁰ π⁺) / N(D⁺ → K⁻ π⁺ π⁺), the ratio of numbers of events observed, and similarly for the D⁻.

A_CP(K_L⁰ K±) in D± → K_L⁰ K±

Table with columns: VALUE (units 10⁻²), EVTS, DOCUMENT ID, TECN, COMMENT. Row: -4.2 ± 3.2 ± 1.2, 650, ABLIKIM, 19M, BES3, e⁺ e⁻ at 3773 MeV

A_CP(K* 2π±) in D⁺ → K⁻ 2π⁺, D⁻ → K⁺ 2π⁻

Table with columns: VALUE (%), EVTS, DOCUMENT ID, TECN, COMMENT. Rows include data for ABZOV, BONVICINI.

••• We do not use the following data for averages, fits, limits, etc. •••

Table with columns: VALUE (%), EVTS, DOCUMENT ID, TECN, COMMENT. Rows include data for MENDEZ, DOBBS.

A_CP(K* π± π± π⁰) in D⁺ → K⁻ π⁺ π⁺ π⁰, D⁻ → K⁺ π⁻ π⁻ π⁰

Table with columns: VALUE (%), DOCUMENT ID, TECN, COMMENT. Row: -0.3 ± 0.6 ± 0.4, BONVICINI, 14, CLEO, All CLEO-c runs

••• We do not use the following data for averages, fits, limits, etc. •••

Table with columns: VALUE (%), DOCUMENT ID, TECN, COMMENT. Row: 1.0 ± 0.9 ± 0.9, DOBBS, 07, CLEO, See BONVICINI 14

A_CP(K_S⁰ π± π⁰) in D⁺ → K_S⁰ π⁺ π⁰, D⁻ → K_S⁰ π⁻ π⁰

Table with columns: VALUE (%), DOCUMENT ID, TECN, COMMENT. Row: -0.1 ± 0.7 ± 0.2, BONVICINI, 14, CLEO, All CLEO-c runs

••• We do not use the following data for averages, fits, limits, etc. •••

Table with columns: VALUE (%), DOCUMENT ID, TECN, COMMENT. Row: 0.3 ± 0.9 ± 0.3, DOBBS, 07, CLEO, See BONVICINI 14

A_CP(K_S⁰ π± η) in D± → K_S⁰ π± η

Table with columns: VALUE (units 10⁻²), EVTS, DOCUMENT ID, TECN, COMMENT. Row: -0.9 ± 2.9 ± 1.0, 1.3k, ABLIKIM, 20V, BES3, e⁺ e⁻, 3773 MeV

A_CP(K_S⁰ π± π⁺ π⁻) in D⁺ → K_S⁰ π⁺ π⁺ π⁻, D⁻ → K_S⁰ π⁻ π⁻ π⁺

Table with columns: VALUE (%), DOCUMENT ID, TECN, COMMENT. Row: 0.0 ± 1.2 ± 0.3, BONVICINI, 14, CLEO, All CLEO-c runs

••• We do not use the following data for averages, fits, limits, etc. •••

Table with columns: VALUE (%), EVTS, DOCUMENT ID, TECN, COMMENT. Row: 0.1 ± 1.1 ± 0.6, DOBBS, 07, CLEO, See BONVICINI 14

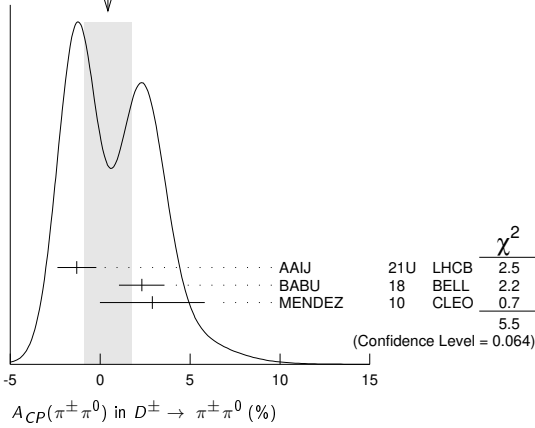
A_CP(K± π± π⁻ π⁰) in D± → K± π± π⁻ π⁰

Table with columns: VALUE (%), EVTS, DOCUMENT ID, TECN, COMMENT. Row: -0.04 ± 0.06 ± 0.01, 350, ABLIKIM, 20Z, BES3, e⁺ e⁻, 3773 MeV

Meson Particle Listings

 D^\pm $A_{CP}(\pi^\pm\pi^0)$ in $D^\pm \rightarrow \pi^\pm\pi^0$

VALUE (%)	EVTS	DOCUMENT ID	TECN	COMMENT
0.4 ± 1.3 OUR AVERAGE	Error	includes scale factor of 1.7.		See the ideogram below.
-1.3 ± 0.9 ± 0.6	28.7k	AAIJ	21U	LHCB pp at 7, 8, 13 TeV
2.31 ± 1.24 ± 0.23	108k	BABU	18	BELL At/near $\Upsilon(4S)$, $\Upsilon(5S)$
2.9 ± 2.9 ± 0.3	2.6k	MENDEZ	10	CLEO e^+e^- at 3774 MeV

WEIGHTED AVERAGE
0.4 ± 1.3 (Error scaled by 1.7) $A_{CP}(\pi^\pm\eta)$ in $D^\pm \rightarrow \pi^\pm\eta$

VALUE (%)	EVTS	DOCUMENT ID	TECN	COMMENT
0.3 ± 0.8 OUR AVERAGE	Error	includes scale factor of 1.2.		
-0.2 ± 0.8 ± 0.4	32.7k	AAIJ	21U	LHCB pp at 13 TeV
+1.74 ± 1.13 ± 0.19		WON	11	BELL $e^+e^- \approx \Upsilon(4S)$
-2.0 ± 2.3 ± 0.3	2.9k	MENDEZ	10	CLEO e^+e^- at 3774 MeV

 $A_{CP}(\pi^\pm\pi^0\eta)$ in $D^\pm \rightarrow \pi^\pm\pi^0\eta$

VALUE (units 10^{-2})	EVTS	DOCUMENT ID	TECN	COMMENT
-5.8 ± 6.6 ± 1.8	381	ABLIKIM	20G	BES3 e^+e^- at 3.773 GeV

 $A_{CP}(\pi^\pm\eta\eta)$ in $D^\pm \rightarrow \pi^\pm\eta\eta$

VALUE (units 10^{-2})	EVTS	DOCUMENT ID	TECN	COMMENT
8.0 ± 8.3 ± 1.9	179	ABLIKIM	20G	BES3 e^+e^- at 3.773 GeV

 $A_{CP}(\pi^\pm\eta'(958))$ in $D^\pm \rightarrow \pi^\pm\eta'(958)$

VALUE (%)	EVTS	DOCUMENT ID	TECN	COMMENT
-0.6 ± 0.7 OUR AVERAGE				
-0.61 ± 0.72 ± 0.54	63k	AAIJ	17AF	LHCB pp at 7, 8 TeV
-0.12 ± 1.12 ± 0.17		WON	11	BELL $e^+e^- \approx \Upsilon(4S)$
-4.0 ± 3.4 ± 0.3	1.0k	MENDEZ	10	CLEO e^+e^- at 3774 MeV

 $A_{CP}(\bar{K}^0/K^0K^\pm)$ in $D^+ \rightarrow \bar{K}^0K^+$, $D^- \rightarrow K^0K^-$

VALUE (%)	EVTS	DOCUMENT ID	TECN	COMMENT
0.11 ± 0.17 OUR AVERAGE				
0.03 ± 0.17 ± 0.14	1.0M	1 AAIJ	14BD	LHCB pp at 7, 8 TeV
0.08 ± 0.28 ± 0.14	277k	KO	13	BELL e^+e^- at $\Upsilon(4S)$
0.46 ± 0.36 ± 0.25	159k	LEES	13E	BABR e^+e^- at $\Upsilon(4S)$

¹ AAIJ 14BD reports its result as $A_{CP}(D^\pm \rightarrow K_S^0\pi^\pm)$ with CP -violation effects in the $K^0 - \bar{K}^0$ system subtracted. It also measures $A_{CP}(D^\pm \rightarrow \bar{K}^0/K^0K^\pm) + A_{CP}(D_S^\pm \rightarrow \bar{K}^0/K^0\pi^\pm) = (0.41 \pm 0.49 \pm 0.26)\%$.

 $A_{CP}(K_S^0K^\pm)$ in $D^\pm \rightarrow K_S^0K^\pm$

VALUE (%)	EVTS	DOCUMENT ID	TECN	COMMENT
-0.01 ± 0.07 OUR AVERAGE				
-0.004 ± 0.061 ± 0.045	6M	AAIJ	19T	LHCB pp at 7, 8, 13 TeV
-1.8 ± 2.7 ± 1.6	780	ABLIKIM	19M	BES3 e^+e^- at 3773 MeV
-0.25 ± 0.28 ± 0.14	277k	KO	13	BELL e^+e^- at $\Upsilon(nS)$
0.13 ± 0.36 ± 0.25	159k	LEES	13E	BABR e^+e^- at $\Upsilon(4S)$
-0.2 ± 1.5 ± 0.9	5.2k	MENDEZ	10	CLEO e^+e^- at 3774 MeV
7.1 ± 6.1 ± 1.2	949	1 LINK	02b	FOCS γ nucleus, $\bar{E}_\gamma \approx 180$ GeV
-0.16 ± 0.58 ± 0.25		KO	10	BELL $e^+e^- \approx \Upsilon(4S)$
6.9 ± 6.0 ± 1.5	949	2 LINK	02b	FOCS γ nucleus, $\bar{E}_\gamma \approx 180$ GeV

¹ LINK 02b measures $N(D^+ \rightarrow K_S^0K^+)/N(D^+ \rightarrow K_S^0\pi^+)$, the ratio of numbers of events observed, and similarly for the D^- .

² LINK 02b measures $N(D^+ \rightarrow K_S^0K^+)/N(D^+ \rightarrow K^-\pi^+\pi^+)$, the ratio of numbers of events observed, and similarly for the D^- .

 $A_{CP}(K_S^0K^\pm\pi^0)$ in $D^\pm \rightarrow K_S^0K^\pm\pi^0$

VALUE (units 10^{-2})	EVTS	DOCUMENT ID	TECN	COMMENT
1.4 ± 3.7 ± 2.4	470	ABLIKIM	19M	BES3 e^+e^- at 3773 MeV

 $A_{CP}(K_L^0K^\pm\pi^0)$ in $D^\pm \rightarrow K_L^0K^\pm\pi^0$

VALUE (units 10^{-2})	EVTS	DOCUMENT ID	TECN	COMMENT
-0.6 ± 4.1 ± 1.7	410	ABLIKIM	19M	BES3 e^+e^- at 3773 MeV

 $A_{CP}(K^+K^-\pi^\pm)$ in $D^\pm \rightarrow K^+K^-\pi^\pm$

See also AAIJ 11G for a search for CP asymmetry in the $D^\pm \rightarrow K^+K^-\pi^\pm$ Dalitz plots using 370k decays and four different binning schemes. No evidence for CP asymmetry was found.

VALUE (%)	EVTS	DOCUMENT ID	TECN	COMMENT
0.37 ± 0.29 OUR AVERAGE				
0.37 ± 0.30 ± 0.15	224k	1 LEES	13F	BABR e^+e^- at $\Upsilon(4S)$
-0.03 ± 0.84 ± 0.29		RUBIN	08	CLEO e^+e^- at 3774 MeV
1.4 ± 1.0 ± 0.8	43k	2 AUBERT	05s	BABR e^+e^- at $\Upsilon(4S)$
0.6 ± 1.1 ± 0.5	14k	3 LINK	00b	FOCS
-1.4 ± 2.9		3 AITALA	97B	E791 $-0.062 < A_{CP} < +0.034$ (90% CL)
-3.1 ± 6.8		3 FRABETTI	94I	E687 $-0.14 < A_{CP} < +0.081$ (90% CL)
-0.1 ± 0.9 ± 0.4		4 BONVICINI	14	CLEO See RUBIN 08
-0.1 ± 1.5 ± 0.8		DOBBS	07	CLEO See BONVICINI 14 and RUBIN 08

••• We do not use the following data for averages, fits, limits, etc. •••

¹ This is the integrated CP asymmetry. LEES 13F also searches for CP asymmetries in four regions of the Dalitz plots (two of which are listed below); in comparisons of binned D^+ and D^- Dalitz plots; in parametrized fits to those plots, including 2-body submodes; and in comparisons of Legendre-polynomial distributions for the K^+K^- and $K^-\pi^+$ systems.

² AUBERT 05s measures $N(D^+ \rightarrow K^+K^-\pi^+)/N(D_S^+ \rightarrow K^+K^-\pi^+)$, the ratio of the numbers of events observed, and similarly for the D^- .

³ FRABETTI 94I, AITALA 98C, and LINK 00b measure $N(D^+ \rightarrow K^-K^+\pi^+)/N(D^+ \rightarrow K^-\pi^+\pi^+)$, the ratio of numbers of events observed, and similarly for the D^- .

⁴ RUBIN 08 performs a dedicated analysis of this decay mode on the same dataset, with slightly better precision. We therefore take it that BONVICINI 14 does not supersede RUBIN 08's A_{CP} result.

 $A_{CP}(K^\pm K^*0)$ in $D^+ \rightarrow K^+K^*0$, $D^- \rightarrow K^-K^*0$

VALUE (%)	EVTS	DOCUMENT ID	TECN	COMMENT
-0.3 ± 0.4 OUR AVERAGE				
-0.3 ± 0.4 ± 0.2	73k	1 LEES	13F	BABR e^+e^- at $\Upsilon(4S)$
-0.4 ± 2.0 ± 0.6		RUBIN	08	CLEO Fit-fraction asymmetry
+0.9 ± 1.7 ± 0.7	11k	2 AUBERT	05s	BABR e^+e^- at $\Upsilon(4S)$
-1.0 ± 5.0		3 AITALA	97B	E791 $-0.092 < A_{CP} < +0.072$ (90% CL)
-12 ± 13		3 FRABETTI	94I	E687 $-0.33 < A_{CP} < +0.094$ (90% CL)

¹ This LEES 13F result is for the $K^\mp\pi^\pm$ mass-squared between 0.4 and 1.0 GeV^2 , and does not actually separate out the K^* .

² AUBERT 05s measures $N(D^+ \rightarrow K^+K^*0)/N(D_S^+ \rightarrow K^+K^-\pi^+)$, the ratio of the numbers of events observed, and similarly for the D^- .

³ FRABETTI 94I and AITALA 97B measure $N(D^+ \rightarrow K^+K^*(892)^0)/N(D^+ \rightarrow K^-\pi^+\pi^+)$, the ratio of numbers of events observed, and similarly for the D^- .

 $A_{CP}(\phi\pi^\pm)$ in $D^\pm \rightarrow \phi\pi^\pm$

VALUE (%)	EVTS	DOCUMENT ID	TECN	COMMENT
0.01 ± 0.09 OUR AVERAGE				Error includes scale factor of 1.8.
0.003 ± 0.040 ± 0.029	55M	AAIJ	19T	LHCB pp at 7, 8, 13 TeV
-0.3 ± 0.3 ± 0.5	97k	1 LEES	13F	BABR e^+e^- at $\Upsilon(4S)$
+0.51 ± 0.28 ± 0.05	237k	STARIC	12	BELL Mainly at $\Upsilon(4S)$
-1.8 ± 1.6 $^{+0.2}_{-0.4}$		RUBIN	08	CLEO Fit-fraction asymmetry
+0.2 ± 1.5 ± 0.6	10k	2 AUBERT	05s	BABR e^+e^- at $\Upsilon(4S)$
-2.8 ± 3.6		3 AITALA	97B	E791 $-0.087 < A_{CP} < +0.031$ (90% CL)
+6.6 ± 8.6		3 FRABETTI	94I	E687 $-0.075 < A_{CP} < +0.21$ (90% CL)

••• We do not use the following data for averages, fits, limits, etc. •••

-0.04 ± 0.14 ± 0.14 1.58M ⁴ AAIJ 13W LHCB pp at 7 TeV

¹ This LEES 13F result is for the K^+K^- mass-squared less than 1.3 GeV^2 and the $K^\mp\pi^\pm$ mass-squared above 1.0 GeV^2 , and does not actually separate out the ϕ .

² AUBERT 05s measures $N(D^+ \rightarrow \phi\pi^+)/N(D_S^+ \rightarrow K^+K^-\pi^+)$, the ratio of the numbers of events observed, and similarly for the D^- .

³ FRABETTI 94I and AITALA 97B measure $N(D^+ \rightarrow \phi\pi^+)/N(D^+ \rightarrow K^-\pi^+\pi^+)$, the ratio of numbers of events observed, and similarly for the D^- .

⁴ See AAIJ 19T.

 $A_{CP}(K^\pm K_S^*(1430)^0)$ in $D^+ \rightarrow K^+K_S^*(1430)^0$, $D^- \rightarrow K^-K_S^*(1430)^0$

VALUE (%)	DOCUMENT ID	TECN	COMMENT
+8 ± 6 $^{+4}_{-2}$	RUBIN	08	CLEO Fit-fraction asymmetry

 $A_{CP}(K^\pm K_2^*(1430)^0)$ in $D^+ \rightarrow K^+K_2^*(1430)^0$, $D^- \rightarrow K^-K_2^*(1430)^0$

VALUE (%)	DOCUMENT ID	TECN	COMMENT
+43 ± 19 $^{+5}_{-18}$	RUBIN	08	CLEO Fit-fraction asymmetry

$A_{CP}(K^\pm K_0^*(700))$ in $D^+ \rightarrow K^+ \bar{K}_0^*(700)$, $D^- \rightarrow K^- K_0^*(700)$

VALUE (%)	DOCUMENT ID	TECN	COMMENT
$-12 \pm 11^{+14}_{-6}$	RUBIN	08	CLEO Fit-fraction asymmetry

$A_{CP}(a_0(1450)^0 \pi^\pm)$ in $D^\pm \rightarrow a_0(1450)^0 \pi^\pm$

VALUE (%)	DOCUMENT ID	TECN	COMMENT
$-19 \pm 12^{+8}_{-11}$	RUBIN	08	CLEO Fit-fraction asymmetry

$A_{CP}(\phi(1680) \pi^\pm)$ in $D^\pm \rightarrow \phi(1680) \pi^\pm$

VALUE (%)	DOCUMENT ID	TECN	COMMENT
$-9 \pm 22 \pm 14$	RUBIN	08	CLEO Fit-fraction asymmetry

$A_{CP}(\pi^+ \pi^- \pi^\pm)$ in $D^\pm \rightarrow \pi^+ \pi^- \pi^\pm$

See also AAIJ 14C for a search for CP violation in $D^\pm \rightarrow \pi^+ \pi^- \pi^\pm$ Dalitz plots using model-independent binned and unbinned methods. No evidence was found.

VALUE (%)	DOCUMENT ID	TECN	COMMENT
-1.7 ± 4.2	¹ AITALA 97B	E791	$-0.086 < A_{CP} < +0.052$ (90% CL)

¹AITALA 97B measure $N(D^+ \rightarrow \pi^+ \pi^- \pi^+)/N(D^+ \rightarrow K^- \pi^+ \pi^+)$, the ratio of numbers of events observed, and similarly for the D^- .

$A_{CP}(\pi^+ \pi^- \pi^\pm \eta)$ in $D^\pm \rightarrow \pi^+ \pi^- \pi^\pm \eta$

VALUE (units 10^{-2})	EVTS	DOCUMENT ID	TECN	COMMENT
$2.5 \pm 5.0 \pm 1.6$	510	ABLIKIM	20V	BES3 $e^+ e^-$, 3773 MeV

$A_{CP}(K_S^0 K^\pm \pi^+ \pi^-)$ in $D^\pm \rightarrow K_S^0 K^\pm \pi^+ \pi^-$

VALUE (%)	EVTS	DOCUMENT ID	TECN	COMMENT
$-4.2 \pm 6.4 \pm 2.2$	523 \pm 32	LINK	05E	FOCS γA , $\bar{E}_\gamma \approx 180$ GeV

$A_{CP}(K^\pm \pi^0)$ in $D^\pm \rightarrow K^\pm \pi^0$

VALUE (%)	EVTS	DOCUMENT ID	TECN	COMMENT
-3 ± 5 OUR AVERAGE				
$-3.2 \pm 4.7 \pm 2.1$	2.5k	AAIJ	21U	LHCB pp at 7, 8, 13 TeV
$-3.5 \pm 10.7 \pm 0.9$	343	MENDEZ	10	CLEO $e^+ e^-$ at 3774 MeV

$A_{CP}(K^\pm \eta)$ in $D^\pm \rightarrow K^\pm \eta$

VALUE (units 10^{-2})	EVTS	DOCUMENT ID	TECN	COMMENT
$-6 \pm 10 \pm 4$	880	AAIJ	21U	LHCB pp at 13 TeV

$D^\pm \chi^2$ TESTS OF CP-VIOLATION (CPV)

We list model-independent searches for local CP violation in phase-space distributions of multi-body decays.

Most of these searches divide phase space (Dalitz plot for 3-body decays, five-dimensional equivalent for 4-body decays) into bins, and perform a χ^2 test comparing normalised yields N_i/\bar{N}_i in CP-conjugate bin pairs i : $\chi^2 = \sum_i (N_i - \alpha \bar{N}_i) / \sigma (N_i - \alpha \bar{N}_i)$. The factor $\alpha = (\sum_j N_j) / (\sum_j \bar{N}_j)$ removes the dependence on phase-space-integrated rate asymmetries. The result is used to obtain the probability (p-value) to obtain the measured χ^2 or larger under the assumption of CP conservation [AUBERT 08A0, BEDIAGA 09]. Alternative methods obtain p-values from other test variables based on unbinned analyses [WILLIAMS 11, AAIJ 14c]. Results can be combined using Fisher's method [MOSTELLER 48].

Local CPV in $D^\pm \rightarrow \pi^+ \pi^- \pi^\pm$

p-value (%)	EVTS	DOCUMENT ID	TECN	COMMENT
78.1	3.1M	¹ AAIJ	14C	LHCB χ^2

¹AAIJ 14c uses binned and unbinned methods, and finds slightly better sensitivity with the former. We took the first value in the table of results for the binned method.

Local CPV in $D^\pm \rightarrow K^+ K^- \pi^\pm$

p-value (%)	EVTS	DOCUMENT ID	TECN	COMMENT
31	OUR EVALUATION			
72	224k	LEES	13F	BABR χ^2
12.7	370k	¹ AAIJ	11G	LHCB χ^2

¹AAIJ 11g publishes results for several binning schemes. We picked the first value in their table of results.

CP VIOLATING ASYMMETRIES OF P-ODD (T-ODD) MOMENTS

$A_{Tviol}(K_S^0 K^\pm \pi^+ \pi^-)$ in $D^\pm \rightarrow K_S^0 K^\pm \pi^+ \pi^-$

$C_T \equiv \bar{p}_{K^+} \cdot (\bar{p}_{\pi^+} \times \bar{p}_{\pi^-})$ is a parity-odd correlation of the K^+ , π^+ , and π^- momenta for the D^+ . $\bar{C}_T \equiv \bar{p}_{K^-} \cdot (\bar{p}_{\pi^-} \times \bar{p}_{\pi^+})$ is the corresponding quantity for the D^- . Then

$A_T \equiv [\Gamma(C_T > 0) - \Gamma(C_T < 0)] / [\Gamma(C_T > 0) + \Gamma(C_T < 0)]$, and

$\bar{A}_T \equiv [\Gamma(-\bar{C}_T > 0) - \Gamma(-\bar{C}_T < 0)] / [\Gamma(-\bar{C}_T > 0) + \Gamma(-\bar{C}_T < 0)]$, and

$A_{Tviol} \equiv \frac{1}{2}(A_T - \bar{A}_T)$. C_T and \bar{C}_T are commonly referred to as T-odd moments, because they are odd under T reversal. However, the T-conjugate process $K_S^0 K^\pm \pi^+ \pi^- \rightarrow D^\pm$ is not accessible, while the P-conjugate process is.

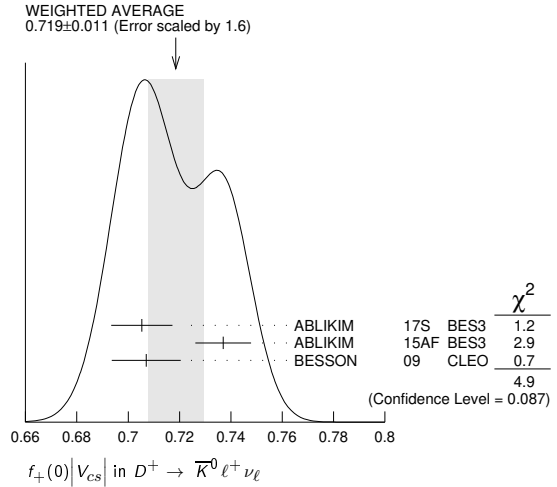
VALUE (units 10^{-3})	EVTS	DOCUMENT ID	TECN	COMMENT
$-12.0 \pm 10.0 \pm 4.6$	21.2 \pm 0.4k	LEES	11E	BABR $e^+ e^- \approx \Upsilon(4S)$
\dots	\dots	\dots	\dots	\dots
$23 \pm 62 \pm 22$	523 \pm 32	LINK	05E	FOCS γA , $\bar{E}_\gamma \approx 180$ GeV

\dots We do not use the following data for averages, fits, limits, etc. \dots

SEMILEPTONIC FORM FACTORS

$f_+(0)|V_{cs}|$ in $D^+ \rightarrow \bar{K}^0 \ell^+ \nu_\ell$

VALUE	DOCUMENT ID	TECN	COMMENT
0.719 \pm 0.011 OUR AVERAGE			Error includes scale factor of 1.6. See the ideogram below.
0.7053 \pm 0.0040 \pm 0.0112	ABLIKIM	17S	BES3 $K_S^0 e^+ \nu_e$ 2-parameter fit
0.737 \pm 0.006 \pm 0.009	¹ ABLIKIM	15AF	BES3 $K_L e^+ \nu_e$ 3-parameter fit
0.707 \pm 0.010 \pm 0.009	² BESSION	09	CLEO $K_S e^+ \nu_e$ 3-parameter fit



¹ABLIKIM 15AF finds 0.728 \pm 0.006 \pm 0.011 for a 2-parameter fit.
²BESSION 09 finds 0.716 \pm 0.007 \pm 0.009 for a 2-parameter fit.

$r_1 \equiv a_1/a_0$ in $D^+ \rightarrow \bar{K}^0 \ell^+ \nu_\ell$

VALUE	EVTS	DOCUMENT ID	TECN	COMMENT
-2.13 \pm 0.14 OUR AVERAGE				
-2.18 \pm 0.14 \pm 0.05		ABLIKIM	17S	BES3 $K_S^0 e^+ \nu_e$ 2-parameter fit
-2.23 \pm 0.42 \pm 0.53	40k	¹ ABLIKIM	15AF	BES3 $K_L e^+ \nu_e$ 3-parameter fit
-1.66 \pm 0.44 \pm 0.10		² BESSION	09	CLEO $K_S e^+ \nu_e$ 3-parameter fit

¹ABLIKIM 15AF finds $r_1 = -1.91 \pm 0.33 \pm 0.28$ for a 2-parameter fit.
²BESSION 09 finds $r_1 = -2.10 \pm 0.25 \pm 0.08$ for 2-parameter fit.

$r_2 \equiv a_2/a_0$ in $D^+ \rightarrow \bar{K}^0 \ell^+ \nu_\ell$

VALUE	EVTS	DOCUMENT ID	TECN	COMMENT
-3 \pm 12 OUR AVERAGE				Error includes scale factor of 1.5.
+11 \pm 9 \pm 9	40k	ABLIKIM	15AF	BES3 $K_L e^+ \nu_e$ 3-parameter fit
-14 \pm 11 \pm 1		BESSION	09	CLEO $K_S e^+ \nu_e$ 3-parameter fit

$f_+(0)|V_{cd}|$ in $D^+ \rightarrow \pi^0 \ell^+ \nu_\ell$

VALUE	DOCUMENT ID	TECN	COMMENT
0.1407 \pm 0.0025 OUR AVERAGE			
0.1400 \pm 0.0026 \pm 0.0007	ABLIKIM	17S	BES3 $\pi^0 e^+ \nu_e$ 2-parameter fit
0.146 \pm 0.007 \pm 0.002	BESSION	09	CLEO $\pi^0 e^+ \nu_e$ 3-parameter fit

$r_1 \equiv a_1/a_0$ in $D^+ \rightarrow \pi^0 \ell^+ \nu_\ell$

VALUE	DOCUMENT ID	TECN	COMMENT
-2.00 \pm 0.13 OUR AVERAGE			
-2.01 \pm 0.13 \pm 0.02	ABLIKIM	17S	BES3 $\pi^0 e^+ \nu_e$ 2-parameter fit
-1.37 \pm 0.88 \pm 0.24	BESSION	09	CLEO $\pi^0 e^+ \nu_e$ 3-parameter fit

$r_2 \equiv a_2/a_0$ in $D^+ \rightarrow \pi^0 \ell^+ \nu_\ell$

VALUE	DOCUMENT ID	TECN	COMMENT
-4 \pm 5 \pm 1			
	BESSION	09	CLEO $\pi^0 e^+ \nu_e$ 3-parameter fit

$f_+(0)|V_{cd}|$ in $D^+ \rightarrow \eta \ell^+ \nu_\ell$ ($\ell = e$ or ν)

VALUE (units 10^{-2})	EVTS	DOCUMENT ID	TECN	COMMENT
8.4 \pm 0.4 OUR AVERAGE				
8.7 \pm 0.8 \pm 0.2	234	ABLIKIM	20T	BES3 $\eta \mu^+ \nu_\mu$, z expansion
7.86 \pm 0.64 \pm 0.21	373	ABLIKIM	18R	BES3 $\eta e^+ \nu_e$, z expansion
8.6 \pm 0.6 \pm 0.1		YELTON	11	CLEO $\eta e^+ \nu_e$, z expansion

$r_1 \equiv a_1/a_0$ in $D^+ \rightarrow \eta e^+ \nu_e$

VALUE	EVTS	DOCUMENT ID	TECN	COMMENT
-5.3 \pm 2.7 OUR AVERAGE				Error includes scale factor of 1.9.
-7.33 \pm 1.69 \pm 0.40	373	ABLIKIM	18R	BES3 z expansion
-1.83 \pm 2.23 \pm 0.28		YELTON	11	CLEO z expansion

$r_V \equiv V(0)/A_1(0)$ in $D^+ \rightarrow \omega e^+ \nu_e$

VALUE	DOCUMENT ID	TECN	COMMENT
1.24 \pm 0.09 \pm 0.06			
	ABLIKIM	15W	BES3 292 fb ⁻¹ , 3773 MeV

Meson Particle Listings

D^\pm

$r_2 \equiv A_2(0)/A_1(0)$ in $D^+ \rightarrow \omega e^+ \nu_e$

VALUE	EVTS	DOCUMENT ID	TECN	COMMENT
$1.06 \pm 0.15 \pm 0.05$		ABLIKIM	15W BES3	292 fb^{-1} , 3773 MeV

$r_V \equiv V(0)/A_1(0)$ in $D^+, D^0 \rightarrow \rho e^+ \nu_e$

VALUE	EVTS	DOCUMENT ID	TECN	COMMENT
1.64 ± 0.10 OUR AVERAGE		Error includes scale factor of 1.2.		
$1.695 \pm 0.083 \pm 0.051$	2.5k	¹ ABLIKIM	19c BES3	$e^+ e^-$ at 3773 MeV
$1.48 \pm 0.15 \pm 0.05$		^{1,2} DOBBS	13 CLEO	$e^+ e^-$ at $\psi(3770)$

¹ Uses both D^+ and D^0 events.
² Using PDG 10 values of V_{cd} and lifetimes, DOBBS 13 gets $A_1(0) = 0.56 \pm 0.01^{+0.02}_{-0.03}$, $A_2(0) = 0.47 \pm 0.06 \pm 0.04$, and $V(0) = 0.84 \pm 0.09^{+0.05}_{-0.06}$.

$r_2 \equiv A_2(0)/A_1(0)$ in $D^+, D^0 \rightarrow \rho e^+ \nu_e$

VALUE	EVTS	DOCUMENT ID	TECN	COMMENT
0.84 ± 0.06 OUR AVERAGE				
$0.845 \pm 0.056 \pm 0.039$	2.5k	¹ ABLIKIM	19c BES3	$e^+ e^-$ at 3773 MeV
$0.83 \pm 0.11 \pm 0.04$		^{1,2} DOBBS	13 CLEO	$e^+ e^-$ at $\psi(3770)$

¹ Uses both D^+ and D^0 events.
² Using PDG 10 values of V_{cd} and lifetimes, DOBBS 13 gets $A_1(0) = 0.56 \pm 0.01^{+0.02}_{-0.03}$, $A_2(0) = 0.47 \pm 0.06 \pm 0.04$, and $V(0) = 0.84 \pm 0.09^{+0.05}_{-0.06}$.

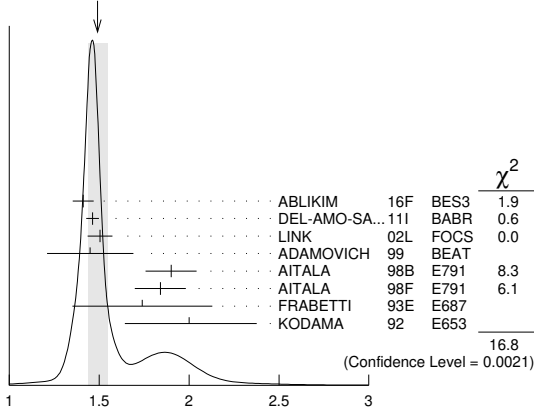
$r_V \equiv V(0)/A_1(0)$ in $D^+ \rightarrow \bar{K}^*(892)^0 \ell^+ \nu_\ell$

See also BRIERE 10 for $\bar{K}^* \ell^+ \nu_\ell$ helicity-basis form-factor measurements.

VALUE	EVTS	DOCUMENT ID	TECN	COMMENT
1.49 ± 0.05 OUR AVERAGE		Error includes scale factor of 2.1. See the ideogram below.		
$1.411 \pm 0.058 \pm 0.007$	16.2k	ABLIKIM	16F BES3	$\bar{K}^*(892)^0 e^+ \nu_e$
$1.463 \pm 0.017 \pm 0.031$		¹ DEL-AMO-SA...111	BABR	
$1.504 \pm 0.057 \pm 0.039$	15k	² LINK	02L FOCUS	$\bar{K}^*(892)^0 \mu^+ \nu_\mu$
$1.45 \pm 0.23 \pm 0.07$	763	ADAMOVICH	99 BEAT	$\bar{K}^*(892)^0 \mu^+ \nu_\mu$
$1.90 \pm 0.11 \pm 0.09$	3000	³ AITALA	98B E791	$\bar{K}^*(892)^0 e^+ \nu_e$
$1.84 \pm 0.11 \pm 0.09$	3034	AITALA	98F E791	$\bar{K}^*(892)^0 \mu^+ \nu_\mu$
$1.74 \pm 0.27 \pm 0.28$	874	FRABETTI	93E E687	$\bar{K}^*(892)^0 \mu^+ \nu_\mu$
$2.00^{+0.34}_{-0.32} \pm 0.16$	305	KODAMA	92 E653	$\bar{K}^*(892)^0 \mu^+ \nu_\mu$
$2.0 \pm 0.6 \pm 0.3$	183	ANJOS	90E E691	$\bar{K}^*(892)^0 e^+ \nu_e$

• • • We do not use the following data for averages, fits, limits, etc. • • •

WEIGHTED AVERAGE
 1.49 ± 0.05 (Error scaled by 2.1)



$r_V \equiv V(0)/A_1(0)$ in $D^+ \rightarrow \bar{K}^*(892)^0 \ell^+ \nu_\ell$

¹ DEL-AMO-SANCHEZ 111 finds the pole mass $m_A = (2.63 \pm 0.10 \pm 0.13) \text{ GeV}$ (m_V is fixed at 2 GeV).
² LINK 02L includes the effects of interference with an S-wave background. This much improves the goodness of fit, but does not much shift the values of the form factors.
³ This is slightly different from the AITALA 98B value: see ref. [5] in AITALA 98F.

$r_2 \equiv A_2(0)/A_1(0)$ in $D^+ \rightarrow \bar{K}^*(892)^0 \ell^+ \nu_\ell$

See also BRIERE 10 for $\bar{K}^* \ell^+ \nu_\ell$ helicity-basis form-factor measurements.

VALUE	EVTS	DOCUMENT ID	TECN	COMMENT
0.802 ± 0.021 OUR AVERAGE				
$0.788 \pm 0.042 \pm 0.008$	16.2k	ABLIKIM	16F BES3	$\bar{K}^*(892)^0 e^+ \nu_e$
$0.801 \pm 0.020 \pm 0.020$		¹ DEL-AMO-SA...111	BABR	
$0.875 \pm 0.049 \pm 0.064$	15k	² LINK	02L FOCUS	$\bar{K}^*(892)^0 \mu^+ \nu_\mu$
$1.00 \pm 0.15 \pm 0.03$	763	ADAMOVICH	99 BEAT	$\bar{K}^*(892)^0 \mu^+ \nu_\mu$
$0.71 \pm 0.08 \pm 0.09$	3000	AITALA	98B E791	$\bar{K}^*(892)^0 e^+ \nu_e$
$0.75 \pm 0.08 \pm 0.09$	3034	AITALA	98F E791	$\bar{K}^*(892)^0 \mu^+ \nu_\mu$
$0.78 \pm 0.18 \pm 0.10$	874	FRABETTI	93E E687	$\bar{K}^*(892)^0 \mu^+ \nu_\mu$
$0.82^{+0.22}_{-0.23} \pm 0.11$	305	KODAMA	92 E653	$\bar{K}^*(892)^0 \mu^+ \nu_\mu$
$0.0 \pm 0.5 \pm 0.2$	183	ANJOS	90E E691	$\bar{K}^*(892)^0 e^+ \nu_e$

• • • We do not use the following data for averages, fits, limits, etc. • • •

¹ DEL-AMO-SANCHEZ 111 finds the pole mass $m_A = (2.63 \pm 0.10 \pm 0.13) \text{ GeV}$ (m_V is fixed at 2 GeV).
² LINK 02L includes the effects of interference with an S-wave background. This much improves the goodness of fit, but does not much shift the values of the form factors.

$r_3 \equiv A_3(0)/A_1(0)$ in $D^+ \rightarrow \bar{K}^*(892)^0 \ell^+ \nu_\ell$

See also BRIERE 10 for $\bar{K}^* \ell^+ \nu_\ell$ helicity-basis form-factor measurements.

VALUE	EVTS	DOCUMENT ID	TECN	COMMENT
$0.04 \pm 0.33 \pm 0.29$	3034	AITALA	98F E791	$\bar{K}^*(892)^0 \mu^+ \nu_\mu$

Γ_L/Γ_T in $D^+ \rightarrow \bar{K}^*(892)^0 \ell^+ \nu_\ell$

See also BRIERE 10 for $\bar{K}^* \ell^+ \nu_\ell$ helicity-basis form-factor measurements.

VALUE	EVTS	DOCUMENT ID	TECN	COMMENT
1.13 ± 0.08 OUR AVERAGE				
$1.09 \pm 0.10 \pm 0.02$	763	ADAMOVICH	99 BEAT	$\bar{K}^*(892)^0 \mu^+ \nu_\mu$
$1.20 \pm 0.13 \pm 0.13$	874	FRABETTI	93E E687	$\bar{K}^*(892)^0 \mu^+ \nu_\mu$
$1.18 \pm 0.18 \pm 0.08$	305	KODA MA	92 E653	$\bar{K}^*(892)^0 \mu^+ \nu_\mu$
$1.8^{+0.6}_{-0.4} \pm 0.3$	183	ANJOS	90E E691	$\bar{K}^*(892)^0 e^+ \nu_e$

• • • We do not use the following data for averages, fits, limits, etc. • • •

Γ_+/ Γ_- in $D^+ \rightarrow \bar{K}^*(892)^0 \ell^+ \nu_\ell$

See also BRIERE 10 for $\bar{K}^* \ell^+ \nu_\ell$ helicity-basis form-factor measurements.

VALUE	EVTS	DOCUMENT ID	TECN	COMMENT
0.22 ± 0.06 OUR AVERAGE		Error includes scale factor of 1.6.		
$0.28 \pm 0.05 \pm 0.02$	763	ADAMOVICH	99 BEAT	$\bar{K}^*(892)^0 \mu^+ \nu_\mu$
$0.16 \pm 0.05 \pm 0.02$	305	KODA MA	92 E653	$\bar{K}^*(892)^0 \mu^+ \nu_\mu$
$0.15^{+0.07}_{-0.05} \pm 0.03$	183	ANJOS	90E E691	$\bar{K}^*(892)^0 e^+ \nu_e$

• • • We do not use the following data for averages, fits, limits, etc. • • •

Amplitude analyses

$D \rightarrow K \pi \pi$ partial wave analyses

Amplitude analyses of D^+ decays to a variety of 4-body kaon or pion final states, fitting simultaneously different partial wave components.

VALUE	DOCUMENT ID	TECN	COMMENT
	ABLIKIM 19AZ BES3		$D^+ \rightarrow K_S^0 \pi^+ \pi^-$

D^\pm REFERENCES

AAIJ 21T JHEP 2106 044	R. Aaij et al.	(LHCb Collab.)
AAIJ 21U JHEP 2106 019	R. Aaij et al.	(LHCb Collab.)
ABLIKIM 21AD PR D104 012006	M. Ablikim et al.	(BESIII Collab.)
ABLIKIM 21BA PR D104 052008	M. Ablikim et al.	(BESIII Collab.)
ABLIKIM 21BB PR D104 072005	M. Ablikim et al.	(BESIII Collab.)
ABUDINEN 21A PRL 127 211801	F. Abudinene et al.	(BELLE II Collab.)
ABLIKIM 20AA PR D102 052003	M. Ablikim et al.	(BESIII Collab.)
ABLIKIM 20AC PR D102 052006	M. Ablikim et al.	(BESIII Collab.)
ABLIKIM 20AF PR D102 112005	M. Ablikim et al.	(BESIII Collab.)
ABLIKIM 20G PR D101 031102	M. Ablikim et al.	(BESIII Collab.)
ABLIKIM 20D PR D101 052009	M. Ablikim et al.	(BESIII Collab.)
ABLIKIM 20H PR D101 072005	M. Ablikim et al.	(BESIII Collab.)
ABLIKIM 20T PRL 124 231801	M. Ablikim et al.	(BESIII Collab.)
ABLIKIM 20V PRL 124 241803	M. Ablikim et al.	(BESIII Collab.)
ABLIKIM 20Z PRL 125 141802	M. Ablikim et al.	(BESIII Collab.)
AAIJ 19G JHEP 1903 176	R. Aaij et al.	(LHCb Collab.)
AAIJ 19H JHEP 1904 063	R. Aaij et al.	(LHCb Collab.)
AAIJ 19T PRL 122 191803	R. Aaij et al.	(LHCb Collab.)
ABLIKIM 19AL PR D99 112002	M. Ablikim et al.	(BESIII Collab.)
ABLIKIM 19AY PR D100 072006	M. Ablikim et al.	(BESIII Collab.)
ABLIKIM 19AZ PR D100 072008	M. Ablikim et al.	(BESIII Collab.)
ABLIKIM 19BG PRL 123 211802	M. Ablikim et al.	(BESIII Collab.)
ABLIKIM 19BH PRL 123 231801	M. Ablikim et al.	(BESIII Collab.)
ABLIKIM 19BI PL B798 135917	M. Ablikim et al.	(BESIII Collab.)
ABLIKIM 19C PRL 122 062001	M. Ablikim et al.	(BESIII Collab.)
ABLIKIM 19M PR D99 032002	M. Ablikim et al.	(BESIII Collab.)
ABLIKIM 18AC PR D98 092009	M. Ablikim et al.	(BESIII Collab.)
ABLIKIM 18AE PRL 121 171803	M. Ablikim et al.	(BESIII Collab.)
ABLIKIM 18F PRL 121 081802	M. Ablikim et al.	(BESIII Collab.)
ABLIKIM 18P PR D97 072015	M. Ablikim et al.	(BESIII Collab.)
ABLIKIM 18R PR D97 092009	M. Ablikim et al.	(BESIII Collab.)
ABLIKIM 18W PR D97 072004	M. Ablikim et al.	(BESIII Collab.)
BABU 18 PR D97 011101	V. Babu et al.	(BELLE Collab.)
AAIJ 17AF PL B771 21	R. Aaij et al.	(LHCb Collab.)
ABLIKIM 17A PL B765 231	M. Ablikim et al.	(BESIII Collab.)
ABLIKIM 17AD PR D96 092002	M. Ablikim et al.	(BESIII Collab.)
ABLIKIM 17M PR D95 071102	M. Ablikim et al.	(BESIII Collab.)
ABLIKIM 17S PR D96 012002	M. Ablikim et al.	(BESIII Collab.)
ABLIKIM 16D PRL 116 082001	M. Ablikim et al.	(BESIII Collab.)
ABLIKIM 16F PR D94 032001	M. Ablikim et al.	(BESIII Collab.)
ABLIKIM 16G EPJ C76 369	M. Ablikim et al.	(BESIII Collab.)
ABLIKIM 16V CP C40 113001	M. Ablikim et al.	(BESIII Collab.)
ABLIKIM 15AF PR D92 112008	M. Ablikim et al.	(BESIII Collab.)
ABLIKIM 15W PR D92 071101	M. Ablikim et al.	(BESIII Collab.)
AAIJ 14BD JHEP 1410 025	R. Aaij et al.	(LHCb Collab.)
AAIJ 14C PL B728 585	R. Aaij et al.	(LHCb Collab.)
ABAZOV 14D PR D90 111102	V.M. Abazov et al.	(DO Collab.)
ABLIKIM 14F PR D89 052001	M. Ablikim et al.	(BESIII Collab.)
ABLIKIM 14E PR D89 051104	M. Ablikim et al.	(BESIII Collab.)
BONVICINI 14 PR D89 072002	G. Bonvicini et al.	(CLEO Collab.)
AAIJ 13AF PL B724 203	R. Aaij et al.	(LHCb Collab.)
AAIJ 13W JHEP 1306 112	R. Aaij et al.	(LHCb Collab.)
DOBBS 13 PRL 110 131802	S. Dobbs et al.	(CLEO Collab.)
KO 13 JHEP 1302 098	B.R. Ko et al.	(BELLE Collab.)
LEES 13E PR D87 052012	J.P. Lees et al.	(BABAR Collab.)
LEES 13F PR D87 052010	J.P. Lees et al.	(BABAR Collab.)
KO Also 12A PRL 109 119903 (errat.)	B.R. Ko et al.	(BELLE Collab.)
	PRL 109 021601	(BELLE Collab.)
STARIC 12 PRL 108 071801	M. Staric et al.	(BELLE Collab.)
AAIJ 11G PR D84 112008	R. Aaij et al.	(LHCb Collab.)
DEL-AMO-SA...11H PR D83 071103	P. del Amo Sanchez et al.	(BABAR Collab.)
DEL-AMO-SA...11I PR D83 072001	P. del Amo Sanchez et al.	(BABAR Collab.)
LEES 11E PR D84 031103	J.P. Lees et al.	(BABAR Collab.)
LEES 11G PR D84 072006	J.P. Lees et al.	(BABAR Collab.)
WILLIAMS 11 PR D84 054015	M. Williams	(LOIC Collab.)
WON 11 PRL 107 221801	E. Won et al.	(BELLE Collab.)
YELTON 11 PR D84 032001	J. Yelton et al.	(CLEO Collab.)
AWASHIN 10A PL B686 84	V.V. Anashin et al.	(VEPP-4M KEKB Collab.)
ASNER 10 PR D81 052007	D.M. Asner et al.	(CLEO Collab.)

Table of meson particle listings for D mesons, including columns for name, mass, width, and production methods.

Table of meson particle listings for D mesons, including columns for name, mass, width, and production methods.

OTHER RELATED PAPERS

Table of other related papers, including authors and journal references.



I(J^P) = 1/2(0^-)

D0 MASS

The fit includes D±, D0, D±, D*±, D*0, D±, D1(2420)0, D±(2460)0, and D±(2536)± mass and mass difference measurements.

Given the recent addition of much more precise measurements, we have omitted all those masses published up through 1990. See any Review before 2015 for those earlier results.

Table of D0 mass measurements with columns: VALUE (MeV), EVTS, DOCUMENT ID, TECN, COMMENT.

1 Obtained by analyzing CLEO-c data but not authored by the CLEO Collaboration. The largest source of error in the TOMARADZE 14 value is from the uncertainties in the K- and K± masses. The systematic error given above is the addition in quadrature of ±0.022 ± 0.053 MeV, where the second error is from those mass uncertainties.
2 The largest source of error in the LEES 13s value is from the uncertainty of the K+ mass. The quoted systematic error is in fact ±0.043 + 3 (mK+ - 493.677), in MeV.

mD± - mD0

The fit includes D±, D0, D±, D*±, D*0, D±, D1(2420)0, D±(2460)0, and D±(2536)± mass and mass difference measurements.

Table of D0 mass difference measurements with columns: VALUE (MeV), DOCUMENT ID, TECN, COMMENT.

D0 MEAN LIFE

Measurements with an error > 10 x 10^-15 s have been omitted from the average.

Table of D0 mean life measurements with columns: VALUE (10^-15 s), EVTS, DOCUMENT ID, TECN, COMMENT.

Meson Particle Listings

 D^0

• • • We do not use the following data for averages, fits, limits, etc. • • •

424 ± 11 ± 7	5118	FRABETTI	91	E687	$K^- \pi^+$, $K^- \pi^+ \pi^+ \pi^-$
417 ± 18 ± 15	890	ALVAREZ	90	NA14	$K^- \pi^+$, $K^- \pi^+ \pi^+ \pi^-$
388 ± 23 ± 21	641	² BARLAG	90c	ACCM	$\pi^- \text{Cu}$ 230 GeV
480 ± 40 ± 30	776	ALBRECHT	88i	ARG	$e^+ e^-$ 10 GeV
422 ± 8 ± 10	4212	RAAB	88	E691	Photoproduction
420 ± 50	90	BARLAG	87b	ACCM	K^- and π^- 200 GeV

¹ABUDINEN 21A determines the lifetime ratio $\tau(D^+)/\tau(D^0) = 2.510 \pm 0.013 \pm 0.007$.

²BARLAG 90c estimate systematic error to be negligible.

See the related review(s):

 $D^0 - \bar{D}^0$ Mixing

$$|m_{D_1^0} - m_{D_2^0}| = x \Gamma$$

The D_1^0 and D_2^0 are the mass eigenstates of the D^0 meson, as described in the note on “ $D^0 - \bar{D}^0$ Mixing,” above. The experiments usually present $x \pm \Delta m/\Gamma$. Then $\Delta m = x \Gamma = x \hbar/\tau$.

“OUR EVALUATION” comes from CPV allowing averages provided by the Heavy Flavor Averaging Group, see the note on “ $D^0 - \bar{D}^0$ Mixing.”

VALUE ($10^{10} \hbar s^{-1}$)	CL%	DOCUMENT ID	TECN	COMMENT
0.997 \pm 0.116 OUR EVALUATION				
0.92 \pm 0.12 OUR AVERAGE				
0.97 \pm 0.14 \pm 0.13		1 AAIJ	21AB LHCB	pp at 13 TeV, $D^0 \rightarrow K_S^0 \pi^+ \pi^-$
0.66 \pm 0.41 \pm 0.37		2 AAIJ	19X LHCB	pp at 7, 8 TeV, $D^0 \rightarrow K_S^0 \pi^+ \pi^-$
- 2.10 \pm 1.29 \pm 0.41		3 AAIJ	18K LHCB	pp at 7, 8, 13 TeV
3.7 \pm 2.9 \pm 1.5		4 AAIJ	16V LHCB	pp at 7 TeV
		5 LEES	16D BABR	$e^+ e^-$, 10.6 GeV
		6 KO	14 BELL	$e^+ e^- \rightarrow \Upsilon(nS)$
1.37 \pm 0.46 \pm 0.18 \pm 0.28		7 PENG	14 BELL	$e^+ e^- \rightarrow \Upsilon(nS)$
		8 AALTONEN	13AE CDF	$p\bar{p}$ at 1.96 TeV
0.39 \pm 0.56 \pm 0.35		9 DEL-AMO-SA...10D	BABR	$e^+ e^-$, 10.6 GeV
		10 AAIJ	17AO LHCB	Repl. by AAIJ 18K
		11 AAIJ	13CE LHCB	Repl. by AAIJ 17AO
		12 AAIJ	13N LHCB	Repl. by AAIJ 13CE
6.4 \pm 1.4 \pm 1.0		13 AUBERT	09AN BABR	$e^+ e^-$ at 10.58 GeV
- 2 \pm 7 \pm 6		14 LOWREY	09	CLEO $e^+ e^-$ at $\psi(3770)$
1.98 \pm 0.73 \pm 0.32 \pm 0.41		15 ZHANG	07B BELL	Repl. by PENG 14
< 7	95	16 ZHANG	06 BELL	$e^+ e^-$
-11 to +22		15 ASNER	05 CLEO	$e^+ e^- \approx 10$ GeV
< 11	90	BITENC	05 BELL	
< 30	90	CRAWFIELD	05 CLEO	
< 7	95	16 LI	05A BELL	See ZHANG 06
< 22	95	17 LINK	05H FOCS	γ nucleus
< 23	95	AUBERT	04Q BABR	
< 11	95	16 AUBERT	03Z BABR	$e^+ e^-$, 10.6 GeV
< 7	95	18 GODANG	00 CLE2	$e^+ e^-$
< 32	90	19,20 AITALA	98 E791	π^- nucleus, 500 GeV
< 24	90	21 AITALA	96C E791	π^- nucleus, 500 GeV
< 21	90	20,22 ANJOS	88c E691	Photoproduction

¹AAIJ 21AB measurement allows for CP violation (none seen).

²AAIJ 19X D^0 come from D^{*+} and $\bar{B} \rightarrow D^0 \mu^- X$ decays (and c.c.). Measurement allows for CP violation (none seen).

³The result was established with D^0 from prompt and secondary D^* . Based on 5 fb⁻¹ of data collected at $\sqrt{s} = 7, 8, 13$ TeV. Assumes no CP violation. Reported $x'^2 = (3.9 \pm 2.7) \times 10^{-5}$ and $y' = (5.28 \pm 0.52) \times 10^{-3}$, where $x' = x \cos(\delta) + y \sin(\delta)$, $y' = y$.

⁴Model-independent measurement of the charm mixing parameters in the decay $D^0 \rightarrow K_S^0 \pi^+ \pi^-$ using 1.0 fb⁻¹ of LHCB data at $\sqrt{s} = 7$ TeV.

⁵Time-dependent amplitude analysis of $D^0 \rightarrow \pi^+ \pi^- \pi^0$.

⁶Based on 976 fb⁻¹ of data collected at $Y(nS)$ resonances. Assumes no CP violation. Reported $x'^2 = (0.09 \pm 0.22) \times 10^{-3}$ and $y' = (4.6 \pm 3.4) \times 10^{-3}$, where $x' = x \cos(\delta) + y \sin(\delta)$, $y' = y \cos(\delta) - x \sin(\delta)$ and δ is the strong phase between $D^0 \rightarrow K^+ \pi^-$ and $\bar{D}^0 \rightarrow K^+ \pi^-$.

⁷The time-dependent Dalitz-plot analysis of $D^0 \rightarrow K_S^0 \pi^+ \pi^-$ is employed. Decay-time information and interference on the Dalitz plot are used to distinguish doubly Cabibbo-suppressed decays from mixing and to measure the relative phase between $D^0 \rightarrow K^+ \pi^-$ and $\bar{D}^0 \rightarrow K^+ \pi^-$. This value allows CP violation and is sensitive to the sign of Δm .

⁸Based on 9.6 fb⁻¹ of data collected at the Tevatron. Assumes no CP violation. Reported $x'^2 = (0.08 \pm 0.18) \times 10^{-3}$ and $y' = (4.3 \pm 4.3) \times 10^{-3}$, where $x' = x \cos(\delta) + y \sin(\delta)$, $y' = y \cos(\delta) - x \sin(\delta)$ and δ is the strong phase between the $D^0 \rightarrow K^+ \pi^-$ and $\bar{D}^0 \rightarrow K^+ \pi^-$.

⁹DEL-AMO-SANCHEZ 10D uses 540,800 $\pm 800 K_S^0 \pi^+ \pi^-$ and 79,900 $\pm 300 K_S^0 K^+ K^-$ events in a time-dependent amplitude analysis of the D^0 and \bar{D}^0 Dalitz plots. No evidence was found for CP violation, and the values here assume no such violation.

¹⁰The result was established with D^0 from prompt and secondary D^* . Based on 3 fb⁻¹ of data collected at $\sqrt{s} = 7, 8$ TeV. Assumes no CP violation. Reported $x'^2 = (3.6 \pm 4.3) \times 10^{-5}$ and $y' = (5.23 \pm 0.84) \times 10^{-3}$, where $x' = x \cos(\delta) + y \sin(\delta)$, $y' = y \cos(\delta) - x \sin(\delta)$ and δ is the strong phase between the $D^0 \rightarrow K^+ \pi^-$ and $\bar{D}^0 \rightarrow K^+ \pi^-$.

¹¹Based on 3 fb⁻¹ of data collected at $\sqrt{s} = 7, 8$ TeV. Assumes no CP violation. Reported $x'^2 = (5.5 \pm 4.9) \times 10^{-4}$ and $y' = (4.8 \pm 1.0) \times 10^{-3}$, where $x' = x \cos(\delta) + y \sin(\delta)$, $y' = y \cos(\delta) - x \sin(\delta)$ and δ is the strong phase between the $D^0 \rightarrow K^+ \pi^-$ and $\bar{D}^0 \rightarrow K^+ \pi^-$.

¹²Based on 1 fb⁻¹ of data collected at $\sqrt{s} = 7$ TeV in 2011. Assumes no CP violation. Reported $x'^2 = (-0.9 \pm 1.3) \times 10^{-4}$ and $y' = (7.2 \pm 2.4) \times 10^{-3}$, where $x' = x \cos(\delta) + y \sin(\delta)$, $y' = y \cos(\delta) - x \sin(\delta)$ and δ is the strong phase between the $D^0 \rightarrow K^+ \pi^-$ and $\bar{D}^0 \rightarrow K^+ \pi^-$.

¹³The AUBERT 09AN values are inferred from the branching ratio $\Gamma(D^0 \rightarrow K^+ \pi^- \pi^0)$ via $\bar{D}^0)/\Gamma(D^0 \rightarrow K^- \pi^+ \pi^0)$ given near the end of this Listings. Mixing is distinguished from DCS decays using decay-time information. Interference between mixing and DCS is allowed. The phase between $D^0 \rightarrow K^+ \pi^- \pi^0$ and $\bar{D}^0 \rightarrow K^+ \pi^- \pi^0$ is assumed to be small. The width difference here is y'' , which is not the same as y_{CP} in the note on $D^0 - \bar{D}^0$ mixing.

¹⁴LOWREY 09 uses quantum correlations in $e^+ e^- \rightarrow D^0 \bar{D}^0$ at the $\psi(3770)$. See below for coherence factors and average relative strong phases for both $D^0 \rightarrow K^- \pi^+ \pi^0$ and $D^0 \rightarrow K^- \pi^- 2\pi^+$. A fit that includes external measurements of charm mixing parameters gets $\Delta m = (2.34 \pm 0.61) \times 10^{10} \hbar s^{-1}$.

¹⁵The ASNER 05 and ZHANG 07B values are from the time-dependent Dalitz-plot analysis of $D^0 \rightarrow K_S^0 \pi^+ \pi^-$. Decay-time information and interference on the Dalitz plot are used to distinguish doubly Cabibbo-suppressed decays from mixing and to measure the relative phase between $D^0 \rightarrow K^+ \pi^-$ and $\bar{D}^0 \rightarrow K^+ \pi^-$. This value allows CP violation and is sensitive to the sign of Δm .

¹⁶The AUBERT 03Z, LI 05A, and ZHANG 06 limits are inferred from the $D^0 - \bar{D}^0$ mixing ratio $\Gamma(K^+ \pi^- \text{ via } \bar{D}^0)/\Gamma(K^- \pi^+)$ given near the end of this D^0 Listings. Decay-time information is used to distinguish DCS decays from $D^0 - \bar{D}^0$ mixing. The limit allows interference between the DCS and mixing ratios, and also allows CP violation. AUBERT 03Z assumes the strong phase between $D^0 \rightarrow K^+ \pi^-$ and $\bar{D}^0 \rightarrow K^+ \pi^-$ amplitudes is small; if an arbitrary phase is allowed, the limit degrades by 20%. The LI 05A and ZHANG 06 limits are valid for an arbitrary strong phase.

¹⁷This LINK 05H limit is inferred from the $D^0 - \bar{D}^0$ mixing ratio $\Gamma(K^+ \pi^- \text{ via } \bar{D}^0)/\Gamma(K^- \pi^+)$ given near the end of this D^0 Listings. Decay-time information is used to distinguish DCS decays from $D^0 - \bar{D}^0$ mixing. The limit allows interference between the DCS and mixing ratios, and also allows CP violation. The strong phase between $D^0 \rightarrow K^+ \pi^-$ and $\bar{D}^0 \rightarrow K^+ \pi^-$ is assumed to be small. If an arbitrary relative strong phase is allowed, the limit degrades by 25%.

¹⁸This GODANG 00 limit is inferred from the $D^0 - \bar{D}^0$ mixing ratio $\Gamma(K^+ \pi^- \text{ via } \bar{D}^0)/\Gamma(K^- \pi^+)$ given near the end of this D^0 Listings. Decay-time information is used to distinguish DCS decays from $D^0 - \bar{D}^0$ mixing. The limit allows interference between the DCS and mixing ratios, and also allows CP violation. The strong phase between $D^0 \rightarrow K^+ \pi^-$ and $\bar{D}^0 \rightarrow K^+ \pi^-$ is assumed to be small. If an arbitrary relative strong phase is allowed, the limit degrades by a factor of two.

¹⁹AITALA 98 allows interference between the doubly Cabibbo-suppressed and mixing amplitudes, and also allows CP violation in this term, but assumes that $A_D = A_R = 0$. See the note on “ $D^0 - \bar{D}^0$ Mixing,” above.

²⁰This limit is inferred from R_M for $f = K^+ \pi^-$ and $f = K^+ \pi^- \pi^+ \pi^-$. See the note on “ $D^0 - \bar{D}^0$ Mixing,” above. Decay-time information is used to distinguish doubly Cabibbo-suppressed decays from $D^0 - \bar{D}^0$ mixing.

²¹This limit is inferred from R_M for $f = K^+ \ell^- \bar{\nu}_\ell$. See the note on “ $D^0 - \bar{D}^0$ Mixing,” above.

²²ANJOS 88c assumes that $y = 0$. See the note on “ $D^0 - \bar{D}^0$ Mixing,” above. Without this assumption, the limit degrades by about a factor of two.

$$(\Gamma_{D_1^0} - \Gamma_{D_2^0})/\Gamma = 2y$$

The D_1^0 and D_2^0 are the mass eigenstates of the D^0 meson, as described in the note on “ $D^0 - \bar{D}^0$ Mixing,” above.

Due to the strong phase difference between $D^0 \rightarrow K^+ \pi^-$ and $\bar{D}^0 \rightarrow K^+ \pi^-$, we exclude from the average those measurements of y' that are inferred from the $D^0 - \bar{D}^0$ mixing ratio $\Gamma(K^+ \pi^- \text{ via } \bar{D}^0)/\Gamma(K^+ \pi^-)$ given near the end of this D^0 Listings.

Some early results have been omitted. See our 2006 Review (Journal of Physics **G33** 1 (2006)).

“OUR EVALUATION” comes from CPV allowing averages provided by the Heavy Flavor Averaging Group, see the note on “ $D^0 - \bar{D}^0$ Mixing.”

VALUE (units 10^{-2})	EVTS	DOCUMENT ID	TECN	COMMENT
1.23 \pm 0.11 OUR EVALUATION				
1.06 \pm 0.16 OUR AVERAGE				Error includes scale factor of 1.1.
0.92 \pm 0.30 \pm 0.28	30.6M	1 AAIJ	21AB LHCB	pp at 13 TeV
1.92 \pm 1.82 \pm 1.29 \pm 1.24	91k	2 NAYAK	20 BELL	$D^0 \rightarrow K_S^0 \omega$
1.14 \pm 0.26 \pm 0.18		3 AAIJ	19 LHCB	pp at 7, 8 TeV
1.48 \pm 0.74	2.3M	4 AAIJ	19X LHCB	$D^0 \rightarrow K_S^0 \pi^+ \pi^-$
		5 AAIJ	18K LHCB	pp at 7, 8, 13 TeV
		6 AAIJ	16V LHCB	pp at 7 TeV
0.06 \pm 0.92 \pm 0.26		7 LEES	16D BABR	$e^+ e^-$, 10.6 GeV
0.4 \pm 1.8 \pm 1.0				

See key on page 1127

Meson Particle Listings

D^0

$2.22 \pm 0.44 \pm 0.18$		8 STARIC	16 BELL	$e^+e^- \rightarrow \Upsilon(nS)$
$-4.0 \pm 2.6 \pm 1.4$		9 ABLIKIM	15D BES3	e^+e^- at $\psi(3770)$
		10 KO	14 BELL	$e^+e^- \rightarrow \Upsilon(nS)$
$0.60 \pm 0.30^{+0.10}_{-0.17}$		11 PENG	14 BELL	$e^+e^- \rightarrow \Upsilon(nS)$
$1.44 \pm 0.36 \pm 0.24$		12 AALTONEN	13AE CDF	$p\bar{p}$ at 1.96 TeV
$0.55 \pm 0.63 \pm 0.41$		13 LEES	13 BABR	$e^+e^- \rightarrow \Upsilon(4S)$
$1.14 \pm 0.40 \pm 0.30$		14 AAIJ	12K LHCb	pp at 7 TeV
$0.22 \pm 1.22 \pm 1.04$		15 DEL-AMO-SA.	10D BABR	e^+e^- , 10.6 GeV
$-1.0 \pm 2.0^{+1.4}_{-1.6}$	18k	16 ZUPANC	09 BELL	$e^+e^- \approx \Upsilon(4S)$
$-2.4 \pm 5.0 \pm 2.8$	3393	17 ABE	02I BELL	$e^+e^- \approx \Upsilon(4S)$
$6.84 \pm 2.78 \pm 1.48$	10k	18 CSORNA	02 CLE2	$e^+e^- \approx \Upsilon(4S)$
$+1.6 \pm 5.8 \pm 2.1$		17 LINK	00 FOCUS	γ nucleus
		17 AITALA	99E E791	$K^-\pi^+$, K^+K^-

- • • We do not use the following data for averages, fits, limits, etc. • • •
- 19 AAIJ 17A LHCb Repl. by AAIJ 18k
- 20 AAIJ 13CE LHCb Repl. by AAIJ 17A0
- 21 AAIJ 13N LHCb Repl. by AAIJ 13CE
- 22 AUBERT 09AI BABR See LEES 13
- 23 AUBERT 09AN BABR e^+e^- at 10.58 GeV
- 24 LOWREY 09 CLEO e^+e^- at $\psi(3770)$
- 25 AALTONEN 08E CDF $p\bar{p}$, $\sqrt{s} = 1.96$ TeV
- 26 AUBERT 08U BABR See AUBERT 09AI
- 27 STARIC 07W BABR $e^+e^- \approx 10.6$ GeV
- 28 ZHANG 07B BELL Repl. by STARIC 16
- 25,29 ZHANG 06 BELL e^+e^-
- 28 ASNER 05 CLEO $e^+e^- \approx 10$ GeV
- 25,29 LI 05A BELL See ZHANG 06
- 25,29 LINK 05H FOCUS γ nucleus
- 30 AUBERT 03P BABR See AUBERT 08U
- 25,29 AUBERT 03Z BABR e^+e^- , 10.6 GeV
- 25 GODANG 00 CLE2 e^+e^-
- 1 AAIJ 21AB analysis of $D^0 \rightarrow K_S^0 \pi^+ \pi^-$ events allows for CP violation (none seen).
- 2 NAYAK 20 reports $(1.92 \pm 1.82 \pm 1.24^{+0.34}_{-0.00}) \times 10^{-2}$ where the last uncertainty is due to possible presence of CP-even decays in the data sample. Extracts $y_{CP} = (\Gamma_{CP^+} - \Gamma_{CP^-}) / (\Gamma_{CP^+} + \Gamma_{CP^-})$ in $D^0 \rightarrow K_S^0 \omega$ versus $\bar{D}^0 \rightarrow K_S^0 \omega$, by measuring the decay lifetime of $D^0 \rightarrow K_S^0 \omega$ with $\omega \rightarrow \pi^+ \pi^- \pi^0$ versus $D^0 \rightarrow K^- \pi^+$. We list $2y_{CP} = 2y$ ($= \Delta\Gamma/\Gamma$) in the absence of CP violation.
- 3 Based on 3 fb^{-1} of data collected at $\sqrt{s} = 7, 8$ TeV. Measures the lifetime difference between $D^0 \rightarrow K^- K^+$ and $D^0 \rightarrow \pi^- \pi^+$ (CP even) decays and $D^0 \rightarrow K^- \pi^+$ (CP mixed) decays, or $y_{CP} = (\Gamma_{CP^+} - \Gamma_{CP^-}) / (\Gamma_{CP^+} + \Gamma_{CP^-})$. The D^0 mesons are required to originate from semimuonic decays of B mesons. We list $2y_{CP} = \Delta\Gamma/\Gamma$.
- 4 AAIJ 19X D^0 come from D^{*+} and $\bar{B}^0 \rightarrow D^0 \mu^- X$ decays (and c.c.) in pp collisions at 7 and 8 TeV. Measurement allows for CP violation (none seen).
- 5 The result was established with D^0 from prompt and secondary D^* . Based on 5 fb^{-1} of data collected at $\sqrt{s} = 7, 8, 13$ TeV. Assumes no CP violation. Reported $x'^2 = (3.9 \pm 2.7) \times 10^{-5}$ and $y' = (5.28 \pm 0.52) \times 10^{-3}$, where $x' = x \cos(\delta) + y \sin(\delta)$, $y' = y \cos(\delta) - x \sin(\delta)$ and δ is the strong phase between the $D^0 \rightarrow K^+ \pi^-$ and $\bar{D}^0 \rightarrow K^+ \pi^-$.
- 6 Model-independent measurement of the charm mixing parameters in the decay $D^0 \rightarrow K_S^0 \pi^+ \pi^-$ using 1.0 fb^{-1} of LHCb data at $\sqrt{s} = 7$ TeV.
- 7 Time-dependent amplitude analysis of $D^0 \rightarrow \pi^+ \pi^- \pi^0$.
- 8 An improved measurement of $\bar{D}^0 - D^0$ mixing and a search for CP violation in D^0 decays to CP-even final states $K^+ K^-$ and $\pi^+ \pi^-$ using the final Belle data sample of 976 fb^{-1} .
- 9 ABLIKIM 15D uses quantum correlations in $e^+e^- \rightarrow D^0 \bar{D}^0$ at the $\psi(3770)$.
- 10 Based on 976 fb^{-1} of data collected at Y(nS) resonances. Assumes no CP violation. Reported $x'^2 = (0.09 \pm 0.22) \times 10^{-3}$ and $y' = (4.6 \pm 3.4) \times 10^{-3}$, where $x' = x \cos(\delta) + y \sin(\delta)$, $y' = y \cos(\delta) - x \sin(\delta)$ and δ is the strong phase between $D^0 \rightarrow K^+ \pi^-$ and $\bar{D}^0 \rightarrow K^+ \pi^-$.
- 11 The time-dependent Dalitz-plot analysis of $D^0 \rightarrow K_S^0 \pi^+ \pi^-$ is employed. Decay-time information and interference on the Dalitz plot are used to distinguish doubly Cabibbo-suppressed decays from mixing and to measure the relative phase between $D^0 \rightarrow K^{*+} \pi^-$ and $\bar{D}^0 \rightarrow K^{*+} \pi^-$. This value allows CP violation and is sensitive to the sign of Δm .
- 12 Based on 9.6 fb^{-1} of data collected at the Tevatron. Assumes no CP violation. Reported $x'^2 = (0.08 \pm 0.18) \times 10^{-3}$ and $y' = (4.3 \pm 4.3) \times 10^{-3}$, where $x' = x \cos(\delta) + y \sin(\delta)$, $y' = y \cos(\delta) - x \sin(\delta)$ and δ is the strong phase between the $D^0 \rightarrow K^+ \pi^-$ and $\bar{D}^0 \rightarrow K^+ \pi^-$.
- 13 Obtained $y_{CP} = (0.72 \pm 0.18 \pm 0.12)\%$ based on three effective D^0 lifetimes measured in $K^{\mp} \pi^{\pm}$, $K^- K^+$, and $\pi^- \pi^+$. We list $2y_{CP} = \Delta\Gamma/\Gamma$.
- 14 Compared the lifetimes of D^0 decay to the CP eigenstate $K^+ K^-$ with D^0 decay to $\pi^+ K^-$. The values here assume no CP violation.
- 15 DEL-AMO-SANCHEZ 10D uses $540,800 \pm 800 K_S^0 \pi^+ \pi^-$ and $79,900 \pm 300 K_S^0 K^+ K^-$ events in a time-dependent amplitude analyses of the D^0 and \bar{D}^0 Dalitz plots. No evidence was found for CP violation, and the values here assume no such violation.
- 16 ZUPANC 09 uses a method based on measuring the mean decay time of $D^0 \rightarrow K_S^0 K^+ K^-$ events for different $K^+ K^-$ mass intervals.

- 17 LINK 00, AITALA 99E, and ABE 02I measure the lifetime difference between $D^0 \rightarrow K^- K^+$ (CP even) decays and $D^0 \rightarrow K^- \pi^+$ (CP mixed) decays, or $y_{CP} = [\Gamma(CP^+) - \Gamma(CP^-)] / [\Gamma(CP^+) + \Gamma(CP^-)]$. We list $2y_{CP} = \Delta\Gamma/\Gamma$.
- 18 CSORNA 02 measures the lifetime difference between $D^0 \rightarrow K^- K^+$ and $\pi^- \pi^+$ (CP even) decays and $D^0 \rightarrow K^- \pi^+$ (CP mixed) decays, or $y_{CP} = [\Gamma(CP^+) - \Gamma(CP^-)] / [\Gamma(CP^+) + \Gamma(CP^-)]$. We list $2y_{CP} = \Delta\Gamma/\Gamma$.
- 19 The result was established with D^0 from prompt and secondary D^* . Based on 3 fb^{-1} of data collected at $\sqrt{s} = 7, 8$ TeV. Assumes no CP violation. Reported $x'^2 = (3.6 \pm 4.3) \times 10^{-5}$ and $y' = (5.23 \pm 0.84) \times 10^{-3}$, where $x' = x \cos(\delta) + y \sin(\delta)$, $y' = y \cos(\delta) - x \sin(\delta)$ and δ is the strong phase between the $D^0 \rightarrow K^+ \pi^-$ and $\bar{D}^0 \rightarrow K^+ \pi^-$.
- 20 Based on 3 fb^{-1} of data collected at $\sqrt{s} = 7, 8$ TeV. Assumes no CP violation. Reported $x'^2 = (5.5 \pm 4.9) \times 10^{-4}$ and $y' = (4.8 \pm 1.0) \times 10^{-3}$, where $x' = x \cos(\delta) + y \sin(\delta)$, $y' = y \cos(\delta) - x \sin(\delta)$ and δ is the strong phase between the $D^0 \rightarrow K^+ \pi^-$ and $\bar{D}^0 \rightarrow K^+ \pi^-$.
- 21 Based on 1 fb^{-1} of data collected at $\sqrt{s} = 7$ TeV in 2011. Assumes no CP violation. Reported $x'^2 = (-0.9 \pm 1.3) \times 10^{-4}$ and $y' = (7.2 \pm 2.4) \times 10^{-3}$, where $x' = x \cos(\delta) + y \sin(\delta)$, $y' = y \cos(\delta) - x \sin(\delta)$ and δ is the strong phase between the $D^0 \rightarrow K^+ \pi^-$ and $\bar{D}^0 \rightarrow K^+ \pi^-$.
- 22 This combines the $y_{CP} = (\tau_{K^+ \pi^-} / \tau_{K^+ K^-}) - 1$ using untagged $K^- \pi^+$ and $K^- K^+$ events of AUBERT 09AI with the disjoint y_{CP} using tagged $K^- \pi^+$, $K^- K^+$, and $\pi^- \pi^+$ events of AUBERT 08U.
- 23 The AUBERT 09AN values are inferred from the branching ratio $\Gamma(D^0 \rightarrow K^+ \pi^- \pi^0 \text{ via } \bar{D}^0) / \Gamma(D^0 \rightarrow K^- \pi^+ \pi^0)$ given near the end of this Listings. Mixing is distinguished from DCS decays using decay-time information. Interference between mixing and DCS is allowed. The phase between $D^0 \rightarrow K^+ \pi^- \pi^0$ and $\bar{D}^0 \rightarrow K^+ \pi^- \pi^0$ is assumed to be small. The width difference here is y'' , which is not the same as y_{CP} in the note on $D^0 - \bar{D}^0$ mixing.
- 24 LOWREY 09 uses quantum correlations in $e^+e^- \rightarrow D^0 \bar{D}^0$ at the $\psi(3770)$. See below for coherence factors and average relative strong phases for both $D^0 \rightarrow K^- \pi^+ \pi^0$ and $D^0 \rightarrow K^- \pi^- 2\pi^+$. A fit that includes external measurements of charm mixing parameters gets $2y = (1.62 \pm 0.32) \times 10^{-2}$.
- 25 The GODANG 00, AUBERT 03Z, LINK 05H, LI 05A, ZHANG 06, AUBERT 07W, and AALTONEN 08E limits are inferred from the $D^0 - \bar{D}^0$ mixing ratio $\Gamma(K^+ \pi^- \text{ via } \bar{D}^0) / \Gamma(K^- \pi^+)$ given near the end of this D^0 Listings. Decay-time information is used to distinguish DCS decays from $D^0 - \bar{D}^0$ mixing. The limits allow interference between the DCS and mixing ratios, and all except AUBERT 07W and AALTONEN 08E also allow CP violation. The phase between $D^0 \rightarrow K^+ \pi^-$ and $\bar{D}^0 \rightarrow K^+ \pi^-$ is assumed to be small. This is a measurement of y' and is not the same as the y_{CP} of our note above on " $D^0 - \bar{D}^0$ Mixing."
- 26 This value combines the results of AUBERT 08U and AUBERT 03P.
- 27 STARIC 07 compares the lifetimes of D^0 decay to the CP eigenstates $K^+ K^-$ and $\pi^+ \pi^-$ with D^0 decay to $K^- \pi^+$.
- 28 The ASNER 05 and ZHANG 07b values are from the time-dependent Dalitz-plot analysis of $D^0 \rightarrow K_S^0 \pi^+ \pi^-$. Decay-time information and interference on the Dalitz plot are used to distinguish doubly Cabibbo-suppressed decays from mixing and to measure the relative phase between $D^0 \rightarrow K^{*+} \pi^-$ and $\bar{D}^0 \rightarrow K^{*+} \pi^-$. This limit allows CP violation.
- 29 The ranges of AUBERT 03Z, LINK 05H, LI 05A, and ZHANG 06 measurements are for 95% confidence level.
- 30 AUBERT 03P measures $Y \equiv 2 \tau^0 / (\tau^+ + \tau^-) - 1$, where τ^0 is the $D^0 \rightarrow K^- \pi^+$ (and $\bar{D}^0 \rightarrow K^+ \pi^-$) lifetime, and τ^+ and τ^- are the D^0 and \bar{D}^0 lifetimes to CP-even states (here $K^- K^+$ and $\pi^- \pi^+$). In the limit of CP conservation, $Y = 0 \equiv \Delta\Gamma / 2\Gamma$. We list $2y = \Delta\Gamma/\Gamma$. AUBERT 03P also uses $\tau^+ - \tau^-$ to get $\Delta Y = -0.008 \pm 0.006 \pm 0.002$.

$|q/p|$

The mass eigenstates D_1^0 and D_2^0 are related to the $C = \pm 1$ states by $|D_{1,2}^0\rangle = p|D^0\rangle + q|\bar{D}^0\rangle$. See the note on " $D^0 - \bar{D}^0$ Mixing" above.

"OUR EVALUATION" comes from CPV allowing averages provided by the Heavy Flavor Averaging Group. This would include as-yet-unpublished results, see the note on " $D^0 - \bar{D}^0$ Mixing."

VALUE	EVTS	DOCUMENT ID	TECN	COMMENT
0.995 ± 0.016 OUR EVALUATION		HFLAV fit; see the note on " $D^0 - \bar{D}^0$ Mixing."		
0.99 ± 0.05 OUR AVERAGE				
0.996 ± 0.052	30.6M	1 AAIJ	21AB LHCb	pp at 13 TeV
$1.05^{+0.22}_{-0.17}$	2.3M	2 AAIJ	19X LHCb	pp at 7, 8 TeV
		3 AAIJ	18k LHCb	pp at 7, 8, 13 TeV
$0.90^{+0.16}_{-0.15}^{+0.08}_{-0.06}$		4 PENG	14 BELL	$e^+e^- \rightarrow \Upsilon(nS)$
		5 AAIJ	13CE LHCb	Repl. by AAIJ 18k
$0.86^{+0.30}_{-0.29}^{+0.10}_{-0.08}$		6 ZHANG	07B BELL	Repl. by PENG 14

- • • We do not use the following data for averages, fits, limits, etc. • • •
- 1 AAIJ 21AB result comes from analysis of $D^0 \rightarrow K_S^0 \pi^+ \pi^-$ events.
- 2 AAIJ 19X measurement comes from analysis of $D^0 \rightarrow K_S^0 \pi^+ \pi^-$ decays. D^0 come from D^{*+} and $\bar{B}^0 \rightarrow D^0 \mu^- X$ decays (and c.c.) in pp collisions at 7 and 8 TeV.
- 3 Based on 5 fb^{-1} of data collected at $\sqrt{s} = 7, 8, 13$ TeV. Allowing for CP violation, the direct CP violation in mixing is reported $1.00 < |q/p| < 1.35$ at the 68.3% CL for the $D^0 \rightarrow K^+ \pi^-$ and $\bar{D}^0 \rightarrow K^+ \pi^-$.
- 4 The time-dependent Dalitz-plot analysis of $D^0 \rightarrow K_S^0 \pi^+ \pi^-$ is employed. Decay-time information and interference on the Dalitz plot are used to distinguish doubly Cabibbo-suppressed decays from mixing and to measure the relative phase between $D^0 \rightarrow K^{*+} \pi^-$ and $\bar{D}^0 \rightarrow K^{*+} \pi^-$. This value allows CP violation and is sensitive to the sign of Δm .

Meson Particle Listings

D^0

⁵ Based on 3 fb⁻¹ of data collected at $\sqrt{s} = 7, 8$ TeV. Allowing for CP violation, the direct CP violation in mixing is reported $0.75 < |q/p| < 1.24$ at the 68.3% CL for the $D^0 \rightarrow K^+ \pi^-$ and $\bar{D}^0 \rightarrow K^+ \pi^-$.

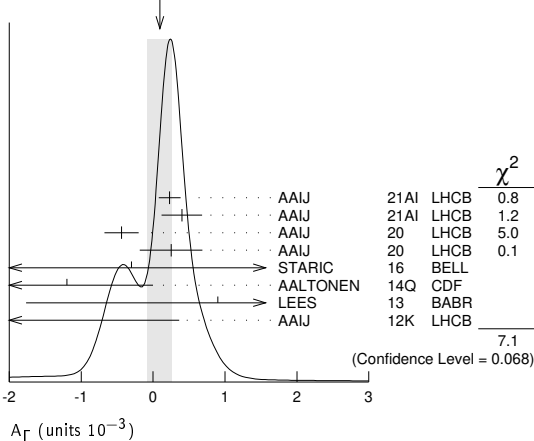
⁶ The phase of p/q is $(-14^{+16}_{-18} \pm 5)^\circ$. The ZHANG 07B value is from the time-dependent Dalitz-plot analysis of $D^0 \rightarrow K_S^0 \pi^+ \pi^-$. Decay-time information and interference on the Dalitz plot are used to distinguish doubly Cabibbo-suppressed decays from mixing and to measure the relative phase between $D^0 \rightarrow K^* \pi^-$ and $\bar{D}^0 \rightarrow K^* \pi^-$. This value allows CP violation.

A_F

A_F is the decay-rate asymmetry for CP-even final states $A_F = (\bar{\tau}_+ - \tau_+) / (\bar{\tau}_+ + \tau_+)$. See the note on " D^0 - \bar{D}^0 Mixing" above.

VALUE (units 10 ⁻³)	EVTS	DOCUMENT ID	TECN	COMMENT
0.089 ± 0.113 OUR EVALUATION				
0.09 ± 0.17 OUR AVERAGE Error includes scale factor of 1.5. See the ideogram below.				
0.23 ± 0.15 ± 0.03		1 AAIJ	21AI LHCb	$D^0 \rightarrow K^+ K^-$
0.40 ± 0.28 ± 0.04		1 AAIJ	21AI LHCb	$D^0 \rightarrow \pi^+ \pi^-$
-0.44 ± 0.23 ± 0.06	21M	2 AAIJ	20 LHCb	$D^0 \rightarrow K^+ K^-$
0.25 ± 0.43 ± 0.07	7M	3 AAIJ	20 LHCb	$D^0 \rightarrow \pi^+ \pi^-$
-0.3 ± 2.0 ± 0.7		4 STARIC	16 BELL	$e^+ e^- \rightarrow \Upsilon(nS)$
-1.2 ± 1.2	1.8M	5 AALTONEN	14Q CDF	$p\bar{p}, \sqrt{s} = 1.96$ TeV
0.9 ± 2.6 ± 0.6	0.7M	LEES	13 BABR	$e^+ e^- \rightarrow \Upsilon(4S)$
-5.9 ± 5.9 ± 2.1		6 AAIJ	12K LHCb	$p\bar{p}$ at 7 TeV, 2010 data.
• • • We do not use the following data for averages, fits, limits, etc. • • •				
-0.30 ± 0.32 ± 0.10	9.6M	6 AAIJ	17AK LHCb	Repl. by AAIJ 20
0.46 ± 0.58 ± 0.12	3.0M	7 AAIJ	17AK LHCb	Repl. by AAIJ 20
-1.34 ± 0.77 ± 0.26	2.3M	8 AAIJ	15AA LHCb	Repl. by AAIJ 20
-0.92 ± 1.45 ± 0.25	0.8M	9 AAIJ	15AA LHCb	Repl. by AAIJ 20
-0.35 ± 0.62 ± 0.12		6 AAIJ	14AL LHCb	Repl. by AAIJ 17AK
0.33 ± 1.06 ± 0.14		7 AAIJ	14AL LHCb	Repl. by AAIJ 17AK
2.6 ± 3.6 ± 0.8		AUBERT	08U BABR	See LEES 13
0.1 ± 3.0 ± 2.5		STARIC	07 BELL	Repl. by STARIC 16
8 ± 6 ± 2		AUBERT	03P BABR	$e^+ e^- \approx \Upsilon(4S)$

WEIGHTED AVERAGE
0.09±0.17 (Error scaled by 1.5)



- Requires D^0 to originate from $D^*(2010)^+ \rightarrow D^0 \pi^+$. AAIJ 21AI measures the parameter $\Delta Y_f \approx -A_F^f$ up to 1% corrections from y_{CP}^f .
- Measured using $D^0 \rightarrow K^+ K^-$ decays, combines measurements with D^0 either from partially reconstructed semileptonic B hadron decays or from $D^{*+} \rightarrow D^0 \pi^+$.
- Measured using $D^0 \rightarrow \pi^+ \pi^-$ decays, combines measurements with D^0 either from partially reconstructed semileptonic B hadron decays or from $D^{*+} \rightarrow D^0 \pi^+$.
- An improved measurement of $\bar{D}^0 - D^0$ mixing and a search for CP violation in D^0 decays to CP-even final states $K^+ K^-$ and $\pi^+ \pi^-$ using the final Belle data sample of 976 fb⁻¹.
- Combined result from $D^0 \rightarrow K^+ K^-$ and $D^0 \rightarrow \pi^+ \pi^-$, with D^0 from $D^{*+} \rightarrow D^0 \pi^+$ (and cc).
- Measured using $D^{*+} \rightarrow D^0 \pi^+$, $D^0 \rightarrow K^+ K^-$ decays (and cc).
- Measured using $D^{*+} \rightarrow D^0 \pi^+$, $D^0 \rightarrow \pi^+ \pi^-$ decays (and cc).
- Measured using $D^0 \rightarrow K^+ K^-$ decays, with D^0 from partially reconstructed semileptonic B hadron decays.
- Measured using $D^0 \rightarrow \pi^+ \pi^-$ decays, with D^0 from partially reconstructed semileptonic B hadron decays.

$\phi_{K_S^0 \pi \pi}$

Parametrizes CP violation in the interference between D^0 mixing and decay. The mass eigenstates D_1^0 and D_2^0 are related to the $C = \pm 1$ states by $|D_{1,2}^0\rangle = p|D^0\rangle + q|\bar{D}^0\rangle$. In the absence of CP violation in the decay, and using the usual phase

convention where CP conservation implies q/p is real, $\phi_{K_S^0 \pi \pi}$ is identical to the decay-mode-independent parameter $\phi = \arg(q/p)$.

VALUE	EVTS	DOCUMENT ID	TECN	COMMENT
0.02 ± 0.04 - 0.05 OUR AVERAGE				
0.056 ± 0.047 - 0.051	30.6M	1 AAIJ	21AB LHCb	$p\bar{p}$ at 13 TeV
-0.09 ± 0.11 - 0.16	2.3M	2 AAIJ	19X LHCb	$p\bar{p}$ at 7, 8 TeV
-0.10 ± 0.19 ± 0.07 - 0.09	1.2M	3 PENG	14 BELL	$e^+ e^-$ at $\Upsilon(4S, 5S)$

- AAIJ 21AB result comes from analysis of $D^0 \rightarrow K_S^0 \pi^+ \pi^-$ events.
- AAIJ 19X result comes from analysis of $D^0 \rightarrow K_S^0 \pi^+ \pi^-$ events. D^0 come from D^{*+} and $\bar{B}^- \rightarrow D^0 \mu^- X$ decays (and c.c.) in $p\bar{p}$ collisions at 7 and 8 TeV.
- PENG 14 reports $-0.10 \pm 0.19 \pm 0.05 \pm 0.05 - 0.07$ value where the last uncertainty is due to the amplitude model. We have added the systematic uncertainties in quadrature.

cos δ

δ is the $D^0 \rightarrow K^+ \pi^-$ relative strong phase.

VALUE	DOCUMENT ID	TECN	COMMENT
0.97 ± 0.11 OUR AVERAGE			
1.02 ± 0.11 ± 0.06	1 ABLIKIM	14c BES3	$e^+ e^- \rightarrow D^0 \bar{D}^0$, 3.77 GeV
0.81 ± 0.22 ± 0.07 - 0.18 - 0.05	2 ASNER	12 CLEO	$e^+ e^- \rightarrow D^0 \bar{D}^0$, 3.77 GeV
1.03 ± 0.31 ± 0.06	3 ASNER	08 CLEO	Repl. by ASNER 12

- • • We do not use the following data for averages, fits, limits, etc. • • •
- Uses quantum correlations in $e^+ e^- \rightarrow D^0 \bar{D}^0$ at the $\psi(3770)$ to measure the asymmetry of the branching fraction of $D^0 \rightarrow K^- \pi^+$ in CP-odd and CP-even eigenstates to be $(12.7 \pm 1.3 \pm 0.7)\%$. A fit that includes external measurements of charm mixing parameters finds the value quoted above.
 - Uses quantum correlations in $e^+ e^- \rightarrow D^0 \bar{D}^0$ at the $\psi(3770)$, where decay rates of CP-tagged $K\pi$ final states depend on the strong phases between the decays of $D^0 \rightarrow K^+ \pi^-$ and $\bar{D}^0 \rightarrow K^+ \pi^-$. The measurements obtained $\sin(\delta) = -0.01 \pm 0.41 \pm 0.04$ and $|\delta| = (10^{+28}_{-53} + 13^{+0}_{-0})^\circ$ as well. A fit that includes external measurements of charm mixing parameters finds $\cos(\delta) = 1.15^{+0.19}_{-0.17} + 0.00_{-0.08}$, $\sin(\delta) = 0.56^{+0.32}_{-0.31} + 0.21_{-0.20}$, and $|\delta| = (18^{+11}_{-17})^\circ$.
 - ASNER 08 uses quantum correlations in $e^+ e^- \rightarrow D^0 \bar{D}^0$ at the $\psi(3770)$, where decay rates of CP-tagged $K\pi$ final states depend on $\cos \delta$ because of interfering amplitudes. The above measurement implies $|\delta| < 75^\circ$ with a confidence level of 95%. A fit that includes external measurements of charm mixing parameters finds $\cos \delta = 1.10 \pm 0.35 \pm 0.07$. See also the note on " D^0 - \bar{D}^0 Mixing" p. 783 in our 2008 Review (PDG 08).

$D^0 \rightarrow K^- \pi^+ \pi^0$ COHERENCE FACTOR $R_{K\pi\pi^0}$

See the note on " D^0 - \bar{D}^0 Mixing" for the definition. $R_{K\pi\pi^0}$ can have any value between 0 and 1. A value near 1 indicates the decay is dominated by a few intermediate states with limited interference.

VALUE	EVTS	DOCUMENT ID	TECN	COMMENT
0.792 ± 0.033 OUR AVERAGE				
0.78 ± 0.04	62.4k	1 ABLIKIM	21AA BES3	$e^+ e^- \rightarrow D^0 \bar{D}^0$ at $\psi(3770)$
0.82 ± 0.06	1,2,3	EVANS	16	$e^+ e^- \rightarrow D^0 \bar{D}^0$ at $\psi(3770)$
0.82 ± 0.07	1,3	LIBBY	14	Repl. by EVANS 16
0.78 ± 0.11 - 0.25	4	LOWREY	09 CLEO	Repl. by LIBBY 14

- • • We do not use the following data for averages, fits, limits, etc. • • •
- Uses quantum correlations in $e^+ e^- \rightarrow D^0 \bar{D}^0$ at the $\psi(3770)$, where the decay rates of CP-tagged $K^- \pi^+ \pi^0$ final states depend on $R_{K\pi\pi^0}$ and $\delta^{K\pi\pi^0}$.
 - A combined fit with a recent LHCb $D^0 \bar{D}^0$ mixing results in AAIJ 16f is also reported to be 0.81 ± 0.06 .
 - Obtained by analyzing CLEO-c data but not authored by the CLEO Collaboration.
 - LOWREY 09 uses quantum correlations in $e^+ e^- \rightarrow D^0 \bar{D}^0$ at the $\psi(3770)$, where the decay rates of CP-tagged $K^- \pi^+ \pi^0$ final states depend on $R_{K\pi\pi^0}$ and $\delta^{K\pi\pi^0}$. A fit that includes external measurements of charm mixing parameters gets $R_{K\pi\pi^0} = 0.84 \pm 0.07$.

$D^0 \rightarrow K^- \pi^+ \pi^0$ AVERAGE RELATIVE STRONG PHASE $\delta^{K\pi\pi^0}$

The quoted value of δ is based on the same sign CP phase of D^0 and \bar{D}^0 convention.

VALUE (°)	EVTS	DOCUMENT ID	TECN	COMMENT
198 ± 10 OUR AVERAGE				
196 ± 14 - 15	62.4k	1 ABLIKIM	21AA BES3	$e^+ e^- \rightarrow D^0 \bar{D}^0$ at $\psi(3770)$
199 ± 13 - 14	1,2,3	EVANS	16	$e^+ e^- \rightarrow D^0 \bar{D}^0$ at $\psi(3770)$
164 ± 20 - 14	1,3	LIBBY	14	Repl. by EVANS 16
239 ± 32 - 28	4	LOWREY	09 CLEO	Repl. by LIBBY 14

- • • We do not use the following data for averages, fits, limits, etc. • • •
- Uses quantum correlations in $e^+ e^- \rightarrow D^0 \bar{D}^0$ at the $\psi(3770)$, where the decay rates of CP-tagged $K^- \pi^+ \pi^0$ final states depend on $R_{K\pi\pi^0}$ and $\delta^{K\pi\pi^0}$.
 - A combined fit with a recent LHCb $D^0 \bar{D}^0$ mixing results in AAIJ 16f is also reported to be 198^{+14}_{-15} degree.
 - Obtained by analyzing CLEO-c data but not authored by the CLEO Collaboration.
 - LOWREY 09 uses quantum correlations in $e^+ e^- \rightarrow D^0 \bar{D}^0$ at the $\psi(3770)$, where the decay rates of CP-tagged $K^- \pi^+ \pi^0$ final states depend on $R_{K\pi\pi^0}$ and $\delta^{K\pi\pi^0}$. A fit that includes external measurements of charm mixing parameters gets $\delta^{K\pi\pi^0} = (227^{+14}_{-17})^\circ$.

$D^0 \rightarrow K^- \pi^- 2\pi^+$ COHERENCE FACTOR $R_{K3\pi}$

See the note on ' D^0 - \bar{D}^0 Mixing' for the definition. $R_{K3\pi}$ can have any value between 0 and 1. A value near 1 indicates the decay is dominated by a few intermediate states with limited interference.

VALUE	EVTS	DOCUMENT ID	TECN	COMMENT
0.52 ± 0.10 -0.09	OUR AVERAGE			
0.52 ± 0.12 -0.10	8.6k	¹ ABLIKIM	21AA BES3	$e^+e^- \rightarrow D^0\bar{D}^0$ at $\psi(3770)$
0.53 ± 0.18 -0.21		^{1,2,3} EVANS	16	$e^+e^- \rightarrow D^0\bar{D}^0$ at $\psi(3770)$, $p\bar{p}$ at 7,8 TeV
• • • We do not use the following data for averages, fits, limits, etc. • • •				
$0.458 \pm 0.010 \pm 0.023$	0.9M,3k	⁴ AAIJ	18AI LHCb	amplitude models
0.32 ± 0.20 -0.28		^{1,3} LIBBY	14	Repl. by EVANS 16
0.36 ± 0.24 -0.30		⁵ LOWREY	09 CLEO	Repl. by LIBBY 14

- ¹ Uses quantum correlations in $e^+e^- \rightarrow D^0\bar{D}^0$ at the $\psi(3770)$, where the decay rates of CP-tagged $K^-\pi^-2\pi^+$ final states depend on $R_{K3\pi}$ and $\delta K3\pi$.
- ² A combined fit with a recent LHCb $D^0\bar{D}^0$ mixing results in AAIJ 16f is also reported, to be $0.43^{+0.17}_{-0.13}$.
- ³ Obtained by analyzing CLEO-c data but not authored by the CLEO Collaboration.
- ⁴ Calculated from amplitude models to $D^0 \rightarrow K^-\pi^-2\pi^+$ and $D^0 \rightarrow K^+\pi^+2\pi^-$ and cc. Reports $0.458 \pm 0.010 \pm 0.012 \pm 0.020$ value where the 3rd uncertainty is the model uncertainty. We combined both systematic uncertainties in quadrature. Because of the importance of model independence in the practical use of the coherence factor, we do not include model-derived results in the average.
- ⁵ LOWREY 09 uses quantum correlations in $e^+e^- \rightarrow D^0\bar{D}^0$ at the $\psi(3770)$, where the decay rates of CP-tagged $K^-\pi^-2\pi^+$ final states depend on $R_{K3\pi}$ and $\delta K3\pi$. A fit that includes external measurements of charm mixing parameters gets $R_{K3\pi} = 0.33^{+0.26}_{-0.23}$.

$D^0 \rightarrow K^- \pi^- 2\pi^+$ AVERAGE RELATIVE STRONG PHASE $\delta K3\pi$

The quoted value of δ is based on the same sign CP phase of D^0 and \bar{D}^0 convention.

VALUE (°)	EVTS	DOCUMENT ID	TECN	COMMENT
149 ± 26 -16	OUR AVERAGE			Error includes scale factor of 1.4.
167 ± 31 -19	8.6k	¹ ABLIKIM	21AA BES3	$e^+e^- \rightarrow D^0\bar{D}^0$ at $\psi(3770)$
125 ± 22 -14		^{1,2,3} EVANS	16	$e^+e^- \rightarrow D^0\bar{D}^0$ at $\psi(3770)$
• • • We do not use the following data for averages, fits, limits, etc. • • •				
255 ± 21 -78		^{1,3} LIBBY	14	Repl. by EVANS 16
118 ± 62 -53		⁴ LOWREY	09 CLEO	Repl. by LIBBY 14

- ¹ Uses quantum correlations in $e^+e^- \rightarrow D^0\bar{D}^0$ at the $\psi(3770)$, where the decay rates of CP-tagged $K^-\pi^-2\pi^+$ final states depend on $R_{K3\pi}$ and $\delta K3\pi$.
- ² A combined fit with a recent LHCb $D^0\bar{D}^0$ mixing results in AAIJ 16f is also reported to be $(128^{+28}_{-17})^\circ$.
- ³ Obtained by analyzing CLEO-c data but not authored by the CLEO Collaboration.
- ⁴ LOWREY 09 uses quantum correlations in $e^+e^- \rightarrow D^0\bar{D}^0$ at the $\psi(3770)$, where the decay rates of CP-tagged $K^-\pi^-2\pi^+$ final states depend on $R_{K3\pi}$ and $\delta K3\pi$. A fit that includes external measurements of charm mixing parameters gets $\delta K3\pi = (114^{+26}_{-23})^\circ$.

$D^0 \rightarrow K^- \pi^- 2\pi^+$, $R_{K3\pi}$ ($y \cos\delta K3\pi - x \sin\delta K3\pi$)

VALUE (10^{-3}TeV^{-1})	EVTS	DOCUMENT ID	TECN	COMMENT
-3.0 ± 0.7	42.5k	¹ AAIJ	16f LHCb	$p\bar{p}$ at 7, 8 TeV

- ¹ From a time-dependent analysis of D mixing in $D^0 \rightarrow K^+\pi^-\pi^+\pi^-$. This result uses external constraints on $R_M = 1/2(x^2 + y^2)$. Without such constraints, AAIJ 16f measure $(0.3 \pm 1.8) \times 10^{-3}$, with a large correlation coefficient to R_M .

$D^0 \rightarrow K_S^0 K^+ \pi^-$ COHERENCE FACTOR $R_{K_S^0 K\pi}$

VALUE	DOCUMENT ID	TECN	COMMENT
0.70 ± 0.08	¹ INSLER	12 CLEO	$e^+e^- \rightarrow D^0\bar{D}^0$ at 3.77 GeV

- ¹ Uses quantum correlations in $e^+e^- \rightarrow D^0\bar{D}^0$ at the $\psi(3770)$, where the signal side D decays to $K_S^0 K\pi$ and the tag-side D decays to $K\pi$, $K\pi\pi\pi$, $K\pi\pi^0$, and 10 additional CP-even, CP-odd, and mixed CP modes involving K_S^0 or K_L^0 .

$D^0 \rightarrow K_S^0 K^+ \pi^-$ AVERAGE RELATIVE STRONG PHASE $\delta K_S^0 K\pi$

The quoted value of δ is based on the same sign CP phase of D^0 and \bar{D}^0 convention.

VALUE (°)	DOCUMENT ID	TECN	COMMENT
0.1 ± 15.7	¹ INSLER	12 CLEO	$e^+e^- \rightarrow D^0\bar{D}^0$ at 3.77 GeV

- ¹ Uses quantum correlations in $e^+e^- \rightarrow D^0\bar{D}^0$ at the $\psi(3770)$, where the signal side D decays to $K_S^0 K\pi$ and the tag-side D decays to $K\pi$, $K\pi\pi\pi$, $K\pi\pi^0$, and 10 additional CP-even, CP-odd, and mixed CP modes involving K_S^0 or K_L^0 .

$D^0 \rightarrow K^* K$ COHERENCE FACTOR $R_{K^* K}$

VALUE	DOCUMENT ID	TECN	COMMENT
0.94 ± 0.12	¹ INSLER	12 CLEO	$e^+e^- \rightarrow D^0\bar{D}^0$ at 3.77 GeV

- ¹ Uses quantum correlations in $e^+e^- \rightarrow D^0\bar{D}^0$ at the $\psi(3770)$, where the signal side D decays to $K_S^0 K\pi$ and the tag-side D decays to $K\pi$, $K\pi\pi\pi$, $K\pi\pi^0$, and 10 additional CP-even, CP-odd, and mixed CP modes involving K_S^0 or K_L^0 .

$D^0 \rightarrow K^* K$ AVERAGE RELATIVE STRONG PHASE $\delta K^* K$

The quoted value of δ is based on the same sign CP phase of D^0 and \bar{D}^0 convention.

VALUE (°)	DOCUMENT ID	TECN	COMMENT
-16.6 ± 18.4	¹ INSLER	12 CLEO	$e^+e^- \rightarrow D^0\bar{D}^0$ at 3.77 GeV

- ¹ Uses quantum correlations in $e^+e^- \rightarrow D^0\bar{D}^0$ at the $\psi(3770)$, where the signal side D decays to $K_S^0 K\pi$ and the tag-side D decays to $K\pi$, $K\pi\pi\pi$, $K\pi\pi^0$, and 10 additional CP-even, CP-odd, and mixed CP modes involving K_S^0 or K_L^0 .

D^0 DECAY MODES

Most decay modes (other than the semileptonic modes) that involve a neutral K meson are now given as K_S^0 modes, not as \bar{K}^0 modes. Nearly always it is a K_S^0 that is measured, and interference between Cabibbo-allowed and doubly Cabibbo-suppressed modes can invalidate the assumption that $2\Gamma(K_S^0) = \Gamma(\bar{K}^0)$.

Mode	Fraction (Γ_i/Γ)	Scale factor/ Confidence level
Topological modes		
Γ_1 0-prongs	[a] (15 \pm 6) %	
Γ_2 2-prongs	(71 \pm 6) %	
Γ_3 4-prongs	[b] (14.6 \pm 0.5) %	
Γ_4 6-prongs	[c] (6.5 \pm 1.3) $\times 10^{-4}$	
Inclusive modes		
Γ_5 e^+ anything	[d] (6.49 \pm 0.11) %	
Γ_6 μ^+ anything	(6.8 \pm 0.6) %	
Γ_7 K^- anything	(54.7 \pm 2.8) %	S=1.3
Γ_8 \bar{K}^0 anything + K^0 anything	(47 \pm 4) %	
Γ_9 K^+ anything	(3.4 \pm 0.4) %	
Γ_{10} $K^*(892)^-$ anything	(15 \pm 9) %	
Γ_{11} $\bar{K}^*(892)^0$ anything	(9 \pm 4) %	
Γ_{12} $K^*(892)^+$ anything	< 3.6 %	CL=90%
Γ_{13} $K^*(892)^0$ anything	(2.8 \pm 1.3) %	
Γ_{14} η anything	(9.5 \pm 0.9) %	
Γ_{15} η' anything	(2.48 \pm 0.27) %	
Γ_{16} ϕ anything	(1.08 \pm 0.04) %	
Γ_{17} invisibles	< 9.4 $\times 10^{-5}$	CL=90%
Semileptonic modes		
Γ_{18} $K^-\ell^+\nu_\ell$		
Γ_{19} $K^-e^+\nu_e$	(3.549 \pm 0.026) %	S=1.2
Γ_{20} $K^-\mu^+\nu_\mu$	(3.41 \pm 0.04) %	
Γ_{21} $K^*(892)^-e^+\nu_e$	(2.15 \pm 0.16) %	
Γ_{22} $K^*(892)^-\mu^+\nu_\mu$	(1.89 \pm 0.24) %	
Γ_{23} $K^-\pi^0e^+\nu_e$	(1.6 \pm 1.3) %	
Γ_{24} $\bar{K}^0\pi^-e^+\nu_e$	(1.44 \pm 0.04) %	
Γ_{25} ($\bar{K}^0\pi^-$) S -wave $e^+\nu_e$	(7.9 \pm 1.7) $\times 10^{-4}$	
Γ_{26} $K^-\pi^+\pi^-e^+\nu_e$	(2.8 \pm 1.4) $\times 10^{-4}$	
Γ_{27} $K_1(1270)^-e^+\nu_e$	(1.01 \pm 0.18) $\times 10^{-3}$	
Γ_{28} $K^-\pi^+\pi^-\mu^+\nu_\mu$	< 1.3 $\times 10^{-3}$	CL=90%
Γ_{29} ($\bar{K}^*(892)\pi^-$) $\mu^+\nu_\mu$	< 1.5 $\times 10^{-3}$	CL=90%
Γ_{30} $\pi^-e^+\nu_e$	(2.91 \pm 0.04) $\times 10^{-3}$	
Γ_{31} $\pi^-\mu^+\nu_\mu$	(2.67 \pm 0.12) $\times 10^{-3}$	S=1.3
Γ_{32} $\pi^-\pi^0e^+\nu_e$	(1.45 \pm 0.07) $\times 10^{-3}$	
Γ_{33} $\rho^-e^+\nu_e$	(1.50 \pm 0.12) $\times 10^{-3}$	S=1.9
Γ_{34} $\rho^-\mu^+\nu_\mu$	(1.35 \pm 0.13) $\times 10^{-3}$	
Γ_{35} $a(980)^-e^+\nu_e$, $a^- \rightarrow \eta\pi^-$	(1.33 \pm 0.34) $\times 10^{-4}$	
Γ_{36} $b_1(1235)^-e^+\nu_e$, $b_1^- \rightarrow \omega\pi^-$	< 1.12 $\times 10^{-4}$	CL=90%
Hadronic modes with one \bar{K}		
Γ_{37} $K^-\pi^+$	(3.947 \pm 0.030) %	S=1.2
Γ_{38} $K_S^0\pi^0$	(1.240 \pm 0.022) %	
Γ_{39} $K_L^0\pi^0$	(10.0 \pm 0.7) $\times 10^{-3}$	
Γ_{40} $K_S^0\pi^+\pi^-$	[e] (2.80 \pm 0.18) %	S=1.1
Γ_{41} $K_S^0\rho^0$	(6.3 \pm 0.6) $\times 10^{-3}$	

Γ ₁₄₉	$f_2(1270)\pi^0, f_2 \rightarrow \pi^+\pi^-$	$(1.97 \pm 0.21) \times 10^{-4}$		Γ ₂₀₅	$a_0(980)^-\pi^+, a_0^- \rightarrow K_S^0 K^-$	$(1.3 \pm 1.4) \times 10^{-4}$	
Γ ₁₅₀	$\pi^+\pi^-\pi^0$ nonresonant	$(1.3 \pm 0.4) \times 10^{-4}$		Γ ₂₀₆	$a_0(1450)^-\pi^+, a_0^- \rightarrow K_S^0 K^-$	$(2.5 \pm 2.0) \times 10^{-5}$	
Γ ₁₅₁	$3\pi^0$	$(2.0 \pm 0.5) \times 10^{-4}$		Γ ₂₀₇	$a_2(1320)^-\pi^+, a_2^- \rightarrow K_S^0 K^-$	$(5 \pm 5) \times 10^{-6}$	
Γ ₁₅₂	$2\pi^+2\pi^-$	$(7.56 \pm 0.20) \times 10^{-3}$		Γ ₂₀₈	$\rho(1450)^-\pi^+, \rho^- \rightarrow K_S^0 K^-$	$(4.6 \pm 2.5) \times 10^{-5}$	
Γ ₁₅₃	$a_1(1260)^+\pi^-, a_1^+ \rightarrow 2\pi^+\pi^-$ total	$(4.53 \pm 0.31) \times 10^{-3}$		Γ ₂₀₉	$K_S^0 K^+\pi^-$	$(2.17 \pm 0.34) \times 10^{-3}$	S=1.1
Γ ₁₅₄	$a_1(1260)^+\pi^-, a_1^+ \rightarrow \rho^0\pi^+$ S-wave	$(3.13 \pm 0.21) \times 10^{-3}$		Γ ₂₁₀	$K^*(892)^0 K_S^0, K^{*0} \rightarrow K^+\pi^-$	$(1.12 \pm 0.21) \times 10^{-4}$	
Γ ₁₅₅	$a_1(1260)^+\pi^-, a_1^+ \rightarrow \rho^0\pi^+$ D-wave	$(1.9 \pm 0.5) \times 10^{-4}$		Γ ₂₁₁	$K^*(892)^- K^+, K^{*-} \rightarrow K_S^0 \pi^-$	$(6.2 \pm 1.0) \times 10^{-4}$	
Γ ₁₅₆	$a_1(1260)^+\pi^-, a_1^+ \rightarrow \sigma\pi^+$	$(6.4 \pm 0.7) \times 10^{-4}$		Γ ₂₁₂	$K^*(1410)^0 K_S^0, K^{*0} \rightarrow K^+\pi^+$	$(5 \pm 8) \times 10^{-5}$	
Γ ₁₅₇	$a_1(1260)^-\pi^+, a_1^- \rightarrow \rho^0\pi^-$ S-wave	$(2.3 \pm 0.9) \times 10^{-4}$		Γ ₂₁₃	$K^*(1410)^- K^+, K^{*-} \rightarrow K_S^0 \pi^-$	$(2.6 \pm 2.0) \times 10^{-4}$	
Γ ₁₅₈	$a_1(1260)^-\pi^+, a_1^- \rightarrow \sigma\pi^-$	$(6.0 \pm 3.4) \times 10^{-5}$		Γ ₂₁₄	$(K^+\pi^-)_{S\text{-wave}} K_S^0$	$(3.7 \pm 1.9) \times 10^{-4}$	
Γ ₁₅₉	$\pi(1300)^+\pi^-, \pi(1300)^+ \rightarrow \sigma\pi^+$	$(5.1 \pm 2.7) \times 10^{-4}$		Γ ₂₁₅	$(K_S^0 \pi^-)_{S\text{-wave}} K^+$	$(1.4 \pm 0.6) \times 10^{-4}$	
Γ ₁₆₀	$\pi(1300)^-\pi^+, \pi(1300)^- \rightarrow \sigma\pi^-$	$(2.3 \pm 2.2) \times 10^{-4}$		Γ ₂₁₆	$a_0(980)^+\pi^-, a_0^+ \rightarrow K_S^0 K^+$	$(6 \pm 4) \times 10^{-4}$	
Γ ₁₆₁	$a_1(1640)^+\pi^-, a_1^+ \rightarrow \rho^0\pi^+$ D-wave	$(3.2 \pm 1.6) \times 10^{-4}$		Γ ₂₁₇	$a_0(1450)^+\pi^-, a_0^+ \rightarrow K_S^0 K^+$	$(3.2 \pm 2.5) \times 10^{-5}$	
Γ ₁₆₂	$a_1(1640)^+\pi^-, a_1^+ \rightarrow \sigma\pi^+$	$(1.8 \pm 1.4) \times 10^{-4}$		Γ ₂₁₈	$\rho(1700)^+\pi^-, \rho^+ \rightarrow K_S^0 K^+$	$(1.1 \pm 0.6) \times 10^{-5}$	
Γ ₁₆₃	$\pi_2(1670)^+\pi^-, \pi_2^+ \rightarrow f_2(1270)^0\pi^+, f_2^0 \rightarrow \pi^+\pi^-$	$(2.0 \pm 0.9) \times 10^{-4}$		Γ ₂₁₉	$K^+ K^- \pi^0$	$(3.42 \pm 0.14) \times 10^{-3}$	
Γ ₁₆₄	$\pi_2(1670)^+\pi^-, \pi_2^+ \rightarrow \sigma\pi^+$	$(2.6 \pm 1.0) \times 10^{-4}$		Γ ₂₂₀	$K^*(892)^+ K^-, K^*(892)^+ \rightarrow K^+\pi^0$	$(1.52 \pm 0.07) \times 10^{-3}$	
Γ ₁₆₅	$2\rho^0$ total	$(1.85 \pm 0.13) \times 10^{-3}$		Γ ₂₂₁	$K^*(892)^- K^+, K^*(892)^- \rightarrow K^-\pi^0$	$(5.4 \pm 0.4) \times 10^{-4}$	
Γ ₁₆₆	$2\rho^0$, parallel helicities	$(8.3 \pm 3.2) \times 10^{-5}$		Γ ₂₂₂	$(K^+\pi^0)_{S\text{-wave}} K^-$	$(2.43 \pm 0.18) \times 10^{-3}$	
Γ ₁₆₇	$2\rho^0$, perpendicular helicities	$(4.8 \pm 0.6) \times 10^{-4}$		Γ ₂₂₃	$(K^-\pi^0)_{S\text{-wave}} K^+$	$(1.3 \pm 0.5) \times 10^{-4}$	
Γ ₁₆₈	$2\rho^0$, longitudinal helicities	$(1.27 \pm 0.10) \times 10^{-3}$		Γ ₂₂₄	$f_0(980)\pi^0, f_0 \rightarrow K^+ K^-$	$(3.6 \pm 0.6) \times 10^{-4}$	
Γ ₁₆₉	$2\rho(770)^0, S\text{-wave}$	$(1.8 \pm 1.3) \times 10^{-4}$		Γ ₂₂₅	$\phi\pi^0, \phi \rightarrow K^+ K^-$	$(6.6 \pm 0.4) \times 10^{-4}$	
Γ ₁₇₀	$2\rho(770)^0, P\text{-wave}$	$(5.3 \pm 1.3) \times 10^{-4}$		Γ ₂₂₆	$K^+ K^- \pi^0$ nonresonant		
Γ ₁₇₁	$2\rho(770)^0, D\text{-wave}$	$(6.2 \pm 3.0) \times 10^{-4}$		Γ ₂₂₇	$2K_S^0 \pi^0$	$< 5.9 \times 10^{-4}$	
Γ ₁₇₂	Resonant $(\pi^+\pi^-)\pi^+\pi^-$ 3-body total	$(1.51 \pm 0.12) \times 10^{-3}$		Γ ₂₂₈	$K^+ K^- \eta$	$(5.9 \pm 1.9) \times 10^{-5}$	
Γ ₁₇₃	$\sigma\pi^+\pi^-$	$(6.2 \pm 0.9) \times 10^{-4}$		Γ ₂₂₉	$\phi(1020)\eta$	$(1.84 \pm 0.12) \times 10^{-4}$	
Γ ₁₇₄	$\sigma\rho(770)^0$	$(5.0 \pm 2.5) \times 10^{-4}$		Γ ₂₃₀	$K^+ K^- \eta$ nonresonant	$(9.9 \pm 0.9) \times 10^{-5}$	
Γ ₁₇₅	$f_0(980)\pi^+\pi^-, f_0 \rightarrow \pi^+\pi^-$	$(1.8 \pm 0.5) \times 10^{-4}$		Γ ₂₃₁	$2K_S^0 \eta$	$(1.3 \pm 0.6) \times 10^{-4}$	
Γ ₁₇₆	$f_2(1270)\pi^+\pi^-, f_2 \rightarrow \pi^+\pi^-$	$(3.7 \pm 0.6) \times 10^{-4}$		Γ ₂₃₂	$K^+ K^- \pi^0 \pi^0$	$(6.9 \pm 0.8) \times 10^{-4}$	
Γ ₁₇₇	$2f_2(1270), f_2 \rightarrow \pi^+\pi^-$	$(1.6 \pm 1.8) \times 10^{-4}$		Γ ₂₃₃	$K^+ K^- \pi^+\pi^-$	$(2.47 \pm 0.11) \times 10^{-3}$	
Γ ₁₇₈	$f_0(1370)\sigma, f_0 \rightarrow \pi^+\pi^-$	$(1.6 \pm 0.5) \times 10^{-3}$		Γ ₂₃₄	$\phi(\pi^+\pi^-)_{S\text{-wave}}, \phi \rightarrow K^+ K^-$	$(10 \pm 5) \times 10^{-5}$	
Γ ₁₇₉	$\pi^+\pi^-2\pi^0$	$(1.02 \pm 0.09) \%$		Γ ₂₃₅	$(\phi\rho^0)_{S\text{-wave}}, \phi \rightarrow K^+ K^-$	$(6.9 \pm 0.6) \times 10^{-4}$	
Γ ₁₈₀	$\eta\pi^0$	[h] $(6.3 \pm 0.6) \times 10^{-4}$	S=1.1	Γ ₂₃₆	$(\phi\rho^0)_{P\text{-wave}}, \phi \rightarrow K^+ K^-$	$(4.0 \pm 1.9) \times 10^{-5}$	
Γ ₁₈₁	$\omega\pi^0$	[h] $(1.17 \pm 0.35) \times 10^{-4}$		Γ ₂₃₇	$(\phi\rho^0)_{D\text{-wave}}, \phi \rightarrow K^+ K^-$	$(4.2 \pm 1.4) \times 10^{-5}$	
Γ ₁₈₂	$\omega\eta$	$(1.98 \pm 0.18) \times 10^{-3}$	S=1.1	Γ ₂₃₈	$K^*(892)^0 \bar{K}^*(892)^0, K^{*0} \rightarrow K^\pm \pi^\mp$		
Γ ₁₈₃	$2\pi^+2\pi^-\pi^0$	$(4.2 \pm 0.5) \times 10^{-3}$		Γ ₂₃₉	$K^+ K^- \rho^0$ 3-body		
Γ ₁₈₄	$\eta\pi^+\pi^-$	[h] $(1.16 \pm 0.07) \times 10^{-3}$		Γ ₂₄₀	$f_0(980)\pi^+\pi^-, f_0 \rightarrow K^+ K^-$		
Γ ₁₈₅	$\omega\pi^+\pi^-$	[h] $(1.33 \pm 0.20) \times 10^{-3}$		Γ ₂₄₁	$(K^*(892)^0 \bar{K}^*(892)^0)_{S\text{-wave}}, K^{*0} \rightarrow K^\pm \pi^\mp$	$(2.24 \pm 0.13) \times 10^{-4}$	
Γ ₁₈₆	$\omega\pi^0\pi^0$	$< 1.10 \times 10^{-3}$	CL=90%	Γ ₂₄₂	$(K^*(892)^0 \bar{K}^*(892)^0)_{P\text{-wave}}, K^{*0} \rightarrow K^\pm \pi^\mp$	$(1.20 \pm 0.08) \times 10^{-4}$	
Γ ₁₈₇	$\eta 2\pi^0$	$(3.8 \pm 1.3) \times 10^{-4}$		Γ ₂₄₃	$(K^*(892)^0 \bar{K}^*(892)^0)_{D\text{-wave}}, K^{*0} \rightarrow K^\pm \pi^\mp$	$(4.7 \pm 0.4) \times 10^{-5}$	
Γ ₁₈₈	$\pi^+\pi^-\pi^0\eta$	$(3.23 \pm 0.22) \times 10^{-3}$		Γ ₂₄₄	$K^*(892)^0 K^\pm \pi^\pm$ 3-body, $K^{*0} \rightarrow K^\pm \pi^\mp$		
Γ ₁₈₉	$3\pi^+3\pi^-$	$(4.3 \pm 1.2) \times 10^{-4}$		Γ ₂₄₅	$K^*(892)^0 (K^-\pi^+)_{S\text{-wave}}$ 3-body, $K^{*0} \rightarrow K^+\pi^-$	$(1.4 \pm 0.6) \times 10^{-4}$	
Γ ₁₉₀	$\eta'(958)\pi^0$	$(9.2 \pm 1.0) \times 10^{-4}$		Γ ₂₄₆	$(K^-\pi^+)_{P\text{-wave}}, (K^+\pi^-)_{S\text{-wave}}$		
Γ ₁₉₁	$\eta'(958)\pi^+\pi^-$	$(4.5 \pm 1.7) \times 10^{-4}$		Γ ₂₄₇	$K_1(1270)^\pm K^\mp, K_1^\pm \rightarrow K^\pm \pi^+ \pi^-$		
Γ ₁₉₂	2η	$(2.11 \pm 0.19) \times 10^{-3}$	S=2.2	Γ ₂₄₈	$K_1(1270)^+ K^-, K_1^+ \rightarrow K^{*0} \pi^+$	$(1.5 \pm 0.5) \times 10^{-4}$	
Γ ₁₉₃	$2\eta\pi^0$	$(7.3 \pm 2.2) \times 10^{-4}$		Γ ₂₄₉	$K^*(1430)^0 \pi^+, K^{*0} \rightarrow K^+\pi^-$	$(2.2 \pm 0.6) \times 10^{-4}$	
Γ ₁₉₄	3η	$< 1.3 \times 10^{-4}$	CL=90%	Γ ₂₅₀	$K_1(1270)^+ K^-, K_1^+ \rightarrow \rho^0 K^+$	$(1.5 \pm 1.2) \times 10^{-5}$	
Γ ₁₉₅	$\eta\eta'(958)$	$(1.01 \pm 0.19) \times 10^{-3}$		Γ ₂₅₁	$K_1(1270)^+ K^-, K_1^+ \rightarrow \omega(782) K^+, \omega \rightarrow \pi^+\pi^-$		
Γ ₁₉₆	$K^+ K^-$	$(4.08 \pm 0.06) \times 10^{-3}$	S=1.6	Γ ₂₅₂	$K_1(1270)^- K^+, K_1^- \rightarrow \bar{K}^{*0} \pi^-$		
Γ ₁₉₇	$2K_S^0$	$(1.41 \pm 0.05) \times 10^{-4}$	S=1.1	Γ ₂₅₃	$K_1(1270)^- K^+, K_1^- \rightarrow \rho^0 K^-$	$(1.3 \pm 0.4) \times 10^{-4}$	
Γ ₁₉₈	$K_S^0 K^- \pi^+$	$(3.3 \pm 0.5) \times 10^{-3}$	S=1.1				
Γ ₁₉₉	$\bar{K}^*(892)^0 K_S^0, \bar{K}^{*0} \rightarrow K^-\pi^+$	$(8.2 \pm 1.6) \times 10^{-5}$					
Γ ₂₀₀	$K^*(892)^+ K^-, K^{*+} \rightarrow K_S^0 \pi^+$	$(1.89 \pm 0.30) \times 10^{-3}$					
Γ ₂₀₁	$\bar{K}^*(1410)^0 K_S^0, \bar{K}^{*0} \rightarrow K^-\pi^+$	$(1.3 \pm 1.9) \times 10^{-4}$					
Γ ₂₀₂	$K^*(1410)^+ K^-, K^{*+} \rightarrow K_S^0 \pi^+$	$(3.2 \pm 1.9) \times 10^{-4}$					
Γ ₂₀₃	$(K^-\pi^+)_{S\text{-wave}} K_S^0$	$(6.0 \pm 2.9) \times 10^{-4}$					
Γ ₂₀₄	$(K_S^0 \pi^+)_{S\text{-wave}} K^-$	$(3.9 \pm 1.0) \times 10^{-4}$					

Meson Particle Listings

 D^0

Γ ₂₅₄	$K_1(1400)^\pm K^\mp, K_1^\pm \rightarrow K^\pm \pi^+ \pi^-$		
Γ ₂₅₅	$K_1(1400)^+ K^-, K_1^+ \rightarrow K^*(892)^0 \pi^+, K^{*0} \rightarrow K^+ \pi^-$	$(4.6 \pm 0.4) \times 10^{-4}$	
Γ ₂₅₆	$K^*(1410)^+ K^-, K^{*+} \rightarrow K^{*0} \pi^+$		
Γ ₂₅₇	$K^*(1410)^- K^+, K^{*-} \rightarrow K^{*0} \pi^-$	$(7.0 \pm 1.1) \times 10^{-5}$	
Γ ₂₅₈	$K_1(1680)^+ K^-, K_1^+ \rightarrow K^{*0} \pi^+, K^{*0} \rightarrow K^+ \pi^-$	$(8.9 \pm 3.2) \times 10^{-5}$	
Γ ₂₅₉	$K^+ K^- \pi^+ \pi^-$ non-resonant	$(2.7 \pm 0.6) \times 10^{-4}$	
Γ ₂₆₀	$2K_S^0 \pi^+ \pi^-$	$(5.3 \pm 0.9) \times 10^{-4}$	
Γ ₂₆₁	$K_S^0 K^- \pi^+ \pi^0$	$(1.32 \pm 0.16) \times 10^{-3}$	
Γ ₂₆₂	$K_S^0 K^+ \pi^- \pi^0$	$(6.5 \pm 0.7) \times 10^{-4}$	
Γ ₂₆₃	$K_S^0 K^- 2\pi^+ \pi^-$	$< 1.4 \times 10^{-4}$	CL=90%
Γ ₂₆₄	$K^+ K^- \pi^+ \pi^- \pi^0$	$(3.1 \pm 2.0) \times 10^{-3}$	

Other $K\bar{K}X$ modes. They include all decay modes of the ϕ, η , and ω .

Γ ₂₆₅	$\phi \pi^0$	$(1.17 \pm 0.04) \times 10^{-3}$	
Γ ₂₆₆	$\phi \eta$	$(1.8 \pm 0.5) \times 10^{-4}$	
Γ ₂₆₇	$\phi \omega$	$(6.5 \pm 1.0) \times 10^{-4}$	

Radiative modes

Γ ₂₆₈	$\rho^0 \gamma$	$(1.82 \pm 0.32) \times 10^{-5}$	
Γ ₂₆₉	$\omega \gamma$	$< 2.4 \times 10^{-4}$	CL=90%
Γ ₂₇₀	$\phi \gamma$	$(2.81 \pm 0.19) \times 10^{-5}$	
Γ ₂₇₁	$\bar{K}^*(892)^0 \gamma$	$(4.1 \pm 0.7) \times 10^{-4}$	

Doubly Cabibbo suppressed (DC) modes or $\Delta C = 2$ forbidden via mixing (CM) modes

Γ ₂₇₂	$K^+ \ell^- \bar{\nu}_\ell$ via \bar{D}^0	$< 2.2 \times 10^{-5}$	CL=90%
Γ ₂₇₃	K^+ or $K^*(892)^+$ $e^- \bar{\nu}_e$ via \bar{D}^0	$< 6 \times 10^{-5}$	CL=90%
Γ ₂₇₄	$K^+ \pi^-$	DC	$(1.50 \pm 0.07) \times 10^{-4}$ S=3.0
Γ ₂₇₅	$K^+ \pi^-$ via DCS		$(1.363 \pm 0.025) \times 10^{-4}$
Γ ₂₇₆	$K^+ \pi^-$ via \bar{D}^0		$< 1.6 \times 10^{-5}$ CL=95%
Γ ₂₇₇	$K_S^0 \pi^+ \pi^-$ in $D^0 \rightarrow \bar{D}^0$		$< 1.8 \times 10^{-4}$ CL=95%
Γ ₂₇₈	$K^*(892)^+ \pi^-, K^{*+} \rightarrow K_S^0 \pi^+$	DC	$(1.13 \pm_{0.34}^{0.60}) \times 10^{-4}$
Γ ₂₇₉	$K_0^*(1430)^+ \pi^-, K_0^{*+} \rightarrow K_S^0 \pi^+$	DC	$< 1.4 \times 10^{-5}$
Γ ₂₈₀	$K_2^*(1430)^+ \pi^-, K_2^{*+} \rightarrow K_S^0 \pi^+$	DC	$< 3.4 \times 10^{-5}$
Γ ₂₈₁	$K^+ \pi^- \pi^0$	DC	$(3.05 \pm 0.15) \times 10^{-4}$
Γ ₂₈₂	$K^+ \pi^- \pi^0$ via \bar{D}^0		$(7.6 \pm_{0.6}^{0.5}) \times 10^{-4}$
Γ ₂₈₃	$K^+ \pi^+ 2\pi^-$ via DCS		$(2.49 \pm 0.07) \times 10^{-4}$
Γ ₂₈₄	$K^+ \pi^+ 2\pi^-$	DC	$(2.65 \pm 0.06) \times 10^{-4}$
Γ ₂₈₅	$K^+ \pi^+ 2\pi^-$ via \bar{D}^0		$(7.9 \pm 3.0) \times 10^{-6}$
Γ ₂₈₆	$K^+ \pi^-$ or $K^+ \pi^+ 2\pi^-$ via \bar{D}^0		
Γ ₂₈₇	μ^- anything via \bar{D}^0		$< 4 \times 10^{-4}$ CL=90%

 $\Delta C = 1$ weak neutral current (CI) modes, Lepton Family number (LF) violating modes, Lepton (L) or Baryon (B) number violating modes

Γ ₂₈₈	$\gamma \gamma$	CI	$< 8.5 \times 10^{-7}$ CL=90%
Γ ₂₈₉	$e^+ e^-$	CI	$< 7.9 \times 10^{-8}$ CL=90%
Γ ₂₉₀	$\mu^+ \mu^-$	CI	$< 6.2 \times 10^{-9}$ CL=90%
Γ ₂₉₁	$\pi^0 e^+ e^-$	CI	$< 4 \times 10^{-6}$ CL=90%
Γ ₂₉₂	$\pi^0 \mu^+ \mu^-$	CI	$< 1.8 \times 10^{-4}$ CL=90%
Γ ₂₉₃	$\eta e^+ e^-$	CI	$< 3 \times 10^{-6}$ CL=90%
Γ ₂₉₄	$\eta \mu^+ \mu^-$	CI	$< 5.3 \times 10^{-4}$ CL=90%
Γ ₂₉₅	$\pi^+ \pi^- e^+ e^-$	CI	$< 7 \times 10^{-6}$ CL=90%
Γ ₂₉₆	$\rho^0 e^+ e^-$	CI	$< 1.0 \times 10^{-4}$ CL=90%
Γ ₂₉₇	$\pi^+ \pi^- \mu^+ \mu^-$	CI	$(9.6 \pm 1.2) \times 10^{-7}$
Γ ₂₉₈	$\pi^+ \pi^- \mu^+ \mu^-$ (non-res)		$< 5.5 \times 10^{-7}$ CL=90%
Γ ₂₉₉	$\rho^0 \mu^+ \mu^-$		$< 2.2 \times 10^{-5}$ CL=90%
Γ ₃₀₀	$\omega e^+ e^-$	CI	$< 6 \times 10^{-6}$ CL=90%
Γ ₃₀₁	$\omega \mu^+ \mu^-$	CI	$< 8.3 \times 10^{-4}$ CL=90%
Γ ₃₀₂	$K^- K^+ e^+ e^-$	CI	$< 1.1 \times 10^{-5}$ CL=90%
Γ ₃₀₃	$\phi e^+ e^-$	CI	$< 5.2 \times 10^{-5}$ CL=90%
Γ ₃₀₄	$K^- K^+ \mu^+ \mu^-$	CI	$(1.54 \pm 0.32) \times 10^{-7}$
Γ ₃₀₅	$K^- K^+ \mu^+ \mu^-$ (non-res)		$< 3.3 \times 10^{-5}$ CL=90%
Γ ₃₀₆	$\phi \mu^+ \mu^-$	CI	$< 3.1 \times 10^{-5}$ CL=90%
Γ ₃₀₇	$\bar{K}^0 e^+ e^-$	[j]	$< 2.4 \times 10^{-5}$ CL=90%

Γ ₃₀₈	$\bar{K}^0 \mu^+ \mu^-$	[i]	$< 2.6 \times 10^{-4}$ CL=90%
Γ ₃₀₉	$K^- \pi^+ e^+ e^-$		
Γ ₃₁₀	$K^- \pi^+ e^+ e^-, 675 < m_{e^+ e^-} < 875 \text{ MeV}$		$(4.0 \pm 0.5) \times 10^{-6}$
Γ ₃₁₁	$K^- \pi^+ e^+ e^-, 1.005 < m_{e^+ e^-} < 1.035 \text{ GeV}$		$< 5 \times 10^{-7}$ CL=90%
Γ ₃₁₂	$\bar{K}^*(892)^0 e^+ e^-$	[i]	$< 4.7 \times 10^{-5}$ CL=90%
Γ ₃₁₃	$K^- \pi^+ \mu^+ \mu^-$	CI	$< 3.59 \times 10^{-4}$ CL=90%
Γ ₃₁₄	$K^- \pi^+ \mu^+ \mu^-, 675 < m_{\mu^+ \mu^-} < 875 \text{ MeV}$		$(4.2 \pm 0.4) \times 10^{-6}$
Γ ₃₁₅	$\bar{K}^*(892)^0 \mu^+ \mu^-$	[i]	$< 2.4 \times 10^{-5}$ CL=90%
Γ ₃₁₆	$\pi^+ \pi^- \pi^0 \mu^+ \mu^-$	CI	$< 8.1 \times 10^{-4}$ CL=90%
Γ ₃₁₇	$\mu^\pm e^\mp$	LF	[j] $< 1.3 \times 10^{-8}$ CL=90%
Γ ₃₁₈	$\pi^0 e^\pm \mu^\mp$	LF	[j] $< 8.0 \times 10^{-7}$ CL=90%
Γ ₃₁₉	$\eta e^\pm \mu^\mp$	LF	[j] $< 2.25 \times 10^{-6}$ CL=90%
Γ ₃₂₀	$\pi^+ \pi^- e^\pm \mu^\mp$	LF	[j] $< 1.71 \times 10^{-6}$ CL=90%
Γ ₃₂₁	$\rho^0 e^\pm \mu^\mp$	LF	[j] $< 5.0 \times 10^{-7}$ CL=90%
Γ ₃₂₂	$\omega e^\pm \mu^\mp$	LF	[j] $< 1.71 \times 10^{-6}$ CL=90%
Γ ₃₂₃	$K^- K^+ e^\pm \mu^\mp$	LF	[j] $< 1.00 \times 10^{-6}$ CL=90%
Γ ₃₂₄	$\phi e^\pm \mu^\mp$	LF	[j] $< 5.1 \times 10^{-7}$ CL=90%
Γ ₃₂₅	$\bar{K}^0 e^\pm \mu^\mp$	LF	[j] $< 1.74 \times 10^{-6}$ CL=90%
Γ ₃₂₆	$K^- \pi^+ e^\pm \mu^\mp$	LF	[j] $< 1.90 \times 10^{-6}$ CL=90%
Γ ₃₂₇	$\bar{K}^*(892)^0 e^\pm \mu^\mp$	LF	[j] $< 1.25 \times 10^{-6}$ CL=90%
Γ ₃₂₈	$2\pi^- 2e^+$	L	$< 9.1 \times 10^{-7}$ CL=90%
Γ ₃₂₉	$2\pi^- 2\mu^+$	L	$< 1.52 \times 10^{-6}$ CL=90%
Γ ₃₃₀	$K^- \pi^- 2e^+$	L	$< 5.0 \times 10^{-7}$ CL=90%
Γ ₃₃₁	$K^- \pi^- 2\mu^+$	L	$< 5.3 \times 10^{-7}$ CL=90%
Γ ₃₃₂	$2K^- 2e^+$	L	$< 3.4 \times 10^{-7}$ CL=90%
Γ ₃₃₃	$2K^- 2\mu^+$	L	$< 1.0 \times 10^{-7}$ CL=90%
Γ ₃₃₄	$\pi^- \pi^- e^+ \mu^+$	L	$< 3.06 \times 10^{-6}$ CL=90%
Γ ₃₃₅	$K^- \pi^- e^+ \mu^+$	L	$< 2.10 \times 10^{-6}$ CL=90%
Γ ₃₃₆	$2K^- e^+ \mu^+$	L	$< 5.8 \times 10^{-7}$ CL=90%
Γ ₃₃₇	$p e^-$	L,B	[k] $< 1.0 \times 10^{-5}$ CL=90%
Γ ₃₃₈	$\bar{p} e^+$	L,B	[l] $< 1.1 \times 10^{-5}$ CL=90%

Γ₃₃₉ Unaccounted decay modes $(35.0 \pm 1.2) \%$ S=1.1

[a] This value is obtained by subtracting the branching fractions for 2-, 4- and 6-prongs from unity.

[b] This is the sum of our $K^- 2\pi^+ \pi^-$, $K^- 2\pi^+ \pi^- \pi^0$, $\bar{K}^0 2\pi^+ 2\pi^-$, $K^+ 2K^- \pi^+$, $2\pi^+ 2\pi^-$, $2\pi^+ 2\pi^- \pi^0$, $K^+ K^- \pi^+ \pi^-$, and $K^+ K^- \pi^+ \pi^- \pi^0$, branching fractions.[c] This is the sum of our $K^- 3\pi^+ 2\pi^-$ and $3\pi^+ 3\pi^-$ branching fractions.[d] The branching fractions for the $K^- e^+ \nu_e$, $K^*(892)^- e^+ \nu_e$, $\pi^- e^+ \nu_e$, and $\rho^- e^+ \nu_e$ modes add up to $6.17 \pm 0.17 \%$.

[e] The branching fraction for this mode may differ from the sum of the submodes that contribute to it, due to interference effects. See the relevant papers.

[f] This is a doubly Cabibbo-suppressed mode.

[g] Submodes of the $D^0 \rightarrow K_S^0 \pi^+ \pi^- \pi^0$ mode with a K^* and/or ρ were studied by COFFMAN 92B, but with only 140 events. With nothing new for 18 years, we refer to our 2008 edition, Physics Letters **B667** 1 (2008), for those results.

[h] This branching fraction includes all the decay modes of the resonance in the final state.

[i] This mode is not a useful test for a $\Delta C=1$ weak neutral current because both quarks must change flavor in this decay.

[j] The value is for the sum of the charge states or particle/antiparticle states indicated.

[k] This limit is for either D^0 or \bar{D}^0 to $p e^-$.[l] This limit is for either D^0 or \bar{D}^0 to $\bar{p} e^+$.

Meson Particle Listings

D^0

$\Gamma(\mu^+ \text{ anything})/\Gamma_{\text{total}}$ Γ_6/Γ

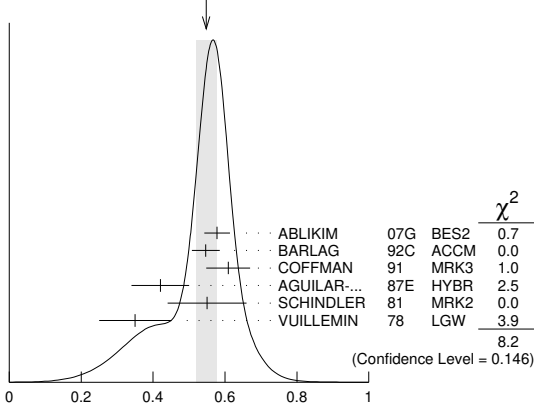
VALUE (%)	EVTs	DOCUMENT ID	TECN	COMMENT
6.8 ± 0.6 OUR FIT				
6.4 ± 0.8 OUR AVERAGE				
6.8 ± 1.5 ± 0.8	79 ± 10	¹ ABLIKIM	08L BES2	$e^+e^- \approx \psi(3772)$
6.5 ± 1.2 ± 0.3	36	KAYIS-TOPAK.05	CHRS	ν_μ emulsion
6.0 ± 0.7 ± 1.2	310	ALBRECHT	96C ARG	$e^+e^- \approx 10 \text{ GeV}$

¹ ABLIKIM 08L finds the ratio of $D^+ \rightarrow \mu^+ X$ and $D^0 \rightarrow \mu^+ X$ branching fractions to be $2.59 \pm 0.70 \pm 0.25$, in accord with the ratio of D^+ and D^0 lifetimes, 2.54 ± 0.02 .

$\Gamma(K^- \text{ anything})/\Gamma_{\text{total}}$ Γ_7/Γ

VALUE	EVTs	DOCUMENT ID	TECN	COMMENT
0.547 ± 0.028 OUR AVERAGE				
0.578 ± 0.016 ± 0.032	2098 ± 59	ABLIKIM	07G BES2	$e^+e^- \approx \psi(3770)$
0.546 ^{+0.039} _{-0.038}		¹ BARLAG	92C ACCM	$\pi^- \text{ Cu } 230 \text{ GeV}$
0.609 ± 0.032 ± 0.052		COFFMAN	91 MRK3	$e^+e^- 3.77 \text{ GeV}$
0.42 ± 0.08		AGUILAR...	87E HYBR	$\pi p, pp 360, 400 \text{ GeV}$
0.55 ± 0.11	121	SCHINDLER	81 MRK2	$e^+e^- 3.771 \text{ GeV}$
0.35 ± 0.10	19	VUILLEMIN	78 LGW	$e^+e^- 3.772 \text{ GeV}$

WEIGHTED AVERAGE
0.547 ± 0.028 (Error scaled by 1.3)



$\Gamma(K^- \text{ anything})/\Gamma_{\text{total}}$

¹ BARLAG 92c computes the branching fraction using topological normalization.

$[\Gamma(K^0 \text{ anything}) + \Gamma(K^0 \text{ anything})]/\Gamma_{\text{total}}$ Γ_8/Γ

VALUE	EVTs	DOCUMENT ID	TECN	COMMENT
0.47 ± 0.04 OUR AVERAGE				
0.476 ± 0.048 ± 0.030	250 ± 25	ABLIKIM	06U BES2	e^+e^- at 3773 MeV
0.455 ± 0.050 ± 0.032		COFFMAN	91 MRK3	$e^+e^- 3.77 \text{ GeV}$

$\Gamma(K^+ \text{ anything})/\Gamma_{\text{total}}$ Γ_9/Γ

VALUE	EVTs	DOCUMENT ID	TECN	COMMENT
0.034 ± 0.004 OUR AVERAGE				
0.035 ± 0.007 ± 0.003	119 ± 23	ABLIKIM	07G BES2	$e^+e^- \approx \psi(3770)$
0.034 ^{+0.007} _{-0.005}		¹ BARLAG	92C ACCM	$\pi^- \text{ Cu } 230 \text{ GeV}$
0.028 ± 0.009 ± 0.004		COFFMAN	91 MRK3	$e^+e^- 3.77 \text{ GeV}$
0.03 ^{+0.05} _{-0.02}		AGUILAR...	87E HYBR	$\pi p, pp 360, 400 \text{ GeV}$
0.08 ± 0.03	25	SCHINDLER	81 MRK2	$e^+e^- 3.771 \text{ GeV}$

¹ BARLAG 92c computes the branching fraction using topological normalization.

$\Gamma(K^*(892)^- \text{ anything})/\Gamma_{\text{total}}$ Γ_{10}/Γ

VALUE	EVTs	DOCUMENT ID	TECN	COMMENT
0.153 ± 0.083 ± 0.019	28 ± 15	ABLIKIM	06U BES2	e^+e^- at 3773 MeV

$\Gamma(K^*(892)^0 \text{ anything})/\Gamma_{\text{total}}$ Γ_{11}/Γ

VALUE	EVTs	DOCUMENT ID	TECN	COMMENT
0.087 ± 0.040 ± 0.012	96 ± 44	ABLIKIM	05P BES	$e^+e^- \approx 3773 \text{ MeV}$

$\Gamma(K^*(892)^+ \text{ anything})/\Gamma_{\text{total}}$ Γ_{12}/Γ

VALUE	CL%	DOCUMENT ID	TECN	COMMENT
< 0.036	90	ABLIKIM	06U BES2	e^+e^- at 3773 MeV

$\Gamma(K^*(892)^0 \text{ anything})/\Gamma_{\text{total}}$ Γ_{13}/Γ

VALUE	EVTs	DOCUMENT ID	TECN	COMMENT
0.028 ± 0.012 ± 0.004	31 ± 12	ABLIKIM	05P BES	$e^+e^- \approx 3773 \text{ MeV}$

$\Gamma(\eta \text{ anything})/\Gamma_{\text{total}}$ Γ_{14}/Γ

This ratio includes η particles from η' decays.

VALUE (%)	EVTs	DOCUMENT ID	TECN	COMMENT
9.5 ± 0.4 ± 0.8	4463 ± 197	HUANG	06B CLEO	e^+e^- at $\psi(3770)$

$\Gamma(\eta' \text{ anything})/\Gamma_{\text{total}}$ Γ_{15}/Γ

VALUE (%)	EVTs	DOCUMENT ID	TECN	COMMENT
2.48 ± 0.17 ± 0.21	299 ± 21	HUANG	06B CLEO	e^+e^- at $\psi(3770)$

$\Gamma(\phi \text{ anything})/\Gamma_{\text{total}}$ Γ_{16}/Γ

VALUE (%)	EVTs	DOCUMENT ID	TECN	COMMENT
1.08 ± 0.04 OUR AVERAGE				
1.091 ± 0.027 ± 0.035	4.1k	ABLIKIM	19AYBES3	e^+e^- at 3773 MeV
1.05 ± 0.08 ± 0.07	368 ± 24	HUANG	06B CLEO	e^+e^- at $\psi(3770)$
• • • We do not use the following data for averages, fits, limits, etc. • • •				
1.71 ^{+0.76} _{-0.71} ± 0.17	9	BAI	00c BES	$e^+e^- \rightarrow D\bar{D}^*, D^*\bar{D}^*$

$\Gamma(\text{invisibles})/\Gamma_{\text{total}}$ Γ_{17}/Γ

VALUE	CL%	DOCUMENT ID	TECN	COMMENT
< 9.4 × 10⁻⁵	90	LAI	17 BELL	e^+e^- at $\Upsilon(nS), n=4,5$

Semileptonic modes

$\Gamma(K^- e^+ \nu_e)/\Gamma_{\text{total}}$ Γ_{19}/Γ

VALUE (%)	EVTs	DOCUMENT ID	TECN	COMMENT
3.549 ± 0.026 OUR FIT				
3.525 ± 0.023 OUR AVERAGE				
3.567 ± 0.031 ± 0.025	4040	ABLIKIM	21BA BES3	e^+e^- at 3.773 GeV
3.505 ± 0.014 ± 0.033	71k	¹ ABLIKIM	15X BES3	2.92 fb ⁻¹ , 3.773 GeV
3.50 ± 0.03 ± 0.04	14.1k	¹ BESSON	09 CLEO	e^+e^- at $\psi(3770)$
3.45 ± 0.10 ± 0.19	1.3k	² WIDHALM	06 BELL	$e^+e^- \approx \Upsilon(4S)$
3.82 ± 0.40 ± 0.27	104	ABLIKIM	04c BES	e^+e^- , 3.773 GeV
3.4 ± 0.5 ± 0.4	55	ADLER	89 MRK3	$e^+e^- 3.77 \text{ GeV}$
• • • We do not use the following data for averages, fits, limits, etc. • • •				
3.56 ± 0.03 ± 0.09		³ DOBBS	08 CLEO	See BESSON 09
3.44 ± 0.10 ± 0.10	1.3k	COAN	05 CLEO	See DOBBS 08

¹ See the form-factor parameters near the end of this D^0 Listing.

² The $\pi^- e^+ \nu_e$ and $K^- e^+ \nu_e$ results of WIDHALM 06 give $|\frac{V_{cd}}{V_{cs}} \cdot \frac{f_{\pi^+}(0)}{f_{K^+}(0)}|^2 = 0.042 \pm 0.003 \pm 0.003$.

³ DOBBS 08 establishes $|\frac{V_{cd}}{V_{cs}} \cdot \frac{f_{\pi^+}(0)}{f_{K^+}(0)}| = 0.188 \pm 0.008 \pm 0.002$ from the D^+ and D^0 decays to $\bar{K} e^+ \nu_e$ and $\pi e^+ \nu_e$.

$\Gamma(K^- e^+ \nu_e)/\Gamma(K^- \pi^+)$ Γ_{19}/Γ_37

VALUE	EVTs	DOCUMENT ID	TECN	COMMENT
0.899 ± 0.009 OUR FIT				
0.930 ± 0.013 OUR AVERAGE				
0.927 ± 0.007 ± 0.012	76k ± 323	¹ AUBERT	07BG BABR	$e^+e^- \approx \Upsilon(4S)$
0.978 ± 0.027 ± 0.044	2510	² BEAN	93c CLE2	$e^+e^- \approx \Upsilon(4S)$
0.90 ± 0.06 ± 0.06	584	³ CRAWFORD	91B CLEO	$e^+e^- \approx 10.5 \text{ GeV}$
0.91 ± 0.07 ± 0.11	250	⁴ ANJOS	89F E691	Photoproduction

¹ The event samples in this AUBERT 07BG result include radiative photons. The $D^0 \rightarrow K^- e^+ \nu_e$ form factor at $q^2 = 0$ is $f_{+}(0) = 0.727 \pm 0.007 \pm 0.005 \pm 0.007$.

² BEAN 93c uses $K^- \mu^+ \nu_\mu$ as well as $K^- e^+ \nu_e$ events and makes a small phase-space adjustment to the number of the μ^+ events to use them as e^+ events. A pole mass of $2.00 \pm 0.12 \pm 0.18 \text{ GeV}/c^2$ is obtained from the q^2 dependence of the decay rate.

³ CRAWFORD 91B uses $K^- e^+ \nu_e$ and $K^- \mu^+ \nu_\mu$ candidates to measure a pole mass of $2.1^{+0.4+0.3}_{-0.2-0.2} \text{ GeV}/c^2$ from the q^2 dependence of the decay rate.

⁴ ANJOS 89F measures a pole mass of $2.1^{+0.4}_{-0.2} \pm 0.2 \text{ GeV}/c^2$ from the q^2 dependence of the decay rate.

$\Gamma(K^- \mu^+ \nu_\mu)/\Gamma_{\text{total}}$ Γ_{20}/Γ

VALUE (%)	EVTs	DOCUMENT ID	TECN	COMMENT
3.41 ± 0.04 OUR FIT				
3.41 ± 0.04 OUR AVERAGE				
3.413 ± 0.019 ± 0.035	47k	ABLIKIM	19B BES3	e^+e^- , 3773 MeV
3.45 ± 0.10 ± 0.21	1249 ± 43	WIDHALM	06 BELL	$e^+e^- \approx \Upsilon(4S)$

$\Gamma(K^- \mu^+ \nu_\mu)/\Gamma(\mu^+ \text{ anything})$ Γ_{20}/Γ_6

VALUE	EVTs	DOCUMENT ID	TECN	COMMENT
0.50 ± 0.04 OUR FIT				
0.472 ± 0.051 ± 0.040				
0.472 ± 0.034 ± 0.028	232	KODA MA	94 E653	π^- emulsion 600 GeV
• • • We do not use the following data for averages, fits, limits, etc. • • •				
0.32 ± 0.05 ± 0.05	124	KODA MA	91 EMUL	pA 800 GeV

$\Gamma(K^- \mu^+ \nu_\mu)/\Gamma(K^- \pi^+)$ Γ_{20}/Γ_37

VALUE	EVTs	DOCUMENT ID	TECN	COMMENT
0.864 ± 0.012 OUR FIT				
0.84 ± 0.04 OUR AVERAGE				
0.852 ± 0.034 ± 0.028	1897	¹ FRABETTI	95G E687	$\gamma \text{Be } \bar{E}_{\gamma} = 220 \text{ GeV}$
0.82 ± 0.13 ± 0.13	338	² FRABETTI	93I E687	$\gamma \text{Be } \bar{E}_{\gamma} = 221 \text{ GeV}$
0.79 ± 0.08 ± 0.09	231	³ CRAWFORD	91B CLEO	$e^+e^- \approx 10.5 \text{ GeV}$

¹ FRABETTI 95G extracts the ratio of form factors $f_{-}(0)/f_{+}(0) = -1.3^{+3.6}_{-3.4} \pm 0.6$, and measures a pole mass of $1.87^{+0.11+0.07}_{-0.08-0.06} \text{ GeV}/c^2$ from the q^2 dependence of the decay rate.

² FRABETTI 93I measures a pole mass of $2.1^{+0.7+0.7}_{-0.3-0.3} \text{ GeV}/c^2$ from the q^2 dependence of the decay rate.

³ CRAWFORD 91B measures a pole mass of $2.00 \pm 0.12 \pm 0.18 \text{ GeV}/c^2$ from the q^2 dependence of the decay rate.

$\Gamma(K^*(892)^- e^+ \nu_e) / \Gamma_{\text{total}}$ Γ_{21} / Γ Both decay modes of the $K^*(892)^-$ are included.

VALUE (%)	EVTS	DOCUMENT ID	TECN	COMMENT
2.15 ± 0.16 OUR FIT				
2.16 ± 0.15 ± 0.08	219 ± 16	¹ COAN	05 CLEO	$e^+ e^-$ at $\psi(3770)$
				¹ COAN 05 uses both $K^- \pi^0$ and $K_S^0 \pi^-$ events.

 $\Gamma(K^*(892)^- e^+ \nu_e) / \Gamma(K_S^0 \pi^- e^+ \nu_e)$ $\Gamma_{21} / \Gamma_{24}$

VALUE (units 10^{-2})	EVTS	DOCUMENT ID	TECN	COMMENT
94.52 ± 0.97 ± 0.62	3.1k	ABLIKIM	19G BES3	$K_S^0 \pi^- e^+ \nu_e$ events

 $\Gamma(K^*(892)^- e^+ \nu_e) / \Gamma(K^0 \pi^+ \pi^-)$ $\Gamma_{21} / \Gamma_{40}$ Unseen decay modes of the $K^*(892)^-$ are included.

VALUE	EVTS	DOCUMENT ID	TECN	COMMENT
0.77 ± 0.07 OUR FIT				
0.76 ± 0.12 ± 0.06	152	¹ BEAN	93c CLE2	$e^+ e^- \approx \gamma(4S)$
				¹ BEAN 93c uses $K^{*-} \mu^+ \nu_\mu$ as well as $K^{*-} e^+ \nu_e$ events and makes a small phase-space adjustment to the number of the μ^+ events to use them as e^+ events.

 $\Gamma(K^*(892)^- \mu^+ \nu_\mu) / \Gamma(K_S^0 \pi^+ \pi^-)$ $\Gamma_{22} / \Gamma_{40}$ Unseen decay modes of the $K^*(892)^-$ are included.

VALUE	EVTS	DOCUMENT ID	TECN	COMMENT
0.674 ± 0.068 ± 0.026	175 ± 17	¹ LINK	05B FOCUS	$\gamma A, \bar{E}_\gamma \approx 180 \text{ GeV}$
				¹ LINK 05B finds that in $D^0 \rightarrow \bar{K}^0 \pi^- \mu^+ \nu_\mu$ the $\bar{K}^0 \pi^-$ system is 6% in S-wave.

 $\Gamma(K^- \pi^0 e^+ \nu_e) / \Gamma_{\text{total}}$ Γ_{23} / Γ

VALUE	EVTS	DOCUMENT ID	TECN	COMMENT
0.016 ± 0.013 ± 0.002	4	¹ BAI	91 MRK3	$e^+ e^- \approx 3.77 \text{ GeV}$

¹ BAI 91 finds that a fraction $0.79^{+0.15+0.09}_{-0.17-0.03}$ of combined D^+ and D^0 decays to $\bar{K} \pi e^+ \nu_e$ (24 events) are $\bar{K}^*(892) e^+ \nu_e$. BAI 91 uses 56 $K^- e^+ \nu_e$ events to measure a pole mass of $1.8 \pm 0.3 \pm 0.2 \text{ GeV}/c^2$ from the q^2 dependence of the decay rate.

 $\Gamma(\bar{K}^0 \pi^- e^+ \nu_e) / \Gamma_{\text{total}}$ Γ_{24} / Γ

VALUE (%)	EVTS	DOCUMENT ID	TECN	COMMENT
1.44 ± 0.04 OUR AVERAGE				
1.434 ± 0.029 ± 0.032	3.1k	ABLIKIM	19G BES3	$e^+ e^-$ at 3773 MeV
2.61 ± 1.04 ± 0.28	9 ± 3	ABLIKIM	06o BES2	$e^+ e^-$ at 3773 MeV
2.8 ± 1.7 ± 0.3	6	¹ BAI	91 MRK3	$e^+ e^- \approx 3.77 \text{ GeV}$

¹ BAI 91 finds that a fraction $0.79^{+0.15+0.09}_{-0.17-0.03}$ of combined D^+ and D^0 decays to $\bar{K} \pi e^+ \nu_e$ (24 events) are $\bar{K}^*(892) e^+ \nu_e$.

 $\Gamma((\bar{K}^0 \pi^-) \text{ s-wave } e^+ \nu_e) / \Gamma(\bar{K}^0 \pi^- e^+ \nu_e)$ $\Gamma_{25} / \Gamma_{24}$

VALUE (units 10^{-2})	EVTS	DOCUMENT ID	TECN	COMMENT
5.51 ± 0.97 ± 0.62	3.1k	ABLIKIM	19G BES3	$K_S^0 \pi^- e^+ \nu_e$ events

 $\Gamma(K^- \pi^+ \pi^- e^+ \nu_e) / \Gamma_{\text{total}}$ Γ_{26} / Γ

VALUE (units 10^{-4})	EVTS	DOCUMENT ID	TECN	COMMENT
2.8 ± 1.4 ± 0.3	8	ARTUSO	07A CLEO	$e^+ e^-$ at $\gamma(3770)$

 $\Gamma(K_1(1270)^- e^+ \nu_e) / \Gamma_{\text{total}}$ Γ_{27} / Γ

VALUE (units 10^{-4})	EVTS	DOCUMENT ID	TECN	COMMENT
10.1 ± 1.8 OUR AVERAGE				
10.9 ± 1.3 ± 0.9 ± 1.2	109	¹ ABLIKIM	21AY BES3	$e^+ e^-$ at 3773 GeV
7.6 ± 4.1 ± 0.9	8	² ARTUSO	07A CLEO	$e^+ e^-$ at $\gamma(3770)$

¹ Uses $B(K_1(1270)^- \rightarrow K^- \pi^+ \pi^-) = (32.9 \pm 3.6)\%$, which is the source of the third uncertainty.

² This ARTUSO 07A result is corrected for all decay modes of the $K_1(1270)^-$.

 $\Gamma(K^- \pi^+ \pi^- \mu^+ \nu_\mu) / \Gamma(K^- \mu^+ \nu_\mu)$ $\Gamma_{28} / \Gamma_{20}$

VALUE	CL%	DOCUMENT ID	TECN	COMMENT
<0.037	90	KODAMA	93B E653	π^- emulsion 600 GeV

 $\Gamma((\bar{K}^*(892) \pi^-) \mu^+ \nu_\mu) / \Gamma(K^- \mu^+ \nu_\mu)$ $\Gamma_{29} / \Gamma_{20}$

VALUE	CL%	DOCUMENT ID	TECN	COMMENT
<0.043	90	¹ KODAMA	93B E653	π^- emulsion 600 GeV

¹ KODAMA 93B searched in $K^- \pi^+ \pi^- \mu^+ \nu_\mu$, but the limit includes other ($\bar{K}^*(892) \pi^-$) charge states.

 $\Gamma(\pi^- e^+ \nu_e) / \Gamma_{\text{total}}$ Γ_{30} / Γ

VALUE (%)	EVTS	DOCUMENT ID	TECN	COMMENT
0.291 ± 0.004 OUR FIT				
0.293 ± 0.004 OUR AVERAGE				
0.295 ± 0.004 ± 0.003	6.3k	¹ ABLIKIM	15x BES3	2.92 fb ⁻¹ , 3773 GeV
0.288 ± 0.008 ± 0.003	1.3k	¹ BESSON	09 CLEO	$e^+ e^-$ at $\psi(3770)$
0.279 ± 0.027 ± 0.016	126	² WIDHALM	06 BELL	$e^+ e^- \approx \gamma(4S)$

• • • We do not use the following data for averages, fits, limits, etc. • • •

0.299 ± 0.011 ± 0.009		³ DOBBS	08 CLEO	See BESSON 09
0.262 ± 0.025 ± 0.008	117	COAN	05 CLEO	See DOBBS 08

¹ See the form-factor parameters near the end of this D^0 Listing.

² The $\pi^- e^+ \nu_e$ and $K^- e^+ \nu_e$ results of WIDHALM 06 give $|\frac{V_{cd}}{V_{cs}} \cdot \frac{f_\pi^+(0)}{f_K^+(0)}|^2 = 0.042 \pm 0.003 \pm 0.003$.

³ DOBBS 08 establishes $|\frac{V_{cd}}{V_{cs}} \cdot \frac{f_\pi^+(0)}{f_K^+(0)}| = 0.188 \pm 0.008 \pm 0.002$ from the D^+ and D^0 decays to $\bar{K} e^+ \nu_e$ and $\pi e^+ \nu_e$.

 $\Gamma(\pi^- e^+ \nu_e) / \Gamma(K^- e^+ \nu_e)$ $\Gamma_{30} / \Gamma_{19}$

VALUE	EVTS	DOCUMENT ID	TECN	COMMENT
0.0821 ± 0.0013 OUR FIT				Error includes scale factor of 1.1.
0.085 ± 0.007 OUR AVERAGE				
0.082 ± 0.006 ± 0.005		¹ HUANG	05 CLEO	$e^+ e^- \approx \gamma(4S)$
0.101 ± 0.020 ± 0.003	91	² FRABETTI	96B E687	$\gamma \text{ Be}, \bar{E}_\gamma \approx 200 \text{ GeV}$
0.103 ± 0.039 ± 0.013	87	³ BUTLER	95 CLE2	< 0.156 (90% CL)

¹ HUANG 05 uses both e and μ events, and makes a small correction to the μ events to make them effectively e events. This result gives $|\frac{V_{cd}}{V_{cs}} \cdot \frac{f_\pi^+(0)}{f_K^+(0)}|^2 = 0.038^{+0.006+0.005}_{-0.007-0.003}$.

² FRABETTI 96B uses both e and μ events, and makes a small correction to the μ events to make them effectively e events. This result gives $|\frac{V_{cd}}{V_{cs}} \cdot \frac{f_\pi^+(0)}{f_K^+(0)}|^2 = 0.050 \pm 0.011 \pm 0.002$.

³ BUTLER 95 has 87 ± 33 $\pi^- e^+ \nu_e$ events. The result gives $|\frac{V_{cd}}{V_{cs}} \cdot \frac{f_\pi^+(0)}{f_K^+(0)}|^2 = 0.052 \pm 0.020 \pm 0.007$.

 $\Gamma(\pi^- e^+ \nu_e) / \Gamma(K^- \pi^+)$ $\Gamma_{30} / \Gamma_{37}$

VALUE (units 10^{-2})	EVTS	DOCUMENT ID	TECN	COMMENT
7.38 ± 0.12 OUR FIT				Error includes scale factor of 1.1.
7.02 ± 0.17 ± 0.23	375k	¹ LEES	15F BABR	347 fb ⁻¹ , 10.58 GeV

¹ See the form-factor parameters near the end of the D^0 Listing.

 $\Gamma(\pi^- \mu^+ \nu_\mu) / \Gamma_{\text{total}}$ Γ_{31} / Γ

VALUE (%)	EVTS	DOCUMENT ID	TECN	COMMENT
0.267 ± 0.012 OUR FIT				Error includes scale factor of 1.3.
0.268 ± 0.012 OUR AVERAGE				Error includes scale factor of 1.2.
0.272 ± 0.008 ± 0.006	2.3k	ABLIKIM	18AE BES3	$e^+ e^-$, 3773 MeV
0.231 ± 0.026 ± 0.019	106 ± 13	WIDHALM	06 BELL	$e^+ e^- \approx \gamma(4S)$

 $\Gamma(\pi^- \mu^+ \nu_\mu) / \Gamma(K^- \mu^+ \nu_\mu)$ $\Gamma_{31} / \Gamma_{20}$

VALUE	EVTS	DOCUMENT ID	TECN	COMMENT
0.0784 ± 0.0035 OUR FIT				Error includes scale factor of 1.2.
0.074 ± 0.008 ± 0.007	288 ± 29	¹ LINK	05 FOCUS	$\gamma A, \bar{E}_\gamma \approx 180 \text{ GeV}$

¹ LINK 05 finds the form-factor ratio $|f_\pi^+(0)/f_K^+(0)|$ to be $0.85 \pm 0.04 \pm 0.04 \pm 0.01$.

 $\Gamma(\pi^- \pi^0 e^+ \nu_e) / \Gamma_{\text{total}}$ Γ_{32} / Γ

VALUE (units 10^{-3})	EVTS	DOCUMENT ID	TECN	COMMENT
1.445 ± 0.058 ± 0.039	1.1k	¹ ABLIKIM	19c BES3	$e^+ e^-$ at 3773 MeV

¹ Seen 100% via $D^0 \rightarrow \rho(770)^- e^+ \nu_e$, and also reported as the branching fraction for $D^0 \rightarrow \rho(770)^- e^+ \nu_e$.

 $\Gamma(\rho^- e^+ \nu_e) / \Gamma_{\text{total}}$ Γ_{33} / Γ

VALUE (units 10^{-3})	EVTS	DOCUMENT ID	TECN	COMMENT
1.50 ± 0.12 OUR AVERAGE				Error includes scale factor of 1.9.
1.445 ± 0.058 ± 0.039	1.1k	¹ ABLIKIM	19c BES3	$e^+ e^-$ at 3773 MeV
1.77 ± 0.12 ± 0.10	305 ± 21	^{2,3} DOBBS	13 CLEO	$e^+ e^-$ at $\psi(3770)$

• • • We do not use the following data for averages, fits, limits, etc. • • •

1.94 ± 0.39 ± 0.13	31 ± 6	COAN	05 CLEO	See DOBBS 13
--------------------	--------	------	---------	--------------

¹ This result is the same as the one reported for $D^0 \rightarrow \pi^- \pi^0 e^+ \nu_e$ which ABLIKIM 19c found to proceed 100% via $D^0 \rightarrow \rho(770)^- e^+ \nu_e$.

² DOBBS 13 finds $\Gamma(D^0 \rightarrow \rho^- e^+ \nu_e) / 2 \Gamma(D^+ \rightarrow \rho^0 e^+ \nu_e) = 1.03 \pm 0.09^{+0.08}_{-0.02}$; isospin invariance predicts the ratio is 1.0.

³ See the D^+ Listings for $D \rightarrow \rho e^+ \nu_e$ form factors.

 $\Gamma(\rho^- \mu^+ \nu_\mu) / \Gamma_{\text{total}}$ Γ_{34} / Γ

VALUE (units 10^{-3})	EVTS	DOCUMENT ID	TECN	COMMENT
1.35 ± 0.09 ± 0.09	570	ABLIKIM	21Bc BES3	$e^+ e^-$ at 3773 GeV

 $\Gamma(a(980)^- e^+ \nu_e, a^- \rightarrow \eta \pi^-) / \Gamma_{\text{total}}$ Γ_{35} / Γ

VALUE (units 10^{-4})	EVTS	DOCUMENT ID	TECN	COMMENT
1.33 ± 0.33 ± 0.29 ± 0.09	26	¹ ABLIKIM	18F BES3	$e^+ e^-$ at 3773 MeV

¹ Signal observed at 6.4 σ C.L.

 $\Gamma(b_1(1235)^- e^+ \nu_e, b_1^- \rightarrow \omega \pi^-) / \Gamma_{\text{total}}$ Γ_{36} / Γ

VALUE	CL%	DOCUMENT ID	TECN	COMMENT
<1.12 × 10⁻⁴	90	ABLIKIM	20AF BES3	$e^+ e^-$, 3773 MeV

Meson Particle Listings

 D^0 Hadronic modes with a single \bar{K} $\Gamma(K^-\pi^+)/\Gamma_{\text{total}}$ Γ_{37}/Γ

VALUE (%)	EVTs	DOCUMENT ID	TECN	COMMENT
3.947±0.030 OUR FIT	Error includes scale factor of 1.2.			
3.909±0.034 OUR AVERAGE				
3.883±0.006±0.051	0.5M	1 ABLIKIM	18w BES3	e^+e^- , 3773 MeV
3.934±0.021±0.061		BONVICINI	14 CLEO	All CLEO-c runs
4.007±0.037±0.072	33.8k	AUBERT	08L BABR	e^+e^- at $\Upsilon(4S)$
3.82±0.07±0.12		2 ARTUSO	98 CLE2	CLEO average
3.90±0.09±0.12	5.4k	3 BARATE	97C ALEP	From Z decays
3.41±0.12±0.28	1.2k	3 ALBRECHT	94F ARG	$e^+e^- \approx \Upsilon(4S)$
3.62±0.34±0.44		3 DECAMP	91J ALEP	From Z decays
••• We do not use the following data for averages, fits, limits, etc. •••				
3.891±0.035±0.069		4 DOBBS	07 CLEO	See BONVICINI 14
3.91±0.08±0.09	10.3k	4 HE	05 CLEO	See DOBBS 07
3.81±0.15±0.16	1.2k	5 ARTUSO	98 CLE2	e^+e^- at $\Upsilon(4S)$
3.69±0.11±0.16		6 COAN	98 CLE2	See ARTUSO 98
4.5±0.6±0.4		7 ALBRECHT	94 ARG	$e^+e^- \approx \Upsilon(4S)$
3.95±0.08±0.17	4.2k	3,8 AKERIB	93 CLE2	See ARTUSO 98
4.5±0.8±0.5	5.6	3 ABACHI	88 HRS	e^+e^- 29 GeV
4.2±0.4±0.4	0.9k	ADLER	88c MRK3	e^+e^- 3.77 GeV
4.1±0.6	0.3k	9 SCHINDLER	81 MRK2	e^+e^- 3.771 GeV
4.3±1.0	130	10 PERUZZI	77 LGW	e^+e^- 3.77 GeV

¹ ABLIKIM 18w measured the combined $K^{\mp}\pi^{\pm}$ branching fraction to be 3.898%. We have subtracted off the doubly Cabibbo-suppressed branching fraction $B(D^0 \rightarrow K^+\pi^-) = (1.50 \pm 0.07) \times 10^{-4}$, even though it is less than one-third of the uncertainty of the combined measurement, in order to treat this as a measurement of $B(D^0 \rightarrow K^-\pi^+)$.

² This combines the CLEO results of ARTUSO 98, COAN 98, and AKERIB 93.

³ ABACHI 88, DECAMP 91J, AKERIB 93, ALBRECHT 94F, and BARATE 97c use $D^*(2010)^+ \rightarrow D^0\pi^+$ decays. The π^+ is both slow and of low p_T with respect to the event thrust axis or nearest jet ($\approx D^{*+}$ direction). The excess number of such π^+ 's over background gives the number of $D^*(2010)^+ \rightarrow D^0\pi^+$ events, and the fraction with $D^0 \rightarrow K^-\pi^+$ gives the $D^0 \rightarrow K^-\pi^+$ branching fraction.

⁴ DOBBS 07 and HE 05 use single- and double-tagged events in an overall fit. DOBBS 07 supersedes HE 05.

⁵ ARTUSO 98, following ALBRECHT 94, uses D^0 mesons from $\bar{B}^0 \rightarrow D^*(2010)^+ X \ell^- \bar{\nu}_\ell$ decays. Our average uses the CLEO average of this value with the values of COAN 98 and AKERIB 93.

⁶ COAN 98 assumes that $\Gamma(B \rightarrow \bar{D} X \ell^+ \nu)/\Gamma(B \rightarrow X \ell^+ \nu) = 1.0 - 3|V_{ub}/V_{cb}|^2 - 0.010 \pm 0.005$, the last term accounting for $\bar{B} \rightarrow D_s^+ K X \ell^- \bar{\nu}$. COAN 98 is included in the CLEO average in ARTUSO 98.

⁷ ALBRECHT 94 uses D^0 mesons from $\bar{B}^0 \rightarrow D^{*+} \ell^- \bar{\nu}_\ell$ decays. This is a different set of events than used by ALBRECHT 94F.

⁸ This AKERIB 93 value includes radiative corrections; without them, the value is $0.0391 \pm 0.0008 \pm 0.0017$. AKERIB 93 is included in the CLEO average in ARTUSO 98.

⁹ SCHINDLER 81 (MARK-2) measures $\sigma(e^+e^- \rightarrow \psi(3770)) \times$ branching fraction to be 0.24 ± 0.02 nb. We use the MARK-3 (ADLER 88c) value of $\sigma = 5.8 \pm 0.5 \pm 0.6$ nb.

¹⁰ PERUZZI 77 (MARK-1) measures $\sigma(e^+e^- \rightarrow \psi(3770)) \times$ branching fraction to be 0.25 ± 0.05 nb. We use the MARK-3 (ADLER 88c) value of $\sigma = 5.8 \pm 0.5 \pm 0.6$ nb.

 $\Gamma(K_S^0\pi^0)/\Gamma_{\text{total}}$ Γ_{38}/Γ

VALUE (%)	EVTs	DOCUMENT ID	TECN	COMMENT
1.240±0.022 OUR FIT				
1.239±0.006±0.027	67k	ABLIKIM	18w BES3	e^+e^- , 3773 MeV
••• We do not use the following data for averages, fits, limits, etc. •••				
1.240±0.017±0.056	614	HE	08 CLEO	See MENDEZ 10

 $\Gamma(K_S^0\pi^0)/[\Gamma(K^-\pi^+) + \Gamma(K^+\pi^-)]$ $\Gamma_{38}/(\Gamma_{37} + \Gamma_{274})$

VALUE (units 10^{-2})	EVTs	DOCUMENT ID	TECN	COMMENT
31.3±0.6 OUR FIT				
30.4±0.3±0.9	20k	MENDEZ	10 CLEO	e^+e^- at 3774 MeV

 $\Gamma(K_S^0\pi^0)/\Gamma(K_S^0\pi^+\pi^-)$ Γ_{38}/Γ_{40}

VALUE	EVTs	DOCUMENT ID	TECN	COMMENT
0.443±0.028 OUR FIT				
0.44±0.02±0.05	1942±64	PROCARIO	93B CLE2	e^+e^- 10.36–10.7 GeV
••• We do not use the following data for averages, fits, limits, etc. •••				
0.34±0.04±0.02	92	1 ALBRECHT	92P ARG	$e^+e^- \approx 10$ GeV
0.36±0.04±0.08	104	KINOSHITA	91 CLEO	$e^+e^- \sim 10.7$ GeV

¹ This value is calculated from numbers in Table 1 of ALBRECHT 92P.

 $\Gamma(K_L^0\pi^0)/\Gamma_{\text{total}}$ Γ_{39}/Γ

VALUE (%)	EVTs	DOCUMENT ID	TECN	COMMENT
0.998±0.049±0.048	1116	1 HE	08 CLEO	e^+e^- at $\psi(3770)$

¹ The difference of HE 08 $D^0 \rightarrow K_L^0\pi^0$ and $K_S^0\pi^0$ branching fractions over the sum is $0.108 \pm 0.025 \pm 0.024$. This is consistent with U-spin symmetry and the Cabibbo angle.

 $\Gamma(K_S^0\pi^+\pi^-)/\Gamma_{\text{total}}$ Γ_{40}/Γ

VALUE (%)	EVTs	DOCUMENT ID	TECN	COMMENT
••• We do not use the following data for averages, fits, limits, etc. •••				
2.52±0.20±0.25	284±22	1 ALBRECHT	94F ARG	$e^+e^- \approx \Upsilon(4S)$
3.2±0.3±0.5		ADLER	87 MRK3	e^+e^- 3.77 GeV
2.6±0.8	32±8	2 SCHINDLER	81 MRK2	e^+e^- 3.771 GeV
4.0±1.2	28	3 PERUZZI	77 LGW	e^+e^- 3.77 GeV

¹ See the footnote on the ALBRECHT 94F measurement of $\Gamma(K^-\pi^+)/\Gamma_{\text{total}}$ for the method used.

² SCHINDLER 81 (MARK-2) measures $\sigma(e^+e^- \rightarrow \psi(3770)) \times$ branching fraction to be 0.30 ± 0.08 nb. We use the MARK-3 (ADLER 88c) value of $\sigma = 5.8 \pm 0.5 \pm 0.6$ nb.

³ PERUZZI 77 (MARK-1) measures $\sigma(e^+e^- \rightarrow \psi(3770)) \times$ branching fraction to be 0.46 ± 0.12 nb. We use the MARK-3 (ADLER 88c) value of $\sigma = 5.8 \pm 0.5 \pm 0.6$ nb.

 $\Gamma(K_S^0\pi^+\pi^-)/\Gamma(K^-\pi^+)$ Γ_{40}/Γ_{37}

VALUE	EVTs	DOCUMENT ID	TECN	COMMENT
0.71±0.05 OUR FIT	Error includes scale factor of 1.1.			
0.81±0.05±0.08	856±35	FRABETTI	94J E687	γ Be $\bar{E}_\gamma = 220$ GeV
••• We do not use the following data for averages, fits, limits, etc. •••				
0.85±0.40	35	AVERY	80 SPEC	$\gamma N \rightarrow D^{*+}$
1.4±0.5	116	PICCOLO	77 MRK1	e^+e^- 4.03, 4.41 GeV

 $\Gamma(K_S^0\rho^0)/\Gamma(K_S^0\pi^+\pi^-)$ Γ_{41}/Γ_{40}

This is the "fit fraction" from the Dalitz-plot analysis.

VALUE	DOCUMENT ID	TECN	COMMENT
0.224±0.017	OUR AVERAGE	Error includes scale factor of 1.7.	
-0.023			
0.210±0.016	1 AUBERT	08AL BABR	Dalitz fit, ≈ 487 k evts
0.264±0.009 ^{+0.010} _{-0.026}	MURAMATSU	02 CLE2	Dalitz fit, 5299 evts
••• We do not use the following data for averages, fits, limits, etc. •••			
0.267±0.011 ^{+0.009} _{-0.028}	ASNER	04A CLEO	See MURAMATSU 02
0.350±0.028±0.067	FRABETTI	94G E687	Dalitz fit, 597 evts
0.227±0.032±0.009	ALBRECHT	93D ARG	Dalitz fit, 440 evts
0.215±0.051±0.037	ANJOS	93 E691	γ Be 90–260 GeV
0.20±0.06±0.03	FRABETTI	92B E687	γ Be, $\bar{E}_\gamma = 221$ GeV
0.12±0.01±0.07	ADLER	87 MRK3	e^+e^- 3.77 GeV

¹ The error on this AUBERT 08AL value includes both statistical and systematic uncertainties; the latter dominates.

² This is the "fit fraction" from the Dalitz-plot analysis.

³ This is the "fit fraction" from the Dalitz-plot analysis.

⁴ The error on this AUBERT 08AL value includes both statistical and systematic uncertainties; the latter dominates.

 $\Gamma(K_S^0\omega, \omega \rightarrow \pi^+\pi^-)/\Gamma(K_S^0\pi^+\pi^-)$ Γ_{42}/Γ_{40}

This is the "fit fraction" from the Dalitz-plot analysis.

VALUE	DOCUMENT ID	TECN	COMMENT
0.0073±0.0020 OUR AVERAGE			
0.009±0.010	1 AUBERT	08AL BABR	Dalitz fit, ≈ 487 k evts
0.0072±0.0018 ^{+0.0010} _{-0.0009}	MURAMATSU	02 CLE2	Dalitz fit, 5299 evts
••• We do not use the following data for averages, fits, limits, etc. •••			
0.0081±0.0019 ^{+0.0018} _{-0.0010}	ASNER	04A CLEO	See MURAMATSU 02

¹ The error on this AUBERT 08AL value includes both statistical and systematic uncertainties; the latter dominates.

 $\Gamma(K_S^0(\pi^+\pi^-)_{S\text{-wave}})/\Gamma(K_S^0\pi^+\pi^-)$ Γ_{43}/Γ_{40}

This is the "fit fraction" from the Dalitz-plot analysis. The $(\pi^+\pi^-)_{S\text{-wave}}$ includes what in isobar models are the $f_0(980)$ and $f_0(1370)$; see the following two data blocks.

VALUE	DOCUMENT ID	TECN	COMMENT
0.119±0.026	1 AUBERT	08AL BABR	Dalitz fit, ≈ 487 k evts
••• We do not use the following data for averages, fits, limits, etc. •••			
0.042±0.005 ^{+0.011} _{-0.005}	ASNER	04A CLEO	See MURAMATSU 02
0.068±0.016±0.018	FRABETTI	94G E687	Dalitz fit, 597 evts
0.046±0.018±0.006	ALBRECHT	93D ARG	Dalitz fit, 440 evts

¹ The error on this AUBERT 08AL value includes both statistical and systematic uncertainties; the latter dominates.

 $\Gamma(K_S^0 f_0(980), f_0 \rightarrow \pi^+\pi^-)/\Gamma(K_S^0\pi^+\pi^-)$ Γ_{44}/Γ_{40}

Fit fraction from the Dalitz plot analyses.

VALUE	DOCUMENT ID	TECN	COMMENT
0.043±0.005^{+0.012}_{-0.006}	MURAMATSU	02 CLE2	Dalitz fit, 5299 evts
••• We do not use the following data for averages, fits, limits, etc. •••			
0.042±0.005 ^{+0.011} _{-0.005}	ASNER	04A CLEO	See MURAMATSU 02
0.068±0.016±0.018	FRABETTI	94G E687	Dalitz fit, 597 evts
0.046±0.018±0.006	ALBRECHT	93D ARG	Dalitz fit, 440 evts

 $\Gamma(K_S^0 f_0(1370), f_0 \rightarrow \pi^+\pi^-)/\Gamma(K_S^0\pi^+\pi^-)$ Γ_{45}/Γ_{40}

This is the "fit fraction" from the Dalitz-plot analysis.

VALUE	DOCUMENT ID	TECN	COMMENT
0.099±0.011^{+0.028}_{-0.044}	MURAMATSU	02 CLE2	Dalitz fit, 5299 evts
••• We do not use the following data for averages, fits, limits, etc. •••			
0.098±0.014 ^{+0.026} _{-0.036}	ASNER	04A CLEO	See MURAMATSU 02
0.077±0.022±0.031	FRABETTI	94G E687	Dalitz fit, 597 evts
0.082±0.028±0.013	ALBRECHT	93D ARG	Dalitz fit, 440 evts

$\Gamma(K_S^0 f_2(1270) \rightarrow \pi^+ \pi^-) / \Gamma(K_S^0 \pi^+ \pi^-)$ $\Gamma_{46} / \Gamma_{40}$

This is the "fit fraction" from the Dalitz-plot analysis.

VALUE	DOCUMENT ID	TECN	COMMENT
0.0032 ± 0.0035 -0.0022 OUR AVERAGE			
0.006 ± 0.007	¹ AUBERT	08AL BABR	Dalitz fit, ≈ 487 k evts
0.0027 ± 0.0015 ± 0.0037 -0.0017	MURAMATSU 02	CLE2	Dalitz fit, 5 299 evts
• • • We do not use the following data for averages, fits, limits, etc. • • •			
0.0036 ± 0.0022 ± 0.0032 -0.0019	ASNER	04A CLEO	See MURAMATSU 02
0.037 ± 0.014 ± 0.017	FRABETTI	94G E687	Dalitz fit, 597 evts
0.050 ± 0.021 ± 0.008	ALBRECHT	93D ARG	Dalitz fit, 440 evts

¹ The error on this AUBERT 08AL value includes both statistical and systematic uncertainties; the latter dominates.

$\Gamma(K^*(892) \pi^+, K^{*-} \rightarrow K_S^0 \pi^-) / \Gamma(K_S^0 \pi^+ \pi^-)$ $\Gamma_{47} / \Gamma_{40}$

This is the "fit fraction" from the Dalitz-plot analysis.

VALUE	DOCUMENT ID	TECN	COMMENT
0.588 ± 0.034 -0.050 OUR AVERAGE			Error includes scale factor of 2.0.
0.557 ± 0.028	¹ AUBERT	08AL BABR	Dalitz fit, ≈ 487 k evts
0.657 ± 0.013 ± 0.018 -0.040	MURAMATSU 02	CLE2	Dalitz fit, 5 299 evts
• • • We do not use the following data for averages, fits, limits, etc. • • •			
0.663 ± 0.013 ± 0.024 -0.043	ASNER	04A CLEO	See MURAMATSU 02
0.625 ± 0.036 ± 0.026	FRABETTI	94G E687	Dalitz fit, 597 evts
0.718 ± 0.042 ± 0.030	ALBRECHT	93D ARG	Dalitz fit, 440 evts
0.480 ± 0.097	ANJOS	93 E691	γ Be 90–260 GeV
0.56 ± 0.04 ± 0.05	ADLER	87 MRK3	$e^+ e^-$ 3.77 GeV

¹ The error on this AUBERT 08AL value includes both statistical and systematic uncertainties; the latter dominates.

$\Gamma(K_S^0(1430) \pi^+, K_0^{*-} \rightarrow K_S^0 \pi^-) / \Gamma(K_S^0 \pi^+ \pi^-)$ $\Gamma_{48} / \Gamma_{40}$

This is the "fit fraction" from the Dalitz-plot analysis.

VALUE	DOCUMENT ID	TECN	COMMENT
0.095 ± 0.014 -0.010 OUR AVERAGE			
0.102 ± 0.015	¹ AUBERT	08AL BABR	Dalitz fit, ≈ 487 k evts
0.073 ± 0.007 ± 0.031 -0.011	MURAMATSU 02	CLE2	Dalitz fit, 5 299 evts
• • • We do not use the following data for averages, fits, limits, etc. • • •			
0.072 ± 0.007 ± 0.014 -0.013	ASNER	04A CLEO	See MURAMATSU 02
0.109 ± 0.027 ± 0.029	FRABETTI	94G E687	Dalitz fit, 597 evts
0.129 ± 0.034 ± 0.021	ALBRECHT	93D ARG	Dalitz fit, 440 evts

¹ The error on this AUBERT 08AL value includes both statistical and systematic uncertainties; the latter dominates.

$\Gamma(K_S^0(1430) \pi^+, K_2^{*-} \rightarrow K_S^0 \pi^-) / \Gamma(K_S^0 \pi^+ \pi^-)$ $\Gamma_{49} / \Gamma_{40}$

This is the "fit fraction" from the Dalitz-plot analysis.

VALUE	DOCUMENT ID	TECN	COMMENT
0.0120 ± 0.0070 -0.0035 OUR AVERAGE			
0.022 ± 0.016	¹ AUBERT	08AL BABR	Dalitz fit, ≈ 487 k evts
0.011 ± 0.002 ± 0.007 -0.003	MURAMATSU 02	CLE2	Dalitz fit, 5 299 evts
• • • We do not use the following data for averages, fits, limits, etc. • • •			
0.011 ± 0.002 ± 0.005 -0.003	ASNER	04A CLEO	See MURAMATSU 02

¹ The error on this AUBERT 08AL value includes both statistical and systematic uncertainties; the latter dominates.

$\Gamma(K^*(1680) \pi^+, K^{*-} \rightarrow K_S^0 \pi^-) / \Gamma(K_S^0 \pi^+ \pi^-)$ $\Gamma_{50} / \Gamma_{40}$

This is the "fit fraction" from the Dalitz-plot analysis.

VALUE	DOCUMENT ID	TECN	COMMENT
0.016 ± 0.013 OUR AVERAGE			
0.007 ± 0.019	¹ AUBERT	08AL BABR	Dalitz fit, ≈ 487 k evts
0.022 ± 0.004 ± 0.018 -0.015	MURAMATSU 02	CLE2	Dalitz fit, 5 299 evts
• • • We do not use the following data for averages, fits, limits, etc. • • •			
0.023 ± 0.005 ± 0.007 -0.014	ASNER	04A CLEO	See MURAMATSU 02

¹ The error on this AUBERT 08AL value includes both statistical and systematic uncertainties; the latter dominates.

$\Gamma(K^*(892) \pi^+, K^{*+} \rightarrow K_S^0 \pi^+) / \Gamma(K_S^0 \pi^+ \pi^-)$ $\Gamma_{51} / \Gamma_{40}$

This is the "fit fraction" from the Dalitz-plot analysis. This is a doubly Cabibbo-suppressed mode.

VALUE (units 10 ⁻³)	DOCUMENT ID	TECN	COMMENT
4.0 ± 2.0 -1.2 OUR AVERAGE			
4.6 ± 2.3	¹ AUBERT	08AL BABR	Dalitz fit, ≈ 487 k evts
3.4 ± 1.3 ± 4.1 -0.4	MURAMATSU 02	CLE2	Dalitz fit, 5 299 evts
• • • We do not use the following data for averages, fits, limits, etc. • • •			
3.4 ± 1.3 ± 3.6 -0.5	ASNER	04A CLEO	See MURAMATSU 02

¹ The error on this AUBERT 08AL value includes both statistical and systematic uncertainties; the latter dominates.

$\Gamma(K_0^{*0}(1430) \pi^-, K_0^{*+} \rightarrow K_S^0 \pi^+) / \Gamma(K_S^0 \pi^+ \pi^-)$ $\Gamma_{52} / \Gamma_{40}$

This is the "fit fraction" from the Dalitz-plot analysis. This is a doubly Cabibbo-suppressed mode.

VALUE	CL%	DOCUMENT ID	TECN	COMMENT
<5 × 10⁻⁴	95	AUBERT	08AL BABR	Dalitz fit, ≈ 487 k evts

$\Gamma(K_2^{*0}(1430) \pi^-, K_2^{*+} \rightarrow K_S^0 \pi^+) / \Gamma(K_S^0 \pi^+ \pi^-)$ $\Gamma_{53} / \Gamma_{40}$

This is the "fit fraction" from the Dalitz-plot analysis. This is a doubly Cabibbo-suppressed mode.

VALUE	CL%	DOCUMENT ID	TECN	COMMENT
<1.2 × 10⁻³	95	AUBERT	08AL BABR	Dalitz fit, ≈ 487 k evts

$\Gamma(K_S^0 \pi^+ \pi^- \text{ nonresonant}) / \Gamma(K_S^0 \pi^+ \pi^-)$ $\Gamma_{54} / \Gamma_{40}$

This is the "fit fraction" from the Dalitz-plot analysis. Neither FRABETTI 94G nor ALBRECHT 93D (quoted in many of the earlier submodes of $K_S^0 \pi^+ \pi^-$) sees evidence for a nonresonant component.

VALUE	DOCUMENT ID	TECN	COMMENT
0.009 ± 0.004 ± 0.020 -0.004	MURAMATSU 02	CLE2	Dalitz fit, 5 299 evts
• • • We do not use the following data for averages, fits, limits, etc. • • •			
0.007 ± 0.007 ± 0.021 0.006	ASNER	04A CLEO	See MURAMATSU 02
0.263 ± 0.024 ± 0.041	ANJOS	93 E691	γ Be 90–260 GeV
0.26 ± 0.08 ± 0.05	FRABETTI	92B E687	γ Be, $E_\gamma = 221$ GeV
0.33 ± 0.05 ± 0.10	ADLER	87 MRK3	$e^+ e^-$ 3.77 GeV

$\Gamma(K^- \pi^+ \pi^0) / \Gamma_{\text{total}}$ Γ_{55} / Γ

VALUE (%)	EVTS	DOCUMENT ID	TECN	COMMENT
• • • We do not use the following data for averages, fits, limits, etc. • • •				
14.57 ± 0.12 ± 0.38		¹ DOBBS	07 CLEO	See BONVICINI 14
14.9 ± 0.3 ± 0.5	19k ± 150	¹ HE	05 CLEO	See DOBBS 07
13.3 ± 1.2 ± 1.3	931	ADLER	88C MRK3	$e^+ e^-$ 3.77 GeV
11.7 ± 4.3	37	² SCHINDLER	81 MRK2	$e^+ e^-$ 3.771 GeV

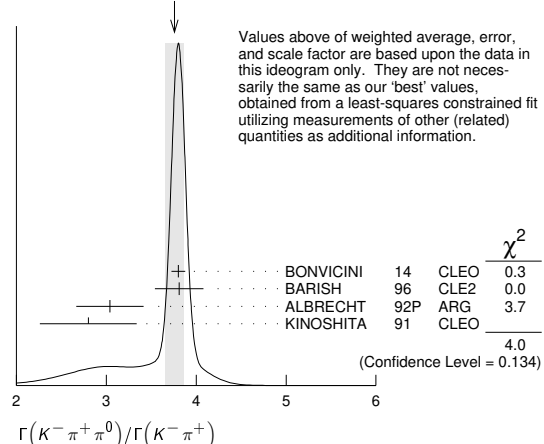
¹ DOBBS 07 and HE 05 use single- and double-tagged events in an overall fit. DOBBS 07 supersedes HE 05.

² SCHINDLER 81 (MARK-2) measures $\sigma(e^+ e^- \rightarrow \psi(3770)) \times$ branching fraction to be 0.68 ± 0.23 nb. We use the MARK-3 (ADLER 88c) value of $\sigma = 5.8 \pm 0.5 \pm 0.6$ nb.

$\Gamma(K^- \pi^+ \pi^0) / \Gamma(K^- \pi^+)$ $\Gamma_{55} / \Gamma_{37}$

VALUE	EVTS	DOCUMENT ID	TECN	COMMENT
3.65 ± 0.13 OUR FIT				Error includes scale factor of 2.1.
3.76 ± 0.10 OUR AVERAGE				Error includes scale factor of 1.4. See the ideogram below.
3.802 ± 0.022 ± 0.073		BONVICINI	14 CLEO	All CLEO-c runs
3.81 ± 0.07 ± 0.26	10k	BARISH	96 CLE2	$e^+ e^- \approx \Upsilon(4S)$
3.04 ± 0.16 ± 0.34	931	¹ ALBRECHT	92P ARG	$e^+ e^- \approx 10$ GeV
2.8 ± 0.14 ± 0.52	1050	KINOSHITA	91 CLEO	$e^+ e^- \sim 10.7$ GeV

WEIGHTED AVERAGE
3.76 ± 0.10 (Error scaled by 1.4)



¹ This value is calculated from numbers in Table 1 of ALBRECHT 92P.

$\Gamma(K^- \rho^+) / \Gamma(K^- \pi^+ \pi^0)$ $\Gamma_{56} / \Gamma_{55}$

This is the "fit fraction" from the Dalitz-plot analysis.

VALUE	DOCUMENT ID	TECN	COMMENT
0.78 ± 0.04 OUR AVERAGE			
0.788 ± 0.019 ± 0.048	KOPP	01 CLE2	Dalitz fit, ≈ 7,000 evts
0.765 ± 0.041 ± 0.054	FRABETTI	94G E687	Dalitz fit, 530 evts
• • • We do not use the following data for averages, fits, limits, etc. • • •			
0.647 ± 0.039 ± 0.150	ANJOS	93 E691	γ Be 90–260 GeV
0.81 ± 0.03 ± 0.06	ADLER	87 MRK3	$e^+ e^-$ 3.77 GeV

$\Gamma(K^- \rho(1700)^+, \rho^+ \rightarrow \pi^+ \pi^0) / \Gamma(K^- \pi^+ \pi^0)$ $\Gamma_{57} / \Gamma_{55}$

This is the "fit fraction" from the Dalitz-plot analysis.

VALUE	DOCUMENT ID	TECN	COMMENT
0.057 ± 0.008 ± 0.009	KOPP	01 CLE2	Dalitz fit, ≈ 7,000 evts

Meson Particle Listings

 D^0 $\Gamma(K^*(892)^-\pi^+, K^*(892)^- \rightarrow K^-\pi^0)/\Gamma(K^-\pi^+\pi^0)$ Γ_{58}/Γ_{55}

This is the "fit fraction" from the Dalitz-plot analysis.

VALUE	DOCUMENT ID	TECN	COMMENT
0.160 ± 0.025 -0.013 OUR AVERAGE			
0.161 ± 0.007 ± 0.027 -0.011	KOPP	01 CLE2	Dalitz fit, ≈ 7,000 evts
0.148 ± 0.028 ± 0.049	FRABETTI	94G E687	Dalitz fit, 530 evts
• • • We do not use the following data for averages, fits, limits, etc. • • •			
0.084 ± 0.011 ± 0.012	ANJOS	93 E691	γ Be 90–260 GeV
0.12 ± 0.02 ± 0.03	ADLER	87 MRK3	e^+e^- 3.77 GeV

 $\Gamma(\bar{K}^*(892)^0\pi^0, \bar{K}^*(892)^0 \rightarrow K^-\pi^+)/\Gamma(K^-\pi^+\pi^0)$ Γ_{59}/Γ_{55}

This is the "fit fraction" from the Dalitz-plot analysis.

VALUE	DOCUMENT ID	TECN	COMMENT
0.135 ± 0.016 OUR AVERAGE			
0.127 ± 0.009 ± 0.016	KOPP	01 CLE2	Dalitz fit, ≈ 7,000 evts
0.165 ± 0.031 ± 0.015	FRABETTI	94G E687	Dalitz fit, 530 evts
• • • We do not use the following data for averages, fits, limits, etc. • • •			
0.142 ± 0.018 ± 0.024	ANJOS	93 E691	γ Be 90–260 GeV
0.13 ± 0.02 ± 0.03	ADLER	87 MRK3	e^+e^- 3.77 GeV

 $\Gamma(K_S^0(1430)^-\pi^+, K_S^0 \rightarrow K^-\pi^0)/\Gamma(K^-\pi^+\pi^0)$ Γ_{60}/Γ_{55}

This is the "fit fraction" from the Dalitz-plot analysis.

VALUE	DOCUMENT ID	TECN	COMMENT
0.033 ± 0.006 ± 0.014	KOPP	01 CLE2	Dalitz fit, ≈ 7,000 evts

 $\Gamma(\bar{K}_S^0(1430)^0\pi^0, \bar{K}_S^0 \rightarrow K^-\pi^+)/\Gamma(K^-\pi^+\pi^0)$ Γ_{61}/Γ_{55}

This is the "fit fraction" from the Dalitz-plot analysis.

VALUE	DOCUMENT ID	TECN	COMMENT
0.041 ± 0.006 -0.009	KOPP	01 CLE2	Dalitz fit, ≈ 7,000 evts

 $\Gamma(K^*(1680)^-\pi^+, K^*(1680)^- \rightarrow K^-\pi^0)/\Gamma(K^-\pi^+\pi^0)$ Γ_{62}/Γ_{55}

This is the "fit fraction" from the Dalitz-plot analysis.

VALUE	DOCUMENT ID	TECN	COMMENT
0.013 ± 0.003 ± 0.004	KOPP	01 CLE2	Dalitz fit, ≈ 7,000 evts

 $\Gamma(K^-\pi^+\pi^0 \text{ nonresonant})/\Gamma(K^-\pi^+\pi^0)$ Γ_{63}/Γ_{55}

This is the "fit fraction" from the Dalitz-plot analysis.

VALUE	EVTS	DOCUMENT ID	TECN	COMMENT
0.080 ± 0.040 -0.014 OUR AVERAGE				
0.075 ± 0.009 ± 0.056 -0.011		KOPP	01 CLE2	Dalitz fit, ≈ 7,000 evts
0.101 ± 0.033 ± 0.040		FRABETTI	94G E687	Dalitz fit, 530 evts
• • • We do not use the following data for averages, fits, limits, etc. • • •				
0.036 ± 0.004 ± 0.018		ANJOS	93 E691	γ Be 90–260 GeV
0.09 ± 0.02 ± 0.04		ADLER	87 MRK3	e^+e^- 3.77 GeV
0.51 ± 0.22	21	SUMMERS	84 E691	Photoproduction

 $\Gamma(K_S^0 2\pi^0)/\Gamma_{\text{total}}$ Γ_{64}/Γ

VALUE (units 10^{-3})	EVTS	DOCUMENT ID	TECN	COMMENT
9.1 ± 1.1 OUR AVERAGE				Error includes scale factor of 2.2.
10.58 ± 0.38 ± 0.73	1259	LOWREY	11 CLEO	e^+e^- ≈ 3.77 GeV
8.34 ± 0.45 ± 0.42		ASNER	08 CLEO	$e^+e^- \rightarrow D^0\bar{D}^0$, 3.77 GeV

 $\Gamma(K_S^0(2\pi^0)_S\text{-wave})/\Gamma(K_S^0 2\pi^0)$ Γ_{65}/Γ_{64}

This is the "fit fraction" from the Dalitz-plot analysis.

VALUE (units 10^{-2})	DOCUMENT ID	TECN	COMMENT
28.9 ± 6.3 ± 3.1	LOWREY	11 CLEO	Dalitz analysis, 1259 evts

 $\Gamma(\bar{K}^*(892)^0\rho^0, \bar{K}^*(892)^0 \rightarrow K_S^0\pi^0)/\Gamma(K_S^0 2\pi^0)$ Γ_{66}/Γ_{38}

This is the "fit fraction" from the Dalitz-plot analysis.

VALUE (units 10^{-2})	DOCUMENT ID	TECN	COMMENT
65.6 ± 5.3 ± 2.5	LOWREY	11 CLEO	Dalitz analysis, 1259 evts
• • • We do not use the following data for averages, fits, limits, etc. • • •			
55 $^{+13}_{-10}$ ± 7	PROCARIO	93B CLE2	Dalitz plot fit, 122 evts

 $\Gamma(\bar{K}^*(1430)^0\pi^0, \bar{K}^*(1430)^0 \rightarrow K_S^0\pi^0)/\Gamma(K_S^0 2\pi^0)$ Γ_{67}/Γ_{64}

This is the "fit fraction" from the Dalitz-plot analysis.

VALUE (units 10^{-2})	DOCUMENT ID	TECN	COMMENT
0.49 ± 0.45 ± 2.51	LOWREY	11 CLEO	Dalitz analysis, 1259 evts

 $\Gamma(\bar{K}^*(1680)^0\pi^0, \bar{K}^*(1680)^0 \rightarrow K_S^0\pi^0)/\Gamma(K_S^0 2\pi^0)$ Γ_{68}/Γ_{64}

This is the "fit fraction" from the Dalitz-plot analysis.

VALUE (units 10^{-2})	DOCUMENT ID	TECN	COMMENT
11.2 ± 2.7 ± 2.5	LOWREY	11 CLEO	Dalitz analysis, 1259 evts

 $\Gamma(K_S^0 f_2(1270), f_2 \rightarrow 2\pi^0)/\Gamma(K_S^0 2\pi^0)$ Γ_{69}/Γ_{64}

This is the "fit fraction" from the Dalitz-plot analysis.

VALUE (units 10^{-2})	DOCUMENT ID	TECN	COMMENT
2.48 ± 0.91 ± 0.78	LOWREY	11 CLEO	Dalitz analysis, 1259 evts

 $\Gamma(2K_S^0, \text{one } K_S^0 \rightarrow 2\pi^0)/\Gamma(K_S^0 2\pi^0)$ Γ_{70}/Γ_{64}

This is the "fit fraction" from the Dalitz-plot analysis.

VALUE (units 10^{-2})	DOCUMENT ID	TECN	COMMENT
3.46 ± 0.92 ± 0.66	LOWREY	11 CLEO	Dalitz analysis, 1259 evts

 $\Gamma(K_S^0 2\pi^0 \text{ nonresonant})/\Gamma(K_S^0 \pi^0)$ Γ_{71}/Γ_{38}

This is the "fit fraction" from the Dalitz-plot analysis.

VALUE	DOCUMENT ID	TECN	COMMENT
• • • We do not use the following data for averages, fits, limits, etc. • • •			
0.37 ± 0.08 ± 0.04	PROCARIO	93B CLE2	Dalitz plot fit, 122 evts

 $\Gamma(K^-\pi^+\pi^-)/\Gamma_{\text{total}}$ Γ_{72}/Γ

VALUE (%)	EVTS	DOCUMENT ID	TECN	COMMENT
• • • We do not use the following data for averages, fits, limits, etc. • • •				
8.30 ± 0.07 ± 0.20		¹ DOBBS	07 CLEO	See BONVICINI 14
8.3 ± 0.2 ± 0.3	15k	¹ HE	05 CLEO	See DOBBS 07
7.9 ± 1.5 ± 0.9		² ALBRECHT	94 ARG	e^+e^- ≈ $\Upsilon(4S)$
6.80 ± 0.27 ± 0.57	1.4k	³ ALBRECHT	94F ARG	e^+e^- ≈ $\Upsilon(4S)$
9.1 ± 0.8 ± 0.8	992	ADLER	88c MRK3	e^+e^- 3.77 GeV
11.7 ± 2.5	185	SCHINDLER	81 MRK2	e^+e^- 3.77 GeV
6.2 ± 1.9	44	PERUZZI	77 LGW	e^+e^- 3.77 GeV

¹ DOBBS 07 and HE 05 use single- and double-tagged events in an overall fit. DOBBS 07 supersedes HE 05.² ALBRECHT 94 uses D^0 mesons from $\bar{B}^0 \rightarrow D^{*+} \ell^- \bar{\nu}_\ell$ decays. This is a different set of events than used by ALBRECHT 94F.³ See the footnote on the ALBRECHT 94F measurement of $\Gamma(K^-\pi^+)/\Gamma_{\text{total}}$ for the method used.⁴ SCHINDLER 81 (MARK-2) measures $\sigma(e^+e^- \rightarrow \psi(3770)) \times$ branching fraction to be 0.68 ± 0.11 nb. We use the MARK-3 (ADLER 88c) value of $\sigma = 5.8 \pm 0.5 \pm 0.6$ nb.⁵ PERUZZI 77 (MARK-1) measures $\sigma(e^+e^- \rightarrow \psi(3770)) \times$ branching fraction to be 0.36 ± 0.10 nb. We use the MARK-3 (ADLER 88c) value of $\sigma = 5.8 \pm 0.5 \pm 0.6$ nb. $\Gamma(K^-\pi^+\pi^-)/\Gamma(K^-\pi^+)$ Γ_{72}/Γ_{37}

VALUE	EVTS	DOCUMENT ID	TECN	COMMENT
2.083 ± 0.031 OUR FIT				
2.087 ± 0.032 OUR AVERAGE				
2.106 ± 0.013 ± 0.032		BONVICINI	14 CLEO	All CLEO-c runs
1.94 ± 0.07 ± 0.09 -0.11		JUN	00 SELX	Σ^- nucleus, 600 GeV
1.7 ± 0.2 ± 0.2	1745	ANJOS	92c E691	γ Be 90–260 GeV
1.90 ± 0.25 ± 0.20	337	ALVAREZ	91B NA14	Photoproduction
2.12 ± 0.16 ± 0.09		BORTOLETT	O88 CLEO	e^+e^- 10.55 GeV
2.17 ± 0.28 ± 0.23		ALBRECHT	85F ARG	e^+e^- 10 GeV
• • • We do not use the following data for averages, fits, limits, etc. • • •				
2.0 ± 0.9	48	BAILEY	86 ACCM	π^- Be fixed target
2.0 ± 1.0	10	BAILEY	83B SPEC	π^- Be $\rightarrow D^0$
2.2 ± 0.8	214	PICCOLO	77 MRK1	e^+e^- 4.03, 4.41 GeV

 $\Gamma(K^-\pi^+\rho^0 \text{ total})/\Gamma(K^-\pi^+\pi^-)$ Γ_{73}/Γ_{72}

VALUE (units 10^{-2})	DOCUMENT ID	TECN	COMMENT
83.5 ± 3.5 OUR AVERAGE			
80 ± 3 ± 5	ANJOS	92c E691	1745 $K^-\pi^+\pi^-$ evts
85.5 ± 3.2 ± 3.0	COFFMAN	92B MRK3	1281 ± 45 $K^-\pi^+\pi^-$ evts

 $\Gamma(K^-\pi^+\rho^0 3\text{-body})/\Gamma(K^-\pi^+\pi^-)$ Γ_{74}/Γ_{72}

VALUE (units 10^{-2})	EVTS	DOCUMENT ID	TECN	COMMENT
7.4 ± 2.0 OUR AVERAGE				
8.4 ± 1.1 ± 2.5	16k	ABLIKIM	17o BES3	$D^0 \rightarrow K^-\pi^+\pi^-$
5 ± 3 ± 2		ANJOS	92c E691	1745 $K^-\pi^+\pi^-$ evts
8.4 ± 2.2 ± 4.0		COFFMAN	92B MRK3	1281 ± 45 $K^-\pi^+\pi^-$ evts

 $\Gamma(\bar{K}^*(892)^0\rho^0, \bar{K}^*(892)^0 \rightarrow K^-\pi^+)/\Gamma(K^-\pi^+\pi^-)$ Γ_{75}/Γ_{72}

VALUE (units 10^{-2})	EVTS	DOCUMENT ID	TECN	COMMENT
12.3 ± 0.6 OUR AVERAGE				
12.3 ± 0.4 ± 0.5	16k	ABLIKIM	17o BES3	$D^0 \rightarrow K^-\pi^+\pi^-$
13 ± 2 ± 2		ANJOS	92c E691	1745 $K^-\pi^+\pi^-$ evts

 $\Gamma(\bar{K}^*(892)^0\rho^0 \text{ transverse}, \bar{K}^*(892)^0 \rightarrow K^-\pi^+)/\Gamma(K^-\pi^+\pi^-)$ Γ_{76}/Γ_{72}

VALUE	EVTS	DOCUMENT ID	TECN	COMMENT
0.142 ± 0.016 ± 0.05	1281	COFFMAN	92B MRK3	$K^-\pi^+\pi^-$ evts

 $\Gamma(K^-\pi^+\rho^0 \text{ total})/\Gamma(K^-\pi^+\pi^-)$ Γ_{77}/Γ_{72}

VALUE (units 10^{-2})	EVTS	DOCUMENT ID	TECN	COMMENT
53 ± 4 OUR AVERAGE				
54.6 ± 2.8 ± 3.7	16k	ABLIKIM	17o BES3	$D^0 \rightarrow K^-\pi^+\pi^-$
47 ± 5 ± 10	1745	ANJOS	92c E691	$K^-\pi^+\pi^-$ evts
49.2 ± 2.4 ± 8.0	1281	COFFMAN	92B MRK3	$K^-\pi^+\pi^-$ evts

 $\Gamma(K_1^-(1270)^-\pi^+, K_1^- \rightarrow K^-\pi^+\pi^- \text{ total})/\Gamma(K^-\pi^+\pi^-)$ Γ_{78}/Γ_{72}

VALUE (units 10^{-2})	EVTS	DOCUMENT ID	TECN	COMMENT
4.8 ± 0.4 OUR AVERAGE				
4.66 ± 0.05 ± 0.39 ± 0.24	891k	¹ AA1J	18aI LHCB	$D^0 \rightarrow K^-\pi^+\pi^-$
6.6 ± 1.9 ± 0.3	1281	COFFMAN	92B MRK3	$K^-\pi^+\pi^-$ evts

¹ The 3rd error is due to the uncertainty in the amplitude model composition.

$\Gamma(K_1(1270)^-\pi^+, K_1^-\pi^+ \rightarrow \bar{K}^*(892)^0\pi^-, \bar{K}^{*0} \rightarrow K^-\pi^+)/\Gamma(K^-2\pi^+\pi^-)$
 Γ_{81}/Γ_{72}

VALUE (units 10 ⁻²)	EVTS	DOCUMENT ID	TECN	COMMENT
0.8 ± 0.2 ± 0.2	16k	ABLIKIM	17o	BES3 D ⁰ → K ⁻ 2π ⁺ π ⁻

$\Gamma(K^-2\pi^+\pi^- \text{ nonresonant})/\Gamma(K^-2\pi^+\pi^-)$
 Γ_{82}/Γ_{72}

VALUE (units 10 ⁻²)	EVTS	DOCUMENT ID	TECN	COMMENT
22.0 ± 0.8 OUR AVERAGE				
22.04 ± 0.28 ± 2.09 ± 1.51	891k	¹ AAIJ	18A1	LHCB D ⁰ → K ⁻ 2π ⁺ π ⁻
21.9 ± 0.6 ± 0.6	16k	² ABLIKIM	17o	BES3 D ⁰ → K ⁻ 2π ⁺ π ⁻
23 ± 2 ± 3	1.7k	ANJOS	92c	E691 D ⁰ → K ⁻ 2π ⁺ π ⁻
24.2 ± 2.5 ± 6.0	1.2k	COFFMAN	92B	MRK3 D ⁰ → K ⁻ 2π ⁺ π ⁻

¹The 3rd error is due to the uncertainty in the amplitude model composition.
²In addition to the 14 ABLIKIM 17o branching ratios we have listed, the paper gives 15 more ratios for mostly non-resonant modes. Four of the 15 have less than 2-standard-deviation significance. Here are some of the omitted modes, with S, P, V, A, and T for scalar, pseudo-scalar, vector, axial-vector, and tensor spin sub-structures: π⁺(K⁻ρ⁰)_P, π⁺(K⁻ρ⁰)_V, π⁺(K⁻*0π⁻)_P, π⁺(K⁻*0π⁻)_V, π⁺(π⁻(K⁻π⁺)_{S-wave})_A, (K⁻π⁺)_V(π⁺π⁻)_S, (K⁻π⁺)_T(π⁺π⁻)_S...

$\Gamma(K_S^0\pi^+\pi^-\pi^0)/\Gamma_{\text{total}}$
 Γ_{83}/Γ

VALUE (%)	EVTS	DOCUMENT ID	TECN	COMMENT
5.2 ± 0.6 OUR FIT				
5.2 ± 1.1 ± 1.2	140	COFFMAN	92B	MRK3 e ⁺ e ⁻ 3.77 GeV
• • • We do not use the following data for averages, fits, limits, etc. • • •				
6.7 ± 1.6 -1.7		¹ BARLAG	92c	ACCM π ⁻ Cu 230 GeV

¹BARLAG 92c computes the branching fraction using topological normalization.

$\Gamma(K_S^0\pi^+\pi^-\pi^0)/\Gamma(K_S^0\pi^+\pi^-)$
 Γ_{83}/Γ_{40}

Branching fractions for submodes of this mode with narrow resonances (the η, ω, η') are fairly well determined (see below). COFFMAN 92B gives fractions of K* and ρ submodes, but with only 140 ± 28 events above background could not determine them with much accuracy. We omit those measurements here; they are in our 2008 Review (Physics Letters **B667** 1 (2008)).

VALUE	EVTS	DOCUMENT ID	TECN	COMMENT
1.85 ± 0.20 OUR FIT				
1.86 ± 0.23 OUR AVERAGE				
1.80 ± 0.20 ± 0.21	190	¹ ALBRECHT	92P	ARG e ⁺ e ⁻ ≈ 10 GeV
2.8 ± 0.8 ± 0.8	46	ANJOS	92c	E691 γBe 90–260 GeV
1.85 ± 0.26 ± 0.30	158	KINOSHITA	91	CLEO e ⁺ e ⁻ ~ 10.7 GeV

¹This value is calculated from numbers in Table 1 of ALBRECHT 92P.

$\Gamma(K^- \pi^+ 2\pi^0)/\Gamma_{\text{total}}$
 Γ_{86}/Γ

VALUE (%)	EVTS	DOCUMENT ID	TECN	COMMENT
8.86 ± 0.13 ± 0.19	6.1k	ABLIKIM	19Ak	BES3 e ⁺ e ⁻ at 3773 MeV
• • • We do not use the following data for averages, fits, limits, etc. • • •				
17.7 ± 2.9		¹ BARLAG	92c	ACCM π ⁻ Cu 230 GeV
14.9 ± 3.7 ± 3.0	24	² ADLER	88c	MRK3 e ⁺ e ⁻ 3.77 GeV
20.9 ^{+7.4} _{-4.3} ± 1.2	9	¹ AGUILAR-...	87F	HYBR πp, pp 360, 400 GeV

¹AGUILAR-BENITEZ 87F and BARLAG 92c compute the branching fraction using topological normalization. They do not distinguish the presence of a third π⁰, and thus are not included in the average.
²ADLER 88c uses an absolute normalization method finding this decay channel opposite a detected D⁰ → K⁺π⁻ in pure D⁰D events.

$\Gamma(K^-2\pi^+\pi^-\pi^0)/\Gamma(K^- \pi^+)$
 Γ_{87}/Γ_{37}

VALUE	EVTS	DOCUMENT ID	TECN	COMMENT
1.09 ± 0.10 OUR FIT				
0.98 ± 0.11 ± 0.11	225	¹ ALBRECHT	92P	ARG e ⁺ e ⁻ ≈ 10 GeV

¹This value is calculated from numbers in Table 1 of ALBRECHT 92P.

$\Gamma(K^-2\pi^+\pi^-\pi^0)/\Gamma(K^-2\pi^+\pi^-)$
 Γ_{87}/Γ_{72}

VALUE	EVTS	DOCUMENT ID	TECN	COMMENT
0.52 ± 0.05 OUR FIT				
0.56 ± 0.07 OUR AVERAGE				
0.55 ± 0.07 ± 0.12 0.09	167	KINOSHITA	91	CLEO e ⁺ e ⁻ ~ 10.7 GeV
0.57 ± 0.06 ± 0.05	180	ANJOS	90d	E691 Photoproduction

$\Gamma(K_S^0\eta\pi^0)/\Gamma_{\text{total}}$
 Γ_{91}/Γ

VALUE (units 10 ⁻³)	EVTS	DOCUMENT ID	TECN	COMMENT
10.06 ± 0.34 ± 0.30	1.1k	ABLIKIM	20v	BES3 e ⁺ e ⁻ , 3773 MeV

$\Gamma(K_S^0\eta\pi^0)/\Gamma(K_S^0\pi^0)$
 Γ_{91}/Γ_{38}

VALUE	EVTS	DOCUMENT ID	TECN	COMMENT
0.46 ± 0.07 ± 0.06	155 ± 22	¹ RUBIN	04	CLEO e ⁺ e ⁻ ≈ 10 GeV

¹The η here is detected in its γγ mode, but other η modes are included in the value given.

$\Gamma(K_S^0 a_0(980), a_0 \rightarrow \eta\pi^0)/\Gamma(K_S^0\eta\pi^0)$
 Γ_{92}/Γ_{91}

VALUE	DOCUMENT ID	TECN	COMMENT
1.19 ± 0.09 ± 0.26	¹ RUBIN	04	CLEO Dalitz fit, 155 evts

¹In addition to K_S⁰a₀(980) and K^{*}(892)⁰η modes, RUBIN 04 finds a fit fraction of 0.246 ± 0.092 ± 0.091 for other, undetermined modes.

$\Gamma(\bar{K}^*(892)^0\eta, \bar{K}^{*0} \rightarrow K_S^0\pi^0)/\Gamma(K_S^0\eta\pi^0)$
 Γ_{93}/Γ_{91}

VALUE	DOCUMENT ID	TECN	COMMENT
0.293 ± 0.062 ± 0.035	¹ RUBIN	04	CLEO Dalitz fit, 155 evts

This is the "fit fraction" from the Dalitz-plot analysis, with interference.
¹See the note on RUBIN 04 in the preceding data block.

$\Gamma(K^- \pi^+ \eta)/\Gamma_{\text{total}}$
 Γ_{94}/Γ

VALUE (units 10 ⁻²)	EVTS	DOCUMENT ID	TECN	COMMENT
1.88 ± 0.05 OUR FIT				Error includes scale factor of 1.4.
1.853 ± 0.025 ± 0.031	6.1k	ABLIKIM	20v	BES3 e ⁺ e ⁻ , 3773 MeV

$\Gamma(K^- \pi^+ \eta)/\Gamma(K^- \pi^+)$
 Γ_{94}/Γ_{37}

VALUE (units 10 ⁻²)	EVTS	DOCUMENT ID	TECN	COMMENT
47.6 ± 1.3 OUR FIT				Error includes scale factor of 1.4.
50.1 ± 2.0 ± 0.2	116k	¹ CHEN	20A	BELL e ⁺ e ⁻ at γ(4S)

¹CHEN 20A reports 0.500 ± 0.002 ± 0.020 ± 0.003 from a measurement of [Γ(D⁰ → K⁻π⁺η)]/Γ(D⁰ → K⁻π⁺) × [B(η → 2γ)] assuming B(η → 2γ) = (39.41 ± 0.20) × 10⁻², which we rescale to our best value B(η → 2γ) = (39.36 ± 0.18) × 10⁻². Our first error is their experiment's error and our second error is the systematic error from using our best value. The third reported uncertainty is the uncertainty from B(η → γγ).

$\Gamma(K^*(892)^0\eta, K^{*0} \rightarrow K^- \pi^+)/\Gamma(K^- \pi^+)$
 Γ_{95}/Γ_{94}

VALUE (units 10 ⁻²)	DOCUMENT ID	TECN	COMMENT
47.61 ± 1.32 ± 0.24 ± 3.64 -0.49 - 2.71	¹ CHEN	20A	BELL e ⁺ e ⁻ at γ(4S)

¹The third uncertainty is due to the uncertainty from the Dalitz model.

$\Gamma(a_0(980)^+ K^-, a_0^+ \rightarrow \eta\pi^+)/\Gamma(K^- \pi^+)$
 Γ_{96}/Γ_{94}

VALUE (units 10 ⁻²)	DOCUMENT ID	TECN	COMMENT
39.28 ± 1.50 ± 1.58 ± 4.38 -0.51 - 3.30	¹ CHEN	20A	BELL e ⁺ e ⁻ at γ(4S)

¹The third uncertainty is due to the uncertainty from the Dalitz model.

$\Gamma(K_2^-(1980)^-\pi^+, K_2^{*-} \rightarrow K^- \eta)/\Gamma_{\text{total}}$
 Γ_{97}/Γ

VALUE (units 10 ⁻⁴)	DOCUMENT ID	TECN	COMMENT
2.2 ± 1.7 -1.9	CHEN	20A	BELL e ⁺ e ⁻ at γ(4S)

$\Gamma(K^- \pi^+ \pi^0 \eta)/\Gamma_{\text{total}}$
 Γ_{98}/Γ

VALUE (units 10 ⁻³)	EVTS	DOCUMENT ID	TECN	COMMENT
4.49 ± 0.22 ± 0.15	580	ABLIKIM	20v	BES3 e ⁺ e ⁻ , 3773 MeV

$\Gamma(K_S^0\pi^+\pi^-\eta)/\Gamma_{\text{total}}$
 Γ_{99}/Γ

VALUE (units 10 ⁻³)	EVTS	DOCUMENT ID	TECN	COMMENT
2.80 ± 0.19 ± 0.10	250	ABLIKIM	20v	BES3 e ⁺ e ⁻ , 3773 MeV

$\Gamma(K_S^0 2\pi^0 \eta)/\Gamma_{\text{total}}$
 Γ_{100}/Γ

VALUE (units 10 ⁻³)	EVTS	DOCUMENT ID	TECN	COMMENT
1.76 ± 0.23 ± 0.13	65	ABLIKIM	20v	BES3 e ⁺ e ⁻ , 3773 MeV

$\Gamma(K_S^0 2\pi^+ 2\pi^-)/\Gamma(K_S^0\pi^+\pi^-)$
 Γ_{101}/Γ_{40}

VALUE	EVTS	DOCUMENT ID	TECN	COMMENT
0.095 ± 0.005 ± 0.007	1283 ± 57	LINK	04d	FOCS γA, E _γ ≈ 180 GeV
• • • We do not use the following data for averages, fits, limits, etc. • • •				
0.07 ± 0.02 ± 0.01	11	¹ ALBRECHT	92P	ARG e ⁺ e ⁻ ≈ 10 GeV
0.149 ± 0.026	56	AMMAR	91	CLEO e ⁺ e ⁻ ≈ 10.5 GeV
0.18 ± 0.07 ± 0.04	6	ANJOS	90d	E691 Photoproduction

¹This value is calculated from numbers in Table 1 of ALBRECHT 92P.

$\Gamma(K_S^0\rho^0\pi^+\pi^-, \text{no } K^*(892)^-)/\Gamma(K_S^0 2\pi^+ 2\pi^-)$
 $\Gamma_{102}/\Gamma_{101}$

VALUE	DOCUMENT ID	TECN	COMMENT
0.40 ± 0.24 ± 0.07	LINK	04d	FOCS γA, E _γ ≈ 180 GeV

$\Gamma(K^*(892)^- 2\pi^+ \pi^-, K^*(892)^- \rightarrow K_S^0\pi^-, \text{no } \rho^0)/\Gamma(K_S^0 2\pi^+ 2\pi^-)$
 $\Gamma_{103}/\Gamma_{101}$

VALUE	DOCUMENT ID	TECN	COMMENT
0.17 ± 0.28 ± 0.02	LINK	04d	FOCS γA, E _γ ≈ 180 GeV

$\Gamma(K^*(892)^-\rho^0\pi^+, K^*(892)^- \rightarrow K_S^0\pi^-)/\Gamma(K_S^0 2\pi^+ 2\pi^-)$
 $\Gamma_{104}/\Gamma_{101}$

VALUE	DOCUMENT ID	TECN	COMMENT
0.60 ± 0.21 ± 0.09	LINK	04d	FOCS γA, E _γ ≈ 180 GeV

$\Gamma(K_S^0 2\pi^+ 2\pi^- \text{ nonresonant})/\Gamma(K_S^0 2\pi^+ 2\pi^-)$
 $\Gamma_{105}/\Gamma_{101}$

VALUE	CL%	DOCUMENT ID	TECN	COMMENT
<0.46	90	LINK	04d	FOCS γA, E _γ ≈ 180 GeV

$\Gamma(K^- 3\pi^+ 2\pi^-)/\Gamma(K^- 2\pi^+ \pi^-)$
 Γ_{107}/Γ_{72}

VALUE (units 10 ⁻³)	EVTS	DOCUMENT ID	TECN	COMMENT
2.70 ± 0.58 ± 0.38	48 ± 10	LINK	04B	FOCS γA, E _γ ≈ 180 GeV

Meson Particle Listings

 D^0

$\Gamma(K_S^0 \eta)/\Gamma_{\text{total}}$ Γ_{108}/Γ
 Unseen decay modes of the η are included.

VALUE (units 10^{-3})	EVTS	DOCUMENT ID	TECN	COMMENT
5.09 ± 0.13 OUR FIT				
5.13 ± 0.07 ± 0.12	9.5k	ABLIKIM	18w BES3	e^+e^- , 3773 MeV
••• We do not use the following data for averages, fits, limits, etc. •••				
4.42 ± 0.15 ± 0.28		ASNER	08 CLEO	See MENDEZ 10

$\Gamma(K_S^0 \eta)/[\Gamma(K^- \pi^+) + \Gamma(K^+ \pi^-)]$ $\Gamma_{108}/(\Gamma_{37} + \Gamma_{274})$
 Unseen decay modes of the η are included.

VALUE (units 10^{-2})	EVTS	DOCUMENT ID	TECN	COMMENT
12.83 ± 0.33 OUR FIT				
12.3 ± 0.3 ± 0.7	2864 ± 65	MENDEZ	10 CLEO	e^+e^- at 3774 MeV

$\Gamma(K_S^0 \eta)/\Gamma(K_S^0 \pi^0)$ Γ_{108}/Γ_{38}
 Unseen decay modes of the η are included.

VALUE	EVTS	DOCUMENT ID	TECN	COMMENT
••• We do not use the following data for averages, fits, limits, etc. •••				
0.32 ± 0.04 ± 0.03	225 ± 30	PROCARIO	93B CLE2	$\eta \rightarrow \gamma\gamma$

$\Gamma(K_S^0 \eta)/\Gamma(K_S^0 \pi^+ \pi^-)$ Γ_{108}/Γ_{40}
 Unseen decay modes of the η are included.

VALUE	EVTS	DOCUMENT ID	TECN	COMMENT
••• We do not use the following data for averages, fits, limits, etc. •••				
0.14 ± 0.02 ± 0.02	80 ± 12	PROCARIO	93B CLE2	$\eta \rightarrow \pi^+ \pi^- \pi^0$

$\Gamma(K_S^0 \omega)/\Gamma_{\text{total}}$ Γ_{109}/Γ
 Unseen decay modes of the ω are included.

VALUE (%)	DOCUMENT ID	TECN	COMMENT
1.11 ± 0.06 OUR FIT			
1.12 ± 0.04 ± 0.05	ASNER	08 CLEO	$e^+e^- \rightarrow D^0 \bar{D}^0$, 3.77 GeV

$\Gamma(K_S^0 \omega)/\Gamma(K^- \pi^+)$ Γ_{109}/Γ_{37}
 Unseen decay modes of the ω are included.

VALUE	DOCUMENT ID	TECN	COMMENT
••• We do not use the following data for averages, fits, limits, etc. •••			
0.50 ± 0.18 ± 0.10	ALBRECHT	89D ARG	e^+e^- 10 GeV

$\Gamma(K_S^0 \omega)/\Gamma(K_S^0 \pi^+ \pi^-)$ Γ_{109}/Γ_{40}
 Unseen decay modes of the ω are included.

VALUE	EVTS	DOCUMENT ID	TECN	COMMENT
0.396 ± 0.032 OUR FIT				Error includes scale factor of 1.1.
0.33 ± 0.09 OUR AVERAGE				Error includes scale factor of 1.1.
0.29 ± 0.08 ± 0.05	16	¹ ALBRECHT	92P ARG	$e^+e^- \approx 10$ GeV
0.54 ± 0.14 ± 0.16	40	KINOSHITA	91 CLEO	$e^+e^- \sim 10.7$ GeV

¹This value is calculated from numbers in Table 1 of ALBRECHT 92P.

$\Gamma(K_S^0 \omega)/\Gamma(K_S^0 \pi^+ \pi^- \pi^0)$ Γ_{109}/Γ_{83}
 Unseen decay modes of the ω are included.

VALUE	DOCUMENT ID	TECN	COMMENT
0.215 ± 0.026 OUR FIT			
0.220 ± 0.048 ± 0.0116	COFFMAN	92B MRK3	1281 ± 45 $K^- 2\pi^+ \pi^-$ evts

$\Gamma(K_S^0 \eta(958))/\Gamma_{\text{total}}$ Γ_{110}/Γ

VALUE (units 10^{-3})	EVTS	DOCUMENT ID	TECN	COMMENT
9.49 ± 0.32 OUR FIT				
9.49 ± 0.20 ± 0.36	3k	ABLIKIM	18w BES3	e^+e^- , 3773 MeV

$\Gamma(K_S^0 \eta(958))/[\Gamma(K^- \pi^+) + \Gamma(K^+ \pi^-)]$ $\Gamma_{110}/(\Gamma_{37} + \Gamma_{274})$
 Unseen decay modes of the $\eta(958)$ are included.

VALUE (units 10^{-2})	EVTS	DOCUMENT ID	TECN	COMMENT
24.0 ± 0.8 OUR FIT				
24.3 ± 0.8 ± 1.1	1321 ± 42	MENDEZ	10 CLEO	e^+e^- at 3774 MeV

$\Gamma(K_S^0 \eta(958))/\Gamma(K_S^0 \pi^+ \pi^-)$ Γ_{110}/Γ_{40}
 Unseen decay modes of the $\eta(958)$ are included.

VALUE	EVTS	DOCUMENT ID	TECN	COMMENT
0.339 ± 0.023 OUR FIT				
0.32 ± 0.04 OUR AVERAGE				
0.31 ± 0.02 ± 0.04	594	PROCARIO	93B CLE2	$\eta' \rightarrow \eta \pi^+ \pi^-$, $\rho^0 \gamma$
0.37 ± 0.13 ± 0.06	18	¹ ALBRECHT	92P ARG	$e^+e^- \approx 10$ GeV

¹This value is calculated from numbers in Table 1 of ALBRECHT 92P.

$\Gamma(\bar{K}^*(892)^0 \pi^+ \pi^- \pi^0)/\Gamma(K^- 2\pi^+ \pi^- \pi^0)$ Γ_{111}/Γ_{87}
 Unseen decay modes of the $\bar{K}^*(892)^0$ are included.

VALUE	DOCUMENT ID	TECN	COMMENT
0.45 ± 0.15 ± 0.15	ANJOS	90D E691	Photoproduction

$\Gamma(\bar{K}^*(892)^0 \eta)/\Gamma_{\text{total}}$ Γ_{112}/Γ

VALUE (units 10^{-2})	DOCUMENT ID	TECN	COMMENT
1.41 ± 0.13 ± 0.01	¹ CHEN	20A BELL	e^+e^- at $\Upsilon(4S)$

¹CHEN 20A reports $(1.41 \pm 0.04 + 0.12 \pm 0.01) \times 10^{-2}$ from a measurement of $[\Gamma(D^0 \rightarrow \bar{K}^*(892)^0 \eta)/\Gamma_{\text{total}}] \times [B(\eta \rightarrow 2\gamma)]$ assuming $B(\eta \rightarrow 2\gamma) = (39.41 \pm 0.20) \times 10^{-2}$, which we rescale to our best value $B(\eta \rightarrow 2\gamma) = (39.36 \pm 0.18) \times 10^{-2}$. Our first error is their experiment's error and our second error is the systematic error from using our best value. The third reported uncertainty is the uncertainty from $B(\eta \rightarrow \gamma\gamma)$.

$\Gamma(\bar{K}^*(892)^0 \eta)/\Gamma(K^- \pi^+)$ Γ_{112}/Γ_{37}
 Unseen decay modes of the $\bar{K}^*(892)^0$ and η are included.

VALUE	EVTS	DOCUMENT ID	TECN	COMMENT
••• We do not use the following data for averages, fits, limits, etc. •••				
0.58 ± 0.19 $^{+0.24}_{-0.28}$	46	KINOSHITA	91 CLEO	$e^+e^- \sim 10.7$ GeV

$\Gamma(\bar{K}^*(892)^0 \eta)/\Gamma(K^- \pi^+ \pi^0)$ Γ_{112}/Γ_{55}
 Unseen decay modes of the $\bar{K}^*(892)^0$ and η are included.

VALUE	EVTS	DOCUMENT ID	TECN	COMMENT
••• We do not use the following data for averages, fits, limits, etc. •••				
0.13 ± 0.02 ± 0.03	214	PROCARIO	93B CLE2	$\bar{K}^{*0} \eta \rightarrow K^- \pi^+ / \gamma\gamma$

$\Gamma(K^- \pi^+ \omega)/\Gamma(K^- \pi^+)$ Γ_{113}/Γ_{37}
 Unseen decay modes of the ω are included.

VALUE	EVTS	DOCUMENT ID	TECN	COMMENT
0.78 ± 0.12 ± 0.10	99	¹ ALBRECHT	92P ARG	$e^+e^- \approx 10$ GeV

¹This value is calculated from numbers in Table 1 of ALBRECHT 92P.

$\Gamma(\bar{K}^*(892)^0 \omega)/\Gamma(K^- \pi^+)$ Γ_{114}/Γ_{37}
 Unseen decay modes of the $\bar{K}^*(892)^0$ and ω are included.

VALUE	EVTS	DOCUMENT ID	TECN	COMMENT
0.28 ± 0.11 ± 0.04	17	¹ ALBRECHT	92P ARG	$e^+e^- \approx 10$ GeV

¹This value is calculated from numbers in Table 1 of ALBRECHT 92P.

$\Gamma(K^- \pi^+ \eta'(958))/\Gamma_{\text{total}}$ Γ_{115}/Γ

VALUE (units 10^{-3})	EVTS	DOCUMENT ID	TECN	COMMENT
6.43 ± 0.15 ± 0.31	2.5k	ABLIKIM	18Ac BES3	e^+e^- , 3773 MeV

$\Gamma(K^- \pi^+ \eta'(958))/\Gamma(K^- 2\pi^+ \pi^-)$ Γ_{115}/Γ_{72}
 Unseen decay modes of the $\eta'(958)$ are included.

VALUE	EVTS	DOCUMENT ID	TECN	COMMENT
0.093 ± 0.014 ± 0.019	286	PROCARIO	93B CLE2	$\eta' \rightarrow \eta \pi^+ \pi^-$, $\rho^0 \gamma$

$\Gamma(K_S^0 \eta'(958) \pi^0)/\Gamma_{\text{total}}$ Γ_{116}/Γ

VALUE (units 10^{-3})	EVTS	DOCUMENT ID	TECN	COMMENT
2.52 ± 0.22 ± 0.15	289	ABLIKIM	18Ac BES3	e^+e^- , 3773 MeV

$\Gamma(\bar{K}^*(892)^0 \eta(958))/\Gamma(K^- \pi^+ \eta(958))$ $\Gamma_{117}/\Gamma_{115}$
 Unseen decay modes of the $\bar{K}^*(892)^0$ are included.

VALUE	CL%	DOCUMENT ID	TECN	COMMENT
<0.15	90	PROCARIO	93B CLE2	

Hadronic modes with three K 's

$\Gamma(K_S^0 K^+ K^-)/\Gamma(K_S^0 \pi^+ \pi^-)$ Γ_{118}/Γ_{40}

VALUE	EVTS	DOCUMENT ID	TECN	COMMENT
0.158 ± 0.001 ± 0.005	14k ± 116	AUBERT,B	05J BABR	$e^+e^- \approx \Upsilon(4S)$
••• We do not use the following data for averages, fits, limits, etc. •••				
0.20 ± 0.05 ± 0.04	47	FRABETTI	92B E687	γ Be, $\bar{E}_\gamma = 221$ GeV
0.170 ± 0.022	136	AMMAR	91 CLEO	$e^+e^- \approx 10.5$ GeV
0.24 ± 0.08		BEBEK	86 CLEO	e^+e^- near $\Upsilon(4S)$
0.185 ± 0.055	52	ALBRECHT	85B ARG	e^+e^- 10 GeV

$\Gamma(K_S^0 a_0(980)^0, a_0^0 \rightarrow K^+ K^-)/\Gamma(K_S^0 K^+ K^-)$ $\Gamma_{119}/\Gamma_{118}$
 This is the "fit fraction" from the Dalitz-plot analysis, with interference.

VALUE	DOCUMENT ID	TECN	COMMENT
0.664 ± 0.016 ± 0.070	AUBERT,B	05J BABR	Dalitz fit, 12540 ± 112 evts

$\Gamma(K^- a_0(980)^+, a_0^+ \rightarrow K^+ K_S^0)/\Gamma(K_S^0 K^+ K^-)$ $\Gamma_{120}/\Gamma_{118}$
 This is the "fit fraction" from the Dalitz-plot analysis, with interference.

VALUE	DOCUMENT ID	TECN	COMMENT
0.134 ± 0.011 ± 0.037	AUBERT,B	05J BABR	Dalitz fit, 12540 ± 112 evts

$\Gamma(K^+ a_0(980)^-, a_0^- \rightarrow K^- K_S^0)/\Gamma(K_S^0 K^+ K^-)$ $\Gamma_{121}/\Gamma_{118}$
 This is a doubly Cabibbo-suppressed mode.

VALUE	CL%	DOCUMENT ID	TECN	COMMENT
<0.025	95	AUBERT,B	05J BABR	Dalitz fit, 12540 ± 112 evts

$\Gamma(K_S^0 f_0(980), f_0 \rightarrow K^+ K^-)/\Gamma(K_S^0 K^+ K^-)$ $\Gamma_{122}/\Gamma_{118}$

VALUE	CL%	DOCUMENT ID	TECN	COMMENT
<0.021	95	AUBERT,B	05J BABR	Dalitz fit, 12540 ± 112 evts

$\Gamma(K_S^0 \phi, \phi \rightarrow K^+ K^-)/\Gamma(K_S^0 K^+ K^-)$ $\Gamma_{123}/\Gamma_{118}$
 This is the "fit fraction" from the Dalitz-plot analysis, with interference.

VALUE	DOCUMENT ID	TECN	COMMENT
0.459 ± 0.007 ± 0.007	AUBERT,B	05J BABR	Dalitz fit, 12540 ± 112 evts

$\Gamma(K_S^0 f_0(1370), f_0 \rightarrow K^+ K^-)/\Gamma(K_S^0 K^+ K^-)$ $\Gamma_{124}/\Gamma_{118}$
 This is the "fit fraction" from the Dalitz-plot analysis, with interference.

VALUE	DOCUMENT ID	TECN	COMMENT
0.038 ± 0.007 ± 0.023	¹ AUBERT,B	05J BABR	Dalitz fit, 12540 ± 112 evts

¹AUBERT,B 05J calls the mode $K_S^0 f_0(1400)$, but insofar as it is seen here at all, it is certainly the same as $f_0(1370)$.

$\Gamma(3K_S^0)/\Gamma_{\text{total}}$		Γ_{125}/Γ	
VALUE (units 10^{-4})	EVTS	DOCUMENT ID	TECN COMMENT
7.5 ± 0.7 OUR FIT			Error includes scale factor of 1.4.
7.21 ± 0.33 ± 0.44	597	ABLIKIM 17A	BES3 $e^+e^- \rightarrow \psi(3770)$

$\Gamma(3K_S^0)/\Gamma(K_S^0\pi^+\pi^-)$		Γ_{125}/Γ_{40}	
VALUE (units 10^{-2})	EVTS	DOCUMENT ID	TECN COMMENT
2.70 ± 0.26 OUR FIT			Error includes scale factor of 1.2.
3.2 ± 0.4 OUR AVERAGE			
3.58 ± 0.54 ± 0.52	170 ± 26	LINK	05A FOCS $\gamma\text{Be}, \bar{E}_\gamma \approx 180 \text{ GeV}$
2.78 ± 0.38 ± 0.48	61	ASNER	96B CLE2 $e^+e^- \approx \Upsilon(4S)$
7.0 ± 2.4 ± 1.2	10 ± 3	FRABETTI	94J E687 $\gamma\text{Be}, \bar{E}_\gamma = 220 \text{ GeV}$
3.2 ± 1.0	22	AMMAR	91 CLEO $e^+e^- \approx 10.5 \text{ GeV}$
3.4 ± 1.4 ± 1.0	5	ALBRECHT	90c ARG $e^+e^- \approx 10 \text{ GeV}$

$\Gamma(K^+2K^-\pi^+)/\Gamma(K^-2\pi^+\pi^-)$		Γ_{126}/Γ_{72}	
VALUE	EVTS	DOCUMENT ID	TECN COMMENT
0.0027 ± 0.0004 OUR AVERAGE			Error includes scale factor of 1.1.
0.00257 ± 0.00034 ± 0.00024	143	LINK	03G FOCS $\gamma A, \bar{E}_\gamma \approx 180 \text{ GeV}$
0.0054 ± 0.0016 ± 0.0008	18	AITALA	01D E791 $\pi^- A, 500 \text{ GeV}$
0.0028 ± 0.0007 ± 0.0001	20	FRABETTI	95c E687 $\gamma \text{Be}, \bar{E}_\gamma \approx 200 \text{ GeV}$

$\Gamma(K^+K^-\bar{K}^*(892)^0, \bar{K}^{*0} \rightarrow K^-\pi^+)/\Gamma(K^+2K^-\pi^+)$		$\Gamma_{127}/\Gamma_{126}$	
VALUE	DOCUMENT ID	TECN	COMMENT
0.20 ± 0.07 ± 0.02	LINK	03G FOCS	$\gamma A, \bar{E}_\gamma \approx 180 \text{ GeV}$

$\Gamma(K^-\pi^+\phi, \phi \rightarrow K^+K^-)/\Gamma(K^+2K^-\pi^+)$		$\Gamma_{128}/\Gamma_{126}$	
VALUE	DOCUMENT ID	TECN	COMMENT
0.18 ± 0.06 ± 0.04	LINK	03G FOCS	$\gamma A, \bar{E}_\gamma \approx 180 \text{ GeV}$

$\Gamma(\phi\bar{K}^*(892)^0, \phi \rightarrow K^+K^-, \bar{K}^{*0} \rightarrow K^-\pi^+)/\Gamma(K^+2K^-\pi^+)$		$\Gamma_{129}/\Gamma_{126}$	
VALUE	DOCUMENT ID	TECN	COMMENT
0.48 ± 0.06 ± 0.01	LINK	03G FOCS	$\gamma A, \bar{E}_\gamma \approx 180 \text{ GeV}$

$\Gamma(K^+2K^-\pi^+ \text{ nonresonant})/\Gamma(K^+2K^-\pi^+)$		$\Gamma_{130}/\Gamma_{126}$	
VALUE	DOCUMENT ID	TECN	COMMENT
0.15 ± 0.06 ± 0.02	LINK	03G FOCS	$\gamma A, \bar{E}_\gamma \approx 180 \text{ GeV}$

$\Gamma(2K_S^0K^\pm\pi^\mp)/\Gamma(K_S^0\pi^+\pi^-)$		Γ_{131}/Γ_{40}	
VALUE (units 10^{-2})	EVTS	DOCUMENT ID	TECN COMMENT
2.12 ± 0.38 ± 0.20	57 ± 10	LINK	05A FOCS $\gamma \text{Be}, \bar{E}_\gamma \approx 180 \text{ GeV}$

Pionic modes

$\Gamma(\pi^+\pi^-)/\Gamma_{\text{total}}$		Γ_{132}/Γ	
VALUE (units 10^{-3})	EVTS	DOCUMENT ID	TECN COMMENT
1.454 ± 0.024 OUR FIT			Error includes scale factor of 1.4.
1.508 ± 0.018 ± 0.022	21k	ABLIKIM 18w	BES3 $e^+e^-, 3773 \text{ MeV}$

$\Gamma(\pi^+\pi^-)/\Gamma(K^-\pi^+)$		Γ_{132}/Γ_{37}	
VALUE (units 10^{-2})	EVTS	DOCUMENT ID	TECN COMMENT
3.68 ± 0.05 OUR FIT			Error includes scale factor of 1.3.
3.59 ± 0.06 OUR AVERAGE			
3.594 ± 0.054 ± 0.040	7334 ± 97	ACOSTA	05c CDF $p\bar{p}, \sqrt{s} = 1.96 \text{ TeV}$
3.53 ± 0.12 ± 0.06	3453	LINK	03 FOCS $\gamma A, \bar{E}_\gamma \approx 180 \text{ GeV}$
3.51 ± 0.16 ± 0.17	710	CSORNA	02 CLE2 $e^+e^- \approx \Upsilon(4S)$
4.0 ± 0.2 ± 0.3	2043	AITALA	98c E791 $\pi^- A, 500 \text{ GeV}$
• • • We do not use the following data for averages, fits, limits, etc. • • •			
3.62 ± 0.10 ± 0.08	2085 ± 54	RUBIN	06 CLEO See MENDEZ 10
3.4 ± 0.7 ± 0.1	76 ± 15	ABLIKIM	05F BES $e^+e^- \approx \psi(3770)$
4.3 ± 0.7 ± 0.3	177	FRABETTI	94c E687 $\gamma\text{Be} \bar{E}_\gamma = 220 \text{ GeV}$
3.48 ± 0.30 ± 0.23	227	SELEN	93 CLE2 $e^+e^- \approx \Upsilon(4S)$
5.5 ± 0.8 ± 0.5	120	ANJOS	91D E691 Photoproduction
5.0 ± 0.7 ± 0.5	110	ALEXANDER	90 CLEO $e^+e^- 10.5\text{--}11 \text{ GeV}$

$\Gamma(\pi^+\pi^-)/[\Gamma(K^-\pi^+) + \Gamma(K^+\pi^-)]$		$\Gamma_{132}/(\Gamma_{37} + \Gamma_{274})$	
VALUE (units 10^{-2})	EVTS	DOCUMENT ID	TECN COMMENT
3.67 ± 0.05 OUR FIT			Error includes scale factor of 1.3.
3.70 ± 0.06 ± 0.09	6210 ± 93	MENDEZ	10 CLEO e^+e^- at 3774 MeV

$\Gamma(2\pi^0)/\Gamma_{\text{total}}$		Γ_{133}/Γ	
VALUE (units 10^{-4})	EVTS	DOCUMENT ID	TECN COMMENT
8.26 ± 0.25 OUR FIT			
8.29 ± 0.30 OUR AVERAGE			
8.24 ± 0.21 ± 0.30	6k	ABLIKIM	15F BES3 e^+e^- at 3.773 GeV
8.4 ± 0.1 ± 0.5	26k	LEES	12L BABR $e^+e^- \approx 10.58 \text{ GeV}$

$\Gamma(2\pi^0)/\Gamma(K^-\pi^+)$		Γ_{133}/Γ_{37}	
VALUE (units 10^{-2})	EVTS	DOCUMENT ID	TECN COMMENT
• • • We do not use the following data for averages, fits, limits, etc. • • •			
2.05 ± 0.13 ± 0.16	499 ± 32	RUBIN	06 CLEO See MENDEZ 10
2.2 ± 0.4 ± 0.4	40	SELEN	93 CLE2 $e^+e^- \rightarrow \Upsilon(4S)$

$\Gamma(2\pi^0)/[\Gamma(K^-\pi^+) + \Gamma(K^+\pi^-)]$		$\Gamma_{133}/(\Gamma_{37} + \Gamma_{274})$	
VALUE (units 10^{-2})	EVTS	DOCUMENT ID	TECN COMMENT
2.08 ± 0.07 OUR FIT			
2.06 ± 0.07 ± 0.10	1567 ± 54	MENDEZ	10 CLEO e^+e^- at 3774 MeV

$\Gamma(\pi^+\pi^-\pi^0)/\Gamma(K^-\pi^+)$		Γ_{134}/Γ_{37}	
VALUE (units 10^{-2})	EVTS	DOCUMENT ID	TECN COMMENT
37.7 ± 1.6 OUR FIT			Error includes scale factor of 2.2.
34.4 ± 0.5 ± 1.2	11k ± 164	RUBIN	06 CLEO e^+e^- at $\psi(3770)$

$\Gamma(\pi^+\pi^-\pi^0)/\Gamma(K^-\pi^+\pi^0)$		Γ_{134}/Γ_{55}	
VALUE (units 10^{-2})	EVTS	DOCUMENT ID	TECN COMMENT
10.32 ± 0.25 OUR FIT			Error includes scale factor of 2.3.
10.41 ± 0.23 OUR AVERAGE			Error includes scale factor of 2.0.
10.12 ± 0.04 ± 0.18	123k ± 490	ARINSTEIN	08 BELL $e^+e^- \approx \Upsilon(4S)$
10.59 ± 0.06 ± 0.13	60k ± 343	AUBERT,B	06x BABR $e^+e^- \approx \Upsilon(4S)$

$\Gamma(\rho^+\pi^-)/\Gamma(\pi^+\pi^-\pi^0)$		$\Gamma_{135}/\Gamma_{134}$	
VALUE (units 10^{-2})	DOCUMENT ID	TECN	COMMENT
68.1 ± 0.6 OUR AVERAGE			
67.8 ± 0.0 ± 0.6	AUBERT	07Bj BABR	Dalitz fit, 45k events
76.3 ± 1.9 ± 2.5	CRONIN-HEN..05	CLEO	$e^+e^- \approx 10 \text{ GeV}$

This is the "fit fraction" from the Dalitz-plot analysis, with interference. See GASPERO 08 and BHATTACHARYA 10a for isospin decompositions of the $D^0 \rightarrow \pi^+\pi^0\pi^-$ Dalitz plot, both based on the amplitudes of AUBERT 07Bj. They quantify the conclusion that the final state is dominantly isospin 0.

$\Gamma(\rho^0\pi^0)/\Gamma(\pi^+\pi^-\pi^0)$		$\Gamma_{136}/\Gamma_{134}$	
VALUE (units 10^{-2})	DOCUMENT ID	TECN	COMMENT
25.9 ± 1.1 OUR AVERAGE			
26.2 ± 0.5 ± 1.1	AUBERT	07Bj BABR	Dalitz fit, 45k events
24.4 ± 2.0 ± 2.1	CRONIN-HEN..05	CLEO	$e^+e^- \approx 10 \text{ GeV}$

This is the "fit fraction" from the Dalitz-plot analysis, with interference.

$\Gamma(\rho^-\pi^+)/\Gamma(\pi^+\pi^-\pi^0)$		$\Gamma_{137}/\Gamma_{134}$	
VALUE (units 10^{-2})	DOCUMENT ID	TECN	COMMENT
34.6 ± 0.8 OUR AVERAGE			
34.6 ± 0.8 ± 0.3	AUBERT	07Bj BABR	Dalitz fit, 45k events
34.5 ± 2.4 ± 1.3	CRONIN-HEN..05	CLEO	$e^+e^- \approx 10 \text{ GeV}$

This is the "fit fraction" from the Dalitz-plot analysis, with interference.

$\Gamma(\rho(1450)^+\pi^-, \rho^+ \rightarrow \pi^+\pi^0)/\Gamma(\pi^+\pi^-\pi^0)$		$\Gamma_{138}/\Gamma_{134}$	
VALUE (units 10^{-2})	DOCUMENT ID	TECN	COMMENT
0.11 ± 0.07 ± 0.12	AUBERT	07Bj BABR	Dalitz fit, 45k events

This is the "fit fraction" from the Dalitz-plot analysis.

$\Gamma(\rho(1450)^0\pi^0, \rho^0 \rightarrow \pi^+\pi^-)/\Gamma(\pi^+\pi^-\pi^0)$		$\Gamma_{139}/\Gamma_{134}$	
VALUE (units 10^{-2})	DOCUMENT ID	TECN	COMMENT
0.30 ± 0.11 ± 0.07	AUBERT	07Bj BABR	Dalitz fit, 45k events

This is the "fit fraction" from the Dalitz-plot analysis.

$\Gamma(\rho(1450)^-\pi^+, \rho^- \rightarrow \pi^-\pi^0)/\Gamma(\pi^+\pi^-\pi^0)$		$\Gamma_{140}/\Gamma_{134}$	
VALUE (units 10^{-2})	DOCUMENT ID	TECN	COMMENT
1.79 ± 0.22 ± 0.12	AUBERT	07Bj BABR	Dalitz fit, 45k events

This is the "fit fraction" from the Dalitz-plot analysis.

$\Gamma(\rho(1700)^+\pi^-, \rho^+ \rightarrow \pi^+\pi^0)/\Gamma(\pi^+\pi^-\pi^0)$		$\Gamma_{141}/\Gamma_{134}$	
VALUE (units 10^{-2})	DOCUMENT ID	TECN	COMMENT
4.1 ± 0.7 ± 0.7	AUBERT	07Bj BABR	Dalitz fit, 45k events

This is the "fit fraction" from the Dalitz-plot analysis.

$\Gamma(\rho(1700)^0\pi^0, \rho^0 \rightarrow \pi^+\pi^-)/\Gamma(\pi^+\pi^-\pi^0)$		$\Gamma_{142}/\Gamma_{134}$	
VALUE (units 10^{-2})	DOCUMENT ID	TECN	COMMENT
5.0 ± 0.6 ± 1.0	AUBERT	07Bj BABR	Dalitz fit, 45k events

This is the "fit fraction" from the Dalitz-plot analysis.

$\Gamma(\rho(1700)^-\pi^+, \rho^- \rightarrow \pi^-\pi^0)/\Gamma(\pi^+\pi^-\pi^0)$		$\Gamma_{143}/\Gamma_{134}$	
VALUE (units 10^{-2})	DOCUMENT ID	TECN	COMMENT
3.2 ± 0.4 ± 0.6	AUBERT	07Bj BABR	Dalitz fit, 45k events

This is the "fit fraction" from the Dalitz-plot analysis.

$\Gamma(f_0(980)\pi^0, f_0 \rightarrow \pi^+\pi^-)/\Gamma(\pi^+\pi^-\pi^0)$		$\Gamma_{144}/\Gamma_{134}$	
VALUE (units 10^{-2})	DOCUMENT ID	TECN	COMMENT
0.25 ± 0.04 ± 0.04	AUBERT	07Bj BABR	Dalitz fit, 45k events

This is the "fit fraction" from the Dalitz-plot analysis.

$\Gamma(f_0(500)\pi^0, f_0 \rightarrow \pi^+\pi^-)/\Gamma(\pi^+\pi^-\pi^0)$		$\Gamma_{145}/\Gamma_{134}$	
VALUE (units 10^{-2})	DOCUMENT ID	TECN	COMMENT
0.82 ± 0.10 ± 0.10	AUBERT	07Bj BABR	Dalitz fit, 45k events

The $f_0(500)$ is the σ . This is the "fit fraction" from the Dalitz-plot analysis.

$\Gamma(f_0(1370)\pi^0, f_0 \rightarrow \pi^+\pi^-)/\Gamma(\pi^+\pi^-\pi^0)$		$\Gamma_{146}/\Gamma_{134}$	
VALUE (units 10^{-2})	DOCUMENT ID	TECN	COMMENT
0.37 ± 0.11 ± 0.09	AUBERT	07Bj BABR	Dalitz fit, 45k events

This is the "fit fraction" from the Dalitz-plot analysis.

Meson Particle Listings

 D^0 $\Gamma(f_0(1500)\pi^0, f_0 \rightarrow \pi^+\pi^-)/\Gamma(\pi^+\pi^-\pi^0)$ $\Gamma_{147}/\Gamma_{134}$

This is the "fit fraction" from the Dalitz-plot analysis.

VALUE (units 10^{-2})	DOCUMENT ID	TECN	COMMENT
$0.39 \pm 0.08 \pm 0.07$	AUBERT	07B J B A B R	Dalitz fit, 45k events

 $\Gamma(f_0(1710)\pi^0, f_0 \rightarrow \pi^+\pi^-)/\Gamma(\pi^+\pi^-\pi^0)$ $\Gamma_{148}/\Gamma_{134}$

This is the "fit fraction" from the Dalitz-plot analysis.

VALUE (units 10^{-2})	DOCUMENT ID	TECN	COMMENT
$0.31 \pm 0.07 \pm 0.08$	AUBERT	07B J B A B R	Dalitz fit, 45k events

 $\Gamma(f_2(1270)\pi^0, f_2 \rightarrow \pi^+\pi^-)/\Gamma(\pi^+\pi^-\pi^0)$ $\Gamma_{149}/\Gamma_{134}$

This is the "fit fraction" from the Dalitz-plot analysis.

VALUE (units 10^{-2})	DOCUMENT ID	TECN	COMMENT
$1.32 \pm 0.08 \pm 0.10$	AUBERT	07B J B A B R	Dalitz fit, 45k events

 $\Gamma(\pi^+\pi^-\pi^0 \text{ nonresonant})/\Gamma(\pi^+\pi^-\pi^0)$ $\Gamma_{150}/\Gamma_{134}$

This is the "fit fraction" from the Dalitz-plot analysis.

VALUE (units 10^{-2})	DOCUMENT ID	TECN	COMMENT
$0.84 \pm 0.21 \pm 0.12$	AUBERT	07B J B A B R	Dalitz fit, 45k events

 $\Gamma(3\pi^0)/\Gamma_{\text{total}}$ Γ_{151}/Γ

VALUE (units 10^{-4})	CL%	EVTS	DOCUMENT ID	TECN	COMMENT
$2.0 \pm 0.4 \pm 0.3$		60	1 ABLIKIM	18x BES3	e^+e^- , 3773 MeV

• • • We do not use the following data for averages, fits, limits, etc. • • •

<3.5	90	RUBIN	06 CLEO	e^+e^- at $\psi(3770)$
------	----	-------	---------	--------------------------

¹ Significance of signal reported by ABLIKIM 18x is 4.8 σ . $\Gamma(2\pi^+2\pi^-)/\Gamma(K^-\pi^+)$ Γ_{152}/Γ_{37}

VALUE (units 10^{-2})	EVTS	DOCUMENT ID	TECN	COMMENT
19.1 ± 0.5 OUR FIT				

$19.1 \pm 0.4 \pm 0.6$	7331 \pm 130	RUBIN	06 CLEO	e^+e^- at $\psi(3770)$
------------------------	----------------	-------	---------	--------------------------

 $\Gamma(2\pi^+2\pi^-)/\Gamma(K^-2\pi^+\pi^-)$ Γ_{152}/Γ_{72}

VALUE (units 10^{-2})	EVTS	DOCUMENT ID	TECN	COMMENT
9.19 ± 0.22 OUR FIT				

9.20 ± 0.26 OUR AVERAGE				
-----------------------------	--	--	--	--

$9.14 \pm 0.18 \pm 0.22$	6360 \pm 115	LINK	07A FOCS	γ Be, $\bar{E}_\gamma \approx 180$ GeV
--------------------------	----------------	------	----------	---

$7.9 \pm 1.8 \pm 0.5$	162	ABLIKIM	05F BES	$e^+e^- \approx \psi(3770)$
-----------------------	-----	---------	---------	-----------------------------

$9.5 \pm 0.7 \pm 0.2$	814	FRABETTI	95c E687	γ Be, $\bar{E}_\gamma \approx 200$ GeV
-----------------------	-----	----------	----------	---

10.2 ± 1.3	345	AMMAR	91 CLEO	$e^+e^- \approx 10.5$ GeV
----------------	-----	-------	---------	---------------------------

• • • We do not use the following data for averages, fits, limits, etc. • • •

$11.5 \pm 2.3 \pm 1.6$	64	ADAMOVICH	92 OMEG	π^- 340 GeV
------------------------	----	-----------	---------	-----------------

$10.8 \pm 2.4 \pm 0.8$	79	FRABETTI	92 E687	γ Be
------------------------	----	----------	---------	-------------

$9.6 \pm 1.8 \pm 0.7$	66	ANJOS	91 E691	γ Be 80–240 GeV
-----------------------	----	-------	---------	------------------------

 $\Gamma(a_1(1260)^+\pi^-, a_1^+ \rightarrow 2\pi^+\pi^- \text{ total})/\Gamma(2\pi^+2\pi^-)$ $\Gamma_{153}/\Gamma_{152}$

This is the fit fraction from the coherent amplitude analysis.

VALUE (units 10^{-2})	DOCUMENT ID	TECN	COMMENT
$60.0 \pm 3.0 \pm 2.4$	LINK	07A FOCS	4-body fit, $\approx 5.7k$ evts

 $\Gamma(a_1(1260)^+\pi^-, a_1^+ \rightarrow \rho^0\pi^+ S\text{-wave})/\Gamma(2\pi^+2\pi^-)$ $\Gamma_{154}/\Gamma_{152}$

This is the fit fraction from the coherent amplitude analysis.

VALUE (units 10^{-2})	DOCUMENT ID	TECN	COMMENT
41.5 ± 2.5 OUR AVERAGE			

$38.1 \pm 2.3 \pm 3.6$		¹ DARGENT	17	4-body fit, 7.3k 4 π evts
------------------------	--	----------------------	----	-------------------------------

$43.3 \pm 2.5 \pm 1.9$		LINK	07A FOCS	4-body fit, $\approx 5.7k$ evts
------------------------	--	------	----------	---------------------------------

¹ Obtained by analyzing CLEO-c data but not authored by the CLEO Collaboration. $\Gamma(a_1(1260)^+\pi^-, a_1^+ \rightarrow \rho^0\pi^+ D\text{-wave})/\Gamma(2\pi^+2\pi^-)$ $\Gamma_{155}/\Gamma_{152}$

This is the fit fraction from the coherent amplitude analysis.

VALUE (units 10^{-2})	DOCUMENT ID	TECN	COMMENT
$2.5 \pm 0.5 \pm 0.4$	LINK	07A FOCS	4-body fit, $\approx 5.7k$ evts

¹ DARGENT 17 using 7.3k events find this contribution negligible. $\Gamma(a_1(1260)^+\pi^-, a_1^+ \rightarrow \sigma\pi^+)/\Gamma(2\pi^+2\pi^-)$ $\Gamma_{156}/\Gamma_{152}$

This is the fit fraction from the coherent amplitude analysis.

VALUE (units 10^{-2})	DOCUMENT ID	TECN	COMMENT
8.4 ± 0.9 OUR AVERAGE			

$10.2 \pm 1.4 \pm 3.3$		¹ DARGENT	17	7.3k 4-body fit, 4 π evts
------------------------	--	----------------------	----	-------------------------------

$8.3 \pm 0.7 \pm 0.6$		LINK	07A FOCS	4-body fit, $\approx 5.7k$ evts
-----------------------	--	------	----------	---------------------------------

¹ Obtained by analyzing CLEO-c data but not authored by the CLEO Collaboration. $\Gamma(a_1(1260)^-\pi^+, a_1^- \rightarrow \rho^0\pi^- S\text{-wave})/\Gamma(2\pi^+2\pi^-)$ $\Gamma_{157}/\Gamma_{152}$

This is the fit fraction from a coherent amplitude analysis.

VALUE (units 10^{-2})	EVTS	DOCUMENT ID	COMMENT
$3.1 \pm 0.6 \pm 1.0$	7.3k	¹ DARGENT	17 4-body fit, 4 π evts

¹ Obtained by analyzing CLEO-c data but not authored by the CLEO Collaboration. $\Gamma(a_1(1260)^-\pi^+, a_1^- \rightarrow \sigma\pi^-)/\Gamma(2\pi^+2\pi^-)$ $\Gamma_{158}/\Gamma_{152}$

This is the fit fraction from a coherent amplitude analysis.

VALUE (units 10^{-2})	EVTS	DOCUMENT ID	COMMENT
$0.8 \pm 0.2 \pm 0.4$	7.3k	¹ DARGENT	17 4-body fit, 4 π evts

¹ Obtained by analyzing CLEO-c data but not authored by the CLEO Collaboration. $\Gamma(\pi(1300)^+\pi^-, \pi(1300)^+ \rightarrow \sigma\pi^+)/\Gamma(2\pi^+2\pi^-)$ $\Gamma_{159}/\Gamma_{152}$

This is the fit fraction from a coherent amplitude analysis.

VALUE (units 10^{-2})	EVTS	DOCUMENT ID	COMMENT
$6.8 \pm 0.9 \pm 3.4$	7.3k	¹ DARGENT	17 4-body fit, 4 π evts

¹ Obtained by analyzing CLEO-c data but not authored by the CLEO Collaboration. $\Gamma(\pi(1300)^-\pi^+, \pi(1300)^- \rightarrow \sigma\pi^-)/\Gamma(2\pi^+2\pi^-)$ $\Gamma_{160}/\Gamma_{152}$

This is the fit fraction from a coherent amplitude analysis.

VALUE (units 10^{-2})	EVTS	DOCUMENT ID	COMMENT
$3.0 \pm 0.6 \pm 2.8$	7.3k	¹ DARGENT	17 4-body fit, 4 π evts

¹ Obtained by analyzing CLEO-c data but not authored by the CLEO Collaboration. $\Gamma(a_1(1640)^+\pi^-, a_1^+ \rightarrow \rho^0\pi^+ D\text{-wave})/\Gamma(2\pi^+2\pi^-)$ $\Gamma_{161}/\Gamma_{152}$

This is the fit fraction from a coherent amplitude analysis.

VALUE (units 10^{-2})	EVTS	DOCUMENT ID	COMMENT
$4.2 \pm 0.6 \pm 2.0$	7.3k	^{1,2} DARGENT	17 4-body fit, 4 π evts

¹ Obtained by analyzing CLEO-c data but not authored by the CLEO Collaboration.² 4-body fit, 4 π evts $\Gamma(a_1(1640)^+\pi^-, a_1^+ \rightarrow \sigma\pi^+)/\Gamma(2\pi^+2\pi^-)$ $\Gamma_{162}/\Gamma_{152}$

This is the fit fraction from a coherent amplitude analysis.

VALUE (units 10^{-2})	EVTS	DOCUMENT ID	COMMENT
$2.4 \pm 0.7 \pm 1.7$	7.3k	¹ DARGENT	17 4-body fit, 4 π evts

¹ Obtained by analyzing CLEO-c data but not authored by the CLEO Collaboration. $\Gamma(\pi_2(1670)^+\pi^-, \pi_2^+ \rightarrow f_2(1270)^0\pi^+, f_2^0 \rightarrow \pi^+\pi^-)/\Gamma(2\pi^+2\pi^-)$ $\Gamma_{163}/\Gamma_{152}$

This is the fit fraction from a coherent amplitude analysis.

VALUE (units 10^{-2})	EVTS	DOCUMENT ID	COMMENT
$2.7 \pm 0.6 \pm 1.1$	7.3k	¹ DARGENT	17 4-body fit, 4 π evts

¹ Obtained by analyzing CLEO-c data but not authored by the CLEO Collaboration. $\Gamma(\pi_2(1670)^+\pi^-, \pi_2^+ \rightarrow \sigma\pi^+)/\Gamma(2\pi^+2\pi^-)$ $\Gamma_{164}/\Gamma_{152}$

This is the fit fraction from a coherent amplitude analysis.

VALUE (units 10^{-2})	EVTS	DOCUMENT ID	COMMENT
$3.5 \pm 0.6 \pm 1.2$	7.3k	¹ DARGENT	17 4-body fit, 4 π evts

¹ Obtained by analyzing CLEO-c data but not authored by the CLEO Collaboration. $\Gamma(2\rho^0 \text{ total})/\Gamma(2\pi^+2\pi^-)$ $\Gamma_{165}/\Gamma_{152}$

This is the fit fraction from the coherent amplitude analysis.

VALUE (units 10^{-2})	DOCUMENT ID	TECN	COMMENT
$24.5 \pm 1.3 \pm 1.0$	LINK	07A FOCS	4-body fit, $\approx 5.7k$ evts

¹ Obtained by analyzing CLEO-c data but not authored by the CLEO Collaboration. $\Gamma(2\rho^0, \text{parallel helicities})/\Gamma(2\pi^+2\pi^-)$ $\Gamma_{166}/\Gamma_{152}$

This is the fit fraction from the coherent amplitude analysis.

VALUE (units 10^{-2})	DOCUMENT ID	TECN	COMMENT
$1.1 \pm 0.3 \pm 0.3$	LINK	07A FOCS	4-body fit, $\approx 5.7k$ evts

 $\Gamma(2\rho^0, \text{perpendicular helicities})/\Gamma(2\pi^+2\pi^-)$ $\Gamma_{167}/\Gamma_{152}$

This is the fit fraction from the coherent amplitude analysis.

VALUE (units 10^{-2})	DOCUMENT ID	TECN	COMMENT
$6.4 \pm 0.6 \pm 0.5$	LINK	07A FOCS	4-body fit, $\approx 5.7k$ evts

 $\Gamma(2\rho^0, \text{longitudinal helicities})/\Gamma(2\pi^+2\pi^-)$ $\Gamma_{168}/\Gamma_{152}$

This is the fit fraction from the coherent amplitude analysis.

VALUE (units 10^{-2})	DOCUMENT ID	TECN	COMMENT
$16.8 \pm 1.0 \pm 0.8$	LINK	07A FOCS	4-body fit, $\approx 5.7k$ evts

 $\Gamma(2\rho(770)^0, S\text{-wave})/\Gamma(2\pi^+2\pi^-)$ $\Gamma_{169}/\Gamma_{152}$

This is the fit fraction from a coherent amplitude analysis.

VALUE (units 10^{-2})	EVTS	DOCUMENT ID	COMMENT
$2.4 \pm 0.7 \pm 1.5$	7.3k	¹ DARGENT	17 4-body fit, 4 π evts

¹ Obtained by analyzing CLEO-c data but not authored by the CLEO Collaboration. $\Gamma(2\rho(770)^0, P\text{-wave})/\Gamma(2\pi^+2\pi^-)$ $\Gamma_{170}/\Gamma_{152}$

This is the fit fraction from a coherent amplitude analysis.

VALUE (units 10^{-2})	EVTS	DOCUMENT ID	COMMENT
$7.0 \pm 0.5 \pm 1.6$	7.3k	¹ DARGENT	17 4-body fit, 4 π evts

¹ Obtained by analyzing CLEO-c data but not authored by the CLEO Collaboration. $\Gamma(2\rho(770)^0, D\text{-wave})/\Gamma(2\pi^+2\pi^-)$ $\Gamma_{171}/\Gamma_{152}$

This is the fit fraction from a coherent amplitude analysis.

VALUE (units 10^{-2})	EVTS	DOCUMENT ID	COMMENT
$8.2 \pm 1.0 \pm 3.9$	7.3k	¹ DARGENT	17 4-body fit, 4 π evts

¹ Obtained by analyzing CLEO-c data but not authored by the CLEO Collaboration. $\Gamma(\text{Resonant } (\pi^+\pi^-)\pi^+\pi^- \text{ 3-body total})/\Gamma(2\pi^+2\pi^-)$ $\Gamma_{172}/\Gamma_{152}$

This is the fit fraction from the coherent amplitude analysis.

VALUE (units 10^{-2})	DOCUMENT ID	TECN	COMMENT
$20.0 \pm 1.2 \pm 1.0$	LINK	07A FOCS	4-body fit, $\approx 5.7k$ evts

$\Gamma(\sigma\pi^+\pi^-)/\Gamma(2\pi^+2\pi^-)$ $\Gamma_{173}/\Gamma_{152}$

This is the fit fraction from the coherent amplitude analysis.

VALUE (units 10^{-2})	EVTS	DOCUMENT ID	TECN	COMMENT
8.2±1.0±0.7	7.3k	LINK	07A	FOCS 4-body fit, $\approx 5.7k$ evts

 $\Gamma(\sigma\rho(770)^0)/\Gamma(2\pi^+2\pi^-)$ $\Gamma_{174}/\Gamma_{152}$

This is the fit fraction from a coherent amplitude analysis.

VALUE (units 10^{-2})	EVTS	DOCUMENT ID	TECN	COMMENT
6.6±1.0±3.2	7.3k	¹ DARGENT	17	4-body fit, 4 π evts

¹ Obtained by analyzing CLEO-c data but not authored by the CLEO Collaboration. $\Gamma(f_0(1370)\sigma, f_0 \rightarrow \pi^+\pi^-)/\Gamma(2\pi^+2\pi^-)$ $\Gamma_{178}/\Gamma_{152}$

This is the fit fraction from the coherent amplitude analysis.

VALUE (units 10^{-2})	EVTS	DOCUMENT ID	TECN	COMMENT
21.2±1.8±6.7	7.3k	¹ DARGENT	17	4-body fit, 4 π evts

¹ Obtained by analyzing CLEO-c data but not authored by the CLEO Collaboration. $\Gamma(f_0(980)\pi^+\pi^-, f_0 \rightarrow \pi^+\pi^-)/\Gamma(2\pi^+2\pi^-)$ $\Gamma_{175}/\Gamma_{152}$

This is the fit fraction from the coherent amplitude analysis.

VALUE (units 10^{-2})	EVTS	DOCUMENT ID	TECN	COMMENT
2.4±0.5±0.4		LINK	07A	FOCS 4-body fit, $\approx 5.7k$ evts

 $\Gamma(f_2(1270)\pi^+\pi^-, f_2 \rightarrow \pi^+\pi^-)/\Gamma(2\pi^+2\pi^-)$ $\Gamma_{176}/\Gamma_{152}$

This is the fit fraction from the coherent amplitude analysis.

VALUE (units 10^{-2})	EVTS	DOCUMENT ID	TECN	COMMENT
4.9±0.6±0.5		LINK	07A	FOCS 4-body fit, $\approx 5.7k$ evts

 $\Gamma(2f_2(1270), f_2 \rightarrow \pi^+\pi^-)/\Gamma(2\pi^+2\pi^-)$ $\Gamma_{177}/\Gamma_{152}$

This is the fit fraction from a coherent amplitude analysis.

VALUE (units 10^{-2})	EVTS	DOCUMENT ID	TECN	COMMENT
2.1±0.5±2.3	7.3k	¹ DARGENT	17	4-body fit, 4 π evts

¹ Obtained by analyzing CLEO-c data but not authored by the CLEO Collaboration. $\Gamma(\pi^+\pi^-2\pi^0)/\Gamma(K^-\pi^+)$ Γ_{179}/Γ_{37}

VALUE (units 10^{-2})	EVTS	DOCUMENT ID	TECN	COMMENT
25.8±1.5±1.8	2724 ± 166	RUBIN	06	CLEO e^+e^- at $\psi(3770)$

 $\Gamma(\eta\pi^0)/\Gamma_{total}$ Γ_{180}/Γ Unseen decay modes of the η are included.

VALUE (units 10^{-4})	EVTS	DOCUMENT ID	TECN	COMMENT
6.3±0.6 OUR FIT				Error includes scale factor of 1.1.
5.8±0.5±0.5	1.7k	ABLIKIM	18L	BES3 e^+e^- , 3773 MeV
••• We do not use the following data for averages, fits, limits, etc. •••				
6.5±0.9±0.4	75	ABLIKIM	16D	BES3 See ABLIKIM 18L
6.4±1.0±0.4	156 ± 24	ARTUSO	08	CLEO See MENDEZ 10

 $\Gamma(\eta\pi^0)/\Gamma(K^-\pi^+)$ Γ_{180}/Γ_{37} Unseen decay modes of the η are included.

VALUE (units 10^{-2})	EVTS	DOCUMENT ID	TECN	COMMENT
••• We do not use the following data for averages, fits, limits, etc. •••				
1.47±0.34±0.11	62 ± 14	RUBIN	06	CLEO See ARTUSO 08

 $\Gamma(\eta\pi^0)/[\Gamma(K^-\pi^+) + \Gamma(K^+\pi^-)]$ $\Gamma_{180}/(\Gamma_{37} + \Gamma_{274})$ Unseen decay modes of the η are included.

VALUE (units 10^{-2})	EVTS	DOCUMENT ID	TECN	COMMENT
1.60±0.14 OUR FIT				Error includes scale factor of 1.1.
1.74±0.15±0.11	481 ± 40	MENDEZ	10	CLEO e^+e^- at 3774 MeV

 $\Gamma(\omega\pi^0)/\Gamma_{total}$ Γ_{181}/Γ Unseen decay modes of the ω are included.

VALUE (units 10^{-4})	EVTS	DOCUMENT ID	TECN	COMMENT
1.17±0.34±0.07	45	ABLIKIM	16D	BES3 e^+e^- , 3773 MeV

 $\Gamma(2\pi^+2\pi^-\pi^0)/\Gamma(K^-\pi^+)$ Γ_{183}/Γ_{37}

VALUE (units 10^{-2})	EVTS	DOCUMENT ID	TECN	COMMENT
10.7±1.2±0.5	1614 ± 171	RUBIN	06	CLEO e^+e^- at $\psi(3770)$

 $\Gamma(\eta\pi^+\pi^-)/\Gamma_{total}$ Γ_{184}/Γ Unseen decay modes of the η are included.

VALUE (units 10^{-4})	EVTS	DOCUMENT ID	TECN	COMMENT
11.6±0.7 OUR AVERAGE				
10.6±1.8±0.7	96	ABLIKIM	20AA	BES3 e^+e^- , 3773 MeV
12.0±0.7±0.4	450	ABLIKIM	20G	BES3 e^+e^- , 3773 MeV
10.9±1.3±0.9	257	ARTUSO	08	CLEO e^+e^- at $\psi(3770)$

 $\Gamma(\eta\pi^+\pi^-)/\Gamma(K^-\pi^+\eta)$ Γ_{184}/Γ_{94}

VALUE (units 10^{-2})	EVTS	DOCUMENT ID	TECN	COMMENT
6.49±0.09±0.12	13k	LI	21G	BELL e^+e^- at $\Upsilon(ns)$

 $\Gamma(\eta2\pi^0)/\Gamma_{total}$ Γ_{187}/Γ

VALUE (units 10^{-4})	CL%	EVTS	DOCUMENT ID	TECN	COMMENT
3.8±1.1±0.7		42	¹ ABLIKIM	18x	BES3 e^+e^- , 3773 MeV
••• We do not use the following data for averages, fits, limits, etc. •••					
<23.8		90	ABLIKIM	20AA	BES3 e^+e^- , 3773 MeV
					¹ Significance of signal reported by ABLIKIM 18x is 3.8 σ .

 $\Gamma(\pi^+\pi^-\pi^0\eta)/\Gamma_{total}$ Γ_{188}/Γ

VALUE (units 10^{-3})	EVTS	DOCUMENT ID	TECN	COMMENT
3.23±0.17±0.14	510	ABLIKIM	20v	BES3 e^+e^- , 3773 MeV

 $\Gamma(\omega\eta)/\Gamma_{total}$ Γ_{182}/Γ

VALUE (units 10^{-3})	EVTS	DOCUMENT ID	TECN	COMMENT
1.98±0.18 OUR AVERAGE				Error includes scale factor of 1.1.
2.15±0.17±0.15	2.2k	ABLIKIM	18L	BES3 e^+e^- , 3773 MeV
1.78±0.19±0.15	600	¹ SMITH	18	e^+e^- , 3773 MeV
				¹ Obtained by analyzing CLEO-c data but not authored by the CLEO Collaboration.

 $\Gamma(\omega\pi^+\pi^-)/\Gamma_{total}$ Γ_{185}/Γ

VALUE (units 10^{-3})	EVTS	DOCUMENT ID	TECN	COMMENT
1.33±0.16±0.12	411	ABLIKIM	20AA	BES3 e^+e^- , 3773 MeV

 $\Gamma(\omega\pi^+\pi^-)/\Gamma(K^-\pi^+)$ Γ_{185}/Γ_{37} Unseen decay modes of the ω are included.

VALUE (units 10^{-2})	EVTS	DOCUMENT ID	TECN	COMMENT
4.1±1.2±0.4	472 ± 132	RUBIN	06	CLEO e^+e^- at $\psi(3770)$

 $\Gamma(\omega\pi^0\pi^0)/\Gamma_{total}$ Γ_{186}/Γ

VALUE	CL%	DOCUMENT ID	TECN	COMMENT
<1.10 × 10⁻³	90	ABLIKIM	20AA	BES3 e^+e^- , 3773 MeV

 $\Gamma(3\pi^+3\pi^-)/\Gamma(K^-2\pi^+\pi^-)$ Γ_{189}/Γ_{72}

VALUE (units 10^{-3})	EVTS	DOCUMENT ID	TECN	COMMENT
5.23±0.59±1.35	149 ± 17	LINK	04B	FOCS $\gamma A, \bar{E}_\gamma \approx 180$ GeV

 $\Gamma(3\pi^+3\pi^-)/\Gamma(K^-3\pi^+2\pi^-)$ $\Gamma_{189}/\Gamma_{107}$

VALUE	DOCUMENT ID	TECN	COMMENT
••• We do not use the following data for averages, fits, limits, etc. •••			
1.93±0.47±0.48	¹ LINK	04B	FOCS $\gamma A, \bar{E}_\gamma \approx 180$ GeV
			¹ This LINK 04B result is not independent of other results in these Listings.

 $\Gamma(\eta'(958)\pi^0)/\Gamma_{total}$ Γ_{190}/Γ Unseen decay modes of the $\eta'(958)$ are included.

VALUE (units 10^{-4})	EVTS	DOCUMENT ID	TECN	COMMENT
9.2±1.0 OUR FIT				
9.3±1.1±0.9	469 ± 56	ABLIKIM	18L	BES3 e^+e^- , 3773 MeV
••• We do not use the following data for averages, fits, limits, etc. •••				
8.1±1.5±0.6	50 ± 9	ARTUSO	08	CLEO See MENDEZ 10

 $\Gamma(\eta'(958)\pi^0)/[\Gamma(K^-\pi^+) + \Gamma(K^+\pi^-)]$ $\Gamma_{190}/(\Gamma_{37} + \Gamma_{274})$ Unseen decay modes of the $\eta'(958)$ are included.

VALUE (units 10^{-2})	EVTS	DOCUMENT ID	TECN	COMMENT
2.32±0.25 OUR FIT				
2.3 ± 0.3 ± 0.2	159 ± 19	MENDEZ	10	CLEO e^+e^- at 3774 MeV

 $\Gamma(\eta'(958)\pi^+\pi^-)/\Gamma_{total}$ Γ_{191}/Γ Unseen decay modes of the $\eta'(958)$ are included.

VALUE (units 10^{-4})	EVTS	DOCUMENT ID	TECN	COMMENT
4.5±1.6±0.5	21 ± 8	ARTUSO	08	CLEO e^+e^- at $\psi(3770)$

 $\Gamma(2\eta)/\Gamma_{total}$ Γ_{192}/Γ Unseen decay modes of the η are included.

VALUE (units 10^{-4})	EVTS	DOCUMENT ID	TECN	COMMENT
21.1±1.9 OUR FIT				Error includes scale factor of 2.2.
22.0±0.7±0.6	3.4k	ABLIKIM	18L	BES3 e^+e^- , 3773 MeV
••• We do not use the following data for averages, fits, limits, etc. •••				
16.7±1.4±1.3	255 ± 22	ARTUSO	08	CLEO See MENDEZ 10

 $\Gamma(2\eta)/[\Gamma(K^-\pi^+) + \Gamma(K^+\pi^-)]$ $\Gamma_{192}/(\Gamma_{37} + \Gamma_{274})$ Unseen decay modes of the η are included.

VALUE (units 10^{-2})	EVTS	DOCUMENT ID	TECN	COMMENT
5.3±0.5 OUR FIT				Error includes scale factor of 2.2.
4.3±0.3±0.4	430 ± 29	MENDEZ	10	CLEO e^+e^- at 3774 MeV

 $\Gamma(2\eta\pi^0)/\Gamma_{total}$ Γ_{193}/Γ

VALUE (units 10^{-4})	EVTS	DOCUMENT ID	TECN	COMMENT
7.3±1.6±1.5	27	¹ ABLIKIM	18x	BES3 e^+e^- , 3773 MeV
				¹ Significance of signal reported by ABLIKIM 18x is 5.5 σ .

Meson Particle Listings

D^0

$\Gamma(3\eta)/\Gamma_{\text{total}}$					Γ_{194}/Γ
VALUE	CL%	DOCUMENT ID	TECN	COMMENT	
$<1.3 \times 10^{-4}$	90	ABLIKIM	18x BES3	e^+e^- , 3773 MeV	

$\Gamma(\eta\eta'(958))/\Gamma_{\text{total}}$					Γ_{195}/Γ
Unseen decay modes of the η and $\eta'(958)$ are included.					
VALUE (units 10^{-4})	EVTS	DOCUMENT ID	TECN	COMMENT	
10.1 ± 1.9 OUR FIT					
9.4 ± 2.5 ± 1.1	158 ± 41	ABLIKIM	18L BES3	e^+e^- , 3773 MeV	
••• We do not use the following data for averages, fits, limits, etc. •••					
12.6 ± 2.5 ± 1.1	46 ± 9	ARTUSO	08 CLEO	See MENDEZ 10	

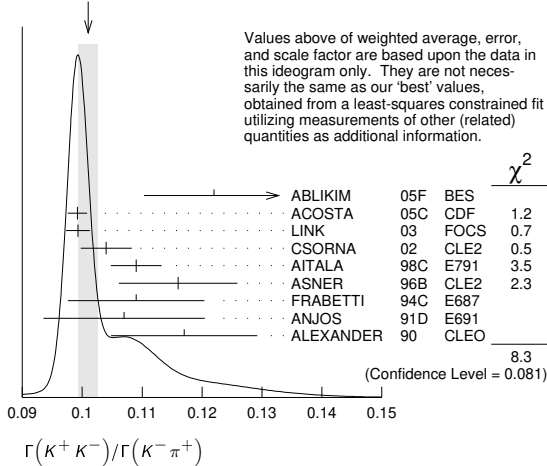
$\Gamma(\eta\eta'(958))/[\Gamma(K^-\pi^+) + \Gamma(K^+\pi^-)]$					$\Gamma_{195}/(\Gamma_{37} + \Gamma_{274})$
Unseen decay modes of the η and $\eta'(958)$ are included.					
VALUE (units 10^{-2})	EVTS	DOCUMENT ID	TECN	COMMENT	
2.5 ± 0.5 OUR FIT					
2.7 ± 0.6 ± 0.3	66 ± 15	MENDEZ	10 CLEO	e^+e^- at 3774 MeV	

————— Hadronic modes with a $K\bar{K}$ pair —————

$\Gamma(K^+K^-)/\Gamma_{\text{total}}$					Γ_{196}/Γ
VALUE (units 10^{-3})	EVTS	DOCUMENT ID	TECN	COMMENT	
4.08 ± 0.06 OUR FIT				Error includes scale factor of 1.6.	
4.233 ± 0.021 ± 0.064	56k	ABLIKIM	18W BES3	e^+e^- , 3773 MeV	
••• We do not use the following data for averages, fits, limits, etc. •••					
4.08 ± 0.08 ± 0.09	4.7k	BONVICINI	08 CLEO	See MENDEZ 10	

$\Gamma(K^+K^-)/\Gamma(K^-\pi^+)$					Γ_{196}/Γ_{37}
VALUE	EVTS	DOCUMENT ID	TECN	COMMENT	
0.1033 ± 0.0013 OUR FIT				Error includes scale factor of 1.6.	
0.1010 ± 0.0016 OUR AVERAGE				Error includes scale factor of 1.4. See the ideogram below.	
0.122 ± 0.011 ± 0.004	242 ± 20	ABLIKIM	05F BES	$e^+e^- \approx \psi(3770)$	
0.0992 ± 0.0011 ± 0.0012	16k ± 200	ACOSTA	05c CDF	$p\bar{p}$, $\sqrt{s}=1.96$ TeV	
0.0993 ± 0.0014 ± 0.0014	11k	LINK	03 FOCS	γ nucleus, $\bar{E}_\gamma \approx 180$ GeV	
0.1040 ± 0.0033 ± 0.0027	1900	CSORNA	02 CLE2	$e^+e^- \approx \Upsilon(4S)$	
0.109 ± 0.003 ± 0.003	3317	AITALA	98c E791	π^- nucleus, 500 GeV	
0.116 ± 0.007 ± 0.007	1102	ASNER	96B CLE2	$e^+e^- \approx \Upsilon(4S)$	
0.109 ± 0.007 ± 0.009	581	FRABETTI	94c E687	γ Be $\bar{E}_\gamma=220$ GeV	
0.107 ± 0.010 ± 0.009	193	ANJOS	91D E691	Photoproduction	
0.117 ± 0.010 ± 0.007	249	ALEXANDER	90 CLEO	e^+e^- 10.5–11 GeV	
••• We do not use the following data for averages, fits, limits, etc. •••					
0.107 ± 0.029 ± 0.015	103	ADAMOVICH	92 OMEG	π^- 340 GeV	
0.138 ± 0.027 ± 0.010	155	FRABETTI	92 E687	γ Be	
0.16 ± 0.05	34	ALVAREZ	91B NA14	Photoproduction	
0.10 ± 0.02 ± 0.01	131	ALBRECHT	90c ARG	$e^+e^- \approx 10$ GeV	
0.122 ± 0.018 ± 0.012	118	BALTRUSAITIS	85E MRK3	e^+e^- 3.77 GeV	
0.113 ± 0.030		ABRAMS	79D MRK2	e^+e^- 3.77 GeV	

WEIGHTED AVERAGE
0.1010 ± 0.0016 (Error scaled by 1.4)



$\Gamma(K^+K^-)/[\Gamma(K^-\pi^+) + \Gamma(K^+\pi^-)]$					$\Gamma_{196}/(\Gamma_{37} + \Gamma_{274})$
VALUE (units 10^{-2})	EVTS	DOCUMENT ID	TECN	COMMENT	
10.29 ± 0.13 OUR FIT				Error includes scale factor of 1.6.	
10.41 ± 0.11 ± 0.12	13.8k	MENDEZ	10 CLEO	e^+e^- at 3774 MeV	

$\Gamma(K^+K^-)/\Gamma(\pi^+\pi^-)$					$\Gamma_{196}/\Gamma_{132}$
The unused results here are redundant with $\Gamma(K^+K^-)/\Gamma(K^-\pi^+)$ and $\Gamma(\pi^+\pi^-)/\Gamma(K^-\pi^+)$ measurements by the same experiments.					
VALUE	EVTS	DOCUMENT ID	TECN	COMMENT	
••• We do not use the following data for averages, fits, limits, etc. •••					
2.760 ± 0.040 ± 0.034	7334	ACOSTA	05c CDF	$p\bar{p}$, $\sqrt{s}=1.96$ TeV	
2.81 ± 0.10 ± 0.06		LINK	03 FOCS	γ nucleus, $\bar{E}_\gamma \approx 180$ GeV	
2.96 ± 0.16 ± 0.15	710	CSORNA	02 CLE2	$e^+e^- \approx \Upsilon(4S)$	
2.75 ± 0.15 ± 0.16		AITALA	98c E791	π^- nucleus, 500 GeV	
2.53 ± 0.46 ± 0.19		FRABETTI	94c E687	γ Be $\bar{E}_\gamma=220$ GeV	
2.23 ± 0.81 ± 0.46		ADAMOVICH	92 OMEG	π^- 340 GeV	
1.95 ± 0.34 ± 0.22		ANJOS	91D E691	Photoproduction	
2.5 ± 0.7		ALBRECHT	90c ARG	$e^+e^- \approx 10$ GeV	
2.35 ± 0.37 ± 0.28		ALEXANDER	90 CLEO	e^+e^- 10.5–11 GeV	

$\Gamma(2K_S^0)/\Gamma_{\text{total}}$					Γ_{197}/Γ
VALUE (units 10^{-4})	EVTS	DOCUMENT ID	TECN	COMMENT	
1.41 ± 0.05 OUR FIT				Error includes scale factor of 1.1.	
1.67 ± 0.11 ± 0.11	576	ABLIKIM	17A BES3	$e^+e^- \rightarrow \psi(3770)$	
••• We do not use the following data for averages, fits, limits, etc. •••					
1.46 ± 0.32 ± 0.09	68 ± 15	BONVICINI	08 CLEO	See MENDEZ 10	

$\Gamma(2K_S^0)/[\Gamma(K^-\pi^+) + \Gamma(K^+\pi^-)]$					$\Gamma_{197}/(\Gamma_{37} + \Gamma_{274})$
VALUE (units 10^{-2})	EVTS	DOCUMENT ID	TECN	COMMENT	
0.357 ± 0.013 OUR FIT				Error includes scale factor of 1.1.	
0.41 ± 0.04 ± 0.02	215 ± 23	MENDEZ	10 CLEO	e^+e^- at 3774 MeV	

$\Gamma(2K_S^0)/\Gamma(K_S^0\pi^+\pi^-)$					Γ_{197}/Γ_{40}
This is the same as $\Gamma(K^0\bar{K}^0)/\Gamma(\bar{K}^0\pi^+\pi^-)$ because $D^0 \rightarrow K_S^0 K_L^0$ is forbidden by CP conservation.					
VALUE (units 10^{-2})	EVTS	DOCUMENT ID	TECN	COMMENT	
0.506 ± 0.034 OUR FIT				Error includes scale factor of 1.1.	
1.20 ± 0.22 OUR AVERAGE					
1.44 ± 0.32 ± 0.16	79 ± 17	LINK	05A FOCS	γ Be, $\bar{E}_\gamma \approx 180$ GeV	
1.01 ± 0.22 ± 0.16	26	ASNER	96B CLE2	$e^+e^- \approx \Upsilon(4S)$	
3.9 ± 1.3 ± 1.3	20 ± 7	FRABETTI	94c E687	γ Be $\bar{E}_\gamma=220$ GeV	
••• We do not use the following data for averages, fits, limits, etc. •••					
2.1 ^{+1.1} _{-0.8} ± 0.2	5	ALEXANDER	90 CLEO	e^+e^- 10.5–11 GeV	

$\Gamma(2K_S^0)/\Gamma(K_S^0\pi^+\pi^0)$					Γ_{197}/Γ_{38}
VALUE (units 10^{-2})	EVTS	DOCUMENT ID	TECN	COMMENT	
1.14 ± 0.04 OUR FIT				Error includes scale factor of 1.1.	
1.101 ± 0.023 ± 0.030	4.8k	DASH	17 BELL	At/near $\Upsilon(4S)$, $\Upsilon(5S)$	

$\Gamma(K_S^0K^-\pi^+)/\Gamma(K^-\pi^+)$					Γ_{198}/Γ_{37}
VALUE	EVTS	DOCUMENT ID	TECN	COMMENT	
0.084 ± 0.013 OUR FIT				Error includes scale factor of 1.1.	
0.08 ± 0.03				¹ ANJOS 91 E691 γ Be 80–240 GeV	
¹ The factor 100 at the top of column 2 of Table I of ANJOS 91 should be omitted.					

$\Gamma(\phi\pi^0)/\Gamma_{\text{total}}$					Γ_{265}/Γ
VALUE (units 10^{-3})	EVTS	DOCUMENT ID	TECN	COMMENT	
1.168 ± 0.028 ± 0.028	3.3k	ABLIKIM	19B BES3	e^+e^- at 3773 MeV	

$\Gamma(\phi\eta)/\Gamma_{\text{total}}$					Γ_{266}/Γ
VALUE (units 10^{-4})	EVTS	DOCUMENT ID	TECN	COMMENT	
1.81 ± 0.46 ± 0.06	102	ABLIKIM	19B BES3	e^+e^- at 3773 MeV	

$\Gamma(K_S^0K^-\pi^+)/\Gamma(K_S^0\pi^+\pi^-)$					Γ_{198}/Γ_{40}
VALUE	EVTS	DOCUMENT ID	TECN	COMMENT	
0.118 ± 0.017 OUR FIT				Error includes scale factor of 1.1.	
0.119 ± 0.021 OUR AVERAGE				Error includes scale factor of 1.3.	
0.108 ± 0.019	61	ANMMAR	91 CLEO	$e^+e^- \approx 10.5$ GeV	
0.16 ± 0.03 ± 0.02	39	ALBRECHT	90c ARG	$e^+e^- \approx 10$ GeV	

$\Gamma(\bar{K}^*(892)^0 K_S^0, \bar{K}^{*0} \rightarrow K^-\pi^+)/\Gamma(K_S^0\pi^+\pi^-)$					$\Gamma_{199}/\Gamma_{198}$
Fit fraction from Dalitz plot analyses. The fraction for the $K_S^0\pi^+$ mass between 792 and 992 MeV is $0.370 \pm 0.003 \pm 0.012$.					
VALUE (units 10^{-2})	EVTS	DOCUMENT ID	TECN	COMMENT	
2.47 ± 0.15 ± 0.23	113k	¹ AAIJ	16N LHCb	Dalitz plot fit	
¹ AAIJ 16N gives results for two S-wave parameterisations. We take the values from the model with LASS parametrization, and the difference as a systematic uncertainty.					

$\Gamma(K^*(892)^+ K^-, K^{*+} \rightarrow K_S^0\pi^+)/\Gamma(K_S^0K^-\pi^+)$					$\Gamma_{200}/\Gamma_{198}$
Fit fraction from Dalitz plot analyses.					
VALUE (units 10^{-2})	EVTS	DOCUMENT ID	TECN	COMMENT	
56.9 ± 0.6 ± 1.1	113k	¹ AAIJ	16N LHCb	Dalitz plot fit	
¹ AAIJ 16N gives results for two S-wave parameterisations. We take the values from the model with LASS parametrization, and the difference as a systematic uncertainty.					

$\Gamma(\overline{K}^*(1410)^0 K_S^0, \overline{K}^{*0} \rightarrow K^- \pi^+) / \Gamma(K_S^0 K^- \pi^+)$ $\Gamma_{201} / \Gamma_{198}$
Fit fraction from Dalitz plot analyses.

VALUE (units 10^{-2})	EVTS	DOCUMENT ID	TECN	COMMENT
3.8 ± 0.5 ± 5.6	113k	¹ AAIJ	16N LHCB	Dalitz plot fit

¹AAIJ 16N gives results for two S-wave parameterisations. We take the values from the model with LASS parametrization, and the difference as a uncertainty (which in this case dominates)

$\Gamma(K^*(1410)^+ K^-, K^{*+} \rightarrow K_S^0 \pi^+) / \Gamma(K_S^0 K^- \pi^+)$ $\Gamma_{202} / \Gamma_{198}$
Fit fraction from Dalitz plot analyses.

VALUE (units 10^{-2})	EVTS	DOCUMENT ID	TECN	COMMENT
9.6 ± 1.1 ± 5.4	113k	¹ AAIJ	16N LHCB	Dalitz plot fit

¹AAIJ 16N gives results for two S-wave parameterisations. We take the values from the model with LASS parametrization, and the difference as a systematic uncertainty (which in this case dominates).

$\Gamma((K^- \pi^+)_{S\text{-wave}} K_S^0) / \Gamma(K_S^0 K^- \pi^+)$ $\Gamma_{203} / \Gamma_{198}$
Fit fraction from Dalitz plot analyses.

VALUE (units 10^{-2})	EVTS	DOCUMENT ID	TECN	COMMENT
18 ± 2 ± 8	113k	¹ AAIJ	16N LHCB	Dalitz plot fit

¹AAIJ 16N gives results for two S-wave parameterisations. We take the values from the model with LASS parametrization, and the difference as a systematic uncertainty (which in this case dominates).

$\Gamma((K_S^0 \pi^+)_{S\text{-wave}} K^-) / \Gamma(K_S^0 K^- \pi^+)$ $\Gamma_{204} / \Gamma_{198}$
Fit fraction from Dalitz plot analyses.

VALUE (units 10^{-2})	EVTS	DOCUMENT ID	TECN	COMMENT
11.7 ± 1.0 ± 2.3	113k	¹ AAIJ	16N LHCB	Dalitz plot fit

¹AAIJ 16N gives results for two S-wave parameterisations. We take the values from the model with LASS parametrization, and the difference as a systematic uncertainty.

$\Gamma(a_0(980)^- \pi^+, a_0^- \rightarrow K_S^0 K^-) / \Gamma(K_S^0 K^- \pi^+)$ $\Gamma_{205} / \Gamma_{198}$
Fit fraction from Dalitz plot analyses.

VALUE (units 10^{-2})	EVTS	DOCUMENT ID	TECN	COMMENT
4.0 ± 0.7 ± 4.1	113k	¹ AAIJ	16N LHCB	Dalitz plot fit

¹AAIJ 16N gives results for two S-wave parameterisations. We take the values from the model with LASS parametrization, and the difference as a systematic uncertainty (which in this case dominates).

$\Gamma(a_0(1450)^- \pi^+, a_0^- \rightarrow K_S^0 K^-) / \Gamma(K_S^0 K^- \pi^+)$ $\Gamma_{206} / \Gamma_{198}$
Fit fraction from Dalitz plot analyses.

VALUE (units 10^{-2})	EVTS	DOCUMENT ID	TECN	COMMENT
0.74 ± 0.15 ± 0.57	113k	¹ AAIJ	16N LHCB	Dalitz plot fit

¹AAIJ 16N gives results for two S-wave parameterisations. We take the values from the model with LASS parametrization, and the difference as a systematic uncertainty (which in this case dominates).

$\Gamma(a_2(1320)^- \pi^+, a_2^- \rightarrow K_S^0 K^-) / \Gamma(K_S^0 K^- \pi^+)$ $\Gamma_{207} / \Gamma_{198}$
Fit fraction from Dalitz plot analyses.

VALUE (units 10^{-2})	EVTS	DOCUMENT ID	TECN	COMMENT
0.15 ± 0.06 ± 0.14	113k	¹ AAIJ	16N LHCB	Dalitz plot fit

¹AAIJ 16N gives results for two S-wave parameterisations. We take the values from the model with LASS parametrization, and the difference as a systematic uncertainty.

$\Gamma(\rho(1450)^- \pi^+, \rho^- \rightarrow K_S^0 K^-) / \Gamma(K_S^0 K^- \pi^+)$ $\Gamma_{208} / \Gamma_{198}$
Fit fraction from Dalitz plot analyses.

VALUE (units 10^{-2})	EVTS	DOCUMENT ID	TECN	COMMENT
1.4 ± 0.2 ± 0.7	113k	¹ AAIJ	16N LHCB	Dalitz plot fit

¹AAIJ 16N gives results for two S-wave parameterisations. We take the values from the model with LASS parametrization, and the difference as a systematic uncertainty.

$\Gamma(K_S^0 K^+ \pi^-) / \Gamma(K^- \pi^+)$ $\Gamma_{209} / \Gamma_{37}$
Fit fraction from Dalitz plot analyses.

VALUE	DOCUMENT ID	TECN	COMMENT
0.05 ± 0.025	¹ ANJOS	91 E691	γ Be 80–240 GeV

¹The factor 100 at the top of column 2 of Table I of ANJOS 91 should be omitted.

$\Gamma(K_S^0 K^+ \pi^-) / \Gamma(K_S^0 \pi^+ \pi^-)$ $\Gamma_{209} / \Gamma_{40}$
Fit fraction from Dalitz plot analyses.

VALUE	EVTS	DOCUMENT ID	TECN	COMMENT
0.098 ± 0.020	55	AMMAR	91 CLEO	$e^+ e^- \approx 10.5$ GeV

$\Gamma(K_S^0 K^+ \pi^-) / \Gamma(K_S^0 K^- \pi^+)$ $\Gamma_{209} / \Gamma_{198}$
Fit fraction from Dalitz plot analyses.

VALUE	EVTS	DOCUMENT ID	TECN	COMMENT
0.654 ± 0.007 OUR FIT				
0.654 ± 0.007 OUR AVERAGE				
0.655 ± 0.004 ± 0.006	76k, 113k	AAIJ	16N LHCB	$\rho\rho$ at 7, 8 TeV
0.592 ± 0.044 ± 0.018		INSLER	12 CLEO	$e^+ e^- \rightarrow D^0 \overline{D}^0$ at 3.77 GeV

$\Gamma(K^*(892)^0 K_S^0, K^{*0} \rightarrow K^+ \pi^-) / \Gamma(\overline{K}^*(892)^0 K_S^0, \overline{K}^{*0} \rightarrow K^- \pi^+)$ $\Gamma_{210} / \Gamma_{199}$
Fit fraction from Dalitz plot analyses.

VALUE	CL%	DOCUMENT ID	TECN	COMMENT
0.356 ± 0.034 ± 0.007		¹ INSLER	12 CLEO	$e^+ e^- \rightarrow D^0 \overline{D}^0$, 3.77 GeV

• • • We do not use the following data for averages, fits, limits, etc. • • •
<0.010 90 AMMAR 91 CLEO $e^+ e^- \approx 10.5$ GeV

¹Uses quantum correlations in $e^+ e^- \rightarrow D^0 \overline{D}^0$ at the $\psi(3770)$, where the signal side D decays to $K_S^0 K \pi$ and the tag-side D decays to $K \pi, K \pi \pi, K \pi \pi^0$, and 10 additional CP-even, CP-odd, and mixed CP modes involving K_S^0 or K_L^0 .

$\Gamma(K^*(892)^0 K_S^0, K^{*0} \rightarrow K^+ \pi^-) / \Gamma(K_S^0 K^+ \pi^-)$ $\Gamma_{210} / \Gamma_{209}$
Fit fraction from Dalitz plot analyses.

VALUE (units 10^{-2})	EVTS	DOCUMENT ID	TECN	COMMENT
5.17 ± 0.21 ± 0.47	76k	¹ AAIJ	16N LHCB	Dalitz plot fit

¹AAIJ 16N gives results for two S-wave parameterisations. We take the values from the model with LASS parametrization, and the difference as a systematic uncertainty.

$\Gamma(K^*(892)^- K^+, K^{*-} \rightarrow K_S^0 \pi^-) / \Gamma(K_S^0 K^+ \pi^-)$ $\Gamma_{211} / \Gamma_{209}$
Fit fraction from Dalitz plot analyses.

VALUE (units 10^{-2})	EVTS	DOCUMENT ID	TECN	COMMENT
28.8 ± 0.4 ± 1.5	76k	¹ AAIJ	16N LHCB	Dalitz plot fit

¹AAIJ 16N gives results for two S-wave parameterisations. We take the values from the model with LASS parametrization, and the difference as a systematic uncertainty.

$\Gamma(K^*(1410)^0 K_S^0, K^{*0} \rightarrow K^+ \pi^+) / \Gamma(K_S^0 K^+ \pi^-)$ $\Gamma_{212} / \Gamma_{209}$
Fit fraction from Dalitz plot analyses.

VALUE (units 10^{-2})	EVTS	DOCUMENT ID	TECN	COMMENT
2.2 ± 0.6 ± 3.7	76k	¹ AAIJ	16N LHCB	Dalitz plot fit

¹AAIJ 16N gives results for two S-wave parameterisations. We take the values from the model with LASS parametrization, and the difference as a systematic uncertainty (which in this case dominates).

$\Gamma(K^*(1410)^- K^+, K^{*-} \rightarrow K_S^0 \pi^-) / \Gamma(K_S^0 K^+ \pi^-)$ $\Gamma_{213} / \Gamma_{209}$
Fit fraction from Dalitz plot analyses.

VALUE (units 10^{-2})	EVTS	DOCUMENT ID	TECN	COMMENT
11.9 ± 1.5 ± 9.1	76k	¹ AAIJ	16N LHCB	Dalitz plot fit

¹AAIJ 16N gives results for two S-wave parameterisations. We take the values from the model with LASS parametrization, and the difference as a systematic uncertainty (which in this case dominates).

$\Gamma((K^+ \pi^-)_{S\text{-wave}} K_S^0) / \Gamma(K_S^0 K^+ \pi^-)$ $\Gamma_{214} / \Gamma_{209}$
Fit fraction from Dalitz plot analyses.

VALUE (units 10^{-2})	EVTS	DOCUMENT ID	TECN	COMMENT
17 ± 2 ± 8	76k	¹ AAIJ	16N LHCB	Dalitz plot fit

¹AAIJ 16N gives results for two S-wave parameterisations. We take the values from the model with LASS parametrization, and the difference as a systematic uncertainty.

$\Gamma((K_S^0 \pi^-)_{S\text{-wave}} K^+) / \Gamma(K_S^0 K^+ \pi^-)$ $\Gamma_{215} / \Gamma_{209}$
Fit fraction from Dalitz plot analyses.

VALUE (units 10^{-2})	EVTS	DOCUMENT ID	TECN	COMMENT
6.3 ± 0.9 ± 2.3	76k	¹ AAIJ	16N LHCB	Dalitz plot fit

¹AAIJ 16N gives results for two S-wave parameterisations. We take the values from the model with LASS parametrization, and the difference as a systematic uncertainty.

$\Gamma(a_0(980)^+ \pi^-, a_0^+ \rightarrow K_S^0 K^+) / \Gamma(K_S^0 K^+ \pi^-)$ $\Gamma_{216} / \Gamma_{209}$
Fit fraction from Dalitz plot analyses.

VALUE (units 10^{-2})	EVTS	DOCUMENT ID	TECN	COMMENT
26 ± 2 ± 18	76k	¹ AAIJ	16N LHCB	Dalitz plot fit

¹AAIJ 16N gives results for two S-wave parameterisations. We take the values from the model with LASS parametrization, and the difference as a systematic uncertainty (which in this case dominates).

$\Gamma(a_0(1450)^+ \pi^-, a_0^+ \rightarrow K_S^0 K^+) / \Gamma(K_S^0 K^+ \pi^-)$ $\Gamma_{217} / \Gamma_{209}$
Fit fraction from Dalitz plot analyses.

VALUE (units 10^{-2})	EVTS	DOCUMENT ID	TECN	COMMENT
1.5 ± 0.3 ± 1.1	76k	¹ AAIJ	16N LHCB	Dalitz plot fit

¹AAIJ 16N gives results for two S-wave parameterisations. We take the values from the model with LASS parametrization, and the difference as a systematic uncertainty (which in this case dominates).

$\Gamma(\rho(1700)^+ \pi^-, \rho^+ \rightarrow K_S^0 K^+) / \Gamma(K_S^0 K^+ \pi^-)$ $\Gamma_{218} / \Gamma_{209}$
Fit fraction from Dalitz plot analyses.

VALUE (units 10^{-2})	EVTS	DOCUMENT ID	TECN	COMMENT
0.53 ± 0.11 ± 0.23	76k	¹ AAIJ	16N LHCB	Dalitz plot fit

¹AAIJ 16N gives results for two S-wave parameterisations. We take the values from the model with LASS parametrization, and the difference as a systematic uncertainty.

$\Gamma(K^+ K^- \pi^0) / \Gamma(K^- \pi^+ \pi^0)$ $\Gamma_{219} / \Gamma_{55}$
Fit fraction from Dalitz plot analyses.

VALUE (units 10^{-2})	EVTS	DOCUMENT ID	TECN	COMMENT
2.37 ± 0.03 ± 0.04	11k ± 122	AUBERT,B	06x BABR	$e^+ e^- \approx \Upsilon(4S)$

• • • We do not use the following data for averages, fits, limits, etc. • • •
0.95 ± 0.26 151 ASNER 96b CLE2 $e^+ e^- \approx \Upsilon(4S)$

Meson Particle Listings

 D^0

$\Gamma(K^*(892)^+K^-, K^*(892)^+ \rightarrow K^+\pi^0)/\Gamma(K^+K^-\pi^0)$ $\Gamma_{220}/\Gamma_{219}$
This is the "fit fraction" from the Dalitz-plot analysis with interference.

VALUE (units 10^{-2})	DOCUMENT ID	TECN	COMMENT
44.4 ± 0.8 ± 0.6	AUBERT	07T	BABR Dalitz fit II, 11k evts

• • • We do not use the following data for averages, fits, limits, etc. • • •

46.1 ± 3.1	1	CAWLFIELD	06A	CLEO	Dalitz fit, 627 ± 30 evts
------------	---	-----------	-----	------	---------------------------

¹The error on this CAWLFIELD 06A result is statistical only.

$\Gamma(K^*(892)^-K^+, K^*(892)^- \rightarrow K^-\pi^0)/\Gamma(K^+K^-\pi^0)$ $\Gamma_{221}/\Gamma_{219}$
This is the "fit fraction" from the Dalitz-plot analysis with interference.

VALUE (units 10^{-2})	DOCUMENT ID	TECN	COMMENT
15.9 ± 0.7 ± 0.6	AUBERT	07T	BABR Dalitz fit II, 11k evts

• • • We do not use the following data for averages, fits, limits, etc. • • •

12.3 ± 2.2	1	CAWLFIELD	06A	CLEO	Dalitz fit, 627 ± 30 evts
------------	---	-----------	-----	------	---------------------------

¹The error on this CAWLFIELD 06A result is statistical only.

$\Gamma((K^+\pi^0)S\text{-wave } K^-)/\Gamma(K^+K^-\pi^0)$ $\Gamma_{222}/\Gamma_{219}$
This is the "fit fraction" from the Dalitz-plot analysis with interference.

VALUE (units 10^{-2})	DOCUMENT ID	TECN	COMMENT	
71.1 ± 3.7 ± 1.9	1	AUBERT	07T	BABR Dalitz fit II, 11k evts

¹The only major difference between fits I and II in the AUBERT 07T analysis is in this mode, where the fit-I fraction is $(16.3 \pm 3.4 \pm 2.1)\%$.

$\Gamma((K^-\pi^0)S\text{-wave } K^+)/\Gamma(K^+K^-\pi^0)$ $\Gamma_{223}/\Gamma_{219}$
This is the "fit fraction" from the Dalitz-plot analysis with interference.

VALUE (units 10^{-2})	DOCUMENT ID	TECN	COMMENT
3.9 ± 0.9 ± 1.0	AUBERT	07T	BABR Dalitz fit II, 11k evts

$\Gamma(f_0(980)\pi^0, f_0 \rightarrow K^+K^-)/\Gamma(K^+K^-\pi^0)$ $\Gamma_{224}/\Gamma_{219}$
This is the "fit fraction" from the Dalitz-plot analysis with interference.

VALUE (units 10^{-2})	DOCUMENT ID	TECN	COMMENT	
10.5 ± 1.1 ± 1.2	1	AUBERT	07T	BABR Dalitz fit II, 11k evts

¹When AUBERT 07T replace the $f_0(980)\pi^0$ mode with $a_0(980)\pi^0$, the fit fraction is a negligibly different $(11.0 \pm 1.5 \pm 1.2)\%$.

$\Gamma(\phi\pi^0, \phi \rightarrow K^+K^-)/\Gamma(K^+K^-\pi^0)$ $\Gamma_{225}/\Gamma_{219}$
This is the "fit fraction" from the Dalitz-plot analysis with interference.

VALUE (units 10^{-2})	DOCUMENT ID	TECN	COMMENT
19.4 ± 0.6 ± 0.5	AUBERT	07T	BABR Dalitz fit II, 11k evts

• • • We do not use the following data for averages, fits, limits, etc. • • •

14.9 ± 1.6	1	CAWLFIELD	06A	CLEO	Dalitz fit, 627 ± 30 evts
------------	---	-----------	-----	------	---------------------------

¹The error on this CAWLFIELD 06A result is statistical only.

$\Gamma(K^+K^-\pi^0\text{ nonresonant})/\Gamma(K^+K^-\pi^0)$ $\Gamma_{226}/\Gamma_{219}$
This is the "fit fraction" from the Dalitz-plot analysis with interference.

VALUE	DOCUMENT ID	TECN	COMMENT	
0.360 ± 0.037	1	CAWLFIELD	06A	CLEO Dalitz fit, 627 ± 30 evts

• • • We do not use the following data for averages, fits, limits, etc. • • •

¹The error is statistical only. CAWLFIELD 06A also fits the Dalitz plot replacing this flat nonresonant background with broad $S\text{-wave } \kappa^\pm \rightarrow K^\pm\pi^0$ resonances. There is no significant improvement in the fit, and $K^*\pi^\mp$ and $\phi\pi^0$ results are not much changed.

$\Gamma(2K_S^0\pi^0)/\Gamma_{\text{total}}$ Γ_{227}/Γ

VALUE	DOCUMENT ID	TECN	COMMENT
<0.00059	ASNER	96B	CLE2 $e^+e^- \approx \mathcal{T}(4S)$

$\Gamma(K^+K^-\eta)/\Gamma_{\text{total}}$ Γ_{228}/Γ

VALUE (units 10^{-4})	EVTS	DOCUMENT ID	TECN	COMMENT
0.59 ± 0.18 ± 0.05	13	ABLIKIM	20V	BES3 e^+e^- , 3773 MeV

$\Gamma(K^+K^-\eta)/\Gamma(K^-\pi^+\eta)$ Γ_{228}/Γ_{94}

VALUE (units 10^{-3})	EVTS	DOCUMENT ID	TECN	COMMENT
9.57^{+0.36}_{-0.33} ± 0.20	1.4k	LI	21G	BELL e^+e^- at $\mathcal{T}(\text{NS})$

$\Gamma(\phi(1020)\eta)/\Gamma(K^-\pi^+\eta)$ Γ_{229}/Γ_{94}

VALUE (units 10^{-3})	EVTS	DOCUMENT ID	TECN	COMMENT	
9.8 ± 0.6 ± 0.1	1.4k	1	LI	21G	BELL e^+e^- at $\mathcal{T}(\text{NS})$

¹LI 21G reports $[\Gamma(D^0 \rightarrow \phi(1020)\eta)/\Gamma(D^0 \rightarrow K^-\pi^+\eta)] \times [\text{B}(\phi(1020) \rightarrow K^+K^-)] = (4.82 \pm 0.23 \pm 0.16) \times 10^{-3}$ which we divide by our best value $\text{B}(\phi(1020) \rightarrow K^+K^-) = (49.1 \pm 0.5) \times 10^{-2}$. Our first error is their experiment's error and our second error is the systematic error from using our best value.

$\Gamma(K^+K^-\eta\text{ nonresonant})/\Gamma(K^-\pi^+\eta)$ Γ_{230}/Γ_{94}

VALUE (units 10^{-3})	EVTS	DOCUMENT ID	TECN	COMMENT
5.26^{+0.45}_{-0.38} ± 0.11	1.4k	LI	21G	BELL e^+e^- at $\mathcal{T}(\text{NS})$

$\Gamma(2K_S^0\eta)/\Gamma_{\text{total}}$ Γ_{231}/Γ

VALUE (units 10^{-4})	EVTS	DOCUMENT ID	TECN	COMMENT
1.33 ± 0.59 ± 0.18	7	ABLIKIM	20V	BES3 e^+e^- , 3773 MeV

$\Gamma(K^+K^-\pi^0\pi^0)/\Gamma_{\text{total}}$ Γ_{232}/Γ

VALUE (units 10^{-4})	EVTS	DOCUMENT ID	TECN	COMMENT
6.9 ± 0.7 ± 0.4	132	ABLIKIM	20Ac	BES3 e^+e^- at 3.773 GeV

$\Gamma(K^+K^-\pi^+\pi^-)/\Gamma(K^-2\pi^+\pi^-)$ Γ_{233}/Γ_{72}

VALUE (units 10^{-2})	EVTS	DOCUMENT ID	TECN	COMMENT	
3.00 ± 0.13 OUR AVERAGE					
2.95 ± 0.11 ± 0.08	2669 ± 101	1	LINK	05G	FOCS γBe , $\overline{E}_\gamma \approx 180$ GeV
3.13 ± 0.37 ± 0.36	136 ± 15		AITALA	98D	E791 π^- nucleus, 500 GeV
3.5 ± 0.4 ± 0.2	244 ± 26		FRABETTI	95c	E687 γBe , $\overline{E}_\gamma \approx 200$ GeV
• • • We do not use the following data for averages, fits, limits, etc. • • •					
4.4 ± 1.8 ± 0.5	19 ± 8		ABLIKIM	05F	BES $e^+e^- \approx \psi(3770)$
4.1 ± 0.7 ± 0.5	114 ± 20		ALBRECHT	94I	ARG $e^+e^- \approx 10$ GeV
3.14 ± 1.0	89 ± 29		ANMMAR	91	CLEO $e^+e^- \approx 10.5$ GeV
2.8 ^{+0.8} _{-0.7}			ANJOS	91	E691 γBe 80–240 GeV

¹LINK 05G uses a smaller, cleaner subset of 1279 ± 48 events for the amplitude analysis that gives the results in the next data blocks.

$\Gamma(\phi(\pi^+\pi^-)S\text{-wave}, \phi \rightarrow K^+K^-)/\Gamma(K^+K^-\pi^+\pi^-)$ $\Gamma_{234}/\Gamma_{233}$
This is the fraction from a coherent amplitude analysis.

VALUE (units 10^{-2})	EVTS	DOCUMENT ID	TECN	COMMENT	
4.0 ± 0.6 ± 2.1	3k	1	DARGENT	17	4-body fit, $K K \pi \pi$ events

• • • We do not use the following data for averages, fits, limits, etc. • • •

10.3 ± 1.0 ± 0.8	3k	2	ARTUSO	12	CLEO 4-body fit, $K K \pi \pi$ events
1 ± 1	1.3k	LINK		05G	FOCS 4-body fit, $K K \pi \pi$ events

¹Obtained by analyzing CLEO data but not authored by the CLEO Collaboration.

²See DARGENT 17

$\Gamma((\phi\rho^0)S\text{-wave}, \phi \rightarrow K^+K^-)/\Gamma(K^+K^-\pi^+\pi^-)$ $\Gamma_{235}/\Gamma_{233}$
This is the fraction from a coherent amplitude analysis.

VALUE (units 10^{-2})	EVTS	DOCUMENT ID	TECN	COMMENT	
28.1 ± 1.3 ± 1.7	2.9k	1,2	DARGENT	17	4-body fit, $K K \pi \pi$ evts

• • • We do not use the following data for averages, fits, limits, etc. • • •

38.3 ± 2.5 ± 3.8		1,3	ARTUSO	12	CLEO Fitting 2959 evts.
29 ± 2 ± 1		LINK		05G	FOCS Fits 1279 ± 48 evts.

¹ARTUSO 12 and DARGENT 17 use the same dataset, but ARTUSO 12 uses a formulation for the D-wave component that is in fact a mix of S- and D-wave, while DARGENT 17 uses a pure D-wave. This explains the discrepancy in their $\rho\phi$ S- and D-wave components.

²Obtained by analyzing CLEO data but not authored by the CLEO Collaboration.

³See DARGENT 17

$\Gamma((\phi\rho^0)P\text{-wave}, \phi \rightarrow K^+K^-)/\Gamma(K^+K^-\pi^+\pi^-)$ $\Gamma_{236}/\Gamma_{233}$
This is the fit fraction from a coherent amplitude analysis.

VALUE (units 10^{-2})	EVTS	DOCUMENT ID	TECN	COMMENT	
1.6 ± 0.3 ± 0.7	2.9k	1	DARGENT	17	4-body fit, $K K \pi \pi$ evts

¹Obtained by analyzing CLEO data but not authored by the CLEO Collaboration.

$\Gamma((\phi\rho^0)D\text{-wave}, \phi \rightarrow K^+K^-)/\Gamma(K^+K^-\pi^+\pi^-)$ $\Gamma_{237}/\Gamma_{233}$

VALUE (units 10^{-2})	EVTS	DOCUMENT ID	TECN	COMMENT	
1.7 ± 0.4 ± 0.4	2.9k	1,2	DARGENT	17	4-body fit, $K K \pi \pi$ evts

• • • We do not use the following data for averages, fits, limits, etc. • • •

3.4 ± 0.7 ± 0.6		1,3	ARTUSO	12	CLEO Fitting 2959 evts.
-----------------	--	-----	--------	----	-------------------------

¹ARTUSO 12 use a formulation for the D-wave component that is in fact a mix of S- and D-wave, while DARGENT 17 uses a pure D-wave.

²Obtained by analyzing CLEO data but not authored by the CLEO Collaboration.

³See DARGENT 17

$\Gamma(K^*(892)^0\overline{K}^*(892)^0, K^*0 \rightarrow K^\pm\pi^\mp)/\Gamma(K^+K^-\pi^+\pi^-)$ $\Gamma_{238}/\Gamma_{233}$
This is the fraction from a coherent amplitude analysis.

VALUE (units 10^{-2})	DOCUMENT ID	TECN	COMMENT
3 ± 2 ± 1	LINK	05G	FOCS Fits 1279 ± 48 evts.

• • • We do not use the following data for averages, fits, limits, etc. • • •

$\Gamma(K^+K^-\rho^0 3\text{-body})/\Gamma(K^+K^-\pi^+\pi^-)$ $\Gamma_{239}/\Gamma_{233}$
This is the fraction from a coherent amplitude analysis.

VALUE (units 10^{-2})	DOCUMENT ID	TECN	COMMENT
2 ± 2 ± 2	LINK	05G	FOCS Fits 1279 ± 48 evts.

• • • We do not use the following data for averages, fits, limits, etc. • • •

$\Gamma(f_0(980)\pi^+\pi^-, f_0 \rightarrow K^+K^-)/\Gamma(K^+K^-\pi^+\pi^-)$ $\Gamma_{240}/\Gamma_{233}$
This is the fraction from a coherent amplitude analysis.

VALUE (units 10^{-2})	DOCUMENT ID	TECN	COMMENT
15 ± 3 ± 2	LINK	05G	FOCS Fits 1279 ± 48 evts.

• • • We do not use the following data for averages, fits, limits, etc. • • •

$$\Gamma((K^*(892)^0 \bar{K}^*(892)^0)_{S\text{-wave}}, K^{*0} \rightarrow K^\pm \pi^\mp) / \Gamma(K^+ K^- \pi^+ \pi^-) \quad \Gamma_{241} / \Gamma_{233}$$

VALUE (units 10^{-2})	EVTS	DOCUMENT ID	TECN	COMMENT
9.06 ± 0.35 OUR AVERAGE				
9.18 ± 0.21 ± 0.28	163k	AAIJ	19c	LHCB 4-body fit, $K K \pi \pi$ evts
4.5 ± 0.8 ± 2.0	3k	¹ DARGENT	17	4-body fit, $K K \pi \pi$ evts
• • • We do not use the following data for averages, fits, limits, etc. • • •				
6.1 ± 0.8 ± 0.9	3k	² ARTUSO	12	CLEO 4-body fit, $K K \pi \pi$ evts
¹ Obtained by analyzing CLEO data but not authored by the CLEO Collaboration.				
² See DARGENT 17				

$$\Gamma((K^*(892)^0 \bar{K}^*(892)^0)_{P\text{-wave}}, K^* \rightarrow K^\pm \pi^\mp) / \Gamma(K^+ K^- \pi^+ \pi^-) \quad \Gamma_{242} / \Gamma_{233}$$

This is the fit fraction from a coherent amplitude analysis.

VALUE (units 10^{-2})	EVTS	DOCUMENT ID	TECN	COMMENT
4.87 ± 0.24 OUR AVERAGE				
4.90 ± 0.16 ± 0.18	163k	AAIJ	19c	LHCB 4-body fit, $K K \pi \pi$ evts
3.6 ± 0.7 ± 1.5	2.9k	¹ DARGENT	17	4-body fit, $K K \pi \pi$ evts
¹ Obtained by analyzing CLEO data but not authored by the CLEO Collaboration.				

$$\Gamma((K^*(892)^0 \bar{K}^*(892)^0)_{D\text{-wave}}, K^* \rightarrow K^\pm \pi^\mp) / \Gamma(K^+ K^- \pi^+ \pi^-) \quad \Gamma_{243} / \Gamma_{233}$$

This is the fit fraction from a coherent amplitude analysis.

VALUE (units 10^{-2})	EVTS	DOCUMENT ID	TECN	COMMENT
1.89 ± 0.13 OUR AVERAGE				
1.85 ± 0.09 ± 0.10	163k	AAIJ	19c	LHCB 4-body fit, $K K \pi \pi$ evts
4.0 ± 0.6 ± 0.7	2.9k	¹ DARGENT	17	4-body fit, $K K \pi \pi$ evts
¹ Obtained by analyzing CLEO data but not authored by the CLEO Collaboration.				

$$\Gamma(K^*(892)^0 K^\mp \pi^\pm \text{ 3-body}, K^{*0} \rightarrow K^\pm \pi^\mp) / \Gamma(K^+ K^- \pi^+ \pi^-) \quad \Gamma_{244} / \Gamma_{233}$$

This is the fraction from a coherent amplitude analysis.

VALUE (units 10^{-2})	DOCUMENT ID	TECN	COMMENT
• • • We do not use the following data for averages, fits, limits, etc. • • •			
11 ± 2 ± 1	LINK	05G	FOCS Fits 1279 ± 48 evts.
¹ Obtained by analyzing CLEO data but not authored by the CLEO Collaboration.			

$$\Gamma(K^*(892)^0 (K^- \pi^+)_{S\text{-wave}} \text{ 3-body}, K^{*0} \rightarrow K^+ \pi^-) / \Gamma(K^+ K^- \pi^+ \pi^-) \quad \Gamma_{245} / \Gamma_{233}$$

This is the fit fraction from a coherent amplitude analysis.

VALUE (units 10^{-2})	EVTS	DOCUMENT ID	TECN	COMMENT
5.8 ± 1.2 ± 2.1	2.9k	¹ DARGENT	17	4-body fit, $K K \pi \pi$ evts
¹ Obtained by analyzing CLEO data but not authored by the CLEO Collaboration.				

$$\Gamma((K^- \pi^+)_{P\text{-wave}}, (K^+ \pi^-)_{S\text{-wave}}) / \Gamma(K^+ K^- \pi^+ \pi^-) \quad \Gamma_{246} / \Gamma_{233}$$

• • • We do not use the following data for averages, fits, limits, etc. • • •

VALUE (units 10^{-2})	DOCUMENT ID	TECN	COMMENT
10.9 ± 1.2 ± 1.7	¹ ARTUSO	12	CLEO Fitting 2959 evts.
¹ See DARGENT 17			

$$\Gamma(K_1(1270)^\pm K^\mp, K_1^\pm \rightarrow K^\pm \pi^+ \pi^-) / \Gamma(K^+ K^- \pi^+ \pi^-) \quad \Gamma_{247} / \Gamma_{233}$$

This is the fraction from a coherent amplitude analysis.

VALUE (units 10^{-2})	DOCUMENT ID	TECN	COMMENT
• • • We do not use the following data for averages, fits, limits, etc. • • •			
33 ± 6 ± 4	¹ LINK	05G	FOCS Fits 1279 ± 48 evts.
¹ This LINK 05G value includes $K_1(1270)^\pm \rightarrow \rho^0 K^\pm, \rightarrow K_0^*(1430)^0 \pi^\pm$, and $K^*(892)^0 \pi^\pm$.			

$$\Gamma(K_1(1270)^+ K^-, K_1^+ \rightarrow K^{*0} \pi^+) / \Gamma(K^+ K^- \pi^+ \pi^-) \quad \Gamma_{248} / \Gamma_{233}$$

VALUE (units 10^{-2})	EVTS	DOCUMENT ID	TECN	COMMENT
5.5 ± 1.4 ± 3.4	3k	¹ DARGENT	17	4-body fit, $K K \pi \pi$ evts
• • • We do not use the following data for averages, fits, limits, etc. • • •				
7.3 ± 0.8 ± 1.9	3k	² ARTUSO	12	CLEO 4-body fit, $K K \pi \pi$ events
¹ Obtained by analyzing CLEO data but not authored by the CLEO Collaboration.				
² See DARGENT 17				

$$\Gamma(K_1(1270)^+ K^-, K_1^+ \rightarrow K^*(1430)^0 \pi^+, K^{*0} \rightarrow K^+ \pi^-) / \Gamma(K^+ K^- \pi^+ \pi^-) \quad \Gamma_{249} / \Gamma_{233}$$

This is the fit fraction from a coherent amplitude analysis.

VALUE (units 10^{-2})	EVTS	DOCUMENT ID	TECN	COMMENT
6.1 ± 1.2 ± 1.8	2.9k	¹ DARGENT	17	4-body fit, $K K \pi \pi$ evts
¹ Obtained by analyzing CLEO data but not authored by the CLEO Collaboration.				

$$\Gamma(K_1(1270)^+ K^-, K_1^+ \rightarrow \rho^0 K^+) / \Gamma(K^+ K^- \pi^+ \pi^-) \quad \Gamma_{250} / \Gamma_{233}$$

VALUE (units 10^{-2})	EVTS	DOCUMENT ID	TECN	COMMENT
9.1 ± 1.5 ± 1.9	2.9k	¹ DARGENT	17	4-body fit, $K K \pi \pi$ evts
• • • We do not use the following data for averages, fits, limits, etc. • • •				
4.7 ± 0.7 ± 0.8		² ARTUSO	12	CLEO Fitting 2959 evts.
¹ Obtained by analyzing CLEO data but not authored by the CLEO Collaboration.				
² See DARGENT 17				

$$\Gamma(K_1(1270)^+ K^-, K_1^+ \rightarrow \omega(782) K^+, \omega \rightarrow \pi^+ \pi^-) / \Gamma(K^+ K^- \pi^+ \pi^-) \quad \Gamma_{251} / \Gamma_{233}$$

This is the fit fraction from a coherent amplitude analysis.

VALUE (units 10^{-2})	EVTS	DOCUMENT ID	TECN	COMMENT
0.6 ± 0.3 ± 0.4	2.9k	¹ DARGENT	17	4-body fit, $K K \pi \pi$ evts
¹ Obtained by analyzing CLEO data but not authored by the CLEO Collaboration.				

$$\Gamma(K_1(1270)^- K^+, K_1^- \rightarrow \bar{K}^{*0} \pi^-) / \Gamma(K^+ K^- \pi^+ \pi^-) \quad \Gamma_{252} / \Gamma_{233}$$

VALUE (units 10^{-2})	DOCUMENT ID	TECN	COMMENT
• • • We do not use the following data for averages, fits, limits, etc. • • •			
0.9 ± 0.3 ± 0.4	¹ ARTUSO	12	CLEO Fitting 2959 evts.
¹ See DARGENT 17			

$$\Gamma(K_1(1270)^- K^+, K_1^- \rightarrow \rho^0 K^-) / \Gamma(K^+ K^- \pi^+ \pi^-) \quad \Gamma_{253} / \Gamma_{233}$$

VALUE (units 10^{-2})	EVTS	DOCUMENT ID	TECN	COMMENT
5.4 ± 0.7 ± 1.3	2.9k	¹ DARGENT	17	4-body fit, $K K \pi \pi$ evts
• • • We do not use the following data for averages, fits, limits, etc. • • •				
6.0 ± 0.8 ± 0.6		² ARTUSO	12	CLEO Fitting 2959 evts.
¹ Obtained by analyzing CLEO data but not authored by the CLEO Collaboration.				
² See DARGENT 17				

$$\Gamma(K_1(1400)^\pm K^\mp, K_1^\pm \rightarrow K^\pm \pi^+ \pi^-) / \Gamma(K^+ K^- \pi^+ \pi^-) \quad \Gamma_{254} / \Gamma_{233}$$

This is the fraction from a coherent amplitude analysis.

VALUE (units 10^{-2})	DOCUMENT ID	TECN	COMMENT
• • • We do not use the following data for averages, fits, limits, etc. • • •			
22 ± 3 ± 4	LINK	05G	FOCS Fits 1279 ± 48 evts.

$$\Gamma(K_1(1400)^+ K^-, K_1^+ \rightarrow K^*(892)^0 \pi^+, K^{*0} \rightarrow K^+ \pi^-) / \Gamma(K^+ K^- \pi^+ \pi^-) \quad \Gamma_{255} / \Gamma_{233}$$

This is the fit fraction from a coherent amplitude analysis.

VALUE (units 10^{-2})	EVTS	DOCUMENT ID	TECN	COMMENT
18.7 ± 1.5 OUR AVERAGE				
19.08 ± 0.60 ± 1.46	163k	AAIJ	19c	LHCB 4-body fit, $K K \pi \pi$ evts
12.4 ± 2.6 ± 6.3	2.9k	¹ DARGENT	17	4-body fit, $K K \pi \pi$ evts
¹ Obtained by analyzing CLEO data but not authored by the CLEO Collaboration.				

$$\Gamma(K^*(1410)^+ K^-, K^{*+} \rightarrow K^{*0} \pi^+) / \Gamma(K^+ K^- \pi^+ \pi^-) \quad \Gamma_{256} / \Gamma_{233}$$

VALUE (units 10^{-2})	DOCUMENT ID	TECN	COMMENT
• • • We do not use the following data for averages, fits, limits, etc. • • •			
4.2 ± 0.7 ± 0.8	^{1,2} ARTUSO	12	CLEO Fitting 2959 evts.
¹ DARGENT 17 find $K^*(1410)^+ \pi^-$ and $K^*(1680)^+ \pi^-$, which both peak outside the $D^0 \rightarrow K K \pi \pi$ kinematic range, effectively indistinguishable; we list their result under $K^*(1680)^+ \pi^-$.			
² See DARGENT 17			

$$\Gamma(K^*(1410)^- K^+, K^{*-} \rightarrow \bar{K}^{*0} \pi^-) / \Gamma(K^+ K^- \pi^+ \pi^-) \quad \Gamma_{257} / \Gamma_{233}$$

VALUE (units 10^{-2})	EVTS	DOCUMENT ID	TECN	COMMENT
2.82 ± 0.19 ± 0.39	163k	AAIJ	19c	LHCB 4-body fit, $K K \pi \pi$ evts
• • • We do not use the following data for averages, fits, limits, etc. • • •				
4.7 ± 0.7 ± 0.7	3k	¹ ARTUSO	12	CLEO 4-body fit, $K K \pi \pi$ evts
¹ See DARGENT 17.				

$$\Gamma(K_1(1680)^+ K^-, K_1^+ \rightarrow K^{*0} \pi^+, K^{*0} \rightarrow K^+ \pi^-) / \Gamma(K^+ K^- \pi^+ \pi^-) \quad \Gamma_{258} / \Gamma_{233}$$

This is the fit fraction from a coherent amplitude analysis.

VALUE (units 10^{-2})	EVTS	DOCUMENT ID	TECN	COMMENT
3.6 ± 0.8 ± 1.0	2.9k	^{1,2} DARGENT	17	4-body fit, $K K \pi \pi$ evts
¹ DARGENT 17 find $K^*(1410)^+ \pi^-$ and $K^*(1680)^+ \pi^-$, which both peak outside the $D^0 \rightarrow K K \pi \pi$ kinematic range, effectively indistinguishable.				
² Obtained by analyzing CLEO data but not authored by the CLEO Collaboration.				

$$\Gamma(K^+ K^- \pi^+ \pi^- \text{ non-resonant}) / \Gamma(K^+ K^- \pi^+ \pi^-) \quad \Gamma_{259} / \Gamma_{233}$$

This is the fit fraction from a coherent amplitude analysis.

VALUE (units 10^{-2})	EVTS	DOCUMENT ID	TECN	COMMENT
11.1 ± 1.2 ± 2.2	2.9k	¹ DARGENT	17	4-body fit, $K K \pi \pi$ evts
¹ Obtained by analyzing CLEO data but not authored by the CLEO Collaboration.				

$$\Gamma(2K_S^0 \pi^+ \pi^-) / \Gamma_{\text{total}} \quad \Gamma_{260} / \Gamma$$

VALUE (units 10^{-4})	EVTS	DOCUMENT ID	TECN	COMMENT
5.3 ± 0.9 ± 0.3	63	ABLIKIM	20Ac	BES3 $e^+ e^-$ at 3.773 GeV

$$\Gamma(2K_S^0 \pi^+ \pi^-) / \Gamma(K_S^0 \pi^+ \pi^-) \quad \Gamma_{260} / \Gamma_{40}$$

VALUE (units 10^{-2})	EVTS	DOCUMENT ID	TECN	COMMENT
4.3 ± 0.8 OUR AVERAGE				
4.16 ± 0.70 ± 0.42	113 ± 21	LINK	05A	FOCS γ Be, $\bar{E}_\gamma \approx 180$ GeV
6.2 ± 2.0 ± 1.6	25	ALBRECHT	94I	ARG $e^+ e^- \approx 10$ GeV

$$\Gamma(K_S^0 K^- \pi^+ \pi^0) / \Gamma_{\text{total}} \quad \Gamma_{261} / \Gamma$$

VALUE (units 10^{-3})	EVTS	DOCUMENT ID	TECN	COMMENT
1.32 ± 0.14 ± 0.07	195	ABLIKIM	20Ac	BES3 $e^+ e^-$ at 3.773 GeV

Meson Particle Listings

D^0

$\Gamma(K_S^0 K^+ \pi^- \pi^0)/\Gamma_{total}$		Γ_{262}/Γ		
VALUE (units 10^{-4})	EVTS	DOCUMENT ID	TECN	COMMENT
$6.5 \pm 0.7 \pm 0.2$	119	ABLIKIM	20AC BES3	$e^+ e^-$ at 3.773 GeV

$\Gamma(K_S^0 K^- 2\pi^+ \pi^-)/\Gamma(K_S^0 2\pi^+ 2\pi^-)$		$\Gamma_{263}/\Gamma_{101}$		
VALUE	CL%	DOCUMENT ID	TECN	COMMENT
<0.054	90	LINK	04D FOCS	$\gamma A, \bar{E}_\gamma \approx 180$ GeV

$\Gamma(K^+ K^- \pi^+ \pi^- \pi^0)/\Gamma_{total}$		Γ_{264}/Γ		
VALUE	CL%	DOCUMENT ID	TECN	COMMENT
0.0031 ± 0.0020		¹ BARLAG	92C ACCM	π^- Cu 230 GeV

¹ BARLAG 92c computes the branching fraction using topological normalization.

$\Gamma(\phi \pi^0)/\Gamma(K^+ K^-)$		$\Gamma_{265}/\Gamma_{196}$		
VALUE	EVTS	DOCUMENT ID	TECN	COMMENT
$0.194 \pm 0.006 \pm 0.009$	1254	TAJIMA	04 BELL	$e^+ e^-$ at $\Upsilon(4S)$

• • • We do not use the following data for averages, fits, limits, etc. • • •

$\Gamma(\phi \eta)/\Gamma(K^+ K^-)$		$\Gamma_{266}/\Gamma_{196}$		
VALUE (units 10^{-2})	EVTS	DOCUMENT ID	TECN	COMMENT
$3.59 \pm 1.14 \pm 0.18$	31	TAJIMA	04 BELL	$e^+ e^-$ at $\Upsilon(4S)$

$\Gamma(\phi \omega)/\Gamma_{total}$		Γ_{267}/Γ			
VALUE (units 10^{-4})	CL%	EVTS	DOCUMENT ID	TECN	COMMENT
$6.48 \pm 0.96 \pm 0.40$		196	¹ ABLIKIM	22 BES3	$e^+ e^-$ at 3.773 GeV
<21	90		ALBRECHT	94i ARG	$e^+ e^- \approx 10$ GeV

• • • We do not use the following data for averages, fits, limits, etc. • • •

¹ ABLIKIM 22 determines the longitudinal polarization fraction of the ϕ and ω , $f_L = 0.00 \pm 0.10 \pm 0.08$, corresponding to $f_L < 0.24$ at 95% CL.

Radiative modes

$\Gamma(\rho^0 \gamma)/\Gamma(\pi^+ \pi^-)$		$\Gamma_{268}/\Gamma_{132}$		
VALUE (units 10^{-2})	EVTS	DOCUMENT ID	TECN	COMMENT
$1.25 \pm 0.21 \pm 0.05$	500	NANUT	17 BELL	$e^+ e^-$ at $\Upsilon(nS)$, $n=2,3,4,5$

$\Gamma(\omega \gamma)/\Gamma_{total}$		Γ_{269}/Γ		
VALUE	CL%	DOCUMENT ID	TECN	COMMENT
$<2.4 \times 10^{-4}$	90	ASNER	98 CLE2	

$\Gamma(\phi \gamma)/\Gamma(K^- \pi^+)$		Γ_{270}/Γ_{37}		
VALUE (units 10^{-4})	EVTS	DOCUMENT ID	TECN	COMMENT
7.1 ± 0.5 OUR FIT				
$7.15 \pm 0.78 \pm 0.69$	243 ± 25	AUBERT	08AZ BABR	$e^+ e^- \approx 10.6$ GeV

$\Gamma(\phi \gamma)/\Gamma(K^+ K^-)$		$\Gamma_{270}/\Gamma_{196}$		
VALUE (units 10^{-3})	EVTS	DOCUMENT ID	TECN	COMMENT
6.9 ± 0.5 OUR FIT				
$6.88 \pm 0.47 \pm 0.21$	524	NANUT	17 BELL	$e^+ e^-$ at $\Upsilon(nS)$, $n=2,3,4,5$
$6.31^{+1.70+0.30}_{-1.48-0.36}$	28	TAJIMA	04 BELL	See NANUT 17

• • • We do not use the following data for averages, fits, limits, etc. • • •

$\Gamma(\bar{K}^*(892)^0 \gamma)/\Gamma(K^- \pi^+)$		Γ_{271}/Γ_{37}		
VALUE (units 10^{-3})	EVTS	DOCUMENT ID	TECN	COMMENT
10.5 ± 1.7 OUR AVERAGE				Error includes scale factor of 3.1.
$11.9 \pm 0.5 \pm 0.5$	9.1k	NANUT	17 BELL	$e^+ e^-$ at $\Upsilon(nS)$, $n=2,3,4,5$
$8.43 \pm 0.51 \pm 0.70$	2.2k	AUBERT	08AZ BABR	$e^+ e^- \approx 10.6$ GeV

Doubly Cabibbo-suppressed / Mixing modes

$\Gamma(K^+ \ell^- \bar{\nu}_\ell \text{ via } \bar{D}^0)/\Gamma(K^- \ell^+ \nu_\ell)$		Γ_{272}/Γ_{18}		
VALUE	CL%	DOCUMENT ID	TECN	COMMENT
$< 6.1 \times 10^{-4}$	90	¹ BITENC	08 BELL	$e^+ e^-$, 10.58 GeV
$<50 \times 10^{-4}$	90	² AITALA	96C E791	π^- nucleus, 500 GeV

• • • We do not use the following data for averages, fits, limits, etc. • • •

¹ The BITENC 08 right-sign sample includes about 15% of $D^0 \rightarrow K^- \pi^0 \ell^+ \nu_\ell$ and other decays.
² AITALA 96c uses $D^{*+} \rightarrow D^0 \pi^+$ (and charge conjugate) decays to identify the charm at production and $D^0 \rightarrow K^- \ell^+ \nu_\ell$ (and charge conjugate) decays to identify the charm at decay.

$$\Gamma(K^+ \text{ or } K^*(892)^+ e^- \bar{\nu}_e \text{ via } \bar{D}^0)/[\Gamma(K^- e^+ \nu_e) + \Gamma(K^*(892)^- e^+ \nu_e)]$$

$$\Gamma_{273}/(\Gamma_{19} + \Gamma_{21})$$

This is a limit on R_M without the complications of possible doubly Cabibbo-suppressed decays that occur when using hadronic modes. The experiments use $D^{*+} \rightarrow D^0 \pi^+$ (and charge conjugate) decays to identify the charm at production and the charge of the e to identify the charm at decay. These limits do not allow CP violation. For the limits on $|m_1 - m_2|$ and $(\Gamma_1 - \Gamma_2)/\Gamma$ that come from the best mixing limit, see near the beginning of these D^0 Listings.

VALUE	CL%	DOCUMENT ID	TECN	COMMENT
<0.001	90	BITENC	05 BELL	$e^+ e^- \approx 10.6$ GeV
$-0.0013 < R < +0.0012$	90	AUBERT	07AB BABR	$e^+ e^- \approx 10.58$ GeV
<0.0078	90	CAWLFIELD	05 CLEO	$e^+ e^- \approx 10.6$ GeV
<0.0042	90	AUBERT,B	04Q BABR	See AUBERT 07AB

• • • We do not use the following data for averages, fits, limits, etc. • • •

$\Gamma(K^+ \pi^-)/\Gamma(K^- \pi^+)$		Γ_{274}/Γ_{37}		
---------------------------------------	--	----------------------------	--	--

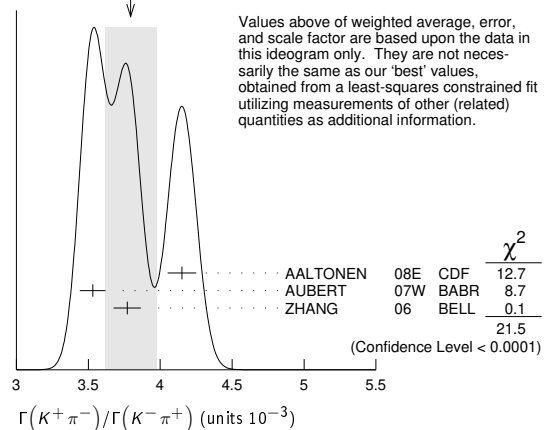
This is R , the time-integrated wrong-sign rate compared to the right-sign rate. See the note on " D^0 - \bar{D}^0 Mixing," near the start of the D^0 Listings.

The experiments here use the charge of the pion in $D^*(2010)^\pm \rightarrow (D^0 \text{ or } \bar{D}^0) \pi^\pm$ decay to tell whether a D^0 or a \bar{D}^0 was born. The $D^0 \rightarrow K^+ \pi^-$ decay can occur directly by doubly Cabibbo-suppressed (DCS) decay, or indirectly by $D^0 \rightarrow \bar{D}^0$ mixing followed by $\bar{D}^0 \rightarrow K^+ \pi^-$ decay. Some of the experiments can use the decay-time information to disentangle the two mechanisms. Here, we list the experimental branching ratio, which if there is no mixing is the DCS ratio. See the next data block for values of the DCS ratio R_D , and the following data block for limits on the mixing ratio R_M . See the section on CP -violating asymmetries near the end of this D^0 Listing for values of A_D , and the note on " D^0 - \bar{D}^0 Mixing" for limits on x' and y' .

Some early limits have been omitted from this Listing; see our 1998 edition (The European Physical Journal **C3** 1 (1998)) and our 2006 edition (Journal of Physics **G33** 1 (2006)).

VALUE (units 10^{-3})	EVTS	DOCUMENT ID	TECN	COMMENT
3.79 ± 0.18 OUR FIT				Error includes scale factor of 3.3.
3.79 ± 0.18 OUR AVERAGE				Error includes scale factor of 3.3. See the ideogram below.
4.15 ± 0.10	$12.7 \pm 0.3k$	¹ AALTONEN	08E CDF	$p\bar{p}$, $\sqrt{s} = 1.96$ TeV
$3.53 \pm 0.08 \pm 0.04$	4030 ± 90	² AUBERT	07W BABR	$e^+ e^- \approx 10.6$ GeV
$3.77 \pm 0.08 \pm 0.05$	4024 ± 88	¹ ZHANG	06 BELL	$e^+ e^-$
$4.05 \pm 0.21 \pm 0.11$	$2.0 \pm 0.1k$	³ ABULENCIA	06x CDF	See AALTONEN 08E
$3.81 \pm 0.17^{+0.08}_{-0.16}$	845 ± 40	² LI	05A BELL	See ZHANG 06
$4.29^{+0.63}_{-0.61} \pm 0.27$	234	⁴ LINK	05H FOCS	γ nucleus
$3.57 \pm 0.22 \pm 0.27$		⁵ AUBERT	03Z BABR	See AUBERT 07W
$4.04 \pm 0.85 \pm 0.25$	149	⁶ LINK	01 FOCS	γ nucleus
$3.32^{+0.63}_{-0.65} \pm 0.40$	45	¹ GODANG	00 CLE2	$e^+ e^-$
$6.8^{+3.4}_{-3.3} \pm 0.7$	34	² AITALA	98 E791	π^- nucl., 500 GeV

WEIGHTED AVERAGE
 3.79 ± 0.18 (Error scaled by 3.3)



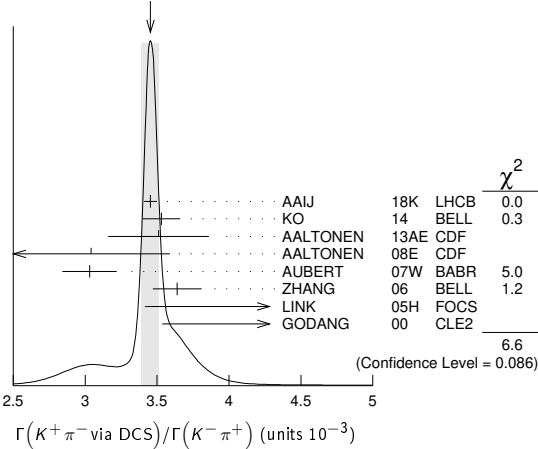
¹ GODANG 00, ZHANG 06, and AALTONEN 08E allow CP violation.
² AITALA 98, LI 05A, and AUBERT 07W assume no CP violation.
³ This ABULENCIA 06x result assumes no mixing.
⁴ This LINK 05H result assumes no mixing but allows CP violation. If neither mixing nor CP violation is allowed, $R = (4.29 \pm 0.63 \pm 0.28) \times 10^{-3}$.
⁵ This AUBERT 03Z result allows CP violation. If CP violation is not allowed, $R = 0.00359 \pm 0.00020 \pm 0.00027$.
⁶ This LINK 01 result assumes no mixing or CP violation.

$\Gamma(K^+\pi^- \text{ via DCS})/\Gamma(K^-\pi^+)$ Γ_{275}/Γ_{37}

This is R_D , the doubly Cabibbo-suppressed ratio when mixing is allowed.

VALUE (units 10^{-3})	EVTS	DOCUMENT ID	TECN	COMMENT
3.45 ± 0.06 OUR AVERAGE	722k			Error includes scale factor of 1.5. See the ideogram below.
3.454 ± 0.040 ± 0.020		1 AAIJ	18K LHCb	pp at 7, 8, 13 TeV
3.53 ± 0.13		2 KO	14 BELL	$e^+e^- \rightarrow \Upsilon(nS)$
3.51 ± 0.35		3 AALTONEN	13AE CDF	$p\bar{p}$ at 1.96 TeV
3.04 ± 0.55	13k	AALTONEN	08E CDF	$p\bar{p}$, $\sqrt{s}=1.96$ TeV
3.03 ± 0.16 ± 0.10	4.0k	4 AUBERT	07W BABR	$e^+e^- \approx 10.6$ GeV
3.64 ± 0.17	4.0k	5 ZHANG	06 BELL	e^+e^-
5.17 $^{+1.47}_{-1.58}$ ± 0.76	234	6 LINK	05H FOCS	γ nucleus
4.8 ± 1.2 ± 0.4	45	7 GODANG	00 CLE2	e^+e^-
• • • We do not use the following data for averages, fits, limits, etc. • • •				
3.533 ± 0.054	236k	8 AAIJ	17A0 LHCb	See AAIJ 18K
3.568 ± 0.066		9 AAIJ	13CE LHCb	pp at 7, 8 TeV
3.52 ± 0.15		10 AAIJ	13N LHCb	Repl. by AAIJ 13CE
2.87 ± 0.37	0.8k	LI	05A BELL	See ZHANG 06

WEIGHTED AVERAGE
3.45 ± 0.06 (Error scaled by 1.5)



- This AAIJ 18K value is for direct and indirect CP violation allowed. The value is the same if either one or the other is not allowed, but in each case the error then is $(0.028 \pm 0.014) \times 10^{-3}$.
- Based on 976 fb^{-1} of data collected at $Y(nS)$ resonances. Assumes no CP violation.
- Based on 9.6 fb^{-1} of data collected at the Tevatron. Assumes no CP violation.
- Result is the same whether or not CP violation is allowed.
- This ZHANG 06 assumes no CP violation.
- This LINK 05H result allows CP violation. Allowing mixing but not CP violation, $R_D = (3.81^{+1.67}_{-1.63} \pm 0.92) \times 10^{-3}$.
- This GODANG 00 result allows CP violation.
- The result was established with D^0 from prompt and secondary D^* assuming no CPV or no direct CPV .
- Based on 3 fb^{-1} of data collected at $\sqrt{s} = 7, 8$ TeV. Assumes no CP violation.
- Based on 1 fb^{-1} of data collected at $\sqrt{s} = 7$ TeV in 2011. Assumes no CP violation.

$\Gamma(K^+\pi^- \text{ via } \bar{D}^0)/\Gamma(K^-\pi^+)$ Γ_{276}/Γ_{37}

This is R_M in the note on " $D^0-\bar{D}^0$ Mixing" near the start of the D^0 Listings. The experiments here (1) use the charge of the pion in $D^*(2010)^\pm \rightarrow (D^0 \text{ or } \bar{D}^0) \pi^\pm$ decay to tell whether a D^0 or a \bar{D}^0 was born; and (2) use the decay-time distribution to disentangle doubly Cabibbo-suppressed decay and mixing. For the limits on $|m_1 - m_2|$ and $(\Gamma_1 - \Gamma_2)/\Gamma$ that come from the best mixing limit, see near the beginning of these D^0 Listings.

VALUE	CL%	DOCUMENT ID	TECN	COMMENT
<0.00040	95	1 ZHANG	06 BELL	e^+e^-
• • • We do not use the following data for averages, fits, limits, etc. • • •				
<0.00046	95	2 LI	05A BELL	See ZHANG 06
<0.0063	95	3 LINK	05H FOCS	γ nucleus
<0.0013	95	4 AUBERT	03Z BABR	e^+e^- , 10.6 GeV
<0.00041	95	5 GODANG	00 CLE2	e^+e^-
<0.0092	95	6 BARATE	98w ALEP	e^+e^- at Z^0
<0.005	90	7 ANJOS	88c E691	Photoproduction

- This ZHANG 06 result allows CP violation, but the result does not change if CP violation is not allowed.
- This LI 05A result allows CP violation. The limit becomes < 0.00042 (95% CL) if CP violation is not allowed.
- LINK 05H obtains the same result whether or not CP violation is allowed.
- This AUBERT 03Z result allows CP violation and assumes that the strong phase between $D^0 \rightarrow K^+\pi^-$ and $\bar{D}^0 \rightarrow K^+\pi^-$ is small, and limits only $D^0 \rightarrow \bar{D}^0$ transitions via off-shell intermediate states. The limit on transitions via on-shell intermediate states is 0.0016.
- This GODANG 00 result allows CP violation and assumes that the strong phase between $D^0 \rightarrow K^+\pi^-$ and $\bar{D}^0 \rightarrow K^+\pi^-$ is small, and limits only $D^0 \rightarrow \bar{D}^0$ transitions via off-shell intermediate states. The limit on transitions via on-shell intermediate states is 0.0017.

- This BARATE 98w result assumes no interference between the DCS and mixing amplitudes ($\gamma' = 0$ in the note on " $D^0-\bar{D}^0$ Mixing" near the start of the D^0 Listings). When interference is allowed, the limit degrades to 0.036 (95%CL).
- This ANJOS 88c result assumes no interference between the DCS and mixing amplitudes ($\gamma' = 0$ in the note on " $D^0-\bar{D}^0$ Mixing" near the start of the D^0 Listings). When interference is allowed, the limit degrades to 0.019.

$\Gamma(K_S^0 \pi^+ \pi^- \text{ in } D^0 \rightarrow \bar{D}^0)/\Gamma(K_S^0 \pi^+ \pi^-)$ Γ_{277}/Γ_{40}

This is R_M in the note on " $D^0-\bar{D}^0$ Mixing" near the start of the D^0 Listings. The experiments here (1) use the charge of the pion in $D^*(2010)^\pm \rightarrow (D^0 \text{ or } \bar{D}^0) \pi^\pm$ decay to tell whether a D^0 or a \bar{D}^0 was born; and (2) use the decay-time distribution to disentangle doubly Cabibbo-suppressed decay and mixing. For the limits on $|m_1 - m_2|$ and $(\Gamma_1 - \Gamma_2)/\Gamma$ that come from the best mixing limit, see near the beginning of these D^0 Listings.

VALUE	CL%	DOCUMENT ID	TECN	COMMENT
<0.0063	95	1 ASNER	05 CLEO	$e^+e^- \approx 10$ GeV

- This ASNER 05 limit allows CP violation. If CP violation is not allowed, the limit is 0.0042 at 95% CL.

$\Gamma(K^+\pi^-\pi^0)/\Gamma(K^-\pi^+\pi^0)$ Γ_{281}/Γ_{55}

The experiments here use the charge of the pion in $D^*(2010)^\pm \rightarrow (D^0 \text{ or } \bar{D}^0) \pi^\pm$ decay to tell whether a D^0 or a \bar{D}^0 was born. The $D^0 \rightarrow K^+\pi^-\pi^0$ decay can occur directly by doubly Cabibbo-suppressed (DCS) decay, or indirectly by $D^0 \rightarrow \bar{D}^0$ mixing followed by $\bar{D}^0 \rightarrow K^+\pi^-\pi^0$ decay.

VALUE (units 10^{-3})	EVTS	DOCUMENT ID	TECN	COMMENT
2.12 ± 0.07 OUR AVERAGE				
2.01 ± 0.11		1 EVANS	16 CLEO	$e^+e^- \rightarrow D^0\bar{D}^0$ at $\psi(3770)$
2.14 ± 0.08 ± 0.08	763	2 AUBERT,B	06N BABR	$e^+e^- \approx \Upsilon(4S)$
2.29 ± 0.15 $^{+0.13}_{-0.09}$	1.9k	TIAN	05B BELL	$e^+e^- \approx \Upsilon(4S)$
4.3 $^{+1.1}_{-1.0}$ ± 0.7	38	BRANDENB...	01 CLE2	$e^+e^- \approx \Upsilon(4S)$

- A combined fit with a recent LHCb $D^0\bar{D}^0$ mixing results in AAIJ 16F is also reported to be $(2.00 \pm 0.11) \times 10^{-3}$.
- This AUBERT,B 06N result assumes no mixing.

$\Gamma(K^+\pi^-\pi^0 \text{ via } \bar{D}^0)/\Gamma(K^-\pi^+\pi^0)$ Γ_{282}/Γ_{55}

This is R_M in the note on " $D^0-\bar{D}^0$ Mixing" near the start of the D^0 Listings. The experiments here (1) use the charge of the pion in $D^*(2010)^\pm \rightarrow (D^0 \text{ or } \bar{D}^0) \pi^\pm$ decay to tell whether a D^0 or a \bar{D}^0 was born; and (2) use the decay-time distribution to disentangle doubly Cabibbo-suppressed decay and mixing. For the limits on $|m_1 - m_2|$ and $(\Gamma_1 - \Gamma_2)/\Gamma$ that come from the best mixing limit, see near the beginning of these D^0 Listings.

VALUE (units 10^{-3})	CL%	DOCUMENT ID	TECN	COMMENT
5.25 $^{+0.25}_{-0.31}$ ± 0.12		AUBERT	09AN BABR	e^+e^- at 10.58 GeV
• • • We do not use the following data for averages, fits, limits, etc. • • •				
<0.54	95	1 AUBERT,B	06N BABR	$e^+e^- \approx \Upsilon(4S)$

- This AUBERT,B 06N limit assumes no CP violation. The measured value corresponding to the limit is $(2.3^{+1.8}_{-1.4} \pm 0.4) \times 10^{-4}$. If CP violation is allowed, this becomes $(1.0^{+2.2}_{-0.7} \pm 0.3) \times 10^{-4}$.

$\Gamma(K^+\pi^+\pi^-\text{ via DCS})/\Gamma(K^-2\pi^+\pi^-)$ Γ_{283}/Γ_{72}

VALUE (units 10^{-3})	EVTS	DOCUMENT ID	TECN	COMMENT
3.03 ± 0.07 OUR AVERAGE				
3.025 ± 0.077	42k,11M	1 AAIJ	16F LHCb	pp at 7, 8 TeV
3.03 ± 0.13		2 EVANS	16 CLEO	$e^+e^- \rightarrow D^0\bar{D}^0$ at $\psi(3770)$

- This result uses external input on the mixing parameters x, y . Without this input, the result is $(3.215 \pm 0.136) \times 10^{-3}$.
- A combined fit with a recent LHCb $D^0\bar{D}^0$ mixing results in AAIJ 16F is also reported to be $(3.01 \pm 0.07) \times 10^{-3}$.

$\Gamma(K^+\pi^+\pi^-)/\Gamma(K^-2\pi^+\pi^-)$ Γ_{284}/Γ_{72}

The experiments here use the charge of the pion in $D^*(2010)^\pm \rightarrow (D^0 \text{ or } \bar{D}^0) \pi^\pm$ decay to tell whether a D^0 or a \bar{D}^0 was born. The $D^0 \rightarrow K^+\pi^+\pi^-$ decay can occur directly by doubly Cabibbo-suppressed (DCS) decay, or indirectly by $D^0 \rightarrow \bar{D}^0$ mixing followed by $\bar{D}^0 \rightarrow K^+\pi^+\pi^-$ decay. Some of the experiments can use the decay-time information to disentangle the two mechanisms. Here, we list the experimental branching ratio, which if there is no mixing is the DCS ratio; in the next data block we give the limits on the mixing ratio.

Some early limits have been omitted from this Listing; see our 1998 edition (EPJ C3 1).

VALUE (units 10^{-3})	CL%	EVTS	DOCUMENT ID	TECN	COMMENT
3.22 ± 0.05 OUR AVERAGE					
3.22 ± 0.05		42k,11M	1 AAIJ	16F LHCb	pp at 7, 8 TeV
3.24 ± 0.08 ± 0.07		3.3k	2 WHITE	13 BELL	$e^+e^- \approx \Upsilon(4S)$
4.4 $^{+1.3}_{-1.2}$ ± 0.4		54	2 DYTMAN	01 CLE2	$e^+e^- \approx \Upsilon(4S)$
2.5 $^{+3.6}_{-3.4}$ ± 0.3			3 AITALA	98 E791	π^- nucl., 500 GeV

Meson Particle Listings

D^0

• • • We do not use the following data for averages, fits, limits, etc. • • •

$3.20 \pm 0.18^{+0.18}_{-0.13}$	1.7k	2	TIAN	05	BELL	See WHITE 13
<18	90	2	AMMAR	91	CLEO	$e^+e^- \approx 10.5$ GeV
<18	90	4	ANJOS	88c	E691	Photoproduction

- ¹ AAIJ 16F result comes from time-dependent analysis that uses external input on the mixing parameters x, y . Without this input, the result is $(3.29 \pm 0.08) \times 10^{-3}$.
- ² AMMAR 91 cannot and DYTMAN 01, TIAN 05 do not distinguish between doubly Cabibbo-suppressed decay and $D^0\text{-}\bar{D}^0$ mixing.
- ³ This AITALA 98 result assumes no $D^0\text{-}\bar{D}^0$ mixing (R_M in the note on " $D^0\text{-}\bar{D}^0$ Mixing"). It becomes $-0.0020^{+0.0117}_{-0.0106} \pm 0.0035$ when mixing is allowed and decay-time information is used to distinguish doubly Cabibbo-suppressed decays from mixing.
- ⁴ ANJOS 88c uses decay-time information to distinguish doubly Cabibbo-suppressed (DCS) decays from $D^0\text{-}\bar{D}^0$ mixing. However, the result assumes no interference between the DCS and mixing amplitudes ($\gamma = 0$ in the note on " $D^0\text{-}\bar{D}^0$ Mixing" near the start of the D^0 Listings). When interference is allowed, the limit degrades to 0.033.

$\Gamma(K^+\pi^+2\pi^- \text{ via } \bar{D}^0)/\Gamma(K^-2\pi^+\pi^-)$ Γ_{285}/Γ_{72}

This is a $D^0\text{-}\bar{D}^0$ mixing limit. The experiments here (1) use the charge of the pion in $D^*(2010)^\pm \rightarrow (D^0 \text{ or } \bar{D}^0)\pi^\pm$ decay to tell whether a D^0 or a \bar{D}^0 was born; and (2) use the decay-time distribution to disentangle doubly Cabibbo-suppressed decay and mixing. For the limits on $|m_{D_1^0} - m_{D_2^0}|$ and $(\Gamma_{D_1^0} - \Gamma_{D_2^0})/\Gamma_{D^0}$ that come from the best mixing limit, see near the beginning of these D^0 Listings.

VALUE (units 10^{-5})	CL%	DOCUMENT ID	TECN	COMMENT
9.6 ± 3.6		¹ AAIJ	16F	LHCB $p\bar{p}$ at 7, 8 TeV

- • • We do not use the following data for averages, fits, limits, etc. • • •
- | | | | | | | |
|-----|----|---|-------|-----|------|-----------------|
| <50 | 90 | 2 | ANJOS | 88c | E691 | Photoproduction |
|-----|----|---|-------|-----|------|-----------------|
- ¹ AAIJ 16F result comes from an unconstrained decay-time dependent fit to the wrong-sign to right-sign decay rates ratio as $(x^2 + y^2)/2$.
 - ² ANJOS 88c uses decay-time information to distinguish doubly Cabibbo-suppressed (DCS) decays from $D^0\text{-}\bar{D}^0$ mixing. However, the result assumes no interference between the DCS and mixing amplitudes ($\gamma = 0$ in the note on " $D^0\text{-}\bar{D}^0$ Mixing" near the start of the D^0 Listings). When interference is allowed, the limit degrades to 0.007.

$\Gamma(K^+\pi^- \text{ or } K^+\pi^+2\pi^- \text{ via } \bar{D}^0)/\Gamma(K^-\pi^+ \text{ or } K^-2\pi^+\pi^-)$ Γ_{286}/Γ_0

This is a $D^0\text{-}\bar{D}^0$ mixing limit. For the limits on $|m_{D_1^0} - m_{D_2^0}|$ and $(\Gamma_{D_1^0} - \Gamma_{D_2^0})/\Gamma_{D^0}$ that come from the best mixing limit, see near the beginning of these D^0 Listings.

VALUE	CL%	DOCUMENT ID	TECN	COMMENT		
<0.0085	90	1	AITALA	98	E791 π^- nucleus, 500 GeV	
<0.0037	90	2	ANJOS	88c	E691	Photoproduction

- • • We do not use the following data for averages, fits, limits, etc. • • •
- ¹ AITALA 98 uses decay-time information to distinguish doubly Cabibbo-suppressed decays from $D^0\text{-}\bar{D}^0$ mixing. The fit allows interference between the two amplitudes, and also allows CP violation in this term. The central value obtained is $0.0039^{+0.0036}_{-0.0032} \pm 0.0016$. When interference is disallowed, the result becomes $0.0021 \pm 0.0009 \pm 0.0002$.
 - ² This combines results of ANJOS 88c on $K^+\pi^-$ and $K^+\pi^-\pi^+\pi^-$ (via \bar{D}^0) reported in the data block above (see footnotes there). It assumes no interference.

$\Gamma(\mu^- \text{ anything via } \bar{D}^0)/\Gamma(\mu^+ \text{ anything})$ Γ_{287}/Γ_6

This is a $D^0\text{-}\bar{D}^0$ mixing limit. See the somewhat better limits above.

VALUE	CL%	DOCUMENT ID	TECN	COMMENT	
<0.0056		90	LOUIS	86	SPEC π^-W 225 GeV

- • • We do not use the following data for averages, fits, limits, etc. • • •
- | | | | | | |
|--------|----|--|-----------|----|-----------------------------------|
| <0.012 | 90 | | BENVENUTI | 85 | CNTR μC , 200 GeV |
| <0.044 | 90 | | BODEK | 82 | SPEC $\pi^-, pFe \rightarrow D^0$ |

Rare or forbidden modes

$\Gamma(\gamma\gamma)/\Gamma_{total}$ Γ_{288}/Γ

$D^0 \rightarrow \gamma\gamma$ is a flavor-changing neutral-current decay, forbidden in the Standard Model at the tree level.

VALUE	CL%	DOCUMENT ID	TECN	COMMENT	
< 8.5 $\times 10^{-7}$		90	NISAR	16	BELL e^+e^- at $\Upsilon(4S)$, $\Upsilon(5S)$

- • • We do not use the following data for averages, fits, limits, etc. • • •
- | | | | | | |
|------------------------|----|--|---------|-----|------------------------------------|
| < 3.8 $\times 10^{-6}$ | 90 | | ABLIKIM | 15F | BES3 e^+e^- at 3.773 GeV |
| < 2.2 $\times 10^{-6}$ | 90 | | LEES | 12L | BABR $e^+e^- \approx 10.58$ GeV |
| < 29 $\times 10^{-6}$ | 90 | | COAN | 03 | CLE2 $e^+e^- \approx \Upsilon(4S)$ |

$\Gamma(e^+e^-)/\Gamma_{total}$ Γ_{289}/Γ

A test for the $\Delta C = 1$ weak neutral current. Allowed by first-order weak interaction combined with electromagnetic interaction.

VALUE	CL%	DOCUMENT ID	TECN	COMMENT	
< 7.9 $\times 10^{-8}$		90	PETRIC	10	BELL $e^+e^- \approx \Upsilon(4S)$

- • • We do not use the following data for averages, fits, limits, etc. • • •
- | | | | | | |
|-------------------------|----|--|------------|-----|------------------------------------|
| < 1.7 $\times 10^{-7}$ | 90 | | LEES | 12Q | BABR $e^+e^- \approx 10.58$ GeV |
| < 1.2 $\times 10^{-6}$ | 90 | | AUBERT,B | 04Y | BABR $e^+e^- \approx \Upsilon(4S)$ |
| < 8.19 $\times 10^{-6}$ | 90 | | PRIPSTEIN | 00 | E789 p nucleus, 800 GeV |
| < 6.2 $\times 10^{-6}$ | 90 | | AITALA | 99G | E791 $\pi^- N$ 500 GeV |
| < 1.3 $\times 10^{-5}$ | 90 | | FREYBERGER | 96 | CLE2 $e^+e^- \approx \Upsilon(4S)$ |
| < 1.3 $\times 10^{-4}$ | 90 | | ADLER | 88 | MRK3 e^+e^- 3.77 GeV |
| < 1.7 $\times 10^{-4}$ | 90 | | ALBRECHT | 88G | ARG e^+e^- 10 GeV |
| < 2.2 $\times 10^{-4}$ | 90 | | HAAS | 88 | CLEO e^+e^- 10 GeV |

$\Gamma(\mu^+\mu^-)/\Gamma_{total}$ Γ_{290}/Γ

A test for the $\Delta C = 1$ weak neutral current. Allowed by first-order weak interaction combined with electromagnetic interaction.

VALUE	CL%	DOCUMENT ID	TECN	COMMENT	
< 6.2 $\times 10^{-9}$		90	AAIJ	13A1	LHCB $p\bar{p}$ at 7 TeV

- • • We do not use the following data for averages, fits, limits, etc. • • •
- | | | | | | |
|--------------------------|----|-------------------|---------------------|---------------------------------|--|
| 0.6–8.1 $\times 10^{-7}$ | 90 | ¹ LEES | 12Q | BABR $e^+e^- \approx 10.58$ GeV | |
| < 2.1 $\times 10^{-7}$ | 90 | | AALTONEN | 10X | CDF $p\bar{p}$, $\sqrt{s} = 1.96$ TeV |
| < 1.4 $\times 10^{-7}$ | 90 | | PETRIC | 10 | BELL $e^+e^- \approx \Upsilon(4S)$ |
| < 2.0 $\times 10^{-6}$ | 90 | | ABT | 04 | HERB pA , 920 GeV |
| < 1.3 $\times 10^{-6}$ | 90 | | AUBERT,B | 04Y | BABR $e^+e^- \approx \Upsilon(4S)$ |
| < 2.5 $\times 10^{-6}$ | 90 | | ACOSTA | 03F | CDF See AALTONEN 10X |
| < 1.56 $\times 10^{-5}$ | 90 | | PRIPSTEIN | 00 | E789 p nucleus, 800 GeV |
| < 5.2 $\times 10^{-6}$ | 90 | | AITALA | 99G | E791 $\pi^- N$ 500 GeV |
| < 4.1 $\times 10^{-6}$ | 90 | | ADAMOVICH | 97 | BEAT π^- Cu, W 350 GeV |
| < 4.2 $\times 10^{-6}$ | 90 | | ALEXOPOU... | 96 | E771 p Si, 800 GeV |
| < 3.4 $\times 10^{-5}$ | 90 | | FREYBERGER | 96 | CLE2 $e^+e^- \approx \Upsilon(4S)$ |
| < 7.6 $\times 10^{-6}$ | 90 | | ADAMOVICH | 95 | BEAT See ADAMOVICH 97 |
| < 4.4 $\times 10^{-5}$ | 90 | | KODA MA | 95 | E653 π^- emulsion 600 GeV |
| < 3.1 $\times 10^{-5}$ | 90 | | ² MISHRA | 94 | E789 -4.1 ± 4.8 events |
| < 7.0 $\times 10^{-5}$ | 90 | | ALBRECHT | 88G | ARG e^+e^- 10 GeV |
| < 1.1 $\times 10^{-5}$ | 90 | | LOUIS | 86 | SPEC π^-W 225 GeV |
| < 3.4 $\times 10^{-4}$ | 90 | | AUBERT | 85 | EMC Deep inelast. $\mu^- N$ |

- ¹ LEES 12Q gives a 2-sided range.
- ² Here MISHRA 94 uses "the statistical approach advocated by the PDG." For an alternate approach, giving a limit of 9×10^{-6} at 90% confidence level, see the paper.

$\Gamma(\pi^0 e^+ e^-)/\Gamma_{total}$ Γ_{291}/Γ

A test for the $\Delta C = 1$ weak neutral current. Allowed by higher-order electroweak interactions.

VALUE	CL%	DOCUMENT ID	TECN	COMMENT	
< 4 $\times 10^{-6}$		90	ABLIKIM	18P	BES3 e^+e^- , 3773 MeV

- • • We do not use the following data for averages, fits, limits, etc. • • •
- | | | | | | |
|------------------------|----|--|------------|----|------------------------------------|
| < 4.5 $\times 10^{-5}$ | 90 | | FREYBERGER | 96 | CLE2 $e^+e^- \approx \Upsilon(4S)$ |
|------------------------|----|--|------------|----|------------------------------------|

$\Gamma(\pi^0 \mu^+ \mu^-)/\Gamma_{total}$ Γ_{292}/Γ

A test for the $\Delta C = 1$ weak neutral current. Allowed by higher-order electroweak interactions.

VALUE	CL%	DOCUMENT ID	TECN	COMMENT	
< 1.8 $\times 10^{-4}$		90	KODA MA	95	E653 π^- emulsion 600 GeV

- • • We do not use the following data for averages, fits, limits, etc. • • •
- | | | | | | |
|------------------------|----|--|------------|----|------------------------------------|
| < 5.4 $\times 10^{-4}$ | 90 | | FREYBERGER | 96 | CLE2 $e^+e^- \approx \Upsilon(4S)$ |
|------------------------|----|--|------------|----|------------------------------------|

$\Gamma(\eta e^+ e^-)/\Gamma_{total}$ Γ_{293}/Γ

A test for the $\Delta C = 1$ weak neutral current. Allowed by higher-order electroweak interactions.

VALUE	CL%	DOCUMENT ID	TECN	COMMENT	
< 3 $\times 10^{-6}$		90	ABLIKIM	18P	BES3 e^+e^- , 3773 MeV

- • • We do not use the following data for averages, fits, limits, etc. • • •
- | | | | | | |
|------------------------|----|--|------------|----|------------------------------------|
| < 1.1 $\times 10^{-4}$ | 90 | | FREYBERGER | 96 | CLE2 $e^+e^- \approx \Upsilon(4S)$ |
|------------------------|----|--|------------|----|------------------------------------|

$\Gamma(\eta \mu^+ \mu^-)/\Gamma_{total}$ Γ_{294}/Γ

A test for the $\Delta C = 1$ weak neutral current. Allowed by higher-order electroweak interactions.

VALUE	CL%	DOCUMENT ID	TECN	COMMENT	
< 5.3 $\times 10^{-4}$		90	FREYBERGER	96	CLE2 $e^+e^- \approx \Upsilon(4S)$

$\Gamma(\pi^+\pi^- e^+ e^-)/\Gamma_{total}$ Γ_{295}/Γ

A test for the $\Delta C = 1$ weak neutral current. Allowed by higher-order electroweak interactions.

VALUE	CL%	DOCUMENT ID	TECN	COMMENT	
< 7 $\times 10^{-6}$		90	ABLIKIM	18P	BES3 e^+e^- , 3773 MeV

- • • We do not use the following data for averages, fits, limits, etc. • • •
- | | | | | | |
|-------------------------|----|--|--------|-----|-------------------------------|
| < 3.73 $\times 10^{-4}$ | 90 | | AITALA | 01c | E791 π^- nucleus, 500 GeV |
|-------------------------|----|--|--------|-----|-------------------------------|

$\Gamma(\rho^0 e^+ e^-)/\Gamma_{total}$ Γ_{296}/Γ

A test for the $\Delta C = 1$ weak neutral current. Allowed by higher-order electroweak interactions.

VALUE	CL%	DOCUMENT ID	TECN	COMMENT	
< 1.0 $\times 10^{-4}$		90	¹ FREYBERGER	96	CLE2 $e^+e^- \approx \Upsilon(4S)$

- • • We do not use the following data for averages, fits, limits, etc. • • •
- | | | | | | |
|-------------------------|----|--|--------|-----|-------------------------------|
| < 1.24 $\times 10^{-4}$ | 90 | | AITALA | 01c | E791 π^- nucleus, 500 GeV |
| < 4.5 $\times 10^{-4}$ | 90 | | HAAS | 88 | CLEO e^+e^- 10 GeV |

- ¹ This FREYBERGER 96 limit is obtained using a phase-space model. The limit changes to $< 1.8 \times 10^{-4}$ using a photon pole amplitude model.

$\Gamma(\pi^+\pi^-\mu^+\mu^-)/\Gamma_{total}$ Γ_{297}/Γ

A test for the $\Delta C = 1$ weak neutral current. Allowed by higher-order electroweak interactions.

VALUE (units 10^{-7})	EVTS	DOCUMENT ID	TECN	COMMENT
$9.64 \pm 0.48 \pm 1.10$	561	¹ AAIJ	17Bg	LHCB $p\bar{p}$ at 8 TeV

- ¹ The second AAIJ 17Bg error is the systematic 0.51×10^{-7} and normalization 0.97×10^{-7} mode errors added in quadrature.

$\Gamma(\pi^+\pi^-\mu^+\mu^- \text{ (non-res)})/\Gamma_{\text{total}}$ Γ_{298}/Γ

VALUE	CL%	DOCUMENT ID	TECN	COMMENT
$<5.5 \times 10^{-7}$	90	¹ AAIJ	14B LHCb	pp at 7 TeV
••• We do not use the following data for averages, fits, limits, etc. •••				
$<3.0 \times 10^{-5}$	90	AITALA	01c E791	π^- nucleus, 500 GeV

¹AAIJ 14B measures this branching-fraction limit relative to the $\pi^+\pi^-\phi, \phi \rightarrow \mu^+\mu^-$ fraction. The above limit excludes the resonant ϕ, ω , and ρ regions, and then fills those gaps with a phase-space model.

 $\Gamma(\rho^0\mu^+\mu^-)/\Gamma_{\text{total}}$ Γ_{299}/Γ

A test for the $\Delta C = 1$ weak neutral current. Allowed by higher-order electroweak interactions.

VALUE	CL%	DOCUMENT ID	TECN	COMMENT
$<2.2 \times 10^{-5}$	90	AITALA	01c E791	π^- nucleus, 500 GeV
••• We do not use the following data for averages, fits, limits, etc. •••				
$<4.9 \times 10^{-4}$	90	¹ FREYBERGER 96	CLE2	$e^+e^- \approx \Upsilon(4S)$
$<2.3 \times 10^{-4}$	90	KODAMA	95 E653	π^- emulsion 600 GeV
$<8.1 \times 10^{-4}$	90	HAAS	88 CLEO	e^+e^- 10 GeV

¹This FREYBERGER 96 limit is obtained using a phase-space model. The limit changes to $<4.5 \times 10^{-4}$ using a photon pole amplitude model.

 $\Gamma(\omega e^+e^-)/\Gamma_{\text{total}}$ Γ_{300}/Γ

A test for the $\Delta C = 1$ weak neutral current. Allowed by higher-order electroweak interactions.

VALUE	CL%	DOCUMENT ID	TECN	COMMENT
$<6 \times 10^{-6}$	90	ABLIKIM	18P BES3	e^+e^- , 3773 MeV
••• We do not use the following data for averages, fits, limits, etc. •••				
$<1.8 \times 10^{-4}$	90	¹ FREYBERGER 96	CLE2	$e^+e^- \approx \Upsilon(4S)$

¹This FREYBERGER 96 limit is obtained using a phase-space model. The limit changes to $<2.7 \times 10^{-4}$ using a photon pole amplitude model.

 $\Gamma(\omega\mu^+\mu^-)/\Gamma_{\text{total}}$ Γ_{301}/Γ

A test for the $\Delta C = 1$ weak neutral current. Allowed by higher-order electroweak interactions.

VALUE	CL%	DOCUMENT ID	TECN	COMMENT
$<8.3 \times 10^{-4}$	90	¹ FREYBERGER 96	CLE2	$e^+e^- \approx \Upsilon(4S)$

¹This FREYBERGER 96 limit is obtained using a phase-space model. The limit changes to $<6.5 \times 10^{-4}$ using a photon pole amplitude model.

 $\Gamma(K^-K^+e^+e^-)/\Gamma_{\text{total}}$ Γ_{302}/Γ

A test for the $\Delta C = 1$ weak neutral current. Allowed by higher-order electroweak interactions.

VALUE	CL%	DOCUMENT ID	TECN	COMMENT
$<1.1 \times 10^{-5}$	90	ABLIKIM	18P BES3	e^+e^- , 3773 MeV
••• We do not use the following data for averages, fits, limits, etc. •••				
$<3.15 \times 10^{-4}$	90	AITALA	01c E791	π^- nucleus, 500 GeV

 $\Gamma(K^-\pi^+e^+e^-, 675 < m_{ee} < 875 \text{ MeV})/\Gamma_{\text{total}}$ Γ_{310}/Γ

VALUE (units 10^{-6})	EVTS	DOCUMENT ID	TECN	COMMENT
$4.0 \pm 0.5 \pm 0.2 \pm 0.1$	68	^{1,2} LEES	19A BABR	e^+e^- near $\Upsilon(4S)$

¹Observation with 9.7 σ significance. The last uncertainty is due to the uncertainty on the branching fraction of the normalization mode, $D^0 \rightarrow K^-\pi^+\pi^+\pi^-$. The second uncertainty is other systematic and is dominated by the model parameterization.

²LEES 19A also sets an upper limit for non-resonant regions, where long-distance effects are expected to be small: $<3.1 \times 10^{-6}$ at 90% CL.

 $\Gamma(K^-\pi^+e^+e^-, 1.005 < m_{ee} < 1.035 \text{ GeV})/\Gamma_{\text{total}}$ Γ_{311}/Γ

VALUE	CL%	DOCUMENT ID	TECN	COMMENT
$<5 \times 10^{-7}$	90	¹ LEES	19A BABR	e^+e^- near $\Upsilon(4S)$

¹LEES 19A also sets an upper limit for non-resonant regions, where long-distance effects are expected to be small: $<3.1 \times 10^{-6}$ at 90% CL.

 $\Gamma(\phi e^+e^-)/\Gamma_{\text{total}}$ Γ_{303}/Γ

A test for the $\Delta C = 1$ weak neutral current. Allowed by higher-order electroweak interactions.

VALUE	CL%	DOCUMENT ID	TECN	COMMENT
$<5.2 \times 10^{-5}$	90	¹ FREYBERGER 96	CLE2	$e^+e^- \approx \Upsilon(4S)$
••• We do not use the following data for averages, fits, limits, etc. •••				
$<5.9 \times 10^{-5}$	90	AITALA	01c E791	π^- nucleus, 500 GeV

¹This FREYBERGER 96 limit is obtained using a phase-space model. The limit changes to $<7.6 \times 10^{-5}$ using a photon pole amplitude model.

 $\Gamma(K^-K^+\mu^+\mu^-)/\Gamma_{\text{total}}$ Γ_{304}/Γ

A test for the $\Delta C = 1$ weak neutral current. Allowed by higher-order electroweak interactions.

VALUE (units 10^{-7})	EVTS	DOCUMENT ID	TECN	COMMENT
$1.54 \pm 0.27 \pm 0.18$	34	¹ AAIJ	17Bg LHCb	pp at 8 TeV

¹The second AAJ 17Bg error is the systematic 0.09×10^{-7} and normalization 0.16×10^{-7} mode errors added in quadrature.

 $\Gamma(K^-K^+\mu^+\mu^- \text{ (non-res)})/\Gamma_{\text{total}}$ Γ_{305}/Γ

VALUE	CL%	DOCUMENT ID	TECN	COMMENT
$<3.3 \times 10^{-5}$	90	AITALA	01c E791	π^- nucleus, 500 GeV

 $\Gamma(\phi\mu^+\mu^-)/\Gamma_{\text{total}}$ Γ_{306}/Γ

A test for the $\Delta C = 1$ weak neutral current. Allowed by higher-order electroweak interactions.

VALUE	CL%	DOCUMENT ID	TECN	COMMENT
$<3.1 \times 10^{-5}$	90	AITALA	01c E791	π^- nucleus, 500 GeV
••• We do not use the following data for averages, fits, limits, etc. •••				
$<4.1 \times 10^{-4}$	90	¹ FREYBERGER 96	CLE2	$e^+e^- \approx \Upsilon(4S)$

¹This FREYBERGER 96 limit is obtained using a phase-space model. The limit changes to $<2.4 \times 10^{-4}$ using a photon pole amplitude model.

 $\Gamma(\bar{K}^0 e^+e^-)/\Gamma_{\text{total}}$ Γ_{307}/Γ

Not a useful test for $\Delta C = 1$ weak neutral current because both quarks must change flavor.

VALUE	CL%	DOCUMENT ID	TECN	COMMENT
$<2.4 \times 10^{-5}$	90	¹ ABLIKIM	18P BES3	e^+e^- , 3773 MeV
••• We do not use the following data for averages, fits, limits, etc. •••				
$<1.1 \times 10^{-4}$	90	FREYBERGER 96	CLE2	$e^+e^- \approx \Upsilon(4S)$
$<1.7 \times 10^{-3}$	90	ADLER	89c MRK3	e^+e^- 3.77 GeV

¹ABLIKIM 18P report a 90% C.L. limit on $D^0 \rightarrow K_S^0 e^+e^-$ of 1.2×10^{-5} which is here interpreted in terms of $D^0 \rightarrow \bar{K}^0 e^+e^-$.

 $\Gamma(\bar{K}^0\mu^+\mu^-)/\Gamma_{\text{total}}$ Γ_{308}/Γ

Not a useful test for $\Delta C = 1$ weak neutral current because both quarks must change flavor.

VALUE	CL%	DOCUMENT ID	TECN	COMMENT
$<2.6 \times 10^{-4}$	90	KODAMA	95 E653	π^- emulsion 600 GeV
••• We do not use the following data for averages, fits, limits, etc. •••				
$<6.7 \times 10^{-4}$	90	FREYBERGER 96	CLE2	$e^+e^- \approx \Upsilon(4S)$

 $\Gamma(K^-\pi^+e^+e^-)/\Gamma_{\text{total}}$ Γ_{309}/Γ

A test for the $\Delta C = 1$ weak neutral current. Allowed by higher-order electroweak interactions.

VALUE	CL%	DOCUMENT ID	TECN	COMMENT
••• We do not use the following data for averages, fits, limits, etc. •••				
$<4.1 \times 10^{-5}$	90	ABLIKIM	18P BES3	see LEES 19A
$<3.85 \times 10^{-4}$	90	AITALA	01c E791	π^- nucleus, 500 GeV

 $\Gamma(\bar{K}^*(892)^0 e^+e^-)/\Gamma_{\text{total}}$ Γ_{312}/Γ

Not a useful test for $\Delta C = 1$ weak neutral current because both quarks must change flavor.

VALUE	CL%	DOCUMENT ID	TECN	COMMENT
$<4.7 \times 10^{-5}$	90	AITALA	01c E791	π^- nucleus, 500 GeV
••• We do not use the following data for averages, fits, limits, etc. •••				
$<1.4 \times 10^{-4}$	90	¹ FREYBERGER 96	CLE2	$e^+e^- \approx \Upsilon(4S)$

¹This FREYBERGER 96 limit is obtained using a phase-space model. The limit changes to $<2.0 \times 10^{-4}$ using a photon pole amplitude model.

 $\Gamma(K^-\pi^+\mu^+\mu^-)/\Gamma_{\text{total}}$ Γ_{313}/Γ

A test for the $\Delta C = 1$ weak neutral current. Allowed by higher-order electroweak interactions.

VALUE	CL%	DOCUMENT ID	TECN	COMMENT
$<3.59 \times 10^{-4}$	90	AITALA	01c E791	π^- nucleus, 500 GeV

 $\Gamma(K^-\pi^+\mu^+\mu^-, 675 < m_{\mu\mu} < 875 \text{ MeV})/\Gamma_{\text{total}}$ Γ_{314}/Γ

VALUE (units 10^{-6})	EVTS	DOCUMENT ID	TECN	COMMENT
$4.17 \pm 0.12 \pm 0.40$	2.4k	¹ AAIJ	16i LHCb	pp at 8 TeV

¹AAIJ 16i uses $B(D^0 \rightarrow K^-\pi^+\pi^+\pi^-) = (8.287 \pm 0.043 \pm 0.200) \times 10^{-2}$ value for the normalization mode.

 $\Gamma(\bar{K}^*(892)^0\mu^+\mu^-)/\Gamma_{\text{total}}$ Γ_{315}/Γ

Not a useful test for $\Delta C = 1$ weak neutral current because both quarks must change flavor.

VALUE	CL%	DOCUMENT ID	TECN	COMMENT
$<2.4 \times 10^{-5}$	90	AITALA	01c E791	π^- nucleus, 500 GeV
••• We do not use the following data for averages, fits, limits, etc. •••				
$<1.18 \times 10^{-3}$	90	¹ FREYBERGER 96	CLE2	$e^+e^- \approx \Upsilon(4S)$

¹This FREYBERGER 96 limit is obtained using a phase-space model. The limit changes to $<1.0 \times 10^{-3}$ using a photon pole amplitude model.

 $\Gamma(\pi^+\pi^-\pi^0\mu^+\mu^-)/\Gamma_{\text{total}}$ Γ_{316}/Γ

A test for the $\Delta C = 1$ weak neutral current. Allowed by higher-order electroweak interactions.

VALUE	CL%	DOCUMENT ID	TECN	COMMENT
$<8.1 \times 10^{-4}$	90	KODAMA	95 E653	π^- emulsion 600 GeV

 $\Gamma(\mu^\pm e^\mp)/\Gamma_{\text{total}}$ Γ_{317}/Γ

A test of lepton family number conservation.

VALUE	CL%	DOCUMENT ID	TECN	COMMENT
$<1.3 \times 10^{-8}$	90	AAIJ	16h LHCb	pp at 7, 8 GeV
••• We do not use the following data for averages, fits, limits, etc. •••				
$<3.3 \times 10^{-7}$	90	LEES	12Q BABR	$e^+e^- \approx 10.58 \text{ GeV}$
$<2.6 \times 10^{-7}$	90	PETRIC	10 BELL	$e^+e^- \approx \Upsilon(4S)$
$<1.1 \times 10^{-7}$	90	AUBERT.B	04Y BABR	$e^+e^- \approx \Upsilon(4S)$
$<1.7 \times 10^{-5}$	90	PRIPSTEIN	00 E789	p nucleus, 800 GeV

Meson Particle Listings

 D^0

$< 8.1 \times 10^{-6}$	90	AITALA	99G	E791	$\pi^- N$	500 GeV
$< 1.9 \times 10^{-5}$	90	¹ FREYBERGER	96	CLE2	$e^+e^- \approx \mathcal{T}(4S)$	
$< 1.0 \times 10^{-4}$	90	ALBRECHT	88G	ARG	e^+e^-	10 GeV
$< 2.7 \times 10^{-4}$	90	HAAS	88	CLEO	e^+e^-	10 GeV
$< 1.2 \times 10^{-4}$	90	BECKER	87C	MRK3	e^+e^-	3.77 GeV
$< 9 \times 10^{-4}$	90	PALKA	87	SIL1	200 GeV	πp
$< 21 \times 10^{-4}$	90	² RILES	87	MRK2	e^+e^-	29 GeV

¹This is the corrected result given in the erratum to FREYBERGER 96.

²RILES 87 assumes $B(D \rightarrow K\pi) = 3.0\%$ and has production model dependency.

$$\Gamma(\pi^0 e^\pm \mu^\mp)/\Gamma_{\text{total}} \quad \Gamma_{318}/\Gamma$$

A test of lepton family number conservation. The value is for the sum of the two charge states.

VALUE	CL%	DOCUMENT ID	TECN	COMMENT
$< 8.0 \times 10^{-7}$	90	LEES	20A	BABR e^+e^- at $\mathcal{T}(4S)$
•••				We do not use the following data for averages, fits, limits, etc. •••
$< 8.6 \times 10^{-5}$	90	FREYBERGER	96	CLE2 $e^+e^- \approx \mathcal{T}(4S)$

$$\Gamma(\eta e^\pm \mu^\mp)/\Gamma_{\text{total}} \quad \Gamma_{319}/\Gamma$$

A test of lepton family number conservation. The value is for the sum of the two charge states.

VALUE	CL%	DOCUMENT ID	TECN	COMMENT
$< 22.5 \times 10^{-7}$	90	¹ LEES	20A	BABR e^+e^- at $\mathcal{T}(4S)$
•••				We do not use the following data for averages, fits, limits, etc. •••
$< 1.0 \times 10^{-4}$	90	FREYBERGER	96	CLE2 $e^+e^- \approx \mathcal{T}(4S)$

¹LEES 20A quotes separate limits $B(D^0 \rightarrow \eta e^\pm \mu^\mp, \eta \rightarrow \gamma\gamma) < 24.0 \times 10^{-7}$ and $B(D^0 \rightarrow \eta e^\pm \mu^\mp, \eta \rightarrow \pi^+\pi^-\pi^0) < 43.0 \times 10^{-7}$.

$$\Gamma(\pi^+\pi^- e^\pm \mu^\mp)/\Gamma_{\text{total}} \quad \Gamma_{320}/\Gamma$$

A test of lepton family-number conservation.

VALUE	CL%	DOCUMENT ID	TECN	COMMENT
$< 1.71 \times 10^{-6}$	90	LEES	20B	BABR e^+e^- at $\mathcal{T}(4S)$
•••				We do not use the following data for averages, fits, limits, etc. •••
$< 1.5 \times 10^{-5}$	90	AITALA	01c	E791 π^- nucleus, 500 GeV

$$\Gamma(\rho^0 e^\pm \mu^\mp)/\Gamma_{\text{total}} \quad \Gamma_{321}/\Gamma$$

A test of lepton family number conservation. The value is for the sum of the two charge states.

VALUE	CL%	DOCUMENT ID	TECN	COMMENT
$< 5.0 \times 10^{-7}$	90	LEES	20A	BABR e^+e^- at $\mathcal{T}(4S)$
•••				We do not use the following data for averages, fits, limits, etc. •••
$< 6.6 \times 10^{-5}$	90	AITALA	01c	E791 π^- nucleus, 500 GeV
$< 4.9 \times 10^{-5}$	90	¹ FREYBERGER	96	CLE2 $e^+e^- \approx \mathcal{T}(4S)$

¹This FREYBERGER 96 limit is obtained using a phase-space model. The limit changes to $< 5.0 \times 10^{-5}$ using a photon pole amplitude model.

$$\Gamma(\omega e^\pm \mu^\mp)/\Gamma_{\text{total}} \quad \Gamma_{322}/\Gamma$$

A test of lepton family number conservation. The value is for the sum of the two charge states.

VALUE	CL%	DOCUMENT ID	TECN	COMMENT
$< 17.1 \times 10^{-7}$	90	LEES	20A	BABR e^+e^- at $\mathcal{T}(4S)$
•••				We do not use the following data for averages, fits, limits, etc. •••
$< 1.2 \times 10^{-4}$	90	¹ FREYBERGER	96	CLE2 $e^+e^- \approx \mathcal{T}(4S)$

¹This FREYBERGER 96 limit is obtained using a phase-space model. The same limit is obtained using a photon pole amplitude model.

$$\Gamma(K^- K^+ e^\pm \mu^\mp)/\Gamma_{\text{total}} \quad \Gamma_{323}/\Gamma$$

A test of lepton family-number conservation.

VALUE	CL%	DOCUMENT ID	TECN	COMMENT
$< 1.00 \times 10^{-6}$	90	LEES	20B	BABR e^+e^- at $\mathcal{T}(4S)$
•••				We do not use the following data for averages, fits, limits, etc. •••
$< 1.8 \times 10^{-4}$	90	AITALA	01c	E791 π^- nucleus, 500 GeV

$$\Gamma(\phi e^\pm \mu^\mp)/\Gamma_{\text{total}} \quad \Gamma_{324}/\Gamma$$

A test of lepton family number conservation. The value is for the sum of the two charge states.

VALUE	CL%	DOCUMENT ID	TECN	COMMENT
$< 5.1 \times 10^{-7}$	90	LEES	20A	BABR e^+e^- at $\mathcal{T}(4S)$
•••				We do not use the following data for averages, fits, limits, etc. •••
$< 4.7 \times 10^{-5}$	90	AITALA	01c	E791 π^- nucleus, 500 GeV
$< 3.4 \times 10^{-5}$	90	¹ FREYBERGER	96	CLE2 $e^+e^- \approx \mathcal{T}(4S)$

¹This FREYBERGER 96 limit is obtained using a phase-space model. The limit changes to $< 3.3 \times 10^{-5}$ using a photon pole amplitude model.

$$\Gamma(K^0 e^\pm \mu^\mp)/\Gamma_{\text{total}} \quad \Gamma_{325}/\Gamma$$

A test of lepton family number conservation. The value is for the sum of the two charge states.

VALUE	CL%	DOCUMENT ID	TECN	COMMENT
$< 17.4 \times 10^{-7}$	90	¹ LEES	20A	BABR e^+e^- at $\mathcal{T}(4S)$
•••				We do not use the following data for averages, fits, limits, etc. •••
$< 1.0 \times 10^{-4}$	90	FREYBERGER	96	CLE2 $e^+e^- \approx \mathcal{T}(4S)$

¹LEES 20A quotes $B(D^0 \rightarrow K_S^0 e^\pm \mu^\mp) < 8.7 \times 10^{-7}$ at 90% CL.

$$\Gamma(K^- \pi^+ e^\pm \mu^\mp)/\Gamma_{\text{total}} \quad \Gamma_{326}/\Gamma$$

A test of lepton family-number conservation.

VALUE	CL%	DOCUMENT ID	TECN	COMMENT
$< 1.90 \times 10^{-6}$	90	LEES	20B	BABR e^+e^- at $\mathcal{T}(4S)$
•••				We do not use the following data for averages, fits, limits, etc. •••
$< 5.53 \times 10^{-4}$	90	AITALA	01c	E791 π^- nucleus, 500 GeV

$$\Gamma(K^*(892)^0 e^\pm \mu^\mp)/\Gamma_{\text{total}} \quad \Gamma_{327}/\Gamma$$

A test of lepton family number conservation. The value is for the sum of the two charge states.

VALUE	CL%	DOCUMENT ID	TECN	COMMENT
$< 12.5 \times 10^{-7}$	90	LEES	20A	BABR e^+e^- at $\mathcal{T}(4S)$
•••				We do not use the following data for averages, fits, limits, etc. •••
$< 8.3 \times 10^{-5}$	90	AITALA	01c	E791 π^- nucleus, 500 GeV
$< 1.0 \times 10^{-4}$	90	¹ FREYBERGER	96	CLE2 $e^+e^- \approx \mathcal{T}(4S)$

¹This FREYBERGER 96 limit is obtained using a phase-space model. The same limit is obtained using a photon pole amplitude model.

$$\Gamma(2\pi^- 2e^+)/\Gamma_{\text{total}} \quad \Gamma_{328}/\Gamma$$

A test of lepton-number conservation.

VALUE	CL%	DOCUMENT ID	TECN	COMMENT
$< 9.1 \times 10^{-7}$	90	LEES	20B	BABR e^+e^- at $\mathcal{T}(4S)$
•••				We do not use the following data for averages, fits, limits, etc. •••
$< 1.12 \times 10^{-4}$	90	¹ AITALA	01c	E791 π^- nucleus, 500 GeV

¹Value includes decay to the charge conjugate state.

$$\Gamma(2\pi^- 2\mu^+)/\Gamma_{\text{total}} \quad \Gamma_{329}/\Gamma$$

A test of lepton-number conservation.

VALUE	CL%	DOCUMENT ID	TECN	COMMENT
$< 1.52 \times 10^{-6}$	90	LEES	20B	BABR e^+e^- at $\mathcal{T}(4S)$
•••				We do not use the following data for averages, fits, limits, etc. •••
$< 2.9 \times 10^{-5}$	90	¹ AITALA	01c	E791 π^- nucleus, 500 GeV

¹Value includes decay to the charge conjugate state.

$$\Gamma(K^- \pi^- 2e^+)/\Gamma_{\text{total}} \quad \Gamma_{330}/\Gamma$$

A test of lepton-number conservation.

VALUE	CL%	DOCUMENT ID	TECN	COMMENT
$< 5.0 \times 10^{-7}$	90	LEES	20B	BABR e^+e^- at $\mathcal{T}(4S)$
•••				We do not use the following data for averages, fits, limits, etc. •••
$< 2.8 \times 10^{-6}$	90	ABLIKIM	19A	BES3 e^+e^- at 3773 MeV
$< 2.06 \times 10^{-4}$	90	¹ AITALA	01c	E791 π^- nucleus, 500 GeV

¹Value includes decay to the charge conjugate state.

$$\Gamma(K^- \pi^- 2\mu^+)/\Gamma_{\text{total}} \quad \Gamma_{331}/\Gamma$$

A test of lepton-number conservation.

VALUE	CL%	DOCUMENT ID	TECN	COMMENT
$< 5.3 \times 10^{-7}$	90	LEES	20B	BABR e^+e^- at $\mathcal{T}(4S)$
•••				We do not use the following data for averages, fits, limits, etc. •••
$< 3.9 \times 10^{-4}$	90	¹ AITALA	01c	E791 π^- nucleus, 500 GeV

¹Value includes decay to the charge conjugate state.

$$\Gamma(2K^- 2e^+)/\Gamma_{\text{total}} \quad \Gamma_{332}/\Gamma$$

A test of lepton-number conservation.

VALUE	CL%	DOCUMENT ID	TECN	COMMENT
$< 3.4 \times 10^{-7}$	90	LEES	20B	BABR e^+e^- at $\mathcal{T}(4S)$
•••				We do not use the following data for averages, fits, limits, etc. •••
$< 1.52 \times 10^{-4}$	90	¹ AITALA	01c	E791 π^- nucleus, 500 GeV

¹Value includes decay to the charge conjugate state.

$$\Gamma(2K^- 2\mu^+)/\Gamma_{\text{total}} \quad \Gamma_{333}/\Gamma$$

A test of lepton-number conservation.

VALUE	CL%	DOCUMENT ID	TECN	COMMENT
$< 1.0 \times 10^{-7}$	90	LEES	20B	BABR e^+e^- at $\mathcal{T}(4S)$
•••				We do not use the following data for averages, fits, limits, etc. •••
$< 9.4 \times 10^{-5}$	90	¹ AITALA	01c	E791 π^- nucleus, 500 GeV

¹Value includes decay to the charge conjugate state.

$$\Gamma(\pi^- \pi^- e^+ \mu^+)/\Gamma_{\text{total}} \quad \Gamma_{334}/\Gamma$$

A test of lepton-number conservation.

VALUE	CL%	DOCUMENT ID	TECN	COMMENT
$< 3.06 \times 10^{-6}$	90	LEES	20B	BABR e^+e^- at $\mathcal{T}(4S)$
•••				We do not use the following data for averages, fits, limits, etc. •••
$< 7.9 \times 10^{-5}$	90	¹ AITALA	01c	E791 π^- nucleus, 500 GeV

¹Value includes decay to the charge conjugate state.

$$\Gamma(K^- \pi^- e^+ \mu^+)/\Gamma_{\text{total}} \quad \Gamma_{335}/\Gamma$$

A test of lepton-number conservation.

VALUE	CL%	DOCUMENT ID	TECN	COMMENT
$< 2.10 \times 10^{-6}$	90	LEES	20B	BABR e^+e^- at $\mathcal{T}(4S)$
•••				We do not use the following data for averages, fits, limits, etc. •••
$< 2.18 \times 10^{-4}$	90	¹ AITALA	01c	E791 π^- nucleus, 500 GeV

¹Value includes decay to the charge conjugate state.

$\Gamma(2K^-e^+\mu^+)/\Gamma_{total}$ **Γ_{336}/Γ**
 A test of lepton-number conservation.

VALUE	CL%	DOCUMENT ID	TECN	COMMENT
<5.8 × 10⁻⁷	90	LEES 20B	BABR	e ⁺ e ⁻ at $\Upsilon(4S)$
••• We do not use the following data for averages, fits, limits, etc. •••				
<5.7 × 10 ⁻⁵	90	¹ AITALA 01c	E791	π^- nucleus, 500 GeV

¹ Value includes decay to the charge conjugate state.

$\Gamma(\rho e^-)/\Gamma_{total}$ **Γ_{337}/Γ**
 A test of baryon- and lepton-number conservation.

VALUE	CL%	DOCUMENT ID	TECN	COMMENT
<1.0 × 10⁻⁵	90	¹ RUBIN 09	CLEO	e ⁺ e ⁻ at $\psi(3770)$

¹ This RUBIN 09 limit is for either $D^0 \rightarrow \rho e^-$ or $\bar{D}^0 \rightarrow \rho e^-$ decay.

$\Gamma(\bar{\rho} e^+)/\Gamma_{total}$ **Γ_{338}/Γ**
 A test of baryon- and lepton-number conservation.

VALUE	CL%	DOCUMENT ID	TECN	COMMENT
<1.1 × 10⁻⁵	90	¹ RUBIN 09	CLEO	e ⁺ e ⁻ at $\psi(3770)$

¹ This RUBIN 09 limit is for either $D^0 \rightarrow \bar{\rho} e^+$ or $\bar{D}^0 \rightarrow \bar{\rho} e^+$ decay.

***D*⁰ CP-VIOLATING DECAY-RATE ASYMMETRIES**

This is the difference between *D*⁰ and \bar{D}^0 partial widths for the decay to state *f*, divided by the sum of the widths:
 $A_{CP}(f) = [\Gamma(D^0 \rightarrow f) - \Gamma(\bar{D}^0 \rightarrow \bar{f})] / [\Gamma(D^0 \rightarrow f) + \Gamma(\bar{D}^0 \rightarrow \bar{f})]$.

$A_{CP}(K^+K^-)$ in $D^0, \bar{D}^0 \rightarrow K^+K^-$

VALUE (%)	EVTS	DOCUMENT ID	TECN	COMMENT
-0.07 ± 0.11 OUR AVERAGE				
0.04 ± 0.12 ± 0.10	4.56M	AALJ 17M	LHCB	pp 7, 8 TeV
-0.24 ± 0.22 ± 0.09	476k	¹ AALTONEN 12B	CDF	$p\bar{p}$, $\sqrt{s}=1.96$ TeV
0.00 ± 0.34 ± 0.13	129k	² AUBERT 08M	BABR	e ⁺ e ⁻ ≈ 10.6 GeV
-0.43 ± 0.30 ± 0.11	120k	³ STARIC 08	BELL	e ⁺ e ⁻ ≈ $\Upsilon(4S)$
+2.0 ± 1.2 ± 0.6		⁴ ACOSTA 05c	CDF	$p\bar{p}$, $\sqrt{s}=1.96$ TeV
0.0 ± 2.2 ± 0.8	3023	⁴ CSORNA 02	CLE2	e ⁺ e ⁻ ≈ $\Upsilon(4S)$
-1.1 ± 2.2 ± 1.5	3330	⁴ LINK 00B	FOCS	
-0.0 ± 4.9 ± 1.2	609	⁴ AITALA 98c	E791	-0.093 <A _{CP} < +0.073 (90% CL)

- We do not use the following data for averages, fits, limits, etc. •••
- 0.06 ± 0.15 ± 0.10 1.8M ¹AALJ 14AK LHCB See AALJ 17M
- ¹ See also “*D*⁰ CP-violating asymmetry differences” at the end of the CP-violating asymmetries.
- ² AUBERT 08M uses corrected numbers of events directly, not ratios with $K^\mp\pi^\pm$ events.
- ³ STARIC 08 uses $D^0 \rightarrow K^-\pi^+$ and $\bar{D}^0 \rightarrow K^+\pi^-$ decays to correct for detector-induced asymmetries.
- ⁴ AITALA 98c, LINK 00B, CSORNA 02, and ACOSTA 05c measure $N(D^0 \rightarrow K^+K^-)/N(D^0 \rightarrow K^-\pi^+)$, the ratio of numbers of events observed, and similarly for the \bar{D}^0 .

$A_{CP}(K_S^0 K_L^0)$ in $D^0, \bar{D}^0 \rightarrow K_S^0 K_L^0$

VALUE (%)	EVTS	DOCUMENT ID	TECN	COMMENT
-1.9 ± 1.1 OUR AVERAGE				Error includes scale factor of 1.1.
-3.1 ± 1.2 ± 0.5	8.1k	¹ AALJ 21X	LHCB	pp at 13 TeV
-0.02 ± 1.53 ± 0.17	5.4k	² DASH 17	BELL	At/near $\Upsilon(4S)$, $\Upsilon(5S)$
-2.9 ± 5.2 ± 2.2	630	AALJ 15AT	LHCB	pp at 7, 8 TeV
-23 ± 19	65	BONVICINI 01	CLE2	e ⁺ e ⁻ ≈ 10.6 GeV
••• We do not use the following data for averages, fits, limits, etc. •••				
2.3 ± 2.8 ± 0.9	1.7k	AALJ 18Av	LHCB	see AALJ 21X

- ¹ AALJ 21X reports a value of $(-3.1 \pm 1.2 \pm 0.4 \pm 0.2) \times 10^{-2}$ where the third uncertainty is from $A_{CP}(K^+K^-) = 0.04 \pm 0.12 \pm 0.10\%$, as measured by LHCB. We have added the systematic uncertainties in quadrature. Supersedes AALJ 18Av.
- ² The systematic uncertainty is dominated by the uncertainty on A_{CP} in the control channel $D^0 \rightarrow K_S^0\pi^0$.

$A_{CP}(\pi^+\pi^-)$ in $D^0, \bar{D}^0 \rightarrow \pi^+\pi^-$

VALUE (%)	EVTS	DOCUMENT ID	TECN	COMMENT
0.13 ± 0.14 OUR AVERAGE				
0.07 ± 0.14 ± 0.11		¹ AALJ 17M	LHCB	pp 7, 8 TeV
0.22 ± 0.24 ± 0.11	215k	² AALTONEN 12B	CDF	$p\bar{p}$, $\sqrt{s}=1.96$ TeV
-0.24 ± 0.52 ± 0.22	63.7k	³ AUBERT 08M	BABR	e ⁺ e ⁻ ≈ 10.6 GeV
0.43 ± 0.52 ± 0.12	51k	⁴ STARIC 08	BELL	e ⁺ e ⁻ ≈ $\Upsilon(4S)$
1.0 ± 1.3 ± 0.6		⁵ ACOSTA 05c	CDF	$p\bar{p}$, $\sqrt{s}=1.96$ TeV
1.9 ± 3.2 ± 0.8	1136	⁵ CSORNA 02	CLE2	e ⁺ e ⁻ ≈ $\Upsilon(4S)$
4.8 ± 3.9 ± 2.5	1177	⁵ LINK 00B	FOCS	
-4.9 ± 7.8 ± 3.0	343	⁵ AITALA 98c	E791	-0.186 <A _{CP} < +0.088 (90% CL)

- We do not use the following data for averages, fits, limits, etc. •••
- 0.20 ± 0.19 ± 0.10 774k ^{2,6}AALJ 14AK LHCB See AALJ 17M
- ¹ AALJ 17M value combines $\Delta A_{CP}(\pi\pi, KK)$ from AALJ 16d, $A_{CP}(KK)$ from AALJ 17M, and $A_{CP}(\pi\pi)$ from AALJ 14AK.
- ² See also “*D*⁰ CP-violating asymmetry differences” at the end of the CP-violating asymmetries.
- ³ AUBERT 08M uses corrected numbers of events directly, not ratios with $K^\mp\pi^\pm$ events.
- ⁴ STARIC 08 uses $D^0 \rightarrow K^-\pi^+$ and $\bar{D}^0 \rightarrow K^+\pi^-$ decays to correct for detector-induced asymmetries.
- ⁵ AITALA 98c, LINK 00B, CSORNA 02, and ACOSTA 05c measure $N(D^0 \rightarrow \pi^+\pi^-)/N(D^0 \rightarrow K^-\pi^+)$, the ratio of numbers of events observed, and similarly for the \bar{D}^0 .
- ⁶ AALJ 14AK uses $\Delta A_{CP}(\pi\pi, KK)$ and $A_{CP}(KK)$ reported in the same paper.

$A_{CP}(\pi^0\pi^0)$ in $D^0, \bar{D}^0 \rightarrow \pi^0\pi^0$

VALUE (%)	EVTS	DOCUMENT ID	TECN	COMMENT
0.0 ± 0.6 OUR AVERAGE				
-0.03 ± 0.64 ± 0.10	34k	NISAR 14	BELL	e ⁺ e ⁻ at/near Υ 's
0.1 ± 4.8	810	BONVICINI 01	CLE2	e ⁺ e ⁻ ≈ 10.6 GeV

$A_{CP}(\rho\gamma)$ in $D^0, \bar{D}^0 \rightarrow \rho\gamma$

VALUE (units 10 ⁻²)	DOCUMENT ID	TECN	COMMENT
5.6 ± 15.2 ± 0.6	NANUT 17	BELL	e ⁺ e ⁻ at $\Upsilon(nS)$, n=2,3,4,5

$A_{CP}(\phi\gamma)$ in $D^0, \bar{D}^0 \rightarrow \phi\gamma$

VALUE (units 10 ⁻²)	DOCUMENT ID	TECN	COMMENT
-9.4 ± 6.6 ± 0.1	NANUT 17	BELL	e ⁺ e ⁻ at $\Upsilon(nS)$, n=2,3,4,5

$A_{CP}(K^*(892)^0\gamma)$ in $D^0, \bar{D}^0 \rightarrow K^*(892)^0\gamma$

VALUE (units 10 ⁻²)	DOCUMENT ID	TECN	COMMENT
-0.3 ± 2.0 ± 0.0	NANUT 17	BELL	e ⁺ e ⁻ at $\Upsilon(nS)$, n=2,3,4,5

$A_{CP}(\pi^+\pi^-\pi^0)$ in $D^0, \bar{D}^0 \rightarrow \pi^+\pi^-\pi^0$

VALUE (%)	EVTS	DOCUMENT ID	TECN	COMMENT
0.3 ± 0.4 OUR AVERAGE				
0.43 ± 1.30	123k ± 490	ARINSTEIN 08	BELL	e ⁺ e ⁻ ≈ $\Upsilon(4S)$
0.31 ± 0.41 ± 0.17	80 ± .3k	¹ AUBERT 08Ao	BABR	e ⁺ e ⁻ ≈ 10.6 GeV
1 ⁺⁹ ₋₇ ± 5		CRONIN-HEN.05	CLEO	e ⁺ e ⁻ ≈ 10 GeV

¹ AUBERT 08Ao report their result using a different sign convention.

$A_{CP}(\eta\pi^-\pi^+)$ in $D^0, \bar{D}^0 \rightarrow \eta\pi^-\pi^+$

VALUE (units 10 ⁻²)	EVTS	DOCUMENT ID	TECN	COMMENT
0.9 ± 1.2 ± 0.5	13k	LI 21G	BELL	e ⁺ e ⁻ at $\Upsilon(nS)$
••• We do not use the following data for averages, fits, limits, etc. •••				
9.6 ± 5.4 ± 1.8	450	ABLIKIM 20G	BES3	e ⁺ e ⁻ at 3.773 GeV

$A_{CP}(\rho(770)^+\pi^- \rightarrow \pi^+\pi^-\pi^0)$ in $D^0 \rightarrow \rho^+\pi^-, \bar{D}^0 \rightarrow \rho^-\pi^+$

VALUE (%)	DOCUMENT ID	TECN	COMMENT
+1.2 ± 0.8 ± 0.3	AUBERT 08Ao	BABR	Table 1, -Col.5/2×Col.2

$A_{CP}(\rho(770)^0\pi^0 \rightarrow \pi^+\pi^-\pi^0)$ in $D^0, \bar{D}^0 \rightarrow \rho^0\pi^0$

VALUE (%)	DOCUMENT ID	TECN	COMMENT
-3.1 ± 2.7 ± 1.2	AUBERT 08Ao	BABR	Table 1, -Col.5/2×Col.2

$A_{CP}(\rho(770)^-\pi^+ \rightarrow \pi^+\pi^-\pi^0)$ in $D^0 \rightarrow \rho^-\pi^+, \bar{D}^0 \rightarrow \rho^+\pi^-$

VALUE (%)	DOCUMENT ID	TECN	COMMENT
-1.0 ± 1.6 ± 0.7	AUBERT 08Ao	BABR	Table 1, -Col.5/2×Col.2

$A_{CP}(\rho(1450)^+\pi^- \rightarrow \pi^+\pi^-\pi^0)$ in $D^0 \rightarrow \rho(1450)^+\pi^-, \bar{D}^0 \rightarrow$ c.c.

VALUE (%)	DOCUMENT ID	TECN	COMMENT
0 ± 50 ± 50	AUBERT 08Ao	BABR	Table 1, -Col.5/2×Col.2

$A_{CP}(\rho(1450)^0\pi^0 \rightarrow \pi^+\pi^-\pi^0)$ in $D^0, \bar{D}^0 \rightarrow \rho(1450)^0\pi^0$

VALUE (%)	DOCUMENT ID	TECN	COMMENT
-17 ± 33 ± 17	AUBERT 08Ao	BABR	Table 1, -Col.5/2×Col.2

$A_{CP}(\rho(1450)^-\pi^+ \rightarrow \pi^+\pi^-\pi^0)$ in $D^0 \rightarrow \rho(1450)^-\pi^+, \bar{D}^0 \rightarrow$ c.c.

VALUE (%)	DOCUMENT ID	TECN	COMMENT
+6 ± 8 ± 3	AUBERT 08Ao	BABR	Table 1, -Col.5/2×Col.2

$A_{CP}(\rho(1700)^+\pi^- \rightarrow \pi^+\pi^-\pi^0)$ in $D^0 \rightarrow \rho(1700)^+\pi^-, \bar{D}^0 \rightarrow$ c.c.

VALUE (%)	DOCUMENT ID	TECN	COMMENT
-5 ± 13 ± 5	AUBERT 08Ao	BABR	Table 1, -Col.5/2×Col.2

$A_{CP}(\rho(1700)^0\pi^0 \rightarrow \pi^+\pi^-\pi^0)$ in $D^0, \bar{D}^0 \rightarrow \rho(1700)^0\pi^0$

VALUE (%)	DOCUMENT ID	TECN	COMMENT
+13 ± 8 ± 3	AUBERT 08Ao	BABR	Table 1, -Col.5/2×Col.2

$A_{CP}(\rho(1700)^-\pi^+ \rightarrow \pi^+\pi^-\pi^0)$ in $D^0 \rightarrow \rho(1700)^-\pi^+, \bar{D}^0 \rightarrow$ c.c.

VALUE (%)	DOCUMENT ID	TECN	COMMENT
+8 ± 10 ± 5	AUBERT 08Ao	BABR	Table 1, -Col.5/2×Col.2

$A_{CP}(f_0(980)\pi^0 \rightarrow \pi^+\pi^-\pi^0)$ in $D^0, \bar{D}^0 \rightarrow f_0(980)\pi^0$

VALUE (%)	DOCUMENT ID	TECN	COMMENT
0 ± 25 ± 25	AUBERT 08Ao	BABR	Table 1, -Col.5/2×Col.2

$A_{CP}(f_0(1370)\pi^0 \rightarrow \pi^+\pi^-\pi^0)$ in $D^0, \bar{D}^0 \rightarrow f_0(1370)\pi^0$

VALUE (%)	DOCUMENT ID	TECN	COMMENT
+25 ± 13 ± 13	AUBERT 08Ao	BABR	Table 1, -Col.5/2×Col.2

$A_{CP}(f_0(1500)\pi^0 \rightarrow \pi^+\pi^-\pi^0)$ in $D^0, \bar{D}^0 \rightarrow f_0(1500)\pi^0$

VALUE (%)	DOCUMENT ID	TECN	COMMENT
0 ± 13 ± 13	AUBERT 08Ao	BABR	Table 1, -Col.5/2×Col.2

$A_{CP}(f_0(1710)\pi^0 \rightarrow \pi^+\pi^-\pi^0)$ in $D^0, \bar{D}^0 \rightarrow f_0(1710)\pi^0$

VALUE (%)	DOCUMENT ID	TECN	COMMENT
0 ± 17 ± 17	AUBERT 08Ao	BABR	Table 1, -Col.5/2×Col.2

Meson Particle Listings

 D^0

VALUE (%)	DOCUMENT ID	TECN	COMMENT
$-4 \pm 4 \pm 4$	AUBERT	08A0 BABR	Table 1, -Col.5/2×Col.2

VALUE (%)	DOCUMENT ID	TECN	COMMENT
$+6 \pm 6 \pm 6$	AUBERT	08A0 BABR	Table 1, -Col.5/2×Col.2

VALUE (%)	DOCUMENT ID	TECN	COMMENT
$-13 \pm 19 \pm 13$	AUBERT	08A0 BABR	Table 1, -Col.5/2×Col.2

VALUE (%)	EVTS	DOCUMENT ID	COMMENT
$0.54 \pm 1.04 \pm 0.51$	7.3k	1,2 DARGENT	17 e^+e^- at $\psi(3770)$

¹ Decay rate asymmetry integrated in decay time and across full 4π phase space.
² Obtained by analyzing CLEO-c data but not authored by the CLEO Collaboration.

VALUE (%)	EVTS	DOCUMENT ID	COMMENT
$4.7 \pm 2.6 \pm 4.9$	7.3k	1 DARGENT	17 4-body fit, 4π evts

¹ Obtained by analyzing CLEO-c data but not authored by the CLEO Collaboration.

VALUE (%)	EVTS	DOCUMENT ID	COMMENT
$13.7 \pm 13.8 \pm 11.4$	7.3k	1 DARGENT	17 4-body fit, 4π evts

¹ Obtained by analyzing CLEO-c data but not authored by the CLEO Collaboration.

VALUE (%)	EVTS	DOCUMENT ID	COMMENT
$-1.6 \pm 12.9 \pm 6.7$	7.3k	1 DARGENT	17 4-body fit, 4π evts

¹ Obtained by analyzing CLEO-c data but not authored by the CLEO Collaboration.

VALUE (%)	EVTS	DOCUMENT ID	COMMENT
$-5.6 \pm 11.9 \pm 27.7$	7.3k	1 DARGENT	17 4-body fit, 4π evts

¹ Obtained by analyzing CLEO-c data but not authored by the CLEO Collaboration.

VALUE (%)	EVTS	DOCUMENT ID	COMMENT
$8.6 \pm 17.8 \pm 19.3$	7.3k	1 DARGENT	17 4-body fit, 4π evts

¹ Obtained by analyzing CLEO-c data but not authored by the CLEO Collaboration.

VALUE (%)	EVTS	DOCUMENT ID	COMMENT
$7.3 \pm 15.1 \pm 10.4$	7.3k	1 DARGENT	17 4-body fit, 4π evts

¹ Obtained by analyzing CLEO-c data but not authored by the CLEO Collaboration.

VALUE (%)	EVTS	DOCUMENT ID	COMMENT
$-14.6 \pm 16.5 \pm 9.4$	7.3k	1 DARGENT	17 4-body fit, 4π evts

¹ Obtained by analyzing CLEO-c data but not authored by the CLEO Collaboration.

VALUE (%)	EVTS	DOCUMENT ID	COMMENT
$2.5 \pm 16.8 \pm 20.8$	7.3k	1 DARGENT	17 4-body fit, 4π evts

¹ Obtained by analyzing CLEO-c data but not authored by the CLEO Collaboration.

VALUE (%)	EVTS	DOCUMENT ID	COMMENT
$-5.6 \pm 5.0 \pm 2.9$	7.3k	1 DARGENT	17 4-body fit, 4π evts

¹ Obtained by analyzing CLEO-c data but not authored by the CLEO Collaboration.

VALUE (%)	EVTS	DOCUMENT ID	COMMENT
$-28.3 \pm 12.3 \pm 20.9$	7.3k	1 DARGENT	17 4-body fit, 4π evts

¹ Obtained by analyzing CLEO-c data but not authored by the CLEO Collaboration.

VALUE (units 10^{-2})	EVTS	DOCUMENT ID	TECN	COMMENT
$-5.5 \pm 5.2 \pm 2.4$	510	ABLIKIM	20v BES3	e^+e^- , 3773 MeV

VALUE (%)	EVTS	DOCUMENT ID	TECN	COMMENT
$-1.00 \pm 1.67 \pm 0.25$	11 ± 0.11k	AUBERT	08A0 BABR	$e^+e^- \approx 10.6$ GeV

VALUE (%)	DOCUMENT ID	TECN	COMMENT
$-0.9 \pm 1.2 \pm 0.4$	1 AUBERT	08A0 BABR	Table 1, -Col.5/2×Col.2

¹ AUBERT 08A0 report their result using a different sign convention.

VALUE (%)	DOCUMENT ID	TECN	COMMENT
$-21 \pm 23 \pm 8$	AUBERT	08A0 BABR	Table 1, -Col.5/2×Col.2

VALUE (%)	DOCUMENT ID	TECN	COMMENT
$+7 \pm 15 \pm 3$	AUBERT	08A0 BABR	Table 1, -Col.5/2×Col.2

VALUE (%)	DOCUMENT ID	TECN	COMMENT
$+1.1 \pm 2.1 \pm 0.5$	AUBERT	08A0 BABR	Table 1, -Col.5/2×Col.2

VALUE (%)	DOCUMENT ID	TECN	COMMENT
$-3 \pm 19 \pm 1$	AUBERT	08A0 BABR	Table 1, -Col.5/2×Col.2

VALUE (%)	DOCUMENT ID	TECN	COMMENT
$-5 \pm 16 \pm 2$	1 AUBERT	08A0 BABR	Table 1, -Col.5/2×Col.2

¹ This AUBERT 08A0 value is obtained when the $a_0(980)^0$ replaces the $f_0(980)$ in the fit.

VALUE (%)	DOCUMENT ID	TECN	COMMENT
$0 \pm 50 \pm 150$	AUBERT	08A0 BABR	Table 1, -Col.5/2×Col.2

VALUE (%)	DOCUMENT ID	TECN	COMMENT
$-5 \pm 4 \pm 1$	AUBERT	08A0 BABR	Table 1, -Col.5/2×Col.2

VALUE (%)	DOCUMENT ID	TECN	COMMENT
$-17 \pm 28 \pm 7$	AUBERT	08A0 BABR	Table 1, -Col.5/2×Col.2

VALUE (%)	DOCUMENT ID	TECN	COMMENT
$-7 \pm 40 \pm 8$	AUBERT	08A0 BABR	Table 1, -Col.5/2×Col.2

VALUE (units 10^{-2})	EVTS	DOCUMENT ID	TECN	COMMENT
$-1.4 \pm 3.3 \pm 1.1$	1.4k	LI	21G BELL	e^+e^- at $\Upsilon(1S)$

VALUE (units 10^{-2})	EVTS	DOCUMENT ID	TECN	COMMENT
$-1.9 \pm 4.4 \pm 0.6$	1.4k	LI	21G BELL	e^+e^- at $\Upsilon(1S)$

VALUE (%)	EVTS	DOCUMENT ID	TECN	COMMENT
-0.20 ± 0.17	OUR AVERAGE			

VALUE (%)	DOCUMENT ID	TECN	COMMENT
$-0.21 \pm 0.16 \pm 0.07$	467k	1 NISAR	14 BELL e^+e^- at/near Υ 's

VALUE (%)	DOCUMENT ID	TECN	COMMENT
0.1 ± 1.3	9099	BONVICINI	01 CLE2 $e^+e^- \approx 10.6$ GeV

••• We do not use the following data for averages, fits, limits, etc. •••

VALUE (%)	DOCUMENT ID	TECN	COMMENT
$-0.28 \pm 0.19 \pm 0.10$	326k	KO	11 BELL See NISAR 14

VALUE (%)	DOCUMENT ID	TECN	COMMENT
-1.8 ± 3.0		BARTELT	95 CLE2 See BONVICINI 01

¹ After subtracting CPV in $K^0 - \bar{K}^0$ mixing, NISAR 14 gets $A_{CP} = (+0.12 \pm 0.16 \pm 0.07)\%$.

VALUE (%)	EVTS	DOCUMENT ID	TECN	COMMENT
$+0.54 \pm 0.51 \pm 0.16$	46k	KO	11 BELL	$e^+e^- \approx \Upsilon(4S)$

VALUE (%)	EVTS	DOCUMENT ID	TECN	COMMENT
$+0.98 \pm 0.67 \pm 0.14$	27k	KO	11 BELL	$e^+e^- \approx \Upsilon(4S)$

VALUE (%)	DOCUMENT ID	TECN	COMMENT
-2.8 ± 9.4	BARTELT	95 CLE2	$-18.2 < A_{CP} < +12.6\%$ (90%CL)

VALUE (%)	EVTS	DOCUMENT ID	TECN	COMMENT
0.2 ± 0.5	OUR AVERAGE			

VALUE (%)	DOCUMENT ID	TECN	COMMENT
-0.01 ± 0.91		AAIJ	18k LHCB pp at 7, 8, 13 TeV

VALUE (%)	DOCUMENT ID	TECN	COMMENT
$0.3 \pm 0.3 \pm 0.6$		BONVICINI	14 CLEO All CLEO-c runs

••• We do not use the following data for averages, fits, limits, etc. •••

VALUE (%)	DOCUMENT ID	TECN	COMMENT
$+0.5 \pm 0.4 \pm 0.9$	150k	MENDEZ	10 CLEO See BONVICINI 14

VALUE (%)	DOCUMENT ID	TECN	COMMENT
$-0.4 \pm 0.5 \pm 0.9$		DOBBS	07 CLEO See BONVICINI 14

$A_{CP}(K^\pm \pi^\mp)$ in $D^0 \rightarrow K^+ \pi^-$, $\bar{D}^0 \rightarrow K^- \pi^+$

VALUE (%)	EVTS	DOCUMENT ID	TECN	COMMENT
- 0.9 ± 1.4 OUR AVERAGE				
- 1.7 ± 1.6		1,2 AAIJ	17A0 LHCb	pp at 7,8 TeV
- 2.1 ± 5.2 ± 1.5	4.0k	AUBERT	07W BABR	$e^+ e^- \approx 10.6$ GeV
+ 2.3 ± 4.7	4.0k	ZHANG	06 BELL	$e^+ e^-$
+18 ± 14 ± 4		4 LINK	05H FOCS	γ nucleus
+ 9.5 ± 6.1 ± 8.3		5 AUBERT	03Z BABR	$e^+ e^-$, 10.6 GeV
+ 2 ± 19 ± 1	45	6 GODANG	00 CLE2	$e^+ e^-$

• • • We do not use the following data for averages, fits, limits, etc. • • •
 - 0.7 ± 1.9 1 AAIJ 13CE LHCb Repl. by AAIJ 17A0
 - 8.0 ± 7.7 0.8k 7 LI 05A BELL See ZHANG 06

¹ Based on 3 fb⁻¹ of data collected at $\sqrt{s} = 7, 8$ TeV. Allowing for CP violation, the direct CP-violation in mixing is reported for the $D^0 \rightarrow K^+ \pi^-$ and $\bar{D}^0 \rightarrow K^+ \pi^-$.
² The CPV is derived from $A_{CP} = (R_D^+ - R_D^0)/(R_D^+ + R_D^0)$.
³ This ZHANG 06 result allows mixing.
⁴ This LINK 05H result assumes no mixing. If mixing is allowed, it becomes $0.13^{+0.33}_{-0.25} \pm 0.10$.
⁵ This AUBERT 03Z limit assumes no mixing. If mixing is allowed, the 95% confidence-level interval is $(-2.8 < A_D < 4.9) \times 10^{-3}$.
⁶ This GODANG 00 result assumes no D^0 - \bar{D}^0 mixing and becomes $-0.43 < A_{CP} < +0.34$ at 95% CL. If mixing is allowed $A_{CP} = -0.01^{+0.16}_{-0.17} \pm 0.01$.
⁷ This LI 05A result allows mixing.

$A_{CP}(K^- \pi^+)$ in $D_{CP(\pm 1)} \rightarrow K^\mp \pi^\pm$

$$A_{CP}(K^- \pi^+) = [B(D_{CP(-)} \rightarrow K^- \pi^+ + c.c.) - B(D_{CP(+)} \rightarrow K^- \pi^+ + c.c.)] / \text{Sum}$$

VALUE (%)	DOCUMENT ID	TECN	COMMENT
12.7 ± 1.3 ± 0.7			
	1 ABLIKIM	14c BES3	$e^+ e^- \rightarrow D^0 \bar{D}^0$, 3.77 GeV

¹ ABLIKIM 14c uses quantum correlations in $e^+ e^- \rightarrow D^0 \bar{D}^0$ at the $\psi(3770)$ to measure the asymmetry of the branching fraction of $D^0 \rightarrow K^- \pi^+$ in CP-odd and CP-even eigenstates. It then extracts the strong-phase difference $\delta_{K\pi}$.

$A_{CP}(K^\mp \pi^\pm \pi^0)$ in $D^0 \rightarrow K^- \pi^+ \pi^0$, $\bar{D}^0 \rightarrow K^+ \pi^- \pi^0$

VALUE (%)	DOCUMENT ID	TECN	COMMENT
0.1 ± 0.5 OUR AVERAGE			
0.1 ± 0.3 ± 0.4	BONVICINI	14 CLEO	All CLEO-c runs
- 3.1 ± 8.6	1 KOPP	01 CLE2	$e^+ e^- \approx 10.6$ GeV

• • • We do not use the following data for averages, fits, limits, etc. • • •
 0.2 ± 0.4 ± 0.8 DOBBS 07 CLEO See BONVICINI 14

¹ KOPP 01 fits separately the D^0 and \bar{D}^0 Dalitz plots and then calculates the integrated difference of normalized densities divided by the integrated sum.

$A_{CP}(K^\pm \pi^\mp \pi^0)$ in $D^0 \rightarrow K^+ \pi^- \pi^0$, $\bar{D}^0 \rightarrow K^- \pi^+ \pi^0$

VALUE (%)	EVTS	DOCUMENT ID	TECN	COMMENT
0 ± 5 OUR AVERAGE				
- 0.6 ± 5.3	1978 ± 104	TIAN	05 BELL	$e^+ e^- \approx 7(45)$
+ 9 ± 25 ± 22	38	BRANDENB...	01 CLE2	$e^+ e^- \approx 7(45)$

$A_{CP}(K_S^0 \pi^+ \pi^-)$ in $D^0, \bar{D}^0 \rightarrow K_S^0 \pi^+ \pi^-$

VALUE (%)	EVTS	DOCUMENT ID	TECN	COMMENT
- 0.1 ± 0.8 OUR AVERAGE				
- 0.05 ± 0.57 ± 0.54	350k	1 AALTONEN	12AD CDF	
- 0.9 ± 2.1 ± 1.6 ± 5.7	4854	2 ASNER	04A CLEO	$e^+ e^- \approx 10$ GeV

¹ This is the overall result of AALTONEN 12AD. Following are the 15 CP fit-fraction asymmetries from the amplitude analysis of the D^0 and $\bar{D}^0 \rightarrow K_S^0 \pi^+ \pi^-$ Dalitz plots.
² This is the overall result of ASNER 04A; CP-violating limits are also given below for each of the 10 resonant submodes found in an amplitude analysis of the D^0 and $\bar{D}^0 \rightarrow K_S^0 \pi^+ \pi^-$ Dalitz plots.

$A_{CP}(K^\mp \pi^\pm \eta)$ in $D^0, \bar{D}^0 \rightarrow K^\mp \pi^\pm \eta$

VALUE (units 10 ⁻²)	EVTS	DOCUMENT ID	TECN	COMMENT
- 1.9 ± 1.3 ± 1.0				
	6.1k	ABLIKIM	20v BES3	$e^+ e^-$, 3773 MeV

$A_{CP}(K_S^0 \pi^0 \eta)$ in $D^0, \bar{D}^0 \rightarrow K_S^0 \pi^0 \eta$

VALUE (units 10 ⁻²)	EVTS	DOCUMENT ID	TECN	COMMENT
- 3.9 ± 3.2 ± 0.8				
	1.1k	ABLIKIM	20v BES3	$e^+ e^-$, 3773 MeV

$A_{CP}(K^\mp \pi^\pm \pi^0 \eta)$ in $D^0, \bar{D}^0 \rightarrow K^\mp \pi^\pm \pi^0 \eta$

VALUE (units 10 ⁻²)	EVTS	DOCUMENT ID	TECN	COMMENT
- 7.9 ± 4.8 ± 2.5				
	580	ABLIKIM	20v BES3	$e^+ e^-$, 3773 MeV

$A_{CP}(K^*(892)^\mp \pi^\pm)$ in $D^0 \rightarrow K^{*-} \pi^+$, $\bar{D}^0 \rightarrow K^{*+} \pi^-$

VALUE (%)	DOCUMENT ID	TECN	COMMENT
+ 0.36 ± 0.33 ± 0.40			
	AALTONEN	12AD CDF	Dalitz fit, ~ 350k evts

• • • We do not use the following data for averages, fits, limits, etc. • • •
 + 2.5 ± 1.9 ± 3.3 ± 0.8 ASNER 04A CLEO Dalitz fit, 4854 evts

$A_{CP}(K^*(892)^\pm \pi^\mp)$ in $D^0 \rightarrow K^{*0} \pi^+ \pi^-$
 This is a doubly Cabibbo-suppressed mode.

VALUE (%)	DOCUMENT ID	TECN	COMMENT
+ 1.0 ± 5.7 ± 2.1			
	AALTONEN	12AD CDF	Dalitz fit, ~ 350k evts

• • • We do not use the following data for averages, fits, limits, etc. • • •
 - 21 ± 42 ± 28 ASNER 04A CLEO Dalitz fit, 4854 evts

$A_{CP}(K_S^0 \rho^0)$ in $D^0 \rightarrow \bar{K}^0 \rho^0, \bar{D}^0 \rightarrow K^0 \rho^0$

VALUE (%)	DOCUMENT ID	TECN	COMMENT
- 0.05 ± 0.50 ± 0.08			
	AALTONEN	12AD CDF	Dalitz fit, ~ 350k evts

• • • We do not use the following data for averages, fits, limits, etc. • • •
 + 3.1 ± 3.8 ± 2.7 ± 2.2 ASNER 04A CLEO Dalitz fit, 4854 evts

$A_{CP}(K_S^0 \omega)$ in $D^0 \rightarrow \bar{K}^0 \omega, \bar{D}^0 \rightarrow K^0 \omega$

VALUE (%)	DOCUMENT ID	TECN	COMMENT
- 12.6 ± 6.0 ± 2.6			
	AALTONEN	12AD CDF	Dalitz fit, ~ 350k evts

• • • We do not use the following data for averages, fits, limits, etc. • • •
 - 26 ± 24 ± 22 ± 4 ASNER 04A CLEO Dalitz fit, 4854 evts

$A_{CP}(K_S^0 f_0(980))$ in $D^0 \rightarrow \bar{K}^0 f_0(980), \bar{D}^0 \rightarrow K^0 f_0(980)$

VALUE (%)	DOCUMENT ID	TECN	COMMENT
- 0.4 ± 2.2 ± 1.6			
	AALTONEN	12AD CDF	Dalitz fit, ~ 350k evts

• • • We do not use the following data for averages, fits, limits, etc. • • •
 - 4.7 ± 11.0 ± 24.9 ± 8.8 ASNER 04A CLEO Dalitz fit, 4854 evts

$A_{CP}(K_S^0 f_2(1270))$ in $D^0 \rightarrow \bar{K}^0 f_2(1270), \bar{D}^0 \rightarrow K^0 f_2(1270)$

VALUE (%)	DOCUMENT ID	TECN	COMMENT
- 4.0 ± 3.4 ± 3.0			
	AALTONEN	12AD CDF	Dalitz fit, ~ 350k evts

• • • We do not use the following data for averages, fits, limits, etc. • • •
 + 34 ± 51 ± 33 ± 79 ASNER 04A CLEO Dalitz fit, 4854 evts

$A_{CP}(K_S^0 f_0(1370))$ in $D^0 \rightarrow \bar{K}^0 f_0(1370), \bar{D}^0 \rightarrow K^0 f_0(1370)$

VALUE (%)	DOCUMENT ID	TECN	COMMENT
- 0.5 ± 4.6 ± 7.7			
	AALTONEN	12AD CDF	Dalitz fit, ~ 350k evts

• • • We do not use the following data for averages, fits, limits, etc. • • •
 + 18 ± 10 ± 13 ± 22 ASNER 04A CLEO Dalitz fit, 4854 evts

$A_{CP}(K_S^0 \rho^0(1450))$ in $D^0 \rightarrow \bar{K}^0 \rho^0(1450), \bar{D}^0 \rightarrow K^0 \rho^0(1450)$

VALUE (%)	DOCUMENT ID	TECN	COMMENT
- 4.1 ± 5.2 ± 8.1			
	AALTONEN	12AD CDF	Dalitz fit, ~ 350k evts

$A_{CP}(K_S^0 f_0(600))$ in $D^0 \rightarrow \bar{K}^0 f_0(600), \bar{D}^0 \rightarrow K^0 f_0(600)$

VALUE (%)	DOCUMENT ID	TECN	COMMENT
- 2.7 ± 2.7 ± 3.6			
	AALTONEN	12AD CDF	Dalitz fit, ~ 350k evts

$A_{CP}(K^*(1410)^\mp \pi^\pm)$ in $D^0 \rightarrow K^*(1410)^- \pi^+$, $\bar{D}^0 \rightarrow K^*(1410)^+ \pi^-$

VALUE (%)	DOCUMENT ID	TECN	COMMENT
- 2.3 ± 5.7 ± 6.4			
	AALTONEN	12AD CDF	Dalitz fit, ~ 350k evts

$A_{CP}(K_0^*(1430)^\mp \pi^\pm)$ in $D^0 \rightarrow K_0^*(1430)^- \pi^+$, $\bar{D}^0 \rightarrow K_0^*(1430)^+ \pi^-$

VALUE (%)	DOCUMENT ID	TECN	COMMENT
4.0 ± 2.4 ± 3.8			
	AALTONEN	12AD CDF	Dalitz fit, ~ 350k evts

• • • We do not use the following data for averages, fits, limits, etc. • • •
 - 0.2 ± 11.3 ± 8.8 ± 5.0 ASNER 04A CLEO Dalitz fit, 4854 evts

$A_{CP}(K_0^*(1430)^\pm \pi^\mp)$ in $D^0 \rightarrow K_0^*(1430)^+ \pi^-$, $\bar{D}^0 \rightarrow K_0^*(1430)^- \pi^+$
 This is a doubly Cabibbo-suppressed mode.

VALUE (%)	DOCUMENT ID	TECN	COMMENT
+ 12 ± 11 ± 10			
	AALTONEN	12AD CDF	Dalitz fit, ~ 350k evts

$A_{CP}(K_2^*(1430)^\mp \pi^\pm)$ in $D^0 \rightarrow K_2^*(1430)^- \pi^+$, $\bar{D}^0 \rightarrow K_2^*(1430)^+ \pi^-$

VALUE (%)	DOCUMENT ID	TECN	COMMENT
+ 2.9 ± 4.0 ± 4.1			
	AALTONEN	12AD CDF	Dalitz fit, ~ 350k evts

• • • We do not use the following data for averages, fits, limits, etc. • • •
 - 7 ± 25 ± 13 ± 26 ASNER 04A CLEO Dalitz fit, 4854 evts

$A_{CP}(K_2^*(1430)^\pm \pi^\mp)$ in $D^0 \rightarrow K_2^*(1430)^+ \pi^-$, $\bar{D}^0 \rightarrow K_2^*(1430)^- \pi^+$
 This is a doubly Cabibbo-suppressed mode.

VALUE (%)	DOCUMENT ID	TECN	COMMENT
- 10 ± 14 ± 29			
	AALTONEN	12AD CDF	Dalitz fit, ~ 350k evts

$A_{CP}(K^*(1680)^\mp \pi^\pm)$ in $D^0 \rightarrow K^*(1680)^- \pi^+$, $\bar{D}^0 \rightarrow K^*(1680)^+ \pi^-$

VALUE (%)	DOCUMENT ID	TECN	COMMENT
+ 0.36 ± 0.33 ± 0.40			
	AALTONEN	12AD CDF	Dalitz fit, ~ 350k evts

• • • We do not use the following data for averages, fits, limits, etc. • • •
 - 36 ± 19 ± 10 ± 35 ASNER 04A CLEO Dalitz fit, 4854 evts

Downloaded from https://academic.oup.com/ptep/article/2022/8/083C01/6651666 by CERN Library user on 11 October 2022

Meson Particle Listings

 D^0 $A_{CP}(K^- \pi^+ \pi^+ \pi^-)$ in $D^0 \rightarrow K^- \pi^+ \pi^+ \pi^-$, $\overline{D}^0 \rightarrow K^+ \pi^- \pi^- \pi^+$

VALUE (%)	DOCUMENT ID	TECN	COMMENT
0.2 ± 0.3 ± 0.4	BONVICINI 14	CLEO	All CLEO-c runs
••• We do not use the following data for averages, fits, limits, etc. •••			
+0.7 ± 0.5 ± 0.9	DOBBS 07	CLEO	See BONVICINI 14

 $A_{CP}(K^\pm \pi^\mp \pi^+ \pi^-)$ in $D^0 \rightarrow K^\pm \pi^- \pi^+ \pi^-$, $\overline{D}^0 \rightarrow K^- \pi^+ \pi^+ \pi^-$

VALUE (%)	EVTS	DOCUMENT ID	TECN	COMMENT
-1.8 ± 4.4	1721 ± 75	TIAN 05	BELL	$e^+ e^- \approx 7(4S)$

 $A_{CP}(K^+ K^- \pi^+ \pi^-)$ in $D^0, \overline{D}^0 \rightarrow K^+ K^- \pi^+ \pi^-$

See also AAIJ 13BR for a search for CP violation in $D^0 \rightarrow K^+ K^- \pi^+ \pi^-$ in binned phase space. No evidence of CP violation was found.

VALUE (%)	EVTS	DOCUMENT ID	TECN	COMMENT
1.3 ± 1.7 OUR AVERAGE				
1.84 ± 1.74 ± 0.3	2.9k	¹ DARGENT 17		$e^+ e^-$
-8.2 ± 5.6 ± 4.7	828 ± 46	LINK 05E	FOCS	$\gamma A, \overline{E}_{\gamma} \approx 180$ GeV
¹ Obtained by analyzing CLEO data but not authored by the CLEO Collaboration.				

 $A_{CP}(K_1^*(1270)^+ K^-)$ in $D^0 \rightarrow K^+ K^- \pi^+ \pi^-$ in $D^0 \rightarrow K_1^*(1270)^+ K^-$, $\overline{D}^0 \rightarrow$ c.c.

Including the full $K_1^*(1270)^+$ phase space accessible in this decay chain, with its various resonance contributions.

VALUE (%)	EVTS	DOCUMENT ID	TECN	COMMENT
-2.3 ± 1.7 OUR AVERAGE				
-2.6 ± 1.7 ± 0.2	163k	AAIJ 19c	LHCB	4-body fit, $K K \pi \pi$ evts
25.3 ± 9.7 ± 12.7	2.9k	¹ DARGENT 17		4-body fit, $K K \pi \pi$ evts
¹ Obtained by analyzing CLEO data but not authored by the CLEO Collaboration.				

 $A_{CP}(K_1^*(1270)^+ K^-)$ in $D^0 \rightarrow K^{*0} \pi^+ K^-$ in $D^0 \rightarrow K_1^*(1270)^+ K^-$, $\overline{D}^0 \rightarrow$ c.c.

VALUE (%)	DOCUMENT ID	TECN	COMMENT
-0.7 ± 10.4	ARTUSO 12	CLEO	Amplitude fit, 2959 evts.

 $A_{CP}(K_1^*(1270)^- K^+)$ in $D^0 \rightarrow \overline{K}^{*0} \pi^- K^+$ in $D^0 \rightarrow K_1^*(1270)^- K^+$, $\overline{D}^0 \rightarrow$ c.c.

VALUE (%)	DOCUMENT ID	TECN	COMMENT
-10.0 ± 31.5	ARTUSO 12	CLEO	Amplitude fit, 2959 evts.

 $A_{CP}(K_1^*(1270)^- K^+)$ in $D^0 \rightarrow K^+ K^- \pi^+ \pi^-$ in $D^0 \rightarrow K_1^*(1270)^- K^+$, $\overline{D}^0 \rightarrow$ c.c.

Including the full $K_1^*(1270)^-$ phase space accessible in this decay chain, with its various resonance contributions.

VALUE (%)	EVTS	DOCUMENT ID	TECN	COMMENT
1.7 ± 3.5 OUR AVERAGE				
3.3 ± 3.5 ± 0.5	163k	AAIJ 19c	LHCB	4-body fit, $K K \pi \pi$ evts
-50.4 ± 12.0 ± 16.1	2.9k	¹ DARGENT 17		4-body fit, $K K \pi \pi$ evts
¹ Obtained by analyzing CLEO data but not authored by the CLEO Collaboration.				

 $A_{CP}(K_1^*(1270)^+ K^-)$ in $D^0 \rightarrow \rho^0 K^+ K^-$ in $D^0 \rightarrow K_1^*(1270)^+ K^-$, $\overline{D}^0 \rightarrow$ c.c.

VALUE (%)	DOCUMENT ID	TECN	COMMENT
-6.5 ± 16.9	ARTUSO 12	CLEO	Amplitude fit, 2959 evts.

 $A_{CP}(K_1^*(1270)^- K^+)$ in $D^0 \rightarrow \rho^0 K^- K^+$ in $D^0 \rightarrow K_1^*(1270)^- K^+$, $\overline{D}^0 \rightarrow$ c.c.

VALUE (%)	DOCUMENT ID	TECN	COMMENT
+9.6 ± 12.9	ARTUSO 12	CLEO	Amplitude fit, 2959 evts.

 $A_{CP}(K_1(1400)^+ K^-)$ in $D^0 \rightarrow K^+ K^- \pi^+ \pi^-$ in $D^0 \rightarrow K_1(1400)^+ K^-$, $\overline{D}^0 \rightarrow$ c.c.

Including the full $K_1(1400)^+$ phase space accessible in this decay chain, with its various resonance contributions.

VALUE (%)	EVTS	DOCUMENT ID	TECN	COMMENT
-4.4 ± 2.1 OUR AVERAGE				
-4.5 ± 2.1 ± 0.3	163k	AAIJ 19c	LHCB	4-body fit, $K K \pi \pi$ evts
9.2 ± 15.2 ± 20.3	2.9k	¹ DARGENT 17		4-body fit, $K K \pi \pi$ evts
¹ Obtained by analyzing CLEO data but not authored by the CLEO Collaboration.				

 $A_{CP}(K^*(1410)^+ K^-)$ in $D^0 \rightarrow K^{*0} \pi^+ K^-$ in $D^0 \rightarrow K^*(1410)^+ K^-$, $\overline{D}^0 \rightarrow$ c.c.

VALUE (%)	DOCUMENT ID	TECN	COMMENT
-20.0 ± 16.8	ARTUSO 12	CLEO	Amplitude fit, 2959 evts.

 $A_{CP}(K^*(1410)^- K^+)$ in $D^0 \rightarrow \overline{K}^{*0} \pi^- K^+$ in $D^0 \rightarrow K^*(1410)^- K^+$, $\overline{D}^0 \rightarrow$ c.c.

VALUE (%)	DOCUMENT ID	TECN	COMMENT
-1.1 ± 13.7	ARTUSO 12	CLEO	Amplitude fit, 2959 evts.

 $A_{CP}(K^*(1680)^+ K^-)$ in $D^0 \rightarrow K^+ K^- \pi^+ \pi^-$ in $D^0 \rightarrow K^*(1680)^+ K^-$, $\overline{D}^0 \rightarrow$ c.c.

Including the full $K^*(1680)^+$ phase space accessible in this decay chain, with its various resonance contributions.

VALUE (%)	EVTS	DOCUMENT ID	TECN	COMMENT
-17.1 ± 21.8 ± 18.5	2.9k	¹ DARGENT 17		4-body fit, $K K \pi \pi$ evts
¹ Obtained by analyzing CLEO data but not authored by the CLEO Collaboration.				

 $A_{CP}(K^{*0} \overline{K}^{*0})$ in $D^0, \overline{D}^0 \rightarrow K^{*0} \overline{K}^{*0}$

VALUE (%)	EVTS	DOCUMENT ID	TECN	COMMENT
-4.6 ± 9.0 ± 11.3	2.9k	¹ DARGENT 17		4-body fit, $K K \pi \pi$ evts
¹ Obtained by analyzing CLEO data but not authored by the CLEO Collaboration.				

 $A_{CP}(K^{*0} \overline{K}^{*0} S\text{-wave})$ in $D^0, \overline{D}^0 \rightarrow K^{*0} \overline{K}^{*0} S\text{-wave}$

VALUE (%)	EVTS	DOCUMENT ID	TECN	COMMENT
-3.9 ± 2.2 OUR AVERAGE				
-4.3 ± 2.2 ± 0.5	163k	AAIJ 19c	LHCB	4-body fit, $K K \pi \pi$ evts
+9.5 ± 13.5	3k	ARTUSO 12	CLEO	4-body fit, $K K \pi \pi$ evts

 $A_{CP}(\phi \rho^0)$ in $D^0, \overline{D}^0 \rightarrow \phi \rho^0$

VALUE (%)	EVTS	DOCUMENT ID	TECN	COMMENT
1.5 ± 4.6 ± 8.0	2.9k	¹ DARGENT 17		4-body fit, $K K \pi \pi$ evts
¹ Obtained by analyzing CLEO data but not authored by the CLEO Collaboration.				

 $A_{CP}(\phi \rho^0 S\text{-wave})$ in $D^0, \overline{D}^0 \rightarrow \phi \rho^0 S\text{-wave}$

VALUE (%)	DOCUMENT ID	TECN	COMMENT
-2.7 ± 5.3	ARTUSO 12	CLEO	Amplitude fit, 2959 evts.

 $A_{CP}(\phi \rho^0 D\text{-wave})$ in $D^0, \overline{D}^0 \rightarrow \phi \rho^0 D\text{-wave}$

VALUE (%)	DOCUMENT ID	TECN	COMMENT
-37.1 ± 19.0	ARTUSO 12	CLEO	Amplitude fit, 2959 evts.

 $A_{CP}(\phi(\pi^+ \pi^-)_{S\text{-wave}})$ in $D^0, \overline{D}^0 \rightarrow \phi(\pi^+ \pi^-)_{S\text{-wave}}$

VALUE (%)	EVTS	DOCUMENT ID	TECN	COMMENT
6 ± 6 OUR AVERAGE				
5.8 ± 6.1 ± 0.8	163k	AAIJ 19c	LHCB	4-body fit, $K K \pi \pi$ evts
-4.0 ± 18.0 ± 44.6	3k	¹ DARGENT 17		4-body fit, $K K \pi \pi$ evts
••• We do not use the following data for averages, fits, limits, etc. •••				
-8.6 ± 10.4	3k	² ARTUSO 12	CLEO	4-body fit, $K K \pi \pi$ evts
¹ Obtained by analyzing CLEO data but not authored by the CLEO Collaboration.				
² see DARGENT 17				

 $A_{CP}(K^*(892)^0(K^- \pi^+)_{S\text{-wave}})$ in $D^0, \overline{D}^0 \rightarrow K^*(892)^0(K^- \pi^+)_{S\text{-wave}}$

VALUE (%)	EVTS	DOCUMENT ID	TECN	COMMENT
-13.1 ± 17.9 ± 31.2	2.9k	¹ DARGENT 17		4-body fit, $K K \pi \pi$ evts
¹ Obtained by analyzing CLEO data but not authored by the CLEO Collaboration.				

 $A_{CP}(K^+ K^- \pi^+ \pi^- \text{ non-resonant})$ in $D^0, \overline{D}^0 \rightarrow K^+ K^- \pi^+ \pi^- \text{ non-resonant}$

VALUE (%)	DOCUMENT ID	TECN	COMMENT
+8.2 ± 10.9 ± 17.1	¹ DARGENT 17		4-body fit, 2.9k $K K \pi \pi$ evts
¹ Obtained by analyzing CLEO data but not authored by the CLEO Collaboration.			

 $A_{CP}((K^- \pi^+)_{P\text{-wave}}(K^+ \pi^-)_{S\text{-wave}})$ in $D^0 \rightarrow (K^- \pi^+)_{P\text{-wave}}(K^+ \pi^-)_{S\text{-wave}}$, $\overline{D}^0 \rightarrow$ c.c.

VALUE (%)	DOCUMENT ID	TECN	COMMENT
+2.7 ± 10.6	ARTUSO 12	CLEO	Amplitude fit, 2959 evts.

 $A_{CP}(K^+ K^- \mu^+ \mu^-)$ in $D^0, \overline{D}^0 \rightarrow K^+ K^- \mu^+ \mu^-$

VALUE (%)	EVTS	DOCUMENT ID	TECN	COMMENT
0 ± 11 ± 2	110	AAIJ 18i	LHCB	pp at 7, 8, 13TeV

 $A_{CP}(\pi^+ \pi^- \mu^+ \mu^-)$ in $D^0, \overline{D}^0 \rightarrow \pi^+ \pi^- \mu^+ \mu^-$

VALUE (%)	EVTS	DOCUMENT ID	TECN	COMMENT
4.9 ± 3.8 ± 0.7	1.1k	AAIJ 18i	LHCB	pp at 7, 8, 13TeV

 D^0 CP-EVEN FRACTIONS

The CP -even fraction F_{\pm} , defined for self-conjugate final states, like the coherence factor is useful for measuring the unitary triangle angle γ in $B \rightarrow DK$ decays. A purely CP -even state has $F_{\pm} = 1$, a CP -odd one has $F_{\pm} = 0$. For details, see NAYAK 15.

 CP -even fraction in $D^0 \rightarrow \pi^+ \pi^- \pi^0$ decays

VALUE (%)	DOCUMENT ID	COMMENT
97.3 ± 1.7	MALDE 15	Uses CLEO data
••• We do not use the following data for averages, fits, limits, etc. •••		
96.8 ± 1.7 ± 0.6	NAYAK 15	see MALDE 15

 CP -even fraction in $D^0 \rightarrow K^+ K^- \pi^0$ decays

VALUE (%)	DOCUMENT ID	COMMENT
73.2 ± 5.5	MALDE 15	Uses CLEO data
••• We do not use the following data for averages, fits, limits, etc. •••		
73.1 ± 5.8 ± 2.1	NAYAK 15	see MALDE 15

 CP -even fraction in $D^0 \rightarrow \pi^+ \pi^- \pi^+ \pi^-$ decays

VALUE (%)	DOCUMENT ID	TECN	COMMENT
76.9 ± 2.1 ± 1.0	¹ HARNEW 18		Uses CLEO-c data
••• We do not use the following data for averages, fits, limits, etc. •••			
72.9 ± 0.9 ± 1.8	^{1,2} DARGENT 17		from amplitude model
73.7 ± 2.8	MALDE 15	CLEO	amplitude model independent

¹ Obtained by analyzing CLEO-c data but not authored by the CLEO Collaboration.

² MALDE 15 and DARGENT 17 use different CLEO data sets, so in principle their results could be averaged. However, given the importance that model-independence has in the use of this value, we exclude the amplitude model-derived result from the average.

CP-even fraction in $D^0 \rightarrow K_S^0 \pi^+ \pi^- \pi^0$ decays

VALUE (%)	DOCUMENT ID	TECN	COMMENT
23.8 ± 1.2 ± 1.2	¹ RESMI	18	Uses CLEO-c data

¹ Obtained by analyzing CLEO-c data but not authored by the CLEO Collaboration.

CP-even fraction in $D^0 \rightarrow K^+ K^- \pi^+ \pi^-$ decays

VALUE (%)	DOCUMENT ID	TECN	COMMENT
75.3 ± 1.8 ± 3.9	¹ DARGENT	17	from amplitude model

¹ Obtained by analyzing CLEO data but not authored by the CLEO Collaboration.

D^0 CP-VIOLATING ASYMMETRY DIFFERENCES

$\Delta A_{CP} = A_{CP}(K^+ K^-) - A_{CP}(\pi^+ \pi^-)$

CP violation in these modes can come from the decay amplitudes (direct) and/or from mixing or interference of mixing and decay (indirect). The difference ΔA_{CP} is primarily sensitive to the direct component, and only retains a second-order dependence on the indirect component for measurements where the mean decay time of the $K^+ K^-$ and $\pi^+ \pi^-$ samples are not identical. The results below are averaged assuming the indirect component can be neglected.

VALUE (%)	EVTS	DOCUMENT ID	TECN	COMMENT
-0.154 ± 0.029	53M,17M	AAIJ	19D	LHCB Time-integrated
••• We do not use the following data for averages, fits, limits, etc. •••				
-0.10 ± 0.08 ± 0.03	6.5M,2.2M	AAIJ	16D	LHCB See AAIJ 19D
0.14 ± 0.16 ± 0.08	2.2M,0.8M	AAIJ	14AK	LHCB See AAIJ 19D
0.49 ± 0.30 ± 0.14	0.56M,0.22M	AAIJ	13AD	LHCB See AAIJ 14AK
-0.82 ± 0.21 ± 0.11	1.4M,0.4M	AAIJ	12G	LHCB See AAIJ 16D
-0.46 ± 0.31 ± 0.12		AALTONEN	12B	CDF See AALTONEN 12o
-0.62 ± 0.21 ± 0.10		AALTONEN	12o	CDF Time-integrated
0.24 ± 0.62 ± 0.26		¹ AUBERT	08M	BABR Time-integrated
-0.86 ± 0.60 ± 0.07	120k	STARIC	08	BELL Time-integrated

¹ Calculated from the AUBERT 08M values of $A_{CP}(K^+ K^-)$ and $A_{CP}(\pi^+ \pi^-)$. The systematic error here combines the systematic errors in quadrature, and therefore somewhat over-estimates it.

D^0 TESTS OF LOCAL CP-VIOLATION (CPV)

We list model-independent searches for local CP violation in phase-space distributions of multi-body decays.

Most of these searches divide phase space (Dalitz plot for 3-body decays, five-dimensional equivalent for 4-body decays) into bins, and perform a χ^2 test comparing normalised yields N_i, \bar{N}_i in CP-conjugate bin pairs i : $\chi^2 = \sum_i (N_i - \alpha \bar{N}_i) / \sigma(N_i - \alpha \bar{N}_i)$. The factor $\alpha = (\sum_i N_i) / (\sum_i \bar{N}_i)$ removes the dependence on phase-space-integrated rate asymmetries. The result is used to obtain the probability (p-value) to obtain the measured χ^2 or larger under the assumption of CP conservation [AUBERT 08Ao, BEDIAGA 09]. Alternative methods obtain p-values from other test variables based on unbinned analyses [WILLIAMS 11, AAIJ 14c]. Results can be combined using Fisher's method [MOSTELLER 48].

Local CPV in $D^0, \bar{D}^0 \rightarrow \pi^+ \pi^- \pi^0$

p-value (%)	EVTS	DOCUMENT ID	TECN	COMMENT
-------------	------	-------------	------	---------

4.9 OUR EVALUATION

2.6	566k	¹ AAIJ	15A	LHCB unbinned method
32.8	82k	AUBERT	08Ao	BABR χ^2

¹ Unusually, AAIJ 15A assigns an uncertainty on the p value of ±0.5%. This results from limited test statistics.

Local CPV in $D^0, \bar{D}^0 \rightarrow \pi^+ \pi^- \pi^+ \pi^-$

p-value (%)	EVTS	DOCUMENT ID	TECN	COMMENT
-------------	------	-------------	------	---------

0.6 ± 0.2 1.0M ¹ AAIJ 17AE LHCB unbinned, P-odd

••• We do not use the following data for averages, fits, limits, etc. •••

4.6 ± 0.5	1.0M	^{2,3} AAIJ	17AE	LHCB unbinned, P-even
41	330k	^{2,4} AAIJ	13BR	LHCB χ^2 , P-even

¹ This AAIJ 17AE value tests CP Violation in P-odd variables.
² This value tests CP Violation in P-even variables.
³ Not included in average as correlation to P-odd measurement using the same data is unclear.
⁴ See AAIJ 17AE.

Local CPV in $D^0, \bar{D}^0 \rightarrow K_S^0 \pi^+ \pi^-$

p-value (%)	EVTS	DOCUMENT ID	TECN	COMMENT
-------------	------	-------------	------	---------

96 350k AALTONEN 12AD CDF χ^2

Local CPV in $D^0, \bar{D}^0 \rightarrow K^+ K^- \pi^0$

p-value (%)	EVTS	DOCUMENT ID	TECN	COMMENT
-------------	------	-------------	------	---------

16.6 11k AUBERT 08Ao BABR χ^2

Local CPV in $D^0, \bar{D}^0 \rightarrow K^+ K^- \pi^+ \pi^-$

p-value (%)	EVTS	DOCUMENT ID	TECN	COMMENT
-------------	------	-------------	------	---------

9.1 57k AAIJ 13BR LHCB χ^2

CP VIOLATING ASYMMETRIES OF P-ODD (T-ODD) MOMENTS

The CP-sensitive P-odd (T-odd) correlation in D^0, \bar{D}^0 decays. The D^0 and \bar{D}^0 are distinguished by the charge of the parent D^* : $D^{*+} \rightarrow D^0 \pi^+$ and $D^{*-} \rightarrow \bar{D}^0 \pi^-$.

$A_{Tviol}(K^+ K^- \pi^+ \pi^-)$ in $D^0, \bar{D}^0 \rightarrow K^+ K^- \pi^+ \pi^-$

$C_T \equiv \vec{p}_{K^+} \cdot (\vec{p}_{\pi^+} \times \vec{p}_{\pi^-})$ is a parity-odd correlation of the K^+ , π^+ , and π^- momenta (evaluated in the D^0 rest frame) for the D^0 . $\overline{C}_T \equiv \vec{p}_{K^-} \cdot (\vec{p}_{\pi^-} \times \vec{p}_{\pi^+})$ is the corresponding quantity for the \bar{D}^0 . Then

$\overline{A}_T \equiv [\Gamma(C_T > 0) - \Gamma(C_T < 0)] / [\Gamma(C_T > 0) + \Gamma(C_T < 0)]$, and

$\overline{A}_T \equiv [\Gamma(-\overline{C}_T > 0) - \Gamma(-\overline{C}_T < 0)] / [\Gamma(-\overline{C}_T > 0) + \Gamma(-\overline{C}_T < 0)]$, and

$A_{Tviol} \equiv \frac{1}{2}(\overline{A}_T - \overline{A}_T)$. C_T and \overline{C}_T are commonly referred to as T-odd moments, because they are odd under T reversal. However, the T-conjugate process $K^+ K^- \pi^+ \pi^- \rightarrow D^0$ is not accessible, while the P-conjugate process is.

VALUE (units 10 ⁻³)	EVTS	DOCUMENT ID	TECN	COMMENT
2.9 ± 2.2 OUR AVERAGE				
5.2 ± 3.7 ± 0.7	110k	¹ KIM	19	BELL $e^+ e^-$ at $\Upsilon(1S) - \Upsilon(6S)$
1.8 ± 2.9 ± 0.4	171k	AAIJ	14BC	LHCB $B \rightarrow D^0 \mu^- X$
1.0 ± 5.1 ± 4.4	47k	DEL-AMO-SA...	10	BABR $e^+ e^- \approx 10.6$ GeV
••• We do not use the following data for averages, fits, limits, etc. •••				
10 ± 57 ± 37	0.8k	LINK	05E	FOCS $\gamma A, \overline{E}_\gamma \approx 180$ GeV

¹ KIM 19 also study CP-violating asymmetries in several other kinematic variables. No evidence for CP violation is found in any of them.

$A_{Tviol}(K_S \pi^+ \pi^- \pi^0)$ in $D^0, \bar{D}^0 \rightarrow K_S \pi^+ \pi^- \pi^0$

VALUE (units 10 ⁻³)	EVTS	DOCUMENT ID	TECN	COMMENT
---------------------------------	------	-------------	------	---------

-0.28 ± 1.38 ± 0.23 745k ¹ PRASANTH 17 BELL $e^+ e^-$ at $\Upsilon(nS)$'s

¹ PRASANTH 17 also measures A_{Tviol} in sub-regions of the $D^0 \rightarrow K_S \pi^+ \pi^- \pi^0$ phase-space. No evidence of T violation is found.

D^0 CPT-VIOLATING DECAY-RATE ASYMMETRIES

$A_{CPT}(K^\mp \pi^\pm)$ in $D^0 \rightarrow K^- \pi^+, \bar{D}^0 \rightarrow K^+ \pi^-$

$A_{CPT}(t)$ is defined in terms of the time-dependent decay probabilities $P(D^0 \rightarrow K^- \pi^+)$ and $\overline{P}(\bar{D}^0 \rightarrow K^+ \pi^-)$ by $A_{CPT}(t) = (\overline{P} - P) / (\overline{P} + P)$. For small mixing parameters $x \equiv \Delta m / \Gamma$ and $y \equiv \Delta \Gamma / 2\Gamma$ (as is the case), and times t , $A_{CPT}(t)$ reduces to $[y \operatorname{Re} \xi - x \operatorname{Im} \xi] / \Gamma t$, where ξ is the CPT-violating parameter.

The following is actually $y \operatorname{Re} \xi - x \operatorname{Im} \xi$.

VALUE	DOCUMENT ID	TECN	COMMENT
-------	-------------	------	---------

0.0083 ± 0.0065 ± 0.0041 LINK 03B FOCS γ nucleus, $\overline{E}_\gamma \approx 180$ GeV

$D^0 \rightarrow K^*(892)^- \ell^+ \nu_\ell$ FORM FACTORS

$r_V \equiv V(0)/A_1(0)$ in $D^0 \rightarrow K^*(892)^- \ell^+ \nu_\ell$

VALUE	EVTS	DOCUMENT ID	TECN	COMMENT
-------	------	-------------	------	---------

1.46 ± 0.07 OUR AVERAGE

1.46 ± 0.07 ± 0.02	3k	ABLIKIM	19G	BES3 $K^*(892)^- e^+ \nu_e$
1.71 ± 0.68 ± 0.34		LINK	05B	FOCS $K^*(892)^- \mu^+ \nu_\mu$

$r_2 \equiv A_2(0)/A_1(0)$ in $D^0 \rightarrow K^*(892)^- \ell^+ \nu_\ell$

VALUE	EVTS	DOCUMENT ID	TECN	COMMENT
-------	------	-------------	------	---------

0.68 ± 0.06 OUR AVERAGE

0.67 ± 0.06 ± 0.01	3k	ABLIKIM	19G	BES3 $K^*(892)^- e^+ \nu_e$
0.91 ± 0.37 ± 0.10		LINK	05B	FOCS $K^*(892)^- \mu^+ \nu_\mu$

$D^0 \rightarrow K^- / \pi^- \ell^+ \nu_\ell$ FORM FACTORS

$f_+(0)$ in $D^0 \rightarrow K^- \ell^+ \nu_\ell$

VALUE	EVTS	DOCUMENT ID	TECN	COMMENT
-------	------	-------------	------	---------

0.736 ± 0.004 OUR AVERAGE

0.7368 ± 0.0026 ± 0.0036	71k	ABLIKIM	15X	BES3 $\ell = e, 2$ -parameter fit
0.727 ± 0.007 ± 0.009		AUBERT	07Bg	BABR $\ell = e, 2$ -parameter fit

$f_+(0) |V_{cb}|$ in $D^0 \rightarrow K^- \ell^+ \nu_\ell$

VALUE	EVTS	DOCUMENT ID	TECN	COMMENT
-------	------	-------------	------	---------

0.7166 ± 0.0030 OUR AVERAGE

0.7133 ± 0.0038 ± 0.0029	47k	ABLIKIM	19B	BES3 $\ell = \mu, 2$ -parameter fit
0.7172 ± 0.0025 ± 0.0035	71k	¹ ABLIKIM	15X	BES3 $\ell = e, 2$ -parameter fit
0.726 ± 0.008 ± 0.004		BESSION	09	CLEO $\ell = e, 3$ -parameter fit

¹ The 3-parameter fit yields $0.7195 \pm 0.0035 \pm 0.0041$.

$r_1 \equiv a_1/a_0$ in $D^0 \rightarrow K^- \ell^+ \nu_\ell$

VALUE	EVTS	DOCUMENT ID	TECN	COMMENT
-------	------	-------------	------	---------

-2.40 ± 0.16 OUR AVERAGE

-2.33 ± 0.16 ± 0.08	71k	¹ ABLIKIM	15X	BES3 $\ell = e, 3$ -parameter fit
-2.65 ± 0.34 ± 0.08		BESSION	09	CLEO $\ell = e, 3$ -parameter fit

¹ The 2-parameter fit yields $-2.23 \pm 0.09 \pm 0.06$.

Meson Particle Listings

 D^0 $r_2 \equiv a_2/a_0$ in $D^0 \rightarrow K^- \ell^+ \nu_\ell$

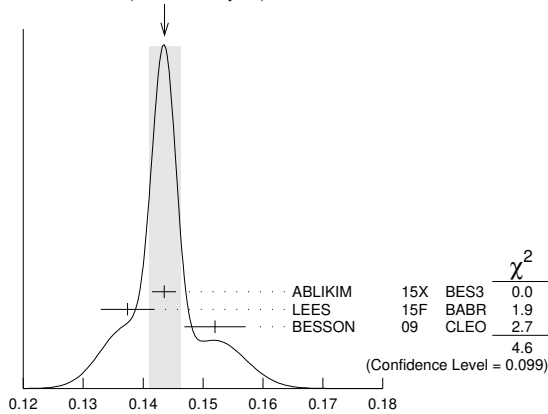
VALUE	EVTS	DOCUMENT ID	TECN	COMMENT
5 ± 4 OUR AVERAGE				
$3.4 \pm 3.9 \pm 2.4$	71k	ABLIKIM	15X BES3	$\ell=e$, 3-parameter fit
$13 \pm 9 \pm 1$		BESSON	09 CLEO	$\ell=e$, 3-parameter fit

 $f_+(0)$ in $D^0 \rightarrow \pi^- \ell^+ \nu_\ell$

VALUE	EVTS	DOCUMENT ID	TECN	COMMENT
$0.6372 \pm 0.0080 \pm 0.0044$ OUR AVERAGE	6.3k	ABLIKIM	15X BES3	$\ell=e$, 2-parameter fit

 $f_+(0)|V_{cd}|$ in $D^0 \rightarrow \pi^- \ell^+ \nu_\ell$

VALUE	EVTS	DOCUMENT ID	TECN	COMMENT
0.1436 ± 0.0026 OUR AVERAGE	Error includes scale factor of 1.5. See the ideogram below.			
$0.1435 \pm 0.0018 \pm 0.0009$	6.3k	¹ ABLIKIM	15X BES3	$\ell=e$, 2-parameter fit
$0.1374 \pm 0.0038 \pm 0.0024$	5.3k	² LEES	15F BABR	$\ell=e$, 3-parameter fit
$0.152 \pm 0.005 \pm 0.001$		BESSON	09 CLEO	$\ell=e$, 3-parameter fit

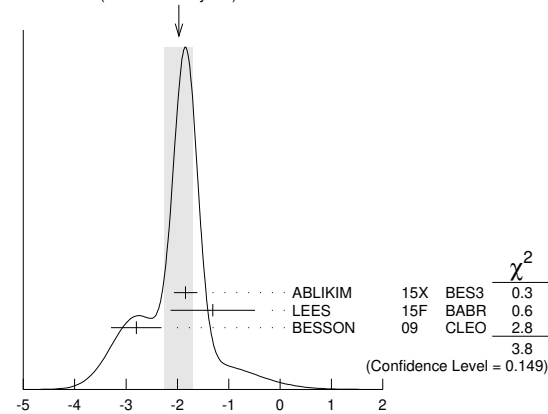
WEIGHTED AVERAGE
0.1436±0.0026 (Error scaled by 1.5) $f_+(0)|V_{cd}|$ in $D^0 \rightarrow \pi^- \ell^+ \nu_\ell$

¹ The 3-parameter fit yields $0.1420 \pm 0.0024 \pm 0.0010$.

² LEES 15F reports a value $0.1374 \pm 0.0038 \pm 0.0022 \pm 0.0009$, where the last uncertainty is due to the uncertainties of the $D^0 \rightarrow K^- \pi^+$ branching fraction.

 $r_1 \equiv a_1/a_0$ in $D^0 \rightarrow \pi^- \ell^+ \nu_\ell$

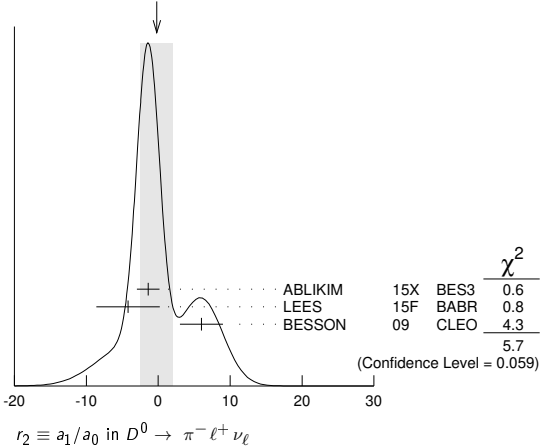
VALUE	EVTS	DOCUMENT ID	TECN	COMMENT
-1.97 ± 0.28 OUR AVERAGE	Error includes scale factor of 1.4. See the ideogram below.			
$-1.84 \pm 0.22 \pm 0.07$	6.3k	¹ ABLIKIM	15X BES3	$\ell=e$, 3-parameter fit
$-1.31 \pm 0.70 \pm 0.43$	5.3k	LEES	15F BABR	$\ell=e$, 3-parameter fit
$-2.80 \pm 0.49 \pm 0.04$		BESSON	09 CLEO	$\ell=e$, 3-parameter fit

WEIGHTED AVERAGE
-1.97±0.28 (Error scaled by 1.4) $r_1 \equiv a_1/a_0$ in $D^0 \rightarrow \pi^- \ell^+ \nu_\ell$

¹ The 2-parameter fit yields $-2.04 \pm 0.08 \pm 0.03$.

 $r_2 \equiv a_1/a_0$ in $D^0 \rightarrow \pi^- \ell^+ \nu_\ell$

VALUE	EVTS	DOCUMENT ID	TECN	COMMENT
-0.2 ± 2.2 OUR AVERAGE	Error includes scale factor of 1.7. See the ideogram below.			
$-1.4 \pm 1.5 \pm 0.5$	6.3k	ABLIKIM	15X BES3	$\ell=e$, 3-parameter fit
$-4.2 \pm 4.0 \pm 1.9$	5.3k	LEES	15F BABR	$\ell=e$, 3-parameter fit
$6 \pm 3 \pm 0$		BESSON	09 CLEO	$\ell=e$, 3-parameter fit

WEIGHTED AVERAGE
-0.2±2.2 (Error scaled by 1.7)

Amplitude analyses

 $D \rightarrow K\pi\pi, D \rightarrow KK\pi\pi$ partial wave analyses

Amplitude analyses of D^0 decays to a variety of 4-body kaon or pion final states, fitting simultaneously different partial wave components.

VALUE	DOCUMENT ID	TECN	COMMENT
¹ AAIJ	19c LHCB		$D^0 \rightarrow K^+ K^- \pi^+ \pi^-$
ABLIKIM	19AK BES3		$D^0 \rightarrow K^- \pi^+ \pi^0 \pi^0$
AAIJ	18AI LHCB		$D^0 \rightarrow K^- \pi^+ \pi^+ \pi^-$
ABLIKIM	17O BES3		$D^0 \rightarrow K^- \pi^+ \pi^+ \pi^-$

¹ AAIJ 19c also provides measurements of CP violation in $D^0 \rightarrow K^+ K^- \pi^+ \pi^-$, with results compatible with CP symmetry.

 D^0 REFERENCES

ABLIKIM	22	PRL 128 011803	M. Ablikim <i>et al.</i>	(BESIII Collab.)
AAIJ	21AB	PRL 127 111801	R. Aaij <i>et al.</i>	(LHCb Collab.)
AAIJ	21AI	PR D104 072010	R. Aaij <i>et al.</i>	(LHCb Collab.)
AAIJ	21X	PR D104 L031102	R. Aaij <i>et al.</i>	(LHCb Collab.)
ABLIKIM	21AA	JHEP 2105 164	M. Ablikim <i>et al.</i>	(BESIII Collab.)
ABLIKIM	21AY	PRL 127 131801	M. Ablikim <i>et al.</i>	(BESIII Collab.)
ABLIKIM	21BA	PR D104 052008	M. Ablikim <i>et al.</i>	(BESIII Collab.)
ABLIKIM	21BC	PR D104 L091103	M. Ablikim <i>et al.</i>	(BESIII Collab.)
ABUDINEN	21A	PRL 127 211801	F. Abudinen <i>et al.</i>	(BELLE II Collab.)
LI	21G	JHEP 2109 075	L.K. Li <i>et al.</i>	(BELLE Collab.)
AAIJ	20	PR D101 012005	R. Aaij <i>et al.</i>	(LHCb Collab.)
ABLIKIM	20AA	PR D102 052003	M. Ablikim <i>et al.</i>	(BESIII Collab.)
ABLIKIM	20AC	PR D102 052006	M. Ablikim <i>et al.</i>	(BESIII Collab.)
ABLIKIM	20AF	PR D102 112005	M. Ablikim <i>et al.</i>	(BESIII Collab.)
ABLIKIM	20G	PR D101 052009	M. Ablikim <i>et al.</i>	(BESIII Collab.)
ABLIKIM	20V	PRL 124 241803	M. Ablikim <i>et al.</i>	(BESIII Collab.)
CHEN	20A	PR D102 012002	Y.Q. Chen <i>et al.</i>	(BELLE Collab.)
LEES	20A	PR D101 112003	J.P. Lees <i>et al.</i>	(BABAR Collab.)
LEES	20B	PRL 124 071802	J.P. Lees <i>et al.</i>	(BABAR Collab.)
NAYAK	20	PR D102 071102	M. Nayak <i>et al.</i>	(BELLE Collab.)
AAIJ	19	PRL 122 011802	R. Aaij <i>et al.</i>	(LHCb Collab.)
AAIJ	19C	JHEP 1902 126	R. Aaij <i>et al.</i>	(LHCb Collab.)
AAIJ	19D	PRL 122 211803	R. Aaij <i>et al.</i>	(LHCb Collab.)
AAIJ	19X	PRL 122 231802	R. Aaij <i>et al.</i>	(LHCb Collab.)
ABLIKIM	19AK	PR D99 092008	M. Ablikim <i>et al.</i>	(BESIII Collab.)
ABLIKIM	19AL	PR D99 112002	M. Ablikim <i>et al.</i>	(BESIII Collab.)
ABLIKIM	19AY	PR D100 072006	M. Ablikim <i>et al.</i>	(BESIII Collab.)
ABLIKIM	19B	PRL 122 011804	M. Ablikim <i>et al.</i>	(BESIII Collab.)
ABLIKIM	19BI	PL B798 135017	M. Ablikim <i>et al.</i>	(BESIII Collab.)
ABLIKIM	19C	PRL 122 062001	M. Ablikim <i>et al.</i>	(BESIII Collab.)
ABLIKIM	19G	PR D99 011103	M. Ablikim <i>et al.</i>	(BESIII Collab.)
KIM	19	PR D99 011104	J.B. Kim <i>et al.</i>	(BELLE Collab.)
LEES	19A	PRL 122 081802	J.P. Lees <i>et al.</i>	(BABAR Collab.)
PDG	19	RPP 2019 at pdg.lbl.gov	M. Tanabashi <i>et al.</i>	(PDG Collab.)
AAIJ	18AI	EPJ C78 443	R. Aaij <i>et al.</i>	(LHCb Collab.)
AAIJ	18AV	JHEP 1811 048	R. Aaij <i>et al.</i>	(LHCb Collab.)
AAIJ	18I	PRL 121 091801	R. Aaij <i>et al.</i>	(LHCb Collab.)
AAIJ	18K	PR D97 031101	R. Aaij <i>et al.</i>	(LHCb Collab.)
ABLIKIM	18AC	PR D98 092009	M. Ablikim <i>et al.</i>	(BESIII Collab.)
ABLIKIM	18AE	PRL 121 171803	M. Ablikim <i>et al.</i>	(BESIII Collab.)
ABLIKIM	18F	PRL 121 081802	M. Ablikim <i>et al.</i>	(BESIII Collab.)
ABLIKIM	18L	PR D97 052005	M. Ablikim <i>et al.</i>	(BESIII Collab.)
ABLIKIM	18P	PR D97 072015	M. Ablikim <i>et al.</i>	(BESIII Collab.)
ABLIKIM	18W	PR D97 072004	M. Ablikim <i>et al.</i>	(BESIII Collab.)
ABLIKIM	18X	PL B781 368	M. Ablikim <i>et al.</i>	(BESIII Collab.)
HARNEW	18	JHEP 1801 144	S. Harnnew <i>et al.</i>	(BRIS, PNNL)
RESMI	18	JHEP 1801 082	P.K. Resmi <i>et al.</i>	
SMITH	18	PR D98 051101	M.J. Smith, D. Cinabro, P. Naik	(LTU, WAYN+)
AAIJ	17AE	PL B769 345	R. Aaij <i>et al.</i>	(LHCb Collab.)
AAIJ	17AK	PRL 118 261803	R. Aaij <i>et al.</i>	(LHCb Collab.)
AAIJ	17AO	PR D95 052004	R. Aaij <i>et al.</i>	(LHCb Collab.)
Also		PR D96 099907 (errata.)	R. Aaij <i>et al.</i>	(LHCb Collab.)
AAIJ	17BG	PRL 119 181805	R. Aaij <i>et al.</i>	(LHCb Collab.)
AAIJ	17M	PL B767 177	R. Aaij <i>et al.</i>	(LHCb Collab.)
ABLIKIM	17A	PL B765 231	M. Ablikim <i>et al.</i>	(BESIII Collab.)
ABLIKIM	17O	PR D95 072010	M. Ablikim <i>et al.</i>	(BESIII Collab.)
DARGENT	17	JHEP 1705 143	P. d'Argent <i>et al.</i>	(HEID, BRIS)
DASH	17	PRL 119 171801	N. Dash <i>et al.</i>	(BELLE Collab.)
LAI	17	PR D95 011102	Y.-T. Lai <i>et al.</i>	(BELLE Collab.)
NANUT	17	PRL 118 051801	T. Nanut <i>et al.</i>	(BELLE Collab.)
PRASANATH	17	PR D95 091101	K. Prasanath <i>et al.</i>	(BELLE Collab.)
AAIJ	16D	PRL 116 131011	R. Aaij <i>et al.</i>	(LHCb Collab.)
AAIJ	16F	PRL 116 241801	R. Aaij <i>et al.</i>	(LHCb Collab.)
AAIJ	16H	PL B754 167	R. Aaij <i>et al.</i>	(LHCb Collab.)
AAIJ	16I	PL B757 558	R. Aaij <i>et al.</i>	(LHCb Collab.)
AAIJ	16N	PR D93 052018	R. Aaij <i>et al.</i>	(LHCb Collab.)

Meson Particle Listings

$D^0, D^{*0}(2007)^0, D^{*0}(2010)^{\pm}$

ALBRECHT	89D	ZPHY C43 181	H. Albrecht et al.	(ARGUS Collab.)
ANJOS	89F	PRL 62 1587	J.C. Anjos et al.	(FNAL E691 Collab.)
ABACHI	88	PL B205 411	S. Abachi et al.	(HRS Collab.)
ADLER	88	PR D37 2023	J. Adler et al.	(Mark III Collab.)
ADLER	88C	PRL 60 89	J. Adler et al.	(Mark III Collab.)
ALBRECHT	88G	PL B209 380	H. Albrecht et al.	(ARGUS Collab.)
ALBRECHT	88I	PL B210 267	H. Albrecht et al.	(ARGUS Collab.)
ANJOS	88C	PRL 60 1239	J.C. Anjos et al.	(FNAL E691 Collab.)
BORTOLETTO	88	PR D37 1719	D. Bortoletto et al.	(CLEO Collab.)
Also		PR D39 1471 (erratum)	D. Bortoletto et al.	(CLEO Collab.)
HAAS	88	PL 60 1614	P. Haas et al.	(CLEO Collab.)
RAAB	88	PR D37 2391	J.R. Raab et al.	(FNAL E691 Collab.)
ADLER	87	PL B196 107	J. Adler et al.	(Mark III Collab.)
AGUILAR...	87E	ZPHY C36 551	M. Aguilar-Benitez et al.	(LEBC-EHS Collab.)
Also		ZPHY C40 321	M. Aguilar-Benitez et al.	(LEBC-EHS Collab.)
AGUILAR...	87F	ZPHY C36 559	M. Aguilar-Benitez et al.	(LEBC-EHS Collab.)
Also		ZPHY C38 520 (erratum)	M. Aguilar-Benitez et al.	(LEBC-EHS Collab.)
BARLAG	87B	ZPHY C37 17	S. Barlag et al.	(ACCMOR Collab.)
BECKER	87C	PL B193 147	J.J. Becker et al.	(Mark III Collab.)
Also		PL B198 590 (erratum)	J.J. Becker et al.	(Mark III Collab.)
PALKA	87	PL B189 238	H. Palka et al.	(ACCMOR Collab.)
RILES	87	PR D35 2914	K. Riles et al.	(Mark II Collab.)
BAILEY	86	ZPHY C30 51	R. Bailey et al.	(ACCMOR Collab.)
BEBEK	86	PRL 56 1893	C. Bebek et al.	(CLEO Collab.)
LOUIS	86	PRL 56 1027	W.C. Louis et al.	(PRIN, CHIC, ISU)
ALBRECHT	85B	PL 158B 525	H. Albrecht et al.	(ARGUS Collab.)
ALBRECHT	85F	PL 150B 235	H. Albrecht et al.	(ARGUS Collab.)
AUBERT	85	PL 155B 461	J.J. Aubert et al.	(EMC Collab.)
BALTRUSAITIS...	85E	PRL 55 150	R.M. Baltrusaitis et al.	(Mark III Collab.)
BENVENUTI	85	PL 158B 531	A.C. Benvenuti et al.	(BCDMS Collab.)
SUMMERS	84	PRL 52 410	D.J. Summers et al.	(UCSB, CARL, COLO+)
BAILEY	83B	PL 132B 237	R. Bailey et al.	(ACCMOR Collab.)
BODEK	82	PL 113B 82	A. Bodek et al.	(ROCH, CIT, CHIC, FNAL+)
SCHINDLER	81	PR D24 78	R.H. Schindler et al.	(Mark II Collab.)
AVERY	80	PRL 44 1309	P. Avery et al.	(ILL, FNAL, COLU)
ABRAMS	79D	PRL 43 481	G.S. Abrams et al.	(Mark II Collab.)
VUILLEMIN	78	PRL 41 1149	V. Vuillemin et al.	(LGW Collab.)
PERUZZI	77	PL 39 1301	I. Peruzzi et al.	(LGW Collab.)
PICCOLO	77	PL 70B 260	M. Piccolo et al.	(Mark I Collab.)
MOSTELLER	48	Am.Stat. 3 No.5 30	R.A. Fisher, F. Mosteller	

OTHER RELATED PAPERS

RICHMAN	95	RMP 67 893	J.D. Richman, P.R. Burchat	(UCSB, STAN)
ROSNER	95	CNPP 21 369	J. Rosner	(CHIC)

$D^*(2007)^0$

$$I(J^P) = \frac{1}{2}(1^-)$$

I, J, P need confirmation.

J consistent with 1, value 0 ruled out (NGUYEN 77).

$D^*(2007)^0$ MASS

The fit includes $D^{\pm}, D^0, D_s^{\pm}, D^{*\pm}, D^{*0}, D_1(2420)^0, D_2^*(2460)^0$, and $D_{s1}(2536)^{\pm}$ mass and mass difference measurements.

VALUE (MeV)	EVTS	DOCUMENT ID	TECN	COMMENT
2006.85 ± 0.05 OUR FIT				Error includes scale factor of 1.1.
•••				We do not use the following data for averages, fits, limits, etc. •••
2006 ± 1.5	1	GOLDBABER 77	MRK1	e^+e^-

¹ From simultaneous fit to $D^*(2010)^+, D^*(2007)^0, D^+$, and D^0 .

$m_{D^*(2007)^0} - m_{D^0}$

The fit includes $D^{\pm}, D^0, D_s^{\pm}, D^{*\pm}, D^{*0}, D_1(2420)^0, D_2^*(2460)^0$, and $D_{s1}(2536)^{\pm}$ mass and mass difference measurements.

VALUE (MeV)	EVTS	DOCUMENT ID	TECN	COMMENT
142.014 ± 0.030 OUR FIT				Error includes scale factor of 1.5.
142.016 ± 0.030 OUR AVERAGE				Error includes scale factor of 1.5.
142.007 ± 0.015 ± 0.014	10k	² TOMARADZE 15	CLEO	$e^+e^- \rightarrow$ hadrons
142.2 ± 0.3 ± 0.2	145	ALBRECHT 95F	ARG	$e^+e^- \rightarrow$ hadrons
142.12 ± 0.05 ± 0.05	1176	BORTOLETTO92B	CLE2	$e^+e^- \rightarrow$ hadrons
•••				We do not use the following data for averages, fits, limits, etc. •••
142.2 ± 2.0		SADROZINSKI 80	CBAL	$D^{*0} \rightarrow D^0\pi^0$
142.7 ± 1.7		³ GOLDBABER 77	MRK1	e^+e^-

² Obtained by analyzing CLEO-c data but not authored by the CLEO Collaboration. This value comes from the average of the results for two decay modes, $D^0 \rightarrow K^-\pi^+$ and $D^0 \rightarrow K^-\pi^+\pi^+$.

³ From simultaneous fit to $D^*(2010)^+, D^*(2007)^0, D^+$, and D^0 .

$D^*(2007)^0$ WIDTH

VALUE (MeV)	CL%	DOCUMENT ID	TECN	COMMENT
<2.1	90	⁴ ABACHI 88B	HRS	$D^{*0} \rightarrow D^+\pi^-$

⁴ Assuming $m_{D^0} = 2007.2 \pm 2.1$ MeV/c².

$D^*(2007)^0$ DECAY MODES

$\bar{D}^*(2007)^0$ modes are charge conjugates of modes below.

Mode	Fraction (Γ_i/Γ)
Γ_1 $D^0\pi^0$	(64.7 ± 0.9) %
Γ_2 $D^0\gamma$	(35.3 ± 0.9) %
Γ_3 $D^0 e^+e^-$	(3.91 ± 0.33) × 10 ⁻³

CONSTRAINED FIT INFORMATION

An overall fit to 2 branching ratios uses 5 measurements and one constraint to determine 2 parameters. The overall fit has a $\chi^2 = 2.5$ for 4 degrees of freedom.

The following off-diagonal array elements are the correlation coefficients $\langle \delta x_i \delta x_j \rangle / (\delta x_i \delta x_j)$, in percent, from the fit to the branching fractions, $x_i \equiv \Gamma_i/\Gamma_{\text{total}}$. The fit constrains the x_i whose labels appear in this array to sum to one.

$$x_2 \begin{bmatrix} -100 \\ x_1 \end{bmatrix}$$

$D^*(2007)^0$ BRANCHING RATIOS

$\Gamma(D^0\pi^0)/\Gamma(D^0\gamma)$	Γ_1/Γ_2
1.83 ± 0.07 OUR FIT	
1.85 ± 0.07 OUR AVERAGE	
1.90 ± 0.07 ± 0.05	4.9k
1.74 ± 0.02 ± 0.13	

Error includes scale factor of 1.1.

VALUE	EVTS	DOCUMENT ID	TECN	COMMENT
1.90 ± 0.07 ± 0.05	4.9k	ABLIKIM 15B	BES3	10.6 $e^+e^- \rightarrow$ hadrons
1.74 ± 0.02 ± 0.13		AUBERT, BE 05G	BABR	10.6 $e^+e^- \rightarrow$ hadrons

$\Gamma(D^0 e^+ e^-)/\Gamma(D^0\gamma)$	Γ_3/Γ_2
11.08 ± 0.76 ± 0.49	
1.90 ± 0.07 ± 0.05	4.9k
1.74 ± 0.02 ± 0.13	

VALUE (units 10 ⁻³)	EVTS	DOCUMENT ID	TECN	COMMENT
11.08 ± 0.76 ± 0.49	421	ABLIKIM 21BD	BES3	4.178 GeV e^+e^-

$\Gamma(D^0\pi^0)/\Gamma_{\text{total}}$	Γ_1/Γ
0.647 ± 0.009 OUR FIT	
•••	
0.655 ± 0.008 ± 0.005	3.2k
0.635 ± 0.003 ± 0.017	69k
0.596 ± 0.035 ± 0.028	858
0.636 ± 0.023 ± 0.033	1097

••• We do not use the following data for averages, fits, limits, etc. •••

VALUE	EVTS	DOCUMENT ID	TECN	COMMENT
0.655 ± 0.008 ± 0.005	3.2k	⁵ ABLIKIM 15B	BES3	$e^+e^- \rightarrow$ hadrons
0.635 ± 0.003 ± 0.017	69k	⁵ AUBERT, BE 05G	BABR	10.6 $e^+e^- \rightarrow$ hadrons
0.596 ± 0.035 ± 0.028	858	⁶ ALBRECHT 95F	ARG	$e^+e^- \rightarrow$ hadrons
0.636 ± 0.023 ± 0.033	1097	⁶ BUTLER 92	CLE2	$e^+e^- \rightarrow$ hadrons

$\Gamma(D^0\gamma)/\Gamma_{\text{total}}$	Γ_2/Γ
0.353 ± 0.009 OUR FIT	
0.381 ± 0.029 OUR AVERAGE	
0.404 ± 0.035 ± 0.028	456
0.364 ± 0.023 ± 0.033	621
0.37 ± 0.08 ± 0.08	

••• We do not use the following data for averages, fits, limits, etc. •••

0.345 ± 0.008 ± 0.005 1.8k ⁵ABLIKIM 15B BES3 $e^+e^- \rightarrow$ hadrons

0.365 ± 0.003 ± 0.017 68k ⁵AUBERT, BE 05G BABR 10.6 $e^+e^- \rightarrow$ hadrons

0.47 ± 0.23 LOW 87 HRS 29 GeV e^+e^-

0.53 ± 0.13 BARTEL 85G JADE e^+e^- , hadrons

0.47 ± 0.12 COLES 82 MRK2 e^+e^-

0.45 ± 0.15 GOLDBABER 77 MRK1 e^+e^-

⁵ Derived from the ratio $\Gamma(D^0\pi^0)/\Gamma(D^0\gamma)$ assuming that the branching fractions of $D^{*0} \rightarrow D^0\pi^0$ and $D^{*0} \rightarrow D^0\gamma$ decays sum to 100%

⁶ The BUTLER 92 and ALBRECHT 95F branching ratios are not independent, they have been constrained by the authors to sum to 100%.

$D^*(2007)^0$ REFERENCES

ABLIKIM 21BD	PR D104 112012	M. Ablikim et al.	(BESIII Collab.)
ABLIKIM 15B	PR D91 031101	M. Ablikim et al.	(BESIII Collab.)
TOMARADZE 15	PR D91 011102	A. Tomaradze et al.	(NWES)
AUBERT, BE 05G	PR D72 091101	B. Aubert et al.	(BABAR Collab.)
ALBRECHT 95F	ZPHY C66 63	H. Albrecht et al.	(ARGUS Collab.)
BORTOLETTO 92B	PRL 69 2046	D. Bortoletto et al.	(CLEO Collab.)
BUTLER 92	PRL 69 2041	F. Butler et al.	(CLEO Collab.)
ABACHI 88B	PL B212 533	S. Abachi et al.	(ANL, IND, MICH, PURD+)
ADLER 88D	PL B208 152	J. Adler et al.	(Mark III Collab.)
LOW 87	PL B183 232	E.H. Low et al.	(HRS Collab.)
BARTEL 85G	PL 161B 197	W. Bartel et al.	(JADE Collab.)
COLES 82	PR D26 2190	M.W. Coles et al.	(LBL, SLAC)
SADROZINSKI 80	Madison Conf. 681	H.F.W. Sadrozinski et al.	(PRIN, CIT+)
GOLDBABER 77	PL 69B 503	G. Goldhaber et al.	(Mark I Collab.)
NGUYEN 77	PRL 39 262	H.K. Nguyen et al.	(LBL, SLAC) J

$D^*(2010)^{\pm}$

$$I(J^P) = \frac{1}{2}(1^-)$$

I, J, P need confirmation.

$D^*(2010)^{\pm}$ MASS

The fit includes $D^{\pm}, D^0, D_s^{\pm}, D^{*\pm}, D^{*0}, D_1(2420)^0, D_2^*(2460)^0$, and $D_{s1}(2536)^{\pm}$ mass and mass difference measurements.

VALUE (MeV)	DOCUMENT ID	TECN	CHG	COMMENT
2101.26 ± 0.05 OUR FIT				

See key on page 1127

Meson Particle Listings

$D^*(2010)^\pm$

••• We do not use the following data for averages, fits, limits, etc. •••
 2008 ±3 1 GOLDHABER 77 MRK1 ± e^+e^-
 2008.6 ±1.0 2 PERUZZI 77 LGW ± e^+e^-
 1 From simultaneous fit to $D^*(2010)^\pm$, $D^*(2007)^0$, D^+ , and D^0 ; not independent of FELDMAN 77B mass difference below.
 2 PERUZZI 77 mass not independent of FELDMAN 77B mass difference below and PERUZZI 77 D^0 mass value.

$m_{D^*(2010)^+} - m_{D^+}$

The fit includes D^\pm , D^0 , D_s^\pm , $D^{*\pm}$, D^{*0} , $D_s^{*\pm}$, $D_1(2420)^0$, $D_2^*(2460)^0$, and $D_{s1}(2536)^\pm$ mass and mass difference measurements.

VALUE (MeV)	EVTS	DOCUMENT ID	TECN	COMMENT
140.603 ±0.015 OUR FIT				
140.602 ±0.014 OUR AVERAGE				
140.6010 ±0.0068 ±0.0129	151k	LEES	17F BABR	$e^+e^- \rightarrow$ hadrons
140.64 ±0.08 ±0.06	620	BORTOLETTO92B	CLE2	$e^+e^- \rightarrow$ hadrons

$m_{D^*(2010)^+} - m_{D^0}$

The fit includes D^\pm , D^0 , D_s^\pm , $D^{*\pm}$, D^{*0} , $D_s^{*\pm}$, $D_1(2420)^0$, $D_2^*(2460)^0$, and $D_{s1}(2536)^\pm$ mass and mass difference measurements.

VALUE (MeV)	EVTS	DOCUMENT ID	TECN	COMMENT
145.4258 ±0.0017 OUR FIT				
145.4258 ±0.0020 OUR AVERAGE				
145.4259 ±0.0004 ±0.0017	312.8k	LEES	13x BABR	$D^{*\pm} \rightarrow D^0 \pi^\pm \rightarrow (K\pi, K3\pi)\pi^\pm$
145.412 ±0.002 ±0.012		ANASTASSOV 02	CLE2	$D^{*\pm} \rightarrow D^0 \pi^\pm \rightarrow (K\pi)\pi^\pm$
145.54 ±0.08	611	3 ADINOLFI 99	BEAT	$D^{*\pm} \rightarrow D^0 \pi^\pm$
145.45 ±0.02		3 BREITWEG 99	ZEUS	$D^{*\pm} \rightarrow D^0 \pi^\pm \rightarrow (K\pi)\pi^\pm$
145.42 ±0.05		3 BREITWEG 99	ZEUS	$D^{*\pm} \rightarrow D^0 \pi^\pm \rightarrow (K^-3\pi)\pi^\pm$
145.5 ±0.15	103	4 ADLOFF 97B	H1	$D^{*\pm} \rightarrow D^0 \pi^\pm$
145.44 ±0.08	152	4 BREITWEG 97	ZEUS	$D^{*\pm} \rightarrow D^0 \pi^\pm$
145.42 ±0.11	199	4 BREITWEG 97	ZEUS	$D^{*0} \rightarrow D^0 \pi^\pm, D^0 \rightarrow K^-3\pi, D^0 \rightarrow K^-3\pi^+$
145.4 ±0.2	48	4 DERRICK 95	ZEUS	$D^{*\pm} \rightarrow D^0 \pi^\pm$
145.39 ±0.06 ±0.03		BARLAG 92B	ACCM	$\pi^- 230$ GeV
145.5 ±0.2	115	4 ALEXANDER 91B	OPAL	$D^{*\pm} \rightarrow D^0 \pi^\pm$
145.30 ±0.06		4 DECAMP 91J	ALEP	$D^{*\pm} \rightarrow D^0 \pi^\pm$
145.40 ±0.05 ±0.10		ABACHI 88B	HRS	$D^{*\pm} \rightarrow D^0 \pi^\pm$
145.46 ±0.07 ±0.03		ALBRECHT 85F	ARG	$D^{*\pm} \rightarrow D^0 \pi^\pm$
145.5 ±0.3	28	BAILEY 83	SPEC	$D^{*\pm} \rightarrow D^0 \pi^\pm$
145.5 ±0.3	60	FITCH 81	SPEC	$\pi^- A$
145.3 ±0.5	30	FELDMAN 77B	MRK1	$D^{*+} \rightarrow D^0 \pi^+$

••• We do not use the following data for averages, fits, limits, etc. •••
 145.4256 ±0.0006 ±0.0017 138.5k LEES 13x BABR $D^{*\pm} \rightarrow D^0 \pi^\pm \rightarrow (K^- \pi^+) \pi^\pm$
 145.4266 ±0.0005 ±0.0019 174.3k LEES 13x BABR $D^{*\pm} \rightarrow D^0 \pi^\pm \rightarrow (K^- 2\pi^+ \pi^-) \pi^\pm$
 145.44 ±0.09 122 4 BREITWEG 97B ZEUS $D^{*0} \rightarrow D^0 \pi^\pm, D^0 \rightarrow K^- \pi^+, D^0 \rightarrow K^- \pi^+$
 145.8 ±1.5 16 AHLEN 83 HRS $D^{*+} \rightarrow D^0 \pi^+$
 145.1 ±1.8 12 BAILEY 83 SPEC $D^{*+} \rightarrow D^0 \pi^+$
 145.1 ±0.5 14 BAILEY 83 SPEC $D^{*+} \rightarrow D^0 \pi^+$
 145.5 ±0.5 14 YELTON 82 MRK2 29 $e^+e^- \rightarrow K^- \pi^+$
 ~145.5 AVERY 80 SPEC γA
 145.2 ±0.6 2 BLIETSCHAU 79 BEBC νp

3 Statistical errors only.
 4 Systematic error not evaluated.

$m_{D^*(2010)^+} - m_{D^*(2007)^0}$

VALUE (MeV)	DOCUMENT ID	TECN	COMMENT
2.6 ±1.8	5 PERUZZI 77	LGW	e^+e^-

••• We do not use the following data for averages, fits, limits, etc. •••
 5 Not independent of FELDMAN 77B mass difference above, PERUZZI 77 D^0 mass, and GOLDHABER 77 $D^*(2007)^0$ mass.

$D^*(2010)^\pm$ WIDTH

VALUE (keV)	CL%	EVTS	DOCUMENT ID	TECN	COMMENT
83.4 ±1.8 OUR AVERAGE					
83.3 ±1.2 ±1.4		312.8k	6 LEES	13x BABR	$D^{*\pm} \rightarrow D^0 \pi^\pm \rightarrow (K\pi, K3\pi)\pi^\pm$
96 ±4 ±22			6 ANASTASSOV 02	CLE2	$D^{*\pm} \rightarrow D^0 \pi^\pm \rightarrow (K\pi)\pi^\pm$

••• We do not use the following data for averages, fits, limits, etc. •••
 83.4 ±1.7 ±1.5 138.5k 6 LEES 13x BABR $D^{*\pm} \rightarrow D^0 \pi^\pm \rightarrow (K^- \pi^+) \pi^\pm$
 83.2 ±1.5 ±2.6 174.3k 6 LEES 13x BABR $D^{*\pm} \rightarrow D^0 \pi^\pm \rightarrow (K^- 2\pi^+ \pi^-) \pi^\pm$
 <131 90 110 BARLAG 92B ACCM $\pi^- 230$ GeV
 6 Ignoring the electromagnetic contribution from $D^{*\pm} \rightarrow D^\pm \gamma$.

$D^*(2010)^\pm$ DECAY MODES

$D^*(2010)^-$ modes are charge conjugates of the modes below.

Mode	Fraction (Γ_i/Γ)
Γ_1 $D^0 \pi^+$	(67.7 ±0.5) %
Γ_2 $D^+ \pi^0$	(30.7 ±0.5) %
Γ_3 $D^+ \gamma$	(1.6 ±0.4) %

CONSTRAINED FIT INFORMATION

An overall fit to 3 branching ratios uses 6 measurements and one constraint to determine 3 parameters. The overall fit has a $\chi^2 = 0.3$ for 4 degrees of freedom.

The following *off-diagonal* array elements are the correlation coefficients $\langle \delta x_i \delta x_j \rangle / (\delta x_i \delta x_j)$, in percent, from the fit to the branching fractions, $x_i \equiv \Gamma_i/\Gamma_{total}$. The fit constrains the x_i whose labels appear in this array to sum to one.

x_2	-62	
x_3	-43	-44
	x_1	x_2

$D^*(2010)^+$ BRANCHING RATIOS

$\Gamma(D^0 \pi^+)/\Gamma_{total}$	VALUE	DOCUMENT ID	TECN	COMMENT	Γ_1/Γ
0.677 ±0.005 OUR FIT					
0.677 ±0.006 OUR AVERAGE					
0.6759 ±0.0029 ±0.0064	7,8,9	BARTELT 98	CLE2	e^+e^-	
0.688 ±0.024 ±0.013		ALBRECHT 95F	ARG	$e^+e^- \rightarrow$ hadrons	
0.681 ±0.010 ±0.013	7	BUTLER 92	CLE2	$e^+e^- \rightarrow$ hadrons	
••• We do not use the following data for averages, fits, limits, etc. •••					
0.57 ±0.04 ±0.04		ADLER 88D	MRK3	e^+e^-	
0.44 ±0.10		COLES 82	MRK2	e^+e^-	
0.6 ±0.15		9 GOLDHABER 77	MRK1	e^+e^-	

$\Gamma(D^+ \pi^0)/\Gamma_{total}$	VALUE	EVTS	DOCUMENT ID	TECN	COMMENT	Γ_2/Γ
0.307 ±0.005 OUR FIT						
0.3073 ±0.0013 ±0.0062						
0.312 ±0.011 ±0.008	1404		ALBRECHT 95F	ARG	$e^+e^- \rightarrow$ hadrons	
0.308 ±0.004 ±0.008	410	7	BUTLER 92	CLE2	$e^+e^- \rightarrow$ hadrons	
0.26 ±0.02 ±0.02			ADLER 88D	MRK3	e^+e^-	
0.34 ±0.07			COLES 82	MRK2	e^+e^-	

$\Gamma(D^+ \gamma)/\Gamma_{total}$	VALUE	CL%	EVTS	DOCUMENT ID	TECN	COMMENT	Γ_3/Γ
0.016 ±0.004 OUR FIT							
0.016 ±0.005 OUR AVERAGE							
0.0168 ±0.0042 ±0.0029			7,8	BARTELT 98	CLE2	e^+e^-	
0.011 ±0.014 ±0.016			12	7 BUTLER 92	CLE2	$e^+e^- \rightarrow$ hadrons	

••• We do not use the following data for averages, fits, limits, etc. •••
 <0.052 90 ALBRECHT 95F ARG $e^+e^- \rightarrow$ hadrons
 0.17 ±0.05 ±0.05 ADLER 88D MRK3 e^+e^-
 0.22 ±0.12 10 COLES 82 MRK2 e^+e^-

7 The branching ratios are not independent, they have been constrained by the authors to sum to 100%.
 8 Systematic error includes theoretical error on the prediction of the ratio of hadronic modes.
 9 Assuming that isospin is conserved in the decay.
 10 Not independent of $\Gamma(D^0 \pi^+)/\Gamma_{total}$ and $\Gamma(D^+ \pi^0)/\Gamma_{total}$ measurement.

$D^*(2010)^\pm$ REFERENCES

LEES 17F	PRL 119 202003	J.P. Lees et al.	(BABAR Collab.)
LEES 13X	PRL 111 111801	J.P. Lees et al.	(BABAR Collab.)
Also	PR D88 052003	J.P. Lees et al.	(BABAR Collab.)
Also	PR D88 079902 (err.)	J.P. Lees et al.	(BABAR Collab.)
ANASTASSOV 02	PR D65 032003	A. Anastassov et al.	(CLEO Collab.)
ADINOLFI 99	NP B547 3	M. Adinolfi et al.	(Beatrice Collab.)
BREITWEG 99	EPJ C6 67	J. Breitweg et al.	(ZEUS Collab.)
BARTELT 98	PRL 80 3919	J. Bartelt et al.	(CLEO Collab.)
ADLOFF 97B	ZPHY C72 593	C. Adloff et al.	(HI Collab.)
BREITWEG 97	PL B401 192	J. Breitweg et al.	(ZEUS Collab.)

Meson Particle Listings

 $D^*(2010)^\pm, D_0^*(2300), D_1(2420)$

BREITWEG	97B	PL B407 402	J. Breitweg <i>et al.</i>	(ZEUS Collab.)
ALBRECHT	95F	ZPHY C66 63	H. Albrecht <i>et al.</i>	(ARGUS Collab.)
DERRICK	95	PL B349 225	M. Derrick <i>et al.</i>	(ZEUS Collab.)
BARLAG	92B	PL B278 480	S. Barlag <i>et al.</i>	(ACCMOR Collab.)
BORTOLETTO	92B	PRL 69 2046	D. Bortoletto <i>et al.</i>	(CLEO Collab.)
BUTLER	92	PRL 69 2041	F. Butler <i>et al.</i>	(CLEO Collab.)
ALEXANDER	91B	PL B262 341	G. Alexander <i>et al.</i>	(OPAL Collab.)
DECAMP	91J	PL B266 218	D. Decamp <i>et al.</i>	(ALEPH Collab.)
ABACHI	88B	PL B212 533	S. Abachi <i>et al.</i>	(ANL, IND, MICH, PURD+)
ADLER	88D	PL B208 152	J. Adler <i>et al.</i>	(Mark III Collab.)
ALBRECHT	85F	PL 150B 235	H. Albrecht <i>et al.</i>	(ARGUS Collab.)
AHLEN	83	PRL 51 1147	S.P. Ahlen <i>et al.</i>	(ANL, IND, LBL+)
BAILEY	83	PL 132B 230	R. Bailey <i>et al.</i>	(AMST, BRIS, CERN, CRAC+)
COLES	82	PR D26 2190	M.W. Coles <i>et al.</i>	(LBL, SLAC)
YELTON	82	PRL 49 430	J.M. Yelton <i>et al.</i>	(SLAC, LBL, UCB+)
FITCH	81	PRL 46 761	V.L. Fitch <i>et al.</i>	(PRIN, SACL, TORI+)
AVERY	80	PRL 44 1309	P. Avery <i>et al.</i>	(ILL, FNAL, COLU)
BLIETSCHAU	79	PL 86B 108	J. Blietschau <i>et al.</i>	(AACH3, BONN, CERN+)
FELDMAN	77B	PL 38 1313	G.J. Feldman <i>et al.</i>	(Mark I Collab.)
GOLDHABER	77	PL 69B 503	G. Goldhaber <i>et al.</i>	(Mark I Collab.)
PERUZZI	77	PRL 39 1301	I. Peruzzi <i>et al.</i>	(LGV Collab.)

 $D_0^*(2300)$

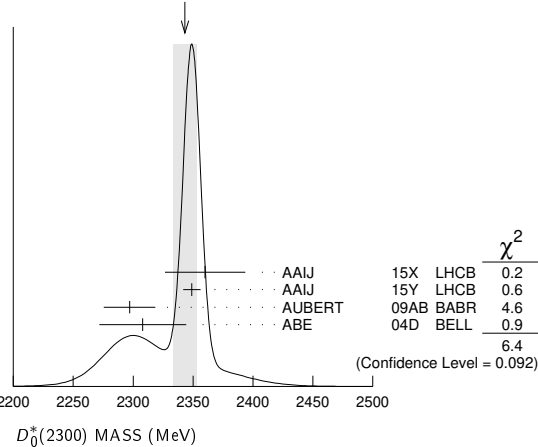
$$I(J^P) = \frac{1}{2}(0^+)$$

was $D_0^*(2400)$

There is a strong evidence that recent data on $B \rightarrow D\pi\pi$ (AAIJ 15Y, AAIJ 16AH) and $B \rightarrow D\pi K$ (AAIJ 14BH, AAIJ 15V, AAIJ 15X) call for two poles in the scalar $I = 1/2$ πD amplitude in this mass range. The data are consistent with a lower pole at $(2105^{+6}_{-8}) - i(102^{+10}_{-11})$ MeV and a higher pole at $(2451^{+35}_{-26}) - i(134^{+7}_{-8})$ MeV (DU 18A, DU 19, DU 21). For details see review on "Heavy Non- $q\bar{q}$ Mesons."

 $D_0^*(2300)$ MASS

VALUE (MeV)	EVTs	DOCUMENT ID	TECN	CHG	COMMENT
2343 ± 10 OUR AVERAGE	Error	includes scale factor of 1.5. See the ideogram below.			
2360 ± 15 ± 30		¹ AAIJ	15X	LHCB	+ $B^0 \rightarrow \bar{D}^0 K^+ \pi^-$
2349 ± 6 ± 4		² AAIJ	15Y	LHCB	+ $B^0 \rightarrow \bar{D}^0 \pi^+ \pi^-$
2297 ± 8 ± 20	3.4k	AUBERT	09AB	BABR	0 $B^- \rightarrow D^+ \pi^- \pi^-$
2308 ± 17 ± 32		ABE	04D	BELL	0 $B^- \rightarrow D^+ \pi^- \pi^-$
••• We do not use the following data for averages, fits, limits, etc. •••					
2354 ± 7 ± 11		³ AAIJ	15Y	LHCB	+ $B^0 \rightarrow \bar{D}^0 \pi^+ \pi^-$
2403 ± 14 ± 35	18.8k	⁴ LINK	04A	FOCS	+ γA
2407 ± 21 ± 35	9.8k	⁴ LINK	04A	FOCS	0 γA

WEIGHTED AVERAGE
2343±10 (Error scaled by 1.5)

- From the Dalitz plot analysis including various K^* and D^{**} mesons as well as broad structures in the $K\pi$ S-wave and the $D\pi$ S- and P-waves.
- Modeling the $\pi^+\pi^-$ S-wave with the Isobar formalism.
- Modeling the $\pi^+\pi^-$ S-wave with the K-matrix formalism.

 $D_0^*(2300)$ WIDTH

VALUE (MeV)	EVTs	DOCUMENT ID	TECN	CHG	COMMENT
229 ± 16 OUR AVERAGE					
255 ± 26 ± 51		¹ AAIJ	15X	LHCB	+ $B^0 \rightarrow \bar{D}^0 K^+ \pi^-$
217 ± 13 ± 13		² AAIJ	15Y	LHCB	+ $B^0 \rightarrow \bar{D}^0 \pi^+ \pi^-$
273 ± 12 ± 48	3.4k	AUBERT	09AB	BABR	0 $B^- \rightarrow D^+ \pi^- \pi^-$
276 ± 21 ± 63		ABE	04D	BELL	0 $B^- \rightarrow D^+ \pi^- \pi^-$

••• We do not use the following data for averages, fits, limits, etc. •••

230 ± 15 ± 21		³ AAIJ	15Y	LHCB	+ $B^0 \rightarrow \bar{D}^0 \pi^+ \pi^-$
283 ± 24 ± 34	18.8k	⁴ LINK	04A	FOCS	+ γA
240 ± 55 ± 59	9.8k	⁴ LINK	04A	FOCS	0 γA

- From the Dalitz plot analysis including various K^* and D^{**} mesons as well as broad structures in the $K\pi$ S-wave and the $D\pi$ S- and P-waves.
- Modeling the $\pi^+\pi^-$ S-wave with the Isobar formalism.
- Modeling the $\pi^+\pi^-$ S-wave with the K-matrix formalism.
- Possibly the feed-down from another state.

 $D_0^*(2300)$ DECAY MODES

Mode	Fraction (Γ_i/Γ)
$\Gamma_1 D\pi^\pm$	seen

$\Gamma(D\pi^\pm)/\Gamma_{total}$	VALUE	EVTs	DOCUMENT ID	TECN	CHG	COMMENT	Γ_1/Γ
seen			AAIJ	15X	LHCB	+ $D^*(2300)^+ \rightarrow D^0 \pi^+$	
seen			AAIJ	15Y	LHCB	+ $D^*(2300)^+ \rightarrow D^0 \pi^+$	
seen	3.4k		AUBERT	09AB	BABR	0 $D^*(2300)^0 \rightarrow D^+ \pi^-$	
seen			ABE	04D	BELL	0 $D^*(2300)^0 \rightarrow D^+ \pi^-$	
seen	18.8k		LINK	04A	FOCS	+ $D^*(2300)^+ \rightarrow D^0 \pi^+$	

 $D_0^*(2300)$ REFERENCES

DU	21	PRL 126 192001	M.-L. Du <i>et al.</i>	
DU	19	PR D99 114002	M.-L. Du, F.-K. Guo, U.-G. Meissner	
DU	18A	PR D98 094018	M.-L. Du <i>et al.</i>	
AAIJ	16AH	PR D94 072001	R. Aaij <i>et al.</i>	(LHCb Collab.)
AAIJ	15V	PR D91 092002	R. Aaij <i>et al.</i>	(LHCb Collab.)
Also	AAIJ	PR D93 119901 (errat.)	R. Aaij <i>et al.</i>	(LHCb Collab.)
AAIJ	15X	PR D92 012012	R. Aaij <i>et al.</i>	(LHCb Collab.)
AAIJ	15Y	PR D92 032002	R. Aaij <i>et al.</i>	(LHCb Collab.)
AAIJ	14BH	PR D90 072003	R. Aaij <i>et al.</i>	(LHCb Collab.)
AUBERT	09AB	PR D79 112004	B. Aubert <i>et al.</i>	(BABAR Collab.)
ABE	04D	PR D69 112002	K. Abe <i>et al.</i>	(BELLE Collab.)
LINK	04A	PL B586 11	J.M. Link <i>et al.</i>	(FOCUS Collab.)

 $D_1(2420)$

$$I(J^P) = \frac{1}{2}(1^+)$$

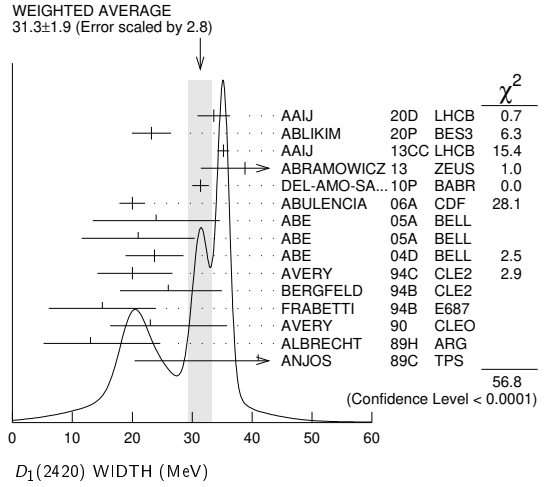
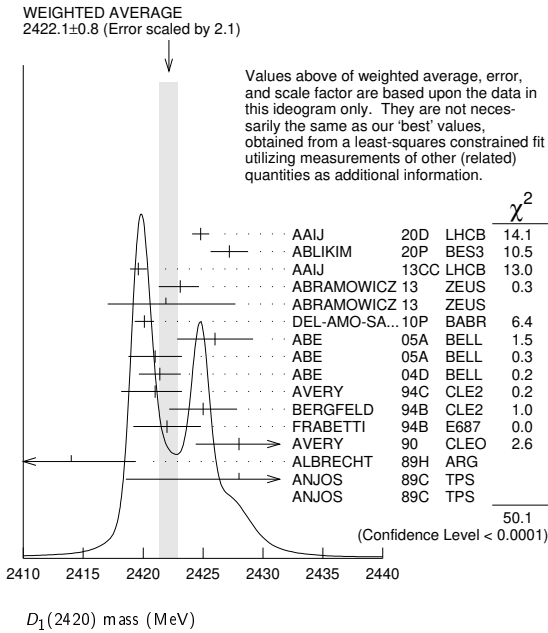
 $D_1(2420)$ MASS

The fit includes $D^\pm, D_0^0, D_s^\pm, D_s^{*+}, D_s^{*0}, D_s^{*\pm}, D_1(2420)^0, D_2^*(2460)^0$, and $D_{s1}(2536)^\pm$ mass and mass difference measurements.

VALUE (MeV)	EVTs	DOCUMENT ID	TECN	CHG	COMMENT	
2422.1 ± 0.6 OUR FIT	Error	includes scale factor of 1.7.				
2422.1 ± 0.8 OUR AVERAGE	Error	includes scale factor of 2.1. See the ideogram below.				
2424.8 ± 0.1 ± 0.7	79k	¹ AAIJ	20D	LHCB	0 $B^- \rightarrow D^{*+} \pi^- \pi^-$	
2427.2 ± 1.0 ± 1.2	4207	ABLIKIM	20P	BES3	+ $e^+ e^- \rightarrow D^{*+} \pi^- \pi^- X$	
2419.6 ± 0.1 ± 0.7	210k	AAIJ	13cc	LHCB	0 $pp \rightarrow D^{*+} \pi^- X$	
2423.1 ± 1.5 ± 0.4	2.7k	² ABRAMOWICZ13	ZEUS	0	$e^\pm p \rightarrow D^{(*)+} \pi^- X$	
2421.9 ± 4.7 ± 3.4	759	³ ABRAMOWICZ13	ZEUS	+	$e^\pm p \rightarrow D^{(*)0} \pi^+ X$	
2420.1 ± 0.1 ± 0.8	103k	DEL-AMO-SA..10P	BABR	0	$e^+ e^- \rightarrow D^{*+} \pi^- X$	
2426 ± 3 ± 1	151	ABE	05A	BELL	0 $B^- \rightarrow D^0 \pi^+ \pi^- \pi^-$	
2428 ± 2 ± 1	124	ABE	05A	BELL	+ $\bar{B}^0 \rightarrow D^+ \pi^+ \pi^- \pi^-$	
2421.4 ± 1.5 ± 0.9		⁴ ABE	04D	BELL	0 $B^- \rightarrow D^{*+} \pi^- \pi^-$	
2421 ± 1 ± 2	± 2	286	AVERY	94c	CLE2	0 $e^+ e^- \rightarrow D^{*+} \pi^- X$
2425 ± 2 ± 2	146	BERGFELD	94B	CLE2	+ $e^+ e^- \rightarrow D^{*0} \pi^+ X$	
2422 ± 2 ± 2	51	FRABETTI	94B	E687	0 $\gamma Be \rightarrow D^{*+} \pi^- X$	
2428 ± 3 ± 2	279	AVERY	90	CLEO	0 $e^+ e^- \rightarrow D^{*+} \pi^- X$	
2414 ± 2 ± 5	171	ALBRECHT	89H	ARG	0 $e^+ e^- \rightarrow D^{*+} \pi^- X$	
2428 ± 8 ± 5	171	ANJOS	89c	TPS	0 $\gamma N \rightarrow D^{*+} \pi^- X$	
2443 ± 7 ± 5	190	ANJOS	89c	TPS	+ $\gamma N \rightarrow D^0 \pi^+ X^0$	
••• We do not use the following data for averages, fits, limits, etc. •••						
2420.5 ± 2.1 ± 0.9	3.1k	⁵ CHEKANOV	09	ZEUS	0 $e^\pm p \rightarrow D^{*+} \pi^- X$	
2421.7 ± 0.7 ± 0.6	7.5k	ABULENCIA	06A	CDF	0 $1900 p\bar{p} \rightarrow D^{*+} \pi^- X$	
2425 ± 3 ± 3	235	⁶ ABREU	98M	DLPH	0 $e^+ e^- \rightarrow D^{*+} \pi^- X$	

- From a full four-body amplitude analysis of the $B^- \rightarrow D^{*+} \pi^- \pi^-$ decay.
- From the combined fit of the $M(D^+ \pi^-)$ and $M(D^{*+} \pi^-)$ distributions. and A_{D_2} fixed to the theoretical prediction of -1 .
- From the fit of the $M(D^0 \pi^+)$ distribution. The widths of the D_1^+ and D_s^{*+} are fixed to 25 MeV and 37 MeV, and A_{D_1} and A_{D_2} are fixed to the theoretical predictions of 3 and -1 , respectively.
- Fit includes the contribution from $D_1^*(2430)^0$.
- Calculated using the mass difference $m(D_1^0) - m(D^{*+})_{PDG}$ reported below and $m(D^{*+})_{PDG} = 2010.27 \pm 0.17$ MeV. The 0.17 MeV uncertainty of the PDG mass value should be added to the experimental uncertainty of 0.9 MeV.

⁶ No systematic error given.



$D_1(2420)$ DECAY MODES

$\bar{D}_1(2420)$ modes are charge conjugates of modes below.

Mode	Fraction (Γ_i/Γ)
Γ_1 $D^*(2007)^0 \pi$	seen
Γ_2 $D \pi^+ \pi^-$	
Γ_3 $D \rho^0$	
Γ_4 $D f_0(500)$	
Γ_5 $D_0^*(2300)^0 \pi$	
Γ_6 $D^0 \pi$	
Γ_7 $D^* \pi^+ \pi^-$	

$D_1(2420)$ BRANCHING RATIOS

Mode	Value	Document ID	TECN	CHG	COMMENT	Γ_i/Γ
$\Gamma(D^*(2007)^0 \pi)/\Gamma_{total}$						
seen		ACKERSTAFF	97W OPAL	0	$e^+e^- \rightarrow D^{*+} \pi^- X$	
seen		AVERY	90 CLEO	0	$e^+e^- \rightarrow D^{*+} \pi^- X$	
seen		ALBRECHT	89H ARG	0	$e^+e^- \rightarrow D^* \pi^- X$	
seen		ANJOS	89c TPS	0	$\gamma N \rightarrow D^{*+} \pi^- X$	
seen		ANJOS	89c TPS	+	$\gamma N \rightarrow D^0 \pi^+ X^0$	

Mode	Value	CL%	Document ID	TECN	CHG	COMMENT	Γ_6/Γ_1
$\Gamma(D^0 \pi)/\Gamma(D^*(2007)^0 \pi)$							
<0.18		90	BERGFELD	94B CLE2	+	$e^+e^- \rightarrow \text{hadrons}$	
•••						We do not use the following data for averages, fits, limits, etc. •••	
<0.24		90	AVERY	90 CLEO	0	$e^+e^- \rightarrow D^+ \pi^- X$	

$D_1(2420)$ POLARIZATION AMPLITUDE A_{D_1}

A polarization amplitude A_{D_1} is a parameter that depends on the initial polarization of the D_1 and is sensitive to a possible S-wave contribution to its decay. For D_1 decays the helicity angle, θ_h , distribution varies like $1 + A_{D_1} \cos^2 \theta_h$, where θ_h is the angle in the D^* rest frame between the two pions emitted by the $D_1 \rightarrow D^* \pi$ and the $D^* \rightarrow D \pi$.

Unpolarized D_1 decaying purely via D-wave is predicted to give $A_{D_1} = 3$.

Mode	Value	EVTS	Document ID	TECN	CHG	COMMENT
5.73 ± 0.25 OUR AVERAGE						
7.8 ^{+6.7} _{-2.7} ± 4.6 ^{+4.6} _{-1.8}	2.7k	1	ABRAMOWICZ13	ZEUS	0	$e^\pm p \rightarrow D^{(*)+} \pi^- X$
5.72 ± 0.25	103k		DEL-AMO-SA...10P	BABR	0	$e^+ e^- \rightarrow D^{*+} \pi^- X$
5.9 ^{+3.0} _{-1.7} ± 2.4 ^{+2.4} _{-1.0}			CHEKANOV	09 ZEUS	0	$e^\pm p \rightarrow D^{*+} \pi^- X$
•••						We do not use the following data for averages, fits, limits, etc. •••
3.30 ± 0.48	210k	2	AAIJ	13cc LHCb	0	$pp \rightarrow D^{*+} \pi^- X$
3.8 ± 0.6 ± 0.8		3	AUBERT	09y BABR	0	$B^+ \rightarrow D_1^0 \ell^+ \nu_\ell$
3.8 ± 0.6 ± 0.8		3	AUBERT	09y BABR	+	$B^0 \rightarrow D_1^- \ell^+ \nu_\ell$
2.74 ^{+1.40} _{-0.93}		4	AVERY	94c CLE2	0	$e^+ e^- \rightarrow D^{*+} \pi^- X$

¹ From the combined fit of the $M(D^+ \pi^-)$ and $M(D^{*+} \pi^-)$ distributions. and A_{D_2} fixed to the theoretical prediction of -1. A pure D-wave not excluded although some S-wave mixing possible.

² Systematic uncertainty not estimated. Resonance parameters fixed.

³ Assuming $\Gamma(\Upsilon(4S) \rightarrow B^+ B^-) / \Gamma(\Upsilon(4S) \rightarrow B^0 \bar{B}^0) = 1.065 \pm 0.026$ and equal partial widths and helicity angle distributions for charged and neutral D_1 mesons.

⁴ Systematic uncertainties not estimated.

$m_{D_1(2420)^0} - m_{D^{*+}}$

The fit includes $D^\pm, D^0, D_s^\pm, D^{* \pm}, D^{*0}, D_s^{* \pm}, D_1(2420)^0, D_2^*(2460)^0$, and $D_{s1}(2536)^\pm$ mass and mass difference measurements.

VALUE (MeV)	EVTS	DOCUMENT ID	TECN	COMMENT
411.8 ± 0.6 OUR FIT				Error includes scale factor of 1.7.
411.5 ± 0.8 OUR AVERAGE				
410.2 ± 2.1 ± 0.9	3.1k	CHEKANOV	09 ZEUS	$e^\pm p \rightarrow D^{*+} \pi^- X$
411.7 ± 0.7 ± 0.4	7.5k	ABULENCIA	06A CDF	1900 $p\bar{p} \rightarrow D^{*+} \pi^- X$

$m_{D_1(2420)^\pm} - m_{D_1(2420)^0}$

VALUE (MeV)	DOCUMENT ID	TECN	COMMENT
4⁺²₋₃ ± 3	BERGFELD	94B CLE2	$e^+ e^- \rightarrow \text{hadrons}$

$D_1(2420)$ WIDTH

VALUE (MeV)	EVTS	DOCUMENT ID	TECN	CHG	COMMENT
31.3 ± 1.9 OUR AVERAGE					Error includes scale factor of 2.8. See the ideogram below.
33.6 ± 0.3 ± 2.7	79k	¹ AAIJ	20D LHCb	0	$B^- \rightarrow D^{*+} \pi^- \pi^-$
23.2 ± 2.3 ± 2.3	4207	ABLIKIM	20P BES3	+	$e^+ e^- \rightarrow D^+ \pi^- \pi^-$
35.2 ± 0.4 ± 0.9	210k	AAIJ	13cc LHCb	0	$pp \rightarrow D^{*+} \pi^- X$
38.8 ± 5.0 ^{+1.9} _{-5.4}	2.7k	² ABRAMOWICZ13	ZEUS	0	$e^\pm p \rightarrow D^{(*)+} \pi^- X$
31.4 ± 0.5 ± 1.3	103k	DEL-AMO-SA...10P	BABR	0	$e^+ e^- \rightarrow D^{*+} \pi^- X$
20.0 ± 1.7 ± 1.3	7.5k	ABULENCIA	06A CDF	0	1900 $p\bar{p} \rightarrow D^{*+} \pi^- X$
24 ± 7 ± 8	151	ABE	05A BELL	0	$B^- \rightarrow D^0 \pi^+ \pi^- \pi^-$
21 ± 5 ± 8	124	ABE	05A BELL	+	$\bar{B}^0 \rightarrow D^+ \pi^+ \pi^- \pi^-$
23.7 ± 2.7 ± 4.0		³ ABE	04D BELL	0	$B^- \rightarrow D^{*+} \pi^- \pi^-$
20 ⁺⁶ ₋₅ ± 3	286	AVERY	94c CLE2	0	$e^+ e^- \rightarrow D^{*+} \pi^- X$
26 ⁺⁸ ₋₇ ± 4	146	BERGFELD	94B CLE2	+	$e^+ e^- \rightarrow D^{*0} \pi^+ X$
15 ± 8 ± 4	51	FRABETTI	94B E687	0	$\gamma Be \rightarrow D^{*+} \pi^- X$
23 ⁺⁸ ₋₆ ± 10 ⁺¹⁰ ₋₃	279	AVERY	90 CLEO	0	$e^+ e^- \rightarrow D^{*+} \pi^- X$
13 ± 6 ± 10 ⁺¹⁰ ₋₅	171	ALBRECHT	89H ARG	0	$e^+ e^- \rightarrow D^{*+} \pi^- X$
41 ± 19 ± 8	190	ANJOS	89c TPS	+	$\gamma N \rightarrow D^0 \pi^+ X^0$
•••					We do not use the following data for averages, fits, limits, etc. •••
53.2 ± 7.2 ^{+3.3} _{-4.9}	3.1k	CHEKANOV	09 ZEUS	0	$e^\pm p \rightarrow D^{*+} \pi^- X$
58 ± 14 ± 10	171	ANJOS	89c TPS	0	$\gamma N \rightarrow D^{*+} \pi^- X$

¹ From a full four-body amplitude analysis of the $B^- \rightarrow D^{*+} \pi^- \pi^-$ decay.

² From the combined fit of the $M(D^+ \pi^-)$ and $M(D^{*+} \pi^-)$ distributions. and A_{D_2} fixed to the theoretical prediction of -1.

³ Fit includes the contribution from $D_1^*(2430)^0$.

Meson Particle Listings

$D_1(2420)$, $D_1(2430)^0$, $D_2^*(2460)$

$D_1(2420)$ REFERENCES

AAIJ	20D	PR D101 032005	R. Aaij <i>et al.</i>	(LHCb Collab.)
ABLIKIM	20P	PL B804 135395	M. Ablikim <i>et al.</i>	(BESIII Collab.)
AAIJ	13CC	JHEP 1309 145	R. Aaij <i>et al.</i>	(LHCb Collab.)
ABRAMOWICZ	13	NP B866 229	H. Abramowicz <i>et al.</i>	(ZEUS Collab.)
DEL-AMO-SA...	10P	PR D82 111101	P. del Amo Sanchez <i>et al.</i>	(BABAR Collab.)
AUBERT	09Y	PRL 103 051803	B. Aubert <i>et al.</i>	(BABAR Collab.)
CHEKANOV	09	EPJ C60 25	S. Chekanov <i>et al.</i>	(ZEUS Collab.)
ABULENCIA	06A	PR D73 051104	A. Abulencia <i>et al.</i>	(CDF Collab.)
ABE	05A	PRL 94 221805	K. Abe <i>et al.</i>	(BELLE Collab.)
ABE	04D	PR D69 112002	K. Abe <i>et al.</i>	(BELLE Collab.)
ABREU	98M	PL B426 231	P. Abreu <i>et al.</i>	(DELPHI Collab.)
ACKERSTAFF	97W	ZPHY C76 425	K. Ackerstaff <i>et al.</i>	(OPAL Collab.)
AVERY	94C	PL B331 236	P. Avery <i>et al.</i>	(CLEO Collab.)
BERGFELD	94B	PL B340 194	T. Bergfeld <i>et al.</i>	(CLEO Collab.)
FRABETTI	94B	PRL 72 324	PL. Frabetti <i>et al.</i>	(FNAL E87 Collab.)
AVERY	90	PR D41 774	P. Avery, D. Besson	(CLEO Collab.)
ALBRECHT	89H	PL B232 398	H. Albrecht <i>et al.</i>	(ARGUS Collab.) JP
ANJOS	89C	PRL 62 1717	J.C. Anjos <i>et al.</i>	(FNAL E691 Collab.)

$D_1(2430)^0$

$$I(J^P) = \frac{1}{2}(1^+)$$

$J^P = 1^+$ determined by AAIJ 20D.

$D_1(2430)^0$ MASS

VALUE (MeV)	EVTS	DOCUMENT ID	TECN	COMMENT
2412 ± 9	OUR AVERAGE			
$2411 \pm 3 \pm 9$	79k	¹ AAIJ	20D LHCb	$B^- \rightarrow D^{*+} \pi^- \pi^-$
$2427 \pm 26 \pm 25$		ABE	04D BELL	$B^- \rightarrow D^{*+} \pi^- \pi^-$
2477 ± 28		² AUBERT	06L BABR	$\bar{B}^0 \rightarrow D^{*+} \omega \pi^-$

• • • We do not use the following data for averages, fits, limits, etc. • • •

¹ From a full four-body amplitude analysis of the $B^- \rightarrow D^{*+} \pi^- \pi^-$ decay.
² Systematic errors not estimated.

$D_1(2430)^0$ WIDTH

VALUE (MeV)	EVTS	DOCUMENT ID	TECN	COMMENT
314 ± 29	OUR AVERAGE			
$309 \pm 9 \pm 28$	79k	¹ AAIJ	20D LHCb	$B^- \rightarrow D^{*+} \pi^- \pi^-$
$384^{+107}_{-75} \pm 74$		ABE	04D BELL	$B^- \rightarrow D^{*+} \pi^- \pi^-$
266 ± 97		² AUBERT	06L BABR	$\bar{B}^0 \rightarrow D^{*+} \omega \pi^-$

• • • We do not use the following data for averages, fits, limits, etc. • • •

¹ From a full four-body amplitude analysis of the $B^- \rightarrow D^{*+} \pi^- \pi^-$ decay.
² Systematic errors not estimated.

$D_1(2430)^0$ DECAY MODES

Mode	Fraction (Γ_i/Γ)
Γ_1 $D^*(2010)^+ \pi^-$	seen

$D_1(2430)^0$ REFERENCES

AAIJ	20D	PR D101 032005	R. Aaij <i>et al.</i>	(LHCb Collab.) JP
AUBERT	06L	PR D74 012001	B. Aubert <i>et al.</i>	(BABAR Collab.)
ABE	04D	PR D69 112002	K. Abe <i>et al.</i>	(BELLE Collab.)

$D_2^*(2460)$

$$I(J^P) = \frac{1}{2}(2^+)$$

$D_2^*(2460)$ MASS

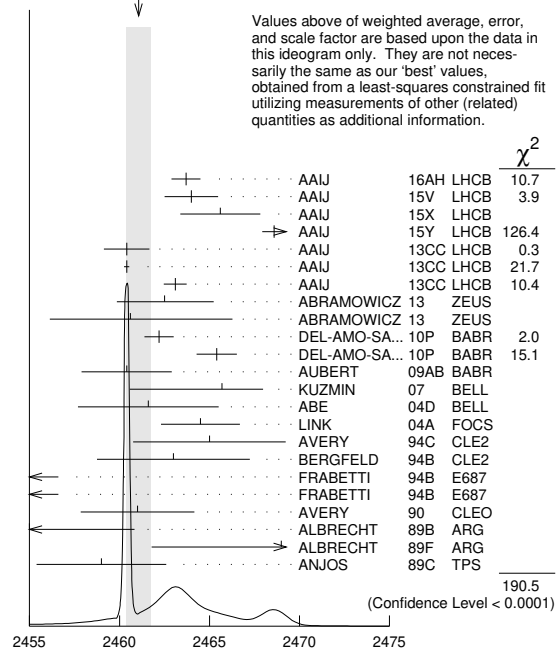
The fit includes D^{\pm} , D^0 , D_s^{\pm} , $D^* \pi^{\pm}$, D^{*0} , D_s^{*+} , $D_1(2420)^0$, $D_2^*(2460)^0$, and $D_{s1}(2536)^{\pm}$ mass and mass difference measurements.

VALUE (MeV)	EVTS	DOCUMENT ID	TECN	CHG	COMMENT
2461.1 ± 0.7	OUR FIT				Error includes scale factor of 6.2.
2461.1 ± 0.7	OUR AVERAGE				Error includes scale factor of 5.2. See the ideogram below.
$2463.7 \pm 0.4 \pm 0.7$	28k	¹ AAIJ	16AH LHCb	0	$B^- \rightarrow D^+ \pi^- \pi^-$
$2464.0 \pm 1.4 \pm 0.5$	2k	² AAIJ	15V LHCb	0	$B^- \rightarrow D^+ K^- \pi^-$
$2465.6 \pm 1.8 \pm 1.3$		³ AAIJ	15X LHCb	+	$B^0 \rightarrow \bar{D}^0 K^+ \pi^-$
$2468.6 \pm 0.6 \pm 0.3$		⁴ AAIJ	15Y LHCb	+	$B^0 \rightarrow \bar{D}^0 \pi^+ \pi^-$
$2460.4 \pm 0.4 \pm 1.2$	82k	AAIJ	13CC LHCb	0	$pp \rightarrow D^{*+} \pi^- X$
$2460.4 \pm 0.1 \pm 0.1$	675k	AAIJ	13CC LHCb	0	$pp \rightarrow D^+ \pi^- X$
$2463.1 \pm 0.2 \pm 0.6$	342k	AAIJ	13CC LHCb	+	$pp \rightarrow D^0 \pi^+ X$
$2462.5 \pm 2.4 \pm 1.3$	2.3k	⁵ ABRAMOWICZ13	ZEUS	0	$e^{\pm} p \rightarrow D^{(*)} \pi^- X$
$2460.6 \pm 4.4 \pm 3.6$	1371	⁶ ABRAMOWICZ13	ZEUS	+	$e^{\pm} p \rightarrow D^{(*)0} \pi^+ X$
$2462.2 \pm 0.1 \pm 0.8$	243k	DEL-AMO-SA..10P	BABR	0	$e^+ e^- \rightarrow D^+ \pi^- X$
$2465.4 \pm 0.2 \pm 1.1$	111k	⁷ DEL-AMO-SA..10P	BABR	+	$e^+ e^- \rightarrow D^0 \pi^+ X$
$2460.4 \pm 1.2 \pm 2.2$	3.4k	AUBERT	09AB BABR	0	$B^- \rightarrow D^+ \pi^- \pi^-$

$2465.7 \pm 1.8^{+1.4}_{-4.8}$	2909	KUZMIN	07 BELL	+	$e^+ e^- \rightarrow \text{hadrons}$
$2461.6 \pm 2.1 \pm 3.3$		⁸ ABE	04D BELL	0	$B^- \rightarrow D^+ \pi^- \pi^-$
$2464.5 \pm 1.1 \pm 1.9$	5.8k	⁸ LINK	04A FOCUS	0	γA
$2465 \pm 3 \pm 3$	486	AVERY	94C CLE2	0	$e^+ e^- \rightarrow D^+ \pi^- X$
$2463 \pm 3 \pm 3$	310	BERGFELD	94B CLE2	+	$e^+ e^- \rightarrow D^0 \pi^+ X$
$2453 \pm 3 \pm 2$	128	FRABETTI	94B E687	0	$\gamma Be \rightarrow D^+ \pi^- X$
$2453 \pm 3 \pm 2$	185	FRABETTI	94B E687	+	$\gamma Be \rightarrow D^0 \pi^+ X$
$2461 \pm 3 \pm 1$	440	AVERY	90 CLEO	0	$e^+ e^- \rightarrow D^{*+} \pi^- X$
$2455 \pm 3 \pm 5$	337	ALBRECHT	89B ARG	0	$e^+ e^- \rightarrow D^+ \pi^- X$
$2469 \pm 4 \pm 6$		ALBRECHT	89F ARG	+	$e^+ e^- \rightarrow D^0 \pi^+ X$
$2459 \pm 3 \pm 2$	153	ANJOS	89C TPS	0	$\gamma N \rightarrow D^+ \pi^- X$
$2468.1 \pm 0.6 \pm 0.5$		⁹ AAIJ	15Y LHCb	+	$B^0 \rightarrow \bar{D}^0 \pi^+ \pi^-$
$2469.1 \pm 3.7^{+1.2}_{-1.3}$	1.5k	¹⁰ CHEKANOV	09 ZEUS	0	$e^{\pm} p \rightarrow D^{(*)} \pi^- X$
$2463.3 \pm 0.6 \pm 0.8$	20k	ABULENCIA	06A CDF	0	$1900 p\bar{p} \rightarrow D^+ \pi^- X$
$2467.6 \pm 1.5 \pm 0.8$	3.5k	¹¹ LINK	04A FOCUS	+	γA
2461 ± 6	126	¹² ABREU	98M DLPH	0	$e^+ e^-$
2466 ± 7	1	ASRATYAN	95 BEBC	0	$53,40 \nu(\bar{\nu}) \rightarrow pX, dX$

• • • We do not use the following data for averages, fits, limits, etc. • • •

WEIGHTED AVERAGE
2461.1±0.7 (Error scaled by 5.2)



$D_2^*(2460)$ mass (MeV)

- From the amplitude analysis in the model describing the $D^+ \pi^-$ wave together with virtual contributions from the $D^{*0}(2007)^0$ and B^{*0} states, and components corresponding to the $D_2^*(2460)^0$, $D_1^*(2680)^0$, $D_3^*(2760)^0$, and $D_2^*(3000)^0$ resonances.
- From the amplitude analysis in the model describing the $D^+ \pi^-$ wave together with virtual contributions from the $D^{*0}(2007)^0$ and B^{*0} states, nonresonant spin-0 and spin-1 components as well as the $D_0^*(2400)^0$, $D_2^*(2460)^0$ and $D_3^*(2760)^0$ resonances.
- From the Dalitz plot analysis including various K^* and D^{**} mesons as well as broad structures in the $K\pi$ S-wave and the $D\pi$ S- and P-waves.
- Modeling the $\pi^+ \pi^-$ S-wave with the Isobar formalism.
- From the combined fit of the $M(D^+ \pi^-)$ and $M(D^{*+} \pi^-)$ distributions. and A_{D_2} fixed to the theoretical prediction of -1 .
- From the fit of the $M(D^0 \pi^+)$ distribution. The widths of the D_1^+ and D_2^{*+} are fixed to 25 MeV and 37 MeV, and A_{D_1} and A_{D_2} are fixed to the theoretical predictions of 3 and -1 , respectively.
- At a fixed width of 50.5 MeV.
- Fit includes the contribution from $D_0^*(2400)^0$.
- Modeling the $\pi^+ \pi^-$ S-wave with the K-matrix formalism.
- Calculated using the mass difference $m(D_2^{*0}) - m(D^{*+})_{PDG}$ reported below and $m(D^{*+})_{PDG} = 2010.27 \pm 0.17$ MeV. The 0.17 MeV uncertainty of the PDG mass value should be added to the experimental uncertainty of $\pm 1.2^{+1.2}_{-1.3}$ MeV.
- Fit includes the contribution from $D_0^*(2400)^{\pm}$. Not independent of the corresponding mass difference measurement, $(m_{D_2^*(2460)^{\pm}} - (m_{D_2^*(2460)^0})$.
- No systematic error given.

See key on page 1127

Meson Particle Listings

 $D_2^*(2460)$ $m_{D_2^*(2460)^0} - m_{D^+}$

The fit includes $D^{\pm}, D^0, D_s^{\pm}, D^{*\pm}, D^{*0}, D_s^{*\pm}, D_1(2420)^0, D_2^*(2460)^0$, and $D_{s1}(2536)^{\pm}$ mass and mass difference measurements.

VALUE (MeV)	EVTS	DOCUMENT ID	TECN	COMMENT
591.5^{+0.7}_{-0.8} OUR FIT				Error includes scale factor of 5.9.
593.9\pm0.6\pm0.5	20k	ABULENCIA	06A	CDF 1900 $p\bar{p} \rightarrow D^+\pi^-X$

 $m_{D_2^*(2460)^0} - m_{D^{*+}}$

The fit includes $D^{\pm}, D^0, D_s^{\pm}, D^{*\pm}, D^{*0}, D_s^{*\pm}, D_1(2420)^0, D_2^*(2460)^0$, and $D_{s1}(2536)^{\pm}$ mass and mass difference measurements.

VALUE (MeV)	EVTS	DOCUMENT ID	TECN	COMMENT
450.9^{+0.7}_{-0.8} OUR FIT				Error includes scale factor of 5.9.
458.8\pm3.7\pm1.2_{-1.3}	1.5k	CHEKANOV	09	ZEUS $e^{\pm}p \rightarrow D^{(*)}\pi^-X$

 $m_{D_2^*(2460)^{\pm}} - m_{D_2^*(2460)^0}$

VALUE (MeV)	DOCUMENT ID	TECN	CHG	COMMENT
3.4\pm1.7 OUR AVERAGE				
3.1 \pm 1.9 \pm 0.9	LINK	04A	FOCS	γA
- 2 \pm 4 \pm 4	BERGFELD	94B	CLE2	$e^+e^- \rightarrow$ hadrons
0 \pm 4	FRABETTI	94B	E687	$\gamma Be \rightarrow D\pi X$
14 \pm 5 \pm 8	ALBRECHT	89F	ARG	$e^+e^- \rightarrow D^0\pi^+X$

 $D_2^*(2460)$ WIDTH

VALUE (MeV)	EVTS	DOCUMENT ID	TECN	CHG	COMMENT
47.3\pm0.8 OUR AVERAGE					Error includes scale factor of 1.5. See the ideogram below.
47.0 \pm 0.8 \pm 1.0	28k	¹ AAIJ	16AH	LHCB	0 $B^- \rightarrow D^+\pi^-\pi^-$
43.8 \pm 2.9 \pm 1.8	2k	² AAIJ	15V	LHCB	0 $B^- \rightarrow D^+K^-\pi^-$
46.0 \pm 3.4 \pm 3.2		³ AAIJ	15X	LHCB	+ $B^0 \rightarrow \bar{D}^0 K^+\pi^-$
47.3 \pm 1.5 \pm 0.7		⁴ AAIJ	15Y	LHCB	+ $B^0 \rightarrow \bar{D}^0 \pi^+\pi^-$
43.2 \pm 1.2 \pm 3.0	82k	AAIJ	13CC	LHCB	0 $pp \rightarrow D^{*+}\pi^-X$
45.6 \pm 0.4 \pm 1.1	675k	AAIJ	13CC	LHCB	0 $pp \rightarrow D^+\pi^-X$
48.6 \pm 1.3 \pm 1.9	342k	AAIJ	13CC	LHCB	+ $pp \rightarrow D^0\pi^+X$
46.6 \pm 8.1 \pm 5.9 _{-3.8}	2.3k	⁵ ABRAMOWICZ13	ZEUS	0	$e^{\pm}p \rightarrow D^{(*)}\pi^-X$
50.5 \pm 0.6 \pm 0.7	243k	DEL-AMO-SA..10P	BABR	0	$e^+e^- \rightarrow D^+\pi^-X$
41.8 \pm 2.5 \pm 2.9	3.4k	AUBERT	09AB	BABR	0 $B^- \rightarrow D^+\pi^-\pi^-$
49.7 \pm 3.8 \pm 6.4	2909	KUZMIN	07	BELL	+ $e^+e^- \rightarrow$ hadrons
49.2 \pm 2.3 \pm 1.3	20k	ABULENCIA	06A	CDF	0 1900 $p\bar{p} \rightarrow D^+\pi^-X$
45.6 \pm 4.4 \pm 6.7		⁶ ABE	04D	BELL	0 $B^- \rightarrow D^+\pi^-\pi^-$
38.7 \pm 5.3 \pm 2.9	5.8k	⁶ LINK	04A	FOCS	0 γA
34.1 \pm 6.5 \pm 4.2	3.5k	⁷ LINK	04A	FOCS	+ γA
28 \pm $\frac{9}{7}$ \pm 6	486	AVERY	94C	CLE2	0 $e^+e^- \rightarrow D^+\pi^-X$
27 \pm $\frac{11}{8}$ \pm 5	310	BERGFELD	94B	CLE2	+ $e^+e^- \rightarrow D^0\pi^+X$
25 \pm 10 \pm 5	128	FRABETTI	94B	E687	0 $\gamma Be \rightarrow D^+\pi^-X$
23 \pm 9 \pm 5	185	FRABETTI	94B	E687	+ $\gamma Be \rightarrow D^0\pi^+X$
20 \pm $\frac{9}{-12}$ \pm $\frac{9}{-10}$	440	AVERY	90	CLEO	0 $e^+e^- \rightarrow D^{*+}\pi^-X$
15 \pm $\frac{13}{-10}$ \pm $\frac{5}{-10}$	337	ALBRECHT	89B	ARG	0 $e^+e^- \rightarrow D^+\pi^-X$
20 \pm 10 \pm 5	153	ANJOS	89C	TPS	0 $\gamma N \rightarrow D^+\pi^-X$
46.0 \pm 1.4 \pm 1.8		⁸ AAIJ	15Y	LHCB	+ $B^0 \rightarrow \bar{D}^0\pi^+\pi^-$

¹ From the amplitude analysis in the model describing the $D^+\pi^-$ wave together with virtual contributions from the $D^*(2007)^0$ and B^{*0} states, and components corresponding to the $D_2^*(2460)^0, D_1^*(2680)^0, D_3^*(2760)^0$, and $D_2^*(3000)^0$ resonances.

² From the amplitude analysis in the model describing the $D^+\pi^-$ wave together with virtual contributions from the $D^*(2007)^0$ and B^{*0} states, nonresonant spin-0 and spin-1 components as well as the $D_0^*(2400)^0, D_2^*(2460)^0$ and $D_1^*(2760)^0$ resonances.

³ From the Dalitz plot analysis including various K^* and D^{**} mesons as well as broad structures in the $K\pi S$ -wave and the $D\pi S$ - and P -waves.

⁴ Modeling the $\pi^+\pi^-\pi^-$ S-wave with the Isobar formalism.

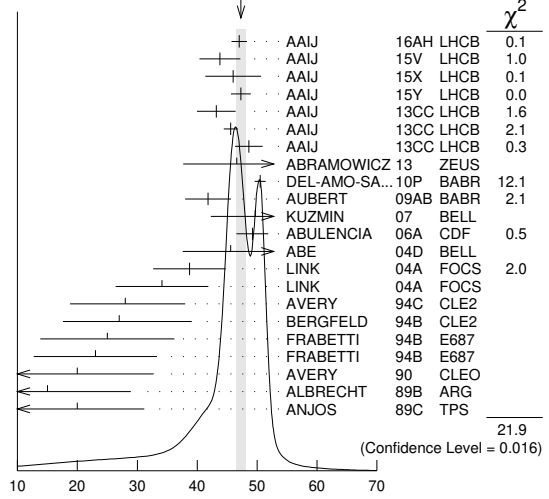
⁵ From the combined fit of the $M(D^+\pi^-)$ and $M(D^{*+}\pi^-)$ distributions. and A_{D_2} fixed to the theoretical prediction of -1 .

⁶ Fit includes the contribution from $D_0^*(2400)^0$.

⁷ Fit includes the contribution from $D_0^*(2400)^{\pm}$.

⁸ Modeling the $\pi^+\pi^-\pi^-$ S-wave with the K-matrix formalism.

WEIGHTED AVERAGE
47.3 \pm 0.8 (Error scaled by 1.5)



$D_2^*(2460)$ width (MeV)

 $D_2^*(2460)$ DECAY MODES

$\bar{D}_2^*(2460)$ modes are charge conjugates of modes below.

Mode	Fraction (Γ_i/Γ)
Γ_1 $D\pi^-$	seen
Γ_2 $D^*(2010)\pi^-$	seen
Γ_3 $D\pi^+\pi^-$	
Γ_4 $D^*\pi^+\pi^-$	

 $D_2^*(2460)$ BRANCHING RATIOS

$\Gamma(D\pi^-)/\Gamma_{total}$	Γ_1/Γ				
VALUE	EVTS	DOCUMENT ID	TECN	CHG	COMMENT
seen	3.4k	AUBERT	09AB	BABR	0 $B^- \rightarrow D^+\pi^-\pi^-$
seen	337	ALBRECHT	89B	ARG	0 $e^+e^- \rightarrow D^+\pi^-X$
seen		ALBRECHT	89F	ARG	+ $e^+e^- \rightarrow D^0\pi^+X$
seen		ANJOS	89C	TPS	0 $\gamma N \rightarrow D^+\pi^-X$

$\Gamma(D^*(2010)\pi^-)/\Gamma_{total}$	Γ_2/Γ			
VALUE	DOCUMENT ID	TECN	CHG	COMMENT
seen	ACKERSTAFF	97W	OPAL	0 $e^+e^- \rightarrow D^{*+}\pi^-X$
seen	AVERY	90	CLEO	0 $e^+e^- \rightarrow D^{*+}\pi^-X$
seen	ALBRECHT	89H	ARG	0 $e^+e^- \rightarrow D^*\pi^-X$

 $\Gamma(D\pi^-)/\Gamma(D^*(2010)\pi^-)$

VALUE	EVTS	DOCUMENT ID	TECN	CHG	COMMENT
1.52\pm0.14 OUR AVERAGE					
1.4 \pm 0.3 \pm 0.3	2.3k	¹ ABRAMOWICZ13	ZEUS	0	$e^{\pm}p \rightarrow D^{(*)}\pi^-X$
1.1 \pm 0.4 \pm $\frac{0.3}{-0.2}$	1371	² ABRAMOWICZ13	ZEUS	+	$e^{\pm}p \rightarrow D^{(*)0}\pi^+X$
1.47 \pm 0.03 \pm 0.16	379k	DEL-AMO-SA..10P	BABR	0	$e^+e^- \rightarrow D^{(*)}\pi^-X$
2.8 \pm 0.8 \pm $\frac{0.5}{-0.6}$	1.5k	CHEKANOV	09	ZEUS	0 $e^{\pm}p \rightarrow D^{(*)}\pi^-X$
2.2 \pm 0.7 \pm 0.6		AVERY	94C	CLE2	0 $e^+e^- \rightarrow D^{*+}\pi^-X$
1.9 \pm 1.1 \pm 0.3		BERGFELD	94B	CLE2	+ $e^+e^- \rightarrow$ hadrons
2.3 \pm 0.8		AVERY	90	CLEO	0 e^+e^-
3.0 \pm 1.1 \pm 1.5		ALBRECHT	89H	ARG	0 $e^+e^- \rightarrow D^*\pi^-X$

• • • We do not use the following data for averages, fits, limits, etc. • • •

1.9 \pm 0.5 ABE 04D BELL 0 $B^- \rightarrow D^{(*)}\pi^-\pi^-$

¹ From the combined fit of the $M(D^+\pi^-)$ and $M(D^{*+}\pi^-)$ distributions. and A_{D_2} fixed to the theoretical prediction of -1 .

² From the fit of the $M(D^0\pi^+)$ distribution. The widths of the D_1^+ and D_2^+ are fixed to 25 MeV and 37 MeV, and A_{D_1} and A_{D_2} are fixed to the theoretical predictions of 3 and -1 , respectively.

Meson Particle Listings

$D_2^*(2460)$, $D_0(2550)^0$, $D_1^*(2600)^0$

$\Gamma(D\pi^-)/[\Gamma(D\pi^-) + \Gamma(D^*(2010)\pi^-)]$ $\Gamma_1/(\Gamma_1+\Gamma_2)$

VALUE	EVTS	DOCUMENT ID	TECN	CHG	COMMENT
• • • We do not use the following data for averages, fits, limits, etc. • • •					
$0.62 \pm 0.03 \pm 0.02$	8414	¹ AUBERT	09Y	BABR 0	$B^+ \rightarrow D_2^{*0} \ell^+ \nu_\ell$
$0.62 \pm 0.03 \pm 0.02$	3361	¹ AUBERT	09Y	BABR +	$\bar{B}^0 \rightarrow D_2^{*+} \ell^- \nu_\ell$
¹ Assuming $\Gamma(\Upsilon(4S) \rightarrow B^+ B^-) / \Gamma(\Upsilon(4S) \rightarrow B^0 \bar{B}^0) = 1.065 \pm 0.026$ and equal partial widths for charged and neutral D_2^* mesons.					

$D_2^*(2460)$ POLARIZATION AMPLITUDE A_{D_2}

A polarization amplitude A_{D_2} is a parameter that depends on the initial polarization of the D_2 . For D_2 decays the helicity angle, θ_H , distribution varies like $1 + A_{D_2} \cos^2(\theta_H)$, where θ_H is the angle in the D^* rest frame between the two pions emitted by the $D_2 \rightarrow D^* \pi$ and $D^* \rightarrow D \pi$.

VALUE	EVTS	DOCUMENT ID	TECN	CHG	COMMENT
• • • We do not use the following data for averages, fits, limits, etc. • • •					
-1.16 ± 0.35	2.3k	¹ ABRAMOWICZ13	ZEUS 0		$e^\pm p \rightarrow D^{(*)+} \pi^- X$
consistent with -1	243k	DEL-AMO-SA...10P	BABR 0		$e^+ e^- \rightarrow D^+ \pi^- X$
$-0.74^{+0.49}_{-0.38}$		² AVERY	94c	CLE2 0	$e^+ e^- \rightarrow D^{*+} \pi^- X$
¹ From the combined fit of the $M(D^+ \pi^-)$ and $M(D^{*+} \pi^-)$ distributions.					
² Systematic uncertainties not estimated.					

$D_2^*(2460)$ REFERENCES

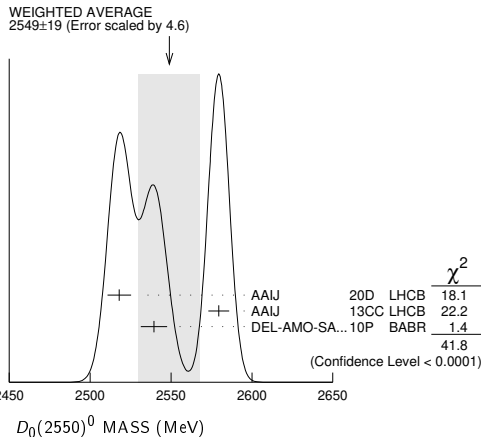
AAIJ	16AH	PR D94 072001	R. Aaij et al.	(LHCb Collab.)
AAIJ	15V	PR D91 092002	R. Aaij et al.	(LHCb Collab.)
Also	PR D93 119901 (errata)	R. Aaij et al.	(LHCb Collab.)	
AAIJ	15X	PR D92 012012	R. Aaij et al.	(LHCb Collab.)
AAIJ	15Y	PR D92 032002	R. Aaij et al.	(LHCb Collab.)
AAIJ	13CC	JHEP 1309 145	R. Aaij et al.	(LHCb Collab.)
ABRAMOWICZ	13	NP B866 229	H. Abramowicz et al.	(ZEUS Collab.)
DEL-AMO-SA...	10P	PR D82 111101	P. del Amo Sanchez et al.	(BABAR Collab.)
AUBERT	09AB	PR D79 112004	B. Aubert et al.	(BABAR Collab.)
AUBERT	09Y	PRL 103 051803	B. Aubert et al.	(BABAR Collab.)
CHEKANOV	09	EPJ C60 25	S. Chekanov et al.	(ZEUS Collab.)
KUZMIN	07	PR D76 012006	A. Kuzmin et al.	(BELLE Collab.)
ABULENCIA	06A	PR D73 051104	A. Abulencia et al.	(CDF Collab.)
ABE	04D	PR D69 112002	K. Abe et al.	(BELLE Collab.)
LINK	04A	PL B586 11	J.M. Link et al.	(FOCUS Collab.)
ABREU	98M	PL B426 231	P. Abreu et al.	(DELPHI Collab.)
ACKERSTAFF	97W	ZPHY C76 425	K. Ackerstaff et al.	(OPAL Collab.)
ASRATYAN	95	ZPHY C68 43	A.E. Asratyan et al.	(BIRM, BELG, CERN+)
AVERY	94C	PL B331 236	P. Avery et al.	(CLEO Collab.)
BERGFELD	94B	PL B340 194	T. Bergfeld et al.	(CLEO Collab.)
FRABETTI	94B	PRL 72 324	P.L. Frabetti et al.	(FNAL E687 Collab.)
AVERY	90	PR D41 774	P. Avery, D. Besson	(CLEO Collab.)
ALBRECHT	89B	PL B221 422	H. Albrecht et al.	(ARGUS Collab.) JP
ALBRECHT	89F	PL B231 208	H. Albrecht et al.	(ARGUS Collab.)
ALBRECHT	89H	PL B232 398	H. Albrecht et al.	(ARGUS Collab.) JP
ANJOS	89C	PRL 62 1717	J.C. Anjos et al.	(FNAL E691 Collab.)

$D_0(2550)^0$ $I(J^P) = \frac{1}{2}(0^-)$

OMITTED FROM SUMMARY TABLE
 $J^P = 0^-$ determined by AAIJ 20D.

$D_0(2550)^0$ MASS

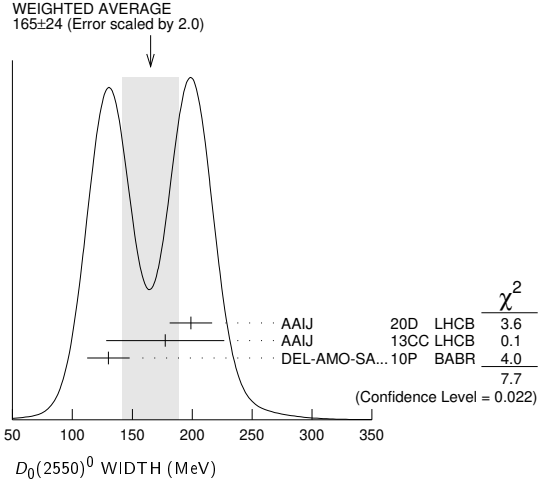
VALUE (MeV)	EVTS	DOCUMENT ID	TECN	CHG	COMMENT
2549 ± 19	OUR AVERAGE	Error includes scale factor of 4.6. See the ideogram below.			
$2518 \pm 2 \pm 7$	79k	¹ AAIJ	20D	LHCB	$B^- \rightarrow D^{*+} \pi^- \pi^-$
$2579.5 \pm 3.4 \pm 5.5$	60k	AAIJ	13cc	LHCB	$pp \rightarrow D^{*+} \pi^- X$
$2539.4 \pm 4.5 \pm 6.8$	34k	DEL-AMO-SA...10P	BABR		$e^+ e^- \rightarrow D^{*+} \pi^- X$



¹ From a full four-body amplitude analysis of the $B^- \rightarrow D^{*+} \pi^- \pi^-$ decay.

$D_0(2550)^0$ WIDTH

VALUE (MeV)	EVTS	DOCUMENT ID	TECN	COMMENT
165 ± 24	OUR AVERAGE	Error includes scale factor of 2.0. See the ideogram below.		
$199 \pm 5 \pm 17$	79k	¹ AAIJ	20D	LHCB $B^- \rightarrow D^{*+} \pi^- \pi^-$
$177.5 \pm 17.8 \pm 46.0$	60k	AAIJ	13cc	LHCB $pp \rightarrow D^{*+} \pi^- X$
$130 \pm 12 \pm 13$	34k	DEL-AMO-SA...10P	BABR	$e^+ e^- \rightarrow D^{*+} \pi^- X$



¹ From a full four-body amplitude analysis of the $B^- \rightarrow D^{*+} \pi^- \pi^-$ decay.

$D_0(2550)^0$ DECAY MODES

Mode	Fraction (Γ_i/Γ)
Γ_1 $D^{*+} \pi^-$	seen

$D_0(2550)^0$ POLARIZATION AMPLITUDE A_{D_0}

A polarization amplitude A_{D_0} is a parameter that depends on the initial polarization of the D_0 . For D_0 decays the helicity angle, θ_H , distribution varies like $1 + A_{D_0} \cos^2(\theta_H)$, where θ_H is the angle in the D_0 rest frame between the two pions emitted in the $D_0 \rightarrow D^* \pi$ and $D^* \rightarrow D \pi$ decays.

VALUE	EVTS	DOCUMENT ID	TECN	COMMENT
• • • We do not use the following data for averages, fits, limits, etc. • • •				
4.2 ± 1.3	60k	¹ AAIJ	13cc	LHCB $pp \rightarrow D^{*+} \pi^- X$
¹ Systematic uncertainty not estimated.				

$D_0(2550)^0$ REFERENCES

AAIJ	20D	PR D101 032005	R. Aaij et al.	(LHCb Collab.) JP
AAIJ	13CC	JHEP 1309 145	R. Aaij et al.	(LHCb Collab.)
DEL-AMO-SA...	10P	PR D82 111101	P. del Amo Sanchez et al.	(BABAR Collab.)

$D_1^*(2600)^0$ $I(J^P) = \frac{1}{2}(1^-)$

OMITTED FROM SUMMARY TABLE
was $D_1^*(2600)$
 $J^P = 1^-$ determined by AAIJ 20D.

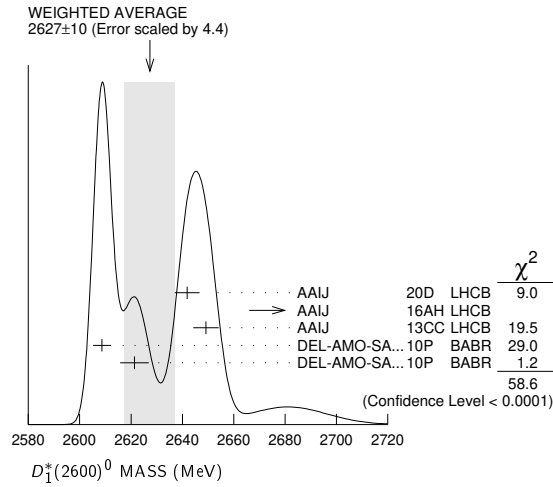
$D_1^*(2600)^0$ MASS

VALUE (MeV)	EVTS	DOCUMENT ID	TECN	CHG	COMMENT
2627 ± 10	OUR AVERAGE	Error includes scale factor of 4.4. See the ideogram below.			
$2641.9 \pm 1.8 \pm 4.5$	79k	¹ AAIJ	20D	LHCB	$B^- \rightarrow D^{*+} \pi^- \pi^-$
$2681.1 \pm 5.6 \pm 14.0$	28k	² AAIJ	16AH	LHCB	$B^- \rightarrow D^+ \pi^- \pi^-$
$2649.2 \pm 3.5 \pm 3.5$	51k	AAIJ	13cc	LHCB	$pp \rightarrow D^{*+} \pi^- X$
$2608.7 \pm 2.4 \pm 2.5$	26k	DEL-AMO-SA...10P	BABR 0		$e^+ e^- \rightarrow D^+ \pi^- X$
$2621.3 \pm 3.7 \pm 4.2$	13k	³ DEL-AMO-SA...10P	BABR +		$e^+ e^- \rightarrow D^0 \pi^+ X$

¹ From a full four-body amplitude analysis of the $B^- \rightarrow D^{*+} \pi^- \pi^-$ decay.
² From the amplitude analysis in the model describing the $D^+ \pi^-$ wave together with virtual contributions from the $D^{*0}(2007)^0$ and B^{*0} states, and components corresponding to the $D_2^*(2460)^0$, $D_1^*(2680)^0$, $D_3^*(2760)^0$, and $D_2^*(3000)^0$ resonances.
³ At a fixed width of 93 MeV.

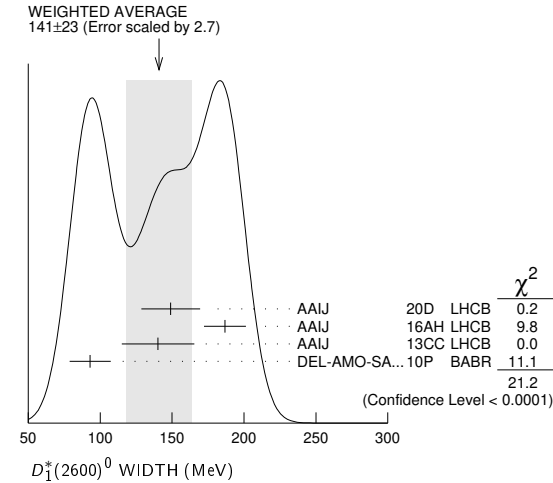
Meson Particle Listings

$D_1^*(2600)^0, D^*(2640)^\pm, D_2(2740)^0$



$D_1^*(2600)^0$ WIDTH

VALUE (MeV)	EVTS	DOCUMENT ID	TECN	COMMENT
141 ± 23 OUR AVERAGE		Error	includes scale factor of 2.7.	See the ideogram below.
149 ± 4 ± 20	79k	¹ AAIJ	20D LHCB	$B^- \rightarrow D^{*+} \pi^- \pi^-$
186.7 ± 8.5 ± 11.9	28k	² AAIJ	16AH LHCB	$B^- \rightarrow D^+ \pi^- \pi^-$
140.2 ± 17.1 ± 18.6	51k	AAIJ	13CC LHCB	$pp \rightarrow D^{*+} \pi^- X$
93 ± 6 ± 13	26k	DEL-AMO-SA...10P	BABR	$e^+ e^- \rightarrow D^+ \pi^- X$



¹ From a full four-body amplitude analysis of the $B^- \rightarrow D^{*+} \pi^- \pi^-$ decay.
² From the amplitude analysis in the model describing the $D^+ \pi^-$ wave together with virtual contributions from the $D^*(2007)^0$ and B^*0 states, and components corresponding to the $D_2^*(2460)^0, D_1^*(2680)^0, D_2^*(2760)^0$, and $D_2^*(3000)^0$ resonances.

$D_1^*(2600)^0$ DECAY MODES

Mode	Fraction (Γ_i/Γ)
Γ_1 $D \pi$	seen
Γ_2 $D^+ \pi^-$	seen
Γ_3 $D^0 \pi^\pm$	seen
Γ_4 $D^* \pi$	seen
Γ_5 $D^{*+} \pi^-$	seen

$D_1^*(2600)^0$ BRANCHING RATIOS

$\Gamma(D^+ \pi^-)/\Gamma(D^{*+} \pi^-)$	VALUE	EVTS	DOCUMENT ID	TECN	COMMENT	Γ_2/Γ_5
	0.32 ± 0.02 ± 0.09	76k	DEL-AMO-SA...10P	BABR	$e^+ e^- \rightarrow D^{(*)+} \pi^- X$	

$D_1^*(2600)^0$ REFERENCES

AAIJ	20D	PR D101 032005	R. Aaij et al.	(LHCb Collab.) JP
AAIJ	16AH	PR D94 072001	R. Aaij et al.	(LHCb Collab.)
AAIJ	13CC	JHEP 1309 145	R. Aaij et al.	(LHCb Collab.)
DEL-AMO-SA...10P	PR D82	111101	P. del Amo Sanchez et al.	(BABAR Collab.)

$D^*(2640)^\pm$

$I(J^P) = \frac{1}{2}(?)^?$

OMITTED FROM SUMMARY TABLE

Seen in Z decays by ABREU 98M. Not seen by ABBIENDI 01N and CHEKANOV 09. Needs confirmation.

$D^*(2640)^\pm$ MASS

VALUE (MeV)	EVTS	DOCUMENT ID	TECN	COMMENT
2637 ± 2 ± 6	66 ± 14	ABREU	98M DLPH	$e^+ e^- \rightarrow D^{*+} \pi^+ \pi^- X$

$D^*(2640)^\pm$ WIDTH

VALUE (MeV)	CL%	DOCUMENT ID	TECN	COMMENT
<15	95	ABREU	98M DLPH	$e^+ e^- \rightarrow D^{*+} \pi^+ \pi^- X$

$D^*(2640)^+$ DECAY MODES

$D^*(2640)^-$ modes are charge conjugates of modes below.

Mode	Fraction (Γ_i/Γ)
Γ_1 $D^*(2010)^+ \pi^+ \pi^-$	seen

$D^*(2640)^\pm$ REFERENCES

CHEKANOV	09	EPJ C60 25	S. Chekanov et al.	(ZEUS Collab.)
ABBIENDI	01N	EPJ C20 445	G. Abbiendi et al.	(OPAL Collab.)
ABREU	98M	PL B426 231	P. Abreu et al.	(DELPHI Collab.)

$D_2(2740)^0$

$I(J^P) = \frac{1}{2}(2^-)$

OMITTED FROM SUMMARY TABLE

was $D(2740)^0$

$J^P = 2^-$ determined by (AAIJ 20D).

$D_2(2740)^0$ MASS

VALUE (MeV)	EVTS	DOCUMENT ID	TECN	COMMENT
2747 ± 6 OUR AVERAGE				
2751 ± 3 ± 7	79k	¹ AAIJ	20D LHCB	$B^- \rightarrow D^{*+} \pi^- \pi^-$
2737.0 ± 3.5 ± 11.2	7.7k	AAIJ	13CC LHCB	$pp \rightarrow D^{*+} \pi^- X$

¹ From a full four-body amplitude analysis of the $B^- \rightarrow D^{*+} \pi^- \pi^-$ decay.

$D_2(2740)^0$ WIDTH

VALUE (MeV)	EVTS	DOCUMENT ID	TECN	COMMENT
88 ± 19 OUR AVERAGE				
102 ± 6 ± 26	79k	¹ AAIJ	20D LHCB	$B^- \rightarrow D^{*+} \pi^- \pi^-$
73.2 ± 13.4 ± 25.0	7.7k	AAIJ	13CC LHCB	$pp \rightarrow D^{*+} \pi^- X$

¹ From a full four-body amplitude analysis of the $B^- \rightarrow D^{*+} \pi^- \pi^-$ decay.

$D_2(2740)^0$ DECAY MODES

Mode	Fraction (Γ_i/Γ)
Γ_1 $D^{*+} \pi^-$	seen

$D_2(2740)^0$ POLARIZATION AMPLITUDE A_{D_J}

A polarization amplitude A_{D_J} is a parameter that depends on the initial polarization of the D_J . For D_J decays the helicity angle, θ_H , distribution varies like $1 + A_{D_J} \cos^2(\theta_H)$, where θ_H is the angle in the D_J rest frame between the two pions emitted in the $D_J \rightarrow D^* \pi$ and $D^* \rightarrow D \pi$ decays.

VALUE	EVTS	DOCUMENT ID	TECN	COMMENT
• • •				We do not use the following data for averages, fits, limits, etc. • • •
3.1 ± 2.2	7.7k	¹ AAIJ	13CC LHCB	$pp \rightarrow D^{*+} \pi^- X$

¹ Systematic uncertainty not estimated.

$D_2(2740)^0$ REFERENCES

AAIJ	20D	PR D101 032005	R. Aaij et al.	(LHCb Collab.) JP
AAIJ	13CC	JHEP 1309 145	R. Aaij et al.	(LHCb Collab.)

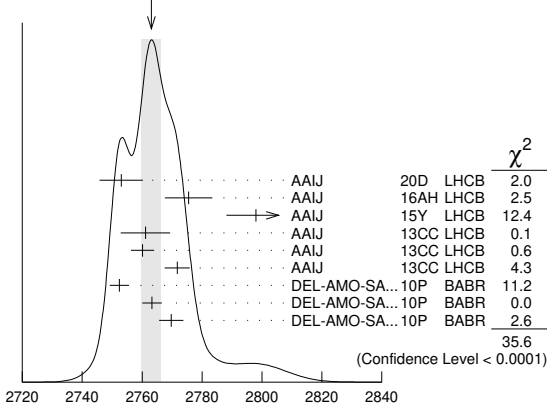
Meson Particle Listings

 $D_3^*(2750)$, $D_1^*(2760)^0$ $D_3^*(2750)$

$$I(J^P) = \frac{1}{2}(3^-)$$

 J^P determined by AAIJ 15Y from the Dalitz plot analysis of $B^0 \rightarrow \bar{D}^0 \pi^+ \pi^-$ decays. $D_3^*(2750)$ MASS

VALUE (MeV)	EVTS	DOCUMENT ID	TECN	CHG	COMMENT
2763.1 ± 3.2 OUR AVERAGE		Error includes scale factor of 2.1. See the ideogram below.			
2753 ± 4 ± 6	79k	¹ AAIJ	20D	LHCB	$B^- \rightarrow D^{*+} \pi^- \pi^-$
2775.5 ± 4.5 ± 6.5	28k	² AAIJ	16AH	LHCB	$B^- \rightarrow D^+ \pi^- \pi^-$
2798 ± 7 ± 7		³ AAIJ	15Y	LHCB	$B^0 \rightarrow \bar{D}^0 \pi^+ \pi^-$
2761.1 ± 5.1 ± 6.5	14k	AAIJ	13CC	LHCB	0 $pp \rightarrow D^{*+} \pi^- X$
2760.1 ± 1.1 ± 3.7	56k	AAIJ	13CC	LHCB	0 $pp \rightarrow D^+ \pi^- X$
2771.7 ± 1.7 ± 3.8	20k	AAIJ	13CC	LHCB	+ $pp \rightarrow D^0 \pi^+ X$
2752.4 ± 1.7 ± 2.7	23.5k	⁴ DEL-AMO-SA...10P	BABR	0	$e^+ e^- \rightarrow D^{*+} \pi^- X$
2763.3 ± 2.3 ± 2.3	11.3k	⁴ DEL-AMO-SA...10P	BABR	0	$e^+ e^- \rightarrow D^+ \pi^- X$
2769.7 ± 3.8 ± 1.5	5.7k	^{4,5} DEL-AMO-SA...10P	BABR	+	$e^+ e^- \rightarrow D^0 \pi^+ X$
• • • We do not use the following data for averages, fits, limits, etc. • • •					
2802 ± 11 ± 10		⁶ AAIJ	15Y	LHCB	$B^0 \rightarrow \bar{D}^0 \pi^+ \pi^-$

WEIGHTED AVERAGE
2763.1 ± 3.2 (Error scaled by 2.1) $D_3^*(2750)$ MASS (MeV)

- From a full four-body amplitude analysis of the $B^- \rightarrow D^{*+} \pi^- \pi^-$ decay.
- From the amplitude analysis in the model describing the $D^+ \pi^-$ wave together with virtual contributions from the $D^*(2007)^0$ and B^*0 states, and components corresponding to the $D_2^*(2460)^0$, $D_1^*(2680)^0$, $D_3^*(2760)^0$, and $D_2^*(3000)^0$ resonances.
- Modeling the $\pi^+ \pi^-$ S-wave with the Isobar formalism.
- The states observed in the $D^* \pi$ and $D \pi$ final states are not necessarily the same.
- At a fixed width of 60.9 MeV.
- Modeling the $\pi^+ \pi^-$ S-wave with the K-matrix formalism.

 $D_3^*(2750)$ WIDTH

VALUE (MeV)	EVTS	DOCUMENT ID	TECN	CHG	COMMENT
66 ± 5 OUR AVERAGE					
66 ± 10 ± 14	79k	¹ AAIJ	20D	LHCB	$B^- \rightarrow D^{*+} \pi^- \pi^-$
95.3 ± 9.6 ± 34.0	28k	² AAIJ	16AH	LHCB	$B^- \rightarrow D^+ \pi^- \pi^-$
105 ± 18 ± 24		³ AAIJ	15Y	LHCB	$B^0 \rightarrow \bar{D}^0 \pi^+ \pi^-$
74.4 ± 3.4 ± 37.0	14k	AAIJ	13CC	LHCB	0 $pp \rightarrow D^{*+} \pi^- X$
74.4 ± 3.4 ± 19.1	56k	AAIJ	13CC	LHCB	0 $pp \rightarrow D^+ \pi^- X$
66.7 ± 6.6 ± 10.5	20k	AAIJ	13CC	LHCB	+ $pp \rightarrow D^0 \pi^+ X$
71 ± 6 ± 11	23.5k	⁴ DEL-AMO-SA...10P	BABR		$e^+ e^- \rightarrow D^{*+} \pi^- X$
60.9 ± 5.1 ± 3.6	11.3k	⁴ DEL-AMO-SA...10P	BABR		$e^+ e^- \rightarrow D^+ \pi^- X$
• • • We do not use the following data for averages, fits, limits, etc. • • •					
154 ± 27 ± 16		⁵ AAIJ	15Y	LHCB	$B^0 \rightarrow \bar{D}^0 \pi^+ \pi^-$

- From a full four-body amplitude analysis of the $B^- \rightarrow D^{*+} \pi^- \pi^-$ decay.
- From the amplitude analysis in the model describing the $D^+ \pi^-$ wave together with virtual contributions from the $D^*(2007)^0$ and B^*0 states, and components corresponding to the $D_2^*(2460)^0$, $D_1^*(2680)^0$, $D_3^*(2760)^0$, and $D_2^*(3000)^0$ resonances.
- Modeling the $\pi^+ \pi^-$ S-wave with the Isobar formalism.
- The states observed in the $D^* \pi$ and $D \pi$ final states are not necessarily the same.
- Modeling the $\pi^+ \pi^-$ S-wave with the K-matrix formalism.

 $D_3^*(2750)$ DECAY MODES

Mode	Fraction (Γ_i/Γ)
Γ_1 $D \pi$	seen
Γ_2 $D^+ \pi^-$	seen
Γ_3 $D^0 \pi^\pm$	seen
Γ_4 $D^* \pi$	seen
Γ_5 $D^{*+} \pi^-$	seen

 $D_3^*(2750)$ BRANCHING RATIOS

$\Gamma(D^+ \pi^-)/\Gamma(D^{*+} \pi^-)$	VALUE	EVTS	DOCUMENT ID	TECN	COMMENT	Γ_2/Γ_5
	0.42 ± 0.05 ± 0.11	34.8k	¹ DEL-AMO-SA...10P	BABR	$e^+ e^- \rightarrow D^{*+} \pi^- X$	

¹ The states observed in the $D^* \pi$ and $D \pi$ final states are not necessarily the same. $D_3^*(2750)$ POLARIZATION AMPLITUDE A_D

A polarization amplitude A_D is a parameter that depends on the initial polarization of the $D_3^*(2750)$. For $D_3^*(2750)$ decays the helicity angle, θ_H , distribution varies like $1 + A_D \cos(\theta_H)$, where θ_H is the angle in the D^* rest frame between the two pions emitted by the $D_3^*(2750) \rightarrow D^* \pi$ and $D^* \rightarrow D \pi$.

VALUE	EVTS	DOCUMENT ID	TECN	COMMENT
• • • We do not use the following data for averages, fits, limits, etc. • • •				
-0.33 ± 0.28	23.5k	¹ DEL-AMO-SA...10P	BABR	$e^+ e^- \rightarrow D^{*+} \pi^- X$

¹ Systematic uncertainties not estimated. The states observed in the $D^* \pi$ and $D \pi$ final states are not necessarily the same. $D_3^*(2750)$ REFERENCES

AAIJ	20D	PR D101 032005	R. Aaij et al.	(LHCB Collab.)
AAIJ	16AH	PR D94 072001	R. Aaij et al.	(LHCB Collab.)
AAIJ	15Y	PR D92 032002	R. Aaij et al.	(LHCB Collab.) JP
AAIJ	13CC	JHEP 1309 145	R. Aaij et al.	(LHCB Collab.)
DEL-AMO-SA...10P	PR D82 111101		P. del Amo Sanchez et al.	(BABAR Collab.)

 $D_1^*(2760)^0$

$$I(J^P) = \frac{1}{2}(1^-)$$

OMITTED FROM SUMMARY TABLE

 J^P determined by AAIJ 15V from the Dalitz plot analysis of $B^- \rightarrow D^+ K^- \pi^-$ decays. $D_1^*(2760)^0$ MASS

VALUE (MeV)	EVTS	DOCUMENT ID	TECN	COMMENT
2781 ± 18 ± 13	2k	¹ AAIJ	15V	LHCB $B^- \rightarrow D^+ K^- \pi^-$

¹ From the amplitude analysis in the model describing the $D^+ \pi^-$ wave together with virtual contributions from the $D^*(2007)^0$ and B^*0 states, nonresonant spin-0 and spin-1 components as well as the $D_0^*(2400)^0$, $D_2^*(2460)^0$ and $D_1^*(2760)^0$ resonances.

 $D_1^*(2760)^0$ WIDTH

VALUE (MeV)	EVTS	DOCUMENT ID	TECN	COMMENT
177 ± 32 ± 21	2k	¹ AAIJ	15V	LHCB $B^- \rightarrow D^+ K^- \pi^-$

¹ From the amplitude analysis in the model describing the $D^+ \pi^-$ wave together with virtual contributions from the $D^*(2007)^0$ and B^*0 states, nonresonant spin-0 and spin-1 components as well as the $D_0^*(2400)^0$, $D_2^*(2460)^0$ and $D_1^*(2760)^0$ resonances.

 $D_1^*(2760)^0$ DECAY MODES

Mode	Fraction (Γ_i/Γ)
Γ_1 $D^+ K^-$	seen

 $D_1^*(2760)^0$ BRANCHING RATIOS

$\Gamma(D^+ K^-)/\Gamma_{\text{total}}$	VALUE	EVTS	DOCUMENT ID	TECN	COMMENT	Γ_1/Γ
			¹ AAIJ	15V	LHCB $B^- \rightarrow D^+ K^- \pi^-$	

¹ From the amplitude analysis in the model describing the $D^+ \pi^-$ wave together with virtual contributions from the $D^*(2007)^0$ and B^*0 states, nonresonant spin-0 and spin-1 components as well as the $D_0^*(2400)^0$, $D_2^*(2460)^0$ and $D_1^*(2760)^0$ resonances.

See key on page 1127

Meson Particle Listings

$D_1^*(2760)^0, D(3000)^0$

$D_1^*(2760)^0$ REFERENCES

AAIJ	15V	PR D91 092002	R. Aaij et al.	(LHCb Collab.) JP
Also		PR D93 119901 (errata.)	R. Aaij et al.	(LHCb Collab.)

$D(3000)^0$

$$I(J^P) = \frac{1}{2}(??)$$

OMITTED FROM SUMMARY TABLE

Both natural- and unnatural-parity components observed depending on the decay mode (AAIJ 13CC).

$D(3000)^0$ MASS

VALUE (MeV)	EVTS	DOCUMENT ID	TECN	COMMENT
3214 ± 29 ± 49	28k	¹ AAIJ	16AH LHCb	$B^- \rightarrow D^+ \pi^- \pi^-$
• • • We do not use the following data for averages, fits, limits, etc. • • •				
2971.8 ± 8.7	9.5k	^{2,3} AAIJ	13CC LHCb	$pp \rightarrow D^{*+} \pi^- X$
3008.1 ± 4.0	17.6k	^{2,4} AAIJ	13CC LHCb	$pp \rightarrow D^+ \pi^- X$

¹ From the amplitude analysis in the model describing the $D^+ \pi^-$ wave together with virtual contributions from the $D^*(2007)^0$ and B^{*0} states, and components corresponding to the $D_2^*(2460)^0$, $D_1^*(2680)^0$, $D_3^*(2760)^0$, and $D_2^*(3000)^0$ resonances.
² Systematic uncertainty not estimated.
³ Unnatural parity preferred.
⁴ Natural parity state. A state $D(3000)^+$ is possibly seen in $D^0 \pi^+$ final state.

$D(3000)^0$ WIDTH

VALUE (MeV)	EVTS	DOCUMENT ID	TECN	COMMENT
186 ± 38 ± 72	28k	⁵ AAIJ	16AH LHCb	$B^- \rightarrow D^+ \pi^- \pi^-$

• • • We do not use the following data for averages, fits, limits, etc. • • •

188.1 ± 44.8	9.5k	^{6,7} AAIJ	13CC LHCb	$pp \rightarrow D^{*+} \pi^- X$
110.5 ± 11.5	17.6k	^{6,8} AAIJ	13CC LHCb	$pp \rightarrow D^+ \pi^- X$

⁵ From the amplitude analysis in the model describing the $D^+ \pi^-$ wave together with virtual contributions from the $D^*(2007)^0$ and B^{*0} states, and components corresponding to the $D_2^*(2460)^0$, $D_1^*(2680)^0$, $D_3^*(2760)^0$, and $D_2^*(3000)^0$ resonances.
⁶ Systematic uncertainty not estimated.
⁷ Unnatural parity preferred.
⁸ Natural parity state. A state $D(3000)^+$ is possibly seen in $D^0 \pi^+$ final state.

$D(3000)^0$ DECAY MODES

Mode	Fraction (Γ_i/Γ)
Γ_1 $D^{*+} \pi^-$	seen

$D(3000)^0$ POLARIZATION AMPLITUDE A_{D_J}

A polarization amplitude A_{D_J} is a parameter that depends on the initial polarization of the D_J . For D_J decays the helicity angle, θ_H , distribution varies like $1 + A_{D_J} \cos^2(\theta_H)$, where θ_H is the angle in the D_J rest frame between the two pions emitted in the $D_J \rightarrow D^* \pi$ and $D^* \rightarrow D \pi$ decays.

VALUE	EVTS	DOCUMENT ID	TECN	COMMENT
• • • We do not use the following data for averages, fits, limits, etc. • • •				
1.5 ± 0.9	9.5k	⁹ AAIJ	13CC LHCb	$pp \rightarrow D^{*+} \pi^- X$
⁹ Systematic uncertainty not estimated.				

$D(3000)^0$ REFERENCES

AAIJ	16AH	PR D94 072001	R. Aaij et al.	(LHCb Collab.)
AAIJ	13CC	JHEP 1309 145	R. Aaij et al.	(LHCb Collab.)

Meson Particle Listings

 D_s^\pm

CHARMED, STRANGE MESONS

(C = ±1, S = ±1)

(including possibly non- $q\bar{q}$ states)

$$D_s^+ = c\bar{s}, D_s^- = \bar{c}s, \text{ similarly for } D_s^{*\prime}s$$

 D_s^\pm

$$I(J^P) = 0(0^-)$$

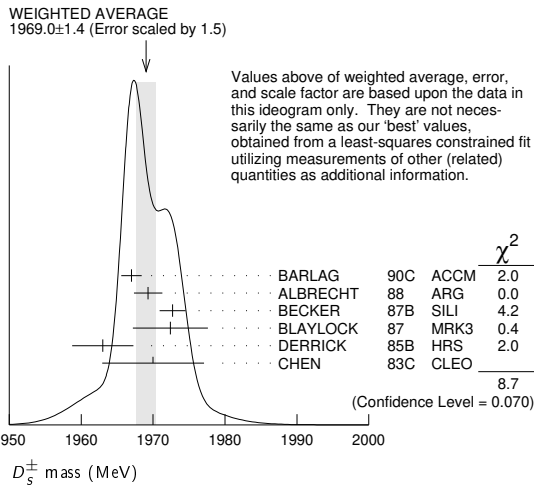
The angular distributions of the decays of the ϕ and $\bar{K}^*(892)^0$ in the $\phi\pi^+$ and $K^+\bar{K}^*(892)^0$ modes strongly indicate that the spin is zero. The parity given is that expected of a $c\bar{s}$ ground state.

 D_s^\pm MASS

The fit includes D_s^\pm , D^0 , $D_s^{*\pm}$, D^{*0} , $D_s^{*\prime\pm}$, $D_1(2420)^0$, $D_2^*(2460)^0$, and $D_{s1}(2536)^\pm$ mass and mass difference measurements. Measurements of the D_s^\pm mass with an error greater than 10 MeV are omitted from the fit and average. A number of early measurements have been omitted altogether.

VALUE (MeV)	EVTS	DOCUMENT ID	TECN	COMMENT
1968.35 ± 0.07 OUR FIT				
1969.0 ± 1.4 OUR AVERAGE				Error includes scale factor of 1.5. See the ideogram below.
1967.0 ± 1.0 ± 1.0	54	BARLAG	90c	ACCM π^- Cu 230 GeV
1969.3 ± 1.4 ± 1.4		ALBRECHT	88	ARG e^+e^- 9.4-10.6 GeV
1972.7 ± 1.5 ± 1.0	21	BECKER	87b	SILI 200 GeV π, K, p
1972.4 ± 3.7 ± 3.7	27	BLAYLOCK	87	MRK3 e^+e^- 4.14 GeV
1963 ± 3 ± 3	30	DERRICK	85b	HRS e^+e^- 29 GeV
1970 ± 5 ± 5	104	CHEN	83c	CLEO e^+e^- 10.5 GeV
••• We do not use the following data for averages, fits, limits, etc. •••				
1968.3 ± 0.7 ± 0.7	290	¹ ANJOS	88	E691 Photoproduction
1980 ± 15	6	USHIDA	86	EMUL ν wideband
1973.6 ± 2.6 ± 3.0	163	ALBRECHT	85d	ARG e^+e^- 10 GeV
1948 ± 28 ± 10	65	AIHARA	84d	TPC e^+e^- 29 GeV
1975 ± 9 ± 10	49	ALTHOFF	84	TASS e^+e^- 14-25 GeV
1975 ± 4	3	BAILEY	84	ACCM hadron ⁺ Be → $\phi\pi^+X$

¹ANJOS 88 enters the fit via $m_{D_s^\pm} - m_{D^\pm}$ (see below).

 **$m_{D_s^\pm} - m_{D^\pm}$**

The fit includes D_s^\pm , D^0 , $D_s^{*\pm}$, D^{*0} , $D_s^{*\prime\pm}$, $D_1(2420)^0$, $D_2^*(2460)^0$, and $D_{s1}(2536)^\pm$ mass and mass difference measurements.

VALUE (MeV)	EVTS	DOCUMENT ID	TECN	COMMENT
98.69 ± 0.05 OUR FIT				
98.69 ± 0.05 OUR AVERAGE				
98.68 ± 0.03 ± 0.04		AAIJ	13v	LHCB $D_s^+ \rightarrow K^+ K^- \pi^+$
99.41 ± 0.38 ± 0.21		ACOSTA	03d	CDF2 $p\bar{p}$, $\sqrt{s} = 1.96$ TeV
98.4 ± 0.1 ± 0.3	48k	AUBERT	02g	BABR $e^+e^- \approx \Upsilon(4S)$
99.5 ± 0.6 ± 0.3		BROWN	94	CLE2 $e^+e^- \approx \Upsilon(4S)$
98.5 ± 1.5	555	CHEN	89	CLEO e^+e^- 10.5 GeV
99.0 ± 0.8	290	ANJOS	88	E691 Photoproduction

 D_s^\pm MEAN LIFE

Measurements with an error greater than 100×10^{-15} s or with fewer than 100 events have been omitted from the Listings.

VALUE (10^{-15} s)	EVTS	DOCUMENT ID	TECN	COMMENT
504 ± 4 OUR AVERAGE				Error includes scale factor of 1.2.
506.4 ± 3.0 ± 1.7 ± 1.7		¹ AAIJ	17An	LHCB pp at 7, 8 TeV
507.4 ± 5.5 ± 5.1	13.6k	LINK	05j	FOCS $\phi\pi^+$ and $\bar{K}^{*0}K^+$
472.5 ± 17.2 ± 6.6	760	IORI	01	SELX 600 GeV Σ^-, π^-, p
518 ± 14 ± 7	1662	AITALA	99	E791 π^- nucleus, 500 GeV
486.3 ± 15.0 ± 4.9 ± 5.1	2167	² BONVICINI	99	CLE2 $e^+e^- \approx \Upsilon(4S)$
475 ± 20 ± 7	900	FRABETTI	93f	E687 γ Be, $\phi\pi^+$
500 ± 60 ± 30	104	FRABETTI	90	E687 γ Be, $\phi\pi^+$
470 ± 40 ± 20	228	RAAB	88	E691 Photoproduction

¹This AAIJ 17An value is derived from the difference between the D_s^- and D^- widths.

The 3rd uncertainty, $\pm 1.7 \times 10^{-15}$ s, arises from the uncertainty of the D^- width.

²BONVICINI 99 obtains 1.19 ± 0.04 for the ratio of D_s^+ to D^0 lifetimes.

 D_s^\pm DECAY MODES

Unless otherwise noted, the branching fractions for modes with a resonance in the final state include all the decay modes of the resonance. D_s^\pm modes are charge conjugates of the modes below.

Mode	Fraction (Γ_i/Γ)	Scale factor/ Confidence level
Inclusive modes		
Γ_1 e^+ semileptonic	[a] (6.33 ± 0.15) %	
Γ_2 π^+ anything	(119.3 ± 1.4) %	
Γ_3 π^- anything	(43.2 ± 0.9) %	
Γ_4 π^0 anything	(123 ± 7) %	
Γ_5 K^- anything	(18.7 ± 0.5) %	
Γ_6 K^+ anything	(28.9 ± 0.7) %	
Γ_7 K_S^0 anything	(19.0 ± 1.1) %	
Γ_8 η anything	[b] (29.9 ± 2.8) %	
Γ_9 ω anything	(6.1 ± 1.4) %	
Γ_{10} η' anything	[c] (10.3 ± 1.4) %	S=1.1
Γ_{11} $f_0(980)$ anything, $f_0 \rightarrow \pi^+\pi^-$	< 1.3	CL=90%
Γ_{12} ϕ anything	(15.7 ± 1.0) %	
Γ_{13} K^+K^- anything	(15.8 ± 0.7) %	
Γ_{14} $K_S^0K^+$ anything	(5.8 ± 0.5) %	
Γ_{15} $K_S^0K^-$ anything	(1.9 ± 0.4) %	
Γ_{16} $2K_S^0$ anything	(1.70 ± 0.32) %	
Γ_{17} $2K^+$ anything	< 2.6	$\times 10^{-3}$ CL=90%
Γ_{18} $2K^-$ anything	< 6	$\times 10^{-4}$ CL=90%
Leptonic and semileptonic modes		
Γ_{19} $e^+\nu_e$	< 8.3	$\times 10^{-5}$ CL=90%
Γ_{20} $\mu^+\nu_\mu$	(5.43 ± 0.15) $\times 10^{-3}$	
Γ_{21} $\tau^+\nu_\tau$	(5.32 ± 0.11) %	
Γ_{22} $\gamma e^+\nu_e$	< 1.3	$\times 10^{-4}$ CL=90%
Γ_{23} $K^+K^-e^+\nu_e$	—	
Γ_{24} $\phi e^+\nu_e$	[d] (2.39 ± 0.16) %	S=1.3
Γ_{25} $\phi\mu^+\nu_\mu$	(1.9 ± 0.5) %	
Γ_{26} $\eta e^+\nu_e + \eta'(958) e^+\nu_e$	[d] (3.03 ± 0.24) %	
Γ_{27} $\eta e^+\nu_e$	[d] (2.32 ± 0.08) %	
Γ_{28} $\eta'(958) e^+\nu_e$	[d] (8.0 ± 0.7) $\times 10^{-3}$	
Γ_{29} $\eta\mu^+\nu_\mu$	(2.4 ± 0.5) %	
Γ_{30} $\eta'(958)\mu^+\nu_\mu$	(1.1 ± 0.5) %	
Γ_{31} $\omega e^+\nu_e$	[e] < 2.0	$\times 10^{-3}$ CL=90%
Γ_{32} $K^0 e^+\nu_e$	(3.4 ± 0.4) $\times 10^{-3}$	
Γ_{33} $K^*(892)^0 e^+\nu_e$	[d] (2.15 ± 0.28) $\times 10^{-3}$	S=1.1
Γ_{34} $f_0(980) e^+\nu_e, f_0 \rightarrow \pi^+\pi^-$		
Γ_{35} $a_0(980)^0 e^+\nu_e, a_0(980)^0 \rightarrow \pi^0\eta$	< 1.2	$\times 10^{-4}$ CL=90%

Hadronic modes with a $K\bar{K}$ pair

Γ_{36} $K^+K_S^0$	(1.453 ± 0.035) %	
Γ_{37} K^+K^0	(1.49 ± 0.06) %	
Γ_{38} $K^+\bar{K}^0$	(2.95 ± 0.14) %	
Γ_{39} $K^+K^-\pi^+$	[f] (5.38 ± 0.10) %	S=1.1
Γ_{40} $\phi\pi^+$	[d,g] (4.5 ± 0.4) %	
Γ_{41} $\phi\pi^+, \phi \rightarrow K^+K^-$	[g] (2.22 ± 0.06) %	
Γ_{42} $K^+\bar{K}^*(892)^0, \bar{K}^{*0} \rightarrow K^-\pi^+$	(2.58 ± 0.06) %	
Γ_{43} $f_0(980)\pi^+, f_0 \rightarrow K^+K^-$	(1.11 ± 0.19) %	

See key on page 1127

Meson Particle Listings

D_S^\pm

Γ_{44}	$f_0(1370)\pi^+, f_0 \rightarrow K^+K^-$	$(7.1 \pm 2.9) \times 10^{-4}$		Γ_{95}	$a_1(1260)^+\eta, a_1^+ \rightarrow$	$(2.5 \pm 0.9) \times 10^{-3}$	
Γ_{45}	$f_0(1710)\pi^+, f_0 \rightarrow K^+K^-$	$(6.7 \pm 2.8) \times 10^{-4}$			$f_0(500)\pi^+, f_0 \rightarrow \pi^+\pi^-$		
Γ_{46}	$K^+\bar{K}_0^*(1430)^0, \bar{K}_0^+ \rightarrow$	$(1.76 \pm 0.25) \times 10^{-3}$		Γ_{96}	$a_0(980)^+\pi^0, a_0^+ \rightarrow$	$(2.2 \pm 0.4) \%$	
	$K^+\pi^+$				$a_0(980)^+\pi^0 \rightarrow \eta\pi^0$		
Γ_{47}	$K^+K_S^0\pi^+$	$(1.52 \pm 0.22) \%$		Γ_{97}	$a_0(980)^+\rho(770)^0, a_0^+ \rightarrow$	$(2.1 \pm 0.9) \times 10^{-3}$	
Γ_{48}	$2K_S^0\pi^+$	$(7.7 \pm 0.6) \times 10^{-3}$			$\eta\pi^+$		
Γ_{49}	$K^0\bar{K}^0\pi^+$	—		Γ_{98}	$\eta(1405)\pi^+, \eta(1405) \rightarrow$	$(2.2 \pm 0.7) \times 10^{-4}$	
Γ_{50}	$K^*(892)^+\bar{K}^0$	[d] $(5.4 \pm 1.2) \%$			$a_0(980)^-\pi^+, a_0^- \rightarrow \eta\pi^-$		
Γ_{51}	$K^+K^-\pi^+\pi^0$	$(5.50 \pm 0.24) \%$	S=1.3	Γ_{99}	$\eta(1405)\pi^+, \eta(1405) \rightarrow$	$(2.2 \pm 0.7) \times 10^{-4}$	
Γ_{52}	$\phi\rho^+$	[d] $(5.59 \pm 0.34) \%$			$a_0(980)^+\pi^-, a_0^+ \rightarrow \eta\pi^+$		
Γ_{53}	$\bar{K}_1(1270)^0K^+, \bar{K}_1(1270)^0 \rightarrow K^-\rho^+$	$(5.7 \pm 0.6) \times 10^{-3}$		Γ_{100}	$f_1(1420)\pi^+, f_1 \rightarrow$	$(5.9 \pm 1.8) \times 10^{-4}$	
Γ_{54}	$\bar{K}_1(1270)^0K^+, \bar{K}_1(1270)^0 \rightarrow K^*(892)\pi$	$(1.31 \pm 0.25) \%$			$a_0(980)^-\pi^+, a_0^- \rightarrow \eta\pi^-$		
Γ_{55}	$\bar{K}_1(1400)^0K^+, \bar{K}_1(1400)^0 \rightarrow K^*(892)\pi$	$(2.0 \pm 0.4) \%$		Γ_{101}	$f_1(1420)\pi^+, f_1 \rightarrow$	$(5.3 \pm 1.8) \times 10^{-4}$	
Γ_{56}	$a_0(980)^0\rho^+, a_0(980)^0 \rightarrow$	$(1.9 \pm 0.4) \times 10^{-3}$			$a_0(980)^+\pi^-, a_0^+ \rightarrow \eta\pi^+$		
Γ_{57}	$f_1(1420)^0\pi^+, f_1(1420)^0 \rightarrow$	$(3.9 \pm 0.7) \times 10^{-3}$		Γ_{102}	$\omega\pi^+\pi^0$	[d] $(2.8 \pm 0.7) \%$	
	K^+K^-			Γ_{103}	$3\pi^+2\pi^-\pi^0$	$(4.9 \pm 3.2) \%$	
Γ_{58}	$f_1(1420)^0\pi^+, f_1(1420)^0 \rightarrow$	$(4.0 \pm 1.4) \times 10^{-4}$		Γ_{104}	$\omega 2\pi^+\pi^-$	[d] $(1.6 \pm 0.5) \%$	
	$a_0(980)^0\pi^0, a_0(980)^0 \rightarrow$			Γ_{105}	$\eta'(958)\pi^+$	[c,d] $(3.94 \pm 0.25) \%$	
	K^+K^-			Γ_{106}	$3\pi^+2\pi^-\pi^0$	—	
Γ_{59}	$\eta(1475)\pi^+, \eta(1475) \rightarrow$	$(7.0 \pm 2.8) \times 10^{-4}$		Γ_{107}	$\omega\eta\pi^+$	[d] $< 2.13 \%$	CL=90%
	$a_0(980)^0\pi^0, a_0(980)^0 \rightarrow$			Γ_{108}	$\eta'(958)\rho^+$	[c,d] $(5.8 \pm 1.5) \%$	
	K^+K^-			Γ_{109}	$\eta'(958)\pi^+\pi^0$	$(5.6 \pm 0.8) \%$	
				Γ_{110}	$\eta'(958)\pi^+\pi^0$ nonresonant	$< 5.1 \%$	CL=90%
Γ_{60}	$K_S^0K^-2\pi^+$	$(1.53 \pm 0.08) \%$	S=1.5	Modes with one or three K's			
Γ_{61}	$K^*(892)^+\bar{K}^*(892)^0$	[d] $(5.64 \pm 0.35) \%$		Γ_{111}	$K^+\pi^0$	$(7.4 \pm 0.5) \times 10^{-4}$	
Γ_{62}	$\eta(1475)K_S^0, \eta \rightarrow$	$(3.4 \pm 1.0) \times 10^{-4}$		Γ_{112}	$K_S^0\pi^+$	$(1.10 \pm 0.05) \times 10^{-3}$	
	$K^*(892)^0\pi^+, K^{*0} \rightarrow$			Γ_{113}	$K^+\eta$	[d] $(1.73 \pm 0.08) \times 10^{-3}$	
	$K^-\pi^+$			Γ_{114}	$K^+\omega$	[d] $(8.7 \pm 2.5) \times 10^{-4}$	
Γ_{63}	$\eta(1475)\pi^+, \eta \rightarrow$	$(3.4 \pm 1.0) \times 10^{-4}$		Γ_{115}	$K^+\eta'(958)$	[d] $(2.64 \pm 0.24) \times 10^{-3}$	
	$\bar{K}^*(892)^+K^-, \bar{K}^{*+} \rightarrow$			Γ_{116}	$K^+\pi^+\pi^-$	$(6.5 \pm 0.4) \times 10^{-3}$	
	$K_S^0\pi^+$			Γ_{117}	$K^+\rho^0$	$(2.5 \pm 0.4) \times 10^{-3}$	
Γ_{64}	$\eta(1475)\pi^+, \eta \rightarrow$	$(1.7 \pm 0.9) \times 10^{-3}$		Γ_{118}	$K^+\rho(1450)^0, \rho^0 \rightarrow \pi^+\pi^-$	$(6.9 \pm 2.4) \times 10^{-4}$	
	$a_0(980)^-\pi^+, a_0^- \rightarrow$			Γ_{119}	$K^*(892)^0\pi^+, K^{*0} \rightarrow K^+\pi^-$	$(1.40 \pm 0.24) \times 10^{-3}$	
	$K_S^0K^-$			Γ_{120}	$K^*(1410)^0\pi^+, K^{*0} \rightarrow$	$(1.22 \pm 0.28) \times 10^{-3}$	
Γ_{65}	$f_1(1285)\pi^+, f_1 \rightarrow$	$(3.4 \pm 0.8) \times 10^{-4}$			$K^+\pi^-$		
	$a_0(980)^-\pi^+, a_0^- \rightarrow$			Γ_{121}	$K^*(1430)^0\pi^+, K^{*0} \rightarrow$	$(5.0 \pm 3.4) \times 10^{-4}$	
	$K_S^0K^-$				$K^+\pi^-$		
Γ_{66}	$K^+K_S^0\pi^+\pi^-$	$(9.5 \pm 0.8) \times 10^{-3}$	S=1.1	Γ_{122}	$K^+\pi^+\pi^-$ nonresonant	$(1.03 \pm 0.34) \times 10^{-3}$	
Γ_{67}	$K^+K^-2\pi^+\pi^-$	$(8.6 \pm 1.5) \times 10^{-3}$		Γ_{123}	$K^0\pi^+\pi^0$	$(1.08 \pm 0.06) \%$	
Γ_{68}	$\phi 2\pi^+\pi^-$	[d] $(1.21 \pm 0.16) \%$		Γ_{124}	$K_S^0 2\pi^+\pi^-$	$(2.8 \pm 1.0) \times 10^{-3}$	
Γ_{69}	$\phi\rho^0\pi^+, \phi \rightarrow K^+K^-$	$(6.4 \pm 1.3) \times 10^{-3}$		Γ_{125}	$K^+\omega\pi^0$	[d] $< 8.2 \times 10^{-3}$	CL=90%
Γ_{70}	$\phi a_1(1260)^+, \phi \rightarrow$	$(7.4 \pm 1.2) \times 10^{-3}$		Γ_{126}	$K^+\omega\pi^+\pi^-$	[d] $< 5.4 \times 10^{-3}$	CL=90%
	$K^+K^-, a_1^+ \rightarrow$			Γ_{127}	$K^+\omega\eta$	[d] $< 7.9 \times 10^{-3}$	CL=90%
	$\rho^0\pi^+$			Γ_{128}	$2K^+K^-$	$(2.15 \pm 0.20) \times 10^{-4}$	
Γ_{71}	$\phi 2\pi^+\pi^-$ non- $\rho, \phi \rightarrow$	$(1.8 \pm 0.7) \times 10^{-3}$		Γ_{129}	$\phi K^+, \phi \rightarrow K^+K^-$	$(8.8 \pm 2.0) \times 10^{-5}$	
	K^+K^-			Doubly Cabibbo-suppressed modes			
Γ_{72}	$K^+K^-\rho^0\pi^+$ non- ϕ	$< 2.6 \times 10^{-4}$	CL=90%	Γ_{130}	$2K^+\pi^-$	$(1.276 \pm 0.031) \times 10^{-4}$	
Γ_{73}	$K^+K^-2\pi^+\pi^-$ nonresonant	$(9 \pm 7) \times 10^{-4}$		Γ_{131}	$K^+K^*(892)^0, K^{*0} \rightarrow$	$(6.0 \pm 3.4) \times 10^{-5}$	
Γ_{74}	$2K_S^0 2\pi^+\pi^-$	$(7.8 \pm 3.3) \times 10^{-4}$			$K^+\pi^-$		
Hadronic modes without K's				Baryon-antibaryon mode			
Γ_{75}	$\pi^+\pi^0$	$< 1.2 \times 10^{-4}$	CL=90%	Γ_{132}	$p\bar{p}$	$(1.22 \pm 0.11) \times 10^{-3}$	
Γ_{76}	$2\pi^+\pi^-$	$(1.08 \pm 0.04) \%$		Γ_{133}	$p\bar{p}e^+\nu_e$	$< 2.0 \times 10^{-4}$	CL=90%
Γ_{77}	$\rho^0\pi^+$	$(1.9 \pm 1.2) \times 10^{-4}$		$\Delta C = 1$ weak neutral current (CI) modes, Lepton family number (LF), or Lepton number (L) violating modes			
Γ_{78}	$\pi^+(\pi^+\pi^-)_{S\text{-wave}}$	[h] $(9.0 \pm 0.4) \times 10^{-3}$		Γ_{134}	$\pi^+e^+e^-$	[j] $< 5.5 \times 10^{-6}$	CL=90%
Γ_{79}	$f_0(980)\pi^+, f_0 \rightarrow \pi^+\pi^-$			Γ_{135}	$\pi^+\phi, \phi \rightarrow e^+e^-$	[j] $(6 \pm 8 \text{ } ^{-4}) \times 10^{-6}$	
Γ_{80}	$f_0(1370)\pi^+, f_0 \rightarrow \pi^+\pi^-$			Γ_{136}	$\pi^+\mu^+\mu^-$	[i] $< 1.8 \times 10^{-7}$	CL=90%
Γ_{81}	$f_0(1500)\pi^+, f_0 \rightarrow \pi^+\pi^-$			Γ_{137}	$K^+e^+e^-$	$< 3.7 \times 10^{-6}$	CL=90%
Γ_{82}	$f_2(1270)\pi^+, f_2 \rightarrow \pi^+\pi^-$	$(1.09 \pm 0.19) \times 10^{-3}$		Γ_{138}	$K^+\mu^+\mu^-$	CI $< 1.4 \times 10^{-7}$	CL=90%
Γ_{83}	$\rho(1450)^0\pi^+, \rho^0 \rightarrow \pi^+\pi^-$	$(2.9 \pm 1.9) \times 10^{-4}$		Γ_{139}	$K^*(892)^+\mu^+\mu^-$	CI $< 1.4 \times 10^{-3}$	CL=90%
Γ_{84}	$\pi^+2\pi^0$	$(6.5 \pm 1.3) \times 10^{-3}$		Γ_{140}	$\pi^+e^+\mu^-$	LF $< 1.1 \times 10^{-6}$	CL=90%
Γ_{85}	$2\pi^+\pi^-\pi^0$	—		Γ_{141}	$\pi^+e^-\mu^+$	LF $< 9.4 \times 10^{-7}$	CL=90%
Γ_{86}	$\eta\pi^+$	[d] $(1.68 \pm 0.09) \%$	S=1.1	Γ_{142}	$K^+e^+\mu^-$	LF $< 7.9 \times 10^{-7}$	CL=90%
Γ_{87}	$\omega\pi^+$	[d] $(1.92 \pm 0.30) \times 10^{-3}$		Γ_{143}	$K^+e^-\mu^+$	LF $< 5.6 \times 10^{-7}$	CL=90%
Γ_{88}	$3\pi^+2\pi^-$	$(7.9 \pm 0.8) \times 10^{-3}$		Γ_{144}	π^-2e^+	L $< 1.4 \times 10^{-6}$	CL=90%
Γ_{89}	$2\pi^+\pi^-2\pi^0$	—		Γ_{145}	$\pi^-2\mu^+$	L $< 8.6 \times 10^{-8}$	CL=90%
Γ_{90}	$\eta\rho^+$	[d] $(8.9 \pm 0.8) \%$		Γ_{146}	$\pi^-e^+\mu^+$	L $< 6.3 \times 10^{-7}$	CL=90%
Γ_{91}	$\eta\pi^+\pi^0$	$(9.5 \pm 0.5) \%$		Γ_{147}	K^-2e^+	L $< 7.7 \times 10^{-7}$	CL=90%
Γ_{92}	$\eta(\pi^+\pi^0)_{P\text{-wave}}$	$(5.1 \pm 3.1) \times 10^{-3}$		Γ_{148}	$K^-2\mu^+$	L $< 2.6 \times 10^{-8}$	CL=90%
Γ_{93}	$2\pi^+\pi^-\eta$	$(3.12 \pm 0.16) \%$		Γ_{149}	$K^-e^+\mu^+$	L $< 2.6 \times 10^{-7}$	CL=90%
Γ_{94}	$a_1(1260)^+\eta, a_1^+ \rightarrow$	$(1.73 \pm 0.16) \%$		Γ_{150}	$K^*(892)^-2\mu^+$	L $< 1.4 \times 10^{-3}$	CL=90%
	$\rho(770)^0\pi^+, \rho^0 \rightarrow \pi^+\pi^-$						

Meson Particle Listings

D_s^\pm

- [a] This is the purely e^+ semileptonic branching fraction: the e^+ fraction from τ^+ decays has been subtracted off. The sum of our (non- τ) e^+ exclusive fractions — an $e^+\nu_e$ with an η, η', ϕ, K^0 , or K^{*0} — is $5.99 \pm 0.31\%$.
- [b] This fraction includes η from η' decays.
- [c] The sum of our exclusive η' fractions — $\eta' e^+\nu_e, \eta' \mu^+\nu_\mu, \eta' \pi^+, \eta' \rho^+$, and $\eta' K^+$ — is $11.8 \pm 1.6\%$.
- [d] This branching fraction includes all the decay modes of the final-state resonance.
- [e] A test for $u\bar{u}$ or $d\bar{d}$ content in the D_s^+ . Neither Cabibbo-favored nor Cabibbo-suppressed decays can contribute, and ω - ϕ mixing is an unlikely explanation for any fraction above about 2×10^{-4} .
- [f] The branching fraction for this mode may differ from the sum of the submodes that contribute to it, due to interference effects. See the relevant papers.
- [g] We decouple the $D_s^+ \rightarrow \phi\pi^+$ branching fraction obtained from mass projections (and used to get some of the other branching fractions) from the $D_s^+ \rightarrow \phi\pi^+, \phi \rightarrow K^+K^-$ branching fraction obtained from the Dalitz-plot analysis of $D_s^+ \rightarrow K^+K^-\pi^+$. That is, the ratio of these two branching fractions is not exactly the $\phi \rightarrow K^+K^-$ branching fraction 0.491.
- [h] This is the average of a model-independent and a K -matrix parametrization of the $\pi^+\pi^-$ S -wave and is a sum over several f_0 mesons.
- [i] This mode is not a useful test for a $\Delta C=1$ weak neutral current because both quarks must change flavor in this decay.
- [j] This is *not* a test for the $\Delta C=1$ weak neutral current, but leads to the $\pi^+\ell^+\ell^-$ final state.

CONSTRAINED FIT INFORMATION

An overall fit to 13 branching ratios uses 21 measurements and one constraint to determine 10 parameters. The overall fit has a $\chi^2 = 11.6$ for 12 degrees of freedom.

The following *off-diagonal* array elements are the correlation coefficients $\langle \delta x_i \delta x_j \rangle / (\delta x_i \delta x_j)$, in percent, from the fit to the branching fractions, $x_i \equiv \Gamma_i / \Gamma_{\text{total}}$. The fit constrains the x_i whose labels appear in this array to sum to one.

x_{39}	27							
x_{51}	8	1						
x_{60}	25	6	15					
x_{66}	20	4	12	46				
x_{76}	17	33	2	7	5			
x_{86}	1	14	-9	-15	-12	6		
x_{87}	0	1	0	-1	0	0	4	
x_{116}	3	20	-6	-9	-7	7	12	0
	x_{36}	x_{39}	x_{51}	x_{60}	x_{66}	x_{76}	x_{86}	x_{87}

See the related review(s):

[D_s[±] Branching Fractions](#)

D_s[±] BRANCHING RATIOS

A number of older, now obsolete results have been omitted. They may be found in earlier editions.

———— Inclusive modes ————

$\Gamma(e^+ \text{ semileptonic}) / \Gamma_{\text{total}}$ Γ_1 / Γ

This is the purely e^+ semileptonic branching fraction: the e^+ fraction from τ^+ decays has been subtracted off.

VALUE (%)	EVTS	DOCUMENT ID	TECN	COMMENT
6.33 ± 0.15 OUR AVERAGE				
6.30 ± 0.13 ± 0.10	17k	^{1,2} ABLIKIM	21AC BES3	e^+e^- at 4.178–4.230 GeV
6.52 ± 0.39 ± 0.15	0.5k	³ ASNER	10 CLEO	e^+e^- at 3774 MeV

¹ ABLIKIM 21AC finds that the ratio of the D_s^+ and D^0 semielectronic widths is $0.790 \pm 0.016 \pm 0.020$.

² ABLIKIM 21AC reports a value of $(6.30 \pm 0.13 \pm 0.09 \pm 0.04) \times 10^{-2}$, where the last uncertainty is an external systematic from $B(D_s^+ \rightarrow \tau\nu)$. We have added the systematic uncertainties in quadrature.

³ Using the D_s^+ and D^0 lifetimes, ASNER 10 finds that the ratio of the D_s^+ and D^0 semileptonic widths is $0.828 \pm 0.051 \pm 0.025$.

$\Gamma(\pi^+ \text{ anything}) / \Gamma_{\text{total}}$ Γ_2 / Γ
Events with two π^+ 's count twice, etc. But π^+ 's from $K_S^0 \rightarrow \pi^+\pi^-$ are not included.

VALUE (%)	DOCUMENT ID	TECN	COMMENT
119.3 ± 1.2 ± 0.7	DOBBS	09 CLEO	e^+e^- at 4170 MeV

$\Gamma(\pi^- \text{ anything}) / \Gamma_{\text{total}}$ Γ_3 / Γ
Events with two π^- 's count twice, etc. But π^- 's from $K_S^0 \rightarrow \pi^+\pi^-$ are not included.

VALUE (%)	DOCUMENT ID	TECN	COMMENT
43.2 ± 0.9 ± 0.3	DOBBS	09 CLEO	e^+e^- at 4170 MeV

$\Gamma(\pi^0 \text{ anything}) / \Gamma_{\text{total}}$ Γ_4 / Γ
Events with two π^0 's count twice, etc. But π^0 's from $K_S^0 \rightarrow 2\pi^0$ are not included.

VALUE (%)	DOCUMENT ID	TECN	COMMENT
123.4 ± 3.8 ± 5.3	DOBBS	09 CLEO	e^+e^- at 4170 MeV

$\Gamma(K^- \text{ anything}) / \Gamma_{\text{total}}$ Γ_5 / Γ

VALUE (%)	DOCUMENT ID	TECN	COMMENT
18.7 ± 0.5 ± 0.2	DOBBS	09 CLEO	e^+e^- at 4170 MeV

$\Gamma(K^+ \text{ anything}) / \Gamma_{\text{total}}$ Γ_6 / Γ

VALUE (%)	DOCUMENT ID	TECN	COMMENT
28.9 ± 0.6 ± 0.3	DOBBS	09 CLEO	e^+e^- at 4170 MeV

$\Gamma(K_S^0 \text{ anything}) / \Gamma_{\text{total}}$ Γ_7 / Γ

VALUE (%)	DOCUMENT ID	TECN	COMMENT
19.0 ± 1.0 ± 0.4	DOBBS	09 CLEO	e^+e^- at 4170 MeV

$\Gamma(\eta \text{ anything}) / \Gamma_{\text{total}}$ Γ_8 / Γ
This ratio includes η particles from η' decays.

VALUE (%)	EVTS	DOCUMENT ID	TECN	COMMENT
29.9 ± 2.2 ± 1.7		DOBBS	09 CLEO	e^+e^- at 4170 MeV
• • • We do not use the following data for averages, fits, limits, etc. • • •				
23.5 ± 3.1 ± 2.0	674 ± 91	HUANG	06B CLEO	See DOBBS 09

$\Gamma(\omega \text{ anything}) / \Gamma_{\text{total}}$ Γ_9 / Γ

VALUE (%)	DOCUMENT ID	TECN	COMMENT
6.1 ± 1.4 ± 0.3	DOBBS	09 CLEO	e^+e^- at 4170 MeV

$\Gamma(\eta' \text{ anything}) / \Gamma_{\text{total}}$ Γ_{10} / Γ

VALUE (%)	EVTS	DOCUMENT ID	TECN	COMMENT
10.3 ± 1.4 OUR AVERAGE	Error includes scale factor of 1.1.			
8.8 ± 1.8 ± 0.5	68	ABLIKIM	15Z BES3	482 pb ⁻¹ , 4009 MeV
11.7 ± 1.7 ± 0.7		DOBBS	09 CLEO	e^+e^- at 4170 MeV
• • • We do not use the following data for averages, fits, limits, etc. • • •				
8.7 ± 1.9 ± 0.8	68	HUANG	06B CLEO	See DOBBS 09

$\Gamma(f_0(980) \text{ anything, } f_0 \rightarrow \pi^+\pi^-) / \Gamma_{\text{total}}$ Γ_{11} / Γ

VALUE (%)	CL%	DOCUMENT ID	TECN	COMMENT
<1.3	90	DOBBS	09 CLEO	e^+e^- at 4170 MeV

$\Gamma(\phi \text{ anything}) / \Gamma_{\text{total}}$ Γ_{12} / Γ

VALUE (%)	EVTS	DOCUMENT ID	TECN	COMMENT
15.7 ± 0.8 ± 0.6		DOBBS	09 CLEO	e^+e^- at 4170 MeV
• • • We do not use the following data for averages, fits, limits, etc. • • •				
16.1 ± 1.2 ± 1.1	398 ± 27	HUANG	06B CLEO	See DOBBS 09

$\Gamma(K^+ K^- \text{ anything}) / \Gamma_{\text{total}}$ Γ_{13} / Γ

VALUE (%)	DOCUMENT ID	TECN	COMMENT
15.8 ± 0.6 ± 0.3	DOBBS	09 CLEO	e^+e^- at 4170 MeV

$\Gamma(K_S^0 K^+ \text{ anything}) / \Gamma_{\text{total}}$ Γ_{14} / Γ

VALUE (%)	DOCUMENT ID	TECN	COMMENT
5.8 ± 0.5 ± 0.1	DOBBS	09 CLEO	e^+e^- at 4170 MeV

$\Gamma(K_S^0 K^- \text{ anything}) / \Gamma_{\text{total}}$ Γ_{15} / Γ

VALUE (%)	DOCUMENT ID	TECN	COMMENT
1.9 ± 0.4 ± 0.1	DOBBS	09 CLEO	e^+e^- at 4170 MeV

$\Gamma(2K_S^0 \text{ anything}) / \Gamma_{\text{total}}$ Γ_{16} / Γ

VALUE (%)	DOCUMENT ID	TECN	COMMENT
1.7 ± 0.3 ± 0.1	DOBBS	09 CLEO	e^+e^- at 4170 MeV

$\Gamma(2K^+ \text{ anything}) / \Gamma_{\text{total}}$ Γ_{17} / Γ

VALUE (%)	DOCUMENT ID	TECN	COMMENT
<0.26	DOBBS	09 CLEO	e^+e^- at 4170 MeV

$\Gamma(2K^- \text{ anything}) / \Gamma_{\text{total}}$ Γ_{18} / Γ

VALUE (%)	DOCUMENT ID	TECN	COMMENT
<0.06	DOBBS	09 CLEO	e^+e^- at 4170 MeV

See key on page 1127

Meson Particle Listings

D_s^+

Leptonic and semileptonic modes

See the related review(s):

Leptonic Decays of Charged Pseudoscalar Mesons

$\Gamma(e^+ \nu_e) / \Gamma_{total}$					Γ_{19} / Γ
VALUE	CL%	DOCUMENT ID	TECN	COMMENT	
$<0.83 \times 10^{-4}$	90	1 ZUPANC	13 BELL	$e^+ e^-$ at $\Upsilon(4S), \Upsilon(5S)$	

• • • We do not use the following data for averages, fits, limits, etc. • • •

$<2.3 \times 10^{-4}$	90	DEL-AMO-SA..10J	BABR	$e^+ e^-$, 10.58 GeV
$<1.2 \times 10^{-4}$	90	ALEXANDER 09	CLEO	$e^+ e^-$ at 4170 MeV
$<1.3 \times 10^{-4}$	90	PEDLAR 07A	CLEO	See ALEXANDER 09

¹ ZUPANC 13 also gives the limit as $< 1.0 \times 10^{-4}$ at 95% CL.

$\Gamma(\mu^+ \nu_\mu) / \Gamma_{total}$					Γ_{20} / Γ
See the note on "Decay Constants of Charged Pseudoscalar Mesons."					
VALUE (units 10^{-3})	EVTS	DOCUMENT ID	TECN	COMMENT	
5.43 ± 0.15 OUR AVERAGE					
5.35 ± 0.13 ± 0.16	2.2k	ABLIKIM	21BE BES3	$e^+ e^-$, 4.178, 4.226 GeV	
5.17 ± 0.75 ± 0.21	69	1 ABLIKIM	16o BES3	$e^+ e^-$ at 4.009 GeV	
5.31 ± 0.28 ± 0.20	492 ± 26	2 ZUPANC	13 BELL	$e^+ e^-$ at $\Upsilon(4S), \Upsilon(5S)$	

6.02 ± 0.38 ± 0.34	275 ± 17	3 DEL-AMO-SA..10J	BABR	$e^+ e^-$, 10.58 GeV
5.65 ± 0.45 ± 0.17	235 ± 14	ALEXANDER 09	CLEO	$e^+ e^-$ at 4170 MeV

• • • We do not use the following data for averages, fits, limits, etc. • • •

5.49 ± 0.16 ± 0.15	1.1k	ABLIKIM	19E BES3	$e^+ e^-$ at 4178 MeV
6.44 ± 0.76 ± 0.57	169 ± 18	4 WIDHALM	08 BELL	See ZUPANC 13
5.94 ± 0.66 ± 0.31	88	5 PEDLAR 07A	CLEO	See ALEXANDER 09
6.8 ± 1.1 ± 1.8	553	6 HEISTER 02I	ALEP	Z decays

¹ ABLIKIM 16o also reports that when constrained by the Standard Model ratio of $\Gamma(D_s^+ \rightarrow \tau^+ \nu_\tau) / \Gamma(D_s^+ \rightarrow \mu^+ \nu_\mu) = 9.76$, the branching fraction is found to be $(0.495 \pm 0.067 \pm 0.026)\%$. The constrained value is used to obtain the decay constant, $f_{D_s^+} = (241.0 \pm 16.3 \pm 6.6)$ MeV.

² ZUPANC 13 uses both $\mu^+ \nu$ and $\tau^+ \nu$ events to get $f_{D_s} = (255.5 \pm 4.2 \pm 5.1)$ MeV.

³ DEL-AMO-SANCHEZ 10J uses $\mu^+ \nu_\mu$ and $\tau^+ \nu_\tau$ events together to get $f_{D_s} = (258.6 \pm 6.4 \pm 7.5)$ MeV.

⁴ WIDHALM 08 gets $f_{D_s} = (275 \pm 16 \pm 12)$ MeV from the branching fraction.

⁵ PEDLAR 07A also fits μ^+ and τ^+ events together and gets an effective $\mu^+ \nu_\mu$ branching fraction of $(6.38 \pm 0.59 \pm 0.33) \times 10^{-3}$

⁶ This HEISTER 02I result is not actually an independent measurement of the absolute $\mu^+ \nu_\mu$ branching fraction, but is in fact based on our $\phi\pi^+$ branching fraction of $3.6 \pm 0.9\%$, so it cannot be included in our overall fit. HEISTER 02I combines its $D_s^+ \rightarrow \tau^+ \nu_\tau$ and $\mu^+ \nu_\mu$ branching fractions to get $f_{D_s} = (285 \pm 19 \pm 40)$ MeV.

$\Gamma(\mu^+ \nu_\mu) / \Gamma(\phi\pi^+)$					$\Gamma_{20} / \Gamma_{40}$
See the note on "Decay Constants of Charged Pseudoscalar Mesons" above.					
VALUE	EVTS	DOCUMENT ID	TECN	COMMENT	

0.143 ± 0.018 ± 0.006	489 ± 55	1 AUBERT	07v BABR	$e^+ e^- \approx \Upsilon(4S)$
0.23 ± 0.06 ± 0.04	18	2 ALEXANDROV 00	BEAT	π^- nucleus, 350 GeV
0.173 ± 0.023 ± 0.035	182	3 CHADHA	98 CLE2	$e^+ e^- \approx \Upsilon(4S)$
0.245 ± 0.052 ± 0.074	39	4 ACOSTA	94 CLE2	See CHADHA 98

¹ AUBERT 07v gets $f_{D_s^+} = (283 \pm 17 \pm 16)$ MeV, using $\Gamma(D_s^+ \rightarrow \phi\pi^+) / \Gamma(\text{total}) = (4.71 \pm 0.46)\%$.

² ALEXANDROV 00 uses $f_D^2 / f_{D_s}^2 = 0.82 \pm 0.09$ from a lattice-gauge-theory calculation to get the relative numbers of $D^+ \rightarrow \mu^+ \nu_\mu$ and $D_s^+ \rightarrow \mu^+ \nu_\mu$ events. The present result leads to $f_{D_s} = (323 \pm 44 \pm 36)$ MeV.

³ CHADHA 98 obtains $f_{D_s} = (280 \pm 19 \pm 28 \pm 34)$ MeV from this measurement, using $\Gamma(D_s^+ \rightarrow \phi\pi^+) / \Gamma(\text{total}) = 0.036 \pm 0.009$.

⁴ ACOSTA 94 obtains $f_{D_s} = (344 \pm 37 \pm 52 \pm 42)$ MeV from this measurement, using $\Gamma(D_s^+ \rightarrow \phi\pi^+) / \Gamma(\text{total}) = 0.037 \pm 0.009$.

$\Gamma(\tau^+ \nu_\tau) / \Gamma_{total}$					Γ_{21} / Γ
See the note on "Decay Constants of Charged Pseudoscalar Mesons" above.					
VALUE (%)	EVTS	DOCUMENT ID	TECN	COMMENT	

5.32 ± 0.11 OUR AVERAGE					
5.29 ± 0.25 ± 0.20	1.7k	1 ABLIKIM	21AF BES3	$e^+ e^-$ at 4.178, 4.226 GeV	
5.27 ± 0.10 ± 0.12	4.9k	2 ABLIKIM	21AZ BES3	$e^+ e^-$ at 4.178, 4.226 GeV	
5.21 ± 0.25 ± 0.17	950	3 ABLIKIM	21BE BES3	$e^+ e^-$ at 4.178, 4.226 GeV	
3.28 ± 1.83 ± 0.37	33	4 ABLIKIM	16o BES3	$e^+ e^-$ at 4.009 GeV	
5.70 ± 0.21 ± 0.31	2.2k	5 ZUPANC	13 BELL	$e^+ e^-$ at $\Upsilon(4S), \Upsilon(5S)$	
4.96 ± 0.37 ± 0.57	748	6 DEL-AMO-SA..10J	BABR	$e^- \bar{\nu}_e \nu_\tau, \mu^- \bar{\nu}_\mu \nu_\tau$	
6.42 ± 0.81 ± 0.18	126	7 ALEXANDER 09	CLEO	$\tau^+ \rightarrow \pi^+ \bar{\nu}_\tau$	
5.52 ± 0.57 ± 0.21	155	7 NAIK 09A	CLEO	$\tau^+ \rightarrow \rho^+ \bar{\nu}_\tau$	
5.30 ± 0.47 ± 0.22	181	7 ONYISI 09	CLEO	$\tau^+ \rightarrow e^+ \nu_e \bar{\nu}_\tau$	

• • • We do not use the following data for averages, fits, limits, etc. • • •

6.17 ± 0.71 ± 0.34	102	8 ECKLUND 08	CLEO	See ONYISI 09
8.0 ± 1.3 ± 0.4	47	8 PEDLAR 07A	CLEO	See ALEXANDER 09
5.79 ± 0.77 ± 1.84	881	9 HEISTER 02I	ALEP	Z decays
7.0 ± 2.1 ± 2.0	22	10 ABBIENDI 01L	OPAL	$D_s^{*+} \rightarrow \gamma D_s^+$ from Z's
7.4 ± 2.8 ± 2.4	16	11 ACCIARRI 97F	L3	$D_s^{*+} \rightarrow \gamma D_s^+$ from Z's

¹ ABLIKIM 21F uses $\tau^+ \rightarrow \pi^+ \pi^0 \bar{\nu}$ decays.

² ABLIKIM 21AZ uses $\tau^+ \rightarrow e^+ \nu_e \bar{\nu}_\tau$ decays.

³ ABLIKIM 21BE uses $\tau^+ \rightarrow e^+ \nu_e \bar{\nu}_\tau$ decays. When constrained by the Standard Model ratio of $\Gamma(D_s^+ \rightarrow \tau^+ \nu_\tau) / \Gamma(D_s^+ \rightarrow \mu^+ \nu_\mu) = 9.75$, the branching fraction is found to be $(5.22 \pm 0.10 \pm 0.14)\%$.

⁴ ABLIKIM 16o also reports that when constrained by the Standard Model ratio of $\Gamma(D_s^+ \rightarrow \tau^+ \nu_\tau) / \Gamma(D_s^+ \rightarrow \mu^+ \nu_\mu) = 9.76$; the branching fraction is found to be $(4.83 \pm 0.65 \pm 0.26)\%$.

⁵ ZUPANC 13 uses both $\mu^+ \nu$ and $\tau^+ \nu$ events to get $f_{D_s} = (255.5 \pm 4.2 \pm 5.1)$ MeV.

⁶ DEL-AMO-SANCHEZ 10J (with a small correction; see LEES 15D) uses $\mu^+ \nu_\mu$ and $\tau^+ \nu_\tau$ events together to get $f_{D_s} = (259.9 \pm 6.6 \pm 7.6)$ MeV.

⁷ ALEXANDER 09, NAIK 09A, and ONYISI 09 use different τ decay modes and are independent. The three papers combined give $f_{D_s} = (259.7 \pm 7.8 \pm 3.4)$ MeV.

⁸ ECKLUND 08 and PEDLAR 07A are independent; ECKLUND 08 uses $\tau^+ \rightarrow e^+ \nu_e \bar{\nu}_\tau$ events, PEDLAR 07A uses $\tau^+ \rightarrow \pi^+ \bar{\nu}_\tau$ events.

⁹ HEISTER 02I combines its $D_s^+ \rightarrow \tau^+ \nu_\tau$ and $\mu^+ \nu_\mu$ branching fractions to get $f_{D_s} = (285 \pm 19 \pm 40)$ MeV.

¹⁰ This ABBIENDI 01L value gives a decay constant f_{D_s} of $(286 \pm 44 \pm 41)$ MeV.

¹¹ The second ACCIARRI 97F error here combines in quadrature systematic (0.016) and normalization (0.018) errors. The branching fraction gives $f_{D_s} = (309 \pm 58 \pm 33 \pm 38)$ MeV.

$\Gamma(\tau^+ \nu_\tau) / \Gamma(\mu^+ \nu_\mu)$					$\Gamma_{21} / \Gamma_{20}$
VALUE	EVTS	DOCUMENT ID	TECN	COMMENT	

• • • We do not use the following data for averages, fits, limits, etc. • • •

10.73 ± 0.69 ± 0.56	2.2k/492	1 ZUPANC	13 BELL	$e^+ e^-$ at $\Upsilon(4S), \Upsilon(5S)$
11.0 ± 1.4 ± 0.6	102	2 ECKLUND 08	CLEO	See ONYISI 09

¹ This ZUPANC 13 ratio is not independent of the separate $\tau\nu$ and $\mu\nu$ fractions listed above.

² This ECKLUND 08 value also uses results from PEDLAR 07A, and it is not independent of other results in these Listings. Combined with earlier CLEO results, the decay constant f_{D_s} is $274 \pm 10 \pm 5$ MeV.

$\Gamma(\gamma e^+ \nu_e) / \Gamma_{total}$					Γ_{22} / Γ
VALUE	CL%	DOCUMENT ID	TECN	COMMENT	

$<1.3 \times 10^{-4}$ 90 ABLIKIM 19AD BES3 for $E_\gamma > 10$ MeV

$\Gamma(K^+ K^- e^+ \nu_e) / \Gamma(K^+ K^- \pi^+)$					$\Gamma_{23} / \Gamma_{39}$
VALUE	EVTS	DOCUMENT ID	TECN	COMMENT	

• • • We do not use the following data for averages, fits, limits, etc. • • •

0.558 ± 0.007 ± 0.016		1 AUBERT	08AN BABR	$e^+ e^-$ at $\Upsilon(4S)$
-----------------------	--	----------	-----------	-----------------------------

¹ This AUBERT 08AN ratio is only for the $K^+ K^-$ mass in the range 1.01–1.03 GeV in the numerator and 1.0095–1.0295 GeV in the denominator.

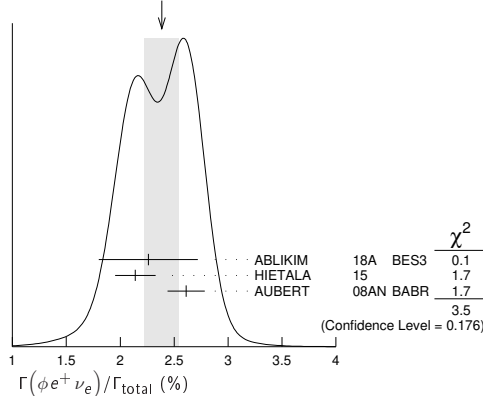
$\Gamma(\phi e^+ \nu_e) / \Gamma_{total}$					Γ_{24} / Γ
See the end of the D_s^+ Listings for measurements of $D_s^+ \rightarrow \phi e^+ \nu_e$ form factors. Unseen decay modes of the ϕ are included.					
VALUE (%)	EVTS	DOCUMENT ID	TECN	COMMENT	

2.39 ± 0.16 OUR AVERAGE				Error includes scale factor of 1.3. See the ideogram below.
2.26 ± 0.45 ± 0.09	26	ABLIKIM	18A BES3	$e^+ e^-$ at 4.009 GeV
2.14 ± 0.17 ± 0.08	207	HIETALA 15		Uses CLEO data
2.61 ± 0.03 ± 0.17	25k	AUBERT	08AN BABR	$e^+ e^-$ at $\Upsilon(4S)$

• • • We do not use the following data for averages, fits, limits, etc. • • •

2.36 ± 0.23 ± 0.13	106	ECKLUND 09	CLEO	See HIETALA 15
2.29 ± 0.37 ± 0.11	45	YELTON 09	CLEO	See ECKLUND 09

WEIGHTED AVERAGE
2.39 ± 0.16 (Error scaled by 1.3)



Meson Particle Listings

D_s^\pm

$\Gamma(\phi e^+ \nu_e)/\Gamma(\phi \pi^+)$ Γ_{24}/Γ_{40}

As noted in the comment column, most of these measurements use $\phi \mu^+ \nu_\mu$ events in addition to or instead of $\phi e^+ \nu_e$ events.

VALUE	EVTS	DOCUMENT ID	TECN	COMMENT
• • • We do not use the following data for averages, fits, limits, etc. • • •				
0.540 ± 0.033 ± 0.048	793	LINK	02J	FOCS Uses $\phi \mu^+ \nu_\mu$
0.54 ± 0.05 ± 0.04	367	BUTLER	94	CLE2 Uses $\phi e^+ \nu_e$ and $\phi \mu^+ \nu_\mu$
0.58 ± 0.17 ± 0.07	97	FRABETTI	93G	E687 Uses $\phi \mu^+ \nu_\mu$
0.57 ± 0.15 ± 0.15	104	ALBRECHT	91	ARG Uses $\phi e^+ \nu_e$
0.49 ± 0.10 $^{+0.10}_{-0.14}$	54	ALEXANDER	90B	CLEO Uses $\phi e^+ \nu_e$ and $\phi \mu^+ \nu_\mu$

$\Gamma(\phi \mu^+ \nu_\mu)/\Gamma_{total}$ Γ_{25}/Γ

VALUE (%)	EVTS	DOCUMENT ID	TECN	COMMENT
1.94 ± 0.53 ± 0.09	22	ABLIKIM	18A	BES3 $e^+ e^-$ at 4.009 GeV

$\Gamma(\eta e^+ \nu_e)/\Gamma_{total}$ Γ_{27}/Γ

Unseen decay modes of the η are included.

VALUE (%)	EVTS	DOCUMENT ID	TECN	COMMENT
2.32 ± 0.08 OUR AVERAGE				
2.323 ± 0.063 ± 0.063	1.8k	ABLIKIM	19S	BES3 $e^+ e^-$ at 4178 MeV
2.30 ± 0.31 ± 0.08	63	ABLIKIM	16T	BES3 $e^+ e^-$ at 4.009 GeV
2.28 ± 0.14 ± 0.19	358	¹ HIETALA	15	Uses CLEO data
• • • We do not use the following data for averages, fits, limits, etc. • • •				
2.48 ± 0.29 ± 0.13	82	YELTON	09	CLEO See HIETALA 15
¹ Obtained by analyzing CLEO-c data but not authored by the CLEO Collaboration.				

$\Gamma(\eta e^+ \nu_e)/\Gamma(\phi e^+ \nu_e)$ Γ_{27}/Γ_{24}

Unseen decay modes of the η and the ϕ are included.

VALUE	EVTS	DOCUMENT ID	TECN	COMMENT
• • • We do not use the following data for averages, fits, limits, etc. • • •				
1.24 ± 0.12 ± 0.15	440	¹ BRANDENB...	95	CLE2 See HIETALA 15
¹ BRANDENBURG 95 uses both e^+ and μ^+ events and makes a phase-space adjustment to use the μ^+ events as e^+ events.				

$\Gamma(\eta'(958) e^+ \nu_e)/\Gamma_{total}$ Γ_{28}/Γ

Unseen decay modes of the $\eta'(958)$ are included.

VALUE (%)	EVTS	DOCUMENT ID	TECN	COMMENT
0.80 ± 0.07 OUR AVERAGE				
0.824 ± 0.073 ± 0.027	261	ABLIKIM	19S	BES3 $e^+ e^-$ at 4178 MeV
0.93 ± 0.30 ± 0.05	14	ABLIKIM	16T	BES3 $e^+ e^-$ at 4009 MeV
0.68 ± 0.15 ± 0.06	20	¹ HIETALA	15	Uses CLEO data
• • • We do not use the following data for averages, fits, limits, etc. • • •				
0.91 ± 0.33 ± 0.05	7.5	YELTON	09	CLEO See HIETALA 15
¹ Obtained by analyzing CLEO-c data but not authored by the CLEO Collaboration.				

$\Gamma(\eta'(958) e^+ \nu_e)/\Gamma(\phi e^+ \nu_e)$ Γ_{28}/Γ_{24}

Unseen decay modes of the resonances are included.

VALUE	EVTS	DOCUMENT ID	TECN	COMMENT
• • • We do not use the following data for averages, fits, limits, etc. • • •				
0.43 ± 0.11 ± 0.07	29	¹ BRANDENB...	95	CLE2 See HIETALA 15
¹ BRANDENBURG 95 uses both e^+ and μ^+ events and makes a phase-space adjustment to use the μ^+ events as e^+ events.				

$[\Gamma(\eta e^+ \nu_e) + \Gamma(\eta'(958) e^+ \nu_e)]/\Gamma(\phi e^+ \nu_e)$ $\Gamma_{26}/\Gamma_{24} = (\Gamma_{27} + \Gamma_{28})/\Gamma_{24}$

Unseen decay modes of the resonances are included.

VALUE	DOCUMENT ID	TECN	COMMENT
• • • We do not use the following data for averages, fits, limits, etc. • • •			
1.67 ± 0.17 ± 0.17	¹ BRANDENB...	95	CLE2 See HIETALA 15
¹ This BRANDENBURG 95 data is redundant with data in previous blocks.			

$\Gamma(\eta \mu^+ \nu_\mu)/\Gamma_{total}$ Γ_{29}/Γ

VALUE (%)	EVTS	DOCUMENT ID	TECN	COMMENT
2.42 ± 0.46 ± 0.11	44	ABLIKIM	18A	BES3 $e^+ e^-$ at 4.009 GeV

$\Gamma(\eta'(958) \mu^+ \nu_\mu)/\Gamma_{total}$ Γ_{30}/Γ

VALUE (%)	EVTS	DOCUMENT ID	TECN	COMMENT
1.06 ± 0.54 ± 0.07	10	ABLIKIM	18A	BES3 $e^+ e^-$ at 4.009 GeV

$\Gamma(\omega e^+ \nu_e)/\Gamma_{total}$ Γ_{31}/Γ

A test for $u\bar{u}$ or $d\bar{d}$ content in the D_s^+ . Neither Cabibbo-favored nor Cabibbo-suppressed decays can contribute, and $\omega - \phi$ mixing is an unlikely explanation for any fraction above about 2×10^{-4} .

VALUE (%)	CL%	DOCUMENT ID	TECN	COMMENT
<0.20	90	MARTIN	11	CLEO $e^+ e^-$ at 4170 MeV

$\Gamma(K^0 e^+ \nu_e)/\Gamma_{total}$ Γ_{32}/Γ

VALUE (%)	EVTS	DOCUMENT ID	TECN	COMMENT
0.34 ± 0.04 OUR AVERAGE				
0.325 ± 0.038 ± 0.016	117	¹ ABLIKIM	19D	BES3 $e^+ e^-$ at 4178 MeV
0.39 ± 0.08 ± 0.03	42	HIETALA	15	Uses CLEO data
• • • We do not use the following data for averages, fits, limits, etc. • • •				
0.37 ± 0.10 ± 0.02	14	YELTON	09	CLEO See HIETALA 15
¹ K^0 reconstructed via $K^0 \rightarrow K_S^0 \rightarrow \pi^+ \pi^-$ decays.				

$\Gamma(K^*(892)^0 e^+ \nu_e)/\Gamma_{total}$ Γ_{33}/Γ

Unseen decay modes of the $K^*(892)^0$ are included.

VALUE (%)	EVTS	DOCUMENT ID	TECN	COMMENT
0.215 ± 0.028 OUR AVERAGE				Error includes scale factor of 1.1.
0.237 ± 0.026 ± 0.020	155	ABLIKIM	19D	BES3 $e^+ e^-$ at 4178 MeV
0.18 ± 0.04 ± 0.01	32	¹ HIETALA	15	$e^+ e^-$ at 4.170 GeV
• • • We do not use the following data for averages, fits, limits, etc. • • •				
0.18 ± 0.07 ± 0.01	7.5	YELTON	09	CLEO See HIETALA 15
¹ Uses CLEO data, but not authored by the CLEO collaboration				

$\Gamma(f_0(980) e^+ \nu_e, f_0 \rightarrow \pi^+ \pi^-)/\Gamma_{total}$ Γ_{34}/Γ

• • • We do not use the following data for averages, fits, limits, etc. • • •

VALUE (%)	EVTS	DOCUMENT ID	TECN	COMMENT
0.13 ± 0.03 ± 0.01	42	¹ HIETALA	15	Uses CLEO data
0.20 ± 0.03 ± 0.01	44	ECKLUND	09	CLEO See HIETALA 15
0.13 ± 0.04 ± 0.01	13	YELTON	09	CLEO See ECKLUND 09
¹ HIETALA 15 uses a tighter cut on the reconstructed $\pi^+ \pi^-$ mass (± 60 MeV around the f^0) than ECKLUND 09. It finds that applying the same tight cut to both analyses gives consistent results.				

$\Gamma(a_0(980)^0 e^+ \nu_e, a_0(980)^0 \rightarrow \pi^0 \eta)/\Gamma_{total}$ Γ_{35}/Γ

VALUE	CL%	DOCUMENT ID	TECN	COMMENT
<1.2 × 10 ⁻⁴	90	ABLIKIM	21Y	BES3 $e^+ e^-$ at 4.178–4.226 GeV

Hadronic modes with a $K\bar{K}$ pair

$\Gamma(K^+ K_S^0)/\Gamma_{total}$ Γ_{36}/Γ

VALUE (%)	EVTS	DOCUMENT ID	TECN	COMMENT
1.453 ± 0.035 OUR FIT				
1.46 ± 0.05 OUR AVERAGE				Error includes scale factor of 1.2.
1.425 ± 0.038 ± 0.031	1.8k	ABLIKIM	19AMBES3	$e^+ e^-$ at 4178 MeV
1.52 ± 0.05 ± 0.03		ONYISI	13	CLEO $e^+ e^-$ at 4.17 GeV
• • • We do not use the following data for averages, fits, limits, etc. • • •				
1.49 ± 0.07 ± 0.05		¹ ALEXANDER	08	CLEO See ONYISI 13
¹ ALEXANDER 08 uses single- and double-tagged events in an overall fit.				

$\Gamma(K^+ K_S^0)/\Gamma(K^+ K^- \pi^+)$ Γ_{36}/Γ_{39}

VALUE (units 10 ⁻²)	EVTS	DOCUMENT ID	TECN	COMMENT
27.55 ± 0.18 ± 0.50	40k	ABLIKIM	20R	BES3 $e^+ e^-$, 4178 ~ 4226 MeV

$\Gamma(K^+ K_S^0)/\Gamma_{total}$ Γ_{37}/Γ

VALUE (%)	EVTS	DOCUMENT ID	TECN	COMMENT
1.485 ± 0.039 ± 0.046	2.3k	ABLIKIM	19AMBES3	$e^+ e^-$ at 4178 MeV

$\Gamma(K^+ \bar{K}^0)/\Gamma_{total}$ Γ_{38}/Γ

VALUE (%)	EVTS	DOCUMENT ID	TECN	COMMENT
2.95 ± 0.11 ± 0.09	2.0k	¹ ZUPANC	13	BELL $e^+ e^-$ at $\Upsilon(4S), \Upsilon(5S)$
¹ ZUPANC 13 finds the \bar{K}^0 from its missing-mass squared, not from $K_S^0 \rightarrow \pi^+ \pi^-$. The DCS ($D_s^+ \rightarrow K^+ K^0$) contribution to this fraction is estimated to be an order of magnitude below the statistical uncertainty.				

$\Gamma(K^+ K^- \pi^+)/\Gamma_{total}$ Γ_{39}/Γ

VALUE (%)	EVTS	DOCUMENT ID	TECN	COMMENT
5.38 ± 0.10 OUR FIT				Error includes scale factor of 1.1.
5.45 ± 0.11 OUR AVERAGE				Error includes scale factor of 1.1.
5.47 ± 0.08 ± 0.13	5.1k	ABLIKIM	21AE	BES3 $e^+ e^-$ at 4.178 GeV
5.55 ± 0.14 ± 0.13		ONYISI	13	CLEO $e^+ e^-$ at 4.17 GeV
5.06 ± 0.15 ± 0.21	4.1k	ZUPANC	13	BELL $e^+ e^-$ at $\Upsilon(4S), \Upsilon(5S)$
5.78 ± 0.20 ± 0.30		DEL-AMO-SA...	10J	BABR $e^+ e^-$, 10.58 GeV
• • • We do not use the following data for averages, fits, limits, etc. • • •				
5.50 ± 0.23 ± 0.16		¹ ALEXANDER	08	CLEO See ONYISI 13
¹ ALEXANDER 08 uses single- and double-tagged events in an overall fit.				

$\Gamma(\phi \pi^+)/\Gamma_{total}$ Γ_{40}/Γ

The results here are model-independent. For earlier, model-dependent results, see our PDG 06 edition. We decouple the $D_s^+ \rightarrow \phi \pi^+$ branching fraction obtained from mass projections (and used to get some of the other branching fractions) from the $D_s^+ \rightarrow \phi \pi^+, \phi \rightarrow K^+ K^-$ branching fraction obtained from the Dalitz-plot analysis of $D_s^+ \rightarrow \phi \pi^+, \phi \rightarrow K^+ K^- \pi^+$. That is, the ratio of these two branching fractions is not exactly the $\phi \rightarrow K^+ K^-$ branching fraction 0.491.

VALUE (%)	EVTS	DOCUMENT ID	TECN	COMMENT
4.5 ± 0.4 OUR AVERAGE				
4.62 ± 0.36 ± 0.51		¹ AUBERT	06N	BABR $e^+ e^-$ at $\Upsilon(4S)$
4.81 ± 0.52 ± 0.38	21.2 ± 19	² AUBERT	05V	BABR $e^+ e^- \approx \Upsilon(4S)$
3.59 ± 0.77 ± 0.48		³ ARTUSO	96	CLE2 $e^+ e^-$ at $\Upsilon(4S)$
• • • We do not use the following data for averages, fits, limits, etc. • • •				
3.9 $^{+5.1}_{-1.9} \pm 1.8$		⁴ BAI	95c	BES $e^+ e^-$ 4.03 GeV

¹ This AUBERT 06N measurement uses $\bar{B}^0 \rightarrow D_s^{(*)-} D^{(*)+}$ and $B^- \rightarrow D_s^{(*)-} D^{(*)+}$ decays, including some from other papers. However, the result is independent of AUBERT 05V.

²AUBERT 05v uses the ratio of $B^0 \rightarrow D^{*-} D_s^{*+}$ events seen in two different ways, in both of which the $D^{*-} \rightarrow \bar{D}^0 \pi^-$ decay is fully reconstructed: (1) The $D_s^{*+} \rightarrow D_s^+ \gamma$, $D_s^+ \rightarrow \phi \pi^+$ decay is fully reconstructed. (2) The number of events in the D_s^+ peak in the missing mass spectrum against the D^{*-} is measured.
³ARTUSO 96 uses partially reconstructed $\bar{B}^0 \rightarrow D^{*+} D_s^{*-}$ decays to get a model-independent value for $\Gamma(D_s^- \rightarrow \phi \pi^-)/\Gamma(D^0 \rightarrow K^- \pi^+)$ of $0.92 \pm 0.20 \pm 0.11$.
⁴BAI 95c uses $e^+ e^- \rightarrow D_s^+ D_s^-$ events in which one or both of the D_s^\pm are observed to obtain the first model-independent measurement of the $D_s^+ \rightarrow \phi \pi^+$ branching fraction, without assumptions about $\sigma(D_s^\pm)$. However, with only two “doubly-tagged” events, the statistical error is very large.

$\Gamma(\phi \pi^+, \phi \rightarrow K^+ K^-)/\Gamma(K^+ K^- \pi^+)$ Γ_{41}/Γ_{39}

This is the “fit fraction” from the Dalitz-plot analysis. We decouple the $D_s^+ \rightarrow \phi \pi^+$ branching fraction obtained from mass projections (and used to get some of the other branching fractions) from the $D_s^+ \rightarrow \phi \pi^+, \phi \rightarrow K^+ K^-$ branching fraction obtained from the Dalitz-plot analysis of $D_s^+ \rightarrow K^+ K^- \pi^+$. That is, the ratio of these two branching fractions is not exactly the $\phi \rightarrow K^+ K^-$ branching fraction 0.491.

VALUE (units 10^{-2})	EVTS	DOCUMENT ID	TECN	COMMENT
41.2 ± 0.7 OUR AVERAGE				
40.5 ± 0.7 ± 0.9	18.6k	ABLIKIM	21AE BES3	$e^+ e^-$ at 4.178 GeV
41.4 ± 0.8 ± 0.5		DEL-AMO-SA...11G	BABR	Dalitz fit, 96k evts
42.2 ± 1.6 ± 0.3		MITCHELL	09A CLEO	Dalitz fit, 12k evts
• • • We do not use the following data for averages, fits, limits, etc. • • •				
39.6 ± 3.3 ± 4.7		FRABETTI	95B E687	Dalitz fit, 701 evts

$\Gamma(K^+ \bar{K}^*(892)^0, \bar{K}^{*0} \rightarrow K^- \pi^+)/\Gamma(K^+ K^- \pi^+)$ Γ_{42}/Γ_{39}

This is the “fit fraction” from the Dalitz-plot analysis.

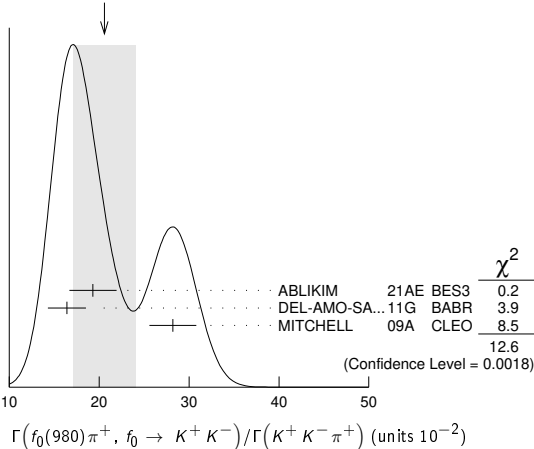
VALUE (units 10^{-2})	EVTS	DOCUMENT ID	TECN	COMMENT
47.9 ± 0.6 OUR AVERAGE				
48.3 ± 0.9 ± 0.6	18.6k	ABLIKIM	21AE BES3	$e^+ e^-$ at 4.178 GeV
47.9 ± 0.5 ± 0.5		DEL-AMO-SA...11G	BABR	Dalitz fit, 96k evts
47.4 ± 1.5 ± 0.4		MITCHELL	09A CLEO	Dalitz fit, 12k evts
• • • We do not use the following data for averages, fits, limits, etc. • • •				
47.8 ± 4.6 ± 4.0		FRABETTI	95B E687	Dalitz fit, 701 evts

$\Gamma(f_0(980) \pi^+, f_0 \rightarrow K^+ K^-)/\Gamma(K^+ K^- \pi^+)$ Γ_{43}/Γ_{39}

This is the “fit fraction” from the Dalitz-plot analysis. This is likely a superposition of $D_s^+ \rightarrow f_0(980) \pi$ and $D_s^+ \rightarrow a_0(980) \pi$ which are indistinguishable in such an analysis.

VALUE (units 10^{-2})	EVTS	DOCUMENT ID	TECN	COMMENT
20.6 ± 3.5 OUR AVERAGE				Error includes scale factor of 2.5. See the ideogram below.
19.3 ± 1.7 ± 2.0	18.6k	ABLIKIM	21AE BES3	$e^+ e^-$ at 4.178 GeV
16.4 ± 0.7 ± 2.0		DEL-AMO-SA...11G	BABR	Dalitz fit, 96k evts
28.2 ± 1.9 ± 1.8		MITCHELL	09A CLEO	Dalitz fit, 12k evts
• • • We do not use the following data for averages, fits, limits, etc. • • •				
11.0 ± 3.5 ± 2.6		FRABETTI	95B E687	Dalitz fit, 701 evts

WEIGHTED AVERAGE
20.6 ± 3.5 (Error scaled by 2.5)

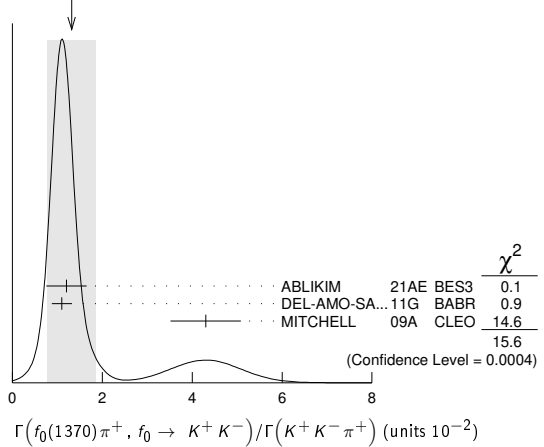


$\Gamma(f_0(1370) \pi^+, f_0 \rightarrow K^+ K^-)/\Gamma(K^+ K^- \pi^+)$ Γ_{44}/Γ_{39}

This is the “fit fraction” from the Dalitz-plot analysis.

VALUE (units 10^{-2})	EVTS	DOCUMENT ID	TECN	COMMENT
1.3 ± 0.5 OUR AVERAGE				Error includes scale factor of 2.8. See the ideogram below.
1.2 ± 0.4 ± 0.2	18.6k	ABLIKIM	21AE BES3	$e^+ e^-$ at 4.178 GeV
1.1 ± 0.1 ± 0.2		DEL-AMO-SA...11G	BABR	Dalitz fit, 96k evts
4.3 ± 0.6 ± 0.5		MITCHELL	09A CLEO	Dalitz fit, 12k evts

WEIGHTED AVERAGE
1.3 ± 0.5 (Error scaled by 2.8)



$\Gamma(f_0(1710) \pi^+, f_0 \rightarrow K^+ K^-)/\Gamma(K^+ K^- \pi^+)$ Γ_{45}/Γ_{39}

This is the “fit fraction” from the Dalitz-plot analysis.

VALUE (units 10^{-2})	EVTS	DOCUMENT ID	TECN	COMMENT
1.3 ± 0.5 OUR AVERAGE				Error includes scale factor of 3.8.
1.9 ± 0.4 ± 0.6	18.6k	ABLIKIM	21AE BES3	$e^+ e^-$ at 4.178 GeV
1.1 ± 0.1 ± 0.1		DEL-AMO-SA...11G	BABR	Dalitz fit, 96k evts
3.4 ± 0.5 ± 0.3		MITCHELL	09A CLEO	Dalitz fit, 12k evts
• • • We do not use the following data for averages, fits, limits, etc. • • •				
3.4 ± 2.3 ± 3.5		FRABETTI	95B E687	Dalitz fit, 701 evts

$\Gamma(K^+ \bar{K}_0^*(1430)^0, \bar{K}_0^{*0} \rightarrow K^- \pi^+)/\Gamma(K^+ K^- \pi^+)$ Γ_{46}/Γ_{39}

This is the “fit fraction” from the Dalitz-plot analysis.

VALUE (units 10^{-2})	EVTS	DOCUMENT ID	TECN	COMMENT
3.3 ± 0.5 OUR AVERAGE				
3.0 ± 0.6 ± 0.5	18.6k	ABLIKIM	21AE BES3	$e^+ e^-$ at 4.178 GeV
2.4 ± 0.3 ± 1.0		DEL-AMO-SA...11G	BABR	Dalitz fit, 96k evts
3.9 ± 0.5 ± 0.5		MITCHELL	09A CLEO	Dalitz fit, 12k evts
• • • We do not use the following data for averages, fits, limits, etc. • • •				
9.3 ± 3.2 ± 3.2		FRABETTI	95B E687	Dalitz fit, 701 evts

$\Gamma(K^+ K_S^0 \pi^0)/\Gamma_{total}$ Γ_{47}/Γ

VALUE (%)	DOCUMENT ID	TECN	COMMENT
1.52 ± 0.09 ± 0.20	ONYISI	13 CLEO	$e^+ e^-$ at 4.17 GeV

$\Gamma(2K_S^0 \pi^+)/\Gamma_{total}$ Γ_{48}/Γ

VALUE (%)	DOCUMENT ID	TECN	COMMENT
0.77 ± 0.05 ± 0.03	ONYISI	13 CLEO	$e^+ e^-$ at 4.17 GeV

$\Gamma(K^*(892) + \bar{K}^0)/\Gamma(\phi \pi^+)$ Γ_{50}/Γ_{40}

Unseen decay modes of the resonances are included.

VALUE	DOCUMENT ID	TECN	COMMENT
1.20 ± 0.21 ± 0.13	CHEN	89 CLEO	$e^+ e^-$ 10 GeV

$\Gamma(K^+ K^- \pi^+ \pi^0)/\Gamma_{total}$ Γ_{51}/Γ

VALUE (%)	EVTS	DOCUMENT ID	TECN	COMMENT
5.50 ± 0.24 OUR FIT				Error includes scale factor of 1.3.
5.51 ± 0.28 OUR AVERAGE				Error includes scale factor of 1.5.

5.42 ± 0.10 ± 0.17	3k	¹ ABLIKIM	21U BES3	$e^+ e^-$ at 4.178–4.226 GeV
6.37 ± 0.21 ± 0.56		ONYISI	13 CLEO	$e^+ e^-$ at 4.17 GeV
• • • We do not use the following data for averages, fits, limits, etc. • • •				
5.65 ± 0.29 ± 0.40		² ALEXANDER	08 CLEO	See ONYISI 13
¹ ABLIKIM 21U uses an amplitude analysis of $D_s^+ \rightarrow K^+ K^- \pi^+ \pi^0$ with 9 components.				
² ALEXANDER 08 uses single- and double-tagged events in an overall fit.				

$\Gamma(\phi \rho^+)/\Gamma_{total}$ Γ_{52}/Γ

VALUE (units 10^{-2})	EVTS	DOCUMENT ID	TECN	COMMENT
5.59 ± 0.15 ± 0.30	3k	¹ ABLIKIM	21U BES3	$e^+ e^-$ at 4.178–4.226 GeV
¹ ABLIKIM 21U uses an amplitude analysis of $D_s^+ \rightarrow K^+ K^- \pi^+ \pi^0$ with 9 components.				

$\Gamma(\bar{K}_1(1270)^0 K^+, \bar{K}_1(1270)^0 \rightarrow K^- \rho^+)/\Gamma_{total}$ Γ_{53}/Γ

VALUE (units 10^{-2})	EVTS	DOCUMENT ID	TECN	COMMENT
0.57 ± 0.05 ± 0.04	3k	¹ ABLIKIM	21U BES3	$e^+ e^-$ at 4.178–4.226 GeV
¹ ABLIKIM 21U uses an amplitude analysis of $D_s^+ \rightarrow K^+ K^- \pi^+ \pi^0$ with 9 components.				

Meson Particle Listings

 D_s^\pm $\Gamma(\bar{K}_1(1270)^0 K^+, \bar{K}_1(1270)^0 \rightarrow K^*(892)\pi)/\Gamma_{\text{total}}$ Γ_{54}/Γ

VALUE (units 10^{-2})	EVTS	DOCUMENT ID	TECN	COMMENT
1.31±0.18±0.18	3k	^{1,2} ABLIKIM	21u	BES3 e^+e^- at 4.178–4.226 GeV

¹ ABLIKIM 21u uses an amplitude analysis of $D_s^+ \rightarrow K^+ K^- \pi^+ \pi^0$ with 9 components.² $\bar{K}_1(1270)^0 \rightarrow K^*(892)\pi$ denotes a sum over $\bar{K}(892)^0 \pi^0$ and $K(892)^- \pi^+$ final states, which are assumed to have relative branching ratio 1/2, as per isospin. $\Gamma(\bar{K}_1(1400)^0 K^+, \bar{K}_1(1400)^0 \rightarrow K^*(892)\pi)/\Gamma_{\text{total}}$ Γ_{55}/Γ

VALUE (units 10^{-2})	EVTS	DOCUMENT ID	TECN	COMMENT
1.98±0.27±0.32	3k	¹ ABLIKIM	21u	BES3 e^+e^- at 4.178–4.226 GeV

¹ $\bar{K}_1(1400)^0 \rightarrow K^*(892)\pi$ denotes a sum over $\bar{K}(892)^0 \pi^0$ and $K(892)^- \pi^+$ final states, which are assumed to have relative branching ratio 1/2, as per isospin. $\Gamma(a_0(980)^0 \rho^+, a_0(980)^0 \rightarrow K^+ K^-)/\Gamma_{\text{total}}$ Γ_{56}/Γ

VALUE (units 10^{-2})	EVTS	DOCUMENT ID	TECN	COMMENT
0.19±0.03±0.03	3k	¹ ABLIKIM	21u	BES3 e^+e^- at 4.178–4.226 GeV

¹ ABLIKIM 21u uses an amplitude analysis of $D_s^+ \rightarrow K^+ K^- \pi^+ \pi^0$ with 9 components. $\Gamma(\bar{K}_1(1420)^0 \pi^+, \bar{K}_1(1420)^0 \rightarrow K^*(892)^- K^\pm)/\Gamma_{\text{total}}$ Γ_{57}/Γ

VALUE (units 10^{-2})	EVTS	DOCUMENT ID	TECN	COMMENT
0.39±0.06±0.03	3k	¹ ABLIKIM	21u	BES3 e^+e^- at 4.178–4.226 GeV

¹ ABLIKIM 21u uses an amplitude analysis of $D_s^+ \rightarrow K^+ K^- \pi^+ \pi^0$ with 9 components. $\Gamma(\bar{K}_1(1420)^0 \pi^+, \bar{K}_1(1420)^0 \rightarrow a_0(980)^0 \pi^0, a_0(980)^0 \rightarrow K^+ K^-)/\Gamma_{\text{total}}$ Γ_{58}/Γ

VALUE (units 10^{-2})	EVTS	DOCUMENT ID	TECN	COMMENT
0.04±0.01±0.01	3k	¹ ABLIKIM	21u	BES3 e^+e^- at 4.178–4.226 GeV

¹ ABLIKIM 21u uses an amplitude analysis of $D_s^+ \rightarrow K^+ K^- \pi^+ \pi^0$ with 9 components. $\Gamma(\eta(1475)\pi^+, \eta(1475) \rightarrow a_0(980)^0 \pi^0, a_0(980)^0 \rightarrow K^+ K^-)/\Gamma_{\text{total}}$ Γ_{59}/Γ

VALUE (units 10^{-2})	EVTS	DOCUMENT ID	TECN	COMMENT
0.07±0.02±0.02	3k	¹ ABLIKIM	21u	BES3 e^+e^- at 4.178–4.226 GeV

¹ ABLIKIM 21u uses an amplitude analysis of $D_s^+ \rightarrow K^+ K^- \pi^+ \pi^0$ with 9 components. $\Gamma(\phi\rho^+)/\Gamma(\phi\pi^+)$ Γ_{52}/Γ_{40}

VALUE	EVTS	DOCUMENT ID	TECN	COMMENT
1.86±0.26^{+0.29}_{-0.40}	253	AVERY	92	CLE2 $e^+e^- \approx 10.5$ GeV

 $\Gamma(K_S^0 K^- 2\pi^+)/\Gamma_{\text{total}}$ Γ_{60}/Γ

VALUE (%)	EVTS	DOCUMENT ID	TECN	COMMENT
1.53±0.08 OUR FIT				Error includes scale factor of 1.5.
1.53±0.11 OUR AVERAGE				Error includes scale factor of 1.8.

1.46±0.05±0.05 1.3k ABLIKIM 21k BES3 e^+e^- at 4.178–4.226 GeV1.69±0.07±0.08 ONYISI 13 CLEO e^+e^- at 4.17 GeV

••• We do not use the following data for averages, fits, limits, etc. •••

1.64±0.10±0.07 ¹ ALEXANDER 08 CLEO See ONYISI 13¹ ALEXANDER 08 uses single- and double-tagged events in an overall fit. $\Gamma(K^*(892)^+ \bar{K}^*(892)^0)/\Gamma(K_S^0 K^- 2\pi^+)$ Γ_{61}/Γ_{60}

VALUE (units 10^{-2})	EVTS	DOCUMENT ID	TECN	COMMENT
40.6±2.9±4.9	1.3k	^{1,2} ABLIKIM	21k	BES3 e^+e^- at 4.178–4.226 GeV

¹ Predominantly S-wave, with a significant D-wave component.² $D_s^+ \rightarrow K_S^0 K^- 2\pi^+$ amplitude analysis with 13 components. $\Gamma(\eta(1475)\pi^+, \eta \rightarrow a_0(980)^- \pi^+, a_0^- \rightarrow K_S^0 K^-)/\Gamma(K_S^0 K^- 2\pi^+)$ Γ_{64}/Γ_{60}

VALUE (units 10^{-2})	EVTS	DOCUMENT ID	TECN	COMMENT
10.8±2.6±5.2	1.3k	¹ ABLIKIM	21k	BES3 e^+e^- at 4.178–4.226 GeV

¹ $D_s^+ \rightarrow K_S^0 K^- 2\pi^+$ amplitude analysis with 13 components. $\Gamma(\eta(1475)K_S^0, \eta \rightarrow K^*(892)^0 \pi^+, K^{*0} \rightarrow K^- \pi^+)/\Gamma(K_S^0 K^- 2\pi^+)$ Γ_{62}/Γ_{60}

VALUE (units 10^{-2})	EVTS	DOCUMENT ID	TECN	COMMENT
2.2±0.6±0.2	1.3k	¹ ABLIKIM	21k	BES3 e^+e^- at 4.178–4.226 GeV

¹ $D_s^+ \rightarrow K_S^0 K^- 2\pi^+$ amplitude analysis with 13 components. $\Gamma(\eta(1475)\pi^+, \eta \rightarrow \bar{K}^*(892)^+ K^-, \bar{K}^{*+} \rightarrow K_S^0 \pi^+)/\Gamma(K_S^0 K^- 2\pi^+)$ Γ_{63}/Γ_{60}

VALUE (units 10^{-2})	EVTS	DOCUMENT ID	TECN	COMMENT
2.2±0.6±0.2	1.3k	¹ ABLIKIM	21k	BES3 e^+e^- at 4.178–4.226 GeV

¹ $D_s^+ \rightarrow K_S^0 K^- 2\pi^+$ amplitude analysis with 13 components. $\Gamma(\bar{K}_1(1285)\pi^+, \bar{K}_1 \rightarrow a_0(980)^- \pi^+, a_0^- \rightarrow K_S^0 K^-)/\Gamma(K_S^0 K^- 2\pi^+)$ Γ_{65}/Γ_{60}

VALUE (units 10^{-2})	EVTS	DOCUMENT ID	TECN	COMMENT
2.2±0.5±0.2	1.3k	¹ ABLIKIM	21k	BES3 e^+e^- at 4.178–4.226 GeV

¹ $D_s^+ \rightarrow K_S^0 K^- 2\pi^+$ amplitude analysis with 13 components. $\Gamma(K^*(892)^+ \bar{K}^*(892)^0)/\Gamma_{\text{total}}$ Γ_{61}/Γ

VALUE (units 10^{-2})	EVTS	DOCUMENT ID	TECN	COMMENT
5.64±0.23±0.27	3k	¹ ABLIKIM	21u	BES3 e^+e^- at 4.178–4.226 GeV

¹ ABLIKIM 21u uses an amplitude analysis of $D_s^+ \rightarrow K^+ K^- \pi^+ \pi^0$ with 9 components. $\Gamma(K^*(892)^+ \bar{K}^*(892)^0)/\Gamma(\phi\pi^+)$ Γ_{61}/Γ_{40}

Unseen decay modes of the resonances are included.

VALUE	DOCUMENT ID	TECN	COMMENT
1.6±0.4±0.4	ALBRECHT	92b	ARG $e^+e^- \approx 10.4$ GeV

 $\Gamma(K^+ K_S^0 \pi^+ \pi^-)/\Gamma_{\text{total}}$ Γ_{66}/Γ

VALUE (%)	DOCUMENT ID	TECN	COMMENT
0.95±0.08 OUR FIT			Error includes scale factor of 1.1.
1.03±0.06±0.08	ONYISI	13	CLEO e^+e^- at 4.17 GeV

 $\Gamma(K^+ K_S^0 \pi^+ \pi^-)/\Gamma(K_S^0 K^- 2\pi^+)$ Γ_{66}/Γ_{60}

VALUE	EVTS	DOCUMENT ID	TECN	COMMENT
0.62 ±0.05 OUR FIT				
0.586±0.052±0.043	476	LINK	01c	FOCS $\gamma A, \bar{E}_\gamma \approx 180$ GeV

 $\Gamma(K^+ K^- 2\pi^+ \pi^-)/\Gamma(K^+ K^- \pi^+)$ Γ_{67}/Γ_{39}

VALUE	EVTS	DOCUMENT ID	TECN	COMMENT
0.160±0.027 OUR AVERAGE				
0.150±0.019±0.025	240	LINK	03d	FOCS $\gamma A, \bar{E}_\gamma \approx 180$ GeV
0.188±0.036±0.040	75	FRABETTI	97c	E687 $\gamma Be, \bar{E}_\gamma \approx 200$ GeV

 $\Gamma(\phi 2\pi^+ \pi^-)/\Gamma(\phi\pi^+)$ Γ_{68}/Γ_{40}

VALUE	EVTS	DOCUMENT ID	TECN	COMMENT
0.269±0.027 OUR AVERAGE				
0.249±0.024±0.021	136	LINK	03d	FOCS $\gamma A, \bar{E}_\gamma \approx 180$ GeV
0.28 ±0.06 ±0.01	40	FRABETTI	97c	E687 $\gamma Be, \bar{E}_\gamma \approx 200$ GeV

$\Gamma(2\pi^+\pi^-)/\Gamma(K^+K^-\pi^+)$ Γ_{76}/Γ_{39}

VALUE	EVTs	DOCUMENT ID	TECN	COMMENT
0.200±0.007 OUR FIT				
0.199±0.004±0.009	≈ 10.5k	AUBERT	09o	BABR $e^+e^- \approx 10.6$ GeV
••• We do not use the following data for averages, fits, limits, etc. •••				
0.265±0.041±0.031	98	FRABETTI	97d	E687 γ Be ≈ 200 GeV

$\Gamma(\rho^0\pi^+)/\Gamma(2\pi^+\pi^-)$ Γ_{77}/Γ_{76}

VALUE	CL%	DOCUMENT ID	TECN	COMMENT
0.018±0.005±0.010		AUBERT	09o	BABR Dalitz fit, ≈ 10.5k evts
••• We do not use the following data for averages, fits, limits, etc. •••				
not seen		LINK	04	FOCS Dalitz fit, 1475 ± 50 evts
0.058±0.023±0.037		AITALA	01A	E791 Dalitz fit, 848 evts
<0.073	90	FRABETTI	97d	E687 γ Be ≈ 200 GeV

$\Gamma(\pi^+(\pi^+\pi^-)_{S\text{-wave}})/\Gamma(2\pi^+\pi^-)$ Γ_{78}/Γ_{76}

This is the "fit fraction" from the Dalitz-plot analysis. See also KLEMP 08, which uses 568 $D_s^+ \rightarrow 3\pi$ decays (over 280 background events) from FNAL E791 to study various parametrizations of the decay amplitudes. The emphasis there is more on S-wave $\pi\pi$ decay products — 20 different solutions are given — than on D_s^+ fit fractions.

VALUE	DOCUMENT ID	TECN	COMMENT
0.833 ± 0.020 OUR AVERAGE			
0.830 ± 0.009 ± 0.019	¹ AUBERT	09o	BABR Dalitz fit, ≈ 10.5k evts
0.8704 ± 0.0560 ± 0.0438	² LINK	04	FOCS Dalitz fit, 1475 ± 50 evts
¹ AUBERT 09o gives the amplitude and phase of the $\pi^+\pi^-$ S-wave in 29 $\pi^+\pi^-$ invariant-mass bins.			
² LINK 04 borrows a K-matrix parametrization from ANISOVICH 03 of the full $\pi\pi$ S-wave isoscalar scattering amplitude to describe the $\pi^+\pi^-$ S-wave component of the $\pi^+\pi^+\pi^-$ state. The fit fraction given above is a sum over five f_0 mesons, the $f_0(980)$, $f_0(1300)$, $f_0(1200-1600)$, $f_0(1500)$, and $f_0(1750)$. See LINK 04 for details and discussion.			

$\Gamma(f_0(980)\pi^+, f_0 \rightarrow \pi^+\pi^-)/\Gamma(2\pi^+\pi^-)$ Γ_{79}/Γ_{76}

This is the "fit fraction" from the Dalitz-plot analysis. See above for the full $\pi^+(\pi^+\pi^-)_{S\text{-wave}}$ fit fraction.

VALUE	DOCUMENT ID	TECN	COMMENT
••• We do not use the following data for averages, fits, limits, etc. •••			
0.565±0.043±0.047	AITALA	01A	E791 Dalitz fit, 848 evts
1.074±0.140±0.043	FRABETTI	97d	E687 γ Be ≈ 200 GeV

$\Gamma(f_0(1370)\pi^+, f_0 \rightarrow \pi^+\pi^-)/\Gamma(2\pi^+\pi^-)$ Γ_{80}/Γ_{76}

This is the "fit fraction" from the Dalitz-plot analysis. See above for the full $\pi^+(\pi^+\pi^-)_{S\text{-wave}}$ fit fraction.

VALUE	DOCUMENT ID	TECN	COMMENT
••• We do not use the following data for averages, fits, limits, etc. •••			
0.324±0.077±0.017	AITALA	01A	E791 Dalitz fit, 848 evts

$\Gamma(f_0(1500)\pi^+, f_0 \rightarrow \pi^+\pi^-)/\Gamma(2\pi^+\pi^-)$ Γ_{81}/Γ_{76}

This is the "fit fraction" from the Dalitz-plot analysis. See above for the full $\pi^+(\pi^+\pi^-)_{S\text{-wave}}$ fit fraction.

VALUE	DOCUMENT ID	TECN	COMMENT
••• We do not use the following data for averages, fits, limits, etc. •••			
0.274±0.114±0.019	¹ FRABETTI	97d	E687 γ Be ≈ 200 GeV
¹ FRABETTI 97d calls this mode $S(1475)\pi^+$, but finds the mass and width of this $S(1475)$ to be in excellent agreement with those of the $f_0(1500)$.			

$\Gamma(f_2(1270)\pi^+, f_2 \rightarrow \pi^+\pi^-)/\Gamma(2\pi^+\pi^-)$ Γ_{82}/Γ_{76}

This is the "fit fraction" from the Dalitz-plot analysis.

VALUE	DOCUMENT ID	TECN	COMMENT
0.101 ± 0.018 OUR AVERAGE			
0.101 ± 0.015 ± 0.011	AUBERT	09o	BABR Dalitz fit, ≈ 10.5k evts
0.0974 ± 0.0449 ± 0.0294	LINK	04	FOCS Dalitz fit, 1475 ± 50 evts
••• We do not use the following data for averages, fits, limits, etc. •••			
0.197 ± 0.033 ± 0.006	AITALA	01A	E791 Dalitz fit, 848 evts
0.123 ± 0.056 ± 0.018	FRABETTI	97d	E687 γ Be ≈ 200 GeV

$\Gamma(\rho(1450)^0\pi^+, \rho^0 \rightarrow \pi^+\pi^-)/\Gamma(2\pi^+\pi^-)$ Γ_{83}/Γ_{76}

This is the "fit fraction" from the Dalitz-plot analysis.

VALUE	DOCUMENT ID	TECN	COMMENT
0.027 ± 0.018 OUR AVERAGE			
0.023 ± 0.008 ± 0.017	AUBERT	09o	BABR Dalitz fit, ≈ 10.5k evts
0.0656 ± 0.0343 ± 0.0440	LINK	04	FOCS Dalitz fit, 1475 ± 50 evts
••• We do not use the following data for averages, fits, limits, etc. •••			
0.044 ± 0.021 ± 0.002	AITALA	01A	E791 Dalitz fit, 848 evts

$\Gamma(\pi^+2\pi^0)/\Gamma_{\text{total}}$ Γ_{84}/Γ

VALUE (%)	EVTs	DOCUMENT ID	TECN	COMMENT
0.65±0.13±0.03	72 ± 16	NAIK	09A	CLEO e^+e^- at 4170 MeV

$\Gamma(2\pi^+\pi^-\pi^0)/\Gamma(\phi\pi^+)$ Γ_{85}/Γ_{40}

VALUE	CL%	DOCUMENT ID	TECN	COMMENT
••• We do not use the following data for averages, fits, limits, etc. •••				
<3.3	90	ANJOS	89e	E691 Photoproduction

$\Gamma(\eta\pi^+)/\Gamma_{\text{total}}$ Γ_{86}/Γ

Unseen decay modes of the η are included.

VALUE (%)	EVTs	DOCUMENT ID	TECN	COMMENT
1.68±0.09 OUR FIT				Error includes scale factor of 1.1.
1.71±0.08 OUR AVERAGE				
1.67±0.08±0.06		ONYISI	13	CLEO e^+e^- at 4.17 GeV
1.82±0.14±0.07	0.8k	ZUPANC	13	BELL e^+e^- at $T(4S), T(5S)$
••• We do not use the following data for averages, fits, limits, etc. •••				
1.58±0.11±0.18		¹ ALEXANDER	08	CLEO See ONYISI 13
¹ ALEXANDER 08 uses single- and double-tagged events in an overall fit.				

$\Gamma(\eta\pi^+)/\Gamma(K^+K_S^0)$ Γ_{86}/Γ_{36}

Unseen decay modes of the η are included.

VALUE	EVTs	DOCUMENT ID	TECN	COMMENT
1.15 ± 0.07 OUR FIT				Error includes scale factor of 1.1.
••• We do not use the following data for averages, fits, limits, etc. •••				
1.236±0.043±0.063	2587 ± 89	MENDEZ	10	CLEO See ONYISI 13

$\Gamma(\eta\pi^+)/\Gamma(\phi\pi^+)$ Γ_{86}/Γ_{40}

Unseen decay modes of the resonances are included.

VALUE	EVTs	DOCUMENT ID	TECN	COMMENT
••• We do not use the following data for averages, fits, limits, etc. •••				
0.48±0.03±0.04	920	JESSOP	98	CLE2 $e^+e^- \approx T(4S)$
0.54±0.09±0.06	165	ALEXANDER	92	CLE2 See JESSOP 98

$\Gamma(\eta\pi^+)/\Gamma(\phi\pi^+, \phi \rightarrow K^+K^-)$ Γ_{86}/Γ_{41}

VALUE (%)	EVTs	DOCUMENT ID	TECN	COMMENT
84.80±0.47±2.64	22k	GUAN	21	BELL $e^+e^- \approx T(4,5S)$

$\Gamma(\eta\pi^+)/\Gamma(K^+K^-\pi^+)$ Γ_{86}/Γ_{39}

VALUE (units 10 ⁻²)	EVTs	DOCUMENT ID	TECN	COMMENT
31.94±0.33±0.49	19.5k	ABLIKIM	20R	BES3 e^+e^- , 4178 ~ 4226 MeV

$\Gamma(2\pi^+\pi^-)/\Gamma_{\text{total}}$ Γ_{93}/Γ

VALUE (units 10 ⁻²)	EVTs	DOCUMENT ID	TECN	COMMENT
3.12±0.13±0.09	2.1k	ABLIKIM	21AR	BES3 e^+e^- at 4.178–4.226 GeV

$\Gamma(a_1(1260)^+\eta, a_1^+ \rightarrow \rho(770)^0\pi^+, \rho^0 \rightarrow \pi^+\pi^-)/\Gamma(2\pi^+\pi^-)$ Γ_{94}/Γ_{93}

VALUE (units 10 ⁻²)	DOCUMENT ID	TECN	COMMENT
55.4±3.9±2.0	¹ ABLIKIM	21AR	BES3 e^+e^- at 4.178–4.226 GeV
¹ $D_s^+ \rightarrow 2\pi^+\pi^-\eta$ amplitude analysis with 11 components.			

$\Gamma(a_1(1260)^+\eta, a_1^+ \rightarrow f_0(500)\pi^+, f_0 \rightarrow \pi^+\pi^-)/\Gamma(2\pi^+\pi^-)$ Γ_{95}/Γ_{93}

VALUE (units 10 ⁻²)	DOCUMENT ID	TECN	COMMENT
8.1±1.9±2.1	¹ ABLIKIM	21AR	BES3 e^+e^- at 4.178–4.226 GeV
¹ $D_s^+ \rightarrow 2\pi^+\pi^-\eta$ amplitude analysis with 11 components.			

$\Gamma(a_0(980)^+\rho(770)^0, a_0^+ \rightarrow \eta\pi^+)/\Gamma(2\pi^+\pi^-)$ Γ_{97}/Γ_{93}

VALUE (units 10 ⁻²)	DOCUMENT ID	TECN	COMMENT
6.7±2.5±1.5	¹ ABLIKIM	21AR	BES3 e^+e^- at 4.178–4.226 GeV
¹ $D_s^+ \rightarrow 2\pi^+\pi^-\eta$ amplitude analysis with 11 components.			

$\Gamma(\eta(1405)\pi^+, \eta(1405) \rightarrow a_0(980)^-\pi^+, a_0^- \rightarrow \eta\pi^-)/\Gamma(2\pi^+\pi^-)$ Γ_{98}/Γ_{93}

VALUE (units 10 ⁻²)	DOCUMENT ID	TECN	COMMENT
0.7±0.2±0.1	¹ ABLIKIM	21AR	BES3 e^+e^- at 4.178–4.226 GeV
¹ $D_s^+ \rightarrow 2\pi^+\pi^-\eta$ amplitude analysis with 11 components.			

$\Gamma(\eta(1405)\pi^+, \eta(1405) \rightarrow a_0(980)^+\pi^-, a_0^+ \rightarrow \eta\pi^+)/\Gamma(2\pi^+\pi^-)$ Γ_{99}/Γ_{93}

VALUE (units 10 ⁻²)	DOCUMENT ID	TECN	COMMENT
0.7±0.2±0.1	¹ ABLIKIM	21AR	BES3 e^+e^- at 4.178–4.226 GeV
¹ $D_s^+ \rightarrow 2\pi^+\pi^-\eta$ amplitude analysis with 11 components.			

$\Gamma(f_1(1420)\pi^+, f_1 \rightarrow a_0(980)^-\pi^+, a_0^- \rightarrow \eta\pi^-)/\Gamma(2\pi^+\pi^-)$ Γ_{100}/Γ_{93}

VALUE (units 10 ⁻²)	DOCUMENT ID	TECN	COMMENT
1.9±0.5±0.3	¹ ABLIKIM	21AR	BES3 e^+e^- at 4.178–4.226 GeV
¹ $D_s^+ \rightarrow 2\pi^+\pi^-\eta$ amplitude analysis with 11 components.			

$\Gamma(f_1(1420)\pi^+, f_1 \rightarrow a_0(980)^+\pi^-, a_0^+ \rightarrow \eta\pi^+)/\Gamma(2\pi^+\pi^-)$ Γ_{101}/Γ_{93}

VALUE (units 10 ⁻²)	DOCUMENT ID	TECN	COMMENT
1.7±0.5±0.3	¹ ABLIKIM	21AR	BES3 e^+e^- at 4.178–4.226 GeV
¹ $D_s^+ \rightarrow 2\pi^+\pi^-\eta$ amplitude analysis with 11 components.			

$\Gamma(\omega\pi^+)/\Gamma_{\text{total}}$ Γ_{87}/Γ

Unseen decay modes of the ω are included.

VALUE (%)	EVTs	DOCUMENT ID	TECN	COMMENT
0.192±0.030 OUR FIT				
0.181±0.032 OUR AVERAGE				
0.177±0.032±0.013	65 ± 12	ABLIKIM	19AH	BES3 e^+e^- at 4.178 GeV
0.21 ± 0.09 ± 0.01	6 ± 2.4	GE	09A	CLEO e^+e^- at 4170 MeV

Meson Particle Listings

 D_s^\pm $\Gamma(\omega\pi^+)/\Gamma(\eta\pi^+)$

Unseen decay modes of the resonances are included.

VALUE	EVTS	DOCUMENT ID	TECN	COMMENT
0.115 ± 0.018 OUR FIT				
0.16 ± 0.04 ± 0.03		BALEST	97 CLE2	$e^+e^- \approx \Upsilon(4S)$

 $\Gamma(3\pi^+2\pi^-)/\Gamma(K^+K^-\pi^+)$

VALUE	EVTS	DOCUMENT ID	TECN	COMMENT
0.146 ± 0.014 OUR AVERAGE				
0.145 ± 0.011 ± 0.010	671	LINK	03b FOCS	$\gamma A, \bar{E}_\gamma \approx 180$ GeV
0.158 ± 0.042 ± 0.031	37	FRABETTI	97c E687	$\gamma Be, \bar{E}_\gamma \approx 200$ GeV

 $\Gamma(\eta\rho^+)/\Gamma_{total}$

Unseen decay modes of the η are included.

VALUE (%)	EVTS	DOCUMENT ID	TECN	COMMENT
8.9 ± 0.6 ± 0.5	328 ± 22	NAIK	09a CLEO	$\eta \rightarrow 2\gamma$

 $\Gamma(\eta\rho^+)/\Gamma(\phi\pi^+)$

Unseen decay modes of the resonances are included.

VALUE	EVTS	DOCUMENT ID	TECN	COMMENT
••• We do not use the following data for averages, fits, limits, etc. •••				
2.98 ± 0.20 ± 0.39	447	JESSOP	98 CLE2	$e^+e^- \approx \Upsilon(4S)$
2.86 ± 0.38 ^{+0.36} _{-0.38}	217	AVERY	92 CLE2	See JESSOP 98

 $\Gamma(\eta\rho^+)/\Gamma(\eta\pi^+\pi^0)$

VALUE (units 10^{-2})	EVTS	DOCUMENT ID	TECN	COMMENT
78.3 ± 5.0 ± 2.1	1.2k	ABLIKIM	19BE BES3	$\eta\pi^+\pi^0$ amplitude analysis

 $\Gamma(\eta\pi^+\pi^0)/\Gamma_{total}$

VALUE (%)	EVTS	DOCUMENT ID	TECN	COMMENT
9.5 ± 0.5 OUR AVERAGE				
9.5 ± 0.28 ± 0.41	2.6k	ABLIKIM	19BE BES3	e^+e^- at 4.178 GeV
9.2 ± 0.4 ± 1.1		ONYISI	13 CLEO	e^+e^- at 4.17 GeV

 $\Gamma(\eta(\pi^+\pi^0)_{P-wave})/\Gamma(\eta\pi^+\pi^0)$

VALUE (units 10^{-2})	EVTS	DOCUMENT ID	TECN	COMMENT
5.4 ± 2.1 ± 2.5	1.2k	ABLIKIM	19BE BES3	$\eta\pi^+\pi^0$ amplitude analysis

 $\Gamma(a_0(980)^+\pi^0, a_0(980)^+ \rightarrow \eta\pi^+\pi^0)/\Gamma(\eta\pi^+\pi^0)$

VALUE (units 10^{-2})	EVTS	DOCUMENT ID	TECN	COMMENT
23.2 ± 2.3 ± 3.3	1.2k	¹ ABLIKIM	19BE BES3	$\eta\pi^+\pi^0$ amplitude analysis

¹ Coherent sum of $D_s^+ \rightarrow a_0^+\pi^0 \rightarrow \eta\pi^+\pi^0$ and $D_s^+ \rightarrow a_0^0\pi^+ \rightarrow \eta\pi^+\pi^0$. ABLIKIM 19BE find $a_0(980)^0 - f(980)$ mixing effects negligibly small in this $D_s^+ \rightarrow \eta\pi^+\pi^0$ Dalitz plot analysis.

 $\Gamma(\omega\pi^+\pi^0)/\Gamma_{total}$

Unseen decay modes of the ω are included.

VALUE (%)	EVTS	DOCUMENT ID	TECN	COMMENT
2.78 ± 0.65 ± 0.25	34 ± 7.9	GE	09a CLEO	e^+e^- at 4170 MeV

 $\Gamma(3\pi^+2\pi^-)/\Gamma_{total}$

VALUE	DOCUMENT ID	TECN	COMMENT
0.049 ± 0.033 -0.030	BARLAG	92c ACCM	π^- 230 GeV

 $\Gamma(\omega 2\pi^+\pi^-)/\Gamma_{total}$

Unseen decay modes of the ω are included.

VALUE (%)	EVTS	DOCUMENT ID	TECN	COMMENT
1.58 ± 0.45 ± 0.09	29 ± 8.2	GE	09a CLEO	e^+e^- at 4170 MeV

 $\Gamma(\eta'(958)\pi^+)/\Gamma_{total}$

Unseen decay modes of the $\eta'(958)$ are included.

VALUE (%)	DOCUMENT ID	TECN	COMMENT
3.94 ± 0.15 ± 0.20	ONYISI	13 CLEO	e^+e^- at 4.17 GeV
••• We do not use the following data for averages, fits, limits, etc. •••			
3.77 ± 0.25 ± 0.30	¹ ALEXANDER	08 CLEO	See ONYISI 13

¹ ALEXANDER 08 uses single- and double-tagged events in an overall fit.

 $\Gamma(\eta'(958)\pi^+)/\Gamma(K^+K_S^0)$

Unseen decay modes of the $\eta'(958)$ are included.

VALUE	EVTS	DOCUMENT ID	TECN	COMMENT
••• We do not use the following data for averages, fits, limits, etc. •••				
2.654 ± 0.088 ± 0.139	1436 ± 47	MENDEZ	10 CLEO	See ONYISI 13

 $\Gamma(\eta'(958)\pi^+)/\Gamma(\phi\pi^+)$

Unseen decay modes of the resonances are included.

VALUE	EVTS	DOCUMENT ID	TECN	COMMENT
••• We do not use the following data for averages, fits, limits, etc. •••				
1.03 ± 0.06 ± 0.07	537	JESSOP	98 CLE2	$e^+e^- \approx \Upsilon(4S)$
1.20 ± 0.15 ± 0.11	281	ALEXANDER	92 CLE2	See JESSOP 98
2.5 ± 1.0 ^{+1.5} _{-0.4}	22	ALVAREZ	91 NA14	Photoproduction
2.5 ± 0.5 ± 0.3	215	ALBRECHT	90d ARG	$e^+e^- \approx 10.4$ GeV

 $\Gamma(\eta'(958)\pi^+)/\Gamma(K^+K^-\pi^+)$

VALUE (units 10^{-2})	EVTS	DOCUMENT ID	TECN	COMMENT
69.4 ± 0.8 ± 3.8	9.9k	ABLIKIM	20R BES3	e^+e^- , 4178 ~ 4226 MeV

 $\Gamma(\omega\eta\pi^+)/\Gamma_{total}$

Unseen decay modes of the ω and η are included.

VALUE	CL%	DOCUMENT ID	TECN	COMMENT
<2.13 × 10⁻²	90	GE	09a CLEO	e^+e^- at 4170 MeV

 $\Gamma(\eta'(958)\rho^+)/\Gamma_{total}$

VALUE (%)	DOCUMENT ID	TECN	COMMENT
5.8 ± 1.4 ± 0.4	ABLIKIM	15z BES3	482 pb ⁻¹ , 4009 MeV

 $\Gamma(\eta'(958)\pi^+)/\Gamma(\phi\pi^+)$

Unseen decay modes of the resonances are included.

VALUE	EVTS	DOCUMENT ID	TECN	COMMENT
••• We do not use the following data for averages, fits, limits, etc. •••				
2.78 ± 0.28 ± 0.30	137	¹ JESSOP	98 CLE2	$e^+e^- \approx \Upsilon(4S)$
3.44 ± 0.62 ^{+0.44} _{-0.46}	68	AVERY	92 CLE2	See JESSOP 98

¹ This JESSOP 98 fraction, when combined with other η' fractions, greatly overshoots the inclusive η' fraction. See the measurement just above, which fits nicely.

 $\Gamma(\eta'(958)\pi^+\pi^0)/\Gamma_{total}$

VALUE (%)	DOCUMENT ID	TECN	COMMENT
5.6 ± 0.5 ± 0.6	ONYISI	13 CLEO	e^+e^- at 4.17 GeV

 $\Gamma(\eta'(958)\pi^+\pi^0 \text{ nonresonant})/\Gamma_{total}$

VALUE	CL%	DOCUMENT ID	TECN	COMMENT
<5.1 × 10⁻²	90	ABLIKIM	15z BES3	482 pb ⁻¹ , 4009 MeV

Modes with one or three K 's $\Gamma(K^+\pi^0)/\Gamma(K^+K_S^0)$

VALUE (units 10^{-2})	EVTS	DOCUMENT ID	TECN	COMMENT
4.2 ± 1.4 ± 0.2	202 ± 70	MENDEZ	10 CLEO	e^+e^- at 4170 MeV
••• We do not use the following data for averages, fits, limits, etc. •••				
5.5 ± 1.3 ± 0.7	141 ± 34	ADAMS	07a CLEO	See MENDEZ 10

 $\Gamma(K^+\pi^0)/\Gamma(K^+K^-\pi^+)$

VALUE (units 10^{-3})	EVTS	DOCUMENT ID	TECN	COMMENT
13.73 ± 0.90 ± 0.33	2.3k	ABLIKIM	20R BES3	e^+e^- , 4178 ~ 4226 MeV

 $\Gamma(K^+\pi^0)/\Gamma(\phi\pi^+, \phi \rightarrow K^+K^-)$

VALUE (%)	EVTS	DOCUMENT ID	TECN	COMMENT
3.28 ± 0.23 ± 0.13	12k	GUAN	21 BELL	$e^+e^- \approx \Upsilon(4,5S)$

 $\Gamma(K_S^0\pi^+)/\Gamma(K^+K_S^0)$

VALUE (units 10^{-2})	EVTS	DOCUMENT ID	TECN	COMMENT
8.12 ± 0.28 OUR AVERAGE				
8.5 ± 0.7 ± 0.2	393 ± 33	MENDEZ	10 CLEO	e^+e^- at 4170 MeV
8.03 ± 0.24 ± 0.19	17.6k ± 481	WON	09 BELL	e^+e^- at $\Upsilon(4S)$
10.4 ± 2.4 ± 1.4	113 ± 26	LINK	08 FOCS	$\gamma A, \bar{E}_\gamma \approx 180$ GeV
••• We do not use the following data for averages, fits, limits, etc. •••				
8.2 ± 0.9 ± 0.2	206 ± 22	ADAMS	07a CLEO	See MENDEZ 10

 $\Gamma(K_S^0\pi^+)/\Gamma(K^+K^-\pi^+)$

VALUE (units 10^{-3})	EVTS	DOCUMENT ID	TECN	COMMENT
20.35 ± 0.62 ± 0.42	2.7k	ABLIKIM	20R BES3	e^+e^- , 4178 ~ 4226 MeV

 $\Gamma(K^+\eta)/\Gamma(K^+K_S^0)$

Unseen decay modes of the η are included.

VALUE (units 10^{-2})	EVTS	DOCUMENT ID	TECN	COMMENT
11.8 ± 2.2 ± 0.6	222 ± 41	MENDEZ	10 CLEO	e^+e^- at 4170 MeV

 $\Gamma(K^+\eta)/\Gamma(\eta\pi^+)$

VALUE (units 10^{-2})	EVTS	DOCUMENT ID	TECN	COMMENT
••• We do not use the following data for averages, fits, limits, etc. •••				
8.9 ± 1.5 ± 0.4	113 ± 18	ADAMS	07a CLEO	See MENDEZ 10

 $\Gamma(K^+\eta)/\Gamma(K^+K^-\pi^+)$

VALUE (units 10^{-2})	EVTS	DOCUMENT ID	TECN	COMMENT
2.97 ± 0.18 ± 0.06	1.8k	ABLIKIM	20R BES3	e^+e^- , 4178 ~ 4226 MeV

 $\Gamma(K^+\eta)/\Gamma(\phi\pi^+, \phi \rightarrow K^+K^-)$

VALUE (%)	EVTS	DOCUMENT ID	TECN	COMMENT
7.81 ± 0.22 ± 0.24	14k	GUAN	21 BELL	$e^+e^- \approx \Upsilon(4,5S)$

See key on page 1127

Meson Particle Listings

D_s^\pm

$\Gamma(K^+\omega)/\Gamma_{total}$ Γ_{114}/Γ
 Unseen decay modes of the ω are included.

VALUE (units 10^{-4})	CL%	EVTS	DOCUMENT ID	TECN	COMMENT
$8.7 \pm 2.4 \pm 0.8$	29	1	ABLIKIM	19AH BES3	e^+e^- at 4.178 GeV

• • • We do not use the following data for averages, fits, limits, etc. • • •

<24	90		GE	09A CLEO	e^+e^- at 4170 MeV
-----	----	--	----	----------	----------------------

¹ Evidence for mode at 4.4 σ .

$\Gamma(K^+\eta(958))/\Gamma(K^+K_S^0)$ Γ_{115}/Γ_{36}
 Unseen decay modes of the $\eta(958)$ are included.

VALUE (units 10^{-2})	EVTS	DOCUMENT ID	TECN	COMMENT
$11.8 \pm 3.6 \pm 0.7$	56 ± 17	MENDEZ	10	CLEO e^+e^- at 4170 MeV

$\Gamma(K^+\eta(958))/\Gamma(\eta(958)\pi^+)$ $\Gamma_{115}/\Gamma_{105}$

VALUE (units 10^{-2})	EVTS	DOCUMENT ID	TECN	COMMENT
$4.2 \pm 1.3 \pm 0.3$	28 ± 9	ADAMS	07A	CLEO See MENDEZ 10

• • • We do not use the following data for averages, fits, limits, etc. • • •

$\Gamma(K^+\eta(958))/\Gamma(K^+K^-\pi^+)$ Γ_{115}/Γ_{39}

VALUE (units 10^{-2})	EVTS	DOCUMENT ID	TECN	COMMENT
$4.91 \pm 0.31 \pm 0.31$	675	ABLIKIM	20R BES3	e^+e^- , 4178 ~ 4226 MeV

$\Gamma(K^+\pi^+\pi^-)/\Gamma_{total}$ Γ_{116}/Γ

VALUE (%)	DOCUMENT ID	TECN	COMMENT
0.65 ± 0.04 OUR FIT			
$0.654 \pm 0.033 \pm 0.025$	ONYISI	13	CLEO e^+e^- at 4.17 GeV

• • • We do not use the following data for averages, fits, limits, etc. • • •

$0.69 \pm 0.05 \pm 0.03$	¹ ALEXANDER	08	CLEO	See ONYISI 13
--------------------------	------------------------	----	------	---------------

¹ ALEXANDER 08 uses single- and double-tagged events in an overall fit.

$\Gamma(K^+\pi^+\pi^-)/\Gamma(K^+K^-\pi^+)$ Γ_{116}/Γ_{39}

VALUE	EVTS	DOCUMENT ID	TECN	COMMENT
0.120 ± 0.007 OUR FIT				
$0.127 \pm 0.007 \pm 0.014$	567 ± 31	LINK	04F	FOCS $\gamma A, \bar{E}_\gamma \approx 180$ GeV

$\Gamma(K^+\rho^0)/\Gamma(K^+\pi^+\pi^-)$ $\Gamma_{117}/\Gamma_{116}$
 This is the "fit fraction" from the Dalitz-plot analysis.

VALUE	DOCUMENT ID	TECN	COMMENT
$0.3883 \pm 0.0531 \pm 0.0261$	LINK	04F	FOCS Dalitz fit, 567 evts

$\Gamma(K^+\rho(1450)^0, \rho^0 \rightarrow \pi^+\pi^-)/\Gamma(K^+\pi^+\pi^-)$ $\Gamma_{118}/\Gamma_{116}$
 This is the "fit fraction" from the Dalitz-plot analysis.

VALUE	DOCUMENT ID	TECN	COMMENT
$0.1062 \pm 0.0351 \pm 0.0104$	LINK	04F	FOCS Dalitz fit, 567 evts

$\Gamma(K^*(892)^0\pi^+, K^{*0} \rightarrow K^+\pi^-)/\Gamma(K^+\pi^+\pi^-)$ $\Gamma_{119}/\Gamma_{116}$
 This is the "fit fraction" from the Dalitz-plot analysis.

VALUE	DOCUMENT ID	TECN	COMMENT
$0.2164 \pm 0.0321 \pm 0.0114$	LINK	04F	FOCS Dalitz fit, 567 evts

$\Gamma(K^*(1410)^0\pi^+, K^{*0} \rightarrow K^+\pi^-)/\Gamma(K^+\pi^+\pi^-)$ $\Gamma_{120}/\Gamma_{116}$
 This is the "fit fraction" from the Dalitz-plot analysis.

VALUE	DOCUMENT ID	TECN	COMMENT
$0.1882 \pm 0.0403 \pm 0.0122$	LINK	04F	FOCS Dalitz fit, 567 evts

$\Gamma(K^*(1430)^0\pi^+, K^{*0} \rightarrow K^+\pi^-)/\Gamma(K^+\pi^+\pi^-)$ $\Gamma_{121}/\Gamma_{116}$
 This is the "fit fraction" from the Dalitz-plot analysis.

VALUE	DOCUMENT ID	TECN	COMMENT
$0.0765 \pm 0.0500 \pm 0.0170$	LINK	04F	FOCS Dalitz fit, 567 evts

$\Gamma(K^+\pi^+\pi^- \text{ nonresonant})/\Gamma(K^+\pi^+\pi^-)$ $\Gamma_{122}/\Gamma_{116}$
 This is the "fit fraction" from the Dalitz-plot analysis.

VALUE	DOCUMENT ID	TECN	COMMENT
$0.1588 \pm 0.0492 \pm 0.0153$	LINK	04F	FOCS Dalitz fit, 567 evts

$\Gamma(K_S^0\pi^+\pi^0)/\Gamma_{total}$ Γ_{123}/Γ

VALUE (%)	EVTS	DOCUMENT ID	TECN	COMMENT
1.08 ± 0.06 OUR AVERAGE				
$1.086 \pm 0.060 \pm 0.030$	666	¹ ABLIKIM	21AB BES3	e^+e^- at 4.178–4.226 GeV
$1.00 \pm 0.18 \pm 0.04$	44	NAIK	09A CLEO	e^+e^- at 4170 MeV

¹ ABLIKIM 21AB uses an amplitude analysis with 5 resonant modes plus one background component, and measures $B(D_S^+ \rightarrow K_S^0\pi^+\pi^0) = (5.43 \pm 0.30 \pm 0.15) \times 10^{-3}$.

$\Gamma(K_S^0 2\pi^+\pi^-)/\Gamma(K_S^0 K^-\pi^+)$ Γ_{124}/Γ_{60}

VALUE	EVTS	DOCUMENT ID	TECN	COMMENT
$0.18 \pm 0.04 \pm 0.05$	179 ± 36	LINK	08	FOCS $\gamma A, \bar{E}_\gamma \approx 180$ GeV

$\Gamma(K^+\omega\pi^0)/\Gamma_{total}$ Γ_{125}/Γ
 Unseen decay modes of the ω are included.

VALUE (%)	CL%	DOCUMENT ID	TECN	COMMENT
<0.82	90	GE	09A	CLEO e^+e^- at 4170 MeV

$\Gamma(K^+\omega\pi^+\pi^-)/\Gamma_{total}$ Γ_{126}/Γ
 Unseen decay modes of the ω are included.

VALUE (%)	CL%	DOCUMENT ID	TECN	COMMENT
<0.54	90	GE	09A	CLEO e^+e^- at 4170 MeV

$\Gamma(K^+\omega\eta)/\Gamma_{total}$ Γ_{127}/Γ
 Unseen decay modes of the ω and η are included.

VALUE (%)	CL%	DOCUMENT ID	TECN	COMMENT
<0.79	90	GE	09A	CLEO e^+e^- at 4170 MeV

$\Gamma(2K^+K^-)/\Gamma(K^+K^-\pi^+)$ Γ_{128}/Γ_{39}

VALUE (units 10^{-3})	EVTS	DOCUMENT ID	TECN	COMMENT
$4.0 \pm 0.3 \pm 0.2$	748 ± 60	DEL-AMO-SA..11g	BABR	$e^+e^- \approx \Upsilon(4S)$

• • • We do not use the following data for averages, fits, limits, etc. • • •

$8.95 \pm 2.12 \pm 2.24$	31	LINK	02i	FOCS $\gamma A, \approx 180$ GeV
--------------------------	----	------	-----	----------------------------------

$\Gamma(\phi K^+, \phi \rightarrow K^+K^-)/\Gamma(2K^+K^-)$ $\Gamma_{129}/\Gamma_{128}$

VALUE	DOCUMENT ID	TECN	COMMENT
$0.41 \pm 0.08 \pm 0.03$	DEL-AMO-SA..11g	BABR	$e^+e^- \approx \Upsilon(4S)$

———— Doubly Cabibbo-suppressed modes ————

$\Gamma(2K^+\pi^-)/\Gamma(K^+K^-\pi^+)$ Γ_{130}/Γ_{39}

VALUE (units 10^{-3})	EVTS	DOCUMENT ID	TECN	COMMENT
2.371 ± 0.034 OUR AVERAGE				
$2.372 \pm 0.024 \pm 0.025$	67k	AAIJ	19g	LHCB pp at 8 TeV
$2.3 \pm 0.3 \pm 0.2$	356 ± 52	DEL-AMO-SA..11g	BABR	$e^+e^- \approx \Upsilon(4S)$
$2.29 \pm 0.28 \pm 0.12$	281 ± 34	KO	09	BELL e^+e^- at $\Upsilon(4S)$
$5.2 \pm 1.7 \pm 1.1$	27 ± 9	LINK	05k	FOCS <0.78%, CL = 90%

$\Gamma(K^+K^*(892)^0, K^{*0} \rightarrow K^+\pi^-)/\Gamma(2K^+\pi^-)$ $\Gamma_{131}/\Gamma_{130}$

VALUE	DOCUMENT ID	TECN	COMMENT
$0.47 \pm 0.22 \pm 0.15$	DEL-AMO-SA..11g	BABR	$e^+e^- \approx \Upsilon(4S)$

———— Baryon-antibaryon mode ————

$\Gamma(\rho\bar{\rho})/\Gamma_{total}$ Γ_{132}/Γ
 This is the only baryonic mode allowed kinematically.

VALUE (units 10^{-3})	EVTS	DOCUMENT ID	TECN	COMMENT
1.22 ± 0.11 OUR AVERAGE				
$1.21 \pm 0.10 \pm 0.05$	193 ± 17	ABLIKIM	19o	BES3 e^+e^- , $E_{cm} = 4178$ MeV
$1.30 \pm 0.36 \pm 0.12$	13.0 ± 3.6	ATHAR	08	CLEO e^+e^- , $E_{cm} \approx 4170$ MeV

$\Gamma(\rho\bar{\rho}e^+\nu_e)/\Gamma_{total}$ Γ_{133}/Γ

VALUE	CL%	DOCUMENT ID	TECN	COMMENT
<2.0 × 10⁻⁴	90	ABLIKIM	19bD	BES3 e^+e^- at 4178 MeV

———— Rare or forbidden modes ————

$\Gamma(\pi^+e^+e^-)/\Gamma_{total}$ Γ_{134}/Γ
 This mode is not a useful test for a $\Delta C=1$ weak neutral current because both quarks must change flavor in this decay.

VALUE	CL%	DOCUMENT ID	TECN	COMMENT
< 5.5 × 10⁻⁶	90	AAIJ	21T	LHCB $1.6 \text{ fb}^{-1} pp$

• • • We do not use the following data for averages, fits, limits, etc. • • •

<1.3 × 10 ⁻⁶	90	LEES	11g	BABR $e^+e^- \approx \Upsilon(4S)$
< 2.2 × 10 ⁻⁵	90	¹ RUBIN	10	CLEO e^+e^- at 4170 MeV
<27 × 10 ⁻⁵	90	AITALA	99g	E791 $\pi^- N$ 500 GeV

¹ This RUBIN 10 limit is for the e^+e^- mass in the continuum away from the $\phi(1020)$. See the next data block.

$\Gamma(\pi^+\phi, \phi \rightarrow e^+e^-)/\Gamma_{total}$ Γ_{135}/Γ
 This is *not* a test for the $\Delta C = 1$ weak neutral current, but leads to the $\pi^+e^+e^-$ final state.

VALUE	EVTS	DOCUMENT ID	TECN	COMMENT
$(6 \pm 8 \pm 1) \times 10^{-6}$	3	RUBIN	10	CLEO e^+e^- at 4170 MeV

$\Gamma(\pi^+\mu^+\mu^-)/\Gamma_{total}$ Γ_{136}/Γ
 This mode is not a useful test for a $\Delta C=1$ weak neutral current because both quarks must change flavor in this decay.

VALUE	CL%	DOCUMENT ID	TECN	COMMENT
<1.8 × 10⁻⁷	90	AAIJ	21T	LHCB $1.6 \text{ fb}^{-1} pp$

• • • We do not use the following data for averages, fits, limits, etc. • • •

<4.1 × 10 ⁻⁷	90	AAIJ	13AF	LHCB pp at 7 TeV
<4.3 × 10 ⁻⁵	90	LEES	11g	BABR $e^+e^- \approx \Upsilon(4S)$
<2.6 × 10 ⁻⁵	90	LINK	03F	FOCS $\gamma A, \bar{E}_\gamma \approx 180$ GeV
<1.4 × 10 ⁻⁴	90	AITALA	99g	E791 $\pi^- N$ 500 GeV
<4.3 × 10 ⁻⁴	90	KODAMA	95	E653 π^- emulsion 600 GeV

Meson Particle Listings

D_s^\pm

$\Gamma(K^+ e^+ e^-)/\Gamma_{total}$ Γ_{137}/Γ
 A test for the $\Delta C=1$ weak neutral current. Allowed by higher-order electroweak interactions.

VALUE	CL%	DOCUMENT ID	TECN	COMMENT
$<3.7 \times 10^{-6}$	90	LEES	11G	BABR $e^+ e^- \approx \mathcal{T}(4S)$
••• We do not use the following data for averages, fits, limits, etc. •••				
$<4.9 \times 10^{-6}$	90	AAIJ	21T	LHCB $1.6 \text{ fb}^{-1} pp$
$<5.2 \times 10^{-5}$	90	RUBIN	10	CLEO $e^+ e^-$ at 4170 MeV
$<1.6 \times 10^{-3}$	90	AITALA	99G	E791 $\pi^- N$ 500 GeV

$\Gamma(K^+ \mu^+ \mu^-)/\Gamma_{total}$ Γ_{138}/Γ
 A test for the $\Delta C=1$ weak neutral current. Allowed by higher-order electroweak interactions.

VALUE	CL%	DOCUMENT ID	TECN	COMMENT
$<1.4 \times 10^{-7}$	90	AAIJ	21T	LHCB $1.6 \text{ fb}^{-1} pp$
••• We do not use the following data for averages, fits, limits, etc. •••				
$<21 \times 10^{-6}$	90	LEES	11G	BABR $e^+ e^- \approx \mathcal{T}(4S)$
$<3.6 \times 10^{-5}$	90	LINK	03F	FOCS $\gamma A, \bar{E}_\gamma \approx 180 \text{ GeV}$
$<1.4 \times 10^{-4}$	90	AITALA	99G	E791 $\pi^- N$ 500 GeV
$<5.9 \times 10^{-4}$	90	KODAMA	95	E653 π^- emulsion 600 GeV

$\Gamma(K^*(892)^+ \mu^+ \mu^-)/\Gamma_{total}$ Γ_{139}/Γ
 A test for the $\Delta C=1$ weak neutral current. Allowed by higher-order electroweak interactions.

VALUE	CL%	DOCUMENT ID	TECN	COMMENT
$<1.4 \times 10^{-3}$	90	KODAMA	95	E653 π^- emulsion 600 GeV

$\Gamma(\pi^+ e^+ \mu^-)/\Gamma_{total}$ Γ_{140}/Γ
 A test of lepton-family-number conservation.

VALUE	CL%	DOCUMENT ID	TECN	COMMENT
$<1.1 \times 10^{-6}$	90	AAIJ	21T	LHCB $1.6 \text{ fb}^{-1} pp$
••• We do not use the following data for averages, fits, limits, etc. •••				
$<12 \times 10^{-6}$	90	LEES	11G	BABR $e^+ e^- \approx \mathcal{T}(4S)$

$\Gamma(\pi^+ e^- \mu^+)/\Gamma_{total}$ Γ_{141}/Γ
 A test of lepton-family-number conservation.

VALUE	CL%	DOCUMENT ID	TECN	COMMENT
$<9.4 \times 10^{-7}$	90	AAIJ	21T	LHCB $1.6 \text{ fb}^{-1} pp$
••• We do not use the following data for averages, fits, limits, etc. •••				
$<20 \times 10^{-6}$	90	LEES	11G	BABR $e^+ e^- \approx \mathcal{T}(4S)$

$\Gamma(K^+ e^+ \mu^-)/\Gamma_{total}$ Γ_{142}/Γ
 A test of lepton-family-number conservation.

VALUE	CL%	DOCUMENT ID	TECN	COMMENT
$<7.9 \times 10^{-7}$	90	AAIJ	21T	LHCB $1.6 \text{ fb}^{-1} pp$
••• We do not use the following data for averages, fits, limits, etc. •••				
$<14 \times 10^{-6}$	90	LEES	11G	BABR $e^+ e^- \approx \mathcal{T}(4S)$

$\Gamma(K^+ e^- \mu^+)/\Gamma_{total}$ Γ_{143}/Γ
 A test of lepton-family-number conservation.

VALUE	CL%	DOCUMENT ID	TECN	COMMENT
$<5.6 \times 10^{-7}$	90	AAIJ	21T	LHCB $1.6 \text{ fb}^{-1} pp$
••• We do not use the following data for averages, fits, limits, etc. •••				
$<9.7 \times 10^{-6}$	90	LEES	11G	BABR $e^+ e^- \approx \mathcal{T}(4S)$

$\Gamma(\pi^- 2e^+)/\Gamma_{total}$ Γ_{144}/Γ
 A test of lepton-number conservation.

VALUE	CL%	DOCUMENT ID	TECN	COMMENT
$<1.4 \times 10^{-6}$	90	AAIJ	21T	LHCB $1.6 \text{ fb}^{-1} pp$
••• We do not use the following data for averages, fits, limits, etc. •••				
$<4.1 \times 10^{-6}$	90	LEES	11G	BABR $e^+ e^- \approx \mathcal{T}(4S)$
$<1.8 \times 10^{-5}$	90	RUBIN	10	CLEO $e^+ e^-$ at 4170 MeV
$<69 \times 10^{-5}$	90	AITALA	99G	E791 $\pi^- N$ 500 GeV

$\Gamma(\pi^- 2\mu^+)/\Gamma_{total}$ Γ_{145}/Γ
 A test of lepton-number conservation.

VALUE	CL%	DOCUMENT ID	TECN	COMMENT
$<8.6 \times 10^{-8}$	90	AAIJ	21T	LHCB $1.6 \text{ fb}^{-1} pp$
••• We do not use the following data for averages, fits, limits, etc. •••				
$<1.2 \times 10^{-7}$	90	AAIJ	13AF	LHCB pp at 7 TeV
$<1.4 \times 10^{-5}$	90	LEES	11G	BABR $e^+ e^- \approx \mathcal{T}(4S)$
$<2.9 \times 10^{-5}$	90	LINK	03F	FOCS $\gamma A, \bar{E}_\gamma \approx 180 \text{ GeV}$
$<8.2 \times 10^{-5}$	90	AITALA	99G	E791 $\pi^- N$ 500 GeV
$<4.3 \times 10^{-4}$	90	KODAMA	95	E653 π^- emulsion 600 GeV

$\Gamma(\pi^- e^+ \mu^+)/\Gamma_{total}$ Γ_{146}/Γ
 A test of lepton-number conservation.

VALUE	CL%	DOCUMENT ID	TECN	COMMENT
$<6.3 \times 10^{-7}$	90	AAIJ	21T	LHCB $1.6 \text{ fb}^{-1} pp$
••• We do not use the following data for averages, fits, limits, etc. •••				
$<8.4 \times 10^{-6}$	90	LEES	11G	BABR $e^+ e^- \approx \mathcal{T}(4S)$
$<7.3 \times 10^{-4}$	90	AITALA	99G	E791 $\pi^- N$ 500 GeV

$\Gamma(K^- 2e^+)/\Gamma_{total}$ Γ_{147}/Γ
 A test of lepton-number conservation.

VALUE	CL%	DOCUMENT ID	TECN	COMMENT
$<7.7 \times 10^{-7}$	90	AAIJ	21T	LHCB $1.6 \text{ fb}^{-1} pp$
••• We do not use the following data for averages, fits, limits, etc. •••				
$<5.2 \times 10^{-6}$	90	LEES	11G	BABR $e^+ e^- \approx \mathcal{T}(4S)$
$<1.7 \times 10^{-5}$	90	RUBIN	10	CLEO $e^+ e^-$ at 4170 MeV
$<63 \times 10^{-5}$	90	AITALA	99G	E791 $\pi^- N$ 500 GeV

$\Gamma(K^- 2\mu^+)/\Gamma_{total}$ Γ_{148}/Γ
 A test of lepton-number conservation.

VALUE	CL%	DOCUMENT ID	TECN	COMMENT
$<2.6 \times 10^{-8}$	90	AAIJ	21T	LHCB $1.6 \text{ fb}^{-1} pp$
••• We do not use the following data for averages, fits, limits, etc. •••				
$<1.3 \times 10^{-5}$	90	LEES	11G	BABR $e^+ e^- \approx \mathcal{T}(4S)$
$<1.3 \times 10^{-5}$	90	LINK	03F	FOCS $\gamma A, \bar{E}_\gamma \approx 180 \text{ GeV}$
$<1.8 \times 10^{-4}$	90	AITALA	99G	E791 $\pi^- N$ 500 GeV
$<5.9 \times 10^{-4}$	90	KODAMA	95	E653 π^- emulsion 600 GeV

$\Gamma(K^- e^+ \mu^+)/\Gamma_{total}$ Γ_{149}/Γ
 A test of lepton-number conservation.

VALUE	CL%	DOCUMENT ID	TECN	COMMENT
$<2.6 \times 10^{-7}$	90	AAIJ	21T	LHCB $1.6 \text{ fb}^{-1} pp$
••• We do not use the following data for averages, fits, limits, etc. •••				
$<6.1 \times 10^{-6}$	90	LEES	11G	BABR $e^+ e^- \approx \mathcal{T}(4S)$
$<6.8 \times 10^{-4}$	90	AITALA	99G	E791 $\pi^- N$ 500 GeV

$\Gamma(K^*(892)^- 2\mu^+)/\Gamma_{total}$ Γ_{150}/Γ
 A test of lepton-number conservation.

VALUE	CL%	DOCUMENT ID	TECN	COMMENT
$<1.4 \times 10^{-3}$	90	KODAMA	95	E653 π^- emulsion 600 GeV

D_s^\pm Amplitude analyses

$D_s^+ \rightarrow K^+ K^- \pi^+$ partial wave analyses

Amplitude analyses of D_s^+ decays to the $K^+ K^- \pi^+$ final state, fitting simultaneously different partial wave components.

VALUE	EVTS	DOCUMENT ID	TECN	COMMENT
seen	18.6k	¹ ABLIKIM	21AE	BES3 $e^+ e^-$ at 4.178 GeV
seen	96k	¹ DEL-AMO-SA.	11G	BABR $e^+ e^-$ at $\mathcal{T}(4S)$
seen	12k	¹ MITCHELL	09A	CLEO $e^+ e^-$ at 4.17 GeV
seen	701	² FRABETTI	95B	E687

- ¹ Amplitude analysis with 6 components.
- ² Amplitude analysis with 5 components.

$D_s^+ \rightarrow 2\pi^+ \pi^- \eta$ partial wave analyses

Amplitude analyses of D_s^+ decays to the $\pi^+ \pi^+ \pi^- \eta$ final state, fitting simultaneously different partial wave components.

VALUE	EVTS	DOCUMENT ID	TECN	COMMENT
seen	2.1k	¹ ABLIKIM	21AR	BES3 $e^+ e^-$ at 4.178–4.226 GeV

- ¹ Amplitude analysis with 11 components.

$D_s^+ \rightarrow (KS)^0 K^- 2\pi^+$ partial wave analyses

Amplitude analyses of D_s^+ decays to the $K_S^0 K^- 2\pi^+$ final state, fitting simultaneously different partial wave components.

VALUE	EVTS	DOCUMENT ID	TECN	COMMENT
seen	1.3k	¹ ABLIKIM	21K	BES3 $e^+ e^-$ at 4.178–4.226 GeV

- ¹ Amplitude analysis with 13 components.

$D_s^+ \rightarrow K^- K^+ \pi^+ \pi^0$ partial wave analyses

Amplitude analyses of D_s^+ decays to the $K^- K^+ \pi^+ \pi^0$ final state, fitting simultaneously different partial wave components.

VALUE	EVTS	DOCUMENT ID	TECN	COMMENT
seen	3k	¹ ABLIKIM	21U	BES3 $e^+ e^-$ at 4.178–4.226 GeV

- ¹ ABLIKIM 21U uses an amplitude analysis with 9 components.

$D_s^+ - D_s^-$ CP-VIOLATING DECAY-RATE ASYMMETRIES

This is the difference between D_s^+ and D_s^- partial widths for the decay to state f , divided by the sum of the widths:

$$A_{CP}(f) = [\Gamma(D_s^+ \rightarrow f) - \Gamma(D_s^- \rightarrow \bar{f})] / [\Gamma(D_s^+ \rightarrow f) + \Gamma(D_s^- \rightarrow \bar{f})].$$

$A_{CP}(\mu^\pm \nu)$ in $D_s^+ \rightarrow \mu^+ \nu, D_s^- \rightarrow \mu^- \bar{\nu}_\mu$

VALUE (%)	EVTS	DOCUMENT ID	TECN	COMMENT
-0.2 ± 2.5 OUR AVERAGE				
$-1.2 \pm 2.5 \pm 1.0$	2.2k	ABLIKIM	21BE	BES3 $e^+ e^-$ at 4.178, 4.226 GeV
4.8 ± 6.1		ALEXANDER	09	CLEO $e^+ e^-$ at 4170 MeV

$A_{CP}(\tau^\pm \nu)$ in $D_s^\pm \rightarrow \tau^\pm \nu_\tau$, $D_s^- \rightarrow \tau^- \bar{\nu}_\tau$

VALUE (%)	EVTS	DOCUMENT ID	TECN	COMMENT
2.9 ± 4.8 ± 1.0	950	¹ ABLIKIM	21BE BES3	e^+e^- at 4.178, 4.226 GeV

¹ABLIKIM 21BE also reports that when constrained by the Standard Model ratio of $\Gamma(D_s^+ \rightarrow \tau^+ \nu_\tau) / \Gamma(D_s^+ \rightarrow \mu^+ \nu_\mu) = 9.75$, the result is $(-0.1 \pm 1.9 \pm 1.0)\%$.

$A_{CP}(K^\pm K_S^0)$ in $D_s^\pm \rightarrow K^\pm K_S^0$

VALUE (%)	EVTS	DOCUMENT ID	TECN	COMMENT
0.09 ± 0.26 OUR AVERAGE				

0.6 ± 2.8 ± 0.6	1.8k	ABLIKIM	19AMBES3	e^+e^- at 4178 MeV
-0.05 ± 0.23 ± 0.24	288k	¹ LEES	13E BABR	e^+e^- at $\Upsilon(4S)$
2.6 ± 1.5 ± 0.6		ONYISI	13 CLEO	e^+e^- at 4.17 GeV
0.12 ± 0.36 ± 0.22		KO	10 BELL	$e^+e^- \approx \Upsilon(4S)$

••• We do not use the following data for averages, fits, limits, etc. •••
 4.7 ± 1.8 ± 0.9 4.0k MENDEZ 10 CLEO See ONYISI 13
 4.9 ± 2.1 ± 0.9 ALEXANDER 08 CLEO See MENDEZ 10

¹LEES 13E finds that after subtracting the contribution due to $K^0 - \bar{K}^0$ mixing, the CP asymmetry is $(+0.28 \pm 0.23 \pm 0.24)\%$.

$A_{CP}(K^\pm K_L^0)$ in $D_s^\pm \rightarrow K^\pm K_L^0$

VALUE (units 10^{-2})	EVTS	DOCUMENT ID	TECN	COMMENT
-1.1 ± 2.6 ± 0.6	2.3k	ABLIKIM	19AMBES3	e^+e^- at 4178 MeV

$A_{CP}(K^+ K^- \pi^\pm)$ in $D_s^\pm \rightarrow K^+ K^- \pi^\pm$

VALUE (%)	DOCUMENT ID	TECN	COMMENT
-0.5 ± 0.8 ± 0.4	ONYISI 13	CLEO	e^+e^- at 4.17 GeV

••• We do not use the following data for averages, fits, limits, etc. •••
 0.3 ± 1.1 ± 0.8 ALEXANDER 08 CLEO See ONYISI 13

$A_{CP}(\phi \pi^\pm)$ in $D_s^\pm \rightarrow \phi \pi^\pm$

VALUE (%)	DOCUMENT ID	TECN	COMMENT
-0.38 ± 0.26 ± 0.08	ABAZOV 14B	D0	$p\bar{p}$ at 1.96 TeV

$A_{CP}(K^\pm K_S^0 \pi^0)$ in $D_s^\pm \rightarrow K^\pm K_S^0 \pi^0$

VALUE (%)	DOCUMENT ID	TECN	COMMENT
-1.6 ± 6.0 ± 1.1	ONYISI 13	CLEO	e^+e^- at 4.17 GeV

$A_{CP}(2K_S^0 \pi^\pm)$ in $D_s^\pm \rightarrow 2K_S^0 \pi^\pm$

VALUE (%)	DOCUMENT ID	TECN	COMMENT
3.1 ± 5.2 ± 0.6	ONYISI 13	CLEO	e^+e^- at 4.17 GeV

$A_{CP}(K^+ K^- \pi^\pm \pi^0)$ in $D_s^\pm \rightarrow K^+ K^- \pi^\pm \pi^0$

VALUE (%)	DOCUMENT ID	TECN	COMMENT
0.0 ± 2.7 ± 1.2	ONYISI 13	CLEO	e^+e^- at 4.17 GeV

••• We do not use the following data for averages, fits, limits, etc. •••
 -5.9 ± 4.2 ± 1.2 ALEXANDER 08 CLEO See ONYISI 13

$A_{CP}(K^\pm K_S^0 \pi^+ \pi^-)$ in $D_s^\pm \rightarrow K^\pm K_S^0 \pi^+ \pi^-$

VALUE (%)	DOCUMENT ID	TECN	COMMENT
-5.7 ± 5.3 ± 0.9	ONYISI 13	CLEO	e^+e^- at 4.17 GeV

$A_{CP}(K_S^0 K^\mp 2\pi^\pm)$ in $D_s^\pm \rightarrow K_S^0 K^\mp 2\pi^\pm$

VALUE (%)	DOCUMENT ID	TECN	COMMENT
4.1 ± 2.7 ± 0.9	ONYISI 13	CLEO	e^+e^- at 4.17 GeV

••• We do not use the following data for averages, fits, limits, etc. •••
 -0.7 ± 3.6 ± 1.1 ALEXANDER 08 CLEO See ONYISI 13

$A_{CP}(\pi^+ \pi^- \pi^\pm)$ in $D_s^\pm \rightarrow \pi^+ \pi^- \pi^\pm$

VALUE (%)	DOCUMENT ID	TECN	COMMENT
-0.7 ± 3.0 ± 0.6	ONYISI 13	CLEO	e^+e^- at 4.17 GeV

••• We do not use the following data for averages, fits, limits, etc. •••
 2.0 ± 4.6 ± 0.7 ALEXANDER 08 CLEO See ONYISI 13

$A_{CP}(\pi^\pm \eta)$ in $D_s^\pm \rightarrow \pi^\pm \eta$

VALUE (%)	EVTS	DOCUMENT ID	TECN	COMMENT
0.3 ± 0.4 OUR AVERAGE				

0.8 ± 0.7 ± 0.5	38k	AAIJ	21U LHCb	pp at 13 TeV
0.2 ± 0.3 ± 0.3	22k	GUAN	21 BELL	$e^+e^- \approx \Upsilon(4,5S)$
1.1 ± 3.0 ± 0.8		ONYISI	13 CLEO	e^+e^- at 4.17 GeV
-4.6 ± 2.9 ± 0.3	2.5k	MENDEZ	10 CLEO	See ONYISI 13
-8.2 ± 5.2 ± 0.8		ALEXANDER	08 CLEO	See MENDEZ 10

$A_{CP}(\pi^\pm \eta')$ in $D_s^\pm \rightarrow \pi^\pm \eta'$

VALUE (%)	EVTS	DOCUMENT ID	TECN	COMMENT
-0.9 ± 0.5 OUR AVERAGE				

-0.82 ± 0.36 ± 0.35	152k	AAIJ	17AF LHCb	pp at 7, 8 TeV
-2.2 ± 2.2 ± 0.6		ONYISI	13 CLEO	e^+e^- at 4.17 GeV
-6.1 ± 3.0 ± 0.3	1.4k	MENDEZ	10 CLEO	See ONYISI 13
-5.5 ± 3.7 ± 1.2		ALEXANDER	08 CLEO	See MENDEZ 10

$A_{CP}(\eta \pi^\pm \pi^0)$ in $D_s^\pm \rightarrow \eta \pi^\pm \pi^0$

VALUE (%)	DOCUMENT ID	TECN	COMMENT
-0.5 ± 3.9 ± 2.0	ONYISI 13	CLEO	e^+e^- at 4.17 GeV

$A_{CP}(\eta' \pi^\pm \pi^0)$ in $D_s^\pm \rightarrow \eta' \pi^\pm \pi^0$

VALUE (%)	DOCUMENT ID	TECN	COMMENT
-0.4 ± 7.4 ± 1.9	ONYISI 13	CLEO	e^+e^- at 4.17 GeV

$A_{CP}(K^\pm \pi^0)$ in $D_s^\pm \rightarrow K^\pm \pi^0$

VALUE (%)	EVTS	DOCUMENT ID	TECN	COMMENT
2 ± 4 OUR AVERAGE				Error includes scale factor of 1.2.

-0.8 ± 3.9 ± 1.2	2.8k	AAIJ	21U LHCb	pp at 7, 8, 13 TeV
6.4 ± 4.4 ± 1.1	12k	GUAN	21 BELL	$e^+e^- \approx \Upsilon(4,5S)$
-26.6 ± 23.8 ± 0.9	202	MENDEZ	10 CLEO	e^+e^- at 4170 MeV
2 ± 29		ADAMS	07A CLEO	See MENDEZ 10

$A_{CP}(K^0 / K^0 \pi^\pm)$ in $D_s^\pm \rightarrow K^0 \pi^+, D_s^- \rightarrow K^0 \pi^-$

VALUE (%)	EVTS	DOCUMENT ID	TECN	COMMENT
0.4 ± 0.5 OUR AVERAGE				

0.38 ± 0.46 ± 0.17	121k	¹ AAIJ	14BD LHCb	pp at 7, 8 TeV
0.3 ± 2.0 ± 0.3	14k	LEES	13E BABR	e^+e^- at $\Upsilon(4S)$
0.61 ± 0.83 ± 0.14	26k	AAIJ	13W LHCb	See AAIJ 14BD

••• We do not use the following data for averages, fits, limits, etc. •••
¹AAIJ 14BD reports its result as $A_{CP}(D_s^\pm \rightarrow K_S^0 K^\pm)$ with CP-violation effects in the $K^0 - \bar{K}^0$ system studied. It also measures $A_{CP}(D^\pm \rightarrow \bar{K}^0 / K^0 K^\pm) + A_{CP}(D_S^\pm \rightarrow \bar{K}^0 / K^0 \pi^\pm) = (0.41 \pm 0.49 \pm 0.26)\%$.

$A_{CP}(K_S^0 \pi^\pm)$ in $D_s^\pm \rightarrow K_S^0 \pi^\pm$

VALUE (%)	EVTS	DOCUMENT ID	TECN	COMMENT
0.20 ± 0.18 OUR AVERAGE				

0.16 ± 0.17 ± 0.05	721k	AAIJ	19T LHCb	pp at 7, 8, 13 TeV
0.6 ± 2.0 ± 0.3	14k	LEES	13E BABR	e^+e^- at $\Upsilon(4S)$
5.45 ± 2.50 ± 0.33		KO	10 BELL	$e^+e^- \approx \Upsilon(4S)$
16.3 ± 7.3 ± 0.3	0.4k	MENDEZ	10 CLEO	e^+e^- at 4170 MeV
27 ± 11		ADAMS	07A CLEO	See MENDEZ 10

$A_{CP}(K^\pm \pi^+ \pi^-)$ in $D_s^\pm \rightarrow K^\pm \pi^+ \pi^-$

VALUE (%)	DOCUMENT ID	TECN	COMMENT
4.5 ± 4.8 ± 0.6	ONYISI 13	CLEO	e^+e^- at 4.17 GeV

••• We do not use the following data for averages, fits, limits, etc. •••
 11.2 ± 7.0 ± 0.9 ALEXANDER 08 CLEO See ONYISI 13

$A_{CP}(K_S^0 \pi^+ \pi^0)$ in $D_s^\pm \rightarrow K_S^0 \pi^+ \pi^0$

VALUE (%)	EVTS	DOCUMENT ID	TECN	COMMENT
2.7 ± 5.5 ± 0.9	666	¹ ABLIKIM	21AB BES3	e^+e^- at 4.178-4.226 GeV

¹ABLIKIM 21AB uses an amplitude analysis with 5 resonant modes plus one background component.

$A_{CP}(K^\pm \eta)$ in $D_s^\pm \rightarrow K^\pm \eta$

VALUE (%)	EVTS	DOCUMENT ID	TECN	COMMENT
1.8 ± 1.9 OUR AVERAGE				

0.9 ± 3.7 ± 1.1	2.5k	AAIJ	21U LHCb	pp at 13 TeV
2.1 ± 2.1 ± 0.4	14k	GUAN	21 BELL	$e^+e^- \approx \Upsilon(4,5S)$
9.3 ± 15.2 ± 0.9	222	MENDEZ	10 CLEO	e^+e^- at 4170 MeV
-20 ± 18		ADAMS	07A CLEO	See MENDEZ 10

$A_{CP}(K^\pm \eta'(958))$ in $D_s^\pm \rightarrow K^\pm \eta'(958)$

VALUE (%)	EVTS	DOCUMENT ID	TECN	COMMENT
6.0 ± 18.9 ± 0.9	56 ± 17	MENDEZ	10 CLEO	e^+e^- at 4170 MeV

••• We do not use the following data for averages, fits, limits, etc. •••
 -17 ± 37 ADAMS 07A CLEO See MENDEZ 10

CP VIOLATING ASYMMETRIES OF P-ODD (T-ODD) MOMENTS

$A_{Tviol}(K_S^0 K^\pm \pi^+ \pi^-)$ in $D_s^\pm \rightarrow K_S^0 K^\pm \pi^+ \pi^-$

$C_T \equiv \bar{p}_{K^+} \cdot (\bar{p}_{\pi^+} \times \bar{p}_{\pi^-})$ is a parity-odd correlation of the K^+ , π^+ , and π^- momenta for the D_s^+ . $\bar{C}_T \equiv \bar{p}_{K^-} \cdot (\bar{p}_{\pi^-} \times \bar{p}_{\pi^+})$ is the corresponding quantity for the D_s^- . Then $A_T \equiv [\Gamma(C_T > 0) - \Gamma(C_T < 0)] / [\Gamma(C_T > 0) + \Gamma(C_T < 0)]$, and $\bar{A}_T \equiv [\Gamma(-\bar{C}_T > 0) - \Gamma(-\bar{C}_T < 0)] / [\Gamma(-\bar{C}_T > 0) + \Gamma(-\bar{C}_T < 0)]$, and $A_{Tviol} \equiv \frac{1}{2}(A_T - \bar{A}_T)$. C_T and \bar{C}_T are commonly referred to as T-odd moments, because they are odd under T reversal. However, the T-conjugate process $K_S^0 K^\pm \pi^+ \pi^- \rightarrow D_s^\pm$ is not accessible, while the P-conjugate process is.

VALUE (units 10^{-3})	EVTS	DOCUMENT ID	TECN	COMMENT
-13.6 ± 7.7 ± 3.4	29.8 ± 0.3k	LEES	11E BABR	$e^+e^- \approx \Upsilon(4S)$

••• We do not use the following data for averages, fits, limits, etc. •••
 -36 ± 67 ± 23 508 ± 34 LINK 05E FOCS $\gamma A, \bar{E}_\gamma \approx 180$ GeV

Meson Particle Listings

D_s^\pm

D_s^+ Semileptonic Form Factors and Decay Constants

$r_2 \equiv A_2(0)/A_1(0)$ in $D_s^+ \rightarrow \phi \ell^+ \nu_\ell$

VALUE	EVTS	DOCUMENT ID	TECN	COMMENT
0.84 ± 0.11 OUR AVERAGE				Error includes scale factor of 2.4.
0.816 ± 0.036 ± 0.030	25 ± 0.5k	¹ AUBERT	08AN BABR	$\phi e^+ \nu_e$
0.713 ± 0.202 ± 0.284	793	LINK	04C FOCS	$\phi \mu^+ \nu_\mu$
1.57 ± 0.25 ± 0.19	271	AITALA	99D E791	$\phi e^+ \nu_e, \phi \mu^+ \nu_\mu$
1.4 ± 0.5 ± 0.3	308	AVERY	94B CLE2	$\phi e^+ \nu_e$
1.1 ± 0.8 ± 0.1	90	FRABETTI	94F E687	$\phi \mu^+ \nu_\mu$
2.1 ^{+0.6} _{-0.5} ± 0.2	19	KODAMA	93 E653	$\phi \mu^+ \nu_\mu$

¹To compare with previous measurements, this AUBERT 08AN value is from a fit that fixes the pole masses at $m_A = 2.5$ GeV/c² and $m_V = 2.1$ GeV/c². A simultaneous fit to r_2, r_V, r_0 (a significant s-wave contribution) and m_A , gives $r_2 = 0.763 \pm 0.071 \pm 0.065$.

$r_V \equiv V(0)/A_1(0)$ in $D_s^+ \rightarrow \phi \ell^+ \nu_\ell$

VALUE	EVTS	DOCUMENT ID	TECN	COMMENT
1.80 ± 0.08 OUR AVERAGE				
1.807 ± 0.046 ± 0.065	25 ± 0.5k	¹ AUBERT	08AN BABR	$\phi e^+ \nu_e$
1.549 ± 0.250 ± 0.148	793	LINK	04C FOCS	$\phi \mu^+ \nu_\mu$
2.27 ± 0.35 ± 0.22	271	AITALA	99D E791	$\phi e^+ \nu_e, \phi \mu^+ \nu_\mu$
0.9 ± 0.6 ± 0.3	308	AVERY	94B CLE2	$\phi e^+ \nu_e$
1.8 ± 0.9 ± 0.2	90	FRABETTI	94F E687	$\phi \mu^+ \nu_\mu$
2.3 ^{+1.1} _{-0.9} ± 0.4	19	KODAMA	93 E653	$\phi \mu^+ \nu_\mu$

¹To compare with previous measurements, this AUBERT 08AN value is from a fit that fixes the pole masses at $m_A = 2.5$ GeV/c² and $m_V = 2.1$ GeV/c². A simultaneous fit to r_2, r_V, r_0 (a significant s-wave contribution) and m_A , gives $r_V = 1.849 \pm 0.060 \pm 0.095$.

Γ_L/Γ_T in $D_s^+ \rightarrow \phi \ell^+ \nu_\ell$

VALUE	EVTS	DOCUMENT ID	TECN	COMMENT
0.72 ± 0.18 OUR AVERAGE				
1.0 ± 0.3 ± 0.2	308	AVERY	94B CLE2	$\phi e^+ \nu_e$
1.0 ± 0.5 ± 0.1	90	¹ FRABETTI	94F E687	$\phi \mu^+ \nu_\mu$
0.54 ± 0.21 ± 0.10	19	¹ KODAMA	93 E653	$\phi \mu^+ \nu_\mu$

¹FRABETTI 94F and KODAMA 93 evaluate Γ_L/Γ_T for a lepton mass of zero.

$f_+(0) |V_{cs}|$ in $D_s^+ \rightarrow \eta e^+ \nu_e$

VALUE	EVTS	DOCUMENT ID	TECN	COMMENT
0.4455 ± 0.0053 ± 0.0044	1.8k	ABLIKIM	19s BES3	$e^+ e^-$ at 4178 MeV

$f_+(0) |V_{cs}|$ in $D_s^+ \rightarrow \eta' e^+ \nu_e$

VALUE	EVTS	DOCUMENT ID	TECN	COMMENT
0.477 ± 0.049 ± 0.011	261	ABLIKIM	19s BES3	$e^+ e^-$ at 4178 MeV

$f_+(0) |V_{cd}|$ in $D_s^+ \rightarrow K^0 e^+ \nu_e$

VALUE	EVTS	DOCUMENT ID	TECN	COMMENT
0.162 ± 0.019 ± 0.003	117	¹ ABLIKIM	19D BES3	$K_S^0 e^+ \nu_e$

¹Using a two parameter fit in the z expansion.

$r_V \equiv V(0)/A_1(0)$ in $D_s^+ \rightarrow K^*(892)^0 e^+ \nu_e$

VALUE	EVTS	DOCUMENT ID	TECN	COMMENT
1.67 ± 0.34 ± 0.16	155	ABLIKIM	19D BES3	$e^+ e^-$ at 4178 MeV

$r_2 \equiv A_2(0)/A_1(0)$ in $D_s^+ \rightarrow K^*(892)^0 e^+ \nu_e$

VALUE	EVTS	DOCUMENT ID	TECN	COMMENT
0.77 ± 0.28 ± 0.07	155	ABLIKIM	19D BES3	$e^+ e^-$ at 4178 MeV

$f_{D_s^+} |V_{cs}|$ in $D_s^+ \rightarrow \mu^+ \nu_\mu$

VALUE (MeV)	EVTS	DOCUMENT ID	TECN	COMMENT
243.1 ± 3.0 ± 3.6 ± 1.0	2.2K	¹ ABLIKIM	21BE BES3	$e^+ e^-$ at 4.178, 4.226 GeV
246.2 ± 3.6 ± 3.5	1.1k	ABLIKIM	19E BES3	$e^+ e^-$ at 4178 MeV

¹The third uncertainty is dominated by the uncertainty of the D_s^+ lifetime.

$f_{D_s^+} |V_{cs}|$ in $D_s^+ \rightarrow \tau^+ \nu_\tau$

VALUE (MeV)	EVTS	DOCUMENT ID	TECN	COMMENT
245.3 ± 3.0 OUR AVERAGE				
251.6 ± 5.9 ± 4.9	1.7k	¹ ABLIKIM	21AF BES3	$e^+ e^-$ at 4.178, 4.226 GeV
244.4 ± 2.3 ± 2.9	4.9k	² ABLIKIM	21AZ BES3	$e^+ e^-$ at 4.178, 4.226 GeV
243.0 ± 5.8 ± 4.0 ± 1.0	950	^{3,4} ABLIKIM	21BE BES3	$e^+ e^-$ at 4.178, 4.226 GeV

¹ABLIKIM 21F uses $\tau^+ \rightarrow \pi^+ \pi^0 \bar{\nu}$ decays.
²ABLIKIM 21AZ uses $\tau^+ \rightarrow e^+ \nu_e \bar{\nu}_\tau$ decays.
³ABLIKIM 21BE uses $\tau^+ \rightarrow e^+ \nu_e \bar{\nu}_\tau$ decays. When constrained by the Standard Model ratio of $\Gamma(D_s^+ \rightarrow \tau^+ \nu_\tau)/\Gamma(D_s^+ \rightarrow \mu^+ \nu_\mu) = 9.75$, the result is $243.2 \pm 2.3 \pm 3.3 \pm 1.0$.

⁴The third uncertainty is dominated by the uncertainty of the D_s^+ lifetime.

D_s^\pm REFERENCES

AJAJ 21T JHEP 2106 044 (LHCb Collab.)
 AJAJ 21U JHEP 2106 019 (LHCb Collab.)
 ABLIKIM 21AB JHEP 2106 181 (BESIII Collab.)
 ABLIKIM 21AC PR D104 012003 (BESIII Collab.)
 ABLIKIM 21AE PR D104 012016 (BESIII Collab.)
 ABLIKIM 21AF PR D104 032001 (BESIII Collab.)
 ABLIKIM 21AR PR D104 L071101 (BESIII Collab.)
 ABLIKIM 21AZ PRL 127 171801 (BESIII Collab.)
 ABLIKIM 21BE PR D104 052009 (BESIII Collab.)
 ABLIKIM 21F PR D103 052011 (BESIII Collab.)
 ABLIKIM 21K PR D103 092006 (BESIII Collab.)
 ABLIKIM 21U PR D104 032011 (BESIII Collab.)
 ABLIKIM 21Y PR D103 092004 (BESIII Collab.)
 GUAN 21 PR D103 112005 (BELLE Collab.)
 ABLIKIM 20R JHEP 2008 146 (BESIII Collab.)
 AJAJ 19G JHEP 1903 176 (LHCb Collab.)
 AJAJ 19T PRL 122 191803 (LHCb Collab.)
 ABLIKIM 19AD PR D99 072002 (BESIII Collab.)
 ABLIKIM 19AH PR D99 091101 (BESIII Collab.)
 ABLIKIM 19AM PR D99 112005 (BESIII Collab.)
 ABLIKIM 19BD PR D100 112008 (BESIII Collab.)
 ABLIKIM 19BE PRL 123 112001 (BESIII Collab.)
 ABLIKIM 19D PRL 122 061801 (BESIII Collab.)
 ABLIKIM 19E PRL 122 071802 (BESIII Collab.)
 ABLIKIM 19O PR D99 031101 (BESIII Collab.)
 ABLIKIM 19S PRL 122 121801 (BESIII Collab.)
 ABLIKIM 18A PR D97 012006 (BESIII Collab.)
 AJAJ 17AF PL B771 21 (LHCb Collab.)
 AJAJ 17AN PRL 119 101801 (LHCb Collab.)
 ABLIKIM 16O PR D94 072004 (BESIII Collab.)
 ABLIKIM 16T PR D94 112003 (BESIII Collab.)
 ABLIKIM 15Z PL B750 466 (BESIII Collab.)
 HIETALA 15 PR D92 012009 (MINN, LUTH, OXF)
 LEES 15D PR D91 019901 (err.) J.P. Lees et al. (BABAR Collab.)
 AJAJ 14BD JHEP 1410 025 (LHCb Collab.)
 ABAZOV 14B PRL 112 111804 (DO Collab.)
 AJAJ 13AF PL B774 203 (LHCb Collab.)
 AJAJ 13V JHEP 1306 065 (LHCb Collab.)
 AJAJ 13W JHEP 1306 112 (LHCb Collab.)
 LEES 13E PR D87 052012 J.P. Lees et al. (BABAR Collab.)
 ONYISI 13 PR D88 032009 P.U.E. Onyisi et al. (CLEO Collab.)
 ZUPANIC 13 JHEP 1309 139 A. Zupanic et al. (BELLE Collab.)
 DEL-AMO-SA... 11G PR D83 052001 P. del Amo Sanchez et al. (BABAR Collab.)
 LEES 11E PR D84 031103 J.P. Lees et al. (BABAR Collab.)
 LEES 11G PR D84 072006 J.P. Lees et al. (BABAR Collab.)
 MARTIN 11 PR D84 012005 L. Martin et al. (CLEO Collab.)
 ASNER 10 PR D81 052007 D.M. Asner et al. (CLEO Collab.)
 DEL-AMO-SA... 10J PR D82 011103 P. del Amo Sanchez et al. (BABAR Collab.)
 Also J.P. Lees et al. (BABAR Collab.)
 KO 10 PRL 104 181602 B.R. Ko et al. (BELLE Collab.)
 MENDEZ 10 PR D81 052013 H. Mendez et al. (CLEO Collab.)
 RUBIN 10 PR D82 092007 P. Rubin et al. (CLEO Collab.)
 ALEXANDER 09 PR D79 052001 J.P. Alexander et al. (CLEO Collab.)
 AUBERT 09O PR D79 032003 B. Aubert et al. (BABAR Collab.)
 DOBBS 09 PR D79 112008 S. Dobbs et al. (CLEO Collab.)
 ECKLUND 09 PR D80 052009 K.M. Ecklund et al. (CLEO Collab.)
 GE 09A PR D80 051102 J.Y. Ge et al. (CLEO Collab.)
 KO 09 PR D80 051102 B.R. Ko et al. (BELLE Collab.)
 MITCHELL 09A PR D79 072008 R.E. Mitchell et al. (CLEO Collab.)
 NAIK 09A PR D80 112004 P. Naik et al. (CLEO Collab.)
 ONYISI 09 PR D79 052002 P.U.E. Onyisi et al. (CLEO Collab.)
 WON 09 PR D80 111101 E. Won et al. (BELLE Collab.)
 YELTON 09 PR D80 052007 J. Yelton et al. (CLEO Collab.)
 ALEXANDER 08 PRL 100 161804 J.P. Alexander et al. (CLEO Collab.)
 ATHAR 08 PRL 100 181802 S.B. Athar et al. (CLEO Collab.)
 AUBERT 08AN PR D78 051101 B. Aubert et al. (BABAR Collab.)
 ECKLUND 08 PR 100 161801 K.M. Ecklund et al. (CLEO Collab.)
 KLEMP 08 EPJ C55 39 E. Klemp, M. Matveev, A.V. Sarantsev (BONN+)
 LINK 08 PR B660 147 J.M. Link et al. (FNAL FOCUS Collab.)
 WIEHAIM 08 PRL 100 241801 L. Wiehaim et al. (FNAL FOCUS Collab.)
 ADAMS 07A PRL 99 191805 G.S. Adams et al. (CLEO Collab.)
 AUBERT 07V PRL 98 141801 B. Aubert et al. (BABAR Collab.)
 PEDLAR 07 PR D76 072002 T.K. Pedlar et al. (CLEO Collab.)
 Also PRL 99 071802 M. Artuso et al. (CLEO Collab.)
 AUBERT 06N PR D74 031103 B. Aubert et al. (BABAR Collab.)
 HUANG 06 PR D74 112005 G.S. Huang et al. (CLEO Collab.)
 PDG 06 JP G33 1 W.-M. Yao et al. (PDG Collab.)
 AUBERT 05E PR D71 091104 B. Aubert et al. (BABAR Collab.)
 LINK 05V PL B622 239 J.M. Link et al. (FNAL FOCUS Collab.)
 LINK 05J PRL 95 052003 J.M. Link et al. (FNAL FOCUS Collab.)
 LINK 05K PL B624 166 J.M. Link et al. (FNAL FOCUS Collab.)
 LINK 04 PL B595 200 J.M. Link et al. (FNAL FOCUS Collab.)
 LINK 04C PL B586 183 J.M. Link et al. (FNAL FOCUS Collab.)
 LINK 04D PL B586 191 J.M. Link et al. (FNAL FOCUS Collab.)
 LINK 04F PL B601 10 J.M. Link et al. (FNAL FOCUS Collab.)
 ACOSTA 03D PR D68 072004 D. Acosta et al. (FNAL CDF-II Collab.)
 ANISOVICH 03 EPJ A16 229 V.V. Anisovich et al. (FNAL FOCUS Collab.)
 LINK 03D PL B561 225 J.M. Link et al. (FNAL FOCUS Collab.)
 LINK 03F PL B572 21 J.M. Link et al. (FNAL FOCUS Collab.)
 AUBERT 02G PR D65 091104 B. Aubert et al. (BABAR Collab.)
 HEISTER 02 PL B528 1 A. Heister et al. (ALEPH Collab.)
 LINK 021 PL B541 227 J.M. Link et al. (FNAL FOCUS Collab.)
 LINK 02J PL B541 243 J.M. Link et al. (FNAL FOCUS Collab.)
 ABBIENDI 01L PL B516 236 G. Abbiendi et al. (OPAL Collab.)
 AITALA 01A PRL 86 765 E.M. Aitala et al. (FNAL E791 Collab.)
 IORI 01 PL B523 22 M. Iori et al. (FNAL SELEX Collab.)
 LINK 01C PRL 87 162001 J.M. Link et al. (FNAL FOCUS Collab.)
 ALEXANDROV 00 PR B478 31 Y. Alexandrov et al. (CERN BEATRICE Collab.)
 AITALA 99 PL B445 449 E.M. Aitala et al. (FNAL E791 Collab.)
 AITALA 99D PL B450 294 E.M. Aitala et al. (FNAL E791 Collab.)
 AITALA 99G PL B462 401 E.M. Aitala et al. (FNAL E791 Collab.)
 BONVICINI 99 PRL 82 4586 G. Bonvicini et al. (CLEO Collab.)
 CHADHA 98 PR D58 032002 M. Chada et al. (CLEO Collab.)
 JESSOP 98 PR D58 052002 C.P. Jessop et al. (CLEO Collab.)
 ACCIARI 97F PL B396 327 M. Acciari et al. (L3 Collab.)
 BALEST 97 PRL 79 1436 R. Balest et al. (CLEO Collab.)
 FRABETTI 97C PL B401 131 P.L. Frabetti et al. (FNAL E687 Collab.)
 FRABETTI 97D PL B407 79 P.L. Frabetti et al. (FNAL E687 Collab.)
 ARTUSO 96 PL B378 364 M. Artuso et al. (CLEO Collab.)
 BAI 95C PR D52 3781 J.Z. Bai et al. (BES Collab.)
 BRANDENB... 95 PRL 75 3804 G.W. Brandenburg et al. (CLEO Collab.)
 FRABETTI 95B PL B351 591 P.L. Frabetti et al. (FNAL E687 Collab.)
 KODAMA 95 PL B345 85 K. Kodama et al. (FNAL E653 Collab.)
 ACOSTA 94 PR D49 5690 D. Acosta et al. (CLEO Collab.)
 AVERY 94B PR B337 405 P. Avery et al. (CLEO Collab.)
 BROWN 94 PR D50 1894 D. Brown et al. (CLEO Collab.)
 BUTLER 94 PL B324 255 F. Butler et al. (CLEO Collab.)
 FRABETTI 94F PL B328 187 P.L. Frabetti et al. (FNAL E687 Collab.)
 FRABETTI 93F PRL 71 827 P.L. Frabetti et al. (FNAL E687 Collab.)

$D_s^\pm, D_s^{*\pm}, D_{s0}^*(2317)^\pm$

Table of experimental data for D_s mesons. Columns include author names, experiment codes (e.g., PL, PRL), and collaboration names (e.g., FNAL E687 Collab., ARGUS Collab.).

OTHER RELATED PAPERS

Table listing other related papers by Richman et al. (UCSB, STAN).

$D_s^{*\pm}$

$I(J^P) = 0(??)$

J^P is natural, width and decay modes consistent with 1^- .

$D_s^{*\pm}$ MASS

The fit includes $D^\pm, D^0, D_s^\pm, D^{*\pm}, D^{*0}, D_1^*(2420)^0, D_2^*(2460)^0$, and $D_{s1}^*(2536)^\pm$ mass and mass difference measurements.

Table with columns: VALUE (MeV), DOCUMENT ID, TECN, COMMENT. Contains fit results: 2112.2 ± 0.4 OUR FIT and 2106.6 ± 2.1 ± 2.7.

$m_{D_s^{*\pm}} - m_{D_s^\pm}$

The fit includes $D^\pm, D^0, D_s^\pm, D^{*\pm}, D^{*0}, D_1^*(2420)^0, D_2^*(2460)^0$, and $D_{s1}^*(2536)^\pm$ mass and mass difference measurements.

Table with columns: VALUE (MeV), EVTS, DOCUMENT ID, TECN, COMMENT. Contains fit results: 143.8 ± 0.4 OUR FIT and 143.9 ± 0.4 OUR AVERAGE.

$D_s^{*\pm}$ WIDTH

Table with columns: VALUE (MeV), CL%, DOCUMENT ID, TECN, COMMENT. Contains fit results: < 1.9 and < 4.5.

D_s^{*+} DECAY MODES

D_s^{*-} modes are charge conjugates of the modes below.

Table with columns: Mode, Fraction (Γ_i/Γ). Lists decay modes like $D_s^+\gamma$ and $D_s^+\pi^0$ with their branching fractions.

CONSTRAINED FIT INFORMATION

An overall fit to 2 branching ratios uses 3 measurements and one constraint to determine 3 parameters. The overall fit has a $\chi^2 = 0.0$ for 1 degrees of freedom.

The following off-diagonal array elements are the correlation coefficients $\langle \delta x_i \delta x_j \rangle / (\delta x_i \delta x_j)$, in percent, from the fit to the branching fractions, $x_i \equiv \Gamma_i / \Gamma_{total}$. The fit constrains the x_i whose labels appear in this array to sum to one.

Correlation matrix for x_2 and x_3 vs x_1 and x_2 .

D_s^{*+} BRANCHING RATIOS

Table for $\Gamma(D_s^{*+}\gamma)/\Gamma_{total}$ and Γ_1/Γ . Includes values like 0.935 ± 0.007 OUR FIT and references to other experiments like ASRATYAN, ALBRECHT, AIHARA, BRANDELIK.

Table for $\Gamma(D_s^{*+}\pi^0)/\Gamma(D_s^{*+}\gamma)$ and Γ_2/Γ_1 . Includes values like 0.062 ± 0.008 OUR FIT and references to AUBERT, BE, GRONBERG.

Table for $\Gamma(D_s^{*+}e^+e^-)/\Gamma(D_s^{*+}\gamma)$ and Γ_3/Γ_1 . Includes values like 7.2 ± 1.7 OUR FIT and reference to CRONIN-HEN..12.

D_{s0}^{*+} REFERENCES

Table listing references for D_{s0}^{*+} from various experiments like CRONIN-HEN., AUBERT, BE, GRONBERG, etc.

$D_{s0}^*(2317)^\pm$

$I(J^P) = 0(0^+)$
 J, P need confirmation.

AUBERT 06P and CHOI 15A do not observe neutral and doubly charged partners of the $D_{s0}^*(2317)^+$. See the review on "Heavy Non- $q\bar{q}$ Mesons."

$D_{s0}^*(2317)^\pm$ MASS

The fit includes $D^\pm, D^0, D_s^\pm, D^{*\pm}, D^{*0}, D_1^*(2420)^0, D_2^*(2460)^0$, and $D_{s1}^*(2536)^\pm$ mass and mass difference measurements.

Table with columns: VALUE (MeV), EVTS, DOCUMENT ID, TECN, COMMENT. Contains fit results: 2317.8 ± 0.5 OUR FIT and 2318.0 ± 0.7 OUR AVERAGE.

1 From a fit of the D_{s0}^* recoil mass where the $D_{s0}^*(2317)$ signal is described with a Crystal Ball function convolved with a Gaussian function.
2 Supersedes AUBERT 03G.
3 Systematic errors not evaluated.

Meson Particle Listings

$D_{s0}^*(2317)^\pm, D_{s1}(2460)^\pm$

⁴ Not independent of the corresponding $m_{D_{s0}^*(2317)} - m_{D_s}$.

⁵ From $D_s^+ \rightarrow K^+ K^- \pi^+$ decay.

⁶ From $D_s^+ \rightarrow K^+ K^- \pi^+ \pi^0$ decay.

$m_{D_{s0}^*(2317)^\pm} - m_{D_s^\pm}$

The fit includes $D^\pm, D^0, D_s^\pm, D^{*\pm}, D^{*0}, D_1(2420)^0, D_2^*(2460)^0$, and $D_{s1}(2536)^\pm$ mass and mass difference measurements.

VALUE (MeV)	EVTS	DOCUMENT ID	TECN	COMMENT
349.4±0.5 OUR FIT 349.2±0.7 OUR AVERAGE				
348.7±0.5±0.7	761	MIKAMI	04	BELL 10.6 e ⁺ e ⁻
350.0±1.2±1.0	135	BESSON	03	CLE2 10.6 e ⁺ e ⁻
351.3±2.1±1.9	24	⁷ KROKOVNY	03B	BELL 10.6 e ⁺ e ⁻
●●● We do not use the following data for averages, fits, limits, etc. ●●●				
349.6±0.4±3.0	1267	^{8,9} AUBERT	03G	BABR 10.6 e ⁺ e ⁻
350.2±1.3	273	^{10,11} AUBERT	03G	BABR 10.6 e ⁺ e ⁻

⁷ Recalculated by us using $m_{D_s^+} = 1968.5 \pm 0.6$ MeV.

⁸ From $D_s^+ \rightarrow K^+ K^- \pi^+$ decay.

⁹ Recalculated by us using $m_{D_s^+} = 1967.20 \pm 0.03$ MeV.

¹⁰ From $D_s^+ \rightarrow K^+ K^- \pi^+ \pi^0$ decay.

¹¹ Recalculated by us using $m_{D_s^+} = 1967.4 \pm 0.2$ MeV. Systematic errors not estimated.

$D_{s0}^*(2317)^\pm$ WIDTH

VALUE (MeV)	CL%	EVTS	DOCUMENT ID	TECN	COMMENT
< 3.8	95	3180	AUBERT	06P	BABR 10.6 e ⁺ e ⁻ → $D_s^0 \pi^0 X$
●●● We do not use the following data for averages, fits, limits, etc. ●●●					
< 4.6	90	761	MIKAMI	04	BELL 10.6 e ⁺ e ⁻
<10			AUBERT	03G	BABR 10.6 e ⁺ e ⁻
< 7	90	135	BESSON	03	CLE2 10.6 e ⁺ e ⁻

$D_{s0}^*(2317)^\pm$ DECAY MODES

$D_{s0}^*(2317)^\pm$ modes are charge conjugates of modes below.

Mode	Fraction (Γ_i/Γ)	Confidence level
Γ_1 $D_s^+ \pi^0$	$(100^{+0}_{-20})\%$	
Γ_2 $D_s^+ \gamma$	< 5 %	90%
Γ_3 $D_s^*(2112)^+ \gamma$	< 6 %	90%
Γ_4 $D_s^+ \gamma \gamma$	< 18 %	95%
Γ_5 $D_s^*(2112)^+ \pi^0$	< 11 %	90%
Γ_6 $D_s^+ \pi^+ \pi^-$	< 4 × 10 ⁻³	90%
Γ_7 $D_s^+ \pi^0 \pi^0$	not seen	

$D_{s0}^*(2317)^\pm$ BRANCHING RATIOS

$\Gamma(D_s^+ \pi^0)/\Gamma_{total}$	Γ_1/Γ	
VALUE	COMMENT	
1.00^{+0.00}_{-0.14} -0.14	47	ABLIKIM 18J BES3 4.6 e ⁺ e ⁻ → $D_s^{*\pm} D_{s0}^*(2317)^\mp$
●●● We do not use the following data for averages, fits, limits, etc. ●●●		
seen	1.5k	AUBERT 03G BABR 10.6 e ⁺ e ⁻

$\Gamma(D_s^+ \gamma)/\Gamma(D_s^+ \pi^0)$	Γ_2/Γ_1	
VALUE	COMMENT	
<0.05	90	MIKAMI 04 BELL 10.6 e ⁺ e ⁻
●●● We do not use the following data for averages, fits, limits, etc. ●●●		
<0.14	95	AUBERT 06P BABR 10.6 e ⁺ e ⁻
<0.052	90	BESSON 03 CLE2 10.6 e ⁺ e ⁻

$\Gamma(D_s^*(2112)^+ \gamma)/\Gamma(D_s^+ \pi^0)$	Γ_3/Γ_1	
VALUE	COMMENT	
<0.059	90	BESSON 03 CLE2 10.6 e ⁺ e ⁻
●●● We do not use the following data for averages, fits, limits, etc. ●●●		
<0.16	95	AUBERT 06P BABR 10.6 e ⁺ e ⁻
<0.18	90	MIKAMI 04 BELL 10.6 e ⁺ e ⁻

$\Gamma(D_s^+ \gamma \gamma)/\Gamma(D_s^+ \pi^0)$	Γ_4/Γ_1	
VALUE	COMMENT	
<0.18	95	AUBERT 06P BABR 10.6 e ⁺ e ⁻
●●● We do not use the following data for averages, fits, limits, etc. ●●●		
not seen		AUBERT 03G BABR 10.6 e ⁺ e ⁻

$\Gamma(D_s^*(2112)^+ \pi^0)/\Gamma(D_s^+ \pi^0)$	Γ_5/Γ_1			
VALUE	CL%	DOCUMENT ID	TECN	COMMENT
<0.11	90	BESSON	03	CLE2 10.6 e ⁺ e ⁻

$\Gamma(D_s^+ \pi^+ \pi^-)/\Gamma(D_s^+ \pi^0)$	Γ_6/Γ_1			
VALUE	CL%	DOCUMENT ID	TECN	COMMENT
<0.004	90	MIKAMI	04	BELL 10.6 e ⁺ e ⁻
●●● We do not use the following data for averages, fits, limits, etc. ●●●				
<0.005	95	AUBERT	06P	BABR 10.6 e ⁺ e ⁻
<0.019	90	BESSON	03	CLE2 10.6 e ⁺ e ⁻

$\Gamma(D_s^+ \pi^0 \pi^0)/\Gamma(D_s^+ \pi^0)$	Γ_7/Γ_1			
VALUE	CL%	DOCUMENT ID	TECN	COMMENT
<0.25	95	AUBERT	06P	BABR 10.6 e ⁺ e ⁻

$D_{s0}^*(2317)^\pm$ REFERENCES

ABLIKIM 18J PR D97 051103	M. Ablikim et al.	(BESIII Collab.)
CHOI 15A PR D91 032011	S.-K. Choi et al.	(BELLE Collab.)
AUBERT 06P PR D74 032007	B. Aubert et al.	(BABAR Collab.)
AUBERT 04E PR D69 031101	B. Aubert et al.	(BABAR Collab.)
AUBERT,B 04S PRL 93 181801	B. Aubert et al.	(BABAR Collab.)
MIKAMI 04 PRL 92 012002	Y. Mikami et al.	(BELLE Collab.)
AUBERT 03G PRL 90 242001	B. Aubert et al.	(BABAR Collab.)
BESSON 03 PR D68 032002	D. Besson et al.	(CLEO Collab.)
KROKOVNY 03B PRL 91 262002	P. Krokovny et al.	(BELLE Collab.)

$D_{s1}(2460)^\pm$ $I(J^P) = 0(1^+)$

See the review on "Heavy Non- $q\bar{q}$ Mesons."

$D_{s1}(2460)^\pm$ MASS

The fit includes $D^\pm, D^0, D_s^\pm, D^{*\pm}, D^{*0}, D_1(2420)^0, D_2^*(2460)^0$, and $D_{s1}(2536)^\pm$ mass and mass difference measurements.

VALUE (MeV)	EVTS	DOCUMENT ID	TECN	COMMENT
2459.5±0.6 OUR FIT				Error includes scale factor of 1.1.
2459.6±0.9 OUR AVERAGE				Error includes scale factor of 1.3.
2460.1±0.2±0.8		¹ AUBERT	06P	BABR 10.6 e ⁺ e ⁻
2458.0±1.0±1.0	195	AUBERT	04E	BABR 10.6 e ⁺ e ⁻
●●● We do not use the following data for averages, fits, limits, etc. ●●●				
2459.5±1.2±3.7	920	AUBERT	06P	BABR 10.6 e ⁺ e ⁻ → $D_s^+ \gamma X$
2458.6±1.0±2.5	560	AUBERT	06P	BABR 10.6 e ⁺ e ⁻ → $D_s^+ \pi^0 \gamma X$
2460.2±0.2±0.8	123	AUBERT	06P	BABR 10.6 e ⁺ e ⁻ → $D_s^+ \pi^+ \pi^- X$
2458.9±1.5	112	² AUBERT,B	04S	BABR $B \rightarrow D_{s1}(2460)^+ \bar{D}^{(*)}$
2461.1±1.6	139	³ AUBERT,B	04S	BABR $B \rightarrow D_{s1}(2460)^+ \bar{D}^{(*)}$
2456.5±1.3±1.3	126	^{4,5} MIKAMI	04	BELL 10.6 e ⁺ e ⁻
2459.5±1.3±2.0	152	^{6,7} MIKAMI	04	BELL 10.6 e ⁺ e ⁻
2459.9±0.9±1.6	60	^{6,7} MIKAMI	04	BELL 10.6 e ⁺ e ⁻
2459.2±1.6±2.0	57	KROKOVNY	03B	BELL 10.6 e ⁺ e ⁻

¹ The average of the values obtained from the $D_s^+ \gamma, D_s^+ \pi^0 \gamma, D_s^+ \pi^+ \pi^-$ final state.

² Systematic errors not evaluated. From the decay to $D_s^{*+} \pi^0$.

³ Systematic errors not evaluated. From the decay to $D_s^{*+} \gamma$.

⁴ Not independent of the corresponding $m_{D_{s1}(2460)^\pm} - m_{D_s^{*\pm}}$.

⁵ Using $m_{D_s^{*+}} = 2112.4 \pm 0.7$ MeV.

⁶ Not independent of the corresponding $m_{D_{s1}(2460)^\pm} - m_{D_s^\pm}$.

⁷ Using $m_{D_s^+} = 1968.5 \pm 0.6$ MeV.

$m_{D_{s1}(2460)^\pm} - m_{D_s^\pm}$

The fit includes $D^\pm, D^0, D_s^\pm, D^{*\pm}, D^{*0}, D_1(2420)^0, D_2^*(2460)^0$, and $D_{s1}(2536)^\pm$ mass and mass difference measurements.

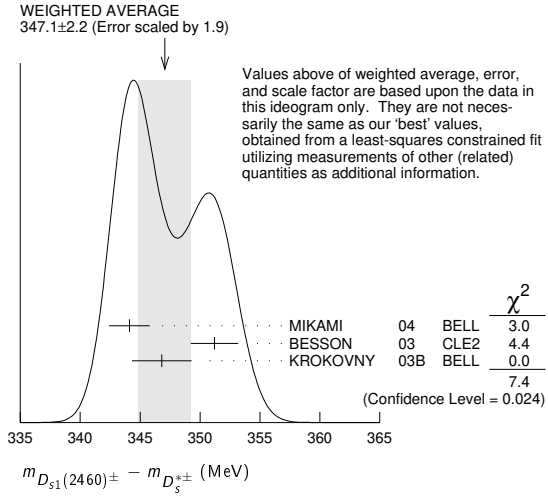
VALUE (MeV)	EVTS	DOCUMENT ID	TECN	COMMENT
347.3±0.7 OUR FIT				Error includes scale factor of 1.2.
347.1±2.2 OUR AVERAGE				Error includes scale factor of 1.9. See the ideogram below.
344.1±1.3±1.1	126	MIKAMI	04	BELL 10.6 e ⁺ e ⁻
351.2±1.7±1.0	41	BESSON	03	CLE2 10.6 e ⁺ e ⁻
346.8±1.6±1.9	57	⁸ KROKOVNY	03B	BELL 10.6 e ⁺ e ⁻
●●● We do not use the following data for averages, fits, limits, etc. ●●●				
<0.16	95	AUBERT	06P	BABR 10.6 e ⁺ e ⁻
<0.18	90	MIKAMI	04	BELL 10.6 e ⁺ e ⁻

⁸ Recalculated by us using $m_{D_s^{*+}} = 2112.4 \pm 0.7$ MeV.

See key on page 1127

Meson Particle Listings

$D_{s1}(2460)^\pm$



$m_{D_{s1}(2460)^\pm} - m_{D_s^\pm}$

The fit includes $D_s^\pm, D^0, D_s^\pm, D^{*\pm}, D^{*0}, D_s^{*±}, D_1(2420)^0, D_2^*(2460)^0,$ and $D_{s1}(2536)^\pm$ mass and mass difference measurements.

VALUE (MeV)	EVTS	DOCUMENT ID	TECN	COMMENT
491.1±0.6 OUR FIT	Error includes scale factor of 1.1.			
491.3±1.4 OUR AVERAGE				
491.0±1.3±1.9	152	⁹ MIKAMI	04 BELL	10.6 e ⁺ e ⁻
491.4±0.9±1.5	60	¹⁰ MIKAMI	04 BELL	10.6 e ⁺ e ⁻

⁹From the decay to $D_s^\pm \pi^\mp \gamma$.
¹⁰From the decay to $D_s^\pm \pi^\mp \pi^\mp$.

$D_{s1}(2460)^\pm$ WIDTH

VALUE (MeV)	CL%	EVTS	DOCUMENT ID	TECN	COMMENT
< 3.5	95	123	AUBERT 06P	BABR	10.6 e ⁺ e ⁻ → $D_s^+ \pi^+ \pi^- X$
< 6.3	95	560	AUBERT 06P	BABR	10.6 e ⁺ e ⁻ → $D_s^+ \pi^0 \gamma X$
<10		195	AUBERT 04E	BABR	10.6 e ⁺ e ⁻
< 5.5	90	126	MIKAMI 04	BELL	10.6 e ⁺ e ⁻
< 7	90	41	BESSON 03	CLE2	10.6 e ⁺ e ⁻

••• We do not use the following data for averages, fits, limits, etc. •••

$D_{s1}(2460)^\pm$ DECAY MODES

$D_{s1}(2460)^\pm$ modes are charge conjugates of the modes below.

Mode	Fraction (Γ_i/Γ)	Scale factor/ Confidence level
Γ_1 $D_s^{*+} \pi^0$	(48 ± 11) %	
Γ_2 $D_s^{*+} \gamma$	(18 ± 4) %	
Γ_3 $D_s^{*+} \pi^+ \pi^-$	(4.3 ± 1.3) %	S=1.1
Γ_4 $D_s^{*+} \gamma$	< 8 %	CL=90%
Γ_5 $D_{s0}^*(2317)^+ \gamma$	(3.7 ± 5.0 / 2.4) %	
Γ_6 $D_s^+ \pi^0$		
Γ_7 $D_s^+ \pi^0 \pi^0$		
Γ_8 $D_s^+ \pi^+ \pi^-$		

CONSTRAINED FIT INFORMATION

An overall fit to 7 branching ratios uses 8 measurements and one constraint to determine 5 parameters. The overall fit has a $\chi^2 = 3.4$ for 4 degrees of freedom.

The following off-diagonal array elements are the correlation coefficients $\langle \delta x_i \delta x_j \rangle / (\delta x_i \delta x_j)$, in percent, from the fit to the branching fractions, $x_i = \Gamma_i / \Gamma_{\text{total}}$. The fit constrains the x_i whose labels appear in this array to sum to one.

x_2	80		
x_3	68	62	
x_5	-3	25	26
	x_1	x_2	x_3

$D_{s1}(2460)^\pm$ BRANCHING RATIOS

$\Gamma(D_s^{*+} \pi^0) / \Gamma_{\text{total}}$	VALUE	CL%	EVTS	DOCUMENT ID	TECN	COMMENT	Γ_1/Γ
0.48±0.11 OUR FIT	11 AUBERT 06N BABR B → $D_{s1}(2460) \pi^0$ ([*])						
0.56±0.13±0.09	••• We do not use the following data for averages, fits, limits, etc. •••						
seen	41		BESSON 03	CLE2	10.6 e ⁺ e ⁻		
	11 Evaluated in AUBERT 06N including measurements from AUBERT,B 04s.						
$\Gamma(D_s^{*+} \gamma) / \Gamma_{\text{total}}$	VALUE	CL%	EVTS	DOCUMENT ID	TECN	COMMENT	Γ_2/Γ
0.18±0.04 OUR FIT	12 AUBERT 06N BABR B → $D_{s1}(2460) \pi^0$ ([*])						
0.16±0.04±0.03	12 Evaluated in AUBERT 06N including measurements from AUBERT,B 04s.						
$\Gamma(D_s^{*+} \gamma) / \Gamma(D_s^{*+} \pi^0)$	VALUE	CL%	EVTS	DOCUMENT ID	TECN	COMMENT	Γ_2/Γ_1
0.38 ± 0.05 OUR FIT	13 AUBERT,B 04s BABR B → $D_{s1}(2460) \pi^0$ ([*])						
0.44 ± 0.09 OUR AVERAGE	••• We do not use the following data for averages, fits, limits, etc. •••						
0.55 ± 0.13 ± 0.08	152		MIKAMI 04	BELL	10.6 e ⁺ e ⁻		
0.38 ± 0.11 ± 0.04	38		KROKOVNY 03B	BELL	10.6 e ⁺ e ⁻		
0.274 ± 0.045 ± 0.020	251		AUBERT,B 04s	BABR	B → $D_{s1}(2460) \pi^0$ ([*])		
< 0.49	90		BESSON 03	CLE2	10.6 e ⁺ e ⁻		
	13 Used by AUBERT 06N in their measurement of $B(D_s^{*+} \pi^0)$ and $B(D_s^{*+} \gamma)$.						
$\Gamma(D_s^{*+} \pi^+ \pi^-) / \Gamma(D_s^{*+} \pi^0)$	VALUE	CL%	EVTS	DOCUMENT ID	TECN	COMMENT	Γ_3/Γ_1
0.090±0.020 OUR FIT	Error includes scale factor of 1.2.						
0.14 ± 0.04 ± 0.02	60 MIKAMI 04 BELL 10.6 e ⁺ e ⁻						
••• We do not use the following data for averages, fits, limits, etc. •••							
<0.08	90		BESSON 03	CLE2	10.6 e ⁺ e ⁻		
$\Gamma(D_s^{*+} \gamma) / \Gamma(D_s^{*+} \pi^0)$	VALUE	CL%	DOCUMENT ID	TECN	COMMENT	Γ_4/Γ_1	
<0.16	90		BESSON 03	CLE2	10.6 e ⁺ e ⁻		
••• We do not use the following data for averages, fits, limits, etc. •••							
<0.31	90		MIKAMI 04	BELL	10.6 e ⁺ e ⁻		
$\Gamma(D_{s0}^*(2317)^+ \gamma) / \Gamma(D_s^{*+} \pi^0)$	VALUE	CL%	DOCUMENT ID	TECN	COMMENT	Γ_5/Γ_1	
<0.22	95		AUBERT 04E	BABR	10.6 e ⁺ e ⁻		
••• We do not use the following data for averages, fits, limits, etc. •••							
<0.58	90		BESSON 03	CLE2	10.6 e ⁺ e ⁻		
$\Gamma(D_s^{*+} \pi^0) / [\Gamma(D_s^{*+} \pi^0) + \Gamma(D_{s0}^*(2317)^+ \gamma)]$	VALUE	CL%	DOCUMENT ID	TECN	COMMENT	$\Gamma_1/(\Gamma_1+\Gamma_5)$	
0.93±0.09 OUR FIT	AUBERT 06P BABR 10.6 e ⁺ e ⁻						
0.97±0.09±0.05							
$\Gamma(D_s^{*+} \gamma) / [\Gamma(D_s^{*+} \pi^0) + \Gamma(D_{s0}^*(2317)^+ \gamma)]$	VALUE	CL%	DOCUMENT ID	TECN	COMMENT	$\Gamma_2/(\Gamma_1+\Gamma_5)$	
0.35 ± 0.04 OUR FIT	AUBERT 06P BABR 10.6 e ⁺ e ⁻						
0.337±0.036±0.038							
$\Gamma(D_s^{*+} \pi^+ \pi^-) / [\Gamma(D_s^{*+} \pi^0) + \Gamma(D_{s0}^*(2317)^+ \gamma)]$	VALUE	CL%	DOCUMENT ID	TECN	COMMENT	$\Gamma_3/(\Gamma_1+\Gamma_5)$	
0.083±0.017 OUR FIT	Error includes scale factor of 1.2.						
0.077±0.013±0.008	AUBERT 06P BABR 10.6 e ⁺ e ⁻						
$\Gamma(D_s^{*+} \gamma) / [\Gamma(D_s^{*+} \pi^0) + \Gamma(D_{s0}^*(2317)^+ \gamma)]$	VALUE	CL%	DOCUMENT ID	TECN	COMMENT	$\Gamma_4/(\Gamma_1+\Gamma_5)$	
<0.24	95		AUBERT 06P	BABR	10.6 e ⁺ e ⁻		
$\Gamma(D_{s0}^*(2317)^+ \gamma) / [\Gamma(D_s^{*+} \pi^0) + \Gamma(D_{s0}^*(2317)^+ \gamma)]$	VALUE	CL%	DOCUMENT ID	TECN	COMMENT	$\Gamma_5/(\Gamma_1+\Gamma_5)$	
<0.25	95		AUBERT 06P	BABR	10.6 e ⁺ e ⁻		
$\Gamma(D_s^+ \pi^0) / [\Gamma(D_s^{*+} \pi^0) + \Gamma(D_{s0}^*(2317)^+ \gamma)]$	VALUE	CL%	DOCUMENT ID	TECN	COMMENT	$\Gamma_6/(\Gamma_1+\Gamma_5)$	
<0.042	95		AUBERT 06P	BABR	10.6 e ⁺ e ⁻		
$\Gamma(D_s^+ \pi^0 \pi^0) / [\Gamma(D_s^{*+} \pi^0) + \Gamma(D_{s0}^*(2317)^+ \gamma)]$	VALUE	CL%	DOCUMENT ID	TECN	COMMENT	$\Gamma_7/(\Gamma_1+\Gamma_5)$	
<0.68	95		AUBERT 06P	BABR	10.6 e ⁺ e ⁻		
$\Gamma(D_s^+ \pi^+ \pi^-) / [\Gamma(D_s^{*+} \pi^0) + \Gamma(D_{s0}^*(2317)^+ \gamma)]$	VALUE	CL%	DOCUMENT ID	TECN	COMMENT	$\Gamma_8/(\Gamma_1+\Gamma_5)$	
<0.33	95		AUBERT 06P	BABR	10.6 e ⁺ e ⁻		

Meson Particle Listings

$D_{s1}(2460)^\pm, D_{s1}(2536)^\pm$

$D_{s1}(2460)^\pm$ REFERENCES

AUBERT	06N	PR D74 031103	B. Aubert et al.	(BABAR Collab.)
AUBERT	06P	PR D74 032007	B. Aubert et al.	(BABAR Collab.)
AUBERT	04E	PR D69 031101	B. Aubert et al.	(BABAR Collab.)
AUBERT,B	04S	PRL 93 181801	B. Aubert et al.	(BABAR Collab.)
MIKAMI	04	PRL 92 012002	Y. Mikami et al.	(BELLE Collab.)
BESSON	03	PR D68 032002	D. Besson et al.	(CLEO Collab.)
KROKOVNY	03B	PRL 91 262002	P. Krokovny et al.	(BELLE Collab.)

$D_{s1}(2536)^\pm$

$J(P) = 0(1^+)$
J, P need confirmation.

Seen in $D^*(2010)^+ K^0, D^*(2007)^0 K^+,$ and $D_s^+ \pi^+ \pi^-$. Not seen in $D^+ K^0$ or $D^0 K^+.$ $J^P = 1^+$ assignment strongly favored.

$D_{s1}(2536)^\pm$ MASS

The fit includes $D^\pm, D^0, D_s^\pm, D^{*\pm}, D^{*0}, D_s^{*\pm}, D_1(2420)^0, D_2^*(2460)^0,$ and $D_{s1}(2536)^\pm$ mass and mass difference measurements.

VALUE (MeV)	EVTS	DOCUMENT ID	TECN	COMMENT
2535.11 ± 0.06 OUR FIT				
2535.21 ± 0.28 OUR AVERAGE				
2537.7 ± 0.5 ± 3.1	24	¹ ABLIKIM	19P BES3	$4.6 e^+ e^- \rightarrow D_s^+ \bar{D}^0 K^-$
2535.7 ± 0.6 ± 0.5	46	² ABAZOV	09G D0	$B_s^0 \rightarrow D_{s1}^- \mu^+ \nu_\mu X$
2534.78 ± 0.31 ± 0.40	182	AUBERT	08B BABR	$B \rightarrow \bar{D}^{(*)} K$
2534.6 ± 0.3 ± 0.7	193	AUBERT	06P BABR	$10.6 e^+ e^- \rightarrow D_s^+ \pi^+ \pi^- X$
2535.3 ± 0.7	92	³ HEISTER	02B ALEP	$e^+ e^- \rightarrow D^{*+} K^0 X,$ $D^{*0} K^+ X$
2534.2 ± 1.2	9	ASRATYAN	94 BEBC	$\nu N \rightarrow D^{*0} X, D^{*0} K^\pm X$
2535 ± 0.6 ± 1	75	FRABETTI	94B E687	$\gamma Be \rightarrow D^{*+} K^0 X,$ $D^{*0} K^+ X$
2535.2 ± 0.5 ± 1.5	28	ALBRECHT	92R ARG	$10.4 e^+ e^- \rightarrow D^{*0} K^+ X$
2536.6 ± 0.7 ± 0.4		AVERY	90 CLEO	$e^+ e^- \rightarrow D^{*+} K^0 X$
2535.9 ± 0.6 ± 2.0		ALBRECHT	89E ARG	$D_{s1}^* \rightarrow D^*(2010) K^0$
● ● ● We do not use the following data for averages, fits, limits, etc. ● ● ●				
2534.1 ± 0.6	116	⁴ AUSHEV	11 BELL	$B \rightarrow D_{s1}(2536) + D^{(*)}$
2535.08 ± 0.01 ± 0.15	8038	⁵ LEES	11B BABR	$10.6 e^+ e^- \rightarrow D^{*+} K_S^0 X$
2535.57 ^{+0.44} _{-0.41} ± 0.10	236	⁶ CHEKANOV	09 ZEUS	$e^\pm p \rightarrow D^{*+} K_S^0 X,$ $D^{*0} K^+ X$
2535.3 ± 0.2 ± 0.5	134	⁷ ALEXANDER	93 CLE2	$e^+ e^- \rightarrow D^{*0} K^+ X$
2534.8 ± 0.6 ± 0.6	44	⁸ ALEXANDER	93 CLE2	$e^+ e^- \rightarrow D^{*+} K^0 X$
2535 ± 28		⁹ ASRATYAN	88 HLBC	$\nu N \rightarrow D_s \gamma \gamma X$

¹ From a fit of the D_s^+ recoil mass distribution with an incoherent sum of the S-wave and D-wave Breit-Wigner line shapes.
² Using the $D^*(2010)^\pm$ mass of 2010.0 ± 0.4 MeV from PDG 06.
³ Calculated using $m(D^*(2010)^\pm) = 2010.0 \pm 0.5$ MeV, $m(D^*(2007)^0) = 2006.7 \pm 0.5$ MeV, and the mass difference below.
⁴ Systematic uncertainties not evaluated.
⁵ Calculated using the mass difference $m(D_{s1}^+) - m(D^{*+})$ PDG below and $m(D^{*+})$ PDG = 2010.25 ± 0.14 MeV. Assuming S-wave decay of the $D_{s1}(2536)$ to $D^{*+} K_S^0$, using a Breit-Wigner line shape corresponding to $L=0$.
⁶ Calculated using the mass difference $m(D_{s1}^+) - m(D^{*+})$ PDG reported below and $m(D^{*+})$ PDG = 2010.27 ± 0.17 MeV.
⁷ Calculated using $m(D^*(2007)^0) = 2006.6 \pm 0.5$ MeV and the mass difference below.
⁸ Calculated using $m(D^*(2010)^\pm) = 2010.1 \pm 0.6$ MeV and the mass difference below.
⁹ Not seen in $D^* K$.

$m_{D_{s1}(2536)^\pm} - m_{D_s^*(2111)}$

The fit includes $D^\pm, D^0, D_s^\pm, D^{*\pm}, D^{*0}, D_s^{*\pm}, D_1(2420)^0, D_2^*(2460)^0,$ and $D_{s1}(2536)^\pm$ mass and mass difference measurements.

VALUE (MeV)	EVTS	DOCUMENT ID	TECN	COMMENT
422.9 ± 0.4 OUR FIT				
424 ± 28				
		ASRATYAN	88 HLBC	$D_s^{*\pm} \gamma$

$m_{D_{s1}(2536)^\pm} - m_{D^*(2010)^\pm}$

The fit includes $D^\pm, D^0, D_s^\pm, D^{*\pm}, D^{*0}, D_s^{*\pm}, D_1(2420)^0, D_2^*(2460)^0,$ and $D_{s1}(2536)^\pm$ mass and mass difference measurements.

VALUE (MeV)	EVTS	DOCUMENT ID	TECN	COMMENT
524.85 ± 0.04 OUR FIT				
524.84 ± 0.04 OUR AVERAGE				
524.83 ± 0.01 ± 0.04	8038	¹⁰ LEES	11B BABR	$10.6 e^+ e^- \rightarrow D^{*+} K_S^0 X$
525.30 ^{+0.44} _{-0.41} ± 0.10	236 ± 30	CHEKANOV	09 ZEUS	$e^\pm p \rightarrow D^{*+} K_S^0 X,$ $D^{*0} K^+ X$

525.3 ± 0.6 ± 0.1	41	HEISTER	02B ALEP	$e^+ e^- \rightarrow D^{*+} K^0 X$
524.7 ± 0.6 ± 0.2	44	ALEXANDER	93 CLE2	$e^+ e^- \rightarrow D^{*+} K_S^0 X$

¹⁰ Assuming S-wave decay of the $D_{s1}(2536)$ to $D^{*+} K_S^0$, using a Breit-Wigner line shape corresponding to $L=0$.

$m_{D_{s1}(2536)^\pm} - m_{D^*(2007)^0}$

The fit includes $D^\pm, D^0, D_s^\pm, D^{*\pm}, D^{*0}, D_s^{*\pm}, D_1(2420)^0, D_2^*(2460)^0,$ and $D_{s1}(2536)^\pm$ mass and mass difference measurements.

VALUE (MeV)	EVTS	DOCUMENT ID	TECN	COMMENT
528.26 ± 0.05 OUR FIT				
Error includes scale factor of 1.2.				
528.68 ± 0.28 OUR AVERAGE				
528.7 ± 1.9 ± 0.5	51	HEISTER	02B ALEP	$e^+ e^- \rightarrow D^{*0} K^+ X$
527.3 ± 2.2	29	ACKERSTAFF	97W OPAL	$e^+ e^- \rightarrow D^{*0} K^+ X$
528.7 ± 0.2 ± 0.2	134	ALEXANDER	93 CLE2	$e^+ e^- \rightarrow D^{*0} K^+ X$

$D_{s1}(2536)^\pm$ WIDTH

VALUE (MeV)	CL% EVTS	DOCUMENT ID	TECN	COMMENT
0.92 ± 0.05 OUR AVERAGE				
1.7 ± 1.2 ± 0.6	24	¹¹ ABLIKIM	19P BES3	$4.6 e^+ e^- \rightarrow D_s^+ \bar{D}^0 K^-$
0.92 ± 0.03 ± 0.04	8038	¹² LEES	11B BABR	$10.6 e^+ e^- \rightarrow D^{*+} K_S^0 X$
● ● ● We do not use the following data for averages, fits, limits, etc. ● ● ●				
0.75 ± 0.23	116	¹³ AUSHEV	11 BELL	$B \rightarrow D_{s1}(2536) + D^{(*)}$
< 2.5	95 193	AUBERT	06P BABR	$10.6 e^+ e^- \rightarrow D_s^+ \pi^+ \pi^- X$
< 3.2	90 75	FRABETTI	94B E687	$\gamma Be \rightarrow D^{*+} K^0 X,$ $D^{*0} K^+ X$
< 2.3	90	ALEXANDER	93 CLEO	$e^+ e^- \rightarrow D^{*0} K^+ X$
< 3.9	90	ALBRECHT	92R ARG	$10.4 e^+ e^- \rightarrow D^{*0} K^+ X$
< 5.44	90	AVERY	90 CLEO	$e^+ e^- \rightarrow D^{*+} K^0 X$
< 4.6	90	ALBRECHT	89E ARG	$D_{s1}^* \rightarrow D^*(2010) K^0$

¹¹ From a fit of the D_s^+ recoil mass distribution with an incoherent sum of the S-wave and S-wave Breit-Wigner line shapes.
¹² Assuming S-wave decay of the $D_{s1}(2536)$ to $D^{*+} K_S^0$, using a Breit-Wigner line shape corresponding to $L=0$.
¹³ Systematic uncertainties not evaluated.

$D_{s1}(2536)^+$ DECAY MODES

Branching fractions are given relative to the one **DEFINED AS 1.** $D_{s1}(2536)^-$ modes are charge conjugates of the modes below.

Mode	Fraction (Γ_i/Γ)	Confidence level
Γ_1 $D^*(2010)^+ K^0$	0.85 ± 0.12	
Γ_2 $(D^*(2010)^+ K^0)_{S-wave}$	0.61 ± 0.09	
Γ_3 $(D^*(2010)^+ K^0)_{D-wave}$		
Γ_4 $D^+ \pi^- K^+$	0.028 ± 0.005	
Γ_5 $D^*(2007)^0 K^+$	DEFINED AS 1	
Γ_6 $D^+ K^0$	< 0.34	90%
Γ_7 $D^0 K^+$	< 0.12	90%
Γ_8 $D_s^{*+} \gamma$	possibly seen	
Γ_9 $D_s^+ \pi^+ \pi^-$	seen	

$D_{s1}(2536)^+$ BRANCHING RATIOS

$\Gamma(D^*(2007)^0 K^+)/\Gamma(D^*(2010)^+ K^0)$	Γ_5/Γ_1			
1.18 ± 0.16 OUR AVERAGE				
0.88 ± 0.24 ± 0.08	116	AUSHEV	11 BELL	$B \rightarrow D_{s1}(2536) + D^{(*)}$
2.3 ± 0.6 ± 0.3	236 ± 30	CHEKANOV	09 ZEUS	$e^\pm p \rightarrow D^{*+} K_S^0 X,$ $D^{*0} K^+ X$
1.32 ± 0.47 ± 0.23	92	¹⁴ HEISTER	02B ALEP	$e^+ e^- \rightarrow D^{*+} K^0 X,$ $D^{*0} K^+ X$
1.9 ^{+1.1} _{-0.9} ± 0.4	35	¹⁴ ACKERSTAFF	97W OPAL	$e^+ e^- \rightarrow D^{*0} K^+ X,$ $D^{*+} K^0 X$
1.1 ± 0.3		ALEXANDER	93 CLEO	$e^+ e^- \rightarrow D^{*0} K^+ X, D^{*+} K^0 X$
1.4 ± 0.3 ± 0.2	15	ALBRECHT	92R ARG	$10.4 e^+ e^- \rightarrow D^{*0} K^+ X, D^{*+} K^0 X$

¹⁴ Ratio of the production rates measured in Z^0 decays.
¹⁵ Evaluated by us from published inclusive cross-sections.

$\Gamma((D^*(2010)^+ K^0)_{S-wave})/\Gamma(D^*(2010)^+ K^0)$	Γ_2/Γ_1			
0.72 ± 0.05 ± 0.01				
	5485	BALAGURA	08 BELL	$10.6 e^+ e^- \rightarrow D^{*+} K^0 X$

$\Gamma(D^+ \pi^- K^+)/\Gamma(D^*(2010)^+ K^0)$	Γ_4/Γ_1			
3.27 ± 0.18 ± 0.37				
	1264	BALAGURA	08 BELL	$10.6 e^+ e^- \rightarrow D^+ \pi^- K^+ X$

See key on page 1127

Meson Particle Listings

 $D_{s1}(2536)^\pm, D_{s2}^*(2573), D_{s0}(2590)^\pm$ $\Gamma(D^+ K^0)/\Gamma(D^*(2010)^+ K^0)$ Γ_6/Γ_1

VALUE	CL%	DOCUMENT ID	TECN	COMMENT
<0.40	90	ALEXANDER 93	CLEO	$e^+ e^- \rightarrow D^{*+} K^0 X$

• • • We do not use the following data for averages, fits, limits, etc. • • •

<0.43	90	ALBRECHT 89E	ARG	$D_{s1}^* \rightarrow D^*(2010) K^0$
-------	----	--------------	-----	--------------------------------------

 $\Gamma(D^0 K^+)/\Gamma(D^*(2007)^0 K^+)$ Γ_7/Γ_5

VALUE	CL%	DOCUMENT ID	TECN	COMMENT
<0.12	90	ALEXANDER 93	CLEO	$e^+ e^- \rightarrow D^{*0} K^+ X$

 $\Gamma(D_s^{*+} \gamma)/\Gamma_{total}$ Γ_8/Γ

VALUE	DOCUMENT ID	TECN	COMMENT
possibly seen	ASRATYAN 88	HLBC	$\nu N \rightarrow D_s \gamma \gamma X$

 $\Gamma(D_s^{*+} \gamma)/\Gamma(D^*(2007)^0 K^+)$ Γ_8/Γ_5

VALUE	CL%	DOCUMENT ID	TECN	COMMENT
<0.42	90	ALEXANDER 93	CLEO	$e^+ e^- \rightarrow D^{*0} K^+ X$

 $\Gamma(D_s^+ \pi^+ \pi^-)/\Gamma_{total}$ Γ_9/Γ

VALUE	DOCUMENT ID	TECN	COMMENT
seen	AUBERT 06P	BABR	$10.6 e^+ e^- \rightarrow D_s^+ \pi^+ \pi^- X$

 $D_{s1}(2536)^\pm$ REFERENCES

ABLIKIM 19P	CP C43 031001	M. Ablikim et al.	(BESIII Collab.)
AUSHEV 11B	PR D83 051102	T. Aushev et al.	(BELLE Collab.)
LEES 11B	PR D83 072003	J.P. Lees et al.	(BABAR Collab.)
ABAZOV 09G	PRL 102 051801	V.M. Abazov et al.	(D0 Collab.)
CHEKANOV 09	EPJ C60 25	S. Chekanov et al.	(ZEUS Collab.)
AUBERT 08B	PR D77 011102	B. Aubert et al.	(BABAR Collab.)
BALAGURA 08	PR D77 032001	V. Balagura et al.	(BELLE Collab.)
AUBERT 06P	PR D74 032007	B. Aubert et al.	(BABAR Collab.)
PDG 06	JP G33 1	W.-M. Yao et al.	(PDG Collab.)
HEISTER 02B	PL B526 34	A. Heister et al.	(ALEPH Collab.)
ACKERSTAFF 97W	ZPHY C76 425	K. Ackerstaff et al.	(OPAL Collab.)
ASRATYAN 94	ZPHY C61 563	A.E. Asratyan et al.	(BIRM, BELG, CERN+)
FRABETTI 94B	PRL 72 324	P.L. Frabetti et al.	(FNAL E687 Collab.)
ALEXANDER 93	PL B303 377	J. Alexander et al.	(CLEO Collab.)
ALBRECHT 92R	PL B297 425	H. Albrecht et al.	(ARGUS Collab.)
AVERY 90	PR D41 774	P. Avery, D. Besson	(CLEO Collab.)
ALBRECHT 89E	PL B230 162	H. Albrecht et al.	(ARGUS Collab.)
ASRATYAN 88	ZPHY C40 483	A.E. Asratyan et al.	(ITEP, SERP)

 $D_{s2}^*(2573)$

$$I(J^P) = 0(2^+)$$

 $D_{s2}^*(2573)$ MASS

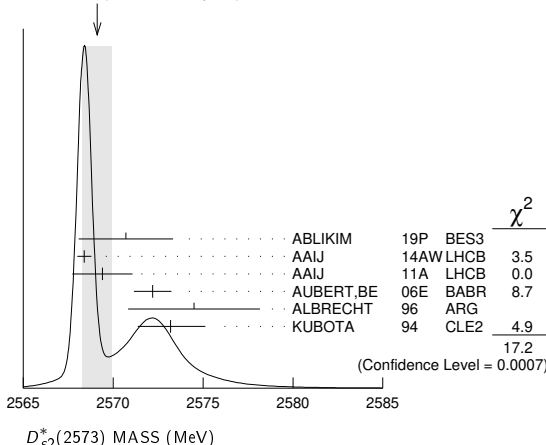
VALUE (MeV)	EVTS	DOCUMENT ID	TECN	COMMENT
-------------	------	-------------	------	---------

2569.1 ± 0.8 OUR AVERAGE Error includes scale factor of 2.4. See the ideogram below.

2570.7 ± 2.0 ± 1.7	62	1 ABLIKIM 19P	BES3	$4.6 e^+ e^- \rightarrow D_s^+ \bar{D}^0 K^-$
2568.39 ± 0.29 ± 0.26		AAIJ 14AW	LHCB	$B_S^0 \rightarrow \bar{D}^0 K^- \pi^+$
2569.4 ± 1.6 ± 0.5	82	AAIJ 11A	LHCB	$B_S \rightarrow D_{s2}^*(2573) \mu \bar{\nu} X$
2572.2 ± 0.3 ± 1.0		AUBERT,BE 06E	BABR	$e^+ e^- \rightarrow D K X$
2574.5 ± 3.3 ± 1.6		ALBRECHT 96	ARG	$e^+ e^- \rightarrow D^0 K^+ X$
2573.2 ± 1.7 ± 1.6	217	KUBOTA 94	CLE2	$e^+ e^- \sim 10.5$ GeV

• • • We do not use the following data for averages, fits, limits, etc. • • •

2570.0 ± 4.3	25	2 EVDOKIMOV 04	SELX	$600 \Sigma^- A \rightarrow D^0 K^+ X$
2568.6 ± 3.2	64	3 HEISTER 02B	ALEP	$e^+ e^- \rightarrow D^0 K^+ X$

WEIGHTED AVERAGE
2569.1±0.8 (Error scaled by 2.4)¹ From a fit of the D_s^+ recoil mass distribution .² Not independent of the mass difference below.³ Calculated using $m_{D_0} = 1864.5 \pm 0.5$ MeV and the mass difference below. $m_{D_{s2}^*(2573)} - m_{D^0}$

VALUE (MeV)	EVTS	DOCUMENT ID	TECN	COMMENT
704 ± 3 ± 1	64	HEISTER 02B	ALEP	$e^+ e^- \rightarrow D^0 K^+ X$

• • • We do not use the following data for averages, fits, limits, etc. • • •

705.4 ± 4.3	25	1 EVDOKIMOV 04	SELX	$600 \Sigma^- A \rightarrow D^0 K^+ X$
-------------	----	----------------	------	--

¹ Systematic errors not estimated. $D_{s2}^*(2573)$ WIDTH

VALUE (MeV)	EVTS	DOCUMENT ID	TECN	COMMENT
-------------	------	-------------	------	---------

16.9 ± 0.7 OUR AVERAGE

17.2 ± 3.6 ± 1.1	62	1 ABLIKIM 19P	BES3	$4.6 e^+ e^- \rightarrow D_s^+ \bar{D}^0 K^-$
16.9 ± 0.5 ± 0.6		AAIJ 14AW	LHCB	$B_S^0 \rightarrow \bar{D}^0 K^- \pi^+$
12.1 ± 4.5 ± 1.6	82	AAIJ 11A	LHCB	$B_S \rightarrow D_{s2}^*(2573) \mu \bar{\nu} X$
27.1 ± 0.6 ± 5.6		AUBERT,BE 06E	BABR	$e^+ e^- \rightarrow D K X$
10.4 ± 8.3 ± 3.0		ALBRECHT 96	ARG	$e^+ e^- \rightarrow D^0 K^+ X$
16 \pm $\frac{+5}{-4}$ ± 3	217	KUBOTA 94	CLE2	$e^+ e^- \sim 10.5$ GeV

• • • We do not use the following data for averages, fits, limits, etc. • • •

14 \pm $\frac{+9}{-6}$	25	2 EVDOKIMOV 04	SELX	$600 \Sigma^- A \rightarrow D^0 K^+ X$
--------------------------	----	----------------	------	--

¹ From a fit of the D_s^+ recoil mass distribution .² Systematic errors not estimated. $D_{s2}^*(2573)^+$ DECAY MODES $D_{s2}^*(2573)^-$ modes are charge conjugates of the modes below.

Mode	Fraction (Γ_i/Γ)
$\Gamma_1 D^0 K^+$	seen
$\Gamma_2 D^*(2007)^0 K^+$	not seen
$\Gamma_3 D^+ K_S^0$	seen
$\Gamma_4 D^{*+} K_S^0$	seen

 $D_{s2}^*(2573)^+$ BRANCHING RATIOS $\Gamma(D^0 K^+)/\Gamma_{total}$ Γ_1/Γ

VALUE	EVTS	DOCUMENT ID	TECN	CHG	COMMENT
-------	------	-------------	------	-----	---------

seen 217 KUBOTA 94 CLE2 ± $e^+ e^- \sim 10.5$ GeV $\Gamma(D^*(2007)^0 K^+)/\Gamma(D^0 K^+)$ Γ_2/Γ_1

VALUE	CL%	DOCUMENT ID	TECN	CHG	COMMENT
-------	-----	-------------	------	-----	---------

<0.33 90 KUBOTA 94 CLE2 + $e^+ e^- \sim 10.5$ GeV $\Gamma(D^{*+} K_S^0)/\Gamma(D^+ K_S^0)$ Γ_4/Γ_3

VALUE	EVTS	DOCUMENT ID	TECN	COMMENT
-------	------	-------------	------	---------

0.044 ± 0.005 ± 0.011 2000 1 AAIJ 16AW LHCB $pp \rightarrow D^{*+} K_S^0 X$ at 7, 8 TeV¹ First observation of the $D_{s2}^*(2573)^+ \rightarrow D^{*+} K_S^0$ decay with a significance of 6.9 σ . $D_{s2}^*(2573)$ REFERENCES

ABLIKIM 19P	CP C43 031001	M. Ablikim et al.	(BESIII Collab.)
AAIJ 16AW	JHEP 1602 133	R. Aaij et al.	(LHCB Collab.)
AAIJ 14AW	PRL 113 162001	R. Aaij et al.	(LHCB Collab.)
AAIJ 11A	PL B698 14	R. Aaij et al.	(LHCB Collab.)
AUBERT,BE 06E	PRL 97 222001	B. Aubert et al.	(BABAR Collab.)
EVDOKIMOV 04	PRL 93 242001	A.V. Evdokimov et al.	(SELEX Collab.)
HEISTER 02B	PL B526 34	A. Heister et al.	(ALEPH Collab.)
ALBRECHT 96	ZPHY C69 405	H. Albrecht et al.	(ARGUS Collab.)
KUBOTA 94	PRL 72 1972	Y. Kubota et al.	(CLEO Collab.)

 $D_{s0}(2590)^+$

$$I(J^P) = 0(0^-)$$

OMITTED FROM SUMMARY TABLE

 $D_{s0}(2590)^+$ MASS

VALUE (MeV)	EVTS	DOCUMENT ID	TECN	COMMENT
-------------	------	-------------	------	---------

2591 ± 6 ± 7 444 1 AAIJ 21A LHCB $B^0 \rightarrow D^-(D^+ K^+ \pi^-)$ ¹ The mass is calculated from the position of the T-matrix pole $D_{s0}(2590)^+$ WIDTH

VALUE (MeV)	EVTS	DOCUMENT ID	TECN	COMMENT
-------------	------	-------------	------	---------

89 ± 16 ± 12 444 1 AAIJ 21A LHCB $B^0 \rightarrow D^-(D^+ K^+ \pi^-)$ ¹ The width is calculated from the position of the T-matrix pole

Meson Particle Listings

$D_{s0}(2590)^+$, $D_{s1}^*(2700)^{\pm}$, $D_{s1}^*(2860)^{\pm}$

$D_{s0}(2590)^+$ DECAY MODES

Mode	Fraction (Γ_i/Γ)
$\Gamma_1 \quad D^+ K^+ \pi^-$	seen

$\Gamma(D^+ K^+ \pi^-)/\Gamma_{total}$	Γ_1/Γ
<u>VALUE</u>	<u>DOCUMENT ID</u>
seen	444 AAIJ

$D_{s0}(2590)^+$ REFERENCES

AAIJ 21A PRL 126 122002 R. Aaij et al. (LHCb Collab.)

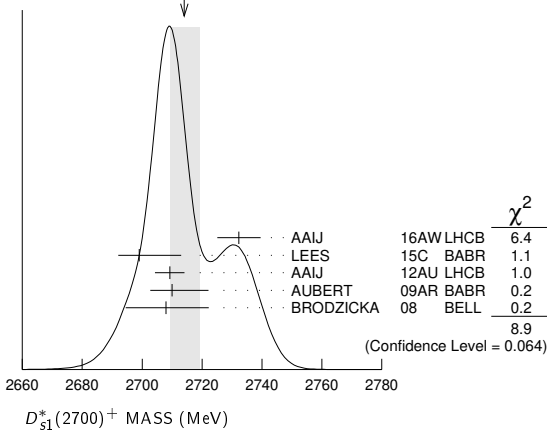
$D_{s1}^*(2700)^{\pm}$ $I(J^P) = 0(1^-)$

$D_{s1}^*(2700)^+$ MASS

VALUE (MeV)	EVTS	DOCUMENT ID	TECN	COMMENT
2714 ± 5 OUR AVERAGE				Error includes scale factor of 1.5. See the ideogram below.
$2732.3 \pm 4.3 \pm 5.8$	15.7k	AAIJ	16AW LHCB	$pp \rightarrow D^{*+} K_S^0 X$ at 7, 8 TeV
$2699 \pm 14 \pm 7$		1 LEES	15c BABR	$B \rightarrow D D^0 K^+$
$2709.2 \pm 1.9 \pm 4.5$	52k	2 AAIJ	12AU LHCB	$pp \rightarrow (D K)^+ X$ at 7 TeV
$2710 \pm 2 \pm 12 \pm 7$	10.4k	3 AUBERT	09AR BABR	$e^+ e^- \rightarrow D^{(*)} K X$
$2708 \pm 9 \pm 11 \pm 10$	182	BRODZICKA	08 BELL	$B^+ \rightarrow D^0 \overline{D}^0 K^+$

- • • We do not use the following data for averages, fits, limits, etc. • • •
- $2694 \pm 8 \pm 13$ LEES 15c BABR $B^0 \rightarrow D^- D^0 K^+$
- $2707 \pm 8 \pm 8$ LEES 15c BABR $B^+ \rightarrow \overline{D}^0 D^0 K^+$
- $2688 \pm 4 \pm 3$ 4 AUBERT, BE 06E BABR $10.6 e^+ e^- \rightarrow D K X$
- ¹From a combined analysis of $B^0 \rightarrow D^- D^0 K^+$ and $B^+ \rightarrow \overline{D}^0 D^0 K^+$.
- ²From the combined fit of the $D^+ K_S^0$ and $D^0 K^+$ modes in the model including the $D_{s2}^*(2573)^+$, $D_{s1}^*(2700)^+$ and spin-0 $D_{s,j}^*(2860)^+$.
- ³From simultaneous fits to the two $D K$ mass spectra and to the total $D^* K$ mass spectrum.
- ⁴Superseded by AUBERT 09AR.

WEIGHTED AVERAGE 2714 ± 5 (Error scaled by 1.5)



$D_{s1}^*(2700)^+$ WIDTH

VALUE (MeV)	EVTS	DOCUMENT ID	TECN	COMMENT
122 ± 10 OUR AVERAGE				
$136 \pm 19 \pm 24$	15.7k	AAIJ	16AW LHCB	$pp \rightarrow D^{*+} K_S^0 X$ at 7, 8 TeV
$127 \pm 24 \pm 19$		1 LEES	15c BABR	$B \rightarrow D D^0 K^+$
$115.8 \pm 7.3 \pm 12.1$	52k	2 AAIJ	12AU LHCB	$pp \rightarrow (D K)^+ X$ at 7 TeV
$149 \pm 7 \pm 39 \pm 52$	10.4k	3 AUBERT	09AR BABR	$e^+ e^- \rightarrow D^{(*)} K X$
$108 \pm 23 \pm 36 \pm 31$	182	BRODZICKA	08 BELL	$B^+ \rightarrow D^0 \overline{D}^0 K^+$

- • • We do not use the following data for averages, fits, limits, etc. • • •
- $145 \pm 24 \pm 22 \pm 14$ LEES 15c BABR $B^0 \rightarrow D^- D^0 K^+$
- $113 \pm 21 \pm 20 \pm 16$ LEES 15c BABR $B^+ \rightarrow \overline{D}^0 D^0 K^+$
- $112 \pm 7 \pm 36$ 4 AUBERT, BE 06E BABR $10.6 e^+ e^- \rightarrow D K X$
- ¹From a combined analysis of $B^0 \rightarrow D^- D^0 K^+$ and $B^+ \rightarrow \overline{D}^0 D^0 K^+$.
- ²From the combined fit of the $D^+ K_S^0$ and $D^0 K^+$ modes in the model including the $D_{s2}^*(2573)^+$, $D_{s1}^*(2700)^+$ and spin-0 $D_{s,j}^*(2860)^+$.
- ³From simultaneous fits to the two $D K$ mass spectra and to the total $D^* K$ mass spectrum.
- ⁴Superseded by AUBERT 09AR.

$D_{s1}^*(2700)^{\pm}$ DECAY MODES

Mode	Fraction (Γ_i/Γ)
$\Gamma_1 \quad D K$	
$\Gamma_2 \quad D^0 K^+$	seen
$\Gamma_3 \quad D^+ K_S^0$	seen
$\Gamma_4 \quad D^* K$	
$\Gamma_5 \quad D^{*0} K^+$	seen
$\Gamma_6 \quad D^{*+} K_S^0$	seen

$D_{s1}^*(2700)^{\pm}$ BRANCHING RATIOS

$\Gamma(D^* K)/\Gamma(DK)$	Γ_4/Γ_1
<u>VALUE</u>	<u>DOCUMENT ID</u>
$0.91 \pm 0.13 \pm 0.12$	1 AUBERT 09AR BABR $e^+ e^- \rightarrow D^{(*)} K X$
¹ From the average of the corresponding ratios with $D^{(*)0} K^+$ and $D^{(*)+} K_S^0$.	
$\Gamma(D^{*0} K^+)/\Gamma(D^0 K^+)$	Γ_5/Γ_2
<u>VALUE</u>	<u>DOCUMENT ID</u>
$0.88 \pm 0.14 \pm 0.14$	1 AUBERT 09AR BABR $e^+ e^- \rightarrow D^{(*)} K X$
¹ From the $D^{*0} K^+$ and $D^0 K^+$, where $D^{*0} \rightarrow D^0 \pi^0$.	
$\Gamma(D^{*+} K_S^0)/\Gamma(D^+ K_S^0)$	Γ_6/Γ_3
<u>VALUE</u>	<u>DOCUMENT ID</u>
$1.14 \pm 0.39 \pm 0.23$	1 AUBERT 09AR BABR $e^+ e^- \rightarrow D^{(*)} K X$
¹ From the $D^{*+} K_S^0$ and $D^+ K_S^0$, where $D^{*+} \rightarrow D^+ \pi^0$.	

$D_{s1}^*(2700)^{\pm}$ REFERENCES

AAIJ 16AW JHEP 1602 133 R. Aaij et al. (LHCb Collab.)
 LEES 15C PR D91 052002 J.P. Lees et al. (BABAR Collab.)
 AAIJ 12AU JHEP 1210 151 R. Aaij et al. (LHCb Collab.)
 AUBERT 09AR PR D80 092003 B. Aubert et al. (BABAR Collab.)
 BRODZICKA 08 PRL 100 092001 J. Brodzicka et al. (BELLE Collab.)
 AUBERT, BE 06E PRL 97 222001 B. Aubert et al. (BABAR Collab.)

$D_{s1}^*(2860)^{\pm}$ $I(J^P) = 0(1^-)$

OMITTED FROM SUMMARY TABLE
 J^P consistent with 1^- from angular analysis of AAIJ 14AW.

$D_{s1}^*(2860)^+$ MASS

VALUE (MeV)	DOCUMENT ID	TECN	COMMENT
$2859 \pm 12 \pm 24$	1 AAIJ	14AW LHCB	$B_s^0 \rightarrow \overline{D}^0 K^- \pi^+$
¹ Separated from the spin-3 component $D_{s3}^*(2860)^-$ by a fit of the helicity angle of the $\overline{D}^0 K^-$ system, with a statistical significance of the spin-3 and spin-1 components in excess of 10 σ .			

$D_{s1}^*(2860)^+$ WIDTH

VALUE (MeV)	DOCUMENT ID	TECN	COMMENT
$159 \pm 23 \pm 77$	1 AAIJ	14AW LHCB	$B_s^0 \rightarrow \overline{D}^0 K^- \pi^+$
¹ Separated from the spin-3 component $D_{s3}^*(2860)^-$ by a fit of the helicity angle of the $\overline{D}^0 K^-$ system, with a statistical significance of the spin-3 and spin-1 components in excess of 10 σ .			

$D_{s1}^*(2860)^{\pm}$ REFERENCES

AAIJ 14AW PRL 113 162001 R. Aaij et al. (LHCb Collab.) JP

See key on page 1127

Meson Particle Listings

 $D_{s3}^*(2860)^\pm, X_0(2900), X_1(2900)$ $D_{s3}^*(2860)^\pm$ $I(J^P) = 0(3^-)$

J^P consistent with 3^- from angular analysis of AAIJ 14AW. Observed by AUBERT, BE 06E and AUBERT 09AR in inclusive production of DK and D^*K in e^+e^- annihilation.

 $D_{s3}^*(2860)^+$ MASS

VALUE (MeV)	EPTS	DOCUMENT ID	TECN	COMMENT
2860.5 ± 2.6 ± 6.5		¹ AAIJ	14AW LHCb	$B_s^0 \rightarrow \bar{D}^0 K^- \pi^+$
• • • We do not use the following data for averages, fits, limits, etc. • • •				
2867.1 ± 4.3 ± 1.9	3.1k	AAIJ	16AW LHCb	$pp \rightarrow D^{*+} K_S^0 X$ at 7, 8 TeV
2866.1 ± 1.0 ± 6.3	36k	^{2,3} AAIJ	12AU LHCb	$pp \rightarrow (DK)^+ X$ at 7 TeV
2862 ± 2 ± 5	3122	^{2,4} AUBERT	09AR BABR	$e^+e^- \rightarrow D^{(*)} K X$
2856.6 ± 1.5 ± 5.0		⁵ AUBERT, BE 06E	BABR	$e^+e^- \rightarrow DKX$

- Separated from the spin-1 component $D_{s1}^*(2860)^-$ by a fit of the helicity angle of the $\bar{D}^0 K^-$ system, with a statistical significance of the spin-3 and spin-1 components in excess of 10σ .
- Possible contribution from the $D_{s1}^*(2860)$ state.
- From the combined fit of the $D^+ K_S^0$ and $D^0 K^+$ modes in the model including the $D_{s2}^*(2573)^+$, $D_{s1}^*(2700)^+$ and spin-0 $D_{sJ}^*(2860)^+$.
- From simultaneous fits to the two DK mass spectra and to the total D^*K mass spectrum.
- Superseded by AUBERT 09AR.

 $D_{s3}^*(2860)^+$ WIDTH

VALUE (MeV)	EPTS	DOCUMENT ID	TECN	COMMENT
53 ± 7 ± 7		¹ AAIJ	14AW LHCb	$B_s^0 \rightarrow \bar{D}^0 K^- \pi^+$
• • • We do not use the following data for averages, fits, limits, etc. • • •				
50 ± 11 ± 13	3.1k	AAIJ	16AW LHCb	$pp \rightarrow D^{*+} K_S^0 X$ at 7, 8 TeV
69.9 ± 3.2 ± 6.6	36k	^{2,3} AAIJ	12AU LHCb	$pp \rightarrow (DK)^+ X$ at 7 TeV
48 ± 3 ± 6	3122	^{2,4} AUBERT	09AR BABR	$e^+e^- \rightarrow D^{(*)} K X$
47 ± 7 ± 10		⁵ AUBERT, BE 06E	BABR	$e^+e^- \rightarrow DKX$

- Separated from the spin-1 component $D_{s1}^*(2860)^-$ by a fit of the helicity angle of the $\bar{D}^0 K^-$ system, with a statistical significance of the spin-3 and spin-1 components in excess of 10σ .
- Possible contribution from the $D_{s1}^*(2860)$ state.
- From the combined fit of the $D^+ K_S^0$ and $D^0 K^+$ modes in the model including the $D_{s2}^*(2573)^+$, $D_{s1}^*(2700)^+$ and spin-0 $D_{sJ}^*(2860)^+$.
- From simultaneous fits to the two DK mass spectra and to the total D^*K mass spectrum.
- Superseded by AUBERT 09AR.

 $D_{s3}^*(2860)^\pm$ DECAY MODES

Mode	Fraction (Γ_i/Γ)
Γ_1 DK	
Γ_2 $D^0 K^+$	seen
Γ_3 $D^+ K_S^0$	seen
Γ_4 $D^* K$	
Γ_5 $D^{*0} K^+$	seen
Γ_6 $D^{*+} K_S^0$	seen

 $D_{s3}^*(2860)^\pm$ BRANCHING RATIOS

$\Gamma(D^*K)/\Gamma(DK)$		Γ_4/Γ_1		
VALUE	EPTS	DOCUMENT ID	TECN	COMMENT
1.10 ± 0.15 ± 0.19	3122	¹ AUBERT	09AR BABR	$e^+e^- \rightarrow D^{(*)} K X$
¹ From the average of the corresponding ratios with $D^{(*)0} K^+$ and $D^{(*)+} K_S^0$.				

$\Gamma(D^{*0} K^+)/\Gamma(D^0 K^+)$		Γ_5/Γ_2		
VALUE	EPTS	DOCUMENT ID	TECN	COMMENT
1.04 ± 0.17 ± 0.20	2241	¹ AUBERT	09AR BABR	$e^+e^- \rightarrow D^{(*)} K X$
¹ From the $D^{*0} K^+$ and $D^0 K^+$, where $D^{*0} \rightarrow D^0 \pi^0$.				

$\Gamma(D^{*+} K_S^0)/\Gamma(D^+ K_S^0)$		Γ_6/Γ_3		
VALUE	EPTS	DOCUMENT ID	TECN	COMMENT
1.38 ± 0.35 ± 0.49	881	¹ AUBERT	09AR BABR	$e^+e^- \rightarrow D^{(*)} K X$
¹ From the $D^{*+} K_S^0$ and $D^+ K_S^0$, where $D^{*+} \rightarrow D^+ \pi^0$.				

 $D_{s3}^*(2860)^\pm$ REFERENCES

AAIJ	16AW JHEP 1602 133	R. Aaij et al.	(LHCb Collab.)
AAIJ	14AW PRL 113 162001	R. Aaij et al.	(LHCb Collab.)
AAIJ	12AU JHEP 1210 151	R. Aaij et al.	(LHCb Collab.)
AUBERT	09AR PR D80 092003	B. Aubert et al.	(BABAR Collab.)
AUBERT, BE	06E PRL 97 222001	B. Aubert et al.	(BABAR Collab.)

 $X_0(2900)$ $I(J^P) = ?(0^+)$

OMITTED FROM SUMMARY TABLE

An exotic state with minimal quark content $\bar{c} d \bar{s} u$. Observed by AAIJ 20AI using full amplitude analysis of $B^+ \rightarrow D^+ D^- K^+$ decays.

 $X_0(2900)$ MASS

VALUE (MeV)	EPTS	DOCUMENT ID	TECN	COMMENT
2866 ± 7 ± 2	1.2k	¹ AAIJ	20AI LHCb	$B^+ \rightarrow D^+ D^- K^+$

- Obtained from the full amplitude analysis. Parameterized with the relativistic Breit-Wigner line shape. Also confirmed by the model-independent analysis of AAIJ 20AF.

 $X_0(2900)$ WIDTH

VALUE (MeV)	EPTS	DOCUMENT ID	TECN	COMMENT
57 ± 12 ± 4	1.2k	¹ AAIJ	20AI LHCb	$B^+ \rightarrow D^+ D^- K^+$

- Obtained from the full amplitude analysis. Parameterized with the relativistic Breit-Wigner line shape. Also confirmed by the model-independent analysis of AAIJ 20AF.

 $X_0(2900)$ DECAY MODES

Mode	Fraction (Γ_i/Γ)
Γ_1 $D^- K^+$	seen

 $X_0(2900)$ BRANCHING RATIOS

$\Gamma(D^- K^+)/\Gamma_{\text{total}}$		Γ_1/Γ	
VALUE	DOCUMENT ID	TECN	COMMENT
seen	AAIJ	20AI LHCb	$B^+ \rightarrow D^+ D^- K^+$

 $X_0(2900)$ REFERENCES

AAIJ	20AF PRL 125 242001	R. Aaij et al.	(LHCb Collab.)
AAIJ	20AI PR D102 112003	R. Aaij et al.	(LHCb Collab.)

 $X_1(2900)$ $I(J^P) = ?(1^-)$

OMITTED FROM SUMMARY TABLE

An exotic state with minimal quark content $\bar{c} d \bar{s} u$. Observed by AAIJ 20AI using full amplitude analysis of $B^+ \rightarrow D^+ D^- K^+$ decays.

 $X_1(2900)$ MASS

VALUE (MeV)	EPTS	DOCUMENT ID	TECN	COMMENT
2904 ± 5 ± 1	1.2k	¹ AAIJ	20AI LHCb	$B^+ \rightarrow D^+ D^- K^+$

- Obtained from the full amplitude analysis. Parameterized with the relativistic Breit-Wigner line shape. Also confirmed by the model-independent analysis of AAIJ 20AF.

 $X_1(2900)$ WIDTH

VALUE (MeV)	EPTS	DOCUMENT ID	TECN	COMMENT
110 ± 11 ± 4	1.2k	¹ AAIJ	20AI LHCb	$B^+ \rightarrow D^+ D^- K^+$

- Obtained from the full amplitude analysis. Parameterized with the relativistic Breit-Wigner line shape. Also confirmed by the model-independent analysis of AAIJ 20AF.

 $X_1(2900)$ DECAY MODES

Mode	Fraction (Γ_i/Γ)
Γ_1 $D^- K^+$	seen

 $X_1(2900)$ BRANCHING RATIOS

$\Gamma(D^- K^+)/\Gamma_{\text{total}}$		Γ_1/Γ	
VALUE	DOCUMENT ID	TECN	COMMENT
seen	AAIJ	20AI LHCb	$B^+ \rightarrow D^+ D^- K^+$

 $X_1(2900)$ REFERENCES

AAIJ	20AF PRL 125 242001	R. Aaij et al.	(LHCb Collab.)
AAIJ	20AI PR D102 112003	R. Aaij et al.	(LHCb Collab.)

Meson Particle Listings

 $D_{sJ}(3040)^\pm$ $D_{sJ}(3040)^\pm$

$$I(J^P) = 0(?^?)$$

OMITTED FROM SUMMARY TABLE

Observed by AUBERT 09AR in inclusive production of $D^* K$ in e^+e^- annihilation.

 $D_{sJ}(3040)^+$ MASS

VALUE (MeV)	DOCUMENT ID	TECN	COMMENT
$3044 \pm 8^{+30}_{-5}$	AUBERT	09AR BABR	$e^+e^- \rightarrow D^* K X$

 $D_{sJ}(3040)^+$ WIDTH

VALUE (MeV)	DOCUMENT ID	TECN	COMMENT
$239 \pm 35^{+46}_{-42}$	AUBERT	09AR BABR	$e^+e^- \rightarrow D^* K X$

 $D_{sJ}(3040)^\pm$ DECAY MODES

Mode
$\Gamma_1 D^* K$
$\Gamma_2 D^{*0} K^+$
$\Gamma_3 D^{*+} K_S^0$

 $D_{sJ}(3040)^\pm$ REFERENCES

AUBERT	09AR PR D80 092003	B. Aubert <i>et al.</i>	(BABAR Collab.)
--------	--------------------	-------------------------	-----------------

BOTTOM MESONS**($B = \pm 1$)** $B^+ = u\bar{b}, B^0 = d\bar{b}, \bar{B}^0 = \bar{d}b, B^- = \bar{u}b$, similarly for B^{*s} **B-particle organization**

Many measurements of B decays involve admixtures of B hadrons. Previously we arbitrarily included such admixtures in the B^\pm section, but because of their importance we have created two new sections: " B^\pm/B^0 Admixture" for $\Upsilon(4S)$ results and " $B^\pm/B^0/B_S^0/b$ -baryon Admixture" for results at higher energies. Most inclusive decay branching fractions and χ_b at high energy are found in the Admixture sections. B^0/\bar{B}^0 mixing data are found in the B^0 section, while B_S^0/\bar{B}_S^0 mixing data and $B-\bar{B}$ mixing data for a B^0/B_S^0 admixture are found in the B_S^0 section. CP -violation data are found in the B^\pm, B^0 , and B^\pm/B^0 Admixture sections. b -baryons are found near the end of the Baryon section. Recently, we also created a new section: " V_{cb} and V_{ub} CKM Matrix Elements."

The organization of the B sections is now as follows, where bullets indicate particle sections and brackets indicate reviews.

[Production and Decay of *b*-flavored Hadrons]

[A Short Note on HFLAV Activities]

- B^\pm
 - mass, mean life
 - branching fractions
 - polarization in B^\pm decay
 - CP violation
- B^0
 - mass, mean life
 - branching fractions
 - [Polarization in B decay]
 - polarization in B^0 decay
 - [$B-\bar{B}$ Mixing]
 - B^0/\bar{B}^0 mixing
 - CP violation
- B^\pm/B^0 Admixture
 - branching fractions, CP violation
 - CP violation
- $B^\pm/B^0/B_S^0/b$ -baryon Admixture
 - mean life
 - production fractions
 - branching fractions
 - χ_b at high energy
 - production fractions in hadronic Z decay
- V_{cb} and V_{ub} CKM Matrix Elements
 - [Determination of V_{cb} and V_{ub}]
- B^*
 - mass
- $B_1(5721)^0$
 - mass
- $B_J^*(5732)$
 - mass, width
- $B_2(5747)^0$
 - mass
- B_S^0
 - mass, mean life
 - branching fractions
 - polarization in B_S^0 decay
 - B_S^0/\bar{B}_S^0 mixing
- B_S^*
 - mass
- $B_{s,J}^*(5850)$
 - mass, width
- B_C^\pm
 - mass, mean life
 - branching fractions

At the end of Baryon Listings:

- Λ_b
 - mass, mean life
 - branching fractions
- Σ_b, Σ_b^*
 - mass
- Ξ_b^0, Ξ_b^-
 - mean life
- Ω_b^-
 - mass, mean life
 - branching fractions
- b -baryon Admixture
 - mean life
 - branching fractions

See the related review(s):[Production and Decay of *b*-flavored Hadrons](#)**HEAVY FLAVOR AVERAGING GROUP**

Revised June 2021 by U. Egede (Monash University) and A. Soffer (Tel Aviv University)

The Heavy Flavor Averaging Group (HFLAV) is an international collaboration of physicists from experiments measuring properties of heavy flavored particles, *i.e.*, hadrons containing b and c quarks, and τ leptons. HFLAV calculates and publishes [1] world average values of quantities such as lifetimes, branching fractions, form factors, mixing parameters, and CP -violating asymmetries. Most parameters concern decays of B and D mesons, and many are related to elements of the Cabibbo-Kobayashi-Maskawa (CKM) quark mixing matrix [2], [3].

HFLAV was originally formed in 2002 to continue the activities of the LEP Heavy Flavor Steering group. Since its inception, a wide range of results have become available from increasingly larger data sets. Consequently, HFLAV has expanded to include eight subgroups:

- b -hadron lifetimes and oscillations, including parameters of CP violation in b mixing;
- decay-time-dependent CP violation in B decays, and angles of the CKM Unitarity Triangle;
- semileptonic decays of b -hadrons ($B \rightarrow X\ell\nu$, $\ell = e, \mu, \tau$), including determinations of the CKM matrix elements $|V_{cb}|$ and $|V_{ub}|$;
- b -hadron decays to hadronic final states containing c -quarks (open charm and charmonium);
- (rarer) b -hadron decays to final states not containing c -quarks, including fully hadronic, semileptonic ($B \rightarrow X\ell\ell, X\nu\bar{\nu}$), leptonic, and radiative decays;
- CP - and T -violating asymmetries of D mesons and $D^0-\bar{D}^0$ mixing;
- c -hadron decays (hadronic, semileptonic, leptonic), properties of excited D states and charm baryons and determination of $|V_{cs}|$ and $|V_{cd}|$;
- τ -lepton physics including branching fractions, tests of lepton universality, determination of $|V_{us}|$, and searches for lepton flavor violation.

Meson Particle Listings

 b -flavored hadrons, B^\pm

Each subgroup has one or two conveners and typically a half-dozen members representing experiments that conduct measurements in that area. Most groups contain representatives from the Belle II and LHCb experiments, and some groups have representatives from the ATLAS, BABAR, Belle, BESIII and CMS experiments. Members of HFLAV are appointed by their respective experimental collaborations. HFLAV has two co-leaders, who are appointed by the managements of Belle II and LHCb.

The averaging procedures used by HFLAV are similar to those of the PDG [4]. When sufficient information is available in publications when calculating world averages, common parameters used for different input measurements are adjusted (rescaled) to common values. The p -value of the fit is provided to indicate the consistency of the measurements included in the average. However, unlike the PDG, when obtaining a world average with a low p -value (*i.e.*, a large χ^2 per degree of freedom), HFLAV does not usually scale the resulting uncertainty. Rather, the systematic uncertainties of the measurements are reviewed with experts from the experiments to understand the discrepancy. Unless inconsistencies among measurements are found, no correction is made to the calculated uncertainty. Close communication between representatives of the experiments and HFLAV members who perform averages helps ensure that measurement uncertainties, known correlations, and systematic effects are properly accounted for. If a special treatment is needed to calculate an average, or if an approximation used in an average calculation might not be sufficiently accurate (*e.g.*, assuming Gaussian uncertainties when the likelihood function is non-Gaussian), a note is included in the HFLAV publication and online documentation to describe this.

In general, HFLAV uses all publicly available results that have written documentation such as a journal publication, preprint, or conference note. These include preliminary results presented at conferences and workshops. However, preliminary results that remain unpublished for an extended period of time, or for which no publication is planned, are not included. A special subset of HFLAV averages are included in the PDG listings; for these averages, only measurements that are published or accepted for publication are used. The averages provided by HFLAV are listed by the PDG as “OUR EVALUATION” with a corresponding note.

All HFLAV averages and input measurements are documented in an approximately biennial journal paper or preprint; the most recent version is Ref. [1]. The latest results and plots are posted on an extensive set of webpages that are updated several times per year; these are available at

<https://hflav.web.cern.ch>.

References:

1. Y. Amhis *et al.* (Heavy Flavor Averaging Group), Eur. Phys. J. **C81**, 226 (2021), [arXiv:1909.12524], updated results and plots available at <https://hflav.web.cern.ch/>.
2. N. Cabibbo, Phys. Rev. Lett. **10**, 531 (1963).

3. M. Kobayashi and T. Maskawa, Prog. Theor. Phys. **49**, 652 (1973).
4. See Section 5 of the “Introduction” to this *Review*.

B^\pm

$$I(J^P) = \frac{1}{2}(0^-)$$

Quantum numbers not measured. Values shown are quark-model predictions.

See also the B^\pm/B^0 ADMIXTURE and $B^\pm/B^0/B_s^0/b$ -baryon ADMIXTURE sections.

 B^\pm MASS

The fit uses m_{B^\pm} , $(m_{B^0} - m_{B^\pm})$, and m_{B^0} to determine m_{B^\pm} , m_{B^0} , and the mass difference.

VALUE (MeV)	EVTS	DOCUMENT ID	TECN	COMMENT
5279.34 ± 0.12 OUR FIT				
5279.25 ± 0.26 OUR AVERAGE				
5279.38 ± 0.11 ± 0.33		1 AAIJ	12E	LHCB $p\bar{p}$ at 7 TeV
5279.10 ± 0.41 ± 0.36		2 ACOSTA	06	CDF $p\bar{p}$ at 1.96 TeV
5279.1 ± 0.4 ± 0.4	526	3 CSORNA	00	CLE2 $e^+e^- \rightarrow \Upsilon(4S)$
5279.1 ± 1.7 ± 1.4	147	ABE	96B	CDF $p\bar{p}$ at 1.8 TeV
••• We do not use the following data for averages, fits, limits, etc. •••				
5278.8 ± 0.54 ± 2.0	362	ALAM	94	CLE2 $e^+e^- \rightarrow \Upsilon(4S)$
5278.3 ± 0.4 ± 2.0		BORTOLETTO92	CLEO	$e^+e^- \rightarrow \Upsilon(4S)$
5280.5 ± 1.0 ± 2.0		4 ALBRECHT	90J	ARG $e^+e^- \rightarrow \Upsilon(4S)$
5275.8 ± 1.3 ± 3.0	32	ALBRECHT	87C	ARG $e^+e^- \rightarrow \Upsilon(4S)$
5278.2 ± 1.8 ± 3.0	12	5 ALBRECHT	87D	ARG $e^+e^- \rightarrow \Upsilon(4S)$
5278.6 ± 0.8 ± 2.0		BEBEK	87	CLEO $e^+e^- \rightarrow \Upsilon(4S)$
1 Uses $B^+ \rightarrow J/\psi K^+$ fully reconstructed decays.				
2 Uses exclusively reconstructed final states containing a $J/\psi \rightarrow \mu^+\mu^-$ decays.				
3 CSORNA 00 uses fully reconstructed 526 $B^+ \rightarrow J/\psi(\ell) K^+$ events and invariant masses without beam constraint.				
4 ALBRECHT 90J assumes 10580 for $\Upsilon(4S)$ mass. Supersedes ALBRECHT 87C and ALBRECHT 87D.				
5 Found using fully reconstructed decays with $J/\psi(1S)$. ALBRECHT 87D assume $m_{\Upsilon(4S)} = 10577$ MeV.				

 B^\pm MEAN LIFE

See $B^\pm/B^0/B_s^0/b$ -baryon ADMIXTURE section for data on B -hadron mean life averaged over species of bottom particles.

“OUR EVALUATION” is an average using rescaled values of the data listed below. The average and rescaling were performed by the Heavy Flavor Averaging Group (HFLAV) and are described at <https://hflav.web.cern.ch/>. The averaging/rescaling procedure takes into account correlations between the measurements and asymmetric lifetime errors.

VALUE (10^{-12} s)	EVTS	DOCUMENT ID	TECN	COMMENT
1.638 ± 0.004 OUR EVALUATION				
1.637 ± 0.004 ± 0.003		AAIJ	14E	LHCB $p\bar{p}$ at 7 TeV
1.639 ± 0.009 ± 0.009		1 AALTONEN	11	CDF $p\bar{p}$ at 1.96 TeV
1.663 ± 0.023 ± 0.015		2 AALTONEN	11B	CDF $p\bar{p}$ at 1.96 TeV
1.635 ± 0.011 ± 0.011		3 ABE	05B	BELL $e^+e^- \rightarrow \Upsilon(4S)$
1.624 ± 0.014 ± 0.018		4 ABDALLAH	04E	DLPH $e^+e^- \rightarrow Z$
1.636 ± 0.058 ± 0.025		5 ACOSTA	02C	CDF $p\bar{p}$ at 1.8 TeV
1.673 ± 0.032 ± 0.023		6 AUBERT	01F	BABR $e^+e^- \rightarrow \Upsilon(4S)$
1.648 ± 0.049 ± 0.035		7 BARATE	00R	ALEP $e^+e^- \rightarrow Z$
1.643 ± 0.037 ± 0.025		8 ABBIENDI	99J	OPAL $e^+e^- \rightarrow Z$
1.637 ± 0.058 ± $\begin{smallmatrix} +0.045 \\ -0.043 \end{smallmatrix}$		7 ABE	98Q	CDF $p\bar{p}$ at 1.8 TeV
1.66 ± 0.06 ± 0.03		8 ACCIARRI	98S	L3 $e^+e^- \rightarrow Z$
1.66 ± 0.06 ± 0.05		8 ABE	97J	SLD $e^+e^- \rightarrow Z$
1.58 ± $\begin{smallmatrix} +0.21 \\ -0.18 \end{smallmatrix}$ ± $\begin{smallmatrix} +0.04 \\ -0.03 \end{smallmatrix}$	94	5 BUSKULIC	96J	ALEP $e^+e^- \rightarrow Z$
1.61 ± 0.16 ± 0.12		7,9 ABREU	95Q	DLPH $e^+e^- \rightarrow Z$
1.72 ± 0.08 ± 0.06		10 ADAM	95	DLPH $e^+e^- \rightarrow Z$
1.52 ± 0.14 ± 0.09		7 AKERS	95T	OPAL $e^+e^- \rightarrow Z$
••• We do not use the following data for averages, fits, limits, etc. •••				
1.695 ± 0.026 ± 0.015		6 ABE	02H	BELL Repl. by ABE 05B
1.68 ± 0.07 ± 0.02		5 ABE	98B	CDF Repl. by ACOSTA 02C
1.56 ± 0.13 ± 0.06		7 ABE	96C	CDF Repl. by ABE 98Q
1.58 ± 0.09 ± 0.03		11 BUSKULIC	96J	ALEP $e^+e^- \rightarrow Z$
1.58 ± 0.09 ± 0.04		7 BUSKULIC	96J	ALEP Repl. by BARATE 00R
1.70 ± 0.09		12 ADAM	95	DLPH $e^+e^- \rightarrow Z$
1.61 ± 0.16 ± 0.05	148	5 ABE	94D	CDF Repl. by ABE 98B
1.30 ± $\begin{smallmatrix} +0.33 \\ -0.29 \end{smallmatrix}$ ± 0.16	92	7 ABREU	93D	DLPH Sup. by ABREU 95Q
1.56 ± 0.19 ± 0.13	134	10 ABREU	93G	DLPH Sup. by ADAM 95
1.51 ± $\begin{smallmatrix} +0.30 \\ -0.28 \end{smallmatrix}$ ± 0.14	59	7 ACTON	93C	OPAL Sup. by AKERS 95T
1.47 ± $\begin{smallmatrix} +0.22 \\ -0.19 \end{smallmatrix}$ ± 0.15	77	7 BUSKULIC	93D	ALEP Sup. by BUSKULIC 96J

1 Measured mean life using fully reconstructed decays ($J/\psi K^{(*)}$).

- 2 Measured using $B^- \rightarrow D^0 \pi^-$ with $D^0 \rightarrow K^- \pi^+$ events that were selected using a silicon vertex trigger.
- 3 Measurement performed using a combined fit of CP -violation, mixing and lifetimes.
- 4 Measurement performed using an inclusive reconstruction and B flavor identification technique.
- 5 Measured mean life using fully reconstructed decays.
- 6 Events are selected in which one B meson is fully reconstructed while the second B meson is reconstructed inclusively.
- 7 Data analyzed using $D/D^* \ell X$ event vertices.
- 8 Data analyzed using charge of secondary vertex.
- 9 ABREU 95Q assumes $B(B^0 \rightarrow D^{*-} \ell^+ \nu_\ell) = 3.2 \pm 1.7\%$.
- 10 Data analyzed using vertex-charge technique to tag B charge.
- 11 Combined result of $D/D^* \ell X$ analysis and fully reconstructed B analysis.
- 12 Combined ABREU 95Q and ADAM 95 result.

τ_{B^\pm}/τ_{B^-}	DOCUMENT ID	TECN	COMMENT
1.002 ± 0.004 ± 0.002	1 AAIJ	14E LHCb	pp at 7 TeV

¹ Measured using $B^\pm \rightarrow J/\psi K^\pm$ decays.

B^\pm DECAY MODES

B^- modes are charge conjugates of the modes below. Modes which do not identify the charge state of the B are listed in the B^\pm/B^0 ADMIXTURE section.

The branching fractions listed below assume 50% $B^0 \bar{B}^0$ and 50% $B^+ B^-$ production at the $T(4S)$. We have attempted to bring older measurements up to date by rescaling their assumed $T(4S)$ production ratio to 50:50 and their assumed D, D_s, D^* , and ψ branching ratios to current values whenever this would affect our averages and best limits significantly.

Indentation is used to indicate a subchannel of a previous reaction. All resonant subchannels have been corrected for resonance branching fractions to the final state so the sum of the subchannel branching fractions can exceed that of the final state.

For inclusive branching fractions, e.g., $B \rightarrow D^\pm X$, the values usually are multiplicities, not branching fractions. They can be greater than one.

Mode	Fraction (Γ_i/Γ)	Scale factor/ Confidence level
Semileptonic and leptonic modes		
Γ_1 $\ell^+ \nu_\ell X$	[a] (10.99 ± 0.28) %	
Γ_2 $e^+ \nu_e X_c$	(10.8 ± 0.4) %	
Γ_3 $\ell^+ \nu_\ell X_u$	(1.65 ± 0.21) × 10 ⁻³	
Γ_4 $D \ell^+ \nu_\ell X$	(9.6 ± 0.7) %	
Γ_5 $\bar{D}^0 \ell^+ \nu_\ell$	[a] (2.30 ± 0.09) %	
Γ_6 $\bar{D}^0 \tau^+ \nu_\tau$	(7.7 ± 2.5) × 10 ⁻³	
Γ_7 $\bar{D}^*(2007)^0 \ell^+ \nu_\ell$	[a] (5.58 ± 0.22) %	
Γ_8 $\bar{D}^*(2007)^0 \tau^+ \nu_\tau$	(1.88 ± 0.20) %	
Γ_9 $D^- \pi^+ \ell^+ \nu_\ell$	(4.4 ± 0.4) × 10 ⁻³	
Γ_{10} $\bar{D}_0^*(2420)^0 \ell^+ \nu_\ell, \bar{D}_0^0 \rightarrow$	(2.5 ± 0.5) × 10 ⁻³	
Γ_{11} $\bar{D}_2^-(2460)^0 \ell^+ \nu_\ell, \bar{D}_2^0 \rightarrow$	(1.53 ± 0.16) × 10 ⁻³	
Γ_{12} $D^*(n) \pi \ell^+ \nu_\ell (n \geq 1)$	(1.85 ± 0.25) %	
Γ_{13} $D^{*-} \pi^+ \ell^+ \nu_\ell$	(6.0 ± 0.4) × 10 ⁻³	
Γ_{14} $\bar{D}_1^-(2420)^0 \ell^+ \nu_\ell, \bar{D}_1^0 \rightarrow$	(3.03 ± 0.20) × 10 ⁻³	
Γ_{15} $\bar{D}_1^{*-} \pi^+ \ell^+ \nu_\ell, \bar{D}_1^0 \rightarrow$	(2.7 ± 0.6) × 10 ⁻³	
Γ_{16} $\bar{D}_2^{*-} \pi^+ \ell^+ \nu_\ell, \bar{D}_2^0 \rightarrow$	(1.01 ± 0.24) × 10 ⁻³	S=2.0
Γ_{17} $\bar{D}^0 \pi^+ \pi^- \ell^+ \nu_\ell$	(1.6 ± 0.4) × 10 ⁻³	
Γ_{18} $\bar{D}^{*0} \pi^+ \pi^- \ell^+ \nu_\ell$	(8 ± 5) × 10 ⁻⁴	
Γ_{19} $D_s^{(*)-} K^+ \ell^+ \nu_\ell$	(6.1 ± 1.0) × 10 ⁻⁴	
Γ_{20} $D_s^- K^+ \ell^+ \nu_\ell$	(3.0 ± 1.4) × 10 ⁻⁴	
Γ_{21} $D_s^{*-} K^+ \ell^+ \nu_\ell$	(2.9 ± 1.9) × 10 ⁻⁴	
Γ_{22} $\pi^0 \ell^+ \nu_\ell$	(7.80 ± 0.27) × 10 ⁻⁵	
Γ_{23} $\pi^0 e^+ \nu_e$		
Γ_{24} $\eta \ell^+ \nu_\ell$	(3.9 ± 0.5) × 10 ⁻⁵	
Γ_{25} $\eta' \ell^+ \nu_\ell$	(2.3 ± 0.8) × 10 ⁻⁵	
Γ_{26} $\omega \ell^+ \nu_\ell$	[a] (1.19 ± 0.09) × 10 ⁻⁴	
Γ_{27} $\omega \mu^+ \nu_\mu$		
Γ_{28} $\rho^0 \ell^+ \nu_\ell$	[a] (1.58 ± 0.11) × 10 ⁻⁴	
Γ_{29} $\pi^+ \pi^- \ell^+ \nu_\ell$	(2.3 ± 0.4) × 10 ⁻⁴	
Γ_{30} $p\bar{p} \ell^+ \nu_\ell$	(5.8 ± 2.6) × 10 ⁻⁶	

Γ_{31} $p\bar{p} \mu^+ \nu_\mu$	(5.32 ± 0.34) × 10 ⁻⁶	
Γ_{32} $p\bar{p} e^+ \nu_e$	(8.2 ± 4.0) × 10 ⁻⁶	
Γ_{33} $e^+ \nu_e$	< 9.8	× 10 ⁻⁷ CL=90%
Γ_{34} $\mu^+ \nu_\mu$	< 8.6	× 10 ⁻⁷ CL=90%
Γ_{35} $\tau^+ \nu_\tau$	(1.09 ± 0.24)	× 10 ⁻⁴ S=1.2
Γ_{36} $\ell^+ \nu_\ell \gamma$	< 3.0	× 10 ⁻⁶ CL=90%
Γ_{37} $e^+ \nu_e \gamma$	< 4.3	× 10 ⁻⁶ CL=90%
Γ_{38} $\mu^+ \nu_\mu \gamma$	< 3.4	× 10 ⁻⁶ CL=90%
Γ_{39} $\mu^+ \mu^- \mu^+ \nu_\mu$	< 1.6	× 10 ⁻⁸ CL=95%

Inclusive modes

Γ_{40} $D^0 X$	(8.6 ± 0.7) %
Γ_{41} $\bar{D}^0 X$	(79 ± 4) %
Γ_{42} $D^+ X$	(2.5 ± 0.5) %
Γ_{43} $D^- X$	(9.9 ± 1.2) %
Γ_{44} $D_s^\pm X$	(7.9 ± 1.4) %
Γ_{45} $D_s^- X$	(1.10 ± 0.40) %
Γ_{46} $A_c^+ X$	(2.1 ± 0.9) %
Γ_{47} $\bar{A}_c^- X$	(2.8 ± 1.1) %
Γ_{48} $\bar{c} X$	(97 ± 4) %
Γ_{49} $c X$	(23.4 ± 2.2) %
Γ_{50} $c/\bar{c} X$	(120 ± 6) %

D, D^* , or D_s modes

Γ_{51} $\bar{D}^0 \pi^+$	(4.68 ± 0.13) × 10 ⁻³	
Γ_{52} $D_{CP(+1)} \pi^+$	[b] (2.05 ± 0.20) × 10 ⁻³	
Γ_{53} $D_{CP(-1)} \pi^+$	[b] (2.1 ± 0.4) × 10 ⁻³	
Γ_{54} $\bar{D}^0 \rho^+$	(1.34 ± 0.18) %	
Γ_{55} $\bar{D}^0 K^+$	(3.69 ± 0.16) × 10 ⁻⁴	
Γ_{56} $D_{CP(+1)} K^+$	[b] (1.83 ± 0.08) × 10 ⁻⁴	
Γ_{57} $D_{CP(-1)} K^+$	[b] (1.99 ± 0.19) × 10 ⁻⁴	
Γ_{58} $D^0 K^+$	(3.64 ± 0.25) × 10 ⁻⁶	
Γ_{59} $[K^- \pi^+]_D K^+$	[c] < 2.8	× 10 ⁻⁷ CL=90%
Γ_{60} $[K^+ \pi^-]_D K^+$	[c] < 2.0	× 10 ⁻⁵ CL=90%
Γ_{61} $[K^- \pi^+ \pi^0]_D K^+$	seen	
Γ_{62} $[K^+ \pi^- \pi^0]_D K^+$	seen	
Γ_{63} $[K^- \pi^+ \pi^+ \pi^-]_D K^+$	seen	
Γ_{64} $[K^+ \pi^- \pi^+ \pi^-]_D K^+$	seen	
Γ_{65} $[\pi^+ \pi^+ \pi^- \pi^-]_D K^+$		
Γ_{66} $[\pi^+ \pi^- \pi^+ \pi^-]_D K^*(892)^+$		
Γ_{67} $[K^- \pi^+]_D K^*(892)^+$	[c]	
Γ_{68} $[K^+ \pi^-]_D K^*(892)^+$	[c]	
Γ_{69} $[K^- \pi^+ \pi^- \pi^+]_D K^*(892)^+$		
Γ_{70} $[K^+ \pi^- \pi^+ \pi^-]_D K^*(892)^+$		
Γ_{71} $[K^- \pi^+]_D \pi^+$	[c] (6.3 ± 1.1) × 10 ⁻⁷	
Γ_{72} $[K^+ \pi^-]_D \pi^+$	(1.7 ± 0.4) × 10 ⁻⁴	
Γ_{73} $[K^- \pi^+ \pi^0]_D \pi^+$	seen	
Γ_{74} $[K^+ \pi^- \pi^0]_D \pi^+$	seen	
Γ_{75} $[K^- \pi^+ \pi^+ \pi^-]_D \pi^+$	seen	
Γ_{76} $[K^+ \pi^- \pi^+ \pi^-]_D \pi^+$	seen	
Γ_{77} $[K^- \pi^+]_{(D\pi)} \pi^+$		
Γ_{78} $[K^+ \pi^-]_{(D\pi)} \pi^+$		
Γ_{79} $[K^- \pi^+]_{(D\gamma)} \pi^+$		
Γ_{80} $[K^+ \pi^-]_{(D\gamma)} \pi^+$		
Γ_{81} $[K^- \pi^+]_{(D\pi)} K^+$		
Γ_{82} $[K^+ \pi^-]_{(D\pi)} K^+$		
Γ_{83} $[K^- \pi^+]_{(D\gamma)} K^+$		
Γ_{84} $[K^+ \pi^-]_{(D\gamma)} K^+$		
Γ_{85} $[\pi^+ \pi^- \pi^0]_D K^-$	(4.6 ± 0.9) × 10 ⁻⁶	
Γ_{86} $[K_S^0 K^+ \pi^-]_D K^+$	seen	
Γ_{87} $[K^*(892)^- K^+]_D K^+$		
Γ_{88} $[K_S^0 K^- \pi^+]_D K^+$	seen	
Γ_{89} $[K^*(892)^+ K^-]_D K^+$	seen	
Γ_{90} $[K_S^0 K^- \pi^+]_D \pi^+$	seen	
Γ_{91} $[K^*(892)^+ K^-]_D \pi^+$	seen	
Γ_{92} $[K_S^0 K^+ \pi^-]_D \pi^+$	seen	
Γ_{93} $[K^*(892)^- K^+]_D \pi^+$	seen	
Γ_{94} $[K^+ K^- \pi^0]_D K^+$		
Γ_{95} $[K^+ K^- \pi^0]_D \pi^+$		
Γ_{96} $[\pi^+ \pi^- \pi^0]_D K^+$		

Meson Particle Listings

B^\pm

Γ ₉₇	$[\pi^+ \pi^- \pi^0]_D \pi^+$		Γ ₁₅₇	$\bar{D}_2^*(2462)^0 \pi^+, \bar{D}_2^{*0} \rightarrow$	$(2.2 \pm 1.1) \times 10^{-4}$
Γ ₉₈	$\bar{D}^0 K^*(892)^+$	$(5.3 \pm 0.4) \times 10^{-4}$		$D^*(2010)^- \pi^+$	
Γ ₉₉	$D_{CP(-)} K^*(892)^+$	[b] $(2.7 \pm 0.8) \times 10^{-4}$	Γ ₁₅₈	$\bar{D}_0^*(2400)^0 \pi^+$	$(6.4 \pm 1.4) \times 10^{-4}$
Γ ₁₀₀	$D_{CP(+)} K^*(892)^+$	[b] $(6.2 \pm 0.7) \times 10^{-4}$		$\times B(\bar{D}_0^*(2400)^0 \rightarrow D^- \pi^+)$	
Γ ₁₀₁	$D^0 K^*(892)^+$	$(5.4 \pm 1.8) \times 10^{-6}$	Γ ₁₅₉	$\bar{D}_1^*(2421)^0 \pi^+, \bar{D}_1^0 \rightarrow D^{*-} \pi^+$	$(7.4 \pm 1.0) \times 10^{-4}$
Γ ₁₀₂	$\bar{D}^0 K^+ \pi^+ \pi^-$	$(5.2 \pm 2.1) \times 10^{-4}$	Γ ₁₆₀	$\bar{D}_2^*(2462)^0 \pi^+, \bar{D}_2^{*0} \rightarrow D^{*-} \pi^+$	$(1.98 \pm 0.30) \times 10^{-4}$
Γ ₁₀₃	$[K^+ \pi^-]_D K^+ \pi^- \pi^+$		Γ ₁₆₁	$\bar{D}_1^*(2427)^0 \pi^+, \bar{D}_1^0 \rightarrow D^{*-} \pi^+$	$(3.5 \pm 0.9) \times 10^{-4}$ S=1.5
Γ ₁₀₄	$[K^- \pi^+]_D K^+ \pi^- \pi^+$		Γ ₁₆₂	$\bar{D}_1^*(2420)^0 \pi^+ \times B(\bar{D}_1^0 \rightarrow$	$< 6 \times 10^{-6}$ CL=90%
Γ ₁₀₅	$D_{CP(+)} K^+ \pi^- \pi^+$			$\bar{D}^{*0} \pi^+ \pi^-)$	
Γ ₁₀₆	$\bar{D}^0 K^+ \bar{K}^0$	$(5.5 \pm 1.6) \times 10^{-4}$	Γ ₁₆₃	$\bar{D}_1^*(2420)^0 \rho^+$	$< 1.4 \times 10^{-3}$ CL=90%
Γ ₁₀₇	$\bar{D}^0 K^+ \bar{K}^*(892)^0$	$(7.5 \pm 1.7) \times 10^{-4}$	Γ ₁₆₄	$\bar{D}_2^*(2460)^0 \pi^+$	$< 1.3 \times 10^{-3}$ CL=90%
Γ ₁₀₈	$\bar{D}^0 \pi^+ \pi^+ \pi^-$	$(5.6 \pm 2.1) \times 10^{-3}$ S=3.6	Γ ₁₆₅	$\bar{D}_2^*(2460)^0 \pi^+ \times B(\bar{D}_2^{*0} \rightarrow$	$< 2.2 \times 10^{-5}$ CL=90%
Γ ₁₀₉	$[K^- \pi^+]_D \pi^+ \pi^- \pi^+$			$\bar{D}^{*0} \pi^+ \pi^-)$	
Γ ₁₁₀	$\bar{D}^0 \pi^+ \pi^+ \pi^-$ nonresonant	$(5 \pm 4) \times 10^{-3}$	Γ ₁₆₆	$\bar{D}_1^*(2680)^0 \pi^+, \bar{D}_1^*(2680)^0 \rightarrow$	$(8.4 \pm 2.1) \times 10^{-5}$
Γ ₁₁₁	$\bar{D}^0 \pi^+ \rho^0$	$(4.2 \pm 3.0) \times 10^{-3}$		$D^- \pi^+$	
Γ ₁₁₂	$\bar{D}^0 a_1(1260)^+$	$(4 \pm 4) \times 10^{-3}$	Γ ₁₆₇	$\bar{D}(2740)^0 \pi^+, \bar{D}^0 \rightarrow$	$(3.3 \pm 1.5) \times 10^{-5}$
Γ ₁₁₃	$\bar{D}^0 \omega \pi^+$	$(4.1 \pm 0.9) \times 10^{-3}$		$D^*(2010)^- \pi^+$	
Γ ₁₁₄	$D^*(2010)^- \pi^+ \pi^+$	$(1.35 \pm 0.22) \times 10^{-3}$	Γ ₁₆₈	$\bar{D}_3^*(2750)^0 \pi^+, \bar{D}_3^{*0} \rightarrow$	$(1.10 \pm 0.32) \times 10^{-5}$
Γ ₁₁₅	$D^*(2010)^- K^+ \pi^+$	$(8.2 \pm 1.4) \times 10^{-5}$		$D^*(2010)^- \pi^+$	
Γ ₁₁₆	$\bar{D}_1^*(2420)^0 \pi^+, \bar{D}_1^0 \rightarrow$	$(8.4 \pm 1.5) \times 10^{-4}$	Γ ₁₆₉	$\bar{D}_3^*(2760)^0 \pi^+, \bar{D}_3^{*0} \rightarrow$	$(1.00 \pm 0.22) \times 10^{-5}$
	$D^*(2010)^- \pi^+$			$D^- \pi^+$	
Γ ₁₁₇	$D^- \pi^+ \pi^+$	$(1.07 \pm 0.05) \times 10^{-3}$	Γ ₁₇₀	$\bar{D}_2^*(3000)^0 \pi^+, \bar{D}_2^{*0} \rightarrow$	$(2.0 \pm 1.4) \times 10^{-6}$
Γ ₁₁₈	$D^- K^+ \pi^+$	$(7.7 \pm 0.5) \times 10^{-5}$		$D^- \pi^+$	
Γ ₁₁₉	$D_0^*(2300)^0 K^+, D_0^{*0} \rightarrow$	$(6.1 \pm 2.4) \times 10^{-6}$	Γ ₁₇₁	$\bar{D}_2^*(2460)^0 \rho^+$	$< 4.7 \times 10^{-3}$ CL=90%
	$D^- \pi^+$		Γ ₁₇₂	$\bar{D}^0 D_s^+$	$(9.0 \pm 0.9) \times 10^{-3}$
Γ ₁₂₀	$D_2^*(2460)^0 K^+, D_2^{*0} \rightarrow$	$(2.32 \pm 0.23) \times 10^{-5}$	Γ ₁₇₃	$D_{s0}^*(2317)^+ \bar{D}^0, D_{s0}^{*+} \rightarrow$	$(8.0 \pm 1.6) \times 10^{-4}$
	$D^- \pi^+$			$D_s^+ \pi^0$	
Γ ₁₂₁	$D_1^*(2760)^0 K^+, D_1^{*0} \rightarrow$	$(3.6 \pm 1.2) \times 10^{-6}$	Γ ₁₇₄	$D_{s0}(2317)^+ \bar{D}^0 \times$	$< 7.6 \times 10^{-4}$ CL=90%
	$D^- \pi^+$			$B(D_{s0}(2317)^+ \rightarrow D_s^{*+} \gamma)$	
Γ ₁₂₂	$D^+ K^0$	$< 2.9 \times 10^{-6}$ CL=90%	Γ ₁₇₅	$D_{s0}(2317)^+ \bar{D}^*(2007)^0 \times$	$(9 \pm 7) \times 10^{-4}$
Γ ₁₂₃	$D^+ K^+ \pi^-$	$(5.6 \pm 1.1) \times 10^{-6}$		$B(D_{s0}(2317)^+ \rightarrow D_s^+ \pi^0)$	
Γ ₁₂₄	$D_2^*(2460)^0 K^+, D_2^{*0} \rightarrow$	$< 6.3 \times 10^{-7}$ CL=90%	Γ ₁₇₆	$D_{s,J}(2457)^+ \bar{D}^0$	$(3.1 \pm 1.0) \times 10^{-3}$
	$D^+ \pi^-$			\times	
Γ ₁₂₅	$D^+ K^{*0}$	$< 4.9 \times 10^{-7}$ CL=90%	Γ ₁₇₇	$D_{s,J}(2457)^+ \bar{D}^0 \times$	$(4.6 \pm 1.3) \times 10^{-4}$
Γ ₁₂₆	$D^+ \bar{K}^{*0}$	$< 1.4 \times 10^{-6}$ CL=90%		$B(D_{s,J}(2457)^+ \rightarrow D_s^+ \gamma)$	
Γ ₁₂₇	$\bar{D}^*(2007)^0 \pi^+$	$(5.18 \pm 0.15) \times 10^{-3}$	Γ ₁₇₈	$D_{s,J}(2457)^+ \bar{D}^0 \times$	$< 2.2 \times 10^{-4}$ CL=90%
Γ ₁₂₈	$\bar{D}_{CP(+)}^{*0} \pi^+$	[d] $(2.9 \pm 0.6) \times 10^{-3}$		$B(D_{s,J}(2457)^+ \rightarrow$	
Γ ₁₂₉	$\bar{D}_{CP(-)}^{*0} \pi^+$	[d] $(2.6 \pm 1.0) \times 10^{-3}$		$D_s^+ \pi^+ \pi^-)$	
Γ ₁₃₀	$\bar{D}^*(2007)^0 \omega \pi^+$	$(4.5 \pm 1.2) \times 10^{-3}$	Γ ₁₇₉	$D_{s,J}(2457)^+ \bar{D}^0 \times$	$< 2.7 \times 10^{-4}$ CL=90%
Γ ₁₃₁	$\bar{D}^*(2007)^0 \rho^+$	$(9.8 \pm 1.7) \times 10^{-3}$		$B(D_{s,J}(2457)^+ \rightarrow D_s^+ \pi^0)$	
Γ ₁₃₂	$\bar{D}^*(2007)^0 K^+$	$(4.20 \pm 0.31) \times 10^{-4}$	Γ ₁₈₀	$D_{s,J}(2457)^+ \bar{D}^0 \times$	$< 9.8 \times 10^{-4}$ CL=90%
				$B(D_{s,J}(2457)^+ \rightarrow D_s^{*+} \gamma)$	
Γ ₁₃₃	$\bar{D}_{CP(+)}^{*0} K^+$	[d] $(2.75 \pm 0.35) \times 10^{-4}$	Γ ₁₈₁	$D_{s,J}(2457)^+ \bar{D}^*(2007)^0$	$(1.20 \pm 0.30) \%$
Γ ₁₃₄	$\bar{D}_{CP(-)}^{*0} K^+$	[d] $(2.31 \pm 0.31) \times 10^{-4}$	Γ ₁₈₂	$D_{s,J}(2457)^+ \bar{D}^*(2007)^0 \times$	$(1.4 \pm 0.7) \times 10^{-3}$
Γ ₁₃₅	$D^*(2007)^0 K^+$	$(4.5 \pm 1.2) \times 10^{-6}$		$B(D_{s,J}(2457)^+ \rightarrow D_s^+ \gamma)$	
Γ ₁₃₆	$\bar{D}^*(2007)^0 K^*(892)^+$	$(8.1 \pm 1.4) \times 10^{-4}$	Γ ₁₈₃	$\bar{D}^0 D_{s1}(2536)^+ \times$	$(4.0 \pm 1.0) \times 10^{-4}$
Γ ₁₃₇	$\bar{D}^*(2007)^0 K^+ \bar{K}^0$	$< 1.06 \times 10^{-3}$ CL=90%		$B(D_{s1}(2536)^+ \rightarrow$	
Γ ₁₃₈	$\bar{D}^*(2007)^0 K^+ \bar{K}^*(892)^0$	$(1.5 \pm 0.4) \times 10^{-3}$		$D^*(2007)^0 K^+ +$	
Γ ₁₃₉	$\bar{D}^*(2007)^0 \pi^+ \pi^+ \pi^-$	$(1.03 \pm 0.12) \%$		$D^*(2010)^+ K^0)$	
Γ ₁₄₀	$\bar{D}^*(2007)^0 a_1(1260)^+$	$(1.9 \pm 0.5) \%$	Γ ₁₈₄	$\bar{D}^0 D_{s1}(2536)^+ \times$	$(2.2 \pm 0.7) \times 10^{-4}$
Γ ₁₄₁	$\bar{D}^*(2007)^0 \pi^- \pi^+ \pi^+ \pi^0$	$(1.8 \pm 0.4) \%$		$B(D_{s1}(2536)^+ \rightarrow$	
Γ ₁₄₂	$\bar{D}^{*0} 3\pi^+ 2\pi^-$	$(5.7 \pm 1.2) \times 10^{-3}$		$D^*(2007)^0 K^+)$	
Γ ₁₄₃	$D^*(2010)^+ \pi^0$	$< 3.6 \times 10^{-6}$	Γ ₁₈₅	$\bar{D}^*(2007)^0 D_{s1}(2536)^+ \times$	$(5.5 \pm 1.6) \times 10^{-4}$
Γ ₁₄₄	$D^*(2010)^+ K^0$	$< 9.0 \times 10^{-6}$ CL=90%		$B(D_{s1}(2536)^+ \rightarrow$	
Γ ₁₄₅	$D^*(2010)^- \pi^+ \pi^+ \pi^0$	$(1.5 \pm 0.7) \%$		$D^*(2007)^0 K^+)$	
Γ ₁₄₆	$D^*(2010)^- \pi^+ \pi^+ \pi^+ \pi^-$	$(2.6 \pm 0.4) \times 10^{-3}$	Γ ₁₈₆	$\bar{D}^0 D_{s1}(2536)^+ \times$	$(2.3 \pm 1.1) \times 10^{-4}$
Γ ₁₄₇	$\bar{D}^{*0} \pi^+$	[e] $(5.7 \pm 1.2) \times 10^{-3}$		$B(D_{s1}(2536)^+ \rightarrow D^{*+} K^0)$	
Γ ₁₄₈	$\bar{D}_1^*(2420)^0 \pi^+$	$(1.5 \pm 0.6) \times 10^{-3}$ S=1.3	Γ ₁₈₇	$\bar{D}^0 D_{s,J}(2700)^+ \times$	$(5.6 \pm 1.8) \times 10^{-4}$ S=1.7
Γ ₁₄₉	$\bar{D}_1^*(2420)^0 \pi^+ \times B(\bar{D}_1^0 \rightarrow$	$(2.5 \pm 1.6) \times 10^{-4}$ S=3.9		$B(D_{s,J}(2700)^+ \rightarrow D^0 K^+)$	
	$\bar{D}^0 \pi^+ \pi^-)$		Γ ₁₈₈	$\bar{D}^{*0} D_{s1}(2536)^+, D_{s1}^+ \rightarrow$	$(3.9 \pm 2.6) \times 10^{-4}$
Γ ₁₅₀	$\bar{D}_1^*(2420)^0 \pi^+ \times B(\bar{D}_1^0 \rightarrow$	$(2.2 \pm 1.0) \times 10^{-4}$		$D^{*+} K^0$	
	$\bar{D}^0 \pi^+ \pi^-$ (nonresonant))		Γ ₁₈₉	$\bar{D}^0 D_{s,J}(2573)^+, D_{s,J}^+ \rightarrow$	$(8 \pm 15) \times 10^{-6}$
Γ ₁₅₁	$\bar{D}_1^*(2430)^0 \pi^+, \bar{D}_1^0 \rightarrow$	$(3.5 \pm 0.6) \times 10^{-4}$		$D^0 K^+$	
	$D^*(2010)^- \pi^+$		Γ ₁₉₀	$\bar{D}^{*0} D_{s,J}(2573), D_{s,J}^+ \rightarrow D^0 K^+$	$< 2 \times 10^{-4}$ CL=90%
Γ ₁₅₂	$\bar{D}(2550)^0 \pi^+, \bar{D}^0 \rightarrow$	$(7.2 \pm 1.4) \times 10^{-5}$	Γ ₁₉₁	$\bar{D}^*(2007)^0 D_{s,J}(2573), D_{s,J}^+ \rightarrow$	$< 5 \times 10^{-4}$ CL=90%
	$D^*(2010)^- \pi^+$			$D^0 K^+$	
Γ ₁₅₃	$\bar{D}_J^*(2600)^0 \pi^+, \bar{D}_J^{*0} \rightarrow$	$(6.8 \pm 1.3) \times 10^{-5}$		$\bar{D}^0 D_s^{*+}$	$(7.6 \pm 1.6) \times 10^{-3}$
	$D^*(2010)^- \pi^+$		Γ ₁₉₂	$\bar{D}^*(2007)^0 D_s^+$	$(8.2 \pm 1.7) \times 10^{-3}$
Γ ₁₅₄	$\bar{D}_2^*(2462)^0 \pi^+, \bar{D}_2^{*0} \rightarrow D^- \pi^+$	$(3.56 \pm 0.24) \times 10^{-4}$	Γ ₁₉₃	$\bar{D}^*(2007)^0 D_s^{*+}$	$(1.71 \pm 0.24) \%$
Γ ₁₅₅	$\bar{D}_2^*(2462)^0 \pi^+, \bar{D}_2^{*0} \rightarrow$	$(2.2 \pm 1.0) \times 10^{-4}$	Γ ₁₉₄	$D_s^{(*)+} \bar{D}^{*0}$	$(2.7 \pm 1.2) \%$
	$\bar{D}^0 \pi^- \pi^+$		Γ ₁₉₅	$\bar{D}^*(2007)^0 D^*(2010)^+$	$(8.1 \pm 1.7) \times 10^{-4}$
Γ ₁₅₆	$\bar{D}_2^*(2462)^0 \pi^+, \bar{D}_2^{*0} \rightarrow$	$< 1.7 \times 10^{-4}$ CL=90%			
	$\bar{D}^0 \pi^- \pi^+$ (nonresonant)				

Γ_{197}	$\bar{D}^0 D^*(2010)^+ + \bar{D}^*(2007)^0 D^+$	< 1.30	%	CL=90%	Γ_{264}	$X(4014)^0 K^+, X^0 \rightarrow \eta_c \pi^0$	< 1.2	$\times 10^{-5}$	CL=90%
Γ_{198}	$\bar{D}^0 D^*(2010)^+$	(3.9 ± 0.5)	$\times 10^{-4}$		Γ_{265}	$Z_c(3900)^0 K^+, Z_c^0 \rightarrow \eta_c \pi^+ \pi^-$	< 4.7	$\times 10^{-5}$	CL=90%
Γ_{199}	$\bar{D}^0 D^+$	(3.8 ± 0.4)	$\times 10^{-4}$		Γ_{266}	$X(4020)^0 K^+, X^0 \rightarrow \eta_c \pi^+ \pi^-$	< 1.6	$\times 10^{-5}$	CL=90%
Γ_{200}	$\bar{D}^0 D^+ K^0$	(1.55 ± 0.21)	$\times 10^{-3}$		Γ_{267}	$\chi_{c1}(3872) K^*(892)^+$	< 6	$\times 10^{-4}$	CL=90%
Γ_{201}	$D^+ \bar{D}^*(2007)^0$	(6.3 ± 1.7)	$\times 10^{-4}$		Γ_{268}	$\chi_{c1}(3872)^+ K^0, \chi_{c1}^+ \rightarrow J/\psi(1S) \pi^+ \pi^0$	[Γ] < 6.1	$\times 10^{-6}$	CL=90%
Γ_{202}	$\bar{D}^*(2007)^0 D^+ K^0$	(2.1 ± 0.5)	$\times 10^{-3}$		Γ_{269}	$\chi_{c1}(3872) K^0 \pi^+$	(2.8 ± 1.2)	$\times 10^{-4}$	
Γ_{203}	$\bar{D}^0 D^*(2010)^+ K^0$	(3.8 ± 0.4)	$\times 10^{-3}$		Γ_{270}	$Z_c(4430)^+ K^0, Z_c^+ \rightarrow J/\psi \pi^+$	< 1.5	$\times 10^{-5}$	CL=95%
Γ_{204}	$\bar{D}^*(2007)^0 D^*(2010)^+ K^0$	(9.2 ± 1.2)	$\times 10^{-3}$		Γ_{271}	$Z_c(4430)^+ K^0, Z_c^+ \rightarrow \psi(2S) \pi^+$	< 4.7	$\times 10^{-5}$	CL=95%
Γ_{205}	$\bar{D}^0 D^0 K^+$	(1.45 ± 0.33)	$\times 10^{-3}$	S=2.6	Γ_{272}	$\psi(4230)^0 K^+, \psi^0 \rightarrow J/\psi \pi^+ \pi^-$	< 1.56	$\times 10^{-5}$	CL=95%
Γ_{206}	$\bar{D}^*(2007)^0 D^0 K^+$	(2.26 ± 0.23)	$\times 10^{-3}$		Γ_{273}	$\chi_{c0}(3915) K^+, \chi_{c0} \rightarrow J/\psi \gamma$	< 1.4	$\times 10^{-5}$	CL=90%
Γ_{207}	$\bar{D}^0 D^*(2007)^0 K^+$	(6.3 ± 0.5)	$\times 10^{-3}$		Γ_{274}	$\chi_{c0}(3915) K^+, \chi_{c0} \rightarrow \chi_{c1}(1P) \pi^0$	< 3.8	$\times 10^{-5}$	CL=90%
Γ_{208}	$\bar{D}^*(2007)^0 D^*(2007)^0 K^+$	(1.12 ± 0.13)	%		Γ_{275}	$X(3930)^0 K^+, X^0 \rightarrow J/\psi \gamma$	< 2.5	$\times 10^{-6}$	CL=90%
Γ_{209}	$D^- D^+ K^+$	(2.2 ± 0.7)	$\times 10^{-4}$		Γ_{276}	$J/\psi(1S) K^+$	(1.020 ± 0.019)	$\times 10^{-3}$	
Γ_{210}	$X_0(2900) D^+, X_0 \rightarrow D^- K^+$	(1.2 ± 0.5)	$\times 10^{-5}$		Γ_{277}	$J/\psi(1S) K^0 \pi^+$	(1.14 ± 0.11)	$\times 10^{-3}$	
Γ_{211}	$X_1(2900) D^+, X_1 \rightarrow D^- K^+$	(6.7 ± 2.3)	$\times 10^{-5}$		Γ_{278}	$J/\psi(1S) K^+ \pi^+ \pi^-$	(8.1 ± 1.3)	$\times 10^{-4}$	S=2.5
Γ_{212}	$D^- D^+ K^+$ nonresonant	(5.3 ± 1.8)	$\times 10^{-5}$		Γ_{279}	$J/\psi(1S) K^+ K^- K^+$	(3.37 ± 0.29)	$\times 10^{-5}$	
Γ_{213}	$D^- D^*(2010)^+ K^+$	(6.3 ± 1.1)	$\times 10^{-4}$		Γ_{280}	$\chi_{c0}(3915) K^+, \chi_{c0} \rightarrow p \bar{p}$	< 7.1	$\times 10^{-8}$	CL=95%
Γ_{214}	$D^*(2010)^- D^+ K^+$	(6.0 ± 1.3)	$\times 10^{-4}$		Γ_{281}	$J/\psi(1S) K^*(892)^+$	(1.43 ± 0.08)	$\times 10^{-3}$	
Γ_{215}	$D^*(2010)^- D^*(2010)^+ K^+$	(1.32 ± 0.18)	$\times 10^{-3}$		Γ_{282}	$J/\psi(1S) K(1270)^+$	(1.8 ± 0.5)	$\times 10^{-3}$	
Γ_{216}	$(\bar{D}^+ + \bar{D}^*)(D + D^*) K$	(4.05 ± 0.30)	%		Γ_{283}	$J/\psi(1S) K(1400)^+$	< 5	$\times 10^{-4}$	CL=90%
Γ_{217}	$D_s^+ \pi^0$	(1.6 ± 0.5)	$\times 10^{-5}$		Γ_{284}	$J/\psi(1S) \eta K^+$	(1.24 ± 0.14)	$\times 10^{-4}$	
Γ_{218}	$D_s^{*+} \pi^0$	< 2.6	$\times 10^{-4}$	CL=90%	Γ_{285}	$\chi_{c1-odd}(3872) K^+, \chi_{c1-odd} \rightarrow J/\psi \eta$	< 3.8	$\times 10^{-6}$	CL=90%
Γ_{219}	$D_s^+ \eta$	< 4	$\times 10^{-4}$	CL=90%	Γ_{286}	$\psi(4160) K^+, \psi \rightarrow J/\psi \eta$	< 7.4	$\times 10^{-6}$	CL=90%
Γ_{220}	$D_s^{*+} \eta$	< 6	$\times 10^{-4}$	CL=90%	Γ_{287}	$J/\psi(1S) \eta' K^+$	< 8.8	$\times 10^{-5}$	CL=90%
Γ_{221}	$D_s^+ \rho^0$	< 3.0	$\times 10^{-4}$	CL=90%	Γ_{288}	$J/\psi(1S) \phi K^+$	(5.0 ± 0.4)	$\times 10^{-5}$	
Γ_{222}	$D_s^{*+} \rho^0$	< 4	$\times 10^{-4}$	CL=90%	Γ_{289}	$J/\psi(1S) K_1(1650), K_1 \rightarrow \phi K^+$	(6 - $\frac{+10}{-6}$)	$\times 10^{-6}$	
Γ_{223}	$D_s^+ \omega$	< 4	$\times 10^{-4}$	CL=90%	Γ_{290}	$J/\psi(1S) K^*(1680)^+, K^* \rightarrow \phi K^+$	(3.4 - $\frac{+1.9}{-2.2}$)	$\times 10^{-6}$	
Γ_{224}	$D_s^{*+} \omega$	< 6	$\times 10^{-4}$	CL=90%	Γ_{291}	$J/\psi(1S) K_2^*(1980), K_2^* \rightarrow \phi K^+$	(1.5 - $\frac{+0.9}{-0.5}$)	$\times 10^{-6}$	
Γ_{225}	$D_s^+ a_1(1260)^0$	< 1.8	$\times 10^{-3}$	CL=90%	Γ_{292}	$J/\psi(1S) K(1830)^+, K(1830)^+ \rightarrow \phi K^+$	(1.3 - $\frac{+1.3}{-1.1}$)	$\times 10^{-6}$	
Γ_{226}	$D_s^{*+} a_1(1260)^0$	< 1.3	$\times 10^{-3}$	CL=90%	Γ_{293}	$\chi_{c1}(4140) K^+, \chi_{c1} \rightarrow J/\psi(1S) \phi$	(10 ± 4)	$\times 10^{-6}$	
Γ_{227}	$D_s^+ K^+ K^-$	(7.2 ± 1.1)	$\times 10^{-6}$		Γ_{294}	$\chi_{c1}(4274) K^+, \chi_{c1} \rightarrow J/\psi(1S) \phi$	(3.6 - $\frac{+2.2}{-1.8}$)	$\times 10^{-6}$	
Γ_{228}	$D_s^+ \phi$	< 4.2	$\times 10^{-7}$	CL=90%	Γ_{295}	$\chi_{c0}(4500) K^+, \chi_c^0 \rightarrow J/\psi(1S) \phi$	(3.3 - $\frac{+2.1}{-1.7}$)	$\times 10^{-6}$	
Γ_{229}	$D_s^{*+} \phi$	< 1.2	$\times 10^{-5}$	CL=90%	Γ_{296}	$\chi_{c0}(4700) K^+, \chi_{c0} \rightarrow J/\psi(1S) \phi$	(6 - $\frac{+5}{-4}$)	$\times 10^{-6}$	
Γ_{230}	$D_s^+ \bar{K}^0$	< 8	$\times 10^{-4}$	CL=90%	Γ_{297}	$J/\psi(1S) \omega K^+$	(3.20 ± $\frac{+0.60}{-0.32}$)	$\times 10^{-4}$	
Γ_{231}	$D_s^{*+} \bar{K}^0$	< 9	$\times 10^{-4}$	CL=90%	Γ_{298}	$\chi_{c0}(3915) K^+, \chi_{c0} \rightarrow J/\psi \omega$	(3.0 - $\frac{+0.9}{-0.7}$)	$\times 10^{-5}$	
Γ_{232}	$D_s^+ \bar{K}^*(892)^0$	< 4.4	$\times 10^{-6}$	CL=90%	Γ_{299}	$J/\psi(1S) \pi^+$	(3.92 ± 0.08)	$\times 10^{-5}$	
Γ_{233}	$D_s^+ K^* K^0$	< 3.5	$\times 10^{-6}$	CL=90%	Γ_{300}	$J/\psi(1S) \pi^+ \pi^+ \pi^+ \pi^- \pi^-$	(1.17 ± 0.13)	$\times 10^{-5}$	
Γ_{234}	$D_s^{*+} \bar{K}^*(892)^0$	< 3.5	$\times 10^{-4}$	CL=90%	Γ_{301}	$\psi(2S) \pi^+ \pi^+ \pi^-$	(1.9 ± 0.4)	$\times 10^{-5}$	
Γ_{235}	$D_s^+ \pi^+ K^+$	(1.80 ± 0.22)	$\times 10^{-4}$		Γ_{302}	$J/\psi(1S) \rho^+$	(4.1 ± 0.5)	$\times 10^{-5}$	S=1.4
Γ_{236}	$D_s^{*-} \pi^+ K^+$	(1.45 ± 0.24)	$\times 10^{-4}$		Γ_{303}	$J/\psi(1S) \pi^+ \pi^0$ nonresonant	< 7.3	$\times 10^{-6}$	CL=90%
Γ_{237}	$D_s^- \pi^+ K^*(892)^+$	< 5	$\times 10^{-3}$	CL=90%	Γ_{304}	$J/\psi(1S) a_1(1260)^+$	< 1.2	$\times 10^{-3}$	CL=90%
Γ_{238}	$D_s^{*-} \pi^+ K^*(892)^+$	< 7	$\times 10^{-3}$	CL=90%	Γ_{305}	$J/\psi(1S) p \bar{p} \pi^+$	< 5.0	$\times 10^{-7}$	CL=90%
Γ_{239}	$D_s^- K^+ K^+$	(9.7 ± 2.1)	$\times 10^{-6}$		Γ_{306}	$J/\psi(1S) p \bar{p} \Lambda$	(1.46 ± 0.12)	$\times 10^{-5}$	
Γ_{240}	$D_s^{*-} K^+ K^+$	< 1.5	$\times 10^{-5}$	CL=90%	Γ_{307}	$J/\psi(1S) \Sigma^0 p$	< 1.1	$\times 10^{-5}$	CL=90%
Charmonium modes					Γ_{308}	$J/\psi(1S) D^+$	< 1.2	$\times 10^{-4}$	CL=90%
Γ_{241}	$\eta_c K^+$	(1.09 ± 0.08)	$\times 10^{-3}$		Γ_{309}	$J/\psi(1S) \bar{D}^0 \pi^+$	< 2.5	$\times 10^{-5}$	CL=90%
Γ_{242}	$\eta_c K^+, \eta_c \rightarrow K_S^0 K^\mp \pi^\pm$	(2.7 ± 0.6)	$\times 10^{-5}$		Γ_{310}	$\psi(2S) \pi^+$	(2.44 ± 0.30)	$\times 10^{-5}$	
Γ_{243}	$\eta_c K^*(892)^+$	(1.1 - $\frac{+0.5}{-0.4}$)	$\times 10^{-3}$		Γ_{311}	$\psi(2S) K^+$	(6.24 ± 0.20)	$\times 10^{-4}$	
Γ_{244}	$\eta_c K^+ \pi^+ \pi^-$	< 3.9	$\times 10^{-4}$	CL=90%	Γ_{312}	$\psi(2S) K^*(892)^+$	(6.7 ± 1.4)	$\times 10^{-4}$	S=1.3
Γ_{245}	$\eta_c K^+ \omega(782)$	< 5.3	$\times 10^{-4}$	CL=90%	Γ_{313}	$\psi(2S) K^0 \pi^+$			
Γ_{246}	$\eta_c K^+ \eta$	< 2.2	$\times 10^{-4}$	CL=90%	Γ_{314}	$\psi(2S) K^+ \pi^+ \pi^-$	(4.3 ± 0.5)	$\times 10^{-4}$	
Γ_{247}	$\eta_c K^+ \pi^0$	< 6.2	$\times 10^{-5}$	CL=90%	Γ_{315}	$\psi(2S) \phi(1020) K^+$	(4.0 ± 0.7)	$\times 10^{-6}$	
Γ_{248}	$\eta_c(2S) K^+$	(4.4 ± 1.0)	$\times 10^{-4}$		Γ_{316}	$\psi(3770) K^+$	(4.3 ± 1.1)	$\times 10^{-4}$	
Γ_{249}	$\eta_c(2S) K^+, \eta_c \rightarrow p \bar{p}$	(3.5 ± 0.8)	$\times 10^{-8}$		Γ_{317}	$\psi(3770) K^+, \psi \rightarrow D^0 \bar{D}^0$	(1.5 ± 0.5)	$\times 10^{-4}$	S=1.4
Γ_{250}	$\eta_c(2S) K^+, \eta_c \rightarrow K_S^0 K^\mp \pi^\pm$	(3.4 - $\frac{+2.3}{-1.6}$)	$\times 10^{-6}$		Γ_{318}	$\psi(3770) K^+, \psi \rightarrow D^+ D^-$	(9.4 ± 3.5)	$\times 10^{-5}$	
Γ_{251}	$\eta_c(2S) K^+, \eta_c \rightarrow p \bar{p} \pi^+ \pi^-$	(1.12 ± 0.18)	$\times 10^{-6}$		Γ_{319}	$\psi(3770) K^+, \psi \rightarrow p \bar{p}$	< 2	$\times 10^{-7}$	CL=95%
Γ_{252}	$h_c(1P) K^+, h_c \rightarrow J/\psi \pi^+ \pi^-$	< 3.4	$\times 10^{-6}$	CL=90%	Γ_{320}	$\psi(4040) K^+$	< 1.3	$\times 10^{-4}$	CL=90%
Γ_{253}	$X(3730)^0 K^+, X^0 \rightarrow \eta_c \eta$	< 4.6	$\times 10^{-5}$	CL=90%					
Γ_{254}	$X(3730)^0 K^+, X^0 \rightarrow \eta_c \pi^0$	< 5.7	$\times 10^{-6}$	CL=90%					
Γ_{255}	$\eta_{c2}(1D) K^+, \eta_{c2} \rightarrow h_c \gamma$	< 3.7	$\times 10^{-5}$	CL=90%					
Γ_{256}	$\eta_{c2}(1D) \pi^+ K_S^0, \eta_{c2} \rightarrow h_c \gamma$	< 1.1	$\times 10^{-4}$	CL=90%					
Γ_{257}	$\psi_2(3823) K^+, \psi_2 \rightarrow J/\psi \pi^+ \pi^-$	(2.8 ± 0.6)	$\times 10^{-7}$						

Meson Particle Listings

B^\pm

Γ ₃₂₁	$\psi(4040) K^+, \psi \rightarrow D^+ D^-$	(1.1 ± 0.5) × 10 ⁻⁵	Γ ₃₈₀	$\rho^0(1450) K^+ \times B(\rho^0(1450) \rightarrow \pi^+ \pi^-)$	< 1.17	× 10 ⁻⁵ CL=90%	
Γ ₃₂₂	$\psi(4160) K^+$	(5.1 ± 2.7) × 10 ⁻⁴	Γ ₃₈₁	$f'_2(1525) K^+ \times B(f'_2(1525) \rightarrow \pi^+ \pi^-)$	< 3.4	× 10 ⁻⁶ CL=90%	
Γ ₃₂₃	$\psi(4160) K^+, \psi \rightarrow \bar{D}^0 D^0$	(8 ± 5) × 10 ⁻⁵	Γ ₃₈₂	$K^+ \rho^0$	(3.7 ± 0.5) × 10 ⁻⁶		
Γ ₃₂₄	$\psi(4160) K^+, \psi \rightarrow D^+ D^-$	(1.5 ± 0.6) × 10 ⁻⁵	Γ ₃₈₃	$K_0^*(1430)^0 \pi^+$	(3.9 ± 0.6) × 10 ⁻⁵	S=1.4	
Γ ₃₂₅	$\psi(4415) K^+, \psi \rightarrow D^+ D^-$	(2.0 ± 0.8) × 10 ⁻⁵	Γ ₃₈₄	$K_2^*(1430)^0 \pi^+$	(5.6 ± 2.2) × 10 ⁻⁶		
Γ ₃₂₆	$\chi_{c0} \pi^+, \chi_{c0} \rightarrow \pi^+ \pi^-$	< 1	Γ ₃₈₅	$K^*(1410)^0 \pi^+$	< 4.5	× 10 ⁻⁵ CL=90%	
Γ ₃₂₇	$\chi_{c0} K^+$	(1.51 ± 0.15) × 10 ⁻⁴	Γ ₃₈₆	$K^*(1680)^0 \pi^+$	< 1.2	× 10 ⁻⁵ CL=90%	
Γ ₃₂₈	$\chi_{c0} K^*(892)^+$	< 2.1	Γ ₃₈₇	$K^+ \pi^0 \pi^0$	(1.62 ± 0.19) × 10 ⁻⁵		
Γ ₃₂₉	$\chi_{c1}(1P) \pi^+$	(2.2 ± 0.5) × 10 ⁻⁵	Γ ₃₈₈	$f_0(980) K^+ \times B(f_0 \rightarrow \pi^0 \pi^0)$	(2.8 ± 0.8) × 10 ⁻⁶		
Γ ₃₃₀	$\chi_{c1}(1P) K^+$	(4.74 ± 0.22) × 10 ⁻⁴	Γ ₃₈₉	$K^- \pi^+ \pi^+$	< 4.6	× 10 ⁻⁸ CL=90%	
Γ ₃₃₁	$\chi_{c1}(1P) K^*(892)^+$	(3.0 ± 0.6) × 10 ⁻⁴	Γ ₃₉₀	$K^- \pi^+ \pi^+$ nonresonant	< 5.6	× 10 ⁻⁵ CL=90%	
Γ ₃₃₂	$\chi_{c1}(1P) K^0 \pi^+$	(5.8 ± 0.4) × 10 ⁻⁴	Γ ₃₉₁	$K_1^+(1270)^0 \pi^+$	< 4.0	× 10 ⁻⁵ CL=90%	
Γ ₃₃₃	$\chi_{c1}(1P) K^+ \pi^0$	(3.29 ± 0.35) × 10 ⁻⁴	Γ ₃₉₂	$K_1^+(1400)^0 \pi^+$	< 3.9	× 10 ⁻⁵ CL=90%	
Γ ₃₃₄	$\chi_{c1}(1P) K^+ \pi^+ \pi^-$	(3.74 ± 0.30) × 10 ⁻⁴	Γ ₃₉₃	$K^0 \pi^+ \pi^0$	< 6.6	× 10 ⁻⁵ CL=90%	
Γ ₃₃₅	$\chi_{c1}(2P) K^+, \chi_{c1}(2P) \rightarrow \pi^+ \pi^- \chi_{c1}(1P)$	< 1.1	Γ ₃₉₄	$K_0^*(1430)^+ \pi^0$	(1.19 ± 0.20) × 10 ⁻⁵		
Γ ₃₃₆	$\chi_{c2} K^+$	(1.1 ± 0.4) × 10 ⁻⁵	Γ ₃₉₅	$K^0 \rho^+$	(7.3 ± 1.0) × 10 ⁻⁶		
Γ ₃₃₇	$\chi_{c2} K^+, \chi_{c2} \rightarrow p \bar{p} \pi^+ \pi^-$	< 1.9	Γ ₃₉₆	$K^*(892)^+ \pi^+ \pi^-$	(7.5 ± 1.0) × 10 ⁻⁵		
Γ ₃₃₈	$\chi_{c2} K^*(892)^+$	< 1.2	Γ ₃₉₇	$K^*(892)^+ \rho^0$	(4.6 ± 1.1) × 10 ⁻⁶		
Γ ₃₃₉	$\chi_{c2} K^0 \pi^+$	(1.16 ± 0.25) × 10 ⁻⁴	Γ ₃₉₈	$K^*(892)^+ f_0(980)$	(4.2 ± 0.7) × 10 ⁻⁶		
Γ ₃₄₀	$\chi_{c2} K^+ \pi^0$	< 6.2	Γ ₃₉₉	$a_1^+ K^0$	(3.5 ± 0.7) × 10 ⁻⁵		
Γ ₃₄₁	$\chi_{c2} K^+ \pi^+ \pi^-$	(1.34 ± 0.19) × 10 ⁻⁴	Γ ₄₀₀	$b_1^+ K^0 \times B(b_1^+ \rightarrow \omega \pi^+)$	(9.6 ± 1.9) × 10 ⁻⁶		
Γ ₃₄₂	$\chi_{c2}(3930) K^+, \chi_{c2} \rightarrow D^+ D^-$	(1.6 ± 0.6) × 10 ⁻⁵	Γ ₄₀₁	$K^*(892)^0 \rho^+$	(9.2 ± 1.5) × 10 ⁻⁶		
Γ ₃₄₃	$\chi_{c2}(3930) \pi^+, \chi_{c2} \rightarrow \pi^+ \pi^-$	< 1	Γ ₄₀₂	$K_1^+(1400)^+ \rho^0$	< 7.8	× 10 ⁻⁴ CL=90%	
Γ ₃₄₄	$h_c(1P) K^+$	(3.7 ± 1.2) × 10 ⁻⁵	Γ ₄₀₃	$K_2^*(1430)^+ \rho^0$	< 1.5	× 10 ⁻³ CL=90%	
Γ ₃₄₅	$h_c(1P) K^+, h_c \rightarrow p \bar{p}$	< 6.4	Γ ₄₀₄	$b_1^+ K^+ \times B(b_1^+ \rightarrow \omega \pi^0)$	(9.1 ± 2.0) × 10 ⁻⁶		
K or K* modes							
Γ ₃₄₆	$K^0 \pi^+$	(2.37 ± 0.08) × 10 ⁻⁵	Γ ₄₀₅	$b_1^+ K^{*0} \times B(b_1^+ \rightarrow \omega \pi^+)$	< 5.9	× 10 ⁻⁶ CL=90%	
Γ ₃₄₇	$K^+ \pi^0$	(1.29 ± 0.05) × 10 ⁻⁵	Γ ₄₀₆	$b_1^0 K^{*+} \times B(b_1^0 \rightarrow \omega \pi^0)$	< 6.7	× 10 ⁻⁶ CL=90%	
Γ ₃₄₈	$\eta' K^+$	(7.04 ± 0.25) × 10 ⁻⁵	Γ ₄₀₇	$K^+ \bar{K}^0$	(1.31 ± 0.17) × 10 ⁻⁶	S=1.2	
Γ ₃₄₉	$\eta' K^*(892)^+$	(4.8 ± 1.8) × 10 ⁻⁶	Γ ₄₀₈	$\bar{K}^0 K^+ \pi^0$	< 2.4	× 10 ⁻⁵ CL=90%	
Γ ₃₅₀	$\eta' K_0^*(1430)^+$	(5.2 ± 2.1) × 10 ⁻⁶	Γ ₄₀₉	$K^+ K_S^0 K_S^0$	(1.05 ± 0.04) × 10 ⁻⁵		
Γ ₃₅₁	$\eta' K_2^*(1430)^+$	(2.8 ± 0.5) × 10 ⁻⁵	Γ ₄₁₀	$f_0(980) K^+, f_0 \rightarrow K_S^0 K_S^0$	(1.47 ± 0.33) × 10 ⁻⁵		
Γ ₃₅₂	ηK^+	(2.4 ± 0.4) × 10 ⁻⁶	Γ ₄₁₁	$f_0(1710) K^+, f_0 \rightarrow K_S^0 K_S^0$	(4.8 ± 4.0) × 10 ⁻⁷		
Γ ₃₅₃	$\eta K^*(892)^+$	(1.93 ± 0.16) × 10 ⁻⁵	Γ ₄₁₂	$K^+ K_S^0 K_S^0$ nonresonant	(2.0 ± 0.4) × 10 ⁻⁵		
Γ ₃₅₄	$\eta K_0^*(1430)^+$	(1.8 ± 0.4) × 10 ⁻⁵	Γ ₄₁₃	$K_S^0 K_S^0 \pi^+$	< 5.1	× 10 ⁻⁷ CL=90%	
Γ ₃₅₅	$\eta K_2^*(1430)^+$	(9.1 ± 3.0) × 10 ⁻⁶	Γ ₄₁₄	$K^+ K^- \pi^+$	(5.2 ± 0.4) × 10 ⁻⁶		
Γ ₃₅₆	$\eta(1295) K^+ \times B(\eta(1295) \rightarrow \eta \pi \pi)$	(2.9 ± 0.8) × 10 ⁻⁶	Γ ₄₁₅	$K^+ K^- \pi^+$ nonresonant	(1.68 ± 0.26) × 10 ⁻⁶		
Γ ₃₅₇	$\eta(1405) K^+ \times B(\eta(1405) \rightarrow \eta \pi \pi)$	< 1.3	Γ ₄₁₆	$K^+ \bar{K}^*(892)^0$	(5.9 ± 0.8) × 10 ⁻⁷		
Γ ₃₅₈	$\eta(1405) K^+ \times B(\eta(1405) \rightarrow K^* K)$	< 1.2	Γ ₄₁₇	$K^+ \bar{K}_0^*(1430)^0$	(3.8 ± 1.3) × 10 ⁻⁷		
Γ ₃₅₉	$\eta(1475) K^+ \times B(\eta(1475) \rightarrow K^* K)$	(1.38 ± 0.21) × 10 ⁻⁵	Γ ₄₁₈	$\pi^+ (K^+ K^-) s\text{-wave}$	(8.5 ± 0.9) × 10 ⁻⁷		
Γ ₃₆₀	$f_1(1285) K^+$	< 2.0	Γ ₄₁₉	$K^+ K^+ \pi^-$	< 1.1	× 10 ⁻⁸ CL=90%	
Γ ₃₆₁	$f_1(1420) K^+ \times B(f_1(1420) \rightarrow \eta \pi \pi)$	< 2.9	Γ ₄₂₀	$K^+ K^+ \pi^-$ nonresonant	< 8.79	× 10 ⁻⁵ CL=90%	
Γ ₃₆₂	$f_1(1420) K^+ \times B(f_1(1420) \rightarrow K^* K)$	< 4.1	Γ ₄₂₁	$f'_2(1525) K^+$	(1.8 ± 0.5) × 10 ⁻⁶	S=1.1	
Γ ₃₆₃	$\phi(1680) K^+ \times B(\phi(1680) \rightarrow K^* K)$	< 3.4	Γ ₄₂₂	$K^+ f_J(2220)$	< 1.18	× 10 ⁻⁵ CL=90%	
Γ ₃₆₄	$f_0(1500) K^+$	(3.7 ± 2.2) × 10 ⁻⁶	Γ ₄₂₃	$K^{*+} \pi^+ K^-$	(9.1 ± 2.9) × 10 ⁻⁷		
Γ ₃₆₅	ωK^+	(6.5 ± 0.4) × 10 ⁻⁶	Γ ₄₂₄	$K^*(892)^+ K^*(892)^0$	< 6.1	× 10 ⁻⁶ CL=90%	
Γ ₃₆₆	$\omega K^*(892)^+$	< 7.4	Γ ₄₂₅	$K^{*+} K^+ \pi^-$	(3.40 ± 0.14) × 10 ⁻⁵	S=1.4	
Γ ₃₆₇	$\omega (K\pi)_0^+$	(2.8 ± 0.4) × 10 ⁻⁵	Γ ₄₂₆	$K^+ K^- K^+$	(8.8 ± 0.7) × 10 ⁻⁶	S=1.1	
Γ ₃₆₈	$\omega K_0^*(1430)^+$	(2.4 ± 0.5) × 10 ⁻⁵	Γ ₄₂₇	$K^+ \phi$	(9.4 ± 3.2) × 10 ⁻⁶		
Γ ₃₆₉	$\omega K_2^*(1430)^+$	(2.1 ± 0.4) × 10 ⁻⁵	Γ ₄₂₈	$f_0(980) K^+ \times B(f_0(980) \rightarrow K^+ K^-)$	< 1.1	× 10 ⁻⁶ CL=90%	
Γ ₃₇₀	$a_0(980)^+ K^0 \times B(a_0(980)^+ \rightarrow \eta \pi^+)$	< 3.9	Γ ₄₂₉	$a_2(1320) K^+ \times B(a_2(1320) \rightarrow K^+ K^-)$	< 1.1	× 10 ⁻⁶ CL=90%	
Γ ₃₇₁	$a_0(980)^0 K^+ \times B(a_0(980)^0 \rightarrow \eta \pi^0)$	< 2.5	Γ ₄₃₀	$X_0(1550) K^+ \times B(X_0(1550) \rightarrow K^+ K^-)$	(4.3 ± 0.7) × 10 ⁻⁶		
Γ ₃₇₂	$K^*(892)^0 \pi^+$	(1.01 ± 0.08) × 10 ⁻⁵	Γ ₄₃₁	$\phi(1680) K^+ \times B(\phi(1680) \rightarrow K^+ K^-)$	< 8	× 10 ⁻⁷ CL=90%	
Γ ₃₇₃	$K^*(892)^+ \pi^0$	(6.8 ± 0.9) × 10 ⁻⁶	Γ ₄₃₂	$f_0(1710) K^+ \times B(f_0(1710) \rightarrow K^+ K^-)$	(1.1 ± 0.6) × 10 ⁻⁶		
Γ ₃₇₄	$K^+ \pi^- \pi^+$	(5.10 ± 0.29) × 10 ⁻⁵	Γ ₄₃₃	$K^+ K^- K^+$ nonresonant	(2.38 ± 0.28) × 10 ⁻⁵		
Γ ₃₇₅	$K^+ \pi^- \pi^+$ nonresonant	(1.63 ± 0.21) × 10 ⁻⁵	Γ ₄₃₄	$K^*(892)^+ K^+ K^-$	(3.6 ± 0.5) × 10 ⁻⁵		
Γ ₃₇₆	$\omega(782) K^+$	(6 ± 9) × 10 ⁻⁶	Γ ₄₃₅	$K^*(892)^+ \phi$	(10.0 ± 2.0) × 10 ⁻⁶	S=1.7	
Γ ₃₇₇	$K^+ f_0(980) \times B(f_0(980) \rightarrow \pi^+ \pi^-)$	(9.4 ± 1.0) × 10 ⁻⁶	Γ ₄₃₆	$\phi(K\pi)_0^+$	(8.3 ± 1.6) × 10 ⁻⁶		
Γ ₃₇₈	$f_2(1270)^0 K^+$	(1.07 ± 0.27) × 10 ⁻⁶	Γ ₄₃₇	$\phi K_1(1270)^+$	(6.1 ± 1.9) × 10 ⁻⁶		
Γ ₃₇₉	$f_0(1370)^0 K^+ \times B(f_0(1370)^0 \rightarrow \pi^+ \pi^-)$	< 1.07	Γ ₄₃₈	$\phi K_1(1400)^+$	< 3.2	× 10 ⁻⁶ CL=90%	
			Γ ₄₃₉	$\phi K^*(1410)^+$	< 4.3	× 10 ⁻⁶ CL=90%	
			Γ ₄₄₀	$\phi K_0^*(1430)^+$	(7.0 ± 1.6) × 10 ⁻⁶		
			Γ ₄₄₁	$\phi K_2^*(1430)^+$	(8.4 ± 2.1) × 10 ⁻⁶		
			Γ ₄₄₂	$\phi K_2^*(1770)^+$	< 1.50	× 10 ⁻⁵ CL=90%	

Γ_{443}	$\phi K_2^*(1820)^+$	< 1.63	$\times 10^{-5}$	CL=90%
Γ_{444}	$a_1^+ K^{*0}$	< 3.6	$\times 10^{-6}$	CL=90%
Γ_{445}	$K^+ \phi$	(4.2 ± 0.8)	$\times 10^{-6}$	S=2.2
Γ_{446}	$\eta' \eta' K^+$	< 2.5	$\times 10^{-5}$	CL=90%
Γ_{447}	$\omega \phi K^+$	< 1.9	$\times 10^{-6}$	CL=90%
Γ_{448}	$X(1812) K^+ \times B(X \rightarrow \omega \phi)$	< 3.2	$\times 10^{-7}$	CL=90%
Γ_{449}	$K^*(892)^+ \gamma$	(3.92 ± 0.22)	$\times 10^{-5}$	S=1.7
Γ_{450}	$K_1(1270)^+ \gamma$	(4.4 + 0.7 - 0.6)	$\times 10^{-5}$	
Γ_{451}	$\eta K^+ \gamma$	(7.9 ± 0.9)	$\times 10^{-6}$	
Γ_{452}	$\eta' K^+ \gamma$	(2.9 + 1.0 - 0.9)	$\times 10^{-6}$	
Γ_{453}	$\phi K^+ \gamma$	(2.7 ± 0.4)	$\times 10^{-6}$	S=1.2
Γ_{454}	$K^+ \pi^- \pi^+ \gamma$	(2.58 ± 0.15)	$\times 10^{-5}$	S=1.3
Γ_{455}	$K^*(892)^0 \pi^+ \gamma$	(2.33 ± 0.12)	$\times 10^{-5}$	
Γ_{456}	$K^+ \rho^0 \gamma$	(8.2 ± 0.9)	$\times 10^{-6}$	
Γ_{457}	$(K^+ \pi^-)_{NR} \pi^+ \gamma$	(9.9 + 1.7 - 2.0)	$\times 10^{-6}$	
Γ_{458}	$K^0 \pi^+ \pi^0 \gamma$	(4.6 ± 0.5)	$\times 10^{-5}$	
Γ_{459}	$K_1(1400)^+ \gamma$	(10 + 5 - 4)	$\times 10^{-6}$	
Γ_{460}	$K^*(1410)^+ \gamma$	(2.7 + 0.8 - 0.6)	$\times 10^{-5}$	
Γ_{461}	$K_0^*(1430)^0 \pi^+ \gamma$	(1.32 + 0.26 - 0.32)	$\times 10^{-6}$	
Γ_{462}	$K_2^*(1430)^+ \gamma$	(1.4 ± 0.4)	$\times 10^{-5}$	
Γ_{463}	$K^*(1680)^+ \gamma$	(6.7 + 1.7 - 1.4)	$\times 10^{-5}$	
Γ_{464}	$K_3^*(1780)^+ \gamma$	< 3.9	$\times 10^{-5}$	CL=90%
Γ_{465}	$K_4^*(2045)^+ \gamma$	< 9.9	$\times 10^{-3}$	CL=90%

Light unflavored meson modes

Γ_{466}	$\rho^+ \gamma$	(9.8 ± 2.5)	$\times 10^{-7}$	
Γ_{467}	$\pi^+ \pi^0$	(5.5 ± 0.4)	$\times 10^{-6}$	S=1.2
Γ_{468}	$\pi^+ \pi^+ \pi^-$	(1.52 ± 0.14)	$\times 10^{-5}$	
Γ_{469}	$\rho^0 \pi^+$	(8.3 ± 1.2)	$\times 10^{-6}$	
Γ_{470}	$\pi^+ f_0(980), f_0 \rightarrow \pi^+ \pi^-$	< 1.5	$\times 10^{-6}$	CL=90%
Γ_{471}	$\pi^+ f_2(1270)$	(2.2 + 0.7 - 0.4)	$\times 10^{-6}$	
Γ_{472}	$\rho(1450)^0 \pi^+, \rho^0 \rightarrow \pi^+ \pi^-$	(1.4 + 0.6 - 0.9)	$\times 10^{-6}$	
Γ_{473}	$\rho(1450)^0 \pi^+, \rho^0 \rightarrow K^+ K^-$	(1.60 ± 0.14)	$\times 10^{-6}$	
Γ_{474}	$f_0(1370) \pi^+, f_0 \rightarrow \pi^+ \pi^-$	< 4.0	$\times 10^{-6}$	CL=90%
Γ_{475}	$f_0(500) \pi^+, f_0 \rightarrow \pi^+ \pi^-$	< 4.1	$\times 10^{-6}$	CL=90%
Γ_{476}	$\pi^+ \pi^- \pi^+$ nonresonant	(5.3 + 1.5 - 1.1)	$\times 10^{-6}$	
Γ_{477}	$\pi^+ \pi^0 \pi^0$	< 8.9	$\times 10^{-4}$	CL=90%
Γ_{478}	$\rho^+ \pi^0$	(1.09 ± 0.14)	$\times 10^{-5}$	
Γ_{479}	$\pi^+ \pi^- \pi^+ \pi^0$	< 4.0	$\times 10^{-3}$	CL=90%
Γ_{480}	$\rho^+ \rho^0$	(2.40 ± 0.19)	$\times 10^{-5}$	
Γ_{481}	$\rho^+ f_0(980), f_0 \rightarrow \pi^+ \pi^-$	< 2.0	$\times 10^{-6}$	CL=90%
Γ_{482}	$a_1(1260)^+ \pi^0$	(2.6 ± 0.7)	$\times 10^{-5}$	
Γ_{483}	$a_1(1260)^0 \pi^+$	(2.0 ± 0.6)	$\times 10^{-5}$	
Γ_{484}	$\omega \pi^+$	(6.9 ± 0.5)	$\times 10^{-6}$	
Γ_{485}	$\omega \rho^+$	(1.59 ± 0.21)	$\times 10^{-5}$	
Γ_{486}	$\eta \pi^+$	(4.02 ± 0.27)	$\times 10^{-6}$	
Γ_{487}	$\eta \rho^+$	(7.0 ± 2.9)	$\times 10^{-6}$	S=2.8
Γ_{488}	$\eta' \pi^+$	(2.7 ± 0.9)	$\times 10^{-6}$	S=1.9
Γ_{489}	$\eta' \rho^+$	(9.7 ± 2.2)	$\times 10^{-6}$	
Γ_{490}	$\phi \pi^+$	(3.2 ± 1.5)	$\times 10^{-8}$	
Γ_{491}	$\phi \rho^+$	< 3.0	$\times 10^{-6}$	CL=90%
Γ_{492}	$a_0(980)^0 \pi^+, a_0^0 \rightarrow \eta \pi^0$	< 5.8	$\times 10^{-6}$	CL=90%
Γ_{493}	$a_0(980)^+ \pi^0, a_0^+ \rightarrow \eta \pi^+$	< 1.4	$\times 10^{-6}$	CL=90%
Γ_{494}	$\pi^+ \pi^+ \pi^+ \pi^- \pi^-$	< 8.6	$\times 10^{-4}$	CL=90%
Γ_{495}	$\rho^0 a_1(1260)^+$	< 6.2	$\times 10^{-4}$	CL=90%
Γ_{496}	$\rho^0 a_2(1320)^+$	< 7.2	$\times 10^{-4}$	CL=90%
Γ_{497}	$b_1^0 \pi^+, b_1^0 \rightarrow \omega \pi^0$	(6.7 ± 2.0)	$\times 10^{-6}$	
Γ_{498}	$b_1^+ \pi^0, b_1^+ \rightarrow \omega \pi^+$	< 3.3	$\times 10^{-6}$	CL=90%
Γ_{499}	$\pi^+ \pi^+ \pi^+ \pi^- \pi^- \pi^0$	< 6.3	$\times 10^{-3}$	CL=90%
Γ_{500}	$b_1^+ \rho^0, b_1^+ \rightarrow \omega \pi^+$	< 5.2	$\times 10^{-6}$	CL=90%
Γ_{501}	$a_1(1260)^+ a_1(1260)^0$	< 1.3	%	CL=90%
Γ_{502}	$b_1^0 \rho^+, b_1^0 \rightarrow \omega \pi^0$	< 3.3	$\times 10^{-6}$	CL=90%

Charged particle (h^\pm) modes

$h^\pm = K^\pm \text{ or } \pi^\pm$

Γ_{503}	$h^+ \pi^0$	(1.6 + 0.7 - 0.6)	$\times 10^{-5}$	
----------------	-------------	---------------------	------------------	--

Γ_{504}	ωh^+	(1.38 + 0.27 - 0.24)	$\times 10^{-5}$	
Γ_{505}	$h^+ X^0$ (Familon)	< 4.9	$\times 10^{-5}$	CL=90%
Γ_{506}	$K^+ X^0, X^0 \rightarrow \mu^+ \mu^-$	< 1	$\times 10^{-7}$	CL=95%

Baryon modes

Γ_{507}	$p \bar{p} \pi^+$	(1.62 ± 0.20)	$\times 10^{-6}$	
Γ_{508}	$p \bar{p} \pi^+$ nonresonant	< 5.3	$\times 10^{-5}$	CL=90%
Γ_{509}	$p \bar{p} \pi^+ \pi^0$	(4.6 ± 1.3)	$\times 10^{-6}$	
Γ_{510}	$p \bar{p} \pi^+ \pi^+ \pi^-$			
Γ_{511}	$p \bar{p} K^+$	(5.9 ± 0.5)	$\times 10^{-6}$	S=1.5
Γ_{512}	$\Theta(1710)^{++} \bar{p}, \Theta^{++} \rightarrow p K^+$	[g] < 9.1	$\times 10^{-8}$	CL=90%
Γ_{513}	$f_J(2220) K^+, f_J \rightarrow p \bar{p}$	[g] < 4.1	$\times 10^{-7}$	CL=90%
Γ_{514}	$\rho \bar{\Lambda}(1520)$	(3.1 ± 0.6)	$\times 10^{-7}$	
Γ_{515}	$p \bar{p} K^+$ nonresonant	< 8.9	$\times 10^{-5}$	CL=90%
Γ_{516}	$p \bar{p} K^*(892)^+$	(3.6 + 0.8 - 0.7)	$\times 10^{-6}$	
Γ_{517}	$f_J(2220) K^{*+}, f_J \rightarrow p \bar{p}$	< 7.7	$\times 10^{-7}$	CL=90%
Γ_{518}	$\rho \bar{\Lambda}$	(2.4 + 1.0 - 0.9)	$\times 10^{-7}$	
Γ_{519}	$\rho \bar{\Lambda} \gamma$	(2.4 + 0.5 - 0.4)	$\times 10^{-6}$	
Γ_{520}	$\rho \bar{\Lambda} \pi^0$	(3.0 + 0.7 - 0.6)	$\times 10^{-6}$	
Γ_{521}	$\rho \bar{\Sigma}^-(1385)^0$	< 4.7	$\times 10^{-7}$	CL=90%
Γ_{522}	$\Delta^+ \bar{\Lambda}$	< 8.2	$\times 10^{-7}$	CL=90%
Γ_{523}	$\rho \bar{\Sigma}^- \gamma$	< 4.6	$\times 10^{-6}$	CL=90%
Γ_{524}	$\rho \bar{\Lambda} \pi^+ \pi^-$	(1.13 ± 0.13)	$\times 10^{-5}$	
Γ_{525}	$p \bar{\Lambda} \pi^+ \pi^-$ nonresonant	(5.9 ± 1.1)	$\times 10^{-6}$	
Γ_{526}	$p \bar{\Lambda} \rho^0, \rho^0 \rightarrow \pi^+ \pi^-$	(4.8 ± 0.9)	$\times 10^{-6}$	
Γ_{527}	$p \bar{\Lambda} f_2(1270), f_2 \rightarrow \pi^+ \pi^-$	(2.0 ± 0.8)	$\times 10^{-6}$	
Γ_{528}	$\rho \bar{\Lambda} K^+ K^-$	(4.1 ± 0.7)	$\times 10^{-6}$	
Γ_{529}	$p \bar{\Lambda} \phi$	(8.0 ± 2.2)	$\times 10^{-7}$	
Γ_{530}	$\bar{p} \Lambda K^+ K^-$	(3.7 ± 0.6)	$\times 10^{-6}$	
Γ_{531}	$\Lambda \bar{\Lambda} \pi^+$	< 9.4	$\times 10^{-7}$	CL=90%
Γ_{532}	$\Lambda \bar{\Lambda} K^+$	(3.4 ± 0.6)	$\times 10^{-6}$	
Γ_{533}	$\Lambda \bar{\Lambda} K^{*+}$	(2.2 + 1.2 - 0.9)	$\times 10^{-6}$	
Γ_{534}	$\Lambda(1520) \bar{\Lambda} K^+$	(2.2 ± 0.7)	$\times 10^{-6}$	
Γ_{535}	$\Lambda \bar{\Lambda}(1520) K^+$	< 2.08	$\times 10^{-6}$	
Γ_{536}	$\bar{\Delta}^0 p$	< 1.38	$\times 10^{-6}$	CL=90%
Γ_{537}	$\Delta^{++} \bar{p}$	< 1.4	$\times 10^{-7}$	CL=90%
Γ_{538}	$D^+ p \bar{p}$	< 1.5	$\times 10^{-5}$	CL=90%
Γ_{539}	$D^*(2010)^+ p \bar{p}$	< 1.5	$\times 10^{-5}$	CL=90%
Γ_{540}	$\bar{D}^0 p \bar{p} \pi^+$	(3.72 ± 0.27)	$\times 10^{-4}$	
Γ_{541}	$\bar{D}^{*0} p \bar{p} \pi^+$	(3.73 ± 0.32)	$\times 10^{-4}$	
Γ_{542}	$D^- p \bar{p} \pi^+ \pi^-$	(1.66 ± 0.30)	$\times 10^{-4}$	
Γ_{543}	$D^{*-} p \bar{p} \pi^+ \pi^-$	(1.86 ± 0.25)	$\times 10^{-4}$	
Γ_{544}	$p \bar{\Lambda}^0 \bar{D}^0$	(1.43 ± 0.32)	$\times 10^{-5}$	
Γ_{545}	$p \bar{\Lambda}^0 \bar{D}^*(2007)^0$	< 5	$\times 10^{-5}$	CL=90%
Γ_{546}	$\bar{\Lambda}_c^- p \pi^+$	(2.3 ± 0.4)	$\times 10^{-4}$	S=2.2
Γ_{547}	$\bar{\Lambda}_c^- \Delta(1232)^{++}$	< 1.9	$\times 10^{-5}$	CL=90%
Γ_{548}	$\bar{\Lambda}_c^- \Delta_X(1600)^{++}$	(4.7 ± 1.0)	$\times 10^{-5}$	
Γ_{549}	$\bar{\Lambda}_c^- \Delta_X(2420)^{++}$	(3.7 ± 0.8)	$\times 10^{-5}$	
Γ_{550}	$(\bar{\Lambda}_c^- p)_s \pi^+$	[h] (3.1 ± 0.7)	$\times 10^{-5}$	
Γ_{551}	$\bar{\Sigma}_c(2520)^0 p$	< 3	$\times 10^{-6}$	CL=90%
Γ_{552}	$\bar{\Sigma}_c(2800)^0 p$	(2.6 ± 0.9)	$\times 10^{-5}$	
Γ_{553}	$\bar{\Lambda}_c^- p \pi^+ \pi^0$	(1.8 ± 0.6)	$\times 10^{-3}$	
Γ_{554}	$\bar{\Lambda}_c^- p \pi^+ \pi^+ \pi^-$	(2.2 ± 0.7)	$\times 10^{-3}$	
Γ_{555}	$\bar{\Lambda}_c^- p \pi^+ \pi^+ \pi^- \pi^0$	< 1.34	%	CL=90%
Γ_{556}	$\Lambda_c^+ \bar{\Lambda}_c^- K^+$	(4.9 ± 0.7)	$\times 10^{-4}$	
Γ_{557}	$\Xi_c(2930) \Lambda_c^+, \Xi_c \rightarrow K^+ \Lambda_c^-$	(1.7 ± 0.5)	$\times 10^{-4}$	
Γ_{558}	$\bar{\Sigma}_c(2455)^0 p$	(2.9 ± 0.7)	$\times 10^{-5}$	
Γ_{559}	$\bar{\Sigma}_c(2455)^0 p \pi^0$	(3.5 ± 1.1)	$\times 10^{-4}$	
Γ_{560}	$\bar{\Sigma}_c(2455)^0 p \pi^- \pi^+$	(3.5 ± 1.1)	$\times 10^{-4}$	
Γ_{561}	$\bar{\Sigma}_c(2455)^- p \pi^+ \pi^+$	(2.37 ± 0.20)	$\times 10^{-4}$	
Γ_{562}	$\bar{\Lambda}_c^-(2593)^- / \bar{\Lambda}_c^-(2625)^- p \pi^+$	< 1.9	$\times 10^{-4}$	CL=90%
Γ_{563}	$\Xi_c^0 \Lambda_c^+$	(9.5 ± 2.3)	$\times 10^{-4}$	
Γ_{564}	$\Xi_c^0 \Lambda_c^+, \Xi_c^0 \rightarrow \Xi^+ \pi^-$	(1.76 ± 0.29)	$\times 10^{-5}$	
Γ_{565}	$\Xi_c^0 \Lambda_c^+, \Xi_c^0 \rightarrow \Lambda K^+ \pi^-$	(1.14 ± 0.26)	$\times 10^{-5}$	
Γ_{566}	$\Xi_c^0 \Lambda_c^+, \Xi_c^0 \rightarrow p K^- K^- \pi^+$	(5.5 ± 1.9)	$\times 10^{-6}$	
Γ_{567}	$\Lambda_c^+ \Xi_c^0$	< 6.5	$\times 10^{-4}$	CL=90%
Γ_{568}	$\Lambda_c^+ \Xi_c^-(2645)^0$	< 7.9	$\times 10^{-4}$	CL=90%
Γ_{569}	$\Lambda_c^+ \Xi_c^-(2790)^0$	(1.1 ± 0.4)	$\times 10^{-3}$	

Meson Particle Listings

B^\pm

Lepton Family number (LF) or Lepton number (L) or Baryon number (B) violating modes, or/and $\Delta B = 1$ weak neutral current (BI) modes

Γ_{570}	$\pi^+ \ell^+ \ell^-$	B1	< 4.9	$\times 10^{-8}$	CL=90%
Γ_{571}	$\pi^+ e^+ e^-$	B1	< 8.0	$\times 10^{-8}$	CL=90%
Γ_{572}	$\pi^+ \mu^+ \mu^-$	B1	(1.78 \pm 0.23)	$\times 10^{-8}$	
Γ_{573}	$\pi^+ \nu \bar{\nu}$	B1	< 1.4	$\times 10^{-5}$	CL=90%
Γ_{574}	$K^+ \ell^+ \ell^-$	B1	[a] (4.7 \pm 0.5)	$\times 10^{-7}$	S=2.3
Γ_{575}	$K^+ e^+ e^-$	B1	(5.6 \pm 0.6)	$\times 10^{-7}$	
Γ_{576}	$K^+ \mu^+ \mu^-$	B1	(4.53 \pm 0.35)	$\times 10^{-7}$	S=1.8
Γ_{577}	$K^+ \mu^+ \mu^-$ nonresonant	B1	(4.37 \pm 0.27)	$\times 10^{-7}$	
Γ_{578}	$K^+ \tau^+ \tau^-$	B1	< 2.25	$\times 10^{-3}$	CL=90%
Γ_{579}	$K^+ \bar{\nu} \nu$	B1	< 1.6	$\times 10^{-5}$	CL=90%
Γ_{580}	$\rho^+ \nu \bar{\nu}$	B1	< 3.0	$\times 10^{-5}$	CL=90%
Γ_{581}	$K^*(892)^+ \ell^+ \ell^-$	B1	[a] (1.01 \pm 0.11)	$\times 10^{-6}$	S=1.1
Γ_{582}	$K^*(892)^+ e^+ e^-$	B1	(1.55 \pm 0.40 / 0.31)	$\times 10^{-6}$	
Γ_{583}	$K^*(892)^+ \mu^+ \mu^-$	B1	(9.6 \pm 1.0)	$\times 10^{-7}$	
Γ_{584}	$K^*(892)^+ \nu \bar{\nu}$	B1	< 4.0	$\times 10^{-5}$	CL=90%
Γ_{585}	$K^+ \pi^+ \pi^- \mu^+ \mu^-$	B1	(4.3 \pm 0.4)	$\times 10^{-7}$	
Γ_{586}	$\phi K^+ \mu^+ \mu^-$	B1	(7.9 \pm 2.1 / 1.7)	$\times 10^{-8}$	
Γ_{587}	$\bar{A} \rho \nu \bar{\nu}$		< 3.0	$\times 10^{-5}$	CL=90%
Γ_{588}	$\pi^+ e^+ \mu^-$	LF	< 6.4	$\times 10^{-3}$	CL=90%
Γ_{589}	$\pi^+ e^- \mu^+$	LF	< 6.4	$\times 10^{-3}$	CL=90%
Γ_{590}	$\pi^+ e^\pm \mu^\mp$	LF	< 1.7	$\times 10^{-7}$	CL=90%
Γ_{591}	$\pi^+ e^+ \tau^-$	LF	< 7.4	$\times 10^{-5}$	CL=90%
Γ_{592}	$\pi^+ e^- \tau^+$	LF	< 2.0	$\times 10^{-5}$	CL=90%
Γ_{593}	$\pi^+ e^\pm \tau^\mp$	LF	< 7.5	$\times 10^{-5}$	CL=90%
Γ_{594}	$\pi^+ \mu^+ \tau^-$	LF	< 6.2	$\times 10^{-5}$	CL=90%
Γ_{595}	$\pi^+ \mu^- \tau^+$	LF	< 4.5	$\times 10^{-5}$	CL=90%
Γ_{596}	$\pi^+ \mu^\pm \tau^\mp$	LF	< 7.2	$\times 10^{-5}$	CL=90%
Γ_{597}	$K^+ e^+ \mu^-$	LF	< 7.0	$\times 10^{-9}$	CL=90%
Γ_{598}	$K^+ e^- \mu^+$	LF	< 6.4	$\times 10^{-9}$	CL=90%
Γ_{599}	$K^+ e^\pm \mu^\mp$	LF	< 9.1	$\times 10^{-8}$	CL=90%
Γ_{600}	$K^+ e^+ \tau^-$	LF	< 4.3	$\times 10^{-5}$	CL=90%
Γ_{601}	$K^+ e^- \tau^+$	LF	< 1.5	$\times 10^{-5}$	CL=90%
Γ_{602}	$K^+ e^\pm \tau^\mp$	LF	< 3.0	$\times 10^{-5}$	CL=90%
Γ_{603}	$K^+ \mu^+ \tau^-$	LF	< 4.5	$\times 10^{-5}$	CL=90%
Γ_{604}	$K^+ \mu^- \tau^+$	LF	< 2.8	$\times 10^{-5}$	CL=90%
Γ_{605}	$K^+ \mu^\pm \tau^\mp$	LF	< 4.8	$\times 10^{-5}$	CL=90%
Γ_{606}	$K^*(892)^+ e^+ \mu^-$	LF	< 1.3	$\times 10^{-6}$	CL=90%
Γ_{607}	$K^*(892)^+ e^- \mu^+$	LF	< 9.9	$\times 10^{-7}$	CL=90%
Γ_{608}	$K^*(892)^+ e^\pm \mu^\mp$	LF	< 1.4	$\times 10^{-6}$	CL=90%
Γ_{609}	$\pi^- e^+ e^+$	L	< 2.3	$\times 10^{-8}$	CL=90%
Γ_{610}	$\pi^- \mu^+ \mu^+$	L	< 4.0	$\times 10^{-9}$	CL=95%
Γ_{611}	$\pi^- e^+ \mu^+$	L	< 1.5	$\times 10^{-7}$	CL=90%
Γ_{612}	$\rho^- e^+ e^+$	L	< 1.7	$\times 10^{-7}$	CL=90%
Γ_{613}	$\rho^- \mu^+ \mu^+$	L	< 4.2	$\times 10^{-7}$	CL=90%
Γ_{614}	$\rho^- e^+ \mu^+$	L	< 4.7	$\times 10^{-7}$	CL=90%
Γ_{615}	$K^- e^+ e^+$	L	< 3.0	$\times 10^{-8}$	CL=90%
Γ_{616}	$K^- \mu^+ \mu^+$	L	< 4.1	$\times 10^{-8}$	CL=90%
Γ_{617}	$K^- e^+ \mu^+$	L	< 1.6	$\times 10^{-7}$	CL=90%
Γ_{618}	$K^*(892)^- e^+ e^+$	L	< 4.0	$\times 10^{-7}$	CL=90%
Γ_{619}	$K^*(892)^- \mu^+ \mu^+$	L	< 5.9	$\times 10^{-7}$	CL=90%
Γ_{620}	$K^*(892)^- e^+ \mu^+$	L	< 3.0	$\times 10^{-7}$	CL=90%
Γ_{621}	$D^- e^+ e^+$	L	< 2.6	$\times 10^{-6}$	CL=90%
Γ_{622}	$D^- e^+ \mu^+$	L	< 1.8	$\times 10^{-6}$	CL=90%
Γ_{623}	$D^- \mu^+ \mu^+$	L	< 6.9	$\times 10^{-7}$	CL=95%
Γ_{624}	$D^* \mu^+ \mu^+$	L	< 2.4	$\times 10^{-6}$	CL=95%
Γ_{625}	$D_s^- \mu^+ \mu^+$	L	< 5.8	$\times 10^{-7}$	CL=95%
Γ_{626}	$\bar{D}^0 \pi^- \mu^+ \mu^+$	L	< 1.5	$\times 10^{-6}$	CL=95%
Γ_{627}	$\Lambda^0 \mu^+$	L,B	< 6	$\times 10^{-8}$	CL=90%
Γ_{628}	$\Lambda^0 e^+$	L,B	< 3.2	$\times 10^{-8}$	CL=90%
Γ_{629}	$\bar{\Lambda}^0 \mu^+$	L,B	< 6	$\times 10^{-8}$	CL=90%
Γ_{630}	$\bar{\Lambda}^0 e^+$	L,B	< 8	$\times 10^{-8}$	CL=90%

- [a] An ℓ indicates an e or a μ mode, not a sum over these modes.
- [b] An $CP(\pm 1)$ indicates the $CP=+1$ and $CP=-1$ eigenstates of the D^0 - \bar{D}^0 system.
- [c] D denotes D^0 or \bar{D}^0 .
- [d] $D_{CP\pm}^0$ decays into $D^0 \pi^0$ with the D^0 reconstructed in CP -even eigenstates $K^+ K^-$ and $\pi^+ \pi^-$.
- [e] \bar{D}^{*} represents an excited state with mass $2.2 < M < 2.8$ GeV/c².
- [f] $\chi_{c1}(3872)^+$ is a hypothetical charged partner of the $\chi_{c1}(3872)$.

[g] $\Theta(1710)^{++}$ is a possible narrow pentaquark state and $G(2220)$ is a possible glueball resonance.
 [h] $(\bar{A}_c^- \rho)_s$ denotes a low-mass enhancement near 3.35 GeV/c².

CONSTRAINED FIT INFORMATION

An overall fit to 3 branching ratios uses 6 measurements and one constraint to determine 3 parameters. The overall fit has a $\chi^2 = 3.7$ for 4 degrees of freedom.

The following *off-diagonal* array elements are the correlation coefficients $\langle \delta x_i \delta x_j \rangle / (\delta x_i \delta x_j)$, in percent, from the fit to the branching fractions, $x_i \equiv \Gamma_i / \Gamma_{total}$. The fit constrains the x_i whose labels appear in this array to sum to one.

x_{407}	10
	$\times 346$

CONSTRAINED FIT INFORMATION

An overall fit to 18 branching ratios uses 58 measurements and one constraint to determine 12 parameters. The overall fit has a $\chi^2 = 64.2$ for 47 degrees of freedom.

The following *off-diagonal* array elements are the correlation coefficients $\langle \delta x_i \delta x_j \rangle / (\delta x_i \delta x_j)$, in percent, from the fit to the branching fractions, $x_i \equiv \Gamma_i / \Gamma_{total}$. The fit constrains the x_i whose labels appear in this array to sum to one.

x_8	33																				
x_{51}	0	0																			
x_{108}	0	0	7																		
x_{149}	0	0	1	13																	
x_{276}	0	0	0	0	0																
x_{281}	0	0	0	0	0	0															
x_{299}	0	0	0	0	0	0	86	0													
x_{311}	0	0	0	0	0	0	40	0	35												
x_{576}	0	0	0	0	0	0	14	0	12	6											
x_{583}	0	0	0	0	0	0	0	5	0	0	0										
	x_7	x_8	x_{51}	x_{108}	x_{149}	x_{276}	x_{281}	x_{299}	x_{311}	x_{576}											

B^+ BRANCHING RATIOS

$\Gamma(\ell^+ \nu_e X) / \Gamma_{total}$ Γ_1 / Γ
 "OUR EVALUATION" is an average using rescaled values of the data listed below. The average and rescaling were performed by the Heavy Flavor Averaging Group (HFLAV) and are described at <https://hflav.web.cern.ch/>. The averaging/rescaling procedure takes into account correlations between the measurements.

VALUE (units 10^{-2})	DOCUMENT ID	TECN	COMMENT
10.99 ± 0.28 OUR EVALUATION	Error includes scale factor of 1.1.		
11.17 ± 0.25 ± 0.28	¹ URQUIJO	07	BELL $e^+ e^- \rightarrow T(4S)$
10.28 ± 0.26 ± 0.39	² AUBERT,B	06Y	BABR $e^+ e^- \rightarrow T(4S)$
10.25 ± 0.57 ± 0.65	³ ARTUSO	97	CLE2 $e^+ e^- \rightarrow T(4S)$
••• We do not use the following data for averages, fits, limits, etc. •••			
11.15 ± 0.26 ± 0.41	⁴ OKABE	05	BELL Repl. by URQUIJO 07
10.1 ± 1.8 ± 1.5	ATHANAS	94	CLE2 Sup. by ARTUSO 97

- 1 URQUIJO 07 report a measurement of $(10.34 \pm 0.23 \pm 0.25)\%$ for the partial branching fraction of $B^+ \rightarrow e^+ \nu_e X_c$ decay with electron energy above 0.6 GeV. We converted the result to $B^+ \rightarrow e^+ \nu_e X$ branching fraction.
- 2 The measurements are obtained for charged and neutral B mesons partial rates of semi-leptonic decay to electrons with momentum above 0.6 GeV/c in the B rest frame. The best precision on the ratio is achieved for a momentum threshold of 1.0 GeV: $B(B^+ \rightarrow e^+ \nu_e X) / B(B^0 \rightarrow e^+ \nu_e X) = 1.074 \pm 0.041 \pm 0.026$.
- 3 ARTUSO 97 uses partial reconstruction of $B \rightarrow D^* \ell \nu_\ell$ and inclusive semileptonic branching ratio from BARISH 96b (0.1049 ± 0.0017 ± 0.0043).
- 4 The measurements are obtained for charged and neutral B mesons partial rates of semi-leptonic decay to electrons with momentum above 0.6 GeV/c in the B rest frame, and their ratio of $B(B^+ \rightarrow e^+ \nu_e X) / B(B^0 \rightarrow e^+ \nu_e X) = 1.08 \pm 0.05 \pm 0.02$.

$\Gamma(e^+ \nu_e X_c) / \Gamma_{total}$ Γ_2 / Γ

VALUE (units 10^{-2})	DOCUMENT ID	TECN	COMMENT
10.79 ± 0.25 ± 0.27	¹ URQUIJO	07	BELL $e^+ e^- \rightarrow T(4S)$
¹ Measure the independent B^+ and B^0 partial branching fractions with electron threshold energies of 0.4 GeV.			

$\Gamma(\ell^+ \nu_\ell X_u) / \Gamma_{total}$ Γ_3 / Γ

Requires $E_\ell^* > 1$ GeV, where E_ℓ^* is lepton energy in B rest frame.

VALUE (units 10^{-3})	DOCUMENT ID	TECN	COMMENT
1.65 ± 0.10 ± 0.18	¹ CAO	21A	BELL $e^+ e^- \rightarrow T(4S)$
¹ The correlation of 50% with $B(B^0 \rightarrow \ell^+ \nu_\ell X_u)$ (lepton energy in B rest frame $E_\ell^* > 1$ GeV) was reported.			

$\Gamma(\overline{D}^0 \ell^+ \nu_\ell)/\Gamma_{\text{total}}$ Γ_5/Γ
 "OUR EVALUATION" is an average using rescaled values of the data listed below. The average and rescaling were performed by the Heavy Flavor Averaging Group (HFLAV) and are described at <https://hflav.web.cern.ch/>. The averaging/rescaling procedure takes into account correlations between the measurements. $\ell = e$ or μ , not sum over e and μ modes.

VALUE (%) DOCUMENT ID TECN COMMENT
2.30 ± 0.09 OUR EVALUATION
2.29 ± 0.08 OUR AVERAGE

2.29 ± 0.08 ± 0.09	¹ AUBERT	10	BABR	$e^+e^- \rightarrow \Upsilon(4S)$
2.34 ± 0.03 ± 0.13	AUBERT	09A	BABR	$e^+e^- \rightarrow \Upsilon(4S)$
2.21 ± 0.13 ± 0.19	² BARTELT	99	CLE2	$e^+e^- \rightarrow \Upsilon(4S)$
1.6 ± 0.6 ± 0.3	³ FULTON	91	CLEO	$e^+e^- \rightarrow \Upsilon(4S)$
2.33 ± 0.09 ± 0.09	¹ AUBERT	08Q	BABR	Repl. by AUBERT 09A
1.94 ± 0.15 ± 0.34	⁴ ATHANAS	97	CLE2	Repl. by BARTELT 99

- ¹ Uses a fully reconstructed B meson as a tag on the recoil side.
- ² Assumes equal production of B^+ and B^0 at the $\Upsilon(4S)$.
- ³ FULTON 91 assumes equal production of $B^0\overline{B}^0$ and B^+B^- at the $\Upsilon(4S)$.
- ⁴ ATHANAS 97 uses missing energy and missing momentum to reconstruct neutrino.

$\Gamma(\overline{D}^0 \ell^+ \nu_\ell)/\Gamma(\ell^+ \nu_\ell X)$ Γ_5/Γ_1

VALUE	DOCUMENT ID	TECN	COMMENT	χ^2	
0.255 ± 0.009 ± 0.009	¹ AUBERT	10	BABR	$e^+e^- \rightarrow \Upsilon(4S)$	0.8
					0.0
					3.7
					4.5

- ¹ Uses a fully reconstructed B meson on the recoil side.

$\Gamma(\overline{D}^0 \ell^+ \nu_\ell)/\Gamma(D \ell^+ \nu_\ell X)$ Γ_5/Γ_4

VALUE	DOCUMENT ID	TECN	COMMENT
0.230 ± 0.020 OUR AVERAGE			
0.25 ± 0.06	¹ AAJ	19AC	LHCB pp at 7 and 8 TeV
0.227 ± 0.014 ± 0.016	² AUBERT	07AN	BABR $e^+e^- \rightarrow \Upsilon(4S)$

- ¹ The relative branching fractions of $B^- \rightarrow D^0, D^{*0}, D^{*0}$ in the $B^- \rightarrow D^0 X \mu^- \overline{\nu}$ channel are determined by fitting the distribution of the missing mass in $\overline{B}_s^{*0} \rightarrow B^- K^+$ decays.
- ² Uses a fully reconstructed B meson on the recoil side.

$\Gamma(\overline{D}^0 \tau^+ \nu_\tau)/\Gamma_{\text{total}}$ Γ_6/Γ

VALUE (units 10^{-2})	DOCUMENT ID	TECN	COMMENT
0.77 ± 0.22 ± 0.12	¹ BOZEK	10	BELL $e^+e^- \rightarrow \Upsilon(4S)$

- ¹ We do not use the following data for averages, fits, limits, etc. ●●●
- 0.67 ± 0.37 ± 0.13 ² AUBERT 08N BABR Repl. by AUBERT 09s
- ¹ Assumes equal production of B^+ and B^0 at the $\Upsilon(4S)$.
- ² Uses a fully reconstructed B meson as a tag on the recoil side.

$\Gamma(\overline{D}^0 \tau^+ \nu_\tau)/\Gamma(\overline{D}^0 \ell^+ \nu_\ell)$ Γ_6/Γ_5

VALUE	DOCUMENT ID	TECN	COMMENT
0.429 ± 0.082 ± 0.052	^{1,2} LEES	12D	BABR $e^+e^- \rightarrow \Upsilon(4S)$

- ¹ We do not use the following data for averages, fits, limits, etc. ●●●
- 0.314 ± 0.170 ± 0.049 ¹ AUBERT 09s BABR Repl. by LEES 12D
- ¹ Uses a fully reconstructed B meson as a tag on the recoil side.
- ² Uses $\tau^+ \rightarrow e^+ \nu_e \overline{\nu}_\tau$ and $\tau^+ \rightarrow \mu^+ \nu_\mu \overline{\nu}_\tau$ and e^+ or μ^+ as ℓ^+ .

$\Gamma(\overline{D}^*(2007)^0 \ell^+ \nu_\ell)/\Gamma_{\text{total}}$ Γ_7/Γ

"OUR EVALUATION" is an average using rescaled values of the data listed below. The average and rescaling were performed by the Heavy Flavor Averaging Group (HFLAV) and are described at <https://hflav.web.cern.ch/>. The averaging/rescaling procedure takes into account correlations between the measurements. $\ell = e$ or μ , not sum over e and μ modes.

VALUE (%) EVTS DOCUMENT ID TECN COMMENT
5.58 ± 0.22 OUR EVALUATION
5.60 ± 0.26 OUR FIT Error includes scale factor of 1.5.
5.58 ± 0.26 OUR AVERAGE Error includes scale factor of 1.5. See the ideogram below.

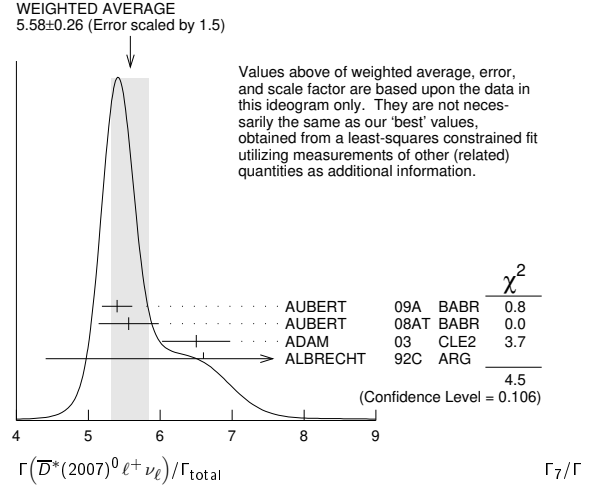
5.40 ± 0.02 ± 0.21	AUBERT	09A	BABR	$e^+e^- \rightarrow \Upsilon(4S)$
5.56 ± 0.08 ± 0.41	¹ AUBERT	08AT	BABR	$e^+e^- \rightarrow \Upsilon(4S)$
6.50 ± 0.20 ± 0.43	² ADAM	03	CLE2	$e^+e^- \rightarrow \Upsilon(4S)$
6.6 ± 1.6 ± 1.5	³ ALBRECHT	92C	ARG	$e^+e^- \rightarrow \Upsilon(4S)$
5.83 ± 0.15 ± 0.30	⁴ AUBERT	08Q	BABR	Repl. by AUBERT 09A
6.50 ± 0.20 ± 0.43	⁵ BRIERE	02	CLE2	$e^+e^- \rightarrow \Upsilon(4S)$
5.13 ± 0.54 ± 0.64	⁶ BARISH	95	CLE2	Repl. by ADAM 03
seen	⁷ SANGHERA	93	CLE2	$e^+e^- \rightarrow \Upsilon(4S)$
4.1 ± 0.8 ± 0.8	⁸ FULTON	91	CLEO	$e^+e^- \rightarrow \Upsilon(4S)$
7.0 ± 1.8 ± 1.4	⁹ ANTREASYAN	90B	CBAL	$e^+e^- \rightarrow \Upsilon(4S)$

- ¹ Measured using the dependence of $B^- \rightarrow D^{*0} e^- \overline{\nu}_e$ decay differential rate and the form factor description by CAPRINI 98.
- ² Simultaneous measurements of both $B^0 \rightarrow D^{*0}(2010)^- \ell \nu$ and $B^+ \rightarrow \overline{D}^*(2007)^0 \ell \nu$.
- ³ ALBRECHT 92C reports $0.058 \pm 0.014 \pm 0.013$. We rescale using the method described in STONE 94 but with the updated PDG 94 $B(D^0 \rightarrow K^- \pi^+)$. Assumes equal production of $B^0\overline{B}^0$ and B^+B^- at the $\Upsilon(4S)$.
- ⁴ Uses a fully reconstructed B meson as a tag on the recoil side.
- ⁵ The results are based on the same analysis and data sample reported in ADAM 03.
- ⁶ BARISH 95 use $B(D^0 \rightarrow K^- \pi^+) = (3.91 \pm 0.08 \pm 0.17)\%$ and $B(D^{*0} \rightarrow D^0 \pi^0) = (63.6 \pm 2.3 \pm 3.3)\%$.

⁷ Combining $\overline{D}^{*0} \ell^+ \nu_\ell$ and $\overline{D}^{*-} \ell^+ \nu_\ell$ SANGHERA 93 test $V-A$ structure and fit the decay angular distributions to obtain $A_{FB} = 3/4 * (\Gamma^- - \Gamma^+)/\Gamma = 0.14 \pm 0.06 \pm 0.03$. Assuming a value of V_{cb} , they measure $V, A_1,$ and A_2 , the three form factors for the $D^* \ell \nu_\ell$ decay, where results are slightly dependent on model assumptions.

⁸ Assumes equal production of $B^0\overline{B}^0$ and B^+B^- at the $\Upsilon(4S)$. Uncorrected for D and D^* branching ratio assumptions.

⁹ ANTREASYAN 90B is average over B and $\overline{D}^*(2010)$ charge states.



$\Gamma(\overline{D}^*(2007)^0 \ell^+ \nu_\ell)/\Gamma(D \ell^+ \nu_\ell X)$ Γ_7/Γ_4

VALUE	DOCUMENT ID	TECN	COMMENT
0.582 ± 0.018 ± 0.030	¹ AUBERT	07AN	BABR $e^+e^- \rightarrow \Upsilon(4S)$

- ¹ Uses a fully reconstructed B meson on the recoil side.

$\Gamma(\overline{D}^*(2007)^0 \tau^+ \nu_\tau)/\Gamma_{\text{total}}$ Γ_8/Γ

VALUE (units 10^{-2})	DOCUMENT ID	TECN	COMMENT
1.88 ± 0.20 OUR FIT			
2.12 ± 0.28 ± 0.29	¹ BOZEK	10	BELL $e^+e^- \rightarrow \Upsilon(4S)$

- ¹ We do not use the following data for averages, fits, limits, etc. ●●●
- 2.25 ± 0.48 ± 0.28 ² AUBERT 08N BABR Repl. by AUBERT 09s
- ¹ Assumes equal production of B^+ and B^0 at the $\Upsilon(4S)$.
- ² Uses a fully reconstructed B meson as a tag on the recoil side.

$\Gamma(\overline{D}^*(2007)^0 \tau^+ \nu_\tau)/\Gamma(\overline{D}^*(2007)^0 \ell^+ \nu_\ell)$ Γ_8/Γ_7

VALUE	DOCUMENT ID	TECN	COMMENT
0.335 ± 0.034 OUR FIT			
0.322 ± 0.032 ± 0.022	^{1,2} LEES	12D	BABR $e^+e^- \rightarrow \Upsilon(4S)$

- ¹ We do not use the following data for averages, fits, limits, etc. ●●●
- 0.346 ± 0.073 ± 0.034 ¹ AUBERT 09s BABR Repl. by LEES 12D
- ¹ Uses a fully reconstructed B meson as a tag on the recoil side.
- ² Uses $\tau^+ \rightarrow e^+ \nu_e \overline{\nu}_\tau$ and $\tau^+ \rightarrow \mu^+ \nu_\mu \overline{\nu}_\tau$ and e^+ or μ^+ as ℓ^+ .

$\Gamma(D^- \pi^+ \ell^+ \nu_\ell)/\Gamma_{\text{total}}$ Γ_9/Γ

VALUE (units 10^{-3})	DOCUMENT ID	TECN	COMMENT
4.4 ± 0.4 OUR AVERAGE			
4.55 ± 0.27 ± 0.39	VOSSEN	18	BELL $e^+e^- \rightarrow \Upsilon(4S)$

- 4.2 ± 0.6 ± 0.3 ¹ AUBERT 08Q BABR $e^+e^- \rightarrow \Upsilon(4S)$
- ¹ We do not use the following data for averages, fits, limits, etc. ●●●
- 4.3 ± 0.6 ± 0.2 ^{1,2} LIVENTSEV 08 BELL Repl. by VOSSEN 18
- 5.6 ± 1.0 ± 0.2 ³ LIVENTSEV 05 BELL Repl. by LIVENTSEV 08

- ¹ Uses a fully reconstructed B meson as a tag on the recoil side.
- ² LIVENTSEV 08 reports $(4.0 \pm 0.4 \pm 0.6) \times 10^{-3}$ from a measurement of $[\Gamma(B^+ \rightarrow D^- \pi^+ \ell^+ \nu_\ell)/\Gamma_{\text{total}}] / [B(B^+ \rightarrow \overline{D}^0 \ell^+ \nu_\ell)]$ assuming $B(B^+ \rightarrow \overline{D}^0 \ell^+ \nu_\ell) = (2.15 \pm 0.22) \times 10^{-2}$, which we rescale to our best value $B(B^+ \rightarrow \overline{D}^0 \ell^+ \nu_\ell) = (2.30 \pm 0.09) \times 10^{-2}$. Our first error is their experiment's error and our second error is the systematic error from using our best value.
- ³ LIVENTSEV 05 reports $[\Gamma(B^+ \rightarrow D^- \pi^+ \ell^+ \nu_\ell)/\Gamma_{\text{total}}] / [B(B^0 \rightarrow D^- \ell^+ \nu_\ell)] = 0.25 \pm 0.03 \pm 0.03$ which we multiply by our best value $B(B^0 \rightarrow D^- \ell^+ \nu_\ell) = (2.24 \pm 0.09) \times 10^{-2}$. Our first error is their experiment's error and our second error is the systematic error from using our best value.

$\Gamma(\overline{D}_s^*(2420)^0 \ell^+ \nu_\ell, \overline{D}_s^{*0} \rightarrow D^- \pi^+)/\Gamma_{\text{total}}$ Γ_{10}/Γ

VALUE (units 10^{-3})	DOCUMENT ID	TECN	COMMENT
2.5 ± 0.5 OUR AVERAGE			
2.6 ± 0.5 ± 0.4	¹ AUBERT	08BL	BABR $e^+e^- \rightarrow \Upsilon(4S)$

- 2.4 ± 0.4 ± 0.6 ¹ LIVENTSEV 08 BELL $e^+e^- \rightarrow \Upsilon(4S)$
- ¹ Uses a fully reconstructed B meson as a tag on the recoil side.

Meson Particle Listings

 B^\pm $\Gamma(\bar{D}_2^*(2460)^0 \ell^+ \nu_\ell, \bar{D}_2^{*0} \rightarrow D^- \pi^+) / \Gamma_{\text{total}}$ Γ_{11} / Γ

VALUE (units 10^{-3})	DOCUMENT ID	TECN	COMMENT
1.53 ± 0.16 OUR AVERAGE			
1.42 ± 0.15 ± 0.15	¹ AUBERT	09Y BABR	$e^+ e^- \rightarrow \Upsilon(4S)$
1.5 ± 0.2 ± 0.2	² AUBERT	08BL BABR	$e^+ e^- \rightarrow \Upsilon(4S)$
2.2 ± 0.3 ± 0.4	² LIVENTSEV	08 BELL	$e^+ e^- \rightarrow \Upsilon(4S)$

¹ Uses a simultaneous fit of all B semileptonic decays without full reconstruction of events. AUBERT 09Y reports $B(B^+ \rightarrow \bar{D}_2^*(2460)^0 \ell^+ \nu_\ell) \cdot B(\bar{D}_2^*(2460)^0 \rightarrow D^{(*)-} \pi^+) = (2.29 \pm 0.23 \pm 0.21) \times 10^{-3}$ and the authors have provided us the individual measurement.

² Uses a fully reconstructed B meson as a tag on the recoil side.

 $\Gamma(D^{(*)-} n \pi \ell^+ \nu_\ell (n \geq 1)) / \Gamma(D \ell^+ \nu_\ell X)$ Γ_{12} / Γ_4

VALUE	DOCUMENT ID	TECN	COMMENT
0.193 ± 0.022 OUR AVERAGE			
0.21 ± 0.07	^{1,2} AAIJ	19AC LHCB	pp at 7 and 8 TeV
0.191 ± 0.013 ± 0.019	³ AUBERT	07AN BABR	$e^+ e^- \rightarrow \Upsilon(4S)$

¹ The relative branching fractions of $B^- \rightarrow D^0, D^{*0}, D^{*0}$ in the $B^- \rightarrow D^0 X \mu^- \bar{\nu}$ channel are determined by fitting the distribution of the missing mass in $\bar{B}_s^{*0} \rightarrow B^- K^+$ decays.

² In this measurement of $f_{D^{*0}} = B(B^- \rightarrow (D^{*0} \rightarrow D^0 X) \mu^- \bar{\nu}) / B(B^- \rightarrow D^0 X \mu^- \bar{\nu})$, D^{*0} refers collectively to L = 1 states $D_0^*(2400), D_1(2420), D_1(2430)$, and $D_2^*(2460)$, as well as other resonances such as radially excited D mesons, and to nonresonant contributions with additional pions.

³ Uses a fully reconstructed B meson on the recoil side.

 $\Gamma(D^{*-} \pi^+ \ell^+ \nu_\ell) / \Gamma_{\text{total}}$ Γ_{13} / Γ

VALUE (units 10^{-3})	DOCUMENT ID	TECN	COMMENT
6.0 ± 0.4 OUR AVERAGE			
6.03 ± 0.43 ± 0.38		VOSSEN	18 BELL $e^+ e^- \rightarrow \Upsilon(4S)$
5.9 ± 0.5 ± 0.4	¹ AUBERT	08Q BABR	$e^+ e^- \rightarrow \Upsilon(4S)$
6.8 ± 1.1 ± 0.3	^{1,2} LIVENTSEV	08 BELL	Repl. by VOSSEN 18
6.0 ± 1.4 ± 0.1	^{3,4} LIVENTSEV	05 BELL	Repl. by LIVENTSEV 08

¹ Uses a fully reconstructed B meson as a tag on the recoil side.

² LIVENTSEV 08 reports $(6.4 \pm 0.8 \pm 0.9) \times 10^{-3}$ from a measurement of $[\Gamma(B^+ \rightarrow D^{*-} \pi^+ \ell^+ \nu_\ell) / \Gamma_{\text{total}}] / [B(B^+ \rightarrow \bar{D}^0 \ell^+ \nu_\ell)]$ assuming $B(B^+ \rightarrow \bar{D}^0 \ell^+ \nu_\ell) = (2.15 \pm 0.22) \times 10^{-2}$, which we rescale to our best value $B(B^+ \rightarrow \bar{D}^0 \ell^+ \nu_\ell) = (2.30 \pm 0.09) \times 10^{-2}$. Our first error is their experiment's error and our second error is the systematic error from using our best value.

³ Excludes D^{*+} contribution to D modes.

⁴ LIVENTSEV 05 reports $[\Gamma(B^+ \rightarrow D^{*-} \pi^+ \ell^+ \nu_\ell) / \Gamma_{\text{total}}] / [B(B^0 \rightarrow D^*(2010)^- \ell^+ \nu_\ell)] = 0.12 \pm 0.02 \pm 0.02$ which we multiply by our best value $B(B^0 \rightarrow D^*(2010)^- \ell^+ \nu_\ell) = (4.97 \pm 0.12) \times 10^{-2}$. Our first error is their experiment's error and our second error is the systematic error from using our best value.

 $\Gamma(\bar{D}_1(2420)^0 \ell^+ \nu_\ell, \bar{D}_1^0 \rightarrow D^{*-} \pi^+) / \Gamma_{\text{total}}$ Γ_{14} / Γ

VALUE (units 10^{-3})	DOCUMENT ID	TECN	COMMENT
3.03 ± 0.20 OUR AVERAGE			
2.97 ± 0.17 ± 0.17	¹ AUBERT	09Y BABR	$e^+ e^- \rightarrow \Upsilon(4S)$
2.9 ± 0.3 ± 0.3	² AUBERT	08BL BABR	$e^+ e^- \rightarrow \Upsilon(4S)$
4.2 ± 0.7 ± 0.7	² LIVENTSEV	08 BELL	$e^+ e^- \rightarrow \Upsilon(4S)$
3.73 ± 0.85 ± 0.57	³ ANASTASSOV	98 CLE2	$e^+ e^- \rightarrow \Upsilon(4S)$

¹ Uses a simultaneous measurement of all B semileptonic decays without full reconstruction of events.

² Uses a fully reconstructed B meson as a tag on the recoil side.

³ Assumes equal production of B^+ and B^0 at the $\Upsilon(4S)$.

 $\Gamma(\bar{D}_1^*(2430)^0 \ell^+ \nu_\ell, \bar{D}_1^{*0} \rightarrow D^{*-} \pi^+) / \Gamma_{\text{total}}$ Γ_{15} / Γ

VALUE (units 10^{-3})	CL%	DOCUMENT ID	TECN	COMMENT
2.7 ± 0.4 ± 0.5		¹ AUBERT	08BL BABR	$e^+ e^- \rightarrow \Upsilon(4S)$
<0.7	90	¹ LIVENTSEV	08 BELL	$e^+ e^- \rightarrow \Upsilon(4S)$

¹ Uses a fully reconstructed B meson as a tag on the recoil side.

 $\Gamma(\bar{D}_2^*(2460)^0 \ell^+ \nu_\ell, \bar{D}_2^{*0} \rightarrow D^{*-} \pi^+) / \Gamma_{\text{total}}$ Γ_{16} / Γ

VALUE (units 10^{-3})	CL%	DOCUMENT ID	TECN	COMMENT
1.01 ± 0.24 OUR AVERAGE	Error includes scale factor of 2.0.			
0.87 ± 0.11 ± 0.07		¹ AUBERT	09Y BABR	$e^+ e^- \rightarrow \Upsilon(4S)$
1.5 ± 0.2 ± 0.2		² AUBERT	08BL BABR	$e^+ e^- \rightarrow \Upsilon(4S)$
1.8 ± 0.6 ± 0.3		² LIVENTSEV	08 BELL	$e^+ e^- \rightarrow \Upsilon(4S)$
<1.6	90	³ ANASTASSOV	98 CLE2	$e^+ e^- \rightarrow \Upsilon(4S)$

¹ Uses a simultaneous fit of all B semileptonic decays without full reconstruction of events. AUBERT 09Y reports $B(B^+ \rightarrow \bar{D}_2^*(2460)^0 \ell^+ \nu_\ell) \cdot B(\bar{D}_2^*(2460)^0 \rightarrow D^{(*)-} \pi^+) = (2.29 \pm 0.23 \pm 0.21) \times 10^{-3}$ and the authors have provided us the individual measurement.

² Uses a fully reconstructed B meson as a tag on the recoil side.

³ Assumes equal production of B^+ and B^0 at the $\Upsilon(4S)$.

 $\Gamma(\bar{D}^0 \pi^+ \pi^- \ell^+ \nu_\ell) / \Gamma(\bar{D}^0 \ell^+ \nu_\ell)$ Γ_{17} / Γ_5

VALUE (units 10^{-2})	DOCUMENT ID	TECN	COMMENT
7.1 ± 1.3 ± 0.8	¹ LEES	16 BABR	$e^+ e^- \rightarrow \Upsilon(4S)$

¹ Measurement used electrons and muons as leptons.

 $\Gamma(\bar{D}^{*0} \pi^+ \pi^- \ell^+ \nu_\ell) / \Gamma(\bar{D}^{*0} \ell^+ \nu_\ell)$ Γ_{18} / Γ_7

VALUE (units 10^{-2})	DOCUMENT ID	TECN	COMMENT
1.4 ± 0.7 ± 0.4	¹ LEES	16 BABR	$e^+ e^- \rightarrow \Upsilon(4S)$

¹ Measurement used electrons and muons as leptons.

 $\Gamma(D_s^{(*)-} K^+ \ell^+ \nu_\ell) / \Gamma_{\text{total}}$ Γ_{19} / Γ

VALUE (units 10^{-4})	DOCUMENT ID	TECN	COMMENT
6.1 ± 1.0 OUR AVERAGE			
5.9 ± 1.2 ± 1.5	¹ STYPULA	12 BELL	$e^+ e^- \rightarrow \Upsilon(4S)$
6.13 $^{+1.04}_{-1.03} \pm 0.67$	¹ DEL-AMO-SA..11L	BABR	$e^+ e^- \rightarrow \Upsilon(4S)$

¹ Assumes equal production of B^+ and B^0 at the $\Upsilon(4S)$.

 $\Gamma(D_s^- K^+ \ell^+ \nu_\ell) / \Gamma_{\text{total}}$ Γ_{20} / Γ

VALUE (units 10^{-4})	DOCUMENT ID	TECN	COMMENT
3.0 ± 0.9 $^{+1.1}_{-0.8}$	¹ STYPULA	12 BELL	$e^+ e^- \rightarrow \Upsilon(4S)$

¹ Assumes equal production of B^+ and B^0 at the $\Upsilon(4S)$.

 $\Gamma(D_s^{*-} K^+ \ell^+ \nu_\ell) / \Gamma_{\text{total}}$ Γ_{21} / Γ

VALUE (units 10^{-4})	DOCUMENT ID	TECN	COMMENT
2.9 ± 1.6 $^{+1.1}_{-1.0}$	^{1,2} STYPULA	12 BELL	$e^+ e^- \rightarrow \Upsilon(4S)$

¹ Assumes equal production of B^+ and B^0 at the $\Upsilon(4S)$.

² STYPULA 12 provides also an upper limit of 0.56×10^{-3} at 90% CL for the same data. Also measures branching fraction of the combined modes of $D_s^- K^+ \ell^+ \nu_\ell$ and $D_s^{*-} K^+ \ell^+ \nu_\ell$ as $B(B^+ \rightarrow D_s^{*-} K^+ \ell^+ \nu_\ell) = (5.9 \pm 1.2 \pm 1.5) \times 10^{-4}$.

 $\Gamma(\pi^0 \ell^+ \nu_\ell) / \Gamma_{\text{total}}$ Γ_{22} / Γ

"OUR EVALUATION" is an average using rescaled values of the data listed below. The average and rescaling were performed by the Heavy Flavor Averaging Group (HFLAV) and are described at <https://hflav.web.cern.ch/>. The averaging/rescaling procedure takes into account correlations between the measurements.

VALUE (units 10^{-4})	DOCUMENT ID	TECN	COMMENT
0.780 ± 0.027 OUR EVALUATION			
0.748 ± 0.029 OUR AVERAGE			
0.80 ± 0.08 ± 0.04	¹ SIBIDANOV	13 BELL	$e^+ e^- \rightarrow \Upsilon(4S)$
0.77 ± 0.04 ± 0.03	² LEES	12AA BABR	$e^+ e^- \rightarrow \Upsilon(4S)$
0.705 ± 0.025 ± 0.035	³ DEL-AMO-SA..11C	BABR	$e^+ e^- \rightarrow \Upsilon(4S)$
0.82 ± 0.09 ± 0.05	³ AUBERT	08AV BABR	$e^+ e^- \rightarrow \Upsilon(4S)$
0.77 ± 0.14 ± 0.08	⁴ HOKUUE	07 BELL	$e^+ e^- \rightarrow \Upsilon(4S)$
0.74 ± 0.05 ± 0.10	⁵ AUBERT,B	05o BABR	Repl. by DEL-AMO-SANCHEZ 11c

¹ The signal events are tagged by a second B meson reconstructed in the fully hadronic decays.

² Uses loose neutrino reconstruction technique. Assumes $B(Y(4S) \rightarrow B^+ B^-) = (51.6 \pm 0.6)\%$ and $B(Y(4S) \rightarrow B^0 \bar{B}^0) = (48.4 \pm 0.6)\%$.

³ Using the isospin symmetry relation, B^+ and B^0 branching fractions are combined.

⁴ The signal events are tagged by a second B meson reconstructed in the semileptonic mode $B \rightarrow D^{(*)} \ell \nu_\ell$.

⁵ B^+ and B^0 decays combined assuming isospin symmetry. Systematic errors include both experimental and form-factor uncertainties.

 $\Gamma(\pi^0 e^+ \nu_e) / \Gamma_{\text{total}}$ Γ_{23} / Γ

VALUE (units 10^{-4})	CL%	DOCUMENT ID	TECN	COMMENT
0.9 ± 0.2 ± 0.2		¹ ALEXANDER	96T CLE2	$e^+ e^- \rightarrow \Upsilon(4S)$
<22	90	ANTREASYSAN 90B	CBAL	$e^+ e^- \rightarrow \Upsilon(4S)$

¹ Derived based in the reported B^0 result by assuming isospin symmetry: $\Gamma(B^0 \rightarrow \pi^- \ell^+ \nu) = 2\Gamma(B^+ \rightarrow \pi^0 \ell^+ \nu)$.

 $\Gamma(\eta \ell^+ \nu_\ell) / \Gamma_{\text{total}}$ Γ_{24} / Γ

VALUE (units 10^{-4})	CL%	DOCUMENT ID	TECN	COMMENT
0.39 ± 0.05 OUR AVERAGE				
0.42 ± 0.11 ± 0.03		¹ BELENO	17 BELL	$e^+ e^- \rightarrow \Upsilon(4S)$
0.38 ± 0.05 ± 0.05		² LEES	12AA BABR	$e^+ e^- \rightarrow \Upsilon(4S)$
0.31 ± 0.06 ± 0.08		² AUBERT	09Q BABR	$e^+ e^- \rightarrow \Upsilon(4S)$
0.64 ± 0.20 ± 0.03		³ AUBERT	08AV BABR	$e^+ e^- \rightarrow \Upsilon(4S)$
0.36 ± 0.05 ± 0.04		² DEL-AMO-SA..11F	BABR	Repl. by LEES 12AA
<1.01	90	⁴ ADAM	07 CLE2	$e^+ e^- \rightarrow \Upsilon(4S)$
0.84 ± 0.31 ± 0.18		⁵ ATHAR	03 CLE2	Repl. by ADAM 07

¹ Uses missing-mass technique by fully reconstructing the hadronic decay chain of the accompanying B .

² Uses loose neutrino reconstruction technique. Assumes $B(\Upsilon(4S) \rightarrow B^+ B^-) = (51.6 \pm 0.6)\%$ and $B(\Upsilon(4S) \rightarrow B^0 \bar{B}^0) = (48.4 \pm 0.6)\%$.

³ Assumes equal production of B⁺ and B⁰ at the T(4S).
⁴ The B⁰ and B⁺ results are combined assuming the isospin, B lifetimes, and relative charged/neutral B production at the T(4S).
⁵ ATHAR 03 reports systematic errors 0.16 ± 0.09, which are experimental systematic and systematic due to model dependence. We combine these in quadrature.

$\Gamma(\eta^{\prime} \ell^+ \nu_{\ell})/\Gamma_{\text{total}}$		Γ_{25}/Γ		
VALUE (units 10 ⁻⁴)	CL%	DOCUMENT ID	TECN	COMMENT
0.23 ± 0.08 OUR AVERAGE				
0.24 ± 0.08 ± 0.03		1 LEES	12AA	BABR e ⁺ e ⁻ → T(4S)
0.04 ± 0.22 ^{+0.05} _{-0.02}		2 AUBERT	08AV	BABR e ⁺ e ⁻ → T(4S)
2.66 ± 0.80 ± 0.56		3 ADAM	07	CLE2 e ⁺ e ⁻ → T(4S)
• • • We do not use the following data for averages, fits, limits, etc. • • •				
<0.72	90	4 BELENO	17	BELL e ⁺ e ⁻ → T(4S)
0.24 ± 0.08 ± 0.03		1 DEL-AMO-SA..11F	BABR	Repl. by LEES 12AA

¹ Uses loose neutrino reconstruction technique. Assumes B(Y(4S) → B⁺B⁻) = (51.6 ± 0.6)% and B(Y(4S) → B⁰B⁰) = (48.4 ± 0.6)%.
² Assumes equal production of B⁺ and B⁰ at the T(4S).
³ The B⁰ and B⁺ results are combined assuming the isospin, B lifetimes, and relative charged/neutral B production at the T(4S). Corresponds to 90% CL interval (1.20–4.46) × 10⁻⁴.
⁴ Uses missing-mass technique by fully reconstructing the hadronic decay chain of the accompanying B.

$\Gamma(\omega \ell^+ \nu_{\ell})/\Gamma_{\text{total}}$		Γ_{26}/Γ		
VALUE (units 10 ⁻⁴)	CL%	DOCUMENT ID	TECN	COMMENT
1.19 ± 0.09 OUR AVERAGE				
1.21 ± 0.14 ± 0.08		1,2 LEES	13A	BABR e ⁺ e ⁻ → T(4S)
1.35 ± 0.21 ± 0.11		3 LEES	13T	BABR e ⁺ e ⁻ → T(4S)
1.07 ± 0.16 ± 0.07		4 SIBIDANOV	13	BELL e ⁺ e ⁻ → T(4S)
1.19 ± 0.16 ± 0.09		2,5 LEES	12AA	BABR e ⁺ e ⁻ → T(4S)
1.3 ± 0.4 ± 0.4		6 SCHWANDA	04	BELL e ⁺ e ⁻ → T(4S)
• • • We do not use the following data for averages, fits, limits, etc. • • •				
1.14 ± 0.16 ± 0.08		2 AUBERT	09Q	BABR Repl. by LEES 13A
<2.1	90	7 BEAN	93B	CLE2 e ⁺ e ⁻ → T(4S)

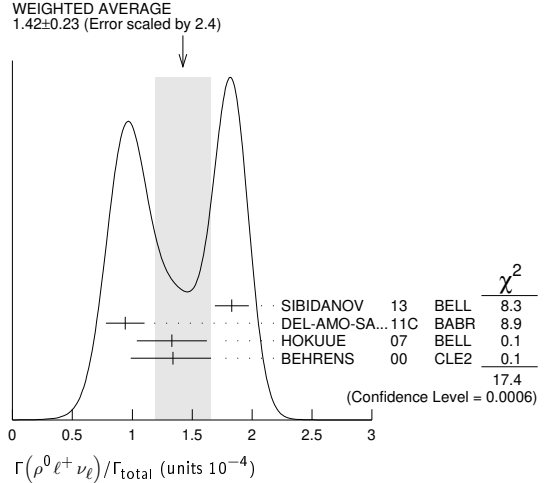
¹ LEES 13A reports (1.21 ± 0.14 ± 0.08) × 10⁻⁴ from a measurement of [Γ(B⁺ → ωℓ⁺ν_ℓ)/Γ_{total}] × [B(ω(782) → π⁺π⁻π⁰)] assuming B(ω(782) → π⁺π⁻π⁰) = (89.2 ± 0.7) × 10⁻².
² Uses B(T(4S) → B⁺B⁻) = (51.6 ± 0.6)% and B(T(4S) → B⁰B⁰) = (48.4 ± 0.6)%.
³ Uses semileptonic tagging. Assumes B(ω → π⁺π⁻π⁰) = (89.2 ± 0.7)% and that the production ratio of B⁺B⁻ to B⁰B⁰ from T(4S) is 1.056 ± 0.028. The partial branching fractions in three bins of q² are also reported.
⁴ The signal events are tagged by a second B meson reconstructed in the fully hadronic decays.
⁵ Uses loose neutrino reconstruction technique.
⁶ Assumes equal production of B⁺ and B⁰ at the T(4S).
⁷ BEAN 93B limit set using ISGW Model. Using isospin and the quark model to combine Γ(ρ⁰ℓ⁺ν_ℓ) and Γ(ρ⁻ℓ⁺ν_ℓ) with this result, they obtain a limit <(1.6–2.7) × 10⁻⁴ at 90% CL for B⁺ → ωℓ⁺ν_ℓ. The range corresponds to the ISGW, WSB, and KS models. An upper limit on |V_{ub}/V_{cb}| < 0.8–0.13 at 90% CL is derived as well.

$\Gamma(\omega \mu^+ \nu_{\mu})/\Gamma_{\text{total}}$		Γ_{27}/Γ		
VALUE	CL%	DOCUMENT ID	TECN	COMMENT
• • • We do not use the following data for averages, fits, limits, etc. • • •				
seen		1 ALBRECHT	91c	ARG

¹ In ALBRECHT 91c, one event is fully reconstructed providing evidence for the b → u transition.

$\Gamma(\rho^0 \ell^+ \nu_{\ell})/\Gamma_{\text{total}}$		Γ_{28}/Γ		
VALUE (units 10 ⁻⁴)	CL%	DOCUMENT ID	TECN	COMMENT
1.58 ± 0.11 OUR EVALUATION				
Error includes scale factor of 2.4. See the ideogram below.				
1.42 ± 0.23 OUR AVERAGE				
1.83 ± 0.10 ± 0.10		1 SIBIDANOV	13	BELL e ⁺ e ⁻ → T(4S)
0.94 ± 0.08 ± 0.14		2 DEL-AMO-SA..11c	BABR	e ⁺ e ⁻ → T(4S)
1.33 ± 0.23 ± 0.18		3 HOKUUE	07	BELL e ⁺ e ⁻ → T(4S)
1.34 ± 0.15 ± 0.28 _{-0.32}		4 BEHRENS	00	CLE2 e ⁺ e ⁻ → T(4S)
• • • We do not use the following data for averages, fits, limits, etc. • • •				
1.16 ± 0.11 ± 0.30		2 AUBERT,B	05o	BABR Repl. by DEL-AMO-SANCHEZ 11c
1.40 ± 0.21 ± 0.32 _{-0.33}		4 BEHRENS	00	CLE2 e ⁺ e ⁻ → T(4S)
1.2 ± 0.2 ± 0.3 _{-0.4}		4 ALEXANDER	96T	CLE2 e ⁺ e ⁻ → T(4S)
<2.1	90	5 BEAN	93B	CLE2 e ⁺ e ⁻ → T(4S)

“OUR EVALUATION” is an average using rescaled values of the data listed below. The average and rescaling were performed by the Heavy Flavor Averaging Group (HFLAV) and are described at <https://hflav.web.cern.ch/>. The averaging/rescaling procedure takes into account correlations between the measurements and asymmetric lifetime errors.



¹ The signal events are tagged by a second B meson reconstructed in the fully hadronic decays.
² B⁺ and B⁰ decays combined assuming isospin symmetry. Systematic errors include both experimental and form-factor uncertainties.
³ The signal events are tagged by a second B meson reconstructed in the semileptonic mode B → D^(*)ℓν_ℓ.
⁴ Derived based in the reported B⁰ result by assuming isospin symmetry: Γ(B⁰ → ρ⁻ℓ⁺ν) = 2Γ(B⁺ → ρ⁰ℓ⁺ν) ≈ 2Γ(B⁺ → ωℓ⁺ν).
⁵ BEAN 93B limit set using ISGW Model. Using isospin and the quark model to combine Γ(ρ⁰ℓ⁺ν_ℓ) and Γ(ρ⁻ℓ⁺ν_ℓ) with this result, they obtain a limit <(1.6–2.7) × 10⁻⁴ at 90% CL for B⁺ → ρ⁰ℓ⁺ν_ℓ. The range corresponds to the ISGW, WSB, and KS models. An upper limit on |V_{ub}/V_{cb}| < 0.8–0.13 at 90% CL is derived as well.

$\Gamma(\pi^+ \pi^- \ell^+ \nu_{\ell})/\Gamma_{\text{total}}$		Γ_{29}/Γ		
VALUE (units 10 ⁻⁵)	CL%	DOCUMENT ID	TECN	COMMENT
22.7^{+1.9}_{-1.6} ± 3.5				
		BELENO	21	BELL e ⁺ e ⁻ → T(4S)

$\Gamma(\rho \bar{p} \ell^+ \nu_{\ell})/\Gamma_{\text{total}}$		Γ_{30}/Γ		
VALUE (units 10 ⁻⁶)	CL%	DOCUMENT ID	TECN	COMMENT
5.8 ± 2.4 ± 0.9				
		1 TIEN	14	BELL e ⁺ e ⁻ → T(4S)

¹ Assumes equal production of B⁺ and B⁰ at the T(4S).

$\Gamma(\rho \bar{p} \mu^+ \nu_{\mu})/\Gamma_{\text{total}}$		Γ_{31}/Γ		
VALUE (units 10 ⁻⁶)	CL%	DOCUMENT ID	TECN	COMMENT
• • • We do not use the following data for averages, fits, limits, etc. • • •				
<8.5	90	1 TIEN	14	BELL e ⁺ e ⁻ → T(4S)

¹ Assumes equal production of B⁺ and B⁰ at the T(4S).

$\Gamma(\rho \bar{p} \mu^+ \nu_{\mu})/\Gamma(J/\psi(1S) K^+)$		Γ_{31}/Γ_{276}		
VALUE (units 10 ⁻³)	CL%	DOCUMENT ID	TECN	COMMENT
5.22 ± 0.31 ± 0.03				
		1 AAIJ	20k	LHCB pp at 7, 8 and 13 TeV

¹ AAIJ 20k reports [Γ(B⁺ → ρ⁺μ⁺ν_μ)/Γ(B⁺ → J/ψ(1S) K⁺)] / [B(J/ψ(1S) → μ⁺μ⁻)] = (8.75 ± 0.39 ± 0.35) × 10⁻² which we multiply by our best value B(J/ψ(1S) → μ⁺μ⁻) = (5.961 ± 0.033) × 10⁻². Our first error is their experiment's error and our second error is the systematic error from using our best value.

$\Gamma(\rho \bar{p} e^+ \nu_e)/\Gamma_{\text{total}}$		Γ_{32}/Γ		
VALUE (units 10 ⁻⁶)	CL%	DOCUMENT ID	TECN	COMMENT
8.2^{+3.7}_{-3.2} ± 0.6				
		1 TIEN	14	BELL e ⁺ e ⁻ → T(4S)
• • • We do not use the following data for averages, fits, limits, etc. • • •				
<5200	90	2 ADAM	03b	CLE2 e ⁺ e ⁻ → T(4S)

¹ Assumes equal production of B⁺ and B⁰ at the T(4S).
² Based on phase-space model; if V–A model is used, the 90% CL upper limit becomes < 1.2 × 10⁻³.

$\Gamma(e^+ \nu_e)/\Gamma_{\text{total}}$		Γ_{33}/Γ		
VALUE (units 10 ⁻⁶)	CL%	DOCUMENT ID	TECN	COMMENT
< 0.98				
• • • We do not use the following data for averages, fits, limits, etc. • • •				
< 3.5	90	2 YOOK	15	BELL e ⁺ e ⁻ → T(4S)
< 8	90	1 AUBERT	10E	BABR e ⁺ e ⁻ → T(4S)
< 1.9	90	1 AUBERT	09V	BABR e ⁺ e ⁻ → T(4S)
< 5.2	90	1 AUBERT	08AD	BABR e ⁺ e ⁻ → T(4S)
<15	90	ARTUSO	95	CLE2 e ⁺ e ⁻ → T(4S)

¹ Assumes equal production of B⁺ and B⁰ at the T(4S).
² Assumes B(T(4S) → B⁺B⁻) = 0.513 ± 0.006.

Meson Particle Listings

 B^\pm

$\Gamma(\mu^+\nu_\mu)/\Gamma_{\text{total}}$		Γ_{34}/Γ			
VALUE (units 10^{-6})	CL%	DOCUMENT ID	TECN	COMMENT	
< 0.86	90	1 PRIM	20 BELL	$e^+e^- \rightarrow \Upsilon(4S)$	
••• We do not use the following data for averages, fits, limits, etc. •••					
0.29 to 1.07	90	2 SIBIDANOV	18 BELL	$e^+e^- \rightarrow \Upsilon(4S)$	
< 2.7	90	3 YOOK	15 BELL	$e^+e^- \rightarrow \Upsilon(4S)$	
< 11	90	4 AUBERT	10E BABR	$e^+e^- \rightarrow \Upsilon(4S)$	
< 1.0	90	4 AUBERT	09V BABR	$e^+e^- \rightarrow \Upsilon(4S)$	
< 5.6	90	4 AUBERT	08AD BABR	$e^+e^- \rightarrow \Upsilon(4S)$	
< 1.7	90	4.5 SATOYAMA	07 BELL	$e^+e^- \rightarrow \Upsilon(4S)$	
< 6.6	90	AUBERT	04O BABR	Repl. by AUBERT 09V	
< 21	90	ARTUSO	95 CLE2	$e^+e^- \rightarrow \Upsilon(4S)$	

- ¹ This is a 90% C.L. upper limit in the frequentist approach. The corresponding upper limit in the Bayesian approach is $< 8.9 \times 10^{-7}$. A 2.8 standard deviation signal above the background is found, with a measured branching fraction $(5.3 \pm 2.0 \pm 0.9) \times 10^{-7}$.
- ² This is a 90% confidence interval in the frequentist approach. A 2.4 standard deviation signal above the background is found, with a measured branching fraction $(6.46 \pm 2.22 \pm 1.60) \times 10^{-7}$.
- ³ Assumes $B(\Upsilon(4S) \rightarrow B^+B^-) = 0.513 \pm 0.006$.
- ⁴ Assumes equal production of B^+ and B^0 at the $\Upsilon(4S)$.
- ⁵ Superseded by SIBIDANOV 18.

$\Gamma(\tau^+\nu_\tau)/\Gamma_{\text{total}}$		Γ_{35}/Γ			
See the note on "Decay Constants of Charged Pseudoscalar Mesons" in the D_s^+ Listings.					
VALUE (units 10^{-4})	CL%	DOCUMENT ID	TECN	COMMENT	
1.09 ± 0.24 OUR AVERAGE		Error includes scale factor of 1.2.			
$1.25 \pm 0.28 \pm 0.27$	1.2	KRONENBIT...15	BELL	$e^+e^- \rightarrow \Upsilon(4S)$	
$0.72 \pm_{-0.25}^{+0.27} \pm 0.11$	3	HARA	13 BELL	$e^+e^- \rightarrow \Upsilon(4S)$	
$1.83 \pm_{-0.49}^{+0.53} \pm 0.24$	2.4	LEES	13K BABR	$e^+e^- \rightarrow \Upsilon(4S)$	
$1.7 \pm 0.8 \pm 0.2$	2.5	AUBERT	10E BABR	$e^+e^- \rightarrow \Upsilon(4S)$	
••• We do not use the following data for averages, fits, limits, etc. •••					
$1.54 \pm_{-0.37}^{+0.38} \pm 0.29$	2.6	HARA	10 BELL	Repl. by KRONENBIT-TER 15	
$1.8 \pm_{-0.8}^{+0.9} \pm 0.45$	2.7	AUBERT	08D BABR	Repl. by LEES 13K	
$0.9 \pm 0.6 \pm 0.1$	2.5	AUBERT	07AL BABR	Repl. by AUBERT 10E	
< 2.6	90	2 AUBERT	06K BABR	$e^+e^- \rightarrow \Upsilon(4S)$	
$1.79 \pm_{-0.49}^{+0.56} \pm 0.46$	2.7	IKADO	06 BELL	Repl. by HARA 13	
< 4.2	90	2 AUBERT,B	05B BABR	Repl. by AUBERT 06K	
< 8.3	90	8 BARATE	01E ALEP	$e^+e^- \rightarrow Z$	
< 8.4	90	2 BROWDER	01 CLE2	$e^+e^- \rightarrow \Upsilon(4S)$	
< 5.7	90	9 ACCIARRI	97F L3	$e^+e^- \rightarrow Z$	
< 104	90	10 ALBRECHT	95D ARG	$e^+e^- \rightarrow \Upsilon(4S)$	
< 22	90	ARTUSO	95 CLE2	$e^+e^- \rightarrow \Upsilon(4S)$	
< 18	90	11 BUSKULIC	95 ALEP	$e^+e^- \rightarrow Z$	

- ¹ Requires one reconstructed semileptonic B decay $B^- \rightarrow D^{(*)0} \ell^- \bar{\nu}_\ell$ in the recoil.
- ² Assumes equal production of B^+ and B^0 at the $\Upsilon(4S)$.
- ³ The authors combine their result with that from HARA 10 obtaining $B(B^- \rightarrow \tau^+ \bar{\nu}_\tau) = (0.96 \pm 0.26) \times 10^{-4}$ and deriving $f_B |V_{ub}| = (7.4 \pm 0.8 \pm 0.5) \times 10^{-4}$ GeV.
- ⁴ Requires a fully reconstructed hadronic B -decay in the recoil. Reports that this result combined with AUBERT 10E value gives $B(B^- \rightarrow \tau^+ \bar{\nu}_\tau) = (1.79 \pm 0.48) \times 10^{-4}$.
- ⁵ Requires one reconstructed semileptonic B decay $B^- \rightarrow D^0 \ell^- \bar{\nu}_\ell X$ in the recoil.
- ⁶ Requires one reconstructed semileptonic B decay $B^- \rightarrow D^{(*)0} \ell^- \bar{\nu}_\ell X$ in the recoil.
- ⁷ The analysis is based on a sample of events with one fully reconstructed tag B in a hadronic decay mode $B^- \rightarrow D^{(*)0} X^-$.
- ⁸ The energy-flow and b -tagging algorithms were used.
- ⁹ ACCIARRI 97F uses missing-energy technique and $f(b \rightarrow B^-) = (38.2 \pm 2.5)\%$.
- ¹⁰ ALBRECHT 95D uses full reconstruction of one B decay as tag.
- ¹¹ BUSKULIC 95 uses same missing-energy technique as in $\bar{B} \rightarrow \tau^+ \nu_\tau X$, but analysis is restricted to endpoint region of missing-energy distribution.

$\Gamma(\ell^+\nu_\ell\gamma)/\Gamma_{\text{total}}$		Γ_{36}/Γ			
VALUE	CL%	DOCUMENT ID	TECN	COMMENT	
< 3.0×10^{-6}	90	1,2 GELB	18 BELL	$e^+e^- \rightarrow \Upsilon(4S)$	
••• We do not use the following data for averages, fits, limits, etc. •••					
< 3.5×10^{-6}	90	2,3 HELLER	15 BELL	$e^+e^- \rightarrow \Upsilon(4S)$	
< 15.6×10^{-6}	90	2 AUBERT	09AT BABR	$e^+e^- \rightarrow \Upsilon(4S)$	
••• We do not use the following data for averages, fits, limits, etc. •••					
¹ Supersedes HELLER 15.					
² Assumes equal production of B^+ and B^0 at the $\Upsilon(4S)$.					
³ Superseded by GELB 18.					

$\Gamma(e^+\nu_e\gamma)/\Gamma_{\text{total}}$		Γ_{37}/Γ			
VALUE	CL%	DOCUMENT ID	TECN	COMMENT	
< 4.3×10^{-6}	90	1,2 GELB	18 BELL	$e^+e^- \rightarrow \Upsilon(4S)$	
••• We do not use the following data for averages, fits, limits, etc. •••					
< 6.1×10^{-6}	90	2,3 HELLER	15 BELL	$e^+e^- \rightarrow \Upsilon(4S)$	
< 17×10^{-6}	90	2 AUBERT	09AT BABR	$e^+e^- \rightarrow \Upsilon(4S)$	
< 200×10^{-6}	90	4 BROWDER	97 CLE2	$e^+e^- \rightarrow \Upsilon(4S)$	
••• We do not use the following data for averages, fits, limits, etc. •••					
¹ Supersedes HELLER 15.					
² Assumes equal production of B^+ and B^0 at the $\Upsilon(4S)$.					
³ Superseded by GELB 18.					
⁴ BROWDER 97 uses the hermiticity of the CLEOII detector to reconstruct the neutrino energy and momentum.					

$\Gamma(\mu^+\nu_\mu\gamma)/\Gamma_{\text{total}}$		Γ_{38}/Γ			
VALUE	CL%	DOCUMENT ID	TECN	COMMENT	
< 3.4×10^{-6}	90	1,2 GELB	18 BELL	$e^+e^- \rightarrow \Upsilon(4S)$	
••• We do not use the following data for averages, fits, limits, etc. •••					
< 3.4×10^{-6}	90	2,3 HELLER	15 BELL	$e^+e^- \rightarrow \Upsilon(4S)$	
< 24×10^{-6}	90	2,4 AUBERT	09AT BABR	$e^+e^- \rightarrow \Upsilon(4S)$	
< 52×10^{-6}	90	5 BROWDER	97 CLE2	$e^+e^- \rightarrow \Upsilon(4S)$	

- ¹ Supersedes HELLER 15.
- ² Assumes equal production of B^+ and B^0 at the $\Upsilon(4S)$.
- ³ Superseded by GELB 18.
- ⁴ Note that the value given by AUBERT 09AT is 24×10^{-6} in the paper abstract, and 26×10^{-6} in the paper itself (Table I).
- ⁵ BROWDER 97 uses the hermiticity of the CLEOII detector to reconstruct the neutrino energy and momentum.

$\Gamma(\mu^+\mu^-\mu^+\nu_\mu)/\Gamma_{\text{total}}$		Γ_{39}/Γ			
VALUE	CL%	DOCUMENT ID	TECN	COMMENT	
< 1.6×10^{-8}	95	1 AAIJ	19P LHCB	pp at 7, 8, 13 TeV	
••• We do not use the following data for averages, fits, limits, etc. •••					
¹ AAIJ 19P limit established for the kinematic region where the lower of the two $M(\mu^+\mu^-)$ is less than $980 \text{ MeV}/c^2$.					

$\Gamma(D^0 X)/\Gamma_{\text{total}}$		Γ_{40}/Γ			
VALUE	CL%	DOCUMENT ID	TECN	COMMENT	
$0.086 \pm 0.006 \pm 0.004$		1 AUBERT	07N BABR	$e^+e^- \rightarrow \Upsilon(4S)$	
••• We do not use the following data for averages, fits, limits, etc. •••					
$0.098 \pm 0.009 \pm 0.006$	1	AUBERT, BE	04B BABR	Repl. by AUBERT 07N	
••• We do not use the following data for averages, fits, limits, etc. •••					
¹ Events are selected by completely reconstructing one B and searching for a reconstructed charmed particle in the rest of the event. The last error includes systematic and charm branching ratio uncertainties.					

$\Gamma(\bar{D}^0 X)/\Gamma_{\text{total}}$		Γ_{41}/Γ			
VALUE	CL%	DOCUMENT ID	TECN	COMMENT	
$0.786 \pm 0.016 \pm_{-0.033}^{+0.034}$		1 AUBERT	07N BABR	$e^+e^- \rightarrow \Upsilon(4S)$	
••• We do not use the following data for averages, fits, limits, etc. •••					
$0.793 \pm 0.025 \pm_{-0.044}^{+0.045}$	1	AUBERT, BE	04B BABR	Repl. by AUBERT 07N	
••• We do not use the following data for averages, fits, limits, etc. •••					
¹ Events are selected by completely reconstructing one B and searching for a reconstructed charmed particle in the rest of the event. The last error includes systematic and charm branching ratio uncertainties.					

$\Gamma(D^0 X)/[\Gamma(D^0 X) + \Gamma(\bar{D}^0 X)]$		$\Gamma_{40}/(\Gamma_{40} + \Gamma_{41})$			
VALUE	CL%	DOCUMENT ID	TECN	COMMENT	
$0.098 \pm 0.007 \pm 0.001$		AUBERT	07N BABR	$e^+e^- \rightarrow \Upsilon(4S)$	
••• We do not use the following data for averages, fits, limits, etc. •••					
$0.110 \pm 0.010 \pm 0.003$		AUBERT, BE	04B BABR	Repl. by AUBERT 07N	

$\Gamma(D^+ X)/\Gamma_{\text{total}}$		Γ_{42}/Γ			
VALUE	CL%	DOCUMENT ID	TECN	COMMENT	
$0.025 \pm 0.005 \pm 0.002$		1 AUBERT	07N BABR	$e^+e^- \rightarrow \Upsilon(4S)$	
••• We do not use the following data for averages, fits, limits, etc. •••					
$0.038 \pm 0.009 \pm 0.005$	1	AUBERT, BE	04B BABR	Repl. by AUBERT 07N	
••• We do not use the following data for averages, fits, limits, etc. •••					
¹ Events are selected by completely reconstructing one B and searching for a reconstructed charmed particle in the rest of the event. The last error includes systematic and charm branching ratio uncertainties.					

$\Gamma(D^- X)/\Gamma_{\text{total}}$		Γ_{43}/Γ			
VALUE	CL%	DOCUMENT ID	TECN	COMMENT	
$0.099 \pm 0.008 \pm 0.009$		1 AUBERT	07N BABR	$e^+e^- \rightarrow \Upsilon(4S)$	
••• We do not use the following data for averages, fits, limits, etc. •••					
$0.098 \pm 0.012 \pm 0.014$	1	AUBERT, BE	04B BABR	Repl. by AUBERT 07N	
••• We do not use the following data for averages, fits, limits, etc. •••					
¹ Events are selected by completely reconstructing one B and searching for a reconstructed charmed particle in the rest of the event. The last error includes systematic and charm branching ratio uncertainties.					

$\Gamma(D^+ X)/[\Gamma(D^+ X) + \Gamma(D^- X)]$		$\Gamma_{42}/(\Gamma_{42} + \Gamma_{43})$			
VALUE	CL%	DOCUMENT ID	TECN	COMMENT	
$0.204 \pm 0.035 \pm 0.001$		AUBERT	07N BABR	$e^+e^- \rightarrow \Upsilon(4S)$	
••• We do not use the following data for averages, fits, limits, etc. •••					
$0.278 \pm 0.052 \pm 0.009$		AUBERT, BE	04B BABR	Repl. by AUBERT 07N	

$\Gamma(D_s^+ X)/\Gamma_{\text{total}}$		Γ_{44}/Γ			
VALUE	CL%	DOCUMENT ID	TECN	COMMENT	
$0.079 \pm 0.006 \pm_{-0.011}^{+0.013}$		1 AUBERT	07N BABR	$e^+e^- \rightarrow \Upsilon(4S)$	
••• We do not use the following data for averages, fits, limits, etc. •••					
$0.143 \pm 0.016 \pm_{-0.034}^{+0.051}$	1	AUBERT, BE	04B BABR	Repl. by AUBERT 07N	
••• We do not use the following data for averages, fits, limits, etc. •••					
¹ Events are selected by completely reconstructing one B and searching for a reconstructed charmed particle in the rest of the event. The last error includes systematic and charm branching ratio uncertainties.					

See key on page 1127

Meson Particle Listings

B^\pm

$\Gamma(D_s^- X)/\Gamma_{total}$ Γ_{45}/Γ
 VALUE CL% DOCUMENT ID TECN COMMENT

$0.011 \pm 0.004 + 0.002$
 $-0.003 - 0.001$ 1 AUBERT 07N BABR $e^+ e^- \rightarrow \Upsilon(4S)$

• • • We do not use the following data for averages, fits, limits, etc. • • •

<0.022 90 1 AUBERT,BE 04B BABR Repl. by AUBERT 07N

1 Events are selected by completely reconstructing one B and searching for a reconstructed charmed particle in the rest of the event. The last error includes systematic and charm branching ratio uncertainties.

$\Gamma(D_s^+ X)/[\Gamma(D_s^+ X) + \Gamma(D_s^- X)]$ $\Gamma_{44}/(\Gamma_{44} + \Gamma_{45})$
 VALUE DOCUMENT ID TECN COMMENT

$0.884 \pm 0.038 \pm 0.002$ AUBERT 07N BABR $e^+ e^- \rightarrow \Upsilon(4S)$

• • • We do not use the following data for averages, fits, limits, etc. • • •

$0.966 \pm 0.039 \pm 0.012$ AUBERT,BE 04B BABR Repl. by AUBERT 07N

$\Gamma(D_s^- X)/[\Gamma(D_s^+ X) + \Gamma(D_s^- X)]$ $\Gamma_{45}/(\Gamma_{44} + \Gamma_{45})$
 VALUE CL% DOCUMENT ID TECN COMMENT

<0.126 90 AUBERT,BE 04B BABR $e^+ e^- \rightarrow \Upsilon(4S)$

$\Gamma(A_c^+ X)/\Gamma_{total}$ Γ_{46}/Γ
 VALUE DOCUMENT ID TECN COMMENT

$0.021 \pm 0.005 \pm 0.008$
 -0.004 1 AUBERT 07N BABR $e^+ e^- \rightarrow \Upsilon(4S)$

• • • We do not use the following data for averages, fits, limits, etc. • • •

$0.029 \pm 0.008 \pm 0.011$
 -0.007 1 AUBERT,BE 04B BABR Repl. by AUBERT 07N

1 Events are selected by completely reconstructing one B and searching for a reconstructed charmed particle in the rest of the event. The last error includes systematic and charm branching ratio uncertainties.

$\Gamma(\bar{A}_c^- X)/\Gamma_{total}$ Γ_{47}/Γ
 VALUE DOCUMENT ID TECN COMMENT

$0.028 \pm 0.005 \pm 0.010$
 -0.007 1 AUBERT 07N BABR $e^+ e^- \rightarrow \Upsilon(4S)$

• • • We do not use the following data for averages, fits, limits, etc. • • •

$0.035 \pm 0.008 \pm 0.013$
 -0.009 1 AUBERT,BE 04B BABR Repl. by AUBERT 07N

1 Events are selected by completely reconstructing one B and searching for a reconstructed charmed particle in the rest of the event. The last error includes systematic and charm branching ratio uncertainties.

$\Gamma(A_c^+ X)/[\Gamma(A_c^+ X) + \Gamma(\bar{A}_c^- X)]$ $\Gamma_{46}/(\Gamma_{46} + \Gamma_{47})$
 VALUE DOCUMENT ID TECN COMMENT

$0.427 \pm 0.071 \pm 0.001$ AUBERT 07N BABR $e^+ e^- \rightarrow \Upsilon(4S)$

• • • We do not use the following data for averages, fits, limits, etc. • • •

$0.452 \pm 0.090 \pm 0.003$ AUBERT,BE 04B BABR Repl. by AUBERT 07N

$\Gamma(\bar{C} X)/\Gamma_{total}$ Γ_{48}/Γ
 VALUE DOCUMENT ID TECN COMMENT

$0.968 \pm 0.019 \pm 0.041$
 -0.039 1 AUBERT 07N BABR $e^+ e^- \rightarrow \Upsilon(4S)$

• • • We do not use the following data for averages, fits, limits, etc. • • •

$0.983 \pm 0.030 \pm 0.054$
 -0.051 1 AUBERT,BE 04B BABR Repl. by AUBERT 07N

1 Events are selected by completely reconstructing one B and searching for a reconstructed charmed particle in the rest of the event. The last error includes systematic and charm branching ratio uncertainties.

$\Gamma(cX)/\Gamma_{total}$ Γ_{49}/Γ
 VALUE DOCUMENT ID TECN COMMENT

$0.234 \pm 0.012 \pm 0.018$
 -0.014 1 AUBERT 07N BABR $e^+ e^- \rightarrow \Upsilon(4S)$

• • • We do not use the following data for averages, fits, limits, etc. • • •

$0.330 \pm 0.022 \pm 0.055$
 -0.037 1 AUBERT,BE 04B BABR Repl. by AUBERT 07N

1 Events are selected by completely reconstructing one B and searching for a reconstructed charmed particle in the rest of the event. The last error includes systematic and charm branching ratio uncertainties.

$\Gamma(c/\bar{c}X)/\Gamma_{total}$ Γ_{50}/Γ
 VALUE DOCUMENT ID TECN COMMENT

$1.202 \pm 0.023 \pm 0.053$
 -0.049 1 AUBERT 07N BABR $e^+ e^- \rightarrow \Upsilon(4S)$

• • • We do not use the following data for averages, fits, limits, etc. • • •

$1.313 \pm 0.037 \pm 0.088$
 -0.075 1 AUBERT,BE 04B BABR Repl. by AUBERT 07N

1 Events are selected by completely reconstructing one B and searching for a reconstructed charmed particle in the rest of the event. The last error includes systematic and charm branching ratio uncertainties.

$\Gamma(\bar{D}^0 \pi^+)/\Gamma_{total}$ Γ_{51}/Γ
 VALUE (units 10^{-3}) EVTS DOCUMENT ID TECN COMMENT

4.68 ± 0.13 OUR FIT
4.70 ± 0.13 OUR AVERAGE

4.34 ± 0.10 ± 0.23 1 KATO 18 BELL $e^+ e^- \rightarrow \Upsilon(4S)$
 4.90 ± 0.07 ± 0.22 2 AUBERT 07H BABR $e^+ e^- \rightarrow \Upsilon(4S)$
 4.9 ± 0.6 ± 0.2 3 ABULENCIA 06J CDF $p\bar{p}$ at 1.96 TeV
 4.49 ± 0.21 ± 0.23 4 AUBERT,BE 06J BABR $e^+ e^- \rightarrow \Upsilon(4S)$
 4.97 ± 0.12 ± 0.29 2,5 AHMED 02B CLE2 $e^+ e^- \rightarrow \Upsilon(4S)$
 5.0 ± 0.7 ± 0.6 54 6 BORTOLETTO92 CLEO $e^+ e^- \rightarrow \Upsilon(4S)$
 5.4 $^{+1.8}_{-1.5} \pm 0.9$ 14 7 BEBEK 87 CLEO $e^+ e^- \rightarrow \Upsilon(4S)$

• • • We do not use the following data for averages, fits, limits, etc. • • •
 4.68 ± 0.26 ± 0.04 8 AUBERT,B 04P BABR Repl. by AUBERT 07H
 5.5 ± 0.4 ± 0.5 304 9 ALAM 94 CLE2 Repl. by AHMED 02B
 2.0 ± 0.8 ± 0.6 12 6 ALBRECHT 90J ARG $e^+ e^- \rightarrow \Upsilon(4S)$
 1.9 ± 1.0 ± 0.6 7 10 ALBRECHT 88K ARG $e^+ e^- \rightarrow \Upsilon(4S)$

1 Measures absolute branching fractions using a missing-mass technique.
 2 Assumes equal production of B^+ and B^0 at the $\Upsilon(4S)$.
 3 ABULENCIA 06J reports $[\Gamma(B^+ \rightarrow \bar{D}^0 \pi^+)/\Gamma_{total}] / [B(B^0 \rightarrow D^- \pi^+)] = 1.97 \pm 0.10 \pm 0.21$ which we multiply by our best value $B(B^0 \rightarrow D^- \pi^+) = (2.51 \pm 0.08) \times 10^{-3}$. Our first error is their experiment's error and our second error is the systematic error from using our best value.
 4 Uses a missing-mass method. Does not depend on D branching fractions or B^+/B^0 production rates.
 5 AHMED 02B reports an additional uncertainty on the branching ratios to account for 4.5% uncertainty on relative production of B^0 and B^+ , which is not included here.
 6 Assumes equal production of B^+ and B^0 at the $\Upsilon(4S)$ and uses the MarkIII branching fractions for the D .
 7 BEBEK 87 value has been updated in BERKELMAN 91 to use same assumptions as noted for BORTOLETTO 92.
 8 AUBERT,B 04P reports $[\Gamma(B^+ \rightarrow \bar{D}^0 \pi^+)/\Gamma_{total}] \times [B(D^0 \rightarrow K^- \pi^+)] = (1.846 \pm 0.032 \pm 0.097) \times 10^{-4}$ which we divide by our best value $B(D^0 \rightarrow K^- \pi^+) = (3.947 \pm 0.030) \times 10^{-2}$. Our first error is their experiment's error and our second error is the systematic error from using our best value.
 9 ALAM 94 assume equal production of B^+ and B^0 at the $\Upsilon(4S)$ and use the CLEOII absolute $B(D^0 \rightarrow K^- \pi^+)$ and the PDG 1992 $B(D^0 \rightarrow K^- \pi^+ \pi^0)/B(D^0 \rightarrow K^- \pi^+)$ and $B(D^0 \rightarrow K^- 2\pi^+ \pi^-)/B(D^0 \rightarrow K^- \pi^+)$.
 10 ALBRECHT 88K assumes $B^0 \bar{B}^0, B^+ B^-$ ratio is 45:55. Superseded by ALBRECHT 90J.

$\Gamma(\bar{D}^0 \rho^+)/\Gamma_{total}$ Γ_{54}/Γ
 VALUE EVTS DOCUMENT ID TECN COMMENT

0.0134 ± 0.0018 OUR AVERAGE
 0.0135 ± 0.0012 ± 0.0015 212 1 ALAM 94 CLE2 $e^+ e^- \rightarrow \Upsilon(4S)$
 0.013 ± 0.004 ± 0.004 19 2 ALBRECHT 90J ARG $e^+ e^- \rightarrow \Upsilon(4S)$

• • • We do not use the following data for averages, fits, limits, etc. • • •
 0.021 ± 0.008 ± 0.009 10 3 ALBRECHT 88K ARG $e^+ e^- \rightarrow \Upsilon(4S)$
 1 ALAM 94 assume equal production of B^+ and B^0 at the $\Upsilon(4S)$ and use the CLEOII absolute $B(D^0 \rightarrow K^- \pi^+)$ and the PDG 1992 $B(D^0 \rightarrow K^- \pi^+ \pi^0)/B(D^0 \rightarrow K^- \pi^+)$ and $B(D^0 \rightarrow K^- 2\pi^+ \pi^-)/B(D^0 \rightarrow K^- \pi^+)$.
 2 Assumes equal production of B^+ and B^0 at the $\Upsilon(4S)$ and uses the MarkIII branching fractions for the D .
 3 ALBRECHT 88K assumes $B^0 \bar{B}^0, B^+ B^-$ ratio is 45:55.

$\Gamma(\bar{D}^0 K^+)/\Gamma(\bar{D}^0 \pi^+)$ Γ_{55}/Γ_{51}
 VALUE (units 10^{-2}) DOCUMENT ID TECN COMMENT

7.89 ± 0.27 OUR AVERAGE Error includes scale factor of 2.3. See the ideogram below.
 7.96 ± 0.03 ± 0.13 AAIJ 21Q LHCB pp at 7, 8, 13 TeV
 6.77 ± 0.23 ± 0.30 HORII 08 BELL $e^+ e^- \rightarrow \Upsilon(4S)$
 8.31 ± 0.35 ± 0.20 AUBERT 04N BABR $e^+ e^- \rightarrow \Upsilon(4S)$
 9.9 $^{+1.4}_{-1.2} \pm 0.6$ BORNHEIM 03 CLE2 $e^+ e^- \rightarrow \Upsilon(4S)$

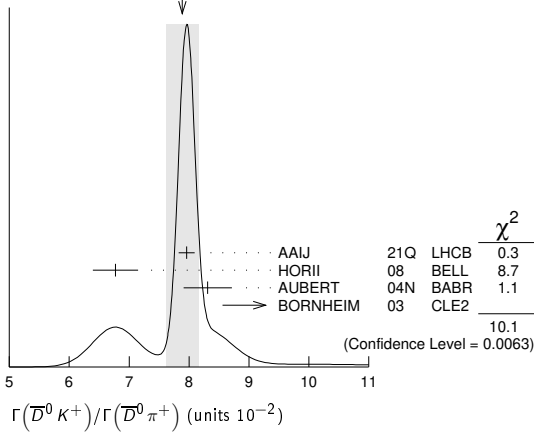
• • • We do not use the following data for averages, fits, limits, etc. • • •
 7.768 ± 0.038 ± 0.066 1,2 AAIJ 18A LHCB pp at 7, 8, 13 TeV
 7.79 ± 0.06 ± 0.19 AAIJ 16L LHCB pp at 7, 8 TeV
 7.93 ± 0.10 ± 0.18 3 AAIJ 16L LHCB pp at 7, 8 TeV
 7.71 ± 0.17 ± 0.26 3 AAIJ 13AE LHCB Repl. by AAIJ 16L
 7.74 ± 0.12 ± 0.19 AAIJ 12M LHCB Repl. by AAIJ 16L
 9.4 ± 0.9 ± 0.7 ABE 03D BELL Repl. by SWAIN 03
 7.7 ± 0.5 ± 0.6 SWAIN 03 BELL Repl. by HORII 08
 7.9 ± 0.9 ± 0.6 ABE 01I BELL Repl. by ABE 03D
 5.5 ± 1.4 ± 0.5 ATHANAS 98 CLE2 Repl. by BORNHEIM 03

1 Supersedes AAIJ 16L.
 2 Superseded by AAIJ 21Q.
 3 Uses $B^\pm \rightarrow [K^\pm \pi^\mp \pi^\pm \pi^-]_D h^\pm$ mode.

Meson Particle Listings

B^\pm

WEIGHTED AVERAGE
7.89±0.27 (Error scaled by 2.3)



$\Gamma(D_{CP(+)} K^+) / \Gamma(D_{CP(+)} \pi^+)$ Γ_{56}/Γ_{52}

VALUE	DOCUMENT ID	TECN	COMMENT
0.089±0.008 OUR AVERAGE			
0.089±0.008±0.003	1,2 ABE	06 BELL	$e^+e^- \rightarrow \Upsilon(4S)$
0.088±0.016±0.005	3 AUBERT	04N BABR	$e^+e^- \rightarrow \Upsilon(4S)$
0.125±0.036±0.010	3 ABE	03D BELL	Repl. by SWAIN 03
0.093±0.018±0.008	3 SWAIN	03 BELL	Repl. by ABE 06

¹ Reports a double ratio of $B(B^+ \rightarrow D_{CP(+)} K^+) / B(B^+ \rightarrow D_{CP(+)} \pi^+)$ and $B(B^+ \rightarrow \bar{D}^0 K^+) / B(B^+ \rightarrow \bar{D}^0 \pi^+)$, $1.13 \pm 0.16 \pm 0.08$. We multiply by our best value of $B(B^+ \rightarrow \bar{D}^0 K^+) / B(B^+ \rightarrow \bar{D}^0 \pi^+) = 0.083 \pm 0.006$. Our first error is their experiment's error and the second error is systematic error from using our best value.

² ABE 06 reports $[\Gamma(B^+ \rightarrow D_{CP(+)} K^+) / \Gamma(B^+ \rightarrow D_{CP(+)} \pi^+)] / [\Gamma(B^+ \rightarrow \bar{D}^0 K^+) / \Gamma(B^+ \rightarrow \bar{D}^0 \pi^+)] = 1.13 \pm 0.06 \pm 0.08$ which we multiply by our best value $\Gamma(B^+ \rightarrow \bar{D}^0 K^+) / \Gamma(B^+ \rightarrow \bar{D}^0 \pi^+) = 0.0789 \pm 0.0027$. Our first error is their experiment's error and our second error is the systematic error from using our best value.

³ $CP=+1$ eigenstate of $D^0 \bar{D}^0$ system is reconstructed via $K^+ K^-$ and $\pi^+ \pi^-$.

$\Gamma(D_{CP(+)} K^+) / \Gamma(\bar{D}^0 K^+)$ Γ_{56}/Γ_{55}

VALUE	DOCUMENT ID	TECN	COMMENT
0.495±0.007 OUR AVERAGE			
0.494±0.008±0.006	1 AAIJ	18A LHCb	pp at 7, 8, 13 TeV
0.496±0.014±0.008	2 AAIJ	18A LHCb	pp at 7, 8, 13 TeV
0.489±0.010±0.009	3 AAIJ	16L LHCb	pp at 7, 8 TeV
0.65 ±0.12 ±0.06	4 AALTONEN	10A CDF	$p\bar{p}$ at 1.96 TeV
0.590±0.045±0.025	5 DEL-AMO-SA..10G	BABR	$e^+e^- \rightarrow \Upsilon(4S)$
0.504±0.019±0.006	6 AAIJ	12M LHCb	Repl. by AAIJ 16L
0.53 ±0.05 ±0.025	AUBERT	08AA BABR	Repl. by DEL-AMO-SANCHEZ 10G
0.45 ±0.06 ±0.02	AUBERT	06J BABR	Repl. by AUBERT 08AA

¹ Uses $D \rightarrow K^+ K^-$ decay mode and reports $R_{CP+} = 0.988 \pm 0.015 \pm 0.011$ which we have divided by 2.

² Uses $D \rightarrow \pi^+ \pi^-$ decay mode and reports $R_{CP+} = 0.992 \pm 0.027 \pm 0.015$ which we have divided by 2.

³ AAIJ 16L reports $R_{CP+} = 0.978 \pm 0.019 \pm 0.018$ which we have divided by 2.

⁴ Reports $R_{CP+} = 2 (B(B^- \rightarrow D_{CP(+)} K^-) + B(B^+ \rightarrow D_{CP(+)} K^+)) / (B(B^- \rightarrow D^0 K^-) + B(B^+ \rightarrow \bar{D}^0 K^+)) = 1.30 \pm 0.24 \pm 0.12$ that we have divided by 2.

⁵ Reports $R_{CP+} = 1.18 \pm 0.09 \pm 0.05$ that we have divided by 2.

⁶ AAIJ 12M reports $R_{CP+} = 1.007 \pm 0.038 \pm 0.012$ which we have divided by 2.

$\Gamma(D_{CP(-)} K^+) / \Gamma(D_{CP(-)} \pi^+)$ Γ_{57}/Γ_{53}

VALUE	DOCUMENT ID	TECN	COMMENT
0.097±0.016±0.007	1 ABE	06 BELL	$e^+e^- \rightarrow \Upsilon(4S)$
0.119±0.028±0.006	2 ABE	03D BELL	Repl. by SWAIN 03
0.108±0.019±0.007	2 SWAIN	03 BELL	Repl. by ABE 06

¹ Reports a double ratio of $B(B^+ \rightarrow D_{CP(-)} K^+) / B(B^+ \rightarrow D_{CP(-)} \pi^+)$ and $B(B^+ \rightarrow \bar{D}^0 K^+) / B(B^+ \rightarrow \bar{D}^0 \pi^+)$, $1.17 \pm 0.14 \pm 0.14$. We multiply by our best value of $B(B^+ \rightarrow \bar{D}^0 K^+) / B(B^+ \rightarrow \bar{D}^0 \pi^+) = 0.083 \pm 0.006$. Our first error is their experiment's error and the second error is systematic error from using our best value.

² $CP=-1$ eigenstate of $D^0 \bar{D}^0$ system is reconstructed via $K_S^0 \pi^0$, $K_S^0 \omega$, $K_S^0 \phi$, $K_S^0 \eta$, and $K_S^0 \eta'$.

$\Gamma(D_{CP(-)} K^+) / \Gamma(\bar{D}^0 K^+)$ Γ_{57}/Γ_{55}

VALUE	DOCUMENT ID	TECN	COMMENT
0.54 ±0.04±0.02	1 DEL-AMO-SA..10G	BABR	$e^+e^- \rightarrow \Upsilon(4S)$
0.515±0.05±0.025	AUBERT	08AA BABR	Repl. by DEL-AMO-SANCHEZ 10G
0.43 ±0.05±0.02	AUBERT	06J BABR	Repl. by AUBERT 08AA

¹ Reports $R_{CP+} = 1.07 \pm 0.08 \pm 0.04$ that we have divided by 2.

$\Gamma(D^0 K^+) / \Gamma(\bar{D}^0 K^+)$ Γ_{58}/Γ_{55}

"OUR EVALUATION" is derived from $r_B(B^+ \rightarrow D^0 K^+)$ data block listed in "CP violation parameters" section.

VALUE (units 10^{-3})	DOCUMENT ID
9.88±0.52 OUR EVALUATION	

$\Gamma([K^- \pi^+]_D K^+) / \Gamma_{total}$ Γ_{59}/Γ

VALUE	CL%	DOCUMENT ID	TECN	COMMENT
<2.8 × 10⁻⁷	90	HORII	08 BELL	$e^+e^- \rightarrow \Upsilon(4S)$
<6.3 × 10 ⁻⁷	90	SAIGO	05 BELL	$e^+e^- \rightarrow \Upsilon(4S)$

$\Gamma([K^- \pi^+]_D K^+) / \Gamma([K^+ \pi^-]_D K^+)$ Γ_{59}/Γ_{60}

VALUE (units 10^{-3})	CL%	DOCUMENT ID	TECN	COMMENT
14 ± 7 OUR AVERAGE	Error includes scale factor of 14.7.			
9.5±0.5±0.3	1 AAIJ	21Q LHCb	pp at 7, 8, 13 TeV	
25.2±0.8±0.4	2 AAIJ	21Q LHCb	pp at 7, 8, 13 TeV	
22.0±8.6±2.6	3 AALTONEN	11AJ CDF	$p\bar{p}$ at 1.96 TeV	
16.3 ^{+4.4+0.7} _{-4.1-1.3}		HORII	11 BELL	$e^+e^- \rightarrow \Upsilon(4S)$
11 ± 6 ± 2		DEL-AMO-SA..10H	BABR	$e^+e^- \rightarrow \Upsilon(4S)$
18.8±1.1±1.0	4 AAIJ	16L LHCb	pp at 7, 8 TeV	
15.2±2.0±0.4	AAIJ	12M LHCb	Repl. by AAIJ 16L	
7.8 ^{+6.2+2.0} _{-5.7+2.8}		HORII	08 BELL	Repl. by HORII 11
<29	90	5 AUBERT	05G BABR	Repl. by DEL-AMO-SANCHEZ 10H
<44	90	6 SAIGO	05 BELL	$e^+e^- \rightarrow \Upsilon(4S)$
<26	90	7 AUBERT,B	04L BABR	Repl. by AUBERT 05G

¹ Uses the ratio of $B^- \rightarrow [K^+ \pi^-]_D K^-$ and $B^- \rightarrow [K^- \pi^+]_D K^-$. AAIJ 21Q gives the charge-averaged rate as 0.0173 ± 0.0006 , where the statistical and systematic uncertainties have been combined according to the correlations between the observables.

² Uses the ratio of $B^+ \rightarrow [K^- \pi^+]_D K^+$ and $B^+ \rightarrow [K^+ \pi^-]_D K^+$. AAIJ 21Q gives the charge-averaged rate as 0.0173 ± 0.0006 , where the statistical and systematic uncertainties have been combined according to the correlations between the observables.

³ AALTONEN 11AJ also measures the ratio separately for $B^+ (R^+(K))$ and $B^- (R^-(K))$ and obtains: $R^+(K) = (42.6 \pm 13.7 \pm 2.8) \times 10^{-3}$, $R^-(K) = (3.8 \pm 10.3 \pm 2.7) \times 10^{-3}$.

⁴ Superseded by AAIJ 21Q.

⁵ AUBERT 05G extract a constraint on the magnitude of the ratio of amplitudes $|A(B^+ \rightarrow D^0 K^+) / A(B^+ \rightarrow \bar{D}^0 K^+)| < 0.23$ at 90% CL (Bayesian). Similar measurements from $B^+ \rightarrow D^{*0} K^+$ are also reported.

⁶ SAIGO 05 extract a constraint on the magnitude of the ratio of amplitudes $|A(B^+ \rightarrow D^0 K^+) / A(B^+ \rightarrow \bar{D}^0 K^+)| < 0.27$ at 90% CL.

⁷ AUBERT,B 04L extract a constraint on the magnitude of the ratio of amplitudes $|A(B^+ \rightarrow D^0 K^+) / A(B^+ \rightarrow \bar{D}^0 K^+)| < 0.22$ at 90% CL.

$\Gamma([K^- \pi^+]_D K^+) / \Gamma([K^+ \pi^-]_D K^+)$ Γ_{61}/Γ_{62}

VALUE (units 10^{-3})	CL%	DOCUMENT ID	TECN	COMMENT
16 ± 4 OUR AVERAGE				
14.0±4.7±2.1	1 AAIJ	15W LHCb	pp at 7, 8 TeV	
19.8±6.2±2.4		NAYAK	13 BELL	$e^+e^- \rightarrow \Upsilon(4S)$
<21	90	2 LEES	11D BABR	$e^+e^- \rightarrow \Upsilon(4S)$
<39	95	3 AUBERT	07BN BABR	Repl. by LEES 11D

¹ Uses $D^0 \rightarrow K^- \pi^+ \pi^0$ for the favored mode, and $D^0 \rightarrow K^+ \pi^- \pi^0$ for the suppressed mode.

² Extracts a constraint on the magnitude of the ratio of amplitudes $|A(B^+ \rightarrow D^0 K^+) / A(B^+ \rightarrow \bar{D}^0 K^+)| < 0.13$ at 95% CL.

³ Extracts a constraint on the magnitude of the ratio of amplitudes $|A(B^+ \rightarrow D^0 K^+) / A(B^+ \rightarrow \bar{D}^0 K^+)| < 0.19$ at 95% CL.

$\Gamma([K^- \pi^+ \pi^+ \pi^-]_D K^+) / \Gamma([K^+ \pi^- \pi^+ \pi^-]_D K^+)$ Γ_{63}/Γ_{64}

VALUE (units 10^{-2})	DOCUMENT ID	TECN	COMMENT
1.40±0.15±0.06	AAIJ	16L LHCb	pp at 7, 8 TeV
1.24±0.27	AAIJ	13AE LHCb	Repl. by AAIJ 16L

¹ We do not use the following data for averages, fits, limits, etc. ●●●

$\Gamma([K^+ \pi^- \pi^+ \pi^-] K^+) / \Gamma([K^+ \pi^- \pi^+ \pi^-]_D K^+)$ Γ_{65}/Γ_{64}

VALUE	DOCUMENT ID	TECN	COMMENT
0.975±0.037±0.019	AAIJ	16L LHCb	pp at 7, 8 TeV

See key on page 1127

Meson Particle Listings

B^{\pm}

$\Gamma([K^-\pi^+]_D K^*(892)^+)/\Gamma([K^+\pi^-]_D K^*(892)^+)$ Γ_{67}/Γ_{68}

VALUE	DOCUMENT ID	TECN	COMMENT
0.012 ± 0.004 OUR AVERAGE			
0.011 ± 0.004 ± 0.001	AAIJ	17B0	LHCB pp at 7, 8, 13 TeV
0.066 ± 0.031 ± 0.010	AUBERT	09AJ	BABR $e^+e^- \rightarrow \Upsilon(4S)$
• • • We do not use the following data for averages, fits, limits, etc. • • •			
0.046 ± 0.031 ± 0.008	AUBERT,B	05V	BABR Repl. by AUBERT 09AJ

$\Gamma([K^-\pi^+\pi^-\pi^+]_D K^*(892)^+)/\Gamma([K^+\pi^-\pi^+\pi^-]_D K^*(892)^+)$ Γ_{69}/Γ_{70}

VALUE	DOCUMENT ID	TECN	COMMENT
0.011 ± 0.005 ± 0.003			
	AAIJ	17B0	LHCB pp at 7, 8, 13 TeV

$\Gamma([K^+\pi^-\pi^+\pi^-]_D K^*(892)^+)/\Gamma([K^+\pi^-\pi^+\pi^-]_D K^*(892)^+)$ Γ_{66}/Γ_{70}

VALUE	DOCUMENT ID	TECN	COMMENT
1.08 ± 0.13 ± 0.03			
	AAIJ	17B0	LHCB pp at 7, 8, 13 TeV

$\Gamma([K^-\pi^+]_D \pi^+)/\Gamma_{total}$ Γ_{71}/Γ

VALUE (units 10^{-7})	DOCUMENT ID	TECN	COMMENT
6.29 $^{+1.02}_{-0.96} \pm 0.37 \pm 0.48$			
	HORII	08	BELL $e^+e^- \rightarrow \Upsilon(4S)$
• • • We do not use the following data for averages, fits, limits, etc. • • •			
6.6 $^{+1.9}_{-1.7} \pm 0.5$	SAIGO	05	BELL Repl. by HORII 08

$\Gamma([K^-\pi^+]_D \pi^+)/\Gamma([K^+\pi^-]_D \pi^+)$ Γ_{71}/Γ_{72}

VALUE (units 10^{-3})	DOCUMENT ID	TECN	COMMENT
3.6 ± 0.5 OUR AVERAGE			Error includes scale factor of 7.9.
4.15 ± 0.08 ± 0.04	¹ AAIJ	21Q	LHCB pp at 7, 8, 13 TeV
3.20 ± 0.07 ± 0.04	² AAIJ	21Q	LHCB pp at 7, 8, 13 TeV
2.8 ± 0.7 ± 0.4	³ AALTONEN	11AJ	CDF $p\bar{p}$ at 1.96 TeV
3.28 $^{+0.38}_{-0.36} \pm 0.12 \pm 0.18$	HORII	11	BELL $e^+e^- \rightarrow \Upsilon(4S)$
3.3 ± 0.6 ± 0.4	DEL-AMO-SA...	10H	BABR $e^+e^- \rightarrow \Upsilon(4S)$
• • • We do not use the following data for averages, fits, limits, etc. • • •			
3.60 ± 0.12 ± 0.09	⁴ AAIJ	16L	LHCB pp at 7, 8 TeV
4.10 ± 0.25 ± 0.05	AAIJ	12M	LHCB Repl. by AAIJ 16L
3.40 $^{+0.55}_{-0.53} \pm 0.15 \pm 0.22$	HORII	08	BELL Repl. by HORII 11
3.5 $^{+1.0}_{-0.9} \pm 0.2$	SAIGO	05	BELL Repl. by HORII 08

- 1 Uses the ratio of $B^- \rightarrow [K^+\pi^-]_D K^-$ and $B^- \rightarrow [K^-\pi^+]_D K^-$. AAJ 21Q gives the charge-averaged rate as 0.00368 ± 0.00007 , where the statistical and systematic uncertainties have been combined according to the correlations between the observables.
- 2 Uses the ratio of $B^+ \rightarrow [K^-\pi^+]_D \pi^+$ and $B^+ \rightarrow [K^+\pi^-]_D \pi^+$. AAJ 21Q gives the charge-averaged rate as 0.00368 ± 0.00007 , where the statistical and systematic uncertainties have been combined according to the correlations between the observables.
- 3 AALTONEN 11AJ also measures the ratio separately for $B^+ (R^+(\pi))$ and $B^- (R^-(\pi))$ and obtains: $R^+(\pi) = (2.4 \pm 1.0 \pm 0.4) \times 10^{-3}$, $R^-(\pi) = (3.1 \pm 1.1 \pm 0.4) \times 10^{-3}$.
- 4 Superseded by AAJ 21Q.

$\Gamma([K^-\pi^+\pi^0]_D \pi^+)/\Gamma([K^+\pi^-\pi^0]_D \pi^+)$ Γ_{73}/Γ_{74}

VALUE (units 10^{-3})	DOCUMENT ID	TECN	COMMENT
2.2 ± 0.4 OUR AVERAGE			
2.35 ± 0.49 ± 0.06	¹ AAIJ	15W	LHCB pp at 7, 8 TeV
1.89 ± 0.54 $^{+0.22}_{-0.25}$	NAYAK	13	BELL $e^+e^- \rightarrow \Upsilon(4S)$
¹ Uses $D^0 \rightarrow K^-\pi^+\pi^0$ for the favored mode, and $D^0 \rightarrow K^+\pi^-\pi^0$ for the suppressed mode.			

$\Gamma([K^-\pi^+\pi^+\pi^-]_D \pi^+)/\Gamma([K^+\pi^-\pi^+\pi^-]_D \pi^+)$ Γ_{75}/Γ_{76}

VALUE (units 10^{-3})	DOCUMENT ID	TECN	COMMENT
3.77 ± 0.18 ± 0.06			
	AAIJ	16L	LHCB pp at 7, 8 TeV
• • • We do not use the following data for averages, fits, limits, etc. • • •			
3.7 ± 0.4	AAIJ	13AE	LHCB Repl. by AAIJ 16L

$\Gamma([K^-\pi^+]_{(D\pi)} \pi^+)/\Gamma([K^+\pi^-]_{(D\pi)} \pi^+)$ Γ_{77}/Γ_{78}

VALUE (units 10^{-3})	DOCUMENT ID	TECN	COMMENT
4.4 ± 0.6 OUR AVERAGE			Error includes scale factor of 1.1.
4.05 ± 0.56 ± 0.59	¹ AAIJ	21Q	LHCB pp at 7, 8, 13 TeV
5.36 ± 0.56 ± 0.58	² AAIJ	21Q	LHCB pp at 7, 8, 13 TeV
3.2 ± 0.9 ± 0.8	DEL-AMO-SA...	10H	BABR $e^+e^- \rightarrow \Upsilon(4S)$
¹ Uses the ratio of $B^- \rightarrow ([K^+\pi^-]_D \pi^0)_{D^*} \pi^-$ and $B^- \rightarrow ([K^-\pi^+]_D \pi^0)_{D^*} \pi^-$, without inclusion of the neutral pion in the reconstruction. AAJ 21Q gives the charge-averaged rate as 0.00471 ± 0.00077 , where the statistical and systematic uncertainties have been combined according to the correlations between the observables.			
² Uses the ratio of $B^+ \rightarrow ([K^+\pi^-]_D \pi^0)_{D^*} \pi^+$ and $B^+ \rightarrow ([K^-\pi^+]_D \pi^0)_{D^*} \pi^+$, without inclusion of the neutral pion in the reconstruction. AAJ 21Q gives the charge-averaged rate as 0.00471 ± 0.00077 , where the statistical and systematic uncertainties have been combined according to the correlations between the observables.			

$\Gamma([K^-\pi^+]_{(D\gamma)} \pi^+)/\Gamma([K^+\pi^-]_{(D\gamma)} \pi^+)$ Γ_{79}/Γ_{80}

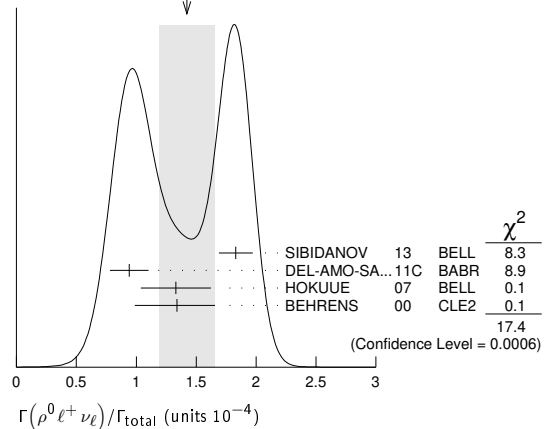
VALUE (units 10^{-3})	DOCUMENT ID	TECN	COMMENT
4.1 ± 1.0 OUR AVERAGE			
4.72 ± 0.92 ± 1.18	¹ AAIJ	21Q	LHCB pp at 7, 8, 13 TeV
4.03 ± 0.91 ± 1.14	² AAIJ	21Q	LHCB pp at 7, 8, 13 TeV
2.7 ± 1.4 ± 2.2	DEL-AMO-SA...	10H	BABR $e^+e^- \rightarrow \Upsilon(4S)$

- 1 Uses the ratio of $B^- \rightarrow ([K^+\pi^-]_{D\gamma})_{D^*} \pi^-$ and $B^- \rightarrow ([K^-\pi^+]_{D\gamma})_{D^*} \pi^-$, without inclusion of the photon in the reconstruction. AAJ 21Q gives the charge-averaged rate as 0.00420 ± 0.00138 , where the statistical and systematic uncertainties have been combined according to the correlations between the observables.
- 2 Uses the ratio of $B^+ \rightarrow ([K^+\pi^-]_{D\gamma})_{D^*} \pi^+$ and $B^+ \rightarrow ([K^-\pi^+]_{D\gamma})_{D^*} \pi^+$, without inclusion of the photon in the reconstruction. AAJ 21Q gives the charge-averaged rate as 0.00420 ± 0.00138 , where the statistical and systematic uncertainties have been combined according to the correlations between the observables.

$\Gamma([K^-\pi^+]_{(D\pi)} K^+)/\Gamma([K^+\pi^-]_{(D\pi)} K^+)$ Γ_{81}/Γ_{82}

VALUE (units 10^{-3})	DOCUMENT ID	TECN	COMMENT
2.8 ± 2.8 OUR AVERAGE			Error includes scale factor of 3.0. See the ideogram below.
20.2 ± 3.5 ± 2.3	¹ AAIJ	21Q	LHCB pp at 7, 8, 13 TeV
3.3 ± 3.5 ± 2.2	² AAIJ	21Q	LHCB pp at 7, 8, 13 TeV
1.8 ± 0.9 ± 0.4	DEL-AMO-SA...	10H	BABR $e^+e^- \rightarrow \Upsilon(4S)$

WEIGHTED AVERAGE
1.42 ± 0.23 (Error scaled by 2.4)



- 1 Uses the ratio of $B^- \rightarrow ([K^+\pi^-]_D \pi^0)_{D^*} K^-$ and $B^- \rightarrow ([K^-\pi^+]_D \pi^0)_{D^*} K^-$, without inclusion of the neutral pion in the reconstruction. AAJ 21Q gives the charge-averaged rate as 0.0118 ± 0.0034 , where the statistical and systematic uncertainties have been combined according to the correlations between the observables.
- 2 Uses the ratio of $B^+ \rightarrow ([K^+\pi^-]_D \pi^0)_{D^*} \pi^+$ and $B^+ \rightarrow ([K^-\pi^+]_D \pi^0)_{D^*} \pi^+$, without inclusion of the neutral pion in the reconstruction. AAJ 21Q gives the charge-averaged rate as 0.0118 ± 0.0034 , where the statistical and systematic uncertainties have been combined according to the correlations between the observables.

$\Gamma([K^-\pi^+]_{(D\gamma)} K^+)/\Gamma([K^+\pi^-]_{(D\gamma)} K^+)$ Γ_{83}/Γ_{84}

VALUE (units 10^{-3})	DOCUMENT ID	TECN	COMMENT
1.4 ± 1.6 OUR AVERAGE			
11.7 ± 21.5 ± 31.3	¹ AAIJ	21Q	LHCB pp at 7, 8, 13 TeV
29.2 ± 21.4 ± 31.2	² AAIJ	21Q	LHCB pp at 7, 8, 13 TeV
1.3 ± 1.4 ± 0.8	DEL-AMO-SA...	10H	BABR $e^+e^- \rightarrow \Upsilon(4S)$

- 1 Uses the ratio of $B^- \rightarrow ([K^+\pi^-]_{D\gamma})_{D^*} K^-$ and $B^- \rightarrow ([K^-\pi^+]_{D\gamma})_{D^*} K^-$, without inclusion of the photon in the reconstruction. AAJ 21Q gives the charge-averaged rate as 0.0163 ± 0.0373 , where the statistical and systematic uncertainties have been combined according to the correlations between the observables.
- 2 Uses the ratio of $B^+ \rightarrow ([K^+\pi^-]_{D\gamma})_{D^*} K^+$ and $B^+ \rightarrow ([K^-\pi^+]_{D\gamma})_{D^*} K^+$, without inclusion of the photon in the reconstruction. AAJ 21Q gives the charge-averaged rate as 0.0163 ± 0.0373 , where the statistical and systematic uncertainties have been combined according to the correlations between the observables.

$\Gamma([\pi^+\pi^-\pi^0]_D K^-)/\Gamma_{total}$ Γ_{85}/Γ

VALUE (units 10^{-6})	DOCUMENT ID	TECN	COMMENT
4.6 ± 0.8 ± 0.4			
	¹ AUBERT	07BJ	BABR $e^+e^- \rightarrow \Upsilon(4S)$
• • • We do not use the following data for averages, fits, limits, etc. • • •			
5.5 ± 1.0 ± 0.7	¹ AUBERT,B	05T	BABR Repl. by AUBERT 07BJ
¹ Assumes equal production of B^+ and B^0 at the $\Upsilon(4S)$.			

Meson Particle Listings

 B^\pm $\Gamma([K_S^0 K^+ \pi^-]_D K^+)/\Gamma([K_S^0 K^+ \pi^-]_D \pi^+)$ Γ_{86}/Γ_{92}

VALUE	DOCUMENT ID	TECN	COMMENT
0.092 ± 0.009 ± 0.004	¹ AAIJ	14v	LHCB <i>pp</i> at 7, 8 TeV

••• We do not use the following data for averages, fits, limits, etc. •••

0.081 ± 0.008 ± 0.004	² AAIJ	20n	LHCB <i>pp</i> at 7, 8, 13 TeV
-----------------------	-------------------	-----	--------------------------------

¹ The analysis uses all of $D \rightarrow K_S^0 K \pi$ Dalitz decays.

² The analysis uses $D \rightarrow K_S^0 K \pi$ Dalitz decays with $K^* K^+$ region excluded.

 $\Gamma([K_S^0 K^- \pi^+]_D K^+)/\Gamma([K_S^0 K^- \pi^+]_D \pi^+)$ Γ_{88}/Γ_{90}

VALUE	DOCUMENT ID	TECN	COMMENT
0.066 ± 0.009 ± 0.002	¹ AAIJ	14v	LHCB <i>pp</i> at 7, 8 TeV

••• We do not use the following data for averages, fits, limits, etc. •••

0.073 ± 0.006 ± 0.002	² AAIJ	20n	LHCB <i>pp</i> at 7, 8, 13 TeV
-----------------------	-------------------	-----	--------------------------------

¹ The analysis uses all of $D \rightarrow K_S^0 K \pi$ Dalitz decays.

² The analysis uses $D \rightarrow K_S^0 K \pi$ Dalitz decays with $K^* K^+$ region excluded.

 $\Gamma([K^*(892)^- K^+]_D K^+)/\Gamma([K^*(892)^- K^+]_D \pi^+)$ Γ_{87}/Γ_{93}

VALUE	DOCUMENT ID	TECN	COMMENT
0.079 ± 0.004 ± 0.002	¹ AAIJ	20n	LHCB <i>pp</i> at 7, 8, 13 TeV

••• We do not use the following data for averages, fits, limits, etc. •••

0.084 ± 0.011 ± 0.003	¹ AAIJ	14v	LHCB Repl. by AAIJ 20n
-----------------------	-------------------	-----	------------------------

¹ The Analysis uses $D \rightarrow K^*(892) K \rightarrow K_S^0 K \pi$ decays.

 $\Gamma([K^*(892)^+ K^-]_D K^+)/\Gamma([K^*(892)^+ K^-]_D \pi^+)$ Γ_{89}/Γ_{91}

VALUE	DOCUMENT ID	TECN	COMMENT
0.062 ± 0.006 ± 0.003	¹ AAIJ	20n	LHCB <i>pp</i> at 7, 8, 13 TeV

••• We do not use the following data for averages, fits, limits, etc. •••

0.056 ± 0.013 ± 0.002	¹ AAIJ	14v	LHCB Repl. by AAIJ 20n
-----------------------	-------------------	-----	------------------------

¹ The Analysis uses $D \rightarrow K^*(892) K \rightarrow K_S^0 K \pi$ decays.

 $\Gamma([K^+ K^- \pi^0]_D K^+)/\Gamma([K^+ K^- \pi^0]_D \pi^+)$ Γ_{94}/Γ_{95}

VALUE	DOCUMENT ID	TECN	COMMENT
0.95 ± 0.22 ± 0.05	¹ AAIJ	15w	LHCB <i>pp</i> at 7, 8 TeV

¹ Uses $D \rightarrow K^+ K^- \pi^0$ mode.

 $\Gamma([\pi^+ \pi^- \pi^0]_D K^+)/\Gamma([\pi^+ \pi^- \pi^0]_D \pi^+)$ Γ_{96}/Γ_{97}

VALUE	DOCUMENT ID	TECN	COMMENT
0.98 ± 0.11 ± 0.05	¹ AAIJ	15w	LHCB <i>pp</i> at 7, 8 TeV

¹ Uses $D \rightarrow \pi^+ \pi^- \pi^0$ mode.

 $\Gamma([K_S^0 K^+ \pi^-]_D \pi^+)/\Gamma([K_S^0 K^+ \pi^-]_D \pi^+)$ Γ_{92}/Γ_{90}

VALUE	DOCUMENT ID	TECN	COMMENT
1.528 ± 0.058 ± 0.025	¹ AAIJ	14v	LHCB <i>pp</i> at 7, 8 TeV

••• We do not use the following data for averages, fits, limits, etc. •••

0.706 ± 0.019 ± 0.009	² AAIJ	20n	LHCB <i>pp</i> at 7, 8, 13 TeV
-----------------------	-------------------	-----	--------------------------------

¹ The analysis uses all of $D \rightarrow K_S^0 K \pi$ Dalitz decays.

² The analysis uses $D \rightarrow K_S^0 K \pi$ Dalitz decays with $K^* K^+$ region excluded.

 $\Gamma([K^*(892)^- K^+]_D \pi^+)/\Gamma([K^*(892)^+ K^-]_D \pi^+)$ Γ_{93}/Γ_{91}

VALUE	DOCUMENT ID	TECN	COMMENT
2.585 ± 0.057 ± 0.019	¹ AAIJ	20n	LHCB <i>pp</i> at 7, 8, 13 TeV

••• We do not use the following data for averages, fits, limits, etc. •••

2.57 ± 0.13 ± 0.06	¹ AAIJ	14v	LHCB Repl. by AAIJ 20n
--------------------	-------------------	-----	------------------------

¹ The Analysis uses $D \rightarrow K^*(892) K \rightarrow K_S^0 K \pi$ decays.

 $\Gamma(\bar{D}^0 K^*(892)^+)/\Gamma_{\text{total}}$ Γ_{98}/Γ

VALUE (units 10 ⁻⁴)	DOCUMENT ID	TECN	COMMENT
5.3 ± 0.4 OUR AVERAGE			

5.29 ± 0.30 ± 0.34	¹ AUBERT	06z	BABR $e^+ e^- \rightarrow \Upsilon(4S)$
--------------------	---------------------	-----	---

6.1 ± 1.6 ± 1.7	¹ MAHAPATRA	02	CLE2 $e^+ e^- \rightarrow \Upsilon(4S)$
-----------------	------------------------	----	---

••• We do not use the following data for averages, fits, limits, etc. •••

6.3 ± 0.7 ± 0.5	¹ AUBERT	04q	BABR Repl. by AUBERT 06z
-----------------	---------------------	-----	--------------------------

¹ Assumes equal production of B^+ and B^0 at the $\Upsilon(4S)$.

 $\Gamma(D_{CP(-)} K^*(892)^+)/\Gamma(\bar{D}^0 K^*(892)^+)$ Γ_{99}/Γ_{98}

VALUE	DOCUMENT ID	TECN	COMMENT
0.515 ± 0.135 ± 0.065	¹ AUBERT	09AJ	BABR $e^+ e^- \rightarrow \Upsilon(4S)$

••• We do not use the following data for averages, fits, limits, etc. •••

0.325 ± 0.13 ± 0.04	² AUBERT,B	05U	BABR Repl. by AUBERT 09AJ
---------------------	-----------------------	-----	---------------------------

¹ The authors report $R_{CP-} = 1.03 \pm 0.27 \pm 0.13$ which is, assuming CP conservation, twice the value of the quoted above branching ratio,

² The authors report $R_{CP-} = 0.65 \pm 0.26 \pm 0.08$ which is, assuming CP conservation, twice the value of the quoted above branching ratio.

 $\Gamma(D_{CP(+)} K^*(892)^+)/\Gamma(\bar{D}^0 K^*(892)^+)$ Γ_{100}/Γ_{98}

VALUE	DOCUMENT ID	TECN	COMMENT
1.16 ± 0.08 OUR AVERAGE			

1.18 ± 0.08 ± 0.02	¹ AAIJ	18x	LHCB <i>pp</i> at 7, 8, 13 TeV
--------------------	-------------------	-----	--------------------------------

1.085 ± 0.175 ± 0.045	² AUBERT	09AJ	BABR $e^+ e^- \rightarrow \Upsilon(4S)$
-----------------------	---------------------	------	---

••• We do not use the following data for averages, fits, limits, etc. •••

1.18 ± 0.08 ± 0.01	³ AAIJ	17Bo	LHCB Repl. by AAIJ 18x
--------------------	-------------------	------	------------------------

0.98 ± 0.20 ± 0.055	⁴ AUBERT,B	05U	BABR Repl. by AUBERT 09AJ
---------------------	-----------------------	-----	---------------------------

¹ Measures the ratio separately for $K^+ K^-$ and $\pi^+ \pi^-$ final states, $R_{KK} = 1.22 \pm 0.09 \pm 0.02$ and $R_{\pi\pi} = 1.08 \pm 0.14 \pm 0.03$, and combines the two results.

² The authors report $R_{CP+} = 2.17 \pm 0.35 \pm 0.09$ which is, assuming CP conservation, twice the value of the quoted above branching ratio,

³ Measures the ratio separately for $K^+ K^-$ and $\pi^+ \pi^-$ final states, $R_{KK} = 1.22 \pm 0.09 \pm 0.01$ and $R_{\pi\pi} = 1.08 \pm 0.14 \pm 0.03$, and combines the two results.

⁴ The authors report $R_{CP+} = 1.96 \pm 0.40 \pm 0.11$ which is, assuming CP conservation, twice the value of the quoted above branching ratio.

 $\Gamma(\bar{D}^0 K^*(892)^+)/\Gamma(\bar{D}^0 K^*(892)^+)$ Γ_{101}/Γ_{98}

"OUR EVALUATION" is derived from $r_{B^+} (B^+ \rightarrow D^0 K^{*+})$ data block listed in "CP violation parameters" section.

VALUE (units 10 ⁻³)	DOCUMENT ID
---------------------------------	-------------

10.2^{+3.2}_{-6.9} OUR EVALUATION

VALUE (units 10 ⁻²)	DOCUMENT ID	TECN	COMMENT
---------------------------------	-------------	------	---------

9.4 ± 1.3 ± 0.9	AAIJ	12t	LHCB <i>pp</i> at 7 TeV
------------------------	------	-----	-------------------------

 $\Gamma(\bar{D}^0 K^+ \pi^+ \pi^-)/\Gamma(\bar{D}^0 \pi^+ \pi^+ \pi^-)$ $\Gamma_{102}/\Gamma_{108}$

VALUE (units 10 ⁻²)	DOCUMENT ID	TECN	COMMENT
---------------------------------	-------------	------	---------

9.4 ± 1.3 ± 0.9	AAIJ	12t	LHCB <i>pp</i> at 7 TeV
------------------------	------	-----	-------------------------

 $\Gamma(D_{CP(+)} K^+ \pi^- \pi^+)/\Gamma([K^+ \pi^-]_D K^+ \pi^- \pi^+)$ $\Gamma_{105}/\Gamma_{103}$

VALUE	DOCUMENT ID	TECN	COMMENT
-------	-------------	------	---------

1.040 ± 0.064	AAIJ	15bc	LHCB <i>pp</i> at 7, 8 TeV
----------------------	------	------	----------------------------

 $\Gamma([K^- \pi^+]_D K^+ \pi^- \pi^+)/\Gamma([K^+ \pi^-]_D K^+ \pi^- \pi^+)$ $\Gamma_{104}/\Gamma_{103}$

VALUE (units 10 ⁻⁴)	DOCUMENT ID	TECN	COMMENT
---------------------------------	-------------	------	---------

85⁺³⁶₋₃₃	AAIJ	15bc	LHCB <i>pp</i> at 7, 8 TeV
---------------------------------------	------	------	----------------------------

 $\Gamma(\bar{D}^0 K^+ \bar{K}^0)/\Gamma_{\text{total}}$ Γ_{106}/Γ

VALUE (units 10 ⁻⁴)	DOCUMENT ID	TECN	COMMENT
---------------------------------	-------------	------	---------

5.5 ± 1.4 ± 0.8	¹ DRUTSKOY	02	BELL $e^+ e^- \rightarrow \Upsilon(4S)$
------------------------	-----------------------	----	---

¹ Assumes equal production of B^+ and B^0 at the $\Upsilon(4S)$.

 $\Gamma(\bar{D}^0 K^+ \bar{K}^*(892)^0)/\Gamma_{\text{total}}$ Γ_{107}/Γ

VALUE (units 10 ⁻⁴)	DOCUMENT ID	TECN	COMMENT
---------------------------------	-------------	------	---------

7.5 ± 1.3 ± 1.1	¹ DRUTSKOY	02	BELL $e^+ e^- \rightarrow \Upsilon(4S)$
------------------------	-----------------------	----	---

¹ Assumes equal production of B^+ and B^0 at the $\Upsilon(4S)$.

 $\Gamma(\bar{D}^0 \pi^+ \pi^+ \pi^-)/\Gamma_{\text{total}}$ Γ_{108}/Γ

VALUE	DOCUMENT ID	TECN	COMMENT
-------	-------------	------	---------

0.0056 ± 0.0021 OUR FIT	Error includes scale factor of 3.6.		
--------------------------------	-------------------------------------	--	--

0.0115 ± 0.0029 ± 0.0021	¹ BORTOLETTO92	CLEO	$e^+ e^- \rightarrow \Upsilon(4S)$
---------------------------------	---------------------------	------	------------------------------------

¹ BORTOLETTO 92 assumes equal production of B^+ and B^0 at the $\Upsilon(4S)$ and uses Mark III branching fractions for the D .

 $\Gamma([K^- \pi^+]_D \pi^+ \pi^- \pi^+)/\Gamma([K^+ \pi^-]_D K^+ \pi^- \pi^+)$ $\Gamma_{109}/\Gamma_{103}$

VALUE (units 10 ⁻⁴)	DOCUMENT ID	TECN	COMMENT
---------------------------------	-------------	------	---------

42.7 ± 5.6	AAIJ	15bc	LHCB <i>pp</i> at 7, 8 TeV
-------------------	------	------	----------------------------

 $\Gamma(\bar{D}^0 \pi^+ \pi^+ \pi^- \text{ nonresonant})/\Gamma_{\text{total}}$ Γ_{110}/Γ

VALUE	DOCUMENT ID	TECN	COMMENT
-------	-------------	------	---------

0.0051 ± 0.0034 ± 0.0023	¹ BORTOLETTO92	CLEO	$e^+ e^- \rightarrow \Upsilon(4S)$
---------------------------------	---------------------------	------	------------------------------------

¹ BORTOLETTO 92 assumes equal production of B^+ and B^0 at the $\Upsilon(4S)$ and uses Mark III branching fractions for the D .

 $\Gamma(\bar{D}^0 \pi^+ \rho^0)/\Gamma_{\text{total}}$ Γ_{111}/Γ

VALUE	DOCUMENT ID	TECN	COMMENT
-------	-------------	------	---------

0.0042 ± 0.0023 ± 0.0020	¹ BORTOLETTO92	CLEO	$e^+ e^- \rightarrow \Upsilon(4S)$
---------------------------------	---------------------------	------	------------------------------------

¹ BORTOLETTO 92 assumes equal production of B^+ and B^0 at the $\Upsilon(4S)$ and uses Mark III branching fractions for the D .

 $\Gamma(\bar{D}^0 a_1(1260)^+)/\Gamma_{\text{total}}$ Γ_{112}/Γ

VALUE	DOCUMENT ID	TECN	COMMENT
-------	-------------	------	---------

0.0045 ± 0.0019 ± 0.0031	¹ BORTOLETTO92	CLEO	$e^+ e^- \rightarrow \Upsilon(4S)$
---------------------------------	---------------------------	------	------------------------------------

¹ BORTOLETTO 92 assumes equal production of B^+ and B^0 at the $\Upsilon(4S)$ and uses Mark III branching fractions for the D .

See key on page 1127

Meson Particle Listings
B \pm

Gamma(B0 omega pi+) / Gamma total
VALUE DOCUMENT_ID TECN COMMENT
0.0041 +/- 0.0007 +/- 0.0006 1 ALEXANDER 01B CLE2 e+ e- -> Gamma(4S)

1 Assumes equal production of B+ and B0 at the Gamma(4S). The signal is consistent with all observed omega pi+ having proceeded through the rho+ resonance at mass 1349 +/- 25 +/- 10 MeV and width 547 +/- 86 +/- 46 MeV.

Gamma(D*(2010)- pi+ pi+) / Gamma total
VALUE (units 10^-3) CL% EVTS DOCUMENT_ID TECN COMMENT
1.35 +/- 0.22 OUR AVERAGE
1.25 +/- 0.08 +/- 0.22 1 ABE 04D BELL e+ e- -> Gamma(4S)
1.9 +/- 0.7 +/- 0.3 14 2 ALAM 94 CLE2 e+ e- -> Gamma(4S)
2.6 +/- 1.4 +/- 0.7 11 3 ALBRECHT 90J ARG e+ e- -> Gamma(4S)
2.4 +/- 1.7 +/- 1.0 +/- 1.6 +/- 0.6 3 4 BEBEK 87 CLEO e+ e- -> Gamma(4S)

• • • We do not use the following data for averages, fits, limits, etc. • • •
<4. 90 5 BORTOLETTO92 CLEO e+ e- -> Gamma(4S)
5. +/- 2. +/- 3. 7 6 ALBRECHT 87C ARG e+ e- -> Gamma(4S)
1 Assumes equal production of B+ and B0 at the Gamma(4S).
2 ALAM 94 assume equal production of B+ and B0 at the Gamma(4S) and use the CLEO II B(D*(2010)+ -> D0 pi+) and absolute B(D0 -> K- pi+) and the PDG 1992 B(D0 -> K- pi+ pi0) / B(D0 -> K- pi+) and B(D0 -> K- 2pi+ pi-) / B(D0 -> K- pi+).
3 Assumes equal production of B+ and B0 at the Gamma(4S) and uses the Mark III branching fractions for the D.
4 BEBEK 87 value has been updated in BERKELMAN 91 to use same assumptions as noted for BORTOLETTO 92.
5 BORTOLETTO 92 assumes equal production of B+ and B0 at the Gamma(4S) and uses Mark III branching fractions for the D and D*(2010). The authors also find the product branching fraction into D** pi followed by D** -> D*(2010) pi to be 0.0014 +/- 0.0008 +/- 0.0003 where D** represents all orbitally excited D mesons.
6 ALBRECHT 87C use PDG 86 branching ratios for D and D*(2010) and assume B(Gamma(4S) -> B+ B-) = 55% and B(Gamma(4S) -> B0 B0) = 45%. Superseded by ALBRECHT 90J.

Gamma(D*(2010)- K+ pi+) / Gamma total
VALUE (units 10^-5) DOCUMENT_ID TECN COMMENT
8.2 +/- 0.3 +/- 1.4 1 AAIJ 17AR LHCB pp at 7, 8 TeV
1 The branching fraction of the normalization mode B+ -> D** pi+ pi+ is rescaled to the updated ratio of Gamma(4S) -> B+ B- to Gamma(4S) -> B0 B0 decay rates of 1.058 +/- 0.024.

Gamma(D*(2010)- K+ pi+) / Gamma(D*(2010)- pi+ pi+)
VALUE (units 10^-2) DOCUMENT_ID TECN COMMENT
6.39 +/- 0.27 +/- 0.48 1 AAIJ 17AR LHCB pp at 7, 8 TeV
1 Uses D** -> D0 pi- and D0 -> K+ pi- decays.

Gamma(D1(2420)0 pi+, D1 -> D*(2010)- pi+) / Gamma total
VALUE (units 10^-4) DOCUMENT_ID TECN COMMENT
8.4 +/- 0.08 +/- 1.46 1 AAIJ 20D LHCB pp at 7, 8, 13 TeV
1 AAIJ 20D used a 4-body amplitude analysis of B- -> D** pi- pi- decays.

Gamma(D1(2420)0 pi+, D1 -> D*(2010)- pi+) / Gamma(D0 pi+ pi+ pi-)
VALUE (units 10^-2) DOCUMENT_ID TECN COMMENT
9.3 +/- 1.6 +/- 0.9 1 AAIJ 11E LHCB pp at 7 TeV
1 AAIJ 11E reports (9.3 +/- 1.6 +/- 0.9) x 10^-2 from a measurement of [Gamma(B+ -> D1(2420)0 pi+, D1 -> D*(2010)- pi+) / Gamma(B+ -> D0 pi+ pi+ pi-)] x [B(D*(2010)+ -> D0 pi+)] assuming B(D*(2010)+ -> D0 pi+) = (67.7 +/- 0.5) x 10^-2.

Gamma(D- pi+ pi+) / Gamma total
VALUE (units 10^-3) CL% EVTS DOCUMENT_ID TECN COMMENT
1.07 +/- 0.05 OUR AVERAGE
1.08 +/- 0.03 +/- 0.05 1 AUBERT 09AB BABR e+ e- -> Gamma(4S)
1.02 +/- 0.04 +/- 0.15 1 ABE 04D BELL e+ e- -> Gamma(4S)
<1.4 90 2 ALAM 94 CLE2 e+ e- -> Gamma(4S)
<7 90 3 BORTOLETTO92 CLEO e+ e- -> Gamma(4S)
2.5 +/- 4.1 +/- 2.4 +/- 2.3 +/- 0.8 1 4 BEBEK 87 CLEO e+ e- -> Gamma(4S)

1 Assumes equal production of B+ and B0 at the Gamma(4S).
2 ALAM 94 assume equal production of B+ and B0 at the Gamma(4S) and use the Mark III B(D+ -> K- 2pi+).
3 BORTOLETTO 92 assumes equal production of B+ and B0 at the Gamma(4S) and uses Mark III branching fractions for the D. The product branching fraction into D0*(2340) pi followed by D0*(2340) -> D pi is < 0.005 at 90%CL and into D2*(2460) followed by D2*(2460) -> D pi is < 0.004 at 90%CL.
4 BEBEK 87 assume the Gamma(4S) decays 43% to B0 B0. B(D- -> K+ pi- pi-) = (9.1 +/- 1.3 +/- 0.4)% is assumed.

Gamma(D- K+ pi+) / Gamma(D- pi+ pi+)
VALUE (units 10^-2) DOCUMENT_ID TECN COMMENT
7.20 +/- 0.19 +/- 0.21 AAIJ 15V LHCB pp at 7, 8 TeV

Gamma(D0*(2300)0 K+, D0* -> D- pi+) / Gamma total
VALUE (units 10^-6) DOCUMENT_ID TECN COMMENT
6.1 +/- 1.9 +/- 1.5 1 AAIJ 15V LHCB pp at 7, 8 TeV
1 Performs the amplitude analysis by fitting the square-Dalitz-plot distribution.

Gamma(D2*(2460)0 K+, D2* -> D- pi+) / Gamma total
VALUE (units 10^-6) DOCUMENT_ID TECN COMMENT
23.2 +/- 1.1 +/- 2.0 1 AAIJ 15V LHCB pp at 7, 8 TeV
1 Performs the amplitude analysis by fitting the square-Dalitz-plot distribution.

Gamma(D1*(2760)0 K+, D1* -> D- pi+) / Gamma total
VALUE (units 10^-6) DOCUMENT_ID TECN COMMENT
3.6 +/- 0.9 +/- 0.8 1 AAIJ 15V LHCB pp at 7, 8 TeV
1 Performs the amplitude analysis by fitting the square-Dalitz-plot distribution.

Gamma(D+ K0) / Gamma total
VALUE (units 10^-6) CL% DOCUMENT_ID TECN COMMENT
<2.9 90 1 DEL-AMO-SA...10k BABR e+ e- -> Gamma(4S)
<5.0 90 1 AUBERT,B 05E BABR Repl. by DEL-AMO-SANCHEZ 10k
1 Assumes equal production of B+ and B0 at the Gamma(4S).

Gamma(D+ K+ pi-) / Gamma(D- K+ pi-)
VALUE (units 10^-2) DOCUMENT_ID TECN COMMENT
7.3 +/- 1.2 +/- 0.7 AAIJ 16M LHCB pp at 7, 8 TeV

Gamma(D2*(2460)0 K+, D2* -> D+ pi-) / Gamma total
VALUE CL% DOCUMENT_ID TECN COMMENT
<6.3 x 10^-7 90 AAIJ 16R LHCB pp at 7, 8 TeV

Gamma(D+ K*0) / Gamma total
VALUE CL% DOCUMENT_ID TECN COMMENT
<4.9 x 10^-7 90 AAIJ 16M LHCB pp at 7, 8 TeV
<1.8 x 10^-6 90 AAIJ 13R LHCB Repl. by AAIJ 16M
<3.0 x 10^-6 90 1 DEL-AMO-SA...10k BABR e+ e- -> Gamma(4S)
1 Assumes equal production of B+ and B0 at the Gamma(4S).

Gamma(D+ K*0) / Gamma total
VALUE (units 10^-6) CL% DOCUMENT_ID TECN COMMENT
<1.4 90 AAIJ 13R LHCB pp at 7 TeV

Gamma(D*(2007)0 pi+) / Gamma total
VALUE (units 10^-3) EVTS DOCUMENT_ID TECN COMMENT
5.18 +/- 0.15 OUR AVERAGE
5.35 +/- 0.04 +/- 0.22 AAIJ 21Q LHCB pp at 7, 8, 13 TeV
4.82 +/- 0.12 +/- 0.35 1 KATO 18 BELL e+ e- -> Gamma(4S)
5.52 +/- 0.17 +/- 0.42 2 AUBERT 07H BABR e+ e- -> Gamma(4S)
5.3 +/- 0.4 +/- 0.1 3,4 AUBERT,BE 06J BABR e+ e- -> Gamma(4S)
4.34 +/- 0.47 +/- 0.18 5 BRANDENB... 98 CLE2 e+ e- -> Gamma(4S)
5.2 +/- 0.7 +/- 0.7 71 6 ALAM 94 CLE2 e+ e- -> Gamma(4S)
7.2 +/- 1.8 +/- 1.6 7 BORTOLETTO92 CLEO e+ e- -> Gamma(4S)
4.0 +/- 1.4 +/- 1.2 9 7 ALBRECHT 90J ARG e+ e- -> Gamma(4S)
4.664 +/- 0.029 +/- 0.268 8 AAIJ 18A LHCB pp at 7, 8, 13 TeV
2.7 +/- 4.4 9 BEBEK 87 CLEO e+ e- -> Gamma(4S)

1 Measures absolute branching fractions using a missing-mass technique.
2 Assumes equal production of B+ and B0 at the Gamma(4S).
3 AUBERT,BE 06J reports [Gamma(B+ -> D*(2007)0 pi+) / Gamma total] / [B(B+ -> D0 pi+)] = 1.14 +/- 0.07 +/- 0.04 which we multiply by our best value B(B+ -> D0 pi+) = (4.68 +/- 0.13) x 10^-3. Our first error is their experiment's error and our second error is the systematic error from using our best value.

4 Uses a missing-mass method. Does not depend on D branching fractions or B+ / B0 production rates.
5 BRANDENBURG 98 assume equal production of B+ and B0 at Gamma(4S) and use the D* reconstruction technique. The first error is their experiment's error and the second error is the systematic error from the PDG 96 value of B(D* -> D pi).
6 ALAM 94 assume equal production of B+ and B0 at the Gamma(4S) and use the CLEO II B(D*(2007)0 -> D0 pi0) and absolute B(D0 -> K- pi+) and the PDG 1992 B(D0 -> K- pi+ pi0) / B(D0 -> K- pi+) and B(D0 -> K- 2pi+ pi-) / B(D0 -> K- pi+).
7 Assumes equal production of B+ and B0 at the Gamma(4S) and uses Mark III branching fractions for the D and D*(2010).
8 Superseded by AAIJ 21Q.
9 This is a derived branching ratio, using the inclusive pion spectrum and other two-body B decays. BEBEK 87 assume the Gamma(4S) decays 43% to B0 B0.

Gamma(D*(2007)0 omega pi+) / Gamma total
VALUE DOCUMENT_ID TECN COMMENT
0.0045 +/- 0.0010 +/- 0.0007 1 ALEXANDER 01B CLE2 e+ e- -> Gamma(4S)
1 Assumes equal production of B+ and B0 at the Gamma(4S). The signal is consistent with all observed omega pi+ having proceeded through the rho+ resonance at mass 1349 +/- 25 +/- 10 MeV and width 547 +/- 86 +/- 46 MeV.

Meson Particle Listings

 B^\pm

$\Gamma(\bar{D}^*(2007)^0 \rho^+)/\Gamma_{\text{total}}$ Γ_{131}/Γ
 VALUE (units 10^{-4}) DOCUMENT ID TECN COMMENT

0.0098 ± 0.0017 OUR AVERAGE
 0.0098 ± 0.0006 ± 0.0017 ¹ CSORNA 03 CLE2 $e^+e^- \rightarrow \Upsilon(4S)$
 0.010 ± 0.006 ± 0.004 7 ² ALBRECHT 90i ARG $e^+e^- \rightarrow \Upsilon(4S)$
 • • • We do not use the following data for averages, fits, limits, etc. • • •
 0.0168 ± 0.0021 ± 0.0028 86 ³ ALAM 94 CLE2 $e^+e^- \rightarrow \Upsilon(4S)$

¹ Assumes equal production of B^0 and B^+ at the $\Upsilon(4S)$ resonance. The second error combines the systematic and theoretical uncertainties in quadrature. CSORNA 03 includes data used in ALAM 94. A full angular fit to three complex helicity amplitudes is performed.

² Assumes equal production of B^+ and B^0 at the $\Upsilon(4S)$ and uses MarkIII branching fractions for the D and $D^*(2010)$.

³ ALAM 94 assume equal production of B^+ and B^0 at the $\Upsilon(4S)$ and use the CLEOII $B(D^*(2007)^0 \rightarrow D^0 \pi^0)$ and absolute $B(D^0 \rightarrow K^- \pi^+)$ and the PDG 1992 $B(D^0 \rightarrow K^- \pi^+ \pi^0)/B(D^0 \rightarrow K^- \pi^+)$ and $B(D^0 \rightarrow K^- 2\pi^+ \pi^-)/B(D^0 \rightarrow K^- \pi^+)$. The nonresonant $\pi^+ \pi^0$ contribution under the ρ^+ is negligible.

$\Gamma(\bar{D}^*(2007)^0 K^+)/\Gamma_{\text{total}}$ Γ_{132}/Γ
 VALUE (units 10^{-4}) DOCUMENT ID TECN COMMENT

4.20 ± 0.31 OUR AVERAGE
 4.21 $^{+0.30}_{-0.26}$ ± 0.12 ¹ AUBERT 05N BABR $e^+e^- \rightarrow \Upsilon(4S)$
 4.0 ± 1.1 ± 0.1 ² ABE 01i BELL $e^+e^- \rightarrow \Upsilon(4S)$

¹ AUBERT 05N reports $[\Gamma(B^+ \rightarrow \bar{D}^*(2007)^0 K^+)/\Gamma_{\text{total}}] / [B(B^+ \rightarrow \bar{D}^*(2007)^0 \pi^+)] = 0.0813 \pm 0.0040 \pm 0.0042$ which we multiply by our best value $B(B^+ \rightarrow \bar{D}^*(2007)^0 \pi^+) = (5.18 \pm 0.15) \times 10^{-3}$. Our first error is their experiment's error and our second error is the systematic error from using our best value.

² ABE 01i reports $[\Gamma(B^+ \rightarrow \bar{D}^*(2007)^0 K^+)/\Gamma_{\text{total}}] / [B(B^+ \rightarrow \bar{D}^*(2007)^0 \pi^+)] = 0.078 \pm 0.019 \pm 0.009$ which we multiply by our best value $B(B^+ \rightarrow \bar{D}^*(2007)^0 \pi^+) = (5.18 \pm 0.15) \times 10^{-3}$. Our first error is their experiment's error and our second error is the systematic error from using our best value.

$\Gamma(\bar{D}_{CP(+)}^{*0} K^+)/\Gamma_{\text{total}}$ Γ_{133}/Γ
 VALUE (units 10^{-4}) DOCUMENT ID TECN COMMENT

2.75 ± 0.29 ± 0.21 OUR AVERAGE
 2.75 ± 0.29 ± 0.21 ¹ AUBERT 08BF BABR $e^+e^- \rightarrow \Upsilon(4S)$
¹ AUBERT 08BF reports $[\Gamma(B^+ \rightarrow \bar{D}_{CP(+)}^{*0} K^+)/\Gamma_{\text{total}}] / [B(B^+ \rightarrow \bar{D}^*(2007)^0 K^+)] = 0.655 \pm 0.065 \pm 0.020$ which we multiply by our best value $B(B^+ \rightarrow \bar{D}^*(2007)^0 K^+) = (4.20 \pm 0.31) \times 10^{-4}$. Our first error is their experiment's error and our second error is the systematic error from using our best value.

$\Gamma(\bar{D}^*(2007)^0 K^+)/\Gamma(\bar{D}^*(2007)^0 \pi^+)$ $\Gamma_{132}/\Gamma_{127}$
 VALUE (units 10^{-2}) DOCUMENT ID TECN COMMENT

8.51 ± 0.12 ± 0.48
 8.51 ± 0.12 ± 0.48 ¹ AAIJ 21q LHCB pp at 7, 8, 13 TeV
 • • • We do not use the following data for averages, fits, limits, etc. • • •
 7.930 ± 0.110 ± 0.560 ² AAIJ 18A LHCB pp at 7, 8, 13 TeV

¹ Uses semi-inclusive reconstruction of $B^+ \rightarrow ([K^+ \pi^-]_{D\gamma/\pi^0})_{D^*} K^+/\pi^+$. Decays of $D^* \rightarrow D\gamma/\pi^0$ are reconstructed without inclusion of π^0 or γ .

² Superseded by AAIJ 21q.

$\Gamma(\bar{D}_{CP(+)}^{*0} K^+)/\Gamma(\bar{D}_{CP(+)}^{*0} \pi^+)$ $\Gamma_{133}/\Gamma_{128}$
 VALUE DOCUMENT ID TECN COMMENT

0.095 ± 0.017 OUR AVERAGE
 0.11 ± 0.02 ± 0.02 ¹ ABE 06 BELL $e^+e^- \rightarrow \Upsilon(4S)$
 0.086 ± 0.021 ± 0.007 ² AUBERT 05N BABR $e^+e^- \rightarrow \Upsilon(4S)$

¹ Reports a double ratio of $B(B^+ \rightarrow D_{CP(+)}^{*0} K^+)/B(B^+ \rightarrow D_{CP(+)}^{*0} \pi^+)$ and $B(B^+ \rightarrow \bar{D}^*(2007)^0 K^+)/B(B^+ \rightarrow \bar{D}^*(2007)^0 \pi^+)$, $1.41 \pm 0.25 \pm 0.06$. We multiply by our best value of $B(B^+ \rightarrow \bar{D}^*(2007)^0 K^+)/B(B^+ \rightarrow \bar{D}^*(2007)^0 \pi^+) = 0.080 \pm 0.011$. Our first error is their experiment's error and the second error is systematic error from using our best value.

² Uses $D^{*0} \rightarrow D^0 \pi^0$ with D^0 reconstructed in the CP -even eigenstates $K^+ K^-$ and $\pi^+ \pi^-$.

$\Gamma(\bar{D}_{CP(-)}^{*0} K^+)/\Gamma_{\text{total}}$ Γ_{134}/Γ
 VALUE (units 10^{-4}) DOCUMENT ID TECN COMMENT

2.31 ± 0.27 ± 0.17 OUR AVERAGE
 2.31 ± 0.27 ± 0.17 ¹ AUBERT 08BF BABR $e^+e^- \rightarrow \Upsilon(4S)$

¹ AUBERT 08BF reports $[\Gamma(B^+ \rightarrow \bar{D}_{CP(-)}^{*0} K^+)/\Gamma_{\text{total}}] / [B(B^+ \rightarrow \bar{D}^*(2007)^0 K^+)] = 0.55 \pm 0.06 \pm 0.02$ which we multiply by our best value $B(B^+ \rightarrow \bar{D}^*(2007)^0 K^+) = (4.20 \pm 0.31) \times 10^{-4}$. Our first error is their experiment's error and our second error is the systematic error from using our best value.

$\Gamma(\bar{D}_{CP(-)}^{*0} K^+)/\Gamma(\bar{D}_{CP(-)}^{*0} \pi^+)$ $\Gamma_{134}/\Gamma_{129}$
 VALUE DOCUMENT ID TECN COMMENT

0.09 ± 0.03 ± 0.01
 0.09 ± 0.03 ± 0.01 ¹ ABE 06 BELL $e^+e^- \rightarrow \Upsilon(4S)$

¹ Reports a double ratio of $B(B^+ \rightarrow (\bar{D}_{CP(-)}^{*0})^0 K^+)/B(B^+ \rightarrow (\bar{D}_{CP(-)}^{*0})^0 \pi^+)$ and $B(B^+ \rightarrow \bar{D}^*(2007)^0 K^+)/B(B^+ \rightarrow \bar{D}^*(2007)^0 \pi^+)$, $1.15 \pm 0.31 \pm 0.12$. We multiply by our best value of $B(B^+ \rightarrow \bar{D}^*(2007)^0 K^+)/B(B^+ \rightarrow \bar{D}^*(2007)^0 \pi^+) = 0.080 \pm 0.011$. Our first error is their experiment's error and the second error is systematic error from using our best value.

$\Gamma(D^*(2007)^0 K^+)/\Gamma(\bar{D}^*(2007)^0 K^+)$ $\Gamma_{135}/\Gamma_{132}$
 "OUR EVALUATION" is derived from $r_{FB}(B^+ \rightarrow D^{*0} K^+)$ data block listed in "CP violation parameters" section.

VALUE (units 10^{-2}) DOCUMENT ID
1.08 $^{+0.27}_{-0.29}$ OUR EVALUATION

$\Gamma(\bar{D}^*(2007)^0 K^*(892)^+)/\Gamma_{\text{total}}$ Γ_{136}/Γ
 VALUE (units 10^{-4}) DOCUMENT ID TECN COMMENT

8.1 ± 1.4 OUR AVERAGE
 8.3 ± 1.1 ± 1.0 ¹ AUBERT 04k BABR $e^+e^- \rightarrow \Upsilon(4S)$
 7.2 ± 2.2 ± 2.6 ² MAHAPATRA 02 CLE2 $e^+e^- \rightarrow \Upsilon(4S)$

¹ Assumes equal production of B^+ and B^0 at the $\Upsilon(4S)$.

² Assumes equal production of B^+ and B^0 at the $\Upsilon(4S)$ and an unpolarized final state.

$\Gamma(\bar{D}^*(2007)^0 K^+ \bar{K}^0)/\Gamma_{\text{total}}$ Γ_{137}/Γ
 VALUE (units 10^{-4}) CL% DOCUMENT ID TECN COMMENT

<10.6 90 ¹ DRUTSKOY 02 BELL $e^+e^- \rightarrow \Upsilon(4S)$
¹ Assumes equal production of B^+ and B^0 at the $\Upsilon(4S)$.

$\Gamma(\bar{D}^*(2007)^0 K^+ \bar{K}^*(892)^0)/\Gamma_{\text{total}}$ Γ_{138}/Γ
 VALUE (units 10^{-4}) DOCUMENT ID TECN COMMENT

15.3 ± 3.1 ± 2.9 ¹ DRUTSKOY 02 BELL $e^+e^- \rightarrow \Upsilon(4S)$
¹ Assumes equal production of B^+ and B^0 at the $\Upsilon(4S)$.

$\Gamma(\bar{D}^*(2007)^0 \pi^+ \pi^+ \pi^-)/\Gamma_{\text{total}}$ Γ_{139}/Γ
 VALUE (units 10^{-2}) EVTS DOCUMENT ID TECN COMMENT

1.03 ± 0.12 OUR AVERAGE
 1.055 ± 0.047 ± 0.129 ¹ MAJUMDER 04 BELL $e^+e^- \rightarrow \Upsilon(4S)$
 0.94 ± 0.20 ± 0.17 48 ^{2,3} ALAM 94 CLE2 $e^+e^- \rightarrow \Upsilon(4S)$

¹ Assumes equal production of B^+ and B^0 at the $\Upsilon(4S)$.

² ALAM 94 assume equal production of B^+ and B^0 at the $\Upsilon(4S)$ and use the CLEOII $B(D^*(2007)^0 \rightarrow D^0 \pi^0)$ and absolute $B(D^0 \rightarrow K^- \pi^+)$ and the PDG 1992 $B(D^0 \rightarrow K^- \pi^+ \pi^0)/B(D^0 \rightarrow K^- \pi^+)$ and $B(D^0 \rightarrow K^- 2\pi^+ \pi^-)/B(D^0 \rightarrow K^- \pi^+)$.

³ The three pion mass is required to be between 1.0 and 1.6 GeV consistent with an a_1 meson. (If this channel is dominated by a_1^+ , the branching ratio for $\bar{D}^{*0} a_1^+$ is twice that for $\bar{D}^{*0} \pi^+ \pi^+ \pi^-$.)

$\Gamma(\bar{D}^*(2007)^0 a_1(1260)^+)/\Gamma_{\text{total}}$ Γ_{140}/Γ
 VALUE DOCUMENT ID TECN COMMENT

0.0188 ± 0.0040 ± 0.0034 ^{1,2} ALAM 94 CLE2 $e^+e^- \rightarrow \Upsilon(4S)$

¹ ALAM 94 value is twice their $\Gamma(\bar{D}^*(2007)^0 \pi^+ \pi^+ \pi^-)/\Gamma_{\text{total}}$ value based on their observation that the three pions are dominantly in the $a_1(1260)$ mass range 1.0 to 1.6 GeV.

² ALAM 94 assume equal production of B^+ and B^0 at the $\Upsilon(4S)$ and use the CLEOII $B(D^*(2007)^0 \rightarrow D^0 \pi^0)$ and absolute $B(D^0 \rightarrow K^- \pi^+)$ and the PDG 1992 $B(D^0 \rightarrow K^- \pi^+ \pi^0)/B(D^0 \rightarrow K^- \pi^+)$ and $B(D^0 \rightarrow K^- 2\pi^+ \pi^-)/B(D^0 \rightarrow K^- \pi^+)$.

$\Gamma(\bar{D}^*(2007)^0 \pi^- \pi^+ \pi^0)/\Gamma_{\text{total}}$ Γ_{141}/Γ
 VALUE DOCUMENT ID TECN COMMENT

0.0180 ± 0.0024 ± 0.0027 ¹ ALEXANDER 01B CLE2 $e^+e^- \rightarrow \Upsilon(4S)$

¹ Assumes equal production of B^+ and B^0 at the $\Upsilon(4S)$. The signal is consistent with all observed $\omega \pi^+$ having proceeded through the ρ^+ resonance at mass $1349 \pm 25 \pm 5$ MeV and width $547 \pm 86 \pm 46$ MeV.

$\Gamma(\bar{D}^{*0} 3\pi^+ 2\pi^-)/\Gamma_{\text{total}}$ Γ_{142}/Γ
 VALUE (units 10^{-3}) DOCUMENT ID TECN COMMENT

5.67 ± 0.91 ± 0.85 ¹ MAJUMDER 04 BELL $e^+e^- \rightarrow \Upsilon(4S)$

¹ Assumes equal production of B^+ and B^0 at the $\Upsilon(4S)$.

$\Gamma(D^*(2010)^+ \pi^0)/\Gamma_{\text{total}}$ Γ_{143}/Γ
 VALUE CL% DOCUMENT ID TECN COMMENT

<3.6 × 10⁻⁶ ¹ IWABUCHI 08 BELL $e^+e^- \rightarrow \Upsilon(4S)$
 • • • We do not use the following data for averages, fits, limits, etc. • • •
 <1.7 × 10⁻⁴ 90 ² BRANDENB... 98 CLE2 $e^+e^- \rightarrow \Upsilon(4S)$

¹ Assumes equal production of B^+ and B^0 at the $\Upsilon(4S)$.

² BRANDENBURG 98 assume equal production of B^+ and B^0 at $\Upsilon(4S)$ and use the D^* partial reconstruction technique. The first error is their experiment's error and the second error is the systematic error from the PDG 96 value of $B(D^* \rightarrow D \pi)$.

$\Gamma(D^*(2010)^+ K^0)/\Gamma_{\text{total}}$ Γ_{144}/Γ
 VALUE CL% DOCUMENT ID TECN COMMENT

<9.0 × 10⁻⁶ 90 ¹ AUBERT,B 05E BABR $e^+e^- \rightarrow \Upsilon(4S)$
 • • • We do not use the following data for averages, fits, limits, etc. • • •
 <9.5 × 10⁻⁵ 90 ¹ GRITSAN 01 CLE2 $e^+e^- \rightarrow \Upsilon(4S)$

¹ Assumes equal production of B^+ and B^0 at the $\Upsilon(4S)$.

See key on page 1127

Meson Particle Listings

B±

$\Gamma(D^*(2010)^-\pi^+\pi^0)/\Gamma_{total}$ Γ_{145}/Γ

Table with columns: VALUE, EVTS, DOCUMENT ID, TECN, COMMENT. Row 1: 0.0152±0.0071±0.0001, 26, 1 ALBRECHT, 90J, ARG, e+e- -> T(4S).

••• We do not use the following data for averages, fits, limits, etc. •••
0.043 ± 0.013 ± 0.026 24 2 ALBRECHT 87c ARG e+e- -> T(4S)

1 ALBRECHT 90J reports 0.018 ± 0.007 ± 0.005 from a measurement of [Γ(B+ -> D*(2010)-π+π0)/Γtotal] × [B(D*(2010)+ -> D0π+)] assuming B(D*(2010)+ -> D0π+) = 0.57 ± 0.06, which we rescale to our best value B(D*(2010)+ -> D0π+) = (67.7 ± 0.5) × 10^-2. Our first error is their experiment's error and our second error is the systematic error from using our best value. Assumes equal production of B+ and B0 at the T(4S) and uses MarkIII branching fractions for the D.

2 ALBRECHT 87c use PDG 86 branching ratios for D and D*(2010) and assume B(T(4S) -> B+B-) = 55% and B(T(4S) -> B0B0) = 45%. Superseded by ALBRECHT 90J.

$\Gamma(D^*(2010)^-\pi^+\pi^+\pi^-)/\Gamma_{total}$ Γ_{146}/Γ

Table with columns: VALUE (units 10^-3), CL%, DOCUMENT ID, TECN, COMMENT. Row 1: 2.56±0.26±0.33, 1 MAJUMDER 04 BELL e+e- -> T(4S).

••• We do not use the following data for averages, fits, limits, etc. •••
<10 90 2 ALBRECHT 90J ARG e+e- -> T(4S)

1 Assumes equal production of B+ and B0 at the T(4S).

2 Assumes equal production of B+ and B0 at the T(4S) and uses MarkIII branching fractions for the D and D*(2010).

$\Gamma(D^{*0}\pi^+)/\Gamma_{total}$ Γ_{147}/Γ

D*0 represents an excited state with mass 2.2 < M < 2.8 GeV/c^2.

Table with columns: VALUE (units 10^-3), DOCUMENT ID, TECN, COMMENT. Row 1: 5.7±1.2±0.2, 1,2 AUBERT,BE 06J BABR e+e- -> T(4S).

1 AUBERT,BE 06J reports [Γ(B+ -> D*0π+)/Γtotal] / [B(B+ -> D0π+)] = 1.22 ± 0.13 ± 0.23 which we multiply by our best value B(B+ -> D0π+) = (4.68 ± 0.13) × 10^-3. Our first error is their experiment's error and our second error is the systematic error from using our best value.

2 Uses a missing-mass method. Does not depend on D branching fractions or B+/B0 production rates.

$\Gamma(D_1^+(2420)^0\pi^+)/\Gamma_{total}$ Γ_{148}/Γ

Table with columns: VALUE, EVTS, DOCUMENT ID, TECN, COMMENT. Row 1: 0.0015±0.0006 OUR AVERAGE, Error includes scale factor of 1.3.

Table with columns: VALUE, EVTS, DOCUMENT ID, TECN, COMMENT. Row 1: 0.0011±0.0005±0.0002, 8, 1 ALAM 94 CLE2 e+e- -> T(4S).

1 ALAM 94 assume equal production of B+ and B0 at the T(4S) and use the CLEOII B(D*(2010)+ -> D0π+) and absolute B(D0 -> K-π+) and the PDG 1992 B(D0 -> K-π+π0)/B(D0 -> K-π+) and assuming B(D1(2420)0 -> D*(2010)π+) = 67%.

2 ALBRECHT 94D assume equal production of B+ and B0 at the T(4S) and use the CLEOII B(D*(2010)+ -> D0π+) assuming B(D1(2420)0 -> D*(2010)π+) = 67%.

$\Gamma(D_1(2420)^0\pi^+ \times B(D_1^0 \rightarrow D^0\pi^+\pi^-))/\Gamma_{total}$ Γ_{149}/Γ

Table with columns: VALUE (units 10^-4), DOCUMENT ID, TECN, COMMENT. Row 1: 2.5 ±1.6 / -1.4 OUR FIT, Error includes scale factor of 3.9.

Table with columns: VALUE, EVTS, DOCUMENT ID, TECN, COMMENT. Row 1: 1.85±0.29±0.35 / -0.55, 1 ABE 05A BELL e+e- -> T(4S).

1 Assumes equal production of B+ and B0 at the T(4S).

$\Gamma(D_1(2420)^0\pi^+ \times B(D_1^0 \rightarrow D^0\pi^+\pi^-))/\Gamma(D^0\pi^+\pi^-)$ $\Gamma_{149}/\Gamma_{108}$

Table with columns: VALUE (units 10^-2), DOCUMENT ID, TECN, COMMENT. Row 1: 4.6±3.3 / -2.7 OUR FIT, Error includes scale factor of 3.9.

Table with columns: VALUE, CL%, DOCUMENT ID, TECN, COMMENT. Row 1: 10.3±1.5±0.9, AAIJ 11E LHCB pp at 7 TeV.

$\Gamma(D_1(2420)^0\pi^+ \times B(D_1^0 \rightarrow D^0\pi^+\pi^- (nonresonant)))/\Gamma(D^0\pi^+\pi^-)$ $\Gamma_{150}/\Gamma_{108}$

Table with columns: VALUE (units 10^-2), DOCUMENT ID, TECN, COMMENT. Row 1: 4.0±0.7±0.5, 1 AAIJ 11E LHCB pp at 7 TeV.

1 Excludes decays where D1(2420)0 -> D*(2010)π+.

$\Gamma(D_1(2430)^0\pi^+, \bar{D}_1^0 \rightarrow D^*(2010)^-\pi^+)/\Gamma_{total}$ Γ_{151}/Γ

Table with columns: VALUE (units 10^-4), DOCUMENT ID, TECN, COMMENT. Row 1: 3.51±0.06±0.61, 1 AAIJ 20D LHCB pp at 7, 8, 13 TeV.

1 AAIJ 20D used a 4-body amplitude analysis of B- -> D*π-π- decays.

$\Gamma(\bar{D}_2^*(2462)^0\pi^+, \bar{D}_2^0 \rightarrow D^-\pi^+)/\Gamma_{total}$ Γ_{154}/Γ

Table with columns: VALUE (units 10^-4), DOCUMENT ID, TECN, COMMENT. Row 1: 3.56±0.24 OUR AVERAGE.

Table with columns: VALUE, CL%, DOCUMENT ID, TECN, COMMENT. Row 1: 3.62±0.06±0.30, 1 AAIJ 16AH LHCB pp at 7, 8 TeV.

2 AUBERT 09AB BABR e+e- -> T(4S)

3.4 ± 0.3 ± 0.72 2 ABE 04D BELL e+e- -> T(4S)

1 Measured using a Dalitz plot analysis of B- -> D+π-π- decays.

2 Assumes equal production of B+ and B0 at the T(4S).

$\Gamma(\bar{D}_2^*(2462)^0\pi^+, \bar{D}_2^0 \rightarrow \bar{D}^0\pi^-\pi^+)/\Gamma(D^0\pi^+\pi^-)$ $\Gamma_{155}/\Gamma_{108}$

Table with columns: VALUE (units 10^-2), DOCUMENT ID, TECN, COMMENT. Row 1: 4.0±1.0±0.4, AAIJ 11E LHCB pp at 7 TeV.

$\Gamma(\bar{D}_2^*(2462)^0\pi^+, \bar{D}_2^0 \rightarrow \bar{D}^0\pi^-\pi^+ (nonresonant))/\Gamma(D^0\pi^+\pi^-)$ $\Gamma_{156}/\Gamma_{108}$

Table with columns: VALUE, CL%, DOCUMENT ID, TECN, COMMENT. Row 1: <3.0 × 10^-2, 90, 1 AAIJ 11E LHCB pp at 7 TeV.

1 Excludes decays where D2*(2462)0 -> D*(2010)π+.

$\Gamma(\bar{D}_2^*(2462)^0\pi^+, \bar{D}_2^0 \rightarrow D^*(2010)^-\pi^+)/\Gamma(D^0\pi^+\pi^-)$ $\Gamma_{157}/\Gamma_{108}$

Table with columns: VALUE (units 10^-2), DOCUMENT ID, TECN, COMMENT. Row 1: 3.9±1.2±0.4, 1 AAIJ 11E LHCB pp at 7 TeV.

1 Uses B(D*(2010)+ -> D0π+) = (67.7 ± 0.5)%.

$\Gamma(\bar{D}_0^*(2400)^0\pi^+ \times B(\bar{D}_0^*(2400)^0 \rightarrow D^-\pi^+))/\Gamma_{total}$ Γ_{158}/Γ

Table with columns: VALUE (units 10^-4), DOCUMENT ID, TECN, COMMENT. Row 1: 6.4±1.4 OUR AVERAGE.

Table with columns: VALUE, CL%, DOCUMENT ID, TECN, COMMENT. Row 1: 6.8±0.3±2.0, 1 AUBERT 09AB BABR e+e- -> T(4S).

6.1±0.6±1.8 1 ABE 04D BELL e+e- -> T(4S)

1 Assumes equal production of B+ and B0 at the T(4S).

$\Gamma(\bar{D}_1(2421)^0\pi^+, \bar{D}_1^0 \rightarrow D^{*-}\pi^+)/\Gamma_{total}$ Γ_{159}/Γ

Table with columns: VALUE (units 10^-4), DOCUMENT ID, TECN, COMMENT. Row 1: 7.4 ± 1.0 OUR AVERAGE.

Table with columns: VALUE, CL%, DOCUMENT ID, TECN, COMMENT. Row 1: 7.95±0.09±1.34, 1 AAIJ 20D LHCB pp at 7, 8, 13 TeV.

6.8 ± 0.7 ± 1.3 2 ABE 04D BELL e+e- -> T(4S)

1 AAIJ 20D used a 4-body amplitude analysis of B- -> D*π-π- decays.

2 Assumes equal production of B+ and B0 at the T(4S).

$\Gamma(\bar{D}_2^*(2462)^0\pi^+, \bar{D}_2^0 \rightarrow D^{*-}\pi^+)/\Gamma_{total}$ Γ_{160}/Γ

Table with columns: VALUE (units 10^-4), DOCUMENT ID, TECN, COMMENT. Row 1: 1.98±0.30 OUR AVERAGE.

Table with columns: VALUE, CL%, DOCUMENT ID, TECN, COMMENT. Row 1: 2.08±0.03±0.37, 1 AAIJ 20D LHCB pp at 7, 8, 13 TeV.

1.8 ± 0.3 ± 0.4 2 ABE 04D BELL e+e- -> T(4S)

1 AAIJ 20D used a 4-body amplitude analysis of B- -> D*π-π- decays.

2 Assumes equal production of B+ and B0 at the T(4S).

$\Gamma(\bar{D}_1^+(2427)^0\pi^+, \bar{D}_1^0 \rightarrow D^{*-}\pi^+)/\Gamma_{total}$ Γ_{161}/Γ

Table with columns: VALUE (units 10^-4), DOCUMENT ID, TECN, COMMENT. Row 1: 3.5 ± 0.9 OUR AVERAGE, Error includes scale factor of 1.5.

Table with columns: VALUE, CL%, DOCUMENT ID, TECN, COMMENT. Row 1: 2.96±0.30±0.63, 1 AAIJ 20D LHCB pp at 7, 8, 13 TeV.

5.0 ± 0.4 ± 1.1 2 ABE 04D BELL e+e- -> T(4S)

1 AAIJ 20D used a 4-body amplitude analysis of B- -> D*π-π- decays.

2 Assumes equal production of B+ and B0 at the T(4S).

$\Gamma(\bar{D}_1(2420)^0\pi^+ \times B(\bar{D}_1^0 \rightarrow \bar{D}^{*0}\pi^+\pi^-))/\Gamma_{total}$ Γ_{162}/Γ

Table with columns: VALUE (units 10^-4), CL%, DOCUMENT ID, TECN, COMMENT. Row 1: <0.06, 90, 1 ABE 05A BELL e+e- -> T(4S).

1 Assumes equal production of B+ and B0 at the T(4S).

$\Gamma(\bar{D}_1^+(2420)^0\rho^+)/\Gamma_{total}$ Γ_{163}/Γ

Table with columns: VALUE, CL%, DOCUMENT ID, TECN, COMMENT. Row 1: <0.0014, 90, 1 ALAM 94 CLE2 e+e- -> T(4S).

1 ALAM 94 assume equal production of B+ and B0 at the T(4S) and use the CLEOII B(D*(2010)+ -> D0π+) assuming B(D1(2420)0 -> D*(2010)π+) = 67%.

$\Gamma(\bar{D}_2^*(2460)^0\pi^+)/\Gamma_{total}$ Γ_{164}/Γ

Table with columns: VALUE, CL%, DOCUMENT ID, TECN, COMMENT. Row 1: <0.0013, 90, 1 ALAM 94 CLE2 e+e- -> T(4S).

••• We do not use the following data for averages, fits, limits, etc. •••

Table with columns: VALUE, CL%, DOCUMENT ID, TECN, COMMENT. Row 1: <0.0028, 90, 2 ALAM 94 CLE2 e+e- -> T(4S).

<0.0023 90 3 ALBRECHT 94D ARG e+e- -> T(4S)

1 ALAM 94 assume equal production of B+ and B0 at the T(4S) and use the MarkIII B(D+ -> K-2π+) and B(D2*(2460)0 -> D+π-) = 30%.

2 ALAM 94 assume equal production of B+ and B0 at the T(4S) and use the MarkIII B(D+ -> K-2π+), the CLEOII B(D*(2010)+ -> D0π+) and B(D2*(2460)0 -> D*(2010)π+) = 20%.

3 ALBRECHT 94D assume equal production of B+ and B0 at the T(4S) and use the CLEOII B(D*(2010)+ -> D0π+) and B(D2*(2460)0 -> D*(2010)π+) = 30%.

$\Gamma(\bar{D}_2^*(2460)^0\pi^+ \times B(\bar{D}_2^0 \rightarrow \bar{D}^{*0}\pi^+\pi^-))/\Gamma_{total}$ Γ_{165}/Γ

Table with columns: VALUE (units 10^-4), CL%, DOCUMENT ID, TECN, COMMENT. Row 1: <0.22, 90, 1 ABE 05A BELL e+e- -> T(4S).

1 Assumes equal production of B+ and B0 at the T(4S).

Downloaded from https://academic.oup.com/ptep/article/2022/8/083C01/6651666 by CERN Library user on 11 October 2022

Meson Particle Listings

B[±]

$\Gamma(\overline{D}_s^*(2460)^0 \rho^+) / \Gamma_{\text{total}}$ Γ_{171} / Γ

VALUE	CL%	DOCUMENT ID	TECN	COMMENT
<0.0047	90	1 ALAM	94 CLE2	e ⁺ e ⁻ → $\Upsilon(4S)$
<0.005	90	2 ALAM	94 CLE2	e ⁺ e ⁻ → $\Upsilon(4S)$

1 ALAM 94 assume equal production of B⁺ and B⁰ at the $\Upsilon(4S)$ and use the Mark III B(D⁺ → K⁻2π⁺) and B(D_{s2}^{*}(2460)⁰ → D⁺π⁻) = 30%.

2 ALAM 94 assume equal production of B⁺ and B⁰ at the $\Upsilon(4S)$ and use the Mark III B(D⁺ → K⁻2π⁺), the CLEO II B(D*(2010)⁺ → D⁰π⁺) and B(D₂^{*}(2460)⁰ → D*(2010)⁺π⁻) = 20%.

$\Gamma(\overline{D}(2550)^0 \pi^+, \overline{D}^0 \rightarrow D^*(2010)^- \pi^+) / \Gamma_{\text{total}}$ Γ_{152} / Γ

VALUE (units 10 ⁻⁴)	DOCUMENT ID	TECN	COMMENT
0.72 ± 0.01 ± 0.14	1 AAIJ	20D LHCb	pp at 7, 8, 13 TeV

1 AAIJ 20D used a 4-body amplitude analysis of B⁻ → D*⁺π⁻π⁻ decays.

$\Gamma(\overline{D}_s^*(2600)^0 \pi^+, \overline{D}_s^0 \rightarrow D^*(2010)^- \pi^+) / \Gamma_{\text{total}}$ Γ_{153} / Γ

VALUE (units 10 ⁻⁴)	DOCUMENT ID	TECN	COMMENT
0.68 ± 0.01 ± 0.13	1 AAIJ	20D LHCb	pp at 7, 8, 13 TeV

1 AAIJ 20D used a 4-body amplitude analysis of B⁻ → D*⁺π⁻π⁻ decays.

$\Gamma(\overline{D}_s^*(2680)^0 \pi^+, \overline{D}_s^0 \rightarrow D^- \pi^+) / \Gamma_{\text{total}}$ Γ_{166} / Γ

VALUE (units 10 ⁻⁴)	DOCUMENT ID	TECN	COMMENT
0.84 ± 0.06 ± 0.20	1 AAIJ	16AH LHCb	pp at 7, 8 TeV

1 Measured using a Dalitz plot analysis of B⁺ → D⁻π⁺π⁺ decays.

$\Gamma(\overline{D}(2740)^0 \pi^+, \overline{D}^0 \rightarrow D^*(2010)^- \pi^+) / \Gamma_{\text{total}}$ Γ_{167} / Γ

VALUE (units 10 ⁻⁴)	DOCUMENT ID	TECN	COMMENT
0.33 ± 0.02 ± 0.15	1 AAIJ	20D LHCb	pp at 7, 8, 13 TeV

1 AAIJ 20D used a 4-body amplitude analysis of B⁻ → D*⁺π⁻π⁻ decays.

$\Gamma(\overline{D}_s^*(2750)^0 \pi^+, \overline{D}_s^0 \rightarrow D^*(2010)^- \pi^+) / \Gamma_{\text{total}}$ Γ_{168} / Γ

VALUE (units 10 ⁻⁴)	DOCUMENT ID	TECN	COMMENT
0.11 ± 0.01 ± 0.03	1 AAIJ	20D LHCb	pp at 7, 8, 13 TeV

1 AAIJ 20D used a 4-body amplitude analysis of B⁻ → D*⁺π⁻π⁻ decays.

$\Gamma(\overline{D}_s^*(2760)^0 \pi^+, \overline{D}_s^0 \rightarrow D^- \pi^+) / \Gamma_{\text{total}}$ Γ_{169} / Γ

VALUE (units 10 ⁻⁵)	DOCUMENT ID	TECN	COMMENT
1.0 ± 0.1 ± 0.2	1 AAIJ	16AH LHCb	pp at 7, 8 TeV

1 Measured using a Dalitz plot analysis of B⁺ → D⁻π⁺π⁺ decays.

$\Gamma(\overline{D}_s^*(3000)^0 \pi^+, \overline{D}_s^0 \rightarrow D^- \pi^+) / \Gamma_{\text{total}}$ Γ_{170} / Γ

VALUE (units 10 ⁻⁶)	DOCUMENT ID	TECN	COMMENT
2 ± 1 ± 1	1 AAIJ	16AH LHCb	pp at 7, 8 TeV

1 Measured using a Dalitz plot analysis of B⁺ → D⁻π⁺π⁺ decays.

$\Gamma(\overline{D}^0 D_s^+) / \Gamma_{\text{total}}$ Γ_{172} / Γ

VALUE (units 10 ⁻³)	DOCUMENT ID	TECN	COMMENT
9.0 ± 0.9 OUR AVERAGE			
8.6 ± 0.2 ± 1.1	1 AAIJ	13AP LHCb	pp at 7 TeV
9.5 ± 2.0 ± 0.8	2 AUBERT	06N BABR	e ⁺ e ⁻ → $\Upsilon(4S)$
9.8 ± 2.6 ± 0.9	3 GIBAUT	96 CLE2	e ⁺ e ⁻ → $\Upsilon(4S)$
14 ± 8 ± 1	4 ALBRECHT	92G ARG	e ⁺ e ⁻ → $\Upsilon(4S)$
13 ± 6 ± 1	5 BORTOLETTO	090 CLEO	e ⁺ e ⁻ → $\Upsilon(4S)$

1 Uses B(B⁰ → D⁻D_{s2}⁺) = (7.2 ± 0.8) × 10⁻³.

2 AUBERT 06N reports (0.92 ± 0.14 ± 0.18) × 10⁻² from a measurement of [$\Gamma(B^+ \rightarrow \overline{D}^0 D_s^+) / \Gamma_{\text{total}}$] × [B(D_{s2}⁺ → φπ⁺)] assuming B(D_{s2}⁺ → φπ⁺) = 0.0462 ± 0.0062, which we rescale to our best value B(D_{s2}⁺ → φπ⁺) = (4.5 ± 0.4) × 10⁻². Our first error is their experiment's error and our second error is the systematic error from using our best value.

3 GIBAUT 96 reports 0.0126 ± 0.0022 ± 0.0025 from a measurement of [$\Gamma(B^+ \rightarrow \overline{D}^0 D_s^+) / \Gamma_{\text{total}}$] × [B(D_{s2}⁺ → φπ⁺)] assuming B(D_{s2}⁺ → φπ⁺) = 0.035, which we rescale to our best value B(D_{s2}⁺ → φπ⁺) = (4.5 ± 0.4) × 10⁻². Our first error is their experiment's error and our second error is the systematic error from using our best value.

4 ALBRECHT 92G reports 0.024 ± 0.012 ± 0.004 from a measurement of [$\Gamma(B^+ \rightarrow \overline{D}^0 D_s^+) / \Gamma_{\text{total}}$] × [B(D_{s2}⁺ → φπ⁺)] assuming B(D_{s2}⁺ → φπ⁺) = 0.027, which we rescale to our best value B(D_{s2}⁺ → φπ⁺) = (4.5 ± 0.4) × 10⁻². Our first error is their experiment's error and our second error is the systematic error from using our best value. Assumes PDG 1990 D⁰ branching ratios, e.g., B(D⁰ → K⁻π⁺) = 3.71 ± 0.25%.

5 BORTOLETTO 90 reports 0.029 ± 0.013 from a measurement of [$\Gamma(B^+ \rightarrow \overline{D}^0 D_s^+) / \Gamma_{\text{total}}$] × [B(D_{s2}⁺ → φπ⁺)] assuming B(D_{s2}⁺ → φπ⁺) = 0.02, which we rescale to our best value B(D_{s2}⁺ → φπ⁺) = (4.5 ± 0.4) × 10⁻². Our first error is their experiment's error and our second error is the systematic error from using our best value.

$\Gamma(D_{s0}^*(2317)^+ \overline{D}^0, D_{s0}^{*+} \rightarrow D_s^+ \pi^0) / \Gamma_{\text{total}}$ Γ_{173} / Γ

VALUE (units 10 ⁻³)	DOCUMENT ID	TECN	COMMENT
0.80^{+0.16}_{-0.13} OUR AVERAGE			

0.80^{+0.17}_{-0.16} ± 0.02 1,2 CHOI 15A BELL e⁺e⁻ → $\Upsilon(4S)$

0.80^{+0.35}_{-0.21} ± 0.07 2,3 AUBERT,B 04s BABR e⁺e⁻ → $\Upsilon(4S)$

• • • We do not use the following data for averages, fits, limits, etc. • • •

0.65^{+0.26}_{-0.24} ± 0.06 2,4 KROKOVNY 03b BELL Repl. by CHOI 15A

1 CHOI 15A reports (8.0^{+1.3}_{-1.2} ± 1.1 ± 0.4) × 10⁻⁴ from a measurement of [$\Gamma(B^+ \rightarrow D_{s0}^*(2317)^+ \overline{D}^0, D_{s0}^{*+} \rightarrow D_s^+ \pi^0) / \Gamma_{\text{total}}$] × [B(D_{s2}⁺ → K⁺K⁻π⁺)] assuming B(D_{s2}⁺ → K⁺K⁻π⁺) = (5.39 ± 0.21) × 10⁻², which we rescale to our best value B(D_{s2}⁺ → K⁺K⁻π⁺) = (5.38 ± 0.10) × 10⁻². Our first error is their experiment's error and our second error is the systematic error from using our best value.

2 Assumes equal production of B⁺ and B⁰ at the $\Upsilon(4S)$.

3 AUBERT,B 04s reports (1.0 ± 0.3^{+0.4}_{-0.2}) × 10⁻³ from a measurement of [$\Gamma(B^+ \rightarrow D_{s0}^*(2317)^+ \overline{D}^0, D_{s0}^{*+} \rightarrow D_s^+ \pi^0) / \Gamma_{\text{total}}$] × [B(D_{s2}⁺ → φπ⁺)] assuming B(D_{s2}⁺ → φπ⁺) = 0.036 ± 0.009, which we rescale to our best value B(D_{s2}⁺ → φπ⁺) = (4.5 ± 0.4) × 10⁻². Our first error is their experiment's error and our second error is the systematic error from using our best value.

4 KROKOVNY 03b reports (0.81^{+0.30}_{-0.27} ± 0.24) × 10⁻³ from a measurement of [$\Gamma(B^+ \rightarrow D_{s0}^*(2317)^+ \overline{D}^0, D_{s0}^{*+} \rightarrow D_s^+ \pi^0) / \Gamma_{\text{total}}$] × [B(D_{s2}⁺ → φπ⁺)] assuming B(D_{s2}⁺ → φπ⁺) = 0.036 ± 0.009, which we rescale to our best value B(D_{s2}⁺ → φπ⁺) = (4.5 ± 0.4) × 10⁻². Our first error is their experiment's error and our second error is the systematic error from using our best value.

$\Gamma(D_{s0}^*(2317)^+ \overline{D}^0 \times B(D_{s0}^*(2317)^+ \rightarrow D_s^{*+} \gamma)) / \Gamma_{\text{total}}$ Γ_{174} / Γ

VALUE (units 10 ⁻³)	CL%	DOCUMENT ID	TECN	COMMENT
<0.76	90	1 KROKOVNY	03b BELL	e ⁺ e ⁻ → $\Upsilon(4S)$

1 Assumes equal production of B⁺ and B⁰ at the $\Upsilon(4S)$.

$\Gamma(D_{s0}^*(2317)^+ \overline{D}^* (2007)^0 \times B(D_{s0}^*(2317)^+ \rightarrow D_s^+ \pi^0)) / \Gamma_{\text{total}}$ Γ_{175} / Γ

VALUE (units 10 ⁻³)	DOCUMENT ID	TECN	COMMENT
0.9 ± 0.6^{+0.4}_{-0.3}	1 AUBERT,B	04s BABR	e ⁺ e ⁻ → $\Upsilon(4S)$

1 Assumes equal production of B⁺ and B⁰ at the $\Upsilon(4S)$.

$\Gamma(D_{s,J}(2457)^+ \overline{D}^0) / \Gamma_{\text{total}}$ Γ_{176} / Γ

VALUE (units 10 ⁻³)	DOCUMENT ID	TECN	COMMENT
3.1 ± 1.0^{+1.0}_{-0.9} OUR AVERAGE			

4.3 ± 1.6 ± 1.3 1 AUBERT 06N BABR e⁺e⁻ → $\Upsilon(4S)$

4.6 ± 1.8_{-1.6} ± 1.0 2,3 AUBERT,B 04s BABR e⁺e⁻ → $\Upsilon(4S)$

2.1 ± 1.1_{-0.9} ± 0.5 2,4 KROKOVNY 03b BELL e⁺e⁻ → $\Upsilon(4S)$

1 Uses a missing-mass method in the events that one of the B mesons is fully reconstructed.

2 Assumes equal production of B⁺ and B⁰ at the $\Upsilon(4S)$.

3 AUBERT,B 04s reports [$\Gamma(B^+ \rightarrow D_{s,J}(2457)^+ \overline{D}^0) / \Gamma_{\text{total}}$] × [B(D_{s1}(2460)⁺ → D_{s2}⁺π⁰)] = (2.2^{+0.8}_{-0.7} ± 0.3) × 10⁻³ which we divide by our best value B(D_{s1}(2460)⁺ → D_{s2}⁺π⁰) = (48 ± 11) × 10⁻². Our first error is their experiment's error and our second error is the systematic error from using our best value.

4 KROKOVNY 03b reports [$\Gamma(B^+ \rightarrow D_{s,J}(2457)^+ \overline{D}^0) / \Gamma_{\text{total}}$] × [B(D_{s1}(2460)⁺ → D_{s2}⁺π⁰)] = (1.0^{+0.5}_{-0.4} ± 0.1) × 10⁻³ which we divide by our best value B(D_{s1}(2460)⁺ → D_{s2}⁺π⁰) = (48 ± 11) × 10⁻². Our first error is their experiment's error and our second error is the systematic error from using our best value.

$\Gamma(D_{s,J}(2457)^+ \overline{D}^0 \times B(D_{s,J}(2457)^+ \rightarrow D_s^+ \gamma)) / \Gamma_{\text{total}}$ Γ_{177} / Γ

VALUE (units 10 ⁻³)	DOCUMENT ID	TECN	COMMENT
0.46^{+0.13}_{-0.11} OUR AVERAGE			

0.48^{+0.19}_{-0.13} ± 0.04 1,2 AUBERT,B 04s BABR e⁺e⁻ → $\Upsilon(4S)$

0.45^{+0.15}_{-0.14} ± 0.04 1,3 KROKOVNY 03b BELL e⁺e⁻ → $\Upsilon(4S)$

1 Assumes equal production of B⁺ and B⁰ at the $\Upsilon(4S)$.

2 AUBERT,B 04s reports (0.6 ± 0.2^{+0.2}_{-0.1}) × 10⁻³ from a measurement of [$\Gamma(B^+ \rightarrow D_{s,J}(2457)^+ \overline{D}^0 \times B(D_{s,J}(2457)^+ \rightarrow D_s^+ \gamma)) / \Gamma_{\text{total}}$] × [B(D_{s2}⁺ → φπ⁺)] assuming B(D_{s2}⁺ → φπ⁺) = 0.036 ± 0.009, which we rescale to our best value B(D_{s2}⁺ → φπ⁺) = (4.5 ± 0.4) × 10⁻². Our first error is their experiment's error and our second error is the systematic error from using our best value.

3 KROKOVNY 03b reports (0.56^{+0.16}_{-0.15} ± 0.17) × 10⁻³ from a measurement of [$\Gamma(B^+ \rightarrow D_{s,J}(2457)^+ \overline{D}^0 \times B(D_{s,J}(2457)^+ \rightarrow D_s^+ \gamma)) / \Gamma_{\text{total}}$] × [B(D_{s2}⁺ → φπ⁺)] assuming B(D_{s2}⁺ → φπ⁺) = 0.036 ± 0.009, which we rescale to our best value B(D_{s2}⁺ → φπ⁺) = (4.5 ± 0.4) × 10⁻². Our first error is their experiment's error and our second error is the systematic error from using our best value.

$\Gamma(D_{sJ}(2457)^+ \bar{D}^0 \times B(D_{sJ}(2457)^+ \rightarrow D_s^+ \pi^+ \pi^-))/\Gamma_{total}$						Γ_{178}/Γ
VALUE (units 10^{-3})	CL%	DOCUMENT ID	TECN	COMMENT		
<0.22	90	¹ KROKOVNY 03B	BELL	$e^+e^- \rightarrow \Upsilon(4S)$		
¹ Assumes equal production of B^+ and B^0 at the $\Upsilon(4S)$.						

$\Gamma(D_{sJ}(2457)^+ \bar{D}^0 \times B(D_{sJ}(2457)^+ \rightarrow D_s^+ \pi^0))/\Gamma_{total}$						Γ_{179}/Γ
VALUE (units 10^{-3})	CL%	DOCUMENT ID	TECN	COMMENT		
<0.27	90	¹ KROKOVNY 03B	BELL	$e^+e^- \rightarrow \Upsilon(4S)$		
¹ Assumes equal production of B^+ and B^0 at the $\Upsilon(4S)$.						

$\Gamma(D_{sJ}(2457)^+ \bar{D}^0 \times B(D_{sJ}(2457)^+ \rightarrow D_s^+ \gamma))/\Gamma_{total}$						Γ_{180}/Γ
VALUE (units 10^{-3})	CL%	DOCUMENT ID	TECN	COMMENT		
<0.98	90	¹ KROKOVNY 03B	BELL	$e^+e^- \rightarrow \Upsilon(4S)$		
¹ Assumes equal production of B^+ and B^0 at the $\Upsilon(4S)$.						

$\Gamma(D_{sJ}(2457)^+ \bar{D}^*(2007)^0)/\Gamma_{total}$						Γ_{181}/Γ
VALUE (units 10^{-3})	CL%	DOCUMENT ID	TECN	COMMENT		
12.0 ± 3.0		OUR AVERAGE				
$11.2 \pm 2.6 \pm 2.0$		¹ AUBERT 06N	BABR	$e^+e^- \rightarrow \Upsilon(4S)$		
$16 \pm 8 \pm 4$		^{2,3} AUBERT,B	04S	BABR $e^+e^- \rightarrow \Upsilon(4S)$		
¹ Uses a missing-mass method in the events that one of the B mesons is fully reconstructed.						
² AUBERT,B 04S reports $[\Gamma(B^+ \rightarrow D_{sJ}(2457)^+ \bar{D}^*(2007)^0)/\Gamma_{total}] \times [B(D_{s1}(2460)^+ \rightarrow D_s^{*+} \pi^0)] = (7.6 \pm 1.7 \pm 3.2/2.4) \times 10^{-3}$ which we divide by our best value $B(D_{s1}(2460)^+ \rightarrow D_s^{*+} \pi^0) = (48 \pm 11) \times 10^{-2}$. Our first error is their experiment's error and our second error is the systematic error from using our best value.						
³ Assumes equal production of B^+ and B^0 at the $\Upsilon(4S)$.						

$\Gamma(D_{sJ}(2457)^+ \bar{D}^*(2007)^0 \times B(D_{sJ}(2457)^+ \rightarrow D_s^+ \gamma))/\Gamma_{total}$						Γ_{182}/Γ
VALUE (units 10^{-3})	CL%	DOCUMENT ID	TECN	COMMENT		
$1.4 \pm 0.4 \pm 0.6$		OUR AVERAGE				
		¹ AUBERT,B	04S	BABR $e^+e^- \rightarrow \Upsilon(4S)$		
¹ Assumes equal production of B^+ and B^0 at the $\Upsilon(4S)$.						

$\Gamma(\bar{D}^0 D_{s1}(2536)^+ \times B(D_{s1}(2536)^+ \rightarrow D^*(2007)^0 K^+))/\Gamma_{total}$						Γ_{184}/Γ
VALUE (units 10^{-4})	CL%	DOCUMENT ID	TECN	COMMENT		
$2.16 \pm 0.52 \pm 0.45$		¹ AUBERT 08B	BABR	$e^+e^- \rightarrow \Upsilon(4S)$		
• • • We do not use the following data for averages, fits, limits, etc. • • •						
<2	90	AUBERT 03X	BABR	Repl. by AUBERT 08B		
¹ Assumes equal production of B^+ and B^0 at the $\Upsilon(4S)$.						

$\Gamma(\bar{D}^0 D_{s1}(2536)^+ \times B(D_{s1}(2536)^+ \rightarrow D^*(2007)^0 K^+ + D^*(2010)^+ K^0))/\Gamma_{total}$						Γ_{183}/Γ
VALUE (units 10^{-4})	CL%	DOCUMENT ID	TECN	COMMENT		
$3.97 \pm 0.85 \pm 0.56$		^{1,2} AUSHEV 11	BELL	$e^+e^- \rightarrow \Upsilon(4S)$		
¹ Uses $\Gamma(D^*(2007)^0 \rightarrow D^0 \pi^0) / \Gamma(D^*(2007)^0 \rightarrow D^0 \gamma) = 1.74 \pm 0.13$ and $\Gamma(D_{s1}(2536)^+ \rightarrow D^*(2007)^0 K^+) / \Gamma(D_{s1}(2536)^+ \rightarrow D^*(2010)^+ K^0) = 1.36 \pm 0.2$						
² Assumes equal production of B^+ and B^0 at the $\Upsilon(4S)$.						

$\Gamma(\bar{D}^*(2007)^0 D_{s1}(2536)^+ \times B(D_{s1}(2536)^+ \rightarrow D^*(2007)^0 K^+))/\Gamma_{total}$						Γ_{185}/Γ
VALUE (units 10^{-4})	CL%	DOCUMENT ID	TECN	COMMENT		
$5.46 \pm 1.17 \pm 1.04$		¹ AUBERT 08B	BABR	$e^+e^- \rightarrow \Upsilon(4S)$		
• • • We do not use the following data for averages, fits, limits, etc. • • •						
<7	90	AUBERT 03X	BABR	Repl. by AUBERT 08B		
¹ Assumes equal production of B^+ and B^0 at the $\Upsilon(4S)$.						

$\Gamma(\bar{D}^0 D_{s1}(2536)^+ \times B(D_{s1}(2536)^+ \rightarrow D^{*+} K^0))/\Gamma_{total}$						Γ_{186}/Γ
VALUE (units 10^{-4})	CL%	DOCUMENT ID	TECN	COMMENT		
$2.30 \pm 0.98 \pm 0.43$		¹ AUBERT 08B	BABR	$e^+e^- \rightarrow \Upsilon(4S)$		
¹ Assumes equal production of B^+ and B^0 at the $\Upsilon(4S)$.						

$\Gamma(\bar{D}^0 D_{sJ}(2700)^+ \times B(D_{sJ}(2700)^+ \rightarrow D^0 K^+))/\Gamma_{total}$						Γ_{187}/Γ
VALUE (units 10^{-4})	CL%	DOCUMENT ID	TECN	COMMENT		
5.6 ± 1.8		OUR AVERAGE				
$5.02 \pm 0.71 \pm 0.93$		¹ LEES 15c	BABR	$e^+e^- \rightarrow \Upsilon(4S)$		
$11.3 \pm 2.2 \pm 1.4$		¹ BRODZICKA 08	BELL	$e^+e^- \rightarrow \Upsilon(4S)$		
-2.8						
¹ Assumes equal production of B^+ and B^0 at the $\Upsilon(4S)$.						

$\Gamma(\bar{D}^{*0} D_{s1}(2536)^+, D_{s1}^+ \rightarrow D^{*+} K^0)/\Gamma_{total}$						Γ_{188}/Γ
VALUE (units 10^{-4})	CL%	DOCUMENT ID	TECN	COMMENT		
$3.92 \pm 2.46 \pm 0.83$		¹ AUBERT 08B	BABR	$e^+e^- \rightarrow \Upsilon(4S)$		
¹ Assumes equal production of B^+ and B^0 at the $\Upsilon(4S)$.						

$\Gamma(\bar{D}^0 D_{sJ}(2573)^+, D_{sJ}^+ \rightarrow D^0 K^+)/\Gamma_{total}$						Γ_{189}/Γ
VALUE (units 10^{-4})	CL%	DOCUMENT ID	TECN	COMMENT		
$0.08 \pm 0.14 \pm 0.05$		¹ LEES 15c	BABR	$e^+e^- \rightarrow \Upsilon(4S)$		
¹ Assumes equal production of B^+ and B^0 at the $\Upsilon(4S)$.						

$\Gamma(\bar{D}^{*0} D_{sJ}(2573), D_{sJ}^+ \rightarrow D^0 K^+)/\Gamma_{total}$						Γ_{190}/Γ
VALUE (units 10^{-4})	CL%	DOCUMENT ID	TECN	COMMENT		
<2	90	AUBERT 03X	BABR	$e^+e^- \rightarrow \Upsilon(4S)$		

$\Gamma(\bar{D}^*(2007)^0 D_{sJ}(2573), D_{sJ}^+ \rightarrow D^0 K^+)/\Gamma_{total}$						Γ_{191}/Γ
VALUE (units 10^{-4})	CL%	DOCUMENT ID	TECN	COMMENT		
<5	90	AUBERT 03X	BABR	$e^+e^- \rightarrow \Upsilon(4S)$		

$\Gamma(\bar{D}^0 D_s^{*+})/\Gamma_{total}$						Γ_{192}/Γ
VALUE	CL%	DOCUMENT ID	TECN	COMMENT		
0.0076 ± 0.0016		OUR AVERAGE				
$0.0079 \pm 0.0017 \pm 0.0007$		¹ AUBERT 06N	BABR	$e^+e^- \rightarrow \Upsilon(4S)$		
$0.0068 \pm 0.0025 \pm 0.0006$		² GIBAUT 96	CLE2	$e^+e^- \rightarrow \Upsilon(4S)$		
$0.010 \pm 0.007 \pm 0.001$		³ ALBRECHT 92G	ARG	$e^+e^- \rightarrow \Upsilon(4S)$		
¹ AUBERT 06N reports $(0.77 \pm 0.15 \pm 0.13) \times 10^{-2}$ from a measurement of $[\Gamma(B^+ \rightarrow \bar{D}^0 D_s^{*+})/\Gamma_{total}] \times [B(D_s^+ \rightarrow \phi \pi^+)]$ assuming $B(D_s^+ \rightarrow \phi \pi^+) = 0.0462 \pm 0.0062$, which we rescale to our best value $B(D_s^+ \rightarrow \phi \pi^+) = (4.5 \pm 0.4) \times 10^{-2}$. Our first error is their experiment's error and our second error is the systematic error from using our best value.						
² GIBAUT 96 reports $0.0087 \pm 0.0027 \pm 0.0017$ from a measurement of $[\Gamma(B^+ \rightarrow \bar{D}^0 D_s^{*+})/\Gamma_{total}] \times [B(D_s^+ \rightarrow \phi \pi^+)]$ assuming $B(D_s^+ \rightarrow \phi \pi^+) = 0.035$, which we rescale to our best value $B(D_s^+ \rightarrow \phi \pi^+) = (4.5 \pm 0.4) \times 10^{-2}$. Our first error is their experiment's error and our second error is the systematic error from using our best value.						
³ ALBRECHT 92G reports $0.016 \pm 0.012 \pm 0.003$ from a measurement of $[\Gamma(B^+ \rightarrow \bar{D}^0 D_s^{*+})/\Gamma_{total}] \times [B(D_s^+ \rightarrow \phi \pi^+)]$ assuming $B(D_s^+ \rightarrow \phi \pi^+) = 0.027$, which we rescale to our best value $B(D_s^+ \rightarrow \phi \pi^+) = (4.5 \pm 0.4) \times 10^{-2}$. Our first error is their experiment's error and our second error is the systematic error from using our best value. Assumes PDG 1990 D^0 branching ratios, e.g., $B(D^0 \rightarrow K^- \pi^+) = 3.71 \pm 0.25\%$.						

$\Gamma(\bar{D}^*(2007)^0 D_s^+)/\Gamma_{total}$						Γ_{193}/Γ
VALUE	CL%	DOCUMENT ID	TECN	COMMENT		
0.0082 ± 0.0017		OUR AVERAGE				
$0.0078 \pm 0.0018 \pm 0.0007$		¹ AUBERT 06N	BABR	$e^+e^- \rightarrow \Upsilon(4S)$		
$0.011 \pm 0.004 \pm 0.001$		² GIBAUT 96	CLE2	$e^+e^- \rightarrow \Upsilon(4S)$		
$0.008 \pm 0.006 \pm 0.001$		³ ALBRECHT 92G	ARG	$e^+e^- \rightarrow \Upsilon(4S)$		
¹ AUBERT 06N reports $(0.76 \pm 0.15 \pm 0.13) \times 10^{-2}$ from a measurement of $[\Gamma(B^+ \rightarrow \bar{D}^*(2007)^0 D_s^+)/\Gamma_{total}] \times [B(D_s^+ \rightarrow \phi \pi^+)]$ assuming $B(D_s^+ \rightarrow \phi \pi^+) = 0.0462 \pm 0.0062$, which we rescale to our best value $B(D_s^+ \rightarrow \phi \pi^+) = (4.5 \pm 0.4) \times 10^{-2}$. Our first error is their experiment's error and our second error is the systematic error from using our best value.						
² GIBAUT 96 reports $0.0140 \pm 0.0043 \pm 0.0035$ from a measurement of $[\Gamma(B^+ \rightarrow \bar{D}^*(2007)^0 D_s^+)/\Gamma_{total}] \times [B(D_s^+ \rightarrow \phi \pi^+)]$ assuming $B(D_s^+ \rightarrow \phi \pi^+) = 0.035$, which we rescale to our best value $B(D_s^+ \rightarrow \phi \pi^+) = (4.5 \pm 0.4) \times 10^{-2}$. Our first error is their experiment's error and our second error is the systematic error from using our best value.						
³ ALBRECHT 92G reports $0.013 \pm 0.009 \pm 0.002$ from a measurement of $[\Gamma(B^+ \rightarrow \bar{D}^*(2007)^0 D_s^+)/\Gamma_{total}] \times [B(D_s^+ \rightarrow \phi \pi^+)]$ assuming $B(D_s^+ \rightarrow \phi \pi^+) = 0.027$, which we rescale to our best value $B(D_s^+ \rightarrow \phi \pi^+) = (4.5 \pm 0.4) \times 10^{-2}$. Our first error is their experiment's error and our second error is the systematic error from using our best value. Assumes PDG 1990 D^0 and $D^*(2007)^0$ branching ratios, e.g., $B(D^0 \rightarrow K^- \pi^+) = 3.71 \pm 0.25\%$ and $B(D^*(2007)^0 \rightarrow D^0 \pi^0) = 55 \pm 6\%$.						

$\Gamma(\bar{D}^*(2007)^0 D_s^{*+})/\Gamma_{total}$						Γ_{194}/Γ
VALUE	CL%	DOCUMENT ID	TECN	COMMENT		
0.0171 ± 0.0024		OUR AVERAGE				
$0.0167 \pm 0.0019 \pm 0.0015$		¹ AUBERT 06N	BABR	$e^+e^- \rightarrow \Upsilon(4S)$		
$0.024 \pm 0.009 \pm 0.002$		² GIBAUT 96	CLE2	$e^+e^- \rightarrow \Upsilon(4S)$		
$0.019 \pm 0.010 \pm 0.002$		³ ALBRECHT 92G	ARG	$e^+e^- \rightarrow \Upsilon(4S)$		
¹ AUBERT 06N reports $(1.62 \pm 0.22 \pm 0.18) \times 10^{-2}$ from a measurement of $[\Gamma(B^+ \rightarrow \bar{D}^*(2007)^0 D_s^{*+})/\Gamma_{total}] \times [B(D_s^+ \rightarrow \phi \pi^+)]$ assuming $B(D_s^+ \rightarrow \phi \pi^+) = 0.0462 \pm 0.0062$, which we rescale to our best value $B(D_s^+ \rightarrow \phi \pi^+) = (4.5 \pm 0.4) \times 10^{-2}$. Our first error is their experiment's error and our second error is the systematic error from using our best value.						
² GIBAUT 96 reports $0.0310 \pm 0.0088 \pm 0.0065$ from a measurement of $[\Gamma(B^+ \rightarrow \bar{D}^*(2007)^0 D_s^{*+})/\Gamma_{total}] \times [B(D_s^+ \rightarrow \phi \pi^+)]$ assuming $B(D_s^+ \rightarrow \phi \pi^+) = 0.035$, which we rescale to our best value $B(D_s^+ \rightarrow \phi \pi^+) = (4.5 \pm 0.4) \times 10^{-2}$. Our first error is their experiment's error and our second error is the systematic error from using our best value.						
³ ALBRECHT 92G reports $0.031 \pm 0.016 \pm 0.005$ from a measurement of $[\Gamma(B^+ \rightarrow \bar{D}^*(2007)^0 D_s^{*+})/\Gamma_{total}] \times [B(D_s^+ \rightarrow \phi \pi^+)]$ assuming $B(D_s^+ \rightarrow \phi \pi^+) = 0.027$, which we rescale to our best value $B(D_s^+ \rightarrow \phi \pi^+) = (4.5 \pm 0.4) \times 10^{-2}$. Our first error is their experiment's error and our second error is the systematic error from using our best value. Assumes PDG 1990 D^0 and $D^*(2007)^0$ branching ratios, e.g., $B(D^0 \rightarrow K^- \pi^+) = 3.71 \pm 0.25\%$ and $B(D^*(2007)^0 \rightarrow D^0 \pi^0) = 55 \pm 6\%$.						

$\Gamma(D_s^{*+} \bar{D}^{*0})/\Gamma_{total}$						Γ_{195}/Γ
VALUE	CL%	DOCUMENT ID	TECN	COMMENT		
$(2.73 \pm 0.93 \pm 0.68) \times 10^{-2}$		¹ AHMED 00B	CLE2	$e^+e^- \rightarrow \Upsilon(4S)$		
¹ AHMED 00B reports their experiment's uncertainties ($\pm 0.78 \pm 0.48 \pm 0.68\%$), where the first error is statistical, the second is systematic, and the third is the uncertainty in the $D_s \rightarrow \phi \pi$ branching fraction. We combine the first two in quadrature.						

Meson Particle Listings

B^\pm

$\Gamma(\bar{D}^*(2007)^0 D^*(2010)^+)/\Gamma_{total}$					Γ_{196}/Γ
VALUE (units 10^{-4})	CL%	DOCUMENT ID	TECN	COMMENT	
8.1±1.2±1.2		¹ AUBERT,B	06A BABR	$e^+e^- \rightarrow \Upsilon(4S)$	
• • •		We do not use the following data for averages, fits, limits, etc. • • •			
<110	90	BARATE	98Q ALEP	$e^+e^- \rightarrow Z$	
		¹ Assumes equal production of B^+ and B^0 at the $\Upsilon(4S)$.			

$[\Gamma(\bar{D}^0 D^*(2010)^+) + \Gamma(\bar{D}^*(2007)^0 D^+)]/\Gamma_{total}$					Γ_{197}/Γ
VALUE (units 10^{-4})	CL%	DOCUMENT ID	TECN	COMMENT	
<130	90	BARATE	98Q ALEP	$e^+e^- \rightarrow Z$	

$\Gamma(\bar{D}^0 D^*(2010)^+)/\Gamma_{total}$					Γ_{198}/Γ
VALUE (units 10^{-4})	CL%	DOCUMENT ID	TECN	COMMENT	
3.9 ± 0.5 OUR AVERAGE					
3.6 ± 0.5 ± 0.4		¹ AUBERT,B	06A BABR	$e^+e^- \rightarrow \Upsilon(4S)$	
4.57 ± 0.71 ± 0.56		¹ MAJUMDER	05 BELL	$e^+e^- \rightarrow \Upsilon(4S)$	
		¹ Assumes equal production of B^+ and B^0 at the $\Upsilon(4S)$.			

$\Gamma(\bar{D}^0 D^+)/\Gamma_{total}$					Γ_{199}/Γ
VALUE (units 10^{-4})	CL%	DOCUMENT ID	TECN	COMMENT	
3.8 ± 0.4 OUR AVERAGE					
3.85 ± 0.31 ± 0.38		¹ ADACHI	08 BELL	$e^+e^- \rightarrow \Upsilon(4S)$	
3.8 ± 0.6 ± 0.5		¹ AUBERT,B	06A BABR	$e^+e^- \rightarrow \Upsilon(4S)$	
• • •		We do not use the following data for averages, fits, limits, etc. • • •			
4.83 ± 0.78 ± 0.58		¹ MAJUMDER	05 BELL	Repl. by ADACHI 08	
<67	90	BARATE	98Q ALEP	$e^+e^- \rightarrow Z$	
		¹ Assumes equal production of B^+ and B^0 at the $\Upsilon(4S)$.			

$\Gamma(\bar{D}^0 D^+ K^0)/\Gamma_{total}$					Γ_{200}/Γ
VALUE (units 10^{-3})	CL%	DOCUMENT ID	TECN	COMMENT	
1.55 ± 0.17 ± 0.13		¹ DEL-AMO-SA..11B	BABR	$e^+e^- \rightarrow \Upsilon(4S)$	
• • •		We do not use the following data for averages, fits, limits, etc. • • •			
<2.8	90	¹ AUBERT	03x BABR	Repl. by DEL-AMO-SANCHEZ 11B	
		¹ Assumes equal production of B^+ and B^0 at the $\Upsilon(4S)$.			

$\Gamma(D^+ \bar{D}^*(2007)^0)/\Gamma_{total}$					Γ_{201}/Γ
VALUE (units 10^{-4})	CL%	DOCUMENT ID	TECN	COMMENT	
6.3 ± 1.4 ± 1.0		¹ AUBERT,B	06A BABR	$e^+e^- \rightarrow \Upsilon(4S)$	
		¹ Assumes equal production of B^+ and B^0 at the $\Upsilon(4S)$.			

$\Gamma(\bar{D}^*(2007)^0 D^+ K^0)/\Gamma_{total}$					Γ_{202}/Γ
VALUE (units 10^{-3})	CL%	DOCUMENT ID	TECN	COMMENT	
2.06 ± 0.38 ± 0.30		¹ DEL-AMO-SA..11B	BABR	$e^+e^- \rightarrow \Upsilon(4S)$	
• • •		We do not use the following data for averages, fits, limits, etc. • • •			
<6.1	90	¹ AUBERT	03x BABR	Repl. by DEL-AMO-SANCHEZ 11B	
		¹ Assumes equal production of B^+ and B^0 at the $\Upsilon(4S)$.			

$\Gamma(\bar{D}^0 D^*(2010)^+ K^0)/\Gamma_{total}$					Γ_{203}/Γ
VALUE (units 10^{-3})	CL%	DOCUMENT ID	TECN	COMMENT	
3.81 ± 0.31 ± 0.23		¹ DEL-AMO-SA..11B	BABR	$e^+e^- \rightarrow \Upsilon(4S)$	
• • •		We do not use the following data for averages, fits, limits, etc. • • •			
5.2 $^{+1.0}_{-0.9}$ ± 0.7		¹ AUBERT	03x BABR	Repl. by DEL-AMO-SANCHEZ 11B	
		¹ Assumes equal production of B^+ and B^0 at the $\Upsilon(4S)$.			

$\Gamma(\bar{D}^*(2007)^0 D^*(2010)^+ K^0)/\Gamma_{total}$					Γ_{204}/Γ
VALUE (units 10^{-3})	CL%	DOCUMENT ID	TECN	COMMENT	
9.17 ± 0.83 ± 0.90		¹ DEL-AMO-SA..11B	BABR	$e^+e^- \rightarrow \Upsilon(4S)$	
• • •		We do not use the following data for averages, fits, limits, etc. • • •			
7.8 $^{+2.3}_{-2.1}$ ± 1.4		¹ AUBERT	03x BABR	Repl. by DEL-AMO-SANCHEZ 11B	
		¹ Assumes equal production of B^+ and B^0 at the $\Upsilon(4S)$.			

$\Gamma(\bar{D}^0 D^0 K^+)/\Gamma_{total}$					Γ_{205}/Γ
VALUE (units 10^{-3})	CL%	DOCUMENT ID	TECN	COMMENT	
1.45 ± 0.33 OUR AVERAGE		Error includes scale factor of 2.6.			
1.31 ± 0.07 ± 0.12		¹ DEL-AMO-SA..11B	BABR	$e^+e^- \rightarrow \Upsilon(4S)$	
2.22 ± 0.22 $^{+0.26}_{-0.24}$		¹ BRODZICKA	08 BELL	$e^+e^- \rightarrow \Upsilon(4S)$	
• • •		We do not use the following data for averages, fits, limits, etc. • • •			
1.17 ± 0.21 ± 0.15		¹ CHISTOV	04 BELL	Repl. by BRODZICKA 08	
1.9 ± 0.3 ± 0.3		¹ AUBERT	03x BABR	Repl. by DEL-AMO-SANCHEZ 11B	
		¹ Assumes equal production of B^+ and B^0 at the $\Upsilon(4S)$.			

$\Gamma(\bar{D}^*(2007)^0 D^0 K^+)/\Gamma_{total}$					Γ_{206}/Γ
VALUE (units 10^{-3})	CL%	DOCUMENT ID	TECN	COMMENT	
2.26 ± 0.16 ± 0.17		¹ DEL-AMO-SA..11B	BABR	$e^+e^- \rightarrow \Upsilon(4S)$	
• • •		We do not use the following data for averages, fits, limits, etc. • • •			
<3.8	90	¹ AUBERT	03x BABR	Repl. by DEL-AMO-SANCHEZ 11B	
		¹ Assumes equal production of B^+ and B^0 at the $\Upsilon(4S)$.			

$\Gamma(\bar{D}^0 D^*(2007)^0 K^+)/\Gamma_{total}$					Γ_{207}/Γ
VALUE (units 10^{-3})	CL%	DOCUMENT ID	TECN	COMMENT	
6.32 ± 0.19 ± 0.45		¹ DEL-AMO-SA..11B	BABR	$e^+e^- \rightarrow \Upsilon(4S)$	
• • •		We do not use the following data for averages, fits, limits, etc. • • •			
4.7 ± 0.7 ± 0.7		¹ AUBERT	03x BABR	Repl. by DEL-AMO-SANCHEZ 11B	
		¹ Assumes equal production of B^+ and B^0 at the $\Upsilon(4S)$.			

$\Gamma(\bar{D}^*(2007)^0 D^*(2007)^0 K^+)/\Gamma_{total}$					Γ_{208}/Γ
VALUE (units 10^{-3})	CL%	DOCUMENT ID	TECN	COMMENT	
11.23 ± 0.36 ± 1.26		¹ DEL-AMO-SA..11B	BABR	$e^+e^- \rightarrow \Upsilon(4S)$	
• • •		We do not use the following data for averages, fits, limits, etc. • • •			
5.3 $^{+1.1}_{-1.0}$ ± 1.2		¹ AUBERT	03x BABR	Repl. by DEL-AMO-SANCHEZ 11B	
		¹ Assumes equal production of B^+ and B^0 at the $\Upsilon(4S)$.			

$\Gamma(D^- D^+ K^+)/\Gamma_{total}$					Γ_{209}/Γ
VALUE (units 10^{-3})	CL%	DOCUMENT ID	TECN	COMMENT	
0.22 ± 0.05 ± 0.05		¹ DEL-AMO-SA..11B	BABR	$e^+e^- \rightarrow \Upsilon(4S)$	
• • •		We do not use the following data for averages, fits, limits, etc. • • •			
<0.90	90	¹ CHISTOV	04 BELL	$e^+e^- \rightarrow \Upsilon(4S)$	
<0.4	90	¹ AUBERT	03x BABR	Repl. by DEL-AMO-SANCHEZ 11B	
		¹ Assumes equal production of B^+ and B^0 at the $\Upsilon(4S)$.			

$\Gamma(X_0(2900) D^+, X_0 \rightarrow D^- K^+)/\Gamma(D^- D^+ K^+)$					$\Gamma_{210}/\Gamma_{209}$
VALUE (units 10^{-2})	CL%	DOCUMENT ID	TECN	COMMENT	
5.6 ± 1.4 ± 0.5		¹ AAIJ	20AI LHCb	pp at 7, 8, 13 TeV	
		¹ Measured in Dalitz plot analysis of $B^+ \rightarrow D^- D^+ K^+$ decays.			

$\Gamma(X_1(2900) D^+, X_1 \rightarrow D^- K^+)/\Gamma(D^- D^+ K^+)$					$\Gamma_{211}/\Gamma_{209}$
VALUE (units 10^{-2})	CL%	DOCUMENT ID	TECN	COMMENT	
30.6 ± 2.4 ± 2.1		¹ AAIJ	20AI LHCb	pp at 7, 8, 13 TeV	
		¹ Measured in Dalitz plot analysis of $B^+ \rightarrow D^- D^+ K^+$ decays.			

$\Gamma(D^- D^+ K^+ \text{ nonresonant})/\Gamma(D^- D^+ K^+)$					$\Gamma_{212}/\Gamma_{209}$
VALUE (units 10^{-2})	CL%	DOCUMENT ID	TECN	COMMENT	
24.2 ± 2.2 ± 0.5		¹ AAIJ	20AI LHCb	pp at 7, 8, 13 TeV	
		¹ Measured in Dalitz plot analysis of $B^+ \rightarrow D^- D^+ K^+$ decays.			

$\Gamma(D^- D^*(2010)^+ K^+)/\Gamma_{total}$					Γ_{213}/Γ
VALUE (units 10^{-3})	CL%	DOCUMENT ID	TECN	COMMENT	
0.63 ± 0.09 ± 0.06		¹ DEL-AMO-SA..11B	BABR	$e^+e^- \rightarrow \Upsilon(4S)$	
• • •		We do not use the following data for averages, fits, limits, etc. • • •			
<0.7	90	¹ AUBERT	03x BABR	Repl. by DEL-AMO-SANCHEZ 11B	
		¹ Assumes equal production of B^+ and B^0 at the $\Upsilon(4S)$.			

$\Gamma(D^- D^*(2010)^+ K^+)/\Gamma(\bar{D}^0 D^0 K^+)$					$\Gamma_{213}/\Gamma_{205}$
VALUE	CL%	DOCUMENT ID	TECN	COMMENT	
0.517 ± 0.015 ± 0.017		¹ AAIJ	20AN LHCb	pp at 7, 8, 13 TeV	
		¹ Uses $D^+ \rightarrow K^- \pi^+ \pi^+$, $D^0 \rightarrow K^- \pi^+$ and $D^0 \rightarrow K^- \pi^+ \pi^+ \pi^-$ decays.			

$\Gamma(D^*(2010)^- D^+ K^+)/\Gamma_{total}$					Γ_{214}/Γ
VALUE (units 10^{-3})	CL%	DOCUMENT ID	TECN	COMMENT	
0.60 ± 0.10 ± 0.08		¹ DEL-AMO-SA..11B	BABR	$e^+e^- \rightarrow \Upsilon(4S)$	
• • •		We do not use the following data for averages, fits, limits, etc. • • •			
1.5 ± 0.3 ± 0.2		¹ AUBERT	03x BABR	Repl. by DEL-AMO-SANCHEZ 11B	
		¹ Assumes equal production of B^+ and B^0 at the $\Upsilon(4S)$.			

$\Gamma(D^*(2010)^- D^+ K^+)/\Gamma(\bar{D}^0 D^0 K^+)$					$\Gamma_{214}/\Gamma_{205}$
VALUE	CL%	DOCUMENT ID	TECN	COMMENT	
0.577 ± 0.016 ± 0.018		¹ AAIJ	20AN LHCb	pp at 7, 8, 13 TeV	
		¹ Uses $D^+ \rightarrow K^- \pi^+ \pi^+$, $D^0 \rightarrow K^- \pi^+$ and $D^0 \rightarrow K^- \pi^+ \pi^+ \pi^-$ decays.			

$\Gamma(D^- D^*(2010)^+ K^+)/\Gamma(D^*(2010)^- D^+ K^+)$					$\Gamma_{213}/\Gamma_{214}$
VALUE	CL%	DOCUMENT ID	TECN	COMMENT	
0.907 ± 0.033 ± 0.014		¹ AAIJ	20AN LHCb	pp at 7, 8, 13 TeV	
		¹ Uses $D^+ \rightarrow K^- \pi^+ \pi^+$, $D^0 \rightarrow K^- \pi^+$ and $D^0 \rightarrow K^- \pi^+ \pi^+ \pi^-$ decays.			

$\Gamma(D^{*0}(2010)^- D^{*0}(2010)^+ K^+)/\Gamma_{\text{total}}$ Γ_{215}/Γ

VALUE (units 10^{-3})	CL%	DOCUMENT ID	TECN	COMMENT
$1.32 \pm 0.13 \pm 0.12$		¹ DEL-AMO-SA..11B	BABR	$e^+e^- \rightarrow \Upsilon(4S)$
••• We do not use the following data for averages, fits, limits, etc. •••				
<1.8	90	¹ AUBERT 03x	BABR	Repl. by DEL-AMO-SANCHEZ 11B

¹ Assumes equal production of B^+ and B^0 at the $\Upsilon(4S)$.

 $\Gamma((\bar{D}^+ + \bar{D}^*) (D + D^*) K)/\Gamma_{\text{total}}$ Γ_{216}/Γ

VALUE (units 10^{-2})	CL%	DOCUMENT ID	TECN	COMMENT
$4.05 \pm 0.11 \pm 0.28$		¹ DEL-AMO-SA..11B	BABR	$e^+e^- \rightarrow \Upsilon(4S)$
••• We do not use the following data for averages, fits, limits, etc. •••				
$3.5 \pm 0.3 \pm 0.5$		¹ AUBERT 03x	BABR	Repl. by DEL-AMO-SANCHEZ 11B

¹ Assumes equal production of B^+ and B^0 at the $\Upsilon(4S)$.

 $\Gamma(D_s^{*0} \pi^0)/\Gamma_{\text{total}}$ Γ_{217}/Γ

VALUE (units 10^{-5})	CL%	DOCUMENT ID	TECN	COMMENT
$1.6^{+0.6}_{-0.5} \pm 0.1$		¹ AUBERT 07M	BABR	$e^+e^- \rightarrow \Upsilon(4S)$
••• We do not use the following data for averages, fits, limits, etc. •••				
<16	90	² ALEXANDER 93B	CLE2	$e^+e^- \rightarrow \Upsilon(4S)$

¹ AUBERT 07M reports $[\Gamma(B^+ \rightarrow D_s^{*0} \pi^0)/\Gamma_{\text{total}}] \times [B(D_s^+ \rightarrow \phi\pi^+)] = (7.0^{+2.4}_{-2.1} \pm 0.6) \times 10^{-7}$ which we divide by our best value $B(D_s^+ \rightarrow \phi\pi^+) = (4.5 \pm 0.4) \times 10^{-2}$. Our first error is their experiment's error and our second error is the systematic error from using our best value.

² ALEXANDER 93B reports $< 2.0 \times 10^{-4}$ from a measurement of $[\Gamma(B^+ \rightarrow D_s^+ \pi^0)/\Gamma_{\text{total}}] \times [B(D_s^+ \rightarrow \phi\pi^+)]$ assuming $B(D_s^+ \rightarrow \phi\pi^+) = 0.037$, which we rescale to our best value $B(D_s^+ \rightarrow \phi\pi^+) = 4.5 \times 10^{-2}$.

 $[\Gamma(D_s^{*+} \pi^0) + \Gamma(D_s^{*+} \pi^+)]/\Gamma_{\text{total}}$ $(\Gamma_{217} + \Gamma_{218})/\Gamma$

VALUE	CL%	DOCUMENT ID	TECN	COMMENT
$<5 \times 10^{-4}$	90	¹ ALBRECHT 93E	ARG	$e^+e^- \rightarrow \Upsilon(4S)$

¹ ALBRECHT 93E reports $< 0.9 \times 10^{-3}$ from a measurement of $[\Gamma(B^+ \rightarrow D_s^{*+} \pi^0) + \Gamma(B^+ \rightarrow D_s^{*+} \pi^+)]/\Gamma_{\text{total}} \times [B(D_s^+ \rightarrow \phi\pi^+)]$ assuming $B(D_s^+ \rightarrow \phi\pi^+) = 0.027$, which we rescale to our best value $B(D_s^+ \rightarrow \phi\pi^+) = 4.5 \times 10^{-2}$.

 $\Gamma(D_s^{*+} \pi^0)/\Gamma_{\text{total}}$ Γ_{218}/Γ

VALUE	CL%	DOCUMENT ID	TECN	COMMENT
$<2.6 \times 10^{-4}$	90	¹ ALEXANDER 93B	CLE2	$e^+e^- \rightarrow \Upsilon(4S)$

¹ ALEXANDER 93B reports $< 3.2 \times 10^{-4}$ from a measurement of $[\Gamma(B^+ \rightarrow D_s^{*+} \pi^0)/\Gamma_{\text{total}}] \times [B(D_s^+ \rightarrow \phi\pi^+)]$ assuming $B(D_s^+ \rightarrow \phi\pi^+) = 0.037$, which we rescale to our best value $B(D_s^+ \rightarrow \phi\pi^+) = 4.5 \times 10^{-2}$.

 $\Gamma(D_s^+ \eta)/\Gamma_{\text{total}}$ Γ_{219}/Γ

VALUE	CL%	DOCUMENT ID	TECN	COMMENT
$<4 \times 10^{-4}$	90	¹ ALEXANDER 93B	CLE2	$e^+e^- \rightarrow \Upsilon(4S)$

¹ ALEXANDER 93B reports $< 4.6 \times 10^{-4}$ from a measurement of $[\Gamma(B^+ \rightarrow D_s^+ \eta)/\Gamma_{\text{total}}] \times [B(D_s^+ \rightarrow \phi\pi^+)]$ assuming $B(D_s^+ \rightarrow \phi\pi^+) = 0.037$, which we rescale to our best value $B(D_s^+ \rightarrow \phi\pi^+) = 4.5 \times 10^{-2}$.

 $\Gamma(D_s^{*+} \eta)/\Gamma_{\text{total}}$ Γ_{220}/Γ

VALUE	CL%	DOCUMENT ID	TECN	COMMENT
$<6 \times 10^{-4}$	90	¹ ALEXANDER 93B	CLE2	$e^+e^- \rightarrow \Upsilon(4S)$

¹ ALEXANDER 93B reports $< 7.5 \times 10^{-4}$ from a measurement of $[\Gamma(B^+ \rightarrow D_s^{*+} \eta)/\Gamma_{\text{total}}] \times [B(D_s^+ \rightarrow \phi\pi^+)]$ assuming $B(D_s^+ \rightarrow \phi\pi^+) = 0.037$, which we rescale to our best value $B(D_s^+ \rightarrow \phi\pi^+) = 4.5 \times 10^{-2}$.

 $\Gamma(D_s^+ \rho^0)/\Gamma_{\text{total}}$ Γ_{221}/Γ

VALUE	CL%	DOCUMENT ID	TECN	COMMENT
$<3.0 \times 10^{-4}$	90	¹ ALEXANDER 93B	CLE2	$e^+e^- \rightarrow \Upsilon(4S)$

¹ ALEXANDER 93B reports $< 3.7 \times 10^{-4}$ from a measurement of $[\Gamma(B^+ \rightarrow D_s^+ \rho^0)/\Gamma_{\text{total}}] \times [B(D_s^+ \rightarrow \phi\pi^+)]$ assuming $B(D_s^+ \rightarrow \phi\pi^+) = 0.037$, which we rescale to our best value $B(D_s^+ \rightarrow \phi\pi^+) = 4.5 \times 10^{-2}$.

 $[\Gamma(D_s^+ \rho^0) + \Gamma(D_s^+ \bar{K}^*(892)^0)]/\Gamma_{\text{total}}$ $(\Gamma_{221} + \Gamma_{232})/\Gamma$

VALUE	CL%	DOCUMENT ID	TECN	COMMENT
$<2.0 \times 10^{-3}$	90	¹ ALBRECHT 93E	ARG	$e^+e^- \rightarrow \Upsilon(4S)$

¹ ALBRECHT 93E reports $< 3.4 \times 10^{-3}$ from a measurement of $[\Gamma(B^+ \rightarrow D_s^+ \rho^0) + \Gamma(B^+ \rightarrow D_s^+ \bar{K}^*(892)^0)]/\Gamma_{\text{total}} \times [B(D_s^+ \rightarrow \phi\pi^+)]$ assuming $B(D_s^+ \rightarrow \phi\pi^+) = 0.027$, which we rescale to our best value $B(D_s^+ \rightarrow \phi\pi^+) = 4.5 \times 10^{-2}$.

 $\Gamma(D_s^{*+} \rho^0)/\Gamma_{\text{total}}$ Γ_{222}/Γ

VALUE	CL%	DOCUMENT ID	TECN	COMMENT
$<4 \times 10^{-4}$	90	¹ ALEXANDER 93B	CLE2	$e^+e^- \rightarrow \Upsilon(4S)$

¹ ALEXANDER 93B reports $< 4.8 \times 10^{-4}$ from a measurement of $[\Gamma(B^+ \rightarrow D_s^{*+} \rho^0)/\Gamma_{\text{total}}] \times [B(D_s^+ \rightarrow \phi\pi^+)]$ assuming $B(D_s^+ \rightarrow \phi\pi^+) = 0.037$, which we rescale to our best value $B(D_s^+ \rightarrow \phi\pi^+) = 4.5 \times 10^{-2}$.

 $[\Gamma(D_s^{*+} \rho^0) + \Gamma(D_s^{*+} \bar{K}^*(892)^0)]/\Gamma_{\text{total}}$ $(\Gamma_{222} + \Gamma_{234})/\Gamma$

VALUE	CL%	DOCUMENT ID	TECN	COMMENT
$<1.2 \times 10^{-3}$	90	¹ ALBRECHT 93E	ARG	$e^+e^- \rightarrow \Upsilon(4S)$

¹ ALBRECHT 93E reports $< 2.0 \times 10^{-3}$ from a measurement of $[\Gamma(B^+ \rightarrow D_s^{*+} \rho^0) + \Gamma(B^+ \rightarrow D_s^{*+} \bar{K}^*(892)^0)]/\Gamma_{\text{total}} \times [B(D_s^+ \rightarrow \phi\pi^+)]$ assuming $B(D_s^+ \rightarrow \phi\pi^+) = 0.027$, which we rescale to our best value $B(D_s^+ \rightarrow \phi\pi^+) = 4.5 \times 10^{-2}$.

 $\Gamma(D_s^+ \omega)/\Gamma_{\text{total}}$ Γ_{223}/Γ

VALUE	CL%	DOCUMENT ID	TECN	COMMENT
$<4 \times 10^{-4}$	90	¹ ALEXANDER 93B	CLE2	$e^+e^- \rightarrow \Upsilon(4S)$
••• We do not use the following data for averages, fits, limits, etc. •••				
$<2.0 \times 10^{-3}$	90	² ALBRECHT 93E	ARG	$e^+e^- \rightarrow \Upsilon(4S)$

¹ ALEXANDER 93B reports $< 4.8 \times 10^{-4}$ from a measurement of $[\Gamma(B^+ \rightarrow D_s^+ \omega)/\Gamma_{\text{total}}] \times [B(D_s^+ \rightarrow \phi\pi^+)]$ assuming $B(D_s^+ \rightarrow \phi\pi^+) = 0.037$, which we rescale to our best value $B(D_s^+ \rightarrow \phi\pi^+) = 4.5 \times 10^{-2}$.

² ALBRECHT 93E reports $< 3.4 \times 10^{-3}$ from a measurement of $[\Gamma(B^+ \rightarrow D_s^+ \omega)/\Gamma_{\text{total}}] \times [B(D_s^+ \rightarrow \phi\pi^+)]$ assuming $B(D_s^+ \rightarrow \phi\pi^+) = 0.027$, which we rescale to our best value $B(D_s^+ \rightarrow \phi\pi^+) = 4.5 \times 10^{-2}$.

 $\Gamma(D_s^{*+} \omega)/\Gamma_{\text{total}}$ Γ_{224}/Γ

VALUE	CL%	DOCUMENT ID	TECN	COMMENT
$<6 \times 10^{-4}$	90	¹ ALEXANDER 93B	CLE2	$e^+e^- \rightarrow \Upsilon(4S)$
••• We do not use the following data for averages, fits, limits, etc. •••				
$<1.1 \times 10^{-3}$	90	² ALBRECHT 93E	ARG	$e^+e^- \rightarrow \Upsilon(4S)$

¹ ALEXANDER 93B reports $< 6.8 \times 10^{-4}$ from a measurement of $[\Gamma(B^+ \rightarrow D_s^{*+} \omega)/\Gamma_{\text{total}}] \times [B(D_s^+ \rightarrow \phi\pi^+)]$ assuming $B(D_s^+ \rightarrow \phi\pi^+) = 0.037$, which we rescale to our best value $B(D_s^+ \rightarrow \phi\pi^+) = 4.5 \times 10^{-2}$.

² ALBRECHT 93E reports $< 1.9 \times 10^{-3}$ from a measurement of $[\Gamma(B^+ \rightarrow D_s^{*+} \omega)/\Gamma_{\text{total}}] \times [B(D_s^+ \rightarrow \phi\pi^+)]$ assuming $B(D_s^+ \rightarrow \phi\pi^+) = 0.027$, which we rescale to our best value $B(D_s^+ \rightarrow \phi\pi^+) = 4.5 \times 10^{-2}$.

 $\Gamma(D_s^{*+} a_1(1260)^0)/\Gamma_{\text{total}}$ Γ_{225}/Γ

VALUE	CL%	DOCUMENT ID	TECN	COMMENT
$<1.8 \times 10^{-3}$	90	¹ ALBRECHT 93E	ARG	$e^+e^- \rightarrow \Upsilon(4S)$

¹ ALBRECHT 93E reports $< 3.0 \times 10^{-3}$ from a measurement of $[\Gamma(B^+ \rightarrow D_s^{*+} a_1(1260)^0)/\Gamma_{\text{total}}] \times [B(D_s^+ \rightarrow \phi\pi^+)]$ assuming $B(D_s^+ \rightarrow \phi\pi^+) = 0.027$, which we rescale to our best value $B(D_s^+ \rightarrow \phi\pi^+) = 4.5 \times 10^{-2}$.

 $\Gamma(D_s^{*+} a_1(1260)^0)/\Gamma_{\text{total}}$ Γ_{226}/Γ

VALUE	CL%	DOCUMENT ID	TECN	COMMENT
$<1.3 \times 10^{-3}$	90	¹ ALBRECHT 93E	ARG	$e^+e^- \rightarrow \Upsilon(4S)$

¹ ALBRECHT 93E reports $< 2.2 \times 10^{-3}$ from a measurement of $[\Gamma(B^+ \rightarrow D_s^{*+} a_1(1260)^0)/\Gamma_{\text{total}}] \times [B(D_s^+ \rightarrow \phi\pi^+)]$ assuming $B(D_s^+ \rightarrow \phi\pi^+) = 0.027$, which we rescale to our best value $B(D_s^+ \rightarrow \phi\pi^+) = 4.5 \times 10^{-2}$.

 $\Gamma(D_s^+ K^+ K^-)/\Gamma(\bar{D}^0 D_s^+)$ $\Gamma_{227}/\Gamma_{172}$

VALUE (units 10^{-4})	CL%	DOCUMENT ID	TECN	COMMENT
$8.0 \pm 0.9 \pm 0.1$		¹ AAJ 18B	LHCB	pp at 7, 8, 13 TeV

¹ AAJ 18B reports $[\Gamma(B^+ \rightarrow D_s^+ K^+ K^-)/\Gamma(B^+ \rightarrow \bar{D}^0 D_s^+)] / [B(D^0 \rightarrow K^+ K^-)] = 0.197 \pm 0.015 \pm 0.017$ which we multiply by our best value $B(D^0 \rightarrow K^+ K^-) = (4.08 \pm 0.06) \times 10^{-3}$. Our first error is their experiment's error and our second error is the systematic error from using our best value.

 $\Gamma(D_s^+ \phi)/\Gamma_{\text{total}}$ Γ_{228}/Γ

VALUE (units 10^{-6})	CL%	DOCUMENT ID	TECN	COMMENT
< 0.42	90	¹ AAJ 18B	LHCB	pp at 7, 8, 13 TeV
••• We do not use the following data for averages, fits, limits, etc. •••				
$1.7^{+1.1}_{-0.7} \pm 0.2$		² AAJ 13R	LHCB	Repl. by AAJ 18B
< 1.9	90	³ AUBERT 06F	BABR	$e^+e^- \rightarrow \Upsilon(4S)$
<1000	90	⁴ ALBRECHT 93E	ARG	$e^+e^- \rightarrow \Upsilon(4S)$
< 260	90	⁵ ALEXANDER 93B	CLE2	$e^+e^- \rightarrow \Upsilon(4S)$

¹ AAJ 18B uses $B^+ \rightarrow D_s^+ \bar{D}^0$ decays for normalization.

² AAJ 13R reports $(1.87^{+1.25}_{-0.73} \pm 0.19 \pm 0.32) \times 10^{-6}$ from a measurement of $[\Gamma(B^+ \rightarrow D_s^+ \phi)/\Gamma_{\text{total}}] / [B(B^+ \rightarrow \bar{D}^0 D_s^+)]$ assuming $B(B^+ \rightarrow \bar{D}^0 D_s^+) = (10.0 \pm 1.7) \times 10^{-3}$, which we rescale to our best value $B(B^+ \rightarrow \bar{D}^0 D_s^+) = (9.0 \pm 0.9) \times 10^{-3}$.

Meson Particle Listings

 B^\pm

Our first error is their experiment's error and our second error is the systematic error from using our best value.

³ Assumes equal production of B^+ and B^0 at the $\Upsilon(4S)$.

⁴ ALBRECHT 93E reports $< 1.7 \times 10^{-3}$ from a measurement of $[\Gamma(B^+ \rightarrow D_s^+ \phi)/\Gamma_{\text{total}}] \times [B(D_s^+ \rightarrow \phi\pi^+)]$ assuming $B(D_s^+ \rightarrow \phi\pi^+) = 0.027$, which we rescale to our best value $B(D_s^+ \rightarrow \phi\pi^+) = 4.5 \times 10^{-2}$.

⁵ ALEXANDER 93B reports $< 3.1 \times 10^{-4}$ from a measurement of $[\Gamma(B^+ \rightarrow D_s^+ \phi)/\Gamma_{\text{total}}] \times [B(D_s^+ \rightarrow \phi\pi^+)]$ assuming $B(D_s^+ \rightarrow \phi\pi^+) = 0.037$, which we rescale to our best value $B(D_s^+ \rightarrow \phi\pi^+) = 4.5 \times 10^{-2}$.

 $\Gamma(D_s^{*+} \phi)/\Gamma_{\text{total}}$ Γ_{229}/Γ

VALUE	CL%	DOCUMENT ID	TECN	COMMENT
$< 1.2 \times 10^{-5}$	90	¹ AUBERT 06F BABR	$e^+e^- \rightarrow \Upsilon(4S)$	

••• We do not use the following data for averages, fits, limits, etc. •••

$< 1.3 \times 10^{-3}$	90	² ALBRECHT 93E ARG	$e^+e^- \rightarrow \Upsilon(4S)$	
------------------------	----	-------------------------------	-----------------------------------	--

$< 3.5 \times 10^{-4}$	90	³ ALEXANDER 93B CLE2	$e^+e^- \rightarrow \Upsilon(4S)$	
------------------------	----	---------------------------------	-----------------------------------	--

¹ Assumes equal production of B^+ and B^0 at the $\Upsilon(4S)$.

² ALBRECHT 93E reports $< 2.1 \times 10^{-3}$ from a measurement of $[\Gamma(B^+ \rightarrow D_s^{*+} \phi)/\Gamma_{\text{total}}] \times [B(D_s^+ \rightarrow \phi\pi^+)]$ assuming $B(D_s^+ \rightarrow \phi\pi^+) = 0.027$, which we rescale to our best value $B(D_s^+ \rightarrow \phi\pi^+) = 4.5 \times 10^{-2}$.

³ ALEXANDER 93B reports $< 4.2 \times 10^{-4}$ from a measurement of $[\Gamma(B^+ \rightarrow D_s^{*+} \phi)/\Gamma_{\text{total}}] \times [B(D_s^+ \rightarrow \phi\pi^+)]$ assuming $B(D_s^+ \rightarrow \phi\pi^+) = 0.037$, which we rescale to our best value $B(D_s^+ \rightarrow \phi\pi^+) = 4.5 \times 10^{-2}$.

 $\Gamma(D_s^+ \bar{K}^0)/\Gamma_{\text{total}}$ Γ_{230}/Γ

VALUE	CL%	DOCUMENT ID	TECN	COMMENT
$< 8 \times 10^{-4}$	90	¹ ALEXANDER 93B CLE2	$e^+e^- \rightarrow \Upsilon(4S)$	

••• We do not use the following data for averages, fits, limits, etc. •••

$< 1.5 \times 10^{-3}$	90	² ALBRECHT 93E ARG	$e^+e^- \rightarrow \Upsilon(4S)$	
------------------------	----	-------------------------------	-----------------------------------	--

¹ ALEXANDER 93B reports $< 10.3 \times 10^{-4}$ from a measurement of $[\Gamma(B^+ \rightarrow D_s^+ \bar{K}^0)/\Gamma_{\text{total}}] \times [B(D_s^+ \rightarrow \phi\pi^+)]$ assuming $B(D_s^+ \rightarrow \phi\pi^+) = 0.037$, which we rescale to our best value $B(D_s^+ \rightarrow \phi\pi^+) = 4.5 \times 10^{-2}$.

² ALBRECHT 93E reports $< 2.5 \times 10^{-3}$ from a measurement of $[\Gamma(B^+ \rightarrow D_s^+ \bar{K}^0)/\Gamma_{\text{total}}] \times [B(D_s^+ \rightarrow \phi\pi^+)]$ assuming $B(D_s^+ \rightarrow \phi\pi^+) = 0.027$, which we rescale to our best value $B(D_s^+ \rightarrow \phi\pi^+) = 4.5 \times 10^{-2}$.

 $\Gamma(D_s^{*+} \bar{K}^0)/\Gamma_{\text{total}}$ Γ_{231}/Γ

VALUE	CL%	DOCUMENT ID	TECN	COMMENT
$< 9 \times 10^{-4}$	90	¹ ALEXANDER 93B CLE2	$e^+e^- \rightarrow \Upsilon(4S)$	

••• We do not use the following data for averages, fits, limits, etc. •••

$< 1.9 \times 10^{-3}$	90	² ALBRECHT 93E ARG	$e^+e^- \rightarrow \Upsilon(4S)$	
------------------------	----	-------------------------------	-----------------------------------	--

¹ ALEXANDER 93B reports $< 10.9 \times 10^{-4}$ from a measurement of $[\Gamma(B^+ \rightarrow D_s^{*+} \bar{K}^0)/\Gamma_{\text{total}}] \times [B(D_s^+ \rightarrow \phi\pi^+)]$ assuming $B(D_s^+ \rightarrow \phi\pi^+) = 0.037$, which we rescale to our best value $B(D_s^+ \rightarrow \phi\pi^+) = 4.5 \times 10^{-2}$.

² ALBRECHT 93E reports $< 3.1 \times 10^{-3}$ from a measurement of $[\Gamma(B^+ \rightarrow D_s^{*+} \bar{K}^0)/\Gamma_{\text{total}}] \times [B(D_s^+ \rightarrow \phi\pi^+)]$ assuming $B(D_s^+ \rightarrow \phi\pi^+) = 0.027$, which we rescale to our best value $B(D_s^+ \rightarrow \phi\pi^+) = 4.5 \times 10^{-2}$.

 $\Gamma(D_s^+ \bar{K}^*(892)^0)/\Gamma_{\text{total}}$ Γ_{232}/Γ

VALUE	CL%	DOCUMENT ID	TECN	COMMENT
$< 4.4 \times 10^{-6}$	90	AAIJ 13R LHCB	pp at 7 TeV	

••• We do not use the following data for averages, fits, limits, etc. •••

$< 4 \times 10^{-4}$	90	¹ ALEXANDER 93B CLE2	$e^+e^- \rightarrow \Upsilon(4S)$	
----------------------	----	---------------------------------	-----------------------------------	--

¹ ALEXANDER 93B reports $< 4.4 \times 10^{-4}$ from a measurement of $[\Gamma(B^+ \rightarrow D_s^+ \bar{K}^*(892)^0)/\Gamma_{\text{total}}] \times [B(D_s^+ \rightarrow \phi\pi^+)]$ assuming $B(D_s^+ \rightarrow \phi\pi^+) = 0.037$, which we rescale to our best value $B(D_s^+ \rightarrow \phi\pi^+) = 4.5 \times 10^{-2}$.

 $\Gamma(D_s^+ K^{*0})/\Gamma_{\text{total}}$ Γ_{233}/Γ

VALUE (units 10^{-6})	CL%	DOCUMENT ID	TECN	COMMENT
< 3.5	90	AAIJ 13R LHCB	pp at 7 TeV	

 $\Gamma(D_s^{*+} \bar{K}^*(892)^0)/\Gamma_{\text{total}}$ Γ_{234}/Γ

VALUE	CL%	DOCUMENT ID	TECN	COMMENT
$< 3.5 \times 10^{-4}$	90	¹ ALEXANDER 93B CLE2	$e^+e^- \rightarrow \Upsilon(4S)$	

¹ ALEXANDER 93B reports $< 4.3 \times 10^{-4}$ from a measurement of $[\Gamma(B^+ \rightarrow D_s^{*+} \bar{K}^*(892)^0)/\Gamma_{\text{total}}] \times [B(D_s^+ \rightarrow \phi\pi^+)]$ assuming $B(D_s^+ \rightarrow \phi\pi^+) = 0.037$, which we rescale to our best value $B(D_s^+ \rightarrow \phi\pi^+) = 4.5 \times 10^{-2}$.

 $\Gamma(D_s^- \pi^+ K^+)/\Gamma_{\text{total}}$ Γ_{235}/Γ

VALUE (units 10^{-4})	CL%	DOCUMENT ID	TECN	COMMENT
1.80 ± 0.22 OUR AVERAGE				
$1.71_{-0.07}^{+0.08} \pm 0.25$		¹ WIECHCZYN...09 BELL	$e^+e^- \rightarrow \Upsilon(4S)$	
$2.02 \pm 0.13 \pm 0.38$		¹ AUBERT 08G BABR	$e^+e^- \rightarrow \Upsilon(4S)$	

••• We do not use the following data for averages, fits, limits, etc. •••

< 7	90	² ALBRECHT 93E ARG	$e^+e^- \rightarrow \Upsilon(4S)$	
-------	----	-------------------------------	-----------------------------------	--

¹ Assumes equal production of B^+ and B^0 at the $\Upsilon(4S)$.

² ALBRECHT 93E reports $< 1.1 \times 10^{-3}$ from a measurement of $[\Gamma(B^+ \rightarrow D_s^- \pi^+ K^+)/\Gamma_{\text{total}}] \times [B(D_s^+ \rightarrow \phi\pi^+)]$ assuming $B(D_s^+ \rightarrow \phi\pi^+) = 0.027$, which we rescale to our best value $B(D_s^+ \rightarrow \phi\pi^+) = 4.5 \times 10^{-2}$.

 $\Gamma(D_s^{*-} \pi^+ K^+)/\Gamma_{\text{total}}$ Γ_{236}/Γ

VALUE (units 10^{-4})	CL%	DOCUMENT ID	TECN	COMMENT
1.45 ± 0.24 OUR AVERAGE				
$1.31_{-0.12}^{+0.13} \pm 0.28$		¹ WIECHCZYN...09 BELL	$e^+e^- \rightarrow \Upsilon(4S)$	
$1.67 \pm 0.16 \pm 0.35$		¹ AUBERT 08G BABR	$e^+e^- \rightarrow \Upsilon(4S)$	

••• We do not use the following data for averages, fits, limits, etc. •••

< 10	90	² ALBRECHT 93E ARG	$e^+e^- \rightarrow \Upsilon(4S)$	
--------	----	-------------------------------	-----------------------------------	--

¹ Assumes equal production of B^+ and B^0 at the $\Upsilon(4S)$.

² ALBRECHT 93E reports $< 1.6 \times 10^{-3}$ from a measurement of $[\Gamma(B^+ \rightarrow D_s^{*-} \pi^+ K^+)/\Gamma_{\text{total}}] \times [B(D_s^+ \rightarrow \phi\pi^+)]$ assuming $B(D_s^+ \rightarrow \phi\pi^+) = 0.027$, which we rescale to our best value $B(D_s^+ \rightarrow \phi\pi^+) = 4.5 \times 10^{-2}$.

 $\Gamma(D_s^- \pi^+ K^*(892)^+)/\Gamma_{\text{total}}$ Γ_{237}/Γ

VALUE	CL%	DOCUMENT ID	TECN	COMMENT
$< 5 \times 10^{-3}$	90	¹ ALBRECHT 93E ARG	$e^+e^- \rightarrow \Upsilon(4S)$	

¹ ALBRECHT 93E reports $< 8.6 \times 10^{-3}$ from a measurement of $[\Gamma(B^+ \rightarrow D_s^- \pi^+ K^*(892)^+)/\Gamma_{\text{total}}] \times [B(D_s^+ \rightarrow \phi\pi^+)]$ assuming $B(D_s^+ \rightarrow \phi\pi^+) = 0.027$, which we rescale to our best value $B(D_s^+ \rightarrow \phi\pi^+) = 4.5 \times 10^{-2}$.

 $\Gamma(D_s^{*-} \pi^+ K^*(892)^+)/\Gamma_{\text{total}}$ Γ_{238}/Γ

VALUE	CL%	DOCUMENT ID	TECN	COMMENT
$< 7 \times 10^{-3}$	90	¹ ALBRECHT 93E ARG	$e^+e^- \rightarrow \Upsilon(4S)$	

¹ ALBRECHT 93E reports $< 1.1 \times 10^{-2}$ from a measurement of $[\Gamma(B^+ \rightarrow D_s^{*-} \pi^+ K^*(892)^+)/\Gamma_{\text{total}}] \times [B(D_s^+ \rightarrow \phi\pi^+)]$ assuming $B(D_s^+ \rightarrow \phi\pi^+) = 0.027$, which we rescale to our best value $B(D_s^+ \rightarrow \phi\pi^+) = 4.5 \times 10^{-2}$.

 $\Gamma(D_s^- K^+ K^+)/\Gamma_{\text{total}}$ Γ_{239}/Γ

VALUE (units 10^{-5})	CL%	DOCUMENT ID	TECN	COMMENT
0.97 ± 0.21 OUR AVERAGE				
$0.93 \pm 0.22 \pm 0.10$		¹ WIECHCZYN...15 BELL	$e^+e^- \rightarrow \Upsilon(4S)$	
$1.1 \pm 0.4 \pm 0.2$		¹ AUBERT 08G BABR	$e^+e^- \rightarrow \Upsilon(4S)$	

¹ Assumes equal production of B^+ and B^0 at the $\Upsilon(4S)$.

 $\Gamma(D_s^- K^+ K^+)/\Gamma_{\text{total}}$ $\Gamma_{239}/\Gamma_{235}$

VALUE	CL%	DOCUMENT ID	TECN	COMMENT
$0.054 \pm 0.013 \pm 0.006$		WIECHCZYN...15 BELL	$e^+e^- \rightarrow \Upsilon(4S)$	

 $\Gamma(D_s^{*-} K^+ K^+)/\Gamma_{\text{total}}$ Γ_{240}/Γ

VALUE (units 10^{-4})	CL%	DOCUMENT ID	TECN	COMMENT
< 0.15	90	¹ AUBERT 08G BABR	$e^+e^- \rightarrow \Upsilon(4S)$	

¹ Assumes equal production of B^+ and B^0 at the $\Upsilon(4S)$.

 $\Gamma(\eta_c K^+)/\Gamma_{\text{total}}$ Γ_{241}/Γ

VALUE (units 10^{-3})	CL%	DOCUMENT ID	TECN	COMMENT
1.09 ± 0.08 OUR AVERAGE				
$0.96 \pm 0.12 \pm 0.06 \pm 0.03$		^{1,2} LEES 20c BABR	$e^+e^- \rightarrow \Upsilon(4S)$	
$0.74_{-0.08}^{+0.09} \pm 0.29$		³ CHILIKIN 19 BELL	$e^+e^- \rightarrow \Upsilon(4S)$	
$1.20 \pm 0.08 \pm 0.07$		¹ KATO 18 BELL	$e^+e^- \rightarrow \Upsilon(4S)$	
$1.25_{-0.20}^{+0.25} \pm 0.12$		⁴ AUBERT,B 05L BABR	$e^+e^- \rightarrow \Upsilon(4S)$	
$1.25 \pm 0.14_{-0.21}^{+0.39}$		⁵ FANG 03 BELL	$e^+e^- \rightarrow \Upsilon(4S)$	
$0.69 \pm 0.26_{-0.21}^{+0.22}$		⁶ EDWARDS 01 CLE2	$e^+e^- \rightarrow \Upsilon(4S)$	

••• We do not use the following data for averages, fits, limits, etc. •••

0.87 ± 0.15		^{1,7} AUBERT 06E BABR	Repl. by LEES 20c
$1.02 \pm 0.12 \pm 0.06$		^{7,8} AUBERT,B 04B BABR	$e^+e^- \rightarrow \Upsilon(4S)$

¹ Measures absolute branching fractions using a missing-mass technique.

² LEES 20c measurement's last uncertainty is due to the used $B(B^\pm \rightarrow K^\pm J/\psi)$ value.

³ CHILIKIN 19 reports $[\Gamma(B^+ \rightarrow \eta_c K^+)/\Gamma_{\text{total}}] \times [B(\eta_c(1S) \rightarrow \pi^+ \pi^- p\bar{p})] = (39.4_{-3.9}^{+4.1} \pm 2.2) \times 10^{-7}$ which we divide by our best value $B(\eta_c(1S) \rightarrow \pi^+ \pi^- p\bar{p}) = (5.3 \pm 2.1) \times 10^{-3}$. Our first error is their experiment's error and our second error is the systematic error from using our best value.

⁴ AUBERT,B 05L reports $[\Gamma(B^+ \rightarrow \eta_c K^+)/\Gamma_{\text{total}}] \times [B(\eta_c(1S) \rightarrow p\bar{p})] = (1.8_{-0.2}^{+0.3} \pm 0.2) \times 10^{-6}$ which we divide by our best value $B(\eta_c(1S) \rightarrow p\bar{p}) = (1.44 \pm 0.14) \times 10^{-3}$. Our first error is their experiment's error and our second error is the systematic error from using our best value.

⁵ Assumes equal production of B^+ and B^0 at the $\Upsilon(4S)$.

⁶ EDWARDS 01 assumes equal production of B^0 and B^+ at the $\Upsilon(4S)$. The correlated uncertainties (28.3%) from $B(J/\psi(1S) \rightarrow \gamma \eta_c)$ in those modes have been accounted for.

⁷ The ratio of $B(B^\pm \rightarrow K^\pm \eta_c) B(\eta_c \rightarrow K\bar{K}\pi) = (7.4 \pm 0.5 \pm 0.7) \times 10^{-5}$ reported in AUBERT,B 04B and $B(B^\pm \rightarrow K^\pm \eta_c) = (8.7 \pm 1.5) \times 10^{-3}$ reported in AUBERT 06E contribute to the determination of $B(\eta_c \rightarrow K\bar{K}\pi)$, which is used by others for normalization.

⁸ AUBERT,B 04B reports $[\Gamma(B^+ \rightarrow \eta_c K^+)/\Gamma_{\text{total}}] \times [B(\eta_c(1S) \rightarrow K\bar{K}\pi)] = (0.074 \pm 0.005 \pm 0.007) \times 10^{-3}$ which we divide by our best value $B(\eta_c(1S) \rightarrow K\bar{K}\pi) = (7.3 \pm 0.4) \times 10^{-2}$. Our first error is their experiment's error and our second error is the systematic error from using our best value.

$\Gamma(B^+ \rightarrow \eta_c K^+)/\Gamma_{\text{total}} \times \Gamma(\eta_c(1S) \rightarrow \gamma\gamma)/\Gamma_{\text{total}}$ Γ_{241}/Γ

VALUE (units 10^{-6})	DOCUMENT ID	TECN	COMMENT
$0.22 \pm 0.09 + 0.04 - 0.07 - 0.02$	1 WICHT	08	BELL $e^+e^- \rightarrow \Upsilon(4S)$

¹ Assumes equal production of B^+ and B^0 at the $\Upsilon(4S)$.

$\Gamma(\eta_c K^+, \eta_c \rightarrow K_S^0 K^\mp \pi^\pm)/\Gamma_{\text{total}}$ Γ_{242}/Γ

VALUE (units 10^{-6})	DOCUMENT ID	TECN	COMMENT
$26.7 \pm 1.4 + 5.7 - 5.5$	1,2 VINOKUROVA	11	BELL $e^+e^- \rightarrow \Upsilon(4S)$

¹ Assumes equal production of B^0 and B^+ from Upsilon(4S) decays.
² VINOKUROVA 11 reports $(26.7 \pm 1.4 + 2.9 - 2.6 \pm 4.9) \times 10^{-6}$, where the first uncertainty is statistical, the second is due to systematics, and the third comes from interference of $\eta_c(1S) \rightarrow K_S^0 K^\pm \pi^\mp$ with nonresonant $K_S^0 K^\pm \pi^\mp$. We combined both systematic uncertainties to single values.

$\Gamma(\eta_c K^*(892)^+)/\Gamma_{\text{total}}$ Γ_{243}/Γ

VALUE (units 10^{-3})	DOCUMENT ID	TECN	COMMENT
$1.1 + 0.5 - 0.4 \pm 0.1$	1,2 AUBERT	07AV	BABR $e^+e^- \rightarrow \Upsilon(4S)$

¹ AUBERT 07AV reports $[\Gamma(B^+ \rightarrow \eta_c K^*(892)^+)/\Gamma_{\text{total}}] \times [B(\eta_c(1S) \rightarrow p\bar{p})] = (1.57 + 0.56 + 0.45 - 0.46 - 0.36) \times 10^{-6}$ which we divide by our best value $B(\eta_c(1S) \rightarrow p\bar{p}) = (1.44 \pm 0.14) \times 10^{-3}$. Our first error is their experiment's error and our second error is the systematic error from using our best value.
² Assumes equal production of B^+ and B^0 at the $\Upsilon(4S)$.

$\Gamma(\eta_c K^+ \pi^+ \pi^-)/\Gamma_{\text{total}}$ Γ_{244}/Γ

VALUE	CL%	DOCUMENT ID	TECN	COMMENT
$<3.9 \times 10^{-4}$	90	VINOKUROVA	15	BELL $e^+e^- \rightarrow \Upsilon(4S)$

$\Gamma(\eta_c K^+ \omega(782))/\Gamma_{\text{total}}$ Γ_{245}/Γ

VALUE	CL%	DOCUMENT ID	TECN	COMMENT
$<5.3 \times 10^{-4}$	90	VINOKUROVA	15	BELL $e^+e^- \rightarrow \Upsilon(4S)$

$\Gamma(\eta_c K^+ \eta)/\Gamma_{\text{total}}$ Γ_{246}/Γ

VALUE	CL%	DOCUMENT ID	TECN	COMMENT
$<2.2 \times 10^{-4}$	90	VINOKUROVA	15	BELL $e^+e^- \rightarrow \Upsilon(4S)$

$\Gamma(\eta_c K^+ \pi^0)/\Gamma_{\text{total}}$ Γ_{247}/Γ

VALUE	CL%	DOCUMENT ID	TECN	COMMENT
$<6.2 \times 10^{-5}$	90	VINOKUROVA	15	BELL $e^+e^- \rightarrow \Upsilon(4S)$

$\Gamma(\eta_c(2S)K^+)/\Gamma_{\text{total}}$ Γ_{248}/Γ

VALUE (units 10^{-4})	DOCUMENT ID	TECN	COMMENT
4.4 ± 1.0 OUR AVERAGE			
$3.5 \pm 1.7 \pm 0.5 \pm 0.1$	1,2 LEES	20c	BABR $e^+e^- \rightarrow \Upsilon(4S)$
$4.8 \pm 1.1 \pm 0.3$	2 KATO	18	BELL $e^+e^- \rightarrow \Upsilon(4S)$

• • • We do not use the following data for averages, fits, limits, etc. • • •
 $3.4 \pm 1.8 \pm 0.3$ ² AUBERT 06E BABR Repl. by LEES 20c
¹ LEES 20c measurement's last uncertainty is due to the used $B(B^\pm \rightarrow K^\pm J/\psi)$ value.
² Measures absolute branching fractions using a missing-mass technique.

$\Gamma(\eta_c(2S)K^+, \eta_c \rightarrow p\bar{p})/\Gamma_{\text{total}}$ Γ_{249}/Γ

VALUE (units 10^{-8})	CL%	DOCUMENT ID	TECN	COMMENT
3.47 ± 0.72 ± 0.26		1 AAIJ	17AD	LHCB pp at 7 and 8 TeV
<10.6	95	2 AAIJ	13s	LHCB Repl. by AAIJ 17AD

• • • We do not use the following data for averages, fits, limits, etc. • • •
¹ Measured relative to $B^+ \rightarrow J/\psi K^+$ decay with charmonia reconstructed in $p\bar{p}$ final state and using $B(B^+ \rightarrow J/\psi K^+) \times B(J/\psi \rightarrow p\bar{p}) = (2.17 \pm 0.08) \times 10^{-6}$. The last uncertainty includes the uncertainty of $B(B^+ \rightarrow J/\psi K^+) \times B(J/\psi \rightarrow p\bar{p})$.
² Measured relative to $B^+ \rightarrow J/\psi K^+$ decay with charmonia reconstructed in $p\bar{p}$ final state and using $B(B^+ \rightarrow J/\psi K^+) = (1.013 \pm 0.034) \times 10^{-3}$ and $B(J/\psi \rightarrow p\bar{p}) = (2.17 \pm 0.07) \times 10^{-3}$.

$\Gamma(\eta_c(2S)K^+, \eta_c \rightarrow p\bar{p}\pi^+\pi^-)/\Gamma_{\text{total}}$ Γ_{251}/Γ

VALUE (units 10^{-7})	DOCUMENT ID	TECN	COMMENT
$11.2 + 1.8 + 0.5 - 1.6 - 0.7$	CHILIKIN	19	BELL $e^+e^- \rightarrow \Upsilon(4S)$

$\Gamma(B^+ \rightarrow h_c(1P)K^+)/\Gamma_{\text{total}} \times \Gamma(h_c(1P) \rightarrow \gamma\eta_c(1S))/\Gamma_{\text{total}}$ $\Gamma_{344}/\Gamma \times \Gamma_{22}^{h_c(1P)}/\Gamma_{h_c(1P)}$

VALUE (units 10^{-4})	CL%	DOCUMENT ID	TECN	COMMENT
<0.48	90	1 AUBERT	08AB	BABR $e^+e^- \rightarrow \Upsilon(4S)$

¹ Uses the production ratio of $(B^+B^-)/(B^0\bar{B}^0) = 1.026 \pm 0.032$ at $\Upsilon(4S)$.

$\Gamma(B^+ \rightarrow \eta_c(2S)K^+)/\Gamma_{\text{total}} \times \Gamma(\eta_c(2S) \rightarrow \gamma\gamma)/\Gamma_{\text{total}}$ $\Gamma_{248}/\Gamma \times \Gamma_{16}^{\eta_c(2S)}/\Gamma_{\eta_c(2S)}$

VALUE (units 10^{-6})	CL%	DOCUMENT ID	TECN	COMMENT
<0.18	90	1 WICHT	08	BELL $e^+e^- \rightarrow \Upsilon(4S)$

¹ Assumes equal production of B^+ and B^0 at the $\Upsilon(4S)$.

$\Gamma(\eta_c(2S)K^+, \eta_c \rightarrow K_S^0 K^\mp \pi^\pm)/\Gamma_{\text{total}}$ Γ_{250}/Γ

VALUE (units 10^{-6})	DOCUMENT ID	TECN	COMMENT
$3.4 + 2.2 + 0.5 - 1.5 - 0.4$	1,2 VINOKUROVA	11	BELL $e^+e^- \rightarrow \Upsilon(4S)$

¹ Assumes equal production of B^0 and B^+ from Upsilon(4S) decays.
² The first uncertainty includes both statistical and interference effects while the second is due to systematics.

$\Gamma(J/\psi(1S)K^+)/\Gamma_{\text{total}}$ Γ_{276}/Γ

VALUE (units 10^{-4})	EVTS	DOCUMENT ID	TECN	COMMENT
10.20 ± 0.19 OUR FIT				
10.18 ± 0.20 OUR AVERAGE				

10.32 ± 0.07 ± 0.24	1	CHOUDHURY	21	BELL $e^+e^- \rightarrow \Upsilon(4S)$
9.4 ± 0.7 ± 0.8	2	CHILIKIN	19	BELL $e^+e^- \rightarrow \Upsilon(4S)$
8.9 ± 0.6 ± 0.5	3	KATO	18	BELL $e^+e^- \rightarrow \Upsilon(4S)$
8.1 ± 1.3 ± 0.7	3	AUBERT	06E	BABR $e^+e^- \rightarrow \Upsilon(4S)$
10.61 ± 0.15 ± 0.48	4	AUBERT	05J	BABR $e^+e^- \rightarrow \Upsilon(4S)$
10.4 ± 1.1 ± 0.1	5	AUBERT,B	05L	BABR $e^+e^- \rightarrow \Upsilon(4S)$
10.2 ± 0.8 ± 0.7	4	JESSOP	97	CLE2 $e^+e^- \rightarrow \Upsilon(4S)$
9.24 ± 3.04 ± 0.05	6	BORTOLETTO	92	CLEO $e^+e^- \rightarrow \Upsilon(4S)$
8.09 ± 3.50 ± 0.04	6	7 ALBRECHT	90J	ARG $e^+e^- \rightarrow \Upsilon(4S)$

• • • We do not use the following data for averages, fits, limits, etc. • • •
 10.1 ± 0.2 ± 0.7 ⁴ ABE 03B BELL Repl. by CHOUDHURY 21
 10.1 ± 0.3 ± 0.5 ⁴ AUBERT 02 BABR Repl. by AUBERT 05J
 11.0 ± 1.5 ± 0.9 ⁵⁹ ⁴ ALAM 94 CLE2 Repl. by JESSOP 97
 22 ± 1.0 ± 2 ⁸ BUSKULIC 92G ALEP $e^+e^- \rightarrow Z$
 7 ± 4 ³ ⁸ ALBRECHT 87D ARG $e^+e^- \rightarrow \Upsilon(4S)$
 10 ± 7 ± 2 ³ ⁹ BEBEK 87 CLEO $e^+e^- \rightarrow \Upsilon(4S)$
 9 ± 5 ³ ¹⁰ ALAM 86 CLEO $e^+e^- \rightarrow \Upsilon(4S)$

¹ CHOUDHURY 21 uses the relative production fraction of charged (r^{\pm}) to neutral (r^0) B mesons at $\Upsilon(4S)$ value of $r^+/r^0 = 1.058 \pm 0.024$.

² CHILIKIN 19 reports $[\Gamma(B^+ \rightarrow J/\psi(1S)K^+)/\Gamma_{\text{total}}] \times [B(J/\psi(1S) \rightarrow p\bar{p}\pi^+\pi^-)] = (56.4 + 3.3 + 2.7 - 3.2 - 2.5) \times 10^{-7}$ which we divide by our best value $B(J/\psi(1S) \rightarrow p\bar{p}\pi^+\pi^-) = (6.0 \pm 0.5) \times 10^{-3}$. Our first error is their experiment's error and our second error is the systematic error from using our best value.

³ Measures absolute branching fractions using a missing-mass technique.
⁴ Assumes equal production of B^+ and B^0 at the $\Upsilon(4S)$.

⁵ AUBERT,B 05L reports $[\Gamma(B^+ \rightarrow J/\psi(1S)K^+)/\Gamma_{\text{total}}] \times [B(J/\psi(1S) \rightarrow p\bar{p})] = (2.2 \pm 0.2 \pm 0.1) \times 10^{-6}$ which we divide by our best value $B(J/\psi(1S) \rightarrow p\bar{p}) = (2.120 \pm 0.029) \times 10^{-3}$. Our first error is their experiment's error and our second error is the systematic error from using our best value.

⁶ BORTOLETTO 92 reports $(8 \pm 2 \pm 2) \times 10^{-4}$ from a measurement of $[\Gamma(B^+ \rightarrow J/\psi(1S)K^+)/\Gamma_{\text{total}}] \times [B(J/\psi(1S) \rightarrow e^+e^-)]$ assuming $B(J/\psi(1S) \rightarrow e^+e^-) = 0.069 \pm 0.009$, which we rescale to our best value $B(J/\psi(1S) \rightarrow e^+e^-) = (5.971 \pm 0.032) \times 10^{-2}$. Our first error is their experiment's error and our second error is the systematic error from using our best value. Assumes equal production of B^+ and B^0 at the $\Upsilon(4S)$.

⁷ ALBRECHT 90J reports $(7 \pm 3 \pm 1) \times 10^{-4}$ from a measurement of $[\Gamma(B^+ \rightarrow J/\psi(1S)K^+)/\Gamma_{\text{total}}] \times [B(J/\psi(1S) \rightarrow e^+e^-)]$ assuming $B(J/\psi(1S) \rightarrow e^+e^-) = 0.069 \pm 0.009$, which we rescale to our best value $B(J/\psi(1S) \rightarrow e^+e^-) = (5.971 \pm 0.032) \times 10^{-2}$. Our first error is their experiment's error and our second error is the systematic error from using our best value. Assumes equal production of B^+ and B^0 at the $\Upsilon(4S)$.

⁸ ALBRECHT 87D assume $B^+B^-/B^0\bar{B}^0$ ratio is 55/45. Superseded by ALBRECHT 90J.

⁹ BEBEK 87 value has been updated in BERKELMAN 91 to use same assumptions as noted for BORTOLETTO 92.

¹⁰ ALAM 86 assumes B^\pm/B^0 ratio is 60/40.

$\Gamma(\eta_c K^+)/\Gamma(J/\psi(1S)K^+)$ $\Gamma_{241}/\Gamma_{276}$

VALUE	DOCUMENT ID	TECN	COMMENT
0.88 ± 0.10 OUR AVERAGE			
$0.85 \pm 0.06 \pm 0.08$	1 AAIJ	13s	LHCB pp at 7 TeV
$1.33 \pm 0.10 \pm 0.43$	2 AUBERT,B	04B	BABR $e^+e^- \rightarrow \Upsilon(4S)$

¹ AAIJ 13s reports $[\Gamma(B^+ \rightarrow \eta_c K^+)/\Gamma(B^+ \rightarrow J/\psi(1S)K^+)] \times [B(\eta_c(1S) \rightarrow p\bar{p})] / [B(J/\psi(1S) \rightarrow p\bar{p})] = 0.578 \pm 0.035 \pm 0.026$ which we multiply or divide by our best values $B(\eta_c(1S) \rightarrow p\bar{p}) = (1.44 \pm 0.14) \times 10^{-3}$, $B(J/\psi(1S) \rightarrow p\bar{p}) = (2.120 \pm 0.029) \times 10^{-3}$. Our first error is their experiment's error and our second error is the systematic error from using our best values.
² Uses BABAR measurement of $B(B^+ \rightarrow J/\psi K^+) = (10.1 \pm 0.3 \pm 0.5) \times 10^{-4}$.

Meson Particle Listings

B^\pm

$$\Gamma(B^+ \rightarrow J/\psi(1S) K^+) / \Gamma_{\text{total}} \times \Gamma(J/\psi(1S) \rightarrow \gamma\gamma) / \Gamma_{\text{total}}$$

$$\Gamma_{276} / \Gamma \times \Gamma_{334}^{J/\psi(1S)} / \Gamma_{J/\psi(1S)}$$

VALUE (units 10^{-6})	CL%	DOCUMENT ID	TECN	COMMENT
<0.16	90	¹ WICHT	08	BELL $e^+e^- \rightarrow \Upsilon(4S)$

¹ Assumes equal production of B^+ and B^0 at the $\Upsilon(4S)$.

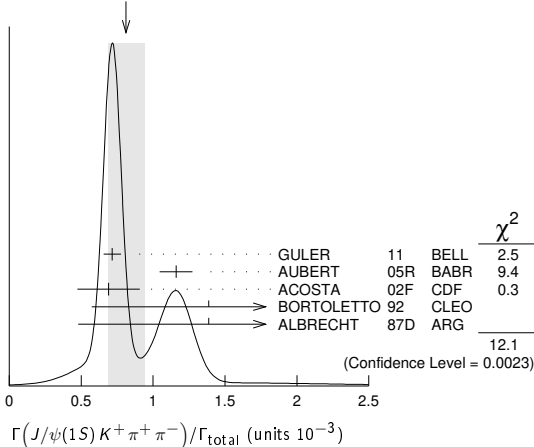
$$\Gamma(J/\psi(1S) K^+ \pi^+ \pi^-) / \Gamma_{\text{total}} \quad \Gamma_{278} / \Gamma$$

VALUE (units 10^{-3})	CL%	EVTS	DOCUMENT ID	TECN	COMMENT
0.81 ± 0.13 OUR AVERAGE					Error includes scale factor of 2.5. See the ideogram below.

0.716 ± 0.010 ± 0.060			¹ GULER	11	BELL $e^+e^- \rightarrow \Upsilon(4S)$
1.16 ± 0.07 ± 0.09			¹ AUBERT	05R	BABR $e^+e^- \rightarrow \Upsilon(4S)$
0.69 ± 0.18 ± 0.12			² ACOSTA	02F	CDF $p\bar{p}$ 1.8 TeV
1.39 ± 0.81 ± 0.01			³ BORTOLETTO	92	CLEO $e^+e^- \rightarrow \Upsilon(4S)$
1.39 ± 0.91 ± 0.01		6	⁴ ALBRECHT	87D	ARG $e^+e^- \rightarrow \Upsilon(4S)$
• • • We do not use the following data for averages, fits, limits, etc. • • •					
<1.8	90		⁵ ALBRECHT	90J	ARG $e^+e^- \rightarrow \Upsilon(4S)$

- Assumes equal production of B^+ and B^0 at the $\Upsilon(4S)$.
- ACOSTA 02F uses as reference of $B(B \rightarrow J/\psi(1S) K^+) = (10.1 \pm 0.6) \times 10^{-4}$. The second error includes the systematic error and the uncertainties of the branching ratio.
- BORTOLETTO 92 reports $(1.2 \pm 0.6 \pm 0.4) \times 10^{-3}$ from a measurement of $[\Gamma(B^+ \rightarrow J/\psi(1S) K^+ \pi^+ \pi^-) / \Gamma_{\text{total}}] \times [B(J/\psi(1S) \rightarrow e^+e^-)]$ assuming $B(J/\psi(1S) \rightarrow e^+e^-) = 0.069 \pm 0.009$, which we rescale to our best value $B(J/\psi(1S) \rightarrow e^+e^-) = (5.971 \pm 0.032) \times 10^{-2}$. Our first error is their experiment's error and our second error is the systematic error from using our best value. Assumes equal production of B^+ and B^0 at the $\Upsilon(4S)$.
- ALBRECHT 87D reports $(1.2 \pm 0.8) \times 10^{-3}$ from a measurement of $[\Gamma(B^+ \rightarrow J/\psi(1S) K^+ \pi^+ \pi^-) / \Gamma_{\text{total}}] \times [B(J/\psi(1S) \rightarrow e^+e^-)]$ assuming $B(J/\psi(1S) \rightarrow e^+e^-) = 0.069 \pm 0.009$, which we rescale to our best value $B(J/\psi(1S) \rightarrow e^+e^-) = (5.971 \pm 0.032) \times 10^{-2}$. Our first error is their experiment's error and our second error is the systematic error from using our best value. They actually report 0.0011 ± 0.0007 assuming $B^+ B^- / B^0 \bar{B}^0$ ratio is 55/45. We rescale to 50/50. Analysis explicitly removes $B^+ \rightarrow \psi(2S) K^+$.
- ALBRECHT 90J reports $< 1.6 \times 10^{-3}$ from a measurement of $[\Gamma(B^+ \rightarrow J/\psi(1S) K^+ \pi^+ \pi^-) / \Gamma_{\text{total}}] \times [B(J/\psi(1S) \rightarrow e^+e^-)]$ assuming $B(J/\psi(1S) \rightarrow e^+e^-) = 0.069$, which we rescale to our best value $B(J/\psi(1S) \rightarrow e^+e^-) = 5.971 \times 10^{-2}$. Assumes equal production of B^+ and B^0 at the $\Upsilon(4S)$.

WEIGHTED AVERAGE
0.81±0.13 (Error scaled by 2.5)



$$\Gamma(J/\psi(1S) K^+ K^- K^+) / \Gamma_{\text{total}} \quad \Gamma_{279} / \Gamma$$

VALUE (units 10^{-6})	DOCUMENT ID	TECN	COMMENT
33.7 ± 2.5 ± 1.4	LEES	15	BABR $e^+e^- \rightarrow \Upsilon(4S)$

$$\Gamma(h_c(1P) K^+, h_c \rightarrow J/\psi \pi^+ \pi^-) / \Gamma_{\text{total}} \quad \Gamma_{252} / \Gamma$$

VALUE	CL%	DOCUMENT ID	TECN	COMMENT
<3.4 × 10⁻⁶	90	¹ AUBERT	05R	BABR $e^+e^- \rightarrow \Upsilon(4S)$

¹ Assumes equal production of B^+ and B^0 at the $\Upsilon(4S)$.

$$\Gamma(X(3730)^0 K^+, X^0 \rightarrow \eta_c \eta) / \Gamma_{\text{total}} \quad \Gamma_{253} / \Gamma$$

VALUE	CL%	DOCUMENT ID	TECN	COMMENT
<4.6 × 10⁻⁵	90	VINOKUROVA	15	BELL $e^+e^- \rightarrow \Upsilon(4S)$

$$\Gamma(X(3730)^0 K^+, X^0 \rightarrow \eta_c \pi^0) / \Gamma_{\text{total}} \quad \Gamma_{254} / \Gamma$$

VALUE	CL%	DOCUMENT ID	TECN	COMMENT
<5.7 × 10⁻⁶	90	VINOKUROVA	15	BELL $e^+e^- \rightarrow \Upsilon(4S)$

$$\Gamma(\eta_{c2}(1D) K^+, \eta_{c2} \rightarrow h_c \gamma) / \Gamma_{\text{total}} \quad \Gamma_{255} / \Gamma$$

VALUE	CL%	DOCUMENT ID	TECN	COMMENT
<3.7 × 10⁻⁵	90	CHILIKIN	20	BELL $e^+e^- \rightarrow \Upsilon(4S)$

$$\Gamma(\eta_{c2}(1D) \pi^+ K_S^0, \eta_{c2} \rightarrow h_c \gamma) / \Gamma_{\text{total}} \quad \Gamma_{256} / \Gamma$$

VALUE	CL%	DOCUMENT ID	TECN	COMMENT
<1.1 × 10⁻⁴	90	CHILIKIN	20	BELL $e^+e^- \rightarrow \Upsilon(4S)$

$$\Gamma(\psi_2(3823) K^+, \psi_2 \rightarrow J/\psi \pi^+ \pi^-) / \Gamma_{\text{total}} \quad \Gamma_{257} / \Gamma$$

VALUE (units 10^{-7})	DOCUMENT ID	TECN	COMMENT
2.82 ± 0.54 ± 0.13	¹ AAIJ	20s	LHCB pp at 7, 8, 13 TeV

¹ The first error is statistic; the second error is the total systematic error.

$$\Gamma(\chi_{c1}(3872) K^+) / \Gamma_{\text{total}} \quad \Gamma_{258} / \Gamma$$

VALUE (units 10^{-4})	CL%	DOCUMENT ID	TECN	COMMENT
2.1 ± 0.6 ± 0.3 ± 0.1		^{1,2} LEES	20c	BABR $e^+e^- \rightarrow \Upsilon(4S)$

- • • We do not use the following data for averages, fits, limits, etc. • • •
- <2.6
- 2.6 ± 0.7 ± 0.9
- <3.2
- 3.3 ± 1.1 ± 1.1
- 3.5 ± 0.8 ± 1.2

- Measures absolute branching fractions using a missing-mass technique.
- LEES 20c measurement's last uncertainty is due to the used $B(B^\pm \rightarrow K^\pm J/\psi)$ value.
- Assumes equal production of B^+ and B^0 at the $\Upsilon(4S)$.
- AUBERT 06 reports $[\Gamma(B^+ \rightarrow \chi_{c1}(3872) K^+) / \Gamma_{\text{total}}] \times [B(\chi_{c1}(3872) \rightarrow \pi^+ \pi^- J/\psi(1S))] = (10.1 \pm 2.5 \pm 1.0) \times 10^{-6}$ which we divide by our best value $B(\chi_{c1}(3872) \rightarrow \pi^+ \pi^- J/\psi(1S)) = (3.8 \pm 1.2) \times 10^{-2}$. Our first error is their experiment's error and our second error is the systematic error from using our best value.
- AUBERT 05R reports $[\Gamma(B^+ \rightarrow \chi_{c1}(3872) K^+) / \Gamma_{\text{total}}] \times [B(\chi_{c1}(3872) \rightarrow \pi^+ \pi^- J/\psi(1S))] = (12.8 \pm 4.1) \times 10^{-6}$ which we divide by our best value $B(\chi_{c1}(3872) \rightarrow \pi^+ \pi^- J/\psi(1S)) = (3.8 \pm 1.2) \times 10^{-2}$. Our first error is their experiment's error and our second error is the systematic error from using our best value.
- CHOI 03 reports $[\Gamma(B^+ \rightarrow \chi_{c1}(3872) K^+) / \Gamma_{\text{total}}] \times [B(\chi_{c1}(3872) \rightarrow \pi^+ \pi^- J/\psi(1S))] = (13.6 \pm 3.0 \pm 0.5) \times 10^{-6}$ which we divide by our best value $B(\chi_{c1}(3872) \rightarrow \pi^+ \pi^- J/\psi(1S)) = (3.8 \pm 1.2) \times 10^{-2}$. Our first error is their experiment's error and our second error is the systematic error from using our best value.

$$\Gamma(\chi_{c1}(3872) K^*(892)^+) / \Gamma_{\text{total}} \quad \Gamma_{267} / \Gamma$$

VALUE	CL%	DOCUMENT ID	TECN	COMMENT
<6 × 10⁻⁴	90	^{1,2} AUBERT	09B	BABR $e^+e^- \rightarrow \Upsilon(4S)$

- • • We do not use the following data for averages, fits, limits, etc. • • •
 - <6 × 10⁻⁴
- AUBERT 09B reports $[\Gamma(B^+ \rightarrow \chi_{c1}(3872) K^*(892)^+) / \Gamma_{\text{total}}] \times [B(\chi_{c1}(3872) \rightarrow \gamma J/\psi)] < 4.8 \times 10^{-6}$ which we divide by our best value $B(\chi_{c1}(3872) \rightarrow \gamma J/\psi) = 8 \times 10^{-3}$.
 - Uses $B(\Upsilon(4S) \rightarrow B^+ B^-) = (51.6 \pm 0.6)\%$ and $B(\Upsilon(4S) \rightarrow B^0 \bar{B}^0) = (48.4 \pm 0.6)\%$.
 - AUBERT 09B reports $[\Gamma(B^+ \rightarrow \chi_{c1}(3872) K^*(892)^+) / \Gamma_{\text{total}}] \times [B(\chi_{c1}(3872) \rightarrow \gamma \psi(2S))] < 28 \times 10^{-6}$ which we divide by our best value $B(\chi_{c1}(3872) \rightarrow \gamma \psi(2S)) = 4.5 \times 10^{-2}$.

$$\Gamma(\chi_{c0}(3915) K^+) / \Gamma_{\text{total}} \quad \Gamma_{259} / \Gamma$$

VALUE	CL%	DOCUMENT ID	TECN	COMMENT
<2.8 × 10⁻⁴	90	¹ KATO	18	BELL $e^+e^- \rightarrow \Upsilon(4S)$

¹ Measures absolute branching fractions using a missing-mass technique.

$$\Gamma(\chi_{c0}(3915) K^+, \chi_{c0} \rightarrow D^+ D^-) / \Gamma(D^- D^+ K^+) \quad \Gamma_{260} / \Gamma_{209}$$

VALUE (units 10^{-2})	DOCUMENT ID	TECN	COMMENT
3.7 ± 0.9 ± 0.2	¹ AAIJ	20A1	LHCB pp at 7, 8, 13 TeV

¹ Measured in Dalitz plot analysis of $B^+ \rightarrow D^- D^+ K^+$ decays.

$$\Gamma(\chi_{c0}(3915) K^+, \chi_{c0} \rightarrow \eta_c \eta) / \Gamma_{\text{total}} \quad \Gamma_{261} / \Gamma$$

VALUE	CL%	DOCUMENT ID	TECN	COMMENT
<4.7 × 10⁻⁵	90	¹ VINOKUROVA	15	BELL $e^+e^- \rightarrow \Upsilon(4S)$

¹ Upper limit is corrected in the Erratum.

$$\Gamma((X\text{chi})_{c0}(3915) K^+, \chi_{c0} \rightarrow \eta_c \pi^0) / \Gamma_{\text{total}} \quad \Gamma_{262} / \Gamma$$

VALUE	CL%	DOCUMENT ID	TECN	COMMENT
<1.7 × 10⁻⁵	90	¹ VINOKUROVA	15	BELL $e^+e^- \rightarrow \Upsilon(4S)$

¹ Upper limit is corrected in the Erratum.

$$\Gamma(X(4014)^0 K^+, X^0 \rightarrow \eta_c \eta) / \Gamma_{\text{total}} \quad \Gamma_{263} / \Gamma$$

VALUE	CL%	DOCUMENT ID	TECN	COMMENT
<3.9 × 10⁻⁵	90	VINOKUROVA	15	BELL $e^+e^- \rightarrow \Upsilon(4S)$

$$\Gamma(X(4014)^0 K^+, X^0 \rightarrow \eta_c \pi^0) / \Gamma_{\text{total}} \quad \Gamma_{264} / \Gamma$$

VALUE	CL%	DOCUMENT ID	TECN	COMMENT
<1.2 × 10⁻⁵	90	VINOKUROVA	15	BELL $e^+e^- \rightarrow \Upsilon(4S)$

See key on page 1127

Meson Particle Listings

B^{\pm}

$\Gamma(Z_c(3900)^0 K^+, Z_c^0 \rightarrow \eta_c \pi^+ \pi^-)/\Gamma_{total}$ Γ_{265}/Γ

VALUE	CL%	DOCUMENT ID	TECN	COMMENT
$<4.7 \times 10^{-5}$	90	VINOKUROVA 15	BELL	$e^+ e^- \rightarrow \Upsilon(4S)$

$\Gamma(X(4020)^0 K^+, X^0 \rightarrow \eta_c \pi^+ \pi^-)/\Gamma_{total}$ Γ_{266}/Γ

VALUE	CL%	DOCUMENT ID	TECN	COMMENT
$<1.6 \times 10^{-5}$	90	VINOKUROVA 15	BELL	$e^+ e^- \rightarrow \Upsilon(4S)$

$\Gamma(\chi_{c1}(3872)^+ K^0, \chi_{c1}^+ \rightarrow J/\psi(1S) \pi^+ \pi^0)/\Gamma_{total}$ Γ_{268}/Γ

VALUE (units 10^{-6})	CL%	DOCUMENT ID	TECN	COMMENT
<6.1	90	1,2 CHOI	11 BELL	$e^+ e^- \rightarrow \Upsilon(4S)$
<22	90	3 AUBERT	05B BABR	$e^+ e^- \rightarrow \Upsilon(4S)$

• • • We do not use the following data for averages, fits, limits, etc. • • •

¹ Assumes $\pi^+ \pi^0$ originates from ρ^+ .
² Assumes equal production of B^+ and B^0 at the $\Upsilon(4S)$.
³ Assumes equal production of B^+ and B^0 at the $\Upsilon(4S)$. The isovector- X hypothesis is excluded with a likelihood test at 1×10^{-4} level.

$\Gamma(\chi_{c1}(3872) K^0 \pi^+)/\Gamma_{total}$ Γ_{269}/Γ

VALUE (units 10^{-4})	CL%	DOCUMENT ID	TECN	COMMENT
$2.8 \pm 0.8 \pm 0.9$		1 BALA	15 BELL	$e^+ e^- \rightarrow \Upsilon(4S)$

¹ BALA 15 reports $[\Gamma(B^+ \rightarrow \chi_{c1}(3872) K^0 \pi^+)/\Gamma_{total}] \times [B(\chi_{c1}(3872) \rightarrow \pi^+ \pi^- J/\psi(1S))] = (10.6 \pm 3.0 \pm 0.9) \times 10^{-6}$ which we divide by our best value $B(\chi_{c1}(3872) \rightarrow \pi^+ \pi^- J/\psi(1S)) = (3.8 \pm 1.2) \times 10^{-2}$. Our first error is their experiment's error and our second error is the systematic error from using our best value.

$\Gamma(Z_c(4430)^+ K^0, Z_c^+ \rightarrow J/\psi \pi^+ \pi^0)/\Gamma_{total}$ Γ_{270}/Γ

VALUE (units 10^{-5})	CL%	DOCUMENT ID	TECN	COMMENT
<1.5	95	1 AUBERT	09AA BABR	$e^+ e^- \rightarrow \Upsilon(4S)$

¹ Assumes equal production of B^+ and B^0 at the $\Upsilon(4S)$.

$\Gamma(Z_c(4430)^+ K^0, Z_c^+ \rightarrow \psi(2S) \pi^+)/\Gamma_{total}$ Γ_{271}/Γ

VALUE (units 10^{-5})	CL%	DOCUMENT ID	TECN	COMMENT
<4.7	95	1 AUBERT	09AA BABR	$e^+ e^- \rightarrow \Upsilon(4S)$

¹ Assumes equal production of B^+ and B^0 at the $\Upsilon(4S)$.

$\Gamma(\psi(4230)^0 K^+, \psi^0 \rightarrow J/\psi \pi^+ \pi^-)/\Gamma_{total}$ Γ_{272}/Γ

VALUE (units 10^{-6})	CL%	DOCUMENT ID	TECN	COMMENT
<15.6	95	1,2 GARG	19 BELL	$e^+ e^- \rightarrow \Upsilon(4S)$

• • • We do not use the following data for averages, fits, limits, etc. • • •

¹ Corresponds to a 90% CL upper limit of $< 14 \times 10^{-6}$.
² Assumes equal production of B^+ and B^0 at the $\Upsilon(4S)$.

$\Gamma(\chi_{c0}(3915) K^+, \chi_{c0} \rightarrow J/\psi \gamma)/\Gamma_{total}$ Γ_{273}/Γ

VALUE (units 10^{-6})	CL%	DOCUMENT ID	TECN	COMMENT
<14	90	1 AUBERT, BE	06M BABR	$e^+ e^- \rightarrow \Upsilon(4S)$

¹ Assumes equal production of B^+ and B^0 at the $\Upsilon(4S)$.

$\Gamma(\chi_{c0}(3915) K^+, \chi_{c0} \rightarrow \chi_{c1}(1P) \pi^0)/\Gamma_{total}$ Γ_{274}/Γ

VALUE	CL%	DOCUMENT ID	TECN	COMMENT
$<3.8 \times 10^{-5}$	90	1 BHARDWAJ	19 BELL	$e^+ e^- \rightarrow \Upsilon(4S)$

¹ Assumes equal production of B^+ and B^0 at the $\Upsilon(4S)$.

$\Gamma(X(3930)^0 K^+, X^0 \rightarrow J/\psi \gamma)/\Gamma_{total}$ Γ_{275}/Γ

VALUE (units 10^{-6})	CL%	DOCUMENT ID	TECN	COMMENT
<2.5	90	1 AUBERT, BE	06M BABR	$e^+ e^- \rightarrow \Upsilon(4S)$

¹ Assumes equal production of B^+ and B^0 at the $\Upsilon(4S)$.

$\Gamma(J/\psi(1S) K^0 \pi^+)/\Gamma_{total}$ Γ_{277}/Γ

VALUE (units 10^{-3})	CL%	DOCUMENT ID	TECN	COMMENT
1.101 ± 0.021		1 AUBERT	09AA BABR	$e^+ e^- \rightarrow \Upsilon(4S)$

• • • We do not use the following data for averages, fits, limits, etc. • • •

¹ Does not report systematic uncertainties.

$\Gamma(J/\psi(1S) K^*(892)^+)/\Gamma_{total}$ Γ_{281}/Γ

For polarization information see the Listings at the end of the " B^0 Branching Ratios" section.

VALUE (units 10^{-3})	EVTS	DOCUMENT ID	TECN	COMMENT
1.43 ± 0.08		OUR FIT		
1.43 ± 0.08		OUR AVERAGE		
$1.78^{+0.36}_{-0.32} \pm 0.02$		1,2 AUBERT	07AV BABR	$e^+ e^- \rightarrow \Upsilon(4S)$
$1.454 \pm 0.047 \pm 0.097$		2 AUBERT	05J BABR	$e^+ e^- \rightarrow \Upsilon(4S)$
$1.28 \pm 0.07 \pm 0.14$		2 ABE	02N BELL	$e^+ e^- \rightarrow \Upsilon(4S)$
$1.41 \pm 0.23 \pm 0.24$		2 JESSOP	97 CLE2	$e^+ e^- \rightarrow \Upsilon(4S)$
$1.58 \pm 0.47 \pm 0.27$		3 ABE	96H CDF	$p\bar{p}$ at 1.8 TeV
$1.50 \pm 1.08 \pm 0.01$		4 BORTOLETTO	092 CLEO	$e^+ e^- \rightarrow \Upsilon(4S)$
$1.85 \pm 1.30 \pm 0.01$	2	5 ALBRECHT	90J ARG	$e^+ e^- \rightarrow \Upsilon(4S)$

• • • We do not use the following data for averages, fits, limits, etc. • • •

$1.37 \pm 0.09 \pm 0.11$ ² AUBERT 02 BABR Repl. by AUBERT 05J Sup. by JESSOP 97

$1.78 \pm 0.51 \pm 0.23$ 13 ² ALAM 94 CLE2

¹ AUBERT 07AV reports $[\Gamma(B^+ \rightarrow J/\psi(1S) K^*(892)^+)/\Gamma_{total}] \times [B(J/\psi(1S) \rightarrow p\bar{p})] = (3.78^{+0.72+0.28}_{-0.64-0.23}) \times 10^{-6}$ which we divide by our best value $B(J/\psi(1S) \rightarrow p\bar{p}) = (2.120 \pm 0.029) \times 10^{-3}$. Our first error is their experiment's error and our second error is the systematic error from using our best value.

² Assumes equal production of B^+ and B^0 at the $\Upsilon(4S)$.

³ ABE 96H assumes that $B(B^+ \rightarrow J/\psi K^+) = (1.02 \pm 0.14) \times 10^{-3}$.

⁴ BORTOLETTO 92 reports $(1.3 \pm 0.9 \pm 0.3) \times 10^{-3}$ from a measurement of $[\Gamma(B^+ \rightarrow J/\psi(1S) K^*(892)^+)/\Gamma_{total}] \times [B(J/\psi(1S) \rightarrow e^+ e^-)]$ assuming $B(J/\psi(1S) \rightarrow e^+ e^-) = 0.069 \pm 0.009$, which we rescale to our best value $B(J/\psi(1S) \rightarrow e^+ e^-) = (5.971 \pm 0.032) \times 10^{-2}$. Our first error is their experiment's error and our second error is the systematic error from using our best value. Assumes equal production of B^+ and B^0 at the $\Upsilon(4S)$.

⁵ ALBRECHT 90J reports $(1.6 \pm 1.1 \pm 0.3) \times 10^{-3}$ from a measurement of $[\Gamma(B^+ \rightarrow J/\psi(1S) K^*(892)^+)/\Gamma_{total}] \times [B(J/\psi(1S) \rightarrow e^+ e^-)]$ assuming $B(J/\psi(1S) \rightarrow e^+ e^-) = 0.069 \pm 0.009$, which we rescale to our best value $B(J/\psi(1S) \rightarrow e^+ e^-) = (5.971 \pm 0.032) \times 10^{-2}$. Our first error is their experiment's error and our second error is the systematic error from using our best value. Assumes equal production of B^+ and B^0 at the $\Upsilon(4S)$.

$\Gamma(J/\psi(1S) K^*(892)^+)/\Gamma(J/\psi(1S) K^+)$ $\Gamma_{281}/\Gamma_{276}$

VALUE	DOCUMENT ID	TECN	COMMENT
1.39 ± 0.09	OUR AVERAGE		
$1.37 \pm 0.05 \pm 0.08$	AUBERT	05J BABR	$e^+ e^- \rightarrow \Upsilon(4S)$
$1.45 \pm 0.20 \pm 0.17$	1 JESSOP	97 CLE2	$e^+ e^- \rightarrow \Upsilon(4S)$
$1.92 \pm 0.60 \pm 0.17$	ABE	96Q CDF	$p\bar{p}$

• • • We do not use the following data for averages, fits, limits, etc. • • •

$1.37 \pm 0.10 \pm 0.08$ ² AUBERT 02 BABR Repl. by AUBERT 05J

¹ JESSOP 97 assumes equal production of B^+ and B^0 at the $\Upsilon(4S)$. The measurement is actually measured as an average over kaon charged and neutral states.
² Assumes equal production of B^+ and B^0 at the $\Upsilon(4S)$.

$\Gamma(J/\psi(1S) K(1270)^+)/\Gamma_{total}$ Γ_{282}/Γ

VALUE (units 10^{-3})	DOCUMENT ID	TECN	COMMENT
$1.80 \pm 0.34 \pm 0.39$	1 ABE	01L BELL	$e^+ e^- \rightarrow \Upsilon(4S)$

¹ Uses the PDG value of $B(B^+ \rightarrow J/\psi(1S) K^+) = (1.00 \pm 0.10) \times 10^{-3}$.

$\Gamma(J/\psi(1S) K(1400)^+)/\Gamma(J/\psi(1S) K(1270)^+)$ $\Gamma_{283}/\Gamma_{282}$

VALUE	CL%	DOCUMENT ID	TECN	COMMENT
<0.30	90	ABE	01L BELL	$e^+ e^- \rightarrow \Upsilon(4S)$

$\Gamma(J/\psi(1S) \eta K^+)/\Gamma_{total}$ Γ_{284}/Γ

VALUE (units 10^{-5})	DOCUMENT ID	TECN	COMMENT
12.4 ± 1.4	OUR AVERAGE		
$12.7 \pm 1.1 \pm 1.1$	1 IWASHITA	14 BELL	$e^+ e^- \rightarrow \Upsilon(4S)$
$10.8 \pm 2.3 \pm 2.4$	1 AUBERT	04Y BABR	$e^+ e^- \rightarrow \Upsilon(4S)$

¹ Assumes equal production of B^+ and B^0 at the $\Upsilon(4S)$.

$\Gamma(\chi_{c1-odd}(3872) K^+, \chi_{c1-odd} \rightarrow J/\psi \eta)/\Gamma_{total}$ Γ_{285}/Γ

VALUE	CL%	DOCUMENT ID	TECN	COMMENT
$<3.8 \times 10^{-6}$	90	IWASHITA	14 BELL	$e^+ e^- \rightarrow \Upsilon(4S)$

$\Gamma(\psi(4160) K^+, \psi \rightarrow J/\psi \eta)/\Gamma_{total}$ Γ_{286}/Γ

VALUE	CL%	DOCUMENT ID	TECN	COMMENT
$<7.4 \times 10^{-6}$	90	IWASHITA	14 BELL	$e^+ e^- \rightarrow \Upsilon(4S)$

$\Gamma(J/\psi(1S) \eta' K^+)/\Gamma_{total}$ Γ_{287}/Γ

VALUE (units 10^{-5})	CL%	DOCUMENT ID	TECN	COMMENT
<8.8	90	1 XIE	07 BELL	$e^+ e^- \rightarrow \Upsilon(4S)$

¹ Assumes equal production of B^+ and B^0 at the $\Upsilon(4S)$.

$\Gamma(J/\psi(1S) \phi K^+)/\Gamma_{total}$ Γ_{288}/Γ

VALUE (units 10^{-5})	DOCUMENT ID	TECN	COMMENT
5.0 ± 0.4	OUR AVERAGE		
$5.00 \pm 0.37 \pm 0.15$	LEES	15 BABR	$e^+ e^- \rightarrow \Upsilon(4S)$
$4.4 \pm 1.4 \pm 0.5$	1 AUBERT	03O BABR	$e^+ e^- \rightarrow \Upsilon(4S)$
$8.8^{+3.5}_{-3.0} \pm 1.3$	2 ANASTASSOV	00 CLE2	$e^+ e^- \rightarrow \Upsilon(4S)$

¹ Assumes equal production of B^+ and B^0 at the $\Upsilon(4S)$.
² ANASTASSOV 00 finds 10 events on a background of 0.5 ± 0.2 . Assumes equal production of B^0 and B^+ at the $\Upsilon(4S)$, a uniform Dalitz plot distribution, isotropic $J/\psi(1S)$ and ϕ decays, and $B(B^+ \rightarrow J/\psi(1S) \phi K^+) = B(B^0 \rightarrow J/\psi(1S) \phi K^0)$.

$\Gamma(J/\psi(1S) K_1(1650), K_1 \rightarrow \phi K^+)/\Gamma(J/\psi(1S) \phi K^+)$ $\Gamma_{289}/\Gamma_{288}$

VALUE	DOCUMENT ID	TECN	COMMENT
$0.12 \pm 0.10^{+0.17}_{-0.06}$	1 AAJ	17 LHCB	pp at 7, 8 TeV

¹ Measured in amplitude analysis of $B^+ \rightarrow J/\psi(1S) \phi K^+$.

Meson Particle Listings

 B^\pm $\Gamma(J/\psi(1S)K^*(1680)^+, K^* \rightarrow \phi K^+)/\Gamma(J/\psi(1S)\phi K^+)$ $\Gamma_{290}/\Gamma_{288}$

VALUE (units 10^{-2})	DOCUMENT ID	TECN	COMMENT
$6.7 \pm 1.9 \pm_{-3.9}^{3.2}$	¹ AAIJ	17	LHCB pp at 7, 8 TeV

¹ Measured in amplitude analysis of $B^+ \rightarrow J/\psi(1S)\phi K^+$. $\Gamma(J/\psi(1S)K_2^*(1980), K_2^* \rightarrow \phi K^+)/\Gamma(J/\psi(1S)\phi K^+)$ $\Gamma_{291}/\Gamma_{288}$

VALUE (units 10^{-2})	DOCUMENT ID	TECN	COMMENT
$2.9 \pm 0.8 \pm_{-0.7}^{1.7}$	¹ AAIJ	17	LHCB pp at 7, 8 TeV

¹ Measured in amplitude analysis of $B^+ \rightarrow J/\psi(1S)\phi K^+$. $\Gamma(J/\psi(1S)K(1830)^+, K(1830)^+ \rightarrow \phi K^+)/\Gamma(J/\psi(1S)\phi K^+)$ $\Gamma_{292}/\Gamma_{288}$

VALUE (units 10^{-2})	DOCUMENT ID	TECN	COMMENT
$2.6 \pm 1.1 \pm_{-1.8}^{2.3}$	¹ AAIJ	17	LHCB pp at 7, 8 TeV

¹ Measured in amplitude analysis of $B^+ \rightarrow J/\psi(1S)\phi K^+$. $\Gamma(\chi_{c1}(4140)K^+, \chi_{c1} \rightarrow J/\psi(1S)\phi)/\Gamma(J/\psi(1S)\phi K^+)$ $\Gamma_{293}/\Gamma_{288}$

VALUE	CL%	DOCUMENT ID	TECN	COMMENT
0.19 ± 0.08 OUR AVERAGE				
0.13 ± 0.032 ± _{-2.0} ^{4.8}		¹ AAIJ	17	LHCB pp at 7, 8 TeV
0.19 ± 0.07 ± 0.04		² ABAZOV	14A	D0 $p\bar{p}$ at 1.96 TeV
••• We do not use the following data for averages, fits, limits, etc. •••				
<0.133	90	LEES	15	BABR $e^+e^- \rightarrow \Upsilon(4S)$
<0.07	90	³ AAIJ	12AA	LHCB pp at 7 TeV

¹ Measured in amplitude analysis of $B^+ \rightarrow J/\psi(1S)\phi K^+$.² Reported a threshold enhancement in the $J/\psi\phi$ mass distribution consistent with the $\chi_{c1}(4140)$ state with a statistical significance of 3.1 standard deviations.³ Branching fractions are normalized to 382 ± 22 events of $B^+ \rightarrow J/\psi\phi K^+$. $\Gamma(\chi_{c1}(4274)K^+, \chi_{c1} \rightarrow J/\psi(1S)\phi)/\Gamma(J/\psi(1S)\phi K^+)$ $\Gamma_{294}/\Gamma_{288}$

VALUE (units 10^{-2})	CL%	DOCUMENT ID	TECN	COMMENT
7.1 ± 2.5 ±_{-2.4}^{3.5}		¹ AAIJ	17	LHCB pp at 7, 8 TeV
••• We do not use the following data for averages, fits, limits, etc. •••				
<18.1	90	LEES	15	BABR $e^+e^- \rightarrow \Upsilon(4S)$
< 8	90	² AAIJ	12AA	LHCB Repl. by AAIJ 17

¹ Measured in amplitude analysis of $B^+ \rightarrow J/\psi(1S)\phi K^+$.² Branching fractions are normalized to 382 ± 22 events of $B^+ \rightarrow J/\psi\phi K^+$. $\Gamma(\chi_{c0}(4500)K^+, \chi_{c0}^0 \rightarrow J/\psi(1S)\phi)/\Gamma(J/\psi(1S)\phi K^+)$ $\Gamma_{295}/\Gamma_{288}$

VALUE (units 10^{-2})	DOCUMENT ID	TECN	COMMENT
$6.6 \pm 2.4 \pm_{-2.3}^{3.5}$	¹ AAIJ	17	LHCB pp at 7, 8 TeV

¹ Measured in amplitude analysis of $B^+ \rightarrow J/\psi(1S)\phi K^+$. $\Gamma(\chi_{c0}(4700)K^+, \chi_{c0} \rightarrow J/\psi(1S)\phi)/\Gamma(J/\psi(1S)\phi K^+)$ $\Gamma_{296}/\Gamma_{288}$

VALUE	DOCUMENT ID	TECN	COMMENT
$0.12 \pm 0.05 \pm_{-0.05}^{0.09}$	¹ AAIJ	17	LHCB pp at 7, 8 TeV

¹ Measured in amplitude analysis of $B^+ \rightarrow J/\psi(1S)\phi K^+$. $\Gamma(J/\psi(1S)\omega K^+)/\Gamma_{total}$ Γ_{297}/Γ

VALUE (units 10^{-4})	DOCUMENT ID	TECN	COMMENT
$3.2 \pm 0.1 \pm_{-0.3}^{0.6}$	¹ DEL-AMO-SA...10b	BABR	$e^+e^- \rightarrow \Upsilon(4S)$

••• We do not use the following data for averages, fits, limits, etc. •••

$3.5 \pm 0.2 \pm 0.4$	¹ AUBERT	08w	BABR Repl. by DEL-AMO-SANCHEZ 10b
-----------------------	---------------------	-----	-----------------------------------

¹ Assumes equal production of B^+ and B^0 at the $\Upsilon(4S)$. $\Gamma(\chi_{c0}(3915)K^+, \chi_{c0} \rightarrow J/\psi\omega)/\Gamma_{total}$ Γ_{298}/Γ

VALUE (units 10^{-5})	DOCUMENT ID	TECN	COMMENT
$3.0 \pm 0.7 \pm_{-0.3}^{0.5}$	¹ DEL-AMO-SA...10b	BABR	$e^+e^- \rightarrow \Upsilon(4S)$

••• We do not use the following data for averages, fits, limits, etc. •••

$4.9 \pm 1.0 \pm_{-0.9}^{0.5}$	¹ AUBERT	08w	BABR Repl. by DEL-AMO-SANCHEZ 10b
--------------------------------	---------------------	-----	-----------------------------------

¹ Assumes equal production of B^+ and B^0 at the $\Upsilon(4S)$. $\Gamma(\chi_{c0}(3915)K^+, \chi_{c0} \rightarrow \rho\bar{\rho})/\Gamma_{total}$ Γ_{280}/Γ

VALUE	CL%	DOCUMENT ID	TECN	COMMENT
$< 7.1 \times 10^{-8}$	95	¹ AAIJ	13s	LHCB pp at 7 TeV

¹ Measured relative to $B^+ \rightarrow J/\psi K^+$ decay with charmonia reconstructed in $p\bar{p}$ final state and using $B(B^+ \rightarrow J/\psi K^+) = (1.013 \pm 0.034) \times 10^{-3}$ and $B(J/\psi \rightarrow p\bar{p}) = (2.17 \pm 0.07) \times 10^{-3}$. $\Gamma(J/\psi(1S)\pi^+)/\Gamma_{total}$ Γ_{299}/Γ

VALUE	DOCUMENT ID	TECN	COMMENT
(3.92 ± 0.08) × 10⁻⁵ OUR FIT			
(3.8 ± 0.6 ± 0.3) × 10⁻⁵	¹ ABE	03b	BELL $e^+e^- \rightarrow \Upsilon(4S)$

¹ Assumes equal production of B^+ and B^0 at the $\Upsilon(4S)$. $\Gamma(J/\psi(1S)\pi^+)/\Gamma(J/\psi(1S)K^+)$ $\Gamma_{299}/\Gamma_{276}$

VALUE (units 10^{-2})	EVTS	DOCUMENT ID	TECN	COMMENT
3.85 ± 0.04 OUR FIT				
3.85 ± 0.04 OUR AVERAGE				
$3.83 \pm 0.03 \pm 0.03$		AAIJ	17o	LHCB pp at 7, 8 TeV
$3.5 \pm 0.3 \pm 1.2$		AABOUD	16L	ATLS pp at 7, 8 TeV
$4.86 \pm 0.82 \pm 0.15$		ABULENCIA	09	CDF $p\bar{p}$ at 1.96 TeV
$5.37 \pm 0.45 \pm 0.11$		AUBERT	04P	BABR $e^+e^- \rightarrow \Upsilon(4S)$
$5.0 \pm_{-1.7}^{+1.9} \pm 0.1$		ABE	96R	CDF $p\bar{p}$ 1.8 TeV
5.2 ± 2.4		BISHAI	96	CLE2 $e^+e^- \rightarrow \Upsilon(4S)$
••• We do not use the following data for averages, fits, limits, etc. •••				
$3.83 \pm 0.11 \pm 0.07$		AAIJ	12AC	LHCB Repl. by AAIJ 17o
$3.91 \pm 0.78 \pm 0.19$		AUBERT	02F	BABR Repl. by AUBERT 04P
4.3 ± 2.3	5	¹ ALEXANDER	95	CLE2 Sup. by BISHAI 96

¹ Assumes equal production of B^+B^- and $B^0\bar{B}^0$ on $\Upsilon(4S)$. $\Gamma(J/\psi(1S)\pi^+\pi^+\pi^-\pi^-)/\Gamma(\psi(2S)K^+)$ $\Gamma_{300}/\Gamma_{311}$

VALUE (units 10^{-2})	DOCUMENT ID	TECN	COMMENT
1.88 ± 0.17 ± 0.09	¹ AAIJ	17k	LHCB pp at 7 and 8 TeV

¹ Contains also the contribution from $B^+ \rightarrow \psi(2S)[\rightarrow J/\psi\pi^+\pi^-]\pi^+\pi^-\pi^-$ decays. $\Gamma(\psi(2S)\pi^+\pi^-\pi^-)/\Gamma(\psi(2S)K^+)$ $\Gamma_{301}/\Gamma_{311}$

VALUE (units 10^{-2})	DOCUMENT ID	TECN	COMMENT
3.04 ± 0.50 ± 0.26	AAIJ	17k	LHCB pp at 7 and 8 TeV

 $\Gamma(J/\psi(1S)\rho^+)/\Gamma_{total}$ Γ_{302}/Γ

VALUE (units 10^{-5})	CL%	DOCUMENT ID	TECN	COMMENT
4.1 ± 0.5 OUR AVERAGE				Error includes scale factor of 1.4.
$3.81 \pm_{-0.24}^{+0.25} \pm 0.35$		AAIJ	19o	LHCB pp at 7 and 8 TeV
$5.0 \pm 0.7 \pm 0.3$		¹ AUBERT	07AC	BABR $e^+e^- \rightarrow \Upsilon(4S)$

••• We do not use the following data for averages, fits, limits, etc. •••

<77	90	BISHAI	96	CLE2 $e^+e^- \rightarrow \Upsilon(4S)$
-----	----	--------	----	--

¹ Assumes equal production of B^+ and B^0 at the $\Upsilon(4S)$. $\Gamma(J/\psi(1S)\pi^+\pi^0 \text{ nonresonant})/\Gamma_{total}$ Γ_{303}/Γ

VALUE (units 10^{-5})	CL%	DOCUMENT ID	TECN	COMMENT
< 0.73	90	¹ AUBERT	07AC	BABR $e^+e^- \rightarrow \Upsilon(4S)$

¹ Assumes equal production of B^+ and B^0 at the $\Upsilon(4S)$. $\Gamma(J/\psi(1S)a_1(1260)^+)/\Gamma_{total}$ Γ_{304}/Γ

VALUE	CL%	DOCUMENT ID	TECN	COMMENT
< 1.2 × 10⁻³	90	BISHAI	96	CLE2 $e^+e^- \rightarrow \Upsilon(4S)$

 $\Gamma(J/\psi(1S)\rho\bar{\rho}\pi^+)/\Gamma_{total}$ Γ_{305}/Γ

VALUE	CL%	DOCUMENT ID	TECN	COMMENT
< 5.0 × 10⁻⁷	90	¹ AAIJ	13z	LHCB pp at 7 TeV

¹ Uses $B(B_S^0 \rightarrow J/\psi(1S)\pi^+\pi^-) = (1.98 \pm 0.20) \times 10^{-4}$. $\Gamma(J/\psi(1S)\rho\bar{\rho})/\Gamma_{total}$ Γ_{306}/Γ

VALUE (units 10^{-6})	CL%	DOCUMENT ID	TECN	COMMENT
14.6 ± 1.2 OUR AVERAGE				
$15.1 \pm 0.8 \pm 1.0$		¹ SIRUNYAN	19CM	CMS pp at 8 TeV
$11.7 \pm 2.8 \pm_{-2.3}^{+1.8}$		² XIE	05	BELL $e^+e^- \rightarrow \Upsilon(4S)$
$12 \pm_{-6}^{+9}$		² AUBERT	03k	BABR $e^+e^- \rightarrow \Upsilon(4S)$

••• We do not use the following data for averages, fits, limits, etc. •••

<41	90	ZANG	04	BELL $e^+e^- \rightarrow \Upsilon(4S)$
-----	----	------	----	--

¹ SIRUNYAN 19CM reports $B(B^+ \rightarrow J/\psi\bar{\Lambda}p)/B(B^+ \rightarrow J/\psi K^*(892)) = (1.054 \pm 0.057 \pm 0.035 \pm 0.011) \times 10^{-2}$ and rescaled with the best value of $B(B^+ \rightarrow J/\psi K^*(892)) = (1.43 \pm 0.08) \times 10^{-3}$, where the last uncertainty is the uncertainty from the branching fractions of $\bar{\Lambda}$ and $K^*(892)$ to reconstructed final states.² Assumes equal production of B^+ and B^0 at the $\Upsilon(4S)$. $\Gamma(J/\psi(1S)\Sigma^0\rho)/\Gamma_{total}$ Γ_{307}/Γ

VALUE	CL%	DOCUMENT ID	TECN	COMMENT
< 1.1 × 10⁻⁵	90	¹ XIE	05	BELL $e^+e^- \rightarrow \Upsilon(4S)$

¹ Assumes equal production of B^+ and B^0 at the $\Upsilon(4S)$. $\Gamma(J/\psi(1S)D^+)/\Gamma_{total}$ Γ_{308}/Γ

VALUE (units 10^{-5})	CL%	DOCUMENT ID	TECN	COMMENT
< 12	90	¹ AUBERT	05u	BABR $e^+e^- \rightarrow \Upsilon(4S)$

¹ Assumes equal production of B^+ and B^0 at the $\Upsilon(4S)$. $\Gamma(J/\psi(1S)D^0\pi^+)/\Gamma_{total}$ Γ_{309}/Γ

VALUE (units 10^{-5})	CL%	DOCUMENT ID	TECN	COMMENT
< 2.5	90	¹ ZHANG	05b	BELL $e^+e^- \rightarrow \Upsilon(4S)$

••• We do not use the following data for averages, fits, limits, etc. •••

<5.2	90	¹ AUBERT	05R	BABR $e^+e^- \rightarrow \Upsilon(4S)$
------	----	---------------------	-----	--

¹ Assumes equal production of B^+ and B^0 at the $\Upsilon(4S)$.

$\Gamma(\psi(2S)\pi^+)/\Gamma_{total}$	Γ_{310}/Γ		
VALUE (units 10^{-5})	DOCUMENT ID	TECN	COMMENT
2.44 ± 0.22 ± 0.20	1 BHARDWAJ	08 BELL	$e^+e^- \rightarrow \Upsilon(4S)$

¹ Assumes equal production of B^+ and B^0 at the $\Upsilon(4S)$.

$\Gamma(\psi(2S)\pi^+)/\Gamma(\psi(2S)K^+)$	$\Gamma_{310}/\Gamma_{311}$		
VALUE (units 10^{-2})	DOCUMENT ID	TECN	COMMENT
3.97 ± 0.29 OUR AVERAGE			
3.95 ± 0.40 ± 0.12	AAIJ	12Ac LHCB	pp at 7 TeV
3.99 ± 0.36 ± 0.17	BHARDWAJ	08 BELL	$e^+e^- \rightarrow \Upsilon(4S)$

$\Gamma(\psi(2S)K^+)/\Gamma_{total}$	Γ_{311}/Γ		
VALUE (units 10^{-4})	DOCUMENT ID	TECN	COMMENT
6.24 ± 0.20 OUR FIT			
6.40 ± 0.34 OUR AVERAGE			
4.6 ± 1.0 ± 0.7	1 LEES	20c BABR	$e^+e^- \rightarrow \Upsilon(4S)$
6.4 ± 1.0 ± 0.4	1 KATO	18 BELL	$e^+e^- \rightarrow \Upsilon(4S)$
6.65 ± 0.17 ± 0.55	2 GULER	11 BELL	$e^+e^- \rightarrow \Upsilon(4S)$
6.17 ± 0.32 ± 0.44	2 AUBERT	05j BABR	$e^+e^- \rightarrow \Upsilon(4S)$
7.8 ± 0.7 ± 0.9	2 RICHICHI	01 CLE2	$e^+e^- \rightarrow \Upsilon(4S)$
18 ± 8 ± 4	5 2 ALBRECHT	90j ARG	$e^+e^- \rightarrow \Upsilon(4S)$

• • • We do not use the following data for averages, fits, limits, etc. • • •

4.9 ± 1.6 ± 0.4

6.9 ± 0.6

6.4 ± 0.5 ± 0.8

6.1 ± 2.3 ± 0.9

<5 at 90% CL

22 ± 17

¹ Measures absolute branching fractions using a missing-mass technique.
² Assumes equal production of B^+ and B^0 at the $\Upsilon(4S)$.
³ ALBRECHT 87D assume $B^+B^-/B^0\bar{B}^0$ ratio is 55/45. Superseded by ALBRECHT 90J.

$\Gamma(\psi(2S)K^+)/\Gamma(J/\psi(1S)K^+)$	$\Gamma_{311}/\Gamma_{276}$		
VALUE	DOCUMENT ID	TECN	COMMENT
0.611 ± 0.019 OUR FIT			
0.605 ± 0.021 OUR AVERAGE			
0.58 ± 0.11 ± 0.02	1 AAIJ	13s LHCB	pp at 7 TeV
0.607 ± 0.018 ± 0.013	2,3 AAIJ	12L LHCB	pp at 7 TeV
0.63 ± 0.05 ± 0.08	ABAZOV	09Y D0	$p\bar{p}$ at 1.96 TeV
0.558 ± 0.082 ± 0.056	ABE	98o CDF	$p\bar{p}$ 1.8 TeV
0.64 ± 0.06 ± 0.07	4 AUBERT	02 BABR	$e^+e^- \rightarrow \Upsilon(4S)$

¹ AAIJ 13s reports $[\Gamma(B^+ \rightarrow \psi(2S)K^+)/\Gamma(B^+ \rightarrow J/\psi(1S)K^+)] \times [B(\psi(2S) \rightarrow p\bar{p}) / [B(J/\psi(1S) \rightarrow p\bar{p})]] = 0.080 \pm 0.012 \pm 0.009$ which we multiply or divide by our best values $B(\psi(2S) \rightarrow p\bar{p}) = (2.94 \pm 0.08) \times 10^{-4}$, $B(J/\psi(1S) \rightarrow p\bar{p}) = (2.120 \pm 0.029) \times 10^{-3}$. Our first error is their experiment's error and our second error is the systematic error from using our best values.
² AAIJ 12L reports $0.594 \pm 0.006 \pm 0.016 \pm 0.015$ from a measurement of $[\Gamma(B^+ \rightarrow \psi(2S)K^+)/\Gamma(B^+ \rightarrow J/\psi(1S)K^+)] \times [B(J/\psi(1S) \rightarrow e^+e^-)] / [B(\psi(2S) \rightarrow e^+e^-)]$ assuming $B(J/\psi(1S) \rightarrow e^+e^-) = (5.94 \pm 0.06) \times 10^{-2}$, $B(\psi(2S) \rightarrow e^+e^-) = (7.72 \pm 0.17) \times 10^{-3}$, which we rescale to our best values $B(J/\psi(1S) \rightarrow e^+e^-) = (5.971 \pm 0.032) \times 10^{-2}$, $B(\psi(2S) \rightarrow e^+e^-) = (7.93 \pm 0.17) \times 10^{-3}$. Our first error is their experiment's error and our second error is the systematic error from using our best values.
³ Assumes $B(J/\psi \rightarrow \mu^+\mu^-) / B(\psi(2S) \rightarrow \mu^+\mu^-) = B(J/\psi \rightarrow e^+e^-) / B(\psi(2S) \rightarrow e^+e^-) = 7.69 \pm 0.19$.
⁴ Assumes equal production of B^+ and B^0 at the $\Upsilon(4S)$.

$\Gamma(\psi(2S)K^*(892)^+)/\Gamma_{total}$	Γ_{312}/Γ		
VALUE (units 10^{-4})	DOCUMENT ID	TECN	COMMENT
6.7 ± 1.4 OUR AVERAGE			Error includes scale factor of 1.3.
5.92 ± 0.85 ± 0.89	1 AUBERT	05j BABR	$e^+e^- \rightarrow \Upsilon(4S)$
9.2 ± 1.9 ± 1.2	1 RICHICHI	01 CLE2	$e^+e^- \rightarrow \Upsilon(4S)$
<30	90	1 ALAM	94 CLE2 Repl. by RICHICHI 01
<35	90	1 BORTOLETTO	92 CLEO $e^+e^- \rightarrow \Upsilon(4S)$
<49	90	1 ALBRECHT	90j ARG $e^+e^- \rightarrow \Upsilon(4S)$

¹ Assumes equal production of B^+ and B^0 at the $\Upsilon(4S)$.

$\Gamma(\psi(2S)K^*(892)^+)/\Gamma(\psi(2S)K^+)$	$\Gamma_{312}/\Gamma_{311}$		
VALUE	DOCUMENT ID	TECN	COMMENT
0.96 ± 0.15 ± 0.09	AUBERT	05j BABR	$e^+e^- \rightarrow \Upsilon(4S)$

$\Gamma(\psi(2S)K^0\pi^+)/\Gamma_{total}$	Γ_{313}/Γ		
VALUE (units 10^{-3})	DOCUMENT ID	TECN	COMMENT
0.588 ± 0.034	1 AUBERT	09AA BABR	$e^+e^- \rightarrow \Upsilon(4S)$

¹ Does not report systematic uncertainties.

$\Gamma(\psi(2S)K^+\pi^+\pi^-)/\Gamma_{total}$	Γ_{314}/Γ		
VALUE (units 10^{-4})	DOCUMENT ID	TECN	COMMENT
4.3 ± 0.5 OUR AVERAGE			
4.31 ± 0.20 ± 0.50	1 GULER	11 BELL	$e^+e^- \rightarrow \Upsilon(4S)$
19 ± 11 ± 4	3 1 ALBRECHT	90j ARG	$e^+e^- \rightarrow \Upsilon(4S)$

¹ Assumes equal production of B^+ and B^0 at the $\Upsilon(4S)$.

$\Gamma(\psi(2S)\phi(1020)K^+)/\Gamma_{total}$	Γ_{315}/Γ		
VALUE (units 10^{-6})	DOCUMENT ID	TECN	COMMENT
4.0 ± 0.4 ± 0.6	1,2 KHACHATRY...	17c CMS	pp at 8 TeV

¹ Measured using $B^+ \rightarrow \psi(2S)K^+$ as a normalization channel. The second error represents total systematic uncertainties including those from branching fractions which were taken from PDG 16 as $B(\phi \rightarrow K^+K^-) = 0.489 \pm 0.005$ and $B(B^+ \rightarrow \psi(2S)K^+) = (6.26 \pm 0.24) \times 10^{-4}$.
² An upper limit on the fraction of the non- ϕ component in $B^+ \rightarrow \psi(2S)K^+K^-K^+$ decays is set as 0.26 at the 95% confidence level.

$\Gamma(\psi(3770)K^+)/\Gamma_{total}$	Γ_{316}/Γ		
VALUE (units 10^{-3})	CL%	DOCUMENT ID	TECN COMMENT
0.43 ± 0.11 OUR AVERAGE			
0.32 ± 0.20 ± 0.05 ± 0.01	1,2	LEES	20c BABR $e^+e^- \rightarrow \Upsilon(4S)$
0.48 ± 0.11 ± 0.07	3	CHISTOV	04 BELL $e^+e^- \rightarrow \Upsilon(4S)$

• • • We do not use the following data for averages, fits, limits, etc. • • •

<0.23

3.5 ± 2.5 ± 0.3

2 KATO

2 AUBERT

18 BELL

06e BABR

$e^+e^- \rightarrow \Upsilon(4S)$

Repl. by LEES 20c

¹ LEES 20c measurement's last uncertainty is due to the used $B(B^\pm \rightarrow K^\pm J/\psi)$ value.
² Measures absolute branching fractions using a missing-mass technique.
³ Assumes equal production of B^+ and B^0 at the $\Upsilon(4S)$.

$\Gamma(\psi(3770)K^+)/\Gamma(D^-D^+K^+)$	$\Gamma_{316}/\Gamma_{209}$		
VALUE	DOCUMENT ID	TECN	COMMENT
0.352 ± 0.035 ± 0.034	1,2 AAIJ	20Ai LHCB	pp at 7, 8, 13 TeV

¹ AAIJ 20Ai reports $[\Gamma(B^+ \rightarrow \psi(3770)K^+)/\Gamma(B^+ \rightarrow D^-D^+K^+)] \times [B(\psi(3770) \rightarrow D^+D^-)] = (14.5 \pm 1.2 \pm 0.8) \times 10^{-2}$ which we divide by our best value $B(\psi(3770) \rightarrow D^+D^-) = (41 \pm 4) \times 10^{-2}$. Our first error is their experiment's error and our second error is the systematic error from using our best value.
² Measured in Dalitz plot analysis of $B^+ \rightarrow D^-D^+K^+$ decays.

$\Gamma(\psi(3770)K^+, \psi \rightarrow D^0\bar{D}^0)/\Gamma_{total}$	Γ_{317}/Γ		
VALUE (units 10^{-4})	DOCUMENT ID	TECN	COMMENT
1.5 ± 0.5 OUR AVERAGE			Error includes scale factor of 1.4.
1.18 ± 0.41 ± 0.15	1 LEES	15c BABR	$e^+e^- \rightarrow \Upsilon(4S)$
2.2 ± 0.5 ± 0.3	1 BRODZICKA	08 BELL	$e^+e^- \rightarrow \Upsilon(4S)$
1.41 ± 0.30 ± 0.22	1 AUBERT	08b BABR	Repl. by LEES 15c
3.4 ± 0.8 ± 0.5	1 CHISTOV	04 BELL	Repl. by BRODZICKA 08

¹ Assumes equal production of B^+ and B^0 at the $\Upsilon(4S)$.

$\Gamma(\psi(3770)K^+, \psi \rightarrow D^+D^-)/\Gamma_{total}$	Γ_{318}/Γ		
VALUE (units 10^{-4})	DOCUMENT ID	TECN	COMMENT
0.94 ± 0.35 OUR AVERAGE			
0.84 ± 0.32 ± 0.21	1 AUBERT	08b BABR	$e^+e^- \rightarrow \Upsilon(4S)$
1.4 ± 0.8 ± 0.2	1 CHISTOV	04 BELL	$e^+e^- \rightarrow \Upsilon(4S)$

¹ Assumes equal production of B^+ and B^0 at the $\Upsilon(4S)$.

$\Gamma(\psi(3770)K^+, \psi \rightarrow p\bar{p})/\Gamma_{total}$	Γ_{319}/Γ		
VALUE	CL%	DOCUMENT ID	TECN COMMENT
<2 × 10⁻⁷	95	1 AAIJ	17Ad LHCB pp at 7 and 8 TeV

¹ Measured relative to $B^+ \rightarrow J/\psi K^+$ decay with charmonia reconstructed in $p\bar{p}$ final state and using $B(B^+ \rightarrow J/\psi K^+) \times B(J/\psi \rightarrow p\bar{p}) = (2.17 \pm 0.08) \times 10^{-6}$.

$\Gamma(\psi(4040)K^+)/\Gamma_{total}$	Γ_{320}/Γ		
VALUE	CL%	DOCUMENT ID	TECN COMMENT
<1.3 × 10⁻⁴	90	AAIJ	13Bc LHCB pp at 7, 8 TeV
<3.0 × 10 ⁻³	90	1 IWASHITA	14 BELL $e^+e^- \rightarrow \Upsilon(4S)$

¹ IWASHITA 14 reports $[\Gamma(B^+ \rightarrow \psi(4040)K^+)/\Gamma_{total}] \times [B(\psi(4040) \rightarrow J/\psi\eta)] < 15.5 \times 10^{-6}$ which we divide by our best value $B(\psi(4040) \rightarrow J/\psi\eta) = 5.2 \times 10^{-3}$.

$\Gamma(\psi(4040)K^+, \psi \rightarrow D^+D^-)/\Gamma(D^-D^+K^+)$	$\Gamma_{321}/\Gamma_{209}$		
VALUE (units 10^{-2})	DOCUMENT ID	TECN	COMMENT
5.0 ± 1.3 ± 0.4	1 AAIJ	20Ai LHCB	pp at 7, 8, 13 TeV

¹ Measured in Dalitz plot analysis of $B^+ \rightarrow D^-D^+K^+$ decays.

$\Gamma(\psi(4160)K^+)/\Gamma_{total}$	Γ_{322}/Γ		
VALUE (units 10^{-4})	DOCUMENT ID	TECN	COMMENT
5.1 ± 1.3 ± 2.5	1 AAIJ	13Bc LHCB	pp at 7, 8 TeV

¹ AAIJ 13Bc reports $[\Gamma(B^+ \rightarrow \psi(4160)K^+)/\Gamma_{total}] \times B(\psi(4160) \rightarrow \mu^+\mu^-) = (3.5 \pm 0.9) \times 10^{-9}$ which we divide by our best value $B(\psi(4160) \rightarrow e^+e^-) = (6.9 \pm 3.3) \times 10^{-6}$ assuming lepton universality. Our first error is their experiment's error and our second error is the systematic error from using our best value.

$\Gamma(\psi(4160)K^+, \psi \rightarrow \bar{D}^0D^0)/\Gamma_{total}$	Γ_{323}/Γ		
VALUE (units 10^{-4})	DOCUMENT ID	TECN	COMMENT
0.84 ± 0.41 ± 0.33	1 LEES	15c BABR	$e^+e^- \rightarrow \Upsilon(4S)$

¹ Assumes equal production of B^+ and B^0 at the $\Upsilon(4S)$.

Meson Particle Listings

B^\pm

$\Gamma(\psi(4160) K^+, \psi \rightarrow D^+ D^-) / \Gamma(D^- D^+ K^+)$ Γ324/Γ209

VALUE (units 10^{-2})	DOCUMENT ID	TECN	COMMENT
6.6 ± 1.5 ± 1.2	¹ AAIJ	20A1	LHCB pp at 7, 8, 13 TeV

¹ Measured in Dalitz plot analysis of $B^+ \rightarrow D^- D^+ K^+$ decays.

$\Gamma(\psi(4415) K^+, \psi \rightarrow D^+ D^-) / \Gamma(D^- D^+ K^+)$ Γ325/Γ209

VALUE (units 10^{-2})	DOCUMENT ID	TECN	COMMENT
9.2 ± 1.4 ± 1.5	¹ AAIJ	20A1	LHCB pp at 7, 8, 13 TeV

¹ Measured in Dalitz plot analysis of $B^+ \rightarrow D^- D^+ K^+$ decays.

$\Gamma(\chi_{c0} \pi^+, \chi_{c0} \rightarrow \pi^+ \pi^-) / \Gamma_{total}$ Γ326/Γ

VALUE (units 10^{-6})	CL%	DOCUMENT ID	TECN	COMMENT
<0.1	90	¹ AUBERT	09L	BABR $e^+ e^- \rightarrow \Upsilon(4S)$
•••				We do not use the following data for averages, fits, limits, etc. •••
<0.3	90	¹ AUBERT,B	05G	BABR Repl. by AUBERT 09L

¹ Assumes equal production of B^+ and B^0 at the $\Upsilon(4S)$.

$\Gamma(\chi_{c0} K^+) / \Gamma_{total}$ Γ327/Γ

VALUE (units 10^{-4})	CL%	DOCUMENT ID	TECN	COMMENT
1.51 ± 0.15 OUR AVERAGE -0.13				
2.0 ± 1.3 ± 0.3 ± 0.1		^{1,2} LEES	20c	BABR $e^+ e^- \rightarrow \Upsilon(4S)$
1.8 ± 0.6 ± 0.6		³ CHILIKIN	19	BELL $e^+ e^- \rightarrow \Upsilon(4S)$
1.84 ± 0.25 ± 0.14		^{4,5} LEES	12o	BABR $e^+ e^- \rightarrow \Upsilon(4S)$
1.68 ± 0.32 ± 0.16		^{4,6} LEES	12o	BABR $e^+ e^- \rightarrow \Upsilon(4S)$
1.8 ± 0.8 ± 0.1		⁷ LEES	11i	BABR $e^+ e^- \rightarrow \Upsilon(4S)$
1.23 ± 0.28 ± 0.05		^{4,8} AUBERT	08A1	BABR $e^+ e^- \rightarrow \Upsilon(4S)$
4.3 ± 2.0 ± 0.2		⁹ AUBERT,BE	06M	BABR $e^+ e^- \rightarrow \Upsilon(4S)$
1.12 ± 0.12 ± 0.30		⁴ GARMASH	06	BELL $e^+ e^- \rightarrow \Upsilon(4S)$

- We do not use the following data for averages, fits, limits, etc. •••
- <3.3 90 ²KATO 18 BELL $e^+ e^- \rightarrow \Upsilon(4S)$
- <2.7 95 10AAIJ 13s LHCB pp at 7 TeV
- <5 90 ^{4,11}WICHT 08 BELL $e^+ e^- \rightarrow \Upsilon(4S)$
- <1.8 90 ²AUBERT 06E BABR $e^+ e^- \rightarrow \Upsilon(4S)$
- 1.84 ± 0.32 ± 0.31 ^{4,12}AUBERT 06o BABR Repl. by LEES 12o
- <8.9 90 ⁴AUBERT 05K BABR $e^+ e^- \rightarrow \Upsilon(4S)$
- 1.39 ± 0.49 ± 0.11 ¹³AUBERT,B 05N BABR Repl. by AUBERT 08A1
- 1.96 ± 0.35 ± 2.00 ⁴GARMASH 05 BELL Repl. by GARMASH 06
- 2.7 ± 0.7 ¹⁴AUBERT 04T BABR Repl. by AUBERT,B 04P
- 3.0 ± 0.8 ± 0.3 ¹⁵AUBERT,B 04P BABR Repl. by AUBERT,B 05N
- 6.0 ± 2.1 ± 1.1 ¹⁶ABE 02B BELL Repl. by GARMASH 05
- <4.8 90 ¹⁷EDWARDS 01 CLE2 $e^+ e^- \rightarrow \Upsilon(4S)$

¹ LEES 20c measurement's last uncertainty is due to the used $B(B^\pm \rightarrow K^\pm J/\psi)$ value.
² Measures absolute branching fractions using a missing-mass technique.
³ CHILIKIN 19 reports $[\Gamma(B^+ \rightarrow \chi_{c0} K^+) / \Gamma_{total}] \times [B(\chi_{c0}(1P) \rightarrow p\bar{p}\pi^+\pi^-)] = (3.7 \pm 1.2 \pm 0.2) \times 10^{-7}$ which we divide by our best value $B(\chi_{c0}(1P) \rightarrow p\bar{p}\pi^+\pi^-) = (2.1 \pm 0.7) \times 10^{-3}$. Our first error is their experiment's error and our second error is the systematic error from using our best value.
⁴ Assumes equal production of B^+ and B^0 at the $\Upsilon(4S)$.
⁵ Measured in the $B^+ \rightarrow K^+ K^0 K^0_S$ decay.
⁶ Measured in the $B^+ \rightarrow K^+ K^0 K^0_S$ decay.
⁷ LEES 11i reports $[\Gamma(B^+ \rightarrow \chi_{c0} K^+) / \Gamma_{total}] \times [B(\chi_{c0}(1P) \rightarrow \pi\pi)] = (1.53 \pm 0.66 \pm 0.27) \times 10^{-6}$ which we divide by our best value $B(\chi_{c0}(1P) \rightarrow \pi\pi) = (8.51 \pm 0.33) \times 10^{-3}$. Our first error is their experiment's error and our second error is the systematic error from using our best value.
⁸ AUBERT 08A1 reports $(0.70 \pm 0.10 \pm 0.12) \times 10^{-6}$ for $B(B^+ \rightarrow \chi_{c0} K^+) \times B(\chi_{c0} \rightarrow \pi^+\pi^-)$. We compute $B(B^+ \rightarrow \chi_{c0} K^+)$ using the PDG value $B(\chi_{c0} \rightarrow \pi\pi) = (8.51 \pm 0.33) \times 10^{-3}$ and 2/3 for the $\pi^+\pi^-$ fraction. Our first error is their experiment's error and the second error is systematic error from using our best value.
⁹ AUBERT,BE 06M reports $[\Gamma(B^+ \rightarrow \chi_{c0} K^+) / \Gamma_{total}] \times [B(\chi_{c0}(1P) \rightarrow \gamma J/\psi(1S))] = (6.1 \pm 2.6 \pm 1.1) \times 10^{-6}$ which we divide by our best value $B(\chi_{c0}(1P) \rightarrow \gamma J/\psi(1S)) = (1.40 \pm 0.05) \times 10^{-2}$. Our first error is their experiment's error and our second error is the systematic error from using our best value. The significance of the observed signal is 2.4 σ .
¹⁰ AAJ 13s reports $[\Gamma(B^+ \rightarrow \chi_{c0} K^+) / \Gamma_{total}] \times [B(\chi_{c0}(1P) \rightarrow p\bar{p})] < 6 \times 10^{-8}$ which we divide by our best value $B(\chi_{c0}(1P) \rightarrow p\bar{p}) = 2.21 \times 10^{-4}$.
¹¹ WICHT 08 reports $[\Gamma(B^+ \rightarrow \chi_{c0} K^+) / \Gamma_{total}] \times [B(\chi_{c0}(1P) \rightarrow \gamma\gamma)] < 0.11 \times 10^{-6}$ which we divide by our best value $B(\chi_{c0}(1P) \rightarrow \gamma\gamma) = 2.04 \times 10^{-4}$.
¹² Measured in the $B^+ \rightarrow K^+ K^- K^+$ decay.
¹³ AUBERT,B 05N reports $(0.66 \pm 0.22 \pm 0.08) \times 10^{-6}$ for $B(B^+ \rightarrow \chi_{c0}^0 K^+) \times B(\chi_{c0}^0 \rightarrow \pi^+\pi^-)$. We compute $B(B^+ \rightarrow \chi_{c0}^0 K^+)$ using the PDG value $B(\chi_{c0}^0 \rightarrow \pi^+\pi^-) = (7.1 \pm 0.6) \times 10^{-3}$ and 2/3 for the $\pi^+\pi^-$ fraction.
¹⁴ The measurement performed using decay channels $\chi_{c0} \rightarrow \pi^+\pi^-$ and $\chi_{c0} \rightarrow K^+ K^-$. The ratio of the branching ratios for these channels is found to be consistent with world average.
¹⁵ AUBERT 04P reports $B(B^+ \rightarrow \chi_{c0} K^+) \times B(\chi_{c0} \rightarrow \pi^+\pi^-) = (1.5 \pm 0.4 \pm 0.1) \times 10^{-6}$ and used PDG value of $B(\chi_{c0} \rightarrow \pi\pi) = (7.4 \pm 0.8) \times 10^{-3}$ and Clebsch-Gordan coefficient to compute $B(B^\pm \rightarrow \chi_{c0} K^+)$.

¹⁶ ABE 02B measures the ratio of $B(B^+ \rightarrow \chi_{c0} K^+) / B(B^+ \rightarrow J/\psi(1S) K^+) = 0.60 \pm 0.21 - 0.18 \pm 0.05 \pm 0.08$, where the third error is due to the uncertainty in the $B(\chi_{c0} \rightarrow \pi^+\pi^-)$, and uses $B(B^+ \rightarrow J/\psi(1S) K^+) = (10.0 \pm 1.0) \times 10^{-4}$ to obtain the result.
¹⁷ EDWARDS 01 assumes equal production of B^0 and B^+ at the $\Upsilon(4S)$. The correlated uncertainties (28.3%) from $B(J/\psi(1S) \rightarrow \gamma\eta_c)$ in those modes have been accounted for.

$\Gamma(\chi_{c0} K^*(892)^+) / \Gamma_{total}$ Γ328/Γ

VALUE (units 10^{-4})	CL%	DOCUMENT ID	TECN	COMMENT
< 2.1	90	¹ AUBERT	08Bd	BABR $e^+ e^- \rightarrow \Upsilon(4S)$
•••				We do not use the following data for averages, fits, limits, etc. •••
<28.6	90	¹ AUBERT	05K	BABR Repl. by AUBERT 08Bd

¹ Assumes equal production of B^+ and B^0 at the $\Upsilon(4S)$.

$\Gamma(\chi_{c1}(1P) \pi^+) / \Gamma_{total}$ Γ329/Γ

VALUE (units 10^{-5})	DOCUMENT ID	TECN	COMMENT
2.2 ± 0.4 ± 0.3	¹ KUMAR	06	BELL $e^+ e^- \rightarrow \Upsilon(4S)$

¹ Assumes equal production of B^+ and B^0 at the $\Upsilon(4S)$.

$\Gamma(\chi_{c1}(1P) K^+) / \Gamma_{total}$ Γ330/Γ

VALUE (units 10^{-4})	DOCUMENT ID	TECN	COMMENT
4.74 ± 0.22 OUR AVERAGE			
4.0 ± 0.8 ± 0.6 ± 0.1	^{1,2} LEES	20c	BABR $e^+ e^- \rightarrow \Upsilon(4S)$
9 ± 3 ± 4	³ CHILIKIN	19	BELL $e^+ e^- \rightarrow \Upsilon(4S)$
5.8 ± 0.9 ± 0.5	¹ KATO	18	BELL $e^+ e^- \rightarrow \Upsilon(4S)$
4.94 ± 0.11 ± 0.33	⁴ BHARDWAJ	11	BELL $e^+ e^- \rightarrow \Upsilon(4S)$
4.5 ± 0.1 ± 0.3	⁵ AUBERT	09b	BABR $e^+ e^- \rightarrow \Upsilon(4S)$
15.5 ± 5.4 ± 2.0	⁶ ACOSTA	02f	CDF $p\bar{p}$ 1.8 TeV
•••			We do not use the following data for averages, fits, limits, etc. •••
8.1 ± 1.4 ± 0.7	¹ AUBERT	06E	BABR Repl. by LEES 20c
5.1 ± 0.4 ± 0.1	⁷ AUBERT,BE	06M	BABR Repl. by AUBERT 09b
4.49 ± 0.19 ± 0.53	⁴ SONI	06	BELL Repl. by BHARDWAJ 11
5.79 ± 0.26 ± 0.65	⁴ AUBERT	05J	BABR Repl. by AUBERT,BE 06M
6.0 ± 0.9 ± 0.2	⁸ AUBERT	02	BABR Repl. by AUBERT 05J
9.7 ± 4.0 ± 0.9	⁴ ALAM	94	CLE2 $e^+ e^- \rightarrow \Upsilon(4S)$
19 ± 13 ± 6	⁹ ALBRECHT	92E	ARG $e^+ e^- \rightarrow \Upsilon(4S)$

¹ Measures absolute branching fractions using a missing-mass technique.
² LEES 20c measurement's last uncertainty is due to the used $B(B^\pm \rightarrow K^\pm J/\psi)$ value.
³ CHILIKIN 19 reports $[\Gamma(B^+ \rightarrow \chi_{c1}(1P) K^+) / \Gamma_{total}] \times [B(\chi_{c1}(1P) \rightarrow p\bar{p}\pi^+\pi^-)] = (4.7 \pm 1.3 \pm 0.4) \times 10^{-7}$ which we divide by our best value $B(\chi_{c1}(1P) \rightarrow p\bar{p}\pi^+\pi^-) = (5.0 \pm 1.9) \times 10^{-4}$. Our first error is their experiment's error and our second error is the systematic error from using our best value.
⁴ Assumes equal production of B^+ and B^0 at the $\Upsilon(4S)$.
⁵ Uses $\chi_{c1,2} \rightarrow J/\psi\gamma$. Assumes $B(\Upsilon(4S) \rightarrow B^+ B^-) = (51.6 \pm 0.6)\%$ and $B(\Upsilon(4S) \rightarrow B^0 \bar{B}^0) = (48.4 \pm 0.6)\%$.
⁶ ACOSTA 02f uses as reference of $B(B \rightarrow J/\psi(1S) K^+) = (10.1 \pm 0.6) \times 10^{-4}$. The second error includes the systematic error and the uncertainties of the branching ratio.
⁷ AUBERT,BE 06M reports $[\Gamma(B^+ \rightarrow \chi_{c1}(1P) K^+) / \Gamma_{total}] \times [B(\chi_{c1}(1P) \rightarrow \gamma J/\psi(1S))] = (1.76 \pm 0.07 \pm 0.12) \times 10^{-4}$ which we divide by our best value $B(\chi_{c1}(1P) \rightarrow \gamma J/\psi(1S)) = (34.3 \pm 1.0) \times 10^{-2}$. Our first error is their experiment's error and our second error is the systematic error from using our best value.
⁸ AUBERT 02 reports $(7.5 \pm 0.9 \pm 0.8) \times 10^{-4}$ from a measurement of $[\Gamma(B^+ \rightarrow \chi_{c1}(1P) K^+) / \Gamma_{total}] \times [B(\chi_{c1}(1P) \rightarrow \gamma J/\psi(1S))]$ assuming $B(\chi_{c1}(1P) \rightarrow \gamma J/\psi(1S)) = 0.273 \pm 0.016$, which we rescale to our best value $B(\chi_{c1}(1P) \rightarrow \gamma J/\psi(1S)) = (34.3 \pm 1.0) \times 10^{-2}$. Our first error is their experiment's error and our second error is the systematic error from using our best value. Assumes equal production of B^+ and B^0 at the $\Upsilon(4S)$.
⁹ ALBRECHT 92E assumes no $\chi_{c2}(1P)$ production and $B(\Upsilon(4S) \rightarrow B^+ B^-) = 50\%$.

$\Gamma(\chi_{c1}(1P) K^+) / \Gamma(J/\psi(1S) K^+)$ Γ330/Γ276

VALUE	DOCUMENT ID	TECN	COMMENT
0.60 ± 0.07 ± 0.02	¹ AUBERT	02	BABR $e^+ e^- \rightarrow \Upsilon(4S)$

¹ AUBERT 02 reports $0.75 \pm 0.08 \pm 0.05$ from a measurement of $[\Gamma(B^+ \rightarrow \chi_{c1}(1P) K^+) / \Gamma(B^+ \rightarrow J/\psi(1S) K^+)] \times [B(\chi_{c1}(1P) \rightarrow \gamma J/\psi(1S))]$ assuming $B(\chi_{c1}(1P) \rightarrow \gamma J/\psi(1S)) = 0.273 \pm 0.016$, which we rescale to our best value $B(\chi_{c1}(1P) \rightarrow \gamma J/\psi(1S)) = (34.3 \pm 1.0) \times 10^{-2}$. Our first error is their experiment's error and our second error is the systematic error from using our best value. Assumes equal production of B^+ and B^0 at the $\Upsilon(4S)$.

$\Gamma(\chi_{c1}(1P) \pi^+) / \Gamma(\chi_{c1}(1P) K^+)$ Γ329/Γ330

VALUE	DOCUMENT ID	TECN	COMMENT
0.043 ± 0.008 ± 0.003	¹ KUMAR	06	BELL $e^+ e^- \rightarrow \Upsilon(4S)$

¹ Assumes equal production of B^+ and B^0 at the $\Upsilon(4S)$.

$\Gamma(\chi_{c1}(1P) K^*(892)^+) / \Gamma_{total}$ Γ331/Γ

VALUE (units 10^{-4})	CL%	DOCUMENT ID	TECN	COMMENT
3.0 ± 0.6 OUR AVERAGE				Error includes scale factor of 1.1.
2.6 ± 0.5 ± 0.4		¹ AUBERT	09b	BABR $e^+ e^- \rightarrow \Upsilon(4S)$
4.05 ± 0.59 ± 0.95		² SONI	06	BELL $e^+ e^- \rightarrow \Upsilon(4S)$
•••				We do not use the following data for averages, fits, limits, etc. •••
2.94 ± 0.95 ± 0.98		² AUBERT	05J	BABR Repl. by AUBERT 09b
<21	90	² ALAM	94	CLE2 $e^+ e^- \rightarrow \Upsilon(4S)$
•••				We do not use the following data for averages, fits, limits, etc. •••
<21				Uses $\chi_{c1,2} \rightarrow J/\psi\gamma$. Assumes $B(\Upsilon(4S) \rightarrow B^+ B^-) = (51.6 \pm 0.6)\%$ and $B(\Upsilon(4S) \rightarrow B^0 \bar{B}^0) = (48.4 \pm 0.6)\%$.
				² Assumes equal production of B^+ and B^0 at the $\Upsilon(4S)$.

$\Gamma(\chi_{c1}(1P)K^*(892)^+)/\Gamma(\chi_{c1}(1P)K^+)$				$\Gamma_{331}/\Gamma_{330}$
VALUE	DOCUMENT ID	TECN	COMMENT	
0.51 ± 0.17 ± 0.16	AUBERT	05j	BABR $e^+e^- \rightarrow \Upsilon(4S)$	

$\Gamma(\chi_{c1}(1P)K^0\pi^+)/\Gamma_{total}$				Γ_{332}/Γ
VALUE (units 10^{-4})	DOCUMENT ID	TECN	COMMENT	
5.75 ± 0.26 ± 0.32	¹ BHARDWAJ	16	BELL $e^+e^- \rightarrow \Upsilon(4S)$	
¹ Assumes equal production of B^+ and B^0 at the $\Upsilon(4S)$.				

$\Gamma(\chi_{c1}(1P)K^0\pi^+)/\Gamma(J/\psi(1S)K^0\pi^+)$				$\Gamma_{332}/\Gamma_{277}$
VALUE	DOCUMENT ID	TECN	COMMENT	
0.503 ± 0.030 ± 0.014	¹ LEES	12b	BABR $e^+e^- \rightarrow \Upsilon(4S)$	
¹ LEES 12b reports $0.501 \pm 0.024 \pm 0.028$ from a measurement of $[\Gamma(B^+ \rightarrow \chi_{c1}(1P)K^0\pi^+)/\Gamma(B^+ \rightarrow J/\psi(1S)K^0\pi^+)] \times [B(\chi_{c1}(1P) \rightarrow \gamma J/\psi(1S))]$ assuming $B(\chi_{c1}(1P) \rightarrow \gamma J/\psi(1S)) = (34.4 \pm 1.5) \times 10^{-2}$, which we rescale to our best value $B(\chi_{c1}(1P) \rightarrow \gamma J/\psi(1S)) = (34.3 \pm 1.0) \times 10^{-2}$. Our first error is their experiment's error and our second error is the systematic error from using our best value.				

$\Gamma(\chi_{c1}(1P)K^+\pi^0)/\Gamma_{total}$				Γ_{333}/Γ
VALUE (units 10^{-4})	DOCUMENT ID	TECN	COMMENT	
3.29 ± 0.29 ± 0.19	¹ BHARDWAJ	16	BELL $e^+e^- \rightarrow \Upsilon(4S)$	
¹ Assumes equal production of B^+ and B^0 at the $\Upsilon(4S)$.				

$\Gamma(\chi_{c1}(1P)K^+\pi^+\pi^-)/\Gamma_{total}$				Γ_{334}/Γ
VALUE (units 10^{-4})	DOCUMENT ID	TECN	COMMENT	
3.74 ± 0.18 ± 0.24	¹ BHARDWAJ	16	BELL $e^+e^- \rightarrow \Upsilon(4S)$	
¹ Assumes equal production of B^+ and B^0 at the $\Upsilon(4S)$.				

$\Gamma(\chi_{c1}(2P)K^+, \chi_{c1}(2P) \rightarrow \pi^+\pi^-\chi_{c1}(1P))/\Gamma_{total}$				Γ_{335}/Γ
VALUE	CL%	DOCUMENT ID	TECN	COMMENT
<1.1 × 10⁻⁵	90	^{1,2} BHARDWAJ	16	BELL $e^+e^- \rightarrow \Upsilon(4S)$
¹ BHARDWAJ 16 analysis fixes mass and width of the $\chi_{c1}(2P)$ state to 3920 MeV and 20 MeV.				
² Assumes equal production of B^+ and B^0 at the $\Upsilon(4S)$.				

$\Gamma(\chi_{c2}K^+)/\Gamma_{total}$				Γ_{336}/Γ
VALUE (units 10^{-5})	CL%	DOCUMENT ID	TECN	COMMENT
1.11 ± 0.36 ± 0.09		¹ BHARDWAJ	11	BELL $e^+e^- \rightarrow \Upsilon(4S)$

• • • We do not use the following data for averages, fits, limits, etc. • • •

< 1.8	90	² AUBERT	09b	BABR $e^+e^- \rightarrow \Upsilon(4S)$
< 20	90	³ AUBERT	06E	BABR $e^+e^- \rightarrow \Upsilon(4S)$
< 2.9	90	¹ SONI	06	BELL Repl. by BHARDWAJ 11
< 3.0	90	¹ AUBERT	05k	BABR Repl. by AUBERT 06e

¹ Assumes equal production of B^+ and B^0 at the $\Upsilon(4S)$.
² Uses $\chi_{c1,2} \rightarrow J/\psi\gamma$. Assumes $B(\Upsilon(4S) \rightarrow B^+B^-) = (51.6 \pm 0.6)\%$ and $B(\Upsilon(4S) \rightarrow B^0\bar{B}^0) = (48.4 \pm 0.6)\%$.
³ Perform measurements of absolute branching fractions using a missing mass technique.

$\Gamma(\chi_{c2}K^+, \chi_{c2} \rightarrow \rho\bar{\rho}\pi^+\pi^-)/\Gamma_{total}$				Γ_{337}/Γ
VALUE	DOCUMENT ID	TECN	COMMENT	
<1.9 × 10⁻⁷	CHILIKIN	19	BELL $e^+e^- \rightarrow \Upsilon(4S)$	

$\Gamma(B^+ \rightarrow \chi_{c2}K^+)/\Gamma_{total} \times \Gamma(\chi_{c2}(1P) \rightarrow \gamma\gamma)/\Gamma_{total}$				$\Gamma_{336}/\Gamma \times \Gamma_{96}^{\chi_{c2}(1P)}/\Gamma_{\chi_{c2}(1P)}$
VALUE (units 10^{-6})	CL%	DOCUMENT ID	TECN	COMMENT
<0.09	90	¹ WICHT	08	BELL $e^+e^- \rightarrow \Upsilon(4S)$
¹ Assumes equal production of B^+ and B^0 at the $\Upsilon(4S)$.				

$\Gamma(\chi_{c2}K^*(892)^+)/\Gamma_{total}$				Γ_{338}/Γ
VALUE	CL%	DOCUMENT ID	TECN	COMMENT
<12 × 10⁻⁵	90	¹ AUBERT	09b	BABR $e^+e^- \rightarrow \Upsilon(4S)$
• • • We do not use the following data for averages, fits, limits, etc. • • •				
<12.7 × 10 ⁻⁵	90	² SONI	06	BELL $e^+e^- \rightarrow \Upsilon(4S)$
< 1.2 × 10 ⁻⁵	90	² AUBERT	05k	BABR Repl. by AUBERT 09b
¹ Uses $\chi_{c1,2} \rightarrow J/\psi\gamma$. Assumes $B(\Upsilon(4S) \rightarrow B^+B^-) = (51.6 \pm 0.6)\%$ and $B(\Upsilon(4S) \rightarrow B^0\bar{B}^0) = (48.4 \pm 0.6)\%$.				
² Assumes equal production of B^+ and B^0 at the $\Upsilon(4S)$.				

$\Gamma(\chi_{c2}K^0\pi^+)/\Gamma_{total}$				Γ_{339}/Γ
VALUE (units 10^{-4})	DOCUMENT ID	TECN	COMMENT	
1.16 ± 0.22 ± 0.12	¹ BHARDWAJ	16	BELL $e^+e^- \rightarrow \Upsilon(4S)$	
¹ Assumes equal production of B^+ and B^0 at the $\Upsilon(4S)$.				

$\Gamma(\chi_{c2}K^+\pi^0)/\Gamma_{total}$				Γ_{340}/Γ
VALUE	CL%	DOCUMENT ID	TECN	COMMENT
<0.62 × 10⁻⁴	90	¹ BHARDWAJ	16	BELL $e^+e^- \rightarrow \Upsilon(4S)$
¹ Assumes equal production of B^+ and B^0 at the $\Upsilon(4S)$.				

$\Gamma(\chi_{c2}K^+\pi^+\pi^-)/\Gamma_{total}$				Γ_{341}/Γ
VALUE (units 10^{-4})	DOCUMENT ID	TECN	COMMENT	
1.34 ± 0.17 ± 0.09	¹ BHARDWAJ	16	BELL $e^+e^- \rightarrow \Upsilon(4S)$	
¹ Assumes equal production of B^+ and B^0 at the $\Upsilon(4S)$.				

$\Gamma(\chi_{c2}(3930)K^+, \chi_{c2} \rightarrow D^+D^-)/\Gamma(D^-D^+K^+)$				$\Gamma_{342}/\Gamma_{209}$
VALUE (units 10^{-2})	DOCUMENT ID	TECN	COMMENT	
7.2 ± 1.2 ± 0.3	¹ AAIJ	20aI	LHCB pp at 7, 8, 13 TeV	
¹ Measured in Dalitz plot analysis of $B^+ \rightarrow D^-D^+K^+$ decays.				

$\Gamma(\chi_{c2}(3930)\pi^+, \chi_{c2} \rightarrow \pi^+\pi^-)/\Gamma_{total}$				Γ_{343}/Γ
VALUE (units 10^{-5})	CL%	DOCUMENT ID	TECN	COMMENT
<0.1	90	¹ AUBERT	09L	BABR $e^+e^- \rightarrow \Upsilon(4S)$
¹ Assumes equal production of B^+ and B^0 at the $\Upsilon(4S)$.				

$\Gamma(h_c(1P)K^+)/\Gamma_{total}$				Γ_{344}/Γ
VALUE (units 10^{-5})	CL%	DOCUMENT ID	TECN	COMMENT
3.7 ± 1.0 ± 0.8		CHILIKIN	19	BELL $e^+e^- \rightarrow \Upsilon(4S)$
• • • We do not use the following data for averages, fits, limits, etc. • • •				
<3.8	90	¹ FANG	06	BELL $e^+e^- \rightarrow \Upsilon(4S)$
¹ Assumes equal production of B^+ and B^0 at the $\Upsilon(4S)$ and $B(h_c \rightarrow \eta_c\gamma) = 50\%$.				

$\Gamma(h_c(1P)K^+, h_c \rightarrow \rho\bar{p})/\Gamma_{total}$				Γ_{345}/Γ
VALUE	CL%	DOCUMENT ID	TECN	COMMENT
<6.4 × 10⁻⁸	95	¹ AAIJ	13s	LHCB pp at 7 TeV
¹ Measured relative to $B^+ \rightarrow J/\psi K^+$ decay with charmonia reconstructed in $p\bar{p}$ final state and using $B(B^+ \rightarrow J/\psi K^+) = (1.013 \pm 0.034) \times 10^{-3}$ and $B(J/\psi \rightarrow \rho\bar{p}) = (2.17 \pm 0.07) \times 10^{-3}$.				

$\Gamma(K^0\pi^+)/\Gamma_{total}$				Γ_{346}/Γ
VALUE (units 10^{-6})	CL%	DOCUMENT ID	TECN	COMMENT
23.7 ± 0.8 OUR FIT				
23.8 ± 0.7 OUR AVERAGE				
23.97 ± 0.53 ± 0.71		¹ DUH	13	BELL $e^+e^- \rightarrow \Upsilon(4S)$
23.9 ± 1.1 ± 1.0		¹ AUBERT, BE	06c	BABR $e^+e^- \rightarrow \Upsilon(4S)$
18.8 ± 3.7 ± 2.1		¹ BORNHEIM	03	CLE2 $e^+e^- \rightarrow \Upsilon(4S)$
18.8 ± 3.3 ± 1.8				
• • • We do not use the following data for averages, fits, limits, etc. • • •				
22.8 ± 0.8 ± 1.3		¹ LIN	07	BELL Repl. by DUH 13
26.0 ± 1.3 ± 1.0		¹ AUBERT, BE	05E	BABR Repl. by AUBERT, BE 06c
22.3 ± 1.7 ± 1.1		¹ AUBERT	04M	BABR Repl. by AUBERT, BE 05E
22.0 ± 1.9 ± 1.1		¹ CHAO	04	BELL Repl. by LIN 07
19.4 ± 3.1 ± 1.6		¹ CASEY	02	BELL Repl. by CHAO 04
13.7 ± 5.7 ± 1.9		¹ ABE	01H	BELL Repl. by CASEY 02
18.2 ± 3.3 ± 2.0		¹ AUBERT	01E	BABR Repl. by AUBERT 04M
18.2 ± 4.6 ± 1.6		¹ CRONIN-HEN..00	CLE2	Repl. by BORNHEIM 03
23 ± 11 ± 3.6		GODANG	98	CLE2 Repl. by CRONIN-HENNESSY 00
< 48	90	ASNER	96	CLE2 Repl. by GODANG 98
<190	90	ALBRECHT	91B	ARG $e^+e^- \rightarrow \Upsilon(4S)$
<100	90	² AVERY	89B	CLEO $e^+e^- \rightarrow \Upsilon(4S)$
<680	90	AVERY	87	CLEO $e^+e^- \rightarrow \Upsilon(4S)$
¹ Assumes equal production of B^+ and B^0 at the $\Upsilon(4S)$. ² AVERY 89b reports $< 9 \times 10^{-5}$ assuming the $\Upsilon(4S)$ decays 43% to $B^0\bar{B}^0$. We rescale to 50%.				

$\Gamma(K^+\pi^0)/\Gamma_{total}$				Γ_{347}/Γ
VALUE (units 10^{-6})	CL%	DOCUMENT ID	TECN	COMMENT
12.9 ± 0.5 OUR AVERAGE				
12.62 ± 0.31 ± 0.56		¹ DUH	13	BELL $e^+e^- \rightarrow \Upsilon(4S)$
13.6 ± 0.6 ± 0.7		¹ AUBERT	07bc	BABR $e^+e^- \rightarrow \Upsilon(4S)$
12.9 ± 2.4 ± 1.2		¹ BORNHEIM	03	CLE2 $e^+e^- \rightarrow \Upsilon(4S)$
12.9 ± 2.2 ± 1.1				
• • • We do not use the following data for averages, fits, limits, etc. • • •				
12.4 ± 0.5 ± 0.6		¹ LIN	07A	BELL Repl. by DUH 13
12.0 ± 0.7 ± 0.6		¹ AUBERT	05L	BABR Repl. by AUBERT 07bc
12.0 ± 1.3 ± 1.3		¹ CHAO	04	BELL Repl. by LIN 07A
12.8 ± 1.2 ± 1.1		¹ AUBERT	03L	BABR Repl. by AUBERT 05L
13.0 ± 2.5 ± 1.3		¹ CASEY	02	BELL Repl. by CHAO 04
16.3 ± 3.5 ± 1.6		¹ ABE	01H	BELL Repl. by CASEY 02
12.0 ± 1.3 ± 1.3		¹ AUBERT	01E	BABR Repl. by AUBERT 03L
10.8 ± 2.1 ± 1.0		¹ AUBERT	01E	BABR Repl. by AUBERT 03L
11.6 ± 3.0 ± 1.4		¹ CRONIN-HEN..00	CLE2	Repl. by BORNHEIM 03
<16	90	GODANG	98	CLE2 Repl. by CRONIN-HENNESSY 00
<14	90	ASNER	96	CLE2 Repl. by GODANG 98
¹ Assumes equal production of B^+ and B^0 at the $\Upsilon(4S)$.				

Meson Particle Listings

 B^\pm $\Gamma(K^+\pi^0)/\Gamma(K^0\pi^+)$ $\Gamma_{347}/\Gamma_{346}$

VALUE	DOCUMENT ID	TECN	COMMENT
0.54 ± 0.03 ± 0.04	LIN	07A	BELL $e^+e^- \rightarrow \Upsilon(4S)$
• • • We do not use the following data for averages, fits, limits, etc. • • •			
2.38 ^{+0.98+0.39} _{-1.10-0.26}	ABE	01H	BELL Repl. by LIN 07A

 $\Gamma(\eta'K^+)/\Gamma_{total}$ Γ_{348}/Γ

VALUE (units 10 ⁻⁶)	DOCUMENT ID	TECN	COMMENT
70.4 ± 2.5 OUR AVERAGE			
71.5 ± 1.3 ± 3.2	¹ AUBERT	09AV	BABR $e^+e^- \rightarrow \Upsilon(4S)$
61 ⁺¹⁰ ₋₈ ± 1	^{1,2} WICHT	08	BELL $e^+e^- \rightarrow \Upsilon(4S)$
69.2 ± 2.2 ± 3.7	¹ SCHUEMANN	06	BELL $e^+e^- \rightarrow \Upsilon(4S)$
80 ⁺¹⁰ ₋₉ ± 7	¹ RICHICHI	00	CLE2 $e^+e^- \rightarrow \Upsilon(4S)$

• • • We do not use the following data for averages, fits, limits, etc. • • •

70.0 ± 1.5 ± 2.8 ¹AUBERT 07AE BABR Repl. by AUBERT 09AV
 68.9 ± 2.0 ± 3.2 ¹AUBERT 05M BABR Repl. by AUBERT 07AE
 76.9 ± 3.5 ± 4.4 ¹AUBERT 03W BABR Repl. by AUBERT 05M
 79⁺¹²₋₁₁ ± 9 ¹ABE 01M BELL Repl. by SCHUEMANN 06
 70 ± 8 ± 5 ¹AUBERT 01G BABR Repl. by AUBERT 03W
 65⁺¹⁵₋₁₄ ± 9 BEHRENS 98 CLE2 Repl. by RICHICHI 00

¹ Assumes equal production of B^+ and B^0 at the $\Upsilon(4S)$.
² WICHT 08 reports $[\Gamma(B^+ \rightarrow \eta'K^+)/\Gamma_{total}] \times [B(\eta'(958) \rightarrow \gamma\gamma)] = (1.40^{+0.16+0.15}_{-0.15-0.12}) \times 10^{-6}$ which we divide by our best value $B(\eta'(958) \rightarrow \gamma\gamma) = (2.307 \pm 0.033) \times 10^{-2}$. Our first error is their experiment's error and our second error is the systematic error from using our best value.

 $\Gamma(\eta'K^*(892)^+)/\Gamma_{total}$ Γ_{349}/Γ

VALUE (units 10 ⁻⁶)	CL%	DOCUMENT ID	TECN	COMMENT
4.8 ± 1.6 ± 0.8		¹ DEL-AMO-SA...10A	BABR	$e^+e^- \rightarrow \Upsilon(4S)$
• • • We do not use the following data for averages, fits, limits, etc. • • •				
4.9 ^{+1.9} _{-1.7} ± 0.8		¹ AUBERT 07E	BABR	Repl. by DEL-AMO-SANCHEZ 10A
< 2.9	90	¹ SCHUEMANN 07	BELL	$e^+e^- \rightarrow \Upsilon(4S)$
< 14	90	¹ AUBERT,B 04D	BABR	Repl. by AUBERT 07E
< 35	90	¹ RICHICHI 00	CLE2	$e^+e^- \rightarrow \Upsilon(4S)$
< 13	90	BEHRENS 98	CLE2	Repl. by RICHICHI 00

¹ Assumes equal production of B^+ and B^0 at the $\Upsilon(4S)$.

 $\Gamma(\eta'K_0^*(1430)^+)/\Gamma_{total}$ Γ_{350}/Γ

VALUE (units 10 ⁻⁶)	DOCUMENT ID	TECN	COMMENT
5.2 ± 1.9 ± 1.0	¹ DEL-AMO-SA...10A	BABR	$e^+e^- \rightarrow \Upsilon(4S)$

¹ Assumes equal production of B^+ and B^0 at the $\Upsilon(4S)$.

 $\Gamma(\eta'K_2^*(1430)^+)/\Gamma_{total}$ Γ_{351}/Γ

VALUE (units 10 ⁻⁶)	DOCUMENT ID	TECN	COMMENT
28.0 ± 4.6 ± 2.6	¹ DEL-AMO-SA...10A	BABR	$e^+e^- \rightarrow \Upsilon(4S)$

¹ Assumes equal production of B^+ and B^0 at the $\Upsilon(4S)$.

 $\Gamma(\eta K^+)/\Gamma_{total}$ Γ_{352}/Γ

VALUE (units 10 ⁻⁶)	CL%	DOCUMENT ID	TECN	COMMENT
2.4 ± 0.4 OUR AVERAGE		Error includes scale factor of 1.7.		
2.12 ± 0.23 ± 0.11		¹ HOI 12	BELL	$e^+e^- \rightarrow \Upsilon(4S)$
2.94 ^{+0.39} _{-0.34} ± 0.21		¹ AUBERT 09AV	BABR	$e^+e^- \rightarrow \Upsilon(4S)$
2.2 ± 2.8 _{-2.2}		¹ RICHICHI 00	CLE2	$e^+e^- \rightarrow \Upsilon(4S)$

• • • We do not use the following data for averages, fits, limits, etc. • • •

2.21 ^{+0.48} _{-0.42} ± 0.01	^{1,2} WICHT	08	BELL	Repl. by HOI 12
3.7 ± 0.4 ± 0.1	¹ AUBERT	07AE	BABR	Repl. by AUBERT 09AV
1.9 ± 0.3 ^{+0.2} _{-0.1}	¹ CHANG	07B	BELL	Repl. by HOI 12
3.3 ± 0.6 ± 0.3	¹ AUBERT,B	05K	BABR	Repl. by AUBERT 07AE
2.1 ± 0.6 ± 0.2	¹ CHANG	05A	BELL	Repl. by CHANG 07B
3.4 ± 0.8 ± 0.2	¹ AUBERT	04H	BABR	Repl. by AUBERT,B 05K
< 14	90	BEHRENS	98	CLE2 Repl. by RICHICHI 00

¹ Assumes equal production of B^+ and B^0 at the $\Upsilon(4S)$.
² WICHT 08 reports $[\Gamma(B^+ \rightarrow \eta K^+)/\Gamma_{total}] \times [B(\eta \rightarrow 2\gamma)] = (0.87^{+0.16+0.10}_{-0.15-0.07}) \times 10^{-6}$ which we divide by our best value $B(\eta \rightarrow 2\gamma) = (39.36 \pm 0.18) \times 10^{-2}$. Our first error is their experiment's error and our second error is the systematic error from using our best value.

 $\Gamma(\eta K^*(892)^+)/\Gamma_{total}$ Γ_{353}/Γ

VALUE (units 10 ⁻⁶)	CL%	DOCUMENT ID	TECN	COMMENT
19.3 ± 1.6 OUR AVERAGE				
19.3 ^{+2.0} _{-1.9} ± 1.5		¹ WANG 07B	BELL	$e^+e^- \rightarrow \Upsilon(4S)$
18.9 ± 1.8 ± 1.3		¹ AUBERT,B 06H	BABR	$e^+e^- \rightarrow \Upsilon(4S)$
26.4 ^{+9.6} _{-8.2} ± 3.3		¹ RICHICHI 00	CLE2	$e^+e^- \rightarrow \Upsilon(4S)$

• • • We do not use the following data for averages, fits, limits, etc. • • •

25.6 ± 4.0 ± 2.4 ¹AUBERT,B 04D BABR Repl. by AUBERT,B 06H
 < 30 90 BEHRENS 98 CLE2 Repl. by RICHICHI 00
¹ Assumes equal production of B^+ and B^0 at the $\Upsilon(4S)$.

 $\Gamma(\eta K_0^*(1430)^+)/\Gamma_{total}$ Γ_{354}/Γ

VALUE (units 10 ⁻⁶)	DOCUMENT ID	TECN	COMMENT
18.2 ± 2.6 ± 2.6	¹ AUBERT,B 06H	BABR	$e^+e^- \rightarrow \Upsilon(4S)$

¹ Assumes equal production of B^+ and B^0 at the $\Upsilon(4S)$.

 $\Gamma(\eta K_2^*(1430)^+)/\Gamma_{total}$ Γ_{355}/Γ

VALUE (units 10 ⁻⁶)	DOCUMENT ID	TECN	COMMENT
9.1 ± 2.7 ± 1.4	¹ AUBERT,B 06H	BABR	$e^+e^- \rightarrow \Upsilon(4S)$

¹ Assumes equal production of B^+ and B^0 at the $\Upsilon(4S)$.

 $\Gamma(\eta(1295)K^+ \times B(\eta(1295) \rightarrow \eta\pi\pi))/\Gamma_{total}$ Γ_{356}/Γ

VALUE (units 10 ⁻⁶)	DOCUMENT ID	TECN	COMMENT
2.9 ± 0.8 ± 0.2	¹ AUBERT 08x	BABR	$e^+e^- \rightarrow \Upsilon(4S)$

¹ Assumes equal production of B^+ and B^0 at the $\Upsilon(4S)$.

 $\Gamma(\eta(1405)K^+ \times B(\eta(1405) \rightarrow \eta\pi\pi))/\Gamma_{total}$ Γ_{357}/Γ

VALUE (units 10 ⁻⁶)	CL%	DOCUMENT ID	TECN	COMMENT
< 1.3	90	¹ AUBERT 08x	BABR	$e^+e^- \rightarrow \Upsilon(4S)$

¹ Assumes equal production of B^+ and B^0 at the $\Upsilon(4S)$.

 $\Gamma(\eta(1405)K^+ \times B(\eta(1405) \rightarrow K^*K))/\Gamma_{total}$ Γ_{358}/Γ

VALUE (units 10 ⁻⁶)	CL%	DOCUMENT ID	TECN	COMMENT
< 1.2	90	¹ AUBERT 08x	BABR	$e^+e^- \rightarrow \Upsilon(4S)$

¹ Assumes equal production of B^+ and B^0 at the $\Upsilon(4S)$.

 $\Gamma(\eta(1475)K^+ \times B(\eta(1475) \rightarrow K^*K))/\Gamma_{total}$ Γ_{359}/Γ

VALUE (units 10 ⁻⁶)	DOCUMENT ID	TECN	COMMENT
13.0 ± 1.8 ± 1.0 1.7 ± 0.6	¹ AUBERT 08x	BABR	$e^+e^- \rightarrow \Upsilon(4S)$

¹ Assumes equal production of B^+ and B^0 at the $\Upsilon(4S)$.

 $\Gamma(\eta_1(1285)K^+)/\Gamma_{total}$ Γ_{360}/Γ

VALUE (units 10 ⁻⁶)	CL%	DOCUMENT ID	TECN	COMMENT
< 2.0	90	¹ AUBERT 08x	BABR	$e^+e^- \rightarrow \Upsilon(4S)$

¹ Assumes equal production of B^+ and B^0 at the $\Upsilon(4S)$.

 $\Gamma(\eta_1(1420)K^+ \times B(\eta_1(1420) \rightarrow \eta\pi\pi))/\Gamma_{total}$ Γ_{361}/Γ

VALUE (units 10 ⁻⁶)	CL%	DOCUMENT ID	TECN	COMMENT
< 2.9	90	¹ AUBERT 08x	BABR	$e^+e^- \rightarrow \Upsilon(4S)$

¹ Assumes equal production of B^+ and B^0 at the $\Upsilon(4S)$.

 $\Gamma(\eta_1(1420)K^+ \times B(\eta_1(1420) \rightarrow K^*K))/\Gamma_{total}$ Γ_{362}/Γ

VALUE (units 10 ⁻⁶)	CL%	DOCUMENT ID	TECN	COMMENT
< 4.1	90	¹ AUBERT 08x	BABR	$e^+e^- \rightarrow \Upsilon(4S)$

¹ Assumes equal production of B^+ and B^0 at the $\Upsilon(4S)$.

 $\Gamma(\phi(1680)K^+ \times B(\phi(1680) \rightarrow K^*K))/\Gamma_{total}$ Γ_{363}/Γ

VALUE (units 10 ⁻⁶)	CL%	DOCUMENT ID	TECN	COMMENT
< 3.4	90	¹ AUBERT 08x	BABR	$e^+e^- \rightarrow \Upsilon(4S)$

¹ Assumes equal production of B^+ and B^0 at the $\Upsilon(4S)$.

 $\Gamma(f_0(1500)K^+)/\Gamma_{total}$ Γ_{364}/Γ

VALUE (units 10 ⁻⁶)	CL%	DOCUMENT ID	TECN	COMMENT
3.7 ± 2.2 OUR AVERAGE				
17 ± 4 ± 12		¹ LEES 120	BABR	$e^+e^- \rightarrow \Upsilon(4S)$
20 ± 10 ± 27		² LEES 120	BABR	$e^+e^- \rightarrow \Upsilon(4S)$
3.2 ^{+2.3} _{-2.3} ± 0.2		^{3,4} AUBERT 08A1	BABR	$e^+e^- \rightarrow \Upsilon(4S)$

• • • We do not use the following data for averages, fits, limits, etc. • • •

< 19 90 ^{4,5}AUBERT,B 05N BABR Repl. by AUBERT 08A1

¹ Measured in the $B^+ \rightarrow K^+K^-K^+$ decay.
² Measured in the $B^+ \rightarrow K^+K_S^0K_S^0$ decay.
³ AUBERT 08A1 reports $B(B^+ \rightarrow f_0(1500)K^+) \cdot B(f_0(1500) \rightarrow \pi^+\pi^-) = (0.73 \pm 0.21^{+0.47}_{-0.48}) \times 10^{-6}$. We divide this result by our best value of $B(f_0(1500) \rightarrow \pi\pi) = (34.5 \pm 2.2) \times 10^{-2}$ multiplied by 2/3 to account for the $\pi^+\pi^-$ fraction. Our first quoted uncertainty is the combined experiment's uncertainty and our second is the systematic uncertainty from using our best value.
⁴ Assumes equal production of B^+ and B^0 at the $\Upsilon(4S)$.
⁵ AUBERT,B 05N reports $B(B^+ \rightarrow f_0(1500)K^+) \cdot B(f_0(1500) \rightarrow \pi^+\pi^-) < 4.4 \times 10^{-6}$. We divide this result by our best value of $B(f_0(1500) \rightarrow \pi\pi) = (34.5 \pm 2.2) \times 10^{-2}$ multiplied by 2/3 to account for the $\pi^+\pi^-$ fraction. Our first quoted uncertainty is the combined experiment's uncertainty and our second is the systematic uncertainty from using our best value.

$\Gamma(\omega K^+)/\Gamma_{total}$ Γ_{365}/Γ

VALUE (units 10^{-6})	CL%	DOCUMENT ID	TECN	COMMENT
6.5 ± 0.4 OUR AVERAGE				
6.8 ± 0.4 ± 0.4		1 CHOBANOVA 14	BELL	$e^+e^- \rightarrow \Upsilon(4S)$
6.3 ± 0.5 ± 0.3		1 AUBERT 07AE	BABR	$e^+e^- \rightarrow \Upsilon(4S)$
3.2 ± $\frac{2.4}{-1.9}$ ± 0.8		1 JESSOP 00	CLE2	$e^+e^- \rightarrow \Upsilon(4S)$
• • • We do not use the following data for averages, fits, limits, etc. • • •				
6.1 ± 0.6 ± 0.4		1 AUBERT,B 06E	BABR	AUBERT 07AE
8.1 ± 0.6 ± 0.6		1 JEN 06	BELL	Repl. by CHOBANOVA 14
4.8 ± 0.8 ± 0.4		1 AUBERT 04H	BABR	Repl. by AUBERT,B 06E
6.5 ± $\frac{1.3}{-1.2}$ ± 0.6		1 WANG 04A	BELL	Repl. by JEN 06
9.2 ± $\frac{2.6}{-2.3}$ ± 1.0		1 LU 02	BELL	Repl. by WANG 04A
<4	90	1 AUBERT 01G	BABR	$e^+e^- \rightarrow \Upsilon(4S)$
1.5 ± $\frac{7}{-6}$ ± 2		1 BERGFELD 98	CLE2	Repl. by JESSOP 00
1 Assumes equal production of B^+ and B^0 at the $\Upsilon(4S)$.				

$\Gamma(\omega K^*(892)^+)/\Gamma_{total}$ Γ_{366}/Γ

VALUE (units 10^{-6})	CL%	DOCUMENT ID	TECN	COMMENT
< 7.4	90	1 AUBERT 09H	BABR	$e^+e^- \rightarrow \Upsilon(4S)$
• • • We do not use the following data for averages, fits, limits, etc. • • •				
< 3.4	90	1 AUBERT,B 06T	BABR	Repl. by AUBERT 09H
< 7.4	90	1 AUBERT 05O	BABR	Repl. by AUBERT,B 06T
<87	90	1 BERGFELD 98	CLE2	
1 Assumes equal production of B^+ and B^0 at the $\Upsilon(4S)$.				

$\Gamma(\omega(K\pi)_0^{*+})/\Gamma_{total}$ Γ_{367}/Γ

($K\pi)_0^{*+}$ is the total S-wave composed of $K_0^*(1430)$ and nonresonant that are described using LASS shape.

VALUE (units 10^{-6})	DOCUMENT ID	TECN	COMMENT
27.5 ± 3.0 ± 2.6	1 AUBERT 09H	BABR	$e^+e^- \rightarrow \Upsilon(4S)$
1 Assumes equal production of B^+ and B^0 at the $\Upsilon(4S)$.			

$\Gamma(\omega K_0^*(1430)^+)/\Gamma_{total}$ Γ_{368}/Γ

VALUE (units 10^{-6})	DOCUMENT ID	TECN	COMMENT
24.0 ± 2.6 ± 4.4	1 AUBERT 09H	BABR	$e^+e^- \rightarrow \Upsilon(4S)$
1 Assumes equal production of B^+ and B^0 at the $\Upsilon(4S)$.			

$\Gamma(\omega K_2^*(1430)^+)/\Gamma_{total}$ Γ_{369}/Γ

VALUE (units 10^{-6})	DOCUMENT ID	TECN	COMMENT
21.5 ± 3.6 ± 2.4	1 AUBERT 09H	BABR	$e^+e^- \rightarrow \Upsilon(4S)$
1 Assumes equal production of B^+ and B^0 at the $\Upsilon(4S)$.			

$\Gamma(a_0(980)^0 K^+ \times B(a_0(980)^0 \rightarrow \eta\pi^0))/\Gamma_{total}$ Γ_{371}/Γ

VALUE (units 10^{-6})	CL%	DOCUMENT ID	TECN	COMMENT
<2.5	90	1 AUBERT,BE 04	BABR	$e^+e^- \rightarrow \Upsilon(4S)$
1 Assumes equal production of charged and neutral B mesons from $\Upsilon(4S)$ decays.				

$\Gamma(a_0(980)^+ K^0 \times B(a_0(980)^+ \rightarrow \eta\pi^+))/\Gamma_{total}$ Γ_{370}/Γ

VALUE (units 10^{-6})	CL%	DOCUMENT ID	TECN	COMMENT
<3.9	90	1 AUBERT,BE 04	BABR	$e^+e^- \rightarrow \Upsilon(4S)$
1 Assumes equal production of charged and neutral B mesons from $\Upsilon(4S)$ decays.				

$\Gamma(K^*(892)^0 \pi^+)/\Gamma_{total}$ Γ_{372}/Γ

VALUE (units 10^{-6})	CL%	DOCUMENT ID	TECN	COMMENT
10.1 ± 0.8 OUR AVERAGE				
10.1 ± 1.7 ± 1.0		1 LEES 17G	BABR	$e^+e^- \rightarrow \Upsilon(4S)$
10.8 ± 0.6 ± $\frac{1.2}{-1.4}$		2 AUBERT 08AI	BABR	$e^+e^- \rightarrow \Upsilon(4S)$
9.67 ± 0.64 ± $\frac{0.81}{-0.89}$		2 GARMASH 06	BELL	$e^+e^- \rightarrow \Upsilon(4S)$
• • • We do not use the following data for averages, fits, limits, etc. • • •				
13.5 ± 1.2 ± $\frac{0.8}{-0.9}$		2 AUBERT,B 05N	BABR	Repl. by AUBERT 08AI
9.8 ± 0.9 ± $\frac{1.1}{-1.2}$		2 GARMASH 05	BELL	Repl. by GARMASH 06
15.5 ± 1.8 ± $\frac{1.5}{-4.0}$		2,3 AUBERT,B 04P	BABR	Repl. by AUBERT,B 05N
19.4 ± $\frac{4.2}{-3.9}$ ± 4.1		4 GARMASH 02	BELL	Repl. by GARMASH 05
<119	90	5 ABE 00C	SLD	$e^+e^- \rightarrow Z$
< 16	90	2 JESSOP 00	CLE2	$e^+e^- \rightarrow \Upsilon(4S)$
<390	90	6 ADAM 96D	DLPH	$e^+e^- \rightarrow Z$
< 41	90	ASNER 96	CLE2	Repl. by JESSOP 00
<480	90	6 ABREU 95N	DLPH	Sup. by ADAM 96D
<170	90	ALBRECHT 91B	ARG	$e^+e^- \rightarrow \Upsilon(4S)$
<150	90	7 AVERY 89B	CLEO	$e^+e^- \rightarrow \Upsilon(4S)$
<260	90	AVERY 87	CLEO	$e^+e^- \rightarrow \Upsilon(4S)$
1 Obtains the result from a Dalitz analysis of $B^+ \rightarrow K_S^0 \pi^+ \pi^0$ decays. The first error is statistical, the second combines all the systematic uncertainties reported in the paper, including signal modelling.				

2 Assumes equal production of B^+ and B^0 at the $\Upsilon(4S)$.
 3 AUBERT 04P also report a branching ratio for $B^+ \rightarrow$ "higher K^* resonances" π^+ , $K^* \rightarrow K^+ \pi^-$, $(25.1 \pm 2.0 \pm \frac{11.0}{-5.7}) \times 10^{-6}$.
 4 Uses a reference decay mode $B^+ \rightarrow \bar{D}^0 \pi^+$ and $\bar{D}^0 \rightarrow K^+ \pi^-$ with $B(B^+ \rightarrow \bar{D}^0 \pi^+) \cdot B(\bar{D}^0 \rightarrow K^+ \pi^-) = (20.3 \pm 2.0) \times 10^{-5}$.
 5 ABE 00C assumes $B(Z \rightarrow b\bar{b}) = (21.7 \pm 0.1)\%$ and the B fractions $f_{B^0} = f_{B^+} = (39.7 \pm \frac{1.8}{-2.2})\%$ and $f_{B_s} = (10.5 \pm \frac{1.8}{-2.2})\%$.
 6 Assumes a B^0, B^- production fraction of 0.39 and a B_s production fraction of 0.12.
 7 AVERY 89B reports $< 1.3 \times 10^{-4}$ assuming the $\Upsilon(4S)$ decays 43% to $B^0 \bar{B}^0$. We rescale to 50%.

$\Gamma(K^*(892)^+ \pi^0)/\Gamma_{total}$ Γ_{373}/Γ

VALUE (units 10^{-6})	CL%	DOCUMENT ID	TECN	COMMENT
6.8 ± 0.9 OUR AVERAGE				
6.4 ± 0.9 ± $\frac{0.4}{-0.5}$		1 LEES 17G	BABR	$e^+e^- \rightarrow \Upsilon(4S)$
8.2 ± 1.5 ± 1.1		2 LEES 11I	BABR	$e^+e^- \rightarrow \Upsilon(4S)$
• • • We do not use the following data for averages, fits, limits, etc. • • •				
6.9 ± 2.0 ± 1.3		2 AUBERT 05X	BABR	Repl. by LEES 11I
<31	90	2 JESSOP 00	CLE2	$e^+e^- \rightarrow \Upsilon(4S)$
<99	90	ASNER 96	CLE2	Repl. by JESSOP 00

1 Obtains the result from a Dalitz analysis of $B^+ \rightarrow K_S^0 \pi^+ \pi^0$ decays. The first error is statistical, the second combines all the systematic uncertainties reported in the paper, including signal modelling.
 2 Assumes equal production of B^+ and B^0 at the $\Upsilon(4S)$.

$\Gamma(K^+ \pi^- \pi^+)/\Gamma(K^+ K^- K^+)$ $\Gamma_{374}/\Gamma_{426}$

VALUE	DOCUMENT ID	TECN	COMMENT
1.703 ± 0.011 ± 0.022	AAIJ	20AJ	LHCB pp at 7 and 8 TeV

$\Gamma(K^+ \pi^- \pi^+)/\Gamma_{total}$ Γ_{374}/Γ

VALUE (units 10^{-6})	DOCUMENT ID	TECN	COMMENT
51.0 ± 2.9 OUR AVERAGE			
54.4 ± 1.1 ± 4.6	1 AUBERT 08AI	BABR	$e^+e^- \rightarrow \Upsilon(4S)$
48.8 ± 1.1 ± 3.6	1 GARMASH 06	BELL	$e^+e^- \rightarrow \Upsilon(4S)$
• • • We do not use the following data for averages, fits, limits, etc. • • •			
64.1 ± 2.4 ± 4.0	1 AUBERT,B 05N	BABR	Repl. by AUBERT 08AI
46.6 ± 2.1 ± 4.3	1 GARMASH 05	BELL	Repl. by GARMASH 06
53.6 ± 3.1 ± 5.1	2 GARMASH 04	BELL	Repl. by GARMASH 05
59.1 ± 3.8 ± 3.2	2 AUBERT 03M	BABR	Repl. by AUBERT,B 05N
55.6 ± 5.8 ± 7.7	3 GARMASH 02	BELL	Repl. by GARMASH 04

1 Assumes equal production of B^+ and B^0 at the $\Upsilon(4S)$.
 2 Assumes equal production of B^0 and B^+ at the $\Upsilon(4S)$; charm and charmonium contributions are subtracted, otherwise no assumptions about intermediate resonances.
 3 Uses a reference decay mode $B^+ \rightarrow \bar{D}^0 \pi^+$ and $\bar{D}^0 \rightarrow K^+ \pi^-$ with $B(B^+ \rightarrow \bar{D}^0 \pi^+) \cdot B(\bar{D}^0 \rightarrow K^+ \pi^-) = (20.3 \pm 2.0) \times 10^{-5}$.

$\Gamma(K^+ \pi^- \pi^+ \text{ nonresonant})/\Gamma_{total}$ Γ_{375}/Γ

VALUE (units 10^{-6})	CL%	DOCUMENT ID	TECN	COMMENT
16.3 ± 2.1 OUR AVERAGE				
9.3 ± 1.0 ± $\frac{6.9}{-1.7}$		1,2 AUBERT 08AI	BABR	$e^+e^- \rightarrow \Upsilon(4S)$
16.9 ± 1.3 ± $\frac{1.7}{-1.6}$		1 GARMASH 06	BELL	$e^+e^- \rightarrow \Upsilon(4S)$
• • • We do not use the following data for averages, fits, limits, etc. • • •				
2.9 ± 0.6 ± $\frac{0.8}{-0.5}$		1 AUBERT,B 05N	BABR	Repl. by AUBERT 08AI
17.3 ± 1.7 ± $\frac{17.2}{-8.0}$		1 GARMASH 05	BELL	Repl. by GARMASH 06
< 17	90	1 AUBERT,B 04P	BABR	Repl. by AUBERT,B 05N
<330	90	3 ADAM 96D	DLPH	$e^+e^- \rightarrow Z$
< 28	90	BERGFELD 96B	CLE2	$e^+e^- \rightarrow \Upsilon(4S)$
<400	90	3 ABREU 95N	DLPH	Sup. by ADAM 96D
<330	90	ALBRECHT 91E	ARG	$e^+e^- \rightarrow \Upsilon(4S)$
<190	90	4 AVERY 89B	CLEO	$e^+e^- \rightarrow \Upsilon(4S)$

1 Assumes equal production of B^+ and B^0 at the $\Upsilon(4S)$.
 2 Calculate the total nonresonant contribution by combining the S-wave composed of $K_0^*(1430)$ and nonresonant that are described using LASS shape.
 3 Assumes a B^0, B^- production fraction of 0.39 and a B_s production fraction of 0.12.
 4 AVERY 89B reports $< 1.7 \times 10^{-4}$ assuming the $\Upsilon(4S)$ decays 43% to $B^0 \bar{B}^0$. We rescale to 50%.

$\Gamma(\omega(782) K^+)/\Gamma_{total}$ Γ_{376}/Γ

VALUE (units 10^{-6})	DOCUMENT ID	TECN	COMMENT
5.9 ± 8.8 ± 0.5 OUR AVERAGE	1,2 AUBERT 08AI	BABR	$e^+e^- \rightarrow \Upsilon(4S)$

1 Assumes equal production of B^+ and B^0 at the $\Upsilon(4S)$.
 2 AUBERT 08AI reports $[\Gamma(B^+ \rightarrow \omega(782) K^+)/\Gamma_{total}] \times [B(\omega(782) \rightarrow \pi^+ \pi^-)] = (0.09 \pm 0.13 \pm \frac{0.036}{-0.045}) \times 10^{-6}$ which we divide by our best value $B(\omega(782) \rightarrow \pi^+ \pi^-) = (1.53 \pm \frac{0.11}{-0.13}) \times 10^{-2}$. Our first error is their experiment's error and our second error is the systematic error from using our best value.

Meson Particle Listings

B^\pm

$\Gamma(K^+ f_0(980) \times B(f_0(980) \rightarrow \pi^+ \pi^-))/\Gamma_{total}$ Γ_{377}/Γ

VALUE (units 10^{-6})	CL%	DOCUMENT ID	TECN	COMMENT
9.4 \pm 1.0	OUR AVERAGE			
10.3 \pm 0.5	\pm 2.0 -1.4	1 AUBERT	08AI BABR	$e^+ e^- \rightarrow \Upsilon(4S)$
8.78 \pm 0.82	\pm 0.85 -1.76	1 GARMASH	06 BELL	$e^+ e^- \rightarrow \Upsilon(4S)$
• • • We do not use the following data for averages, fits, limits, etc. • • •				
9.47 \pm 0.97	\pm 0.62 -0.88	1 AUBERT,B	05N BABR	Repl. by AUBERT 08AI
7.55 \pm 1.24	\pm 1.63 -1.18	1 GARMASH	05 BELL	Repl. by GARMASH 06
9.2 \pm 1.2	\pm 2.1 -2.6	2 AUBERT,B	04P BABR	Repl. by AUBERT,B 05N
9.6 \pm 2.5	\pm 3.7 -2.3	3 GARMASH	02 BELL	Repl. by GARMASH 05
<80	90	4 AVERY	89B CLEO	$e^+ e^- \rightarrow \Upsilon(4S)$

- Assumes equal production of B^+ and B^0 at the $\Upsilon(4S)$.
- AUBERT,B 04P also reports $B(B^+ \rightarrow \text{"higher } f^0 \text{ resonances"} \pi^+, f(980)^0 \rightarrow \pi^+ \pi^-) = (3.2 \pm 1.2 \pm 2.9) \times 10^{-6}$.
- Uses a reference decay mode $B^+ \rightarrow \bar{D}^0 \pi^+$ and $\bar{D}^0 \rightarrow K^+ \pi^-$ with $B(B^+ \rightarrow \bar{D}^0 \pi^+) \times B(\bar{D}^0 \rightarrow K^+ \pi^-) = (20.3 \pm 2.0) \times 10^{-5}$. Only charged pions from the $f_0(980)$ are used.
- AVERY 89B reports $< 7 \times 10^{-5}$ assuming the $\Upsilon(4S)$ decays 43% to $B^0 \bar{B}^0$. We rescale to 50%.

$\Gamma(f_2(1270)^0 K^+)/\Gamma_{total}$ Γ_{378}/Γ

VALUE (units 10^{-6})	CL%	DOCUMENT ID	TECN	COMMENT
1.07 \pm 0.27	OUR AVERAGE			
0.89 \pm 0.38	\pm 0.01 -0.33	1,2 AUBERT	08AI BABR	$e^+ e^- \rightarrow \Upsilon(4S)$
1.33 \pm 0.30	\pm 0.23 -0.34	1 GARMASH	06 BELL	$e^+ e^- \rightarrow \Upsilon(4S)$
• • • We do not use the following data for averages, fits, limits, etc. • • •				
<16	90	3 AUBERT,B	05N BABR	Repl. by AUBERT 08AI
< 2.3	90	4 GARMASH	05 BELL	Repl. by GARMASH 06

- Assumes equal production of B^+ and B^0 at the $\Upsilon(4S)$.
- AUBERT 08AI reports $(0.50 \pm 0.15 \pm 0.15) \times 10^{-6}$ for $B(B^+ \rightarrow f_2(1270) K^+) \times B(f_2(1270) \rightarrow \pi^+ \pi^-)$. We compute $B(B^+ \rightarrow f_2(1270) K^+)$ using the PDG value $B(f_2(1270) \rightarrow \pi^+ \pi^-) = (84.2 \pm 2.9) \times 10^{-2}$ and 2/3 for the $\pi^+ \pi^-$ fraction. Our first error is their experiment's error and the second error is systematic error from using our best value.
- AUBERT,B 05N reports 8.9×10^{-6} at 90% CL for $B(B^+ \rightarrow f_2(1270) K^+) \times B(f_2(1270) \rightarrow \pi^+ \pi^-)$. We rescaled it using the PDG value $B(f_2(1270) \rightarrow \pi^+ \pi^-) = 84.7\%$ and 2/3 for the $\pi^+ \pi^-$ fraction.
- GARMASH 05 reports 1.3×10^{-6} at 90% CL for $B(B^+ \rightarrow f_2(1270) K^+) \times B(f_2(1270) \rightarrow \pi^+ \pi^-)$. We rescaled it using the PDG value $B(f_2(1270) \rightarrow \pi^+ \pi^-) = 84.7\%$ and 2/3 for the $\pi^+ \pi^-$ fraction.

$\Gamma(f_0(1370)^0 K^+ \times B(f_0(1370)^0 \rightarrow \pi^+ \pi^-))/\Gamma_{total}$ Γ_{379}/Γ

VALUE	CL%	DOCUMENT ID	TECN	COMMENT
<10.7 $\times 10^{-6}$	90	1 AUBERT,B	05N BABR	$e^+ e^- \rightarrow \Upsilon(4S)$

- Assumes equal production of B^+ and B^0 at the $\Upsilon(4S)$.

$\Gamma(\rho^0(1450) K^+ \times B(\rho^0(1450) \rightarrow \pi^+ \pi^-))/\Gamma_{total}$ Γ_{380}/Γ

VALUE	CL%	DOCUMENT ID	TECN	COMMENT
<11.7 $\times 10^{-6}$	90	1 AUBERT,B	05N BABR	$e^+ e^- \rightarrow \Upsilon(4S)$

- Assumes equal production of B^+ and B^0 at the $\Upsilon(4S)$.

$\Gamma(f_2'(1525) K^+ \times B(f_2'(1525) \rightarrow \pi^+ \pi^-))/\Gamma_{total}$ Γ_{381}/Γ

VALUE	CL%	DOCUMENT ID	TECN	COMMENT
<3.4 $\times 10^{-6}$	90	1 AUBERT,B	05N BABR	$e^+ e^- \rightarrow \Upsilon(4S)$

- Assumes equal production of B^+ and B^0 at the $\Upsilon(4S)$.

$\Gamma(K^+ \rho^0)/\Gamma_{total}$ Γ_{382}/Γ

VALUE (units 10^{-6})	CL%	DOCUMENT ID	TECN	COMMENT
3.7 \pm 0.5	OUR AVERAGE			
3.56 \pm 0.45	\pm 0.57 -0.46	1 AUBERT	08AI BABR	$e^+ e^- \rightarrow \Upsilon(4S)$
3.89 \pm 0.47	\pm 0.43 -0.41	1 GARMASH	06 BELL	$e^+ e^- \rightarrow \Upsilon(4S)$
• • • We do not use the following data for averages, fits, limits, etc. • • •				
5.07 \pm 0.75	\pm 0.55 -0.88	1 AUBERT,B	05N BABR	Repl. by AUBERT 08AI
4.78 \pm 0.75	\pm 1.01 -0.97	1 GARMASH	05 BELL	Repl. by GARMASH 06
< 6.2	90	2 AUBERT,B	04P BABR	Repl. by AUBERT,B 05N
< 12	90	3 GARMASH	02 BELL	$e^+ e^- \rightarrow \Upsilon(4S)$
< 86	90	4 ABE	00C SLD	$e^+ e^- \rightarrow Z$
< 17	90	1 JESSOP	00 CLE2	$e^+ e^- \rightarrow \Upsilon(4S)$
<120	90	5 ADAM	96D DLPH	$e^+ e^- \rightarrow Z$
< 19	90	ASNER	96 CLE2	Repl. by JESSOP 00
<190	90	5 ABREU	95N DLPH	Sup. by ADAM 96D
<180	90	ALBRECHT	91B ARG	$e^+ e^- \rightarrow \Upsilon(4S)$
< 80	90	6 AVERY	89B CLEO	$e^+ e^- \rightarrow \Upsilon(4S)$
<260	90	AVERY	87 CLEO	$e^+ e^- \rightarrow \Upsilon(4S)$

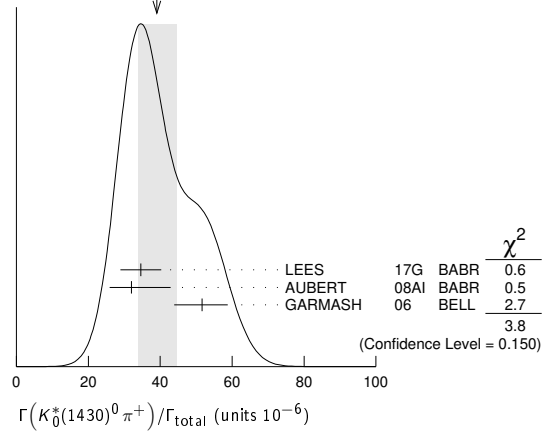
- Assumes equal production of B^+ and B^0 at the $\Upsilon(4S)$.

- AUBERT 04P reports a central value of $(3.9 \pm 1.2 \pm 1.3) \times 10^{-6}$ for this branching ratio.
- Uses a reference decay mode $B^+ \rightarrow \bar{D}^0 \pi^+$ and $\bar{D}^0 \rightarrow K^+ \pi^-$ with $B(B^+ \rightarrow \bar{D}^0 \pi^+) \times B(\bar{D}^0 \rightarrow K^+ \pi^-) = (20.3 \pm 2.0) \times 10^{-5}$.
- ABE 00c assumes $B(Z \rightarrow b\bar{b}) = (21.7 \pm 0.1)\%$ and the B fractions $f_{B^0} = f_{B^+} = (39.7 \pm 1.8)\%$ and $f_{B_s} = (10.5 \pm 1.8)\%$.
- Assumes production fractions $f_{B^0} = f_{B^-} = 0.39$ and $f_{B_s} = 0.12$.
- AVERY 89B reports $< 7 \times 10^{-5}$ assuming the $\Upsilon(4S)$ decays 43% to $B^0 \bar{B}^0$. We rescale to 50%.

$\Gamma(K_0^*(1430)^0 \pi^+)/\Gamma_{total}$ Γ_{383}/Γ

VALUE (units 10^{-6})	CL%	DOCUMENT ID	TECN	COMMENT
39 \pm 6	OUR AVERAGE			Error includes scale factor of 1.4. See the ideogram below.
34.6 \pm 3.3	\pm 4.6	1 LEES	17G BABR	$e^+ e^- \rightarrow \Upsilon(4S)$
32.0 \pm 1.2	\pm 10.8 6.0	2 AUBERT	08AI BABR	$e^+ e^- \rightarrow \Upsilon(4S)$
51.6 \pm 1.7	\pm 7.0 -7.5	2 GARMASH	06 BELL	$e^+ e^- \rightarrow \Upsilon(4S)$
• • • We do not use the following data for averages, fits, limits, etc. • • •				
44.4 \pm 2.2	\pm 5.3	2,3 AUBERT,B	05N BABR	Repl. by AUBERT 08AI
45.0 \pm 2.9	\pm 15.0 -10.7	2 GARMASH	05 BELL	Repl. by GARMASH 06

WEIGHTED AVERAGE
39+6-5 (Error scaled by 1.4)



- Obtains the result from a Dalitz analysis of $B^+ \rightarrow K_0^* \pi^+ \pi^0$ decays. The first error is statistical, the second combines all the systematic uncertainties reported in the paper, including signal modelling.
- Assumes equal production of B^+ and B^0 at the $\Upsilon(4S)$.
- See erratum: AUBERT, BE 06A.

$\Gamma(K_2^*(1430)^0 \pi^+)/\Gamma_{total}$ Γ_{384}/Γ

VALUE (units 10^{-6})	CL%	DOCUMENT ID	TECN	COMMENT
5.6 \pm 2.2 \pm 0.1		1,2 AUBERT	08AI BABR	$e^+ e^- \rightarrow \Upsilon(4S)$
• • • We do not use the following data for averages, fits, limits, etc. • • •				
< 23	90	3 AUBERT,B	05N BABR	Repl. by AUBERT 08AI
< 6.9	90	4 GARMASH	05 BELL	$e^+ e^- \rightarrow \Upsilon(4S)$
<680	90	ALBRECHT	91B ARG	$e^+ e^- \rightarrow \Upsilon(4S)$

- Assumes equal production of B^+ and B^0 at the $\Upsilon(4S)$.
- AUBERT 08AI reports $(1.85 \pm 0.41 \pm 0.61) \times 10^{-6}$ for $B(B^+ \rightarrow K_2^*(1430)^0 \pi^+) \times B(K_2^*(1430)^0 \rightarrow K^+ \pi^-)$. We compute $B(B^+ \rightarrow K_2^*(1430)^0 \pi^+)$ using the PDG value $B(K_2^*(1430)^0 \rightarrow K\pi) = (49.9 \pm 1.2) \times 10^{-2}$ and 2/3 for the $K^+ \pi^-$ fraction. Our first error is their experiment's error and the second error is systematic error from using our best value.
- AUBERT,B 05N reports 7.7×10^{-6} at 90% CL for $B(B^+ \rightarrow K_2^*(1430)^0 \pi^+) \times B(K_2^*(1430)^0 \rightarrow K^+ \pi^-)$. We rescaled it using the PDG value $B(K_2^*(1430)^0 \rightarrow K\pi) = 49.9\%$ and 2/3 for the $K^+ \pi^-$ fraction.
- GARMASH 05 reports 2.3×10^{-6} at 90% CL for $B(B^+ \rightarrow K_2^*(1430)^0 \pi^+) \times B(K_2^*(1430)^0 \rightarrow K^+ \pi^-)$. We rescaled it using the PDG value $B(K_2^*(1430)^0 \rightarrow K\pi) = 49.9\%$ and 2/3 for the $K^+ \pi^-$ mode.

$\Gamma(K^*(1410)^0 \pi^+)/\Gamma_{total}$ Γ_{385}/Γ

VALUE (units 10^{-6})	CL%	DOCUMENT ID	TECN	COMMENT
<45	90	1 GARMASH	05 BELL	$e^+ e^- \rightarrow \Upsilon(4S)$

- GARMASH 05 reports 2.0×10^{-6} at 90% CL for $B(B^+ \rightarrow K^*(1410)^0 \pi^+) \times B(K^*(1410)^0 \rightarrow K^+ \pi^-)$. We rescaled it using the PDG value $B(K^*(1410)^0 \rightarrow K\pi) = 6.6\%$ and 2/3 for the $K^+ \pi^-$ mode.

$\Gamma(K^*(1680)^0 \pi^+)/\Gamma_{total}$ Γ_{386}/Γ

VALUE (units 10^{-6})	CL%	DOCUMENT ID	TECN	COMMENT
<12	90	¹ GARMASH 05	BELL	$e^+e^- \rightarrow \Upsilon(4S)$
••• We do not use the following data for averages, fits, limits, etc. •••				
<15	90	² AUBERT,B 05N	BABR	$e^+e^- \rightarrow \Upsilon(4S)$
¹ GARMASH 05 reports 3.1×10^{-6} at 90% CL for $B(B^+ \rightarrow K^*(1680)^0 \pi^+) \times B(K^*(1680)^0 \rightarrow K^+ \pi^-)$. We rescaled it using the PDG value $B(K^*(1680)^0 \rightarrow K^+ \pi^-) = 38.7\%$ and 2/3 for the $K^+ \pi^-$ mode.				
² AUBERT,B 05N reports 3.8×10^{-6} at 90% CL for $B(B^+ \rightarrow K^*(1680)^0 \pi^+) \times B(K^*(1680)^0 \rightarrow K^+ \pi^-)$. We rescaled it using the PDG value $B(K^*(1680)^0 \rightarrow K^+ \pi^-) = 38.7\%$ and 2/3 for the $K^+ \pi^-$ fraction.				

$\Gamma(K^+ \pi^0 \pi^0)/\Gamma_{total}$ Γ_{387}/Γ

VALUE (units 10^{-6})	DOCUMENT ID	TECN	COMMENT
16.2 ± 1.2 ± 1.5	¹ LEES 11i	BABR	$e^+e^- \rightarrow \Upsilon(4S)$
¹ Assumes equal production of B^+ and B^0 at the $\Upsilon(4S)$.			

$\Gamma(f_0(980) K^+ \times B(f_0 \rightarrow \pi^0 \pi^0))/\Gamma_{total}$ Γ_{388}/Γ

VALUE (units 10^{-6})	DOCUMENT ID	TECN	COMMENT
2.8 ± 0.6 ± 0.5	¹ LEES 11i	BABR	$e^+e^- \rightarrow \Upsilon(4S)$
¹ Assumes equal production of B^+ and B^0 at the $\Upsilon(4S)$.			

$\Gamma(K^- \pi^+ \pi^+)/\Gamma_{total}$ Γ_{389}/Γ

VALUE	CL%	DOCUMENT ID	TECN	COMMENT
< 4.6 × 10⁻⁸	90	AAIJ 17E	LHCB	pp at 7, 8 TeV
••• We do not use the following data for averages, fits, limits, etc. •••				
<9.5 × 10 ⁻⁷	90	¹ AUBERT 08BE	BABR	$e^+e^- \rightarrow \Upsilon(4S)$
<4.5 × 10 ⁻⁶	90	¹ GARMASH 04	BELL	$e^+e^- \rightarrow \Upsilon(4S)$
<1.8 × 10 ⁻⁶	90	² AUBERT 03M	BABR	Repl. by AUBERT 08BE
<7.0 × 10 ⁻⁶	90	³ GARMASH 02	BELL	$e^+e^- \rightarrow \Upsilon(4S)$
¹ Assumes equal production of B^+ and B^0 at the $\Upsilon(4S)$.				
² Assumes equal production of B^0 and B^+ at the $\Upsilon(4S)$; charm and charmonium contributions are subtracted, otherwise no assumptions about intermediate resonances.				
³ Uses a reference decay mode $B^+ \rightarrow \bar{D}^0 \pi^+$ and $\bar{D}^0 \rightarrow K^+ \pi^-$ with $B(B^+ \rightarrow \bar{D}^0 \pi^+) \cdot B(\bar{D}^0 \rightarrow K^+ \pi^-) = (20.3 \pm 2.0) \times 10^{-5}$.				

$\Gamma(K^- \pi^+ \pi^+ \text{ nonresonant})/\Gamma_{total}$ Γ_{390}/Γ

VALUE (units 10^{-6})	CL%	DOCUMENT ID	TECN	COMMENT
< 56	90	BERGFELD 96B	CLE2	$e^+e^- \rightarrow \Upsilon(4S)$

$\Gamma(K_1(1270)^0 \pi^+)/\Gamma_{total}$ Γ_{391}/Γ

VALUE	CL%	DOCUMENT ID	TECN	COMMENT
< 4.0 × 10⁻⁵	90	¹ AUBERT 10D	BABR	$e^+e^- \rightarrow \Upsilon(4S)$
¹ Assumes equal production of B^+ and B^0 at the $\Upsilon(4S)$.				

$\Gamma(K_1(1400)^0 \pi^+)/\Gamma_{total}$ Γ_{392}/Γ

VALUE	CL%	DOCUMENT ID	TECN	COMMENT
< 3.9 × 10⁻⁵	90	¹ AUBERT 10D	BABR	$e^+e^- \rightarrow \Upsilon(4S)$
••• We do not use the following data for averages, fits, limits, etc. •••				
<2.6 × 10 ⁻³	90	ALBRECHT 91B	ARG	$e^+e^- \rightarrow \Upsilon(4S)$
¹ Assumes equal production of B^+ and B^0 at the $\Upsilon(4S)$.				

$\Gamma(K^0 \pi^+ \pi^0)/\Gamma_{total}$ Γ_{393}/Γ

VALUE (units 10^{-6})	CL%	DOCUMENT ID	TECN	COMMENT
31.8 ± 1.8 ± 6.3 2.1		¹ LEES 17G	BABR	$e^+e^- \rightarrow \Upsilon(4S)$
< 66	90	² ECKHART 02	CLE2	$e^+e^- \rightarrow \Upsilon(4S)$
¹ Obtains the result from a Dalitz analysis of $B^+ \rightarrow K_S^0 \pi^+ \pi^0$ decays. The first error is statistical, the second combines all the systematic uncertainties reported in the paper, including signal modelling.				
² Assumes equal production of B^+ and B^0 at the $\Upsilon(4S)$.				

$\Gamma(K^0 \rho^+)/\Gamma_{total}$ Γ_{395}/Γ

VALUE (units 10^{-6})	CL%	DOCUMENT ID	TECN	COMMENT
7.3 ± 1.0 1.2		OUR AVERAGE		
6.5 ± 1.1 ± 0.8 -1.9		¹ LEES 17G	BABR	$e^+e^- \rightarrow \Upsilon(4S)$
8.0 ± 1.4 ± 0.6 -1.3		AUBERT 07Z	BABR	$e^+e^- \rightarrow \Upsilon(4S)$
••• We do not use the following data for averages, fits, limits, etc. •••				
<48	90	ASNER 96	CLE2	$e^+e^- \rightarrow \Upsilon(4S)$
¹ Obtains the result from a Dalitz analysis of $B^+ \rightarrow K_S^0 \pi^+ \pi^0$ decays. The first error is statistical, the second combines all the systematic uncertainties reported in the paper, including signal modelling.				

$\Gamma(K_S^0(1430)^+ \pi^0)/\Gamma_{total}$ Γ_{394}/Γ

VALUE (units 10^{-6})	DOCUMENT ID	TECN	COMMENT
11.9 ± 1.7 ± 1.0 1.6	¹ LEES 17G	BABR	$e^+e^- \rightarrow \Upsilon(4S)$
¹ Obtains the result from a Dalitz analysis of $B^+ \rightarrow K_S^0 \pi^+ \pi^0$ decays. The first error is statistical, the second combines all the systematic uncertainties reported in the paper, including signal modelling.			

$\Gamma(K^*(892)^+ \pi^+ \pi^-)/\Gamma_{total}$ Γ_{396}/Γ

VALUE (units 10^{-6})	CL%	DOCUMENT ID	TECN	COMMENT
75.3 ± 6.0 ± 8.1		¹ AUBERT,B 06U	BABR	$e^+e^- \rightarrow \Upsilon(4S)$
••• We do not use the following data for averages, fits, limits, etc. •••				
<1100	90	ALBRECHT 91E	ARG	$e^+e^- \rightarrow \Upsilon(4S)$
¹ Assumes equal production of B^+ and B^0 at the $\Upsilon(4S)$.				

$\Gamma(K^*(892)^+ \rho^0)/\Gamma_{total}$ Γ_{397}/Γ

VALUE (units 10^{-6})	CL%	DOCUMENT ID	TECN	COMMENT
4.6 ± 1.0 ± 0.4		¹ DEL-AMO-SA...11D	BABR	$e^+e^- \rightarrow \Upsilon(4S)$
••• We do not use the following data for averages, fits, limits, etc. •••				
< 6.1	90	¹ AUBERT,B 06G	BABR	Repl. by DEL-AMO-SANCHEZ 11D
10.6 ± 3.0 ± 2.4 -2.6		¹ AUBERT 03v	BABR	Repl. by AUBERT,B 06G
< 74	90	² GODANG 02	CLE2	$e^+e^- \rightarrow \Upsilon(4S)$
<900	90	ALBRECHT 91B	ARG	$e^+e^- \rightarrow \Upsilon(4S)$
¹ Assumes equal production of B^+ and B^0 at the $\Upsilon(4S)$.				
² Assumes a helicity 00 configuration. For a helicity 11 configuration, the limit decreases to 4.9×10^{-5} .				

$\Gamma(K^*(892)^+ f_0(980))/\Gamma_{total}$ Γ_{398}/Γ

VALUE (units 10^{-6})	DOCUMENT ID	TECN	COMMENT
4.2 ± 0.6 ± 0.3	¹ DEL-AMO-SA...11D	BABR	$e^+e^- \rightarrow \Upsilon(4S)$
••• We do not use the following data for averages, fits, limits, etc. •••			
5.2 ± 1.2 ± 0.5	¹ AUBERT,B 06G	BABR	Repl. by DEL-AMO-SANCHEZ 11D
¹ Assumes equal production of B^+ and B^0 at the $\Upsilon(4S)$.			

$\Gamma(a_1^+ K^0)/\Gamma_{total}$ Γ_{399}/Γ

VALUE (units 10^{-6})	DOCUMENT ID	TECN	COMMENT
34.9 ± 5.0 ± 4.4	^{1,2} AUBERT 08F	BABR	$e^+e^- \rightarrow \Upsilon(4S)$
¹ Assumes equal production of B^+ and B^0 at the $\Upsilon(4S)$.			
² Assumes a_1^\pm decays only to 3π and $B(a_1^\pm \rightarrow \pi^\pm \pi^+ \pi^\pm) = 0.5$.			

$\Gamma(b_1^+ K^0 \times B(b_1^+ \rightarrow \omega \pi^+))/\Gamma_{total}$ Γ_{400}/Γ

VALUE (units 10^{-6})	DOCUMENT ID	TECN	COMMENT
9.6 ± 1.7 ± 0.9	¹ AUBERT 08AG	BABR	$e^+e^- \rightarrow \Upsilon(4S)$
¹ Assumes equal production of B^+ and B^0 at the $\Upsilon(4S)$.			

$\Gamma(K^*(892)^0 \rho^+)/\Gamma_{total}$ Γ_{401}/Γ

VALUE (units 10^{-6})	DOCUMENT ID	TECN	COMMENT
9.2 ± 1.5	OUR AVERAGE		
9.6 ± 1.7 ± 1.5	¹ AUBERT,B 06G	BABR	$e^+e^- \rightarrow \Upsilon(4S)$
8.9 ± 1.7 ± 1.2	¹ ZHANG 05D	BELL	$e^+e^- \rightarrow \Upsilon(4S)$
¹ Assumes equal production of B^+ and B^0 at the $\Upsilon(4S)$.			

$\Gamma(K_1(1400)^+ \rho^0)/\Gamma_{total}$ Γ_{402}/Γ

VALUE	CL%	DOCUMENT ID	TECN	COMMENT
< 7.8 × 10⁻⁴	90	ALBRECHT 91B	ARG	$e^+e^- \rightarrow \Upsilon(4S)$

$\Gamma(K_S^0(1430)^+ \rho^0)/\Gamma_{total}$ Γ_{403}/Γ

VALUE	CL%	DOCUMENT ID	TECN	COMMENT
< 1.5 × 10⁻³	90	ALBRECHT 91B	ARG	$e^+e^- \rightarrow \Upsilon(4S)$

$\Gamma(b_1^0 K^+ \times B(b_1^0 \rightarrow \omega \pi^0))/\Gamma_{total}$ Γ_{404}/Γ

VALUE (units 10^{-6})	DOCUMENT ID	TECN	COMMENT
9.1 ± 1.7 ± 1.0	¹ AUBERT 07B1	BABR	$e^+e^- \rightarrow \Upsilon(4S)$
¹ Assumes equal production of B^+ and B^0 at the $\Upsilon(4S)$.			

$\Gamma(b_1^+ K^{*0} \times B(b_1^+ \rightarrow \omega \pi^+))/\Gamma_{total}$ Γ_{405}/Γ

VALUE	CL%	DOCUMENT ID	TECN	COMMENT
< 5.9 × 10⁻⁶	90	¹ AUBERT 09AF	BABR	$e^+e^- \rightarrow \Upsilon(4S)$
¹ Assumes equal production of B^+ and B^0 at the $\Upsilon(4S)$.				

$\Gamma(b_1^0 K^{*+} \times B(b_1^0 \rightarrow \omega \pi^0))/\Gamma_{total}$ Γ_{406}/Γ

VALUE	CL%	DOCUMENT ID	TECN	COMMENT
< 6.7 × 10⁻⁶	90	¹ AUBERT 09AF	BABR	$e^+e^- \rightarrow \Upsilon(4S)$
¹ Assumes equal production of B^+ and B^0 at the $\Upsilon(4S)$.				

$\Gamma(K^+ \bar{K}^0)/\Gamma_{total}$ Γ_{407}/Γ

VALUE (units 10^{-6})	CL%	DOCUMENT ID	TECN	COMMENT
1.31 ± 0.17		OUR FIT Error includes scale factor of 1.2.		
1.19 ± 0.18		OUR AVERAGE		
1.11 ± 0.19 ± 0.05		¹ DUH 13	BELL	$e^+e^- \rightarrow \Upsilon(4S)$
1.61 ± 0.44 ± 0.09		¹ AUBERT,BE 06c	BABR	$e^+e^- \rightarrow \Upsilon(4S)$
••• We do not use the following data for averages, fits, limits, etc. •••				
1.22 ± 0.32 ± 0.13 -0.28 - 0.16		¹ LIN 07	BELL	Repl. by DUH 13
1.0 ± 0.4 ± 0.1		¹ ABE 05G	BELL	Repl. by LIN 07
1.5 ± 0.5 ± 0.1		¹ AUBERT,BE 05E	BABR	Repl. by AUBERT,BE 06c

Meson Particle Listings

B^\pm

< 2.5	90	¹ AUBERT	04M	BABR	Repl. by AUBERT, BE 05E
< 3.3	90	¹ CHAO	04	BELL	$e^+e^- \rightarrow \Upsilon(4S)$
< 3.3	90	¹ BORNHEIM	03	CLE2	$e^+e^- \rightarrow \Upsilon(4S)$
< 2.0	90	¹ CASEY	02	BELL	Repl. by CHAO 04
< 5.0	90	¹ ABE	01H	BELL	$e^+e^- \rightarrow \Upsilon(4S)$
< 2.4	90	¹ AUBERT	01E	BABR	$e^+e^- \rightarrow \Upsilon(4S)$
< 5.1	90	¹ CRONIN-HEN...	00	CLE2	$e^+e^- \rightarrow \Upsilon(4S)$
< 21	90	GODANG	98	CLE2	Repl. by CRONIN-HENNESSY 00

¹ Assumes equal production of B^+ and B^0 at the $\Upsilon(4S)$.

$\Gamma(K^+ \bar{K}^0)/\Gamma(K^0 \pi^+)$				$\Gamma_{407}/\Gamma_{346}$
VALUE	DOCUMENT ID	TECN	COMMENT	
0.055 ± 0.007 OUR FIT			Error includes scale factor of 1.2.	
0.064 ± 0.009 ± 0.004	AAIJ	13Bs	LHCB pp at 7 TeV	

$\Gamma(\bar{K}^0 K^+ \pi^0)/\Gamma_{total}$				Γ_{408}/Γ
VALUE	CL%	DOCUMENT ID	TECN	COMMENT
< 24 × 10⁻⁶	90	¹ ECKHART	02	CLE2 $e^+e^- \rightarrow \Upsilon(4S)$

¹ Assumes equal production of B^+ and B^0 at the $\Upsilon(4S)$.

$\Gamma(K^+ K_S^0 K_S^0)/\Gamma_{total}$				Γ_{409}/Γ
VALUE (units 10 ⁻⁶)	DOCUMENT ID	TECN	COMMENT	
10.5 ± 0.4 OUR AVERAGE				
10.42 ± 0.43 ± 0.22	¹ KALIYAR	19	BELL $e^+e^- \rightarrow \Upsilon(4S)$	
10.6 ± 0.5 ± 0.3	^{1,2} LEES	12o	BABR $e^+e^- \rightarrow \Upsilon(4S)$	

• • • We do not use the following data for averages, fits, limits, etc. • • •

10.7 ± 1.2 ± 1.0	¹ AUBERT, B	04v	BABR	Repl. by LEES 12o
13.4 ± 1.9 ± 1.5	¹ GARMASH	04	BELL	Repl. by KALIYAR 19

¹ Assumes equal production of B^+ and B^0 at the $\Upsilon(4S)$.
² All intermediate charmonium and charm resonances are removed, except of χ_{c0} .

$\Gamma(f_0(980) K^+, f_0 \rightarrow K_S^0 K_S^0)/\Gamma_{total}$				Γ_{410}/Γ
VALUE (units 10 ⁻⁶)	DOCUMENT ID	TECN	COMMENT	
14.7 ± 2.8 ± 1.8	¹ LEES	12o	BABR $e^+e^- \rightarrow \Upsilon(4S)$	

¹ Assumes equal production of B^+ and B^0 at the $\Upsilon(4S)$.

$\Gamma(f_0(1710) K^+, f_0 \rightarrow K_S^0 K_S^0)/\Gamma_{total}$				Γ_{411}/Γ
VALUE (units 10 ⁻⁶)	DOCUMENT ID	TECN	COMMENT	
0.40 ± 0.40 ± 0.11	¹ LEES	12o	BABR $e^+e^- \rightarrow \Upsilon(4S)$	

¹ Assumes equal production of B^+ and B^0 at the $\Upsilon(4S)$.

$\Gamma(K^+ K_S^0 K_S^0 \text{ nonresonant})/\Gamma_{total}$				Γ_{412}/Γ
VALUE (units 10 ⁻⁶)	DOCUMENT ID	TECN	COMMENT	
19.8 ± 3.7 ± 2.5	¹ LEES	12o	BABR $e^+e^- \rightarrow \Upsilon(4S)$	

¹ Assumes equal production of B^+ and B^0 at the $\Upsilon(4S)$.

$\Gamma(K_S^0 K_S^0 \pi^+)/\Gamma_{total}$				Γ_{413}/Γ
VALUE	CL%	DOCUMENT ID	TECN	COMMENT
< 5.1 × 10⁻⁷	90	¹ AUBERT	09j	BABR $e^+e^- \rightarrow \Upsilon(4S)$

• • • We do not use the following data for averages, fits, limits, etc. • • •

< 8.7 × 10 ⁻⁷	¹ KALIYAR	19	BELL	$e^+e^- \rightarrow \Upsilon(4S)$
< 3.2 × 10 ⁻⁶	90	¹ GARMASH	04	BELL $e^+e^- \rightarrow \Upsilon(4S)$

¹ Assumes equal production of B^+ and B^0 at the $\Upsilon(4S)$.

$\Gamma(K^+ K^- \pi^+)/\Gamma(K^+ K^- K^+)$				$\Gamma_{414}/\Gamma_{426}$
VALUE	DOCUMENT ID	TECN	COMMENT	
0.151 ± 0.004 ± 0.008	AAIJ	20Aj	LHCB pp at 7 and 8 TeV	

$\Gamma(K^+ K^- \pi^+)/\Gamma_{total}$				Γ_{414}/Γ
VALUE (units 10 ⁻⁶)	CL%	DOCUMENT ID	TECN	COMMENT
5.2 ± 0.4 OUR AVERAGE				
5.38 ± 0.40 ± 0.35	^{1,2} HSU	17	BELL	$e^+e^- \rightarrow \Upsilon(4S)$
5.0 ± 0.5 ± 0.5	² AUBERT	07Bv	BABR	$e^+e^- \rightarrow \Upsilon(4S)$

• • • We do not use the following data for averages, fits, limits, etc. • • •

< 13	90	² GARMASH	04	BELL $e^+e^- \rightarrow \Upsilon(4S)$
< 6.3	90	^{2,3} AUBERT	03M	BABR Repl. by AUBERT 07Bv
< 12	90	⁴ GARMASH	02	BELL $e^+e^- \rightarrow \Upsilon(4S)$

¹ HSU 17 provides also measurement as a function of $K^+ K^-$ invariant mass.
² Assumes equal production of B^+ and B^0 at the $\Upsilon(4S)$.
³ Charm and charmonium contributions are subtracted, otherwise no assumptions about intermediate resonances.
⁴ Uses a reference decay mode $B^+ \rightarrow \bar{D}^0 \pi^+$ and $\bar{D}^0 \rightarrow K^+ \pi^-$ with $B(B^+ \rightarrow \bar{D}^0 \pi^+) \cdot B(\bar{D}^0 \rightarrow K^+ \pi^-) = (20.3 \pm 2.0) \times 10^{-5}$.

$\Gamma(K^+ K^- \pi^+ \text{ nonresonant})/\Gamma_{total}$				Γ_{415}/Γ
VALUE (units 10 ⁻⁶)	CL%	DOCUMENT ID	TECN	COMMENT
1.68 ± 0.23 ± 0.13		¹ AAIJ	19AL	LHCB pp at 7, 8 TeV

• • • We do not use the following data for averages, fits, limits, etc. • • •

< 75	90	BERGFELD	96B	CLE2 $e^+e^- \rightarrow \Upsilon(4S)$
¹ AAIJ 19AL reports $0.323 \pm 0.015 \pm 0.041$ fit fraction for $B^+ \rightarrow K^+ K^- \pi^+$ nonresonant from the amplitude analysis of $B^\pm \rightarrow \pi^\pm K^+ K^-$ decays. We use the PDG 19 value $B(B^+ \rightarrow K^+ K^- \pi^+) = (5.2 \pm 0.4) \times 10^{-6}$ to obtain $B(B^+ \rightarrow K^+ K^- \pi^+ \text{ nonresonant})$. Our first error is the experiment's error and the second error is systematic error from using our best value.				

$\Gamma(K^+ \bar{K}^*(892)^0)/\Gamma_{total}$				Γ_{416}/Γ
VALUE (units 10 ⁻⁷)	CL%	DOCUMENT ID	TECN	COMMENT
5.9 ± 0.6 ± 0.5		¹ AAIJ	19AL	LHCB pp at 7, 8 TeV

• • • We do not use the following data for averages, fits, limits, etc. • • •

< 11	90	² AUBERT	07AR	BABR $e^+e^- \rightarrow \Upsilon(4S)$
< 1290	90	ABBIENDI	00B	OPAL $e^+e^- \rightarrow Z$
< 1380	90	³ ABE	00C	SLD $e^+e^- \rightarrow Z$
< 53	90	² JESSOP	00	CLE2 $e^+e^- \rightarrow \Upsilon(4S)$

¹ AAIJ 19AL reports $(7.5 \pm 0.6 \pm 0.5) \times 10^{-2}$ fit fraction for $B^+ \rightarrow K^+ \bar{K}^*(892)^0$ from the amplitude analysis of $B^\pm \rightarrow \pi^\pm K^+ K^-$ decays. We use the PDG 19 value $B(B^+ \rightarrow K^+ K^- \pi^+) = (5.2 \pm 0.4) \times 10^{-6}$ to obtain $B(B^+ \rightarrow K^+ \bar{K}^*(892)^0)$, $\bar{K}^*(892)^0 \rightarrow K^+ \pi^-$. We compute $B(B^+ \rightarrow K^+ \bar{K}^*(892)^0)$ using 2/3 of $B(\bar{K}^*(892)^0 \rightarrow (K\pi)^0) = (99.754 \pm 0.021)\%$ for the $K^+ \pi^-$ fraction. Our first error is the experiment's error and the second error is systematic error from using our best value.
² Assumes equal production of B^+ and B^0 at the $\Upsilon(4S)$.
³ ABE 00c assumes $B(Z \rightarrow b\bar{b}) = (21.7 \pm 0.1)\%$ and the B fractions $f_{B^0} = f_{B^+} = (39.7 \pm 1.8)\%$ and $f_{B_s} = (10.5 \pm 1.8)\%$.

$\Gamma(K^+ \bar{K}_0^*(1430)^0)/\Gamma_{total}$				Γ_{417}/Γ
VALUE (units 10 ⁻⁶)	CL%	DOCUMENT ID	TECN	COMMENT
0.38 ± 0.12 ± 0.05		¹ AAIJ	19AL	LHCB pp at 7, 8 TeV

• • • We do not use the following data for averages, fits, limits, etc. • • •

< 2.2	90	² AUBERT	07AR	BABR $e^+e^- \rightarrow \Upsilon(4S)$
¹ AAIJ 19AL reports $(4.5 \pm 0.7 \pm 1.2) \times 10^{-2}$ for fit fraction for $B^+ \rightarrow K^+ \bar{K}_0^*(1430)^0$ from the amplitude analysis of $B^\pm \rightarrow \pi^\pm K^+ K^-$ decays. We use the PDG 19 value $B(B^+ \rightarrow K^+ K^- \pi^+) = (5.2 \pm 0.4) \times 10^{-6}$ to obtain $B(B^+ \rightarrow K^+ \bar{K}_0^*(1430)^0)$, $\bar{K}_0^*(1430)^0 \rightarrow K^+ \pi^-$. We compute $B(B^+ \rightarrow K^+ \bar{K}_0^*(1430)^0)$ using 2/3 of PDG 19 value $B(K_S^*(1430)^0 \rightarrow K\pi) = (93 \pm 10)\%$ for the $K^+ \pi^-$ fraction. Our first error is the experiment's error and the second error is systematic error from using our best value. ² Assumes equal production of B^+ and B^0 at the $\Upsilon(4S)$.				

$\Gamma(\rho(1450)^0 \pi^+, \rho^0 \rightarrow K^+ K^-)/\Gamma_{total}$				Γ_{473}/Γ
VALUE (units 10 ⁻⁶)	CL%	DOCUMENT ID	TECN	COMMENT
1.60 ± 0.08 ± 0.12		¹ AAIJ	19AL	LHCB pp at 7, 8 TeV

¹ AAIJ 19AL reports $0.307 \pm 0.012 \pm 0.009$ fit fraction for $B^+ \rightarrow \rho(1450)^0 \pi^+$ from the amplitude analysis of $B^\pm \rightarrow \pi^\pm K^+ K^-$ decays. We use the PDG 19 value $B(B^+ \rightarrow K^+ K^- \pi^+) = (5.2 \pm 0.4) \times 10^{-6}$ to obtain $B(B^+ \rightarrow \rho(1450)^0 \pi^+)$, $\rho(1450)^0 \rightarrow K^+ K^-$. Our first error is the experiment's error and the second error is systematic error from using our best value.

$\Gamma(\pi^+ (K^+ K^-) S\text{-wave})/\Gamma_{total}$				Γ_{418}/Γ
VALUE (units 10 ⁻⁷)	CL%	DOCUMENT ID	TECN	COMMENT
8.53 ± 0.67 ± 0.66		¹ AAIJ	19AL	LHCB pp at 7, 8 TeV

¹ AAIJ 19AL reports $0.164 \pm 0.008 \pm 0.01$ fit fraction for $B^+ \rightarrow \pi^+ (K^+ K^-)_{S\text{-wave}}$ in the region of $0.95 < m(K^+ K^-) < 1.42$ GeV/c² from the amplitude analysis of $B^\pm \rightarrow \pi^\pm K^+ K^-$ decays. We use the PDG 19 value $B(B^+ \rightarrow K^+ K^- \pi^+) = (5.2 \pm 0.4) \times 10^{-6}$ to obtain $B(B^+ \rightarrow \pi^+ (K^+ K^-)_{S\text{-wave}})$. Our first error is the experiment's error and the second error is systematic error from using our best value.

$\Gamma(K^+ K^+ \pi^-)/\Gamma_{total}$				Γ_{419}/Γ
VALUE	CL%	DOCUMENT ID	TECN	COMMENT
< 1.1 × 10⁻⁸	90	AAIJ	17E	LHCB pp at 7, 8 TeV

• • • We do not use the following data for averages, fits, limits, etc. • • •

< 1.6 × 10 ⁻⁷	90	¹ AUBERT	08BE	BABR $e^+e^- \rightarrow \Upsilon(4S)$
< 2.4 × 10 ⁻⁶	90	¹ GARMASH	04	BELL $e^+e^- \rightarrow \Upsilon(4S)$
< 1.3 × 10 ⁻⁶	90	² AUBERT	03M	BABR Repl. by AUBERT 08BE
< 3.2 × 10 ⁻⁶	90	³ GARMASH	02	BELL $e^+e^- \rightarrow \Upsilon(4S)$

¹ Assumes equal production of B^+ and B^0 at the $\Upsilon(4S)$.
² Assumes equal production of B^0 and B^+ at the $\Upsilon(4S)$; charm and charmonium contributions are subtracted, otherwise no assumptions about intermediate resonances.
³ Uses a reference decay mode $B^+ \rightarrow \bar{D}^0 \pi^+$ and $\bar{D}^0 \rightarrow K^+ \pi^-$ with $B(B^+ \rightarrow \bar{D}^0 \pi^+) \cdot B(\bar{D}^0 \rightarrow K^+ \pi^-) = (20.3 \pm 2.0) \times 10^{-5}$.

$\Gamma(K^+ K^+ \pi^- \text{ nonresonant})/\Gamma_{\text{total}}$ Γ_{420}/Γ

VALUE (units 10^{-6})	CL%	DOCUMENT ID	TECN	COMMENT
<87.9	90	ABBIENDI	00B	OPAL $e^+ e^- \rightarrow Z$

$\Gamma(f_2'(1525) K^+)/\Gamma_{\text{total}}$ Γ_{421}/Γ

VALUE (units 10^{-6})	CL%	DOCUMENT ID	TECN	COMMENT
1.8 ± 0.5 OUR AVERAGE				Error includes scale factor of 1.1.
1.56 ± 0.36 ± 0.30		1,2 LEES	120	BABR $e^+ e^- \rightarrow \Upsilon(4S)$
2.8 ± 0.9 ± 0.5		1,3 LEES	120	BABR $e^+ e^- \rightarrow \Upsilon(4S)$

• • • We do not use the following data for averages, fits, limits, etc. • • •

<8 90 1,4 GARMASH 05 BELL $e^+ e^- \rightarrow \Upsilon(4S)$

¹ Assumes equal production of B^+ and B^0 at the $\Upsilon(4S)$.
² Measured in the $B^+ \rightarrow K^+ K^- K^+$ decay.
³ Measured in the $B^+ \rightarrow K^+ K_S^0 K_S^0$ decay.
⁴ GARMASH 05 reports $B(B^+ \rightarrow f_2'(1525) K^+) \cdot B(f_2'(1525) \rightarrow K^+ K^-) < 4.9 \times 10^{-6}$ at 90% CL. We divide this result by our best value of $B(f_2'(1525) \rightarrow K \bar{K}) = 87.6 \times 10^{-2}$ multiplied by 2/3 to account for the $K^+ K^-$ fraction.

$\Gamma(K^+ f_J(2220))/\Gamma_{\text{total}}$ Γ_{422}/Γ

VALUE (units 10^{-6})	CL%	DOCUMENT ID	TECN	COMMENT
not seen		1 HUANG	03	BELL $e^+ e^- \rightarrow \Upsilon(4S)$

¹ No evidence is found for such decay and set a limit on $B(B^+ \rightarrow f_J(2220) \times B(f_J(2220) \rightarrow \phi\phi) < 1.2 \times 10^{-6}$ at 90%CL where the $f_J(2220)$ is a possible glueball state.

$\Gamma(K^*+ \pi^+ K^-)/\Gamma_{\text{total}}$ Γ_{423}/Γ

VALUE (units 10^{-6})	CL%	DOCUMENT ID	TECN	COMMENT
<11.8	90	1 AUBERT,B	06U	BABR $e^+ e^- \rightarrow \Upsilon(4S)$

¹ Assumes equal production of B^+ and B^0 at the $\Upsilon(4S)$.

$\Gamma(K^*(892)+ K^*(892)^0)/\Gamma_{\text{total}}$ Γ_{424}/Γ

VALUE (units 10^{-6})	CL%	DOCUMENT ID	TECN	COMMENT
0.91 ± 0.29 OUR AVERAGE				
0.77 ± 0.35 ± 0.12		1 GOH	15	BELL $e^+ e^- \rightarrow \Upsilon(4S)$
1.2 ± 0.5 ± 0.1		2 AUBERT	09F	BABR $e^+ e^- \rightarrow \Upsilon(4S)$

• • • We do not use the following data for averages, fits, limits, etc. • • •

<71 90 3 GODANG 02 CLE2 $e^+ e^- \rightarrow \Upsilon(4S)$

¹ Signal significance is 2.7 standard deviations. This measurement corresponds to an upper limit of $< 1.31 \times 10^{-6}$ at 90% CL.
² Signal significance is 3.7 standard deviations.
³ Assumes a helicity 00 configuration. For a helicity 11 configuration, the limit decreases to 4.8×10^{-5} .

$\Gamma(K^*+ K^+ \pi^-)/\Gamma_{\text{total}}$ Γ_{425}/Γ

VALUE (units 10^{-6})	CL%	DOCUMENT ID	TECN	COMMENT
<6.1	90	1 AUBERT,B	06U	BABR $e^+ e^- \rightarrow \Upsilon(4S)$

¹ Assumes equal production of B^+ and B^0 at the $\Upsilon(4S)$.

$\Gamma(K^+ K^- K^+)/\Gamma_{\text{total}}$ Γ_{426}/Γ

VALUE (units 10^{-6})	CL%	DOCUMENT ID	TECN	COMMENT
34.0 ± 1.4 OUR AVERAGE				Error includes scale factor of 1.4.
34.6 ± 0.6 ± 0.9		1,2 LEES	120	BABR $e^+ e^- \rightarrow \Upsilon(4S)$
30.6 ± 1.2 ± 2.3		1 GARMASH	05	BELL $e^+ e^- \rightarrow \Upsilon(4S)$

• • • We do not use the following data for averages, fits, limits, etc. • • •

35.2 ± 0.9 ± 1.6 1 AUBERT 060 BABR Repl. by LEES 120
 32.8 ± 1.8 ± 2.8 1 GARMASH 04 BELL Repl. by GARMASH 05
 29.6 ± 2.1 ± 1.6 3 AUBERT 03M BABR Repl. by AUBERT 060
 35.3 ± 3.7 ± 4.5 4 GARMASH 02 BELL Repl. by GARMASH 04
 <200 90 5 ADAM 96D DLPH $e^+ e^- \rightarrow Z$
 <320 90 5 ABREU 95N DLPH Sup. by ADAM 96D
 <350 90 ALBRECHT 91E ARG $e^+ e^- \rightarrow \Upsilon(4S)$

¹ Assumes equal production of B^+ and B^0 at the $\Upsilon(4S)$.
² All intermediate charmonium and charm resonances are removed, except of χ_{c0} .
³ Assumes equal production of B^0 and B^+ at the $\Upsilon(4S)$; charm and charmonium contributions are subtracted, otherwise no assumptions about intermediate resonances.
⁴ Uses a reference decay mode $B^+ \rightarrow \bar{D}^0 \pi^+$ and $\bar{D}^0 \rightarrow K^+ \pi^-$ with $B(B^+ \rightarrow \bar{D}^0 \pi^+) \cdot B(\bar{D}^0 \rightarrow K^+ \pi^-) = (20.3 \pm 2.0) \times 10^{-5}$.
⁵ Assumes B^0 and B^- production fractions of 0.39, and B_s production fraction of 0.12.

$\Gamma(K^+ \phi)/\Gamma_{\text{total}}$ Γ_{427}/Γ

VALUE (units 10^{-6})	CL%	DOCUMENT ID	TECN	COMMENT
8.8 ± 0.7 OUR AVERAGE				Error includes scale factor of 1.1.
9.2 ± 0.4 ± 0.7		1 LEES	120	BABR $e^+ e^- \rightarrow \Upsilon(4S)$
7.6 ± 1.3 ± 0.6		2 ACOSTA	05J	CDF $p\bar{p}$ at 1.96 TeV
9.60 ± 0.92 ± 1.05		1 GARMASH	05	BELL $e^+ e^- \rightarrow \Upsilon(4S)$
5.5 ± 2.1 ± 0.6		1 BRIERE	01	CLE2 $e^+ e^- \rightarrow \Upsilon(4S)$

• • • We do not use the following data for averages, fits, limits, etc. • • •

8.4 ± 0.7 ± 0.7		1 AUBERT	060	BABR Repl. by LEES 120
10.0 ± 0.9 ± 0.8		1 AUBERT	04A	BABR Repl. by AUBERT 060
9.4 ± 1.1 ± 0.7		1 CHEN	03B	BELL Repl. by GARMASH 05
14.6 ± 3.0 ± 2.8		3 GARMASH	02	BELL Repl. by CHEN 03B
7.7 ± 1.6 ± 1.4		1 AUBERT	01D	BABR $e^+ e^- \rightarrow \Upsilon(4S)$
<144	90	4 ABE	00c	SLD $e^+ e^- \rightarrow Z$
< 5	90	1 BERGFELD	98	CLE2
<280	90	5 ADAM	96D	DLPH $e^+ e^- \rightarrow Z$
< 12	90	ASNER	96	CLE2 $e^+ e^- \rightarrow \Upsilon(4S)$
<440	90	6 ABREU	95N	DLPH Sup. by ADAM 96D
<180	90	ALBRECHT	91B	ARG $e^+ e^- \rightarrow \Upsilon(4S)$
< 90	90	7 AVERY	89B	CLEO $e^+ e^- \rightarrow \Upsilon(4S)$
<210	90	AVERY	87	CLEO $e^+ e^- \rightarrow \Upsilon(4S)$

¹ Assumes equal production of B^+ and B^0 at the $\Upsilon(4S)$.
² Uses $B(B^+ \rightarrow J/\psi K^+) = (1.00 \pm 0.04) \times 10^{-3}$ and $B(J/\psi \rightarrow \mu^+ \mu^-) = 0.0588 \pm 0.0010$.
³ Uses a reference decay mode $B^+ \rightarrow \bar{D}^0 \pi^+$ and $\bar{D}^0 \rightarrow K^+ \pi^-$ with $B(B^+ \rightarrow \bar{D}^0 \pi^+) \cdot B(\bar{D}^0 \rightarrow K^+ \pi^-) = (20.3 \pm 2.0) \times 10^{-5}$.
⁴ ABE 00c assumes $B(Z \rightarrow b\bar{b}) = (21.7 \pm 0.1)\%$ and the B fractions $f_{B^0} = f_{B^+} = (39.7 \pm 1.8)_{-2.2}^{\pm 1.8}\%$ and $f_{B_s} = (10.5 \pm 1.8)_{-2.2}^{\pm 1.8}\%$.
⁵ ADAM 96D assumes $f_{B^0} = f_{B^-} = 0.39$ and $f_{B_s} = 0.12$.
⁶ Assumes a B^0, B^- production fraction of 0.39 and a B_s production fraction of 0.12.
⁷ AVERY 89B reports $< 8 \times 10^{-5}$ assuming the $\Upsilon(4S)$ decays 43% to $B^0 \bar{B}^0$. We rescale to 50%.

$\Gamma(f_0(980) K^+ \times B(f_0(980) \rightarrow K^+ K^-))/\Gamma_{\text{total}}$ Γ_{428}/Γ

VALUE (units 10^{-6})	CL%	DOCUMENT ID	TECN	COMMENT
9.4 ± 1.6 ± 2.8		1 LEES	120	BABR $e^+ e^- \rightarrow \Upsilon(4S)$

• • • We do not use the following data for averages, fits, limits, etc. • • •

6.5 ± 2.5 ± 1.6		1 AUBERT	060	BABR $e^+ e^- \rightarrow \Upsilon(4S)$
<2.9	90	1 GARMASH	05	BELL $e^+ e^- \rightarrow \Upsilon(4S)$

¹ Assumes equal production of B^+ and B^0 at the $\Upsilon(4S)$.

$\Gamma(a_2(1320) K^+ \times B(a_2(1320) \rightarrow K^+ K^-))/\Gamma_{\text{total}}$ Γ_{429}/Γ

VALUE (units 10^{-6})	CL%	DOCUMENT ID	TECN	COMMENT
<1.1 × 10⁻⁶	90	1 GARMASH	05	BELL $e^+ e^- \rightarrow \Upsilon(4S)$

¹ Assumes equal production of B^+ and B^0 at the $\Upsilon(4S)$.

$\Gamma(X_0(1550) K^+ \times B(X_0(1550) \rightarrow K^+ K^-))/\Gamma_{\text{total}}$ Γ_{430}/Γ

$X_0(1550)$ is a possible spin zero state near 1.55 GeV/ c^2 invariant mass of $K^+ K^-$.

VALUE (units 10^{-6})	CL%	DOCUMENT ID	TECN	COMMENT
4.3 ± 0.6 ± 0.3		1 AUBERT	060	BABR $e^+ e^- \rightarrow \Upsilon(4S)$

¹ Assumes equal production of B^+ and B^0 at the $\Upsilon(4S)$.

$\Gamma(\phi(1680) K^+ \times B(\phi(1680) \rightarrow K^+ K^-))/\Gamma_{\text{total}}$ Γ_{431}/Γ

VALUE (units 10^{-6})	CL%	DOCUMENT ID	TECN	COMMENT
<0.8 × 10⁻⁶	90	1 GARMASH	05	BELL $e^+ e^- \rightarrow \Upsilon(4S)$

¹ Assumes equal production of B^+ and B^0 at the $\Upsilon(4S)$.

$\Gamma(f_0(1710) K^+ \times B(f_0(1710) \rightarrow K^+ K^-))/\Gamma_{\text{total}}$ Γ_{432}/Γ

VALUE (units 10^{-6})	CL%	DOCUMENT ID	TECN	COMMENT
1.12 ± 0.25 ± 0.50		1 LEES	120	BABR $e^+ e^- \rightarrow \Upsilon(4S)$

• • • We do not use the following data for averages, fits, limits, etc. • • •

1.7 ± 1.0 ± 0.3 1 AUBERT 060 BABR Repl. by LEES 120

¹ Assumes equal production of B^+ and B^0 at the $\Upsilon(4S)$.

$\Gamma(K^+ K^- K^+ \text{ nonresonant})/\Gamma_{\text{total}}$ Γ_{433}/Γ

VALUE (units 10^{-6})	CL%	DOCUMENT ID	TECN	COMMENT
23.8 ± 2.8 OUR AVERAGE				
22.8 ± 2.7 ± 7.6		1 LEES	120	BABR $e^+ e^- \rightarrow \Upsilon(4S)$
24.0 ± 1.5 ± 2.6		1 GARMASH	05	BELL $e^+ e^- \rightarrow \Upsilon(4S)$

• • • We do not use the following data for averages, fits, limits, etc. • • •

50.0 ± 6.0 ± 4.0		1 AUBERT	060	BABR Repl. by LEES 120
<38	90	BERGFELD	96B	CLE2 $e^+ e^- \rightarrow \Upsilon(4S)$

¹ Assumes equal production of B^+ and B^0 at the $\Upsilon(4S)$.

$\Gamma(K^*(892)+ K^+ K^-)/\Gamma_{\text{total}}$ Γ_{434}/Γ

VALUE (units 10^{-6})	CL%	DOCUMENT ID	TECN	COMMENT
36.2 ± 3.3 ± 3.6		1 AUBERT,B	06U	BABR $e^+ e^- \rightarrow \Upsilon(4S)$

• • • We do not use the following data for averages, fits, limits, etc. • • •

<1600	90	ALBRECHT	91E	ARG $e^+ e^- \rightarrow \Upsilon(4S)$
-------	----	----------	-----	--

¹ Assumes equal production of B^+ and B^0 at the $\Upsilon(4S)$.

Meson Particle Listings

B^\pm

$\Gamma(K^*(892)^+\phi)/\Gamma_{total}$ Γ_{435}/Γ

VALUE (units 10^{-6})	CL%	DOCUMENT ID	TECN	COMMENT
10.0 ± 2.0 OUR AVERAGE		Error includes scale factor of 1.7.		
11.2 ± 1.0 ± 0.9		¹ AUBERT	07BA	BABR $e^+e^- \rightarrow \Upsilon(4S)$
6.7 $^{+2.1+0.7}_{-1.9-1.0}$		¹ CHEN	03B	BELL $e^+e^- \rightarrow \Upsilon(4S)$

• • • We do not use the following data for averages, fits, limits, etc. • • •

12.7 $^{+2.2}_{-2.0} \pm 1.1$		¹ AUBERT	03V	BABR Repl. by AUBERT 07BA
9.7 $^{+4.2}_{-3.4} \pm 1.7$		¹ AUBERT	01D	BABR Repl. by AUBERT 03V
< 22.5	90	¹ BRIERE	01	CLE2 $e^+e^- \rightarrow \Upsilon(4S)$
< 41	90	¹ BERGFELD	98	CLE2
< 70	90	ASNER	96	CLE2 $e^+e^- \rightarrow \Upsilon(4S)$
< 1300	90	ALBRECHT	91B	ARG $e^+e^- \rightarrow \Upsilon(4S)$

¹ Assumes equal production of B^+ and B^0 at the $\Upsilon(4S)$.

$\Gamma(\phi(K\pi)_0^{*+})/\Gamma_{total}$ Γ_{436}/Γ

($K\pi)_0^{*+}$ is the total S-wave composed of $K_0^*(1430)$ and nonresonant that are described using LASS shape.

VALUE (units 10^{-6})	DOCUMENT ID	TECN	COMMENT
8.3 ± 1.4 ± 0.8	¹ AUBERT	08BI	BABR $e^+e^- \rightarrow \Upsilon(4S)$

¹ Assumes equal production of B^+ and B^0 at the $\Upsilon(4S)$.

$\Gamma(\phi K_1(1270)^+)/\Gamma_{total}$ Γ_{437}/Γ

VALUE (units 10^{-6})	DOCUMENT ID	TECN	COMMENT
6.1 ± 1.6 ± 1.1	¹ AUBERT	08BI	BABR $e^+e^- \rightarrow \Upsilon(4S)$

¹ Assumes equal production of B^+ and B^0 at the $\Upsilon(4S)$.

$\Gamma(\phi K_1(1400)^+)/\Gamma_{total}$ Γ_{438}/Γ

VALUE (units 10^{-6})	CL%	DOCUMENT ID	TECN	COMMENT
< 3.2	90	¹ AUBERT	08BI	BABR $e^+e^- \rightarrow \Upsilon(4S)$

• • • We do not use the following data for averages, fits, limits, etc. • • •

< 1100	90	ALBRECHT	91B	ARG $e^+e^- \rightarrow \Upsilon(4S)$
--------	----	----------	-----	---------------------------------------

¹ Assumes equal production of B^+ and B^0 at the $\Upsilon(4S)$.

$\Gamma(\phi K^*(1410)^+)/\Gamma_{total}$ Γ_{439}/Γ

VALUE (units 10^{-6})	CL%	DOCUMENT ID	TECN	COMMENT
< 4.3	90	¹ AUBERT	08BI	BABR $e^+e^- \rightarrow \Upsilon(4S)$

¹ Assumes equal production of B^+ and B^0 at the $\Upsilon(4S)$.

$\Gamma(\phi K_0^*(1430)^+)/\Gamma_{total}$ Γ_{440}/Γ

VALUE (units 10^{-6})	DOCUMENT ID	TECN	COMMENT
7.0 ± 1.3 ± 0.9	¹ AUBERT	08BI	BABR $e^+e^- \rightarrow \Upsilon(4S)$

¹ Assumes equal production of B^+ and B^0 at the $\Upsilon(4S)$.

$\Gamma(\phi K_2^*(1430)^+)/\Gamma_{total}$ Γ_{441}/Γ

VALUE (units 10^{-6})	CL%	DOCUMENT ID	TECN	COMMENT
8.4 ± 1.8 ± 1.0		¹ AUBERT	08BI	BABR $e^+e^- \rightarrow \Upsilon(4S)$

• • • We do not use the following data for averages, fits, limits, etc. • • •

< 3400	90	ALBRECHT	91B	ARG $e^+e^- \rightarrow \Upsilon(4S)$
--------	----	----------	-----	---------------------------------------

¹ Assumes equal production of B^+ and B^0 at the $\Upsilon(4S)$.

$\Gamma(\phi K_2^*(1770)^+)/\Gamma_{total}$ Γ_{442}/Γ

VALUE (units 10^{-6})	CL%	DOCUMENT ID	TECN	COMMENT
< 15.0	90	¹ AUBERT	08BI	BABR $e^+e^- \rightarrow \Upsilon(4S)$

¹ Assumes equal production of B^+ and B^0 at the $\Upsilon(4S)$.

$\Gamma(\phi K_2^*(1820)^+)/\Gamma_{total}$ Γ_{443}/Γ

VALUE (units 10^{-6})	CL%	DOCUMENT ID	TECN	COMMENT
< 16.3	90	¹ AUBERT	08BI	BABR $e^+e^- \rightarrow \Upsilon(4S)$

¹ Assumes equal production of B^+ and B^0 at the $\Upsilon(4S)$.

$\Gamma(a_1^+ K^{*0})/\Gamma_{total}$ Γ_{444}/Γ

VALUE (units 10^{-6})	CL%	DOCUMENT ID	TECN	COMMENT
< 3.6	90	^{1,2} DEL-AMO-SA..10I	BABR	$e^+e^- \rightarrow \Upsilon(4S)$

¹ Assumes $B(a_1^+ \rightarrow \pi^+ \pi^+ \pi^-) = 0.5$

² Assumes equal production of B^+ and B^0 at the $\Upsilon(4S)$.

$\Gamma(K^+\phi)/\Gamma_{total}$ Γ_{445}/Γ

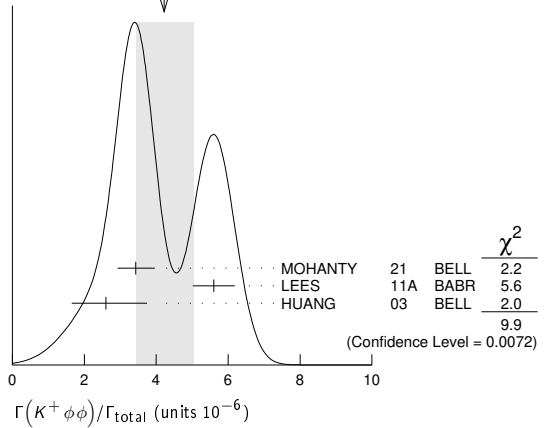
VALUE (units 10^{-6})	DOCUMENT ID	TECN	COMMENT
4.2 ± 0.8 OUR AVERAGE	Error includes scale factor of 2.2. See the ideogram below.		

3.4 $^{+0.48}_{-0.46} \pm 0.22$	¹ MOHANTY	21	BELL $e^+e^- \rightarrow \Upsilon(4S)$
5.6 ± 0.5 ± 0.3	¹ LEES	11A	BABR $e^+e^- \rightarrow \Upsilon(4S)$
2.6 $^{+1.1}_{-0.9} \pm 0.3$	¹ HUANG	03	BELL $e^+e^- \rightarrow \Upsilon(4S)$

• • • We do not use the following data for averages, fits, limits, etc. • • •

7.5 ± 1.0 ± 0.7	¹ AUBERT, BE	06H	BABR Repl. by LEES 11A
-----------------	-------------------------	-----	------------------------

WEIGHTED AVERAGE
4.2 ± 0.8 (Error scaled by 2.2)



¹ Assumes equal production of B^0 and B^+ at the $\Upsilon(4S)$ and the $\phi\phi$ invariant mass below 2.85 GeV/ c^2 .

$\Gamma(\eta'\eta'K^+)/\Gamma_{total}$ Γ_{446}/Γ

VALUE (units 10^{-6})	CL%	DOCUMENT ID	TECN	COMMENT
< 25	90	¹ AUBERT, B	06P	BABR $e^+e^- \rightarrow \Upsilon(4S)$

¹ Assumes equal production of B^+ and B^0 at the $\Upsilon(4S)$.

$\Gamma(\omega\phi K^+)/\Gamma_{total}$ Γ_{447}/Γ

VALUE (units 10^{-6})	CL%	DOCUMENT ID	TECN	COMMENT
< 1.9	90	¹ LIU	09	BELL $e^+e^- \rightarrow \Upsilon(4S)$

¹ Assumes equal production of B^+ and B^0 at the $\Upsilon(4S)$.

$\Gamma(X(1812)K^+ \times B(X \rightarrow \omega\phi))/\Gamma_{total}$ Γ_{448}/Γ

VALUE (units 10^{-6})	CL%	DOCUMENT ID	TECN	COMMENT
< 0.32	90	¹ LIU	09	BELL $e^+e^- \rightarrow \Upsilon(4S)$

¹ Assumes equal production of B^+ and B^0 at the $\Upsilon(4S)$.

$\Gamma(K^*(892)^+\gamma)/\Gamma_{total}$ Γ_{449}/Γ

VALUE (units 10^{-5})	CL%	DOCUMENT ID	TECN	COMMENT
3.92 ± 0.22 OUR AVERAGE		Error includes scale factor of 1.7.		

3.76 ± 0.10 ± 0.12	¹ HORIGUCHI	17	BELL $e^+e^- \rightarrow \Upsilon(4S)$
4.22 ± 0.14 ± 0.16	² AUBERT	09AO	BABR $e^+e^- \rightarrow \Upsilon(4S)$
3.76 $^{+0.89}_{-0.83} \pm 0.28$	³ COAN	00	CLE2 $e^+e^- \rightarrow \Upsilon(4S)$

• • • We do not use the following data for averages, fits, limits, etc. • • •

3.87 ± 0.28 ± 0.26	⁴ AUBERT, BE	04A	BABR Repl. by AUBERT 09AO	
4.25 ± 0.31 ± 0.24	³ NAKAO	04	BELL Repl. by HORIGUCHI 17	
3.83 ± 0.62 ± 0.22	³ AUBERT	02C	BABR Repl. by AUBERT, BE 04A	
5.7 ± 3.1 ± 1.1	⁵ AMMAR	93	CLE2 Repl. by COAN 00	
< 55	90	⁶ ALBRECHT	89G	ARG $e^+e^- \rightarrow \Upsilon(4S)$
< 55	90	⁶ AVERY	89B	CLEO $e^+e^- \rightarrow \Upsilon(4S)$
< 180	90	AVERY	87	CLEO $e^+e^- \rightarrow \Upsilon(4S)$

¹ Uses $B(\Upsilon(4S) \rightarrow B^+B^-) = (51.4 \pm 0.6)\%$ and $B(\Upsilon(4S) \rightarrow B^0\bar{B}^0) = (48.6 \pm 0.6)\%$.

² Uses $B(\Upsilon(4S) \rightarrow B^+B^-) = (51.6 \pm 0.6)\%$ and $B(\Upsilon(4S) \rightarrow B^0\bar{B}^0) = (48.4 \pm 0.6)\%$.

³ Assumes equal production of B^+ and B^0 at the $\Upsilon(4S)$.

⁴ Uses the production ratio of charged and neutral B from $\Upsilon(4S)$ decays $R^{+0} = 1.006 \pm 0.048$.

⁵ AMMAR 93 observed 4.1 ± 2.3 events above background.

⁶ Assumes the $\Upsilon(4S)$ decays 43% to $B^0\bar{B}^0$.

$\Gamma(K_1(1270)^+\gamma)/\Gamma_{total}$ Γ_{450}/Γ

VALUE (units 10^{-5})	CL%	DOCUMENT ID	TECN	COMMENT
4.4 $^{+0.7}_{-0.6}$ OUR AVERAGE				

4.41 $^{+0.63}_{-0.44} \pm 0.58$	^{1,2} DEL-AMO-SA..16	BABR	$e^+e^- \rightarrow \Upsilon(4S)$
4.3 ± 0.9 ± 0.9	³ YANG	05	BELL $e^+e^- \rightarrow \Upsilon(4S)$

• • • We do not use the following data for averages, fits, limits, etc. • • •

< 9.9	90	³ NISHIDA	02	BELL Repl. by YANG 05
< 730	90	⁴ ALBRECHT	89G	ARG $e^+e^- \rightarrow \Upsilon(4S)$

¹ Requires $M_{K\pi\pi} < 1.8$ GeV/ c^2 .

² Uses $B(\Upsilon(4S) \rightarrow B^+B^-) = 0.513 \pm 0.006$.

³ Assumes equal production of B^+ and B^0 at the $\Upsilon(4S)$.

⁴ ALBRECHT 89G reports < 0.0066 assuming the $\Upsilon(4S)$ decays 45% to $B^0\bar{B}^0$. We rescale to 50%.

$\Gamma(\eta K^+\gamma)/\Gamma_{total}$ Γ_{451}/Γ

VALUE (units 10^{-6})	DOCUMENT ID	TECN	COMMENT
7.9 ± 0.9 OUR AVERAGE			

7.7 ± 1.0 ± 0.4	^{1,2} AUBERT	09	BABR $e^+e^- \rightarrow \Upsilon(4S)$
8.4 ± 1.5 $^{+1.2}_{-0.9}$	^{2,3} NISHIDA	05	BELL $e^+e^- \rightarrow \Upsilon(4S)$

See key on page 1127

Meson Particle Listings

B^\pm

• • • We do not use the following data for averages, fits, limits, etc. • • •
 $10.0 \pm 1.3 \pm 0.5$ ^{1,2}AUBERT,B 06M BABR Repl. by AUBERT 09

- ¹ $m_{\eta K} < 3.25 \text{ GeV}/c^2$.
- ² Assumes equal production of B^+ and B^0 at the $\Upsilon(4S)$.
- ³ $m_{\eta K} < 2.4 \text{ GeV}/c^2$

$\Gamma(\eta' K^+ \gamma)/\Gamma_{\text{total}}$		Γ_{452}/Γ	
VALUE (units 10^{-6})	DOCUMENT ID	TECN	COMMENT
2.9 ± 1.0	OUR AVERAGE		

$3.6 \pm 1.2 \pm 0.4$ ^{1,2} WEDD 10 BELL $e^+ e^- \rightarrow \Upsilon(4S)$
 $1.9 \pm 1.5 \pm 0.1$ ^{1,3} AUBERT,B 06M BABR $e^+ e^- \rightarrow \Upsilon(4S)$

- ¹ Assumes equal production of B^+ and B^0 at the $\Upsilon(4S)$.
- ² $m_{\eta' K} < 3.4 \text{ GeV}/c^2$.
- ³ Set the upper limit of 4.2×10^{-6} at 90% CL with $m_{\eta' K} < 3.25 \text{ GeV}/c^2$.

$\Gamma(\phi K^+ \gamma)/\Gamma_{\text{total}}$		Γ_{453}/Γ	
VALUE (units 10^{-6})	DOCUMENT ID	TECN	COMMENT
2.7 ± 0.4	OUR AVERAGE		Error includes scale factor of 1.2.

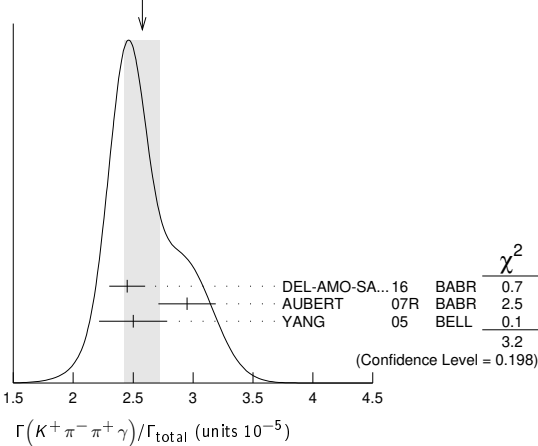
$2.48 \pm 0.30 \pm 0.24$ ¹ SAHOO 11A BELL $e^+ e^- \rightarrow \Upsilon(4S)$
 $3.5 \pm 0.6 \pm 0.4$ ¹ AUBERT 07Q BABR $e^+ e^- \rightarrow \Upsilon(4S)$
 • • • We do not use the following data for averages, fits, limits, etc. • • •
 $3.4 \pm 0.9 \pm 0.4$ ¹ DRUTSKOY 04 BELL Repl. by SAHOO 11A

- ¹ Assumes equal production of B^+ and B^0 at $\Upsilon(4S)$.

$\Gamma(K^+ \pi^- \pi^+ \gamma)/\Gamma_{\text{total}}$		Γ_{454}/Γ	
VALUE (units 10^{-5})	DOCUMENT ID	TECN	COMMENT
2.56 ± 0.15	OUR AVERAGE		Error includes scale factor of 1.3. See the ideogram below.

$2.45 \pm 0.09 \pm 0.12$ ^{1,2} DEL-AMO-SA..16 BABR $e^+ e^- \rightarrow \Upsilon(4S)$
 $2.95 \pm 0.13 \pm 0.20$ ^{1,3} AUBERT 07R BABR $e^+ e^- \rightarrow \Upsilon(4S)$
 $2.50 \pm 0.18 \pm 0.22$ ^{3,4} YANG 05 BELL $e^+ e^- \rightarrow \Upsilon(4S)$
 • • • We do not use the following data for averages, fits, limits, etc. • • •
 $2.4 \pm 0.5 \pm 0.4$ ^{3,5} NISHIDA 02 BELL Repl. by YANG 05

WEIGHTED AVERAGE
 2.58 ± 0.15 (Error scaled by 1.3)



- ¹ $M_{K\pi\pi} < 1.8 \text{ GeV}/c^2$.
- ² Uses $B(\Upsilon(4S) \rightarrow B^+ B^-) = 0.513 \pm 0.006$.
- ³ Assumes equal production of B^+ and B^0 at the $\Upsilon(4S)$.
- ⁴ $M_{K\pi\pi} < 2.0 \text{ GeV}/c^2$.
- ⁵ $M_{K\pi\pi} < 2.4 \text{ GeV}/c^2$.

$\Gamma(K^*(892)^0 \pi^+ \gamma)/\Gamma_{\text{total}}$		Γ_{455}/Γ	
VALUE (units 10^{-5})	DOCUMENT ID	TECN	COMMENT
2.33 ± 0.12	OUR AVERAGE		

$2.34 \pm 0.09 \pm 0.08$ ^{1,2} DEL-AMO-SA..16 BABR $e^+ e^- \rightarrow \Upsilon(4S)$
 $2.0 \pm 0.7 \pm 0.2$ ^{3,4} NISHIDA 02 BELL $e^+ e^- \rightarrow \Upsilon(4S)$

- ¹ Requires $M_{K\pi\pi} < 1.8 \text{ GeV}/c^2$.
- ² Uses $B(\Upsilon(4S) \rightarrow B^+ B^-) = 0.513 \pm 0.006$.
- ³ Assumes equal production of B^+ and B^0 at the $\Upsilon(4S)$.
- ⁴ $M_{K\pi\pi} < 2.4 \text{ GeV}/c^2$.

$\Gamma(K^+ \rho^0 \gamma)/\Gamma_{\text{total}}$		Γ_{456}/Γ	
VALUE (units 10^{-6})	CL%	DOCUMENT ID	TECN COMMENT
$8.2 \pm 0.4 \pm 0.8$		^{1,2} DEL-AMO-SA..16	BABR $e^+ e^- \rightarrow \Upsilon(4S)$

• • • We do not use the following data for averages, fits, limits, etc. • • •
 < 20 90 ^{3,4} NISHIDA 02 BELL $e^+ e^- \rightarrow \Upsilon(4S)$
¹ Requires $M_{K\pi\pi} < 1.8 \text{ GeV}/c^2$.
² Uses $B(\Upsilon(4S) \rightarrow B^+ B^-) = 0.513 \pm 0.006$.
³ Assumes equal production of B^+ and B^0 at the $\Upsilon(4S)$.
⁴ $M_{K\pi\pi} < 2.4 \text{ GeV}/c^2$.

$\Gamma((K^+ \pi^-)_{NR} \pi^+ \gamma)/\Gamma_{\text{total}}$		Γ_{457}/Γ	
VALUE (units 10^{-6})	CL%	DOCUMENT ID	TECN COMMENT
$9.9 \pm 0.7 \pm 1.5$		^{1,2} DEL-AMO-SA..16	BABR $e^+ e^- \rightarrow \Upsilon(4S)$

• • • We do not use the following data for averages, fits, limits, etc. • • •
 < 9.2 90 ^{3,4} NISHIDA 02 BELL $e^+ e^- \rightarrow \Upsilon(4S)$
¹ Requires $M_{K\pi\pi} < 1.8 \text{ GeV}/c^2$.
² Uses $B(\Upsilon(4S) \rightarrow B^+ B^-) = 0.513 \pm 0.006$.
³ Assumes equal production of B^+ and B^0 at the $\Upsilon(4S)$.
⁴ $M_{K\pi\pi} < 2.4 \text{ GeV}/c^2$.

$\Gamma(K^0 \pi^+ \pi^0 \gamma)/\Gamma_{\text{total}}$		Γ_{458}/Γ	
VALUE (units 10^{-5})	DOCUMENT ID	TECN	COMMENT
$4.56 \pm 0.42 \pm 0.31$		^{1,2} AUBERT 07R	BABR $e^+ e^- \rightarrow \Upsilon(4S)$

- ¹ $M_{K\pi\pi} < 1.8 \text{ GeV}/c^2$.
- ² Assumes equal production of B^+ and B^0 at the $\Upsilon(4S)$.

$\Gamma(K_1^*(1400)^+ \gamma)/\Gamma_{\text{total}}$		Γ_{459}/Γ	
VALUE (units 10^{-6})	CL%	DOCUMENT ID	TECN COMMENT
$9.7 \pm 4.6 \pm 2.9$		^{1,2} DEL-AMO-SA..16	BABR $e^+ e^- \rightarrow \Upsilon(4S)$

• • • We do not use the following data for averages, fits, limits, etc. • • •
 < 15 90 ³ YANG 05 BELL $e^+ e^- \rightarrow \Upsilon(4S)$
 < 50 90 ³ NISHIDA 02 BELL Repl. by YANG 05
 < 2200 90 ⁴ ALBRECHT 89G ARG $e^+ e^- \rightarrow \Upsilon(4S)$
¹ Requires $M_{K\pi\pi} < 1.8 \text{ GeV}/c^2$.
² Uses $B(\Upsilon(4S) \rightarrow B^+ B^-) = 0.513 \pm 0.006$.
³ Assumes equal production of B^+ and B^0 at the $\Upsilon(4S)$.
⁴ ALBRECHT 89G reports < 0.0020 assuming the $\Upsilon(4S)$ decays 45% to $B^0 \bar{B}^0$. We rescale to 50%.

$\Gamma(K^*(1410)^+ \gamma)/\Gamma_{\text{total}}$		Γ_{460}/Γ	
VALUE (units 10^{-5})	DOCUMENT ID	TECN	COMMENT
$2.71 \pm 0.54 \pm 0.59$		^{1,2} DEL-AMO-SA..16	BABR $e^+ e^- \rightarrow \Upsilon(4S)$

- ¹ Requires $M_{K\pi\pi} < 1.8 \text{ GeV}/c^2$.
- ² Uses $B(\Upsilon(4S) \rightarrow B^+ B^-) = 0.513 \pm 0.006$.

$\Gamma(K_0^*(1430)^0 \pi^+ \gamma)/\Gamma_{\text{total}}$		Γ_{461}/Γ	
VALUE (units 10^{-6})	DOCUMENT ID	TECN	COMMENT
$1.32 \pm 0.09 \pm 0.24$		^{1,2} DEL-AMO-SA..16	BABR $e^+ e^- \rightarrow \Upsilon(4S)$

- ¹ Requires $M_{K\pi\pi} < 1.8 \text{ GeV}/c^2$.
- ² Uses $B(\Upsilon(4S) \rightarrow B^+ B^-) = 0.513 \pm 0.006$.

$\Gamma(K_2^*(1430)^+ \gamma)/\Gamma_{\text{total}}$		Γ_{462}/Γ	
VALUE (units 10^{-5})	CL%	DOCUMENT ID	TECN COMMENT
1.4 ± 0.4	OUR AVERAGE		

$0.87 \pm 0.70 \pm 0.87$ ^{1,2} DEL-AMO-SA..16 BABR $e^+ e^- \rightarrow \Upsilon(4S)$
 $1.45 \pm 0.40 \pm 0.15$ ³ AUBERT,B 04U BABR $e^+ e^- \rightarrow \Upsilon(4S)$
 • • • We do not use the following data for averages, fits, limits, etc. • • •
 < 140 90 ⁴ ALBRECHT 89G ARG $e^+ e^- \rightarrow \Upsilon(4S)$

- ¹ Requires $M_{K\pi\pi} < 1.8 \text{ GeV}/c^2$.
- ² Uses $B(\Upsilon(4S) \rightarrow B^+ B^-) = 0.513 \pm 0.006$.
- ³ Assumes equal production of B^+ and B^0 at the $\Upsilon(4S)$.
- ⁴ ALBRECHT 89G reports < 0.0013 assuming the $\Upsilon(4S)$ decays 45% to $B^0 \bar{B}^0$. We rescale to 50%.

$\Gamma(K^*(1680)^+ \gamma)/\Gamma_{\text{total}}$		Γ_{463}/Γ	
VALUE (units 10^{-5})	CL%	DOCUMENT ID	TECN COMMENT
$6.67 \pm 0.93 \pm 1.44$		^{1,2} DEL-AMO-SA..16	BABR $e^+ e^- \rightarrow \Upsilon(4S)$

• • • We do not use the following data for averages, fits, limits, etc. • • •
 < 190 90 ³ ALBRECHT 89G ARG $e^+ e^- \rightarrow \Upsilon(4S)$
¹ Requires $M_{K\pi\pi} < 1.8 \text{ GeV}/c^2$.
² Uses $B(\Upsilon(4S) \rightarrow B^+ B^-) = 0.513 \pm 0.006$.
³ ALBRECHT 89G reports < 0.0017 assuming the $\Upsilon(4S)$ decays 45% to $B^0 \bar{B}^0$. We rescale to 50%.

Meson Particle Listings

B^\pm

$\Gamma(K_S^0(1780)^+ \gamma)/\Gamma_{total}$ Γ_{464}/Γ

VALUE (units 10^{-6})	CL%	DOCUMENT ID	TECN	COMMENT
< 39	90	1,2 NISHIDA	05 BELL	$e^+ e^- \rightarrow \Upsilon(4S)$
••• We do not use the following data for averages, fits, limits, etc. •••				
<5500	90	3 ALBRECHT	89G ARG	$e^+ e^- \rightarrow \Upsilon(4S)$
¹ Assumes equal production of B^+ and B^0 at the $\Upsilon(4S)$. ² Uses $B(K_S^0(1780) \rightarrow \eta K) = 0.11^{+0.05}_{-0.04}$. ³ ALBRECHT 89G reports < 0.005 assuming the $\Upsilon(4S)$ decays 45% to $B^0 \bar{B}^0$. We rescale to 50%.				

$\Gamma(K_S^0(2045)^+ \gamma)/\Gamma_{total}$ Γ_{465}/Γ

VALUE	CL%	DOCUMENT ID	TECN	COMMENT
<0.0099	90	1 ALBRECHT	89G ARG	$e^+ e^- \rightarrow \Upsilon(4S)$
¹ ALBRECHT 89G reports < 0.0090 assuming the $\Upsilon(4S)$ decays 45% to $B^0 \bar{B}^0$. We rescale to 50%.				

$\Gamma(\rho^+ \gamma)/\Gamma_{total}$ Γ_{466}/Γ

VALUE (units 10^{-6})	CL%	DOCUMENT ID	TECN	COMMENT
0.98 ± 0.25 OUR AVERAGE				
1.20 ± 0.42 ± 0.20		1 AUBERT	08BH BABR	$e^+ e^- \rightarrow \Upsilon(4S)$
0.87 ± 0.29 ± 0.09 -0.27 -0.11		1 TANIGUCHI	08 BELL	$e^+ e^- \rightarrow \Upsilon(4S)$
••• We do not use the following data for averages, fits, limits, etc. •••				
1.10 ± 0.37 ± 0.09 -0.33		1 AUBERT	07L BABR	Repl. by AUBERT 08BH
0.55 ± 0.42 ± 0.09 -0.36 -0.08		1 MOHAPATRA	06 BELL	Repl. by TANIGUCHI 08
0.9 ± 0.6 ± 0.1 -0.5	90	1 AUBERT	05 BABR	Repl. by AUBERT 07L
< 2.2	90	1 MOHAPATRA	05 BELL	$e^+ e^- \rightarrow \Upsilon(4S)$
< 2.1	90	1 AUBERT	04C BABR	$e^+ e^- \rightarrow \Upsilon(4S)$
<13	90	1,2 COAN	00 CLE2	$e^+ e^- \rightarrow \Upsilon(4S)$
¹ Assumes equal production of B^+ and B^0 at $\Upsilon(4S)$. ² No evidence for a nonresonant $K \pi \gamma$ contamination was seen; the central value assumes no contamination.				

$\Gamma(\pi^+ \pi^0)/\Gamma_{total}$ Γ_{467}/Γ

VALUE (units 10^{-6})	CL%	DOCUMENT ID	TECN	COMMENT
5.5 ± 0.4 OUR AVERAGE				Error includes scale factor of 1.2.
5.86 ± 0.26 ± 0.38		1 DUH	13 BELL	$e^+ e^- \rightarrow \Upsilon(4S)$
5.02 ± 0.46 ± 0.29		1 AUBERT	07bc BABR	$e^+ e^- \rightarrow \Upsilon(4S)$
4.6 ± 1.8 ± 0.6 -1.6 -0.7		1 BORNHEIM	03 CLE2	$e^+ e^- \rightarrow \Upsilon(4S)$
••• We do not use the following data for averages, fits, limits, etc. •••				
6.5 ± 0.4 ± 0.4		1 LIN	07A BELL	Repl. by DUH 13
5.8 ± 0.6 ± 0.4		1 AUBERT	05L BABR	Repl. by AUBERT 07bc
5.0 ± 1.2 ± 0.5		1 CHAO	04 BELL	Repl. by LIN 07A
5.5 ± 1.0 ± 0.6 -1.9		1 AUBERT	03L BABR	Repl. by AUBERT 05L
7.4 ± 2.3 ± 0.9 -2.2		1 CASEY	02 BELL	Repl. by CHAO 04
< 13.4	90	1 ABE	01H BELL	$e^+ e^- \rightarrow \Upsilon(4S)$
< 9.6	90	1 AUBERT	01E BABR	$e^+ e^- \rightarrow \Upsilon(4S)$
< 12.7	90	1 CRONIN-HEN.	00 CLE2	$e^+ e^- \rightarrow \Upsilon(4S)$
< 20	90	GODANG	98 CLE2	Repl. by CRONIN-HENNESSY 00
< 17	90	ASNER	96 CLE2	Repl. by GODANG 98
< 240	90	1 ALBRECHT	90B ARG	$e^+ e^- \rightarrow \Upsilon(4S)$
<2300	90	2 BEBEK	87 CLEO	$e^+ e^- \rightarrow \Upsilon(4S)$
¹ Assumes equal production of B^+ and B^0 at the $\Upsilon(4S)$. ² BEBEK 87 assume the $\Upsilon(4S)$ decays 43% to $B^0 \bar{B}^0$.				

$\Gamma(\pi^+ \pi^0)/\Gamma(K^0 \pi^+)$ $\Gamma_{467}/\Gamma_{346}$

VALUE	DOCUMENT ID	TECN	COMMENT
0.285 ± 0.02 ± 0.02	LIN	07A BELL	$e^+ e^- \rightarrow \Upsilon(4S)$

$\Gamma(\pi^+ \pi^+ \pi^-)/\Gamma(K^+ K^- K^+)$ $\Gamma_{468}/\Gamma_{426}$

VALUE	DOCUMENT ID	TECN	COMMENT
0.488 ± 0.005 ± 0.009	AAIJ	20AJ LHCB	pp at 7 and 8 TeV

$\Gamma(\pi^+ \pi^+ \pi^-)/\Gamma_{total}$ Γ_{468}/Γ

VALUE (units 10^{-6})	CL%	DOCUMENT ID	TECN	COMMENT
15.2 ± 0.6 ± 1.3 -1.2		1 AUBERT	09L BABR	$e^+ e^- \rightarrow \Upsilon(4S)$
••• We do not use the following data for averages, fits, limits, etc. •••				
16.2 ± 1.2 ± 0.9		1 AUBERT,B	05G BABR	Repl. by AUBERT 09L
10.9 ± 3.3 ± 1.6		1 AUBERT	03M BABR	Repl. by AUBERT 05G
<130	90	2 ADAM	96D DLPH	$e^+ e^- \rightarrow Z$
<220	90	3 ABREU	95N DLPH	Sup. by ADAM 96D
<450	90	4 ALBRECHT	90B ARG	$e^+ e^- \rightarrow \Upsilon(4S)$
<190	90	5 BORTOLETTO89	CLEO	$e^+ e^- \rightarrow \Upsilon(4S)$
¹ Assumes equal production of B^0 and B^+ at the $\Upsilon(4S)$; charm and charmonium contributions are subtracted, otherwise no assumptions about intermediate resonances. ² ADAM 96D assumes $f_{B^0} = f_{B^-} = 0.39$ and $f_{B_s} = 0.12$. ³ Assumes a B^0, B^- production fraction of 0.39 and a B_s production fraction of 0.12. ⁴ ALBRECHT 90B limit assumes equal production of $B^0 \bar{B}^0$ and $B^+ B^-$ at $\Upsilon(4S)$. ⁵ BORTOLETTO 89 reports < 1.7×10^{-4} assuming the $\Upsilon(4S)$ decays 43% to $B^0 \bar{B}^0$. We rescale to 50%.				

$\Gamma(\rho^0 \pi^+)/\Gamma_{total}$ Γ_{469}/Γ

VALUE (units 10^{-6})	CL%	DOCUMENT ID	TECN	COMMENT
8.3 ± 1.2 OUR AVERAGE				
8.1 ± 0.7 ± 1.3 -2.0 -1.6		1 AUBERT	09L BABR	$e^+ e^- \rightarrow \Upsilon(4S)$
8.0 ± 2.3 ± 0.7		1 GORDON	02 BELL	$e^+ e^- \rightarrow \Upsilon(4S)$
10.4 ± 3.3 ± 2.1 -3.4		1 JESSOP	00 CLE2	$e^+ e^- \rightarrow \Upsilon(4S)$
••• We do not use the following data for averages, fits, limits, etc. •••				
8.8 ± 1.0 ± 0.6 -0.9		1 AUBERT,B	05G BABR	Repl. by AUBERT 09L
9.5 ± 1.1 ± 0.9		1 AUBERT	04Z BABR	Repl. by AUBERT 05G
< 83	90	2 ABE	00c SLD	$e^+ e^- \rightarrow Z$
<160	90	3 ADAM	96D DLPH	$e^+ e^- \rightarrow Z$
< 43	90	ASNER	96 CLE2	Repl. by JESSOP 00
<260	90	4 ABREU	95N DLPH	Sup. by ADAM 96D
<150	90	1 ALBRECHT	90B ARG	$e^+ e^- \rightarrow \Upsilon(4S)$
<170	90	5 BORTOLETTO89	CLEO	$e^+ e^- \rightarrow \Upsilon(4S)$
<230	90	5 BEBEK	87 CLEO	$e^+ e^- \rightarrow \Upsilon(4S)$
<600	90	GILES	84 CLEO	Repl. by BEBEK 87

¹ Assumes equal production of B^+ and B^0 at the $\Upsilon(4S)$.
² ABE 00c assumes $B(Z \rightarrow b\bar{b}) = (21.7 \pm 0.1)\%$ and the B fractions $f_{B^0} = f_{B^+} = (39.7 \pm 1.8, 2.2)\%$ and $f_{B_s} = (10.5 \pm 1.8, 2.2)\%$.
³ ADAM 96D assumes $f_{B^0} = f_{B^-} = 0.39$ and $f_{B_s} = 0.12$.
⁴ Assumes a B^0, B^- production fraction of 0.39 and a B_s production fraction of 0.12.
⁵ Papers assume the $\Upsilon(4S)$ decays 43% to $B^0 \bar{B}^0$. We rescale to 50%.

$[\Gamma(K^*(892)^0 \pi^+) + \Gamma(\rho^0 \pi^+)]/\Gamma_{total}$ $(\Gamma_{372} + \Gamma_{469})/\Gamma$

VALUE (units 10^{-6})	DOCUMENT ID	TECN	COMMENT
170 ± 120 ± 20	1 ADAM	96D DLPH	$e^+ e^- \rightarrow Z$

¹ ADAM 96D assumes $f_{B^0} = f_{B^-} = 0.39$ and $f_{B_s} = 0.12$.

$\Gamma(\pi^+ f_0(980), f_0 \rightarrow \pi^+ \pi^-)/\Gamma_{total}$ Γ_{470}/Γ

VALUE (units 10^{-6})	CL%	DOCUMENT ID	TECN	COMMENT
< 1.5	90	1 AUBERT	09L BABR	$e^+ e^- \rightarrow \Upsilon(4S)$
••• We do not use the following data for averages, fits, limits, etc. •••				
< 3.0	90	1 AUBERT,B	05G BABR	Repl. by AUBERT 09L
<140	90	2 BORTOLETTO89	CLEO	$e^+ e^- \rightarrow \Upsilon(4S)$

¹ Assumes equal production of B^+ and B^0 at the $\Upsilon(4S)$.
² BORTOLETTO 89 reports < 1.2×10^{-4} assuming the $\Upsilon(4S)$ decays 43% to $B^0 \bar{B}^0$. We rescale to 50%.

$\Gamma(\pi^+ f_2(1270))/\Gamma_{total}$ Γ_{471}/Γ

VALUE (units 10^{-6})	CL%	DOCUMENT ID	TECN	COMMENT
2.2 ± 0.7 ± 0.4 OUR AVERAGE				
17.0 ± 2.4 ± 2.1		1 AAJ	19AL LHCB	pp at 7, 8 TeV
1.60 ± 0.67 ± 0.02 -0.44 -0.06		2,3 AUBERT	09L BABR	$e^+ e^- \rightarrow \Upsilon(4S)$

••• We do not use the following data for averages, fits, limits, etc. •••

4.10 ± 1.28 ± 0.04 -0.14		3,4 AUBERT,B	05G BABR	Repl. by AUBERT 09L
<240	90	5 BORTOLETTO89	CLEO	$e^+ e^- \rightarrow \Upsilon(4S)$

¹ AAJ 19AL reports 0.075 ± 0.008 ± 0.007 fit fraction for $B^+ \rightarrow f_2(1270) \pi^+$ from the amplitude analysis of $B^\pm \rightarrow \pi^\pm K^+ K^-$ decays. We use the PDG 19 value $B(B^+ \rightarrow K^+ K^- \pi^+) = (5.2 \pm 0.4) \times 10^{-6}$ to obtain $B(B^+ \rightarrow f_2(1270) \pi^+, f_2(1270) \rightarrow K^+ K^-)$. We compute $B(B^+ \rightarrow f_2(1270) \pi^+)$ using 1/2 of PDG 19 value of $B(f_2(1270) \rightarrow K \bar{K}) = (4.6 \pm 0.5, 0.4)\%$ for $K^+ K^-$ fraction. Our first error is the experiment's error and the second error is systematic error from using our best value.
² AUBERT 09L reports $[\Gamma(B^+ \rightarrow \pi^+ f_2(1270))/\Gamma_{total}] \times [B(f_2(1270) \rightarrow \pi^+ \pi^-)] = (0.9 \pm 0.2 \pm 0.1 \pm 0.3, 0.1) \times 10^{-6}$ which we divide by our best value $B(f_2(1270) \rightarrow \pi^+ \pi^-) = (56.2 \pm 1.9, 0.6) \times 10^{-2}$. Our first error is their experiment's error and our second error is the systematic error from using our best value.
³ Assumes equal production of B^+ and B^0 at the $\Upsilon(4S)$.
⁴ AUBERT,B 05G reports $[\Gamma(B^+ \rightarrow \pi^+ f_2(1270))/\Gamma_{total}] \times [B(f_2(1270) \rightarrow \pi^+ \pi^-)] = (2.3 \pm 0.6 \pm 0.4) \times 10^{-6}$ which we divide by our best value $B(f_2(1270) \rightarrow \pi^+ \pi^-) = (56.2 \pm 1.9, 0.6) \times 10^{-2}$. Our first error is their experiment's error and our second error is the systematic error from using our best value.
⁵ BORTOLETTO 89 reports < 2.1×10^{-4} assuming the $\Upsilon(4S)$ decays 43% to $B^0 \bar{B}^0$. We rescale to 50%.

$\Gamma(\rho(1450)^0 \pi^+, \rho^0 \rightarrow \pi^+ \pi^-)/\Gamma_{total}$ Γ_{472}/Γ

VALUE (units 10^{-6})	CL%	DOCUMENT ID	TECN	COMMENT
1.4 ± 0.4 ± 0.5 ± 0.8		1 AUBERT	09L BABR	$e^+ e^- \rightarrow \Upsilon(4S)$

••• We do not use the following data for averages, fits, limits, etc. •••

<2.3	90	1 AUBERT,B	05G BABR	Repl. by AUBERT 09L
------	----	------------	----------	---------------------

¹ Assumes equal production of B^+ and B^0 at the $\Upsilon(4S)$.

See key on page 1127

Meson Particle Listings

B^{\pm}

$\Gamma(f_0(1370)\pi^+, f_0 \rightarrow \pi^+\pi^-)/\Gamma_{total}$ Γ_{474}/Γ

VALUE (units 10^{-6})	CL%	DOCUMENT ID	TECN	COMMENT
<4.0	90	¹ AUBERT 09L	BABR	$e^+e^- \rightarrow \Upsilon(4S)$
••• We do not use the following data for averages, fits, limits, etc. •••				
<3.0	90	¹ AUBERT,B 05G	BABR	Repl. by AUBERT 09L
¹ Assumes equal production of B^+ and B^0 at the $\Upsilon(4S)$.				

$\Gamma(f_0(500)\pi^+, f_0 \rightarrow \pi^+\pi^-)/\Gamma_{total}$ Γ_{475}/Γ

VALUE (units 10^{-6})	CL%	DOCUMENT ID	TECN	COMMENT
<4.1	90	¹ AUBERT,B 05G	BABR	$e^+e^- \rightarrow \Upsilon(4S)$
¹ Assumes equal production of B^+ and B^0 at the $\Upsilon(4S)$.				

$\Gamma(\pi^+\pi^-\pi^+\text{nonresonant})/\Gamma_{total}$ Γ_{476}/Γ

VALUE (units 10^{-6})	CL%	DOCUMENT ID	TECN	COMMENT
$5.3 \pm 0.7_{-0.8}$		¹ AUBERT 09L	BABR	$e^+e^- \rightarrow \Upsilon(4S)$
••• We do not use the following data for averages, fits, limits, etc. •••				
< 4.6	90	¹ AUBERT,B 05G	BABR	Repl. by AUBERT 09L
<41	90	BERGFELD 96B	CLE2	$e^+e^- \rightarrow \Upsilon(4S)$
¹ Assumes equal production of B^+ and B^0 at the $\Upsilon(4S)$.				

$\Gamma(\pi^+\pi^0\pi^0)/\Gamma_{total}$ Γ_{477}/Γ

VALUE	CL%	DOCUMENT ID	TECN	COMMENT
$<8.9 \times 10^{-4}$	90	¹ ALBRECHT 90B	ARG	$e^+e^- \rightarrow \Upsilon(4S)$
¹ ALBRECHT 90B limit assumes equal production of $B^0\bar{B}^0$ and B^+B^- at $\Upsilon(4S)$.				

$\Gamma(\rho^+\pi^0)/\Gamma_{total}$ Γ_{478}/Γ

VALUE (units 10^{-6})	CL%	DOCUMENT ID	TECN	COMMENT
10.9 ± 1.4 OUR AVERAGE				
$10.2 \pm 1.4 \pm 0.9$		¹ AUBERT 07X	BABR	$e^+e^- \rightarrow \Upsilon(4S)$
$13.2 \pm 2.3_{-1.9}$		¹ ZHANG 05A	BELL	$e^+e^- \rightarrow \Upsilon(4S)$
••• We do not use the following data for averages, fits, limits, etc. •••				
$10.9 \pm 1.9 \pm 1.9$		¹ AUBERT 04Z	BABR	Repl. by AUBERT 07X
< 43	90	^{1,2} JESSOP 00	CLE2	$e^+e^- \rightarrow \Upsilon(4S)$
< 77	90	ASNER 96	CLE2	Repl. by JESSOP 00
<550	90	¹ ALBRECHT 90B	ARG	$e^+e^- \rightarrow \Upsilon(4S)$
¹ Assumes equal production of B^+ and B^0 at the $\Upsilon(4S)$.				
² Assumes no nonresonant contributions of $B^+ \rightarrow \pi^+\pi^0\pi^0$.				

$\Gamma(\pi^+\pi^-\pi^+\pi^0)/\Gamma_{total}$ Γ_{479}/Γ

VALUE	CL%	DOCUMENT ID	TECN	COMMENT
$<4.0 \times 10^{-3}$	90	¹ ALBRECHT 90B	ARG	$e^+e^- \rightarrow \Upsilon(4S)$
¹ ALBRECHT 90B limit assumes equal production of $B^0\bar{B}^0$ and B^+B^- at $\Upsilon(4S)$.				

$\Gamma(\rho^+\rho^0)/\Gamma_{total}$ Γ_{480}/Γ

VALUE (units 10^{-6})	CL%	DOCUMENT ID	TECN	COMMENT
24.0 ± 1.9 OUR AVERAGE				
$23.7 \pm 1.4 \pm 1.4$		¹ AUBERT 09G	BABR	$e^+e^- \rightarrow \Upsilon(4S)$
$31.7 \pm 7.1_{+3.8_{-6.7}}$		^{1,2} ZHANG 03B	BELL	$e^+e^- \rightarrow \Upsilon(4S)$
••• We do not use the following data for averages, fits, limits, etc. •••				
$16.8 \pm 2.2 \pm 2.3$		¹ AUBERT,BE 06G	BABR	Repl. by AUBERT 09G
$22.5_{-5.4}^{+5.7} \pm 5.8$		¹ AUBERT 03V	BABR	Repl. by AUBERT,BE 06G
< 1000	90	¹ ALBRECHT 90B	ARG	$e^+e^- \rightarrow \Upsilon(4S)$
¹ Assumes equal production of B^+ and B^0 at the $\Upsilon(4S)$.				
² The systematic error includes the error associated with the helicity-mix uncertainty.				

$\Gamma(\rho^+ f_0(980), f_0 \rightarrow \pi^+\pi^-)/\Gamma_{total}$ Γ_{481}/Γ

VALUE (units 10^{-6})	CL%	DOCUMENT ID	TECN	COMMENT
<2.0	90	¹ AUBERT 09G	BABR	$e^+e^- \rightarrow \Upsilon(4S)$
••• We do not use the following data for averages, fits, limits, etc. •••				
<1.9	90	¹ AUBERT,BE 06G	BABR	Repl. by AUBERT 09G
¹ Assumes equal production of B^+ and B^0 at the $\Upsilon(4S)$.				

$\Gamma(a_1(1260)^+\pi^0)/\Gamma_{total}$ Γ_{482}/Γ

VALUE (units 10^{-6})	CL%	DOCUMENT ID	TECN	COMMENT
26.4 ± 5.4 ± 4.1				
<1700	90	^{1,2} AUBERT 07BL	BABR	$e^+e^- \rightarrow \Upsilon(4S)$
••• We do not use the following data for averages, fits, limits, etc. •••				
<1700	90	¹ ALBRECHT 90B	ARG	$e^+e^- \rightarrow \Upsilon(4S)$
¹ Assumes equal production of B^+ and B^0 at the $\Upsilon(4S)$.				
² Assumes a_1^+ decays only to 3π and $B(a_1^+ \rightarrow \pi^\pm\pi^\mp\pi^+) = 0.5$.				

$\Gamma(a_1(1260)^0\pi^+)/\Gamma_{total}$ Γ_{483}/Γ

VALUE (units 10^{-6})	CL%	DOCUMENT ID	TECN	COMMENT
20.4 ± 4.7 ± 3.4				
<900	90	^{1,2} AUBERT 07BL	BABR	$e^+e^- \rightarrow \Upsilon(4S)$
••• We do not use the following data for averages, fits, limits, etc. •••				
<900	90	¹ ALBRECHT 90B	ARG	$e^+e^- \rightarrow \Upsilon(4S)$
¹ Assumes equal production of B^+ and B^0 at the $\Upsilon(4S)$.				
² Assumes a_1^0 decays only to 3π and $B(a_1^0 \rightarrow \pi^\pm\pi^\mp\pi^0) = 1.0$.				

$\Gamma(\omega\pi^+)/\Gamma_{total}$ Γ_{484}/Γ

VALUE (units 10^{-6})	CL%	DOCUMENT ID	TECN	COMMENT
6.9 ± 0.5 OUR AVERAGE				
$6.7 \pm 0.5 \pm 0.4$		¹ AUBERT 07AE	BABR	$e^+e^- \rightarrow \Upsilon(4S)$
$6.9 \pm 0.6 \pm 0.5$		¹ JEN 06	BELL	$e^+e^- \rightarrow \Upsilon(4S)$
$11.3_{-2.9}^{+3.3} \pm 1.4$		¹ JESSOP 00	CLE2	$e^+e^- \rightarrow \Upsilon(4S)$
••• We do not use the following data for averages, fits, limits, etc. •••				
$6.1 \pm 0.7 \pm 0.4$		¹ AUBERT,B 06E	BABR	Repl. by AUBERT 07AE
$5.5 \pm 0.9 \pm 0.5$		¹ AUBERT 04H	BABR	Repl. by AUBERT,B 06E
$5.7_{-1.3}^{+1.4} \pm 0.6$		¹ WANG 04A	BELL	Repl. by JEN 06
$4.2_{-1.8}^{+2.0} \pm 0.5$		¹ LU 02	BELL	Repl. by WANG 04A
$6.6_{-1.8}^{+2.1} \pm 0.7$		¹ AUBERT 01G	BABR	Repl. by AUBERT 04H
< 23	90	¹ BERGFELD 98	CLE2	Repl. by JESSOP 00
<400	90	¹ ALBRECHT 90B	ARG	$e^+e^- \rightarrow \Upsilon(4S)$
¹ Assumes equal production of B^+ and B^0 at the $\Upsilon(4S)$.				

$\Gamma(\omega\rho^+)/\Gamma_{total}$ Γ_{485}/Γ

VALUE (units 10^{-6})	CL%	DOCUMENT ID	TECN	COMMENT
15.9 ± 1.6 ± 1.4				
$10.6 \pm 2.1_{-1.0}^{+1.6}$		¹ AUBERT 09H	BABR	$e^+e^- \rightarrow \Upsilon(4S)$
$12.6_{-3.3}^{+3.7} \pm 1.6$		¹ AUBERT,B 06T	BABR	Repl. by AUBERT 09H
<61	90	¹ AUBERT 05O	BABR	Repl. by AUBERT,B 06T
<61	90	¹ BERGFELD 98	CLE2	
¹ Assumes equal production of B^+ and B^0 at the $\Upsilon(4S)$.				

$\Gamma(\eta\pi^+)/\Gamma_{total}$ Γ_{486}/Γ

VALUE (units 10^{-6})	CL%	DOCUMENT ID	TECN	COMMENT
4.02 ± 0.27 OUR AVERAGE				
$4.07 \pm 0.26 \pm 0.21$		¹ HOI 12	BELL	$e^+e^- \rightarrow \Upsilon(4S)$
$4.00 \pm 0.40 \pm 0.24$		¹ AUBERT 09AV	BABR	$e^+e^- \rightarrow \Upsilon(4S)$
$1.2_{-1.2}^{+2.8}$		¹ RICHICHI 00	CLE2	$e^+e^- \rightarrow \Upsilon(4S)$
••• We do not use the following data for averages, fits, limits, etc. •••				
$5.0 \pm 0.5 \pm 0.3$		¹ AUBERT 07AE	BABR	Repl. by AUBERT 09AV
$4.2 \pm 0.4 \pm 0.2$		¹ CHANG 07B	BELL	Repl. by HOI 12
$5.1 \pm 0.6 \pm 0.3$		¹ AUBERT,B 05K	BABR	Repl. by AUBERT 07AE
$4.8 \pm 0.7 \pm 0.3$		¹ CHANG 05A	BELL	Repl. by CHANG 07B
$5.3 \pm 1.0 \pm 0.3$		¹ AUBERT 04H	BABR	Repl. by AUBERT,B 05K
< 15	90	BEHRENS 98	CLE2	Repl. by RICHICHI 00
<700	90	¹ ALBRECHT 90B	ARG	$e^+e^- \rightarrow \Upsilon(4S)$
¹ Assumes equal production of B^+ and B^0 at the $\Upsilon(4S)$.				

$\Gamma(\eta\rho^+)/\Gamma_{total}$ Γ_{487}/Γ

VALUE (units 10^{-6})	CL%	DOCUMENT ID	TECN	COMMENT
7.0 ± 2.9 OUR AVERAGE				Error includes scale factor of 2.8.
$9.9 \pm 1.2 \pm 0.8$		¹ AUBERT 08AH	BABR	$e^+e^- \rightarrow \Upsilon(4S)$
$4.1_{-1.3}^{+1.4} \pm 0.4$		¹ WANG 07B	BELL	$e^+e^- \rightarrow \Upsilon(4S)$
••• We do not use the following data for averages, fits, limits, etc. •••				
$8.4 \pm 1.9 \pm 1.1$		¹ AUBERT,B 05K	BABR	Repl. by AUBERT 08AH
<14	90	¹ AUBERT,B 04D	BABR	Repl. by AUBERT,B 05K
<15	90	¹ RICHICHI 00	CLE2	$e^+e^- \rightarrow \Upsilon(4S)$
<32	90	BEHRENS 98	CLE2	Repl. by RICHICHI 00
¹ Assumes equal production of B^+ and B^0 at the $\Upsilon(4S)$.				

$\Gamma(\eta'\pi^+)/\Gamma_{total}$ Γ_{488}/Γ

VALUE (units 10^{-6})	CL%	DOCUMENT ID	TECN	COMMENT
2.7 ± 0.9 OUR AVERAGE				Error includes scale factor of 1.9.
$3.5 \pm 0.6 \pm 0.2$		¹ AUBERT 09AV	BABR	$e^+e^- \rightarrow \Upsilon(4S)$
$1.76_{-0.62}^{+0.67} \pm 0.15$		¹ SCHUEMANN 06	BELL	$e^+e^- \rightarrow \Upsilon(4S)$
••• We do not use the following data for averages, fits, limits, etc. •••				
$3.9 \pm 0.7 \pm 0.3$		¹ AUBERT 07AE	BABR	Repl. by AUBERT 09AV
$4.0 \pm 0.8 \pm 0.4$		¹ AUBERT,B 05K	BABR	Repl. by AUBERT 07AE
< 4.5	90	¹ AUBERT 04H	BABR	Repl. by AUBERT,B 05K
< 7.0	90	¹ ABE 01M	BELL	$e^+e^- \rightarrow \Upsilon(4S)$
<12	90	¹ AUBERT 01G	BABR	$e^+e^- \rightarrow \Upsilon(4S)$
<12	90	¹ RICHICHI 00	CLE2	$e^+e^- \rightarrow \Upsilon(4S)$
<31	90	BEHRENS 98	CLE2	Repl. by RICHICHI 00
¹ Assumes equal production of B^+ and B^0 at the $\Upsilon(4S)$.				

$\Gamma(\eta'\rho^+)/\Gamma_{total}$ Γ_{489}/Γ

VALUE (units 10^{-6})	CL%	DOCUMENT ID	TECN	COMMENT
9.7 ± 1.9 ± 1.1				
<900	90	¹ DEL-AMO-SA...10A	BABR	$e^+e^- \rightarrow \Upsilon(4S)$

Meson Particle Listings

 B^\pm

• • • We do not use the following data for averages, fits, limits, etc. • • •

VALUE (units 10^{-8})	CL%	DOCUMENT ID	TECN	COMMENT
$8.7^{+3.1+2.3}_{-2.8-1.3}$		¹ AUBERT 07E	BABR	Repl. by DEL-AMO-SANCHEZ 10A
< 5.8	90	¹ SCHUEMANN 07	BELL	$e^+e^- \rightarrow \Upsilon(4S)$
< 22	90	¹ AUBERT,B 04D	BABR	Repl. by AUBERT 07E
< 33	90	¹ RICHICHI 00	CLE2	$e^+e^- \rightarrow \Upsilon(4S)$
< 47	90	BEHRENS 98	CLE2	Repl. by RICHICHI 00

¹ Assumes equal production of B^+ and B^0 at the $\Upsilon(4S)$.

$\Gamma(\phi\pi^+)/\Gamma_{\text{total}}$ Γ_{490}/Γ				
VALUE (units 10^{-8})	CL%	DOCUMENT ID	TECN	COMMENT
$3.2 \pm 1.5 \pm 0.3$		¹ AAIJ 19AL	LHCB	pp at 7, 8 TeV

• • • We do not use the following data for averages, fits, limits, etc. • • •

VALUE (units 10^{-8})	CL%	DOCUMENT ID	TECN	COMMENT
< 15	90	² AAIJ 14A	LHCB	Repl. by AAIJ 19AL
< 33	90	³ KIM 12A	BELL	$e^+e^- \rightarrow \Upsilon(4S)$
< 24	90	³ AUBERT,B 06C	BABR	$e^+e^- \rightarrow \Upsilon(4S)$
< 41	90	³ AUBERT 04A	BABR	Repl. by AUBERT,B 06C
< 140	90	³ AUBERT 01D	BABR	$e^+e^- \rightarrow \Upsilon(4S)$
< 15 300	90	⁴ ABE 00C	SLD	$e^+e^- \rightarrow Z$
< 500	90	³ BERGFELD 98	CLE2	

¹ AAIJ 19AL reports $(0.3 \pm 0.1 \pm 0.1) \times 10^{-2}$ fit fraction for $B^+ \rightarrow \phi(1020)\pi^+$ from the amplitude analysis of $B^\pm \rightarrow \pi^\pm K^+ K^-$ decays. We use the PDG 19 value $B(B^+ \rightarrow K^+ K^- \pi^+) = (5.2 \pm 0.4) \times 10^{-6}$ to obtain $B(B^+ \rightarrow \phi(1020)\pi^+, \phi(1020) \rightarrow K^+ K^-)$. We compute $B(B^+ \rightarrow \phi(1020)\pi^+)$ using the PDG 19 value of $B(\phi(1020) \rightarrow K^+ K^-) = (49.2 \pm 0.5)\%$. Our first error is the experiment's error and the second error is systematic error from using our best value.

² Measures $B(B^+ \rightarrow \phi\pi^+)/B(B^+ \rightarrow \phi K^+) < 0.018$ at 90% C.L. and assumes $B(B^+ \rightarrow \phi K^+) = (8.8^{+0.7}_{-0.6}) \times 10^{-6}$.

³ Assumes equal production of B^+ and B^0 at the $\Upsilon(4S)$.

⁴ ABE 00c assumes $B(Z \rightarrow b\bar{b}) = (21.7 \pm 0.1)\%$ and the B fractions $f_{B^0} = f_{B^+} = (39.7^{+1.8}_{-2.2})\%$ and $f_{B_s} = (10.5^{+1.8}_{-2.2})\%$.

$\Gamma(\phi\rho^+)/\Gamma_{\text{total}}$ Γ_{491}/Γ				
VALUE (units 10^{-6})	CL%	DOCUMENT ID	TECN	COMMENT
< 3.0	90	¹ AUBERT 08BK	BABR	$e^+e^- \rightarrow \Upsilon(4S)$

• • • We do not use the following data for averages, fits, limits, etc. • • •

VALUE (units 10^{-6})	CL%	DOCUMENT ID	TECN	COMMENT
< 16		¹ BERGFELD 98	CLE2	

¹ Assumes equal production of B^+ and B^0 at the $\Upsilon(4S)$.

$\Gamma(a_0(980)^0\pi^+, a_0^0 \rightarrow \eta\pi^0)/\Gamma_{\text{total}}$ Γ_{492}/Γ				
VALUE (units 10^{-6})	CL%	DOCUMENT ID	TECN	COMMENT
< 5.8	90	¹ AUBERT,BE 04	BABR	$e^+e^- \rightarrow \Upsilon(4S)$

¹ Assumes equal production of charged and neutral B mesons from $\Upsilon(4S)$ decays.

$\Gamma(a_0(980)^+\pi^0, a_0^+ \rightarrow \eta\pi^+)/\Gamma_{\text{total}}$ Γ_{493}/Γ				
VALUE (units 10^{-6})	CL%	DOCUMENT ID	TECN	COMMENT
< 1.4	90	¹ AUBERT 08A	BABR	$e^+e^- \rightarrow \Upsilon(4S)$

¹ Assumes equal production of B^+ and B^0 at the $\Upsilon(4S)$.

$\Gamma(\pi^+\pi^+\pi^+\pi^-\pi^-)/\Gamma_{\text{total}}$ Γ_{494}/Γ				
VALUE	CL%	DOCUMENT ID	TECN	COMMENT
< 8.6×10^{-4}	90	¹ ALBRECHT 90B	ARG	$e^+e^- \rightarrow \Upsilon(4S)$

¹ ALBRECHT 90B limit assumes equal production of $B^0\bar{B}^0$ and B^+B^- at $\Upsilon(4S)$.

$\Gamma(\rho^0 a_1(1260)^+)/\Gamma_{\text{total}}$ Γ_{495}/Γ				
VALUE	CL%	DOCUMENT ID	TECN	COMMENT
< 6.2×10^{-4}	90	¹ BORTOLETTO89	CLEO	$e^+e^- \rightarrow \Upsilon(4S)$

• • • We do not use the following data for averages, fits, limits, etc. • • •

VALUE	CL%	DOCUMENT ID	TECN	COMMENT
< 6.0×10^{-4}	90	² ALBRECHT 90B	ARG	$e^+e^- \rightarrow \Upsilon(4S)$
< 3.2×10^{-3}	90	¹ BEBEK 87	CLEO	$e^+e^- \rightarrow \Upsilon(4S)$

¹ BORTOLETTO 89 reports $< 5.4 \times 10^{-4}$ assuming the $\Upsilon(4S)$ decays 43% to $B^0\bar{B}^0$. We rescale to 50%.

² ALBRECHT 90B limit assumes equal production of $B^0\bar{B}^0$ and B^+B^- at $\Upsilon(4S)$.

$\Gamma(\rho^0 a_2(1320)^+)/\Gamma_{\text{total}}$ Γ_{496}/Γ				
VALUE	CL%	DOCUMENT ID	TECN	COMMENT
< 7.2×10^{-4}	90	¹ BORTOLETTO89	CLEO	$e^+e^- \rightarrow \Upsilon(4S)$

• • • We do not use the following data for averages, fits, limits, etc. • • •

VALUE	CL%	DOCUMENT ID	TECN	COMMENT
< 2.6×10^{-3}	90	² BEBEK 87	CLEO	$e^+e^- \rightarrow \Upsilon(4S)$

¹ BORTOLETTO 89 reports $< 6.3 \times 10^{-4}$ assuming the $\Upsilon(4S)$ decays 43% to $B^0\bar{B}^0$. We rescale to 50%.

² BEBEK 87 reports $< 2.3 \times 10^{-3}$ assuming the $\Upsilon(4S)$ decays 43% to $B^0\bar{B}^0$. We rescale to 50%.

$\Gamma(b_1^0\pi^+, b_1^0 \rightarrow \omega\pi^0)/\Gamma_{\text{total}}$ Γ_{497}/Γ				
VALUE (units 10^{-6})	CL%	DOCUMENT ID	TECN	COMMENT
$6.7 \pm 1.7 \pm 1.0$		¹ AUBERT 07BI	BABR	$e^+e^- \rightarrow \Upsilon(4S)$

¹ Assumes equal production of B^+ and B^0 at the $\Upsilon(4S)$.

$\Gamma(b_1^+\pi^0, b_1^+ \rightarrow \omega\pi^+)/\Gamma_{\text{total}}$ Γ_{498}/Γ				
VALUE (units 10^{-6})	CL%	DOCUMENT ID	TECN	COMMENT
< 3.3	90	¹ AUBERT 08AG	BABR	$e^+e^- \rightarrow \Upsilon(4S)$

¹ Assumes equal production of B^+ and B^0 at the $\Upsilon(4S)$.

$\Gamma(\pi^+\pi^+\pi^+\pi^-\pi^-)/\Gamma_{\text{total}}$ Γ_{499}/Γ				
VALUE	CL%	DOCUMENT ID	TECN	COMMENT
< 6.3×10^{-3}	90	¹ ALBRECHT 90B	ARG	$e^+e^- \rightarrow \Upsilon(4S)$

¹ ALBRECHT 90B limit assumes equal production of $B^0\bar{B}^0$ and B^+B^- at $\Upsilon(4S)$.

$\Gamma(b_1^+\rho^0, b_1^+ \rightarrow \omega\pi^+)/\Gamma_{\text{total}}$ Γ_{500}/Γ				
VALUE	CL%	DOCUMENT ID	TECN	COMMENT
< 5.2×10^{-6}	90	¹ AUBERT 09AF	BABR	$e^+e^- \rightarrow \Upsilon(4S)$

¹ Assumes equal production of B^+ and B^0 at the $\Upsilon(4S)$.

$\Gamma(b_1^0\rho^+, b_1^0 \rightarrow \omega\pi^0)/\Gamma_{\text{total}}$ Γ_{502}/Γ				
VALUE	CL%	DOCUMENT ID	TECN	COMMENT
< 3.3×10^{-6}	90	¹ AUBERT 09AF	BABR	$e^+e^- \rightarrow \Upsilon(4S)$

¹ Assumes equal production of B^+ and B^0 at the $\Upsilon(4S)$.

$\Gamma(a_1(1260)^+ a_1(1260)^0)/\Gamma_{\text{total}}$ Γ_{501}/Γ				
VALUE	CL%	DOCUMENT ID	TECN	COMMENT
< 1.3×10^{-2}	90	¹ ALBRECHT 90B	ARG	$e^+e^- \rightarrow \Upsilon(4S)$

¹ ALBRECHT 90B limit assumes equal production of $B^0\bar{B}^0$ and B^+B^- at $\Upsilon(4S)$.

$\Gamma(h^+\pi^0)/\Gamma_{\text{total}}$ Γ_{503}/Γ				
VALUE (units 10^{-6})	CL%	DOCUMENT ID	TECN	COMMENT
$16^{+6}_{-5} \pm 3.6$		GODANG 98	CLE2	$e^+e^- \rightarrow \Upsilon(4S)$

$h^+ = K^+$ or π^+

$\Gamma(\omega h^+)/\Gamma_{\text{total}}$ Γ_{504}/Γ				
VALUE (units 10^{-6})	CL%	DOCUMENT ID	TECN	COMMENT
$13.8^{+2.7}_{-2.4}$ OUR AVERAGE				

VALUE	CL%	DOCUMENT ID	TECN	COMMENT
$13.4^{+3.3}_{-2.9} \pm 1.1$		¹ LU 02	BELL	$e^+e^- \rightarrow \Upsilon(4S)$
$14.3^{+3.6}_{-3.2} \pm 2.0$		¹ JESSOP 00	CLE2	$e^+e^- \rightarrow \Upsilon(4S)$

• • • We do not use the following data for averages, fits, limits, etc. • • •

VALUE	CL%	DOCUMENT ID	TECN	COMMENT
$25^{+8}_{-7} \pm 3$		¹ BERGFELD 98	CLE2	Repl. by JESSOP 00

¹ Assumes equal production of B^+ and B^0 at the $\Upsilon(4S)$.

$\Gamma(h^+X^0(\text{Familon}))/\Gamma_{\text{total}}$ Γ_{505}/Γ				
VALUE (units 10^{-6})	CL%	DOCUMENT ID	TECN	COMMENT
< 49	90	¹ AMMAR 01B	CLE2	$e^+e^- \rightarrow \Upsilon(4S)$

¹ AMMAR 01B searched for the two-body decay of the B meson to a massless neutral feebly-interacting particle X^0 such as the familon, the Nambu-Goldstone boson associated with a spontaneously broken global family symmetry.

$\Gamma(K^+X^0, X^0 \rightarrow \mu^+\mu^-)/\Gamma_{\text{total}}$ Γ_{506}/Γ				
VALUE	CL%	DOCUMENT ID	TECN	COMMENT
< 1×10^{-7}	95	¹ AAIJ 17AQ	LHCB	pp at 7, 8 TeV

X^0 stands here for a long-lived scalar particle.

¹ AAIJ 17AQ searched for a long-lived scalar particle $X^0 \rightarrow \mu^+\mu^-$ in the mass range 250–4700 MeV and lifetime range 0.1–1000 ps. The limit is between 10^{-7} and 2×10^{-10} in these ranges except in vetoed mass regions around K_S^0 , J/ψ , $\psi(2S)$, and $\psi(3770)$.

$\Gamma(\rho\bar{\rho}\pi^+)/\Gamma_{\text{total}}$ Γ_{507}/Γ				
VALUE (units 10^{-6})	CL%	DOCUMENT ID	TECN	COMMENT
1.62 ± 0.20 OUR AVERAGE				

VALUE	CL%	DOCUMENT ID	TECN	COMMENT
$1.60^{+0.22}_{-0.19} \pm 0.12$		^{1,2,3} WEI 08	BELL	$e^+e^- \rightarrow \Upsilon(4S)$
$1.69 \pm 0.29 \pm 0.26$		¹ AUBERT 07AV	BABR	$e^+e^- \rightarrow \Upsilon(4S)$

• • • We do not use the following data for averages, fits, limits, etc. • • •

VALUE	CL%	DOCUMENT ID	TECN	COMMENT
$1.07 \pm 0.11 \pm 0.11$		⁴ AAIJ 14AF	LHCB	pp at 7, 8 TeV
$3.06^{+0.73}_{-0.62} \pm 0.37$		^{1,3} WANG 04	BELL	Repl. by WEI 08

< 3.7 90 ^{1,2} ABE 02K BELL Repl. by WANG 04

< 500 90 ⁵ ABREU 95N DLPH Repl. by ADAM 96D

< 160 90 ⁶ BEBEK 89F CLEO $e^+e^- \rightarrow \Upsilon(4S)$

570 $\pm 150 \pm 210$ ⁷ ALBRECHT 88F ARG $e^+e^- \rightarrow \Upsilon(4S)$

¹ Assumes equal production of B^+ and B^0 at the $\Upsilon(4S)$.

² Explicitly vetoes resonant production of $\rho\bar{\rho}$ from Charmonium states.

³ Also provides results with $m_{\rho\bar{\rho}} < 2.85$ GeV/ c^2 and angular asymmetry of $\rho\bar{\rho}$ system.

⁴ Requires $m_{\rho\bar{\rho}} < 2.85$ GeV/ c^2 .

⁵ Assumes a B^0, B^- production fraction of 0.39 and a B_s production fraction of 0.12.

⁶ BEBEK 89 reports $< 1.4 \times 10^{-4}$ assuming the $\Upsilon(4S)$ decays 43% to $B^0\bar{B}^0$. We rescale to 50%.

⁷ ALBRECHT 88F reports $(5.2 \pm 1.4 \pm 1.9) \times 10^{-4}$ assuming the $\Upsilon(4S)$ decays 45% to $B^0\bar{B}^0$. We rescale to 50%.

$\Gamma(\rho\pi^+\text{nonresonant})/\Gamma_{\text{total}}$		Γ_{508}/Γ	
VALUE (units 10 ⁻⁶)	CL%	DOCUMENT ID	TECN COMMENT
<53	90	BERGFELD	96B CLE2 e ⁺ e ⁻ → $\Upsilon(4S)$

$\Gamma(\rho\pi^+\pi^0)/\Gamma_{\text{total}}$		Γ_{509}/Γ	
VALUE (units 10 ⁻⁶)	CL%	DOCUMENT ID	TECN COMMENT
4.58 ± 1.17 ± 0.67		1 CHU	20 BELL e ⁺ e ⁻ → $\Upsilon(4S)$
1 Assumes equal production of B ⁰ and B ⁺ from $\Upsilon(4S)$ decays. This measurement is quoted for M(π ⁺ π ⁰) < 1.3 GeV.			

$\Gamma(\rho\pi^+\pi^+\pi^-)/\Gamma_{\text{total}}$		Γ_{510}/Γ	
VALUE	CL%	DOCUMENT ID	TECN COMMENT
<5.2 × 10 ⁻⁴	90	1 ALBRECHT	88F ARG e ⁺ e ⁻ → $\Upsilon(4S)$
1 ALBRECHT 88F reports < 4.7 × 10 ⁻⁴ assuming the $\Upsilon(4S)$ decays 45% to B ⁰ \bar{B}^0 . We rescale to 50%.			

$\Gamma(\rho\pi^+K^+)/\Gamma_{\text{total}}$		Γ_{511}/Γ	
VALUE (units 10 ⁻⁶)	CL%	DOCUMENT ID	TECN COMMENT
5.9 ± 0.5 OUR AVERAGE		Error includes scale factor of 1.5.	
5.54 ^{+0.27} _{-0.25} ± 0.36		1,2,3 WEI	08 BELL e ⁺ e ⁻ → $\Upsilon(4S)$
6.7 ± 0.5 ± 0.4		1,3 AUBERT,B	05L BABR e ⁺ e ⁻ → $\Upsilon(4S)$
• • • We do not use the following data for averages, fits, limits, etc. • • •			
4.59 ^{+0.38} _{-0.34} ± 0.50		1,2,3 WANG	05A BELL Repl. by WEI 08
5.66 ^{+0.67} _{-0.57} ± 0.62		1,2,3 WANG	04 BELL Repl. by WANG 05A
4.3 ^{+1.1} _{-0.9} ± 0.5		1,2 ABE	02k BELL Repl. by WANG 04
1 Assumes equal production of B ⁺ and B ⁰ at the $\Upsilon(4S)$. 2 Explicitly vetoes resonant production of $\rho\bar{p}$ from Charmonium states. 3 Provides also results with m _{ρ\bar{p}} < 2.85 GeV/c ² and angular asymmetry of $\rho\bar{p}$ system.			

$\Gamma(\rho\pi^+K^+)/\Gamma(J/\psi(1S)K^+)$		$\Gamma_{511}/\Gamma_{276}$	
VALUE	CL%	DOCUMENT ID	TECN COMMENT
0.0104 ± 0.0005 ± 0.0001		1,2 AAIJ	13s LHCB pp at 7 TeV
1 AAIJ 13s reports [Γ(B ⁺ → ρπ ⁺ K ⁺)/Γ(B ⁺ → J/ψ(1S)K ⁺)] / [B(J/ψ(1S) → ρπ ⁺)] = 4.91 ± 0.19 ± 0.14 which we multiply by our best value B(J/ψ(1S) → ρπ ⁺) = (2.120 ± 0.029) × 10 ⁻³ . Our first error is their experiment's error and our second error is the systematic error from using our best value. 2 Measurement includes contribution where ρπ ⁺ is produced in charmonia decays.			

$\Gamma(\Theta(1710)^{++}\bar{p}, \Theta^{++} \rightarrow \rho K^+)/\Gamma_{\text{total}}$		Γ_{512}/Γ	
VALUE (units 10 ⁻⁶)	CL%	DOCUMENT ID	TECN COMMENT
<0.091	90	1 WANG	05A BELL e ⁺ e ⁻ → $\Upsilon(4S)$
• • • We do not use the following data for averages, fits, limits, etc. • • •			
<0.1	90	1,2 AUBERT,B	05L BABR e ⁺ e ⁻ → $\Upsilon(4S)$
1 Assumes equal production of B ⁺ and B ⁰ at the $\Upsilon(4S)$. 2 Provides upper limits depending on the pentaquark masses between 1.43 to 2.0 GeV/c ² .			

$\Gamma(f_J(2220)K^+, f_J \rightarrow \rho\bar{p})/\Gamma_{\text{total}}$		Γ_{513}/Γ	
VALUE (units 10 ⁻⁶)	CL%	DOCUMENT ID	TECN COMMENT
<0.41	90	1 WANG	05A BELL e ⁺ e ⁻ → $\Upsilon(4S)$
1 Assumes equal production of B ⁺ and B ⁰ at the $\Upsilon(4S)$.			

$\Gamma(\rho\bar{A}(1520))/\Gamma_{\text{total}}$		Γ_{514}/Γ	
VALUE (units 10 ⁻⁷)	CL%	DOCUMENT ID	TECN COMMENT
3.15 ± 0.48 ± 0.27		1 AAIJ	14AF LHCB pp at 7, 8 TeV
• • • We do not use the following data for averages, fits, limits, etc. • • •			
3.9 ^{+1.0} _{-0.9} ± 0.3		1 AAIJ	13AU LHCB Repl. by AAIJ 14AF
<15	90	2 AUBERT,B	05L BABR e ⁺ e ⁻ → $\Upsilon(4S)$
1 Uses B(B ⁺ → J/ψK ⁺) = (1.016 ± 0.033) × 10 ⁻³ , B(J/ψ → ρπ ⁺) = (2.17 ± 0.07) × 10 ⁻³ and B(A(1520) → K ⁻ ρ) = 0.234 ± 0.016. 2 Assumes equal production of B ⁺ and B ⁰ at the $\Upsilon(4S)$.			

$\Gamma(\rho\pi^+K^*\text{nonresonant})/\Gamma_{\text{total}}$		Γ_{515}/Γ	
VALUE (units 10 ⁻⁶)	CL%	DOCUMENT ID	TECN COMMENT
<89	90	BERGFELD	96B CLE2 e ⁺ e ⁻ → $\Upsilon(4S)$

$\Gamma(\rho\pi^+K^*(892^+)/\Gamma_{\text{total}}$		Γ_{516}/Γ	
VALUE (units 10 ⁻⁶)	CL%	DOCUMENT ID	TECN COMMENT
3.6 ^{+0.8} _{-0.7} OUR AVERAGE			
3.38 ^{+0.73} _{-0.60} ± 0.39		1,2 CHEN	08c BELL e ⁺ e ⁻ → $\Upsilon(4S)$
5.3 ± 1.5 ± 1.3		2 AUBERT	07AV BABR e ⁺ e ⁻ → $\Upsilon(4S)$
• • • We do not use the following data for averages, fits, limits, etc. • • •			
10.3 ^{+3.6} _{-2.8} ± 1.3		2,3 WANG	04 BELL Repl. by CHEN 08c
1 Explicitly vetoes resonant production of $\rho\bar{p}$ from charmonium states. 2 Assumes equal production of B ⁺ and B ⁰ at the $\Upsilon(4S)$. 3 Explicitly vetoes resonant production of $\rho\bar{p}$ from charmonium states. The branching fraction for M _{ρ\bar{p}} < 2.85 GeV/c ² is also reported.			

$\Gamma(f_J(2220)K^{*+}, f_J \rightarrow \rho\bar{p})/\Gamma_{\text{total}}$		Γ_{517}/Γ	
VALUE (units 10 ⁻⁶)	CL%	DOCUMENT ID	TECN COMMENT
<0.77	90	1 AUBERT	07AV BABR e ⁺ e ⁻ → $\Upsilon(4S)$
1 Assumes equal production of B ⁺ and B ⁰ at the $\Upsilon(4S)$.			

$\Gamma(\rho\bar{A})/\Gamma_{\text{total}}$		Γ_{518}/Γ	
VALUE (units 10 ⁻⁶)	CL%	DOCUMENT ID	TECN COMMENT
0.24 ^{+0.10} _{-0.08} ± 0.03		1 AAIJ	17R LHCB pp at 7, 8 TeV
• • • We do not use the following data for averages, fits, limits, etc. • • •			
< 0.32	90	2 TSAI	07 BELL e ⁺ e ⁻ → $\Upsilon(4S)$
< 0.49	90	2 CHANG	05 BELL Repl. by TSAI 07
< 1.5	90	2 BORNHEIM	03 CLE2 e ⁺ e ⁻ → $\Upsilon(4S)$
< 2.2	90	2 ABE	02O BELL e ⁺ e ⁻ → $\Upsilon(4S)$
< 2.6	90	2 COAN	99 CLE2 e ⁺ e ⁻ → $\Upsilon(4S)$
< 60	90	3 AVERY	89B CLEO e ⁺ e ⁻ → $\Upsilon(4S)$
< 93	90	4 ALBRECHT	88F ARG e ⁺ e ⁻ → $\Upsilon(4S)$

1 Statistical significance of the signal is 4.1 standard deviations where the normalisation is based on B(B⁺ → K_S⁰π⁺) = (11.895 ± 0.375) × 10⁻⁰⁶.
 2 Assumes equal production of B⁺ and B⁰ at the $\Upsilon(4S)$.
 3 AVERY 89B reports < 5 × 10⁻⁵ assuming the $\Upsilon(4S)$ decays 43% to B⁰ \bar{B}^0 . We rescale to 50%.
 4 ALBRECHT 88F reports < 8.5 × 10⁻⁵ assuming the $\Upsilon(4S)$ decays 45% to B⁰ \bar{B}^0 . We rescale to 50%.

$\Gamma(\rho\bar{A}\gamma)/\Gamma_{\text{total}}$		Γ_{519}/Γ	
VALUE (units 10 ⁻⁶)	CL%	DOCUMENT ID	TECN COMMENT
2.45 ^{+0.44} _{-0.38} ± 0.22		1 WANG	07c BELL e ⁺ e ⁻ → $\Upsilon(4S)$
• • • We do not use the following data for averages, fits, limits, etc. • • •			
2.16 ^{+0.58} _{-0.53} ± 0.20		1 LEE	05 BELL Repl. by WANG 07c
< 3.9	90	2 EDWARDS	03 CLE2 e ⁺ e ⁻ → $\Upsilon(4S)$

1 Assumes equal production of B⁺ and B⁰ at the $\Upsilon(4S)$.
 2 Corresponds to E_γ > 1.5 GeV. The limit changes to 3.3 × 10⁻⁶ for E_γ > 2.0 GeV.

$\Gamma(\rho\bar{A}\pi^0)/\Gamma_{\text{total}}$		Γ_{520}/Γ	
VALUE (units 10 ⁻⁶)	CL%	DOCUMENT ID	TECN COMMENT
3.00 ^{+0.61} _{-0.53} ± 0.33		1 WANG	07c BELL e ⁺ e ⁻ → $\Upsilon(4S)$
1 Assumes equal production of B ⁺ and B ⁰ at the $\Upsilon(4S)$.			

$\Gamma(\rho\Sigma(1385)^0)/\Gamma_{\text{total}}$		Γ_{521}/Γ	
VALUE (units 10 ⁻⁶)	CL%	DOCUMENT ID	TECN COMMENT
<0.47	90	1 WANG	07c BELL e ⁺ e ⁻ → $\Upsilon(4S)$
1 Assumes equal production of B ⁺ and B ⁰ at the $\Upsilon(4S)$.			

$\Gamma(\Delta^+\bar{A})/\Gamma_{\text{total}}$		Γ_{522}/Γ	
VALUE (units 10 ⁻⁶)	CL%	DOCUMENT ID	TECN COMMENT
<0.82	90	1 WANG	07c BELL e ⁺ e ⁻ → $\Upsilon(4S)$
1 Assumes equal production of B ⁺ and B ⁰ at the $\Upsilon(4S)$.			

$\Gamma(\rho\Sigma\gamma)/\Gamma_{\text{total}}$		Γ_{523}/Γ	
VALUE (units 10 ⁻⁶)	CL%	DOCUMENT ID	TECN COMMENT
<4.6	90	1 LEE	05 BELL e ⁺ e ⁻ → $\Upsilon(4S)$
• • • We do not use the following data for averages, fits, limits, etc. • • •			
<7.9	90	2 EDWARDS	03 CLE2 e ⁺ e ⁻ → $\Upsilon(4S)$
1 Assumes equal production of B ⁺ and B ⁰ at the $\Upsilon(4S)$. 2 Corresponds to E _γ > 1.5 GeV. The limit changes to 6.4 × 10 ⁻⁶ for E _γ > 2.0 GeV.			

$\Gamma(\rho\bar{A}\pi^+\pi^-)/\Gamma_{\text{total}}$		Γ_{524}/Γ	
VALUE (units 10 ⁻⁶)	CL%	DOCUMENT ID	TECN COMMENT
11.28 ^{+0.91} _{-0.72} ± 1.03		1 CHEN	09c BELL e ⁺ e ⁻ → $\Upsilon(4S)$
• • • We do not use the following data for averages, fits, limits, etc. • • •			
<200	90	2 ALBRECHT	88F ARG e ⁺ e ⁻ → $\Upsilon(4S)$
1 Assumes equal production of B ⁺ and B ⁰ at the $\Upsilon(4S)$. 2 ALBRECHT 88F reports < 1.8 × 10 ⁻⁴ assuming the $\Upsilon(4S)$ decays 45% to B ⁰ \bar{B}^0 . We rescale to 50%.			

$\Gamma(\rho\bar{A}\pi^+\pi^-\text{nonresonant})/\Gamma_{\text{total}}$		Γ_{525}/Γ	
VALUE (units 10 ⁻⁶)	CL%	DOCUMENT ID	TECN COMMENT
5.92 ^{+0.88} _{-0.84} ± 0.69		1 CHEN	09c BELL e ⁺ e ⁻ → $\Upsilon(4S)$
1 Assumes equal production of B ⁺ and B ⁰ at the $\Upsilon(4S)$.			

$\Gamma(\rho\bar{A}\rho^0, \rho^0 \rightarrow \pi^+\pi^-)/\Gamma_{\text{total}}$		Γ_{526}/Γ	
VALUE (units 10 ⁻⁶)	CL%	DOCUMENT ID	TECN COMMENT
4.78 ^{+0.67} _{-0.64} ± 0.60		1 CHEN	09c BELL e ⁺ e ⁻ → $\Upsilon(4S)$
1 Assumes equal production of B ⁺ and B ⁰ at the $\Upsilon(4S)$.			

Meson Particle Listings

B^\pm

$\Gamma(\rho\bar{\Lambda}\eta_2(1270), \eta_2 \rightarrow \pi^+\pi^-)/\Gamma_{\text{total}}$	Γ_{527}/Γ			
VALUE (units 10^{-6})	DOCUMENT ID	TECN	COMMENT	
$2.03^{+0.77}_{-0.72} \pm 0.27$	¹ CHEN	09c	BELL	$e^+e^- \rightarrow \Upsilon(4S)$

¹ Assumes equal production of B^+ and B^0 at the $\Upsilon(4S)$.

$\Gamma(\rho\bar{\Lambda}K+K^-)/\Gamma_{\text{total}}$	Γ_{528}/Γ			
VALUE (units 10^{-6})	DOCUMENT ID	TECN	COMMENT	
$4.10^{+0.45}_{-0.43} \pm 0.50$	¹ LU	19	BELL	$e^+e^- \rightarrow \Upsilon(4S)$

¹ Assumes equal production of B^+ and B^0 at the $\Upsilon(4S)$.

$\Gamma(\rho\bar{\Lambda}\phi)/\Gamma_{\text{total}}$	Γ_{529}/Γ			
VALUE (units 10^{-6})	DOCUMENT ID	TECN	COMMENT	
$0.795 \pm 0.209 \pm 0.077$	¹ LU	19	BELL	$e^+e^- \rightarrow \Upsilon(4S)$

¹ Assumes equal production of B^+ and B^0 at the $\Upsilon(4S)$.

$\Gamma(\bar{p}\Lambda K+K^-)/\Gamma_{\text{total}}$	Γ_{530}/Γ			
VALUE (units 10^{-6})	DOCUMENT ID	TECN	COMMENT	
$3.70^{+0.39}_{-0.37} \pm 0.44$	¹ LU	19	BELL	$e^+e^- \rightarrow \Upsilon(4S)$

¹ Assumes equal production of B^+ and B^0 at the $\Upsilon(4S)$.

$\Gamma(\Lambda\bar{\Lambda}\pi^+)/\Gamma_{\text{total}}$	Γ_{531}/Γ			
VALUE (units 10^{-6})	CL%	DOCUMENT ID	TECN	COMMENT
<0.94	90	^{1,2} CHANG	09	BELL Repl. by CHANG 09
• • • We do not use the following data for averages, fits, limits, etc. • • •				
<2.8	90	² LEE	04	BELL $e^+e^- \rightarrow \Upsilon(4S)$

¹ For $m_{\Lambda\bar{\Lambda}} < 2.85$ GeV/c².

² Assumes equal production of B^+ and B^0 at the $\Upsilon(4S)$.

$\Gamma(\Lambda\bar{\Lambda}K^+)/\Gamma_{\text{total}}$	Γ_{532}/Γ			
VALUE (units 10^{-6})	DOCUMENT ID	TECN	COMMENT	
$3.38^{+0.41}_{-0.36} \pm 0.41$	^{1,2} CHANG	09	BELL	$e^+e^- \rightarrow \Upsilon(4S)$
• • • We do not use the following data for averages, fits, limits, etc. • • •				
$2.91^{+0.9}_{-0.70} \pm 0.38$	² LEE	04	BELL	Repl. by CHANG 09

¹ Excluding charmonium events in $2.85 < m_{\Lambda\bar{\Lambda}} < 3.128$ GeV/c² and $3.315 < m_{\Lambda\bar{\Lambda}} < 3.735$ GeV/c². Measurements in various $m_{\Lambda\bar{\Lambda}}$ bins are also reported.

² Assumes equal production of B^+ and B^0 at the $\Upsilon(4S)$.

$\Gamma(\Lambda\bar{\Lambda}K^+)/\Gamma_{\text{total}}$	Γ_{533}/Γ			
VALUE (units 10^{-6})	DOCUMENT ID	TECN	COMMENT	
$2.19^{+1.13}_{-0.88} \pm 0.33$	^{1,2} CHANG	09	BELL	$e^+e^- \rightarrow \Upsilon(4S)$

¹ For $m_{\Lambda\bar{\Lambda}} < 2.85$ GeV/c².

² Assumes equal production of B^+ and B^0 at the $\Upsilon(4S)$.

$\Gamma(\Lambda(1520)\bar{\Lambda}K^+)/\Gamma_{\text{total}}$	Γ_{534}/Γ			
VALUE (units 10^{-6})	DOCUMENT ID	TECN	COMMENT	
$2.23 \pm 0.63 \pm 0.25$	¹ LU	19	BELL	$e^+e^- \rightarrow \Upsilon(4S)$

¹ Assumes equal production of B^+ and B^0 at the $\Upsilon(4S)$.

$\Gamma(\Lambda\bar{\Lambda}(1520)K^+)/\Gamma_{\text{total}}$	Γ_{535}/Γ			
VALUE	DOCUMENT ID	TECN	COMMENT	
$<2.08 \times 10^{-6}$	¹ LU	19	BELL	$e^+e^- \rightarrow \Upsilon(4S)$

¹ Assumes equal production of B^+ and B^0 at the $\Upsilon(4S)$.

$\Gamma(\bar{D}^0\rho)/\Gamma_{\text{total}}$	Γ_{536}/Γ			
VALUE (units 10^{-6})	CL%	DOCUMENT ID	TECN	COMMENT
< 1.38	90	¹ WEI	08	BELL $e^+e^- \rightarrow \Upsilon(4S)$
• • • We do not use the following data for averages, fits, limits, etc. • • •				
<380	90	² BORTOLETTO89	CLEO	$e^+e^- \rightarrow \Upsilon(4S)$

¹ Assumes equal production of B^+ and B^0 at the $\Upsilon(4S)$.

² BORTOLETTO 89 reports $< 3.3 \times 10^{-4}$ assuming the $\Upsilon(4S)$ decays 43% to $B^0\bar{B}^0$. We rescale to 50%.

$\Gamma(\Delta^{++}\bar{p})/\Gamma_{\text{total}}$	Γ_{537}/Γ			
VALUE (units 10^{-6})	CL%	DOCUMENT ID	TECN	COMMENT
< 0.14	90	¹ WEI	08	BELL $e^+e^- \rightarrow \Upsilon(4S)$
• • • We do not use the following data for averages, fits, limits, etc. • • •				
<150	90	² BORTOLETTO89	CLEO	$e^+e^- \rightarrow \Upsilon(4S)$

¹ Assumes equal production of B^+ and B^0 at the $\Upsilon(4S)$.

² BORTOLETTO 89 reports $< 1.3 \times 10^{-4}$ assuming the $\Upsilon(4S)$ decays 43% to $B^0\bar{B}^0$. We rescale to 50%.

$\Gamma(D^+\rho\bar{p})/\Gamma_{\text{total}}$	Γ_{538}/Γ			
VALUE	CL%	DOCUMENT ID	TECN	COMMENT
$<1.5 \times 10^{-5}$	90	¹ ABE	02w	BELL $e^+e^- \rightarrow \Upsilon(4S)$

¹ Assumes equal production of B^+ and B^0 at the $\Upsilon(4S)$.

$\Gamma(D^{*+}(2010)\rho\bar{p})/\Gamma_{\text{total}}$	Γ_{539}/Γ			
VALUE	CL%	DOCUMENT ID	TECN	COMMENT
$<1.5 \times 10^{-5}$	90	¹ ABE	02w	BELL $e^+e^- \rightarrow \Upsilon(4S)$

¹ Assumes equal production of B^+ and B^0 at the $\Upsilon(4S)$.

$\Gamma(\bar{D}^0\rho\bar{p}\pi^+)/\Gamma_{\text{total}}$	Γ_{540}/Γ			
VALUE (units 10^{-4})	DOCUMENT ID	TECN	COMMENT	
$3.72 \pm 0.11 \pm 0.25$	^{1,2} DEL-AMO-SA..12	BABR	$e^+e^- \rightarrow \Upsilon(4S)$	

¹ Uses the values of D and D^* branching fractions from PDG 08.

² Assumes equal production of B^+ and B^0 at the $\Upsilon(4S)$.

$\Gamma(\bar{D}^{*0}\rho\bar{p}\pi^+)/\Gamma_{\text{total}}$	Γ_{541}/Γ			
VALUE (units 10^{-4})	DOCUMENT ID	TECN	COMMENT	
$3.73 \pm 0.17 \pm 0.27$	^{1,2} DEL-AMO-SA..12	BABR	$e^+e^- \rightarrow \Upsilon(4S)$	

¹ Uses the values of D and D^* branching fractions from PDG 08.

² Assumes equal production of B^+ and B^0 at the $\Upsilon(4S)$.

$\Gamma(D^-\rho\bar{p}\pi^+\pi^-)/\Gamma_{\text{total}}$	Γ_{542}/Γ			
VALUE (units 10^{-4})	DOCUMENT ID	TECN	COMMENT	
$1.66 \pm 0.13 \pm 0.27$	^{1,2} DEL-AMO-SA..12	BABR	$e^+e^- \rightarrow \Upsilon(4S)$	

¹ Uses the values of D and D^* branching fractions from PDG 08.

² Assumes equal production of B^+ and B^0 at the $\Upsilon(4S)$.

$\Gamma(D^{*-}\rho\bar{p}\pi^+\pi^-)/\Gamma_{\text{total}}$	Γ_{543}/Γ			
VALUE (units 10^{-4})	DOCUMENT ID	TECN	COMMENT	
$1.86 \pm 0.16 \pm 0.19$	^{1,2} DEL-AMO-SA..12	BABR	$e^+e^- \rightarrow \Upsilon(4S)$	

¹ Uses the values of D and D^* branching fractions from PDG 08.

² Assumes equal production of B^+ and B^0 at the $\Upsilon(4S)$.

$\Gamma(\rho\bar{\Lambda}^0\bar{D}^0)/\Gamma_{\text{total}}$	Γ_{544}/Γ			
VALUE (units 10^{-5})	DOCUMENT ID	TECN	COMMENT	
$1.43^{+0.28}_{-0.25} \pm 0.18$	^{1,2} CHEN	11F	BELL	$e^+e^- \rightarrow \Upsilon(4S)$

¹ Uses $B(\Lambda \rightarrow p\pi^-) = 63.9 \pm 0.5\%$, $B(D^0 \rightarrow K^-\pi^+) = 3.89 \pm 0.05\%$, and $B(D^0 \rightarrow K^-\pi^+\pi^0) = 13.9 \pm 0.5\%$.

² Assumes equal production of B^0 and B^+ from Upsilon(4S) decays.

$\Gamma(\rho\bar{\Lambda}^0\bar{D}^*(2007)^0)/\Gamma_{\text{total}}$	Γ_{545}/Γ			
VALUE (units 10^{-5})	CL%	DOCUMENT ID	TECN	COMMENT
<5	90	^{1,2,3} CHEN	11F	BELL $e^+e^- \rightarrow \Upsilon(4S)$

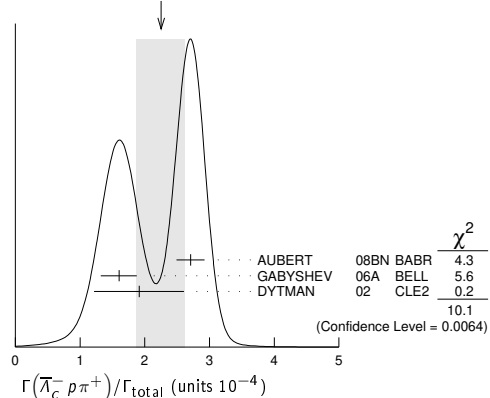
¹ CHEN 11F reports $< 4.8 \times 10^{-5}$ from a measurement of $[\Gamma(B^+ \rightarrow \rho\bar{\Lambda}^0\bar{D}^*(2007)^0)/\Gamma_{\text{total}}] / [B(D^*(2007)^0 \rightarrow D^0\pi^0)]$ assuming $B(D^*(2007)^0 \rightarrow D^0\pi^0) = (61.9 \pm 2.9) \times 10^{-2}$, which we rescale to our best value $B(D^*(2007)^0 \rightarrow D^0\pi^0) = 64.7 \times 10^{-2}$.

² Uses $B(\Lambda \rightarrow p\pi^-) = 63.9 \pm 0.5\%$ and $B(D^0 \rightarrow K^-\pi^+) = 3.89 \pm 0.05\%$.

³ Assumes equal production of B^0 and B^+ from Upsilon(4S) decays.

$\Gamma(\bar{\Lambda}_c^-\rho\pi^+)/\Gamma_{\text{total}}$	Γ_{546}/Γ			
VALUE (units 10^{-4})	DOCUMENT ID	TECN	COMMENT	
2.3 ± 0.4	OUR AVERAGE			
$2.71 \pm 0.16 \pm 0.14$	^{1,2} AUBERT	08BN	BABR	$e^+e^- \rightarrow \Upsilon(4S)$
$1.60 \pm 0.20 \pm 0.08$	^{1,3} GABYSHEV	06A	BELL	$e^+e^- \rightarrow \Upsilon(4S)$
$1.9 \pm 0.5 \pm 0.1$	^{1,4} DYTMAN	02	CLE2	$e^+e^- \rightarrow \Upsilon(4S)$
• • • We do not use the following data for averages, fits, limits, etc. • • •				
$1.5 \pm 0.4 \pm 0.1$	^{1,5} GABYSHEV	02	BELL	Repl. by GABYSHEV 06A
$6.2^{+2.3}_{-2.0} \pm 1.6$	^{1,6} FU	97	CLE2	Repl. by DYTMAN 02

WEIGHTED AVERAGE
2.3±0.4 (Error scaled by 2.2)



- ¹ Assumes equal production of B^+ and B^0 at the $\Upsilon(4S)$.
² AUBERT 08BN reports $(3.4 \pm 0.1 \pm 0.9) \times 10^{-4}$ from a measurement of $[\Gamma(B^+ \rightarrow \bar{\Lambda}_c^- p \pi^+)/\Gamma_{\text{total}}] \times [B(\Lambda_c^+ \rightarrow p K^- \pi^+)]$ assuming $B(\Lambda_c^+ \rightarrow p K^- \pi^+) = (5.0 \pm 1.3) \times 10^{-2}$, which we rescale to our best value $B(\Lambda_c^+ \rightarrow p K^- \pi^+) = (6.28 \pm 0.32) \times 10^{-2}$. Our first error is their experiment's error and our second error is the systematic error from using our best value.
³ GABYSHEV 06A reports $(2.01 \pm 0.15 \pm 0.20) \times 10^{-4}$ from a measurement of $[\Gamma(B^+ \rightarrow \bar{\Lambda}_c^- p \pi^+)/\Gamma_{\text{total}}] \times [B(\Lambda_c^+ \rightarrow p K^- \pi^+)]$ assuming $B(\Lambda_c^+ \rightarrow p K^- \pi^+) = 0.05$, which we rescale to our best value $B(\Lambda_c^+ \rightarrow p K^- \pi^+) = (6.28 \pm 0.32) \times 10^{-2}$. Our first error is their experiment's error and our second error is the systematic error from using our best value.
⁴ DYTMAN 02 reports $(2.4^{+0.63}_{-0.62}) \times 10^{-4}$ from a measurement of $[\Gamma(B^+ \rightarrow \bar{\Lambda}_c^- p \pi^+)/\Gamma_{\text{total}}] \times [B(\Lambda_c^+ \rightarrow p K^- \pi^+)]$ assuming $B(\Lambda_c^+ \rightarrow p K^- \pi^+) = 0.05$, which we rescale to our best value $B(\Lambda_c^+ \rightarrow p K^- \pi^+) = (6.28 \pm 0.32) \times 10^{-2}$. Our first error is their experiment's error and our second error is the systematic error from using our best value.
⁵ GABYSHEV 02 reports $(1.87^{+0.51}_{-0.49}) \times 10^{-4}$ from a measurement of $[\Gamma(B^+ \rightarrow \bar{\Lambda}_c^- p \pi^+)/\Gamma_{\text{total}}] \times [B(\Lambda_c^+ \rightarrow p K^- \pi^+)]$ assuming $B(\Lambda_c^+ \rightarrow p K^- \pi^+) = 0.05$, which we rescale to our best value $B(\Lambda_c^+ \rightarrow p K^- \pi^+) = (6.28 \pm 0.32) \times 10^{-2}$. Our first error is their experiment's error and our second error is the systematic error from using our best value.
⁶ FU 97 uses PDG 96 values of Λ_c branching fraction.

$\Gamma(\bar{\Lambda}_c^- \Delta(1232)^+)/\Gamma_{\text{total}}$ Γ_{547}/Γ

VALUE (units 10^{-5})	CL%	DOCUMENT ID	TECN	COMMENT
<1.9	90	GABYSHEV	06A	BELL $e^+e^- \rightarrow \Upsilon(4S)$

$\Gamma(\bar{\Lambda}_c^- \Delta_X(1600)^+)/\Gamma_{\text{total}}$ Γ_{548}/Γ

VALUE (units 10^{-5})	CL%	DOCUMENT ID	TECN	COMMENT
4.7 ± 0.9 ± 0.2		1 GABYSHEV	06A	BELL $e^+e^- \rightarrow \Upsilon(4S)$

- ¹ GABYSHEV 06A reports $(5.9 \pm 1.0 \pm 0.6) \times 10^{-5}$ from a measurement of $[\Gamma(B^+ \rightarrow \bar{\Lambda}_c^- \Delta_X(1600)^+)/\Gamma_{\text{total}}] \times [B(\Lambda_c^+ \rightarrow p K^- \pi^+)]$ assuming $B(\Lambda_c^+ \rightarrow p K^- \pi^+) = 0.05$, which we rescale to our best value $B(\Lambda_c^+ \rightarrow p K^- \pi^+) = (6.28 \pm 0.32) \times 10^{-2}$. Our first error is their experiment's error and our second error is the systematic error from using our best value.

$\Gamma(\bar{\Lambda}_c^- \Delta_X(2420)^+)/\Gamma_{\text{total}}$ Γ_{549}/Γ

VALUE (units 10^{-5})	CL%	DOCUMENT ID	TECN	COMMENT
3.7 ± 0.9 ± 0.2		1 GABYSHEV	06A	BELL $e^+e^- \rightarrow \Upsilon(4S)$

- ¹ GABYSHEV 06A reports $(4.7^{+1.0}_{-0.9} \pm 0.4) \times 10^{-5}$ from a measurement of $[\Gamma(B^+ \rightarrow \bar{\Lambda}_c^- \Delta_X(2420)^+)/\Gamma_{\text{total}}] \times [B(\Lambda_c^+ \rightarrow p K^- \pi^+)]$ assuming $B(\Lambda_c^+ \rightarrow p K^- \pi^+) = 0.05$, which we rescale to our best value $B(\Lambda_c^+ \rightarrow p K^- \pi^+) = (6.28 \pm 0.32) \times 10^{-2}$. Our first error is their experiment's error and our second error is the systematic error from using our best value.

$\Gamma((\bar{\Lambda}_c^- p)_s \pi^+)/\Gamma_{\text{total}}$ Γ_{550}/Γ
 $(\bar{\Lambda}_c^- p)_s$ denotes a low-mass enhancement near 3.35 GeV/c².

VALUE (units 10^{-5})	CL%	DOCUMENT ID	TECN	COMMENT
3.1 ± 0.7 ± 0.2		1 GABYSHEV	06A	BELL $e^+e^- \rightarrow \Upsilon(4S)$

- ¹ GABYSHEV 06A reports $(3.9^{+0.8}_{-0.7} \pm 0.4) \times 10^{-5}$ from a measurement of $[\Gamma(B^+ \rightarrow (\bar{\Lambda}_c^- p)_s \pi^+)/\Gamma_{\text{total}}] \times [B(\Lambda_c^+ \rightarrow p K^- \pi^+)]$ assuming $B(\Lambda_c^+ \rightarrow p K^- \pi^+) = 0.05$, which we rescale to our best value $B(\Lambda_c^+ \rightarrow p K^- \pi^+) = (6.28 \pm 0.32) \times 10^{-2}$. Our first error is their experiment's error and our second error is the systematic error from using our best value.

$\Gamma(\bar{\Sigma}_c(2520)^0 p)/\Gamma_{\text{total}}$ Γ_{551}/Γ

VALUE (units 10^{-5})	CL%	DOCUMENT ID	TECN	COMMENT
<0.3	90	1,2 AUBERT	08BN	BABR $e^+e^- \rightarrow \Upsilon(4S)$

- • • We do not use the following data for averages, fits, limits, etc. • • •
 <2.7 90 1,2 GABYSHEV 06A BELL $e^+e^- \rightarrow \Upsilon(4S)$
 <4.6 90 1,2 GABYSHEV 02 BELL Repl. by GABYSHEV 06A
¹ Assumes equal production of B^+ and B^0 at the $\Upsilon(4S)$.
² Uses the value for $\Lambda_c \rightarrow p K^- \pi^+$ branching ratio $(5.0 \pm 1.3)\%$.

$\Gamma(\bar{\Sigma}_c(2520)^0 p)/\Gamma(\bar{\Lambda}_c^- p \pi^+)$ $\Gamma_{551}/\Gamma_{546}$

VALUE (units 10^{-3})	CL%	DOCUMENT ID	TECN	COMMENT
<9	90	AUBERT	08BN	BABR $e^+e^- \rightarrow \Upsilon(4S)$

$\Gamma(\bar{\Sigma}_c(2800)^0 p)/\Gamma_{\text{total}}$ Γ_{552}/Γ

VALUE (units 10^{-5})	CL%	DOCUMENT ID	TECN	COMMENT
2.6 ± 0.7 ± 0.4		1 AUBERT	08BN	BABR $e^+e^- \rightarrow \Upsilon(4S)$

- ¹ AUBERT 08BN reports $[\Gamma(B^+ \rightarrow \bar{\Sigma}_c(2800)^0 p)/\Gamma_{\text{total}}] / [B(B^+ \rightarrow \bar{\Lambda}_c^- p \pi^+)] = 0.117 \pm 0.023 \pm 0.024$ which we multiply by our best value $B(B^+ \rightarrow \bar{\Lambda}_c^- p \pi^+) = (2.3 \pm 0.4) \times 10^{-4}$. Our first error is their experiment's error and our second error is the systematic error from using our best value.

$\Gamma(\bar{\Lambda}_c^- p \pi^+ \pi^0)/\Gamma_{\text{total}}$ Γ_{553}/Γ

VALUE (units 10^{-3})	CL%	DOCUMENT ID	TECN	COMMENT
1.81 ± 0.29 ± 0.52 0.50		1,2 DYTMAN	02	CLE2 $e^+e^- \rightarrow \Upsilon(4S)$
• • • We do not use the following data for averages, fits, limits, etc. • • •				
<3.12	90	3 FU	97	CLE2 $e^+e^- \rightarrow \Upsilon(4S)$

- ¹ Assumes equal production of B^+ and B^0 at the $\Upsilon(4S)$.
² DYTMAN 02 measurement uses $B(\Lambda_c^- \rightarrow \bar{p} K^+ \pi^-) = 5.0 \pm 1.3\%$. The second error includes the systematic and the uncertainty of the branching ratio.
³ FU 97 uses PDG 96 values of Λ_c branching ratio.

$\Gamma(\bar{\Lambda}_c^- p \pi^+ \pi^+ \pi^-)/\Gamma_{\text{total}}$ Γ_{554}/Γ

VALUE (units 10^{-3})	CL%	DOCUMENT ID	TECN	COMMENT
2.25 ± 0.25 ± 0.63 0.61		1,2 DYTMAN	02	CLE2 $e^+e^- \rightarrow \Upsilon(4S)$
• • • We do not use the following data for averages, fits, limits, etc. • • •				
<1.46	90	3 FU	97	CLE2 $e^+e^- \rightarrow \Upsilon(4S)$

- ¹ Assumes equal production of B^+ and B^0 at the $\Upsilon(4S)$.
² DYTMAN 02 measurement uses $B(\Lambda_c^- \rightarrow \bar{p} K^+ \pi^-) = 5.0 \pm 1.3\%$. The second error includes the systematic and the uncertainty of the branching ratio.
³ FU 97 uses PDG 96 values of Λ_c branching ratio.

$\Gamma(\bar{\Lambda}_c^- p \pi^+ \pi^+ \pi^- \pi^0)/\Gamma_{\text{total}}$ Γ_{555}/Γ

VALUE (units 10^{-2})	CL%	DOCUMENT ID	TECN	COMMENT
<1.34 × 10⁻²		1 FU	97	CLE2 $e^+e^- \rightarrow \Upsilon(4S)$
1 FU 97 uses PDG 96 values of Λ_c branching ratio.				

$\Gamma(\Lambda_c^+ \Lambda_c^- K^+)/\Gamma_{\text{total}}$ Γ_{556}/Γ

VALUE (units 10^{-4})	CL%	DOCUMENT ID	TECN	COMMENT
4.9 ± 0.7 OUR AVERAGE				
4.80 ± 0.43 ± 0.60		LI	18A	BELL $e^+e^- \rightarrow \Upsilon(4S)$
9.1 ± 4.5 ± 0.5		1,2 AUBERT	08H	BABR $e^+e^- \rightarrow \Upsilon(4S)$
• • • We do not use the following data for averages, fits, limits, etc. • • •				
6.3 ± 2.5 ± 0.3		2,3 GABYSHEV	06	BELL Repl. by LI 18A.

- ¹ AUBERT 08H reports $(1.14 \pm 0.15 \pm 0.62) \times 10^{-3}$ from a measurement of $[\Gamma(B^+ \rightarrow \Lambda_c^+ \Lambda_c^- K^+)/\Gamma_{\text{total}}] \times [B(\Lambda_c^+ \rightarrow p K^- \pi^+)]$ assuming $B(\Lambda_c^+ \rightarrow p K^- \pi^+) = (5.0 \pm 1.3) \times 10^{-2}$, which we rescale to our best value $B(\Lambda_c^+ \rightarrow p K^- \pi^+) = (6.28 \pm 0.32) \times 10^{-2}$. Our first error is their experiment's error and our second error is the systematic error from using our best value.
² Assumes equal production of B^+ and B^0 at the $\Upsilon(4S)$.
³ GABYSHEV 06 reports $(7.9^{+1.0}_{-0.9} \pm 3.6) \times 10^{-4}$ from a measurement of $[\Gamma(B^+ \rightarrow \Lambda_c^+ \Lambda_c^- K^+)/\Gamma_{\text{total}}] \times [B(\Lambda_c^+ \rightarrow p K^- \pi^+)]$ assuming $B(\Lambda_c^+ \rightarrow p K^- \pi^+) = (5.0 \pm 1.3) \times 10^{-2}$, which we rescale to our best value $B(\Lambda_c^+ \rightarrow p K^- \pi^+) = (6.28 \pm 0.32) \times 10^{-2}$. Our first error is their experiment's error and our second error is the systematic error from using our best value.

$\Gamma(\Xi_c(2930) \Lambda_c^+, \Xi_c \rightarrow K^+ \Lambda_c^-)/\Gamma_{\text{total}}$ Γ_{557}/Γ

VALUE (units 10^{-4})	CL%	DOCUMENT ID	TECN	COMMENT
1.73 ± 0.45 ± 0.21		1 LI	18A	BELL $e^+e^- \rightarrow \Upsilon(4S)$

- ¹ The $\Xi_c(2930)$ is found in its decay to $K^- \Lambda_c^+$ in $B^- \rightarrow K^- \Lambda_c^- \Lambda_c^+$ with a significance more than 5 sigma.

$\Gamma(\bar{\Sigma}_c(2455)^0 p)/\Gamma_{\text{total}}$ Γ_{558}/Γ

VALUE (units 10^{-5})	CL%	DOCUMENT ID	TECN	COMMENT
2.9 ± 0.6 ± 0.2 0.1		1,2 GABYSHEV	06A	BELL $e^+e^- \rightarrow \Upsilon(4S)$

- • • We do not use the following data for averages, fits, limits, etc. • • •
 <8.3 90 1,3 DYTMAN 02 CLE2 $e^+e^- \rightarrow \Upsilon(4S)$
 <9.3 90 1,4 GABYSHEV 02 BELL Repl. by GABYSHEV 06A
¹ Assumes equal production of B^+ and B^0 at the $\Upsilon(4S)$.
² GABYSHEV 06A reports $(3.7 \pm 0.7 \pm 0.4) \times 10^{-5}$ from a measurement of $[\Gamma(B^+ \rightarrow \bar{\Sigma}_c(2455)^0 p)/\Gamma_{\text{total}}] \times [B(\Lambda_c^+ \rightarrow p K^- \pi^+)]$ assuming $B(\Lambda_c^+ \rightarrow p K^- \pi^+) = 0.05$, which we rescale to our best value $B(\Lambda_c^+ \rightarrow p K^- \pi^+) = (6.28 \pm 0.32) \times 10^{-2}$. Our first error is their experiment's error and our second error is the systematic error from using our best value.
³ DYTMAN 02 measurement uses $B(\Lambda_c^- \rightarrow \bar{p} K^+ \pi^-) = 5.0 \pm 1.3\%$. The second error includes the systematic and the uncertainty of the branching ratio.
⁴ Uses the value for $\Lambda_c \rightarrow p K^- \pi^+$ branching ratio $(5.0 \pm 1.3)\%$.

$\Gamma(\bar{\Sigma}_c(2455)^0 p)/\Gamma(\bar{\Lambda}_c^- p \pi^+)$ $\Gamma_{558}/\Gamma_{546}$

VALUE (units 10^{-3})	CL%	DOCUMENT ID	TECN	COMMENT
0.123 ± 0.012 ± 0.008		1 AUBERT	08BN	BABR $e^+e^- \rightarrow \Upsilon(4S)$

- ¹ Assumes equal production of B^+ and B^0 at the $\Upsilon(4S)$.

Meson Particle Listings

 B^{\pm} $\Gamma(\overline{\Sigma}_c(2455)^0 p \pi^0) / \Gamma_{\text{total}}$ Γ_{559} / Γ

VALUE (units 10^{-4})	DOCUMENT ID	TECN	COMMENT
$3.5 \pm 1.1 \pm 0.2$	1,2 DYTMAN 02	CLE2	$e^+ e^- \rightarrow \Upsilon(4S)$

¹DYTMAN 02 reports $(4.4 \pm 1.4) \times 10^{-4}$ from a measurement of $[\Gamma(B^+ \rightarrow \overline{\Sigma}_c(2455)^0 p \pi^0) / \Gamma_{\text{total}}] \times [B(\Lambda_c^+ \rightarrow p K^- \pi^+)]$ assuming $B(\Lambda_c^+ \rightarrow p K^- \pi^+) = 0.05$, which we rescale to our best value $B(\Lambda_c^+ \rightarrow p K^- \pi^+) = (6.28 \pm 0.32) \times 10^{-2}$. Our first error is their experiment's error and our second error is the systematic error from using our best value.

²Assumes equal production of B^+ and B^0 at the $\Upsilon(4S)$.

 $\Gamma(\overline{\Sigma}_c(2455)^0 p \pi^- \pi^+) / \Gamma_{\text{total}}$ Γ_{560} / Γ

VALUE (units 10^{-4})	DOCUMENT ID	TECN	COMMENT
$3.5 \pm 1.0 \pm 0.2$	1,2 DYTMAN 02	CLE2	$e^+ e^- \rightarrow \Upsilon(4S)$

¹DYTMAN 02 reports $(4.4 \pm 1.3) \times 10^{-4}$ from a measurement of $[\Gamma(B^+ \rightarrow \overline{\Sigma}_c(2455)^0 p \pi^- \pi^+) / \Gamma_{\text{total}}] \times [B(\Lambda_c^+ \rightarrow p K^- \pi^+)]$ assuming $B(\Lambda_c^+ \rightarrow p K^- \pi^+) = 0.05$, which we rescale to our best value $B(\Lambda_c^+ \rightarrow p K^- \pi^+) = (6.28 \pm 0.32) \times 10^{-2}$. Our first error is their experiment's error and our second error is the systematic error from using our best value.

²Assumes equal production of B^+ and B^0 at the $\Upsilon(4S)$.

 $\Gamma(\overline{\Sigma}_c(2455)^- p \pi^+ \pi^+) / \Gamma_{\text{total}}$ Γ_{561} / Γ

VALUE (units 10^{-4})	DOCUMENT ID	TECN	COMMENT
2.37 ± 0.20 OUR AVERAGE			

$2.37 \pm 0.16^{+0.13}_{-0.12}$	1,2 LEES	12Z	BABR $e^+ e^- \rightarrow \Upsilon(4S)$
$2.2 \pm 0.8 \pm 0.1$	1,3 DYTMAN 02	CLE2	$e^+ e^- \rightarrow \Upsilon(4S)$

¹Assumes equal production of B^+ and B^0 at the $\Upsilon(4S)$.

²LEES 12Z reports $(2.98 \pm 0.16 \pm 0.15 \pm 0.77) \times 10^{-4}$ from a measurement of $[\Gamma(B^+ \rightarrow \overline{\Sigma}_c(2455)^- p \pi^+ \pi^+) / \Gamma_{\text{total}}] \times [B(\Lambda_c^+ \rightarrow p K^- \pi^+)]$ assuming $B(\Lambda_c^+ \rightarrow p K^- \pi^+) = (5.0 \pm 1.3) \times 10^{-2}$, which we rescale to our best value $B(\Lambda_c^+ \rightarrow p K^- \pi^+) = (6.28 \pm 0.32) \times 10^{-2}$. Our first error is their experiment's error and our second error is the systematic error from using our best value.

³DYTMAN 02 reports $(2.8 \pm 0.9 \pm 0.5 \pm 0.7) \times 10^{-4}$ from a measurement of $[\Gamma(B^+ \rightarrow \overline{\Sigma}_c(2455)^- p \pi^+ \pi^+) / \Gamma_{\text{total}}] \times [B(\Lambda_c^+ \rightarrow p K^- \pi^+)]$ assuming $B(\Lambda_c^+ \rightarrow p K^- \pi^+) = (5.0 \pm 1.3) \times 10^{-2}$, which we rescale to our best value $B(\Lambda_c^+ \rightarrow p K^- \pi^+) = (6.28 \pm 0.32) \times 10^{-2}$. Our first error is their experiment's error and our second error is the systematic error from using our best value.

 $\Gamma(\overline{\Lambda}_c(2593)^- / \overline{\Lambda}_c(2625)^- p \pi^+) / \Gamma_{\text{total}}$ Γ_{562} / Γ

VALUE	CL%	DOCUMENT ID	TECN	COMMENT
$< 1.9 \times 10^{-4}$	90	1,2 DYTMAN 02	CLE2	$e^+ e^- \rightarrow \Upsilon(4S)$

¹Assumes equal production of B^+ and B^0 at the $\Upsilon(4S)$.

²DYTMAN 02 measurement uses $B(\Lambda_c^- \rightarrow \overline{p} K^+ \pi^-) = 5.0 \pm 1.3\%$. The second error includes the systematic and the uncertainty of the branching ratio.

 $\Gamma(\Xi_c^0 \Lambda_c^+) / \Gamma_{\text{total}}$ Γ_{563} / Γ

VALUE (units 10^{-4})	DOCUMENT ID	TECN	COMMENT
$9.51 \pm 2.10 \pm 0.88$	1 LI	19A	BELL $e^+ e^- \rightarrow \Upsilon(4S)$

¹First measured the absolute branching fraction using a missing-mass technique.

 $\Gamma(\Xi_c^0 \Lambda_c^+, \Xi_c^0 \rightarrow \Xi^+ \pi^-) / \Gamma_{\text{total}}$ Γ_{564} / Γ

VALUE (units 10^{-5})	DOCUMENT ID	TECN	COMMENT
1.76 ± 0.29 OUR AVERAGE			

$1.71 \pm 0.28 \pm 0.15$	1 LI	19A	BELL $e^+ e^- \rightarrow \Upsilon(4S)$
$2.0 \pm 0.7 \pm 0.1$	2,3 AUBERT 08H	BABR	$e^+ e^- \rightarrow \Upsilon(4S)$

• • • We do not use the following data for averages, fits, limits, etc. • • •

$4.5^{+1.8}_{-1.5} \pm 0.2$	3,4 CHISTOV 06A	BELL	Repl. by LI 19A
-----------------------------	-----------------	------	-----------------

¹Using a hadronic B -tagging method based on a full reconstruction.

²AUBERT 08H reports $(2.51 \pm 0.89 \pm 0.61) \times 10^{-5}$ from a measurement of $[\Gamma(B^+ \rightarrow \Xi_c^0 \Lambda_c^+, \Xi_c^0 \rightarrow \Xi^+ \pi^-) / \Gamma_{\text{total}}] \times [B(\Lambda_c^+ \rightarrow p K^- \pi^+)]$ assuming $B(\Lambda_c^+ \rightarrow p K^- \pi^+) = (5.0 \pm 1.3) \times 10^{-2}$, which we rescale to our best value $B(\Lambda_c^+ \rightarrow p K^- \pi^+) = (6.28 \pm 0.32) \times 10^{-2}$. Our first error is their experiment's error and our second error is the systematic error from using our best value.

³Assumes equal production of B^+ and B^0 at the $\Upsilon(4S)$.

⁴CHISTOV 06A reports $(5.6^{+1.9}_{-1.5} \pm 1.9) \times 10^{-5}$ from a measurement of $[\Gamma(B^+ \rightarrow \Xi_c^0 \Lambda_c^+, \Xi_c^0 \rightarrow \Xi^+ \pi^-) / \Gamma_{\text{total}}] \times [B(\Lambda_c^+ \rightarrow p K^- \pi^+)]$ assuming $B(\Lambda_c^+ \rightarrow p K^- \pi^+) = (5.0 \pm 1.3) \times 10^{-2}$, which we rescale to our best value $B(\Lambda_c^+ \rightarrow p K^- \pi^+) = (6.28 \pm 0.32) \times 10^{-2}$. Our first error is their experiment's error and our second error is the systematic error from using our best value.

 $\Gamma(\Xi_c^0 \Lambda_c^+, \Xi_c^0 \rightarrow \Lambda K^+ \pi^-) / \Gamma_{\text{total}}$ Γ_{565} / Γ

VALUE (units 10^{-3})	DOCUMENT ID	TECN	COMMENT
1.14 ± 0.26 OUR AVERAGE			

$1.11 \pm 0.26 \pm 0.10$	1 LI	19A	BELL $e^+ e^- \rightarrow \Upsilon(4S)$
$1.4 \pm 0.8 \pm 0.1$	2,3 AUBERT 08H	BABR	$e^+ e^- \rightarrow \Upsilon(4S)$

• • • We do not use the following data for averages, fits, limits, etc. • • •

$3.2^{+1.1}_{-0.9} \pm 0.2$	3,4 CHISTOV 06A	BELL	Repl. by LI 19A
-----------------------------	-----------------	------	-----------------

¹Using a hadronic B -tagging method based on a full reconstruction.

²AUBERT 08H reports $(1.70 \pm 0.93 \pm 0.53) \times 10^{-5}$ from a measurement of $[\Gamma(B^+ \rightarrow \Xi_c^0 \Lambda_c^+, \Xi_c^0 \rightarrow \Lambda K^+ \pi^-) / \Gamma_{\text{total}}] \times [B(\Lambda_c^+ \rightarrow p K^- \pi^+)]$ assuming $B(\Lambda_c^+ \rightarrow p K^- \pi^+) = (5.0 \pm 1.3) \times 10^{-2}$, which we rescale to our best value $B(\Lambda_c^+ \rightarrow p K^- \pi^+) = (6.28 \pm 0.32) \times 10^{-2}$. Our first error is their experiment's error and our second error is the systematic error from using our best value.

³Assumes equal production of B^+ and B^0 at the $\Upsilon(4S)$.

⁴CHISTOV 06A reports $(4.0^{+1.1}_{-0.9} \pm 1.3) \times 10^{-5}$ from a measurement of $[\Gamma(B^+ \rightarrow \Xi_c^0 \Lambda_c^+, \Xi_c^0 \rightarrow \Lambda K^+ \pi^-) / \Gamma_{\text{total}}] \times [B(\Lambda_c^+ \rightarrow p K^- \pi^+)]$ assuming $B(\Lambda_c^+ \rightarrow p K^- \pi^+) = (5.0 \pm 1.3) \times 10^{-2}$, which we rescale to our best value $B(\Lambda_c^+ \rightarrow p K^- \pi^+) = (6.28 \pm 0.32) \times 10^{-2}$. Our first error is their experiment's error and our second error is the systematic error from using our best value.

 $\Gamma(\Xi_c^0 \Lambda_c^+, \Xi_c^0 \rightarrow p K^- K^- \pi^+) / \Gamma_{\text{total}}$ Γ_{566} / Γ

VALUE (units 10^{-6})	DOCUMENT ID	TECN	COMMENT
$5.47 \pm 1.78 \pm 0.57$	1 LI	19A	BELL $e^+ e^- \rightarrow \Upsilon(4S)$

¹Using a hadronic B -tagging method based on a full reconstruction.

 $\Gamma(\Lambda_c^+ \Xi_c^0) / \Gamma_{\text{total}}$ Γ_{567} / Γ

VALUE	CL%	DOCUMENT ID	TECN	COMMENT
$< 6.5 \times 10^{-4}$	90	1 LI	19G	BELL $e^+ e^- \rightarrow \Upsilon(4S)$

¹Uses fully reconstructed B^+ meson on tag side and recoil against Λ_c^+ on signal side.

 $\Gamma(\Lambda_c^+ \Xi_c^-(2645)^0) / \Gamma_{\text{total}}$ Γ_{568} / Γ

VALUE	CL%	DOCUMENT ID	TECN	COMMENT
$< 7.9 \times 10^{-4}$	90	1 LI	19G	BELL $e^+ e^- \rightarrow \Upsilon(4S)$

¹Uses fully reconstructed B^+ meson on tag side and recoil against Λ_c^+ on signal side.

 $\Gamma(\Lambda_c^+ \Xi_c^-(2790)^0) / \Gamma_{\text{total}}$ Γ_{569} / Γ

VALUE (units 10^{-3})	DOCUMENT ID	TECN	COMMENT
$1.1 \pm 0.4 \pm 0.2$	1 LI	19G	BELL $e^+ e^- \rightarrow \Upsilon(4S)$

¹Uses fully reconstructed B^+ meson on tag side and recoil against Λ_c^+ on signal side.

 $\Gamma(\pi^+ \ell^+ \ell^-) / \Gamma_{\text{total}}$ Γ_{570} / Γ

VALUE	CL%	DOCUMENT ID	TECN	COMMENT
$< 4.9 \times 10^{-8}$	90	1 WEI	08A	BELL $e^+ e^- \rightarrow \Upsilon(4S)$

• • • We do not use the following data for averages, fits, limits, etc. • • •

$< 6.6 \times 10^{-8}$	90	1 LEES	13M	BABR $e^+ e^- \rightarrow \Upsilon(4S)$
$< 1.2 \times 10^{-7}$	90	1 AUBERT	07AG	BABR $e^+ e^- \rightarrow \Upsilon(4S)$

¹Assumes equal production of B^+ and B^0 at the $\Upsilon(4S)$.

 $\Gamma(\pi^+ e^+ e^-) / \Gamma_{\text{total}}$ Γ_{571} / Γ

Test for $\Delta B=1$ weak neutral current. Allowed by higher-order electroweak interactions.

VALUE	CL%	DOCUMENT ID	TECN	COMMENT
$< 8.0 \times 10^{-8}$	90	1 WEI	08A	BELL $e^+ e^- \rightarrow \Upsilon(4S)$

• • • We do not use the following data for averages, fits, limits, etc. • • •

$< 12.5 \times 10^{-8}$	90	1 LEES	13M	BABR $e^+ e^- \rightarrow \Upsilon(4S)$
$< 18 \times 10^{-8}$	90	1 AUBERT	07AG	BABR $e^+ e^- \rightarrow \Upsilon(4S)$
$< 3.9 \times 10^{-3}$	90	2 WEIR	90B	MRK2 $e^+ e^-$ 29 GeV

¹Assumes equal production of B^+ and B^0 at the $\Upsilon(4S)$.

²WEIR 90B assumes B^+ production cross section from LUND.

 $\Gamma(\pi^+ \mu^+ \mu^-) / \Gamma_{\text{total}}$ Γ_{572} / Γ

Test for $\Delta B=1$ weak neutral current. Allowed by higher-order electroweak interactions.

VALUE (units 10^{-8})	CL%	DOCUMENT ID	TECN	COMMENT
$1.78 \pm 0.22 \pm 0.03$		1 AAJ	15AR	LHCB pp at 7, 8 TeV

• • • We do not use the following data for averages, fits, limits, etc. • • •

< 5.5	90	2 LEES	13M	BABR $e^+ e^- \rightarrow \Upsilon(4S)$
$2.3 \pm 0.6 \pm 0.1$		AAJ	12AY	LHCB Repl. by AAJ 15AR
< 6.9	90	2 WEI	08A	BELL $e^+ e^- \rightarrow \Upsilon(4S)$
< 28	90	2 AUBERT	07AG	BABR $e^+ e^- \rightarrow \Upsilon(4S)$

¹AAJ 15AR reports $(1.83 \pm 0.24 \pm 0.05) \times 10^{-8}$ from a measurement of $[\Gamma(B^+ \rightarrow \pi^+ \mu^+ \mu^-) / \Gamma_{\text{total}}] / [B(B^+ \rightarrow J/\psi(1S) K^+)] / [B(J/\psi(1S) \rightarrow \mu^+ \mu^-)]$ assuming $B(B^+ \rightarrow J/\psi(1S) K^+) = (1.05 \pm 0.05) \times 10^{-3}$, $B(J/\psi(1S) \rightarrow \mu^+ \mu^-) = (5.961 \pm 0.033) \times 10^{-2}$, which we rescale to our best values $B(B^+ \rightarrow J/\psi(1S) K^+) = (1.020 \pm 0.019) \times 10^{-3}$, $B(J/\psi(1S) \rightarrow \mu^+ \mu^-) = (5.961 \pm 0.033) \times 10^{-2}$. Our first error is their experiment's error and our second error is the systematic error from using our best values.

²Assumes equal production of B^+ and B^0 at the $\Upsilon(4S)$.

 $\Gamma(\pi^+ \mu^+ \mu^-) / \Gamma(K^+ \mu^+ \mu^-)$ $\Gamma_{572} / \Gamma_{576}$

VALUE	DOCUMENT ID	TECN	COMMENT
$0.053 \pm 0.014 \pm 0.001$	AAJ	12AY	LHCB Repl. by AAJ 15AR

• • • We do not use the following data for averages, fits, limits, etc. • • •

 $\Gamma(\pi^+ \nu \nu) / \Gamma_{\text{total}}$ Γ_{573} / Γ

Test for $\Delta B=1$ weak neutral current. Allowed by higher-order electroweak interactions.

VALUE	CL%	DOCUMENT ID	TECN	COMMENT
$< 1.4 \times 10^{-5}$	90	1 GRYGIER	17	BELL $e^+ e^- \rightarrow \Upsilon(4S)$

• • • We do not use the following data for averages, fits, limits, etc. • • •

$<9.8 \times 10^{-5}$	90	1 LUTZ	13 BELL	$e^+e^- \rightarrow \Upsilon(4S)$
$<1.7 \times 10^{-4}$	90	1 CHEN	07D BELL	$e^+e^- \rightarrow \Upsilon(4S)$
$<1.0 \times 10^{-4}$	90	1 AUBERT	05H BABR	$e^+e^- \rightarrow \Upsilon(4S)$

¹ Assumes equal production of B^+ and B^0 at the $\Upsilon(4S)$.

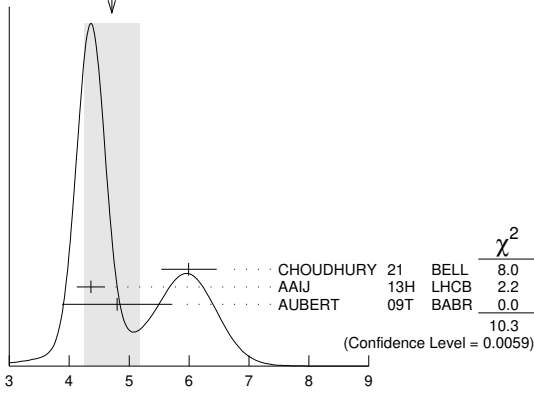
$\Gamma(K^+ \ell^+ \ell^-)/\Gamma_{total}$ Γ_{574}/Γ
 Test for $\Delta B=1$ weak neutral current. Allowed by higher-order electroweak interactions.

VALUE (units 10^{-7})	DOCUMENT ID	TECN	COMMENT
4.7 ± 0.5 OUR AVERAGE	Error includes scale factor of 2.3. See the ideogram below.		
5.99 ^{+0.45} _{-0.43} ± 0.14	CHOU DHURY 21	BELL	$e^+e^- \rightarrow \Upsilon(4S)$
4.36 ± 0.15 ± 0.18	1 AAIJ	13H LHCB	pp at 7 TeV
4.8 ± 0.9 ± 0.2	2 AUBERT	09T BABR	$e^+e^- \rightarrow \Upsilon(4S)$

• • • We do not use the following data for averages, fits, limits, etc. • • •

5.3 ^{+0.6} _{-0.5} ± 0.3	2,3 WEI	09A BELL	$e^+e^- \rightarrow \Upsilon(4S)$
3.8 ^{+0.9} _{-0.8} ± 0.2	2 AUBERT,B	06J BABR	Repl. by AUBERT 09T
5.3 ^{+1.1} _{-1.0} ± 0.3	2 ISHIKAWA	03 BELL	Repl. by WEI 09A

WEIGHTED AVERAGE
4.7±0.5 (Error scaled by 2.3)



- ¹ Uses $B(B^+ \rightarrow J/\psi K^+ \rightarrow \mu^+ \mu^- K^+) = (6.01 \pm 0.21) \times 10^{-5}$.
- ² Assumes equal production of B^+ and B^0 at the $\Upsilon(4S)$.
- ³ Superseded by CHOU DHURY 21.

$\Gamma(K^+ e^+ e^-)/\Gamma_{total}$ Γ_{575}/Γ
 Test for $\Delta B=1$ weak neutral current. Allowed by higher-order electroweak interactions.

VALUE (units 10^{-7})	CL%	DOCUMENT ID	TECN	COMMENT
5.6 ± 0.6 OUR AVERAGE		Error includes scale factor of 1.8.		
5.75 ^{+0.64} _{-0.61} ± 0.15		CHOU DHURY 21	BELL	$e^+e^- \rightarrow \Upsilon(4S)$
5.1 ^{+1.2} _{-1.1} ± 0.2		1 AUBERT	09T BABR	$e^+e^- \rightarrow \Upsilon(4S)$

• • • We do not use the following data for averages, fits, limits, etc. • • •

5.7 ^{+0.9} _{-0.8} ± 0.3	1,2 WEI	09A BELL	$e^+e^- \rightarrow \Upsilon(4S)$
4.2 ^{+1.2} _{-1.1} ± 0.2	1 AUBERT,B	06J BABR	Repl. by AUBERT 09T
10.5 ^{+2.5} _{-2.2} ± 0.7	1 AUBERT	03U BABR	Repl. by AUBERT,B 06J
6.3 ^{+1.9} _{-1.7} ± 0.3	3 ISHIKAWA	03 BELL	Repl. by WEI 09A
<14	90	1 ABE	02 BELL $e^+e^- \rightarrow \Upsilon(4S)$
<9	90	1 AUBERT	02L BABR $e^+e^- \rightarrow \Upsilon(4S)$
<24	90	4 ANDERSON	01B CLE2 $e^+e^- \rightarrow \Upsilon(4S)$

- ¹ Assumes equal production of B^+ and B^0 at the $\Upsilon(4S)$.
- ² Superseded by CHOU DHURY 21.
- ³ Assumes equal production of B^0 and B^+ at $\Upsilon(4S)$. The second error is a total of systematic uncertainties including model dependence.
- ⁴ The result is for di-lepton masses above 0.5 GeV.

$\Gamma(K^+ \mu^+ \mu^-)/\Gamma_{total}$ Γ_{576}/Γ
 Test for $\Delta B=1$ weak neutral current. Allowed by higher-order electroweak interactions.

VALUE (units 10^{-7})	CL%	DOCUMENT ID	TECN	COMMENT
4.53 ± 0.35 OUR FIT		Error includes scale factor of 1.8.		
4.5 ± 0.6 OUR AVERAGE		Error includes scale factor of 2.9.		
6.24 ^{+0.65} _{-0.61} ± 0.16		CHOU DHURY 21	BELL	$e^+e^- \rightarrow \Upsilon(4S)$
4.29 ± 0.07 ± 0.21		1 AAIJ	14M LHCB	pp at 7, 8 TeV
4.1 ^{+1.6} _{-1.5} ± 0.2		2 AUBERT	09T BABR	$e^+e^- \rightarrow \Upsilon(4S)$

• • • We do not use the following data for averages, fits, limits, etc. • • •

4.36 ± 0.15 ± 0.18	3 AAIJ	13H LHCB	Repl. by AAIJ 14M
5.3 ^{+0.8} _{-0.7} ± 0.3	2,4 WEI	09A BELL	$e^+e^- \rightarrow \Upsilon(4S)$
3.1 ^{+1.5} _{-1.2} ± 0.3	2 AUBERT,B	06J BABR	Repl. by AUBERT 09T
0.7 ^{+1.9} _{-1.1} ± 0.2	2 AUBERT	03U BABR	Repl. by AUBERT,B 06J
4.5 ^{+1.4} _{-1.2} ± 0.3	5 ISHIKAWA	03 BELL	Repl. by WEI 09A
9.8 ^{+4.6} _{-3.6} ± 1.6	2 ABE	02 BELL	Repl. by ISHIKAWA 03
< 12	90	2 AUBERT	02L BABR $e^+e^- \rightarrow \Upsilon(4S)$
< 36.8	90	6 ANDERSON	01B CLE2 $e^+e^- \rightarrow \Upsilon(4S)$
< 52	90	7 AFFOLDER	99B CDF $p\bar{p}$ at 1.8 TeV
< 100	90	8 ABE	96L CDF Repl. by AFFOLDER 99B
< 2400	90	9 ALBRECHT	91E ARG $e^+e^- \rightarrow \Upsilon(4S)$
< 64000	90	10 WEIR	90B MRK2 $e^+e^- 29$ GeV
< 1700	90	11 AVERY	89B CLEO $e^+e^- \rightarrow \Upsilon(4S)$
< 3800	90	12 AVERY	87 CLEO $e^+e^- \rightarrow \Upsilon(4S)$

- ¹ Uses $B(B^+ \rightarrow J/\psi(1S) K^+) = (0.998 \pm 0.014 \pm 0.040) \times 10^{-3}$ for normalization.
- ² Assumes equal production of B^+ and B^0 at the $\Upsilon(4S)$.
- ³ Uses $B(B^+ \rightarrow J/\psi K^+ \rightarrow \mu^+ \mu^- K^+) = (6.01 \pm 0.21) \times 10^{-5}$.
- ⁴ Superseded by CHOU DHURY 21.
- ⁵ Assumes equal production of B^0 and B^+ at $\Upsilon(4S)$. The second error is a total of systematic uncertainties including model dependence.
- ⁶ The result is for di-lepton masses above 0.5 GeV.
- ⁷ AFFOLDER 99B measured relative to $B^+ \rightarrow J/\psi(1S) K^+$.
- ⁸ ABE 96L measured relative to $B^+ \rightarrow J/\psi(1S) K^+$ using PDG 94 branching ratios.
- ⁹ ALBRECHT 91E reports $< 2.2 \times 10^{-4}$ assuming the $\Upsilon(4S)$ decays 45% to $B^0 \bar{B}^0$. We rescale to 50%.
- ¹⁰ WEIR 90B assumes B^+ production cross section from LUND.
- ¹¹ AVERY 89B reports $< 1.5 \times 10^{-4}$ assuming the $\Upsilon(4S)$ decays 43% to $B^0 \bar{B}^0$. We rescale to 50%.
- ¹² AVERY 87 reports $< 3.2 \times 10^{-4}$ assuming the $\Upsilon(4S)$ decays 40% to $B^0 \bar{B}^0$. We rescale to 50%.

$\Gamma(K^+ \mu^+ \mu^- \text{nonresonant})/\Gamma_{total}$ Γ_{577}/Γ
 Test for $\Delta B=1$ weak neutral current. Allowed by higher-order electroweak interactions.

VALUE (units 10^{-7})	DOCUMENT ID	TECN	COMMENT
4.37 ± 0.15 ± 0.23	1 AAIJ	17Y LHCB	pp at 7, 8 TeV

¹ Measured in amplitude analysis using model including short-distance $K^+ \mu^+ \mu^-$ and $\rho(770), \omega(782), \phi(1020), J/\psi, \psi(2S), \psi(3770), \psi(4040), \psi(4160),$ and $\psi(4415)$ contributions.

$\Gamma(K^+ \tau^+ \tau^-)/\Gamma_{total}$ Γ_{578}/Γ
 Test for $\Delta B=1$ weak neutral current. Allowed by higher-order electroweak interactions.

VALUE	CL%	DOCUMENT ID	TECN	COMMENT
< 2.25 × 10⁻³	90	1,2 LEES	17 BABR	$e^+e^- \rightarrow \Upsilon(4S)$

- ¹ Uses only leptonic decays of τ and the quoted limit combines the final states $K^+ e^+ e^-$, $K^+ \mu^+ \mu^-$, and $K^+ \tau^+ \tau^-$.
- ² If observed events are interpreted as a signal the branching fraction measurement becomes $(1.31^{+0.66+0.35}_{-0.61-0.25}) \times 10^{-3}$.

$\Gamma(K^+ \mu^+ \mu^-)/\Gamma(J/\psi(1S) K^+)$ $\Gamma_{576}/\Gamma_{276}$
 Test for $\Delta B=1$ weak neutral current. Allowed by higher-order electroweak interactions.

VALUE (units 10^{-3})	DOCUMENT ID	TECN	COMMENT
0.444 ± 0.034 OUR FIT	Error includes scale factor of 1.7.		
0.46 ± 0.04 ± 0.02	AALTONEN 11A1	CDF	$p\bar{p}$ at 1.96 TeV
0.38 ± 0.05 ± 0.02	AALTONEN 11L	CDF	Repl. by AALTONEN 11A1
0.59 ± 0.15 ± 0.03	AALTONEN 09B	CDF	Repl. by AALTONEN 11L

• • • We do not use the following data for averages, fits, limits, etc. • • •

< 4.1 × 10 ⁻⁵	90	3 ABUDINEN	21 BEL2	$e^+e^- \rightarrow \Upsilon(4S)$
< 1.9 × 10 ⁻⁵	90	1,4 GRYGIER	17 BELL	$e^+e^- \rightarrow \Upsilon(4S)$
< 5.5 × 10 ⁻⁵	90	1 LUTZ	13 BELL	$e^+e^- \rightarrow \Upsilon(4S)$
< 1.3 × 10 ⁻⁵	90	1 DEL-AMO-SA.10	BABR	Repl. by LEES 13I
< 1.4 × 10 ⁻⁵	90	1 CHEN	07D BELL	$e^+e^- \rightarrow \Upsilon(4S)$
< 5.2 × 10 ⁻⁵	90	1 AUBERT	05H BABR	$e^+e^- \rightarrow \Upsilon(4S)$
< 2.4 × 10 ⁻⁴	90	1 BROWDER	01 CLE2	$e^+e^- \rightarrow \Upsilon(4S)$

- ¹ Assumes equal production of B^+ and B^0 at the $\Upsilon(4S)$.
- ² Also reported a limit $< 3.7 \times 10^{-5}$ at 90% CL obtained using a fully reconstructed hadronic B -tag evnets.
- ³ Using an inclusive tagging method that exploits not only the properties of the $B^+ \rightarrow K^+ \nu \tau$ decay, but also the inclusive properties of the other B meson in the event.
- ⁴ The result was reported in arXiv:1702.03224, but missing from the publication by mistake.

$\Gamma(\rho^+ \nu \tau)/\Gamma_{total}$ Γ_{580}/Γ
 Test for $\Delta B=1$ weak neutral current. Allowed by higher-order electroweak interaction.

VALUE	CL%	DOCUMENT ID	TECN	COMMENT
< 3.0 × 10⁻⁵	90	1 GRYGIER	17 BELL	$e^+e^- \rightarrow \Upsilon(4S)$

• • • We do not use the following data for averages, fits, limits, etc. • • •

< 2.13 × 10 ⁻⁴	90	1 LUTZ	13 BELL	$e^+e^- \rightarrow \Upsilon(4S)$
< 1.5 × 10 ⁻⁴	90	1 CHEN	07D BELL	Repl. by LUTZ 13

¹ Assumes equal production of B^+ and B^0 at the $\Upsilon(4S)$.

Meson Particle Listings

 B^\pm

$\Gamma(K^*(892)+\ell^+\ell^-)/\Gamma_{\text{total}}$ Γ_{581}/Γ
Test for $\Delta B=1$ weak neutral current. Allowed by higher-order electroweak interactions.

VALUE (units 10^{-7})	CL%	DOCUMENT ID	TECN	COMMENT
10.1 ± 1.1 OUR AVERAGE				Error includes scale factor of 1.1.
9.24 ± 0.93 ± 0.67		AAIJ	14M LHCb	pp at 7, 8 TeV
14.0 $^{+4.0}_{-3.7}$ ± 0.9		¹ AUBERT	09T BABR	$e^+e^- \rightarrow \Upsilon(4S)$
12.4 $^{+2.3}_{-2.1}$ ± 1.3		¹ WEI	09A BELL	$e^+e^- \rightarrow \Upsilon(4S)$
• • • We do not use the following data for averages, fits, limits, etc. • • •				
11.6 ± 1.9		² AAIJ	12AH LHCb	Repl. by AAIJ 14M
7.3 $^{+5.0}_{-4.2}$ ± 2.1		¹ AUBERT,B	06J BABR	Repl. by AUBERT 09T
<22	90	¹ ISHIKAWA	03 BELL	$e^+e^- \rightarrow \Upsilon(4S)$
¹ Assumes equal production of B^+ and B^0 at the $\Upsilon(4S)$.				
² Measured in $B^+ \rightarrow K^*(892)+\mu^+\mu^-$ decays.				

$\Gamma(K^*(892)+e^+e^-)/\Gamma_{\text{total}}$ Γ_{592}/Γ
Test for $\Delta B=1$ weak neutral current. Allowed by higher-order electroweak interactions.

VALUE (units 10^{-7})	CL%	DOCUMENT ID	TECN	COMMENT
15.5 $^{+4.0}_{-3.1}$ OUR AVERAGE				
13.8 $^{+4.7}_{-4.2}$ ± 0.8		¹ AUBERT	09T BABR	$e^+e^- \rightarrow \Upsilon(4S)$
17.3 $^{+5.0}_{-4.2}$ ± 2.0		¹ WEI	09A BELL	$e^+e^- \rightarrow \Upsilon(4S)$
• • • We do not use the following data for averages, fits, limits, etc. • • •				
7.5 $^{+7.6}_{-6.5}$ ± 3.8		¹ AUBERT,B	06J BABR	Repl. by AUBERT 09T
2.0 $^{+13.4}_{-8.7}$ ± 2.8		¹ AUBERT	03U BABR	$e^+e^- \rightarrow \Upsilon(4S)$
< 46	90	² ISHIKAWA	03 BELL	$e^+e^- \rightarrow \Upsilon(4S)$
< 89	90	¹ ABE	02 BELL	Repl. by ISHIKAWA 03
< 95	90	¹ AUBERT	02L BABR	$e^+e^- \rightarrow \Upsilon(4S)$
<6900	90	³ ALBRECHT	91E ARG	$e^+e^- \rightarrow \Upsilon(4S)$
¹ Assumes equal production of B^+ and B^0 at the $\Upsilon(4S)$.				
² Assumes equal production of B^0 and B^+ at $\Upsilon(4S)$. The second error is a total of systematic uncertainties including model dependence.				
³ ALBRECHT 91E reports $< 6.3 \times 10^{-4}$ assuming the $\Upsilon(4S)$ decays 45% to $B^0\bar{B}^0$. We rescale to 50%.				

$\Gamma(K^*(892)+\mu^+\mu^-)/\Gamma_{\text{total}}$ Γ_{583}/Γ
Test for $\Delta B=1$ weak neutral current. Allowed by higher-order electroweak interactions.

VALUE (units 10^{-7})	CL%	DOCUMENT ID	TECN	COMMENT
9.6 ± 1.0 OUR FIT				
9.6 ± 1.1 OUR AVERAGE				
9.24 ± 0.93 ± 0.67		¹ AAIJ	14M LHCb	pp at 7, 8 TeV
14.6 $^{+7.9}_{-7.5}$ ± 1.2		² AUBERT	09T BABR	$e^+e^- \rightarrow \Upsilon(4S)$
11.1 $^{+3.2}_{-2.7}$ ± 1.0		² WEI	09A BELL	$e^+e^- \rightarrow \Upsilon(4S)$
• • • We do not use the following data for averages, fits, limits, etc. • • •				
11.6 ± 1.9		AAIJ	12AH LHCb	Repl. by AAIJ 14M
9.7 $^{+9.4}_{-6.9}$ ± 1.4		² AUBERT,B	06J BABR	Repl. by AUBERT 09T
30.7 $^{+25.8}_{-17.8}$ ± 4.2		² AUBERT	03U BABR	$e^+e^- \rightarrow \Upsilon(4S)$
6.5 $^{+6.9}_{-5.3}$ ± 1.5		³ ISHIKAWA	03 BELL	Repl. by WEI 09A
< 39	90	² ABE	02 BELL	Repl. by ISHIKAWA 03
<170	90	² AUBERT	02L BABR	$e^+e^- \rightarrow \Upsilon(4S)$
¹ Uses $B(B^+ \rightarrow J/\psi(1S)K^*(892)^+) = (1.431 \pm 0.027 \pm 0.090) \times 10^{-3}$ for normalization.				
² Assumes equal production of B^+ and B^0 at the $\Upsilon(4S)$.				
³ Assumes equal production of B^0 and B^+ at $\Upsilon(4S)$. The second error is a total of systematic uncertainties including model dependence. The 90% C.L. upper limit is 2.2×10^{-6} .				

$\Gamma(K^*(892)+\mu^+\mu^-)/\Gamma(J/\psi(1S)K^*(892)^+)$ $\Gamma_{583}/\Gamma_{281}$
VALUE (units 10^{-3})

VALUE (units 10^{-3})	DOCUMENT ID	TECN	COMMENT
0.67 ± 0.08 OUR FIT			
0.67 ± 0.22 ± 0.04	AALTONEN	11Al CDF	$p\bar{p}$ at 1.96 TeV

$\Gamma(K^*(892)+\nu\bar{\nu})/\Gamma_{\text{total}}$ Γ_{584}/Γ
Test for $\Delta B=1$ weak neutral current. Allowed by higher-order electroweak interaction.

VALUE	CL%	DOCUMENT ID	TECN	COMMENT
<4.0 × 10⁻⁵	90	¹ LUTZ	13 BELL	$e^+e^- \rightarrow \Upsilon(4S)$
• • • We do not use the following data for averages, fits, limits, etc. • • •				
<6.1 × 10 ⁻⁵	90	¹ GRYGIER	17 BELL	$e^+e^- \rightarrow \Upsilon(4S)$
<6.4 × 10 ⁻⁵	90	^{1,2} LEES	13l BABR	$e^+e^- \rightarrow \Upsilon(4S)$
<8 × 10 ⁻⁵	90	AUBERT	08bc BABR	Repl. by LEES 13l
<1.4 × 10 ⁻⁴	90	¹ CHEN	07D BELL	$e^+e^- \rightarrow \Upsilon(4S)$
¹ Assumes equal production of B^+ and B^0 at the $\Upsilon(4S)$.				
² Also reported a limit $< 11.6 \times 10^{-5}$ at 90% CL obtained using a fully reconstructed hadronic B -tag events.				

$\Gamma(K^+\pi^+\pi^-\mu^+\mu^-)/\Gamma(\psi(2S)K^+)$ $\Gamma_{585}/\Gamma_{311}$
VALUE (units 10^{-4})

VALUE (units 10^{-4})	DOCUMENT ID	TECN	COMMENT
6.95 $^{+0.46}_{-0.43}$ ± 0.34	AAIJ	14AZ LHCb	pp at 7, 8 TeV

$\Gamma(\phi K^+\mu^+\mu^-)/\Gamma(J/\psi(1S)\phi K^+)$ $\Gamma_{586}/\Gamma_{288}$
VALUE (units 10^{-3})

VALUE (units 10^{-3})	DOCUMENT ID	TECN	COMMENT
1.58 $^{+0.36}_{-0.32}$ - 0.07	AAIJ	14AZ LHCb	pp at 7, 8 TeV

$\Gamma(\bar{\Lambda}p\nu\bar{\nu})/\Gamma_{\text{total}}$ Γ_{587}/Γ
VALUE

VALUE	CL%	DOCUMENT ID	TECN	COMMENT
<3.0 × 10⁻⁵	90	¹ LEES	19c BABR	$e^+e^- \rightarrow \Upsilon(4S)$

¹ Signal candidates are identified by first fully reconstructing B^+ in one of many possible exclusive decays to hadronic final states.

$\Gamma(\pi^+e^+\mu^-)/\Gamma_{\text{total}}$ Γ_{588}/Γ
Test of lepton family number conservation.

VALUE	CL%	DOCUMENT ID	TECN	COMMENT
<0.0064	90	¹ WEIR	90B MRK2	e^+e^- 29 GeV

¹ WEIR 90B assumes B^+ production cross section from LUND.

$\Gamma(\pi^+e^-\mu^+)/\Gamma_{\text{total}}$ Γ_{589}/Γ
Test of lepton family number conservation.

VALUE	CL%	DOCUMENT ID	TECN	COMMENT
<0.0064	90	¹ WEIR	90B MRK2	e^+e^- 29 GeV

¹ WEIR 90B assumes B^+ production cross section from LUND.

$\Gamma(\pi^+e^\pm\mu^\mp)/\Gamma_{\text{total}}$ Γ_{590}/Γ
VALUE

VALUE	CL%	DOCUMENT ID	TECN	COMMENT
<1.7 × 10⁻⁷	90	¹ AUBERT	07Ag BABR	$e^+e^- \rightarrow \Upsilon(4S)$

¹ Assumes equal production of B^+ and B^0 at the $\Upsilon(4S)$.

$\Gamma(\pi^+e^+\tau^-)/\Gamma_{\text{total}}$ Γ_{591}/Γ
Test of lepton family number conservation.

VALUE (units 10^{-6})	CL%	DOCUMENT ID	TECN	COMMENT
<74	90	¹ LEES	12P BABR	$e^+e^- \rightarrow \Upsilon(4S)$

¹ Uses a fully reconstructed hadronic B decay as a tag on the recoil side.

$\Gamma(\pi^+e^-\tau^+)/\Gamma_{\text{total}}$ Γ_{592}/Γ
Test of lepton family number conservation.

VALUE (units 10^{-6})	CL%	DOCUMENT ID	TECN	COMMENT
<20	90	¹ LEES	12P BABR	$e^+e^- \rightarrow \Upsilon(4S)$

¹ Uses a fully reconstructed hadronic B decay as a tag on the recoil side.

$\Gamma(\pi^+e^\pm\tau^\mp)/\Gamma_{\text{total}}$ Γ_{593}/Γ
Test of lepton family number conservation.

VALUE (units 10^{-6})	CL%	DOCUMENT ID	TECN	COMMENT
<75	90	^{1,2} LEES	12P BABR	$e^+e^- \rightarrow \Upsilon(4S)$

¹ Assumes $B(B^+ \rightarrow h^+\ell^+\tau^-) = B(B^+ \rightarrow h^+\ell^-\tau^+)$.

² Uses a fully reconstructed hadronic B decay as a tag on the recoil side.

$\Gamma(\pi^+\mu^+\tau^-)/\Gamma_{\text{total}}$ Γ_{594}/Γ
Test of lepton family number conservation.

VALUE (units 10^{-6})	CL%	DOCUMENT ID	TECN	COMMENT
<62	90	¹ LEES	12P BABR	$e^+e^- \rightarrow \Upsilon(4S)$

¹ Uses a fully reconstructed hadronic B decay as a tag on the recoil side.

$\Gamma(\pi^+\mu^-\tau^+)/\Gamma_{\text{total}}$ Γ_{595}/Γ
Test of lepton family number conservation.

VALUE (units 10^{-6})	CL%	DOCUMENT ID	TECN	COMMENT
<45	90	¹ LEES	12P BABR	$e^+e^- \rightarrow \Upsilon(4S)$

¹ Uses a fully reconstructed hadronic B decay as a tag on the recoil side.

$\Gamma(\pi^+\mu^\pm\tau^\mp)/\Gamma_{\text{total}}$ Γ_{596}/Γ
Test of lepton family number conservation.

VALUE (units 10^{-6})	CL%	DOCUMENT ID	TECN	COMMENT
<72	90	^{1,2} LEES	12P BABR	$e^+e^- \rightarrow \Upsilon(4S)$

¹ Assumes $B(B^+ \rightarrow h^+\ell^+\tau^-) = B(B^+ \rightarrow h^+\ell^-\tau^+)$.

² Uses a fully reconstructed hadronic B decay as a tag on the recoil side.

$\Gamma(K^+e^+\mu^-)/\Gamma_{\text{total}}$ Γ_{597}/Γ
Test of lepton family number conservation.

VALUE	CL%	DOCUMENT ID	TECN	COMMENT
<6.4 × 10⁻⁹	90	AAIJ	19AM LHCb	pp at 7, 8 TeV

• • • We do not use the following data for averages, fits, limits, etc. • • •

<3.0 × 10⁻⁸ 90 CHOUDHURY 21 BELL $e^+e^- \rightarrow \Upsilon(4S)$

<0.91 × 10⁻⁷ 90 ¹AUBERT,B 06J BABR $e^+e^- \rightarrow \Upsilon(4S)$

<8 × 10⁻⁷ 90 ¹AUBERT 02L BABR Repl. by AUBERT,B 06J

<6.4 × 10⁻³ 90 ²WEIR 90B MRK2 e^+e^- 29 GeV

¹ Assumes equal production of B^+ and B^0 at the $\Upsilon(4S)$.

² WEIR 90B assumes B^+ production cross section from LUND.

• • • We do not use the following data for averages, fits, limits, etc. • • •
 $< 8.5 \times 10^{-8}$ 90 CHOUDHURY 21 BELL $e^+e^- \rightarrow \Upsilon(4S)$
 $< 1.3 \times 10^{-7}$ 90 1 AUBERT,B 06J BABR $e^+e^- \rightarrow \Upsilon(4S)$
 $< 6.4 \times 10^{-3}$ 90 2 WEIR 90B MRK2 $e^+e^- 29 \text{ GeV}$

¹ Assumes equal production of B^+ and B^0 at the $\Upsilon(4S)$.
² WEIR 90B assumes B^+ production cross section from LUND.

$\Gamma(K^+ e^{\pm} \mu^{\mp})/\Gamma_{\text{total}}$ Γ_{599}/Γ

VALUE (units 10^{-7})	CL%	DOCUMENT ID	TECN	COMMENT
<0.91	90	1 AUBERT,B 06J	BABR	$e^+e^- \rightarrow \Upsilon(4S)$

¹ Assumes equal production of B^+ and B^0 at the $\Upsilon(4S)$.

$\Gamma(K^+ K^{\pm} \tau^{\mp})/\Gamma_{\text{total}}$ Γ_{600}/Γ

Test of lepton family number conservation.

VALUE (units 10^{-6})	CL%	DOCUMENT ID	TECN	COMMENT
<43	90	1 LEES 12P	BABR	$e^+e^- \rightarrow \Upsilon(4S)$

¹ Uses a fully reconstructed hadronic B decay as a tag on the recoil side.

$\Gamma(K^+ e^- \tau^+)/\Gamma_{\text{total}}$ Γ_{601}/Γ

Test of lepton family number conservation.

VALUE (units 10^{-6})	CL%	DOCUMENT ID	TECN	COMMENT
<15	90	1 LEES 12P	BABR	$e^+e^- \rightarrow \Upsilon(4S)$

¹ Uses a fully reconstructed hadronic B decay as a tag on the recoil side.

$\Gamma(K^+ e^{\pm} \tau^{\mp})/\Gamma_{\text{total}}$ Γ_{602}/Γ

Test of lepton family number conservation.

VALUE (units 10^{-6})	CL%	DOCUMENT ID	TECN	COMMENT
<30	90	1,2 LEES 12P	BABR	$e^+e^- \rightarrow \Upsilon(4S)$

¹ Assumes $B(B^+ \rightarrow h^+ \ell^+ \tau^-) = B(B^+ \rightarrow h^+ \ell^- \tau^+)$.

² Uses a fully reconstructed hadronic B decay as a tag on the recoil side.

$\Gamma(K^+ \mu^+ \tau^-)/\Gamma_{\text{total}}$ Γ_{603}/Γ

Test of lepton family number conservation.

VALUE (units 10^{-6})	CL%	DOCUMENT ID	TECN	COMMENT
<45	90	1 LEES 12P	BABR	$e^+e^- \rightarrow \Upsilon(4S)$

¹ Uses a fully reconstructed hadronic B decay as a tag on the recoil side.

$\Gamma(K^+ \mu^- \tau^+)/\Gamma_{\text{total}}$ Γ_{604}/Γ

Test of lepton family number conservation.

VALUE	CL%	DOCUMENT ID	TECN	COMMENT
<2.8 $\times 10^{-5}$	90	1 LEES 12P	BABR	$e^+e^- \rightarrow \Upsilon(4S)$

• • • We do not use the following data for averages, fits, limits, etc. • • •

$< 3.9 \times 10^{-5}$	90	2 AAIJ 20P	LHCB	pp at 7, 8, 13 TeV
------------------------	----	------------	------	----------------------

¹ Uses a fully reconstructed hadronic B decay as a tag on the recoil side.

² Uses the $B_{s2}^0 \rightarrow B^+ K^-$ decays for kinematic constraints.

$\Gamma(K^+ \mu^{\pm} \tau^{\mp})/\Gamma_{\text{total}}$ Γ_{605}/Γ

Test of lepton family number conservation.

VALUE (units 10^{-6})	CL%	DOCUMENT ID	TECN	COMMENT
<48	90	1,2 LEES 12P	BABR	$e^+e^- \rightarrow \Upsilon(4S)$

• • • We do not use the following data for averages, fits, limits, etc. • • •

< 77	90	1 AUBERT 07AZ	BABR	Repl. by LEES 12P
--------	----	---------------	------	-------------------

¹ Uses a fully reconstructed hadronic B decay as a tag on the recoil side.

² Assumes $B(B^+ \rightarrow h^+ \ell^+ \tau^-) = B(B^+ \rightarrow h^+ \ell^- \tau^+)$.

$\Gamma(K^*(892)^+ e^+ \mu^-)/\Gamma_{\text{total}}$ Γ_{606}/Γ

VALUE (units 10^{-7})	CL%	DOCUMENT ID	TECN	COMMENT
<13	90	1 AUBERT,B 06J	BABR	$e^+e^- \rightarrow \Upsilon(4S)$

¹ Assumes equal production of B^+ and B^0 at the $\Upsilon(4S)$.

$\Gamma(K^*(892)^+ e^- \mu^+)/\Gamma_{\text{total}}$ Γ_{607}/Γ

VALUE (units 10^{-7})	CL%	DOCUMENT ID	TECN	COMMENT
<9.9	90	1 AUBERT,B 06J	BABR	$e^+e^- \rightarrow \Upsilon(4S)$

¹ Assumes equal production of B^+ and B^0 at the $\Upsilon(4S)$.

$\Gamma(K^*(892)^+ e^{\pm} \mu^{\mp})/\Gamma_{\text{total}}$ Γ_{608}/Γ

Test of lepton family number conservation.

VALUE	CL%	DOCUMENT ID	TECN	COMMENT
<1.4 $\times 10^{-6}$	90	1 AUBERT,B 06J	BABR	$e^+e^- \rightarrow \Upsilon(4S)$

• • • We do not use the following data for averages, fits, limits, etc. • • •

$< 7.9 \times 10^{-6}$	90	1 AUBERT 02L	BABR	Repl. by AUBERT,B 06J
------------------------	----	--------------	------	-----------------------

¹ Assumes equal production of B^+ and B^0 at the $\Upsilon(4S)$.

$\Gamma(\pi^- e^+ e^+)/\Gamma_{\text{total}}$ Γ_{609}/Γ

Test of total lepton number conservation.

VALUE	CL%	DOCUMENT ID	TECN	COMMENT
<2.3 $\times 10^{-8}$	90	1 LEES 12J	BABR	$e^+e^- \rightarrow \Upsilon(4S)$

• • • We do not use the following data for averages, fits, limits, etc. • • •

$< 1.6 \times 10^{-6}$	90	1 EDWARDS 02B	CLE2	$e^+e^- \rightarrow \Upsilon(4S)$
------------------------	----	---------------	------	-----------------------------------

< 0.0039	90	2 WEIR 90B	MRK2	$e^+e^- 29 \text{ GeV}$
------------	----	------------	------	-------------------------

¹ Assumes equal production of B^+ and B^0 at the $\Upsilon(4S)$.

² WEIR 90B assumes B^+ production cross section from LUND.

$\Gamma(\pi^- \mu^+ \mu^+)/\Gamma_{\text{total}}$ Γ_{610}/Γ

Test of total lepton number conservation.

VALUE	CL%	DOCUMENT ID	TECN	COMMENT
< 4.0 $\times 10^{-9}$	95	1 AAIJ 14AC	LHCB	pp at 7, 8 TeV

• • • We do not use the following data for averages, fits, limits, etc. • • •

$< 1.3 \times 10^{-8}$	95	2 AAIJ 12AD	LHCB	Repl. by AAIJ 14AC
------------------------	----	-------------	------	--------------------

$< 4.4 \times 10^{-8}$	90	1 AAIJ 12C	LHCB	pp at 7 TeV
------------------------	----	------------	------	---------------

$< 10.7 \times 10^{-8}$	90	3 LEES 12J	BABR	$e^+e^- \rightarrow \Upsilon(4S)$
-------------------------	----	------------	------	-----------------------------------

$< 1.4 \times 10^{-6}$	90	3 EDWARDS 02B	CLE2	$e^+e^- \rightarrow \Upsilon(4S)$
------------------------	----	---------------	------	-----------------------------------

$< 9.1 \times 10^{-3}$	90	4 WEIR 90B	MRK2	$e^+e^- 29 \text{ GeV}$
------------------------	----	------------	------	-------------------------

¹ Uses $B^+ \rightarrow J/\psi K^+$, $J/\psi \rightarrow \mu^+ \mu^-$ mode for normalization. Obtains neutrino-mass-dependent upper limits in the range $0.4\text{--}4.0 \times 10^{-9}$. This limit is applicable for Majorana neutrino lifetime $< 1 \text{ ps}$.

² Uses $B^+ \rightarrow J/\psi K^+$, $J/\psi \rightarrow \mu^+ \mu^-$ mode for normalization. Obtains neutrino-mass-dependent upper limits in the range $0.4\text{--}1.0 \times 10^{-8}$.

³ Assumes equal production of B^+ and B^0 at the $\Upsilon(4S)$.

⁴ WEIR 90B assumes B^+ production cross section from LUND.

$\Gamma(\pi^- e^- \mu^+)/\Gamma_{\text{total}}$ Γ_{611}/Γ

Test of total lepton number conservation.

VALUE	CL%	DOCUMENT ID	TECN	COMMENT
<1.5 $\times 10^{-7}$	90	1 LEES 14A	BABR	$e^+e^- \rightarrow \Upsilon(4S)$

• • • We do not use the following data for averages, fits, limits, etc. • • •

$< 1.3 \times 10^{-6}$	90	1 EDWARDS 02B	CLE2	$e^+e^- \rightarrow \Upsilon(4S)$
------------------------	----	---------------	------	-----------------------------------

< 0.0064	90	2 WEIR 90B	MRK2	$e^+e^- 29 \text{ GeV}$
------------	----	------------	------	-------------------------

¹ Assumes equal production of B^+ and B^0 at the $\Upsilon(4S)$.

² WEIR 90B assumes B^+ production cross section from LUND.

$\Gamma(\rho^- e^+ e^+)/\Gamma_{\text{total}}$ Γ_{612}/Γ

Test of total lepton number conservation.

VALUE (units 10^{-6})	CL%	DOCUMENT ID	TECN	COMMENT
<0.17	90	1 LEES 14A	BABR	$e^+e^- \rightarrow \Upsilon(4S)$

• • • We do not use the following data for averages, fits, limits, etc. • • •

< 2.6	90	1 EDWARDS 02B	CLE2	$e^+e^- \rightarrow \Upsilon(4S)$
---------	----	---------------	------	-----------------------------------

¹ Assumes equal production of B^+ and B^0 at the $\Upsilon(4S)$.

$\Gamma(\rho^- \mu^+ \mu^+)/\Gamma_{\text{total}}$ Γ_{613}/Γ

Test of total lepton number conservation.

VALUE (units 10^{-6})	CL%	DOCUMENT ID	TECN	COMMENT
<0.42	90	LEES 14A	BABR	$e^+e^- \rightarrow \Upsilon(4S)$

• • • We do not use the following data for averages, fits, limits, etc. • • •

< 5.0	90	1 EDWARDS 02B	CLE2	$e^+e^- \rightarrow \Upsilon(4S)$
---------	----	---------------	------	-----------------------------------

¹ Assumes equal production of B^+ and B^0 at the $\Upsilon(4S)$.

$\Gamma(\rho^- e^+ \mu^+)/\Gamma_{\text{total}}$ Γ_{614}/Γ

Test of total lepton number conservation.

VALUE (units 10^{-6})	CL%	DOCUMENT ID	TECN	COMMENT
<0.47	90	1 LEES 14A	BABR	$e^+e^- \rightarrow \Upsilon(4S)$

• • • We do not use the following data for averages, fits, limits, etc. • • •

< 3.3	90	1 EDWARDS 02B	CLE2	$e^+e^- \rightarrow \Upsilon(4S)$
---------	----	---------------	------	-----------------------------------

¹ Assumes equal production of B^+ and B^0 at the $\Upsilon(4S)$.

$\Gamma(K^- e^+ e^+)/\Gamma_{\text{total}}$ Γ_{615}/Γ

Test of total lepton number conservation.

VALUE	CL%	DOCUMENT ID	TECN	COMMENT
<3.0 $\times 10^{-8}$	90	1 LEES 12J	BABR	$e^+e^- \rightarrow \Upsilon(4S)$

• • • We do not use the following data for averages, fits, limits, etc. • • •

$< 1.0 \times 10^{-6}$	90	1 EDWARDS 02B	CLE2	$e^+e^- \rightarrow \Upsilon(4S)$
------------------------	----	---------------	------	-----------------------------------

< 0.0039	90	2 WEIR 90B	MRK2	$e^+e^- 29 \text{ GeV}$
------------	----	------------	------	-------------------------

¹ Assumes equal production of B^+ and B^0 at the $\Upsilon(4S)$.

² WEIR 90B assumes B^+ production cross section from LUND.

$\Gamma(K^- \mu^+ \mu^+)/\Gamma_{\text{total}}$ Γ_{616}/Γ

Test of total lepton number conservation.

VALUE	CL%	DOCUMENT ID	TECN	COMMENT
<4.1 $\times 10^{-8}$	90	AAIJ 12C	LHCB	pp at 7 TeV

• • • We do not use the following data for averages, fits, limits, etc. • • •

$< 6.7 \times 10^{-8}$	90	1 LEES 12J	BABR	$e^+e^- \rightarrow \Upsilon(4S)$
------------------------	----	------------	------	-----------------------------------

$< 1.8 \times 10^{-6}$	90	1 EDWARDS 02B	CLE2	$e^+e^- \rightarrow \Upsilon(4S)$
------------------------	----	---------------	------	-----------------------------------

$< 9.1 \times 10^{-3}$	90	2 WEIR 90B	MRK2	$e^+e^- 29 \text{ GeV}$
------------------------	----	------------	------	-------------------------

¹ Assumes equal production of B^+ and B^0 at the $\Upsilon(4S)$.

² WEIR 90B assumes B^+ production cross section from LUND.

$\Gamma(K^- e^+ \mu^+)/\Gamma_{\text{total}}$ Γ_{617}/Γ

Test of total lepton number conservation.

VALUE	CL%	DOCUMENT ID	TECN	COMMENT
<1.6 $\times 10^{-7}$	90	1 LEES 14A	BABR	$e^+e^- \rightarrow \Upsilon(4S)$

• • • We do not use the following data for averages, fits, limits, etc. • • •

$< 2.0 \times 10^{-6}$	90	1 EDWARDS 02B	CLE2	$e^+e^- \rightarrow \Upsilon(4S)$
------------------------	----	---------------	------	-----------------------------------

< 0.0064	90	2 WEIR 90B	MRK2	$e^+e^- 29 \text{ GeV}$
------------	----	------------	------	-------------------------

¹ Assumes equal production of B^+ and B^0 at the $\Upsilon(4S)$.

² WEIR 90B assumes B^+ production cross section from LUND.

Meson Particle Listings

 B^\pm

$\Gamma(K^*(892)^- e^+ e^-)/\Gamma_{\text{total}}$ Γ_{618}/Γ
 Test of total lepton number conservation.

VALUE (units 10^{-6})	CL%	DOCUMENT ID	TECN	COMMENT
<0.40	90	¹ LEES	14A	BABR $e^+ e^- \rightarrow \Upsilon(4S)$
•••				We do not use the following data for averages, fits, limits, etc. •••
<2.8	90	¹ EDWARDS	02B	CLE2 $e^+ e^- \rightarrow \Upsilon(4S)$
				¹ Assumes equal production of B^+ and B^0 at the $\Upsilon(4S)$.

$\Gamma(K^*(892)^- \mu^+ \mu^-)/\Gamma_{\text{total}}$ Γ_{619}/Γ
 Test of total lepton number conservation.

VALUE (units 10^{-6})	CL%	DOCUMENT ID	TECN	COMMENT
<0.59	90	¹ LEES	14A	BABR $e^+ e^- \rightarrow \Upsilon(4S)$
•••				We do not use the following data for averages, fits, limits, etc. •••
<8.3	90	¹ EDWARDS	02B	CLE2 $e^+ e^- \rightarrow \Upsilon(4S)$
				¹ Assumes equal production of B^+ and B^0 at the $\Upsilon(4S)$.

$\Gamma(K^*(892)^- e^+ \mu^-)/\Gamma_{\text{total}}$ Γ_{620}/Γ
 Test of total lepton number conservation.

VALUE (units 10^{-6})	CL%	DOCUMENT ID	TECN	COMMENT
<0.30	90	¹ LEES	14A	BABR $e^+ e^- \rightarrow \Upsilon(4S)$
•••				We do not use the following data for averages, fits, limits, etc. •••
<4.4	90	¹ EDWARDS	02B	CLE2 $e^+ e^- \rightarrow \Upsilon(4S)$
				¹ Assumes equal production of B^+ and B^0 at the $\Upsilon(4S)$.

$\Gamma(D^- e^+ e^-)/\Gamma_{\text{total}}$ Γ_{621}/Γ

VALUE	CL%	DOCUMENT ID	TECN	COMMENT
<2.6 $\times 10^{-6}$	90	¹ LEES	14A	BABR $e^+ e^- \rightarrow \Upsilon(4S)$
<2.6 $\times 10^{-6}$	90	^{1,2} SEON	11B	BELL $e^+ e^- \rightarrow \Upsilon(4S)$
				¹ Assumes equal production of B^0 and B^+ from Upsilon(4S) decays. ² Uses $D^- \rightarrow K^+ \pi^- \pi^-$ mode and 3-body phase-space hypothesis for the signal decays.

$\Gamma(D^- e^+ \mu^-)/\Gamma_{\text{total}}$ Γ_{622}/Γ

VALUE	CL%	DOCUMENT ID	TECN	COMMENT
<1.8 $\times 10^{-6}$	90	^{1,2} SEON	11B	BELL $e^+ e^- \rightarrow \Upsilon(4S)$
•••				We do not use the following data for averages, fits, limits, etc. •••
<2.1 $\times 10^{-6}$	90	¹ LEES	14A	BABR $e^+ e^- \rightarrow \Upsilon(4S)$
				¹ Assumes equal production of B^0 and B^+ from Upsilon(4S) decays. ² Uses $D^- \rightarrow K^+ \pi^- \pi^-$ mode and 3-body phase-space hypothesis for the signal decays.

$\Gamma(D^- \mu^+ \mu^-)/\Gamma_{\text{total}}$ Γ_{623}/Γ

VALUE	CL%	DOCUMENT ID	TECN	COMMENT
< 6.9 $\times 10^{-7}$	95	¹ AAIJ	12AD	LHCB pp at 7 TeV
•••				We do not use the following data for averages, fits, limits, etc. •••
<17 $\times 10^{-7}$	90	² LEES	14A	BABR $e^+ e^- \rightarrow \Upsilon(4S)$
< 1.1 $\times 10^{-6}$	90	^{2,3} SEON	11B	BELL $e^+ e^- \rightarrow \Upsilon(4S)$
				¹ Uses $B^+ \rightarrow \psi(2S) K^+$, $\psi(2S) \rightarrow J/\psi \pi^+ \pi^-$ mode for normalization. ² Assumes equal production of B^0 and B^+ from Upsilon(4S) decays. ³ Uses $D^- \rightarrow K^+ \pi^- \pi^-$ mode and 3-body phase-space hypothesis for the signal decays.

$\Gamma(D^{*-} \mu^+ \mu^-)/\Gamma_{\text{total}}$ Γ_{624}/Γ

VALUE	CL%	DOCUMENT ID	TECN	COMMENT
<2.4 $\times 10^{-6}$	95	¹ AAIJ	12AD	LHCB pp at 7 TeV
				¹ Uses $B^+ \rightarrow \psi(2S) K^+$, $\psi(2S) \rightarrow J/\psi \pi^+ \pi^-$ mode for normalization.

$\Gamma(D_s^- \mu^+ \mu^-)/\Gamma_{\text{total}}$ Γ_{625}/Γ

VALUE	CL%	DOCUMENT ID	TECN	COMMENT
<5.8 $\times 10^{-7}$	95	¹ AAIJ	12AD	LHCB pp at 7 TeV
				¹ Uses $B^+ \rightarrow \psi(2S) K^+$, $\psi(2S) \rightarrow J/\psi \pi^+ \pi^-$ mode for normalization. Obtains neutrino-mass-dependent upper limits in the range $1.5-8.0 \times 10^{-7}$.

$\Gamma(D^0 \pi^- \mu^+ \mu^-)/\Gamma_{\text{total}}$ Γ_{626}/Γ

VALUE	CL%	DOCUMENT ID	TECN	COMMENT
<1.5 $\times 10^{-6}$	95	¹ AAIJ	12AD	LHCB pp at 7 TeV
				¹ Uses $B^+ \rightarrow \psi(2S) K^+$, $\psi(2S) \rightarrow J/\psi \pi^+ \pi^-$ mode for normalization. Obtains neutrino-mass-dependent upper limits in the range $0.3-1.5 \times 10^{-6}$.

$\Gamma(\Lambda^0 \mu^+)/\Gamma_{\text{total}}$ Γ_{627}/Γ

VALUE	CL%	DOCUMENT ID	TECN	COMMENT
<6 $\times 10^{-8}$	90	^{1,2} DEL-AMO-SA..11k	BABR	$e^+ e^- \rightarrow \Upsilon(4S)$
				¹ DEL-AMO-SANCHEZ 11k reports $< 6.1 \times 10^{-8}$ from a measurement of $[\Gamma(B^+ \rightarrow \Lambda^0 \mu^+)/\Gamma_{\text{total}}] \times [B(\Lambda \rightarrow p \pi^-)]$ assuming $B(\Lambda \rightarrow p \pi^-) = (63.9 \pm 0.5) \times 10^{-2}$. ² Uses $B(\Upsilon(4S) \rightarrow B^0 \bar{B}^0) = (51.6 \pm 0.6)\%$ and $B(\Upsilon(4S) \rightarrow B^+ B^-) = (48.4 \pm 0.6)\%$.

$\Gamma(\Lambda^0 e^+)/\Gamma_{\text{total}}$ Γ_{628}/Γ

VALUE	CL%	DOCUMENT ID	TECN	COMMENT
<3.2 $\times 10^{-8}$	90	^{1,2} DEL-AMO-SA..11k	BABR	$e^+ e^- \rightarrow \Upsilon(4S)$
				¹ DEL-AMO-SANCHEZ 11k reports $< 3.2 \times 10^{-8}$ from a measurement of $[\Gamma(B^+ \rightarrow \Lambda^0 e^+)/\Gamma_{\text{total}}] \times [B(\Lambda \rightarrow p \pi^-)]$ assuming $B(\Lambda \rightarrow p \pi^-) = (63.9 \pm 0.5) \times 10^{-2}$. ² Uses $B(\Upsilon(4S) \rightarrow B^0 \bar{B}^0) = (51.6 \pm 0.6)\%$ and $B(\Upsilon(4S) \rightarrow B^+ B^-) = (48.4 \pm 0.6)\%$.

$\Gamma(\Lambda^0 \mu^+)/\Gamma_{\text{total}}$ Γ_{629}/Γ

VALUE	CL%	DOCUMENT ID	TECN	COMMENT
<6 $\times 10^{-8}$	90	^{1,2} DEL-AMO-SA..11k	BABR	$e^+ e^- \rightarrow \Upsilon(4S)$
				¹ DEL-AMO-SANCHEZ 11k reports $< 6.2 \times 10^{-8}$ from a measurement of $[\Gamma(B^+ \rightarrow \Lambda^0 \mu^+)/\Gamma_{\text{total}}] \times [B(\Lambda \rightarrow p \pi^-)]$ assuming $B(\Lambda \rightarrow p \pi^-) = (63.9 \pm 0.5) \times 10^{-2}$. ² Uses $B(\Upsilon(4S) \rightarrow B^0 \bar{B}^0) = (51.6 \pm 0.6)\%$ and $B(\Upsilon(4S) \rightarrow B^+ B^-) = (48.4 \pm 0.6)\%$.

$\Gamma(\Lambda^0 e^+)/\Gamma_{\text{total}}$ Γ_{630}/Γ

VALUE	CL%	DOCUMENT ID	TECN	COMMENT
<8 $\times 10^{-8}$	90	^{1,2} DEL-AMO-SA..11k	BABR	$e^+ e^- \rightarrow \Upsilon(4S)$
				¹ DEL-AMO-SANCHEZ 11k reports $< 8.1 \times 10^{-8}$ from a measurement of $[\Gamma(B^+ \rightarrow \Lambda^0 e^+)/\Gamma_{\text{total}}] \times [B(\Lambda \rightarrow p \pi^-)]$ assuming $B(\Lambda \rightarrow p \pi^-) = (63.9 \pm 0.5) \times 10^{-2}$. ² Uses $B(\Upsilon(4S) \rightarrow B^0 \bar{B}^0) = (51.6 \pm 0.6)\%$ and $B(\Upsilon(4S) \rightarrow B^+ B^-) = (48.4 \pm 0.6)\%$.

POLARIZATION IN B^+ DECAY

In decays involving two vector mesons, one can distinguish among the states in which meson polarizations are both longitudinal (L) or both are transverse and parallel (||) or perpendicular (\perp) to each other with the parameters Γ_L/Γ , Γ_{\perp}/Γ , and the relative phases $\phi_{||}$ and ϕ_{\perp} . See the definitions in the note on "Polarization in B Decays" review in the B^0 Particle Listings.

Γ_L/Γ in $B^+ \rightarrow \bar{D}^{*0} \rho^+$

VALUE	DOCUMENT ID	TECN	COMMENT
0.892 \pm 0.018 \pm 0.016	CSORNA	03	CLE2 $e^+ e^- \rightarrow \Upsilon(4S)$

Γ_L/Γ in $B^+ \rightarrow \bar{D}^{*0} K^{*+}$

VALUE	DOCUMENT ID	TECN	COMMENT
0.86 \pm 0.06 \pm 0.03	AUBERT	04k	BABR $e^+ e^- \rightarrow \Upsilon(4S)$

Γ_L/Γ in $B^+ \rightarrow J/\psi K^{*+}$

VALUE	DOCUMENT ID	TECN	COMMENT
0.604 \pm 0.015 \pm 0.018	ITOH	05	BELL $e^+ e^- \rightarrow \Upsilon(4S)$

Γ_{\perp}/Γ in $B^+ \rightarrow J/\psi K^{*+}$

VALUE	DOCUMENT ID	TECN	COMMENT
0.180 \pm 0.014 \pm 0.010	ITOH	05	BELL $e^+ e^- \rightarrow \Upsilon(4S)$

Γ_L/Γ in $B^+ \rightarrow \omega K^{*+}$

VALUE	DOCUMENT ID	TECN	COMMENT
0.41 \pm 0.18 \pm 0.05	AUBERT	09H	BABR $e^+ e^- \rightarrow \Upsilon(4S)$

Γ_L/Γ in $B^+ \rightarrow \omega K_2^*(1430)^+$

VALUE	DOCUMENT ID	TECN	COMMENT
0.56 \pm 0.10 \pm 0.04	AUBERT	09H	BABR $e^+ e^- \rightarrow \Upsilon(4S)$

Γ_L/Γ in $B^+ \rightarrow K^{*+} \bar{K}^{*0}$

VALUE	DOCUMENT ID	TECN	COMMENT
0.82 \pm 0.15 \pm 0.21 OUR AVERAGE			

1.06 \pm 0.30 \pm 0.14			¹ GOH	15	BELL	$e^+ e^- \rightarrow \Upsilon(4S)$
0.75 \pm 0.16 \pm 0.03			^{2,3} AUBERT	09F	BABR	$e^+ e^- \rightarrow \Upsilon(4S)$

¹ Signal significance 2.7 standard deviations.
² Signal significance 3.7 standard deviations.
³ Assumes equal production of B^+ and B^0 at the $\Upsilon(4S)$.

Γ_L/Γ in $B^+ \rightarrow \phi K^*(892)^+$

VALUE	DOCUMENT ID	TECN	COMMENT
0.50 \pm 0.05 OUR AVERAGE			

0.49 \pm 0.05 \pm 0.03	AUBERT	07BA	BABR	$e^+ e^- \rightarrow \Upsilon(4S)$
0.52 \pm 0.08 \pm 0.03	CHEN	05A	BELL	$e^+ e^- \rightarrow \Upsilon(4S)$
•••				We do not use the following data for averages, fits, limits, etc. •••
0.46 \pm 0.12 \pm 0.03	AUBERT	03v	BABR	Repl. by AUBERT 07BA

Γ_{\perp}/Γ in $B^+ \rightarrow \phi K^{*+}$

VALUE	DOCUMENT ID	TECN	COMMENT
0.20 \pm 0.05 OUR AVERAGE			

0.21 \pm 0.05 \pm 0.02	AUBERT	07BA	BABR	$e^+ e^- \rightarrow \Upsilon(4S)$
0.19 \pm 0.08 \pm 0.02	CHEN	05A	BELL	$e^+ e^- \rightarrow \Upsilon(4S)$

$\phi_{||}$ in $B^+ \rightarrow \phi K^{*+}$

VALUE ($^\circ$)	DOCUMENT ID	TECN	COMMENT
2.34 \pm 0.18 OUR AVERAGE			

2.47 \pm 0.20 \pm 0.07	AUBERT	07BA	BABR	$e^+ e^- \rightarrow \Upsilon(4S)$
2.10 \pm 0.28 \pm 0.04	CHEN	05A	BELL	$e^+ e^- \rightarrow \Upsilon(4S)$

ϕ_{\perp} in $B^+ \rightarrow \phi K^{*+}$

VALUE ($^\circ$)	DOCUMENT ID	TECN	COMMENT
2.58 \pm 0.17 OUR AVERAGE			

2.69 \pm 0.20 \pm 0.03	AUBERT	07BA	BABR	$e^+ e^- \rightarrow \Upsilon(4S)$
2.31 \pm 0.30 \pm 0.07	CHEN	05A	BELL	$e^+ e^- \rightarrow \Upsilon(4S)$

$\delta_0(B^+ \rightarrow \phi K^{*+})$	DOCUMENT ID	TECN	COMMENT
VALUE (rad)			
$3.07 \pm 0.18 \pm 0.06$	AUBERT	07BA BABR	$e^+ e^- \rightarrow \Upsilon(4S)$

$A_{CP}^0(B^+ \rightarrow \phi K^{*+})$	DOCUMENT ID	TECN	COMMENT
VALUE			
$0.17 \pm 0.11 \pm 0.02$	AUBERT	07BA BABR	$e^+ e^- \rightarrow \Upsilon(4S)$

$A_{CP}^{\perp}(B^+ \rightarrow \phi K^{*+})$	DOCUMENT ID	TECN	COMMENT
VALUE			
$0.22 \pm 0.24 \pm 0.08$	AUBERT	07BA BABR	$e^+ e^- \rightarrow \Upsilon(4S)$

$\Delta\phi_{\parallel}(B^+ \rightarrow \phi K^{*+})$	DOCUMENT ID	TECN	COMMENT
VALUE (rad)			
$0.07 \pm 0.20 \pm 0.05$	AUBERT	07BA BABR	$e^+ e^- \rightarrow \Upsilon(4S)$

$\Delta\phi_{\perp}(B^+ \rightarrow \phi K^{*+})$	DOCUMENT ID	TECN	COMMENT
VALUE (rad)			
$0.19 \pm 0.20 \pm 0.07$	AUBERT	07BA BABR	$e^+ e^- \rightarrow \Upsilon(4S)$

$\Delta\delta_0(B^+ \rightarrow \phi K^{*+})$	DOCUMENT ID	TECN	COMMENT
VALUE (rad)			
$0.20 \pm 0.18 \pm 0.03$	AUBERT	07BA BABR	$e^+ e^- \rightarrow \Upsilon(4S)$

Γ_L/Γ in $B^+ \rightarrow \phi K_1(1270)^+$	DOCUMENT ID	TECN	COMMENT
VALUE			
$0.46 \pm 0.12 \pm 0.06$ -0.13 ± 0.07	AUBERT	08BI BABR	$e^+ e^- \rightarrow \Upsilon(4S)$

Γ_L/Γ in $B^+ \rightarrow \phi K_2^*(1430)^+$	DOCUMENT ID	TECN	COMMENT
VALUE			
$0.80 \pm 0.09 \pm 0.03$ -0.10 ± 0.03	AUBERT	08BI BABR	$e^+ e^- \rightarrow \Upsilon(4S)$

$\delta_0(B^+ \rightarrow \phi K_2^*(1430)^+)$	DOCUMENT ID	TECN	COMMENT
VALUE (rad)			
$3.59 \pm 0.19 \pm 0.12$	AUBERT	08BI BABR	$e^+ e^- \rightarrow \Upsilon(4S)$

$\Delta\delta_0(B^+ \rightarrow \phi K_2^*(1430)^+)$	DOCUMENT ID	TECN	COMMENT
VALUE (rad)			
$-0.05 \pm 0.19 \pm 0.06$	AUBERT	08BI BABR	$e^+ e^- \rightarrow \Upsilon(4S)$

Γ_L/Γ in $B^+ \rightarrow \rho^0 K^*(892)^+$	DOCUMENT ID	TECN	COMMENT
VALUE			
$0.78 \pm 0.12 \pm 0.03$	DEL-AMO-SA...11D	BABR	$e^+ e^- \rightarrow \Upsilon(4S)$

• • • We do not use the following data for averages, fits, limits, etc. • • •

Γ_L/Γ in $B^+ \rightarrow K^*(892)^0 \rho^+$	DOCUMENT ID	TECN	COMMENT
VALUE			
$0.96 \pm 0.04 \pm 0.04$ -0.15 ± 0.04	AUBERT	03V BABR	Repl. by DEL-AMO-SANCHEZ 11D

Γ_L/Γ in $B^+ \rightarrow K^*(892)^0 \rho^+$	DOCUMENT ID	TECN	COMMENT
VALUE			
0.48 ± 0.08 OUR AVERAGE			
$0.52 \pm 0.10 \pm 0.04$	AUBERT,B	06G BABR	$e^+ e^- \rightarrow \Upsilon(4S)$
$0.43 \pm 0.11 \pm 0.05$ -0.02 ± 0.02	ZHANG	05D BELL	$e^+ e^- \rightarrow \Upsilon(4S)$

Γ_L/Γ in $B^+ \rightarrow \mu^+ \mu^- K^*(892)^+ (1.0 < q^2 < 8.68 \text{ GeV}^2/c^4)$	DOCUMENT ID	TECN	COMMENT
VALUE			
$0.60 \pm 0.31 \pm 0.13$ -0.25 ± 0.13	¹ SIRUNYAN	21AC CMS	pp at 8 TeV

¹ SIRUNYAN 21AC measurement is performed in $1.0 < q^2 < 8.68 \text{ GeV}^2/c^4$. Reports also measurements in several other q^2 intervals.

Γ_L/Γ in $B^+ \rightarrow \mu^+ \mu^- K^*(892)^+ (1.1 < q^2 < 6.0 \text{ GeV}^2/c^4)$	DOCUMENT ID	TECN	COMMENT
VALUE			
$0.59 \pm 0.09 \pm 0.03$	¹ AAIJ	21J LHCB	pp at 7, 8, 13 TeV

¹ The full set of CP-averaged angular observables is measured as a function of the q^2 . The measured Γ_L is related to the polarisation of the $K^*(892)^+$.

Γ_L/Γ in $B^+ \rightarrow \mu^+ \mu^- K^*(892)^+ (10.09 < q^2 < 12.86 \text{ GeV}^2/c^4)$	DOCUMENT ID	TECN	COMMENT
VALUE			
$0.88 \pm 0.10 \pm 0.05$ -0.13 ± 0.05	¹ SIRUNYAN	21AC CMS	pp at 8 TeV

¹ SIRUNYAN 21AC measurement is performed in $10.09 < q^2 < 12.86 \text{ GeV}^2/c^4$. Reports also measurements in several other q^2 intervals.

Γ_L/Γ in $B^+ \rightarrow \mu^+ \mu^- K^*(892)^+ (14.18 < q^2 < 19.0 \text{ GeV}^2/c^4)$	DOCUMENT ID	TECN	COMMENT
VALUE			
$0.55 \pm 0.13 \pm 0.06$ -0.10 ± 0.06	¹ SIRUNYAN	21AC CMS	pp at 8 TeV

¹ SIRUNYAN 21AC measurement is performed in $14.18 < q^2 < 19.0 \text{ GeV}^2/c^4$. Reports also measurements in several other q^2 intervals.

Γ_L/Γ in $B^+ \rightarrow \mu^+ \mu^- K^*(892)^+ (15.0 < q^2 < 19.0 \text{ GeV}^2/c^4)$	DOCUMENT ID	TECN	COMMENT
VALUE			
$0.40 \pm 0.13 \pm 0.03$ -0.11 ± 0.03	¹ AAIJ	21J LHCB	pp at 7, 8, 13 TeV

¹ The full set of CP-averaged angular observables is measured as a function of the q^2 . The measured Γ_L is related to the polarisation of the $K^*(892)^+$.

Γ_L/Γ in $B^+ \rightarrow \rho^+ \rho^0$	DOCUMENT ID	TECN	COMMENT
VALUE			
0.950 ± 0.016 OUR AVERAGE			
$0.950 \pm 0.015 \pm 0.006$	AUBERT	09G BABR	$e^+ e^- \rightarrow \Upsilon(4S)$
$0.948 \pm 0.106 \pm 0.021$	ZHANG	03B BELL	$e^+ e^- \rightarrow \Upsilon(4S)$

• • • We do not use the following data for averages, fits, limits, etc. • • •

$0.905 \pm 0.042 \pm 0.023$ -0.027	AUBERT,BE	06G BABR	Repl. by AUBERT 09G
$0.97 \pm 0.03 \pm 0.04$ -0.07	AUBERT	03V BABR	Repl. by AUBERT,BE 06G

Γ_L/Γ in $B^+ \rightarrow \omega \rho^+$	DOCUMENT ID	TECN	COMMENT
VALUE			
0.90 ± 0.05 ± 0.03	AUBERT	09H BABR	$e^+ e^- \rightarrow \Upsilon(4S)$

• • • We do not use the following data for averages, fits, limits, etc. • • •

$0.82 \pm 0.11 \pm 0.02$	AUBERT,B	06T BABR	Repl. by AUBERT 09H
$0.88 \pm 0.12 \pm 0.03$ -0.15 ± 0.03	AUBERT	05O BABR	Repl. by AUBERT,B 06T

Γ_L/Γ in $B^+ \rightarrow \rho^+ \bar{p} K^*(892)^+$	DOCUMENT ID	TECN	COMMENT
VALUE			
0.32 ± 0.17 ± 0.09	CHEN	08C BELL	$e^+ e^- \rightarrow \Upsilon(4S)$

CP VIOLATION

A_{CP} is defined as

$$\frac{B(B^- \rightarrow \bar{f}) - B(B^+ \rightarrow f)}{B(B^- \rightarrow \bar{f}) + B(B^+ \rightarrow f)}$$

the CP-violation charge asymmetry of exclusive B^- and B^+ decay.

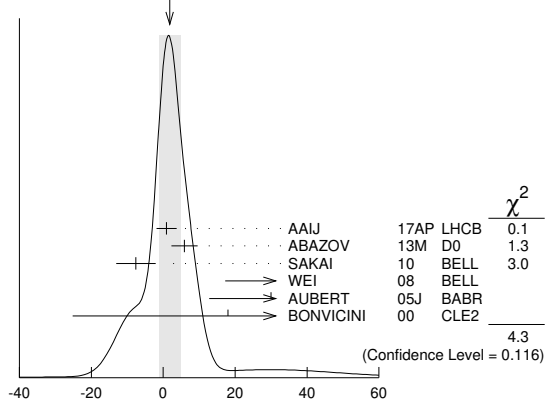
$A_{CP}(B^+ \rightarrow J/\psi(1S)K^+)$

VALUE (units 10^{-3})	DOCUMENT ID	TECN	COMMENT
1.8 ± 3.0 OUR AVERAGE			Error includes scale factor of 1.5. See the ideogram below.
$0.9 \pm 2.7 \pm 0.7$	AAIJ	17AP LHCB	pp at 7, 8 TeV
$5.9 \pm 3.6 \pm 0.7$	ABAZOV	13M D0	$p\bar{p}$ at 1.96 TeV
$-7.6 \pm 5.0 \pm 2.2$	SAKAI	10 BELL	$e^+ e^- \rightarrow \Upsilon(4S)$
$90 \pm 70 \pm 20$	¹ WEI	08 BELL	$e^+ e^- \rightarrow \Upsilon(4S)$
$30 \pm 14 \pm 10$	² AUBERT	05J BABR	$e^+ e^- \rightarrow \Upsilon(4S)$
$18 \pm 43 \pm 4$	³ BONVICINI	00 CLE2	$e^+ e^- \rightarrow \Upsilon(4S)$

• • • We do not use the following data for averages, fits, limits, etc. • • •

$7.5 \pm 6.1 \pm 3.0$	⁴ ABAZOV	08O D0	Repl. by ABAZOV 13M
$30 \pm 15 \pm 6$	AUBERT	04P BABR	Repl. by AUBERT 05J
$-26 \pm 22 \pm 17$	ABE	03B BELL	Repl. by SAKAI 10
$3 \pm 30 \pm 4$	AUBERT	02F BABR	Repl. by AUBERT 04P

WEIGHTED AVERAGE
1.8 ± 3.0 (Error scaled by 1.5)



$A_{CP}(B^+ \rightarrow J/\psi(1S)K^+)$ (units 10^{-3})

¹ Uses $B^+ \rightarrow J/\psi K^+$, where $J/\psi \rightarrow p\bar{p}$.
² The result reported corresponds to $-A_{CP}$.
³ A +0.3% correction is applied due to a slightly higher reconstruction efficiency for the positive kaons.
⁴ Uses $J/\psi \rightarrow \mu^+ \mu^-$ decay.

Meson Particle Listings

 B^\pm $A_{CP}(B^+ \rightarrow J/\psi(1S)\pi^+)$

VALUE (units 10^{-2})	DOCUMENT ID	TECN	COMMENT
1.8 ± 1.2 OUR AVERAGE	Error includes scale factor of 1.3.		
1.91 ± 0.89 ± 0.16	¹ AAIJ	17o	LHCB pp at 7, 8 TeV
- 4.2 ± 4.4 ± 0.9	ABAZOV	13M	D0 $p\bar{p}$ at 1.96 TeV
12.3 ± 8.5 ± 0.4	AUBERT	04P	BABR $e^+e^- \rightarrow \Upsilon(4S)$
- 2.3 ± 16.4 ± 1.5	ABE	03B	BELL $e^+e^- \rightarrow \Upsilon(4S)$
• • • We do not use the following data for averages, fits, limits, etc. • • •			
0.5 ± 2.7 ± 1.1	² AAIJ	12Ac	LHCB Repl. by AAIJ 17o
- 9 ± 8 ± 3	³ ABAZOV	08o	D0 Repl. by ABAZOV 13M
1 ± 22 ± 1	AUBERT	02F	BABR Repl. by AUBERT 04P
¹ Obtained by using LHCb measurement of $A_{CP}(B^+ \rightarrow J/\psi K^+) = (0.09 \pm 0.27 \pm 0.07) \times 10^{-2}$ of AAIJ 17AP.			
² Uses $A_{CP}(B^+ \rightarrow J/\psi K^+) = 0.001 \pm 0.007$ to extract production asymmetry.			
³ Uses $J/\psi \rightarrow \mu^+\mu^-$ decay.			

 $A_{CP}(B^+ \rightarrow J/\psi\rho^+)$

VALUE	DOCUMENT ID	TECN	COMMENT
-0.05 ± 0.05 OUR AVERAGE			
-0.045 ^{+0.056} _{-0.057} ± 0.008	AAIJ	19o	LHCB pp at 7 and 8 TeV
-0.11 ± 0.12 ± 0.08	AUBERT	07Ac	BABR $e^+e^- \rightarrow \Upsilon(4S)$

 $A_{CP}(B^+ \rightarrow J/\psi K^*(892)^+)$

VALUE	DOCUMENT ID	TECN	COMMENT
-0.048 ± 0.029 ± 0.016	¹ AUBERT	05J	BABR $e^+e^- \rightarrow \Upsilon(4S)$
¹ The result reported corresponds to $-A_{CP}$.			

 $A_{CP}(B^+ \rightarrow \eta_c K^+)$

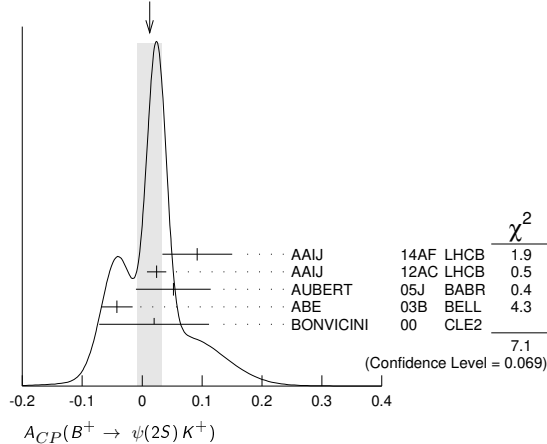
VALUE	DOCUMENT ID	TECN	COMMENT
0.01 ± 0.07 OUR AVERAGE	Error includes scale factor of 2.2.		
0.040 ± 0.034 ± 0.004	¹ AAIJ	14AF	LHCB pp at 7, 8 TeV
-0.16 ± 0.08 ± 0.02	¹ WEI	08	BELL $e^+e^- \rightarrow \Upsilon(4S)$
• • • We do not use the following data for averages, fits, limits, etc. • • •			
0.046 ± 0.057 ± 0.007	¹ AAIJ	13AU	LHCB Repl. by AAIJ 14AF
¹ Uses $B^+ \rightarrow \eta_c K^+$, where $\eta_c \rightarrow p\bar{p}$.			

 $A_{CP}(B^+ \rightarrow \psi(2S)\pi^+)$

VALUE	DOCUMENT ID	TECN	COMMENT
0.03 ± 0.06 OUR AVERAGE			
0.048 ± 0.090 ± 0.011	¹ AAIJ	12Ac	LHCB pp at 7 TeV
0.022 ± 0.085 ± 0.016	BHARDWAJ	08	BELL $e^+e^- \rightarrow \Upsilon(4S)$
¹ Uses $A_{CP}(B^+ \rightarrow J/\psi K^+) = 0.001 \pm 0.007$ to extract production asymmetry.			

 $A_{CP}(B^+ \rightarrow \psi(2S)K^+)$

VALUE	DOCUMENT ID	TECN	COMMENT
0.012 ± 0.020 OUR AVERAGE	Error includes scale factor of 1.5. See the ideogram below.		
0.092 ± 0.058 ± 0.004	¹ AAIJ	14AF	LHCB pp at 7, 8 TeV
0.024 ± 0.014 ± 0.008	² AAIJ	12Ac	LHCB pp at 7 TeV
0.052 ± 0.059 ± 0.020	AUBERT	05J	BABR $e^+e^- \rightarrow \Upsilon(4S)$
-0.042 ± 0.020 ± 0.017	ABE	03B	BELL $e^+e^- \rightarrow \Upsilon(4S)$
0.02 ± 0.091 ± 0.01	³ BONVICINI	00	CLE2 $e^+e^- \rightarrow \Upsilon(4S)$
• • • We do not use the following data for averages, fits, limits, etc. • • •			
-0.002 ± 0.123 ± 0.012	^{1,2} AAIJ	13AU	LHCB Repl. by AAIJ 14AF

WEIGHTED AVERAGE
0.012 ± 0.020 (Error scaled by 1.5) $A_{CP}(B^+ \rightarrow \psi(2S)K^+)$

- ¹ Uses $\psi(2S) \rightarrow p\bar{p}$ decays.
² Uses $A_{CP}(B^+ \rightarrow J/\psi K^+) = 0.001 \pm 0.007$ to extract production asymmetry.
³ A +0.3% correction is applied due to a slightly higher reconstruction efficiency for the positive kaons.

 $A_{CP}(B^+ \rightarrow \psi(2S)K^*(892)^+)$

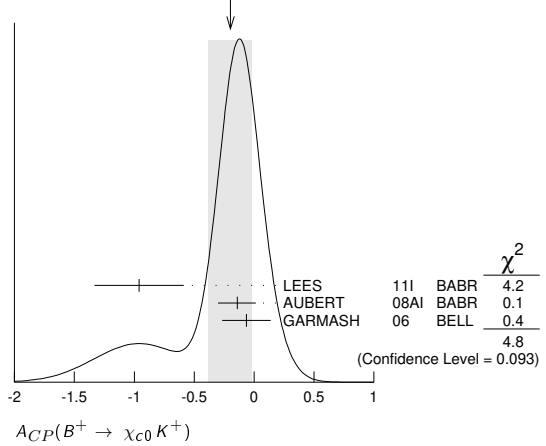
VALUE	DOCUMENT ID	TECN	COMMENT
0.077 ± 0.207 ± 0.051	¹ AUBERT	05J	BABR $e^+e^- \rightarrow \Upsilon(4S)$
¹ The result reported corresponds to $-A_{CP}$.			

 $A_{CP}(B^+ \rightarrow \chi_{c1}(1P)\pi^+)$

VALUE	DOCUMENT ID	TECN	COMMENT
0.07 ± 0.18 ± 0.02	KUMAR	06	BELL $e^+e^- \rightarrow \Upsilon(4S)$

 $A_{CP}(B^+ \rightarrow \chi_{c0}K^+)$

VALUE	DOCUMENT ID	TECN	COMMENT
-0.20 ± 0.18 OUR AVERAGE	Error includes scale factor of 1.5. See the ideogram below.		
-0.96 ± 0.37 ± 0.04	LEES	11i	BABR $e^+e^- \rightarrow \Upsilon(4S)$
-0.14 ± 0.15 ^{+0.03} _{-0.06}	AUBERT	08Ai	BABR $e^+e^- \rightarrow \Upsilon(4S)$
-0.065 ± 0.20 ^{+0.035} _{-0.024}	GARMASH	06	BELL $e^+e^- \rightarrow \Upsilon(4S)$

WEIGHTED AVERAGE
-0.20 ± 0.18 (Error scaled by 1.5) $A_{CP}(B^+ \rightarrow \chi_{c0}K^+)$ $A_{CP}(B^+ \rightarrow \chi_{c1}K^+)$

VALUE	DOCUMENT ID	TECN	COMMENT
-0.009 ± 0.033 OUR AVERAGE			
-0.01 ± 0.03 ± 0.02	KUMAR	06	BELL $e^+e^- \rightarrow \Upsilon(4S)$
-0.003 ± 0.076 ± 0.017	¹ AUBERT	05J	BABR $e^+e^- \rightarrow \Upsilon(4S)$
¹ The result reported corresponds to $-A_{CP}$.			

 $A_{CP}(B^+ \rightarrow \chi_{c1}K^*(892)^+)$

VALUE	DOCUMENT ID	TECN	COMMENT
0.471 ± 0.378 ± 0.268	¹ AUBERT	05J	BABR $e^+e^- \rightarrow \Upsilon(4S)$
¹ The result reported corresponds to $-A_{CP}$.			

 $A_{CP}(B^+ \rightarrow D^0 \ell^+ \nu_\ell)$

VALUE (units 10^{-2})	DOCUMENT ID	TECN	COMMENT
-0.14 ± 0.14 ± 0.14	¹ ABAZOV	17A	D0 $p\bar{p}$ at 1.96 TeV
¹ Uses $D^0 \rightarrow K^-\pi^+$ decays and $f(B^+) = 0.56 \pm 0.01$ from 10.4 fb ⁻¹ of Run II data.			

 $A_{CP}(B^+ \rightarrow \bar{D}^0 \pi^+)$

VALUE	DOCUMENT ID	TECN	COMMENT
-0.007 ± 0.007 OUR AVERAGE			
-0.006 ± 0.005 ± 0.010	¹ AAIJ	13AE	LHCB pp at 7 TeV
-0.008 ± 0.008	ABE	06	BELL $e^+e^- \rightarrow \Upsilon(4S)$
¹ Uses $B^\pm \rightarrow [K^\pm \pi^\mp \pi^\pm \pi^\mp]_D h^\pm$ mode.			

 $A_{CP}(B^+ \rightarrow D_{CP(+)}\pi^+)$

VALUE	DOCUMENT ID	TECN	COMMENT
-0.0080 ± 0.0024 OUR AVERAGE			
-0.008 ± 0.002 ± 0.002	¹ AAIJ	21q	LHCB pp at 7, 8, 13 TeV
-0.0098 ± 0.0043 ± 0.0021	AAIJ	16L	LHCB pp at 7, 8 TeV
0.035 ± 0.024	ABE	06	BELL $e^+e^- \rightarrow \Upsilon(4S)$
• • • We do not use the following data for averages, fits, limits, etc. • • •			
-0.008 ± 0.003 ± 0.002	^{2,3} AAIJ	18A	LHCB pp at 7, 8, 13 TeV
-0.008 ± 0.006 ± 0.002	^{3,4} AAIJ	18A	LHCB pp at 7, 8, 13 TeV
¹ Uses $D \rightarrow K^+K^-$ and $D \rightarrow \pi^+\pi^-$ decay modes.			
² Uses $D \rightarrow K^+K^-$ decay mode.			
³ Superseded by AAIJ 21q.			
⁴ Uses $D \rightarrow \pi^+\pi^-$ decay mode.			

 $A_{CP}(B^+ \rightarrow D_{CP(-)}\pi^+)$

VALUE	DOCUMENT ID	TECN	COMMENT
0.017 ± 0.026	ABE	06	BELL $e^+e^- \rightarrow \Upsilon(4S)$

 $A_{CP}([K^\mp \pi^\pm \pi^\pm \pi^\mp]_D \pi^+)$

VALUE	DOCUMENT ID	TECN	COMMENT
0.023 ± 0.048 ± 0.005	AAIJ	16L	LHCB pp at 7, 8 TeV
• • • We do not use the following data for averages, fits, limits, etc. • • •			
0.13 ± 0.10	AAIJ	13AE	LHCB Repl. by AAIJ 16L

$A_{CP}(B^+ \rightarrow [\pi^+\pi^+\pi^-\pi^-]_D K^+)$

VALUE	DOCUMENT ID	TECN	COMMENT
$0.100 \pm 0.034 \pm 0.018$	AAIJ	16L	LHCB pp at 7, 8 TeV

$A_{CP}(B^+ \rightarrow [\pi^+\pi^-\pi^+\pi^-]_D K^*(892)^+)$

VALUE	DOCUMENT ID	TECN	COMMENT
$0.02 \pm 0.11 \pm 0.01$	AAIJ	17B0	LHCB pp at 7, 8, 13 TeV

$A_{CP}(B^+ \rightarrow \bar{D}^0 K^+)$

VALUE	DOCUMENT ID	TECN	COMMENT
-0.017 ± 0.005 OUR AVERAGE			
$-0.019 \pm 0.005 \pm 0.002$	1 AAIJ	18A	LHCB pp at 7, 8, 13 TeV
$-0.0194 \pm 0.0072 \pm 0.0060$	AAIJ	16L	LHCB pp at 7, 8 TeV
$0.010 \pm 0.026 \pm 0.005$	2 AAIJ	15W	LHCB pp at 7, 8 TeV
0.066 ± 0.036	ABE	06	BELL $e^+e^- \rightarrow \Upsilon(4S)$
••• We do not use the following data for averages, fits, limits, etc. •••			
$0.000 \pm 0.012 \pm 0.002$	3 AAIJ	16L	LHCB pp at 7, 8 TeV
$-0.029 \pm 0.020 \pm 0.018$	3 AAIJ	13AE	LHCB Repl. by AAIJ 16L
$0.003 \pm 0.080 \pm 0.037$	4 ABE	03D	BELL Repl. by SWAIN 03
$0.04 \pm 0.06 \pm 0.03$	5 SWAIN	03	BELL Repl. by ABE 06
1 Supersedes AAIJ 16L.			
2 Uses $D^0 \rightarrow K^-\pi^+\pi^0$ for the favored mode, and $D^0 \rightarrow K^+\pi^-\pi^0$ for the suppressed mode.			
3 Uses $B^\pm \rightarrow [K^\pm\pi^\mp\pi^+\pi^-]_D h^\pm$ mode.			
4 Corresponds to 90% confidence range $-0.15 < A_{CP} < 0.16$.			
5 Corresponds to 90% confidence range $-0.07 < A_{CP} < 0.15$.			

$A_{CP}([K^\mp\pi^\pm\pi^+\pi^-]_D K^+)$

VALUE	DOCUMENT ID	TECN	COMMENT
$-0.313 \pm 0.102 \pm 0.038$	AAIJ	16L	LHCB pp at 7, 8 TeV
••• We do not use the following data for averages, fits, limits, etc. •••			
-0.42 ± 0.22	AAIJ	13AE	LHCB Repl. by AAIJ 16L

$A_{CP}(B^+ \rightarrow [\pi^+\pi^+\pi^-\pi^-]_D \pi^+)$

VALUE (units 10^{-3})	DOCUMENT ID	TECN	COMMENT
$-4.1 \pm 7.9 \pm 2.4$	AAIJ	16L	LHCB pp at 7, 8 TeV

$A_{CP}(B^+ \rightarrow [K^-\pi^+]_D K^+)$

VALUE	DOCUMENT ID	TECN	COMMENT
-0.58 ± 0.21 OUR AVERAGE			
$-0.82 \pm 0.44 \pm 0.09$	AALTONEN	11AJ	CDF $p\bar{p}$ at 1.96 TeV
$-0.39 \pm 0.26 \pm 0.04$	HORII	11	BELL $e^+e^- \rightarrow \Upsilon(4S)$
$-0.86 \pm 0.47 \pm 0.12$	DEL-AMO-SA...10H	BABR	$e^+e^- \rightarrow \Upsilon(4S)$
••• We do not use the following data for averages, fits, limits, etc. •••			
$-0.1 \pm 0.8 \pm 0.4$	HORII	08	BELL Repl. by HORII 11
$+0.88 \pm 0.77 \pm 0.06$	SAIGO	05	BELL Repl. by HORII 08

$A_{CP}(B^+ \rightarrow [K^-\pi^+\pi^0]_D K^+)$

VALUE	DOCUMENT ID	TECN	COMMENT
0.07 ± 0.30 OUR AVERAGE			Error includes scale factor of 1.5.
$-0.20 \pm 0.27 \pm 0.04$	1 AAIJ	15W	LHCB pp at 7, 8 TeV
$0.41 \pm 0.30 \pm 0.05$	NAYAK	13	BELL $e^+e^- \rightarrow \Upsilon(4S)$
1 Uses $D^0 \rightarrow K^-\pi^+\pi^0$ for the favored mode, and $D^0 \rightarrow K^+\pi^-\pi^0$ for the suppressed mode.			

$A_{CP}(B^+ \rightarrow [K^+K^-\pi^0]_D K^+)$

VALUE	DOCUMENT ID	TECN	COMMENT
$0.30 \pm 0.20 \pm 0.02$	1 AAIJ	15W	LHCB pp at 7, 8 TeV
1 Uses $D \rightarrow K^+K^-\pi^0$ mode.			

$A_{CP}(B^+ \rightarrow [\pi^+\pi^-\pi^0]_D K^+)$

VALUE	DOCUMENT ID	TECN	COMMENT
$0.054 \pm 0.091 \pm 0.011$	1 AAIJ	15W	LHCB pp at 7, 8 TeV
1 Uses $D \rightarrow \pi^+\pi^-\pi^0$ mode.			

$A_{CP}(B^+ \rightarrow \bar{D}^0 K^*(892)^+)$

VALUE	DOCUMENT ID	TECN	COMMENT
-0.007 ± 0.019 OUR AVERAGE			
$-0.004 \pm 0.023 \pm 0.008$	1 AAIJ	17B0	LHCB pp at 7, 8, 13 TeV
$-0.013 \pm 0.031 \pm 0.009$	2 AAIJ	17B0	LHCB pp at 7, 8, 13 TeV
1 Uses $B^\pm \rightarrow [K^\pm\pi^\mp]_D K^*(892)^\pm$ decay mode.			
2 Uses $B^\pm \rightarrow [K^\pm\pi^\mp\pi^+\pi^-]_D K^*(892)^\pm$ decay mode.			

$A_{CP}(B^+ \rightarrow [K^-\pi^+]_D K^*(892)^+)$

VALUE	DOCUMENT ID	TECN	COMMENT
-0.75 ± 0.16 OUR AVERAGE			
$-0.81 \pm 0.17 \pm 0.04$	AAIJ	17B0	LHCB pp at 7, 8, 13 TeV
$-0.34 \pm 0.43 \pm 0.16$	AUBERT	09AJ	BABR $e^+e^- \rightarrow \Upsilon(4S)$
••• We do not use the following data for averages, fits, limits, etc. •••			
$-0.22 \pm 0.61 \pm 0.17$	AUBERT,B	05V	BABR Repl. by AUBERT 09AJ

$A_{CP}(B^+ \rightarrow [K^-\pi^+\pi^-\pi^+]_D K^*(892)^+)$

VALUE	DOCUMENT ID	TECN	COMMENT
$-0.45 \pm 0.21 \pm 0.14$	AAIJ	17B0	LHCB pp at 7, 8, 13 TeV

$A_{CP}(B^+ \rightarrow [K^-\pi^+]_D \pi^+)$

VALUE	DOCUMENT ID	TECN	COMMENT
0.00 ± 0.09 OUR AVERAGE			
$0.13 \pm 0.25 \pm 0.02$	AALTONEN	11AJ	CDF $p\bar{p}$ at 1.96 TeV
$-0.04 \pm 0.11 \pm 0.02$	HORII	11	BELL $e^+e^- \rightarrow \Upsilon(4S)$
$0.03 \pm 0.17 \pm 0.04$	DEL-AMO-SA...10H	BABR	$e^+e^- \rightarrow \Upsilon(4S)$
••• We do not use the following data for averages, fits, limits, etc. •••			
$-0.02 \pm 0.15 \pm 0.04$	HORII	08	BELL Repl. by HORII 11
$+0.30 \pm 0.29 \pm 0.06$	SAIGO	05	BELL Repl. by HORII 08

$A_{CP}(B^+ \rightarrow [K^-\pi^+\pi^0]_D \pi^+)$

VALUE	DOCUMENT ID	TECN	COMMENT
0.35 ± 0.16 OUR AVERAGE			
$0.438 \pm 0.190 \pm 0.011$	1 AAIJ	15W	LHCB pp at 7, 8 TeV
$0.16 \pm 0.27 \pm 0.03$	NAYAK	13	BELL $e^+e^- \rightarrow \Upsilon(4S)$
1 Uses $D^0 \rightarrow K^-\pi^+\pi^0$ for the favored mode, and $D^0 \rightarrow K^+\pi^-\pi^0$ for the suppressed mode.			

$A_{CP}(B^+ \rightarrow [K^+K^-\pi^0]_D \pi^+)$

VALUE	DOCUMENT ID	TECN	COMMENT
$-0.030 \pm 0.040 \pm 0.005$	1 AAIJ	15W	LHCB pp at 7, 8 TeV
1 Uses $D \rightarrow K^+K^-$ mode.			

$A_{CP}(B^+ \rightarrow [\pi^+\pi^-\pi^0]_D \pi^+)$

VALUE	DOCUMENT ID	TECN	COMMENT
$-0.016 \pm 0.020 \pm 0.004$	1 AAIJ	15W	LHCB pp at 7, 8 TeV
1 Uses $D \rightarrow \pi^+\pi^-$ mode.			

$A_{CP}(B^+ \rightarrow [K^-\pi^+]_{(D\pi)} \pi^+)$

VALUE	DOCUMENT ID	TECN	COMMENT
$-0.09 \pm 0.27 \pm 0.05$	DEL-AMO-SA...10H	BABR	$e^+e^- \rightarrow \Upsilon(4S)$

$A_{CP}(B^+ \rightarrow [K^-\pi^+]_{(D\gamma)} \pi^+)$

VALUE	DOCUMENT ID	TECN	COMMENT
$-0.65 \pm 0.55 \pm 0.22$	DEL-AMO-SA...10H	BABR	$e^+e^- \rightarrow \Upsilon(4S)$

$A_{CP}(B^+ \rightarrow [K^-\pi^+]_{(D\pi)} K^+)$

VALUE	DOCUMENT ID	TECN	COMMENT
$0.77 \pm 0.35 \pm 0.12$	DEL-AMO-SA...10H	BABR	$e^+e^- \rightarrow \Upsilon(4S)$

$A_{CP}(B^+ \rightarrow [K^-\pi^+]_{(D\gamma)} K^+)$

VALUE	DOCUMENT ID	TECN	COMMENT
$0.36 \pm 0.94 \pm 0.25$	DEL-AMO-SA...10H	BABR	$e^+e^- \rightarrow \Upsilon(4S)$

$A_{CP}(B^+ \rightarrow [\pi^+\pi^-\pi^0]_D K^+)$

VALUE	DOCUMENT ID	TECN	COMMENT
$-0.02 \pm 0.15 \pm 0.03$	1 AUBERT	07BJ	BABR $e^+e^- \rightarrow \Upsilon(4S)$
$-0.02 \pm 0.16 \pm 0.03$	AUBERT,B	05T	BABR Repl. by AUBERT 07BJ
••• We do not use the following data for averages, fits, limits, etc. •••			
1 Uses a Dalitz plot analysis of $D^0 \rightarrow \pi^+\pi^-\pi^0$. Also reports the one-sigma regions: $0.06 < r_B < 0.78, -30^\circ < \gamma < 76^\circ$, and $-27^\circ < \delta < 78^\circ$.			

$A_{CP}(B^+ \rightarrow [K_S^0 K^+ \pi^-]_D K^+)$

VALUE	DOCUMENT ID	TECN	COMMENT
$0.095 \pm 0.089 \pm 0.018$	1 AAIJ	20N	LHCB pp at 7, 8, 13 TeV
$0.040 \pm 0.091 \pm 0.018$	2 AAIJ	14V	LHCB Repl. by AAIJ 20N
••• We do not use the following data for averages, fits, limits, etc. •••			
1 The analysis uses $D \rightarrow K_S^0 K \pi$ Dalitz decays with $K^* K^+$ region excluded.			
2 The analysis uses all of $D \rightarrow K_S^0 K \pi$ Dalitz decays.			

$A_{CP}(B^+ \rightarrow [K_S^0 K^-\pi^+]_D K^+)$

VALUE	DOCUMENT ID	TECN	COMMENT
$-0.038 \pm 0.075 \pm 0.011$	1 AAIJ	20N	LHCB pp at 7, 8, 13 TeV
$0.233 \pm 0.129 \pm 0.024$	2 AAIJ	14V	LHCB Repl. by AAIJ 20N
••• We do not use the following data for averages, fits, limits, etc. •••			
1 The analysis uses $D \rightarrow K_S^0 K \pi$ Dalitz decays with $K^* K^+$ region excluded.			
2 The analysis uses all of $D \rightarrow K_S^0 K \pi$ Dalitz decays.			

$A_{CP}(B^+ \rightarrow [K_S^0 K^-\pi^+]_D \pi^+)$

VALUE	DOCUMENT ID	TECN	COMMENT
$0.003 \pm 0.015 \pm 0.003$	1 AAIJ	20N	LHCB pp at 7, 8, 13 TeV
$-0.052 \pm 0.029 \pm 0.017$	2 AAIJ	14V	LHCB Repl. by AAIJ 20N
••• We do not use the following data for averages, fits, limits, etc. •••			
1 The analysis uses $D \rightarrow K_S^0 K \pi$ Dalitz decays with $K^* K^+$ region excluded.			
2 The analysis uses all of $D \rightarrow K_S^0 K \pi$ Dalitz decays.			

Meson Particle Listings

 B^\pm $A_{CP}(B^+ \rightarrow [K_S^0 K^+ \pi^-]_D \pi^+)$

VALUE	DOCUMENT ID	TECN	COMMENT
$-0.034 \pm 0.020 \pm 0.003$	¹ AAIJ	20N	LHCB pp at 7, 8, 13 TeV
$-0.025 \pm 0.024 \pm 0.010$	² AAIJ	14v	LHCB Repl. by AAIJ 20N

¹ The analysis uses $D \rightarrow K_S^0 K \pi$ Dalitz decays with $K^{*-} K^+$ region excluded.
² The analysis uses all of $D \rightarrow K_S^0 K \pi$ Dalitz decays.

 $A_{CP}(B^+ \rightarrow [K^*(892)^- K^+]_D K^+)$

VALUE	DOCUMENT ID	TECN	COMMENT
$0.084 \pm 0.049 \pm 0.008$	¹ AAIJ	20N	LHCB pp at 7, 8, 13 TeV
$0.026 \pm 0.109 \pm 0.029$	¹ AAIJ	14v	LHCB Repl. by AAIJ 20N

¹ The Analysis uses $D \rightarrow K^*(892) K \rightarrow K_S^0 K \pi$ decays.

 $A_{CP}(B^+ \rightarrow [K^*(892)^+ K^-]_D K^+)$

VALUE	DOCUMENT ID	TECN	COMMENT
$0.021 \pm 0.094 \pm 0.017$	¹ AAIJ	20N	LHCB pp at 7, 8, 13 TeV
$0.336 \pm 0.208 \pm 0.026$	¹ AAIJ	14v	LHCB Repl. by AAIJ 20N

¹ The Analysis uses $D \rightarrow K^*(892) K \rightarrow K_S^0 K \pi$ decays.

 $A_{CP}(B^+ \rightarrow [K^*(892)^+ K^-]_D \pi^+)$

VALUE	DOCUMENT ID	TECN	COMMENT
$0.007 \pm 0.017 \pm 0.003$	¹ AAIJ	20N	LHCB pp at 7, 8, 13 TeV
$-0.054 \pm 0.043 \pm 0.017$	¹ AAIJ	14v	LHCB Repl. by AAIJ 20N

¹ The Analysis uses $D \rightarrow K^*(892) K \rightarrow K_S^0 K \pi$ decays.

 $A_{CP}(B^+ \rightarrow [K^*(892)^- K^+]_D \pi^+)$

VALUE	DOCUMENT ID	TECN	COMMENT
$-0.020 \pm 0.011 \pm 0.003$	¹ AAIJ	20N	LHCB pp at 7, 8, 13 TeV
$-0.012 \pm 0.028 \pm 0.010$	¹ AAIJ	14v	LHCB Repl. by AAIJ 20N

¹ The Analysis uses $D \rightarrow K^*(892) K \rightarrow K_S^0 K \pi$ decays.

 $A_{CP}(B^+ \rightarrow D_{CP(+1)} K^+)$

VALUE	DOCUMENT ID	TECN	COMMENT
0.132 ± 0.015 OUR AVERAGE	Error includes scale factor of 1.8.		
$0.136 \pm 0.009 \pm 0.001$	¹ AAIJ	21q	LHCB pp at 7, 8, 13 TeV
$0.097 \pm 0.018 \pm 0.009$	AAIJ	16L	LHCB pp at 7, 8 TeV
$0.39 \pm 0.17 \pm 0.04$	AALTONEN	10A	CDF $p\bar{p}$ at 1.96 TeV
$0.25 \pm 0.06 \pm 0.02$	² DEL-AMO-SA...10G	BABR	$e^+ e^- \rightarrow \Upsilon(4S)$
$0.06 \pm 0.14 \pm 0.05$	ABE	06	BELL $e^+ e^- \rightarrow \Upsilon(4S)$
$0.126 \pm 0.014 \pm 0.002$	^{3,4} AAIJ	18A	LHCB pp at 7, 8, 13 TeV
$0.115 \pm 0.025 \pm 0.007$	^{4,5} AAIJ	18A	LHCB pp at 7, 8, 13 TeV
$0.145 \pm 0.032 \pm 0.010$	⁶ AAIJ	12M	LHCB Repl. by AAIJ 16L
$0.27 \pm 0.09 \pm 0.04$	AUBERT	08AA	BABR Repl. by DEL-AMO-SANCHEZ 10G
$0.35 \pm 0.13 \pm 0.04$	AUBERT	06J	BABR Repl. by AUBERT 08AA
$0.07 \pm 0.17 \pm 0.06$	AUBERT	04N	BABR Repl. by AUBERT 06J
$0.29 \pm 0.26 \pm 0.05$	⁷ ABE	03D	BELL Repl. by SWAIN 03
$0.06 \pm 0.19 \pm 0.04$	⁸ SWAIN	03	BELL Repl. by ABE 06

- ¹ Uses $D \rightarrow K^+ K^-$ and $D \rightarrow \pi^+ \pi^-$ decay modes.
² Reports the first evidence for direct CP violation in $B \rightarrow DK$ decays with 3.6 standard deviations.
³ Uses $D \rightarrow K^+ K^-$ decay mode.
⁴ Superseded by AAIJ 21q.
⁵ Uses $D \rightarrow \pi^+ \pi^-$ decay mode.
⁶ AAIJ 12M reports an evidence of direct CP violation in $B^\pm \rightarrow DK^\pm$ decays with a total significance of 5.8 σ .
⁷ Corresponds to 90% confidence range $-0.14 < A_{CP} < 0.73$.
⁸ Corresponds to 90% confidence range $-0.26 < A_{CP} < 0.38$.

 $A_{ADS}(B^+ \rightarrow DK^+)$

$$A_{ADS}(B^+ \rightarrow DK^+) = \frac{(R_K^- - R_K^+)}{(R_K^- + R_K^+)} \text{ where}$$

$$R_K^- = \Gamma(B^- \rightarrow [K^+ \pi^-]_D K^-) / \Gamma(B^- \rightarrow [K^- \pi^+]_D K^-) \text{ and}$$

$$R_K^+ = \Gamma(B^+ \rightarrow [K^- \pi^+]_D K^+) / \Gamma(B^+ \rightarrow [K^+ \pi^-]_D K^+)$$

VALUE	DOCUMENT ID	TECN	COMMENT
-0.451 ± 0.026	¹ AAIJ	21q	LHCB pp at 7, 8, 13 TeV
$-0.403 \pm 0.056 \pm 0.011$	² AAIJ	16L	LHCB pp at 7, 8 TeV
$-0.52 \pm 0.15 \pm 0.02$	AAIJ	12M	LHCB Repl. by AAIJ 16L

¹ The statistical and systematic uncertainties have been combined according to the correlations between the R_K^- and R_K^+ observables.
² Superseded by AAIJ 21q.

 $A_{ADS}(B^+ \rightarrow D\pi^+)$

$$A_{ADS}(B^+ \rightarrow D\pi^+) = \frac{(R_\pi^- - R_\pi^+)}{(R_\pi^- + R_\pi^+)} \text{ where}$$

$$R_\pi^- = \Gamma(B^- \rightarrow [K^+ \pi^-]_D \pi^-) / \Gamma(B^- \rightarrow [K^- \pi^+]_D \pi^-) \text{ and}$$

$$R_\pi^+ = \Gamma(B^+ \rightarrow [K^- \pi^+]_D \pi^+) / \Gamma(B^+ \rightarrow [K^+ \pi^-]_D \pi^+)$$

VALUE	DOCUMENT ID	TECN	COMMENT
0.129 ± 0.014	¹ AAIJ	21q	LHCB pp at 7, 8, 13 TeV
$0.100 \pm 0.031 \pm 0.009$	² AAIJ	16L	LHCB pp at 7, 8 TeV
$0.143 \pm 0.062 \pm 0.011$	AAIJ	12M	LHCB Repl. by AAIJ 16L

¹ The statistical and systematic uncertainties have been combined according to the correlations between the R_π^- and R_π^+ observables.
² Superseded by AAIJ 21q.

 $A_{ADS}(B^+ \rightarrow D^*(D\gamma)K^+)$

$$A_{ADS}(B^+ \rightarrow D^*(D\gamma)K^+) = (R_K^- - R_K^+) / (R_K^- + R_K^+), \text{ where}$$

$$R_K^- = \Gamma(B^- \rightarrow (\gamma[K^+ \pi^-]_D)_{D^*} K^-) / \Gamma(B^- \rightarrow (\gamma[K^- \pi^+]_D)_{D^*} K^-) \text{ and}$$

$$R_K^+ = \Gamma(B^+ \rightarrow (\gamma[K^- \pi^+]_D)_{D^*} K^+) / \Gamma(B^+ \rightarrow (\gamma[K^+ \pi^-]_D)_{D^*} K^+)$$

VALUE	DOCUMENT ID	TECN	COMMENT
-0.558 ± 1.349	¹ AAIJ	21q	LHCB pp at 7, 8, 13 TeV

¹ The statistical and systematic uncertainties have been combined according to the correlations between the R_K^- and R_K^+ observables.

 $A_{ADS}(B^+ \rightarrow D^*(D\pi^0)K^+)$

$$A_{ADS}(B^+ \rightarrow D^*(D\pi^0)K^+) = (R_K^- - R_K^+) / (R_K^- + R_K^+), \text{ where}$$

$$R_K^- = \Gamma(B^- \rightarrow ([K^+ \pi^-]_{D\pi^0})_{D^*} K^-) / \Gamma(B^- \rightarrow ([K^- \pi^+]_{D\pi^0})_{D^*} K^-) \text{ and}$$

$$R_K^+ = \Gamma(B^+ \rightarrow ([K^- \pi^+]_{D\pi^0})_{D^*} K^+) / \Gamma(B^+ \rightarrow ([K^+ \pi^-]_{D\pi^0})_{D^*} K^+)$$

VALUE	DOCUMENT ID	TECN	COMMENT
0.717 ± 0.286	¹ AAIJ	21q	LHCB pp at 7, 8, 13 TeV

¹ The statistical and systematic uncertainties have been combined according to the correlations between the R_K^- and R_K^+ observables.

 $A_{ADS}(B^+ \rightarrow D^*(D\gamma)\pi^+)$

$$A_{ADS}(B^+ \rightarrow D^*(D\gamma)\pi^+) = (R_\pi^- - R_\pi^+) / (R_\pi^- + R_\pi^+), \text{ where}$$

$$R_\pi^- = \Gamma(B^- \rightarrow (\gamma[K^+ \pi^-]_D)_{D^*} \pi^-) / \Gamma(B^- \rightarrow (\gamma[K^- \pi^+]_D)_{D^*} \pi^-) \text{ and}$$

$$R_\pi^+ = \Gamma(B^+ \rightarrow (\gamma[K^- \pi^+]_D)_{D^*} \pi^+) / \Gamma(B^+ \rightarrow (\gamma[K^+ \pi^-]_D)_{D^*} \pi^+)$$

VALUE	DOCUMENT ID	TECN	COMMENT
0.079 ± 0.128	¹ AAIJ	21q	LHCB pp at 7, 8, 13 TeV

¹ The statistical and systematic uncertainties have been combined according to the correlations between the R_π^- and R_π^+ observables.

 $A_{ADS}(B^+ \rightarrow D^*(D\pi^0)\pi^+)$

$$A_{ADS}(B^+ \rightarrow D^*(D\pi^0)\pi^+) = (R_\pi^- - R_\pi^+) / (R_\pi^- + R_\pi^+), \text{ where}$$

$$R_\pi^- = \Gamma(B^- \rightarrow ([K^+ \pi^-]_{D\pi^0})_{D^*} \pi^-) / \Gamma(B^- \rightarrow ([K^- \pi^+]_{D\pi^0})_{D^*} \pi^-) \text{ and}$$

$$R_\pi^+ = \Gamma(B^+ \rightarrow ([K^- \pi^+]_{D\pi^0})_{D^*} \pi^+) / \Gamma(B^+ \rightarrow ([K^+ \pi^-]_{D\pi^0})_{D^*} \pi^+)$$

VALUE	DOCUMENT ID	TECN	COMMENT
-0.140 ± 0.059	¹ AAIJ	21q	LHCB pp at 7, 8, 13 TeV

¹ The statistical and systematic uncertainties have been combined according to the correlations between the R_π^- and R_π^+ observables.

 $A_{ADS}(B^+ \rightarrow [K^- \pi^+]_D K^+ \pi^- \pi^+)$

VALUE	DOCUMENT ID	TECN	COMMENT
-0.33 ± 0.36	AAIJ	15bc	LHCB pp at 7, 8 TeV

 $A_{ADS}(B^+ \rightarrow [K^- \pi^+]_D \pi^+ \pi^- \pi^+)$

VALUE	DOCUMENT ID	TECN	COMMENT
-0.013 ± 0.087	AAIJ	15bc	LHCB pp at 7, 8 TeV

 $A_{CP}(B^+ \rightarrow D_{CP(-1)} K^+)$

VALUE	DOCUMENT ID	TECN	COMMENT
-0.10 ± 0.07 OUR AVERAGE			
$-0.09 \pm 0.07 \pm 0.02$	DEL-AMO-SA...10G	BABR	$e^+ e^- \rightarrow \Upsilon(4S)$
$-0.12 \pm 0.14 \pm 0.05$	ABE	06	BELL $e^+ e^- \rightarrow \Upsilon(4S)$
$-0.09 \pm 0.09 \pm 0.02$	AUBERT	08AA	BABR Repl. by DEL-AMO-SANCHEZ 10G
$-0.06 \pm 0.13 \pm 0.04$	AUBERT	06J	BABR Repl. by AUBERT 08AA
$-0.22 \pm 0.24 \pm 0.04$	¹ ABE	03D	BELL Repl. by SWAIN 03
$-0.19 \pm 0.17 \pm 0.05$	² SWAIN	03	BELL Repl. by ABE 06

¹ Corresponds to 90% confidence range $-0.62 < A_{CP} < 0.18$.
² Corresponds to 90% confidence range $-0.47 < A_{CP} < 0.11$.

 $A_{CP}(B^+ \rightarrow [K^+ K^-]_D K^+ \pi^- \pi^+)$

VALUE	DOCUMENT ID	TECN	COMMENT
-0.045 ± 0.064 ± 0.011	AAIJ	15bc	LHCB pp at 7, 8 TeV

VALUE	DOCUMENT ID	TECN	COMMENT
$A_{CP}(B^+ \rightarrow [\pi^+\pi^-]_D K^+ \pi^- \pi^+)$	AAIJ	15bc	LHCB pp at 7, 8 TeV
$-0.054 \pm 0.101 \pm 0.011$			

VALUE	DOCUMENT ID	TECN	COMMENT
$A_{CP}(B^+ \rightarrow [K^- \pi^+]_D K^+ \pi^- \pi^+)$	AAIJ	15bc	LHCB pp at 7, 8 TeV
$0.013 \pm 0.019 \pm 0.013$			

VALUE	DOCUMENT ID	TECN	COMMENT
$A_{CP}(B^+ \rightarrow [K^+ K^-]_D \pi^+ \pi^- \pi^+)$	AAIJ	15bc	LHCB pp at 7, 8 TeV
$-0.019 \pm 0.011 \pm 0.010$			

VALUE	DOCUMENT ID	TECN	COMMENT
$A_{CP}(B^+ \rightarrow [\pi^+\pi^-]_D \pi^+ \pi^- \pi^+)$	AAIJ	15bc	LHCB pp at 7, 8 TeV
$-0.013 \pm 0.016 \pm 0.010$			

VALUE	DOCUMENT ID	TECN	COMMENT
$A_{CP}(B^+ \rightarrow [K^- \pi^+]_D \pi^+ \pi^- \pi^+)$	AAIJ	15bc	LHCB pp at 7, 8 TeV
$-0.002 \pm 0.003 \pm 0.011$			

VALUE	DOCUMENT ID	TECN	COMMENT
$A_{CP}(B^+ \rightarrow \bar{D}^{*0} \pi^+)$			
-0.004 ± 0.0021 OUR AVERAGE			Error includes scale factor of 1.1.
$-0.004 \pm 0.004 \pm 0.001$	¹ AAIJ	21q	LHCB pp at 7, 8, 13 TeV
$0.001 \pm 0.002 \pm 0.001$	² AAIJ	21q	LHCB pp at 7, 8, 13 TeV
-0.014 ± 0.015	ABE	06	BELL $e^+e^- \rightarrow \Upsilon(4S)$
• • • We do not use the following data for averages, fits, limits, etc. • • •			
$0.000 \pm 0.006 \pm 0.001$	^{1,3} AAIJ	18a	LHCB pp at 7, 8, 13 TeV
$0.002 \pm 0.003 \pm 0.001$	^{2,3} AAIJ	18a	LHCB pp at 7, 8, 13 TeV
¹ Uses $D^{*0} \rightarrow D^0 \gamma$ decay mode.			
² Uses $D^{*0} \rightarrow D^0 \pi^0$ decay mode.			
³ Superseded by AAJ 21q.			

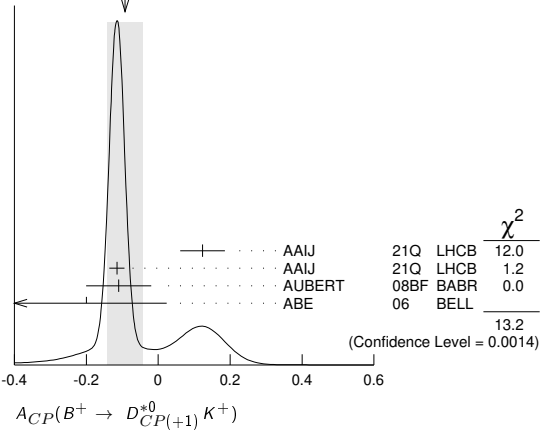
VALUE	DOCUMENT ID	TECN	COMMENT
$A_{CP}(B^+ \rightarrow (D_{CP(+1)}^{*0})^0 \pi^+)$			
0.010 ± 0.007 OUR AVERAGE			
$0.000 \pm 0.014 \pm 0.006$	¹ AAIJ	21q	LHCB pp at 7, 8, 13 TeV
$0.013 \pm 0.007 \pm 0.003$	² AAIJ	21q	LHCB pp at 7, 8, 13 TeV
-0.021 ± 0.045	ABE	06	BELL $e^+e^- \rightarrow \Upsilon(4S)$
• • • We do not use the following data for averages, fits, limits, etc. • • •			
$-0.003 \pm 0.017 \pm 0.002$	^{1,3} AAIJ	18a	LHCB pp at 7, 8, 13 TeV
$0.025 \pm 0.010 \pm 0.003$	^{2,3} AAIJ	18a	LHCB pp at 7, 8, 13 TeV
¹ Uses $D^{*0} \rightarrow D^0 \gamma$ decay mode.			
² Uses $D^{*0} \rightarrow D^0 \pi^0$ decay mode.			
³ Superseded by AAJ 21q.			

VALUE	DOCUMENT ID	TECN	COMMENT
$A_{CP}(B^+ \rightarrow (D_{CP(-1)}^{*0})^0 \pi^+)$			
-0.090 ± 0.051	ABE	06	BELL $e^+e^- \rightarrow \Upsilon(4S)$

VALUE	DOCUMENT ID	TECN	COMMENT
$A_{CP}(B^+ \rightarrow D^{*0} K^+)$			
0.012 ± 0.010 OUR AVERAGE			Error includes scale factor of 1.5.
$-0.004 \pm 0.014 \pm 0.003$	¹ AAIJ	21q	LHCB pp at 7, 8, 13 TeV
$0.020 \pm 0.007 \pm 0.003$	² AAIJ	21q	LHCB pp at 7, 8, 13 TeV
$-0.06 \pm 0.04 \pm 0.01$	AUBERT	08BF	BABR $e^+e^- \rightarrow \Upsilon(4S)$
-0.089 ± 0.086	ABE	06	BELL $e^+e^- \rightarrow \Upsilon(4S)$
• • • We do not use the following data for averages, fits, limits, etc. • • •			
$0.001 \pm 0.021 \pm 0.007$	^{1,3} AAIJ	18a	LHCB pp at 7, 8, 13 TeV
$0.006 \pm 0.012 \pm 0.004$	^{2,3} AAIJ	18a	LHCB pp at 7, 8, 13 TeV
¹ Uses $D^{*0} \rightarrow D^0 \gamma$ decay mode.			
² Uses $D^{*0} \rightarrow D^0 \pi^0$ decay mode.			
³ Superseded by AAJ 21q.			

VALUE	DOCUMENT ID	TECN	COMMENT
$A_{CP}(B^+ \rightarrow D_{CP(+1)}^{*0} K^+)$			
-0.09 ± 0.05 OUR AVERAGE			Error includes scale factor of 2.6. See the ideogram below.
$0.123 \pm 0.054 \pm 0.031$	¹ AAIJ	21q	LHCB pp at 7, 8, 13 TeV
$-0.115 \pm 0.019 \pm 0.009$	² AAIJ	21q	LHCB pp at 7, 8, 13 TeV
$-0.11 \pm 0.09 \pm 0.01$	AUBERT	08BF	BABR $e^+e^- \rightarrow \Upsilon(4S)$
$-0.20 \pm 0.22 \pm 0.04$	ABE	06	BELL $e^+e^- \rightarrow \Upsilon(4S)$
• • • We do not use the following data for averages, fits, limits, etc. • • •			
$0.276 \pm 0.094 \pm 0.047$	^{1,3} AAIJ	18a	LHCB pp at 7, 8, 13 TeV
$-0.151 \pm 0.033 \pm 0.011$	^{2,3} AAIJ	18a	LHCB pp at 7, 8, 13 TeV
$-0.10 \pm 0.23 \pm 0.03$	AUBERT	05N	BABR Repl. by AUBERT 08BF
			¹ Uses $D^{*0} \rightarrow D^0 \gamma$ decay mode.
			² Uses $D^{*0} \rightarrow D^0 \pi^0$ decay mode.
			³ Superseded by AAJ 21q.

WEIGHTED AVERAGE
-0.09±0.05 (Error scaled by 2.6)



VALUE	DOCUMENT ID	TECN	COMMENT
$A_{CP}(B^+ \rightarrow D_{CP(-1)}^{*0} K^+)$			
0.07 ± 0.10 OUR AVERAGE			
$+0.06 \pm 0.10 \pm 0.02$	AUBERT	08BF	BABR $e^+e^- \rightarrow \Upsilon(4S)$
$+0.13 \pm 0.30 \pm 0.08$	ABE	06	BELL $e^+e^- \rightarrow \Upsilon(4S)$

VALUE	DOCUMENT ID	TECN	COMMENT
$A_{CP}(B^+ \rightarrow D_{CP(+1)} K^*(892)^+)$			
0.08 ± 0.06 OUR AVERAGE			
$0.08 \pm 0.06 \pm 0.01$	¹ AAIJ	17Bo	LHCB pp at 7, 8, 13 TeV
$0.09 \pm 0.13 \pm 0.06$	AUBERT	09AJ	BABR $e^+e^- \rightarrow \Upsilon(4S)$
• • • We do not use the following data for averages, fits, limits, etc. • • •			
$-0.08 \pm 0.19 \pm 0.08$	AUBERT,B	05U	BABR Repl. by AUBERT 09AJ

¹ Measures the asymmetry separately for K^+K^- and $\pi^+\pi^-$ final states, $A(KK) = 0.06 \pm 0.07 \pm 0.01$ and $A(\pi\pi) = 0.15 \pm 0.13 \pm 0.01$, and combines the two results. The value of $A(\pi\pi)$ was updated in AAJ 18x.

VALUE	DOCUMENT ID	TECN	COMMENT
$A_{CP}(B^+ \rightarrow D_{CP(-1)} K^*(892)^+)$			
$-0.23 \pm 0.21 \pm 0.07$	AUBERT	09AJ	BABR $e^+e^- \rightarrow \Upsilon(4S)$
• • • We do not use the following data for averages, fits, limits, etc. • • •			
$-0.26 \pm 0.40 \pm 0.12$	AUBERT,B	05U	BABR Repl. by AUBERT 09AJ

VALUE	DOCUMENT ID	TECN	COMMENT
$A_{CP}(B^+ \rightarrow D_s^+ \phi)$			
$-0.01 \pm 0.41 \pm 0.03$	AAIJ	13R	LHCB pp at 7 TeV

VALUE (%)	DOCUMENT ID	TECN	COMMENT
$A_{CP}(B^+ \rightarrow D_s^+ \bar{D}^0)$			
$-0.4 \pm 0.5 \pm 0.5$	AAIJ	18w	LHCB pp at 7, 8 TeV

VALUE	DOCUMENT ID	TECN	COMMENT
$A_{CP}(B^+ \rightarrow D^{*+} \bar{D}^0)$			
$-0.15 \pm 0.11 \pm 0.02$	AUBERT,B	06A	BABR $e^+e^- \rightarrow \Upsilon(4S)$

VALUE	DOCUMENT ID	TECN	COMMENT
$A_{CP}(B^+ \rightarrow D^{*+} \bar{D}^0)$			
$-0.06 \pm 0.13 \pm 0.02$	AUBERT,B	06A	BABR $e^+e^- \rightarrow \Upsilon(4S)$

VALUE	DOCUMENT ID	TECN	COMMENT
$A_{CP}(B^+ \rightarrow D^+ \bar{D}^{*0})$			
$0.13 \pm 0.18 \pm 0.04$	AUBERT,B	06A	BABR $e^+e^- \rightarrow \Upsilon(4S)$

VALUE	DOCUMENT ID	TECN	COMMENT
$A_{CP}(B^+ \rightarrow D^+ \bar{D}^0)$			
0.016 ± 0.025 OUR AVERAGE			
$0.023 \pm 0.027 \pm 0.004$	AAIJ	18w	LHCB pp at 7, 8 TeV
$0.00 \pm 0.08 \pm 0.02$	ADACHI	08	BELL $e^+e^- \rightarrow \Upsilon(4S)$
$-0.13 \pm 0.14 \pm 0.02$	AUBERT,B	06A	BABR $e^+e^- \rightarrow \Upsilon(4S)$

VALUE	DOCUMENT ID	TECN	COMMENT
$A_{CP}(B^+ \rightarrow K_S^0 \pi^+)$			
-0.017 ± 0.016 OUR AVERAGE			
$-0.022 \pm 0.025 \pm 0.010$	AAIJ	13Bs	LHCB pp at 7 TeV
$-0.011 \pm 0.021 \pm 0.006$	DUH	13	BELL $e^+e^- \rightarrow \Upsilon(4S)$
$-0.029 \pm 0.039 \pm 0.010$	¹ AUBERT,BE	06c	BABR $e^+e^- \rightarrow \Upsilon(4S)$
0.18 ± 0.24	² CHEN	00	CLE2 $e^+e^- \rightarrow \Upsilon(4S)$

Meson Particle Listings

 B^\pm

••• We do not use the following data for averages, fits, limits, etc. •••

0.03 ± 0.03 ± 0.01	LIN	07	BELL	Repl. by DUH 13
-0.09 ± 0.05 ± 0.01	³ AUBERT, BE	05E	BABR	Repl. by AUBERT, BE 06c
0.05 ± 0.05 ± 0.01	⁴ CHAO	05A	BELL	Repl. by LIN 07
-0.05 ± 0.08 ± 0.01	⁵ AUBERT	04M	BABR	Repl. by AUBERT, BE 05E
0.07 + 0.09 + 0.01 -0.08 - 0.03	⁶ UNNO	03	BELL	Repl. by CHAO 05A
0.46 ± 0.15 ± 0.02	⁷ CASEY	02	BELL	Repl. by UNNO 03
0.098 + 0.430 + 0.020 -0.343 - 0.063	⁸ ABE	01K	BELL	Repl. by CASEY 02
-0.21 ± 0.18 ± 0.03	⁹ AUBERT	01E	BABR	Repl. by AUBERT 04M

¹ Corresponds to 90% confidence range $-0.092 < A_{CP} < 0.036$.

² Corresponds to 90% confidence range $-0.22 < A_{CP} < 0.56$.

³ Corresponds to 90% confidence range $-0.16 < A_{CP} < -0.02$.

⁴ Corresponds to 90% confidence range $-0.04 < A_{CP} < 0.13$.

⁵ Corresponds to 90% confidence range $-0.18 < A_{CP} < 0.08$.

⁶ Corresponds to 90% confidence range $-0.10 < A_{CP} < +0.22$.

⁷ Corresponds to 90% confidence range $+0.19 < A_{CP} < +0.72$.

⁸ Corresponds to 90% confidence range $-0.53 < A_{CP} < 0.82$.

⁹ Corresponds to 90% confidence range $-0.51 < A_{CP} < 0.09$.

 $A_{CP}(B^+ \rightarrow K^+ \pi^0)$

VALUE	DOCUMENT ID	TECN	COMMENT
0.030 ± 0.013 OUR AVERAGE			
0.025 ± 0.015 ± 0.007	AAIJ	21H	LHCB pp at 13 TeV
0.043 ± 0.024 ± 0.002	DUH	13	BELL $e^+e^- \rightarrow \Upsilon(4S)$
0.030 ± 0.039 ± 0.010	AUBERT	07Bc	BABR $e^+e^- \rightarrow \Upsilon(4S)$
-0.29 ± 0.23	¹ CHEN	00	CLE2 $e^+e^- \rightarrow \Upsilon(4S)$

••• We do not use the following data for averages, fits, limits, etc. •••

0.07 ± 0.03 ± 0.01	LIN	08	BELL	Repl. by DUH 13
0.06 ± 0.06 ± 0.01	² AUBERT	05L	BABR	Repl. by AUBERT 07Bc
0.06 ± 0.06 ± 0.02	² CHAO	05A	BELL	Repl. by CHAO 04B
0.04 ± 0.05 ± 0.02	³ CHAO	04B	BELL	Repl. by LIN 08
-0.09 ± 0.09 ± 0.01	⁴ AUBERT	03L	BABR	Repl. by AUBERT 05L
-0.02 ± 0.19 ± 0.02	⁵ CASEY	02	BELL	Repl. by CHAO 04B
-0.059 + 0.222 + 0.055 -0.196 - 0.017	⁶ ABE	01K	BELL	Repl. by CASEY 02
0.00 ± 0.18 ± 0.04	⁷ AUBERT	01E	BABR	Repl. by AUBERT 03L

¹ Corresponds to 90% confidence range $-0.67 < A_{CP} < 0.09$.

² Corresponds to a 90% CL interval of $-0.06 < A_{CP} < 0.18$.

³ Corresponds to 90% CL interval of $-0.05 < A_{CP} < 0.13$.

⁴ Corresponds to 90% confidence range $-0.24 < A_{CP} < 0.06$.

⁵ Corresponds to 90% confidence range $-0.35 < A_{CP} < +0.30$.

⁶ Corresponds to 90% confidence range $-0.40 < A_{CP} < 0.36$.

⁷ Corresponds to 90% confidence range $-0.30 < A_{CP} < +0.30$.

 $A_{CP}(B^+ \rightarrow \eta' K^+)$

VALUE	DOCUMENT ID	TECN	COMMENT
0.004 ± 0.011 OUR AVERAGE			
-0.002 ± 0.012 ± 0.006	¹ AAIJ	15o	LHCB pp at 7, 8 TeV
0.008 + 0.017 + 0.009 -0.018	AUBERT	09AV	BABR $e^+e^- \rightarrow \Upsilon(4S)$
0.028 ± 0.028 ± 0.021	SCHUEMANN	06	BELL $e^+e^- \rightarrow \Upsilon(4S)$
0.03 ± 0.12	² CHEN	00	CLE2 $e^+e^- \rightarrow \Upsilon(4S)$

••• We do not use the following data for averages, fits, limits, etc. •••

0.010 ± 0.022 ± 0.006	AUBERT	07AE	BABR	Repl. by AUBERT 09AV
0.033 ± 0.028 ± 0.005	³ AUBERT	05M	BABR	Repl. by AUBERT 07AE
0.037 ± 0.045 ± 0.011	⁴ AUBERT	03W	BABR	Repl. by AUBERT 05M
-0.11 ± 0.11 ± 0.02	⁵ AUBERT	02E	BABR	Repl. by AUBERT 05M
-0.015 ± 0.070 ± 0.009	⁶ CHEN	02B	BELL	Repl. by SCHUEMANN 06
0.06 ± 0.15 ± 0.01	⁷ ABE	01M	BELL	Repl. by CHEN 02B

¹ Obtained using $A_{CP}(B^\pm \rightarrow J/\psi K^\pm) = (0.3 \pm 0.6) \times 10^{-2}$.

² Corresponds to 90% confidence range $-0.17 < A_{CP} < 0.23$.

³ Corresponds to 90% confidence range $-0.012 < A_{CP} < 0.078$.

⁴ Corresponds to 90% confidence range $-0.04 < A_{CP} < 0.11$.

⁵ Corresponds to 90% confidence range $-0.28 < A_{CP} < 0.07$.

⁶ Corresponds to 90% confidence range $-0.13 < A_{CP} < 0.10$.

⁷ Corresponds to 90% confidence range $-0.20 < A_{CP} < 0.32$.

 $A_{CP}(B^+ \rightarrow \eta' K^*(892)^+)$

VALUE	DOCUMENT ID	TECN	COMMENT
-0.26 ± 0.27 ± 0.02	DEL-AMO-SA...10A	BABR	$e^+e^- \rightarrow \Upsilon(4S)$

••• We do not use the following data for averages, fits, limits, etc. •••

-0.30 + 0.33 + 0.02 -0.37	¹ AUBERT	07E	BABR	Repl. by DEL-AMO-SANCHEZ 10A
------------------------------	---------------------	-----	------	------------------------------

¹ Reports A_{CP} with the opposite sign convention.

 $A_{CP}(B^+ \rightarrow \eta' K_0^*(1430)^+)$

VALUE	DOCUMENT ID	TECN	COMMENT
0.06 ± 0.20 ± 0.02	DEL-AMO-SA...10A	BABR	$e^+e^- \rightarrow \Upsilon(4S)$

VALUE	DOCUMENT ID	TECN	COMMENT
0.15 ± 0.13 ± 0.02	DEL-AMO-SA...10A	BABR	$e^+e^- \rightarrow \Upsilon(4S)$

VALUE	DOCUMENT ID	TECN	COMMENT
0.027 ± 0.008 OUR AVERAGE			
0.025 ± 0.004 ± 0.008	¹ AAIJ	14Bo	LHCB pp at 7, 8 TeV
0.028 ± 0.020 ± 0.023	AUBERT	08Al	BABR $e^+e^- \rightarrow \Upsilon(4S)$
0.049 ± 0.026 ± 0.020	GARMASH	06	BELL $e^+e^- \rightarrow \Upsilon(4S)$

 $A_{CP}(B^+ \rightarrow \eta K^+)$

VALUE	DOCUMENT ID	TECN	COMMENT
-0.37 ± 0.08 OUR AVERAGE			
-0.38 ± 0.11 ± 0.01	HOI	12	BELL $e^+e^- \rightarrow \Upsilon(4S)$
-0.36 ± 0.11 ± 0.03	AUBERT	09AV	BABR $e^+e^- \rightarrow \Upsilon(4S)$

••• We do not use the following data for averages, fits, limits, etc. •••

-0.22 ± 0.11 ± 0.01	AUBERT	07AE	BABR	Repl. by AUBERT 09AV
-0.39 ± 0.16 ± 0.03	CHANG	07B	BELL	Repl. by HOI 12
-0.20 ± 0.15 ± 0.01	AUBERT, B	05K	BABR	Repl. by AUBERT 07AE
-0.49 ± 0.31 ± 0.07	CHANG	05A	BELL	Repl. by CHANG 07B
-0.52 ± 0.24 ± 0.01	AUBERT	04H	BABR	Repl. by AUBERT, B 05K

 $A_{CP}(B^+ \rightarrow \eta K^*(892)^+)$

VALUE	DOCUMENT ID	TECN	COMMENT
0.02 ± 0.06 OUR AVERAGE			
0.03 ± 0.10 ± 0.01	WANG	07B	BELL $e^+e^- \rightarrow \Upsilon(4S)$
0.01 ± 0.08 ± 0.02	AUBERT, B	06H	BABR $e^+e^- \rightarrow \Upsilon(4S)$

••• We do not use the following data for averages, fits, limits, etc. •••

0.13 ± 0.14 ± 0.02	AUBERT, B	04D	BABR	Repl. by AUBERT, B 06H
--------------------	-----------	-----	------	------------------------

 $A_{CP}(B^+ \rightarrow \eta K_0^*(1430)^+)$

VALUE	DOCUMENT ID	TECN	COMMENT
0.05 ± 0.13 ± 0.02	AUBERT, B	06H	BABR $e^+e^- \rightarrow \Upsilon(4S)$

VALUE	DOCUMENT ID	TECN	COMMENT
0.02 ± 0.04 OUR AVERAGE			
-0.03 ± 0.04 ± 0.01	CHOBANOVA	14	BELL $e^+e^- \rightarrow \Upsilon(4S)$
-0.01 ± 0.07 ± 0.01	AUBERT	07AE	BABR $e^+e^- \rightarrow \Upsilon(4S)$

••• We do not use the following data for averages, fits, limits, etc. •••

0.05 ± 0.09 ± 0.01	AUBERT, B	06E	BABR	Repl. by AUBERT 07AE
0.05 + 0.08 + 0.01 -0.07	JEN	06	BELL	Repl. by CHOBANOVA 14
-0.09 ± 0.17 ± 0.01	AUBERT	04H	BABR	Repl. by AUBERT, B 06E
0.06 + 0.21 + 0.18 -0.18	¹ WANG	04A	BELL	Repl. by JEN 06
-0.21 ± 0.28 ± 0.03	² LU	02	BELL	Repl. by WANG 04A

 $A_{CP}(B^+ \rightarrow \omega K^+)$

VALUE	DOCUMENT ID	TECN	COMMENT
-0.02 ± 0.04 OUR AVERAGE			
-0.03 ± 0.04 ± 0.01	CHOBANOVA	14	BELL $e^+e^- \rightarrow \Upsilon(4S)$
-0.01 ± 0.07 ± 0.01	AUBERT	07AE	BABR $e^+e^- \rightarrow \Upsilon(4S)$

••• We do not use the following data for averages, fits, limits, etc. •••

0.05 ± 0.09 ± 0.01	AUBERT, B	06E	BABR	Repl. by AUBERT 07AE
0.05 + 0.08 + 0.01 -0.07	JEN	06	BELL	Repl. by CHOBANOVA 14
-0.09 ± 0.17 ± 0.01	AUBERT	04H	BABR	Repl. by AUBERT, B 06E
0.06 + 0.21 + 0.18 -0.18	¹ WANG	04A	BELL	Repl. by JEN 06
-0.21 ± 0.28 ± 0.03	² LU	02	BELL	Repl. by WANG 04A

¹ Corresponds to 90% CL interval $0.15 < A_{CP} < 0.90$

² Corresponds to 90% confidence range $-0.70 < A_{CP} < +0.38$.

 $A_{CP}(B^+ \rightarrow \omega K^{*+})$

VALUE	DOCUMENT ID	TECN	COMMENT
+0.29 ± 0.35 ± 0.02	AUBERT	09H	BABR $e^+e^- \rightarrow \Upsilon(4S)$

VALUE	DOCUMENT ID	TECN	COMMENT
0.02 ± 0.04 OUR AVERAGE			
-0.03 ± 0.04 ± 0.01	CHOBANOVA	14	BELL $e^+e^- \rightarrow \Upsilon(4S)$
-0.01 ± 0.07 ± 0.01	AUBERT	07AE	BABR $e^+e^- \rightarrow \Upsilon(4S)$

••• We do not use the following data for averages, fits, limits, etc. •••

0.05 ± 0.09 ± 0.01	AUBERT, B	06E	BABR	Repl. by AUBERT 07AE
0.05 + 0.08 + 0.01 -0.07	JEN	06	BELL	Repl. by CHOBANOVA 14
-0.09 ± 0.17 ± 0.01	AUBERT	04H	BABR	Repl. by AUBERT, B 06E
0.06 + 0.21 + 0.18 -0.18	¹ WANG	04A	BELL	Repl. by JEN 06
-0.21 ± 0.28 ± 0.03	² LU	02	BELL	Repl. by WANG 04A

 $A_{CP}(B^+ \rightarrow \omega K_0^*(1430)^+)$

VALUE	DOCUMENT ID	TECN	COMMENT
+0.14 ± 0.15 ± 0.02	AUBERT	09H	BABR $e^+e^- \rightarrow \Upsilon(4S)$

VALUE	DOCUMENT ID	TECN	COMMENT
0.04 ± 0.011 OUR AVERAGE			
-0.002 ± 0.012 ± 0.006	¹ AAIJ	15o	LHCB pp at 7, 8 TeV
0.008 + 0.017 + 0.009 -0.018	AUBERT	09AV	BABR $e^+e^- \rightarrow \Upsilon(4S)$
0.028 ± 0.028 ± 0.021	SCHUEMANN	06	BELL $e^+e^- \rightarrow \Upsilon(4S)$
0.03 ± 0.12	² CHEN	00	CLE2 $e^+e^- \rightarrow \Upsilon(4S)$

••• We do not use the following data for averages, fits, limits, etc. •••

0.010 ± 0.022 ± 0.006	AUBERT	07AE	BABR	Repl. by AUBERT 09AV
0.033 ± 0.028 ± 0.005	³ AUBERT	05M	BABR	Repl. by AUBERT 07AE
0.037 ± 0.045 ± 0.011	⁴ AUBERT	03W	BABR	Repl. by AUBERT 05M
-0.11 ± 0.11 ± 0.02	⁵ AUBERT	02E	BABR	Repl. by AUBERT 05M
-0.015 ± 0.070 ± 0.009	⁶ CHEN	02B	BELL	Repl. by SCHUEMANN 06
0.06 ± 0.15 ± 0.01	⁷ ABE	01M	BELL	Repl. by CHEN 02B

¹ Obtains the result from a Dalitz analysis of $B^+ \rightarrow K_S^0 \pi^+ \pi^0$ decays. The first error is statistical, the second combines all the systematic uncertainties reported in the paper, including signal modelling.

 $A_{CP}(B^+ \rightarrow K^*(892)^+ \pi^0)$

VALUE	DOCUMENT ID	TECN	COMMENT
-0.39 ± 0.21 OUR AVERAGE			Error includes scale factor of 1.6.
-0.52 ± 0.14 + 0.06 -0.05	¹ LEES	17G	BABR $e^+e^- \rightarrow \Upsilon(4S)$
-0.06 ± 0.24 ± 0.04	LEES	11i	BABR $e^+e^- \rightarrow \Upsilon(4S)$

••• We do not use the following data for averages, fits, limits, etc. •••

0.04 ± 0.29 ± 0.05	AUBERT	05X	BABR	Repl. by LEES 11i
--------------------	--------	-----	------	-------------------

¹ Obtains the result from a Dalitz analysis of $B^+ \rightarrow K_S^0 \pi^+ \pi^0$ decays. The first error is statistical, the second combines all the systematic uncertainties reported in the paper, including signal modelling.

 $A_{CP}(B^+ \rightarrow K^+ \pi^- \pi^+)$

VALUE	DOCUMENT ID	TECN	COMMENT
0.027 ± 0.008 OUR AVERAGE			
0.025 ± 0.004 ± 0.008	¹ AAIJ	14Bo	LHCB pp at 7, 8 TeV
0.028 ± 0.020 ± 0.023	AUBERT	08Al	BABR $e^+e^- \rightarrow \Upsilon(4S)$
0.049 ± 0.026 ± 0.020	GARMASH	06	BELL $e^+e^- \rightarrow \Upsilon(4S)$

See key on page 1127

Meson Particle Listings
 B^\pm

• • • We do not use the following data for averages, fits, limits, etc. • • •

$0.032 \pm 0.008 \pm 0.008$	AAIJ	13AZ	LHCB	Repl. by AAIJ 14Bo
$-0.013 \pm 0.037 \pm 0.011$	AUBERT,B	05N	BABR	Repl. by AUBERT 08Ai
$0.01 \pm 0.07 \pm 0.03$	AUBERT	03M	BABR	Repl. by AUBERT,B 05N

¹ AAIJ 14Bo reports also CP asymmetries in restricted regions of phase space. $A_{CP}(B^+ \rightarrow K^+ K^- K^+ \text{nonresonant})$

VALUE	DOCUMENT ID	TECN	COMMENT
$0.060 \pm 0.044 \pm 0.019$	LEES	12o	BABR $e^+ e^- \rightarrow \Upsilon(4S)$

 $A_{CP}(B^+ \rightarrow f(980)^0 K^+)$

VALUE	DOCUMENT ID	TECN	COMMENT
$-0.08 \pm 0.08 \pm 0.04$	¹ LEES	12o	BABR $e^+ e^- \rightarrow \Upsilon(4S)$

¹ Measured in the $B^+ \rightarrow K^+ K^- K^+$ decay. $A_{CP}(B^+ \rightarrow f_2(1270) K^+)$

VALUE	DOCUMENT ID	TECN	COMMENT
-0.68 ± 0.19 OUR AVERAGE			

$-0.85 \pm 0.22 \pm 0.26$	AUBERT	08Ai	BABR $e^+ e^- \rightarrow \Upsilon(4S)$
$-0.59 \pm 0.22 \pm 0.036$	GARMASH	06	BELL $e^+ e^- \rightarrow \Upsilon(4S)$

 $A_{CP}(B^+ \rightarrow f_0(1500) K^+)$

VALUE	DOCUMENT ID	TECN	COMMENT
$0.28 \pm 0.26 \pm 0.15$	AUBERT	08Ai	BABR $e^+ e^- \rightarrow \Upsilon(4S)$

 $A_{CP}(B^+ \rightarrow f_2'(1525)^0 K^+)$

VALUE	DOCUMENT ID	TECN	COMMENT
-0.08 ± 0.05 OUR AVERAGE			

$0.18 \pm 0.18 \pm 0.04$	¹ LEES	11i	BABR $e^+ e^- \rightarrow \Upsilon(4S)$
$-0.106 \pm 0.050 \pm 0.036$	AUBERT	08Ai	BABR $e^+ e^- \rightarrow \Upsilon(4S)$
$-0.077 \pm 0.065 \pm 0.046$	GARMASH	06	BELL $e^+ e^- \rightarrow \Upsilon(4S)$

• • • We do not use the following data for averages, fits, limits, etc. • • •

$0.14 \pm 0.10 \pm 0.04$	² LEES	12o	BABR $e^+ e^- \rightarrow \Upsilon(4S)$
$-0.31 \pm 0.25 \pm 0.08$	³ AUBERT	06o	BABR Repl. by LEES 12o
$0.088 \pm 0.095 \pm 0.097$	AUBERT,B	05N	BABR Repl. by AUBERT 08Ai

¹ Measured in $B^+ \rightarrow f_0 K^+$ with $f_0 \rightarrow \pi^0 \pi^0$ decay.² Measured in the $B^+ \rightarrow K^+ K^- K^+$ decay assuming $A_{CP}(B^+ \rightarrow f_2'(1525)^0 K^+) = A_{CP}(B^+ \rightarrow f_0(1500)^0 K^+) = A_{CP}(B^+ \rightarrow f_0(1710)^0 K^+)$ ³ Measured in the $B^+ \rightarrow K^+ K^- K^+$ decay. $A_{CP}(B^+ \rightarrow \rho^0 K^+)$

VALUE	DOCUMENT ID	TECN	COMMENT
0.37 ± 0.10 OUR AVERAGE			

$0.44 \pm 0.10 \pm 0.06$	AUBERT	08Ai	BABR $e^+ e^- \rightarrow \Upsilon(4S)$
$0.30 \pm 0.11 \pm 0.11$	GARMASH	06	BELL $e^+ e^- \rightarrow \Upsilon(4S)$

• • • We do not use the following data for averages, fits, limits, etc. • • •

$0.32 \pm 0.13 \pm 0.10$	AUBERT,B	05N	BABR Repl. by AUBERT 08Ai
--------------------------	----------	-----	---------------------------

 $A_{CP}(B^+ \rightarrow K^0 \pi^+ \pi^0)$

VALUE	DOCUMENT ID	TECN	COMMENT
$0.07 \pm 0.05 \pm 0.04$	¹ LEES	17G	BABR $e^+ e^- \rightarrow \Upsilon(4S)$

¹ Obtains the result from a Dalitz analysis of $B^+ \rightarrow K_S^0 \pi^+ \pi^0$ decays. The first error is statistical, the second combines all the systematic uncertainties reported in the paper, including signal modelling. $A_{CP}(B^+ \rightarrow K_S^0(1430)^0 \pi^+)$

VALUE	DOCUMENT ID	TECN	COMMENT
0.061 ± 0.032 OUR AVERAGE			

$0.14 \pm 0.10 \pm 0.14$	¹ LEES	17G	BABR $e^+ e^- \rightarrow \Upsilon(4S)$
--------------------------	-------------------	-----	---

$0.032 \pm 0.035 \pm 0.034$	AUBERT	08Ai	BABR $e^+ e^- \rightarrow \Upsilon(4S)$
$0.076 \pm 0.038 \pm 0.028$	GARMASH	06	BELL $e^+ e^- \rightarrow \Upsilon(4S)$

• • • We do not use the following data for averages, fits, limits, etc. • • •

$-0.064 \pm 0.032 \pm 0.023$	AUBERT,B	05N	BABR Repl. by AUBERT 08Ai
------------------------------	----------	-----	---------------------------

¹ Obtains the result from a Dalitz analysis of $B^+ \rightarrow K_S^0 \pi^+ \pi^0$ decays. The first error is statistical, the second combines all the systematic uncertainties reported in the paper, including signal modelling. $A_{CP}(B^+ \rightarrow K_S^0(1430)^+ \pi^0)$

VALUE	DOCUMENT ID	TECN	COMMENT
$0.26 \pm 0.12 \pm 0.14$	¹ LEES	17G	BABR $e^+ e^- \rightarrow \Upsilon(4S)$

¹ Obtains the result from a Dalitz analysis of $B^+ \rightarrow K_S^0 \pi^+ \pi^0$ decays. The first error is statistical, the second combines all the systematic uncertainties reported in the paper, including signal modelling. $A_{CP}(B^+ \rightarrow K_S^0(1430)^0 \pi^+)$

VALUE	DOCUMENT ID	TECN	COMMENT
$0.05 \pm 0.23 \pm 0.18$	AUBERT	08Ai	BABR $e^+ e^- \rightarrow \Upsilon(4S)$

 $A_{CP}(B^+ \rightarrow K^+ \pi^0 \pi^0)$

VALUE	DOCUMENT ID	TECN	COMMENT
$-0.06 \pm 0.06 \pm 0.04$	LEES	11i	BABR $e^+ e^- \rightarrow \Upsilon(4S)$

 $A_{CP}(B^+ \rightarrow K^0 \rho^+)$

VALUE	DOCUMENT ID	TECN	COMMENT
-0.03 ± 0.15 OUR AVERAGE			

$0.21 \pm 0.19 \pm 0.24$	¹ LEES	17G	BABR $e^+ e^- \rightarrow \Upsilon(4S)$
$-0.12 \pm 0.17 \pm 0.02$	AUBERT	07Z	BABR $e^+ e^- \rightarrow \Upsilon(4S)$

¹ Obtains the result from a Dalitz analysis of $B^+ \rightarrow K_S^0 \pi^+ \pi^0$ decays. The first error is statistical, the second combines all the systematic uncertainties reported in the paper, including signal modelling. $A_{CP}(B^+ \rightarrow K^+ \pi^+ \pi^-)$

VALUE	DOCUMENT ID	TECN	COMMENT
$0.07 \pm 0.07 \pm 0.04$	AUBERT,B	06U	BABR $e^+ e^- \rightarrow \Upsilon(4S)$

 $A_{CP}(B^+ \rightarrow \rho^0 K^*(892)^+)$

VALUE	DOCUMENT ID	TECN	COMMENT
$0.31 \pm 0.13 \pm 0.03$	DEL-AMO-SA..11d	BABR	$e^+ e^- \rightarrow \Upsilon(4S)$

• • • We do not use the following data for averages, fits, limits, etc. • • •

$0.20 \pm 0.32 \pm 0.04$	AUBERT	03v	BABR Repl. by DEL-AMO-SANCHEZ 11d
--------------------------	--------	-----	-----------------------------------

 $A_{CP}(B^+ \rightarrow K^*(892)^+ f_0(980))$

VALUE	DOCUMENT ID	TECN	COMMENT
$-0.15 \pm 0.12 \pm 0.03$	DEL-AMO-SA..11d	BABR	$e^+ e^- \rightarrow \Upsilon(4S)$

• • • We do not use the following data for averages, fits, limits, etc. • • •

$-0.34 \pm 0.21 \pm 0.03$	AUBERT,B	06G	BABR Repl. by DEL-AMO-SANCHEZ 11d
---------------------------	----------	-----	-----------------------------------

 $A_{CP}(B^+ \rightarrow a_1^+ K^0)$

VALUE	DOCUMENT ID	TECN	COMMENT
$+0.12 \pm 0.11 \pm 0.02$	AUBERT	08F	BABR $e^+ e^- \rightarrow \Upsilon(4S)$

 $A_{CP}(B^+ \rightarrow b_1^+ K^0)$

VALUE	DOCUMENT ID	TECN	COMMENT
$-0.03 \pm 0.15 \pm 0.02$	AUBERT	08AG	BABR $e^+ e^- \rightarrow \Upsilon(4S)$

 $A_{CP}(B^+ \rightarrow K^*(892)^0 \rho^+)$

VALUE	DOCUMENT ID	TECN	COMMENT
$-0.01 \pm 0.16 \pm 0.02$	AUBERT,B	06G	BABR $e^+ e^- \rightarrow \Upsilon(4S)$

 $A_{CP}(B^+ \rightarrow b_1^0 K^+)$

VALUE	DOCUMENT ID	TECN	COMMENT
$-0.46 \pm 0.20 \pm 0.02$	AUBERT	07Bi	BABR $e^+ e^- \rightarrow \Upsilon(4S)$

 $A_{CP}(B^+ \rightarrow K^0 K^+)$

VALUE	DOCUMENT ID	TECN	COMMENT
0.04 ± 0.14 OUR AVERAGE			

$0.014 \pm 0.168 \pm 0.002$	DUH	13	BELL $e^+ e^- \rightarrow \Upsilon(4S)$
$0.10 \pm 0.26 \pm 0.03$	¹ AUBERT,BE	06c	BABR $e^+ e^- \rightarrow \Upsilon(4S)$

• • • We do not use the following data for averages, fits, limits, etc. • • •

$0.13 \pm 0.23 \pm 0.02$	LIN	07	BELL Repl. by DUH 13
$0.15 \pm 0.33 \pm 0.03$	² AUBERT,BE	05E	BABR Repl. by AUBERT,BE 06c

¹ Corresponds to 90% confidence range $-0.31 < A_{CP} < 0.54$.² Corresponds to 90% confidence range $-0.43 < A_{CP} < 0.68$. $A_{CP}(B^+ \rightarrow K_S^0 K^+)$

VALUE	DOCUMENT ID	TECN	COMMENT
$-0.21 \pm 0.14 \pm 0.01$	AAIJ	13Bs	LHCB pp at 7 TeV

 $A_{CP}(B^+ \rightarrow K^+ K_S^0 K_S^0)$

VALUE	DOCUMENT ID	TECN	COMMENT
0.025 ± 0.031 OUR AVERAGE			

$0.016 \pm 0.039 \pm 0.009$	KALIYAR	19	BELL $e^+ e^- \rightarrow \Upsilon(4S)$
$0.04 \pm 0.04 \pm 0.02$	LEES	12o	BABR $e^+ e^- \rightarrow \Upsilon(4S)$

• • • We do not use the following data for averages, fits, limits, etc. • • •

$-0.04 \pm 0.11 \pm 0.02$	¹ AUBERT,B	04V	BABR Repl. by LEES 12o
---------------------------	-----------------------	-----	------------------------

¹ Corresponds to 90% confidence range $-0.23 < A_{CP} < 0.15$. $A_{CP}(B^+ \rightarrow K^+ K^- \pi^+)$

VALUE	DOCUMENT ID	TECN	COMMENT
-0.122 ± 0.021 OUR AVERAGE			

$-0.170 \pm 0.073 \pm 0.017$	¹ HSU	17	BELL $e^+ e^- \rightarrow \Upsilon(4S)$
$-0.123 \pm 0.017 \pm 0.014$	² AAIJ	14Bo	LHCB pp at 7, 8 TeV
$0.00 \pm 0.10 \pm 0.03$	AUBERT	07Bb	BABR $e^+ e^- \rightarrow \Upsilon(4S)$

Meson Particle Listings

 B^\pm

• • • We do not use the following data for averages, fits, limits, etc. • • •

$-0.141 \pm 0.040 \pm 0.019$ ³AAIJ 14 LHCb Repl. by AAIJ 14B0

¹HSU 17 provides also measurement as a function of K^+K^- invariant mass.

²AAIJ 14B0 reports also CP asymmetries in restricted regions of phase space.

³AAIJ 14 reports $A_{CP}(B^+ \rightarrow K^+K^-\pi^+) = -0.648 \pm 0.070 \pm 0.013 \pm 0.007$ in the Dalitz plot region of $m_{K^+K^-}^2 < 1.5 \text{ GeV}^2/c^4$. The third uncertainty is due to the CP asymmetry of the $B^\pm \rightarrow J/\psi K^\pm$ reference mode uncertainty.

 $A_{CP}(B^+ \rightarrow K^+K^-\pi^+ \text{ nonresonant})$

VALUE	DOCUMENT ID	TECN	COMMENT
$-0.107 \pm 0.053 \pm 0.035$	¹ AAIJ 19AL LHCb		pp at 7, 8 TeV

¹ Uses amplitude analysis of $B^\pm \rightarrow \pi^\pm K^+K^-$ decays.

 $A_{CP}(B^+ \rightarrow K^+\bar{K}^*(892)^0)$

VALUE	DOCUMENT ID	TECN	COMMENT
$0.123 \pm 0.087 \pm 0.045$	¹ AAIJ 19AL LHCb		pp at 7, 8 TeV

¹ Uses amplitude analysis of $B^\pm \rightarrow \pi^\pm K^+K^-$ decays.

 $A_{CP}(B^+ \rightarrow K^+\bar{K}_0^*(1430)^0)$

VALUE	DOCUMENT ID	TECN	COMMENT
$0.104 \pm 0.149 \pm 0.088$	¹ AAIJ 19AL LHCb		pp at 7, 8 TeV

¹ Uses amplitude analysis of $B^\pm \rightarrow \pi^\pm K^+K^-$ decays.

 $A_{CP}(B^+ \rightarrow \phi\pi^+)$

VALUE	DOCUMENT ID	TECN	COMMENT
$0.098 \pm 0.436 \pm 0.266$	¹ AAIJ 19AL LHCb		pp at 7, 8 TeV

¹ Uses amplitude analysis of $B^\pm \rightarrow \pi^\pm K^+K^-$ decays.

 $A_{CP}(B^+ \rightarrow \pi^+(K^+K^-)_S\text{-wave})$

VALUE	DOCUMENT ID	TECN	COMMENT
$-0.664 \pm 0.038 \pm 0.019$	¹ AAIJ 19AL LHCb		pp at 7, 8 TeV

¹ Uses amplitude analysis of $B^\pm \rightarrow \pi^\pm K^+K^-$ decays in the $\pi\pi - KK$ rescattering mass region of $0.95 < m(K^+K^-) < 1.42 \text{ GeV}/c^2$.

 $A_{CP}(B^+ \rightarrow K^+K^-K^+)$

VALUE	DOCUMENT ID	TECN	COMMENT
-0.033 ± 0.008 OUR AVERAGE			
$-0.036 \pm 0.004 \pm 0.007$	¹ AAIJ 14B0 LHCb		pp at 7, 8 TeV
$-0.017^{+0.019}_{-0.014} \pm 0.014$	² LEES 120 BABR		$e^+e^- \rightarrow \Upsilon(4S)$

• • • We do not use the following data for averages, fits, limits, etc. • • •

$-0.043 \pm 0.009 \pm 0.008$ AAJJ 13AZ LHCb Repl. by AAJJ 14B0
 $-0.017 \pm 0.026 \pm 0.015$ AUBERT 060 BABR Repl. by LEES 120
 $0.02 \pm 0.07 \pm 0.03$ AUBERT 03M BABR Repl. by AUBERT 060

¹AAIJ 14B0 reports also CP asymmetries in restricted regions of phase space.

²All intermediate charmonium and charm resonances are removed, except of χ_{c0} .

 $A_{CP}(B^+ \rightarrow \phi K^+)$

VALUE	DOCUMENT ID	TECN	COMMENT
0.024 ± 0.028 OUR AVERAGE			Error includes scale factor of 2.3.
$0.017 \pm 0.011 \pm 0.006$	¹ AAIJ 150 LHCb		pp at 7, 8 TeV
$0.128 \pm 0.044 \pm 0.013$	LEES 120 BABR		$e^+e^- \rightarrow \Upsilon(4S)$
$-0.07 \pm 0.17^{+0.03}_{-0.02}$	ACOSTA 05J CDF		$p\bar{p}$ at 1.96 TeV
$0.01 \pm 0.12 \pm 0.05$	² CHEN 03B BELL		$e^+e^- \rightarrow \Upsilon(4S)$

• • • We do not use the following data for averages, fits, limits, etc. • • •

$0.022 \pm 0.021 \pm 0.009$ AAJJ 14A LHCb Repl. by AAJJ 150
 $0.00 \pm 0.08 \pm 0.02$ AUBERT 060 BABR Repl. by LEES 120
 $0.04 \pm 0.09 \pm 0.01$ ³AUBERT 04A BABR Repl. by AUBERT 060
 $-0.05 \pm 0.20 \pm 0.03$ ⁴AUBERT 02E BABR $e^+e^- \rightarrow \Upsilon(4S)$

¹ Obtained using $A_{CP}(B^\pm \rightarrow J/\psi K^\pm) = (0.3 \pm 0.6) \times 10^{-2}$.

² Corresponds to 90% confidence range $-0.20 < A_{CP} < 0.22$.

³ Corresponds to 90% confidence range $-0.10 < A_{CP} < 0.18$.

⁴ Corresponds to 90% confidence range $-0.37 < A_{CP} < 0.28$.

 $A_{CP}(B^+ \rightarrow X_0(1550)K^+)$

VALUE	DOCUMENT ID	TECN	COMMENT
$-0.04 \pm 0.07 \pm 0.02$	¹ AUBERT 060 BABR		$e^+e^- \rightarrow \Upsilon(4S)$

¹ Measured in the $B^+ \rightarrow K^+K^-K^+$ decay.

 $A_{CP}(B^+ \rightarrow K^{*+}K^+K^-)$

VALUE	DOCUMENT ID	TECN	COMMENT
$0.11 \pm 0.08 \pm 0.03$	AUBERT,B 06U BABR		$e^+e^- \rightarrow \Upsilon(4S)$

 $A_{CP}(B^+ \rightarrow \phi K^*(892)^+)$

VALUE	DOCUMENT ID	TECN	COMMENT
-0.01 ± 0.06 OUR AVERAGE			
$0.00 \pm 0.09 \pm 0.04$	AUBERT 07BA BABR		$e^+e^- \rightarrow \Upsilon(4S)$
$-0.02 \pm 0.14 \pm 0.03$	¹ CHEN 05A BELL		$e^+e^- \rightarrow \Upsilon(4S)$

• • • We do not use the following data for averages, fits, limits, etc. • • •

$0.16 \pm 0.17 \pm 0.03$ AUBERT 03V BABR Repl. by AUBERT 07BA
 $-0.13 \pm 0.29^{+0.08}_{-0.11}$ ²CHEN 03B BELL Repl. by CHEN 05A
 $-0.43^{+0.36}_{-0.30} \pm 0.06$ ³AUBERT 02E BABR Repl. by AUBERT 03V

¹ Corresponds to 90% confidence range $-0.25 < A_{CP} < 0.22$.

² Corresponds to 90% confidence range $-0.64 < A_{CP} < 0.36$.

³ Corresponds to 90% confidence range $-0.88 < A_{CP} < 0.18$.

 $A_{CP}(B^+ \rightarrow \phi(K\pi)_0^{*+})$

VALUE	DOCUMENT ID	TECN	COMMENT
$0.04 \pm 0.15 \pm 0.04$	AUBERT 08B1 BABR		$e^+e^- \rightarrow \Upsilon(4S)$

 $A_{CP}(B^+ \rightarrow \phi K_1(1270)^+)$

VALUE	DOCUMENT ID	TECN	COMMENT
$0.15 \pm 0.19 \pm 0.05$	AUBERT 08B1 BABR		$e^+e^- \rightarrow \Upsilon(4S)$

 $A_{CP}(B^+ \rightarrow \phi K_2^*(1430)^+)$

VALUE	DOCUMENT ID	TECN	COMMENT
$-0.23 \pm 0.19 \pm 0.06$	AUBERT 08B1 BABR		$e^+e^- \rightarrow \Upsilon(4S)$

 $A_{CP}(B^+ \rightarrow K^+\phi\phi)$

VALUE	DOCUMENT ID	TECN	COMMENT
-0.08 ± 0.07 OUR AVERAGE			
$-0.02 \pm 0.11 \pm 0.11$	¹ MOHANTY 21 BELL		$e^+e^- \rightarrow \Upsilon(4S)$
$-0.10 \pm 0.08 \pm 0.02$	¹ LEES 11A BABR		$e^+e^- \rightarrow \Upsilon(4S)$

¹ Assumes $m_{\phi\phi} < 2.85 \text{ GeV}/c^2$.

 $A_{CP}(B^+ \rightarrow K^+[\phi\phi]\eta_c)$

VALUE	DOCUMENT ID	TECN	COMMENT
0.10 ± 0.08 OUR AVERAGE			
$0.12 \pm 0.12 \pm 0.01$	¹ MOHANTY 21 BELL		$e^+e^- \rightarrow \Upsilon(4S)$
$0.09 \pm 0.10 \pm 0.02$	¹ LEES 11A BABR		$e^+e^- \rightarrow \Upsilon(4S)$

¹ $m_{\phi\phi}$ is consistent with η_c mass in $[2.94, 3.02] \text{ GeV}/c^2$.

 $A_{CP}(B^+ \rightarrow K^*(892)^+\gamma)$

VALUE	DOCUMENT ID	TECN	COMMENT
0.014 ± 0.018 OUR AVERAGE			
$0.011 \pm 0.023 \pm 0.003$	¹ HORIGUCHI 17 BELL		$e^+e^- \rightarrow \Upsilon(4S)$
$0.018 \pm 0.028 \pm 0.007$	AUBERT 09A0 BABR		$e^+e^- \rightarrow \Upsilon(4S)$

¹ Uses $B(\Upsilon(4S) \rightarrow B^+B^-) = (51.4 \pm 0.6)\%$ and $B(\Upsilon(4S) \rightarrow B^0\bar{B}^0) = (48.6 \pm 0.6)\%$.

 $A_{CP}(B^+ \rightarrow \chi_{s1}\gamma)$

VALUE	DOCUMENT ID	TECN	COMMENT
$0.0275 \pm 0.0184 \pm 0.0032$	¹ WATANUKI 19 BELL		$e^+e^- \rightarrow \Upsilon(4S)$

¹ Using a sum-of-exclusive technique with $m_{X_s} < 2.8 \text{ GeV}/c^2$.

 $A_{CP}(B^+ \rightarrow \eta K^+\gamma)$

VALUE	DOCUMENT ID	TECN	COMMENT
-0.12 ± 0.07 OUR AVERAGE			
$-0.09 \pm 0.10 \pm 0.01$	¹ AUBERT 09 BABR		$e^+e^- \rightarrow \Upsilon(4S)$
$-0.16 \pm 0.09 \pm 0.06$	² NIISHIDA 05 BELL		$e^+e^- \rightarrow \Upsilon(4S)$

• • • We do not use the following data for averages, fits, limits, etc. • • •

$-0.09 \pm 0.12 \pm 0.01$ ¹AUBERT,B 06M BABR Repl. by AUBERT 09

¹ $m_{\eta K} < 3.25 \text{ GeV}/c^2$.

² $m_{\eta K} < 2.4 \text{ GeV}/c^2$

 $A_{CP}(B^+ \rightarrow \phi K^+\gamma)$

VALUE	DOCUMENT ID	TECN	COMMENT
-0.13 ± 0.11 OUR AVERAGE			Error includes scale factor of 1.1.
$-0.03 \pm 0.11 \pm 0.08$	SAHOO 11A BELL		$e^+e^- \rightarrow \Upsilon(4S)$
$-0.26 \pm 0.14 \pm 0.05$	AUBERT 07Q BABR		$e^+e^- \rightarrow \Upsilon(4S)$

 $A_{CP}(B^+ \rightarrow \rho^+\gamma)$

VALUE	DOCUMENT ID	TECN	COMMENT
$-0.11 \pm 0.32 \pm 0.09$	TANIGUCHI 08 BELL		$e^+e^- \rightarrow \Upsilon(4S)$

 $A_{CP}(B^+ \rightarrow \pi^+\pi^0)$

VALUE	DOCUMENT ID	TECN	COMMENT
0.03 ± 0.04 OUR AVERAGE			
$0.025 \pm 0.043 \pm 0.007$	DUH 13 BELL		$e^+e^- \rightarrow \Upsilon(4S)$
$0.03 \pm 0.08 \pm 0.01$	AUBERT 07Bc BABR		$e^+e^- \rightarrow \Upsilon(4S)$

• • • We do not use the following data for averages, fits, limits, etc. • • •

$0.07 \pm 0.06 \pm 0.01$ LIN 08 BELL Repl. by DUH 13
 $-0.01 \pm 0.10 \pm 0.02$ ¹AUBERT 05L BABR Repl. by AUBERT 07Bc
 $0.00 \pm 0.10 \pm 0.02$ ²CHAO 05A BELL Repl. by CHAO 04B
 $-0.02 \pm 0.10 \pm 0.01$ ³CHAO 04B BELL Repl. by LIN 08
 $-0.03^{+0.18}_{-0.17} \pm 0.02$ ⁴AUBERT 03L BABR Repl. by AUBERT 05L

⁵ CASEY 02 BELL Repl. by CHAO 04B

¹ Corresponds to a 90% CL interval of $-0.19 < A_{CP} < 0.21$.

² Corresponds to a 90% CL interval of $-0.17 < A_{CP} < 0.16$.

³ This corresponds to 90% CL interval of $-0.18 < A_{CP} < 0.14$.

⁴ Corresponds to 90% confidence range $-0.32 < A_{CP} < 0.27$.

⁵ Corresponds to 90% confidence range $-0.23 < A_{CP} < +0.86$.

 $A_{CP}(B^+ \rightarrow \pi^+\pi^-\pi^+)$

VALUE	DOCUMENT ID	TECN	COMMENT
0.057 ± 0.013 OUR AVERAGE			
$0.058 \pm 0.008 \pm 0.011$	¹ AAIJ 14B0 LHCb		pp at 7, 8 TeV
$0.032 \pm 0.044^{+0.040}_{-0.037}$	AUBERT 09L BABR		$e^+e^- \rightarrow \Upsilon(4S)$

• • • We do not use the following data for averages, fits, limits, etc. • • •
 0.117 ± 0.021 ± 0.011 ² AAIJ 14 LHCb Repl. by AAIJ 14B0
 -0.007 ± 0.077 ± 0.025 AUBERT,B 05G BABR Repl. by AUBERT 09L
 -0.39 ± 0.33 ± 0.12 AUBERT 03M BABR Repl. by AUBERT 05G
¹ AAIJ 14B0 reports also CP asymmetries in restricted regions of phase space.
² AAIJ 14 reports $A_{CP}(B^+ \rightarrow \pi^+ \pi^- \pi^+) = 0.584 \pm 0.082 \pm 0.027 \pm 0.007$ in the Dalitz plot region of $m_{\pi^+ \pi^-}^2 > 15 \text{ GeV}^2/c^4$ or $m_{\pi^+ \pi^-}^2 < 0.4 \text{ GeV}^2/c^4$. The third uncertainty is due to the CP asymmetry of the $B^\pm \rightarrow J/\psi K^\pm$ reference mode uncertainty.

$A_{CP}(B^+ \rightarrow \rho^0 \pi^+)$

VALUE	DOCUMENT ID	TECN	COMMENT
0.009 ± 0.019 OUR AVERAGE			
0.007 ± 0.011 ± 0.016	¹ AAIJ	20A LHCb	pp at 7, 8 TeV
0.18 ± 0.07 ^{+0.05} _{-0.15}	AUBERT	09L BABR	e ⁺ e ⁻ → $\Upsilon(4S)$

• • • We do not use the following data for averages, fits, limits, etc. • • •
 -0.074 ± 0.120 ^{+0.035} _{-0.055} AUBERT,B 05G BABR Repl. by AUBERT 09L
 -0.19 ± 0.11 ± 0.02 AUBERT 04Z BABR Repl. by AUBERT,B 05G
¹ This result is obtained with an amplitude analysis of $B^+ \rightarrow \pi^+ \pi^+ \pi^-$ decays, using the isobar model within the mass range $1.0 < m(\pi^+ \pi^-) < 1.5 \text{ GeV}$ to describe the $\pi^+ \pi^-$ S-wave contribution.

$A_{CP}(B^+ \rightarrow f_2(1270) \pi^+)$

VALUE	DOCUMENT ID	TECN	COMMENT
0.40 ± 0.06 OUR AVERAGE			
0.468 ± 0.061 ± 0.046	¹ AAIJ	20A LHCb	pp at 7, 8 TeV
0.267 ± 0.102 ± 0.048	² AAIJ	19AL LHCb	pp at 7, 8 TeV
0.41 ± 0.25 ^{+0.18} _{-0.15}	AUBERT	09L BABR	e ⁺ e ⁻ → $\Upsilon(4S)$

• • • We do not use the following data for averages, fits, limits, etc. • • •
 -0.004 ± 0.247 ^{+0.028} _{-0.032} AUBERT,B 05G BABR Repl. by AUBERT 09L
¹ This result is obtained with an amplitude analysis of $B^+ \rightarrow \pi^+ \pi^+ \pi^-$ decays, using the isobar model within the mass range $1.0 < m(\pi^+ \pi^-) < 1.5 \text{ GeV}$ to describe the $\pi^+ \pi^-$ S-wave contribution.
² Uses amplitude analysis of $B^\pm \rightarrow \pi^\pm K^+ K^-$ decays.

$A_{CP}(B^+ \rightarrow \rho^0(1450) \pi^+)$

VALUE	DOCUMENT ID	TECN	COMMENT
-0.11 ± 0.05 OUR AVERAGE			
-0.129 ± 0.033 ± 0.359	¹ AAIJ	20A LHCb	pp at 7, 8 TeV
-0.109 ± 0.044 ± 0.024	² AAIJ	19AL LHCb	pp at 7, 8 TeV
-0.06 ± 0.28 ^{+0.23} _{-0.40}	AUBERT	09L BABR	e ⁺ e ⁻ → $\Upsilon(4S)$

¹ This result is obtained with an amplitude analysis of $B^+ \rightarrow \pi^+ \pi^+ \pi^-$ decays, using the isobar model within the mass range $1.0 < m(\pi^+ \pi^-) < 1.5 \text{ GeV}$ to describe the $\pi^+ \pi^-$ S-wave contribution.
² Uses amplitude analysis of $B^\pm \rightarrow \pi^\pm K^+ K^-$ decays.

$A_{CP}(B^+ \rightarrow \rho_3(1690) \pi^+)$

VALUE	DOCUMENT ID	TECN	COMMENT
-0.801 ± 0.114 ± 0.253			
	¹ AAIJ	20A LHCb	pp at 7, 8 TeV

¹ This result is obtained with an amplitude analysis of $B^+ \rightarrow \pi^+ \pi^+ \pi^-$ decays, using the isobar model within the mass range $1.0 < m(\pi^+ \pi^-) < 1.5 \text{ GeV}$ to describe the $\pi^+ \pi^-$ S-wave contribution.

$A_{CP}(B^+ \rightarrow f_0(1370) \pi^+)$

VALUE	DOCUMENT ID	TECN	COMMENT
0.72 ± 0.15 ± 0.16	AUBERT	09L BABR	e ⁺ e ⁻ → $\Upsilon(4S)$

$A_{CP}(B^+ \rightarrow \pi^+ \pi^- \pi^+ \text{ nonresonant})$

VALUE	DOCUMENT ID	TECN	COMMENT
-0.14 ± 0.14 ^{+0.18} _{-0.08}	AUBERT	09L BABR	e ⁺ e ⁻ → $\Upsilon(4S)$

$A_{CP}(B^+ \rightarrow \rho^+ \pi^0)$

VALUE	DOCUMENT ID	TECN	COMMENT
0.02 ± 0.11 OUR AVERAGE			
-0.01 ± 0.13 ± 0.02	AUBERT	07X BABR	e ⁺ e ⁻ → $\Upsilon(4S)$
0.06 ± 0.17 ^{+0.04} _{-0.05}	ZHANG	05A BELL	e ⁺ e ⁻ → $\Upsilon(4S)$

• • • We do not use the following data for averages, fits, limits, etc. • • •
 0.24 ± 0.16 ± 0.06 AUBERT 04Z BABR Repl. by AUBERT 07X

$A_{CP}(B^+ \rightarrow \rho^+ \rho^0)$

VALUE	DOCUMENT ID	TECN	COMMENT
-0.05 ± 0.05 OUR AVERAGE			
-0.054 ± 0.055 ± 0.010	AUBERT	09G BABR	e ⁺ e ⁻ → $\Upsilon(4S)$
0.00 ± 0.22 ± 0.03	ZHANG	03B BELL	e ⁺ e ⁻ → $\Upsilon(4S)$

• • • We do not use the following data for averages, fits, limits, etc. • • •
 -0.12 ± 0.13 ± 0.10 AUBERT,BE 06G BABR Repl. by AUBERT 09G
 -0.19 ± 0.23 ± 0.03 AUBERT 03V BABR Repl. by AUBERT,BE 06G

$A_{CP}(B^+ \rightarrow \omega \pi^+)$

VALUE	DOCUMENT ID	TECN	COMMENT
-0.04 ± 0.05 OUR AVERAGE			
-0.048 ± 0.065 ± 0.038	¹ AAIJ	20A LHCb	pp at 7, 8 TeV
-0.02 ± 0.08 ± 0.01	AUBERT	07AE BABR	e ⁺ e ⁻ → $\Upsilon(4S)$
-0.02 ± 0.09 ± 0.01	JEN	06 BELL	e ⁺ e ⁻ → $\Upsilon(4S)$
-0.34 ± 0.25	² CHEN	00 CLE2	e ⁺ e ⁻ → $\Upsilon(4S)$

• • • We do not use the following data for averages, fits, limits, etc. • • •
 -0.01 ± 0.10 ± 0.01 AUBERT,B 06E BABR Repl. by AUBERT 07AE
 0.03 ± 0.16 ± 0.01 AUBERT 04H BABR Repl. by AUBERT,B 06E
 0.50 ^{+0.23} _{-0.20} ± 0.02 ³ WANG 04A BELL Repl. by JEN 06
 -0.01 ^{+0.29} _{-0.31} ± 0.03 ⁴ AUBERT 02E BABR Repl. by AUBERT 04H

¹ This result is obtained with an amplitude analysis of $B^+ \rightarrow \pi^+ \pi^+ \pi^-$ decays, using the isobar model within the mass range $1.0 < m(\pi^+ \pi^-) < 1.5 \text{ GeV}$ to describe the $\pi^+ \pi^-$ S-wave contribution.
² Corresponds to 90% confidence range $-0.75 < A_{CP} < 0.07$.
³ Corresponds to 90% CL interval $-0.25 < A_{CP} < 0.41$.
⁴ Corresponds to 90% confidence range $-0.50 < A_{CP} < 0.46$.

$A_{CP}(B^+ \rightarrow \omega \rho^+)$

VALUE	DOCUMENT ID	TECN	COMMENT
-0.20 ± 0.09 ± 0.02	AUBERT	09H BABR	e ⁺ e ⁻ → $\Upsilon(4S)$

• • • We do not use the following data for averages, fits, limits, etc. • • •
 0.04 ± 0.18 ± 0.02 AUBERT,B 06T BABR Repl. by AUBERT 09H
 0.05 ± 0.26 ± 0.02 AUBERT 05O BABR Repl. by AUBERT,B 06T

$A_{CP}(B^+ \rightarrow \eta \pi^+)$

VALUE	DOCUMENT ID	TECN	COMMENT
-0.14 ± 0.07 OUR AVERAGE			Error includes scale factor of 1.4.
-0.19 ± 0.06 ± 0.01	HOI	12 BELL	e ⁺ e ⁻ → $\Upsilon(4S)$
-0.03 ± 0.09 ± 0.03	AUBERT	09AV BABR	e ⁺ e ⁻ → $\Upsilon(4S)$

• • • We do not use the following data for averages, fits, limits, etc. • • •
 -0.08 ± 0.10 ± 0.01 AUBERT 07AE BABR Repl. by AUBERT 09AV
 -0.23 ± 0.09 ± 0.02 CHANG 07B BELL Repl. by HOI 12
 -0.13 ± 0.12 ± 0.01 AUBERT,B 05K BABR Repl. by AUBERT 07AE
 0.07 ± 0.15 ± 0.03 CHANG 05A BELL Repl. by CHANG 07B
 -0.44 ± 0.18 ± 0.01 AUBERT 04H BABR Repl. by AUBERT,B 05K

$A_{CP}(B^+ \rightarrow \eta \rho^+)$

VALUE	DOCUMENT ID	TECN	COMMENT
0.11 ± 0.11 OUR AVERAGE			
0.13 ± 0.11 ± 0.02	AUBERT	08AH BABR	e ⁺ e ⁻ → $\Upsilon(4S)$
-0.04 ^{+0.34} _{-0.32} ± 0.01	WANG	07B BELL	e ⁺ e ⁻ → $\Upsilon(4S)$

• • • We do not use the following data for averages, fits, limits, etc. • • •
 0.02 ± 0.18 ± 0.02 AUBERT,B 05K BABR Repl. by AUBERT 08AH

$A_{CP}(B^+ \rightarrow \eta' \pi^+)$

VALUE	DOCUMENT ID	TECN	COMMENT
0.06 ± 0.16 OUR AVERAGE			
0.03 ± 0.17 ± 0.02	AUBERT	09AV BABR	e ⁺ e ⁻ → $\Upsilon(4S)$
0.20 ^{+0.37} _{-0.36} ± 0.04	SCHUEMANN	06 BELL	e ⁺ e ⁻ → $\Upsilon(4S)$

• • • We do not use the following data for averages, fits, limits, etc. • • •
 0.21 ± 0.17 ± 0.01 AUBERT 07AE BABR Repl. by AUBERT 09AV
 0.14 ± 0.16 ± 0.01 AUBERT,B 05K BABR Repl. by AUBERT 07AE

$A_{CP}(B^+ \rightarrow \eta' \rho^+)$

VALUE	DOCUMENT ID	TECN	COMMENT
0.26 ± 0.17 ± 0.02	DEL-AMO-SA...	10A BABR	e ⁺ e ⁻ → $\Upsilon(4S)$

• • • We do not use the following data for averages, fits, limits, etc. • • •
 0.04 ± 0.28 ± 0.02 ¹ AUBERT 07E BABR Repl. by DEL-AMO-SANCHEZ 10A

¹ Reports A_{CP} with the opposite sign convention.

$A_{CP}(B^+ \rightarrow b_1^0 \pi^+)$

VALUE	DOCUMENT ID	TECN	COMMENT
+0.05 ± 0.16 ± 0.02	AUBERT	07BI BABR	e ⁺ e ⁻ → $\Upsilon(4S)$

$A_{CP}(B^+ \rightarrow \rho \bar{p} \pi^+)$

VALUE	DOCUMENT ID	TECN	COMMENT
0.00 ± 0.04 OUR AVERAGE			
-0.02 ± 0.05 ± 0.02	¹ WEI	08 BELL	e ⁺ e ⁻ → $\Upsilon(4S)$
+0.04 ± 0.07 ± 0.04	AUBERT	07AV BABR	e ⁺ e ⁻ → $\Upsilon(4S)$

• • • We do not use the following data for averages, fits, limits, etc. • • •
 -0.16 ± 0.22 ± 0.01 WANG 04 BELL Repl. by WEI 08

¹ Requires $m_{\rho \bar{p}} < 2.85 \text{ GeV}/c^2$.

$A_{CP}(B^+ \rightarrow \rho \bar{p} K^+)$

VALUE	DOCUMENT ID	TECN	COMMENT
0.00 ± 0.04 OUR AVERAGE			Error includes scale factor of 2.2.
0.021 ± 0.020 ± 0.004	¹ AAIJ	14AF LHCb	pp at 7, 8 TeV
-0.17 ± 0.10 ± 0.02	¹ WEI	08 BELL	e ⁺ e ⁻ → $\Upsilon(4S)$
-0.16 ^{+0.07} _{-0.08} ± 0.04	¹ AUBERT,B	05L BABR	e ⁺ e ⁻ → $\Upsilon(4S)$

Meson Particle Listings

 B^\pm

• • • We do not use the following data for averages, fits, limits, etc. • • •

$-0.047 \pm 0.036 \pm 0.007$	¹ AAIJ	13AU LHCb	Repl. by AAIJ 14AF
$-0.05 \pm 0.11 \pm 0.01$	WANG	04 BELL	Repl. by WEI 08

¹ Requires $m_{p\bar{p}} < 2.85 \text{ GeV}/c^2$.

 $A_{CP}(B^+ \rightarrow p\bar{p}K^*(892)^+)$

VALUE	DOCUMENT ID	TECN	COMMENT
0.21 ± 0.16 OUR AVERAGE	Error includes scale factor of 1.4.		
$-0.01 \pm 0.19 \pm 0.02$	CHEN	08c BELL	$e^+e^- \rightarrow \Upsilon(4S)$
$+0.32 \pm 0.13 \pm 0.05$	AUBERT	07AV BABR	$e^+e^- \rightarrow \Upsilon(4S)$

 $A_{CP}(B^+ \rightarrow p\bar{p}\gamma)$

VALUE	DOCUMENT ID	TECN	COMMENT
$+0.17 \pm 0.16 \pm 0.05$	WANG	07c BELL	$e^+e^- \rightarrow \Upsilon(4S)$

 $A_{CP}(B^+ \rightarrow p\bar{p}\pi^0)$

VALUE	DOCUMENT ID	TECN	COMMENT
$+0.01 \pm 0.17 \pm 0.04$	WANG	07c BELL	$e^+e^- \rightarrow \Upsilon(4S)$

 $A_{CP}(B^+ \rightarrow K^+\ell^+\ell^-)$

VALUE	DOCUMENT ID	TECN	COMMENT
-0.02 ± 0.08 OUR AVERAGE			
$-0.03 \pm 0.14 \pm 0.01$	¹ LEES	12s BABR	$e^+e^- \rightarrow \Upsilon(4S)$
$-0.18 \pm 0.18 \pm 0.01$	AUBERT	09T BABR	$e^+e^- \rightarrow \Upsilon(4S)$
$+0.04 \pm 0.10 \pm 0.02$	WEI	09A BELL	$e^+e^- \rightarrow \Upsilon(4S)$

• • • We do not use the following data for averages, fits, limits, etc. • • •

$-0.07 \pm 0.22 \pm 0.02$	AUBERT,B	06j BABR	Repl. by AUBERT 09T
---------------------------	----------	----------	---------------------

¹ Measured in the union of $0.10 < q^2 < 8.12 \text{ GeV}^2/c^4$ and $q^2 > 10.11 \text{ GeV}^2/c^4$. LEES 12s reports also individual measurements $A_{CP}(B^+ \rightarrow K^+\ell^+\ell^-) = 0.02 \pm 0.18 \pm 0.01$ for $0.10 < q^2 < 8.12 \text{ GeV}^2/c^4$ and $A_{CP}(B^+ \rightarrow K^+\ell^+\ell^-) = -0.06 \pm 0.22 \pm 0.01$ for $q^2 > 10.11 \text{ GeV}^2/c^4$.

 $A_{CP}(B^+ \rightarrow K^+e^+e^-)$

VALUE	DOCUMENT ID	TECN	COMMENT
$+0.14 \pm 0.14 \pm 0.03$	WEI	09A BELL	$e^+e^- \rightarrow \Upsilon(4S)$

 $A_{CP}(B^+ \rightarrow K^+\mu^+\mu^-)$

VALUE	DOCUMENT ID	TECN	COMMENT
0.011 ± 0.017 OUR AVERAGE			
$0.012 \pm 0.017 \pm 0.001$	AAIJ	14AN LHCb	pp at 7, 8 TeV
$-0.05 \pm 0.13 \pm 0.03$	WEI	09A BELL	$e^+e^- \rightarrow \Upsilon(4S)$

• • • We do not use the following data for averages, fits, limits, etc. • • •

$0.000 \pm 0.033 \pm 0.009$	AAIJ	13BN LHCb	Repl. by AAIJ 14AN
-----------------------------	------	-----------	--------------------

 $A_{CP}(B^+ \rightarrow \pi^+\mu^+\mu^-)$

VALUE	DOCUMENT ID	TECN	COMMENT
$-0.11 \pm 0.12 \pm 0.01$	AAIJ	15AR LHCb	pp at 7, 8 TeV

 $A_{CP}(B^+ \rightarrow K^*\ell^+\ell^-)$

VALUE	DOCUMENT ID	TECN	COMMENT
-0.09 ± 0.14 OUR AVERAGE			
0.01 ± 0.26	AUBERT	09T BABR	$e^+e^- \rightarrow \Upsilon(4S)$
-0.24 ± 0.02			
-0.13 ± 0.17	WEI	09A BELL	$e^+e^- \rightarrow \Upsilon(4S)$
0.16 ± 0.01			

• • • We do not use the following data for averages, fits, limits, etc. • • •

$0.03 \pm 0.23 \pm 0.03$	AUBERT,B	06j BABR	Repl. by AUBERT 09T
--------------------------	----------	----------	---------------------

 $A_{CP}(B^+ \rightarrow K^*e^+e^-)$

VALUE	DOCUMENT ID	TECN	COMMENT
$-0.14 \pm 0.23 \pm 0.02$	WEI	09A BELL	$e^+e^- \rightarrow \Upsilon(4S)$

 $A_{CP}(B^+ \rightarrow K^*\mu^+\mu^-)$

VALUE	DOCUMENT ID	TECN	COMMENT
$-0.12 \pm 0.24 \pm 0.02$	WEI	09A BELL	$e^+e^- \rightarrow \Upsilon(4S)$

CP VIOLATION PARAMETERS IN $B^+ \rightarrow DK^+$ AND SIMILAR DECAYS

The parameters r_{B^+} and δ_{B^+} are the magnitude ratio and strong phase difference between the amplitudes of $A(B^+ \rightarrow \bar{D}^{(*)0}K^{(*)+})$ and $A(B^+ \rightarrow D^{(*)0}K^{(*)+})$. The measured observables are defined as $x_\pm = r_{B^+} \cos(\delta_{B^+} \pm \gamma)$ and $y_\pm = r_{B^+} \sin(\delta_{B^+} \pm \gamma)$, and can be used to measure the CKM angle γ .

"OUR EVALUATION" is provided by the Heavy Flavor Averaging Group (HFLAV). It is derived from combinations of their results on $B^+ \rightarrow DK^+$ and related processes.

 γ

For angle $\gamma(\phi_3)$ of the CKM unitarity triangle, see the review on "CP Violation" in the Reviews section.

"OUR EVALUATION" is provided by the Heavy Flavor Averaging Group (HFLAV).

VALUE (°) CL% DOCUMENT ID TECN COMMENT

 $65.9^{+3.3}_{-3.5}$ OUR EVALUATION

• • • We do not use the following data for averages, fits, limits, etc. • • •

$65.4^{+3.8}_{-4.2}$	¹ AAIJ	21AM LHCb	pp at 7, 8, 13 TeV
$68.7^{+5.2}_{-5.1}$	² AAIJ	21L LHCb	pp at 7, 8, 13 TeV
44 ± 12	^{3,4} AAIJ	21M LHCb	pp at 7, 8, 13 TeV
$5.7^{+10.2}_{-8.8} \pm 6.7$	⁵ RESMI	19 BELL	$e^+e^- \rightarrow \Upsilon(4S)$
87^{+11}_{-12}	⁶ AAIJ	18AD LHCb	Repl. by AAIJ 21L
128^{+17}_{-22}	⁷ AAIJ	18U LHCb	pp at 7, 8 TeV
$5-86$ or $185-266$	⁸ AAIJ	18Z LHCb	pp at 7, 8 TeV
80^{+21}_{-22}	⁹ AAIJ	16AA LHCb	Repl. by AAIJ 16Z
$72.2^{+6.8}_{-7.3}$	¹⁰ AAIJ	16AQ LHCb	Repl. by AAIJ 21AM
71 ± 20	^{11,12} AAIJ	16Z LHCb	pp at 7, 8 TeV
74^{+20}_{-19}	AAIJ	15Bc LHCb	pp at 7, 8 TeV
$63.5^{+7.2}_{-6.7}$	^{13,14} AAIJ	15K LHCb	pp at 7, 8 TeV
62^{+15}_{-14}	¹⁵ AAIJ	14BA LHCb	Repl. by AAIJ 21L
84^{+49}_{-42}	¹⁶ AAIJ	14BE LHCb	Repl. by AAIJ 14BA
115^{+28}_{-43}	¹⁷ AAIJ	14BF LHCb	Repl. by AAIJ 18U
$72.6^{+9.7}_{-17.2}$	¹⁸ AAIJ	13AK LHCb	Repl. by AAIJ 21AM
69^{+17}_{-16}	¹⁹ LEES	13B BABR	$e^+e^- \rightarrow \Upsilon(4S)$
44^{+43}_{-38}	^{20,21} AAIJ	12AQ LHCb	Repl. by AAIJ 13AK
$77.3^{+15.1}_{-14.9} \pm 5.9$	^{21,22} AIHARA	12 BELL	$e^+e^- \rightarrow \Upsilon(4S)$
$68^{+14} \pm 5$	²³ DEL-AMO-SA..10F	BABR	Repl. by LEES 13B
7 ± 173	²⁴ DEL-AMO-SA..10G	BABR	$e^+e^- \rightarrow \Upsilon(4S)$
$78.4^{+10.8}_{-11.6} \pm 9.6$	²⁵ POLUEKTOV	10 BELL	$e^+e^- \rightarrow \Upsilon(4S)$
162 ± 56	²⁶ AUBERT	09R BABR	$e^+e^- \rightarrow \Upsilon(4S)$
$76^{+22}_{-23} \pm 7.1$	²⁷ AUBERT	08AL BABR	Repl. by DEL-AMO-SANCHEZ 10F
$53^{+15}_{-18} \pm 10$	²⁸ POLUEKTOV	06 BELL	Repl. by POLUEKTOV 10
$70 \pm 31^{+18}_{-15}$	²⁹ AUBERT,B	05Y BABR	Repl. by AUBERT 08AL
$77^{+17}_{-19} \pm 17$	³⁰ POLUEKTOV	04 BELL	Repl. by POLUEKTOV 06

¹ AAIJ 21AM presents a combination of existing measurements from LHCb collaboration. It includes also charm mixing parameters.

² Uses binned Dalitz plot analysis of $D \rightarrow K_S^0 \pi^+ \pi^-$ and $K_S^0 K^+ K^-$ from $B^\pm \rightarrow DK^\pm$ modes. Strong phase measurements from CLEO-c and BES-III of the D decay over the Dalitz plot are used as input. Value is modulo 180° .

³ Measured in $B_S^0 \rightarrow D_S^\pm K^\mp \pi^\pm \pi^\mp$ decays in restricted phase space with $m(K^+ \pi^+ \pi^-) < 1950 \text{ MeV}$, $m(K^+ \pi^-) < 1200 \text{ MeV}$ and $m(\pi^+ \pi^-) < 1200 \text{ MeV}$. The value is modulo 180° .

⁴ A model-independent coherence factor for the decay $B_S \rightarrow D_S K \pi \pi$ (in the restricted phase space region) is also reported.

⁵ Uses binned analysis of $D \rightarrow K_S^0 \pi^+ \pi^- \pi^0$ from $B^\pm \rightarrow DK^\pm$ modes over the phase space. Strong phase measurements from RESMI 18 analysis of CLEO-c data of the D decay over the phase space binning are used as input.

⁶ Uses binned Dalitz plot analysis of $D \rightarrow K_S^0 \pi^+ \pi^-$ and $K_S^0 K^+ K^-$ from $B^\pm \rightarrow DK^\pm$ modes. Strong phase measurements from CLEO-c of the D decay over the Dalitz plot are used as input.

⁷ Measured in $B_S^0 \rightarrow D_S^\mp K^\pm$ decays, constraining $-2\beta_S$ by the measurement of $\phi_S = 0.030 \pm 0.033$ from HFLAV. The value is modulo 180° .

⁸ AAIJ 18Z reports the intervals $(5-86)^\circ$ or $(185-266)^\circ$ at 68% C.L. The extraction uses the time dependent CP violation measurement in $B^0 \rightarrow D^\mp \pi^\pm$ decays with external input and some theoretical assumptions.

⁹ Uses Dalitz plot analysis of $D \rightarrow K_S^0 \pi^+ \pi^-$ decays coming from $B^0 \rightarrow DK^*(892)^0$ modes. Measures $r_{B^0} = 0.39 \pm 0.13$, and $\delta_{B^0} = 197^{+24}_{-20}$ degrees.

¹⁰ A combination of measurements from analyses of time-integrated $B^+ \rightarrow DK^+$, $B^0 \rightarrow DK^{(*)0}$, $B^0 \rightarrow DK^+ \pi^-$, and $B^+ \rightarrow DK^+ \pi^+$ tree-level decays. In addition, results from a time-dependent analysis of $B_S^0 \rightarrow D_S K$ decays are included.

¹¹ A model-independent binned Dalitz plot analysis of the decays $B^0 \rightarrow DK^{*0}$, with $D \rightarrow K_S^0 \pi^+ \pi^-$ and $D \rightarrow K_S^0 K^+ K^-$. The results cannot be combined with the model-dependent analysis of the same dataset reported in AAIJ 16AA.

¹² Angle γ required to satisfy $0 < \gamma < 180$ degrees.

¹³ Obtained by measuring time-dependent CP asymmetry in $B_S^0 \rightarrow K^+ K^-$ and using a U-spin relation between $B_S^0 \rightarrow K^+ K^-$ and $B^0 \rightarrow \pi^+ \pi^-$.

¹⁴ Results are also presented using additional inputs on $B^0 \rightarrow \pi^0 \pi^0$ and $B^+ \rightarrow \pi^+ \pi^0$ decays from other experiments and isospin symmetry assumptions. The dependence of the results on the maximum allowed amount of U-spin breaking up to 50% is also included.

¹⁵ Uses binned Dalitz plot analysis of $B^+ \rightarrow DK^+$ decays, with $D \rightarrow K_S^0 \pi^+ \pi^-$ and $D \rightarrow K_S^0 K^+ K^-$. Strong phase measurements from CLEO-c (LIBBY 10) of the D

- decay over the Dalitz plot are used as input. Solution that satisfies $0 < \gamma < 180$ is chosen.
- 16 AAIJ 14BE uses model-dependent analysis of $D \rightarrow K_S^0 \pi^+ \pi^-$ amplitudes. The model is the same as in DEL-AMO-SANCHEZ 10F.
- 17 Measured in $B_S^0 \rightarrow D_S^+ K^\pm$ decays, constraining $-2\beta_S$ by the measurement of $\phi_S = 0.01 \pm 0.07 \pm 0.0$ from AAIJ 13AR. The value is modulo 180° at 68% CL.
- 18 Presents a confidence region $55.4^\circ < \gamma < 82.3^\circ$ at 68% CL with best fit value 72.6° and includes both statistical and systematic uncertainties. The corresponding 95% CL is $40.2^\circ < \gamma < 92.7^\circ$. The value is determined from combination of measurements using D meson decaying to $K^+ K^-$, $\pi^+ \pi^-$, $K^\pm \pi^\mp$, $K_S^0 \pi^+ \pi^-$, $K_S^0 K^+ K^-$, and $K^\pm \pi^\mp \pi^\pm \pi^\mp$. Combines $B^\pm \rightarrow D K^\pm$ and $B^\pm \rightarrow D \pi^\pm$.
- 19 Reports combination of published measurements using GGSZ, GLW, and ADS methods. Reports also 2σ range of $41-102^\circ$ and a 5.9σ significance for $\gamma(B^+ \rightarrow D^{(*)0} K^{(*)+}) \neq 0$ hypothesis.
- 20 Reports combined statistical and systematic uncertainties.
- 21 Uses binned Dalitz plot of $\overline{D}^0 \rightarrow K_S^0 \pi^+ \pi^-$ decays from $B^+ \rightarrow \overline{D}^0 K^+$. Measurement of strong phases in $\overline{D}^0 \rightarrow K_S^0 \pi^+ \pi^-$ Dalitz plot from LIBBY 10 is used as input.
- 22 We combined the systematics in quadrature. The authors report separately the contribution to the systematic uncertainty due to the uncertainty on the bin-averaged strong phase difference between D^0 and \overline{D}^0 amplitudes.
- 23 Uses Dalitz plot analysis of $\overline{D}^0 \rightarrow K_S^0 \pi^+ \pi^-$, $K_S^0 K^+ K^-$ decays from $B^+ \rightarrow D^{(*)} K^+$, $D K^{*+}$ modes. The corresponding two standard deviation interval for γ is $39^\circ < \gamma < 98^\circ$. CP conservation in the combined result is ruled out with a significance of 3.5 standard deviations.
- 24 Reports confidence intervals for the CKM angle γ from the measured values of the GLW parameters using $B^\pm \rightarrow D K^\pm$ decays with D mesons decaying to non-CP($K\pi$), CP-even ($K^+ K^-$, $\pi^+ \pi^-$), and CP-odd ($K_S^0 \pi^0$, $K_S^0 \omega$) states.
- 25 Uses Dalitz plot analysis of $\overline{D}^0 \rightarrow K_S^0 \pi^+ \pi^-$ decays from $B^+ \rightarrow D^{(*)} K^+$ modes. The corresponding two standard deviation interval for γ is $54.2^\circ < \gamma < 100.5^\circ$. CP conservation in the combined result is ruled out with a significance of 3.5 standard deviations.
- 26 Uses Dalitz plot analysis of $D^0 \rightarrow K_S^0 \pi^+ \pi^-$ decays coming from $B^0 \rightarrow D^0 K^{*0}$ modes. The corresponding 95% CL interval is $77^\circ < \gamma < 247^\circ$. A 180 degree ambiguity is implied.
- 27 Uses Dalitz plot analysis of $\overline{D}^0 \rightarrow K_S^0 \pi^+ \pi^-$ and $\overline{D}^0 \rightarrow K_S^0 K^+ K^-$ decays coming from $B^\pm \rightarrow D^{(*)} K^{(*)\pm}$ modes. The corresponding two standard deviation interval is $29^\circ < \gamma < 122^\circ$.
- 28 Uses a Dalitz plot analysis of the $\overline{D}^0 \rightarrow K_S^0 \pi^+ \pi^-$ decays; Combines the $D K^+$, $D^* K^+$ and $D K^{*+}$ modes. The corresponding two standard deviations interval for gamma is $8^\circ < \gamma < 111^\circ$.
- 29 Uses a Dalitz plot analysis of neutral $D \rightarrow K_S^0 \pi^+ \pi^-$ decays coming from $B^\pm \rightarrow D K^\pm$ and $B^\pm \rightarrow D^{*0} K^\pm$ followed by $D^{*0} \rightarrow D \pi^0$, $D \gamma$. The corresponding two standard deviations interval for gamma is $12^\circ < \gamma < 137^\circ$. AUBERT,B 05Y also reports the amplitude ratios and the strong phases.
- 30 Uses a Dalitz plot analysis of the 3-body $D \rightarrow K_S^0 \pi^+ \pi^-$ decays coming from $B^\pm \rightarrow D K^\pm$ and $B^\pm \rightarrow D^* K^\pm$ followed by $D^* \rightarrow D \pi^0$; here we use D to denote that the neutral D meson produced in the decay is an admixture of D^0 and \overline{D}^0 . The corresponding two standard deviations interval for γ is $26^\circ < \gamma < 126^\circ$. POLUEKTOV 04 also reports the amplitude ratios and the strong phases.

$r_B(B^+ \rightarrow D^0 K^+)$

r_B and δ_B are the amplitude ratio and relative strong phase between the amplitudes of $A(B^+ \rightarrow D^0 K^+)$ and $A(B^+ \rightarrow \overline{D}^0 K^+)$,

"OUR EVALUATION" is provided by the Heavy Flavor Averaging Group (HFLAV).

VALUE	CL%	DOCUMENT ID	TECN	COMMENT
0.0994 ± 0.0026		OUR EVALUATION		
0.0904 ^{+0.0077} _{-0.0075}		1 AAIJ	21L LHCb	pp at 7, 8, 13 TeV
0.323 ± 0.147 ± 0.056		2 RESMI	19 BELL	$e^+ e^- \rightarrow \Upsilon(4S)$
0.086 ^{+0.013} _{-0.014}		3 AAIJ	18AD LHCb	Repl. by AAIJ 21L
0.080 ^{+0.019} _{-0.021}		4 AAIJ	14BA LHCb	Repl. by AAIJ 21L
0.06 ± 0.04		5 AAIJ	14BE LHCb	Repl. by AAIJ 14BA
0.097 ± 0.011		6 AAIJ	13AE LHCb	pp at 7 TeV
0.092 ^{+0.013} _{-0.012}		7 LEES	13B BABR	$e^+ e^- \rightarrow \Upsilon(4S)$
0.07 ± 0.04		8,9 AAIJ	12AQ LHCb	pp at 7 TeV
0.145 ± 0.030 ± 0.015		9,10 AIHARA	12 BELL	$e^+ e^- \rightarrow \Upsilon(4S)$
<0.13		11 LEES	11D BABR	$e^+ e^- \rightarrow \Upsilon(4S)$
0.096 ± 0.029 ± 0.006		12 DEL-AMO-SA..10F	BABR	Repl. by LEES 13B
0.095 ^{+0.051} _{-0.041}		13 DEL-AMO-SA..10H	BABR	Repl. by LEES 13B
0.160 ± 0.040 ± 0.051 _{-0.038 -0.015}		14 POLUEKTOV	10 BELL	$e^+ e^- \rightarrow \Upsilon(4S)$
0.086 ± 0.032 ± 0.015		15 AUBERT	08AL BABR	Repl. by DEL-AMO-SANCHEZ 10F
<0.19		90 HORII	08 BELL	$e^+ e^- \rightarrow \Upsilon(4S)$
0.159 ^{+0.054} _{-0.050} ± 0.050		16 POLUEKTOV	06 BELL	Repl. by POLUEKTOV 10
0.12 ± 0.08 ± 0.05		17 AUBERT,B	05Y BABR	Repl. by AUBERT 08AL

- 1 Uses binned analysis of $D \rightarrow K_S^0 \pi^+ \pi^- \pi^0$ from $B^\pm \rightarrow D K^\pm$ modes over the phase space. Strong phase measurements from CLEO-c and BES-III data of the D decay over the phase space binning are used as input.
- 2 Uses binned analysis of $D \rightarrow K_S^0 \pi^+ \pi^- \pi^0$ from $B^\pm \rightarrow D K^\pm$ modes over the phase space. Strong phase measurements from RESMI 18 analysis of CLEO-c data of the D decay over the phase space binning are used as input.

- 3 Uses binned Dalitz plot analysis of $D \rightarrow K_S^0 \pi^+ \pi^-$ and $K_S^0 K^+ K^-$ from $B^\pm \rightarrow D K^\pm$ modes. Strong phase measurements from CLEO-c of the D decay over the Dalitz plot are used as input.
- 4 Uses binned Dalitz plot analysis of $B^+ \rightarrow D K^+$ decays, with $D \rightarrow K_S^0 \pi^+ \pi^-$ and $D \rightarrow K_S^0 K^+ K^-$. Strong phase measurements from CLEO-c (LIBBY 10) of the D decay over the Dalitz plot are used as input.
- 5 AAIJ 14BE uses model-dependent analysis of $D \rightarrow K_S^0 \pi^+ \pi^-$ amplitudes. The model is the same as in DEL-AMO-SANCHEZ 10F.
- 6 Uses $B^\pm \rightarrow [K^\pm \pi^\mp \pi^\pm \pi^\mp]_D h^\pm$ mode.
- 7 Reports combination of published measurements using GGSZ, GLW, and ADS methods.
- 8 Reports combined statistical and systematic uncertainties.
- 9 Uses binned Dalitz plot of $\overline{D}^0 \rightarrow K_S^0 \pi^+ \pi^-$ decays from $B^+ \rightarrow \overline{D}^0 K^+$. Measurement of strong phases in $\overline{D}^0 \rightarrow K_S^0 \pi^+ \pi^-$ Dalitz plot from LIBBY 10 is used as input.
- 10 We combined the systematics in quadrature. The authors report separately the contribution to the systematic uncertainty due to the uncertainty on the bin-averaged strong phase difference between D^0 and \overline{D}^0 amplitudes.
- 11 Uses decays of neutral D to $K^- \pi^+ \pi^0$.
- 12 Uses Dalitz plot analysis of $\overline{D}^0 \rightarrow K_S^0 \pi^+ \pi^-$, $K_S^0 K^+ K^-$ decays from $B^+ \rightarrow D^{(*)} K^{(*)+}$ modes. The corresponding two standard deviation interval is $0.037 < r_B < 0.155$.
- 13 Uses the Cabibbo suppressed decay of $B^+ \rightarrow \overline{D} K^+$ followed by $\overline{D} \rightarrow K^- \pi^+$.
- 14 Uses Dalitz plot analysis of $\overline{D}^0 \rightarrow K_S^0 \pi^+ \pi^-$ decays from $B^+ \rightarrow D^0 K^+$ modes. The corresponding two standard deviation interval is $0.084 < r_B < 0.239$.
- 15 Uses Dalitz plot analysis of $\overline{D}^0 \rightarrow K_S^0 \pi^+ \pi^-$ and $\overline{D}^0 \rightarrow K_S^0 K^+ K^-$ decays coming from $B^\pm \rightarrow D^{(*)} K^{(*)\pm}$ modes.
- 16 Uses a Dalitz plot analysis of the $\overline{D}^0 \rightarrow K_S^0 \pi^+ \pi^-$ decays; Combines the $D K^+$, $D^* K^+$ and $D K^{*+}$ modes.
- 17 Uses a Dalitz analysis of neutral D decays to $K_S^0 \pi^+ \pi^-$ in the processes $B^\pm \rightarrow D^{(*)} K^\pm$, $D^* \rightarrow D \pi^0$, $D \gamma$.

$\delta_B(B^+ \rightarrow D^0 K^+)$

"OUR EVALUATION" is provided by the Heavy Flavor Averaging Group (HFLAV).

VALUE (°)	DOCUMENT ID	TECN	COMMENT
-----------	-------------	------	---------

127.7^{+3.6}_{-3.9} OUR EVALUATION

• • • We do not use the following data for averages, fits, limits, etc. • • •

118.3 ^{+5.5} _{-5.6}	1 AAIJ	21L LHCb	pp at 7, 8, 13 TeV
83.4 ^{+18.3} _{-16.6} ± 5.1	2 RESMI	19 BELL	$e^+ e^- \rightarrow \Upsilon(4S)$
101 ± 11	3 AAIJ	18AD LHCb	Repl. by AAIJ 21L
134 ⁺¹⁴ ₋₁₅	4 AAIJ	14BA LHCb	Repl. by AAIJ 21L
115 ⁺⁴¹ ₋₅₁	5 AAIJ	14BE LHCb	Repl. by AAIJ 14BA
105 ⁺¹⁶ ₋₁₇	6 LEES	13B BABR	$e^+ e^- \rightarrow \Upsilon(4S)$
137 ⁺³⁵ ₋₄₆	7,8 AAIJ	12AQ LHCb	pp at 7 TeV
129.9 ± 15.0 ± 6.0	8,9 AIHARA	12 BELL	$e^+ e^- \rightarrow \Upsilon(4S)$
119 ⁺¹⁹ ₋₂₀ ± 4	10 DEL-AMO-SA..10F	BABR	Repl. by LEES 13B
136.7 ^{+13.0} _{-15.8} ± 23.2	11 POLUEKTOV	10 BELL	$e^+ e^- \rightarrow \Upsilon(4S)$
109 ⁺²⁷ ₋₃₀ ± 8	12 AUBERT	08AL BABR	Repl. by DEL-AMO-SANCHEZ 10F
145.7 ^{+19.0} _{-19.7} ± 23.1	13 POLUEKTOV	06 BELL	Repl. by POLUEKTOV 10
104 ± 45 ± 23 ₋₃₂	14 AUBERT,B	05Y BABR	Repl. by AUBERT 08AL

- 1 Uses binned Dalitz plot analysis of $D \rightarrow K_S^0 \pi^+ \pi^-$ and $K_S^0 K^+ K^-$ from $B^\pm \rightarrow D K^\pm$ modes. Strong phase measurements from CLEO-c and BES-III of the D decay over the Dalitz plot are used as input. Value is modulo 180° .
- 2 Uses binned analysis of $D \rightarrow K_S^0 \pi^+ \pi^- \pi^0$ from $B^\pm \rightarrow D K^\pm$ modes over the phase space. Strong phase measurements from RESMI 18 analysis of CLEO-c data of the D decay over the phase space binning are used as input.
- 3 Uses binned Dalitz plot analysis of $D \rightarrow K_S^0 \pi^+ \pi^-$ and $K_S^0 K^+ K^-$ from $B^\pm \rightarrow D K^\pm$ modes. Strong phase measurements from CLEO-c of the D decay over the Dalitz plot are used as input.
- 4 Uses binned Dalitz plot analysis of $B^+ \rightarrow D K^+$ decays, with $D \rightarrow K_S^0 \pi^+ \pi^-$ and $D \rightarrow K_S^0 K^+ K^-$. Strong phase measurements from CLEO-c (LIBBY 10) of the D decay over the Dalitz plot are used as input.
- 5 AAIJ 14BE uses model-dependent analysis of $D \rightarrow K_S^0 \pi^+ \pi^-$ amplitudes. The model is the same as in DEL-AMO-SANCHEZ 10F.
- 6 Reports combination of published measurements using GGSZ, GLW, and ADS methods.
- 7 Reports combined statistical and systematic uncertainties.
- 8 Uses binned Dalitz plot of $\overline{D}^0 \rightarrow K_S^0 \pi^+ \pi^-$ decays from $B^+ \rightarrow \overline{D}^0 K^+$. Measurement of strong phases in $\overline{D}^0 \rightarrow K_S^0 \pi^+ \pi^-$ Dalitz plot from LIBBY 10 is used as input.
- 9 We combined the systematics in quadrature. The authors report separately the contribution to the systematic uncertainty due to the uncertainty on the bin-averaged strong phase difference between D^0 and \overline{D}^0 amplitudes.
- 10 Uses Dalitz plot analysis of $\overline{D}^0 \rightarrow K_S^0 \pi^+ \pi^-$, $K_S^0 K^+ K^-$ decays from $B^+ \rightarrow D^{(*)} K^{(*)+}$ modes. The corresponding two standard deviation interval is $75^\circ < \delta_B < 157^\circ$.
- 11 Uses Dalitz plot analysis of $\overline{D}^0 \rightarrow K_S^0 \pi^+ \pi^-$ decays from $B^+ \rightarrow \overline{D}^0 K^+$ modes. The corresponding two standard deviation interval is $102.2^\circ < \delta_B < 162.3^\circ$.

Meson Particle Listings

 B^\pm

- ¹² Uses Dalitz plot analysis of $\overline{D}^0 \rightarrow K_S^0 \pi^+ \pi^-$ and $\overline{D}^0 \rightarrow K_S^0 K^+ K^-$ decays coming from $B^\pm \rightarrow D^{(*)} K^{(*)\pm}$ modes.
- ¹³ Uses a Dalitz plot analysis of the $\overline{D}^0 \rightarrow K_S^0 \pi^+ \pi^-$ decays; Combines the $D K^+$, $D^* K^+$ and $D K^{*+}$ modes.
- ¹⁴ Uses a Dalitz analysis of neutral D decays to $K_S^0 \pi^+ \pi^-$ in the processes $B^\pm \rightarrow D^{(*)} K^\pm$, $D^* \rightarrow D \pi^0$, $D \gamma$.

 $r_B(B^+ \rightarrow D^0 \pi^+)$

VALUE (units 10^{-3})	DOCUMENT ID	TECN	COMMENT
--------------------------	-------------	------	---------

• • • We do not use the following data for averages, fits, limits, etc. • • •

5.0 ± 1.7 ¹ AAIJ 21L LHCb pp at 7, 8, 13 TeV

- ¹ Uses binned Dalitz plot analysis of $D \rightarrow K_S^0 \pi^+ \pi^-$ and $K_S^0 K^+ K^-$ from $B^\pm \rightarrow D \pi^\pm$ modes. Strong phase measurements from CLEO-c and BES-III of the D decay over the Dalitz plot are used as input.

 $\delta_B(B^+ \rightarrow D^0 \pi^+)$

VALUE (°)	DOCUMENT ID	TECN	COMMENT
-----------	-------------	------	---------

• • • We do not use the following data for averages, fits, limits, etc. • • •

291 \pm 24 ¹ AAIJ 21L LHCb pp at 7, 8, 13 TeV

- ¹ Uses binned Dalitz plot analysis of $D \rightarrow K_S^0 \pi^+ \pi^-$ and $K_S^0 K^+ K^-$ from $B^\pm \rightarrow D \pi^\pm$ modes. Strong phase measurements from CLEO-c and BES-III of the D decay over the Dalitz plot are used as input. Value is modulo 180°.

 $r_B(B^+ \rightarrow D^0 K^{*+})$

r_B and δ_B are the amplitude ratio and relative strong phase between the amplitudes of $A_{CP}(B^+ \rightarrow D^0 K^{*+})$ and $A_{CP}(B^+ \rightarrow \overline{D}^0 K^{*+})$.

"OUR EVALUATION" is provided by the Heavy Flavor Averaging Group (HFLAV).

VALUE	DOCUMENT ID	TECN	COMMENT
-------	-------------	------	---------

0.101 \pm 0.016 OUR EVALUATION

• • • We do not use the following data for averages, fits, limits, etc. • • •

0.143 \pm 0.048 ¹ LEES 13B BABR $e^+ e^- \rightarrow \Upsilon(4S)$

0.166 \pm 0.073 ² DEL-AMO-SA...10F BABR Repl. by LEES 13B

0.31 \pm 0.07 ³ AUBERT 09AJ BABR Repl. by LEES 13B

0.181 \pm 0.088 \pm 0.042 ⁴ AUBERT 08AL BABR Repl. by AUBERT 09AJ

0.564 \pm 0.216 \pm 0.093 ⁵ POLUEKTOV 06 BELL $e^+ e^- \rightarrow \Upsilon(4S)$

- ¹ Reports combination of published measurements using GGSZ, GLW, and ADS methods.
- ² DEL-AMO-SANCHEZ 10F reports $r_B \cdot k = 0.149 \pm 0.066$ for $k = 0.9$.
- ³ Obtained by combining the GLW and ADS methods. The 2-sigma range corresponds to [0.17, 0.43].
- ⁴ Uses Dalitz plot analysis of $\overline{D}^0 \rightarrow K_S^0 \pi^+ \pi^-$ and $\overline{D}^0 \rightarrow K_S^0 K^+ K^-$ decays coming from $B^\pm \rightarrow D^{(*)} K^{(*)\pm}$ modes.
- ⁵ Uses a Dalitz plot analysis of the $\overline{D}^0 \rightarrow K_S^0 \pi^+ \pi^-$ decays; Combines the $D K^+$, $D^* K^+$ and $D K^{*+}$ modes.

 $\delta_B(B^+ \rightarrow D^0 K^{*+})$

"OUR EVALUATION" is provided by the Heavy Flavor Averaging Group (HFLAV).

VALUE (°)	DOCUMENT ID	TECN	COMMENT
-----------	-------------	------	---------

48 \pm 59 OUR EVALUATION

• • • We do not use the following data for averages, fits, limits, etc. • • •

101 \pm 43 ¹ LEES 13B BABR $e^+ e^- \rightarrow \Upsilon(4S)$

111 \pm 32 DEL-AMO-SA...10F BABR Repl. by LEES 13B

104 \pm 39 \pm 18 ² AUBERT 08AL BABR Repl. by LEES 13B

242.6 \pm 20.2 \pm 23.2 \pm 49.4 ³ POLUEKTOV 06 BELL $e^+ e^- \rightarrow \Upsilon(4S)$

- ¹ Reports combination of published measurements using GGSZ, GLW, and ADS methods.
- ² Uses Dalitz plot analysis of $\overline{D}^0 \rightarrow K_S^0 \pi^+ \pi^-$ and $\overline{D}^0 \rightarrow K_S^0 K^+ K^-$ decays coming from $B^\pm \rightarrow D^{(*)} K^{(*)\pm}$ modes.
- ³ Uses a Dalitz plot analysis of the $\overline{D}^0 \rightarrow K_S^0 \pi^+ \pi^-$ decays; Combines the $D K^+$, $D^* K^+$ and $D K^{*+}$ modes.

 $r_B(B^+ \rightarrow D^{*0} K^+)$

r_B and δ_B are the amplitude ratio and relative strong phase between the amplitudes of $A(B^+ \rightarrow D^{*0} K^+)$ and $A(B^+ \rightarrow \overline{D}^{*0} K^+)$.

"OUR EVALUATION" is provided by the Heavy Flavor Averaging Group (HFLAV).

VALUE	DOCUMENT ID	TECN	COMMENT
-------	-------------	------	---------

0.104 \pm 0.013 OUR EVALUATION

• • • We do not use the following data for averages, fits, limits, etc. • • •

0.106 \pm 0.019 ¹ LEES 13B BABR $e^+ e^- \rightarrow \Upsilon(4S)$

0.133 \pm 0.042 \pm 0.013 ² DEL-AMO-SA...10F BABR Repl. by LEES 13B

0.096 \pm 0.035 ³ DEL-AMO-SA...10H BABR Repl. by LEES 13B

0.196 \pm 0.072 \pm 0.064 ⁴ POLUEKTOV 10 BELL $e^+ e^- \rightarrow \Upsilon(4S)$

0.135 \pm 0.050 \pm 0.012 ⁵ AUBERT 08AL BABR Repl. by DEL-AMO-SANCHEZ 10F

0.175 \pm 0.108 \pm 0.050 ⁶ POLUEKTOV 06 BELL Repl. by POLUEKTOV 10

0.17 \pm 0.10 \pm 0.04 ⁷ AUBERT,B 05Y BABR Repl. by AUBERT 08AL

- ¹ Reports combination of published measurements using GGSZ, GLW, and ADS methods.
- ² Uses Dalitz plot analysis of $\overline{D}^0 \rightarrow K_S^0 \pi^+ \pi^-$, $K_S^0 K^+ K^-$ decays from $B^+ \rightarrow D^{(*)} K^{(*)+}$ modes. The corresponding two standard deviation interval is $0.049 < r_B^* < 0.215$.

³ Uses the Cabibbo suppressed decay of $B^+ \rightarrow \overline{D}^* K^+$ followed by $\overline{D}^* \rightarrow \overline{D} \pi^0$ or $\overline{D} \gamma$, and $\overline{D} \rightarrow K^- \pi^+$.

⁴ Uses Dalitz plot analysis of $\overline{D}^0 \rightarrow K_S^0 \pi^+ \pi^-$ decays from $B^+ \rightarrow D^{*0} K^+$ modes. The corresponding two standard deviation interval is $0.061 < r_B^* < 0.271$.

⁵ Uses Dalitz plot analysis of $\overline{D}^0 \rightarrow K_S^0 \pi^+ \pi^-$ and $\overline{D}^0 \rightarrow K_S^0 K^+ K^-$ decays coming from $B^\pm \rightarrow D^{(*)} K^{(*)\pm}$ modes.

⁶ Uses a Dalitz plot analysis of the $\overline{D}^0 \rightarrow K_S^0 \pi^+ \pi^-$ decays; Combines the $D K^+$, $D^* K^+$ and $D K^{*+}$ modes.

⁷ Uses a Dalitz analysis of neutral D decays to $K_S^0 \pi^+ \pi^-$ in the processes $B^\pm \rightarrow D^{(*)} K^\pm$, $D^* \rightarrow D \pi^0$, $D \gamma$.

 $\delta_B(B^+ \rightarrow D^{*0} K^+)$

"OUR EVALUATION" is provided by the Heavy Flavor Averaging Group (HFLAV).

VALUE (°)	DOCUMENT ID	TECN	COMMENT
-----------	-------------	------	---------

314.8 \pm 9.9 OUR EVALUATION

• • • We do not use the following data for averages, fits, limits, etc. • • •

294 \pm 21 ¹ LEES 13B BABR $e^+ e^- \rightarrow \Upsilon(4S)$

278 \pm 21 \pm 6 ² DEL-AMO-SA...10F BABR Repl. by LEES 13B

341.9 \pm 18.0 \pm 23.1 ³ POLUEKTOV 10 BELL $e^+ e^- \rightarrow \Upsilon(4S)$

297 \pm 27 \pm 6.4 ⁴ AUBERT 08AL BABR Repl. by DEL-AMO-SANCHEZ 10F

302.0 \pm 33.8 \pm 23.7 ⁵ POLUEKTOV 06 BELL Repl. by POLUEKTOV 10

296 \pm 41 \pm 20 ⁶ AUBERT,B 05Y BABR Repl. by AUBERT 08AL

¹ Reports combination of published measurements using GGSZ, GLW, and ADS methods. We added 360° to the value of $(-66 \pm 21)^\circ$ quoted by LEES 13B.

² Uses Dalitz plot analysis of $\overline{D}^0 \rightarrow K_S^0 \pi^+ \pi^-$, $K_S^0 K^+ K^-$ decays from $B^+ \rightarrow D^{(*)} K^{(*)+}$ modes. The corresponding two standard deviation interval is $236^\circ < \delta_B^* < 322^\circ$.

³ Uses Dalitz plot analysis of $\overline{D}^0 \rightarrow K_S^0 \pi^+ \pi^-$ decays from $B^+ \rightarrow D^* K^+$ modes. The corresponding two standard deviation interval is $296.5^\circ < \delta_B^* < 382.7^\circ$.

⁴ Uses Dalitz plot analysis of $\overline{D}^0 \rightarrow K_S^0 \pi^+ \pi^-$ and $\overline{D}^0 \rightarrow K_S^0 K^+ K^-$ decays coming from $B^\pm \rightarrow D^{(*)} K^{(*)\pm}$ modes.

⁵ Uses a Dalitz plot analysis of the $\overline{D}^0 \rightarrow K_S^0 \pi^+ \pi^-$ decays; Combines the $D K^+$, $D^* K^+$ and $D K^{*+}$ modes.

⁶ Uses a Dalitz analysis of neutral D decays to $K_S^0 \pi^+ \pi^-$ in the processes $B^\pm \rightarrow D^{(*)} K^\pm$, $D^* \rightarrow D \pi^0$, $D \gamma$.

PARTIAL BRANCHING FRACTIONS

 $B(B^+ \rightarrow K^{*+} \ell^+ \ell^-) (q^2 < 2.0 \text{ GeV}^2/c^4)$

VALUE (units 10^{-7})	DOCUMENT ID	TECN	COMMENT
--------------------------	-------------	------	---------

1.4 \pm 0.5 OUR AVERAGE

1.37 \pm 0.60 AAIJ 12AH LHCb pp at 7 TeV

1.30 \pm 0.98 \pm 0.14 AALTONEN 11AI CDF $p\overline{p}$ at 1.96 TeV

 $B(B^+ \rightarrow K^{*+} \ell^+ \ell^-) (2.0 < q^2 < 4.3 \text{ GeV}^2/c^4)$

VALUE (units 10^{-7})	DOCUMENT ID	TECN	COMMENT
--------------------------	-------------	------	---------

1.1 \pm 0.5 OUR AVERAGE

1.24 \pm 0.60 AAIJ 12AH LHCb pp at 7 TeV

0.71 \pm 1.00 \pm 0.15 AALTONEN 11AI CDF $p\overline{p}$ at 1.96 TeV

 $B(B^+ \rightarrow K^{*+} \ell^+ \ell^-) (4.3 < q^2 < 8.68 \text{ GeV}^2/c^4)$

VALUE (units 10^{-7})	DOCUMENT ID	TECN	COMMENT
--------------------------	-------------	------	---------

2.4 \pm 0.8 OUR AVERAGE

2.50 \pm 0.88 AAIJ 12AH LHCb pp at 7 TeV

1.71 \pm 1.58 \pm 0.49 AALTONEN 11AI CDF $p\overline{p}$ at 1.96 TeV

 $B(B^+ \rightarrow K^{*+} \ell^+ \ell^-) (10.09 < q^2 < 12.86 \text{ GeV}^2/c^4)$

VALUE (units 10^{-7})	DOCUMENT ID	TECN	COMMENT
--------------------------	-------------	------	---------

2.1 \pm 0.6 OUR AVERAGE

2.13 \pm 0.72 AAIJ 12AH LHCb pp at 7 TeV

1.97 \pm 0.99 \pm 0.22 AALTONEN 11AI CDF $p\overline{p}$ at 1.96 TeV

$B(B^+ \rightarrow K^{*+} \ell^+ \ell^-)$ ($14.18 < q^2 < 16.0 \text{ GeV}^2/c^4$)

VALUE (units 10^{-7})	DOCUMENT ID	TECN	COMMENT
0.86^{+0.40}_{-0.32} OUR AVERAGE			
1.00 ^{+0.47} _{-0.38}	AAIJ	12AH LHCb	pp at 7 TeV
0.52 \pm 0.61 \pm 0.09	AALTONEN	11AI CDF	$p\bar{p}$ at 1.96 TeV

$B(B^+ \rightarrow K^{*+} \ell^+ \ell^-)$ ($15.0 < q^2 < 19.0 \text{ GeV}^2/c^4$)

VALUE (units 10^{-7})	DOCUMENT ID	TECN	COMMENT
1.78^{+0.32}_{-0.29} OUR AVERAGE			
2.9 ^{+1.0} _{-0.8} \pm 0.3	1 WEHLE	21 BELL	$e^+e^- \rightarrow \Upsilon(4S)$
2.1 ^{+1.2} _{-1.0} \pm 0.2	2 WEHLE	21 BELL	$e^+e^- \rightarrow \Upsilon(4S)$
1.58 ^{+0.32} _{-0.29} \pm 0.11	3 AAIJ	14M LHCb	pp at 7, 8 TeV

1 Measured with $\mu^+ \mu^-$ as lepton pair.
 2 Measured with $e^+ e^-$ as lepton pair.
 3 Uses $B(B^+ \rightarrow J/\psi(1S) K^*(892)^+) = (1.431 \pm 0.027 \pm 0.090) \times 10^{-3}$ for normalization and $\mu^+ \mu^-$ as a lepton pair.

$B(B^+ \rightarrow K^{*+} \ell^+ \ell^-)$ ($q^2 > 16.0 \text{ GeV}^2/c^4$)

VALUE (units 10^{-7})	DOCUMENT ID	TECN	COMMENT
1.3\pm0.4 OUR AVERAGE			
1.25 \pm 0.46	AAIJ	12AH LHCb	pp at 7 TeV
1.57 \pm 0.96 \pm 0.17	AALTONEN	11AI CDF	$p\bar{p}$ at 1.96 TeV

$B(B^+ \rightarrow K^{*+} \ell^+ \ell^-)$ ($1.0 < q^2 < 6.0 \text{ GeV}^2/c^4$)

VALUE (units 10^{-7})	DOCUMENT ID	TECN	COMMENT
1.72^{+0.40}_{-0.32} OUR AVERAGE			
1.2 ^{+0.9} _{-0.7} \pm 0.2	1,2 WEHLE	21 BELL	$e^+e^- \rightarrow \Upsilon(4S)$
1.7 ^{+1.0} _{-1.0} \pm 0.2	2,3 WEHLE	21 BELL	$e^+e^- \rightarrow \Upsilon(4S)$
1.79 ^{+0.41} _{-0.37} \pm 0.13	4 AAIJ	14M LHCb	pp at 7, 8 TeV
2.57 \pm 1.61 \pm 0.40	AALTONEN	11AI CDF	$p\bar{p}$ at 1.96 TeV
••• We do not use the following data for averages, fits, limits, etc. •••			
2.90 ^{+0.90} _{-0.85}	AAIJ	12AH LHCb	Repl. by AAIJ 14M

1 Measured with $\mu^+ \mu^-$ as lepton pair.
 2 Result is determined for the range $1.1 < q^2 < 6.0 \text{ GeV}^2/c^4$.
 3 Measured with $e^+ e^-$ as lepton pair.
 4 Uses $B(B^+ \rightarrow J/\psi(1S) K^*(892)^+) = (1.431 \pm 0.027 \pm 0.090) \times 10^{-3}$ for normalization and $\mu^+ \mu^-$ as a lepton pair. Measured in $1.1 < q^2 < 6.0 \text{ GeV}^2/c^4$.

$B(B^+ \rightarrow K^{*+} \ell^+ \ell^-)$ ($0.0 < q^2 < 4.3 \text{ GeV}^2/c^4$)

VALUE (units 10^{-7})	DOCUMENT ID	TECN	COMMENT
2.01\pm1.39\pm0.27	AALTONEN	11AI CDF	$p\bar{p}$ at 1.96 TeV

$B(B^+ \rightarrow K^{*+} \mu^+ \mu^-) / B(B^+ \rightarrow K^{*+} e^+ e^-)$ ($0.045 < q^2 < 1.1 \text{ GeV}^2/c^4$)

VALUE	DOCUMENT ID	TECN	COMMENT
0.62^{+0.60}_{-0.36} \pm 0.07	WEHLE	21 BELL	$e^+e^- \rightarrow \Upsilon(4S)$

$B(B^+ \rightarrow K^{*+} \mu^+ \mu^-) / B(B^+ \rightarrow K^{*+} e^+ e^-)$ ($1.1 < q^2 < 6.0 \text{ GeV}^2/c^4$)

VALUE	DOCUMENT ID	TECN	COMMENT
0.72^{+0.99}_{-0.44} \pm 0.14	WEHLE	21 BELL	$e^+e^- \rightarrow \Upsilon(4S)$

$B(B^+ \rightarrow K^{*+} \mu^+ \mu^-) / B(B^+ \rightarrow K^{*+} e^+ e^-)$ ($15.0 < q^2 < 19.0 \text{ GeV}^2/c^4$)

VALUE	DOCUMENT ID	TECN	COMMENT
1.40^{+1.99}_{-0.68} \pm 0.11	WEHLE	21 BELL	$e^+e^- \rightarrow \Upsilon(4S)$

$B(B^+ \rightarrow K^+ \ell^+ \ell^-)$ ($q^2 < 2.0 \text{ GeV}^2/c^4$)

VALUE (units 10^{-7})	DOCUMENT ID	TECN	COMMENT
0.51\pm0.08 OUR AVERAGE			Error includes scale factor of 1.5.
0.556 \pm 0.053 \pm 0.027	1 AAIJ	13H LHCb	pp at 7 TeV
0.36 \pm 0.11 \pm 0.03	AALTONEN	11AI CDF	$p\bar{p}$ at 1.96 TeV
1 Measured in $0.05 < q^2 < 2.0 \text{ GeV}^2/c^4$ range.			

$B(B^+ \rightarrow K^+ \ell^+ \ell^-)$ ($2.0 < q^2 < 4.3 \text{ GeV}^2/c^4$)

VALUE (units 10^{-7})	DOCUMENT ID	TECN	COMMENT
0.60\pm0.07 OUR AVERAGE			Error includes scale factor of 1.3.
0.573 \pm 0.053 \pm 0.023	AAIJ	13H LHCb	pp at 7 TeV
0.80 \pm 0.15 \pm 0.05	AALTONEN	11AI CDF	$p\bar{p}$ at 1.96 TeV

$B(B^+ \rightarrow K^+ \ell^+ \ell^-)$ ($4.3 < q^2 < 8.68 \text{ GeV}^2/c^4$)

VALUE (units 10^{-7})	DOCUMENT ID	TECN	COMMENT
1.03\pm0.07 OUR AVERAGE			
1.003 \pm 0.070 \pm 0.039	AAIJ	13H LHCb	pp at 7 TeV
1.18 \pm 0.19 \pm 0.09	AALTONEN	11AI CDF	$p\bar{p}$ at 1.96 TeV

$B(B^+ \rightarrow K^+ \ell^+ \ell^-)$ ($10.09 < q^2 < 12.86 \text{ GeV}^2/c^4$)

VALUE (units 10^{-7})	DOCUMENT ID	TECN	COMMENT
0.58\pm0.05 OUR AVERAGE			
0.565 \pm 0.050 \pm 0.022	AAIJ	13H LHCb	pp at 7 TeV
0.68 \pm 0.12 \pm 0.05	AALTONEN	11AI CDF	$p\bar{p}$ at 1.96 TeV

$B(B^+ \rightarrow K^+ \ell^+ \ell^-)$ ($14.18 < q^2 < 16.0 \text{ GeV}^2/c^4$)

VALUE (units 10^{-7})	DOCUMENT ID	TECN	COMMENT
0.40\pm0.05 OUR AVERAGE			Error includes scale factor of 1.4.
0.377 \pm 0.036 \pm 0.015	AAIJ	13H LHCb	pp at 7 TeV
0.53 \pm 0.10 \pm 0.03	AALTONEN	11AI CDF	$p\bar{p}$ at 1.96 TeV

$B(B^+ \rightarrow K^+ \ell^+ \ell^-)$ ($16.0 < q^2 < 18.0 \text{ GeV}^2/c^4$)

VALUE (units 10^{-7})	DOCUMENT ID	TECN	COMMENT
0.354\pm0.036\pm0.018	AAIJ	13H LHCb	pp at 7 TeV

$B(B^+ \rightarrow K^+ \ell^+ \ell^-)$ ($18.0 < q^2 < 22.0 \text{ GeV}^2/c^4$)

VALUE (units 10^{-7})	DOCUMENT ID	TECN	COMMENT
0.312\pm0.040\pm0.016	AAIJ	13H LHCb	pp at 7 TeV
F_H is a fractional contribution of (pseudo) scalar and tensor amplitudes to the decay width in the massless muon approximation.			

$B(B^+ \rightarrow K^+ \ell^+ \ell^-)$ ($15.0 < q^2 < 22.0 \text{ GeV}^2/c^4$)

VALUE (units 10^{-7})	DOCUMENT ID	TECN	COMMENT
0.85\pm0.03\pm0.04	1 AAIJ	14M LHCb	pp at 7, 8 TeV
1 Uses $B(B^+ \rightarrow J/\psi(1S) K^+) = (0.998 \pm 0.014 \pm 0.040) \times 10^{-3}$ for normalization and $\mu^+ \mu^-$ as a lepton pair.			

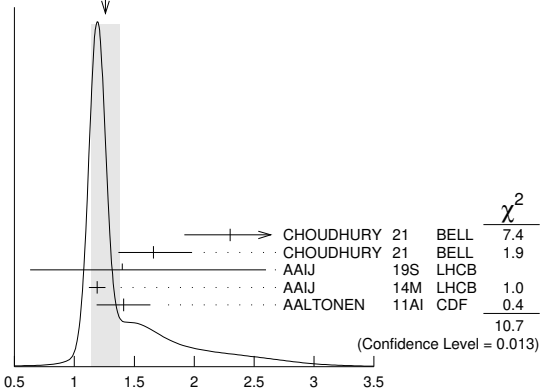
$B(B^+ \rightarrow K^+ \ell^+ \ell^-)$ ($16.0 < q^2 < 16.0 \text{ GeV}^2/c^4$)

VALUE (units 10^{-7})	DOCUMENT ID	TECN	COMMENT
0.48\pm0.11\pm0.03	AALTONEN	11AI CDF	$p\bar{p}$ at 1.96 TeV

$B(B^+ \rightarrow K^+ \ell^+ \ell^-)$ ($1.0 < q^2 < 6.0 \text{ GeV}^2/c^4$)

VALUE (units 10^{-7})	DOCUMENT ID	TECN	COMMENT
1.26\pm0.12 OUR AVERAGE			Error includes scale factor of 1.9. See the ideogram below.
2.30 ^{+0.41} _{-0.38} \pm 0.05	1 CHOUDHURY	21 BELL	$e^+e^- \rightarrow \Upsilon(4S)$
1.66 ^{+0.32} _{-0.29} \pm 0.04	2 CHOUDHURY	21 BELL	$e^+e^- \rightarrow \Upsilon(4S)$
1.40 ^{+0.98} _{-0.34} \pm 0.69	3 AAIJ	19S LHCb	pp at 7, 8, 13 TeV
1.19 \pm 0.034 \pm 0.059	4 AAIJ	14M LHCb	pp at 7, 8 TeV
1.41 \pm 0.20 \pm 0.10	AALTONEN	11AI CDF	$p\bar{p}$ at 1.96 TeV
••• We do not use the following data for averages, fits, limits, etc. •••			
1.56 ^{+0.19} _{-0.15} ^{+0.06} _{-0.04}	5 AAIJ	14AR LHCb	pp at 7, 8 TeV
1.205 \pm 0.085 \pm 0.070	AAIJ	13H LHCb	Repl. by AAIJ 14M

WEIGHTED AVERAGE
1.26 \pm 0.12 (Error scaled by 1.9)



$B(B^+ \rightarrow K^+ \ell^+ \ell^-)$ ($1.0 < q^2 < 6.0 \text{ GeV}^2/c^4$) (units 10^{-7})

1 Measured for $B^+ \rightarrow K^+ \mu^+ \mu^-$ decays. Measurements in other q^2 bins are also reported.
 2 Measured for $B^+ \rightarrow K^+ e^+ e^-$ decays. Measurements in other q^2 bins are also reported.
 3 Measured by taking the ratio of the branching fraction from $B^+ \rightarrow K^+ e^+ e^-$ and $B^+ \rightarrow J/\psi(e^+ e^-) K^+$ decays and multiplying it by the measured value of $B^+ \rightarrow J/\psi K^+$ and $J/\psi \rightarrow e^+ e^-$ as in PDG 18. The branching fraction of $B^+ \rightarrow K^+ e^+ e^-$ is determined in the region $1.1 < q^2 < 6 \text{ GeV}^2/c^4$.
 4 Uses $B(B^+ \rightarrow J/\psi(1S) K^+) = (0.998 \pm 0.014 \pm 0.040) \times 10^{-3}$ for normalization and $\mu^+ \mu^-$ for leptons. Measured for $1.1 < q^2 < 6.0 \text{ GeV}^2/c^4$.
 5 Measured by taking the ratio of the branching fraction from $B^+ \rightarrow K^+ e^+ e^-$ and $B^+ \rightarrow J/\psi(e^+ e^-) K^+$ decays and multiplying it by the measured value of $B^+ \rightarrow J/\psi K^+$ and $J/\psi \rightarrow e^+ e^-$ as in PDG 12. The branching fraction of $B^+ \rightarrow K^+ e^+ e^-$ is determined in the region $1 < q^2 < 6 \text{ GeV}^2/c^4$.

Meson Particle Listings

 B^\pm $B(B^+ \rightarrow K^+ \mu^+ \mu^-) / B(B^+ \rightarrow K^+ e^+ e^-) (1.0 < q^2 < 6.0 \text{ GeV}^2/c^4)$

VALUE	DOCUMENT ID	TECN	COMMENT
0.86 ± 0.06 OUR AVERAGE			
1.39 ^{+0.36} _{-0.33} ± 0.02	1 CHOUDHURY 21	BELL	$e^+ e^- \rightarrow \Upsilon(4S)$
0.846 ^{+0.060+0.016} _{-0.054-0.014}	2 AAIJ	19s LHCb	pp at 7, 8, 13 TeV
0.745 ^{+0.090} _{-0.074} ± 0.036	3 AAIJ	14AR LHCb	pp at 7, 8 TeV

¹ Measurements in other q^2 bins are also reported.

² The ratio is determined using the relative branching fractions of the decays $B^+ \rightarrow K^+ \ell^+ \ell^-$ and $B^+ \rightarrow J/\psi(\rightarrow \ell^+ \ell^-) K^+$, with $\ell = e, \mu$. Measured for the region $1.1 < q^2 < 6.0 \text{ GeV}^2/c^4$.

³ The ratio is determined using the relative branching fractions of the decays $B^+ \rightarrow K^+ \ell^+ \ell^-$ and $B^+ \rightarrow J/\psi(\rightarrow \ell^+ \ell^-) K^+$, with $\ell = e, \mu$.

 $B(B^+ \rightarrow K^+ \ell^+ \ell^-) (0.0 < q^2 < 4.3 \text{ GeV}^2/c^4)$

VALUE (units 10^{-7})	DOCUMENT ID	TECN	COMMENT
1.13 ± 0.19 ± 0.08	AALTONEN	11AI CDF	$p\bar{p}$ at 1.96 TeV

 $B(B^+ \rightarrow K^+ \pi^+ \pi^- \mu^+ \mu^-) (1.00 < q^2 < 6.00 \text{ GeV}^2/c^4)$

VALUE (units 10^{-7})	DOCUMENT ID	TECN	COMMENT
1.38^{+0.15}_{-0.14} ± 0.08	AAIJ	14AZ LHCb	pp at 7, 8 TeV

 $B(B^+ \rightarrow K^+ \pi^+ \pi^- \mu^+ \mu^-) (0.10 < q^2 < 2.00 \text{ GeV}^2/c^4)$

VALUE (units 10^{-7})	DOCUMENT ID	TECN	COMMENT
1.33^{+0.13}_{-0.12} ± 0.09	AAIJ	14AZ LHCb	pp at 7, 8 TeV

 $B(B^+ \rightarrow K^+ \pi^+ \pi^- \mu^+ \mu^-) (2.00 < q^2 < 4.30 \text{ GeV}^2/c^4)$

VALUE (units 10^{-8})	DOCUMENT ID	TECN	COMMENT
5.38^{+0.94}_{-0.87} ± 0.35	AAIJ	14AZ LHCb	pp at 7, 8 TeV

 $B(B^+ \rightarrow K^+ \pi^+ \pi^- \mu^+ \mu^-) (4.30 < q^2 < 8.68 \text{ GeV}^2/c^4)$

VALUE (units 10^{-7})	DOCUMENT ID	TECN	COMMENT
1.01^{+0.12}_{-0.13} ± 0.09	AAIJ	14AZ LHCb	pp at 7, 8 TeV

 $B(B^+ \rightarrow K^+ \pi^+ \pi^- \mu^+ \mu^-) (10.09 < q^2 < 12.86 \text{ GeV}^2/c^4)$

VALUE (units 10^{-8})	DOCUMENT ID	TECN	COMMENT
5.07^{+0.94}_{-0.89} ± 0.47	AAIJ	14AZ LHCb	pp at 7, 8 TeV

 $B(B^+ \rightarrow K^+ \pi^+ \pi^- \mu^+ \mu^-) (14.18 < q^2 < 19.00 \text{ GeV}^2/c^4)$

VALUE (units 10^{-8})	DOCUMENT ID	TECN	COMMENT
0.48^{+0.39}_{-0.29} ± 0.05	AAIJ	14AZ LHCb	pp at 7, 8 TeV

 $B(B^+ \rightarrow \pi^+ \mu^+ \mu^-) / B(B^+ \rightarrow K^+ \mu^+ \mu^-) (1.00 < q^2 < 6.00 \text{ GeV}^2/c^4)$

VALUE (units 10^{-2})	DOCUMENT ID	TECN	COMMENT
3.8 ± 0.9 ± 0.1	AAIJ	15AR LHCb	pp at 7, 8 TeV

 $B(B^+ \rightarrow \pi^+ \mu^+ \mu^-) (1.00 < q^2 < 6.00 \text{ GeV}^2/c^4)$

VALUE (units 10^{-3})	DOCUMENT ID	TECN	COMMENT
4.55^{+1.05}_{-1.00} ± 0.15	AAIJ	15AR LHCb	pp at 7, 8 TeV

 $B(B^+ \rightarrow \pi^+ \mu^+ \mu^-) (15.00 < q^2 < 22.00 \text{ GeV}^2/c^4)$

VALUE (units 10^{-3})	DOCUMENT ID	TECN	COMMENT
3.29^{+0.84}_{-0.70} ± 0.07	AAIJ	15AR LHCb	pp at 7, 8 TeV

 $B(B^+ \rightarrow \pi^+ \mu^+ \mu^-) / B(B^+ \rightarrow K^+ \mu^+ \mu^-) (15.0 < q^2 < 22.0 \text{ GeV}^2/c^4)$

VALUE (units 10^{-2})	DOCUMENT ID	TECN	COMMENT
3.7 ± 0.8 ± 0.1	AAIJ	15AR LHCb	pp at 7, 8 TeV

 $A_{FB}(B^+ \rightarrow K^+ \mu^+ \mu^-) (1.1 < q^2 < 6.0 \text{ GeV}^2/c^4)$

A_{FB} is the forward-backward angular asymmetry of the lepton pair in $B \rightarrow K^{(*)} \ell^+ \ell^-$ decay as defined in B^+, B^0 admixture particle listings.

VALUE	DOCUMENT ID	TECN	COMMENT
-0.003 ± 0.017 OUR AVERAGE			
-0.14 ^{+0.07} _{-0.06} ± 0.03	1 SIRUNYAN	18DX CMS	pp at 8 TeV
0.005 ± 0.015 ± 0.010	2 AAIJ	14o LHCb	pp at 7, 8 TeV
0.02 ^{+0.05} _{-0.03} ± 0.02	AAIJ	13H LHCb	Repl. by AAIJ 14o

¹ Measurement is performed in $1.0 < q^2 < 6.0 \text{ GeV}^2/c^4$. SIRUNYAN 18DX reports also measurements in several other q^2 intervals.

² AAIJ 14o reports 68% C.L. interval, which we encode as midpoint with uncertainty as half of the width of interval.

 $A_{FB}(B^+ \rightarrow K^+ \mu^+ \mu^-) (15.0 < q^2 < 22.0 \text{ GeV}^2/c^4)$

VALUE	DOCUMENT ID	TECN	COMMENT
-0.015 ± 0.015 ± 0.01	1 AAIJ	14o LHCb	pp at 7, 8 TeV

¹ AAIJ 14o reports 68% C.L. interval, which we encode as midpoint with uncertainty as half of the width of interval.

 $F_H(B^+ \rightarrow K^+ \mu^+ \mu^-) (1.1 < q^2 < 6.0 \text{ GeV}^2/c^4)$

F_H is a fractional contribution of (pseudo) scalar and tensor amplitudes to the decay width in the massless muon approximation.

VALUE	DOCUMENT ID	TECN	COMMENT
0.04 ± 0.04 OUR AVERAGE			
0.38 ^{+0.17} _{-0.21} ± 0.09	1 SIRUNYAN	18DX CMS	pp at 8 TeV
0.03 ± 0.03 ± 0.02	2 AAIJ	14o LHCb	pp at 7, 8 TeV
0.05 ^{+0.08+0.04} _{-0.05-0.02}	AAIJ	13H LHCb	Repl. by AAIJ 14o

¹ Measurement is performed in $1.0 < q^2 < 6.0 \text{ GeV}^2/c^4$. SIRUNYAN 18DX reports also measurements in several other q^2 intervals.

² AAIJ 14o reports 68% C.L. interval, which we encode as midpoint with uncertainty as half of the width of interval.

 $F_H(B^+ \rightarrow K^+ \mu^+ \mu^-) (15.0 < q^2 < 22.0 \text{ GeV}^2/c^4)$

F_H is a fractional contribution of (pseudo) scalar and tensor amplitudes to the decay width in the massless muon approximation.

VALUE	DOCUMENT ID	TECN	COMMENT
0.035 ± 0.035 ± 0.02	1 AAIJ	14o LHCb	pp at 7, 8 TeV

¹ AAIJ 14o reports 68% C.L. interval, which we encode as midpoint with uncertainty as half of the width of interval.

FORWARD-BACKWARD ASYMMETRIES

The forward-backward asymmetry is defined as $A_{FB} = [N(q_{FB} > 0) - N(q_{FB} < 0)] / [N(q_{FB} > 0) + N(q_{FB} < 0)]$, where $q_{FB} = -q_B \cdot \text{sgn}(\eta_B)$ with q_B as the B hadron electric charge, η_B as its pseudorapidity, and $\text{sgn}(\eta_B)$ as a sign function of η_B .

 $A_{FB}(B^\pm \rightarrow J/\psi K^\pm)$

VALUE (units 10^{-2})	DOCUMENT ID	TECN	COMMENT
-0.24 ± 0.41 ± 0.19	ABAZOV	15 D0	$p\bar{p}$ at 1.96 TeV

 $A_{FB}(B^\pm \rightarrow K^*(892)^+ \mu^+ \mu^-) (1.0 < q^2 < 8.68 \text{ GeV}^2/c^4)$

VALUE	DOCUMENT ID	TECN	COMMENT
-0.14^{+0.32}_{-0.35} ± 0.17	1,2 SIRUNYAN	21Ac CMS	pp at 8 TeV

¹ SIRUNYAN 21Ac measurement is performed in $1.0 < q^2 < 8.68 \text{ GeV}^2/c^4$. Reports also measurements in several other q^2 intervals.

² A_{FB} is defined with respect to $\mu^+ \mu^-$ direction and not the B direction.

 $A_{FB}(B^\pm \rightarrow K^*(892)^+ \mu^+ \mu^-) (1.1 < q^2 < 6.0 \text{ GeV}^2/c^4)$

VALUE	DOCUMENT ID	TECN	COMMENT
-0.08^{+0.07}_{-0.06} ± 0.02	1 AAIJ	21J LHCb	pp at 7, 8, 13 TeV

¹ The full set of CP-averaged angular observables is measured as a function of the q^2 . The A_{FB} is measured related to the dimuon system.

 $A_{FB}(B^\pm \rightarrow K^*(892)^+ \mu^+ \mu^-) (10.09 < q^2 < 12.86 \text{ GeV}^2/c^4)$

VALUE	DOCUMENT ID	TECN	COMMENT
0.09^{+0.16}_{-0.11} ± 0.04	1,2 SIRUNYAN	21Ac CMS	pp at 8 TeV

¹ SIRUNYAN 21Ac measurement is performed in $10.09 < q^2 < 12.86 \text{ GeV}^2/c^4$. Reports also measurements in several other q^2 intervals.

² A_{FB} is defined with respect to $\mu^+ \mu^-$ direction and not the B direction.

 $A_{FB}(B^\pm \rightarrow K^*(892)^+ \mu^+ \mu^-) (14.18 < q^2 < 19.0 \text{ GeV}^2/c^4)$

VALUE	DOCUMENT ID	TECN	COMMENT
0.33^{+0.11}_{-0.07} ± 0.05	1,2 SIRUNYAN	21Ac CMS	pp at 8 TeV

¹ SIRUNYAN 21Ac measurement is performed in $14.18 < q^2 < 19.0 \text{ GeV}^2/c^4$. Reports also measurements in several other q^2 intervals.

² A_{FB} is defined with respect to $\mu^+ \mu^-$ direction and not the B direction.

 $A_{FB}(B^\pm \rightarrow K^*(892)^+ \mu^+ \mu^-) (15.0 < q^2 < 19.0 \text{ GeV}^2/c^4)$

VALUE	DOCUMENT ID	TECN	COMMENT
0.31 ± 0.06 ± 0.04	1 AAIJ	21J LHCb	pp at 7, 8, 13 TeV

¹ The full set of CP-averaged angular observables is measured as a function of the q^2 . The A_{FB} is measured related to the dimuon system.

 $A_P(B^+) = [\sigma(B^-) - \sigma(B^+)] / [\sigma(B^-) + \sigma(B^+)]$

VALUE (units 10^{-3})	DOCUMENT ID	TECN	COMMENT
-5.2 ± 1.9 OUR AVERAGE			
-4.1 ± 4.9 ± 1.0	1 AAIJ	17AP LHCb	pp at 7 TeV
-5.3 ± 3.1 ± 1.0	1 AAIJ	17AP LHCb	pp at 8 TeV

Production asymmetries

See key on page 1127

Meson Particle Listings B±

-2.3±2.4±3.7 2 AAIJ 17Bf LHCB pp at 7 TeV
-7.4±1.5±3.2 2 AAIJ 17Bf LHCB pp at 8 TeV
1 AAIJ 17AP uses B+ -> D0 pi+ decays with B+ transverse momenta pT and rapidities y in the region of 2 < pT < 30 GeV/c and 2.1 < y < 4.5.
2 AAIJ 17Bf uses B+ -> J/psi K+ decays with B+ transverse momenta pT and rapidities y in the region of 0 < pT < 30 GeV/c and 2.1 < y < 4.5.

B± REFERENCES

AAIJ 21AM JHEP 2112 141
AAIJ 21H PRL 126 091802
AAIJ 21J PRL 126 161802
AAIJ 21L JHEP 2102 167
AAIJ 21M JHEP 2103 137
AAIJ 21Q JHEP 2104 081
ABUDINEN 21 PRL 127 181802
BELENO 21 PR D103 112001
CAO 21A PR D104 012008
CHOUDHURY 21 S JHEP 2103 105
MOHANTY 21 PR D103 052013
SIRUNYAN 21AC JHEP 2104 124
WEHLE 21 PRL 126 161801
AAIJ 20A PRL 124 031801
Also
AAIJ 20AI PR D101 012006
AAIJ 20AJ PR D102 112003
AAIJ 20AK JHEP 2012 139
AAIJ 20D PR D101 032005
AAIJ 20K JHEP 2003 146
AAIJ 20N JHEP 2006 058
AAIJ 20P JHEP 2006 129
AAIJ 20S JHEP 2008 123
CHILIKIN 20 JHEP 2005 034
CHU 20 PR D101 052012
LEES 20C PRL 124 152001
PRIM 20 PR D101 032007
AAIJ 19AC PR D99 092009
AAIJ 19AL PRL 123 231802
AAIJ 19AM PRL 123 241802
AAIJ 19O EPJ C79 537
AAIJ 19P EPJ C79 675
AAIJ 19S PRL 122 191801
BHARDWAJ 19 PR D99 111101
CHILIKIN 19 PR D100 012001
GARG 19 PR D99 071102
KALIYAR 19 PR D99 031102
LEES 19C PR D100 111101
LI 19A PRL 122 082001
LU 19G PR D100 112010
LU 19 PR D99 032003
PDG 19 RPP 2019 at pdg.lbl.gov
RESMI 19 JHEP 1910 178
SIRUNYAN 19CM JHEP 1912 100
WATANUKI 19 PR D99 032012
AAIJ 18A PL B777 16
AAIJ 18AD JHEP 1808 176
Also
AAIJ 18B JHEP 1801 131
AAIJ 18U JHEP 1803 059
AAIJ 18W JHEP 1805 160
AAIJ 18X JHEP 1805 067
AAIJ 18Z JHEP 1806 084
GELB 18 PR D98 112016
KATO 18 PR D97 012005
LI 18A EPJ C78 252
PDG 18 PR D98 030001
RESMI 18 JHEP 1801 082
SIBIDANOV 18 PRL 121 031801
SIRUNYAN 18DX PR D98 112011
VOSSEN 18 PR D98 012005
AAIJ 17A PR D95 012002
AAIJ 17AD PL B769 305
AAIJ 17AP PR D95 052005
AAIJ 17AQ PR D95 071101
AAIJ 17AR PR D96 011101
AAIJ 17BF PL B774 139
AAIJ 17BO JHEP 1711 156
AAIJ 17E PL B765 307
AAIJ 17K EPJ C77 72
AAIJ 17O JHEP 1703 036
AAIJ 17R JHEP 1704 162
AAIJ 17Y EPJ C77 161
ABAZOV 17A PR D95 031101
V.M. Abazov et al.
BELENO 17 PR D96 091102
C. Beleno et al.
GRYGIER 17 PR D96 091101
J. Grygier et al.
HORIGUCHI 17 PRL 119 191802
T. Horiguchi et al.
HSU 17 PR D96 031101
C.-L. Hsu et al.
KHACHATRYAN 17C PL B764 66
V. Khachatryan et al.
LEES 17 PRL 118 031802
J.P. Lees et al.
LEES 17G PR D96 072001
J.P. Lees et al.
AABOUD 16L EPJ C76 513
M. Aaboud et al.
AAIJ 16AA JHEP 1608 137
R. Aaij et al.
AAIJ 16B PR D94 072001
R. Aaij et al.
AAIJ 16A JHEP 1612 087
R. Aaij et al.
AAIJ 16L PL B760 117
R. Aaij et al.
AAIJ 16M PR D93 051101
R. Aaij et al.
AAIJ 16R PR D93 119902
R. Aaij et al.
AAIJ 16Z JHEP 1606 131
R. Aaij et al.
BHARDWAJ 16 PR D93 052016
V. Bhardwaj et al.
DEL-AMO-SA... 16 PR D93 052013
P. del Amo Sanchez et al.
LEES 16 PRL 116 041801
J.P. Lees et al.
PDG 16 CP C40 100001
C. Patrignani et al.
AAIJ 15AR JHEP 1510 034
R. Aaij et al.
AAIJ 15B PR D92 112005
R. Aaij et al.
AAIJ 15K PL B741 1
R. Aaij et al.
AAIJ 15O PRL 115 051801
R. Aaij et al.
AAIJ 15V PR D91 092002
R. Aaij et al.
Also
AAIJ 15W PR D93 119901 (err.)
R. Aaij et al.
AAIJ 15 PR D91 112014
R. Aaij et al.
ABAZOV 15 PRL 114 051803
V.M. Abazov et al.
BALA 15 PR D91 051101
A. Bala et al.
CHOI 15A PR D91 092011
S.-K. Choi et al.
GOH 15 PR D91 071101
Y.-M. Goh et al.
HELLER 15 PR D91 112009
A. Heller et al.
KRONENBIT... 15 PR D92 051102
B. Kronenbiter et al.
LEES 15 PR D91 012003
J.P. Lees et al.
LEES 15C PR D91 052002
J.P. Lees et al.

VINOKUROVA 15 JHEP 1506 132
Also
WIECHCZYNS... 15 PR D91 032008 (err.)
YOOK 15 PR D91 052016
AAIJ 14 PL 112 011801
AAIJ 14A PL B728 85
AAIJ 14AC PRL 112 131802
AAIJ 14AF PRL 113 141801
AAIJ 14AN JHEP 1409 177
AAIJ 14AR PRL 113 151601
AAIJ 14AZ JHEP 1410 064
AAIJ 14BA JHEP 1410 097
AAIJ 14BE NP B888 169
AAIJ 14BF JHEP 1411 060
AAIJ 14B PR D90 112004
AAIJ 14E JHEP 1404 114
AAIJ 14M JHEP 1406 133
AAIJ 14O JHEP 1405 082
AAIJ 14P PL B733 36
ABAZOV 14A PR D89 012004
V.M. Abazov et al.
CHOBANOVA 14 PR D90 012002
V. Chobanova et al.
IWASHITA 14 PTEP 2014 043C01
T. Iwashita et al.
LEES 14A PR D89 011102
J.P. Lees et al.
TIEN 14 PR D89 011101
K.-J. Tien et al.
AAIJ 13AE PL B723 44
R. Aaij et al.
AAIJ 13AK PL B726 151
R. Aaij et al.
AAIJ 13AP PR D87 092007
R. Aaij et al.
AAIJ 13AR PR D87 112010
R. Aaij et al.
AAIJ 13AU PR D88 052015
R. Aaij et al.
AAIJ 13AZ PRL 111 103801
R. Aaij et al.
AAIJ 13B PRL 111 112003
R. Aaij et al.
AAIJ 13BN PRL 111 151801
R. Aaij et al.
AAIJ 13BS PL B726 646
R. Aaij et al.
AAIJ 13H JHEP 1302 105
R. Aaij et al.
AAIJ 13R JHEP 1302 043
R. Aaij et al.
AAIJ 13S EPJ C73 2462
R. Aaij et al.
AAIJ 13Z JHEP 1309 006
R. Aaij et al.
ABAZOV 13M PRL 110 241801
V.M. Abazov et al.
DUH 13 PR D87 031103
Y. T. Duh et al.
HARA 13 PRL 110 131801
K. Hara et al.
LEES 13A PR D87 032004
J.P. Lees et al.
LEES 13B PR D87 052015
J.P. Lees et al.
LEES 13I PR D87 112005
J.P. Lees et al.
LEES 13K PR D88 031102
J.P. Lees et al.
LEES 13M PR D88 032012
J.P. Lees et al.
LEES 13T PR D88 072006
J.P. Lees et al.
LUTZ 13 PR D87 111103
O. Lutz et al.
NAYAK 13 PR D88 091104
M. Nayak et al.
SIBIDANOV 13 PR D88 032005
A. Sibidanov et al.
AAIJ 12AA PR D85 091103
R. Aaij et al.
AAIJ 12AC PR D85 091105
R. Aaij et al.
AAIJ 12AD PR D85 112004
R. Aaij et al.
AAIJ 12AF JHEP 1207 133
R. Aaij et al.
AAIJ 12AG PL B718 43
R. Aaij et al.
AAIJ 12AY JHEP 1212 125
R. Aaij et al.
AAIJ 12C PRL 108 101601
R. Aaij et al.
AAIJ 12E PL B708 241
R. Aaij et al.
AAIJ 12L EPJ C72 2118
R. Aaij et al.
AAIJ 12M PL B712 203
R. Aaij et al.
Also
PL B713 351 (err.)
R. Aaij et al.
AAIJ 12T PRL 108 161801
R. Aaij et al.
AIHARA 12 PR D85 112014
H. Aihara et al.
DEL-AMO-SA... 12 PR D85 092017
P. del Amo Sanchez et al.
HORI 12 PR 108 031801
J. Horii et al.
KIM 12A PR D86 031101
J. Kim et al.
LEES 12AA PR D86 092004
J.P. Lees et al.
LEES 12B PR D85 052003
J.P. Lees et al.
LEES 12D PRL 109 101802
J.P. Lees et al.
Also
PR D88 072012
J.P. Lees et al.
LEES 12J PR D85 071103
J.P. Lees et al.
LEES 12K PR D85 112010
J.P. Lees et al.
LEES 12P PR D86 012004
J.P. Lees et al.
LEES 12S PR D86 032012
J.P. Lees et al.
LEES 12T PR D86 091102
J.P. Lees et al.
STYPUALA 12 PR D86 010001
J. Styputala et al.
AAIJ 11E PR D84 092001
R. Aaij et al.
Also
PR D85 039904 (err.)
R. Aaij et al.
AALTONEN 11 PRL 106 121804
T. Aaltonen et al.
AALTONEN 11A PRL 107 201802
T. Aaltonen et al.
AALTONEN 11B PR D84 091504
T. Aaltonen et al.
AALTONEN 11A PR D83 032008
T. Aaltonen et al.
AALTONEN 11L PRL 106 161801
T. Aaltonen et al.
AUSHEV 11 PR D83 051102
T. Aushev et al.
BHARDWAJ 11 PRL 107 091803
V. Bhardwaj et al.
CHEN 11F PR D84 071501
P. Chen et al.
CHOI 11 PR D84 052004
S.-K. Choi et al.
DEL-AMO-SA... 11B PR D83 032004
P. del Amo Sanchez et al.
DEL-AMO-SA... 11C PR D83 032007
P. del Amo Sanchez et al.
DEL-AMO-SA... 11D PR D83 051101
P. del Amo Sanchez et al.
DEL-AMO-SA... 11E PR D83 052011
P. del Amo Sanchez et al.
DEL-AMO-SA... 11K PR D83 091101
P. del Amo Sanchez et al.
DEL-AMO-SA... 11L PRL 107 041804
P. del Amo Sanchez et al.
GULER 11 PR D83 032005
H. Guler et al.
HORII 11 PRL 106 231803
Y. Horii et al.
LEES 11A PR D84 012001
J.P. Lees et al.
LEES 11B PR D84 012002
J.P. Lees et al.
LEES 11I PR D84 092007
J.P. Lees et al.
SAHOO 11A PR D84 071101
H. Sahoo et al.
SEON 11 PR D84 071106
O. Seon et al.
VINOKUROVA 11 PL B706 139
A. Vinokurova et al.
AALTONEN 10A PR D81 031105
T. Aaltonen et al.
AUBERT 10 PRL 104 011802
B. Aubert et al.
AUBERT 10D PR D81 052009
B. Aubert et al.
AUBERT 10E PR D81 051101
B. Aubert et al.
BOZEK 10 PR D82 072005
A. Bozek et al.
DEL-AMO-SA... 10A PR D82 011502
P. del Amo Sanchez et al.
DEL-AMO-SA... 10B PR D82 011101
P. del Amo Sanchez et al.
DEL-AMO-SA... 10F PRL 105 121801
P. del Amo Sanchez et al.
DEL-AMO-SA... 10G PR D82 072004
P. del Amo Sanchez et al.
DEL-AMO-SA... 10H PR D82 072006
P. del Amo Sanchez et al.
DEL-AMO-SA... 10I PR D82 091101
P. del Amo Sanchez et al.
DEL-AMO-SA... 10K PR D82 092006
P. del Amo Sanchez et al.
DEL-AMO-SA... 10Q PR D82 112002
P. del Amo Sanchez et al.
HARA 10 PR D82 071101
K. Hara et al.
LIBBY 10 PR D82 112006
J. Libby et al.
POLUEKTOV 10 PR D81 112002
A. Poluektov et al.
SAKAI 10 PR D82 091104
K. Sakai et al.
WEDD 10 PR D81 111104
R. Wedd et al.
AALTONEN 09B PR D79 011104
T. Aaltonen et al.
ABAZOV 09Y PR D79 111102
V.M. Abazov et al.
ABULENCIA 09 PR D79 112003
A. Abulencia et al.

Downloaded from https://academic.oup.com/ptep/article/2022/8/083C01/6651666 by CERN Library user on 11 October 2022

See key on page 1127

Meson Particle Listings

B^\pm, B^0

AUBERT	03K	PRL 90 231801	B. Aubert et al.	(BABAR Collab.)
AUBERT	03L	PRL 91 021801	B. Aubert et al.	(BABAR Collab.)
AUBERT	03M	PRL 91 051801	B. Aubert et al.	(BABAR Collab.)
AUBERT	03O	PRL 91 071801	B. Aubert et al.	(BABAR Collab.)
AUBERT	03U	PRL 91 221802	B. Aubert et al.	(BABAR Collab.)
AUBERT	03V	PRL 91 171802	B. Aubert et al.	(BABAR Collab.)
AUBERT	03W	PRL 91 161801	B. Aubert et al.	(BABAR Collab.)
AUBERT	03X	PR D68 092001	B. Aubert et al.	(BABAR Collab.)
BORNHEIM	03	PR D68 052002	A. Bornheim et al.	(CLEO Collab.)
CHEN	05B	PRL 91 201801	K.-F. Chen et al.	(BELLE Collab.)
CHOI	03	PRL 91 262001	S.-K. Choi et al.	(BELLE Collab.)
CSORNA	03	PR D67 112002	S.E. Csorna et al.	(CLEO Collab.)
EDWARDS	03	PR D68 011102	K.W. Edwards et al.	(CLEO Collab.)
FANG	03	PRL 90 071801	F. Fang et al.	(BELLE Collab.)
HUANG	03	PRL 91 241802	H.-C. Huang et al.	(BELLE Collab.)
ISHIKAWA	03	PRL 91 216101	A. Ishikawa et al.	(BELLE Collab.)
KROKOVNY	03B	PRL 91 262002	P. Krokovny et al.	(BELLE Collab.)
SWAIN	03	PR D68 051101	S.K. Swain et al.	(BELLE Collab.)
UNNO	03	PR D68 011103	Y. Unno et al.	(BELLE Collab.)
ZHANG	03B	PRL 91 221801	J. Zhang et al.	(BELLE Collab.)
ABE	02	PRL 88 021801	K. ABE et al.	(BELLE Collab.)
ABE	02B	PRL 88 031802	K. ABE et al.	(BELLE Collab.)
ABE	02H	PRL 88 171801	K. ABE et al.	(BELLE Collab.)
ABE	02K	PRL 88 181803	K. ABE et al.	(BELLE Collab.)
ABE	02N	PL B538 11	K. ABE et al.	(BELLE Collab.)
ABE	02O	PR D65 091103	K. ABE et al.	(BELLE Collab.)
ABE	02W	PRL 89 151802	K. ABE et al.	(BELLE Collab.)
ACOSTA	02C	PR D65 092009	D. Acosta et al.	(CDF Collab.)
ACOSTA	02F	PR D66 052005	D. Acosta et al.	(CDF Collab.)
AHMED	02B	PR D66 031101	S. Ahmed et al.	(CLEO Collab.)
AUBERT	02	PR D65 032001	B. Aubert et al.	(BABAR Collab.)
AUBERT	02C	PRL 88 101805	B. Aubert et al.	(BABAR Collab.)
AUBERT	02E	PR D65 051101	B. Aubert et al.	(BABAR Collab.)
AUBERT	02F	PR D65 091101	B. Aubert et al.	(BABAR Collab.)
AUBERT	02L	PRL 88 241801	B. Aubert et al.	(BABAR Collab.)
BRIERE	02	PRL 89 081803	R. Briere et al.	(CLEO Collab.)
CASEY	02	PR D66 092002	B.C.K. Casey et al.	(BELLE Collab.)
CHEN	02B	PL B546 196	K.-F. Chen et al.	(BELLE Collab.)
DRUTSKOY	02	PL B542 171	A. Drutskoy et al.	(BELLE Collab.)
DYTMAN	02	PR D66 091101	S.A. Dytman et al.	(CLEO Collab.)
ECKHART	02	PRL 89 251801	Y. Eckhart et al.	(CLEO Collab.)
EDWARDS	02B	PR D65 111102	K.W. Edwards et al.	(CLEO Collab.)
GABYSHEV	02	PR D66 091102	N. Gabyshev et al.	(BELLE Collab.)
GARMASH	02	PR D65 092005	A. Garmash et al.	(BELLE Collab.)
GODANG	02	PRL 88 021802	R. Godang et al.	(CLEO Collab.)
GORDON	02	PL B542 183	A. Gordon et al.	(BELLE Collab.)
LU	02	PRL 89 191801	R.-S. Lu et al.	(BELLE Collab.)
MAHAPATRA	02	PRL 88 101803	R. Mahapatra et al.	(CLEO Collab.)
NISHIDA	02	PRL 89 231801	S. Nishida et al.	(BELLE Collab.)
ABE	01H	PRL 87 101801	K. ABE et al.	(BELLE Collab.)
ABE	01I	PRL 87 111801	K. ABE et al.	(BELLE Collab.)
ABE	01K	PR D64 071101	K. ABE et al.	(BELLE Collab.)
ABE	01L	PRL 87 161401	K. ABE et al.	(BELLE Collab.)
ABE	01M	PL B517 309	K. ABE et al.	(BELLE Collab.)
ALEXANDER	01B	PR D64 092001	J.P. Alexander et al.	(CLEO Collab.)
AMMAR	01B	PRL 87 271801	R. Ammar et al.	(CLEO Collab.)
ANDERSON	01B	PRL 87 181803	S. Anderson et al.	(CLEO Collab.)
AUBERT	01D	PRL 87 151801	B. Aubert et al.	(BABAR Collab.)
AUBERT	01E	PRL 87 151802	B. Aubert et al.	(BABAR Collab.)
AUBERT	01F	PRL 87 201803	B. Aubert et al.	(BABAR Collab.)
AUBERT	01G	PRL 87 221802	B. Aubert et al.	(BABAR Collab.)
BARATE	01E	EPJ C19 213	R. Barate et al.	(ALEPH Collab.)
BRIERE	01	PRL 86 3718	R.A. Briere et al.	(CLEO Collab.)
BROWDER	01	PRL 86 2450	T.E. Browder et al.	(CLEO Collab.)
EDWARDS	01	PRL 86 30	K.W. Edwards et al.	(CLEO Collab.)
GRITSAN	01	PR D64 077501	A. Gritsan et al.	(CLEO Collab.)
RICHICHI	01	PR D63 031103	S.J. Richichi et al.	(CLEO Collab.)
ABBBIENDI	00B	PL B476 233	G. Abbiendi et al.	(OPAL Collab.)
ABE	00C	PR D62 071101	K. ABE et al.	(SLD Collab.)
AHMED	00B	PR D62 112003	S. Ahmed et al.	(CLEO Collab.)
ANASTASSOV	00	PRL 84 1393	A. Anastassov et al.	(CLEO Collab.)
BARATE	00R	PL B492 275	R. Barate et al.	(ALEPH Collab.)
BEHRENS	00	PR D61 052001	B.H. Behrens et al.	(CLEO Collab.)
BONVICINI	00	PRL 84 5940	G. Bonvicini et al.	(CLEO Collab.)
CHEN	00	PRL 85 325	K. Chen et al.	(CLEO Collab.)
COAN	00	PRL 84 5283	T.E. Coan et al.	(CLEO Collab.)
CRONIN-HEN	00	PRL 85 515	D. Cronin-Hennessy et al.	(CLEO Collab.)
CSORNA	00	PR D61 111101	S.E. Csorna et al.	(CLEO Collab.)
JESSOP	00	PRL 85 2881	C.P. Jessop et al.	(CLEO Collab.)
RICHICHI	00	PRL 85 520	S.J. Richichi et al.	(CLEO Collab.)
ABBBIENDI	99J	EPJ C12 609	G. Abbiendi et al.	(OPAL Collab.)
AFFOLDER	99B	PRL 83 3378	T. Affolder et al.	(CDF Collab.)
BARTELT	99	PRL 82 3746	J. Bartelt et al.	(CLEO Collab.)
COAN	99	PR D59 111101	T.E. Coan et al.	(CLEO Collab.)
ABE	98B	PR D57 5382	F. ABE et al.	(CDF Collab.)
ABE	98O	PR D58 072001	F. ABE et al.	(CDF Collab.)
ABE	98Q	PR D58 092002	F. ABE et al.	(CDF Collab.)
ACCIARRI	98S	PL B438 417	M. Acciari et al.	(L3 Collab.)
ANASTASSOV	98	PRL 80 4127	A. Anastassov et al.	(CLEO Collab.)
ATHANAS	98	PRL 80 5493	M. Athanas et al.	(CLEO Collab.)
BARATE	98Q	EPJ C4 387	R. Barate et al.	(ALEPH Collab.)
BEHRENS	98	PRL 80 3710	B.H. Behrens et al.	(CLEO Collab.)
BERGFELD	98	PRL 81 272	T. Bergfeld et al.	(CLEO Collab.)
BRANDENBURG	98	PRL 80 2762	G. Brandenburg et al.	(CLEO Collab.)
CAPRINI	98	NP B530 153	I. Caprini, L. Lelouch, M. Neubert	(BCIP, CERN)
GODANG	98	PRL 80 3456	R. Godang et al.	(CLEO Collab.)
ABE	97J	PRL 77 590	K. ABE et al.	(SLD Collab.)
ACCIARRI	97F	PL B396 327	M. Acciari et al.	(L3 Collab.)
ARTUSO	97	PL B399 321	M. Artuso et al.	(CLEO Collab.)
ATHANAS	97	PRL 79 2208	M. Athanas et al.	(CLEO Collab.)
BROWDER	97	PR D56 11	T. Browder et al.	(CLEO Collab.)
FU	97	PRL 79 3125	X. Fu et al.	(CLEO Collab.)
JESSOP	97	PRL 79 4533	C.P. Jessop et al.	(CLEO Collab.)
ABE	96B	PR D53 3496	F. ABE et al.	(CDF Collab.)
ABE	96C	PRL 76 4462	F. ABE et al.	(CDF Collab.)
ABE	96H	PRL 76 2015	F. ABE et al.	(CDF Collab.)
ABE	96L	PRL 76 4675	F. ABE et al.	(CDF Collab.)
ABE	96Q	PR D54 6596	F. ABE et al.	(CDF Collab.)
ABE	96R	PRL 77 5176	F. ABE et al.	(CDF Collab.)
ADAM	96D	ZPHY C72 207	W. Adam et al.	(DELPHI Collab.)
ALEXANDER	96T	PRL 77 5000	J.P. Alexander et al.	(CLEO Collab.)
ASNER	96	PR D53 1039	D.M. Asner et al.	(CLEO Collab.)
BARISH	96B	PRL 76 1570	B.C. Barish et al.	(CLEO Collab.)
BERGFELD	96B	PRL 77 4503	T. Bergfeld et al.	(CLEO Collab.)
BISHAI	96	PL B369 186	M. Bishai et al.	(CLEO Collab.)
BUSKULIC	96J	ZPHY C71 31	D. Buskulic et al.	(ALEPH Collab.)
GIBAUT	96	PR D53 4734	D. Gibaut et al.	(CLEO Collab.)
PDG	96	PR D54 11	R. M. Barnett et al.	(PDG Collab.)
ABREU	95N	PL B357 255	P. Abreu et al.	(DELPHI Collab.)
ABREU	95Q	ZPHY C68 13	P. Abreu et al.	(DELPHI Collab.)
ADAM	95	ZPHY C68 363	W. Adam et al.	(DELPHI Collab.)

AKERS	95T	ZPHY C67 379	R. Akers et al.	(OPAL Collab.)
ALBRECHT	95D	PL B353 554	H. Albrecht et al.	(ARGUS Collab.)
ALEXANDER	95P	PL B341 435	J. Alexander et al.	(CLEO Collab.)
	Also	PL B347 469 (erratum)	J. Alexander et al.	(CLEO Collab.)
ARTUSO	95	PRL 75 785	M. Artuso et al.	(CLEO Collab.)
BARISH	95	PR D51 1014	B.C. Barish et al.	(CLEO Collab.)
BUSKULIC	95	PL B343 444	D. Buskulic et al.	(ALEPH Collab.)
ABE	94D	PRL 72 3456	F. ABE et al.	(CDF Collab.)
ALAM	94	PR D50 43	M.S. Alam et al.	(CLEO Collab.)
ALBRECHT	94D	PL B335 526	H. Albrecht et al.	(ARGUS Collab.)
ATHANAS	94	PRL 73 3503	M. Athanas et al.	(CLEO Collab.)
	Also	PRL 74 3090 (erratum)	M. Athanas et al.	(CLEO Collab.)
PDG	94	PR D50 1173	L. Montanet et al.	(CERN, LBL, BOST+)
STONE	94	HEPSY 93-11	S. Stone	
	Published in	B Decays, 2nd Edition, World Scientific, Singapore		
ABREU	93D	ZPHY C57 181	P. Abreu et al.	(DELPHI Collab.)
ABREU	93G	PL B312 253	P. Abreu et al.	(DELPHI Collab.)
ACTON	93C	PL B307 247	P.D. Acton et al.	(OPAL Collab.)
ALBRECHT	93E	ZPHY C00 11	H. Albrecht et al.	(ARGUS Collab.)
ALEXANDER	93B	PL B319 365	J. Alexander et al.	(CLEO Collab.)
AMMAR	93	PRL 71 674	R. Ammar et al.	(CLEO Collab.)
BEAN	93B	PRL 70 2681	A. Bean et al.	(CLEO Collab.)
BUSKULIC	93D	PL B307 194	D. Buskulic et al.	(ALEPH Collab.)
	Also	PL B325 537 (erratum)	D. Buskulic et al.	(ALEPH Collab.)
SANGHERA	93	PR D47 791	S. Sanghera et al.	(CLEO Collab.)
ALBRECHT	92C	PL B275 195	H. Albrecht et al.	(ARGUS Collab.)
ALBRECHT	92E	PL B277 209	H. Albrecht et al.	(ARGUS Collab.)
ALBRECHT	92G	ZPHY C54 1	H. Albrecht et al.	(ARGUS Collab.)
BORTOLETTO	92	PR D45 215	D. Bortoletto et al.	(CLEO Collab.)
BUSKULIC	92G	PL B295 326	D. Buskulic et al.	(ALEPH Collab.)
ALBRECHT	91B	PL B254 288	H. Albrecht et al.	(ARGUS Collab.)
ALBRECHT	91C	PL B255 297	H. Albrecht et al.	(ARGUS Collab.)
ALBRECHT	91E	PL B262 148	H. Albrecht et al.	(ARGUS Collab.)
BERKELMAN	91	ARNPS 41 1	K. Berkelman, S. Stone	(CORN, SYRA)

B⁰

$$I(J^P) = \frac{1}{2}(0^{-})$$

Quantum numbers not measured. Values shown are quark-model predictions.

See also the B^\pm/B^0 ADMIXTURE and $B^\pm/B^0/B^0_s/b$ -baryon ADMIXTURE sections.

See the Note "Production and Decay of b-flavored Hadrons" at the beginning of the B^\pm Particle Listings and the Note on " $B^0\text{-}\bar{B}^0$ Mixing" near the end of the B^0 Particle Listings.

B⁰ MASS

The fit uses $m_{B^{\pm}}$, ($m_{B^0} - m_{B^+}$), and m_{B^0} to determine m_{B^+} , m_{B^0} , and the mass difference.

VALUE (MeV)	EVTS	DOCUMENT ID	TECN	COMMENT
5279.66 ± 0.12 OUR FIT				
5279.63 ± 0.20 OUR AVERAGE				
5279.74 ± 0.30 ± 0.10		¹ AAIJ	19U LHCb	pp at 7, 8, 13 TeV
5279.6 ± 0.2 ± 0.1		² AAD	13U ATLAS	pp at 7 TeV
5279.58 ± 0.15 ± 0.28		³ AAIJ	12E LHCb	pp at 7 TeV
5279.63 ± 0.53 ± 0.33		⁴ ACOSTA	06 CDF	$p\bar{p}$ at 1.96 TeV
5279.1 ± 0.7 ± 0.3	135	⁵ CSORNA	00 CLE2	$e^+e^- \rightarrow \Upsilon(4S)$
5281.3 ± 2.2 ± 1.4	51	ABE	96B CDF	$p\bar{p}$ at 1.8 TeV
● ● ● We do not use the following data for averages, fits, limits, etc. ● ● ●				
5279.2 ± 0.54 ± 2.0	340	ALAM	94 CLE2	$e^+e^- \rightarrow \Upsilon(4S)$
5278.0 ± 0.4 ± 2.0		BORTOLETTO	09E CLE2	$e^+e^- \rightarrow \Upsilon(4S)$
5279.6 ± 0.7 ± 2.0	40	⁶ ALBRECHT	90J ARG	$e^+e^- \rightarrow \Upsilon(4S)$
5278.2 ± 1.0 ± 3.0	40	ALBRECHT	87C ARG	$e^+e^- \rightarrow \Upsilon(4S)$
5279.5 ± 1.6 ± 3.0	7	⁷ ALBRECHT	87D ARG	$e^+e^- \rightarrow \Upsilon(4S)$
5280.6 ± 0.8 ± 2.0		BEBEK	87 CLEO	$e^+e^- \rightarrow \Upsilon(4S)$

- ¹ Uses $B^0 \rightarrow J/\psi p\bar{p}$ decays.
- ² Measured with $B^0_d \rightarrow J/\psi(\mu^+\mu^-) K_S^0(\pi^+\pi^-)$ decays.
- ³ Uses $B^0 \rightarrow J/\psi K^0$ fully reconstructed decays.
- ⁴ Uses exclusively reconstructed final states containing a $J/\psi \rightarrow \mu^+\mu^-$ decays.
- ⁵ CSORNA 00 uses fully reconstructed 135 $B^0 \rightarrow J/\psi^{(l)} K_S^0$ events and invariant masses without beam constraint.
- ⁶ ALBRECHT 90J assumes 10580 for $\Upsilon(4S)$ mass. Supersedes ALBRECHT 87C and ALBRECHT 87D.
- ⁷ Found using fully reconstructed decays with J/ψ . ALBRECHT 87D assume $m_{\Upsilon(4S)} = 10577$ MeV.

Meson Particle Listings

B^0

VALUE (MeV)	DOCUMENT ID	TECN	COMMENT
$m_{B^0} - m_{B^+}$			
0.32 ± 0.05 OUR FIT			
0.33 ± 0.05 OUR AVERAGE			
$0.57 \pm 0.49 \pm 0.10$	1 SIRUNYAN	18DF CMS	pp at 8 TeV
$0.20 \pm 0.17 \pm 0.11$	1 AAIJ	12E LHCb	pp at 7 TeV
$0.33 \pm 0.05 \pm 0.03$	2 AUBERT	08AF BABR	$e^+e^- \rightarrow \Upsilon(4S)$
$0.53 \pm 0.67 \pm 0.14$	1 ACOSTA	06 CDF	$p\bar{p}$ at 1.96 TeV
$0.41 \pm 0.25 \pm 0.19$	ALAM	94 CLE2	$e^+e^- \rightarrow \Upsilon(4S)$
$-0.4 \pm 0.6 \pm 0.5$	BORTOLETTO	92 CLEO	$e^+e^- \rightarrow \Upsilon(4S)$
$-0.9 \pm 1.2 \pm 0.5$	ALBRECHT	90J ARG	$e^+e^- \rightarrow \Upsilon(4S)$
$2.0 \pm 1.1 \pm 0.3$	3 BEBEK	87 CLEO	$e^+e^- \rightarrow \Upsilon(4S)$

1 Uses exclusively reconstructed final states containing a $J/\psi \rightarrow \mu^+\mu^-$ decay.
 2 Uses the B -momentum distributions in the e^+e^- rest frame.
 3 BEBEK 87 actually measure the difference between half of E_{cm} and the B^\pm or B^0 mass, so the $m_{B^0} - m_{B^\pm}$ is more accurate. Assume $m_{\Upsilon(4S)} = 10580$ MeV.

$m_{B_H^0} - m_{B_L^0}$

See the $B^0\text{-}\bar{B}^0$ MIXING PARAMETERS section near the end of these B^0 Listings.

B^0 MEAN LIFE

See $B^\pm/B^0/B_s^0/b$ -baryon ADMIXTURE section for data on B -hadron mean life averaged over species of bottom particles.

“OUR EVALUATION” is an average using rescaled values of the data listed below. The average and rescaling were performed by the Heavy Flavor Averaging Group (HFLAV) and are described at <https://hflav.web.cern.ch/>. The averaging/rescaling procedure takes into account correlations between the measurements and asymmetric lifetime errors.

VALUE (10^{-12} s)	EVTS	DOCUMENT ID	TECN	COMMENT
1.519 ± 0.004 OUR EVALUATION				
$1.515 \pm 0.005 \pm 0.006$		1 SIRUNYAN	18BY CMS	pp at 8 TeV
$1.534 \pm 0.019 \pm 0.021$		2 ABAZOV	15A D0	$p\bar{p}$ at 1.96 TeV
$1.499 \pm 0.013 \pm 0.005$		3 AAIJ	14E LHCb	pp at 7 TeV
$1.524 \pm 0.006 \pm 0.004$		4 AAIJ	14E LHCb	pp at 7 TeV
$1.524 \pm 0.011 \pm 0.004$		5 AAIJ	14R LHCb	pp at 7 TeV
$1.509 \pm 0.012 \pm 0.018$		6 AAD	13U ATLAS	pp at 7 TeV
$1.508 \pm 0.025 \pm 0.043$		3 ABAZOV	12U D0	$p\bar{p}$ at 1.96 TeV
$1.507 \pm 0.010 \pm 0.008$		7 AALTONEN	11 CDF	$p\bar{p}$ at 1.96 TeV
$1.414 \pm 0.018 \pm 0.034$		8 ABAZOV	09E D0	$p\bar{p}$ at 1.96 TeV
$1.504 \pm 0.013 \pm 0.018$		9 AUBERT	06G BABR	$e^+e^- \rightarrow \Upsilon(4S)$
$1.531 \pm 0.021 \pm 0.031$		11 ABDALLAH	04E DLPH	$e^+e^- \rightarrow Z$
$1.523 \pm 0.024 \pm 0.022$		12 AUBERT	03C BABR	$e^+e^- \rightarrow \Upsilon(4S)$
$1.533 \pm 0.034 \pm 0.038$		13 AUBERT	03H BABR	$e^+e^- \rightarrow \Upsilon(4S)$
$1.497 \pm 0.073 \pm 0.032$		14 ACOSTA	02C CDF	$p\bar{p}$ at 1.8 TeV
$1.529 \pm 0.012 \pm 0.029$		15 AUBERT	02H BABR	$e^+e^- \rightarrow \Upsilon(4S)$
$1.546 \pm 0.032 \pm 0.022$		16 AUBERT	01F BABR	$e^+e^- \rightarrow \Upsilon(4S)$
$1.541 \pm 0.028 \pm 0.023$		15 ABBIENDI,G	00B OPAL	$e^+e^- \rightarrow Z$
$1.518 \pm 0.053 \pm 0.034$		17 BARATE	00R ALEP	$e^+e^- \rightarrow Z$
$1.523 \pm 0.057 \pm 0.053$		18 ABBIENDI	99J OPAL	$e^+e^- \rightarrow Z$
$1.474 \pm 0.039 \pm 0.052$		17 ABE	98Q CDF	$p\bar{p}$ at 1.8 TeV
$1.52 \pm 0.06 \pm 0.04$		18 ACCIARRI	98S L3	$e^+e^- \rightarrow Z$
$1.64 \pm 0.08 \pm 0.08$		18 ABE	97J SLD	$e^+e^- \rightarrow Z$
$1.532 \pm 0.041 \pm 0.040$		19 ABREU	97F DLPH	$e^+e^- \rightarrow Z$
$1.25 \pm 0.15 \pm 0.05$	121	14 BUSKULIC	96J ALEP	$e^+e^- \rightarrow Z$
$1.49 \pm 0.17 \pm 0.08$		20 BUSKULIC	96J ALEP	$e^+e^- \rightarrow Z$
$1.61 \pm 0.14 \pm 0.08$		17,21 ABREU	95Q DLPH	$e^+e^- \rightarrow Z$
$1.63 \pm 0.14 \pm 0.13$		22 ADAM	95 DLPH	$e^+e^- \rightarrow Z$
$1.53 \pm 0.12 \pm 0.08$		17,23 AKERS	95T OPAL	$e^+e^- \rightarrow Z$

••• We do not use the following data for averages, fits, limits, etc. •••

$1.501 \pm 0.078 \pm 0.050$		3 ABAZOV	07S D0	Repl. by ABAZOV 12u
$1.524 \pm 0.030 \pm 0.016$		3 ABULENCIA	07A CDF	Repl. by AALTONEN 11
$1.473 \pm 0.052 \pm 0.023$		8 ABAZOV	05B D0	Repl. by ABAZOV 05w
$1.40 \pm 0.11 \pm 0.03$		3 ABAZOV	05C D0	Repl. by ABAZOV 07S
$1.530 \pm 0.043 \pm 0.023$		8 ABAZOV	05W D0	Repl. by ABAZOV 09E
$1.54 \pm 0.05 \pm 0.02$		24 ACOSTA	05 CDF	Repl. by AALTONEN 11
$1.554 \pm 0.030 \pm 0.019$		16 ABE	02H BELL	Repl. by ABE 05B
$1.58 \pm 0.09 \pm 0.02$		14 ABE	98B CDF	Repl. by ACOSTA 02C
$1.54 \pm 0.08 \pm 0.06$		17 ABE	96C CDF	Repl. by ABE 98Q
$1.55 \pm 0.06 \pm 0.03$		25 BUSKULIC	96J ALEP	$e^+e^- \rightarrow Z$
$1.61 \pm 0.07 \pm 0.04$		17 BUSKULIC	96J ALEP	Repl. by BARATE 00R

1.62 ± 0.12		26 ADAM	95 DLPH	$e^+e^- \rightarrow Z$
$1.57 \pm 0.18 \pm 0.08$	121	14 ABE	94D CDF	Repl. by ABE 98B
$1.17 \pm 0.29 \pm 0.16$		96	17 ABREU	93D DLPH Sup. by ABREU 95Q
$1.55 \pm 0.25 \pm 0.18$		76	22 ABREU	93G DLPH Sup. by ADAM 95
$1.51 \pm 0.24 \pm 0.12$		78	17 ACTON	93C OPAL Sup. by AKERS 95T
$1.52 \pm 0.20 \pm 0.07$		77	17 BUSKULIC	93D ALEP Sup. by BUSKULIC 96J
$1.20 \pm 0.16 \pm 0.14$		15	27 WAGNER	90 MRK2 $E_{cm}^{ee} = 29$ GeV
$0.82 \pm 0.57 \pm 0.27$			28 AVERILL	89 HRS $E_{cm}^{ee} = 29$ GeV

1 Measured using $B^0 \rightarrow J/\psi K^*(892)^0$ and $B^0 \rightarrow J/\psi K_S^0$ decays.
 2 Measured using $B^0 \rightarrow D^-\mu^+\nu X$ decays.
 3 Measured mean life using $B^0 \rightarrow J/\psi K_S^0$ decays.
 4 Measured using $B^0 \rightarrow J/\psi K^*0$ decays.
 5 Measured using $B^0 \rightarrow K^+\pi^-$ decays.
 6 Measured with $B_d^0 \rightarrow J/\psi(\mu^+\mu^-) K_S^0(\pi^+\pi^-)$ decays.
 7 Measured mean life using fully reconstructed decays ($J/\psi K^*$).
 8 Measured mean life using $B^0 \rightarrow J/\psi K^*0$ decays.
 9 Measured using a simultaneous fit of the B^0 lifetime and $\bar{B}^0 B^0$ oscillation frequency Δm_d in the partially reconstructed $B^0 \rightarrow D^*\pi^+$ decays.
 10 Measurement performed using a combined fit of CP -violation, mixing and lifetimes.
 11 Measurement performed using an inclusive reconstruction and B flavor identification technique.
 12 AUBERT 03C uses a sample of approximately 14,000 exclusively reconstructed $B^0 \rightarrow D^*(2010)^-\ell\nu$ and simultaneously measures the lifetime and oscillation frequency.
 13 Measurement performed with decays $B^0 \rightarrow D^*\pi^+$ and $B^0 \rightarrow D^*\rho^+$ using a partial reconstruction technique.
 14 Measured mean life using fully reconstructed decays.
 15 Data analyzed using partially reconstructed $\bar{B}^0 \rightarrow D^*\ell^-\bar{\nu}$ decays.
 16 Events are selected in which one B meson is fully reconstructed while the second B meson is reconstructed inclusively.
 17 Data analyzed using $D/D^*\ell X$ event vertices.
 18 Data analyzed using charge of secondary vertex.
 19 Data analyzed using inclusive $D/D^*\ell X$.
 20 Measured mean life using partially reconstructed $D^{*-}\pi^+ X$ vertices.
 21 ABREU 95Q assumes $B(B^0 \rightarrow D^{*-}\ell^+\nu_\ell) = 3.2 \pm 1.7\%$.
 22 Data analyzed using vertex-charge technique to tag B charge.
 23 AKERS 95T assumes $B(B^0 \rightarrow D_s^{(*)}D^0)$ = $5.0 \pm 0.9\%$ to find B^+/B^0 yield.
 24 Measured using the time-dependent angular analysis of $B_d^0 \rightarrow J/\psi K^*0$ decays.
 25 Combined result of $D/D^*\ell X$ analysis, fully reconstructed B analysis, and partially reconstructed $D^{*-}\pi^+ X$ analysis.
 26 Combined ABREU 95Q and ADAM 95 result.
 27 WAGNER 90 tagged B^0 mesons by their decays into $D^{*-}e^+\nu$ and $D^{*-}\mu^+\nu$ where the D^{*-} is tagged by its decay into π^-D^0 .
 28 AVERILL 89 is an estimate of the B^0 mean lifetime assuming that $B^0 \rightarrow D^{*+} + X$ always.

τ_{B^0}/τ_{B^+}

VALUE	DOCUMENT ID	TECN	COMMENT
$1.000 \pm 0.008 \pm 0.009$	1 AAIJ	14E LHCb	pp at 7 TeV

1 Measured using $B^0 \rightarrow J/\psi K^*0$ decays.

MEAN LIFE RATIO τ_{B^+}/τ_{B^0}

τ_{B^+}/τ_{B^0} (direct measurements)

“OUR EVALUATION” is an average using rescaled values of the data listed below. The average and rescaling were performed by the Heavy Flavor Averaging Group (HFLAV) and are described at <https://hflav.web.cern.ch/>. The averaging/rescaling procedure takes into account correlations between the measurements and asymmetric lifetime errors.

VALUE	EVTS	DOCUMENT ID	TECN	COMMENT
1.076 ± 0.004 OUR EVALUATION				
$1.074 \pm 0.005 \pm 0.003$		1 AAIJ	14E LHCb	pp at 7 TeV
$1.088 \pm 0.009 \pm 0.004$		2 AALTONEN	11 CDF	$p\bar{p}$ at 1.96 TeV
$1.080 \pm 0.016 \pm 0.014$		3 ABAZOV	05D D0	$p\bar{p}$ at 1.96 TeV
$1.066 \pm 0.008 \pm 0.008$		4 ABE	05B BELL	$e^+e^- \rightarrow \Upsilon(4S)$
$1.060 \pm 0.021 \pm 0.024$		5 ABDALLAH	04E DLPH	$e^+e^- \rightarrow Z$
$1.093 \pm 0.066 \pm 0.028$		6 ACOSTA	02C CDF	$p\bar{p}$ at 1.8 TeV
$1.082 \pm 0.026 \pm 0.012$		7 AUBERT	01F BABR	$e^+e^- \rightarrow \Upsilon(4S)$
$1.085 \pm 0.059 \pm 0.018$		3 BARATE	00R ALEP	$e^+e^- \rightarrow Z$
$1.079 \pm 0.064 \pm 0.041$		8 ABBIENDI	99J OPAL	$e^+e^- \rightarrow Z$
$1.110 \pm 0.056 \pm 0.033$		3 ABE	98Q CDF	$p\bar{p}$ at 1.8 TeV
$1.09 \pm 0.07 \pm 0.03$		8 ACCIARRI	98S L3	$e^+e^- \rightarrow Z$
$1.01 \pm 0.07 \pm 0.06$		8 ABE	97J SLD	$e^+e^- \rightarrow Z$
$1.27 \pm 0.23 \pm 0.03$		6 BUSKULIC	96J ALEP	$e^+e^- \rightarrow Z$
$1.00 \pm 0.17 \pm 0.10$		3,9 ABREU	95Q DLPH	$e^+e^- \rightarrow Z$
$1.06 \pm 0.13 \pm 0.10$		10 ADAM	95 DLPH	$e^+e^- \rightarrow Z$
$0.99 \pm 0.14 \pm 0.05$		3,11 AKERS	95T OPAL	$e^+e^- \rightarrow Z$

• • • We do not use the following data for averages, fits, limits, etc. • • •

1.091 ± 0.023 ± 0.014	7	ABE	02H	BELL	Repl. by ABE 05B	
1.06 ± 0.07 ± 0.02	6	ABE	98B	CDF	Repl. by ACOSTA 02C	
1.01 ± 0.11 ± 0.02	3	ABE	96C	CDF	Repl. by ABE 98Q	
1.03 ± 0.08 ± 0.02	12	BUSKULIC	96J	ALEP	e ⁺ e ⁻ → Z	
0.98 ± 0.08 ± 0.03	3	BUSKULIC	96J	ALEP	Repl. by BARATE 00R	
1.02 ± 0.16 ± 0.05	269	6	ABE	94D	CDF	Repl. by ABE 98B
1.11 ± 0.51 ± 0.11	188	3	ABREU	93D	DLPH	Sup. by ABREU 95Q
1.01 ± 0.29 ± 0.12	253	10	ABREU	93G	DLPH	Sup. by ADAM 95
1.0 ± 0.33 ± 0.08	130		ACTON	93C	OPAL	Sup. by AKERS 95T
0.96 ± 0.19 ± 0.18	154	3	BUSKULIC	93D	ALEP	Sup. by BUSKULIC 96J
-0.39 ± 0.22						
-0.25 ± 0.12						
-0.15 ± 0.12						

- Measured using $B \rightarrow J/\psi K^{(*)}$ decays.
- Measured mean life using fully reconstructed decays ($J/\psi K^{(*)}$).
- Data analyzed using $D/D^* \mu X$ vertices.
- Measurement performed using a combined fit of CP -violation, mixing and lifetimes.
- Measurement performed using an inclusive reconstruction and B flavor identification technique.
- Measured using fully reconstructed decays.
- Events are selected in which one B meson is fully reconstructed while the second B meson is reconstructed inclusively.
- Data analyzed using charge of secondary vertex.
- ABREU 95Q assumes $B(B^0 \rightarrow D^{*-} \ell^+ \nu_\ell) = 3.2 \pm 1.7\%$.
- Data analyzed using vertex-charge technique to tag B charge.
- AKERS 95T assumes $B(B^0 \rightarrow D_s^{(*)} D^{(*)}) = 5.0 \pm 0.9\%$ to find B^+/B^0 yield.
- Combined result of $D/D^* \ell X$ analysis and fully reconstructed B analysis.

τ_{B^+}/τ_{B^0} (inferred from branching fractions)

These measurements are inferred from the branching fractions for semileptonic decay or other spectator-dominated decays by assuming that the rates for such decays are equal for B^0 and B^+ . We do not use measurements which assume equal production of B^0 and B^+ because of the large uncertainty in the production ratio.

“OUR EVALUATION” has been obtained by the Heavy Flavor Averaging Group (HFLAV) by taking into account correlations between measurements.

VALUE	CL%	EVTS	DOCUMENT ID	TECN	COMMENT
1.076 ± 0.034					OUR EVALUATION
1.07 ± 0.04					OUR AVERAGE
1.07 ± 0.04 ± 0.03			URQUIJO 07	BELL	e ⁺ e ⁻ → $\Upsilon(4S)$
1.067 ± 0.041 ± 0.033			AUBERT,B	06Y	BABR e ⁺ e ⁻ → $\Upsilon(4S)$
• • • We do not use the following data for averages, fits, limits, etc. • • •					
0.95 ± 0.117 ± 0.091			1	ARTUSO 97	CLE2 e ⁺ e ⁻ → $\Upsilon(4S)$
1.15 ± 0.17 ± 0.06			2	JESSOP 97	CLE2 e ⁺ e ⁻ → $\Upsilon(4S)$
0.93 ± 0.18 ± 0.12			3	ATHANAS 94	CLE2 Sup. by ARTUSO 97
0.91 ± 0.27 ± 0.21			4	ALBRECHT 92C	ARG e ⁺ e ⁻ → $\Upsilon(4S)$
1.0 ± 0.4	29	4,5	ALBRECHT 92G	ARG	e ⁺ e ⁻ → $\Upsilon(4S)$
0.89 ± 0.19 ± 0.13			4	FULTON 91	CLEO e ⁺ e ⁻ → $\Upsilon(4S)$
1.00 ± 0.23 ± 0.14			4	ALBRECHT 89L	ARG e ⁺ e ⁻ → $\Upsilon(4S)$
0.49 to 2.3	90		6	BEAN 87B	CLEO e ⁺ e ⁻ → $\Upsilon(4S)$

- ARTUSO 97 uses partial reconstruction of $B \rightarrow D^* \ell \nu_\ell$ and independent of B^0 and B^+ production fraction.
- Assumes equal production of B^+ and B^0 at the $\Upsilon(4S)$.
- ATHANAS 94 uses events tagged by fully reconstructed B^- decays and partially or fully reconstructed B^0 decays.
- Assumes equal production of B^0 and B^+ .
- ALBRECHT 92G data analyzed using $B \rightarrow D_s \bar{D}, D_s \bar{D}^*, D_s^* \bar{D}, D_s^* \bar{D}^*$ events.
- BEAN 87B assume the fraction of $B^0 \bar{B}^0$ events at the $\Upsilon(4S)$ is 0.41.

$\Delta\Gamma_{B_d^0}/\Gamma_{B_d^0}$

$\Gamma_{B_d^0}$ and $\Delta\Gamma_{B_d^0}$ are the decay rate average and difference between two B_d^0 CP eigenstates (light – heavy). The λ_{CP} characterizes B^0 and \bar{B}^0 decays to states of charmonium plus K_L^0 , see the review on “ CP Violation” in the reviews section.

“OUR EVALUATION” has been obtained by the Heavy Flavor Averaging Group (HFLAV) by taking into account correlations between measurements.

VALUE (units 10 ⁻²)	CL%	DOCUMENT ID	TECN	COMMENT
0.1 ± 1.0				OUR EVALUATION
0.1 ± 1.0				OUR AVERAGE
3.4 ± 2.3 ± 2.4		1	SIRUNYAN 18BY	CMS pp at 8 TeV
- 0.1 ± 1.1 ± 0.9		2	AABOUD 16G	ATLS pp at 7, 8 TeV
- 4.4 ± 2.5 ± 1.1		3	AJLI 14E	LHCB pp at 7 TeV
1.7 ± 1.8 ± 1.1		4	HIGUCHI 12	BELL e ⁺ e ⁻ → $\Upsilon(4S)$
0.8 ± 3.7 ± 1.8		5	AUBERT,B	04C BABR e ⁺ e ⁻ → $\Upsilon(4S)$
0 ± 9		6	ABDALLAH 03B	DLPH e ⁺ e ⁻ → Z
• • • We do not use the following data for averages, fits, limits, etc. • • •				
0.50 ± 1.38			ABAHOV 14	D0 $p\bar{p}$ at 1.96 TeV
< 80	95	7	BEHRENS 00B	CLE2 e ⁺ e ⁻ → $\Upsilon(4S)$

- Measured using $B^0 \rightarrow J/\psi K^*(892)^0$ and $B^0 \rightarrow J/\psi K_S^0$ decays, and assuming $\beta = 21.9 \pm 0.7$ degrees.
- Measured from the ratio of decay time distributions of $B^0 \rightarrow J/\psi K_S^0$ and $B^0 \rightarrow J/\psi K^{*0}$ decays.
- Measured using the effective lifetimes of $B^0 \rightarrow J/\psi K_S^0$ and $B^0 \rightarrow J/\psi K^{*0}$ decays.
- Reports $-\Delta\Gamma_d/\Gamma_d$ using $B^0 \rightarrow J/\psi K_S^0, J/\psi K_L^0, D^- \pi^+, D^{*-} \pi^+, D^{*-} \rho^+$, and $D^{*-} \ell^+ \nu$ decays.
- Corresponds to 90% confidence range [-0.084, 0.068].
- Used the measured $\tau_{B^0} = 1.55 \pm 0.03$ ps. Corresponds to an upper limit of < 0.18 at 95% C.L.
- BEHRENS 00B uses high-momentum lepton tags and partially reconstructed $\bar{B}^0 \rightarrow D^{*+} \pi^-, \rho^-$ decays to determine the flavor of the B meson. Assumes $\Delta_{md}=0.478 \pm 0.018$ ps⁻¹ and $\tau_{B^0}=1.548 \pm 0.032$ ps.

B⁰ DECAY MODES

\bar{B}^0 modes are charge conjugates of the modes below. Reactions indicate the weak decay vertex and do not include mixing. Modes which do not identify the charge state of the B are listed in the B^\pm/B^0 ADMIXTURE section.

The branching fractions listed below assume 50% $B^0 \bar{B}^0$ and 50% $B^+ B^-$ production at the $\Upsilon(4S)$. We have attempted to bring older measurements up to date by rescaling their assumed $\Upsilon(4S)$ production ratio to 50:50 and their assumed D, D_s, D^* , and ψ branching ratios to current values whenever this would affect our averages and best limits significantly.

Indentation is used to indicate a subchannel of a previous reaction. All resonant subchannels have been corrected for resonance branching fractions to the final state so the sum of the subchannel branching fractions can exceed that of the final state.

For inclusive branching fractions, e.g., $B \rightarrow D^\pm X$, the values usually are multiplicities, not branching fractions. They can be greater than one.

Mode	Fraction (Γ_i/Γ)	Scale factor/ Confidence level
Γ_1 $\ell^+ \nu_\ell X$	[a] (10.33 ± 0.28) %	
Γ_2 $e^+ \nu_e X_c$	(10.1 ± 0.4) %	
Γ_3 $\ell^+ \nu_\ell X_u$	(1.51 ± 0.19) × 10 ⁻³	
Γ_4 $D \ell^+ \nu_\ell X$	(9.3 ± 0.8) %	
Γ_5 $D^- \ell^+ \nu_\ell$	[a] (2.24 ± 0.09) %	
Γ_6 $D^- \tau^+ \nu_\tau$	(1.05 ± 0.23) %	
Γ_7 $D^*(2010)^- \ell^+ \nu_\ell$	[a] (4.97 ± 0.12) %	
Γ_8 $D^*(2010)^- \tau^+ \nu_\tau$	(1.58 ± 0.09) %	S=1.1
Γ_9 $\bar{D}^0 \pi^- \ell^+ \nu_\ell$	(4.1 ± 0.5) × 10 ⁻³	
Γ_{10} $D_0^*(2300)^- \ell^+ \nu_\ell, D_0^{*-} \rightarrow$	(3.0 ± 1.2) × 10 ⁻³	S=1.8
Γ_{11} $\bar{D}_2^0 \pi^-$ $D_2^*(2460)^- \ell^+ \nu_\ell, D_2^{*-} \rightarrow$	(1.21 ± 0.33) × 10 ⁻³	S=1.8
Γ_{12} $\bar{D}^{*0} \pi^-$ $\bar{D}^{*0} \pi^- \ell^+ \nu_\ell$ (n ≥ 1)	(2.3 ± 0.5) %	
Γ_{13} $\bar{D}^{*0} \pi^- \ell^+ \nu_\ell$	(5.8 ± 0.8) × 10 ⁻³	S=1.4
Γ_{14} $D_1(2420)^- \ell^+ \nu_\ell, D_1^- \rightarrow$ $\bar{D}^{*0} \pi^-$	(2.80 ± 0.28) × 10 ⁻³	
Γ_{15} $D_1'(2430)^- \ell^+ \nu_\ell, D_1'^- \rightarrow$ $\bar{D}^{*0} \pi^-$	(3.1 ± 0.9) × 10 ⁻³	
Γ_{16} $D_2^*(2460)^- \ell^+ \nu_\ell, D_2^{*-} \rightarrow$ $\bar{D}^{*0} \pi^-$	(6.8 ± 1.2) × 10 ⁻⁴	
Γ_{17} $D^- \pi^+ \pi^- \ell^+ \nu_\ell$	(1.3 ± 0.5) × 10 ⁻³	
Γ_{18} $D^{*-} \pi^+ \pi^- \ell^+ \nu_\ell$	(1.4 ± 0.5) × 10 ⁻³	
Γ_{19} $\rho^- \ell^+ \nu_\ell$	[a] (2.94 ± 0.21) × 10 ⁻⁴	
Γ_{20} $\pi^- \ell^+ \nu_\ell$	[a] (1.50 ± 0.06) × 10 ⁻⁴	
Γ_{21} $\pi^- \mu^+ \nu_\mu$		
Γ_{22} $\pi^- \tau^+ \nu_\tau$	< 2.5 × 10 ⁻⁴	CL=90%

Inclusive modes

Γ_{23} $K^\pm X$	(78 ± 8) %	
Γ_{24} $D^0 X$	(8.1 ± 1.5) %	
Γ_{25} $\bar{D}^0 X$	(47.4 ± 2.8) %	
Γ_{26} $D^+ X$	< 3.9 %	CL=90%
Γ_{27} $D^- X$	(36.9 ± 3.3) %	
Γ_{28} $D_s^+ X$	(10.3 ± 2.1 / 1.8) %	
Γ_{29} $D_s^- X$	< 2.6 %	CL=90%
Γ_{30} $A_c^+ X$	< 3.1 %	CL=90%
Γ_{31} $\bar{A}_c^- X$	(5.0 ± 2.1 / 1.5) %	
Γ_{32} $\bar{c} X$	(95 ± 5) %	
Γ_{33} $c X$	(24.6 ± 3.1) %	
Γ_{34} $\bar{c}/c X$	(119 ± 6) %	

Meson Particle Listings

B^0

D, D*, or D_s modes

Γ ₃₅	$D^- \pi^+$	(2.51 ± 0.08) × 10 ⁻³		Γ ₉₅	$D_{s0}(2317)^+ D^-$, $D_{s0}^+ \rightarrow D_s^{*+} \gamma$	< 9.5	× 10 ⁻⁴	CL=90%
Γ ₃₆	$D^- \rho^+$	(7.6 ± 1.2) × 10 ⁻³		Γ ₉₆	$D_{s0}(2317)^+ D^*(2010)^-$, $D_{s0}^+ \rightarrow D_s^+ \pi^0$	(1.5 ± 0.6) × 10 ⁻³		
Γ ₃₇	$D^- K^0 \pi^+$	(4.9 ± 0.9) × 10 ⁻⁴		Γ ₉₇	$D_{sJ}(2457)^+ D^-$	(3.5 ± 1.1) × 10 ⁻³		
Γ ₃₈	$D^- K^*(892)^+$	(4.5 ± 0.7) × 10 ⁻⁴		Γ ₉₈	$D_{sJ}(2457)^+ D^-$, $D_{sJ}^+ \rightarrow D_s^+ \gamma$	(6.5 ± 1.7) × 10 ⁻⁴		
Γ ₃₉	$D^- \omega \pi^+$	(2.8 ± 0.6) × 10 ⁻³		Γ ₉₉	$D_{sJ}(2457)^+ D^-$, $D_{sJ}^+ \rightarrow D_s^{*+} \gamma$	< 6.0	× 10 ⁻⁴	CL=90%
Γ ₄₀	$D^- K^+$	(2.05 ± 0.08) × 10 ⁻⁴		Γ ₁₀₀	$D_{sJ}(2457)^+ D^-$, $D_{sJ}^+ \rightarrow D_s^+ \pi^+ \pi^-$	< 2.0	× 10 ⁻⁴	CL=90%
Γ ₄₁	$D^- K^+ \pi^+ \pi^-$	(3.5 ± 0.8) × 10 ⁻⁴		Γ ₁₀₁	$D_{sJ}(2457)^+ D^-$, $D_{sJ}^+ \rightarrow D_s^+ \pi^0$	< 3.6	× 10 ⁻⁴	CL=90%
Γ ₄₂	$D^- K^+ \bar{K}^0$	< 3.1	× 10 ⁻⁴	CL=90%				
Γ ₄₃	$D^- K^+ \bar{K}^*(892)^0$	(8.8 ± 1.9) × 10 ⁻⁴		Γ ₁₀₂	$D^*(2010)^- D_{sJ}(2457)^+$	(9.3 ± 2.2) × 10 ⁻³		
Γ ₄₄	$\bar{D}^0 \pi^+ \pi^-$	(8.8 ± 0.5) × 10 ⁻⁴		Γ ₁₀₃	$D_{sJ}(2457)^+ D^*(2010)$, $D_{sJ}^+ \rightarrow D_s^+ \gamma$	(2.3 ± 0.9) × 10 ⁻³		
Γ ₄₅	$D^*(2010)^- \pi^+$	(2.74 ± 0.13) × 10 ⁻³		Γ ₁₀₄	$D^- D_{s1}(2536)^+$, $D_{s1}^+ \rightarrow D^{*0} K^+ + D^{*+} K^0$	(2.8 ± 0.7) × 10 ⁻⁴		
Γ ₄₆	$\bar{D}^0 K^+ K^-$	(6.1 ± 0.5) × 10 ⁻⁵		Γ ₁₀₅	$D^- D_{s1}(2536)^+$, $D_{s1}^+ \rightarrow D^{*0} K^+$	(1.7 ± 0.6) × 10 ⁻⁴		
Γ ₄₇	$D^- \pi^+ \pi^+ \pi^-$	(6.0 ± 0.6) × 10 ⁻³		Γ ₁₀₆	$D^- D_{s1}(2536)^+$, $D_{s1}^+ \rightarrow D^{*+} K^0$	(2.6 ± 1.1) × 10 ⁻⁴		
Γ ₄₈	($D^- \pi^+ \pi^+ \pi^-$) nonresonant	(3.9 ± 1.9) × 10 ⁻³		Γ ₁₀₇	$D^*(2010)^- D_{s1}(2536)^+$, $D_{s1}^+ \rightarrow D^{*0} K^+ + D^{*+} K^0$	(5.0 ± 1.4) × 10 ⁻⁴		
Γ ₄₉	$D^- \pi^+ \rho^0$	(1.1 ± 1.0) × 10 ⁻³		Γ ₁₀₈	$D^*(2010)^- D_{s1}(2536)^+$, $D_{s1}^+ \rightarrow D_s^{*+} \pi^0$	(3.3 ± 1.1) × 10 ⁻⁴		
Γ ₅₀	$D^- a_1(1260)^+$	(6.0 ± 3.3) × 10 ⁻³		Γ ₁₀₉	$D^{*-} D_{s1}(2536)^+$, $D_{s1}^+ \rightarrow D^{*+} K^0$	(5.0 ± 1.7) × 10 ⁻⁴		
Γ ₅₁	$D^*(2010)^- \pi^+ \pi^0$	(1.5 ± 0.5) %		Γ ₁₁₀	$D^- D_{sJ}(2573)^+$, $D_{sJ}^+ \rightarrow D^0 K^+$	(3.4 ± 1.8) × 10 ⁻⁵		
Γ ₅₂	$D^*(2010)^- \rho^+$	(6.8 ± 0.9) × 10 ⁻³		Γ ₁₁₁	$D^*(2010)^- D_{sJ}(2573)^+$, $D_{sJ}^+ \rightarrow D^0 K^+$	< 2	× 10 ⁻⁴	CL=90%
Γ ₅₃	$D^*(2010)^- K^+$	(2.12 ± 0.15) × 10 ⁻⁴		Γ ₁₁₂	$D^- D_{sJ}(2700)^+$, $D_{sJ}^+ \rightarrow D^0 K^+$	(7.1 ± 1.2) × 10 ⁻⁴		
Γ ₅₄	$D^*(2010)^- K^0 \pi^+$	(3.0 ± 0.8) × 10 ⁻⁴		Γ ₁₁₃	$D^+ \pi^-$	(7.3 ± 1.2) × 10 ⁻⁷		
Γ ₅₅	$D^*(2010)^- K^*(892)^+$	(3.3 ± 0.6) × 10 ⁻⁴		Γ ₁₁₄	$D_s^+ \pi^-$	(2.03 ± 0.18) × 10 ⁻⁵		
Γ ₅₆	$D^*(2010)^- K^+ \bar{K}^0$	< 4.7	× 10 ⁻⁴	CL=90%				
Γ ₅₇	$D^*(2010)^- K^+ \bar{K}^*(892)^0$	(1.29 ± 0.33) × 10 ⁻³		Γ ₁₁₅	$D_s^+ \pi^-$	(2.1 ± 0.4) × 10 ⁻⁵		S=1.4
Γ ₅₈	$D^*(2010)^- \pi^+ \pi^+ \pi^-$	(7.21 ± 0.29) × 10 ⁻³		Γ ₁₁₆	$D_s^+ \rho^-$	< 2.4	× 10 ⁻⁵	CL=90%
Γ ₅₉	($D^*(2010)^- \pi^+ \pi^+ \pi^-$) non-resonant	(0.0 ± 2.5) × 10 ⁻³		Γ ₁₁₇	$D_s^+ \rho^-$	(4.1 ± 1.3) × 10 ⁻⁵		
Γ ₆₀	$D^*(2010)^- \pi^+ \rho^0$	(5.7 ± 3.2) × 10 ⁻³		Γ ₁₁₈	$D_s^+ a_0^-$	< 1.9	× 10 ⁻⁵	CL=90%
Γ ₆₁	$D^*(2010)^- a_1(1260)^+$	(1.30 ± 0.27) %		Γ ₁₁₉	$D_s^+ a_0^-$	< 3.6	× 10 ⁻⁵	CL=90%
Γ ₆₂	$\bar{D}_1(2420)^0 \pi^- \pi^+$, $\bar{D}_1^0 \rightarrow D^{*-} \pi^+$	(1.47 ± 0.35) × 10 ⁻⁴		Γ ₁₂₀	$D_s^+ a_1(1260)^-$	< 2.1	× 10 ⁻³	CL=90%
Γ ₆₃	$D^*(2010)^- K^+ \pi^- \pi^+$	(4.7 ± 0.4) × 10 ⁻⁴		Γ ₁₂₁	$D_s^+ a_1(1260)^-$	< 1.7	× 10 ⁻³	CL=90%
Γ ₆₄	$D^*(2010)^- \pi^+ \pi^+ \pi^- \pi^0$	(1.76 ± 0.27) %		Γ ₁₂₂	$D_s^+ a_2^-$	< 1.9	× 10 ⁻⁴	CL=90%
Γ ₆₅	$D^{*-} 3\pi^+ 2\pi^-$	(4.7 ± 0.9) × 10 ⁻³		Γ ₁₂₃	$D_s^+ a_2^-$	< 2.0	× 10 ⁻⁴	CL=90%
Γ ₆₆	$D^*(2010)^- \omega \pi^+$	(2.46 ± 0.18) × 10 ⁻³	S=1.2	Γ ₁₂₄	$D_s^- K^+$	(2.7 ± 0.5) × 10 ⁻⁵		S=2.7
Γ ₆₇	$\bar{D}_1(2430)^0 \omega$, $\bar{D}_1^0 \rightarrow D^{*-} \pi^+$	(2.7 ± 0.8) × 10 ⁻⁴		Γ ₁₂₅	$D_s^- K^+$	(2.19 ± 0.30) × 10 ⁻⁵		
Γ ₆₈	$D^{*-} \rho(1450)^+$, $\rho^+ \rightarrow \omega \pi^+$	(1.07 ± 0.40) × 10 ⁻³		Γ ₁₂₆	$D_s^- K^*(892)^+$	(3.5 ± 1.0) × 10 ⁻⁵		
Γ ₆₉	$\bar{D}_1(2420)^0 \omega$, $\bar{D}_1^0 \rightarrow D^{*-} \pi^+$	(7.0 ± 2.2) × 10 ⁻⁵		Γ ₁₂₇	$D_s^- K^*(892)^+$	(3.2 ± 1.5) × 10 ⁻⁵		
Γ ₇₀	$\bar{D}_2^*(2460)^0 \omega$, $\bar{D}_2^0 \rightarrow D^{*-} \pi^+$	(4.0 ± 1.4) × 10 ⁻⁵		Γ ₁₂₈	$D_s^- \pi^+ K^0$	(9.7 ± 1.4) × 10 ⁻⁵		
Γ ₇₁	$D^{*-} b_1(1235)^+$, $b_1^+ \rightarrow \omega \pi^+$	< 7	× 10 ⁻⁵	CL=90%				
Γ ₇₂	$\bar{D}^{*-} \pi^+$	[b] (1.9 ± 0.9) × 10 ⁻³		Γ ₁₂₉	$D_s^- \pi^+ K^0$	< 1.10	× 10 ⁻⁴	CL=90%
Γ ₇₃	$D_1(2420)^- \pi^+$, $D_1^- \rightarrow D^- \pi^+ \pi^-$	(9.9 ± 2.0) × 10 ⁻⁵		Γ ₁₃₀	$D_s^- K^+ \pi^+ \pi^-$	(1.7 ± 0.5) × 10 ⁻⁴		
Γ ₇₄	$D_1(2420)^- \pi^+$, $D_1^- \rightarrow D^- \pi^+ \pi^-$	< 3.3	× 10 ⁻⁵	CL=90%				
Γ ₇₅	$\bar{D}_2^*(2460)^- \pi^+$, $(D_2^*)^- \rightarrow D^0 \pi^-$	(2.38 ± 0.16) × 10 ⁻⁴		Γ ₁₃₁	$D_s^- \pi^+ K^*(892)^0$	< 3.0	× 10 ⁻³	CL=90%
Γ ₇₆	$\bar{D}_0^*(2400)^- \pi^+$, $(D_0^*)^- \rightarrow D^0 \pi^-$	(7.6 ± 0.8) × 10 ⁻⁵		Γ ₁₃₂	$D_s^- \pi^+ K^*(892)^0$	< 1.6	× 10 ⁻³	CL=90%
Γ ₇₇	$D_2^*(2460)^- \pi^+$, $(D_2^*)^- \rightarrow D^{*-} \pi^+ \pi^-$	< 2.4	× 10 ⁻⁵	CL=90%				
Γ ₇₈	$\bar{D}_2^*(2460)^- \rho^+$	< 4.9	× 10 ⁻³	CL=90%				
Γ ₇₉	$D^0 \bar{D}^0$	(1.4 ± 0.7) × 10 ⁻⁵		Γ ₁₃₃	$\bar{D}^0 K^0$	(5.2 ± 0.7) × 10 ⁻⁵		
Γ ₈₀	$D^{*0} \bar{D}^0$	< 2.9	× 10 ⁻⁴	CL=90%				
Γ ₈₁	$D^- D^+$	(2.11 ± 0.18) × 10 ⁻⁴		Γ ₁₃₄	$\bar{D}^0 K^+ \pi^-$	(8.8 ± 1.7) × 10 ⁻⁵		
Γ ₈₂	$D^\pm D^{*\mp}$ (CP-averaged)	(6.1 ± 0.6) × 10 ⁻⁴		Γ ₁₃₅	$\bar{D}^0 K^*(892)^0$	(4.5 ± 0.6) × 10 ⁻⁵		
Γ ₈₃	$D^- D_s^+$	(7.2 ± 0.8) × 10 ⁻³		Γ ₁₃₆	$\bar{D}^0 K^*(1410)^0$	< 6.7	× 10 ⁻⁵	CL=90%
Γ ₈₄	$D^*(2010)^- D_s^+$	(8.0 ± 1.1) × 10 ⁻³		Γ ₁₃₇	$\bar{D}^0 K_0^*(1430)^0$	(7 ± 7) × 10 ⁻⁶		
Γ ₈₅	$D^- D_s^{*+}$	(7.4 ± 1.6) × 10 ⁻³		Γ ₁₃₈	$\bar{D}^0 K_2^*(1430)^0$	(2.1 ± 0.9) × 10 ⁻⁵		
Γ ₈₆	$D^*(2010)^- D_s^{*+}$	(1.77 ± 0.14) %		Γ ₁₃₉	$D_0^*(2300)^- K^+$, $D_0^{*-} \rightarrow \bar{D}^0 \pi^-$	(1.9 ± 0.9) × 10 ⁻⁵		
Γ ₈₇	$D_{s0}(2317)^- K^+$, $D_{s0}^- \rightarrow D_s^- \pi^0$	(4.2 ± 1.4) × 10 ⁻⁵		Γ ₁₄₀	$D_2^*(2460)^- K^+$, $D_2^{*-} \rightarrow \bar{D}^0 \pi^-$	(2.03 ± 0.35) × 10 ⁻⁵		
Γ ₈₈	$D_{s0}(2317)^- \pi^+$, $D_{s0}^- \rightarrow D_s^- \pi^0$	< 2.5	× 10 ⁻⁵	CL=90%				
Γ ₈₉	$D_{sJ}(2457)^- K^+$, $D_{sJ}^- \rightarrow D_s^- \pi^0$	< 9.4	× 10 ⁻⁶	CL=90%				
Γ ₉₀	$D_{sJ}(2457)^- \pi^+$, $D_{sJ}^- \rightarrow D_s^- \pi^0$	< 4.0	× 10 ⁻⁶	CL=90%				
Γ ₉₁	$D_s^- D_s^+$	< 3.6	× 10 ⁻⁵	CL=90%				
Γ ₉₂	$D_s^- D_s^+$	< 1.3	× 10 ⁻⁴	CL=90%				
Γ ₉₃	$D_s^- D_s^+$	< 2.4	× 10 ⁻⁴	CL=90%				
Γ ₉₄	$D_{s0}^+(2317)^+ D^-$, $D_{s0}^+ \rightarrow D_s^+ \pi^0$	(1.06 ± 0.16) × 10 ⁻³	S=1.1	Γ ₁₄₂	$\bar{D}^0 K^+ \pi^-$ nonresonant	< 3.7	× 10 ⁻⁵	CL=90%
				Γ ₁₄₃	$[K^+ K^-]_D K^*(892)^0$	(4.2 ± 0.7) × 10 ⁻⁵		
				Γ ₁₄₄	$[\pi^+ \pi^-]_D K^*(892)^0$	(6.0 ± 1.1) × 10 ⁻⁵		
				Γ ₁₄₅	$[\pi^+ K^-]_D K^*(892)^0$			
				Γ ₁₄₆	$[K^+ \pi^-]_D K^*(892)^0$			
				Γ ₁₄₇	$[\pi^+ \pi^- \pi^+ \pi^-]_D K^{*0}$	(4.6 ± 0.9) × 10 ⁻⁵		

Γ ₁₄₈	$[\pi^+ K^- \pi^+ \pi^-]_D K^{*0}$			Γ ₂₁₅	$J/\psi(1S)\rho^0$	$(2.55 \pm_{-0.16}^{+0.18}) \times 10^{-5}$	
Γ ₁₄₉	$[K^+ \pi^- \pi^+ \pi^-]_D K^{*0}$			Γ ₂₁₆	$J/\psi(1S)f_0(980), f_0 \rightarrow \pi^+ \pi^-$	$< 1.1 \times 10^{-6}$	CL=90%
Γ ₁₅₀	$\bar{D}^0 \pi^0$	$(2.63 \pm 0.14) \times 10^{-4}$		Γ ₂₁₇	$J/\psi(1S)\rho(1450)^0, \rho^0 \rightarrow \pi \pi$	$(2.9 \pm_{-0.7}^{+1.6}) \times 10^{-6}$	
Γ ₁₅₁	$\bar{D}^0 \rho^0$	$(3.21 \pm 0.21) \times 10^{-4}$		Γ ₂₁₈	$J/\psi\rho(1700)^0, \rho^0 \rightarrow \pi^+ \pi^-$	$(2.0 \pm 1.3) \times 10^{-6}$	
Γ ₁₅₂	$\bar{D}^0 f_2$	$(1.56 \pm 0.21) \times 10^{-4}$		Γ ₂₁₉	$J/\psi(1S)\omega$	$(1.8 \pm_{-0.5}^{+0.7}) \times 10^{-5}$	
Γ ₁₅₃	$\bar{D}^0 \eta$	$(2.36 \pm 0.32) \times 10^{-4}$	S=2.5	Γ ₂₂₀	$J/\psi(1S)K^+ K^-$	$(2.54 \pm 0.35) \times 10^{-6}$	
Γ ₁₅₄	$\bar{D}^0 \eta'$	$(1.38 \pm 0.16) \times 10^{-4}$	S=1.3	Γ ₂₂₁	$J/\psi(1S)a_0(980), a_0 \rightarrow K^+ K^-$	$(4.7 \pm 3.4) \times 10^{-7}$	
Γ ₁₅₅	$\bar{D}^0 \omega$	$(2.54 \pm 0.16) \times 10^{-4}$		Γ ₂₂₂	$J/\psi(1S)\phi$	$< 1.1 \times 10^{-7}$	CL=90%
Γ ₁₅₆	$D^0 \phi$	$< 2.3 \times 10^{-6}$	CL=95%	Γ ₂₂₃	$J/\psi(1S)\eta'(958)$	$(7.6 \pm 2.4) \times 10^{-6}$	
Γ ₁₅₇	$D^0 K^+ \pi^-$	$(5.3 \pm 3.2) \times 10^{-6}$		Γ ₂₂₄	$J/\psi(1S)K^0 \pi^+ \pi^-$	$(4.5 \pm 0.4) \times 10^{-4}$	
Γ ₁₅₈	$D^0 K^*(892)^0$	$(3.0 \pm 0.6) \times 10^{-6}$		Γ ₂₂₅	$J/\psi(1S)K^0 K^- \pi^+ + c.c.$	$< 2.1 \times 10^{-5}$	CL=90%
Γ ₁₅₉	$\bar{D}^{*0} \gamma$	$< 2.5 \times 10^{-5}$	CL=90%	Γ ₂₂₆	$J/\psi(1S)K^0 K^+ K^-$	$(2.5 \pm 0.7) \times 10^{-5}$	S=1.8
Γ ₁₆₀	$\bar{D}^*(2007)^0 \pi^0$	$(2.2 \pm 0.6) \times 10^{-4}$	S=2.6	Γ ₂₂₇	$J/\psi(1S)K^0 K^\pm \pi^\mp$		
Γ ₁₆₁	$\bar{D}^*(2007)^0 \rho^0$	$< 5.1 \times 10^{-4}$	CL=90%	Γ ₂₂₈	$J/\psi(1S)K^0 \rho^0$	$(5.4 \pm 3.0) \times 10^{-4}$	
Γ ₁₆₂	$\bar{D}^*(2007)^0 \eta$	$(2.3 \pm 0.6) \times 10^{-4}$	S=2.8	Γ ₂₂₉	$J/\psi(1S)K^*(892)^+ \pi^-$	$(8 \pm 4) \times 10^{-4}$	
Γ ₁₆₃	$\bar{D}^*(2007)^0 \eta'$	$(1.40 \pm 0.22) \times 10^{-4}$		Γ ₂₃₀	$J/\psi(1S)\pi^+ \pi^- \pi^+ \pi^-$	$(1.44 \pm 0.12) \times 10^{-5}$	
Γ ₁₆₄	$\bar{D}^*(2007)^0 \pi^+ \pi^-$	$(6.2 \pm 2.2) \times 10^{-4}$		Γ ₂₃₁	$J/\psi(1S)f_1(1285)$	$(8.4 \pm 2.1) \times 10^{-6}$	
Γ ₁₆₅	$\bar{D}^*(2007)^0 K^0$	$(3.6 \pm 1.2) \times 10^{-5}$		Γ ₂₃₂	$J/\psi(1S)K^*(892)^0 \pi^+ \pi^-$	$(6.6 \pm 2.2) \times 10^{-4}$	
Γ ₁₆₆	$\bar{D}^*(2007)^0 K^*(892)^0$	$< 6.9 \times 10^{-5}$	CL=90%	Γ ₂₃₃	$\eta_{c2}(1D)K_S^0, \eta_{c2} \rightarrow h_c \gamma$	$< 3.5 \times 10^{-5}$	CL=90%
Γ ₁₆₇	$D^*(2007)^0 K^*(892)^0$	$< 4.0 \times 10^{-5}$	CL=90%	Γ ₂₃₄	$\eta_{c2}(1D)\pi^- K^+, \eta_{c2} \rightarrow h_c \gamma$	$< 1.0 \times 10^{-4}$	CL=90%
Γ ₁₆₈	$D^*(2007)^0 \pi^+ \pi^+ \pi^- \pi^-$	$(2.7 \pm 0.5) \times 10^{-3}$		Γ ₂₃₅	$\chi_{c1}(3872)^- K^+$	$< 5 \times 10^{-4}$	CL=90%
Γ ₁₆₉	$D^*(2010)^+ D^*(2010)^-$	$(8.0 \pm 0.6) \times 10^{-4}$		Γ ₂₃₆	$\chi_{c1}(3872)^- K^+, \chi_{c1}(3872)^- \rightarrow J/\psi(1S)\pi^- \pi^0$	$[c] < 4.2 \times 10^{-6}$	CL=90%
Γ ₁₇₀	$\bar{D}^*(2007)^0 \omega$	$(3.6 \pm 1.1) \times 10^{-4}$	S=3.1	Γ ₂₃₇	$\chi_{c1}(3872)K^0$	$(1.1 \pm 0.4) \times 10^{-4}$	
Γ ₁₇₁	$D^*(2010)^+ D^-$	$(6.1 \pm 1.5) \times 10^{-4}$	S=1.6	Γ ₂₃₈	$\chi_{c1}(3872)K^*(892)^0$	$(1.0 \pm 0.5) \times 10^{-4}$	
Γ ₁₇₂	$D^*(2007)^0 \bar{D}^*(2007)^0$	$< 9 \times 10^{-5}$	CL=90%	Γ ₂₃₉	$\chi_{c1}(3872)K^+ \pi^-$	$(2.1 \pm 0.8) \times 10^{-4}$	
Γ ₁₇₃	$D^- D^0 K^+$	$(1.07 \pm 0.11) \times 10^{-3}$		Γ ₂₄₀	$\chi_{c1}(3872)\gamma$	$< 1.3 \times 10^{-5}$	CL=90%
Γ ₁₇₄	$D^- D^*(2007)^0 K^+$	$(3.5 \pm 0.4) \times 10^{-3}$		Γ ₂₄₁	$Z_c(4430)^\pm K^\mp, Z_c^\pm \rightarrow \psi(2S)\pi^\pm$	$(6.0 \pm_{-2.4}^{+3.0}) \times 10^{-5}$	
Γ ₁₇₅	$D^*(2010)^- D^0 K^+$	$(2.47 \pm 0.21) \times 10^{-3}$		Γ ₂₄₂	$Z_c(4430)^\pm K^\mp, Z_c^\pm \rightarrow J/\psi\pi^\pm$	$(5.4 \pm_{-1.2}^{+4.0}) \times 10^{-6}$	
Γ ₁₇₆	$D^*(2010)^- D^*(2007)^0 K^+$	$(1.06 \pm 0.09) \%$		Γ ₂₄₃	$Z_c(3900)^\pm K^\mp, Z_c^\pm \rightarrow J/\psi\pi^\pm$	$< 9 \times 10^{-7}$	
Γ ₁₇₇	$D^- D^+ K^0$	$(7.5 \pm 1.7) \times 10^{-4}$		Γ ₂₄₄	$Z_c(4200)^\pm K^\mp, X^\pm \rightarrow J/\psi\pi^\pm$	$(2.2 \pm_{-0.8}^{+1.3}) \times 10^{-5}$	
Γ ₁₇₈	$D^*(2010)^- D^+ K^0 + D^- D^*(2010)^+ K^0$	$(6.4 \pm 0.5) \times 10^{-3}$		Γ ₂₄₅	$J/\psi(1S)p\bar{p}$	$(4.5 \pm 0.6) \times 10^{-7}$	
Γ ₁₇₉	$D^*(2010)^- D^*(2010)^+ K^0$	$(8.1 \pm 0.7) \times 10^{-3}$		Γ ₂₄₆	$J/\psi(1S)\gamma$	$< 1.5 \times 10^{-6}$	CL=90%
Γ ₁₈₀	$D^{*-} D_{s1}(2536)^+, D_{s1}^+ \rightarrow D^{*+} K^0$	$(8.0 \pm 2.4) \times 10^{-4}$		Γ ₂₄₇	$J/\psi(1S)\bar{D}^0$	$< 1.3 \times 10^{-5}$	CL=90%
Γ ₁₈₁	$\bar{D}^0 D^0 K^0$	$(2.7 \pm 1.1) \times 10^{-4}$		Γ ₂₄₈	$\psi(2S)\pi^0$	$(1.17 \pm 0.19) \times 10^{-5}$	
Γ ₁₈₂	$D^0 \bar{D}^0 K^+ \pi^-$	$(3.5 \pm 0.5) \times 10^{-4}$		Γ ₂₄₉	$\psi(2S)K^0$	$(5.8 \pm 0.5) \times 10^{-4}$	
Γ ₁₈₃	$\bar{D}^0 D^*(2007)^0 K^0 + \bar{D}^*(2007)^0 D^0 K^0$	$(1.1 \pm 0.5) \times 10^{-3}$		Γ ₂₅₀	$\psi(3770)K^0, \psi \rightarrow \bar{D}^0 D^0$	$< 1.23 \times 10^{-4}$	CL=90%
Γ ₁₈₄	$\bar{D}^*(2007)^0 D^*(2007)^0 K^0$	$(2.4 \pm 0.9) \times 10^{-3}$		Γ ₂₅₁	$\psi(3770)K^0, \psi \rightarrow D^- D^+$	$< 1.88 \times 10^{-4}$	CL=90%
Γ ₁₈₅	$(\bar{D} + \bar{D}^*)(D + D^*)K$	$(3.68 \pm 0.26) \%$		Γ ₂₅₂	$\psi(2S)\pi^+ \pi^-$	$(2.24 \pm 0.35) \times 10^{-5}$	
Charmonium modes				Γ ₂₅₃	$\psi(2S)K^+ \pi^-$	$(5.8 \pm 0.4) \times 10^{-4}$	
Γ ₁₈₆	$\eta_c K^0$	$(8.0 \pm 1.1) \times 10^{-4}$		Γ ₂₅₄	$\psi(2S)K^*(892)^0$	$(5.9 \pm 0.4) \times 10^{-4}$	
Γ ₁₈₇	$\eta_c(1S)K^+ \pi^-$	$(6.0 \pm 0.7) \times 10^{-4}$		Γ ₂₅₅	$\chi_{c0} K^0$	$(1.9 \pm 0.4) \times 10^{-4}$	
Γ ₁₈₈	$\eta_c(1S)K^+ \pi^- (NR)$	$(6.2 \pm 1.3) \times 10^{-5}$		Γ ₂₅₆	$\chi_{c0} K^*(892)^0$	$(1.7 \pm 0.4) \times 10^{-4}$	
Γ ₁₈₉	$X(4100)^- K^+, X^- \rightarrow \eta_c \pi^-$	$(2.0 \pm 1.0) \times 10^{-5}$		Γ ₂₅₇	$\chi_{c1} \pi^0$	$(1.12 \pm 0.28) \times 10^{-5}$	
Γ ₁₉₀	$\eta_c(1S)K^*(1410)^0$	$(1.9 \pm 1.5) \times 10^{-4}$		Γ ₂₅₈	$\chi_{c1} K^0$	$(3.95 \pm 0.27) \times 10^{-4}$	
Γ ₁₉₁	$\eta_c(1S)K_0^*(1430)^0$	$(1.6 \pm 0.4) \times 10^{-4}$		Γ ₂₅₉	$\chi_{c1} \pi^- K^+$	$(4.97 \pm 0.30) \times 10^{-4}$	
Γ ₁₉₂	$\eta_c(1S)K_2^*(1430)^0$	$(5.0 \pm_{-2.7}^{+2.3}) \times 10^{-5}$		Γ ₂₆₀	$\chi_{c1} K^*(892)^0$	$(2.38 \pm 0.19) \times 10^{-4}$	S=1.2
Γ ₁₉₃	$\eta_c(1S)K^*(1680)^0$	$(3 \pm 4) \times 10^{-5}$		Γ ₂₆₁	$X(4051)^- K^+, X^- \rightarrow \chi_{c1} \pi^-$	$(3.0 \pm_{-1.8}^{+4.0}) \times 10^{-5}$	
Γ ₁₉₄	$\eta_c(1S)K_0^*(1950)^0$	$(4.4 \pm_{-4.0}^{+3.0}) \times 10^{-5}$		Γ ₂₆₂	$X(4248)^- K^+, X^- \rightarrow \chi_{c1} \pi^-$	$(4.0 \pm_{-1.0}^{+20.0}) \times 10^{-5}$	
Γ ₁₉₅	$\eta_c K^*(892)^0$	$(5.2 \pm_{-0.9}^{+0.8}) \times 10^{-4}$	S=1.6	Γ ₂₆₃	$\chi_{c1} \pi^+ \pi^- K^0$	$(3.2 \pm 0.5) \times 10^{-4}$	
Γ ₁₉₆	$\eta_c(2S)K_S^0, \eta_c \rightarrow p\bar{p}\pi^+ \pi^-$	$(4.2 \pm_{-1.2}^{+1.4}) \times 10^{-7}$		Γ ₂₆₄	$\chi_{c1} \pi^- \pi^0 K^+$	$(3.5 \pm 0.6) \times 10^{-4}$	
Γ ₁₉₇	$\eta_c(2S)K^{*0}$	$< 3.9 \times 10^{-4}$	CL=90%	Γ ₂₆₅	$\chi_{c2} K^0$	$< 1.5 \times 10^{-5}$	CL=90%
Γ ₁₉₈	$h_c(1P)K_S^0$	$< 1.4 \times 10^{-5}$		Γ ₂₆₆	$\chi_{c2} K^*(892)^0$	$(4.9 \pm 1.2) \times 10^{-5}$	S=1.1
Γ ₁₉₉	$h_c(1P)K^{*0}$	$< 4 \times 10^{-4}$	CL=90%	Γ ₂₆₇	$\chi_{c2} \pi^- K^+$	$(7.2 \pm 1.0) \times 10^{-5}$	
Γ ₂₀₀	$J/\psi(1S)K^0$	$(8.91 \pm 0.21) \times 10^{-4}$		Γ ₂₆₈	$\chi_{c2} \pi^+ \pi^- K^0$	$< 1.70 \times 10^{-4}$	CL=90%
Γ ₂₀₁	$J/\psi(1S)K^+ \pi^-$	$(1.15 \pm 0.05) \times 10^{-3}$		Γ ₂₆₉	$\chi_{c2} \pi^- \pi^0 K^+$	$< 7.4 \times 10^{-5}$	CL=90%
Γ ₂₀₂	$J/\psi(1S)K^*(892)^0$	$(1.27 \pm 0.05) \times 10^{-3}$		Γ ₂₇₀	$\psi(4660)K^0, \psi \rightarrow \Lambda_c^+ \Lambda_c^-$	$< 2.3 \times 10^{-4}$	CL=90%
Γ ₂₀₃	$J/\psi(1S)\eta K_S^0$	$(5.4 \pm 0.9) \times 10^{-5}$		Γ ₂₇₁	$\psi(4230)^0 K^0, \psi^0 \rightarrow J/\psi\pi^+ \pi^-$	$< 1.7 \times 10^{-5}$	CL=90%
Γ ₂₀₄	$J/\psi(1S)\eta' K_S^0$	$< 2.5 \times 10^{-5}$	CL=90%				
Γ ₂₀₅	$J/\psi(1S)\phi K^0$	$(4.9 \pm 1.0) \times 10^{-5}$	S=1.3				
Γ ₂₀₆	$J/\psi(1S)\omega K^0$	$(2.3 \pm 0.4) \times 10^{-4}$					
Γ ₂₀₇	$\chi_{c0}(3915), \chi_{c0} \rightarrow J/\psi\omega$	$(2.1 \pm 0.9) \times 10^{-5}$					
Γ ₂₀₈	$J/\psi(1S)K(1270)^0$	$(1.3 \pm 0.5) \times 10^{-3}$					
Γ ₂₀₉	$J/\psi(1S)\pi^0$	$(1.66 \pm 0.10) \times 10^{-5}$					
Γ ₂₁₀	$J/\psi(1S)\eta$	$(1.08 \pm 0.23) \times 10^{-5}$	S=1.5				
Γ ₂₁₁	$J/\psi(1S)\pi^+ \pi^-$	$(4.00 \pm 0.15) \times 10^{-5}$					
Γ ₂₁₂	$J/\psi(1S)\pi^+ \pi^-$ nonresonant	$< 1.2 \times 10^{-5}$	CL=90%				
Γ ₂₁₃	$J/\psi(1S)f_0(500), f_0 \rightarrow \pi \pi$	$(8.8 \pm_{-1.6}^{+1.2}) \times 10^{-6}$					
Γ ₂₁₄	$J/\psi(1S)f_2$	$(3.3 \pm_{-0.6}^{+0.5}) \times 10^{-6}$	S=1.5				
				K or K* modes			
				Γ ₂₇₂	$K^+ \pi^-$	$(1.96 \pm 0.05) \times 10^{-5}$	
				Γ ₂₇₃	$K^0 \pi^0$	$(9.9 \pm 0.5) \times 10^{-6}$	
				Γ ₂₇₄	$\eta' K^0$	$(6.6 \pm 0.4) \times 10^{-5}$	S=1.4
				Γ ₂₇₅	$\eta' K^*(892)^0$	$(2.8 \pm 0.6) \times 10^{-6}$	
				Γ ₂₇₆	$\eta' K_0^*(1430)^0$	$(6.3 \pm 1.6) \times 10^{-6}$	

Meson Particle Listings

B^0

Γ ₂₇₇	$\eta' K_2^*(1430)^0$	(1.37 ± 0.32) × 10 ⁻⁵		Γ ₃₄₃	$K^+ K^- \pi^0$	(2.2 ± 0.6) × 10 ⁻⁶	
Γ ₂₇₈	ηK^0	(1.23 ^{+0.27} _{-0.24}) × 10 ⁻⁶		Γ ₃₄₄	$K_S^0 K_S^0 \pi^0$	< 9	CL=90%
Γ ₂₇₉	$\eta K^*(892)^0$	(1.59 ± 0.10) × 10 ⁻⁵		Γ ₃₄₅	$K_S^0 K_S^0 \eta$	< 1.0	CL=90%
Γ ₂₈₀	$\eta K_0^*(1430)^0$	(1.10 ± 0.22) × 10 ⁻⁵		Γ ₃₄₆	$K_S^0 K_S^0 \eta'$	< 2.0	CL=90%
Γ ₂₈₁	$\eta K_2^*(1430)^0$	(9.6 ± 2.1) × 10 ⁻⁶		Γ ₃₄₇	$K^0 K^+ K^-$	(2.68 ± 0.11) × 10 ⁻⁵	
Γ ₂₈₂	ωK^0	(4.8 ± 0.4) × 10 ⁻⁶		Γ ₃₄₈	$K^0 \phi$	(7.3 ± 0.7) × 10 ⁻⁶	
Γ ₂₈₃	$a_0(980)^0 K^0, a_0^0 \rightarrow \eta \pi^0$	< 7.8	CL=90%	Γ ₃₄₉	$f_0(980) K^0, f_0 \rightarrow K^+ K^-$	(7.0 ^{+3.5} _{-3.0}) × 10 ⁻⁶	
Γ ₂₈₄	$b_1^0 K^0, b_1^0 \rightarrow \omega \pi^0$	< 7.8	CL=90%	Γ ₃₅₀	$f_0(1500) K^0$	(1.3 ^{+0.7} _{-0.5}) × 10 ⁻⁵	
Γ ₂₈₅	$a_0(980)^\pm K^\mp, a_0^\pm \rightarrow \eta \pi^\pm$	< 1.9	CL=90%	Γ ₃₅₁	$f_2'(1525)^0 K^0$	(3 ⁺⁵ ₋₄) × 10 ⁻⁷	
Γ ₂₈₆	$b_1^- K^+, b_1^- \rightarrow \omega \pi^-$	(7.4 ± 1.4) × 10 ⁻⁶		Γ ₃₅₂	$f_0(1710) K^0, f_0 \rightarrow K^+ K^-$	(4.4 ± 0.9) × 10 ⁻⁶	
Γ ₂₈₇	$b_1^0 K^*, b_1^0 \rightarrow \omega \pi^0$	< 8.0	CL=90%	Γ ₃₅₃	$K^0 K^+ K^-$ nonresonant	(3.3 ± 1.0) × 10 ⁻⁵	
Γ ₂₈₈	$b_1^- K^*, b_1^- \rightarrow \omega \pi^-$	< 5.0	CL=90%	Γ ₃₅₄	$K_S^0 K_S^0 K_S^0$	(6.0 ± 0.5) × 10 ⁻⁶	S=1.1
Γ ₂₈₉	$a_0(1450)^\pm K^\mp, a_0^\pm \rightarrow \eta \pi^\pm$	< 3.1	CL=90%	Γ ₃₅₅	$f_0(980) K^0, f_0 \rightarrow K_S^0 K_S^0$	(2.7 ± 1.8) × 10 ⁻⁶	
Γ ₂₉₀	$K_S^0 X^0$ (Familon)	< 5.3	CL=90%	Γ ₃₅₆	$f_0(1710) K^0, f_0 \rightarrow K_S^0 K_S^0$	(5.0 ^{+5.0} _{-2.6}) × 10 ⁻⁷	
Γ ₂₉₁	$\omega K^*(892)^0$	(2.0 ± 0.5) × 10 ⁻⁶		Γ ₃₅₇	$f_2(2010) K^0, f_2 \rightarrow K_S^0 K_S^0$	(5 ± 6) × 10 ⁻⁷	
Γ ₂₉₂	$\omega (K\pi)_0^0$	(1.84 ± 0.25) × 10 ⁻⁵		Γ ₃₅₈	$K_S^0 K_S^0 K_S^0$ nonresonant	(1.33 ± 0.31) × 10 ⁻⁵	
Γ ₂₉₃	$\omega K_0^*(1430)^0$	(1.60 ± 0.34) × 10 ⁻⁵		Γ ₃₅₉	$K_S^0 K_S^0 K_S^0$	< 1.6	CL=90%
Γ ₂₉₄	$\omega K_2^*(1430)^0$	(1.01 ± 0.23) × 10 ⁻⁵		Γ ₃₆₀	$K^*(892)^0 K^+ K^-$	(2.75 ± 0.26) × 10 ⁻⁵	
Γ ₂₉₅	$\omega K^+ \pi^-$ nonresonant	(5.1 ± 1.0) × 10 ⁻⁶		Γ ₃₆₁	$K^*(892)^0 \phi$	(1.00 ± 0.05) × 10 ⁻⁵	
Γ ₂₉₆	$K^+ \pi^- \pi^0$	(3.78 ± 0.32) × 10 ⁻⁵		Γ ₃₆₂	$K^+ K^- \pi^+ \pi^-$ nonresonant	< 7.17	CL=90%
Γ ₂₉₇	$K^+ \rho^-$	(7.0 ± 0.9) × 10 ⁻⁶		Γ ₃₆₃	$K^*(892)^0 K^- \pi^+$	(4.5 ± 1.3) × 10 ⁻⁶	
Γ ₂₉₈	$K^+ \rho(1450)^-$	(2.4 ± 1.2) × 10 ⁻⁶		Γ ₃₆₄	$K^*(892)^0 \bar{K}^*(892)^0$	(8.3 ± 2.4) × 10 ⁻⁷	S=1.5
Γ ₂₉₉	$K^+ \rho(1700)^-$	(6 ± 7) × 10 ⁻⁷		Γ ₃₆₅	$K^+ K^+ \pi^- \pi^-$ nonresonant	< 6.0	CL=90%
Γ ₃₀₀	$(K^+ \pi^- \pi^0)$ nonresonant	(2.8 ± 0.6) × 10 ⁻⁶		Γ ₃₆₆	$K^*(892)^0 K^+ \pi^-$	< 2.2	CL=90%
Γ ₃₀₁	$(K\pi)_0^+ \pi^-, (K\pi)_0^{*+} \rightarrow$ $K^+ \pi^0$	(3.4 ± 0.5) × 10 ⁻⁵		Γ ₃₆₇	$K^*(892)^0 K^*(892)^0$	< 2	CL=90%
Γ ₃₀₂	$(K\pi)_0^+ \pi^0, (K\pi)_0^0 \rightarrow$ $K^+ \pi^-$	(8.6 ± 1.7) × 10 ⁻⁶		Γ ₃₆₈	$K^*(892)^+ K^*(892)^-$	< 2.0	CL=90%
Γ ₃₀₃	$K_2^*(1430)^0 \pi^0$	< 4.0	CL=90%	Γ ₃₆₉	$K_1(1400)^0 \phi$	< 5.0	CL=90%
Γ ₃₀₄	$K^*(1680)^0 \pi^0$	< 7.5	CL=90%	Γ ₃₇₀	$\phi (K\pi)_0^0$	(4.3 ± 0.4) × 10 ⁻⁶	
Γ ₃₀₅	$K_x^0 \pi^0$	[d] (6.1 ± 1.6) × 10 ⁻⁶		Γ ₃₇₁	$\phi (K\pi)_0^0 (1.60 < m_{K\pi} < 2.15)$	[f] < 1.7	CL=90%
Γ ₃₀₆	$K^0 \pi^+ \pi^-$	(4.97 ± 0.18) × 10 ⁻⁵		Γ ₃₇₂	$K_0^*(1430)^0 K^- \pi^+$	< 3.18	CL=90%
Γ ₃₀₇	$K^0 \pi^+ \pi^-$ nonresonant	(1.39 ^{+0.26} _{-0.18}) × 10 ⁻⁵	S=1.6	Γ ₃₇₃	$K_0^*(1430)^0 \bar{K}^*(892)^0$	< 3.3	CL=90%
Γ ₃₀₈	$K^0 \rho^0$	(3.4 ± 1.1) × 10 ⁻⁶	S=2.3	Γ ₃₇₄	$K_0^*(1430)^0 \bar{K}_0^*(1430)^0$	< 8.4	CL=90%
Γ ₃₀₉	$K^*(892)^+ \pi^-$	(7.5 ± 0.4) × 10 ⁻⁶		Γ ₃₇₅	$K_0^*(1430)^0 \phi$	(3.9 ± 0.8) × 10 ⁻⁶	
Γ ₃₁₀	$K_0^*(1430)^+ \pi^-$	(3.3 ± 0.7) × 10 ⁻⁵	S=2.0	Γ ₃₇₆	$K_0^*(1430)^0 K^*(892)^0$	< 1.7	CL=90%
Γ ₃₁₁	$K_x^+ \pi^-$	[d] (5.1 ± 1.6) × 10 ⁻⁶		Γ ₃₇₇	$K_0^*(1430)^0 K_0^*(1430)^0$	< 4.7	CL=90%
Γ ₃₁₂	$K^*(1410)^+ \pi^-, K^{*+} \rightarrow$ $K^0 \pi^+$	< 3.8	CL=90%	Γ ₃₇₈	$K^*(1680)^0 \phi$	< 3.5	CL=90%
Γ ₃₁₃	$(K\pi)_0^{*+} \pi^-, (K\pi)_0^{*+} \rightarrow$ $K^0 \pi^+$	(1.62 ± 0.13) × 10 ⁻⁵		Γ ₃₇₉	$K^*(1780)^0 \phi$	< 2.7	CL=90%
Γ ₃₁₄	$f_0(980) K^0, f_0 \rightarrow \pi^+ \pi^-$	(8.1 ± 0.8) × 10 ⁻⁶	S=1.3	Γ ₃₈₀	$K^*(2045)^0 \phi$	< 1.53	CL=90%
Γ ₃₁₅	$K^0 f_0(500)$	(1.6 ^{+2.5} _{-1.6}) × 10 ⁻⁷		Γ ₃₈₁	$K_2^*(1430)^0 \rho^0$	< 1.1	CL=90%
Γ ₃₁₆	$K^0 f_0(1500)$	(1.3 ± 0.8) × 10 ⁻⁶		Γ ₃₈₂	$K_2^*(1430)^0 \phi$	(6.8 ± 0.9) × 10 ⁻⁶	S=1.2
Γ ₃₁₇	$f_2(1270) K^0$	(2.7 ^{+1.3} _{-1.2}) × 10 ⁻⁶		Γ ₃₈₃	$K^0 \phi \phi$	(3.7 ± 0.7) × 10 ⁻⁶	S=1.3
Γ ₃₁₈	$f_x(1300) K^0, f_x \rightarrow \pi^+ \pi^-$	(1.8 ± 0.7) × 10 ⁻⁶		Γ ₃₈₄	$\eta' \eta' K^0$	< 3.1	CL=90%
Γ ₃₁₉	$K^*(892)^0 \pi^0$	(3.3 ± 0.6) × 10 ⁻⁶		Γ ₃₈₅	$\eta K^0 \gamma$	(7.6 ± 1.8) × 10 ⁻⁶	
Γ ₃₂₀	$K_2^*(1430)^+ \pi^-$	(3.65 ± 0.34) × 10 ⁻⁶		Γ ₃₈₆	$\eta' K^0 \gamma$	< 6.4	CL=90%
Γ ₃₂₁	$K^*(1680)^+ \pi^-$	(1.41 ± 0.10) × 10 ⁻⁵		Γ ₃₈₇	$K^0 \phi \gamma$	(2.7 ± 0.7) × 10 ⁻⁶	
Γ ₃₂₂	$K^+ \pi^- \pi^+ \pi^-$	[e] < 2.3	CL=90%	Γ ₃₈₈	$K^+ \pi^- \gamma$	(4.6 ± 1.4) × 10 ⁻⁶	
Γ ₃₂₃	$\rho^0 K^+ \pi^-$	(2.8 ± 0.7) × 10 ⁻⁶		Γ ₃₈₉	$K^*(892)^0 \gamma$	(4.18 ± 0.25) × 10 ⁻⁵	S=2.1
Γ ₃₂₄	$f_0(980) K^+ \pi^-, f_0 \rightarrow \pi \pi$	(1.4 ^{+0.5} _{-0.6}) × 10 ⁻⁶		Γ ₃₉₀	$K^*(1410) \gamma$	< 1.3	CL=90%
Γ ₃₂₅	$K^+ \pi^- \pi^+ \pi^-$ nonresonant	< 2.1	CL=90%	Γ ₃₉₁	$K^+ \pi^- \gamma$ nonresonant	< 2.6	CL=90%
Γ ₃₂₆	$K^*(892)^0 \pi^+ \pi^-$	(5.5 ± 0.5) × 10 ⁻⁵		Γ ₃₉₂	$K^*(892)^0 X(214), X \rightarrow \mu^+ \mu^-$	[g] < 2.26	CL=90%
Γ ₃₂₇	$K^*(892)^0 \rho^0$	(3.9 ± 1.3) × 10 ⁻⁶	S=1.9	Γ ₃₉₃	$K^0 \pi^+ \pi^- \gamma$	(1.99 ± 0.18) × 10 ⁻⁵	
Γ ₃₂₈	$K^*(892)^0 f_0(980), f_0 \rightarrow \pi \pi$	(3.9 ^{+2.1} _{-1.8}) × 10 ⁻⁶	S=3.9	Γ ₃₉₄	$K^+ \pi^- \pi^0 \gamma$	(4.1 ± 0.4) × 10 ⁻⁵	
Γ ₃₂₉	$K_1(1270)^+ \pi^-$	< 3.0	CL=90%	Γ ₃₉₅	$K_1(1270)^0 \gamma$	< 5.8	CL=90%
Γ ₃₃₀	$K_1(1400)^+ \pi^-$	< 2.7	CL=90%	Γ ₃₉₆	$K_1(1400)^0 \gamma$	< 1.2	CL=90%
Γ ₃₃₁	$a_1(1260)^- K^+$	[e] (1.6 ± 0.4) × 10 ⁻⁵		Γ ₃₉₇	$K_2^*(1430)^0 \gamma$	(1.24 ± 0.24) × 10 ⁻⁵	
Γ ₃₃₂	$K^*(892)^+ \rho^-$	(1.03 ± 0.26) × 10 ⁻⁵		Γ ₃₉₈	$K^*(1680)^0 \gamma$	< 2.0	CL=90%
Γ ₃₃₃	$K_0^*(1430)^+ \rho^-$	(2.8 ± 1.2) × 10 ⁻⁵		Γ ₃₉₉	$K_3^*(1780)^0 \gamma$	< 8.3	CL=90%
Γ ₃₃₄	$K_1(1400)^0 \rho^0$	< 3.0	CL=90%	Γ ₄₀₀	$K_4^*(2045)^0 \gamma$	< 4.3	CL=90%
Γ ₃₃₅	$K_0^*(1430)^0 \rho^0$	(2.7 ± 0.6) × 10 ⁻⁵		Light unflavored meson modes			
Γ ₃₃₆	$K_0^*(1430)^0 f_0(980), f_0 \rightarrow \pi \pi$	(2.7 ± 0.9) × 10 ⁻⁶		Γ ₄₀₁	$\rho^0 \gamma$	(8.6 ± 1.5) × 10 ⁻⁷	
Γ ₃₃₇	$K_2^*(1430)^0 f_0(980), f_0 \rightarrow \pi \pi$	(8.6 ± 2.0) × 10 ⁻⁶		Γ ₄₀₂	$\rho^0 X(214), X \rightarrow \mu^+ \mu^-$	[g] < 1.73	CL=90%
Γ ₃₃₈	$K^+ K^-$	(7.8 ± 1.5) × 10 ⁻⁸		Γ ₄₀₃	$\omega \gamma$	(4.4 ^{+1.8} _{-1.6}) × 10 ⁻⁷	
Γ ₃₃₉	$K^0 \bar{K}^0$	(1.21 ± 0.16) × 10 ⁻⁶		Γ ₄₀₄	$\phi \gamma$	< 1.0	CL=90%
Γ ₃₄₀	$K^0 K^- \pi^+$	(6.7 ± 0.5) × 10 ⁻⁶		Γ ₄₀₅	$\pi^+ \pi^-$	(5.12 ± 0.19) × 10 ⁻⁶	
Γ ₃₄₁	$K^*(892)^\pm K^\mp$	< 4	CL=90%	Γ ₄₀₆	$\pi^0 \pi^0$	(1.59 ± 0.26) × 10 ⁻⁶	S=1.4
Γ ₃₄₂	$\bar{K}^{*0} K^0 + K^{*0} \bar{K}^0$	< 9.6	CL=90%	Γ ₄₀₇	$\eta \pi^0$	(4.1 ± 1.7) × 10 ⁻⁷	
				Γ ₄₀₈	$\eta \eta$	< 1.0	CL=90%
				Γ ₄₀₉	$\eta' \pi^0$	(1.2 ± 0.6) × 10 ⁻⁶	S=1.7
				Γ ₄₁₀	$\eta' \eta'$	< 1.7	CL=90%
				Γ ₄₁₁	$\eta' \eta$	< 1.2	CL=90%

- • • We do not use the following data for averages, fits, limits, etc. • • •
- 2.21±0.11±0.12 2 AUBERT 08Q BABR Repl. by AUBERT 10
- 2.13±0.12±0.39 ABE 02E BELL Repl. by GLATTAUER 16
- 1.87±0.15±0.32 5 ATHANAS 97 CLE2 Repl. by BARTELT 99
- 1.8 ±0.6 ±0.3 6 FULTON 91 CLEO $e^+e^- \rightarrow \Upsilon(4S)$
- 2.0 ±0.7 ±0.6 7 ALBRECHT 89J ARG $e^+e^- \rightarrow \Upsilon(4S)$

- 1 Uses a fully reconstructed B meson as a tag on the recoil side while the other, on the signal side, is partially reconstructed from $B \rightarrow D\ell\nu$.
- 2 Uses a fully reconstructed B meson as a tag on the recoil side.
- 3 Assumes equal production of B^+ and B^0 at the $\Upsilon(4S)$.
- 4 BUSKULIC 97 assumes fraction (B^+) = fraction (B^0) = (37.8 ± 2.2)% and PDG 96 values for B lifetime and branching ratio of D^* and D decays.
- 5 ATHANAS 97 uses missing energy and missing momentum to reconstruct neutrino.
- 6 FULTON 91 assumes assuming equal production of B^0 and B^+ at the $\Upsilon(4S)$ and uses Mark III D and D^* branching ratios.
- 7 ALBRECHT 89J reports 0.018 ± 0.006 ± 0.005. We rescale using the method described in STONE 94 but with the updated PDG 94 $B(D^0 \rightarrow K^-\pi^+)$.

$\Gamma(D^-\ell^+\nu_\ell)/\Gamma(\ell^+\nu_\ell X)$ Γ_5/Γ_1

VALUE	DOCUMENT ID	TECN	COMMENT
0.230±0.011±0.011	1 AUBERT	10 BABR	$e^+e^- \rightarrow \Upsilon(4S)$

1 Uses a fully reconstructed B meson on the recoil side.

$\Gamma(D^-\ell^+\nu_\ell)/\Gamma(D\ell^+\nu_\ell X)$ Γ_5/Γ_4

VALUE	DOCUMENT ID	TECN	COMMENT
0.215±0.016±0.013	1 AUBERT	07AN BABR	$e^+e^- \rightarrow \Upsilon(4S)$

1 Uses a fully reconstructed B meson on the recoil side.

$\Gamma(D^-\tau^+\nu_\tau)/\Gamma_{total}$ Γ_6/Γ

VALUE (units 10 ⁻²)	DOCUMENT ID	TECN	COMMENT
1.04±0.35±0.18	1 AUBERT	08N BABR	Repl. by AUBERT 09s

- • • We do not use the following data for averages, fits, limits, etc. • • •
- 1 Uses a fully reconstructed B meson as a tag on the recoil side.

$\Gamma(D^-\tau^+\nu_\tau)/\Gamma(D^-\ell^+\nu_\ell)$ Γ_6/Γ_5

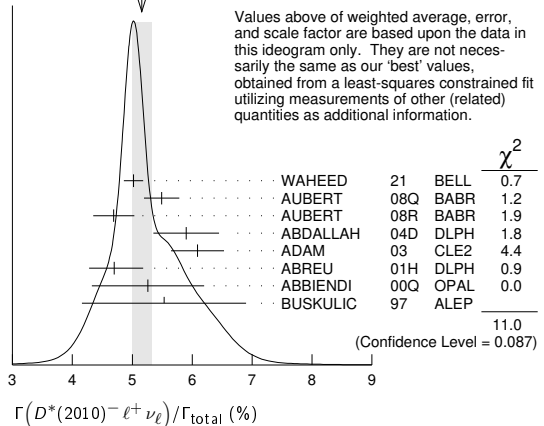
VALUE	DOCUMENT ID	TECN	COMMENT
0.469±0.084±0.053	1,2 LEES	12D BABR	$e^+e^- \rightarrow \Upsilon(4S)$

- • • We do not use the following data for averages, fits, limits, etc. • • •
- 1 AUBERT 09s BABR Repl. by LEES 12D
- 1 Uses a fully reconstructed B meson as a tag on the recoil side.
- 2 Uses $\tau^+ \rightarrow e^+\nu_e\bar{\nu}_\tau$ and $\tau^+ \rightarrow \mu^+\nu_\mu\bar{\nu}_\tau$ and e^+ or μ^+ as ℓ^+ .

$\Gamma(D^*(2010)^-\ell^+\nu_\ell)/\Gamma_{total}$ Γ_7/Γ
 "OUR EVALUATION" is an average using rescaled values of the data listed below. The average and rescaling were performed by the Heavy Flavor Averaging Group (HFLAV) and are described at <https://hflav.web.cern.ch/>. The averaging/rescaling procedure takes into account correlations between the measurements.

VALUE (%)	EVTS	DOCUMENT ID	TECN	COMMENT	
4.97±0.12 OUR EVALUATION		This value assumes isospin symmetry.			
5.14±0.15 OUR FIT		Error includes scale factor of 1.3.			
5.16±0.16 OUR AVERAGE		Error includes scale factor of 1.4. See the ideogram below.			
5.02±0.02±0.16	1	WAHEED 21	BELL	$e^+e^- \rightarrow \Upsilon(4S)$	
5.49±0.16±0.25	2	AUBERT 08Q	BABR	$e^+e^- \rightarrow \Upsilon(4S)$	
4.69±0.04±0.34	3	AUBERT 08R	BABR	$e^+e^- \rightarrow \Upsilon(4S)$	
5.90±0.22±0.50	4	ABDALLAH 04D	DLPH	$e^+e^- \rightarrow Z^0$	
6.09±0.19±0.40	5	ADAM 03	CLE2	$e^+e^- \rightarrow \Upsilon(4S)$	
4.70±0.13±0.36	6	ABREU 01H	DLPH	$e^+e^- \rightarrow Z$	
5.26±0.20±0.46	7	ABBIENDI 00Q	OPAL	$e^+e^- \rightarrow Z$	
5.53±0.26±0.52	8	BUSKULIC 97	ALEP	$e^+e^- \rightarrow Z$	
• • • We do not use the following data for averages, fits, limits, etc. • • •					
4.90±0.02±0.16	1	WAHEED 19	BELL	Repl. by WAHEED 21	
4.58±0.03±0.26	1	DUNGEL 10	BELL	Repl. by WAHEED 19	
4.90±0.07±0.36	4	AUBERT 05E	BABR	Repl. by AUBERT 08R	
5.39±0.11±0.34	9	ABDALLAH 04D	DLPH	$e^+e^- \rightarrow Z^0$	
4.59±0.23±0.40	10	ABE 02F	BELL	Repl. by DUNGEL 10	
6.09±0.19±0.40	11	BRIERE 02	CLE2	$e^+e^- \rightarrow \Upsilon(4S)$	
5.08±0.21±0.66	12	ACKERSTAFF 97G	OPAL	Repl. by ABBIENDI 00Q	
5.52±0.17±0.68	13	ABREU 96P	DLPH	Repl. by ABREU 01H	
4.49±0.32±0.39	376	BARISH 95	CLE2	Repl. by ADAM 03	
5.18±0.30±0.62	410	BUSKULIC 95N	ALEP	Sup. by BUSKULIC 97	
4.5 ±0.3 ±0.4	16	ALBRECHT 94	ARG	$e^+e^- \rightarrow \Upsilon(4S)$	
4.7 ±0.5 ±0.5	235	ALBRECHT 93	ARG	$e^+e^- \rightarrow \Upsilon(4S)$	
seen	398	SANGHERA 93	CLE2	$e^+e^- \rightarrow \Upsilon(4S)$	
7.0 ±1.8 ±1.4	19	ANTREASIAN 90B	CBAL	$e^+e^- \rightarrow \Upsilon(4S)$	
6.0 ±1.0 ±1.4	20	ALBRECHT 89C	ARG	$e^+e^- \rightarrow \Upsilon(4S)$	
4.0 ±0.4 ±0.6	21	ALBRECHT 89J	ARG	$e^+e^- \rightarrow \Upsilon(4S)$	
7.0 ±1.2 ±1.9	47	BORTOLETTO 89B	CLEO	$e^+e^- \rightarrow \Upsilon(4S)$	
		23	ALBRECHT 87J	ARG	$e^+e^- \rightarrow \Upsilon(4S)$

WEIGHTED AVERAGE
5.16±0.16 (Error scaled by 1.4)



- 1 WAHEED 21 uses fully reconstructed $D^{*+}\ell^+\nu$ events ($\ell = e$ or μ).
- 2 Uses a fully reconstructed B meson as a tag on the recoil side.
- 3 Measured using fully reconstructed D^* sample and a simultaneous fit to the Caprini-Lellouch-Neubert form factor parameters: $\rho^2 = 1.191 \pm 0.048 \pm 0.028$, $R_1(1) = 1.429 \pm 0.061 \pm 0.044$, and $R_2(1) = 0.827 \pm 0.038 \pm 0.022$.
- 4 Measured using fully reconstructed D^* sample.
- 5 Uses the combined fit of both $B^0 \rightarrow D^*(2010)^-\ell\nu$ and $B^+ \rightarrow \bar{D}^*(2007)^0\ell\nu$ samples.
- 6 ABREU 01H measured using about 5000 partial reconstructed D^* sample.
- 7 ABBIENDI 00Q assumes the fraction $B(b \rightarrow B^0) = (39.7^{+1.3}_{-2.2})\%$. This result is an average of two methods using exclusive and partial D^* reconstruction.
- 8 BUSKULIC 97 assumes fraction (B^+) = fraction (B^0) = (37.8 ± 2.2)% and PDG 96 values for B lifetime and D^* and D branching fractions.
- 9 Combines with previous partial reconstructed D^* measurement.
- 10 Assumes equal production of B^+ and B^0 at the $\Upsilon(4S)$.
- 11 The results are based on the same analysis and data sample reported in ADAM 03.
- 12 ACKERSTAFF 97G assumes fraction (B^+) = fraction (B^0) = (37.8 ± 2.2)% and PDG 96 values for B lifetime and branching ratio of D^* and D decays.
- 13 ABREU 96P result is the average of two methods using exclusive and partial D^* reconstruction.
- 14 BARISH 95 use $B(D^0 \rightarrow K^-\pi^+) = (3.91 \pm 0.08 \pm 0.17)\%$ and $B(D^{*+} \rightarrow D^0\pi^+) = (68.1 \pm 1.0 \pm 1.3)\%$.
- 15 BUSKULIC 95N assumes fraction (B^+) = fraction (B^0) = $38.2 \pm 1.3 \pm 2.2\%$ and $\tau_{B^0} = 1.58 \pm 0.06$ ps. $\Gamma(D^{*+}\ell^+\nu_\ell)/\Gamma_{total} = [5.18 - 0.13(\text{fraction}(B^0) - 38.2) - 1.5(\tau_{B^0} - 1.58)]\%$.
- 16 ALBRECHT 94 assumes $B(D^{*+} \rightarrow D^0\pi^+) = 68.1 \pm 1.0 \pm 1.3\%$. Uses partial reconstruction of D^{*+} and is independent of D^0 branching ratios.
- 17 ALBRECHT 93 reports 0.052 ± 0.005 ± 0.006. We rescale using the method described in STONE 94 but with the updated PDG 94 $B(D^0 \rightarrow K^-\pi^+)$. We have taken their average e and μ value. They also obtain $\alpha = 2\Gamma^0/(\Gamma^- + \Gamma^+) - 1 = 1.1 \pm 0.4 \pm 0.2$, $A_{FB} = 3/4 * (\Gamma^- - \Gamma^+)/\Gamma = 0.2 \pm 0.08 \pm 0.06$ and a value of $|V_{cb}| = 0.036 - 0.045$ depending on model assumptions.
- 18 Combining $\bar{D}^{*0}\ell^+\nu_\ell$ and $\bar{D}^{*+}\ell^+\nu_\ell$ SANGHERA 93 test $V-A$ structure and fit the decay angular distributions to obtain $A_{FB} = 3/4 * (\Gamma^- - \Gamma^+)/\Gamma = 0.14 \pm 0.06 \pm 0.03$. Assuming a value of V_{cb} , they measure V, A_1 , and A_2 , the three form factors for the $D^*\ell\nu_\ell$ decay, where results are slightly dependent on model assumptions.
- 19 ANTREASIAN 90B is average over B and $\bar{D}^*(2010)$ charge states.
- 20 The measurement of ALBRECHT 89C suggests a D^* polarization γ_L/γ_T of 0.85 ± 0.45, or $\alpha = 0.7 \pm 0.9$.
- 21 ALBRECHT 89J is ALBRECHT 87J value rescaled using $B(D^*(2010)^- \rightarrow D^0\pi^-) = 0.57 \pm 0.04 \pm 0.04$. Superseded by ALBRECHT 93.
- 22 We have taken average of the the BORTOLETTO 89B values for electrons and muons, 0.046 ± 0.005 ± 0.007. We rescale using the method described in STONE 94 but with the updated PDG 94 $B(D^0 \rightarrow K^-\pi^+)$. The measurement suggests a D^* polarization parameter value $\alpha = 0.65 \pm 0.66 \pm 0.25$.
- 23 ALBRECHT 87J assume μ - e universality, the $B(\Upsilon(4S) \rightarrow B^0\bar{B}^0) = 0.45$, the $B(D^0 \rightarrow K^-\pi^+) = (0.042 \pm 0.004 \pm 0.004)$, and the $B(D^*(2010)^- \rightarrow D^0\pi^-) = 0.49 \pm 0.08$. Superseded by ALBRECHT 89J.

$\Gamma(D^*(2010)^-\ell^+\nu_\ell)/\Gamma(D\ell^+\nu_\ell X)$ Γ_7/Γ_4

VALUE	DOCUMENT ID	TECN	COMMENT
0.537±0.031±0.036	1 AUBERT	07AN BABR	$e^+e^- \rightarrow \Upsilon(4S)$

1 Uses a fully reconstructed B meson on the recoil side.

$\Gamma(D^*(2010)^-\tau^+\nu_\tau)/\Gamma_{total}$ Γ_8/Γ

VALUE (units 10 ⁻²)	DOCUMENT ID	TECN	COMMENT
1.58±0.09 OUR FIT		Error includes scale factor of 1.1.	
1.48±0.18 OUR AVERAGE		Error includes scale factor of 1.1.	
1.42±0.094±0.140	1	AAIJ 18D	LHCb pp at 7, 8 TeV
2.02 ^{+0.40} _{-0.37} ±0.37	2	MATYJA 07	BELL $e^+e^- \rightarrow \Upsilon(4S)$

Meson Particle Listings

B^0

• • • We do not use the following data for averages, fits, limits, etc. • • •
 1.11±0.51 ±0.06 ³ AUBERT 08N BABR Repl. by AUBERT 09s

- ¹ Normalizes to $B(B^0 \rightarrow D^*(2010)^- \pi^+ \pi^- \pi^+) = (7.214 \pm 0.28) \times 10^{-3}$.
- ² Observed in the recoil of the accompanying B meson.
- ³ Uses a fully reconstructed B meson as a tag on the recoil side.

$\Gamma(D^*(2010)^- \tau^+ \nu_\tau) / \Gamma(D^*(2010)^- \ell^+ \nu_\ell)$ Γ_8 / Γ_7

VALUE	DOCUMENT ID	TECN	COMMENT
0.308±0.016 OUR FIT			
0.315±0.018 OUR AVERAGE			
0.291±0.019±0.029	¹ AAIJ	18D	LHCB pp at 7, 8 TeV
0.302±0.030±0.011	² SATO	16B	BELL $e^+e^- \rightarrow \Upsilon(4S)$
0.336±0.027±0.030	³ AAIJ	15Q	LHCB pp at 7, 8 TeV
0.355±0.039±0.021	^{4,5} LEES	12D	BABR $e^+e^- \rightarrow \Upsilon(4S)$

• • • We do not use the following data for averages, fits, limits, etc. • • •
 0.207±0.095±0.008 ⁴ AUBERT 09s BABR Repl. by LEES 12D

- ¹ Uses $\tau^+ \rightarrow \pi^+ \pi^- \pi^+ \bar{\nu}_\tau$ and $\tau^+ \rightarrow \pi^+ \pi^- \pi^+ \pi^0 \bar{\nu}_\tau$, and μ^+ as ℓ^+ .
- ² Uses semileptonic B decay events for tagging and $\tau^+ \rightarrow \ell^+ \nu_\ell \bar{\nu}_\tau$ mode.
- ³ Uses $\tau^+ \rightarrow \mu^+ \nu_\mu \bar{\nu}_\tau$ and μ^+ as ℓ^+ .
- ⁴ Uses a fully reconstructed B meson as a tag on the recoil side.
- ⁵ Uses $\tau^+ \rightarrow e^+ \nu_e \bar{\nu}_\tau$ and $\tau^+ \rightarrow \mu^+ \nu_\mu \bar{\nu}_\tau$ and e^+ or μ^+ as ℓ^+ .

$\Gamma(D^*(2010)^- \tau^+ \nu_\tau) / \Gamma(D^*(2010)^- \pi^+ \pi^+ \pi^-)$ Γ_8 / Γ_{58}

VALUE	DOCUMENT ID	TECN	COMMENT
1.97±0.13±0.18	¹ AAIJ	18D	LHCB pp at 7, 8 TeV

- ¹ Uses $\tau^+ \rightarrow \pi^+ \pi^- \pi^+ \bar{\nu}_\tau$ and $\tau^+ \rightarrow \pi^+ \pi^- \pi^+ \pi^0 \bar{\nu}_\tau$ modes.

$\Gamma(\bar{D}^0 \pi^- \ell^+ \nu_\ell) / \Gamma_{total}$ Γ_9 / Γ

VALUE (units 10^{-3})	DOCUMENT ID	TECN	COMMENT
4.1 ±0.5 OUR AVERAGE			
4.05±0.36±0.41			VOSSEN 18 BELL $e^+e^- \rightarrow \Upsilon(4S)$
4.3 ±0.8 ±0.3	¹ AUBERT	08Q	BABR $e^+e^- \rightarrow \Upsilon(4S)$

• • • We do not use the following data for averages, fits, limits, etc. • • •
 4.4 ±0.9 ±0.2 ^{1,2} LIVENTSEV 08 BELL Repl. by VOSSEN 18
 3.4 ±1.0 ±0.1 ³ LIVENTSEV 05 BELL Repl. by LIVENTSEV 08

- ¹ Uses a fully reconstructed B meson as a tag on the recoil side.
- ² LIVENTSEV 08 reports $(4.2 \pm 0.7 \pm 0.6) \times 10^{-3}$ from a measurement of $[\Gamma(B^0 \rightarrow \bar{D}^0 \pi^- \ell^+ \nu_\ell) / \Gamma_{total}] / [B(B^0 \rightarrow D^- \ell^+ \nu_\ell)]$ assuming $B(B^0 \rightarrow D^- \ell^+ \nu_\ell) = (2.12 \pm 0.20) \times 10^{-2}$, which we rescale to our best value $B(B^0 \rightarrow D^- \ell^+ \nu_\ell) = (2.24 \pm 0.09) \times 10^{-2}$. Our first error is their experiment's error and our second error is the systematic error from using our best value.
- ³ LIVENTSEV 05 reports $[\Gamma(B^0 \rightarrow \bar{D}^0 \pi^- \ell^+ \nu_\ell) / \Gamma_{total}] / [B(B^+ \rightarrow \bar{D}^0 \ell^+ \nu_\ell)] = 0.15 \pm 0.03 \pm 0.03$ which we multiply by our best value $B(B^+ \rightarrow \bar{D}^0 \ell^+ \nu_\ell) = (2.30 \pm 0.09) \times 10^{-2}$. Our first error is their experiment's error and our second error is the systematic error from using our best value.

$\Gamma(D_0^*(2300)^- \ell^+ \nu_\ell, D_0^{*-} \rightarrow \bar{D}^0 \pi^-) / \Gamma_{total}$ Γ_{10} / Γ

VALUE (units 10^{-3})	DOCUMENT ID	TECN	COMMENT
3.0±1.2 OUR AVERAGE			Error includes scale factor of 1.8.
4.4±0.8±0.6	¹ AUBERT	08BL	BABR $e^+e^- \rightarrow \Upsilon(4S)$
2.0±0.7±0.5	¹ LIVENTSEV	08	BELL $e^+e^- \rightarrow \Upsilon(4S)$

- ¹ Uses a fully reconstructed B meson as a tag on the recoil side.

$\Gamma(D_2^*(2460)^- \ell^+ \nu_\ell, D_2^{*-} \rightarrow \bar{D}^0 \pi^-) / \Gamma_{total}$ Γ_{11} / Γ

VALUE (units 10^{-3})	DOCUMENT ID	TECN	COMMENT
1.21±0.33 OUR AVERAGE			Error includes scale factor of 1.8.
1.10±0.17±0.08	¹ AUBERT	09Y	BABR $e^+e^- \rightarrow \Upsilon(4S)$
2.2 ±0.4 ±0.4	² LIVENTSEV	08	BELL $e^+e^- \rightarrow \Upsilon(4S)$

- ¹ Uses a simultaneous fit of all B semileptonic decays without full reconstruction of events. AUBERT 09Y reports $B(B^0 \rightarrow \bar{D}_2^*(2460)^- \ell^+ \nu_\ell) \cdot B(\bar{D}_2^*(2460)^- \rightarrow \bar{D}^{(*)0} \pi^-) = (1.77 \pm 0.26 \pm 0.11) \times 10^{-3}$ and the authors have provided us the individual measurement.
- ² Uses a fully reconstructed B meson as a tag on the recoil side.

$\Gamma(\bar{D}^{(*)} n \pi \ell^+ \nu_\ell (n \geq 1)) / \Gamma(D \ell^+ \nu_\ell X)$ Γ_{12} / Γ_4

VALUE	DOCUMENT ID	TECN	COMMENT
0.248±0.032±0.030	¹ AUBERT	07AN	BABR $e^+e^- \rightarrow \Upsilon(4S)$

- ¹ Uses a fully reconstructed B meson on the recoil side.

$\Gamma(\bar{D}^{*0} \pi^- \ell^+ \nu_\ell) / \Gamma_{total}$ Γ_{13} / Γ

VALUE (units 10^{-3})	DOCUMENT ID	TECN	COMMENT
5.8 ±0.8 OUR AVERAGE			Error includes scale factor of 1.4.
6.46±0.53±0.52			VOSSEN 18 BELL $e^+e^- \rightarrow \Upsilon(4S)$
4.8 ±0.8 ±0.4	¹ AUBERT	08Q	BABR $e^+e^- \rightarrow \Upsilon(4S)$

- • • We do not use the following data for averages, fits, limits, etc. • • •
- 5.9 ±2.3 ±0.2 ^{1,2} LIVENTSEV 08 BELL Repl. by VOSSEN 18
- 5.6 ±1.2 ±0.2 ^{3,4} LIVENTSEV 05 BELL Repl. by LIVENTSEV 08
- ¹ Uses a fully reconstructed B meson as a tag on the recoil side.
- ² LIVENTSEV 08 reports $(5.6 \pm 2.1 \pm 0.8) \times 10^{-3}$ from a measurement of $[\Gamma(B^0 \rightarrow \bar{D}^{*0} \pi^- \ell^+ \nu_\ell) / \Gamma_{total}] / [B(B^0 \rightarrow D^- \ell^+ \nu_\ell)]$ assuming $B(B^0 \rightarrow D^- \ell^+ \nu_\ell) = (2.12 \pm 0.20) \times 10^{-2}$, which we rescale to our best value $B(B^0 \rightarrow D^- \ell^+ \nu_\ell) = (2.24 \pm 0.09) \times$

10^{-2} . Our first error is their experiment's error and our second error is the systematic error from using our best value.

³ Excludes D^{*+} contribution to $D \pi$ modes.
⁴ LIVENTSEV 05 reports $[\Gamma(B^0 \rightarrow \bar{D}^{*0} \pi^- \ell^+ \nu_\ell) / \Gamma_{total}] / [B(B^+ \rightarrow \bar{D}^*(2007)^0 \ell^+ \nu_\ell)] = 0.10 \pm 0.02 \pm 0.01$ which we multiply by our best value $B(B^+ \rightarrow \bar{D}^*(2007)^0 \ell^+ \nu_\ell) = (5.58 \pm 0.22) \times 10^{-2}$. Our first error is their experiment's error and our second error is the systematic error from using our best value.

$\Gamma(D_1(2420)^- \ell^+ \nu_\ell, D_1^- \rightarrow \bar{D}^{*0} \pi^-) / \Gamma_{total}$ Γ_{14} / Γ

VALUE (units 10^{-3})	DOCUMENT ID	TECN	COMMENT
2.80±0.28 OUR AVERAGE			
2.78±0.24±0.25	¹ AUBERT	09Y	BABR $e^+e^- \rightarrow \Upsilon(4S)$
2.7 ±0.4 ±0.3	² AUBERT	08BL	BABR $e^+e^- \rightarrow \Upsilon(4S)$
5.4 ±1.9 ±0.9	² LIVENTSEV	08	BELL $e^+e^- \rightarrow \Upsilon(4S)$

- ¹ Uses a simultaneous measurement of all B semileptonic decays without full reconstruction of events.
- ² Uses a fully reconstructed B meson as a tag on the recoil side.

$\Gamma(D_1'(2430)^- \ell^+ \nu_\ell, D_1'^- \rightarrow \bar{D}^{*0} \pi^-) / \Gamma_{total}$ Γ_{15} / Γ

VALUE (units 10^{-3})	CL%	DOCUMENT ID	TECN	COMMENT
3.1±0.7±0.5		¹ AUBERT	08BL	BABR $e^+e^- \rightarrow \Upsilon(4S)$

• • • We do not use the following data for averages, fits, limits, etc. • • •
 <5.0 90 ¹ LIVENTSEV 08 BELL $e^+e^- \rightarrow \Upsilon(4S)$

- ¹ Uses a fully reconstructed B meson as a tag on the recoil side.

$\Gamma(D_2^*(2460)^- \ell^+ \nu_\ell, D_2^{*-} \rightarrow \bar{D}^{*0} \pi^-) / \Gamma_{total}$ Γ_{16} / Γ

VALUE (units 10^{-3})	CL%	DOCUMENT ID	TECN	COMMENT
0.68±0.12 OUR AVERAGE				
0.67±0.12±0.05		¹ AUBERT	09Y	BABR $e^+e^- \rightarrow \Upsilon(4S)$
0.7 ±0.2 ±0.2		² AUBERT	08BL	BABR $e^+e^- \rightarrow \Upsilon(4S)$

• • • We do not use the following data for averages, fits, limits, etc. • • •
 <3.0 90 ² LIVENTSEV 08 BELL $e^+e^- \rightarrow \Upsilon(4S)$

- ¹ Uses a simultaneous fit of all B semileptonic decays without full reconstruction of events. AUBERT 09Y reports $B(B^0 \rightarrow \bar{D}_2^*(2460)^- \ell^+ \nu_\ell) \cdot B(\bar{D}_2^*(2460)^- \rightarrow \bar{D}^{(*)0} \pi^-) = (1.77 \pm 0.26 \pm 0.11) \times 10^{-3}$ and the authors have provided us the individual measurement.
- ² Uses a fully reconstructed B meson as a tag on the recoil side.

$\Gamma(D^- \pi^+ \pi^- \ell^+ \nu_\ell) / \Gamma(D^- \ell^+ \nu_\ell)$ Γ_{17} / Γ_5

VALUE (units 10^{-2})	DOCUMENT ID	TECN	COMMENT
5.8±1.8±1.2	¹ LEES	16	BABR $e^+e^- \rightarrow \Upsilon(4S)$

- ¹ Measurement used electrons and muons as leptons.

$\Gamma(D^{*-} \pi^+ \pi^- \ell^+ \nu_\ell) / \Gamma(D^*(2010)^- \ell^+ \nu_\ell)$ Γ_{18} / Γ_7

VALUE (units 10^{-2})	DOCUMENT ID	TECN	COMMENT
2.8±0.8±0.6	¹ LEES	16	BABR $e^+e^- \rightarrow \Upsilon(4S)$

- ¹ Measurement used electrons and muons as leptons.

$\Gamma(\rho^- \ell^+ \nu_\ell) / \Gamma_{total}$ Γ_{19} / Γ

$\ell = e$ or μ , not sum over e and μ modes.

"OUR EVALUATION" has been obtained by the Heavy Flavor Averaging Group (HFLAV) by including both B^0 and B^+ decays. The average assumes equality of the semileptonic decay width for these isospin conjugate states.

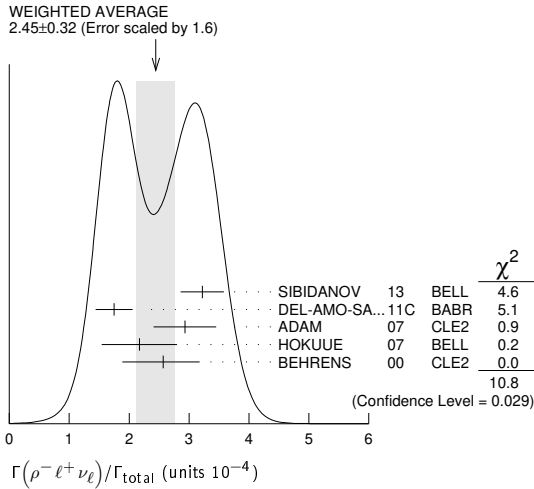
2.94±0.11±0.18 OUR EVALUATION

VALUE (units 10^{-4})	CL%	DOCUMENT ID	TECN	COMMENT
2.45±0.32 OUR AVERAGE				Error includes scale factor of 1.6. See the ideogram below.
3.22±0.27±0.24		¹ SIBIDANOV	13	BELL $e^+e^- \rightarrow \Upsilon(4S)$
1.75±0.15±0.27		² DEL-AMO-SA...	11C	BABR $e^+e^- \rightarrow \Upsilon(4S)$
2.93±0.37±0.37		³ ADAM	07	CLE2 $e^+e^- \rightarrow \Upsilon(4S)$
2.17±0.54±0.32		⁴ HOKUUE	07	BELL $e^+e^- \rightarrow \Upsilon(4S)$
2.57±0.29 ^{+0.53} _{-0.62}		⁵ BEHRENS	00	CLE2 $e^+e^- \rightarrow \Upsilon(4S)$

• • • We do not use the following data for averages, fits, limits, etc. • • •
 2.14±0.21±0.56 ² AUBERT,B 05o BABR Repl. by DEL-AMO-SANCHEZ 11c
 2.17±0.34^{+0.62}_{-0.68} ⁶ ATHAR 03 CLE2 Repl. by ADAM 07
 3.29±0.42±0.72 ⁷ AUBERT 03E BABR Repl. by AUBERT,B 05o
 2.69±0.41^{+0.61}_{-0.64} ⁸ BEHRENS 00 CLE2 $e^+e^- \rightarrow \Upsilon(4S)$
 2.5 ±0.4 ^{+0.7}_{-0.9} ⁹ ALEXANDER 96T CLE2 Repl. by BEHRENS 00
 <4.1 90 ¹⁰ BEAN 93B CLE2 $e^+e^- \rightarrow \Upsilon(4S)$

- ¹ The signal events are tagged by a second B meson reconstructed in the fully hadronic decays.
- ² B^+ and B^0 decays combined assuming isospin symmetry. Systematic errors include both experimental and form-factor uncertainties.
- ³ The B^0 and B^+ results are combined assuming the isospin, B lifetimes, and relative charged/neutral B production at the $\Upsilon(4S)$.
- ⁴ The signal events are tagged by a second B meson reconstructed in the semileptonic mode $B \rightarrow D^{(*)} \ell \nu_\ell$.
- ⁵ Averaging with ALEXANDER 96T results including experimental and theoretical correlations considered, BEHRENS 00 reports systematic errors $\pm 0.33 \pm 0.41$, where the second error is theoretical model dependence. We combine these in quadrature.

- ⁶ ATHAR 03 reports systematic errors $^{+0.47}_{-0.50} \pm 0.41 \pm 0.01$, which are experimental systematic, systematic due to residual form-factor uncertainties in the signal, and systematic due to residual form-factor uncertainties in the cross-feed modes, respectively. We combine these in quadrature.
- ⁷ Uses isospin constraints and extrapolation to all electron energies according to five different form-factor calculations. The second error combines the systematic and theoretical uncertainties in quadrature.
- ⁸ BEHRENS 00 reports $^{+0.35}_{-0.40} \pm 0.50$, where the second error is the theoretical model dependence. We combine these in quadrature. B^+ and B^0 decays combined using isospin symmetry: $\Gamma(B^0 \rightarrow \rho^- \ell^+ \nu) = 2\Gamma(B^+ \rightarrow \rho^0 \ell^+ \nu) \approx 2\Gamma(B^+ \rightarrow \omega \ell^+ \nu)$. No evidence for $\omega \ell \nu$ is reported.
- ⁹ ALEXANDER 96T reports $^{+0.5}_{-0.7} \pm 0.5$ where the second error is the theoretical model dependence. We combine these in quadrature. B^+ and B^0 decays combined using isospin symmetry: $\Gamma(B^0 \rightarrow \rho^- \ell^+ \nu) = 2\Gamma(B^+ \rightarrow \rho^0 \ell^+ \nu) \approx 2\Gamma(B^+ \rightarrow \omega \ell^+ \nu)$. No evidence for $\omega \ell \nu$ is reported.
- ¹⁰ BEAN 93B limit set using ISGW Model. Using isospin and the quark model to combine $\Gamma(\rho^0 \ell^+ \nu)$ and $\Gamma(\omega \ell^+ \nu)$ with this result, they obtain a limit $<(1.6-2.7) \times 10^{-4}$ at 90% CL for $B^+ \rightarrow (\omega \text{ or } \rho^0) \ell^+ \nu$. The range corresponds to the ISGW, WSB, and KS models. An upper limit on $|V_{ub}/V_{cb}| < 0.08-0.13$ at 90% CL is derived as well.



Γ(π⁻ℓ⁺ν_ℓ)/Γ_{total} **Γ₂₀/Γ**

"OUR EVALUATION" is provided by the Heavy Flavor Averaging Group (HFLAV) and the procedure is described at <https://hflav.web.cern.ch/>.

VALUE (units 10 ⁻⁴)	DOCUMENT ID	TECN	COMMENT
1.50 ± 0.06 OUR EVALUATION			
1.46 ± 0.04 OUR AVERAGE			
1.49 ± 0.09 ± 0.07	¹ SIBIDANOV 13	BELL	e ⁺ e ⁻ → T(4S)
1.47 ± 0.05 ± 0.06	^{2,3} LEES 12AA	BABR	e ⁺ e ⁻ → T(4S)
1.41 ± 0.05 ± 0.07	⁴ DEL-AMO-SA...11C	BABR	e ⁺ e ⁻ → T(4S)
1.49 ± 0.04 ± 0.07	² HA 11	BELL	e ⁺ e ⁻ → T(4S)
1.54 ± 0.17 ± 0.09	⁴ AUBERT 08AV	BABR	e ⁺ e ⁻ → T(4S)
1.37 ± 0.15 ± 0.11	^{5,6} ADAM 07	CLE2	e ⁺ e ⁻ → T(4S)
1.38 ± 0.19 ± 0.14	⁷ HOKUUE 07	BELL	e ⁺ e ⁻ → T(4S)
• • • We do not use the following data for averages, fits, limits, etc. • • •			
1.42 ± 0.05 ± 0.08	² DEL-AMO-SA...11F	BABR	Repl. by LEES 12AA
1.46 ± 0.07 ± 0.08	⁸ AUBERT 07J	BABR	Repl. by DEL-AMO-SANCHEZ 11F
1.33 ± 0.17 ± 0.11	⁹ AUBERT,B 06K	BABR	Repl. by AUBERT 08AV
1.38 ± 0.10 ± 0.18	¹⁰ AUBERT,B 05o	BABR	Repl. by DEL-AMO-SANCHEZ 11c
1.33 ± 0.18 ± 0.13	¹¹ ATHAR 03	CLE2	Repl. by ADAM 07
1.8 ± 0.4 ± 0.4	¹² ALEXANDER 96T	CLE2	Repl. by ATHAR 03

- ¹ The signal events are tagged by a second B meson reconstructed in the fully hadronic decays.
- ² Uses loose neutrino reconstruction technique. Assumes $B(T(4S) \rightarrow B^+ B^-) = (51.6 \pm 0.6)\%$ and $B(T(4S) \rightarrow B^0 \bar{B}^0) = (48.4 \pm 0.6)\%$.
- ³ Reports also a branching fraction value $B(B^0 \rightarrow \pi^- \ell^+ \nu) = (1.45 \pm 0.04 \pm 0.06) \times 10^{-4}$ from the decays of B^+ and B^0 that are combined using the isospin symmetry relation.
- ⁴ Using the isospin symmetry relation, B^+ and B^0 branching fractions are combined.
- ⁵ The B^0 and B^+ results are combined assuming the isospin, B lifetimes, and relative charged/neutral B production at the $T(4S)$.
- ⁶ Also report the rate for $q^2 > 16 \text{ GeV}^2$ of $(0.41 \pm 0.08 \pm 0.04) \times 10^{-4}$ from which they obtain $|V_{ub}| = 3.6 \pm 0.4 \pm 0.2^{+0.6}_{-0.4}$ (last error is from theory).
- ⁷ The signal events are tagged by a second B meson reconstructed in the semileptonic mode $B \rightarrow D^{(*)} \ell \nu$.
- ⁸ The analysis uses events in which the signal B decays are reconstructed with an innovative loose neutrino reconstruction technique.
- ⁹ The signals are tagged by a second B meson reconstructed in a semileptonic or hadronic decay. The B^0 and B^+ results are combined assuming the isospin symmetry.
- ¹⁰ B^+ and B^0 decays combined assuming isospin symmetry. Systematic errors include both experimental and form-factor uncertainties.

- ¹¹ ATHAR 03 reports systematic errors $0.11 \pm 0.01 \pm 0.07$, which are experimental systematic, systematic due to residual form-factor uncertainties in the signal, and systematic due to residual form-factor uncertainties in the cross-feed modes, respectively. We combine these in quadrature.
- ¹² ALEXANDER 96T gives systematic errors $\pm 0.3 \pm 0.2$ where the second error reflects the estimated model dependence. We combine these in quadrature. Assumes isospin symmetry: $\Gamma(B^0 \rightarrow \pi^- \ell^+ \nu) = 2 \times \Gamma(B^+ \rightarrow \pi^0 \ell^+ \nu)$.

Γ(π⁻μ⁺ν_μ)/Γ_{total} **Γ₂₁/Γ**

VALUE	DOCUMENT ID	TECN	COMMENT
• • • We do not use the following data for averages, fits, limits, etc. • • •			
seen	¹ ALBRECHT 91c	ARG	
¹ In ALBRECHT 91c, one event is fully reconstructed providing evidence for the $b \rightarrow u$ transition.			

Γ(π⁻τ⁺ν_τ)/Γ_{total} **Γ₂₂/Γ**

VALUE	CL%	DOCUMENT ID	TECN	COMMENT
<2.5 × 10⁻⁴	90	¹ HAMER 16	BELL	e ⁺ e ⁻ → T(4S)
¹ Assumes equal production of B^+ and B^0 at the $T(4S)$.				

Γ(K[±]X)/Γ_{total} **Γ₂₃/Γ**

VALUE	DOCUMENT ID	TECN	COMMENT
0.78 ± 0.08	¹ ALBRECHT 96D	ARG	e ⁺ e ⁻ → T(4S)
¹ Average multiplicity.			

Γ(D⁰X)/Γ_{total} **Γ₂₄/Γ**

VALUE	DOCUMENT ID	TECN	COMMENT
0.081 ± 0.014 ± 0.005	¹ AUBERT 07N	BABR	e ⁺ e ⁻ → T(4S)
• • • We do not use the following data for averages, fits, limits, etc. • • •			
0.063 ± 0.019 ± 0.005	¹ AUBERT,BE 04B	BABR	Repl. by AUBERT 07N
¹ Events are selected by completely reconstructing one B and searching for a reconstructed charmed particle in the rest of the event. The last error includes systematic and charm branching ratio uncertainties.			

Γ(D⁰X)/Γ_{total} **Γ₂₅/Γ**

VALUE	DOCUMENT ID	TECN	COMMENT
0.474 ± 0.020 ± 0.020 -0.019	¹ AUBERT 07N	BABR	e ⁺ e ⁻ → T(4S)
• • • We do not use the following data for averages, fits, limits, etc. • • •			
0.511 ± 0.031 ± 0.028	¹ AUBERT,BE 04B	BABR	Repl. by AUBERT 07N
¹ Events are selected by completely reconstructing one B and searching for a reconstructed charmed particle in the rest of the event. The last error includes systematic and charm branching ratio uncertainties.			

Γ(D⁰X)/[Γ(D⁰X) + Γ(D⁰X)] **Γ₂₄/[Γ₂₄ + Γ₂₅]**

VALUE	DOCUMENT ID	TECN	COMMENT
0.146 ± 0.022 ± 0.006	AUBERT 07N	BABR	e ⁺ e ⁻ → T(4S)
• • • We do not use the following data for averages, fits, limits, etc. • • •			
0.110 ± 0.031 ± 0.008	AUBERT,BE 04B	BABR	Repl. by AUBERT 07N

Γ(D⁺X)/Γ_{total} **Γ₂₆/Γ**

VALUE	CL%	DOCUMENT ID	TECN	COMMENT
<0.039	90	¹ AUBERT 07N	BABR	e ⁺ e ⁻ → T(4S)
• • • We do not use the following data for averages, fits, limits, etc. • • •				
<0.051	90	¹ AUBERT,BE 04B	BABR	Repl. by AUBERT 07N
¹ Events are selected by completely reconstructing one B and searching for a reconstructed charmed particle in the rest of the event. The last error includes systematic and charm branching ratio uncertainties.				

Γ(D⁻X)/Γ_{total} **Γ₂₇/Γ**

VALUE	DOCUMENT ID	TECN	COMMENT
0.369 ± 0.016 ± 0.030 -0.027	¹ AUBERT 07N	BABR	e ⁺ e ⁻ → T(4S)
• • • We do not use the following data for averages, fits, limits, etc. • • •			
0.397 ± 0.030 ± 0.040 -0.038	¹ AUBERT,BE 04B	BABR	Repl. by AUBERT 07N
¹ Events are selected by completely reconstructing one B and searching for a reconstructed charmed particle in the rest of the event. The last error includes systematic and charm branching ratio uncertainties.			

Γ(D⁺X)/[Γ(D⁺X) + Γ(D⁻X)] **Γ₂₆/[Γ₂₆ + Γ₂₇]**

VALUE	DOCUMENT ID	TECN	COMMENT
0.058 ± 0.028 ± 0.006	AUBERT 07N	BABR	e ⁺ e ⁻ → T(4S)
• • • We do not use the following data for averages, fits, limits, etc. • • •			
0.055 ± 0.040 ± 0.006	AUBERT,BE 04B	BABR	Repl. by AUBERT 07N

Γ(D_s[±]X)/Γ_{total} **Γ₂₈/Γ**

VALUE	DOCUMENT ID	TECN	COMMENT
0.103 ± 0.012 ± 0.017 -0.014	¹ AUBERT 07N	BABR	e ⁺ e ⁻ → T(4S)
• • • We do not use the following data for averages, fits, limits, etc. • • •			
0.109 ± 0.021 ± 0.039 -0.024	¹ AUBERT,BE 04B	BABR	Repl. by AUBERT 07N
¹ Events are selected by completely reconstructing one B and searching for a reconstructed charmed particle in the rest of the event. The last error includes systematic and charm branching ratio uncertainties.			

Meson Particle Listings

B^0

$\Gamma(D_s^- X)/\Gamma_{total}$ Γ_{29}/Γ

VALUE	CL%	DOCUMENT ID	TECN	COMMENT
<0.026	90	¹ AUBERT	07N	BABR $e^+e^- \rightarrow \Upsilon(4S)$
••• We do not use the following data for averages, fits, limits, etc. •••				
<0.087	90	¹ AUBERT,BE	04B	BABR Repl. by AUBERT 07N

¹ Events are selected by completely reconstructing one B and searching for a reconstructed charmed particle in the rest of the event. The last error includes systematic and charm branching ratio uncertainties.

$\Gamma(D_s^+ X)/[\Gamma(D_s^+ X) + \Gamma(D_s^- X)]$ $\Gamma_{28}/(\Gamma_{28} + \Gamma_{29})$

VALUE	DOCUMENT ID	TECN	COMMENT
0.879 ± 0.066 ± 0.005	AUBERT	07N	BABR $e^+e^- \rightarrow \Upsilon(4S)$
••• We do not use the following data for averages, fits, limits, etc. •••			
0.733 ± 0.092 ± 0.010	AUBERT,BE	04B	BABR Repl. by AUBERT 07N

$\Gamma(A_c^+ X)/\Gamma_{total}$ Γ_{30}/Γ

VALUE	CL%	DOCUMENT ID	TECN	COMMENT
<0.031	90	¹ AUBERT	07N	BABR $e^+e^- \rightarrow \Upsilon(4S)$
••• We do not use the following data for averages, fits, limits, etc. •••				
<0.038	90	¹ AUBERT,BE	04B	BABR Repl. by AUBERT 07N

¹ Events are selected by completely reconstructing one B and searching for a reconstructed charmed particle in the rest of the event. The last error includes systematic and charm branching ratio uncertainties.

$\Gamma(\bar{A}_c^+ X)/\Gamma_{total}$ Γ_{31}/Γ

VALUE	DOCUMENT ID	TECN	COMMENT
0.05 ± 0.010 ± 0.019 -0.011	¹ AUBERT	07N	BABR $e^+e^- \rightarrow \Upsilon(4S)$
••• We do not use the following data for averages, fits, limits, etc. •••			
0.049 ± 0.017 ± 0.018 -0.011	¹ AUBERT,BE	04B	BABR Repl. by AUBERT 07N

¹ Events are selected by completely reconstructing one B and searching for a reconstructed charmed particle in the rest of the event. The last error includes systematic and charm branching ratio uncertainties.

$\Gamma(A_c^+ X)/[\Gamma(A_c^+ X) + \Gamma(\bar{A}_c^+ X)]$ $\Gamma_{30}/(\Gamma_{30} + \Gamma_{31})$

VALUE	DOCUMENT ID	TECN	COMMENT
0.243 ± 0.119 ± 0.003 -0.121	AUBERT	07N	BABR $e^+e^- \rightarrow \Upsilon(4S)$
••• We do not use the following data for averages, fits, limits, etc. •••			
0.286 ± 0.142 ± 0.007	AUBERT,BE	04B	BABR Repl. by AUBERT 07N

$\Gamma(\Upsilon X)/\Gamma_{total}$ Γ_{32}/Γ

VALUE	DOCUMENT ID	TECN	COMMENT
0.947 ± 0.030 ± 0.045 -0.040	¹ AUBERT	07N	BABR $e^+e^- \rightarrow \Upsilon(4S)$
••• We do not use the following data for averages, fits, limits, etc. •••			
1.039 ± 0.051 ± 0.063 -0.058	¹ AUBERT,BE	04B	BABR Repl. by AUBERT 07N

¹ Events are selected by completely reconstructing one B and searching for a reconstructed charmed particle in the rest of the event. The last error includes systematic and charm branching ratio uncertainties.

$\Gamma(cX)/\Gamma_{total}$ Γ_{33}/Γ

VALUE	DOCUMENT ID	TECN	COMMENT
0.246 ± 0.024 ± 0.021 -0.017	¹ AUBERT	07N	BABR $e^+e^- \rightarrow \Upsilon(4S)$
••• We do not use the following data for averages, fits, limits, etc. •••			
0.237 ± 0.036 ± 0.041 -0.027	¹ AUBERT,BE	04B	BABR Repl. by AUBERT 07N

¹ Events are selected by completely reconstructing one B and searching for a reconstructed charmed particle in the rest of the event. The last error includes systematic and charm branching ratio uncertainties.

$\Gamma(\Upsilon/cX)/\Gamma_{total}$ Γ_{34}/Γ

VALUE	DOCUMENT ID	TECN	COMMENT
1.193 ± 0.030 ± 0.053 -0.049	¹ AUBERT	07N	BABR $e^+e^- \rightarrow \Upsilon(4S)$
••• We do not use the following data for averages, fits, limits, etc. •••			
1.276 ± 0.062 ± 0.088 -0.074	¹ AUBERT,BE	04B	BABR Repl. by AUBERT 07N

¹ Events are selected by completely reconstructing one B and searching for a reconstructed charmed particle in the rest of the event. The last error includes systematic and charm branching ratio uncertainties.

$\Gamma(D^- \pi^+)/\Gamma_{total}$ Γ_{35}/Γ

VALUE (units 10^{-3})	EVTS	DOCUMENT ID	TECN	COMMENT
2.51 ± 0.08 OUR FIT				
2.56 ± 0.08 OUR AVERAGE				
2.48 ± 0.01 ± 0.10		WAHEED	22	BELL $e^+e^- \rightarrow \Upsilon(4S)$
2.55 ± 0.05 ± 0.16		¹ AUBERT	07H	BABR $e^+e^- \rightarrow \Upsilon(4S)$
3.03 ± 0.23 ± 0.23		² AUBERT,BE	06J	BABR $e^+e^- \rightarrow \Upsilon(4S)$
2.68 ± 0.12 ± 0.24		^{1,3} AHMED	02B	CLE2 $e^+e^- \rightarrow \Upsilon(4S)$
2.7 ± 0.6 ± 0.5		⁴ BORTOLETTO	092	CLEO $e^+e^- \rightarrow \Upsilon(4S)$
4.8 ± 1.1 ± 1.1	22	⁵ ALBRECHT	90J	ARG $e^+e^- \rightarrow \Upsilon(4S)$
5.1 ± 2.8 ± 1.3 -2.5 -1.2	4	⁶ BEBEK	87	CLEO $e^+e^- \rightarrow \Upsilon(4S)$

••• We do not use the following data for averages, fits, limits, etc. •••

2.73 ± 0.19 ± 0.05		^{1,7} AUBERT,B	04o	BABR Repl. by AUBERT 07H
2.83 ± 0.42 ± 0.05	81	⁸ ALAM	94	CLE2 Repl. by AHMED 02b
3.1 ± 1.3 ± 1.0	7	⁵ ALBRECHT	88k	ARG $e^+e^- \rightarrow \Upsilon(4S)$

- Assumes equal production of B^+ and B^0 at the $\Upsilon(4S)$.
- Uses a missing-mass method. Does not depend on D branching fractions or B^+/B^0 production rates.
- AHMED 02b reports an additional uncertainty on the branching ratios to account for 4.5% uncertainty on relative production of B^0 and B^+ , which is not included here.
- BORTOLETTO 92 assumes equal production of B^+ and B^0 at the $\Upsilon(4S)$ and uses Mark III branching fractions for the D .
- ALBRECHT 88k assumes $B^0\bar{B}^0:B^+B^-$ production ratio is 45:55. Superseded by ALBRECHT 90J which assumes 50:50.
- BEBEK 87 value has been updated in BERKELMAN 91 to use same assumptions as noted for BORTOLETTO 92.
- AUBERT,B 04o reports $[\Gamma(B^0 \rightarrow D^- \pi^+)/\Gamma_{total}] \times [B(D^+ \rightarrow K_S^0 \pi^+)] = (42.7 \pm 2.1 \pm 2.2) \times 10^{-6}$ which we divide by our best value $B(D^+ \rightarrow K_S^0 \pi^+) = (1.562 \pm 0.031) \times 10^{-2}$. Our first error is their experiment's error and our second error is the systematic error from using our best value.
- ALAM 94 reports $[\Gamma(B^0 \rightarrow D^- \pi^+)/\Gamma_{total}] \times [B(D^+ \rightarrow K^- 2\pi^+)] = (0.265 \pm 0.032 \pm 0.023) \times 10^{-3}$ which we divide by our best value $B(D^+ \rightarrow K^- 2\pi^+) = (9.38 \pm 0.16) \times 10^{-2}$. Our first error is their experiment's error and our second error is the systematic error from using our best value. Assumes equal production of B^+ and B^0 at the $\Upsilon(4S)$.

$\Gamma(D^- \ell^+ \nu_\ell)/\Gamma(D^- \pi^+)$ Γ_5/Γ_{35}

VALUE	DOCUMENT ID	TECN	COMMENT
9.9 ± 1.0 ± 0.9	AALTONEN	09E	CDF $p\bar{p}$ at 1.96 TeV

$\Gamma(D^- \rho^+)/\Gamma_{total}$ Γ_{36}/Γ

VALUE	EVTS	DOCUMENT ID	TECN	COMMENT
0.0076 ± 0.0012 OUR AVERAGE				
0.0075 ± 0.0013 ± 0.0001	79	¹ ALAM	94	CLE2 $e^+e^- \rightarrow \Upsilon(4S)$
0.009 ± 0.005 ± 0.003	9	² ALBRECHT	90J	ARG $e^+e^- \rightarrow \Upsilon(4S)$
••• We do not use the following data for averages, fits, limits, etc. •••				
0.022 ± 0.012 ± 0.009	6	² ALBRECHT	88k	ARG $e^+e^- \rightarrow \Upsilon(4S)$

- ALAM 94 reports $[\Gamma(B^0 \rightarrow D^- \rho^+)/\Gamma_{total}] \times [B(D^+ \rightarrow K^- 2\pi^+)] = 0.000704 \pm 0.000096 \pm 0.000070$ which we divide by our best value $B(D^+ \rightarrow K^- 2\pi^+) = (9.38 \pm 0.16) \times 10^{-2}$. Our first error is their experiment's error and our second error is the systematic error from using our best value. Assumes equal production of B^+ and B^0 at the $\Upsilon(4S)$.
- ALBRECHT 88k assumes $B^0\bar{B}^0:B^+B^-$ production ratio is 45:55. Superseded by ALBRECHT 90J which assumes 50:50.

$\Gamma(D^- K^0 \pi^+)/\Gamma_{total}$ Γ_{37}/Γ

VALUE (units 10^{-4})	DOCUMENT ID	TECN	COMMENT
4.9 ± 0.7 ± 0.5	¹ AUBERT,BE	05B	BABR $e^+e^- \rightarrow \Upsilon(4S)$
¹ Assumes equal production of B^+ and B^0 at the $\Upsilon(4S)$.			

$\Gamma(D^- K^*(892^+)/\Gamma_{total}$ Γ_{38}/Γ

VALUE (units 10^{-4})	DOCUMENT ID	TECN	COMMENT
4.5 ± 0.7 OUR AVERAGE			
4.6 ± 0.6 ± 0.5	¹ AUBERT,BE	05B	BABR $e^+e^- \rightarrow \Upsilon(4S)$
3.7 ± 1.5 ± 1.0	¹ MAHAPATRA	02	CLE2 $e^+e^- \rightarrow \Upsilon(4S)$
¹ Assumes equal production of B^+ and B^0 at the $\Upsilon(4S)$.			

$\Gamma(D^- \omega \pi^+)/\Gamma_{total}$ Γ_{39}/Γ

VALUE	DOCUMENT ID	TECN	COMMENT
0.0028 ± 0.0005 ± 0.0004	¹ ALEXANDER	01B	CLE2 $e^+e^- \rightarrow \Upsilon(4S)$
¹ Assumes equal production of B^+ and B^0 at the $\Upsilon(4S)$. The signal is consistent with all observed $\omega \pi^+$ having proceeded through the ρ^{++} resonance at mass $1349 \pm 25 \pm 5$ MeV and width $547 \pm 86 \pm 46$ MeV.			

$\Gamma(D^- K^+)/\Gamma(D^- \pi^+)$ Γ_{40}/Γ_{35}

VALUE (units 10^{-2})	DOCUMENT ID	TECN	COMMENT
8.19 ± 0.20 OUR AVERAGE			
8.19 ± 0.20 ± 0.23	WAHEED	22	BELL $e^+e^- \rightarrow \Upsilon(4S)$
8.22 ± 0.11 ± 0.25	AAIJ	13P	LHCB $p\bar{p}$ at 7 TeV
6.8 ± 1.5 ± 0.7	ABE	01I	BELL $e^+e^- \rightarrow \Upsilon(4S)$

$\Gamma(D^- K^+ \pi^+ \pi^-)/\Gamma(D^- \pi^+ \pi^+ \pi^-)$ Γ_{41}/Γ_{47}

VALUE (units 10^{-2})	DOCUMENT ID	TECN	COMMENT
5.9 ± 1.1 ± 0.5	AAIJ	12T	LHCB $p\bar{p}$ at 7 TeV

$\Gamma(D^- K^+ \bar{K}^0)/\Gamma_{total}$ Γ_{42}/Γ

VALUE (units 10^{-4})	CL%	DOCUMENT ID	TECN	COMMENT
<3.1	90	¹ DRUTSKOY	02	BELL $e^+e^- \rightarrow \Upsilon(4S)$
¹ Assumes equal production of B^+ and B^0 at the $\Upsilon(4S)$.				

$\Gamma(D^- K^+ \bar{K}^*(892^0))/\Gamma_{total}$ Γ_{43}/Γ

VALUE (units 10^{-4})	DOCUMENT ID	TECN	COMMENT
8.8 ± 1.1 ± 1.5	¹ DRUTSKOY	02	BELL $e^+e^- \rightarrow \Upsilon(4S)$
¹ Assumes equal production of B^+ and B^0 at the $\Upsilon(4S)$.			

See key on page 1127

Meson Particle Listings

B^0

$\Gamma(\bar{D}^0 \pi^+ \pi^-)/\Gamma_{total}$ Γ_{44}/Γ

VALUE (units 10^{-4})	CL% EVTS	DOCUMENT ID	TECN	COMMENT
8.8 ± 0.5 OUR AVERAGE				
8.95 ± 0.15 ± 0.52		1 AAIJ	15Y	LHCB pp at 7, 8 TeV
8.4 ± 0.4 ± 0.8		2 KUZMIN	07	BELL $e^+e^- \rightarrow \Upsilon(4S)$
• • • We do not use the following data for averages, fits, limits, etc. • • •				
8.0 ± 0.6 ± 1.5		2,3 SATPATHY	03	BELL Repl. by KUZMIN 07
< 16	90	2 ALAM	94	CLE2 $e^+e^- \rightarrow \Upsilon(4S)$
< 70	90	4 BORTOLETTO92	CLEO	$e^+e^- \rightarrow \Upsilon(4S)$
< 340	90	5 BEBEK	87	CLEO $e^+e^- \rightarrow \Upsilon(4S)$
700 ± 500	5	6 BEHREND	83	CLEO $e^+e^- \rightarrow \Upsilon(4S)$

¹ The second uncertainty combines in quadrature all systematic uncertainties quoted in the paper. AAIJ 15Y reports $B(B^0 \rightarrow \bar{D}^0 \pi^+ \pi^-) = (8.46 \pm 0.14 \pm 0.49) \times 10^{-4}$ in the kinematic region $m(\bar{D}^0 \pi^\pm) > 2.1$ GeV which we corrected to the full phase-space dividing by 0.945 from Belle.

² Assumes equal production of B^+ and B^0 at the $\Upsilon(4S)$.

³ No assumption about the intermediate mechanism is made in the analysis.

⁴ BORTOLETTO 92 assumes equal production of B^+ and B^0 at the $\Upsilon(4S)$ and uses Mark III branching fractions for the D . The product branching fraction into $D_0^*(2340)\pi$ followed by $D_0^*(2340) \rightarrow D^0\pi$ is < 0.0001 at 90% CL and into $D_2^*(2460)$ followed by $D_2^*(2460) \rightarrow D^0\pi$ is < 0.0004 at 90% CL.

⁵ BEBEK 87 assume the $\Upsilon(4S)$ decays 43% to $B^0\bar{B}^0$. We rescale to 50%. $B(D^0 \rightarrow K^-\pi^+) = (4.2 \pm 0.4 \pm 0.4)\%$ and $B(D^0 \rightarrow K^-\pi^+\pi^+) = (9.1 \pm 0.8 \pm 0.8)\%$ were used.

⁶ Corrected by us using assumptions: $B(D^0 \rightarrow K^-\pi^+) = (0.042 \pm 0.006)$ and $B(\Upsilon(4S) \rightarrow B^0\bar{B}^0) = 50\%$. The product branching ratio is $B(B^0 \rightarrow \bar{D}^0 \pi^+ \pi^-)B(\bar{D}^0 \rightarrow K^+\pi^-) = (0.39 \pm 0.26) \times 10^{-2}$.

$\Gamma(D^*(2010)^-\pi^+)/\Gamma_{total}$ Γ_{45}/Γ

VALUE (units 10^{-3})	EVTS	DOCUMENT ID	TECN	COMMENT
2.74 ± 0.13 OUR AVERAGE				
2.79 ± 0.08 ± 0.17		1 AUBERT	07H	BABR $e^+e^- \rightarrow \Upsilon(4S)$
2.48 ± 0.34 ± 0.08		2,3 AUBERT, BE	06J	BABR $e^+e^- \rightarrow \Upsilon(4S)$
2.81 ± 0.24 ± 0.05		4 BRANDENB...	98	CLE2 $e^+e^- \rightarrow \Upsilon(4S)$
2.6 ± 0.3 ± 0.4	82	5 ALAM	94	CLE2 $e^+e^- \rightarrow \Upsilon(4S)$
3.37 ± 0.96 ± 0.02		6 BORTOLETTO92	CLEO	$e^+e^- \rightarrow \Upsilon(4S)$
2.36 ± 0.88 ± 0.02	12	7 ALBRECHT	90J	ARG $e^+e^- \rightarrow \Upsilon(4S)$
2.36 +1.50 ± 0.02 -1.10	5	8 BEBEK	87	CLEO $e^+e^- \rightarrow \Upsilon(4S)$
• • • We do not use the following data for averages, fits, limits, etc. • • •				
10 ± 4 ± 1	8	9 AKERS	94J	OPAL $e^+e^- \rightarrow Z$
2.7 ± 1.4 ± 1.0	5	10 ALBRECHT	87c	ARG $e^+e^- \rightarrow \Upsilon(4S)$
3.5 ± 2 ± 2		11 ALBRECHT	86F	ARG $e^+e^- \rightarrow \Upsilon(4S)$
17 ± 5 ± 5	41	12 GILES	84	CLEO $e^+e^- \rightarrow \Upsilon(4S)$

¹ Assumes equal production of B^+ and B^0 at the $\Upsilon(4S)$.

² AUBERT, BE 06J reports $[\Gamma(B^0 \rightarrow D^*(2010)^-\pi^+)/\Gamma_{total}] / [B(B^0 \rightarrow D^-\pi^+)] = 0.99 \pm 0.11 \pm 0.08$ which we multiply by our best value $B(B^0 \rightarrow D^-\pi^+) = (2.51 \pm 0.08) \times 10^{-3}$. Our first error is their experiment's error and our second error is the systematic error from using our best value.

³ Uses a missing-mass method. Does not depend on D branching fractions or B^+/\bar{B}^0 production rates.

⁴ BRANDENBURG 98 assume equal production of B^+ and B^0 at $\Upsilon(4S)$ and use the D^* reconstruction technique. The first error is their experiment's error and the second error is the systematic error from the PDG 96 value of $B(D^* \rightarrow D\pi)$.

⁵ ALAM 94 assume equal production of B^+ and B^0 at the $\Upsilon(4S)$ and use the CLEO II $B(D^*(2010)^+ \rightarrow D^0\pi^+)$ and absolute $B(D^0 \rightarrow K^-\pi^+)$ and the PDG 1992 $B(D^0 \rightarrow K^-\pi^+\pi^0)/B(D^0 \rightarrow K^-\pi^+)$ and $B(D^0 \rightarrow K^-2\pi^+\pi^-)/B(D^0 \rightarrow K^-\pi^+)$.

⁶ BORTOLETTO 92 reports $(4.0 \pm 1.0 \pm 0.7) \times 10^{-3}$ from a measurement of $[\Gamma(B^0 \rightarrow D^*(2010)^-\pi^+)/\Gamma_{total}] \times [B(D^*(2010)^+ \rightarrow D^0\pi^+)]$ assuming $B(D^*(2010)^+ \rightarrow D^0\pi^+) = 0.57 \pm 0.06$, which we rescale to our best value $B(D^*(2010)^+ \rightarrow D^0\pi^+) = (67.7 \pm 0.5) \times 10^{-2}$. Our first error is their experiment's error and our second error is the systematic error from using our best value. Assumes equal production of B^+ and B^0 at the $\Upsilon(4S)$ and uses Mark III branching fractions for the D .

⁷ ALBRECHT 90J reports $(2.8 \pm 0.9 \pm 0.6) \times 10^{-3}$ from a measurement of $[\Gamma(B^0 \rightarrow D^*(2010)^-\pi^+)/\Gamma_{total}] \times [B(D^*(2010)^+ \rightarrow D^0\pi^+)]$ assuming $B(D^*(2010)^+ \rightarrow D^0\pi^+) = 0.57 \pm 0.06$, which we rescale to our best value $B(D^*(2010)^+ \rightarrow D^0\pi^+) = (67.7 \pm 0.5) \times 10^{-2}$. Our first error is their experiment's error and our second error is the systematic error from using our best value. Assumes equal production of B^+ and B^0 at the $\Upsilon(4S)$ and uses Mark III branching fractions for the D .

⁸ BEBEK 87 reports $(2.8^{+1.5+1.0}_{-1.2-0.6}) \times 10^{-3}$ from a measurement of $[\Gamma(B^0 \rightarrow D^*(2010)^-\pi^+)/\Gamma_{total}] \times [B(D^*(2010)^+ \rightarrow D^0\pi^+)]$ assuming $B(D^*(2010)^+ \rightarrow D^0\pi^+) = 0.57 \pm 0.06$, which we rescale to our best value $B(D^*(2010)^+ \rightarrow D^0\pi^+) = (67.7 \pm 0.5) \times 10^{-2}$. Our first error is their experiment's error and our second error is the systematic error from using our best value. Updated in BERKELMAN 91 to use same assumptions as noted for BORTOLETTO 92 and ALBRECHT 90J.

⁹ Assumes $B(Z \rightarrow b\bar{b}) = 0.217$ and 38% B_d production fraction.

¹⁰ ALBRECHT 87c use PDG 86 branching ratios for D and $D^*(2010)$ and assume $B(\Upsilon(4S) \rightarrow B^+B^-) = 55\%$ and $B(\Upsilon(4S) \rightarrow B^0\bar{B}^0) = 45\%$. Superseded by ALBRECHT 90J.

¹¹ ALBRECHT 86F uses pseudomass that is independent of D^0 and D^+ branching ratios.

¹² Assumes $B(D^*(2010)^+ \rightarrow D^0\pi^+) = 0.60^{+0.08}_{-0.15}$. Assumes $B(\Upsilon(4S) \rightarrow B^0\bar{B}^0) = 0.40 \pm 0.02$. Does not depend on D branching ratios.

$\Gamma(D^*(2010)^-\ell^+\nu_\ell)/\Gamma(D^*(2010)^-\pi^+)$ Γ_7/Γ_{45}

VALUE	DOCUMENT ID	TECN	COMMENT
16.5 ± 2.3 ± 1.1	AALTONEN	09E	CDF $p\bar{p}$ at 1.96 TeV

$\Gamma(\bar{D}^0 K^+ K^-)/\Gamma(\bar{D}^0 \pi^+ \pi^-)$ Γ_{46}/Γ_{44}

VALUE	DOCUMENT ID	TECN	COMMENT
0.069 ± 0.004 ± 0.003	AAIJ	18Az	LHCB pp at 7, 8 TeV
• • • We do not use the following data for averages, fits, limits, etc. • • •			
0.056 ± 0.011 ± 0.007	AAIJ	12A	LHCB pp at 7 TeV, Repl. by AAIJ 18Az

$\Gamma(D^-\pi^+\pi^+\pi^-)/\Gamma_{total}$ Γ_{47}/Γ

VALUE	DOCUMENT ID	TECN	COMMENT
0.0060 ± 0.0006 OUR FIT			
0.0080 ± 0.0021 ± 0.0014	1 BORTOLETTO92	CLEO	$e^+e^- \rightarrow \Upsilon(4S)$
1 BORTOLETTO 92 assumes equal production of B^+ and B^0 at the $\Upsilon(4S)$ and uses Mark III branching fractions for the D .			

$\Gamma(D^-\pi^+\pi^+\pi^-)/\Gamma(D^-\pi^+)$ Γ_{47}/Γ_{35}

VALUE	DOCUMENT ID	TECN	COMMENT
2.39 ± 0.23 OUR FIT			
2.38 ± 0.11 ± 0.21	AAIJ	11E	LHCB pp at 7 TeV

$\Gamma((D^-\pi^+\pi^+\pi^-)_{nonresonant})/\Gamma_{total}$ Γ_{48}/Γ

VALUE	DOCUMENT ID	TECN	COMMENT
0.0039 ± 0.0014 ± 0.0013	1 BORTOLETTO92	CLEO	$e^+e^- \rightarrow \Upsilon(4S)$
1 BORTOLETTO 92 assumes equal production of B^+ and B^0 at the $\Upsilon(4S)$ and uses Mark III branching fractions for the D .			

$\Gamma(D^-\pi^+\rho^0)/\Gamma_{total}$ Γ_{49}/Γ

VALUE	DOCUMENT ID	TECN	COMMENT
0.0011 ± 0.0009 ± 0.0004	1 BORTOLETTO92	CLEO	$e^+e^- \rightarrow \Upsilon(4S)$
1 BORTOLETTO 92 assumes equal production of B^+ and B^0 at the $\Upsilon(4S)$ and uses Mark III branching fractions for the D .			

$\Gamma(D^-\pi_1(1260)^+)/\Gamma_{total}$ Γ_{50}/Γ

VALUE	DOCUMENT ID	TECN	COMMENT
0.0060 ± 0.0022 ± 0.0024	1 BORTOLETTO92	CLEO	$e^+e^- \rightarrow \Upsilon(4S)$
1 BORTOLETTO 92 assumes equal production of B^+ and B^0 at the $\Upsilon(4S)$ and uses Mark III branching fractions for the D .			

$\Gamma(D^*(2010)^-\pi^+\pi^0)/\Gamma_{total}$ Γ_{51}/Γ

VALUE	EVTS	DOCUMENT ID	TECN	COMMENT
0.0152 ± 0.0052 ± 0.0001	51	1 ALBRECHT	90J	ARG $e^+e^- \rightarrow \Upsilon(4S)$
• • • We do not use the following data for averages, fits, limits, etc. • • •				
0.015 ± 0.008 ± 0.008	8	2 ALBRECHT	87c	ARG $e^+e^- \rightarrow \Upsilon(4S)$

¹ ALBRECHT 90J reports $0.018 \pm 0.004 \pm 0.005$ from a measurement of $[\Gamma(B^0 \rightarrow D^*(2010)^-\pi^+\pi^0)/\Gamma_{total}] \times [B(D^*(2010)^+ \rightarrow D^0\pi^+)]$ assuming $B(D^*(2010)^+ \rightarrow D^0\pi^+) = 0.57 \pm 0.06$, which we rescale to our best value $B(D^*(2010)^+ \rightarrow D^0\pi^+) = (67.7 \pm 0.5) \times 10^{-2}$. Our first error is their experiment's error and our second error is the systematic error from using our best value. Assumes equal production of B^+ and B^0 at the $\Upsilon(4S)$ and uses Mark III branching fractions for the D .

² ALBRECHT 87c use PDG 86 branching ratios for D and $D^*(2010)$ and assume $B(\Upsilon(4S) \rightarrow B^+B^-) = 55\%$ and $B(\Upsilon(4S) \rightarrow B^0\bar{B}^0) = 45\%$. Superseded by ALBRECHT 90J.

$\Gamma(D^*(2010)^-\rho^+)/\Gamma_{total}$ Γ_{52}/Γ

VALUE (units 10^{-3})	EVTS	DOCUMENT ID	TECN	COMMENT
6.8 ± 0.9 OUR AVERAGE				
6.8 ± 0.3 ± 0.9		1,2 CSORNA	03	CLE2 $e^+e^- \rightarrow \Upsilon(4S)$
16.0 ± 11.3 ± 0.1		3 BORTOLETTO92	CLEO	$e^+e^- \rightarrow \Upsilon(4S)$
5.89 ± 3.52 ± 0.04	19	4 ALBRECHT	90J	ARG $e^+e^- \rightarrow \Upsilon(4S)$
• • • We do not use the following data for averages, fits, limits, etc. • • •				
7.4 ± 1.0 ± 1.4	76	2,5 MATVIENKO	15	BELL $e^+e^- \rightarrow \Upsilon(4S)$
81 ± 29 ± 59	19	6,7 ALAM	94	CLE2 $e^+e^- \rightarrow \Upsilon(4S)$
		8 CHEN	85	CLEO $e^+e^- \rightarrow \Upsilon(4S)$

¹ The second error combines the systematic and theoretical uncertainties in quadrature. CSORNA 03 includes data used in ALAM 94. A full angular fit to three complex helicity amplitudes is performed.

² Assumes equal production of B^0 and B^+ at the $\Upsilon(4S)$ resonance.

³ BORTOLETTO 92 reports $0.019 \pm 0.008 \pm 0.011$ from a measurement of $[\Gamma(B^0 \rightarrow D^*(2010)^-\rho^+)/\Gamma_{total}] \times [B(D^*(2010)^+ \rightarrow D^0\pi^+)]$ assuming $B(D^*(2010)^+ \rightarrow D^0\pi^+) = 0.57 \pm 0.06$, which we rescale to our best value $B(D^*(2010)^+ \rightarrow D^0\pi^+) = (67.7 \pm 0.5) \times 10^{-2}$. Our first error is their experiment's error and our second error is the systematic error from using our best value. Assumes equal production of B^+ and B^0 at the $\Upsilon(4S)$ and uses Mark III branching fractions for the D .

⁴ ALBRECHT 90J reports $0.007 \pm 0.003 \pm 0.003$ from a measurement of $[\Gamma(B^0 \rightarrow D^*(2010)^-\rho^+)/\Gamma_{total}] \times [B(D^*(2010)^+ \rightarrow D^0\pi^+)]$ assuming $B(D^*(2010)^+ \rightarrow D^0\pi^+) = 0.57 \pm 0.06$, which we rescale to our best value $B(D^*(2010)^+ \rightarrow D^0\pi^+) = (67.7 \pm 0.5) \times 10^{-2}$. Our first error is their experiment's error and our second error is the systematic error from using our best value. Assumes equal production of B^+ and B^0 at the $\Upsilon(4S)$ and uses Mark III branching fractions for the D .

Meson Particle Listings

 B^0

- ⁵ MATVIENKO 15 reports $B(B^0 \rightarrow D^*(2010)^-\rho^+, \rho^+ \rightarrow \omega\pi^+) = (1.48 \pm 0.27 + 0.15 - 0.09 - 0.21) \times 10^{-3}$. The last uncertainty is a model one.
- ⁶ ALAM 94 assume equal production of B^+ and B^0 at the $\Upsilon(4S)$ and use the CLEOII $B(D^*(2010)^+ \rightarrow D^0\pi^+)$ and absolute $B(D^0 \rightarrow K^-\pi^+)$ and the PDG 1992 $B(D^0 \rightarrow K^-\pi^+\pi^0)/B(D^0 \rightarrow K^-\pi^+)$ and $B(D^0 \rightarrow K^-2\pi^+\pi^-)/B(D^0 \rightarrow K^-\pi^+)$.
- ⁷ This decay is nearly completely longitudinally polarized, $\Gamma_L/\Gamma = (93 \pm 5 \pm 5)\%$, as expected from the factorization hypothesis (ROSNER 90). The nonresonant $\pi^+\pi^0$ contribution under the ρ^+ is less than 9% at 90% CL.
- ⁸ Uses $B(D^* \rightarrow D^0\pi^+) = 0.6 \pm 0.15$ and $B(\Upsilon(4S) \rightarrow B^0\bar{B}^0) = 0.4$. Does not depend on D branching ratios.

$\Gamma(D^*(2010)^- K^+)/\Gamma_{\text{total}}$	Γ_{53}/Γ		
VALUE (units 10^{-4})	DOCUMENT ID	TECN	COMMENT
2.12 ± 0.15 OUR AVERAGE			
2.12 ± 0.12 ± 0.10	¹ AUBERT	06A	BABR $e^+e^- \rightarrow \Upsilon(4S)$
2.0 ± 0.4 ± 0.1	² ABE	01i	BELL $e^+e^- \rightarrow \Upsilon(4S)$

- ¹ AUBERT 06A reports $[\Gamma(B^0 \rightarrow D^*(2010)^- K^+)/\Gamma_{\text{total}}] / [B(B^0 \rightarrow D^*(2010)^-\pi^+)] = 0.0776 \pm 0.0034 \pm 0.0029$ which we multiply by our best value $B(B^0 \rightarrow D^*(2010)^-\pi^+) = (2.74 \pm 0.13) \times 10^{-3}$. Our first error is their experiment's error and our second error is the systematic error from using our best value.
- ² ABE 01i reports $[\Gamma(B^0 \rightarrow D^*(2010)^- K^+)/\Gamma_{\text{total}}] / [B(B^0 \rightarrow D^*(2010)^-\pi^+)] = 0.074 \pm 0.015 \pm 0.006$ which we multiply by our best value $B(B^0 \rightarrow D^*(2010)^-\pi^+) = (2.74 \pm 0.13) \times 10^{-3}$. Our first error is their experiment's error and our second error is the systematic error from using our best value.

$\Gamma(D^*(2010)^- K^+)/\Gamma(D^*(2010)^-\pi^+)$	Γ_{53}/Γ_{45}		
VALUE	DOCUMENT ID	TECN	COMMENT
(7.76 ± 0.34 ± 0.26) × 10⁻²	AALJ	13A0	LHCB pp at 7 TeV

$\Gamma(D^*(2010)^- K^0\pi^+)/\Gamma_{\text{total}}$	Γ_{54}/Γ		
VALUE (units 10^{-4})	DOCUMENT ID	TECN	COMMENT
3.0 ± 0.7 ± 0.3			
	¹ AUBERT, BE	05B	BABR $e^+e^- \rightarrow \Upsilon(4S)$

- ¹ Assumes equal production of B^+ and B^0 at the $\Upsilon(4S)$.

$\Gamma(D^*(2010)^- K^*(892)^+)/\Gamma_{\text{total}}$	Γ_{55}/Γ		
VALUE (units 10^{-4})	DOCUMENT ID	TECN	COMMENT
3.3 ± 0.6 OUR AVERAGE			
3.2 ± 0.6 ± 0.3	¹ AUBERT, BE	05B	BABR $e^+e^- \rightarrow \Upsilon(4S)$
3.8 ± 1.3 ± 0.8	² MAHAPATRA	02	CLE2 $e^+e^- \rightarrow \Upsilon(4S)$

- ¹ Assumes equal production of B^+ and B^0 at the $\Upsilon(4S)$.
- ² Assumes equal production of B^+ and B^0 at the $\Upsilon(4S)$ and an unpolarized final state.

$\Gamma(D^*(2010)^- K^+\bar{K}^0)/\Gamma_{\text{total}}$	Γ_{56}/Γ		
VALUE (units 10^{-4})	CL%	DOCUMENT ID	TECN COMMENT
<4.7	90	¹ DRUTSKOY	02 BELL $e^+e^- \rightarrow \Upsilon(4S)$

$\Gamma(D^*(2010)^- K^+\bar{K}^*(892)^0)/\Gamma_{\text{total}}$	Γ_{57}/Γ		
VALUE (units 10^{-4})	DOCUMENT ID	TECN	COMMENT
12.9 ± 2.2 ± 2.5			
	¹ DRUTSKOY	02	BELL $e^+e^- \rightarrow \Upsilon(4S)$

- ¹ Assumes equal production of B^+ and B^0 at the $\Upsilon(4S)$.

$\Gamma(D^*(2010)^-\pi^+\pi^+\pi^-)/\Gamma_{\text{total}}$	Γ_{58}/Γ		
VALUE (units 10^{-3})	CL%	DOCUMENT ID	TECN COMMENT
7.21 ± 0.29 OUR AVERAGE			
7.26 ± 0.11 ± 0.31		¹ LEES	16H BABR $e^+e^- \rightarrow \Upsilon(4S)$
6.81 ± 0.23 ± 0.72		² MAJUMDER	04 BELL $e^+e^- \rightarrow \Upsilon(4S)$
6.3 ± 1.0 ± 1.1		^{3,4} ALAM	94 CLE2 $e^+e^- \rightarrow \Upsilon(4S)$
13.4 ± 3.6 ± 0.1		⁵ BORTOLETTO	92 CLEO $e^+e^- \rightarrow \Upsilon(4S)$
10.1 ± 4.1 ± 0.1		⁶ ALBRECHT	90J ARG $e^+e^- \rightarrow \Upsilon(4S)$

- • • We do not use the following data for averages, fits, limits, etc. • • •

33 ± 9 ± 16	⁷ ALBRECHT	87c	ARG $e^+e^- \rightarrow \Upsilon(4S)$
<42	⁸ BEBEK	87	CLEO $e^+e^- \rightarrow \Upsilon(4S)$

- ¹ Assumes $B(\Upsilon(4S) \rightarrow B^0\bar{B}^0) = 0.486 \pm 0.006$.
- ² Assumes equal production of B^+ and B^0 at the $\Upsilon(4S)$.
- ³ ALAM 94 assume equal production of B^+ and B^0 at the $\Upsilon(4S)$ and use the CLEOII $B(D^*(2010)^+ \rightarrow D^0\pi^+)$ and absolute $B(D^0 \rightarrow K^-\pi^+)$ and the PDG 1992 $B(D^0 \rightarrow K^-\pi^+\pi^0)/B(D^0 \rightarrow K^-\pi^+)$ and $B(D^0 \rightarrow K^-2\pi^+\pi^-)/B(D^0 \rightarrow K^-\pi^+)$.
- ⁴ The three pion mass is required to be between 1.0 and 1.6 GeV consistent with an a_1 meson. (If this channel is dominated by a_1^+ , the branching ratio for $\bar{D}^{*-}a_1^+$ is twice that for $\bar{D}^{*-}\pi^+\pi^+\pi^-$.)

- ⁵ BORTOLETTO 92 reports $0.0159 \pm 0.0028 \pm 0.0037$ from a measurement of $[\Gamma(B^0 \rightarrow D^*(2010)^-\pi^+\pi^+\pi^-)/\Gamma_{\text{total}}] \times [B(D^*(2010)^+ \rightarrow D^0\pi^+)]$ assuming $B(D^*(2010)^+ \rightarrow D^0\pi^+) = 0.57 \pm 0.06$, which we rescale to our best value $B(D^*(2010)^+ \rightarrow D^0\pi^+) = (67.7 \pm 0.5) \times 10^{-2}$. Our first error is their experiment's error and our second error is the systematic error from using our best value. Assumes equal production of B^+ and B^0 at the $\Upsilon(4S)$ and uses MarkIII branching fractions for the D .

- ⁶ ALBRECHT 90J reports $0.012 \pm 0.003 \pm 0.004$ from a measurement of $[\Gamma(B^0 \rightarrow D^*(2010)^-\pi^+\pi^+\pi^-)/\Gamma_{\text{total}}] \times [B(D^*(2010)^+ \rightarrow D^0\pi^+)]$ assuming $B(D^*(2010)^+ \rightarrow D^0\pi^+) = 0.57 \pm 0.06$, which we rescale to our best value

$B(D^*(2010)^+ \rightarrow D^0\pi^+) = (67.7 \pm 0.5) \times 10^{-2}$. Our first error is their experiment's error and our second error is the systematic error from using our best value. Assumes equal production of B^+ and B^0 at the $\Upsilon(4S)$ and uses MarkIII branching fractions for the D .

- ⁷ ALBRECHT 87c use PDG 86 branching ratios for D and $D^*(2010)$ and assume $B(\Upsilon(4S) \rightarrow B^+B^-) = 55\%$ and $B(\Upsilon(4S) \rightarrow B^0\bar{B}^0) = 45\%$. Superseded by ALBRECHT 90J.

- ⁸ BEBEK 87 value has been updated in BERKELMAN 91 to use same assumptions as noted for BORTOLETTO 92.

$\Gamma((D^*(2010)^-\pi^+\pi^+\pi^-)_{\text{nonresonant}})/\Gamma_{\text{total}}$	Γ_{59}/Γ		
VALUE	DOCUMENT ID	TECN	COMMENT
0.0000 ± 0.0019 ± 0.0016			
	¹ BORTOLETTO	92	CLEO $e^+e^- \rightarrow \Upsilon(4S)$

- ¹ BORTOLETTO 92 assumes equal production of B^+ and B^0 at the $\Upsilon(4S)$ and uses MarkIII branching fractions for the D and $D^*(2010)$.

$\Gamma(D^*(2010)^-\pi^+\rho^0)/\Gamma_{\text{total}}$	Γ_{60}/Γ		
VALUE	DOCUMENT ID	TECN	COMMENT
0.00573 ± 0.00317 ± 0.00004			
	¹ BORTOLETTO	92	CLEO $e^+e^- \rightarrow \Upsilon(4S)$

- ¹ BORTOLETTO 92 reports $0.0068 \pm 0.0032 \pm 0.0021$ from a measurement of $[\Gamma(B^0 \rightarrow D^*(2010)^-\pi^+\rho^0)/\Gamma_{\text{total}}] \times [B(D^*(2010)^+ \rightarrow D^0\pi^+)]$ assuming $B(D^*(2010)^+ \rightarrow D^0\pi^+) = 0.57 \pm 0.06$, which we rescale to our best value $B(D^*(2010)^+ \rightarrow D^0\pi^+) = (67.7 \pm 0.5) \times 10^{-2}$. Our first error is their experiment's error and our second error is the systematic error from using our best value. Assumes equal production of B^+ and B^0 at the $\Upsilon(4S)$ and uses MarkIII branching fractions for the D .

$\Gamma(D^*(2010)^- a_1(1260)^+)/\Gamma_{\text{total}}$	Γ_{61}/Γ		
VALUE	DOCUMENT ID	TECN	COMMENT
0.0130 ± 0.0027 OUR AVERAGE			
0.0126 ± 0.0020 ± 0.0022	^{1,2} ALAM	94	CLE2 $e^+e^- \rightarrow \Upsilon(4S)$
0.0152 ± 0.0070 ± 0.0001	³ BORTOLETTO	92	CLEO $e^+e^- \rightarrow \Upsilon(4S)$

- ¹ ALAM 94 value is twice their $\Gamma(D^*(2010)^-\pi^+\pi^+\pi^-)/\Gamma_{\text{total}}$ value based on their observation that the three pions are dominantly in the $a_1(1260)$ mass range 1.0 to 1.6 GeV.

- ² ALAM 94 assume equal production of B^+ and B^0 at the $\Upsilon(4S)$ and use the CLEOII $B(D^*(2010)^+ \rightarrow D^0\pi^+)$ and absolute $B(D^0 \rightarrow K^-\pi^+)$ and the PDG 1992 $B(D^0 \rightarrow K^-\pi^+\pi^0)/B(D^0 \rightarrow K^-\pi^+)$ and $B(D^0 \rightarrow K^-2\pi^+\pi^-)/B(D^0 \rightarrow K^-\pi^+)$.

- ³ BORTOLETTO 92 reports $0.018 \pm 0.006 \pm 0.006$ from a measurement of $[\Gamma(B^0 \rightarrow D^*(2010)^- a_1(1260)^+)/\Gamma_{\text{total}}] \times [B(D^*(2010)^+ \rightarrow D^0\pi^+)]$ assuming $B(D^*(2010)^+ \rightarrow D^0\pi^+) = 0.57 \pm 0.06$, which we rescale to our best value $B(D^*(2010)^+ \rightarrow D^0\pi^+) = (67.7 \pm 0.5) \times 10^{-2}$. Our first error is their experiment's error and our second error is the systematic error from using our best value. Assumes equal production of B^+ and B^0 at the $\Upsilon(4S)$ and uses MarkIII branching fractions for the D .

$\Gamma(\bar{D}_1^*(2420)^0\pi^-\pi^+, \bar{D}_1^0 \rightarrow D^{*-}\pi^+)/\Gamma(D^*(2010)^-\pi^+\pi^+\pi^-)$	Γ_{62}/Γ_{58}		
VALUE	DOCUMENT ID	TECN	COMMENT
(2.04 ± 0.42 ± 0.22) × 10⁻²	AALJ	13A0	LHCB pp at 7 TeV

$\Gamma(D^*(2010)^- K^+\pi^-\pi^+)/\Gamma(D^*(2010)^-\pi^+\pi^+\pi^-)$	Γ_{63}/Γ_{58}		
VALUE	DOCUMENT ID	TECN	COMMENT
(6.47 ± 0.37 ± 0.35) × 10⁻²	AALJ	13A0	LHCB pp at 7 TeV

$\Gamma(D^*(2010)^-\pi^+\pi^+\pi^-)/\Gamma_{\text{total}}$	Γ_{64}/Γ		
VALUE	EVTS	DOCUMENT ID	TECN COMMENT
0.0176 ± 0.0027 OUR AVERAGE			
0.0172 ± 0.0014 ± 0.0024		¹ ALEXANDER	01B CLE2 $e^+e^- \rightarrow \Upsilon(4S)$
0.0345 ± 0.0181 ± 0.0003	28	² ALBRECHT	90J ARG $e^+e^- \rightarrow \Upsilon(4S)$

- ¹ Assumes equal production of B^+ and B^0 at the $\Upsilon(4S)$. The signal is consistent with all observed $\omega\pi^+$ having proceeded through the ρ^+ resonance at mass $1349 \pm 25^{+10}_{-5}$ MeV and width $547 \pm 86^{+46}_{-45}$ MeV.

- ² ALBRECHT 90J reports $0.041 \pm 0.015 \pm 0.016$ from a measurement of $[\Gamma(B^0 \rightarrow D^*(2010)^-\pi^+\pi^+\pi^-)/\Gamma_{\text{total}}] \times [B(D^*(2010)^+ \rightarrow D^0\pi^+)]$ assuming $B(D^*(2010)^+ \rightarrow D^0\pi^+) = 0.57 \pm 0.06$, which we rescale to our best value $B(D^*(2010)^+ \rightarrow D^0\pi^+) = (67.7 \pm 0.5) \times 10^{-2}$. Our first error is their experiment's error and our second error is the systematic error from using our best value. Assumes equal production of B^+ and B^0 at the $\Upsilon(4S)$ and uses MarkIII branching fractions for the D .

$\Gamma(D^{*-}3\pi^2)/\Gamma_{\text{total}}$	Γ_{65}/Γ		
VALUE (units 10^{-3})	DOCUMENT ID	TECN	COMMENT
4.72 ± 0.59 ± 0.71			
	¹ MAJUMDER	04	BELL $e^+e^- \rightarrow \Upsilon(4S)$

- ¹ Assumes equal production of B^+ and B^0 at the $\Upsilon(4S)$.

$\Gamma(D^*(2010)^-\omega\pi^+)/\Gamma_{\text{total}}$	Γ_{66}/Γ		
VALUE (units 10^{-3})	DOCUMENT ID	TECN	COMMENT
2.46 ± 0.18 OUR AVERAGE			Error includes scale factor of 1.2.
2.31 ± 0.11 ± 0.14	¹ MATVIENKO	15	BELL $e^+e^- \rightarrow \Upsilon(4S)$
2.88 ± 0.21 ± 0.31	¹ AUBERT	06L	BABR $e^+e^- \rightarrow \Upsilon(4S)$
2.9 ± 0.3 ± 0.4	^{1,2} ALEXANDER	01B	CLE2 $e^+e^- \rightarrow \Upsilon(4S)$

- ¹ Assumes equal production of B^+ and B^0 at the $\Upsilon(4S)$.

- ² The signal is consistent with all observed $\omega\pi^+$ having proceeded through the ρ^+ resonance at mass $1349 \pm 25^{+10}_{-5}$ MeV and width $547 \pm 86^{+46}_{-45}$ MeV.

See key on page 1127

Meson Particle Listings

B^0

$\Gamma(\bar{D}_1(2430)^0 \omega, \bar{D}_1^0 \rightarrow D^{*-} \pi^+) / \Gamma_{\text{total}}$ Γ_{67} / Γ

VALUE (units 10^{-4})	DOCUMENT ID	TECN	COMMENT
2.7^{+0.8}_{-0.4} OUR AVERAGE			
2.5 ± 0.4 ^{+0.8} _{-0.2}	1,2 MATVIENKO	15	BELL $e^+ e^- \rightarrow \Upsilon(4S)$
4.1 ± 1.2 ± 1.1	3 AUBERT	06L	BABR $e^+ e^- \rightarrow \Upsilon(4S)$
1 Assumes equal production of B^+ and B^0 . 2 The measurement is obtained by amplitude analysis of $B^0 \rightarrow D^{*-} \omega \pi^+$. The second uncertainty combines in quadrature experimental systematic and model uncertainties. 3 Obtained by fitting the events with $\cos \theta_{D^*} < 0.5$ and scaling up the result by a factor of 4/3. No interference effects between $B^0 \rightarrow D_1^0 \omega$ and $D^{*-} \omega \pi^+$ are assumed.			

$\Gamma(D^{*-} \rho(1450)^+, \rho^+ \rightarrow \omega \pi^+) / \Gamma_{\text{total}}$ Γ_{68} / Γ

VALUE (units 10^{-3})	DOCUMENT ID	TECN	COMMENT
1.07^{+0.15+0.40}_{-0.31-0.13}			
1.2 ± 0.1 ± 0.4	1,2 MATVIENKO	15	BELL $e^+ e^- \rightarrow \Upsilon(4S)$
1 Obtained by amplitude analysis of $\bar{B}^0 \rightarrow D^{*-} \omega \pi^+$. The second uncertainty combines in quadrature experimental systematic and model uncertainties. 2 Assumes equal production of B^0 and B^+ at $\Upsilon(4S)$.			

$\Gamma(\bar{D}_1(2420)^0 \omega, \bar{D}_1^0 \rightarrow D^{*-} \pi^+) / \Gamma_{\text{total}}$ Γ_{69} / Γ

VALUE (units 10^{-4})	DOCUMENT ID	TECN	COMMENT
0.7 ± 0.2 ± 0.1			
0.7 ± 0.2 ± 0.1	1,2 MATVIENKO	15	BELL $e^+ e^- \rightarrow \Upsilon(4S)$
1 Obtained by amplitude analysis of $\bar{B}^0 \rightarrow D^{*-} \omega \pi^+$. The second uncertainty combines in quadrature experimental systematic and model uncertainties. 2 Assumes equal production of B^0 and B^+ at $\Upsilon(4S)$.			

$\Gamma(\bar{D}_2^*(2460)^0 \omega, \bar{D}_2^0 \rightarrow D^{*-} \pi^+) / \Gamma_{\text{total}}$ Γ_{70} / Γ

VALUE (units 10^{-4})	DOCUMENT ID	TECN	COMMENT
0.4 ± 0.1 ± 0.1			
0.4 ± 0.1 ± 0.1	1,2 MATVIENKO	15	BELL $e^+ e^- \rightarrow \Upsilon(4S)$
1 Obtained by amplitude analysis of $\bar{B}^0 \rightarrow D^{*-} \omega \pi^+$. The second uncertainty combines in quadrature experimental systematic and model uncertainties. 2 Assumes equal production of B^0 and B^+ at $\Upsilon(4S)$.			

$\Gamma(D^{*-} b_1(1235)^+, b_1^+ \rightarrow \omega \pi^+) / \Gamma_{\text{total}}$ Γ_{71} / Γ

VALUE	CL%	DOCUMENT ID	TECN	COMMENT
<0.7 × 10⁻⁴				
<0.7 × 10 ⁻⁴	90	1 MATVIENKO	15	BELL $e^+ e^- \rightarrow \Upsilon(4S)$
1 Assumes equal production of B^0 and B^+ at $\Upsilon(4S)$.				

$\Gamma(\bar{D}^{*-} \pi^+) / \Gamma_{\text{total}}$ Γ_{72} / Γ

D^{*-} represents an excited state with mass $2.2 < M < 2.8$ GeV/ c^2 .

VALUE (units 10^{-3})	DOCUMENT ID	TECN	COMMENT
1.9 ± 0.9 ± 0.1			
1.9 ± 0.9 ± 0.1	1,2 AUBERT, BE	06J	BABR $e^+ e^- \rightarrow \Upsilon(4S)$
1 AUBERT, BE 06J reports $[\Gamma(B^0 \rightarrow \bar{D}^{*-} \pi^+) / \Gamma_{\text{total}}] / [B(B^0 \rightarrow D^- \pi^+)] = 0.77 \pm 0.22 \pm 0.29$ which we multiply by our best value $B(B^0 \rightarrow D^- \pi^+) = (2.51 \pm 0.08) \times 10^{-3}$. Our first error is their experiment's error and our second error is the systematic error from using our best value. 2 Uses a missing-mass method. Does not depend on D branching fractions or B^+ / B^0 production rates.			

$\Gamma(D_1(2420)^- \pi^+, D_1^- \rightarrow D^- \pi^+ \pi^-) / \Gamma_{\text{total}}$ Γ_{73} / Γ

VALUE (units 10^{-4})	DOCUMENT ID	TECN	COMMENT
0.99^{+0.20}_{-0.25} OUR FIT			
0.89 ± 0.15 ^{+0.17} _{-0.32}	1 ABE	05A	BELL $e^+ e^- \rightarrow \Upsilon(4S)$
1 Assumes equal production of B^+ and B^0 at the $\Upsilon(4S)$.			

$\Gamma(D_1(2420)^- \pi^+, D_1^- \rightarrow D^- \pi^+ \pi^-) / \Gamma(D^- \pi^+ \pi^-)$ $\Gamma_{73} / \Gamma_{47}$

VALUE (units 10^{-2})	DOCUMENT ID	TECN	COMMENT
1.7 ± 0.4 OUR FIT			
2.1 ± 0.5 ^{+0.3} _{-0.5}	AAIJ	11E	LHCB pp at 7 TeV

$\Gamma(D_1(2420)^- \pi^+, D_1^- \rightarrow D^{*-} \pi^+ \pi^-) / \Gamma_{\text{total}}$ Γ_{74} / Γ

VALUE (units 10^{-4})	CL%	DOCUMENT ID	TECN	COMMENT
<0.33				
<0.33	90	1 ABE	05A	BELL $e^+ e^- \rightarrow \Upsilon(4S)$
1 Assumes equal production of B^+ and B^0 at the $\Upsilon(4S)$.				

$\Gamma(D^*(2010)^- \pi^+ \pi^+ \pi^-) / \Gamma(D^*(2010)^- \pi^+)$ $\Gamma_{58} / \Gamma_{45}$

VALUE	DOCUMENT ID	TECN	COMMENT
2.64 ± 0.04 ± 0.13			
2.64 ± 0.04 ± 0.13	AAIJ	13A0	LHCB pp at 7 TeV

$\Gamma(\bar{D}_2^*(2460)^- \pi^+, (D_2^*)^- \rightarrow D^0 \pi^-) / \Gamma_{\text{total}}$ Γ_{75} / Γ

VALUE (units 10^{-4})	CL%	DOCUMENT ID	TECN	COMMENT
2.38 ± 0.16 OUR AVERAGE				
2.44 ± 0.07 ± 0.16	1	AAIJ	15Y	LHCB pp at 7, 8 TeV
2.15 ± 0.17 ± 0.31	2,3	KUZMIN	07	BELL $e^+ e^- \rightarrow \Upsilon(4S)$
••• We do not use the following data for averages, fits, limits, etc. ••• <14.7 90 2 ALAM 94 CLE2 $e^+ e^- \rightarrow \Upsilon(4S)$				
1 Result obtained using the isobar formalism. The second uncertainty combines in quadrature all systematic uncertainties quoted in the paper. 2 Assumes equal production of B^+ and B^0 at the $\Upsilon(4S)$. 3 Our second uncertainty combines systematics and model errors quoted in the paper.				

$\Gamma(\bar{D}_2^*(2400)^- \pi^+, (D_2^*)^- \rightarrow D^0 \pi^-) / \Gamma_{\text{total}}$ Γ_{76} / Γ

VALUE (units 10^{-4})	DOCUMENT ID	TECN	COMMENT
0.76 ± 0.08 OUR AVERAGE			
0.77 ± 0.05 ± 0.06	1	AAIJ	15Y LHCB pp at 7, 8 TeV
0.60 ± 0.13 ± 0.27	2,3	KUZMIN	07 BELL $e^+ e^- \rightarrow \Upsilon(4S)$
1 Result obtained using the isobar formalism. The second uncertainty combines in quadrature all systematic uncertainties quoted in the paper. 2 Assumes equal production of B^+ and B^0 at the $\Upsilon(4S)$. 3 Our second uncertainty combines systematics and model errors quoted in the paper.			

$\Gamma(D_2^*(2460)^- \pi^+, (D_2^*)^- \rightarrow D^{*-} \pi^+ \pi^-) / \Gamma_{\text{total}}$ Γ_{77} / Γ

VALUE (units 10^{-4})	CL%	DOCUMENT ID	TECN	COMMENT
<0.24				
<0.24	90	1 ABE	05A	BELL $e^+ e^- \rightarrow \Upsilon(4S)$
1 Assumes equal production of B^+ and B^0 at the $\Upsilon(4S)$.				

$\Gamma(\bar{D}_2^*(2460)^- \rho^+) / \Gamma_{\text{total}}$ Γ_{78} / Γ

VALUE	CL%	DOCUMENT ID	TECN	COMMENT
<0.0049				
<0.0049	90	1 ALAM	94	CLE2 $e^+ e^- \rightarrow \Upsilon(4S)$
1 ALAM 94 assumes equal production of B^+ and B^0 at the $\Upsilon(4S)$ and use the CLEO II absolute $B(D^0 \rightarrow K^- \pi^+)$ and $B(D_2^*(2460)^+ \rightarrow D^0 \pi^+) = 30\%$.				

$\Gamma(D^0 \bar{D}^0) / \Gamma_{\text{total}}$ Γ_{79} / Γ

VALUE (units 10^{-4})	CL%	DOCUMENT ID	TECN	COMMENT
0.14 ± 0.06 ± 0.03				
0.14 ± 0.06 ± 0.03	1	AAIJ	13AP	LHCB pp at 7 TeV
••• We do not use the following data for averages, fits, limits, etc. •••				
<0.43	90	2	ADACHI	08 BELL $e^+ e^- \rightarrow \Upsilon(4S)$
<0.6	90	2	AUBERT, B	06A BABR $e^+ e^- \rightarrow \Upsilon(4S)$
1 Uses $B(B^0 \rightarrow D^- D^+) = (2.11 \pm 0.31) \times 10^{-4}$ and $B(B^+ \rightarrow \bar{D}^0 D_s^+) = (10.1 \pm 1.7) \times 10^{-3}$. 2 Assumes equal production of B^+ and B^0 at the $\Upsilon(4S)$.				

$\Gamma(D^{*0} \bar{D}^0) / \Gamma_{\text{total}}$ Γ_{80} / Γ

VALUE (units 10^{-4})	CL%	DOCUMENT ID	TECN	COMMENT
<2.9				
<2.9	90	1	AUBERT, B	06A BABR $e^+ e^- \rightarrow \Upsilon(4S)$
1 Assumes equal production of B^+ and B^0 at the $\Upsilon(4S)$.				

$\Gamma(D^- D^+) / \Gamma_{\text{total}}$ Γ_{81} / Γ

VALUE (units 10^{-4})	CL%	DOCUMENT ID	TECN	COMMENT
2.11 ± 0.18 OUR AVERAGE				
2.12 ± 0.16 ± 0.18	1	ROHRKEN	12	BELL $e^+ e^- \rightarrow \Upsilon(4S)$
1.97 ± 0.20 ± 0.20	1	FRATINA	07	BELL $e^+ e^- \rightarrow \Upsilon(4S)$
2.8 ± 0.4 ± 0.5	1	AUBERT, B	06A	BABR $e^+ e^- \rightarrow \Upsilon(4S)$
••• We do not use the following data for averages, fits, limits, etc. •••				
1.91 ± 0.51 ± 0.30	1	MAJUMDER	05	BELL Repl. by FRATINA 07
< 9.4	90	1	LIPELES	00 CLE2 $e^+ e^- \rightarrow \Upsilon(4S)$
<59	90	1	BARATE	98Q ALEP $e^+ e^- \rightarrow Z$
<12	90	1	ASNER	97 CLE2 $e^+ e^- \rightarrow \Upsilon(4S)$
1 Assumes equal production of B^+ and B^0 at the $\Upsilon(4S)$.				

$\Gamma(D^\pm D^{*\mp} (CP\text{-averaged})) / \Gamma_{\text{total}}$ Γ_{82} / Γ

VALUE (units 10^{-4})	DOCUMENT ID	TECN	COMMENT
6.14 ± 0.29 ± 0.50			
6.14 ± 0.29 ± 0.50	1	ROHRKEN	12 BELL $e^+ e^- \rightarrow \Upsilon(4S)$
1 Assumes equal production of B^+ and B^0 at the $\Upsilon(4S)$.			

$\Gamma(D^- D_s^+) / \Gamma_{\text{total}}$ Γ_{83} / Γ

VALUE	EVTS	DOCUMENT ID	TECN	COMMENT
0.0072 ± 0.0008 OUR AVERAGE				
0.0073 ± 0.0004 ± 0.0007	1	ZUPANC	07	BELL $e^+ e^- \rightarrow \Upsilon(4S)$
0.0066 ± 0.0014 ± 0.0006	2	AUBERT	06N	BABR $e^+ e^- \rightarrow \Upsilon(4S)$
0.0068 ± 0.0024 ± 0.0006	3	GIBAUT	96	CLE2 $e^+ e^- \rightarrow \Upsilon(4S)$
0.010 ± 0.009 ± 0.001	4	ALBRECHT	92G	ARG $e^+ e^- \rightarrow \Upsilon(4S)$
0.0053 ± 0.0030 ± 0.0005	5	BORTOLETTO92	CLEO	$e^+ e^- \rightarrow \Upsilon(4S)$
••• We do not use the following data for averages, fits, limits, etc. •••				
0.012 ± 0.007	3	6	BORTOLETTO90	CLEO $e^+ e^- \rightarrow \Upsilon(4S)$
1 ZUPANC 07 reports $(7.5 \pm 0.2 \pm 1.1) \times 10^{-3}$ from a measurement of $[\Gamma(B^0 \rightarrow D^- D_s^+) / \Gamma_{\text{total}}] \times [B(D_s^+ \rightarrow \phi \pi^+) / B(D_s^+ \rightarrow \phi \pi^+)]$ assuming $B(D_s^+ \rightarrow \phi \pi^+) = (4.4 \pm 0.6) \times 10^{-2}$, which we rescale to our best value $B(D_s^+ \rightarrow \phi \pi^+) = (4.5 \pm 0.4) \times 10^{-2}$. Our first error is their experiment's error and our second error is the systematic error from using our best value. 2 AUBERT 06N reports $(0.64 \pm 0.13 \pm 0.10) \times 10^{-2}$ from a measurement of $[\Gamma(B^0 \rightarrow D^- D_s^+) / \Gamma_{\text{total}}] \times [B(D_s^+ \rightarrow \phi \pi^+) / B(D_s^+ \rightarrow \phi \pi^+)]$ assuming $B(D_s^+ \rightarrow \phi \pi^+) = 0.0462 \pm 0.0062$, which we rescale to our best value $B(D_s^+ \rightarrow \phi \pi^+) = (4.5 \pm 0.4) \times 10^{-2}$. Our first error is their experiment's error and our second error is the systematic error from using our best value. 3 GIBAUT 96 reports $0.0087 \pm 0.0024 \pm 0.0020$ from a measurement of $[\Gamma(B^0 \rightarrow D^- D_s^+) / \Gamma_{\text{total}}] \times [B(D_s^+ \rightarrow \phi \pi^+) / B(D_s^+ \rightarrow \phi \pi^+)]$ assuming $B(D_s^+ \rightarrow \phi \pi^+) = 0.035$, which we rescale to our best value $B(D_s^+ \rightarrow \phi \pi^+) = (4.5 \pm 0.4) \times 10^{-2}$. Our first error is their experiment's error and our second error is the systematic error from using our best value.				

Meson Particle Listings

B^0

⁴ ALBRECHT 92G reports $0.017 \pm 0.013 \pm 0.006$ from a measurement of $[\Gamma(B^0 \rightarrow D^- D_s^+)/\Gamma_{\text{total}}] \times [B(D_s^+ \rightarrow \phi\pi^+)]$ assuming $B(D_s^+ \rightarrow \phi\pi^+) = 0.027$, which we rescale to our best value $B(D_s^+ \rightarrow \phi\pi^+) = (4.5 \pm 0.4) \times 10^{-2}$. Our first error is their experiment's error and our second error is the systematic error from using our best value. Assumes PDG 1990 D^+ branching ratios, e.g., $B(D^+ \rightarrow K^- 2\pi^+) = 7.7 \pm 1.0\%$.

⁵ BORTOLETTO 92 reports $0.0080 \pm 0.0045 \pm 0.0030$ from a measurement of $[\Gamma(B^0 \rightarrow D^- D_s^+)/\Gamma_{\text{total}}] \times [B(D_s^+ \rightarrow \phi\pi^+)]$ assuming $B(D_s^+ \rightarrow \phi\pi^+) = 0.030 \pm 0.011$, which we rescale to our best value $B(D_s^+ \rightarrow \phi\pi^+) = (4.5 \pm 0.4) \times 10^{-2}$. Our first error is their experiment's error and our second error is the systematic error from using our best value. Assumes equal production of B^+ and B^0 at the $\Upsilon(4S)$ and uses Mark III branching fractions for the D .

⁶ BORTOLETTO 90 assume $B(D_s \rightarrow \phi\pi^+) = 2\%$. Superseded by BORTOLETTO 92.

$\Gamma(D^*(2010)^- D_s^+)/\Gamma_{\text{total}}$		Γ_{84}/Γ		
VALUE	EVTS	DOCUMENT ID	TECN	COMMENT
0.0080 ± 0.0011 OUR AVERAGE				
0.0073 ± 0.0013 ± 0.0007		¹ AUBERT	06N BABR	$e^+e^- \rightarrow \Upsilon(4S)$
0.0083 ± 0.0015 ± 0.0007		² AUBERT	03i BABR	$e^+e^- \rightarrow \Upsilon(4S)$
0.0088 ± 0.0017 ± 0.0008		³ AHMED	00B CLE2	$e^+e^- \rightarrow \Upsilon(4S)$
0.008 ± 0.006 ± 0.001		⁴ ALBRECHT	92G ARG	$e^+e^- \rightarrow \Upsilon(4S)$
0.011 ± 0.006 ± 0.001		⁵ BORTOLETTO92	CLEO	$e^+e^- \rightarrow \Upsilon(4S)$
••• We do not use the following data for averages, fits, limits, etc. •••				
0.0072 ± 0.0022 ± 0.0006		⁶ GIBAUT	96 CLE2	Repl. by AHMED 00B
0.024 ± 0.014		³ BORTOLETTO90	CLEO	$e^+e^- \rightarrow \Upsilon(4S)$

¹ AUBERT 06N reports $(0.71 \pm 0.13 \pm 0.09) \times 10^{-2}$ from a measurement of $[\Gamma(B^0 \rightarrow D^*(2010)^- D_s^+)/\Gamma_{\text{total}}] \times [B(D_s^+ \rightarrow \phi\pi^+)]$ assuming $B(D_s^+ \rightarrow \phi\pi^+) = 0.0462 \pm 0.0062$, which we rescale to our best value $B(D_s^+ \rightarrow \phi\pi^+) = (4.5 \pm 0.4) \times 10^{-2}$. Our first error is their experiment's error and our second error is the systematic error from using our best value.

² AUBERT 03i reports $0.0103 \pm 0.0014 \pm 0.0013$ from a measurement of $[\Gamma(B^0 \rightarrow D^*(2010)^- D_s^+)/\Gamma_{\text{total}}] \times [B(D_s^+ \rightarrow \phi\pi^+)]$ assuming $B(D_s^+ \rightarrow \phi\pi^+) = 0.036$, which we rescale to our best value $B(D_s^+ \rightarrow \phi\pi^+) = (4.5 \pm 0.4) \times 10^{-2}$. Our first error is their experiment's error and our second error is the systematic error from using our best value.

³ AHMED 00B reports $0.0110 \pm 0.0018 \pm 0.0011$ from a measurement of $[\Gamma(B^0 \rightarrow D^*(2010)^- D_s^+)/\Gamma_{\text{total}}] \times [B(D_s^+ \rightarrow \phi\pi^+)]$ assuming $B(D_s^+ \rightarrow \phi\pi^+) = 0.036$, which we rescale to our best value $B(D_s^+ \rightarrow \phi\pi^+) = (4.5 \pm 0.4) \times 10^{-2}$. Our first error is their experiment's error and our second error is the systematic error from using our best value.

⁴ ALBRECHT 92G reports $0.014 \pm 0.010 \pm 0.003$ from a measurement of $[\Gamma(B^0 \rightarrow D^*(2010)^- D_s^+)/\Gamma_{\text{total}}] \times [B(D_s^+ \rightarrow \phi\pi^+)]$ assuming $B(D_s^+ \rightarrow \phi\pi^+) = 0.027$, which we rescale to our best value $B(D_s^+ \rightarrow \phi\pi^+) = (4.5 \pm 0.4) \times 10^{-2}$. Our first error is their experiment's error and our second error is the systematic error from using our best value. Assumes PDG 1990 D^+ and $D^*(2010)^+$ branching ratios, e.g., $B(D^0 \rightarrow K^- \pi^+) = 3.71 \pm 0.25\%$, $B(D^+ \rightarrow K^- 2\pi^+) = 7.1 \pm 1.0\%$, and $B(D^*(2010)^+ \rightarrow D^0 \pi^+) = 55 \pm 4\%$.

⁵ BORTOLETTO 92 reports $0.016 \pm 0.009 \pm 0.006$ from a measurement of $[\Gamma(B^0 \rightarrow D^*(2010)^- D_s^+)/\Gamma_{\text{total}}] \times [B(D_s^+ \rightarrow \phi\pi^+)]$ assuming $B(D_s^+ \rightarrow \phi\pi^+) = 0.030 \pm 0.011$, which we rescale to our best value $B(D_s^+ \rightarrow \phi\pi^+) = (4.5 \pm 0.4) \times 10^{-2}$. Our first error is their experiment's error and our second error is the systematic error from using our best value. Assumes equal production of B^+ and B^0 at the $\Upsilon(4S)$ and uses Mark III branching fractions for the D and $D^*(2010)$.

⁶ GIBAUT 96 reports $0.0093 \pm 0.0023 \pm 0.0016$ from a measurement of $[\Gamma(B^0 \rightarrow D^*(2010)^- D_s^+)/\Gamma_{\text{total}}] \times [B(D_s^+ \rightarrow \phi\pi^+)]$ assuming $B(D_s^+ \rightarrow \phi\pi^+) = 0.035$, which we rescale to our best value $B(D_s^+ \rightarrow \phi\pi^+) = (4.5 \pm 0.4) \times 10^{-2}$. Our first error is their experiment's error and our second error is the systematic error from using our best value.

⁷ BORTOLETTO 90 assume $B(D_s \rightarrow \phi\pi^+) = 2\%$. Superseded by BORTOLETTO 92.

$\Gamma(D^- D_s^+)/\Gamma_{\text{total}}$		Γ_{85}/Γ		
VALUE	EVTS	DOCUMENT ID	TECN	COMMENT
0.0074 ± 0.0016 OUR AVERAGE				
0.0071 ± 0.0016 ± 0.0006		¹ AUBERT	06N BABR	$e^+e^- \rightarrow \Upsilon(4S)$
0.0078 ± 0.0032 ± 0.0007		² GIBAUT	96 CLE2	$e^+e^- \rightarrow \Upsilon(4S)$
0.016 ± 0.012 ± 0.001		³ ALBRECHT	92G ARG	$e^+e^- \rightarrow \Upsilon(4S)$

¹ AUBERT 06N reports $(0.69 \pm 0.16 \pm 0.09) \times 10^{-2}$ from a measurement of $[\Gamma(B^0 \rightarrow D^- D_s^+)/\Gamma_{\text{total}}] \times [B(D_s^+ \rightarrow \phi\pi^+)]$ assuming $B(D_s^+ \rightarrow \phi\pi^+) = 0.0462 \pm 0.0062$, which we rescale to our best value $B(D_s^+ \rightarrow \phi\pi^+) = (4.5 \pm 0.4) \times 10^{-2}$. Our first error is their experiment's error and our second error is the systematic error from using our best value.

² GIBAUT 96 reports $0.0100 \pm 0.0035 \pm 0.0022$ from a measurement of $[\Gamma(B^0 \rightarrow D^- D_s^+)/\Gamma_{\text{total}}] \times [B(D_s^+ \rightarrow \phi\pi^+)]$ assuming $B(D_s^+ \rightarrow \phi\pi^+) = 0.035$, which we rescale to our best value $B(D_s^+ \rightarrow \phi\pi^+) = (4.5 \pm 0.4) \times 10^{-2}$. Our first error is their experiment's error and our second error is the systematic error from using our best value.

³ ALBRECHT 92G reports $0.027 \pm 0.017 \pm 0.009$ from a measurement of $[\Gamma(B^0 \rightarrow D^- D_s^+)/\Gamma_{\text{total}}] \times [B(D_s^+ \rightarrow \phi\pi^+)]$ assuming $B(D_s^+ \rightarrow \phi\pi^+) = 0.027$, which we rescale to our best value $B(D_s^+ \rightarrow \phi\pi^+) = (4.5 \pm 0.4) \times 10^{-2}$. Our first error is their experiment's error and our second error is the systematic error from using our best value. Assumes PDG 1990 D^+ branching ratios, e.g., $B(D^+ \rightarrow K^- 2\pi^+) = 7.7 \pm 1.0\%$.

$\Gamma(D^*(2010)^- D_s^+)/\Gamma_{\text{total}}$		Γ_{86}/Γ		
VALUE	DOCUMENT ID	TECN	COMMENT	
0.0177 ± 0.0014 OUR AVERAGE				
0.0173 ± 0.0018 ± 0.0015	¹ AUBERT	06N BABR	$e^+e^- \rightarrow \Upsilon(4S)$	
0.0188 ± 0.0009 ± 0.0017	² AUBERT	05v BABR	$e^+e^- \rightarrow \Upsilon(4S)$	
0.0158 ± 0.0027 ± 0.0014	³ AUBERT	03i BABR	$e^+e^- \rightarrow \Upsilon(4S)$	
0.015 ± 0.004 ± 0.001	⁴ AHMED	00B CLE2	$e^+e^- \rightarrow \Upsilon(4S)$	
0.016 ± 0.009 ± 0.001	⁵ ALBRECHT	92G ARG	$e^+e^- \rightarrow \Upsilon(4S)$	
••• We do not use the following data for averages, fits, limits, etc. •••				
0.016 ± 0.005 ± 0.001	⁶ GIBAUT	96 CLE2	Repl. by AHMED 00B	

¹ AUBERT 06N reports $(1.68 \pm 0.21 \pm 0.19) \times 10^{-2}$ from a measurement of $[\Gamma(B^0 \rightarrow D^*(2010)^- D_s^+)/\Gamma_{\text{total}}] \times [B(D_s^+ \rightarrow \phi\pi^+)]$ assuming $B(D_s^+ \rightarrow \phi\pi^+) = 0.0462 \pm 0.0062$, which we rescale to our best value $B(D_s^+ \rightarrow \phi\pi^+) = (4.5 \pm 0.4) \times 10^{-2}$. Our first error is their experiment's error and our second error is the systematic error from using our best value.

² A partial reconstruction technique is used and the result is independent of the particle decay rate of D_s^+ meson. It also provides a model-independent determination of $B(D_s^+ \rightarrow \phi\pi^+) = (4.81 \pm 0.52 \pm 0.38)\%$.

³ AUBERT 03i reports $0.0197 \pm 0.0015 \pm 0.0030$ from a measurement of $[\Gamma(B^0 \rightarrow D^*(2010)^- D_s^+)/\Gamma_{\text{total}}] \times [B(D_s^+ \rightarrow \phi\pi^+)]$ assuming $B(D_s^+ \rightarrow \phi\pi^+) = 0.036$, which we rescale to our best value $B(D_s^+ \rightarrow \phi\pi^+) = (4.5 \pm 0.4) \times 10^{-2}$. Our first error is their experiment's error and our second error is the systematic error from using our best value.

⁴ AHMED 00B reports $0.0182 \pm 0.0037 \pm 0.0025$ from a measurement of $[\Gamma(B^0 \rightarrow D^*(2010)^- D_s^+)/\Gamma_{\text{total}}] \times [B(D_s^+ \rightarrow \phi\pi^+)]$ assuming $B(D_s^+ \rightarrow \phi\pi^+) = 0.036$, which we rescale to our best value $B(D_s^+ \rightarrow \phi\pi^+) = (4.5 \pm 0.4) \times 10^{-2}$. Our first error is their experiment's error and our second error is the systematic error from using our best value.

⁵ ALBRECHT 92G reports $0.026 \pm 0.014 \pm 0.006$ from a measurement of $[\Gamma(B^0 \rightarrow D^*(2010)^- D_s^+)/\Gamma_{\text{total}}] \times [B(D_s^+ \rightarrow \phi\pi^+)]$ assuming $B(D_s^+ \rightarrow \phi\pi^+) = 0.027$, which we rescale to our best value $B(D_s^+ \rightarrow \phi\pi^+) = (4.5 \pm 0.4) \times 10^{-2}$. Our first error is their experiment's error and our second error is the systematic error from using our best value. Assumes PDG 1990 D^+ and $D^*(2010)^+$ branching ratios, e.g., $B(D^0 \rightarrow K^- \pi^+) = 3.71 \pm 0.25\%$, $B(D^+ \rightarrow K^- 2\pi^+) = 7.1 \pm 1.0\%$, and $B(D^*(2010)^+ \rightarrow D^0 \pi^+) = 55 \pm 4\%$.

$\Gamma(D^*(2010)^- D_s^+)/\Gamma_{\text{total}}$		Γ_{86}/Γ_{84}		
VALUE	DOCUMENT ID	TECN	COMMENT	
2.19 ± 0.08 ± 0.02	¹ AAJ	21s LHCB	pp at 13 TeV	

¹ AAJ 21s reports $[\Gamma(B^0 \rightarrow D^*(2010)^- D_s^+)/\Gamma(B^0 \rightarrow D^*(2010)^- D_s^+)] \times [B(D_s^+ \rightarrow D_s^+ \gamma)] = 2.045 \pm 0.022 \pm 0.071$ which we divide by our best value $B(D_s^+ \rightarrow D_s^+ \gamma) = (93.5 \pm 0.7) \times 10^{-2}$. Our first error is their experiment's error and our second error is the systematic error from using our best value.

$[\Gamma(D^*(2010)^- D_s^+) + \Gamma(D^*(2010)^- D_s^{*+})]/\Gamma_{\text{total}}$		$(\Gamma_{84} + \Gamma_{86})/\Gamma$		
VALUE (units 10^{-2})	EVTS	DOCUMENT ID	TECN	COMMENT
2.5 ± 0.4 OUR AVERAGE				
2.40 ± 0.35 ± 0.22		¹ AUBERT	03i BABR	$e^+e^- \rightarrow \Upsilon(4S)$
3.3 ± 0.9 ± 0.3		² BORTOLETTO90	CLEO	$e^+e^- \rightarrow \Upsilon(4S)$

¹ AUBERT 03i reports $(3.00 \pm 0.19 \pm 0.39) \times 10^{-2}$ from a measurement of $[\Gamma(B^0 \rightarrow D^*(2010)^- D_s^+) + \Gamma(B^0 \rightarrow D^*(2010)^- D_s^{*+})]/\Gamma_{\text{total}}] \times [B(D_s^+ \rightarrow \phi\pi^+)]$ assuming $B(D_s^+ \rightarrow \phi\pi^+) = 0.036$, which we rescale to our best value $B(D_s^+ \rightarrow \phi\pi^+) = (4.5 \pm 0.4) \times 10^{-2}$. Our first error is their experiment's error and our second error is the systematic error from using our best value.

² BORTOLETTO 90 reports $(7.5 \pm 2.0) \times 10^{-2}$ from a measurement of $[\Gamma(B^0 \rightarrow D^*(2010)^- D_s^+) + \Gamma(B^0 \rightarrow D^*(2010)^- D_s^{*+})]/\Gamma_{\text{total}}] \times [B(D_s^+ \rightarrow \phi\pi^+)]$ assuming $B(D_s^+ \rightarrow \phi\pi^+) = 0.02$, which we rescale to our best value $B(D_s^+ \rightarrow \phi\pi^+) = (4.5 \pm 0.4) \times 10^{-2}$. Our first error is their experiment's error and our second error is the systematic error from using our best value.

$\Gamma(D_{S0}(2317)^- K^+, D_{S0}^- \rightarrow D_s^- \pi^0)/\Gamma_{\text{total}}$		Γ_{87}/Γ		
VALUE (units 10^{-5})	DOCUMENT ID	TECN	COMMENT	
4.2 ± 1.3 ± 0.4	¹ DRUTSKOY	05 BELL	$e^+e^- \rightarrow \Upsilon(4S)$	

¹ DRUTSKOY 05 reports $(5.3^{+1.5}_{-1.3} \pm 1.6) \times 10^{-5}$ from a measurement of $[\Gamma(B^0 \rightarrow D_{S0}(2317)^- K^+, D_{S0}^- \rightarrow D_s^- \pi^0)/\Gamma_{\text{total}}] \times [B(D_s^+ \rightarrow \phi\pi^+)]$ assuming $B(D_s^+ \rightarrow \phi\pi^+) = 0.036 \pm 0.009$, which we rescale to our best value $B(D_s^+ \rightarrow \phi\pi^+) = (4.5 \pm 0.4) \times 10^{-2}$. Our first error is their experiment's error and our second error is the systematic error from using our best value.

$\Gamma(D_{S0}(2317)^- \pi^+, D_{S0}^- \rightarrow D_s^- \pi^0)/\Gamma_{\text{total}}$		Γ_{88}/Γ		
VALUE (units 10^{-5})	CL%	DOCUMENT ID	TECN	COMMENT
<2.5	90	¹ DRUTSKOY	05 BELL	$e^+e^- \rightarrow \Upsilon(4S)$

¹ Assumes equal production of B^+ and B^0 at the $\Upsilon(4S)$.

$\Gamma(D_{sJ}(2457)^- K^+, D_{sJ}^- \rightarrow D_s^- \pi^0)/\Gamma_{total}$					Γ_{89}/Γ
VALUE (units 10^{-5})	CL%	DOCUMENT ID	TECN	COMMENT	
<0.94	90	1 DRUTSKOY 05	BELL	$e^+ e^- \rightarrow \Upsilon(4S)$	
1 Assumes equal production of B^+ and B^0 at the $\Upsilon(4S)$.					

$\Gamma(D_{sJ}(2457)^- \pi^+, D_{sJ}^- \rightarrow D_s^- \pi^0)/\Gamma_{total}$					Γ_{90}/Γ
VALUE (units 10^{-5})	CL%	DOCUMENT ID	TECN	COMMENT	
<0.40	90	1 DRUTSKOY 05	BELL	$e^+ e^- \rightarrow \Upsilon(4S)$	
1 Assumes equal production of B^+ and B^0 at the $\Upsilon(4S)$.					

$\Gamma(D_s^- D_s^+)/\Gamma_{total}$					Γ_{91}/Γ
VALUE	CL%	DOCUMENT ID	TECN	COMMENT	
< 3.6×10^{-5}	90	1 ZUPANC 07	BELL	$e^+ e^- \rightarrow \Upsilon(4S)$	
• • • We do not use the following data for averages, fits, limits, etc. • • •					
< 10×10^{-5}	90	1 AUBERT,BE 05F	BABR	$e^+ e^- \rightarrow \Upsilon(4S)$	
1 Assumes equal production of B^+ and B^0 at the $\Upsilon(4S)$.					

$\Gamma(D_s^{*-} D_s^+)/\Gamma_{total}$					Γ_{92}/Γ
VALUE	CL%	DOCUMENT ID	TECN	COMMENT	
< 1.3×10^{-4}	90	1 AUBERT,BE 05F	BABR	$e^+ e^- \rightarrow \Upsilon(4S)$	
1 Assumes equal production of B^+ and B^0 at the $\Upsilon(4S)$.					

$\Gamma(D_s^{*-} D_s^{*+})/\Gamma_{total}$					Γ_{93}/Γ
VALUE	CL%	DOCUMENT ID	TECN	COMMENT	
< 2.4×10^{-4}	90	1 AUBERT,BE 05F	BABR	$e^+ e^- \rightarrow \Upsilon(4S)$	
1 Assumes equal production of B^+ and B^0 at the $\Upsilon(4S)$.					

$\Gamma(D_{s0}^*(2317)^+ D^-, D_{s0}^{*+} \rightarrow D_s^+ \pi^0)/\Gamma_{total}$					Γ_{94}/Γ
VALUE (units 10^{-3})	CL%	DOCUMENT ID	TECN	COMMENT	
1.06 ± 0.16 OUR AVERAGE		Error includes scale factor of 1.1.			
$0.99^{+0.19}_{-0.15} \pm 0.03$		1,2 CHOI 15A	BELL	$e^+ e^- \rightarrow \Upsilon(4S)$	
$1.4^{+0.5}_{-0.4} \pm 0.1$		2,3 AUBERT,B 04s	BABR	$e^+ e^- \rightarrow \Upsilon(4S)$	
• • • We do not use the following data for averages, fits, limits, etc. • • •					
$0.69^{+0.29}_{-0.24} \pm 0.06$		2,4 KROKOVNY 03B	BELL	Repl. by CHOI 15A	

1 CHOI 15A reports $(10.2^{+1.3}_{-1.2} \pm 1.0 \pm 0.4) \times 10^{-4}$ from a measurement of $[\Gamma(B^0 \rightarrow D_{s0}^*(2317)^+ D^-, D_{s0}^{*+} \rightarrow D_s^+ \pi^0)/\Gamma_{total}] \times [B(D_s^+ \rightarrow K^+ K^- \pi^+)] \times [B(D^+ \rightarrow K^- 2\pi^+)]$ assuming $B(D_s^+ \rightarrow K^+ K^- \pi^+) = (5.39 \pm 0.21) \times 10^{-2}$, $B(D^+ \rightarrow K^- 2\pi^+) = (9.13 \pm 0.19) \times 10^{-2}$, which we rescale to our best values $B(D_s^+ \rightarrow K^+ K^- \pi^+) = (5.38 \pm 0.10) \times 10^{-2}$, $B(D^+ \rightarrow K^- 2\pi^+) = (9.38 \pm 0.16) \times 10^{-2}$. Our first error is their experiment's error and our second error is the systematic error from using our best values.

2 Assumes equal production of B^+ and B^0 at the $\Upsilon(4S)$.

3 AUBERT,B 04s reports $(1.8 \pm 0.4^{+0.7}_{-0.5}) \times 10^{-3}$ from a measurement of $[\Gamma(B^0 \rightarrow D_{s0}^*(2317)^+ D^-, D_{s0}^{*+} \rightarrow D_s^+ \pi^0)/\Gamma_{total}] \times [B(D_s^+ \rightarrow \phi \pi^+)]$ assuming $B(D_s^+ \rightarrow \phi \pi^+) = 0.036 \pm 0.009$, which we rescale to our best value $B(D_s^+ \rightarrow \phi \pi^+) = (4.5 \pm 0.4) \times 10^{-2}$. Our first error is their experiment's error and our second error is the systematic error from using our best value.

4 KROKOVNY 03B reports $(0.86^{+0.33}_{-0.26} \pm 0.26) \times 10^{-3}$ from a measurement of $[\Gamma(B^0 \rightarrow D_{s0}^*(2317)^+ D^-, D_{s0}^{*+} \rightarrow D_s^+ \pi^0)/\Gamma_{total}] \times [B(D_s^+ \rightarrow \phi \pi^+)]$ assuming $B(D_s^+ \rightarrow \phi \pi^+) = 0.036 \pm 0.009$, which we rescale to our best value $B(D_s^+ \rightarrow \phi \pi^+) = (4.5 \pm 0.4) \times 10^{-2}$. Our first error is their experiment's error and our second error is the systematic error from using our best value.

$\Gamma(D_{s0}(2317)^+ D^-, D_{s0}^+ \rightarrow D_s^{*+} \gamma)/\Gamma_{total}$					Γ_{95}/Γ
VALUE (units 10^{-3})	CL%	DOCUMENT ID	TECN	COMMENT	
<0.95	90	1 KROKOVNY 03B	BELL	$e^+ e^- \rightarrow \Upsilon(4S)$	
1 Assumes equal production of B^+ and B^0 at the $\Upsilon(4S)$.					

$\Gamma(D_{s0}(2317)^+ D^*(2010)^-, D_{s0}^+ \rightarrow D_s^+ \pi^0)/\Gamma_{total}$					Γ_{96}/Γ
VALUE (units 10^{-3})	CL%	DOCUMENT ID	TECN	COMMENT	
1.5 ± 0.4 ± 0.5		1 AUBERT,B 04s	BABR	$e^+ e^- \rightarrow \Upsilon(4S)$	
1 Assumes equal production of B^+ and B^0 at the $\Upsilon(4S)$.					

$\Gamma(D_{sJ}(2457)^+ D^-)/\Gamma_{total}$					Γ_{97}/Γ
VALUE (units 10^{-3})	CL%	DOCUMENT ID	TECN	COMMENT	
3.5 ± 1.1 OUR AVERAGE					
$2.6 \pm 1.5 \pm 0.7$		1 AUBERT 06N	BABR	$e^+ e^- \rightarrow \Upsilon(4S)$	
$4.8^{+2.2}_{-1.6} \pm 1.1$		2,3 AUBERT,B 04s	BABR	$e^+ e^- \rightarrow \Upsilon(4S)$	
$3.9^{+1.5}_{-1.3} \pm 0.9$		2,4 KROKOVNY 03B	BELL	$e^+ e^- \rightarrow \Upsilon(4S)$	

1 Uses a missing-mass method in the events that one of the B mesons is fully reconstructed.

2 Assumes equal production of B^+ and B^0 at the $\Upsilon(4S)$.

3 AUBERT,B 04s reports $[\Gamma(B^0 \rightarrow D_{sJ}(2457)^+ D^-)/\Gamma_{total}] \times [B(D_{s1}(2460)^+ \rightarrow D_s^+ \pi^0)] = (2.3^{+1.0}_{-0.7} \pm 0.3) \times 10^{-3}$ which we divide by our best value $B(D_{s1}(2460)^+ \rightarrow D_s^+ \pi^0) = (48 \pm 11) \times 10^{-2}$.

$D_s^{*+} \pi^0 = (48 \pm 11) \times 10^{-2}$. Our first error is their experiment's error and our second error is the systematic error from using our best value.

4 KROKOVNY 03B reports $[\Gamma(B^0 \rightarrow D_{sJ}(2457)^+ D^-)/\Gamma_{total}] \times [B(D_{s1}(2460)^+ \rightarrow D_s^+ \pi^0)] = (1.9^{+0.7}_{-0.6} \pm 0.2) \times 10^{-3}$ which we divide by our best value $B(D_{s1}(2460)^+ \rightarrow D_s^+ \pi^0) = (48 \pm 11) \times 10^{-2}$. Our first error is their experiment's error and our second error is the systematic error from using our best value.

$\Gamma(D_{sJ}(2457)^+ D^-, D_{sJ}^+ \rightarrow D_s^+ \gamma)/\Gamma_{total}$					Γ_{98}/Γ
VALUE (units 10^{-3})	CL%	DOCUMENT ID	TECN	COMMENT	
0.65 ± 0.17 ± 0.14 OUR AVERAGE					
$0.64^{+0.24}_{-0.16} \pm 0.06$		1,2 AUBERT,B 04s	BABR	$e^+ e^- \rightarrow \Upsilon(4S)$	
$0.66^{+0.21}_{-0.19} \pm 0.06$		1,3 KROKOVNY 03B	BELL	$e^+ e^- \rightarrow \Upsilon(4S)$	

1 Assumes equal production of B^+ and B^0 at the $\Upsilon(4S)$.

2 AUBERT,B 04s reports $(0.8 \pm 0.2^{+0.3}_{-0.2}) \times 10^{-3}$ from a measurement of $[\Gamma(B^0 \rightarrow D_{sJ}(2457)^+ D^-, D_{sJ}^+ \rightarrow D_s^+ \gamma)/\Gamma_{total}] \times [B(D_s^+ \rightarrow \phi \pi^+)]$ assuming $B(D_s^+ \rightarrow \phi \pi^+) = 0.036 \pm 0.009$, which we rescale to our best value $B(D_s^+ \rightarrow \phi \pi^+) = (4.5 \pm 0.4) \times 10^{-2}$. Our first error is their experiment's error and our second error is the systematic error from using our best value.

3 KROKOVNY 03B reports $(0.82^{+0.22}_{-0.19} \pm 0.25) \times 10^{-3}$ from a measurement of $[\Gamma(B^0 \rightarrow D_{sJ}(2457)^+ D^-, D_{sJ}^+ \rightarrow D_s^+ \gamma)/\Gamma_{total}] \times [B(D_s^+ \rightarrow \phi \pi^+)]$ assuming $B(D_s^+ \rightarrow \phi \pi^+) = 0.036 \pm 0.009$, which we rescale to our best value $B(D_s^+ \rightarrow \phi \pi^+) = (4.5 \pm 0.4) \times 10^{-2}$. Our first error is their experiment's error and our second error is the systematic error from using our best value.

$\Gamma(D_{sJ}(2457)^+ D^-, D_{sJ}^+ \rightarrow D_s^+ \gamma)/\Gamma_{total}$					Γ_{99}/Γ
VALUE (units 10^{-3})	CL%	DOCUMENT ID	TECN	COMMENT	
<0.60	90	1 KROKOVNY 03B	BELL	$e^+ e^- \rightarrow \Upsilon(4S)$	
1 Assumes equal production of B^+ and B^0 at the $\Upsilon(4S)$.					

$\Gamma(D_{sJ}(2457)^+ D^-, D_{sJ}^+ \rightarrow D_s^+ \pi^+ \pi^-)/\Gamma_{total}$					Γ_{100}/Γ
VALUE (units 10^{-3})	CL%	DOCUMENT ID	TECN	COMMENT	
<0.20	90	1 KROKOVNY 03B	BELL	$e^+ e^- \rightarrow \Upsilon(4S)$	
1 Assumes equal production of B^+ and B^0 at the $\Upsilon(4S)$.					

$\Gamma(D_{sJ}(2457)^+ D^-, D_{sJ}^+ \rightarrow D_s^+ \pi^0)/\Gamma_{total}$					Γ_{101}/Γ
VALUE (units 10^{-3})	CL%	DOCUMENT ID	TECN	COMMENT	
<0.36	90	1 KROKOVNY 03B	BELL	$e^+ e^- \rightarrow \Upsilon(4S)$	
1 Assumes equal production of B^+ and B^0 at the $\Upsilon(4S)$.					

$\Gamma(D^*(2010)^- D_{sJ}(2457)^+)/\Gamma_{total}$					Γ_{102}/Γ
VALUE (units 10^{-3})	CL%	DOCUMENT ID	TECN	COMMENT	
9.3 ± 2.2 OUR AVERAGE					
$8.8 \pm 2.0 \pm 1.4$		1 AUBERT 06N	BABR	$e^+ e^- \rightarrow \Upsilon(4S)$	
$11^{+5}_{-4} \pm 3$		2,3 AUBERT,B 04s	BABR	$e^+ e^- \rightarrow \Upsilon(4S)$	

1 Uses a missing-mass method in the events that one of the B mesons is fully reconstructed.

2 AUBERT,B 04s reports $[\Gamma(B^0 \rightarrow D^*(2010)^- D_{sJ}(2457)^+)/\Gamma_{total}] \times [B(D_{s1}(2460)^+ \rightarrow D_s^+ \pi^0)] = (5.5 \pm 1.2^{+2.2}_{-1.6}) \times 10^{-3}$ which we divide by our best value $B(D_{s1}(2460)^+ \rightarrow D_s^+ \pi^0) = (48 \pm 11) \times 10^{-2}$. Our first error is their experiment's error and our second error is the systematic error from using our best value.

3 Assumes equal production of B^+ and B^0 at the $\Upsilon(4S)$.

$\Gamma(D_{sJ}(2457)^+ D^*(2010)^-, D_{sJ}^+ \rightarrow D_s^+ \gamma)/\Gamma_{total}$					Γ_{103}/Γ
VALUE (units 10^{-3})	CL%	DOCUMENT ID	TECN	COMMENT	
2.3 ± 0.3 ± 0.9 ± 0.6		1 AUBERT,B 04s	BABR	$e^+ e^- \rightarrow \Upsilon(4S)$	
1 Assumes equal production of B^+ and B^0 at the $\Upsilon(4S)$.					

$[\Gamma(D^- D_{s1}(2536)^+, D_{s1}^+ \rightarrow D^{*0} K^+) + \Gamma(D^{*+} K^0)]/\Gamma_{total}$					$\Gamma_{104}/\Gamma = (\Gamma_{105} + \Gamma_{106})/\Gamma$
VALUE (units 10^{-4})	CL%	DOCUMENT ID	TECN	COMMENT	
2.75 ± 0.62 ± 0.36		1,2 AUSHEV 11	BELL	$e^+ e^- \rightarrow \Upsilon(4S)$	
1 Uses $\Gamma(D^*(2007)^0 \rightarrow D^0 \pi^0) / \Gamma(D^*(2007)^0 \rightarrow D^0 \gamma) = 1.74 \pm 0.13$ and $\Gamma(D_{s1}(2536)^+ \rightarrow D^*(2007)^0 K^+) / \Gamma(D_{s1}(2536)^+ \rightarrow D^*(2010)^+ K^0) = 1.36 \pm 0.2$.					
2 Assumes equal production of B^+ and B^0 at the $\Upsilon(4S)$.					

$\Gamma(D^- D_{s1}(2536)^+, D_{s1}^+ \rightarrow D^{*0} K^+)/\Gamma_{total}$					Γ_{105}/Γ
VALUE (units 10^{-4})	CL%	DOCUMENT ID	TECN	COMMENT	
1.71 ± 0.48 ± 0.32		1 AUBERT 08B	BABR	$e^+ e^- \rightarrow \Upsilon(4S)$	
• • • We do not use the following data for averages, fits, limits, etc. • • •					
<5	90	AUBERT 03X	BABR	Repl. by AUBERT 08B	
1 Assumes equal production of B^+ and B^0 at the $\Upsilon(4S)$.					

$\Gamma(D^- D_{s1}(2536)^+, D_{s1}^+ \rightarrow D^{*+} K^0)/\Gamma_{total}$					Γ_{106}/Γ
VALUE (units 10^{-4})	CL%	DOCUMENT ID	TECN	COMMENT	
2.61 ± 1.03 ± 0.31		1 AUBERT 08B	BABR	$e^+ e^- \rightarrow \Upsilon(4S)$	
1 Assumes equal production of B^+ and B^0 at the $\Upsilon(4S)$.					

Meson Particle Listings

 B^0

$$\frac{\Gamma(D^*(2010) - D_{s1}(2536)^+, D_{s1}^+ \rightarrow D^{*0} K^+) + \Gamma(D^{*+} K^0)}{\Gamma_{107}/\Gamma = (\Gamma_{108} + \Gamma_{109})/\Gamma}$$

VALUE (units 10^{-4})	DOCUMENT ID	TECN	COMMENT
5.01 ± 1.21 ± 0.70	1,2 AUSHEV	11	BELL $e^+ e^- \rightarrow \Upsilon(4S)$

¹ Uses $\Gamma(D^*(2007)^0 \rightarrow D^0 \pi^0) / \Gamma(D^*(2007)^0 \rightarrow D^0 \gamma) = 1.74 \pm 0.13$ and $\Gamma(D_{s1}(2536)^+ \rightarrow D^*(2007)^0 K^+) / \Gamma(D_{s1}(2536)^+ \rightarrow D^*(2010)^+ K^0) = 1.36 \pm 0.2$.

² Assumes equal production of B^+ and B^0 at the $\Upsilon(4S)$.

$$\Gamma(D^*(2010) - D_{s1}(2536)^+, D_{s1}^+ \rightarrow D^{*0} K^+)/\Gamma_{108}/\Gamma$$

VALUE (units 10^{-4})	CL%	DOCUMENT ID	TECN	COMMENT
3.32 ± 0.88 ± 0.66		1 AUBERT	08B	BABR $e^+ e^- \rightarrow \Upsilon(4S)$

• • • We do not use the following data for averages, fits, limits, etc. • • •

<7 90 AUBERT 03X BABR Repl. by AUBERT 08B

¹ Assumes equal production of B^+ and B^0 at the $\Upsilon(4S)$.

$$\Gamma(D^* - D_{s1}(2536)^+, D_{s1}^+ \rightarrow D^{*+} K^0)/\Gamma_{109}/\Gamma$$

VALUE (units 10^{-4})	DOCUMENT ID	TECN	COMMENT
5.00 ± 1.51 ± 0.67	1 AUBERT	08B	BABR $e^+ e^- \rightarrow \Upsilon(4S)$

¹ Assumes equal production of B^+ and B^0 at the $\Upsilon(4S)$.

$$\Gamma(D^- D_{sJ}(2573)^+, D_{sJ}^+ \rightarrow D^0 K^+)/\Gamma_{110}/\Gamma$$

VALUE (units 10^{-5})	CL%	DOCUMENT ID	TECN	COMMENT
3.4 ± 1.7 ± 0.5		1 LEES	15C	BABR $e^+ e^- \rightarrow \Upsilon(4S)$

• • • We do not use the following data for averages, fits, limits, etc. • • •

<10 90 AUBERT 03X BABR $e^+ e^- \rightarrow \Upsilon(4S)$

¹ Assumes equal production of B^+ and B^0 at the $\Upsilon(4S)$.

$$\Gamma(D^*(2010) - D_{sJ}(2573)^+, D_{sJ}^+ \rightarrow D^0 K^+)/\Gamma_{111}/\Gamma$$

VALUE (units 10^{-4})	CL%	DOCUMENT ID	TECN	COMMENT
<2		90	AUBERT	03X BABR $e^+ e^- \rightarrow \Upsilon(4S)$

¹ Assumes equal production of B^+ and B^0 at the $\Upsilon(4S)$.

$$\Gamma(D^- D_{sJ}(2700)^+, D_{sJ}^+ \rightarrow D^0 K^+)/\Gamma_{112}/\Gamma$$

VALUE (units 10^{-4})	DOCUMENT ID	TECN	COMMENT
7.14 ± 0.96 ± 0.69	1 LEES	15C	BABR $e^+ e^- \rightarrow \Upsilon(4S)$

¹ Assumes equal production of B^+ and B^0 at the $\Upsilon(4S)$.

$$\Gamma(D^+ \pi^-)/\Gamma_{113}/\Gamma$$

VALUE (units 10^{-7})	DOCUMENT ID	TECN	COMMENT
7.3 ± 1.2 ± 0.2	1,2 DAS	10	BELL $e^+ e^- \rightarrow \Upsilon(4S)$

¹ DAS 10 reports $[\Gamma(B^0 \rightarrow D^+ \pi^-)/\Gamma_{\text{total}}] / [B(B^0 \rightarrow D^- \pi^+)] = (2.92 \pm 0.38 \pm 0.31) \times 10^{-4}$ which we multiply by our best value $B(B^0 \rightarrow D^- \pi^+) = (2.51 \pm 0.08) \times 10^{-3}$. Our first error is their experiment's error and our second error is the systematic error from using our best value.

² Derived using $\tan(\theta_C) f_D/f_{D_s} \sqrt{B(B^0 \rightarrow D_s^+ \pi^-)/B(B^0 \rightarrow D^- \pi^+)}$ by assuming the flavor SU(3) symmetry, where θ_C is the Cabibbo angle, f_D (f_{D_s}) is the D (D_s) meson decay constant.

$$\Gamma(D_s^+ \pi^-)/\Gamma_{114}/\Gamma$$

VALUE (units 10^{-6})	CL%	DOCUMENT ID	TECN	COMMENT
20.3 ± 1.8 OUR FIT				
21.6 ± 2.6 OUR AVERAGE				

19.9 ± 2.6 ± 1.8 1 DAS 10 BELL $e^+ e^- \rightarrow \Upsilon(4S)$

25 ± 4 ± 2 1 AUBERT 08AJ BABR $e^+ e^- \rightarrow \Upsilon(4S)$

• • • We do not use the following data for averages, fits, limits, etc. • • •

14.0 ± 3.5 ± 1.3 2 AUBERT 07K BABR Repl. by AUBERT 08AJ

25 ± 9 ± 2 3 AUBERT 03D BABR Repl. by AUBERT 07K

19 ± 9 ± 2 4 KROKOVNY 02 BELL Repl. by DAS 10

< 220 90 5 ALEXANDER 93B CLE2 $e^+ e^- \rightarrow \Upsilon(4S)$

< 1300 90 6 BORTOLETTO 90 CLEO $e^+ e^- \rightarrow \Upsilon(4S)$

¹ Assumes equal production of B^+ and B^0 at the $\Upsilon(4S)$.

² AUBERT 07K reports $[\Gamma(B^0 \rightarrow D_s^+ \pi^-)/\Gamma_{\text{total}}] \times [B(D_s^+ \rightarrow \phi \pi^+)] = (0.63 \pm 0.15 \pm 0.05) \times 10^{-6}$ which we divide by our best value $B(D_s^+ \rightarrow \phi \pi^+) = (4.5 \pm 0.4) \times 10^{-2}$. Our first error is their experiment's error and our second error is the systematic error from using our best value.

³ AUBERT 03D reports $[\Gamma(B^0 \rightarrow D_s^+ \pi^-)/\Gamma_{\text{total}}] \times [B(D_s^+ \rightarrow \phi \pi^+)] = (1.13 \pm 0.33 \pm 0.21) \times 10^{-6}$ which we divide by our best value $B(D_s^+ \rightarrow \phi \pi^+) = (4.5 \pm 0.4) \times 10^{-2}$. Our first error is their experiment's error and our second error is the systematic error from using our best value.

⁴ KROKOVNY 02 reports $[\Gamma(B^0 \rightarrow D_s^+ \pi^-)/\Gamma_{\text{total}}] \times [B(D_s^+ \rightarrow \phi \pi^+)] = (0.86_{-0.30}^{+0.37} \pm 0.11) \times 10^{-6}$ which we divide by our best value $B(D_s^+ \rightarrow \phi \pi^+) = (4.5 \pm 0.4) \times 10^{-2}$. Our first error is their experiment's error and our second error is the systematic error from using our best value.

⁵ ALEXANDER 93B reports $< 270 \times 10^{-6}$ from a measurement of $[\Gamma(B^0 \rightarrow D_s^+ \pi^-)/\Gamma_{\text{total}}] \times [B(D_s^+ \rightarrow \phi \pi^+)]$ assuming $B(D_s^+ \rightarrow \phi \pi^+) = 0.037$, which we rescale to our best value $B(D_s^+ \rightarrow \phi \pi^+) = 4.5 \times 10^{-2}$.

⁶ BORTOLETTO 90 assume $B(D_s \rightarrow \phi \pi^+) = 2\%$.

$$\frac{\Gamma(D_s^+ \pi^-) + \Gamma(D_s^- K^+)}{\Gamma_{\text{total}}} (\Gamma_{114} + \Gamma_{124})/\Gamma$$

VALUE	CL%	DOCUMENT ID	TECN	COMMENT
< 1.0 × 10⁻³		90	1 ALBRECHT	93E ARG $e^+ e^- \rightarrow \Upsilon(4S)$

¹ ALBRECHT 93E reports $< 1.7 \times 10^{-3}$ from a measurement of $[\Gamma(B^0 \rightarrow D_s^+ \pi^-) + \Gamma(B^0 \rightarrow D_s^- K^+)]/\Gamma_{\text{total}} \times [B(D_s^+ \rightarrow \phi \pi^+)]$ assuming $B(D_s^+ \rightarrow \phi \pi^+) = 0.027$, which we rescale to our best value $B(D_s^+ \rightarrow \phi \pi^+) = 4.5 \times 10^{-2}$.

$$\Gamma(D_s^+ \pi^-)/\Gamma(D^- \pi^+) \Gamma_{114}/\Gamma_{35}$$

VALUE (units 10^{-3})	DOCUMENT ID	TECN	COMMENT
8.1 ± 0.7 OUR FIT			
7.7 ± 0.7 ± 0.6	AAIJ	21W	LHCb pp at 7, 8, 13 TeV

$$\Gamma(D_s^{*+} \pi^-)/\Gamma_{\text{total}} \Gamma_{115}/\Gamma$$

VALUE (units 10^{-5})	CL%	DOCUMENT ID	TECN	COMMENT
2.1 ± 0.4 OUR AVERAGE				Error includes scale factor of 1.4.

1.75 ± 0.34 ± 0.20 1 JOSHI 10 BELL $e^+ e^- \rightarrow \Upsilon(4S)$

2.6 $^{+0.5}_{-0.4}$ ± 0.2 1 AUBERT 08AJ BABR $e^+ e^- \rightarrow \Upsilon(4S)$

• • • We do not use the following data for averages, fits, limits, etc. • • •

2.9 ± 0.7 ± 0.3 2 AUBERT 07K BABR Repl. by AUBERT 08AJ

< 4.1 90 AUBERT 03D BABR Repl. by AUBERT 07K

< 40 90 3 ALEXANDER 93B CLE2 $e^+ e^- \rightarrow \Upsilon(4S)$

¹ Assumes equal production of B^+ and B^0 at the $\Upsilon(4S)$.

² AUBERT 07K reports $[\Gamma(B^0 \rightarrow D_s^{*+} \pi^-)/\Gamma_{\text{total}}] \times [B(D_s^+ \rightarrow \phi \pi^+)] = (1.32 \pm 0.27 \pm 0.15) \times 10^{-6}$ which we divide by our best value $B(D_s^+ \rightarrow \phi \pi^+) = (4.5 \pm 0.4) \times 10^{-2}$. Our first error is their experiment's error and our second error is the systematic error from using our best value.

³ ALEXANDER 93B reports $< 44 \times 10^{-5}$ from a measurement of $[\Gamma(B^0 \rightarrow D_s^{*+} \pi^-)/\Gamma_{\text{total}}] \times [B(D_s^+ \rightarrow \phi \pi^+)]$ assuming $B(D_s^+ \rightarrow \phi \pi^+) = 0.037$, which we rescale to our best value $B(D_s^+ \rightarrow \phi \pi^+) = 4.5 \times 10^{-2}$.

$$\frac{\Gamma(D_s^{*+} \pi^-) + \Gamma(D_s^{*+} K^+)}{\Gamma_{\text{total}}} (\Gamma_{115} + \Gamma_{125})/\Gamma$$

VALUE	CL%	DOCUMENT ID	TECN	COMMENT
< 7 × 10⁻⁴		90	1 ALBRECHT	93E ARG $e^+ e^- \rightarrow \Upsilon(4S)$

¹ ALBRECHT 93E reports $< 1.2 \times 10^{-3}$ from a measurement of $[\Gamma(B^0 \rightarrow D_s^{*+} \pi^-) + \Gamma(B^0 \rightarrow D_s^{*+} K^+)]/\Gamma_{\text{total}} \times [B(D_s^+ \rightarrow \phi \pi^+)]$ assuming $B(D_s^+ \rightarrow \phi \pi^+) = 0.027$, which we rescale to our best value $B(D_s^+ \rightarrow \phi \pi^+) = 4.5 \times 10^{-2}$.

$$\Gamma(D_s^+ \rho^-)/\Gamma_{\text{total}} \Gamma_{116}/\Gamma$$

VALUE (units 10^{-9})	CL%	DOCUMENT ID	TECN	COMMENT
< 2.4		90	1 AUBERT	08AJ BABR $e^+ e^- \rightarrow \Upsilon(4S)$

• • • We do not use the following data for averages, fits, limits, etc. • • •

< 130 90 2 ALBRECHT 93E ARG $e^+ e^- \rightarrow \Upsilon(4S)$

< 50 90 3 ALEXANDER 93B CLE2 $e^+ e^- \rightarrow \Upsilon(4S)$

¹ Assumes equal production of B^+ and B^0 at the $\Upsilon(4S)$.

² ALBRECHT 93E reports $< 2.2 \times 10^{-3}$ from a measurement of $[\Gamma(B^0 \rightarrow D_s^+ \rho^-)/\Gamma_{\text{total}}] \times [B(D_s^+ \rightarrow \phi \pi^+)]$ assuming $B(D_s^+ \rightarrow \phi \pi^+) = 0.027$, which we rescale to our best value $B(D_s^+ \rightarrow \phi \pi^+) = 4.5 \times 10^{-2}$.

³ ALEXANDER 93B reports $< 6.6 \times 10^{-4}$ from a measurement of $[\Gamma(B^0 \rightarrow D_s^+ \rho^-)/\Gamma_{\text{total}}] \times [B(D_s^+ \rightarrow \phi \pi^+)]$ assuming $B(D_s^+ \rightarrow \phi \pi^+) = 0.037$, which we rescale to our best value $B(D_s^+ \rightarrow \phi \pi^+) = 4.5 \times 10^{-2}$.

$$\Gamma(D_s^{*+} \rho^-)/\Gamma_{\text{total}} \Gamma_{117}/\Gamma$$

VALUE (units 10^{-9})	CL%	DOCUMENT ID	TECN	COMMENT
4.1 ± 1.3 ± 0.4		1 AUBERT	08AJ BABR	$e^+ e^- \rightarrow \Upsilon(4S)$

• • • We do not use the following data for averages, fits, limits, etc. • • •

< 150 90 2 ALBRECHT 93E ARG $e^+ e^- \rightarrow \Upsilon(4S)$

< 60 90 3 ALEXANDER 93B CLE2 $e^+ e^- \rightarrow \Upsilon(4S)$

¹ Assumes equal production of B^+ and B^0 at the $\Upsilon(4S)$.

² ALBRECHT 93E reports $< 2.5 \times 10^{-3}$ from a measurement of $[\Gamma(B^0 \rightarrow D_s^{*+} \rho^-)/\Gamma_{\text{total}}] \times [B(D_s^+ \rightarrow \phi \pi^+)]$ assuming $B(D_s^+ \rightarrow \phi \pi^+) = 0.027$, which we rescale to our best value $B(D_s^+ \rightarrow \phi \pi^+) = 4.5 \times 10^{-2}$.

³ ALEXANDER 93B reports $< 7.4 \times 10^{-4}$ from a measurement of $[\Gamma(B^0 \rightarrow D_s^{*+} \rho^-)/\Gamma_{\text{total}}] \times [B(D_s^+ \rightarrow \phi \pi^+)]$ assuming $B(D_s^+ \rightarrow \phi \pi^+) = 0.037$, which we rescale to our best value $B(D_s^+ \rightarrow \phi \pi^+) = 4.5 \times 10^{-2}$.

$$\Gamma(D_s^+ \phi_0)/\Gamma_{\text{total}} \Gamma_{118}/\Gamma$$

VALUE (units 10^{-9})	CL%	DOCUMENT ID	TECN	COMMENT
< 1.9		90	1 AUBERT	06X BABR $e^+ e^- \rightarrow \Upsilon(4S)$

¹ Assumes equal production of B^+ and B^0 at the $\Upsilon(4S)$.

$\Gamma(D_s^{*+} a_0^-)/\Gamma_{total}$		Γ_{119}/Γ			
VALUE (units 10^{-5})	CL%	DOCUMENT ID	TECN	COMMENT	
<3.6	90	¹ AUBERT	06X	BABR	$e^+e^- \rightarrow \Upsilon(4S)$
¹ Assumes equal production of B^+ and B^0 at the $\Upsilon(4S)$.					

$\Gamma(D_s^+ a_1(1260)^-)/\Gamma_{total}$		Γ_{120}/Γ			
VALUE	CL%	DOCUMENT ID	TECN	COMMENT	
<2.1 $\times 10^{-3}$	90	¹ ALBRECHT	93E	ARG	$e^+e^- \rightarrow \Upsilon(4S)$
¹ ALBRECHT 93E reports $< 3.5 \times 10^{-3}$ from a measurement of $[\Gamma(B^0 \rightarrow D_s^+ a_1(1260)^-)/\Gamma_{total}] \times [B(D_s^+ \rightarrow \phi\pi^+)]$ assuming $B(D_s^+ \rightarrow \phi\pi^+) = 0.027$, which we rescale to our best value $B(D_s^+ \rightarrow \phi\pi^+) = 4.5 \times 10^{-2}$.					

$\Gamma(D_s^{*+} a_1(1260)^-)/\Gamma_{total}$		Γ_{121}/Γ			
VALUE	CL%	DOCUMENT ID	TECN	COMMENT	
<1.7 $\times 10^{-3}$	90	¹ ALBRECHT	93E	ARG	$e^+e^- \rightarrow \Upsilon(4S)$
¹ ALBRECHT 93E reports $< 2.9 \times 10^{-3}$ from a measurement of $[\Gamma(B^0 \rightarrow D_s^{*+} a_1(1260)^-)/\Gamma_{total}] \times [B(D_s^+ \rightarrow \phi\pi^+)]$ assuming $B(D_s^+ \rightarrow \phi\pi^+) = 0.027$, which we rescale to our best value $B(D_s^+ \rightarrow \phi\pi^+) = 4.5 \times 10^{-2}$.					

$\Gamma(D_s^+ a_2^-)/\Gamma_{total}$		Γ_{122}/Γ			
VALUE (units 10^{-5})	CL%	DOCUMENT ID	TECN	COMMENT	
<19	90	¹ AUBERT	06X	BABR	$e^+e^- \rightarrow \Upsilon(4S)$
¹ Assumes equal production of B^+ and B^0 at the $\Upsilon(4S)$.					

$\Gamma(D_s^{*+} a_2^-)/\Gamma_{total}$		Γ_{123}/Γ			
VALUE (units 10^{-5})	CL%	DOCUMENT ID	TECN	COMMENT	
<20	90	¹ AUBERT	06X	BABR	$e^+e^- \rightarrow \Upsilon(4S)$
¹ Assumes equal production of B^+ and B^0 at the $\Upsilon(4S)$.					

$\Gamma(D_s^- K^+)/\Gamma_{total}$		Γ_{124}/Γ			
VALUE (units 10^{-6})	CL%	DOCUMENT ID	TECN	COMMENT	
27 \pm 5 OUR FIT		Error includes scale factor of 2.7.			
22 \pm 5 OUR AVERAGE		Error includes scale factor of 1.8.			
19.1 \pm 2.4 \pm 1.7		¹ DAS	10	BELL	$e^+e^- \rightarrow \Upsilon(4S)$
29 \pm 4 \pm 2		¹ AUBERT	08AJ	BABR	$e^+e^- \rightarrow \Upsilon(4S)$
• • • We do not use the following data for averages, fits, limits, etc. • • •					
27 \pm 5 \pm 2		² AUBERT	07K	BABR	Repl. by AUBERT 08AJ
26 \pm 10 \pm 2		³ AUBERT	03D	BABR	Repl. by AUBERT 07K
36 \pm 11 \pm 3		⁴ KROKOVNY	02	BELL	Repl. by DAS 10
< 190	90	⁵ ALEXANDER	93B	CLE2	$e^+e^- \rightarrow \Upsilon(4S)$
<1300	90	⁶ BORTOLETTO90	CLEO	$e^+e^- \rightarrow \Upsilon(4S)$	
¹ Assumes equal production of B^+ and B^0 at the $\Upsilon(4S)$.					
² AUBERT 07K reports $[\Gamma(B^0 \rightarrow D_s^- K^+)/\Gamma_{total}] \times [B(D_s^+ \rightarrow \phi\pi^+)] = (1.21 \pm 0.17 \pm 0.11) \times 10^{-6}$ which we divide by our best value $B(D_s^+ \rightarrow \phi\pi^+) = (4.5 \pm 0.4) \times 10^{-2}$. Our first error is their experiment's error and our second error is the systematic error from using our best value.					
³ AUBERT 03D reports $[\Gamma(B^0 \rightarrow D_s^- K^+)/\Gamma_{total}] \times [B(D_s^+ \rightarrow \phi\pi^+)] = (1.16 \pm 0.36 \pm 0.24) \times 10^{-6}$ which we divide by our best value $B(D_s^+ \rightarrow \phi\pi^+) = (4.5 \pm 0.4) \times 10^{-2}$. Our first error is their experiment's error and our second error is the systematic error from using our best value.					
⁴ KROKOVNY 02 reports $[\Gamma(B^0 \rightarrow D_s^- K^+)/\Gamma_{total}] \times [B(D_s^+ \rightarrow \phi\pi^+)] = (1.61^{+0.45}_{-0.38} \pm 0.21) \times 10^{-6}$ which we divide by our best value $B(D_s^+ \rightarrow \phi\pi^+) = (4.5 \pm 0.4) \times 10^{-2}$. Our first error is their experiment's error and our second error is the systematic error from using our best value.					
⁵ ALEXANDER 93B reports $< 230 \times 10^{-6}$ from a measurement of $[\Gamma(B^0 \rightarrow D_s^- K^+)/\Gamma_{total}] \times [B(D_s^+ \rightarrow \phi\pi^+)]$ assuming $B(D_s^+ \rightarrow \phi\pi^+) = 0.037$, which we rescale to our best value $B(D_s^+ \rightarrow \phi\pi^+) = 4.5 \times 10^{-2}$.					
⁶ BORTOLETTO 90 assume $B(D_s \rightarrow \phi\pi^+) = 2\%$.					

$\Gamma(D_s^{*-} K^+)/\Gamma_{total}$		Γ_{125}/Γ			
VALUE (units 10^{-5})	CL%	DOCUMENT ID	TECN	COMMENT	
2.19 \pm 0.30 OUR AVERAGE					
2.02 \pm 0.33 \pm 0.22		¹ JOSHI	10	BELL	$e^+e^- \rightarrow \Upsilon(4S)$
2.4 \pm 0.4 \pm 0.2		¹ AUBERT	08AJ	BABR	$e^+e^- \rightarrow \Upsilon(4S)$
• • • We do not use the following data for averages, fits, limits, etc. • • •					
2.2 \pm 0.6 \pm 0.2		² AUBERT	07K	BABR	Repl. by AUBERT 08AJ
< 2.5	90	AUBERT	03D	BABR	Repl. by AUBERT 07K
<14	90	³ ALEXANDER	93B	CLE2	$e^+e^- \rightarrow \Upsilon(4S)$
¹ Assumes equal production of B^+ and B^0 at the $\Upsilon(4S)$.					
² AUBERT 07K reports $[\Gamma(B^0 \rightarrow D_s^{*-} K^+)/\Gamma_{total}] \times [B(D_s^+ \rightarrow \phi\pi^+)] = (0.97 \pm 0.24 \pm 0.12) \times 10^{-6}$ which we divide by our best value $B(D_s^+ \rightarrow \phi\pi^+) = (4.5 \pm 0.4) \times 10^{-2}$. Our first error is their experiment's error and our second error is the systematic error from using our best value.					
³ ALEXANDER 93B reports $< 17 \times 10^{-5}$ from a measurement of $[\Gamma(B^0 \rightarrow D_s^{*-} K^+)/\Gamma_{total}] \times [B(D_s^+ \rightarrow \phi\pi^+)]$ assuming $B(D_s^+ \rightarrow \phi\pi^+) = 0.037$, which we rescale to our best value $B(D_s^+ \rightarrow \phi\pi^+) = 4.5 \times 10^{-2}$.					

$\Gamma(D_s^- K^+)/\Gamma(D^- \pi^+)$		Γ_{124}/Γ_{35}			
VALUE (units 10^{-2})	CL%	DOCUMENT ID	TECN	COMMENT	
1.09 \pm 0.19 OUR FIT		Error includes scale factor of 2.7.			
1.29 \pm 0.05 \pm 0.08		AAIJ	15Ac	LHCB	pp at 7, 8 TeV

$\Gamma(D_s^- K^*(892)^+)/\Gamma_{total}$		Γ_{126}/Γ			
VALUE (units 10^{-5})	CL%	DOCUMENT ID	TECN	COMMENT	
3.5 \pm 1.0 \pm 0.4		¹ AUBERT	08AJ	BABR	$e^+e^- \rightarrow \Upsilon(4S)$
• • • We do not use the following data for averages, fits, limits, etc. • • •					
<280	90	² ALBRECHT	93E	ARG	$e^+e^- \rightarrow \Upsilon(4S)$
< 80	90	³ ALEXANDER	93B	CLE2	$e^+e^- \rightarrow \Upsilon(4S)$

¹ Assumes equal production of B^+ and B^0 at the $\Upsilon(4S)$.
² ALBRECHT 93E reports $< 4.6 \times 10^{-3}$ from a measurement of $[\Gamma(B^0 \rightarrow D_s^- K^*(892)^+)/\Gamma_{total}] \times [B(D_s^+ \rightarrow \phi\pi^+)]$ assuming $B(D_s^+ \rightarrow \phi\pi^+) = 0.027$, which we rescale to our best value $B(D_s^+ \rightarrow \phi\pi^+) = 4.5 \times 10^{-2}$.
³ ALEXANDER 93B reports $< 9.7 \times 10^{-4}$ from a measurement of $[\Gamma(B^0 \rightarrow D_s^- K^*(892)^+)/\Gamma_{total}] \times [B(D_s^+ \rightarrow \phi\pi^+)]$ assuming $B(D_s^+ \rightarrow \phi\pi^+) = 0.037$, which we rescale to our best value $B(D_s^+ \rightarrow \phi\pi^+) = 4.5 \times 10^{-2}$.

$\Gamma(D_s^{*-} K^*(892)^+)/\Gamma_{total}$		Γ_{127}/Γ			
VALUE (units 10^{-5})	CL%	DOCUMENT ID	TECN	COMMENT	
3.2 \pm 1.4 \pm 0.4		¹ AUBERT	08AJ	BABR	$e^+e^- \rightarrow \Upsilon(4S)$
• • • We do not use the following data for averages, fits, limits, etc. • • •					
<350	90	² ALBRECHT	93E	ARG	$e^+e^- \rightarrow \Upsilon(4S)$
< 90	90	³ ALEXANDER	93B	CLE2	$e^+e^- \rightarrow \Upsilon(4S)$

¹ Assumes equal production of B^+ and B^0 at the $\Upsilon(4S)$.
² ALBRECHT 93E reports $< 5.8 \times 10^{-3}$ from a measurement of $[\Gamma(B^0 \rightarrow D_s^{*-} K^*(892)^+)/\Gamma_{total}] \times [B(D_s^+ \rightarrow \phi\pi^+)]$ assuming $B(D_s^+ \rightarrow \phi\pi^+) = 0.027$, which we rescale to our best value $B(D_s^+ \rightarrow \phi\pi^+) = 4.5 \times 10^{-2}$.
³ ALEXANDER 93B reports $< 11.0 \times 10^{-4}$ from a measurement of $[\Gamma(B^0 \rightarrow D_s^{*-} K^*(892)^+)/\Gamma_{total}] \times [B(D_s^+ \rightarrow \phi\pi^+)]$ assuming $B(D_s^+ \rightarrow \phi\pi^+) = 0.037$, which we rescale to our best value $B(D_s^+ \rightarrow \phi\pi^+) = 4.5 \times 10^{-2}$.

$\Gamma(D_s^- \pi^+ K^0)/\Gamma_{total}$		Γ_{128}/Γ			
VALUE (units 10^{-4})	CL%	DOCUMENT ID	TECN	COMMENT	
0.97 \pm 0.14 OUR AVERAGE					
0.94 \pm 0.12 \pm 0.10		¹ WIEHCZYN...	15	BELL	$e^+e^- \rightarrow \Upsilon(4S)$
1.10 \pm 0.26 \pm 0.20		¹ AUBERT	08G	BABR	$e^+e^- \rightarrow \Upsilon(4S)$
• • • We do not use the following data for averages, fits, limits, etc. • • •					
<40	90	² ALBRECHT	93E	ARG	$e^+e^- \rightarrow \Upsilon(4S)$

¹ Assumes equal production of B^+ and B^0 at the $\Upsilon(4S)$.
² ALBRECHT 93E reports $< 7.3 \times 10^{-3}$ from a measurement of $[\Gamma(B^0 \rightarrow D_s^- \pi^+ K^0)/\Gamma_{total}] \times [B(D_s^+ \rightarrow \phi\pi^+)]$ assuming $B(D_s^+ \rightarrow \phi\pi^+) = 0.027$, which we rescale to our best value $B(D_s^+ \rightarrow \phi\pi^+) = 4.5 \times 10^{-2}$.

$\Gamma(D_s^{*-} \pi^+ K^0)/\Gamma_{total}$		Γ_{129}/Γ			
VALUE (units 10^{-4})	CL%	DOCUMENT ID	TECN	COMMENT	
< 1.10	90	¹ AUBERT	08G	BABR	$e^+e^- \rightarrow \Upsilon(4S)$
• • • We do not use the following data for averages, fits, limits, etc. • • •					
<25	90	² ALBRECHT	93E	ARG	$e^+e^- \rightarrow \Upsilon(4S)$

¹ Assumes equal production of B^+ and B^0 at the $\Upsilon(4S)$.
² ALBRECHT 93E reports $< 4.2 \times 10^{-3}$ from a measurement of $[\Gamma(B^0 \rightarrow D_s^{*-} \pi^+ K^0)/\Gamma_{total}] \times [B(D_s^+ \rightarrow \phi\pi^+)]$ assuming $B(D_s^+ \rightarrow \phi\pi^+) = 0.027$, which we rescale to our best value $B(D_s^+ \rightarrow \phi\pi^+) = 4.5 \times 10^{-2}$.

$\Gamma(D_s^- K^+ \pi^+ \pi^-)/\Gamma_{total}$		Γ_{130}/Γ			
VALUE (units 10^{-4})	CL%	DOCUMENT ID	TECN	COMMENT	
1.71 \pm 0.31 \pm 0.34		¹ AAIJ	12Ax	LHCB	pp at 7 TeV
¹ AAIJ 12Ax reports $[\Gamma(B^0 \rightarrow D_s^- K^+ \pi^+ \pi^-)/\Gamma_{total}] / [B(D_s^0 \rightarrow D_s^- K^+ \pi^+ \pi^-)] = 0.54 \pm 0.07 \pm 0.07$ which we multiply by our best value $B(D_s^0 \rightarrow D_s^- K^+ \pi^+ \pi^-) = (3.2 \pm 0.6) \times 10^{-4}$. Our first error is their experiment's error and our second error is the systematic error from using our best value.					

$\Gamma(D_s^- \pi^+ K^*(892)^0)/\Gamma_{total}$		Γ_{131}/Γ			
VALUE	CL%	DOCUMENT ID	TECN	COMMENT	
<3.0 $\times 10^{-3}$		¹ ALBRECHT	93E	ARG	$e^+e^- \rightarrow \Upsilon(4S)$
¹ ALBRECHT 93E reports $< 5.0 \times 10^{-3}$ from a measurement of $[\Gamma(B^0 \rightarrow D_s^- \pi^+ K^*(892)^0)/\Gamma_{total}] \times [B(D_s^+ \rightarrow \phi\pi^+)]$ assuming $B(D_s^+ \rightarrow \phi\pi^+) = 0.027$, which we rescale to our best value $B(D_s^+ \rightarrow \phi\pi^+) = 4.5 \times 10^{-2}$.					

Meson Particle Listings

B^0

$\Gamma(D_s^{*-}\pi^+K^*(892)^0)/\Gamma_{total}$					Γ_{132}/Γ
VALUE	CL%	DOCUMENT ID	TECN	COMMENT	

<1.6 × 10⁻³ 90 1 ALBRECHT 93E ARG e⁺e⁻ → $\Upsilon(4S)$
 1 ALBRECHT 93E reports < 2.7 × 10⁻³ from a measurement of $[\Gamma(B^0 \rightarrow D_s^{*-}\pi^+K^*(892)^0)/\Gamma_{total}] \times [B(B^0 \rightarrow \phi\pi^+)]$ assuming $B(D_s^+ \rightarrow \phi\pi^+) = 0.027$, which we rescale to our best value $B(D_s^+ \rightarrow \phi\pi^+) = 4.5 \times 10^{-2}$.

$\Gamma(\bar{D}^0 K^0)/\Gamma_{total}$					Γ_{133}/Γ
VALUE (units 10 ⁻⁵)		DOCUMENT ID	TECN	COMMENT	

5.2 ± 0.7 OUR AVERAGE
 5.3 ± 0.7 ± 0.3 1 AUBERT,B 06L BABR e⁺e⁻ → $\Upsilon(4S)$
 5.0^{+1.3}_{-1.2} ± 0.6 1 KROKOVNY 03 BELL e⁺e⁻ → $\Upsilon(4S)$
 1 Assumes equal production of B⁺ and B⁰ at the $\Upsilon(4S)$.

$\Gamma(\bar{D}^0 K^+ \pi^-)/\Gamma_{total}$					Γ_{134}/Γ
VALUE (units 10 ⁻⁶)		DOCUMENT ID	TECN	COMMENT	

88 ± 15 ± 9 1 AUBERT 06A BABR e⁺e⁻ → $\Upsilon(4S)$
 1 Assumes equal production of B⁺ and B⁰ at the $\Upsilon(4S)$.

$\Gamma(\bar{D}^0 K^+ \pi^-)/\Gamma(\bar{D}^0 \pi^+ \pi^-)$					Γ_{134}/Γ_{44}
VALUE		DOCUMENT ID	TECN	COMMENT	

0.106 ± 0.007 ± 0.008 AAIJ 13AQ LHCB pp at 7 TeV

$\Gamma(\bar{D}^0 K^*(892)^0)/\Gamma_{total}$					Γ_{135}/Γ
VALUE (units 10 ⁻⁵)		DOCUMENT ID	TECN	COMMENT	

4.5 ± 0.6 OUR AVERAGE
 5.4 ± 0.3 ± 1.1 1,2 AAIJ 15X LHCB pp at 7, 8 TeV
 4.0 ± 0.7 ± 0.3 3 AUBERT,B 06L BABR e⁺e⁻ → $\Upsilon(4S)$
 4.8^{+1.1}_{-1.0} ± 0.5 3 KROKOVNY 03 BELL e⁺e⁻ → $\Upsilon(4S)$
 • • • We do not use the following data for averages, fits, limits, etc. • • •
 5.7 ± 0.9 ± 0.6 3 AUBERT 06A BABR Repl. by AUBERT,B 06L

1 AAIJ 15X reports (5.13 ± 0.20 ± 0.15 ± 0.24 ± 0.60) × 10⁻⁵ from a measurement of $[\Gamma(B^0 \rightarrow \bar{D}^0 K^*(892)^0)/\Gamma_{total}] \times [B(B^0 \rightarrow \bar{D}^0 K^+ \pi^-)]$ assuming $B(B^0 \rightarrow \bar{D}^0 K^+ \pi^-) = (9.2 \pm 0.6 \pm 0.7 \pm 0.6) \times 10^{-5}$, which we rescale to our best value $B(B^0 \rightarrow \bar{D}^0 K^+ \pi^-) = (8.8 \pm 1.7) \times 10^{-5}$. Our first error is their experiment's error and our second error is the systematic error from using our best value.
 2 Measured via amplitude analysis of B⁰ → $\bar{D}^0 K^+ \pi^-$, which excludes contribution from decay via D*(2010)⁻ resonance.
 3 Assumes equal production of B⁺ and B⁰ at the $\Upsilon(4S)$.

$\Gamma(\bar{D}^0 K^*(1410)^0)/\Gamma_{total}$					Γ_{136}/Γ
VALUE	CL%	DOCUMENT ID	TECN	COMMENT	

<6.7 × 10⁻⁵ 90 1 AAIJ 15X LHCB pp at 7, 8 TeV
 1 Measured via amplitude analysis of B⁰ → $\bar{D}^0 K^+ \pi^-$, which excludes contribution from decay via D*(2010)⁻ resonance.

$\Gamma(\bar{D}^0 K_0^*(1430)^0)/\Gamma_{total}$					Γ_{137}/Γ
VALUE (units 10 ⁻⁵)		DOCUMENT ID	TECN	COMMENT	

0.7 ± 0.7 ± 0.1 1,2 AAIJ 15X LHCB pp at 7, 8 TeV
 1 AAIJ 15X reports (0.71 ± 0.27 ± 0.33 ± 0.47 ± 0.08) × 10⁻⁵ from a measurement of $[\Gamma(B^0 \rightarrow \bar{D}^0 K_0^*(1430)^0)/\Gamma_{total}] \times [B(B^0 \rightarrow \bar{D}^0 K^+ \pi^-)]$ assuming $B(B^0 \rightarrow \bar{D}^0 K^+ \pi^-) = (9.2 \pm 0.6 \pm 0.7 \pm 0.6) \times 10^{-5}$, which we rescale to our best value $B(B^0 \rightarrow \bar{D}^0 K^+ \pi^-) = (8.8 \pm 1.7) \times 10^{-5}$. Our first error is their experiment's error and our second error is the systematic error from using our best value.
 2 Measured via amplitude analysis of B⁰ → $\bar{D}^0 K^+ \pi^-$, which excludes contribution from decay via D*(2010)⁻ resonance.

$\Gamma(\bar{D}^0 K_2^*(1430)^0)/\Gamma_{total}$					Γ_{138}/Γ
VALUE (units 10 ⁻⁵)		DOCUMENT ID	TECN	COMMENT	

2.1 ± 0.8 ± 0.4 1,2 AAIJ 15X LHCB pp at 7, 8 TeV
 1 AAIJ 15X reports (2.04 ± 0.45 ± 0.30 ± 0.54 ± 0.25) × 10⁻⁵ from a measurement of $[\Gamma(B^0 \rightarrow \bar{D}^0 K_2^*(1430)^0)/\Gamma_{total}] \times [B(B^0 \rightarrow \bar{D}^0 K^+ \pi^-)]$ assuming $B(B^0 \rightarrow \bar{D}^0 K^+ \pi^-) = (9.2 \pm 0.6 \pm 0.7 \pm 0.6) \times 10^{-5}$, which we rescale to our best value $B(B^0 \rightarrow \bar{D}^0 K^+ \pi^-) = (8.8 \pm 1.7) \times 10^{-5}$. Our first error is their experiment's error and our second error is the systematic error from using our best value.
 2 Measured via amplitude analysis of B⁰ → $\bar{D}^0 K^+ \pi^-$, which excludes contribution from decay via D*(2010)⁻ resonance.

$\Gamma(D_0^*(2300)^- K^+, D_0^{*-} \rightarrow \bar{D}^0 \pi^-)/\Gamma_{total}$					Γ_{139}/Γ
VALUE (units 10 ⁻⁵)		DOCUMENT ID	TECN	COMMENT	

1.9 ± 0.8 ± 0.4 1,2 AAIJ 15X LHCB pp at 7, 8 TeV
 1 AAIJ 15X reports (1.77 ± 0.26 ± 0.19 ± 0.67 ± 0.20) × 10⁻⁵ from a measurement of $[\Gamma(B^0 \rightarrow D_0^*(2300)^- K^+, D_0^{*-} \rightarrow \bar{D}^0 \pi^-)/\Gamma_{total}] \times [B(B^0 \rightarrow \bar{D}^0 K^+ \pi^-)]$ assuming $B(B^0 \rightarrow \bar{D}^0 K^+ \pi^-) = (9.2 \pm 0.6 \pm 0.7 \pm 0.6) \times 10^{-5}$, which we rescale to our best value $B(B^0 \rightarrow \bar{D}^0 K^+ \pi^-) = (8.8 \pm 1.7) \times 10^{-5}$. Our first error is their experiment's error and our second error is the systematic error from using our best value.
 2 Measured via amplitude analysis of B⁰ → $\bar{D}^0 K^+ \pi^-$, which excludes contribution from decay via D*(2010)⁻ resonance.

$\Gamma(D_2^*(2460)^- K^+, D_2^{*-} \rightarrow \bar{D}^0 \pi^-)/\Gamma_{total}$					Γ_{140}/Γ
VALUE (units 10 ⁻⁶)		DOCUMENT ID	TECN	COMMENT	

20.3 ± 3.5 OUR AVERAGE
 22 ± 2 ± 4 1,2 AAIJ 15X LHCB pp at 7, 8 TeV
 18.3 ± 4.0 ± 3.1 3 AUBERT 06A BABR e⁺e⁻ → $\Upsilon(4S)$
 1 AAIJ 15X reports (2.12 ± 0.10 ± 0.11 ± 0.11 ± 0.25) × 10⁻⁵ from a measurement of $[\Gamma(B^0 \rightarrow D_2^*(2460)^- K^+, D_2^{*-} \rightarrow \bar{D}^0 \pi^-)/\Gamma_{total}] \times [B(B^0 \rightarrow \bar{D}^0 K^+ \pi^-)]$ assuming $B(B^0 \rightarrow \bar{D}^0 K^+ \pi^-) = (9.2 \pm 0.6 \pm 0.7 \pm 0.6) \times 10^{-5}$, which we rescale to our best value $B(B^0 \rightarrow \bar{D}^0 K^+ \pi^-) = (8.8 \pm 1.7) \times 10^{-5}$. Our first error is their experiment's error and our second error is the systematic error from using our best value.
 2 Measured via amplitude analysis of B⁰ → $\bar{D}^0 K^+ \pi^-$, which excludes contribution from decay via D*(2010)⁻ resonance.
 3 Assumes equal production of B⁺ and B⁰ at the $\Upsilon(4S)$.

$\Gamma(D_3^*(2760)^- K^+, D_3^{*-} \rightarrow \bar{D}^0 \pi^-)/\Gamma_{total}$					Γ_{141}/Γ
VALUE	CL%	DOCUMENT ID	TECN	COMMENT	

<0.10 × 10⁻⁵ 90 1 AAIJ 15X LHCB pp at 7, 8 TeV
 1 Measured via amplitude analysis of B⁰ → $\bar{D}^0 K^+ \pi^-$, which excludes contribution from decay via D*(2010)⁻ resonance.

$\Gamma(\bar{D}^0 K^+ \pi^- \text{ nonresonant})/\Gamma_{total}$					Γ_{142}/Γ
VALUE (units 10 ⁻⁶)	CL%	DOCUMENT ID	TECN	COMMENT	

<37 90 1 AUBERT 06A BABR e⁺e⁻ → $\Upsilon(4S)$
 1 Assumes equal production of B⁺ and B⁰ at the $\Upsilon(4S)$.

$\Gamma([\pi^+ K^-]_D K^*(892)^0)/\Gamma(\bar{D}^0 K^*(892)^0)$					$\Gamma_{143}/\Gamma_{135}$
VALUE		DOCUMENT ID	TECN	COMMENT	

0.92 ± 0.10 ± 0.02 AAIJ 19N LHCB pp at 7, 8, 13 TeV
 • • • We do not use the following data for averages, fits, limits, etc. • • •
 1.05^{+0.17}_{-0.15} ± 0.04 AAIJ 14BN LHCB Repl. by AAIJ 16s
 1.36^{+0.37}_{-0.32} ± 0.07 AAIJ 13L LHCB Repl. by AAIJ 14BN

$\Gamma([\pi^+ \pi^-]_D K^*(892)^0)/\Gamma(\bar{D}^0 K^*(892)^0)$					$\Gamma_{144}/\Gamma_{135}$
VALUE		DOCUMENT ID	TECN	COMMENT	

1.32 ± 0.19 ± 0.03 AAIJ 19N LHCB pp at 7, 8, 13 TeV
 • • • We do not use the following data for averages, fits, limits, etc. • • •
 1.21^{+0.28}_{-0.25} ± 0.05 AAIJ 14BN LHCB Repl. by AAIJ 16s

$\Gamma([\pi^+ K^-]_D K^*(892)^0)/\Gamma([K^+ \pi^-]_D K^*(892)^0)$					$\Gamma_{145}/\Gamma_{146}$
VALUE		DOCUMENT ID	TECN	COMMENT	

0.080 ± 0.015 ± 0.002 AAIJ 19N LHCB pp at 7, 8, 13 TeV

$\Gamma([\pi^+ \pi^- \pi^+ \pi^-]_D K^*(892)^0)/\Gamma(\bar{D}^0 K^*(892)^0)$					$\Gamma_{147}/\Gamma_{135}$
VALUE		DOCUMENT ID	TECN	COMMENT	

1.01 ± 0.16 ± 0.04 AAIJ 19N LHCB pp at 7, 8, 13 TeV

$\Gamma([\pi^+ K^- \pi^+ \pi^-]_D K^*(892)^0)/\Gamma([K^+ \pi^- \pi^+ \pi^-]_D K^*(892)^0)$					$\Gamma_{148}/\Gamma_{149}$
VALUE		DOCUMENT ID	TECN	COMMENT	

0.073 ± 0.018 ± 0.002 AAIJ 19N LHCB pp at 7, 8, 13 TeV

$\Gamma(\bar{D}^0 \rho^0)/\Gamma_{total}$					Γ_{150}/Γ
VALUE (units 10 ⁻⁴)	CL%	DOCUMENT ID	TECN	COMMENT	

2.63 ± 0.14 OUR AVERAGE
 2.69 ± 0.09 ± 0.13 1 LEES 11M BABR e⁺e⁻ → $\Upsilon(4S)$
 2.25 ± 0.14 ± 0.35 1 BLYTH 06 BELL e⁺e⁻ → $\Upsilon(4S)$
 2.74^{+0.36}_{-0.32} ± 0.55 1 COAN 02 CLE2 e⁺e⁻ → $\Upsilon(4S)$
 • • • We do not use the following data for averages, fits, limits, etc. • • •
 2.9 ± 0.2 ± 0.3 1 AUBERT 04B BABR Repl. by LEES 11M
 3.1 ± 0.4 ± 0.5 1 ABE 02J BELL Repl. by BLYTH 06
 <1.2 90 2 NEMAT1 98 CLE2 Repl. by COAN 02
 <4.8 90 3 ALAM 94 CLE2 Repl. by NEMAT1 98

1 Assumes equal production of B⁺ and B⁰ at the $\Upsilon(4S)$.
 2 NEMAT1 98 assumes equal production of B⁺ and B⁰ at the $\Upsilon(4S)$ and use the PDG 96 values for D⁰, D^{*0}, η, η', and ω branching fractions.
 3 ALAM 94 assume equal production of B⁺ and B⁰ at the $\Upsilon(4S)$ and use the CLEO II absolute B(D⁰ → K⁻π⁺) and the PDG 1992 B(D⁰ → K⁻π⁺π⁰)/B(D⁰ → K⁻π⁺) and B(D⁰ → K⁻2π⁺π⁻)/B(D⁰ → K⁻π⁺).

$\Gamma(\bar{D}^0 \rho^0)/\Gamma_{total}$					Γ_{151}/Γ
VALUE (units 10 ⁻⁴)	CL%	DOCUMENT ID	TECN	COMMENT	

3.21 ± 0.21 OUR AVERAGE
 3.21 ± 0.10 ± 0.21 1 AAIJ 15Y LHCB pp at 7, 8 TeV
 3.19 ± 0.20 ± 0.45 2,3 KUZMIN 07 BELL e⁺e⁻ → $\Upsilon(4S)$
 • • • We do not use the following data for averages, fits, limits, etc. • • •
 2.9 ± 1.0 ± 0.4 2 SATPATHY 03 BELL Repl. by KUZMIN 07
 < 3.9 90 4 NEMAT1 98 CLE2 e⁺e⁻ → $\Upsilon(4S)$
 < 5.5 90 5 ALAM 94 CLE2 Repl. by NEMAT1 98

See key on page 1127

Meson Particle Listings

B^0

< 6.0 90 6 BORTOLETTO92 CLEO $e^+e^- \rightarrow \Upsilon(4S)$
 <27.0 90 7 ALBRECHT 88k ARG $e^+e^- \rightarrow \Upsilon(4S)$

- ¹ Measured using isobar formalism in the decay chain $B^0 \rightarrow \bar{D}^0 \rho(770)$, $\rho \rightarrow \pi^+\pi^-$ assuming $B(\rho(770) \rightarrow \pi^+\pi^-) = 1$. The second uncertainty combines in quadrature all systematic uncertainties quoted in the paper.
² Assumes equal production of B^+ and B^0 at the $\Upsilon(4S)$.
³ Our second uncertainty combines systematics and model errors quoted in the paper.
⁴ NEMATI 98 assumes equal production of B^+ and B^0 at the $\Upsilon(4S)$ and use the PDG 96 values for D^0 , D^{*0} , η , η' , and ω branching fractions.
⁵ ALAM 94 assume equal production of B^+ and B^0 at the $\Upsilon(4S)$ and use the CLEOII absolute $B(D^0 \rightarrow K^-\pi^+)$ and the PDG 1992 $B(D^0 \rightarrow K^-\pi^+\pi^0)/B(D^0 \rightarrow K^-\pi^+)$ and $B(D^0 \rightarrow K^-2\pi^+\pi^-)/B(D^0 \rightarrow K^-\pi^+)$.
⁶ BORTOLETTO 92 assumes equal production of B^+ and B^0 at the $\Upsilon(4S)$ and uses Mark III branching fractions for the D .
⁷ ALBRECHT 88k reports < 0.003 assuming $B^0\bar{B}^0:B^+B^-$ production ratio is 45:55. We rescale to 50%.

$\Gamma(\bar{D}^0 f_2)/\Gamma_{total}$ Γ_{152}/Γ

VALUE (units 10^{-4})	DOCUMENT ID	TECN	COMMENT
1.56 ± 0.21 OUR AVERAGE			
1.68 ± 0.11 ± 0.21	¹ AAJ	15Y	LHCB pp at 7, 8 TeV
1.20 ± 0.18 ± 0.38	^{2,3} KUZMIN	07	BELL $e^+e^- \rightarrow \Upsilon(4S)$

¹ Result obtained using the isobar formalism. The second uncertainty combines in quadrature all systematic uncertainties quoted in the paper. Measured in the decay chain $B^0 \rightarrow \bar{D}^0 f_2(1270)$, $f_2 \rightarrow \pi^+\pi^-$.
² Assumes equal production of B^+ and B^0 at the $\Upsilon(4S)$.
³ Our second uncertainty combines systematics and model errors quoted in the paper.

$\Gamma(\bar{D}^0 \eta)/\Gamma_{total}$ Γ_{153}/Γ

VALUE (units 10^{-4})	CL%	DOCUMENT ID	TECN	COMMENT
2.36 ± 0.32 OUR AVERAGE				Error includes scale factor of 2.5.
2.53 ± 0.09 ± 0.11		¹ LEES	11M	BABR $e^+e^- \rightarrow \Upsilon(4S)$
1.77 ± 0.16 ± 0.21		¹ BLYTH	06	BELL $e^+e^- \rightarrow \Upsilon(4S)$
• • • We do not use the following data for averages, fits, limits, etc. • • •				
2.5 ± 0.2 ± 0.3		¹ AUBERT	04B	BABR Repl. by LEES 11M
1.4 $^{+0.5}_{-0.4}$ ± 0.3		¹ ABE	02J	BELL Repl. by BLYTH 06
<1.3	90	² NEMATI	98	CLE2 $e^+e^- \rightarrow \Upsilon(4S)$
<6.8	90	³ ALAM	94	CLE2 Repl. by NEMATI 98

- ¹ Assumes equal production of B^+ and B^0 at the $\Upsilon(4S)$.
² NEMATI 98 assumes equal production of B^+ and B^0 at the $\Upsilon(4S)$ and use the PDG 96 values for D^0 , D^{*0} , η , η' , and ω branching fractions.
³ ALAM 94 assume equal production of B^+ and B^0 at the $\Upsilon(4S)$ and use the CLEOII absolute $B(D^0 \rightarrow K^-\pi^+)$ and the PDG 1992 $B(D^0 \rightarrow K^-\pi^+\pi^0)/B(D^0 \rightarrow K^-\pi^+)$ and $B(D^0 \rightarrow K^-2\pi^+\pi^-)/B(D^0 \rightarrow K^-\pi^+)$.

$\Gamma(\bar{D}^0 \eta')/\Gamma_{total}$ Γ_{154}/Γ

VALUE (units 10^{-4})	CL%	DOCUMENT ID	TECN	COMMENT
1.38 ± 0.16 OUR AVERAGE				Error includes scale factor of 1.3.
1.48 ± 0.13 ± 0.07		¹ LEES	11M	BABR $e^+e^- \rightarrow \Upsilon(4S)$
1.14 ± 0.20 $^{+0.10}_{-0.13}$		¹ SCHUMANN	05	BELL $e^+e^- \rightarrow \Upsilon(4S)$
• • • We do not use the following data for averages, fits, limits, etc. • • •				
1.7 ± 0.4 ± 0.2		¹ AUBERT	04B	BABR Repl. by LEES 11M
<9.4	90	² NEMATI	98	CLE2 $e^+e^- \rightarrow \Upsilon(4S)$
<8.6	90	³ ALAM	94	CLE2 Repl. by NEMATI 98

- ¹ Assumes equal production of B^+ and B^0 at the $\Upsilon(4S)$.
² NEMATI 98 assumes equal production of B^+ and B^0 at the $\Upsilon(4S)$ and use the PDG 96 values for D^0 , D^{*0} , η , η' , and ω branching fractions.
³ ALAM 94 assume equal production of B^+ and B^0 at the $\Upsilon(4S)$ and use the CLEOII absolute $B(D^0 \rightarrow K^-\pi^+)$ and the PDG 1992 $B(D^0 \rightarrow K^-\pi^+\pi^0)/B(D^0 \rightarrow K^-\pi^+)$ and $B(D^0 \rightarrow K^-2\pi^+\pi^-)/B(D^0 \rightarrow K^-\pi^+)$.

$\Gamma(\bar{D}^0 \eta')/\Gamma(\bar{D}^0 \eta)$ $\Gamma_{154}/\Gamma_{153}$

VALUE	DOCUMENT ID	TECN	COMMENT
0.54 ± 0.07 ± 0.01	LEES	11M	BABR $e^+e^- \rightarrow \Upsilon(4S)$
• • • We do not use the following data for averages, fits, limits, etc. • • •			
0.7 ± 0.2 ± 0.1	AUBERT	04B	BABR Repl. by LEES 11M

$\Gamma(\bar{D}^0 \omega)/\Gamma_{total}$ Γ_{155}/Γ

VALUE (units 10^{-4})	CL%	DOCUMENT ID	TECN	COMMENT
2.54 ± 0.16 OUR AVERAGE				
2.75 ± 0.72 ± 0.35		¹ AAJ	15Y	LHCB pp at 7, 8 TeV
2.57 ± 0.11 ± 0.14		² LEES	11M	BABR $e^+e^- \rightarrow \Upsilon(4S)$
2.37 ± 0.23 ± 0.28		² BLYTH	06	BELL $e^+e^- \rightarrow \Upsilon(4S)$
• • • We do not use the following data for averages, fits, limits, etc. • • •				
3.0 ± 0.3 ± 0.4		² AUBERT	04B	BABR Repl. by LEES 11M
1.8 ± 0.5 $^{+0.4}_{-0.3}$		² ABE	02J	BELL Repl. by BLYTH 06
<5.1	90	³ NEMATI	98	CLE2 $e^+e^- \rightarrow \Upsilon(4S)$
<6.3	90	⁴ ALAM	94	CLE2 Repl. by NEMATI 98

- ¹ Result obtained using the isobar model. The second uncertainty combines in quadrature all systematic uncertainties quoted in the paper.
² Assumes equal production of B^+ and B^0 at the $\Upsilon(4S)$.

³ NEMATI 98 assumes equal production of B^+ and B^0 at the $\Upsilon(4S)$ and use the PDG 96 values for D^0 , D^{*0} , η , η' , and ω branching fractions.
⁴ ALAM 94 assume equal production of B^+ and B^0 at the $\Upsilon(4S)$ and use the CLEOII absolute $B(D^0 \rightarrow K^-\pi^+)$ and the PDG 1992 $B(D^0 \rightarrow K^-\pi^+\pi^0)/B(D^0 \rightarrow K^-\pi^+)$ and $B(D^0 \rightarrow K^-2\pi^+\pi^-)/B(D^0 \rightarrow K^-\pi^+)$.

$\Gamma(D^0 \phi)/\Gamma_{total}$ Γ_{156}/Γ

VALUE	CL%	DOCUMENT ID	TECN	COMMENT
< 2.3 × 10⁻⁶	95	AAIJ	18AY	LHCB pp at 7 and 8 TeV
• • • We do not use the following data for averages, fits, limits, etc. • • •				
<11.6 × 10 ⁻⁶	90	¹ AUBERT	07A0	BABR $e^+e^- \rightarrow \Upsilon(4S)$

¹ Assumes equal production of B^+ and B^0 at the $\Upsilon(4S)$.

$\Gamma(D^0 K^+\pi^-)/\Gamma_{total}$ Γ_{157}/Γ

VALUE (units 10^{-6})	CL%	DOCUMENT ID	TECN	COMMENT
• • • We do not use the following data for averages, fits, limits, etc. • • •				
<19	90	¹ AUBERT	06A	BABR Repl. by AUBERT 09AE

¹ Assumes equal production of B^+ and B^0 at the $\Upsilon(4S)$.

$\Gamma(D^0 K^+\pi^-)/\Gamma(\bar{D}^0 K^+\pi^-)$ $\Gamma_{157}/\Gamma_{134}$

VALUE	DOCUMENT ID	TECN	COMMENT
0.060 ± 0.034 OUR AVERAGE			
0.045 $^{+0.056+0.028}_{-0.050-0.018}$	^{1,2} NEGISHI	12	BELL $e^+e^- \rightarrow \Upsilon(4S)$
0.068 ± 0.042	³ AUBERT	09AE	BABR $e^+e^- \rightarrow \Upsilon(4S)$

¹ Assumes equal production of B^0 and B^+ at $\Upsilon(4S)$.
² Uses $D^0 \rightarrow K^-\pi^+$ mode. Restricts $K^+\pi^-$ mass within ± 50 MeV of the nominal K^*0 mass. Corresponds to the upper limit, < 0.16 at 95% CL.
³ Reports a signal at the level of 2.5 standard deviations after combining results from $D^0 \rightarrow K^+\pi^-$, $K^+\pi^-\pi^0$, and $K^+\pi^-\pi^+\pi^-$.

$\Gamma(D^0 K^*(892)^0)/\Gamma_{total}$ Γ_{158}/Γ

VALUE (units 10^{-5})	CL%	DOCUMENT ID	TECN	COMMENT
• • • We do not use the following data for averages, fits, limits, etc. • • •				
<1.1	90	¹ AUBERT,B	06L	BABR $e^+e^- \rightarrow \Upsilon(4S)$
<1.8	90	¹ KROKOVNY	03	BELL $e^+e^- \rightarrow \Upsilon(4S)$

¹ Assumes equal production of B^+ and B^0 at the $\Upsilon(4S)$.

$\Gamma(D^0 K^*(892)^0)/\Gamma(\bar{D}^0 K^*(892)^0)$ $\Gamma_{158}/\Gamma_{135}$

"OUR EVALUATION" is derived from $r_{B^0}(B^0 \rightarrow D K^*0)$ data block listed in "CP violation parameters" section.

VALUE (units 10^{-2})	DOCUMENT ID
6.6 $^{+1.1}_{-1.2}$ OUR EVALUATION	

$\Gamma(\bar{D}^{*0} \gamma)/\Gamma_{total}$ Γ_{159}/Γ

VALUE	CL%	DOCUMENT ID	TECN	COMMENT
<2.5 × 10⁻⁵	90	¹ AUBERT,B	05Q	BABR $e^+e^- \rightarrow \Upsilon(4S)$
• • • We do not use the following data for averages, fits, limits, etc. • • •				
<5.0 × 10 ⁻⁵	90	¹ ARTUSO	00	CLE2 $e^+e^- \rightarrow \Upsilon(4S)$

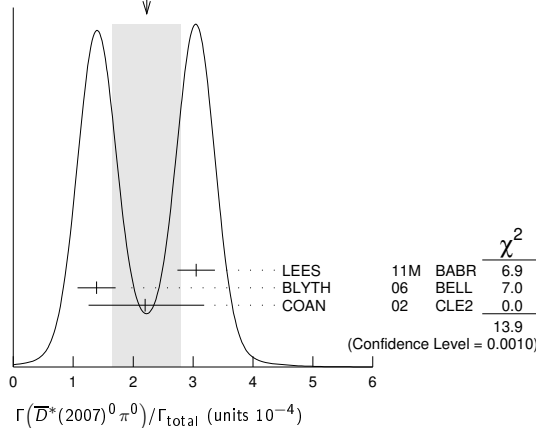
¹ Assumes equal production of B^+ and B^0 at the $\Upsilon(4S)$.

$\Gamma(\bar{D}^* (2007)^0 \pi^0)/\Gamma_{total}$ Γ_{160}/Γ

VALUE (units 10^{-4})	CL%	DOCUMENT ID	TECN	COMMENT
2.2 ± 0.6 OUR AVERAGE				Error includes scale factor of 2.6. See the ideogram below.
3.05 ± 0.14 ± 0.28		¹ LEES	11M	BABR $e^+e^- \rightarrow \Upsilon(4S)$
1.39 ± 0.18 ± 0.26		¹ BLYTH	06	BELL $e^+e^- \rightarrow \Upsilon(4S)$
2.20 $^{+0.59}_{-0.52}$ ± 0.79		¹ COAN	02	CLE2 $e^+e^- \rightarrow \Upsilon(4S)$
• • • We do not use the following data for averages, fits, limits, etc. • • •				
2.9 ± 0.4 ± 0.5		¹ AUBERT	04B	BABR Repl. by LEES 11M
2.7 $^{+0.8+0.5}_{-0.7-0.6}$		¹ ABE	02J	BELL Repl. by BLYTH 06
<4.4	90	² NEMATI	98	CLE2 Repl. by COAN 02
<9.7	90	³ ALAM	94	CLE2 Repl. by NEMATI 98

- ¹ Assumes equal production of B^+ and B^0 at the $\Upsilon(4S)$.
² NEMATI 98 assumes equal production of B^+ and B^0 at the $\Upsilon(4S)$ and use the PDG 96 values for D^0 , D^{*0} , η , η' , and ω branching fractions.
³ ALAM 94 assume equal production of B^+ and B^0 at the $\Upsilon(4S)$ and use the CLEOII $B(D^*(2007)^0 \rightarrow D^0 \pi^0)$ and absolute $B(D^0 \rightarrow K^-\pi^+)$ and the PDG 1992 $B(D^0 \rightarrow K^-\pi^+\pi^0)/B(D^0 \rightarrow K^-\pi^+)$ and $B(D^0 \rightarrow K^-2\pi^+\pi^-)/B(D^0 \rightarrow K^-\pi^+)$.

Meson Particle Listings

 B^0 WEIGHTED AVERAGE
2.2±0.6 (Error scaled by 2.6) $\Gamma(D^0 \pi^0) / \Gamma(D^*(2007)^0 \pi^0)$ $\Gamma_{150} / \Gamma_{160}$

VALUE	DOCUMENT ID	TECN	COMMENT
0.90 ± 0.08 OUR AVERAGE			
0.88 ± 0.05 ± 0.06	LEES	11M BABR	$e^+ e^- \rightarrow \Upsilon(4S)$
1.62 ± 0.23 ± 0.35	BLYTH	06 BELL	$e^+ e^- \rightarrow \Upsilon(4S)$
••• We do not use the following data for averages, fits, limits, etc. •••			
1.0 ± 0.1 ± 0.2	AUBERT	04B BABR	Repl. by LEES 11M

 $\Gamma(D^*(2007)^0 \rho^0) / \Gamma_{total}$ Γ_{161} / Γ

VALUE	CL%	DOCUMENT ID	TECN	COMMENT
<5.1 × 10⁻⁴	90	1 SATPATHY	03 BELL	$e^+ e^- \rightarrow \Upsilon(4S)$
••• We do not use the following data for averages, fits, limits, etc. •••				
<0.00056	90	2 NEMAT1	98 CLE2	$e^+ e^- \rightarrow \Upsilon(4S)$
<0.00117	90	3 ALAM	94 CLE2	Repl. by NEMAT1 98

- Assumes equal production of B^+ and B^0 at the $\Upsilon(4S)$.
- NEMAT1 98 assumes equal production of B^+ and B^0 at the $\Upsilon(4S)$ and use the PDG 96 values for D^0 , D^{*0} , η , η' , and ω branching fractions.
- ALAM 94 assume equal production of B^+ and B^0 at the $\Upsilon(4S)$ and use the CLEO II $B(D^*(2007)^0 \rightarrow D^0 \pi^0)$ and absolute $B(D^0 \rightarrow K^- \pi^+)$ and the PDG 1992 $B(D^0 \rightarrow K^- \pi^+ \pi^0) / B(D^0 \rightarrow K^- \pi^+)$ and $B(D^0 \rightarrow K^- 2\pi^+ \pi^-) / B(D^0 \rightarrow K^- \pi^+)$.

 $\Gamma(D^*(2007)^0 \eta) / \Gamma_{total}$ Γ_{162} / Γ

VALUE (units 10 ⁻⁴)	CL%	DOCUMENT ID	TECN	COMMENT
2.3 ± 0.6 OUR AVERAGE		Error includes scale factor of 2.8.		
2.69 ± 0.14 ± 0.23		1 LEES	11M BABR	$e^+ e^- \rightarrow \Upsilon(4S)$
1.40 ± 0.28 ± 0.26		1 BLYTH	06 BELL	$e^+ e^- \rightarrow \Upsilon(4S)$
••• We do not use the following data for averages, fits, limits, etc. •••				
2.6 ± 0.4 ± 0.4		1 AUBERT	04B BABR	Repl. by LEES 11M
<4.6	90	1 ABE	02J BELL	$e^+ e^- \rightarrow \Upsilon(4S)$
<2.6	90	2 NEMAT1	98 CLE2	$e^+ e^- \rightarrow \Upsilon(4S)$
<6.9	90	3 ALAM	94 CLE2	Repl. by NEMAT1 98

- Assumes equal production of B^+ and B^0 at the $\Upsilon(4S)$.
- NEMAT1 98 assumes equal production of B^+ and B^0 at the $\Upsilon(4S)$ and use the PDG 96 values for D^0 , D^{*0} , η , η' , and ω branching fractions.
- ALAM 94 assume equal production of B^+ and B^0 at the $\Upsilon(4S)$ and use the CLEO II $B(D^*(2007)^0 \rightarrow D^0 \pi^0)$ and absolute $B(D^0 \rightarrow K^- \pi^+)$ and the PDG 1992 $B(D^0 \rightarrow K^- \pi^+ \pi^0) / B(D^0 \rightarrow K^- \pi^+)$ and $B(D^0 \rightarrow K^- 2\pi^+ \pi^-) / B(D^0 \rightarrow K^- \pi^+)$.

 $\Gamma(D^0 \eta) / \Gamma(D^*(2007)^0 \eta)$ $\Gamma_{153} / \Gamma_{162}$

VALUE	DOCUMENT ID	TECN	COMMENT
0.99 ± 0.10 OUR AVERAGE			
0.97 ± 0.07 ± 0.07	LEES	11M BABR	$e^+ e^- \rightarrow \Upsilon(4S)$
1.27 ± 0.29 ± 0.25	BLYTH	06 BELL	$e^+ e^- \rightarrow \Upsilon(4S)$
••• We do not use the following data for averages, fits, limits, etc. •••			
0.9 ± 0.2 ± 0.1	AUBERT	04B BABR	Repl. by LEES 11M

 $\Gamma(D^*(2007)^0 \eta') / \Gamma(D^*(2007)^0 \eta)$ $\Gamma_{163} / \Gamma_{162}$

VALUE	DOCUMENT ID	TECN	COMMENT
0.61 ± 0.14 ± 0.02	LEES	11M BABR	$e^+ e^- \rightarrow \Upsilon(4S)$
••• We do not use the following data for averages, fits, limits, etc. •••			
0.5 ± 0.3 ± 0.1	AUBERT	04B BABR	Repl. by LEES 11M

 $\Gamma(D^*(2007)^0 \eta') / \Gamma_{total}$ Γ_{163} / Γ

VALUE (units 10 ⁻⁴)	CL%	DOCUMENT ID	TECN	COMMENT
1.40 ± 0.22 OUR AVERAGE				
1.48 ± 0.22 ± 0.13		1 LEES	11M BABR	$e^+ e^- \rightarrow \Upsilon(4S)$
1.21 ± 0.34 ± 0.22		1 SCHUMANN	05 BELL	$e^+ e^- \rightarrow \Upsilon(4S)$

••• We do not use the following data for averages, fits, limits, etc. •••

1.3 ± 0.7 ± 0.2	1,2 AUBERT	04B BABR	Repl. by LEES 11M
<14	90	BRANDENB...	98 CLE2 $e^+ e^- \rightarrow \Upsilon(4S)$
<19	90	3 NEMAT1	98 CLE2 $e^+ e^- \rightarrow \Upsilon(4S)$
<27	90	4 ALAM	94 CLE2 Repl. by NEMAT1 98

1 Assumes equal production of B^+ and B^0 at the $\Upsilon(4S)$.2 Reports an upper limit $< 2.6 \times 10^{-4}$ at 90% CL.3 NEMAT1 98 assumes equal production of B^+ and B^0 at the $\Upsilon(4S)$ and use the PDG 96 values for D^0 , D^{*0} , η , η' , and ω branching fractions.4 ALAM 94 assume equal production of B^+ and B^0 at the $\Upsilon(4S)$ and use the CLEO II $B(D^*(2007)^0 \rightarrow D^0 \pi^0)$ and absolute $B(D^0 \rightarrow K^- \pi^+)$ and the PDG 1992 $B(D^0 \rightarrow K^- \pi^+ \pi^0) / B(D^0 \rightarrow K^- \pi^+)$ and $B(D^0 \rightarrow K^- 2\pi^+ \pi^-) / B(D^0 \rightarrow K^- \pi^+)$. $\Gamma(D^0 \eta') / \Gamma(D^*(2007)^0 \eta')$ $\Gamma_{154} / \Gamma_{163}$

VALUE	DOCUMENT ID	TECN	COMMENT
0.96 ± 0.18 ± 0.06	LEES	11M BABR	$e^+ e^- \rightarrow \Upsilon(4S)$
••• We do not use the following data for averages, fits, limits, etc. •••			
1.3 ± 0.8 ± 0.2	AUBERT	04B BABR	Repl. by LEES 11M

 $\Gamma(D^*(2007)^0 \pi^+ \pi^-) / \Gamma_{total}$ Γ_{164} / Γ

VALUE	DOCUMENT ID	TECN	COMMENT
(6.2 ± 1.2 ± 1.8) × 10⁻⁴	1,2 SATPATHY	03 BELL	$e^+ e^- \rightarrow \Upsilon(4S)$

1 Assumes equal production of B^+ and B^0 at the $\Upsilon(4S)$.

2 No assumption about the intermediate mechanism is made in the analysis.

 $\Gamma(D^*(2007)^0 K^0) / \Gamma_{total}$ Γ_{165} / Γ

VALUE (units 10 ⁻⁵)	CL%	DOCUMENT ID	TECN	COMMENT
3.6 ± 1.2 ± 0.3		1 AUBERT,B	06L BABR	$e^+ e^- \rightarrow \Upsilon(4S)$

••• We do not use the following data for averages, fits, limits, etc. •••

<6.6 90 1 KROKOVNY 03 BELL $e^+ e^- \rightarrow \Upsilon(4S)$ 1 Assumes equal production of B^+ and B^0 at the $\Upsilon(4S)$. $\Gamma(D^*(2007)^0 K^*(892)^0) / \Gamma_{total}$ Γ_{166} / Γ

VALUE	CL%	DOCUMENT ID	TECN	COMMENT
<6.9 × 10⁻⁵	90	1 KROKOVNY	03 BELL	$e^+ e^- \rightarrow \Upsilon(4S)$

1 Assumes equal production of B^+ and B^0 at the $\Upsilon(4S)$. $\Gamma(D^*(2007)^0 K^*(892)^0) / \Gamma_{total}$ Γ_{167} / Γ

VALUE	CL%	DOCUMENT ID	TECN	COMMENT
<4.0 × 10⁻⁵	90	1 KROKOVNY	03 BELL	$e^+ e^- \rightarrow \Upsilon(4S)$

1 Assumes equal production of B^+ and B^0 at the $\Upsilon(4S)$. $\Gamma(D^*(2007)^0 \pi^+ \pi^+ \pi^- \pi^-) / \Gamma_{total}$ Γ_{168} / Γ

VALUE (units 10 ⁻³)	DOCUMENT ID	TECN	COMMENT
2.7 ± 0.5 OUR AVERAGE			
2.60 ± 0.47 ± 0.37	1 MAJUMDER	04 BELL	$e^+ e^- \rightarrow \Upsilon(4S)$
3.0 ± 0.7 ± 0.6	1 EDWARDS	02 CLE2	$e^+ e^- \rightarrow \Upsilon(4S)$

1 Assumes equal production of B^+ and B^0 at the $\Upsilon(4S)$. $\Gamma(D^*(2007)^0 \pi^+ \pi^+ \pi^- \pi^-) / \Gamma(D^*(2010)^- \pi^+ \pi^+ \pi^- \pi^-)$ $\Gamma_{168} / \Gamma_{64}$

VALUE	DOCUMENT ID	TECN	COMMENT
0.17 ± 0.04 ± 0.02	1 EDWARDS	02 CLE2	$e^+ e^- \rightarrow \Upsilon(4S)$

1 Assumes equal production of B^+ and B^0 at the $\Upsilon(4S)$. $\Gamma(D^*(2010)^+ D^*(2010)^-) / \Gamma_{total}$ Γ_{169} / Γ

VALUE (units 10 ⁻⁴)	CL%	DOCUMENT ID	TECN	COMMENT
8.0 ± 0.6 OUR AVERAGE				
7.82 ± 0.38 ± 0.63		1 KRONENBIT...	12 BELL	$e^+ e^- \rightarrow \Upsilon(4S)$
8.1 ± 0.6 ± 1.0		1 AUBERT,B	06A BABR	$e^+ e^- \rightarrow \Upsilon(4S)$
9.9 +4.2 -3.3 ± 1.2		1 LIPELES	00 CLE2	$e^+ e^- \rightarrow \Upsilon(4S)$
••• We do not use the following data for averages, fits, limits, etc. •••				
8.1 ± 0.8 ± 1.1		1 MIYAKE	05 BELL	Repl. by KRONENBIT-TER 12
8.3 ± 1.6 ± 1.2		1,2 AUBERT	02M BABR	Repl. by AUBERT,B 06B
6.2 +4.0 -2.9 ± 1.0		3 ARTUSO	99 CLE2	Repl. by LIPELES 00
<61	90	4 BARATE	98Q ALEP	$e^+ e^- \rightarrow Z$
<22	90	5 ASNER	97 CLE2	Repl. by ARTUSO 99

1 Assumes equal production of B^+ and B^0 at the $\Upsilon(4S)$.2 AUBERT 02M also assumes the measured CP -odd fraction of the final states is $0.22 \pm 0.18 \pm 0.03$.3 ARTUSO 99 uses $B(\Upsilon(4S) \rightarrow B^0 \bar{B}^0) = (48 \pm 4)\%$.4 BARATE 98Q (ALEPH) observes 2 events with an expected background of 0.10 ± 0.03 which corresponds to a branching ratio of $(2.3^{+1.9}_{-1.2} \pm 0.4) \times 10^{-3}$.5 ASNER 97 at CLEO observes 1 event with an expected background of 0.022 ± 0.011 . This corresponds to a branching ratio of $(5.3^{+7.1}_{-3.7} \pm 1.0) \times 10^{-4}$.

$\Gamma(\bar{D}^*(2007)^0\omega)/\Gamma_{total}$ Γ_{170}/Γ

VALUE (units 10^{-4})	CL%	DOCUMENT ID	TECN	COMMENT
3.6 ± 1.1 OUR AVERAGE		Error includes scale factor of 3.1.		
4.55 ± 0.24 ± 0.39		¹ LEES	11M BABR	$e^+e^- \rightarrow \Upsilon(4S)$
2.29 ± 0.39 ± 0.40		¹ BLYTH	06 BELL	$e^+e^- \rightarrow \Upsilon(4S)$
• • • We do not use the following data for averages, fits, limits, etc. • • •				
4.2 ± 0.7 ± 0.9	90	¹ AUBERT	04B BABR	Repl. by LEES 11M
< 7.9	90	¹ ABE	02J BELL	$e^+e^- \rightarrow \Upsilon(4S)$
< 7.4	90	² NEMAT1	98 CLE2	$e^+e^- \rightarrow \Upsilon(4S)$
< 21	90	³ ALAM	94 CLE2	Repl. by NEMAT1 98

- ¹ Assumes equal production of B^+ and B^0 at the $\Upsilon(4S)$.
- ² NEMAT1 98 assumes equal production of B^+ and B^0 at the $\Upsilon(4S)$ and use the PDG 96 values for D^0 , D^{*0} , η , η' , and ω branching fractions.
- ³ ALAM 94 assume equal production of B^+ and B^0 at the $\Upsilon(4S)$ and use the CLEO II B($D^*(2007)^0 \rightarrow D^0\pi^0$) and absolute B($D^0 \rightarrow K^-\pi^+$) and the PDG 1992 B($D^0 \rightarrow K^-\pi^+\pi^0$)/B($D^0 \rightarrow K^-\pi^+$) and B($D^0 \rightarrow K^-\pi^+\pi^-$)/B($D^0 \rightarrow K^-\pi^+$).

$\Gamma(\bar{D}^0\omega)/\Gamma(\bar{D}^*(2007)^0\omega)$ $\Gamma_{155}/\Gamma_{170}$

VALUE	DOCUMENT ID	TECN	COMMENT
0.58 ± 0.06 OUR AVERAGE			
0.56 ± 0.04 ± 0.04	LEES	11M BABR	$e^+e^- \rightarrow \Upsilon(4S)$
1.04 ± 0.20 ± 0.17	BLYTH	06 BELL	$e^+e^- \rightarrow \Upsilon(4S)$
• • • We do not use the following data for averages, fits, limits, etc. • • •			
0.7 ± 0.1 ± 0.1	AUBERT	04B BABR	Repl. by LEES 11M

$\Gamma(D^*(2010)^+D^-)/\Gamma_{total}$ Γ_{171}/Γ

VALUE (units 10^{-4})	CL%	DOCUMENT ID	TECN	COMMENT
6.1 ± 1.5 OUR AVERAGE		Error includes scale factor of 1.6.		
5.7 ± 0.7 ± 0.7		¹ AUBERT,B	06A BABR	$e^+e^- \rightarrow \Upsilon(4S)$
11.7 ± 2.6 ^{+2.2} _{-2.5}		^{1,2} ABE	02Q BELL	$e^+e^- \rightarrow \Upsilon(4S)$
• • • We do not use the following data for averages, fits, limits, etc. • • •				
8.8 ± 1.0 ± 1.3		¹ AUBERT	03J BABR	Repl. by AUBERT,B 06B
14.8 ± 3.8 ^{+2.8} _{-3.1}		^{1,3} ABE	02Q BELL	$e^+e^- \rightarrow \Upsilon(4S)$
< 6.3	90	¹ LIPELES	00 CLE2	$e^+e^- \rightarrow \Upsilon(4S)$
< 56	90	BARATE	98Q ALEP	$e^+e^- \rightarrow Z$
< 18	90	ASNER	97 CLE2	$e^+e^- \rightarrow \Upsilon(4S)$

- ¹ Assumes equal production of B^+ and B^0 at the $\Upsilon(4S)$.
- ² The measurement is performed using fully reconstructed D^* and D^+ decays.
- ³ The measurement is performed using a partial reconstruction technique for the D^* and fully reconstructed D^+ decays as a cross check.

$\Gamma(D^*(2007)^0\bar{D}^*(2007)^0)/\Gamma_{total}$ Γ_{172}/Γ

VALUE (units 10^{-4})	CL%	DOCUMENT ID	TECN	COMMENT
< 0.9	90	¹ AUBERT,B	06A BABR	$e^+e^- \rightarrow \Upsilon(4S)$
• • • We do not use the following data for averages, fits, limits, etc. • • •				
< 270	90	BARATE	98Q ALEP	$e^+e^- \rightarrow Z$

- ¹ Assumes equal production of B^+ and B^0 at the $\Upsilon(4S)$.

$\Gamma(D^-D^0K^+)/\Gamma_{total}$ Γ_{173}/Γ

VALUE (units 10^{-3})	DOCUMENT ID	TECN	COMMENT
1.07 ± 0.07 ± 0.09	¹ DEL-AMO-SA..11B	BABR	$e^+e^- \rightarrow \Upsilon(4S)$
• • • We do not use the following data for averages, fits, limits, etc. • • •			
1.7 ± 0.3 ± 0.3	¹ AUBERT	03X BABR	Repl. by DEL-AMO-SANCHEZ 11B

- ¹ Assumes equal production of B^+ and B^0 at the $\Upsilon(4S)$.

$\Gamma(D^-D^*(2007)^0K^+)/\Gamma_{total}$ Γ_{174}/Γ

VALUE (units 10^{-3})	DOCUMENT ID	TECN	COMMENT
3.46 ± 0.18 ± 0.37	¹ DEL-AMO-SA..11B	BABR	$e^+e^- \rightarrow \Upsilon(4S)$
• • • We do not use the following data for averages, fits, limits, etc. • • •			
4.6 ± 0.7 ± 0.7	¹ AUBERT	03X BABR	Repl. by DEL-AMO-SANCHEZ 11B

- ¹ Assumes equal production of B^+ and B^0 at the $\Upsilon(4S)$.

$\Gamma(D^*(2010)^-D^0K^+)/\Gamma_{total}$ Γ_{175}/Γ

VALUE (units 10^{-3})	DOCUMENT ID	TECN	COMMENT
2.47 ± 0.10 ± 0.18	¹ DEL-AMO-SA..11B	BABR	$e^+e^- \rightarrow \Upsilon(4S)$
• • • We do not use the following data for averages, fits, limits, etc. • • •			
3.1 ^{+0.4} _{-0.3} ± 0.4	¹ AUBERT	03X BABR	Repl. by DEL-AMO-SANCHEZ 11B

- ¹ Assumes equal production of B^+ and B^0 at the $\Upsilon(4S)$.

$\Gamma(D^*(2010)^-D^0K^+)/\Gamma(D^-D^0K^+)$ $\Gamma_{175}/\Gamma_{173}$

VALUE	DOCUMENT ID	TECN	COMMENT
1.754 ± 0.028 ± 0.038	¹ AAIJ	20AN LHCB	pp at 7, 8, 13 TeV

- ¹ Uses $D^+ \rightarrow K^-\pi^+\pi^+$, $D^0 \rightarrow K^-\pi^+$ and $D^0 \rightarrow K^-\pi^+\pi^-\pi^-$ decays.

$\Gamma(D^*(2010)^-D^*(2007)^0K^+)/\Gamma_{total}$ Γ_{176}/Γ

VALUE (units 10^{-3})	DOCUMENT ID	TECN	COMMENT
10.6 ± 0.33 ± 0.86	¹ DEL-AMO-SA..11B	BABR	$e^+e^- \rightarrow \Upsilon(4S)$
• • • We do not use the following data for averages, fits, limits, etc. • • •			
11.8 ± 1.0 ± 1.7	¹ AUBERT	03X BABR	Repl. by DEL-AMO-SANCHEZ 11B

- ¹ Assumes equal production of B^+ and B^0 at the $\Upsilon(4S)$.

$\Gamma(D^-D^+K^0)/\Gamma_{total}$ Γ_{177}/Γ

VALUE (units 10^{-3})	CL%	DOCUMENT ID	TECN	COMMENT
0.75 ± 0.12 ± 0.12		¹ DEL-AMO-SA..11B	BABR	$e^+e^- \rightarrow \Upsilon(4S)$
• • • We do not use the following data for averages, fits, limits, etc. • • •				
< 1.7	90	¹ AUBERT	03X BABR	Repl. by DEL-AMO-SANCHEZ 11B

- ¹ Assumes equal production of B^+ and B^0 at the $\Upsilon(4S)$.

$[\Gamma(D^*(2010)^-D^+K^0) + \Gamma(D^-D^*(2010)^+K^0)]/\Gamma_{total}$ Γ_{178}/Γ

VALUE (units 10^{-3})	DOCUMENT ID	TECN	COMMENT
6.41 ± 0.36 ± 0.39	¹ DEL-AMO-SA..11B	BABR	$e^+e^- \rightarrow \Upsilon(4S)$
• • • We do not use the following data for averages, fits, limits, etc. • • •			
6.5 ± 1.2 ± 1.0	¹ AUBERT	03X BABR	Repl. by DEL-AMO-SANCHEZ 11B

- ¹ Assumes equal production of B^+ and B^0 at the $\Upsilon(4S)$.

$\Gamma(D^*(2010)^-D^*(2010)^+K^0)/\Gamma_{total}$ Γ_{179}/Γ

VALUE (units 10^{-3})	DOCUMENT ID	TECN	COMMENT
8.1 ± 0.7 OUR AVERAGE			
8.26 ± 0.43 ± 0.67	¹ DEL-AMO-SA..11B	BABR	$e^+e^- \rightarrow \Upsilon(4S)$
6.8 ± 0.8 ± 1.4	^{1,2} DALSENO	07 BELL	$e^+e^- \rightarrow \Upsilon(4S)$
8.8 ± 0.8 ± 1.4	^{1,2} AUBERT,B	06Q BABR	$e^+e^- \rightarrow \Upsilon(4S)$
• • • We do not use the following data for averages, fits, limits, etc. • • •			
8.8 ^{+1.5} _{-1.4} ± 1.3	¹ AUBERT	03X BABR	Repl. by AUBERT,B 06Q

- ¹ Assumes equal production of B^+ and B^0 at the $\Upsilon(4S)$.
- ² The result is rescaled by a factor of 2 to convert from K_S^0 to K^0 .

$\Gamma(D^{*-}D_{s1}(2536)^+, D_{s1}^+ \rightarrow D^{*+}K^0)/\Gamma_{total}$ Γ_{180}/Γ

VALUE (units 10^{-4})	DOCUMENT ID	TECN	COMMENT
8.0 ± 2.4 OUR AVERAGE			
7.6 ^{+4.8+1.6} _{-4.2-1.4}	^{1,2} DALSENO	07 BELL	$e^+e^- \rightarrow \Upsilon(4S)$
8.2 ± 2.6 ± 1.2	^{1,2} AUBERT,B	06Q BABR	$e^+e^- \rightarrow \Upsilon(4S)$

- ¹ Assumes equal production of B^+ and B^0 at the $\Upsilon(4S)$.
- ² The result is rescaled by a factor of 2 to convert from K_S^0 to K^0 .

$\Gamma(\bar{D}^0D^0K^0)/\Gamma_{total}$ Γ_{181}/Γ

VALUE (units 10^{-3})	CL%	DOCUMENT ID	TECN	COMMENT
0.27 ± 0.10 ± 0.05		¹ DEL-AMO-SA..11B	BABR	$e^+e^- \rightarrow \Upsilon(4S)$
• • • We do not use the following data for averages, fits, limits, etc. • • •				
< 1.4	90	¹ AUBERT	03X BABR	Repl. by DEL-AMO-SANCHEZ 11B

- ¹ Assumes equal production of B^+ and B^0 at the $\Upsilon(4S)$.

$\Gamma(D^0\bar{D}^0K^+\pi^-)/\Gamma(D^*(2010)^-D^0K^+)$ $\Gamma_{182}/\Gamma_{175}$

VALUE (%)	DOCUMENT ID	TECN	COMMENT
14.2 ± 1.1 ± 1.0	¹ AAIJ	20AG LHCB	pp at 7, 8, and 13 TeV

- ¹ AAIJ 20AG excluded contributions from $B^0 \rightarrow D^{*-}D^0K^+$ transitions with $D^{*-} \rightarrow \bar{D}^0\pi^-$.

$[\Gamma(\bar{D}^0D^*(2007)^0K^0) + \Gamma(\bar{D}^*(2007)^0D^0K^0)]/\Gamma_{total}$ Γ_{183}/Γ

VALUE (units 10^{-3})	CL%	DOCUMENT ID	TECN	COMMENT
1.08 ± 0.32 ± 0.36		¹ DEL-AMO-SA..11B	BABR	$e^+e^- \rightarrow \Upsilon(4S)$
• • • We do not use the following data for averages, fits, limits, etc. • • •				
< 3.7	90	¹ AUBERT	03X BABR	Repl. by DEL-AMO-SANCHEZ 11B

- ¹ Assumes equal production of B^+ and B^0 at the $\Upsilon(4S)$.

$\Gamma(\bar{D}^*(2007)^0D^*(2007)^0K^0)/\Gamma_{total}$ Γ_{184}/Γ

VALUE (units 10^{-3})	CL%	DOCUMENT ID	TECN	COMMENT
2.40 ± 0.55 ± 0.67		¹ DEL-AMO-SA..11B	BABR	$e^+e^- \rightarrow \Upsilon(4S)$
• • • We do not use the following data for averages, fits, limits, etc. • • •				
< 6.6	90	¹ AUBERT	03X BABR	Repl. by DEL-AMO-SANCHEZ 11B

- ¹ Assumes equal production of B^+ and B^0 at the $\Upsilon(4S)$.

$\Gamma((\bar{D}^+\bar{D}^*)(D^+D^*)K)/\Gamma_{total}$ Γ_{185}/Γ

VALUE (units 10^{-2})	DOCUMENT ID	TECN	COMMENT
3.68 ± 0.10 ± 0.24	¹ DEL-AMO-SA..11B	BABR	$e^+e^- \rightarrow \Upsilon(4S)$
• • • We do not use the following data for averages, fits, limits, etc. • • •			
4.3 ± 0.3 ± 0.6	¹ AUBERT	03X BABR	Repl. by DEL-AMO-SANCHEZ 11B

- ¹ Assumes equal production of B^+ and B^0 at the $\Upsilon(4S)$.

Meson Particle Listings

B^0

$\Gamma(\eta_c K^0)/\Gamma_{\text{total}}$	Γ_{186}/Γ		
VALUE (units 10^{-3})	DOCUMENT ID	TECN	COMMENT
0.80 ± 0.11 OUR AVERAGE			
$0.71^{+0.12}_{-0.10} \pm 0.28$	1 CHILIKIN	19	BELL $e^+e^- \rightarrow \Upsilon(4S)$
$0.58^{+0.20+0.06}_{-0.18-0.05}$	2,3 AUBERT	07AV	BABR $e^+e^- \rightarrow \Upsilon(4S)$
$0.89 \pm 0.15 \pm 0.05$	2,4 AUBERT,B	04B	BABR $e^+e^- \rightarrow \Upsilon(4S)$
$1.23 \pm 0.23^{+0.40}_{-0.41}$	2 FANG	03	BELL $e^+e^- \rightarrow \Upsilon(4S)$
$1.09^{+0.55}_{-0.42} \pm 0.33$	5 EDWARDS	01	CLE2 $e^+e^- \rightarrow \Upsilon(4S)$

¹ CHILIKIN 19 reports $[\Gamma(B^0 \rightarrow \eta_c K^0)/\Gamma_{\text{total}}] \times [B(\eta_c(1S) \rightarrow \pi^+\pi^-\rho\bar{\rho})] = (38.0^{+6.4+1.3}_{-2.9-4.7}) \times 10^{-7}$ which we divide by our best value $B(\eta_c(1S) \rightarrow \pi^+\pi^-\rho\bar{\rho}) = (5.3 \pm 2.1) \times 10^{-3}$. Our first error is their experiment's error and our second error is the systematic error from using our best value.

² Assumes equal production of B^+ and B^0 at the $\Upsilon(4S)$.

³ AUBERT 07AV reports $[\Gamma(B^0 \rightarrow \eta_c K^0)/\Gamma_{\text{total}}] \times [B(\eta_c(1S) \rightarrow \rho\bar{\rho})] = (0.83^{+0.28}_{-0.26} \pm 0.05) \times 10^{-6}$ which we divide by our best value $B(\eta_c(1S) \rightarrow \rho\bar{\rho}) = (1.44 \pm 0.14) \times 10^{-3}$. Our first error is their experiment's error and our second error is the systematic error from using our best value.

⁴ AUBERT,B 04B reports $[\Gamma(B^0 \rightarrow \eta_c K^0)/\Gamma_{\text{total}}] \times [B(\eta_c(1S) \rightarrow K\bar{K}\pi)] = (0.0648 \pm 0.0085 \pm 0.0071) \times 10^{-3}$ which we divide by our best value $B(\eta_c(1S) \rightarrow K\bar{K}\pi) = (7.3 \pm 0.4) \times 10^{-2}$. Our first error is their experiment's error and our second error is the systematic error from using our best value.

⁵ EDWARDS 01 assumes equal production of B^0 and B^+ at the $\Upsilon(4S)$. The correlated uncertainties (28.3)% from $B(J/\psi(1S) \rightarrow \gamma\eta_c)$ in those modes have been accounted for.

$\Gamma(\eta_c K^0)/\Gamma(J/\psi(1S) K^0)$	$\Gamma_{186}/\Gamma_{200}$		
VALUE	DOCUMENT ID	TECN	COMMENT
$1.39 \pm 0.20 \pm 0.45$	1 AUBERT,B	04B	BABR $e^+e^- \rightarrow \Upsilon(4S)$

¹ Uses BABAR measurement of $B(B^0 \rightarrow J/\psi K^0) = (8.5 \pm 0.5 \pm 0.6) \times 10^{-4}$.

$\Gamma(\eta_c(1S) K^+\pi^-)/\Gamma(J/\psi(1S) K^+\pi^-)$	$\Gamma_{187}/\Gamma_{201}$		
VALUE	DOCUMENT ID	TECN	COMMENT
$0.53 \pm 0.03 \pm 0.05$	1 AAIJ	18AN	LHCB pp at 7, 8, 13 TeV

¹ AAIJ 18AN reports $[\Gamma(B^0 \rightarrow \eta_c(1S) K^+\pi^-)/\Gamma(B^0 \rightarrow J/\psi(1S) K^+\pi^-)] \times [B(\eta_c(1S) \rightarrow \rho\bar{\rho})] / [B(J/\psi(1S) \rightarrow \rho\bar{\rho})] = 0.357 \pm 0.015 \pm 0.008$ which we multiply or divide by our best values $B(\eta_c(1S) \rightarrow \rho\bar{\rho}) = (1.44 \pm 0.14) \times 10^{-3}$, $B(J/\psi(1S) \rightarrow \rho\bar{\rho}) = (2.120 \pm 0.029) \times 10^{-3}$. Our first error is their experiment's error and our second error is the systematic error from using our best values.

$\Gamma(\eta_c(1S) K^*(1410)^0)/\Gamma(\eta_c(1S) K^+\pi^-)$	$\Gamma_{190}/\Gamma_{187}$		
VALUE (units 10^{-2})	DOCUMENT ID	TECN	COMMENT
$32 \pm 24 \pm 6$	1 AAIJ	18AN	LHCB pp at 7, 8, 13 TeV

¹ AAIJ 18AN reports $[\Gamma(B^0 \rightarrow \eta_c(1S) K^*(1410)^0)/\Gamma(B^0 \rightarrow \eta_c(1S) K^+\pi^-)] \times [B(K^*(1410) \rightarrow K\pi)] = 0.021 \pm 0.011 \pm 0.011$ which we divide by our best value $B(K^*(1410) \rightarrow K\pi) = (6.6 \pm 1.3) \times 10^{-2}$. Our first error is their experiment's error and our second error is the systematic error from using our best value.

$\Gamma(\eta_c(1S) K^+\pi^-(NR))/\Gamma(\eta_c(1S) K^+\pi^-)$	$\Gamma_{188}/\Gamma_{187}$		
VALUE (units 10^{-2})	DOCUMENT ID	TECN	COMMENT
$10.3 \pm 1.4^{+1.0}_{-1.2}$	AAIJ	18AN	LHCB pp at 7, 8, 13 TeV

$\Gamma(\eta_c(1S) K_0^*(1430)^0)/\Gamma(\eta_c(1S) K^+\pi^-)$	$\Gamma_{191}/\Gamma_{187}$		
VALUE (units 10^{-2})	DOCUMENT ID	TECN	COMMENT
$27 \pm 5 \pm 3$	1 AAIJ	18AN	LHCB pp at 7, 8, 13 TeV

¹ AAIJ 18AN reports $[\Gamma(B^0 \rightarrow \eta_c(1S) K_0^*(1430)^0)/\Gamma(B^0 \rightarrow \eta_c(1S) K^+\pi^-)] \times [B(K_0^*(1430) \rightarrow K\pi)] = 0.253 \pm 0.035^{+0.035}_{-0.028}$ which we divide by our best value $B(K_0^*(1430) \rightarrow K\pi) = (93 \pm 10) \times 10^{-2}$. Our first error is their experiment's error and our second error is the systematic error from using our best value.

$\Gamma(\eta_c(1S) K_2^*(1430)^0)/\Gamma(\eta_c(1S) K^+\pi^-)$	$\Gamma_{192}/\Gamma_{187}$		
VALUE (units 10^{-2})	DOCUMENT ID	TECN	COMMENT
$8.2 \pm 3.6^{+0.2}_{-4.4}$	1 AAIJ	18AN	LHCB pp at 7, 8, 13 TeV

¹ AAIJ 18AN reports $[\Gamma(B^0 \rightarrow \eta_c(1S) K_2^*(1430)^0)/\Gamma(B^0 \rightarrow \eta_c(1S) K^+\pi^-)] \times [B(K_2^*(1430) \rightarrow K\pi)] = 0.041 \pm 0.015^{+0.010}_{-0.016}$ which we divide by our best value $B(K_2^*(1430) \rightarrow K\pi) = (49.9 \pm 1.2) \times 10^{-2}$. Our first error is their experiment's error and our second error is the systematic error from using our best value.

$\Gamma(\eta_c(1S) K^*(1680)^0)/\Gamma(\eta_c(1S) K^+\pi^-)$	$\Gamma_{193}/\Gamma_{187}$		
VALUE (units 10^{-2})	DOCUMENT ID	TECN	COMMENT
$5.7 \pm 6.5^{+0.4}_{-6.8}$	1 AAIJ	18AN	LHCB pp at 7, 8, 13 TeV

¹ AAIJ 18AN reports $[\Gamma(B^0 \rightarrow \eta_c(1S) K^*(1680)^0)/\Gamma(B^0 \rightarrow \eta_c(1S) K^+\pi^-)] \times [B(K^*(1680) \rightarrow K\pi)] = 0.022 \pm 0.020^{+0.015}_{-0.017}$ which we divide by our best value $B(K^*(1680) \rightarrow K\pi) = (38.7 \pm 2.5) \times 10^{-2}$. Our first error is their experiment's error and our second error is the systematic error from using our best value.

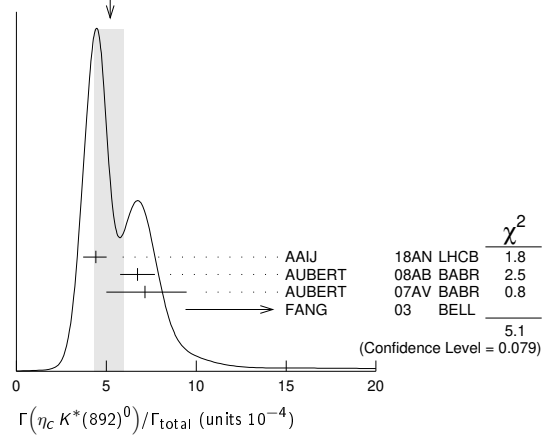
$\Gamma(\eta_c(1S) K_0^*(1950)^0)/\Gamma(\eta_c(1S) K^+\pi^-)$	$\Gamma_{194}/\Gamma_{187}$		
VALUE (units 10^{-2})	DOCUMENT ID	TECN	COMMENT
$7^{+4}_{-6} \pm 2$	1 AAIJ	18AN	LHCB pp at 7, 8, 13 TeV

¹ AAIJ 18AN reports $[\Gamma(B^0 \rightarrow \eta_c(1S) K_0^*(1950)^0)/\Gamma(B^0 \rightarrow \eta_c(1S) K^+\pi^-)] \times [B(K_0^*(1950) \rightarrow K^-\pi^+)] = 0.038 \pm 0.018^{+0.014}_{-0.025}$ which we divide by our best value $B(K_0^*(1950) \rightarrow K^-\pi^+) = (52 \pm 14) \times 10^{-2}$. Our first error is their experiment's error and our second error is the systematic error from using our best value.

$\Gamma(X(4100)^- K^+, X^- \rightarrow \eta_c \pi^-)/\Gamma(\eta_c(1S) K^+\pi^-)$	$\Gamma_{189}/\Gamma_{187}$		
VALUE (units 10^{-2})	DOCUMENT ID	TECN	COMMENT
$3.3 \pm 1.1^{+1.2}_{-1.1}$	AAIJ	18AN	LHCB pp at 7, 8, 13 TeV

$\Gamma(\eta_c K^*(892)^0)/\Gamma_{\text{total}}$	Γ_{195}/Γ		
VALUE (units 10^{-4})	DOCUMENT ID	TECN	COMMENT
$5.2^{+0.8}_{-0.9}$ OUR AVERAGE			Error includes scale factor of 1.6. See the ideogram below.
$4.42 \pm 0.24^{+0.54}_{-0.66}$	1 AAIJ	18AN	LHCB pp at 7, 8, 13 TeV
$6.7 \pm 0.8 \pm 0.5$	2,3 AUBERT	08AB	BABR $e^+e^- \rightarrow \Upsilon(4S)$
$7.2^{+2.2}_{-2.0} \pm 0.7$	4,5 AUBERT	07AV	BABR $e^+e^- \rightarrow \Upsilon(4S)$
$16.2 \pm 3.2^{+5.5}_{-6.0}$	5 FANG	03	BELL $e^+e^- \rightarrow \Upsilon(4S)$

WEIGHTED AVERAGE
5.2+0.8-0.9 (Error scaled by 1.6)



¹ AAIJ 18AN reports $B(B^0 \rightarrow \eta_c K^*(892)^0, K^*(892)^0 \rightarrow K^+\pi^-) = (2.95 \pm 0.16^{+0.36}_{-0.44}) \times 10^{-4}$ using the fitted fraction of $0.514 \pm 0.019^{+0.017}_{-0.048}$ from Dalitz decay of $B(B^0 \rightarrow \eta_c K^+\pi^-) = (5.73 \pm 0.24 \pm 0.67) \times 10^{-4}$ and corrected for $B(K^*(892)^0 \rightarrow K^+\pi^-) = 2/3$.

² AUBERT 08AB reports $[\Gamma(B^0 \rightarrow \eta_c K^*(892)^0)/\Gamma_{\text{total}}] / [B(B^+ \rightarrow \eta_c K^+)] = 0.62 \pm 0.06 \pm 0.05$ which we multiply by our best value $B(B^+ \rightarrow \eta_c K^+) = (1.09 \pm 0.08) \times 10^{-3}$. Our first error is their experiment's error and our second error is the systematic error from using our best value.

³ Uses the production ratio of $(B^+B^-)/(B^0\bar{B}^0) = 1.026 \pm 0.032$ at $\Upsilon(4S)$.

⁴ AUBERT 07AV reports $[\Gamma(B^0 \rightarrow \eta_c K^*(892)^0)/\Gamma_{\text{total}}] \times [B(\eta_c(1S) \rightarrow \rho\bar{\rho})] = (1.03^{+0.27}_{-0.24} \pm 0.17) \times 10^{-6}$ which we divide by our best value $B(\eta_c(1S) \rightarrow \rho\bar{\rho}) = (1.44 \pm 0.14) \times 10^{-3}$. Our first error is their experiment's error and our second error is the systematic error from using our best value.

⁵ Assumes equal production of B^+ and B^0 at the $\Upsilon(4S)$.

$\Gamma(\eta_c(2S) K_0^0, \eta_c \rightarrow \rho\bar{\rho}\pi^+\pi^-)/\Gamma_{\text{total}}$	Γ_{196}/Γ		
VALUE (units 10^{-7})	DOCUMENT ID	TECN	COMMENT
$4.2 \pm 1.4^{+0.3}_{-1.2-0.3}$	CHILIKIN	19	BELL $e^+e^- \rightarrow \Upsilon(4S)$

$\Gamma(\eta_c(2S) K^*0)/\Gamma_{\text{total}}$	Γ_{197}/Γ			
VALUE (units 10^{-4})	CL%	DOCUMENT ID	TECN	COMMENT
<3.9	90	1 AUBERT	08AB	BABR $e^+e^- \rightarrow \Upsilon(4S)$

¹ Uses the production ratio of $(B^+B^-)/(B^0\bar{B}^0) = 1.026 \pm 0.032$ at $\Upsilon(4S)$.

$\Gamma(h_c(1P) K_0^0)/\Gamma_{\text{total}}$	Γ_{198}/Γ		
VALUE	DOCUMENT ID	TECN	COMMENT
$<1.4 \times 10^{-5}$	CHILIKIN	19	BELL $e^+e^- \rightarrow \Upsilon(4S)$

$\Gamma(B^0 \rightarrow h_c(1P) K^*0)/\Gamma_{\text{total}} \times \Gamma(h_c(1P) \rightarrow \gamma\eta_c(1S))/\Gamma_{\text{total}}$	$\Gamma_{199}/\Gamma \times \Gamma_{22}^{h_c(1P)}/\Gamma_{h_c(1P)}$			
VALUE (units 10^{-4})	CL%	DOCUMENT ID	TECN	COMMENT
<2.2	90	1 AUBERT	08AB	BABR $e^+e^- \rightarrow \Upsilon(4S)$

¹ Uses the production ratio of $(B^+B^-)/(B^0\bar{B}^0) = 1.026 \pm 0.032$ at $\Upsilon(4S)$.

$\Gamma(\eta_c K^*(892)^0)/\Gamma(\eta_c K^0)$		$\Gamma_{195}/\Gamma_{186}$		
VALUE	DOCUMENT ID	TECN	COMMENT	
1.33 ± 0.36^{+0.24}_{-0.33}	FANG	03	BELL	e ⁺ e ⁻ → $\Upsilon(4S)$

$\Gamma(J/\psi(1S) K^0)/\Gamma_{total}$		Γ_{200}/Γ		
VALUE (units 10 ⁻⁴)	DOCUMENT ID	TECN	COMMENT	

8.91 ± 0.21 OUR FIT				
8.91 ± 0.21 OUR AVERAGE				
9.02 ± 0.10 ± 0.26	1	CHOUDHURY 21	BELL	e ⁺ e ⁻ → $\Upsilon(4S)$
8.1 ± 0.9 ± 0.6	2	CHILIKIN 19	BELL	e ⁺ e ⁻ → $\Upsilon(4S)$
8.8 ^{+1.4} _{-1.3} ± 0.1	3,4	AUBERT 07AV	BABR	e ⁺ e ⁻ → $\Upsilon(4S)$
8.69 ± 0.22 ± 0.30	4	AUBERT 05J	BABR	e ⁺ e ⁻ → $\Upsilon(4S)$
9.5 ± 0.8 ± 0.6	4	AVERY 00	CLE2	e ⁺ e ⁻ → $\Upsilon(4S)$
11.5 ± 2.3 ± 1.7	5	ABE 96H	CDF	p \bar{p} at 1.8 TeV
6.93 ± 4.07 ± 0.04	6	BORTOLETTO92	CLEO	e ⁺ e ⁻ → $\Upsilon(4S)$
9.24 ± 7.21 ± 0.05	2, 7	ALBRECHT 90J	ARG	e ⁺ e ⁻ → $\Upsilon(4S)$

• • • We do not use the following data for averages, fits, limits, etc. • • •

7.9 ± 0.4 ± 0.9	4	ABE 03B	BELL	Repl. by CHOUDHURY 21
8.3 ± 0.4 ± 0.5	4	AUBERT 02	BABR	Repl. by AUBERT 05J
8.5 ^{+1.4} _{-1.2} ± 0.6	4	JESSOP 97	CLE2	Repl. by AVERY 00
7.5 ± 2.4 ± 0.8	10, 6	ALAM 94	CLEO	Sup. by JESSOP 97
<50	90	ALAM 86	CLEO	e ⁺ e ⁻ → $\Upsilon(4S)$

- 1 CHOUDHURY 21 uses the relative production fraction of charged (f[±]) to neutral (f⁰) B mesons at $\Upsilon(4S)$ value of f[±]/f⁰ = 1.058 ± 0.024.
- 2 CHILIKIN 19 reports $[\Gamma(B^0 \rightarrow J/\psi(1S) K^0)/\Gamma_{total}] \times [B(J/\psi(1S) \rightarrow p\bar{p}\pi^+\pi^-)] = (48.6^{+4.6+2.4}_{-4.4-2.6}) \times 10^{-7}$ which we divide by our best value B(J/ψ(1S) → p \bar{p} π⁺π⁻) = (6.0 ± 0.5) × 10⁻³. Our first error is their experiment's error and our second error is the systematic error from using our best value.
- 3 AUBERT 07AV reports $[\Gamma(B^0 \rightarrow J/\psi(1S) K^0)/\Gamma_{total}] \times [B(J/\psi(1S) \rightarrow p\bar{p})] = (1.87^{+0.28}_{-0.26} \pm 0.07) \times 10^{-6}$ which we divide by our best value B(J/ψ(1S) → p \bar{p}) = (2.120 ± 0.029) × 10⁻³. Our first error is their experiment's error and our second error is the systematic error from using our best value.
- 4 Assumes equal production of B⁺ and B⁰ at the $\Upsilon(4S)$.
- 5 ABE 96H assumes that B(B⁺ → J/ψ K⁺) = (1.02 ± 0.14) × 10⁻³.
- 6 BORTOLETTO 92 reports (6 ± 3 ± 2) × 10⁻⁴ from a measurement of $[\Gamma(B^0 \rightarrow J/\psi(1S) K^0)/\Gamma_{total}] \times [B(J/\psi(1S) \rightarrow e^+e^-)]$ assuming B(J/ψ(1S) → e⁺e⁻) = 0.069 ± 0.009, which we rescale to our best value B(J/ψ(1S) → e⁺e⁻) = (5.971 ± 0.032) × 10⁻². Our first error is their experiment's error and our second error is the systematic error from using our best value. Assumes equal production of B⁺ and B⁰ at the $\Upsilon(4S)$.
- 7 ALBRECHT 90J reports (8 ± 6 ± 2) × 10⁻⁴ from a measurement of $[\Gamma(B^0 \rightarrow J/\psi(1S) K^0)/\Gamma_{total}] \times [B(J/\psi(1S) \rightarrow e^+e^-)]$ assuming B(J/ψ(1S) → e⁺e⁻) = 0.069 ± 0.009, which we rescale to our best value B(J/ψ(1S) → e⁺e⁻) = (5.971 ± 0.032) × 10⁻². Our first error is their experiment's error and our second error is the systematic error from using our best value. Assumes equal production of B⁺ and B⁰ at the $\Upsilon(4S)$.

$\Gamma(J/\psi(1S) K^+\pi^-)/\Gamma_{total}$		Γ_{201}/Γ		
VALUE (units 10 ⁻³)	DOCUMENT ID	TECN	COMMENT	

1.15 ± 0.05 OUR AVERAGE				
1.15 ± 0.01 ± 0.05		CHILIKIN 14	BELL	$\bar{B}^0 \rightarrow J/\psi K^-\pi^+$
1.16 ± 0.56 ± 0.01	1	BORTOLETTO92	CLEO	e ⁺ e ⁻ → $\Upsilon(4S)$

- • • We do not use the following data for averages, fits, limits, etc. • • •
- | | | | | | |
|---------------|----|-------------|--------------|--|--|
| 1.079 ± 0.011 | 2 | AUBERT 09AA | BABR | e ⁺ e ⁻ → $\Upsilon(4S)$ | |
| <1.3 | 90 | 3 | ALBRECHT 87D | ARG | e ⁺ e ⁻ → $\Upsilon(4S)$ |
| <6.3 | 90 | 4 | GILES 84 | CLEO | e ⁺ e ⁻ → $\Upsilon(4S)$ |
- 1 BORTOLETTO 92 reports (1.0 ± 0.4 ± 0.3) × 10⁻³ from a measurement of $[\Gamma(B^0 \rightarrow J/\psi(1S) K^+\pi^-)/\Gamma_{total}] \times [B(J/\psi(1S) \rightarrow e^+e^-)]$ assuming B(J/ψ(1S) → e⁺e⁻) = 0.069 ± 0.009, which we rescale to our best value B(J/ψ(1S) → e⁺e⁻) = (5.971 ± 0.032) × 10⁻². Our first error is their experiment's error and our second error is the systematic error from using our best value. Assumes equal production of B⁺ and B⁰ at the $\Upsilon(4S)$.
 - 2 Does not report systematic uncertainties.
 - 3 ALBRECHT 87D assume B⁺B⁻/B⁰ \bar{B}^0 ratio is 55/45. Kπ system is specifically selected as nonresonant.

$\Gamma(J/\psi(1S) K^*(892)^0)/\Gamma_{total}$		Γ_{202}/Γ		
VALUE (units 10 ⁻³)	DOCUMENT ID	TECN	COMMENT	

1.27 ± 0.05 OUR FIT				
1.28 ± 0.05 OUR AVERAGE				
1.19 ± 0.01 ± 0.08		CHILIKIN 14	BELL	$\bar{B}^0 \rightarrow J/\psi K^-\pi^+$
1.33 ^{+0.22} _{-0.21} ± 0.02	1,2	AUBERT 07AV	BABR	e ⁺ e ⁻ → $\Upsilon(4S)$
1.309 ± 0.026 ± 0.077	2	AUBERT 05J	BABR	e ⁺ e ⁻ → $\Upsilon(4S)$
1.29 ± 0.05 ± 0.13	2	ABE 02N	BELL	e ⁺ e ⁻ → $\Upsilon(4S)$
1.74 ± 0.20 ± 0.18	3	ABE 98O	CDF	p \bar{p} 1.8 TeV
1.32 ± 0.17 ± 0.17	4	JESSOP 97	CLE2	e ⁺ e ⁻ → $\Upsilon(4S)$
1.27 ± 0.65 ± 0.01	5	BORTOLETTO92	CLEO	e ⁺ e ⁻ → $\Upsilon(4S)$
1.27 ± 0.60 ± 0.01	6	ALBRECHT 80J	ARG	e ⁺ e ⁻ → $\Upsilon(4S)$
4.04 ± 1.81 ± 0.02	5, 7	BEBEK 97	CLEO	e ⁺ e ⁻ → $\Upsilon(4S)$

- • • We do not use the following data for averages, fits, limits, etc. • • •
- | | | | | |
|--------------------|-------|--------------|------|--|
| 1.24 ± 0.05 ± 0.09 | 2 | AUBERT 02 | BABR | Repl. by AUBERT 05J |
| 1.36 ± 0.27 ± 0.22 | 8 | ABE 96H | CDF | Sup. by ABE 98O |
| 1.69 ± 0.31 ± 0.18 | 29, 9 | ALAM 94 | CLE2 | Sup. by JESSOP 97 |
| | 10 | ALBRECHT 94G | ARG | e ⁺ e ⁻ → $\Upsilon(4S)$ |
| 4.0 ± 0.30 | 11 | ALBAJAR 91E | UA1 | E _{cm} ^{pp} = 630 GeV |
| 3.3 ± 0.18 | 12 | ALBRECHT 87D | ARG | e ⁺ e ⁻ → $\Upsilon(4S)$ |
| 4.1 ± 0.18 | 5, 13 | ALAM 86 | CLEO | Repl. by BEBEK 87 |
- 1 AUBERT 07AV reports $[\Gamma(B^0 \rightarrow J/\psi(1S) K^*(892)^0)/\Gamma_{total}] \times [B(J/\psi(1S) \rightarrow p\bar{p})] = (2.82^{+0.30+0.36}_{-0.28-0.35}) \times 10^{-6}$ which we divide by our best value B(J/ψ(1S) → p \bar{p}) = (2.120 ± 0.029) × 10⁻³. Our first error is their experiment's error and our second error is the systematic error from using our best value.
 - 2 Assumes equal production of B⁺ and B⁰ at the $\Upsilon(4S)$.
 - 3 ABE 98O reports $[B(B^0 \rightarrow J/\psi(1S) K^*(892)^0)]/[B(B^+ \rightarrow J/\psi(1S) K^+)] = 1.76 \pm 0.14 \pm 0.15$. We multiply by our best value B(B⁺ → J/ψ(1S) K⁺) = (9.9 ± 1.0) × 10⁻⁴. Our first error is their experiment's error and our second error is the systematic error from using our best value.
 - 4 Assumes equal production of B⁺ and B⁰ at the $\Upsilon(4S)$.
 - 5 BORTOLETTO 92 reports (1.1 ± 0.5 ± 0.3) × 10⁻³ from a measurement of $[\Gamma(B^0 \rightarrow J/\psi(1S) K^*(892)^0)/\Gamma_{total}] \times [B(J/\psi(1S) \rightarrow e^+e^-)]$ assuming B(J/ψ(1S) → e⁺e⁻) = 0.069 ± 0.009, which we rescale to our best value B(J/ψ(1S) → e⁺e⁻) = (5.971 ± 0.032) × 10⁻². Our first error is their experiment's error and our second error is the systematic error from using our best value. Assumes equal production of B⁺ and B⁰ at the $\Upsilon(4S)$.
 - 6 ALBRECHT 90J reports (1.1 ± 0.5 ± 0.2) × 10⁻³ from a measurement of $[\Gamma(B^0 \rightarrow J/\psi(1S) K^*(892)^0)/\Gamma_{total}] \times [B(J/\psi(1S) \rightarrow e^+e^-)]$ assuming B(J/ψ(1S) → e⁺e⁻) = 0.069 ± 0.009, which we rescale to our best value B(J/ψ(1S) → e⁺e⁻) = (5.971 ± 0.032) × 10⁻². Our first error is their experiment's error and our second error is the systematic error from using our best value. Assumes equal production of B⁺ and B⁰ at the $\Upsilon(4S)$.
 - 7 BEBEK 87 reports (3.5 ± 1.6 ± 0.3) × 10⁻³ from a measurement of $[\Gamma(B^0 \rightarrow J/\psi(1S) K^*(892)^0)/\Gamma_{total}] \times [B(J/\psi(1S) \rightarrow e^+e^-)]$ assuming B(J/ψ(1S) → e⁺e⁻) = 0.069 ± 0.009, which we rescale to our best value B(J/ψ(1S) → e⁺e⁻) = (5.971 ± 0.032) × 10⁻². Our first error is their experiment's error and our second error is the same assumptions.
 - 8 ABE 96H assumes that B(B⁺ → J/ψ K⁺) = (1.02 ± 0.14) × 10⁻³.
 - 9 The neutral and charged B events together are predominantly longitudinally polarized. $\Gamma_{\perp}/\Gamma = 0.080 \pm 0.08 \pm 0.05$. This can be compared with a prediction using HQET, 0.73 (KRAMER 92). This polarization indicates that the B → ψ K* decay is dominated by the CP = -1 CP eigenstate. Assumes equal production of B⁺ and B⁰ at the $\Upsilon(4S)$.
 - 10 ALBRECHT 94G measures the polarization in the vector-vector decay to be predominantly longitudinal, $\Gamma_{\perp}/\Gamma = 0.03 \pm 0.16 \pm 0.15$ making the neutral decay a CP eigenstate when the K*0 decays through K_S⁰π⁰.
 - 11 ALBAJAR 91E assumes B_d⁰ production fraction of 36%.
 - 12 ALBRECHT 87D assume B⁺B⁻/B⁰ \bar{B}^0 ratio is 55/45. Superseded by ALBRECHT 90J.
 - 13 ALAM 86 assumes B[±]B⁰ ratio is 60/40. The observation of the decay B⁺ → J/ψ K*(892)⁺ (HAAS 85) has been retracted in this paper.

$\Gamma(J/\psi(1S) K^*(892)^0)/\Gamma(J/\psi(1S) K^0)$		$\Gamma_{202}/\Gamma_{200}$		
VALUE	DOCUMENT ID	TECN	COMMENT	

1.50 ± 0.09 OUR AVERAGE				
1.51 ± 0.05 ± 0.08		AUBERT 05J	BABR	e ⁺ e ⁻ → $\Upsilon(4S)$
1.39 ± 0.36 ± 0.10		ABE 96Q	CDF	p \bar{p}

• • • We do not use the following data for averages, fits, limits, etc. • • •

1.49 ± 0.10 ± 0.08	1	AUBERT 02	BABR	Repl. by AUBERT 05J
--------------------	---	-----------	------	---------------------

1 Assumes equal production of B⁺ and B⁰ at the $\Upsilon(4S)$.

$\Gamma(J/\psi(1S) \eta K_S^0)/\Gamma_{total}$		Γ_{203}/Γ		
VALUE (units 10 ⁻⁵)	DOCUMENT ID	TECN	COMMENT	

5.4 ± 0.9 OUR AVERAGE				
5.22 ± 0.78 ± 0.49	1	IWASHITA 14	BELL	e ⁺ e ⁻ → $\Upsilon(4S)$
8.4 ± 2.6 ± 2.7	1	AUBERT 04Y	BABR	e ⁺ e ⁻ → $\Upsilon(4S)$

1 Assumes equal production of B⁺ and B⁰ at the $\Upsilon(4S)$.

$\Gamma(J/\psi(1S) \eta' K_S^0)/\Gamma_{total}$		Γ_{204}/Γ		
VALUE (units 10 ⁻⁵)	DOCUMENT ID	TECN	COMMENT	

<2.5	90	1	XIE 07	BELL	e ⁺ e ⁻ → $\Upsilon(4S)$
----------------	----	---	--------	------	--

1 Assumes equal production of B⁺ and B⁰ at the $\Upsilon(4S)$.

$\Gamma(J/\psi(1S) \omega K^0)/\Gamma_{total}$		Γ_{206}/Γ		
VALUE (units 10 ⁻⁴)	DOCUMENT ID	TECN	COMMENT	

2.3 ± 0.3 ± 0.3	1	DEL-AMO-SA...10B	BABR	e ⁺ e ⁻ → $\Upsilon(4S)$
------------------------	---	------------------	------	--

• • • We do not use the following data for averages, fits, limits, etc. • • •

3.1 ± 0.6 ± 0.3	1	AUBERT 08W	BABR	Repl. by DEL-AMO-SANCHEZ 10B
-----------------	---	------------	------	------------------------------

1 Assumes equal production of B⁺ and B⁰ at the $\Upsilon(4S)$.

Meson Particle Listings

 B^0 $\Gamma(\chi_{c0}(3915), \chi_{c0} \rightarrow J/\psi\omega)/\Gamma_{\text{total}}$ Γ_{207}/Γ

VALUE (units 10^{-5})	DOCUMENT ID	TECN	COMMENT
$2.1 \pm 0.9 \pm 0.3$	¹ DEL-AMO-SA.10B	BABR	$e^+e^- \rightarrow \Upsilon(4S)$

• • • We do not use the following data for averages, fits, limits, etc. • • •

$1.3^{+1.3}_{-1.1} \pm 0.2$	^{1,2} AUBERT	08w	BABR Repl. by DEL-AMO-SANCHEZ 10B
-----------------------------	-----------------------	-----	-----------------------------------

¹ Assumes equal production of B^+ and B^0 at the $\Upsilon(4S)$.

² Corresponds to upper limit of 3.9×10^{-5} at 90% CL.

 $\Gamma(J/\psi(1S)\phi K^0)/\Gamma_{\text{total}}$ Γ_{205}/Γ

VALUE (units 10^{-5})	DOCUMENT ID	TECN	COMMENT
4.9 ± 1.0 OUR AVERAGE	Error includes scale factor of 1.3.		
$4.43 \pm 0.76 \pm 0.19$	LEES	15	BABR $e^+e^- \rightarrow \Upsilon(4S)$
$10.2 \pm 3.8 \pm 1.0$	¹ AUBERT	03o	BABR $e^+e^- \rightarrow \Upsilon(4S)$
$8.8^{+3.5}_{-3.0} \pm 1.3$	² ANASTASSOV	00	CLE2 $e^+e^- \rightarrow \Upsilon(4S)$

¹ Assumes equal production of B^+ and B^0 at the $\Upsilon(4S)$.

² ANASTASSOV 00 finds 10 events on a background of 0.5 ± 0.2 . Assumes equal production of B^0 and B^+ at the $\Upsilon(4S)$, a uniform Dalitz plot distribution, isotropic $J/\psi(1S)$ and ϕ decays, and $B(B^+ \rightarrow J/\psi(1S)\phi K^+) = B(B^0 \rightarrow J/\psi(1S)\phi K^0)$.

 $\Gamma(J/\psi(1S)K(1270)^0)/\Gamma_{\text{total}}$ Γ_{208}/Γ

VALUE (units 10^{-3})	DOCUMENT ID	TECN	COMMENT
$1.30 \pm 0.34 \pm 0.32$	¹ ABE	01L	BELL $e^+e^- \rightarrow \Upsilon(4S)$

¹ Assumes equal production of B^+ and B^0 at the $\Upsilon(4S)$ and uses the PDG value of $B(B^+ \rightarrow J/\psi(1S)K^+) = (1.00 \pm 0.10) \times 10^{-3}$.

 $\Gamma(J/\psi(1S)\pi^0)/\Gamma_{\text{total}}$ Γ_{209}/Γ

VALUE (units 10^{-5})	CL%	DOCUMENT ID	TECN	COMMENT
1.66 ± 0.10 OUR AVERAGE				
$1.62 \pm 0.11 \pm 0.06$		¹ PAL	18	BELL $e^+e^- \rightarrow \Upsilon(4S)$
$1.69 \pm 0.14 \pm 0.07$		¹ AUBERT	08AU	BABR $e^+e^- \rightarrow \Upsilon(4S)$
$2.5^{+1.1}_{-0.9} \pm 0.2$		¹ AVERY	00	CLE2 $e^+e^- \rightarrow \Upsilon(4S)$

• • • We do not use the following data for averages, fits, limits, etc. • • •

$1.94 \pm 0.22 \pm 0.17$		¹ AUBERT,B	06B	BABR Repl. by AUBERT 08AU
$2.3 \pm 0.5 \pm 0.2$		¹ ABE	03B	BELL Repl. by PAL 18
$2.0 \pm 0.6 \pm 0.2$		¹ AUBERT	02	BABR Repl. by AUBERT,B 06B
< 32	90	² ACCIARRI	97C	L3
< 5.8	90	BISHAI	96	CLE2 Sup. by AVERY 00
< 690	90	¹ ALEXANDER	95	CLE2 Sup. by BISHAI 96

¹ Assumes equal production of B^+ and B^0 at the $\Upsilon(4S)$.

² ACCIARRI 97C assumes B^0 production fraction ($39.5 \pm 4.0\%$) and B_S ($12.0 \pm 3.0\%$).

 $\Gamma(J/\psi(1S)\eta)/\Gamma_{\text{total}}$ Γ_{210}/Γ

VALUE (units 10^{-6})	CL%	DOCUMENT ID	TECN	COMMENT
10.8 ± 2.3 OUR AVERAGE		Error includes scale factor of 1.5.		
$7.3 \pm 2.5 \pm 1.3$		¹ AAJ	15D	LHCB pp at 7, 8 TeV
$12.3^{+1.8}_{-1.7} \pm 0.7$		^{2,3} CHANG	12	BELL $e^+e^- \rightarrow \Upsilon(4S)$

• • • We do not use the following data for averages, fits, limits, etc. • • •

$9.5 \pm 1.7 \pm 0.8$		³ CHANG	07A	BELL Repl. by CHANG 12
< 27	90	³ AUBERT	03o	BABR $e^+e^- \rightarrow \Upsilon(4S)$
< 1200	90	⁴ ACCIARRI	97C	L3

¹ AAJ 15D reports $[\Gamma(B^0 \rightarrow J/\psi(1S)\eta)/\Gamma_{\text{total}}] / [B(B_S^0 \rightarrow J/\psi(1S)\eta)] = (1.85 \pm 0.61 \pm 0.14) \times 10^{-2}$ which we multiply by our best value $B(B_S^0 \rightarrow J/\psi(1S)\eta) = (4.0 \pm 0.7) \times 10^{-4}$. Our first error is their experiment's error and our second error is the systematic error from using our best value.

² Reconstructs η in $\gamma\gamma$ and $\pi^+\pi^-\pi^0$ decays.

³ Assumes equal production of B^+ and B^0 at the $\Upsilon(4S)$.

⁴ ACCIARRI 97C assumes B^0 production fraction ($39.5 \pm 4.0\%$) and B_S ($12.0 \pm 3.0\%$).

 $\Gamma(J/\psi(1S)\pi^+\pi^-)/\Gamma_{\text{total}}$ Γ_{211}/Γ

VALUE (units 10^{-5})	DOCUMENT ID	TECN	COMMENT
4.00 ± 0.15 OUR AVERAGE			
$3.98 \pm 0.14 \pm 0.07$	^{1,2} AAJ	13M	LHCB pp at 7 TeV
$4.6 \pm 0.7 \pm 0.6$	³ AUBERT	03B	BABR $e^+e^- \rightarrow \Upsilon(4S)$

¹ AAJ 13M reports $(3.97 \pm 0.09 \pm 0.11 \pm 0.16) \times 10^{-5}$ from a measurement of $[\Gamma(B^0 \rightarrow J/\psi(1S)\pi^+\pi^-)/\Gamma_{\text{total}}] / [B(B^+ \rightarrow J/\psi(1S)K^+)]$ assuming $B(B^+ \rightarrow J/\psi(1S)K^+) = (1.018 \pm 0.042) \times 10^{-3}$, which we rescale to our best value $B(B^+ \rightarrow J/\psi(1S)K^+) = (1.020 \pm 0.019) \times 10^{-3}$. Our first error is their experiment's error and our second error is the systematic error from using our best value.

² AAJ 13M does not report correlations between various measurements of the $J/\psi\pi\pi$ final state.

³ Assumes equal production of B^+ and B^0 at the $\Upsilon(4S)$.

 $\Gamma(J/\psi(1S)\pi^+\pi^- \text{ nonresonant})/\Gamma_{\text{total}}$ Γ_{212}/Γ

VALUE (units 10^{-5})	CL%	DOCUMENT ID	TECN	COMMENT
< 1.2	90	¹ AUBERT	07AC	BABR $e^+e^- \rightarrow \Upsilon(4S)$

¹ Assumes equal production of B^+ and B^0 at the $\Upsilon(4S)$.

 $\Gamma(J/\psi(1S)\eta_0(500), \eta_0 \rightarrow \pi\pi)/\Gamma_{\text{total}}$ Γ_{213}/Γ

VALUE (units 10^{-6})	DOCUMENT ID	TECN	COMMENT
$8.8 \pm 0.5^{+1.1}_{-1.5}$	¹ AAJ	14x	LHCB pp at 7, 8 TeV

• • • We do not use the following data for averages, fits, limits, etc. • • •

$6.4^{+2.5}_{-1.1} \pm 0.2$	^{2,3} AAJ	13M	LHCB Repl. by AAJ 14x
-----------------------------	--------------------	-----	-----------------------

¹ AAJ 14x uses Dalitz plot analysis of $B^0 \rightarrow J/\psi\pi^+\pi^-$.

² AAJ 13M reports $(6.4 \pm 0.8^{+2.4}_{-0.8}) \times 10^{-6}$ from a measurement of $[\Gamma(B^0 \rightarrow J/\psi(1S)\eta_0(500), \eta_0 \rightarrow \pi\pi)/\Gamma_{\text{total}}] / [B(B^0 \rightarrow J/\psi(1S)\pi^+\pi^-)]$ assuming $B(B^0 \rightarrow J/\psi(1S)\pi^+\pi^-) = (3.97 \pm 0.09 \pm 0.11 \pm 0.16) \times 10^{-5}$, which we rescale to our best value $B(B^0 \rightarrow J/\psi(1S)\pi^+\pi^-) = (4.00 \pm 0.15) \times 10^{-5}$. Our first error is their experiment's error and our second error is the systematic error from using our best value.

³ AAJ 13M does not report correlations between various measurements of the $J/\psi\pi\pi$ final state. Measured in Dalitz plot like analysis of $B^0 \rightarrow J/\psi\pi^+\pi^-$.

 $\Gamma(J/\psi(1S)f_2)/\Gamma_{\text{total}}$ Γ_{214}/Γ

VALUE (units 10^{-5})	CL%	DOCUMENT ID	TECN	COMMENT
$0.33^{+0.05}_{-0.06}$ OUR AVERAGE		Error includes scale factor of 1.5.		

$0.30 \pm 0.03^{+0.02}_{-0.03}$		¹ AAJ	14x	LHCB pp at 7, 8 TeV
---------------------------------	--	------------------	-----	-----------------------

$0.42 \pm 0.06 \pm 0.02$		^{2,3} AAJ	13M	LHCB pp at 7 TeV
--------------------------	--	--------------------	-----	--------------------

• • • We do not use the following data for averages, fits, limits, etc. • • •

< 0.5	90	^{4,5} AUBERT	07AC	BABR $e^+e^- \rightarrow \Upsilon(4S)$
---------	----	-----------------------	------	--

¹ AAJ 14x uses Dalitz plot analysis of $B^0 \rightarrow J/\psi\pi^+\pi^-$.

² AAJ 13M reports $[\Gamma(B^0 \rightarrow J/\psi(1S)f_2)/\Gamma_{\text{total}}] \times [B(f_2(1270) \rightarrow \pi\pi)] = (3.5 \pm 0.4 \pm 0.4) \times 10^{-6}$ from a measurement of $[\Gamma(B^0 \rightarrow J/\psi(1S)f_2)/\Gamma_{\text{total}}] \times [B(f_2(1270) \rightarrow \pi\pi)] / [B(B^0 \rightarrow J/\psi(1S)\pi^+\pi^-)]$ assuming $B(B^0 \rightarrow J/\psi(1S)\pi^+\pi^-) = (3.97 \pm 0.09 \pm 0.11 \pm 0.16) \times 10^{-5}$, which we rescale to our best values $B(f_2(1270) \rightarrow \pi\pi) = (84.2^{+2.9}_{-0.9}) \times 10^{-2}$, $B(B^0 \rightarrow J/\psi(1S)\pi^+\pi^-) = (4.00 \pm 0.15) \times 10^{-5}$. Our first error is their experiment's error and our second error is the systematic error from using our best values.

³ AAJ 13M does not report correlations between various measurements of the $J/\psi\pi\pi$ final state. Measured in Dalitz plot like analysis of $B^0 \rightarrow J/\psi\pi^+\pi^-$.

⁴ AUBERT 07AC reports $[\Gamma(B^0 \rightarrow J/\psi(1S)f_2)/\Gamma_{\text{total}}] \times [B(f_2(1270) \rightarrow \pi\pi)] < 0.46 \times 10^{-5}$ which we divide by our best value $B(f_2(1270) \rightarrow \pi\pi) = 84.2 \times 10^{-2}$.

⁵ Assumes equal production of B^+ and B^0 at the $\Upsilon(4S)$.

 $\Gamma(J/\psi(1S)\rho^0)/\Gamma_{\text{total}}$ Γ_{215}/Γ

VALUE (units 10^{-5})	CL%	DOCUMENT ID	TECN	COMMENT
$2.55^{+0.18}_{-0.16}$ OUR AVERAGE				

$2.50 \pm 0.10^{+0.18}_{-0.15}$		¹ AAJ	14x	LHCB pp at 7, 8 TeV
---------------------------------	--	------------------	-----	-----------------------

$2.7 \pm 0.3 \pm 0.2$		² AUBERT	07AC	BABR $e^+e^- \rightarrow \Upsilon(4S)$
-----------------------	--	---------------------	------	--

• • • We do not use the following data for averages, fits, limits, etc. • • •

$2.51^{+0.22}_{-0.23} \pm 0.10$		^{3,4} AAJ	13M	LHCB Repl. by AAJ 14x
---------------------------------	--	--------------------	-----	-----------------------

$1.6 \pm 0.6 \pm 0.4$		² AUBERT	03B	BABR Repl. by AUBERT 07AC
-----------------------	--	---------------------	-----	---------------------------

< 25	90	BISHAI	96	CLE2 $e^+e^- \rightarrow \Upsilon(4S)$
--------	----	--------	----	--

¹ AAJ 14x uses Dalitz plot analysis of $B^0 \rightarrow J/\psi\pi^+\pi^-$. We assume $B(\rho(770)^0 \rightarrow \pi^+\pi^-) = 100\%$.

² Assumes equal production of B^+ and B^0 at the $\Upsilon(4S)$.

³ AAJ 13M reports $(2.49^{+0.20+0.16}_{-0.13-0.23}) \times 10^{-5}$ from a measurement of $[\Gamma(B^0 \rightarrow J/\psi(1S)\rho^0)/\Gamma_{\text{total}}] / [B(B^0 \rightarrow J/\psi(1S)\pi^+\pi^-)]$ assuming $B(B^0 \rightarrow J/\psi(1S)\pi^+\pi^-) = (3.97 \pm 0.09 \pm 0.11 \pm 0.16) \times 10^{-5}$, which we rescale to our best value $B(B^0 \rightarrow J/\psi(1S)\pi^+\pi^-) = (4.00 \pm 0.15) \times 10^{-5}$. Our first error is their experiment's error and our second error is the systematic error from using our best value.

⁴ AAJ 13M does not report correlations between various measurements of the $J/\psi\pi\pi$ final state. Measured in Dalitz plot like analysis of $B^0 \rightarrow J/\psi\pi^+\pi^-$. Assumes $B(\rho(770)^0 \rightarrow \pi\pi) = 100\%$.

 $\Gamma(J/\psi(1S)\eta_0(980), \eta_0 \rightarrow \pi^+\pi^-)/\Gamma_{\text{total}}$ Γ_{216}/Γ

VALUE	CL%	DOCUMENT ID	TECN	COMMENT
$< 1.1 \times 10^{-6}$	90	¹ AAJ	13M	LHCB pp at 7 TeV

¹ AAJ 13M does not provide correlations between various measurements of the $J/\psi\pi^+\pi^-$ final state. The measurements were obtained from a Dalitz plot like analysis of $B^0 \rightarrow J/\psi\pi^+\pi^-$. Also reports $\Gamma(J/\psi(1S)\eta_0(980), \eta_0 \rightarrow \pi^+\pi^-)/\Gamma_{\text{total}} = (6.1^{+3.1+1.7}_{-2.0-1.4}) \times 10^{-6}$.

 $\Gamma(J/\psi(1S)\rho(1450)^0, \rho^0 \rightarrow \pi\pi)/\Gamma_{\text{total}}$ Γ_{217}/Γ

VALUE (units 10^{-6})	DOCUMENT ID	TECN	COMMENT
$2.9^{+1.5}_{-0.7}$ OUR AVERAGE			

$4.6 \pm 1.1 \pm 1.9$		¹ AAJ	14x	LHCB pp at 7, 8 TeV
-----------------------	--	------------------	-----	-----------------------

$2.1^{+2.4}_{-0.7} \pm 0.1$		^{2,3} AAJ	13M	LHCB pp at 7 TeV
-----------------------------	--	--------------------	-----	--------------------

¹ AAJ 14x uses Dalitz plot analysis of $B^0 \rightarrow J/\psi\pi^+\pi^-$.

² AAJ 13M reports $(2.1^{+1.0+2.2}_{-0.6-0.4}) \times 10^{-6}$ from a measurement of $[\Gamma(B^0 \rightarrow J/\psi(1S)\rho(1450)^0, \rho^0 \rightarrow \pi\pi)/\Gamma_{\text{total}}] / [B(B^0 \rightarrow J/\psi(1S)\pi^+\pi^-)]$ assuming $B(B^0 \rightarrow J/\psi(1S)\pi^+\pi^-) = (3.97 \pm 0.09 \pm 0.11 \pm 0.16) \times 10^{-5}$, which we rescale

See key on page 1127

Meson Particle Listings

B^0

to our best value $B(B^0 \rightarrow J/\psi(1S)\pi^+\pi^-) = (4.00 \pm 0.15) \times 10^{-5}$. Our first error is their experiment's error and our second error is the systematic error from using our best value.

³ AAIJ 13M does not report correlations between various measurements of the $J/\psi\pi\pi$ final state. Measured in Dalitz plot like analysis of $B^0 \rightarrow J/\psi\pi^+\pi^-$.

$\Gamma(J/\psi\rho(1700)^0, \rho^0 \rightarrow \pi^+\pi^-)/\Gamma_{total}$ Γ_{218}/Γ

VALUE (units 10^{-6})	DOCUMENT ID	TECN	COMMENT
$2.0 \pm 0.5 \pm 1.2$	¹ AAIJ	14x	LHCB pp at 7, 8 TeV

¹ AAIJ 14x uses Dalitz plot analysis of $B^0 \rightarrow J/\psi\pi^+\pi^-$.

$\Gamma(J/\psi(1S)\omega)/\Gamma_{total}$ Γ_{219}/Γ

VALUE (units 10^{-5})	CL%	DOCUMENT ID	TECN	COMMENT
$1.8 \pm 0.7 \pm 0.1$		¹ AAIJ	14x	LHCB pp at 7, 8 TeV

• • • We do not use the following data for averages, fits, limits, etc. • • •

<27	90	BISHAI	96	CLE2 $e^+e^- \rightarrow \Upsilon(4S)$
-----	----	--------	----	--

¹ AAIJ 14x reports $[\Gamma(B^0 \rightarrow J/\psi(1S)\omega)/\Gamma_{total}] \times [B(\omega(782) \rightarrow \pi^+\pi^-)] = (2.7_{-0.6}^{+0.8+0.7} \pm 0.7) \times 10^{-7}$ which we divide by our best value $B(\omega(782) \rightarrow \pi^+\pi^-) = (1.53_{-0.13}^{+0.11}) \times 10^{-2}$. Our first error is their experiment's error and our second error is the systematic error from using our best value.

$\Gamma(J/\psi(1S)\omega)/\Gamma(J/\psi(1S)\rho^0)$ $\Gamma_{219}/\Gamma_{215}$

VALUE	DOCUMENT ID	TECN	COMMENT
$0.61 \pm 0.24 \pm 0.31$ -0.14 ± 0.16	^{1,2} AAIJ	13M	LHCB pp at 7 TeV

¹ AAIJ 13M reports $0.61 \pm 0.24 \pm 0.31$ from a measurement of $[\Gamma(B^0 \rightarrow J/\psi(1S)\omega)/\Gamma(B^0 \rightarrow J/\psi(1S)\rho^0)] \times [B(\omega(782) \rightarrow \pi^+\pi^-)]$ assuming $B(\omega(782) \rightarrow \pi^+\pi^-) = (1.53_{-0.13}^{+0.11}) \times 10^{-2}$.

² AAIJ 13M does not report correlations between various measurements of the $J/\psi\pi\pi$ final state. Measured in Dalitz plot like analysis of $B^0 \rightarrow J/\psi\pi^+\pi^-$. Assumes $B(\rho(770)^0 \rightarrow \pi\pi) = 100\%$.

$\Gamma(J/\psi(1S)\omega)/\Gamma(J/\psi(1S)\rho^0)$ $\Gamma_{219}/\Gamma_{215}$

VALUE	DOCUMENT ID	TECN	COMMENT
$0.89 \pm 0.19 \pm 0.07$ -0.13	AAIJ	13A	LHCB pp at 7 TeV

$\Gamma(J/\psi(1S)K^+K^-)/\Gamma_{total}$ Γ_{220}/Γ

VALUE (units 10^{-6})	DOCUMENT ID	TECN	COMMENT
$2.54 \pm 0.35 \pm 0.05$	¹ AAIJ	13BT	LHCB pp at 7 TeV

¹ AAIJ 13BT reports $(2.53 \pm 0.31 \pm 0.19) \times 10^{-6}$ from a measurement of $[\Gamma(B^0 \rightarrow J/\psi(1S)K^+K^-)/\Gamma_{total}] / [B(B^+ \rightarrow J/\psi(1S)K^+)]$ assuming $B(B^+ \rightarrow J/\psi(1S)K^+) = (1.018 \pm 0.042) \times 10^{-3}$, which we rescale to our best value $B(B^+ \rightarrow J/\psi(1S)K^+) = (1.020 \pm 0.019) \times 10^{-3}$. Our first error is their experiment's error and our second error is the systematic error from using our best value.

$\Gamma(J/\psi(1S)a_0(980), a_0 \rightarrow K^+K^-)/\Gamma_{total}$ Γ_{221}/Γ

VALUE (units 10^{-6})	DOCUMENT ID	TECN	COMMENT
$0.470 \pm 0.331 \pm 0.072$	¹ AAIJ	13BT	LHCB pp at 7 TeV

¹ AAIJ 13BT uses $B(\bar{B}^0 \rightarrow J/\psi K^+K^-) = (2.53 \pm 0.31 \pm 0.19) \times 10^{-6}$ to derive this result. It also reports the equivalent upper limit of $< 9.0 \times 10^{-7}$ at 90% CL.

$\Gamma(J/\psi(1S)\phi)/\Gamma_{total}$ Γ_{222}/Γ

VALUE	CL%	DOCUMENT ID	TECN	COMMENT
$< 1.1 \times 10^{-7}$		90	AAIJ	21K LHCB pp at 7, 8, 13 TeV

• • • We do not use the following data for averages, fits, limits, etc. • • •

<10.1 $\times 10^{-7}$	90	LEES	15	BABR $e^+e^- \rightarrow \Upsilon(4S)$
< 1.9 $\times 10^{-7}$	90	¹ AAIJ	13BT	LHCB pp at 7 TeV
< 9.4 $\times 10^{-7}$	90	² LIU	08I	BELL $e^+e^- \rightarrow \Upsilon(4S)$
< 9.2 $\times 10^{-6}$	90	² AUBERT	03o	BABR $e^+e^- \rightarrow \Upsilon(4S)$

¹ AAIJ 13BT uses $B(B^0 \rightarrow J/\psi(1S)K^+K^-) = (2.53 \pm 0.31 \pm 0.19) \times 10^{-6}$ and $B(\phi \rightarrow K^+K^-) = (48.9 \pm 0.5)\%$ to obtain this result.

² Assumes equal production of B^+ and B^0 at the $\Upsilon(4S)$.

$\Gamma(J/\psi(1S)\eta'(958))/\Gamma_{total}$ Γ_{223}/Γ

VALUE (units 10^{-6})	CL%	DOCUMENT ID	TECN	COMMENT
$7.6 \pm 2.2 \pm 1.0$		¹ AAIJ	15D	LHCB pp at 7, 8 TeV

• • • We do not use the following data for averages, fits, limits, etc. • • •

< 7.4	90	^{2,3} CHANG	12	BELL $e^+e^- \rightarrow \Upsilon(4S)$
< 63	90	³ AUBERT	03o	BABR $e^+e^- \rightarrow \Upsilon(4S)$

¹ AAIJ 15D reports $[\Gamma(B^0 \rightarrow J/\psi(1S)\eta'(958))/\Gamma_{total}] / [B(B_s^0 \rightarrow J/\psi(1S)\eta')] = (2.28 \pm 0.65 \pm 0.16) \times 10^{-2}$ which we multiply by our best value $B(B_s^0 \rightarrow J/\psi(1S)\eta') = (3.3 \pm 0.4) \times 10^{-4}$. Our first error is their experiment's error and our second error is the systematic error from using our best value.

² Reconstructs $\eta'(985)$ in $(\eta\pi^+ + \pi^-\eta)$ and $\rho(770)$ decays.

³ Assumes equal production of B^+ and B^0 at the $\Upsilon(4S)$.

$\Gamma(J/\psi(1S)\eta)/\Gamma(J/\psi(1S)\eta'(958))$ $\Gamma_{210}/\Gamma_{223}$

VALUE	DOCUMENT ID	TECN	COMMENT
$1.111 \pm 0.475 \pm 0.062$	¹ AAIJ	15D	LHCB pp at 7, 8 TeV

¹ Uses $J/\psi \rightarrow \mu^+\mu^-$, $\eta' \rightarrow \rho^0\gamma$, and $\eta' \rightarrow \eta\pi^+\pi^-$ decays.

$\Gamma(J/\psi(1S)K^0\pi^+\pi^-)/\Gamma(J/\psi(1S)K^0)$ $\Gamma_{224}/\Gamma_{200}$

VALUE	DOCUMENT ID	TECN	COMMENT
0.50 ± 0.04 OUR AVERAGE			
0.493 $\pm 0.034 \pm 0.027$	AAIJ	14L	LHCB pp at 7 TeV
1.24 $\pm 0.40 \pm 0.15$	AFFOLDER	02B	CDF $p\bar{p}$ 1.8 TeV

$\Gamma(J/\psi(1S)K^0K^+K^-)/\Gamma_{total}$ Γ_{226}/Γ

VALUE (units 10^{-6})	DOCUMENT ID	TECN	COMMENT
25 ± 7 OUR AVERAGE			Error includes scale factor of 1.8.
34.9 $\pm 6.7 \pm 1.5$	LEES	15	BABR $e^+e^- \rightarrow \Upsilon(4S)$
20.2 $\pm 4.3 \pm 1.9$	¹ AAIJ	14L	LHCB pp at 7 TeV

¹ Measured with $B(B^0 \rightarrow J/\psi K_S^0 K^+K^-) / B(B^0 \rightarrow J/\psi K_S^0)$ using PDG 12 for the involved branching fractions.

$\Gamma(J/\psi(1S)K^0K^-\pi^+ + c.c.)/\Gamma_{total}$ Γ_{225}/Γ

VALUE	CL%	DOCUMENT ID	TECN	COMMENT
$< 21 \times 10^{-6}$	90	¹ AAIJ	14L	LHCB pp at 7 TeV

¹ Measured with $B(B^0 \rightarrow J/\psi K_S^0 K^\pm\pi^\mp) / B(B^0 \rightarrow J/\psi K_S^0\pi^+\pi^-)$ using PDG 12 values for the involved branching fractions.

$\Gamma(J/\psi(1S)K^0\rho^0)/\Gamma_{total}$ Γ_{228}/Γ

VALUE (units 10^{-4})	DOCUMENT ID	TECN	COMMENT
$5.4 \pm 2.9 \pm 0.9$	¹ AFFOLDER	02B	CDF $p\bar{p}$ 1.8 TeV

¹ Uses $B^0 \rightarrow J/\psi(1S)K_S^0$ decay as a reference and $B(B^0 \rightarrow J/\psi(1S)K^0) = 8.3 \times 10^{-4}$.

$\Gamma(J/\psi(1S)K^*(892)^+\pi^-)/\Gamma_{total}$ Γ_{229}/Γ

VALUE (units 10^{-4})	DOCUMENT ID	TECN	COMMENT
$7.7 \pm 4.1 \pm 1.3$	¹ AFFOLDER	02B	CDF $p\bar{p}$ 1.8 TeV

¹ Uses $B^0 \rightarrow J/\psi(1S)K_S^0$ decay as a reference and $B(B^0 \rightarrow J/\psi(1S)K^0) = 8.3 \times 10^{-4}$.

$\Gamma(J/\psi(1S)\pi^+\pi^-\pi^+\pi^-)/\Gamma(J/\psi(1S)\pi^+\pi^-)$ $\Gamma_{230}/\Gamma_{211}$

VALUE	DOCUMENT ID	TECN	COMMENT
$0.361 \pm 0.017 \pm 0.021$	¹ AAIJ	14Y	LHCB pp at 7, 8 TeV

¹ Excludes contributions from $\psi(2S)$ and $\chi_{c1}(3872)$ decaying to $J/\psi(1S)\pi^+\pi^-$.

$\Gamma(J/\psi(1S)f_1(1285))/\Gamma_{total}$ Γ_{231}/Γ

VALUE (units 10^{-6})	DOCUMENT ID	TECN	COMMENT
$8.4 \pm 2.1 \pm 0.5$	¹ AAIJ	14Y	LHCB pp at 7, 8 TeV

¹ AAIJ 14Y reports $(8.37 \pm 1.95 \pm 0.71 \pm 0.35) \times 10^{-6}$ from a measurement of $[\Gamma(B^0 \rightarrow J/\psi(1S)f_1(1285))/\Gamma_{total}] \times [B(f_1(1285) \rightarrow 2\pi^+2\pi^-)]$ assuming $B(f_1(1285) \rightarrow 2\pi^+2\pi^-) = 0.11 \pm 0.007$, which we rescale to our best value $B(f_1(1285) \rightarrow 2\pi^+2\pi^-) = (10.9 \pm 0.6) \times 10^{-2}$. Our first error is their experiment's error and our second error is the systematic error from using our best value.

$\Gamma(J/\psi(1S)K^*(892)^0\pi^+\pi^-)/\Gamma_{total}$ Γ_{232}/Γ

VALUE (units 10^{-4})	DOCUMENT ID	TECN	COMMENT
$6.6 \pm 1.9 \pm 1.1$	¹ AFFOLDER	02B	CDF $p\bar{p}$ 1.8 TeV

¹ Uses $B^0 \rightarrow J/\psi(1S)K^*(892)^0$ decay as a reference and $B(B^0 \rightarrow J/\psi(1S)K^0) = 12.4 \times 10^{-4}$.

$\Gamma(\eta_{c2}(1D)K_S^0, \eta_{c2} \rightarrow h_c\gamma)/\Gamma_{total}$ Γ_{233}/Γ

VALUE	CL%	DOCUMENT ID	TECN	COMMENT
$< 3.5 \times 10^{-5}$		90	CHILIKIN	20 BELL $e^+e^- \rightarrow \Upsilon(4S)$

$\Gamma(\eta_{c2}(1D)\pi^-K^+, \eta_{c2} \rightarrow h_c\gamma)/\Gamma_{total}$ Γ_{234}/Γ

VALUE	CL%	DOCUMENT ID	TECN	COMMENT
$< 1.0 \times 10^{-4}$		90	CHILIKIN	20 BELL $e^+e^- \rightarrow \Upsilon(4S)$

$\Gamma(\chi_{c1}(3872)K^0)/\Gamma_{total}$ Γ_{237}/Γ

VALUE (units 10^{-4})	CL%	DOCUMENT ID	TECN	COMMENT
1.1 ± 0.4 OUR AVERAGE				
1.05 $\pm 0.31 \pm 0.34$		¹ CHOI	11	BELL $e^+e^- \rightarrow \Upsilon(4S)$
1.4 $\pm 0.7 \pm 0.7$		² DEL-AMO-SA.	10B	BABR $e^+e^- \rightarrow \Upsilon(4S)$

• • • We do not use the following data for averages, fits, limits, etc. • • •

<2.8	90	^{3,4} BHARDWAJ	11	BELL $e^+e^- \rightarrow \Upsilon(4S)$
2.6 $\pm 1.3 \pm 0.6$		^{4,5} AUSHEV	10	BELL $e^+e^- \rightarrow \Upsilon(4S)$
<6	90	^{6,7} AUBERT	09B	BABR $e^+e^- \rightarrow \Upsilon(4S)$
6.1 $\pm 3.1 \pm 1.5$		^{4,6,8} AUBERT	08B	BABR $e^+e^- \rightarrow \Upsilon(4S)$
<1.6	90	⁹ AUBERT	08Y	BABR $e^+e^- \rightarrow \Upsilon(4S)$
<2.7	90	¹⁰ AUBERT	06	BABR Repl. by AUBERT 08Y
3.4 $\pm 1.6 \pm 1.4$ -1.3		^{11,12} GOKHROO	06	BELL $e^+e^- \rightarrow \Upsilon(4S)$

¹ CHOI 11 reports $[\Gamma(B^0 \rightarrow \chi_{c1}(3872)K^0)/\Gamma_{total}] / [B(B^+ \rightarrow \chi_{c1}(3872)K^+)] = 0.50 \pm 0.14 \pm 0.04$ which we multiply by our best value $B(B^+ \rightarrow \chi_{c1}(3872)K^+) = (2.1 \pm 0.7) \times 10^{-4}$. Our first error is their experiment's error and our second error is the systematic error from using our best value.

² DEL-AMO-SANCHEZ 10B reports $[\Gamma(B^0 \rightarrow \chi_{c1}(3872)K^0)/\Gamma_{total}] \times [B(\chi_{c1}(3872) \rightarrow \omega J/\psi(1S))] = (6 \pm 3 \pm 1) \times 10^{-6}$ which we divide by our best value $B(\chi_{c1}(3872) \rightarrow \omega J/\psi(1S)) = (4.3 \pm 2.1) \times 10^{-2}$. Our first error is their experiment's error and our second error is the systematic error from using our best value.

Meson Particle Listings

B^0

- ³ BHARDWAJ 11 reports $[\Gamma(B^0 \rightarrow \chi_{c1}(3872) K^0)/\Gamma_{\text{total}}] \times [B(\chi_{c1}(3872) \rightarrow \gamma J/\psi)] < 2.4 \times 10^{-6}$ which we divide by our best value $B(\chi_{c1}(3872) \rightarrow \gamma J/\psi) = 8 \times 10^{-3}$.
- ⁴ Assumes equal production of B^+ and B^0 at the $\Upsilon(4S)$.
- ⁵ AUSHEV 10 reports $[\Gamma(B^0 \rightarrow \chi_{c1}(3872) K^0)/\Gamma_{\text{total}}] \times [B(\chi_{c1}(3872) \rightarrow \overline{D}^{*0} D^0)] = (0.97 \pm 0.46 \pm 0.13) \times 10^{-4}$ which we divide by our best value $B(\chi_{c1}(3872) \rightarrow \overline{D}^{*0} D^0) = (37 \pm 9) \times 10^{-2}$. Our first error is their experiment's error and our second error is the systematic error from using our best value.
- ⁶ Uses $B(\Upsilon(4S) \rightarrow B^+ B^-) = (51.6 \pm 0.6)\%$ and $B(\Upsilon(4S) \rightarrow B^0 \overline{B}^0) = (48.4 \pm 0.6)\%$.
- ⁷ AUBERT 09b reports $[\Gamma(B^0 \rightarrow \chi_{c1}(3872) K^0)/\Gamma_{\text{total}}] \times [B(\chi_{c1}(3872) \rightarrow \gamma J/\psi)] < 4.9 \times 10^{-6}$ which we divide by our best value $B(\chi_{c1}(3872) \rightarrow \gamma J/\psi) = 8 \times 10^{-3}$.
- ⁸ AUBERT 08b reports $[\Gamma(B^0 \rightarrow \chi_{c1}(3872) K^0)/\Gamma_{\text{total}}] \times [B(\chi_{c1}(3872) \rightarrow \overline{D}^{*0} D^0)] = (2.22 \pm 1.05 \pm 0.42) \times 10^{-4}$ which we divide by our best value $B(\chi_{c1}(3872) \rightarrow \overline{D}^{*0} D^0) = (37 \pm 9) \times 10^{-2}$. Our first error is their experiment's error and our second error is the systematic error from using our best value.
- ⁹ AUBERT 08y reports $[\Gamma(B^0 \rightarrow \chi_{c1}(3872) K^0)/\Gamma_{\text{total}}] \times [B(\chi_{c1}(3872) \rightarrow \pi^+ \pi^- J/\psi(1S))] < 6.0 \times 10^{-6}$ which we divide by our best value $B(\chi_{c1}(3872) \rightarrow \pi^+ \pi^- J/\psi(1S)) = 3.8 \times 10^{-2}$.
- ¹⁰ AUBERT 06 reports $[\Gamma(B^0 \rightarrow \chi_{c1}(3872) K^0)/\Gamma_{\text{total}}] \times [B(\chi_{c1}(3872) \rightarrow \pi^+ \pi^- J/\psi(1S))] < 10.3 \times 10^{-6}$ which we divide by our best value $B(\chi_{c1}(3872) \rightarrow \pi^+ \pi^- J/\psi(1S)) = 3.8 \times 10^{-2}$.
- ¹¹ GOKHROO 06 reports $[\Gamma(B^0 \rightarrow \chi_{c1}(3872) K^0)/\Gamma_{\text{total}}] \times [B(\chi_{c1}(3872) \rightarrow D^0 \overline{D}^0 \pi^0)] = (1.66 \pm 0.70 \pm 0.37) \times 10^{-4}$ which we divide by our best value $B(\chi_{c1}(3872) \rightarrow D^0 \overline{D}^0 \pi^0) = (49 \pm 18) \times 10^{-2}$. Our first error is their experiment's error and our second error is the systematic error from using our best value.
- ¹² Measure the near-threshold enhancements in the $(D^0 \overline{D}^0 \pi^0)$ system at a mass $3875.2 \pm 0.7 \pm 1.6 \pm 0.8$ MeV/ c^2 .

$\Gamma(\chi_{c1}(3872) K^+ K^-)/\Gamma_{\text{total}}$		Γ_{235}/Γ	
VALUE	CL%	DOCUMENT ID	TECN COMMENT
$< 5 \times 10^{-4}$	90	1 AUBERT 06e	BABR $e^+ e^- \rightarrow \Upsilon(4S)$

¹ Perform measurements of absolute branching fractions using a missing mass technique.

$\Gamma(\chi_{c1}(3872) K^+ K^-, \chi_{c1}(3872) K^- K^+ \rightarrow J/\psi(1S) \pi^+ \pi^-)/\Gamma_{\text{total}}$		Γ_{236}/Γ	
VALUE (units 10^{-6})	CL%	DOCUMENT ID	TECN COMMENT
< 4.2	90	1,2 CHOI 11	BELL $e^+ e^- \rightarrow \Upsilon(4S)$

- • • We do not use the following data for averages, fits, limits, etc. • • •
- < 5.4
- 90 2,3 AUBERT 05b BABR $e^+ e^- \rightarrow \Upsilon(4S)$
- ¹ Assumes $\pi^+ \pi^0$ originates from ρ^+ .
- ² Assumes equal production of B^+ and B^0 at the $\Upsilon(4S)$.
- ³ The isovector-X hypothesis is excluded with a likelihood test at 1×10^{-4} level.

$\Gamma(\chi_{c1}(3872) K^*(892)^0)/\Gamma_{\text{total}}$		Γ_{238}/Γ	
VALUE (units 10^{-4})	CL%	DOCUMENT ID	TECN COMMENT
$1.0 \pm 0.4 \pm 0.3$		1 BALA 15	BELL $e^+ e^- \rightarrow \Upsilon(4S)$

- • • We do not use the following data for averages, fits, limits, etc. • • •
- < 3.3
- 90 2,3 AUBERT 09b BABR $e^+ e^- \rightarrow \Upsilon(4S)$
- < 1.0
- 90 3,4 AUBERT 09b BABR $e^+ e^- \rightarrow \Upsilon(4S)$
- ¹ BALA 15 reports $[\Gamma(B^0 \rightarrow \chi_{c1}(3872) K^*(892)^0)/\Gamma_{\text{total}}] \times [B(\chi_{c1}(3872) \rightarrow \pi^+ \pi^- J/\psi(1S))] = (4.0 \pm 1.5 \pm 0.3) \times 10^{-6}$ which we divide by our best value $B(\chi_{c1}(3872) \rightarrow \pi^+ \pi^- J/\psi(1S)) = (3.8 \pm 1.2) \times 10^{-2}$. Our first error is their experiment's error and our second error is the systematic error from using our best value.
- ² AUBERT 09b reports $[\Gamma(B^0 \rightarrow \chi_{c1}(3872) K^*(892)^0)/\Gamma_{\text{total}}] \times [B(\chi_{c1}(3872) \rightarrow \gamma J/\psi)] < 2.8 \times 10^{-6}$ which we divide by our best value $B(\chi_{c1}(3872) \rightarrow \gamma J/\psi) = 8 \times 10^{-3}$.
- ³ Uses $B(\Upsilon(4S) \rightarrow B^+ B^-) = (51.6 \pm 0.6)\%$ and $B(\Upsilon(4S) \rightarrow B^0 \overline{B}^0) = (48.4 \pm 0.6)\%$.
- ⁴ AUBERT 09b reports $[\Gamma(B^0 \rightarrow \chi_{c1}(3872) K^*(892)^0)/\Gamma_{\text{total}}] \times [B(\chi_{c1}(3872) \rightarrow \gamma \psi(2S))] < 4.4 \times 10^{-6}$ which we divide by our best value $B(\chi_{c1}(3872) \rightarrow \gamma \psi(2S)) = 4.5 \times 10^{-2}$.

$\Gamma(\chi_{c1}(3872) K^+ \pi^-)/\Gamma_{\text{total}}$		Γ_{239}/Γ	
VALUE (units 10^{-4})	CL%	DOCUMENT ID	TECN COMMENT
$2.1 \pm 0.4 \pm 0.7$		1,2 BALA 15	BELL $e^+ e^- \rightarrow \Upsilon(4S)$

- ¹ BALA 15 reports $[\Gamma(B^0 \rightarrow \chi_{c1}(3872) K^+ \pi^-)/\Gamma_{\text{total}}] \times [B(\chi_{c1}(3872) \rightarrow \pi^+ \pi^- J/\psi(1S))] = (7.9 \pm 1.3 \pm 0.4) \times 10^{-6}$ which we divide by our best value $B(\chi_{c1}(3872) \rightarrow \pi^+ \pi^- J/\psi(1S)) = (3.8 \pm 1.2) \times 10^{-2}$. Our first error is their experiment's error and our second error is the systematic error from using our best value.
- ² Assumes equal production of B^+ and B^0 at the $\Upsilon(4S)$.

$\Gamma(\chi_{c1}(3872) \gamma)/\Gamma_{\text{total}}$		Γ_{240}/Γ	
VALUE	CL%	DOCUMENT ID	TECN COMMENT
$< 1.3 \times 10^{-5}$	90	1,2 CHOU 19	BELL $e^+ e^- \rightarrow \Upsilon(4S)$

- ¹ Assumes equal production of B^+ and B^0 at $\Upsilon(4S)$.
- ² CHOU 19 reports $[\Gamma(B^0 \rightarrow \chi_{c1}(3872) \gamma)/\Gamma_{\text{total}}] \times [B(\chi_{c1}(3872) \rightarrow \pi^+ \pi^- J/\psi(1S))] < 5.1 \times 10^{-7}$ which we divide by our best value $B(\chi_{c1}(3872) \rightarrow \pi^+ \pi^- J/\psi(1S)) = 3.8 \times 10^{-2}$.

$\Gamma(Z_c(4430)^\pm K^\mp, Z_c^\pm \rightarrow \psi(2S) \pi^\pm)/\Gamma_{\text{total}}$		Γ_{241}/Γ	
VALUE (units 10^{-5})	CL%	DOCUMENT ID	TECN COMMENT
$6.0 \pm 1.7 \pm 2.5$ $-2.0 - 1.4$		CHILIKIN 13	BELL $e^+ e^- \rightarrow \Upsilon(4S)$

- • • We do not use the following data for averages, fits, limits, etc. • • •
- < 3.1
- 95 1 AUBERT 09AA BABR $e^+ e^- \rightarrow \Upsilon(4S)$
- $3.2 \pm 1.8 \pm 5.3$
 $-0.9 - 1.6$
- 1 MIZUK 09 BELL $e^+ e^- \rightarrow \Upsilon(4S)$
- $4.1 \pm 1.0 \pm 1.4$
- 1,2 CHOI 08 BELL Repl. by MIZUK 09
- ¹ Assumes equal production of B^+ and B^0 at the $\Upsilon(4S)$.
- ² Establishes the $(Z_c 4430)^+$ with a significance of 6.5 sigma. Needs confirmation.

$\Gamma(Z_c(4430)^\pm K^\mp, Z_c^\pm \rightarrow J/\psi \pi^\pm)/\Gamma_{\text{total}}$		Γ_{242}/Γ	
VALUE (units 10^{-6})	CL%	DOCUMENT ID	TECN COMMENT
$5.4 \pm 4.0 \pm 1.1$ $-1.0 - 0.6$		CHILIKIN 14	BELL $\overline{B}^0 \rightarrow J/\psi K^- \pi^+$

- • • We do not use the following data for averages, fits, limits, etc. • • •
- < 4
- 95 1 AUBERT 09AA BABR $e^+ e^- \rightarrow \Upsilon(4S)$
- ¹ Assumes equal production of B^+ and B^0 at the $\Upsilon(4S)$.

$\Gamma(Z_c(3900)^\pm K^\mp, Z_c^\pm \rightarrow J/\psi \pi^\pm)/\Gamma_{\text{total}}$		Γ_{243}/Γ	
VALUE	CL%	DOCUMENT ID	TECN COMMENT
$< 9 \times 10^{-7}$		CHILIKIN 14	BELL $\overline{B}^0 \rightarrow J/\psi K^- \pi^+$

$\Gamma(Z_c(4200)^\pm K^\mp, X^\pm \rightarrow J/\psi \pi^\pm)/\Gamma_{\text{total}}$		Γ_{244}/Γ	
VALUE (units 10^{-5})	CL%	DOCUMENT ID	TECN COMMENT
$2.2 \pm 0.7 \pm 1.1$ $-0.5 - 0.6$		CHILIKIN 14	BELL $\overline{B}^0 \rightarrow J/\psi K^- \pi^+$

$\Gamma(Z_c(3900)^\pm K^\mp, Z_c^\pm \rightarrow J/\psi \pi^\pm)/\Gamma(J/\psi(1S) K^*(892)^0)$		$\Gamma_{243}/\Gamma_{202}$	
VALUE	CL%	DOCUMENT ID	TECN COMMENT
$< 1.5 \times 10^{-2}$	90	ABAZOV 18b	D0 $p\overline{p}$ at 1.96 TeV

$\Gamma(J/\psi(1S) p\overline{p})/\Gamma_{\text{total}}$		Γ_{245}/Γ	
VALUE (units 10^{-7})	CL%	DOCUMENT ID	TECN COMMENT
$4.51 \pm 0.40 \pm 0.44$		1 AAIJ 19u	LHCB pp at 7, 8, 13 TeV

- • • We do not use the following data for averages, fits, limits, etc. • • •
- < 5.2
- 90 2 AAIJ 13z
- LHCB Repl. by AAIJ 19u
- < 8.3
- 90 3 XIE 05
- BELL $e^+ e^- \rightarrow \Upsilon(4S)$
- < 19
- 90 3 AUBERT 03k
- BABR $e^+ e^- \rightarrow \Upsilon(4S)$
- ¹ Measured relative to $B_S^0 \rightarrow J/\psi \phi$ assuming $B(B_S^0 \rightarrow J/\psi \phi) = (10.5 \pm 0.13 \pm 0.64) \times 10^{-4}$ and taking into account small $K^+ K^- S$ -wave contribution. Measurement assumes $f_s/f_d = 0.259 \pm 0.015$ for 7, 8 TeV data and f_s/f_d multiplied by 1.068 ± 0.046 for 13 TeV data.
- ² Uses $B(B_S^0 \rightarrow J/\psi(1S) \pi^+ \pi^-) = (1.98 \pm 0.20) \times 10^{-4}$.
- ³ Assumes equal production of B^+ and B^0 at the $\Upsilon(4S)$.

$\Gamma(J/\psi(1S) \gamma)/\Gamma_{\text{total}}$		Γ_{246}/Γ	
VALUE (units 10^{-6})	CL%	DOCUMENT ID	TECN COMMENT
< 1.5	90	1 AAIJ 15bB	LHCB pp at 7, 8 TeV

- • • We do not use the following data for averages, fits, limits, etc. • • •
- < 1.6
- 90 2 AUBERT,B 04T
- BABR $e^+ e^- \rightarrow \Upsilon(4S)$
- ¹ Branching fractions of normalization modes $B^0 \rightarrow J/\psi \gamma$ taken from PDG 14. Uses $f_s/f_d = 0.259 \pm 0.015$.
- ² Assumes equal production of B^+ and B^0 at the $\Upsilon(4S)$.

$\Gamma(J/\psi(1S) \overline{D}^0)/\Gamma_{\text{total}}$		Γ_{247}/Γ	
VALUE (units 10^{-5})	CL%	DOCUMENT ID	TECN COMMENT
< 1.3	90	1 AUBERT 05u	BABR $e^+ e^- \rightarrow \Upsilon(4S)$

- • • We do not use the following data for averages, fits, limits, etc. • • •
- < 2.0
- 90 1 ZHANG 05b
- BELL $e^+ e^- \rightarrow \Upsilon(4S)$
- ¹ Assumes equal production of B^+ and B^0 at the $\Upsilon(4S)$.

$\Gamma(\psi(2S) \pi^0)/\Gamma_{\text{total}}$		Γ_{248}/Γ	
VALUE (units 10^{-5})	CL%	DOCUMENT ID	TECN COMMENT
$1.17 \pm 0.17 \pm 0.08$		1 CHOBANOVA 16	BELL $e^+ e^- \rightarrow \Upsilon(4S)$

- ¹ Assumes equal production of B^+ and B^0 at the $\Upsilon(4S)$.

$\Gamma(\psi(2S) K^0)/\Gamma_{\text{total}}$		Γ_{249}/Γ	
VALUE (units 10^{-4})	CL%	DOCUMENT ID	TECN COMMENT
5.8 ± 0.5		OUR FIT	
5.8 ± 0.5		OUR AVERAGE	

- 4.7 $\pm 0.7 \pm 0.7$
- 1 AAIJ 14L
- LHCB pp at 7 TeV
- 6.46 $\pm 0.65 \pm 0.51$
- 2 AUBERT 05j
- BABR $e^+ e^- \rightarrow \Upsilon(4S)$
- 6.7 ± 1.1
- 2 ABE 03b
- BELL $e^+ e^- \rightarrow \Upsilon(4S)$
- 5.0 $\pm 1.1 \pm 0.6$
- 2 RICHICHI 01
- CLE2 $e^+ e^- \rightarrow \Upsilon(4S)$
- • • We do not use the following data for averages, fits, limits, etc. • • •
- 6.9 $\pm 1.1 \pm 1.1$
- 2 AUBERT 02
- BABR Repl. by AUBERT 05j
- < 8
- 90 2 ALAM 94
- CLE2 $e^+ e^- \rightarrow \Upsilon(4S)$
- < 15
- 90 2 BORTOLETTI 09Q
- CLEO $e^+ e^- \rightarrow \Upsilon(4S)$
- < 28
- 90 2 ALBRECHT 90j
- ARG $e^+ e^- \rightarrow \Upsilon(4S)$

- ¹ Measured with $B(B^0 \rightarrow \psi(2S) K_S^0) \times B(\psi(2S) \rightarrow J/\psi \pi^+ \pi^-) / B(B^0 \rightarrow J/\psi K_S^0)$ using PDG 12 values for the involved branching fractions.
- ² Assumes equal production of B^+ and B^0 at the $\Upsilon(4S)$.

See key on page 1127

Meson Particle Listings

B^0

$\Gamma(\psi(2S)K^0)/\Gamma(J/\psi(1S)K^0)$ $\Gamma_{249}/\Gamma_{200}$

VALUE	DOCUMENT ID	TECN	COMMENT
$0.82 \pm 0.13 \pm 0.12$	¹ AUBERT 02	BABR	$e^+e^- \rightarrow \Upsilon(4S)$

¹ Assumes equal production of B^+ and B^0 at the $\Upsilon(4S)$.

$\Gamma(\psi(3770)K^0, \psi \rightarrow \bar{D}^0 D^0)/\Gamma_{total}$ Γ_{250}/Γ

VALUE (units 10^{-4})	CL%	DOCUMENT ID	TECN	COMMENT
< 1.23	90	¹ AUBERT 08B	BABR	$e^+e^- \rightarrow \Upsilon(4S)$

¹ Assumes equal production of B^+ and B^0 at the $\Upsilon(4S)$.

$\Gamma(\psi(3770)K^0, \psi \rightarrow D^- D^+)/\Gamma_{total}$ Γ_{251}/Γ

VALUE (units 10^{-4})	CL%	DOCUMENT ID	TECN	COMMENT
< 1.88	90	¹ AUBERT 08B	BABR	$e^+e^- \rightarrow \Upsilon(4S)$

¹ Assumes equal production of B^+ and B^0 at the $\Upsilon(4S)$.

$\Gamma(\psi(2S)\pi^+\pi^-)/\Gamma(J/\psi(1S)\pi^+\pi^-)$ $\Gamma_{252}/\Gamma_{211}$

VALUE	DOCUMENT ID	TECN	COMMENT
$0.56 \pm 0.07 \pm 0.05$	¹ AAIJ 13AA	LHCB	pp at 7 TeV

¹ Assuming lepton universality for dimuon decay modes of J/ψ and $\psi(2S)$ mesons, the ratio $B(J/\psi \rightarrow \mu^+\mu^-)/B(\psi(2S) \rightarrow \mu^+\mu^-) = B(J/\psi \rightarrow e^+e^-)/B(\psi(2S) \rightarrow e^+e^-) = 7.69 \pm 0.19$ was used.

$\Gamma(\psi(2S)K^+\pi^-)/\Gamma_{total}$ Γ_{253}/Γ

VALUE (units 10^{-4})	CL%	DOCUMENT ID	TECN	COMMENT
5.80 ± 0.39		^{1,2} CHILIKIN 13	BELL	$e^+e^- \rightarrow \Upsilon(4S)$

• • • We do not use the following data for averages, fits, limits, etc. • • •

5.57 ± 0.16	³ AUBERT 09AA	BABR	$e^+e^- \rightarrow \Upsilon(4S)$
$5.68 \pm 0.13 \pm 0.42$	² MIZUK 09	BELL	$e^+e^- \rightarrow \Upsilon(4S)$
< 10	90	² ALBRECHT 90J	ARG $e^+e^- \rightarrow \Upsilon(4S)$

¹ Combines measurements with $\psi(2S) \rightarrow \ell^+\ell^-$ with measurement from MIZUK 09 which uses $\psi(2S) \rightarrow J/\psi\pi^+\pi^-$.

² Assumes equal production of B^+ and B^0 at the $\Upsilon(4S)$.

³ Does not report systematic uncertainties.

$\Gamma(\psi(2S)K^*(892)^0)/\Gamma_{total}$ Γ_{254}/Γ

VALUE (units 10^{-4})	CL%	DOCUMENT ID	TECN	COMMENT
5.9 ± 0.4		OUR FIT		

6.0 ± 0.5 **OUR AVERAGE** Error includes scale factor of 1.1.

$5.55 \pm 0.22 \pm 0.41$ $-0.23 - 0.84$	¹ CHILIKIN 13	BELL	$e^+e^- \rightarrow \Upsilon(4S)$
$6.49 \pm 0.59 \pm 0.97$	¹ AUBERT 05J	BABR	$e^+e^- \rightarrow \Upsilon(4S)$
$7.6 \pm 1.1 \pm 1.0$	¹ RICHICHI 01	CLE2	$e^+e^- \rightarrow \Upsilon(4S)$
$9.0 \pm 2.2 \pm 0.9$	² ABE 98a	CDF	$p\bar{p}$ 1.8 TeV

• • • We do not use the following data for averages, fits, limits, etc. • • •

$5.52 \pm 0.35 \pm 0.53$ $-0.32 - 0.58$	¹ MIZUK 09	BELL	$e^+e^- \rightarrow \Upsilon(4S)$
< 19	90	¹ ALAM 94	CLE2 Repl. by RICHICHI 01
$14 \pm 8 \pm 4$	¹ BORTOLETTO 92	CLEO	$e^+e^- \rightarrow \Upsilon(4S)$
< 23	90	¹ ALBRECHT 90J	ARG $e^+e^- \rightarrow \Upsilon(4S)$

¹ Assumes equal production of B^+ and B^0 at the $\Upsilon(4S)$.

² ABE 98a reports $[B(B^0 \rightarrow \psi(2S)K^*(892)^0)]/[B(B^+ \rightarrow J/\psi(1S)K^+)] = 0.908 \pm 0.194 \pm 0.10$. We multiply by our best value $B(B^+ \rightarrow J/\psi(1S)K^+) = (9.9 \pm 1.0) \times 10^{-4}$. Our first error is their experiment's error and our second error is the systematic error from using our best value.

$\Gamma(\psi(2S)K^*(892)^0)/\Gamma(J/\psi(1S)K^*(892)^0)$ $\Gamma_{254}/\Gamma_{202}$

VALUE	DOCUMENT ID	TECN	COMMENT
$0.487 \pm 0.018 \pm 0.011$	^{1,2} AAIJ 12L	LHCB	pp at 7 TeV

¹ AAIJ 12L reports $0.476 \pm 0.014 \pm 0.010 \pm 0.012$ from a measurement of $[\Gamma(B^0 \rightarrow \psi(2S)K^*(892)^0)/\Gamma(B^0 \rightarrow J/\psi(1S)K^*(892)^0)] \times [B(J/\psi(1S) \rightarrow e^+e^-)] / [B(\psi(2S) \rightarrow e^+e^-)]$ assuming $B(J/\psi(1S) \rightarrow e^+e^-) = (5.94 \pm 0.06) \times 10^{-2}$, $B(\psi(2S) \rightarrow e^+e^-) = (7.72 \pm 0.17) \times 10^{-3}$, which we rescale to our best values $B(J/\psi(1S) \rightarrow e^+e^-) = (5.971 \pm 0.032) \times 10^{-2}$, $B(\psi(2S) \rightarrow e^+e^-) = (7.93 \pm 0.17) \times 10^{-3}$. Our first error is their experiment's error and our second error is the systematic error from using our best values.

² Assumes $B(J/\psi \rightarrow \mu^+\mu^-) / B(\psi(2S) \rightarrow \mu^+\mu^-) = B(J/\psi \rightarrow e^+e^-) / B(\psi(2S) \rightarrow e^+e^-) = 7.69 \pm 0.19$.

$\Gamma(\psi(2S)K^*(892)^0)/\Gamma(\psi(2S)K^0)$ $\Gamma_{254}/\Gamma_{249}$

VALUE	DOCUMENT ID	TECN	COMMENT
1.02 ± 0.10	OUR FIT		
$1.00 \pm 0.14 \pm 0.09$	AUBERT 05J	BABR	$e^+e^- \rightarrow \Upsilon(4S)$

$\Gamma(\chi_{c0}K^0)/\Gamma_{total}$ Γ_{255}/Γ

VALUE (units 10^{-6})	CL%	DOCUMENT ID	TECN	COMMENT
195 ± 42 -36 ± 11		¹ AAIJ 18F	LHCB	pp at 7, 8 TeV

• • • We do not use the following data for averages, fits, limits, etc. • • •

145 ± 103 -85 ± 8	2,3	LEES 12i	BABR	$e^+e^- \rightarrow \Upsilon(4S)$
$148 \pm 30 \pm 13$	2,4	LEES 12o	BABR	$e^+e^- \rightarrow \Upsilon(4S)$
142 ± 55 -44 ± 22	2,5	AUBERT 09AU	BABR	$e^+e^- \rightarrow \Upsilon(4S)$
< 113	90	⁵ GARMASH 07	BELL	$e^+e^- \rightarrow \Upsilon(4S)$
< 1240	90	² AUBERT 05K	BABR	$e^+e^- \rightarrow \Upsilon(4S)$
< 500	90	⁶ EDWARDS 01	CLE2	$e^+e^- \rightarrow \Upsilon(4S)$

¹ AAIJ 18F uses Dalitz plot analysis of the $B^0 \rightarrow K_S^0\pi^+\pi^-$ final state decays. For the branching fraction of the reference mode, the PDG 18 average $B(B^0 \rightarrow K_S^0\pi^+\pi^-) = (4.96 \pm 0.20) \times 10^{-5}$ is used. We compute $B(B^0 \rightarrow \chi_{c0}K^0)$ using the PDG value $B(\chi_{c0} \rightarrow \pi\pi) = (8.51 \pm 0.33) \times 10^{-3}$ and 2/3 for the $\pi^+\pi^-$ fraction. Our first error is their experiment's error and the second error is systematic error from using our best value.

² Assumes equal production of B^+ and B^0 at the $\Upsilon(4S)$.

³ LEES 12i reports $[\Gamma(B^0 \rightarrow \chi_{c0}K^0)/\Gamma_{total}] \times [B(\chi_{c0}(1P) \rightarrow K_S^0K_S^0)] = (0.46 \pm 0.25 \pm 0.21) \times 10^{-6}$ which we divide by our best value $B(\chi_{c0}(1P) \rightarrow K_S^0K_S^0) = (3.16 \pm 0.17) \times 10^{-3}$. Our first error is their experiment's error and our second error is the systematic error from using our best value.

⁴ Measured in the $B^0 \rightarrow K_S^0K^+K^-$ decay.

⁵ Uses Dalitz plot analysis of the $B^0 \rightarrow K^0\pi^+\pi^-$ final state decays.

⁶ EDWARDS 01 assumes equal production of B^0 and B^+ at the $\Upsilon(4S)$. The correlated uncertainties (28.3%) from $B(J/\psi(1S) \rightarrow \gamma\eta_c)$ in those modes have been accounted for.

$\Gamma(\chi_{c0}K^*(892)^0)/\Gamma_{total}$ Γ_{256}/Γ

VALUE (units 10^{-4})	CL%	DOCUMENT ID	TECN	COMMENT
$1.7 \pm 0.3 \pm 0.2$		¹ AUBERT 08BD	BABR	$e^+e^- \rightarrow \Upsilon(4S)$

• • • We do not use the following data for averages, fits, limits, etc. • • •

< 7.7	90	¹ AUBERT 05K	BABR	Repl. by AUBERT 08BD
---------	----	-------------------------	------	----------------------

¹ Assumes equal production of B^+ and B^0 at the $\Upsilon(4S)$.

$\Gamma(\chi_{c1}\pi^0)/\Gamma_{total}$ Γ_{257}/Γ

VALUE (units 10^{-5})	CL%	DOCUMENT ID	TECN	COMMENT
$1.12 \pm 0.25 \pm 0.12$		¹ KUMAR 08	BELL	$e^+e^- \rightarrow \Upsilon(4S)$

¹ Assumes equal production of B^+ and B^0 at the $\Upsilon(4S)$.

$\Gamma(\chi_{c1}K^0)/\Gamma_{total}$ Γ_{258}/Γ

VALUE (units 10^{-4})	CL%	DOCUMENT ID	TECN	COMMENT
3.95 ± 0.27		OUR AVERAGE		

15 ± 5 -4 ± 6	¹ CHILIKIN 19	BELL	$e^+e^- \rightarrow \Upsilon(4S)$
3.78 ± 0.17 -0.16 ± 0.33	² BHARDWAJ 11	BELL	$e^+e^- \rightarrow \Upsilon(4S)$
$4.2 \pm 0.3 \pm 0.3$	³ AUBERT 09B	BABR	$e^+e^- \rightarrow \Upsilon(4S)$
3.1 ± 1.5 -1.1 ± 0.1	⁴ AVERY 00	CLE2	$e^+e^- \rightarrow \Upsilon(4S)$

• • • We do not use the following data for averages, fits, limits, etc. • • •

$3.51 \pm 0.33 \pm 0.45$	² SONI 06	BELL	Repl. by BHARDWAJ 11
$4.53 \pm 0.41 \pm 0.51$	² AUBERT 05J	BABR	Repl. by AUBERT 09B
$4.3 \pm 1.4 \pm 0.1$	⁵ AUBERT 02	BABR	Repl. by AUBERT 05J
< 27	90	² ALAM 94	CLE2 $e^+e^- \rightarrow \Upsilon(4S)$

¹ CHILIKIN 19 reports $[\Gamma(B^0 \rightarrow \chi_{c1}K^0)/\Gamma_{total}] \times [B(\chi_{c1}(1P) \rightarrow p\bar{p}\pi^+\pi^-)] = (7.4 \pm 2.4 \pm 0.6) \times 10^{-7}$ which we divide by our best value $B(\chi_{c1}(1P) \rightarrow p\bar{p}\pi^+\pi^-) = (5.0 \pm 1.9) \times 10^{-4}$. Our first error is their experiment's error and our second error is the systematic error from using our best value.

² Assumes equal production of B^+ and B^0 at the $\Upsilon(4S)$.

³ Uses $\chi_{c1,2} \rightarrow J/\psi\gamma$. Assumes $B(\Upsilon(4S) \rightarrow B^+B^-) = (51.6 \pm 0.6)\%$ and $B(\Upsilon(4S) \rightarrow B^0\bar{B}^0) = (48.4 \pm 0.6)\%$.

⁴ AVERY 00 reports $(3.9 \pm 1.9 \pm 0.4) \times 10^{-4}$ from a measurement of $[\Gamma(B^0 \rightarrow \chi_{c1}K^0)/\Gamma_{total}] \times [B(\chi_{c1}(1P) \rightarrow \gamma J/\psi(1S))] \times [B(\chi_{c1}(1P) \rightarrow \gamma J/\psi(1S))] = 0.273 \pm 0.016$, which we rescale to our best value $B(\chi_{c1}(1P) \rightarrow \gamma J/\psi(1S)) = (34.3 \pm 1.0) \times 10^{-2}$. Our first error is their experiment's error and our second error is the systematic error from using our best value. Assumes equal production of B^+ and B^0 at the $\Upsilon(4S)$.

⁵ AUBERT 02 reports $(5.4 \pm 1.4 \pm 1.1) \times 10^{-4}$ from a measurement of $[\Gamma(B^0 \rightarrow \chi_{c1}K^0)/\Gamma_{total}] \times [B(\chi_{c1}(1P) \rightarrow \gamma J/\psi(1S))] \times [B(\chi_{c1}(1P) \rightarrow \gamma J/\psi(1S))] = 0.273 \pm 0.016$, which we rescale to our best value $B(\chi_{c1}(1P) \rightarrow \gamma J/\psi(1S)) = (34.3 \pm 1.0) \times 10^{-2}$. Our first error is their experiment's error and our second error is the systematic error from using our best value. Assumes equal production of B^+ and B^0 at the $\Upsilon(4S)$.

$\Gamma(\chi_{c1}K^0)/\Gamma(J/\psi(1S)K^0)$ $\Gamma_{258}/\Gamma_{200}$

VALUE	DOCUMENT ID	TECN	COMMENT
$0.53 \pm 0.16 \pm 0.01$	¹ AUBERT 02	BABR	$e^+e^- \rightarrow \Upsilon(4S)$

¹ AUBERT 02 reports $0.66 \pm 0.11 \pm 0.17$ from a measurement of $[\Gamma(B^0 \rightarrow \chi_{c1}K^0)/\Gamma(B^0 \rightarrow J/\psi(1S)K^0)] \times [B(\chi_{c1}(1P) \rightarrow \gamma J/\psi(1S))] \times [B(\chi_{c1}(1P) \rightarrow \gamma J/\psi(1S))] = 0.273 \pm 0.016$, which we rescale to our best value $B(\chi_{c1}(1P) \rightarrow \gamma J/\psi(1S)) = (34.3 \pm 1.0) \times 10^{-2}$. Our first error is their experiment's error and our second error is the systematic error from using our best value. Assumes equal production of B^+ and B^0 at the $\Upsilon(4S)$.

Meson Particle Listings

 B^0 $\Gamma(\chi_{c1} \pi^- K^+)/\Gamma_{\text{total}}$ Γ_{259}/Γ

VALUE (units 10^{-4})	DOCUMENT ID	TECN	COMMENT
4.97 ± 0.12 ± 0.28	¹ BHARDWAJ 16	BELL	$e^+ e^- \rightarrow \Upsilon(4S)$
• • • We do not use the following data for averages, fits, limits, etc. • • •			
3.83 ± 0.10 ± 0.39	¹ MIZUK 08	BELL	Repl. by BHARDWAJ 16
¹ Assumes equal production of B^+ and B^0 at the $\Upsilon(4S)$.			

 $\Gamma(\chi_{c1} \pi^- K^+)/\Gamma(J/\psi(1S) K^+ \pi^-)$ $\Gamma_{259}/\Gamma_{201}$

VALUE	DOCUMENT ID	TECN	COMMENT
0.476 ± 0.021 ± 0.013	¹ LEES 12B	BABR	
¹ LEES 12B reports $0.474 \pm 0.013 \pm 0.026$ from a measurement of $[\Gamma(B^0 \rightarrow \chi_{c1} \pi^- K^+)/\Gamma(B^0 \rightarrow J/\psi(1S) K^+ \pi^-)] \times [B(\chi_{c1}(1P) \rightarrow \gamma J/\psi(1S))]$ assuming $B(\chi_{c1}(1P) \rightarrow \gamma J/\psi(1S)) = (34.4 \pm 1.5) \times 10^{-2}$, which we rescale to our best value $B(\chi_{c1}(1P) \rightarrow \gamma J/\psi(1S)) = (34.3 \pm 1.0) \times 10^{-2}$. Our first error is their experiment's error and our second error is the systematic error from using our best value.			

 $\Gamma(\chi_{c1} K^*(892)^0)/\Gamma_{\text{total}}$ Γ_{260}/Γ

VALUE (units 10^{-4})	CL%	DOCUMENT ID	TECN	COMMENT
2.38 ± 0.19 OUR FIT				Error includes scale factor of 1.2.
2.22 ± 0.40 OUR AVERAGE				Error includes scale factor of 1.6.

2.5 ± 0.2 ± 0.2	¹ AUBERT 09B	BABR	$e^+ e^- \rightarrow \Upsilon(4S)$
1.73 ± 0.15 ± 0.34	² MIZUK 08	BELL	$e^+ e^- \rightarrow \Upsilon(4S)$
• • • We do not use the following data for averages, fits, limits, etc. • • •			
3.14 ± 0.34 ± 0.72	² SONI 06	BELL	Repl. by MIZUK 08
3.27 ± 0.42 ± 0.64	² AUBERT 05J	BABR	Repl. by AUBERT 09B
3.8 ± 1.3 ± 0.1	³ AUBERT 02	BABR	Repl. by AUBERT 05J
<21	90	⁴ ALAM 94	CLE2 $e^+ e^- \rightarrow \Upsilon(4S)$

¹ Uses $\chi_{c1,2} \rightarrow J/\psi \gamma$. Assumes $B(\Upsilon(4S) \rightarrow B^+ B^-) = (51.6 \pm 0.6)\%$ and $B(\Upsilon(4S) \rightarrow B^0 \bar{B}^0) = (48.4 \pm 0.6)\%$.

² Assumes equal production of B^+ and B^0 at the $\Upsilon(4S)$.

³ AUBERT 02 reports $(4.8 \pm 1.4 \pm 0.9) \times 10^{-4}$ from a measurement of $[\Gamma(B^0 \rightarrow \chi_{c1} K^*(892)^0)/\Gamma_{\text{total}}] \times [B(\chi_{c1}(1P) \rightarrow \gamma J/\psi(1S))]$ assuming $B(\chi_{c1}(1P) \rightarrow \gamma J/\psi(1S)) = 0.273 \pm 0.016$, which we rescale to our best value $B(\chi_{c1}(1P) \rightarrow \gamma J/\psi(1S)) = (34.3 \pm 1.0) \times 10^{-2}$. Our first error is their experiment's error and our second error is the systematic error from using our best value. Assumes equal production of B^+ and B^0 at the $\Upsilon(4S)$.

⁴ BORTOLETTO 92 assumes equal production of B^+ and B^0 at the $\Upsilon(4S)$.

 $\Gamma(\chi_{c1} K^*(892)^0)/\Gamma(J/\psi(1S) K^*(892)^0)$ $\Gamma_{260}/\Gamma_{202}$

VALUE (units 10^{-2})	DOCUMENT ID	TECN	COMMENT
18.8 ± 1.5 OUR FIT			Error includes scale factor of 1.1.
19.8 ± 1.1 ± 1.5	¹ AAIJ 13Ac	LHCb	pp at 7 TeV
¹ Uses $B(\chi_{c1} \rightarrow J/\psi \gamma) = (34.4 \pm 1.5)\%$.			

 $\Gamma(\chi_{c1} K^*(892)^0)/\Gamma(\chi_{c1} K^0)$ $\Gamma_{260}/\Gamma_{258}$

VALUE	DOCUMENT ID	TECN	COMMENT
0.72 ± 0.11 ± 0.12	AUBERT 05J	BABR	$e^+ e^- \rightarrow \Upsilon(4S)$
• • • We do not use the following data for averages, fits, limits, etc. • • •			
0.89 ± 0.34 ± 0.17	¹ AUBERT 02	BABR	Repl. by AUBERT 05J
¹ Assumes equal production of B^+ and B^0 at the $\Upsilon(4S)$.			

 $\Gamma(X(4051)^- K^+, X^- \rightarrow \chi_{c1} \pi^-)/\Gamma_{\text{total}}$ Γ_{261}/Γ

VALUE (units 10^{-5})	CL%	DOCUMENT ID	TECN	COMMENT
3.0 ± 1.5 ± 3.7 OUR FIT				
0.8 ± 1.6				
• • • We do not use the following data for averages, fits, limits, etc. • • •				
<1.8	90	^{1,2} LEES 12B	BABR	
¹ Assumes equal production of B^+ and B^0 at the $\Upsilon(4S)$.				
² Uses $\chi_{c1} \rightarrow J/\psi \gamma$ mode. Uses $\chi_{c1} \rightarrow J/\psi \gamma$ mode. Finds a good description of the data without this $B^0 \rightarrow X(4051)^+ K^-$ decay mode in a fit.				

 $\Gamma(X(4248)^- K^+, X^- \rightarrow \chi_{c1} \pi^-)/\Gamma_{\text{total}}$ Γ_{262}/Γ

VALUE (units 10^{-5})	CL%	DOCUMENT ID	TECN	COMMENT
4.0 ± 2.3 ± 19.7 OUR FIT				
-0.9 ± 0.5				
• • • We do not use the following data for averages, fits, limits, etc. • • •				
<4.0	90	^{1,2} LEES 12B	BABR	
¹ Assumes equal production of B^+ and B^0 at the $\Upsilon(4S)$.				
² Uses $\chi_{c1} \rightarrow J/\psi \gamma$ mode. Finds a good description of the data without this $B^0 \rightarrow X(4248)^+ K^-$ decay mode in a fit.				

 $\Gamma(\chi_{c1} \pi^+ \pi^- K^0)/\Gamma_{\text{total}}$ Γ_{263}/Γ

VALUE (units 10^{-4})	DOCUMENT ID	TECN	COMMENT
3.16 ± 0.35 ± 0.32	¹ BHARDWAJ 16	BELL	$e^+ e^- \rightarrow \Upsilon(4S)$
¹ Assumes equal production of B^+ and B^0 at the $\Upsilon(4S)$.			

 $\Gamma(\chi_{c1} \pi^- \pi^0 K^+)/\Gamma_{\text{total}}$ Γ_{264}/Γ

VALUE (units 10^{-4})	DOCUMENT ID	TECN	COMMENT
3.52 ± 0.52 ± 0.24	¹ BHARDWAJ 16	BELL	$e^+ e^- \rightarrow \Upsilon(4S)$
¹ Assumes equal production of B^+ and B^0 at the $\Upsilon(4S)$.			

 $\Gamma(\chi_{c2} K^0)/\Gamma_{\text{total}}$ Γ_{265}/Γ

VALUE	CL%	DOCUMENT ID	TECN	COMMENT
<1.5 × 10⁻⁵	90	¹ BHARDWAJ 11	BELL	$e^+ e^- \rightarrow \Upsilon(4S)$
• • • We do not use the following data for averages, fits, limits, etc. • • •				
<2.8 × 10 ⁻⁵	90	² AUBERT 09B	BABR	$e^+ e^- \rightarrow \Upsilon(4S)$
<2.6 × 10 ⁻⁵	90	¹ SONI 06	BELL	Repl. by BHARDWAJ 11
<4.1 × 10 ⁻⁵	90	¹ AUBERT 05K	BABR	$e^+ e^- \rightarrow \Upsilon(4S)$

¹ Assumes equal production of B^+ and B^0 at the $\Upsilon(4S)$.

² Uses $\chi_{c1,2} \rightarrow J/\psi \gamma$. Assumes $B(\Upsilon(4S) \rightarrow B^+ B^-) = (51.6 \pm 0.6)\%$ and $B(\Upsilon(4S) \rightarrow B^0 \bar{B}^0) = (48.4 \pm 0.6)\%$.

 $\Gamma(\chi_{c2} K^*(892)^0)/\Gamma_{\text{total}}$ Γ_{266}/Γ

VALUE (units 10^{-5})	CL%	DOCUMENT ID	TECN	COMMENT
4.9 ± 1.2 OUR FIT				Error includes scale factor of 1.1.
6.6 ± 1.8 ± 0.5				
• • • We do not use the following data for averages, fits, limits, etc. • • •				
<7.1	90	² SONI 06	BELL	$e^+ e^- \rightarrow \Upsilon(4S)$
<3.6	90	² AUBERT 05K	BABR	Repl. by AUBERT 09B

¹ Uses $\chi_{c1,2} \rightarrow J/\psi \gamma$. Assumes $B(\Upsilon(4S) \rightarrow B^+ B^-) = (51.6 \pm 0.6)\%$ and $B(\Upsilon(4S) \rightarrow B^0 \bar{B}^0) = (48.4 \pm 0.6)\%$.

² Assumes equal production of B^+ and B^0 at the $\Upsilon(4S)$.

 $\Gamma(\chi_{c2} K^*(892)^0)/\Gamma(\chi_{c1} K^*(892)^0)$ $\Gamma_{266}/\Gamma_{260}$

VALUE (units 10^{-2})	DOCUMENT ID	TECN	COMMENT
20 ± 5 OUR FIT			Error includes scale factor of 1.1.
17.1 ± 5.0 ± 2.0	¹ AAIJ 13Ac	LHCb	pp at 7 TeV
¹ Uses $B(\chi_{c1} \rightarrow J/\psi \gamma)/B(\chi_{c2} \rightarrow J/\psi \gamma) = 1.76 \pm 0.11$.			

 $\Gamma(\chi_{c2} \pi^- K^+)/\Gamma_{\text{total}}$ Γ_{267}/Γ

VALUE (units 10^{-4})	DOCUMENT ID	TECN	COMMENT
0.72 ± 0.09 ± 0.05	¹ BHARDWAJ 16	BELL	$e^+ e^- \rightarrow \Upsilon(4S)$
¹ Assumes equal production of B^+ and B^0 at the $\Upsilon(4S)$.			

 $\Gamma(\chi_{c2} \pi^+ \pi^- K^0)/\Gamma_{\text{total}}$ Γ_{268}/Γ

VALUE	CL%	DOCUMENT ID	TECN	COMMENT
<1.70 × 10⁻⁴	90	¹ BHARDWAJ 16	BELL	$e^+ e^- \rightarrow \Upsilon(4S)$
¹ Assumes equal production of B^+ and B^0 at the $\Upsilon(4S)$.				

 $\Gamma(\chi_{c2} \pi^- \pi^0 K^+)/\Gamma_{\text{total}}$ Γ_{269}/Γ

VALUE	CL%	DOCUMENT ID	TECN	COMMENT
<0.74 × 10⁻⁴	90	¹ BHARDWAJ 16	BELL	$e^+ e^- \rightarrow \Upsilon(4S)$
¹ Assumes equal production of B^+ and B^0 at the $\Upsilon(4S)$.				

 $\Gamma(\psi(4660) K^0, \psi \rightarrow \Lambda_c^+ \Lambda_c^-)/\Gamma_{\text{total}}$ Γ_{270}/Γ

VALUE	CL%	DOCUMENT ID	TECN	COMMENT
<2.3 × 10⁻⁴	90	¹ LI 18D	BELL	$e^+ e^- \rightarrow \Upsilon(4S)$
¹ Assumes $B(\Upsilon(4S) \rightarrow B^0 \bar{B}^0) = 48.6 \pm 0.6\%$ and $B(\Lambda_c^+ \rightarrow p K^- \pi^+) = 6.23 \pm 0.33\%$.				

 $\Gamma(\psi(4230)^0 K^0, \psi^0 \rightarrow J/\psi \pi^+ \pi^-)/\Gamma_{\text{total}}$ Γ_{271}/Γ

VALUE	CL%	DOCUMENT ID	TECN	COMMENT
<17 × 10⁻⁶	90	¹ GARG 19	BELL	$e^+ e^- \rightarrow \Upsilon(4S)$
¹ Assumes equal production of B^0 and B^+ at the $\Upsilon(4S)$.				

 $\Gamma(K^+ \pi^-)/\Gamma_{\text{total}}$ Γ_{272}/Γ

VALUE (units 10^{-6})	CL%	DOCUMENT ID	TECN	COMMENT
19.6 ± 0.5 OUR FIT				
19.6 ± 0.5 OUR AVERAGE				
20.00 ± 0.34 ± 0.60		¹ DUH 13	BELL	$e^+ e^- \rightarrow \Upsilon(4S)$
19.1 ± 0.6 ± 0.6		¹ AUBERT 07B	BABR	$e^+ e^- \rightarrow \Upsilon(4S)$
18.0 ± 2.3 ± 1.2		¹ BORNHEIM 03	CLE2	$e^+ e^- \rightarrow \Upsilon(4S)$
• • • We do not use the following data for averages, fits, limits, etc. • • •				
19.9 ± 0.4 ± 0.8		¹ LIN 07A	BELL	Repl. by DUH 13
18.5 ± 1.0 ± 0.7		¹ CHAO 04	BELL	Repl. by LIN 07A
17.9 ± 0.9 ± 0.7		¹ AUBERT 02Q	BABR	Repl. by AUBERT 07B
22.5 ± 1.9 ± 1.8		¹ CASEY 02	BELL	Repl. by CHAO 04
19.3 ± 3.4 ± 1.5		¹ ABE 01H	BELL	Repl. by CASEY 02
16.7 ± 1.6 ± 1.3		¹ AUBERT 01E	BABR	Repl. by AUBERT 02Q
< 6.6	90	² ABE 00C	SLD	$e^+ e^- \rightarrow Z$
17.2 ± 2.5 ± 1.2		¹ CRONIN-HEN..00	CLE2	Repl. by BORNHEIM 03
15 ± 5 ± 1.4		GODANG 98	CLE2	Repl. by CRONIN-HENNESSY 00
24 ± 17 ± 2		³ ADAM 96D	DLPH	$e^+ e^- \rightarrow Z$
< 17	90	ASNER 96	CLE2	Sup. by ADAM 96D
< 30	90	⁴ BUSKULIC 96V	ALEP	$e^+ e^- \rightarrow Z$
< 90	90	⁵ ABREU 95N	DLPH	Sup. by ADAM 96D
< 81	90	⁶ AKERS 94L	OPAL	$e^+ e^- \rightarrow Z$

See key on page 1127

Meson Particle Listings B⁰

Table with columns for value, document ID, TECN, and COMMENT. Rows include BATTLE, ALBRECHT, AVERY, and AVERY with various decay channels like e+e- to gamma(4S).

- 1 Assumes equal production of B+ and B0 at the gamma(4S).
2 ABE 00c assumes B(Z -> bD-bar) = (21.7 +/- 0.1)% and the B fractions fB0 = fB+ = ...
3 ADAM 96D assumes fB0 = fB- = 0.39 and fBs = 0.12. Contributions from B0 and Bs decays cannot be separated.
4 BUSKULIC 96v assumes PDG 96 production fractions for B0, B+, Bs, b baryons.
5 Assumes a B0, B- production fraction of 0.39 and a Bs production fraction of 0.12.
6 Assumes B(Z -> bD-bar) = 0.217 and B0D (Bs) fraction 39.5% (12%).
7 BATTLE 93 assumes equal production of B0B0-bar and B+B- at gamma(4S).
8 Assumes the gamma(4S) decays 43% to B0B0-bar.

Gamma(K+ pi-)/Gamma(K0 pi0) and Gamma(K+ pi-)/Gamma(K0 pi0) tables. Includes OUR AVERAGE values and individual data points with document IDs like LIN, ABE, and ASNER.

Gamma(K+ pi- + pi+ pi-)/Gamma total table. Includes OUR AVERAGE value and individual data points with document IDs like ADAM, ASNER, and BATTLE.

Gamma(K0 pi0)/Gamma total table. Includes OUR AVERAGE value and individual data points with document IDs like DUH, LEES, BORNHEIM, FUJIKAWA, AUBERT, LIN, CHAO, CASEY, ABE, AUBERT, CRONIN-HEN., GODANG, and ASNER.

Gamma(eta K0)/Gamma total table. Includes OUR AVERAGE value and individual data points with document IDs like AUBERT, SCHUEMANN, RICHICHI, AUBERT, AUBERT, ABE, AUBERT, and BEHRENS.

Gamma(eta* K*(892)0)/Gamma total table. Includes OUR AVERAGE value and individual data points with document IDs like SATO, DEL-AMO-SA., AUBERT, SCHUEMANN, AUBERT, RICHICHI, and BEHRENS.

Gamma(eta* K0*(1430)0)/Gamma total table. Includes OUR AVERAGE value and individual data points with document IDs like DEL-AMO-SA.

Gamma(eta* K2*(1430)0)/Gamma total table. Includes OUR AVERAGE value and individual data points with document IDs like DEL-AMO-SA.

Gamma(eta K0)/Gamma total table. Includes OUR AVERAGE value and individual data points with document IDs like HOI, AUBERT, CHANG, AUBERT, CHANG, AUBERT, RICHICHI, and BEHRENS.

Gamma(eta K*(892)0)/Gamma total table. Includes OUR AVERAGE value and individual data points with document IDs like WANG, AUBERT, RICHICHI, AUBERT, and BEHRENS.

Gamma(eta K0*(1430)0)/Gamma total table. Includes OUR AVERAGE value and individual data points with document IDs like AUBERT.

Gamma(eta K2*(1430)0)/Gamma total table. Includes OUR AVERAGE value and individual data points with document IDs like AUBERT.

Gamma(omega K0)/Gamma total table. Includes OUR AVERAGE value and individual data points with document IDs like CHOBANOVA, AUBERT, JESSOP, AUBERT, JEN, AUBERT, WANG, AUBERT, and BERGFELD.

Meson Particle Listings

 B^0 $\Gamma(a_0(980)^0 K^0, a_0^0 \rightarrow \eta \pi^0)/\Gamma_{\text{total}}$ Γ_{283}/Γ

VALUE (units 10^{-6})	CL%	DOCUMENT ID	TECN	COMMENT
<7.8	90	¹ AUBERT,BE	04	BABR $e^+e^- \rightarrow \Upsilon(4S)$

¹ Assumes equal production of charged and neutral B mesons at $\Upsilon(4S)$.

 $\Gamma(b_1^0 K^0, b_1^0 \rightarrow \omega \pi^0)/\Gamma_{\text{total}}$ Γ_{284}/Γ

VALUE (units 10^{-6})	CL%	DOCUMENT ID	TECN	COMMENT
<7.8	90	¹ AUBERT	08AQ	BABR $e^+e^- \rightarrow \Upsilon(4S)$

¹ Assumes equal production of B^+ and B^0 at the $\Upsilon(4S)$.

 $\Gamma(a_0(980)^\pm K^\mp, a_0^\pm \rightarrow \eta \pi^\pm)/\Gamma_{\text{total}}$ Γ_{285}/Γ

VALUE (units 10^{-6})	CL%	DOCUMENT ID	TECN	COMMENT
<1.9	90	¹ AUBERT	07Y	BABR $e^+e^- \rightarrow \Upsilon(4S)$
•••		We do not use the following data for averages, fits, limits, etc. •••		
<2.1	90	¹ AUBERT,BE	04	BABR Repl. by AUBERT 07Y

¹ Assumes equal production of B^+ and B^0 at the $\Upsilon(4S)$.

 $\Gamma(b_1^- K^+, b_1^- \rightarrow \omega \pi^-)/\Gamma_{\text{total}}$ Γ_{286}/Γ

VALUE (units 10^{-6})	CL%	DOCUMENT ID	TECN	COMMENT
$7.4 \pm 1.0 \pm 1.0$		¹ AUBERT	07BI	BABR $e^+e^- \rightarrow \Upsilon(4S)$

¹ Assumes equal production of B^+ and B^0 at the $\Upsilon(4S)$.

 $\Gamma(b_1^0 K^{*0}, b_1^0 \rightarrow \omega \pi^0)/\Gamma_{\text{total}}$ Γ_{287}/Γ

VALUE	CL%	DOCUMENT ID	TECN	COMMENT
< 8.0×10^{-6}	90	¹ AUBERT	09AF	BABR $e^+e^- \rightarrow \Upsilon(4S)$

¹ Assumes equal production of B^+ and B^0 at the $\Upsilon(4S)$.

 $\Gamma(b_1^- K^{*+}, b_1^- \rightarrow \omega \pi^-)/\Gamma_{\text{total}}$ Γ_{288}/Γ

VALUE	CL%	DOCUMENT ID	TECN	COMMENT
< 5.0×10^{-6}	90	¹ AUBERT	09AF	BABR $e^+e^- \rightarrow \Upsilon(4S)$

¹ Assumes equal production of B^+ and B^0 at the $\Upsilon(4S)$.

 $\Gamma(a_0(1450)^\pm K^\mp, a_0^\pm \rightarrow \eta \pi^\pm)/\Gamma_{\text{total}}$ Γ_{289}/Γ

VALUE (units 10^{-6})	CL%	DOCUMENT ID	TECN	COMMENT
<3.1	90	¹ AUBERT	07Y	BABR $e^+e^- \rightarrow \Upsilon(4S)$

¹ Assumes equal production of B^+ and B^0 at the $\Upsilon(4S)$.

 $\Gamma(K_S^0 X^0 (\text{Familon}))/\Gamma_{\text{total}}$ Γ_{290}/Γ

VALUE (units 10^{-6})	CL%	DOCUMENT ID	TECN	COMMENT
<53	90	¹ AMMAR	01B	CLE2 $e^+e^- \rightarrow \Upsilon(4S)$

¹ AMMAR 01B searched for the two-body decay of the B meson to a massless neutral feebly-interacting particle X^0 such as the familon, the Nambu-Goldstone boson associated with a spontaneously broken global family symmetry.

 $\Gamma(\omega K^*(892)^0)/\Gamma_{\text{total}}$ Γ_{291}/Γ

VALUE (units 10^{-6})	CL%	DOCUMENT ID	TECN	COMMENT
2.0 ± 0.5 OUR AVERAGE				
$2.2 \pm 0.6 \pm 0.2$		¹ AUBERT	09H	BABR $e^+e^- \rightarrow \Upsilon(4S)$
$1.8 \pm 0.7 \pm 0.3$		¹ GOLDENZWE..08	BELL	$e^+e^- \rightarrow \Upsilon(4S)$
•••		We do not use the following data for averages, fits, limits, etc. •••		
< 4.2	90	¹ AUBERT,B	06T	BABR Repl. by AUBERT 09H
< 6.0	90	¹ AUBERT	05O	BABR Repl. by AUBERT,B 06T
< 23	90	¹ BERGFELD	98	CLE2

¹ Assumes equal production of B^+ and B^0 at the $\Upsilon(4S)$.

 $\Gamma(\omega (K\pi)_0^{*0})/\Gamma_{\text{total}}$ Γ_{292}/Γ

$(K\pi)_0^{*0}$ is the total S-wave composed of $K_0^*(1430)$ and nonresonant that are described using LASS shape.

VALUE (units 10^{-6})	CL%	DOCUMENT ID	TECN	COMMENT
$18.4 \pm 1.8 \pm 1.7$		¹ AUBERT	09H	BABR $e^+e^- \rightarrow \Upsilon(4S)$

¹ Assumes equal production of B^+ and B^0 at the $\Upsilon(4S)$.

 $\Gamma(\omega K_0^*(1430)^0)/\Gamma_{\text{total}}$ Γ_{293}/Γ

VALUE (units 10^{-6})	CL%	DOCUMENT ID	TECN	COMMENT
$16.0 \pm 1.6 \pm 3.0$		¹ AUBERT	09H	BABR $e^+e^- \rightarrow \Upsilon(4S)$

¹ Assumes equal production of B^+ and B^0 at the $\Upsilon(4S)$.

 $\Gamma(\omega K_2^*(1430)^0)/\Gamma_{\text{total}}$ Γ_{294}/Γ

VALUE (units 10^{-6})	CL%	DOCUMENT ID	TECN	COMMENT
$10.1 \pm 2.0 \pm 1.1$		¹ AUBERT	09H	BABR $e^+e^- \rightarrow \Upsilon(4S)$

¹ Assumes equal production of B^+ and B^0 at the $\Upsilon(4S)$.

 $\Gamma(\omega K^+ \pi^- \text{ nonresonant})/\Gamma_{\text{total}}$ Γ_{295}/Γ

VALUE (units 10^{-6})	CL%	DOCUMENT ID	TECN	COMMENT
$5.1 \pm 0.7 \pm 0.7$		^{1,2} GOLDENZWE..08	BELL	$e^+e^- \rightarrow \Upsilon(4S)$

¹ Assumes equal production of B^+ and B^0 at the $\Upsilon(4S)$.
² For the $K\pi$ mass range 0.755–1.250 GeV/ c^2 , excluding $K^*(892)$.

 $\Gamma(K^+ \pi^- \pi^0)/\Gamma_{\text{total}}$ Γ_{296}/Γ

VALUE (units 10^{-6})	CL%	DOCUMENT ID	TECN	COMMENT
37.8 ± 3.2 OUR AVERAGE				
$38.5 \pm 1.0 \pm 3.9$		^{1,2} LEES	11	BABR $e^+e^- \rightarrow \Upsilon(4S)$
$36.6^{+4.2}_{-4.3} \pm 3.0$		¹ CHANG	04	BELL $e^+e^- \rightarrow \Upsilon(4S)$
•••		We do not use the following data for averages, fits, limits, etc. •••		
$35.7^{+2.6}_{-1.5} \pm 2.2$		¹ AUBERT	08AQ	BABR Repl. by LEES 11
<40	90	¹ ECKHART	02	CLE2 $e^+e^- \rightarrow \Upsilon(4S)$

¹ Assumes equal production of B^+ and B^0 at the $\Upsilon(4S)$.
² Uses Dalitz plot analysis of $B^0 \rightarrow K^+ \pi^- \pi^0$ decays.

 $\Gamma(K^+ \rho^-)/\Gamma_{\text{total}}$ Γ_{297}/Γ

VALUE (units 10^{-6})	CL%	DOCUMENT ID	TECN	COMMENT
7.0 ± 0.9 OUR AVERAGE				
$6.6 \pm 0.5 \pm 0.8$		^{1,2} LEES	11	BABR $e^+e^- \rightarrow \Upsilon(4S)$
$15.1^{+3.4}_{-3.3} \pm 2.4$		¹ CHANG	04	BELL $e^+e^- \rightarrow \Upsilon(4S)$
•••		We do not use the following data for averages, fits, limits, etc. •••		
$8.0^{+0.8}_{-1.3} \pm 0.6$		¹ AUBERT	08AQ	BABR Repl. by LEES 11
$7.3^{+1.3}_{-1.2} \pm 1.3$		¹ AUBERT	03T	BABR Repl. by AUBERT 08AQ
<32	90	¹ JESSOP	00	CLE2 $e^+e^- \rightarrow \Upsilon(4S)$
<35	90	ASNER	96	CLE2 Repl. by JESSOP 00

¹ Assumes equal production of B^+ and B^0 at the $\Upsilon(4S)$.
² Uses Dalitz plot analysis of $B^0 \rightarrow K^+ \pi^- \pi^0$ decays.

 $\Gamma(K^+ \rho(1450)^-)/\Gamma_{\text{total}}$ Γ_{298}/Γ

VALUE (units 10^{-6})	CL%	DOCUMENT ID	TECN	COMMENT
$2.4 \pm 1.0 \pm 0.6$		^{1,2} LEES	11	BABR $e^+e^- \rightarrow \Upsilon(4S)$
•••		We do not use the following data for averages, fits, limits, etc. •••		
<2.1	90	¹ AUBERT	08AQ	BABR Repl. by LEES 11

¹ Assumes equal production of B^+ and B^0 at the $\Upsilon(4S)$.
² Uses Dalitz plot analysis of $B^0 \rightarrow K^+ \pi^- \pi^0$ decays.

 $\Gamma(K^+ \rho(1700)^-)/\Gamma_{\text{total}}$ Γ_{299}/Γ

VALUE (units 10^{-6})	CL%	DOCUMENT ID	TECN	COMMENT
$0.6 \pm 0.6 \pm 0.4$		^{1,2} LEES	11	BABR $e^+e^- \rightarrow \Upsilon(4S)$
•••		We do not use the following data for averages, fits, limits, etc. •••		
<1.1	90	¹ AUBERT	08AQ	BABR Repl. by LEES 11

¹ Assumes equal production of B^+ and B^0 at the $\Upsilon(4S)$.
² Uses Dalitz plot analysis of $B^0 \rightarrow K^+ \pi^- \pi^0$ decays.

 $\Gamma((K^+ \pi^- \pi^0) \text{ nonresonant})/\Gamma_{\text{total}}$ Γ_{300}/Γ

VALUE (units 10^{-6})	CL%	DOCUMENT ID	TECN	COMMENT
$2.8 \pm 0.5 \pm 0.4$		^{1,2} LEES	11	BABR $e^+e^- \rightarrow \Upsilon(4S)$
•••		We do not use the following data for averages, fits, limits, etc. •••		
$4.4 \pm 0.9 \pm 0.5$		¹ AUBERT	08AQ	BABR Repl. by LEES 11
<9.4	90	¹ CHANG	04	BELL $e^+e^- \rightarrow \Upsilon(4S)$

¹ Assumes equal production of B^+ and B^0 at the $\Upsilon(4S)$.
² Uses Dalitz plot analysis of $B^0 \rightarrow K^+ \pi^- \pi^0$ decays. The quoted value is only for the flat part of the non-resonant component.

 $\Gamma((K\pi)_0^{*+} \pi^-, (K\pi)_0^{*+} \rightarrow K^+ \pi^0)/\Gamma_{\text{total}}$ Γ_{301}/Γ

$(K\pi)_0^{*+}$ is the total S-wave composed of $K_0^*(1430)$ and nonresonant that are described using LASS shape.

VALUE (units 10^{-6})	CL%	DOCUMENT ID	TECN	COMMENT
$34.2 \pm 2.4 \pm 4.1$		^{1,2} LEES	11	BABR $e^+e^- \rightarrow \Upsilon(4S)$

••• We do not use the following data for averages, fits, limits, etc. •••

VALUE (units 10^{-6})	CL%	DOCUMENT ID	TECN	COMMENT
$9.4^{+1.1}_{-1.3} \pm 2.3$		¹ AUBERT	08AQ	BABR Repl. by LEES 11

¹ Assumes equal production of B^+ and B^0 at the $\Upsilon(4S)$.
² Uses Dalitz plot analysis of $B^0 \rightarrow K^+ \pi^- \pi^0$ decays.

 $\Gamma((K\pi)_0^{*0} \pi^0, (K\pi)_0^{*0} \rightarrow K^+ \pi^-)/\Gamma_{\text{total}}$ Γ_{302}/Γ

$(K\pi)_0^{*0}$ is the total S-wave composed of $K_0^*(1430)$ and nonresonant that are described using LASS shape.

VALUE (units 10^{-6})	CL%	DOCUMENT ID	TECN	COMMENT
$8.6 \pm 1.1 \pm 1.3$		^{1,2} LEES	11	BABR $e^+e^- \rightarrow \Upsilon(4S)$

••• We do not use the following data for averages, fits, limits, etc. •••

VALUE (units 10^{-6})	CL%	DOCUMENT ID	TECN	COMMENT
$8.7^{+1.1}_{-0.9} \pm 2.8$		¹ AUBERT	08AQ	BABR Repl. by LEES 11

¹ Assumes equal production of B^+ and B^0 at the $\Upsilon(4S)$.
² Uses Dalitz plot analysis of $B^0 \rightarrow K^+ \pi^- \pi^0$ decays.

 $\Gamma(K_2^*(1430)^0 \pi^0)/\Gamma_{\text{total}}$ Γ_{303}/Γ

VALUE (units 10^{-6})	CL%	DOCUMENT ID	TECN	COMMENT
<4.0	90	¹ AUBERT	08AQ	BABR $e^+e^- \rightarrow \Upsilon(4S)$

¹ Assumes equal production of B^+ and B^0 at the $\Upsilon(4S)$.

Meson Particle Listings
B⁰

Γ(K*(1680)⁰π⁰)/Γ_{total} Γ₃₀₄/Γ

VALUE (units 10 ⁻⁶)	CL%	DOCUMENT ID	TECN	COMMENT
<7.5	90	¹ AUBERT	08AQ BABR	e ⁺ e ⁻ → γ(4S)

¹ Assumes equal production of B⁺ and B⁰ at the γ(4S).

Γ(K_x⁰π⁰)/Γ_{total} Γ₃₀₅/Γ
K_x⁰ stands for the possible candidates of K*(1410), K₀^{*}(1430) and K₂^{*}(1430).

VALUE (units 10 ⁻⁶)	DOCUMENT ID	TECN	COMMENT
6.1 +1.6 +0.5 -1.5 -0.6	¹ CHANG 04 BELL		e ⁺ e ⁻ → γ(4S)

¹ Assumes equal production of B⁺ and B⁰ at the γ(4S).

Γ(K⁰π⁺π⁻)/Γ_{total} Γ₃₀₆/Γ

VALUE (units 10 ⁻⁶)	CL%	DOCUMENT ID	TECN	COMMENT
49.7 ± 1.8 OUR FIT				
49.6 ± 2.0 OUR AVERAGE				
50.2 ± 1.5 ± 1.8		¹ AUBERT 09AU BABR		e ⁺ e ⁻ → γ(4S)
47.5 ± 2.4 ± 3.7		² GARMASH 07 BELL		e ⁺ e ⁻ → γ(4S)
50 +10 -9 ±7		¹ ECKHART 02 CLE2		e ⁺ e ⁻ → γ(4S)

• • • We do not use the following data for averages, fits, limits, etc. • • •

43.0 ± 2.3 ± 2.3		¹ AUBERT 06i BABR	Repl. by AUBERT 09AU
43.7 ± 3.8 ± 3.4		¹ AUBERT,B 04o BABR	Repl. by AUBERT 06i
45.4 ± 5.2 ± 5.9		¹ GARMASH 04 BELL	Repl. by GARMASH 07
<440	90	ALBRECHT 91E ARG	e ⁺ e ⁻ → γ(4S)

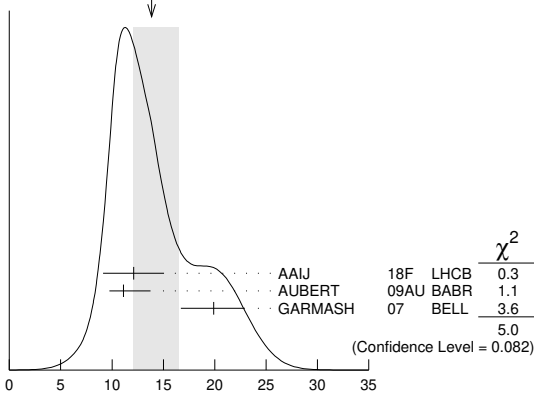
¹ Assumes equal production of B⁺ and B⁰ at the γ(4S).

² Uses Dalitz plot analysis of the B⁰ → K⁰π⁺π⁻ final state decays.

Γ(K⁰π⁺π⁻ nonresonant)/Γ_{total} Γ₃₀₇/Γ

VALUE (units 10 ⁻⁶)	DOCUMENT ID	TECN	COMMENT
13.9 ± 2.6 OUR AVERAGE			Error includes scale factor of 1.6. See the ideogram below.
12.1 ± 0.6 ± 2.9	¹ AAIJ 18F LHCB		pp at 7, 8 TeV
11.1 ± 2.5 ± 0.9	² AUBERT 09AU BABR		e ⁺ e ⁻ → γ(4S)
19.9 ± 2.5 +1.7 -2.0	³ GARMASH 07 BELL		e ⁺ e ⁻ → γ(4S)

WEIGHTED AVERAGE
13.9±2.6-1.8 (Error scaled by 1.6)



¹ Uses Dalitz plot analysis of the B⁰ → K_S⁰π⁺π⁻ final state decays. For the branching fraction of the reference mode, the PDG 18 average B(B⁰ → K_S⁰π⁺π⁻) = (4.96 ± 0.20) × 10⁻⁵ is used.

² Assumes equal production of B⁺ and B⁰ at the γ(4S).

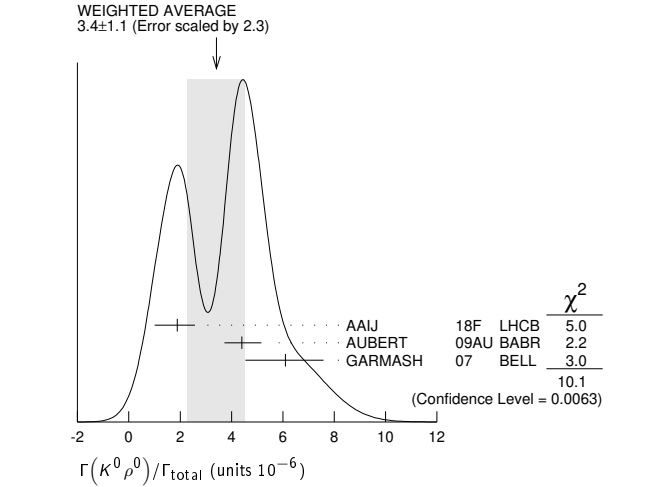
³ Uses Dalitz plot analysis of the B⁰ → K⁰π⁺π⁻ final state decays.

Γ(K⁰ρ⁰)/Γ_{total} Γ₃₀₈/Γ

VALUE (units 10 ⁻⁶)	CL%	DOCUMENT ID	TECN	COMMENT
3.4 ± 1.1 OUR AVERAGE				Error includes scale factor of 2.3. See the ideogram below.
1.89 +0.55 +0.40 -0.79 ±0.40		¹ AAIJ 18F LHCB		pp at 7, 8 TeV
4.4 +0.7 ±0.3 -0.6		² AUBERT 09AU BABR		e ⁺ e ⁻ → γ(4S)
6.1 ± 1.0 +1.1 -1.2		³ GARMASH 07 BELL		e ⁺ e ⁻ → γ(4S)

• • • We do not use the following data for averages, fits, limits, etc. • • •

4.9 ± 0.8 ± 0.9		² AUBERT 07f BABR	Repl. by AUBERT 09Au
<39	90	ASNER 96 CLEO	e ⁺ e ⁻ → γ(4S)
<320	90	ALBRECHT 91B ARG	e ⁺ e ⁻ → γ(4S)
<500	90	⁴ AVERY 89B CLEO	e ⁺ e ⁻ → γ(4S)



¹ Uses Dalitz plot analysis of the B⁰ → K_S⁰π⁺π⁻ final state decays. For the branching fraction of the reference mode, the PDG 18 average B(B⁰ → K_S⁰π⁺π⁻) = (4.96 ± 0.20) × 10⁻⁵ is used.

² Assumes equal production of B⁺ and B⁰ at the γ(4S).

³ Uses Dalitz plot analysis of the B⁰ → K⁰π⁺π⁻ final state decays.

⁴ AVERY 89B reports < 5.8 × 10⁻⁴ assuming the γ(4S) decays 43% to B⁰ \bar{B}^0 . We rescale to 50%.

Γ(K*(892)⁺π⁻)/Γ_{total} Γ₃₀₉/Γ

VALUE (units 10 ⁻⁶)	CL%	DOCUMENT ID	TECN	COMMENT
7.5 ± 0.4 OUR AVERAGE				
7.02 ± 0.30 ± 0.45		¹ AAIJ 18F LHCB		pp at 7, 8 TeV
8.0 ± 1.1 ± 0.8		^{2,3} LEES 11 BABR		e ⁺ e ⁻ → γ(4S)
8.3 +0.9 +0.8 -0.8		^{3,4} AUBERT 09AU BABR		e ⁺ e ⁻ → γ(4S)
8.4 ± 1.1 +1.0 -0.9		⁴ GARMASH 07 BELL		e ⁺ e ⁻ → γ(4S)
16 +6 -5 ±2		³ ECKHART 02 CLE2		e ⁺ e ⁻ → γ(4S)

• • • We do not use the following data for averages, fits, limits, etc. • • •

12.6 +2.7 +0.9 -1.6 ±0.9		^{2,3} AUBERT 08AQ BABR	Repl. by LEES 11
11.0 ± 1.5 ± 0.71		³ AUBERT 06i BABR	Repl. by AUBERT 09AU
12.9 ± 2.4 ± 1.4		³ AUBERT,B 04o BABR	Repl. by AUBERT 06i
14.8 +4.6 +2.8 -4.4 -1.3		³ CHANG 04 BELL	Repl. by GARMASH 07
<72	90	ASNER 96 CLE2	e ⁺ e ⁻ → γ(4S)
<620	90	ALBRECHT 91B ARG	e ⁺ e ⁻ → γ(4S)
<380	90	⁵ AVERY 89B CLEO	e ⁺ e ⁻ → γ(4S)
<560	90	⁶ AVERY 87 CLEO	e ⁺ e ⁻ → γ(4S)

¹ Uses Dalitz plot analysis of the B⁰ → K_S⁰π⁺π⁻ final state decays. For the branching fraction of the reference mode, the PDG 18 average B(B⁰ → K_S⁰π⁺π⁻) = (4.96 ± 0.20) × 10⁻⁵ is used.

² Uses Dalitz plot analysis of B⁰ → K⁺π⁻π⁰ decays.

³ Assumes equal production of B⁺ and B⁰ at the γ(4S).

⁴ Uses Dalitz plot analysis of the B⁰ → K⁰π⁺π⁻ final state decays.

⁵ AVERY 89B reports < 4.4 × 10⁻⁴ assuming the γ(4S) decays 43% to B⁰ \bar{B}^0 . We rescale to 50%.

⁶ AVERY 87 reports < 7 × 10⁻⁴ assuming the γ(4S) decays 40% to B⁰ \bar{B}^0 . We rescale to 50%.

Γ(K₀^{*}(1430)⁺π⁻)/Γ_{total} Γ₃₁₀/Γ

VALUE (units 10 ⁻⁶)	DOCUMENT ID	TECN	COMMENT
33 ± 7 OUR AVERAGE			Error includes scale factor of 2.0.
29.9 +2.3 +3.6 -1.7 ±3.6	^{1,2} AUBERT 09AU BABR		e ⁺ e ⁻ → γ(4S)
49.7 ± 3.8 +6.8 -8.2	² GARMASH 07 BELL		e ⁺ e ⁻ → γ(4S)

¹ Assumes equal production of B⁺ and B⁰ at the γ(4S).

² Uses Dalitz plot analysis of the B⁰ → K⁰π⁺π⁻ final state decays.

Γ(K_x⁺π⁻)/Γ_{total} Γ₃₁₁/Γ
K_x⁺ stands for the possible candidates of K*(1410), K₀^{*}(1430) and K₂^{*}(1430).

VALUE (units 10 ⁻⁶)	DOCUMENT ID	TECN	COMMENT
5.1 ± 1.5 +0.6 -0.7	¹ CHANG 04 BELL		e ⁺ e ⁻ → γ(4S)

¹ Assumes equal production of B⁺ and B⁰ at the γ(4S).

Γ(K*(1410)⁺π⁻, K⁺π⁻ → K⁰π⁺)/Γ_{total} Γ₃₁₂/Γ

VALUE (units 10 ⁻⁶)	CL%	DOCUMENT ID	TECN	COMMENT
<3.8	90	¹ GARMASH 07 BELL		e ⁺ e ⁻ → γ(4S)

¹ Uses Dalitz plot analysis of the B⁰ → K⁰π⁺π⁻ final state decays.

Meson Particle Listings

B^0

$\Gamma((K\pi)_0^{*+}, (K\pi)_0^{*+} \rightarrow K^0\pi^+)/\Gamma_{\text{total}}$ Γ_{313}/Γ

VALUE (units 10^{-6})	DOCUMENT ID	TECN	COMMENT
16.2 ± 0.69 ± 1.15	¹ AAIJ	18F LHCb	pp at 7, 8 TeV

¹ Uses Dalitz plot analysis of the $B^0 \rightarrow K_S^0 \pi^+ \pi^-$ final state decays. $(K\pi)_0^{*+}$ is the S-wave component of $K^0 \pi^+$. For the branching fraction of the reference mode, the PDG 18 average $B(B^0 \rightarrow K_S^0 \pi^+ \pi^-) = (4.96 \pm 0.20) \times 10^{-5}$ is used.

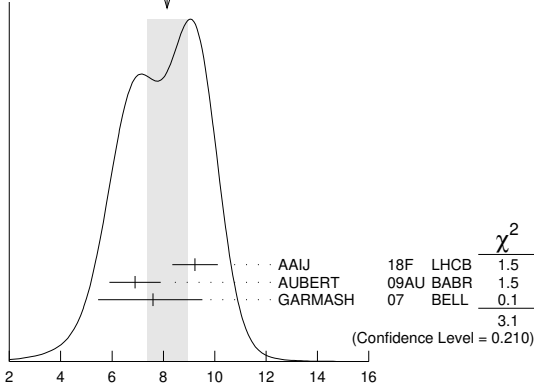
$\Gamma(f_0(980)K^0, f_0 \rightarrow \pi^+\pi^-)/\Gamma_{\text{total}}$ Γ_{314}/Γ

VALUE (units 10^{-6})	CL%	DOCUMENT ID	TECN	COMMENT
8.1 ± 0.8	OUR AVERAGE	Error includes scale factor of 1.3. See the ideogram below.		

9.23 ± 0.40 ± 0.79	¹ AAIJ	18F LHCb	pp at 7, 8 TeV
6.9 ± 0.8 ± 0.6	² AUBERT	09AU BABR	$e^+e^- \rightarrow \Upsilon(4S)$
7.6 ± 1.7 ^{+0.9} _{-1.3}	³ GARMASH	07 BELL	$e^+e^- \rightarrow \Upsilon(4S)$

• • • We do not use the following data for averages, fits, limits, etc. • • •
 5.5 ± 0.7 ± 0.6 ² AUBERT 06i BABR Repl. by AUBERT 09AU
 <360 90 ⁴ AVERY 89B CLEO $e^+e^- \rightarrow \Upsilon(4S)$

WEIGHTED AVERAGE
8.1 ± 0.8 (Error scaled by 1.3)



$\Gamma(f_0(980)K^0, f_0 \rightarrow \pi^+\pi^-)/\Gamma_{\text{total}}$ (units 10^{-6})

¹ Uses Dalitz plot analysis of the $B^0 \rightarrow K_S^0 \pi^+ \pi^-$ final state decays. For the branching fraction of the reference mode, the PDG 18 average $B(B^0 \rightarrow K_S^0 \pi^+ \pi^-) = (4.96 \pm 0.20) \times 10^{-5}$ is used.
² Assumes equal production of B^+ and B^0 at the $\Upsilon(4S)$.
³ Uses Dalitz plot analysis of the $B^0 \rightarrow K^0 \pi^+ \pi^-$ final state decays.
⁴ AVERY 89B reports $< 4.2 \times 10^{-4}$ assuming the $\Upsilon(4S)$ decays 43% to $B^0 \bar{B}^0$. We rescale to 50%.

$\Gamma(K^0 f_0(500))/\Gamma_{\text{total}}$ Γ_{315}/Γ

VALUE (units 10^{-6})	DOCUMENT ID	TECN	COMMENT
0.16 ^{+0.20} _{-0.04} ± 0.15	¹ AAIJ	18F LHCb	pp at 7, 8 TeV

¹ Uses Dalitz plot analysis of the $B^0 \rightarrow K_S^0 \pi^+ \pi^-$ final state decays. For the branching fraction of the reference mode, the PDG 18 average $B(B^0 \rightarrow K_S^0 \pi^+ \pi^-) = (4.96 \pm 0.20) \times 10^{-5}$ is used.

$\Gamma(K^0 f_0(1500))/\Gamma_{\text{total}}$ Γ_{316}/Γ

VALUE (units 10^{-6})	DOCUMENT ID	TECN	COMMENT
1.29 ± 0.27 ± 0.70	¹ AAIJ	18F LHCb	pp at 7, 8 TeV

¹ Uses Dalitz plot analysis of the $B^0 \rightarrow K_S^0 \pi^+ \pi^-$ final state decays. For the branching fraction of the reference mode, the PDG 18 average $B(B^0 \rightarrow K_S^0 \pi^+ \pi^-) = (4.96 \pm 0.20) \times 10^{-5}$ is used.

$\Gamma(f_2(1270)K^0)/\Gamma_{\text{total}}$ Γ_{317}/Γ

VALUE (units 10^{-6})	CL%	DOCUMENT ID	TECN	COMMENT
2.7 ^{+1.0} _{-0.8} ± 0.9		¹ AUBERT	09AU BABR	$e^+e^- \rightarrow \Upsilon(4S)$

• • • We do not use the following data for averages, fits, limits, etc. • • •
 <2.5 90 ² GARMASH 07 BELL $e^+e^- \rightarrow \Upsilon(4S)$
¹ Assumes equal production of B^+ and B^0 at the $\Upsilon(4S)$.
² GARMASH 07 reports $B(B^0 \rightarrow f_2(1270)K^0) \times B(f_2(1270) \rightarrow \pi^+\pi^-) < 1.4 \times 10^{-6}$ using Dalitz plot analysis. We compute $B(B^0 \rightarrow f_2(1270)K^0)$ using the PDG value $B(f_2(1270) \rightarrow \pi\pi) = 84.2 \times 10^{-2}$ and 2/3 for the $\pi^+\pi^-$ fraction.

$\Gamma(f_x(1300)K^0, f_x \rightarrow \pi^+\pi^-)/\Gamma_{\text{total}}$ Γ_{318}/Γ

VALUE (units 10^{-6})	DOCUMENT ID	TECN	COMMENT
1.81 ^{+0.55} _{-0.45} ± 0.48	¹ AUBERT	09AU BABR	$e^+e^- \rightarrow \Upsilon(4S)$

¹ Assumes equal production of B^+ and B^0 at the $\Upsilon(4S)$.

$\Gamma(K^*(892)^0\pi^0)/\Gamma_{\text{total}}$ Γ_{319}/Γ

VALUE (units 10^{-6})	CL%	DOCUMENT ID	TECN	COMMENT
3.3 ± 0.5 ± 0.4		^{1,2} LEES	11 BABR	$e^+e^- \rightarrow \Upsilon(4S)$

• • • We do not use the following data for averages, fits, limits, etc. • • •
 3.6 ± 0.7 ± 0.4 ^{1,2} AUBERT 08AQ BABR Repl. by LEES 11
 < 3.5 90 ² CHANG 04 BELL $e^+e^- \rightarrow \Upsilon(4S)$
 < 3.6 90 JESSOP 00 CLE2 $e^+e^- \rightarrow \Upsilon(4S)$
 < 28 90 ASNER 96 CLE2 Repl. by JESSOP 00

¹ Uses Dalitz plot analysis of $B^0 \rightarrow K^+\pi^-\pi^0$ decays.
² Assumes equal production of B^+ and B^0 at the $\Upsilon(4S)$.

$\Gamma(K_S^*(1430)^+\pi^-)/\Gamma_{\text{total}}$ Γ_{320}/Γ

VALUE (units 10^{-6})	CL%	DOCUMENT ID	TECN	COMMENT
3.65 ^{+0.15} _{-0.12} ± 0.31		¹ AAIJ	18F LHCb	pp at 7, 8 TeV

• • • We do not use the following data for averages, fits, limits, etc. • • •
 < 16.2 90 ^{2,3} AUBERT 08AQ BABR $e^+e^- \rightarrow \Upsilon(4S)$
 < 6 90 ⁴ GARMASH 07 BELL $e^+e^- \rightarrow \Upsilon(4S)$
 < 18 90 ³ GARMASH 04 BELL Repl. by GARMASH 07
 < 2600 90 ALBRECHT 91B ARG $e^+e^- \rightarrow \Upsilon(4S)$

¹ Uses Dalitz plot analysis of the $B^0 \rightarrow K_S^0 \pi^+ \pi^-$ final state decays. We compute $B(B^0 \rightarrow K_S^*(1430)^+\pi^-)$ using the PDG 18 value $B(K_S^*(1430) \rightarrow K\pi) = 49.9 \times 10^{-2}$ and 2/3 for the $K^0 \pi^+$ fraction. For the branching fraction of the reference mode, the PDG 18 average $B(B^0 \rightarrow K_S^0 \pi^+ \pi^-) = (4.96 \pm 0.20) \times 10^{-5}$ is used.
² Uses Dalitz plot analysis of $B^0 \rightarrow K^+\pi^-\pi^0$ decays.
³ Assumes equal production of B^+ and B^0 at the $\Upsilon(4S)$.
⁴ GARMASH 07 reports $B(B^0 \rightarrow K_S^*(1430)^+\pi^-) \times B(K_S^*(1430) \rightarrow K^0 \pi^+) < 2.1 \times 10^{-6}$ using Dalitz plot analysis. We compute $B(B^0 \rightarrow K_S^*(1430)^+\pi^-)$ using the PDG value $B(K_S^*(1430) \rightarrow K\pi) = 49.9 \times 10^{-2}$ and 2/3 for the $K^0 \pi^+$ fraction.

$\Gamma(K^*(1680)^+\pi^-)/\Gamma_{\text{total}}$ Γ_{321}/Γ

VALUE (units 10^{-6})	CL%	DOCUMENT ID	TECN	COMMENT
14.1 ± 0.58 ± 0.84		¹ AAIJ	18F LHCb	pp at 7, 8 TeV

• • • We do not use the following data for averages, fits, limits, etc. • • •
 < 25 90 ^{2,3} AUBERT 08AQ BABR $e^+e^- \rightarrow \Upsilon(4S)$
 < 10 90 ⁴ GARMASH 07 BELL $e^+e^- \rightarrow \Upsilon(4S)$

¹ Uses Dalitz plot analysis of the $B^0 \rightarrow K_S^0 \pi^+ \pi^-$ final state decays. We compute $B(B^0 \rightarrow K_S^*(1680)^+\pi^-)$ using the PDG 18 value $B(K_S^*(1680) \rightarrow K\pi) = (49.9 \pm 1.2) \times 10^{-2}$ and 2/3 for the $K^0 \pi^+$ fraction. For the branching fraction of the reference mode, the PDG 18 average $B(B^0 \rightarrow K_S^0 \pi^+ \pi^-) = (4.96 \pm 0.20) \times 10^{-5}$ is used.
² Uses Dalitz plot analysis of $B^0 \rightarrow K^+\pi^-\pi^0$ decays.
³ Assumes equal production of B^+ and B^0 at the $\Upsilon(4S)$.
⁴ GARMASH 07 reports $B(B^0 \rightarrow K^*(1680)^+\pi^-) \times B(K^*(1680) \rightarrow K^0 \pi^+) < 2.6 \times 10^{-6}$ using Dalitz plot analysis. We compute $B(B^0 \rightarrow K^*(1680)^+\pi^-)$ using the PDG value $B(K^*(1680) \rightarrow K\pi) = 38.7 \times 10^{-2}$ and 2/3 for the $K^0 \pi^+$ fraction.

$\Gamma(K^+\pi^-\pi^+\pi^-)/\Gamma_{\text{total}}$ Γ_{322}/Γ

VALUE	CL%	DOCUMENT ID	TECN	COMMENT
< 2.3 × 10⁻⁴	90	¹ ADAM	96D DLPH	$e^+e^- \rightarrow Z$

• • • We do not use the following data for averages, fits, limits, etc. • • •
 < 2.1 × 10⁻⁴ 90 ² ABREU 95N DLPH Sup. by ADAM 96D
¹ ADAM 96D assumes $f_{B^0} = f_{B^-} = 0.39$ and $f_{B_s} = 0.12$. Contributions from B^0 and B_s decays cannot be separated. Limits are given for the weighted average of the decay rates for the two neutral B mesons.
² Assumes a B^0, B^- production fraction of 0.39 and a B_s production fraction of 0.12. Contributions from B^0 and B_s decays cannot be separated. Limits are given for the weighted average of the decay rates for the two neutral B mesons.

$\Gamma(\rho^0 K^+\pi^-)/\Gamma_{\text{total}}$ Γ_{323}/Γ

VALUE (units 10^{-6})	DOCUMENT ID	TECN	COMMENT
2.8 ± 0.5 ± 0.5	^{1,2} KYEONG	09 BELL	$e^+e^- \rightarrow \Upsilon(4S)$

¹ Assumes equal production of B^+ and B^0 at the $\Upsilon(4S)$.
² Required $0.75 < m_{K^+\pi^-} < 1.20 \text{ GeV}/c^2$.

$\Gamma(f_0(980)K^+\pi^-, f_0 \rightarrow \pi\pi)/\Gamma_{\text{total}}$ Γ_{324}/Γ

VALUE (units 10^{-6})	DOCUMENT ID	TECN	COMMENT
1.4 ± 0.4 ^{+0.3} _{-0.4}	^{1,2} KYEONG	09 BELL	$e^+e^- \rightarrow \Upsilon(4S)$

¹ Assumes equal production of B^+ and B^0 at the $\Upsilon(4S)$.
² Required $0.75 < m_{K^+\pi^-} < 1.2 \text{ GeV}/c^2$.

$\Gamma(K^+\pi^-\pi^+\pi^- \text{ nonresonant})/\Gamma_{\text{total}}$ Γ_{325}/Γ

VALUE	CL%	DOCUMENT ID	TECN	COMMENT
< 2.1 × 10⁻⁶	90	^{1,2} KYEONG	09 BELL	$e^+e^- \rightarrow \Upsilon(4S)$

¹ Assumes equal production of B^+ and B^0 at the $\Upsilon(4S)$.
² Required $0.55 < m_{\pi^+\pi^-} < 1.42$ and $0.75 < m_{K^+\pi^-} < 1.20 \text{ GeV}/c^2$.

See key on page 1127

Meson Particle Listings

B^0

$\Gamma(K^*(892)^0 \pi^+ \pi^-) / \Gamma_{total}$ **Γ_{326} / Γ**

VALUE (units 10^{-6})	CL%	DOCUMENT ID	TECN	COMMENT
$54.5 \pm 2.9 \pm 4.3$		1 AUBERT	07As BABR	$e^+ e^- \rightarrow \Upsilon(4S)$
• • • We do not use the following data for averages, fits, limits, etc. • • •				
$4.5^{+1.1+0.9}_{-1.0-1.6}$		1,2 KYEONG	09 BELL	$e^+ e^- \rightarrow \Upsilon(4S)$
<1400	90	ALBRECHT	91E ARG	$e^+ e^- \rightarrow \Upsilon(4S)$

1 Assumes equal production of B^+ and B^0 at the $\Upsilon(4S)$.
2 Required $0.55 < m_{\pi^+ \pi^-} < 1.42$ GeV/ c^2 .

$\Gamma(K_S^0(1430)^+ \rho^-) / \Gamma_{total}$ **Γ_{333} / Γ**

VALUE (units 10^{-6})	DOCUMENT ID	TECN	COMMENT
$28 \pm 10 \pm 6$	1 LEES	12K BABR	$e^+ e^- \rightarrow \Upsilon(4S)$

1 Assumes equal production of B^+ and B^0 at the $\Upsilon(4S)$.

$\Gamma(K_1(1400)^0 \rho^0) / \Gamma_{total}$ **Γ_{334} / Γ**

VALUE	CL%	DOCUMENT ID	TECN	COMMENT
< 3.0×10^{-3}	90	ALBRECHT	91B ARG	$e^+ e^- \rightarrow \Upsilon(4S)$

$\Gamma(K_S^0(1430)^0 \rho^0) / \Gamma_{total}$ **Γ_{335} / Γ**

VALUE (units 10^{-6})	DOCUMENT ID	TECN	COMMENT
$27 \pm 4 \pm 4$	1 LEES	12K BABR	$e^+ e^- \rightarrow \Upsilon(4S)$

1 Assumes equal production of B^+ and B^0 at the $\Upsilon(4S)$.

$\Gamma(K^*(892)^0 \rho^0) / \Gamma_{total}$ **Γ_{327} / Γ**

VALUE (units 10^{-6})	CL%	DOCUMENT ID	TECN	COMMENT
3.9 ± 1.3 OUR AVERAGE		Error includes scale factor of 1.9.		
$5.1 \pm 0.6^{+0.6}_{-0.8}$		1 LEES	12K BABR	$e^+ e^- \rightarrow \Upsilon(4S)$
$2.1^{+0.8+0.9}_{-0.7-0.5}$		1 KYEONG	09 BELL	$e^+ e^- \rightarrow \Upsilon(4S)$
• • • We do not use the following data for averages, fits, limits, etc. • • •				
$5.6 \pm 0.9 \pm 1.3$		1 AUBERT,B	06G BABR	Repl. by LEES 12K
< 34	90	2 GODANG	02 CLE2	$e^+ e^- \rightarrow \Upsilon(4S)$
< 286	90	3 ABE	00c SLD	$e^+ e^- \rightarrow Z$
< 460	90	ALBRECHT	91B ARG	$e^+ e^- \rightarrow \Upsilon(4S)$
< 580	90	4 AVERY	89B CLEO	$e^+ e^- \rightarrow \Upsilon(4S)$
< 960	90	5 AVERY	87 CLEO	$e^+ e^- \rightarrow \Upsilon(4S)$

$\Gamma(K_S^0(1430)^0 f_0(980), f_0 \rightarrow \pi \pi) / \Gamma_{total}$ **Γ_{336} / Γ**

VALUE (units 10^{-6})	DOCUMENT ID	TECN	COMMENT
$2.7 \pm 0.7 \pm 0.6$	1 LEES	12K BABR	$e^+ e^- \rightarrow \Upsilon(4S)$

1 Assumes equal production of B^+ and B^0 at the $\Upsilon(4S)$.

$\Gamma(K_S^0(1430)^0 f_0(980), f_0 \rightarrow \pi \pi) / \Gamma_{total}$ **Γ_{337} / Γ**

VALUE (units 10^{-6})	DOCUMENT ID	TECN	COMMENT
$8.6 \pm 1.7 \pm 1.0$	1 LEES	12K BABR	$e^+ e^- \rightarrow \Upsilon(4S)$

1 Assumes equal production of B^+ and B^0 at the $\Upsilon(4S)$.

1 Assumes equal production of B^+ and B^0 at the $\Upsilon(4S)$.
2 Assumes a helicity 00 configuration. For a helicity 11 configuration, the limit decreases to 2.4×10^{-5} .
3 ABE 00c assumes $B(Z \rightarrow b\bar{b}) = (21.7 \pm 0.1)\%$ and the B fractions $f_{B^0} = f_{B^+} = (39.7^{+1.8}_{-2.2})\%$ and $f_{B_s} = (10.5^{+1.8}_{-2.2})\%$.
4 AVERY 89B reports $< 6.7 \times 10^{-4}$ assuming the $\Upsilon(4S)$ decays 43% to $B^0 \bar{B}^0$. We rescale to 50%.
5 AVERY 87 reports $< 1.2 \times 10^{-3}$ assuming the $\Upsilon(4S)$ decays 40% to $B^0 \bar{B}^0$. We rescale to 50%.

$\Gamma(K^+ K^-) / \Gamma_{total}$ **Γ_{338} / Γ**

VALUE (units 10^{-8})	CL%	DOCUMENT ID	TECN	COMMENT
$7.80 \pm 1.27 \pm 0.84$		1 AAJJ	17G LHCB	pp at 7 and 8 TeV
• • • We do not use the following data for averages, fits, limits, etc. • • •				
10	$\pm 8 \pm 4$	2,3 DUH	13 BELL	$e^+ e^- \rightarrow \Upsilon(4S)$
12	$+ 8$ $- 7 \pm 1$	4 AAJJ	12AR LHCB	Repl. by AAJJ 17G
23	$\pm 10 \pm 10$	5 AALTONEN	12L CDF	$p\bar{p}$ at 1.96 TeV
< 70	90	6 AALTONEN	09c CDF	Repl. by AALTONEN 12L
< 50	90	3 AUBERT	07B BABR	$e^+ e^- \rightarrow \Upsilon(4S)$
< 41	90	7 LIN	07 BELL	Repl. by DUH 13
< 180	90	7 ABULENCIA,A	06D CDF	Repl. by AALTONEN 09c
< 37	90	ABE	05G BELL	Repl. by LIN 07
< 70	90	CHAO	04 BELL	$e^+ e^- \rightarrow \Upsilon(4S)$
< 80	90	3 BORNHEIM	03 CLE2	$e^+ e^- \rightarrow \Upsilon(4S)$
< 60	90	3 AUBERT	02Q BABR	$e^+ e^- \rightarrow \Upsilon(4S)$
< 90	90	3 CASEY	02 BELL	$e^+ e^- \rightarrow \Upsilon(4S)$
< 270	90	3 ABE	01H BELL	$e^+ e^- \rightarrow \Upsilon(4S)$
< 250	90	3 AUBERT	01E BABR	$e^+ e^- \rightarrow \Upsilon(4S)$
< 6600	90	8 ABE	00c SLD	$e^+ e^- \rightarrow Z$
< 190	90	3 CRONIN-HEN.	00 CLE2	$e^+ e^- \rightarrow \Upsilon(4S)$
< 430	90	GODANG	98 CLE2	Repl. by CRONIN-HENNESSY 00
< 4600	90	9 ADAM	96D DLPH	$e^+ e^- \rightarrow Z$
< 400	90	ASNER	96 CLE2	Repl. by GODANG 98
< 1800	90	10 BUSKULIC	96V ALEP	$e^+ e^- \rightarrow Z$
< 12000	90	11 ABREU	95N DLPH	Sup. by ADAM 96D
< 700	90	3 BATTLE	93 CLE2	$e^+ e^- \rightarrow \Upsilon(4S)$

1 Supersedes results of AAJJ 12AR.
2 DUH 13 reports also for the same data $B(B^0 \rightarrow K^+ K^-) < 0.20 \times 10^{-6}$ at 90% CL.
3 Assumes equal production of B^+ and B^0 at the $\Upsilon(4S)$.
4 AAJJ 12AR reports $[\Gamma(B^0 \rightarrow K^+ K^-) / \Gamma_{total}] / [B(B_s^0 \rightarrow K^+ K^-)] / [\Gamma(\bar{B} \rightarrow B_s^0) / \Gamma(\bar{B} \rightarrow B^0)] = 0.018^{+0.008}_{-0.007} \pm 0.009$ which we multiply by our best values $B(B_s^0 \rightarrow K^+ K^-) = (2.66 \pm 0.22) \times 10^{-5}$, $\Gamma(\bar{B} \rightarrow B_s^0) / \Gamma(\bar{B} \rightarrow B^0) = 0.246 \pm 0.023$. Our first error is their experiment's error and our second error is the systematic error from using our best values.
5 Reported a central value of $(0.23 \pm 0.10 \pm 0.10) \times 10^{-6}$ using $B(B^0 \rightarrow K^+ \pi^-) = (19.4 \pm 0.6) \times 10^{-6}$.
6 Obtains this result from $B(K^+ K^-) / B(K^+ \pi^-) = 0.020 \pm 0.008 \pm 0.006$, assuming $B(B^0 \rightarrow K^+ \pi^-) = (19.4 \pm 0.6) \times 10^{-6}$.
7 ABULENCIA,A 06D obtains this from $\Gamma(K^+ K^-) / \Gamma(K^+ \pi^-) < 0.10$ at 90% CL, assuming $B(B^0 \rightarrow K^+ \pi^-) = (18.9 \pm 0.7) \times 10^{-6}$.
8 ABE 00c assumes $B(Z \rightarrow b\bar{b}) = (21.7 \pm 0.1)\%$ and the B fractions $f_{B^0} = f_{B^+} = (39.7^{+1.8}_{-2.2})\%$ and $f_{B_s} = (10.5^{+1.8}_{-2.2})\%$.
9 ADAM 96D assumes $f_{B^0} = f_{B^-} = 0.39$ and $f_{B_s} = 0.12$. Contributions from B^0 and B_s decays cannot be separated. Limits are given for the weighted average of the decay rates for the two neutral B mesons.
10 BUSKULIC 96V assumes PDG 96 production fractions for B^0, B^+, B_s, b baryons.
11 Assumes a B^0, B^- production fraction of 0.39 and a B_s production fraction of 0.12. Contributions from B^0 and B_s^0 decays cannot be separated. Limits are given for the weighted average of the decay rates for the two neutral B mesons.

$\Gamma(K^*(892)^0 f_0(980), f_0 \rightarrow \pi \pi) / \Gamma_{total}$ **Γ_{328} / Γ**

VALUE (units 10^{-6})	CL%	DOCUMENT ID	TECN	COMMENT
$3.9^{+2.1}_{-1.8}$ OUR AVERAGE		Error includes scale factor of 3.9.		
$5.7 \pm 0.6 \pm 0.4$		1 LEES	12K BABR	$e^+ e^- \rightarrow \Upsilon(4S)$
$1.4^{+0.6+0.6}_{-0.5-0.4}$		1,2 KYEONG	09 BELL	$e^+ e^- \rightarrow \Upsilon(4S)$
• • • We do not use the following data for averages, fits, limits, etc. • • •				
< 4.3	90	1 AUBERT,B	06G BABR	$e^+ e^- \rightarrow \Upsilon(4S)$
< 170	90	3 AVERY	89B CLEO	$e^+ e^- \rightarrow \Upsilon(4S)$

$\Gamma(K_1(1270)^+ \pi^-) / \Gamma_{total}$ **Γ_{329} / Γ**

VALUE	CL%	DOCUMENT ID	TECN	COMMENT
< 3.0×10^{-5}	90	1 AUBERT	10D BABR	$e^+ e^- \rightarrow \Upsilon(4S)$

1 Assumes equal production of B^+ and B^0 at the $\Upsilon(4S)$.

$\Gamma(K_1(1400)^+ \pi^-) / \Gamma_{total}$ **Γ_{330} / Γ**

VALUE	CL%	DOCUMENT ID	TECN	COMMENT
< 2.7×10^{-5}	90	1 AUBERT	10D BABR	$e^+ e^- \rightarrow \Upsilon(4S)$
• • • We do not use the following data for averages, fits, limits, etc. • • •				
< 1.1×10^{-3}	90	ALBRECHT	91B ARG	$e^+ e^- \rightarrow \Upsilon(4S)$

1 Assumes equal production of B^+ and B^0 at the $\Upsilon(4S)$.

$\Gamma(a_1(1260)^- K^+) / \Gamma_{total}$ **Γ_{331} / Γ**

VALUE (units 10^{-6})	CL%	DOCUMENT ID	TECN	COMMENT
$16.3 \pm 2.9 \pm 2.3$		1,2 AUBERT	08F BABR	$e^+ e^- \rightarrow \Upsilon(4S)$
• • • We do not use the following data for averages, fits, limits, etc. • • •				
< 230	90	3 ADAM	96D DLPH	$e^+ e^- \rightarrow Z$
< 390	90	4 ABREU	95N DLPH	Sup. by ADAM 96D

1 Assumes equal production of B^+ and B^0 at the $\Upsilon(4S)$.
2 Assumes a_1^\pm decays only to 3π and $B(a_1^\pm \rightarrow \pi^\pm \pi^\mp \pi^\pm) = 0.5$.
3 ADAM 96D assumes $f_{B^0} = f_{B^-} = 0.39$ and $f_{B_s} = 0.12$. Contributions from B^0 and B_s decays cannot be separated. Limits are given for the weighted average of the decay rates for the two neutral B mesons.
4 Assumes a B^0, B^- production fraction of 0.39 and a B_s production fraction of 0.12. Contributions from B^0 and B_s^0 decays cannot be separated. Limits are given for the weighted average of the decay rates for the two neutral B mesons.

$\Gamma(K^*(892)^+ \rho^-) / \Gamma_{total}$ **Γ_{332} / Γ**

VALUE (units 10^{-6})	CL%	DOCUMENT ID	TECN	COMMENT
$10.3 \pm 2.3 \pm 1.3$		1 LEES	12K BABR	$e^+ e^- \rightarrow \Upsilon(4S)$
• • • We do not use the following data for averages, fits, limits, etc. • • •				
< 12.0	90	1 AUBERT,B	06G BABR	Repl. by LEES 12K

1 Assumes equal production of B^+ and B^0 at the $\Upsilon(4S)$.

$\Gamma(K^0 \bar{K}^0) / \Gamma_{total}$ **Γ_{339} / Γ**

VALUE (units 10^{-6})	CL%	DOCUMENT ID	TECN	COMMENT
1.21 ± 0.16 OUR AVERAGE				
$1.26 \pm 0.19 \pm 0.05$		1 DUH	13 BELL	$e^+ e^- \rightarrow \Upsilon(4S)$
$1.08 \pm 0.28 \pm 0.11$		1 AUBERT,BE	06c BABR	$e^+ e^- \rightarrow \Upsilon(4S)$

Meson Particle Listings

B^0

• • • We do not use the following data for averages, fits, limits, etc. • • •

$0.87^{+0.25}_{-0.20} \pm 0.09$	1	LIN	07	BELL	Repl. by DUH 13
$0.8 \pm 0.3 \pm 0.9$	1	ABE	05G	BELL	Repl. by LIN 07
$1.19^{+0.40}_{-0.35} \pm 0.13$	1	AUBERT, BE	05E	BABR	Repl. by AUBERT, BE 06c
< 1.8	90	1	AUBERT	04M	BABR $e^+e^- \rightarrow \Upsilon(4S)$
< 1.5	90	1	CHAO	04	BELL Repl. by ABE 05G
< 3.3	90	1	BORNHEIM	03	CLE2 $e^+e^- \rightarrow \Upsilon(4S)$
< 4.1	90	1	CASEY	02	BELL $e^+e^- \rightarrow \Upsilon(4S)$
< 17	90	1	GODANG	98	CLE2 $e^+e^- \rightarrow \Upsilon(4S)$

¹ Assumes equal production of B^+ and B^0 at the $\Upsilon(4S)$.

$\Gamma(K^0 \bar{K}^0)/\Gamma(K^0 \phi)$ $\Gamma_{339}/\Gamma_{348}$

VALUE	DOCUMENT ID	TECN	COMMENT
$0.17 \pm 0.08 \pm 0.02$	1	AAIJ	20F LHCb pp at 7, 8, 13 TeV

¹ Observed signal with a significance of 3.5 σ .

$\Gamma(K^0 K^- \pi^+)/\Gamma_{total}$ Γ_{340}/Γ

VALUE (units 10^{-6})	CL%	DOCUMENT ID	TECN	COMMENT
6.7 ± 0.5 OUR FIT				
7.0 ± 0.6 OUR AVERAGE				
$7.2 \pm 0.7 \pm 0.3$	1	LAI	19	BELL $e^+e^- \rightarrow \Upsilon(4S)$
$6.4 \pm 1.0 \pm 0.6$	1	DEL-AMO-SA.	10E	BABR $e^+e^- \rightarrow \Upsilon(4S)$

• • • We do not use the following data for averages, fits, limits, etc. • • •

< 18	90	1	GARMASH	04	BELL $e^+e^- \rightarrow \Upsilon(4S)$
< 21	90	1	ECKHART	02	CLE2 $e^+e^- \rightarrow \Upsilon(4S)$

¹ Assumes equal production of B^+ and B^0 at the $\Upsilon(4S)$.

$\Gamma(K^*(892)^\pm K^\mp)/\Gamma_{total}$ Γ_{341}/Γ

VALUE	CL%	DOCUMENT ID	TECN	COMMENT
$< 0.4 \times 10^{-6}$	90	AAIJ	14BMLHCb	pp at 7 TeV

$\Gamma(K^0 K^- \pi^+)/\Gamma(K^0 \pi^+ \pi^-)$ $\Gamma_{340}/\Gamma_{306}$

VALUE	DOCUMENT ID	TECN	COMMENT
0.134 ± 0.011 OUR FIT			
$0.123 \pm 0.009 \pm 0.015$	AAIJ	17BP	LHCb pp at 7, 8 TeV
• • • We do not use the following data for averages, fits, limits, etc. • • •			
$0.128 \pm 0.017 \pm 0.009$	AAIJ	13BP	LHCb Repl. by AAIJ 17BP

$[\Gamma(K^* K^0) + \Gamma(K^* \bar{K}^0)]/\Gamma_{total}$ Γ_{342}/Γ

VALUE (units 10^{-6})	CL%	DOCUMENT ID	TECN	COMMENT
< 0.96	90	1	AAIJ	16 LHCb pp at 7 TeV

• • • We do not use the following data for averages, fits, limits, etc. • • •

< 1.9	90	2	AUBERT, BE	06N	BABR $e^+e^- \rightarrow \Upsilon(4S)$
-------	----	---	------------	-----	--

¹ Assumes $B(B^0 \rightarrow K^0 \pi^+ \pi^-) = (4.96 \pm 0.20) \times 10^{-5}$.

² Assumes equal production of B^+ and B^0 at the $\Upsilon(4S)$.

$\Gamma(K^+ K^- \pi^0)/\Gamma_{total}$ Γ_{343}/Γ

VALUE (units 10^{-6})	CL%	DOCUMENT ID	TECN	COMMENT	
$2.17 \pm 0.60 \pm 0.24$		1	GAUR	13	BELL $e^+e^- \rightarrow \Upsilon(4S)$

• • • We do not use the following data for averages, fits, limits, etc. • • •

< 19	90	1	ECKHART	02	CLE2 $e^+e^- \rightarrow \Upsilon(4S)$
------	----	---	---------	----	--

¹ Assumes equal production of B^+ and B^0 at the $\Upsilon(4S)$.

$\Gamma(K_S^0 K_S^0 \pi^0)/\Gamma_{total}$ Γ_{344}/Γ

VALUE	CL%	DOCUMENT ID	TECN	COMMENT	
$< 0.9 \times 10^{-6}$	90	1	AUBERT	09AD	BABR $e^+e^- \rightarrow \Upsilon(4S)$

¹ Assumes equal production of B^+ and B^0 at the $\Upsilon(4S)$.

$\Gamma(K_S^0 K_S^0 \eta)/\Gamma_{total}$ Γ_{345}/Γ

VALUE	CL%	DOCUMENT ID	TECN	COMMENT	
$< 1.0 \times 10^{-6}$	90	1	AUBERT	09AD	BABR $e^+e^- \rightarrow \Upsilon(4S)$

¹ Assumes equal production of B^+ and B^0 at the $\Upsilon(4S)$.

$\Gamma(K_S^0 K_S^0 \eta')/\Gamma_{total}$ Γ_{346}/Γ

VALUE	CL%	DOCUMENT ID	TECN	COMMENT	
$< 2.0 \times 10^{-6}$	90	1	AUBERT	09AD	BABR $e^+e^- \rightarrow \Upsilon(4S)$

¹ Assumes equal production of B^+ and B^0 at the $\Upsilon(4S)$.

$\Gamma(K^0 K^+ K^-)/\Gamma_{total}$ Γ_{347}/Γ

VALUE (units 10^{-6})	CL%	DOCUMENT ID	TECN	COMMENT
26.8 ± 1.1 OUR FIT				
26.6 ± 1.2 OUR AVERAGE				
$26.5 \pm 0.9 \pm 0.8$	1,2	LEES	12b	BABR $e^+e^- \rightarrow \Upsilon(4S)$
$28.3 \pm 3.3 \pm 4.0$	1	GARMASH	04	BELL $e^+e^- \rightarrow \Upsilon(4S)$

• • • We do not use the following data for averages, fits, limits, etc. • • •

$23.8 \pm 2.0 \pm 1.6$	1	AUBERT, B	04V	BABR	Repl. by LEES 12b
< 1300	90	1	ALBRECHT	91E	ARG $e^+e^- \rightarrow \Upsilon(4S)$

¹ Assumes equal production of B^+ and B^0 at the $\Upsilon(4S)$.

² All intermediate charmonium and charm resonances are removed, except of χ_{c0} .

$\Gamma(K^0 K^+ K^-)/\Gamma(K^0 \pi^+ \pi^-)$ $\Gamma_{347}/\Gamma_{306}$

VALUE	DOCUMENT ID	TECN	COMMENT
0.539 ± 0.025 OUR FIT			
$0.549 \pm 0.018 \pm 0.033$	AAIJ	17BP	LHCb pp at 7, 8 TeV

• • • We do not use the following data for averages, fits, limits, etc. • • •

$0.385 \pm 0.031 \pm 0.023$	AAIJ	13BP	LHCb Repl. by AAIJ 17BP
-----------------------------	------	------	-------------------------

$\Gamma(K^0 \phi)/\Gamma_{total}$ Γ_{348}/Γ

VALUE (units 10^{-6})	CL%	DOCUMENT ID	TECN	COMMENT
7.3 ± 0.7 OUR AVERAGE				
$7.1 \pm 0.6^{+0.4}_{-0.3}$	1	LEES	12b	BABR $e^+e^- \rightarrow \Upsilon(4S)$
$9.0^{+2.2}_{-1.8} \pm 0.7$	1	CHEN	03B	BELL $e^+e^- \rightarrow \Upsilon(4S)$

• • • We do not use the following data for averages, fits, limits, etc. • • •

$8.4^{+1.5}_{-1.3} \pm 0.5$	1	AUBERT	04A	BABR	Repl. by LEES 12b
$8.1^{+3.1}_{-2.5} \pm 0.8$	1	AUBERT	01D	BABR	$e^+e^- \rightarrow \Upsilon(4S)$
< 12.3	90	1	BRIERE	01	CLE2 $e^+e^- \rightarrow \Upsilon(4S)$
< 31	90	1	BERGFELD	98	CLE2
< 88	90	1	ASNER	96	CLE2 $e^+e^- \rightarrow \Upsilon(4S)$
< 720	90	1	ALBRECHT	91B	ARG $e^+e^- \rightarrow \Upsilon(4S)$
< 420	90	2	AVERY	89B	CLEO $e^+e^- \rightarrow \Upsilon(4S)$
< 1000	90	3	AVERY	87	CLEO $e^+e^- \rightarrow \Upsilon(4S)$

¹ Assumes equal production of B^+ and B^0 at the $\Upsilon(4S)$.

² AVERY 89B reports $< 4.9 \times 10^{-4}$ assuming the $\Upsilon(4S)$ decays 43% to $B^0 \bar{B}^0$. We rescale to 50%.

³ AVERY 87 reports $< 1.3 \times 10^{-3}$ assuming the $\Upsilon(4S)$ decays 40% to $B^0 \bar{B}^0$. We rescale to 50%.

$\Gamma(f_0(980) K^0, f_0 \rightarrow K^+ K^-)/\Gamma_{total}$ Γ_{349}/Γ

VALUE (units 10^{-6})	DOCUMENT ID	TECN	COMMENT	
$7.0^{+2.6}_{-1.8} \pm 2.4$	1	LEES	12b	BABR $e^+e^- \rightarrow \Upsilon(4S)$

¹ Assumes equal production of B^+ and B^0 at the $\Upsilon(4S)$.

$\Gamma(f_0(1500) K^0)/\Gamma_{total}$ Γ_{350}/Γ

VALUE (units 10^{-6})	DOCUMENT ID	TECN	COMMENT	
$13.3^{+5.8}_{-4.4} \pm 3.2$	1	LEES	12b	BABR $e^+e^- \rightarrow \Upsilon(4S)$

¹ Assumes equal production of B^+ and B^0 at the $\Upsilon(4S)$.

$\Gamma(f_2'(1525)^0 K^0)/\Gamma_{total}$ Γ_{351}/Γ

VALUE (units 10^{-6})	DOCUMENT ID	TECN	COMMENT	
$0.29^{+0.27}_{-0.18} \pm 0.36$	1	LEES	12b	BABR $e^+e^- \rightarrow \Upsilon(4S)$

¹ Assumes equal production of B^+ and B^0 at the $\Upsilon(4S)$.

$\Gamma(f_0(1710) K^0, f_0 \rightarrow K^+ K^-)/\Gamma_{total}$ Γ_{352}/Γ

VALUE (units 10^{-6})	DOCUMENT ID	TECN	COMMENT	
$4.4 \pm 0.7 \pm 0.5$	1	LEES	12b	BABR $e^+e^- \rightarrow \Upsilon(4S)$

¹ Assumes equal production of B^+ and B^0 at the $\Upsilon(4S)$.

$\Gamma(K^0 K^+ K^- \text{ nonresonant})/\Gamma_{total}$ Γ_{353}/Γ

VALUE (units 10^{-6})	DOCUMENT ID	TECN	COMMENT	
$33 \pm 5 \pm 9$	1	LEES	12b	BABR $e^+e^- \rightarrow \Upsilon(4S)$

¹ Assumes equal production of B^+ and B^0 at the $\Upsilon(4S)$.

$\Gamma(K_S^0 K_S^0 K_S^0)/\Gamma_{total}$ Γ_{354}/Γ

VALUE (units 10^{-6})	DOCUMENT ID	TECN	COMMENT	
6.0 ± 0.5 OUR AVERAGE			Error includes scale factor of 1.1.	
$6.19 \pm 0.48 \pm 0.19$	1	LEES	12b	BABR $e^+e^- \rightarrow \Upsilon(4S)$
$4.2^{+1.6}_{-1.3} \pm 0.8$	1	GARMASH	04	BELL $e^+e^- \rightarrow \Upsilon(4S)$

• • • We do not use the following data for averages, fits, limits, etc. • • •

$6.9^{+0.9}_{-0.8} \pm 0.6$	1	AUBERT, B	05	BABR	Repl. by LEES 12b
-----------------------------	---	-----------	----	------	-------------------

¹ Assumes equal production of B^+ and B^0 at the $\Upsilon(4S)$.

$\Gamma(f_0(980) K^0, f_0 \rightarrow K_S^0 K_S^0)/\Gamma_{total}$ Γ_{355}/Γ

VALUE (units 10^{-6})	DOCUMENT ID	TECN	COMMENT	
$2.7^{+1.3}_{-1.2} \pm 1.3$	1,2	LEES	12b	BABR $e^+e^- \rightarrow \Upsilon(4S)$

¹ Assumes equal production of B^+ and B^0 at the $\Upsilon(4S)$.

² Uses Dalitz plot analysis of the $B^0 \rightarrow K_S^0 K_S^0 K_S^0$ decay.

$\Gamma(f_0(1710) K^0, f_0 \rightarrow K_S^0 K_S^0)/\Gamma_{total}$ Γ_{356}/Γ

VALUE (units 10^{-6})	DOCUMENT ID	TECN	COMMENT	
$0.50^{+0.46}_{-0.24} \pm 0.11$	1,2	LEES	12b	BABR $e^+e^- \rightarrow \Upsilon(4S)$

¹ Assumes equal production of B^+ and B^0 at the $\Upsilon(4S)$.

² Uses Dalitz plot analysis of the $B^0 \rightarrow K_S^0 K_S^0 K_S^0$ decay.

$\Gamma(B^0(210)K^0, \bar{B}^0 \rightarrow K_S^0 K_S^0)/\Gamma_{total}$ **Γ_{357}/Γ**

VALUE (units 10 ⁻⁶)	DOCUMENT ID	TECN	COMMENT
0.54 ± 0.21 ± 0.20 ± 0.52	1,2 LEES	12i	BABR e ⁺ e ⁻ → $\Upsilon(4S)$

¹ Assumes equal production of B⁺ and B⁰ at the $\Upsilon(4S)$.
² Uses Dalitz plot analysis of the B⁰ → K_S⁰K_S⁰ decay.

$\Gamma(K_S^0 K_S^0 K_S^0 \text{ nonresonant})/\Gamma_{total}$ **Γ_{358}/Γ**

VALUE (units 10 ⁻⁶)	DOCUMENT ID	TECN	COMMENT
13.3 ± 2.2 ± 2.3 ± 2.2	1,2 LEES	12i	BABR e ⁺ e ⁻ → $\Upsilon(4S)$

¹ Assumes equal production of B⁺ and B⁰ at the $\Upsilon(4S)$.
² Uses Dalitz plot analysis of the B⁰ → K_S⁰K_S⁰K_S⁰ decay.

$\Gamma(K_S^0 K_S^0 K_L^0)/\Gamma_{total}$ **Γ_{359}/Γ**

VALUE (units 10 ⁻⁶)	CL%	DOCUMENT ID	TECN	COMMENT
<16	90	1 AUBERT,B	06R	BABR e ⁺ e ⁻ → $\Upsilon(4S)$

¹ Assumes equal production of B⁺ and B⁰ at the $\Upsilon(4S)$.

$\Gamma(K^*(892)^0 K^+ K^-)/\Gamma_{total}$ **Γ_{360}/Γ**

VALUE (units 10 ⁻⁶)	CL%	DOCUMENT ID	TECN	COMMENT
27.5 ± 1.3 ± 2.2		1 AUBERT	07As	BABR e ⁺ e ⁻ → $\Upsilon(4S)$
<610	90	ALBRECHT	91E	ARG e ⁺ e ⁻ → $\Upsilon(4S)$

••• We do not use the following data for averages, fits, limits, etc. •••

¹ Assumes equal production of B⁺ and B⁰ at the $\Upsilon(4S)$.

$\Gamma(K^*(892)^0 \phi)/\Gamma_{total}$ **Γ_{361}/Γ**

VALUE (units 10 ⁻⁶)	CL%	DOCUMENT ID	TECN	COMMENT
10.0 ± 0.5 OUR FIT				
10.0 ± 0.5 OUR AVERAGE				
10.4 ± 0.5 ± 0.6		1 PRIM	13	BELL e ⁺ e ⁻ → $\Upsilon(4S)$
9.7 ± 0.5 ± 0.5		1 AUBERT	08Bg	BABR e ⁺ e ⁻ → $\Upsilon(4S)$
11.5 ± 4.5 ± 1.8 ± 3.7 ± 1.7		1 BRIERE	01	CLE2 e ⁺ e ⁻ → $\Upsilon(4S)$

••• We do not use the following data for averages, fits, limits, etc. •••

9.2 ± 0.7 ± 0.6		1 AUBERT	07D	BABR Repl. by AUBERT 08Bg
9.2 ± 0.9 ± 0.5		1 AUBERT,B	04W	BABR Repl. by AUBERT 07D
11.2 ± 1.3 ± 0.8		1 AUBERT	03V	BABR Repl. by AUBERT,B 04W
10.0 ± 1.6 ± 0.7 ± 1.5 ± 0.8		1 CHEN	03B	BELL Repl. by PRIM 13
8.7 ± 2.5 ± 2.1 ± 1.1		1 AUBERT	01D	BABR Repl. by AUBERT 03V
<384	90	2 ABE	00c	SLD e ⁺ e ⁻ → Z
< 21	90	1 BERGFELD	98	CLE2
< 43	90	ASNER	96	CLE2 e ⁺ e ⁻ → $\Upsilon(4S)$
<320	90	ALBRECHT	91B	ARG e ⁺ e ⁻ → $\Upsilon(4S)$
<380	90	3 AVERY	89B	CLE0 e ⁺ e ⁻ → $\Upsilon(4S)$
<380	90	4 AVERY	87	CLE0 e ⁺ e ⁻ → $\Upsilon(4S)$

¹ Assumes equal production of B⁺ and B⁰ at the $\Upsilon(4S)$.
² ABE 00c assumes B(Z → b \bar{b})=(21.7 ± 0.1)% and the B fractions f_{B⁰}=f_{B⁺}=(39.7 ± 1.8 ± 2.2)% and f_{B_S⁻}=(10.5 ± 2.2)%.
³ AVERY 89B reports < 4.4 × 10⁻⁴ assuming the $\Upsilon(4S)$ decays 43% to B⁰B⁰. We rescale to 50%.
⁴ AVERY 87 reports < 4.7 × 10⁻⁴ assuming the $\Upsilon(4S)$ decays 40% to B⁰B⁰. We rescale to 50%.

$\Gamma(K^+ K^- \pi^+ \pi^- \text{ nonresonant})/\Gamma_{total}$ **Γ_{362}/Γ**

VALUE (units 10 ⁻⁶)	CL%	DOCUMENT ID	TECN	COMMENT
<71.7	90	1,2 CHIANG	10	BELL e ⁺ e ⁻ → $\Upsilon(4S)$

¹ Measured in the range 0.7 < m_{K π} < 1.7 and corrected using PS assumption for the full K π mass range.
² Assumes equal production of B⁺ and B⁰ at the $\Upsilon(4S)$.

$\Gamma(K^*(892)^0 K^- \pi^+)/\Gamma_{total}$ **Γ_{363}/Γ**

VALUE (units 10 ⁻⁶)	DOCUMENT ID	TECN	COMMENT
4.5 ± 1.3 OUR AVERAGE			
2.1 ± 5.63 ± 4.85 ± 5.26 ± 4.75	1,2 CHIANG	10	BELL e ⁺ e ⁻ → $\Upsilon(4S)$
4.6 ± 1.1 ± 0.8	2 AUBERT	07As	BABR e ⁺ e ⁻ → $\Upsilon(4S)$

¹ Measured in the range 0.7 < m_{K π} < 1.7 and corrected using PS assumption for the full K π mass range. The quoted result is equivalent to the upper limit of < 13.9 × 10⁻⁶ at 90% CL.
² Assumes equal production of B⁺ and B⁰ at the $\Upsilon(4S)$.

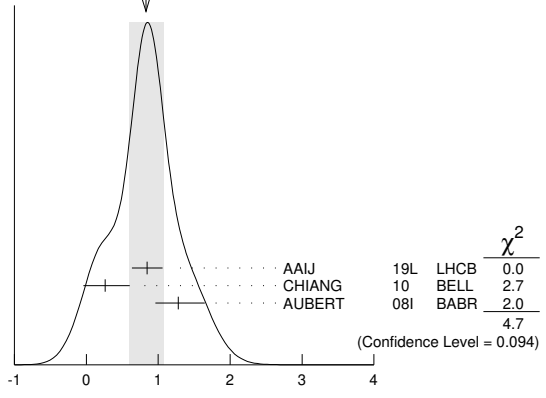
$\Gamma(K^*(892)^0 \bar{K}^*(892)^0)/\Gamma_{total}$ **Γ_{364}/Γ**

VALUE (units 10 ⁻⁶)	CL%	DOCUMENT ID	TECN	COMMENT
0.83 ± 0.24 OUR AVERAGE				Error includes scale factor of 1.5. See the ideogram below.
0.85 ± 0.07 ± 0.20		1 AAIJ	19L	LHCB pp at 7 and 8 TeV
0.26 ± 0.33 ± 0.10 ± 0.29 ± 0.08		2,3 CHIANG	10	BELL e ⁺ e ⁻ → $\Upsilon(4S)$
1.28 ± 0.35 ± 0.30 ± 0.11		3 AUBERT	08i	BABR e ⁺ e ⁻ → $\Upsilon(4S)$

••• We do not use the following data for averages, fits, limits, etc. •••

< 22	90	4 GODA NG	02	CLE2	e ⁺ e ⁻ → $\Upsilon(4S)$
<469	90	5 ABE	00c	SLD	e ⁺ e ⁻ → Z

WEIGHTED AVERAGE
0.83±0.24 (Error scaled by 1.5)



¹ AAIJ 19L reports $[\Gamma(B^0 \rightarrow K^*(892)^0 \bar{K}^*(892)^0)/\Gamma_{total}] / [B(B_S^0 \rightarrow \bar{K}^*(892)^0 K^*(892)^0)] = 0.0758 \pm 0.0057 \pm 0.0030$ which we multiply by our best value $B(B_S^0 \rightarrow \bar{K}^*(892)^0 K^*(892)^0) = (1.11 \pm 0.27) \times 10^{-5}$. Our first error is their experiment's error and our second error is the systematic error from using our best value.
² Measured in the range 0.7 < m_{K π} < 1.7 and corrected using PS assumption for the full K π mass range. The quoted result is equivalent to the upper limit of < 0.8 × 10⁻⁶ at 90% CL.
³ Assumes equal production of B⁺ and B⁰ at the $\Upsilon(4S)$.
⁴ Assumes a helicity 00 configuration. For a helicity 11 configuration, the limit decreases to 1.9 × 10⁻⁵.
⁵ ABE 00c assumes B(Z → b \bar{b})=(21.7 ± 0.1)% and the B fractions f_{B⁰}=f_{B⁺}=(39.7 ± 1.8 ± 2.2)% and f_{B_S⁻}=(10.5 ± 2.2)%.

$\Gamma(K^+ K^+ \pi^- \pi^- \text{ nonresonant})/\Gamma_{total}$ **Γ_{365}/Γ**

VALUE (units 10 ⁻⁶)	CL%	DOCUMENT ID	TECN	COMMENT
<6.0	90	1 CHIANG	10	BELL e ⁺ e ⁻ → $\Upsilon(4S)$

¹ Assumes equal production of B⁺ and B⁰ at the $\Upsilon(4S)$.

$\Gamma(K^*(892)^0 K^+ \pi^-)/\Gamma_{total}$ **Γ_{366}/Γ**

VALUE (units 10 ⁻⁶)	CL%	DOCUMENT ID	TECN	COMMENT
<2.2		1 AUBERT	07As	BABR e ⁺ e ⁻ → $\Upsilon(4S)$
<7.6	90	1 CHIANG	10	BELL e ⁺ e ⁻ → $\Upsilon(4S)$

¹ Assumes equal production of B⁺ and B⁰ at the $\Upsilon(4S)$.

$\Gamma(K^*(892)^0 K^*(892)^0)/\Gamma_{total}$ **Γ_{367}/Γ**

VALUE (units 10 ⁻⁶)	CL%	DOCUMENT ID	TECN	COMMENT
< 0.2	90	1 CHIANG	10	BELL e ⁺ e ⁻ → $\Upsilon(4S)$

••• We do not use the following data for averages, fits, limits, etc. •••

< 0.41	90	1 AUBERT	08i	BABR e ⁺ e ⁻ → $\Upsilon(4S)$
<37	90	2 GODA NG	02	CLE2 e ⁺ e ⁻ → $\Upsilon(4S)$

¹ Assumes equal production of B⁺ and B⁰ at the $\Upsilon(4S)$.
² Assumes a helicity 00 configuration. For a helicity 11 configuration, the limit decreases to 2.9 × 10⁻⁵.

$\Gamma(K^*(892)^+ K^*(892)^-)/\Gamma_{total}$ **Γ_{368}/Γ**

VALUE (units 10 ⁻⁶)	CL%	DOCUMENT ID	TECN	COMMENT
< 2.0	90	1 AUBERT	08AP	BABR e ⁺ e ⁻ → $\Upsilon(4S)$

••• We do not use the following data for averages, fits, limits, etc. •••

<141	90	2 GODA NG	02	CLE2 e ⁺ e ⁻ → $\Upsilon(4S)$
------	----	-----------	----	---

¹ Assumes equal production of B⁺ and B⁰ at the $\Upsilon(4S)$.
² Assumes a helicity 00 configuration. For a helicity 11 configuration, the limit decreases to 8.9 × 10⁻⁵.

$\Gamma(K_1(1400)^0 \phi)/\Gamma_{total}$ **Γ_{369}/Γ**

VALUE	CL%	DOCUMENT ID	TECN	COMMENT
<5.0 × 10⁻³	90	ALBRECHT	91B	ARG e ⁺ e ⁻ → $\Upsilon(4S)$

$\Gamma(\phi(K\pi)_0^0)/\Gamma_{total}$ **Γ_{370}/Γ**

This decay refers to the coherent sum of resonant and nonresonant J^P = 0⁺ K π components with 1.13 < m_{K π} < 1.53 GeV/c².

VALUE (units 10 ⁻⁶)	DOCUMENT ID	TECN	COMMENT
4.3 ± 0.4 OUR AVERAGE			
4.3 ± 0.4 ± 0.4	1 PRIM	13	BELL e ⁺ e ⁻ → $\Upsilon(4S)$
4.3 ± 0.6 ± 0.4	1 AUBERT	08Bg	BABR e ⁺ e ⁻ → $\Upsilon(4S)$

Meson Particle Listings

 B^0

- We do not use the following data for averages, fits, limits, etc. •••

$5.0 \pm 0.8 \pm 0.3$ ¹AUBERT 07D BABR Repl. by AUBERT 08BG

¹ Assumes equal production of B^+ and B^0 at the $\Upsilon(4S)$.

$$\Gamma(\phi(K\pi)_0^0(1.60 < m_{K\pi} < 2.15))/\Gamma_{\text{total}} \quad \Gamma_{371}/\Gamma$$

This decay refers to the coherent sum of resonant and nonresonant $J^P = 0^+ K\pi$ components with $1.60 < m_{K\pi} < 2.15 \text{ GeV}/c^2$.

VALUE (units 10^{-6})	CL%	DOCUMENT ID	TECN	COMMENT
<1.7	90	¹ AUBERT 07A0 BABR		$e^+e^- \rightarrow \Upsilon(4S)$

¹ Assumes equal production of B^+ and B^0 at the $\Upsilon(4S)$.

$$\Gamma(K_0^*(1430)^0 K^- \pi^+)/\Gamma_{\text{total}} \quad \Gamma_{372}/\Gamma$$

VALUE (units 10^{-6})	CL%	DOCUMENT ID	TECN	COMMENT
<31.8	90	^{1,2} CHIANG 10 BELL		$e^+e^- \rightarrow \Upsilon(4S)$

¹ Measured in the range $0.7 < m_{K\pi} < 1.7$ and corrected using PS assumption for the full $K\pi$ mass range.

² Assumes equal production of B^+ and B^0 at the $\Upsilon(4S)$.

$$\Gamma(K_0^*(1430)^0 \bar{K}^*(892)^0)/\Gamma_{\text{total}} \quad \Gamma_{373}/\Gamma$$

VALUE (units 10^{-6})	CL%	DOCUMENT ID	TECN	COMMENT
<3.3	90	^{1,2} CHIANG 10 BELL		$e^+e^- \rightarrow \Upsilon(4S)$

¹ Measured in the range $0.7 < m_{K\pi} < 1.7$ and corrected using PS assumption for the full $K\pi$ mass range.

² Assumes equal production of B^+ and B^0 at the $\Upsilon(4S)$.

$$\Gamma(K_0^*(1430)^0 \bar{K}_0^*(1430)^0)/\Gamma_{\text{total}} \quad \Gamma_{374}/\Gamma$$

VALUE (units 10^{-6})	CL%	DOCUMENT ID	TECN	COMMENT
<8.4	90	^{1,2} CHIANG 10 BELL		$e^+e^- \rightarrow \Upsilon(4S)$

¹ Measured in the range $0.7 < m_{K\pi} < 1.7$ and corrected using PS assumption for the full $K\pi$ mass range.

² Assumes equal production of B^+ and B^0 at the $\Upsilon(4S)$.

$$\Gamma(K_0^*(1430)^0 \phi)/\Gamma_{\text{total}} \quad \Gamma_{375}/\Gamma$$

VALUE (units 10^{-6})	CL%	DOCUMENT ID	TECN	COMMENT
$3.9 \pm 0.5 \pm 0.6$		¹ AUBERT 08BG BABR		$e^+e^- \rightarrow \Upsilon(4S)$

- We do not use the following data for averages, fits, limits, etc. •••

$4.6 \pm 0.7 \pm 0.6$ ¹AUBERT 07D BABR Repl. by AUBERT 08BG
seen ²AUBERT,B 04W BABR Repl. by AUBERT 07D

¹ Assumes equal production of B^+ and B^0 at the $\Upsilon(4S)$.

² Observed 181 ± 17 events with statistical significance greater than 10σ .

$$\Gamma(K_0^*(1430)^0 K^*(892)^0)/\Gamma_{\text{total}} \quad \Gamma_{376}/\Gamma$$

VALUE (units 10^{-6})	CL%	DOCUMENT ID	TECN	COMMENT
<1.7	90	¹ CHIANG 10 BELL		$e^+e^- \rightarrow \Upsilon(4S)$

¹ Assumes equal production of B^+ and B^0 at the $\Upsilon(4S)$.

$$\Gamma(K_0^*(1430)^0 K_0^*(1430)^0)/\Gamma_{\text{total}} \quad \Gamma_{377}/\Gamma$$

VALUE (units 10^{-6})	CL%	DOCUMENT ID	TECN	COMMENT
<4.7	90	¹ CHIANG 10 BELL		$e^+e^- \rightarrow \Upsilon(4S)$

¹ Assumes equal production of B^+ and B^0 at the $\Upsilon(4S)$.

$$\Gamma(K^*(1680)^0 \phi)/\Gamma_{\text{total}} \quad \Gamma_{378}/\Gamma$$

VALUE (units 10^{-6})	CL%	DOCUMENT ID	TECN	COMMENT
<3.5	90	¹ AUBERT 07A0 BABR		$e^+e^- \rightarrow \Upsilon(4S)$

¹ Assumes equal production of B^+ and B^0 at the $\Upsilon(4S)$.

$$\Gamma(K^*(1780)^0 \phi)/\Gamma_{\text{total}} \quad \Gamma_{379}/\Gamma$$

VALUE (units 10^{-6})	CL%	DOCUMENT ID	TECN	COMMENT
<2.7	90	¹ AUBERT 07A0 BABR		$e^+e^- \rightarrow \Upsilon(4S)$

¹ Assumes equal production of B^+ and B^0 at the $\Upsilon(4S)$.

$$\Gamma(K^*(2045)^0 \phi)/\Gamma_{\text{total}} \quad \Gamma_{380}/\Gamma$$

VALUE (units 10^{-6})	CL%	DOCUMENT ID	TECN	COMMENT
<15.3	90	¹ AUBERT 07A0 BABR		$e^+e^- \rightarrow \Upsilon(4S)$

¹ Assumes equal production of B^+ and B^0 at the $\Upsilon(4S)$.

$$\Gamma(K_2^*(1430)^0 \rho^0)/\Gamma_{\text{total}} \quad \Gamma_{381}/\Gamma$$

VALUE (units 10^{-6})	CL%	DOCUMENT ID	TECN	COMMENT
<1.1 $\times 10^3$	90	ALBRECHT 91B ARG		$e^+e^- \rightarrow \Upsilon(4S)$

$$\Gamma(K_2^*(1430)^0 \phi)/\Gamma_{\text{total}} \quad \Gamma_{382}/\Gamma$$

VALUE (units 10^{-6})	CL%	DOCUMENT ID	TECN	COMMENT
6.8 ± 0.9 OUR AVERAGE		Error includes scale factor of 1.2.		

$5.5^{+0.9}_{-0.7} \pm 1.0$ ¹PRIM 13 BELL $e^+e^- \rightarrow \Upsilon(4S)$

$7.5 \pm 0.9 \pm 0.5$ ¹AUBERT 08BG BABR $e^+e^- \rightarrow \Upsilon(4S)$

- We do not use the following data for averages, fits, limits, etc. •••

$7.8 \pm 1.1 \pm 0.6$ ¹AUBERT 07D BABR Repl. by AUBERT 08BG
seen ²AUBERT,B 04W BABR Repl. by AUBERT 07D

¹ Assumes equal production of B^+ and B^0 at the $\Upsilon(4S)$.

² The angular distribution of $B \rightarrow \phi K^*(1430)$ provides evidence with statistical significance of 3.2σ .

$$\Gamma(K^0 \phi \phi)/\Gamma_{\text{total}} \quad \Gamma_{383}/\Gamma$$

VALUE (units 10^{-6})	CL%	DOCUMENT ID	TECN	COMMENT
3.7 ± 0.7 OUR AVERAGE		Error includes scale factor of 1.3.		

$3.02^{+0.75}_{-0.66} \pm 0.20$ ¹MOHANTY 21 BELL $e^+e^- \rightarrow \Upsilon(4S)$

$4.5 \pm 0.8 \pm 0.3$ ¹LEES 11A BABR $e^+e^- \rightarrow \Upsilon(4S)$

- We do not use the following data for averages, fits, limits, etc. •••

$4.1^{+1.7}_{-1.4} \pm 0.4$ ¹AUBERT,BE 06H BABR Repl. by LEES 11A

¹ Assumes equal production of B^0 and B^+ at the $\Upsilon(4S)$ and the $\phi\phi$ invariant mass below $2.85 \text{ GeV}/c^2$.

$$\Gamma(\eta'/\eta' K^0)/\Gamma_{\text{total}} \quad \Gamma_{384}/\Gamma$$

VALUE (units 10^{-6})	CL%	DOCUMENT ID	TECN	COMMENT
<31	90	¹ AUBERT,B 06P BABR		$e^+e^- \rightarrow \Upsilon(4S)$

¹ Assumes equal production of B^+ and B^0 at the $\Upsilon(4S)$.

$$\Gamma(\eta K^0 \gamma)/\Gamma_{\text{total}} \quad \Gamma_{385}/\Gamma$$

VALUE (units 10^{-6})	CL%	DOCUMENT ID	TECN	COMMENT
7.6 ± 1.8 OUR AVERAGE				

$7.1^{+2.1}_{-2.0} \pm 0.4$ ^{1,2}AUBERT 09 BABR $e^+e^- \rightarrow \Upsilon(4S)$

$8.7^{+3.1+1.9}_{-2.7-1.6}$ ^{2,3}NISHIDA 05 BELL $e^+e^- \rightarrow \Upsilon(4S)$

- We do not use the following data for averages, fits, limits, etc. •••

$11.3^{+2.8}_{-1.6} \pm 0.6$ ^{1,2}AUBERT,B 06M BABR Repl. by AUBERT 09

¹ $m_{\eta K} < 3.25 \text{ GeV}/c^2$.

² Assumes equal production of B^+ and B^0 at the $\Upsilon(4S)$.

³ $m_{\eta' K} < 2.4 \text{ GeV}/c^2$.

$$\Gamma(\eta' K^0 \gamma)/\Gamma_{\text{total}} \quad \Gamma_{386}/\Gamma$$

VALUE (units 10^{-6})	CL%	DOCUMENT ID	TECN	COMMENT
<6.4	90	^{1,2} WEDD 10 BELL		$e^+e^- \rightarrow \Upsilon(4S)$

- We do not use the following data for averages, fits, limits, etc. •••

<6.6 ^{1,3}AUBERT,B 06M BABR $e^+e^- \rightarrow \Upsilon(4S)$

¹ Assumes equal production of B^+ and B^0 at the $\Upsilon(4S)$.

² $m_{\eta' K} < 3.4 \text{ GeV}/c^2$.

³ $m_{\eta' K} < 3.25 \text{ GeV}/c^2$.

$$\Gamma(K^0 \phi \gamma)/\Gamma_{\text{total}} \quad \Gamma_{387}/\Gamma$$

VALUE (units 10^{-6})	CL%	DOCUMENT ID	TECN	COMMENT
$2.74 \pm 0.60 \pm 0.32$		¹ SAHOO 11A BELL		$e^+e^- \rightarrow \Upsilon(4S)$

- We do not use the following data for averages, fits, limits, etc. •••

<2.7 ¹AUBERT 07Q BABR $e^+e^- \rightarrow \Upsilon(4S)$

<8.3 ¹DRUTSKOY 04 BELL $e^+e^- \rightarrow \Upsilon(4S)$

¹ Assumes equal production of B^+ and B^0 at the $\Upsilon(4S)$.

$$\Gamma(K^+ \pi^- \pi^-)/\Gamma_{\text{total}} \quad \Gamma_{388}/\Gamma$$

VALUE	DOCUMENT ID	TECN	COMMENT
$(4.6^{+1.3+0.5}_{-1.2-0.7}) \times 10^{-6}$	^{1,2} NISHIDA 02 BELL		$e^+e^- \rightarrow \Upsilon(4S)$

¹ Assumes equal production of B^+ and B^0 at the $\Upsilon(4S)$.

² $1.25 \text{ GeV}/c^2 < m_{K\pi} < 1.6 \text{ GeV}/c^2$

$$\Gamma(K^*(892)^0 \gamma)/\Gamma_{\text{total}} \quad \Gamma_{389}/\Gamma$$

VALUE (units 10^{-6})	CL%	DOCUMENT ID	TECN	COMMENT
41.8 ± 2.5 OUR AVERAGE		Error includes scale factor of 2.1.		

$39.6 \pm 0.7 \pm 1.4$ ¹HORIGUCHI 17 BELL $e^+e^- \rightarrow \Upsilon(4S)$

$44.7 \pm 1.0 \pm 1.6$ ²AUBERT 09A0 BABR $e^+e^- \rightarrow \Upsilon(4S)$

$45.5^{+7.2}_{-6.8} \pm 3.4$ ³COAN 00 CLE2 $e^+e^- \rightarrow \Upsilon(4S)$

- We do not use the following data for averages, fits, limits, etc. •••

$39.2 \pm 2.0 \pm 2.4$ ⁴AUBERT,BE 04A BABR Repl. by AUBERT 09A0

$40.1 \pm 2.1 \pm 1.7$ ⁵NAKAO 04 BELL Repl. by HORIGUCHI 17

< 110 ⁹⁰ ACOSTA 02G CDF $p\bar{p}$ at 1.8 TeV

$42.3 \pm 4.0 \pm 2.2$ ⁵AUBERT 02C BABR Repl. by AUBERT,BE 04A

< 210 ⁹⁰ ADAM 96D DLPH $e^+e^- \rightarrow Z$

< 40 $\pm 17 \pm 8$ ⁷AMMAR 93 CLE2 Repl. by COAN 00

< 420 ⁹⁰ ALBRECHT 89G ARG $e^+e^- \rightarrow \Upsilon(4S)$

< 240 ⁹⁰ AVERY 89B CLE0 $e^+e^- \rightarrow \Upsilon(4S)$

< 2100 ⁹⁰ AVERY 87 CLE0 $e^+e^- \rightarrow \Upsilon(4S)$

¹ Uses $B(\Upsilon(4S) \rightarrow B^+ B^-) = (51.4 \pm 0.6)\%$ and $B(\Upsilon(4S) \rightarrow B^0 \bar{B}^0) = (48.6 \pm 0.6)\%$.

² Uses $B(\Upsilon(4S) \rightarrow B^+ B^-) = (51.6 \pm 0.6)\%$ and $B(\Upsilon(4S) \rightarrow B^0 \bar{B}^0) = (48.4 \pm 0.6)\%$.

³ Assumes equal production of B^+ and B^0 at the $\Upsilon(4S)$. No evidence for a nonresonant $K\pi\gamma$ contamination was seen; the central value assumes no contamination.

⁴ Uses the production ratio of charged and neutral B from $\Upsilon(4S)$ decays $R^{+}/0 = 1.006 \pm 0.048$.

⁵ Assumes equal production of B^+ and B^0 at the $\Upsilon(4S)$.

⁶ ADAM 96D assumes $f_{B^0} = f_{B^-} = 0.39$ and $f_{B_s} = 0.12$.

⁷ AMMAR 93 observed 6.6 ± 2.8 events above background.

⁸ AVERY 89B reports $< 2.8 \times 10^{-4}$ assuming the $\Upsilon(4S)$ decays 43% to $B^0 \bar{B}^0$. We rescale to 50%.

$\Gamma(K^*(1410)\gamma)/\Gamma_{total}$					Γ_{390}/Γ
VALUE	CL%	DOCUMENT ID	TECN	COMMENT	
$<1.3 \times 10^{-4}$	90	¹ NISHIDA	02	BELL $e^+e^- \rightarrow \Upsilon(4S)$	

¹ Assumes equal production of B⁺ and B⁰ at the $\Upsilon(4S)$.

$\Gamma(K^+\pi^-\gamma \text{ nonresonant})/\Gamma_{total}$					Γ_{391}/Γ
VALUE	CL%	DOCUMENT ID	TECN	COMMENT	
$<2.6 \times 10^{-6}$	90	^{1,2} NISHIDA	02	BELL $e^+e^- \rightarrow \Upsilon(4S)$	

¹ Assumes equal production of B⁺ and B⁰ at the $\Upsilon(4S)$.
² $1.25 \text{ GeV}/c^2 < M_{K\pi} < 1.6 \text{ GeV}/c^2$

$\Gamma(K^*(892)^0 X(214), X \rightarrow \mu^+\mu^-)/\Gamma_{total}$					Γ_{392}/Γ
VALUE (units 10^{-8})	CL%	DOCUMENT ID	TECN	COMMENT	
<2.26	90	^{1,2} HYUN	10	BELL $e^+e^- \rightarrow \Upsilon(4S)$	

X(214) is a hypothetical particle of mass 214 MeV/c² reported by the HyperCP experiment (PARK 05)
¹ Assumes equal production of B⁺ and B⁰ at the $\Upsilon(4S)$.
² Based on scalar nature of X particle. With a vector X assumption, the upper limit is 2.27×10^{-8} .

$\Gamma(K^0\pi^+\pi^-)/\Gamma_{total}$					Γ_{393}/Γ
VALUE (units 10^{-9})	CL%	DOCUMENT ID	TECN	COMMENT	
1.99 ± 0.18 OUR AVERAGE					
$2.05 \pm 0.20^{+0.26}_{-0.22}$		^{1,2} DEL-AMO-SA...	16	BABR $e^+e^- \rightarrow \Upsilon(4S)$	
$1.85 \pm 0.21 \pm 0.12$		^{1,3} AUBERT	07R	BABR $e^+e^- \rightarrow \Upsilon(4S)$	
$2.40 \pm 0.4 \pm 0.3$		^{3,4} YANG	05	BELL $e^+e^- \rightarrow \Upsilon(4S)$	

¹ $M_{K\pi\pi} < 1.8 \text{ GeV}/c^2$.
² Uses $B(\Upsilon(4S) \rightarrow B^+B^-) = 0.513 \pm 0.006$.
³ Assumes equal production of B⁺ and B⁰ at the $\Upsilon(4S)$.
⁴ $M_{K\pi\pi} < 2.0 \text{ GeV}/c^2$.

$\Gamma(K^+\pi^-\pi^0\gamma)/\Gamma_{total}$					Γ_{394}/Γ
VALUE (units 10^{-5})	CL%	DOCUMENT ID	TECN	COMMENT	
$4.07 \pm 0.22 \pm 0.31$		^{1,2} AUBERT	07R	BABR $e^+e^- \rightarrow \Upsilon(4S)$	

¹ $M_{K\pi\pi} < 1.8 \text{ GeV}/c^2$.
² Assumes equal production of B⁺ and B⁰ at the $\Upsilon(4S)$.

$\Gamma(K_1(1270)^0\gamma)/\Gamma_{total}$					Γ_{395}/Γ
VALUE (units 10^{-5})	CL%	DOCUMENT ID	TECN	COMMENT	
< 5.8	90	¹ YANG	05	BELL $e^+e^- \rightarrow \Upsilon(4S)$	

• • • We do not use the following data for averages, fits, limits, etc. • • •
 <700 90 ² ALBRECHT 89G ARG $e^+e^- \rightarrow \Upsilon(4S)$
¹ Assumes equal production of B⁺ and B⁰ at the $\Upsilon(4S)$.
² ALBRECHT 89G reports < 0.0078 assuming the $\Upsilon(4S)$ decays 45% to $B^0\bar{B}^0$. We rescale to 50%.

$\Gamma(K_1(1400)^0\gamma)/\Gamma_{total}$					Γ_{396}/Γ
VALUE (units 10^{-5})	CL%	DOCUMENT ID	TECN	COMMENT	
< 1.2	90	¹ YANG	05	BELL $e^+e^- \rightarrow \Upsilon(4S)$	

• • • We do not use the following data for averages, fits, limits, etc. • • •
 <430 90 ² ALBRECHT 89G ARG $e^+e^- \rightarrow \Upsilon(4S)$
¹ Assumes equal production of B⁺ and B⁰ at the $\Upsilon(4S)$.
² ALBRECHT 89G reports < 0.0048 assuming the $\Upsilon(4S)$ decays 45% to $B^0\bar{B}^0$. We rescale to 50%.

$\Gamma(K_2^*(1430)^0\gamma)/\Gamma_{total}$					Γ_{397}/Γ
VALUE (units 10^{-5})	CL%	DOCUMENT ID	TECN	COMMENT	
1.24 ± 0.24 OUR AVERAGE					
$1.22 \pm 0.25 \pm 0.10$		¹ AUBERT,B	04U	BABR $e^+e^- \rightarrow \Upsilon(4S)$	
$1.3 \pm 0.5 \pm 0.1$		¹ NISHIDA	02	BELL $e^+e^- \rightarrow \Upsilon(4S)$	

• • • We do not use the following data for averages, fits, limits, etc. • • •
 <40 90 ² ALBRECHT 89G ARG $e^+e^- \rightarrow \Upsilon(4S)$
¹ Assumes equal production of B⁺ and B⁰ at the $\Upsilon(4S)$.
² ALBRECHT 89G reports $< 4.4 \times 10^{-4}$ assuming the $\Upsilon(4S)$ decays 45% to $B^0\bar{B}^0$. We rescale to 50%.

$\Gamma(K^*(1680)^0\gamma)/\Gamma_{total}$					Γ_{398}/Γ
VALUE	CL%	DOCUMENT ID	TECN	COMMENT	
<0.0020	90	¹ ALBRECHT	89G	ARG $e^+e^- \rightarrow \Upsilon(4S)$	

¹ ALBRECHT 89G reports < 0.0022 assuming the $\Upsilon(4S)$ decays 45% to $B^0\bar{B}^0$. We rescale to 50%.

$\Gamma(K_3^*(1780)^0\gamma)/\Gamma_{total}$					Γ_{399}/Γ
VALUE (units 10^{-6})	CL%	DOCUMENT ID	TECN	COMMENT	
< 83	90	^{1,2} NISHIDA	05	BELL $e^+e^- \rightarrow \Upsilon(4S)$	

• • • We do not use the following data for averages, fits, limits, etc. • • •
 <10000 90 ³ ALBRECHT 89G ARG $e^+e^- \rightarrow \Upsilon(4S)$
¹ Assumes equal production of B⁺ and B⁰ at the $\Upsilon(4S)$.
² Uses $B(K_3^*(1780) \rightarrow \eta K) = 0.11^{+0.05}_{-0.04}$.
³ ALBRECHT 89G reports < 0.011 assuming the $\Upsilon(4S)$ decays 45% to $B^0\bar{B}^0$. We rescale to 50%.

$\Gamma(K_2^*(2045)^0\gamma)/\Gamma_{total}$					Γ_{400}/Γ
VALUE	CL%	DOCUMENT ID	TECN	COMMENT	
<0.0043	90	¹ ALBRECHT	89G	ARG $e^+e^- \rightarrow \Upsilon(4S)$	

¹ ALBRECHT 89G reports < 0.0048 assuming the $\Upsilon(4S)$ decays 45% to $B^0\bar{B}^0$. We rescale to 50%.

$\Gamma(\rho^0\gamma)/\Gamma_{total}$					Γ_{401}/Γ
VALUE (units 10^{-6})	CL%	DOCUMENT ID	TECN	COMMENT	
0.86 ± 0.15 OUR AVERAGE					
$0.97^{+0.24}_{-0.22} \pm 0.06$		¹ AUBERT	08BH	BABR $e^+e^- \rightarrow \Upsilon(4S)$	
$0.78^{+0.17+0.09}_{-0.16-0.10}$		¹ TANIGUCHI	08	BELL $e^+e^- \rightarrow \Upsilon(4S)$	

• • • We do not use the following data for averages, fits, limits, etc. • • •
 $0.79^{+0.22}_{-0.20} \pm 0.06$ ¹ AUBERT 07L BABR Repl. by AUBERT 08BH
 $1.25^{+0.37+0.07}_{-0.33-0.06}$ ¹ MOHAPATRA 06 BELL Repl. by TANIGUCHI 08
 $0.0 \pm 0.2 \pm 0.1$ 90 ¹ AUBERT 05 BABR Repl. by AUBERT 07L
 < 0.8 90 ¹ MOHAPATRA 05 BELL $e^+e^- \rightarrow \Upsilon(4S)$
 < 1.2 90 ¹ AUBERT 04c BABR $e^+e^- \rightarrow \Upsilon(4S)$
 < 17 90 ¹ COAN 00 CLE2 $e^+e^- \rightarrow \Upsilon(4S)$
¹ Assumes equal production of B⁺ and B⁰ at the $\Upsilon(4S)$.

$\Gamma(\rho^0 X(214), X \rightarrow \mu^+\mu^-)/\Gamma_{total}$					Γ_{402}/Γ
VALUE (units 10^{-8})	CL%	DOCUMENT ID	TECN	COMMENT	
<1.73	90	^{1,2} HYUN	10	BELL $e^+e^- \rightarrow \Upsilon(4S)$	

X(214) is a hypothetical particle of mass 214 MeV/c² reported by the HyperCP experiment (PARK 05)
¹ Assumes equal production of B⁺ and B⁰ at the $\Upsilon(4S)$.
² The result is the same for a scalar or vector X particle.

$\Gamma(\rho^0\gamma)/\Gamma(K^*(892)^0\gamma)$					$\Gamma_{401}/\Gamma_{389}$
VALUE (units 10^{-2})	CL%	DOCUMENT ID	TECN	COMMENT	
$2.06^{+0.45+0.14}_{-0.43-0.16}$		TANIGUCHI	08	BELL $e^+e^- \rightarrow \Upsilon(4S)$	

$\Gamma(\omega\gamma)/\Gamma_{total}$					Γ_{403}/Γ
VALUE (units 10^{-6})	CL%	DOCUMENT ID	TECN	COMMENT	
$0.44^{+0.18}_{-0.16}$ OUR AVERAGE					
$0.50^{+0.27}_{-0.23} \pm 0.09$		¹ AUBERT	08BH	BABR $e^+e^- \rightarrow \Upsilon(4S)$	
$0.40^{+0.19}_{-0.17} \pm 0.13$		¹ TANIGUCHI	08	BELL $e^+e^- \rightarrow \Upsilon(4S)$	

• • • We do not use the following data for averages, fits, limits, etc. • • •
 $0.40^{+0.24}_{-0.20} \pm 0.05$ ¹ AUBERT 07L BABR Repl. by AUBERT 08BH
 $0.56^{+0.34+0.05}_{-0.27-0.10}$ ¹ MOHAPATRA 06 BELL Repl. by TANIGUCHI 08
 <1.0 90 ¹ AUBERT 05 BABR Repl. by AUBERT 07L
 <0.8 90 ¹ MOHAPATRA 05 BELL Repl. by MOHAPATRA 06
 <1.0 90 ¹ AUBERT 04c BABR $e^+e^- \rightarrow \Upsilon(4S)$
 <9.2 90 ¹ COAN 00 CLE2 $e^+e^- \rightarrow \Upsilon(4S)$
¹ Assumes equal production of B⁺ and B⁰ at the $\Upsilon(4S)$.

$\Gamma(\phi\gamma)/\Gamma_{total}$					Γ_{404}/Γ
VALUE	CL%	DOCUMENT ID	TECN	COMMENT	
$<1.0 \times 10^{-7}$	90	¹ KING	16	BELL $e^+e^- \rightarrow \Upsilon(4S)$	

• • • We do not use the following data for averages, fits, limits, etc. • • •
 $<8.5 \times 10^{-7}$ 90 ¹ AUBERT,BE 05c BABR $e^+e^- \rightarrow \Upsilon(4S)$
 $<3.3 \times 10^{-6}$ 90 ¹ COAN 00 CLE2 $e^+e^- \rightarrow \Upsilon(4S)$
¹ Assumes equal production of B⁺ and B⁰ at the $\Upsilon(4S)$.

$\Gamma(\pi^+\pi^-)/\Gamma_{total}$					Γ_{405}/Γ
VALUE (units 10^{-6})	CL%	DOCUMENT ID	TECN	COMMENT	
5.12 ± 0.19 OUR FIT					
5.13 ± 0.24 OUR AVERAGE					
$5.04 \pm 0.21 \pm 0.18$		¹ DUH	13	BELL $e^+e^- \rightarrow \Upsilon(4S)$	
$5.5 \pm 0.4 \pm 0.3$		¹ AUBERT	07B	BABR $e^+e^- \rightarrow \Upsilon(4S)$	
$4.5^{+1.4+0.5}_{-1.2-0.4}$		¹ BORNHEIM	03	CLE2 $e^+e^- \rightarrow \Upsilon(4S)$	

• • • We do not use the following data for averages, fits, limits, etc. • • •
 $5.1 \pm 0.2 \pm 0.2$ ¹ LIN 07A BELL Repl. by DUH 13
 $4.4 \pm 0.6 \pm 0.3$ ¹ CHAO 04 BELL Repl. by LIN 07A
 $4.7 \pm 0.6 \pm 0.2$ ¹ AUBERT 02Q BABR Repl. by AUBERT 07b
 $5.4 \pm 1.2 \pm 0.5$ ¹ CASEY 02 BELL Repl. by CHAO 04
 $5.6^{+2.3+0.4}_{-2.0-0.5}$ ¹ ABE 01H BELL Repl. by CASEY 02
 $4.1 \pm 1.0 \pm 0.7$ ¹ AUBERT 01E BABR Repl. by AUBERT 02Q
 < 67 90 ² ABE 00c SLD $e^+e^- \rightarrow Z$
 $4.3^{+1.6}_{-1.4} \pm 0.5$ ¹ CRONIN-HEN..00 CLE2 Repl. by BORNHEIM 03
 < 15 90 GODANG 98 CLE2 Repl. by CRONIN-HENNESSY 00
 < 45 90 ³ ADAM 96D DLPH $e^+e^- \rightarrow Z$

Meson Particle Listings

 B^0

< 20	90	ASNER	96	CLE2	Repl. by GODANG 98
< 41	90	⁴ BUSKULIC	96V	ALEP	$e^+e^- \rightarrow Z$
< 55	90	⁵ ABREU	95N	DLPH	Sup. by ADAM 96D
< 47	90	⁶ AKERS	94L	OPAL	$e^+e^- \rightarrow Z$
< 29	90	¹ BATTLE	93	CLE2	$e^+e^- \rightarrow \Upsilon(4S)$
<130	90	¹ ALBRECHT	90B	ARG	$e^+e^- \rightarrow \Upsilon(4S)$
< 77	90	⁷ BORTOLETTO	089	CLEO	$e^+e^- \rightarrow \Upsilon(4S)$
<260	90	⁷ BEBEK	87	CLEO	$e^+e^- \rightarrow \Upsilon(4S)$
<500	90	GILES	84	CLEO	$e^+e^- \rightarrow \Upsilon(4S)$

¹ Assumes equal production of B^+ and B^0 at the $\Upsilon(4S)$.² ABE 00c assumes $B(Z \rightarrow b\bar{b}) = (21.7 \pm 0.1)\%$ and the B fractions $f_{B^0} = f_{B^+} = (39.7^{+1.8}_{-2.2})\%$ and $f_{B_s} = (10.5^{+1.8}_{-2.2})\%$.³ ADAM 96D assumes $f_{B^0} = f_{B^-} = 0.39$ and $f_{B_s} = 0.12$.⁴ BUSKULIC 96V assumes PDG 96 production fractions for B^0 , B^+ , B_s , b baryons.⁵ Assumes a B^0 , B^- production fraction of 0.39 and a B_s production fraction of 0.12.⁶ Assumes $B(Z \rightarrow b\bar{b}) = 0.217$ and B^0_d (B^0_s) fraction 39.5% (12%).⁷ Paper assumes the $\Upsilon(4S)$ decays 43% to $B^0\bar{B}^0$. We rescale to 50%. $\Gamma(\pi^+\pi^-)/\Gamma(K^+\pi^-)$ $\Gamma_{405}/\Gamma_{272}$

VALUE	DOCUMENT ID	TECN	COMMENT
0.261 ± 0.010 OUR FIT			
0.261 ± 0.015 OUR AVERAGE			
$0.262 \pm 0.009 \pm 0.017$	AAIJ	12AR LHCb	pp at 7 TeV
$0.259 \pm 0.017 \pm 0.016$	AALTONEN	11N CDF	$p\bar{p}$ at 1.96 TeV
• • • We do not use the following data for averages, fits, limits, etc. • • •			
$0.21 \pm 0.05 \pm 0.03$	ABULENCIA,A	06D CDF	Repl. by AALTONEN 11N

 $\Gamma(\pi^0\pi^0)/\Gamma_{total}$ Γ_{406}/Γ

VALUE (units 10^{-6})	CL%	DOCUMENT ID	TECN	COMMENT
1.59 ± 0.26 OUR AVERAGE				Error includes scale factor of 1.4.
$1.31 \pm 0.19 \pm 0.19$		¹ JULIUS	17	BELL $e^+e^- \rightarrow \Upsilon(4S)$
$1.83 \pm 0.21 \pm 0.13$		¹ LEES	13D	BABR $e^+e^- \rightarrow \Upsilon(4S)$
• • • We do not use the following data for averages, fits, limits, etc. • • •				
$1.47 \pm 0.25 \pm 0.12$		¹ AUBERT	07Bc	BABR Repl. by LEES 13D
$1.17 \pm 0.32 \pm 0.10$		¹ AUBERT	05L	BABR Repl. by AUBERT 07Bc
$2.3^{+0.4}_{-0.5} \pm 0.3$		¹ CHAO	05	BELL Repl. by JULIUS 17
< 3.6	90	¹ AUBERT	03L	BABR $e^+e^- \rightarrow \Upsilon(4S)$
$2.1 \pm 0.6 \pm 0.3$		¹ AUBERT	03s	BABR Repl. by AUBERT 05L
< 4.4	90	¹ BORNHEIM	03	CLE2 $e^+e^- \rightarrow \Upsilon(4S)$
$1.7 \pm 0.6 \pm 0.2$		¹ LEE	03	BELL Repl. by CHAO 05
< 5.7	90	¹ ASNER	02	CLE2 $e^+e^- \rightarrow \Upsilon(4S)$
< 6.4	90	¹ CASEY	02	BELL $e^+e^- \rightarrow \Upsilon(4S)$
< 9.3	90	GODANG	98	CLE2 Repl. by ASNER 02
< 9.1	90	ASNER	96	CLE2 Repl. by GODANG 98
<60	90	² ACCIARRI	95H L3	$e^+e^- \rightarrow Z$

¹ Assumes equal production of B^+ and B^0 at the $\Upsilon(4S)$.² ACCIARRI 95H assumes $f_{B^0} = 39.5 \pm 4.0$ and $f_{B_s} = 12.0 \pm 3.0\%$. $\Gamma(\eta\pi^0)/\Gamma_{total}$ Γ_{407}/Γ

VALUE (units 10^{-6})	CL%	DOCUMENT ID	TECN	COMMENT
$0.41^{+0.17+0.05}_{-0.15-0.07}$		^{1,2} PAL	15	BELL $e^+e^- \rightarrow \Upsilon(4S)$
• • • We do not use the following data for averages, fits, limits, etc. • • •				
< 1.5	90	² AUBERT	08AH	BABR $e^+e^- \rightarrow \Upsilon(4S)$
< 1.3	90	² AUBERT	06W	BABR Repl. by AUBERT 08AH
< 2.5	90	² CHANG	05A	BELL Repl. by PAL 15
< 2.5	90	² AUBERT,B	04D	BABR Repl. by AUBERT 06W
< 2.9	90	² RICHICHI	00	CLE2 $e^+e^- \rightarrow \Upsilon(4S)$
< 8	90	BEHRENS	98	CLE2 Repl. by RICHICHI 00
< 250	90	³ ACCIARRI	95H L3	$e^+e^- \rightarrow Z$
<1800	90	² ALBRECHT	90B	ARG $e^+e^- \rightarrow \Upsilon(4S)$

¹ PAL 15 signal significance is 3.0 standard deviations. The measurement corresponds to 90% CL upper limit of $< 6.5 \times 10^{-7}$.² Assumes equal production of B^+ and B^0 at the $\Upsilon(4S)$.³ ACCIARRI 95H assumes $f_{B^0} = 39.5 \pm 4.0$ and $f_{B_s} = 12.0 \pm 3.0\%$. $\Gamma(\eta\eta)/\Gamma_{total}$ Γ_{408}/Γ

VALUE (units 10^{-6})	CL%	DOCUMENT ID	TECN	COMMENT
< 1.0	90	¹ AUBERT	09AV	BABR $e^+e^- \rightarrow \Upsilon(4S)$
• • • We do not use the following data for averages, fits, limits, etc. • • •				
< 1.8	90	¹ AUBERT,B	06V	BABR Repl. by AUBERT 09AV
< 2.0	90	¹ CHANG	05A	BELL $e^+e^- \rightarrow \Upsilon(4S)$
< 2.8	90	¹ AUBERT,B	04X	BABR $e^+e^- \rightarrow \Upsilon(4S)$
< 18	90	BEHRENS	98	CLE2 $e^+e^- \rightarrow \Upsilon(4S)$
<410	90	² ACCIARRI	95H L3	$e^+e^- \rightarrow Z$

¹ Assumes equal production of B^+ and B^0 at the $\Upsilon(4S)$.² ACCIARRI 95H assumes $f_{B^0} = 39.5 \pm 4.0$ and $f_{B_s} = 12.0 \pm 3.0\%$. $\Gamma(\eta'\pi^0)/\Gamma_{total}$ Γ_{409}/Γ

VALUE (units 10^{-6})	CL%	DOCUMENT ID	TECN	COMMENT
1.2 ± 0.6 OUR AVERAGE				Error includes scale factor of 1.7.
$0.9 \pm 0.4 \pm 0.1$		¹ AUBERT	08AH	BABR $e^+e^- \rightarrow \Upsilon(4S)$
$2.8 \pm 1.0 \pm 0.3$		¹ SCHUEMANN	06	BELL $e^+e^- \rightarrow \Upsilon(4S)$
• • • We do not use the following data for averages, fits, limits, etc. • • •				
$0.8^{+0.8}_{-0.6} \pm 0.1$		¹ AUBERT	06W	BABR Repl. by AUBERT 08AH
$1.0^{+1.4}_{-1.0} \pm 0.8$	90	¹ AUBERT,B	04D	BABR Repl. by AUBERT 06W
< 5.7	90	¹ RICHICHI	00	CLE2 $e^+e^- \rightarrow \Upsilon(4S)$
< 11	90	BEHRENS	98	CLE2 Repl. by RICHICHI 00

¹ Assumes equal production of B^+ and B^0 at the $\Upsilon(4S)$. $\Gamma(\eta'\eta)/\Gamma_{total}$ Γ_{410}/Γ

VALUE (units 10^{-6})	CL%	DOCUMENT ID	TECN	COMMENT
< 1.7	90	¹ AUBERT	09AV	BABR $e^+e^- \rightarrow \Upsilon(4S)$
• • • We do not use the following data for averages, fits, limits, etc. • • •				
< 6.5	90	¹ SCHUEMANN	07	BELL $e^+e^- \rightarrow \Upsilon(4S)$
< 2.4	90	¹ AUBERT,B	06V	BABR Repl. by AUBERT 09AV
<10	90	¹ AUBERT,B	04X	BABR Repl. by AUBERT,B 06V
<47	90	BEHRENS	98	CLE2 $e^+e^- \rightarrow \Upsilon(4S)$

¹ Assumes equal production of B^+ and B^0 at the $\Upsilon(4S)$. $\Gamma(\eta'\eta)/\Gamma_{total}$ Γ_{411}/Γ

VALUE (units 10^{-6})	CL%	DOCUMENT ID	TECN	COMMENT
< 1.2	90	¹ AUBERT	08AH	BABR $e^+e^- \rightarrow \Upsilon(4S)$
• • • We do not use the following data for averages, fits, limits, etc. • • •				
< 4.5	90	¹ SCHUEMANN	07	BELL $e^+e^- \rightarrow \Upsilon(4S)$
< 1.7	90	¹ AUBERT	06W	BABR Repl. by AUBERT 08AH
< 4.6	90	¹ AUBERT,B	04X	BABR $e^+e^- \rightarrow \Upsilon(4S)$
<27	90	BEHRENS	98	CLE2 $e^+e^- \rightarrow \Upsilon(4S)$

¹ Assumes equal production of B^+ and B^0 at the $\Upsilon(4S)$. $\Gamma(\eta'\rho^0)/\Gamma_{total}$ Γ_{412}/Γ

VALUE (units 10^{-6})	CL%	DOCUMENT ID	TECN	COMMENT
< 1.3	90	¹ SCHUEMANN	07	BELL $e^+e^- \rightarrow \Upsilon(4S)$
• • • We do not use the following data for averages, fits, limits, etc. • • •				
< 2.8	90	¹ DEL-AMO-SA...	10A	BABR $e^+e^- \rightarrow \Upsilon(4S)$
< 3.7	90	AUBERT	07E	BABR Repl. by DEL-AMO-SANCHEZ 10A
< 4.3	90	¹ AUBERT,B	04D	BABR Repl. by AUBERT 07E
<12	90	¹ RICHICHI	00	CLE2 $e^+e^- \rightarrow \Upsilon(4S)$
<23	90	BEHRENS	98	CLE2 Repl. by RICHICHI 00

¹ Assumes equal production of B^+ and B^0 at the $\Upsilon(4S)$. $\Gamma(\eta'\eta_0(980), \eta_0 \rightarrow \pi^+\pi^-)/\Gamma_{total}$ Γ_{413}/Γ

VALUE (units 10^{-6})	CL%	DOCUMENT ID	TECN	COMMENT
< 0.9	90	¹ DEL-AMO-SA...	10A	BABR $e^+e^- \rightarrow \Upsilon(4S)$
• • • We do not use the following data for averages, fits, limits, etc. • • •				
<1.5	90	AUBERT	07E	BABR Repl. by DEL-AMO-SANCHEZ 10A

¹ Assumes equal production of B^+ and B^0 at the $\Upsilon(4S)$. $\Gamma(\eta\rho^0)/\Gamma_{total}$ Γ_{414}/Γ

VALUE (units 10^{-6})	CL%	DOCUMENT ID	TECN	COMMENT
< 1.5	90	¹ AUBERT	07Y	BABR $e^+e^- \rightarrow \Upsilon(4S)$
• • • We do not use the following data for averages, fits, limits, etc. • • •				
< 1.9	90	¹ WANG	07B	BELL $e^+e^- \rightarrow \Upsilon(4S)$
< 1.5	90	¹ AUBERT,B	04D	BABR Repl. by AUBERT 07Y
<10	90	¹ RICHICHI	00	CLE2 $e^+e^- \rightarrow \Upsilon(4S)$
<13	90	BEHRENS	98	CLE2 Repl. by RICHICHI 00

¹ Assumes equal production of B^+ and B^0 at the $\Upsilon(4S)$. $\Gamma(\eta\eta_0(980), \eta_0 \rightarrow \pi^+\pi^-)/\Gamma_{total}$ Γ_{415}/Γ

VALUE (units 10^{-6})	CL%	DOCUMENT ID	TECN	COMMENT
< 0.4	90	¹ AUBERT	07Y	BABR $e^+e^- \rightarrow \Upsilon(4S)$

¹ Assumes equal production of B^+ and B^0 at the $\Upsilon(4S)$. $\Gamma(\omega\eta)/\Gamma_{total}$ Γ_{416}/Γ

VALUE (units 10^{-6})	CL%	DOCUMENT ID	TECN	COMMENT
$0.94^{+0.35}_{-0.30} \pm 0.09$		¹ AUBERT	09AV	BABR $e^+e^- \rightarrow \Upsilon(4S)$
• • • We do not use the following data for averages, fits, limits, etc. • • •				
< 1.9	90	¹ AUBERT,B	05k	BABR Repl. by AUBERT 09AV
$4.0^{+1.3}_{-1.2} \pm 0.4$		¹ AUBERT,B	04X	BABR Repl. by AUBERT,B 05k
<12	90	¹ BERGFELD	98	CLE2

¹ Assumes equal production of B^+ and B^0 at the $\Upsilon(4S)$.

$\Gamma(\omega\eta)/\Gamma_{total}$ Γ_{417}/Γ

VALUE (units 10 ⁻⁶)	CL%	DOCUMENT ID	TECN	COMMENT
$1.01^{+0.46}_{-0.38} \pm 0.09$		¹ AUBERT	09AV BABR	e ⁺ e ⁻ → $\Upsilon(4S)$
• • • We do not use the following data for averages, fits, limits, etc. • • •				
< 2.2	90	¹ SCHUEMANN	07 BELL	e ⁺ e ⁻ → $\Upsilon(4S)$
< 2.8	90	¹ AUBERT,B	04X BABR	e ⁺ e ⁻ → $\Upsilon(4S)$
< 60	90	¹ BERGFELD	98 CLE2	
¹ Assumes equal production of B ⁺ and B ⁰ at the $\Upsilon(4S)$.				

$\Gamma(\omega\rho^0)/\Gamma_{total}$ Γ_{418}/Γ

VALUE (units 10 ⁻⁶)	CL%	DOCUMENT ID	TECN	COMMENT
< 1.6	90	¹ AUBERT	09H BABR	e ⁺ e ⁻ → $\Upsilon(4S)$
• • • We do not use the following data for averages, fits, limits, etc. • • •				
< 1.5	90	¹ AUBERT,B	06T BABR	Repl. by AUBERT 09H
< 3.3	90	¹ AUBERT	05O BABR	Repl. by AUBERT,B 06T
< 11	90	¹ BERGFELD	98 CLE2	
¹ Assumes equal production of B ⁺ and B ⁰ at the $\Upsilon(4S)$.				

$\Gamma(\omega f_0(980), f_0 \rightarrow \pi^+\pi^-)/\Gamma_{total}$ Γ_{419}/Γ

VALUE (units 10 ⁻⁶)	CL%	DOCUMENT ID	TECN	COMMENT
< 1.5	90	¹ AUBERT	09H BABR	e ⁺ e ⁻ → $\Upsilon(4S)$
• • • We do not use the following data for averages, fits, limits, etc. • • •				
< 1.5	90	¹ AUBERT,B	06T BABR	Repl. by AUBERT 09H
¹ Assumes equal production of B ⁺ and B ⁰ at the $\Upsilon(4S)$.				

$\Gamma(\omega\omega)/\Gamma_{total}$ Γ_{420}/Γ

VALUE (units 10 ⁻⁶)	CL%	DOCUMENT ID	TECN	COMMENT
$1.2 \pm 0.3^{+0.3}_{-0.2}$		¹ LEES	14 BABR	e ⁺ e ⁻ → $\Upsilon(4S)$
• • • We do not use the following data for averages, fits, limits, etc. • • •				
< 4.0	90	¹ AUBERT,B	06T BABR	Repl. by LEES 14
< 19	90	¹ BERGFELD	98 CLE2	
¹ Assumes equal production of B ⁺ and B ⁰ at the $\Upsilon(4S)$.				

$\Gamma(\phi\pi^0)/\Gamma_{total}$ Γ_{421}/Γ

VALUE (units 10 ⁻⁶)	CL%	DOCUMENT ID	TECN	COMMENT
< 0.15	90	¹ KIM	12A BELL	e ⁺ e ⁻ → $\Upsilon(4S)$
• • • We do not use the following data for averages, fits, limits, etc. • • •				
< 0.28	90	¹ AUBERT,B	06c BABR	e ⁺ e ⁻ → $\Upsilon(4S)$
< 1.0	90	¹ AUBERT,B	04D BABR	Repl. by AUBERT,B 06c
< 5	90	¹ BERGFELD	98 CLE2	
¹ Assumes equal production of B ⁺ and B ⁰ at the $\Upsilon(4S)$.				

$\Gamma(\phi\eta)/\Gamma_{total}$ Γ_{422}/Γ

VALUE (units 10 ⁻⁶)	CL%	DOCUMENT ID	TECN	COMMENT
< 0.5	90	¹ AUBERT	09AV BABR	e ⁺ e ⁻ → $\Upsilon(4S)$
• • • We do not use the following data for averages, fits, limits, etc. • • •				
< 0.6	90	¹ AUBERT,B	06v BABR	Repl. by AUBERT 09AV
< 1.0	90	¹ AUBERT,B	04X BABR	Repl. by AUBERT,B 06v
< 9	90	¹ BERGFELD	98 CLE2	
¹ Assumes equal production of B ⁺ and B ⁰ at the $\Upsilon(4S)$.				

$\Gamma(\phi\eta')/\Gamma_{total}$ Γ_{423}/Γ

VALUE (units 10 ⁻⁶)	CL%	DOCUMENT ID	TECN	COMMENT
< 0.5	90	¹ SCHUEMANN	07 BELL	e ⁺ e ⁻ → $\Upsilon(4S)$
• • • We do not use the following data for averages, fits, limits, etc. • • •				
< 1.1	90	¹ AUBERT	09AV BABR	e ⁺ e ⁻ → $\Upsilon(4S)$
< 1.0	90	¹ AUBERT,B	06v BABR	Repl. by AUBERT 09AV
< 4.5	90	¹ AUBERT,B	04X BABR	Repl. by AUBERT,B 06v
< 31	90	¹ BERGFELD	98 CLE2	
¹ Assumes equal production of B ⁺ and B ⁰ at the $\Upsilon(4S)$.				

$\Gamma(\phi\pi^+\pi^-)/\Gamma_{total}$ Γ_{424}/Γ

VALUE (units 10 ⁻⁷)	CL%	DOCUMENT ID	TECN	COMMENT
$1.82 \pm 0.25 \pm 0.43$		¹ AAIJ	17A LHCB	pp at 7, 8 TeV
¹ Signal evidence is 4.5 standard deviations.				

$\Gamma(\phi\rho^0)/\Gamma_{total}$ Γ_{425}/Γ

VALUE (units 10 ⁻⁶)	CL%	DOCUMENT ID	TECN	COMMENT
< 0.33	90	¹ AUBERT	08BK BABR	e ⁺ e ⁻ → $\Upsilon(4S)$
• • • We do not use the following data for averages, fits, limits, etc. • • •				
< 15.6	90	² ABE	00c SLD	e ⁺ e ⁻ → Z
< 13	90	¹ BERGFELD	98 CLE2	
¹ Assumes equal production of B ⁺ and B ⁰ at the $\Upsilon(4S)$.				
² ABE 00c assumes B(Z → b \bar{b})=(21.7 ± 0.1)% and the B fractions f _{B⁰} =f _{B⁺} =(39.7 ^{+1.8} _{-2.2})% and f _{B_s} =(10.5 ^{+1.8} _{-2.2})%.				

$\Gamma(\phi f_0(980), f_0 \rightarrow \pi^+\pi^-)/\Gamma_{total}$ Γ_{426}/Γ

VALUE (units 10 ⁻⁶)	CL%	DOCUMENT ID	TECN	COMMENT
< 0.38	90	¹ AUBERT	08BK BABR	e ⁺ e ⁻ → $\Upsilon(4S)$
¹ Assumes equal production of B ⁺ and B ⁰ at the $\Upsilon(4S)$.				

$\Gamma(\phi\omega)/\Gamma_{total}$ Γ_{427}/Γ

VALUE (units 10 ⁻⁶)	CL%	DOCUMENT ID	TECN	COMMENT
< 0.7	90	¹ LEES	14 BABR	e ⁺ e ⁻ → $\Upsilon(4S)$
• • • We do not use the following data for averages, fits, limits, etc. • • •				
< 1.2	90	¹ AUBERT,B	06T BABR	Repl. by LEES 14
< 21	90	¹ BERGFELD	98 CLE2	
¹ Assumes equal production of B ⁺ and B ⁰ at the $\Upsilon(4S)$.				

$\Gamma(\phi\phi)/\Gamma_{total}$ Γ_{428}/Γ

VALUE (units 10 ⁻⁶)	CL%	DOCUMENT ID	TECN	COMMENT
< 2.7 × 10 ⁻⁸	90	AAIJ	19AP LHCB	pp at 7, 8 and 13 TeV
• • • We do not use the following data for averages, fits, limits, etc. • • •				
< 2.8 × 10 ⁻⁸	90	AAIJ	15As LHCB	Repl. by AAIJ 19AP
< 2 × 10 ⁻⁷	90	¹ AUBERT	08BK BABR	e ⁺ e ⁻ → $\Upsilon(4S)$
< 1.5 × 10 ⁻⁶	90	¹ AUBERT,B	04X BABR	Repl. by AUBERT 08BK
< 3.21 × 10 ⁻⁴	90	² ABE	00c SLD	e ⁺ e ⁻ → Z
< 1.2 × 10 ⁻⁵	90	¹ BERGFELD	98 CLE2	
< 3.9 × 10 ⁻⁵	90	ASNER	96 CLE2	e ⁺ e ⁻ → $\Upsilon(4S)$
¹ Assumes equal production of B ⁺ and B ⁰ at the $\Upsilon(4S)$.				
² ABE 00c assumes B(Z → b \bar{b})=(21.7 ± 0.1)% and the B fractions f _{B⁰} =f _{B⁺} =(39.7 ^{+1.8} _{-2.2})% and f _{B_s} =(10.5 ^{+1.8} _{-2.2})%.				

$\Gamma(a_0(980)^\pm\pi^\mp, a_0^\pm \rightarrow \eta\pi^\pm)/\Gamma_{total}$ Γ_{429}/Γ

VALUE (units 10 ⁻⁶)	CL%	DOCUMENT ID	TECN	COMMENT
< 3.1	90	¹ AUBERT	07Y BABR	e ⁺ e ⁻ → $\Upsilon(4S)$
• • • We do not use the following data for averages, fits, limits, etc. • • •				
< 5.1	90	¹ AUBERT,BE	04 BABR	Repl. by AUBERT 07Y
¹ Assumes equal production of B ⁺ and B ⁰ at the $\Upsilon(4S)$.				

$\Gamma(a_0(1450)^\pm\pi^\mp, a_0^\pm \rightarrow \eta\pi^\pm)/\Gamma_{total}$ Γ_{430}/Γ

VALUE (units 10 ⁻⁶)	CL%	DOCUMENT ID	TECN	COMMENT
< 2.3	90	¹ AUBERT	07Y BABR	e ⁺ e ⁻ → $\Upsilon(4S)$
¹ Assumes equal production of B ⁺ and B ⁰ at the $\Upsilon(4S)$.				

$\Gamma(\pi^+\pi^-\pi^0)/\Gamma_{total}$ Γ_{431}/Γ

VALUE	CL%	DOCUMENT ID	TECN	COMMENT
< 7.2 × 10 ⁻⁴	90	¹ ALBRECHT	90B ARG	e ⁺ e ⁻ → $\Upsilon(4S)$
¹ ALBRECHT 90B limit assumes equal production of B ⁰ \bar{B}^0 and B ⁺ B ⁻ at $\Upsilon(4S)$.				

$\Gamma(\rho^0\pi^0)/\Gamma_{total}$ Γ_{432}/Γ

VALUE (units 10 ⁻⁶)	CL%	DOCUMENT ID	TECN	COMMENT
2.0 ± 0.5 OUR AVERAGE				
3.0 ± 0.5 ± 0.7		^{1,2} KUSAKA	08 BELL	e ⁺ e ⁻ → $\Upsilon(4S)$
1.4 ± 0.6 ± 0.3		¹ AUBERT	04Z BABR	e ⁺ e ⁻ → $\Upsilon(4S)$
1.6 ^{+2.0} _{-1.4} ± 0.8		¹ JESSOP	00 CLEO	e ⁺ e ⁻ → $\Upsilon(4S)$
• • • We do not use the following data for averages, fits, limits, etc. • • •				
3.12 ^{+0.88} _{-0.82} ± 0.76		¹ DRAGIC	06 BELL	Repl. by KUSAKA 08
5.1 ± 1.6 ± 0.9		¹ DRAGIC	04 BELL	Repl. by DRAGIC 06
< 5.3	90	¹ GORDON	02 BELL	Repl. by DRAGIC 04
< 24	90	ASNER	96 CLEO	Repl. by JESSOP 00
< 400	90	¹ ALBRECHT	90B ARG	e ⁺ e ⁻ → $\Upsilon(4S)$
¹ Assumes equal production of B ⁺ and B ⁰ at the $\Upsilon(4S)$.				
² This is the first measurement that excludes contributions from $\rho(1450)$ and $\rho(1570)$ resonances.				

$\Gamma(\rho^\mp\pi^\pm)/\Gamma_{total}$ Γ_{433}/Γ

VALUE (units 10 ⁻⁶)	CL%	DOCUMENT ID	TECN	COMMENT
23.0 ± 2.3 OUR AVERAGE				
22.6 ± 1.1 ± 4.4		^{1,2} KUSAKA	08 BELL	e ⁺ e ⁻ → $\Upsilon(4S)$
22.6 ± 1.8 ± 2.2		¹ AUBERT	03T BABR	e ⁺ e ⁻ → $\Upsilon(4S)$
27.6 ^{+8.4} _{-7.4} ± 4.2		¹ JESSOP	00 CLE2	e ⁺ e ⁻ → $\Upsilon(4S)$
• • • We do not use the following data for averages, fits, limits, etc. • • •				
20.8 ^{+6.0} _{-6.3} ± 3.1		¹ GORDON	02 BELL	Repl. by KUSAKA 08
< 88	90	ASNER	96 CLE2	Repl. by JESSOP 00
< 520	90	¹ ALBRECHT	90B ARG	e ⁺ e ⁻ → $\Upsilon(4S)$
< 5200	90	³ BEBEK	87 CLEO	e ⁺ e ⁻ → $\Upsilon(4S)$
¹ Assumes equal production of B ⁺ and B ⁰ at the $\Upsilon(4S)$.				
² This is the first measurement that excludes contributions from $\rho(1450)$ and $\rho(1570)$ resonances.				
³ BEBEK 87 reports < 6.1 × 10 ⁻³ assuming the $\Upsilon(4S)$ decays 43% to B ⁰ \bar{B}^0 . We rescale to 50%.				

Meson Particle Listings

 B^0 $\Gamma(\pi^+\pi^-\pi^+\pi^-)/\Gamma_{\text{total}}$ Γ_{434}/Γ

VALUE	CL%	DOCUMENT ID	TECN	COMMENT
$<11.2 \times 10^{-6}$	90	¹ VANHOEFER 14	BELL	$e^+e^- \rightarrow \Upsilon(4S)$
••• We do not use the following data for averages, fits, limits, etc. •••				
$<23.1 \times 10^{-6}$	90	¹ AUBERT 08BB	BABR	$e^+e^- \rightarrow \Upsilon(4S)$
$<19.3 \times 10^{-6}$	90	¹ CHIANG 08	BELL	Repl. by VANHOEFER 14
$<2.3 \times 10^{-4}$	90	² ADAM 96D	DLPH	$e^+e^- \rightarrow Z$
$<2.8 \times 10^{-4}$	90	³ ABREU 95N	DLPH	Sup. by ADAM 96D
$<6.7 \times 10^{-4}$	90	¹ ALBRECHT 90B	ARG	$e^+e^- \rightarrow \Upsilon(4S)$

- ¹ Assumes equal production of B^+ and B^0 at the $\Upsilon(4S)$.
² ADAM 96D assumes $f_{B^0} = f_{B^-} = 0.39$ and $f_{B_s} = 0.12$.
³ Assumes a B^0 , B^- production fraction of 0.39 and a B_s production fraction of 0.12.

 $\Gamma(\rho^0\pi^+\pi^-)/\Gamma_{\text{total}}$ Γ_{435}/Γ

VALUE (units 10^{-6})	CL%	DOCUMENT ID	TECN	COMMENT
<8.8	90	¹ AUBERT 08BB	BABR	$e^+e^- \rightarrow \Upsilon(4S)$
••• We do not use the following data for averages, fits, limits, etc. •••				
<12.0	90	¹ VANHOEFER 14	BELL	$e^+e^- \rightarrow \Upsilon(4S)$
<12.0	90	¹ CHIANG 08	BELL	Repl. by VANHOEFER 14

- ¹ Assumes equal production of B^+ and B^0 at the $\Upsilon(4S)$.

 $\Gamma(\rho^0\rho^0)/\Gamma_{\text{total}}$ Γ_{436}/Γ

VALUE (units 10^{-6})	CL%	DOCUMENT ID	TECN	COMMENT
0.96 ± 0.15 OUR FIT				
0.97 ± 0.24 OUR AVERAGE				
$1.02 \pm 0.30 \pm 0.15$		^{1,2} VANHOEFER 14	BELL	$e^+e^- \rightarrow \Upsilon(4S)$
$0.92 \pm 0.32 \pm 0.14$		² AUBERT 08BB	BABR	$e^+e^- \rightarrow \Upsilon(4S)$
••• We do not use the following data for averages, fits, limits, etc. •••				
$0.4 \pm 0.4 \pm 0.2$		² CHIANG 08	BELL	Repl. by VANHOEFER 14
$1.07 \pm 0.33 \pm 0.19$		² AUBERT 07G	BABR	Repl. by AUBERT 08BB
<1.1	90	² AUBERT 05I	BABR	Repl. by AUBERT 07G
<2.1	90	² AUBERT 03V	BABR	Repl. by AUBERT 05I
<18	90	³ GODANG 02	CLE2	$e^+e^- \rightarrow \Upsilon(4S)$
<136	90	⁴ ABE 00C	SLD	$e^+e^- \rightarrow Z$
<280	90	² ALBRECHT 90B	ARG	$e^+e^- \rightarrow \Upsilon(4S)$
<290	90	⁵ BORTOLETTO 89	CLEO	$e^+e^- \rightarrow \Upsilon(4S)$
<430	90	⁵ BEBEK 87	CLEO	$e^+e^- \rightarrow \Upsilon(4S)$

- ¹ Signal significance 3.4 standard deviations.
² Assumes equal production of B^+ and B^0 at the $\Upsilon(4S)$.
³ Assumes a helicity 00 configuration. For a helicity 11 configuration, the limit decreases to 1.4×10^{-5} .
⁴ ABE 00C assumes $B(Z \rightarrow b\bar{b}) = (21.7 \pm 0.1)\%$ and the B fractions $f_{B^0} = f_{B^+} = (39.7 \pm 1.8 \pm 2.2)\%$ and $f_{B_s} = (10.5 \pm 1.8 \pm 2.2)\%$.
⁵ Paper assumes the $\Upsilon(4S)$ decays 43% to $B^0\bar{B}^0$. We rescale to 50%.

 $\Gamma(\rho^0\rho^0)/\Gamma(K^*(892)^0\phi)$ $\Gamma_{436}/\Gamma_{361}$

VALUE (units 10^{-2})	DOCUMENT ID	TECN	COMMENT
9.5 ± 1.5 OUR FIT			
9.4 ± 1.7 ± 0.9	AAIJ 15T	LHCB	pp at 7, 8 TeV

 $\Gamma(f_0(980)\pi^+\pi^-, f_0 \rightarrow \pi^+\pi^-)/\Gamma_{\text{total}}$ Γ_{437}/Γ

VALUE	CL%	DOCUMENT ID	TECN	COMMENT
$<3.0 \times 10^{-6}$	90	¹ VANHOEFER 14	BELL	$e^+e^- \rightarrow \Upsilon(4S)$
••• We do not use the following data for averages, fits, limits, etc. •••				
$<3.8 \times 10^{-6}$	90	¹ CHIANG 08	BELL	$e^+e^- \rightarrow \Upsilon(4S)$

- ¹ Assumes equal production of B^+ and B^0 at the $\Upsilon(4S)$.

 $\Gamma(\rho^0 f_0(980), f_0 \rightarrow \pi^+\pi^-)/\Gamma_{\text{total}}$ Γ_{438}/Γ

VALUE (units 10^{-7})	CL%	DOCUMENT ID	TECN	COMMENT
7.8 ± 2.2 ± 1.1		^{1,2} VANHOEFER 14	BELL	$e^+e^- \rightarrow \Upsilon(4S)$
••• We do not use the following data for averages, fits, limits, etc. •••				
<8.1	90	AAIJ 15T	LHCB	pp at 7, 8 TeV
<4.0	90	² AUBERT 08BB	BABR	$e^+e^- \rightarrow \Upsilon(4S)$
<3	90	² CHIANG 08	BELL	Repl. by VANHOEFER 14
<5.3	90	² AUBERT 07G	BABR	Repl. by AUBERT 08BB

- ¹ Signal significance of 3.1 standard deviations.
² Assumes equal production of B^+ and B^0 at the $\Upsilon(4S)$.

 $\Gamma(f_0(980)f_0(980), f_0 \rightarrow \pi^+\pi^-, f_0 \rightarrow \pi^+\pi^-)/\Gamma_{\text{total}}$ Γ_{439}/Γ

VALUE (units 10^{-6})	CL%	DOCUMENT ID	TECN	COMMENT
<0.19	90	¹ AUBERT 08BB	BABR	$e^+e^- \rightarrow \Upsilon(4S)$
••• We do not use the following data for averages, fits, limits, etc. •••				
<0.2	90	¹ VANHOEFER 14	BELL	$e^+e^- \rightarrow \Upsilon(4S)$
<0.1	90	¹ CHIANG 08	BELL	Repl. by VANHOEFER 14
<0.16	90	¹ AUBERT 07G	BABR	Repl. by AUBERT 08BB

- ¹ Assumes equal production of B^+ and B^0 at the $\Upsilon(4S)$.

 $\Gamma(f_0(980)f_0(980), f_0 \rightarrow \pi^+\pi^-, f_0 \rightarrow K^+K^-)/\Gamma_{\text{total}}$ Γ_{440}/Γ

VALUE (units 10^{-6})	CL%	DOCUMENT ID	TECN	COMMENT
<0.23	90	¹ AUBERT 08BK	BABR	$e^+e^- \rightarrow \Upsilon(4S)$

- ¹ Assumes equal production of B^+ and B^0 at the $\Upsilon(4S)$.

 $\Gamma(a_1(1260)\pi^\pm\pi^\pm)/\Gamma_{\text{total}}$ Γ_{441}/Γ

VALUE (units 10^{-6})	CL%	DOCUMENT ID	TECN	COMMENT
26 ± 5 OUR AVERAGE				
$22.2 \pm 2.0 \pm 2.8$		^{1,2} DALSENO 12	BELL	$e^+e^- \rightarrow \Upsilon(4S)$
$33.2 \pm 3.8 \pm 3.0$		^{2,3} AUBERT 06V	BABR	$e^+e^- \rightarrow \Upsilon(4S)$
Error includes scale factor of 1.9.				
••• We do not use the following data for averages, fits, limits, etc. •••				
<630	90	² ALBRECHT 90B	ARG	$e^+e^- \rightarrow \Upsilon(4S)$
<490	90	⁴ BORTOLETTO 89	CLEO	$e^+e^- \rightarrow \Upsilon(4S)$
<1000	90	⁴ BEBEK 87	CLEO	$e^+e^- \rightarrow \Upsilon(4S)$

- ¹ DALSENO 12 reports $B(B^0 \rightarrow a_1^\pm\pi^\mp) B(a_1^\pm \rightarrow \pi^\pm\pi^\mp\pi^-) = (11.1 \pm 1.0 \pm 1.4) \times 10^{-6}$ which we rescaled assuming $a_1(1260)$ decays only to 3π and $B(a_1^\pm \rightarrow \pi^\pm\pi^\mp\pi^-) = 0.5$.
² Assumes equal production of B^+ and B^0 at the $\Upsilon(4S)$.
³ Assumes $a_1(1260)$ decays only to 3π and $B(a_1^\pm \rightarrow \pi^\pm\pi^\mp\pi^\pm) = 0.5$.
⁴ Paper assumes the $\Upsilon(4S)$ decays 43% to $B^0\bar{B}^0$. We rescale to 50%.

 $\Gamma(a_2(1320)\pi^\pm\pi^\pm)/\Gamma_{\text{total}}$ Γ_{442}/Γ

VALUE	CL%	DOCUMENT ID	TECN	COMMENT
$<6.3 \times 10^{-6}$	90	¹ DALSENO 12	BELL	$e^+e^- \rightarrow \Upsilon(4S)$
••• We do not use the following data for averages, fits, limits, etc. •••				
$<3.0 \times 10^{-4}$	90	² BORTOLETTO 89	CLEO	$e^+e^- \rightarrow \Upsilon(4S)$
$<1.4 \times 10^{-3}$	90	² BEBEK 87	CLEO	$e^+e^- \rightarrow \Upsilon(4S)$

- ¹ DALSENO 12 reports $B(B^0 \rightarrow a_2^\pm\pi^\mp) B(a_2^\pm \rightarrow \pi^\pm\pi^\mp\pi^-) < 2.2 \times 10^{-6}$ which we rescaled using $B(a_2^\pm \rightarrow \pi^\pm\pi^\mp\pi^-) = 1/2 B(a_2^\pm \rightarrow 3\pi) = 0.35 \pm 0.013$.
² Paper assumes the $\Upsilon(4S)$ decays 43% to $B^0\bar{B}^0$. We rescale to 50%.

 $\Gamma(\pi^+\pi^-\pi^0\pi^0)/\Gamma_{\text{total}}$ Γ_{443}/Γ

VALUE	CL%	DOCUMENT ID	TECN	COMMENT
$<3.1 \times 10^{-3}$	90	¹ ALBRECHT 90B	ARG	$e^+e^- \rightarrow \Upsilon(4S)$

- ¹ ALBRECHT 90B limit assumes equal production of $B^0\bar{B}^0$ and B^+B^- at $\Upsilon(4S)$.

 $\Gamma(\rho^+\rho^-)/\Gamma_{\text{total}}$ Γ_{444}/Γ

VALUE (units 10^{-6})	CL%	DOCUMENT ID	TECN	COMMENT
27.7 ± 1.9 OUR AVERAGE				
$28.3 \pm 1.5 \pm 1.5$		¹ VANHOEFER 16	BELL	$e^+e^- \rightarrow \Upsilon(4S)$
$25.5 \pm 2.1 \pm 3.6$		¹ AUBERT 07BF	BABR	$e^+e^- \rightarrow \Upsilon(4S)$
$22.8 \pm 3.8 \pm 2.3$		¹ SOMOV 06	BELL	Repl. by VANHOEFER 16
$25 \pm 7 \pm 5$		¹ AUBERT 04G	BABR	Repl. by AUBERT, B 04R
$30 \pm 4 \pm 5$		^{1,2} AUBERT, B 04R	BABR	Repl. by AUBERT 07BF
<2200	90	¹ ALBRECHT 90B	ARG	$e^+e^- \rightarrow \Upsilon(4S)$

- We do not use the following data for averages, fits, limits, etc. •••
¹ Assumes equal production of B^+ and B^0 at the $\Upsilon(4S)$.
² The quoted result is obtained after combining with AUBERT 04G result by AUBERT 04R alone gives $(33 \pm 4 \pm 5) \times 10^{-6}$.

 $\Gamma(a_1(1260)^0\pi^0)/\Gamma_{\text{total}}$ Γ_{445}/Γ

VALUE	CL%	DOCUMENT ID	TECN	COMMENT
$<1.1 \times 10^{-3}$	90	¹ ALBRECHT 90B	ARG	$e^+e^- \rightarrow \Upsilon(4S)$

- ¹ ALBRECHT 90B limit assumes equal production of $B^0\bar{B}^0$ and B^+B^- at $\Upsilon(4S)$.

 $\Gamma(\omega\pi^0)/\Gamma_{\text{total}}$ Γ_{446}/Γ

VALUE (units 10^{-6})	CL%	DOCUMENT ID	TECN	COMMENT
<0.5	90	¹ AUBERT 08AH	BABR	$e^+e^- \rightarrow \Upsilon(4S)$
••• We do not use the following data for averages, fits, limits, etc. •••				
<2.0	90	¹ JEN 06	BELL	$e^+e^- \rightarrow \Upsilon(4S)$
<1.2	90	¹ AUBERT, B 04D	BABR	Repl. by AUBERT 08AH
<1.9	90	¹ WANG 04A	BELL	$e^+e^- \rightarrow \Upsilon(4S)$
<3	90	¹ AUBERT 01G	BABR	$e^+e^- \rightarrow \Upsilon(4S)$
<5.5	90	¹ JESSOP 00	CLE2	$e^+e^- \rightarrow \Upsilon(4S)$
<14	90	¹ BERGFELD 98	CLE2	Repl. by JESSOP 00
<460	90	² ALBRECHT 90B	ARG	$e^+e^- \rightarrow \Upsilon(4S)$

- ¹ Assumes equal production of B^+ and B^0 at the $\Upsilon(4S)$.
² ALBRECHT 90B limit assumes equal production of $B^0\bar{B}^0$ and B^+B^- at $\Upsilon(4S)$.

 $\Gamma(\pi^+\pi^-\pi^-\pi^0)/\Gamma_{\text{total}}$ Γ_{447}/Γ

VALUE	CL%	DOCUMENT ID	TECN	COMMENT
$<9.0 \times 10^{-3}$	90	¹ ALBRECHT 90B	ARG	$e^+e^- \rightarrow \Upsilon(4S)$

- ¹ ALBRECHT 90B limit assumes equal production of $B^0\bar{B}^0$ and B^+B^- at $\Upsilon(4S)$.

Meson Particle Listings

B^0

$\Gamma(a_1(1260)^+ \rho^-)/\Gamma_{total}$		Γ_{448}/Γ			
VALUE (units 10^{-6})	CL%	DOCUMENT ID	TECN	COMMENT	
< 61	90	1,2 AUBERT,B	060	BABR	$e^+e^- \rightarrow \Upsilon(4S)$
<ul style="list-style-type: none"> ••• We do not use the following data for averages, fits, limits, etc. ••• 					
<3400	90	1 ALBRECHT	90B	ARG	$e^+e^- \rightarrow \Upsilon(4S)$
<ol style="list-style-type: none"> Assumes equal production of B^+ and B^0 at the $\Upsilon(4S)$. Assumes $a_1(1260)$ decays only to 3π and $B(a_1^\pm \rightarrow \pi^\pm \pi^\mp \pi^\pm) = 0.5$. 					

$\Gamma(a_1(1260)^0 \rho^0)/\Gamma_{total}$		Γ_{449}/Γ			
VALUE	CL%	DOCUMENT ID	TECN	COMMENT	
<2.4 × 10 ⁻³	90	1 ALBRECHT	90B	ARG	$e^+e^- \rightarrow \Upsilon(4S)$
<ol style="list-style-type: none"> ALBRECHT 90B limit assumes equal production of $B^0\bar{B}^0$ and B^+B^- at $\Upsilon(4S)$. 					

$\Gamma(b_1^{\mp} \pi^\pm, b_1^{\mp} \rightarrow \omega \pi^\mp)/\Gamma_{total}$		Γ_{450}/Γ			
VALUE (units 10^{-6})	CL%	DOCUMENT ID	TECN	COMMENT	
10.9 ± 1.2 ± 0.9		1 AUBERT	07B1	BABR	$e^+e^- \rightarrow \Upsilon(4S)$
<ol style="list-style-type: none"> Assumes equal production of B^+ and B^0 at the $\Upsilon(4S)$. 					

$\Gamma(b_1^0 \pi^0, b_1^0 \rightarrow \omega \pi^0)/\Gamma_{total}$		Γ_{451}/Γ			
VALUE (units 10^{-6})	CL%	DOCUMENT ID	TECN	COMMENT	
<1.9	90	1 AUBERT	08AG	BABR	$e^+e^- \rightarrow \Upsilon(4S)$
<ol style="list-style-type: none"> Assumes equal production of B^+ and B^0 at the $\Upsilon(4S)$. 					

$\Gamma(b_1^- \rho^+, b_1^- \rightarrow \omega \pi^-)/\Gamma_{total}$		Γ_{452}/Γ			
VALUE	CL%	DOCUMENT ID	TECN	COMMENT	
<1.4 × 10 ⁻⁶	90	1 AUBERT	09AF	BABR	$e^+e^- \rightarrow \Upsilon(4S)$
<ol style="list-style-type: none"> Assumes equal production of B^+ and B^0 at the $\Upsilon(4S)$. 					

$\Gamma(b_1^0 \rho^0, b_1^0 \rightarrow \omega \pi^0)/\Gamma_{total}$		Γ_{453}/Γ			
VALUE	CL%	DOCUMENT ID	TECN	COMMENT	
<3.4 × 10 ⁻⁶	90	1 AUBERT	09AF	BABR	$e^+e^- \rightarrow \Upsilon(4S)$
<ol style="list-style-type: none"> Assumes equal production of B^+ and B^0 at the $\Upsilon(4S)$. 					

$\Gamma(\pi^+ \pi^+ \pi^+ \pi^- \pi^- \pi^-)/\Gamma_{total}$		Γ_{454}/Γ			
VALUE	CL%	DOCUMENT ID	TECN	COMMENT	
<3.0 × 10 ⁻³	90	1 ALBRECHT	90B	ARG	$e^+e^- \rightarrow \Upsilon(4S)$
<ol style="list-style-type: none"> ALBRECHT 90B limit assumes equal production of $B^0\bar{B}^0$ and B^+B^- at $\Upsilon(4S)$. 					

$\Gamma(a_1(1260)^+ a_1(1260)^-, a_1^+ \rightarrow 2\pi^+ \pi^-, a_1^- \rightarrow 2\pi^- \pi^+)/\Gamma_{total}$		Γ_{455}/Γ			
VALUE (units 10^{-6})	CL%	DOCUMENT ID	TECN	COMMENT	
11.8 ± 2.6 ± 1.6		1 AUBERT	09AL	BABR	$e^+e^- \rightarrow \Upsilon(4S)$
<ul style="list-style-type: none"> ••• We do not use the following data for averages, fits, limits, etc. ••• 					
<6000	90	1 ALBRECHT	90B	ARG	$e^+e^- \rightarrow \Upsilon(4S)$
<2800	90	2 BORTOLETTO89	CLEO	$e^+e^- \rightarrow \Upsilon(4S)$	
<ol style="list-style-type: none"> Assumes equal production of $B^0\bar{B}^0$ and B^+B^- at $\Upsilon(4S)$. BORTOLETTO 89 reports $< 3.2 \times 10^{-3}$ assuming the $\Upsilon(4S)$ decays 43% to $B^0\bar{B}^0$. We rescale to 50%. 					

$\Gamma(\pi^+ \pi^+ \pi^+ \pi^- \pi^- \pi^- \pi^0)/\Gamma_{total}$		Γ_{456}/Γ			
VALUE	CL%	DOCUMENT ID	TECN	COMMENT	
<1.1 × 10 ⁻²	90	1 ALBRECHT	90B	ARG	$e^+e^- \rightarrow \Upsilon(4S)$
<ol style="list-style-type: none"> ALBRECHT 90B limit assumes equal production of $B^0\bar{B}^0$ and B^+B^- at $\Upsilon(4S)$. 					

$\Gamma(p\bar{p})/\Gamma_{total}$		Γ_{457}/Γ			
VALUE (units 10^{-8})	CL%	DOCUMENT ID	TECN	COMMENT	
1.25 ± 0.27 ± 0.18		1 AAIJ	17B1	LHCb	pp at 7 and 8 TeV
<ul style="list-style-type: none"> ••• We do not use the following data for averages, fits, limits, etc. ••• 					
1.47 ^{+0.62+0.35} _{-0.51-0.14}		2 AAIJ	13BQ	LHCb	Repl. by AAIJ 17B1
< 11	90	3 TSAI	07	BELL	$e^+e^- \rightarrow \Upsilon(4S)$
< 41	90	3 CHANG	05	BELL	$e^+e^- \rightarrow \Upsilon(4S)$
< 27	90	3 AUBERT	04U	BABR	$e^+e^- \rightarrow \Upsilon(4S)$
< 140	90	3 BORNHEIM	03	CLE2	$e^+e^- \rightarrow \Upsilon(4S)$
< 120	90	3 ABE	02o	BELL	$e^+e^- \rightarrow \Upsilon(4S)$
< 700	90	3 COAN	99	CLE2	$e^+e^- \rightarrow \Upsilon(4S)$
< 1800	90	4 BUSKULIC	96v	ALEP	$e^+e^- \rightarrow Z$
<35000	90	5 ABREU	95N	DLPH	Sup. by ADAM 96D
< 3400	90	6 BORTOLETTO89	CLEO	$e^+e^- \rightarrow \Upsilon(4S)$	
<12000	90	7 ALBRECHT	88F	ARG	$e^+e^- \rightarrow \Upsilon(4S)$
<17000	90	6 BEBEK	87	CLEO	$e^+e^- \rightarrow \Upsilon(4S)$

- Uses normalization mode $B(B^0 \rightarrow K^+ \pi^-) = (19.6 \pm 0.5) \times 10^{-6}$.
- Uses normalization mode $B(B^0 \rightarrow K^+ \pi^-) = (19.55 \pm 0.54) \times 10^{-6}$.
- Assumes equal production of B^+ and B^0 at the $\Upsilon(4S)$.
- BUSKULIC 96v assumes PDG 96 production fractions for B^0, B^+, B_s, b baryons.
- Assumes a B^0, B^- production fraction of 0.39 and a B_s production fraction of 0.12.
- Paper assumes the $\Upsilon(4S)$ decays 43% to $B^0\bar{B}^0$. We rescale to 50%.
- ALBRECHT 88F reports $< 1.3 \times 10^{-4}$ assuming the $\Upsilon(4S)$ decays 45% to $B^0\bar{B}^0$. We rescale to 50%.

$\Gamma(p\bar{p}\pi^+\pi^-)/\Gamma_{total}$		Γ_{458}/Γ			
VALUE (units 10^{-6})	CL%	DOCUMENT ID	TECN	COMMENT	
2.87 ± 0.15 ± 0.11		1,2 AAIJ	17B1	LHCb	pp at 7, 8 TeV
<ul style="list-style-type: none"> ••• We do not use the following data for averages, fits, limits, etc. ••• 					
0.83 ± 0.17 ± 0.17		3 CHU	20	BELL	$e^+e^- \rightarrow \Upsilon(4S)$
<950	90	4 ABREU	95N	DLPH	Sup. by ADAM 96D
<250	90	5 BEBEK	89	CLEO	$e^+e^- \rightarrow \Upsilon(4S)$
540 ± 180 ± 200		6 ALBRECHT	88F	ARG	$e^+e^- \rightarrow \Upsilon(4S)$

- AAIJ 17B1 reports $[\Gamma(B^0 \rightarrow p\bar{p}\pi^+\pi^-)/\Gamma_{total}] / [B(B^0 \rightarrow J/\psi(1S) K^*(892)^0)] / [B(J/\psi(1S) \rightarrow p\bar{p})] / [B(K^*(892) \rightarrow (K\pi)^\pm)] = 1.07 \pm 0.04 \pm 0.04$ which we multiply by our best values $B(B^0 \rightarrow J/\psi(1S) K^*(892)^0) = (1.27 \pm 0.05) \times 10^{-3}$, $B(J/\psi(1S) \rightarrow p\bar{p}) = (2.120 \pm 0.029) \times 10^{-3}$, $B(K^*(892) \rightarrow (K\pi)^\pm) = (99.902 \pm 0.009) \times 10^{-2}$. Our first error is their experiment's error and our second error is the systematic error from using our best values.
- The branching ratio is given for $m_{p\bar{p}} < 2.85$ GeV.
- Assumes equal production of B^0 and B^+ from $\Upsilon(4S)$ decays. This measurement is quoted for $M(\pi^+\pi^-) < 1.22$ GeV excluding the $0.46 < M(\pi^+\pi^-) < 0.53$ GeV region.
- Assumes a B^0, B^- production fraction of 0.39 and a B_s production fraction of 0.12.
- BEBEK 89 reports $< 2.9 \times 10^{-4}$ assuming the $\Upsilon(4S)$ decays 43% to $B^0\bar{B}^0$. We rescale to 50%.
- ALBRECHT 88F reports $6.0 \pm 2.0 \pm 2.2$ assuming the $\Upsilon(4S)$ decays 45% to $B^0\bar{B}^0$. We rescale to 50%.

$\Gamma(p\bar{p}\pi^+\pi^-)/\Gamma(p\bar{p}K^+\pi^-)$		$\Gamma_{458}/\Gamma_{459}$			
VALUE	CL%	DOCUMENT ID	TECN	COMMENT	
0.46 ± 0.02 ± 0.02		1 AAIJ	17B1	LHCb	pp at 7, 8 TeV
<ol style="list-style-type: none"> The ratio is given for $m_{p\bar{p}} < 2.85$ GeV. 					

$\Gamma(p\bar{p}K^0)/\Gamma_{total}$		Γ_{460}/Γ			
VALUE (units 10^{-6})	CL%	DOCUMENT ID	TECN	COMMENT	
2.66 ± 0.32 OUR AVERAGE					
2.51 ^{+0.35} _{-0.29} ± 0.21		1,2 CHEN	08c	BELL	$e^+e^- \rightarrow \Upsilon(4S)$
3.0 ± 0.5 ± 0.3		2 AUBERT	07AV	BABR	$e^+e^- \rightarrow \Upsilon(4S)$
<ul style="list-style-type: none"> ••• We do not use the following data for averages, fits, limits, etc. ••• 					
2.40 ^{+0.64} _{-0.44} ± 0.28		2,3,4 WANG	05A	BELL	Repl. by CHEN 08c
1.88 ^{+0.77} _{-0.60} ± 0.23		2,3,5 WANG	04	BELL	Repl. by WANG 05A
<7.2	90	2,3 ABE	02k	BELL	Repl. by WANG 04

- Explicitly vetoes resonant production of $p\bar{p}$ from charmonium states.
- Assumes equal production of B^+ and B^0 at the $\Upsilon(4S)$.
- Explicitly vetoes resonant production of $p\bar{p}$ from charmonium states and pK^0 production from Λ_c .
- Provides also results with $M_{p\bar{p}} < 2.85$ GeV/ c^2 and angular asymmetry of $p\bar{p}$ system.
- The branching fraction for $M_{p\bar{p}} < 2.85$ is also reported.

$\Gamma(\Theta(1540)^+ p, \Theta^+ \rightarrow pK_S^0)/\Gamma_{total}$		Γ_{461}/Γ			
VALUE (units 10^{-6})	CL%	DOCUMENT ID	TECN	COMMENT	
<0.05	90	1 AUBERT	07AV	BABR	$e^+e^- \rightarrow \Upsilon(4S)$
<ul style="list-style-type: none"> ••• We do not use the following data for averages, fits, limits, etc. ••• 					
<0.23	90	1 WANG	05A	BELL	$e^+e^- \rightarrow \Upsilon(4S)$
<ol style="list-style-type: none"> Assumes equal production of B^+ and B^0 at the $\Upsilon(4S)$. 					

$\Gamma(f_j(2220) K^0, f_j \rightarrow p\bar{p})/\Gamma_{total}$		Γ_{462}/Γ			
VALUE (units 10^{-6})	CL%	DOCUMENT ID	TECN	COMMENT	
<0.45	90	1 AUBERT	07AV	BABR	$e^+e^- \rightarrow \Upsilon(4S)$
<ol style="list-style-type: none"> Assumes equal production of B^+ and B^0 at the $\Upsilon(4S)$. 					

$\Gamma(p\bar{p}K^+\pi^-)/\Gamma_{total}$		Γ_{459}/Γ			
VALUE (units 10^{-6})	CL%	DOCUMENT ID	TECN	COMMENT	
6.3 ± 0.5 ± 0.2		1,2 AAIJ	17B1	LHCb	pp at 7, 8 TeV
<ol style="list-style-type: none"> AAIJ 17B1 reports $[\Gamma(B^0 \rightarrow p\bar{p}K^+\pi^-)/\Gamma_{total}] / [B(B^0 \rightarrow J/\psi(1S) K^*(892)^0)] / [B(J/\psi(1S) \rightarrow p\bar{p})] / [B(K^*(892) \rightarrow (K\pi)^\pm)] = 2.34 \pm 0.12 \pm 0.12$ which we multiply by our best values $B(B^0 \rightarrow J/\psi(1S) K^*(892)^0) = (1.27 \pm 0.05) \times 10^{-3}$, $B(J/\psi(1S) \rightarrow p\bar{p}) = (2.120 \pm 0.029) \times 10^{-3}$, $B(K^*(892) \rightarrow (K\pi)^\pm) = (99.902 \pm 0.009) \times 10^{-2}$. Our first error is their experiment's error and our second error is the systematic error from using our best values. The branching ratio is given for $m_{p\bar{p}} < 2.85$ GeV. 					

$\Gamma(p\bar{p}K^*(892)^0)/\Gamma_{total}$		Γ_{463}/Γ			
VALUE (units 10^{-6})	CL%	DOCUMENT ID	TECN	COMMENT	
1.24 ^{+0.28} _{-0.25} OUR AVERAGE					
1.18 ^{+0.29} _{-0.25} ± 0.11		1,2 CHEN	08c	BELL	$e^+e^- \rightarrow \Upsilon(4S)$
1.47 ± 0.45 ± 0.40		2 AUBERT	07AV	BABR	$e^+e^- \rightarrow \Upsilon(4S)$
<ul style="list-style-type: none"> ••• We do not use the following data for averages, fits, limits, etc. ••• 					
<7.6	90	2 WANG	04	BELL	$e^+e^- \rightarrow \Upsilon(4S)$

- Explicitly vetoes resonant production of $p\bar{p}$ from charmonium states.
- Assumes equal production of B^+ and B^0 at the $\Upsilon(4S)$.

Meson Particle Listings

 B^0

$\Gamma(p\bar{p}\pi^0)/\Gamma_{\text{total}}$	Γ_{466}/Γ			
VALUE (units 10^{-7})	DOCUMENT ID	TECN	COMMENT	
$5.0 \pm 1.8 \pm 0.6$	PAL	19	BELL	$e^+e^- \rightarrow \Upsilon(4S)$

$\Gamma(f_J(2220)K_0^* f_J \rightarrow p\bar{p})/\Gamma_{\text{total}}$	Γ_{464}/Γ			
VALUE (units 10^{-6})	CL%	DOCUMENT ID	TECN	COMMENT
<0.15	90	¹ AUBERT	07AV BABR	$e^+e^- \rightarrow \Upsilon(4S)$
¹ Assumes equal production of B^+ and B^0 at the $\Upsilon(4S)$.				

$\Gamma(p\bar{p}K^+K^-)/\Gamma_{\text{total}}$	Γ_{465}/Γ			
VALUE (units 10^{-8})	DOCUMENT ID	TECN	COMMENT	
$12.1 \pm 3.1 \pm 0.5$	^{1,2} AAIJ	17BD LHCB	pp at 7, 8 TeV	
¹ AAIJ 17BD reports $[\Gamma(B^0 \rightarrow p\bar{p}K^+K^-)/\Gamma_{\text{total}}] / [B(B^0 \rightarrow J/\psi(1S)K^*(892)^0)] / [B(J/\psi(1S) \rightarrow p\bar{p})] / [B(K^*(892) \rightarrow (K\pi)^\pm)] = 0.045 \pm 0.011 \pm 0.004$ which we multiply by our best values $B(B^0 \rightarrow J/\psi(1S)K^*(892)^0) = (1.27 \pm 0.05) \times 10^{-3}$, $B(J/\psi(1S) \rightarrow p\bar{p}) = (2.120 \pm 0.029) \times 10^{-3}$, $B(K^*(892) \rightarrow (K\pi)^\pm) = (99.902 \pm 0.009) \times 10^{-2}$. Our first error is their experiment's error and our second error is the systematic error from using our best values.				
² The branching ratio is given for $m_{p\bar{p}} < 2.85$ GeV.				

$\Gamma(p\bar{p}K^+K^-)/\Gamma(p\bar{p}K^+\pi^-)$	$\Gamma_{465}/\Gamma_{459}$			
VALUE (%)	DOCUMENT ID	TECN	COMMENT	
$1.9 \pm 0.5 \pm 0.2$	¹ AAIJ	17BD LHCB	pp at 7, 8 TeV	
¹ The ratio is given for $m_{p\bar{p}} < 2.85$ GeV.				

$\Gamma(p\bar{p}p\bar{p})/\Gamma_{\text{total}}$	Γ_{467}/Γ			
VALUE	CL%	DOCUMENT ID	TECN	COMMENT
$<2.0 \times 10^{-7}$	90	¹ LEES	18c BABR	$e^+e^- \rightarrow \Upsilon(4S)$
¹ Assumes equal production of B^+ and B^0 at the $\Upsilon(4S)$.				

$\Gamma(p\bar{\Lambda}\pi^-)/\Gamma_{\text{total}}$	Γ_{468}/Γ			
VALUE (units 10^{-6})	CL%	DOCUMENT ID	TECN	COMMENT
3.14 ± 0.29 OUR AVERAGE				
$3.07 \pm 0.31 \pm 0.23$		¹ AUBERT	09AC BABR	$e^+e^- \rightarrow \Upsilon(4S)$
$3.23 \pm 0.33 \pm 0.29$		¹ WANG	07c BELL	$e^+e^- \rightarrow \Upsilon(4S)$
• • • We do not use the following data for averages, fits, limits, etc. • • •				
$2.62 \pm 0.44 \pm 0.31$		^{1,2} WANG	05A BELL	Repl. by WANG 07c
$3.97 \pm 1.00 \pm 0.56$		¹ WANG	03A BELL	Repl. by WANG 05A
<13	90	¹ COAN	99 CLE2	$e^+e^- \rightarrow \Upsilon(4S)$
<180	90	³ ALBRECHT	88F ARG	$e^+e^- \rightarrow \Upsilon(4S)$
¹ Assumes equal production of B^+ and B^0 at the $\Upsilon(4S)$.				
² Provides also results with $m_{p\bar{p}} < 2.85$ GeV/ c^2 and angular asymmetry of $p\bar{\Lambda}$ system.				
³ ALBRECHT 88F reports $<2.0 \times 10^{-4}$ assuming the $\Upsilon(4S)$ decays 45% to $B^0\bar{B}^0$. We rescale to 50%.				

$\Gamma(p\bar{\Lambda}\pi^- \gamma)/\Gamma_{\text{total}}$	Γ_{469}/Γ			
VALUE	CL%	DOCUMENT ID	TECN	COMMENT
$<6.5 \times 10^{-7}$	90	¹ LAI	14 BELL	$e^+e^- \rightarrow \Upsilon(4S)$
¹ Assumes equal production of B^+ and B^0 at the $\Upsilon(4S)$.				

$\Gamma(p\bar{\Sigma}^-(1385^-))/\Gamma_{\text{total}}$	Γ_{470}/Γ			
VALUE (units 10^{-6})	CL%	DOCUMENT ID	TECN	COMMENT
<0.26	90	¹ WANG	07c BELL	$e^+e^- \rightarrow \Upsilon(4S)$
¹ Assumes equal production of B^+ and B^0 at the $\Upsilon(4S)$.				

$[\Gamma(\Delta(1232)^+ \bar{p}) + \Gamma(\Delta(1232)^- p)]/\Gamma_{\text{total}}$	Γ_{471}/Γ			
VALUE	DOCUMENT ID	TECN	COMMENT	
$<1.6 \times 10^{-6}$	PAL	19	BELL	$e^+e^- \rightarrow \Upsilon(4S)$

$\Gamma(\Delta^0 \bar{\Lambda})/\Gamma_{\text{total}}$	Γ_{472}/Γ			
VALUE (units 10^{-6})	CL%	DOCUMENT ID	TECN	COMMENT
<0.93	90	¹ WANG	07c BELL	$e^+e^- \rightarrow \Upsilon(4S)$
¹ Assumes equal production of B^+ and B^0 at the $\Upsilon(4S)$.				

$\Gamma(p\bar{\Lambda}K^-)/\Gamma_{\text{total}}$	Γ_{473}/Γ			
VALUE (units 10^{-6})	CL%	DOCUMENT ID	TECN	COMMENT
<0.82	90	¹ WANG	03 BELL	$e^+e^- \rightarrow \Upsilon(4S)$
¹ Assumes equal production of B^+ and B^0 at the $\Upsilon(4S)$.				

$\Gamma(p\bar{\Lambda}D^-)/\Gamma_{\text{total}}$	Γ_{474}/Γ			
VALUE (units 10^{-6})	DOCUMENT ID	TECN	COMMENT	
$25.1 \pm 2.6 \pm 3.5$	¹ CHANG	15	BELL	$e^+e^- \rightarrow \Upsilon(4S)$
¹ Assumes equal production of B^+ and B^0 at the $\Upsilon(4S)$.				

$\Gamma(p\bar{\Lambda}D^{*-})/\Gamma_{\text{total}}$	Γ_{475}/Γ			
VALUE (units 10^{-6})	DOCUMENT ID	TECN	COMMENT	
$33.6 \pm 6.3 \pm 4.4$	¹ CHANG	15	BELL	$e^+e^- \rightarrow \Upsilon(4S)$
¹ Assumes equal production of B^+ and B^0 at the $\Upsilon(4S)$.				

$\Gamma(p\bar{\Sigma}^0 \pi^-)/\Gamma_{\text{total}}$	Γ_{476}/Γ			
VALUE	CL%	DOCUMENT ID	TECN	COMMENT
$<3.8 \times 10^{-6}$	90	¹ WANG	03 BELL	$e^+e^- \rightarrow \Upsilon(4S)$
¹ Assumes equal production of B^+ and B^0 at the $\Upsilon(4S)$.				

$\Gamma(\bar{\Lambda}\Lambda)/\Gamma_{\text{total}}$	Γ_{477}/Γ			
VALUE (units 10^{-6})	CL%	DOCUMENT ID	TECN	COMMENT
<0.32	90	¹ TSAI	07 BELL	$e^+e^- \rightarrow \Upsilon(4S)$
• • • We do not use the following data for averages, fits, limits, etc. • • •				
<0.69	90	¹ CHANG	05 BELL	Repl. by TSAI 07
<1.2	90	¹ BORNHEIM	03 CLE2	$e^+e^- \rightarrow \Upsilon(4S)$
<1.0	90	¹ ABE	02O BELL	Repl. by CHANG 05
<3.9	90	¹ COAN	99 CLE2	$e^+e^- \rightarrow \Upsilon(4S)$
¹ Assumes equal production of B^+ and B^0 at the $\Upsilon(4S)$.				

$\Gamma(\bar{\Lambda}\Lambda K^0)/\Gamma_{\text{total}}$	Γ_{478}/Γ			
VALUE (units 10^{-6})	DOCUMENT ID	TECN	COMMENT	
$4.76 \pm 0.84 \pm 0.68 \pm 0.61$	^{1,2} CHANG	09	BELL	$e^+e^- \rightarrow \Upsilon(4S)$
¹ Excluding charmonium events in $2.85 < m_{\Lambda\bar{\Lambda}} < 3.128$ GeV/ c^2 and $3.315 < m_{\Lambda\bar{\Lambda}} < 3.735$ GeV/ c^2 . Measurements in various $m_{\Lambda\bar{\Lambda}}$ bins are also reported.				
² Assumes equal production of B^+ and B^0 at the $\Upsilon(4S)$.				

$\Gamma(\bar{\Lambda}\Lambda K^{*0})/\Gamma_{\text{total}}$	Γ_{479}/Γ			
VALUE (units 10^{-6})	DOCUMENT ID	TECN	COMMENT	
$2.46 \pm 0.87 \pm 0.34$	^{1,2} CHANG	09	BELL	$e^+e^- \rightarrow \Upsilon(4S)$
¹ Excluding charmonium events in $2.85 < m_{\Lambda\bar{\Lambda}} < 3.128$ GeV/ c^2 and $3.315 < m_{\Lambda\bar{\Lambda}} < 3.735$ GeV/ c^2 . Measurements in various $m_{\Lambda\bar{\Lambda}}$ bins are also reported.				
² Assumes equal production of B^+ and B^0 at the $\Upsilon(4S)$.				

$\Gamma(\bar{\Lambda}\Lambda D^0)/\Gamma_{\text{total}}$	Γ_{480}/Γ			
VALUE (units 10^{-5})	DOCUMENT ID	TECN	COMMENT	
$1.00 \pm 0.30 \pm 0.26$ OUR AVERAGE				
$0.98 \pm 0.29 \pm 0.19$	^{1,2} LEES	14b	BABR	$e^+e^- \rightarrow \Upsilon(4S)$
$1.05 \pm 0.57 \pm 0.14$	² CHANG	09	BELL	$e^+e^- \rightarrow \Upsilon(4S)$
¹ Evidence for 3.4 st. dev. signal significance.				
² Assumes equal production of B^+ and B^0 at the $\Upsilon(4S)$.				

$\Gamma(D^0 \Sigma^0 \bar{\Lambda} + \text{c.c.})/\Gamma_{\text{total}}$	Γ_{481}/Γ			
VALUE	CL%	DOCUMENT ID	TECN	COMMENT
$<3.1 \times 10^{-5}$	90	^{1,2} LEES	14b	BABR $e^+e^- \rightarrow \Upsilon(4S)$
¹ Here $\Sigma^0 \rightarrow \Lambda\gamma$.				
² Assumes equal production of B^+ and B^0 at the $\Upsilon(4S)$.				

$\Gamma(\Delta^0 \bar{\Sigma}^0)/\Gamma_{\text{total}}$	Γ_{482}/Γ			
VALUE	CL%	DOCUMENT ID	TECN	COMMENT
<0.0015	90	¹ BORTOLETTO89	CLEO	$e^+e^- \rightarrow \Upsilon(4S)$
¹ BORTOLETTO 89 reports <0.0018 assuming $\Upsilon(4S)$ decays 43% to $B^0\bar{B}^0$. We rescale to 50%.				

$\Gamma(\Delta^{++} \bar{\Delta}^{--})/\Gamma_{\text{total}}$	Γ_{483}/Γ			
VALUE	CL%	DOCUMENT ID	TECN	COMMENT
$<1.1 \times 10^{-4}$	90	¹ BORTOLETTO89	CLEO	$e^+e^- \rightarrow \Upsilon(4S)$
¹ BORTOLETTO 89 reports $<1.3 \times 10^{-4}$ assuming $\Upsilon(4S)$ decays 43% to $B^0\bar{B}^0$. We rescale to 50%.				

$\Gamma(D^0 p\bar{p})/\Gamma_{\text{total}}$	Γ_{484}/Γ			
VALUE (units 10^{-4})	DOCUMENT ID	TECN	COMMENT	
1.04 ± 0.07 OUR AVERAGE				
$1.02 \pm 0.04 \pm 0.06$	^{1,2} DEL-AMO-SA..12	BABR	$e^+e^- \rightarrow \Upsilon(4S)$	
$1.18 \pm 0.15 \pm 0.16$	² ABE	02W BELL	$e^+e^- \rightarrow \Upsilon(4S)$	
• • • We do not use the following data for averages, fits, limits, etc. • • •				
$1.13 \pm 0.06 \pm 0.08$	² AUBERT,B	06s BABR	Repl. by DEL-AMO-SANCHEZ 12	
¹ Uses the values of D and D^* branching fractions from PDG 08.				
² Assumes equal production of B^+ and B^0 at the $\Upsilon(4S)$.				

$\Gamma(D_s^- \bar{\Lambda} p)/\Gamma_{\text{total}}$	Γ_{485}/Γ			
VALUE (units 10^{-5})	DOCUMENT ID	TECN	COMMENT	
$2.8 \pm 0.8 \pm 0.3$	^{1,2} MEDVEDEVA	07	BELL	$e^+e^- \rightarrow \Upsilon(4S)$
¹ Assumes equal production of B^+ and B^0 at the $\Upsilon(4S)$.				
² MEDVEDEVA 07 reports $(2.9 \pm 0.7 \pm 0.5 \pm 0.4) \times 10^{-5}$ from a measurement of $[\Gamma(B^0 \rightarrow D_s^- \bar{\Lambda} p)/\Gamma_{\text{total}}] \times [B(D_s^+ \rightarrow \phi\pi^+) / B(D_s^+ \rightarrow \phi\pi^+)]$ assuming $B(D_s^+ \rightarrow \phi\pi^+) = (4.4 \pm 0.6) \times 10^{-2}$, which we rescale to our best value $B(D_s^+ \rightarrow \phi\pi^+) = (4.5 \pm 0.4) \times 10^{-2}$. Our first error is their experiment's error and our second error is the systematic error from using our best value.				

Γ(D*(2007)⁰ p p̄)/Γ_{total} Γ₄₈₆/Γ

Table with columns: VALUE (units 10⁻⁴), DOCUMENT ID, TECN, COMMENT. Includes 'OUR AVERAGE' and data from DEL-AMO-SA...12 and ABE.

• • • We do not use the following data for averages, fits, limits, etc. • • •
1.01 ± 0.10 ± 0.09 2 AUBERT,B 06s BABR Repl. by DEL-AMO-SANCHEZ 12
1 Uses the values of D and D* branching fractions from PDG 08.
2 Assumes equal production of B+ and B0 at the T(4S).

Γ(D*(2010)- p p̄)/Γ_{total} Γ₄₈₇/Γ

Table with columns: VALUE (units 10⁻⁴), DOCUMENT ID, TECN, COMMENT. Includes 'OUR AVERAGE' and data from ANDERSON 01.

1 Assumes equal production of B+ and B0 at the T(4S).

Γ(D- p p̄ π+)/Γ_{total} Γ₄₈₈/Γ

Table with columns: VALUE (units 10⁻⁴), DOCUMENT ID, TECN, COMMENT. Includes 'OUR AVERAGE' and data from DEL-AMO-SA...12 and AUBERT,B.

• • • We do not use the following data for averages, fits, limits, etc. • • •
1 Uses the values of D and D* branching fractions from PDG 08.
2 Assumes equal production of B+ and B0 at the T(4S).

Γ(D*(2010)- p p̄ π+)/Γ_{total} Γ₄₈₉/Γ

Table with columns: VALUE (units 10⁻⁴), DOCUMENT ID, TECN, COMMENT. Includes 'OUR AVERAGE' and data from DEL-AMO-SA...12 and ANDERSON 01.

• • • We do not use the following data for averages, fits, limits, etc. • • •
4.81 ± 0.22 ± 0.44 2 AUBERT,B 06s BABR Repl. by DEL-AMO-SANCHEZ 12
1 Uses the values of D and D* branching fractions from PDG 08.
2 Assumes equal production of B+ and B0 at the T(4S).

Γ(D0 p p̄ π+ π-)/Γ_{total} Γ₄₉₀/Γ

Table with columns: VALUE (units 10⁻⁴), DOCUMENT ID, TECN, COMMENT. Includes 'OUR AVERAGE' and data from DEL-AMO-SA...12.

1 Uses the values of D and D* branching fractions from PDG 08.
2 Assumes equal production of B+ and B0 at the T(4S).

Γ(D*0 p p̄ π+ π-)/Γ_{total} Γ₄₉₁/Γ

Table with columns: VALUE (units 10⁻⁴), DOCUMENT ID, TECN, COMMENT. Includes 'OUR AVERAGE' and data from DEL-AMO-SA...12.

1 Uses the values of D and D* branching fractions from PDG 08.
2 Assumes equal production of B+ and B0 at the T(4S).

Γ(Θc p̄ π+, Θc → D* p)/Γ_{total} Γ₄₉₂/Γ

Table with columns: VALUE (units 10⁻⁶), CL%, DOCUMENT ID, TECN, COMMENT. Includes 'OUR AVERAGE' and data from AUBERT,B.

1 Assumes equal production of B+ and B0 at the T(4S).

Γ(Θc p̄ π+, Θc → D* π)/Γ_{total} Γ₄₉₃/Γ

Table with columns: VALUE (units 10⁻⁶), CL%, DOCUMENT ID, TECN, COMMENT. Includes 'OUR AVERAGE' and data from AUBERT,B.

1 Assumes equal production of B+ and B0 at the T(4S).

Γ(Σc-- Δ++)/Γ_{total} Γ₄₉₄/Γ

Table with columns: VALUE (units 10⁻⁴), CL%, DOCUMENT ID, TECN, COMMENT. Includes 'OUR AVERAGE' and data from PROCARIO 94.

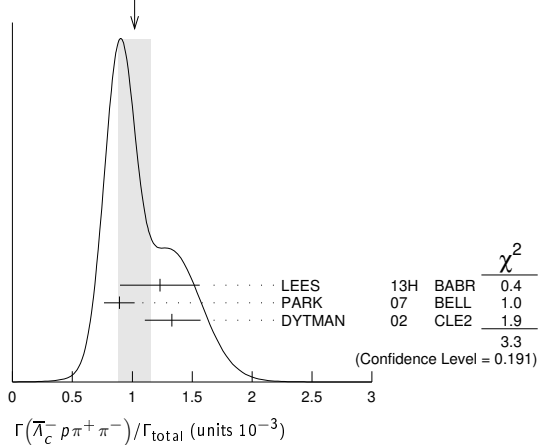
1 PROCARIO 94 reports < 0.0012 from a measurement of [Γ(B0 → Σc-- Δ++)/Γtotal] × [B(Λc+ → p K- π+)] assuming B(Λc+ → p K- π+) = 0.043, which we rescale to our best value B(Λc+ → p K- π+) = 6.28 × 10-2.

Γ(Λc- p π+ π-)/Γ_{total} Γ₄₉₅/Γ

Table with columns: VALUE (units 10-3), DOCUMENT ID, TECN, COMMENT. Includes 'OUR AVERAGE' and data from LEES, BELL, and DYTMAN.

• • • We do not use the following data for averages, fits, limits, etc. • • •
0.88 ± 0.16 ± 0.05 5 GABYSHEV 02 BELL Repl. by PARK 07
1.33 +0.46 -0.42 6 FU 97 CLE2 Repl. by DYTMAN 02

WEIGHTED AVERAGE 1.02±0.14 (Error scaled by 1.3)



1 Assumes equal production of B+ and B0 at the T(4S).
2 Uses Λc+ → p K- π+ mode. The second error includes the uncertainty of the branching fraction of the Λc decay, B(Λc+ → p K- π+) = (5.0 ± 1.3)%.
3 PARK 07 reports (11.2 ± 0.5 ± 3.2) × 10-4 from a measurement of [Γ(B0 → Λc- p π+ π-)/Γtotal] × [B(Λc+ → p K- π+)] assuming B(Λc+ → p K- π+) = (5.0 ± 1.3) × 10-2, which we rescale to our best value B(Λc+ → p K- π+) = (6.28 ± 0.32) × 10-2. Our first error is their experiment's error and our second error is the systematic error from using our best value.
4 DYTMAN 02 reports (1.67 +0.27 -0.25) × 10-3 from a measurement of [Γ(B0 → Λc- p π+ π-)/Γtotal] × [B(Λc+ → p K- π+)] assuming B(Λc+ → p K- π+) = 0.05, which we rescale to our best value B(Λc+ → p K- π+) = (6.28 ± 0.32) × 10-2. Our first error is their experiment's error and our second error is the systematic error from using our best value.
5 GABYSHEV 02 reports (1.1 ± 0.2) × 10-3 from a measurement of [Γ(B0 → Λc- p π+ π-)/Γtotal] × [B(Λc+ → p K- π+)] assuming B(Λc+ → p K- π+) = 0.05, which we rescale to our best value B(Λc+ → p K- π+) = (6.28 ± 0.32) × 10-2. Our first error is their experiment's error and our second error is the systematic error from using our best value.
6 FU 97 uses PDG 96 values of Λc branching fraction.

Γ(Λc- p)/Γ_{total} Γ₄₉₆/Γ

Table with columns: VALUE (units 10-3), CL%, DOCUMENT ID, TECN, COMMENT. Includes 'OUR AVERAGE' and data from AUBERT and GABYSHEV.

• • • We do not use the following data for averages, fits, limits, etc. • • •
2.10 +0.67 +0.77 -0.55 -0.46 1,4 AUBERT 07AV BABR Repl. by AUBERT 08BN
< 9 90 1,5 DYTMAN 02 CLE2 e+ e- → T(4S)
< 3.1 90 1,4 GABYSHEV 02 BELL e+ e- → T(4S)
< 21 90 6 FU 97 CLE2 e+ e- → T(4S)

1 Assumes equal production of B+ and B0 at the T(4S).
2 AUBERT 08BN reports (1.89 ± 0.21 ± 0.49) × 10-9 from a measurement of [Γ(B0 → Λc- p)/Γtotal] × [B(Λc+ → p K- π+)] assuming B(Λc+ → p K- π+) = (5.0 ± 1.3) × 10-2, which we rescale to our best value B(Λc+ → p K- π+) = (6.28 ± 0.32) × 10-2. Our first error is their experiment's error and our second error is the systematic error from using our best value.
3 The second error for GABYSHEV 03 includes the systematic and the error of Λc → p K+ π- decay branching fraction.
4 Uses the value for Λc → p K- π+ branching ratio (5.0 ± 1.3)%.
5 DYTMAN 02 measurement uses B(Λc- → p K+ π-) = 5.0 ± 1.3%. The second error includes the systematic and the uncertainty of the branching ratio.
6 FU 97 uses PDG 96 values of Λc branching ratio.

Γ(Λc- p π0)/Γ_{total} Γ₄₉₇/Γ

Table with columns: VALUE (units 10-4), CL%, DOCUMENT ID, TECN, COMMENT. Includes 'OUR AVERAGE' and data from AUBERT and FU.

• • • We do not use the following data for averages, fits, limits, etc. • • •
1 AUBERT 10H reports (1.94 ± 0.17 ± 0.52) × 10-4 from a measurement of [Γ(B0 → Λc- p π0)/Γtotal] × [B(Λc+ → p K- π+)] assuming B(Λc+ → p K- π+) = (5.0 ± 1.3) × 10-2, which we rescale to our best value B(Λc+ → p K- π+) = (6.28 ± 0.32) × 10-2. Our first error is their experiment's error and our second error is the systematic error from using our best value.
2 Assumes equal production of B+ and B0 at the T(4S).
3 FU 97 uses PDG 96 values of Λc branching ratio.

Meson Particle Listings

 B^0 $\Gamma(\Lambda_c^- p K^+ K^-)/\Gamma_{\text{total}}$ Γ_{510}/Γ

VALUE (units 10^{-5})	DOCUMENT ID	TECN	COMMENT
$2.0 \pm 0.4 \pm 0.1$	1,2 LEES	15B	BABR $e^+ e^- \rightarrow \Upsilon(4S)$

- ¹ LEES 15B reports $[\Gamma(B^0 \rightarrow \Lambda_c^- p K^+ K^-)/\Gamma_{\text{total}}] \times [\text{B}(\Lambda_c^+ \rightarrow p K^- \pi^+)] = (12.5 \pm 2.0 \pm 1.0) \times 10^{-7}$ which we divide by our best value $\text{B}(\Lambda_c^+ \rightarrow p K^- \pi^+) = (6.28 \pm 0.32) \times 10^{-2}$. Our first error is their experiment's error and our second error is the systematic error from using our best value.
- ² Assumes equal production of B^+ and B^0 at the $\Upsilon(4S)$.

 $\Gamma(\Lambda_c^- \rho \phi)/\Gamma_{\text{total}}$ Γ_{511}/Γ

VALUE	CL%	DOCUMENT ID	TECN	COMMENT
$<1.0 \times 10^{-5}$	90	1,2 LEES	15B	BABR $e^+ e^- \rightarrow \Upsilon(4S)$

- ¹ LEES 15B reports $<1.2 \times 10^{-5}$ from a measurement of $[\Gamma(B^0 \rightarrow \Lambda_c^- \rho \phi)/\Gamma_{\text{total}}] \times [\text{B}(\Lambda_c^+ \rightarrow p K^- \pi^+)]$ assuming $\text{B}(\Lambda_c^+ \rightarrow p K^- \pi^+) = (5.0 \pm 1.3) \times 10^{-2}$, which we rescale to our best value $\text{B}(\Lambda_c^+ \rightarrow p K^- \pi^+) = 6.28 \times 10^{-2}$.
- ² Assumes equal production of B^+ and B^0 at the $\Upsilon(4S)$.

 $\Gamma(\Sigma_c(2455)^- p)/\Gamma_{\text{total}}$ Γ_{498}/Γ

VALUE (units 10^{-6})	DOCUMENT ID	TECN	COMMENT
<24	1,2 AUBERT	10H	BABR $e^+ e^- \rightarrow \Upsilon(4S)$

- ¹ AUBERT 10H reports $[\Gamma(B^0 \rightarrow \Sigma_c(2455)^- p)/\Gamma_{\text{total}}] \times [\text{B}(\Lambda_c^+ \rightarrow p K^- \pi^+)] < 1.5 \times 10^{-6}$ which we divide by our best value $\text{B}(\Lambda_c^+ \rightarrow p K^- \pi^+) = 6.28 \times 10^{-2}$.
- ² Assumes equal production of B^+ and B^0 at the $\Upsilon(4S)$.

 $\Gamma(\Lambda_c^- p \pi^+ \pi^- \pi^0)/\Gamma_{\text{total}}$ Γ_{499}/Γ

VALUE	CL%	DOCUMENT ID	TECN	COMMENT
$<5.07 \times 10^{-3}$	90	1 FU	97	CLE2 $e^+ e^- \rightarrow \Upsilon(4S)$

- ¹ FU 97 uses PDG 96 values of Λ_c branching ratio.

 $\Gamma(\Lambda_c^- p \pi^+ \pi^- \pi^+ \pi^-)/\Gamma_{\text{total}}$ Γ_{500}/Γ

VALUE	CL%	DOCUMENT ID	TECN	COMMENT
$<2.74 \times 10^{-3}$	90	1 FU	97	CLE2 $e^+ e^- \rightarrow \Upsilon(4S)$

- ¹ FU 97 uses PDG 96 values of Λ_c branching ratio.

 $\Gamma(\Lambda_c^- p \pi^+ \pi^- (\text{nonresonant}))/\Gamma_{\text{total}}$ Γ_{501}/Γ

VALUE (units 10^{-4})	DOCUMENT ID	TECN	COMMENT
5.5 ± 1.0 OUR AVERAGE	Error includes scale factor of 1.3.		
$7.9 \pm 0.4 \pm 2.0$	1,2 LEES	13H	BABR $e^+ e^- \rightarrow \Upsilon(4S)$
$5.1 \pm 0.8 \pm 0.3$	1,3 PARK	07	BELL $e^+ e^- \rightarrow \Upsilon(4S)$

- ¹ Assumes equal production of B^+ and B^0 at the $\Upsilon(4S)$.
- ² Uses $\Lambda_c^+ \rightarrow p K^- \pi^+$ mode. The second error includes the uncertainty of the branching fraction of the Λ_c decay, $\text{B}(\Lambda_c^+ \rightarrow p K^- \pi^+) = (5.0 \pm 1.3)\%$.
- ³ PARK 07 reports $(6.4 \pm 0.4 \pm 1.9) \times 10^{-4}$ from a measurement of $[\Gamma(B^0 \rightarrow \Lambda_c^- p \pi^+ \pi^- (\text{nonresonant}))/\Gamma_{\text{total}}] \times [\text{B}(\Lambda_c^+ \rightarrow p K^- \pi^+)]$ assuming $\text{B}(\Lambda_c^+ \rightarrow p K^- \pi^+) = (5.0 \pm 1.3) \times 10^{-2}$, which we rescale to our best value $\text{B}(\Lambda_c^+ \rightarrow p K^- \pi^+) = (6.28 \pm 0.32) \times 10^{-2}$. Our first error is their experiment's error and our second error is the systematic error from using our best value.

 $\Gamma(\Sigma_c(2520)^- p \pi^+)/\Gamma_{\text{total}}$ Γ_{502}/Γ

VALUE (units 10^{-4})	DOCUMENT ID	TECN	COMMENT
1.02 ± 0.18 OUR AVERAGE			
$1.15 \pm 0.10 \pm 0.30$	1,2 LEES	13H	BABR $e^+ e^- \rightarrow \Upsilon(4S)$
$0.96 \pm 0.21 \pm 0.05$	1,3 PARK	07	BELL $e^+ e^- \rightarrow \Upsilon(4S)$
$1.3 \pm 0.5 \pm 0.1$	4 GABYSHEV	02	BELL Repl. by PARK 07

- ¹ Assumes equal production of B^+ and B^0 at the $\Upsilon(4S)$.
- ² Uses $\Lambda_c^+ \rightarrow p K^- \pi^+$ mode. The second error includes the uncertainty of the branching fraction of the Λ_c decay, $\text{B}(\Lambda_c^+ \rightarrow p K^- \pi^+) = (5.0 \pm 1.3)\%$.
- ³ PARK 07 reports $(1.2 \pm 0.1 \pm 0.4) \times 10^{-4}$ from a measurement of $[\Gamma(B^0 \rightarrow \Sigma_c(2520)^- p \pi^+)/\Gamma_{\text{total}}] \times [\text{B}(\Lambda_c^+ \rightarrow p K^- \pi^+)]$ assuming $\text{B}(\Lambda_c^+ \rightarrow p K^- \pi^+) = (5.0 \pm 1.3) \times 10^{-2}$, which we rescale to our best value $\text{B}(\Lambda_c^+ \rightarrow p K^- \pi^+) = (6.28 \pm 0.32) \times 10^{-2}$. Our first error is their experiment's error and our second error is the systematic error from using our best value.
- ⁴ GABYSHEV 02 reports $(1.63^{+0.64}_{-0.58}) \times 10^{-4}$ from a measurement of $[\Gamma(B^0 \rightarrow \Sigma_c(2520)^- p \pi^+)/\Gamma_{\text{total}}] \times [\text{B}(\Lambda_c^+ \rightarrow p K^- \pi^+)]$ assuming $\text{B}(\Lambda_c^+ \rightarrow p K^- \pi^+) = 0.05$, which we rescale to our best value $\text{B}(\Lambda_c^+ \rightarrow p K^- \pi^+) = (6.28 \pm 0.32) \times 10^{-2}$. Our first error is their experiment's error and our second error is the systematic error from using our best value.

 $\Gamma(\Sigma_c(2520)^0 p \pi^-)/\Gamma_{\text{total}}$ Γ_{503}/Γ

VALUE	CL%	DOCUMENT ID	TECN	COMMENT
$<0.31 \times 10^{-4}$	90	1,2 LEES	13H	BABR $e^+ e^- \rightarrow \Upsilon(4S)$
$<0.38 \times 10^{-4}$	90	1 PARK	07	BELL $e^+ e^- \rightarrow \Upsilon(4S)$
$<1.21 \times 10^{-4}$	90	1,2 GABYSHEV	02	BELL Repl. by PARK 07

- ¹ Assumes equal production of B^+ and B^0 at the $\Upsilon(4S)$.
- ² Uses the value for $\Lambda_c \rightarrow p K^- \pi^+$ branching ratio $(5.0 \pm 1.3)\%$.

 $\Gamma(\Sigma_c(2455)^0 N^0, N^0 \rightarrow p \pi^-)/\Gamma_{\text{total}}$ Γ_{505}/Γ

VALUE (units 10^{-4})	DOCUMENT ID	TECN	COMMENT
$0.64 \pm 0.16 \pm 0.03$	1,2 KIM	08	BELL $e^+ e^- \rightarrow \Upsilon(4S)$

- N^0 is the $N(1440) P_{11}$ or $N(1535) S_{11}$ or an admixture of the two baryonic states.
- ¹ Assumes equal production of B^+ and B^0 at the $\Upsilon(4S)$.
- ² KIM 08 reports $(0.80 \pm 0.15 \pm 0.25) \times 10^{-4}$ from a measurement of $[\Gamma(B^0 \rightarrow \Sigma_c(2455)^0 N^0, N^0 \rightarrow p \pi^-)/\Gamma_{\text{total}}] \times [\text{B}(\Lambda_c^+ \rightarrow p K^- \pi^+)]$ assuming $\text{B}(\Lambda_c^+ \rightarrow p K^- \pi^+) = (5.0 \pm 1.3) \times 10^{-2}$, which we rescale to our best value $\text{B}(\Lambda_c^+ \rightarrow p K^- \pi^+) = (6.28 \pm 0.32) \times 10^{-2}$. Our first error is their experiment's error and our second error is the systematic error from using our best value.

 $\Gamma(\Sigma_c(2455)^0 p \pi^-)/\Gamma_{\text{total}}$ Γ_{504}/Γ

VALUE (units 10^{-4})	CL%	DOCUMENT ID	TECN	COMMENT
1.08 ± 0.16 OUR AVERAGE				
$0.91 \pm 0.07 \pm 0.24$		1,2 LEES	13H	BABR $e^+ e^- \rightarrow \Upsilon(4S)$
$1.12 \pm 0.21 \pm 0.06$		1,3 PARK	07	BELL $e^+ e^- \rightarrow \Upsilon(4S)$
$1.8 \pm 0.6 \pm 0.1$		4 DYTMAN	02	CLE2 $e^+ e^- \rightarrow \Upsilon(4S)$

- We do not use the following data for averages, fits, limits, etc. **•••**
- $0.38^{+0.37}_{-0.33} \pm 0.02$ 90 ⁵ GABYSHEV 02 BELL Repl. by PARK 07

- ¹ Assumes equal production of B^+ and B^0 at the $\Upsilon(4S)$.
- ² Uses $\Lambda_c^+ \rightarrow p K^- \pi^+$ mode. The second error includes the uncertainty of the branching fraction of the Λ_c decay, $\text{B}(\Lambda_c^+ \rightarrow p K^- \pi^+) = (5.0 \pm 1.3)\%$.
- ³ PARK 07 reports $(1.4 \pm 0.2 \pm 0.4) \times 10^{-4}$ from a measurement of $[\Gamma(B^0 \rightarrow \Sigma_c(2455)^0 p \pi^-)/\Gamma_{\text{total}}] \times [\text{B}(\Lambda_c^+ \rightarrow p K^- \pi^+)]$ assuming $\text{B}(\Lambda_c^+ \rightarrow p K^- \pi^+) = (5.0 \pm 1.3) \times 10^{-2}$, which we rescale to our best value $\text{B}(\Lambda_c^+ \rightarrow p K^- \pi^+) = (6.28 \pm 0.32) \times 10^{-2}$. Our first error is their experiment's error and our second error is the systematic error from using our best value.
- ⁴ DYTMAN 02 reports $(2.2 \pm 0.7) \times 10^{-4}$ from a measurement of $[\Gamma(B^0 \rightarrow \Sigma_c(2455)^0 p \pi^-)/\Gamma_{\text{total}}] \times [\text{B}(\Lambda_c^+ \rightarrow p K^- \pi^+)]$ assuming $\text{B}(\Lambda_c^+ \rightarrow p K^- \pi^+) = 0.05$, which we rescale to our best value $\text{B}(\Lambda_c^+ \rightarrow p K^- \pi^+) = (6.28 \pm 0.32) \times 10^{-2}$. Our first error is their experiment's error and our second error is the systematic error from using our best value.
- ⁵ GABYSHEV 02 reports $(0.48^{+0.46}_{-0.41}) \times 10^{-4}$ from a measurement of $[\Gamma(B^0 \rightarrow \Sigma_c(2455)^0 p \pi^-)/\Gamma_{\text{total}}] \times [\text{B}(\Lambda_c^+ \rightarrow p K^- \pi^+)]$ assuming $\text{B}(\Lambda_c^+ \rightarrow p K^- \pi^+) = 0.05$, which we rescale to our best value $\text{B}(\Lambda_c^+ \rightarrow p K^- \pi^+) = (6.28 \pm 0.32) \times 10^{-2}$. Our first error is their experiment's error and our second error is the systematic error from using our best value.

 $\Gamma(\Sigma_c(2455)^- p \pi^+)/\Gamma_{\text{total}}$ Γ_{506}/Γ

VALUE (units 10^{-4})	DOCUMENT ID	TECN	COMMENT
1.83 ± 0.24 OUR AVERAGE			
$2.13 \pm 0.10 \pm 0.56$	1,2 LEES	13H	BABR $e^+ e^- \rightarrow \Upsilon(4S)$
$1.67 \pm 0.25^{+0.09}_{-0.08}$	1,3 PARK	07	BELL $e^+ e^- \rightarrow \Upsilon(4S)$
$2.9 \pm 0.9^{+0.2}_{-0.1}$	4 DYTMAN	02	CLE2 $e^+ e^- \rightarrow \Upsilon(4S)$

- We do not use the following data for averages, fits, limits, etc. **•••**
- $1.9^{+0.6}_{-0.5} \pm 0.1$ ⁵ GABYSHEV 02 BELL Repl. by PARK 07

 $\Gamma(\Sigma_c(2455)^- p \pi^+)/\Gamma_{\text{total}}$ Γ_{507}/Γ

VALUE (units 10^{-5})	DOCUMENT ID	TECN	COMMENT
$3.4 \pm 0.7 \pm 0.2$	1,2 AUBERT	09AG	BABR $e^+ e^- \rightarrow \Upsilon(4S)$

- ¹ AUBERT 09AG reports $(4.33 \pm 0.82 \pm 0.33 \pm 1.13) \times 10^{-5}$ from a measurement of $[\Gamma(B^0 \rightarrow \Lambda_c^- p K^+ \pi^-)/\Gamma_{\text{total}}] \times [\text{B}(\Lambda_c^+ \rightarrow p K^- \pi^+)]$ assuming $\text{B}(\Lambda_c^+ \rightarrow p K^- \pi^+) = (5.0 \pm 1.3) \times 10^{-2}$, which we rescale to our best value $\text{B}(\Lambda_c^+ \rightarrow p K^- \pi^+) = (6.28 \pm 0.32) \times 10^{-2}$. Our first error is their experiment's error and our second error is the systematic error from using our best value.
- ² Assumes equal production of B^+ and B^0 at the $\Upsilon(4S)$.

 $\Gamma(\Lambda_c^- p K^+ \pi^-)/\Gamma_{\text{total}}$ Γ_{507}/Γ

VALUE (units 10^{-5})	DOCUMENT ID	TECN	COMMENT
$3.4 \pm 0.7 \pm 0.2$	1,2 AUBERT	09AG	BABR $e^+ e^- \rightarrow \Upsilon(4S)$

- ¹ AUBERT 09AG reports $(4.33 \pm 0.82 \pm 0.33 \pm 1.13) \times 10^{-5}$ from a measurement of $[\Gamma(B^0 \rightarrow \Lambda_c^- p K^+ \pi^-)/\Gamma_{\text{total}}] \times [\text{B}(\Lambda_c^+ \rightarrow p K^- \pi^+)]$ assuming $\text{B}(\Lambda_c^+ \rightarrow p K^- \pi^+) = (5.0 \pm 1.3) \times 10^{-2}$, which we rescale to our best value $\text{B}(\Lambda_c^+ \rightarrow p K^- \pi^+) = (6.28 \pm 0.32) \times 10^{-2}$. Our first error is their experiment's error and our second error is the systematic error from using our best value.
- ² Assumes equal production of B^+ and B^0 at the $\Upsilon(4S)$.

$\Gamma(\Sigma_c(2455)^{--} \rho K^+, \Sigma_c^{--} \rightarrow \bar{\Lambda}_c^- \pi^-) / \Gamma_{\text{total}}$ Γ_{508}/Γ

VALUE (units 10 ⁻⁵)	DOCUMENT ID	TECN	COMMENT
$0.88 \pm 0.25 \pm 0.05$ -0.04	1,2 AUBERT	09AG BABR	$e^+ e^- \rightarrow \Upsilon(4S)$

- ¹ AUBERT 09AG reports $(1.11 \pm 0.30 \pm 0.09 \pm 0.29) \times 10^{-5}$ from a measurement of $[\Gamma(B^0 \rightarrow \Sigma_c(2455)^{--} \rho K^+, \Sigma_c^{--} \rightarrow \bar{\Lambda}_c^- \pi^-) / \Gamma_{\text{total}}] \times [B(\Lambda_c^+ \rightarrow \rho K^- \pi^+)]$ assuming $B(\Lambda_c^+ \rightarrow \rho K^- \pi^+) = (5.0 \pm 1.3) \times 10^{-2}$, which we rescale to our best value $B(\Lambda_c^+ \rightarrow \rho K^- \pi^+) = (6.28 \pm 0.32) \times 10^{-2}$. Our first error is their experiment's error and our second error is the systematic error from using our best value.
- ² Assumes equal production of B^+ and B^0 at the $\Upsilon(4S)$.

 $\Gamma(\Lambda_c^- \rho K^*(892)^0) / \Gamma_{\text{total}}$ Γ_{509}/Γ

VALUE (units 10 ⁻⁵)	CL%	DOCUMENT ID	TECN	COMMENT
<2.42	90	1 AUBERT	09AG BABR	$e^+ e^- \rightarrow \Upsilon(4S)$

- ¹ Assumes equal production of B^+ and B^0 at the $\Upsilon(4S)$.

 $\Gamma(\Lambda_c^- \rho \bar{p} \bar{p}) / \Gamma_{\text{total}}$ Γ_{512}/Γ

VALUE (units 10 ⁻⁶)	DOCUMENT ID	TECN	COMMENT
<2.8	1 LEES	14c BABR	$e^+ e^- \rightarrow \Upsilon(4S)$

- ¹ Assumes equal production of B^+ and B^0 at the $\Upsilon(4S)$ and $B(\Lambda_c^+ \rightarrow \rho K^- \pi^+) = 0.050 \pm 0.013$.

 $\Gamma(\bar{\Lambda}_c^- \Lambda K^+) / \Gamma_{\text{total}}$ Γ_{513}/Γ

VALUE (units 10 ⁻⁵)	DOCUMENT ID	TECN	COMMENT
$4.8 \pm 1.1 \pm 0.2$ -0.3	1,2 LEES	11f BABR	$e^+ e^- \rightarrow \Upsilon(4S)$

- ¹ Assumes equal production of B^0 and B^+ from Upsilon(4S) decays.
- ² LEES 11f reports $(3.8 \pm 0.8 \pm 0.2 \pm 1.0) \times 10^{-5}$ from a measurement of $[\Gamma(B^0 \rightarrow \bar{\Lambda}_c^- \Lambda K^+) / \Gamma_{\text{total}}] / [B(\Lambda_c^+ \rightarrow \rho K^- \pi^+) / [B(\Lambda \rightarrow p \pi^-)]]$ assuming $B(\Lambda_c^+ \rightarrow \rho K^- \pi^+) = (5.0 \pm 1.3) \times 10^{-2}$, $B(\Lambda \rightarrow p \pi^-) = (63.9 \pm 0.5) \times 10^{-2}$, which we rescale to our best values $B(\Lambda_c^+ \rightarrow \rho K^- \pi^+) = (6.28 \pm 0.32) \times 10^{-2}$, $B(\Lambda \rightarrow p \pi^-) = (63.9 \pm 0.5) \times 10^{-2}$. Our first error is their experiment's error and our second error is the systematic error from using our best values. The reported uncertainties are statistical, systematic, and $\bar{\Lambda}_c^-$ branching fraction uncertainty.

 $\Gamma(\bar{\Lambda}_c^- \Lambda_c^+) / \Gamma_{\text{total}}$ Γ_{514}/Γ

VALUE (units 10 ⁻⁵)	CL%	DOCUMENT ID	TECN	COMMENT
<1.6	95	1 AAJ	14AA LHCB	pp at 7 TeV
<6.2	90	2 UCHIDA	08 BELL	$e^+ e^- \rightarrow \Upsilon(4S)$

- ¹ Uses $B(\bar{B}^0 \rightarrow D^+ D_s^-) = (7.2 \pm 0.8) \times 10^{-3}$.
- ² Assumes equal production of B^+ and B^0 at the $\Upsilon(4S)$.

 $\Gamma(\bar{\Lambda}_c(2593)^- / \bar{\Lambda}_c(2625)^- \rho) / \Gamma_{\text{total}}$ Γ_{515}/Γ

VALUE	CL%	DOCUMENT ID	TECN	COMMENT
$<1.1 \times 10^{-4}$	90	1,2 DYTMAN	02 CLE2	$e^+ e^- \rightarrow \Upsilon(4S)$

- ¹ Assumes equal production of B^+ and B^0 at the $\Upsilon(4S)$.
- ² DYTMAN 02 measurement uses $B(\Lambda_c^- \rightarrow \bar{p} K^+ \pi^-) = 5.0 \pm 1.3\%$. The second error includes the systematic and the uncertainty of the branching ratio.

 $\Gamma(\Xi_c^- \Lambda_c^+) / \Gamma_{\text{total}}$ Γ_{516}/Γ

VALUE (units 10 ⁻³)	DOCUMENT ID	TECN	COMMENT
$1.2 \pm 0.7 \pm 0.3$	1,2 LI	19c BELL	$e^+ e^- \rightarrow \Upsilon(4S)$

- ¹ Uses fully reconstructed B^0 on tag side with recoil against Λ_c^+ .
- ² LI 19c reports $(1.16 \pm 0.74 \pm 0.33) \times 10^{-3}$ from a measurement of $[\Gamma(B^0 \rightarrow \Xi_c^- \Lambda_c^+) / \Gamma_{\text{total}}] \times [B(\Lambda_c^+ \rightarrow \rho K^- \pi^+)]$ assuming $B(\Lambda_c^+ \rightarrow \rho K^- \pi^+) = (6.28 \pm 0.32) \times 10^{-2}$.

 $\Gamma(\Xi_c^- \Lambda_c^+, \Xi_c^- \rightarrow \Xi^+ \pi^- \pi^-) / \Gamma_{\text{total}}$ Γ_{517}/Γ

VALUE (units 10 ⁻⁵)	DOCUMENT ID	TECN	COMMENT
2.4 ± 1.1 OUR AVERAGE	Error includes scale factor of 1.8.		

VALUE (units 10 ⁻⁵)	DOCUMENT ID	TECN	COMMENT
$3.3 \pm 0.7 \pm 0.3$	1 LI	19c BELL	$e^+ e^- \rightarrow \Upsilon(4S)$
$1.2 \pm 0.9 \pm 0.1$	2,3 AUBERT	08H BABR	$e^+ e^- \rightarrow \Upsilon(4S)$
$7.4 \pm 3.3 \pm 0.4$ -2.7	3,4 CHISTOV	06A BELL	Repl. by LI 19c

- ¹ LI 19c reports $(3.32 \pm 0.74 \pm 0.33) \times 10^{-5}$ from a measurement of $[\Gamma(B^0 \rightarrow \Xi_c^- \Lambda_c^+, \Xi_c^- \rightarrow \Xi^+ \pi^- \pi^-) / \Gamma_{\text{total}}] \times [B(\Lambda_c^+ \rightarrow \rho K^- \pi^+)]$ assuming $B(\Lambda_c^+ \rightarrow \rho K^- \pi^+) = (6.28 \pm 0.32) \times 10^{-2}$.
- ² AUBERT 08H reports $(1.5 \pm 1.07 \pm 0.44) \times 10^{-5}$ from a measurement of $[\Gamma(B^0 \rightarrow \Xi_c^- \Lambda_c^+, \Xi_c^- \rightarrow \Xi^+ \pi^- \pi^-) / \Gamma_{\text{total}}] \times [B(\Lambda_c^+ \rightarrow \rho K^- \pi^+)]$ assuming $B(\Lambda_c^+ \rightarrow \rho K^- \pi^+) = (5.0 \pm 1.3) \times 10^{-2}$, which we rescale to our best value $B(\Lambda_c^+ \rightarrow \rho K^- \pi^+) = (6.28 \pm 0.32) \times 10^{-2}$. Our first error is their experiment's error and our second error is the systematic error from using our best value.
- ³ Assumes equal production of B^+ and B^0 at the $\Upsilon(4S)$.
- ⁴ CHISTOV 06A reports $(9.3 \pm 3.7 \pm 3.1) \times 10^{-5}$ from a measurement of $[\Gamma(B^0 \rightarrow \Xi_c^- \Lambda_c^+, \Xi_c^- \rightarrow \Xi^+ \pi^- \pi^-) / \Gamma_{\text{total}}] \times [B(\Lambda_c^+ \rightarrow \rho K^- \pi^+)]$ assuming $B(\Lambda_c^+ \rightarrow \rho K^- \pi^+) = (5.0 \pm 1.3) \times 10^{-2}$, which we rescale to our best value $B(\Lambda_c^+ \rightarrow \rho K^- \pi^+) = (6.28 \pm 0.32) \times 10^{-2}$. Our first error is their experiment's error and our second error is the systematic error from using our best value.

 $\Gamma(\Xi_c^- \Lambda_c^+, \Xi_c^- \rightarrow \bar{p} K^+ \pi^-) / \Gamma_{\text{total}}$ Γ_{518}/Γ

VALUE (units 10 ⁻⁶)	DOCUMENT ID	TECN	COMMENT
$5.3 \pm 1.5 \pm 0.7$	1 LI	19c BELL	$e^+ e^- \rightarrow \Upsilon(4S)$

- ¹ LI 19c reports $(5.27 \pm 1.51 \pm 0.69) \times 10^{-6}$ from a measurement of $[\Gamma(B^0 \rightarrow \Xi_c^- \Lambda_c^+, \Xi_c^- \rightarrow \bar{p} K^+ \pi^-) / \Gamma_{\text{total}}] \times [B(\Lambda_c^+ \rightarrow \rho K^- \pi^+)]$ assuming $B(\Lambda_c^+ \rightarrow \rho K^- \pi^+) = (6.28 \pm 0.32) \times 10^{-2}$.

 $\Gamma(\Lambda_c^+ \Lambda_c^- K^0) / \Gamma_{\text{total}}$ Γ_{519}/Γ

VALUE (units 10 ⁻⁴)	DOCUMENT ID	TECN	COMMENT
4.0 ± 0.9 OUR AVERAGE			

VALUE (units 10 ⁻⁴)	DOCUMENT ID	TECN	COMMENT
$3.99 \pm 0.76 \pm 0.51$	1 LI	18D BELL	$e^+ e^- \rightarrow \Upsilon(4S)$
$3.8 \pm 3.1 \pm 2.1$	2,3 AUBERT	08H BABR	$e^+ e^- \rightarrow \Upsilon(4S)$
$7.9 \pm 2.9 \pm 4.3$ -2.3	2,3 GABYSHEV	06 BELL	Repl. by LI 18D

- ¹ Assumes $B(\Upsilon(4S) \rightarrow B^0 \bar{B}^0) = 48.6 \pm 0.6\%$ and $B(\Lambda_c^+ \rightarrow \rho K^- \pi^+) = 6.23 \pm 0.33\%$.
- ² Assumes $B(\Lambda_c^+ \rightarrow \rho K^- \pi^+) = 5.0 \pm 1.3\%$.
- ³ Assumes equal production of B^+ and B^0 at the $\Upsilon(4S)$.
- • • We do not use the following data for averages, fits, limits, etc. • • •

 $\Gamma(\Xi_c(2930)^- \Lambda_c^+, \Xi_c^- \rightarrow \Lambda_c^- K^0) / \Gamma_{\text{total}}$ Γ_{520}/Γ

VALUE (units 10 ⁻⁴)	DOCUMENT ID	TECN	COMMENT
$2.37 \pm 0.51 \pm 0.31$	1 LI	18D BELL	$e^+ e^- \rightarrow \Upsilon(4S)$

- ¹ Assumes $B(\Upsilon(4S) \rightarrow B^0 \bar{B}^0) = 48.6 \pm 0.6\%$ and $B(\Lambda_c^+ \rightarrow \rho K^- \pi^+) = 6.23 \pm 0.33\%$.

 $\Gamma(\gamma\gamma) / \Gamma_{\text{total}}$ Γ_{521}/Γ

Test for $\Delta B=1$ weak neutral current. Allowed by higher-order electroweak interactions.

VALUE	CL%	DOCUMENT ID	TECN	COMMENT
$<3.2 \times 10^{-7}$	90	1 DEL-AMO-SA..11A	BABR	$e^+ e^- \rightarrow \Upsilon(4S)$
$<6.2 \times 10^{-7}$	90	1 VILLA	06 BELL	$e^+ e^- \rightarrow \Upsilon(4S)$
$<1.7 \times 10^{-6}$	90	1 AUBERT	01I BABR	$e^+ e^- \rightarrow \Upsilon(4S)$
$<3.9 \times 10^{-5}$	90	2 ACCIARRI	95I L3	$e^+ e^- \rightarrow Z$

- ¹ Assumes equal production of B^+ and B^0 at the $\Upsilon(4S)$.
- ² ACCIARRI 95I assumes $f_{B^0} = 39.5 \pm 4.0$ and $f_{B^+} = 12.0 \pm 3.0\%$.

 $\Gamma(e^+ e^-) / \Gamma_{\text{total}}$ Γ_{522}/Γ

Test for $\Delta B=1$ weak neutral current. Allowed by higher-order electroweak interactions.

VALUE	CL%	DOCUMENT ID	TECN	COMMENT
$<2.5 \times 10^{-9}$	90	1 AAJ	20W LHCB	pp at 7, 8, 13 TeV
$<8.3 \times 10^{-8}$	90	AALTONEN	09P CDF	$p\bar{p}$ at 1.96 TeV
$<11.3 \times 10^{-8}$	90	2 AUBERT	08P BABR	$e^+ e^- \rightarrow \Upsilon(4S)$
$<6.1 \times 10^{-8}$	90	2 AUBERT	05W BABR	Repl. by AUBERT 08P
$<1.9 \times 10^{-7}$	90	2 CHANG	03 BELL	$e^+ e^- \rightarrow \Upsilon(4S)$
$<8.3 \times 10^{-7}$	90	2 BERGFELD	00B CLE2	$e^+ e^- \rightarrow \Upsilon(4S)$
$<1.4 \times 10^{-5}$	90	3 ACCIARRI	97B L3	$e^+ e^- \rightarrow Z$
$<5.9 \times 10^{-6}$	90	AMMAR	94 CLE2	Repl. by BERGFELD 00B
$<2.6 \times 10^{-5}$	90	4 AVERY	89B CLEO	$e^+ e^- \rightarrow \Upsilon(4S)$
$<7.6 \times 10^{-5}$	90	5 ALBRECHT	87D ARG	$e^+ e^- \rightarrow \Upsilon(4S)$
$<6.4 \times 10^{-5}$	90	6 AVERY	87 CLEO	$e^+ e^- \rightarrow \Upsilon(4S)$
$<3 \times 10^{-4}$	90	GILES	84 CLEO	Repl. by AVERY 87

- ¹ Assumes no contribution from $B_s^0 \rightarrow e^+ e^-$ decays.
- ² Assumes equal production of B^+ and B^0 at the $\Upsilon(4S)$.
- ³ ACCIARRI 97B assume PDG 96 production fractions for B^+ , B^0 , B_s , and Λ_b .
- ⁴ AVERY 89B reports $<3 \times 10^{-5}$ assuming the $\Upsilon(4S)$ decays 43% to $B^0 \bar{B}^0$. We rescale to 50%.
- ⁵ ALBRECHT 87D reports $<8.5 \times 10^{-5}$ assuming the $\Upsilon(4S)$ decays 45% to $B^0 \bar{B}^0$. We rescale to 50%.
- ⁶ AVERY 87 reports $<8 \times 10^{-5}$ assuming the $\Upsilon(4S)$ decays 40% to $B^0 \bar{B}^0$. We rescale to 50%.

 $\Gamma(e^+ e^- \gamma) / \Gamma_{\text{total}}$ Γ_{523}/Γ

Test for $\Delta B=1$ weak neutral current. Allowed by higher-order electroweak interactions.

VALUE	CL%	DOCUMENT ID	TECN	COMMENT
$<1.2 \times 10^{-7}$	90	AUBERT	08c BABR	$e^+ e^- \rightarrow \Upsilon(4S)$

 $\Gamma(\mu^+ \mu^-) / \Gamma_{\text{total}}$ Γ_{524}/Γ

Test for $\Delta B=1$ weak neutral current. Allowed by higher-order electroweak interactions.

VALUE (units 10 ⁻³)	CL%	DOCUMENT ID	TECN	COMMENT
0.07 ± 0.13 -0.11 OUR AVERAGE	Error includes scale factor of 1.8.			

VALUE (units 10 ⁻³)	CL%	DOCUMENT ID	TECN	COMMENT
$0.12 \pm 0.08 \pm 0.01$ -0.07		1 AAJ	22 LHCB	pp at 7, 8, 13 TeV
-0.19 ± 0.16		2,3 AABOUD	19L ATLS	pp at 7, 8, 13 TeV
<0.36	95	4 SIRUNYAN	20AG	pp at 7, 8, 13 TeV
$0.15 \pm 0.12 \pm 0.02$ $-0.10 - 0.01$		5 AAJ	17AI LHCB	Repl. by AAJ 22
-0.25 ± 0.20		6 AABOUD	16L ATLS	Repl. by AABOUD 19L
0.39 ± 0.16 -0.14		7 KHACHATRY..15BE	LHC	pp at 7, 8 TeV
<0.80	90	8 AAJ	13B LHCB	Repl. by AAJ 13BA
<0.63	90	9 AAJ	13BA LHCB	Repl. by KHACHATRYAN 15BE

- • • We do not use the following data for averages, fits, limits, etc. • • •

Meson Particle Listings

 B^0

CL%	TECN	DOCUMENT ID	COMMENT
< 3.8	90	¹⁰ AALTONEN 13F CDF	$p\bar{p}$ at 1.96 TeV
$0.35^{+0.21}_{-0.18}$		¹¹ CHATRCHYAN13AW CMS	Repl. by SIRUN-YAN 20AG
< 2.6	90	⁸ AAIJ 12A LHCB	Repl. by AAIJ 12W
< 0.81	90	¹² AAIJ 12W LHCB	Repl. by AAIJ 13B
< 1.4	90	¹² CHATRCHYAN12A CMS	pp at 7 TeV
< 12	90	¹³ AAIJ 11B LHCB	Repl. by AAIJ 12A
< 5.0	90	¹² AALTONEN 11AG CDF	$p\bar{p}$ at 1.96 TeV
< 3.7	90	¹² CHATRCHYAN11T CMS	Repl. by CHA-TRCHYAN 12A

- ¹ Corresponds to a 95% CL upper limit of $< 2.6 \times 10^{-10}$.
² Corresponds to a 95% CL upper limit of $< 2.1 \times 10^{-10}$.
³ Uses normalization mode $B(B^+ \rightarrow J/\psi K^+) = (1.010 \pm 0.029) \times 10^{-3}$ and B production ratio $f(b \rightarrow B_s^0)/f(b \rightarrow B^0) = 0.256 \pm 0.013$.
⁴ Uses normalization mode $B(B^+ \rightarrow J/\psi K^+) = (1.01 \pm 0.03) \times 10^{-3}$.
⁵ Corresponds to a 95% CL upper limit of $< 3.4 \times 10^{-10}$.
⁶ This value is obtained from a profile-likelihood fit, see Fig. 9. It corresponds to an upper limit of $< 0.42 \times 10^{-9}$ at 95% C.L.
⁷ Derived from the combined fit to CMS and LHCb data. Uncertainty includes both statistical and systematic component. Also reports $B(B^0 \rightarrow \mu^+ \mu^-)/B(B_s^0 \rightarrow \mu^+ \mu^-) = 0.14^{+0.08}_{-0.06}$.
⁸ Uses $B(B^+ \rightarrow J/\psi K^+ \rightarrow \mu^+ \mu^- K^+) = (6.01 \pm 0.21) \times 10^{-5}$ and $B(B^0 \rightarrow K^+ \pi^-) = (1.94 \pm 0.06) \times 10^{-5}$ for normalization.
⁹ Reports also a limit of $< 7.4 \times 10^{-10}$ at 95% CL. Uses normalization modes $B^+ \rightarrow J/\psi K^+ \rightarrow \mu^+ \mu^- K^+$ and $B^0 \rightarrow K^+ \pi^-$.
¹⁰ Uses normalization mode $B(B^+ \rightarrow J/\psi K^+) = (10.22 \pm 0.35) \times 10^{-4}$.
¹¹ Reports also a limit of $< 9.2 \times 10^{-10}$ at 90% CL. and uses $B(B^+ \rightarrow J/\psi K^+ \rightarrow \mu^+ \mu^- K^+) = (6.0 \pm 0.2) \times 10^{-5}$ for normalization.
¹² Uses $B(B^+ \rightarrow J/\psi K^+ \rightarrow \mu^+ \mu^- K^+) = (6.01 \pm 0.21) \times 10^{-5}$.
¹³ Uses B production ratio $f(\bar{b} \rightarrow B^+)/f(\bar{b} \rightarrow B_s^0) = 3.71 \pm 0.47$ and three normalization modes.

CL%	TECN	DOCUMENT ID	COMMENT
< 2.0×10^{-9}	95	¹ AAIJ 22 LHCB	pp at 7, 8, 13 TeV
$< 1.6 \times 10^{-7}$	90	² AUBERT 08c BABR	$e^+e^- \rightarrow \Upsilon(4S)$

Test for $\Delta B=1$ weak neutral current. Allowed by higher-order electroweak interactions.

••• We do not use the following data for averages, fits, limits, etc. •••

¹ The exclusion is limited to the range $m_{\mu\mu} > 4.9$ GeV/ c^2 .

CL%	TECN	DOCUMENT ID	COMMENT
< 2.1×10^{-3}	95	¹ AAIJ 17AJ LHCB	pp at 7, 8 TeV
< 1.1×10^{-3}	90	² AUBERT 06s BABR	$e^+e^- \rightarrow \Upsilon(4S)$

Test for $\Delta B=1$ weak neutral current. Allowed by higher-order electroweak interactions.

••• We do not use the following data for averages, fits, limits, etc. •••

¹ Assuming no contribution from $B_s^0 \rightarrow \tau^+ \tau^-$.
² Assumes equal production of B^+ and B^0 at the $\Upsilon(4S)$.

CL%	TECN	DOCUMENT ID	COMMENT
< 6.9×10^{-10}	95	AAIJ 17N LHCB	pp at 7, 8 TeV
< 5.3×10^{-9}	90	¹ AAIJ 13AW LHCB	Repl. by AAIJ 17N

Also reports a limit of $< 6.6 \times 10^{-9}$ at 95% CL.

CL%	TECN	DOCUMENT ID	COMMENT
< 6.0×10^{-10}	95	AAIJ 17N LHCB	pp at 7, 8 TeV
< 5.1×10^{-9}	90	¹ AAIJ 13AW LHCB	Repl. by AAIJ 17N

Here S and P are the hypothetical scalar and pseudoscalar particles with masses of 2.5 GeV/ c^2 and 214.3 MeV/ c^2 , respectively.

••• We do not use the following data for averages, fits, limits, etc. •••

¹ Also reports a limit of $< 6.3 \times 10^{-9}$ at 95% CL.

CL%	TECN	DOCUMENT ID	COMMENT
< 5.3×10^{-8}	90	¹ LEES 13M BABR	$e^+e^- \rightarrow \Upsilon(4S)$
< 1.5×10^{-7}	90	¹ WEI 08A BELL	$e^+e^- \rightarrow \Upsilon(4S)$
< 1.2×10^{-7}	90	¹ AUBERT 07AG BABR	Repl. by LEES 13M

Assumes equal production of B^+ and B^0 at the $\Upsilon(4S)$.

CL%	TECN	DOCUMENT ID	COMMENT
< 0.9×10^{-5}	90	¹ GRYGIER 17 BELL	$e^+e^- \rightarrow \Upsilon(4S)$
< 6.9×10^{-5}	90	¹ LUTZ 13 BELL	$e^+e^- \rightarrow \Upsilon(4S)$
< 2.2×10^{-4}	90	¹ CHEN 07D BELL	Repl. by LUTZ 13

Test for $\Delta B=1$ weak neutral current. Allowed by higher-order electroweak interaction.

••• We do not use the following data for averages, fits, limits, etc. •••

¹ Assumes equal production of B^+ and B^0 at the $\Upsilon(4S)$.

CL%	TECN	DOCUMENT ID	COMMENT
< 8.4×10^{-8}	90	¹ LEES 13M BABR	$e^+e^- \rightarrow \Upsilon(4S)$
< 2.3×10^{-7}	90	¹ WEI 08A BELL	$e^+e^- \rightarrow \Upsilon(4S)$
< 1.4×10^{-7}	90	¹ AUBERT 07AG BABR	Repl. by LEES 13M

Assumes equal production of B^+ and B^0 at the $\Upsilon(4S)$.

CL%	TECN	DOCUMENT ID	COMMENT
< 6.9×10^{-8}	90	¹ LEES 13M BABR	$e^+e^- \rightarrow \Upsilon(4S)$
< 1.8×10^{-7}	90	¹ WEI 08A BELL	$e^+e^- \rightarrow \Upsilon(4S)$
< 5.1×10^{-7}	90	¹ AUBERT 07AG BABR	$e^+e^- \rightarrow \Upsilon(4S)$

Assumes equal production of B^+ and B^0 at the $\Upsilon(4S)$.

CL%	TECN	DOCUMENT ID	COMMENT
< 6.4×10^{-8}	90	¹ LEES 13M BABR	$e^+e^- \rightarrow \Upsilon(4S)$

Assumes equal production of B^+ and B^0 at the $\Upsilon(4S)$.

CL%	TECN	DOCUMENT ID	COMMENT
< 10.8×10^{-8}	90	¹ LEES 13M BABR	$e^+e^- \rightarrow \Upsilon(4S)$

Assumes equal production of B^+ and B^0 at the $\Upsilon(4S)$.

CL%	TECN	DOCUMENT ID	COMMENT
< 11.2×10^{-8}	90	¹ LEES 13M BABR	$e^+e^- \rightarrow \Upsilon(4S)$

Assumes equal production of B^+ and B^0 at the $\Upsilon(4S)$.

CL%	TECN	DOCUMENT ID	COMMENT
3.3 ± 0.6	OUR AVERAGE		
$3.51^{+0.69}_{-0.60} \pm 0.10$		CHOUDHURY 21 BELL	$e^+e^- \rightarrow \Upsilon(4S)$
$2.1^{+1.5}_{-1.3} \pm 0.2$		¹ AUBERT 09T BABR	$e^+e^- \rightarrow \Upsilon(4S)$
$3.4^{+0.9}_{-0.8} \pm 0.2$		^{1,2} WEI 09A BELL	$e^+e^- \rightarrow \Upsilon(4S)$
$2.9^{+1.6}_{-1.3} \pm 0.3$		¹ AUBERT,B 06J BABR	Repl. by AUBERT 09T
< 6.8	90	¹ ISHIKAWA 03 BELL	$e^+e^- \rightarrow \Upsilon(4S)$

Assumes equal production of B^0 and B^+ at $\Upsilon(4S)$.
² Superseded by CHOUDHURY 21.

CL%	TECN	DOCUMENT ID	COMMENT
$2.5^{+1.1}_{-0.9}$	OUR AVERAGE		Error includes scale factor of 1.3.
$3.1^{+1.0}_{-0.9} \pm 0.08$		CHOUDHURY 21 BELL	$e^+e^- \rightarrow \Upsilon(4S)$
$0.8^{+1.5}_{-1.2} \pm 0.1$		¹ AUBERT 09T BABR	$e^+e^- \rightarrow \Upsilon(4S)$
$2.0^{+1.4}_{-1.0} \pm 0.1$		^{1,2} WEI 09A BELL	$e^+e^- \rightarrow \Upsilon(4S)$
$1.3^{+1.6}_{-1.1} \pm 0.2$		¹ AUBERT,B 06J BABR	Repl. by AUBERT 09T
$2.1^{+2.3}_{-1.6} \pm 0.8$		¹ AUBERT 03U BABR	$e^+e^- \rightarrow \Upsilon(4S)$
< 5.4	90	³ ISHIKAWA 03 BELL	$e^+e^- \rightarrow \Upsilon(4S)$
< 27	90	¹ ABE 02 BELL	Repl. by ISHIKAWA 03
< 38	90	¹ AUBERT 02L BABR	$e^+e^- \rightarrow \Upsilon(4S)$
< 84.5	90	⁴ ANDERSON 01B CLE2	$e^+e^- \rightarrow \Upsilon(4S)$
< 3000	90	ALBRECHT 91E ARG	$e^+e^- \rightarrow \Upsilon(4S)$
< 5200	90	⁵ AVERY 87 CLEO	$e^+e^- \rightarrow \Upsilon(4S)$

Assumes equal production of B^+ and B^0 at the $\Upsilon(4S)$.
² Superseded by CHOUDHURY 21.
³ Assumes equal production of B^0 and B^+ at $\Upsilon(4S)$.
⁴ The result is for di-lepton masses above 0.5 GeV.
⁵ AVERY 87 reports $< 6.5 \times 10^{-4}$ assuming the $\Upsilon(4S)$ decays 40% to $B^0 \bar{B}^0$. We rescale to 50%.

CL%	TECN	DOCUMENT ID	COMMENT
< 2.6×10^{-5}	90	¹ GRYGIER 17 BELL	$e^+e^- \rightarrow \Upsilon(4S)$
< 4.9×10^{-5}	90	^{1,2} LEES 13I BABR	$e^+e^- \rightarrow \Upsilon(4S)$
< 19.4×10^{-5}	90	¹ LUTZ 13 BELL	$e^+e^- \rightarrow \Upsilon(4S)$
< 5.6×10^{-5}	90	¹ DEL-AMO-SA...10Q BABR	Repl. by LEES 13I
< 1.6×10^{-4}	90	¹ CHEN 07D BELL	$e^+e^- \rightarrow \Upsilon(4S)$

Test for $\Delta B=1$ weak neutral current. Allowed by higher-order electroweak interaction.

••• We do not use the following data for averages, fits, limits, etc. •••

¹ Assumes equal production of B^+ and B^0 at the $\Upsilon(4S)$.
² Also reported a limit $< 8.1 \times 10^{-5}$ at 90% CL obtained using a fully reconstructed hadronic B -tag evnets.

CL%	TECN	DOCUMENT ID	COMMENT
< 2.6×10^{-5}	90	¹ GRYGIER 17 BELL	$e^+e^- \rightarrow \Upsilon(4S)$
< 4.9×10^{-5}	90	^{1,2} LEES 13I BABR	$e^+e^- \rightarrow \Upsilon(4S)$
< 19.4×10^{-5}	90	¹ LUTZ 13 BELL	$e^+e^- \rightarrow \Upsilon(4S)$
< 5.6×10^{-5}	90	¹ DEL-AMO-SA...10Q BABR	Repl. by LEES 13I
< 1.6×10^{-4}	90	¹ CHEN 07D BELL	$e^+e^- \rightarrow \Upsilon(4S)$

Test for $\Delta B=1$ weak neutral current. Allowed by higher-order electroweak interaction.

••• We do not use the following data for averages, fits, limits, etc. •••

¹ Assumes equal production of B^+ and B^0 at the $\Upsilon(4S)$.
² Also reported a limit $< 8.1 \times 10^{-5}$ at 90% CL obtained using a fully reconstructed hadronic B -tag evnets.

$\Gamma(\rho^0 \nu \bar{\nu})/\Gamma_{\text{total}}$ Γ_{540}/Γ
Test for $\Delta B=1$ weak neutral current. Allowed by higher-order electroweak interaction.

Table with columns: VALUE (units 10^-5), CL%, DOCUMENT ID, TECN, COMMENT. Includes entries for GRYGIER, BELL, LUTZ, CHEN.

$\Gamma(K^0 \mu^+ \mu^-)/\Gamma_{\text{total}}$ Γ_{538}/Γ
Test for $\Delta B=1$ weak neutral current. Allowed by higher-order electroweak interactions.

Table with columns: VALUE (units 10^-7), CL%, DOCUMENT ID, TECN, COMMENT. Includes OUR FIT and OUR AVERAGE values, and entries for CHOU DHURY, AAIJ, WEI, AUBERT, B, ABE, ANDERSON, ALBRECHT, AVERY.

1 Uses B(B^0 -> J/psi(1S) K^0) = (0.928 +/- 0.013 +/- 0.037) x 10^-3 for normalization.
2 Assumes equal production of B+ and B0 at the T(4S).
3 Superseded by CHOU DHURY 21.
4 Assumes equal production of B0 and B+ at T(4S). The second error is a total of systematic uncertainties including model dependence.
5 The result is for di-lepton masses above 0.5 GeV.
6 AVERY 87 reports < 4.5 x 10^-4 assuming the T(4S) decays 40% to B0 B0-bar. We rescale to 50%.

$\Gamma(K^0 \mu^+ \mu^-)/\Gamma(J/\psi(1S) K^0)$ $\Gamma_{538}/\Gamma_{200}$

Table with columns: VALUE (units 10^-3), DOCUMENT ID, TECN, COMMENT. Includes OUR FIT and OUR AVERAGE values, and entry for AALTONEN.

$\Gamma(K^*(892)^0 e^+ e^-)/\Gamma_{\text{total}}$ Γ_{541}/Γ
Test for $\Delta B=1$ weak neutral current. Allowed by higher-order electroweak interactions.

Table with columns: VALUE (units 10^-7), DOCUMENT ID, TECN, COMMENT. Includes OUR AVERAGE value, and entries for AUBERT, WEI.

$\Gamma(K^*(892)^0 e^+ e^-)/\Gamma_{\text{total}}$ Γ_{542}/Γ
Test for $\Delta B=1$ weak neutral current. Allowed by higher-order electroweak interactions.

Table with columns: VALUE (units 10^-7), CL%, DOCUMENT ID, TECN, COMMENT. Includes OUR AVERAGE value, and entries for AUBERT, WEI, AUBERT, B, AUBERT, ISHIKAWA, ABE, AUBERT, ALBRECHT.

1 Assumes equal production of B+ and B0 at the T(4S).
2 Assumes equal production of B0 and B+ at T(4S).

$\Gamma(K^*(892)^0 \mu^+ \mu^-)/\Gamma_{\text{total}}$ Γ_{543}/Γ
Test for $\Delta B=1$ weak neutral current. Allowed by higher-order electroweak interactions.

Table with columns: VALUE (units 10^-7), CL%, DOCUMENT ID, TECN, COMMENT. Includes OUR FIT and OUR AVERAGE values, and entries for AAIJ, AUBERT, WEI, AAIJ, AUBERT, B, AUBERT, ISHIKAWA, ABE, AUBERT, AFFOLDER.

1 Uses B(B^0 -> J/psi K*(892)^0) = (1.19 +/- 0.01 +/- 0.08) x 10^-3. The second error is the total systematic uncertainty.
2 Assumes equal production of B+ and B0 at the T(4S).
3 Assumes equal production of B0 and B+ at T(4S). The second error is a total of systematic uncertainties including model dependence.
4 AFFOLDER 99B measured relative to B0 -> J/psi(1S) K*(892)^0.

$\Gamma(K^*(892)^0 \mu^+ \mu^-)/\Gamma(J/\psi(1S) K^*(892)^0)$ $\Gamma_{543}/\Gamma_{202}$

Table with columns: VALUE (units 10^-3), DOCUMENT ID, TECN, COMMENT. Includes OUR FIT and OUR AVERAGE values, and entries for AALTONEN.

$\Gamma(K^*(892)^0 \chi, \chi \rightarrow \mu^+ \mu^-)/\Gamma_{\text{total}}$ Γ_{544}/Γ

Table with columns: VALUE, CL%, DOCUMENT ID, TECN, COMMENT. Includes entry for AAIJ.

$\Gamma(\pi^+ \pi^- \mu^+ \mu^-)/\Gamma_{\text{total}}$ Γ_{545}/Γ

Table with columns: VALUE (units 10^-8), DOCUMENT ID, TECN, COMMENT. Includes entry for AAIJ.

$\Gamma(K^*(892)^0 \nu \bar{\nu})/\Gamma_{\text{total}}$ Γ_{546}/Γ
Test for $\Delta B=1$ weak neutral current. Allowed by higher-order electroweak interactions.

Table with columns: VALUE, CL%, DOCUMENT ID, TECN, COMMENT. Includes entry for GRYGIER, and entries for LEES, LUTZ, AUBERT, CHEN, ADAM.

$\Gamma(\text{invisible})/\Gamma_{\text{total}}$ Γ_{547}/Γ

Table with columns: VALUE (units 10^-5), CL%, DOCUMENT ID, TECN, COMMENT. Includes entry for LEES, and entries for KU, HSU, AUBERT, B.

1 Uses the fully reconstructed B0 -> D(*) - l+ nu_l events as a tag.
2 Identified by fully reconstructing a hadronic decay of the accompanying B meson.
3 Identified by fully reconstructing a hadronic decay of the accompanying B meson and requiring no other particles in the event.

Meson Particle Listings

 B^0 $\Gamma(\nu\bar{\nu})/\Gamma_{\text{total}}$ Γ_{548}/Γ

VALUE (units 10^{-5})	CL%	DOCUMENT ID	TECN	COMMENT
<1.6	90	¹ KU	20	BELL $e^+e^- \rightarrow \Upsilon(4S)$
•••		We do not use the following data for averages, fits, limits, etc. •••		
<1.7	90	² LEES	12T	BABR $e^+e^- \rightarrow \Upsilon(4S)$
<4.7	90	² AUBERT,B	04J	BABR Repl. by LEES 12T

¹ Identified by fully reconstructing a hadronic decay of the accompanying B meson.
² Uses the fully reconstructed $B^0 \rightarrow D^{(*)-} \ell^+ \nu_{\ell}$ events as a tag.

 $\Gamma(\phi\nu\bar{\nu})/\Gamma_{\text{total}}$ Γ_{549}/Γ

Test for $\Delta B = 1$ weak neutral current. Allowed by higher-order electroweak interaction.

VALUE	CL%	DOCUMENT ID	TECN	COMMENT
<1.27 $\times 10^{-4}$	90	¹ LUTZ	13	BELL $e^+e^- \rightarrow \Upsilon(4S)$
•••		We do not use the following data for averages, fits, limits, etc. •••		
<5.8 $\times 10^{-5}$	90	¹ CHEN	07D	BELL Repl. by LUTZ 13

¹ Assumes equal production of B^+ and B^0 at the $\Upsilon(4S)$.

 $\Gamma(e^{\pm}\mu^{\mp})/\Gamma_{\text{total}}$ Γ_{550}/Γ

Test of lepton family number conservation. Allowed by higher-order electroweak interactions.

VALUE	CL%	DOCUMENT ID	TECN	COMMENT
< 1.0 $\times 10^{-9}$	90	¹ AAIJ	18T	LHCB pp at 7, 8 TeV
•••		We do not use the following data for averages, fits, limits, etc. •••		
< 2.8 $\times 10^{-9}$	90	² AAIJ	13BMLHCB	Repl. by AAIJ 18T
< 6.4 $\times 10^{-8}$	90	AALTONEN	09P	CDF $p\bar{p}$ at 1.96 TeV
< 9.2 $\times 10^{-8}$	90	³ AUBERT	08P	BABR $e^+e^- \rightarrow \Upsilon(4S)$
< 1.8 $\times 10^{-7}$	90	³ AUBERT	05W	BABR $e^+e^- \rightarrow \Upsilon(4S)$
< 1.7 $\times 10^{-7}$	90	³ CHANG	03	BELL $e^+e^- \rightarrow \Upsilon(4S)$
< 15 $\times 10^{-7}$	90	³ BERGFELD	00B	CLE2 $e^+e^- \rightarrow \Upsilon(4S)$
< 3.5 $\times 10^{-6}$	90	ABE	98V	CDF $p\bar{p}$ at 1.8 TeV
< 1.6 $\times 10^{-5}$	90	⁴ ACCIARRI	97B	L3 $e^+e^- \rightarrow Z$
< 5.9 $\times 10^{-6}$	90	AMMAR	94	CLE2 $e^+e^- \rightarrow \Upsilon(4S)$
< 3.4 $\times 10^{-5}$	90	⁵ AVERY	89B	CLEO $e^+e^- \rightarrow \Upsilon(4S)$
< 4.5 $\times 10^{-5}$	90	⁶ ALBRECHT	87D	ARG $e^+e^- \rightarrow \Upsilon(4S)$
< 7.7 $\times 10^{-5}$	90	⁷ AVERY	87	CLEO $e^+e^- \rightarrow \Upsilon(4S)$
< 3 $\times 10^{-4}$	90	GILES	84	CLEO Repl. by AVERY 87

¹ AAIJ 18T uses normalization modes $B(B^0 \rightarrow K^+\pi^-) = (19.6 \pm 0.5) \times 10^{-6}$ and $B(B^+ \rightarrow J/\psi K^+) = (1.026 \pm 0.031) \times 10^{-3}$.
² Uses normalization mode $B(B^0 \rightarrow K^+\pi^-) = (19.4 \pm 0.6) \times 10^{-6}$.
³ Assumes equal production of B^+ and B^0 at the $\Upsilon(4S)$.
⁴ ACCIARRI 97B assume PDG 96 production fractions for B^+ , B^0 , B_s , and Λ_b .
⁵ Paper assumes the $\Upsilon(4S)$ decays 43% to $B^0\bar{B}^0$. We rescale to 50%.
⁶ ALBRECHT 87D reports $< 5 \times 10^{-5}$ assuming the $\Upsilon(4S)$ decays 45% to $B^0\bar{B}^0$. We rescale to 50%.
⁷ AVERY 87 reports $< 9 \times 10^{-5}$ assuming the $\Upsilon(4S)$ decays 40% to $B^0\bar{B}^0$. We rescale to 50%.

 $\Gamma(\pi^0 e^{\pm}\mu^{\mp})/\Gamma_{\text{total}}$ Γ_{551}/Γ

VALUE	CL%	DOCUMENT ID	TECN	COMMENT
<1.4 $\times 10^{-7}$	90	¹ AUBERT	07AG	BABR $e^+e^- \rightarrow \Upsilon(4S)$

¹ Assumes equal production of B^+ and B^0 at the $\Upsilon(4S)$.

 $\Gamma(K^0 e^{\pm}\mu^{\mp})/\Gamma_{\text{total}}$ Γ_{552}/Γ

Test of lepton family number conservation.

VALUE	CL%	DOCUMENT ID	TECN	COMMENT
< 3.8 $\times 10^{-8}$	90	CHOUDHURY	21	BELL $e^+e^- \rightarrow \Upsilon(4S)$
•••		We do not use the following data for averages, fits, limits, etc. •••		
< 2.7 $\times 10^{-7}$	90	¹ AUBERT,B	06J	BABR $e^+e^- \rightarrow \Upsilon(4S)$
<40 $\times 10^{-7}$	90	¹ AUBERT	02L	BABR Repl. by AUBERT,B 06J

¹ Assumes equal production of B^+ and B^0 at the $\Upsilon(4S)$.

 $\Gamma(K^*(892)^0 e^+ \mu^-)/\Gamma_{\text{total}}$ Γ_{553}/Γ

VALUE (units 10^{-7})	CL%	DOCUMENT ID	TECN	COMMENT
<1.6	90	¹ SANDILYA	18	BELL $e^+e^- \rightarrow \Upsilon(4S)$
•••		We do not use the following data for averages, fits, limits, etc. •••		
<5.3	90	² AUBERT,B	06J	BABR $e^+e^- \rightarrow \Upsilon(4S)$

¹ Uses $B(\Upsilon(4S) \rightarrow B^0\bar{B}^0) = 0.486 \pm 0.006$.
² Assumes equal production of B^0 and B^+ at $\Upsilon(4S)$.

 $\Gamma(K^*(892)^0 e^- \mu^+)/\Gamma_{\text{total}}$ Γ_{554}/Γ

VALUE (units 10^{-7})	CL%	DOCUMENT ID	TECN	COMMENT
<1.2	90	¹ SANDILYA	18	BELL $e^+e^- \rightarrow \Upsilon(4S)$
•••		We do not use the following data for averages, fits, limits, etc. •••		
<3.4	90	² AUBERT,B	06J	BABR $e^+e^- \rightarrow \Upsilon(4S)$

¹ Uses $B(\Upsilon(4S) \rightarrow B^0\bar{B}^0) = 0.486 \pm 0.006$.
² Assumes equal production of B^0 and B^+ at $\Upsilon(4S)$.

 $\Gamma(K^*(892)^0 e^{\pm}\mu^{\mp})/\Gamma_{\text{total}}$ Γ_{555}/Γ

Test of lepton family number conservation.

VALUE (units 10^{-7})	CL%	DOCUMENT ID	TECN	COMMENT
< 1.8	90	¹ SANDILYA	18	BELL $e^+e^- \rightarrow \Upsilon(4S)$
•••		We do not use the following data for averages, fits, limits, etc. •••		
< 5.8	90	² AUBERT,B	06J	BABR $e^+e^- \rightarrow \Upsilon(4S)$
<34	90	² AUBERT	02L	BABR Repl. by AUBERT,B 06J

¹ Uses $B(\Upsilon(4S) \rightarrow B^0\bar{B}^0) = 0.486 \pm 0.006$.
² Assumes equal production of B^+ and B^0 at the $\Upsilon(4S)$.

 $\Gamma(e^{\pm}\tau^{\mp})/\Gamma_{\text{total}}$ Γ_{556}/Γ

Test of lepton family number conservation. Allowed by higher-order electroweak interactions.

VALUE	CL%	DOCUMENT ID	TECN	COMMENT
<1.6 $\times 10^{-5}$	90	¹ ATMACAN	21	BELL $e^+e^- \rightarrow \Upsilon(4S)$
•••		We do not use the following data for averages, fits, limits, etc. •••		
<2.8 $\times 10^{-5}$	90	² AUBERT	08AD	BABR $e^+e^- \rightarrow \Upsilon(4S)$
<1.1 $\times 10^{-4}$	90	BORNHEIM	04	CLE2 $e^+e^- \rightarrow \Upsilon(4S)$
<5.3 $\times 10^{-4}$	90	AMMAR	94	CLE2 Repl. by BORNHEIM 04

¹ Uses events in which one B meson is fully reconstructed in a hadronic decay mode.
² Assumes equal production of B^+ and B^0 at the $\Upsilon(4S)$.

 $\Gamma(\mu^{\pm}\tau^{\mp})/\Gamma_{\text{total}}$ Γ_{557}/Γ

Test of lepton family number conservation. Allowed by higher-order electroweak interactions.

VALUE	CL%	DOCUMENT ID	TECN	COMMENT
<1.4 $\times 10^{-5}$	95	¹ AAIJ	19AK	LHCB pp at 7, 8 TeV
•••		We do not use the following data for averages, fits, limits, etc. •••		
<1.5 $\times 10^{-5}$	90	² ATMACAN	21	BELL $e^+e^- \rightarrow \Upsilon(4S)$
<2.2 $\times 10^{-5}$	90	³ AUBERT	08AD	BABR $e^+e^- \rightarrow \Upsilon(4S)$
<3.8 $\times 10^{-5}$	90	BORNHEIM	04	CLE2 $e^+e^- \rightarrow \Upsilon(4S)$
<8.3 $\times 10^{-4}$	90	AMMAR	94	CLE2 Repl. by BORNHEIM 04

¹ Assuming no contribution from $B_s^0 \rightarrow \mu^{\pm}\tau^{\mp}$.
² Uses events in which one B meson is fully reconstructed in a hadronic decay mode.
³ Assumes equal production of B^+ and B^0 at the $\Upsilon(4S)$.

 $\Gamma(\Lambda_c^+ \mu^-)/\Gamma_{\text{total}}$ Γ_{558}/Γ

VALUE	CL%	DOCUMENT ID	TECN	COMMENT
<1.4 $\times 10^{-6}$	90	^{1,2} DEL-AMO-SA...	11k	BABR $e^+e^- \rightarrow \Upsilon(4S)$

¹ DEL-AMO-SANCHEZ 11k reports $< 180 \times 10^{-8}$ from a measurement of $[\Gamma(B^0 \rightarrow \Lambda_c^+ \mu^-)/\Gamma_{\text{total}}] \times [B(\Lambda_c^+ \rightarrow pK^-\pi^+)]$ assuming $B(\Lambda_c^+ \rightarrow pK^-\pi^+) = (5.0 \pm 1.3) \times 10^{-2}$, which we rescale to our best value $B(\Lambda_c^+ \rightarrow pK^-\pi^+) = 6.28 \times 10^{-2}$.
² Uses $B(\Upsilon(4S) \rightarrow B^0\bar{B}^0) = (51.6 \pm 0.6)\%$ and $B(\Upsilon(4S) \rightarrow B^+B^-) = (48.4 \pm 0.6)\%$.

 $\Gamma(\Lambda_c^+ e^-)/\Gamma_{\text{total}}$ Γ_{559}/Γ

VALUE	CL%	DOCUMENT ID	TECN	COMMENT
<4 $\times 10^{-6}$	90	^{1,2} DEL-AMO-SA...	11k	BABR $e^+e^- \rightarrow \Upsilon(4S)$

¹ DEL-AMO-SANCHEZ 11k reports $< 520 \times 10^{-8}$ from a measurement of $[\Gamma(B^0 \rightarrow \Lambda_c^+ e^-)/\Gamma_{\text{total}}] \times [B(\Lambda_c^+ \rightarrow pK^-\pi^+)]$ assuming $B(\Lambda_c^+ \rightarrow pK^-\pi^+) = (5.0 \pm 1.3) \times 10^{-2}$, which we rescale to our best value $B(\Lambda_c^+ \rightarrow pK^-\pi^+) = 6.28 \times 10^{-2}$.
² Uses $B(\Upsilon(4S) \rightarrow B^0\bar{B}^0) = (51.6 \pm 0.6)\%$ and $B(\Upsilon(4S) \rightarrow B^+B^-) = (48.4 \pm 0.6)\%$.

 B_s^0 CROSS-PARTICLE BRANCHING RATIOS $\Gamma([K^+K^-]_D K^*(892)^0)/\Gamma_{\text{total}} \times B(B_s^0 \rightarrow [K^+K^-]_D K^*(892)^0)$ $\Gamma_{143}/\Gamma \times B$

VALUE	DOCUMENT ID	TECN	COMMENT
0.10 $\pm 0.02 \pm 0.01$	AAIJ	14BN	LHCB pp at 7, 8 TeV

 $\Gamma([\pi^+\pi^-]_D K^*(892)^0)/\Gamma_{\text{total}} \times B(B_s^0 \rightarrow [\pi^+\pi^-]_D K^*(892)^0)$ $\Gamma_{144}/\Gamma \times B$

VALUE	DOCUMENT ID	TECN	COMMENT
0.15 $\pm 0.04 \pm 0.01$	AAIJ	14BN	LHCB pp at 7, 8 TeV

See the related review(s):

Polarization in B Decays

POLARIZATION IN B^0 DECAY

In decays involving two vector mesons, one can distinguish among the states in which meson polarizations are both longitudinal (L) or both are transverse and parallel (\parallel) or perpendicular (\perp) to each other with the parameters Γ_L/Γ , Γ_{\perp}/Γ , and the relative phases ϕ_{\parallel} and ϕ_{\perp} . See the definitions in the note on "Polarization in B Decays" review in the B^0 Particle Listings.

 Γ_L/Γ in $B^0 \rightarrow J/\psi(1S)K^*(892)^0$

VALUE	EVTS	DOCUMENT ID	TECN	COMMENT
0.571 ± 0.007 OUR AVERAGE				
0.572 $\pm 0.006 \pm 0.014$		¹ AAIJ	13AT	LHCB pp at 7 TeV
0.587 $\pm 0.011 \pm 0.013$		² ABAZOV	09E	D0 $p\bar{p}$ at 1.96 TeV
0.556 $\pm 0.009 \pm 0.010$		³ AUBERT	07AD	BABR $e^+e^- \rightarrow \Upsilon(4S)$
0.562 $\pm 0.026 \pm 0.018$		ACOSTA	05	CDF $p\bar{p}$ at 1.96 TeV
0.574 $\pm 0.012 \pm 0.009$		ITOH	05	BELL $e^+e^- \rightarrow \Upsilon(4S)$
0.59 $\pm 0.06 \pm 0.01$		⁴ AFFOLDER	00N	CDF $p\bar{p}$ at 1.8 TeV
0.52 $\pm 0.07 \pm 0.04$		⁵ JESSOP	97	CLE2 $e^+e^- \rightarrow \Upsilon(4S)$
0.65 $\pm 0.10 \pm 0.04$	65	ABE	95Z	CDF $p\bar{p}$ at 1.8 TeV
0.97 $\pm 0.16 \pm 0.15$	13	⁶ ALBRECHT	94G	ARG $e^+e^- \rightarrow \Upsilon(4S)$

See key on page 1127

Meson Particle Listings

B^0

• • • We do not use the following data for averages, fits, limits, etc. • • •

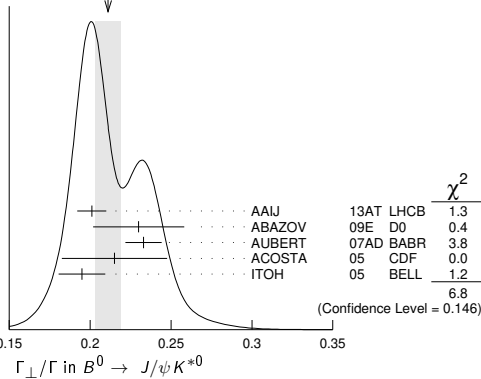
$0.566 \pm 0.012 \pm 0.005$	³ AUBERT	05P BABR	Repl. by AUBERT 07AD
$0.62 \pm 0.02 \pm 0.03$	⁷ ABE	02N BELL	Repl. by ITOH 05
$0.597 \pm 0.028 \pm 0.024$	⁸ AUBERT	01H BABR	Repl. by AUBERT 07AD
$0.80 \pm 0.08 \pm 0.05$	⁴² ALAM	94 CLE2	Sup. by JESSOP 97

- ¹ AAIJ 13AT obtains $\Gamma_{\parallel}/\Gamma = 0.227 \pm 0.004 \pm 0.011$. The relation $1 = (\Gamma_L + \Gamma_{\perp} + \Gamma_{\parallel})/\Gamma$ is used to obtain Γ_L/Γ .
- ² Measured the angular and lifetime parameters for the time-dependent angular untagged decays $B_d^0 \rightarrow J/\psi K^{*0}$ and $B_s^0 \rightarrow J/\psi \phi$.
- ³ Obtained by combining the B^0 and B^+ modes.
- ⁴ AFFOLDER 00N measurements are based on 190 B^0 candidates obtained from a data sample of 89 pb^{-1} . The P -wave fraction is found to be $0.13^{+0.12}_{-0.09} \pm 0.06$.
- ⁵ JESSOP 97 is the average over a mixture of B^0 and B^+ decays. The P -wave fraction is found to be $0.16 \pm 0.08 \pm 0.04$.
- ⁶ Averaged over an admixture of B^0 and B^+ decays.
- ⁷ Averaged over an admixture of B^0 and B^+ decays and the P wave fraction is $(19 \pm 2 \pm 3)\%$.
- ⁸ Averaged over an admixture of B^0 and B^- decays and the P wave fraction is $(16.0 \pm 3.2 \pm 1.4) \times 10^{-2}$.

Γ_{\perp}/Γ in $B^0 \rightarrow J/\psi K^{*0}$

VALUE	DOCUMENT ID	TECN	COMMENT
0.211 ± 0.008 OUR AVERAGE	Error includes scale factor of 1.3. See the ideogram below.		
$0.201 \pm 0.004 \pm 0.008$	AAIJ	13AT LHCB	pp at 7 TeV
$0.230 \pm 0.013 \pm 0.025$	¹ ABAZOV	09E D0	$p\bar{p}$ at 1.96 TeV
$0.233 \pm 0.010 \pm 0.005$	² AUBERT	07AD BABR	$e^+e^- \rightarrow \Upsilon(4S)$
$0.215 \pm 0.032 \pm 0.006$	ACOSTA	05 CDF	$p\bar{p}$ at 1.96 TeV
$0.195 \pm 0.012 \pm 0.008$	ITOH	05 BELL	$e^+e^- \rightarrow \Upsilon(4S)$

WEIGHTED AVERAGE
 0.211 ± 0.008 (Error scaled by 1.3)

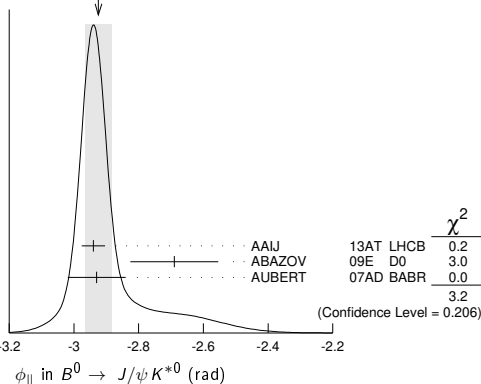


- ¹ Measured the angular and lifetime parameters for the time-dependent angular untagged decays $B_d^0 \rightarrow J/\psi K^{*0}$ and $B_s^0 \rightarrow J/\psi \phi$.
- ² Obtained by combining the B^0 and B^+ modes.

ϕ_{\parallel} in $B^0 \rightarrow J/\psi K^{*0}$

VALUE (rad)	DOCUMENT ID	TECN	COMMENT
-2.92 ± 0.04 OUR AVERAGE	Error includes scale factor of 1.3. See the ideogram below.		
$-2.94 \pm 0.02 \pm 0.03$	AAIJ	13AT LHCB	pp at 7 TeV
$-2.69 \pm 0.08 \pm 0.11$	¹ ABAZOV	09E D0	$p\bar{p}$ at 1.96 TeV
$-2.93 \pm 0.08 \pm 0.04$	² AUBERT	07AD BABR	$e^+e^- \rightarrow \Upsilon(4S)$

WEIGHTED AVERAGE
 -2.92 ± 0.04 (Error scaled by 1.3)

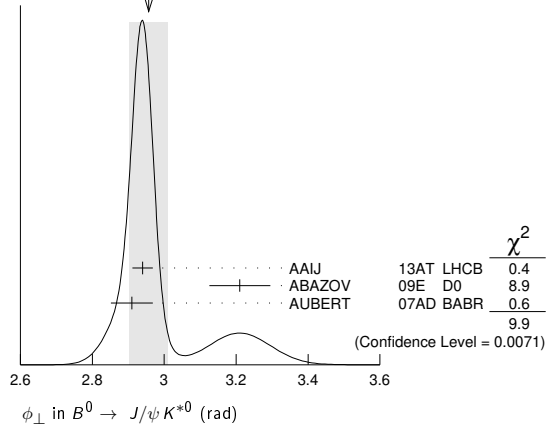


- ¹ Obtained ϕ_{\parallel} as $\delta_2 - \delta_1$, assuming they are uncorrelated.
- ² Obtained by combining the B^0 and B^+ modes.

ϕ_{\perp} in $B^0 \rightarrow J/\psi K^{*0}$

VALUE (rad)	DOCUMENT ID	TECN	COMMENT
2.96 ± 0.05 OUR AVERAGE	Error includes scale factor of 2.2. See the ideogram below.		
$2.94 \pm 0.02 \pm 0.02$	AAIJ	13AT LHCB	pp at 7 TeV
$3.21 \pm 0.06 \pm 0.06$	ABAZOV	09E D0	$p\bar{p}$ at 1.96 TeV
$2.91 \pm 0.05 \pm 0.03$	¹ AUBERT	07AD BABR	$e^+e^- \rightarrow \Upsilon(4S)$

WEIGHTED AVERAGE
 2.96 ± 0.05 (Error scaled by 2.2)



- ¹ Obtained by combining the B^0 and B^+ modes.

Γ_L/Γ in $B^0 \rightarrow \psi(2S) K^*(892)^0$

VALUE	DOCUMENT ID	TECN	COMMENT
$0.463^{+0.028}_{-0.040}$ OUR AVERAGE			
$0.455^{+0.031+0.014}_{-0.029-0.049}$	CHILIKIN	13 BELL	$e^+e^- \rightarrow \Upsilon(4S)$
$0.48 \pm 0.05 \pm 0.02$	¹ AUBERT	07AD BABR	$e^+e^- \rightarrow \Upsilon(4S)$
$0.45 \pm 0.11 \pm 0.04$	² RICHICHI	01 CLE2	$e^+e^- \rightarrow \Upsilon(4S)$
$0.448^{+0.040+0.040}_{-0.027-0.053}$	MIZUK	09 BELL	$e^+e^- \rightarrow \Upsilon(4S)$

• • • We do not use the following data for averages, fits, limits, etc. • • •

- ¹ Obtained by combining the B^0 and B^+ modes.
- ² Averages between charged and neutral B mesons.

Γ_{\perp}/Γ in $B^0 \rightarrow \psi(2S) K^{*0}$

VALUE	DOCUMENT ID	TECN	COMMENT
$0.30 \pm 0.06 \pm 0.02$	¹ AUBERT	07AD BABR	$e^+e^- \rightarrow \Upsilon(4S)$

- ¹ Obtained by combining the B^0 and B^+ modes.

ϕ_{\parallel} in $B^0 \rightarrow \psi(2S) K^{*0}$

VALUE (rad)	DOCUMENT ID	TECN	COMMENT
$-2.8 \pm 0.4 \pm 0.1$	¹ AUBERT	07AD BABR	$e^+e^- \rightarrow \Upsilon(4S)$

- ¹ Obtained by combining the B^0 and B^+ modes.

ϕ_{\perp} in $B^0 \rightarrow \psi(2S) K^{*0}$

VALUE (rad)	DOCUMENT ID	TECN	COMMENT
$2.8 \pm 0.3 \pm 0.1$	¹ AUBERT	07AD BABR	$e^+e^- \rightarrow \Upsilon(4S)$

- ¹ Obtained by combining the B^0 and B^+ modes.

Γ_L/Γ in $B^0 \rightarrow \chi_{c1} K^*(892)^0$

VALUE	DOCUMENT ID	TECN	COMMENT
$0.83^{+0.06}_{-0.08}$ OUR AVERAGE	Error includes scale factor of 1.3.		
$0.947^{+0.038+0.046}_{-0.048-0.099}$	MIZUK	08 BELL	$e^+e^- \rightarrow \Upsilon(4S)$
$0.77 \pm 0.07 \pm 0.04$	¹ AUBERT	07AD BABR	$e^+e^- \rightarrow \Upsilon(4S)$

- ¹ Obtained by combining the B^0 and B^+ modes.

Γ_{\perp}/Γ in $B^0 \rightarrow \chi_{c1} K^*(892)^0$

VALUE	DOCUMENT ID	TECN	COMMENT
$0.03 \pm 0.04 \pm 0.02$	¹ AUBERT	07AD BABR	$e^+e^- \rightarrow \Upsilon(4S)$

- ¹ Obtained by combining the B^0 and B^+ modes.

ϕ_{\parallel} in $B^0 \rightarrow \chi_{c1} K^*(892)^0$

VALUE (rad)	DOCUMENT ID	TECN	COMMENT
$0.0 \pm 0.3 \pm 0.1$	¹ AUBERT	07AD BABR	$e^+e^- \rightarrow \Upsilon(4S)$

- ¹ Obtained by combining the B^0 and B^+ modes.

Meson Particle Listings

 B^0 Γ_L/Γ in $B^0 \rightarrow D_s^{*+} D^{*-}$

VALUE	DOCUMENT ID	TECN	COMMENT
0.574±0.014 OUR AVERAGE			
0.578±0.010±0.011	¹ AAIJ	21s	LHCB pp at 13 TeV
0.519±0.050±0.028	² AUBERT	03i	BABR $e^+e^- \rightarrow \Upsilon(4S)$
0.506±0.139±0.036	AHMED	00B	CLE2 $e^+e^- \rightarrow \Upsilon(4S)$
¹ AAIJ 21s uses $D_s^{*+} \rightarrow D_s^+ \gamma$ decays.			
² Measurement performed using partial reconstruction of D^{*-} decay.			

 $|H_{\pm}|$ in $B^0 \rightarrow D_s^{*+} D^{*-}$

H_+ , H_- define parity-even (\parallel) and parity-odd (\perp) polarization transversity amplitudes
 $A_{\parallel,\perp} = (H_+ \pm H_-)/\sqrt{2}$.

VALUE	DOCUMENT ID	TECN	COMMENT
0.195±0.022±0.032	¹ AAIJ	21s	BELL pp at 13 TeV
¹ AAIJ 21s uses $D_s^{*+} \rightarrow D_s^+ \gamma$ decays.			

 $|H_{\pm}|$ in $B^0 \rightarrow D_s^{*+} D^{*-}$

H_+ , H_- define parity-even (\parallel) and parity-odd (\perp) polarization transversity amplitudes
 $A_{\parallel,\perp} = (H_+ \pm H_-)/\sqrt{2}$.

VALUE	DOCUMENT ID	TECN	COMMENT
0.620±0.011±0.013	¹ AAIJ	21s	LHCB pp at 13 TeV
¹ AAIJ 21s uses $D_s^{*+} \rightarrow D_s^+ \gamma$ decays.			

 ϕ_+ in $B^0 \rightarrow D_s^{*+} D^{*-}$

VALUE	DOCUMENT ID	TECN	COMMENT
-0.046±0.102±0.020	¹ AAIJ	21s	LHCB pp at 13 TeV
¹ AAIJ 21s uses $D_s^{*+} \rightarrow D_s^+ \gamma$ decays.			

 ϕ_- in $B^0 \rightarrow D_s^{*+} D^{*-}$

VALUE	DOCUMENT ID	TECN	COMMENT
0.108±0.170±0.051	¹ AAIJ	21s	LHCB pp at 13 TeV
¹ AAIJ 21s uses $D_s^{*+} \rightarrow D_s^+ \gamma$ decays.			

 Γ_L/Γ in $B^0 \rightarrow D^{*-} \rho^+$

VALUE	EVTS	DOCUMENT ID	TECN	COMMENT
0.885±0.016±0.012		CSORNA	03	CLE2 $e^+e^- \rightarrow \Upsilon(4S)$
••• We do not use the following data for averages, fits, limits, etc. •••				
0.93 ± 0.05 ± 0.05	76	ALAM	94	CLE2 $e^+e^- \rightarrow \Upsilon(4S)$

 Γ_L/Γ in $B^0 \rightarrow D_s^{*+} \rho^-$

VALUE	DOCUMENT ID	TECN	COMMENT
0.84^{+0.26}_{-0.28}±0.13	¹ AUBERT	08AJ	BABR $e^+e^- \rightarrow \Upsilon(4S)$
¹ Assumes equal production of B^+ and B^0 at the $\Upsilon(4S)$.			

 Γ_L/Γ in $B^0 \rightarrow D_s^{*+} K^{*-}$

VALUE	DOCUMENT ID	TECN	COMMENT
0.92^{+0.37}_{-0.31}±0.07	¹ AUBERT	08AJ	BABR $e^+e^- \rightarrow \Upsilon(4S)$
¹ Assumes equal production of B^+ and B^0 at the $\Upsilon(4S)$.			

 Γ_L/Γ in $B^0 \rightarrow D^{*+} D^{*-}$

VALUE	DOCUMENT ID	TECN	COMMENT
0.624±0.029±0.011	KRONENBIT...12	BELL	$e^+e^- \rightarrow \Upsilon(4S)$
••• We do not use the following data for averages, fits, limits, etc. •••			
0.57 ± 0.08 ± 0.02	MIYAKE	05	BELL Repl. by KRONENBITTER 12

 Γ_{\perp}/Γ in $B^0 \rightarrow D^{*+} D^{*-}$

VALUE	DOCUMENT ID	TECN	COMMENT
0.147±0.019 OUR AVERAGE			
0.138±0.024±0.006	KRONENBIT...12	BELL	$e^+e^- \rightarrow \Upsilon(4S)$
0.158±0.028±0.006	AUBERT	09c	BABR $e^+e^- \rightarrow \Upsilon(4S)$
••• We do not use the following data for averages, fits, limits, etc. •••			
0.125±0.043±0.023	VERVINK	09	BELL Repl. by KRONENBITTER 12
0.143±0.034±0.008	AUBERT	07B0	BABR Repl. by AUBERT 09c
0.125±0.044±0.007	AUBERT,BE	05A	BABR Repl. by AUBERT 07B0
0.19 ± 0.08 ± 0.01	MIYAKE	05	BELL Repl. by VERVINK 09
0.063±0.055±0.009	AUBERT	03Q	BABR Repl. by AUBERT,BE 05A

 Γ_L/Γ in $B^0 \rightarrow \bar{D}^{*0} \omega$

VALUE	DOCUMENT ID	TECN	COMMENT
0.665±0.047±0.015	LEES	11M	BABR $e^+e^- \rightarrow \Upsilon(4S)$

 Γ_L/Γ in $B^0 \rightarrow \bar{D}_1(2430)^0 \omega$

VALUE (%)	DOCUMENT ID	TECN	COMMENT
63.0±9.1^{+5.5}_{-6.0}	^{1,2} MATVIENKO	15	BELL $e^+e^- \rightarrow \Upsilon(4S)$

¹ Obtained by amplitude analysis of $\bar{B}^0 \rightarrow D^{*-} \omega \pi^+$. The second uncertainty combines in quadrature experimental systematic and model uncertainties.

² Assumes equal production of B^0 and B^+ at $\Upsilon(4S)$.

 Γ_L/Γ in $B^0 \rightarrow \bar{D}_1(2420)^0 \omega$

VALUE (%)	DOCUMENT ID	TECN	COMMENT
67.1±11.7^{+2.3}_{-5.0}	^{1,2} MATVIENKO	15	BELL $e^+e^- \rightarrow \Upsilon(4S)$
¹ Obtained by amplitude analysis of $\bar{B}^0 \rightarrow D^{*-} \omega \pi^+$. The second uncertainty combines in quadrature experimental systematic and model uncertainties.			
² Assumes equal production of B^0 and B^+ at $\Upsilon(4S)$.			

 Γ_L/Γ in $B^0 \rightarrow \bar{D}_2^*(2460)^0 \omega$

VALUE (%)	DOCUMENT ID	TECN	COMMENT
76.0±18.3^{+3.5}_{-8.5}-2.8	^{1,2} MATVIENKO	15	BELL $e^+e^- \rightarrow \Upsilon(4S)$
¹ Obtained by amplitude analysis of $\bar{B}^0 \rightarrow D^{*-} \omega \pi^+$. The second uncertainty combines in quadrature experimental systematic and model uncertainties.			
² Assumes equal production of B^0 and B^+ at $\Upsilon(4S)$.			

 Γ_L/Γ in $B^0 \rightarrow D^{*-} \omega \pi^+$

VALUE	DOCUMENT ID	TECN	COMMENT
0.654±0.042±0.016	¹ AUBERT	06L	BABR $e^+e^- \rightarrow \Upsilon(4S)$
¹ Invariant mass of the $[\omega \pi]$ system is restricted in the region 1.1 and 1.9 GeV.			

 Γ_L/Γ in $B^0 \rightarrow \omega K^{*0}$

VALUE	DOCUMENT ID	TECN	COMMENT
0.69±0.11 OUR AVERAGE			
0.68±0.17±0.16	AAIJ	19J	LHCB pp at 7, 8 TeV
0.72±0.14±0.02	AUBERT	09H	BABR $e^+e^- \rightarrow \Upsilon(4S)$
0.56±0.29 ^{+0.18} _{-0.08}	GOLDENZWE..08	BELL	$e^+e^- \rightarrow \Upsilon(4S)$

 Γ_{\perp}/Γ in $B^0 \rightarrow \omega K^{*0}(892)^0$

VALUE	DOCUMENT ID	TECN	COMMENT
0.10±0.09±0.09	AAIJ	19J	LHCB pp at 7, 8 TeV

 A_{CP}^0 in $B^0 \rightarrow \omega K^{*0}(892)^0$

VALUE	DOCUMENT ID	TECN	COMMENT
-0.13±0.27±0.13	AAIJ	19J	LHCB pp at 7, 8 TeV

 A_{CP}^{\perp} in $B^0 \rightarrow \omega K^{*0}(892)^0$

VALUE	DOCUMENT ID	TECN	COMMENT
0.3±0.8±0.4	AAIJ	19J	LHCB pp at 7, 8 TeV

 A_{CP}^{\parallel} in $B^0 \rightarrow \omega K^{*0}(892)^0$

VALUE	DOCUMENT ID	TECN	COMMENT
0.26±0.55±0.22	AAIJ	19J	LHCB pp at 7, 8 TeV

 ϕ_0 in $B^0 \rightarrow \omega K^{*0}(892)^0$

VALUE	DOCUMENT ID	TECN	COMMENT
-0.86±0.29±0.71	AAIJ	19J	LHCB pp at 7, 8 TeV

 ϕ_{\perp} in $B^0 \rightarrow \omega K^{*0}(892)^0$

VALUE	DOCUMENT ID	TECN	COMMENT
1.6±0.4±0.6	AAIJ	19J	LHCB pp at 7, 8 TeV

 ϕ_{\parallel} in $B^0 \rightarrow \omega K^{*0}(892)^0$

VALUE	DOCUMENT ID	TECN	COMMENT
-1.83±0.29±0.32	AAIJ	19J	LHCB pp at 7, 8 TeV

 Γ_L/Γ in $B^0 \rightarrow \omega K_2^*(1430)^0$

VALUE	DOCUMENT ID	TECN	COMMENT
0.45±0.12±0.02	AUBERT	09H	BABR $e^+e^- \rightarrow \Upsilon(4S)$

 Γ_L/Γ in $B^0 \rightarrow K^{*0} \bar{K}^{*0}$

VALUE	DOCUMENT ID	TECN	COMMENT
0.74 ± 0.05 OUR AVERAGE			
0.724±0.051±0.016	¹ AAIJ	19L	LHCB pp at 7 and 8 TeV
0.80 ^{+0.10} _{-0.12} ± 0.06	AUBERT	08I	BABR $e^+e^- \rightarrow \Upsilon(4S)$

¹ Untagged and time-integrated analysis within 150 MeV of the K^{*0} mass.

 Γ_L/Γ in $B^0 \rightarrow \phi K^{*0}(892)^0$

VALUE	DOCUMENT ID	TECN	COMMENT
0.497±0.017 OUR AVERAGE			
0.497±0.019±0.015	AAIJ	14AM	LHCB pp at 7 TeV
0.499±0.030±0.018	PRIM	13	BELL $e^+e^- \rightarrow \Upsilon(4S)$
0.494±0.034±0.013	AUBERT	08BG	BABR $e^+e^- \rightarrow \Upsilon(4S)$
••• We do not use the following data for averages, fits, limits, etc. •••			
0.506±0.040±0.015	AUBERT	07D	BABR Repl. by AUBERT 08BG
0.45 ± 0.05 ± 0.02	CHEN	05A	BELL Repl. by PRIM 13
0.52 ± 0.05 ± 0.02	¹ AUBERT,B	04W	BABR Repl. by AUBERT 07D
0.65 ± 0.07 ± 0.02	AUBERT	03V	BABR Repl. by AUBERT,B 04W
0.41 ± 0.10 ± 0.04	CHEN	03B	BELL Repl. by CHEN 05A

¹ AUBERT,B 04W also measures the fraction of parity-odd transverse contribution $f_{\perp} = 0.22 \pm 0.05 \pm 0.02$ and the phases of the parity-even and parity-odd transverse amplitudes relative to the longitudinal amplitude.

Γ_{\perp}/Γ in $B^0 \rightarrow \phi K^*(892)^0$

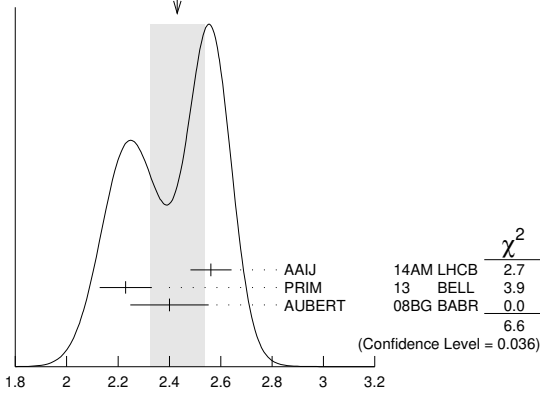
VALUE	DOCUMENT ID	TECN	COMMENT
0.224 ± 0.015 OUR AVERAGE			
0.221 ± 0.016 ± 0.013	AAIJ	14AM LHCb	pp at 7 TeV
0.238 ± 0.026 ± 0.008	PRIM	13 BELL	e ⁺ e ⁻ → $\Upsilon(4S)$
0.212 ± 0.032 ± 0.013	AUBERT	08BG BABR	e ⁺ e ⁻ → $\Upsilon(4S)$
••• We do not use the following data for averages, fits, limits, etc. •••			
0.227 ± 0.038 ± 0.013	AUBERT	07D BABR	Repl. by AUBERT 08Bg
0.31 ^{+0.06} _{-0.05} ± 0.02	¹ CHEN	05A BELL	Repl. by PRIM 13
0.22 ± 0.05 ± 0.02	AUBERT,B	04W BABR	Repl. by AUBERT 07D

¹ This quantity was recalculated by the BELLE authors from numbers in the original paper.

ϕ_{\parallel} in $B^0 \rightarrow \phi K^*(892)^0$

VALUE (rad)	DOCUMENT ID	TECN	COMMENT
2.43 ± 0.11 OUR AVERAGE			Error includes scale factor of 1.8. See the ideogram below.
2.562 ± 0.069 ± 0.040	AAIJ	14AM LHCb	pp at 7 TeV
2.23 ± 0.10 ± 0.02	PRIM	13 BELL	e ⁺ e ⁻ → $\Upsilon(4S)$
2.40 ± 0.13 ± 0.08	AUBERT	08BG BABR	e ⁺ e ⁻ → $\Upsilon(4S)$
••• We do not use the following data for averages, fits, limits, etc. •••			
2.31 ± 0.14 ± 0.08	AUBERT	07D BABR	Repl. by AUBERT 08Bg
2.40 ^{+0.28} _{-0.24} ± 0.07	¹ CHEN	05A BELL	Repl. by PRIM 13
2.34 ^{+0.23} _{-0.20} ± 0.05	AUBERT,B	04W BABR	Repl. by AUBERT 07D

WEIGHTED AVERAGE
2.43 ± 0.11 (Error scaled by 1.8)

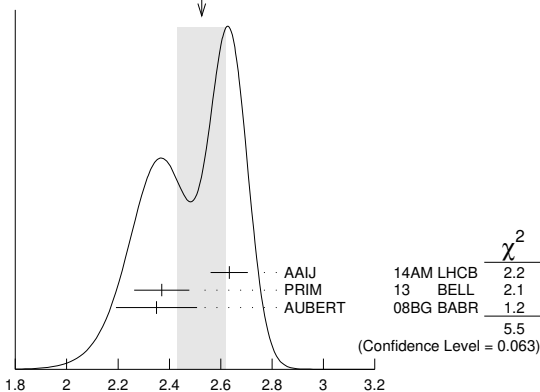


¹ This quantity was recalculated by the BELLE authors from numbers in the original paper.

ϕ_{\perp} in $B^0 \rightarrow \phi K^*(892)^0$

VALUE (rad)	DOCUMENT ID	TECN	COMMENT
2.53 ± 0.09 OUR AVERAGE			Error includes scale factor of 1.7. See the ideogram below.
2.633 ± 0.062 ± 0.037	AAIJ	14AM LHCb	pp at 7 TeV
2.37 ± 0.10 ± 0.04	PRIM	13 BELL	e ⁺ e ⁻ → $\Upsilon(4S)$
2.35 ± 0.13 ± 0.09	AUBERT	08BG BABR	e ⁺ e ⁻ → $\Upsilon(4S)$
••• We do not use the following data for averages, fits, limits, etc. •••			
2.24 ± 0.15 ± 0.09	AUBERT	07D BABR	Repl. by AUBERT 08Bg
2.51 ± 0.25 ± 0.06	¹ CHEN	05A BELL	Repl. by PRIM 13
2.47 ± 0.25 ± 0.05	AUBERT,B	04W BABR	Repl. by AUBERT 07D

WEIGHTED AVERAGE
2.53 ± 0.09 (Error scaled by 1.7)



¹ This quantity was recalculated by the BELLE authors from numbers in the original paper.

$\delta_0(B^0 \rightarrow \phi K^*(892)^0)$

VALUE (rad)	DOCUMENT ID	TECN	COMMENT
2.88 ± 0.10 OUR AVERAGE			
2.91 ± 0.10 ± 0.08	PRIM	13 BELL	e ⁺ e ⁻ → $\Upsilon(4S)$
2.82 ± 0.15 ± 0.09	AUBERT	08BG BABR	e ⁺ e ⁻ → $\Upsilon(4S)$
••• We do not use the following data for averages, fits, limits, etc. •••			
2.78 ± 0.17 ± 0.09	AUBERT	07D BABR	Repl. by AUBERT 08Bg

A_{CP}^0 in $B^0 \rightarrow \phi K^*(892)^0$

VALUE	DOCUMENT ID	TECN	COMMENT
-0.007 ± 0.030 OUR AVERAGE			
-0.003 ± 0.038 ± 0.005	AAIJ	14AM LHCb	pp at 7 TeV
-0.030 ± 0.061 ± 0.007	PRIM	13 BELL	e ⁺ e ⁻ → $\Upsilon(4S)$
0.01 ± 0.07 ± 0.02	AUBERT	08BG BABR	e ⁺ e ⁻ → $\Upsilon(4S)$
••• We do not use the following data for averages, fits, limits, etc. •••			
-0.03 ± 0.08 ± 0.02	AUBERT	07D BABR	Repl. by AUBERT 08Bg
0.13 ± 0.12 ± 0.04	¹ CHEN	05A BELL	Repl. by PRIM 13
-0.06 ± 0.10 ± 0.01	AUBERT,B	04W BABR	Repl. by AUBERT 07D

¹ This quantity was recalculated by the BELLE authors from numbers in the original paper.

A_{CP}^{\perp} in $B^0 \rightarrow \phi K^*(892)^0$

VALUE	DOCUMENT ID	TECN	COMMENT
-0.02 ± 0.06 OUR AVERAGE			
0.047 ± 0.074 ± 0.009	AAIJ	14AM LHCb	pp at 7 TeV
-0.14 ± 0.11 ± 0.01	PRIM	13 BELL	e ⁺ e ⁻ → $\Upsilon(4S)$
-0.04 ± 0.15 ± 0.06	AUBERT	08BG BABR	e ⁺ e ⁻ → $\Upsilon(4S)$
••• We do not use the following data for averages, fits, limits, etc. •••			
-0.03 ± 0.16 ± 0.05	AUBERT	07D BABR	Repl. by AUBERT 08Bg
-0.20 ± 0.18 ± 0.04	¹ CHEN	05A BELL	Repl. by PRIM 13
-0.10 ± 0.24 ± 0.05	AUBERT,B	04W BABR	Repl. by AUBERT 07D

¹ This quantity was recalculated by the BELLE authors from numbers in the original paper.

$\Delta\phi_{\parallel}$ in $B^0 \rightarrow \phi K^*(892)^0$

VALUE (rad)	DOCUMENT ID	TECN	COMMENT
0.05 ± 0.05 OUR AVERAGE			
0.045 ± 0.069 ± 0.015	AAIJ	14AM LHCb	pp at 7 TeV
-0.02 ± 0.10 ± 0.01	PRIM	13 BELL	e ⁺ e ⁻ → $\Upsilon(4S)$
0.22 ± 0.12 ± 0.08	AUBERT	08BG BABR	e ⁺ e ⁻ → $\Upsilon(4S)$
••• We do not use the following data for averages, fits, limits, etc. •••			
0.24 ± 0.14 ± 0.08	AUBERT	07D BABR	Repl. by AUBERT 08Bg
-0.32 ± 0.27 ± 0.07	¹ CHEN	05A BELL	Repl. by PRIM 13
0.27 ^{+0.20} _{-0.23} ± 0.05	AUBERT,B	04W BABR	Repl. by AUBERT 07D

¹ This quantity was recalculated by the BELLE authors from numbers in the original paper.

$\Delta\phi_{\perp}$ in $B^0 \rightarrow \phi K^*(892)^0$

VALUE (rad)	DOCUMENT ID	TECN	COMMENT
0.08 ± 0.05 OUR AVERAGE			
0.062 ± 0.062 ± 0.005	AAIJ	14AM LHCb	pp at 7 TeV
0.05 ± 0.10 ± 0.02	PRIM	13 BELL	e ⁺ e ⁻ → $\Upsilon(4S)$
0.21 ± 0.13 ± 0.08	AUBERT	08BG BABR	e ⁺ e ⁻ → $\Upsilon(4S)$
••• We do not use the following data for averages, fits, limits, etc. •••			
0.19 ± 0.15 ± 0.08	AUBERT	07D BABR	Repl. by AUBERT 08Bg
-0.30 ± 0.25 ± 0.06	¹ CHEN	05A BELL	Repl. by PRIM 13
0.36 ± 0.25 ± 0.05	AUBERT,B	04W BABR	Repl. by AUBERT 07D

¹ This quantity was recalculated by the BELLE authors from numbers in the original paper.

$\Delta\delta_0(B^0 \rightarrow \phi K^*(892)^0)$

VALUE (rad)	DOCUMENT ID	TECN	COMMENT
0.13 ± 0.09 OUR AVERAGE			
0.08 ± 0.10 ± 0.01	PRIM	13 BELL	e ⁺ e ⁻ → $\Upsilon(4S)$
0.27 ± 0.14 ± 0.08	AUBERT	08BG BABR	e ⁺ e ⁻ → $\Upsilon(4S)$
••• We do not use the following data for averages, fits, limits, etc. •••			
0.21 ± 0.17 ± 0.08	AUBERT	07D BABR	Repl. by AUBERT 08Bg

$\Delta\phi_{00}(B^0 \rightarrow \phi K_0^*(1430)^0)$

VALUE (rad)	DOCUMENT ID	TECN	COMMENT
0.28 ± 0.42 ± 0.04	AUBERT	08BG BABR	e ⁺ e ⁻ → $\Upsilon(4S)$

Γ_{\perp}/Γ in $B^0 \rightarrow \phi K_2^*(1430)^0$

VALUE	DOCUMENT ID	TECN	COMMENT
0.913^{+0.028}_{-0.050} OUR AVERAGE			
0.918 ^{+0.029} _{-0.060} ± 0.012	PRIM	13 BELL	e ⁺ e ⁻ → $\Upsilon(4S)$
0.901 ^{+0.046} _{-0.058} ± 0.037	AUBERT	08BG BABR	e ⁺ e ⁻ → $\Upsilon(4S)$
••• We do not use the following data for averages, fits, limits, etc. •••			
0.853 ^{+0.061} _{-0.069} ± 0.036	AUBERT	07D BABR	Repl. by AUBERT 08Bg

Meson Particle Listings

B^0

Γ_{\perp}/Γ in $B^0 \rightarrow \phi K_2^*(1430)^0$

VALUE	DOCUMENT ID	TECN	COMMENT
0.027\pm0.031\pm0.025 OUR AVERAGE	Error includes scale factor of 1.1.		
0.056 \pm 0.050 \pm 0.009	PRIM	13	BELL $e^+e^- \rightarrow \Upsilon(4S)$
0.002 \pm 0.018 \pm 0.031	AUBERT	08B6	BABR $e^+e^- \rightarrow \Upsilon(4S)$
••• We do not use the following data for averages, fits, limits, etc. •••			
0.045 \pm 0.049 \pm 0.013	AUBERT	07D	BABR Repl. by AUBERT 08B6

ϕ_{\parallel} in $B^0 \rightarrow \phi K_2^*(1430)^0$

VALUE (rad)	DOCUMENT ID	TECN	COMMENT
4.0\pm0.4 OUR AVERAGE			
3.76 \pm 2.88 \pm 1.32	PRIM	13	BELL $e^+e^- \rightarrow \Upsilon(4S)$
3.96 \pm 0.38 \pm 0.06	AUBERT	08B6	BABR $e^+e^- \rightarrow \Upsilon(4S)$
••• We do not use the following data for averages, fits, limits, etc. •••			
2.90 \pm 0.39 \pm 0.06	AUBERT	07D	BABR Repl. by AUBERT 08B6

ϕ_{\perp} in $B^0 \rightarrow \phi K_2^*(1430)^0$

VALUE (rad)	DOCUMENT ID	TECN	COMMENT
4.45\pm0.43\pm0.13	PRIM	13	BELL $e^+e^- \rightarrow \Upsilon(4S)$
••• We do not use the following data for averages, fits, limits, etc. •••			
5.72 \pm 0.55 \pm 0.11	AUBERT	07D	BABR Repl. by AUBERT 08B6

$\delta_0(B^0 \rightarrow \phi K_2^*(1430)^0)$

VALUE (rad)	DOCUMENT ID	TECN	COMMENT
3.46\pm0.14 OUR AVERAGE			
3.53 \pm 0.11 \pm 0.19	PRIM	13	BELL $e^+e^- \rightarrow \Upsilon(4S)$
3.41 \pm 0.13 \pm 0.13	AUBERT	08B6	BABR $e^+e^- \rightarrow \Upsilon(4S)$
••• We do not use the following data for averages, fits, limits, etc. •••			
3.54 \pm 0.12 \pm 0.06	AUBERT	07D	BABR Repl. by AUBERT 08B6

A_{CP}^0 in $B^0 \rightarrow \phi K_2^*(1430)^0$

VALUE	DOCUMENT ID	TECN	COMMENT
-0.03\pm0.04 OUR AVERAGE			
-0.016 \pm 0.066 \pm 0.008	PRIM	13	BELL $e^+e^- \rightarrow \Upsilon(4S)$
-0.05 \pm 0.06 \pm 0.01	AUBERT	08B6	BABR $e^+e^- \rightarrow \Upsilon(4S)$

A_{CP}^{\perp} in $B^0 \rightarrow \phi K_2^*(1430)^0$

VALUE	DOCUMENT ID	TECN	COMMENT
-0.01\pm0.85\pm0.09	PRIM	13	BELL $e^+e^- \rightarrow \Upsilon(4S)$

$\Delta\phi_{\parallel}(B^0 \rightarrow \phi K_2^*(1430)^0)$

VALUE (rad)	DOCUMENT ID	TECN	COMMENT
-0.9\pm0.4 OUR AVERAGE			
-0.02 \pm 1.08 \pm 1.01	PRIM	13	BELL $e^+e^- \rightarrow \Upsilon(4S)$
-1.00 \pm 0.38 \pm 0.09	AUBERT	08B6	BABR $e^+e^- \rightarrow \Upsilon(4S)$

$\Delta\phi_{\perp}(B^0 \rightarrow \phi K_2^*(1430)^0)$

VALUE	DOCUMENT ID	TECN	COMMENT
-0.19\pm0.42\pm0.11	PRIM	13	BELL $e^+e^- \rightarrow \Upsilon(4S)$

$\Delta\delta_0$ in $B^0 \rightarrow \phi K_2^*(1430)^0$

VALUE (rad)	DOCUMENT ID	TECN	COMMENT
0.08\pm0.09 OUR AVERAGE			
0.06 \pm 0.11 \pm 0.02	PRIM	13	BELL $e^+e^- \rightarrow \Upsilon(4S)$
0.11 \pm 0.13 \pm 0.06	AUBERT	08B6	BABR $e^+e^- \rightarrow \Upsilon(4S)$

Γ_L/Γ in $B^0 \rightarrow K^*(892)^0 \rho^0$

VALUE	DOCUMENT ID	TECN	COMMENT
0.173\pm0.026 OUR AVERAGE			
0.164 \pm 0.015 \pm 0.022	AAIJ	19J	LHCB pp at 7, 8 TeV
0.40 \pm 0.08 \pm 0.11	LEES	12K	BABR $e^+e^- \rightarrow \Upsilon(4S)$
••• We do not use the following data for averages, fits, limits, etc. •••			
0.57 \pm 0.09 \pm 0.08	AUBERT,B	06G	BABR Repl. by LEES 12K

Γ_{\perp}/Γ in $B^0 \rightarrow K^*(892)^0 \rho^0$

VALUE	DOCUMENT ID	TECN	COMMENT
0.401\pm0.016\pm0.037	AAIJ	19J	LHCB pp at 7, 8 TeV

A_{CP}^0 in $B^0 \rightarrow K^*(892)^0 \rho^0$

VALUE	DOCUMENT ID	TECN	COMMENT
-0.62\pm0.09\pm0.09	AAIJ	19J	LHCB pp at 7, 8 TeV

A_{CP}^{\perp} in $B^0 \rightarrow K^*(892)^0 \rho^0$

VALUE	DOCUMENT ID	TECN	COMMENT
0.050\pm0.039\pm0.015	AAIJ	19J	LHCB pp at 7, 8 TeV

A_{CP}^{\parallel} in $B^0 \rightarrow K^*(892)^0 \rho^0$

VALUE	DOCUMENT ID	TECN	COMMENT
0.188\pm0.037\pm0.022	AAIJ	19J	LHCB pp at 7, 8 TeV

ϕ_0 in $B^0 \rightarrow K^*(892)^0 \rho^0$

VALUE	DOCUMENT ID	TECN	COMMENT
1.57\pm0.08\pm0.18	AAIJ	19J	LHCB pp at 7, 8 TeV

ϕ_{\perp} in $B^0 \rightarrow K^*(892)^0 \rho^0$

VALUE	DOCUMENT ID	TECN	COMMENT
-2.365\pm0.032\pm0.054	AAIJ	19J	LHCB pp at 7, 8 TeV

ϕ_{\parallel} in $B^0 \rightarrow K^*(892)^0 \rho^0$

VALUE	DOCUMENT ID	TECN	COMMENT
0.795\pm0.030\pm0.068	AAIJ	19J	LHCB pp at 7, 8 TeV

Γ_L/Γ in $B^0 \rightarrow K^* \rho^-$

VALUE	DOCUMENT ID	TECN	COMMENT
0.38\pm0.13\pm0.03	LEES	12K	BABR $e^+e^- \rightarrow \Upsilon(4S)$

Γ_L/Γ in $B^0 \rightarrow \rho^+ \rho^-$

VALUE	DOCUMENT ID	TECN	COMMENT
0.990\pm0.021\pm0.019 OUR AVERAGE			

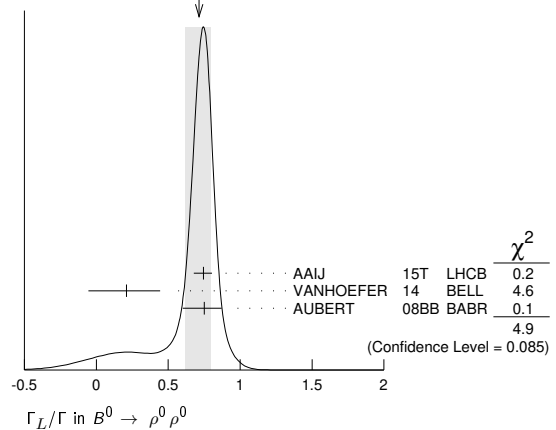
0.988 \pm 0.012 \pm 0.023	VANHOEFER	16	BELL $e^+e^- \rightarrow \Upsilon(4S)$
0.992 \pm 0.024 \pm 0.026 \pm 0.013	AUBERT	07BF	BABR $e^+e^- \rightarrow \Upsilon(4S)$
••• We do not use the following data for averages, fits, limits, etc. •••			
0.941 \pm 0.034 \pm 0.030	SOMOV	06	BELL Repl. by VANHOEFER 16
0.978 \pm 0.014 \pm 0.021 \pm 0.029	AUBERT,B	05C	BABR Repl. by AUBERT 07BF
0.98 \pm 0.02 \pm 0.03	AUBERT	04G	BABR Repl. by AUBERT,B 04R
0.99 \pm 0.03 \pm 0.04 \pm 0.03	AUBERT,B	04R	BABR Repl. by AUBERT,B 05C

Γ_L/Γ in $B^0 \rightarrow \rho^0 \rho^0$

VALUE	DOCUMENT ID	TECN	COMMENT
0.71\pm0.08\pm0.09 OUR AVERAGE	Error includes scale factor of 1.6. See the ideogram below.		

0.745 \pm 0.048 \pm 0.034	AAIJ	15T	LHCB pp at 7, 8 TeV
0.21 \pm 0.18 \pm 0.22	VANHOEFER	14	BELL $e^+e^- \rightarrow \Upsilon(4S)$
0.75 \pm 0.11 \pm 0.05	AUBERT	08BB	BABR $e^+e^- \rightarrow \Upsilon(4S)$
••• We do not use the following data for averages, fits, limits, etc. •••			
0.87 \pm 0.13 \pm 0.04	AUBERT	07G	BABR Repl. by AUBERT 08BB

WEIGHTED AVERAGE
0.71+0.08-0.09 (Error scaled by 1.6)



Γ_L/Γ in $B^0 \rightarrow a_1(1260)^+ a_1(1260)^-$

VALUE	DOCUMENT ID	TECN	COMMENT
0.31\pm0.22\pm0.10	AUBERT	09AL	BABR $e^+e^- \rightarrow \Upsilon(4S)$

Γ_L/Γ in $B^0 \rightarrow \rho^0 \bar{K}^*(892)^0$

VALUE	DOCUMENT ID	TECN	COMMENT
1.01\pm0.13\pm0.03	CHEN	08c	BELL $e^+e^- \rightarrow \Upsilon(4S)$

Γ_L/Γ in $B^0 \rightarrow \Lambda \bar{\Lambda} K^*(892)^0$

VALUE	DOCUMENT ID	TECN	COMMENT
0.60\pm0.22\pm0.08	CHANG	09	BELL $e^+e^- \rightarrow \Upsilon(4S)$

VALUE	DOCUMENT ID	TECN	COMMENT
0.504 ± 0.06 ± 0.04	1 AABOUD	18BY ATLS	pp at 8 TeV

¹ A set of angular parameters obtained for this decay is also presented.

VALUE	DOCUMENT ID	TECN	COMMENT
0.044 ± 0.026 ± 0.014	1 AAIJ	20AO LHCB	pp at 7, 8, 13 TeV
0.16 ± 0.06 ± 0.03	2 AAIJ	15Z LHCB	Repl. by AAIJ 20AO

¹ Determined in the effective dielectron invariant mass range 0.0008 < q² < 0.257 GeV²/c⁴.
² Determined in the effective dielectron invariant mass range 0.002 < q² < 1.120 GeV²/c⁴.

VALUE	DOCUMENT ID	TECN	COMMENT
0.11 ± 0.10 ± 0.02	1 AAIJ	20AO LHCB	pp at 7, 8, 13 TeV
-0.23 ± 0.23 ± 0.05	2 AAIJ	15Z LHCB	Repl. by AAIJ 20AO

¹ Determined in the effective dielectron invariant mass range 0.0008 < q² < 0.257 GeV²/c⁴.
² Determined in the effective dielectron invariant mass range 0.002 < q² < 1.120 GeV²/c⁴.

VALUE	DOCUMENT ID	TECN	COMMENT
0.02 ± 0.10 ± 0.01	1 AAIJ	20AO LHCB	pp at 7, 8, 13 TeV
0.14 ± 0.22 ± 0.05	2 AAIJ	15Z LHCB	Repl. by AAIJ 20AO

¹ Determined in the effective dielectron invariant mass range 0.0008 < q² < 0.257 GeV²/c⁴.
² Determined in the effective dielectron invariant mass range 0.002 < q² < 1.120 GeV²/c⁴.

VALUE	DOCUMENT ID	TECN	COMMENT
-0.06 ± 0.08 ± 0.02	1 AAIJ	20AO LHCB	pp at 7, 8, 13 TeV
0.10 ± 0.18 ± 0.05	2 AAIJ	15Z LHCB	Repl. by AAIJ 20AO

¹ Determined in the effective dielectron invariant mass range 0.0008 < q² < 0.257 GeV²/c⁴.
² Determined in the effective dielectron invariant mass range 0.002 < q² < 1.120 GeV²/c⁴.

See the related review(s):

B⁰ — \bar{B}^0 MixingB⁰- \bar{B}^0 MIXING PARAMETERS

For a discussion of B⁰- \bar{B}^0 mixing see the note on “B⁰- \bar{B}^0 Mixing” in the B⁰ Particle Listings above.

χ_d is a measure of the time-integrated B⁰- \bar{B}^0 mixing probability that a produced B⁰(\bar{B}^0) decays as a \bar{B}^0 (B⁰). Mixing violates $\Delta B \neq 2$ rule.

$$\chi_d = \frac{x_d^2}{2(1+x_d^2)}$$

$$\chi_d = \frac{\Delta m_{B^0}}{\Gamma_{B^0}} = (m_{B_H^0} - m_{B_L^0}) \tau_{B^0}$$

where H, L stand for heavy and light states of two B⁰ CP eigenstates and $\tau_{B^0} = \frac{1}{0.5(\Gamma_{B_H^0} + \Gamma_{B_L^0})}$.

 χ_d

This B⁰- \bar{B}^0 mixing parameter is the probability (integrated over time) that a produced B⁰ (or \bar{B}^0) decays as a \bar{B}^0 (or B⁰), e.g. for inclusive lepton decays

$$\chi_d = \frac{\Gamma(B^0 \rightarrow \ell^+ X \text{ (via } \bar{B}^0))}{\Gamma(B^0 \rightarrow \ell^+ X)} = \frac{\Gamma(\bar{B}^0 \rightarrow \ell^+ X \text{ (via } B^0))}{\Gamma(\bar{B}^0 \rightarrow \ell^+ X)}$$

Where experiments have measured the parameter $r = \chi/(1-\chi)$, we have converted to χ . Mixing violates the $\Delta B \neq 2$ rule.

Note that the measurement of χ at energies higher than the $\Upsilon(4S)$ have not separated χ_d from χ_s where the subscripts indicate B⁰($\bar{B}^0 d$) or B_s⁰(\bar{B}_s^0). They are listed in the B[±]/B_s⁰/B_s[±]/b-baryon ADMIXTURE section.

The experiments at $\Upsilon(4S)$ make an assumption about the B⁰- \bar{B}^0 fraction and about the ratio of the B[±] and B⁰ semileptonic branching ratios (usually that it equals one).

“OUR EVALUATION” is an average using rescaled values of the data listed below. The average and rescaling were performed by the Heavy Flavor Averaging Group (HFLAV) and are described at <https://hflav.web.cern.ch/>. The averaging/rescaling procedure takes into account correlations between the measurements, includes χ_d calculated from Δm_{B^0} and τ_{B^0} .

VALUE	CL%	DOCUMENT ID	TECN	COMMENT
0.1858 ± 0.0011		OUR EVALUATION		
0.182 ± 0.015		OUR AVERAGE		
0.198 ± 0.013 ± 0.014		1 BEHRENS	00B CLE2	e ⁺ e ⁻ → $\Upsilon(4S)$
0.16 ± 0.04 ± 0.04		2 ALBRECHT	94 ARG	e ⁺ e ⁻ → $\Upsilon(4S)$
0.149 ± 0.023 ± 0.022		3 BARTELT	93 CLE2	e ⁺ e ⁻ → $\Upsilon(4S)$
0.171 ± 0.048		4 ALBRECHT	92L ARG	e ⁺ e ⁻ → $\Upsilon(4S)$

• • • We do not use the following data for averages, fits, limits, etc. • • •

0.20 ± 0.13 ± 0.12	5 ALBRECHT	96D ARG	e ⁺ e ⁻ → $\Upsilon(4S)$
0.19 ± 0.07 ± 0.09	6 ALBRECHT	96D ARG	e ⁺ e ⁻ → $\Upsilon(4S)$
0.24 ± 0.12	7 ELSEN	90 JADE	e ⁺ e ⁻ 35–44 GeV
0.158 ^{+0.052} _{-0.059}	8 ARTUSO	89 CLEO	e ⁺ e ⁻ → $\Upsilon(4S)$
0.17 ± 0.05	9 ALBRECHT	87I ARG	e ⁺ e ⁻ → $\Upsilon(4S)$
< 0.19	90 BEAN	87B CLEO	e ⁺ e ⁻ → $\Upsilon(4S)$
< 0.27	90 10 AVERY	84 CLEO	e ⁺ e ⁻ → $\Upsilon(4S)$

- ¹ BEHRENS 00B uses high-momentum lepton tags and partially reconstructed \bar{B}^0 → D*⁺π⁻, ρ⁻ decays to determine the flavor of the B meson.
² ALBRECHT 94 reports r=0.194 ± 0.062 ± 0.054. We convert to χ for comparison. Uses tagged events (lepton + pion from D*⁺).
³ BARTELT 93 analysis performed using tagged events (lepton+pion from D*⁺). Using dilepton events they obtain 0.157 ± 0.016^{+0.033}_{-0.028}.
⁴ ALBRECHT 92L is a combined measurement employing several lepton-based techniques. It uses all previous ARGUS data in addition to new data and therefore supersedes ALBRECHT 87I. A value of r = 20.6 ± 7.0% is directly measured. The value can be used to measure x = $\Delta M/\Gamma$ = 0.72 ± 0.15 for the B_d meson. Assumes $f_{+/-}/f_0 = 1.0 \pm 0.05$ and uses $\tau_{B^{\pm}}/\tau_{B^0} = (0.95 \pm 0.14)(f_{+/-}/f_0)$.
⁵ Uses D*⁺K[±] correlations.
⁶ Uses (D*⁺ℓ⁻) K[±] correlations.
⁷ These experiments see a combination of B_s and B_d mesons.
⁸ ALBRECHT 87I is inclusive measurement with like-sign dileptons, with tagged B decays plus leptons, and one fully reconstructed event. Measures r=0.21 ± 0.08. We convert to χ for comparison. Superseded by ALBRECHT 92L.
⁹ BEAN 87B measured r < 0.24; we converted to χ .
¹⁰ Same-sign dilepton events. Limit assumes semileptonic BR for B⁺ and B⁰ equal. If B⁰/B[±] ratio < 0.58, no limit exists. The limit was corrected in BEAN 87B from r < 0.30 to r < 0.37. We converted this limit to χ .

 $\Delta m_{B^0} = m_{B_H^0} - m_{B_L^0}$

Δm_{B^0} is a measure of 2π times the B⁰- \bar{B}^0 oscillation frequency in time-dependent mixing experiments.

“OUR EVALUATION” is an average using rescaled values of the data listed below. The average and rescaling were performed by the Heavy Flavor Averaging Group (HFLAV) and are described at <https://hflav.web.cern.ch/>. The averaging/rescaling procedure takes into account correlations between the measurements and includes Δm_d calculated from χ_d measured at $\Upsilon(4S)$.

VALUE (10 ¹² s ⁻¹)	DOCUMENT ID	TECN	COMMENT
0.5065 ± 0.0019	OUR EVALUATION		
0.5050 ± 0.0021 ± 0.0010	1 AAIJ	16AV LHCB	pp at 7, 8 TeV
0.503 ± 0.011 ± 0.013	2 AAIJ	13CF LHCB	pp at 7 TeV
0.5156 ± 0.0051 ± 0.0033	3 AAIJ	13F LHCB	pp at 7 TeV
0.499 ± 0.032 ± 0.003	4 AAIJ	12I LHCB	pp at 7 TeV
0.506 ± 0.020 ± 0.016	5 ABZOV	06W D0	pp at 1.96 TeV
0.511 ± 0.007 ^{+0.007} _{-0.006}	6 AUBERT	06G BABR	e ⁺ e ⁻ → $\Upsilon(4S)$
0.511 ± 0.005 ± 0.006	7 ABE	05B BELL	e ⁺ e ⁻ → $\Upsilon(4S)$
0.531 ± 0.025 ± 0.007	8 ABDALLAH	03B DLPH	e ⁺ e ⁻ → Z
0.492 ± 0.018 ± 0.013	9 AUBERT	03C BABR	e ⁺ e ⁻ → $\Upsilon(4S)$
0.503 ± 0.008 ± 0.010	10 HASTINGS	03 BELL	e ⁺ e ⁻ → $\Upsilon(4S)$
0.509 ± 0.017 ± 0.020	11 ZHENG	03 BELL	e ⁺ e ⁻ → $\Upsilon(4S)$
0.516 ± 0.016 ± 0.010	12 AUBERT	02I BABR	e ⁺ e ⁻ → $\Upsilon(4S)$
0.493 ± 0.012 ± 0.009	13 AUBERT	02J BABR	e ⁺ e ⁻ → $\Upsilon(4S)$
0.497 ± 0.024 ± 0.025	14 ABBIENDI,G	00B OPAL	e ⁺ e ⁻ → Z
0.503 ± 0.064 ± 0.071	15 ABE	99K CDF	pp at 1.8 TeV
0.500 ± 0.052 ± 0.043	16 ABE	99Q CDF	pp at 1.8 TeV
0.516 ± 0.099 ^{+0.029} _{-0.035}	17 AFFOLDER	99C CDF	pp at 1.8 TeV
0.471 ± 0.078 ^{+0.033} _{-0.068}	18 ABE	98C CDF	pp at 1.8 TeV
0.458 ± 0.046 ± 0.032	19 ACCIARRI	98D L3	e ⁺ e ⁻ → Z
0.437 ± 0.043 ± 0.044	20 ACCIARRI	98D L3	e ⁺ e ⁻ → Z
0.472 ± 0.049 ± 0.053	21 ACCIARRI	98D L3	e ⁺ e ⁻ → Z
0.523 ± 0.072 ± 0.043	22 ABREU	97N DLPH	e ⁺ e ⁻ → Z
0.493 ± 0.042 ± 0.027	20 ABREU	97N DLPH	e ⁺ e ⁻ → Z
0.499 ± 0.053 ± 0.015	23 ABREU	97N DLPH	e ⁺ e ⁻ → Z
0.480 ± 0.040 ± 0.051	19 ABREU	97N DLPH	e ⁺ e ⁻ → Z
0.444 ± 0.029 ^{+0.020} _{-0.017}	20 ACKERSTAFF	97U OPAL	e ⁺ e ⁻ → Z
0.430 ± 0.043 ^{+0.028} _{-0.030}	19 ACKERSTAFF	97V OPAL	e ⁺ e ⁻ → Z
0.482 ± 0.044 ± 0.024	24 BUSKULIC	97D ALEP	e ⁺ e ⁻ → Z
0.404 ± 0.045 ± 0.027	20 BUSKULIC	97D ALEP	e ⁺ e ⁻ → Z
0.452 ± 0.039 ± 0.044	19 BUSKULIC	97D ALEP	e ⁺ e ⁻ → Z
0.539 ± 0.060 ± 0.024	25 ALEXANDER	96V OPAL	e ⁺ e ⁻ → Z
0.567 ± 0.089 ^{+0.029} _{-0.023}	26 ALEXANDER	96V OPAL	e ⁺ e ⁻ → Z
0.516 ± 0.016 ± 0.010	27 AUBERT	02N BABR	e ⁺ e ⁻ → $\Upsilon(4S)$
0.494 ± 0.012 ± 0.015	28 HARA	02 BELL	Repl. by ABE 05B
0.528 ± 0.017 ± 0.011	29 TOMURA	02 BELL	Repl. by ABE 05B
0.463 ± 0.008 ± 0.016	13 ABE	01D BELL	Repl. by HASTINGS 03
0.444 ± 0.028 ± 0.028	30 ACCIARRI	98D L3	e ⁺ e ⁻ → Z
0.497 ± 0.035	31 ABREU	97N DLPH	e ⁺ e ⁻ → Z

• • • We do not use the following data for averages, fits, limits, etc. • • •

Meson Particle Listings

B^0

VALUE	DOCUMENT ID	TECN	COMMENT
0.467 ± 0.022 +0.017 -0.015	32 ACKERSTAFF 97V	OPAL	$e^+e^- \rightarrow Z$
0.446 ± 0.032	33 BUSKULIC 97D	ALEP	$e^+e^- \rightarrow Z$
0.531 +0.050 -0.046 ± 0.078	34 ABREU 96Q	DLPH	Sup. by ABREU 97N
0.496 +0.055 -0.051 ± 0.043	19 ACCIARRI 96E	L3	Repl. by ACCIARRI 98D
0.548 ± 0.050 +0.023 -0.019	35 ALEXANDER 96V	OPAL	$e^+e^- \rightarrow Z$
0.496 ± 0.046	36 AKERS 95J	OPAL	Repl. by ACKERSTAFF 97V
0.462 +0.040 +0.052 -0.053 -0.035	19 AKERS 95J	OPAL	Repl. by ACKERSTAFF 97V
0.50 ± 0.12 ± 0.06	22 ABREU 94M	DLPH	Sup. by ABREU 97N
0.508 ± 0.075 ± 0.025	25 AKERS 94C	OPAL	Repl. by ALEXANDER 96V
0.57 ± 0.11 ± 0.02	26 AKERS 94H	OPAL	Repl. by ALEXANDER 96V
0.50 +0.07 +0.11 -0.06 -0.10	19 BUSKULIC 94B	ALEP	Sup. by BUSKULIC 97D
0.52 +0.10 +0.04 -0.11 -0.03	26 BUSKULIC 93K	ALEP	Sup. by BUSKULIC 97D

- Uses semileptonic decays of $B^0 \rightarrow D^- \mu^+ \nu_\mu X$ and $B^0 \rightarrow D^{(*)-} \mu^+ \nu_\mu X$, where the D mesons are reconstructed in $D^- \rightarrow K^+ \pi^- \pi^-$ and $D^{(*)-} \rightarrow \bar{D}^0 \pi^-$ with $\bar{D}^0 \rightarrow K^+ \pi^-$.
- Uses semileptonic decays of $B^0 \rightarrow D^- \mu^+ \nu_\mu X$ where the D^- mesons are reconstructed in $D^- \rightarrow K^+ K^- \pi^-$.
- Measured using $B^0 \rightarrow D^- \pi^+$ and $B^0 \rightarrow J/\psi K^*(892)^0$ decays.
- Measured using $B^0 \rightarrow D^- \pi^+$.
- Uses opposite-side flavor-tagging with $B \rightarrow D^{(*)} \mu \nu_\mu X$ events.
- Measured using a simultaneous fit of the B^0 lifetime and $\bar{B}^0 B^0$ oscillation frequency Δm_d in the partially reconstructed $B^0 \rightarrow D^{*-} \ell \nu$ decays.
- Measurement performed using a combined fit of CP -violation, mixing and lifetimes.
- Events with a high transverse momentum lepton were removed and an inclusively reconstructed vertex was required.
- AUBERT 03c uses a sample of approximately 14,000 exclusively reconstructed $B^0 \rightarrow D^*(2010)^- \ell \nu$ and simultaneously measures the lifetime and oscillation frequency.
- HASTINGS 03 measurement based on the time evolution of dilepton events. It also reports $f_+/f_0 = 1.01 \pm 0.03 \pm 0.09$ and CPT violation parameters in B^0 - \bar{B}^0 mixing.
- ZHENG 03 data analyzed using partially reconstructed $\bar{B}^0 \rightarrow D^{*-} \pi^+$ decay and a flavor tag based on the charge of the lepton from the accompanying B decay.
- Uses a tagged sample of fully-reconstructed neutral B decays at $\Upsilon(4S)$.
- Measured based on the time evolution of dilepton events in $\Upsilon(4S)$ decays.
- Data analyzed using partially reconstructed $\bar{B}^0 \rightarrow D^{*+} \ell^- \bar{\nu}$ decay and a combination of flavor tags from the rest of the event.
- Uses di-muon events.
- Uses jet-charge and lepton-flavor tagging.
- Uses $\ell^- D^{*+} \ell$ events.
- Uses π - B in the same side.
- Uses ℓ - ℓ .
- Uses ℓ - Q_{hem} .
- Uses ℓ - ℓ with impact parameters.
- Uses $D^{*\pm} Q_{\text{hem}}$.
- Uses $\pi_s^\pm \ell$ - Q_{hem} .
- Uses $D^{*\pm} \ell/Q_{\text{hem}}$.
- Uses $D^{*\pm} \ell$ - Q_{hem} .
- Uses $D^{*\pm} \ell$.
- AUBERT 02N result based on the same analysis and data sample reported in AUBERT 02I.
- Uses a tagged sample of B^0 decays reconstructed in the mode $B^0 \rightarrow D^* \ell \nu$.
- Uses a tagged sample of fully-reconstructed hadronic B^0 decays at $\Upsilon(4S)$.
- ACCIARRI 98D combines results from ℓ - ℓ , ℓ - Q_{hem} , and ℓ - ℓ with impact parameters.
- ABREU 97N combines results from $D^{*\pm} Q_{\text{hem}}$, ℓ - Q_{hem} , $\pi_s^\pm \ell$ - Q_{hem} , and $D^{*\pm} Q_{\text{hem}}$.
- ACKERSTAFF 97V combines results from ℓ - ℓ , ℓ - Q_{hem} , $D^{*-} \ell$, and $D^{*+} Q_{\text{hem}}$.
- BUSKULIC 97D combines results from $D^{*\pm} \ell/Q_{\text{hem}}$, ℓ - Q_{hem} , and ℓ - ℓ .
- ABREU 96Q analysis performed using lepton, kaon, and jet-charge tags.
- ALEXANDER 96V combines results from $D^{*\pm} \ell$ and $D^{*\pm} \ell$ - Q_{hem} .
- AKERS 95J combines results from charge measurement, $D^{*\pm} \ell$ - Q_{hem} and ℓ - ℓ .

$\chi_d = \Delta m_{B^0} / \Gamma_{B^0}$

"OUR EVALUATION" is an average using rescaled values of the data listed below. The average and rescaling were performed by the Heavy Flavor Averaging Group (HFLAV) and are described at <https://hflav.web.cern.ch/>. The averaging/rescaling procedure takes into account correlations between the measurements and includes Δm_d calculated from χ_d measured at $\Upsilon(4S)$.

VALUE	DOCUMENT ID
0.769 ± 0.004 OUR EVALUATION	

$\text{Re}(\lambda_{CP} / |\lambda_{CP}|) \text{Re}(z)$

The λ_{CP} characterizes B^0 and \bar{B}^0 decays to states of charmonium plus K_S^0 . Parameter z is used to describe CPT violation in mixing, see the review on "CP Violation" in the reviews section.

VALUE	DOCUMENT ID	TECN	COMMENT
0.047 ± 0.022 ± 0.003	1 LEES	16E	BABR $e^+e^- \rightarrow \Upsilon(4S)$

- • • We do not use the following data for averages, fits, limits, etc. • • •
- | VALUE | DOCUMENT ID | TECN | COMMENT |
|-----------------------|-------------|------|------------------------|
| 0.014 ± 0.035 ± 0.034 | 2 AUBERT,B | 04C | BABR Repl. by LEES 16E |
- The first uncertainty is the uncertainty from $\text{Re}(z)$ and the second uncertainty is from $\text{Re}(\lambda/|\lambda|)$.
 - Corresponds to 90% confidence range $[-0.072, 0.101]$.

$\Delta\Gamma \text{Re}(z)$

VALUE (ps ⁻¹)	DOCUMENT ID	TECN	COMMENT
-0.0071 ± 0.0039 ± 0.0020	AUBERT	06T	BABR $e^+e^- \rightarrow \Upsilon(4S)$

$\text{Re}(z)$

VALUE (units 10 ⁻²)	DOCUMENT ID	TECN	COMMENT
-4 ± 4 OUR AVERAGE	Error includes scale factor of 1.4.		

- | | | | |
|------------------|-----------|-----|--|
| -6.5 ± 2.8 ± 1.4 | 1 LEES | 16E | BABR $e^+e^- \rightarrow \Upsilon(4S)$ |
| 1.9 ± 3.7 ± 3.3 | 2 HIGUCHI | 12 | BELL $e^+e^- \rightarrow \Upsilon(4S)$ |
- • • We do not use the following data for averages, fits, limits, etc. • • •
- | | | | |
|------------|------------|----|--------------------------|
| 0 ± 12 ± 1 | 3 HASTINGS | 03 | BELL Repl. by HIGUCHI 12 |
|------------|------------|----|--------------------------|
- Measurement uses decays $B^0/\bar{B}^0 \rightarrow c\bar{c}K_S^0/K_L^0$.
 - Measured using $B^0 \rightarrow J/\psi K_S^0, J/\psi K_L^0, D^- \pi^+, D^{*-} \pi^+, D^{*-} \rho^+$, and $D^{*-} \ell^+ \nu$ decays.
 - Measured using inclusive dilepton events from B^0 decay.

$\text{Im}(z)$

VALUE (units 10 ⁻²)	DOCUMENT ID	TECN	COMMENT
-0.8 ± 0.4 OUR AVERAGE			

- | | | | |
|---------------------|-----------|-----|--|
| 1.0 ± 3.0 ± 1.3 | 1 LEES | 16E | BABR $e^+e^- \rightarrow \Upsilon(4S)$ |
| -0.57 ± 0.33 ± 0.33 | 2 HIGUCHI | 12 | BELL $e^+e^- \rightarrow \Upsilon(4S)$ |
| -1.39 ± 0.73 ± 0.32 | 3 AUBERT | 06T | BABR $e^+e^- \rightarrow \Upsilon(4S)$ |
- • • We do not use the following data for averages, fits, limits, etc. • • •
- | | | | |
|-----------------|------------|-----|--------------------------|
| 3.8 ± 2.9 ± 2.5 | 4 AUBERT,B | 04C | BABR Repl. by AUBERT 06T |
| -3 ± 1 ± 3 | 5 HASTINGS | 03 | BELL Repl. by HIGUCHI 12 |
- Measurement uses decays $B^0/\bar{B}^0 \rightarrow c\bar{c}K_S^0/K_L^0$.
 - Measured using $B^0 \rightarrow J/\psi K_S^0, J/\psi K_L^0, D^- \pi^+, D^{*-} \pi^+, D^{*-} \rho^+$, and $D^{*-} \ell^+ \nu$ decays.
 - Measurement uses $B^0/\bar{B}^0 \rightarrow \ell^+ X/\ell^- X$ decays. Assuming $\Delta\Gamma = 0$, the result becomes $\text{Im}(z) = (-0.37 \pm 0.54) \times 10^{-2}$.
 - Corresponds to 90% confidence range $[-0.028, 0.104]$.
 - Measured using inclusive dilepton events from B^0 decay.

CP VIOLATION PARAMETERS

$\text{Re}(\epsilon_{B^0})/(1+|\epsilon_{B^0}|^2)$

CP impurity in B_d^0 system. It is obtained from either $a_{\ell\ell}$, the charge asymmetry in like-sign dilepton events or a_{CP} , the time-dependent asymmetry of inclusive B^0 and \bar{B}^0 decays.

"OUR EVALUATION" is an average obtained by the Heavy Flavor Averaging Group (HFLAV) and described at <https://hflav.web.cern.ch/>. It is the result of a fit to B_d and B_s CP asymmetries, which includes the B_d measurements listed below and the B_s measurements listed in the B_s section, taking into account correlations between those measurements.

VALUE (units 10 ⁻³)	DOCUMENT ID	TECN	COMMENT
-0.5 ± 0.4 OUR EVALUATION			
-0.1 ± 0.4 OUR AVERAGE			

- | | | | |
|----------------------------|----------|------|--|
| -0.05 ± 0.48 ± 0.75 | 1 AAIJ | 15F | LHCb pp at 7, 8 TeV |
| -0.975 ± 0.875 ± 0.475 | 2 LEES | 15A | BABR $e^+e^- \rightarrow \Upsilon(4S)$ |
| 1.55 ± 1.05 | 3 ABAZOV | 14 | D0 $p\bar{p}$ at 1.96 TeV |
| 0.15 ± 0.42 +0.94
-0.81 | 4 LEES | 13N | BABR $e^+e^- \rightarrow \Upsilon(4S)$ |
| -1.7 ± 1.1 ± 0.4 | 5 ABAZOV | 12Ac | D0 $p\bar{p}$ at 1.96 TeV |
| 0.4 ± 1.3 ± 0.9 | 6 AUBERT | 06T | BABR $e^+e^- \rightarrow \Upsilon(4S)$ |
| -0.3 ± 2.0 ± 2.1 | 7 NAKANO | 06 | BELL $e^+e^- \rightarrow \Upsilon(4S)$ |
| 3.5 ± 10.3 ± 1.5 | 8 JAFFE | 01 | CLE2 $e^+e^- \rightarrow \Upsilon(4S)$ |
- • • We do not use the following data for averages, fits, limits, etc. • • •
- | | | | |
|-------------------|---------------|-----|--|
| -0.3 ± 1.3 | 9 ABAZOV | 11U | D0 Repl. by ABAZOV 14 |
| -2.3 ± 1.1 ± 0.8 | 10 ABAZOV | 06S | D0 Repl. by ABAZOV 11U |
| -14.7 ± 6.7 ± 5.7 | 11 AUBERT,B | 04C | BABR Repl. by AUBERT 06T |
| 1.2 ± 2.9 ± 3.6 | 2 AUBERT | 02K | BABR Repl. by LEES 15A |
| -3.2 ± 6.5 | 12 BARATE | 01D | ALEP $e^+e^- \rightarrow Z$ |
| 4 ± 18 ± 3 | 13 BEHRENS | 00B | CLE2 Repl. by JAFFE 01 |
| 1.2 ± 13.8 ± 3.2 | 14 ABBIENDI | 99J | OPAL $e^+e^- \rightarrow Z$ |
| 2 ± 7 ± 3 | 15 ACKERSTAFF | 97U | OPAL $e^+e^- \rightarrow Z$ |
| < 45 | 16 BARTELT | 93 | CLE2 $e^+e^- \rightarrow \Upsilon(4S)$ |

- AAIJ 15F uses semileptonic B^0 decays in the inclusive final states $D^- \mu^+$ and $D^{*-} \mu^+$, where the D^- meson decays into the $K^+ \pi^- \pi^-$ final state, and the D^{*-} meson into the $\bar{D}^0 (\rightarrow K^+ \pi^-) \pi^-$ final state. Reports $A_{SL}^d = (-0.02 \pm 0.19 \pm 0.30)\%$, which equals to $4\text{Re}(\epsilon_{B^0})/(1+|\epsilon_{B^0}|^2)$.
- Uses the charge asymmetry in like-sign dilepton events. LEES 15A reports $A_{SL}^d = (-3.9 \pm 3.5 \pm 1.9) \times 10^{-3}$.
- ABAZOV 14 uses the dimuon charge asymmetry with different impact parameters from which it reports $A_{SL}^d = (-0.62 \pm 0.42) \times 10^{-2}$.
- Uses $B^0 \rightarrow D^{*-} X \ell^+ \nu_\ell$ and a kaon-tagged sample which yields measurement of $A_{SL}^d = (0.06 \pm 0.17 +0.38 -0.32)\%$, corresponding to $\Delta_{CP} = 1-|q/p| = (0.29 \pm 0.84 +1.88 -1.61) \times 10^{-3}$.
- ABAZOV 12Ac uses $B^0 \rightarrow D^- \mu^+ X$ and $B^0 \rightarrow D^*(2010)^- \mu^+ X$ decays without initial state flavor tagging which yields measurement of $A_{SL}^d = (6.8 \pm 4.5 \pm 1.4) \times 10^{-3}$.
- AUBERT 06T reports $|q/p|-1 = (-0.8 \pm 2.7 \pm 1.9) \times 10^{-3}$. We convert to $(1-|q/p|^2)/4$.

- 7 Uses the charge asymmetry in like-sign dilepton events and reports |q/p| = 1.0005 ± 0.0040 ± 0.0043.
8 JAFFE 01 finds a_ell ell = 0.013 ± 0.050 ± 0.005 and combines with the previous BEHRENS 00b independent measurement.
9 ABAZOV 11u uses the dimuon charge asymmetry with different impact parameters from which it reports A_SL^d = (-1.2 ± 5.2) x 10^-3.
10 Uses the dimuon charge asymmetry.
11 AUBERT 04c reports |q/p| = 1.029 ± 0.013 ± 0.011 and we converted it to (1 - |q/p|^2)/4.
12 BARATE 01d measured by investigating time-dependent asymmetries in semileptonic and fully inclusive B_d^0 decays.
13 BEHRENS 00b uses high-momentum lepton tags and partially reconstructed B^0 -> D^*+ pi-, rho- decays to determine the flavor of the B meson.
14 Data analyzed using the time-dependent asymmetry of inclusive B^0 decay. The production flavor of B^0 mesons is determined using both the jet charge and the charge of secondary vertex in the opposite hemisphere.
15 ACKERSTAFF 97u assumes CPT and is based on measuring the charge asymmetry in a sample of B^0 decays defined by lepton and Q_hem tags. If CPT is not invoked, Re(epsilon_B) = -0.006 ± 0.010 ± 0.006 is found. The indirect CPT violation parameter is determined to Im(delta B) = -0.020 ± 0.016 ± 0.006.
16 BARTELT 93 finds a_ell ell = 0.031 ± 0.096 ± 0.032 which corresponds to |a_ell ell| < 0.18, which yields the above |Re(epsilon_B0)/(1+|epsilon_B0|^2)|.

A_T/CP

A_T/CP is defined as

P(B0 -> B0) - P(B0 -> B0_bar) / (P(B0 -> B0) + P(B0 -> B0_bar))

the CPT invariant asymmetry between the oscillation probabilities P(B0 -> B0) and P(B0 -> B0_bar).

Table with columns: VALUE, DOCUMENT ID, TECN, COMMENT. Row 1: 0.005 ± 0.012 ± 0.014, 1 AUBERT, 02k BABR, e+ e- -> gamma(4S)

ACP(B0 -> D*(2010)+ D-)

ACP is defined as

(B(B0 -> D*) - B(B0 -> f)) / (B(B0 -> D*) + B(B0 -> f))

the CP-violation charge asymmetry of exclusive B0 and B0_bar decay.

Table with columns: VALUE, DOCUMENT ID, TECN, COMMENT. Rows include: 0.013 ± 0.014 OUR AVERAGE, 0.008 ± 0.014 ± 0.006, 0.06 ± 0.05 ± 0.02, 0.008 ± 0.048 ± 0.013, 0.07 ± 0.08 ± 0.04, -0.12 ± 0.06 ± 0.02, -0.03 ± 0.10 ± 0.02, -0.03 ± 0.11 ± 0.05

ACP(B0 -> [K+ K-]D K*(892)0)

Table with columns: VALUE, DOCUMENT ID, TECN, COMMENT. Row 1: -0.05 ± 0.10 ± 0.01, AAIJ, 19N LHCB, pp at 7, 8, 13 TeV

ACP(B0 -> [K+ pi-]D K*(892)0)

Table with columns: VALUE, DOCUMENT ID, TECN, COMMENT. Row 1: 0.047 ± 0.027 ± 0.010, AAIJ, 19N LHCB, pp at 7, 8, 13 TeV

ACP(B0 -> [K+ pi- pi+ pi-]D K*(892)0)

Table with columns: VALUE, DOCUMENT ID, TECN, COMMENT. Row 1: 0.037 ± 0.032 ± 0.010, AAIJ, 19N LHCB, pp at 7, 8, 13 TeV

ACP(B0 -> [K- pi+]D K*(892)0)

Table with columns: VALUE, DOCUMENT ID, TECN, COMMENT. Row 1: 0.19 ± 0.19 ± 0.01, AAIJ, 19N LHCB, pp at 7, 8, 13 TeV

ACP(B0 -> [K- pi+ pi+ pi-]D K*(892)0)

Table with columns: VALUE, DOCUMENT ID, TECN, COMMENT. Row 1: -0.01 ± 0.24 ± 0.01, AAIJ, 19N LHCB, pp at 7, 8, 13 TeV

R_d^+ = Gamma(B0 -> [pi+ K-]D K*0) / Gamma(B0 -> [pi- K+]D K*0)

Table with columns: VALUE, DOCUMENT ID, TECN, COMMENT. Row 1: 0.064 ± 0.021 ± 0.002, AAIJ, 19N LHCB, pp at 7, 8, 13 TeV

R_d^- = Gamma(B0 -> [pi- K+]D K*0) / Gamma(B0 -> [pi+ K-]D K*0)

Table with columns: VALUE, DOCUMENT ID, TECN, COMMENT. Row 1: 0.095 ± 0.021 ± 0.003, AAIJ, 19N LHCB, pp at 7, 8, 13 TeV

ACP(B0 -> [pi+ pi-]D K*(892)0)

Table with columns: VALUE, DOCUMENT ID, TECN, COMMENT. Row 1: -0.18 ± 0.14 ± 0.01, AAIJ, 19N LHCB, pp at 7, 8, 13 TeV

ACP(B0 -> [pi+ pi- pi+ pi-]D K*(892)0)

Table with columns: VALUE, DOCUMENT ID, TECN, COMMENT. Row 1: -0.03 ± 0.15 ± 0.01, AAIJ, 19N LHCB, pp at 7, 8, 13 TeV

R_d^+ = Gamma(B0 -> [pi+ K- pi+ pi-]D K*0) / Gamma(B0 -> [pi- K+ pi+ pi-]D K*0)

Table with columns: VALUE, DOCUMENT ID, TECN, COMMENT. Row 1: 0.074 ± 0.026 ± 0.002, AAIJ, 19N LHCB, pp at 7, 8, 13 TeV

R_d^- = Gamma(B0 -> [pi- K+ pi+ pi-]D K*0) / Gamma(B0 -> [pi+ K- pi+ pi-]D K*0)

Table with columns: VALUE, DOCUMENT ID, TECN, COMMENT. Row 1: 0.072 ± 0.025 ± 0.003, AAIJ, 19N LHCB, pp at 7, 8, 13 TeV

ACP(B0 -> K+ pi-)

Table with columns: VALUE, DOCUMENT ID, TECN, COMMENT. Row 1: -0.0834 ± 0.0032 OUR AVERAGE, -0.0824 ± 0.0033 ± 0.0033, -0.084 ± 0.004 ± 0.003, -0.083 ± 0.013 ± 0.004, -0.069 ± 0.014 ± 0.007, -0.107 ± 0.016 ± 0.006 ± 0.004, -0.04 ± 0.16, -0.080 ± 0.007 ± 0.003, -0.088 ± 0.011 ± 0.008, -0.086 ± 0.023 ± 0.009, -0.094 ± 0.018 ± 0.008, -0.107 ± 0.018 ± 0.007 ± 0.004, -0.013 ± 0.078 ± 0.012, -0.088 ± 0.035 ± 0.013, -0.133 ± 0.030 ± 0.009, -0.101 ± 0.025 ± 0.005, -0.07 ± 0.08 ± 0.02, -0.102 ± 0.050 ± 0.016, -0.06 ± 0.09 ± 0.01 ± 0.02, 0.044 ± 0.186 ± 0.018 ± 0.167 ± 0.021, -0.19 ± 0.10 ± 0.03

- 1 Corresponds to 90% confidence range -0.30 < ACP < 0.22.
2 Corresponds to a 90% CL interval of -0.15 < ACP < -0.03.
3 Based on a total signal yield of N(K- pi+) + N(K+ pi-) = 1606 ± 51 events.
4 CHAO 04b reports significance of 3.9 standard deviation for deviation of ACP from zero.
5 Corresponds to 90% confidence range -0.21 < ACP < 0.07.
6 Corresponds to 90% confidence range -0.188 < ACP < -0.016.
7 Corresponds to 90% confidence range -0.21 < ACP < +0.09.
8 Corresponds to 90% confidence range -0.25 < ACP < 0.37.
9 Corresponds to 90% confidence range -0.35 < ACP < -0.03.

ACP(B0 -> eta' K*(892)0)

Table with columns: VALUE, DOCUMENT ID, TECN, COMMENT. Row 1: -0.07 ± 0.18 OUR AVERAGE, -0.22 ± 0.29 ± 0.07, 0.02 ± 0.23 ± 0.02, 0.08 ± 0.25 ± 0.02

1 Reports ACP with the opposite sign convention.

ACP(B0 -> eta' K0*(1430)0)

Table with columns: VALUE, DOCUMENT ID, TECN, COMMENT. Row 1: -0.19 ± 0.17 ± 0.02, DEL-AMO-SA..10A, BABR, e+ e- -> gamma(4S)

ACP(B0 -> eta' K2*(1430)0)

Table with columns: VALUE, DOCUMENT ID, TECN, COMMENT. Row 1: 0.14 ± 0.18 ± 0.02, DEL-AMO-SA..10A, BABR, e+ e- -> gamma(4S)

ACP(B0 -> eta K*(892)0)

Table with columns: VALUE, DOCUMENT ID, TECN, COMMENT. Row 1: 0.19 ± 0.05 OUR AVERAGE, 0.17 ± 0.08 ± 0.01, 0.21 ± 0.06 ± 0.02, 0.02 ± 0.11 ± 0.02

Meson Particle Listings

 B^0 $A_{CP}(B^0 \rightarrow \eta K_0^*(1430)^0)$

VALUE	DOCUMENT ID	TECN	COMMENT
$0.06 \pm 0.13 \pm 0.02$	AUBERT,B	06H	BABR $e^+e^- \rightarrow \Upsilon(4S)$

 $A_{CP}(B^0 \rightarrow \eta K_2^*(1430)^0)$

VALUE	DOCUMENT ID	TECN	COMMENT
$-0.07 \pm 0.19 \pm 0.02$	AUBERT,B	06H	BABR $e^+e^- \rightarrow \Upsilon(4S)$

 $A_{CP}(B^0 \rightarrow b_1 K^+)$

VALUE	DOCUMENT ID	TECN	COMMENT
$-0.07 \pm 0.12 \pm 0.02$	AUBERT	07B1	BABR $e^+e^- \rightarrow \Upsilon(4S)$

 $A_{CP}(B^0 \rightarrow \omega K^*0)$

VALUE	DOCUMENT ID	TECN	COMMENT
$0.45 \pm 0.25 \pm 0.02$	AUBERT	09H	BABR $e^+e^- \rightarrow \Upsilon(4S)$

 $A_{CP}(B^0 \rightarrow \omega(K\pi)_0^*0)$

VALUE	DOCUMENT ID	TECN	COMMENT
$-0.07 \pm 0.09 \pm 0.02$	AUBERT	09H	BABR $e^+e^- \rightarrow \Upsilon(4S)$

 $A_{CP}(B^0 \rightarrow \omega K_2^*(1430)^0)$

VALUE	DOCUMENT ID	TECN	COMMENT
$-0.37 \pm 0.17 \pm 0.02$	AUBERT	09H	BABR $e^+e^- \rightarrow \Upsilon(4S)$

 $A_{CP}(B^0 \rightarrow K^+\pi^-\pi^0)$

VALUE (units 10^{-2})	DOCUMENT ID	TECN	COMMENT
0 ± 6 OUR AVERAGE			

$-3.0^{+4.5}_{-5.1} \pm 5.5$	¹ AUBERT	08AQ	BABR $e^+e^- \rightarrow \Upsilon(4S)$
$7 \pm 11 \pm 1$	² CHANG	04	BELL $e^+e^- \rightarrow \Upsilon(4S)$

- ¹ Uses Dalitz plot analysis of $B^0 \rightarrow K^+\pi^-\pi^0$ decays.
² Corresponds to 90% confidence range $-0.12 < A_{CP} < 0.26$.

 $A_{CP}(B^0 \rightarrow \rho^- K^+)$

VALUE	DOCUMENT ID	TECN	COMMENT
0.20 ± 0.11 OUR AVERAGE			

$0.20 \pm 0.09 \pm 0.08$	¹ LEES	11	BABR $e^+e^- \rightarrow \Upsilon(4S)$
$0.22^{+0.22}_{-0.23} \pm 0.06$	² CHANG	04	BELL $e^+e^- \rightarrow \Upsilon(4S)$

- • • We do not use the following data for averages, fits, limits, etc. • • •

$0.11^{+0.14}_{-0.15} \pm 0.07$	¹ AUBERT	08AQ	BABR Repl. by LEES 11
$-0.28 \pm 0.17 \pm 0.08$	³ AUBERT	03T	BABR Repl. by AUBERT 08AQ

- ¹ Uses Dalitz plot analysis of $B^0 \rightarrow K^+\pi^-\pi^0$ decays.
² Corresponds to 90% confidence range $-0.18 < A_{CP} < 0.64$.
³ The result reported corresponds to $-A_{CP}$.

 $A_{CP}(B^0 \rightarrow \rho(1450)^- K^+)$

VALUE	DOCUMENT ID	TECN	COMMENT
$-0.10 \pm 0.32 \pm 0.09$	¹ LEES	11	BABR $e^+e^- \rightarrow \Upsilon(4S)$

- ¹ Uses Dalitz plot analysis of $B^0 \rightarrow K^+\pi^-\pi^0$ decays.

 $A_{CP}(B^0 \rightarrow \rho(1700)^- K^+)$

VALUE	DOCUMENT ID	TECN	COMMENT
$-0.36 \pm 0.57 \pm 0.23$	¹ LEES	11	BABR $e^+e^- \rightarrow \Upsilon(4S)$

- ¹ Uses Dalitz plot analysis of $B^0 \rightarrow K^+\pi^-\pi^0$ decays.

 $A_{CP}(B^0 \rightarrow K^+\pi^-\pi^0 \text{ nonresonant})$

VALUE	DOCUMENT ID	TECN	COMMENT
$0.10 \pm 0.16 \pm 0.08$	¹ LEES	11	BABR $e^+e^- \rightarrow \Upsilon(4S)$

- • • We do not use the following data for averages, fits, limits, etc. • • •

$0.23^{+0.19}_{-0.27} \pm 0.11$	¹ AUBERT	08AQ	BABR Repl. by LEES 11
---------------------------------	---------------------	------	-----------------------

- ¹ Uses Dalitz plot analysis of $B^0 \rightarrow K^+\pi^-\pi^0$ decays. The quoted value is only for the flat part of the non-resonant component.

 $A_{CP}(B^0 \rightarrow K^0\pi^+\pi^-)$

VALUE	DOCUMENT ID	TECN	COMMENT
$-0.01 \pm 0.05 \pm 0.01$	¹ AUBERT	09AU	BABR $e^+e^- \rightarrow \Upsilon(4S)$

- ¹ Uses Dalitz plot analysis of $B^0 \rightarrow K^0\pi^+\pi^-$ decays and the first of two equivalent solutions is used.

 $A_{CP}(B^0 \rightarrow K^*(892)^+\pi^-)$

VALUE	DOCUMENT ID	TECN	COMMENT
-0.27 ± 0.04 OUR AVERAGE			

$-0.308 \pm 0.060 \pm 0.016$	¹ AAIJ	18F	LHCB pp at 7, 8 TeV
$-0.29 \pm 0.11 \pm 0.02$	² LEES	11	BABR $e^+e^- \rightarrow \Upsilon(4S)$
$-0.21 \pm 0.10 \pm 0.02$	^{3,4} AUBERT	09AU	BABR $e^+e^- \rightarrow \Upsilon(4S)$
$-0.21 \pm 0.11 \pm 0.07$	⁵ DALSENSO	09	BELL $e^+e^- \rightarrow \Upsilon(4S)$
$0.26^{+0.33}_{-0.34} \pm 0.10$	⁶ EISENSTEIN	03	CLE2 $e^+e^- \rightarrow \Upsilon(4S)$

- • • We do not use the following data for averages, fits, limits, etc. • • •

$-0.19^{+0.20}_{-0.15} \pm 0.04$	² AUBERT	08AQ	BABR Repl. by LEES 11
$-0.11 \pm 0.14 \pm 0.05$	³ AUBERT	06I	BABR Repl. by AUBERT 09AU
$0.23 \pm 0.18^{+0.09}_{-0.06}$	AUBERT,B	04O	BABR Repl. by AUBERT 06I

- ¹ Uses Dalitz plot analysis of the $B^0 \rightarrow K_S^0\pi^+\pi^-$ final state decays.

- ² Uses Dalitz plot analysis of $B^0 \rightarrow K^+\pi^-\pi^0$ decays.

- ³ Uses Dalitz plot analysis of $B^0 \rightarrow K^0\pi^+\pi^-$ decays.

- ⁴ The first of two equivalent solutions is used.

- ⁵ Uses Dalitz plot analysis of $B^0 \rightarrow K^0\pi^+\pi^-$ decays and the first of two consistent solutions that may be preferred.

- ⁶ Corresponds to 90% confidence range $-0.31 < A_{CP} < 0.78$.

 $A_{CP}(B^0 \rightarrow (K\pi)_0^{*+}\pi^-)$

VALUE	DOCUMENT ID	TECN	COMMENT
0.02 ± 0.04 OUR AVERAGE			

$-0.032 \pm 0.047 \pm 0.031$	¹ AAIJ	18F	LHCB pp at 7, 8 TeV
$0.07 \pm 0.14 \pm 0.01$	² LEES	11	BABR $e^+e^- \rightarrow \Upsilon(4S)$
$0.09 \pm 0.07 \pm 0.03$	³ AUBERT	09AU	BABR $e^+e^- \rightarrow \Upsilon(4S)$

- • • We do not use the following data for averages, fits, limits, etc. • • •

$0.17^{+0.11}_{-0.16} \pm 0.22$	² AUBERT	08AQ	BABR Repl. by LEES 11
---------------------------------	---------------------	------	-----------------------

- ¹ Uses Dalitz plot analysis of the $B^0 \rightarrow K_S^0\pi^+\pi^-$ final states decays.

- ² Uses Dalitz plot analysis of $B^0 \rightarrow K^+\pi^-\pi^0$ decays.

- ³ Uses Dalitz plot analysis of $B^0 \rightarrow K^0\pi^+\pi^-$ decays and the first of two equivalent solutions is used.

 $A_{CP}(B^0 \rightarrow K_2^*(1430)^+\pi^-)$

VALUE	DOCUMENT ID	TECN	COMMENT
$-0.29 \pm 0.22 \pm 0.09$	¹ AAIJ	18F	LHCB pp at 7, 8 TeV

- ¹ Uses Dalitz plot analysis of the $B^0 \rightarrow K_S^0\pi^+\pi^-$ final state decays.

 $A_{CP}(B^0 \rightarrow K^*(1680)^+\pi^-)$

VALUE	DOCUMENT ID	TECN	COMMENT
$-0.07 \pm 0.13 \pm 0.04$	¹ AAIJ	18F	LHCB pp at 7, 8 TeV

- ¹ Uses Dalitz plot analysis of the $B^0 \rightarrow K_S^0\pi^+\pi^-$ final state decays.

 $A_{CP}(B^0 \rightarrow f_0(980)K_S^0)$

VALUE	DOCUMENT ID	TECN	COMMENT
$0.28 \pm 0.27 \pm 0.15$	¹ AAIJ	18F	LHCB pp at 7, 8 TeV

- ¹ Uses Dalitz plot analysis of the $B^0 \rightarrow K_S^0\pi^+\pi^-$ final state decays.

 $A_{CP}(B^0 \rightarrow (K\pi)_0^{*0}\pi^0)$

VALUE	DOCUMENT ID	TECN	COMMENT
$-0.15 \pm 0.10 \pm 0.04$	¹ LEES	11	BABR $e^+e^- \rightarrow \Upsilon(4S)$

- • • We do not use the following data for averages, fits, limits, etc. • • •

$-0.22 \pm 0.12^{+0.30}_{-0.29}$	¹ AUBERT	08AQ	BABR Repl. by LEES 11
----------------------------------	---------------------	------	-----------------------

- ¹ Uses Dalitz plot analysis of $B^0 \rightarrow K^+\pi^-\pi^0$ decays.

 $A_{CP}(B^0 \rightarrow K^*0\pi^0)$

VALUE	DOCUMENT ID	TECN	COMMENT
$-0.15 \pm 0.12 \pm 0.04$	¹ LEES	11	BABR $e^+e^- \rightarrow \Upsilon(4S)$

- • • We do not use the following data for averages, fits, limits, etc. • • •

$-0.09^{+0.21}_{-0.24} \pm 0.09$	¹ AUBERT	08AQ	BABR Repl. by LEES 11
----------------------------------	---------------------	------	-----------------------

- ¹ Uses Dalitz plot analysis of $B^0 \rightarrow K^+\pi^-\pi^0$ decays.

 $A_{CP}(B^0 \rightarrow K^*(892)^0\pi^+\pi^-)$

VALUE	DOCUMENT ID	TECN	COMMENT
$0.07 \pm 0.04 \pm 0.03$	AUBERT	07As	BABR $e^+e^- \rightarrow \Upsilon(4S)$

 $A_{CP}(B^0 \rightarrow K^*(892)^0\rho^0)$

VALUE	DOCUMENT ID	TECN	COMMENT
$-0.06 \pm 0.09 \pm 0.02$	LEES	12K	BABR $e^+e^- \rightarrow \Upsilon(4S)$

- • • We do not use the following data for averages, fits, limits, etc. • • •

$0.09 \pm 0.19 \pm 0.02$	AUBERT,B	06G	BABR Repl. by LEES 12K
--------------------------	----------	-----	------------------------

 $A_{CP}(B^0 \rightarrow K^*0f_0(980))$

VALUE	DOCUMENT ID	TECN	COMMENT
$0.07 \pm 0.10 \pm 0.02$	LEES	12K	BABR $e^+e^- \rightarrow \Upsilon(4S)$

- • • We do not use the following data for averages, fits, limits, etc. • • •

$-0.17 \pm 0.28 \pm 0.02$	AUBERT,B	06G	BABR Repl. by LEES 12K
---------------------------	----------	-----	------------------------

 $A_{CP}(B^0 \rightarrow K^{*+}\rho^-)$

VALUE	DOCUMENT ID	TECN	COMMENT
$0.21 \pm 0.15 \pm 0.02$	LEES	12K	BABR $e^+e^- \rightarrow \Upsilon(4S)$

$A_{CP}(B^0 \rightarrow K^*(892)^0 K^+ K^-)$

VALUE	DOCUMENT ID	TECN	COMMENT
$0.01 \pm 0.05 \pm 0.02$	AUBERT	07As	BABR $e^+ e^- \rightarrow \Upsilon(4S)$

 $A_{CP}(B^0 \rightarrow a_1^- K^+)$

VALUE	DOCUMENT ID	TECN	COMMENT
$-0.16 \pm 0.12 \pm 0.01$	AUBERT	08F	BABR $e^+ e^- \rightarrow \Upsilon(4S)$

 $A_{CP}(B^0 \rightarrow K^0 K^0)$

VALUE	DOCUMENT ID	TECN	COMMENT
$-0.58^{+0.73}_{-0.66} \pm 0.04$	LIN	07	BELL $e^+ e^- \rightarrow \Upsilon(4S)$

 $A_{CP}(B^0 \rightarrow K^*(892)^0 \phi)$

VALUE	DOCUMENT ID	TECN	COMMENT
0.00 ± 0.04 OUR AVERAGE			
$-0.007 \pm 0.048 \pm 0.021$	PRIM	13	BELL $e^+ e^- \rightarrow \Upsilon(4S)$
$0.01 \pm 0.06 \pm 0.03$	AUBERT	08Bg	BABR $e^+ e^- \rightarrow \Upsilon(4S)$
••• We do not use the following data for averages, fits, limits, etc. •••			
$-0.03 \pm 0.07 \pm 0.03$	AUBERT	07D	BABR Repl. by AUBERT 08Bg
$0.02 \pm 0.09 \pm 0.02$	1 CHEN	05A	BELL Repl. by PRIM 13
$-0.01 \pm 0.09 \pm 0.02$	AUBERT,B	04W	BABR Repl. by AUBERT 07D
$0.04 \pm 0.12 \pm 0.02$	AUBERT	03V	BABR Repl. by AUBERT 04W
$0.07 \pm 0.15 \pm 0.05$	2 CHEN	03B	BELL Repl. by CHEN 05A
$0.00 \pm 0.27 \pm 0.03$	3 AUBERT	02E	BABR Repl. by AUBERT 03V

¹ Corresponds to 90% confidence range $-0.14 < A_{CP} < 0.17$.

² Corresponds to 90% confidence range $-0.18 < A_{CP} < 0.33$.

³ Corresponds to 90% confidence range $-0.44 < A_{CP} < 0.44$.

 $A_{CP}(B^0 \rightarrow K^*(892)^0 K^- \pi^+)$

VALUE	DOCUMENT ID	TECN	COMMENT
$0.22 \pm 0.33 \pm 0.20$	AUBERT	07As	BABR $e^+ e^- \rightarrow \Upsilon(4S)$

 $A_{CP}(B^0 \rightarrow \phi(K\pi)_0^0)$

VALUE	DOCUMENT ID	TECN	COMMENT
0.12 ± 0.08 OUR AVERAGE			
$0.093 \pm 0.094 \pm 0.017$	PRIM	13	BELL $e^+ e^- \rightarrow \Upsilon(4S)$
$0.20 \pm 0.14 \pm 0.06$	AUBERT	08Bg	BABR $e^+ e^- \rightarrow \Upsilon(4S)$
••• We do not use the following data for averages, fits, limits, etc. •••			
$0.17 \pm 0.15 \pm 0.03$	AUBERT	07D	BABR Repl. by AUBERT 08Bg

 $A_{CP}(B^0 \rightarrow \phi K_2^*(1430)^0)$

VALUE	DOCUMENT ID	TECN	COMMENT
-0.11 ± 0.10 OUR AVERAGE			
$-0.155^{+0.152}_{-0.133} \pm 0.033$	PRIM	13	BELL $e^+ e^- \rightarrow \Upsilon(4S)$
$-0.08 \pm 0.12 \pm 0.05$	AUBERT	08Bg	BABR $e^+ e^- \rightarrow \Upsilon(4S)$
••• We do not use the following data for averages, fits, limits, etc. •••			
$-0.12 \pm 0.14 \pm 0.04$	AUBERT	07D	BABR Repl. by AUBERT 08Bg

 $A_{CP}(B^0 \rightarrow K^*(892)^0 \gamma)$

VALUE	DOCUMENT ID	TECN	COMMENT
-0.006 ± 0.011 OUR AVERAGE			
$-0.013 \pm 0.017 \pm 0.004$	1 HORIGUCHI	17	BELL $e^+ e^- \rightarrow \Upsilon(4S)$
$0.008 \pm 0.017 \pm 0.009$	AAIJ	13	LHCB pp at 7 TeV
$-0.016 \pm 0.022 \pm 0.007$	AUBERT	09Ao	BABR $e^+ e^- \rightarrow \Upsilon(4S)$
¹ Uses $B(\Upsilon(4S) \rightarrow B^+ B^-) = (51.4 \pm 0.6)\%$ and $B(\Upsilon(4S) \rightarrow B^0 \bar{B}^0) = (48.6 \pm 0.6)\%$.			

 $A_{CP}(B^0 \rightarrow K_2^*(1430)^0 \gamma)$

VALUE	DOCUMENT ID	TECN	COMMENT
$-0.08 \pm 0.15 \pm 0.01$	AUBERT,B	04u	BABR $e^+ e^- \rightarrow \Upsilon(4S)$

 $A_{CP}(B^0 \rightarrow X_s \gamma)$

VALUE	DOCUMENT ID	TECN	COMMENT
$-0.0094 \pm 0.0174 \pm 0.0047$	1 WATA NUKI	19	BELL $e^+ e^- \rightarrow \Upsilon(4S)$
¹ Using a sum-of-exclusive technique with $m_{X_s} < 2.8 \text{ GeV}/c^2$.			

 $A_{CP}(B^0 \rightarrow \rho^+ \pi^-)$

VALUE	DOCUMENT ID	TECN	COMMENT
0.13 ± 0.06 OUR AVERAGE			Error includes scale factor of 1.1.
$0.09^{+0.05}_{-0.06} \pm 0.04$	1 LEES	13J	BABR $e^+ e^- \rightarrow \Upsilon(4S)$
$0.21 \pm 0.08 \pm 0.04$	1 KUSAKA	07	BELL $e^+ e^- \rightarrow \Upsilon(4S)$
••• We do not use the following data for averages, fits, limits, etc. •••			
$0.03 \pm 0.07 \pm 0.04$	AUBERT	07AA	BABR Repl. by LEES 13J
$-0.02 \pm 0.16^{+0.05}_{-0.02}$	WANG	05	BELL Repl. by KUSAKA 07
$-0.18 \pm 0.08 \pm 0.03$	AUBERT	03T	BABR Repl. by AUBERT 07AA

¹ Uses time-dependent Dalitz plot analysis of $B^0 \rightarrow \pi^+ \pi^- \pi^0$ decays.

 $A_{CP}(B^0 \rightarrow \rho^- \pi^+)$

VALUE	DOCUMENT ID	TECN	COMMENT
-0.08 ± 0.08 OUR AVERAGE			
$-0.12 \pm 0.08^{+0.04}_{-0.05}$	1 LEES	13J	BABR $e^+ e^- \rightarrow \Upsilon(4S)$
$0.08 \pm 0.16 \pm 0.11$	1 KUSAKA	07	BELL $e^+ e^- \rightarrow \Upsilon(4S)$
••• We do not use the following data for averages, fits, limits, etc. •••			
$-0.37 \pm 0.16^{+0.09}_{-0.10}$	AUBERT	07AA	BABR Repl. by LEES 13J
$-0.53 \pm 0.29^{+0.09}_{-0.04}$	WANG	05	BELL Repl. by KUSAKA 07
¹ Uses time-dependent Dalitz plot analysis of $B^0 \rightarrow \pi^+ \pi^- \pi^0$ decays.			

 $A_{CP}(B^0 \rightarrow a_1(1260)^\pm \pi^\mp)$

VALUE	DOCUMENT ID	TECN	COMMENT
-0.07 ± 0.06 OUR AVERAGE			
$-0.06 \pm 0.05 \pm 0.07$	DALSENO	12	BELL $e^+ e^- \rightarrow \Upsilon(4S)$
$-0.07 \pm 0.07 \pm 0.02$	AUBERT	07o	BABR $e^+ e^- \rightarrow \Upsilon(4S)$

 $A_{CP}(B^0 \rightarrow b_1^- \pi^+)$

VALUE	DOCUMENT ID	TECN	COMMENT
$-0.05 \pm 0.10 \pm 0.02$	AUBERT	07Bi	BABR $e^+ e^- \rightarrow \Upsilon(4S)$

 $A_{CP}(B^0 \rightarrow \rho \bar{\rho} K^*(892)^0)$

VALUE	DOCUMENT ID	TECN	COMMENT
0.05 ± 0.12 OUR AVERAGE			
$-0.08 \pm 0.20 \pm 0.02$	CHEN	08c	BELL $e^+ e^- \rightarrow \Upsilon(4S)$
$0.11 \pm 0.13 \pm 0.06$	AUBERT	07AV	BABR $e^+ e^- \rightarrow \Upsilon(4S)$

 $A_{CP}(B^0 \rightarrow \rho \bar{\rho} \pi^-)$

VALUE	DOCUMENT ID	TECN	COMMENT
0.04 ± 0.07 OUR AVERAGE			
$0.10 \pm 0.10 \pm 0.02$	AUBERT	09Ac	BABR $e^+ e^- \rightarrow \Upsilon(4S)$
$-0.02 \pm 0.10 \pm 0.03$	WANG	07c	BELL $e^+ e^- \rightarrow \Upsilon(4S)$

 $A_{CP}(B^0 \rightarrow K^{*0} \ell^+ \ell^-)$

VALUE	DOCUMENT ID	TECN	COMMENT
-0.05 ± 0.10 OUR AVERAGE			
$0.02 \pm 0.20 \pm 0.02$	AUBERT	09T	BABR $e^+ e^- \rightarrow \Upsilon(4S)$
$-0.08 \pm 0.12 \pm 0.02$	WEI	09A	BELL $e^+ e^- \rightarrow \Upsilon(4S)$

 $A_{CP}(B^0 \rightarrow K^{*0} e^+ e^-)$

VALUE	DOCUMENT ID	TECN	COMMENT
$-0.21 \pm 0.19 \pm 0.02$	WEI	09A	BELL $e^+ e^- \rightarrow \Upsilon(4S)$

 $A_{CP}(B^0 \rightarrow K^{*0} \mu^+ \mu^-)$

VALUE	DOCUMENT ID	TECN	COMMENT
-0.034 ± 0.024 OUR AVERAGE			
$-0.035 \pm 0.024 \pm 0.003$	AAIJ	14AN	LHCB pp at 7, 8 TeV
$0.00 \pm 0.15 \pm 0.03$	WEI	09A	BELL $e^+ e^- \rightarrow \Upsilon(4S)$
••• We do not use the following data for averages, fits, limits, etc. •••			
$-0.072 \pm 0.040 \pm 0.005$	AAIJ	13E	LHCB Repl. by AAIJ 14AN

 $C_{D^*(2010)^- D^+} (B^0 \rightarrow D^*(2010)^- D^+)$

VALUE	DOCUMENT ID	TECN	COMMENT
-0.02 ± 0.08 OUR AVERAGE			
$-0.028 \pm 0.130 \pm 0.026$	1 AAIJ	20L	LHCB pp at 7, 8, 13 TeV
$-0.13 \pm 0.16 \pm 0.05$	2 ROHRKEN	12	BELL $e^+ e^- \rightarrow \Upsilon(4S)$
$0.00 \pm 0.17 \pm 0.03$	AUBERT	09c	BABR $e^+ e^- \rightarrow \Upsilon(4S)$
$0.23 \pm 0.25 \pm 0.06$	3 AUSHEV	04	BELL $e^+ e^- \rightarrow \Upsilon(4S)$
••• We do not use the following data for averages, fits, limits, etc. •••			
$0.23 \pm 0.15 \pm 0.04$	AUBERT	07Ai	BABR Repl. by AUBERT 09c
$0.17 \pm 0.24 \pm 0.04$	AUBERT,B	05z	BABR Repl. by AUBERT 07Ai
$-0.22 \pm 0.37 \pm 0.10$	AUBERT	03j	BABR Repl. by AUBERT,B 05z

¹ AAIJ 20L reports the measurements of $C = -0.059 \pm 0.092 \pm 0.020$ and $\Delta C = -0.031 \pm 0.092 \pm 0.016$ such that $C_{D^*(2010)^- D^+} = C - \Delta C$.

² ROHRKEN 12 reports the measurements of $C = -0.01 \pm 0.11 \pm 0.04$ and $\Delta C = 0.12 \pm 0.11 \pm 0.03$ such that $C_{D^*(2010)^- D^+} = C - \Delta C$.

³ Combines results from fully and partially reconstructed $B^0 \rightarrow D^{*\pm} D^\mp$ decays.

 $S_{D^*(2010)^- D^+} (B^0 \rightarrow D^*(2010)^- D^+)$

VALUE	DOCUMENT ID	TECN	COMMENT
-0.83 ± 0.09 OUR AVERAGE			
$-0.880 \pm 0.107 \pm 0.022$	1 AAIJ	20L	LHCB pp at 7, 8, 13 TeV
$-0.65 \pm 0.22 \pm 0.07$	2 ROHRKEN	12	BELL $e^+ e^- \rightarrow \Upsilon(4S)$
$-0.73 \pm 0.23 \pm 0.050$	AUBERT	09c	BABR $e^+ e^- \rightarrow \Upsilon(4S)$
$-0.96 \pm 0.43 \pm 0.12$	3 AUSHEV	04	BELL $e^+ e^- \rightarrow \Upsilon(4S)$
••• We do not use the following data for averages, fits, limits, etc. •••			
$-0.44 \pm 0.22 \pm 0.06$	AUBERT	07Ai	BABR Repl. by AUBERT 09c
$-0.29 \pm 0.33 \pm 0.07$	AUBERT,B	05z	BABR Repl. by AUBERT 07Ai
$-0.24 \pm 0.69 \pm 0.12$	AUBERT	03j	BABR Repl. by AUBERT,B 05z

¹ AAIJ 20L reports the measurements of $S = -0.861 \pm 0.077 \pm 0.019$ and $\Delta S = 0.019 \pm 0.075 \pm 0.012$ such that $S_{D^*(2010)^- D^+} = S - \Delta S$.

² ROHRKEN 12 reports the measurements of $S = -0.78 \pm 0.15 \pm 0.05$ and $\Delta S = -0.13 \pm 0.15 \pm 0.04$ such that $S_{D^*(2010)^- D^+} = S - \Delta S$.

³ Combines results from fully and partially reconstructed $B^0 \rightarrow D^{*\pm} D^\mp$ decays.

Meson Particle Listings

B^0

$C_{D^*(2010)+D^-} (B^0 \rightarrow D^{*+}(2010)+D^-)$

VALUE	DOCUMENT ID	TECN	COMMENT
-0.03 ± 0.09 OUR AVERAGE	Error includes scale factor of 1.1.		
-0.090 ± 0.130 ± 0.026	¹ AAIJ	20L LHCB	pp at 7, 8, 13 TeV
0.11 ± 0.14 ± 0.06	² ROHRKEN	12 BELL	$e^+e^- \rightarrow \Upsilon(4S)$
0.08 ± 0.17 ± 0.04	AUBERT	09c BABR	$e^+e^- \rightarrow \Upsilon(4S)$
-0.37 ± 0.22 ± 0.06	³ AUSHEV	04 BELL	$e^+e^- \rightarrow \Upsilon(4S)$

• • • We do not use the following data for averages, fits, limits, etc. • • •

0.18 ± 0.15 ± 0.04	AUBERT	07Al BABR	Repl. by AUBERT 09c
0.09 ± 0.25 ± 0.06	AUBERT,B	05Z BABR	Repl. by AUBERT 07Al
-0.47 ± 0.40 ± 0.12	AUBERT	03J BABR	Repl. by AUBERT,B 05Z

¹AAIJ 20L reports the measurements of $C = -0.059 \pm 0.092 \pm 0.020$ and $\Delta C = -0.031 \pm 0.092 \pm 0.016$ such that $C_{D^*(2010)+D^-} = C + \Delta C$.

²ROHRKEN 12 reports the measurements of $C = -0.01 \pm 0.11 \pm 0.04$ and $\Delta C = 0.12 \pm 0.11 \pm 0.03$ such that $C_{D^*(2010)+D^-} = C + \Delta C$.

³Combines results from fully and partially reconstructed $B^0 \rightarrow D^{*+}D^-$ decays.

$S_{D^*(2010)+D^-} (B^0 \rightarrow D^{*+}(2010)+D^-)$

VALUE	DOCUMENT ID	TECN	COMMENT
-0.80 ± 0.09 OUR AVERAGE	Error includes scale factor of 1.1.		
-0.842 ± 0.107 ± 0.022	¹ AAIJ	20L LHCB	pp at 7, 8, 13 TeV
-0.90 ± 0.21 ± 0.07	² ROHRKEN	12 BELL	$e^+e^- \rightarrow \Upsilon(4S)$
-0.62 ± 0.21 ± 0.03	AUBERT	09c BABR	$e^+e^- \rightarrow \Upsilon(4S)$
-0.55 ± 0.39 ± 0.12	³ AUSHEV	04 BELL	$e^+e^- \rightarrow \Upsilon(4S)$

• • • We do not use the following data for averages, fits, limits, etc. • • •

-0.79 ± 0.21 ± 0.06	AUBERT	07Al BABR	Repl. by AUBERT 09c
-0.54 ± 0.35 ± 0.07	AUBERT,B	05Z BABR	Repl. by AUBERT 07Al
-0.82 ± 0.75 ± 0.14	AUBERT	03J BABR	Repl. by AUBERT,B 05Z

¹AAIJ 20L reports the measurements of $S = -0.861 \pm 0.077 \pm 0.019$ and $\Delta S = 0.019 \pm 0.075 \pm 0.012$ such that $S_{D^*(2010)+D^-} = S + \Delta S$.

²ROHRKEN 12 reports the measurements of $S = -0.78 \pm 0.15 \pm 0.05$ and $\Delta S = -0.13 \pm 0.15 \pm 0.04$ such that $S_{D^*(2010)+D^-} = S + \Delta S$.

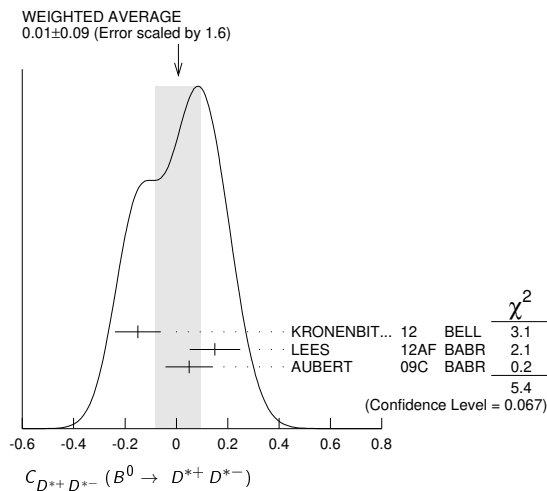
³Combines results from fully and partially reconstructed $B^0 \rightarrow D^{*+}D^-$ decays.

$C_{D^{*+}D^{*-}} (B^0 \rightarrow D^{*+}D^{*-})$

VALUE	DOCUMENT ID	TECN	COMMENT
0.01 ± 0.09 OUR AVERAGE	Error includes scale factor of 1.6. See the ideogram below.		
-0.15 ± 0.08 ± 0.04	^{1,2} KRONENBIT... 12	BELL	$e^+e^- \rightarrow \Upsilon(4S)$
+0.15 ± 0.09 ± 0.04	³ LEES	12AF BABR	$e^+e^- \rightarrow \Upsilon(4S)$
0.05 ± 0.09 ± 0.02	AUBERT	09c BABR	$e^+e^- \rightarrow \Upsilon(4S)$

• • • We do not use the following data for averages, fits, limits, etc. • • •

-0.15 ± 0.13 ± 0.04	² VERVINK	09 BELL	Repl. by KRONENBITTER 12
-0.02 ± 0.11 ± 0.02	¹ AUBERT	07Bo BABR	Repl. by AUBERT 09c
0.26 ± 0.26 ± 0.06	² MIYAKE	05 BELL	Repl. by VERVINK 09
0.28 ± 0.23 ± 0.02	⁴ AUBERT	03Q BABR	Repl. by AUBERT 07Bo



¹Assumes both CP -even and CP -odd states having the CP asymmetry.

²Belle Collab. quotes $A_{D^{*+}D^{*-}}$ which is equal to $-C_{D^{*+}D^{*-}}$.

³Measured partially reconstructed candidates when one D^0 meson is not explicitly reconstructed. Analysis does not separate CP -even and CP -odd component.

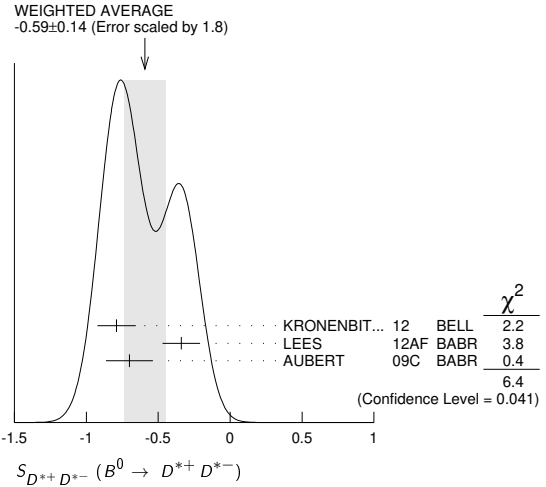
⁴AUBERT 03Q reports $|\lambda| = 0.75 \pm 0.19 \pm 0.02$ and $\text{Im}(\lambda) = 0.05 \pm 0.29 \pm 0.10$. We convert them to S and C parameters taking into account correlations.

$S_{D^{*+}D^{*-}} (B^0 \rightarrow D^{*+}D^{*-})$

VALUE	DOCUMENT ID	TECN	COMMENT
-0.59 ± 0.14 OUR AVERAGE	Error includes scale factor of 1.8. See the ideogram below.		
-0.79 ± 0.13 ± 0.03	¹ KRONENBIT... 12	BELL	$e^+e^- \rightarrow \Upsilon(4S)$
-0.34 ± 0.12 ± 0.05	² LEES	12AF BABR	$e^+e^- \rightarrow \Upsilon(4S)$
-0.70 ± 0.16 ± 0.03	¹ AUBERT	09c BABR	$e^+e^- \rightarrow \Upsilon(4S)$

• • • We do not use the following data for averages, fits, limits, etc. • • •

-0.96 ± 0.25 ^{+0.13} _{-0.16}	VERVINK	09 BELL	Repl. by KRONENBITTER 12
-0.66 ± 0.19 ± 0.04	¹ AUBERT	07Bo BABR	Repl. by AUBERT 09c
-0.75 ± 0.56 ± 0.12	MIYAKE	05 BELL	Repl. by VERVINK 09
0.06 ± 0.37 ± 0.13	³ AUBERT	03Q BABR	Repl. by AUBERT 07Bo



¹Assumes both CP -even and CP -odd states having the CP asymmetry.

²Measured partially reconstructed candidates when one D^0 meson is not explicitly reconstructed. Analysis does not separate CP -even and CP -odd component.

³AUBERT 03Q reports $|\lambda| = 0.75 \pm 0.19 \pm 0.02$ and $\text{Im}(\lambda) = 0.05 \pm 0.29 \pm 0.10$. We convert them to S and C parameters taking into account correlations.

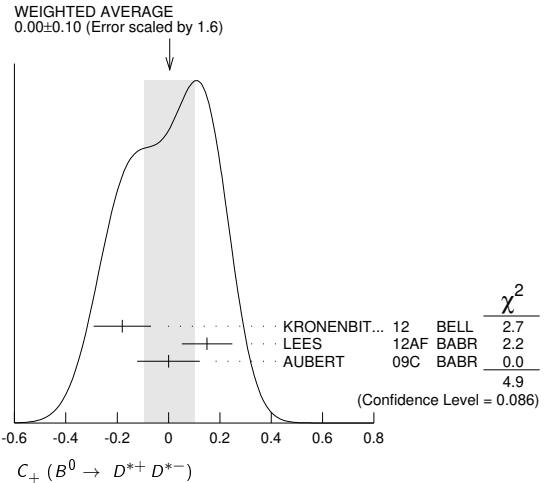
$C_+(B^0 \rightarrow D^{*+}D^{*-})$

See the note in the $C_{\pi\pi}$ datablock, but for CP even final state.

VALUE	DOCUMENT ID	TECN	COMMENT
0.00 ± 0.10 OUR AVERAGE	Error includes scale factor of 1.6. See the ideogram below.		
-0.18 ± 0.10 ± 0.05	¹ KRONENBIT... 12	BELL	$e^+e^- \rightarrow \Upsilon(4S)$
+0.15 ± 0.09 ± 0.04	² LEES	12AF BABR	$e^+e^- \rightarrow \Upsilon(4S)$
0.00 ± 0.12 ± 0.02	AUBERT	09c BABR	$e^+e^- \rightarrow \Upsilon(4S)$

• • • We do not use the following data for averages, fits, limits, etc. • • •

-0.05 ± 0.14 ± 0.02	AUBERT	07Bo BABR	Repl. by AUBERT 09c
0.06 ± 0.17 ± 0.03	³ AUBERT, BE	05A BABR	Repl. by AUBERT 07Bo



¹Belle Collab. quotes $A_{D^{*+}D^{*-}}$ which is equal to $-C_{D^{*+}D^{*-}}$.

²Measured partially reconstructed candidates when one D^0 meson is not explicitly reconstructed. Extracted under assumption of equal C_+ and C_- .

³AUBERT, BE 05A reports a CP -odd fraction $R_{\perp} = 0.125 \pm 0.044 \pm 0.007$.

$S_+(B^0 \rightarrow D^{*+}D^{*-})$

See the note in the $S_{\pi\pi}$ datablock, but for CP even final state.

VALUE	DOCUMENT ID	TECN	COMMENT
-0.73 ± 0.09 OUR AVERAGE	Error includes scale factor of 1.8. See the ideogram below.		
-0.81 ± 0.13 ± 0.03	KRONENBIT... 12	BELL	$e^+e^- \rightarrow \Upsilon(4S)$
-0.49 ± 0.18 ± 0.08	¹ LEES	12AF BABR	$e^+e^- \rightarrow \Upsilon(4S)$
-0.76 ± 0.16 ± 0.04	AUBERT	09c BABR	$e^+e^- \rightarrow \Upsilon(4S)$

See key on page 1127

Meson Particle Listings

B^0

••• We do not use the following data for averages, fits, limits, etc. •••
 $-0.72 \pm 0.19 \pm 0.05$ AUBERT 07B0 BABR Repl. by AUBERT 09c
 $-0.75 \pm 0.25 \pm 0.03$ ²AUBERT,BE 05A BABR Repl. by AUBERT 07B0
¹ Measured partially reconstructed candidates when one D^0 meson is not explicitly reconstructed. Analysis does not separate CP-even and CP-odd component. Value is obtained from $S = -0.34 \pm 0.12 \pm 0.05$ using $S = S_+ (1 - 2 R_\perp)$ with $R_\perp = 0.158 \pm 0.029$.
² AUBERT,BE 05A reports a CP-odd fraction $R_\perp = 0.125 \pm 0.044 \pm 0.007$.

$C_-(B^0 \rightarrow D^{*+} D^{*-})$
 See the note in the $C_{\pi\pi}$ datablock, but for CP odd final state.

VALUE	DOCUMENT ID	TECN	COMMENT
0.19 ± 0.31 OUR AVERAGE			
$0.05 \pm 0.39 \pm 0.08$	¹ KRONENBIT...12	BELL	$e^+ e^- \rightarrow \Upsilon(4S)$
$0.41 \pm 0.49 \pm 0.08$	AUBERT 09c	BABR	$e^+ e^- \rightarrow \Upsilon(4S)$

••• We do not use the following data for averages, fits, limits, etc. •••
 $0.23 \pm 0.67 \pm 0.10$ AUBERT 07B0 BABR Repl. by AUBERT 09c
 $-0.20 \pm 0.96 \pm 0.11$ ²AUBERT,BE 05A BABR Repl. by AUBERT 07B0
¹ Belle Collab. quotes $A_{D^{*+} D^{*-}}$ which is equal to $-C_{D^{*+} D^{*-}}$.
² AUBERT,BE 05A reports a CP-odd fraction $R_\perp = 0.125 \pm 0.044 \pm 0.007$.

$S_-(B^0 \rightarrow D^{*+} D^{*-})$
 See the note in the $S_{\pi\pi}$ datablock, but for CP odd final state.

VALUE	DOCUMENT ID	TECN	COMMENT
0.1 ± 1.6 OUR AVERAGE			Error includes scale factor of 3.5.
$1.52 \pm 0.62 \pm 0.12$	KRONENBIT...12	BELL	$e^+ e^- \rightarrow \Upsilon(4S)$
$-1.80 \pm 0.70 \pm 0.16$	AUBERT 09c	BABR	$e^+ e^- \rightarrow \Upsilon(4S)$

••• We do not use the following data for averages, fits, limits, etc. •••
 $-1.83 \pm 1.04 \pm 0.23$ AUBERT 07B0 BABR Repl. by AUBERT 09c
 $-1.75 \pm 1.78 \pm 0.22$ ¹AUBERT,BE 05A BABR Repl. by AUBERT 07B0
¹ AUBERT,BE 05A reports a CP-odd fraction $R_\perp = 0.125 \pm 0.044 \pm 0.007$.

$C(B^0 \rightarrow D^*(2010)^+ D^*(2010)^- K_S^0)$

VALUE	DOCUMENT ID	TECN	COMMENT
$0.01 \pm 0.28 \pm 0.09$	¹ DALSENO 07	BELL	$e^+ e^- \rightarrow \Upsilon(4S)$

¹ Reports value of A which is equal to $-C$.

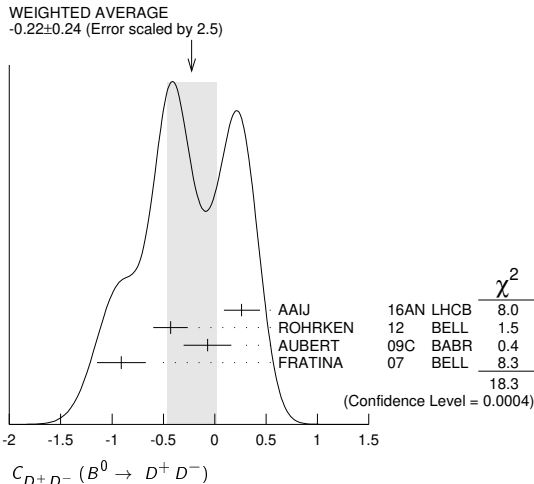
$S(B^0 \rightarrow D^*(2010)^+ D^*(2010)^- K_S^0)$

VALUE	DOCUMENT ID	TECN	COMMENT
$0.06 \pm 0.45 \pm 0.06$	¹ DALSENO 07	BELL	$e^+ e^- \rightarrow \Upsilon(4S)$

¹ This value includes an unknown CP dilution factor D due to possible contributions from intermediate resonances and different partial waves.

$C_{D^+ D^-}(B^0 \rightarrow D^+ D^-)$

VALUE	DOCUMENT ID	TECN	COMMENT
-0.22 ± 0.24 OUR AVERAGE			Error includes scale factor of 2.5. See the ideogram below.
$0.26 \pm 0.18 \pm 0.02$	AAIJ 16AN	LHCB	pp at 7, 8 TeV
$-0.43 \pm 0.16 \pm 0.05$	ROHRKEN 12	BELL	$e^+ e^- \rightarrow \Upsilon(4S)$
$-0.07 \pm 0.23 \pm 0.03$	AUBERT 09c	BABR	$e^+ e^- \rightarrow \Upsilon(4S)$
$-0.91 \pm 0.23 \pm 0.06$	¹ FRATINA 07	BELL	$e^+ e^- \rightarrow \Upsilon(4S)$
$0.11 \pm 0.22 \pm 0.07$	AUBERT 07A1	BABR	Repl. by AUBERT 09c
$0.11 \pm 0.35 \pm 0.06$	AUBERT,B 05Z	BABR	Repl. by AUBERT 07A1



¹ The paper reports A, which is equal to $-C$.

$S_{D^+ D^-}(B^0 \rightarrow D^+ D^-)$

VALUE	DOCUMENT ID	TECN	COMMENT
$-0.76 \pm 0.15 \pm 0.13$ OUR AVERAGE			Error includes scale factor of 1.2.
$-0.54 \pm 0.17 \pm 0.16$	AAIJ 16AN	LHCB	pp at 7, 8 TeV
$-1.06 \pm 0.21 \pm 0.14$	ROHRKEN 12	BELL	$e^+ e^- \rightarrow \Upsilon(4S)$
$-0.63 \pm 0.36 \pm 0.05$	AUBERT 09c	BABR	$e^+ e^- \rightarrow \Upsilon(4S)$
$-1.13 \pm 0.37 \pm 0.09$	FRATINA 07	BELL	$e^+ e^- \rightarrow \Upsilon(4S)$
••• We do not use the following data for averages, fits, limits, etc. •••			
$-0.54 \pm 0.34 \pm 0.06$	AUBERT 07A1	BABR	Repl. by AUBERT 09c
$-0.29 \pm 0.63 \pm 0.06$	AUBERT,B 05Z	BABR	Repl. by AUBERT 07A1

$C_{J/\psi(1S)\pi^0}(B^0 \rightarrow J/\psi(1S)\pi^0)$

VALUE	DOCUMENT ID	TECN	COMMENT
0.03 ± 0.17 OUR AVERAGE			Error includes scale factor of 1.5.
$0.15 \pm 0.14 \pm 0.04$	¹ PAL 18	BELL	$e^+ e^- \rightarrow \Upsilon(4S)$
$-0.20 \pm 0.19 \pm 0.03$	AUBERT 08AU	BABR	$e^+ e^- \rightarrow \Upsilon(4S)$
••• We do not use the following data for averages, fits, limits, etc. •••			
$-0.08 \pm 0.16 \pm 0.05$	¹ LEE 08A	BELL	Repl. by PAL 18
$-0.21 \pm 0.26 \pm 0.06$	AUBERT,B 06B	BABR	Repl. by AUBERT 08AU
$0.01 \pm 0.29 \pm 0.03$	¹ KATAOKA 04	BELL	Repl. by LEE 08A
$0.38 \pm 0.41 \pm 0.09$	AUBERT 03N	BABR	Repl. by AUBERT,B 06B

¹ BELLE Collab. quotes $A_{J/\psi\pi^0}$ which is equal to $-C_{J/\psi\pi^0}$.

$S_{J/\psi(1S)\pi^0}(B^0 \rightarrow J/\psi(1S)\pi^0)$

VALUE	DOCUMENT ID	TECN	COMMENT
-0.89 ± 0.32 OUR AVERAGE			Error includes scale factor of 2.2.
$-0.59 \pm 0.19 \pm 0.03$	PAL 18	BELL	$e^+ e^- \rightarrow \Upsilon(4S)$
$-1.23 \pm 0.21 \pm 0.04$	AUBERT 08AU	BABR	$e^+ e^- \rightarrow \Upsilon(4S)$
••• We do not use the following data for averages, fits, limits, etc. •••			
$-0.65 \pm 0.21 \pm 0.05$	LEE 08A	BELL	Repl. by PAL 18
$-0.68 \pm 0.30 \pm 0.04$	AUBERT,B 06B	BABR	Repl. by AUBERT 08AU
$-0.72 \pm 0.42 \pm 0.09$	KATAOKA 04	BELL	Repl. by LEE 08A
$0.05 \pm 0.49 \pm 0.16$	AUBERT 03N	BABR	Repl. by AUBERT,B 06B

$C(B^0 \rightarrow J/\psi(1S)\rho^0)$

VALUE	DOCUMENT ID	TECN	COMMENT
$-0.063 \pm 0.056 \pm 0.019 \pm 0.014$	¹ AAIJ 15J	LHCB	pp at 7, 8 TeV

¹ Time-dependent CP violation is measured in the $B^0 \rightarrow J/\psi\rho^0$ and was used to limit the size of penguin amplitude contributions to ϕ_S in $B_S^0 \rightarrow J/\psi\phi$ decays to be between $[-1.05^\circ, 1.18^\circ]$ at 95% confidence level.

$S(B^0 \rightarrow J/\psi(1S)\rho^0)$

VALUE	DOCUMENT ID	TECN	COMMENT
$-0.66 \pm 0.13 \pm 0.09 \pm 0.12 \pm 0.03$	¹ AAIJ 15J	LHCB	pp at 7, 8 TeV

¹ Time-dependent CP violation is measured in the $B^0 \rightarrow J/\psi\rho^0$ and was used to limit the size of penguin amplitude contributions to ϕ_S in $B_S^0 \rightarrow J/\psi\phi$ decays to be between $[-1.05^\circ, 1.18^\circ]$ at 95% confidence level.

$C_{D_{CP}^{(*)} h^0}(B^0 \rightarrow D_{CP}^{(*)} h^0)$

VALUE	DOCUMENT ID	TECN	COMMENT
$-0.02 \pm 0.07 \pm 0.03$	¹ ABDESSALAM 15		$e^+ e^- \rightarrow \Upsilon(4S)$

••• We do not use the following data for averages, fits, limits, etc. •••
 $-0.23 \pm 0.16 \pm 0.04$ AUBERT 07AJ BABR Repl. by ABDESSALAM 15
¹ BABAR and BELLE combined analysis uses CP-eigenstate decay modes $D^0 \rightarrow K^+ K^-$, $K_S^0 \pi^0$, $K_S^0 \omega$, and $h^0 = \pi^0, \eta, \omega$.

$S_{D_{CP}^{(*)} h^0}(B^0 \rightarrow D_{CP}^{(*)} h^0)$

VALUE	DOCUMENT ID	TECN	COMMENT
$-0.66 \pm 0.10 \pm 0.06$	¹ ABDESSALAM 15		$e^+ e^- \rightarrow \Upsilon(4S)$

••• We do not use the following data for averages, fits, limits, etc. •••
 $-0.56 \pm 0.23 \pm 0.05$ AUBERT 07AJ BABR Repl. by ABDESSALAM 15
¹ BABAR and BELLE combined analysis uses CP-eigenstate decay modes $D^0 \rightarrow K^+ K^-$, $K_S^0 \pi^0$, $K_S^0 \omega$, and $h^0 = \pi^0, \eta, \omega$.

$C_{K^0 \pi^0}(B^0 \rightarrow K^0 \pi^0)$

VALUE	DOCUMENT ID	TECN	COMMENT
0.00 ± 0.13 OUR AVERAGE			Error includes scale factor of 1.4.
$-0.14 \pm 0.13 \pm 0.06$	¹ FUJIKAWA 10A	BELL	$e^+ e^- \rightarrow \Upsilon(4S)$
$0.13 \pm 0.13 \pm 0.03$	AUBERT 09I	BABR	$e^+ e^- \rightarrow \Upsilon(4S)$

••• We do not use the following data for averages, fits, limits, etc. •••
 $0.24 \pm 0.15 \pm 0.03$ AUBERT 08E BABR Repl. by AUBERT 09I
 $0.05 \pm 0.14 \pm 0.05$ ¹ CHAO 07 BELL Repl. by FUJIKAWA 10A
 $0.06 \pm 0.18 \pm 0.03$ AUBERT 05Y BABR Repl. by AUBERT 08E

Meson Particle Listings

 B^0

$-0.16 \pm 0.29 \pm 0.05$	^{1,2} CHAO	05A	BELL	Repl. by CHEN 05B
$0.11 \pm 0.20 \pm 0.09$	¹ CHEN	05B	BELL	Repl. by CHAO 07
$-0.03 \pm 0.36 \pm 0.11$	¹ AUBERT	04M	BABR	Repl. by AUBERT,B 04M
$0.40 \pm 0.27 \pm 0.09$	³ AUBERT,B	04M	BABR	Repl. by AUBERT 05Y

¹ Reports A which is equal to $-C$.

² Corresponds to a 90% CL interval of $-0.33 < A_{CP} < 0.64$.

³ Based on a total signal yield of 122 ± 16 events.

 $S_{K^0 \pi^0} (B^0 \rightarrow K^0 \pi^0)$

VALUE	DOCUMENT ID	TECN	COMMENT
0.58 ± 0.17 OUR AVERAGE			
$0.67 \pm 0.31 \pm 0.08$	FUJIKAWA	10A	BELL $e^+ e^- \rightarrow \Upsilon(4S)$
$0.55 \pm 0.20 \pm 0.03$	AUBERT	09I	BABR $e^+ e^- \rightarrow \Upsilon(4S)$
••• We do not use the following data for averages, fits, limits, etc. •••			
$0.40 \pm 0.23 \pm 0.03$	AUBERT	08E	BABR Repl. by AUBERT 09I
$0.33 \pm 0.35 \pm 0.08$	CHAO	07	BELL Repl. by FUJIKAWA 10A
$0.35 \pm 0.30 \pm 0.33 \pm 0.04$	AUBERT	05Y	BABR Repl. by AUBERT 08E
$0.32 \pm 0.61 \pm 0.13$	CHEN	05B	BELL Repl. by CHAO 07
$0.48 \pm 0.38 \pm 0.06$	¹ AUBERT,B	04M	BABR Repl. by AUBERT 05Y

¹ Based on a total signal yield of 122 ± 16 events.

 $C_{\eta'(958) K_S^0} (B^0 \rightarrow \eta'(958) K_S^0)$

See updated measurements in $C_{\eta' K^0}$

VALUE	DOCUMENT ID	TECN	COMMENT
-0.04 ± 0.20 OUR AVERAGE			Error includes scale factor of 2.5.
$-0.21 \pm 0.10 \pm 0.02$	AUBERT	05M	BABR $e^+ e^- \rightarrow \Upsilon(4S)$
$0.19 \pm 0.11 \pm 0.05$	¹ CHEN	05B	BELL $e^+ e^- \rightarrow \Upsilon(4S)$
••• We do not use the following data for averages, fits, limits, etc. •••			
$-0.26 \pm 0.22 \pm 0.03$	¹ ABE	03C	BELL Repl. by ABE 03H
$0.01 \pm 0.16 \pm 0.04$	¹ ABE	03H	BELL Repl. by CHEN 05B
$0.10 \pm 0.22 \pm 0.04$	AUBERT	03W	BABR Repl. by AUBERT 05M
$-0.13 \pm 0.32 \pm 0.06$	¹ CHEN	02B	BELL Repl. by ABE 03C

¹ BELLE Collab. quotes $A_{\eta'(958) K_S^0}$ which is equal to $-C_{\eta'(958) K_S^0}$.

 $S_{\eta'(958) K_S^0} (B^0 \rightarrow \eta'(958) K_S^0)$

See updated measurements in $S_{\eta' K^0}$

VALUE	DOCUMENT ID	TECN	COMMENT
0.43 ± 0.17 OUR AVERAGE			Error includes scale factor of 1.5.
$0.30 \pm 0.14 \pm 0.02$	AUBERT	05M	BABR $e^+ e^- \rightarrow \Upsilon(4S)$
$0.65 \pm 0.18 \pm 0.04$	CHEN	05B	BELL $e^+ e^- \rightarrow \Upsilon(4S)$
••• We do not use the following data for averages, fits, limits, etc. •••			
$0.71 \pm 0.37 \pm 0.05$	ABE	03C	BELL Repl. by ABE 03H
$0.43 \pm 0.27 \pm 0.05$	ABE	03H	BELL Repl. by CHEN 05B
$0.02 \pm 0.34 \pm 0.03$	AUBERT	03W	BABR Repl. by AUBERT 05M
$0.28 \pm 0.55 \pm 0.07$	CHEN	02B	BELL Repl. by ABE 03C

 $C_{\eta' K^0} (B^0 \rightarrow \eta' K^0)$

VALUE	DOCUMENT ID	TECN	COMMENT
-0.06 ± 0.04 OUR AVERAGE			
$-0.03 \pm 0.05 \pm 0.04$	¹ SANTELJ	14	BELL $e^+ e^- \rightarrow \Upsilon(4S)$
$-0.08 \pm 0.06 \pm 0.02$	AUBERT	09I	BABR $e^+ e^- \rightarrow \Upsilon(4S)$
••• We do not use the following data for averages, fits, limits, etc. •••			
$-0.16 \pm 0.07 \pm 0.03$	² AUBERT	07A	BABR Repl. by AUBERT 09I
$0.01 \pm 0.07 \pm 0.05$	^{1,2} CHEN	07	BELL Repl. by SANTELJ 14
¹ The paper reports A, which is equal to $-C$.			
² The mixing-induced CP violation is reported with a significance of more than 5 standard deviations in this $b \rightarrow s$ penguin dominated mode.			

 $S_{\eta' K^0} (B^0 \rightarrow \eta' K^0)$

VALUE	DOCUMENT ID	TECN	COMMENT
0.63 ± 0.06 OUR AVERAGE			
$0.68 \pm 0.07 \pm 0.03$	SANTELJ	14	BELL $e^+ e^- \rightarrow \Upsilon(4S)$
$0.57 \pm 0.08 \pm 0.02$	AUBERT	09I	BABR $e^+ e^- \rightarrow \Upsilon(4S)$
••• We do not use the following data for averages, fits, limits, etc. •••			
$0.58 \pm 0.10 \pm 0.03$	¹ AUBERT	07A	BABR Repl. by AUBERT 09I
$0.64 \pm 0.10 \pm 0.04$	¹ CHEN	07	BELL Repl. by SANTELJ 14
¹ The mixing-induced CP violation is reported with a significance of more than 5 standard deviations in this $b \rightarrow s$ penguin dominated mode.			

 $C_{\omega K_S^0} (B^0 \rightarrow \omega K_S^0)$

VALUE	DOCUMENT ID	TECN	COMMENT
0.0 ± 0.4 OUR AVERAGE			Error includes scale factor of 3.0.
$0.36 \pm 0.19 \pm 0.05$	¹ CHOBANOVA	14	BELL $e^+ e^- \rightarrow \Upsilon(4S)$
$-0.52 \pm 0.22 \pm 0.03$	AUBERT	09I	BABR $e^+ e^- \rightarrow \Upsilon(4S)$
••• We do not use the following data for averages, fits, limits, etc. •••			
$0.09 \pm 0.29 \pm 0.06$	¹ CHAO	07	BELL Repl. by CHOBANOVA 14
$-0.55 \pm 0.28 \pm 0.03$	AUBERT,B	06E	BABR Repl. by AUBERT 09I
$-0.27 \pm 0.48 \pm 0.15$	¹ CHEN	05B	BELL Repl. by CHAO 07
¹ Belle Collab. quotes $A_{\omega K_S^0}$ which is equal to $-C_{\omega K_S^0}$.			

 $S_{\omega K_S^0} (B^0 \rightarrow \omega K_S^0)$

VALUE	DOCUMENT ID	TECN	COMMENT
0.70 ± 0.21 OUR AVERAGE			
$0.91 \pm 0.32 \pm 0.05$	CHOBANOVA	14	BELL $e^+ e^- \rightarrow \Upsilon(4S)$
$0.55 \pm 0.26 \pm 0.02$	AUBERT	09I	BABR $e^+ e^- \rightarrow \Upsilon(4S)$
••• We do not use the following data for averages, fits, limits, etc. •••			
$0.11 \pm 0.46 \pm 0.07$	CHAO	07	BELL Repl. by CHOBANOVA 14
$0.51 \pm 0.35 \pm 0.02$	AUBERT,B	06E	BABR Repl. by AUBERT 09I
$0.76 \pm 0.65 \pm 0.13$	CHEN	05B	BELL Repl. by CHAO 07

 $C (B^0 \rightarrow K_S^0 \pi^0 \pi^0)$

VALUE	DOCUMENT ID	TECN	COMMENT
-0.21 ± 0.20 OUR AVERAGE			
$-0.28 \pm 0.21 \pm 0.04$	¹ YUSA	19	BELL $e^+ e^- \rightarrow \Upsilon(4S)$
$0.23 \pm 0.52 \pm 0.13$	AUBERT	07AQ	BABR $e^+ e^- \rightarrow \Upsilon(4S)$
¹ Reports value of A which is equal to $-C$.			

 $S (B^0 \rightarrow K_S^0 \pi^0 \pi^0)$

VALUE	DOCUMENT ID	TECN	COMMENT
$0.89 \pm 0.27 \pm 0.30$ OUR AVERAGE			
$0.92 \pm 0.27 \pm 0.11$	YUSA	19	BELL $e^+ e^- \rightarrow \Upsilon(4S)$
$0.72 \pm 0.71 \pm 0.08$	AUBERT	07AQ	BABR $e^+ e^- \rightarrow \Upsilon(4S)$

 $C_{\rho^0 K_S^0} (B^0 \rightarrow \rho^0 K_S^0)$

VALUE	DOCUMENT ID	TECN	COMMENT
-0.04 ± 0.20 OUR AVERAGE			
$-0.05 \pm 0.26 \pm 0.10$	¹ AUBERT	09AU	BABR $e^+ e^- \rightarrow \Upsilon(4S)$
$-0.03 \pm 0.24 \pm 0.23 \pm 0.15$	^{2,3} DALSENO	09	BELL $e^+ e^- \rightarrow \Upsilon(4S)$
••• We do not use the following data for averages, fits, limits, etc. •••			
$0.64 \pm 0.41 \pm 0.20$	AUBERT	07F	BABR Repl. by AUBERT 09AU
¹ Uses Dalitz plot analysis of $B^0 \rightarrow K^0 \pi^+ \pi^-$ decays and the first of two equivalent solutions is used.			
² Quotes $A_{\rho^0 (KS)^0}$ which is equal to $-C_{\rho^0 K_S^0}$.			
³ Uses Dalitz plot analysis of $B^0 \rightarrow K^0 \pi^+ \pi^-$ decays and the first of two consistent solutions that may be preferred.			

 $S_{\rho^0 K_S^0} (B^0 \rightarrow \rho^0 K_S^0)$

VALUE	DOCUMENT ID	TECN	COMMENT
$0.50 \pm 0.17 \pm 0.21$ OUR AVERAGE			
$0.35 \pm 0.26 \pm 0.31 \pm 0.07$	¹ AUBERT	09AU	BABR $e^+ e^- \rightarrow \Upsilon(4S)$
$0.64 \pm 0.19 \pm 0.25 \pm 0.13$	² DALSENO	09	BELL $e^+ e^- \rightarrow \Upsilon(4S)$
••• We do not use the following data for averages, fits, limits, etc. •••			
$0.20 \pm 0.52 \pm 0.24$	AUBERT	07F	BABR Repl. by AUBERT 09AU
¹ Uses Dalitz plot analysis of $B^0 \rightarrow K^0 \pi^+ \pi^-$ decays and the first of two equivalent solutions is used.			
² Uses Dalitz plot analysis of $B^0 \rightarrow K^0 \pi^+ \pi^-$ decays and the first of two consistent solutions that may be preferred.			

 $C_{f_0(980) K_S^0} (B^0 \rightarrow f_0(980) K_S^0)$

VALUE	DOCUMENT ID	TECN	COMMENT
0.29 ± 0.20 OUR AVERAGE			
$0.28 \pm 0.24 \pm 0.09$	¹ LEES	12o	BABR $e^+ e^- \rightarrow \Upsilon(4S)$
$0.30 \pm 0.29 \pm 0.14$	^{2,3} NAKAHAMA	10	BELL $e^+ e^- \rightarrow \Upsilon(4S)$
••• We do not use the following data for averages, fits, limits, etc. •••			
$0.08 \pm 0.19 \pm 0.05$	⁴ AUBERT	09AU	BABR Repl. by LEES 12o
$0.06 \pm 0.17 \pm 0.11$	^{2,5} DALSENO	09	BELL Repl. by NAKAHAMA 10
$-0.41 \pm 0.23 \pm 0.07$	² AUBERT	07AX	BABR Repl. by AUBERT 09AU
$0.15 \pm 0.15 \pm 0.07$	² CHAO	07	BELL Repl. by DALSENO 09
$0.39 \pm 0.27 \pm 0.09$	² CHEN	05B	BELL Repl. by CHAO 07
¹ Uses Dalitz plot analysis of the $B^0 \rightarrow K_S^0 K^+ K^-$ decay.			
² Quotes $A_{f_0(980) K_S^0}$ which is equal to $-C_{f_0(980) K_S^0}$.			
³ Uses Dalitz plot analysis of $B^0 \rightarrow K_S^0 K^+ K^-$ decays and the first of four consistent solutions that may be preferred.			
⁴ Uses Dalitz plot analysis of $B^0 \rightarrow K^0 \pi^+ \pi^-$ decays and the first of two equivalent solutions is used.			
⁵ Uses Dalitz plot analysis of $B^0 \rightarrow K^0 \pi^+ \pi^-$ decays and the first of two consistent solutions that may be preferred.			

 $S_{f_0(980) K_S^0} (B^0 \rightarrow f_0(980) K_S^0)$

VALUE	DOCUMENT ID	TECN	COMMENT
-0.50 ± 0.16 OUR AVERAGE			
$-0.55 \pm 0.18 \pm 0.12$	¹ LEES	12o	BABR $e^+ e^- \rightarrow \Upsilon(4S)$
$-0.43 \pm 0.22 \pm 0.14$	² DALSENO	09	BELL $e^+ e^- \rightarrow \Upsilon(4S)$

• • • We do not use the following data for averages, fits, limits, etc. • • •

$-0.96^{+0.21}_{-0.04} \pm 0.04$	³ AUBERT	09AU BABR	Repl. by LEES 12o
$-0.25 \pm 0.26 \pm 0.10$	⁴ AUBERT	07AX BABR	Repl. by AUBERT 09AU
$0.18 \pm 0.23 \pm 0.11$	CHAO	07 BELL	Repl. by DALSENO 09
$0.47 \pm 0.41 \pm 0.08$	CHEN	05B BELL	Repl. by CHAO 07

¹ Uses Dalitz plot analysis of the $B^0 \rightarrow K_S^0 K^+ K^-$ decay.

² Uses Dalitz plot analysis of $B^0 \rightarrow K^0 \pi^+ \pi^-$ decays and the first of two consistent solutions that may be preferred.

³ Uses Dalitz plot analysis of $B^0 \rightarrow K^0 \pi^+ \pi^-$ decays and the first of two equivalent solutions is used.

⁴ Reports β_{eff} . We quote S obtained from epaps: E-PRLTAO-99-076741.

$S_{f_2(1270) K_S^0} (B^0 \rightarrow f_2(1270) K_S^0)$

VALUE	DOCUMENT ID	TECN	COMMENT
$-0.48 \pm 0.52 \pm 0.12$	¹ AUBERT	09AU BABR	$e^+ e^- \rightarrow \Upsilon(4S)$

¹ Uses Dalitz plot analysis of $B^0 \rightarrow K^0 \pi^+ \pi^-$ decays and the first of two equivalent solutions is used.

$C_{f_2(1270) K_S^0} (B^0 \rightarrow f_2(1270) K_S^0)$

VALUE	DOCUMENT ID	TECN	COMMENT
$0.28^{+0.35}_{-0.40} \pm 0.11$	¹ AUBERT	09AU BABR	$e^+ e^- \rightarrow \Upsilon(4S)$

¹ Uses Dalitz plot analysis of $B^0 \rightarrow K^0 \pi^+ \pi^-$ decays and the first of two equivalent solutions is used.

$S_{f_x(1300) K_S^0} (B^0 \rightarrow f_x(1300) K_S^0)$

VALUE	DOCUMENT ID	TECN	COMMENT
$-0.20 \pm 0.52 \pm 0.10$	¹ AUBERT	09AU BABR	$e^+ e^- \rightarrow \Upsilon(4S)$

¹ Uses Dalitz plot analysis of $B^0 \rightarrow K^0 \pi^+ \pi^-$ decays and the first of two equivalent solutions is used.

$C_{f_x(1300) K_S^0} (B^0 \rightarrow f_x(1300) K_S^0)$

VALUE	DOCUMENT ID	TECN	COMMENT
$0.13^{+0.33}_{-0.35} \pm 0.10$	¹ AUBERT	09AU BABR	$e^+ e^- \rightarrow \Upsilon(4S)$

¹ Uses Dalitz plot analysis of $B^0 \rightarrow K^0 \pi^+ \pi^-$ decays and the first of two equivalent solutions is used.

$S_{K^0 \pi^+ \pi^-} (B^0 \rightarrow K^0 \pi^+ \pi^- \text{ nonresonant})$

VALUE	DOCUMENT ID	TECN	COMMENT
$-0.01 \pm 0.31 \pm 0.10$	¹ AUBERT	09AU BABR	$e^+ e^- \rightarrow \Upsilon(4S)$

¹ Uses Dalitz plot analysis of $B^0 \rightarrow K^0 \pi^+ \pi^-$ decays and the first of two equivalent solutions is used.

$C_{K^0 \pi^+ \pi^-} (B^0 \rightarrow K^0 \pi^+ \pi^- \text{ nonresonant})$

VALUE	DOCUMENT ID	TECN	COMMENT
$0.01 \pm 0.25 \pm 0.08$	¹ AUBERT	09AU BABR	$e^+ e^- \rightarrow \Upsilon(4S)$

¹ Uses Dalitz plot analysis of $B^0 \rightarrow K^0 \pi^+ \pi^-$ decays and the first of two equivalent solutions is used.

$C_{K_S^0 K_S^0} (B^0 \rightarrow K_S^0 K_S^0)$

VALUE	DOCUMENT ID	TECN	COMMENT
0.0 ± 0.4 OUR AVERAGE	Error includes scale factor of 1.4.		
$0.38 \pm 0.38 \pm 0.05$	¹ NAKAHAMA	08 BELL	$e^+ e^- \rightarrow \Upsilon(4S)$
$-0.40 \pm 0.41 \pm 0.06$	AUBERT, BE	06c BABR	$e^+ e^- \rightarrow \Upsilon(4S)$

¹ Reports $A_{K_S^0 K_S^0}$ which equals to $-C_{K_S^0 K_S^0}$.

$S_{K_S^0 K_S^0} (B^0 \rightarrow K_S^0 K_S^0)$

VALUE	DOCUMENT ID	TECN	COMMENT
-0.8 ± 0.5 OUR AVERAGE			
$-0.38^{+0.69}_{-0.77} \pm 0.09$	NAKAHAMA	08 BELL	$e^+ e^- \rightarrow \Upsilon(4S)$
$-1.28^{+0.80}_{-0.73} \pm 0.11$	AUBERT, BE	06c BABR	$e^+ e^- \rightarrow \Upsilon(4S)$

$C_{K^+ K^- K_S^0} (B^0 \rightarrow K^+ K^- K_S^0 \text{ nonresonant})$

VALUE	DOCUMENT ID	TECN	COMMENT
0.06 ± 0.08 OUR AVERAGE			
$0.02 \pm 0.09 \pm 0.03$	^{1,2} LEES	12o BABR	$e^+ e^- \rightarrow \Upsilon(4S)$
$0.14 \pm 0.11 \pm 0.09$	^{3,4} NAKAHAMA	10 BELL	$e^+ e^- \rightarrow \Upsilon(4S)$

• • • We do not use the following data for averages, fits, limits, etc. • • •

$0.054 \pm 0.102 \pm 0.060$	^{3,5} AUBERT	07AX BABR	Repl. by LEES 12o
$0.09 \pm 0.10 \pm 0.05$	^{3,5} CHAO	07 BELL	Repl. by NAKAHAMA 10
$0.10 \pm 0.14 \pm 0.04$	⁵ AUBERT	05T BABR	Repl. by AUBERT 07AX
$0.09 \pm 0.12 \pm 0.07$	³ CHEN	05B BELL	Repl. by CHAO 07
$-0.10 \pm 0.19 \pm 0.10$	⁵ AUBERT, B	04V BABR	Repl. by AUBERT 05T
$0.40 \pm 0.33 \pm 0.28$	³ ABE	03C BELL	Repl. by ABE 03H
$0.17 \pm 0.16 \pm 0.04$	^{3,5} ABE	03H BELL	Repl. by CHEN 05B

¹ Uses Dalitz plot analysis of the $B^0 \rightarrow K_S^0 K^+ K^-$ decay.

² This measurement is performed on all the isobar components, excluding ϕK_S^0 and $\eta(980) K_S^0$.

³ Quotes $A_{K^+ K^- K_S^0}$ which is equal to $-C_{K^+ K^- K_S^0}$.

⁴ Uses Dalitz plot analysis of $B^0 \rightarrow K_S^0 K^+ K^-$ decays and the first of four consistent solutions that may be preferred.

⁵ Excludes the events from $B^0 \rightarrow \phi K_S^0$ decay. The results are derived from a combined sample of $K^+ K^- K_S^0$ and $K^+ K^- K_L^0$ decays.

$S_{K^+ K^- K_S^0} (B^0 \rightarrow K^+ K^- K_S^0 \text{ nonresonant})$

VALUE	DOCUMENT ID	TECN	COMMENT
-0.66 ± 0.11 OUR AVERAGE			
$-0.65 \pm 0.12 \pm 0.03$	^{1,2} LEES	12o BABR	$e^+ e^- \rightarrow \Upsilon(4S)$
$-0.68 \pm 0.15^{+0.21}_{-0.13}$	³ CHAO	07 BELL	$e^+ e^- \rightarrow \Upsilon(4S)$

• • • We do not use the following data for averages, fits, limits, etc. • • •

$-0.764 \pm 0.111^{+0.071}_{-0.040}$	^{3,4} AUBERT	07AX BABR	Repl. by LEES 12o
$-0.42 \pm 0.17 \pm 0.03$	^{3,5} AUBERT	05T BABR	Repl. by AUBERT 07AX
$-0.49 \pm 0.18 \pm 0.04$	CHEN	05B BELL	Repl. by CHAO 07
$-0.56 \pm 0.25 \pm 0.04$	^{3,6} AUBERT, B	04V BABR	Repl. by AUBERT 05T
$-0.49 \pm 0.43 \pm 0.11$	ABE	03C BELL	Repl. by ABE 03H
$-0.51 \pm 0.26 \pm 0.05$	^{3,7} ABE	03H BELL	Repl. by CHEN 05B

¹ Uses Dalitz plot analysis of the $B^0 \rightarrow K_S^0 K^+ K^-$ decay.

² This measurement is performed on all the isobar components, excluding ϕK_S^0 and $\eta(980) K_S^0$. Note that the nonresonant component is not a CP eigenstate.

³ Excludes events from $B^0 \rightarrow \phi K_S^0$ decay. The results are derived from a combined sample of $K^+ K^- K_S^0$ and $K^+ K^- K_L^0$ decays.

⁴ Reports β_{eff} . We quote S obtained from epaps: E-PRLTAO-99-076741.

⁵ The measured CP -even final states fraction is $0.89 \pm 0.08 \pm 0.06$.

⁶ The measured CP -even final states fraction is $0.98 \pm 0.15 \pm 0.04$.

⁷ The measured CP -even final states fraction is $1.03 \pm 0.15 \pm 0.05$.

$C_{K^+ K^- K_S^0} (B^0 \rightarrow K^+ K^- K_S^0 \text{ inclusive})$

VALUE	DOCUMENT ID	TECN	COMMENT
$0.015 \pm 0.077 \pm 0.053$	^{1,2} AUBERT	07AX BABR	$e^+ e^- \rightarrow \Upsilon(4S)$

¹ Measured using full Dalitz plot fit including ϕ component.

² The results are derived from a combined sample of $K^+ K^- K_S^0$ and $K^+ K^- K_L^0$ decays.

$S_{K^+ K^- K_S^0} (B^0 \rightarrow K^+ K^- K_S^0 \text{ inclusive})$

VALUE	DOCUMENT ID	TECN	COMMENT
$-0.647 \pm 0.116 \pm 0.040$	¹ AUBERT	07AX BABR	$e^+ e^- \rightarrow \Upsilon(4S)$

¹ Measured using full Dalitz plot fit including ϕ component.

$C_{\phi K_S^0} (B^0 \rightarrow \phi K_S^0)$

VALUE	DOCUMENT ID	TECN	COMMENT
0.01 ± 0.14 OUR AVERAGE			
$0.05 \pm 0.18 \pm 0.05$	¹ LEES	12o BABR	$e^+ e^- \rightarrow \Upsilon(4S)$
$-0.04 \pm 0.20 \pm 0.10$	^{2,3} NAKAHAMA	10 BELL	$e^+ e^- \rightarrow \Upsilon(4S)$

• • • We do not use the following data for averages, fits, limits, etc. • • •

$0.08 \pm 0.18 \pm 0.04$	^{2,4} AUBERT	07AX BABR	Repl. by LEES 12o
$-0.07 \pm 0.15 \pm 0.05$	^{2,4} CHEN	07 BELL	Repl. by NAKAHAMA 10
$0.00 \pm 0.23 \pm 0.05$	⁴ AUBERT	05T BABR	Repl. by AUBERT 07AX
$-0.08 \pm 0.22 \pm 0.09$	^{2,4} CHEN	05B BELL	Repl. by CHEN 07
$0.01 \pm 0.33 \pm 0.10$	⁴ AUBERT, B	04G BABR	Repl. by AUBERT 05T
$0.56 \pm 0.41 \pm 0.16$	² ABE	03C BELL	Repl. by ABE 03H
$0.15 \pm 0.29 \pm 0.07$	² ABE	03H BELL	Repl. by CHEN 05B

¹ Uses Dalitz plot analysis of the $B^0 \rightarrow K_S^0 K^+ K^-$ decay.

² Quotes $A_{\phi K_S^0}$ which is equal to $-C_{\phi K_S^0}$.

³ Uses Dalitz plot analysis of $B^0 \rightarrow K_S^0 K^+ K^-$ decays and the first of four consistent solutions that may be preferred.

⁴ Result combines B -meson final states ϕK_S^0 and ϕK_L^0 by assuming $S_{\phi K_S^0} = -S_{\phi K_L^0}$.

$S_{\phi K_S^0} (B^0 \rightarrow \phi K_S^0)$

VALUE	DOCUMENT ID	TECN	COMMENT
0.59 ± 0.14 OUR AVERAGE			
$0.66 \pm 0.17 \pm 0.07$	¹ LEES	12o BABR	$e^+ e^- \rightarrow \Upsilon(4S)$
$0.50 \pm 0.21 \pm 0.06$	² CHEN	07 BELL	$e^+ e^- \rightarrow \Upsilon(4S)$

• • • We do not use the following data for averages, fits, limits, etc. • • •

$0.21 \pm 0.26 \pm 0.11$	^{2,3} AUBERT	07AX BABR	Repl. by LEES 12o
$0.50 \pm 0.25^{+0.07}_{-0.04}$	² AUBERT	05T BABR	Repl. by AUBERT 07AX
$0.08 \pm 0.33 \pm 0.09$	² CHEN	05B BELL	Repl. by CHEN 07
$0.47 \pm 0.34^{+0.08}_{-0.06}$	² AUBERT, B	04G BABR	Repl. by AUBERT 05T
$-0.73 \pm 0.64 \pm 0.22$	ABE	03C BELL	Repl. by ABE 03H
$-0.96 \pm 0.50^{+0.09}_{-0.11}$	ABE	03H BELL	Repl. by CHEN 05B

¹ Uses Dalitz plot analysis of the $B^0 \rightarrow K_S^0 K^+ K^-$ decay.

² Result combines B -meson final states ϕK_S^0 and ϕK_L^0 by assuming $S_{\phi K_S^0} = -S_{\phi K_L^0}$.

³ Reports β_{eff} . We quote S obtained from epaps: E-PRLTAO-99-076741.

Meson Particle Listings

 B^0 $C_{K_S K_S K_S}(B^0 \rightarrow K_S K_S K_S)$

VALUE	DOCUMENT ID	TECN	COMMENT
-0.14 ± 0.12 OUR AVERAGE			
$-0.12 \pm 0.16 \pm 0.05$	1 KANG 21	BELL	$e^+ e^- \rightarrow \Upsilon(4S)$
$-0.17 \pm 0.18 \pm 0.04$	LEES 12i	BABR	$e^+ e^- \rightarrow \Upsilon(4S)$
• • • We do not use the following data for averages, fits, limits, etc. • • •			
$0.02 \pm 0.21 \pm 0.05$	AUBERT 07AT	BABR	Repl. by LEES 12i
$-0.31 \pm 0.20 \pm 0.07$	1 CHEN 07	BELL	Repl. by KANG 21
$-0.34 \pm 0.28 \pm 0.05$	AUBERT,B 05	BABR	Repl. by AUBERT 07AT
$-0.54 \pm 0.34 \pm 0.09$	1 SUMISAWA 05	BELL	Repl. by CHEN 07
1 KANG 21 quotes $A_{K_S^0 K_S^0 K_S^0}$ which is equal to $-C_{K_S^0 K_S^0 K_S^0}$.			

 $S_{K_S K_S K_S}(B^0 \rightarrow K_S K_S K_S)$

VALUE	DOCUMENT ID	TECN	COMMENT
-0.82 ± 0.17 OUR AVERAGE			
$-0.71 \pm 0.23 \pm 0.05$	KANG 21	BELL	$e^+ e^- \rightarrow \Upsilon(4S)$
$-0.94 \pm 0.24 \pm 0.06$	LEES 12i	BABR	$e^+ e^- \rightarrow \Upsilon(4S)$
• • • We do not use the following data for averages, fits, limits, etc. • • •			
$-0.71 \pm 0.24 \pm 0.04$	AUBERT 07AT	BABR	Repl. by LEES 12i
$0.30 \pm 0.32 \pm 0.08$	CHEN 07	BELL	Repl. by KANG 21
$-0.71 \pm 0.38 \pm 0.04$	AUBERT,B 05	BABR	Repl. by AUBERT 07AT
$1.26 \pm 0.68 \pm 0.20$	SUMISAWA 05	BELL	Repl. by CHEN 07.

 $C_{K_S^0 \pi^0 \gamma}(B^0 \rightarrow K_S^0 \pi^0 \gamma)$

VALUE	DOCUMENT ID	TECN	COMMENT
$0.36 \pm 0.33 \pm 0.04$	1 AUBERT 08BA	BABR	$e^+ e^- \rightarrow \Upsilon(4S)$
• • • We do not use the following data for averages, fits, limits, etc. • • •			
$0.20 \pm 0.20 \pm 0.06$	2,3 USHIRODA 06	BELL	$e^+ e^- \rightarrow \Upsilon(4S)$
$-1.0 \pm 0.5 \pm 0.2$	1 AUBERT,B 05P	BABR	Repl. by AUBERT 08BA
$-0.03 \pm 0.34 \pm 0.11$	3 USHIRODA 05	BELL	Repl. by USHIRODA 06
1 Requires $1.1 < M_{K_S^0 \pi^0} < 1.8$ GeV/c ² .			
2 Requires $M_{K_S^0 \pi^0} < 1.8$ GeV/c ² .			
3 Reports $A_{K_S^0 \pi^0 \gamma}$, which is $-C_{K_S^0 \pi^0 \gamma}$.			

 $S_{K_S^0 \pi^0 \gamma}(B^0 \rightarrow K_S^0 \pi^0 \gamma)$

VALUE	DOCUMENT ID	TECN	COMMENT
$-0.78 \pm 0.59 \pm 0.09$	1 AUBERT 08BA	BABR	$e^+ e^- \rightarrow \Upsilon(4S)$
• • • We do not use the following data for averages, fits, limits, etc. • • •			
$-0.10 \pm 0.31 \pm 0.07$	2 USHIRODA 06	BELL	$e^+ e^- \rightarrow \Upsilon(4S)$
$0.9 \pm 1.0 \pm 0.2$	1 AUBERT,B 05P	BABR	Repl. by AUBERT 08BA
$-0.58 \pm 0.46 \pm 0.11$	USHIRODA 05	BELL	Repl. by USHIRODA 06
1 Requires $1.1 < M_{K_S^0 \pi^0} < 1.8$ GeV/c ² .			
2 Requires $M_{K_S^0 \pi^0} < 1.8$ GeV/c ² .			

 $C_{K_S^0 \pi^+ \pi^- \gamma}(B^0 \rightarrow K_S^0 \pi^+ \pi^- \gamma)$

VALUE	DOCUMENT ID	TECN	COMMENT
$-0.39 \pm 0.20 \pm 0.03$	1 DEL-AMO-SA..16	BABR	$e^+ e^- \rightarrow \Upsilon(4S)$
• • • We do not use the following data for averages, fits, limits, etc. • • •			
$-0.10 \pm 0.31 \pm 0.07$	2 USHIRODA 06	BELL	$e^+ e^- \rightarrow \Upsilon(4S)$
$0.9 \pm 1.0 \pm 0.2$	1 AUBERT,B 05P	BABR	Repl. by AUBERT 08BA
$-0.58 \pm 0.46 \pm 0.11$	USHIRODA 05	BELL	Repl. by USHIRODA 06
1 Requires $1.1 < M_{K_S^0 \pi^0} < 1.8$ GeV/c ² .			
2 Requires $M_{K_S^0 \pi^0} < 1.8$ GeV/c ² .			

 $S_{K_S^0 \pi^+ \pi^- \gamma}(B^0 \rightarrow K_S^0 \pi^+ \pi^- \gamma)$

VALUE	DOCUMENT ID	TECN	COMMENT
$0.14 \pm 0.25 \pm 0.03$	1 DEL-AMO-SA..16	BABR	$e^+ e^- \rightarrow \Upsilon(4S)$
• • • We do not use the following data for averages, fits, limits, etc. • • •			
$-0.40 \pm 0.23 \pm 0.03$	AUBERT,B 05P	BABR	Repl. by AUBERT 08BA
$-0.57 \pm 0.32 \pm 0.09$	3 AUBERT,B 04Z	BABR	Repl. by AUBERT,B 05P
1 Requires $0.8 < M_{K_S^0 \pi^0} < 1.0$ GeV/c ² .			
2 Reports value of A which is equal to $-C$.			
3 Based on a total signal of 105 ± 14 events with $K^*(892)^0 \rightarrow K_S^0 \pi^0$ only.			

 $C_{K^*(892)^0 \gamma}(B^0 \rightarrow K^*(892)^0 \gamma)$

VALUE	DOCUMENT ID	TECN	COMMENT
-0.04 ± 0.16 OUR AVERAGE			
$-0.14 \pm 0.16 \pm 0.03$	1 AUBERT 08BA	BABR	$e^+ e^- \rightarrow \Upsilon(4S)$
$0.20 \pm 0.24 \pm 0.05$	1,2 USHIRODA 06	BELL	$e^+ e^- \rightarrow \Upsilon(4S)$
• • • We do not use the following data for averages, fits, limits, etc. • • •			
$-0.40 \pm 0.23 \pm 0.03$	AUBERT,B 05P	BABR	Repl. by AUBERT 08BA
$-0.57 \pm 0.32 \pm 0.09$	3 AUBERT,B 04Z	BABR	Repl. by AUBERT,B 05P
1 Requires $0.8 < M_{K_S^0 \pi^0} < 1.0$ GeV/c ² .			
2 Reports value of A which is equal to $-C$.			
3 Based on a total signal of 105 ± 14 events with $K^*(892)^0 \rightarrow K_S^0 \pi^0$ only.			

 $S_{K^*(892)^0 \gamma}(B^0 \rightarrow K^*(892)^0 \gamma)$

VALUE	DOCUMENT ID	TECN	COMMENT
-0.15 ± 0.22 OUR AVERAGE			
$-0.03 \pm 0.29 \pm 0.03$	1 AUBERT 08BA	BABR	$e^+ e^- \rightarrow \Upsilon(4S)$
$-0.32 \pm 0.36 \pm 0.05$	1 USHIRODA 06	BELL	$e^+ e^- \rightarrow \Upsilon(4S)$

• • • We do not use the following data for averages, fits, limits, etc. • • •

$-0.21 \pm 0.40 \pm 0.05$	AUBERT,B 05P	BABR	Repl. by AUBERT 08BA
$-0.79 \pm 0.63 \pm 0.10$	2 USHIRODA 05	BELL	Repl. by USHIRODA 06
$0.25 \pm 0.63 \pm 0.14$	3 AUBERT,B 04Z	BABR	Repl. by AUBERT,B 05P
1 Requires $0.8 < M_{K_S^0 \pi^0} < 1.0$ GeV/c ² .			
2 Assumes $C(B^0 \rightarrow K^*(892)^0 \gamma) = 0$.			
3 Based on a total signal of 105 ± 14 events with $K^*(892)^0 \rightarrow K_S^0 \pi^0$ only.			

 $C_{\eta K^0 \gamma}(B^0 \rightarrow \eta K^0 \gamma)$

VALUE	DOCUMENT ID	TECN	COMMENT
0.1 ± 0.4 OUR AVERAGE			
$0.48 \pm 0.41 \pm 0.07$	1,2 NAKANO 18	BELL	$e^+ e^- \rightarrow \Upsilon(4S)$
$-0.32 \pm 0.40 \pm 0.07$	3 AUBERT 09	BABR	$e^+ e^- \rightarrow \Upsilon(4S)$
1 Assuming $m_{\eta K_S^0} < 2.1$ GeV.			
2 Reversed the sign for C=-A.			
3 Assuming $m_{\eta K} < 3.25$ GeV.			

 $S_{\eta K^0 \gamma}(B^0 \rightarrow \eta K^0 \gamma)$

VALUE	DOCUMENT ID	TECN	COMMENT
-0.5 ± 0.5 OUR AVERAGE			
$-1.32 \pm 0.77 \pm 0.36$	1 NAKANO 18	BELL	$e^+ e^- \rightarrow \Upsilon(4S)$
$-0.18 \pm 0.49 \pm 0.12$	2 AUBERT 09	BABR	$e^+ e^- \rightarrow \Upsilon(4S)$
1 Assuming $m_{\eta K_S^0} < 2.1$ GeV.			
2 Assuming $m_{\eta K} < 3.25$ GeV.			

 $C_{K^0 \phi \gamma}(B^0 \rightarrow K^0 \phi \gamma)$

VALUE	DOCUMENT ID	TECN	COMMENT
$-0.35 \pm 0.58 \pm 0.10$	1 SAHOO 11A	BELL	$e^+ e^- \rightarrow \Upsilon(4S)$
1 Reports value of A, which is equal to $-C$.			

 $S_{K^0 \phi \gamma}(B^0 \rightarrow K^0 \phi \gamma)$

VALUE	DOCUMENT ID	TECN	COMMENT
$0.74 \pm 0.72 \pm 0.10$	SAHOO 11A	BELL	$e^+ e^- \rightarrow \Upsilon(4S)$
-1.05 ± 0.24			

 $C(B^0 \rightarrow K_S^0 \rho^0 \gamma)$

VALUE	DOCUMENT ID	TECN	COMMENT
$-0.05 \pm 0.18 \pm 0.06$	1,2 LI 08F	BELL	$e^+ e^- \rightarrow \Upsilon(4S)$
1 Requires $M_{K_S^0 \pi^+ \pi^-} < 1.8$ GeV/c ² and $0.6 < M_{\pi^+ \pi^-} < 0.9$ GeV/c ² .			
2 Reports value of A_{eff} which is equal to $-C$, and includes the non-resonant $\pi^+ \pi^-$ contribution in the ρ^0 region.			

 $S(B^0 \rightarrow K_S^0 \rho^0 \gamma)$

VALUE	DOCUMENT ID	TECN	COMMENT
-0.04 ± 0.23 OUR AVERAGE			
$-0.18 \pm 0.32 \pm 0.06$	1 DEL-AMO-SA..16	BABR	$e^+ e^- \rightarrow \Upsilon(4S)$
$0.11 \pm 0.33 \pm 0.05$	2 LI 08F	BELL	$e^+ e^- \rightarrow \Upsilon(4S)$
1 Requires $M_{K \pi \pi} < 1.8$ GeV/c ² , 0.6 GeV/c ² $< m_{\pi^+ \pi^-} < 0.9$ GeV/c ² , $m_{K \pi} < 0.845$ GeV/c ² or $m_{K \pi} > 0.945$ GeV/c ² .			
2 Requires $M_{K \pi \pi} < 1.8$ GeV/c ² .			

 $C(B^0 \rightarrow \rho^0 \gamma)$

VALUE	DOCUMENT ID	TECN	COMMENT
$0.44 \pm 0.49 \pm 0.14$	1 USHIRODA 08	BELL	$e^+ e^- \rightarrow \Upsilon(4S)$
1 Reports value of A which is equal to $-C$.			

 $S(B^0 \rightarrow \rho^0 \gamma)$

VALUE	DOCUMENT ID	TECN	COMMENT
$-0.83 \pm 0.65 \pm 0.18$	USHIRODA 08	BELL	$e^+ e^- \rightarrow \Upsilon(4S)$

 $C_{\pi \pi}(B^0 \rightarrow \pi^+ \pi^-)$

$C_{\pi \pi}$ is defined as $(1 - |\lambda|^2)/(1 + |\lambda|^2)$, where the quantity $\lambda = q/p \bar{A}_f/A_f$ is a phase convention independent observable quantity for the final state f . For details, see the review on "CP Violation" in the Reviews section.

VALUE	DOCUMENT ID	TECN	COMMENT
-0.314 ± 0.030 OUR AVERAGE			
$-0.311 \pm 0.045 \pm 0.015$	AAIJ 21o	LHCB	pp at 13 TeV
$-0.34 \pm 0.06 \pm 0.01$	AAIJ 18o	LHCB	pp at 7, 8 TeV
$-0.33 \pm 0.06 \pm 0.03$	1 DALSENO 13	BELL	$e^+ e^- \rightarrow \Upsilon(4S)$
$-0.25 \pm 0.08 \pm 0.02$	LEES 13D	BABR	$e^+ e^- \rightarrow \Upsilon(4S)$
• • • We do not use the following data for averages, fits, limits, etc. • • •			
$-0.38 \pm 0.15 \pm 0.02$	AAIJ 13Bo	LHCB	Repl. by AAJ 18o
$-0.21 \pm 0.09 \pm 0.02$	AUBERT 07AF	BABR	Repl. by LEES 13D
$-0.55 \pm 0.08 \pm 0.05$	1 ISHINO 07	BELL	Repl. by DALSENO 13
$-0.56 \pm 0.12 \pm 0.06$	1 ABE 05D	BELL	Repl. by ISHINO 07
$-0.09 \pm 0.15 \pm 0.04$	AUBERT,BE 05	BABR	Repl. by AUBERT 07AF

-0.58 ± 0.15 ± 0.07	¹ ABE	04E	BELL	Repl. by ABE 05D
-0.77 ± 0.27 ± 0.08	¹ ABE	03G	BELL	Repl. by ABE 04E.
-0.94 ± 0.31 ± 0.09	¹ ABE	02M	BELL	Repl. by ABE 03G
-0.25 ± 0.45 ± 0.14	² AUBERT	02D	BABR	Repl. by AUBERT 02Q
-0.30 ± 0.25 ± 0.04	³ AUBERT	02Q	BABR	Repl. by AUBERT, BE 05

¹ Paper reports $A_{\pi\pi}$ which equals to $-C_{\pi\pi}$.
² Corresponds to 90% confidence range $-1.0 < C_{\pi\pi} < 0.47$.
³ Corresponds to 90% confidence range $-0.72 < C_{\pi\pi} < 0.12$.

S_{ππ}(B⁰ → π⁺π⁻)

$S_{\pi\pi} = 2\text{Im}\lambda/(1+|\lambda|^2)$, see the note in the $C_{\pi\pi}$ datablock above.

VALUE	DOCUMENT ID	TECN	COMMENT
-0.670 ± 0.030 OUR AVERAGE			
-0.706 ± 0.042 ± 0.013	AAIJ	21o	LHCB pp at 13 TeV
-0.63 ± 0.05 ± 0.01	AAIJ	18o	LHCB pp at 7, 8 TeV
-0.64 ± 0.08 ± 0.03	¹ DALSENO	13	BELL e ⁺ e ⁻ → T(4S)
-0.68 ± 0.10 ± 0.03	LEES	13D	BABR e ⁺ e ⁻ → T(4S)
••• We do not use the following data for averages, fits, limits, etc. •••			
-0.71 ± 0.13 ± 0.02	AAIJ	13Bo	LHCB Repl. by AAIJ 18o
-0.60 ± 0.11 ± 0.03	AUBERT	07AF	BABR Repl. by LEES 13D
-0.61 ± 0.10 ± 0.04	ISHINO	07	BELL Repl. by DALSENO 13
-0.67 ± 0.16 ± 0.06	² ABE	05D	BELL Repl. by ISHINO 07
-0.30 ± 0.17 ± 0.03	AUBERT, BE	05	BABR Repl. by AUBERT 07AF
-1.00 ± 0.21 ± 0.07	³ ABE	04E	BELL Repl. by ABE 05D
-1.23 ± 0.41 ± 0.08	ABE	03G	BELL Repl. by ABE 04E.
-1.21 ± 0.38 ± 0.16	ABE	02M	BELL Repl. by ABE 03G
0.03 ± 0.52 ± 0.11	⁴ AUBERT	02D	BABR Repl. by AUBERT 02Q
0.02 ± 0.34 ± 0.05	⁵ AUBERT	02Q	BABR Repl. by AUBERT, BE 05

¹ An isospin analysis using other BELLE measurements, disfavors the region of 23.8° < φ₂ < 66.8° at 68% CL.
² Rule out the CP-conserving case, $C_{\pi\pi} = S_{\pi\pi} = 0$, at the 5.4 sigma level.
³ Rule out the CP-conserving case, $C_{\pi\pi} = S_{\pi\pi} = 0$, at the 5.2 sigma level.
⁴ Corresponds to 90% confidence range $-0.89 < S_{\pi\pi} < 0.85$.
⁵ Corresponds to 90% confidence range $-0.54 < S_{\pi\pi} < 0.58$.

C_{π⁰π⁰}(B⁰ → π⁰π⁰)

VALUE	DOCUMENT ID	TECN	COMMENT
-0.33 ± 0.22 OUR AVERAGE			
-0.14 ± 0.36 ± 0.10	¹ JULIUS	17	BELL e ⁺ e ⁻ → T(4S)
-0.43 ± 0.26 ± 0.05	LEES	13D	BABR e ⁺ e ⁻ → T(4S)
••• We do not use the following data for averages, fits, limits, etc. •••			
-0.49 ± 0.35 ± 0.05	AUBERT	07Bc	BABR Repl. by LEES 13D
-0.12 ± 0.56 ± 0.06	² AUBERT	05L	BABR Repl. by AUBERT 07Bc
-0.44 ± 0.53 ± 0.17	¹ CHAO	05	BELL Repl. by JULIUS 17

¹ BELLE Collab. quotes $A_{\pi^0\pi^0}$ which is equal to $-C_{\pi^0\pi^0}$.
² Corresponds to a 90% CL interval of $-0.88 < A_{CP} < 0.64$.

C_{ρπ}(B⁰ → ρ⁺π⁻)

VALUE	DOCUMENT ID	TECN	COMMENT
-0.03 ± 0.07 OUR AVERAGE			Error includes scale factor of 1.2.
-0.016 ± 0.059 ± 0.036	¹ LEES	13J	BABR e ⁺ e ⁻ → T(4S)
-0.13 ± 0.09 ± 0.05	¹ KUSAKA	07	BELL e ⁺ e ⁻ → T(4S)
••• We do not use the following data for averages, fits, limits, etc. •••			
0.15 ± 0.09 ± 0.05	AUBERT	07AA	BABR Repl. by LEES 13J
0.25 ± 0.17 ± 0.02	WANG	05	BELL Repl. by KUSAKA 07
0.36 ± 0.18 ± 0.04	AUBERT	03T	BABR Repl. by AUBERT 07AA

¹ Uses time-dependent Dalitz plot analysis of B⁰ → π⁺π⁻π⁰ decays.

S_{ρπ}(B⁰ → ρ⁺π⁻)

VALUE	DOCUMENT ID	TECN	COMMENT
0.05 ± 0.07 OUR AVERAGE			
0.053 ± 0.081 ± 0.034	¹ LEES	13J	BABR e ⁺ e ⁻ → T(4S)
0.06 ± 0.13 ± 0.05	¹ KUSAKA	07	BELL e ⁺ e ⁻ → T(4S)
••• We do not use the following data for averages, fits, limits, etc. •••			
-0.03 ± 0.11 ± 0.04	AUBERT	07AA	BABR Repl. by LEES 13J
-0.28 ± 0.23 ± 0.08	WANG	05	BELL Repl. by KUSAKA 07
0.19 ± 0.24 ± 0.03	AUBERT	03T	BABR Repl. by AUBERT 07AA

¹ Uses time-dependent Dalitz plot analysis of B⁰ → π⁺π⁻π⁰ decays.

ΔC_{ρπ}(B⁰ → ρ⁺π⁻)

ΔC_{ρπ} describes the asymmetry between the rates Γ(B⁰ → ρ⁺π⁻) + Γ(B⁰ → ρ⁻π⁺) and Γ(B⁰ → ρ⁻π⁺) + Γ(B⁰ → ρ⁺π⁻).

VALUE	DOCUMENT ID	TECN	COMMENT
0.27 ± 0.06 OUR AVERAGE			
0.234 ± 0.061 ± 0.048	¹ LEES	13J	BABR e ⁺ e ⁻ → T(4S)
0.36 ± 0.10 ± 0.05	¹ KUSAKA	07	BELL e ⁺ e ⁻ → T(4S)

••• We do not use the following data for averages, fits, limits, etc. •••

0.39 ± 0.09 ± 0.09	AUBERT	07AA	BABR Repl. by LEES 13J
0.38 ± 0.18 ± 0.02	WANG	05	BELL Repl. by KUSAKA 07
0.28 ± 0.18 ± 0.04	AUBERT	03T	BABR Repl. by AUBERT 07AA

¹ Uses time-dependent Dalitz plot analysis of B⁰ → π⁺π⁻π⁰ decays.

ΔS_{ρπ}(B⁰ → ρ⁺π⁻)

ΔS_{ρπ} is related to the strong phase difference between the amplitudes contributing to B⁰ → ρ⁺π⁻.

VALUE	DOCUMENT ID	TECN	COMMENT
0.01 ± 0.08 OUR AVERAGE			
0.054 ± 0.082 ± 0.039	¹ LEES	13J	BABR e ⁺ e ⁻ → T(4S)
-0.08 ± 0.13 ± 0.05	¹ KUSAKA	07	BELL e ⁺ e ⁻ → T(4S)
••• We do not use the following data for averages, fits, limits, etc. •••			
-0.01 ± 0.14 ± 0.06	AUBERT	07AA	BABR Repl. by LEES 13J
-0.30 ± 0.24 ± 0.09	WANG	05	BELL Repl. by KUSAKA 07
0.15 ± 0.25 ± 0.03	AUBERT	03T	BABR Repl. by AUBERT 07AA

¹ Uses time-dependent Dalitz plot analysis of B⁰ → π⁺π⁻π⁰ decays.

C_{ρ⁰π⁰}(B⁰ → ρ⁰π⁰)

VALUE	DOCUMENT ID	TECN	COMMENT
0.27 ± 0.24 OUR AVERAGE			
0.19 ± 0.23 ± 0.15	¹ LEES	13J	BABR e ⁺ e ⁻ → T(4S)
0.49 ± 0.36 ± 0.28	^{1,2} KUSAKA	07	BELL e ⁺ e ⁻ → T(4S)
••• We do not use the following data for averages, fits, limits, etc. •••			
-0.10 ± 0.40 ± 0.53	AUBERT	07AA	BABR Repl. by LEES 13J
0.53 ± 0.67 ± 0.10	² DRAGIC	06	BELL Repl. by KUSAKA 07
-0.84 ± 0.15			

¹ Uses time-dependent Dalitz plot analysis of B⁰ → π⁺π⁻π⁰ decays.

² Quotes $A_{\rho^0\pi^0}$ which is equal to $-C_{\rho^0\pi^0}$.

S_{ρπ⁰}(B⁰ → ρ⁰π⁰)

VALUE	DOCUMENT ID	TECN	COMMENT
-0.23 ± 0.34 OUR AVERAGE			
-0.37 ± 0.34 ± 0.20	¹ LEES	13J	BABR e ⁺ e ⁻ → T(4S)
-0.17 ± 0.57 ± 0.35	¹ KUSAKA	07	BELL e ⁺ e ⁻ → T(4S)

••• We do not use the following data for averages, fits, limits, etc. •••

0.04 ± 0.44 ± 0.18 AUBERT 07AA BABR Repl. by LEES 13J

¹ Uses time-dependent Dalitz plot analysis of B⁰ → π⁺π⁻π⁰ decays.

C_{a₁π}(B⁰ → a₁(1260)⁺π⁻)

VALUE	DOCUMENT ID	TECN	COMMENT
-0.05 ± 0.11 OUR AVERAGE			
-0.01 ± 0.11 ± 0.09	DALSENO	12	BELL e ⁺ e ⁻ → T(4S)
-0.10 ± 0.15 ± 0.09	AUBERT	07o	BABR e ⁺ e ⁻ → T(4S)

S_{a₁π}(B⁰ → a₁(1260)⁺π⁻)

VALUE	DOCUMENT ID	TECN	COMMENT
-0.2 ± 0.4 OUR AVERAGE			Error includes scale factor of 3.2.
-0.51 ± 0.14 ± 0.08	DALSENO	12	BELL e ⁺ e ⁻ → T(4S)
0.37 ± 0.21 ± 0.07	AUBERT	07o	BABR e ⁺ e ⁻ → T(4S)

ΔC_{a₁π}(B⁰ → a₁(1260)⁺π⁻)

ΔC_{a₁π} describes the asymmetry between the rates Γ(B⁰ → a₁⁺π⁻) + Γ(B⁰ → a₁⁻π⁺) and Γ(B⁰ → a₁⁻π⁺) + Γ(B⁰ → a₁⁺π⁻).

VALUE	DOCUMENT ID	TECN	COMMENT
0.43 ± 0.14 OUR AVERAGE			Error includes scale factor of 1.3.
0.54 ± 0.11 ± 0.07	DALSENO	12	BELL e ⁺ e ⁻ → T(4S)
0.26 ± 0.15 ± 0.07	AUBERT	07o	BABR e ⁺ e ⁻ → T(4S)

ΔS_{a₁π}(B⁰ → a₁(1260)⁺π⁻)

ΔS_{a₁π} is related to the strong phase difference between the amplitudes contributing to B⁰ → a₁π decays.

VALUE	DOCUMENT ID	TECN	COMMENT
-0.11 ± 0.12 OUR AVERAGE			
-0.09 ± 0.14 ± 0.06	DALSENO	12	BELL e ⁺ e ⁻ → T(4S)
-0.14 ± 0.21 ± 0.06	AUBERT	07o	BABR e ⁺ e ⁻ → T(4S)

C(B⁰ → b₁⁻K⁺)

VALUE	DOCUMENT ID	TECN	COMMENT
-0.22 ± 0.23 ± 0.05			
	AUBERT	07B1	BABR e ⁺ e ⁻ → T(4S)

ΔC(B⁰ → b₁⁻π⁺)

VALUE	DOCUMENT ID	TECN	COMMENT
-1.04 ± 0.23 ± 0.08			
	AUBERT	07B1	BABR e ⁺ e ⁻ → T(4S)

C_{ρρ}(B⁰ → ρ⁰π⁰)

VALUE	DOCUMENT ID	TECN	COMMENT
0.2 ± 0.8 ± 0.3			
	AUBERT	08B8	BABR e ⁺ e ⁻ → T(4S)

Meson Particle Listings

 B^0 $S_{\rho\rho}(B^0 \rightarrow \rho^0\rho^0)$

VALUE	DOCUMENT ID	TECN	COMMENT
$0.3 \pm 0.7 \pm 0.2$	AUBERT	08BB	BABR $e^+e^- \rightarrow \Upsilon(4S)$

 $C_{\rho\rho}(B^0 \rightarrow \rho^+\rho^-)$

VALUE	DOCUMENT ID	TECN	COMMENT
0.00 ± 0.09 OUR AVERAGE			
$0.00 \pm 0.10 \pm 0.06$	¹ VANHOEFER 16	BELL	$e^+e^- \rightarrow \Upsilon(4S)$
$0.01 \pm 0.15 \pm 0.06$	AUBERT	07BF	BABR $e^+e^- \rightarrow \Upsilon(4S)$
••• We do not use the following data for averages, fits, limits, etc. •••			
$-0.16 \pm 0.21 \pm 0.08$	¹ SOMOV 07	BELL	Repl. by VANHOEFER 16
$-0.00 \pm 0.30 \pm 0.09$	¹ SOMOV 06	BELL	Repl. by SOMOV 07
$-0.03 \pm 0.18 \pm 0.09$	AUBERT,B	05C	BABR Repl. by AUBERT 07BF
$-0.17 \pm 0.27 \pm 0.14$	AUBERT,B	04R	BABR Repl. by AUBERT,B 05C

¹ BELLE Collab. quotes A_{CP} which is equal to $-C$.

 $S_{\rho\rho}(B^0 \rightarrow \rho^+\rho^-)$

VALUE	DOCUMENT ID	TECN	COMMENT
-0.14 ± 0.13 OUR AVERAGE			
$-0.13 \pm 0.15 \pm 0.05$	VANHOEFER 16	BELL	$e^+e^- \rightarrow \Upsilon(4S)$
$-0.17 \pm 0.20 \pm 0.05$	AUBERT	07BF	BABR $e^+e^- \rightarrow \Upsilon(4S)$
••• We do not use the following data for averages, fits, limits, etc. •••			
$0.19 \pm 0.30 \pm 0.08$	SOMOV 07	BELL	Repl. by VANHOEFER 16
$0.08 \pm 0.41 \pm 0.09$	SOMOV 06	BELL	Repl. by SOMOV 07
$-0.33 \pm 0.24 \pm 0.08$	AUBERT,B	05C	BABR Repl. by AUBERT 07BF
$-0.42 \pm 0.42 \pm 0.14$	AUBERT,B	04R	BABR Repl. by AUBERT,B 05C

 $|\lambda|(B^0 \rightarrow J/\psi K^*(892)^0)$

VALUE	CL%	DOCUMENT ID	TECN	COMMENT
<0.25	95	¹ AUBERT,B	04H	BABR $e^+e^- \rightarrow \Upsilon(4S)$

¹ Uses the measured cosine coefficients C and \bar{C} and assumes $|q/p| = 1$.

 $\cos 2\beta(B^0 \rightarrow J/\psi K^*(892)^0)$

$\beta(\phi_1)$ is one of the angles of CKM unitarity triangle, see the review on "CP" Violation in the Reviews section.

VALUE	DOCUMENT ID	TECN	COMMENT
1.7 ± 0.7 OUR AVERAGE			Error includes scale factor of 1.6.

2.72 ± 0.50	¹ AUBERT	05P	BABR $e^+e^- \rightarrow \Upsilon(4S)$
0.79 ± 0.27			
$0.87 \pm 0.74 \pm 0.12$	² ITOH	05	BELL $e^+e^- \rightarrow \Upsilon(4S)$

¹ The measurement is obtained when $\sin 2\beta$ is fixed to 0.726 and the sign of $\cos 2\beta$ is positive with 86% confidence level.

² The measurement is obtained with $\sin 2\beta$ fixed to 0.731.

 $\cos 2\beta(B^0 \rightarrow [K_S^0\pi^+\pi^-]_{D^{(*)}} h^0)$

VALUE	DOCUMENT ID	TECN	COMMENT
$0.91 \pm 0.22 \pm 0.11$	¹ ADACHI 18		$e^+e^- \rightarrow \Upsilon(4S)$

••• We do not use the following data for averages, fits, limits, etc. •••

$1.06 \pm 0.33 \pm 0.21$	² VOROBYEV 16	BELL	$e^+e^- \rightarrow \Upsilon(4S)$
$0.42 \pm 0.49 \pm 0.16$	³ AUBERT 07BH	BABR	$e^+e^- \rightarrow \Upsilon(4S)$
$1.87 \pm 0.40 \pm 0.22$	⁴ KROKOVNY 06	BELL	Repl. by VOROBYEV 16
-0.53 ± 0.32			

¹ Analyzes joint data sample of Belle and BaBar using Dalitz plot analysis of $D \rightarrow K_S^0\pi^+\pi^-$; the second error combines experimental systematic uncertainty and the Dalitz plot model uncertainty.

² A model-independent measurement uses the binned Dalitz plot technique.

³ AUBERT 07BH evaluates the likelihoods for the positive and negative solutions assuming $\sin(2\beta_{eff}) = 0.678$. It quotes $L_+/L_- / (L_+ + L_-) = 0.86$ corresponding to a likelihood ratio of $L_+/L_- = 6.14$ in favor of the positive solution.

⁴ KROKOVNY 06 evaluates the likelihoods for the positive and negative solutions assuming $\sin(2\beta_{eff}) = 0.689$. It quotes $L_+/L_- / (L_+ + L_-) = 0.983$ corresponding to a likelihood ratio of $L_+/L_- = 57.8$ in favor of the positive solution.

 $(S_+ + S_-)/2(B^0 \rightarrow D^{*-}\pi^+)$

$$S_{\pm} = -\frac{2\text{Im}(\lambda_{\pm})}{1+|\lambda_{\pm}|^2} \text{ where } \lambda_{+} \text{ and } \lambda_{-} \text{ are defined in the } C_{\pi\pi} \text{ datablock above for } B^0 \rightarrow D^{*-}\pi^+ \text{ and } \bar{B}^0 \rightarrow D^{*+}\pi^-.$$

VALUE	DOCUMENT ID	TECN	COMMENT
-0.039 ± 0.011 OUR AVERAGE			

$-0.046 \pm 0.013 \pm 0.015$	¹ BAHINIPATI 11	BELL	$e^+e^- \rightarrow \Upsilon(4S)$
$-0.040 \pm 0.023 \pm 0.010$	² AUBERT 06Y	BABR	$e^+e^- \rightarrow \Upsilon(4S)$
$-0.034 \pm 0.014 \pm 0.009$	¹ AUBERT 05Z	BABR	$e^+e^- \rightarrow \Upsilon(4S)$
••• We do not use the following data for averages, fits, limits, etc. •••			
$-0.039 \pm 0.020 \pm 0.013$	³ RONGA 06	BELL	Repl. by BAHINIPATI 11
$-0.030 \pm 0.028 \pm 0.018$	¹ GERSHON 05	BELL	Repl. by RONGA 06
$-0.068 \pm 0.038 \pm 0.020$	² AUBERT 04V	BABR	Repl. by AUBERT 06Y
$-0.063 \pm 0.024 \pm 0.014$	¹ AUBERT 04W	BABR	Repl. by AUBERT 05Z
$0.060 \pm 0.040 \pm 0.019$	² SARANGI 04	BELL	Repl. by RONGA 06

¹ Uses partially reconstructed $B^0 \rightarrow D^{*\pm}\pi^{\mp}$ decays.

² Uses fully reconstructed $B^0 \rightarrow D^{*\pm}\pi^{\mp}$ decays.

³ Combines the results from fully reconstructed and partially reconstructed $D^*\pi$ events by taking weighted averages. Assumes that systematic errors from physics parameters and fit biases in the two measurements are 100% correlated.

 $(S_- - S_+)/2(B^0 \rightarrow D^{*-}\pi^+)$

VALUE	DOCUMENT ID	TECN	COMMENT
-0.009 ± 0.015 OUR AVERAGE			
$-0.015 \pm 0.013 \pm 0.015$	¹ BAHINIPATI 11	BELL	$e^+e^- \rightarrow \Upsilon(4S)$
$0.049 \pm 0.042 \pm 0.015$	² AUBERT 06Y	BABR	$e^+e^- \rightarrow \Upsilon(4S)$
$-0.019 \pm 0.022 \pm 0.013$	¹ AUBERT 05Z	BABR	$e^+e^- \rightarrow \Upsilon(4S)$
••• We do not use the following data for averages, fits, limits, etc. •••			
$-0.011 \pm 0.020 \pm 0.013$	³ RONGA 06	BELL	Repl. by BAHINIPATI 11
$-0.005 \pm 0.028 \pm 0.018$	¹ GERSHON 05	BELL	Repl. by RONGA 06
$0.031 \pm 0.070 \pm 0.033$	² AUBERT 04V	BABR	Repl. by AUBERT 06Y
$-0.004 \pm 0.037 \pm 0.014$	¹ AUBERT 04W	BABR	Repl. by AUBERT 05Z
$0.049 \pm 0.040 \pm 0.019$	² SARANGI 04	BELL	Repl. by RONGA 06

¹ Uses partially reconstructed $B^0 \rightarrow D^{*\pm}\pi^{\mp}$ decays.

² Uses fully reconstructed $B^0 \rightarrow D^{*\pm}\pi^{\mp}$ decays.

³ Combines the results from fully reconstructed and partially reconstructed $D^*\pi$ events by taking weighted averages. Assumes that systematic errors from physics parameters and fit biases in the two measurements are 100% correlated.

 $(S_+ + S_-)/2(B^0 \rightarrow D^-\pi^+)$

VALUE	DOCUMENT ID	TECN	COMMENT
-0.046 ± 0.023 OUR AVERAGE			
$-0.010 \pm 0.023 \pm 0.07$	¹ AUBERT 06Y	BABR	$e^+e^- \rightarrow \Upsilon(4S)$
$-0.050 \pm 0.021 \pm 0.012$	² RONGA 06	BELL	$e^+e^- \rightarrow \Upsilon(4S)$
••• We do not use the following data for averages, fits, limits, etc. •••			
$-0.022 \pm 0.038 \pm 0.020$	¹ AUBERT 04V	BABR	Repl. by AUBERT 06Y
$-0.062 \pm 0.037 \pm 0.018$	¹ SARANGI 04	BELL	Repl. by RONGA 06

¹ Uses fully reconstructed $B^0 \rightarrow D^{\pm}\pi^{\mp}$ decays.

² Combines the results from fully reconstructed and partially reconstructed $D\pi$ events by taking weighted averages. Assumes that systematic errors from physics parameters and fit biases in the two measurements are 100% correlated.

 $(S_- - S_+)/2(B^0 \rightarrow D^-\pi^+)$

VALUE	DOCUMENT ID	TECN	COMMENT
-0.022 ± 0.021 OUR AVERAGE			
$-0.033 \pm 0.042 \pm 0.012$	¹ AUBERT 06Y	BABR	$e^+e^- \rightarrow \Upsilon(4S)$
$-0.019 \pm 0.021 \pm 0.012$	² RONGA 06	BELL	$e^+e^- \rightarrow \Upsilon(4S)$
••• We do not use the following data for averages, fits, limits, etc. •••			
$0.025 \pm 0.068 \pm 0.033$	¹ AUBERT 04V	BABR	Repl. by AUBERT 06Y
$-0.025 \pm 0.037 \pm 0.018$	¹ SARANGI 04	BELL	Repl. by RONGA 06

¹ Uses fully reconstructed $B^0 \rightarrow D^{\pm}\pi^{\mp}$ decays.

² Combines the results from fully reconstructed and partially reconstructed $D\pi$ events by taking weighted averages. Assumes that systematic errors from physics parameters and fit biases in the two measurements are 100% correlated.

 $S_+(B^0 \rightarrow D^-\pi^+)$

VALUE	DOCUMENT ID	TECN	COMMENT
$0.058 \pm 0.020 \pm 0.011$	¹ AAIJ 18Z	LHCB	pp at 7, 8 TeV

¹ Measured in the simultaneous analysis of $B^0 \rightarrow D^{\mp}\pi^{\pm}$ decays. AAIJ 18Z reports a statistical (systematic) correlation of 0.6 (-0.41) with the measured value of $S_-(B^0 \rightarrow D^+\pi^-)$.

 $S_-(B^0 \rightarrow D^+\pi^-)$

VALUE	DOCUMENT ID	TECN	COMMENT
$0.038 \pm 0.020 \pm 0.007$	¹ AAIJ 18Z	LHCB	pp at 7, 8 TeV

¹ Measured in the simultaneous analysis of $B^0 \rightarrow D^{\mp}\pi^{\pm}$ decays. AAIJ 18Z reports a statistical (systematic) correlation of 0.6 (-0.41) with the measured value of $S_+(B^0 \rightarrow D^-\pi^+)$.

 $(S_+ + S_-)/2(B^0 \rightarrow D^-\rho^+)$

VALUE	DOCUMENT ID	TECN	COMMENT
$-0.024 \pm 0.031 \pm 0.009$	¹ AUBERT 06Y	BABR	$e^+e^- \rightarrow \Upsilon(4S)$

¹ Uses fully reconstructed $B^0 \rightarrow D^-\rho^+$ decays.

 $(S_- - S_+)/2(B^0 \rightarrow D^-\rho^+)$

VALUE	DOCUMENT ID	TECN	COMMENT
$-0.098 \pm 0.055 \pm 0.018$	¹ AUBERT 06Y	BABR	$e^+e^- \rightarrow \Upsilon(4S)$

¹ Uses fully reconstructed $B^0 \rightarrow D^-\rho^+$ decays.

 $C_{\eta_c K_S^0}(B^0 \rightarrow \eta_c K_S^0)$

VALUE	DOCUMENT ID	TECN	COMMENT
$0.080 \pm 0.124 \pm 0.029$	AUBERT 09K	BABR	$e^+e^- \rightarrow \Upsilon(4S)$

 $S_{\eta_c K_S^0}(B^0 \rightarrow \eta_c K_S^0)$

VALUE	DOCUMENT ID	TECN	COMMENT
$0.925 \pm 0.160 \pm 0.057$	AUBERT 09K	BABR	$e^+e^- \rightarrow \Upsilon(4S)$

See key on page 1127

Meson Particle Listings

B^0

$C_{c\bar{c}K^{(*)0}}(B^0 \rightarrow c\bar{c}K^{(*)0})$

"OUR EVALUATION" is an average using rescaled values of the data listed below. The average and rescaling were performed by the Heavy Flavor Averaging Group (HFLAV) and are described at <https://hflav.web.cern.ch/>. The averaging/rescaling procedure takes into account correlations between the measurements.

VALUE (units 10^{-2})	DOCUMENT ID	TECN	COMMENT
-0.5 ± 1.5 OUR EVALUATION			
0.0 ± 1.4 OUR AVERAGE			
-1.7 ± 2.9	1,2 AAIJ	17BN LHCb	pp at 7, 8 TeV
$-0.6 \pm 1.6 \pm 1.2$	3 ADACHI	12A BELL	$e^+e^- \rightarrow \Upsilon(4S)$
$-29 \begin{smallmatrix} +53 \\ -44 \end{smallmatrix} \pm 6$	4 AUBERT	09AU BABR	$e^+e^- \rightarrow \Upsilon(4S)$
$2.4 \pm 2.0 \pm 1.6$	5 AUBERT	09K BABR	$e^+e^- \rightarrow \Upsilon(4S)$
• • • We do not use the following data for averages, fits, limits, etc. • • •			
$-4 \pm 7 \pm 5$	6 SAHOO	08 BELL	Repl. by ADACHI 12A
$4.9 \pm 2.3 \pm 1.8$	5 AUBERT	07AY BABR	Repl. by AUBERT 09K
$-1.8 \pm 2.1 \pm 1.4$	7 CHEN	07 BELL	Repl. by ADACHI 12A
$-0.7 \pm 4.1 \pm 3.3$	8 ABE	05B BELL	Repl. by CHEN 07
$5.1 \pm 3.2 \pm 1.4$	9 AUBERT	05F BABR	Repl. by AUBERT 07AY
$5.1 \pm 5.1 \pm 2.6$	10 ABE	02Z BELL	Repl. by ABE 05B
$5.3 \pm 5.4 \pm 3.2$	11 AUBERT	02P BABR	Repl. by AUBERT 05F

- Measurement based on $B^0 \rightarrow J/\psi K_S^0$, $B^0 \rightarrow \psi(2S) K_S^0$ with $J/\psi \rightarrow \mu^+ \mu^-$, $J/\psi \rightarrow e^+ e^-$ and $\psi(2S) \rightarrow \mu^+ \mu^-$.
- AAIJ 17BN provides the correlation coefficient $\rho=0.42$ between the uncertainties of $S_{B^0 \rightarrow c\bar{c}K^{(*)0}}(B^0 \rightarrow c\bar{c}K^{(*)0})$ and $C_{c\bar{c}K^{(*)0}}(B^0 \rightarrow c\bar{c}K^{(*)0})$ measurements.
- Measurement based on $B^0 \rightarrow J/\psi K_S^0$, $B^0 \rightarrow \psi(2S) K_S^0$, $B^0 \rightarrow J/\psi K_L^0$, and $B^0 \rightarrow \chi_{c1}(1P) K_S^0$ decays.
- Uses Dalitz plot analysis of $B^0 \rightarrow K^0 \pi^+ \pi^-$ decays and the first of two equivalent solutions is used.
- Measurement based on $B^0 \rightarrow c\bar{c}K^{(*)0}$ decays.
- Reports value of A of $B^0 \rightarrow \psi(2S) K^0$ which is equal to $-C$.
- Reports value of A of $B^0 \rightarrow J/\psi K^0$ which is equal to $-C$.
- Measurement based on $152 \times 10^6 B\bar{B}$ pairs.
- Measurement based on $227 \times 10^6 B\bar{B}$ pairs.
- Measured with both $\eta_f = \pm 1$ samples.
- Measured with the high purity of $\eta_f = -1$ samples.

$\sin(2\beta)$

For a discussion of CP violation, see the review on " CP Violation" in the Reviews section. $\sin(2\beta)$ is a measure of the CP -violating amplitude in the $B_d^0 \rightarrow J/\psi(1S) K_S^0$.

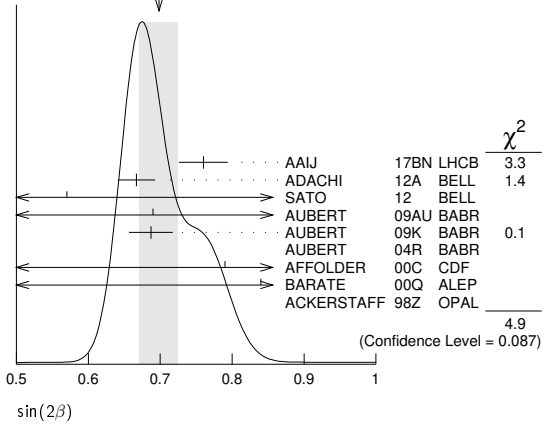
"OUR EVALUATION" is an average using rescaled values of the data listed below. The average and rescaling were performed by the Heavy Flavor Averaging Group (HFLAV) and are described at <https://hflav.web.cern.ch/>. The averaging/rescaling procedure takes into account correlations between the measurements.

VALUE	DOCUMENT ID	TECN	COMMENT
0.699 ± 0.017 OUR EVALUATION			
0.698 ± 0.027 OUR AVERAGE			
0.760 ± 0.034	1,2 AAIJ	17BN LHCb	pp at 7, 8 TeV
$0.667 \pm 0.023 \pm 0.012$	3 ADACHI	12A BELL	$e^+e^- \rightarrow \Upsilon(4S)$
$0.57 \pm 0.58 \pm 0.06$	4 SATO	12 BELL	$e^+e^- \rightarrow \Upsilon(5S)$
$0.69 \pm 0.52 \pm 0.08$	5 AUBERT	09AU BABR	$e^+e^- \rightarrow \Upsilon(4S)$
$0.687 \pm 0.028 \pm 0.012$	6 AUBERT	09K BABR	$e^+e^- \rightarrow \Upsilon(4S)$
$1.56 \pm 0.42 \pm 0.21$	7 AUBERT	04R BABR	$e^+e^- \rightarrow \Upsilon(4S)$
$0.79 \begin{smallmatrix} +0.41 \\ -0.44 \end{smallmatrix} \pm 0.16$	8 AFFOLDER	00C CDF	$p\bar{p}$ at 1.8 TeV
$0.84 \begin{smallmatrix} +0.82 \\ -1.04 \end{smallmatrix} \pm 0.16$	9 BARATE	00Q ALEP	$e^+e^- \rightarrow Z$
$3.2 \begin{smallmatrix} +1.8 \\ -2.0 \end{smallmatrix} \pm 0.5$	10 ACKERSTAFF	98Z OPAL	$e^+e^- \rightarrow Z$
• • • We do not use the following data for averages, fits, limits, etc. • • •			
$0.72 \pm 0.09 \pm 0.03$	11 SAHOO	08 BELL	Repl. by ADACHI 12A
$0.714 \pm 0.032 \pm 0.018$	6 AUBERT	07AY BABR	Repl. by AUBERT 09K
$0.642 \pm 0.031 \pm 0.017$	CHEN	07 BELL	Repl. by ADACHI 12A
$0.728 \pm 0.056 \pm 0.023$	12 ABE	05B BELL	Repl. by CHEN 07
$0.722 \pm 0.040 \pm 0.023$	13 AUBERT	05F BABR	Repl. by AUBERT 07AY
$0.99 \pm 0.14 \pm 0.06$	14 ABE	02U BELL	$e^+e^- \rightarrow \Upsilon(4S)$
$0.719 \pm 0.074 \pm 0.035$	15 ABE	02Z BELL	Repl. by ABE 05B
$0.59 \pm 0.14 \pm 0.05$	16 AUBERT	02N BABR	$e^+e^- \rightarrow \Upsilon(4S)$
$0.741 \pm 0.067 \pm 0.034$	17 AUBERT	02P BABR	Repl. by AUBERT 05F
$0.58 \begin{smallmatrix} +0.32 \\ -0.34 \end{smallmatrix} \pm 0.10$	ABASHIAN	01 BELL	Repl. by ABE 01G
$0.99 \pm 0.14 \pm 0.06$	18 ABE	01G BELL	Repl. by ABE 02Z
$0.34 \pm 0.20 \pm 0.05$	AUBERT	01 BABR	Repl. by AUBERT 01B
$0.59 \pm 0.14 \pm 0.05$	18 AUBERT	01B BABR	Repl. by AUBERT 02P
$1.8 \pm 1.1 \pm 0.3$	19 ABE	98U CDF	Repl. by AFFOLDER 00C

- Measurement based on $B^0 \rightarrow J/\psi K_S^0$, $B^0 \rightarrow \psi(2S) K_S^0$ with $J/\psi \rightarrow \mu^+ \mu^-$, $J/\psi \rightarrow e^+ e^-$ and $\psi(2S) \rightarrow \mu^+ \mu^-$.
- AAIJ 17BN provides the correlation coefficient $\rho = 0.42$ between the uncertainties of $\sin(2\beta)$ and $\cos(2\beta)$ measurements.
- Measurement based on $B^0 \rightarrow J/\psi K_S^0$, $B^0 \rightarrow \psi(2S) K_S^0$, $B^0 \rightarrow J/\psi K_L^0$, and $B^0 \rightarrow \chi_{c1}(1P) K_S^0$ decays.
- SATO 12 uses 121 fb^{-1} data collected on $Y(5S)$ resonance. Uses the " $B - \pi$ tagging" where $B\pi^+$ and $B\pi^-$ tagged $J/\psi K_S^0$ events are compared.
- Uses Dalitz plot analysis of $B^0 \rightarrow K^0 \pi^+ \pi^-$ decays and the first of two equivalent solutions.
- Measurement based on $B^0 \rightarrow c\bar{c}K^{(*)0}$ decays.

- Measurement in which the J/ψ decays to hadrons or to muons that do not satisfy the standard identification criteria.
- AFFOLDER 00c uses about 400 $B^0 \rightarrow J/\psi(1S) K_S^0$ events. The production flavor of B^0 was determined using three tagging algorithms: a same-side tag, a jet-charge tag, and a soft-lepton tag.
- BARATE 00Q uses 23 candidates for $B^0 \rightarrow J/\psi(1S) K_S^0$ decays. A combination of jet-charge, vertex-charge, and same-side tagging techniques were used to determine the B^0 production flavor.
- ACKERSTAFF 98z uses 24 candidates for $B_d^0 \rightarrow J/\psi(1S) K_S^0$ decay. A combination of jet-charge and vertex-charge techniques were used to tag the B_d^0 production flavor.
- Based on $B^0 \rightarrow \psi(2S) K_S^0$ decays.
- Measurement based on $152 \times 10^6 B\bar{B}$ pairs.
- Measurement based on $227 \times 10^6 B\bar{B}$ pairs.
- ABE 02U result is based on the same analysis and data sample reported in ABE 01G.
- ABE 02Z result is based on $85 \times 10^6 B\bar{B}$ pairs.
- AUBERT 02N result based on the same analysis and data sample reported in AUBERT 01B.
- AUBERT 02P result is based on $88 \times 10^6 B\bar{B}$ pairs.
- First observation of CP violation in B^0 meson system.
- ABE 98u uses $198 \pm 17 B_d^0 \rightarrow J/\psi(1S) K^0$ events. The production flavor of B^0 was determined using the same side tagging technique.

WEIGHTED AVERAGE
 0.698 ± 0.027 (Error scaled by 1.6)



$C_{J/\psi(nS)K^0}(B^0 \rightarrow J/\psi(nS)K^0)$

"OUR EVALUATION" is an average using rescaled values of the data listed below. The average and rescaling were performed by the Heavy Flavor Averaging Group (HFLAV) and are described at <https://hflav.web.cern.ch/>. The averaging/rescaling procedure takes into account correlations between the measurements.

VALUE (units 10^{-2})	DOCUMENT ID	TECN	COMMENT
-0.8 ± 1.7 OUR EVALUATION			
-0.5 ± 1.6 OUR AVERAGE			
-1.7 ± 2.9	1,2 AAIJ	17BN LHCb	pp at 7, 8 TeV
$1.5 \pm 2.1 \begin{smallmatrix} +2.3 \\ -4.5 \end{smallmatrix}$	3,4 ADACHI	12A BELL	$e^+e^- \rightarrow \Upsilon(4S)$
$-10.4 \pm 5.5 \begin{smallmatrix} +2.7 \\ -4.7 \end{smallmatrix}$	4,5 ADACHI	12A BELL	$e^+e^- \rightarrow \Upsilon(4S)$
$-1.9 \pm 2.6 \begin{smallmatrix} +4.1 \\ -1.7 \end{smallmatrix}$	4,6 ADACHI	12A BELL	$e^+e^- \rightarrow \Upsilon(4S)$
$8.9 \pm 7.6 \pm 2.0$	5 AUBERT	09K BABR	$e^+e^- \rightarrow \Upsilon(4S)$
$1.6 \pm 2.3 \pm 1.8$	AUBERT	09K BABR	$e^+e^- \rightarrow \Upsilon(4S)$
• • • We do not use the following data for averages, fits, limits, etc. • • •			
-1.4 ± 3.0	7 AAIJ	17BN LHCb	pp at 7, 8 TeV
$-5 \pm 10 \pm 1$	8 AAIJ	17BN LHCb	pp at 7, 8 TeV
$-3.8 \pm 3.2 \pm 0.5$	9 AAIJ	15N LHCb	Repl. by AAIJ 17BN
$3 \pm 9 \pm 1$	10 AAIJ	13K LHCb	Repl. by AAIJ 15N
$-4 \pm 7 \pm 5$	4,5 SAHOO	08 BELL	Repl. by ADACHI 12A
$-1.8 \pm 2.1 \pm 1.4$	4 CHEN	07 BELL	Repl. by ADACHI 12A

- Measurement based on $B^0 \rightarrow J/\psi K_S^0$, $B^0 \rightarrow \psi(2S) K_S^0$ with $J/\psi \rightarrow \mu^+ \mu^-$, $J/\psi \rightarrow e^+ e^-$ and $\psi(2S) \rightarrow \mu^+ \mu^-$.
- AAIJ 17BN provides the correlation coefficient $\rho = 0.42$ between the uncertainties of $S_{J/\psi(nS)K^0}(B^0 \rightarrow J/\psi(nS)K^0)$ and $C_{J/\psi(nS)K^0}(B^0 \rightarrow J/\psi(nS)K^0)$ measurements.
- Uses $B^0 \rightarrow J/\psi K_S^0$ decays.
- The paper reports A , which is equal to $-C$.
- Uses $B^0 \rightarrow \psi(2S) K_S^0$ decays.
- Uses $B^0 \rightarrow J/\psi K_L^0$ decays.
- Measurement based on $B^0 \rightarrow J/\psi K_S^0$ with $J/\psi \rightarrow \mu^+ \mu^-$ and $J/\psi \rightarrow e^+ e^-$.
- Measurement based on $B^0 \rightarrow \psi(2S) K_S^0$ with $\psi(2S) \rightarrow \mu^+ \mu^-$.
- AAIJ 15N uses 41,560 flavor-tagged $B_d^0 \rightarrow J/\psi K_S^0$ events from 3 fb^{-1} of integrated luminosity. Provides the correlation coefficient $\rho = 0.483$ between the statistical uncertainties of $S_{J/\psi(nS)K^0}$ and $C_{J/\psi(nS)K^0}$ measurements.
- AAIJ 13K uses 8200 flavor-tagged $B_d^0 \rightarrow J/\psi K_S^0$ events from 1 fb^{-1} of integrated luminosity. Provides the correlation coefficient $\rho = 0.42$ between the statistical uncertainties of $S_{J/\psi(nS)K^0}(B^0 \rightarrow J/\psi(nS)K^0)$ and $C_{J/\psi(nS)K^0}(B^0 \rightarrow J/\psi(nS)K^0)$ measurements.

Meson Particle Listings

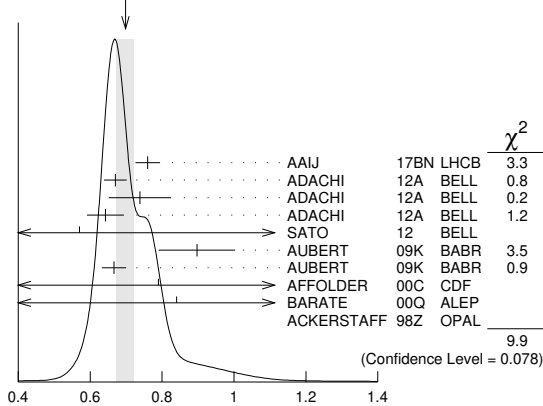
B^0

$S_{J/\psi(nS)K^0} (B^0 \rightarrow J/\psi(nS)K^0)$

"OUR EVALUATION" is an average using rescaled values of the data listed below. The average and rescaling were performed by the Heavy Flavor Averaging Group (HFLAV) and are described at <https://hflav.web.cern.ch/>. The averaging/rescaling procedure takes into account correlations between the measurements.

VALUE	DOCUMENT ID	TECN	COMMENT
0.701 ± 0.017 OUR EVALUATION			
0.698 ± 0.024 OUR AVERAGE			Error includes scale factor of 1.4. See the ideogram below.
0.760 ± 0.034	^{1,2} AAIJ	17BN LHCB	pp at 7, 8 TeV
0.670 ± 0.029 ± 0.013	³ ADACHI	12A BELL	$e^+e^- \rightarrow \Upsilon(4S)$
0.738 ± 0.079 ± 0.036	⁴ ADACHI	12A BELL	$e^+e^- \rightarrow \Upsilon(4S)$
0.642 ± 0.047 ± 0.021	⁵ ADACHI	12A BELL	$e^+e^- \rightarrow \Upsilon(4S)$
0.57 ± 0.58 ± 0.06	⁶ SATO	12 BELL	$e^+e^- \rightarrow \Upsilon(5S)$
0.897 ± 0.100 ± 0.036	⁴ AUBERT	09K BABR	$e^+e^- \rightarrow \Upsilon(4S)$
0.666 ± 0.031 ± 0.013	AUBERT	09K BABR	$e^+e^- \rightarrow \Upsilon(4S)$
0.79 ^{+0.41} _{-0.44}	⁷ AFFOLDER	00C CDF	$p\bar{p}$ at 1.8 TeV
0.84 ^{+0.82} _{-1.04} ± 0.16	⁸ BARATE	00Q ALEP	$e^+e^- \rightarrow Z$
3.2 ^{+1.8} _{-2.0} ± 0.5	⁹ ACKERSTAFF	98Z OPAL	$e^+e^- \rightarrow Z$
• • • We do not use the following data for averages, fits, limits, etc. • • •			
0.75 ± 0.04	¹⁰ AAIJ	17BN LHCB	pp at 7, 8 TeV
0.84 ± 0.10 ± 0.01	¹¹ AAIJ	17BN LHCB	pp at 7, 8 TeV
0.731 ± 0.035 ± 0.020	¹² AAIJ	15N LHCB	Repl. by AAIJ 17BN
0.73 ± 0.07 ± 0.04	¹³ AAIJ	13K LHCB	Repl. by AAIJ 15N
0.650 ± 0.029 ± 0.018	¹⁴ SAHOO	08 BELL	Repl. by ADACHI 12A
0.72 ± 0.09 ± 0.03	⁴ SAHOO	08 BELL	Repl. by ADACHI 12A
0.642 ± 0.031 ± 0.017	CHEN	07 BELL	Repl. by ADACHI 12A

WEIGHTED AVERAGE
0.698 ± 0.024 (Error scaled by 1.4)



$S_{J/\psi(nS)K^0} (B^0 \rightarrow J/\psi(nS)K^0)$

- Measurement based on $B^0 \rightarrow J/\psi K_S^0$, $B^0 \rightarrow \psi(2S) K_S^0$ with $J/\psi \rightarrow \mu^+ \mu^-$, $J/\psi \rightarrow e^+ e^-$ and $\psi(2S) \rightarrow \mu^+ \mu^-$.
- AAIJ 17BN provides the correlation coefficient $\rho = 0.42$ between the uncertainties of $S_{J/\psi(nS)K^0} (B^0 \rightarrow J/\psi(nS)K^0)$ and $C_{J/\psi(nS)K^0} (B^0 \rightarrow J/\psi(nS)K^0)$ measurements.
- Uses $B^0 \rightarrow J/\psi K_S^0$ decays.
- Based on $B^0 \rightarrow \psi(2S) K_S^0$ decays.
- Uses $B^0 \rightarrow J/\psi K_S^0$ decays.
- SATO 12 uses 121 fb⁻¹ data collected at $\Upsilon(5S)$ resonance. Uses the " $B - \pi$ tagging" where $B\pi^+$ and $B\pi^-$ tagged $J/\psi K_S^0$ events are compared.
- AFFOLDER 00C uses about 400 $B^0 \rightarrow J/\psi(1S) K_S^0$ events. The production flavor of B^0 was determined using three tagging algorithms: a same-side tag, a jet-charge tag, and a soft-lepton tag.
- BARATE 00Q uses 23 candidates for $B^0 \rightarrow J/\psi(1S) K_S^0$ decays. A combination of jet-charge, vertex-charge, and same-side tagging techniques were used to determine the B^0 production flavor.
- ACKERSTAFF 98Z uses 24 candidates for $B_d^0 \rightarrow J/\psi(1S) K_S^0$ decay. A combination of jet-charge and vertex-charge techniques were used to tag the B_d^0 production flavor.
- Measurement based on $B^0 \rightarrow J/\psi K_S^0$ with $J/\psi \rightarrow \mu^+ \mu^-$ and $J/\psi \rightarrow e^+ e^-$.
- Measurement based on $B^0 \rightarrow \psi(2S) K_S^0$ with $\psi(2S) \rightarrow \mu^+ \mu^-$.
- AAIJ 15N uses 41,560 flavor-tagged $B_d \rightarrow J/\psi K_S^0$ events from 3 fb⁻¹ of integrated luminosity. Provides the correlation coefficient $\rho = 0.483$ between the statistical uncertainties of and measurements.
- AAIJ 13K uses 8200 flavor-tagged $B_d \rightarrow J/\psi K_S^0$ events from 1 fb⁻¹ of integrated luminosity. Provides the correlation coefficient $\rho = 0.42$ between the statistical uncertainties of $S_{J/\psi(nS)K^0} (B^0 \rightarrow J/\psi(nS)K^0)$ and $C_{J/\psi(nS)K^0} (B^0 \rightarrow J/\psi(nS)K^0)$ measurements.
- Combined result of CHEN 07 and SAHOO 08.

$C_{J/\psi K^*0} (B^0 \rightarrow J/\psi K^*0)$

VALUE	DOCUMENT ID	TECN	COMMENT
0.025 ± 0.083 ± 0.054	¹ AUBERT	09K BABR	$e^+e^- \rightarrow \Upsilon(4S)$
¹ Based on $B^0 \rightarrow J/\psi K^*0$, $K^*0 \rightarrow K_S^0 \pi^0$.			

$S_{J/\psi K^*0} (B^0 \rightarrow J/\psi K^*0)$

VALUE	DOCUMENT ID	TECN	COMMENT
0.601 ± 0.239 ± 0.087	^{1,2} AUBERT	09K BABR	$e^+e^- \rightarrow \Upsilon(4S)$
¹ Based on $B^0 \rightarrow J/\psi K^*0$, $K^*0 \rightarrow K_S^0 \pi^0$.			
² This $S_{J/\psi K^*0}$ value has been corrected for the dilution of the $\sin(\Delta M \Delta t)$ coefficient of the CP asymmetry by a factor of $1 - R_{\perp}$, which arises from the mixture of CP -even and CP -odd B decay amplitudes.			

$C_{\chi_{c0} K_S^0} (B^0 \rightarrow \chi_{c0} K_S^0)$

VALUE	DOCUMENT ID	TECN	COMMENT
-0.29 ^{+0.53}_{-0.44} ± 0.06	¹ AUBERT	09AU BABR	$e^+e^- \rightarrow \Upsilon(4S)$
¹ Uses Dalitz plot analysis of $B^0 \rightarrow K^0 \pi^+ \pi^-$ decays and the first of two equivalent solutions is used.			

$S_{\chi_{c0} K_S^0} (B^0 \rightarrow \chi_{c0} K_S^0)$

VALUE	DOCUMENT ID	TECN	COMMENT
-0.69 ± 0.52 ± 0.08	¹ AUBERT	09AU BABR	$e^+e^- \rightarrow \Upsilon(4S)$
¹ Uses Dalitz plot analysis of $B^0 \rightarrow K^0 \pi^+ \pi^-$ decays and the first of two equivalent solutions is used.			

$C_{\chi_{c1} K_S^0} (B^0 \rightarrow \chi_{c1} K_S^0)$

VALUE	DOCUMENT ID	TECN	COMMENT
0.06 ± 0.07 OUR AVERAGE			
0.017 ± 0.083 ^{+0.026} _{-0.046}	ADACHI	12A BELL	$e^+e^- \rightarrow \Upsilon(4S)$
0.129 ± 0.109 ± 0.025	AUBERT	09K BABR	$e^+e^- \rightarrow \Upsilon(4S)$

$S_{\chi_{c1} K_S^0} (B^0 \rightarrow \chi_{c1} K_S^0)$

VALUE	DOCUMENT ID	TECN	COMMENT
0.63 ± 0.10 OUR AVERAGE			
0.640 ± 0.117 ± 0.040	ADACHI	12A BELL	$e^+e^- \rightarrow \Upsilon(4S)$
0.614 ± 0.160 ± 0.040	AUBERT	09K BABR	$e^+e^- \rightarrow \Upsilon(4S)$

$\sin(2\beta_{\text{eff}}) (B^0 \rightarrow \phi K^0)$

VALUE	DOCUMENT ID	TECN	COMMENT
0.22 ± 0.27 ± 0.12	AUBERT	07AX BABR	$e^+e^- \rightarrow \Upsilon(4S)$
• • • We do not use the following data for averages, fits, limits, etc. • • •			
0.50 ± 0.25 ^{+0.07} _{-0.04}	¹ AUBERT	05T BABR	Repl. by AUBERT 07AX
¹ Obtained by constraining $C = 0$.			

$\sin(2\beta_{\text{eff}}) (B^0 \rightarrow \phi K_S^0(1430)^0)$

VALUE	DOCUMENT ID	TECN	COMMENT
0.97 ^{+0.03}_{-0.52}	¹ AUBERT	08BG BABR	$e^+e^- \rightarrow \Upsilon(4S)$
¹ Measured using the CP -violation phase difference $\Delta\phi_{00}$ between the B and \bar{B} decay amplitude.			

$\sin(2\beta_{\text{eff}}) (B^0 \rightarrow K^+ K^- K_S^0)$

VALUE	DOCUMENT ID	TECN	COMMENT
0.77 ± 0.11 ^{+0.07}_{-0.04}	AUBERT	07AX BABR	$e^+e^- \rightarrow \Upsilon(4S)$
• • • We do not use the following data for averages, fits, limits, etc. • • •			
0.55 ± 0.22 ± 0.12	¹ AUBERT	05T BABR	Repl. by AUBERT 07AX
¹ Obtained by constraining $C = 0$.			

$\sin(2\beta_{\text{eff}}) (B^0 \rightarrow [K_S^0 \pi^+ \pi^-]_{D^{(*)}} h^0)$

VALUE	DOCUMENT ID	TECN	COMMENT
0.80 ± 0.14 ± 0.07	¹ ADACHI	18	$e^+e^- \rightarrow \Upsilon(4S)$
• • • We do not use the following data for averages, fits, limits, etc. • • •			
0.43 ± 0.27 ± 0.08	² VOROBYEV	16 BELL	$e^+e^- \rightarrow \Upsilon(4S)$
0.29 ± 0.34 ± 0.06	AUBERT	07BH BABR	$e^+e^- \rightarrow \Upsilon(4S)$
0.78 ± 0.44 ± 0.22	KROKOVNY	06 BELL	Repl. by VOROBYEV 16
¹ Analyzes joint data sample of Belle and BaBar using Dalitz plot analysis of $D \rightarrow K_S^0 \pi^+ \pi^-$; the second error combines experimental systematic uncertainty and the Dalitz plot model uncertainty.			
² A model-independent measurement uses the binned Dalitz plot technique.			

$\beta_{\text{eff}} (B^0 \rightarrow [K_S^0 \pi^+ \pi^-]_{D^{(*)}} h^0)$

VALUE (°)	DOCUMENT ID	TECN	COMMENT
22.5 ± 4.4 ± 1.3	¹ ADACHI	18	$e^+e^- \rightarrow \Upsilon(4S)$
• • • We do not use the following data for averages, fits, limits, etc. • • •			
11.7 ± 7.8 ± 2.1	² VOROBYEV	16 BELL	$e^+e^- \rightarrow \Upsilon(4S)$
¹ Analyzes joint data sample of Belle and BaBar using Dalitz plot analysis of $D \rightarrow K_S^0 \pi^+ \pi^-$; the second error combines experimental systematic uncertainty and the Dalitz plot model uncertainty.			
² A model-independent measurement uses the binned Dalitz plot technique.			

$2\beta_{\text{eff}} (B^0 \rightarrow J/\psi \rho^0)$

VALUE (°)	DOCUMENT ID	TECN	COMMENT
41.7 ± 9.6 ^{+2.8}_{-6.3}	AAIJ	15J LHCB	pp at 7, 8 TeV

$|\lambda| (B^0 \rightarrow [K_S^0 \pi^+ \pi^-]_{D^{(*)}} h^0)$

VALUE	DOCUMENT ID	TECN	COMMENT
1.01 ± 0.08 ± 0.02	AUBERT	07BH BABR	$e^+ e^- \rightarrow \Upsilon(4S)$

$|\sin(2\beta + \gamma)|$
 β (ϕ_1) and γ (ϕ_3) are angles of CKM unitarity triangle, see the review on "CP Violation" in the Reviews section.

VALUE	CL%	DOCUMENT ID	TECN	COMMENT
>0.40	90	1 AUBERT	06Y BABR	$e^+ e^- \rightarrow \Upsilon(4S)$
••• We do not use the following data for averages, fits, limits, etc. •••				
>0.77	68	2 AAIJ	18z LHCb	pp at 7, 8 TeV
>0.13	95	3 RONGA	06 BELL	$e^+ e^- \rightarrow \Upsilon(4S)$
>0.07	95	3 RONGA	06 BELL	$e^+ e^- \rightarrow \Upsilon(4S)$
>0.35	90	4 AUBERT	05z BABR	$e^+ e^- \rightarrow \Upsilon(4S)$
>0.69	68	5 AUBERT	04V BABR	$e^+ e^- \rightarrow \Upsilon(4S)$
>0.58	95	6 AUBERT	04W BABR	Repl. by AUBERT 05z

- 1 Uses fully reconstructed $B^0 \rightarrow D^{(*)} \pi^\pm \pi^\mp$ and $D^\pm \rho^\mp$ decays and some theoretical assumptions.
- 2 Uses a time dependent CP violation measurement in $B^0 \rightarrow D^\mp \pi^\pm$ decays with external input and some theoretical assumptions.
- 3 Combines the results from fully reconstructed and partially reconstructed $D^{(*)} \pi$ events by taking weighted averages. Assumes that systematic errors from physics parameters and fit biases in the two measurements are 100% correlated.
- 4 Uses partially reconstructed $B^0 \rightarrow D^{*\pm} \pi^\mp$ decays and some theoretical assumptions.
- 5 Uses fully reconstructed $B^0 \rightarrow D^{(*)} \pi^\pm \pi^\mp$ decays and some theoretical assumptions, such as the SU(3) symmetry relation.
- 6 Combining this measurement with the results from AUBERT 04V for fully reconstructed $B^0 \rightarrow D^{(*)} \pi^\pm \pi^\mp$ and some theoretical assumptions, such as the SU(3) symmetry relation.

$2\beta + \gamma$

VALUE (°)	DOCUMENT ID	TECN	COMMENT
83 ± 53 ± 20	1 AUBERT	08AC BABR	$e^+ e^- \rightarrow \Upsilon(4S)$

- 1 Used a time-dependent Dalitz-plot analysis of $B^0 \rightarrow D^\mp K^0 \pi^\pm$ assuming the ratio of the $b \rightarrow u$ and $b \rightarrow c$ decay amplitudes to be 0.3.

α
 For angle $\alpha(\phi_2)$ of the CKM unitarity triangle, see the review on "CP violation" in the reviews section.

"OUR EVALUATION" is provided by the Heavy Flavor Averaging Group (HFLAV).

VALUE (°)	DOCUMENT ID	TECN	COMMENT
85.2^{+4.8}_{-4.3} OUR EVALUATION			

••• We do not use the following data for averages, fits, limits, etc. •••

93.7 ± 10.6	1 VANHOEFER	16 BELL	$e^+ e^- \rightarrow \Upsilon(4S)$
84.9 ± 13.5	1 VANHOEFER	14 BELL	Repl. by VANHOEFER 16
79 ± 7 ± 11	2 AUBERT	10D BABR	$e^+ e^- \rightarrow \Upsilon(4S)$
92.4 ^{+6.0} _{-6.5}	1 AUBERT	09G BABR	$e^+ e^- \rightarrow \Upsilon(4S)$
78.6 ± 7.3	3 AUBERT	07O BABR	$e^+ e^- \rightarrow \Upsilon(4S)$
88 ± 17	4 SOMOV	06 BELL	Repl. by VANHOEFER 14
100 ± 13	5 AUBERT,B	05c BABR	Repl. by AUBERT 09G
102 ⁺¹⁶ ₋₁₂ ± 14	6 AUBERT,B	04r BABR	Repl. by AUBERT,B 05c

- 1 Based on an isospin analysis of the $B \rightarrow \rho\rho$ system.
- 2 Obtained using the time dependent analysis of $B^0 \rightarrow a_1(1260)^\pm \pi^\mp$ and branching fraction measurements of $B \rightarrow a_1(1260) K$ and $B \rightarrow K_1 \pi$. Uses SU(3) flavor relations.
- 3 The angle α_{eff} is obtained using the measured CP parameters of $B^0 \rightarrow a_1(1260)^\pm \pi^\mp$ and choosing one of the four solutions that is compatible with the result of SM-based fits.
- 4 Obtained using isospin relation and selecting a solution closest to the CKM best fit average; the 90% CL allowed interval is $59^\circ < \phi_2 (\equiv \alpha) < 115^\circ$.
- 5 Obtained using isospin relation and selecting a solution closest to the CKM best fit average; 90% CL allowed interval is $79^\circ < \alpha < 123^\circ$.
- 6 Obtained from the measured CP parameters of the longitudinal polarization by selecting the solution closest to the CKM best fit central value of $\alpha = 95^\circ - 98^\circ$.

CP VIOLATION PARAMETERS IN $B^0 \rightarrow D^0 K^{*0}$ DECAY

The parameters r_{B^0} and δ_{B^0} are the magnitude ratio and strong phase difference between the amplitudes of $A(B^0 \rightarrow D^0 K^{*0})$ and $A(B^0 \rightarrow \bar{D}^0 K^{*0})$. The measured observables are defined as $x_\pm = r_{B^0} \cos(\delta_{B^0} \pm \gamma)$ and $y_\pm = r_{B^0} \sin(\delta_{B^0} \pm \gamma)$ where γ is the CKM angle γ .

"OUR EVALUATION" is provided by the Heavy Flavor Averaging Group (HFLAV). The CKM angle γ is listed in the B^+ section for "CP VIOLATION PARAMETERS IN $B^+ \rightarrow D K^+$ AND SIMILAR DECAYS."

$x_+(B^0 \rightarrow DK^{*0})$

VALUE	DOCUMENT ID	TECN	COMMENT
0.04 ± 0.17 OUR AVERAGE			
0.04 ± 0.16 ± 0.11	1 AAIJ	16s LHCb	pp at 7, 8 TeV
0.05 ± 0.35 ± 0.02	AAIJ	16z LHCb	pp at 7, 8 TeV

- We do not use the following data for averages, fits, limits, etc. •••
- | | | | |
|--------------------|--------|-----------|-------------------|
| 0.05 ± 0.24 ± 0.04 | 2 AAIJ | 16AA LHCb | Repl. by AAIJ 16z |
|--------------------|--------|-----------|-------------------|
- 1 Uses Dalitz plof of $B^0 \rightarrow DK^+ \pi^-$ with $D \rightarrow K^+ K^-, \pi^+ \pi^-,$ or $K^+ \pi^-$.
 - 2 Uses Dalitz plot analysis of $D \rightarrow K_S^0 \pi^+ \pi^-$ decays coming from $B^0 \rightarrow DK^*(892)^0$ modes.

$x_-(B^0 \rightarrow DK^{*0})$

VALUE	DOCUMENT ID	TECN	COMMENT
-0.16 ± 0.14 OUR AVERAGE			
-0.02 ± 0.13 ± 0.14	1 AAIJ	16s LHCb	pp at 7, 8 TeV
-0.31 ± 0.20 ± 0.04	AAIJ	16z LHCb	pp at 7, 8 TeV

- We do not use the following data for averages, fits, limits, etc. •••
- | | | | |
|---------------------|--------|-----------|-------------------|
| -0.15 ± 0.14 ± 0.03 | 2 AAIJ | 16AA LHCb | Repl. by AAIJ 16z |
|---------------------|--------|-----------|-------------------|
- 1 Uses Dalitz plot of $B^0 \rightarrow DK^+ \pi^-$ with $D \rightarrow K^+ K^-, \pi^+ \pi^-,$ or $K^+ \pi^-$.
 - 2 Uses Dalitz plot analysis of $D \rightarrow K_S^0 \pi^+ \pi^-$ decays coming from $B^0 \rightarrow DK^*(892)^0$ modes.

$y_+(B^0 \rightarrow DK^{*0})$

VALUE	DOCUMENT ID	TECN	COMMENT
-0.68 ± 0.22 OUR AVERAGE			
-0.47 ± 0.28 ± 0.22	1 AAIJ	16s LHCb	pp at 7, 8 TeV
-0.81 ± 0.28 ± 0.06	AAIJ	16z LHCb	pp at 7, 8 TeV

- We do not use the following data for averages, fits, limits, etc. •••
- | | | | |
|--|--------|-----------|-------------------|
| -0.65 ^{+0.24} _{-0.23} ± 0.08 | 2 AAIJ | 16AA LHCb | Repl. by AAIJ 16z |
|--|--------|-----------|-------------------|
- 1 Uses Dalitz plof of $B^0 \rightarrow DK^+ \pi^-$ with $D \rightarrow K^+ K^-, \pi^+ \pi^-,$ or $K^+ \pi^-$.
 - 2 Uses Dalitz plot analysis of $D \rightarrow K_S^0 \pi^+ \pi^-$ decays coming from $B^0 \rightarrow DK^*(892)^0$ modes.

$y_-(B^0 \rightarrow DK^{*0})$

VALUE	DOCUMENT ID	TECN	COMMENT
0.20 ± 0.25 OUR AVERAGE			Error includes scale factor of 1.2.
-0.35 ± 0.26 ± 0.41	1 AAIJ	16s LHCb	pp at 7, 8 TeV
0.31 ± 0.21 ± 0.05	AAIJ	16z LHCb	pp at 7, 8 TeV

- We do not use the following data for averages, fits, limits, etc. •••
- | | | | |
|--------------------|--------|-----------|-------------------|
| 0.25 ± 0.15 ± 0.06 | 2 AAIJ | 16AA LHCb | Repl. by AAIJ 16z |
|--------------------|--------|-----------|-------------------|
- 1 Uses Dalitz plof of $B^0 \rightarrow DK^+ \pi^-$ with $D \rightarrow K^+ K^-, \pi^+ \pi^-,$ or $K^+ \pi^-$.
 - 2 Uses Dalitz plot analysis of $D \rightarrow K_S^0 \pi^+ \pi^-$ decays coming from $B^0 \rightarrow DK^*(892)^0$ modes.

$r_{B^0}(B^0 \rightarrow DK^{*0})$
 "OUR EVALUATION" is provided by the Heavy Flavor Averaging Group (HFLAV).

VALUE	DOCUMENT ID	TECN	COMMENT
0.257^{+0.021}_{-0.023} OUR EVALUATION			

- We do not use the following data for averages, fits, limits, etc. •••
- | | | | |
|-------------|--------|-----------|-------------------|
| 0.39 ± 0.13 | 1 AAIJ | 16AA LHCb | Repl. by AAIJ 16z |
| 0.56 ± 0.17 | 2 AAIJ | 16z LHCb | pp at 7, 8 TeV |
- 1 Uses Dalitz plot analysis of $D \rightarrow K_S^0 \pi^+ \pi^-$ decays coming from $B^0 \rightarrow DK^*(892)^0$ modes.
 - 2 Measurement is performed with $K^+ \pi^-$ masses within 50 MeV of the K^{*0} mass and an absolute value of the cosine of the K^{*0} helicity angle greater than 0.4. Angle γ is required to satisfy $0 < \gamma < 180$ degrees.

$\delta_{B^0}(B^0 \rightarrow DK^{*0})$
 "OUR EVALUATION" is provided by the Heavy Flavor Averaging Group (HFLAV).

VALUE (°)	DOCUMENT ID	TECN	COMMENT
194.1^{+9.6}_{-8.8} OUR EVALUATION			

- We do not use the following data for averages, fits, limits, etc. •••
- | | | | |
|-----------------------------------|--------|-----------|-------------------|
| 197 ⁺²⁴ ₋₂₀ | 1 AAIJ | 16AA LHCb | Repl. by AAIJ 16z |
| 204 ⁺²¹ ₋₂₀ | 2 AAIJ | 16z LHCb | pp at 7, 8 TeV |
- 1 Uses Dalitz plot analysis of $D \rightarrow K_S^0 \pi^+ \pi^-$ decays coming from $B^0 \rightarrow DK^*(892)^0$ modes.
 - 2 Measurement is performed with $K^+ \pi^-$ masses within 50 MeV of the K^{*0} mass and an absolute value of the cosine of the K^{*0} helicity angle greater than 0.4. Angle γ is required to satisfy $0 < \gamma < 180$ degrees.

T and CPT VIOLATION PARAMETERS

Measured values of the T -, CP -, and CPT -asymmetry parameters, defined as the differences in $S_{\alpha,\beta}^\pm$ and $C_{\alpha,\beta}^\pm$ between symmetry-transformed transitions. The indices $\alpha = \ell^+, \ell^-$ and $\beta = K_S^0, K_L^0$ stand for reconstructed the flavor final state and the CP final states from $\Upsilon(4S)$ decay. The sign \pm indicates whether the decay to the flavor final state α occurs before or after the decay to the CP final state.

Alternatively, violations of CPT symmetry and Lorentz invariance are searched for by studying interference effects in B^0 mixing. Results are expressed in terms of the standard model extension parameter Δa , which describes the difference between the couplings of the valence quarks within B^0 meson with the Lorentz-violating fields.

$\Delta S_T^+(S_{\ell^-, K_S^0}^- - S_{\ell^+, K_S^0}^+)$

VALUE	DOCUMENT ID	TECN	COMMENT
-1.37 ± 0.14 ± 0.06	LEES	12W BABR	$e^+ e^- \rightarrow \Upsilon(4S)$

$\Delta S_T^-(S_{\ell^-, K_S^0}^+ - S_{\ell^+, K_S^0}^-)$

VALUE	DOCUMENT ID	TECN	COMMENT
1.17 ± 0.18 ± 0.11	LEES	12W BABR	$e^+ e^- \rightarrow \Upsilon(4S)$

Meson Particle Listings

B^0

ΔC_{τ}^+ ($C_{\ell^-, K_S^0}^- - C_{\ell^+, K_S^0}^+$)

VALUE	DOCUMENT ID	TECN	COMMENT
0.10 ± 0.14 ± 0.08	LEES	12W	BABR $e^+ e^- \rightarrow \Upsilon(4S)$

ΔC_{τ}^- ($C_{\ell^-, K_S^0}^+ - C_{\ell^+, K_S^0}^-$)

VALUE	DOCUMENT ID	TECN	COMMENT
0.04 ± 0.14 ± 0.08	LEES	12W	BABR $e^+ e^- \rightarrow \Upsilon(4S)$

ΔS_{CP}^+ ($S_{\ell^-, K_S^0}^+ - S_{\ell^+, K_S^0}^+$)

VALUE	DOCUMENT ID	TECN	COMMENT
-1.30 ± 0.11 ± 0.07	LEES	12W	BABR $e^+ e^- \rightarrow \Upsilon(4S)$

ΔS_{CP}^- ($S_{\ell^-, K_S^0}^- - S_{\ell^+, K_S^0}^-$)

VALUE	DOCUMENT ID	TECN	COMMENT
1.33 ± 0.12 ± 0.06	LEES	12W	BABR $e^+ e^- \rightarrow \Upsilon(4S)$

ΔC_{CP}^+ ($C_{\ell^+, K_S^0}^+ - C_{\ell^+, K_S^0}^+$)

VALUE	DOCUMENT ID	TECN	COMMENT
0.07 ± 0.09 ± 0.03	LEES	12W	BABR $e^+ e^- \rightarrow \Upsilon(4S)$

ΔC_{CP}^- ($C_{\ell^-, K_S^0}^- - C_{\ell^+, K_S^0}^-$)

VALUE	DOCUMENT ID	TECN	COMMENT
0.08 ± 0.10 ± 0.04	LEES	12W	BABR $e^+ e^- \rightarrow \Upsilon(4S)$

ΔS_{CPT}^+ ($S_{\ell^+, K_S^0}^- - S_{\ell^+, K_S^0}^+$)

VALUE	DOCUMENT ID	TECN	COMMENT
0.16 ± 0.21 ± 0.09	LEES	12W	BABR $e^+ e^- \rightarrow \Upsilon(4S)$

ΔS_{CPT}^- ($S_{\ell^+, K_S^0}^+ - S_{\ell^+, K_S^0}^-$)

VALUE	DOCUMENT ID	TECN	COMMENT
-0.03 ± 0.13 ± 0.06	LEES	12W	BABR $e^+ e^- \rightarrow \Upsilon(4S)$

ΔC_{CPT}^+ ($C_{\ell^+, K_S^0}^- - C_{\ell^+, K_S^0}^+$)

VALUE	DOCUMENT ID	TECN	COMMENT
0.14 ± 0.15 ± 0.07	LEES	12W	BABR $e^+ e^- \rightarrow \Upsilon(4S)$

ΔC_{CPT}^- ($C_{\ell^+, K_S^0}^+ - C_{\ell^+, K_S^0}^-$)

VALUE	DOCUMENT ID	TECN	COMMENT
0.03 ± 0.12 ± 0.08	LEES	12W	BABR $e^+ e^- \rightarrow \Upsilon(4S)$

Δa_{\parallel} CPT parameter in B^0 mixing

VALUE (10^{-15} GeV)	DOCUMENT ID	TECN	COMMENT
-0.10 ± 0.82 ± 0.54	¹ AAIJ	16E	LHCB $p\bar{p}$ at 7, 8 TeV

¹ Uses $B^0 \rightarrow J/\psi K_S^0$ decays.

Δa_{\perp} CPT parameter in B^0 mixing

VALUE (10^{-13} GeV)	DOCUMENT ID	TECN	COMMENT
-0.20 ± 0.22 ± 0.04	¹ AAIJ	16E	LHCB $p\bar{p}$ at 7, 8 TeV

¹ Uses $B^0 \rightarrow J/\psi K_S^0$ decays.

Δa_{χ} CPT parameter in B^0 mixing

VALUE (10^{-15} GeV)	DOCUMENT ID	TECN	COMMENT
+1.97 ± 1.30 ± 0.29	¹ AAIJ	16E	LHCB $p\bar{p}$ at 7, 8 TeV

¹ Uses $B^0 \rightarrow J/\psi K_S^0$ decays.

Δa_{γ} CPT parameter in B^0 mixing

VALUE (10^{-15} GeV)	DOCUMENT ID	TECN	COMMENT
+0.44 ± 1.26 ± 0.29	¹ AAIJ	16E	LHCB $p\bar{p}$ at 7, 8 TeV

¹ Uses $B^0 \rightarrow J/\psi K_S^0$ decays.

$B^0 \rightarrow D^{*-} \ell^+ \nu_{\ell}$ FORM FACTORS

R_1 (form factor ratio $\sim V/A_1$)

VALUE	DOCUMENT ID	TECN	COMMENT
1.239 ± 0.029 OUR AVERAGE			

1.229 ± 0.028 ± 0.009	¹ WAHEED	19	BELL $e^+ e^- \rightarrow \Upsilon(4S)$
1.56 ± 0.07 ± 0.15	AUBERT	09A	BABR $e^+ e^- \rightarrow \Upsilon(4S)$
1.18 ± 0.30 ± 0.12	DUBOSCQ	96	CLE2 $e^+ e^- \rightarrow \Upsilon(4S)$

• • • We do not use the following data for averages, fits, limits, etc. • • •

1.401 ± 0.034 ± 0.018	¹ DUNGEL	10	BELL Repl. by WAHEED 19
1.429 ± 0.061 ± 0.044	AUBERT	08R	BABR Repl. by AUBERT 09A
1.396 ± 0.060 ± 0.044	AUBERT,B	06Z	BABR Repl. by AUBERT 08R

¹ Uses fully reconstructed $D^{*-} \ell^+ \nu$ events ($\ell = e$ or μ).

R_2 (form factor ratio $\sim A_2/A_1$)

VALUE	DOCUMENT ID	TECN	COMMENT
0.84 ± 0.04 OUR AVERAGE			Error includes scale factor of 1.8.

0.852 ± 0.021 ± 0.006	¹ WAHEED	19	BELL $e^+ e^- \rightarrow \Upsilon(4S)$
0.66 ± 0.05 ± 0.09	AUBERT	09A	BABR $e^+ e^- \rightarrow \Upsilon(4S)$
0.71 ± 0.22 ± 0.07	DUBOSCQ	96	CLE2 $e^+ e^- \rightarrow \Upsilon(4S)$

• • • We do not use the following data for averages, fits, limits, etc. • • •

0.864 ± 0.024 ± 0.008	¹ DUNGEL	10	BELL Repl. by WAHEED 19
0.827 ± 0.038 ± 0.022	AUBERT	08R	BABR Repl. by AUBERT 09A
0.885 ± 0.040 ± 0.026	AUBERT,B	06Z	BABR Repl. by AUBERT 08R

¹ Uses fully reconstructed $D^{*-} \ell^+ \nu$ events ($\ell = e$ or μ).

$\rho_{A_1}^2$ (form factor slope)

VALUE	DOCUMENT ID	TECN	COMMENT
1.12 ± 0.04 OUR AVERAGE			Error includes scale factor of 1.5.

1.106 ± 0.031 ± 0.007	¹ WAHEED	19	BELL $e^+ e^- \rightarrow \Upsilon(4S)$
1.22 ± 0.02 ± 0.07	AUBERT	09A	BABR $e^+ e^- \rightarrow \Upsilon(4S)$
0.91 ± 0.15 ± 0.06	DUBOSCQ	96	CLE2 $e^+ e^- \rightarrow \Upsilon(4S)$

• • • We do not use the following data for averages, fits, limits, etc. • • •

1.214 ± 0.034 ± 0.009	¹ DUNGEL	10	BELL Repl. by WAHEED 19
1.191 ± 0.048 ± 0.028	AUBERT	08R	BABR Repl. by AUBERT 09A
1.145 ± 0.059 ± 0.046	AUBERT,B	06Z	BABR Repl. by AUBERT 08R

¹ Uses fully reconstructed $D^{*-} \ell^+ \nu$ events ($\ell = e$ or μ).

PARTIAL BRANCHING FRACTIONS IN $B^0 \rightarrow K^{*0} \ell^+ \ell^-$

$B(B^0 \rightarrow K^{*0} e^+ e^-)$ ($0.0009 < q^2 < 1.0$ GeV²/c⁴)

VALUE (units 10^{-7})	DOCUMENT ID	TECN	COMMENT
3.1^{+0.9}_{-0.8} ± 0.2 ± 0.2	¹ AAIJ	13U	LHCB $p\bar{p}$ at 7 TeV

¹ The last uncertainty is due to uncertainties of $B(B^0 \rightarrow J/\psi K^{*0})$ and $B(J/\psi \rightarrow e^+ e^-)$ branching fraction measurements.

$B(B^0 \rightarrow K^{*0} \ell^+ \ell^-)$ ($0.1 < q^2 < 2.0$ GeV²/c⁴)

VALUE (units 10^{-7})	DOCUMENT ID	TECN	COMMENT
1.24^{+0.23}_{-0.27} OUR AVERAGE			Error includes scale factor of 1.6.

1.14 ± 0.11 ^{+0.11} _{-0.15}	AAIJ	13Y	LHCB $p\bar{p}$ at 7 TeV, $K^{*0} \mu^+ \mu^-$
1.80 ± 0.36 ± 0.11	AALTONEN	11A1	CDF $p\bar{p}$ at 1.96 TeV

• • • We do not use the following data for averages, fits, limits, etc. • • •

0.48 ^{+0.14} _{-0.12} ± 0.04	¹ CHATRCHYAN	13BL	CMS $p\bar{p}$ at 7 TeV
1.16 ± 0.23 ± 0.11	AAIJ	12U	LHCB Repl. by AAIJ 13Y

¹ CHATRCHYAN 13BL uses, for this bin, $1.0 < q^2 < 2.0$ GeV²/c⁴.

$B(B^0 \rightarrow K^{*0} \ell^+ \ell^-)$ ($2.0 < q^2 < 4.3$ GeV²/c⁴)

VALUE (units 10^{-7})	DOCUMENT ID	TECN	COMMENT
0.76 ± 0.07 OUR AVERAGE			

0.759 ± 0.115 ± 0.046	KHACHATRY..	16D	CMS $p\bar{p}$ at 8 TeV
0.69 ± 0.07 ± 0.09	AAIJ	13Y	LHCB $p\bar{p}$ at 7 TeV, $K^{*0} \mu^+ \mu^-$
0.87 ± 0.16 ± 0.07	CHATRCHYAN	13BL	CMS $p\bar{p}$ at 7 TeV
0.84 ± 0.28 ± 0.06	AALTONEN	11A1	CDF $p\bar{p}$ at 1.96 TeV

• • • We do not use the following data for averages, fits, limits, etc. • • •

0.78 ± 0.21 ± 0.05	AAIJ	12U	LHCB Repl. by AAIJ 13Y
--------------------	------	-----	------------------------

$B(B^0 \rightarrow K^{*0} \ell^+ \ell^-)$ ($4.3 < q^2 < 8.68$ GeV²/c⁴)

VALUE (units 10^{-7})	DOCUMENT ID	TECN	COMMENT
1.87 ± 0.21 OUR AVERAGE			

2.15 ± 0.18 ^{+0.22} _{-0.28}	AAIJ	13Y	LHCB $p\bar{p}$ at 7 TeV, $K^{*0} \mu^+ \mu^-$
1.62 ± 0.31 ± 0.18	CHATRCHYAN	13BL	CMS $p\bar{p}$ at 7 TeV
1.73 ± 0.43 ± 0.15	AALTONEN	11A1	CDF $p\bar{p}$ at 1.96 TeV

• • • We do not use the following data for averages, fits, limits, etc. • • •

3.02 ± 0.35 ± 0.22	AAIJ	12U	LHCB Repl. by AAIJ 13Y
--------------------	------	-----	------------------------

$B(B^0 \rightarrow K^{*0} \ell^+ \ell^-)$ ($10.09 < q^2 < 12.86$ GeV²/c⁴)

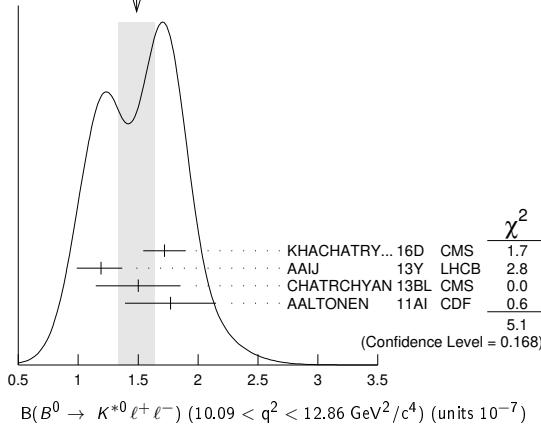
VALUE (units 10^{-7})	DOCUMENT ID	TECN	COMMENT
1.49 ± 0.15 OUR AVERAGE			Error includes scale factor of 1.3. See the ideogram below.

1.72 ± 0.11 ± 0.14	KHACHATRY..	16D	CMS $p\bar{p}$ at 8 TeV
1.19 ± 0.11 ^{+0.14} _{-0.17}	AAIJ	13Y	LHCB $p\bar{p}$ at 7 TeV, $K^{*0} \mu^+ \mu^-$
1.50 ± 0.25 ± 0.25	CHATRCHYAN	13BL	CMS $p\bar{p}$ at 7 TeV
1.77 ± 0.36 ± 0.12	AALTONEN	11A1	CDF $p\bar{p}$ at 1.96 TeV

• • • We do not use the following data for averages, fits, limits, etc. • • •

1.52 ± 0.25 ± 0.19	AAIJ	12U	LHCB Repl. by AAIJ 13Y
--------------------	------	-----	------------------------

WEIGHTED AVERAGE
1.49±0.15 (Error scaled by 1.3)



B(B⁰ → K^{*0} ℓ⁺ ℓ⁻) (14.18 < q² < 16.0 GeV²/c⁴)

VALUE (units 10 ⁻⁷)	DOCUMENT ID	TECN	COMMENT
1.09±0.10 OUR AVERAGE	Error includes scale factor of 1.1.		
1.22±0.11±0.09	KHACHATRY...16D	CMS	pp at 8 TeV
1.02±0.11 ^{+0.11} _{-0.15}	AAIJ	13Y LHCb	pp at 7 TeV, K ^{*0} μ ⁺ μ ⁻
0.84 ^{+0.16} _{-0.15} ±0.09	CHATRCHYAN13BL	CMS	pp at 7 TeV
1.34±0.26±0.08	AALTONEN	11AI CDF	p̄p̄ at 1.96 TeV
••• We do not use the following data for averages, fits, limits, etc. •••			
1.15±0.20±0.09	AAIJ	12U LHCb	Repl. by AAIJ 13Y

B(B⁰ → K^{*0} ℓ⁺ ℓ⁻) (16.0 < q² < 19.0 GeV²/c⁴)

VALUE (units 10 ⁻⁷)	DOCUMENT ID	TECN	COMMENT
1.27±0.09 OUR AVERAGE			
1.26±0.09±0.09	KHACHATRY...16D	CMS	pp at 8 TeV
1.23±0.12 ^{+0.15} _{-0.18}	AAIJ	13Y LHCb	pp at 7 TeV, K ^{*0} μ ⁺ μ ⁻
1.56±0.18±0.15	CHATRCHYAN13BL	CMS	pp at 7 TeV
0.97±0.26±0.07	AALTONEN	11AI CDF	p̄p̄ at 1.96 TeV
••• We do not use the following data for averages, fits, limits, etc. •••			
1.50±0.24±0.15	AAIJ	12U LHCb	Repl. by AAIJ 13Y

B(B⁰ → K^{*}(892)⁰ ℓ⁺ ℓ⁻) (15.0 < q² < 19.0 GeV²/c⁴)

VALUE (units 10 ⁻⁷)	DOCUMENT ID	TECN	COMMENT
1.80 ±0.13 OUR AVERAGE			
2.2 ^{+0.5} _{-0.4} ±0.2	¹ WEHLE	21 BELL	e ⁺ e ⁻ → γ(4S)
2.0 ^{+0.6} _{-0.5} ±0.2	² WEHLE	21 BELL	e ⁺ e ⁻ → γ(4S)
1.744 ^{+0.072} _{-0.076} ±0.123	¹ AAIJ	17Q LHCb	pp at 7, 8 TeV
••• We do not use the following data for averages, fits, limits, etc. •••			
1.95 ^{+0.08} _{-0.09} ±0.13	¹ AAIJ	16A0 LHCb	Repl. by AAIJ 17Q

¹ Measured with μ⁺ μ⁻ as lepton pair.
² Measured with e⁺ e⁻ as lepton pair.

B(B⁰ → K^{*0} ℓ⁺ ℓ⁻) (1.0 < q² < 6.0 GeV²/c⁴)

VALUE (units 10 ⁻⁷)	DOCUMENT ID	TECN	COMMENT
1.74±0.11 OUR AVERAGE			
1.9 ^{+0.6} _{-0.5} ±0.3	^{1,2} WEHLE	21 BELL	e ⁺ e ⁻ → γ(4S)
1.8 ^{+0.6} _{-0.6} ±0.2	^{1,3} WEHLE	21 BELL	e ⁺ e ⁻ → γ(4S)
1.68±0.083±0.12	^{1,2} AAIJ	17Q LHCb	pp at 7, 8 TeV
1.90±0.20	² KHACHATRY...16D	CMS	pp at 7, 8 TeV
1.42±0.41 ±0.12	² AALTONEN	11AI CDF	p̄p̄ at 1.96 TeV
••• We do not use the following data for averages, fits, limits, etc. •••			
1.92 ^{+0.10} _{-0.09} ±0.14	AAIJ	16A0 LHCb	Repl. by AAIJ 17Q
1.70±0.15 ^{+0.20} _{-0.25}	AAIJ	13Y LHCb	Repl. by AAIJ 16A0
2.20±0.30 ±0.20	CHATRCHYAN13BL	CMS	Repl. by KHACHATRYAN 16D
2.10±0.30 ±0.15	AAIJ	12U LHCb	Repl. by AAIJ 13Y

¹ Result is determined for the range 1.1 < q² < 6.0 GeV²/c⁴.
² Measured with μ⁺ μ⁻ as lepton pair.
³ Measured with e⁺ e⁻ as lepton pair.

B(B⁰ → K^{*0} ℓ⁺ ℓ⁻) (0.0 < q² < 4.3 GeV²/c⁴)

VALUE (units 10 ⁻⁷)	DOCUMENT ID	TECN	COMMENT
2.60±0.45 ±0.17	AALTONEN	11AI CDF	p̄p̄ at 1.96 TeV

B(B⁰ → K^{*0} μ⁺ μ⁻)/B(B⁰ → K^{*0} e⁺ e⁻) (0.045 < q² < 1.1 GeV²/c⁴)

VALUE	DOCUMENT ID	TECN	COMMENT
0.65^{+0.11}_{-0.07} OUR AVERAGE			
0.46 ^{+0.55} _{-0.27} ±0.13	WEHLE	21 BELL	e ⁺ e ⁻ → γ(4S)
0.66 ^{+0.11} _{-0.07} ±0.03	AAIJ	17W LHCb	pp at 7, 8 TeV

B(B⁰ → K^{*0} μ⁺ μ⁻)/B(B⁰ → K^{*0} e⁺ e⁻) (1.1 < q² < 6.0 GeV²/c⁴)

VALUE	DOCUMENT ID	TECN	COMMENT
0.71^{+0.12}_{-0.08} OUR AVERAGE			
1.06 ^{+0.63} _{-0.38} ±0.13	WEHLE	21 BELL	e ⁺ e ⁻ → γ(4S)
0.69 ^{+0.11} _{-0.07} ±0.05	AAIJ	17W LHCb	pp at 7, 8 TeV

B(B⁰ → K^{*0} μ⁺ μ⁻)/B(B⁰ → K^{*0} e⁺ e⁻) (15.0 < q² < 19.0 GeV²/c⁴)

VALUE	DOCUMENT ID	TECN	COMMENT
1.12^{+0.61}_{-0.36} ±0.10	WEHLE	21 BELL	e ⁺ e ⁻ → γ(4S)

B(B⁰ → K⁰ ℓ⁺ ℓ⁻) (q² < 2.0 GeV²/c⁴)

VALUE (units 10 ⁻⁷)	DOCUMENT ID	TECN	COMMENT
0.24^{+0.22}_{-0.20} OUR AVERAGE			
0.21 ^{+0.27} _{-0.23}	AAIJ	12AH LHCb	pp at 7 TeV
0.31±0.37±0.02	AALTONEN	11AI CDF	p̄p̄ at 1.96 TeV

B(B⁰ → K⁰ ℓ⁺ ℓ⁻) (2.0 < q² < 4.3 GeV²/c⁴)

VALUE (units 10 ⁻⁷)	DOCUMENT ID	TECN	COMMENT
0.24^{+0.35}_{-0.30} OUR AVERAGE	Error includes scale factor of 1.6.		
0.07 ^{+0.25} _{-0.21}	AAIJ	12AH LHCb	pp at 7 TeV
0.93±0.49±0.07	AALTONEN	11AI CDF	p̄p̄ at 1.96 TeV

B(B⁰ → K⁰ ℓ⁺ ℓ⁻) (4.3 < q² < 8.68 GeV²/c⁴)

VALUE (units 10 ⁻⁷)	DOCUMENT ID	TECN	COMMENT
1.08±0.27 OUR AVERAGE			
1.23±0.31	AAIJ	12AH LHCb	pp at 7 TeV
0.66±0.51±0.05	AALTONEN	11AI CDF	p̄p̄ at 1.96 TeV

B(B⁰ → K⁰ ℓ⁺ ℓ⁻) (10.09 < q² < 12.86 GeV²/c⁴)

VALUE (units 10 ⁻⁷)	DOCUMENT ID	TECN	COMMENT
0.27±0.27 OUR AVERAGE	Error includes scale factor of 1.8.		
0.50 ^{+0.22} _{-0.19}	AAIJ	12AH LHCb	pp at 7 TeV
-0.03±0.22±0.01	AALTONEN	11AI CDF	p̄p̄ at 1.96 TeV

B(B⁰ → K⁰ ℓ⁺ ℓ⁻) (14.18 < q² < 16.0 GeV²/c⁴)

VALUE (units 10 ⁻⁷)	DOCUMENT ID	TECN	COMMENT
0.29^{+0.21}_{-0.15} OUR AVERAGE	Error includes scale factor of 1.8.		
0.20 ^{+0.13} _{-0.09}	AAIJ	12AH LHCb	pp at 7 TeV
0.73±0.26±0.06	AALTONEN	11AI CDF	p̄p̄ at 1.96 TeV

B(B⁰ → K⁰ ℓ⁺ ℓ⁻) (q² > 16.0 GeV²/c⁴)

VALUE (units 10 ⁻⁷)	DOCUMENT ID	TECN	COMMENT
0.31^{+0.16}_{-0.12} OUR AVERAGE			
0.35 ^{+0.44} _{-0.14}	AAIJ	12AH LHCb	pp at 7 TeV
0.21±0.18±0.16	AALTONEN	11AI CDF	p̄p̄ at 1.96 TeV

B(B⁰ → K⁰ ℓ⁺ ℓ⁻) (1.0 < q² < 6.0 GeV²/c⁴)

VALUE (units 10 ⁻⁷)	DOCUMENT ID	TECN	COMMENT
0.91^{+0.15}_{-0.13} OUR AVERAGE			
0.62 ^{+0.44} _{-0.32} ±0.02	¹ CHOUDHURY	21 BELL	e ⁺ e ⁻ → γ(4S)
1.12 ^{+0.50} _{-0.40} ±0.04	² CHOUDHURY	21 BELL	e ⁺ e ⁻ → γ(4S)
0.916 ^{+0.172} _{-0.157} ±0.004	³ AAIJ	14M LHCb	pp at 7, 8 TeV
0.98 ±0.61 ±0.08	AALTONEN	11AI CDF	p̄p̄ at 1.96 TeV
••• We do not use the following data for averages, fits, limits, etc. •••			
0.65 ^{+0.45} _{-0.35}	AAIJ	12AH LHCb	Repl. by AAIJ 14M

¹ Measured for B⁰ → K_S⁰ μ⁺ μ⁻ decays. Measurements in other q² bins are also reported.
² Measured for B⁰ → K_S⁰ e⁺ e⁻ decays. Measurements in other q² bins are also reported.
³ Uses B(B⁰ → J/ψ(1S) K⁰) = (0.928 ± 0.013 ± 0.037) × 10⁻³ for normalisation and μ⁺ μ⁻ as a lepton pair. Measured in 1.1 < q² < 6.0 GeV²/c⁴.

Meson Particle Listings

B^0

$B(B^0 \rightarrow K^0 \mu^+ \mu^-) / B(B^0 \rightarrow K^0 e^+ e^-) (1.0 < q^2 < 6.0 \text{ GeV}^2/c^4)$

VALUE	DOCUMENT ID	TECN	COMMENT
$0.55^{+0.46}_{-0.34} \pm 0.01$	1 CHOUHURY 21	BELL	$e^+ e^- \rightarrow \Upsilon(4S)$

¹ Measured from the ratio of $K_S^0 \mu^+ \mu^-$ and $K_S^0 e^+ e^-$. Measurements in other q^2 bins are also reported.

$B(B^0 \rightarrow K^0 \ell^+ \ell^-) (0.0 < q^2 < 4.3 \text{ GeV}^2/c^4)$

VALUE (units 10^{-7})	DOCUMENT ID	TECN	COMMENT
$1.27 \pm 0.62 \pm 0.10$	AALTONEN 11A1	CDF	$p\bar{p}$ at 1.96 TeV

$B(B^0 \rightarrow K^0 \ell^+ \ell^-) (15.0 < q^2 < 22.0 \text{ GeV}^2/c^4)$

VALUE (units 10^{-7})	DOCUMENT ID	TECN	COMMENT
$0.67^{+0.11}_{-0.11} \pm 0.04$	¹ AAIJ 14M	LHCB	pp at 7, 8 TeV

¹ Uses $B(B^0 \rightarrow J/\psi(1S) K^0) = (0.928 \pm 0.013 \pm 0.037) \times 10^{-3}$ for normalisation and $\mu^+ \mu^-$ as a lepton pair.

$B(B^0 \rightarrow K_{S,2}^*(1430)^0 \mu^+ \mu^-) (1.10 < q^2 < 6.00 \text{ GeV}^2/c^4)$

VALUE (units 10^{-8})	DOCUMENT ID	TECN	COMMENT
$4.02 \pm 0.44 \pm 0.31$	^{1,2} AAIJ 16AP	LHCB	pp at 7, 8 TeV

¹ Measured the differential branching fraction and angular moments of the decay $B^0 \rightarrow K^+ \pi^- \mu^+ \mu^-$ in the $K^+ \pi^-$ invariant mass region $1330 < m(K^+ \pi^-) < 1530 \text{ MeV}/c^2$.
² The reported value is converted from the measured $dB/dq^2 = (0.82 \pm 0.09 \pm 0.063) \times 10^{-8} (\text{GeV}^2/c^4)^{-1}$ by multiplying by the $\Delta q^2 = 4.9 \text{ GeV}^2/c^4$ range.

$F_H(B^0 \rightarrow K^0 \mu^+ \mu^-) (1.1 < q^2 < 6.0 \text{ GeV}^2/c^4)$

F_H is a fractional contribution of (pseudo) scalar and tensor amplitudes to the decay width in the massless muon approximation.

VALUE	DOCUMENT ID	TECN	COMMENT
$0.76 \pm 0.46 \pm 0.09$	¹ AAIJ 14O	LHCB	pp at 7, 8 TeV

¹ AAIJ 14O reports 68% C.L. interval, which we encode as midpoint with uncertainty as half of the width of interval.

$F_H(B^0 \rightarrow K^0 \mu^+ \mu^-) (15.0 < q^2 < 22.0 \text{ GeV}^2/c^4)$

VALUE	DOCUMENT ID	TECN	COMMENT
$0.34 \pm 0.25 \pm 0.03$	¹ AAIJ 14O	LHCB	pp at 7, 8 TeV

¹ AAIJ 14O reports 68% C.L. interval, which we encode as midpoint with uncertainty as half of the width of interval.

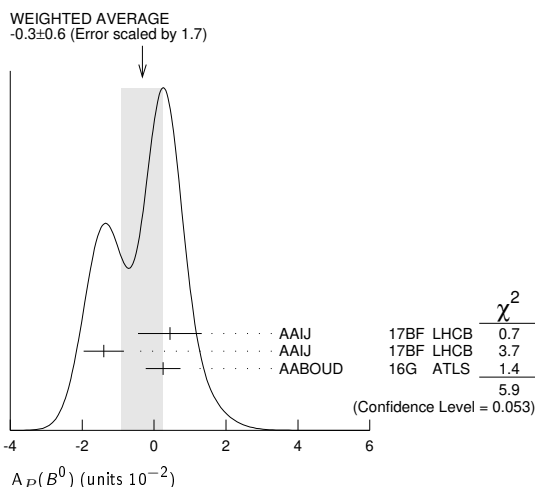
PRODUCTION ASYMMETRIES

$A_P(B^0)$

$$A_P(B^0) = [\sigma(\bar{B}^0) - \sigma(B^0)] / [\sigma(\bar{B}^0) + \sigma(B^0)]$$

VALUE (units 10^{-2})	DOCUMENT ID	TECN	COMMENT
-0.3 ± 0.6 OUR AVERAGE	Error includes scale factor of 1.7. See the ideogram below.		
$0.44 \pm 0.88 \pm 0.11$	¹ AAIJ 17BF	LHCB	pp at 7 TeV
$-1.40 \pm 0.55 \pm 0.10$	¹ AAIJ 17BF	LHCB	pp at 8 TeV
$0.25 \pm 0.48 \pm 0.05$	² AABOUD 16G	ATLS	pp at 7, 8 TeV
$-0.35 \pm 0.76 \pm 0.28$	³ AAIJ 14BP	LHCB	Repl. by AAIJ 17BF, pp at 7 TeV

• • • We do not use the following data for averages, fits, limits, etc. • • •



¹ AAIJ 17BF uses $B^0 \rightarrow J/\psi K^{*0}$ decays with B^0 transverse momenta p_T and rapidities y in the region of $0 < p_T < 30 \text{ GeV}/c$ and $2.1 < y < 4.5$.
² Based on time-dependent analysis of $B^0 \rightarrow J/\psi K^{*0}$ decay in kinematic range $p_T > 10 \text{ GeV}/c$ and $|\eta| < 2.5$.
³ Based on time-dependent analysis of $B^0 \rightarrow J/\psi K^{*0}$ and $B^0 \rightarrow D^- \pi^+$ in kinematic range $4 < p_T < 30 \text{ GeV}/c$ and $2.5 < \eta < 4.5$.

$A(B^0 + \bar{B}^0)$ in $K_S^0 K^\mp \pi^\pm$

$$A(B^0 + \bar{B}^0) = [n(K_S^0 K^- \pi^+) - n(K_S^0 K^+ \pi^-)] / [n(K_S^0 K^- \pi^+) + n(K_S^0 K^+ \pi^-)]$$

VALUE (units 10^{-2})	DOCUMENT ID	TECN	COMMENT
$-8.5 \pm 8.9 \pm 0.2$	LAI 19	BELL	$e^+ e^- \rightarrow \Upsilon(4S)$

B^0 REFERENCES

AAIJ 22	PRL 128 041801	R. Aaij et al.	(LHCB Collab.)
Also	PR D105 012010	R. Aaij et al.	(LHCB Collab.)
WAHEED 22	PR D105 012003	E. Waheed et al.	(Belle Collab.)
AAIJ 21K	CP C45 043001	R. Aaij et al.	(LHCB Collab.)
AAIJ 21O	JHEP 2103 075	R. Aaij et al.	(LHCB Collab.)
AAIJ 21S	JHEP 2106 177	R. Aaij et al.	(LHCB Collab.)
AAIJ 21W	EPJ C81 314	R. Aaij et al.	(LHCB Collab.)
ATMACAN 21	PR D104 1091105	H. Atmacan et al.	(Belle Collab.)
CAO 21A	PR D104 012008	L. Cao et al.	(BELLE Collab.)
CHOUHURY 21	JHEP 2103 105	S. Choudhury et al.	(BELLE Collab.)
KANG 21	PR D103 032003	K.H. Kang et al.	(BELLE Collab.)
MOHANTY 21	PR D103 052013	S. Mohanty et al.	(Belle Collab.)
WAHEED 21	PR D103 079901	E. Waheed et al.	(BELLE Collab.)
WEHLE 21	PRL 126 161801	S. Wehle et al.	(BELLE Collab.)
AAIJ 20AG	PR D102 051102	R. Aaij et al.	(LHCB Collab.)
AAIJ 20AN	JHEP 2012 139	R. Aaij et al.	(LHCB Collab.)
AAIJ 20AO	JHEP 2012 081	R. Aaij et al.	(LHCB Collab.)
AAIJ 20F	PR D102 012011	R. Aaij et al.	(LHCB Collab.)
AAIJ 20L	JHEP 2003 147	R. Aaij et al.	(LHCB Collab.)
AAIJ 20W	PRL 124 211802	R. Aaij et al.	(LHCB Collab.)
CHILKIN 20	JHEP 2005 034	K. Chilikin et al.	(BELLE Collab.)
CHU 20	PR D101 052012	K. Chu et al.	(BELLE Collab.)
KU 20	PR D102 012003	Y. Ku et al.	(BELLE Collab.)
SIRUNYAN 20AG	JHEP 2004 188	A.M. Sirunyan et al.	(CMS Collab.)
AABOUD 19L	JHEP 1904 098	M. Aaboud et al.	(ATLAS Collab.)
AAIJ 19AK	PRL 123 211801	R. Aaij et al.	(LHCB Collab.)
AAIJ 19AP	JHEP 1912 155	R. Aaij et al.	(LHCB Collab.)
AAIJ 19J	JHEP 1905 026	R. Aaij et al.	(LHCB Collab.)
AAIJ 19L	JHEP 1907 032	R. Aaij et al.	(LHCB Collab.)
AAIJ 19N	JHEP 1908 041	R. Aaij et al.	(LHCB Collab.)
AAIJ 19U	PRL 122 191804	R. Aaij et al.	(LHCB Collab.)
CHILKIN 19	PR D100 012001	K. Chilikin et al.	(BELLE Collab.)
CHOU 19	PR D100 012002	P.-C. Chou et al.	(BELLE Collab.)
GARG 19	PR D99 071102	R. Garg et al.	(BELLE Collab.)
LAI 19	PR D100 011101	Y.-T. Lai et al.	(BELLE Collab.)
LI 19C	PR D100 031101	Y.B. Li et al.	(BELLE Collab.)
PAL 19	PR D99 091104	B. Pal et al.	(BELLE Collab.)
WAHEED 19	PR D100 052007	E. Waheed et al.	(BELLE Collab.)
WATANUKI 19	PR D99 032012	S. Watanuki et al.	(BELLE Collab.)
YUSA 19	PR D99 011102	Y. Yusa et al.	(BELLE Collab.)
AABOUD 18BY	JHEP 1810 047	M. Aaboud et al.	(ATLAS Collab.)
AAIJ 18AN	EPJ C78 1011	R. Aaij et al.	(BABAR Collab.)
AAIJ 18AY	PR D98 071103	R. Aaij et al.	(LHCB Collab.)
AAIJ 18AZ	PR D98 072006	R. Aaij et al.	(LHCB Collab.)
AAIJ 18D	PRL 120 171802	R. Aaij et al.	(LHCB Collab.)
AAIJ 18F	PRL 120 261801	R. Aaij et al.	(LHCB Collab.)
AAIJ 18O	PR D98 032004	R. Aaij et al.	(LHCB Collab.)
AAIJ 18T	JHEP 1803 078	R. Aaij et al.	(LHCB Collab.)
AAIJ 18Z	JHEP 1806 084	R. Aaij et al.	(LHCB Collab.)
ABAZOV 18B	PR D98 052010	V.M. Abazov et al.	(DO Collab.)
ADACHI 18	PR D98 122012	I. Adachi et al.	(BELLE and BABAR Collab.)
Also	PRL 121 261801	I. Adachi et al.	(BELLE and BABAR Collab.)
LEES 18C	PR D98 071102	J.P. Lees et al.	(BABAR Collab.)
LI 18D	EPJ C78 928	Y.B. Li et al.	(BELLE Collab.)
NAKANO 18	PR D97 092003	H. Nakano et al.	(BELLE Collab.)
PAL 18	PR D98 112008	B. Pal et al.	(BELLE Collab.)
PDG 18	PR D98 030001	M. Tanabashi et al.	(PDG Collab.)
SANDILYA 18	PR D98 071101	S. Sandilya et al.	(BELLE Collab.)
SIRUNYAN 18BY	EPJ C78 457	A.M. Sirunyan et al.	(CMS Collab.)
SIRUNYAN 18DF	EPJ C78 939	A.M. Sirunyan et al.	(CMS Collab.)
VOSSEN 18	PR D98 012005	A. Vossen et al.	(BELLE Collab.)
AAIJ 17A	PR D95 012006	R. Aaij et al.	(LHCB Collab.)
AAIJ 17AI	PRL 118 191801	R. Aaij et al.	(LHCB Collab.)
AAIJ 17AJ	PRL 118 251802	R. Aaij et al.	(LHCB Collab.)
AAIJ 17BD	PR D96 051103	R. Aaij et al.	(LHCB Collab.)
AAIJ 17BF	PL B774 139	R. Aaij et al.	(LHCB Collab.)
AAIJ 17BJ	PRL 119 232001	R. Aaij et al.	(LHCB Collab.)
AAIJ 17BN	JHEP 1711 170	R. Aaij et al.	(LHCB Collab.)
AAIJ 17BP	JHEP 1711 027	R. Aaij et al.	(LHCB Collab.)
AAIJ 17G	PRL 118 081801	R. Aaij et al.	(LHCB Collab.)
AAIJ 17N	JHEP 1703 001	R. Aaij et al.	(LHCB Collab.)
AAIJ 17Q	JHEP 1704 142	R. Aaij et al.	(LHCB Collab.)
AAIJ 17W	JHEP 1708 055	R. Aaij et al.	(LHCB Collab.)
GRYGIER 17	PR D96 091101	J. Grygier et al.	(BELLE Collab.)
HORIGUCHI 17	PRL 119 191802	T. Horiguchi et al.	(BELLE Collab.)
JULIUS 17	PR D96 032007	T. Julius et al.	(BELLE Collab.)
AABOUD 16G	JHEP 1606 081	M. Aaboud et al.	(ATLAS Collab.)
AABOUD 16L	EPJ C76 513	M. Aaboud et al.	(ATLAS Collab.)
AAIJ 16	JHEP 1601 012	R. Aaij et al.	(LHCB Collab.)
AAIJ 16AA	JHEP 1608 137	R. Aaij et al.	(LHCB Collab.)
AAIJ 16AN	PRL 117 261801	R. Aaij et al.	(LHCB Collab.)
AAIJ 16AO	JHEP 1611 047	R. Aaij et al.	(LHCB Collab.)
AAIJ 16AP	JHEP 1612 065	R. Aaij et al.	(LHCB Collab.)
AAIJ 16AV	EPJ C76 412	R. Aaij et al.	(LHCB Collab.)
AAIJ 16E	PRL 116 241601	R. Aaij et al.	(LHCB Collab.)
AAIJ 16S	PR D93 112018	R. Aaij et al.	(LHCB Collab.)
AAIJ 16Z	JHEP 1606 131	R. Aaij et al.	(LHCB Collab.)
BHARDWAJ 16	PR D93 052016	V. Bhardwaj et al.	(BELLE Collab.)
CHOBANOVA 16	PR D93 031101	V. Chobanova et al.	(BELLE Collab.)
DEL-AMO-SA... 16	PR D93 052013	P. del Amo Sanchez et al.	(BABAR Collab.)
GLATTAUER 16	PR D93 032006	R. Glattauer et al.	(BELLE Collab.)
HAMER 16	PR D93 032007	P. Hamer et al.	(BELLE Collab.)
KHACHATRYAN... 16D	PL B753 424	V. Khachatryan et al.	(CMS Collab.)
KING 16	PR D93 111101	Z. King et al.	(BELLE Collab.)
LEES 16	PRL 116 041801	J.P. Lees et al.	(BABAR Collab.)
LEES 16E	PR D94 011101	J.P. Lees et al.	(BABAR Collab.)
LEES 16H	PR D94 091101	J.P. Lees et al.	(BABAR Collab.)
SATO 16B	PR D94 072007	Y. Saito et al.	(BELLE Collab.)
VANHOEFER 16	PR D93 032010	P. Vanhoefer et al.	(BELLE Collab.)
Also	PR D94 099903 (err.)	P. Vanhoefer et al.	(BELLE Collab.)
VOROBYEV 16	PR D94 052004	V. Vorobyev et al.	(BELLE Collab.)
AAIJ 15AC	JHEP 1505 019	R. Aaij et al.	(LHCB Collab.)
AAIJ 15AS	JHEP 1510 053	R. Aaij et al.	(LHCB Collab.)
AAIJ 15AZ	PRL 115 161802	R. Aaij et al.	(LHCB Collab.)
AAIJ 15BB	PR D92 112002	R. Aaij et al.	(LHCB Collab.)
AAIJ 15D	JHEP 1501 024	R. Aaij et al.	(LHCB Collab.)
AAIJ 15F	PRL 114 041601	R. Aaij et al.	(LHCB Collab.)
AAIJ 15J	PL B742 38	R. Aaij et al.	(LHCB Collab.)
AAIJ 15N	PRL 115 031601	R. Aaij et al.	(LHCB Collab.)
AAIJ 15Q	PRL 115 111803	R. Aaij et al.	(LHCB Collab.)
AAIJ 15S	PL B743 46	R. Aaij et al.	(LHCB Collab.)

See key on page 1127

Meson Particle Listings

B⁰

Table listing meson particles with columns for particle name, mass, production method, and associated researchers/institutions. Includes entries for various B mesons and their decays.

Downloaded from https://academic.oup.com/ptep/article/2022/8/083C01/6651666 by CERN Library user on 11 October 2022

Meson Particle Listings

$B^0, B^\pm/B^0$ ADMIXTURE

BUSKULIC 93D	PL B307 194	D. Buskulic et al.	(ALEPH Collab.)
Also	PL B325 537 (erratum)	D. Buskulic et al.	(ALEPH Collab.)
BUSKULIC 93K	PL B313 498	D. Buskulic et al.	(ALEPH Collab.)
SANGHERA 93	PR D47 791	S. Sanghera et al.	(CLEO Collab.)
ALBRECHT 92C	PL B275 195	H. Albrecht et al.	(ARGUS Collab.)
ALBRECHT 92G	ZPHY C54 1	H. Albrecht et al.	(ARGUS Collab.)
ALBRECHT 92L	ZPHY C55 357	H. Albrecht et al.	(ARGUS Collab.)
BORTOLETTO 92	PR D45 21	D. Bortoletto et al.	(CLEO Collab.)
HENDERSON 92	PR D45 2212	S. Henderson et al.	(CLEO Collab.)
KRAMER 92	PL B279 181	G. Kramer, W.F. Palmer	(HAMB, OSU)
ALBAJAR 91E	PL B273 540	C. Albajar et al.	(UA1 Collab.)
ALBRECHT 91B	PL B254 288	H. Albrecht et al.	(ARGUS Collab.)
ALBRECHT 91C	PL B255 297	H. Albrecht et al.	(ARGUS Collab.)
ALBRECHT 91E	PL B262 148	H. Albrecht et al.	(ARGUS Collab.)
BERKELMAN 91	ARNPS 41 1	K. Berkelman, S. Stone	(CORN, SYRA)
"Decays of B Mesons"			
FULTON 91	PR D43 651	R. Fulton et al.	(CLEO Collab.)
ALBRECHT 90B	PL B241 278	H. Albrecht et al.	(ARGUS Collab.)
ALBRECHT 90J	ZPHY C48 543	H. Albrecht et al.	(ARGUS Collab.)
ANTREASYAN 90B	ZPHY C48 553	D. Antreasyan et al.	(Crystal Ball Collab.)
BORTOLETTO 90	PRL 64 2117	D. Bortoletto et al.	(CLEO Collab.)
ELSEN 90	ZPHY C46 349	E. Elsen et al.	(JADE Collab.)
ROSNER 90	PR D42 3732	J.L. Rosner	
WAGNER 90	PRL 64 1095	S.R. Wagner et al.	(Mark II Collab.)
ALBRECHT 89C	PL B219 121	H. Albrecht et al.	(ARGUS Collab.)
ALBRECHT 89G	PL B229 304	H. Albrecht et al.	(ARGUS Collab.)
ALBRECHT 89J	PL B229 175	H. Albrecht et al.	(ARGUS Collab.)
ALBRECHT 89L	PL B232 554	H. Albrecht et al.	(ARGUS Collab.)
ARTUSO 89	PRL 62 2233	M. Artuso et al.	(CLEO Collab.)
AVERILL 89	PR D39 123	D.A. Averill et al.	(HRS Collab.)
AVERY 89B	PL B223 470	P. Avery et al.	(CLEO Collab.)
BEBEK 89	PRL 62 9	C. Bebek et al.	(CLEO Collab.)
BORTOLETTO 89	PRL 62 2436	D. Bortoletto et al.	(CLEO Collab.)
BORTOLETTO 89B	PRL 63 1667	D. Bortoletto et al.	(CLEO Collab.)
ALBRECHT 88F	PL B209 119	H. Albrecht et al.	(ARGUS Collab.)
ALBRECHT 88K	PL B215 424	H. Albrecht et al.	(ARGUS Collab.)
ALBRECHT 87C	PL B185 218	H. Albrecht et al.	(ARGUS Collab.)
ALBRECHT 87D	PL B199 451	H. Albrecht et al.	(ARGUS Collab.)
ALBRECHT 87I	PL B192 245	H. Albrecht et al.	(ARGUS Collab.)
ALBRECHT 87J	PL B197 452	H. Albrecht et al.	(ARGUS Collab.)
AVERY 87	PL B183 429	P. Avery et al.	(CLEO Collab.)
BEAN 87B	PRL 58 183	A. Bean et al.	(CLEO Collab.)
BEBEK 87	PR D36 1289	C. Bebek et al.	(CLEO Collab.)
ALAM 86	PR D34 3279	M.S. Alam et al.	(CLEO Collab.)
ALBRECHT 86F	PL B182 95	H. Albrecht et al.	(ARGUS Collab.)
PDG 86	PL 170B 1	M. Aguilar-Benitez et al.	(CERN, CIT+)
CHEN 85	PR D31 2386	A. Chen et al.	(CLEO Collab.)
HAAS 85	PRL 55 1248	J. Haas et al.	(CLEO Collab.)
AVERY 84	PRL 53 1309	P. Avery et al.	(CLEO Collab.)
GILES 84	PR D30 2279	R. Giles et al.	(CLEO Collab.)
BEHRENDIS 83	PRL 50 881	S. Behrendis et al.	(CLEO Collab.)

B^\pm/B^0 ADMIXTURE

B DECAY MODES

The branching fraction measurements are for an admixture of B mesons at the $T(4S)$. The values quoted assume that $B(T(4S) \rightarrow B\bar{B}) = 100\%$.

For inclusive branching fractions, e.g., $B \rightarrow D^\pm$ anything, the treatment of multiple D 's in the final state must be defined. One possibility would be to count the number of events with one-or-more D 's and divide by the total number of B 's. Another possibility would be to count the total number of D 's and divide by the total number of B 's, which is the definition of average multiplicity. The two definitions are identical if only one D is allowed in the final state. Even though the "one-or-more" definition seems sensible, for practical reasons inclusive branching fractions are almost always measured using the multiplicity definition. For heavy final state particles, authors call their results inclusive branching fractions while for light particles some authors call their results multiplicities. In the B sections, we list all results as inclusive branching fractions, adopting a multiplicity definition. This means that inclusive branching fractions can exceed 100% and that inclusive partial widths can exceed total widths, just as inclusive cross sections can exceed total cross section.

\bar{B} modes are charge conjugates of the modes below. Reactions indicate the weak decay vertex and do not include mixing.

Mode	Fraction (Γ_i/Γ)	Scale factor/ Confidence level
Semileptonic and leptonic modes		
Γ_1	$e^+ \nu_e$ anything	[a]
Γ_2	$\mu^+ \nu_\mu$ anything	[a]
Γ_3	$\ell^+ \nu_\ell$ anything	[a,b] (10.84 ± 0.16) %
Γ_4	$D^- \ell^+ \nu_\ell$ anything	[b] (2.6 ± 0.5) %
Γ_5	$\bar{D}^0 \ell^+ \nu_\ell$ anything	[b] (7.3 ± 1.5) %
Γ_6	$\bar{D} \ell^+ \nu_\ell$	(2.42 ± 0.12) %
Γ_7	$D^{*-} \ell^+ \nu_\ell$ anything	[c] (6.7 ± 1.3) × 10 ⁻³
Γ_8	$D^{*0} \ell^+ \nu_\ell$ anything	
Γ_9	$\bar{D}^* \ell^+ \nu_\ell$	[d] (4.95 ± 0.11) %
Γ_{10}	$\bar{D}^{**} \ell^+ \nu_\ell$	[b,e] (2.7 ± 0.7) %
Γ_{11}	$\bar{D}_1(2420) \ell^+ \nu_\ell$ anything	(3.8 ± 1.3) × 10 ⁻³ S=2.4
Γ_{12}	$\bar{D} \pi \ell^+ \nu_\ell$ anything + $\bar{D}^* \pi \ell^+ \nu_\ell$ anything	(2.6 ± 0.5) % S=1.5
Γ_{13}	$\bar{D} \pi \ell^+ \nu_\ell$ anything	(1.5 ± 0.6) %
Γ_{14}	$\bar{D}^* \pi \ell^+ \nu_\ell$ anything	(1.9 ± 0.4) %
Γ_{15}	$\bar{D}_2^*(2460) \ell^+ \nu_\ell$ anything	(4.4 ± 1.6) × 10 ⁻³

Γ_{16}	$D^{*-} \pi^+ \ell^+ \nu_\ell$ anything	(1.00 ± 0.34) %
Γ_{17}	$\bar{D} \pi^+ \pi^- \ell^+ \nu_\ell$	(1.62 ± 0.32) × 10 ⁻³
Γ_{18}	$\bar{D}^* \pi^+ \pi^- \ell^+ \nu_\ell$	(9.4 ± 3.2) × 10 ⁻⁴
Γ_{19}	$D_s^- \ell^+ \nu_\ell$ anything	[b] < 7 × 10 ⁻³ CL=90%
Γ_{20}	$D_s^- \ell^+ \nu_\ell K^+$ anything	[b] < 5 × 10 ⁻³ CL=90%
Γ_{21}	$D_s^- \ell^+ \nu_\ell K^0$ anything	[b] < 7 × 10 ⁻³ CL=90%
Γ_{22}	$X_c \ell^+ \nu_\ell$	(10.65 ± 0.16) %
Γ_{23}	$X_u \ell^+ \nu_\ell$	(1.91 ± 0.27) × 10 ⁻³
Γ_{24}	$X_u e^+ \nu_e$	(1.57 ± 0.19) × 10 ⁻³
Γ_{25}	$X_u \mu^+ \nu_\mu$	(1.62 ± 0.21) × 10 ⁻³
Γ_{26}	$K^+ \ell^+ \nu_\ell$ anything	[b] (6.3 ± 0.6) %
Γ_{27}	$K^- \ell^+ \nu_\ell$ anything	[b] (10 ± 4) × 10 ⁻³
Γ_{28}	$K^0/\bar{K}^0 \ell^+ \nu_\ell$ anything	[b] (4.6 ± 0.5) %
Γ_{29}	$\bar{D}^* \tau^+ \nu_\tau$	(8.2 ± 0.8) × 10 ⁻³
Γ_{30}	$\bar{D}^* \tau^+ \nu_\tau$	(1.46 ± 0.08) %

D, D*, or D_s modes

Γ_{31}	D^\pm anything	(23.1 ± 1.2) %	S=1.3
Γ_{32}	D^0/\bar{D}^0 anything	(61.6 ± 2.9) %	
Γ_{33}	$D^*(2010)^\pm$ anything	(22.5 ± 1.5) %	
Γ_{34}	$\bar{D}^*(2007)^0$ anything	(26.0 ± 2.7) %	
Γ_{35}	D_s^\pm anything	[f] (8.3 ± 0.8) %	
Γ_{36}	$D_s^{*\pm}$ anything	(6.3 ± 1.0) %	
Γ_{37}	$D_s^\pm \bar{D}^*(*)$	(3.4 ± 0.6) %	
Γ_{38}	$\bar{D} \bar{D}_{s0}(2317)$	seen	
Γ_{39}	$\bar{D} \bar{D}_{sJ}(2457)$	seen	
Γ_{40}	$D^{(*)} \bar{D}^{(*)} K^0 + D^{(*)} \bar{D}^{(*)} K^\pm$ [fg]	(7.1 ± 2.7) % (-1.7) %	
Γ_{41}	$b \rightarrow c \bar{c} s$	(22 ± 4) %	
Γ_{42}	$D_s^{(*)} \bar{D}^{(*)}$	[fg] (3.9 ± 0.4) %	
Γ_{43}	$D^* D^*(2010)^\pm$	[f] < 5.9 × 10 ⁻³ CL=90%	
Γ_{44}	$D^* D^*(2010)^\pm + D^* D^\pm$	[f] < 5.5 × 10 ⁻³ CL=90%	
Γ_{45}	$D D^\pm$	[f] < 3.1 × 10 ⁻³ CL=90%	
Γ_{46}	$D_s^{(*)\pm} \bar{D}^{(*)} X (n\pi^\pm)$	[fg] (9 ± 5) % (-4) %	
Γ_{47}	$\bar{D}^*(2010) \gamma$	< 1.1 × 10 ⁻³ CL=90%	
Γ_{48}	$D_s^\pm \pi^-, D_s^{*+} \pi^-, D_s^\pm \rho^-, D_s^{*+} \rho^-, D_s^\pm \pi^0, D_s^{*+} \pi^0, D_s^\pm \eta, D_s^{*+} \eta, D_s^\pm \rho^0, D_s^{*+} \rho^0, D_s^\pm \omega, D_s^{*+} \omega$	[f] < 4 × 10 ⁻⁴ CL=90%	
Γ_{49}	$D_{s1}(2536)^+$ anything	< 9.5 × 10 ⁻³ CL=90%	

Charmonium modes

Γ_{50}	$J/\psi(1S)$ anything	(1.094 ± 0.032) %	S=1.1
Γ_{51}	$J/\psi(1S)$ (direct) anything	(7.8 ± 0.4) × 10 ⁻³	S=1.1
Γ_{52}	$\psi(2S)$ anything	(3.07 ± 0.21) × 10 ⁻³	
Γ_{53}	$\chi_{c1}(1P)$ anything	(3.55 ± 0.27) × 10 ⁻³	S=1.3
Γ_{54}	$\chi_{c1}(1P)$ (direct) anything	(3.08 ± 0.19) × 10 ⁻³	
Γ_{55}	$\chi_{c2}(1P)$ anything	(10.0 ± 1.7) × 10 ⁻⁴	S=1.6
Γ_{56}	$\chi_{c2}(1P)$ (direct) anything	(7.5 ± 1.1) × 10 ⁻⁴	
Γ_{57}	$\eta_c(1S)$ anything	< 9 × 10 ⁻³ CL=90%	
Γ_{58}	$K \chi_{c1}(3872)$	(2.3 ± 0.7) × 10 ⁻⁴	
Γ_{59}	$K X(3940), X \rightarrow D^{*0} D^0$	< 6.7 × 10 ⁻⁵ CL=90%	
Γ_{60}	$K \chi_{c0}(3915), \chi_{c0} \rightarrow \omega J/\psi$	[b] (7.1 ± 3.4) × 10 ⁻⁵	

K or K* modes

Γ_{61}	K^\pm anything	[f] (78.9 ± 2.5) %
Γ_{62}	K^+ anything	(66 ± 5) %
Γ_{63}	K^- anything	(13 ± 4) %
Γ_{64}	K^0/\bar{K}^0 anything	[f] (64 ± 4) %
Γ_{65}	$K^*(892)^\pm$ anything	(18 ± 6) %
Γ_{66}	$K^*(892)^0/\bar{K}^*(892)^0$ anything	[f] (14.6 ± 2.6) %
Γ_{67}	$K^*(892) \gamma$	(4.2 ± 0.6) × 10 ⁻⁵
Γ_{68}	$\eta K \gamma$	(8.5 ± 1.8) × 10 ⁻⁶ (-1.6) %
Γ_{69}	$K_1(1400) \gamma$	< 1.27 × 10 ⁻⁴ CL=90%
Γ_{70}	$K_2^*(1430) \gamma$	(1.7 ± 0.6) × 10 ⁻⁵ (-0.5) %
Γ_{71}	$K_2(1770) \gamma$	< 1.2 × 10 ⁻³ CL=90%
Γ_{72}	$K_3^*(1780) \gamma$	< 3.7 × 10 ⁻⁵ CL=90%
Γ_{73}	$K_4^*(2045) \gamma$	< 1.0 × 10 ⁻³ CL=90%
Γ_{74}	$K \eta'(958)$	(8.3 ± 1.1) × 10 ⁻⁵
Γ_{75}	$K^*(892) \eta'(958)$	(4.1 ± 1.1) × 10 ⁻⁶
Γ_{76}	$K \eta$	< 5.2 × 10 ⁻⁶ CL=90%
Γ_{77}	$K^*(892) \eta$	(1.8 ± 0.5) × 10 ⁻⁵

See key on page 1127

Meson Particle Listings

B^\pm/B^0 ADMIXTURE

Γ_{78}	$K\phi\phi$	(2.3 ± 0.9) × 10 ⁻⁶	
Γ_{79}	$\bar{b} \rightarrow \bar{s}\gamma$	(3.49 ± 0.19) × 10 ⁻⁴	
Γ_{80}	$\bar{b} \rightarrow \bar{d}\gamma$	(9.2 ± 3.0) × 10 ⁻⁶	
Γ_{81}	$\bar{b} \rightarrow \bar{s}g\text{gluon}$	< 6.8 %	CL=90%
Γ_{82}	η anything	(2.6 $\begin{smallmatrix} +0.5 \\ -0.8 \end{smallmatrix}$) × 10 ⁻⁴	
Γ_{83}	η' anything	(4.2 ± 0.9) × 10 ⁻⁴	
Γ_{84}	K^+ gluon (charmless)	< 1.87 × 10 ⁻⁴	CL=90%
Γ_{85}	K^0 gluon (charmless)	(1.9 ± 0.7) × 10 ⁻⁴	

Light unflavored meson modes

Γ_{86}	$\rho\gamma$	(1.39 ± 0.25) × 10 ⁻⁶	S=1.2
Γ_{87}	$\rho/\omega\gamma$	(1.30 ± 0.23) × 10 ⁻⁶	S=1.2
Γ_{88}	π^\pm anything [f]	(358 ± 7) %	
Γ_{89}	π^0 anything	(235 ± 11) %	
Γ_{90}	η anything	(17.6 ± 1.6) %	
Γ_{91}	ρ^0 anything	(21 ± 5) %	
Γ_{92}	ω anything	< 81 %	CL=90%
Γ_{93}	ϕ anything	(3.43 ± 0.12) %	
Γ_{94}	$\phi K^*(892)$	< 2.2 × 10 ⁻⁵	CL=90%
Γ_{95}	$\bar{b} \rightarrow \bar{d}$ gluon		
Γ_{96}	π^+ gluon (charmless)	(3.7 ± 0.8) × 10 ⁻⁴	

Baryon modes

Γ_{97}	$\Lambda_c^+ / \bar{\Lambda}_c^-$ anything	(3.6 ± 0.4) %	
Γ_{98}	Λ_c^+ anything	< 1.3 %	CL=90%
Γ_{99}	$\bar{\Lambda}_c^-$ anything	< 7 %	CL=90%
Γ_{100}	$\bar{\Lambda}_c^- \ell^+$ anything	< 9 × 10 ⁻⁴	CL=90%
Γ_{101}	$\bar{\Lambda}_c^- e^+$ anything	< 1.8 × 10 ⁻³	CL=90%
Γ_{102}	$\bar{\Lambda}_c^- \mu^+$ anything	< 1.4 × 10 ⁻³	CL=90%
Γ_{103}	$\bar{\Lambda}_c^- p$ anything	(2.04 ± 0.33) %	
Γ_{104}	$\bar{\Lambda}_c^- p e^+ \nu_e$	< 8 × 10 ⁻⁴	CL=90%
Γ_{105}	$\bar{\Sigma}_c^-$ anything	(3.3 ± 1.7) × 10 ⁻³	
Γ_{106}	$\bar{\Sigma}_c^-$ anything	< 8 × 10 ⁻³	CL=90%
Γ_{107}	$\bar{\Sigma}_c^0$ anything	(3.7 ± 1.7) × 10 ⁻³	
Γ_{108}	$\bar{\Sigma}_c^0 N (N = p \text{ or } n)$	< 1.2 × 10 ⁻³	CL=90%
Γ_{109}	Ξ_c^0 anything, $\Xi_c^0 \rightarrow \Xi^- \pi^+$	(1.93 ± 0.30) × 10 ⁻⁴	S=1.1
Γ_{110}	$\Xi_c^+, \Xi_c^+ \rightarrow \Xi^- \pi^+ \pi^+$	(4.5 $\begin{smallmatrix} +1.3 \\ -1.2 \end{smallmatrix}$) × 10 ⁻⁴	
Γ_{111}	p/\bar{p} anything [f]	(8.0 ± 0.4) %	
Γ_{112}	p/\bar{p} (direct) anything [f]	(5.5 ± 0.5) %	
Γ_{113}	$\bar{p} e^+ \nu_e$ anything	< 5.9 × 10 ⁻⁴	CL=90%
Γ_{114}	$\Lambda/\bar{\Lambda}$ anything [f]	(4.0 ± 0.5) %	
Γ_{115}	Λ anything	seen	
Γ_{116}	$\bar{\Lambda}$ anything	seen	
Γ_{117}	Ξ^- / Ξ^+ anything [f]	(2.7 ± 0.6) × 10 ⁻³	
Γ_{118}	baryons anything	(6.8 ± 0.6) %	
Γ_{119}	$p\bar{p}$ anything	(2.47 ± 0.23) %	
Γ_{120}	$\Lambda\bar{p}/\bar{\Lambda}p$ anything [f]	(2.5 ± 0.4) %	
Γ_{121}	$\Lambda\bar{\Lambda}$ anything	< 5 × 10 ⁻³	CL=90%

Lepton Family number (LF) violating modes or $\Delta B = 1$ weak neutral current (B_I) modes

Γ_{122}	$s e^+ e^-$	B_I	(6.7 ± 1.7) × 10 ⁻⁶	S=2.0
Γ_{123}	$s \mu^+ \mu^-$	B_I	(4.3 ± 1.0) × 10 ⁻⁶	
Γ_{124}	$s \ell^+ \ell^-$	B_I [b]	(5.8 ± 1.3) × 10 ⁻⁶	S=1.8
Γ_{125}	$\pi \ell^+ \ell^-$	B_I	< 5.9 × 10 ⁻⁸	CL=90%
Γ_{126}	$\pi e^+ e^-$	B_I	< 1.10 × 10 ⁻⁷	CL=90%
Γ_{127}	$\pi \mu^+ \mu^-$	B_I	< 5.0 × 10 ⁻⁸	CL=90%
Γ_{128}	$K e^+ e^-$	B_I	(4.4 ± 0.6) × 10 ⁻⁷	
Γ_{129}	$K^*(892) e^+ e^-$	B_I	(1.19 ± 0.20) × 10 ⁻⁶	S=1.2
Γ_{130}	$K \mu^+ \mu^-$	B_I	(4.4 ± 0.4) × 10 ⁻⁷	
Γ_{131}	$K^*(892) \mu^+ \mu^-$	B_I	(1.06 ± 0.09) × 10 ⁻⁶	
Γ_{132}	$K \ell^+ \ell^-$	B_I	(4.8 ± 0.4) × 10 ⁻⁷	
Γ_{133}	$K^*(892) \ell^+ \ell^-$	B_I	(1.05 ± 0.10) × 10 ⁻⁶	
Γ_{134}	$K \nu \bar{\nu}$	B_I	< 1.6 × 10 ⁻⁵	CL=90%
Γ_{135}	$K^* \nu \bar{\nu}$	B_I	< 2.7 × 10 ⁻⁵	CL=90%
Γ_{136}	$\pi \nu \bar{\nu}$	B_I	< 8 × 10 ⁻⁶	CL=90%
Γ_{137}	$\rho \nu \bar{\nu}$	B_I	< 2.8 × 10 ⁻⁵	CL=90%
Γ_{138}	$s e^\pm \mu^\mp$	LF [f]	< 2.2 × 10 ⁻⁵	CL=90%
Γ_{139}	$\pi e^\pm \mu^\mp$	LF	< 9.2 × 10 ⁻⁸	CL=90%
Γ_{140}	$\rho e^\pm \mu^\mp$	LF	< 3.2 × 10 ⁻⁶	CL=90%
Γ_{141}	$K e^\pm \mu^\mp$	LF	< 3.8 × 10 ⁻⁸	CL=90%
Γ_{142}	$K^*(892) e^\pm \mu^\mp$	LF	< 5.1 × 10 ⁻⁷	CL=90%

[a] These values are model dependent.

[b] An ℓ indicates an e or a μ mode, not a sum over these modes.

[c] Here "anything" means at least one particle observed.

[d] This is a $B(B^0 \rightarrow D^{*-} \ell^+ \nu_\ell)$ value.

[e] D^{**} stands for the sum of the $D(1^1P_1)$, $D(1^3P_0)$, $D(1^3P_1)$, $D(1^3P_2)$, $D(2^1S_0)$, and $D(2^1S_1)$ resonances.

[f] The value is for the sum of the charge states or particle/antiparticle states indicated.

[g] $D^{(*)}\bar{D}^{(*)}$ stands for the sum of $D^* \bar{D}^*$, $D^* \bar{D}$, $D \bar{D}^*$, and $D \bar{D}$.

[h] $X(3915)$ denotes a near-threshold enhancement in the $\omega J/\psi$ mass spectrum.

[i] Inclusive branching fractions have a multiplicity definition and can be greater than 100%.

B^\pm/B^0 ADMIXTURE BRANCHING RATIOS

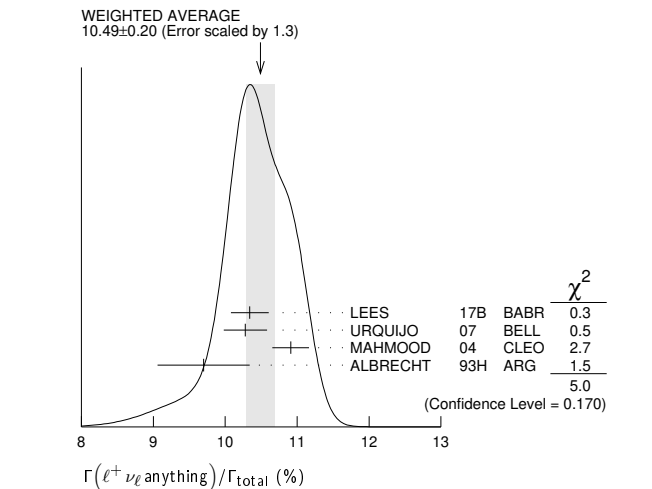
$\Gamma(\ell^+ \nu_\ell \text{ anything})/\Gamma_{\text{total}}$

These branching fraction values are model dependent.

Γ_3/Γ

"OUR EVALUATION" assumes lepton universality and is an average using rescaled values of the data listed below. The average and rescaling were performed by the Heavy Flavor Averaging Group (HFLAV) and are described at <https://hflav.web.cern.ch/>. The averaging/rescaling procedure takes into account correlations between the measurements.

VALUE (%)	DOCUMENT ID	TECN	COMMENT
10.84 ± 0.16 OUR EVALUATION			
10.49 ± 0.20 OUR AVERAGE			Error includes scale factor of 1.3. See the ideogram below.
10.34 ± 0.04 ± 0.26	¹ LEES	17B	BABR $e^+ e^- \rightarrow \Upsilon(4S)$
10.28 ± 0.18 ± 0.24	² URQUIJO	07	BELL $e^+ e^- \rightarrow \Upsilon(4S)$
10.91 ± 0.09 ± 0.24	³ MAHMOOD	04	CLEO $e^+ e^- \rightarrow \Upsilon(4S)$
9.7 ± 0.5 ± 0.4	⁴ ALBRECHT	93H	ARG $e^+ e^- \rightarrow \Upsilon(4S)$
9.96 ± 0.19 ± 0.32	⁵ AUBERT,B	06Y	BABR Repl. by LEES 17B
10.85 ± 0.21 ± 0.36	⁶ OKABE	05	BELL Repl. by URQUIJO 07
10.83 ± 0.16 ± 0.06	⁷ AUBERT	04X	BABR Repl. by AUBERT,B 06Y
10.36 ± 0.06 ± 0.23	⁸ AUBERT,B	04A	BABR $e^+ e^- \rightarrow \Upsilon(4S)$
10.87 ± 0.18 ± 0.30	⁹ AUBERT	03	BABR Repl. by AUBERT 04X
10.90 ± 0.12 ± 0.49	¹⁰ ABE	02Y	BELL Repl. by OKABE 05
10.49 ± 0.17 ± 0.43	¹¹ BARISH	96B	CLE2 Repl. by MAHMOOD 04
10.80 ± 0.20 ± 0.56	¹² HENDERSON	92	CLEO $e^+ e^- \rightarrow \Upsilon(4S)$
10.0 ± 0.4 ± 0.3	¹³ YANAGISAWA	91	CSB2 $e^+ e^- \rightarrow \Upsilon(4S)$
10.3 ± 0.6 ± 0.2	¹⁴ ALBRECHT	90H	ARG Direct e at $\Upsilon(4S)$
10.0 ± 0.6 ± 0.2	¹⁵ ALBRECHT	90H	ARG Direct μ at $\Upsilon(4S)$
11.7 ± 0.4 ± 1.0	¹⁶ WACHS	89	CBAL Direct e at $\Upsilon(4S)$
12.0 ± 0.7 ± 0.5	CHEN	84	CLEO Direct e at $\Upsilon(4S)$
10.8 ± 0.6 ± 1.0	CHEN	84	CLEO Direct μ at $\Upsilon(4S)$
11.2 ± 0.9 ± 1.0	LEVMAN	84	CUSB Direct μ at $\Upsilon(4S)$
13.2 ± 0.8 ± 1.4	¹⁷ KLOPFEN...	83B	CUSB Direct e at $\Upsilon(4S)$



¹ LEES 17B measurement is obtained from semileptonic decays to electrons. The result is averaged over B^\pm and B^0 mesons, assuming lepton universality.

² URQUIJO 07 report a measurement of $(10.07 \pm 0.18 \pm 0.21)\%$ for the partial branching fraction of $B \rightarrow e \nu_e X_c$ decay with electron energy above 0.6 GeV. We converted the result to $B \rightarrow e \nu_e X$ branching fraction.

³ Uses charge and angular correlations in $\Upsilon(4S)$ events with a high-momentum lepton and an additional electron.

⁴ ALBRECHT 93H analysis performed using tagged semileptonic decays of the B . This technique is almost model independent for the lepton branching ratio.

Meson Particle Listings

B^\pm/B^0 ADMIXTURE

- ⁵ The measurements are obtained for charged and neutral B mesons partial rates of semileptonic decay to electrons with momentum above 0.6 GeV/c in the B rest frame. The best precision on the ratio is achieved for a momentum threshold of 1.0 GeV: $B(B^+ \rightarrow e^+ \nu_e X) / B(B^0 \rightarrow e^+ \nu_e X) = 1.074 \pm 0.041 \pm 0.026$.
- ⁶ The measurements are obtained for charged and neutral B mesons partial rates of semileptonic decay to electrons with momentum above 0.6 GeV/c in the B rest frame, and their ratio of $B(B^+ \rightarrow e^+ \nu_e X) / B(B^0 \rightarrow e^+ \nu_e X) = 1.08 \pm 0.05 \pm 0.02$.
- ⁷ The semileptonic branching ratio, $|V_{cb}|$ and other heavy-quark parameters are determined from a simultaneous fit to moments of the hadronic-mass and lepton-energy distribution.
- ⁸ Uses the high-momentum lepton tag method and requires the electron energy above 0.6 GeV.
- ⁹ Uses the high-momentum lepton tag method. They also report $|V_{cb}| = 0.0423 \pm 0.0007(\text{exp}) \pm 0.0020(\text{theo.})$.
- ¹⁰ Uses the high-momentum lepton tag method. ABE 02Y also reports $|V_{cb}| = 0.0408 \pm 0.0010(\text{exp}) \pm 0.0025(\text{theo.})$. The second error is due to uncertainties of theoretical inputs.
- ¹¹ BARISH 96B analysis performed using tagged semileptonic decays of the B . This technique is almost model independent for the lepton branching ratio.
- ¹² HENDERSON 92 measurement employs e and μ . The systematic error contains 0.004 in quadrature from model dependence. The authors average a variation of the Isgur, Scora, Grinstein, and Wise model with that of the Altarelli-Cabibbo-Corbò-Maiani-Martinelli model for semileptonic decays to correct the acceptance.
- ¹³ YANAGISAWA 91 also measures an average semileptonic branching ratio at the $\Upsilon(5S)$ of 9.6–10.5% depending on assumptions about the relative production of different B meson species.
- ¹⁴ ALBRECHT 90H uses the model of ALTARELLI 82 to correct over all lepton momenta. 0.99 ± 0.006 is obtained using ISGUR 89B.
- ¹⁵ ALBRECHT 90H uses the model of ALTARELLI 82 to correct over all lepton momenta. 0.97 ± 0.006 is obtained using ISGUR 89B.
- ¹⁶ Using data above $p(e) = 2.4$ GeV, WACHS 89 determine $\sigma(B \rightarrow e\nu\mu)/\sigma(B \rightarrow e\nu\text{charm}) < 0.065$ at 90% CL.
- ¹⁷ Ratio $\sigma(b \rightarrow e\nu\mu)/\sigma(b \rightarrow e\nu\text{charm}) < 0.055$ at CL = 90%.

$\Gamma(D^- \ell^+ \nu_\ell \text{ anything}) / \Gamma(\ell^+ \nu_\ell \text{ anything})$ Γ_4/Γ_3

VALUE	DOCUMENT ID	TECN	COMMENT
0.26 ± 0.07 ± 0.04	¹ FULTON 91	CLEO	$e^+ e^- \rightarrow \Upsilon(4S)$

¹ FULTON 91 uses $B(D^+ \rightarrow K^- \pi^+ \pi^+) = (9.1 \pm 1.3 \pm 0.4)\%$ as measured by MARK III.

$\Gamma(D^0 \ell^+ \nu_\ell \text{ anything}) / \Gamma(\ell^+ \nu_\ell \text{ anything})$ Γ_5/Γ_3

VALUE	DOCUMENT ID	TECN	COMMENT
0.67 ± 0.09 ± 0.10	¹ FULTON 91	CLEO	$e^+ e^- \rightarrow \Upsilon(4S)$

¹ FULTON 91 uses $B(D^0 \rightarrow K^- \pi^+) = (4.2 \pm 0.4 \pm 0.4)\%$ as measured by MARK III.

$\Gamma(D^{\pm} \ell^+ \nu_\ell) / \Gamma(\ell^+ \nu_\ell \text{ anything})$ Γ_6/Γ_3

VALUE	DOCUMENT ID	TECN	COMMENT
0.223 ± 0.006 ± 0.009	¹ AUBERT 10	BABR	$e^+ e^- \rightarrow \Upsilon(4S)$

¹ Uses a fully reconstructed B meson as a tag on the recoil side.

$\Gamma(D^{*-} \ell^+ \nu_\ell \text{ anything}) / \Gamma_{\text{total}}$ Γ_7/Γ

VALUE (units 10^{-2})	DOCUMENT ID	TECN	COMMENT
0.67 ± 0.08 ± 0.10	ABDALLAH 04b	DLPH	$e^+ e^- \rightarrow Z^0$

• • • We do not use the following data for averages, fits, limits, etc. • • •

$0.6 \pm 0.3 \pm 0.1$	¹ BARISH 95	CLE2	$e^+ e^- \rightarrow \Upsilon(4S)$
-----------------------	------------------------	------	------------------------------------

¹ BARISH 95 use $B(D^0 \rightarrow K^- \pi^+) = (3.91 \pm 0.08 \pm 0.17)\%$ and $B(D^{*+} \rightarrow D^0 \pi^+) = (68.1 \pm 1.0 \pm 1.3)\%$.

$\Gamma(D^{*0} \ell^+ \nu_\ell \text{ anything}) / \Gamma_{\text{total}}$ Γ_8/Γ

VALUE (units 10^{-2})	DOCUMENT ID	TECN	COMMENT
$0.6 \pm 0.6 \pm 0.1$	¹ BARISH 95	CLE2	$e^+ e^- \rightarrow \Upsilon(4S)$

¹ BARISH 95 use $B(D^0 \rightarrow K^- \pi^+) = (3.91 \pm 0.08 \pm 0.17)\%$, $B(D^{*+} \rightarrow D^0 \pi^+) = (68.1 \pm 1.0 \pm 1.3)\%$, $B(D^{*0} \rightarrow D^0 \pi^0) = (63.6 \pm 2.3 \pm 3.3)\%$.

$\Gamma(D^{**} \ell^+ \nu_\ell) / \Gamma_{\text{total}}$ Γ_{10}/Γ

D^{**} stands for the sum of the $D(1^1 P_1)$, $D(1^3 P_0)$, $D(1^3 P_1)$, $D(1^3 P_2)$, $D(2^1 S_0)$, and $D(2^1 S_1)$ resonances. $\ell = e$ or μ , not sum over e and μ modes.

VALUE	CL%	EVTs	DOCUMENT ID	TECN	COMMENT
0.027 ± 0.005 ± 0.005	63		¹ ALBRECHT 93	ARG	$e^+ e^- \rightarrow \Upsilon(4S)$

• • • We do not use the following data for averages, fits, limits, etc. • • •

< 0.028	95		² BARISH 95	CLE2	$e^+ e^- \rightarrow \Upsilon(4S)$
-----------	----	--	------------------------	------	------------------------------------

¹ ALBRECHT 93 assumes the GISW model to correct for unseen modes. Using the BHKT model, the result becomes $0.023 \pm 0.006 \pm 0.004$. Assumes $B(D^{*+} \rightarrow D^0 \pi^+) = 68.1\%$, $B(D^0 \rightarrow K^- \pi^+) = 3.65\%$, $B(D^0 \rightarrow K^- \pi^+ \pi^- \pi^+) = 7.5\%$. We have taken their average e and μ value.

² BARISH 95 use $B(D^0 \rightarrow K^- \pi^+) = (3.91 \pm 0.08 \pm 0.17)\%$, assume all nonresonant channels are zero, and use GISW model for relative abundances of D^{**} states.

$\Gamma(\bar{D}_1(2420) \ell^+ \nu_\ell \text{ anything}) / \Gamma_{\text{total}}$ Γ_{11}/Γ

VALUE	DOCUMENT ID	TECN	COMMENT
0.0038 ± 0.0013 OUR AVERAGE	Error includes scale factor of 2.4.		
0.0033 ± 0.0006	¹ ABAZOV 05o	D0	$p\bar{p}$ at 1.96 TeV
0.0074 ± 0.0016	² BUSKULIC 97b	ALEP	$e^+ e^- \rightarrow Z$

• • • We do not use the following data for averages, fits, limits, etc. • • •

seen	³ BUSKULIC 95b	ALEP	Repl. by BUSKULIC 97b
------	---------------------------	------	-----------------------

- ¹ Assumes $B(D_1 \rightarrow D^* \pi) = 1$, $B(D_1 \rightarrow D^* \pi^\pm) = 2/3$, and $B(b \rightarrow B) = 0.397$.
- ² BUSKULIC 97b assumes $B(D_1(2420) \rightarrow D^* \pi) = 1$, $B(D_1(2420) \rightarrow D^* \pi^\pm) = 2/3$, and $B(b \rightarrow B) = 0.378 \pm 0.022$.
- ³ BUSKULIC 95b reports $f_B \times B(B \rightarrow \bar{D}_1(2420)^0 \ell^+ \nu_\ell \text{ anything}) \times B(\bar{D}_1(2420)^0 \rightarrow \bar{D}^*(2010)^- \pi^+) = (2.04 \pm 0.58 \pm 0.34)10^{-3}$, where f_B is the production fraction for a single B charge state.

$[\Gamma(\bar{D} \pi \ell^+ \nu_\ell \text{ anything}) + \Gamma(\bar{D}^* \pi \ell^+ \nu_\ell \text{ anything})] / \Gamma_{\text{total}}$ Γ_{12}/Γ

VALUE	DOCUMENT ID	TECN	COMMENT
0.026 ± 0.005 OUR AVERAGE	Error includes scale factor of 1.5.		
$0.0340 \pm 0.0052 \pm 0.0032$	¹ ABREU 00r	DLPH	$e^+ e^- \rightarrow Z$
$0.0226 \pm 0.0029 \pm 0.0033$	² BUSKULIC 97b	ALEP	$e^+ e^- \rightarrow Z$

- ¹ Assumes no contribution from B_S and b baryons. Further assumes contributions from single pion ($D \pi$ and $D^* \pi$) states only, allowing isospin conservation to relate the relative π^0 and π^\pm rates.
- ² BUSKULIC 97b assumes $B(b \rightarrow B) = 0.378 \pm 0.022$ and uses isospin invariance by assuming that all observed $D^0 \pi^+$, $D^{*0} \pi^+$, $D^+ \pi^+$, and $D^{*+} \pi^+$ are from D^{**} states. A correction has been applied to account for the production of B_S^0 and Λ_b^0 .

$\Gamma(\bar{D} \pi \ell^+ \nu_\ell \text{ anything}) / \Gamma_{\text{total}}$ Γ_{13}/Γ

VALUE	DOCUMENT ID	TECN	COMMENT
0.0154 ± 0.0061	ABREU 00r	DLPH	$e^+ e^- \rightarrow Z$

$\Gamma(\bar{D}^* \pi \ell^+ \nu_\ell \text{ anything}) / \Gamma_{\text{total}}$ Γ_{14}/Γ

VALUE	DOCUMENT ID	TECN	COMMENT
0.0186 ± 0.0038	ABREU 00r	DLPH	$e^+ e^- \rightarrow Z$

$\Gamma(\bar{D}_2^*(2460) \ell^+ \nu_\ell \text{ anything}) / \Gamma_{\text{total}}$ Γ_{15}/Γ

VALUE	CL%	DOCUMENT ID	TECN	COMMENT
0.0044 ± 0.0016		¹ ABAZOV 05o	D0	$p\bar{p}$ at 1.96 TeV

• • • We do not use the following data for averages, fits, limits, etc. • • •

< 0.0065	95	² BUSKULIC 97b	ALEP	$e^+ e^- \rightarrow Z$
not seen		³ BUSKULIC 95b	ALEP	$e^+ e^- \rightarrow Z$

- ¹ Assumes $B(D_2^* \rightarrow D^* \pi^\pm) = 0.30 \pm 0.06$ and $B(b \rightarrow B) = 0.397$.
- ² A revised number based on BUSKULIC 97b which assumes $B(D_2^*(2460) \rightarrow D^* \pi^\pm) = 0.20$ and $B(b \rightarrow B) = 0.378 \pm 0.022$.
- ³ BUSKULIC 95b reports $f_B \times B(B \rightarrow \bar{D}_2^*(2460)^0 \ell^+ \nu_\ell \text{ anything}) \times B(\bar{D}_2^*(2460)^0 \rightarrow \bar{D}^*(2010)^- \pi^+) \leq 0.81 \times 10^{-3}$ at CL=95%, where f_B is the production fraction for a single B charge state.

$\Gamma(B \rightarrow \bar{D}_2^*(2460) \ell^+ \nu_\ell \text{ anything}) \times B(D_2^*(2460) \rightarrow D^{*-} \pi^+) / \Gamma(B \rightarrow \bar{D}_1(2420) \ell^+ \nu_\ell \text{ anything}) \times B(\bar{D}_1(2420) \rightarrow D^{*-} \pi^+)$

VALUE	DOCUMENT ID	TECN	COMMENT
0.39 ± 0.09 ± 0.12	ABAZOV 05o	D0	$p\bar{p}$ at 1.96 TeV

$\Gamma(D^{*-} \pi^+ \ell^+ \nu_\ell \text{ anything}) / \Gamma_{\text{total}}$ Γ_{16}/Γ

Includes resonant and nonresonant contributions.

VALUE (units 10^{-3})	DOCUMENT ID	TECN	COMMENT
10.0 ± 2.7 ± 2.1	¹ BUSKULIC 95b	ALEP	$e^+ e^- \rightarrow Z$

¹ BUSKULIC 95b reports $f_B \times B(B \rightarrow \bar{D}^*(2010)^- \pi^+ \ell^+ \nu_\ell \text{ anything}) = (3.7 \pm 1.0 \pm 0.7)10^{-3}$. Above value assumes $f_B = 0.37 \pm 0.03$.

$\Gamma(\bar{D} \pi^+ \pi^- \ell^+ \nu_\ell) / \Gamma(\bar{D} \ell^+ \nu_\ell)$ Γ_{17}/Γ_6

VALUE (units 10^{-2})	DOCUMENT ID	TECN	COMMENT
6.7 ± 1.0 ± 0.8	¹ LEES 16	BABR	$e^+ e^- \rightarrow \Upsilon(4S)$

¹ Measurement used electrons and muons as leptons.

$\Gamma(\bar{D}^* \pi^+ \pi^- \ell^+ \nu_\ell) / \Gamma(\bar{D}^* \ell^+ \nu_\ell)$ Γ_{18}/Γ_9

VALUE (units 10^{-2})	DOCUMENT ID	TECN	COMMENT
1.9 ± 0.5 ± 0.4	¹ LEES 16	BABR	$e^+ e^- \rightarrow \Upsilon(4S)$

¹ Measurement used electrons and muons as leptons.

$\Gamma(D_S^- \ell^+ \nu_\ell \text{ anything}) / \Gamma_{\text{total}}$ Γ_{19}/Γ

VALUE	CL%	DOCUMENT ID	TECN	COMMENT
$< 7 \times 10^{-3}$	90	¹ ALBRECHT 93E	ARG	$e^+ e^- \rightarrow \Upsilon(4S)$

¹ ALBRECHT 93E reports < 0.012 from a measurement of $[\Gamma(B \rightarrow D_S^- \ell^+ \nu_\ell \text{ anything}) / \Gamma_{\text{total}}] \times [B(D_S^+ \rightarrow \phi \pi^+)]$ assuming $B(D_S^+ \rightarrow \phi \pi^+) = 0.027$, which we rescale to our best value $B(D_S^+ \rightarrow \phi \pi^+) = 4.5 \times 10^{-2}$.

See key on page 1127

Meson Particle Listings

B^\pm/B^0 ADMIXTURE

$\Gamma(D_s^- \ell^+ \nu_\ell K^+ \text{ anything})/\Gamma_{\text{total}}$ Γ_{20}/Γ

VALUE	CL%	DOCUMENT ID	TECN	COMMENT
$<5 \times 10^{-3}$	90	¹ ALBRECHT	93E ARG	$e^+e^- \rightarrow \Upsilon(4S)$
¹ ALBRECHT ^{93E} reports < 0.008 from a measurement of $[\Gamma(B \rightarrow D_s^- \ell^+ \nu_\ell K^+ \text{ anything})/\Gamma_{\text{total}}] \times [B(D_s^+ \rightarrow \phi\pi^+)]$ assuming $B(D_s^+ \rightarrow \phi\pi^+) = 0.027$, which we rescale to our best value $B(D_s^+ \rightarrow \phi\pi^+) = 4.5 \times 10^{-2}$.				

$\Gamma(D_s^- \ell^+ \nu_\ell K^0 \text{ anything})/\Gamma_{\text{total}}$ Γ_{21}/Γ

VALUE	CL%	DOCUMENT ID	TECN	COMMENT
$<7 \times 10^{-3}$	90	¹ ALBRECHT	93E ARG	$e^+e^- \rightarrow \Upsilon(4S)$
¹ ALBRECHT ^{93E} reports < 0.012 from a measurement of $[\Gamma(B \rightarrow D_s^- \ell^+ \nu_\ell K^0 \text{ anything})/\Gamma_{\text{total}}] \times [B(D_s^+ \rightarrow \phi\pi^+)]$ assuming $B(D_s^+ \rightarrow \phi\pi^+) = 0.027$, which we rescale to our best value $B(D_s^+ \rightarrow \phi\pi^+) = 4.5 \times 10^{-2}$.				

$\Gamma(X_c \ell^+ \nu_\ell)/\Gamma_{\text{total}}$ Γ_{22}/Γ

"OUR EVALUATION" is an average using rescaled values of the data listed below. The average and rescaling were performed by the Heavy Flavor Averaging Group (HFLAV) and are described at <https://hflav.web.cern.ch/>. The averaging/rescaling procedure takes into account correlations between the measurements.

VALUE (%)	DOCUMENT ID	TECN	COMMENT
10.65 ± 0.16 OUR EVALUATION			
10.29 ± 0.19 OUR AVERAGE			
$10.18 \pm 0.03 \pm 0.24$	¹ LEES	17B BABR	$e^+e^- \rightarrow \Upsilon(4S)$
$10.44 \pm 0.19 \pm 0.22$	² URQUIJO	07 BELL	$e^+e^- \rightarrow \Upsilon(4S)$
• • • We do not use the following data for averages, fits, limits, etc. • • •			
$10.64 \pm 0.17 \pm 0.06$	³ AUBERT	10A BABR	Repl. by LEES 17B
$10.61 \pm 0.16 \pm 0.06$	⁴ AUBERT	04X BABR	Repl. by AUBERT 10A

- The measurement is obtained from semileptonic decays to electrons $B \rightarrow X_c e \nu$, and using a theoretical model (GAMBINO 07, GAMBINO 11) to predict the contribution from $B \rightarrow X_c e \nu$. The result is averaged over B^\pm and B^0 mesons, assuming lepton universality.
- Measured the independent B^+ and B^0 partial branching fractions with electron energy above 0.4 GeV.
- Obtained from a combined fit to the moments of observed spectra in inclusive $B \rightarrow X_c \ell^+ \nu_\ell$ decay.
- The semileptonic branching ratio, $|V_{cb}|$ and other heavy-quark parameters are determined from a simultaneous fit to moments of the hadronic-mass and lepton-energy distribution.

$\Gamma(X_u \ell^+ \nu_\ell)/\Gamma_{\text{total}}$ Γ_{23}/Γ

"OUR EVALUATION" is an average using rescaled values of the data listed below. The average and rescaling were performed by the Heavy Flavor Averaging Group (HFLAV) and are described at <https://hflav.web.cern.ch/>. The averaging/rescaling procedure takes into account correlations between the measurements.

VALUE (units 10^{-3})	DOCUMENT ID	TECN	COMMENT
1.91 ± 0.27 OUR EVALUATION			
$1.85 \pm 0.08 \pm 0.19$	¹ CAO	21A BELL	$e^+e^- \rightarrow \Upsilon(4S)$
$1.665 \pm 0.087 \pm_{-0.094}^{+0.103}$	² LEES	17B BABR	$e^+e^- \rightarrow \Upsilon(4S)$
$2.01 \pm 0.15 \pm 0.25$	³ LEES	12R BABR	$e^+e^- \rightarrow \Upsilon(4S)$
$2.53 \pm 0.24 \pm 0.24$	⁴ AUBERT.B	05X BABR	$e^+e^- \rightarrow \Upsilon(4S)$
$2.80 \pm 0.52 \pm 0.41$	⁵ LIMOSANI	05 BELL	$e^+e^- \rightarrow \Upsilon(4S)$
$1.77 \pm 0.29 \pm 0.38$	⁶ BORNHEIM	02 CLE2	$e^+e^- \rightarrow \Upsilon(4S)$
• • • We do not use the following data for averages, fits, limits, etc. • • •			
$1.963 \pm 0.173 \pm 0.159$	⁷ URQUIJO	10 BELL	Repl. by CAO 21A
$1.18 \pm 0.09 \pm 0.07$	⁸ AUBERT	08AS BABR	Repl. by LEES 12R
$2.27 \pm 0.26 \pm_{-0.33}^{+0.37}$	⁹ AUBERT	06H BABR	Repl. by LEES 17B
$2.24 \pm 0.27 \pm 0.47$	^{10,11} AUBERT	04I BABR	Repl. by AUBERT.B 05X

- Measures several partial branching fractions in different phase space regions. The most inclusive result of the full branching fraction is obtained in the region for lepton energy in B rest frame $E_\ell^+ > 1$ GeV, where the measured partial branching fraction is $\Delta B = (1.59 \pm 0.07 \pm 0.16) \times 10^{-3}$. The acceptance in that region is reported to be 0.86.
- Obtained from the partial rate $\Delta B = (1.554 \pm 0.082 \pm_{-0.086}^{+0.095}) \times 10^{-3}$ for the electron momentum interval of 0.8–2.7 GeV/c based on GGOU1 method ($X_c \ell \nu$, m_c constraint fit of SF parameters).
- Measures several partial branching fractions in different phase space regions. The most precise result on the full branching fraction is obtained in the region for lepton momentum in B rest frame $p_\ell^+ > 1$ GeV/c, where the measured partial branching fraction is $\Delta B = (1.80 \pm 0.13 \pm 0.15) \times 10^{-3}$. The acceptance in that region is reported in a private communication by the Authors to be 0.894. The corresponding $|V_{ub}|$ from the BLNP method is $(4.28 \pm 0.15 \pm 0.18 \pm 0.19) \times 10^{-3}$, where the last uncertainty comes from theoretical prediction.
- Determined from the partial rate $\Delta B = (4.41 \pm 0.42 \pm 0.42) \times 10^{-4}$ measured for electron energy > 2 GeV and hadronic mass squared < 3.5 GeV², and calculated acceptance 0.174 in that region. The V_{ub} is measured as $(4.41 \pm 0.30 \pm_{-0.47}^{+0.65} \pm 0.28) \times 10^{-3}$.
- Uses electrons in the momentum interval 1.9–2.6 GeV/c in the center-of-mass frame. The V_{ub} is found to be $(5.08 \pm 0.47 \pm_{-0.48}^{+0.49}) \times 10^{-3}$.
- BORNHEIM 02 uses the observed yield of leptons from semileptonic B decays in the end-point momentum interval 2.2–2.6 GeV/c with recent CLEO-2 data on $B \rightarrow X_c \gamma$. The V_{ub} is found to be $(4.08 \pm 0.34 \pm 0.53) \times 10^{-3}$.

⁷ Uses a multivariate analysis method and requires lepton momentum in the B rest frame, $p_\ell^+ > 1.0$ GeV/c.

⁸ Measures several partial branching fractions in different phase space regions. The most precise result is obtained in the region for hadronic mass $M_{X_c} < 1.55$ GeV/c², and is $\Delta B = (1.18 \pm 0.09 \pm 0.07) \times 10^{-3}$. The corresponding $|V_{ub}|$ from the BLNP method is $(4.27 \pm 0.16 \pm 0.13 \pm 0.30) \times 10^{-3}$, where the last uncertainty comes from the theoretical prediction of the partial rate in the given phase-space region.

⁹ Obtained from the partial rate $\Delta B = (0.572 \pm 0.041 \pm 0.065) \times 10^{-3}$ for the electron momentum interval of 2.0–2.6 GeV/c based on BLNP method.

¹⁰ Used BaBar measurement of Semileptonic branching fraction $B(B \rightarrow X_c \ell \nu_\ell) = (10.87 \pm 0.18 \pm 0.30)\%$ to convert the ratio of rates to branching fraction.

¹¹ The third error includes the systematics and theoretical errors summed in quadrature.

$\Gamma(X_u \ell^+ \nu_\ell)/\Gamma(\ell^+ \nu_\ell \text{ anything})$ Γ_{23}/Γ_3

ℓ denotes e or μ , not the sum. These experiments measure this ratio in very limited momentum intervals.

VALUE (units 10^{-2})	CL%	EVTS	DOCUMENT ID	TECN	COMMENT
$2.06 \pm 0.25 \pm 0.42$			¹ AUBERT	04I BABR	$e^+e^- \rightarrow \Upsilon(4S)$
• • • We do not use the following data for averages, fits, limits, etc. • • •					
			² ALBRECHT	94C ARG	$e^+e^- \rightarrow \Upsilon(4S)$
		107	³ BARTELT	93B CLE2	$e^+e^- \rightarrow \Upsilon(4S)$
		77	⁴ ALBRECHT	91C ARG	$e^+e^- \rightarrow \Upsilon(4S)$
		41	⁵ ALBRECHT	90 ARG	$e^+e^- \rightarrow \Upsilon(4S)$
		76	⁶ FULTON	90 CLEO	$e^+e^- \rightarrow \Upsilon(4S)$
<4.0	90		⁷ BEHRENDIS	87 CLEO	$e^+e^- \rightarrow \Upsilon(4S)$
<4.0	90		CHEN	84 CLEO	Direct e at $\Upsilon(4S)$
<5.5	90		KLOPFEN...	83B CUSB	Direct e at $\Upsilon(4S)$

¹ The third error includes the systematics and theoretical errors summed in quadrature.

² ALBRECHT 94C find $\Gamma(b \rightarrow c)/\Gamma(b \rightarrow \text{all}) = 0.99 \pm 0.02 \pm 0.04$.

³ BARTELT 93B (CLEO II) measures an excess of $107 \pm 15 \pm 11$ leptons in the lepton momentum interval 2.3–2.6 GeV/c which is attributed to $b \rightarrow u \ell \nu_\ell$. This corresponds to a model-dependent partial branching ratio ΔB_{ub} between $(1.15 \pm 0.16 \pm 0.15) \times 10^{-4}$, as evaluated using the KS model (KOERNER 88), and $(1.54 \pm 0.22 \pm 0.20) \times 10^{-4}$ using the ACCMM model (ARTUSO 93). The corresponding values of $|V_{ub}/V_{cb}|$ are 0.056 ± 0.006 and 0.076 ± 0.008 , respectively.

⁴ ALBRECHT 91C result supersedes ALBRECHT 90. Two events are fully reconstructed providing evidence for the $b \rightarrow u$ transition. Using the model of ALTARELLI 82, they obtain $|V_{ub}/V_{cb}| = 0.11 \pm 0.012$ from 77 leptons in the 2.3–2.6 GeV momentum range.

⁵ ALBRECHT 90 observes 41 ± 10 excess e and μ (lepton) events in the momentum interval $p = 2.3\text{--}2.6$ GeV signaling the presence of the $b \rightarrow u$ transition. The events correspond to a model-dependent measurement of $|V_{ub}/V_{cb}| = 0.10 \pm 0.01$.

⁶ FULTON 90 observe 76 ± 20 excess e and μ (lepton) events in the momentum interval $p = 2.4\text{--}2.6$ GeV signaling the presence of the $b \rightarrow u$ transition. The average branching ratio, $(1.8 \pm 0.4 \pm 0.3) \times 10^{-4}$, corresponds to a model-dependent measurement of approximately $|V_{ub}/V_{cb}| = 0.1$ using $B(b \rightarrow c \ell \nu) = 10.2 \pm 0.2 \pm 0.7\%$.

⁷ The quoted possible limits range from 0.018 to 0.04 for the ratio, depending on which model or momentum range is chosen. We select the most conservative limit they have calculated. This corresponds to a limit on $|V_{ub}/V_{cb}| < 0.20$. While the endpoint technique employed is more robust than their previous results in CHEN 84, these results do not provide a numerical improvement in the limit.

$\Gamma(X_u e^+ \nu_e)/\Gamma_{\text{total}}$ Γ_{24}/Γ

Requires $E_e^+ > 1$ GeV, where E_e^+ is e^+ energy in B rest frame.

VALUE (units 10^{-3})	DOCUMENT ID	TECN	COMMENT
$1.57 \pm 0.10 \pm 0.16$	¹ CAO	21A BELL	$e^+e^- \rightarrow \Upsilon(4S)$

¹ The correlation of 53% with $B(B \rightarrow X_u \mu^+ \nu_\mu)$ (lepton energy in B rest frame $E_{\mu^+} > 1$ GeV) is reported.

$\Gamma(X_u \mu^+ \nu_\mu)/\Gamma_{\text{total}}$ Γ_{25}/Γ

Requires $E_\mu^+ > 1$ GeV, where E_μ^+ is μ^+ energy in B rest frame.

VALUE (units 10^{-3})	DOCUMENT ID	TECN	COMMENT
$1.62 \pm 0.10 \pm 0.18$	¹ CAO	21A BELL	$e^+e^- \rightarrow \Upsilon(4S)$

¹ The correlation of 53% with $B(B \rightarrow X_u e^+ \nu_e)$ (lepton energy in B rest frame $E_{e^+} > 1$ GeV) is reported.

$\Gamma(K^+ \ell^+ \nu_\ell \text{ anything})/\Gamma(\ell^+ \nu_\ell \text{ anything})$ Γ_{26}/Γ_3

ℓ denotes e or μ , not the sum.

VALUE	DOCUMENT ID	TECN	COMMENT
0.58 ± 0.05 OUR AVERAGE			
$0.594 \pm 0.021 \pm 0.056$	ALBRECHT	94C ARG	$e^+e^- \rightarrow \Upsilon(4S)$
$0.54 \pm 0.07 \pm 0.06$	¹ ALAM	87B CLEO	$e^+e^- \rightarrow \Upsilon(4S)$

¹ ALAM 87B measurement relies on lepton-kaon correlations.

$\Gamma(K^- \ell^+ \nu_\ell \text{ anything})/\Gamma(\ell^+ \nu_\ell \text{ anything})$ Γ_{27}/Γ_3

ℓ denotes e or μ , not the sum.

VALUE	DOCUMENT ID	TECN	COMMENT
0.092 ± 0.035 OUR AVERAGE			
$0.086 \pm 0.011 \pm 0.044$	ALBRECHT	94C ARG	$e^+e^- \rightarrow \Upsilon(4S)$
$0.10 \pm 0.05 \pm 0.02$	¹ ALAM	87B CLEO	$e^+e^- \rightarrow \Upsilon(4S)$

¹ ALAM 87B measurement relies on lepton-kaon correlations.

Meson Particle Listings

B^\pm/B^0 ADMIXTURE

$\Gamma(K^0/\bar{K}^0 \ell^+ \nu_\ell \text{ anything})/\Gamma(\ell^+ \nu_\ell \text{ anything})$ Γ_{28}/Γ_3

ℓ denotes e or μ , not the sum. Sum over K^0 and \bar{K}^0 states.

VALUE	DOCUMENT ID	TECN	COMMENT
0.42 ± 0.05 OUR AVERAGE			
0.452 ± 0.038 ± 0.056	1 ALBRECHT 94c	ARG	$e^+e^- \rightarrow \Upsilon(4S)$
0.39 ± 0.06 ± 0.04	2 ALAM 87b	CLEO	$e^+e^- \rightarrow \Upsilon(4S)$

1 ALBRECHT 94c assume a K^0/\bar{K}^0 multiplicity twice that of K_S^0 .
2 ALAM 87b measurement relies on lepton-kaon correlations.

$\Gamma(\bar{D}^+ \tau^+ \nu_\tau)/\Gamma(\bar{D}^+ \ell^+ \nu_\ell)$ Γ_{29}/Γ_6

“OUR EVALUATION” is an average using rescaled values of the data listed below. The average and rescaling were performed by the Heavy Flavor Averaging Group (HFLAV) and are described at <https://hflav.web.cern.ch/>. The averaging/rescaling procedure takes into account correlations between the measurements.

VALUE (units 10^{-2})	DOCUMENT ID	TECN	COMMENT
33.9 ± 3.0 OUR EVALUATION			
35 ± 4 OUR AVERAGE			Error includes scale factor of 1.2.
30.7 ± 3.7 ± 1.6	1 CARIA 20	BELL	$e^+e^- \rightarrow \Upsilon(4S)$
37.5 ± 6.4 ± 2.6	2,3 HUSCHLE 15	BELL	$e^+e^- \rightarrow \Upsilon(4S)$
44.0 ± 5.8 ± 4.2	2,3 LEES 12d	BABR	$e^+e^- \rightarrow \Upsilon(4S)$

• • • We do not use the following data for averages, fits, limits, etc. • • •
4.16 ± 11.7 ± 5.2 2 AUBERT 08N BABR Repl. by LEES 12d

1 The tag-side B meson is reconstructed in a semileptonic decay mode and the signal-side τ is reconstructed in a purely leptonic decay. The Belle combination of HUSCHLE 15 and CARIA 20 yields $R(D) = (32.6 \pm 3.4) \times 10^{-2}$.
2 Uses a fully reconstructed B meson as a tag on the recoil side.
3 Uses $\tau^+ \rightarrow e^+ \nu_e \bar{\nu}_\tau$ and $\tau^+ \rightarrow \mu^+ \nu_\mu \bar{\nu}_\tau$ and e^+ or μ^+ as ℓ^+ . Obtained from simultaneous fit to B^+ and B^0 assuming isospin symmetry.

$\Gamma(\bar{D}^* \tau^+ \nu_\tau)/\Gamma(\bar{D}^* \ell^+ \nu_\ell)$ Γ_{30}/Γ_9

“OUR EVALUATION” is an average using rescaled values of the data listed below. The average and rescaling were performed by the Heavy Flavor Averaging Group (HFLAV) and are described at <https://hflav.web.cern.ch/>. The averaging/rescaling procedure takes into account correlations between the measurements.

VALUE (units 10^{-2})	DOCUMENT ID	TECN	COMMENT
29.5 ± 1.4 OUR EVALUATION			
29.6 ± 1.6 OUR AVERAGE			
28.3 ± 1.8 ± 1.4	1 CARIA 20	BELL	$e^+e^- \rightarrow \Upsilon(4S)$
27.0 ± 3.5 ± 2.8 ± 2.5	2 HIROSE 17	BELL	$e^+e^- \rightarrow \Upsilon(4S)$
29.3 ± 3.8 ± 1.5	3 HUSCHLE 15	BELL	$e^+e^- \rightarrow \Upsilon(4S)$
33.2 ± 2.4 ± 1.8	3 LEES 12d	BABR	$e^+e^- \rightarrow \Upsilon(4S)$

• • • We do not use the following data for averages, fits, limits, etc. • • •
29.7 ± 5.6 ± 1.8 4 AUBERT 08N BABR Repl. by LEES 12d

1 The tag-side B meson is reconstructed in a semileptonic decay mode and the signal-side τ is reconstructed in a purely leptonic decay. The Belle combination of HUSCHLE 15, HIROSE 17, and CARIA 20 yields $R(D^*) = 0.238 \pm 0.018$.
2 Uses a fully reconstructed B meson as a tag on the recoil side.
3 Uses $\tau^+ \rightarrow e^+ \nu_e \bar{\nu}_\tau$ and $\tau^+ \rightarrow \mu^+ \nu_\mu \bar{\nu}_\tau$ and e^+ or μ^+ as ℓ^+ . Obtained from simultaneous fit to B^+ and B^0 assuming isospin symmetry. Uses a fully reconstructed B meson as a tag on the recoil side.
4 Uses a fully reconstructed B meson as a tag on the recoil side. The results are normalized to the B^+ decay rate.

$\langle n_c \rangle$

VALUE	DOCUMENT ID	TECN	COMMENT
1.10 ± 0.05	1 GIBBONS 97b	CLE2	$e^+e^- \rightarrow \Upsilon(4S)$

• • • We do not use the following data for averages, fits, limits, etc. • • •
0.98 ± 0.16 ± 0.12 2 ALAM 87b CLEO $e^+e^- \rightarrow \Upsilon(4S)$

1 GIBBONS 97b from charm counting using $B(D_S^+ \rightarrow \phi \pi) = 0.036 \pm 0.009$ and $B(L_C^+ \rightarrow p K^- \pi^+) = 0.044 \pm 0.006$.
2 From the difference between K^- and K^+ widths. ALAM 87b measurement relies on lepton-kaon correlations. It does not consider the possibility of $B\bar{B}$ mixing. We have thus removed it from the average.

$\Gamma(D^\pm \text{ anything})/\Gamma_{\text{total}}$ Γ_{31}/Γ

VALUE	EVTS	DOCUMENT ID	TECN	COMMENT
0.231 ± 0.012 OUR AVERAGE				
0.230 ± 0.012 ± 0.004	1 GIBBONS 97b	CLE2	$e^+e^- \rightarrow \Upsilon(4S)$	
0.241 ± 0.037 ± 0.004	2 BORTOLETTO92	CLEO	$e^+e^- \rightarrow \Upsilon(4S)$	
0.223 ± 0.051 ± 0.004	3 ALBRECHT 91H	ARG	$e^+e^- \rightarrow \Upsilon(4S)$	

• • • We do not use the following data for averages, fits, limits, etc. • • •
0.203 ± 0.048 ± 0.003 20k 4 BORTOLETTO87 CLEO Sup. by BORTOLETTO 92

1 GIBBONS 97b reports $[\Gamma(B \rightarrow D^\pm \text{ anything})/\Gamma_{\text{total}}] \times [B(D^+ \rightarrow K^- 2\pi^+)] = 0.0216 \pm 0.0008 \pm 0.00082$ which we divide by our best value $B(D^+ \rightarrow K^- 2\pi^+) = (9.38 \pm 0.16) \times 10^{-2}$. Our first error is their experiment's error and our second error is the systematic error from using our best value.
2 BORTOLETTO 92 reports $[\Gamma(B \rightarrow D^\pm \text{ anything})/\Gamma_{\text{total}}] \times [B(D^+ \rightarrow K^- 2\pi^+)] = 0.0226 \pm 0.0030 \pm 0.0018$ which we divide by our best value $B(D^+ \rightarrow K^- 2\pi^+) = (9.38 \pm 0.16) \times 10^{-2}$. Our first error is their experiment's error and our second error is the systematic error from using our best value.
3 ALBRECHT 91H reports $[\Gamma(B \rightarrow D^\pm \text{ anything})/\Gamma_{\text{total}}] \times [B(D^+ \rightarrow K^- 2\pi^+)] = 0.0209 \pm 0.0027 \pm 0.0040$ which we divide by our best value $B(D^+ \rightarrow K^- 2\pi^+) =$

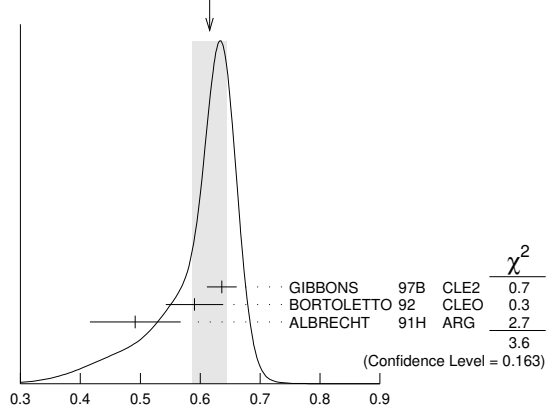
$(9.38 \pm 0.16) \times 10^{-2}$. Our first error is their experiment's error and our second error is the systematic error from using our best value.
4 BORTOLETTO 87 reports $[\Gamma(B \rightarrow D^\pm \text{ anything})/\Gamma_{\text{total}}] \times [B(D^+ \rightarrow K^- 2\pi^+)] = 0.019 \pm 0.004 \pm 0.002$ which we divide by our best value $B(D^+ \rightarrow K^- 2\pi^+) = (9.38 \pm 0.16) \times 10^{-2}$. Our first error is their experiment's error and our second error is the systematic error from using our best value.

$\Gamma(D^0/\bar{D}^0 \text{ anything})/\Gamma_{\text{total}}$ Γ_{32}/Γ

VALUE	EVTS	DOCUMENT ID	TECN	COMMENT
0.616 ± 0.029 OUR AVERAGE				Error includes scale factor of 1.3. See the ideogram below.
0.636 ± 0.024 ± 0.005	1 GIBBONS 97b	CLE2	$e^+e^- \rightarrow \Upsilon(4S)$	
0.590 ± 0.047 ± 0.005	2 BORTOLETTO92	CLEO	$e^+e^- \rightarrow \Upsilon(4S)$	
0.492 ± 0.074 ± 0.004	3 ALBRECHT 91H	ARG	$e^+e^- \rightarrow \Upsilon(4S)$	

• • • We do not use the following data for averages, fits, limits, etc. • • •
0.532 ± 0.065 ± 0.004 21k 4 BORTOLETTO87 CLEO $e^+e^- \rightarrow \Upsilon(4S)$
0.608 ± 0.183 ± 0.005 5 GREEN 83 CLEO Repl. by BORTOLETTO 87

WEIGHTED AVERAGE
0.616 ± 0.029 (Error scaled by 1.3)



1 GIBBONS 97b reports $[\Gamma(B \rightarrow D^0/\bar{D}^0 \text{ anything})/\Gamma_{\text{total}}] \times [B(D^0 \rightarrow K^- \pi^+)] = 0.0251 \pm 0.0006 \pm 0.00075$ which we divide by our best value $B(D^0 \rightarrow K^- \pi^+) = (3.947 \pm 0.030) \times 10^{-2}$. Our first error is their experiment's error and our second error is the systematic error from using our best value.
2 BORTOLETTO 92 reports $[\Gamma(B \rightarrow D^0/\bar{D}^0 \text{ anything})/\Gamma_{\text{total}}] \times [B(D^0 \rightarrow K^- \pi^+)] = 0.0233 \pm 0.0012 \pm 0.0014$ which we divide by our best value $B(D^0 \rightarrow K^- \pi^+) = (3.947 \pm 0.030) \times 10^{-2}$. Our first error is their experiment's error and our second error is the systematic error from using our best value.
3 ALBRECHT 91H reports $[\Gamma(B \rightarrow D^0/\bar{D}^0 \text{ anything})/\Gamma_{\text{total}}] \times [B(D^0 \rightarrow K^- \pi^+)] = 0.0194 \pm 0.0015 \pm 0.0025$ which we divide by our best value $B(D^0 \rightarrow K^- \pi^+) = (3.947 \pm 0.030) \times 10^{-2}$. Our first error is their experiment's error and our second error is the systematic error from using our best value.
4 BORTOLETTO 87 reports $[\Gamma(B \rightarrow D^0/\bar{D}^0 \text{ anything})/\Gamma_{\text{total}}] \times [B(D^0 \rightarrow K^- \pi^+)] = 0.0210 \pm 0.0015 \pm 0.0021$ which we divide by our best value $B(D^0 \rightarrow K^- \pi^+) = (3.947 \pm 0.030) \times 10^{-2}$. Our first error is their experiment's error and our second error is the systematic error from using our best value.
5 GREEN 83 reports $[\Gamma(B \rightarrow D^0/\bar{D}^0 \text{ anything})/\Gamma_{\text{total}}] \times [B(D^0 \rightarrow K^- \pi^+)] = 0.024 \pm 0.006 \pm 0.004$ which we divide by our best value $B(D^0 \rightarrow K^- \pi^+) = (3.947 \pm 0.030) \times 10^{-2}$. Our first error is their experiment's error and our second error is the systematic error from using our best value.

$\Gamma(D^- \ell^+ \nu_\ell \text{ anything})/\Gamma(\bar{D}^0 \ell^+ \nu_\ell \text{ anything})$ Γ_4/Γ_5

VALUE	DOCUMENT ID	TECN	COMMENT
0.359 ± 0.006 ± 0.009	1 AAIJ 19AD	LHCb	pp at 13 TeV

1 AAIJ 19AD uses $D^0 \rightarrow K^- \pi^+$ and $D^+ \rightarrow K^- \pi^+ \pi^+$ modes.

$\Gamma(D^*(2010)^\pm \text{ anything})/\Gamma_{\text{total}}$ Γ_{33}/Γ

VALUE	EVTS	DOCUMENT ID	TECN	COMMENT
0.225 ± 0.015 OUR AVERAGE				
0.247 ± 0.019 ± 0.01	1 GIBBONS 97b	CLE2	$e^+e^- \rightarrow \Upsilon(4S)$	
0.205 ± 0.019 ± 0.007	2 ALBRECHT 96d	ARG	$e^+e^- \rightarrow \Upsilon(4S)$	
0.230 ± 0.028 ± 0.009	3 BORTOLETTO92	CLEO	$e^+e^- \rightarrow \Upsilon(4S)$	

• • • We do not use the following data for averages, fits, limits, etc. • • •
0.283 ± 0.053 ± 0.002 4 ALBRECHT 91H ARG Sup. by ALBRECHT 96d
0.22 ± 0.04 ± 0.07 ± 0.04 5200 5 BORTOLETTO87 CLEO $e^+e^- \rightarrow \Upsilon(4S)$
0.27 ± 0.06 ± 0.08 ± 0.06 510 6 CSORNA 85 CLEO Repl. by BORTOLETTO 87

1 GIBBONS 97b reports $B(B \rightarrow D^*(2010)^\pm \text{ anything}) = 0.239 \pm 0.015 \pm 0.014 \pm 0.009$ using CLEO measured D and D^* branching fractions. We rescale to our PDG 96 values of D and D^* branching ratios. Our first error is their experiment's error and our second error is the systematic error from using our best value.
2 ALBRECHT 96d reports $B(B \rightarrow D^*(2010)^\pm \text{ anything}) = 0.196 \pm 0.019$ using CLEO measured $B(D^*(2010)^+ \rightarrow D^0 \pi^+) = 0.681 \pm 0.01 \pm 0.013$, $B(D^0 \rightarrow K^- \pi^+) = 0.0401 \pm 0.0014$, $B(D^0 \rightarrow K^- \pi^+ \pi^+ \pi^-) = 0.081 \pm 0.005$. We rescale to our PDG 96

See key on page 1127

Meson Particle Listings

B^\pm/B^0 ADMIXTURE

values of D and D^* branching ratios. Our first error is their experiment's error and our second error is the systematic error from using our best value.

³ BORTOLETTO 92 reports $B(B \rightarrow D^*(2010)^+ \text{ anything}) = 0.25 \pm 0.03 \pm 0.04$ using MARK II $B(D^*(2010)^+ \rightarrow D^0 \pi^+) = 0.57 \pm 0.06$ and $B(D^0 \rightarrow K^- \pi^+) = 0.042 \pm 0.008$. We rescale to our PDG 96 values of D and D^* branching ratios. Our first error is their experiment's error and our second error is the systematic error from using our best value.

⁴ ALBRECHT 91H reports $0.348 \pm 0.060 \pm 0.035$ from a measurement of $[\Gamma(B \rightarrow D^*(2010)^\pm \text{ anything})/\Gamma_{\text{total}}] \times [B(D^*(2010)^+ \rightarrow D^0 \pi^+)]$ assuming $B(D^*(2010)^+ \rightarrow D^0 \pi^+) = 0.55 \pm 0.04$, which we rescale to our best value $B(D^*(2010)^+ \rightarrow D^0 \pi^+) = (67.7 \pm 5) \times 10^{-2}$. Our first error is their experiment's error and our second error is the systematic error from using our best value. Uses the PDG 90 $B(D^0 \rightarrow K^- \pi^+) = 0.0371 \pm 0.0025$.

⁵ BORTOLETTO 87 uses old MARK III (BALTRUSAITIS 86E) branching ratios $B(D^0 \rightarrow K^- \pi^+) = 0.056 \pm 0.004 \pm 0.003$ and also assumes $B(D^*(2010)^+ \rightarrow D^0 \pi^+) = 0.60^{+0.08}_{-0.15}$. The product branching ratio for $B(B \rightarrow D^*(2010)^+) B(D^*(2010)^+ \rightarrow D^0 \pi^+)$ is $0.13 \pm 0.02 \pm 0.012$. Superseded by BORTOLETTO 92.

⁶ $V-A$ momentum spectrum used to extrapolate below $p = 1$ GeV. We correct the value assuming $B(D^0 \rightarrow K^- \pi^+) = 0.042 \pm 0.006$ and $B(D^{*+} \rightarrow D^0 \pi^+) = 0.6^{+0.08}_{-0.15}$. The product branching fraction is $B(B \rightarrow D^{*+} X) \cdot B(D^{*+} \rightarrow \pi^+ D^0) \cdot B(D^0 \rightarrow K^- \pi^+) = (68 \pm 15 \pm 9) \times 10^{-4}$.

$\Gamma(\bar{D}^*(2007)^0 \text{ anything})/\Gamma_{\text{total}}$ Γ₃₄/Γ

VALUE	DOCUMENT ID	TECN	COMMENT
0.263 ± 0.023 ± 0.015	¹ GIBBONS 97B	CLE2	$e^+ e^- \rightarrow \Upsilon(4S)$

¹ GIBBONS 97B reports $B(B \rightarrow \bar{D}^*(2007)^0 \text{ anything}) = 0.247 \pm 0.012 \pm 0.018 \pm 0.018$ using CLEO measured D and D^* branching fractions. We rescale to our PDG 96 values of D and D^* branching ratios. Our first error is their experiment's error and our second error is the systematic error from using our best value.

$\Gamma(D_s^\pm \text{ anything})/\Gamma_{\text{total}}$ Γ₃₅/Γ

VALUE	DOCUMENT ID	TECN	COMMENT
0.083 ± 0.008 OUR AVERAGE			
0.089 ± 0.010 ± 0.008	¹ ARTUSO 05B	CLE2	$e^+ e^- \rightarrow \Upsilon(5S)$
0.087 ± 0.005 ± 0.008	² AUBERT 02G	BABR	$e^+ e^- \rightarrow \Upsilon(4S)$
0.065 ± 0.011 ± 0.006	³ ALBRECHT 92G	ARG	$e^+ e^- \rightarrow \Upsilon(4S)$
0.068 ± 0.010 ± 0.006	⁴ BORTOLETTO90	CLEO	$e^+ e^- \rightarrow \Upsilon(4S)$
0.085 ± 0.022 ± 0.008	⁵ HAAS 86	CLEO	$e^+ e^- \rightarrow \Upsilon(4S)$

• • • We do not use the following data for averages, fits, limits, etc. • • •

0.094 ± 0.007 ± 0.008	⁶ GIBAUT 96	CLE2	Repl. by ARTUSO 05B
0.094 ± 0.024 ± 0.008	⁷ ALBRECHT 87H	ARG	$e^+ e^- \rightarrow \Upsilon(4S)$

¹ ARTUSO 05B reports $0.0905 \pm 0.0025 \pm 0.0140$ from a measurement of $[\Gamma(B \rightarrow D_s^\pm \text{ anything})/\Gamma_{\text{total}}] \times [B(D_s^\pm \rightarrow \phi \pi^\pm)]$ assuming $B(D_s^\pm \rightarrow \phi \pi^\pm) = (4.4 \pm 0.5) \times 10^{-2}$, which we rescale to our best value $B(D_s^\pm \rightarrow \phi \pi^\pm) = (4.5 \pm 0.4) \times 10^{-2}$. Our first error is their experiment's error and our second error is the systematic error from using our best value.

² AUBERT 02G reports $[\Gamma(B \rightarrow D_s^\pm \text{ anything})/\Gamma_{\text{total}}] \times [B(D_s^\pm \rightarrow \phi \pi^\pm)] = 0.00393 \pm 0.00007 \pm 0.00021$ which we divide by our best value $B(D_s^\pm \rightarrow \phi \pi^\pm) = (4.5 \pm 0.4) \times 10^{-2}$. Our first error is their experiment's error and our second error is the systematic error from using our best value.

³ ALBRECHT 92G reports $[\Gamma(B \rightarrow D_s^\pm \text{ anything})/\Gamma_{\text{total}}] \times [B(D_s^\pm \rightarrow \phi \pi^\pm)] = 0.00292 \pm 0.00039 \pm 0.00031$ which we divide by our best value $B(D_s^\pm \rightarrow \phi \pi^\pm) = (4.5 \pm 0.4) \times 10^{-2}$. Our first error is their experiment's error and our second error is the systematic error from using our best value.

⁴ BORTOLETTO 90 reports $[\Gamma(B \rightarrow D_s^\pm \text{ anything})/\Gamma_{\text{total}}] \times [B(D_s^\pm \rightarrow \phi \pi^\pm)] = 0.00306 \pm 0.00047$ which we divide by our best value $B(D_s^\pm \rightarrow \phi \pi^\pm) = (4.5 \pm 0.4) \times 10^{-2}$. Our first error is their experiment's error and our second error is the systematic error from using our best value.

⁵ HAAS 86 reports $[\Gamma(B \rightarrow D_s^\pm \text{ anything})/\Gamma_{\text{total}}] \times [B(D_s^\pm \rightarrow \phi \pi^\pm)] = 0.0038 \pm 0.0010$ which we divide by our best value $B(D_s^\pm \rightarrow \phi \pi^\pm) = (4.5 \pm 0.4) \times 10^{-2}$. Our first error is their experiment's error and our second error is the systematic error from using our best value. $64 \pm 22\%$ decays are 2-body.

⁶ GIBAUT 96 reports $0.1211 \pm 0.0039 \pm 0.0088$ from a measurement of $[\Gamma(B \rightarrow D_s^\pm \text{ anything})/\Gamma_{\text{total}}] \times [B(D_s^\pm \rightarrow \phi \pi^\pm)]$ assuming $B(D_s^\pm \rightarrow \phi \pi^\pm) = 0.035$, which we rescale to our best value $B(D_s^\pm \rightarrow \phi \pi^\pm) = (4.5 \pm 0.4) \times 10^{-2}$. Our first error is their experiment's error and our second error is the systematic error from using our best value.

⁷ ALBRECHT 87H reports $[\Gamma(B \rightarrow D_s^\pm \text{ anything})/\Gamma_{\text{total}}] \times [B(D_s^\pm \rightarrow \phi \pi^\pm)] = 0.0042 \pm 0.0009 \pm 0.0006$ which we divide by our best value $B(D_s^\pm \rightarrow \phi \pi^\pm) = (4.5 \pm 0.4) \times 10^{-2}$. Our first error is their experiment's error and our second error is the systematic error from using our best value. $46 \pm 16\%$ of $B \rightarrow D_s X$ decays are 2-body. Superseded by ALBRECHT 92G.

$\Gamma(D_s^\pm \text{ anything})/\Gamma_{\text{total}}$ Γ₃₆/Γ

VALUE	DOCUMENT ID	TECN	COMMENT
0.063 ± 0.009 ± 0.006	¹ AUBERT 02G	BABR	$e^+ e^- \rightarrow \Upsilon(4S)$

¹ AUBERT 02G reports $[\Gamma(B \rightarrow D_s^\pm \text{ anything})/\Gamma_{\text{total}}] \times [B(D_s^\pm \rightarrow \phi \pi^\pm)] = 0.00284 \pm 0.00029 \pm 0.00025$ which we divide by our best value $B(D_s^\pm \rightarrow \phi \pi^\pm) = (4.5 \pm 0.4) \times 10^{-2}$. Our first error is their experiment's error and our second error is the systematic error from using our best value.

$\Gamma(D_s^\pm \bar{D}^{(*)})/\Gamma(D_s^\pm \text{ anything})$ Γ₃₇/Γ₃₆

Sum over modes

VALUE	DOCUMENT ID	TECN	COMMENT
0.533 ± 0.037 ± 0.037	AUBERT 02G	BABR	$e^+ e^- \rightarrow \Upsilon(4S)$

$\Gamma(\bar{D} D_{s0}(2317))/\Gamma_{\text{total}}$ Γ₃₈/Γ

VALUE	DOCUMENT ID	TECN	COMMENT
seen	¹ KROKOVNY 03B	BELL	$e^+ e^- \rightarrow \Upsilon(4S)$

¹ The product branching ratio for $B(B \rightarrow \bar{D} D_{s0}(2317)^+) \times B(D_{s0}(2317)^+ \rightarrow D_s \pi^0)$ is measured to be $(8.5^{+2.1}_{-1.9} \pm 2.6) \times 10^{-4}$.

$\Gamma(\bar{D} D_{sJ}(2457))/\Gamma_{\text{total}}$ Γ₃₉/Γ

VALUE	DOCUMENT ID	TECN	COMMENT
seen	¹ KROKOVNY 03B	BELL	$e^+ e^- \rightarrow \Upsilon(4S)$

¹ The product branching ratio for $B(B \rightarrow \bar{D} D_{sJ}(2457)^+) \times B(D_{sJ}(2457)^+ \rightarrow D_s^* \pi^0, D_s^* \gamma)$ are measured to be $(17.8^{+4.5}_{-3.9} \pm 5.3) \times 10^{-4}$ and $(6.7^{+1.3}_{-1.2} \pm 2.0) \times 10^{-4}$, respectively.

$[\Gamma(D^{(*)} \bar{D}^{(*)} K^0) + \Gamma(D^{(*)} \bar{D}^{(*)} K^\pm)]/\Gamma_{\text{total}}$ Γ₄₀/Γ

VALUE	DOCUMENT ID	TECN	COMMENT
0.071 ± 0.025 ± 0.010 -0.015 - 0.009	¹ BARATE 98Q	ALEP	$e^+ e^- \rightarrow Z$

¹ The systematic error includes the uncertainties due to the charm branching ratios.

$\Gamma(b \rightarrow c \bar{c} s)/\Gamma_{\text{total}}$ Γ₄₁/Γ

VALUE	DOCUMENT ID	TECN	COMMENT
0.219 ± 0.037	¹ COAN 98	CLE2	$e^+ e^- \rightarrow \Upsilon(4S)$

¹ COAN 98 uses $D-\ell$ correlation.

$\Gamma(D_s^{(*)} \bar{D}^{(*)})/\Gamma(D_s^\pm \text{ anything})$ Γ₄₂/Γ₃₅

Sum over modes.

VALUE	DOCUMENT ID	TECN	COMMENT
0.469 ± 0.017 OUR AVERAGE			
0.464 ± 0.013 ± 0.015	AUBERT 02G	BABR	$e^+ e^- \rightarrow \Upsilon(4S)$
0.56 ± 0.21 ± 0.09 -0.15 - 0.08	¹ BARATE 98Q	ALEP	$e^+ e^- \rightarrow Z$
0.457 ± 0.019 ± 0.037	GIBAUT 96	CLE2	$e^+ e^- \rightarrow \Upsilon(4S)$
0.58 ± 0.07 ± 0.09	ALBRECHT 92G	ARG	$e^+ e^- \rightarrow \Upsilon(4S)$
0.56 ± 0.10	BORTOLETTO90	CLEO	$e^+ e^- \rightarrow \Upsilon(4S)$

¹ BARATE 98Q measures $B(B \rightarrow D_s^{(*)} \bar{D}^{(*)}) = 0.056^{+0.021+0.009+0.019}_{-0.015-0.008-0.011}$, where the third error results from the uncertainty on the different D branching ratios and is dominated by the uncertainty on $B(D_s^\pm \rightarrow \phi \pi^\pm)$. We divide $B(B \rightarrow D_s^{(*)} \bar{D}^{(*)})$ by our best value of $B(B \rightarrow D_s \text{ anything}) = 0.1 \pm 0.025$.

$\Gamma(D^* D^*(2010)^\pm)/\Gamma_{\text{total}}$ Γ₄₃/Γ

VALUE	CL%	DOCUMENT ID	TECN	COMMENT
< 5.9 × 10⁻³	90	BARATE 98Q	ALEP	$e^+ e^- \rightarrow Z$

$[\Gamma(D D^*(2010)^\pm) + \Gamma(D^* D^\pm)]/\Gamma_{\text{total}}$ Γ₄₄/Γ

VALUE	CL%	DOCUMENT ID	TECN	COMMENT
< 5.5 × 10⁻³	90	BARATE 98Q	ALEP	$e^+ e^- \rightarrow Z$

$\Gamma(D D^\pm)/\Gamma_{\text{total}}$ Γ₄₅/Γ

VALUE	CL%	DOCUMENT ID	TECN	COMMENT
< 3.1 × 10⁻³	90	BARATE 98Q	ALEP	$e^+ e^- \rightarrow Z$

$\Gamma(D_s^{(*)} \pm \bar{D}^{(*)} X (n\pi^\pm))/\Gamma_{\text{total}}$ Γ₄₆/Γ

VALUE	DOCUMENT ID	TECN	COMMENT
0.094 ± 0.040 ± 0.034 -0.031 - 0.024	¹ BARATE 98Q	ALEP	$e^+ e^- \rightarrow Z$

¹ The systematic error includes the uncertainties due to the charm branching ratios.

$\Gamma(\bar{D}^*(2010)\gamma)/\Gamma_{\text{total}}$ Γ₄₇/Γ

VALUE	CL%	DOCUMENT ID	TECN	COMMENT
< 1.1 × 10⁻³	90	¹ LESIAK 92	CBAL	$e^+ e^- \rightarrow \Upsilon(4S)$

¹ LESIAK 92 set a limit on the inclusive process $B(b \rightarrow s\gamma) < 2.8 \times 10^{-3}$ at 90% CL for the range of masses of 892–2045 MeV, independent of assumptions about s -quark hadronization.

$\Gamma(D_s^\pm \pi^-, D_s^{*+} \pi^-, D_s^\pm \rho^-, D_s^{*+} \rho^-, D_s^\pm \pi^0, D_s^{*+} \pi^0, D_s^\pm \eta, D_s^{*+} \eta, D_s^\pm \rho^0, D_s^{*+} \rho^0, D_s^\pm \omega, D_s^{*+} \omega)/\Gamma_{\text{total}}$ Γ₄₈/Γ

Sum over modes.

VALUE	CL%	DOCUMENT ID	TECN	COMMENT
< 4 × 10⁻⁴	90	¹ ALEXANDER 93B	CLE2	$e^+ e^- \rightarrow \Upsilon(4S)$

¹ ALEXANDER 93B reports $< 4.8 \times 10^{-4}$ from a measurement of $[\Gamma(B \rightarrow D_s^\pm \pi^-, D_s^{*+} \pi^-, D_s^\pm \rho^-, D_s^{*+} \rho^-, D_s^\pm \pi^0, D_s^{*+} \pi^0, D_s^\pm \eta, D_s^{*+} \eta, D_s^\pm \rho^0, D_s^{*+} \rho^0, D_s^\pm \omega, D_s^{*+} \omega)/\Gamma_{\text{total}}] \times [B(D_s^\pm \rightarrow \phi \pi^\pm)]$ assuming $B(D_s^\pm \rightarrow \phi \pi^\pm) = 0.037$, which we rescale to our best value $B(D_s^\pm \rightarrow \phi \pi^\pm) = 4.5 \times 10^{-2}$. This branching ratio limit provides a model-dependent upper limit $|V_{ub}|/|V_{cb}| < 0.16$ at CL=90%.

Meson Particle Listings

B^\pm/B^0 ADMIXTURE

$\Gamma(D_{s1}(2536)^+ \text{ anything})/\Gamma_{\text{total}}$ Γ_{49}/Γ

$D_{s1}(2536)^+$ is the narrow P -wave D_s^+ meson with $J^P = 1^+$.

VALUE	CL%	DOCUMENT ID	TECN	COMMENT
<0.0095	90	¹ BISHAI	98	CLE2 $e^+e^- \rightarrow \Upsilon(4S)$

¹ Assuming factorization, the decay constant $f_{D_{s1}^+}$ is at least a factor of 2.5 times smaller than $f_{D_s^+}$.

$\Gamma(J/\psi(1S) \text{ anything})/\Gamma_{\text{total}}$ Γ_{50}/Γ

VALUE (units 10^{-2})	EVTs	DOCUMENT ID	TECN	COMMENT
1.094 ± 0.032 OUR AVERAGE		Error includes scale factor of 1.1.		
1.057 ± 0.012 ± 0.040		¹ AUBERT	03F	BABR $e^+e^- \rightarrow \Upsilon(4S)$
1.121 ± 0.013 ± 0.042		ANDERSON	02	CLE2 $e^+e^- \rightarrow \Upsilon(4S)$
1.29 ± 0.45 ± 0.01	27	² MASCHMANN	90	CBAL $e^+e^- \rightarrow \Upsilon(4S)$
1.24 ± 0.27 ± 0.01	120	³ ALBRECHT	87D	ARG $e^+e^- \rightarrow \Upsilon(4S)$
1.35 ± 0.24 ± 0.01	52	⁴ ALAM	86	CLEO $e^+e^- \rightarrow \Upsilon(4S)$
• • • We do not use the following data for averages, fits, limits, etc. • • •				
1.12 ± 0.06 ± 0.01	1489	⁵ BALEST	95B	CLE2 $e^+e^- \rightarrow \Upsilon(4S)$
1.4 $\begin{smallmatrix} +0.6 \\ -0.5 \end{smallmatrix}$	7	⁶ ALBRECHT	85H	ARG $e^+e^- \rightarrow \Upsilon(4S)$
1.1 ± 0.21 ± 0.23	46	⁷ HAAS	85	CLEO Repl. by ALAM 86

- ¹ AUBERT 03F also reports the momentum distribution and helicity of $J/\psi \rightarrow \ell^+ \ell^-$ in the $\Upsilon(4S)$ center-of-mass frame.
- ² MASCHMANN 90 reports $(1.12 \pm 0.33 \pm 0.25) \times 10^{-2}$ from a measurement of $[\Gamma(B \rightarrow J/\psi(1S) \text{ anything})/\Gamma_{\text{total}}] \times [B(J/\psi(1S) \rightarrow e^+e^-)]$ assuming $B(J/\psi(1S) \rightarrow e^+e^-) = 0.069 \pm 0.009$, which we rescale to our best value $B(J/\psi(1S) \rightarrow e^+e^-) = (5.971 \pm 0.032) \times 10^{-2}$. Our first error is their experiment's error and our second error is the systematic error from using our best value.
- ³ ALBRECHT 87D reports $(1.07 \pm 0.16 \pm 0.22) \times 10^{-2}$ from a measurement of $[\Gamma(B \rightarrow J/\psi(1S) \text{ anything})/\Gamma_{\text{total}}] \times [B(J/\psi(1S) \rightarrow e^+e^-)]$ assuming $B(J/\psi(1S) \rightarrow e^+e^-) = 0.069 \pm 0.009$, which we rescale to our best value $B(J/\psi(1S) \rightarrow e^+e^-) = (5.971 \pm 0.032) \times 10^{-2}$. Our first error is their experiment's error and our second error is the systematic error from using our best value. ALBRECHT 87D find the branching ratio for J/ψ not from $\psi(2S)$ to be 0.0081 ± 0.0023.
- ⁴ ALAM 86 reports $(1.09 \pm 0.16 \pm 0.21) \times 10^{-2}$ from a measurement of $[\Gamma(B \rightarrow J/\psi(1S) \text{ anything})/\Gamma_{\text{total}}] \times [B(J/\psi(1S) \rightarrow \mu^+\mu^-)]$ assuming $B(J/\psi(1S) \rightarrow \mu^+\mu^-) = 0.074 \pm 0.012$, which we rescale to our best value $B(J/\psi(1S) \rightarrow \mu^+\mu^-) = (5.961 \pm 0.033) \times 10^{-2}$. Our first error is their experiment's error and our second error is the systematic error from using our best value.
- ⁵ BALEST 95B reports $(1.12 \pm 0.04 \pm 0.06) \times 10^{-2}$ from a measurement of $[\Gamma(B \rightarrow J/\psi(1S) \text{ anything})/\Gamma_{\text{total}}] \times [B(J/\psi(1S) \rightarrow e^+e^-)]$ assuming $B(J/\psi(1S) \rightarrow e^+e^-) = 0.0599 \pm 0.0025$, which we rescale to our best value $B(J/\psi(1S) \rightarrow e^+e^-) = (5.971 \pm 0.032) \times 10^{-2}$. Our first error is their experiment's error and our second error is the systematic error from using our best value. They measure $J/\psi(1S) \rightarrow e^+e^-$ and $\mu^+\mu^-$ and use PDG 1994 values for the branching fractions. The rescaling is the same for either mode so we use e^+e^- .
- ⁶ Statistical and systematic errors were added in quadrature. ALBRECHT 85H also report a CL = 90% limit of 0.007 for $B \rightarrow J/\psi(1S) + X$ where $m_X < 1$ GeV.
- ⁷ Dimuon and dielectron events used.

$\Gamma(J/\psi(1S) \text{ (direct) anything})/\Gamma_{\text{total}}$ Γ_{51}/Γ

VALUE	DOCUMENT ID	TECN	COMMENT
0.0078 ± 0.0004 OUR AVERAGE	Error includes scale factor of 1.1.		
0.00740 ± 0.00023 ± 0.00043	¹ AUBERT	03F	BABR $e^+e^- \rightarrow \Upsilon(4S)$
0.00813 ± 0.00017 ± 0.00037	² ANDERSON	02	CLE2 $e^+e^- \rightarrow \Upsilon(4S)$
• • • We do not use the following data for averages, fits, limits, etc. • • •			
0.0080 ± 0.0008	³ BALEST	95B	CLE2 $e^+e^- \rightarrow \Upsilon(4S)$

- ¹ AUBERT 03F also reports the helicity of $J/\psi \rightarrow \ell^+ \ell^-$ produced directly in B decay.
- ² Also reports the measurement of $J/\psi \rightarrow \ell^+ \ell^-$ polarization produced directly from B decay.
- ³ BALEST 95B assume PDG 1994 values for sub mode branching ratios. $J/\psi(1S)$ mesons are reconstructed in $J/\psi(1S) \rightarrow e^+e^-$ and $J/\psi(1S) \rightarrow \mu^+\mu^-$. The $B \rightarrow J/\psi(1S)X$ branching ratio contains $J/\psi(1S)$ mesons directly from B decays and also from feeddown through $\psi(2S) \rightarrow J/\psi(1S)$, $\chi_{c1}(1P) \rightarrow J/\psi(1S)$, or $\chi_{c2}(1P) \rightarrow J/\psi(1S)$. Using the measured inclusive rates, BALEST 95B corrects for the feeddown and finds the $B \rightarrow J/\psi(1S) \text{ (direct) } X$ branching ratio.

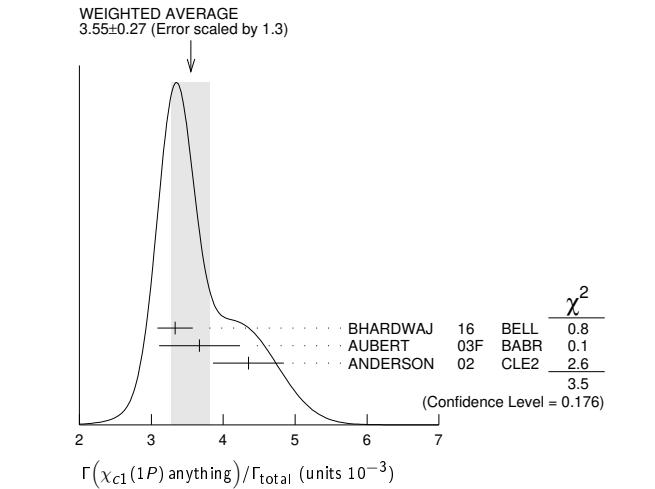
$\Gamma(\psi(2S) \text{ anything})/\Gamma_{\text{total}}$ Γ_{52}/Γ

VALUE	EVTs	DOCUMENT ID	TECN	COMMENT
0.00307 ± 0.00021 OUR AVERAGE		Error includes scale factor of 1.1.		
0.00297 ± 0.00020 ± 0.00020		AUBERT	03F	BABR $e^+e^- \rightarrow \Upsilon(4S)$
0.00316 ± 0.00014 ± 0.00028		¹ ANDERSON	02	CLE2 $e^+e^- \rightarrow \Upsilon(4S)$
0.0046 ± 0.0017 ± 0.0011	8	ALBRECHT	87D	ARG $e^+e^- \rightarrow \Upsilon(4S)$
• • • We do not use the following data for averages, fits, limits, etc. • • •				
0.0034 ± 0.0004 ± 0.0003	240	² BALEST	95B	CLE2 $e^+e^- \rightarrow \Upsilon(4S)$

- ¹ Also reports the measurement of $\psi(2S) \rightarrow \ell^+ \ell^-$ polarization produced directly from B decay.
- ² BALEST 95B assume PDG 1994 values for sub mode branching ratios. They find $B(B \rightarrow \psi(2S)X, \psi(2S) \rightarrow \ell^+ \ell^-) = 0.30 \pm 0.05 \pm 0.04$ and $B(B \rightarrow \psi(2S)X, \psi(2S) \rightarrow J/\psi(1S) \pi^+ \pi^-) = 0.37 \pm 0.05 \pm 0.05$. Weighted average is quoted for $B(B \rightarrow \psi(2S)X)$.

$\Gamma(\chi_{c1}(1P) \text{ anything})/\Gamma_{\text{total}}$ Γ_{53}/Γ

VALUE (units 10^{-3})	EVTs	DOCUMENT ID	TECN	COMMENT
3.55 ± 0.27 OUR AVERAGE		Error includes scale factor of 1.3. See the ideogram below.		
3.33 ± 0.05 ± 0.24		¹ BHARDWAJ	16	BELL $e^+e^- \rightarrow \Upsilon(4S)$
3.67 ± 0.35 ± 0.44		AUBERT	03F	BABR $e^+e^- \rightarrow \Upsilon(4S)$
4.35 ± 0.29 ± 0.40		ANDERSON	02	CLE2 $e^+e^- \rightarrow \Upsilon(4S)$
• • • We do not use the following data for averages, fits, limits, etc. • • •				
3.63 ± 0.22 ± 0.34		² ABE	02L	BELL Repl. by BHARDWAJ 16
3.30 ± 0.35 ± 0.09		³ CHEN	01	CLE2 $e^+e^- \rightarrow \Upsilon(4S)$
4.0 ± 0.6 ± 0.4	112	⁴ BALEST	95B	CLE2 Repl. by CHEN 01
10.5 ± 3.5 ± 2.5		⁵ ALBRECHT	92E	ARG $e^+e^- \rightarrow \Upsilon(4S)$



- ¹ Assumes equal production of B^+ and B^0 at the $\Upsilon(4S)$.
- ² ABE 02L uses PDG 01 values for $B(J/\psi(1S) \rightarrow \ell^+ \ell^-)$ and $B(\chi_{c1,c2} \rightarrow J/\psi(1S)\gamma)$.
- ³ CHEN 01 reports $0.00414 \pm 0.00031 \pm 0.00040$ from a measurement of $[\Gamma(B \rightarrow \chi_{c1}(1P) \text{ anything})/\Gamma_{\text{total}}] \times [B(\chi_{c1}(1P) \rightarrow \gamma J/\psi(1S))]$ assuming $B(\chi_{c1}(1P) \rightarrow \gamma J/\psi(1S)) = 0.273 \pm 0.016$, which we rescale to our best value $B(\chi_{c1}(1P) \rightarrow \gamma J/\psi(1S)) = (34.3 \pm 1.0) \times 10^{-2}$. Our first error is their experiment's error and our second error is the systematic error from using our best value. Assumes equal production of B^+ and B^0 at the $\Upsilon(4S)$.
- ⁴ BALEST 95B assume $B(\chi_{c1}(1P) \rightarrow J/\psi(1S)\gamma) = (27.3 \pm 1.6) \times 10^{-2}$, the PDG 1994 value. Fit to ψ -photon invariant mass distribution allows for a $\chi_{c1}(1P)$ and a $\chi_{c2}(1P)$ component.
- ⁵ ALBRECHT 92E assumes no $\chi_{c2}(1P)$ production.

$\Gamma(\chi_{c1}(1P) \text{ (direct) anything})/\Gamma_{\text{total}}$ Γ_{54}/Γ

VALUE (units 10^{-3})	DOCUMENT ID	TECN	COMMENT
3.08 ± 0.19 OUR AVERAGE	Error includes scale factor of 1.6. See the ideogram below.		
3.03 ± 0.05 ± 0.24	¹ BHARDWAJ	16	BELL $e^+e^- \rightarrow \Upsilon(4S)$
3.41 ± 0.35 ± 0.42	AUBERT	03F	BABR $e^+e^- \rightarrow \Upsilon(4S)$
3.1 ± 0.4 ± 0.1	² CHEN	01	CLE2 $e^+e^- \rightarrow \Upsilon(4S)$
• • • We do not use the following data for averages, fits, limits, etc. • • •			
3.32 ± 0.22 ± 0.34	³ ABE	02L	BELL Repl. by BHARDWAJ 16
3.7 ± 0.7	⁴ BALEST	95B	CLE2 Repl. by CHEN 01

- ¹ Assumes equal production of B^+ and B^0 at the $\Upsilon(4S)$.
- ² CHEN 01 reports $0.00383 \pm 0.00031 \pm 0.00040$ from a measurement of $[\Gamma(B \rightarrow \chi_{c1}(1P) \text{ (direct) anything})/\Gamma_{\text{total}}] \times [B(\chi_{c1}(1P) \rightarrow \gamma J/\psi(1S))]$ assuming $B(\chi_{c1}(1P) \rightarrow \gamma J/\psi(1S)) = 0.273 \pm 0.016$, which we rescale to our best value $B(\chi_{c1}(1P) \rightarrow \gamma J/\psi(1S)) = (34.3 \pm 1.0) \times 10^{-2}$. Our first error is their experiment's error and our second error is the systematic error from using our best value. Assumes equal production of B^+ and B^0 at the $\Upsilon(4S)$.
- ³ ABE 02L uses PDG 01 values for $B(J/\psi(1S) \rightarrow \ell^+ \ell^-)$ and $B(\chi_{c1,c2} \rightarrow J/\psi(1S)\gamma)$.
- ⁴ BALEST 95B assume PDG 1994 values. $J/\psi(1S)$ mesons are reconstructed in the e^+e^- and $\mu^+\mu^-$ modes. The $B \rightarrow \chi_{c1}(1P)X$ branching ratio contains $\chi_{c1}(1P)$ mesons directly from B decays and also from feeddown through $\psi(2S) \rightarrow \chi_{c1}(1P)\gamma$. Using the measured inclusive rates, BALEST 95B corrects for the feeddown and finds the $B \rightarrow \chi_{c1}(1P) \text{ (direct) } X$ branching ratio.

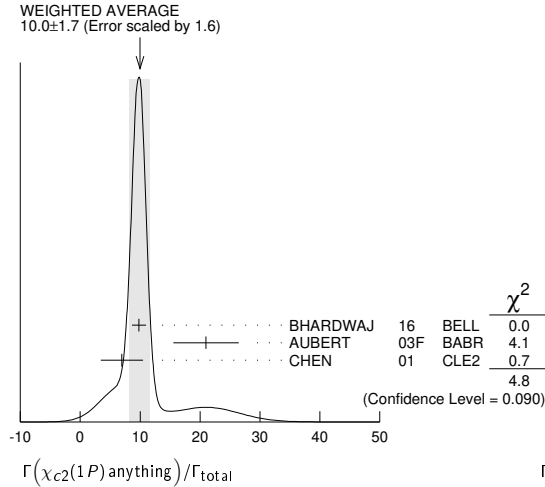
$\Gamma(\chi_{c2}(1P) \text{ anything})/\Gamma_{\text{total}}$ Γ_{55}/Γ

VALUE (units 10^{-4})	CL%	DOCUMENT ID	TECN	COMMENT
10.0 ± 1.7 OUR AVERAGE		Error includes scale factor of 1.6. See the ideogram below.		
9.8 ± 0.6 ± 1.0		¹ BHARDWAJ	16	BELL $e^+e^- \rightarrow \Upsilon(4S)$
21.0 ± 4.5 ± 3.1		AUBERT	03F	BABR $e^+e^- \rightarrow \Upsilon(4S)$
7.0 ± 3.5 ± 0.2		² CHEN	01	CLE2 $e^+e^- \rightarrow \Upsilon(4S)$
• • • We do not use the following data for averages, fits, limits, etc. • • •				
18.0 $\begin{smallmatrix} +2.3 \\ -2.8 \end{smallmatrix}$ ± 2.6		³ ABE	02L	BELL Repl. by BHARDWAJ 16
<38	90	⁴ BALEST	95B	CLE2 Repl. by CHEN 01
¹ Assumes equal production of B^+ and B^0 at the $\Upsilon(4S)$.				

²CHEN 01 reports $(9.8 \pm 4.8 \pm 1.5) \times 10^{-4}$ from a measurement of $[\Gamma(B \rightarrow \chi_{c2}(1P)\text{anything})/\Gamma_{\text{total}}] \times [B(\chi_{c2}(1P) \rightarrow \gamma J/\psi(1S))]$ assuming $B(\chi_{c2}(1P) \rightarrow \gamma J/\psi(1S)) = 0.135 \pm 0.011$, which we rescale to our best value $B(\chi_{c2}(1P) \rightarrow \gamma J/\psi(1S)) = (19.0 \pm 0.5) \times 10^{-2}$. Our first error is their experiment's error and our second error is the systematic error from using our best value. Assumes equal production of B^+ and B^0 at the $\Upsilon(4S)$.

³ABE 02L uses PDG 01 values for $B(J/\psi(1S) \rightarrow \ell^+ \ell^-)$ and $B(\chi_{c1,c2} \rightarrow J/\psi(1S)\gamma)$.

⁴BALEST 95B assume $B(\chi_{c2}(1P) \rightarrow J/\psi(1S)\gamma) = (13.5 \pm 1.1) \times 10^{-2}$, the PDG 1994 value. $J/\psi(1S)$ mesons are reconstructed in the e^+e^- and $\mu^+\mu^-$ modes, and PDG 1994 branching fractions are used. If interpreted as signal, the 35 ± 13 events correspond to $B(B \rightarrow \chi_{c2}(1P)X) = (0.25 \pm 0.10 \pm 0.03) \times 10^{-2}$.



$\Gamma(\chi_{c2}(1P)\text{ (direct) anything})/\Gamma_{\text{total}}$ Γ_{56}/Γ

VALUE (units 10^{-3})	DOCUMENT ID	TECN	COMMENT
0.75 ± 0.11 OUR AVERAGE			
0.70 ± 0.06 ± 0.10	¹ BHARDWAJ 16	BELL	$e^+e^- \rightarrow \Upsilon(4S)$
1.90 ± 0.45 ± 0.29	AUBERT 03F	BABR	$e^+e^- \rightarrow \Upsilon(4S)$
••• We do not use the following data for averages, fits, limits, etc. •••			
1.53 ^{+0.23} _{-0.28} ± 0.27	² ABE	02L BELL	Repl. by BHARDWAJ 16

¹Assumes equal production of B^+ and B^0 at the $\Upsilon(4S)$.

²ABE 02L uses PDG 01 values for $B(J/\psi(1S) \rightarrow \ell^+ \ell^-)$ and $B(\chi_{c1,c2} \rightarrow J/\psi(1S)\gamma)$.

$\Gamma(\eta_{c1}(1S)\text{ anything})/\Gamma_{\text{total}}$ Γ_{57}/Γ

VALUE	CL%	DOCUMENT ID	TECN	COMMENT
<0.009	90	¹ BALEST 95B	CLE2	$e^+e^- \rightarrow \Upsilon(4S)$

¹BALEST 95B assume PDG 1994 values for sub mode branching ratios. $J/\psi(1S)$ mesons are reconstructed in $J/\psi(1S) \rightarrow e^+e^-$ and $J/\psi(1S) \rightarrow \mu^+\mu^-$. Search region $2960 < m_{\eta_{c1}(1S)} < 3010$ MeV/ c^2 .

$\Gamma(K\chi_{c1}(3872))/\Gamma_{\text{total}}$ Γ_{58}/Γ

VALUE (units 10^{-4})	DOCUMENT ID	TECN	COMMENT
2.3 ± 0.7 OUR AVERAGE			
2.2 ± 0.6 ± 0.5	¹ AUSHEV 10	BELL	$e^+e^- \rightarrow \Upsilon(4S)$
2.5 ^{+0.8} _{-0.9} ± 1.0	^{2,3} GOKHROO 06	BELL	$e^+e^- \rightarrow \Upsilon(4S)$

¹AUSHEV 10 reports $[\Gamma(B \rightarrow K\chi_{c1}(3872))/\Gamma_{\text{total}}] \times [B(\chi_{c1}(3872) \rightarrow \bar{D}^{*0}D^0)] = (0.80 \pm 0.20 \pm 0.10) \times 10^{-4}$ which we divide by our best value $B(\chi_{c1}(3872) \rightarrow \bar{D}^{*0}D^0) = (37 \pm 9) \times 10^{-2}$. Our first error is their experiment's error and our second error is the systematic error from using our best value.

²GOKHROO 06 reports $[\Gamma(B \rightarrow K\chi_{c1}(3872))/\Gamma_{\text{total}}] \times [B(\chi_{c1}(3872) \rightarrow D^0\bar{D}^0\pi^0)] = (1.22 \pm 0.31^{+0.23}_{-0.30}) \times 10^{-4}$ which we divide by our best value $B(\chi_{c1}(3872) \rightarrow D^0\bar{D}^0\pi^0) = (49⁺¹⁸₋₂₀) \times 10^{-2}$. Our first error is their experiment's error and our second error is the systematic error from using our best value.

³Measure the near-threshold enhancements in the $(D^0\bar{D}^0\pi^0)$ system at a mass $3875.2 \pm 0.7^{+0.3}_{-1.6} \pm 0.8$ MeV/ c^2 .

$\Gamma(KX(3940), X \rightarrow D^{*0}D^0)/\Gamma_{\text{total}}$ Γ_{59}/Γ

VALUE (units 10^{-4})	CL%	DOCUMENT ID	TECN	COMMENT
<0.67	90	AUSHEV 10	BELL	$e^+e^- \rightarrow \Upsilon(4S)$

$\Gamma(K\chi_{c0}(3915), \chi_{c0} \rightarrow \omega J/\psi)/\Gamma_{\text{total}}$ Γ_{60}/Γ

VALUE (units 10^{-5})	DOCUMENT ID	TECN	COMMENT
7.1 ± 1.3 ± 3.1	¹ CHOI 05	BELL	$e^+e^- \rightarrow \Upsilon(4S)$

¹CHOI 05 reports the observation of a near-threshold enhancement in the $\omega J/\psi$ mass spectrum in exclusive $B \rightarrow K\omega J/\psi$. The new state, denoted as $\chi_{c0}(3915)$, is measured to have a mass of $3943 \pm 11 \pm 13$ GeV/ c^2 and a width $\Gamma = 87 \pm 22 \pm 26$ MeV.

$\Gamma(K^\pm\text{ anything})/\Gamma_{\text{total}}$ Γ_{61}/Γ

VALUE	DOCUMENT ID	TECN	COMMENT
0.789 ± 0.025 OUR AVERAGE			
0.82 ± 0.01 ± 0.05	ALBRECHT 94C	ARG	$e^+e^- \rightarrow \Upsilon(4S)$
0.775 ± 0.015 ± 0.025	¹ ALBRECHT 93I	ARG	$e^+e^- \rightarrow \Upsilon(4S)$
0.85 ± 0.07 ± 0.09	ALAM 87B	CLEO	$e^+e^- \rightarrow \Upsilon(4S)$
••• We do not use the following data for averages, fits, limits, etc. •••			
seen	² BRODY 82	CLEO	$e^+e^- \rightarrow \Upsilon(4S)$
seen	³ GIANNINI 82	CUSB	$e^+e^- \rightarrow \Upsilon(4S)$

¹ALBRECHT 93I value is not independent of the sum of $B \rightarrow K^+$ anything and $B \rightarrow K^-$ anything ALBRECHT 94C values.

²Assuming $\Upsilon(4S) \rightarrow B\bar{B}$, a total of $3.38 \pm 0.34 \pm 0.68$ kaons per $\Upsilon(4S)$ decay is found (the second error is systematic). In the context of the standard B -decay model, this leads to a value for $(b\text{-quark} \rightarrow c\text{-quark})/(b\text{-quark} \rightarrow \text{all})$ of $1.09 \pm 0.33 \pm 0.13$.

³GIANNINI 82 at CESR-CUSB observed 1.58 ± 0.35 K^0 per hadronic event much higher than 0.82 ± 0.10 below threshold. Consistent with predominant $b \rightarrow cX$ decay.

$\Gamma(K^+\text{ anything})/\Gamma_{\text{total}}$ Γ_{62}/Γ

VALUE	DOCUMENT ID	TECN	COMMENT
0.66 ± 0.05	¹ ALBRECHT 94C	ARG	$e^+e^- \rightarrow \Upsilon(4S)$
••• We do not use the following data for averages, fits, limits, etc. •••			
0.620 ± 0.013 ± 0.038	² ALBRECHT 94C	ARG	$e^+e^- \rightarrow \Upsilon(4S)$
0.66 ± 0.05 ± 0.07	² ALAM 87B	CLEO	$e^+e^- \rightarrow \Upsilon(4S)$

¹Measurement relies on lepton-kaon correlations. It is for the weak decay vertex and does not include mixing of the neutral B meson. Mixing effects were corrected for by assuming a mixing parameter r of $(18.1 \pm 4.3)\%$.

²Measurement relies on lepton-kaon correlations. It includes production through mixing of the neutral B meson.

$\Gamma(K^-\text{ anything})/\Gamma_{\text{total}}$ Γ_{63}/Γ

VALUE	DOCUMENT ID	TECN	COMMENT
0.13 ± 0.04	¹ ALBRECHT 94C	ARG	$e^+e^- \rightarrow \Upsilon(4S)$
••• We do not use the following data for averages, fits, limits, etc. •••			
0.165 ± 0.011 ± 0.036	² ALBRECHT 94C	ARG	$e^+e^- \rightarrow \Upsilon(4S)$
0.19 ± 0.05 ± 0.02	² ALAM 87B	CLEO	$e^+e^- \rightarrow \Upsilon(4S)$

¹Measurement relies on lepton-kaon correlations. It is for the weak decay vertex and does not include mixing of the neutral B meson. Mixing effects were corrected for by assuming a mixing parameter r of $(18.1 \pm 4.3)\%$.

²Measurement relies on lepton-kaon correlations. It includes production through mixing of the neutral B meson.

$\Gamma(K^0/\bar{K}^0\text{ anything})/\Gamma_{\text{total}}$ Γ_{64}/Γ

VALUE	DOCUMENT ID	TECN	COMMENT
0.64 ± 0.04 OUR AVERAGE			
0.642 ± 0.010 ± 0.042	¹ ALBRECHT 94C	ARG	$e^+e^- \rightarrow \Upsilon(4S)$
0.63 ± 0.06 ± 0.06	ALAM 87B	CLEO	$e^+e^- \rightarrow \Upsilon(4S)$

¹ALBRECHT 94C assume a K^0/\bar{K}^0 multiplicity twice that of K_S^0 .

$\Gamma(K^*(892)^\pm\text{ anything})/\Gamma_{\text{total}}$ Γ_{65}/Γ

VALUE	DOCUMENT ID	TECN	COMMENT
0.182 ± 0.054 ± 0.024	ALBRECHT 94I	ARG	$e^+e^- \rightarrow \Upsilon(4S)$

$\Gamma(K^*(892)^0/\bar{K}^{*0}\text{ anything})/\Gamma_{\text{total}}$ Γ_{66}/Γ

VALUE	DOCUMENT ID	TECN	COMMENT
0.146 ± 0.016 ± 0.020	ALBRECHT 94I	ARG	$e^+e^- \rightarrow \Upsilon(4S)$

$\Gamma(K^*(892)\gamma)/\Gamma_{\text{total}}$ Γ_{67}/Γ

VALUE (units 10^{-5})	CL%	DOCUMENT ID	TECN	COMMENT
4.24 ± 0.54 ± 0.32	90	¹ COAN 00	CLE2	$e^+e^- \rightarrow \Upsilon(4S)$
••• We do not use the following data for averages, fits, limits, etc. •••				
<150	90	² LESIAK 92	CBAL	$e^+e^- \rightarrow \Upsilon(4S)$
<24	90	ALBRECHT 88H	ARG	$e^+e^- \rightarrow \Upsilon(4S)$

¹An average of $B(B^+ \rightarrow K^*(892)^+\gamma)$ and $B(B^0 \rightarrow K^*(892)^0\gamma)$ measurements reported in COAN 00 by assuming full correlated systematic errors.

²LESIAK 92 set a limit on the inclusive process $B(b \rightarrow s\gamma) < 2.8 \times 10^{-3}$ at 90% CL for the range of masses of 892–2045 MeV, independent of assumptions about s-quark hadronization.

$\Gamma(\eta K\gamma)/\Gamma_{\text{total}}$ Γ_{68}/Γ

VALUE (units 10^{-6})	DOCUMENT ID	TECN	COMMENT
8.5 ± 1.3^{+1.2}_{-0.9}	¹ NISHIDA 05	BELL	$e^+e^- \rightarrow \Upsilon(4S)$

¹ $m_{\eta K} < 2.4$ GeV/ c^2

$\Gamma(K_1(1400)\gamma)/\Gamma_{\text{total}}$ Γ_{69}/Γ

VALUE	CL%	DOCUMENT ID	TECN	COMMENT
<12.7 × 10⁻⁵	90	¹ COAN 00	CLE2	$e^+e^- \rightarrow \Upsilon(4S)$
••• We do not use the following data for averages, fits, limits, etc. •••				
< 1.6 × 10 ⁻³	90	² LESIAK 92	CBAL	$e^+e^- \rightarrow \Upsilon(4S)$
< 4.1 × 10 ⁻⁴	90	ALBRECHT 88H	ARG	$e^+e^- \rightarrow \Upsilon(4S)$

¹Assumes equal production of B^+ and B^0 at the $\Upsilon(4S)$.

²LESIAK 92 set a limit on the inclusive process $B(b \rightarrow s\gamma) < 2.8 \times 10^{-3}$ at 90% CL for the range of masses of 892–2045 MeV, independent of assumptions about s-quark hadronization.

Meson Particle Listings

 B^\pm/B^0 ADMIXTURE $\Gamma(K_S^*(1430)\gamma)/\Gamma_{\text{total}}$ Γ_{70}/Γ

VALUE (units 10^{-5})	CL%	DOCUMENT ID	TECN	COMMENT
$1.66 \pm_{-0.53}^{+0.59} \pm 0.13$		¹ COAN	00	CLE2 $e^+e^- \rightarrow \Upsilon(4S)$

••• We do not use the following data for averages, fits, limits, etc. •••

<83 90 ALBRECHT 88H ARG $e^+e^- \rightarrow \Upsilon(4S)$

¹ COAN 00 obtains a fitted signal yield of $15.9^{+5.7}_{-5.2}$ events. A search for contamination by $K^*(1410)$ yielded a rate consistent with 0; the central value assumes no contamination.

 $\Gamma(K_2(1770)\gamma)/\Gamma_{\text{total}}$ Γ_{71}/Γ

VALUE	CL%	DOCUMENT ID	TECN	COMMENT
$<1.2 \times 10^{-3}$	90	¹ LESIAK	92	CBAL $e^+e^- \rightarrow \Upsilon(4S)$

¹ LESIAK 92 set a limit on the inclusive process $B(b \rightarrow s\gamma) < 2.8 \times 10^{-3}$ at 90% CL for the range of masses of 892–2045 MeV, independent of assumptions about s-quark hadronization.

 $\Gamma(K_S^*(1780)\gamma)/\Gamma_{\text{total}}$ Γ_{72}/Γ

VALUE	CL%	DOCUMENT ID	TECN	COMMENT
$<3.7 \times 10^{-5}$	90	¹ NISHIDA	05	BELL $e^+e^- \rightarrow \Upsilon(4S)$

••• We do not use the following data for averages, fits, limits, etc. •••

<3.0 $\times 10^{-3}$ 90 ALBRECHT 88H ARG $e^+e^- \rightarrow \Upsilon(4S)$

¹ Uses $B(K_S^*(1780) \rightarrow \eta K) = 0.11^{+0.05}_{-0.04}$.

 $\Gamma(K_S^*(2045)\gamma)/\Gamma_{\text{total}}$ Γ_{73}/Γ

VALUE	CL%	DOCUMENT ID	TECN	COMMENT
$<1.0 \times 10^{-3}$	90	¹ LESIAK	92	CBAL $e^+e^- \rightarrow \Upsilon(4S)$

¹ LESIAK 92 set a limit on the inclusive process $B(b \rightarrow s\gamma) < 2.8 \times 10^{-3}$ at 90% CL for the range of masses of 892–2045 MeV, independent of assumptions about s-quark hadronization.

 $\Gamma(K\eta'(958))/\Gamma_{\text{total}}$ Γ_{74}/Γ

VALUE	CL%	DOCUMENT ID	TECN	COMMENT
$(8.3^{+0.9}_{-0.8} \pm 0.7) \times 10^{-5}$		¹ RICHICHI	00	CLE2 $e^+e^- \rightarrow \Upsilon(4S)$

¹ Assumes equal production of B^+ and B^0 at the $\Upsilon(4S)$.

 $\Gamma(K^*(892)\eta(958))/\Gamma_{\text{total}}$ Γ_{75}/Γ

VALUE (units 10^{-6})	CL%	DOCUMENT ID	TECN	COMMENT
$4.1^{+1.0}_{-0.9} \pm 0.5$		¹ AUBERT	07E	BABR $e^+e^- \rightarrow \Upsilon(4S)$

••• We do not use the following data for averages, fits, limits, etc. •••

<22 90 ¹ RICHICHI 00 CLE2 $e^+e^- \rightarrow \Upsilon(4S)$

¹ Assumes equal production of B^+ and B^0 at the $\Upsilon(4S)$.

 $\Gamma(K\eta)/\Gamma_{\text{total}}$ Γ_{76}/Γ

VALUE	CL%	DOCUMENT ID	TECN	COMMENT
$<5.2 \times 10^{-6}$	90	¹ RICHICHI	00	CLE2 $e^+e^- \rightarrow \Upsilon(4S)$

¹ Assumes equal production of B^+ and B^0 at the $\Upsilon(4S)$.

 $\Gamma(K^*(892)\eta)/\Gamma_{\text{total}}$ Γ_{77}/Γ

VALUE	CL%	DOCUMENT ID	TECN	COMMENT
$(1.80^{+0.49}_{-0.43} \pm 0.18) \times 10^{-5}$		¹ RICHICHI	00	CLE2 $e^+e^- \rightarrow \Upsilon(4S)$

¹ Assumes equal production of B^+ and B^0 at the $\Upsilon(4S)$.

 $\Gamma(K\phi\phi)/\Gamma_{\text{total}}$ Γ_{78}/Γ

VALUE (units 10^{-6})	CL%	DOCUMENT ID	TECN	COMMENT
$2.3^{+0.9}_{-0.8} \pm 0.3$		¹ HUANG	03	BELL $e^+e^- \rightarrow \Upsilon(4S)$

¹ Assumes equal production of charged and neutral B meson pairs and isospin symmetry.

 $\Gamma(B \rightarrow \bar{\Sigma}\gamma)/\Gamma_{\text{total}}$ Γ_{79}/Γ

VALUE (units 10^{-4})	DOCUMENT ID	TECN	COMMENT
3.49 ± 0.19 OUR AVERAGE			

3.75 ± 0.18 ± 0.35	^{1,2} SAITO	15	BELL $e^+e^- \rightarrow \Upsilon(4S)$
3.52 ± 0.20 ± 0.51	^{1,3} LEES	12v	BABR $e^+e^- \rightarrow \Upsilon(4S)$
3.32 ± 0.16 ± 0.31	^{1,4} LEES	12v	BABR $e^+e^- \rightarrow \Upsilon(4S)$
3.47 ± 0.15 ± 0.40	^{1,5} LIMOSANI	09	BELL $e^+e^- \rightarrow \Upsilon(4S)$
3.29 ± 0.91 ± 0.64	^{1,6} AUBERT	08o	BABR $e^+e^- \rightarrow \Upsilon(4S)$
3.90 ± 0.44 ± 0.29	^{1,7} CHEN	01c	CLE2 $e^+e^- \rightarrow \Upsilon(4S)$
•••	•••	•••	•••
2.30 ± 0.08 ± 0.30	⁸ DEL-AMO-SA...10M	BABR	$e^+e^- \rightarrow \Upsilon(4S)$
4.3 ± 0.3 ± 0.7	⁹ AUBERT	09u	BABR Repl. by DEL-AMO-SANCHEZ 10m
3.92 ± 0.31 ± 0.47	^{1,10} AUBERT,BE	06b	BABR Repl. by LEES 12v
3.49 ± 0.20 ± 0.59 ± 0.46	^{1,11} AUBERT,B	05R	BABR Repl. by LEES 12u
3.50 ± 0.32 ± 0.31	^{1,12} KOPPENBURG	04	BELL Repl. by LIMOSANI 09
3.36 ± 0.53 ± 0.65 ± 0.68	¹³ ABE	01F	BELL Repl. by SAITO 15
2.32 ± 0.57 ± 0.35	ALAM	95	CLE2 Repl. by CHEN 01c

¹ We extrapolate the measured value to $E_\gamma > 1.6$ GeV using the method of BUCHMUELLER 06 (average of three theoretical models).

² SAITO 15 measured $(3.51 \pm 0.17 \pm 0.33) \times 10^{-4}$ using a sum-of-exclusive approach in which 38 of the hadronic final states with $m_{X_S} < 2.8$ GeV/ c^2 are reconstructed. The cut of minimum photon energy is $E_\gamma > 1.9$ GeV.

³ Reports $(3.29 \pm 0.19 \pm 0.48) \times 10^{-4}$ for $E_\gamma > 1.9$ GeV.

⁴ Reports $(3.21 \pm 0.15 \pm 0.29 \pm 0.08) \times 10^{-4}$ for $1.8 < E_\gamma < 2.8$ GeV, where the last systematic uncertainty is for model dependency. Results with other cutoffs are also reported.

⁵ The measurement reported is $(3.45 \pm 0.15 \pm 0.40) \times 10^{-4}$ for $E_\gamma > 1.7$ GeV.

⁶ Uses a fully reconstructed B meson as a tag on the recoil side. The measurement reported is $(3.66 \pm 0.85 \pm 0.60) \times 10^{-4}$ for $E_\gamma > 1.9$ GeV.

⁷ The measurement reported is $(3.21 \pm 0.43^{+0.32}_{-0.29}) \times 10^{-4}$ for $E_\gamma > 2.0$ GeV.

⁸ Measured using sums of seven exclusive final states $B \rightarrow X_{d(s)}\gamma$ where $X_{d(s)}$ is a nonstrange (strange) charmless hadronic system in mass range 0.5–2.0 GeV/ c^2 .

⁹ Measured using sums of seven exclusive final states $B \rightarrow X_{d(s)}\gamma$ where $X_{d(s)}$ is a nonstrange (strange) charmless hadronic system in mass range 0.6–1.8 GeV/ c^2 .

¹⁰ The measurement reported is $(3.67 \pm 0.29 \pm 0.45) \times 10^{-4}$ for $E_\gamma > 1.9$ GeV.

¹¹ The measurement reported is $(3.27 \pm 0.18^{+0.55}_{-0.42}) \times 10^{-4}$ for $E_\gamma > 1.9$ GeV.

¹² The measurement reported is $(3.55 \pm 0.32 \pm 0.32) \times 10^{-4}$ for $E_\gamma > 1.8$ GeV.

¹³ ABE 01F reports their systematic errors $(\pm 0.42^{+0.50}_{-0.54}) \times 10^{-4}$, where the second error is due to the theoretical uncertainty. We combine them in quadrature.

 $\Gamma(B \rightarrow \bar{\Sigma}\gamma)/\Gamma_{\text{total}}$ Γ_{80}/Γ

VALUE (units 10^{-6})	DOCUMENT ID	TECN	COMMENT
9.2 ± 2.0 ± 2.3	¹ DEL-AMO-SA...10M	BABR	$e^+e^- \rightarrow \Upsilon(4S)$

••• We do not use the following data for averages, fits, limits, etc. •••

14 ± 5 ± 4 ² AUBERT 09u BABR Repl. by DEL-AMO-SANCHEZ 10m

¹ Measured using sums of seven exclusive final states $B \rightarrow X_{d(s)}\gamma$ where $X_{d(s)}$ is a nonstrange (strange) charmless hadronic system in mass range 0.5–2.0 GeV/ c^2 .

² Measured using sums of seven exclusive final states $B \rightarrow X_{d(s)}\gamma$ where $X_{d(s)}$ is a nonstrange (strange) charmless hadronic system in mass range 0.6–1.8 GeV/ c^2 .

 $\Gamma(B \rightarrow \bar{\Sigma}\gamma)/\Gamma(B \rightarrow \bar{\Sigma}\gamma)$ Γ_{80}/Γ_{79}

VALUE	DOCUMENT ID	TECN	COMMENT
0.040 ± 0.009 ± 0.010	¹ DEL-AMO-SA...10M	BABR	$e^+e^- \rightarrow \Upsilon(4S)$

••• We do not use the following data for averages, fits, limits, etc. •••

0.033 ± 0.013 ± 0.009 ² AUBERT 09u BABR Repl. by DEL-AMO-SANCHEZ 10m

¹ Measured using sums of seven exclusive final states $B \rightarrow X_{d(s)}\gamma$ where $X_{d(s)}$ is a nonstrange (strange) charmless hadronic system in mass range 0.5–2.0 GeV/ c^2 .

² Measured using sums of seven exclusive final states $B \rightarrow X_{d(s)}\gamma$ where $X_{d(s)}$ is a nonstrange (strange) charmless hadronic system in mass range 0.6–1.8 GeV/ c^2 .

 $\Gamma(B \rightarrow \bar{\Sigma}gluon)/\Gamma_{\text{total}}$ Γ_{81}/Γ

VALUE	CL%	EVTS	DOCUMENT ID	TECN	COMMENT
<0.068		90	¹ COAN	98	CLE2 $e^+e^- \rightarrow \Upsilon(4S)$

••• We do not use the following data for averages, fits, limits, etc. •••

<0.08 2 ² ALBRECHT 95d ARG $e^+e^- \rightarrow \Upsilon(4S)$

¹ COAN 98 uses D - ℓ correlation.

² ALBRECHT 95d use full reconstruction of one B decay as tag. Two candidate events for charmless B decay can be interpreted as either $b \rightarrow sgluon$ or $b \rightarrow u$ transition. If interpreted as $B \rightarrow sgluon$ they find a branching ratio of ~ 0.026 or the upper limit quoted above. Result is highly model dependent.

 $\Gamma(\eta \text{ anything})/\Gamma_{\text{total}}$ Γ_{82}/Γ

VALUE (units 10^{-4})	CL%	DOCUMENT ID	TECN	COMMENT
2.61 ± 0.30 ± 0.44 ± 0.74		¹ NISHIMURA	10	BELL $e^+e^- \rightarrow \Upsilon(4S)$

••• We do not use the following data for averages, fits, limits, etc. •••

1.69 ± 0.29 ± 0.36 ± 0.62 ² NISHIMURA 10 BELL $e^+e^- \rightarrow \Upsilon(4S)$

<4.4 90 ³ BROWDER 98 CLE2 $e^+e^- \rightarrow \Upsilon(4S)$

¹ Uses $B \rightarrow \eta X_S$ with $0.4 < m_{X_S} < 2.6$ GeV/ c^2 .

² Uses $B \rightarrow \eta X_S$ with $1.8 < m_{X_S} < 2.6$ GeV/ c^2 .

³ BROWDER 98 search for high momentum $B \rightarrow \eta X_S$ between 2.1 and 2.7 GeV/ c .

 $\Gamma(\eta' \text{ anything})/\Gamma_{\text{total}}$ Γ_{83}/Γ

VALUE (units 10^{-4})	DOCUMENT ID	TECN	COMMENT
4.2 ± 0.9 OUR AVERAGE			

3.9 ± 0.8 ± 0.9 ¹ AUBERT,B 04F BABR $e^+e^- \rightarrow \Upsilon(4S)$

4.6 ± 1.1 ± 0.6 ² BONVICINI 03 CLE2 $e^+e^- \rightarrow \Upsilon(4S)$

••• We do not use the following data for averages, fits, limits, etc. •••

6.2 ± 1.6 ± 1.3 ± 2.0 ³ BROWDER 98 CLE2 $e^+e^- \rightarrow \Upsilon(4S)$

¹ AUBERT,B 04F reports branching ratio $B \rightarrow \eta' X_S$ for high momentum η' between 2.0 and 2.7 GeV/ c in the $\Upsilon(4S)$ center-of-mass frame. X_S represents a recoil system consisting of a kaon and zero to four pions.

² BONVICINI 03 observed a signal of 61.2 ± 13.9 events in $B \rightarrow \eta' X_{nc}$ production for high momentum η' between 2.0 and 2.7 GeV/ c in the $\Upsilon(4S)$ center-of-mass frame. The X_{nc} denotes "charmless" hadronic states recoiling against η' . The second error combines systematic and background subtraction uncertainties in quadrature.

³ BROWDER 98 observed a signal of 39.0 ± 11.6 events in high momentum $B \rightarrow \eta' X_S$ production between 2.0 and 2.7 GeV/ c . The branching fraction is based on the interpretation of $b \rightarrow sg$, where the last error includes additional uncertainties due to the color-suppressed $b \rightarrow$ backgrounds.

$\Gamma(K^+ \text{ gluon (charmless)})/\Gamma_{\text{total}}$					Γ_{84}/Γ
VALUE (units 10^{-4})	CL%	DOCUMENT ID	TECN	COMMENT	
<1.87	90	¹ DEL-AMO-SA..11	BABR	$e^+e^- \rightarrow \Upsilon(4S)$	
¹ $B \rightarrow K^+ X$ with $m_X < 1.69 \text{ GeV}/c^2$.					

$\Gamma(K^0 \text{ gluon (charmless)})/\Gamma_{\text{total}}$					Γ_{85}/Γ
VALUE (units 10^{-4})	CL%	DOCUMENT ID	TECN	COMMENT	
$1.95 \pm 0.51 \pm 0.50$		¹ DEL-AMO-SA..11	BABR	$e^+e^- \rightarrow \Upsilon(4S)$	
¹ $B \rightarrow K^0 X$ with $m_X < 1.69 \text{ GeV}/c^2$.					

$\Gamma(\rho\gamma)/\Gamma_{\text{total}}$					Γ_{86}/Γ
VALUE (units 10^{-6})	CL%	DOCUMENT ID	TECN	COMMENT	
1.39 ± 0.25 OUR AVERAGE		Error includes scale factor of 1.2.			
$1.73^{+0.34}_{-0.32} \pm 0.17$		^{1,2} AUBERT	08BH	BABR	$e^+e^- \rightarrow \Upsilon(4S)$
$1.21^{+0.24}_{-0.22} \pm 0.12$		^{1,2} TANIGUCHI	08	BELL	$e^+e^- \rightarrow \Upsilon(4S)$
• • • We do not use the following data for averages, fits, limits, etc. • • •					
$1.36^{+0.29}_{-0.27} \pm 0.10$		^{1,3} AUBERT	07L	BABR	Repl. by AUBERT 08BH
< 1.9	90	^{1,3} AUBERT	04c	BABR	Repl. by AUBERT 07L
< 14	90	^{1,4} COAN	00	CLE2	$e^+e^- \rightarrow \Upsilon(4S)$

- ¹ Assumes equal production of B^+ and B^0 at the $\Upsilon(4S)$.
² Assumes $\Gamma(B \rightarrow \rho\gamma) = \Gamma(B^+ \rightarrow \rho^+\gamma) = 2\Gamma(B^0 \rightarrow \rho^0\gamma)$ and uses lifetime ratio of $\tau_{B^+}/\tau_{B^0} = 1.071 \pm 0.009$.
³ Assumes $\Gamma(B \rightarrow \rho\gamma) = \Gamma(B^+ \rightarrow \rho^+\gamma) = 2\Gamma(B^0 \rightarrow \rho^0\gamma)$ and uses lifetime ratio of $\tau_{B^+}/\tau_{B^0} = 1.083 \pm 0.017$.
⁴ COAN 00 reports $B(B \rightarrow \rho\gamma)/B(B \rightarrow K^*(892)\gamma) < 0.32$ at 90%CL and scaled by the central value of $B(B \rightarrow K^*(892)\gamma) = (4.24 \pm 0.54 \pm 0.32) \times 10^{-5}$.

$\Gamma(\rho\gamma)/\Gamma(K^*(892)\gamma)$					Γ_{86}/Γ_{67}
VALUE (units 10^{-2})	CL%	DOCUMENT ID	TECN	COMMENT	
$3.02^{+0.60+0.26}_{-0.55-0.28}$		TANIGUCHI	08	BELL	$e^+e^- \rightarrow \Upsilon(4S)$

$\Gamma(\rho/\omega\gamma)/\Gamma_{\text{total}}$					Γ_{87}/Γ
VALUE (units 10^{-6})	CL%	DOCUMENT ID	TECN	COMMENT	
1.30 ± 0.23 OUR AVERAGE		Error includes scale factor of 1.2.			
$1.63^{+0.30}_{-0.28} \pm 0.16$		^{1,2,3} AUBERT	08BH	BABR	$e^+e^- \rightarrow \Upsilon(4S)$
$1.14 \pm 0.20^{+0.10}_{-0.12}$		^{1,3} TANIGUCHI	08	BELL	$e^+e^- \rightarrow \Upsilon(4S)$

- • • We do not use the following data for averages, fits, limits, etc. • • •
- | | | | | | |
|----------------------------------|----|------------------------|-----|------|-----------------------------------|
| $1.25^{+0.25}_{-0.24} \pm 0.09$ | | ⁴ AUBERT | 07L | BABR | Repl. by AUBERT 08BH |
| $1.32^{+0.34+0.10}_{-0.31-0.09}$ | | ⁴ MOHAPATRA | 06 | BELL | Repl. by TANIGUCHI 08 |
| $0.6 \pm 0.3 \pm 0.1$ | | ⁴ AUBERT | 05 | BABR | Repl. by AUBERT 07L |
| < 1.4 | 90 | ⁴ MOHAPATRA | 05 | BELL | $e^+e^- \rightarrow \Upsilon(4S)$ |
- ¹ Assumes $\Gamma(B \rightarrow \rho\gamma) = \Gamma(B^+ \rightarrow \rho^+\gamma) = 2\Gamma(B^0 \rightarrow \rho^0\gamma)$ and uses lifetime ratio of $\tau_{B^+}/\tau_{B^0} = 1.071 \pm 0.009$.
² Also reports $|V_{td}/V_{ts}| = 0.233^{+0.025+0.022}_{-0.024-0.021}$.
³ Assumes equal production of B^+ and B^0 at the $\Upsilon(4S)$.
⁴ Assumes $\Gamma(B \rightarrow \rho\gamma) = \Gamma(B^+ \rightarrow \rho^+\gamma) = 2\Gamma(B^0 \rightarrow \rho^0\gamma)$ and uses lifetime ratio of $\tau_{B^+}/\tau_{B^0} = 1.083 \pm 0.017$.

$\Gamma(\rho/\omega\gamma)/\Gamma(K^*(892)\gamma)$					Γ_{87}/Γ_{67}
VALUE (units 10^{-2})	CL%	DOCUMENT ID	TECN	COMMENT	
$2.84 \pm 0.50^{+0.27}_{-0.29}$		¹ TANIGUCHI	08	BELL	$e^+e^- \rightarrow \Upsilon(4S)$

- • • We do not use the following data for averages, fits, limits, etc. • • •
- | | | | | | |
|---------|----|-----------|----|------|-----------------------|
| < 3.5 | 90 | MOHAPATRA | 05 | BELL | Repl. by TANIGUCHI 08 |
|---------|----|-----------|----|------|-----------------------|
- ¹ Also reports $|V_{td}/V_{ts}| = 0.195^{+0.020}_{-0.019} \pm 0.015$.

$\Gamma(\pi^\pm \text{ anything})/\Gamma_{\text{total}}$					Γ_{88}/Γ
VALUE	CL%	DOCUMENT ID	TECN	COMMENT	
$3.585 \pm 0.025 \pm 0.070$		¹ ALBRECHT	93i	ARG	$e^+e^- \rightarrow \Upsilon(4S)$
¹ ALBRECHT 93 excludes π^\pm from K_S^0 and Λ decays. If included, they find $4.105 \pm 0.025 \pm 0.080$.					

$\Gamma(\pi^0 \text{ anything})/\Gamma_{\text{total}}$					Γ_{89}/Γ
VALUE	CL%	DOCUMENT ID	TECN	COMMENT	
$2.35 \pm 0.02 \pm 0.11$		¹ ABE	01J	BELL	$e^+e^- \rightarrow \Upsilon(4S)$
¹ From fully inclusive π^0 yield with no corrections from decays of K_S^0 or other particles.					

$\Gamma(\eta \text{ anything})/\Gamma_{\text{total}}$					Γ_{90}/Γ
VALUE	CL%	DOCUMENT ID	TECN	COMMENT	
$0.176 \pm 0.011 \pm 0.012$		KUBOTA	96	CLE2	$e^+e^- \rightarrow \Upsilon(4S)$

$\Gamma(\rho^0 \text{ anything})/\Gamma_{\text{total}}$					Γ_{91}/Γ
VALUE	CL%	DOCUMENT ID	TECN	COMMENT	
$0.208 \pm 0.042 \pm 0.032$		ALBRECHT	94J	ARG	$e^+e^- \rightarrow \Upsilon(4S)$

$\Gamma(\omega \text{ anything})/\Gamma_{\text{total}}$					Γ_{92}/Γ
VALUE	CL%	DOCUMENT ID	TECN	COMMENT	
< 0.81	90	ALBRECHT	94J	ARG	$e^+e^- \rightarrow \Upsilon(4S)$

$\Gamma(\phi \text{ anything})/\Gamma_{\text{total}}$					Γ_{93}/Γ
VALUE	CL%	DOCUMENT ID	TECN	COMMENT	
0.0343 ± 0.0012 OUR AVERAGE					
$0.0353 \pm 0.0005 \pm 0.0030$		HUANG	07	CLEO	$e^+e^- \rightarrow \Upsilon(4S)$
$0.0341 \pm 0.0006 \pm 0.0012$		AUBERT	04s	BABR	$e^+e^- \rightarrow \Upsilon(4S)$
$0.0390 \pm 0.0030 \pm 0.0035$		ALBRECHT	94J	ARG	$e^+e^- \rightarrow \Upsilon(4S)$
$0.023 \pm 0.006 \pm 0.005$		BORTOLETTO	086	CLEO	$e^+e^- \rightarrow \Upsilon(4S)$

$\Gamma(\phi K^*(892))/\Gamma_{\text{total}}$					Γ_{94}/Γ
VALUE	CL%	DOCUMENT ID	TECN	COMMENT	
$< 2.2 \times 10^{-5}$	90	¹ BERGFELD	98	CLE2	
¹ Assumes equal production of B^+ and B^0 at the $\Upsilon(4S)$.					

$\Gamma(\pi^+ \text{ gluon (charmless)})/\Gamma_{\text{total}}$					Γ_{96}/Γ
VALUE (units 10^{-4})	CL%	DOCUMENT ID	TECN	COMMENT	
$3.72^{+0.50}_{-0.47} \pm 0.59$		¹ DEL-AMO-SA..11	BABR	$e^+e^- \rightarrow \Upsilon(4S)$	
¹ $B \rightarrow \pi^+ X$ with $m_X < 1.71 \text{ GeV}/c^2$.					

$\Gamma(\Lambda_c^+ / \bar{\Lambda}_c^- \text{ anything})/\Gamma_{\text{total}}$					Γ_{97}/Γ
VALUE (%)	CL%	DOCUMENT ID	TECN	COMMENT	
$3.59 \pm 0.32^{+0.19}_{-0.18}$		¹ AUBERT	07c	BABR	$e^+e^- \rightarrow \Upsilon(4S)$
• • • We do not use the following data for averages, fits, limits, etc. • • •					
$6.4 \pm 0.8 \pm 0.8$		² CRAWFORD	92	CLEO	$e^+e^- \rightarrow \Upsilon(4S)$
14 ± 9		³ ALBRECHT	88e	ARG	$e^+e^- \rightarrow \Upsilon(4S)$
< 11.2	90	⁴ ALAM	87	CLEO	$e^+e^- \rightarrow \Upsilon(4S)$

- ¹ AUBERT 07c reports $0.045 \pm 0.003 \pm 0.012$ from a measurement of $[\Gamma(B \rightarrow \Lambda_c^+ / \bar{\Lambda}_c^- \text{ anything})/\Gamma_{\text{total}}] \times [B(\Lambda_c^+ \rightarrow pK^- \pi^+)]$ assuming $B(\Lambda_c^+ \rightarrow pK^- \pi^+) = (5.0 \pm 1.3) \times 10^{-2}$, which we rescale to our best value $B(\Lambda_c^+ \rightarrow pK^- \pi^+) = (6.28 \pm 0.32) \times 10^{-2}$. Our first error is their experiment's error and our second error is the systematic error from using our best value.
² CRAWFORD 92 result derived from lepton baryon correlations. Assumes all charmed baryons in B^0 and B^\pm decay are Λ_c .
³ ALBRECHT 88e measured $B(B \rightarrow \Lambda_c^+ X) \cdot B(\Lambda_c^+ \rightarrow pK^- \pi^+) = (0.30 \pm 0.12 \pm 0.06)\%$ and used $B(\Lambda_c^+ \rightarrow pK^- \pi^+) = (2.2 \pm 1.0)\%$ from ABRAMS 80 to obtain above number.
⁴ Assuming all baryons result from charmed baryons, ALAM 86 conclude the branching fraction is $7.4 \pm 2.9\%$. The limit given above is model independent.

$\Gamma(\Lambda_c^+ \text{ anything})/\Gamma(\bar{\Lambda}_c^- \text{ anything})$					Γ_{98}/Γ_{99}
VALUE	CL%	DOCUMENT ID	TECN	COMMENT	
$0.19 \pm 0.13 \pm 0.04$		¹ AMMAR	97	CLE2	$e^+e^- \rightarrow \Upsilon(4S)$
¹ AMMAR 97 uses a high-momentum lepton tag ($P_\ell > 1.4 \text{ GeV}/c^2$).					

$\Gamma(\bar{\Lambda}_c^- \mu^+ \text{ anything})/\Gamma(\bar{\Lambda}_c^- \text{ anything})$					Γ_{102}/Γ_{99}
VALUE (units 10^{-2})	CL%	DOCUMENT ID	TECN	COMMENT	
$-2.0 \pm 2.0 \pm 1.9$		LEES	12	BABR	$e^+e^- \rightarrow \Upsilon(4S)$

$\Gamma(\bar{\Lambda}_c^- \ell^+ \text{ anything})/\Gamma(\Lambda_c^+ / \bar{\Lambda}_c^- \text{ anything})$					Γ_{100}/Γ_{97}
VALUE	CL%	DOCUMENT ID	TECN	COMMENT	
$< 2.5 \times 10^{-2}$	90	¹ LEES	12	BABR	$e^+e^- \rightarrow \Upsilon(4S)$
¹ LEES 12 quotes also the measurement $\Gamma(B \rightarrow \bar{\Lambda}_c^- \ell^+ \text{ anything})/\Gamma(B \rightarrow \Lambda_c^+ / \bar{\Lambda}_c^- \text{ anything}) = (1.2 \pm 0.7 \pm 0.4) \times 10^{-2}$.					

$\Gamma(\bar{\Lambda}_c^- e^+ \text{ anything})/\Gamma(\Lambda_c^+ / \bar{\Lambda}_c^- \text{ anything})$					Γ_{101}/Γ_{97}
VALUE	CL%	DOCUMENT ID	TECN	COMMENT	
< 0.05	90	¹ BONVICINI	98	CLE2	$e^+e^- \rightarrow \Upsilon(4S)$
¹ BONVICINI 98 uses the electron with momentum above $0.6 \text{ GeV}/c$.					

$\Gamma(\bar{\Lambda}_c^- e^+ \text{ anything})/\Gamma(\bar{\Lambda}_c^- \text{ anything})$					Γ_{101}/Γ_{99}
VALUE (units 10^{-2})	CL%	DOCUMENT ID	TECN	COMMENT	
$2.5 \pm 1.1 \pm 0.6$		¹ LEES	12	BABR	$e^+e^- \rightarrow \Upsilon(4S)$
¹ Uses the full reconstruction of the recoiling B in a hadronic decay as a tag.					

$\Gamma(\bar{\Lambda}_c^- \ell^+ \text{ anything})/\Gamma(\bar{\Lambda}_c^- \text{ anything})$					Γ_{100}/Γ_{99}
VALUE	CL%	DOCUMENT ID	TECN	COMMENT	
$< 3.5 \times 10^{-2}$	90	¹ LEES	12	BABR	$e^+e^- \rightarrow \Upsilon(4S)$
¹ LEES 12 quotes also the measurement $\Gamma(B \rightarrow \bar{\Lambda}_c^- \ell^+ \text{ anything})/\Gamma(B \rightarrow \bar{\Lambda}_c^- \text{ anything}) = (1.7 \pm 1.0 \pm 0.6) \times 10^{-2}$.					

$\Gamma(\bar{\Lambda}_c^- p \text{ anything})/\Gamma(\Lambda_c^+ / \bar{\Lambda}_c^- \text{ anything})$					Γ_{103}/Γ_{97}
VALUE	CL%	DOCUMENT ID	TECN	COMMENT	
$0.57 \pm 0.05 \pm 0.05$		BONVICINI	98	CLE2	$e^+e^- \rightarrow \Upsilon(4S)$

Meson Particle Listings

B^\pm/B^0 ADMIXTURE

$\Gamma(\bar{A}_c^- p e^+ \nu_e)/\Gamma(\bar{A}_c^- p \text{ anything})$ $\Gamma_{104}/\Gamma_{103}$

VALUE	CL%	DOCUMENT ID	TECN	COMMENT
<0.04	90	¹ BONVICINI 98	CLE2	$e^+e^- \rightarrow \Upsilon(4S)$

¹BONVICINI 98 uses the electron with momentum above 0.6 GeV/c.

$\Gamma(\bar{S}_c^- \text{ anything})/\Gamma_{\text{total}}$ Γ_{105}/Γ

VALUE	EVTS	DOCUMENT ID	TECN	COMMENT
0.0033 ± 0.0017 ± 0.0002	77	¹ PROCARIO 94	CLE2	$e^+e^- \rightarrow \Upsilon(4S)$

¹PROCARIO 94 reports $[\Gamma(B \rightarrow \bar{S}_c^- \text{ anything})/\Gamma_{\text{total}}] \times [B(\Lambda_c^+ \rightarrow p K^- \pi^+)] = 0.00021 \pm 0.00008 \pm 0.00007$ which we divide by our best value $B(\Lambda_c^+ \rightarrow p K^- \pi^+) = (6.28 \pm 0.32) \times 10^{-2}$. Our first error is their experiment's error and our second error is the systematic error from using our best value.

$\Gamma(\bar{S}_c^- \text{ anything})/\Gamma_{\text{total}}$ Γ_{106}/Γ

VALUE	CL%	DOCUMENT ID	TECN	COMMENT
<8 × 10 ⁻³	90	¹ PROCARIO 94	CLE2	$e^+e^- \rightarrow \Upsilon(4S)$

¹PROCARIO 94 reports $[\Gamma(B \rightarrow \bar{S}_c^- \text{ anything})/\Gamma_{\text{total}}] \times [B(\Lambda_c^+ \rightarrow p K^- \pi^+)] < 0.00048$ which we divide by our best value $B(\Lambda_c^+ \rightarrow p K^- \pi^+) = 6.28 \times 10^{-2}$.

$\Gamma(\bar{S}_c^0 \text{ anything})/\Gamma_{\text{total}}$ Γ_{107}/Γ

VALUE	EVTS	DOCUMENT ID	TECN	COMMENT
0.0037 ± 0.0017 ± 0.0002	76	¹ PROCARIO 94	CLE2	$e^+e^- \rightarrow \Upsilon(4S)$

¹PROCARIO 94 reports $[\Gamma(B \rightarrow \bar{S}_c^0 \text{ anything})/\Gamma_{\text{total}}] \times [B(\Lambda_c^+ \rightarrow p K^- \pi^+)] = 0.00023 \pm 0.00008 \pm 0.00007$ which we divide by our best value $B(\Lambda_c^+ \rightarrow p K^- \pi^+) = (6.28 \pm 0.32) \times 10^{-2}$. Our first error is their experiment's error and our second error is the systematic error from using our best value.

$\Gamma(\bar{S}_c^0 N(N = p \text{ or } n))/\Gamma_{\text{total}}$ Γ_{108}/Γ

VALUE	CL%	DOCUMENT ID	TECN	COMMENT
<1.2 × 10 ⁻³	90	¹ PROCARIO 94	CLE2	$e^+e^- \rightarrow \Upsilon(4S)$

¹PROCARIO 94 reports < 0.0017 from a measurement of $[\Gamma(B \rightarrow \bar{S}_c^0 N(N = p \text{ or } n))/\Gamma_{\text{total}}] \times [B(\Lambda_c^+ \rightarrow p K^- \pi^+)]$ assuming $B(\Lambda_c^+ \rightarrow p K^- \pi^+) = 0.043$, which we rescale to our best value $B(\Lambda_c^+ \rightarrow p K^- \pi^+) = 6.28 \times 10^{-2}$.

$\Gamma(\Xi_c^0 \text{ anything}, \Xi_c^0 \rightarrow \Xi^- \pi^+)/\Gamma_{\text{total}}$ Γ_{109}/Γ

VALUE (units 10 ⁻³)	DOCUMENT ID	TECN	COMMENT
0.193 ± 0.030 OUR AVERAGE	Error includes scale factor of 1.1.		
0.211 ± 0.019 ± 0.025	¹ AUBERT,B 05M	BABR	$e^+e^- \rightarrow \Upsilon(4S)$
0.144 ± 0.048 ± 0.021	² BARISH 97	CLE2	$e^+e^- \rightarrow \Upsilon(4S)$

¹The yield is obtained by requiring the momentum $P < 2.15$ GeV/c.
²BARISH 97 find 79 ± 27 Ξ_c^0 events.

$\Gamma(\Xi_c^+, \Xi_c^+ \rightarrow \Xi^- \pi^+ \pi^+)/\Gamma_{\text{total}}$ Γ_{110}/Γ

VALUE (units 10 ⁻³)	DOCUMENT ID	TECN	COMMENT
0.453 ± 0.096 ± 0.095 ± 0.065	¹ BARISH 97	CLE2	$e^+e^- \rightarrow \Upsilon(4S)$

¹BARISH 97 find 125 ± 28 Ξ_c^+ events.

$\Gamma(p/\bar{p} \text{ anything})/\Gamma_{\text{total}}$ Γ_{111}/Γ

Includes p and \bar{p} from Λ and $\bar{\Lambda}$ decay.

VALUE	EVTS	DOCUMENT ID	TECN	COMMENT
0.080 ± 0.004 OUR AVERAGE				
0.080 ± 0.005 ± 0.005		ALBRECHT 93i	ARG	$e^+e^- \rightarrow \Upsilon(4S)$
0.080 ± 0.005 ± 0.003		CRAWFORD 92	CLEO	$e^+e^- \rightarrow \Upsilon(4S)$
0.082 ± 0.005 ± 0.013 ± 0.010	2163	¹ ALBRECHT 89k	ARG	$e^+e^- \rightarrow \Upsilon(4S)$

• • • We do not use the following data for averages, fits, limits, etc. • • •

>0.021		² ALAM 83B	CLEO	$e^+e^- \rightarrow \Upsilon(4S)$
--------	--	-----------------------	------	-----------------------------------

¹ALBRECHT 89k include direct and nondirect protons.
²ALAM 83B reported their result as $> 0.036 \pm 0.006 \pm 0.009$. Data are consistent with equal yields of p and \bar{p} . Using assumed yields below cut, $B(B \rightarrow p + X) = 0.03$ not including protons from Λ decays.

$\Gamma(p/\bar{p} \text{ (direct) anything})/\Gamma_{\text{total}}$ Γ_{112}/Γ

VALUE	EVTS	DOCUMENT ID	TECN	COMMENT
0.055 ± 0.005 OUR AVERAGE				
0.055 ± 0.005 ± 0.0035		ALBRECHT 93i	ARG	$e^+e^- \rightarrow \Upsilon(4S)$
0.056 ± 0.006 ± 0.005		CRAWFORD 92	CLEO	$e^+e^- \rightarrow \Upsilon(4S)$
0.055 ± 0.016	1220	¹ ALBRECHT 89k	ARG	$e^+e^- \rightarrow \Upsilon(4S)$

¹ALBRECHT 89k subtract contribution of Λ decay from the inclusive proton yield.

$\Gamma(\bar{p} e^+ \nu_e \text{ anything})/\Gamma_{\text{total}}$ Γ_{113}/Γ

VALUE	CL%	DOCUMENT ID	TECN	COMMENT
< 5.9 × 10 ⁻⁴	90	¹ ADAM 03B	CLE2	$e^+e^- \rightarrow \Upsilon(4S)$

• • • We do not use the following data for averages, fits, limits, etc. • • •

<16 × 10 ⁻⁴	90	ALBRECHT 90H	ARG	$e^+e^- \rightarrow \Upsilon(4S)$
------------------------	----	--------------	-----	-----------------------------------

¹Based on $V-A$ model.

$\Gamma(\Lambda/\bar{\Lambda} \text{ anything})/\Gamma_{\text{total}}$ Γ_{114}/Γ

VALUE	EVTS	DOCUMENT ID	TECN	COMMENT
0.040 ± 0.005 OUR AVERAGE				
0.038 ± 0.004 ± 0.006	2998	CRAWFORD 92	CLEO	$e^+e^- \rightarrow \Upsilon(4S)$
0.042 ± 0.005 ± 0.006	943	ALBRECHT 89k	ARG	$e^+e^- \rightarrow \Upsilon(4S)$

• • • We do not use the following data for averages, fits, limits, etc. • • •

0.022 ± 0.003 ± 0.0022		¹ ACKERSTAFF 97N	OPAL	$e^+e^- \rightarrow Z$
>0.011		² ALAM 83B	CLEO	$e^+e^- \rightarrow \Upsilon(4S)$

¹ACKERSTAFF 97N assumes $B(b \rightarrow B) = 0.868 \pm 0.041$, i.e., an admixture of B^0, B^\pm , and B_s .
²ALAM 83B reported their result as $> 0.022 \pm 0.007 \pm 0.004$. Values are for $(B(\Lambda X) + B(\bar{\Lambda} X))/2$. Data are consistent with equal yields of p and \bar{p} . Using assumed yields below cut, $B(B \rightarrow \Lambda X) = 0.03$.

$\Gamma(\Lambda \text{ anything})/\Gamma(\bar{\Lambda} \text{ anything})$ $\Gamma_{115}/\Gamma_{116}$

VALUE	DOCUMENT ID	TECN	COMMENT
0.43 ± 0.09 ± 0.07	¹ AMMAR 97	CLE2	$e^+e^- \rightarrow \Upsilon(4S)$

¹AMMAR 97 uses a high-momentum lepton tag ($P_\ell > 1.4$ GeV/c²).

$\Gamma(\Xi^-/\Xi^+ \text{ anything})/\Gamma_{\text{total}}$ Γ_{117}/Γ

VALUE	EVTS	DOCUMENT ID	TECN	COMMENT
0.0027 ± 0.0006 OUR AVERAGE				
0.0027 ± 0.0005 ± 0.0004	147	CRAWFORD 92	CLEO	$e^+e^- \rightarrow \Upsilon(4S)$
0.0028 ± 0.0014	54	ALBRECHT 89k	ARG	$e^+e^- \rightarrow \Upsilon(4S)$

$\Gamma(\text{baryons anything})/\Gamma_{\text{total}}$ Γ_{118}/Γ

VALUE	DOCUMENT ID	TECN	COMMENT
0.068 ± 0.005 ± 0.003	¹ ALBRECHT 92o	ARG	$e^+e^- \rightarrow \Upsilon(4S)$

• • • We do not use the following data for averages, fits, limits, etc. • • •

0.076 ± 0.014	² ALBRECHT 89k	ARG	$e^+e^- \rightarrow \Upsilon(4S)$
---------------	---------------------------	-----	-----------------------------------

¹ALBRECHT 92o result is from simultaneous analysis of p and Λ yields, $p\bar{p}$ and $\Lambda\bar{\Lambda}$ correlations, and various lepton-baryon and lepton-baryon-antibaryon correlations. Supersedes ALBRECHT 89k.
²ALBRECHT 89k obtain this result by adding their measurements (5.5 ± 1.6)% for direct protons and (4.2 ± 0.5 ± 0.6)% for inclusive Λ production. They then assume (5.5 ± 1.6)% for neutron production and add it in also. Since each B decay has two baryons, they divide by 2 to obtain (7.6 ± 1.4)%.

$\Gamma(p\bar{p} \text{ anything})/\Gamma_{\text{total}}$ Γ_{119}/Γ

Includes p and \bar{p} from Λ and $\bar{\Lambda}$ decay.

VALUE	EVTS	DOCUMENT ID	TECN	COMMENT
0.0247 ± 0.0023 OUR AVERAGE				
0.024 ± 0.001 ± 0.004		CRAWFORD 92	CLEO	$e^+e^- \rightarrow \Upsilon(4S)$
0.025 ± 0.002 ± 0.002	918	ALBRECHT 89k	ARG	$e^+e^- \rightarrow \Upsilon(4S)$

$\Gamma(p\bar{p} \text{ anything})/\Gamma(p/\bar{p} \text{ anything})$ $\Gamma_{119}/\Gamma_{111}$

Includes p and \bar{p} from Λ and $\bar{\Lambda}$ decay.

VALUE	DOCUMENT ID	TECN	COMMENT
0.30 ± 0.02 ± 0.05	¹ CRAWFORD 92	CLEO	$e^+e^- \rightarrow \Upsilon(4S)$

• • • We do not use the following data for averages, fits, limits, etc. • • •

¹CRAWFORD 92 value is not independent of their $\Gamma(p\bar{p} \text{ anything})/\Gamma_{\text{total}}$ value.

$\Gamma(\Lambda\bar{\Lambda}/\bar{\Lambda} p \text{ anything})/\Gamma_{\text{total}}$ Γ_{120}/Γ

Includes p and \bar{p} from Λ and $\bar{\Lambda}$ decay.

VALUE	EVTS	DOCUMENT ID	TECN	COMMENT
0.025 ± 0.004 OUR AVERAGE				
0.029 ± 0.005 ± 0.005		CRAWFORD 92	CLEO	$e^+e^- \rightarrow \Upsilon(4S)$
0.023 ± 0.004 ± 0.003	165	ALBRECHT 89k	ARG	$e^+e^- \rightarrow \Upsilon(4S)$

$\Gamma(\Lambda\bar{\Lambda}/\bar{\Lambda} p \text{ anything})/\Gamma(\Lambda/\bar{\Lambda} \text{ anything})$ $\Gamma_{120}/\Gamma_{114}$

Includes p and \bar{p} from Λ and $\bar{\Lambda}$ decay.

VALUE	DOCUMENT ID	TECN	COMMENT
0.76 ± 0.11 ± 0.08	¹ CRAWFORD 92	CLEO	$e^+e^- \rightarrow \Upsilon(4S)$

• • • We do not use the following data for averages, fits, limits, etc. • • •

¹CRAWFORD 92 value is not independent of their $[\Gamma(\Lambda\bar{p} \text{ anything}) + \Gamma(\bar{\Lambda} p \text{ anything})]/\Gamma_{\text{total}}$ value.

$\Gamma(\bar{\Lambda} \text{ anything})/\Gamma_{\text{total}}$ Γ_{121}/Γ

VALUE	CL%	EVTS	DOCUMENT ID	TECN	COMMENT
<0.005	90		CRAWFORD 92	CLEO	$e^+e^- \rightarrow \Upsilon(4S)$

• • • We do not use the following data for averages, fits, limits, etc. • • •

<0.0088	90	12	ALBRECHT 89k	ARG	$e^+e^- \rightarrow \Upsilon(4S)$
---------	----	----	--------------	-----	-----------------------------------

$\Gamma(\bar{\Lambda} \text{ anything})/\Gamma(\Lambda/\bar{\Lambda} \text{ anything})$ $\Gamma_{121}/\Gamma_{114}$

VALUE	CL%	DOCUMENT ID	TECN	COMMENT
<0.13	90	¹ CRAWFORD 92	CLEO	$e^+e^- \rightarrow \Upsilon(4S)$

• • • We do not use the following data for averages, fits, limits, etc. • • •

¹CRAWFORD 92 value is not independent of their $\Gamma(\bar{\Lambda} \text{ anything})/\Gamma_{\text{total}}$ value.

See key on page 1127

Meson Particle Listings
 B^\pm/B^0 ADMIXTURE $\Gamma(s e^+ e^-)/\Gamma_{total}$
Test for $\Delta B = 1$ weak neutral current. Allowed by higher-order electroweak interactions.

VALUE (units 10^{-6})	CL%	DOCUMENT ID	TECN	COMMENT
6.7 ± 1.7 OUR AVERAGE				Error includes scale factor of 2.0.
7.69 ^{+0.82+0.71} _{-0.77-0.60}		¹ LEES	14D	BABR $e^+ e^- \rightarrow \Upsilon(4S)$
4.04 ± 1.30 ^{+0.87} _{-0.83}		² IWASAKI	05	BELL $e^+ e^- \rightarrow \Upsilon(4S)$

• • • We do not use the following data for averages, fits, limits, etc. • • •

6.0 ± 1.7 ± 1.3		² AUBERT,B	04I	BABR Repl. by LEES 14D
5.0 ± 2.3 ^{+1.3} _{-1.1}		² KANEKO	03	BELL Repl. by IWASAKI 05
< 57	90	GLENN	98	CLEO $e^+ e^- \rightarrow \Upsilon(4S)$
< 50000	90	BEBEK	81	CLEO $e^+ e^- \rightarrow \Upsilon(4S)$

¹ Measured from sum of exclusive modes through K^+ , $K^+\pi^0$, $K^+\pi^-$, $K^+\pi^-\pi^0$, $K^+\pi^-\pi^+$, K_S^0 , $K_S^0\pi^0$, $K_S^0\pi^+$, $K_S^0\pi^+\pi^0$, and $K_S^0\pi^+\pi^-$ corrected for unobserved modes.
² Requires $M_{\ell^+\ell^-} > 0.2 \text{ GeV}/c^2$.

 $\Gamma(s \mu^+ \mu^-)/\Gamma_{total}$
Test for $\Delta B = 1$ weak neutral current. Allowed by higher-order electroweak interactions.

VALUE (units 10^{-6})	CL%	DOCUMENT ID	TECN	COMMENT
4.3 ± 1.0 OUR AVERAGE				
4.41 ^{+1.31+0.63} _{-1.17-0.50}		¹ LEES	14D	BABR $e^+ e^- \rightarrow \Upsilon(4S)$
4.13 ± 1.05 ^{+0.85} _{-0.81}		² IWASAKI	05	BELL $e^+ e^- \rightarrow \Upsilon(4S)$

• • • We do not use the following data for averages, fits, limits, etc. • • •

5.0 ± 2.8 ± 1.2		AUBERT,B	04I	BABR Repl. by LEES 14D
7.9 ± 2.1 ^{+2.1} _{-1.5}		KANEKO	03	BELL Repl. by IWASAKI 05
< 58	90	GLENN	98	CLEO $e^+ e^- \rightarrow \Upsilon(4S)$
< 17000	90	CHADWICK	81	CLEO $e^+ e^- \rightarrow \Upsilon(4S)$

¹ Measured from sum of exclusive modes through K^+ , $K^+\pi^0$, $K^+\pi^-$, $K^+\pi^-\pi^0$, $K^+\pi^-\pi^+$, K_S^0 , $K_S^0\pi^0$, $K_S^0\pi^+$, $K_S^0\pi^+\pi^0$, and $K_S^0\pi^+\pi^-$ corrected for unobserved modes.
² Requires $M_{\ell^+\ell^-} > 0.2 \text{ GeV}/c^2$.

 $[\Gamma(s e^+ e^-) + \Gamma(s \mu^+ \mu^-)]/\Gamma_{total}$
Test for $\Delta B = 1$ weak neutral current. Allowed by higher-order electroweak interactions.

VALUE	CL%	DOCUMENT ID	TECN	COMMENT
< 4.2 × 10⁻⁵	90	GLENN	98	CLEO $e^+ e^- \rightarrow \Upsilon(4S)$

• • • We do not use the following data for averages, fits, limits, etc. • • •

< 0.0024	90	¹ BEAN	87	CLEO Repl. by GLENN 98
< 0.0062	90	² AVERY	84	CLEO Repl. by BEAN 87

¹ BEAN 87 reports $[(\mu^+\mu^-) + (e^+e^-)]/2$ and we converted it.
² Determine ratio of B^+ to B^0 semileptonic decays to be in the range 0.25–2.9.

 $\Gamma(s \ell^+ \ell^-)/\Gamma_{total}$
Test for $\Delta B = 1$ weak neutral current.

VALUE (units 10^{-6})	CL%	DOCUMENT ID	TECN	COMMENT
5.8 ± 1.3 OUR AVERAGE				Error includes scale factor of 1.8.
6.73 ^{+0.70+0.60} _{-0.64-0.56}		¹ LEES	14D	BABR $e^+ e^- \rightarrow \Upsilon(4S)$
4.11 ± 0.83 ± 0.85 _{-0.81}		² IWASAKI	05	BELL $e^+ e^- \rightarrow \Upsilon(4S)$

• • • We do not use the following data for averages, fits, limits, etc. • • •

5.6 ± 1.5 ± 1.3		³ AUBERT,B	04I	BABR Repl. by LEES 14D
6.1 ± 1.4 ^{+1.4} _{-1.1}		³ KANEKO	03	BELL Repl. by IWASAKI 05

¹ Measured from sum of exclusive modes through K^+ , $K^+\pi^0$, $K^+\pi^-$, $K^+\pi^-\pi^0$, $K^+\pi^-\pi^+$, K_S^0 , $K_S^0\pi^0$, $K_S^0\pi^+$, $K_S^0\pi^+\pi^0$, and $K_S^0\pi^+\pi^-$ corrected for unobserved modes.
² Requires $M_{\ell^+\ell^-} > 0.2 \text{ GeV}/c^2$.
³ Requires $M_{e^+e^-} > 0.2 \text{ GeV}/c^2$.

 $\Gamma(\pi \ell^+ \ell^-)/\Gamma_{total}$
Test for $\Delta B = 1$ weak neutral current.

VALUE	CL%	DOCUMENT ID	TECN	COMMENT
< 5.9 × 10⁻⁸	90	¹ LEES	13M	BABR $e^+ e^- \rightarrow \Upsilon(4S)$

• • • We do not use the following data for averages, fits, limits, etc. • • •

< 6.2 × 10 ⁻⁸	90	¹ WEI	08A	BELL $e^+ e^- \rightarrow \Upsilon(4S)$
< 9.1 × 10 ⁻⁸	90	¹ AUBERT	07AG	BABR $e^+ e^- \rightarrow \Upsilon(4S)$

¹ Assumes equal production of B^+ and B^0 at the $\Upsilon(4S)$.

 $\Gamma(\pi e^+ e^-)/\Gamma_{total}$

VALUE	CL%	DOCUMENT ID	TECN	COMMENT
< 11.0 × 10⁻⁸	90	¹ LEES	13M	BABR $e^+ e^- \rightarrow \Upsilon(4S)$

¹ Assumes equal production of B^+ and B^0 at the $\Upsilon(4S)$.

 $\Gamma(\pi \mu^+ \mu^-)/\Gamma_{total}$

VALUE	CL%	DOCUMENT ID	TECN	COMMENT
< 5.0 × 10⁻⁸	90	¹ LEES	13M	BABR $e^+ e^- \rightarrow \Upsilon(4S)$

¹ Assumes equal production of B^+ and B^0 at the $\Upsilon(4S)$.

 $\Gamma(K e^+ e^-)/\Gamma_{total}$
Test for $\Delta B = 1$ weak neutral current. Allowed by higher-order electroweak interactions.

VALUE (units 10^{-7})	CL%	DOCUMENT ID	TECN	COMMENT
4.4 ± 0.6 OUR AVERAGE				
3.9 ^{+0.9} _{-0.8} ± 0.2		¹ AUBERT	09T	BABR $e^+ e^- \rightarrow \Upsilon(4S)$
4.8 ^{+0.8} _{-0.7} ± 0.3		¹ WEI	09A	BELL $e^+ e^- \rightarrow \Upsilon(4S)$

• • • We do not use the following data for averages, fits, limits, etc. • • •

3.3 ^{+0.9} _{-0.8} ± 0.2		¹ AUBERT,B	06J	BABR Repl. by AUBERT 09T
7.4 ^{+1.8} _{-1.6} ± 0.5		¹ AUBERT	03U	BABR Repl. by AUBERT,B 06J
4.8 ^{+1.5} _{-1.3} ± 0.3		^{1,2} ISHIKAWA	03	BELL Repl. by WEI 09A
< 13	90	ABE	02	BELL Repl. by ISHIKAWA 03

¹ Assumes equal production of B^+ and B^0 at the $\Upsilon(4S)$.

² The second error is a total of systematic uncertainties including model dependence.

 $\Gamma(K^*(892) e^+ e^-)/\Gamma_{total}$
Test for $\Delta B = 1$ weak neutral current. Allowed by higher-order electroweak interactions.

VALUE (units 10^{-7})	CL%	DOCUMENT ID	TECN	COMMENT
11.9 ± 2.0 OUR AVERAGE				Error includes scale factor of 1.2.
9.9 ^{+2.3} _{-2.1} ± 0.6		¹ AUBERT	09T	BABR $e^+ e^- \rightarrow \Upsilon(4S)$
13.9 ^{+2.3} _{-2.0} ± 1.2		¹ WEI	09A	BELL $e^+ e^- \rightarrow \Upsilon(4S)$

• • • We do not use the following data for averages, fits, limits, etc. • • •

9.7 ^{+3.0} _{-2.7} ± 1.4		¹ AUBERT,B	06J	BABR Repl. by AUBERT 09T
9.8 ^{+5.0} _{-4.2} ± 1.1		¹ AUBERT	03U	BABR Repl. by AUBERT,B 06J
14.9 ^{+5.2+1.2} _{-4.6-1.3}		² ISHIKAWA	03	BELL Repl. by WEI 09A
< 56	90	ABE	02	BELL Repl. by ISHIKAWA 03

¹ Assumes equal production of B^+ and B^0 at the $\Upsilon(4S)$.

² Assumes equal production of B^0 and B^+ at $\Upsilon(4S)$. The second error is a total of systematic uncertainties including model dependence.

 $\Gamma(K \mu^+ \mu^-)/\Gamma_{total}$
Test for $\Delta B = 1$ weak neutral current. Allowed by higher-order electroweak interactions.

VALUE (units 10^{-7})	CL%	DOCUMENT ID	TECN	COMMENT
4.4 ± 0.4 OUR AVERAGE				
4.2 ± 0.4 ± 0.2		AALTONEN	11AI	CDF $p\bar{p}$ at 1.96 TeV
4.1 ^{+1.3} _{-1.2} ± 0.2		¹ AUBERT	09T	BABR $e^+ e^- \rightarrow \Upsilon(4S)$
5.0 ± 0.6 ± 0.3		¹ WEI	09A	BELL $e^+ e^- \rightarrow \Upsilon(4S)$

• • • We do not use the following data for averages, fits, limits, etc. • • •

3.5 ^{+1.3} _{-1.1} ± 0.3		¹ AUBERT,B	06J	BABR Repl. by AUBERT 09T
4.5 ^{+2.3} _{-1.9} ± 0.4		¹ AUBERT	03U	BABR Repl. by AUBERT,B 06J
4.8 ^{+1.2} _{-1.1} ± 0.4		^{1,2} ISHIKAWA	03	BELL Repl. by WEI 09A
9.9 ^{+4.0+1.3} _{-3.2-1.0}		ABE	02	BELL Repl. by ISHIKAWA 03

¹ Assumes equal production of B^+ and B^0 at the $\Upsilon(4S)$.

² The second error is a total of systematic uncertainties including model dependence.

 $\Gamma(K \mu^+ \mu^-)/\Gamma(K e^+ e^-)$

VALUE	CL%	DOCUMENT ID	TECN	COMMENT
1.01^{+0.19}_{-0.16} OUR AVERAGE				
1.03 ^{+0.28} _{-0.24} ± 0.01		¹ CHOUDHURY	21	BELL $e^+ e^- \rightarrow \Upsilon(4S)$
1.00 ^{+0.31} _{-0.25} ± 0.07		² LEES	12S	BABR $e^+ e^- \rightarrow \Upsilon(4S)$
0.96 ^{+0.44} _{-0.34} ± 0.05		AUBERT	09T	BABR $e^+ e^- \rightarrow \Upsilon(4S)$

• • • We do not use the following data for averages, fits, limits, etc. • • •

1.03 ± 0.19 ± 0.06		³ WEI	09A	BELL $e^+ e^- \rightarrow \Upsilon(4S)$
1.06 ± 0.48 ± 0.08		AUBERT,B	06J	BABR Repl. by AUBERT 09T

¹ For $1.0 < q^2 < 6.0 \text{ GeV}^2/c^4$. Measurements in other q^2 bins are also reported.

² Measured in the union of $0.10 < q^2 < 8.12 \text{ GeV}^2/c^4$ and $q^2 > 10.11 \text{ GeV}^2/c^4$. LEES 12S reports also individual measurements $\Gamma(B \rightarrow K \mu^+ \mu^-)/\Gamma(B \rightarrow K e^+ e^-) = 0.74^{+0.40}_{-0.31} \pm 0.06$ for $0.10 < q^2 < 8.12 \text{ GeV}^2/c^4$ and $\Gamma(B \rightarrow K \mu^+ \mu^-)/\Gamma(B \rightarrow K e^+ e^-) = 1.43^{+0.65}_{-0.44} \pm 0.12$ for $q^2 > 10.11 \text{ GeV}^2/c^4$.

³ Superseded by CHOUDHURY 21.

 $\Gamma(K^*(892) \mu^+ \mu^-)/\Gamma_{total}$
Test for $\Delta B = 1$ weak neutral current. Allowed by higher-order electroweak interactions.

VALUE (units 10^{-7})	CL%	DOCUMENT ID	TECN	COMMENT
10.6 ± 0.9 OUR AVERAGE				
10.1 ± 1.0 ± 0.5		AALTONEN	11AI	CDF $p\bar{p}$ at 1.96 TeV
13.5 ^{+3.5} _{-3.3} ± 1.0		¹ AUBERT	09T	BABR $e^+ e^- \rightarrow \Upsilon(4S)$
11.0 ^{+1.6} _{-1.4} ± 0.8		¹ WEI	09A	BELL $e^+ e^- \rightarrow \Upsilon(4S)$

Meson Particle Listings

 B^\pm/B^0 ADMIXTURE

••• We do not use the following data for averages, fits, limits, etc. •••

VALUE	CL%	DOCUMENT ID	TECN	COMMENT
$8.8^{+3.5}_{-3.0} \pm 1.2$		¹ AUBERT,B 06j BABR		Repl. by AUBERT 09T
$12.7^{+7.6}_{-6.1} \pm 1.6$		¹ AUBERT 03u BABR		Repl. by AUBERT,B 06j
$11.7^{+3.6}_{-3.1} \pm 1.0$		² ISHIKAWA 03 BELL		Repl. by WEI 09A
<31	90	ABE 02 BELL		Repl. by ISHIKAWA 03

¹ Assumes equal production of B^+ and B^0 at the $\Upsilon(4S)$.

² Assumes equal production of B^0 and B^+ at $\Upsilon(4S)$. The second error is a total of systematic uncertainties including model dependence.

$\Gamma(K^*(892)\mu^+\mu^-)/\Gamma(K^*(892)e^+e^-)$ $\Gamma_{131}/\Gamma_{129}$

VALUE	CL%	DOCUMENT ID	TECN	COMMENT
0.98 ± 0.15 OUR AVERAGE				
$1.13^{+0.34}_{-0.26} \pm 0.10$		¹ LEES 12s BABR		$e^+e^- \rightarrow \Upsilon(4S)$
$1.37^{+0.53}_{-0.40} \pm 0.09$		AUBERT 09T BABR		$e^+e^- \rightarrow \Upsilon(4S)$
$0.83 \pm 0.17 \pm 0.08$		WEI 09A BELL		$e^+e^- \rightarrow \Upsilon(4S)$

••• We do not use the following data for averages, fits, limits, etc. •••

$0.91 \pm 0.45 \pm 0.06$		AUBERT,B 06j BABR		Repl. by AUBERT 09T
--------------------------	--	-------------------	--	---------------------

¹ Measured in the union of $0.10 < q^2 < 8.12 \text{ GeV}^2/c^4$ and $q^2 > 10.11 \text{ GeV}^2/c^4$. LEES 12s reports also individual measurements $\Gamma(B \rightarrow K^*(892)\mu^+\mu^-)/\Gamma(B \rightarrow K^*(892)e^+e^-) = 1.06^{+0.48}_{-0.33} \pm 0.08$ for $0.10 < q^2 < 8.12 \text{ GeV}^2/c^4$ and $\Gamma(B \rightarrow K^*(892)\mu^+\mu^-)/\Gamma(B \rightarrow K^*(892)e^+e^-) = 1.18^{+0.55}_{-0.37} \pm 0.11$ for $q^2 > 10.11 \text{ GeV}^2/c^4$.

$\Gamma(K\ell^+\ell^-)/\Gamma_{\text{total}}$ Γ_{132}/Γ

Test for $\Delta B = 1$ weak neutral current. Allowed by higher-order electroweak interactions.

VALUE (units 10^{-7})	CL%	DOCUMENT ID	TECN	COMMENT
4.8 ± 0.4 OUR AVERAGE				
$4.7 \pm 0.6 \pm 0.2$		LEES 12s BABR		$e^+e^- \rightarrow \Upsilon(4S)$
$4.8^{+0.5}_{-0.4} \pm 0.3$		WEI 09A BELL		$e^+e^- \rightarrow \Upsilon(4S)$

••• We do not use the following data for averages, fits, limits, etc. •••

$3.9 \pm 0.7 \pm 0.2$		¹ AUBERT 09T BABR		Repl. by LEES 12s
$3.4 \pm 0.7 \pm 0.2$		¹ AUBERT,B 06j BABR		Repl. by AUBERT 09T
$6.5^{+1.4}_{-1.3} \pm 0.4$		² AUBERT 03u BABR		Repl. by AUBERT,B 06j
$4.8^{+1.0}_{-0.9} \pm 0.3$		³ ISHIKAWA 03 BELL		Repl. by WEI 09A
$7.5^{+2.5}_{-2.1} \pm 0.6$		⁴ ABE 02 BELL		Repl. by ISHIKAWA 03
< 5.1	90	¹ AUBERT 02L BABR		$e^+e^- \rightarrow \Upsilon(4S)$
< 17	90	⁵ ANDERSON 01B CLE2		$e^+e^- \rightarrow \Upsilon(4S)$

¹ Assumes equal production of B^+ and B^0 at the $\Upsilon(4S)$.

² Assumes all four $B \rightarrow K\ell^+\ell^-$ modes having equal partial widths in the fit.

³ Assumes equal production rate for charge and neutral B meson pairs, isospin invariance, lepton universality for $B \rightarrow K\ell^+\ell^-$, and $B(B \rightarrow K^*(892)\mu^+\mu^-) = 1.33$. The second error is total systematic uncertainties including model dependence.

⁴ Assumes lepton universality.

⁵ The result is for di-lepton masses above 0.5 GeV.

$\Gamma(K^*(892)\ell^+\ell^-)/\Gamma_{\text{total}}$ Γ_{133}/Γ

Test for $\Delta B = 1$ weak neutral current. Allowed by higher-order electroweak interactions.

VALUE (units 10^{-7})	CL%	DOCUMENT ID	TECN	COMMENT
10.5 ± 1.0 OUR AVERAGE				
$10.2^{+1.4}_{-1.3} \pm 0.5$		LEES 12s BABR		$e^+e^- \rightarrow \Upsilon(4S)$
$10.7^{+1.1}_{-1.0} \pm 0.9$		WEI 09A BELL		$e^+e^- \rightarrow \Upsilon(4S)$

••• We do not use the following data for averages, fits, limits, etc. •••

$11.1^{+1.9}_{-1.8} \pm 0.7$		¹ AUBERT 09T BABR		Repl. by LEES 12s
$7.8^{+1.9}_{-1.7} \pm 1.1$		¹ AUBERT,B 06j BABR		Repl. by AUBERT 09T
$8.8^{+3.3}_{-2.9} \pm 1.0$		² AUBERT 03u BABR		Repl. by AUBERT,B 06j
$11.5^{+2.6}_{-2.4} \pm 0.8$		³ ISHIKAWA 03 BELL		Repl. by WEI 09A
< 31	90	^{1,4} AUBERT 02L BABR		Repl. by AUBERT 03u
< 33	90	⁵ ANDERSON 01B CLE2		$e^+e^- \rightarrow \Upsilon(4S)$

¹ Assumes equal production of B^+ and B^0 at the $\Upsilon(4S)$.

² Assumes the partial width ratio of electron and muon modes to be $\Gamma(B \rightarrow K^*(892)e^+e^-)/\Gamma(B \rightarrow K^*(892)\mu^+\mu^-) = 1.33$.

³ Assumes equal production rate for charge and neutral B meson pairs, isospin invariance, lepton universality for $B \rightarrow K\ell^+\ell^-$, and $B(B \rightarrow K^*(892)\mu^+\mu^-) = 1.33$. The second error is total systematic uncertainties including model dependence.

⁴ For averaging $K^*(892)\mu^+\mu^-$ and $K^*(892)e^+e^-$ modes, AUBERT 02L assumed $B(B \rightarrow K^*(892)e^+e^-)/B(B \rightarrow K^*(892)\mu^+\mu^-) = 1.2$.

⁵ The result is for di-lepton masses above 0.5 GeV.

$\Gamma(K\nu\bar{\nu})/\Gamma_{\text{total}}$ Γ_{134}/Γ

Test for $\Delta B = 1$ weak neutral current.

VALUE	CL%	DOCUMENT ID	TECN	COMMENT
< 1.6 × 10⁻⁵				
	90	¹ GRYGIER 17 BELL		$e^+e^- \rightarrow \Upsilon(4S)$

••• We do not use the following data for averages, fits, limits, etc. •••

< 1.7 × 10 ⁻⁵	90	^{1,2} LEES 13i BABR		$e^+e^- \rightarrow \Upsilon(4S)$
< 1.4 × 10 ⁻⁵	90	¹ DEL-AMO-SA...10Q BABR		Repl. by LEES 13i

¹ Assumes equal production of B^+ and B^0 at the $\Upsilon(4S)$.

² Also reported a limit < 3.2 × 10⁻⁵ at 90% CL obtained using a fully reconstructed hadronic B -tag events.

$\Gamma(K^*\nu\bar{\nu})/\Gamma_{\text{total}}$ Γ_{135}/Γ

Test for $\Delta B = 1$ weak neutral current.

VALUE	CL%	DOCUMENT ID	TECN	COMMENT
< 2.7 × 10⁻⁵				
	90	¹ GRYGIER 17 BELL		$e^+e^- \rightarrow \Upsilon(4S)$

••• We do not use the following data for averages, fits, limits, etc. •••

< 7.6 × 10 ⁻⁵	90	^{1,2} LEES 13i BABR		$e^+e^- \rightarrow \Upsilon(4S)$
< 8 × 10 ⁻⁵	90	AUBERT 08Bc BABR		Repl. by LEES 13i

¹ Assumes equal production of B^+ and B^0 at the $\Upsilon(4S)$.

² Also reported a limit < 7.9 × 10⁻⁵ at 90% CL obtained using a fully reconstructed hadronic B -tag events.

$\Gamma(\pi\nu\bar{\nu})/\Gamma_{\text{total}}$ Γ_{136}/Γ

VALUE	CL%	DOCUMENT ID	TECN	COMMENT
< 0.8 × 10⁻⁵				
	90	¹ GRYGIER 17 BELL		$e^+e^- \rightarrow \Upsilon(4S)$

¹ Assumes equal production of B^+ and B^0 at the $\Upsilon(4S)$.

$\Gamma(\rho\nu\bar{\nu})/\Gamma_{\text{total}}$ Γ_{137}/Γ

VALUE	CL%	DOCUMENT ID	TECN	COMMENT
< 2.8 × 10⁻⁵				
	90	¹ GRYGIER 17 BELL		$e^+e^- \rightarrow \Upsilon(4S)$

¹ Assumes equal production of B^+ and B^0 at the $\Upsilon(4S)$.

$\Gamma(s e^\pm \mu^\mp)/\Gamma_{\text{total}}$ Γ_{138}/Γ

Test for lepton family number conservation. Allowed by higher-order electroweak interactions.

VALUE	CL%	DOCUMENT ID	TECN	COMMENT
< 2.2 × 10⁻⁵				
	90	GLENN 98 CLEO		$e^+e^- \rightarrow \Upsilon(4S)$

$\Gamma(\pi e^\pm \mu^\mp)/\Gamma_{\text{total}}$ Γ_{139}/Γ

Test for lepton family number conservation.

VALUE	CL%	DOCUMENT ID	TECN	COMMENT
< 9.2 × 10⁻⁸				
	90	¹ AUBERT 07Ag BABR		$e^+e^- \rightarrow \Upsilon(4S)$

••• We do not use the following data for averages, fits, limits, etc. •••

< 1.6 × 10 ⁻⁶	90	¹ EDWARDS 02B CLE2		$e^+e^- \rightarrow \Upsilon(4S)$
--------------------------	----	-------------------------------	--	-----------------------------------

¹ Assumes equal production of B^+ and B^0 at the $\Upsilon(4S)$.

$\Gamma(\rho e^\pm \mu^\mp)/\Gamma_{\text{total}}$ Γ_{140}/Γ

Test for lepton family number conservation.

VALUE	CL%	DOCUMENT ID	TECN	COMMENT
< 3.2 × 10⁻⁶				
	90	¹ EDWARDS 02B CLE2		$e^+e^- \rightarrow \Upsilon(4S)$

¹ Assumes equal production of B^+ and B^0 at the $\Upsilon(4S)$.

$\Gamma(K e^\pm \mu^\mp)/\Gamma_{\text{total}}$ Γ_{141}/Γ

Test for lepton family number conservation.

VALUE (units 10^{-7})	CL%	DOCUMENT ID	TECN	COMMENT
< 0.38				
	90	¹ AUBERT,B 06j BABR		$e^+e^- \rightarrow \Upsilon(4S)$

••• We do not use the following data for averages, fits, limits, etc. •••

< 16	90	¹ EDWARDS 02B CLE2		$e^+e^- \rightarrow \Upsilon(4S)$
------	----	-------------------------------	--	-----------------------------------

¹ Assumes equal production of B^+ and B^0 at the $\Upsilon(4S)$.

$\Gamma(K^*(892) e^\pm \mu^\mp)/\Gamma_{\text{total}}$ Γ_{142}/Γ

Test for lepton family number conservation.

VALUE (units 10^{-7})	CL%	DOCUMENT ID	TECN	COMMENT
< 5.1				
	90	¹ AUBERT,B 06j BABR		$e^+e^- \rightarrow \Upsilon(4S)$

••• We do not use the following data for averages, fits, limits, etc. •••

< 62	90	¹ EDWARDS 02B CLE2		$e^+e^- \rightarrow \Upsilon(4S)$
------	----	-------------------------------	--	-----------------------------------

¹ Assumes equal production of B^+ and B^0 at the $\Upsilon(4S)$.

CP VIOLATION

A_{CP} is defined as

$$\frac{B(\bar{B} \rightarrow \bar{\tau}) - B(B \rightarrow \tau)}{B(\bar{B} \rightarrow \bar{\tau}) + B(B \rightarrow \tau)}$$

the CP -violation charge asymmetry of inclusive B^\pm and B^0 decay.

$A_{CP}(B \rightarrow K^*(892)\gamma)$

VALUE	CL%	DOCUMENT ID	TECN	COMMENT
-0.003 ± 0.011 OUR AVERAGE				
-0.004 ± 0.014 ± 0.003		¹ HORIGUCHI 17 BELL		$e^+e^- \rightarrow \Upsilon(4S)$
-0.003 ± 0.017 ± 0.007		² AUBERT 09A BABR		$e^+e^- \rightarrow \Upsilon(4S)$
0.08 ± 0.13 ± 0.03		³ COAN 00 CLE2		$e^+e^- \rightarrow \Upsilon(4S)$

Meson Particle Listings

B^\pm/B^0 ADMIXTURE

- We do not use the following data for averages, fits, limits, etc. •••
 - $-0.013 \pm 0.036 \pm 0.010$ ⁴ AUBERT,BE 04A BABR Repl. by AUBERT 09A0
 - $-0.015 \pm 0.044 \pm 0.012$ ³ NAKAO 04 BELL Repl. by Horiguchi 17
 - $-0.044 \pm 0.076 \pm 0.012$ ⁵ AUBERT 02c BABR Repl. by AUBERT, BE 04A
- ¹ Uses $B(\Upsilon(4S) \rightarrow B^+B^-) = (51.4 \pm 0.6)\%$ and $B(\Upsilon(4S) \rightarrow B^0\bar{B}^0) = (48.6 \pm 0.6)\%$.
- ² Corresponds to a 90% CL interval $-0.033 < A_{CP} < 0.028$.
- ³ Assumes equal production of B^+ and B^0 at the $\Upsilon(4S)$.
- ⁴ Corresponds to a 90% CL allowed region, $-0.074 < A_{CP} < 0.049$.
- ⁵ A 90% CL range is $-0.170 < A_{CP} < 0.082$.

$A_{CP}(B \rightarrow s\gamma)$

VALUE	DOCUMENT ID	TECN	COMMENT
0.015 ± 0.011 OUR AVERAGE			
$0.0144 \pm 0.0128 \pm 0.0011$	¹ WATANUKI 19 BELL		$e^+e^- \rightarrow \Upsilon(4S)$
$0.017 \pm 0.019 \pm 0.010$	² LEES 14k BABR		$e^+e^- \rightarrow \Upsilon(4S)$

- We do not use the following data for averages, fits, limits, etc. •••
- $-0.011 \pm 0.030 \pm 0.014$ ³ AUBERT 08BJ BABR Repl. by LEES 14k
- $0.025 \pm 0.050 \pm 0.015$ ⁴ AUBERT,B 04E BABR Repl. by AUBERT 08BJ
- $0.002 \pm 0.050 \pm 0.030$ ⁵ NISHIDA 04 BELL Repl. by WATANUKI 19

¹ Using a sum-of-exclusive technique with $m_{X_S} < 2.8$ GeV/c².

² Measured with 16 exclusively reconstructed $B \rightarrow X_S\gamma$ decays with $0.6 < m_{X_S} < 2.0$ GeV/c² (ten charged and six neutral self-tagging B modes).

³ Uses a sum of exclusively reconstructed $B \rightarrow X_S$ decay modes, with X_S mass between 0.6 and 2.8 GeV/c².

⁴ Corresponds to $-0.06 < A_{CP} < 0.11$ at 90% CL.

⁵ This measurement is performed inclusively for recoil mass X_S less than 2.1 GeV, which corresponds to $-0.093 < A_{CP} < 0.096$ at 90% CL.

$A_{CP}(B \rightarrow (s+d)\gamma)$

VALUE	DOCUMENT ID	TECN	COMMENT
0.010 ± 0.031 OUR AVERAGE			
$0.022 \pm 0.039 \pm 0.009$	¹ PESANTEZ 15 BELL		$e^+e^- \rightarrow \Upsilon(4S)$
$0.057 \pm 0.060 \pm 0.018$	LEES 12v BABR		$e^+e^- \rightarrow \Upsilon(4S)$
$-0.10 \pm 0.18 \pm 0.05$	² AUBERT 080 BABR		$e^+e^- \rightarrow \Upsilon(4S)$
$-0.110 \pm 0.115 \pm 0.017$	AUBERT, BE 06b BABR		$e^+e^- \rightarrow \Upsilon(4S)$
$-0.079 \pm 0.108 \pm 0.022$	³ COAN 01 CLE2		$e^+e^- \rightarrow \Upsilon(4S)$

¹ Assumes equal production of B^+ and B^0 at the $\Upsilon(4S)$. Uses an opposite side lepton tag. Requires center-of-mass frame $E_\gamma > 2.1$ GeV.

² Uses a fully reconstructed B meson as a tag on the recoil side. Requires $E_\gamma > 2.2$ GeV.

³ Corresponds to $-0.27 < A_{CP} < 0.10$ at 90% CL.

$A_{CP}(B \rightarrow X_S \ell^+ \ell^-)$

VALUE	DOCUMENT ID	TECN	COMMENT
$0.04 \pm 0.11 \pm 0.01$	¹ LEES 14d BABR		$e^+e^- \rightarrow \Upsilon(4S)$

- We do not use the following data for averages, fits, limits, etc. •••
- $-0.22 \pm 0.26 \pm 0.02$ ² AUBERT,B 04i BABR Repl. by LEES 14d

¹ Measured from sum of exclusive modes through K^+ , $K^+\pi^0$, $K^+\pi^-$, $K^+\pi^-\pi^0$, $K^+\pi^-\pi^+$, $K_S^0\pi^+$, and $K_S^0\pi^+\pi^0$.

² The final state flavor is determined by the kaon and pion charges where modes with $X_S = K_S^0$, $K_S^0\pi^0$ or $K_S^0\pi^+\pi^-$ are not used.

$A_{CP}(B \rightarrow X_S \ell^+ \ell^-) (1.0 < q^2 < 6.0 \text{ GeV}^2/c^4)$

VALUE	DOCUMENT ID	TECN	COMMENT
$-0.06 \pm 0.22 \pm 0.01$	¹ LEES 14d BABR		$e^+e^- \rightarrow \Upsilon(4S)$

¹ Measured from sum of exclusive modes through K^+ , $K^+\pi^0$, $K^+\pi^-$, $K^+\pi^-\pi^0$, $K^+\pi^-\pi^+$, $K_S^0\pi^+$, and $K_S^0\pi^+\pi^0$.

$A_{CP}(B \rightarrow X_S \ell^+ \ell^-) (10.1 < q^2 < 12.9 \text{ or } q^2 > 14.2 \text{ GeV}^2/c^4)$

VALUE	DOCUMENT ID	TECN	COMMENT
$0.19^{+0.18}_{-0.17} \pm 0.01$	¹ LEES 14d BABR		$e^+e^- \rightarrow \Upsilon(4S)$

¹ Measured from sum of exclusive modes through K^+ , $K^+\pi^0$, $K^+\pi^-$, $K^+\pi^-\pi^0$, $K^+\pi^-\pi^+$, $K_S^0\pi^+$, and $K_S^0\pi^+(\pi^-\pi^0)$.

$A_{CP}(B \rightarrow K^* e^+ e^-)$

VALUE	DOCUMENT ID	TECN	COMMENT
$-0.18 \pm 0.15 \pm 0.01$	WEI 09A BELL		$e^+e^- \rightarrow \Upsilon(4S)$

$A_{CP}(B \rightarrow K^* \mu^+ \mu^-)$

VALUE	DOCUMENT ID	TECN	COMMENT
$-0.03 \pm 0.13 \pm 0.02$	WEI 09A BELL		$e^+e^- \rightarrow \Upsilon(4S)$

$A_{CP}(B \rightarrow K^* \ell^+ \ell^-)$

VALUE	DOCUMENT ID	TECN	COMMENT
-0.04 ± 0.07 OUR AVERAGE			
$0.03 \pm 0.13 \pm 0.01$	¹ LEES 12s BABR		$e^+e^- \rightarrow \Upsilon(4S)$
$+0.01^{+0.16}_{-0.15} \pm 0.01$	AUBERT 09T BABR		$e^+e^- \rightarrow \Upsilon(4S)$
$-0.10 \pm 0.10 \pm 0.01$	WEI 09A BELL		$e^+e^- \rightarrow \Upsilon(4S)$

¹ Measured in the union of $0.10 < q^2 < 8.12 \text{ GeV}^2/c^4$ and $q^2 > 10.11 \text{ GeV}^2/c^4$. LEES 12s reports also individual measurements $A_{CP}(B \rightarrow K^* \ell^+ \ell^-) = -0.13^{+0.18}_{-0.19} \pm 0.01$ for $0.10 < q^2 < 8.12 \text{ GeV}^2/c^4$ and $A_{CP}(B \rightarrow K^* \ell^+ \ell^-) = 0.16^{+0.18}_{-0.19} \pm 0.01$ for $q^2 > 10.11 \text{ GeV}^2/c^4$.

$A_{CP}(B \rightarrow \eta \text{ anything})$

VALUE	DOCUMENT ID	TECN	COMMENT
$-0.13 \pm 0.04^{+0.02}_{-0.03}$	¹ NISHIMURA 10 BELL		$e^+e^- \rightarrow \Upsilon(4S)$

¹ Uses $B \rightarrow \eta X_S$ with $0.4 < m_{X_S} < 2.6 \text{ GeV}/c^2$.

$\Delta A_{CP}(X_S \gamma) = A_{CP}(B^\pm \rightarrow X_S \gamma) - A_{CP}(B^0 \rightarrow X_S \gamma)$

This is the isospin difference of the CP asymmetries.

VALUE	DOCUMENT ID	TECN	COMMENT
0.041 ± 0.023 OUR AVERAGE			
$0.0369 \pm 0.0265 \pm 0.0076$	¹ WATANUKI 19 BELL		$e^+e^- \rightarrow \Upsilon(4S)$
$0.050 \pm 0.039 \pm 0.015$	² LEES 14k BABR		$e^+e^- \rightarrow \Upsilon(4S)$

¹ Using a sum-of-exclusive technique with $m_{X_S} < 2.8 \text{ GeV}/c^2$.

² Measured with 16 exclusively reconstructed $B \rightarrow X_S \gamma$ decays with $0.6 < m_{X_S} < 2.0 \text{ GeV}/c^2$ (ten charged and six neutral self-tagging B modes).

$\bar{A}_{CP}(B \rightarrow X_S \gamma) = (A_{CP}(B^+ \rightarrow X_S \gamma) + A_{CP}(B^0 \rightarrow X_S \gamma))/2$

VALUE	DOCUMENT ID	TECN	COMMENT
$0.0091 \pm 0.0121 \pm 0.0013$	¹ WATANUKI 19 BELL		$e^+e^- \rightarrow \Upsilon(4S)$

¹ Using a sum-of-exclusive technique with $m_{X_S} < 2.8 \text{ GeV}/c^2$.

$\Delta A_{CP}(B \rightarrow K^* \gamma) = A_{CP}(B^+ \rightarrow K^{*0} \gamma) - A_{CP}(B^0 \rightarrow K^{*0} \gamma)$

This is the isospin difference of the CP asymmetries.

VALUE	DOCUMENT ID	TECN	COMMENT
$0.024 \pm 0.028 \pm 0.005$	¹ Horiguchi 17 BELL		$e^+e^- \rightarrow \Upsilon(4S)$

¹ Uses $B(\Upsilon(4S) \rightarrow B^+B^-) = (51.4 \pm 0.6)\%$ and $B(\Upsilon(4S) \rightarrow B^0\bar{B}^0) = (48.6 \pm 0.6)\%$.

$\bar{A}_{CP}(B \rightarrow K^* \gamma) = (A_{CP}(B^+ \rightarrow K^{*0} \gamma) + A_{CP}(B^0 \rightarrow K^{*0} \gamma))/2$

This is the average CP asymmetry.

VALUE	DOCUMENT ID	TECN	COMMENT
$-0.001 \pm 0.014 \pm 0.003$	¹ Horiguchi 17 BELL		$e^+e^- \rightarrow \Upsilon(4S)$

¹ Uses $B(\Upsilon(4S) \rightarrow B^+B^-) = (51.4 \pm 0.6)\%$ and $B(\Upsilon(4S) \rightarrow B^0\bar{B}^0) = (48.6 \pm 0.6)\%$.

POLARIZATION IN B DECAY

In decays involving two vector mesons, one can distinguish among the states in which meson polarizations are both longitudinal (L) or both are transverse and parallel (\parallel) or perpendicular (\perp) to each other with the parameters Γ_L/Γ , Γ_\parallel/Γ , and the relative phases ϕ_\parallel and ϕ_\perp . See the definitions in the note on "Polarization in B Decays" review in the B^0 Particle Listings.

$F_L(B \rightarrow K^* \ell^+ \ell^-) (q^2 > 0.1 \text{ GeV}^2/c^4)$

VALUE	DOCUMENT ID	TECN	COMMENT
$0.63^{+0.18}_{-0.19} \pm 0.05$	¹ AUBERT,B 06j BABR		$e^+e^- \rightarrow \Upsilon(4S)$

¹ Results with different q^2 cuts are also reported.

$F_L(B \rightarrow K^* \ell^+ \ell^-) (m_{\ell\ell} < 2.5 \text{ GeV}/c^2)$

VALUE	DOCUMENT ID	TECN	COMMENT
$0.35 \pm 0.16 \pm 0.04$	AUBERT 09N BABR		$e^+e^- \rightarrow \Upsilon(4S)$

$F_L(B \rightarrow K^* \ell^+ \ell^-) (m_{\ell\ell} > 3.2 \text{ GeV}/c^2)$

VALUE	DOCUMENT ID	TECN	COMMENT
$0.71^{+0.20}_{-0.22} \pm 0.04$	AUBERT 09N BABR		$e^+e^- \rightarrow \Upsilon(4S)$

$F_L(B \rightarrow K^* \ell^+ \ell^-) (0.10 < q^2 < 0.98 \text{ GeV}^2/c^4)$

VALUE	DOCUMENT ID	TECN	COMMENT
$0.263^{+0.045}_{-0.044} \pm 0.017$	AAIJ 16b LHCB		pp at 7, 8 TeV

$F_L(B \rightarrow K^* \ell^+ \ell^-) (1.1 < q^2 < 2.5 \text{ GeV}^2/c^4)$

VALUE	DOCUMENT ID	TECN	COMMENT
$0.660^{+0.083}_{-0.077} \pm 0.022$	AAIJ 16b LHCB		pp at 7, 8 TeV

$F_L(B \rightarrow K^* \ell^+ \ell^-) (0.1 < q^2 < 2.0 \text{ GeV}^2/c^4)$

VALUE	DOCUMENT ID	TECN	COMMENT
$0.34^{+0.08}_{-0.07}$ OUR AVERAGE			

$0.37^{+0.10}_{-0.09} \pm 0.03$	AAIJ 13y LHCB		pp at 7 TeV, $K^{*0} \mu^+ \mu^-$
$0.30 \pm 0.16 \pm 0.02$	AALTONEN 12i CDF		$p\bar{p}$ at 1.96 TeV
$0.29^{+0.21}_{-0.18} \pm 0.02$	WEI 09A BELL		$e^+e^- \rightarrow \Upsilon(4S)$

- We do not use the following data for averages, fits, limits, etc. •••
- $0.60^{+0.00}_{-0.28} \pm 0.19$ ¹ CHATRCHYAN 13BL CMS pp at 7 TeV
- $0.00^{+0.13}_{-0.00} \pm 0.02$ AAIJ 12u LHCB Repl. by AAIJ 13y
- $0.53^{+0.32}_{-0.34} \pm 0.07$ AALTONEN 11L CDF Repl. by AALTONEN 12i

¹ CHATRCHYAN 13BL uses, for this bin, $1.0 < q^2 < 2.0 \text{ GeV}^2/c^4$.

Meson Particle Listings

 B^\pm/B^0 ADMIXTURE $F_L(B \rightarrow K^* \ell^+ \ell^-)$ ($2.0 < q^2 < 4.3 \text{ GeV}^2/c^4$)

VALUE	DOCUMENT ID	TECN	COMMENT
0.77 ± 0.05 OUR AVERAGE			
0.876 ^{+0.109} _{-0.097} ± 0.017	¹ AAIJ 16B	LHCB	pp at 7, 8 TeV
0.80 ± 0.08 ± 0.06	KHACHATRY...16D	CMS	pp at 8 TeV
0.74 ^{+0.10} _{-0.09} ± 0.02	AAIJ 13Y	LHCB	pp at 7 TeV, $K^{*0} \mu^+ \mu^-$
0.65 ± 0.17 ± 0.03	CHATRCHYAN13BL	CMS	pp at 7 TeV
0.37 ^{+0.25} _{-0.24} ± 0.10	AALTONEN 12I	CDF	$p\bar{p}$ at 1.96 TeV
0.71 ± 0.24 ± 0.05	WEI 09A	BELL	$e^+ e^- \rightarrow \Upsilon(4S)$
• • • We do not use the following data for averages, fits, limits, etc. • • •			
0.77 ± 0.15 ± 0.03	AAIJ 12U	LHCB	Repl. by AAIJ 13Y
0.40 ^{+0.32} _{-0.33} ± 0.08	AALTONEN 11L	CDF	Repl. by AALTONEN 12I

¹ Measured in $2.5 < q^2 < 4.0 \text{ GeV}^2/c^4$.

 $F_L(B \rightarrow K^* \ell^+ \ell^-)$ ($4.0 < q^2 < 6.0 \text{ GeV}^2/c^4$)

VALUE	DOCUMENT ID	TECN	COMMENT
0.611 ± 0.052 ± 0.017	AAIJ 16B	LHCB	pp at 7, 8 TeV

 $F_L(B \rightarrow K^* \ell^+ \ell^-)$ ($6.0 < q^2 < 8.0 \text{ GeV}^2/c^4$)

VALUE	DOCUMENT ID	TECN	COMMENT
0.579 ± 0.046 ± 0.015	AAIJ 16B	LHCB	pp at 7, 8 TeV

 $F_L(B \rightarrow K^* \ell^+ \ell^-)$ ($4.3 < q^2 < 8.6 \text{ GeV}^2/c^4$)

VALUE	DOCUMENT ID	TECN	COMMENT
0.64 ± 0.06 OUR AVERAGE			
0.57 ± 0.07 ± 0.03	AAIJ 13Y	LHCB	pp at 7 TeV, $K^{*0} \mu^+ \mu^-$
0.81 ^{+0.13} _{-0.12} ± 0.05	CHATRCHYAN13BL	CMS	pp at 7 TeV
0.68 ^{+0.15} _{-0.17} ± 0.09	AALTONEN 12I	CDF	$p\bar{p}$ at 1.96 TeV
0.64 ^{+0.23} _{-0.24} ± 0.07	WEI 09A	BELL	$e^+ e^- \rightarrow \Upsilon(4S)$
• • • We do not use the following data for averages, fits, limits, etc. • • •			
0.60 ^{+0.06} _{-0.07} ± 0.01	AAIJ 12U	LHCB	Repl. by AAIJ 13Y
0.82 ^{+0.19} _{-0.23} ± 0.07	AALTONEN 11L	CDF	Repl. by AALTONEN 12I

 $F_L(B \rightarrow K^* \ell^+ \ell^-)$ ($10.09 < q^2 < 12.86 \text{ GeV}^2/c^4$)

VALUE	DOCUMENT ID	TECN	COMMENT
0.448 ± 0.033 OUR AVERAGE			
0.493 ^{+0.049} _{-0.047} ± 0.013	¹ AAIJ 16B	LHCB	pp at 7, 8 TeV
0.39 ± 0.05 ± 0.04	KHACHATRY...16D	CMS	pp at 8 TeV
0.48 ^{+0.08} _{-0.09} ± 0.03	AAIJ 13Y	LHCB	pp at 7 TeV, $K^{*0} \mu^+ \mu^-$
0.45 ^{+0.10} _{-0.11} ± 0.04	CHATRCHYAN13BL	CMS	pp at 7 TeV
0.47 ± 0.14 ± 0.03	AALTONEN 12I	CDF	$p\bar{p}$ at 1.96 TeV
0.17 ^{+0.17} _{-0.15} ± 0.03	WEI 09A	BELL	$e^+ e^- \rightarrow \Upsilon(4S)$
• • • We do not use the following data for averages, fits, limits, etc. • • •			
0.41 ± 0.11 ± 0.03	AAIJ 12U	LHCB	Repl. by AAIJ 13Y
0.31 ^{+0.19} _{-0.18} ± 0.02	AALTONEN 11L	CDF	Repl. by AALTONEN 12I

¹ Measured in $11.0 < q^2 < 12.5 \text{ GeV}^2/c^4$.

 $F_L(B \rightarrow K^* \ell^+ \ell^-)$ ($15.0 < q^2 < 17.0 \text{ GeV}^2/c^4$)

VALUE	DOCUMENT ID	TECN	COMMENT
0.349 ± 0.039 ± 0.009	AAIJ 16B	LHCB	pp at 7, 8 TeV

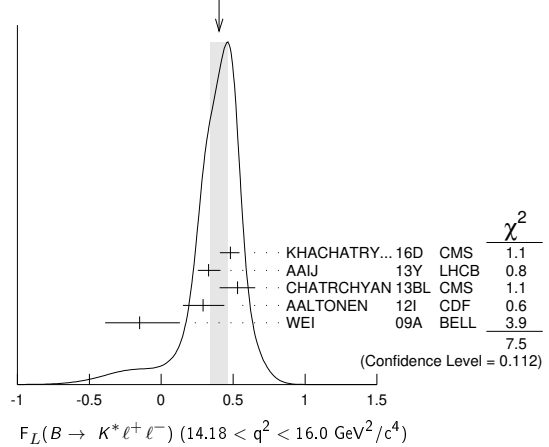
 $F_L(B \rightarrow K^* \ell^+ \ell^-)$ ($17.0 < q^2 < 19.0 \text{ GeV}^2/c^4$)

VALUE	DOCUMENT ID	TECN	COMMENT
0.354 ± 0.049 ± 0.025	AAIJ 16B	LHCB	pp at 7, 8 TeV

 $F_L(B \rightarrow K^* \ell^+ \ell^-)$ ($14.18 < q^2 < 16.0 \text{ GeV}^2/c^4$)

VALUE	DOCUMENT ID	TECN	COMMENT
0.40 ± 0.06 OUR AVERAGE			
0.48 ^{+0.05} _{-0.06} ± 0.04	KHACHATRY...16D	CMS	pp at 8 TeV
0.33 ^{+0.08} _{-0.07} ± 0.02	AAIJ 13Y	LHCB	pp at 7 TeV, $K^{*0} \mu^+ \mu^-$
0.53 ± 0.12 ± 0.03	CHATRCHYAN13BL	CMS	pp at 7 TeV
0.29 ^{+0.14} _{-0.13} ± 0.05	AALTONEN 12I	CDF	$p\bar{p}$ at 1.96 TeV
-0.15 ^{+0.27} _{-0.23} ± 0.07	WEI 09A	BELL	$e^+ e^- \rightarrow \Upsilon(4S)$
• • • We do not use the following data for averages, fits, limits, etc. • • •			
0.37 ± 0.09 ± 0.05	AAIJ 12U	LHCB	Repl. by AAIJ 13Y
0.55 ^{+0.17} _{-0.18} ± 0.02	AALTONEN 11L	CDF	Repl. by AALTONEN 12I

WEIGHTED AVERAGE
0.40 ± 0.06 (Error scaled by 1.4)

 $F_L(B \rightarrow K^* \ell^+ \ell^-)$ ($16.0 < q^2 < 19.0 \text{ GeV}^2/c^4$)

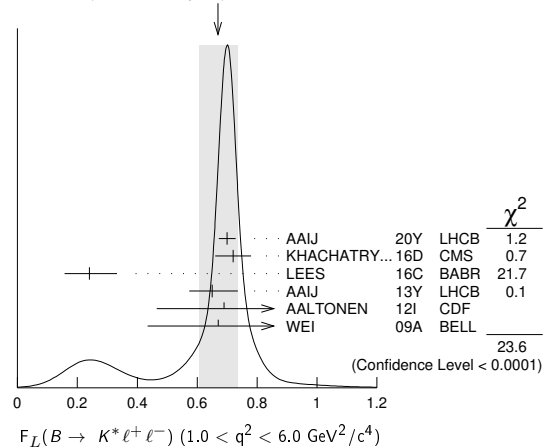
VALUE	DOCUMENT ID	TECN	COMMENT
0.350 ± 0.019 OUR AVERAGE			
0.345 ± 0.020 ± 0.007	¹ AAIJ 20Y	LHCB	pp at 7, 8, 13 TeV
0.38 ^{+0.05} _{-0.06} ± 0.04	KHACHATRY...16D	CMS	pp at 8 TeV
0.38 ± 0.09 ± 0.03	AAIJ 13Y	LHCB	pp at 7 TeV, $K^{*0} \mu^+ \mu^-$
0.44 ± 0.07 ± 0.03	CHATRCHYAN13BL	CMS	pp at 7 TeV
0.20 ± 0.19 ± 0.05	AALTONEN 12I	CDF	$p\bar{p}$ at 1.96 TeV
0.12 ± 0.15 ± 0.02	WEI 09A	BELL	$e^+ e^- \rightarrow \Upsilon(4S)$
• • • We do not use the following data for averages, fits, limits, etc. • • •			
0.344 ^{+0.028} _{-0.030} ± 0.008	¹ AAIJ 16B	LHCB	Repl. by AAIJ 20Y
0.26 ± 0.10 ± 0.03	AAIJ 12U	LHCB	Repl. by AAIJ 13Y
0.09 ± 0.18 ± 0.03	AALTONEN 11L	CDF	Repl. by AALTONEN 12I

¹ Measured in $15.0 < q^2 < 19.0 \text{ GeV}^2/c^4$.

 $F_L(B \rightarrow K^* \ell^+ \ell^-)$ ($1.0 < q^2 < 6.0 \text{ GeV}^2/c^4$)

VALUE	DOCUMENT ID	TECN	COMMENT
0.67 ± 0.07 OUR AVERAGE			
0.700 ± 0.025 ± 0.013	¹ AAIJ 20Y	LHCB	pp at 7, 8, 13 TeV
0.72 ± 0.06	KHACHATRY...16D	CMS	pp at 7, 8 TeV
0.24 ± 0.09 ± 0.02	² LEES 16C	BABR	$e^+ e^- \rightarrow \Upsilon(4S)$
0.65 ± 0.08 ± 0.03	AAIJ 13Y	LHCB	pp at 7 TeV, $K^{*0} \mu^+ \mu^-$
0.69 ± 0.19 ± 0.08	AALTONEN 12I	CDF	$p\bar{p}$ at 1.96 TeV
0.67 ± 0.23 ± 0.05	WEI 09A	BELL	$e^+ e^- \rightarrow \Upsilon(4S)$
• • • We do not use the following data for averages, fits, limits, etc. • • •			
0.690 ^{+0.035} _{-0.036} ± 0.017	¹ AAIJ 16B	LHCB	Repl. by AAIJ 20Y
0.68 ± 0.10 ± 0.02	CHATRCHYAN13BL	CMS	Repl. by KHACHATRYAN 16D
0.55 ± 0.10 ± 0.03	AAIJ 12U	LHCB	Repl. by AAIJ 13Y
0.50 ± 0.27 ± 0.03	AALTONEN 11L	CDF	Repl. by AALTONEN 12I

WEIGHTED AVERAGE
0.67 ± 0.07 (Error scaled by 2.8)



¹ Measured in $1.1 < q^2 < 6.0 \text{ GeV}^2/c^4$.

² Measured by combining B^0 and B^+ with e and μ as leptons. Results are also provided separately for B^0 and B^+ .

$F_L(B \rightarrow K^* \ell^+ \ell^-)$ ($0.0 < q^2 < 4.3 \text{ GeV}^2/c^4$)

VALUE	DOCUMENT ID	TECN	COMMENT
$0.33^{+0.14}_{-0.13} \pm 0.03$	AALTONEN	12I	CDF $p\bar{p}$ at 1.96 TeV
••• We do not use the following data for averages, fits, limits, etc. •••			
$0.47^{+0.23}_{-0.24} \pm 0.03$	AALTONEN	11L	CDF Repl. by AALTONEN 12I

$P_\tau(B \rightarrow D^* \tau^+ \nu_\tau)$

Measures difference in decay widths with positive and negative τ^+ helicities normalized to the sum of those decay widths.

VALUE	DOCUMENT ID	TECN	COMMENT
$-0.38 \pm 0.51^{+0.21}_{-0.16}$	¹ HIROSE	17	BELL $e^+ e^- \rightarrow \Upsilon(4S)$
¹ Uses a fully reconstructed B meson as a tag on the recoil side.			

PARTIAL BRANCHING FRACTIONS IN $B \rightarrow K^{(*)} \ell^+ \ell^-$

$B(B \rightarrow K^* \ell^+ \ell^-)$ ($q^2 < 2.0 \text{ GeV}^2/c^4$)

VALUE (units 10^{-7})	DOCUMENT ID	TECN	COMMENT
1.68 ± 0.23 OUR AVERAGE			
$1.89^{+0.52}_{-0.46} \pm 0.06$	¹ LEES	12s	BABR $e^+ e^- \rightarrow \Upsilon(4S)$
$1.73 \pm 0.33 \pm 0.10$	AALTONEN	11AI	CDF $p\bar{p}$ at 1.96 TeV
$1.46^{+0.40}_{-0.35} \pm 0.11$	WEI	09A	BELL $e^+ e^- \rightarrow \Upsilon(4S)$
••• We do not use the following data for averages, fits, limits, etc. •••			
$0.98 \pm 0.40 \pm 0.09$	AALTONEN	11L	CDF Repl. by AALTONEN 11AI
¹ The value reported here from LEES 12s refers to $0.1 < q^2 < 2.0 \text{ GeV}^2/c^2$.			

$B(B \rightarrow K^* \ell^+ \ell^-)$ ($2.0 < q^2 < 4.3 \text{ GeV}^2/c^4$)

VALUE (units 10^{-7})	DOCUMENT ID	TECN	COMMENT
0.87 ± 0.17 OUR AVERAGE			
$0.95^{+0.35}_{-0.30} \pm 0.04$	LEES	12s	BABR $e^+ e^- \rightarrow \Upsilon(4S)$
$0.82 \pm 0.26 \pm 0.06$	AALTONEN	11AI	CDF $p\bar{p}$ at 1.96 TeV
$0.86^{+0.31}_{-0.27} \pm 0.07$	WEI	09A	BELL $e^+ e^- \rightarrow \Upsilon(4S)$
••• We do not use the following data for averages, fits, limits, etc. •••			
$1.00 \pm 0.38 \pm 0.09$	AALTONEN	11L	CDF Repl. by AALTONEN 11AI

$B(B \rightarrow K^* \ell^+ \ell^-)$ ($4.3 < q^2 < 8.68 \text{ GeV}^2/c^4$)

VALUE (units 10^{-7})	DOCUMENT ID	TECN	COMMENT
1.67 ± 0.29 OUR AVERAGE			
$1.82^{+0.56}_{-0.52} \pm 0.09$	¹ LEES	12s	BABR $e^+ e^- \rightarrow \Upsilon(4S)$
$1.72 \pm 0.41 \pm 0.14$	AALTONEN	11AI	CDF $p\bar{p}$ at 1.96 TeV
$1.37^{+0.47}_{-0.42} \pm 0.39$	WEI	09A	BELL $e^+ e^- \rightarrow \Upsilon(4S)$
••• We do not use the following data for averages, fits, limits, etc. •••			
$1.69 \pm 0.57 \pm 0.15$	AALTONEN	11L	CDF Repl. by AALTONEN 11AI
¹ The value reported here from LEES 12s refers to $4.3 < q^2 < 8.12 \text{ GeV}^2/c^2$.			

$B(B \rightarrow K^* \ell^+ \ell^-)$ ($10.09 < q^2 < 12.86 \text{ GeV}^2/c^4$)

VALUE (units 10^{-7})	DOCUMENT ID	TECN	COMMENT
1.93 ± 0.25 OUR AVERAGE			
$1.86^{+0.52}_{-0.48} \pm 0.10$	¹ LEES	12s	BABR $e^+ e^- \rightarrow \Upsilon(4S)$
$1.77 \pm 0.34 \pm 0.11$	AALTONEN	11AI	CDF $p\bar{p}$ at 1.96 TeV
$2.24^{+0.44}_{-0.40} \pm 0.19$	WEI	09A	BELL $e^+ e^- \rightarrow \Upsilon(4S)$
••• We do not use the following data for averages, fits, limits, etc. •••			
$1.97 \pm 0.47 \pm 0.17$	AALTONEN	11L	CDF Repl. by AALTONEN 11AI
¹ The value reported here from LEES 12s refers to $10.11 < q^2 < 12.89 \text{ GeV}^2/c^2$.			

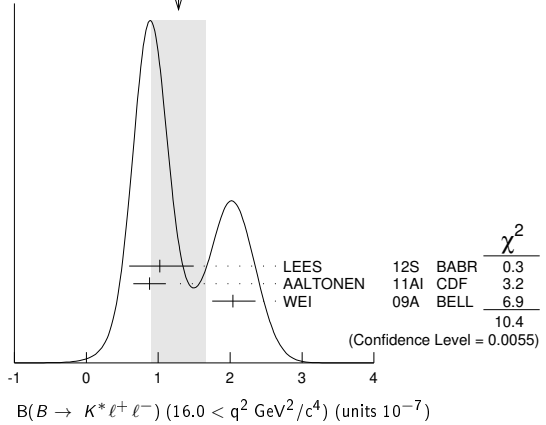
$B(B \rightarrow K^* \ell^+ \ell^-)$ ($14.18 < q^2 < 16.0 \text{ GeV}^2/c^4$)

VALUE (units 10^{-7})	DOCUMENT ID	TECN	COMMENT
1.21 ± 0.17 OUR AVERAGE			
$1.46^{+0.41}_{-0.36} \pm 0.06$	¹ LEES	12s	BABR $e^+ e^- \rightarrow \Upsilon(4S)$
$1.21 \pm 0.24 \pm 0.07$	AALTONEN	11AI	CDF $p\bar{p}$ at 1.96 TeV
$1.05^{+0.29}_{-0.26} \pm 0.08$	WEI	09A	BELL $e^+ e^- \rightarrow \Upsilon(4S)$
••• We do not use the following data for averages, fits, limits, etc. •••			
$1.51 \pm 0.36 \pm 0.13$	AALTONEN	11L	CDF Repl. by AALTONEN 11AI
¹ The value reported here from LEES 12s refers to $14.21 < q^2 < 16.0 \text{ GeV}^2/c^2$.			

$B(B \rightarrow K^* \ell^+ \ell^-)$ ($16.0 < q^2 \text{ GeV}^2/c^4$)

VALUE (units 10^{-7})	DOCUMENT ID	TECN	COMMENT
1.3 ± 0.4 OUR AVERAGE			Error includes scale factor of 2.3. See the ideogram below.
$1.02^{+0.47}_{-0.42} \pm 0.06$	LEES	12s	BABR $e^+ e^- \rightarrow \Upsilon(4S)$
$0.88 \pm 0.22 \pm 0.05$	AALTONEN	11AI	CDF $p\bar{p}$ at 1.96 TeV
$2.04^{+0.27}_{-0.24} \pm 0.16$	WEI	09A	BELL $e^+ e^- \rightarrow \Upsilon(4S)$
••• We do not use the following data for averages, fits, limits, etc. •••			
$1.35 \pm 0.37 \pm 0.12$	AALTONEN	11L	CDF Repl. by AALTONEN 11AI

WEIGHTED AVERAGE
 1.3 ± 0.4 (Error scaled by 2.3)



$B(B \rightarrow K^* \ell^+ \ell^-)$ ($1.0 < q^2 < 6.0 \text{ GeV}^2/c^4$)

VALUE (units 10^{-7})	DOCUMENT ID	TECN	COMMENT
1.64 ± 0.26 OUR AVERAGE			
$2.05^{+0.53}_{-0.48} \pm 0.07$	LEES	12s	BABR $e^+ e^- \rightarrow \Upsilon(4S)$
$1.48 \pm 0.39 \pm 0.12$	AALTONEN	11AI	CDF $p\bar{p}$ at 1.96 TeV
$1.49^{+0.45}_{-0.40} \pm 0.12$	WEI	09A	BELL $e^+ e^- \rightarrow \Upsilon(4S)$
••• We do not use the following data for averages, fits, limits, etc. •••			
$1.60 \pm 0.54 \pm 0.14$	AALTONEN	11L	CDF Repl. by AALTONEN 11AI

$B(B \rightarrow K^* \ell^+ \ell^-)$ ($0.0 < q^2 < 4.3 \text{ GeV}^2/c^4$)

VALUE (units 10^{-7})	DOCUMENT ID	TECN	COMMENT
$2.53 \pm 0.43 \pm 0.15$	AALTONEN	11AI	CDF $p\bar{p}$ at 1.96 TeV
••• We do not use the following data for averages, fits, limits, etc. •••			
$1.98 \pm 0.55 \pm 0.18$	AALTONEN	11L	CDF Repl. by AALTONEN 11AI

$B(B^+ \rightarrow K^* \mu^+ \mu^-) / B(B^+ \rightarrow K^* e^+ e^-)$ ($0.045 < q^2 < 1.1 \text{ GeV}^2/c^4$)

VALUE	DOCUMENT ID	TECN	COMMENT
$0.52^{+0.36}_{-0.26} \pm 0.05$	WEHLE	21	BELL $e^+ e^- \rightarrow \Upsilon(4S)$

$B(B^+ \rightarrow K^* \mu^+ \mu^-) / B(B^+ \rightarrow K^* e^+ e^-)$ ($1.1 < q^2 < 6.0 \text{ GeV}^2/c^4$)

VALUE	DOCUMENT ID	TECN	COMMENT
$0.96^{+0.45}_{-0.29} \pm 0.11$	WEHLE	21	BELL $e^+ e^- \rightarrow \Upsilon(4S)$

$B(B^+ \rightarrow K^* \mu^+ \mu^-) / B(B^+ \rightarrow K^* e^+ e^-)$ ($15.0 < q^2 < 19.0 \text{ GeV}^2/c^4$)

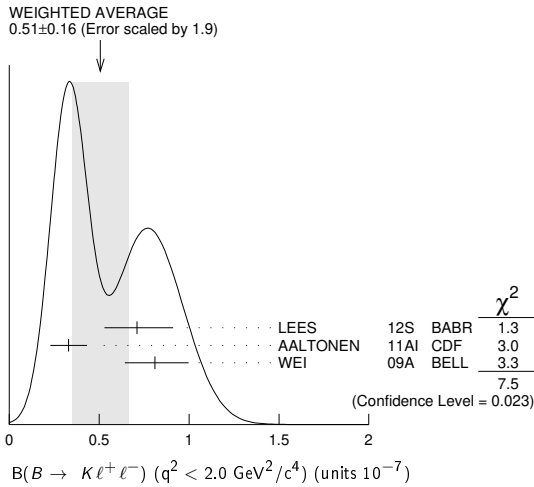
VALUE	DOCUMENT ID	TECN	COMMENT
$1.18^{+0.52}_{-0.32} \pm 0.10$	WEHLE	21	BELL $e^+ e^- \rightarrow \Upsilon(4S)$

$B(B \rightarrow K \ell^+ \ell^-)$ ($q^2 < 2.0 \text{ GeV}^2/c^4$)

VALUE (units 10^{-7})	DOCUMENT ID	TECN	COMMENT
0.51 ± 0.16 OUR AVERAGE			Error includes scale factor of 1.9. See the ideogram below.
$0.71^{+0.20}_{-0.18} \pm 0.02$	¹ LEES	12s	BABR $e^+ e^- \rightarrow \Upsilon(4S)$
$0.33 \pm 0.10 \pm 0.02$	AALTONEN	11AI	CDF $p\bar{p}$ at 1.96 TeV
$0.81^{+0.18}_{-0.16} \pm 0.05$	WEI	09A	BELL $e^+ e^- \rightarrow \Upsilon(4S)$
••• We do not use the following data for averages, fits, limits, etc. •••			
$0.38 \pm 0.16 \pm 0.03$	AALTONEN	11L	CDF Repl. by AALTONEN 11AI
¹ The value reported here from LEES 12s refers to $0.1 < q^2 < 2.0 \text{ GeV}^2/c^2$.			

Meson Particle Listings

B^\pm/B^0 ADMIXTURE



$B(B \rightarrow K \ell^+ \ell^-)$ ($2.0 < q^2 < 4.3 \text{ GeV}^2/c^4$)

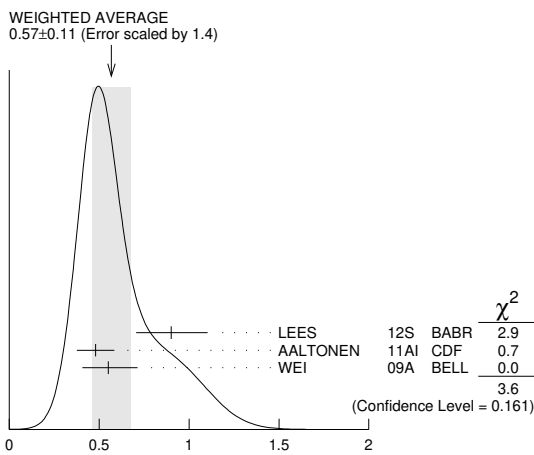
VALUE (units 10^{-7})	DOCUMENT ID	TECN	COMMENT
0.57±0.10 0.09 OUR AVERAGE	Error includes scale factor of 1.2.		
0.49 $^{+0.15}_{-0.13}$ ± 0.01	LEES	12s	BABR $e^+ e^- \rightarrow \Upsilon(4S)$
0.77 ± 0.14 ± 0.05	AALTONEN	11A1	CDF $p\bar{p}$ at 1.96 TeV
0.46 $^{+0.14}_{-0.12}$ ± 0.03	WEI	09A	BELL $e^+ e^- \rightarrow \Upsilon(4S)$
••• We do not use the following data for averages, fits, limits, etc. •••			
0.58 ± 0.19 ± 0.04	AALTONEN	11L	CDF Repl. by AALTONEN 11A1

$B(B \rightarrow K \ell^+ \ell^-)$ ($4.3 < q^2 < 8.68 \text{ GeV}^2/c^4$)

VALUE (units 10^{-7})	DOCUMENT ID	TECN	COMMENT
1.00±0.11 OUR AVERAGE			
0.94 $^{+0.20}_{-0.19}$ ± 0.02	¹ LEES	12s	BABR $e^+ e^- \rightarrow \Upsilon(4S)$
1.05 ± 0.17 ± 0.07	AALTONEN	11A1	CDF $p\bar{p}$ at 1.96 TeV
1.00 $^{+0.19}_{-0.18}$ ± 0.06	WEI	09A	BELL $e^+ e^- \rightarrow \Upsilon(4S)$
••• We do not use the following data for averages, fits, limits, etc. •••			
0.93 ± 0.25 ± 0.06	AALTONEN	11L	CDF Repl. by AALTONEN 11A1
¹ The value reported here from LEES 12s refers to $4.3 < q^2 < 8.12 \text{ GeV}^2/c^2$.			

$B(B \rightarrow K \ell^+ \ell^-)$ ($10.09 < q^2 < 12.86 \text{ GeV}^2/c^4$)

VALUE (units 10^{-7})	DOCUMENT ID	TECN	COMMENT
0.57±0.11 OUR AVERAGE	Error includes scale factor of 1.4. See the ideogram below.		
0.90 $^{+0.20}_{-0.19}$ ± 0.04	¹ LEES	12s	BABR $e^+ e^- \rightarrow \Upsilon(4S)$
0.48 ± 0.10 ± 0.03	AALTONEN	11A1	CDF $p\bar{p}$ at 1.96 TeV
0.55 $^{+0.16}_{-0.14}$ ± 0.03	WEI	09A	BELL $e^+ e^- \rightarrow \Upsilon(4S)$
••• We do not use the following data for averages, fits, limits, etc. •••			
0.72 ± 0.17 ± 0.05	AALTONEN	11L	CDF Repl. by AALTONEN 11A1



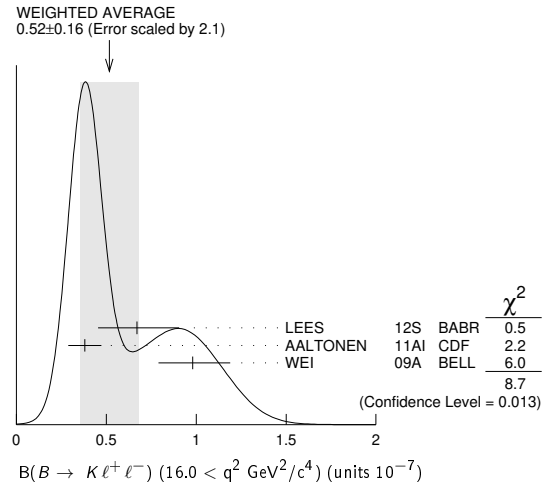
¹ The value reported here from LEES 12s refers to $10.11 < q^2 < 12.89 \text{ GeV}^2/c^2$.

$B(B \rightarrow K \ell^+ \ell^-)$ ($14.18 < q^2 < 16.0 \text{ GeV}^2/c^4$)

VALUE (units 10^{-7})	DOCUMENT ID	TECN	COMMENT
0.49±0.07 OUR AVERAGE			
0.49 $^{+0.15}_{-0.14}$ ± 0.02	¹ LEES	12s	BABR $e^+ e^- \rightarrow \Upsilon(4S)$
0.52 ± 0.09 ± 0.03	AALTONEN	11A1	CDF $p\bar{p}$ at 1.96 TeV
0.38 $^{+0.19}_{-0.12}$ ± 0.02	WEI	09A	BELL $e^+ e^- \rightarrow \Upsilon(4S)$
••• We do not use the following data for averages, fits, limits, etc. •••			
0.38 ± 0.12 ± 0.03	AALTONEN	11L	CDF Repl. by AALTONEN 11A1
¹ The value reported here from LEES 12s refers to $14.21 < q^2 < 16.0 \text{ GeV}^2/c^2$.			

$B(B \rightarrow K \ell^+ \ell^-)$ ($16.0 < q^2 \text{ GeV}^2/c^4$)

VALUE (units 10^{-7})	DOCUMENT ID	TECN	COMMENT
0.52±0.16 OUR AVERAGE	Error includes scale factor of 2.1. See the ideogram below.		
0.67 $^{+0.23}_{-0.21}$ ± 0.05	LEES	12s	BABR $e^+ e^- \rightarrow \Upsilon(4S)$
0.38 ± 0.09 ± 0.02	AALTONEN	11A1	CDF $p\bar{p}$ at 1.96 TeV
0.98 $^{+0.20}_{-0.18}$ ± 0.06	WEI	09A	BELL $e^+ e^- \rightarrow \Upsilon(4S)$
••• We do not use the following data for averages, fits, limits, etc. •••			
0.35 ± 0.13 ± 0.02	AALTONEN	11L	CDF Repl. by AALTONEN 11A1



$B(B \rightarrow K \ell^+ \ell^-)$ ($1.0 < q^2 < 6.0 \text{ GeV}^2/c^4$)

VALUE (units 10^{-7})	DOCUMENT ID	TECN	COMMENT
1.33±0.13 OUR AVERAGE			
1.36 $^{+0.27}_{-0.24}$ ± 0.03	LEES	12s	BABR $e^+ e^- \rightarrow \Upsilon(4S)$
1.29 ± 0.18 ± 0.08	AALTONEN	11A1	CDF $p\bar{p}$ at 1.96 TeV
1.36 $^{+0.23}_{-0.21}$ ± 0.08	WEI	09A	BELL $e^+ e^- \rightarrow \Upsilon(4S)$
••• We do not use the following data for averages, fits, limits, etc. •••			
1.01 ± 0.26 ± 0.07	AALTONEN	11L	CDF Repl. by AALTONEN 11A1

$B(B \rightarrow K \ell^+ \ell^-)$ ($0.0 < q^2 < 4.3 \text{ GeV}^2/c^4$)

VALUE (units 10^{-7})	DOCUMENT ID	TECN	COMMENT
1.07±0.17±0.07	AALTONEN	11A1	CDF $p\bar{p}$ at 1.96 TeV
••• We do not use the following data for averages, fits, limits, etc. •••			
0.96 ± 0.25 ± 0.06	AALTONEN	11L	CDF Repl. by AALTONEN 11A1

$B(B \rightarrow X_s \ell^+ \ell^-)$ ($1.0 < q^2 < 6.0 \text{ GeV}^2/c^4$)

VALUE (units 10^{-6})	DOCUMENT ID	TECN	COMMENT
1.60$^{+0.41}_{-0.39}$ ± 0.25 -0.22	¹ LEES	14D	BABR $e^+ e^- \rightarrow \Upsilon(4S)$
¹ Measured from sum of exclusive modes through K^+ , $K^+\pi^0$, $K^+\pi^-$, $K^+\pi^-\pi^0$, $K^+\pi^-\pi^+$, $K_S^0\pi^0$, $K_S^0\pi^+$, $K_S^0\pi^+\pi^0$, and $K_S^0\pi^+\pi^-$ corrected for unobserved modes.			

$B(B \rightarrow X_s e^+ e^-)$ ($1.0 < q^2 < 6.0 \text{ GeV}^2/c^4$)

VALUE (units 10^{-6})	DOCUMENT ID	TECN	COMMENT
1.93$^{+0.47}_{-0.45}$ ± 0.28 -0.24	¹ LEES	14D	BABR $e^+ e^- \rightarrow \Upsilon(4S)$
¹ Measured from sum of exclusive modes through K^+ , $K^+\pi^0$, $K^+\pi^-$, $K^+\pi^-\pi^0$, $K^+\pi^-\pi^+$, $K_S^0\pi^0$, $K_S^0\pi^+$, $K_S^0\pi^+\pi^0$, and $K_S^0\pi^+\pi^-$ corrected for unobserved modes.			

$B(B \rightarrow X_s \mu^+ \mu^-)$ ($1.0 < q^2 < 6.0 \text{ GeV}^2/c^4$)

VALUE (units 10^{-6})	DOCUMENT ID	TECN	COMMENT
0.66$^{+0.82}_{-0.76}$ ± 0.31 -0.25	¹ LEES	14D	BABR $e^+ e^- \rightarrow \Upsilon(4S)$
¹ Measured from sum of exclusive modes through K^+ , $K^+\pi^0$, $K^+\pi^-$, $K^+\pi^-\pi^0$, $K^+\pi^-\pi^+$, $K_S^0\pi^0$, $K_S^0\pi^+$, $K_S^0\pi^+\pi^0$, and $K_S^0\pi^+\pi^-$ corrected for unobserved modes.			

See key on page 1127

Meson Particle Listings
 B^\pm/B^0 ADMIXTURE

$B(B \rightarrow X_s \ell^+ \ell^-) (14.2 < q^2 \text{ GeV}^2/c^4)$

VALUE (units 10^{-6})	DOCUMENT ID	TECN	COMMENT
$0.57^{+0.16+0.03}_{-0.15-0.02}$	1 LEES	14D	BABR $e^+e^- \rightarrow \Upsilon(4S)$

¹ Measured from sum of exclusive modes through $K^+, K^+\pi^0, K^+\pi^-, K^+\pi^-\pi^0, K^+\pi^-\pi^+, K_S^0, K_S^0\pi^0, K_S^0\pi^+, K_S^0\pi^+\pi^0$, and $K_S^0\pi^+\pi^-$ corrected for unobserved modes.

$B(B \rightarrow X_s e^+ e^-) (14.2 < q^2 \text{ GeV}^2/c^4)$

VALUE (units 10^{-6})	DOCUMENT ID	TECN	COMMENT
$0.56^{+0.19+0.03}_{-0.18-0.03}$	1 LEES	14D	BABR $e^+e^- \rightarrow \Upsilon(4S)$

¹ Measured from sum of exclusive modes through $K^+, K^+\pi^0, K^+\pi^-, K^+\pi^-\pi^0, K^+\pi^-\pi^+, K_S^0, K_S^0\pi^0, K_S^0\pi^+, K_S^0\pi^+\pi^0$, and $K_S^0\pi^+\pi^-$ corrected for unobserved modes.

$B(B \rightarrow X_s \mu^+ \mu^-) (14.2 < q^2 \text{ GeV}^2/c^4)$

VALUE (units 10^{-6})	DOCUMENT ID	TECN	COMMENT
$0.60^{+0.31+0.05}_{-0.29-0.04}$	1 LEES	14D	BABR $e^+e^- \rightarrow \Upsilon(4S)$

¹ Measured from sum of exclusive modes through $K^+, K^+\pi^0, K^+\pi^-, K^+\pi^-\pi^0, K^+\pi^-\pi^+, K_S^0, K_S^0\pi^0, K_S^0\pi^+, K_S^0\pi^+\pi^0$, and $K_S^0\pi^+\pi^-$ corrected for unobserved modes.

LEPTON (HADRON) FORWARD-BACKWARD ASYMMETRY
IN $B \rightarrow K^{(*)} \ell^+ \ell^- (B \rightarrow K/\pi h^+ h^-)$ DECAY

The forward-backward angular asymmetry of the lepton pair in $B \rightarrow K^{(*)} \ell^+ \ell^- (B \rightarrow K/\pi h^+ h^-)$ decay is defined as

$$A_{FB}(s) = \frac{N(\cos\theta > 0) - N(\cos\theta < 0)}{N(\cos\theta > 0) + N(\cos\theta < 0)},$$

where $s=q^2/m_B^2$, and θ is the angle of the $\ell^- (h^-)$ with respect to the flight direction of the B meson, measured in the dilepton (dihadron) rest frame. In addition, the fraction of longitudinal polarization F_L of the K^* and F_S , the relative contribution from scalar and pseudoscalar penguin amplitudes in $B \rightarrow K \ell^+ \ell^-$, can be measured from the angular distribution of its decay products.

$A_{FB}(B \rightarrow K^* \ell^+ \ell^-) (q^2 > 0.1 \text{ GeV}^2/c^4)$

VALUE	CL%	DOCUMENT ID	TECN	COMMENT
$0.50 \pm 0.15 \pm 0.02$		1 ISHIKAWA	06 BELL	$e^+e^- \rightarrow \Upsilon(4S)$

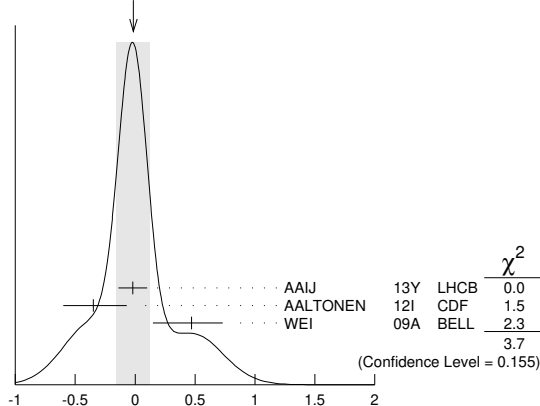
••• We do not use the following data for averages, fits, limits, etc. •••
>0.55 95 2 AUBERT,B 06J BABR $e^+e^- \rightarrow \Upsilon(4S)$
¹ Using an unbinned max. likelihood fits to the M_{bc} distribution in five q^2 bins for $\cos\theta > 0$ and $\cos\theta < 0$.
² Results with different q^2 cuts are also reported.

$A_{FB}(B \rightarrow K^* \ell^+ \ell^-) (0.1 < q^2 < 2.0 \text{ GeV}^2/c^4)$

VALUE	DOCUMENT ID	TECN	COMMENT
-0.01 ± 0.14 OUR AVERAGE	Error includes scale factor of 1.4. See the ideogram below.		
$-0.02 \pm 0.12 \pm 0.01$	AAIJ	13Y LHCb	pp at 7 TeV, $K^{*0} \mu^+ \mu^-$
$-0.35^{+0.26}_{-0.23} \pm 0.10$	AALTONEN	12I CDF	$p\bar{p}$ at 1.96 TeV
$0.47^{+0.26}_{-0.32} \pm 0.03$	WEI	09A BELL	$e^+e^- \rightarrow \Upsilon(4S)$

••• We do not use the following data for averages, fits, limits, etc. •••
 $-0.29^{+0.37}_{-0.00} \pm 0.18$ 1 CHATRCHYAN13BL CMS pp at 7 TeV
 $-0.15 \pm 0.20 \pm 0.06$ AAJJ 12U LHCb Repl. by AAJJ13Y
 $0.13^{+1.65}_{-0.75} \pm 0.25$ AALTONEN 11L CDF Repl. by AALTONEN12I

WEIGHTED AVERAGE
 -0.01 ± 0.14 (Error scaled by 1.4)



$A_{FB}(B \rightarrow K^* \ell^+ \ell^-) (0.1 < q^2 < 2.0 \text{ GeV}^2/c^4)$

¹ CHATRCHYAN 13BL uses, for this bin, $1.0 < q^2 < 2.0 \text{ GeV}^2/c^4$.

$A_{FB}(B \rightarrow K^* \ell^+ \ell^-) (m_{\ell\ell} < 2.5 \text{ GeV}/c^2)$

VALUE	DOCUMENT ID	TECN	COMMENT
$0.24^{+0.18}_{-0.23} \pm 0.05$	AUBERT	09N BABR	$e^+e^- \rightarrow \Upsilon(4S)$

$A_{FB}(B \rightarrow K^* \ell^+ \ell^-) (m_{\ell\ell} > 3.2 \text{ GeV}/c^2)$

VALUE	DOCUMENT ID	TECN	COMMENT
$0.76^{+0.52}_{-0.32} \pm 0.07$	AUBERT	09N BABR	$e^+e^- \rightarrow \Upsilon(4S)$

$A_{FB}(B \rightarrow K^* \ell^+ \ell^-) (0.10 < q^2 < 0.98 \text{ GeV}^2/c^4)$

VALUE	DOCUMENT ID	TECN	COMMENT
$-0.003^{+0.058}_{-0.057} \pm 0.009$	AAIJ	16B LHCb	pp at 7, 8 TeV

$A_{FB}(B \rightarrow K^* \ell^+ \ell^-) (1.1 < q^2 < 2.5 \text{ GeV}^2/c^4)$

VALUE	DOCUMENT ID	TECN	COMMENT
$-0.191^{+0.068}_{-0.080} \pm 0.012$	AAIJ	16B LHCb	pp at 7, 8 TeV

$A_{FB}(B \rightarrow K^* \ell^+ \ell^-) (2.0 < q^2 < 4.3 \text{ GeV}^2/c^4)$

VALUE	DOCUMENT ID	TECN	COMMENT
-0.14 ± 0.05 OUR AVERAGE			
$-0.118^{+0.082}_{-0.090} \pm 0.007$	1 AAJJ	16B LHCb	pp at 7, 8 TeV
$-0.12^{+0.15}_{-0.17} \pm 0.05$	KHACHATRY..16D	CMS	pp at 8 TeV
$-0.20 \pm 0.08 \pm 0.01$	AAIJ	13Y LHCb	pp at 7 TeV, $K^{*0} \mu^+ \mu^-$
$-0.07 \pm 0.20 \pm 0.02$	CHATRCHYAN13BL	CMS	pp at 7 TeV
$0.29^{+0.32}_{-0.35} \pm 0.15$	AALTONEN	12I CDF	$p\bar{p}$ at 1.96 TeV
$0.11^{+0.31}_{-0.36} \pm 0.07$	WEI	09A BELL	$e^+e^- \rightarrow \Upsilon(4S)$
••• We do not use the following data for averages, fits, limits, etc. •••			
$0.05^{+0.16}_{-0.20} \pm 0.04$	AAIJ	12U LHCb	Repl. by AAJJ13Y
$0.19^{+0.40}_{-0.41} \pm 0.14$	AALTONEN	11L CDF	Repl. by AALTONEN12I

¹ Measured in $2.5 < q^2 < 4.0 \text{ GeV}^2/c^4$.

$A_{FB}(B \rightarrow K^* \ell^+ \ell^-) (0.0 < q^2 < 4.3 \text{ GeV}^2/c^4)$

VALUE	DOCUMENT ID	TECN	COMMENT
$-0.08^{+0.21}_{-0.20} \pm 0.05$	AALTONEN	12I CDF	$p\bar{p}$ at 1.96 TeV
••• We do not use the following data for averages, fits, limits, etc. •••			
$0.21^{+0.31}_{-0.33} \pm 0.05$	AALTONEN	11L CDF	Repl. by AALTONEN12I

$A_{FB}(B \rightarrow K^* \ell^+ \ell^-) (4.0 < q^2 < 6.0 \text{ GeV}^2/c^4)$

VALUE	DOCUMENT ID	TECN	COMMENT
$0.025^{+0.051}_{-0.052} \pm 0.004$	AAIJ	16B LHCb	pp at 7, 8 TeV

$A_{FB}(B \rightarrow K^* \ell^+ \ell^-) (6.0 < q^2 < 8.0 \text{ GeV}^2/c^4)$

VALUE	DOCUMENT ID	TECN	COMMENT
$0.152^{+0.041}_{-0.040} \pm 0.008$	AAIJ	16B LHCb	pp at 7, 8 TeV

$A_{FB}(B \rightarrow K^* \ell^+ \ell^-) (1.0 < q^2 < 6.0 \text{ GeV}^2/c^4)$

VALUE	DOCUMENT ID	TECN	COMMENT
-0.078 ± 0.022 OUR AVERAGE	Error includes scale factor of 1.1.		
$-0.073 \pm 0.021 \pm 0.002$	1 AAJJ	20Y LHCb	pp at 7, 8, 13 TeV
-0.12 ± 0.08	KHACHATRY..16D	CMS	pp at 7, 8 TeV
$0.21^{+0.10+0.07}_{-0.15-0.09}$	2 LEES	16c BABR	$e^+e^- \rightarrow \Upsilon(4S)$
$-0.17 \pm 0.06 \pm 0.01$	AAIJ	13Y LHCb	pp at 7 TeV, $K^{*0} \mu^+ \mu^-$
$0.29^{+0.20}_{-0.23} \pm 0.07$	AALTONEN	12I CDF	$p\bar{p}$ at 1.96 TeV
$0.26^{+0.27}_{-0.30} \pm 0.07$	WEI	09A BELL	$e^+e^- \rightarrow \Upsilon(4S)$
••• We do not use the following data for averages, fits, limits, etc. •••			
$-0.075^{+0.032}_{-0.034} \pm 0.007$	1 AAJJ	16B LHCb	Repl. by AAJJ20Y
0.55 ± 0.43	3 SATO	16 BELL	$e^+e^- \rightarrow \Upsilon(4S)$
$-0.07 \pm 0.12 \pm 0.01$	CHATRCHYAN13BL	CMS	Repl. by KHACHATRYAN 16d
$-0.06^{+0.13}_{-0.14} \pm 0.07$	AAIJ	12U LHCb	Repl. by AAJJ13Y
$0.43^{+0.36}_{-0.37} \pm 0.06$	AALTONEN	11L CDF	Repl. by AALTONEN12I

¹ Measured in $1.1 < q^2 < 6.0 \text{ GeV}^2/c^4$.

² Measured by combining B^0 and B^+ with e and μ as leptons. Results are also provided separately for B^0 and B^+ .

³ Uses $K^* \rightarrow K^-\pi^+, K^-\pi^0, K_S^0\pi^-$ in the range $M(K\pi) < 1.1 \text{ GeV}/c^2$. Uncertainty is statistical only.

Meson Particle Listings

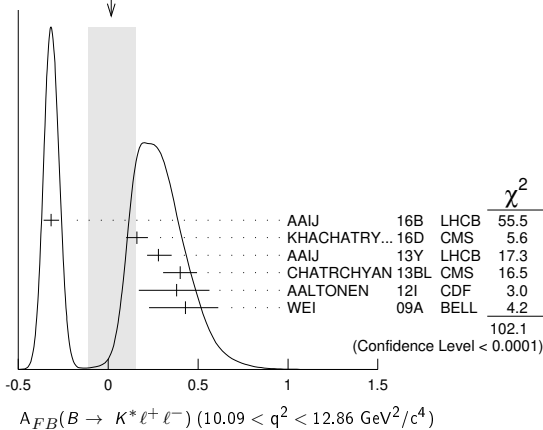
 B^\pm/B^0 ADMIXTURE $A_{FB}(B \rightarrow K^* \ell^+ \ell^-)$ ($4.3 < q^2 < 8.6 \text{ GeV}^2/c^4$)

VALUE	DOCUMENT ID	TECN	COMMENT
$0.13^{+0.06}_{-0.05}$ OUR AVERAGE	Error includes scale factor of 1.1.		
$0.16^{+0.06}_{-0.05} \pm 0.01$	AAIJ	13Y LHCb	pp at 7 TeV, $K^{*0} \mu^+ \mu^-$
$-0.01 \pm 0.11 \pm 0.03$	CHATRCHYAN13BL	CMS	pp at 7 TeV
$0.01 \pm 0.20 \pm 0.09$	AALTONEN	12I CDF	$p\bar{p}$ at 1.96 TeV
$0.45^{+0.15}_{-0.21} \pm 0.15$	WEI	09A BELL	$e^+ e^- \rightarrow \Upsilon(4S)$
• • • We do not use the following data for averages, fits, limits, etc. • • •			
$0.27^{+0.06}_{-0.08} \pm 0.02$	AAIJ	12U LHCb	Repl. by AAIJ 13Y
$-0.06^{+0.30}_{-0.28} \pm 0.05$	AALTONEN	11L CDF	Repl. by AALTONEN 12I

 $A_{FB}(B \rightarrow K^* \ell^+ \ell^-)$ ($10.09 < q^2 < 12.86 \text{ GeV}^2/c^4$)

VALUE	DOCUMENT ID	TECN	COMMENT
0.02 ± 0.13 OUR AVERAGE	Error includes scale factor of 4.5. See the ideogram below.		
$-0.318^{+0.044}_{-0.040} \pm 0.009$	¹ AAIJ	16B LHCb	pp at 7, 8 TeV
$0.16 \pm 0.06 \pm 0.01$	KHACHATRY...16D	CMS	pp at 8 TeV
$0.28 \pm 0.07 \pm 0.02$	AAIJ	13Y LHCb	pp at 7 TeV, $K^{*0} \mu^+ \mu^-$
$0.40 \pm 0.08 \pm 0.05$	CHATRCHYAN13BL	CMS	pp at 7 TeV
$0.38 \pm 0.16 \pm 0.09$	AALTONEN	12I CDF	$p\bar{p}$ at 1.96 TeV
$0.43 \pm 0.18 \pm 0.03$	WEI	09A BELL	$e^+ e^- \rightarrow \Upsilon(4S)$
• • • We do not use the following data for averages, fits, limits, etc. • • •			
$0.27^{+0.11}_{-0.13} \pm 0.02$	AAIJ	12U LHCb	Repl. by AAIJ 13Y
$0.66 \pm 0.23 \pm 0.07$	AALTONEN	11L CDF	Repl. by AALTONEN 12I

WEIGHTED AVERAGE
 0.02 ± 0.13 (Error scaled by 4.5)

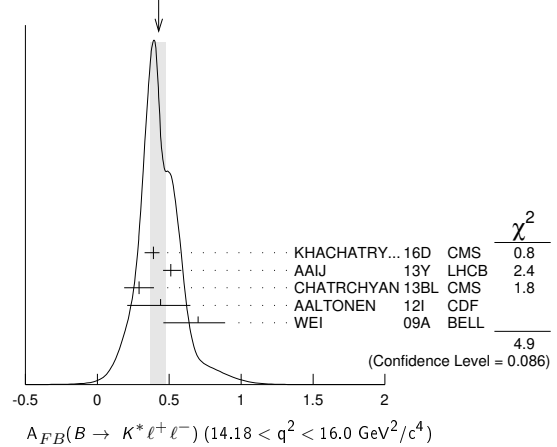


¹ Measured in $11.0 < q^2 < 12.5 \text{ GeV}^2/c^4$.

 $A_{FB}(B \rightarrow K^* \ell^+ \ell^-)$ ($14.18 < q^2 < 16.0 \text{ GeV}^2/c^4$)

VALUE	DOCUMENT ID	TECN	COMMENT
$0.43^{+0.05}_{-0.06}$ OUR AVERAGE	Error includes scale factor of 1.6. See the ideogram below.		
$0.39^{+0.04}_{-0.06} \pm 0.01$	KHACHATRY...16D	CMS	pp at 8 TeV
$0.51^{+0.07}_{-0.05} \pm 0.02$	AAIJ	13Y LHCb	pp at 7 TeV, $K^{*0} \mu^+ \mu^-$
$0.29 \pm 0.09 \pm 0.05$	CHATRCHYAN13BL	CMS	pp at 7 TeV
$0.44^{+0.19}_{-0.21} \pm 0.10$	AALTONEN	12I CDF	$p\bar{p}$ at 1.96 TeV
$0.70^{+0.16}_{-0.22} \pm 0.10$	WEI	09A BELL	$e^+ e^- \rightarrow \Upsilon(4S)$
• • • We do not use the following data for averages, fits, limits, etc. • • •			
$0.47^{+0.06}_{-0.08} \pm 0.03$	AAIJ	12U LHCb	Repl. by AAIJ 13Y
$0.42 \pm 0.16 \pm 0.09$	AALTONEN	11L CDF	Repl. by AALTONEN 12I

WEIGHTED AVERAGE
 $0.43 \pm 0.05 - 0.06$ (Error scaled by 1.6)

 $A_{FB}(B \rightarrow K^* \ell^+ \ell^-)$ ($15.0 < q^2 < 17.0 \text{ GeV}^2/c^4$)

VALUE	DOCUMENT ID	TECN	COMMENT
$0.411^{+0.41}_{-0.037} \pm 0.008$	AAIJ	16B LHCb	pp at 7, 8 TeV

 $A_{FB}(B \rightarrow K^* \ell^+ \ell^-)$ ($17.0 < q^2 < 19.0 \text{ GeV}^2/c^4$)

VALUE	DOCUMENT ID	TECN	COMMENT
$0.305^{+0.049}_{-0.048} \pm 0.013$	AAIJ	16B LHCb	pp at 7, 8 TeV

 $A_{FB}(B \rightarrow K^* \ell^+ \ell^-)$ ($16.0 < q^2 < 19.0 \text{ GeV}^2/c^4$)

VALUE	DOCUMENT ID	TECN	COMMENT
0.362 ± 0.019 OUR AVERAGE			
$0.353 \pm 0.020 \pm 0.010$	¹ AAIJ	20Y LHCb	pp at 7, 8, 13 TeV
$0.35 \pm 0.07 \pm 0.01$	KHACHATRY...16D	CMS	pp at 8 TeV
$0.30 \pm 0.08^{+0.01}_{-0.02}$	AAIJ	13Y LHCb	pp at 7 TeV, $K^{*0} \mu^+ \mu^-$
$0.41 \pm 0.05 \pm 0.03$	CHATRCHYAN13BL	CMS	pp at 7 TeV
$0.65^{+0.17}_{-0.18} \pm 0.16$	AALTONEN	12I CDF	$p\bar{p}$ at 1.96 TeV
$0.66^{+0.11}_{-0.16} \pm 0.04$	WEI	09A BELL	$e^+ e^- \rightarrow \Upsilon(4S)$
• • • We do not use the following data for averages, fits, limits, etc. • • •			
$0.355 \pm 0.027 \pm 0.009$	¹ AAIJ	16B LHCb	Repl. by AAIJ 20Y
$0.16^{+0.11}_{-0.13} \pm 0.06$	AAIJ	12U LHCb	Repl. by AAIJ 13Y
$0.70^{+0.16}_{-0.25} \pm 0.10$	AALTONEN	11L CDF	Repl. by AALTONEN 12I

¹ Measured in $15.0 < q^2 < 19.0 \text{ GeV}^2/c^4$.

 $A_{FB}(B \rightarrow K \ell^+ \ell^-)$ ($q^2 > 0.1 \text{ GeV}^2/c^4$)

VALUE	DOCUMENT ID	TECN	COMMENT
0.11 ± 0.12 OUR AVERAGE			
$0.15^{+0.21}_{-0.23} \pm 0.08$	¹ AUBERT,B	06J BABR	$e^+ e^- \rightarrow \Upsilon(4S)$
$0.10 \pm 0.14 \pm 0.01$	² ISHIKAWA	06 BELL	$e^+ e^- \rightarrow \Upsilon(4S)$
• • • We do not use the following data for averages, fits, limits, etc. • • •			
¹ Results with different q^2 cuts are also reported.			
² Using an unbinned max. likelihood fits to the M_{bc} distribution in five q^2 bins for $\cos \theta > 0$ and $\cos \theta < 0$.			

 $A_{FB}(B \rightarrow K \ell^+ \ell^-)$ ($q^2 < 2.0 \text{ GeV}^2/c^4$)

VALUE	DOCUMENT ID	TECN	COMMENT
$0.00^{+0.06}_{-0.05}$ OUR AVERAGE			
$0.00^{+0.06+0.03}_{-0.05-0.01}$	AAIJ	13H LHCb	pp at 7 TeV
$0.13^{+0.42}_{-0.43} \pm 0.07$	AALTONEN	12I CDF	$p\bar{p}$ at 1.96 TeV
$0.06^{+0.32}_{-0.35} \pm 0.02$	WEI	09A BELL	$e^+ e^- \rightarrow \Upsilon(4S)$
• • • We do not use the following data for averages, fits, limits, etc. • • •			
$-0.15^{+0.46}_{-0.39} \pm 0.08$	AALTONEN	11L CDF	Repl. by AALTONEN 12I

 $A_{FB}(B \rightarrow K \ell^+ \ell^-)$ ($2.0 < q^2 < 4.3 \text{ GeV}^2/c^4$)

VALUE	DOCUMENT ID	TECN	COMMENT
$0.09^{+0.10}_{-0.07}$ OUR AVERAGE	Error includes scale factor of 1.4.		
$0.07^{+0.08+0.02}_{-0.05-0.01}$	AAIJ	13H LHCb	pp at 7 TeV
$0.32^{+0.15}_{-0.16} \pm 0.05$	AALTONEN	12I CDF	$p\bar{p}$ at 1.96 TeV
$-0.43^{+0.38}_{-0.40} \pm 0.09$	WEI	09A BELL	$e^+ e^- \rightarrow \Upsilon(4S)$

See key on page 1127

Meson Particle Listings

B^\pm/B^0 ADMIXTURE

••• We do not use the following data for averages, fits, limits, etc. •••

$0.72^{+0.40}_{-0.35} \pm 0.07$ AALTONEN 11L CDF Repl. by AALTONEN 12i

$A_{FB}(B \rightarrow K\ell^+\ell^-)$ ($0.0 < q^2 < 4.3 \text{ GeV}^2/c^4$)

VALUE	DOCUMENT ID	TECN	COMMENT
$0.31 \pm 0.16 \pm 0.04$	AALTONEN 12i	CDF	$p\bar{p}$ at 1.96 TeV

••• We do not use the following data for averages, fits, limits, etc. •••

$0.36^{+0.24}_{-0.26} \pm 0.06$ AALTONEN 11L CDF Repl. by AALTONEN 12i

$A_{FB}(B \rightarrow K\ell^+\ell^-)$ ($1.0 < q^2 < 6.0 \text{ GeV}^2/c^4$)

VALUE	DOCUMENT ID	TECN	COMMENT
$0.034^{+0.040}_{-0.029}$ OUR AVERAGE			

$0.02^{+0.05}_{-0.03} \pm 0.02$ AAIJ 13H LHCB pp at 7 TeV

$0.13 \pm 0.09 \pm 0.02$ AALTONEN 12i CDF $p\bar{p}$ at 1.96 TeV

$-0.04^{+0.13}_{-0.16} \pm 0.05$ WEI 09A BELL $e^+e^- \rightarrow \Upsilon(4S)$

••• We do not use the following data for averages, fits, limits, etc. •••

0.00 ± 0.13 SATO 16 BELL $e^+e^- \rightarrow \Upsilon(4S)$

$0.08^{+0.27}_{-0.22} \pm 0.07$ AALTONEN 11L CDF Repl. by AALTONEN 12i

¹ Statistical uncertainty only.

$A_{FB}(B \rightarrow K\ell^+\ell^-)$ ($4.3 < q^2 < 8.6 \text{ GeV}^2/c^4$)

VALUE	DOCUMENT ID	TECN	COMMENT
$-0.04^{+0.04}_{-0.05}$ OUR AVERAGE			

$-0.02^{+0.03}_{-0.05} \pm 0.03$ AAIJ 13H LHCB pp at 7 TeV

$0.01^{+0.13}_{-0.10} \pm 0.01$ AALTONEN 12i CDF $p\bar{p}$ at 1.96 TeV

$-0.20^{+0.12}_{-0.14} \pm 0.03$ WEI 09A BELL $e^+e^- \rightarrow \Upsilon(4S)$

••• We do not use the following data for averages, fits, limits, etc. •••

$-0.20^{+0.17}_{-0.28} \pm 0.03$ AALTONEN 11L CDF Repl. by AALTONEN 12i

$A_{FB}(B \rightarrow K\ell^+\ell^-)$ ($10.09 < q^2 < 12.86 \text{ GeV}^2/c^4$)

VALUE	DOCUMENT ID	TECN	COMMENT
-0.05 ± 0.06 OUR AVERAGE			

$-0.03 \pm 0.07 \pm 0.01$ AAIJ 13H LHCB pp at 7 TeV

$-0.03^{+0.11}_{-0.10} \pm 0.04$ AALTONEN 12i CDF $p\bar{p}$ at 1.96 TeV

$-0.21^{+0.17}_{-0.15} \pm 0.06$ WEI 09A BELL $e^+e^- \rightarrow \Upsilon(4S)$

••• We do not use the following data for averages, fits, limits, etc. •••

$-0.10^{+0.17}_{-0.15} \pm 0.07$ AALTONEN 11L CDF Repl. by AALTONEN 12i

$A_{FB}(B \rightarrow K\ell^+\ell^-)$ ($14.18 < q^2 < 16.0 \text{ GeV}^2/c^4$)

VALUE	DOCUMENT ID	TECN	COMMENT
$-0.02^{+0.07}_{-0.05}$ OUR AVERAGE			

$-0.01^{+0.12}_{-0.06} \pm 0.01$ AAIJ 13H LHCB pp at 7 TeV

$-0.05^{+0.09}_{-0.11} \pm 0.03$ AALTONEN 12i CDF $p\bar{p}$ at 1.96 TeV

$0.04^{+0.32}_{-0.26} \pm 0.05$ WEI 09A BELL $e^+e^- \rightarrow \Upsilon(4S)$

••• We do not use the following data for averages, fits, limits, etc. •••

$0.03^{+0.49}_{-0.16} \pm 0.04$ AALTONEN 11L CDF Repl. by AALTONEN 12i

$A_{FB}(B \rightarrow K\ell^+\ell^-)$ ($16.0 < q^2 < 18.0 \text{ GeV}^2/c^4$)

VALUE	DOCUMENT ID	TECN	COMMENT
$-0.09^{+0.07}_{-0.09} \pm 0.02$	AAIJ 13H LHCB		pp at 7 TeV

$A_{FB}(B \rightarrow K\ell^+\ell^-)$ ($18.0 < q^2 < 22.0 \text{ GeV}^2/c^4$)

VALUE	DOCUMENT ID	TECN	COMMENT
$0.02 \pm 0.11 \pm 0.01$	AAIJ 13H LHCB		pp at 7 TeV

$A_{FB}(B \rightarrow K\ell^+\ell^-)$ ($q^2 > 16.0 \text{ GeV}^2/c^4$)

VALUE	DOCUMENT ID	TECN	COMMENT
$0.04^{+0.09}_{-0.07}$ OUR AVERAGE			

$0.09^{+0.17}_{-0.13} \pm 0.03$ AALTONEN 12i CDF $p\bar{p}$ at 1.96 TeV

$0.02^{+0.11}_{-0.08} \pm 0.02$ WEI 09A BELL $e^+e^- \rightarrow \Upsilon(4S)$

••• We do not use the following data for averages, fits, limits, etc. •••

$0.07^{+0.30}_{-0.23} \pm 0.02$ AALTONEN 11L CDF Repl. by AALTONEN 12i

$A_{FB}(B \rightarrow X_s\ell^+\ell^-)$ ($1.0 < q^2 < 6.0 \text{ GeV}^2/c^4$)

VALUE	DOCUMENT ID	TECN	COMMENT
0.74 ± 0.54	SATO 16 BELL		$e^+e^- \rightarrow \Upsilon(4S)$

¹ Uses the sum of 10 exclusive X_s modes in the range $M(X_s) > 1.1 \text{ GeV}/c^2$. Uncertainty is statistical only.

$F_S(B \rightarrow K\ell^+\ell^-)$ ($q^2 > 0.1 \text{ GeV}^2/c^4$)

VALUE	DOCUMENT ID	TECN	COMMENT
$0.81^{+0.58}_{-0.61} \pm 0.46$	AUBERT,B 06j	BABR	$e^+e^- \rightarrow \Upsilon(4S)$

¹ Results with different q^2 cuts are also reported.

$A_{FB}(B \rightarrow K\rho\bar{\rho})$ ($m_{\rho\bar{\rho}} < 2.85 \text{ GeV}/c^2$)

VALUE	DOCUMENT ID	TECN	COMMENT
$0.495 \pm 0.012 \pm 0.007$	AAIJ 14AF LHCB		pp at 7, 8 TeV

¹ Measured in $B^+ \rightarrow K^+\rho\bar{\rho}$ decays.

$A_{FB}(B \rightarrow \pi\rho\bar{\rho})$ ($m_{\rho\bar{\rho}} < 2.85 \text{ GeV}/c^2$)

VALUE	DOCUMENT ID	TECN	COMMENT
$-0.409 \pm 0.033 \pm 0.006$	AAIJ 14AF LHCB		pp at 7, 8 TeV

¹ Measured in $B^+ \rightarrow \pi^+\rho\bar{\rho}$ decays.

ISOSPIN ASYMMETRY

Δ_0_- is defined as

$$\frac{\Gamma(\bar{B}^0 \rightarrow f_d) - \Gamma(B^- \rightarrow f_d)}{\Gamma(\bar{B}^0 \rightarrow f_d) + \Gamma(B^- \rightarrow f_d)}$$

the isospin asymmetry of inclusive neutral and charged B decay.

$\Delta_0_-(B \rightarrow X_s\gamma)$

VALUE	DOCUMENT ID	TECN	COMMENT
-0.005 ± 0.020 OUR AVERAGE			

$-0.0048 \pm 0.0149 \pm 0.0150$ WATANUKI 19 BELL $e^+e^- \rightarrow \Upsilon(4S)$

$-0.006 \pm 0.058 \pm 0.026$ AUBERT,B 05R BABR $e^+e^- \rightarrow \Upsilon(4S)$

¹ Using a sum-of-exclusive technique with $m_{X_s} < 2.8 \text{ GeV}/c^2$.

$\Delta_0_-(B \rightarrow X_{s+d}\gamma)$

VALUE	DOCUMENT ID	TECN	COMMENT
$-0.06 \pm 0.15 \pm 0.07$	AUBERT 08o	BABR	$e^+e^- \rightarrow \Upsilon(4S)$

¹ Uses a fully reconstructed B meson as a tag on the recoil side. The result is for $E_\gamma > 2.2 \text{ GeV}$.

$\Delta_0_+(B \rightarrow K^*(892)\gamma)$

Δ_0_+ describes the isospin asymmetry between $\Gamma(B^0 \rightarrow K^*(892)^0\gamma)$ and $\Gamma(B^+ \rightarrow K^*(892)^+\gamma)$.

VALUE	DOCUMENT ID	TECN	COMMENT
0.063 ± 0.017 OUR AVERAGE			

$0.062 \pm 0.015 \pm 0.013$ HORIGUCHI 17 BELL $e^+e^- \rightarrow \Upsilon(4S)$

$0.066 \pm 0.021 \pm 0.022$ AUBERT 09a0 BABR $e^+e^- \rightarrow \Upsilon(4S)$

••• We do not use the following data for averages, fits, limits, etc. •••

$0.050 \pm 0.045 \pm 0.037$ AUBERT,BE 04A BABR Repl. by AUBERT 09a0

$0.012 \pm 0.044 \pm 0.026$ NAKAO 04 BELL Repl. by HORIGUCHI 17

¹ Uses $B(\Upsilon(4S) \rightarrow B^+B^-) = (51.4 \pm 0.6)\%$ and $B(\Upsilon(4S) \rightarrow B^0\bar{B}^0) = (48.6 \pm 0.6)\%$.

² Uses the production ratio of charged and neutral B from $\Upsilon(4S)$ decays and the lifetime ratio $\tau_{B^+}/\tau_{B^0} = 1.071 \pm 0.009$. The 90% CL interval is $0.017 < \Delta_0_+ < 0.116$.

³ Uses the production ratio of charged and neutral B from $\Upsilon(4S)$ decays $R^{+0} = 1.006 \pm 0.048$ and the lifetime ratio of $\tau_{B^+}/\tau_{B^0} = 1.083 \pm 0.017$. The 90% CL interval is $-0.046 < \Delta_0_+ < 0.146$.

$\Delta_{\rho\gamma} = \Gamma(B^+ \rightarrow \rho^+\gamma) / (2 \cdot \Gamma(B^0 \rightarrow \rho^0\gamma)) - 1$

VALUE	DOCUMENT ID	TECN	COMMENT
-0.46 ± 0.17 OUR AVERAGE			

$-0.43^{+0.25}_{-0.22} \pm 0.10$ AUBERT 08BH BABR $e^+e^- \rightarrow \Upsilon(4S)$

$-0.48^{+0.21}_{-0.19} \pm 0.09$ TANIGUCHI 08 BELL $e^+e^- \rightarrow \Upsilon(4S)$

$\Delta_0_-(B \rightarrow K\ell^+\ell^-)$

VALUE	DOCUMENT ID	TECN	COMMENT
-0.15 ± 0.06 OUR AVERAGE			Error includes scale factor of 1.2.

$-0.31^{+0.13}_{-0.11} \pm 0.01$ CHOUDHURY 21 BELL $e^+e^- \rightarrow \Upsilon(4S)$

$-0.10^{+0.08}_{-0.09} \pm 0.02$ AAIJ 14M LHCB pp at 7, 8 TeV

$-0.09^{+0.08}_{-0.08} \pm 0.02$ AAIJ 14M LHCB pp at 7, 8 TeV

$-0.58^{+0.29}_{-0.37} \pm 0.02$ LEES 12S BABR $e^+e^- \rightarrow \Upsilon(4S)$

••• We do not use the following data for averages, fits, limits, etc. •••

$-0.35^{+0.23}_{-0.27}$ AAIJ 12AH LHCB Repl. by AAIJ 14M

$-1.43^{+0.56}_{-0.85} \pm 0.05$ AUBERT 09T BABR Repl. by LEES 12S

$-0.31^{+0.17}_{-0.14} \pm 0.08$ WEI 09A BELL $e^+e^- \rightarrow \Upsilon(4S)$

¹ For $1.0 < q^2 < 6.0 \text{ GeV}^2/c^4$ using both $\mu^+\mu^-$ and e^+e^- as a lepton pair. Measurements in other q^2 bins are also reported.

² For $1.1 < q^2 < 6.0 \text{ GeV}^2/c^4$ using $\mu^+\mu^-$ as a lepton pair and assuming isospin symmetry for the $B \rightarrow J/\psi(1S)K$. Measurements in other q^2 bins are also reported.

³ For $15.0 < q^2 < 19.0 \text{ GeV}^2/c^4$ using $\mu^+\mu^-$ as a lepton pair and assuming isospin symmetry for the $B \rightarrow J/\psi(1S)K$. Measurements in other q^2 bins are also reported.

⁴ For $0.10 < q^2 < 8.12 \text{ GeV}^2/c^4$. Measurements in other q^2 bins are also reported.

Meson Particle Listings

 B^\pm/B^0 ADMIXTURE⁵ For $1 < q^2 < 6 \text{ GeV}^2/c^4$.⁶ For $0.1 < m_{\ell^+ \ell^-}^2 < 7.02 \text{ GeV}^2/c^4$.⁷ Assumes equal production of B^+ and B^0 at the $\Upsilon(4S)$.⁸ Superseded by CHODHURY 21.⁹ For $q^2 < 8.68 \text{ GeV}^2/c^4$. $\Delta_0(B \rightarrow K^* \ell^+ \ell^-)$

VALUE	DOCUMENT ID	TECN	COMMENT
-0.03 ± 0.08 OUR AVERAGE	Error includes scale factor of 1.2.		
$0.00 \pm 0.12 \pm 0.02$	1 AAIJ	14M LHCB	$p\bar{p}$ at 7, 8 TeV
$0.06 \pm 0.10 \pm 0.02$	2 AAIJ	14M LHCB	$p\bar{p}$ at 7, 8 TeV
$-0.25 \pm 0.20 \pm 0.03$	3 LEES	12s BABR	$e^+ e^- \rightarrow \Upsilon(4S)$
$-0.29 \pm 0.16 \pm 0.09$	4 WEI	09A BELL	$e^+ e^- \rightarrow \Upsilon(4S)$
• • • We do not use the following data for averages, fits, limits, etc. • • •			
-0.15 ± 0.16	5 AAIJ	12AH LHCB	Repl. by AAIJ 14M
$-0.56 \pm 0.17 \pm 0.03$	6,7 AUBERT	09T BABR	Repl. by LEES 12s

¹ For $1.1 < q^2 < 6.0 \text{ GeV}^2/c^4$ using $\mu^+ \mu^-$ as a lepton pair and assuming isospin symmetry for the $B(B \rightarrow J/\psi(1S) K^*(892))$. Measurements in other q^2 bins are also reported.² For $15.0 < q^2 < 22.0 \text{ GeV}^2/c^4$ using $\mu^+ \mu^-$ as a lepton pair and assuming isospin symmetry for the $B(B \rightarrow J/\psi(1S) K^*(892))$. Measurements in other q^2 bins are also reported.³ For $0.10 < q^2 < 8.12 \text{ GeV}^2/c^4$. Measurements in other q^2 bins are also reported.⁴ For $q^2 < 8.68 \text{ GeV}^2/c^4$.⁵ For $1 < q^2 < 6 \text{ GeV}^2/c^4$.⁶ For $0.1 < m_{\ell^+ \ell^-}^2 < 7.02 \text{ GeV}^2/c^4$.⁷ Assumes equal production of B^+ and B^0 at the $\Upsilon(4S)$. $\Delta_0(B \rightarrow K^{(*)} \ell^+ \ell^-)$

VALUE	DOCUMENT ID	TECN	COMMENT
-0.45 ± 0.17 OUR AVERAGE	Error includes scale factor of 1.7.		
$-0.64 \pm 0.15 \pm 0.03$	1,2 AUBERT	09T BABR	$e^+ e^- \rightarrow \Upsilon(4S)$
$-0.30 \pm 0.12 \pm 0.08$	3 WEI	09A BELL	$e^+ e^- \rightarrow \Upsilon(4S)$

¹ For $0.1 < m_{\ell^+ \ell^-}^2 < 7.02 \text{ GeV}^2/c^4$.² Assumes equal production of B^+ and B^0 at the $\Upsilon(4S)$.³ For $q^2 < 8.68 \text{ GeV}^2/c^4$. $B \rightarrow X_c \ell \nu$ HADRONIC MASS MOMENTS $\langle M_X^2 - \overline{M}_D^2 \rangle$ (First Moments)

VALUE (GeV^2)	DOCUMENT ID	TECN	COMMENT
0.36 ± 0.08 OUR AVERAGE	Error includes scale factor of 1.8.		
$0.467 \pm 0.038 \pm 0.068$	1 ACOSTA	05F CDF	$p\bar{p}$ at 1.96 TeV
$0.293 \pm 0.012 \pm 0.058$	2 CSORNA	04 CLE2	$e^+ e^- \rightarrow \Upsilon(4S)$
• • • We do not use the following data for averages, fits, limits, etc. • • •			
$0.251 \pm 0.023 \pm 0.062$	3 CRONIN-HEN..01B	CLE2	$e^+ e^- \rightarrow \Upsilon(4S)$

¹ Moments are measured with a minimum lepton momentum of 0.7 GeV/c in the B rest frame;² Uses minimum lepton energy of 1.5 GeV and also reports moments with $E_\ell > 1.0 \text{ GeV}$.³ The leptons are required to have $E_\ell > 1.5 \text{ GeV}/c$. $\langle M_X^2 \rangle$ (First Moments)

VALUE (GeV^2)	DOCUMENT ID	TECN	COMMENT
4.156 ± 0.029 OUR AVERAGE			
$4.144 \pm 0.028 \pm 0.022$	1 SCHWANDA	07 BELL	$e^+ e^- \rightarrow \Upsilon(4S)$
$4.18 \pm 0.04 \pm 0.03$	1 AUBERT,B	04 BABR	$e^+ e^- \rightarrow \Upsilon(4S)$

¹ The leptons are required to have $E_\ell > 1.5 \text{ GeV}/c$. $\langle (M_X^2 - \overline{M}_X^2)^2 \rangle$ (Second Moments)

VALUE (GeV^4)	DOCUMENT ID	TECN	COMMENT
0.55 ± 0.08 OUR AVERAGE			
$0.515 \pm 0.061 \pm 0.064$	1 SCHWANDA	07 BELL	$e^+ e^- \rightarrow \Upsilon(4S)$
$0.629 \pm 0.031 \pm 0.143$	2 CSORNA	04 CLE2	$e^+ e^- \rightarrow \Upsilon(4S)$
• • • We do not use the following data for averages, fits, limits, etc. • • •			
$1.05 \pm 0.26 \pm 0.13$	3 ACOSTA	05F CDF	$p\bar{p}$ at 1.96 TeV
$0.576 \pm 0.048 \pm 0.168$	1 CRONIN-HEN..01B	CLE2	$e^+ e^- \rightarrow \Upsilon(4S)$

¹ The leptons are required to have $E_\ell > 1.5 \text{ GeV}/c$.² Uses minimum lepton energy of 1.5 GeV and also reports moments with $E_\ell > 1.0 \text{ GeV}$.³ Moments are measured with a minimum lepton momentum of 0.7 GeV/c in the B rest frame; $\langle (M_X^2 - \overline{M}_D^2)^2 \rangle$ (Second Moments)

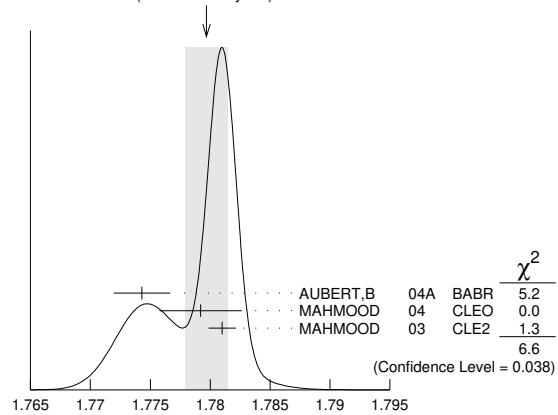
VALUE (GeV^4)	DOCUMENT ID	TECN	COMMENT
$0.639 \pm 0.056 \pm 0.178$	1 CRONIN-HEN..01B	CLE2	$e^+ e^- \rightarrow \Upsilon(4S)$

¹ The leptons are required to have $E_\ell > 1.5 \text{ GeV}/c$. $B \rightarrow X_c \ell \nu$ LEPTON MOMENTUM MOMENTS $R_0 (\Gamma_{E_\ell > 1.7 \text{ GeV}} / \Gamma_{E_\ell > 1.5 \text{ GeV}})$

VALUE	DOCUMENT ID	TECN	COMMENT
$0.6187 \pm 0.0014 \pm 0.0016$	1 MAHMOOD	03 CLE2	$e^+ e^- \rightarrow \Upsilon(4S)$

¹ The leptons are required to have $E_\ell > 1.5 \text{ GeV}$ in the B rest frame. $R_1 (\langle E_\ell \rangle_{E_\ell > 1.5 \text{ GeV}})$

VALUE	DOCUMENT ID	TECN	COMMENT
1.7797 ± 0.0018 OUR AVERAGE	Error includes scale factor of 1.8. See the ideogram below.		
$1.7743 \pm 0.0019 \pm 0.0014$	1 AUBERT,B	04A BABR	$e^+ e^- \rightarrow \Upsilon(4S)$
$1.7792 \pm 0.0021 \pm 0.0027$	2 MAHMOOD	04 CLEO	$e^+ e^- \rightarrow \Upsilon(4S)$
$1.7810 \pm 0.0007 \pm 0.0009$	3 MAHMOOD	03 CLE2	$e^+ e^- \rightarrow \Upsilon(4S)$

WEIGHTED AVERAGE
 1.7797 ± 0.0018 (Error scaled by 1.8) $R_1 (\langle E_\ell \rangle_{E_\ell > 1.5 \text{ GeV}})$ ¹ The leptons are required to have $E_\ell > 1.5 \text{ GeV}$ in the B rest frame. The result with $E_\ell > 0.6 \text{ GeV}$ is also given.² Uses $E_e > 1.5 \text{ GeV}$ and also reports moments with other minimum minimum E_e conditions, as low as $E_e > 0.6 \text{ GeV}$.³ The leptons are required to have $E_\ell > 1.5 \text{ GeV}$ in the B rest frame. $R_2 (\langle E_\ell^2 - \overline{E}_\ell^2 \rangle_{E_\ell > 1.5 \text{ GeV}})$

VALUE (10^{-3} GeV^2)	DOCUMENT ID	TECN	COMMENT
30.8 ± 0.8 OUR AVERAGE			
$30.3 \pm 0.9 \pm 0.5$	1 AUBERT,B	04A BABR	$e^+ e^- \rightarrow \Upsilon(4S)$
$31.6 \pm 0.8 \pm 1.0$	2 MAHMOOD	04 CLEO	$e^+ e^- \rightarrow \Upsilon(4S)$

¹ The leptons are required to have $E_\ell > 1.5 \text{ GeV}$ in the B rest frame. The result with $E_\ell > 0.6 \text{ GeV}$ is also given.² Uses $E_e > 1.5 \text{ GeV}$ and also reports moments with other minimum minimum E_e conditions, as low as $E_e > 0.6 \text{ GeV}$. $R_3 (\langle E_\ell^3 - \overline{E}_\ell^3 \rangle_{E_\ell > 1.5 \text{ GeV}})$

VALUE (10^{-3} GeV^3)	DOCUMENT ID	TECN	COMMENT
$2.12 \pm 0.47 \pm 0.20$	1 AUBERT,B	04A BABR	$e^+ e^- \rightarrow \Upsilon(4S)$

¹ The leptons are required to have $E_\ell > 1.5 \text{ GeV}$ in the B rest frame. The result with $E_\ell > 0.6 \text{ GeV}$ is also given. $B \rightarrow X_s \gamma$ PHOTON ENERGY MOMENTS $\langle E_\gamma \rangle$

VALUE (GeV)	DOCUMENT ID	TECN	COMMENT
2.314 ± 0.011 OUR AVERAGE			
$2.346 \pm 0.018 \pm 0.027$	1,2 LEES	12U BABR	$e^+ e^- \rightarrow \Upsilon(4S)$
$2.304 \pm 0.014 \pm 0.017$	2,3 LEES	12V BABR	$e^+ e^- \rightarrow \Upsilon(4S)$
$2.311 \pm 0.009 \pm 0.015$	3 LIMOSANI	09 BELL	$e^+ e^- \rightarrow \Upsilon(4S)$
$2.289 \pm 0.058 \pm 0.027$	3,4 AUBERT	08B BABR	$e^+ e^- \rightarrow \Upsilon(4S)$
$2.309 \pm 0.023 \pm 0.023$	2,3 SCHWANDA	08 BELL	$e^+ e^- \rightarrow \Upsilon(4S)$
• • • We do not use the following data for averages, fits, limits, etc. • • •			
$2.288 \pm 0.025 \pm 0.023$	3 AUBERT,BE	06B BABR	Repl. by LEES 12V

¹ LEES 12U uses $E_\gamma > 1.897 \text{ GeV}$ to calculate the moments; the moments are used to calculate the HQET parameters $m_b = 4.579 \pm 0.032 \text{ GeV}/c^2$ and $\mu_\pi^2 = 0.257 \pm 0.034 \text{ GeV}^2$ in the shape function model. The same HQET parameters are also determined in the kinetic model.² Results for different E_γ threshold values are also measured.³ The result is for $E_\gamma > 1.9 \text{ GeV}$.⁴ Uses a fully reconstructed B meson as a tag on the recoil side.

See key on page 1127

Meson Particle Listings
B±/B0 ADMIXTURE

⟨Eγ²⟩ - ⟨Eγ⟩²

Table with columns: VALUE (10⁻² GeV²), DOCUMENT ID, TECN, COMMENT. Includes entries for LEES, LIMOSANI, AUBERT, and SCHWANDA.

••• We do not use the following data for averages, fits, limits, etc.
1 LEES 12U uses Eγ > 1.897 GeV to calculate the moments; the moments are used to calculate the HQET parameters mb = 4.579 + 0.032 - 0.029 GeV/c² and μπ² = 0.257 + 0.034 - 0.039 GeV² in the shape function model. The same HQET parameters are also determined in the kinetic model.
2 Results for different Eγ threshold values are also measured.
3 The result is for Eγ > 1.9 GeV.
4 Uses a fully reconstructed B meson as a tag on the recoil side.

B±/B0 ADMIXTURE REFERENCES

Large table of references for B±/B0 admixture, listing authors, document IDs, and technical details.

Large table of references for B±/B0 admixture, listing authors, document IDs, and technical details.

Downloaded from https://academic.oup.com/ptep/article/2022/8/083C01/6651666 by CERN Library user on 11 October 2022

Meson Particle Listings

 B^\pm/B^0 ADMIXTURE, $B^\pm/B^0/B_s^0/b$ -baryon ADMIXTURE

BORTOLETTO	86	PRL 56 800	D. Bortoletto et al.	(CLEO Collab.)
HAAS	86	PRL 56 2781	J. Haas et al.	(CLEO Collab.)
ALBRECHT	85H	PL 162B 395	H. Albrecht et al.	(ARGUS Collab.)
CSORNA	85	PRL 54 1894	S.E. Csorna et al.	(CLEO Collab.)
HAAS	85	PRL 55 1248	J. Haas et al.	(CLEO Collab.)
AVERY	84	PRL 53 1309	P. Avery et al.	(CLEO Collab.)
CHEN	84	PRL 52 1084	A. Chen et al.	(CLEO Collab.)
LEVMAN	84	PL 141B 271	G.M. Levman et al.	(CUSB Collab.)
ALAM	83B	PRL 51 1143	M.S. Alam et al.	(CLEO Collab.)
GREEN	83	PRL 51 347	J. Green et al.	(CLEO Collab.)
KLOPFEN...	83B	PL 130B 444	C. Klopfenstein et al.	(CUSB Collab.)
ALTARELLI	82	NP B208 365	G. Altarelli et al.	(ROMA, INFN, FRAS)
BRODY	82	PRL 48 1070	A.D. Brody et al.	(CLEO Collab.)
GIANNINI	82	NP B206 1	G. Giannini et al.	(CUSB Collab.)
BEBEK	81	PRL 46 84	C. Bebek et al.	(CLEO Collab.)
CHADWICK	81	PRL 46 88	K. Chadwick et al.	(CLEO Collab.)
ABRAMS	80	PRL 44 10	G.S. Abrams et al.	(SLAC, LBL)

 $B^\pm/B^0/B_s^0/b$ -baryon ADMIXTURE $B^\pm/B^0/B_s^0/b$ -baryon ADMIXTURE MEAN LIFE

Each measurement of the B mean life is an average over an admixture of various bottom mesons and baryons which decay weakly. Different techniques emphasize different admixtures of produced particles, which could result in a different B mean life.

"OUR EVALUATION" is an average using rescaled values of the data listed below. The average and rescaling were performed by the Heavy Flavor Averaging Group (HFLAV) and are described at <https://hflav.web.cern.ch/>. This is a weighted average of the lifetimes of the five main b -hadron species (B^+ , B^0 , B_s^0 , B_{sH}^0 , and Λ_b) that assumes the production fractions in Z decays (given at the end of this section) and equal production fractions of B_{sH}^0 and B_{sL}^0 mesons.

VALUE (10^{-12} s)	EVTS	DOCUMENT ID	TECN	COMMENT
1.5672 ± 0.0029 OUR EVALUATION				
• • • We do not use the following data for averages, fits, limits, etc. • • •				
1.570 ± 0.005 ± 0.008		¹ ABDALLAH	04E DLPH	$e^+e^- \rightarrow Z$
1.533 ± 0.015 +0.035 -0.031		² ABE	98B CDF	$p\bar{p}$ at 1.8 TeV
1.549 ± 0.009 ± 0.015		³ ACCIARRI	98 L3	$e^+e^- \rightarrow Z$
1.611 ± 0.010 ± 0.027		⁴ ACKERSTAFF	97F OPAL	$e^+e^- \rightarrow Z$
1.582 ± 0.011 ± 0.027		⁴ ABREU	96E DLPH	$e^+e^- \rightarrow Z$
1.575 ± 0.010 ± 0.026		⁵ ABREU	96E DLPH	$e^+e^- \rightarrow Z$
1.533 ± 0.013 ± 0.0229.8k		⁶ BUSKULIC	96F ALEP	$e^+e^- \rightarrow Z$
1.564 ± 0.030 ± 0.036		⁷ ABE,K	95B SLD	$e^+e^- \rightarrow Z$
1.542 ± 0.021 ± 0.045		⁸ ABREU	94L DLPH	$e^+e^- \rightarrow Z$
1.50 +0.24 -0.21 ± 0.03		⁹ ABREU	94P DLPH	$e^+e^- \rightarrow Z$
1.46 ± 0.06 ± 0.06 5344		¹⁰ ABE	93J CDF	Repl. by ABE 98B
1.23 +0.14 -0.13 ± 0.15 188		¹¹ ABREU	93D DLPH	Sup. by ABREU 94L
1.49 ± 0.11 ± 0.12 253		¹² ABREU	93G DLPH	Sup. by ABREU 94L
1.51 +0.16 -0.14 ± 0.11 130		¹³ ACTON	93C OPAL	$e^+e^- \rightarrow Z$
1.523 ± 0.034 ± 0.038 372		¹⁴ ACTON	93L OPAL	$e^+e^- \rightarrow Z$
1.535 ± 0.035 ± 0.028 357		¹⁴ ADRIANI	93K L3	Repl. by ACCIARRI 98
1.511 ± 0.022 ± 0.078		¹⁵ BUSKULIC	93O ALEP	$e^+e^- \rightarrow Z$
1.28 ± 0.10		¹⁶ ABREU	92 DLPH	Sup. by ABREU 94L
1.37 ± 0.07 ± 0.06 1354		¹⁷ ACTON	92 OPAL	Sup. by ACTON 93L
1.49 ± 0.03 ± 0.06		¹⁸ BUSKULIC	92F ALEP	Sup. by BUSKULIC 96F
1.35 +0.19 -0.17 ± 0.05		¹⁹ BUSKULIC	92G ALEP	$e^+e^- \rightarrow Z$
1.32 ± 0.08 ± 0.09 1386		²⁰ ADEVA	91H L3	Sup. by ADRIANI 93K
1.32 +0.31 -0.25 ± 0.15 37		²¹ ALEXANDER	91G OPAL	$e^+e^- \rightarrow Z$
1.29 ± 0.06 ± 0.10 2973		²² DECAMP	91C ALEP	Sup. by BUSKULIC 92F
1.36 +0.25 -0.23 ± 0.15		²³ HAGEMANN	90 JADE	$E_{cm}^{ee} = 35$ GeV
1.13 ± 0.15		²⁴ LYONS	90 RVUE	
1.35 ± 0.10 ± 0.24		BRAUNSCH...	89B TASS	$E_{cm}^{ee} = 35$ GeV
0.98 ± 0.12 ± 0.13		ONG	89 MRK2	$E_{cm}^{ee} = 29$ GeV
1.17 +0.27 +0.17 -0.22 -0.16 ± 0.15		KLEM	88 DLCO	$E_{cm}^{ee} = 29$ GeV
1.29 ± 0.20 ± 0.21		²⁵ ASH	87 MAC	$E_{cm}^{ee} = 29$ GeV
1.02 +0.42 -0.39 ± 0.15	301	²⁶ BROM	87 HRS	$E_{cm}^{ee} = 29$ GeV

¹ Measurement performed using an inclusive reconstruction and B flavor identification technique.

² Measured using inclusive $J/\psi(1S) \rightarrow \mu^+\mu^-$ vertex.

³ ACCIARRI 98 uses inclusively reconstructed secondary vertex and lepton impact parameter.

⁴ ACKERSTAFF 97F uses inclusively reconstructed secondary vertices.

⁵ Combines ABREU 96E secondary vertex result with ABREU 94L impact parameter result.

⁶ BUSKULIC 96F analyzed using 3D impact parameter.

⁷ ABE,K 95B uses an inclusive topological technique.

⁸ ABREU 94L uses charged particle impact parameters. Their result from inclusively reconstructed secondary vertices is superseded by ABREU 96E.

⁹ From proper time distribution of $b \rightarrow J/\psi(1S)$ anything.

¹⁰ ABE 93J analyzed using $J/\psi(1S) \rightarrow \mu\mu$ vertices.

¹¹ ABREU 93D data analyzed using $D/D^*\ell$ anything event vertices.

¹² ABREU 93G data analyzed using charged and neutral vertices.

¹³ ACTON 93C analysed using $D/D^*\ell$ anything event vertices.

¹⁴ ACTON 93L and ADRIANI 93K analyzed using lepton (e and μ) impact parameter at Z .

¹⁵ BUSKULIC 93O analyzed using dipole method.

¹⁶ ABREU 92 is combined result of muon and hadron impact parameter analyses. Hadron tracks gave $(12.7 \pm 0.4 \pm 1.2) \times 10^{-13}$ s for an admixture of B species weighted by production fraction and mean charge multiplicity, while muon tracks gave $(13.0 \pm 1.0 \pm 0.8) \times 10^{-13}$ s for an admixture weighted by production fraction and semileptonic branching fraction.

¹⁷ ACTON 92 is combined result of muon and electron impact parameter analyses.

¹⁸ BUSKULIC 92F uses the lepton impact parameter distribution for data from the 1991 run.

¹⁹ BUSKULIC 92G use $J/\psi(1S)$ tags to measure the average b lifetime. This is comparable to other methods only if the $J/\psi(1S)$ branching fractions of the different b -flavored hadrons are in the same ratio.

²⁰ Using $Z \rightarrow e^+X$ or μ^+X , ADEVA 91H determined the average lifetime for an admixture of B hadrons from the impact parameter distribution of the lepton.

²¹ Using $Z \rightarrow J/\psi(1S)X$, $J/\psi(1S) \rightarrow \ell^+\ell^-$, ALEXANDER 91G determined the average lifetime for an admixture of B hadrons from the decay point of the $J/\psi(1S)$.

²² Using $Z \rightarrow eX$ or μX , DECAMP 91C determines the average lifetime for an admixture of B hadrons from the signed impact parameter distribution of the lepton.

²³ HAGEMANN 90 uses electrons and muons in an impact parameter analysis.

²⁴ LYONS 90 combine the results of the B lifetime measurements of ONG 89, BRAUN-SCHWEIG 89B, KLEM 88, and ASH 87, and JADE data by private communication. They use statistical techniques which include variation of the error with the mean life, and possible correlations between the systematic errors. This result is not independent of the measured results used in our average.

²⁵ We have combined an overall scale error of 15% in quadrature with the systematic error of ± 0.7 to obtain ± 2.1 systematic error.

²⁶ Statistical and systematic errors were combined by BROM 87.

CHARGED b -HADRON ADMIXTURE MEAN LIFE

VALUE (10^{-12} s)	DOCUMENT ID	TECN	COMMENT
1.72 ± 0.08 ± 0.06	¹ ADAM	95 DLPH	$e^+e^- \rightarrow Z$
¹ ADAM 95 data analyzed using vertex-charge technique to tag b -hadron charge.			

NEUTRAL b -HADRON ADMIXTURE MEAN LIFE

VALUE (10^{-12} s)	DOCUMENT ID	TECN	COMMENT
1.58 ± 0.11 ± 0.09	¹ ADAM	95 DLPH	$e^+e^- \rightarrow Z$
¹ ADAM 95 data analyzed using vertex-charge technique to tag b -hadron charge.			

MEAN LIFE RATIO $\tau_{\text{charged } b\text{-hadron}}/\tau_{\text{neutral } b\text{-hadron}}$

VALUE	DOCUMENT ID	TECN	COMMENT
1.09 +0.11 -0.10 ± 0.08	¹ ADAM	95 DLPH	$e^+e^- \rightarrow Z$
¹ ADAM 95 data analyzed using vertex-charge technique to tag b -hadron charge.			

 $|\Delta\tau_b|/\tau_{b,\bar{b}}$

$\tau_{b,\bar{b}}$ and $|\Delta\tau_b|$ are the mean life average and difference between b and \bar{b} hadrons.

VALUE	DOCUMENT ID	TECN	COMMENT
-0.001 ± 0.012 ± 0.008	¹ ABBIENDI	99J OPAL	$e^+e^- \rightarrow Z$
¹ Data analyzed using both the jet charge and the charge of secondary vertex in the opposite hemisphere.			

 \bar{b} PRODUCTION FRACTIONS AND DECAY MODES

The branching fraction measurements are for an admixture of B mesons and baryons at energies above the $T(4S)$. Only the highest energy results (LHC, LEP, Tevatron, $SppS$) are used in the branching fraction averages. In the following, we assume that the production fractions are the same at the LHC, LEP, and at the Tevatron.

For inclusive branching fractions, e.g., $B \rightarrow D^\pm$ anything, the values usually are multiplicities, not branching fractions. They can be greater than one.

The modes below are listed for a \bar{b} initial state. b modes are their charge conjugates. Reactions indicate the weak decay vertex and do not include mixing.

Mode	Fraction (Γ_i/Γ)	Scale factor/ Confidence level
------	--------------------------------	-----------------------------------

PRODUCTION FRACTIONS

The production fractions for weakly decaying b -hadrons at high energy have been calculated from the best values of mean lives, mixing parameters, and branching fractions in this edition by the Heavy Flavor Averaging Group (HFLAV) as described in the note " B^0/\bar{B}^0 Mixing" in the B^0 Particle Listings. We no longer provide world averages of the b -hadron production fractions, where results from LEP, Tevatron and LHC are averaged together; indeed the available data (from CDF and LHCb) shows that the fractions depend on the kinematics (in particular the p_T) of the produced b hadron. Hence we would like to list the fractions in Z decays instead, which are well-defined physics observables. The production fractions in $p\bar{p}$ collisions at the Tevatron are also listed at the end of the section. Values assume

$$\begin{aligned} B(\bar{b} \rightarrow B^+) &= B(\bar{b} \rightarrow B^0) \\ B(\bar{b} \rightarrow B^+) + B(\bar{b} \rightarrow B^0) + B(\bar{b} \rightarrow B_s^0) + B(b \rightarrow b\text{-baryon}) &= 100\%. \end{aligned}$$

The correlation coefficients between production fractions are also reported:

$$\begin{aligned} \text{cor}(B_s^0, b\text{-baryon}) &= 0.064 \\ \text{cor}(B_s^0, B^\pm=B^0) &= -0.633 \\ \text{cor}(b\text{-baryon}, B^\pm=B^0) &= -0.813. \end{aligned}$$

The notation for production fractions varies in the literature ($f_d, d_{B^0}, f(b \rightarrow \bar{B}^0), B_f(b \rightarrow \bar{B}^0)$). We use our own branching fraction notation here, $B(\bar{b} \rightarrow B^0)$.

Note these production fractions are b -hadronization fractions, not the conventional branching fractions of b -quark to a B -hadron, which may have considerable dependence on the initial and final state kinematic and production environment.

Γ_1	B^+	(40.8 ± 0.7) %
Γ_2	B^0	(40.8 ± 0.7) %
Γ_3	B_s^0	(10.0 ± 0.8) %
Γ_4	B_c^+	
Γ_5	b -baryon	(8.4 ± 1.1) %

DECAY MODES

Semileptonic and leptonic modes

Γ_6	ν anything	(23.1 ± 1.5) %	
Γ_7	$\ell^+ \nu_\ell$ anything	[a] (10.69 ± 0.22) %	
Γ_8	$e^+ \nu_e$ anything	(10.86 ± 0.35) %	
Γ_9	$\mu^+ \nu_\mu$ anything	(10.95 ± $\frac{0.29}{0.25}$) %	
Γ_{10}	$D^- \ell^+ \nu_\ell$ anything	[a] (2.2 ± 0.4) %	S=1.9
Γ_{11}	$D^- \pi^+ \ell^+ \nu_\ell$ anything	(4.9 ± 1.9) × 10 ⁻³	
Γ_{12}	$D^- \pi^- \ell^+ \nu_\ell$ anything	(2.6 ± 1.6) × 10 ⁻³	
Γ_{13}	$\bar{D}^0 \ell^+ \nu_\ell$ anything	[a] (6.79 ± 0.34) %	
Γ_{14}	$\bar{D}^0 \pi^- \ell^+ \nu_\ell$ anything	(1.07 ± 0.27) %	
Γ_{15}	$\bar{D}^0 \pi^+ \ell^+ \nu_\ell$ anything	(2.3 ± 1.6) × 10 ⁻³	
Γ_{16}	$D^{*-} \ell^+ \nu_\ell$ anything	[a] (2.75 ± 0.19) %	
Γ_{17}	$D^{*-} \pi^- \ell^+ \nu_\ell$ anything	(6 ± 7) × 10 ⁻⁴	
Γ_{18}	$D^{*-} \pi^+ \ell^+ \nu_\ell$ anything	(4.8 ± 1.0) × 10 ⁻³	
Γ_{19}	$\bar{D}_j^0 \ell^+ \nu_\ell$ anything × B($\bar{D}_j^0 \rightarrow D^{*+} \pi^-$)	[a,b] (2.6 ± 0.9) × 10 ⁻³	
Γ_{20}	$D_j^- \ell^+ \nu_\ell$ anything × B($D_j^- \rightarrow D^0 \pi^-$)	[a,b] (7.0 ± 2.3) × 10 ⁻³	
Γ_{21}	$\bar{D}_2^*(2460)^0 \ell^+ \nu_\ell$ anything × B($\bar{D}_2^*(2460)^0 \rightarrow$ $D^{*-} \pi^+$)	< 1.4 × 10 ⁻³	CL=90%
Γ_{22}	$D_2^*(2460)^- \ell^+ \nu_\ell$ anything × B($D_2^*(2460)^- \rightarrow$ $D^0 \pi^-$)	(4.2 ± $\frac{1.5}{1.8}$) × 10 ⁻³	
Γ_{23}	$\bar{D}_2^*(2460)^0 \ell^+ \nu_\ell$ anything × B($\bar{D}_2^*(2460)^0 \rightarrow$ $D^- \pi^+$)	(1.6 ± 0.8) × 10 ⁻³	
Γ_{24}	charmless $\ell \bar{\nu}_\ell$	[a] (1.7 ± 0.5) × 10 ⁻³	
Γ_{25}	$\tau^+ \nu_\tau$ anything	(2.41 ± 0.23) %	
Γ_{26}	$D^{*-} \tau \nu_\tau$ anything	(9 ± 4) × 10 ⁻³	
Γ_{27}	$\bar{c} \rightarrow \ell^- \bar{\nu}_\ell$ anything	[a] (8.02 ± 0.19) %	
Γ_{28}	$c \rightarrow \ell^+ \nu$ anything	(1.6 ± $\frac{0.4}{0.5}$) %	

Charmed meson and baryon modes

Γ_{29}	\bar{D}^0 anything	(58.7 ± 2.8) %	
Γ_{30}	$D^0 D_s^\pm$ anything	[c] (9.1 ± $\frac{4.0}{2.8}$) %	
Γ_{31}	$D^\mp D_s^\pm$ anything	[c] (4.0 ± $\frac{2.3}{1.8}$) %	
Γ_{32}	$\bar{D}^0 D^0$ anything	[c] (5.1 ± $\frac{2.0}{1.8}$) %	
Γ_{33}	$D^0 D^\pm$ anything	[c] (2.7 ± $\frac{1.8}{1.6}$) %	
Γ_{34}	$D^\pm D^\mp$ anything	[c] < 9 × 10 ⁻³	CL=90%
Γ_{35}	D^0 anything		
Γ_{36}	D^+ anything		
Γ_{37}	D^- anything	(22.7 ± 1.6) %	
Γ_{38}	$D^*(2010)^+$ anything	(17.3 ± 2.0) %	
Γ_{39}	$D_1(2420)^0$ anything	(5.0 ± 1.5) %	
Γ_{40}	$D^*(2010)^\mp D_s^\pm$ anything	[c] (3.3 ± $\frac{1.6}{1.3}$) %	
Γ_{41}	$D^0 D^*(2010)^\pm$ anything	[c] (3.0 ± $\frac{1.1}{0.9}$) %	
Γ_{42}	$D^*(2010)^\pm D^\mp$ anything	[c] (2.5 ± $\frac{1.2}{1.0}$) %	
Γ_{43}	$D^*(2010)^\pm D^*(2010)^\mp$ anything	[c] (1.2 ± 0.4) %	
Γ_{44}	$\bar{D} D$ anything	(10 ± $\frac{11}{10}$) %	
Γ_{45}	$D_2^*(2460)^0$ anything	(4.7 ± 2.7) %	
Γ_{46}	D_c^- anything	(14.7 ± 2.1) %	
Γ_{47}	D_s^+ anything	(10.1 ± 3.1) %	
Γ_{48}	Λ_c^+ anything	(7.7 ± 1.1) %	
Γ_{49}	\bar{c}/c anything	[d] (116.2 ± 3.2) %	

Charmonium modes

Γ_{50}	$J/\psi(1S)$ anything	(1.16 ± 0.10) %	
Γ_{51}	$\psi(2S)$ anything	(3.06 ± 0.30) × 10 ⁻³	
Γ_{52}	$\chi_{c0}(1P)$ anything	(1.5 ± 0.6) %	
Γ_{53}	$\chi_{c1}(1P)$ anything	(1.4 ± 0.4) %	
Γ_{54}	$\chi_{c2}(1P)$ anything	(6.2 ± 2.9) × 10 ⁻³	
Γ_{55}	$\chi_c(2P)$ anything, $\chi_c \rightarrow \phi\phi$	< 2.8 × 10 ⁻⁷	CL=95%
Γ_{56}	$\eta_c(1S)$ anything	(5.6 ± 0.9) × 10 ⁻³	
Γ_{57}	$\eta_c(2S)$ anything, $\eta_c \rightarrow \phi\phi$	(3.9 ± 1.4) × 10 ⁻⁷	
Γ_{58}	$\chi_{c1}(3872)$ anything, $\chi_{c1} \rightarrow \phi\phi$	< 4.5 × 10 ⁻⁷	CL=95%
Γ_{59}	$\chi_{c0}(3915)$ anything, $\chi_{c0} \rightarrow \phi\phi$	< 3.1 × 10 ⁻⁷	CL=95%

K or K* modes

Γ_{60}	$\bar{s}\gamma$	(3.1 ± 1.1) × 10 ⁻⁴	
Γ_{61}	$\bar{s}\bar{\nu}$	B1 < 6.4 × 10 ⁻⁴	CL=90%
Γ_{62}	K^\pm anything	(74 ± 6) %	
Γ_{63}	K_S^0 anything	(29.0 ± 2.9) %	

Pion modes

Γ_{64}	π^\pm anything	(397 ± 21) %	
Γ_{65}	π^0 anything	[d] (278 ± 60) %	
Γ_{66}	ϕ anything	(2.82 ± 0.23) %	

Baryon modes

Γ_{67}	p/\bar{p} anything	(13.1 ± 1.1) %	
Γ_{68}	$\Lambda/\bar{\Lambda}$ anything	(5.9 ± 0.6) %	
Γ_{69}	b -baryon anything	(10.2 ± 2.8) %	
Γ_{70}	$\bar{\Lambda}_b^0$ anything		
Γ_{71}	Ξ_b^+ anything		

Other modes

Γ_{72}	charged anything	[d] (497 ± 7) %	
Γ_{73}	hadron ⁺ hadron ⁻	(1.7 ± $\frac{1.0}{0.7}$) × 10 ⁻⁵	
Γ_{74}	charmless	(7 ± 21) × 10 ⁻³	

 $\Delta B = 1$ weak neutral current (B1) modes

Γ_{75}	$e^+ e^-$ anything		
Γ_{76}	$\mu^+ \mu^-$ anything	B1 < 3.2 × 10 ⁻⁴	CL=90%
Γ_{77}	$\nu\bar{\nu}$ anything		

[a] An ℓ indicates an e or a μ mode, not a sum over these modes.

[b] D_j represents an unresolved mixture of pseudoscalar and tensor D^{**} (P -wave) states.

[c] The value is for the sum of the charge states or particle/antiparticle states indicated.

[d] Inclusive branching fractions have a multiplicity definition and can be greater than 100%.

Meson Particle Listings

 $B^\pm/B^0/B_s^0/b$ -baryon ADMIXTURE $B^\pm/B^0/B_s^0/b$ -baryon ADMIXTURE BRANCHING RATIOS

$\Gamma(B^+)/\Gamma_{\text{total}}$ Γ_1/Γ
 "OUR EVALUATION" is an average from Z decay obtained by the Heavy Flavor Averaging Group (HFLAV) as described at <https://hflav.web.cern.ch/>.

VALUE	DOCUMENT ID	TECN	COMMENT
0.408 ± 0.007 OUR EVALUATION			
0.4099 ± 0.0082 ± 0.0111	¹ ABDALLAH	03k DLPH	$e^+e^- \rightarrow Z$

¹ The analysis is based on a neural network, to estimate the charge of the weakly-decaying b-hadron by distinguishing its decay products from particles produced at the primary vertex.

$\Gamma(B^+)/\Gamma(B^0)$ Γ_1/Γ_2

VALUE	DOCUMENT ID	TECN	COMMENT
1.054 ± 0.018⁺ 0.062⁻	AALTONEN	08N CDF	$p\bar{p}$ at 1.96 TeV

$\Gamma(B_s^0)/\Gamma(B^+)$ Γ_3/Γ_1

VALUE	DOCUMENT ID	TECN	COMMENT
• • • We do not use the following data for averages, fits, limits, etc. • • •			
0.121 ± 0.002 ± 0.005	^{1,2} AAIJ	20v LHCb	pp at 7 TeV
0.124 ± 0.002 ± 0.005	^{1,3} AAIJ	20v LHCb	pp at 8 TeV
0.130 ± 0.002 ± 0.005	^{1,4,5} AAIJ	20v LHCb	pp at 13 TeV

¹ AAIJ 20v measures the average value using the observed $B_s^0 \rightarrow J/\psi\phi$ and $B^+ \rightarrow J/\psi K^+$ yields, over the ranges b-hadron p_T of 0.5 and 40 GeV and η of 2.0 and 6.5. The value is not used in averages as BR-related systematic uncertainties are not evaluated.

² AAIJ 20v reports $[\Gamma(\bar{B} \rightarrow B_s^0)/\Gamma(\bar{B} \rightarrow B^+)] \times [B(B_s^0 \rightarrow J/\psi(1S)\phi)] / [B(B^+ \rightarrow J/\psi(1S)K^+)] = 0.1238 \pm 0.0010 \pm 0.0022$ which we multiply or divide by our best values $B(B_s^0 \rightarrow J/\psi(1S)\phi) = (1.04 \pm 0.04) \times 10^{-3}$, $B(B^+ \rightarrow J/\psi(1S)K^+) = (1.020 \pm 0.019) \times 10^{-3}$. Our first error is their experiment's error and our second error is the systematic error from using our best values.

³ AAIJ 20v reports $[\Gamma(\bar{B} \rightarrow B_s^0)/\Gamma(\bar{B} \rightarrow B^+)] \times [B(B_s^0 \rightarrow J/\psi(1S)\phi)] / [B(B^+ \rightarrow J/\psi(1S)K^+)] = 0.1270 \pm 0.0007 \pm 0.0022$ which we multiply or divide by our best values $B(B_s^0 \rightarrow J/\psi(1S)\phi) = (1.04 \pm 0.04) \times 10^{-3}$, $B(B^+ \rightarrow J/\psi(1S)K^+) = (1.020 \pm 0.019) \times 10^{-3}$. Our first error is their experiment's error and our second error is the systematic error from using our best values.

⁴ AAIJ 20v reports the results in two different data sets, and we quote here the weighted average.

⁵ AAIJ 20v reports $[\Gamma(\bar{B} \rightarrow B_s^0)/\Gamma(\bar{B} \rightarrow B^+)] \times [B(B_s^0 \rightarrow J/\psi(1S)\phi)] / [B(B^+ \rightarrow J/\psi(1S)K^+)] = 0.1326 \pm 0.0007 \pm 0.0023$ which we multiply or divide by our best values $B(B_s^0 \rightarrow J/\psi(1S)\phi) = (1.04 \pm 0.04) \times 10^{-3}$, $B(B^+ \rightarrow J/\psi(1S)K^+) = (1.020 \pm 0.019) \times 10^{-3}$. Our first error is their experiment's error and our second error is the systematic error from using our best values.

$\Gamma(B_s^0)/[\Gamma(B^+) + \Gamma(B^0)]$ $\Gamma_3/(\Gamma_1+\Gamma_2)$
 "OUR EVALUATION" is an average from Z decay obtained by the Heavy Flavor Averaging Group (HFLAV) as described at <https://hflav.web.cern.ch/>.

VALUE	DOCUMENT ID	TECN	COMMENT
0.1230 ± 0.0115 OUR EVALUATION			
• • • We do not use the following data for averages, fits, limits, etc. • • •			
0.122 ± 0.006	¹ AAIJ	19AD LHCb	pp at 13 TeV
0.134 ± 0.004 ⁺ 0.011 ⁻	² AAIJ	12j LHCb	pp at 7 TeV
0.1265 ± 0.0085 ± 0.0131	³ AAIJ	11f LHCb	pp at 7 TeV
0.128 ⁺ 0.011 ⁻ ± 0.011	⁴ AALTONEN	08N CDF	$p\bar{p}$ at 1.96 TeV
0.213 ± 0.068	⁵ AFFOLDER	00E CDF	$p\bar{p}$ at 1.8 TeV
0.21 ± 0.036 ⁺ 0.038 ⁻	⁶ ABE	99p CDF	$p\bar{p}$ at 1.8 TeV

¹ AAIJ 19AD measured the average value using b-hadron semileptonic decays and assuming isospin symmetry for b-hadron p_T of 4 and 25 GeV and η of 2 and 5.

² AAIJ 12j measured this value using b-hadron semileptonic decays and assuming isospin symmetry.

³ AAIJ 11f measured $f_s/f_d = 0.253 \pm 0.017 \pm 0.017 \pm 0.020$, where the errors are statistical, systematic, and theoretical. We divide their value by 2. Our second error combines systematic and theoretical uncertainties.

⁴ AALTONEN 08N reports $[\Gamma(\bar{B} \rightarrow B_s^0)/\Gamma(\bar{B} \rightarrow B^+) + \Gamma(\bar{B} \rightarrow B^0)] \times [B(D_s^+ \rightarrow \phi\pi^+)] = (5.76 \pm 0.18⁺ 0.45⁻ 0.42) \times 10^{-3}$ which we divide by our best value $B(D_s^+ \rightarrow \phi\pi^+) = (4.5 \pm 0.4) \times 10^{-2}$. Our first error is their experiment's error and our second error is the systematic error from using our best value.

⁵ AFFOLDER 00E uses several electron-charm final states in $b \rightarrow ce^-X$.

⁶ ABE 99p uses the numbers of $K^*(892)^0$, $K^*(892)^+$, and $\phi(1020)$ events produced in association with the double semileptonic decays $b \rightarrow c\mu^-X$ with $c \rightarrow s\mu^+X$.

$\Gamma(B_s^0)/\Gamma(B^0)$ Γ_3/Γ_2
 "OUR EVALUATION" has been provided by the Heavy Flavor Averaging Group (HFLAV, <https://hflav.web.cern.ch/>).

VALUE	DOCUMENT ID	TECN	COMMENT
0.246 ± 0.023 OUR EVALUATION			
0.239 ± 0.016 OUR AVERAGE			
0.240 ± 0.004 ± 0.020	¹ AAD	15CM ATLAS	pp at 7 TeV
0.238 ± 0.004 ± 0.026	² AAIJ	13P LHCb	pp at 7 TeV

• • • We do not use the following data for averages, fits, limits, etc. • • •

0.2385 ± 0.0075	³ AAIJ	21Y LHCb	pp at 8 TeV
0.2539 ± 0.0079	³ AAIJ	21Y LHCb	pp at 13 TeV
0.2390 ± 0.0076	³ AAIJ	21Y LHCb	pp at 7 TeV

¹ AAD 15CM measurement is derived from the observed $B_s^0 \rightarrow J/\psi\phi$ and $B_d^0 \rightarrow J/\psi K^{*0}$ yields and a recent theory prediction of $B(B_s^0 \rightarrow J/\psi\phi)/B(B_d^0 \rightarrow J/\psi K^{*0})$. The second uncertainty combines in quadrature systematic and theoretical uncertainties.

² AAIJ 13P studies also separately the $p_T(B)$ and $\eta(B)$ dependency of $\Gamma(\bar{B} \rightarrow B_s^0)/\Gamma(\bar{B} \rightarrow B^0)$, finding $f_s/f_d(p_T) = (0.256 \pm 0.020) + (-2.0 \pm 0.6) 10^{-3} / \text{GeV}/c (p_T - \langle p_T \rangle)$ and $f_s/f_d(\eta) = (0.256 \pm 0.020) + (0.005 \pm 0.006) (\eta - \langle \eta \rangle)$, where $\langle p_T \rangle = 10.4 \text{ GeV}/c$ and $\langle \eta \rangle = 3.28$. AAIJ 13P reports the measurement as $0.238 \pm 0.004 \pm 0.015 \pm 0.021$ where the last uncertainty is theoretical.

³ AAIJ 21Y uses hadronic decays $B^0 \rightarrow D^- \pi^+$, $B^0 \rightarrow D^- K^+$, $B_s^0 \rightarrow D_s^- \pi^+$ and $B_s^0 \rightarrow J/\psi\phi$ as well as semileptonic B^0 and B_s^0 decays. Measured within the p_T range [0.5,40] GeV/c, η range [2, 6.4].

$\Gamma(B_c^+)/[\Gamma(B^+) + \Gamma(B^0)]$ $\Gamma_4/(\Gamma_1+\Gamma_2)$

VALUE (units 10^{-3})	DOCUMENT ID	TECN	COMMENT
3.7 ± 0.6 OUR AVERAGE			
3.63 ± 0.08 ± 0.87	¹ AAIJ	19Al LHCb	pp at 7 TeV
3.78 ± 0.04 ± 0.90	¹ AAIJ	19Al LHCb	pp at 13 TeV

¹ Measured using B_c^+ semileptonic decays.

$\Gamma(b\text{-baryon})/[\Gamma(B^+) + \Gamma(B^0)]$ $\Gamma_5/(\Gamma_1+\Gamma_2)$
 "OUR EVALUATION" is an average from Z decay obtained by the Heavy Flavor Averaging Group (HFLAV) as described at <https://hflav.web.cern.ch/>.

VALUE	DOCUMENT ID	TECN	COMMENT
0.103 ± 0.015 OUR EVALUATION			
• • • We do not use the following data for averages, fits, limits, etc. • • •			
0.259 ± 0.018	¹ AAIJ	19AD LHCb	pp at 13 TeV
0.305 ± 0.010 ± 0.081	² AAIJ	12j LHCb	pp at 7 TeV
0.31 ± 0.11 ⁺ 0.12 ⁻ 0.08	³ AALTONEN	09E CDF	$p\bar{p}$ at 1.8 TeV
0.22 ± 0.08 ⁺ 0.01 ⁻	⁴ AALTONEN	08N CDF	$p\bar{p}$ at 1.96 TeV
0.118 ± 0.042	^{3,5} AFFOLDER	00E CDF	$p\bar{p}$ at 1.8 TeV

¹ AAIJ 19AD measured the average value for Λ_b^0 using semileptonic decays and assuming isospin symmetry for b-hadron p_T of 4 and 25 GeV and η of 2 and 5.

² AAIJ 12j measured the ratio to be $(0.404 \pm 0.017 \pm 0.027 \pm 0.105) \times [1 - (0.031 \pm 0.004 \pm 0.003) \times p_T]$ using b-hadron semileptonic decays where the p_T is the momentum of charmed hadron-muon pair in GeV/c. We quote their weighted average value where the second error combines systematic and the error on $B(\Lambda_c^+ \rightarrow pK^- \pi^+)$.

³ AALTONEN 09E errata to the measurement reported in AFFOLDER 00E using the p_T spectra from fully reconstructed B^0 and Λ_b decays.

⁴ AALTONEN 08N reports $[\Gamma(\bar{B} \rightarrow b\text{-baryon})/[\Gamma(\bar{B} \rightarrow B^+) + \Gamma(\bar{B} \rightarrow B^0)]] \times [B(\Lambda_c^+ \rightarrow pK^- \pi^+)] = (14.1 \pm 0.6⁺ 5.3⁻ 4.4) \times 10^{-3}$ which we divide by our best value $B(\Lambda_c^+ \rightarrow pK^- \pi^+) = (6.28 \pm 0.32) \times 10^{-2}$. Our first error is their experiment's error and our second error is the systematic error from using our best value.

⁵ AFFOLDER 00E uses several electron-charm final states in $b \rightarrow ce^-X$.

$\Gamma(\nu\text{anything})/\Gamma_{\text{total}}$ Γ_6/Γ

VALUE	DOCUMENT ID	TECN	COMMENT
0.2308 ± 0.0077 ± 0.0124	^{1,2} ACCIARRI	96c L3	$e^+e^- \rightarrow Z$

¹ ACCIARRI 96c assumes relative b semileptonic decay rates $e:\mu:\tau$ of 1:1:0.25. Based on missing-energy spectrum.

² Assumes Standard Model value for R_B .

$\Gamma(e^+ \nu_e \text{anything})/\Gamma_{\text{total}}$ Γ_7/Γ
 "OUR EVALUATION" is an average of the data listed below, excluding all asymmetry measurements, performed by the LEP Electroweak Working Group as described in the "Note on the Z boson" in the Z Particle Listings.

VALUE	DOCUMENT ID	TECN	COMMENT
0.1069 ± 0.0022 OUR EVALUATION			
0.1064 ± 0.0016 OUR AVERAGE			
0.1070 ± 0.0010 ± 0.0035	¹ HEISTER	02G ALEP	$e^+e^- \rightarrow Z$
0.1070 ± 0.0008 ⁺ 0.0037 ⁻ 0.0049	² ABREU	01L DLPH	$e^+e^- \rightarrow Z$
0.1083 ± 0.0010 ⁺ 0.0028 ⁻ 0.0024	³ ABBIENDI	00E OPAL	$e^+e^- \rightarrow Z$
0.1016 ± 0.0013 ± 0.0030	⁴ ACCIARRI	00 L3	$e^+e^- \rightarrow Z$
0.1085 ± 0.0012 ± 0.0047	^{5,6} ACCIARRI	96c L3	$e^+e^- \rightarrow Z$
• • • We do not use the following data for averages, fits, limits, etc. • • •			
0.1106 ± 0.0039 ± 0.0022	⁷ ABREU	95D DLPH	$e^+e^- \rightarrow Z$
0.114 ± 0.003 ± 0.004	⁸ BUSKULIC	94G ALEP	$e^+e^- \rightarrow Z$
0.100 ± 0.007 ± 0.007	⁹ ABREU	93C DLPH	$e^+e^- \rightarrow Z$
0.105 ± 0.006 ± 0.005	¹⁰ AKERS	93B OPAL	Repl. by ABBI- ENDI 00E

¹ Uses the combination of lepton transverse momentum spectrum and the correlation between the charge of the lepton and opposite jet charge. The first error is statistic and the second error is the total systematic error including the modeling.

² The experimental systematic and model uncertainties are combined in quadrature.

³ ABBIENDI 00E result is determined by comparing the distribution of several kinematic variables of leptonic events in a lifetime tagged $Z \rightarrow b\bar{b}$ sample using artificial neural

Meson Particle Listings

$B^\pm/B^0/B_s^0$ b -baryon ADMIXTURE

network techniques. The first error is statistic; the second error is the total systematic error.

⁴ ACCIARRI 00 result obtained from a combined fit of $R_b = \Gamma(Z \rightarrow b\bar{b})/\Gamma(Z \rightarrow \text{hadrons})$ and $B(b \rightarrow \ell\nu X)$, using double-tagging method.

⁵ ACCIARRI 96c result obtained by a fit to the single lepton spectrum.

⁶ Assumes Standard Model value for R_B .

⁷ ABREU 95D give systematic errors ± 0.0019 (model) and 0.0012 (R_c). We combine these in quadrature.

⁸ BUSKULIC 94G uses e and μ events. This value is from a global fit to the lepton p and p_T (relative to jet) spectra which also determines the b and c production fractions, the fragmentation functions, and the forward-backward asymmetries. This branching ratio depends primarily on the ratio of dileptons to single leptons at high p_T , but the lower p_T portion of the lepton spectrum is included in the global fit to reduce the model dependence. The model dependence is ± 0.0026 and is included in the systematic error.

⁹ ABREU 93c event count includes $e\bar{e}$ events. Combining $e\bar{e}$, $\mu\mu$, and $e\mu$ events, they obtain $0.100 \pm 0.007 \pm 0.007$.

¹⁰ AKERS 93B analysis performed using single and dilepton events.

$\Gamma(e^+ \nu_e \text{ anything})/\Gamma_{\text{total}}$					Γ_8/Γ
VALUE	EVTS	DOCUMENT ID	TECN	COMMENT	

0.1086 ± 0.0035 OUR AVERAGE					
0.1078 ± 0.0008 ^{+0.0050} _{-0.0046}		¹ ABBIENDI	00E OPAL	$e^+e^- \rightarrow Z$	
0.1089 ± 0.0020 ± 0.0051		^{2,3} ACCIARRI	96c L3	$e^+e^- \rightarrow Z$	
0.107 ± 0.015 ± 0.007	260	⁴ ABREU	93c DLPH	$e^+e^- \rightarrow Z$	
0.138 ± 0.032 ± 0.008		⁵ ADEVA	91c L3	$e^+e^- \rightarrow Z$	
• • • We do not use the following data for averages, fits, limits, etc. • • •					
0.086 ± 0.027 ± 0.008		⁶ ABE	93E VNS	$E_{\text{cm}}^{ee} = 58 \text{ GeV}$	
0.109 ^{+0.014} _{-0.013} ± 0.0055	2719	⁷ AKERS	93B OPAL	Repl. by ABBIENDI 00E	
0.111 ± 0.028 ± 0.026		BEHREND	90D CELL	$E_{\text{cm}}^{ee} = 43 \text{ GeV}$	
0.150 ± 0.011 ± 0.022		BEHREND	90D CELL	$E_{\text{cm}}^{ee} = 35 \text{ GeV}$	
0.112 ± 0.009 ± 0.011		ONG	88 MRK2	$E_{\text{cm}}^{ee} = 29 \text{ GeV}$	
0.149 ^{+0.022} _{-0.019}		PAL	86 DLCO	$E_{\text{cm}}^{ee} = 29 \text{ GeV}$	
0.110 ± 0.018 ± 0.010		AIHARA	85 TPC	$E_{\text{cm}}^{ee} = 29 \text{ GeV}$	
0.111 ± 0.034 ± 0.040		ALTHOFF	84J TASS	$E_{\text{cm}}^{ee} = 34.6 \text{ GeV}$	
0.146 ± 0.028		KOOP	84 DLCO	Repl. by PAL 86	
0.116 ± 0.021 ± 0.017		NELSON	83 MRK2	$E_{\text{cm}}^{ee} = 29 \text{ GeV}$	

¹ ABBIENDI 00E result is determined by comparing the distribution of several kinematic variables of leptonic events in a lifetime tagged $Z \rightarrow b\bar{b}$ sample using artificial neural network techniques. The first error is statistic; the second error is the total systematic error.

² ACCIARRI 96c result obtained by a fit to the single lepton spectrum.

³ Assumes Standard Model value for R_B .

⁴ ABREU 93c event count includes $e\bar{e}$ events. Combining $e\bar{e}$, $\mu\mu$, and $e\mu$ events, they obtain $0.100 \pm 0.007 \pm 0.007$.

⁵ ADEVA 91c measure the average $B(b \rightarrow eX)$ branching ratio using single and double tagged b enhanced Z events. Combining e and μ results, they obtain $0.113 \pm 0.010 \pm 0.006$. Constraining the initial number of b quarks by the Standard Model prediction ($378 \pm 3 \text{ MeV}$) for the decay of the Z into $b\bar{b}$, the electron result gives $0.112 \pm 0.004 \pm 0.008$. They obtain $0.119 \pm 0.003 \pm 0.006$ when e and μ results are combined. Used to measure the $b\bar{b}$ width itself, this electron result gives $370 \pm 12 \pm 24 \text{ MeV}$ and combined with the muon result gives $385 \pm 7 \pm 22 \text{ MeV}$.

⁶ ABE 93E experiment also measures forward-backward asymmetries and fragmentation functions for b and c .

⁷ AKERS 93B analysis performed using single and dilepton events.

$\Gamma(\mu^+ \nu_\mu \text{ anything})/\Gamma_{\text{total}}$					Γ_9/Γ
VALUE	EVTS	DOCUMENT ID	TECN	COMMENT	

0.1095 ± 0.0029 OUR AVERAGE					
0.1096 ± 0.0008 ^{+0.0034} _{-0.0027}		¹ ABBIENDI	00E OPAL	$e^+e^- \rightarrow Z$	
0.1082 ± 0.0015 ± 0.0059		^{2,3} ACCIARRI	96c L3	$e^+e^- \rightarrow Z$	
0.110 ± 0.012 ± 0.007	656	⁴ ABREU	93c DLPH	$e^+e^- \rightarrow Z$	
0.113 ± 0.012 ± 0.006		⁵ ADEVA	91c L3	$e^+e^- \rightarrow Z$	
• • • We do not use the following data for averages, fits, limits, etc. • • •					
0.122 ± 0.006 ± 0.007		³ UENO	96 AMY	e^+e^- at 57.9 GeV	
0.101 ^{+0.010} _{-0.009} ± 0.0055	4248	⁶ AKERS	93B OPAL	Repl. by ABBIENDI 00E	
0.104 ± 0.023 ± 0.016		BEHREND	90D CELL	$E_{\text{cm}}^{ee} = 43 \text{ GeV}$	
0.148 ± 0.010 ± 0.016		BEHREND	90D CELL	$E_{\text{cm}}^{ee} = 35 \text{ GeV}$	
0.118 ± 0.012 ± 0.010		ONG	88 MRK2	$E_{\text{cm}}^{ee} = 29 \text{ GeV}$	
0.117 ± 0.016 ± 0.015		BARTEL	87 JADE	$E_{\text{cm}}^{ee} = 34.6 \text{ GeV}$	
0.114 ± 0.018 ± 0.025		BARTEL	85J JADE	Repl. by BARTEL 87	
0.117 ± 0.028 ± 0.010		ALTHOFF	84G TASS	$E_{\text{cm}}^{ee} = 34.5 \text{ GeV}$	
0.105 ± 0.015 ± 0.013		ADEVA	83B MRKJ	$E_{\text{cm}}^{ee} = 33\text{-}38.5 \text{ GeV}$	
0.155 ^{+0.054} _{-0.029}		FERNANDEZ	83D MAC	$E_{\text{cm}}^{ee} = 29 \text{ GeV}$	

¹ ABBIENDI 00E result is determined by comparing the distribution of several kinematic variables of leptonic events in a lifetime tagged $Z \rightarrow b\bar{b}$ sample using artificial neural network techniques. The first error is statistic; the second error is the total systematic error.

² ACCIARRI 96c result obtained by a fit to the single lepton spectrum.

³ Assumes Standard Model value for R_B .

⁴ ABREU 93c event count includes $\mu\mu$ events. Combining $e\bar{e}$, $\mu\mu$, and $e\mu$ events, they obtain $0.100 \pm 0.007 \pm 0.007$.

⁵ ADEVA 91c measure the average $B(b \rightarrow eX)$ branching ratio using single and double tagged b enhanced Z events. Combining e and μ results, they obtain $0.113 \pm 0.010 \pm 0.006$. Constraining the initial number of b quarks by the Standard Model prediction ($378 \pm 3 \text{ MeV}$) for the decay of the Z into $b\bar{b}$, the muon result gives $0.123 \pm 0.003 \pm 0.006$. They obtain $0.119 \pm 0.003 \pm 0.006$ when e and μ results are combined. Used to measure the $b\bar{b}$ width itself, this muon result gives $394 \pm 9 \pm 22 \text{ MeV}$ and combined with the electron result gives $385 \pm 7 \pm 22 \text{ MeV}$.

⁶ AKERS 93B analysis performed using single and dilepton events.

$\Gamma(D^- \ell^+ \nu_\ell \text{ anything})/\Gamma_{\text{total}}$					Γ_{10}/Γ
VALUE	DOCUMENT ID	TECN	COMMENT		

0.022 ± 0.004 OUR AVERAGE				Error includes scale factor of 1.9.
0.0272 ± 0.0028 ± 0.0018	¹ ABREU	00R DLPH	$e^+e^- \rightarrow Z$	
0.0194 ± 0.0025 ± 0.0003	² AKERS	95Q OPAL	$e^+e^- \rightarrow Z$	

¹ ABREU 00R reports their experiment's uncertainties $\pm 0.0019 \pm 0.0016 \pm 0.0018$, where the first error is statistical, the second is systematic, and the third is the uncertainty due to the D branching fraction. We combine first two in quadrature.

² AKERS 95Q reports $[\Gamma(\bar{D} \rightarrow D^- \ell^+ \nu_\ell \text{ anything})/\Gamma_{\text{total}}] \times [B(D^+ \rightarrow K^- 2\pi^+)] = (1.82 \pm 0.20 \pm 0.12) \times 10^{-3}$ which we divide by our best value $B(D^+ \rightarrow K^- 2\pi^+) = (9.38 \pm 0.16) \times 10^{-2}$. Our first error is their experiment's error and our second error is the systematic error from using our best value.

$\Gamma(D^- \pi^+ \ell^+ \nu_\ell \text{ anything})/\Gamma_{\text{total}}$					Γ_{11}/Γ
VALUE	DOCUMENT ID	TECN	COMMENT		

0.0049 ± 0.0018 ± 0.0007				
	ABREU	00R DLPH	$e^+e^- \rightarrow Z$	

$\Gamma(D^- \pi^- \ell^+ \nu_\ell \text{ anything})/\Gamma_{\text{total}}$					Γ_{12}/Γ
VALUE	DOCUMENT ID	TECN	COMMENT		

0.0026 ± 0.0015 ± 0.0004				
	ABREU	00R DLPH	$e^+e^- \rightarrow Z$	

$\Gamma(\bar{D}^0 \ell^+ \nu_\ell \text{ anything})/\Gamma_{\text{total}}$					Γ_{13}/Γ
VALUE	DOCUMENT ID	TECN	COMMENT		

0.0679 ± 0.0034 OUR AVERAGE				
0.0704 ± 0.0040 ± 0.0017	¹ ABREU	00R DLPH	$e^+e^- \rightarrow Z$	
0.0638 ± 0.0056 ± 0.0005	² AKERS	95Q OPAL	$e^+e^- \rightarrow Z$	

¹ ABREU 00R reports their experiment's uncertainties $\pm 0.0034 \pm 0.0036 \pm 0.0017$, where the first error is statistical, the second is systematic, and the third is the uncertainty due to the D branching fraction. We combine first two in quadrature.

² AKERS 95Q reports $[\Gamma(\bar{D} \rightarrow \bar{D}^0 \ell^+ \nu_\ell \text{ anything})/\Gamma_{\text{total}}] \times [B(D^0 \rightarrow K^- \pi^+)] = (2.52 \pm 0.14 \pm 0.17) \times 10^{-3}$ which we divide by our best value $B(D^0 \rightarrow K^- \pi^+) = (3.947 \pm 0.030) \times 10^{-2}$. Our first error is their experiment's error and our second error is the systematic error from using our best value.

$\Gamma(\bar{D}^0 \pi^- \ell^+ \nu_\ell \text{ anything})/\Gamma_{\text{total}}$					Γ_{14}/Γ
VALUE	DOCUMENT ID	TECN	COMMENT		

0.0107 ± 0.0025 ± 0.0011				
	ABREU	00R DLPH	$e^+e^- \rightarrow Z$	

$\Gamma(\bar{D}^0 \pi^+ \ell^+ \nu_\ell \text{ anything})/\Gamma_{\text{total}}$					Γ_{15}/Γ
VALUE	DOCUMENT ID	TECN	COMMENT		

0.0023 ± 0.0015 ± 0.0004				
	ABREU	00R DLPH	$e^+e^- \rightarrow Z$	

$\Gamma(D^{*-} \ell^+ \nu_\ell \text{ anything})/\Gamma_{\text{total}}$					Γ_{16}/Γ
VALUE	DOCUMENT ID	TECN	COMMENT		

0.0275 ± 0.0019 OUR AVERAGE				
0.0275 ± 0.0021 ± 0.0009	¹ ABREU	00R DLPH	$e^+e^- \rightarrow Z$	
0.0276 ± 0.0027 ± 0.0011	² AKERS	95Q OPAL	$e^+e^- \rightarrow Z$	

¹ ABREU 00R reports their experiment's uncertainties $\pm 0.0017 \pm 0.0013 \pm 0.0009$, where the first error is statistical, the second is systematic, and the third is the uncertainty due to the D branching fraction. We combine first two in quadrature.

² AKERS 95Q reports $[B(\bar{D} \rightarrow D^{*+} \ell^+ \nu_\ell X) \times B(D^{*+} \rightarrow D^0 \pi^+) \times B(D^0 \rightarrow K^- \pi^+)] = ((7.53 \pm 0.47 \pm 0.56) \times 10^{-4})$ and uses $B(D^{*+} \rightarrow D^0 \pi^+) = 0.681 \pm 0.013$ and $B(D^0 \rightarrow K^- \pi^+) = 0.0401 \pm 0.0014$ to obtain the above result. The first error is the experiments error and the second error is the systematic error from the D^{*+} and D^0 branching ratios.

$\Gamma(D^{*-} \pi^- \ell^+ \nu_\ell \text{ anything})/\Gamma_{\text{total}}$					Γ_{17}/Γ
VALUE	DOCUMENT ID	TECN	COMMENT		

0.0006 ± 0.0007 ± 0.0002				
	ABREU	00R DLPH	$e^+e^- \rightarrow Z$	

$\Gamma(D^{*-} \pi^+ \ell^+ \nu_\ell \text{ anything})/\Gamma_{\text{total}}$					Γ_{18}/Γ
VALUE	DOCUMENT ID	TECN	COMMENT		

0.0048 ± 0.0009 ± 0.0005				
	ABREU	00R DLPH	$e^+e^- \rightarrow Z$	

$\Gamma(\bar{D}_j^0 \ell^+ \nu_\ell \text{ anything} \times B(\bar{D}_j^0 \rightarrow D^{*+} \pi^-))/\Gamma_{\text{total}}$					Γ_{19}/Γ
VALUE (units 10^{-3})	DOCUMENT ID	TECN	COMMENT		

2.64 ± 0.79 ± 0.39				
	ABBIENDI	03M OPAL	$e^+e^- \rightarrow Z$	

• • • We do not use the following data for averages, fits, limits, etc. • • •

6.1 ± 1.3 ± 1.3	AKERS	95Q OPAL	Repl. by ABBIENDI 03M	
-----------------	-------	----------	-----------------------	--

$\Gamma(D_j^- \ell^+ \nu_\ell \text{ anything} \times B(D_j^- \rightarrow D^0 \pi^-))/\Gamma_{\text{total}}$					Γ_{20}/Γ
VALUE (units 10^{-3})	DOCUMENT ID	TECN	COMMENT		

7.0 ± 1.9 ± 1.2				
	AKERS	95Q OPAL	$e^+e^- \rightarrow Z$	

Meson Particle Listings

 $B^\pm/B^0/B_s^0/b$ -baryon ADMIXTURE

$\Gamma(\overline{D}_2^*(2460)^0 \ell^+ \nu_\ell \text{ anything} \times B(\overline{D}_2^*(2460)^0 \rightarrow D^{*-} \pi^+))/\Gamma_{\text{total}}$		Γ_{21}/Γ	
VALUE (units 10^{-3})	CL%	DOCUMENT ID	TECN COMMENT
<1.4	90	ABBIENDI	03M OPAL $e^+ e^- \rightarrow Z$

$\Gamma(D_2^*(2460)^- \ell^+ \nu_\ell \text{ anything} \times B(D_2^*(2460)^- \rightarrow D^0 \pi^-))/\Gamma_{\text{total}}$		Γ_{22}/Γ	
VALUE (units 10^{-3})		DOCUMENT ID	TECN COMMENT
$4.2 \pm 1.3^{+0.7}_{-1.2}$		AKERS	95Q OPAL $e^+ e^- \rightarrow Z$

$\Gamma(\overline{D}_2^*(2460)^0 \ell^+ \nu_\ell \text{ anything} \times B(\overline{D}_2^*(2460)^0 \rightarrow D^- \pi^+))/\Gamma_{\text{total}}$		Γ_{23}/Γ	
VALUE (units 10^{-3})		DOCUMENT ID	TECN COMMENT
$1.6 \pm 0.7 \pm 0.3$		AKERS	95Q OPAL $e^+ e^- \rightarrow Z$

$\Gamma(\text{charmless } \ell \nu_\ell)/\Gamma_{\text{total}}$		Γ_{24}/Γ	
"OUR EVALUATION" is an average of the data listed below performed by the LEP Heavy Flavour Steering Group. The averaging procedure takes into account correlations between the measurements.			

VALUE	DOCUMENT ID	TECN	COMMENT
0.00171 ± 0.00052 OUR EVALUATION			
0.0017 ± 0.0004 OUR AVERAGE			
0.00163 ± 0.00053 ± 0.00055 -0.00062	1 ABBIENDI	01R OPAL	$e^+ e^- \rightarrow Z$
0.00157 ± 0.00035 ± 0.00055	2 ABREU	00D DLPH	$e^+ e^- \rightarrow Z$
0.00173 ± 0.00055 ± 0.00055	3 BARATE	99G ALEP	$e^+ e^- \rightarrow Z$
0.0033 ± 0.0010 ± 0.0017	4 ACCIARRI	98K L3	$e^+ e^- \rightarrow Z$

- Obtained from the best fit of the MC simulated events to the data based on the $b \rightarrow X_{\ell} \ell \nu$ neutral network output distributions.
- ABREU 00D result obtained from a fit to the numbers of decays in $b \rightarrow u$ enriched and depleted samples and their lepton spectra, and assuming $|V_{cb}| = 0.0384 \pm 0.0033$ and $\tau_b = 1.564 \pm 0.014$ ps.
- Uses lifetime tagged $b\bar{b}$ sample.
- ACCIARRI 98K assumes $R_b = 0.2174 \pm 0.0009$ at Z decay.

$\Gamma(\tau^+ \nu_\tau \text{ anything})/\Gamma_{\text{total}}$		Γ_{25}/Γ	
VALUE (units 10^{-2})	EVTS	DOCUMENT ID	TECN COMMENT
2.41 ± 0.23 OUR AVERAGE			
2.78 ± 0.18 ± 0.51		1 ABBIENDI	01Q OPAL $e^+ e^- \rightarrow Z$
2.43 ± 0.20 ± 0.25		2 BARATE	01E ALEP $e^+ e^- \rightarrow Z$
2.19 ± 0.24 ± 0.39		3 ABREU	00C DLPH $e^+ e^- \rightarrow Z$
1.7 ± 0.5 ± 1.1		4,5 ACCIARRI	96C L3 $e^+ e^- \rightarrow Z$
2.4 ± 0.7 ± 0.8	1032	6 ACCIARRI	94C L3 $e^+ e^- \rightarrow Z$
• • • We do not use the following data for averages, fits, limits, etc. • • •			
2.75 ± 0.30 ± 0.37	405	7 BUSKULIC	95 ALEP Repl. by BARATE 01E
4.08 ± 0.76 ± 0.62		BUSKULIC	93B ALEP Repl. by BUSKULIC 95

- ABBIENDI 01Q uses a missing energy technique.
- The energy-flow and b -tagging algorithms were used.
- Uses the missing energy in $Z \rightarrow b\bar{b}$ decays without identifying leptons.
- ACCIARRI 96C result obtained from missing energy spectrum.
- Assumes Standard Model value for R_b .
- This is a direct result using tagged $b\bar{b}$ events at the Z, but species are not separated.
- BUSKULIC 95 uses missing-energy technique.

$\Gamma(D^{*-} \tau \nu_\tau \text{ anything})/\Gamma_{\text{total}}$		Γ_{26}/Γ	
VALUE		DOCUMENT ID	TECN COMMENT
(0.88 ± 0.31 ± 0.28) × 10⁻²		1 BARATE	01E ALEP $e^+ e^- \rightarrow Z$

- The energy-flow and b -tagging algorithms were used.

$\Gamma(\overline{b} \rightarrow \overline{c} \rightarrow \ell^+ \nu_\ell \text{ anything})/\Gamma_{\text{total}}$		Γ_{27}/Γ	
"OUR EVALUATION" is an average of the data listed below, excluding all asymmetry measurements, performed by the LEP Electroweak Working Group as described in the "Note on the Z boson" in the Z Particle Listings.			

VALUE	DOCUMENT ID	TECN	COMMENT
0.0802 ± 0.0019 OUR EVALUATION			
0.0817 ± 0.0020 OUR AVERAGE			
0.0818 ± 0.0015 ± 0.0024 -0.0026	1 HEISTER	02G ALEP	$e^+ e^- \rightarrow Z$
0.0798 ± 0.0022 ± 0.0025 -0.0029	2 ABREU	01L DLPH	$e^+ e^- \rightarrow Z$
0.0840 ± 0.0016 ± 0.0039 -0.0036	3 ABBIENDI	00E OPAL	$e^+ e^- \rightarrow Z$
• • • We do not use the following data for averages, fits, limits, etc. • • •			
0.0770 ± 0.0097 ± 0.0046	4 ABREU	95D DLPH	$e^+ e^- \rightarrow Z$
0.082 ± 0.003 ± 0.012	5 BUSKULIC	94G ALEP	$e^+ e^- \rightarrow Z$
0.077 ± 0.004 ± 0.007	6 AKERS	93B OPAL	Repl. by ABBI- ENDI 00E

- Uses the combination of lepton transverse momentum spectrum and the correlation between the charge of the lepton and opposite jet charge. The first error is statistic and the second error is the total systematic error including the modeling.
- The experimental systematic and model uncertainties are combined in quadrature.
- ABBIENDI 00E result is determined by comparing the distribution of several kinematic variables of leptonic events in a lifetime tagged $Z \rightarrow b\bar{b}$ sample using artificial neural network techniques. The first error is statistic; the second error is the total systematic error.
- ABREU 95D give systematic errors ± 0.0033 (model) and 0.0032 (R_c). We combine these in quadrature. This result is from the same global fit as their $\Gamma(\overline{b} \rightarrow \ell^+ \nu_\ell X)$ data.
- BUSKULIC 94G uses e and μ events. This value is from the same global fit as their $\Gamma(\overline{b} \rightarrow \ell^+ \nu_\ell \text{ anything})/\Gamma_{\text{total}}$ data.
- AKERS 93B analysis performed using single and dilepton events.

$\Gamma(c \rightarrow \ell^+ \nu \text{ anything})/\Gamma_{\text{total}}$		Γ_{28}/Γ	
VALUE		DOCUMENT ID	TECN COMMENT
0.0161 ± 0.0020 ± 0.0034 -0.0047		1 ABREU	01L DLPH $e^+ e^- \rightarrow Z$

- The experimental systematic and model uncertainties are combined in quadrature.

$\Gamma(\overline{D}^0 \text{ anything})/\Gamma_{\text{total}}$		Γ_{29}/Γ	
VALUE		DOCUMENT ID	TECN COMMENT
0.587 ± 0.028 ± 0.005		1 BUSKULIC	96Y ALEP $e^+ e^- \rightarrow Z$

- BUSKULIC 96Y reports 0.605 ± 0.024 ± 0.016 from a measurement of $[\Gamma(\overline{D} \rightarrow \overline{D}^0 \text{ anything})/\Gamma_{\text{total}}] \times [B(D^0 \rightarrow K^- \pi^+)]$ assuming $B(D^0 \rightarrow K^- \pi^+) = 0.0383$, which we rescale to our best value $B(D^0 \rightarrow K^- \pi^+) = (3.947 \pm 0.030) \times 10^{-2}$. Our first error is their experiment's error and our second error is the systematic error from using our best value.

$\Gamma(D^0 D_s^\pm \text{ anything})/\Gamma_{\text{total}}$		Γ_{30}/Γ	
VALUE		DOCUMENT ID	TECN COMMENT
0.091 ± 0.020 ± 0.034 -0.018 - 0.022		1 BARATE	98Q ALEP $e^+ e^- \rightarrow Z$

- The systematic error includes the uncertainties due to the charm branching ratios.

$\Gamma(D^\mp D_s^\pm \text{ anything})/\Gamma_{\text{total}}$		Γ_{31}/Γ	
VALUE		DOCUMENT ID	TECN COMMENT
0.040 ± 0.017 ± 0.016 -0.014 - 0.011		1 BARATE	98Q ALEP $e^+ e^- \rightarrow Z$

- The systematic error includes the uncertainties due to the charm branching ratios.

$[\Gamma(D^0 D_s^\pm \text{ anything}) + \Gamma(D^\mp D_s^\pm \text{ anything})]/\Gamma_{\text{total}}$		$(\Gamma_{30} + \Gamma_{31})/\Gamma$	
VALUE		DOCUMENT ID	TECN COMMENT
0.131 ± 0.026 ± 0.048 -0.022 - 0.031		1 BARATE	98Q ALEP $e^+ e^- \rightarrow Z$

- The systematic error includes the uncertainties due to the charm branching ratios.

$\Gamma(\overline{D}^0 D^0 \text{ anything})/\Gamma_{\text{total}}$		Γ_{32}/Γ	
VALUE		DOCUMENT ID	TECN COMMENT
0.051 ± 0.016 ± 0.012 -0.014 - 0.011		1 BARATE	98Q ALEP $e^+ e^- \rightarrow Z$

- The systematic error includes the uncertainties due to the charm branching ratios.

$\Gamma(D^0 D^\pm \text{ anything})/\Gamma_{\text{total}}$		Γ_{33}/Γ	
VALUE		DOCUMENT ID	TECN COMMENT
0.027 ± 0.015 ± 0.010 -0.013 - 0.009		1 BARATE	98Q ALEP $e^+ e^- \rightarrow Z$

- The systematic error includes the uncertainties due to the charm branching ratios.

$[\Gamma(\overline{D}^0 D^0 \text{ anything}) + \Gamma(D^0 D^\pm \text{ anything})]/\Gamma_{\text{total}}$		$(\Gamma_{32} + \Gamma_{33})/\Gamma$	
VALUE		DOCUMENT ID	TECN COMMENT
0.078 ± 0.020 ± 0.018 -0.018 - 0.016		1 BARATE	98Q ALEP $e^+ e^- \rightarrow Z$

- The systematic error includes the uncertainties due to the charm branching ratios.

$\Gamma(D^\pm D^\mp \text{ anything})/\Gamma_{\text{total}}$		Γ_{34}/Γ	
VALUE	CL%	DOCUMENT ID	TECN COMMENT
<0.009	90	BARATE	98Q ALEP $e^+ e^- \rightarrow Z$

$[\Gamma(D^0 \text{ anything}) + \Gamma(D^+ \text{ anything})]/\Gamma_{\text{total}}$		$(\Gamma_{35} + \Gamma_{36})/\Gamma$	
VALUE		DOCUMENT ID	TECN COMMENT
0.093 ± 0.017 ± 0.014		1 ABDALLAH	03E DLPH $e^+ e^- \rightarrow Z$

- The second error is the total of systematic uncertainties including the branching fractions used in the measurement.

$\Gamma(D^- \text{ anything})/\Gamma_{\text{total}}$		Γ_{37}/Γ	
VALUE		DOCUMENT ID	TECN COMMENT
0.227 ± 0.016 ± 0.004		1 BUSKULIC	96Y ALEP $e^+ e^- \rightarrow Z$

- BUSKULIC 96Y reports 0.234 ± 0.013 ± 0.010 from a measurement of $[\Gamma(\overline{D} \rightarrow D^- \text{ anything})/\Gamma_{\text{total}}] \times [B(D^+ \rightarrow K^- 2\pi^+)]$ assuming $B(D^+ \rightarrow K^- 2\pi^+) = 0.091$, which we rescale to our best value $B(D^+ \rightarrow K^- 2\pi^+) = (9.38 \pm 0.16) \times 10^{-2}$. Our first error is their experiment's error and our second error is the systematic error from using our best value.

$\Gamma(D^*(2010)^+ \text{ anything})/\Gamma_{\text{total}}$		Γ_{38}/Γ	
VALUE		DOCUMENT ID	TECN COMMENT
0.173 ± 0.016 ± 0.012		1 ACKERSTAFF	98E OPAL $e^+ e^- \rightarrow Z$

- Uses lepton tags to select $Z \rightarrow b\bar{b}$ events.

$\Gamma(D_1(2420)^0 \text{ anything})/\Gamma_{\text{total}}$		Γ_{39}/Γ	
VALUE		DOCUMENT ID	TECN COMMENT
0.050 ± 0.014 ± 0.006		1 ACKERSTAFF	97W OPAL $e^+ e^- \rightarrow Z$

- ACKERSTAFF 97W assumes $B(D_1^*(2460)^0 \rightarrow D^{*+} \pi^-) = 0.21 \pm 0.04$ and $\Gamma_{b\overline{b}}/\Gamma_{\text{hadrons}} = 0.216$ at Z decay.

$\Gamma(D^*(2010)^\mp D_s^\pm \text{ anything})/\Gamma_{\text{total}}$	DOCUMENT ID	TECN	COMMENT	Γ_{40}/Γ
VALUE $0.033 \pm 0.010 + 0.012$ $-0.009 - 0.009$	1	BARATE	98Q ALEP $e^+e^- \rightarrow Z$	

¹ The systematic error includes the uncertainties due to the charm branching ratios.

$\Gamma(D^0 D^*(2010)^\pm \text{ anything})/\Gamma_{\text{total}}$	DOCUMENT ID	TECN	COMMENT	Γ_{41}/Γ
VALUE $0.030 \pm 0.009 + 0.007$ $-0.008 - 0.005$	1	BARATE	98Q ALEP $e^+e^- \rightarrow Z$	

¹ The systematic error includes the uncertainties due to the charm branching ratios.

$\Gamma(D^*(2010)^\pm D^\mp \text{ anything})/\Gamma_{\text{total}}$	DOCUMENT ID	TECN	COMMENT	Γ_{42}/Γ
VALUE $0.025 \pm 0.019 + 0.006$ $-0.009 - 0.005$	1	BARATE	98Q ALEP $e^+e^- \rightarrow Z$	

¹ The systematic error includes the uncertainties due to the charm branching ratios.

$\Gamma(D^*(2010)^\pm D^*(2010)^\mp \text{ anything})/\Gamma_{\text{total}}$	DOCUMENT ID	TECN	COMMENT	Γ_{43}/Γ
VALUE 0.012 ± 0.004 -0.003 ± 0.002	1	BARATE	98Q ALEP $e^+e^- \rightarrow Z$	

¹ The systematic error includes the uncertainties due to the charm branching ratios.

$\Gamma(\bar{D} D \text{ anything})/\Gamma_{\text{total}}$	DOCUMENT ID	TECN	COMMENT	Γ_{44}/Γ
VALUE $0.10 \pm 0.032 + 0.107$ -0.095	1	ABBIENDI	04I OPAL $e^+e^- \rightarrow Z$	

¹ Measurement performed using an inclusive identification of B mesons and the D candidates.

$\Gamma(D_s^*(2460)^0 \text{ anything})/\Gamma_{\text{total}}$	DOCUMENT ID	TECN	COMMENT	Γ_{45}/Γ
VALUE $0.047 \pm 0.024 \pm 0.013$	1	ACKERSTAFF	97W OPAL $e^+e^- \rightarrow Z$	

¹ ACKERSTAFF 97W assumes $B(D_s^*(2460)^0 \rightarrow D^* \pi^+) = 0.21 \pm 0.04$ and $\Gamma_{b\bar{D}}/\Gamma_{\text{hadrons}} = 0.216$ at Z decay.

$\Gamma(D_s^- \text{ anything})/\Gamma_{\text{total}}$	DOCUMENT ID	TECN	COMMENT	Γ_{46}/Γ
VALUE $0.147 \pm 0.017 \pm 0.013$	1	BUSKULIC	96Y ALEP $e^+e^- \rightarrow Z$	

¹ BUSKULIC 96Y reports $0.183 \pm 0.019 \pm 0.009$ from a measurement of $[\Gamma(\bar{D} \rightarrow D_s^- \text{ anything})/\Gamma_{\text{total}}] \times [B(D_s^+ \rightarrow \phi \pi^+)]$ assuming $B(D_s^+ \rightarrow \phi \pi^+) = 0.036$, which we rescale to our best value $B(D_s^+ \rightarrow \phi \pi^+) = (4.5 \pm 0.4) \times 10^{-2}$. Our first error is their experiment's error and our second error is the systematic error from using our best value.

$\Gamma(D_s^+ \text{ anything})/\Gamma_{\text{total}}$	DOCUMENT ID	TECN	COMMENT	Γ_{47}/Γ
VALUE $0.101 \pm 0.010 \pm 0.029$	1	ABDALLAH	03E DLPH $e^+e^- \rightarrow Z$	

¹ The second error is the total of systematic uncertainties including the branching fractions used in the measurement.

$\Gamma(b \rightarrow \Lambda_c^+ \text{ anything})/\Gamma_{\text{total}}$	DOCUMENT ID	TECN	COMMENT	Γ_{48}/Γ
VALUE $0.077 \pm 0.011 \pm 0.004$	1	BUSKULIC	96Y ALEP $e^+e^- \rightarrow Z$	

¹ BUSKULIC 96Y reports $0.110 \pm 0.014 \pm 0.006$ from a measurement of $[\Gamma(b \rightarrow \Lambda_c^+ \text{ anything})/\Gamma_{\text{total}}] \times [B(\Lambda_c^+ \rightarrow p K^- \pi^+)]$ assuming $B(\Lambda_c^+ \rightarrow p K^- \pi^+) = 0.044$, which we rescale to our best value $B(\Lambda_c^+ \rightarrow p K^- \pi^+) = (6.28 \pm 0.32) \times 10^{-2}$. Our first error is their experiment's error and our second error is the systematic error from using our best value.

$\Gamma(\bar{\tau}/c \text{ anything})/\Gamma_{\text{total}}$	DOCUMENT ID	TECN	COMMENT	Γ_{49}/Γ
VALUE 1.162 ± 0.032 OUR AVERAGE				

1.12 ± 0.11 -0.10	1	ABBIENDI	04I OPAL $e^+e^- \rightarrow Z$	
1.166 $\pm 0.031 \pm 0.080$	2	ABREU	00 DLPH $e^+e^- \rightarrow Z$	
1.147 ± 0.041	3	ABREU	98D DLPH $e^+e^- \rightarrow Z$	
1.230 $\pm 0.036 \pm 0.065$	4	BUSKULIC	96Y ALEP $e^+e^- \rightarrow Z$	

¹ Measurement performed using an inclusive identification of B mesons and the D candidates.

² Evaluated via summation of exclusive and inclusive channels.

³ ABREU 98D results are extracted from a fit to the b -tagging probability distribution based on the impact parameter.

⁴ BUSKULIC 96Y assumes PDG 96 production fractions for B^0, B^+, B_s, b baryons, and PDG 96 branching ratios for charm decays. This is sum of their inclusive $\bar{D}^0, D^-, \bar{D}_s^-,$ and Λ_c branching ratios, corrected to include inclusive Ξ_c and charmonium.

$\Gamma(J/\psi(1S) \text{ anything})/\Gamma_{\text{total}}$	CL% EVTS	DOCUMENT ID	TECN	COMMENT	Γ_{50}/Γ
VALUE (units 10^{-2}) 1.16 ± 0.10 OUR AVERAGE					

1.12 $\pm 0.12 \pm 0.10$		1	ABREU	94P DLPH $e^+e^- \rightarrow Z$	
1.16 $\pm 0.16 \pm 0.14$	121	2	ADRIANI	93J L3 $e^+e^- \rightarrow Z$	
1.21 $\pm 0.13 \pm 0.08$			BUSKULIC	92G ALEP $e^+e^- \rightarrow Z$	

• • • We do not use the following data for averages, fits, limits, etc. • • •

1.3 $\pm 0.2 \pm 0.2$		3	ADRIANI	92 L3 $e^+e^- \rightarrow Z$	
<4.9	90		MATTEUZZI	83 MRK2 $E_{\text{cm}}^{\text{ee}} = 29$ GeV	

¹ ABREU 94P is an inclusive measurement from b decays at the Z . Uses $J/\psi(1S) \rightarrow e^+e^-$ and $\mu^+\mu^-$ channels. Assumes $\Gamma(Z \rightarrow b\bar{b})/\Gamma_{\text{hadron}} = 0.22$.

² ADRIANI 93J is an inclusive measurement from b decays at the Z . Uses $J/\psi(1S) \rightarrow \mu^+\mu^-$ and $J/\psi(1S) \rightarrow e^+e^-$ channels.

³ ADRIANI 92 measurement is an inclusive result for $B(Z \rightarrow J/\psi(1S) X) = (4.1 \pm 0.7 \pm 0.3) \times 10^{-3}$ which is used to extract the b -hadron contribution to $J/\psi(1S)$ production.

$\Gamma(\psi(2S) \text{ anything})/\Gamma_{\text{total}}$	DOCUMENT ID	TECN	COMMENT	Γ_{51}/Γ
VALUE $0.0048 \pm 0.0022 \pm 0.0010$	1	ABREU	94P DLPH $e^+e^- \rightarrow Z$	

• • • We do not use the following data for averages, fits, limits, etc. • • •

¹ ABREU 94P is an inclusive measurement from b decays at the Z . Uses $\psi(2S) \rightarrow J/\psi(1S) \pi^+ \pi^-, J/\psi(1S) \rightarrow \mu^+ \mu^-$ channels. Assumes $\Gamma(Z \rightarrow b\bar{b})/\Gamma_{\text{hadron}} = 0.22$.

$\Gamma(\psi(2S) \text{ anything})/\Gamma(J/\psi(1S) \text{ anything})$	DOCUMENT ID	TECN	COMMENT	Γ_{51}/Γ_{50}
VALUE 0.263 ± 0.013 OUR AVERAGE				

¹ AAJJ 20G LHCb pp at 13 TeV
^{2,3} AAJJ 12BD LHCb pp at 7 TeV
^{4,5} CHATRCHYAN 12AK CMS pp at 7 TeV

¹ The first error is statistic; the second error is the total systematic error.

² AAJJ 12BD reports $B(b \rightarrow \psi(2S) X) = (3.08 \pm 0.07 \pm 0.36 \pm 0.27) \times 10^{-3}$ and we divided our best value of $B(b \rightarrow \psi(1S) X) = (1.16 \pm 0.10) \times 10^{-2}$ as the ratio listed here.

³ Assumes lepton universality imposing $B(\psi(2s) \rightarrow \mu^+ \mu^-) = B(\psi(2s) \rightarrow e^+ e^-)$.

⁴ CHATRCHYAN 12AK really reports $\Gamma_{51}/\Gamma = (3.08 \pm 0.12 \pm 0.13 \pm 0.42) \times 10^{-3}$ assuming PDG 10 value of $\Gamma_{50}/\Gamma = (1.16 \pm 0.10) \times 10^{-2}$ which we present as a ratio of $\Gamma_{51}/\Gamma_{50} = (26.5 \pm 1.0 \pm 1.1 \pm 2.8) \times 10^{-2}$.

⁵ CHATRCHYAN 12AK reports $(26.5 \pm 1.0 \pm 1.1 \pm 2.8) \times 10^{-2}$ from a measurement of $[\Gamma(\bar{D} \rightarrow \psi(2S) \text{ anything})/\Gamma(\bar{D} \rightarrow J/\psi(1S) \text{ anything})] \times [B(\psi(2S) \rightarrow \mu^+ \mu^-)] / [B(J/\psi(1S) \rightarrow \mu^+ \mu^-)]$ assuming $B(\psi(2S) \rightarrow \mu^+ \mu^-) = (7.7 \pm 0.8) \times 10^{-3}$, $B(J/\psi(1S) \rightarrow \mu^+ \mu^-) = (5.93 \pm 0.06) \times 10^{-2}$, which we rescale to our best values $B(\psi(2S) \rightarrow \mu^+ \mu^-) = (8.0 \pm 0.6) \times 10^{-3}$, $B(J/\psi(1S) \rightarrow \mu^+ \mu^-) = (5.961 \pm 0.033) \times 10^{-2}$. Our first error is their experiment's error and our second error is the systematic error from using our best values.

$\Gamma(\chi_{c0}(1P) \text{ anything})/\Gamma(\eta_c(1S) \text{ anything})$	DOCUMENT ID	TECN	COMMENT	Γ_{52}/Γ_{56}
VALUE $0.32 \pm 0.06 \pm 0.05$	1	AAJJ	17BB LHCb pp at 7, 8 TeV	

¹ AAJJ 17BB reports $[\Gamma(\bar{D} \rightarrow \chi_{c0}(1P) \text{ anything})/\Gamma(\bar{D} \rightarrow \eta_c(1S) \text{ anything})] / [B(\eta_c(1S) \rightarrow \phi \phi)] \times [B(\chi_{c0}(1P) \rightarrow \phi \phi)] = 0.147 \pm 0.023 \pm 0.011$ which we multiply or divide by our best values $B(\eta_c(1S) \rightarrow \phi \phi) = (1.74 \pm 0.19) \times 10^{-3}$, $B(\chi_{c0}(1P) \rightarrow \phi \phi) = (8.0 \pm 0.7) \times 10^{-4}$. Our first error is their experiment's error and our second error is the systematic error from using our best values.

$\Gamma(\chi_{c1}(1P) \text{ anything})/\Gamma_{\text{total}}$	EVTS	DOCUMENT ID	TECN	COMMENT	Γ_{53}/Γ
VALUE 0.014 ± 0.004 OUR AVERAGE					

0.0112 ± 0.0057 -0.0050 ± 0.0003	1	ABREU	94P DLPH $e^+e^- \rightarrow Z$	
0.019 $\pm 0.007 \pm 0.001$	19	2	ADRIANI	93J L3 $e^+e^- \rightarrow Z$

¹ ABREU 94P reports $0.014 \pm 0.006 \pm 0.002$ from a measurement of $[\Gamma(\bar{D} \rightarrow \chi_{c1}(1P) \text{ anything})/\Gamma_{\text{total}}] \times [B(\chi_{c1}(1P) \rightarrow \gamma J/\psi(1S))] / [B(\chi_{c1}(1P) \rightarrow \gamma J/\psi(1S))] = 0.273 \pm 0.016$, which we rescale to our best value $B(\chi_{c1}(1P) \rightarrow \gamma J/\psi(1S)) = (34.3 \pm 1.0) \times 10^{-2}$. Our first error is their experiment's error and our second error is the systematic error from using our best value. Assumes no $\chi_{c2}(1P)$ and $\Gamma(Z \rightarrow b\bar{b})/\Gamma_{\text{hadron}} = 0.22$.

² ADRIANI 93J reports $0.024 \pm 0.009 \pm 0.002$ from a measurement of $[\Gamma(\bar{D} \rightarrow \chi_{c1}(1P) \text{ anything})/\Gamma_{\text{total}}] \times [B(\chi_{c1}(1P) \rightarrow \gamma J/\psi(1S))] / [B(\chi_{c1}(1P) \rightarrow \gamma J/\psi(1S))] = 0.273 \pm 0.016$, which we rescale to our best value $B(\chi_{c1}(1P) \rightarrow \gamma J/\psi(1S)) = (34.3 \pm 1.0) \times 10^{-2}$. Our first error is their experiment's error and our second error is the systematic error from using our best value.

$\Gamma(\chi_{c1}(1P) \text{ anything})/\Gamma(J/\psi(1S) \text{ anything})$	EVTS	DOCUMENT ID	TECN	COMMENT	Γ_{53}/Γ_{50}
VALUE 1.92 ± 0.82	121	1	ADRIANI	93J L3 $e^+e^- \rightarrow Z$	

• • • We do not use the following data for averages, fits, limits, etc. • • •

¹ ADRIANI 93J is a ratio of inclusive measurements from b decays at the Z using only the $J/\psi(1S) \rightarrow \mu^+ \mu^-$ channel since some systematics cancel.

Meson Particle Listings

$B^\pm/B^0/B_s^0/b$ -baryon ADMIXTURE

$\Gamma(\chi_{c1}(1P)\text{ anything})/\Gamma(\chi_{c0}(1P)\text{ anything})$ Γ_{53}/Γ_{52}

VALUE	DOCUMENT ID	TECN	COMMENT
0.96 ± 0.21 ± 0.15	¹ AAIJ	17Bb LHCb	pp at 7, 8 TeV

¹ AAIJ 17Bb reports $[\Gamma(\bar{b} \rightarrow \chi_{c1}(1P)\text{ anything})/\Gamma(\bar{b} \rightarrow \chi_{c0}(1P)\text{ anything})] / [B(\chi_{c0}(1P) \rightarrow \phi\phi) \times B(\chi_{c1}(1P) \rightarrow \phi\phi)] = 0.50 \pm 0.11 \pm 0.01$ which we multiply or divide by our best values $B(\chi_{c0}(1P) \rightarrow \phi\phi) = (8.0 \pm 0.7) \times 10^{-4}$, $B(\chi_{c1}(1P) \rightarrow \phi\phi) = (4.2 \pm 0.5) \times 10^{-4}$. Our first error is their experiment's error and our second error is the systematic error from using our best values.

$\Gamma(\chi_{c1}(1P)\text{ anything})/\Gamma(\eta_c(1S)\text{ anything})$ Γ_{53}/Γ_{56}

VALUE	DOCUMENT ID	TECN	COMMENT
0.31 ± 0.07 ± 0.05	¹ AAIJ	17Bb LHCb	pp at 7, 8 TeV

¹ AAIJ 17Bb reports $[\Gamma(\bar{b} \rightarrow \chi_{c1}(1P)\text{ anything})/\Gamma(\bar{b} \rightarrow \eta_c(1S)\text{ anything})] / [B(\eta_c(1S) \rightarrow \phi\phi) \times B(\chi_{c1}(1P) \rightarrow \phi\phi)] = 0.073 \pm 0.016 \pm 0.006$ which we multiply or divide by our best values $B(\eta_c(1S) \rightarrow \phi\phi) = (1.74 \pm 0.19) \times 10^{-3}$, $B(\chi_{c1}(1P) \rightarrow \phi\phi) = (4.2 \pm 0.5) \times 10^{-4}$. Our first error is their experiment's error and our second error is the systematic error from using our best values.

$\Gamma(\chi_{c2}(1P)\text{ anything})/\Gamma(\chi_{c0}(1P)\text{ anything})$ Γ_{54}/Γ_{52}

VALUE	DOCUMENT ID	TECN	COMMENT
0.42 ± 0.08 ± 0.05	¹ AAIJ	17Bb LHCb	pp at 7, 8 TeV

¹ AAIJ 17Bb reports $[\Gamma(\bar{b} \rightarrow \chi_{c2}(1P)\text{ anything})/\Gamma(\bar{b} \rightarrow \chi_{c0}(1P)\text{ anything})] / [B(\chi_{c0}(1P) \rightarrow \phi\phi) \times B(\chi_{c2}(1P) \rightarrow \phi\phi)] = 0.56 \pm 0.10 \pm 0.01$ which we multiply or divide by our best values $B(\chi_{c0}(1P) \rightarrow \phi\phi) = (8.0 \pm 0.7) \times 10^{-4}$, $B(\chi_{c2}(1P) \rightarrow \phi\phi) = (1.06 \pm 0.09) \times 10^{-3}$. Our first error is their experiment's error and our second error is the systematic error from using our best values.

$\Gamma(\chi_{c2}(1P)\text{ anything})/\Gamma(\eta_c(1S)\text{ anything})$ Γ_{54}/Γ_{56}

VALUE	DOCUMENT ID	TECN	COMMENT
0.133 ± 0.023 ± 0.018	¹ AAIJ	17Bb LHCb	pp at 7, 8 TeV

¹ AAIJ 17Bb reports $[\Gamma(\bar{b} \rightarrow \chi_{c2}(1P)\text{ anything})/\Gamma(\bar{b} \rightarrow \eta_c(1S)\text{ anything})] / [B(\eta_c(1S) \rightarrow \phi\phi) \times B(\chi_{c2}(1P) \rightarrow \phi\phi)] = 0.081 \pm 0.013 \pm 0.005$ which we multiply or divide by our best values $B(\eta_c(1S) \rightarrow \phi\phi) = (1.74 \pm 0.19) \times 10^{-3}$, $B(\chi_{c2}(1P) \rightarrow \phi\phi) = (1.06 \pm 0.09) \times 10^{-3}$. Our first error is their experiment's error and our second error is the systematic error from using our best values.

$\Gamma(\chi_c(2P)\text{ anything, } \chi_c \rightarrow \phi\phi)/\Gamma_{total}$ Γ_{55}/Γ

VALUE	CL%	DOCUMENT ID	TECN	COMMENT
<2.8 × 10⁻⁷	95	AAIJ	17Bb LHCb	pp at 7, 8 TeV

$\Gamma(\eta_c(1S)\text{ anything})/\Gamma(J/\psi(1S)\text{ anything})$ Γ_{56}/Γ_{50}

VALUE	DOCUMENT ID	TECN	COMMENT
0.48 ± 0.03 ± 0.06	AAIJ	20H LHCb	pp at 13 TeV

$\Gamma(\eta_c(2S)\text{ anything, } \eta_c \rightarrow \phi\phi)/\Gamma(\eta_c(1S)\text{ anything})$ Γ_{57}/Γ_{56}

VALUE (units 10 ⁻⁵)	DOCUMENT ID	TECN	COMMENT
7.0 ± 2.0 ± 0.8	¹ AAIJ	17Bb LHCb	pp at 7, 8 TeV

¹ AAIJ 17Bb reports $[\Gamma(\bar{b} \rightarrow \eta_c(2S)\text{ anything, } \eta_c \rightarrow \phi\phi)/\Gamma(\bar{b} \rightarrow \eta_c(1S)\text{ anything})] / [B(\eta_c(1S) \rightarrow \phi\phi)] = 0.040 \pm 0.011 \pm 0.004$ which we multiply by our best value $B(\eta_c(1S) \rightarrow \phi\phi) = (1.74 \pm 0.19) \times 10^{-3}$. Our first error is their experiment's error and our second error is the systematic error from using our best value.

$\Gamma(\chi_{c1}(3872)\text{ anything, } \chi_{c1} \rightarrow \phi\phi)/\Gamma_{total}$ Γ_{58}/Γ

VALUE	CL%	DOCUMENT ID	TECN	COMMENT
<4.5 × 10⁻⁷	95	AAIJ	17Bb LHCb	pp at 7, 8 TeV

$\Gamma(\chi_{c0}(3915)\text{ anything, } \chi_{c0} \rightarrow \phi\phi)/\Gamma_{total}$ Γ_{59}/Γ

VALUE	CL%	DOCUMENT ID	TECN	COMMENT
<3.1 × 10⁻⁷	95	AAIJ	17Bb LHCb	pp at 7, 8 TeV

$\Gamma(\bar{\Sigma}^0)/\Gamma_{total}$ Γ_{60}/Γ

VALUE (units 10 ⁻⁴)	CL%	DOCUMENT ID	TECN	COMMENT
3.11 ± 0.80 ± 0.72		¹ BARATE	98i ALEP	$e^+e^- \rightarrow Z$

••• We do not use the following data for averages, fits, limits, etc. •••
 < 5.4 90 ² ADAM 96d DLPH $e^+e^- \rightarrow Z$
 < 12 90 ³ ADRIANI 93L L3 $e^+e^- \rightarrow Z$

¹ BARATE 98i uses lifetime tagged $Z \rightarrow b\bar{b}$ sample.
² ADAM 96d assumes $f_{B^0} = f_{B^-} = 0.39$ and $f_{B_s} = 0.12$.
³ ADRIANI 93L result is for $\bar{b} \rightarrow \bar{\Sigma}^0$ is performed inclusively.

$\Gamma(\bar{\Sigma}^0\nu)/\Gamma_{total}$ Γ_{61}/Γ

VALUE	CL%	DOCUMENT ID	TECN	COMMENT
<6.4 × 10⁻⁴	90	¹ BARATE	01E ALEP	$e^+e^- \rightarrow Z$

¹ The energy-flow and b -tagging algorithms were used.

$\Gamma(K^\pm\text{ anything})/\Gamma_{total}$ Γ_{62}/Γ

VALUE	DOCUMENT ID	TECN	COMMENT
0.74 ± 0.06 OUR AVERAGE			
0.72 ± 0.02 ± 0.06	BARATE	98v ALEP	$e^+e^- \rightarrow Z$
0.88 ± 0.05 ± 0.18	ABREU	95c DLPH	$e^+e^- \rightarrow Z$

$\Gamma(K_S^0\text{ anything})/\Gamma_{total}$ Γ_{63}/Γ

VALUE	DOCUMENT ID	TECN	COMMENT
0.290 ± 0.011 ± 0.027	ABREU	95c DLPH	$e^+e^- \rightarrow Z$

$\Gamma(\pi^\pm\text{ anything})/\Gamma_{total}$ Γ_{64}/Γ

VALUE	DOCUMENT ID	TECN	COMMENT
3.97 ± 0.02 ± 0.21	BARATE	98v ALEP	$e^+e^- \rightarrow Z$

$\Gamma(\pi^0\text{ anything})/\Gamma_{total}$ Γ_{65}/Γ

VALUE	DOCUMENT ID	TECN	COMMENT
2.78 ± 0.15 ± 0.60	¹ ADAM	96 DLPH	$e^+e^- \rightarrow Z$

¹ ADAM 96 measurement obtained from a fit to the rapidity distribution of $\pi^{0,s}$ in $Z \rightarrow bb$ events.

$\Gamma(\phi\text{ anything})/\Gamma_{total}$ Γ_{66}/Γ

VALUE	DOCUMENT ID	TECN	COMMENT
0.0282 ± 0.0013 ± 0.0019	ABBIENDI	00z OPAL	$e^+e^- \rightarrow Z$

$\Gamma(\rho/\omega\text{ anything})/\Gamma_{total}$ Γ_{67}/Γ

VALUE	DOCUMENT ID	TECN	COMMENT
0.131 ± 0.011 OUR AVERAGE			
0.131 ± 0.004 ± 0.011	BARATE	98v ALEP	$e^+e^- \rightarrow Z$
0.141 ± 0.018 ± 0.056	ABREU	95c DLPH	$e^+e^- \rightarrow Z$

$\Gamma(\Lambda/\bar{\Lambda}\text{ anything})/\Gamma_{total}$ Γ_{68}/Γ

VALUE	DOCUMENT ID	TECN	COMMENT
0.059 ± 0.006 OUR AVERAGE			
0.0587 ± 0.0046 ± 0.0048	ACKERSTAFF	97N OPAL	$e^+e^- \rightarrow Z$
0.059 ± 0.007 ± 0.009	ABREU	95c DLPH	$e^+e^- \rightarrow Z$

$\Gamma(b\text{-baryon anything})/\Gamma_{total}$ Γ_{69}/Γ

VALUE	DOCUMENT ID	TECN	COMMENT
0.102 ± 0.007 ± 0.027	¹ BARATE	98v ALEP	$e^+e^- \rightarrow Z$

¹ BARATE 98v assumes $B(B_S \rightarrow pX) = 8 \pm 4\%$ and $B(b\text{-baryon} \rightarrow pX) = 58 \pm 6\%$.

$\Gamma(\Xi_b^\pm\text{ anything})/\Gamma(\bar{\Lambda}_b^0\text{ anything})$ Γ_{71}/Γ_{70}

VALUE (units 10 ⁻²)	DOCUMENT ID	TECN	COMMENT
7.3 ± 1.7 OUR AVERAGE			
6.7 ± 0.5 ± 2.1	¹ AAIJ	19Ab LHCb	pp at 7 and 8 TeV
8.2 ± 0.7 ± 2.6	¹ AAIJ	19Ab LHCb	pp at 13 TeV

¹ Measured from $R = [B(\bar{b} \rightarrow \Xi_b^\pm) \times B(\Xi_b^\pm \rightarrow J/\psi \Xi^\pm)] / [B(\bar{b} \rightarrow \bar{\Lambda}_b^0) \times B(\bar{\Lambda}_b^0 \rightarrow J/\psi \bar{\Lambda}^0)]$ and assumes $\Gamma_{\Xi_b^\pm} \rightarrow J/\psi \Xi^\pm / \Gamma_{\bar{\Lambda}_b^0} \rightarrow J/\psi \bar{\Lambda}^0 = 3/2$ related through SU(3) flavor symmetry.

$\Gamma(\text{charged anything})/\Gamma_{total}$ Γ_{72}/Γ

VALUE	DOCUMENT ID	TECN	COMMENT
4.97 ± 0.03 ± 0.06	¹ ABREU	98H DLPH	$e^+e^- \rightarrow Z$

••• We do not use the following data for averages, fits, limits, etc. •••
 5.84 ± 0.04 ± 0.38 ABREU 95c DLPH Repl. by ABREU 98H

¹ ABREU 98H measurement excludes the contribution from K^0 and Λ decay.

$\Gamma(\text{hadron}^+\text{ hadron}^-)/\Gamma_{total}$ Γ_{73}/Γ

VALUE (units 10 ⁻⁵)	DOCUMENT ID	TECN	COMMENT
1.7 ± 1.0 ± 0.2	^{1,2} BUSKULIC	96v ALEP	$e^+e^- \rightarrow Z$

¹ BUSKULIC 96v assumes PDG 96 production fractions for B^0, B^+, B_s^+, b baryons.
² Average branching fraction of weakly decaying B hadrons into two long-lived charged hadrons, weighted by their production cross section and lifetimes.

$\Gamma(\text{charmless})/\Gamma_{total}$ Γ_{74}/Γ

VALUE	DOCUMENT ID	TECN	COMMENT
0.007 ± 0.021	¹ ABREU	98D DLPH	$e^+e^- \rightarrow Z$

¹ ABREU 98D results are extracted from a fit to the b -tagging probability distribution based on the impact parameter. The expected hidden charm contribution of 0.026 ± 0.004 has been subtracted.

$\Gamma(\mu^+\mu^-\text{ anything})/\Gamma_{total}$ Γ_{76}/Γ

VALUE	CL%	DOCUMENT ID	TECN	COMMENT
<3.2 × 10⁻⁴	90	ABBOTT	98B D0	$p\bar{p}$ 1.8 TeV

••• We do not use the following data for averages, fits, limits, etc. •••
 < 5.0 × 10⁻⁵ 90 ¹ ALBAJAR 91c UA1 $E_{cm}^{pp} = 630$ GeV
 < 0.02 95 ALTHOFF 84G TASS $E_{cm}^{ee} = 34.5$ GeV
 < 0.007 95 ADEVA 83 MRKJ $E_{cm}^{ee} = 30\text{--}38$ GeV
 < 0.007 95 BARTEL 83B JADE $E_{cm}^{ee} = 33\text{--}37$ GeV

¹ Both ABBOTT 98B and GLENN 98 claim that the efficiency quoted in ALBAJAR 91c was overestimated by a large factor.

$[\Gamma(e^+e^-\text{ anything}) + \Gamma(\mu^+\mu^-\text{ anything})]/\Gamma_{total}$ $(\Gamma_{75} + \Gamma_{76})/\Gamma$

VALUE	CL%	DOCUMENT ID	TECN	COMMENT
<0.008	90	MATTEUZZI	83 MRK2	$E_{cm}^{ee} = 29$ GeV

••• We do not use the following data for averages, fits, limits, etc. •••

$\Gamma(\nu\bar{\nu}\text{anything})/\Gamma_{\text{total}}$	DOCUMENT ID	TECN	COMMENT
$<3.9 \times 10^{-4}$	1 GROSSMAN 96	RVUE	$e^+e^- \rightarrow Z$
$<1.8 \times 10^{-3}$ at CL=90% using conservative simplifying assumptions.	1 GROSSMAN 96		limit is derived from the ALEPH BUSKULIC 95 limit $B^+ \rightarrow \tau^+ \nu_\tau$

χ_b AT HIGH ENERGY

For a discussion of $B\text{-}\bar{B}$ mixing, see the note on " $B^0\text{-}\bar{B}^0$ Mixing" in the B^0 Particle Listings.

χ_b is the average $B\text{-}\bar{B}$ mixing parameter at high-energy $\chi_b = f'_d \chi_d + f'_s \chi_s$ where f'_d and f'_s are the fractions of B^0 and B_s^0 hadrons in an unbiased sample of semileptonic b -hadron decays.

"OUR EVALUATION" is an average using rescaled values of the data listed below. The average and rescaling were performed by the Heavy Flavor Averaging Group (HFLAV) and are described at <https://hflav.web.cern.ch/>. The averaging/rescaling procedure takes into account correlations between the measurements.

VALUE	EVTS	DOCUMENT ID	TECN	COMMENT
0.1284 ± 0.0069 OUR EVALUATION				
0.129 ± 0.004 OUR AVERAGE				
0.132 ± 0.001 ± 0.024		1 ABAZOV 06s	D0	$p\bar{p}$ at 1.96 TeV
0.152 ± 0.007 ± 0.011		2 ACOSTA 04A	CDF	$p\bar{p}$ at 1.8 TeV
0.1312 ± 0.0049 ± 0.0042		3 ABBIENDI 03P	OPAL	$e^+e^- \rightarrow Z$
0.127 ± 0.013 ± 0.006		4 ABREU 01L	DLPH	$e^+e^- \rightarrow Z$
0.1192 ± 0.0068 ± 0.0051		5 ACCIARRI 99D	L3	$e^+e^- \rightarrow Z$
0.121 ± 0.016 ± 0.006		6 ABREU 94J	DLPH	$e^+e^- \rightarrow Z$
0.114 ± 0.014 ± 0.008		7 BUSKULIC 94G	ALEP	$e^+e^- \rightarrow Z$
0.129 ± 0.022		8 BUSKULIC 92b	ALEP	$e^+e^- \rightarrow Z$
0.176 ± 0.031 ± 0.032	1112	9 ABE 91G	CDF	$p\bar{p}$ 1.8 TeV
0.148 ± 0.029 ± 0.017		10 ALBAJAR 91D	UA1	$p\bar{p}$ 630 GeV
$\bullet\bullet\bullet$ We do not use the following data for averages, fits, limits, etc. $\bullet\bullet\bullet$				
0.131 ± 0.020 ± 0.016		11 ABE 97I	CDF	Repl. by ACOSTA 04A
0.1107 ± 0.0062 ± 0.0055		12 ALEXANDER 96	OPAL	Rep. by ABBIENDI 03P
0.136 ± 0.037 ± 0.040		13 UENO 96	AMY	e^+e^- at 57.9 GeV
0.144 ± 0.014 ± 0.017 ± 0.011		14 ABREU 94F	DLPH	Sup. by ABREU 94J
0.131 ± 0.014		15 ABREU 94J	DLPH	$e^+e^- \rightarrow Z$
0.123 ± 0.012 ± 0.008		ACCIARRI 94D	L3	Repl. by ACCIARRI 99D
0.157 ± 0.020 ± 0.032		16 ALBAJAR 94	UA1	$\sqrt{s} = 630$ GeV
0.121 ± 0.044 ± 0.017	1665	17 ABREU 93c	DLPH	Sup. by ABREU 94J
0.143 ± 0.022 ± 0.007		18 AKERS 93b	OPAL	Sup. by ALEXANDER 96
0.145 ± 0.041 ± 0.035 ± 0.018		19 ACTON 92c	OPAL	$e^+e^- \rightarrow Z$
0.121 ± 0.017 ± 0.006		20 ADEVA 92c	L3	Sup. by ACCIARRI 94D
0.132 ± 0.22 ± 0.015 ± 0.012	823	21 DECAMP 91	ALEP	$e^+e^- \rightarrow Z$
0.178 ± 0.049 ± 0.040 ± 0.020		22 ADEVA 90P	L3	$e^+e^- \rightarrow Z$
0.17 ± 0.15 ± 0.08	23,24	WEIR 90	MRK2	e^+e^- 29 GeV
0.21 ± 0.29 ± 0.15	23	BAND 88	MAC	$E_{\text{cm}}^e = 29$ GeV
>0.02 at 90% CL	23	BAND 88	MAC	$E_{\text{cm}}^e = 29$ GeV
0.121 ± 0.047	23,25	ALBAJAR 87c	UA1	Repl. by ALBAJAR 91D
<0.12 at 90% CL	23,26	SCHAAD 85	MRK2	$E_{\text{cm}}^e = 29$ GeV

1 Uses the dimuon charge asymmetry. Averaged over the mix of b -flavored hadrons.
 2 Measurement performed using events containing a dimuon or an e/μ pair.
 3 The average B mixing parameter is determined simultaneously with b and c forward-backward asymmetries in the fit.
 4 The experimental systematic and model uncertainties are combined in quadrature.
 5 ACCIARRI 99D uses maximum-likelihood fits to extract χ_b as well as the A_{FB}^b in $Z \rightarrow b\bar{b}$ events containing prompt leptons.
 6 This ABREU 94J result is from 5182 $\ell\ell$ and 279 $\ell\ell$ events. The systematic error includes 0.004 for model dependence.
 7 BUSKULIC 94G data analyzed using ee , $e\mu$, and $\mu\mu$ events.
 8 BUSKULIC 92b uses a jet charge technique combined with electrons and muons.
 9 ABE 91G measurement of χ is done with $e\mu$ and ee events.
 10 ALBAJAR 91D measurement of χ is done with dimuons.
 11 Uses di-muon events.
 12 ALEXANDER 96 uses a maximum likelihood fit to simultaneously extract χ as well as the forward-backward asymmetries in $e^+e^- \rightarrow Z \rightarrow b\bar{b}$ and $c\bar{c}$.
 13 UENO 96 extracted χ from the energy dependence of the forward-backward asymmetry.
 14 ABREU 94F uses the average electric charge sum of the jets recoiling against a b -quark jet tagged by a high p_T muon. The result is for $\bar{\chi} = f_d \chi_d + 0.9 f_s \chi_s$.
 15 This ABREU 94J result combines $\ell\ell$, $\ell\ell$, and jet-charge ℓ (ABREU 94F) analyses. It is for $\bar{\chi} = f_d \chi_d + 0.9 f_s \chi_s$.
 16 ALBAJAR 94 uses dimuon events. Not independent of ALBAJAR 91D.
 17 ABREU 93c data analyzed using ee , $e\mu$, and $\mu\mu$ events.

18 AKERS 93b analysis performed using dilepton events.
 19 ACTON 92c uses electrons and muons. Superseded by AKERS 93b.
 20 ADEVA 92c uses electrons and muons.
 21 DECAMP 91 done with opposite and like-sign dileptons. Superseded by BUSKULIC 92b.
 22 ADEVA 90P measurement uses ee , $\mu\mu$, and $e\mu$ events from 118k events at the Z. Superseded by ADEVA 92c.
 23 These experiments are not in the average because the combination of B_s and B_d mesons which they see could differ from those at higher energy.
 24 The WEIR 90 measurement supersedes the limit obtained in SCHAAD 85. The 90% CL are 0.06 and 0.38.
 25 ALBAJAR 87c measured $\chi = (\bar{B}^0 \rightarrow B^0 \rightarrow \mu^+ X)$ divided by the average production weighted semileptonic branching fraction for B hadrons at 546 and 630 GeV.
 26 Limit is average probability for hadron containing B quark to produce a positive lepton.

CP VIOLATION PARAMETERS in semileptonic b -hadron decays.

$\text{Re}(\epsilon_b) / (1 + |\epsilon_b|^2)$

CP impurity in semileptonic b -hadron decays.

VALUE (units 10^{-3})	DOCUMENT ID	TECN	COMMENT
$\bullet\bullet\bullet$ We do not use the following data for averages, fits, limits, etc. $\bullet\bullet\bullet$			
$-6.2 \pm 5.2 \pm 4.7$	1 AABOUD 17E	ATLS	pp at 8 TeV
$-1.24 \pm 0.38 \pm 0.18$	2 ABAZOV 14	D0	$p\bar{p}$ at 1.96 TeV
$-1.97 \pm 0.43 \pm 0.23$	3 ABAZOV 11U	D0	Repl. by ABAZOV 14
$-2.39 \pm 0.63 \pm 0.37$	4 ABAZOV 10H	D0	Repl. by ABAZOV 11U
1 AABOUD 17E reports a measurement of charge asymmetry of $A_{SL}^b = (-25 \pm 21 \pm 19) \times 10^{-3}$ in lepton + jets $t\bar{t}$ events in which a b -hadron decays semileptonically to a soft muon.			
2 ABAZOV 14 reports a measurement of like-sign dimuon charge asymmetry of $A_{SL}^b = (-4.96 \pm 1.53 \pm 0.72) \times 10^{-3}$ in semileptonic b -hadron decays.			
3 ABAZOV 11U reports a measurement of like-sign dimuon charge asymmetry of $A_{SL}^b = (-7.87 \pm 1.72 \pm 0.93) \times 10^{-3}$ in semileptonic b -hadron decays.			
4 ABAZOV 10H reports a measurement of like-sign dimuon charge asymmetry of $A_{SL}^b = (-9.57 \pm 2.51 \pm 1.46) \times 10^{-3}$ in semileptonic b -hadron decays. Using the measured production ratio of B_d^0 and B_s^0 , and the asymmetry of $B_d^0 A_{SL}^d = (-4.7 \pm 4.6) \times 10^{-3}$ measured from B -factories, they obtain the asymmetry for B_s^0 as $A_{SL}^b = (-14.6 \pm 7.5) \times 10^{-3}$.			

B-HADRON PRODUCTION FRACTIONS IN $p\bar{p}$ COLLISIONS AT Tevatron

The production fractions for b -hadrons in $p\bar{p}$ collisions at the Tevatron have been calculated from the best values of mean lifetimes, mixing parameters, and branching fractions in this edition by the Heavy Flavor Averaging Group (HFLAV) (see <https://hflav.web.cern.ch/>).

The values reported below assume:

$$f(\bar{b} \rightarrow B^+) = f(\bar{b} \rightarrow B^0)$$

$$f(\bar{b} \rightarrow B^+) + f(\bar{b} \rightarrow B^0) + f(\bar{b} \rightarrow B_s^0) + f(b \rightarrow b\text{-baryon}) = 1$$

The values are:

$$f(\bar{b} \rightarrow B^+) = f(\bar{b} \rightarrow B^0) = 0.344 \pm 0.021$$

$$f(\bar{b} \rightarrow B_s^0) = 0.115 \pm 0.013$$

$$f(b \rightarrow b\text{-baryon}) = 0.198 \pm 0.046$$

$$f(\bar{b} \rightarrow B_s^0) / f(\bar{b} \rightarrow B^0) = 0.334 \pm 0.041$$

and their correlation coefficients are:

$$\text{cor}(B_s^0, b\text{-baryon}) = -0.429$$

$$\text{cor}(B_s^0, B^+ = B^0) = +0.159$$

$$\text{cor}(b\text{-baryon}, B^+ = B^0) = -0.960$$

as obtained with the Tevatron average of time-integrated mixing parameter $\bar{\chi} = 0.147 \pm 0.011$.

PRODUCTION ASYMMETRIES

$A_C^{b\bar{b}}$

$$A_C^{b\bar{b}} = [N(\Delta y > 0) - N(\Delta y < 0)] / [N(\Delta y > 0) + N(\Delta y < 0)]$$

with $\Delta y = |y_b| - |y_{\bar{b}}|$ where $y_{b/\bar{b}}$ is rapidity of b or \bar{b} quarks.

VALUE (units 10^{-2})	DOCUMENT ID	TECN	COMMENT
Average is meaningless.			
$0.4 \pm 0.4 \pm 0.3$	1 AAJ 14As	LHCb	pp at 7 TeV
$2.0 \pm 0.9 \pm 0.6$	2 AAJ 14As	LHCb	pp at 7 TeV
$1.6 \pm 1.7 \pm 0.6$	3 AAJ 14As	LHCb	pp at 7 TeV

1 Measured for $40 < M(b\bar{b}) < 75$ GeV/ c^2 .
 2 Measured for $75 < M(b\bar{b}) < 105$ GeV/ c^2 .
 3 Measured for $M(b\bar{b}) > 105$ GeV/ c^2 .

$B^\pm/B^0/B_s^0/b$ -baryon ADMIXTURE REFERENCES

AAJ 21Y	PR D104 032005	R. Aaij et al.	(LHCb Collab.)
AAJ 20G	EPJ C80 185	R. Aaij et al.	(LHCb Collab.)
AAJ 20H	EPJ C80 191	R. Aaij et al.	(LHCb Collab.)
AAJ 20V	PRL 124 122002	R. Aaij et al.	(LHCb Collab.)
AAJ 19AB	PR D99 052006	R. Aaij et al.	(LHCb Collab.)
AAJ 19AD	PR D100 031102	R. Aaij et al.	(LHCb Collab.)
AAJ 19AI	PR D100 112006	R. Aaij et al.	(LHCb Collab.)
AABOUD 17E	JHEP 1702 071	M. Aaboud et al.	(ATLAS Collab.)
AAJ 17BB	EPJ C77 609	R. Aaij et al.	(LHCb Collab.)
AAD 15CM	PRL 115 262001	G. Aad et al.	(ATLAS Collab.)
AAJ 14AS	PRL 113 082003	R. Aaij et al.	(LHCb Collab.)

Meson Particle Listings

$B^\pm/B^0/B_s^0/b$ -baryon ADMIXTURE, V_{cb} and V_{ub} CKM Matrix Elements

ABAZOV	14	PR D89 012002	V.M. Abazov et al.	(DO Collab.)
AAUJ	13P	JHEP 1304 001	R. Aaij et al.	(LHCb Collab.)
AAUJ	12B	EPJ C72 2100	R. Aaij et al.	(LHCb Collab.)
Also		EPJ C80 49 (errata.)	R. Aaij et al.	(LHCb Collab.)
AAUJ	12J	PR D85 032008	R. Aaij et al.	(LHCb Collab.)
CHATRCHYAN	12AK	JHEP 1202 011	S. Chatrchyan et al.	(CMS Collab.)
AAUJ	11F	PRL 107 211801	R. Aaij et al.	(LHCb Collab.)
ABAZOV	11U	PR D84 052007	V.M. Abazov et al.	(DO Collab.)
ABAZOV	10H	PRL 105 081801	V.M. Abazov et al.	(DO Collab.)
Also		PR D82 032001	V.M. Abazov et al.	(DO Collab.)
PDG	10	JP G37 075021	K. Nakamura et al.	(PDG Collab.)
AALTONEN	09E	PR D79 032001	T. Aaltonen et al.	(CDF Collab.)
AALTONEN	08N	PR D77 072003	T. Aaltonen et al.	(CDF Collab.)
ABAZOV	06S	PR D74 092001	V.M. Abazov et al.	(DO Collab.)
ABBIENDI	04I	EPJ C35 149	G. Abbiendi et al.	(OPAL Collab.)
ABDALLAH	04E	EPJ C33 307	J. Abdallah et al.	(DELPHI Collab.)
ACOSTA	04A	PR D69 012002	D. Acosta et al.	(CDF Collab.)
ABBIENDI	03M	EPJ C30 467	G. Abbiendi et al.	(OPAL Collab.)
ABBIENDI	03P	PL B577 18	G. Abbiendi et al.	(OPAL Collab.)
ABDALLAH	03E	PL B561 26	J. Abdallah et al.	(DELPHI Collab.)
ABDALLAH	03K	PL B576 29	J. Abdallah et al.	(DELPHI Collab.)
HEISTER	02G	EPJ C22 613	A. Heister et al.	(ALEPH Collab.)
ABBIENDI	01Q	PL B520 1	G. Abbiendi et al.	(OPAL Collab.)
ABBIENDI	01R	EPJ C21 399	G. Abbiendi et al.	(OPAL Collab.)
ABREU	01L	EPJ C20 455	P. Abreu et al.	(DELPHI Collab.)
BARATE	01E	EPJ C19 213	R. Barate et al.	(ALEPH Collab.)
ABBIENDI	00E	EPJ C13 225	G. Abbiendi et al.	(OPAL Collab.)
ABBIENDI	00Z	PL B492 13	G. Abbiendi et al.	(OPAL Collab.)
ABREU	00	EPJ C12 225	P. Abreu et al.	(DELPHI Collab.)
ABREU	00C	PL B496 43	P. Abreu et al.	(DELPHI Collab.)
ABREU	00D	PL B478 14	P. Abreu et al.	(DELPHI Collab.)
ABREU	00R	PR B475 407	P. Abreu et al.	(DELPHI Collab.)
ACCIARRI	00	EPJ C13 47	M. Acciari et al.	(L3 Collab.)
AFFOLDER	00E	PRL 84 1663	T. Affolder et al.	(CDF Collab.)
ABBIENDI	99J	EPJ C12 609	G. Abbiendi et al.	(OPAL Collab.)
ABE	99P	PR D60 092005	F. Abe et al.	(CDF Collab.)
ACCIARRI	99D	PL B448 152	M. Acciari et al.	(L3 Collab.)
BARATE	99G	EPJ C6 555	R. Barate et al.	(ALEPH Collab.)
ABBOTT	98B	PL B423 419	B. Abbott et al.	(DO Collab.)
ABE	98B	PR D57 5382	F. Abe et al.	(CDF Collab.)
ABREU	98D	PL B426 193	P. Abreu et al.	(DELPHI Collab.)
ABREU	98H	PL B425 399	P. Abreu et al.	(DELPHI Collab.)
ACCIARRI	98	PL B416 220	M. Acciari et al.	(L3 Collab.)
ACCIARRI	98K	PL B406 174	M. Acciari et al.	(L3 Collab.)
ACKERSTAFF	98E	EPJ C1 439	K. Ackerstaff et al.	(OPAL Collab.)
BARATE	98I	PL B429 169	R. Barate et al.	(ALEPH Collab.)
BARATE	98Q	EPJ C4 387	R. Barate et al.	(ALEPH Collab.)
BARATE	98V	EPJ C5 205	R. Barate et al.	(ALEPH Collab.)
GLENN	98	PRL 80 2289	S. Glenn et al.	(CLEO Collab.)
ABE	97I	PR D55 2546	F. Abe et al.	(CDF Collab.)
ACKERSTAFF	97F	ZPHY C73 397	K. Ackerstaff et al.	(OPAL Collab.)
ACKERSTAFF	97N	ZPHY C74 423	K. Ackerstaff et al.	(OPAL Collab.)
ACKERSTAFF	97W	ZPHY C76 425	K. Ackerstaff et al.	(OPAL Collab.)
ABREU	96E	PL B377 195	P. Abreu et al.	(DELPHI Collab.)
ACCIARRI	96C	ZPHY C71 379	M. Acciari et al.	(L3 Collab.)
ADAM	96	ZPHY C69 561	W. Adam et al.	(DELPHI Collab.)
ADAM	96D	ZPHY C72 207	W. Adam et al.	(DELPHI Collab.)
ALEXANDER	96	ZPHY C70 357	G. Alexander et al.	(OPAL Collab.)
BUSKULIC	96F	PL B369 151	D. Buskalic et al.	(ALEPH Collab.)
BUSKULIC	96V	PL B384 471	D. Buskalic et al.	(ALEPH Collab.)
BUSKULIC	96Y	PL B388 648	D. Buskalic et al.	(ALEPH Collab.)
GROSSMAN	96	NP B465 369	Y. Grossman, Z. Ligeti, E. Nardi	(REHO, CIT)
Also		NP B480 753 (erratum)	Y. Grossman, Z. Ligeti, E. Nardi	(REHO, CIT)
PDG	96	PR D54 1	R. M. Barnett et al.	(PDG Collab.)
UENO	96	PL B381 365	K. Ueno et al.	(AMT Collab.)
ABE-K	95B	PRL 75 3624	K. Abe et al.	(SLD Collab.)
ABREU	95C	PL B347 447	P. Abreu et al.	(DELPHI Collab.)
ABREU	95D	ZPHY C66 323	P. Abreu et al.	(DELPHI Collab.)
ADAM	95	ZPHY C68 363	W. Adam et al.	(DELPHI Collab.)
AKERS	95Q	ZPHY C67 57	R. Akers et al.	(OPAL Collab.)
BUSKULIC	95	PL B343 444	D. Buskalic et al.	(ALEPH Collab.)
ABREU	94F	PL B322 459	P. Abreu et al.	(DELPHI Collab.)
ABREU	94J	PL B332 488	P. Abreu et al.	(DELPHI Collab.)
ABREU	94L	ZPHY C63 3	P. Abreu et al.	(DELPHI Collab.)
ABREU	94P	PL B341 109	P. Abreu et al.	(DELPHI Collab.)
ACCIARRI	94C	PL B352 201	M. Acciari et al.	(L3 Collab.)
ACCIARRI	94D	PL B305 542	M. Acciari et al.	(L3 Collab.)
ALBAJAR	94	ZPHY C61 41	C. Albajar et al.	(UA1 Collab.)
BUSKULIC	94G	ZPHY C62 179	D. Buskalic et al.	(ALEPH Collab.)
ABE	93E	PL B313 288	K. Abe et al.	(VENUS Collab.)
ABE	93J	PRL 71 3421	F. Abe et al.	(CDF Collab.)
ABREU	93C	PL B301 145	P. Abreu et al.	(DELPHI Collab.)
ABREU	93D	ZPHY C57 181	P. Abreu et al.	(DELPHI Collab.)
ABREU	93G	PL B312 253	P. Abreu et al.	(DELPHI Collab.)
ACTON	93C	PL B307 247	P.D. Acton et al.	(OPAL Collab.)
ACTON	93L	ZPHY C60 217	P.D. Acton et al.	(OPAL Collab.)
ADRIANI	93J	PL B317 467	O. Adriani et al.	(L3 Collab.)
ADRIANI	93K	PL B317 474	O. Adriani et al.	(L3 Collab.)
ADRIANI	93L	PL B317 637	O. Adriani et al.	(L3 Collab.)
AKERS	93B	ZPHY C60 199	R. Akers et al.	(OPAL Collab.)
BUSKULIC	93B	PL B298 479	D. Buskalic et al.	(ALEPH Collab.)
BUSKULIC	93O	PL B314 459	D. Buskalic et al.	(ALEPH Collab.)
ABREU	92	ZPHY C53 567	P. Abreu et al.	(DELPHI Collab.)
ACTON	92	PL B274 513	D.P. Acton et al.	(OPAL Collab.)
ACTON	92C	PL B276 379	D.P. Acton et al.	(OPAL Collab.)
ADEVA	92C	PL B288 395	B. Adeva et al.	(L3 Collab.)
ADRIANI	92	PL B288 412	O. Adriani et al.	(L3 Collab.)
BUSKULIC	92B	PL B284 177	D. Buskalic et al.	(ALEPH Collab.)
BUSKULIC	92F	PL B295 174	D. Buskalic et al.	(ALEPH Collab.)
BUSKULIC	92G	PL B295 396	D. Buskalic et al.	(ALEPH Collab.)
ABE	91G	PRL 67 3351	F. Abe et al.	(CDF Collab.)
ADEVA	91C	PL B261 177	B. Adeva et al.	(L3 Collab.)
ADEVA	91H	PL B270 111	B. Adeva et al.	(L3 Collab.)
ALBAJAR	91C	PL B262 163	C. Albajar et al.	(UA1 Collab.)
ALBAJAR	91D	PL B262 171	C. Albajar et al.	(UA1 Collab.)
ALEXANDER	91G	PL B266 485	G. Alexander et al.	(OPAL Collab.)
DECAMP	91	PL B258 236	D. Decamp et al.	(ALEPH Collab.)
DECAMP	91C	PL B257 492	D. Decamp et al.	(ALEPH Collab.)
ADEVA	90P	PL B252 703	B. Adeva et al.	(L3 Collab.)
BEHREND	90D	ZPHY C47 333	H.J. Behrend et al.	(CELLO Collab.)
HAGEMANN	90	ZPHY C48 401	J. Hagemann et al.	(JADE Collab.)
LYONS	90	PR D41 982	L. Lyons, A.J. Martin, D.H. Saxon	(OXF, BRIS+)
WEIR	90	PL B240 289	A.J. Weir et al.	(Mark II Collab.)
BRAUNSCH...	89B	ZPHY C44 1	R. Braunschweig et al.	(TASSO Collab.)
ONG	89	PRL 62 1236	R.A. Ong et al.	(Mark II Collab.)
BAND	88	PL B200 221	H.R. Band et al.	(MAC Collab.)
KLEM	88	PR D37 41	D.E. Klem et al.	(DELCO Collab.)
ONG	88	PRL 60 2587	R.A. Ong et al.	(Mark II Collab.)
ALBAJAR	87C	PL B186 247	C. Albajar et al.	(UA1 Collab.)
ASH	87	PRL 58 640	W.W. Ash et al.	(MAC Collab.)
BARTEL	87	ZPHY C33 339	W. Bartel et al.	(JADE Collab.)
BROM	87	PL B195 301	J.M. Brom et al.	(HRS Collab.)

PAL	86	PR D33 2708	T. Pal et al.	(DELCO Collab.)
AIHARA	85	ZPHY C27 39	H. Aihara et al.	(TPC Collab.)
BARTEL	85J	PL 163B 277	W. Bartel et al.	(JADE Collab.)
SCHAAED	85	PL 160B 188	T. Schaad et al.	(Mark II Collab.)
ALTHOFF	84G	ZPHY C22 219	M. Althoff et al.	(TASSO Collab.)
ALTHOFF	84J	PL 146B 443	M. Althoff et al.	(TASSO Collab.)
KOOP	84	PRL 52 970	D.E. Koop et al.	(DELCO Collab.)
ADEVA	83	PRL 50 739	B. Adeva et al.	(Mark-J Collab.)
ADEVA	83B	PRL 51 443	B. Adeva et al.	(Mark-J Collab.)
BARTEL	83B	PL 132B 241	W. Bartel et al.	(JADE Collab.)
FERNANDEZ	83D	PRL 50 2054	E. Fernandez et al.	(MAC Collab.)
MATTEUZZI	83	PRL 129B 141	C. Matteuzzi et al.	(Mark II Collab.)
NELSON	83	PRL 50 1542	M.E. Nelson et al.	(Mark II Collab.)

V_{cb} and V_{ub} CKM Matrix Elements

OMITTED FROM SUMMARY TABLE

See the related review(s):
Semileptonic B Hadron Decays, Determination of V_{cb} and V_{ub}

V_{cb} MEASUREMENTS

For the discussion of V_{cb} measurements, which is not repeated here, see the review on "Determination of $|V_{cb}|$ and $|V_{ub}|$."

The CKM matrix element $|V_{cb}|$ can be determined by studying the rate of the semileptonic decay $B \rightarrow D^{(*)} \ell \nu$ as a function of the recoil kinematics of $D^{(*)}$ mesons. Taking advantage of theoretical constraints on the normalization and a linear ω dependence of the form factors ($F(\omega)$, $G(\omega)$) provided by Heavy Quark Effective Theory (HQET), the $|V_{cb}| \times F(\omega)$ and ρ^2 can be simultaneously extracted from data, where ω is the scalar product of the two-meson four velocities, $F(1)$ is the form factor at zero recoil ($\omega=1$) and ρ^2 is the slope. Using the theoretical input of $F(1)$, a value of $|V_{cb}|$ can be obtained.

"OUR EVALUATION" is an average using rescaled values of the data listed below. The average and rescaling were performed by the Heavy Flavor Averaging Group (HFAG) and are described at <https://hfag.web.cern.ch/>. The averaging/rescaling procedure takes into account correlations between the measurements.

$|V_{cb}| \times F(1)$ (from $B^0 \rightarrow D^{*+} \ell^+ \nu$)

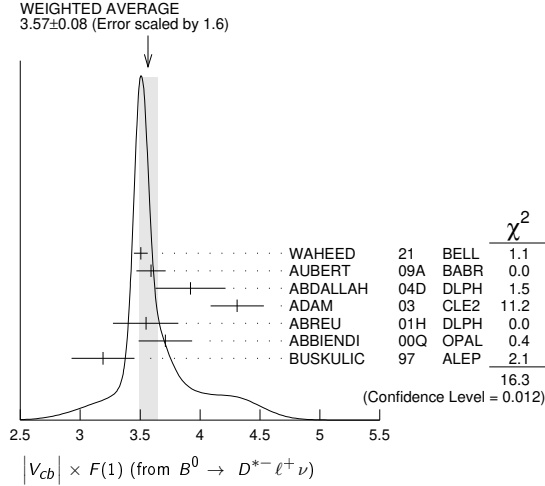
VALUE (units 10^{-2})	DOCUMENT ID	TECN	COMMENT
3.500 ± 0.036 OUR EVALUATION	with $\rho^2 = 1.121 \pm 0.024$ and a correlation of 0.317. The fitted χ^2 is 42.2 for 23 degrees of freedom.		
3.57 ± 0.08 OUR AVERAGE	Error includes scale factor of 1.66. See the ideogram below.		
$3.506 \pm 0.015 \pm 0.056$	¹ WAHEED	21	BELL $e^+e^- \rightarrow T(4S)$
$3.59 \pm 0.02 \pm 0.12$	² AUBERT	09A	BABR $e^+e^- \rightarrow T(4S)$
$3.92 \pm 0.18 \pm 0.23$	³ ABDALLAH	04D	DLPH $e^+e^- \rightarrow Z^0$
$4.31 \pm 0.13 \pm 0.18$	⁴ ADAM	03	CLE2 $e^+e^- \rightarrow T(4S)$
$3.55 \pm 0.14 \pm 0.23$ -0.24	⁵ ABREU	01H	DLPH $e^+e^- \rightarrow Z$
$3.71 \pm 0.10 \pm 0.20$	⁶ ABBIENDI	00Q	OPAL $e^+e^- \rightarrow Z$
$3.19 \pm 0.18 \pm 0.19$	⁷ BUSKULIC	97	ALEP $e^+e^- \rightarrow Z$
••• We do not use the following data for averages, fits, limits, etc. •••			
$3.483 \pm 0.015 \pm 0.056$	¹ WAHEED	19	BELL Repl. by WAHEED 21
$3.46 \pm 0.02 \pm 0.10$	⁸ DUNGEL	10	BELL Repl. by WAHEED 19
$3.59 \pm 0.06 \pm 0.14$	⁹ AUBERT	08AT	BABR Repl. by AUBERT 09A
$3.44 \pm 0.03 \pm 0.11$	¹⁰ AUBERT	08R	BABR Repl. by AUBERT 09A
$3.55 \pm 0.03 \pm 0.16$	¹¹ AUBERT	05E	BABR Repl. by AUBERT 08R
$3.77 \pm 0.11 \pm 0.19$	¹² ABDALLAH	04D	DLPH $e^+e^- \rightarrow Z^0$
$3.54 \pm 0.19 \pm 0.18$	¹³ ABE	02F	BELL Repl. by DUNGEL 10
$4.31 \pm 0.13 \pm 0.18$	¹⁴ BRIERE	02	CLE2 $e^+e^- \rightarrow T(4S)$
$3.28 \pm 0.19 \pm 0.22$	ACKERSTAFF	97G	OPAL Repl. by ABBIENDI 00Q
$3.50 \pm 0.19 \pm 0.23$	¹⁵ ABREU	96P	DLPH Repl. by ABREU 01H
$3.51 \pm 0.19 \pm 0.20$	¹⁶ BARISH	95N	CLE2 Repl. by ADAM 03
$3.14 \pm 0.23 \pm 0.25$	BUSKULIC	95N	ALEP Repl. by BUSKULIC 97
¹ WAHEED 21 uses fully reconstructed $D^{*+} \ell^+ \nu$ events ($\ell = e$ or μ) and $\eta_{EW} = 1.0066$. ² Obtained from a global fit to $B \rightarrow D^{*+} \ell \nu$ events, with reconstructed D^0 ℓ and $D^+ \ell$ final states and $\rho^2 = 1.22 \pm 0.02 \pm 0.07$. ³ Measurement using fully reconstructed D^* sample with a $\rho^2 = 1.32 \pm 0.15 \pm 0.33$. ⁴ Average of the $B^0 \rightarrow D^{*+}(2010) \ell^+ \nu$ and $B^+ \rightarrow \bar{D}^{*+}(2007) \ell^+ \nu$ modes with $\rho^2 = 1.61 \pm 0.09 \pm 0.21$ and $\tilde{r}_{+-} = 0.521 \pm 0.012$. ⁵ ABREU 01H measured using about 5000 partial reconstructed D^* sample with a $\rho^2 = 1.34 \pm 0.14 \pm 0.24$ -0.22 . ⁶ ABBIENDI 00Q: measured using both inclusively and exclusively reconstructed D^{*+} samples with a $\rho^2 = 1.21 \pm 0.12 \pm 0.20$. The statistical and systematic correlations between $ V_{cb} \times F(1)$ and ρ^2 are 0.90 and 0.54 respectively. ⁷ BUSKULIC 97: measured using exclusively reconstructed D^{*+} with a $a^2 = 0.31 \pm 0.17 \pm 0.08$. The statistical correlation is 0.92. ⁸ Uses fully reconstructed $D^{*+} \ell^+ \nu$ events ($\ell = e$ or μ). ⁹ Measured using the dependence of $B^- \rightarrow D^{*0} e^- \bar{\nu}_e$ decay differential rate and the form factor description by CAPRINI 98 with $\rho^2 = 1.16 \pm 0.06 \pm 0.08$.			

See key on page 1127

Meson Particle Listings

V_{cb} and V_{ub} CKM Matrix Elements, B^*

- ¹⁰ Measured using fully reconstructed D^* sample and a simultaneous fit to the Caprini-Lellouch-Neubert form factor parameters: $\rho^2 = 1.191 \pm 0.048 \pm 0.028$, $R_1(1) = 1.429 \pm 0.061 \pm 0.044$, and $R_2(1) = 0.827 \pm 0.038 \pm 0.022$.
- ¹¹ Measurement using fully reconstructed D^* sample with a $\rho^2 = 1.29 \pm 0.03 \pm 0.27$.
- ¹² Combines with previous partial reconstructed D^* measurement with a $\rho^2 = 1.39 \pm 0.10 \pm 0.33$.
- ¹³ Measured using exclusive $B^0 \rightarrow D^*(892)^- e^+ \nu$ decays with $\rho^2 = 1.35 \pm 0.17 \pm 0.19$ and a correlation of 0.91.
- ¹⁴ BRIERE 02 result is based on the same analysis and data sample reported in ADAM 03.
- ¹⁵ ABREU 96P: measured using both inclusively and exclusively reconstructed $D^{*\pm}$ samples.
- ¹⁶ BARISH 95: measured using both exclusive reconstructed $B^0 \rightarrow D^{*-} \ell^+ \nu$ and $B^+ \rightarrow D^{*0} \ell^+ \nu$ samples. They report their experiment's uncertainties $\pm 0.0019 \pm 0.0018 \pm 0.0008$, where the first error is statistical, the second is systematic, and the third is the uncertainty in the lifetimes. We combine the last two in quadrature.



$|V_{cb}| \times G(1)$ (from $B \rightarrow D^- \ell^+ \nu$)

VALUE	DOCUMENT ID	TECN	COMMENT
0.04153 ± 0.00098 OUR EVALUATION	with $\rho^2 = 1.129 \pm 0.033$ and a correlation of 0.758. The fitted χ^2 is 4.6 for 8 degrees of freedom.		
0.0422 ± 0.0010 OUR AVERAGE			
0.04229 ± 0.00137	¹ GLATTAUER 16	BELL	$e^+ e^- \rightarrow \Upsilon(4S)$
0.0423 ± 0.0019 ± 0.0014	² AUBERT 10	BABR	$e^+ e^- \rightarrow \Upsilon(4S)$
0.0431 ± 0.0008 ± 0.0023	³ AUBERT 09A	BABR	$e^+ e^- \rightarrow \Upsilon(4S)$
0.0416 ± 0.0047 ± 0.0037	⁴ BARTELT 99	CLE2	$e^+ e^- \rightarrow \Upsilon(4S)$
0.0278 ± 0.0068 ± 0.0065	⁵ BUSKULIC 97	ALEP	$e^+ e^- \rightarrow Z$
• • • We do not use the following data for averages, fits, limits, etc. • • •			
0.0411 ± 0.0044 ± 0.0052	⁶ ABE 02E	BELL	Repl. by GLATTAUER 16
0.0337 ± 0.0044 ± 0.0072 ± 0.0049	⁷ ATHANAS 97	CLE2	Repl. by BARTELT 99

- ¹ Obtained from a fit to the combined partially reconstructed $B \rightarrow \bar{D} \ell \nu \ell$ sample while tagged by the other fully reconstructed B meson in the event. Also reports fitted $\rho^2 = 1.09 \pm 0.05$.
- ² Obtained from a fit to the combined $B \rightarrow \bar{D} \ell^+ \nu \ell$ sample in which a hadronic decay of the second B meson is fully reconstructed and $\rho^2 = 1.20 \pm 0.09 \pm 0.04$.
- ³ Obtained from a global fit to $B \rightarrow D^{(*)} \ell \nu \ell$ events, with reconstructed $D^0 \ell$ and $D^+ \ell$ final states and $\rho^2 = 1.20 \pm 0.04 \pm 0.07$.
- ⁴ BARTELT 99: measured using both exclusive reconstructed $B^0 \rightarrow D^- \ell^+ \nu$ and $B^+ \rightarrow D^0 \ell^+ \nu$ samples.
- ⁵ BUSKULIC 97: measured using exclusively reconstructed D^\pm with a $\rho^2 = -0.05 \pm 0.53 \pm 0.38$. The statistical correlation is 0.99.
- ⁶ Using the missing energy and momentum to extract kinematic information about the undetected neutrino in the $B^0 \rightarrow D^- \ell^+ \nu$ decay.
- ⁷ ATHANAS 97: measured using both exclusive reconstructed $B^0 \rightarrow D^- \ell^+ \nu$ and $B^+ \rightarrow D^0 \ell^+ \nu$ samples with a $\rho^2 = 0.59 \pm 0.22 \pm 0.12^{+0.59}_{-0}$. They report their experiment's uncertainties $\pm 0.0044 \pm 0.0048^{+0.0053}_{-0.0012}$, where the first error is statistical, the second is systematic, and the third is the uncertainty due to the form factor model variations. We combine the last two in quadrature.

$|V_{cb}|$ (from $D_s^{*-} \mu^+ \nu_\mu$)

VALUE (units 10^{-3})	DOCUMENT ID	TECN	COMMENT
41.4 ± 0.6 ± 0.9 ± 1.2	¹ AAIJ 20E	LHCB	pp at 7, 8 TeV

¹ Measured from an inclusive sample of $D_s^{*-} \mu^+$ candidates using CNL parameterization of the form factor. AAIJ 20E provides also measurement of $|V_{cb}| = (42.3 \pm 0.8 \pm 0.9 \pm 1.2) \times 10^{-3}$ using BGL parameterization of the form factor. The third uncertainty is due to the external inputs used in the measurement.

V_{ub} MEASUREMENTS

For the discussion of V_{ub} measurements, which is not repeated here, see the review on "Determination of $|V_{cb}|$ and $|V_{ub}|$."

The CKM matrix element $|V_{ub}|$ can be determined by studying the rate of the charmless semileptonic decay $b \rightarrow u \ell \nu$. The relevant branching ratio measurements based on exclusive and inclusive decays can be found in the B Listings, and are not repeated here.

V_{cb} and V_{ub} CKM Matrix Elements REFERENCES

WAHEED 21 PR D103 079901	E. Waheed <i>et al.</i>	(BELLE Collab.)
AAJ 20E PR D101 072004	R. Aaij <i>et al.</i>	(LHCb Collab.)
WAHEED 19 PR D100 052007	E. Waheed <i>et al.</i>	(BELLE Collab.)
GLATTAUER 16 PR D93 032006	R. Glattauer <i>et al.</i>	(BELLE Collab.)
AUBERT 10 PRL 104 011802	B. Aubert <i>et al.</i>	(BABAR Collab.)
DUNGEL 10 PR D82 112007	W. Dungenl <i>et al.</i>	(BELLE Collab.)
AUBERT 09A PR D79 012002	B. Aubert <i>et al.</i>	(BABAR Collab.)
AUBERT 08AT PRL 100 231803	B. Aubert <i>et al.</i>	(BABAR Collab.)
AUBERT 08R PR D77 032002	B. Aubert <i>et al.</i>	(BABAR Collab.)
AUBERT 05E PR D71 051502	B. Aubert <i>et al.</i>	(BABAR Collab.)
ABDALLAH 04D EPJ C33 213	J. Abdallah <i>et al.</i>	(DELPHI Collab.)
ADAM 03 PR D67 032001	N.E. Adam <i>et al.</i>	(CLEO Collab.)
ABE 02E PL B526 258	K. Abe <i>et al.</i>	(BELLE Collab.)
ABE 02F PL B526 247	K. Abe <i>et al.</i>	(BELLE Collab.)
BRIERE 02 PRL 89 081803	R. Briere <i>et al.</i>	(CLEO Collab.)
ABREU 01H PL B510 55	P. Abreu <i>et al.</i>	(DELPHI Collab.)
ABBIENDI 00Q PL B482 15	G. Abbiendi <i>et al.</i>	(OPAL Collab.)
BARTELT 99 PRL 82 3746	J. Bartelt <i>et al.</i>	(CLEO Collab.)
CAPRINI 98 NP B530 153	L. Caprini, L. Lellouch, M. Neubert	(BCIP, CERN)
ACKERSTAFF 97G PL B395 128	K. Ackerstaff <i>et al.</i>	(OPAL Collab.)
ATHANAS 97 PRL 79 2208	M. Athanas <i>et al.</i>	(CLEO Collab.)
BUSKULIC 97 PL B395 373	D. Buskulic <i>et al.</i>	(ALEPH Collab.)
ABREU 96P ZPHY C71 539	P. Abreu <i>et al.</i>	(DELPHI Collab.)
BARISH 95 PR D51 1014	B.C. Barish <i>et al.</i>	(CLEO Collab.)
BUSKULIC 95N PL B359 236	D. Buskulic <i>et al.</i>	(ALEPH Collab.)



$$I(J^P) = \frac{1}{2}(1^-)$$

I, J, P need confirmation.

Quantum numbers shown are quark-model predictions.

B^* MASS

From mass difference below and the average of our B masses ($m_{B^\pm} + m_{B^0}$)/2.

VALUE (MeV)	DOCUMENT ID
5324.71 ± 0.21 OUR FIT	

$m_{B^*} - m_B$	
VALUE (MeV)	DOCUMENT ID TECN COMMENT
45.21 ± 0.26 OUR FIT	
45.42 ± 0.26 OUR AVERAGE	Includes data from the datablock that follows this one.
46.2 ± 0.3 ± 0.8	¹ ACKERSTAFF 97M OPAL $e^+ e^- \rightarrow Z$
45.3 ± 0.35 ± 0.87	4227 ¹ BUSKULIC 96D ALEP $E_{cm}^{ee} = 88-94$ GeV
45.5 ± 0.3 ± 0.8	¹ ABREU 95R DLPH $E_{cm}^{ee} = 88-94$ GeV
46.3 ± 1.9	1378 ¹ ACCIARRI 95B L3 $E_{cm}^{ee} = 88-94$ GeV
46.4 ± 0.3 ± 0.8	² AKERIB 91 CLE2 $e^+ e^- \rightarrow \gamma X$
45.6 ± 0.8	² WU 91 CSB2 $e^+ e^- \rightarrow \gamma X, \gamma \ell X$
45.4 ± 1.0	³ LEE-FRANZINI 90 CSB2 $e^+ e^- \rightarrow \Upsilon(5S)$
• • • We do not use the following data for averages, fits, limits, etc. • • •	
52 ± 2 ± 4	1400 ⁴ HAN 85 CUSB $e^+ e^- \rightarrow \gamma e X$

- ¹ u, d, s flavor averaged.
- ² These papers report E_γ in the B^* center of mass. The $m_{B^*} - m_B$ is 0.2 MeV higher. $E_{cm} = 10.61-10.7$ GeV. Admixture of B^0 and B^+ mesons, but not B_s .
- ³ LEE-FRANZINI 90 value is for an admixture of B^0 and B^+ . They measure $46.7 \pm 0.4 \pm 0.2$ MeV for an admixture of $B^0, B^+,$ and B_s , and use the shape of the photon line to separate the above value.
- ⁴ HAN 85 is for $E_{cm} = 10.6-11.2$ GeV, giving an admixture of $B^0, B^+,$ and B_s .

$m_{B^{*+}} - m_{B^+}$

VALUE (MeV)	DOCUMENT ID	TECN	COMMENT
45.37 ± 0.21 OUR FIT			
45.01 ± 0.30 ± 0.23	⁵ AAIJ 13o	LHCB	pp at 7 TeV

⁵ Obtained the mass difference between $B^{*+} K^-$ and $B^+ K^-$ from $B_{S_2}^*(5840)^0$ decay.

$$|(m_{B^{*+}} - m_{B^+}) - (m_{B^{*0}} - m_{B^0})|$$

VALUE (MeV)	CL%	DOCUMENT ID	TECN	COMMENT
<6	95	ABREU 95R	DLPH	$E_{cm}^{ee} = 88-94$ GeV

$m_{B^{*0}} - m_{B^0}$

VALUE (MeV)	DOCUMENT ID	TECN	COMMENT
0.91 ± 0.24 ± 0.09	⁶ SIRUNYAN 18DF	CMS	pp at 8 TeV

⁶ Uses exclusively reconstructed final states containing a $J/\psi \rightarrow \mu^+ \mu^-$ decay.

Meson Particle Listings

$B^*, B_1(5721), B_J^*(5732)$

B^* DECAY MODES

Mode	Fraction (Γ_i/Γ)
$\Gamma_1 \quad B\gamma$	seen

B^* REFERENCES

SIRUNYAN 18DF EPJ C78 939	A.M. Sirunyan <i>et al.</i>	(CMS Collab.)
AAIJ 13O PRL 110 151803	R. Aaij <i>et al.</i>	(LHCb Collab.)
ACKERSTAFF 97M ZPHY C74 413	K. Ackerstaff <i>et al.</i>	(OPAL Collab.)
BUSKULIC 96D ZPHY C69 393	D. Buskulic <i>et al.</i>	(ALEPH Collab.)
ABREU 95B PL B345 589	P. Abreu <i>et al.</i>	(DELPHI Collab.)
ACCIARRI 95B PL B345 589	M. Acciari <i>et al.</i>	(L3 Collab.)
AKERIB 91 PRL 67 1692	D.S. Akarib <i>et al.</i>	(CLEO Collab.)
WU 91 PL B273 177	Q.W. Wu <i>et al.</i>	(CUSB II Collab.)
LEE-FRANZINI 90 PRL 65 2947	J. Lee-Franzini <i>et al.</i>	(CUSB II Collab.)
HAN 85 PRL 55 36	K. Han <i>et al.</i>	(COLU, LSU, MPIM, STON)

$B_1(5721)$

$$I(J^P) = \frac{1}{2}(1^+)$$

I, J, P need confirmation.

Quantum numbers shown are quark-model predictions.

$B_1(5721)$ MASS

$B_1(5721)^+$ mass

OUR FIT uses m_{B^+0} and $m_{B_1^+} - m_{B^+0}$ to determine $m_{B_1(5721)^+}$.

VALUE (MeV)	DOCUMENT ID
$5725.9^{+2.5}_{-2.7}$ OUR FIT	

$m_{B_1^+} - m_{B^+0}$

VALUE (MeV)	EVTS	DOCUMENT ID	TECN	COMMENT
$401.2^{+2.4}_{-2.7}$ OUR FIT				

$401.2^{+2.4}_{-2.7}$ OUR AVERAGE

$400.5 \pm 1.8 \pm 3.1$	8k	¹ AAIJ	15AB LHCb	$p\bar{p}$ at 7, 8 TeV
$402 \pm 3 \pm 1_3$		² AALTONEN	14i CDF	$p\bar{p}$ at 1.96 TeV

¹ AAIJ 15AB reports $[m_{B_1^+} - m_{B^+0}] - (m_{B^+0} - m_{B^0}) - m_{\pi^+} = 260.9 \pm 1.8 \pm 3.1$

MeV which we adjust by the π^+ mass and assume $(m_{B^+0} - m_{B^0}) = (m_{B^+} - m_{B^+0}) = 45.01 \pm 0.30 \pm 0.23$ MeV. The masses inside the square brackets were measured for each candidate event.

² AALTONEN 14i reports $m_{B_1(5721)^+} - m_{B^+0} - m_{\pi^+} = 262 \pm 3^{+1}_3$ MeV which we adjusted by the π^+ mass.

$B_1(5721)^0$ mass

OUR FIT uses mass differences measurements listed below to determine the $m_{B_1(5721)^0}$.

VALUE (MeV)	DOCUMENT ID
5726.1 ± 1.3 OUR FIT	Error includes scale factor of 1.2.

$m_{B_1^0} - m_{B^+}$

VALUE (MeV)	DOCUMENT ID	TECN	COMMENT
446.7 ± 1.3 OUR FIT	Error includes scale factor of 1.2.		
$441.5 \pm 2.4 \pm 1.3$	¹ ABAZOV	07T D0	$p\bar{p}$ at 1.96 TeV

••• We do not use the following data for averages, fits, limits, etc. •••

$446.2^{+1.9+1.0}_{-2.1-1.2}$	¹ AALTONEN	09D CDF	Repl. by AALTONEN 14i
-------------------------------	-----------------------	---------	-----------------------

¹ Observed in $B_1^0 \rightarrow B^{*+} \pi^-$.

$m_{B_1^0} - m_{B^{*+}}$

VALUE (MeV)	EVTS	DOCUMENT ID	TECN	COMMENT
401.4 ± 1.2 OUR FIT	Error includes scale factor of 1.2.			

402.8 ± 1.1 OUR AVERAGE

$403.4 \pm 0.7 \pm 1.5$	35k	¹ AAIJ	15AB LHCb	$p\bar{p}$ at 7, 8 TeV
$402.3 \pm 0.9 \pm 1.1_{-1.2}$		² AALTONEN	14i CDF	$p\bar{p}$ at 1.96 TeV

¹ AAIJ 15AB reports $[m_{B_1^0} - m_{B^+}] - (m_{B^{*+}} - m_{B^+}) - m_{\pi^-} = 263.9 \pm 0.7 \pm 1.4$

MeV which we adjust by the π^- mass and $(m_{B^{*+}} - m_{B^+}) = 45.01 \pm 0.30 \pm 0.23$ MeV. The masses inside the square brackets were measured for each candidate event.

² AALTONEN 14i reports $m_{B_1(5721)^0} - m_{B^{*+}} - m_{\pi^-} = 262.7 \pm 0.9^{+1.1}_{-1.2}$ MeV which we adjusted by the π^- mass.

$B_1(5721)$ WIDTH

$B_1(5721)^+$ width

VALUE (MeV)	EVTS	DOCUMENT ID	TECN	COMMENT
31 ± 6 OUR AVERAGE	Error includes scale factor of 1.1.			
$29.1 \pm 3.6 \pm 4.3$	8k	AAIJ	15AB LHCb	$p\bar{p}$ at 7, 8 TeV
$49^{+12}_{-10} \pm 2_{-13}$		AALTONEN	14i CDF	$p\bar{p}$ at 1.96 TeV

$B_1(5721)^0$ width

VALUE (MeV)	EVTS	DOCUMENT ID	TECN	COMMENT
27.5 ± 3.4 OUR AVERAGE	Error includes scale factor of 1.1.			
$30.1 \pm 1.5 \pm 3.5$	35k	AAIJ	15AB LHCb	$p\bar{p}$ at 7, 8 TeV
$23 \pm 3 \pm 4$		AALTONEN	14i CDF	$p\bar{p}$ at 1.96 TeV

$B_1(5721)$ DECAY MODES

Mode	Fraction (Γ_i/Γ)
$\Gamma_1 \quad B^* \pi$	seen

$\Gamma(B^* \pi)/\Gamma_{total}$

VALUE	DOCUMENT ID	TECN	CHG	COMMENT
seen	AAIJ	15AB LHCb	± 0	$p\bar{p}$ at 7, 8 TeV
seen	AALTONEN	14i CDF	\pm	$p\bar{p}$ at 1.96 TeV
seen	AALTONEN	09D CDF	0	$p\bar{p}$ at 1.96 TeV
seen	¹ ABAZOV	07T D0	0	$p\bar{p}$ at 1.96 TeV

¹ Observed in $B_1^0 \rightarrow B^{*+} \pi^-$ with $B^{*+} \rightarrow B^+ \gamma$ and $B^+ \rightarrow J/\psi \pi^+$.

$B_1(5721)$ REFERENCES

AAIJ 15AB JHEP 1504 024	R. Aaij <i>et al.</i>	(LHCb Collab.)
AALTONEN 14i PR D90 012013	T. Aaltonen <i>et al.</i>	(CDF Collab.)
AALTONEN 09D PRL 102 102003	T. Aaltonen <i>et al.</i>	(CDF Collab.)
ABAZOV 07T PRL 99 172001	V.M. Abazov <i>et al.</i>	(D0 Collab.)

$B_J^*(5732)$

$$I(J^P) = ?(??)$$

OMITTED FROM SUMMARY TABLE

also known as B^{**}

Signal can be interpreted as stemming from several narrow and broad resonances.

$B_J^*(5732)$ MASS

VALUE (MeV)	EVTS	DOCUMENT ID	TECN	COMMENT
5698 ± 8 OUR AVERAGE	Error includes scale factor of 1.2.			

5710 ± 20 ¹ AFFOLDER 01F CDF $p\bar{p}$ at 1.8 TeV

5695^{+17}_{-19} ² BARATE 98L ALEP $e^+e^- \rightarrow Z$

$5704 \pm 4 \pm 10$ 1944 ³ BUSKULIC 96D ALEP $E_{cm}^{e^+e^-} = 88-94$ GeV

$5732 \pm 5 \pm 20$ 2157 ABREU 95B DLPH $E_{cm}^{e^+e^-} = 88-94$ GeV

5681 ± 11 1738 AKERS 95E OPAL $E_{cm}^{e^+e^-} = 88-94$ GeV

••• We do not use the following data for averages, fits, limits, etc. •••

5713 ± 2 ⁴ ACCIARRI 99N L3 $e^+e^- \rightarrow Z$

¹ AFFOLDER 01F uses the reconstructed B meson through semileptonic decay channels. The fraction of light B mesons that are produced at $L=1$ B^{**} states is measured to be $0.28 \pm 0.06 \pm 0.03$.

² BARATE 98L uses fully reconstructed B mesons to search for B^{**} production in the $B \pi^\pm$ system. In the framework of heavy quark symmetry (HQSS), they also measured the mass of B_2^* to be 5739^{+8+6}_{-11-4} MeV/ c^2 and the relative production rate of $B(b \rightarrow B_2^* \rightarrow B^{(*)} \pi)/B(b \rightarrow B_{u,d}) = (31 \pm 9^{+6}_{-5})\%$.

³ Using $m_{B \pi^-} - m_B = 424 \pm 4 \pm 10$ MeV.

⁴ ACCIARRI 99N uses inclusive reconstructed B mesons to search for B^{**} production in the $B^{(*)} \pi^\pm$ system. In the framework of HQET, they measured the mass of B_1^* and B_2^* to be $5670 \pm 10 \pm 13$ MeV and $5768 \pm 5 \pm 6$ with the $B(b \rightarrow B^{**}) = (32 \pm 3 \pm 6) \times 10^{-2}$. They also reported the evidence for the existence of an excited B -meson state or mixture of states in the region 5.9–6.0 GeV.

$B_J^*(5732)$ WIDTH

VALUE (MeV)	EVTS	DOCUMENT ID	TECN	COMMENT
128 ± 18 OUR AVERAGE				
145 ± 28	2157	ABREU	95B DLPH	$E_{cm}^{e^+e^-} = 88-94$ GeV
116 ± 24	1738	AKERS	95E OPAL	$E_{cm}^{e^+e^-} = 88-94$ GeV

$B_J^*(5732)$ DECAY MODES

Mode	Fraction (Γ_i/Γ)
$\Gamma_1 \quad B^* \pi + B \pi$	seen
$\Gamma_2 \quad B^* \pi(X)$	[a] (85 ± 29) %

[a] X refers to decay modes with or without additional accompanying decay particles.

Meson Particle Listings

$B_2^*(5732)$, $B_2^*(5747)$, $B_J(5840)$

 $B_2^*(5732)$ BRANCHING RATIOS

X refers to decay modes with or without additional accompanying decay particles.

$\Gamma(B^*\pi(X))/\Gamma_{\text{total}}$	DOCUMENT ID	TECN	COMMENT	Γ_2/Γ
$0.85^{+0.26}_{-0.27} \pm 0.12$	ABBIENDI	02E	OPAL $e^+e^- \rightarrow Z$	

 $B_2^*(5732)$ REFERENCES

ABBIENDI 02E	EPJ C23 437	G. Abbiendi et al.	(OPAL Collab.)
AFFOLDER 01F	PR D64 072002	T. Affolder et al.	(CDF Collab.)
ACCIARRI 99N	PL B465 323	M. Acciari et al.	(L3 Collab.)
BARATE 98L	PL B425 215	R. Barate et al.	(ALEPH Collab.)
BUSKULIC 96D	ZPHY C69 393	D. Buskulic et al.	(ALEPH Collab.)
ABREU 95B	PL B345 598	P. Abreu et al.	(DELPHI Collab.)
AKERS 95E	ZPHY C66 19	R. Akers et al.	(OPAL Collab.)

 $B_2^*(5747)$

$$I(J^P) = \frac{1}{2}(2^+)$$

I, J, P need confirmation.

Quantum numbers shown are quark-model predictions.

 $B_2^*(5747)$ MASS **$B_2^*(5747)^+$ mass**

OUR FIT uses m_{B^0} and $m_{B_2^{*+}} - m_{B^0}$ to determine $m_{B_2^*(5747)^+}$.

VALUE (MeV)	DOCUMENT ID
5737.2 ± 0.7 OUR FIT	

 $m_{B_2^{*+}} - m_{B^0}$

VALUE (MeV)	EVTS	DOCUMENT ID	TECN	COMMENT
457.5 ± 0.7 OUR FIT				
457.5 ± 0.7 OUR AVERAGE				
457.62 ± 0.72 ± 0.40	4k	¹ AAIJ	15AB LHCB	$p\bar{p}$ at 7, 8 TeV
457.3 ± 1.3 $^{+0.3}_{-0.9}$		² AALTONEN	14i CDF	$p\bar{p}$ at 1.96 TeV

¹ AAIJ 15AB reports $[m_{B_2^{*+}} - m_{B^0}] - m_{\pi^+} = 318.1 \pm 0.7 \pm 0.4$ MeV which we adjust by the π^+ mass. The masses inside the square brackets were measured for each candidate event.

² AALTONEN 14i reports $m_{B_2^*(5747)^+} - m_{B^0} - m_{\pi^+} = 317.7 \pm 1.2 \pm 0.3$ MeV which we adjusted by the π^+ mass.

 $B_2^*(5747)^0$ mass

OUR FIT uses m_{B^+} , m_{B^0} and $m_{B_2^{*+}} - m_{B^+}$, and mass differences below to determine $m_{B_2^*(5747)^0}$. The -0.659 correlation between statistical uncertainties of $m_{B^0} - m_{B^+}$ and $m_{B_2^{*0}} - m_{B^0}$ measurements reported by ABAZOV 07T is taken into account.

VALUE (MeV)	DOCUMENT ID
5739.5 ± 0.7 OUR FIT	Error includes scale factor of 1.4.

 $m_{B_2^{*0}} - m_{B^0}$

VALUE (MeV)	DOCUMENT ID	TECN	COMMENT
13.4 ± 1.4 OUR FIT	Error includes scale factor of 1.3.		
26.2 ± 3.1 ± 0.9	¹ ABAZOV	07T D0	$p\bar{p}$ at 1.96 TeV

••• We do not use the following data for averages, fits, limits, etc. •••

14.9 $^{+2.2+1.2}_{-2.5-1.4}$	¹ AALTONEN	09D CDF	Repl. by AALTONEN 14i
-------------------------------	-----------------------	---------	-----------------------

¹ Observed in $B_2^{*0} \rightarrow B^{*+}\pi^-$ and $B_2^{*0} \rightarrow B^+\pi^-$.

 $m_{B_2^{*0}} - m_{B^+}$

VALUE (MeV)	EVTS	DOCUMENT ID	TECN	COMMENT
460.2 ± 0.6 OUR FIT	Error includes scale factor of 1.4.			
459.9 ± 0.8 OUR AVERAGE	Error includes scale factor of 1.8.			
460.18 ± 0.37 ± 0.33	17k	¹ AAIJ	15AB LHCB	$p\bar{p}$ at 7, 8 TeV
457.5 ± 1.2 $^{+0.8}_{-0.9}$		² AALTONEN	14i CDF	$p\bar{p}$ at 1.96 TeV

¹ AAIJ 15AB reports $[m_{B_2^{*0}} - m_{B^+}] - m_{\pi^-} = 320.6 \pm 0.4 \pm 0.3$ MeV which we adjust by the π^- mass. The masses inside the square brackets were measured for each candidate event.

² AALTONEN 14i reports $m_{B_2^*(5747)^0} - m_{B^+} - m_{\pi^-} = 317.9 \pm 1.2 \pm 0.8$ MeV which we adjusted by the π^- mass.

 $B_2^*(5747)$ WIDTH **$B_2^*(5747)^+$ width**

VALUE (MeV)	EVTS	DOCUMENT ID	TECN	COMMENT
20 ± 5 OUR AVERAGE	Error includes scale factor of 2.2.			
23.6 ± 2.0 ± 2.1	4k	AAIJ	15AB LHCB	$p\bar{p}$ at 7, 8 TeV
11 $^{+4}_{-3}$ $^{+3}_{-4}$		AALTONEN	14i CDF	$p\bar{p}$ at 1.96 TeV

 $B_2^*(5747)^0$ width

VALUE (MeV)	EVTS	DOCUMENT ID	TECN	COMMENT
24.2 ± 1.7 OUR AVERAGE				
24.5 ± 1.0 ± 1.5	17k	AAIJ	15AB LHCB	$p\bar{p}$ at 7, 8 TeV
22 $^{+3}_{-2}$ $^{+4}_{-5}$		AALTONEN	14i CDF	$p\bar{p}$ at 1.96 TeV
••• We do not use the following data for averages, fits, limits, etc. •••				
22.7 $^{+3.8+3.2}_{-3.2-10.2}$		AALTONEN	09D CDF	Repl. by AALTONEN 14i

 $B_2^*(5747)$ DECAY MODES

Mode	Fraction (Γ_i/Γ)
Γ_1 $B\pi$	seen
Γ_2 $B^*\pi$	seen

$\Gamma(B\pi)/\Gamma_{\text{total}}$	DOCUMENT ID	TECN	CHG	COMMENT
seen	AAIJ	15AB LHCB	±0	$p\bar{p}$ at 7, 8 TeV
seen	AALTONEN	14i CDF	±	$p\bar{p}$ at 1.96 TeV
seen	AALTONEN	09D CDF	0	$p\bar{p}$ at 1.96 TeV
seen	ABAZOV	07T D0	0	$p\bar{p}$ at 1.96 TeV

$\Gamma(B^*\pi)/\Gamma_{\text{total}}$	DOCUMENT ID	TECN	CHG	COMMENT
seen	AAIJ	15AB LHCB	±0	$p\bar{p}$ at 7, 8 TeV
seen	AALTONEN	09D CDF	0	$p\bar{p}$ at 1.96 TeV
seen	ABAZOV	07T D0	0	$p\bar{p}$ at 1.96 TeV

$\Gamma(B^*\pi)/\Gamma(B\pi)$	DOCUMENT ID	TECN	CHG	COMMENT
0.84 ± 0.27 OUR AVERAGE				
0.71 ± 0.14 ± 0.30	17k	AAIJ	15AB LHCB	0 $p\bar{p}$ at 7, 8 TeV
1.0 ± 0.5 ± 0.8	4k	AAIJ	15AB LHCB	± $p\bar{p}$ at 7, 8 TeV
1.10 ± 0.42 ± 0.31		¹ ABAZOV	07T D0	0 $p\bar{p}$ at 1.96 TeV

¹ Converted from measured ratio of $R = B(B_2^{*0} \rightarrow B^{*+}\pi^-) / B(B_2^{*0} \rightarrow B^*(*)\pi^-) = 0.475 \pm 0.095 \pm 0.069$.

 $B_2^*(5747)$ REFERENCES

AAIJ 15AB	JHEP 1504 024	R. Aaij et al.	(LHCb Collab.)
AALTONEN 14I	PR D90 012013	T. Aaltonen et al.	(CDF Collab.)
AALTONEN 09D	PRL 102 102003	T. Aaltonen et al.	(CDF Collab.)
ABAZOV 07T	PRL 99 172001	V.M. Abazov et al.	(D0 Collab.)

 $B_J(5840)$

$$I(J^P) = \frac{1}{2}(??)$$

I, J, P need confirmation.

OMITTED FROM SUMMARY TABLE
Quantum numbers shown are quark-model predictions.

 $B_J(5840)$ MASS **$B_J(5840)^+$ MASS**

OUR FIT uses m_{B^0} and $m_{B_J(5840)^+} - m_{B^0}$ to determine $m_{B_J(5840)^+}$.

VALUE (MeV)	DOCUMENT ID
5851 ± 19 OUR FIT	

 $m_{B_J(5840)^+} - m_{B^0}$

VALUE (MeV)	EVTS	DOCUMENT ID	TECN	COMMENT
571 ± 19 OUR FIT				
571 ± 13 ± 14	7k	¹ AAIJ	15AB LHCB	$p\bar{p}$ at 7, 8 TeV
••• We do not use the following data for averages, fits, limits, etc. •••				
595 ± 26 ± 14	7k	² AAIJ	15AB LHCB	$p\bar{p}$ at 7, 8 TeV

¹ AAIJ 15AB reports $[m_{B_J^+} - m_{B^0}] - m_{\pi^+} = 431 \pm 13 \pm 14$ MeV which we adjust by the π^+ mass. The masses inside the square brackets were measured for each candidate event. The result assumes $P = (-1)^J$ and uses two relativistic Breit-Wigner functions in the fit for mass difference.

² AAIJ 15AB reports $[m_{B_J^+} - m_{B^0}] - m_{\pi^+} = 455 \pm 26 \pm 14$ MeV which we adjust by the π^+ mass. The masses inside the square brackets were measured for each candidate event. The result assumes $P = (-1)^J$ and uses three relativistic Breit-Wigner functions in the fit for mass difference.

 $m_{B_J(5840)^+} - m_{B^+}$

VALUE (MeV)	EVTS	DOCUMENT ID	TECN	COMMENT
••• We do not use the following data for averages, fits, limits, etc. •••				
565 ± 15 ± 14	7k	¹ AAIJ	15AB LHCB	$p\bar{p}$ at 7, 8 TeV
¹ AAIJ 15AB reports $[m_{B_J^+} - m_{B^0}] - (m_{B^+} - m_{B^0}) - m_{\pi^+} = 425 \pm 15 \pm 14$ MeV which we adjust by the π^+ mass. The masses inside the square brackets were measured for each candidate event. The result assumes $P = -(-1)^J$, $(m_{B^0} - m_{B^+}) = (m_{B^+} - m_{B^0}) = 45.01 \pm 0.30 \pm 0.23$ MeV, and uses three relativistic Breit-Wigner functions in the fit for mass difference.				

Meson Particle Listings

$B_J(5840)$, $B_J(5970)$

$B_J(5840)^0$ MASS

OUR FIT uses m_{B^+} and $m_{B_J(5840)^0} - m_{B^+}$ to determine $m_{B_J(5840)^0}$.

VALUE (MeV)	DOCUMENT ID
5863 ± 9 OUR FIT	

$m_{B_J(5840)^0} - m_{B^+}$

VALUE (MeV)	EVTS	DOCUMENT ID	TECN	COMMENT
584 ± 9 OUR FIT				

584 ± 5 ± 7 12k 1 AAIJ 15AB LHCB pp at 7, 8 TeV

• • • We do not use the following data for averages, fits, limits, etc. • • •

610 ± 22 ± 7 12k 2 AAIJ 15AB LHCB pp at 7, 8 TeV

¹ AAIJ 15AB reports $[m_{B_J^0} - m_{B^+}] - m_{\pi^-} = 444 \pm 5 \pm 7$ MeV which we adjust by

the π^- mass. The masses inside the square brackets were measured for each candidate event. The result assumes $P = (-1)^J$ and uses two relativistic Breit-Wigner functions in the fit for mass difference.

² AAIJ 15AB reports $[m_{B_J^0} - m_{B^+}] - m_{\pi^-} = 471 \pm 22 \pm 7$ MeV which we adjust by

the π^- mass. The masses inside the square brackets were measured for each candidate event. The result assumes $P = (-1)^J$ and uses three relativistic Breit-Wigner functions in the fit for mass difference.

$m_{B_J(5840)^0} - m_{B^{*+}}$

VALUE (MeV)	EVTS	DOCUMENT ID	TECN	COMMENT
584 ± 5 ± 7	12k	1 AAIJ	15AB LHCB	pp at 7, 8 TeV

• • • We do not use the following data for averages, fits, limits, etc. • • •

584 ± 5 ± 7 12k 1 AAIJ 15AB LHCB pp at 7, 8 TeV

¹ AAIJ 15AB reports $[m_{B_J^0} - m_{B^{*+}}] - (m_{B^{*+}} - m_{B^+}) - m_{\pi^-} = 444 \pm 5 \pm 7$ MeV

which we adjust by the π^- mass. The masses inside the square brackets were measured for each candidate event. The result assumes $P = (-1)^J$, $(m_{B^{*+}} - m_{B^+}) = 45.01 \pm 0.30 \pm 0.23$ MeV, and uses three relativistic Breit-Wigner functions in the fit for mass difference.

$B_J(5840)$ WIDTH

$B_J(5840)^+$ WIDTH

VALUE (MeV)	EVTS	DOCUMENT ID	TECN	COMMENT
224 ± 24 ± 80	7k	1 AAIJ	15AB LHCB	pp at 7, 8 TeV

• • • We do not use the following data for averages, fits, limits, etc. • • •

215 ± 27 ± 80 7k 2 AAIJ 15AB LHCB pp at 7, 8 TeV

229 ± 27 ± 80 7k 3 AAIJ 15AB LHCB pp at 7, 8 TeV

¹ Assuming $P = (-1)^J$ and using two relativistic Breit-Wigner functions in the fit for mass difference.

² Assuming $P = (-1)^J$ and using three relativistic Breit-Wigner functions in the fit for mass difference.

³ Assuming $P = -(-1)^J$ and using three relativistic Breit-Wigner functions in the fit for mass difference.

$B_J(5840)^0$ WIDTH

VALUE (MeV)	EVTS	DOCUMENT ID	TECN	COMMENT
127 ± 17 ± 34	12k	1 AAIJ	15AB LHCB	pp at 7, 8 TeV

• • • We do not use the following data for averages, fits, limits, etc. • • •

107 ± 20 ± 34 12k 2 AAIJ 15AB LHCB pp at 7, 8 TeV

119 ± 17 ± 34 12k 3 AAIJ 15AB LHCB pp at 7, 8 TeV

¹ Assuming $P = (-1)^J$ and using two relativistic Breit-Wigner functions in the fit for mass difference.

² Assuming $P = (-1)^J$ and using three relativistic Breit-Wigner functions in the fit for mass difference.

³ Assuming $P = -(-1)^J$ and using three relativistic Breit-Wigner functions in the fit for mass difference.

$B_J(5840)$ DECAY MODES

Mode	Fraction (Γ_j/Γ)
Γ_1 $B^* \pi$	seen
Γ_2 $B \pi$	possibly seen

$B_J(5840)$ BRANCHING RATIOS

$\Gamma(B^* \pi)/\Gamma_{total}$	Γ_1/Γ
seen	7k AAIJ 15AB LHCB \pm pp at 7, 8 TeV
seen	12k AAIJ 15AB LHCB 0 pp at 7, 8 TeV

$\Gamma(B \pi)/\Gamma_{total}$	Γ_2/Γ
possibly seen	7k 1 AAIJ 15AB LHCB \pm pp at 7, 8 TeV
possibly seen	1 AAIJ 15AB LHCB 0 pp at 7, 8 TeV

¹ A $B \pi$ decay is forbidden from a $P = -(-1)^J$ parent, whereas $B^* \pi$ is allowed.

$B_J(5840)$ REFERENCES

$B_J(5970)$

$$I(J^P) = \frac{1}{2}(??)$$

I, J, P need confirmation.

Quantum numbers shown are quark-model predictions.

$B_J(5970)$ MASS

$B_J(5970)^+$ MASS

OUR FIT uses m_{B^0} and $m_{B_J(5970)^+} - m_{B^0}$ to determine $m_{B_J(5970)^+}$.

VALUE (MeV)	DOCUMENT ID
5964 ± 5 OUR FIT	

$m_{B_J(5970)^+} - m_{B^0}$

VALUE (MeV)	EVTS	DOCUMENT ID	TECN	COMMENT
685 ± 5 OUR FIT				

685 ± 5 OUR AVERAGE

685.3 ± 4.1 ± 2.5 2k 1 AAIJ 15AB LHCB pp at 7, 8 TeV

681 ± 5 ± 12 1.4k 2 AALTONEN 14i CDF $p\bar{p}$ at 1.96 TeV

• • • We do not use the following data for averages, fits, limits, etc. • • •

686.8 ± 4.5 ± 2.5 2k 3 AAIJ 15AB LHCB pp at 7, 8 TeV

¹ AAIJ 15AB reports $[m_{B_J^+} - m_{B^0}] - m_{\pi^+} = 545.8 \pm 4.1 \pm 2.5$ MeV which we adjust by

the π^+ mass. The masses inside the square brackets were measured for each candidate event. The result assumes $P = (-1)^J$ and uses two relativistic Breit-Wigner functions in the fit for mass difference.

² AALTONEN 14i reports $m_{B_J(5970)^+} - m_{B^0} - m_{\pi^+} = 541 \pm 5 \pm 12$ MeV which we

adjusted by the π^+ mass.

³ AAIJ 15AB reports $[m_{B_J^+} - m_{B^0}] - m_{\pi^+} = 547 \pm 5 \pm 3$ MeV which we adjust by

the π^+ mass. The masses inside the square brackets were measured for each candidate event. The result assumes $P = (-1)^J$ and uses three relativistic Breit-Wigner functions in the fit for mass difference.

$m_{B_J(5970)^+} - m_{B^{*0}}$

VALUE (MeV)	EVTS	DOCUMENT ID	TECN	COMMENT
686.0 ± 4.0 ± 2.5	2k	1 AAIJ	15AB LHCB	pp at 7, 8 TeV

• • • We do not use the following data for averages, fits, limits, etc. • • •

686.0 ± 4.0 ± 2.5 2k 1 AAIJ 15AB LHCB pp at 7, 8 TeV

¹ AAIJ 15AB reports $[m_{B_J^+} - m_{B^{*0}}] - (m_{B^{*0}} - m_{B^0}) - m_{\pi^+} = 547 \pm 4 \pm 3$ MeV which

we adjust by the π^+ mass. The masses inside the square brackets were measured for each candidate event. The result assumes $P = (-1)^J$, $(m_{B^{*0}} - m_{B^0}) = (m_{B^{*+}} - m_{B^+}) = 45.01 \pm 0.30 \pm 0.23$ MeV, and uses three relativistic Breit-Wigner functions in the fit for mass difference.

$B_J(5970)^0$ MASS

OUR FIT uses m_{B^+} and $m_{B_J(5970)^0} - m_{B^+}$ to determine $m_{B_J(5970)^0}$.

VALUE (MeV)	DOCUMENT ID
5971 ± 5 OUR FIT	

$m_{B_J(5970)^0} - m_{B^+}$

VALUE (MeV)	EVTS	DOCUMENT ID	TECN	COMMENT
691 ± 5 OUR FIT				

691 ± 5 OUR AVERAGE

689.9 ± 2.9 ± 5.1 10k 1 AAIJ 15AB LHCB pp at 7, 8 TeV

698 ± 5 ± 12 2.6k 2 AALTONEN 14i CDF $p\bar{p}$ at 1.96 TeV

• • • We do not use the following data for averages, fits, limits, etc. • • •

714.3 ± 6.4 ± 5.1 10k 3 AAIJ 15AB LHCB pp at 7, 8 TeV

¹ AAIJ 15AB reports $[m_{B_J^0} - m_{B^+}] - m_{\pi^-} = 550.4 \pm 2.9 \pm 5.1$ MeV which we adjust by

the π^- mass. The masses inside the square brackets were measured for each candidate event. The result assumes $P = (-1)^J$ and uses two relativistic Breit-Wigner functions in the fit for mass difference.

² AALTONEN 14i reports $m_{B_J(5970)^0} - m_{B^+} - m_{\pi^-} = 558 \pm 5 \pm 12$ MeV which we

adjusted by the π^- mass.

³ AAIJ 15AB reports $[m_{B_J^0} - m_{B^+}] - m_{\pi^-} = 575 \pm 6 \pm 5$ MeV which we adjust by

the π^- mass. The masses inside the square brackets were measured for each candidate event. The result assumes $P = (-1)^J$ and uses three relativistic Breit-Wigner functions in the fit for mass difference.

$m_{B_J(5970)^0} - m_{B^{*+}}$

VALUE (MeV)	EVTS	DOCUMENT ID	TECN	COMMENT
691.6 ± 3.7 ± 5.1	10k	1 AAIJ	15AB LHCB	pp at 7, 8 TeV

• • • We do not use the following data for averages, fits, limits, etc. • • •

691.6 ± 3.7 ± 5.1 10k 1 AAIJ 15AB LHCB pp at 7, 8 TeV

¹ AAIJ 15AB reports $[m_{B_J^0} - m_{B^{*+}}] - (m_{B^{*+}} - m_{B^+}) - m_{\pi^-} = 552 \pm 4 \pm 5$ MeV

which we adjust by the π^- mass. The masses inside the square brackets were measured for each candidate event. The result assumes $P = -(-1)^J$, $(m_{B^{*+}} - m_{B^+}) = 45.01 \pm 0.30 \pm 0.23$ MeV, and uses three relativistic Breit-Wigner functions in the fit for mass difference.

See key on page 1127

Meson Particle Listings

 $B_J(5970)$ $B_J(5970)$ WIDTH $B_J(5970)^+$ WIDTH

VALUE (MeV)	EVTS	DOCUMENT ID	TECN	COMMENT
62±20 OUR AVERAGE				
63±15±17	2k	¹ AAIJ	15AB LHCB	pp at 7, 8 TeV
60 ⁺³⁰ ₋₂₀ ±40	1.4k	AALTONEN	14i CDF	$p\bar{p}$ at 1.96 TeV

• • • We do not use the following data for averages, fits, limits, etc. • • •

61±14±17	2k	² AAIJ	15AB LHCB	pp at 7, 8 TeV
61±15±17	2k	³ AAIJ	15AB LHCB	pp at 7, 8 TeV

¹ Assuming $P = (-1)^J$ and using two relativistic Breit-Wigner functions in the fit for mass difference.

² Assuming $P = (-1)^J$ and using three relativistic Breit-Wigner functions in the fit for mass difference.

³ Assuming $P = -(-1)^J$ and using three relativistic Breit-Wigner functions in the fit for mass difference.

 $B_J(5970)^0$ WIDTH

VALUE (MeV)	EVTS	DOCUMENT ID	TECN	COMMENT
81±12 OUR AVERAGE				
82± 8± 9	10k	¹ AAIJ	15AB LHCB	pp at 7, 8 TeV
70 ⁺³⁰ ₋₂₀ ±30	2.6k	AALTONEN	14i CDF	$p\bar{p}$ at 1.96 TeV

• • • We do not use the following data for averages, fits, limits, etc. • • •

56± 7± 9	10k	² AAIJ	15AB LHCB	pp at 7, 8 TeV
82±10± 9	10k	³ AAIJ	15AB LHCB	pp at 7, 8 TeV

¹ Assuming $P = (-1)^J$ and using two relativistic Breit-Wigner functions in the fit for mass difference.

² Assuming $P = (-1)^J$ and using three relativistic Breit-Wigner functions in the fit for mass difference.

³ Assuming $P = -(-1)^J$ and using three relativistic Breit-Wigner functions in the fit for mass difference.

 $B_J(5970)$ DECAY MODES

Mode	Fraction (Γ_j/Γ)
Γ_1 $B\pi$	possibly seen
Γ_2 $B^*\pi$	seen

 $B_J(5970)$ BRANCHING RATIOS

$\Gamma(B\pi)/\Gamma_{\text{total}}$	VALUE	EVTS	DOCUMENT ID	TECN	CHG	COMMENT	Γ_1/Γ
possibly seen		2k	¹ AAIJ	15AB LHCB	±	pp at 7, 8 TeV	
possibly seen		10k	¹ AAIJ	15AB LHCB	0	pp at 7, 8 TeV	
possibly seen		2.6k	AALTONEN	14i CDF	0	$p\bar{p}$ at 1.96 TeV	
possibly seen		1.4k	AALTONEN	14i CDF	±	$p\bar{p}$ at 1.96 TeV	

¹ A $B\pi$ decay is forbidden from a $P = -(-1)^J$ parent, whereas $B^*\pi$ is allowed.

$\Gamma(B^*\pi)/\Gamma_{\text{total}}$	VALUE	EVTS	DOCUMENT ID	TECN	CHG	COMMENT	Γ_2/Γ
seen		10k	AAIJ	15AB LHCB	0	pp at 7, 8 TeV	
seen		2k	AAIJ	15AB LHCB	±	pp at 7, 8 TeV	
seen		2.6k	AALTONEN	14i CDF	0	$p\bar{p}$ at 1.96 TeV	
seen		1.4k	AALTONEN	14i CDF	±	$p\bar{p}$ at 1.96 TeV	

 $B_J(5970)$ REFERENCES

AAIJ	15AB JHEP 1504 024	R. Aaij <i>et al.</i>	(LHCb Collab.)
AALTONEN	14i PR D90 012013	T. Aaltonen <i>et al.</i>	(CDF Collab.)

Meson Particle Listings

 B_s^0 **BOTTOM, STRANGE MESONS** $(B = \pm 1, S = \mp 1)$ $B_s^0 = s\bar{b}, \bar{B}_s^0 = \bar{s}b$, similarly for B_s^{*0} s B_s^0

$$I(J^P) = 0(0^-)$$

I, J, P need confirmation. Quantum numbers shown are quark-model predictions.

 B_s^0 MASS

VALUE (MeV)	EVTS	DOCUMENT ID	TECN	COMMENT
5366.92 ± 0.10 OUR FIT				
5366.91 ± 0.11 OUR AVERAGE				
5366.98 ± 0.07 ± 0.13		1 AAIJ	21C LHCb	pp at 7, 8, 13 TeV
5366.85 ± 0.19 ± 0.13		2 AAIJ	19U LHCb	pp at 7, 8, 13 TeV
5366.83 ± 0.25 ± 0.27		3 AAIJ	18AC LHCb	pp at 7, 8, 13 TeV
5367.08 ± 0.38 ± 0.15	128	4 AAIJ	16U LHCb	pp at 7, 8 TeV
5366.90 ± 0.28 ± 0.23		5 AAIJ	12E LHCb	pp at 7 TeV
5364.4 ± 1.3 ± 0.7		LOUVOT	09 BELL	$e^+e^- \rightarrow \Upsilon(5S)$
5366.01 ± 0.73 ± 0.33		6 ACOSTA	06 CDF	$p\bar{p}$ at 1.96 TeV
5369.9 ± 2.3 ± 1.3	32	7 ABE	96B CDF	$p\bar{p}$ at 1.8 TeV
5374 ± 16 ± 2	3	ABREU	94D DLPH	$e^+e^- \rightarrow Z$
5359 ± 19 ± 7	1	7 AKERS	94J OPAL	$e^+e^- \rightarrow Z$
5368.6 ± 5.6 ± 1.5	2	BUSKULIC	93G ALEP	$e^+e^- \rightarrow Z$
••• We do not use the following data for averages, fits, limits, etc. •••				
5370 ± 1 ± 3		DRUTSKOY	07A BELL	Repl. by LOUVOT 09
5370 ± 40	6	8 AKERS	94J OPAL	$e^+e^- \rightarrow Z$
5383.3 ± 4.5 ± 5.0	14	ABE	93F CDF	Repl. by ABE 96B

- Uses $B_s^0 \rightarrow J/\psi \pi^+ \pi^- K^+ K^-$ decays.
- Uses $B_s^0 \rightarrow J/\psi p\bar{p}$ decays.
- Uses $B_s^0 \rightarrow \chi_{c1} K^+ K^-$ mode.
- Uses $J/\psi \rightarrow \mu^+ \mu^-, \phi \rightarrow K^+ K^-$ decays, and observes 128 ± 13 events of $B_s^0 \rightarrow J/\psi \phi$.
- Uses $B_s^0 \rightarrow J/\psi \phi$ fully reconstructed decays.
- Uses exclusively reconstructed final states containing a $J/\psi \rightarrow \mu^+ \mu^-$ decays.
- From the decay $B_s^0 \rightarrow J/\psi(1S) \phi$.
- From the decay $B_s^0 \rightarrow D_s^- \pi^+$.

$$m_{B_s^0} - m_B$$

m_B is the average of our B masses ($m_{B^\pm} + m_{B^0}$)/2.

VALUE (MeV)	CL%	DOCUMENT ID	TECN	COMMENT
87.42 ± 0.14 OUR FIT				
87.42 ± 0.24 OUR AVERAGE				
87.60 ± 0.44 ± 0.09		1 AAIJ	15U LHCb	pp at 7, 8 TeV
87.42 ± 0.30 ± 0.09		2 AAIJ	12E LHCb	pp at 7 TeV
86.64 ± 0.80 ± 0.08		3 ACOSTA	06 CDF	$p\bar{p}$ at 1.96 TeV

- We use the following data for averages but not for fits. •••
- | | | | | |
|------------------|--|-----|---------|-----------------------|
| 89.7 ± 2.7 ± 1.2 | | ABE | 96B CDF | $p\bar{p}$ at 1.8 TeV |
|------------------|--|-----|---------|-----------------------|
- We do not use the following data for averages, fits, limits, etc. •••
- | | | | | |
|-----------|----|--------------|---------|-----------------------------------|
| 80 to 130 | 68 | LEE-FRANZINI | 90 CSB2 | $e^+e^- \rightarrow \Upsilon(5S)$ |
|-----------|----|--------------|---------|-----------------------------------|
- The reported result is $m_{B_s^0} - m_{B^0} = 87.45 \pm 0.44 \pm 0.09$ MeV. We convert it to the mass difference with respect to the average of $(m_{B^\pm} + m_{B^0})/2$. Uses the mode $B_s^0 \rightarrow \psi(2S) K^- \pi^+$.
 - The reported result is $m_{B_s^0} - m_{B^+} = 87.52 \pm 0.30 \pm 0.12$ MeV. We convert it to the mass difference with respect to the average of $(m_{B^\pm} + m_{B^0})/2$.
 - The reported result is $m_{B_s^0} - m_{B^0} = 86.38 \pm 0.90 \pm 0.06$ MeV. We convert it to the mass difference with respect to the average of $(m_{B^\pm} + m_{B^0})/2$.

$$m_{B_{SH}^0} - m_{B_{SL}^0}$$

See the $B_s^0 - \bar{B}_s^0$ MIXING section near the end of these B_s^0 Listings.

 B_s^0 MEAN LIFE

"OUR EVALUATION" is provided by the Heavy Flavor Averaging Group (HFLAV, <https://hflav.web.cern.ch/>).

The mean B_s^0 lifetime is defined and computed as $1/\Gamma_{B_s^0}$, where $\Gamma_{B_s^0}$ is the average decay width of the B_s^0 mass eigenstates.

VALUE (10^{-12} s)	EVTS	DOCUMENT ID	TECN	COMMENT
1.520 ± 0.005 OUR EVALUATION				

••• We do not use the following data for averages, fits, limits, etc. •••

1.518 ± 0.041 ± 0.027		1 AALTONEN	11AP CDF	$p\bar{p}$ at 1.96 TeV
1.398 ± 0.044 ± 0.028		2 ABAZOV	06V D0	$p\bar{p}$ at 1.96 TeV
1.42 ± 0.14 ± 0.03		3 ABREU	00Y DLPH	$e^+e^- \rightarrow Z$
1.53 ± 0.16 ± 0.07		4 ABREU,P	00G DLPH	$e^+e^- \rightarrow Z$
1.36 ± 0.09 ± 0.06		5 ABE	99D CDF	$p\bar{p}$ at 1.8 TeV
1.72 ± 0.20 ± 0.18		6 ACKERSTAFF	98F OPAL	$e^+e^- \rightarrow Z$
1.50 ± 0.16 ± 0.04		5 ACKERSTAFF	98G OPAL	$e^+e^- \rightarrow Z$
1.47 ± 0.14 ± 0.08		4 BARATE	98C ALEP	$e^+e^- \rightarrow Z$
1.51 ± 0.11		7 BARATE	98C ALEP	$e^+e^- \rightarrow Z$
1.56 ± 0.29 ± 0.08		5 ABREU	96F DLPH	Repl. by ABREU 00Y
1.65 ± 0.34 ± 0.12		4 ABREU	96F DLPH	Repl. by ABREU 00Y
1.76 ± 0.20 ± 0.15		8 ABREU	96F DLPH	Repl. by ABREU 00Y
1.60 ± 0.26 ± 0.13		9 ABREU	96F DLPH	Repl. by ABREU,P 00G
1.67 ± 0.14		10 ABREU	96F DLPH	$e^+e^- \rightarrow Z$
1.61 ± 0.30 ± 0.18	90	4 BUSKULIC	96E ALEP	Repl. by BARATE 98C
1.54 ± 0.14 ± 0.04		5 BUSKULIC	96M ALEP	$e^+e^- \rightarrow Z$
1.42 ± 0.27 ± 0.11	76	5 ABE	95R CDF	Repl. by ABE 99D
1.74 ± 1.08 ± 0.07	8	11 ABE	95R CDF	Sup. by ABE 96N
1.54 ± 0.25 ± 0.06	79	5 AKERS	95G OPAL	Repl. by ACKERSTAFF 98G
1.59 ± 0.17 ± 0.03	134	5 BUSKULIC	95O ALEP	Sup. by BUSKULIC 96M
0.96 ± 0.37	41	12 ABREU	94E DLPH	Sup. by ABREU 96F
1.92 ± 0.45 ± 0.04	31	5 BUSKULIC	94C ALEP	Sup. by BUSKULIC 95O
1.13 ± 0.35 ± 0.09	22	5 ACTON	93H OPAL	Sup. by AKERS 95G

- AALTONEN 11AP combines the fully reconstructed $B_s^0 \rightarrow D_s^- \pi^+$ decays and partially reconstructed $B_s^0 \rightarrow D_s X$ decays.
- Measured using $D_s \mu^+$ vertices.
- Uses $D_s^- \ell^+$, and $\phi \ell^+$ vertices.
- Measured using D_s hadron vertices.
- Measured using $D_s^- \ell^+$ vertices.
- ACKERSTAFF 98F use fully reconstructed $D_s^- \rightarrow \phi \pi^-$ and $D_s^- \rightarrow K^*0 K^-$ in the inclusive B_s^0 decay.
- Combined results from $D_s^- \ell^+$ and D_s hadron.
- Measured using $\phi \ell$ vertices.
- Measured using inclusive D_s vertices.
- Combined result for the four ABREU 96F methods.
- Exclusive reconstruction of $B_s^0 \rightarrow \psi \phi$.
- ABREU 94E uses the flight-distance distribution of D_s vertices, ϕ -lepton vertices, and $D_s \mu$ vertices.

 $\Gamma_{B_s^0}$

"OUR EVALUATION" is an average performed by the Heavy Flavor Averaging Group (HFLAV, <https://hflav.web.cern.ch/>) as described in our "Review on $B - \bar{B}$ Mixing" in the B^0 section of these Listings. It includes the measurements of $\Gamma_{B_s^0}$ and $\Delta \Gamma_{B_s^0}$ listed in this section, as well as constraints from effective lifetimes with pure CP modes and flavor-specific modes.

VALUE (10^{12} s $^{-1}$)	DOCUMENT ID	TECN	COMMENT
0.6578 ± 0.0024 OUR EVALUATION			Error includes scale factor of 2.6.
0.662 ± 0.004 OUR AVERAGE			Error includes scale factor of 2.7. See the ideogram below.
0.6703 ± 0.0014 ± 0.0018	1 AAD	21AE ATLS	pp at 7, 8, 13 TeV
0.608 ± 0.018 ± 0.012	2 AAIJ	21AN LHCb	pp at 7, 8 TeV
0.6590 ± 0.0032 ± 0.0023	1 SIRUNYAN	21E CMS	pp at 8, 13 TeV
0.6563 ± 0.0021	3 AAIJ	19Q LHCb	pp at 7, 8, 13 TeV
0.668 ± 0.011 ± 0.006	4 AAIJ	16AK LHCb	pp at 7, 8 TeV
0.654 ± 0.008 ± 0.004	1 AALTONEN	12AJ CDF	$p\bar{p}$ at 1.96 TeV
0.693 ± 0.018 ± 0.017	1 ABAZOV	12D D0	$p\bar{p}$ at 1.96 TeV

••• We do not use the following data for averages, fits, limits, etc. •••

0.6531 ± 0.0042 ± 0.0026	1 SIRUNYAN	21E CMS	pp at 13 TeV
0.650 ± 0.006 ± 0.004	3 AAIJ	17V LHCb	Repl. by AAIJ 19Q
0.675 ± 0.003 ± 0.003	1 AAD	16AP ATLS	Repl. by AAD 21AE
0.6704 ± 0.0043 ± 0.0055	1 KHACHATRY...	16S CMS	pp at 8 TeV
0.6603 ± 0.0027 ± 0.0015	5 AAIJ	15I LHCb	Repl. by AAIJ 19Q
0.677 ± 0.007 ± 0.004	1 AAD	14U ATLS	Repl. by AAD 16AP
0.661 ± 0.004 ± 0.006	6 AAIJ	13AR LHCb	Repl. by AAIJ 15I
0.677 ± 0.007 ± 0.004	1 AAD	12CV ATLS	Repl. by AAD 14U

See key on page 1127

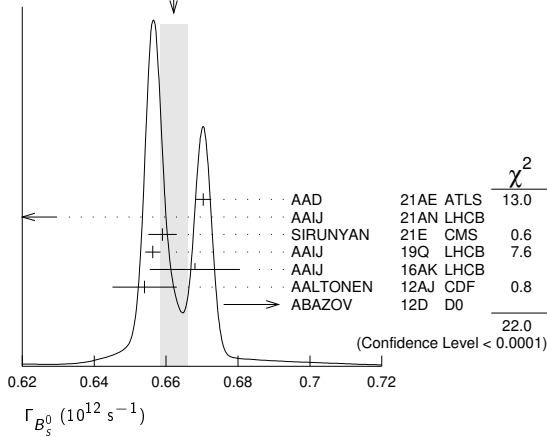
Meson Particle Listings

B_s^0

0.657 ± 0.009 ± 0.008	¹ AAIJ	12d LHCb	Repl. by AAIJ 13AR
0.654 ± 0.011 ± 0.005	^{1,7} AALTONEN	12d CDF	Repl. by AALTONEN 12AJ
0.672 ± 0.027 ± 0.013	¹ ABAZOV	09E D0	Repl. by ABAZOV 08AM
0.658 ± 0.017 ± 0.009	^{1,8} AALTONEN	08J CDF	Repl. by AALTONEN 12D
0.658 ± 0.022 ± 0.004	¹ ABAZOV	08AMD0	Repl. by ABAZOV 12D
0.658 ± 0.035 ± 0.0130 -0.004	^{1,8} ABAZOV	07 D0	Repl. by ABAZOV 09E
0.714 ± 0.007 ± 0.010 -0.008	^{1,8} ACOSTA	05 CDF	Repl. by AALTONEN 08J

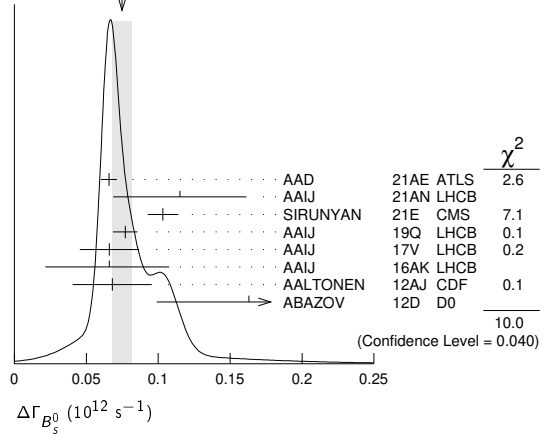
0.19 ± 0.07 ± 0.02 -0.01	^{1,11} ABAZOV	08AMD0	Repl. by ABAZOV 12D
0.12 ± 0.08 ± 0.10 ± 0.02	^{10,12} ABAZOV	07 D0	Repl. by ABAZOV 07N
0.13 ± 0.09	¹³ ABAZOV	07N D0	Repl. by ABAZOV 09E
0.47 ± 0.19 ± 0.01 -0.24	¹⁰ ACOSTA	05 CDF	Repl. by AALTONEN 08J

WEIGHTED AVERAGE
0.662±0.004 (Error scaled by 2.7)



- Measured using a time-dependent angular analysis of $B_s^0 \rightarrow J/\psi \phi$ decays.
- Measured using a time-dependent angular analysis of $B_s^0 \rightarrow J/\psi \phi$ decays with $J/\psi \rightarrow e^+ e^-$.
- Measured using time-dependent angular analysis of $B_s^0 \rightarrow J/\psi K^+ K^-$ in the region $m(KK) > 1.05$ GeV.
- Measured using a time-dependent angular analysis of $B_s^0 \rightarrow \psi(2S) \phi$ decays.
- Measured using a time-dependent angular analysis of $B_s^0 \rightarrow J/\psi K^+ K^-$ decays.
- Measured using a combined time-dependent angular analysis of $B_s^0 \rightarrow J/\psi K^+ K^-$ and $B_s^0 \rightarrow J/\psi \pi^+ \pi^-$ decays.
- Assuming CPV phase $\phi_s = -0.04$.
- Assuming CPV phase $\phi_s = 0$.

WEIGHTED AVERAGE
0.075±0.007 (Error scaled by 1.6)



- Measured using the time-dependent angular analysis of $B_s^0 \rightarrow J/\psi \phi$ decays.
- Measured using a time-dependent angular analysis of $B_s^0 \rightarrow J/\psi \phi$ decays with $J/\psi \rightarrow e^+ e^-$.
- Measured using time-dependent angular analysis of $B_s^0 \rightarrow J/\psi K^+ K^-$ decays.
- Measured using time-dependent angular analysis of $B_s^0 \rightarrow J/\psi K^+ K^-$ in the region $m(KK) > 1.05$ GeV.
- Measured using time-dependent angular analysis of $B_s^0 \rightarrow \psi(2S) \phi$ decays.
- The error includes both statistical and systematic uncertainties.
- AAIJ 13AR result comes from a combined fit to $B_s^0 \rightarrow J/\psi K^+ K^-$ and $B_s^0 \rightarrow J/\psi \pi^+ \pi^-$ data sets. Also reports $\Delta\Gamma_s = 0.100 \pm 0.016 \pm 0.003 \text{ ps}^{-1}$ from a fit to $B_s^0 \rightarrow J/\psi K^+ K^-$ decays.
- Uses the time-dependent angular analysis of $B_s^0 \rightarrow J/\psi \phi$ decays and assuming CP-violating angle $\beta_s(B^0 \rightarrow J/\psi \phi) = 0.02$.
- Measured the angular and lifetime parameters for the time-dependent angular untagged decays $B_d^0 \rightarrow J/\psi K^{*0}$ and $B_s^0 \rightarrow J/\psi \phi$.
- Measured using the time-dependent angular analysis of $B_s^0 \rightarrow J/\psi \phi$ decays and assuming CP-violating phase $\phi_s = 0$.
- Obtains 90% CL interval $-0.06 < \Delta\Gamma_s < 0.30$.
- ABAZOV 07 reports $0.17 \pm 0.09 \pm 0.02$ with CP-violating phase ϕ_s as a free parameter.
- Combines D^0 measurements of time-dependent angular distributions in $B_s^0 \rightarrow J/\psi \phi$ and charge asymmetry in semileptonic decays. There is a 4-fold ambiguity in the solution.

$\Delta\Gamma_{B_s^0}$

“OUR EVALUATION” is an average performed by the Heavy Flavor Averaging Group (HFLAV, <https://hflav.web.cern.ch/>) as described in our “Review on $B-\bar{B}$ Mixing” in the B^0 section of these Listings. It includes the measurements of Γ_{B^0} and $\Delta\Gamma_{B^0}$ listed in this section, as well as constraints from effective lifetimes with pure CP modes and flavor-specific modes.

VALUE (10^{12} s^{-1})	DOCUMENT ID	TECN	COMMENT
0.084 ± 0.005 OUR EVALUATION	Error includes scale factor of 1.7.		
0.075 ± 0.007 OUR AVERAGE	Error includes scale factor of 1.6. See the ideogram below.		
0.0657 ± 0.0043 ± 0.0037	¹ AAD	21AE ATLS	$p\bar{p}$ at 7, 8, 13 TeV
0.115 ± 0.045 ± 0.011	² AAIJ	21AN LHCb	$p\bar{p}$ at 7, 8 TeV
0.1032 ± 0.0095 ± 0.0048	¹ SIRUNYAN	21E CMS	$p\bar{p}$ at 8, 13 TeV
0.077 ± 0.008 ± 0.003	³ AAIJ	19Q LHCb	$p\bar{p}$ at 13 TeV
0.066 ± 0.018 ± 0.010	⁴ AAIJ	17V LHCb	$p\bar{p}$ at 7, 8 TeV
0.066 ± 0.041 ± 0.007 -0.044	⁵ AAIJ	16AK LHCb	$p\bar{p}$ at 7, 8 TeV
0.068 ± 0.026 ± 0.009	¹ AALTONEN	12AJ CDF	$p\bar{p}$ at 1.96 TeV
0.163 ± 0.065 ± 0.064 -0.064	^{1,6} ABAZOV	12D D0	$p\bar{p}$ at 1.96 TeV
• • • We do not use the following data for averages, fits, limits, etc. • • •			
0.114 ± 0.014 ± 0.007	¹ SIRUNYAN	21E CMS	$p\bar{p}$ at 13 TeV
0.085 ± 0.011 ± 0.007	¹ AAD	16AP ATLS	Repl. by AAD 21AE
0.095 ± 0.013 ± 0.007	¹ KHACHATRYAN	16S CMS	$p\bar{p}$ at 8 TeV
0.0805 ± 0.0091 ± 0.0032	³ AAIJ	15I LHCb	Repl. by AAIJ 19Q
0.053 ± 0.021 ± 0.010	¹ AAD	14U ATLS	Repl. by AAD 16AP
0.106 ± 0.011 ± 0.007	⁷ AAIJ	13AR LHCb	Repl. by AAIJ 15I
0.053 ± 0.021 ± 0.010	¹ AAD	12CV ATLS	Repl. by AAD 14U
0.123 ± 0.029 ± 0.011	¹ AAIJ	12D LHCb	Repl. by AAIJ 13AR
0.075 ± 0.035 ± 0.006	⁸ AALTONEN	12D CDF	Repl. by AALTONEN 12AJ
0.085 ± 0.072 ± 0.001 -0.078	⁹ ABAZOV	09E D0	Repl. by ABAZOV 08AM
0.076 ± 0.059 ± 0.006 -0.063	¹⁰ AALTONEN	08J CDF	Repl. by AALTONEN 12D

$\Delta\Gamma_{B_s^0}/\Gamma_{B_s^0}$

$\Gamma_{B_s^0}$ and $\Delta\Gamma_{B_s^0}$ are the decay rate average and difference between two B_s^0 CP eigenstates (light – heavy).

“OUR EVALUATION” is provided by the Heavy Flavor Averaging Group (HFLAV, <https://hflav.web.cern.ch/>). It is derived from the averages of $\Gamma_{B_s^0}$ and $\Delta\Gamma_{B_s^0}$ (and their correlation).

VALUE	CL%	DOCUMENT ID	TECN	COMMENT
0.128 ± 0.007 OUR EVALUATION	• • • We do not use the following data for averages, fits, limits, etc. • • •			
0.090 ± 0.009 ± 0.023		¹ ESEN	13 BELL	$e^+ e^- \rightarrow \Upsilon(5S)$
		² AAIJ	12D LHCb	$p\bar{p}$ at 7 TeV
		³ AALTONEN	12D CDF	$p\bar{p}$ at 1.96 TeV
		⁴ ABAZOV	12D D0	$p\bar{p}$ at 1.96 TeV
0.147 ± 0.036 ± 0.042 -0.030 -0.041		¹ ESEN	10 BELL	$e^+ e^- \rightarrow \Upsilon(5S)$
0.072 ± 0.021 ± 0.022		⁵ ABAZOV	09I D0	$p\bar{p}$ at 1.96 TeV
> 0.012	95	⁵ AALTONEN	08F CDF	$p\bar{p}$ at 1.96 TeV
0.116 ± 0.09 ± 0.010 -0.10		⁶ AALTONEN	08J CDF	Repl. by AALTONEN 12D
0.079 ± 0.038 ± 0.031 -0.035 -0.030		⁵ ABAZOV	07Y D0	Repl. by ABAZOV 09I
0.24 ± 0.28 ± 0.03 -0.38 -0.04		^{6,7} ABAZOV	05W D0	Repl. by ABAZOV 08AM
0.65 ± 0.25 ± 0.01 -0.33		⁶ ACOSTA	05 CDF	Repl. by AALTONEN 08J
< 0.46	95	⁸ ABREU	00Y DLPH	$e^+ e^- \rightarrow Z$

Meson Particle Listings

B_S^0

<0.69	95	9 ABREU,P	00G DLPH	$e^+e^- \rightarrow Z$
0.25 $\begin{smallmatrix} +0.21 \\ -0.14 \end{smallmatrix}$		10 BARATE	00K ALEP	$e^+e^- \rightarrow Z$
<0.83	95	11 ABE	99D CDF	$p\bar{p}$ at 1.8 TeV
<0.67	95	12 ACCIARRI	98S L3	$e^+e^- \rightarrow Z$

- Assumes CP violation is negligible.
- Measured using the time-dependent angular analysis of $B_S^0 \rightarrow J/\psi\phi$ decays.
- Uses the time-dependent angular analysis of $B_S^0 \rightarrow J/\psi\phi$ decays and assuming CP-violating angle $\beta_S(B^0 \rightarrow J/\psi\phi) = 0.02$.
- Measured using fully reconstructed $B_S \rightarrow J/\psi\phi$ decays.
- Assumes $2 B(B_S^0 \rightarrow D_S^{(*)} D_S^{(*)}) \approx \Delta\Gamma_S^{CP} / \Gamma_S$.
- Measured using the time-dependent angular analysis of $B_S^0 \rightarrow J/\psi\phi$ decays.
- Uses $|A_0|^2 - |A_{||}|^2 = 0.355 \pm 0.066$ from ACOSTA 05.
- Uses $D_S^- \ell^+$, and $\phi\ell^+$ vertices.
- Measured using D_S hadron vertices.
- Uses $\phi\phi$ correlations from $B_S^0 \rightarrow D_S^{(*)} + D_S^{(*)-}$.
- ABE 99D assumes $\tau_{B_S^0} = 1.55 \pm 0.05$ ps.
- ACCIARRI 98S assumes $\tau_{B_S^0} = 1.49 \pm 0.06$ ps and PDG 98 values of b production fraction.

B_{sH}^0 MEAN LIFE

B_{sH}^0 is the heavy mass state of two B_S^0 CP eigenstates.

"OUR EVALUATION" is provided by the Heavy Flavor Averaging Group (HFLAV, <https://hflav.web.cern.ch/>). It is derived from the averages of $\Gamma_{B_S^0}$ and $\Delta\Gamma_{B_S^0}$ (and their correlation).

VALUE (10^{-12} s)	DOCUMENT ID	TECN	COMMENT
1.624 ± 0.009 OUR EVALUATION			
• • • We do not use the following data for averages, fits, limits, etc. • • •			
2.07 ± 0.29 ± 0.03	1 AAIJ	22 LHCB	pp at 7, 8, 13 TeV
1.70 $\begin{smallmatrix} +0.60 \\ -0.43 \end{smallmatrix}$ ± 0.09	1 SIRUNYAN	20AG CMS	pp at 7, 8, 13 TeV
1.677 ± 0.034 ± 0.011	2 SIRUNYAN	18BY CMS	pp at 8 TeV
2.04 ± 0.44 ± 0.05	1 AAIJ	17AI LHCB	pp at 7, 8, 13 TeV
1.70 ± 0.14 ± 0.05	3 ABAZOV	16C D0	$p\bar{p}$ at 1.96 TeV
1.75 ± 0.12 ± 0.07	4 AAIJ	13AB LHCB	pp at 7 TeV
1.652 ± 0.024 ± 0.024	5 AAIJ	13AR LHCB	pp at 7 TeV
1.700 ± 0.040 ± 0.026	6 AAIJ	12AN LHCB	pp at 7 TeV
	7 AALTONEN	12D CDF	$p\bar{p}$ at 1.96 TeV
1.70 $\begin{smallmatrix} +0.12 \\ -0.11 \end{smallmatrix}$ ± 0.03	6 AALTONEN	11AB CDF	$p\bar{p}$ at 1.96 TeV
1.613 $\begin{smallmatrix} +0.123 \\ -0.113 \end{smallmatrix}$	8,9 AALTONEN	08J CDF	Repl. by AALTONEN 12D
1.58 $\begin{smallmatrix} +0.39 \\ -0.42 \end{smallmatrix}$ $\begin{smallmatrix} +0.01 \\ -0.02 \end{smallmatrix}$	9 ABAZOV	05W D0	Repl. by ABAZOV 08AM
2.07 $\begin{smallmatrix} +0.58 \\ -0.46 \end{smallmatrix}$ ± 0.03	9 ACOSTA	05 CDF	Repl. by AALTONEN 08J

- Measured using $B_S \rightarrow \mu^+ \mu^-$ decays which, in the Standard Model, correspond to B_{sH}^0 decays. Assumes $-2 \text{Re}(\lambda)/(1 + |\lambda|^2) = 1$.
- Measured using $B_S^0 \rightarrow J/\psi\pi^+\pi^-$ decays with $0.9240 < m(\pi\pi) < 1.0204$ GeV, which is dominated by the $f_0(980)$ resonance, making it a CP-odd state.
- Measured using $J/\psi\pi^+\pi^-$ mode with $0.880 < m(\pi\pi) < 1.080$ GeV/ c^2 , which is mostly $J/\psi f_0(980)$ mode, a pure CP-odd final state.
- Measured using a pure CP-odd final state $J/\psi K_S^0$ with the assumption that contributions from penguin diagrams are small.
- Measured using $B_S \rightarrow J/\psi\pi^+\pi^-$ decays which, in the limit of $\phi_S = 0$ and $|\lambda| = 1$, correspond to B_{sH}^0 decays.
- Measured using a pure CP-odd final state $J/\psi f_0(980)$.
- Uses the time-dependent angular analysis of $B_S^0 \rightarrow J/\psi\phi$ decays assuming CP-violating angle $\beta_S(B^0 \rightarrow J/\psi\phi) = 0.02$.
- Obtained from $\Delta\Gamma_S$ and Γ_S fit with a correlation of 0.6.
- Measured using the time-dependent angular analysis of $B_S^0 \rightarrow J/\psi\phi$ decays.

B_{sL}^0 MEAN LIFE

B_{sL}^0 is the light mass state of two B_S^0 CP eigenstates.

"OUR EVALUATION" is provided by the Heavy Flavor Averaging Group (HFLAV, <https://hflav.web.cern.ch/>). It is derived from the averages of $\Gamma_{B_S^0}$ and $\Delta\Gamma_{B_S^0}$ (and their correlation).

VALUE (10^{-12} s)	DOCUMENT ID	TECN	COMMENT
1.429 ± 0.007 OUR EVALUATION			
• • • We do not use the following data for averages, fits, limits, etc. • • •			
1.40 ± 0.02	1 SIRUNYAN	18BY CMS	pp at 8 TeV
1.479 ± 0.034 ± 0.011	2 AAIJ	16AL LHCB	pp at 7, 8 TeV
1.379 ± 0.026 ± 0.017	3 AAIJ	14F LHCB	pp at 7, 8 TeV
1.407 ± 0.016 ± 0.007	4 AAIJ	14R LHCB	pp at 7 TeV
1.440 ± 0.096 ± 0.009	4 AAIJ	12 LHCB	Repl. by AAIJ 14R
1.455 ± 0.046 ± 0.006	4 AAIJ	12R LHCB	Repl. by AAIJ 14R

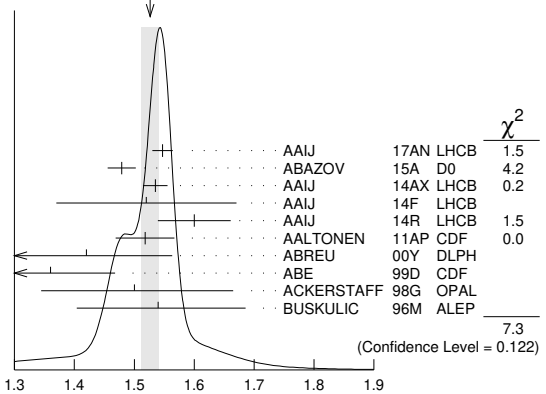
	5 AALTONEN	12D CDF	$p\bar{p}$ at 1.96 TeV
1.437 $\begin{smallmatrix} +0.054 \\ -0.047 \end{smallmatrix}$	6,7 AALTONEN	08J CDF	Repl. by AALTONEN 12D
1.24 $\begin{smallmatrix} +0.14 \\ -0.11 \end{smallmatrix}$ $\begin{smallmatrix} +0.01 \\ -0.02 \end{smallmatrix}$	7 ABAZOV	05W D0	Repl. by ABAZOV 08AM
1.05 $\begin{smallmatrix} +0.16 \\ -0.13 \end{smallmatrix}$ ± 0.02	7 ACOSTA	05 CDF	Repl. by AALTONEN 08J
1.27 ± 0.33 ± 0.08	8 BARATE	00K ALEP	$e^+e^- \rightarrow Z$

- Measured using results in SIRUNYAN 18BY for the heavy B_S^0 lifetime obtained from $B_S^0 \rightarrow J/\psi\pi^+\pi^-$ decays and the average effective $B_S^0 \rightarrow J/\psi\phi$ lifetime, and magnitude squared of the CP-odd amplitude $|A_{\perp}|^2 = 0.250 \pm 0.006$. The uncertainty includes all statistical and systematic contributions.
- Measured using $B_S^0 \rightarrow J/\psi\eta$ decays.
- Measured using $B_S^0 \rightarrow D_S^- D_S^+$. The effective lifetime is translated into a decay width of $\Gamma_L = 0.725 \pm 0.014 \pm 0.009$ ps $^{-1}$.
- Measured using $B_S^0 \rightarrow K^+ K^-$ decays. There may still be CPV in the decay.
- Uses the time-dependent angular analysis of $B_S^0 \rightarrow J/\psi\phi$ decays and assuming CP-violating angle $\beta_S(B^0 \rightarrow J/\psi\phi) = 0.02$.
- Obtained from $\Delta\Gamma_S$ and Γ_S fit with a correlation of 0.6.
- Measured using the time-dependent angular analysis of $B_S^0 \rightarrow J/\psi\phi$ decays.
- Uses $\phi\phi$ correlations from $B_S^0 \rightarrow D_S^{(*)} + D_S^{(*)-}$.

B_S^0 MEAN LIFE (Flavor specific)

VALUE (10^{-12} s)	DOCUMENT ID	TECN	COMMENT
1.527 ± 0.011 OUR EVALUATION			
1.526 ± 0.015 OUR AVERAGE			Error includes scale factor of 1.3. See the ideogram below.
1.547 ± 0.013 ± 0.011	1 AAIJ	17AN LHCB	pp at 7, 8 TeV
1.479 ± 0.010 ± 0.021	2 ABAZOV	15A D0	$p\bar{p}$ at 1.96 TeV
1.535 ± 0.015 ± 0.014	3 AAIJ	14AX LHCB	pp at 7 TeV
1.52 ± 0.15 ± 0.01	4 AAIJ	14F LHCB	pp at 7, 8 TeV
1.60 ± 0.06 ± 0.01	5 AAIJ	14R LHCB	pp at 7 TeV
1.518 ± 0.041 ± 0.027	6 AALTONEN	11AP CDF	$p\bar{p}$ at 1.96 TeV
1.42 $\begin{smallmatrix} +0.14 \\ -0.13 \end{smallmatrix}$ ± 0.03	7 ABREU	00Y DLPH	$e^+e^- \rightarrow Z$
1.36 ± 0.09 $\begin{smallmatrix} +0.06 \\ -0.05 \end{smallmatrix}$	8 ABE	99D CDF	$p\bar{p}$ at 1.8 TeV
1.50 $\begin{smallmatrix} +0.16 \\ -0.15 \end{smallmatrix}$ ± 0.04	8 ACKERSTAFF	98G OPAL	$e^+e^- \rightarrow Z$
1.54 $\begin{smallmatrix} +0.14 \\ -0.13 \end{smallmatrix}$ ± 0.04	8 BUSKULIC	96M ALEP	$e^+e^- \rightarrow Z$
• • • We do not use the following data for averages, fits, limits, etc. • • •			
1.398 ± 0.044 $\begin{smallmatrix} +0.028 \\ -0.025 \end{smallmatrix}$	9 ABAZOV	06V D0	Repl. by ABAZOV 15A

WEIGHTED AVERAGE
1.526 ± 0.015 (Error scaled by 1.3)



B_S^0 MEAN LIFE (Flavor specific) (10^{-12} s)

- AAIJ 17AN value was measured using $B_S^0 \rightarrow D_S^{(*)-} \mu^+ \nu_\mu$ decays relative to $B^0 \rightarrow D^{(*)-} \mu^+ \nu_\mu$ decays.
- Measured using $B_S^0 \rightarrow D_S^- \mu^+ \nu_\mu X$ decays.
- Measured using the $B_S^0 \rightarrow D_S^- \pi^+$ decays.
- Measured using $B_S^0 \rightarrow D^+ D_S^-$.
- Measured using $B_S^0 \rightarrow \pi^+ K^-$ decays.
- AALTONEN 11AP combines the fully reconstructed $B_S^0 \rightarrow D_S^- \pi^+$ decays and partially reconstructed $B_S^0 \rightarrow D_S X$ decays.
- Uses $D_S^- \ell^+$, and $\phi\ell^+$ vertices.
- Measured using $D_S^- \ell^+$ vertices.
- Measured using $D_S^- \mu^+$ vertices.

B_S^0 MEAN LIFE ($B_S \rightarrow J/\psi\phi$)

VALUE (10^{-12} s)	DOCUMENT ID	TECN	COMMENT
1.480 ± 0.007 OUR EVALUATION			
1.480 ± 0.007 OUR AVERAGE			
1.481 ± 0.007 ± 0.005	1 SIRUNYAN	18BY CMS	pp at 8 TeV
1.480 ± 0.011 ± 0.005	1 AAIJ	14E LHCB	pp at 7 TeV
1.444 $^{+0.098}_{-0.090}$ ± 0.020	1 ABAZOV	05B D0	$p\bar{p}$ at 1.96 TeV
1.34 $^{+0.23}_{-0.19}$ ± 0.05	2 ABE	98B CDF	$p\bar{p}$ at 1.8 TeV
• • • We do not use the following data for averages, fits, limits, etc. • • •			
1.39 $^{+0.13}_{-0.16}$ ± 0.01	2 ABAZOV	05W D0	$p\bar{p}$ at 1.96 TeV
1.34 $^{+0.23}_{-0.19}$ ± 0.05	3 ABE	96N CDF	Repl. by ABE 98B
1 Measured using fully reconstructed $B_S \rightarrow J/\psi\phi$ decays.			
2 Measured using the time-dependent angular analysis of $B_S^0 \rightarrow J/\psi\phi$ decays.			
3 ABE 96N uses 58 ± 12 exclusive $B_S \rightarrow J/\psi\phi$ events.			

$\tau_{B_S^0}/\tau_{B^0}$ MEAN LIFE RATIO

VALUE	DOCUMENT ID	TECN	COMMENT
0.980 ± 0.006 ± 0.003	1 SIRUNYAN	18BY CMS	pp at 8 TeV
1 Measured using $B_S^0 \rightarrow J/\psi\phi(1020)$ and $B^0 \rightarrow J/\psi K^*(892)^0$ decays.			

$\Gamma_{B_S^0} - \Gamma_{B^0}$

VALUE (10^{12} s $^{-1}$)	DOCUMENT ID	TECN	COMMENT
-0.0041 ± 0.0024 ± 0.0015	1 AAIJ	19Q LHCB	pp at 13 TeV
1 Measured using time-dependent angular analysis of $B_S^0 \rightarrow J/\psi K^+ K^-$ decays.			

$\Gamma_{B_{SH}^0} - \Gamma_{B^0}$

VALUE (10^{12} s $^{-1}$)	DOCUMENT ID	TECN	COMMENT
-0.05 ± 0.004 ± 0.004	1 AAIJ	19AF LHCB	pp at 7, 8, 13 TeV
1 Measured in $B_S^0 \rightarrow J/\psi\pi^+\pi^-$ decays.			

B_S^0 DECAY MODES

These branching fractions all scale with $B(\bar{b} \rightarrow B_S^0)$.

The branching fraction $B(B_S^0 \rightarrow D_S^- \ell^+ \nu_\ell \text{ anything})$ is not a pure measurement since the measured product branching fraction $B(\bar{b} \rightarrow B_S^0) \times B(B_S^0 \rightarrow D_S^- \ell^+ \nu_\ell \text{ anything})$ was used to determine $B(\bar{b} \rightarrow B_S^0)$, as described in the note on " B^0 - \bar{B}^0 Mixing"

For inclusive branching fractions, e.g., $B \rightarrow D^\pm \text{ anything}$, the values usually are multiplicities, not branching fractions. They can be greater than one.

Mode	Fraction (Γ_i/Γ)	Scale factor/ Confidence level
Γ_1 $D_S^- \text{ anything}$	(62 ± 6) %	
Γ_2 $\ell \nu_\ell X$	(9.6 ± 0.8) %	
Γ_3 $e^+ \nu X^-$	(9.1 ± 0.8) %	
Γ_4 $\mu^+ \nu X^-$	(10.2 ± 1.0) %	
Γ_5 $D_S^- \ell^+ \nu_\ell \text{ anything}$	[a] (8.1 ± 1.3) %	
Γ_6 $D_S^{*-} \ell^+ \nu_\ell \text{ anything}$	(5.4 ± 1.1) %	
Γ_7 $D_S^- \mu^+ \nu_\mu$	(2.44 ± 0.23) %	
Γ_8 $D_S^{*-} \mu^+ \nu_\mu$	(5.3 ± 0.5) %	
Γ_9 $D_{S1}(2536)^- \mu^+ \nu_\mu, D_{S1}^- \rightarrow D^{*-} K_S^0$	(2.7 ± 0.7) × 10 $^{-3}$	
Γ_{10} $D_{S1}(2536)^- X \mu^+ \nu, D_{S1}^- \rightarrow \bar{D}^0 K^+$	(4.4 ± 1.3) × 10 $^{-3}$	
Γ_{11} $D_{S2}(2573)^- X \mu^+ \nu, D_{S2}^- \rightarrow \bar{D}^0 K^+$	(2.7 ± 1.0) × 10 $^{-3}$	
Γ_{12} $K^- \mu^+ \nu_\mu$	(1.06 ± 0.09) × 10 $^{-4}$	
Γ_{13} $D_S^- \pi^+$	(2.98 ± 0.14) × 10 $^{-3}$	
Γ_{14} $D_S^- \rho^+$	(6.8 ± 1.4) × 10 $^{-3}$	
Γ_{15} $D_S^- \pi^+ \pi^+ \pi^-$	(6.1 ± 1.0) × 10 $^{-3}$	
Γ_{16} $D_{S1}(2536)^- \pi^+, D_{S1}^- \rightarrow D_S^- \pi^+ \pi^-$	(2.4 ± 0.8) × 10 $^{-5}$	
Γ_{17} $D_S^\mp K^\pm$	(2.25 ± 0.12) × 10 $^{-4}$	
Γ_{18} $D_S^- K^+ \pi^+ \pi^-$	(3.2 ± 0.6) × 10 $^{-4}$	
Γ_{19} $D_S^+ D_S^-$	(4.4 ± 0.5) × 10 $^{-3}$	
Γ_{20} $D_S^- D^+$	(2.8 ± 0.5) × 10 $^{-4}$	
Γ_{21} $D^+ D^-$	(2.2 ± 0.6) × 10 $^{-4}$	
Γ_{22} $D^{*+} D^-$		

Γ_{23} $D^{*-} D^+$		
Γ_{24} $D^0 \bar{D}^0$	(1.9 ± 0.5) × 10 $^{-4}$	
Γ_{25} $D_S^{*-} \pi^+$	(1.9 $^{+0.5}_{-0.4}$) × 10 $^{-3}$	
Γ_{26} $D_S^{*\mp} K^\pm$	(1.32 $^{+0.40}_{-0.32}$) × 10 $^{-4}$	
Γ_{27} $D_S^{*-} \rho^+$	(9.5 ± 2.0) × 10 $^{-3}$	
Γ_{28} $D_S^{*+} D_S^- + D_S^{*-} D_S^+$	(1.39 ± 0.17) %	
Γ_{29} $D_S^{*+} D_S^{*-}$	(1.44 ± 0.21) %	S=1.1
Γ_{30} $D_S^{*(*)+} D_S^{*-}$	(4.5 ± 1.4) %	
Γ_{31} $D_S^{*-} D_S^+$	(3.9 ± 0.8) × 10 $^{-4}$	
Γ_{32} $\bar{D}^{*0} \bar{K}^0$	(2.8 ± 1.1) × 10 $^{-4}$	
Γ_{33} $\bar{D}^0 \bar{K}^0$	(4.3 ± 0.9) × 10 $^{-4}$	
Γ_{34} $\bar{D}^0 K^- \pi^+$	(1.04 ± 0.13) × 10 $^{-3}$	
Γ_{35} $\bar{D}^0 \bar{K}^*(892)^0$	(4.4 ± 0.6) × 10 $^{-4}$	
Γ_{36} $\bar{D}^0 \bar{K}^*(1410)$	(3.9 ± 3.5) × 10 $^{-4}$	
Γ_{37} $\bar{D}^0 \bar{K}_0^*(1430)$	(3.0 ± 0.7) × 10 $^{-4}$	
Γ_{38} $\bar{D}^0 \bar{K}_2^*(1430)$	(1.1 ± 0.4) × 10 $^{-4}$	
Γ_{39} $\bar{D}^0 \bar{K}^*(1680)$	< 7.8 × 10 $^{-5}$	CL=90%
Γ_{40} $\bar{D}^0 \bar{K}_0^*(1950)$	< 1.1 × 10 $^{-4}$	CL=90%
Γ_{41} $\bar{D}^0 \bar{K}_2^*(1780)$	< 2.6 × 10 $^{-5}$	CL=90%
Γ_{42} $\bar{D}^0 \bar{K}_4^*(2045)$	< 3.1 × 10 $^{-5}$	CL=90%
Γ_{43} $\bar{D}^0 K^- \pi^+$ (non-resonant)	(2.1 ± 0.8) × 10 $^{-4}$	
Γ_{44} $D_{S2}^*(2573)^- \pi^+, D_{S2}^- \rightarrow \bar{D}^0 K^-$	(2.6 ± 0.4) × 10 $^{-4}$	
Γ_{45} $D_{S1}^*(2700)^- \pi^+, D_{S1}^- \rightarrow \bar{D}^0 K^-$	(1.6 ± 0.8) × 10 $^{-5}$	
Γ_{46} $D_{S1}^*(2860)^- \pi^+, D_{S1}^- \rightarrow \bar{D}^0 K^-$	(5 ± 4) × 10 $^{-5}$	
Γ_{47} $D_{S3}^*(2860)^- \pi^+, D_{S3}^- \rightarrow \bar{D}^0 K^-$	(2.2 ± 0.6) × 10 $^{-5}$	
Γ_{48} $\bar{D}^0 K^+ K^-$	(5.6 ± 0.9) × 10 $^{-5}$	
Γ_{49} $\bar{D}^0 f_0(980)$	< 3.1 × 10 $^{-6}$	CL=90%
Γ_{50} $\bar{D}^0 \phi$	(3.0 ± 0.5) × 10 $^{-5}$	
Γ_{51} $\bar{D}^{*0} \phi$	(3.7 ± 0.6) × 10 $^{-5}$	
Γ_{52} $D^{*\mp} \pi^\pm$	< 6.1 × 10 $^{-6}$	CL=90%
Γ_{53} $\eta_c \phi$	(5.0 ± 0.9) × 10 $^{-4}$	
Γ_{54} $\eta' X_{S\bar{S}}$		
Γ_{55} $\eta_c \pi^+ \pi^-$	(1.8 ± 0.7) × 10 $^{-4}$	
Γ_{56} $J/\psi(1S) \phi$	(1.04 ± 0.04) × 10 $^{-3}$	
Γ_{57} $J/\psi(1S) \phi \phi$	(1.20 $^{+0.14}_{-0.16}$) × 10 $^{-5}$	
Γ_{58} $J/\psi(1S) \pi^0$	< 1.2 × 10 $^{-3}$	CL=90%
Γ_{59} $J/\psi(1S) \eta$	(4.0 ± 0.7) × 10 $^{-4}$	S=1.4
Γ_{60} $J/\psi(1S) K_S^0$	(1.92 ± 0.14) × 10 $^{-5}$	
Γ_{61} $J/\psi(1S) \bar{K}^*(892)^0$	(4.1 ± 0.4) × 10 $^{-5}$	
Γ_{62} $J/\psi(1S) \eta'$	(3.3 ± 0.4) × 10 $^{-4}$	
Γ_{63} $J/\psi(1S) \pi^+ \pi^-$	(2.02 ± 0.17) × 10 $^{-4}$	S=1.7
Γ_{64} $J/\psi(1S) f_0(500), f_0 \rightarrow \pi^+ \pi^-$	< 4 × 10 $^{-6}$	CL=90%
Γ_{65} $J/\psi(1S) \rho, \rho \rightarrow \pi^+ \pi^-$	< 3.4 × 10 $^{-6}$	CL=90%
Γ_{66} $J/\psi(1S) f_0(980), f_0 \rightarrow \pi^+ \pi^-$	(1.24 ± 0.15) × 10 $^{-4}$	S=2.1
Γ_{67} $J/\psi(1S) f_2(1270), f_2 \rightarrow \pi^+ \pi^-$	(1.0 ± 0.4) × 10 $^{-6}$	
Γ_{68} $J/\psi(1S) f_2(1270)_0, f_2 \rightarrow \pi^+ \pi^-$	(7.3 ± 1.7) × 10 $^{-7}$	
Γ_{69} $J/\psi(1S) f_2(1270)_\parallel, f_2 \rightarrow \pi^+ \pi^-$	(1.05 ± 0.33) × 10 $^{-6}$	
Γ_{70} $J/\psi(1S) f_2(1270)_\perp, f_2 \rightarrow \pi^+ \pi^-$	(1.3 ± 0.7) × 10 $^{-6}$	
Γ_{71} $J/\psi(1S) f_0(1370), f_0 \rightarrow \pi^+ \pi^-$	(4.4 $^{+0.6}_{-4.0}$) × 10 $^{-5}$	
Γ_{72} $J/\psi(1S) f_0(1500), f_0 \rightarrow \pi^+ \pi^-$	(2.04 $^{+0.32}_{-0.24}$) × 10 $^{-5}$	
Γ_{73} $J/\psi(1S) f'_2(1525)_0, f'_2 \rightarrow \pi^+ \pi^-$	(1.03 ± 0.22) × 10 $^{-6}$	
Γ_{74} $J/\psi(1S) f'_2(1525)_\parallel, f'_2 \rightarrow \pi^+ \pi^-$	(1.2 $^{+2.6}_{-0.8}$) × 10 $^{-7}$	
Γ_{75} $J/\psi(1S) f'_2(1525)_\perp, f'_2 \rightarrow \pi^+ \pi^-$	(5 ± 4) × 10 $^{-7}$	
Γ_{76} $J/\psi(1S) f_0(1790), f_0 \rightarrow \pi^+ \pi^-$	(4.9 $^{+10.0}_{-1.0}$) × 10 $^{-6}$	
Γ_{77} $J/\psi(1S) \pi^+ \pi^-$ (nonresonant)	(1.74 $^{+1.10}_{-0.34}$) × 10 $^{-5}$	
Γ_{78} $J/\psi(1S) \bar{K}^0 \pi^+ \pi^-$	< 4.4 × 10 $^{-5}$	CL=90%
Γ_{79} $J/\psi(1S) K^+ K^-$	(7.9 ± 0.7) × 10 $^{-4}$	

Meson Particle Listings

B_s^0			
Γ_{80}	$J/\psi(1S) K^0 K^- \pi^+ + \text{c.c.}$	$(9.5 \pm 1.3) \times 10^{-4}$	
Γ_{81}	$J/\psi(1S) \bar{K}^0 K^+ K^-$	$< 1.2 \times 10^{-5}$	CL=90%
Γ_{82}	$J/\psi K^*(892)^0 \bar{K}^*(892)^0$	$(1.10 \pm 0.09) \times 10^{-4}$	
Γ_{83}	$J/\psi(1S) f_2'(1525)$	$(2.6 \pm 0.6) \times 10^{-4}$	
Γ_{84}	$J/\psi(1S) \rho \bar{\rho}$	$(3.6 \pm 0.4) \times 10^{-6}$	
Γ_{85}	$J/\psi(1S) \gamma$	$< 7.3 \times 10^{-6}$	CL=90%
Γ_{86}	$J/\psi(1S) \pi^+ \pi^- \pi^+ \pi^-$	$(7.5 \pm 0.8) \times 10^{-5}$	
Γ_{87}	$J/\psi(1S) f_1(1285)$	$(7.2 \pm 1.4) \times 10^{-5}$	
Γ_{88}	$\psi(2S) \eta$	$(3.3 \pm 0.9) \times 10^{-4}$	
Γ_{89}	$\psi(2S) \eta'$	$(1.29 \pm 0.35) \times 10^{-4}$	
Γ_{90}	$\psi(2S) \pi^+ \pi^-$	$(6.9 \pm 1.2) \times 10^{-5}$	
Γ_{91}	$\psi(2S) \phi$	$(5.2 \pm 0.4) \times 10^{-4}$	
Γ_{92}	$\psi(2S) K^- \pi^+$	$(3.1 \pm 0.4) \times 10^{-5}$	
Γ_{93}	$\psi(2S) \bar{K}^*(892)^0$	$(3.3 \pm 0.5) \times 10^{-5}$	
Γ_{94}	$\chi_{c1} \phi$	$(1.97 \pm 0.25) \times 10^{-4}$	
Γ_{95}	$\chi_{c1} K^+ K^-$		
Γ_{96}	$\chi_{c2} K^+ K^-$		
Γ_{97}	$\chi_{c1}(3872) \phi$	$(1.1 \pm 0.4) \times 10^{-4}$	
Γ_{98}	$\chi_{c1}(3872)(K^+ K^-)_{\text{non-}\phi}$	$(8.6 \pm 3.5) \times 10^{-5}$	
Γ_{99}	$\pi^+ \pi^-$	$(7.0 \pm 1.0) \times 10^{-7}$	
Γ_{100}	$\pi_0^0 \pi^0$	$< 2.1 \times 10^{-4}$	CL=90%
Γ_{101}	$\eta \pi^0$	$< 1.0 \times 10^{-3}$	CL=90%
Γ_{102}	$\eta \eta$	$< 1.43 \times 10^{-4}$	CL=90%
Γ_{103}	$\rho^0 \rho^0$	$< 3.20 \times 10^{-4}$	CL=90%
Γ_{104}	$\eta' \eta$	$< 6.5 \times 10^{-5}$	CL=90%
Γ_{105}	$\eta' \eta'$	$(3.3 \pm 0.7) \times 10^{-5}$	
Γ_{106}	$\eta' \phi$	$< 8.2 \times 10^{-7}$	CL=90%
Γ_{107}	$\phi f_0(980), f_0(980) \rightarrow \pi^+ \pi^-$	$(1.12 \pm 0.21) \times 10^{-6}$	
Γ_{108}	$\phi f_2(1270), f_2(1270) \rightarrow \pi^+ \pi^-$	$(6.1 \pm 1.8) \times 10^{-7}$	
Γ_{109}	$\phi \rho^0$	$(2.7 \pm 0.8) \times 10^{-7}$	
Γ_{110}	$\phi \pi^+ \pi^-$	$(3.5 \pm 0.5) \times 10^{-6}$	
Γ_{111}	$\phi \phi$	$(1.85 \pm 0.14) \times 10^{-5}$	
Γ_{112}	$\phi \phi \phi$	$(2.2 \pm 0.6) \times 10^{-6}$	
Γ_{113}	$\pi^+ K^-$	$(5.8 \pm 0.7) \times 10^{-6}$	
Γ_{114}	$K^+ K^-$	$(2.66 \pm 0.22) \times 10^{-5}$	
Γ_{115}	$K^0 \bar{K}^0$	$(1.76 \pm 0.31) \times 10^{-5}$	
Γ_{116}	$K^0 \pi^+ \pi^-$	$(9.5 \pm 2.1) \times 10^{-6}$	
Γ_{117}	$K^0 K^+ \pi^-$	$(8.4 \pm 0.9) \times 10^{-5}$	
Γ_{118}	$K^*(892)^- \pi^+$	$(2.9 \pm 1.1) \times 10^{-6}$	
Γ_{119}	$K^*(892)^\pm K^\mp$	$(1.9 \pm 0.5) \times 10^{-5}$	
Γ_{120}	$K_0^*(1430)^\pm K^\mp$	$(3.1 \pm 2.5) \times 10^{-5}$	
Γ_{121}	$K_2^*(1430)^\pm K^\mp$	$(1.0 \pm 1.7) \times 10^{-5}$	
Γ_{122}	$K^*(892)^0 \bar{K}^0 + \text{c.c.}$	$(2.0 \pm 0.6) \times 10^{-5}$	
Γ_{123}	$K_0^*(1430) \bar{K}^0 + \text{c.c.}$	$(3.3 \pm 1.0) \times 10^{-5}$	
Γ_{124}	$K_2^*(1430) \bar{K}^0 + \text{c.c.}$	$(1.7 \pm 2.2) \times 10^{-5}$	
Γ_{125}	$K_0^*(892)^0 \bar{K}^0 + \text{c.c.}$	$(1.6 \pm 0.4) \times 10^{-5}$	
Γ_{126}	$K^0 K^+ K^-$	$(1.3 \pm 0.6) \times 10^{-6}$	
Γ_{127}	$\bar{K}^*(892)^0 \rho^0$	$< 7.67 \times 10^{-4}$	CL=90%
Γ_{128}	$\bar{K}^*(892)^0 K^*(892)^0$	$(1.11 \pm 0.27) \times 10^{-5}$	
Γ_{129}	$K^*(892)^0 \bar{K}_2^*(1430)^0$		
Γ_{130}	$K_2^*(1430)^0 \bar{K}^*(892)^0$		
Γ_{131}	$K_2^*(1430)^0 \bar{K}_2^*(1430)^0$		
Γ_{132}	$\phi K^*(892)^0$	$(1.14 \pm 0.30) \times 10^{-6}$	
Γ_{133}	$\rho \bar{\rho}$	$< 1.5 \times 10^{-8}$	CL=90%
Γ_{134}	$\rho \bar{\rho} K^+ K^-$	$(4.5 \pm 0.5) \times 10^{-6}$	
Γ_{135}	$\rho \bar{\rho} K^+ \pi^-$	$(1.39 \pm 0.26) \times 10^{-6}$	
Γ_{136}	$\rho \bar{\rho} \pi^+ \pi^-$	$(4.3 \pm 2.0) \times 10^{-7}$	
Γ_{137}	$\rho \bar{\rho} K^- + \text{c.c.}$	$(5.5 \pm 1.0) \times 10^{-6}$	
Γ_{138}	$\Lambda_c^- \Lambda \pi^+$	$(3.6 \pm 1.6) \times 10^{-4}$	
Γ_{139}	$\Lambda_c^- \Lambda_c^+$	$< 8.0 \times 10^{-5}$	CL=95%
Lepton Family number (LF) violating modes or $\Delta B = 1$ weak neutral current (BI) modes			
Γ_{140}	$\gamma \gamma$	$< 3.1 \times 10^{-6}$	CL=90%
Γ_{141}	$\phi \gamma$	$(3.4 \pm 0.4) \times 10^{-5}$	
Γ_{142}	$\mu^+ \mu^-$	$(3.01 \pm 0.35) \times 10^{-9}$	
Γ_{143}	$e^+ e^-$	$< 9.4 \times 10^{-9}$	CL=90%
Γ_{144}	$\tau^+ \tau^-$	$< 6.8 \times 10^{-3}$	CL=95%
Γ_{145}	$\mu^+ \mu^- \mu^+ \mu^-$	$< 2.5 \times 10^{-9}$	CL=95%
Γ_{146}	$S P, S \rightarrow \mu^+ \mu^-, P \rightarrow \mu^+ \mu^-$	$[b] < 2.2 \times 10^{-9}$	CL=95%
Γ_{147}	$\phi(1020) \mu^+ \mu^-$	$(8.4 \pm 0.4) \times 10^{-7}$	
Γ_{148}	$f_2'(1525) \mu^+ \mu^-$	$(1.62 \pm 0.22) \times 10^{-7}$	
Γ_{149}	$\bar{K}^*(892)^0 \mu^+ \mu^-$	$B1 (2.9 \pm 1.1) \times 10^{-8}$	
Γ_{150}	$\pi^+ \pi^- \mu^+ \mu^-$	$B1 (8.4 \pm 1.7) \times 10^{-8}$	
Γ_{151}	$\phi \nu \bar{\nu}$	$B1 < 5.4 \times 10^{-3}$	CL=90%
Γ_{152}	$e^\pm \mu^\mp$	$LF [c] < 5.4 \times 10^{-9}$	CL=90%
Γ_{153}	$\mu^\pm \tau^\mp$	$LF < 4.2 \times 10^{-5}$	CL=95%

[a] Not a pure measurement. See note at head of B_s^0 Decay Modes.
[b] Here S and P are the hypothetical scalar and pseudoscalar particles with masses of 2.5 GeV/c² and 214.3 MeV/c², respectively.
[c] The value is for the sum of the charge states or particle/antiparticle states indicated.

CONSTRAINED FIT INFORMATION
An overall fit to 12 branching ratios uses 20 measurements and one constraint to determine 8 parameters. The overall fit has a $\chi^2 = 26.9$ for 13 degrees of freedom.

The following *off-diagonal* array elements are the correlation coefficients $\langle \delta x_i \delta x_j \rangle / (\delta x_i \delta x_j)$, in percent, from the fit to the branching fractions, $x_i \equiv \Gamma_i / \Gamma_{\text{total}}$. The fit constrains the x_i whose labels appear in this array to sum to one.

x_{15}	17					
x_{17}	82	14				
x_{56}	0	0	0			
x_{63}	0	0	0	43		
x_{66}	0	0	0	31	52	
x_{111}	0	0	0	15	6	5
	x_{13}	x_{15}	x_{17}	x_{56}	x_{63}	x_{66}

B_s^0 BRANCHING RATIOS

$\Gamma(D_s^- \text{ anything}) / \Gamma_{\text{total}}$	Γ_1 / Γ		
VALUE	EVTS	DOCUMENT ID	TECN COMMENT
0.62 ± 0.06 OUR AVERAGE			
0.602 ± 0.058 ± 0.023		1 WANG 22	BELL $e^+ e^- \rightarrow \Upsilon(5S)$
0.91 ± 0.18 ± 0.41		2 DRUTSKOY 07	BELL $e^+ e^- \rightarrow \Upsilon(4S)$
0.81 ± 0.24 ± 0.22	90	3 BUSKULIC 96E	ALEP $e^+ e^- \rightarrow Z$
1.56 ± 0.58 ± 0.44	147	4 ACTON 92N	OPAL $e^+ e^- \rightarrow Z$
<p>1 WANG 22 selects the B_s events by tagging the accompanying B_s via partial reconstruction of the semileptonic decays $B_s \rightarrow D_s X \ell^+ \nu$.</p> <p>2 The extraction of this result takes into account the correlation between the measurements of $B(\Upsilon(5S) \rightarrow D_s X)$ and $B(\Upsilon(5S) \rightarrow D^0 X)$.</p> <p>3 BUSKULIC 96E separate $c\bar{c}$ and $b\bar{b}$ sources of D_s^+ mesons using a lifetime tag, subtract generic $\bar{b} \rightarrow W^+ \rightarrow D_s^+$ events, and obtain $B(\bar{b} \rightarrow B_s^0) \times B(B_s^0 \rightarrow D_s^- \text{ anything}) = 0.088 \pm 0.020 \pm 0.020$ assuming $B(D_s \rightarrow \phi\pi) = (3.5 \pm 0.4) \times 10^{-2}$ and PDG 1994 values for the relative partial widths to other D_s channels. We evaluate using our current values $B(\bar{b} \rightarrow B_s^0) = 0.107 \pm 0.014$ and $B(D_s \rightarrow \phi\pi) = 0.036 \pm 0.009$. Our first error is their experiment's and our second error is that due to $B(\bar{b} \rightarrow B_s^0)$ and $B(D_s \rightarrow \phi\pi)$.</p> <p>4 ACTON 92N assume that excess of 147 ± 48 D_s^0 events over that expected from $B^0, B^+,$ and $c\bar{c}$ is all from B_s^0 decay. The product branching fraction is measured to be $B(\bar{b} \rightarrow B_s^0) B(B_s^0 \rightarrow D_s^- \text{ anything}) \times B(D_s^- \rightarrow \phi\pi^-) = (5.9 \pm 1.9 \pm 1.1) \times 10^{-3}$. We evaluate using our current values $B(\bar{b} \rightarrow B_s^0) = 0.107 \pm 0.014$ and $B(D_s \rightarrow \phi\pi) = 0.036 \pm 0.009$. Our first error is their experiment's and our second error is that due to $B(\bar{b} \rightarrow B_s^0)$ and $B(D_s \rightarrow \phi\pi)$.</p>			
$\Gamma(\ell \nu X) / \Gamma_{\text{total}}$	Γ_2 / Γ		
VALUE (units 10^{-2})	DOCUMENT ID	TECN	COMMENT
9.6 ± 0.8 OUR AVERAGE			
9.6 ± 0.4 ± 0.7	1 OSWALD 13	BELL	$e^+ e^- \rightarrow \Upsilon(5S)$
9.5 ^{+2.5+1.1} _{-2.0-1.9}	2 LEES 12A	BABR	$e^+ e^-$
<p>1 The measurement corresponds to the average of the electron and muon branching fractions.</p> <p>2 The measurement corresponds to a branching fraction where the lepton originates from bottom decay and is the average between the electron and muon branching fractions. LEES 12A uses the correlation of the production of ϕ mesons in association with a lepton in $e^+ e^-$ data taken at center-of-mass energies between 10.54 and 11.2 GeV.</p>			
$\Gamma(e^+ \nu X^-) / \Gamma_{\text{total}}$	Γ_3 / Γ		
VALUE (units 10^{-2})	DOCUMENT ID	TECN	COMMENT
9.1 ± 0.5 ± 0.6	OSWALD 13	BELL	$e^+ e^- \rightarrow \Upsilon(5S)$
$\Gamma(\mu^+ \nu X^-) / \Gamma_{\text{total}}$	Γ_4 / Γ		
VALUE (units 10^{-2})	DOCUMENT ID	TECN	COMMENT
10.2 ± 0.6 ± 0.8	OSWALD 13	BELL	$e^+ e^- \rightarrow \Upsilon(5S)$

$\Gamma(D_s^- \ell^+ \nu_\ell \text{ anything})/\Gamma_{\text{total}}$ Γ_5/Γ
 The values and averages in this section serve only to show what values result if one assumes our $B(\bar{b} \rightarrow B_s^0)$. They cannot be thought of as measurements since the underlying product branching fractions were also used to determine $B(\bar{b} \rightarrow B_s^0)$ as described in the note on "Production and Decay of b -Flavored Hadrons."

VALUE (units 10^{-2})	EVTS	DOCUMENT ID	TECN	COMMENT
8.1 ± 1.3 OUR AVERAGE				
8.2 ± 0.2 ± 1.5		1 OSWALD	15 BELL	$e^+e^- \rightarrow \Upsilon(5S)$
7.6 ± 1.2 ± 2.1	134	2 BUSKULIC	950 ALEP	$e^+e^- \rightarrow Z$
10.7 ± 4.3 ± 2.9		3 ABREU	92M DLPH	$e^+e^- \rightarrow Z$
10.3 ± 3.6 ± 2.8	18	4 ACTON	92N OPAL	$e^+e^- \rightarrow Z$
• • • We do not use the following data for averages, fits, limits, etc. • • •				
13 ± 4 ± 4	27	5 BUSKULIC	92E ALEP	$e^+e^- \rightarrow Z$

¹ Obtains $B_s \rightarrow D_s X e \nu$, and $D_s X \mu \nu$ separately, then combines them by assuming systematic uncertainties are fully correlated, except for the one on lepton identification. The third uncertainty adds in quadrature systematic uncertainties from external sources (number of B_s events, and $D_s^{(*)}$ branching fractions). OSWALD 15 also measures the cross-section $\sigma(e^+e^- \rightarrow B_s^{(*)} \bar{B}_s^{(*)}) = 53.8 \pm 1.4 \pm 5.3$ pb at $\sqrt{s} = 10.86$ GeV.

² BUSKULIC 950 use $D_s \ell$ correlations. The measured product branching ratio is $B(\bar{b} \rightarrow B_s) \times B(B_s \rightarrow D_s^- \ell^+ \nu_\ell \text{ anything}) = (0.82 \pm 0.09^{+0.13}_{-0.14})\%$ assuming $B(D_s \rightarrow \phi\pi) = (3.5 \pm 0.4) \times 10^{-2}$ and PDG 1994 values for the relative partial widths to the six other D_s channels used in this analysis. Combined with results from $\Upsilon(4S)$ experiments this can be used to extract $B(\bar{b} \rightarrow B_s) = (11.0 \pm 1.2^{+2.5}_{-2.6})\%$. We evaluate using our current values $B(\bar{b} \rightarrow B_s^0) = 0.107 \pm 0.014$ and $B(D_s \rightarrow \phi\pi) = 0.036 \pm 0.009$. Our first error is their experiment's and our second error is that due to $B(\bar{b} \rightarrow B_s^0)$ and $B(D_s \rightarrow \phi\pi)$.

³ ABREU 92M measured muons only and obtained product branching ratio $B(Z \rightarrow b \text{ or } \bar{b}) \times B(\bar{b} \rightarrow B_s) \times B(B_s \rightarrow D_s \mu^+ \nu_\mu \text{ anything}) \times B(D_s \rightarrow \phi\pi) = (18 \pm 8) \times 10^{-5}$. We evaluate using our current values $B(\bar{b} \rightarrow B_s^0) = 0.107 \pm 0.014$ and $B(D_s \rightarrow \phi\pi) = 0.036 \pm 0.009$. Our first error is their experiment's and our second error is that due to $B(\bar{b} \rightarrow B_s^0)$ and $B(D_s \rightarrow \phi\pi)$. We use $B(Z \rightarrow b \text{ or } \bar{b}) = 2B(Z \rightarrow b \bar{b}) = 2 \times (0.2212 \pm 0.0019)$.

⁴ ACTON 92N is measured using $D_s \rightarrow \phi\pi^+$ and $K^*(892)^0 K^+$ events. The product branching fraction measured is measured to be $B(\bar{b} \rightarrow B_s^0) B(B_s^0 \rightarrow D_s^- \ell^+ \nu_\ell \text{ anything}) \times B(D_s^- \rightarrow \phi\pi^-) = (3.9 \pm 1.1 \pm 0.8) \times 10^{-4}$. We evaluate using our current values $B(\bar{b} \rightarrow B_s^0) = 0.107 \pm 0.014$ and $B(D_s \rightarrow \phi\pi) = 0.036 \pm 0.009$. Our first error is their experiment's and our second error is that due to $B(\bar{b} \rightarrow B_s^0)$ and $B(D_s \rightarrow \phi\pi)$.

⁵ BUSKULIC 92E is measured using $D_s \rightarrow \phi\pi^+$ and $K^*(892)^0 K^+$ events. They use $2.7 \pm 0.7\%$ for the $\phi\pi^+$ branching fraction. The average product branching fraction is measured to be $B(\bar{b} \rightarrow B_s^0) B(B_s^0 \rightarrow D_s^- \ell^+ \nu_\ell \text{ anything}) = 0.020 \pm 0.0055^{+0.005}_{-0.006}$. We evaluate using our current values $B(\bar{b} \rightarrow B_s^0) = 0.107 \pm 0.014$ and $B(D_s \rightarrow \phi\pi) = 0.036 \pm 0.009$. Our first error is their experiment's and our second error is that due to $B(\bar{b} \rightarrow B_s^0)$ and $B(D_s \rightarrow \phi\pi)$. Superseded by BUSKULIC 950.

$\Gamma(D_s^{*-} \ell^+ \nu_\ell \text{ anything})/\Gamma_{\text{total}}$ Γ_6/Γ
 VALUE (units 10^{-2})

DOCUMENT ID	TECN	COMMENT
1 OSWALD	15 BELL	$e^+e^- \rightarrow \Upsilon(5S)$

5.4 ± 0.4 ± 1.0

¹ Obtains $B_s \rightarrow D_s^* X e \nu$, and $D_s^* X \mu \nu$ separately, then combines them by assuming systematic uncertainties are fully correlated, except for the one on lepton identification. The third uncertainty adds in quadrature systematic uncertainties from external sources (number of B_s events, and $D_s^{(*)}$ branching fractions). OSWALD 15 also measures the cross-section $\sigma(e^+e^- \rightarrow B_s^{(*)} \bar{B}_s^{(*)}) = 53.8 \pm 1.4 \pm 5.3$ pb at $\sqrt{s} = 10.86$ GeV.

$\Gamma(D_s^- \mu^+ \nu_\mu)/\Gamma_{\text{total}}$ Γ_7/Γ
 VALUE (units 10^{-2})

DOCUMENT ID	TECN	COMMENT
1 AAIJ	20E LHCB	pp at 7, 8 TeV

2.44 ± 0.21 ± 0.10

¹ AAIJ 20E reports $[\Gamma(B_s^0 \rightarrow D_s^- \mu^+ \nu_\mu)/\Gamma_{\text{total}}] / [B(B^0 \rightarrow D^- \ell^+ \nu_\ell)] = 1.09 \pm 0.05 \pm 0.06 \pm 0.05$ which we multiply by our best value $B(B^0 \rightarrow D^- \ell^+ \nu_\ell) = (2.24 \pm 0.09) \times 10^{-2}$. Our first error is their experiment's error and our second error is the systematic error from using our best value.

$\Gamma(D_s^{*-} \mu^+ \nu_\mu)/\Gamma_{\text{total}}$ Γ_8/Γ
 VALUE (units 10^{-2})

DOCUMENT ID	TECN	COMMENT
1 AAIJ	20E LHCB	pp at 7, 8 TeV

5.3 ± 0.5 ± 0.1

¹ AAIJ 20E reports $[\Gamma(B_s^0 \rightarrow D_s^{*-} \mu^+ \nu_\mu)/\Gamma_{\text{total}}] / [B(B^0 \rightarrow D^*(2010)^- \ell^+ \nu_\ell)] = 1.06 \pm 0.05 \pm 0.07 \pm 0.05$ which we multiply by our best value $B(B^0 \rightarrow D^*(2010)^- \ell^+ \nu_\ell) = (4.97 \pm 0.12) \times 10^{-2}$. Our first error is their experiment's error and our second error is the systematic error from using our best value.

$\Gamma(D_s^- \mu^+ \nu_\mu)/\Gamma(D_s^{*-} \mu^+ \nu_\mu)$ Γ_7/Γ_8
 VALUE

DOCUMENT ID	TECN	COMMENT
1 AAIJ	20E LHCB	pp at 7, 8 TeV

0.464 ± 0.013 ± 0.043

¹ AAIJ 20E value is not independent of other reported measurements.

$\Gamma(D_{s1}(2536)^- \mu^+ \nu_\mu, D_{s1}^- \rightarrow D^{*-} K_S^0)/\Gamma_{\text{total}}$ Γ_9/Γ
 VALUE (units 10^{-3})

DOCUMENT ID	TECN	COMMENT
1 ABAZOV	09G D0	$p\bar{p}$ at 1.96 TeV

2.7 ± 0.7 ± 0.2

¹ ABAZOV 09G reports $[\Gamma(B_s^0 \rightarrow D_{s1}(2536)^- \mu^+ \nu_\mu, D_{s1}^- \rightarrow D^{*-} K_S^0)/\Gamma_{\text{total}}] \times [B(\bar{b} \rightarrow B_s^0)] = (2.66 \pm 0.52 \pm 0.45) \times 10^{-4}$ which we divide by our best value $B(\bar{b} \rightarrow B_s^0) = (10.0 \pm 0.8) \times 10^{-2}$. Our first error is their experiment's error and our second error is the systematic error from using our best value.

$\Gamma(D_{s1}(2536)^- X \mu^+ \nu, D_{s1}^- \rightarrow \bar{D}^0 K^+)/\Gamma(D_s^- \ell^+ \nu_\ell \text{ anything})$ Γ_{10}/Γ_5
 VALUE (units 10^{-2})

DOCUMENT ID	TECN	COMMENT
AAIJ	11A LHCB	pp at 7 TeV

5.4 ± 1.2 ± 0.5

$\Gamma(D_{s2}(2573)^- X \mu^+ \nu, D_{s2}^- \rightarrow \bar{D}^0 K^+)/\Gamma(D_s^- \ell^+ \nu_\ell \text{ anything})$ Γ_{11}/Γ_5
 VALUE (units 10^{-2})

DOCUMENT ID	TECN	COMMENT
AAIJ	11A LHCB	pp at 7 TeV

3.3 ± 1.0 ± 0.4

$\Gamma(D_{s1}(2536)^- X \mu^+ \nu, D_{s1}^- \rightarrow \bar{D}^0 K^+)/\Gamma(D_{s2}(2573)^- X \mu^+ \nu, D_{s2}^- \rightarrow \bar{D}^0 K^+)$ Γ_{10}/Γ_{11}
 VALUE

DOCUMENT ID	TECN	COMMENT
1 AAIJ	11A LHCB	pp at 7 TeV

0.61 ± 0.14 ± 0.05

¹ Not independent of other AAIJ 11A measurements.

$\Gamma(K^- \mu^+ \nu_\mu)/\Gamma(D_s^- \mu^+ \nu_\mu)$ Γ_{12}/Γ_7
 VALUE (units 10^{-3})

DOCUMENT ID	TECN	COMMENT
1,2 AAIJ	21G LHCB	pp at 8 TeV

4.89 ± 0.21 ± 0.25

¹ AAIJ 21G measures $B(B_s^0 \rightarrow K^- \mu^+ \nu_\mu)/B(B_s^0 \rightarrow D_s^- \mu^+ \nu_\mu) = (4.89 \pm 0.21^{+0.20}_{-0.21} \pm 0.14) \times 10^{-3}$ over the whole q^2 range, where the last uncertainty is due to the $D_s^- \rightarrow K^+ K^- \pi^-$ branching fraction.

² AAIJ 21G reports this branching ratio for $q^2 < 7$ GeV² as $(1.66 \pm 0.08 \pm 0.07 \pm 0.05) \times 10^{-3}$ and for $q^2 > 7$ GeV² as $(3.25 \pm 0.21^{+0.16}_{-0.17} \pm 0.09) \times 10^{-3}$.

$\Gamma(K^- \mu^+ \nu_\mu)/\Gamma_{\text{total}}$ Γ_{12}/Γ
 VALUE (units 10^{-4})

DOCUMENT ID	TECN	COMMENT
1 AAIJ	21G LHCB	pp at 8 TeV

1.06 ± 0.05 ± 0.08

¹ The total systematic error includes D_s^- branching fractions, B_s^0 lifetime, $|V_{cb}|$, and $B_s^0 \rightarrow D_s^-$ form factor integral uncertainties.

$\Gamma(D_s^- \pi^+)/\Gamma_{\text{total}}$ Γ_{13}/Γ
 VALUE (units 10^{-3})

DOCUMENT ID	TECN	COMMENT
1 AAIJ	21Y LHCB	pp at 7, 8, 13 TeV
2 LOUVOT	09 BELL	$e^+e^- \rightarrow \Upsilon(5S)$
3 ABULENCIA	07c CDF	$p\bar{p}$ at 1.96 TeV

2.98 ± 0.14 OUR FIT
2.97 ± 0.13 OUR AVERAGE

2.96 ± 0.10 ± 0.09
 3.6 ± 0.5 ± 0.5
 2.8 ± 0.6 ± 0.1
 • • • We do not use the following data for averages, fits, limits, etc. • • •

4 AAIJ	12AG LHCB	Repl. by AAIJ 21Y
6 DRUTSKOY	07A BELL	Repl. by LOUVOT 09
5 ABULENCIA	06J CDF	Repl. by ABULENCIA 07c
6 AKERS	94J OPAL	$e^+e^- \rightarrow Z$
1 BUSKULIC	93G ALEP	$e^+e^- \rightarrow Z$

¹ AAIJ 21Y reports $[\Gamma(B_s^0 \rightarrow D_s^- \pi^+)/\Gamma_{\text{total}}] / [B(B^0 \rightarrow D^- \pi^+)] = 1.18 \pm 0.04$ which we multiply by our best value $B(B^0 \rightarrow D^- \pi^+) = (2.51 \pm 0.08) \times 10^{-3}$. Our first error is their experiment's error and our second error is the systematic error from using our best value.

² LOUVOT 09 reports $(3.67^{+0.35+0.65}_{-0.33-0.645}) \times 10^{-3}$ from a measurement of $[\Gamma(B_s^0 \rightarrow D_s^- \pi^+)/\Gamma_{\text{total}}] \times [B(\Upsilon(10860) \rightarrow B_s^{(*)} \bar{B}_s^{(*)})]$ assuming $B(\Upsilon(10860) \rightarrow B_s^{(*)} \bar{B}_s^{(*)}) = (19.5 \pm 2.6) \times 10^{-2}$, which we rescale to our best value $B(\Upsilon(10860) \rightarrow B_s^{(*)} \bar{B}_s^{(*)}) = (20.1 \pm 3.1) \times 10^{-2}$. Our first error is their experiment's error and our second error is the systematic error from using our best value.

³ ABULENCIA 07c reports $[\Gamma(B_s^0 \rightarrow D_s^- \pi^+)/\Gamma_{\text{total}}] / [B(B^0 \rightarrow D^- \pi^+)] = 1.13 \pm 0.08 \pm 0.23$ which we multiply by our best value $B(B^0 \rightarrow D^- \pi^+) = (2.51 \pm 0.08) \times 10^{-3}$. Our first error is their experiment's error and our second error is the systematic error from using our best value.

⁴ AAIJ 12AG reports $(2.95 \pm 0.05 \pm 0.17^{+0.18}_{-0.22}) \times 10^{-3}$ where the last uncertainty comes from the semileptonic f_1/f_0 measurement. We combined the systematics in quadrature.

⁵ ABULENCIA 06J reports $[\Gamma(B_s^0 \rightarrow D_s^- \pi^+)/\Gamma_{\text{total}}] / [B(B^0 \rightarrow D^- \pi^+)] = 1.32 \pm 0.18 \pm 0.38$ which we multiply by our best value $B(B^0 \rightarrow D^- \pi^+) = (2.51 \pm 0.08) \times 10^{-3}$. Our first error is their experiment's error and our second error is the systematic error from using our best value.

⁶ AKERS 94J uses ≤ 6 events and measures the limit on the product branching fraction $f(\bar{b} \rightarrow B_s^0) \cdot B(B_s^0 \rightarrow D_s^- \pi^+) < 1.3\%$ at CL = 90%. We divide by our current value $B(\bar{b} \rightarrow B_s^0) = 0.105$.

$\Gamma(D_s^- \rho^+)/\Gamma(D_s^- \pi^+)$ Γ_{14}/Γ_{13}
 VALUE

DOCUMENT ID	TECN	COMMENT
LOUVOT	10 BELL	$e^+e^- \rightarrow \Upsilon(5S)$

2.3 ± 0.4 ± 0.2

Meson Particle Listings

 B_S^0 $\Gamma(D_S^- \pi^+ \pi^+ \pi^-) / \Gamma_{\text{total}}$ Γ_{15} / Γ

VALUE (units 10^{-3})	DOCUMENT ID	TECN	COMMENT
6.1 ± 1.0 OUR FIT			
6.3 ± 1.4 ± 0.6	¹ ABULENCIA 07c	CDF	$p\bar{p}$ at 1.96 TeV

¹ ABULENCIA 07c reports $[\Gamma(B_S^0 \rightarrow D_S^- \pi^+ \pi^+ \pi^-) / \Gamma_{\text{total}}] / [B(B^0 \rightarrow D^- \pi^+ \pi^+ \pi^-)] = 1.05 \pm 0.10 \pm 0.22$ which we multiply by our best value $B(B^0 \rightarrow D^- \pi^+ \pi^+ \pi^-) = (6.0 \pm 0.6) \times 10^{-3}$. Our first error is their experiment's error and our second error is the systematic error from using our best value.

 $\Gamma(D_S^- \pi^+ \pi^+ \pi^-) / \Gamma(D_S^- \pi^+)$ $\Gamma_{15} / \Gamma_{13}$

VALUE	DOCUMENT ID	TECN	COMMENT
2.05 ± 0.33 OUR FIT			
2.01 ± 0.37 ± 0.20	AAIJ	11e	LHCB pp at 7 TeV

 $\Gamma(D_{S1}(2536)^- \pi^+, D_{S1}^- \rightarrow D_S^- \pi^+ \pi^-) / \Gamma(D_S^- \pi^+ \pi^-)$ $\Gamma_{16} / \Gamma_{15}$

VALUE (units 10^{-3})	DOCUMENT ID	TECN	COMMENT
4.0 ± 1.0 ± 0.4	AAIJ	12ax	LHCB pp at 7 TeV

 $\Gamma(D_S^\mp K^\pm) / \Gamma_{\text{total}}$ Γ_{17} / Γ

VALUE (units 10^{-4})	DOCUMENT ID	TECN	COMMENT
2.25 ± 0.12 OUR FIT			
2.3	¹ LOUVOT 09	BELL	$e^+ e^- \rightarrow \Upsilon(5S)$

¹ LOUVOT 09 reports $(2.4 \pm 1.2 \pm 0.42) \times 10^{-4}$ from a measurement of $[\Gamma(B_S^0 \rightarrow D_S^\mp K^\pm) / \Gamma_{\text{total}}] \times [B(\Upsilon(10860) \rightarrow B_S^{(*)} \bar{B}_S^{(*)})]$ assuming $B(\Upsilon(10860) \rightarrow B_S^{(*)} \bar{B}_S^{(*)}) = (19.5 \pm 2.6) \times 10^{-2}$, which we rescale to our best value $B(\Upsilon(10860) \rightarrow B_S^{(*)} \bar{B}_S^{(*)}) = (20.1 \pm 3.1) \times 10^{-2}$. Our first error is their experiment's error and our second error is the systematic error from using our best value.

 $\Gamma(D_S^\mp K^\pm) / \Gamma(D_S^- \pi^+)$ $\Gamma_{17} / \Gamma_{13}$

VALUE (units 10^{-2})	DOCUMENT ID	TECN	COMMENT
7.55 ± 0.24 OUR FIT			
7.55 ± 0.24 OUR AVERAGE			
7.52 ± 0.15 ± 0.19	AAIJ	15ac	LHCB pp at 7, 8 TeV
9.7 ± 1.8 ± 0.9	AALTONEN	09aQ	CDF $p\bar{p}$ at 1.96 TeV
• • •			We do not use the following data for averages, fits, limits, etc. • • •
6.46 ± 0.43 ± 0.25	AAIJ	12ag	LHCB Repl. by AAIJ 15Ac

 $\Gamma(D_S^- K^+ \pi^+ \pi^-) / \Gamma(D_S^- \pi^+ \pi^-)$ $\Gamma_{18} / \Gamma_{15}$

VALUE (units 10^{-2})	DOCUMENT ID	TECN	COMMENT
5.2 ± 0.5 ± 0.3	AAIJ	12ax	LHCB pp at 7 TeV

 $\Gamma(D_S^+ D_S^-) / \Gamma_{\text{total}}$ Γ_{19} / Γ

VALUE (units 10^{-3})	CL%	DOCUMENT ID	TECN	COMMENT
4.4 ± 0.5 OUR AVERAGE				
4.0 ± 0.2 ± 0.5		¹ AAIJ	13AP	LHCB pp at 7 TeV
5.8 ± 1.1 ± 1.3		² ESEN	13	BELL $e^+ e^- \rightarrow \Upsilon(5S)$
5.4 ± 0.8 ± 0.8		³ AALTONEN	12c	CDF $p\bar{p}$ at 1.96 TeV
• • •				We do not use the following data for averages, fits, limits, etc. • • •
10.3 ± 3.9 ± 2.6		⁴ ESEN	10	BELL Repl. by ESEN 13
10.4 ± 3.5 ± 1.1		⁵ AALTONEN	08f	CDF Repl. by AALTONEN 12c
<67	90	DRUTSKOY	07a	BELL Repl. by ESEN 10

¹ Uses $B(B^0 \rightarrow D^- D_S^+) = (7.2 \pm 0.8) \times 10^{-3}$.

² Use $\Upsilon(5S) \rightarrow B_S^* \bar{B}_S^*$ decays assuming $B(\Upsilon(5S) \rightarrow B_S^* \bar{B}_S^*) = (17.1 \pm 3.0)\%$ and $\Gamma(\Upsilon(5S) \rightarrow B_S^* \bar{B}_S^*) / \Gamma(\Upsilon(5S) \rightarrow B_S^{(*)} \bar{B}_S^{(*)}) = (87.0 \pm 1.7)\%$.

³ AALTONEN 12c reports $(f_S / f_d) (B(B_S^0 \rightarrow D_S^+ D_S^-) / B(B^0 \rightarrow D^- D_S^+)) = 0.183 \pm 0.021 \pm 0.017$. We multiply this result by our best value of $B(B^0 \rightarrow D^- D_S^+) = (7.2 \pm 0.8) \times 10^{-3}$ and divide by our best value of f_S / f_d , where $1/2 f_S / f_d = 0.1230 \pm 0.0115$. Our first quoted uncertainty is the combined experiment's uncertainty and our second is the systematic uncertainty from using our best values.

⁴ Uses $\Upsilon(10860) \rightarrow B_S^* \bar{B}_S^*$ assuming $B(\Upsilon(10860) \rightarrow B_S^{(*)} \bar{B}_S^{(*)}) = (19.3 \pm 2.9)\%$ and $\Gamma(\Upsilon(10860) \rightarrow B_S^* \bar{B}_S^*) / \Gamma(\Upsilon(10860) \rightarrow B_S^{(*)} \bar{B}_S^{(*)}) = (90.1 \pm 3.8)\%$.

⁵ AALTONEN 08f reports $[\Gamma(B_S^0 \rightarrow D_S^+ D_S^-) / \Gamma_{\text{total}}] / [B(B^0 \rightarrow D^- D_S^+)] = 1.44 \pm 0.48 \pm 0.44$ which we multiply by our best value $B(B^0 \rightarrow D^- D_S^+) = (7.2 \pm 0.8) \times 10^{-3}$. Our first error is their experiment's error and our second error is the systematic error from using our best value.

 $\Gamma(D_S^- D^+) / \Gamma_{\text{total}}$ Γ_{20} / Γ

VALUE (units 10^{-4})	DOCUMENT ID	TECN	COMMENT
2.8 ± 0.4 ± 0.3			
• • •			We do not use the following data for averages, fits, limits, etc. • • •
3.6 ± 0.6 ± 0.5	² AAIJ	13AP	LHCB Repl. by AAIJ 14AA

¹ AAIJ 14AA reports $[\Gamma(B_S^0 \rightarrow D_S^- D^+) / \Gamma_{\text{total}}] / [B(B^0 \rightarrow D^- D_S^+)] = 0.038 \pm 0.004 \pm 0.003$ which we multiply by our best value $B(B^0 \rightarrow D^- D_S^+) = (7.2 \pm 0.8) \times 10^{-3}$. Our first error is their experiment's error and our second error is the systematic error from using our best value.

² Uses $B(B^0 \rightarrow D^- D_S^+) = (7.2 \pm 0.8) \times 10^{-3}$.

 $\Gamma(D^+ D^-) / \Gamma_{\text{total}}$ Γ_{21} / Γ

VALUE (units 10^{-4})	DOCUMENT ID	TECN	COMMENT
2.2 ± 0.4 ± 0.4			
• • •			We do not use the following data for averages, fits, limits, etc. • • •
1.7 × 10 ⁻³	¹ AAIJ	13AP	LHCB pp at 7 TeV

¹ Uses $B(B^0 \rightarrow D^- D^+) = (2.11 \pm 0.31) \times 10^{-4}$ and $B(B^+ \rightarrow \bar{D}^0 D_S^+) = (10.1 \pm 1.7) \times 10^{-3}$.

 $\Gamma(D^0 \bar{D}^0) / \Gamma_{\text{total}}$ Γ_{24} / Γ

VALUE (units 10^{-4})	DOCUMENT ID	TECN	COMMENT
1.9 ± 0.3 ± 0.4			
• • •			We do not use the following data for averages, fits, limits, etc. • • •
1.7 × 10 ⁻³	¹ AAIJ	13AP	LHCB pp at 7 TeV

¹ Uses $B(B^0 \rightarrow D^- D^+) = (2.11 \pm 0.31) \times 10^{-4}$ and $B(B^+ \rightarrow \bar{D}^0 D_S^+) = (10.1 \pm 1.7) \times 10^{-3}$.

 $\Gamma(D_S^{*-} \pi^+) / \Gamma(D_S^- \pi^+)$ $\Gamma_{25} / \Gamma_{13}$

VALUE	DOCUMENT ID	TECN	COMMENT
0.65 ± 0.15 ± 0.07	LOUVOT	10	BELL $e^+ e^- \rightarrow \Upsilon(5S)$

 $\Gamma(D_S^{*\mp} K^\pm) / \Gamma(D_S^- \pi^+)$ $\Gamma_{26} / \Gamma_{25}$

VALUE	DOCUMENT ID	TECN	COMMENT
0.068 ± 0.005 ± 0.003 ± 0.002	AAIJ	15Ad	LHCB pp at 7, 8 TeV

 $\Gamma(D_S^- \rho^+) / \Gamma(D_S^- \pi^+)$ $\Gamma_{27} / \Gamma_{13}$

VALUE	DOCUMENT ID	TECN	COMMENT
3.2 ± 0.6 ± 0.3	LOUVOT	10	BELL $e^+ e^- \rightarrow \Upsilon(5S)$

 $\Gamma(D_S^- \rho^+) / \Gamma(D_S^- \rho^+)$ $\Gamma_{27} / \Gamma_{14}$

VALUE	DOCUMENT ID	TECN	COMMENT	
• • •			We do not use the following data for averages, fits, limits, etc. • • •	
1.4 ± 0.3 ± 0.1	¹ LOUVOT	10	BELL $e^+ e^- \rightarrow \Upsilon(5S)$	
• • •			We do not use the following data for averages, fits, limits, etc. • • •	
<121	90	DRUTSKOY	07a	BELL Repl. by ESEN 10

¹ Not independent of other LOUVOT 10 measurements.

 $[\Gamma(D_S^{*+} D_S^-) + \Gamma(D_S^{*-} D_S^+)] / \Gamma_{\text{total}}$ Γ_{28} / Γ

VALUE (units 10^{-3})	CL%	DOCUMENT ID	TECN	COMMENT
13.9 ± 1.7 OUR AVERAGE				
13.6 ± 1.0 ± 1.4		¹ AAIJ	16P	LHCB pp at 7 TeV
17.6 ± 2.3 ± 4.0		² ESEN	13	BELL $e^+ e^- \rightarrow \Upsilon(5S)$
12.5 ± 1.7 ± 1.8		³ AALTONEN	12c	CDF $p\bar{p}$ at 1.96 TeV
• • •				We do not use the following data for averages, fits, limits, etc. • • •
27.5 ± 8.3 ± 6.9		⁴ ESEN	10	BELL Repl. by ESEN 13
<121	90	DRUTSKOY	07a	BELL Repl. by ESEN 10

¹ AAIJ 16P reports $[\Gamma(B_S^0 \rightarrow D_S^{*+} D_S^-) + \Gamma(D_S^{*-} D_S^+)] / \Gamma_{\text{total}} / [B(B^0 \rightarrow D^- D_S^+)] = 1.88 \pm 0.08 \pm 0.12$ which we multiply by our best value $B(B^0 \rightarrow D^- D_S^+) = (7.2 \pm 0.8) \times 10^{-3}$. Our first error is their experiment's error and our second error is the systematic error from using our best value.

² Use $\Upsilon(5S) \rightarrow B_S^* \bar{B}_S^*$ decays assuming $B(\Upsilon(5S) \rightarrow B_S^* \bar{B}_S^*) = (17.1 \pm 3.0)\%$ and $\Gamma(\Upsilon(5S) \rightarrow B_S^* \bar{B}_S^*) / \Gamma(\Upsilon(5S) \rightarrow B_S^{(*)} \bar{B}_S^{(*)}) = (87.0 \pm 1.7)\%$.

³ AALTONEN 12c reports $(f_S / f_d) (B(B_S^0 \rightarrow D_S^{*+} D_S^- + D_S^{*-} D_S^+) / B(B^0 \rightarrow D^- D_S^+)) = 0.424 \pm 0.046 \pm 0.035$. We multiply this result by our best value of $B(B^0 \rightarrow D^- D_S^+) = (7.2 \pm 0.8) \times 10^{-3}$ and divide by our best value of f_S / f_d , where $1/2 f_S / f_d = 0.1230 \pm 0.0115$. Our first quoted uncertainty is the combined experiment's uncertainty and our second is the systematic uncertainty from using our best values.

⁴ Uses $\Upsilon(10860) \rightarrow B_S^* \bar{B}_S^*$ assuming $B(\Upsilon(10860) \rightarrow B_S^{(*)} \bar{B}_S^{(*)}) = (19.3 \pm 2.9)\%$ and $\Gamma(\Upsilon(10860) \rightarrow B_S^* \bar{B}_S^*) / \Gamma(\Upsilon(10860) \rightarrow B_S^{(*)} \bar{B}_S^{(*)}) = (90.1 \pm 3.8)\%$.

 $\Gamma(D_S^{*+} D_S^{*-}) / \Gamma_{\text{total}}$ Γ_{29} / Γ

VALUE (units 10^{-3})	CL%	DOCUMENT ID	TECN	COMMENT
14.4 ± 2.1 OUR AVERAGE				Error includes scale factor of 1.1.
12.7 ± 1.3 ± 1.4		¹ AAIJ	16P	LHCB pp at 7 TeV
19.8 ± 3.3 ± 5.2		² ESEN	13	BELL $e^+ e^- \rightarrow \Upsilon(5S)$
19.2 ± 2.9 ± 2.7		³ AALTONEN	12c	CDF $p\bar{p}$ at 1.96 TeV
• • •				We do not use the following data for averages, fits, limits, etc. • • •
30.8 ± 12.2 ± 8.5		⁴ ESEN	10	BELL Repl. by ESEN 13
<257	90	DRUTSKOY	07a	BELL Repl. by ESEN 10

¹ AAIJ 16P reports $[\Gamma(B_S^0 \rightarrow D_S^{*+} D_S^{*-}) / \Gamma_{\text{total}}] / [B(B^0 \rightarrow D^- D_S^+)] = 1.76 \pm 0.11 \pm 0.14$ which we multiply by our best value $B(B^0 \rightarrow D^- D_S^+) = (7.2 \pm 0.8) \times 10^{-3}$. Our first error is their experiment's error and our second error is the systematic error from using our best value.

² Use $\Upsilon(5S) \rightarrow B_S^* \bar{B}_S^*$ decays assuming $B(\Upsilon(5S) \rightarrow B_S^* \bar{B}_S^*) = (17.1 \pm 3.0)\%$ and $\Gamma(\Upsilon(5S) \rightarrow B_S^* \bar{B}_S^*) / \Gamma(\Upsilon(5S) \rightarrow B_S^{(*)} \bar{B}_S^{(*)}) = (87.0 \pm 1.7)\%$.

³ AALTONEN 12c reports $(f_S / f_d) (B(B_S^0 \rightarrow D_S^{*+} D_S^{*-}) / B(B^0 \rightarrow D^- D_S^+)) = 0.654 \pm 0.072 \pm 0.065$. We multiply this result by our best value of $B(B^0 \rightarrow D^- D_S^+) = (7.2 \pm 0.8) \times 10^{-3}$ and divide by our best value of f_S / f_d , where $1/2 f_S / f_d = 0.1230 \pm 0.0115$. Our first quoted uncertainty is the combined experiment's uncertainty and our second is the systematic uncertainty from using our best values.

⁴ Uses $\Upsilon(10860) \rightarrow B_S^* \bar{B}_S^*$ assuming $B(\Upsilon(10860) \rightarrow B_S^{(*)} \bar{B}_S^{(*)}) = (19.3 \pm 2.9)\%$ and $\Gamma(\Upsilon(10860) \rightarrow B_S^* \bar{B}_S^*) / \Gamma(\Upsilon(10860) \rightarrow B_S^{(*)} \bar{B}_S^{(*)}) = (90.1 \pm 3.8)\%$.

$\Gamma(D_S^{(*)+} D_S^{(*)-})/\Gamma_{\text{total}}$ Γ_{30}/Γ

“OUR EVALUATION” is an average using rescaled values of the data listed below. The average and rescaling were performed by the Heavy Flavor Averaging Group (HFLAV, <https://hflav.web.cern.ch/>) and are described at <https://hflav.web.cern.ch/>. The averaging/rescaling procedure takes into account correlations between the measurements.

VALUE (%)	CL%	DOCUMENT ID	TECN	COMMENT
4.5 ± 1.4		OUR EVALUATION		
3.4 ± 0.4		OUR AVERAGE		
3.07 ± 0.22 ± 0.33		1 AAIJ	16P LHCb	pp at 7 TeV
4.32 ^{+0.42+1.04} _{-0.39-1.03}		2 ESEN	13 BELL	$e^+e^- \rightarrow \Upsilon(5S)$
3.7 ± 0.4 ± 0.5		3 AALTONEN	12C CDF	$p\bar{p}$ at 1.96 TeV
3.5 ± 1.0 ± 1.1		4 ABAZOV	09I D0	$p\bar{p}$ at 1.96 TeV
14 ± 6 ± 3		5,6 BARATE	00K ALEP	$e^+e^- \rightarrow Z$
6.85 ^{+1.53+1.79} _{-1.30-1.80}		7,8 ESEN	10 BELL	Repl. by ESEN 13
3.9 ^{+1.9+1.6} _{-1.7-1.5}		4 ABAZOV	07Y D0	Repl. by ABAZOV 09I
<0.218	90	BARATE	98Q ALEP	$e^+e^- \rightarrow Z$

¹ AAIJ 16P reports $[\Gamma(B_S^0 \rightarrow D_S^{(*)+} D_S^{(*)-})/\Gamma_{\text{total}}] / [B(B^0 \rightarrow D^- D_S^+)] = 4.24 \pm 0.14 \pm 0.27$ which we multiply by our best value $B(B^0 \rightarrow D^- D_S^+) = (7.2 \pm 0.8) \times 10^{-3}$. Our first error is their experiment's error and our second error is the systematic error from using our best value.

² Use $\Upsilon(5S) \rightarrow B_S^* \bar{B}_S^*$ decays assuming $B(\Upsilon(5S) \rightarrow B_S^* \bar{B}_S^*) = (17.1 \pm 3.0)\%$ and $\Gamma(\Upsilon(5S) \rightarrow B_S^* \bar{B}_S^*) / \Gamma(\Upsilon(5S) \rightarrow B_S^{(*)} \bar{B}_S^{(*)}) = (87.0 \pm 1.7)\%$.

³ AALTONEN 12C reports $(f_S/f_D) (B(B_S^0 \rightarrow D_S^{(*)+} D_S^{(*)-}) / B(B^0 \rightarrow D^- D_S^+)) = 1.261 \pm 0.095 \pm 0.112$. We multiply this result by our best value of $B(B^0 \rightarrow D^- D_S^+) = (7.2 \pm 0.8) \times 10^{-3}$ and divide by our best value of f_S/f_D , where $1/2 f_S/f_D = 0.1230 \pm 0.0115$. Our first quoted uncertainty is the combined experiment's uncertainty and our second is the systematic uncertainty from using our best values.

⁴ Uses the final states where $D_S^+ \rightarrow \phi\pi^+$ and $D_S^- \rightarrow \phi\mu^- \bar{\nu}_\mu$.

⁵ Reports $B(B_S^0(\text{short}) \rightarrow D_S^{(*)+} D_S^{(*)-}) = (0.23 \pm 0.10 \pm 0.05) \cdot [0.17/B(D_S \rightarrow \phi\chi)]^2$ assuming $B(B_S^0 \rightarrow B_S^0(\text{short})) = 50\%$. We use our best value of $B(D_S \rightarrow \phi\chi) = 15.7 \pm 1.0\%$ to obtain the quoted result.

⁶ Uses $\phi\phi$ correlations from $B_S^0(\text{short}) \rightarrow D_S^{(*)+} D_S^{(*)-}$.

⁷ Sum of exclusive $B_S \rightarrow D_S^+ D_S^-$, $B_S \rightarrow D_S^{\pm} D_S^{\mp}$ and $B_S \rightarrow D_S^{*+} D_S^{*-}$.

⁸ Uses $\Upsilon(10860) \rightarrow B_S^* \bar{B}_S^*$ assuming $B(\Upsilon(10860) \rightarrow B_S^{(*)} \bar{B}_S^{(*)}) = (19.3 \pm 2.9)\%$ and $\Gamma(\Upsilon(10860) \rightarrow B_S^* \bar{B}_S^*) / \Gamma(\Upsilon(10860) \rightarrow B_S^{(*)} \bar{B}_S^{(*)}) = (90.1^{+3.8}_{-4.0})\%$.

 $\Gamma(D^{*+} D_S^+)/\Gamma_{\text{total}}$ Γ_{31}/Γ

VALUE (units 10^{-4})	DOCUMENT ID	TECN	COMMENT
3.9 ± 0.6 ± 0.5	1 AAIJ	21S LHCb	pp at 13 TeV

¹ AAIJ 21S reports $[\Gamma(B_S^0 \rightarrow D^{*+} D_S^+)/\Gamma_{\text{total}}] / [B(B^0 \rightarrow D^*(2010)^- D_S^+)] = 0.049 \pm 0.006 \pm 0.0036$ which we multiply by our best value $B(B^0 \rightarrow D^*(2010)^- D_S^+) = (8.0 \pm 1.1) \times 10^{-3}$. Our first error is their experiment's error and our second error is the systematic error from using our best value.

 $[\Gamma(D^{*+} D^-) + \Gamma(D^{*-} D^+)]/\Gamma_{\text{total}}$ $(\Gamma_{22} + \Gamma_{23})/\Gamma$

VALUE (units 10^{-5})	DOCUMENT ID	TECN	COMMENT
8.4 ± 1.1 ± 0.8	1 AAIJ	21N LHCb	pp at 7, 8, 13 TeV

¹ AAIJ 21N reports $[\Gamma(B_S^0 \rightarrow D^{*+} D^-) + \Gamma(B_S^0 \rightarrow D^{*-} D^+)]/\Gamma_{\text{total}} / [B(B^0 \rightarrow D^{\pm} D^{*\mp} (CP\text{-averaged}))] = 0.137 \pm 0.017 \pm 0.006$ which we multiply by our best value $B(B^0 \rightarrow D^{\pm} D^{*\mp} (CP\text{-averaged})) = (6.1 \pm 0.6) \times 10^{-4}$. Our first error is their experiment's error and our second error is the systematic error from using our best value.

 $\Gamma(\bar{D}^{*0} K^0)/\Gamma_{\text{total}}$ Γ_{32}/Γ

VALUE (units 10^{-4})	DOCUMENT ID	TECN	COMMENT
2.8 ± 1.0 ± 0.5	1 AAIJ	16c LHCb	pp at 7, 8 TeV

¹ Measured and normalized to the $B_S^0 \rightarrow \bar{D}^{*0} K_S^0$ decay with $f_S/f_D = 0.259 \pm 0.015$. Signal significance is 4.4 standard deviations.

 $\Gamma(\bar{D}^0 K^0)/\Gamma_{\text{total}}$ Γ_{33}/Γ

VALUE (units 10^{-4})	DOCUMENT ID	TECN	COMMENT
4.3 ± 0.5 ± 0.7	1 AAIJ	16c LHCb	pp at 7, 8 TeV

¹ Measured and normalized to the $B^0 \rightarrow \bar{D}^0 K_S^0$ decay with $f_S/f_D = 0.259 \pm 0.015$.

 $\Gamma(\bar{D}^0 K^- \pi^+)/\Gamma_{\text{total}}$ Γ_{34}/Γ

VALUE (units 10^{-4})	DOCUMENT ID	TECN	COMMENT
10.4 ± 1.1 ± 0.5	1 AAIJ	13aQ LHCb	pp at 7 TeV

¹ AAIJ 13aQ reports $[\Gamma(B_S^0 \rightarrow \bar{D}^0 K^- \pi^+)/\Gamma_{\text{total}}] / [B(B^0 \rightarrow \bar{D}^0 \pi^+ \pi^-)] = 1.18 \pm 0.05 \pm 0.12$ which we multiply by our best value $B(B^0 \rightarrow \bar{D}^0 \pi^+ \pi^-) = (8.8 \pm 0.5) \times 10^{-4}$. Our first error is their experiment's error and our second error is the systematic error from using our best value.

 $\Gamma(\bar{D}^0 \bar{K}^*(892)^0)/\Gamma_{\text{total}}$ Γ_{35}/Γ

VALUE (units 10^{-4})	DOCUMENT ID	TECN	COMMENT
4.4 ± 0.6	OUR AVERAGE		

4.29 ± 0.09 ± 0.65	¹ AAIJ	14BH LHCb	pp at 7, 8 TeV
4.7 ± 1.2 ± 0.3	² AAIJ	11D LHCb	pp at 7 TeV

• • • We do not use the following data for averages, fits, limits, etc. • • •

¹ Uses Dalitz plot analysis of $B_S^0 \rightarrow \bar{D}^0 K^- \pi^+$ decays.
² AAIJ 11D reports $[\Gamma(B_S^0 \rightarrow \bar{D}^0 \bar{K}^*(892)^0)/\Gamma_{\text{total}}] / [B(B^0 \rightarrow \bar{D}^0 \rho^0)] = 1.48 \pm 0.34 \pm 0.19$ which we multiply by our best value $B(B^0 \rightarrow \bar{D}^0 \rho^0) = (3.21 \pm 0.21) \times 10^{-4}$. Our first error is their experiment's error and our second error is the systematic error from using our best value.
³ AAIJ 13BX reports $[\Gamma(B_S^0 \rightarrow \bar{D}^0 \bar{K}^*(892)^0)/\Gamma_{\text{total}}] / [B(B^0 \rightarrow \bar{D}^0 K^*(892)^0)] = 7.8 \pm 0.7 \pm 0.3 \pm 0.6$ which we multiply by our best value $B(B^0 \rightarrow \bar{D}^0 K^*(892)^0) = (4.5 \pm 0.6) \times 10^{-5}$. Our first error is their experiment's error and our second error is the systematic error from using our best value.

 $\Gamma(\bar{D}^0 \bar{K}^*(1410))/\Gamma_{\text{total}}$ Γ_{36}/Γ

VALUE (units 10^{-5})	DOCUMENT ID	TECN	COMMENT
38.6 ± 11.4 ± 33.3	¹ AAIJ	14BH LHCb	pp at 7, 8 TeV

¹ Uses Dalitz plot analysis of $B_S^0 \rightarrow \bar{D}^0 K^- \pi^+$ decays.

 $\Gamma(\bar{D}^0 \bar{K}_0^*(1430))/\Gamma_{\text{total}}$ Γ_{37}/Γ

VALUE (units 10^{-5})	DOCUMENT ID	TECN	COMMENT
30.0 ± 2.4 ± 6.8	¹ AAIJ	14BH LHCb	pp at 7, 8 TeV

¹ Uses Dalitz plot analysis of $B_S^0 \rightarrow \bar{D}^0 K^- \pi^+$ decays. Corresponds to the resonant $K_0^*(1430)$ part of LASS parametrization.

 $\Gamma(\bar{D}^0 \bar{K}_2^*(1430))/\Gamma_{\text{total}}$ Γ_{38}/Γ

VALUE (units 10^{-5})	DOCUMENT ID	TECN	COMMENT
11.1 ± 1.8 ± 3.8	¹ AAIJ	14BH LHCb	pp at 7, 8 TeV

¹ Uses Dalitz plot analysis of $B_S^0 \rightarrow \bar{D}^0 K^- \pi^+$ decays.

 $\Gamma(\bar{D}^0 \bar{K}^*(1680))/\Gamma_{\text{total}}$ Γ_{39}/Γ

VALUE (units 10^{-5})	CL%	DOCUMENT ID	TECN	COMMENT
<7.8	90	¹ AAIJ	14BH LHCb	pp at 7, 8 TeV

¹ Uses Dalitz plot analysis of $B_S^0 \rightarrow \bar{D}^0 K^- \pi^+$ decays.

 $\Gamma(\bar{D}^0 \bar{K}_0^*(1950))/\Gamma_{\text{total}}$ Γ_{40}/Γ

VALUE (units 10^{-5})	CL%	DOCUMENT ID	TECN	COMMENT
<11	90	¹ AAIJ	14BH LHCb	pp at 7, 8 TeV

¹ Uses Dalitz plot analysis of $B_S^0 \rightarrow \bar{D}^0 K^- \pi^+$ decays.

 $\Gamma(\bar{D}^0 \bar{K}_3^*(1780))/\Gamma_{\text{total}}$ Γ_{41}/Γ

VALUE (units 10^{-5})	CL%	DOCUMENT ID	TECN	COMMENT
<2.6	90	¹ AAIJ	14BH LHCb	pp at 7, 8 TeV

¹ Uses Dalitz plot analysis of $B_S^0 \rightarrow \bar{D}^0 K^- \pi^+$ decays.

 $\Gamma(\bar{D}^0 \bar{K}_4^*(2045))/\Gamma_{\text{total}}$ Γ_{42}/Γ

VALUE (units 10^{-5})	CL%	DOCUMENT ID	TECN	COMMENT
<3.1	90	¹ AAIJ	14BH LHCb	pp at 7, 8 TeV

¹ Uses Dalitz plot analysis of $B_S^0 \rightarrow \bar{D}^0 K^- \pi^+$ decays.

 $\Gamma(\bar{D}^0 K^- \pi^+ (\text{non-resonant}))/\Gamma_{\text{total}}$ Γ_{43}/Γ

VALUE (units 10^{-5})	DOCUMENT ID	TECN	COMMENT
20.6 ± 3.8 ± 7.3	¹ AAIJ	14BH LHCb	pp at 7, 8 TeV

¹ Uses Dalitz plot analysis of $B_S^0 \rightarrow \bar{D}^0 K^- \pi^+$ decays. Corresponds to the non-resonant part of the LASS parametrization.

 $\Gamma(D_{S2}^*(2573)^- \pi^+, D_{S2}^* \rightarrow \bar{D}^0 K^-)/\Gamma_{\text{total}}$ Γ_{44}/Γ

VALUE (units 10^{-5})	DOCUMENT ID	TECN	COMMENT
25.7 ± 0.7 ± 4.0	¹ AAIJ	14BH LHCb	pp at 7, 8 TeV

¹ Uses Dalitz plot analysis of $B_S^0 \rightarrow \bar{D}^0 K^- \pi^+$ decays.

 $\Gamma(D_{S1}^*(2700)^- \pi^+, D_{S1}^* \rightarrow \bar{D}^0 K^-)/\Gamma_{\text{total}}$ Γ_{45}/Γ

VALUE (units 10^{-5})	DOCUMENT ID	TECN	COMMENT
1.6 ± 0.4 ± 0.7	¹ AAIJ	14BH LHCb	pp at 7, 8 TeV

¹ Uses Dalitz plot analysis of $B_S^0 \rightarrow \bar{D}^0 K^- \pi^+$ decays.

 $\Gamma(D_{S1}^*(2860)^- \pi^+, D_{S1}^* \rightarrow \bar{D}^0 K^-)/\Gamma_{\text{total}}$ Γ_{46}/Γ

VALUE (units 10^{-5})	DOCUMENT ID	TECN	COMMENT
5.0 ± 1.2 ± 3.4	¹ AAIJ	14BH LHCb	pp at 7, 8 TeV

¹ Uses Dalitz plot analysis of $B_S^0 \rightarrow \bar{D}^0 K^- \pi^+$ decays.

Meson Particle Listings

B_S^0

$\Gamma(D_{s3}^{*+}(2860)^-\pi^+, D_{s3}^{*+} \rightarrow \bar{D}^0 K^-)/\Gamma_{total}$				Γ_{47}/Γ
VALUE (units 10^{-5})	DOCUMENT ID	TECN	COMMENT	
$2.2 \pm 0.1 \pm 0.6$	¹ AAIJ	14BH	LHCB pp at 7, 8 TeV	

¹ Uses Dalitz plot analysis of $B_S^0 \rightarrow \bar{D}^0 K^- \pi^+$ decays.

$\Gamma(\bar{D}^0 K^+ K^-)/\Gamma_{total}$				Γ_{48}/Γ
VALUE (units 10^{-5})	DOCUMENT ID	TECN	COMMENT	
$5.6 \pm 0.7 \pm 0.5$	¹ AAIJ	18AZ	LHCB pp at 7, 8 TeV	

- • • We do not use the following data for averages, fits, limits, etc. • • •
- $5.5 \pm 2.0 \pm 0.5$ ^{2,3} AAIJ 12AMLHCB Repl. by AAIJ 18AZ
- ¹ AAIJ 18AZ reports $[\Gamma(B_S^0 \rightarrow \bar{D}^0 K^+ K^-)/\Gamma_{total}] / [B(B^0 \rightarrow \bar{D}^0 K^+ K^-)] = 0.930 \pm 0.089 \pm 0.069$ which we multiply by our best value $B(B^0 \rightarrow \bar{D}^0 K^+ K^-) = (6.1 \pm 0.5) \times 10^{-5}$. Our first error is their experiment's error and our second error is the systematic error from using our best value.
- ² AAIJ 12AM reports $[\Gamma(B_S^0 \rightarrow \bar{D}^0 K^+ K^-)/\Gamma_{total}] / [B(B^0 \rightarrow \bar{D}^0 K^+ K^-)] = 0.90 \pm 0.27 \pm 0.20$ which we multiply by our best value $B(B^0 \rightarrow \bar{D}^0 K^+ K^-) = (6.1 \pm 0.5) \times 10^{-5}$. Our first error is their experiment's error and our second error is the systematic error from using our best value.
- ³ Uses $B(b \rightarrow B_S^0)/B(b \rightarrow B^0) = 0.267_{-0.020}^{+0.023}$ measured by the same authors.

$\Gamma(\bar{D}^0 f_0(980))/\Gamma_{total}$				Γ_{49}/Γ
VALUE	CL%	DOCUMENT ID	TECN	COMMENT
$<3.1 \times 10^{-6}$	90	AAIJ	15AG	LHCB pp at 7, 8 TeV

$\Gamma(\bar{D}^0 \phi)/\Gamma_{total}$				Γ_{50}/Γ
VALUE (units 10^{-5})	DOCUMENT ID	TECN	COMMENT	
$3.0 \pm 0.4 \pm 0.2$	¹ AAIJ	18AY	LHCB pp at 7 and 8 TeV	

¹ AAIJ 18AY reports $[\Gamma(B_S^0 \rightarrow \bar{D}^0 \phi)/\Gamma_{total}] / [B(B^0 \rightarrow \bar{D}^0 \pi^+ \pi^-)] = (3.4 \pm 0.4 \pm 0.3) \times 10^{-2}$ which we multiply by our best value $B(B^0 \rightarrow \bar{D}^0 \pi^+ \pi^-) = (8.8 \pm 0.5) \times 10^{-4}$. Our first error is their experiment's error and our second error is the systematic error from using our best value.

$\Gamma(\bar{D}^0 \phi)/\Gamma(\bar{D}^0 K^*(892)^0)$				Γ_{50}/Γ_{35}
VALUE	DOCUMENT ID	TECN	COMMENT	
$0.069 \pm 0.013 \pm 0.007$	AAIJ	13Bx	LHCB Repl. by AAIJ 18AY	

$\Gamma(\bar{D}^{*0} \phi)/\Gamma_{total}$				Γ_{51}/Γ
VALUE (units 10^{-5})	DOCUMENT ID	TECN	COMMENT	
$3.7 \pm 0.6 \pm 0.2$	¹ AAIJ	18AY	LHCB pp at 7 and 8 TeV	

¹ AAIJ 18AY reports $[\Gamma(B_S^0 \rightarrow \bar{D}^{*0} \phi)/\Gamma_{total}] / [B(B^0 \rightarrow \bar{D}^0 \pi^+ \pi^-)] = (4.2 \pm 0.5 \pm 0.4) \times 10^{-2}$ which we multiply by our best value $B(B^0 \rightarrow \bar{D}^0 \pi^+ \pi^-) = (8.8 \pm 0.5) \times 10^{-4}$. Our first error is their experiment's error and our second error is the systematic error from using our best value.

$\Gamma(D^{*+} \pi^\pm)/\Gamma_{total}$				Γ_{52}/Γ
VALUE	CL%	DOCUMENT ID	TECN	COMMENT
$<6.1 \times 10^{-6}$	90	¹ AAIJ	13AL	LHCB pp at 7 TeV

¹ Uses $f_s/f_d = 0.256 \pm 0.020$ and $B(B^0 \rightarrow D^{*+} \pi^-) = (2.76 \pm 0.13) \times 10^{-3}$.

$\Gamma(\eta_c \phi)/\Gamma_{total}$				Γ_{53}/Γ
VALUE (units 10^{-4})	DOCUMENT ID	TECN	COMMENT	
$5.01 \pm 0.53 \pm 0.68$	¹ AAIJ	17U	LHCB pp at 7, 8 TeV	

¹ The last uncertainty includes the limited knowledge of the external branching fractions where the η_c is reconstructed in the $p\bar{p}, K^+ K^- \pi^+ \pi^-, \pi^+ \pi^- \pi^+ \pi^-,$ and $K^+ K^- K^+ K^-$ decays and $\phi(1020) \rightarrow K^+ K^-$.

$\Gamma(\eta_c \pi^+ \pi^-)/\Gamma_{total}$				Γ_{55}/Γ
VALUE (units 10^{-4})	DOCUMENT ID	TECN	COMMENT	
$1.76 \pm 0.59 \pm 0.31$	¹ AAIJ	17U	LHCB pp at 7, 8 TeV	

¹ The last uncertainty includes the limited knowledge of the external branching fractions where the η_c is reconstructed in the $p\bar{p}, K^+ K^- \pi^+ \pi^-, \pi^+ \pi^- \pi^+ \pi^-,$ and $K^+ K^- K^+ K^-$ decays. The significance of the signal, including systematic uncertainties, is 4.6 standard deviations.

$\Gamma(J/\psi(1S) \phi)/\Gamma_{total}$				Γ_{56}/Γ
VALUE (units 10^{-3})	EVTS	DOCUMENT ID	TECN	COMMENT
1.04 ± 0.04 OUR FIT				
1.04 ± 0.04 OUR AVERAGE				
$1.037 \pm 0.032 \pm 0.022$		¹ AAIJ	21Y	LHCB pp at 7, 8, 13 TeV
$1.25 \pm 0.07 \pm 0.23$		² THORNE	13	BELL $e^+ e^- \rightarrow \Upsilon(5S)$
$1.5 \pm 0.5 \pm 0.1$		³ ABE	96Q	CDF $p\bar{p}$

- • • We do not use the following data for averages, fits, limits, etc. • • •
- $1.050 \pm 0.013 \pm 0.104$ ⁴ AAIJ 13AN LHCB Repl. by AAIJ 21Y
- <6 ⁵ AKERS 94I OPAL $e^+ e^- \rightarrow Z$
- seen ¹⁴ ⁶ ABE 93F CDF $p\bar{p}$ at 1.8 TeV
- seen ¹ ⁷ ACTON 92N OPAL Sup. by AKERS 94J

¹ AAIJ 21Y reports $[\Gamma(B_S^0 \rightarrow J/\psi(1S) \phi)/\Gamma_{total}] \times [B(\phi(1020) \rightarrow K^+ K^-)] = (5.01 \pm 0.16 \pm 0.17) \times 10^{-4}$ from a measurement of $[\Gamma(B_S^0 \rightarrow J/\psi(1S) \phi)/\Gamma_{total}] \times [B(\phi(1020) \rightarrow K^+ K^-)] / [B(B^+ \rightarrow J/\psi(1S) K^+)]$ assuming $B(B^+ \rightarrow J/\psi(1S) K^+) = (1.003 \pm 0.035) \times 10^{-3}$, which we rescale to our best values $B(\phi(1020) \rightarrow K^+ K^-) = (49.1 \pm 0.5) \times 10^{-2}$, $B(B^+ \rightarrow J/\psi(1S) K^+) = (1.020 \pm 0.019) \times 10^{-3}$. Our first error is their experiment's error and our second error is the systematic error from using our best values.

- ² THORNE 13 uses $f_s = (17.2 \pm 3.0)\%$ as the fraction of $\Upsilon(5S)$ decaying to $B_S^{(*)} \bar{B}_S^{(*)}$.
- ³ ABE 96Q reports $[\Gamma(B_S^0 \rightarrow J/\psi(1S) \phi)/\Gamma_{total}] \times [\Gamma(\bar{B} \rightarrow B_S^0) / (\Gamma(\bar{B} \rightarrow B^+) + \Gamma(\bar{B} \rightarrow B^0))] = (0.185 \pm 0.055 \pm 0.020) \times 10^{-3}$ which we divide by our best value $\Gamma(\bar{B} \rightarrow B_S^0) / [\Gamma(\bar{B} \rightarrow B^+) + \Gamma(\bar{B} \rightarrow B^0)] = 0.1230 \pm 0.0115$. Our first error is their experiment's error and our second error is the systematic error from using our best value.
- ⁴ AAIJ 13AN uses $f_s/f_d = 0.256 \pm 0.020$ and $B(B^+ \rightarrow J/\psi K^+) = (10.18 \pm 0.42) \times 10^{-4}$.
- ⁵ AKERS 94J sees one event and measures the limit on the product branching fraction $f(\bar{B} \rightarrow B_S^0) \cdot B(B_S^0 \rightarrow J/\psi(1S) \phi) < 7 \times 10^{-4}$ at CL = 90%. We divide by $B(\bar{B} \rightarrow B_S^0) = 0.112$.
- ⁶ ABE 93F measured using $J/\psi(1S) \rightarrow \mu^+ \mu^-$ and $\phi \rightarrow K^+ K^-$.
- ⁷ In ACTON 92N a limit on the product branching fraction is measured to be $f(\bar{B} \rightarrow B_S^0) \cdot B(B_S^0 \rightarrow J/\psi(1S) \phi) \leq 0.22 \times 10^{-2}$.

$\Gamma(J/\psi(1S) \phi \phi)/\Gamma(J/\psi(1S) \phi)$				Γ_{57}/Γ_{56}
VALUE (units 10^{-2})	EVTS	DOCUMENT ID	TECN	COMMENT
$1.15 \pm 0.12 \pm 0.05$	128	¹ AAIJ	16U	LHCB pp at 7, 8 TeV

¹ Uses $J/\psi \rightarrow \mu^+ \mu^-, \phi \rightarrow K^+ K^-$ decays, and observes 128 ± 13 events of $B_S^0 \rightarrow J/\psi \phi \phi$.

$\Gamma(J/\psi(1S) \pi^0)/\Gamma_{total}$				Γ_{58}/Γ
VALUE	CL%	DOCUMENT ID	TECN	COMMENT
$<1.2 \times 10^{-3}$	90	¹ ACCIARRI	97c	L3

¹ ACCIARRI 97c assumes B^0 production fraction $(39.5 \pm 4.0\%)$ and B_S $(12.0 \pm 3.0\%)$.

$\Gamma(J/\psi(1S) \eta)/\Gamma_{total}$				Γ_{59}/Γ
VALUE (units 10^{-4})	CL%	DOCUMENT ID	TECN	COMMENT
4.0 ± 0.7 OUR AVERAGE				Error includes scale factor of 1.4.
$3.6_{-0.6}^{+0.5}$	$_{-0.2}^{+0.3}$	¹ AAIJ	13A	LHCB pp at 7 TeV
5.10 ± 0.50	$_{-0.63}^{+1.17}$	² LI	12	BELL $e^+ e^- \rightarrow \Upsilon(4S)$

- • • We do not use the following data for averages, fits, limits, etc. • • •
- <38 ³ ACCIARRI 97c L3

¹ AAIJ 13A reports $[\Gamma(B_S^0 \rightarrow J/\psi(1S) \eta)/\Gamma_{total}] / [B(B^0 \rightarrow J/\psi(1S) \rho^0)] = 14.0 \pm 1.2_{-1.5}^{+1.1}$ which we multiply by our best value $B(B^0 \rightarrow J/\psi(1S) \rho^0) = (2.55_{-0.16}^{+0.18}) \times 10^{-5}$. Our first error is their experiment's error and our second error is the systematic error from using our best value.

- ² Observed for the first time with significances over 10σ . The second error are total systematic uncertainties including the error on $N(B_S^{(*)} \bar{B}_S^{(*)})$.
- ³ ACCIARRI 97c assumes B^0 production fraction $(39.5 \pm 4.0\%)$ and B_S $(12.0 \pm 3.0\%)$.

$\Gamma(J/\psi(1S) K_S^0)/\Gamma_{total}$				Γ_{60}/Γ
VALUE (units 10^{-5})	DOCUMENT ID	TECN	COMMENT	
1.92 ± 0.14 OUR AVERAGE				
$1.92 \pm 0.14 \pm 0.05$	¹ AAIJ	15AL	LHCB pp at 7, 8 TeV	
$2.0 \pm 0.4 \pm 0.2$	² AALTONEN	11A	CDF $p\bar{p}$ at 1.96 TeV	

- • • We do not use the following data for averages, fits, limits, etc. • • •
- $2.03 \pm 0.16 \pm 0.20$ ³ AAIJ 13AB LHCB Repl. by AAIJ 15AL
- $2.03 \pm 0.26 \pm 0.20$ ⁴ AAIJ 12O LHCB Repl. by AAIJ 13AB

¹ AAIJ 15AL reports $[\Gamma(B_S^0 \rightarrow J/\psi(1S) K_S^0)/\Gamma_{total}] / [B(B^0 \rightarrow J/\psi(1S) K_S^0)] = (4.31 \pm 0.17 \pm 0.12 \pm 0.25) \times 10^{-2}$ which we multiply by our best value $B(B^0 \rightarrow J/\psi(1S) K_S^0) = (4.45 \pm 0.11) \times 10^{-4}$. Our first error is their experiment's error and our second error is the systematic error from using our best value.

² AALTONEN 11A reports $[\Gamma(B_S^0 \rightarrow J/\psi(1S) K_S^0)/\Gamma_{total}] \times [B(\bar{B} \rightarrow B_S^0)] / [B(\bar{B} \rightarrow B^0)] / [B(B^0 \rightarrow J/\psi(1S) K_S^0)] = (1.09 \pm 0.19 \pm 0.11) \times 10^{-2}$ which we multiply or divide by our best values $B(\bar{B} \rightarrow B_S^0) = (10.0 \pm 0.8) \times 10^{-2}$, $B(\bar{B} \rightarrow B^0) = (40.8 \pm 0.7) \times 10^{-2}$, $B(B^0 \rightarrow J/\psi(1S) K_S^0) = 1/2 \times B(B^0 \rightarrow J/\psi(1S) K^0) = 1/2 \times (8.91 \pm 0.21) \times 10^{-4}$. Our first error is their experiment's error and our second error is the systematic error from using our best values.

See key on page 1127

Meson Particle Listings

B_s^0

³ AAIJ 13AB reports $(1.97 \pm 0.14 \pm 0.07 \pm 0.15 \pm 0.08) \times 10^{-5}$ from a measurement of $[\Gamma(B_s^0 \rightarrow J/\psi(1S) K_S^0)/\Gamma_{total}] / [B(B^0 \rightarrow J/\psi(1S) K^0)] \times [\Gamma(\bar{B} \rightarrow B^0)/\Gamma(\bar{B} \rightarrow B^0)]$ assuming $B(B^0 \rightarrow J/\psi(1S) K^0) = (8.98 \pm 0.35) \times 10^{-4}$, $\Gamma(\bar{B} \rightarrow B^0)/\Gamma(\bar{B} \rightarrow B^0) = 0.256 \pm 0.020$, which we rescale to our best values $B(B^0 \rightarrow J/\psi(1S) K^0) = (8.91 \pm 0.21) \times 10^{-4}$, $\Gamma(\bar{B} \rightarrow B^0)/\Gamma(\bar{B} \rightarrow B^0) = 0.246 \pm 0.023$. Our first error is their experiment's error and our second error is the systematic error from using our best values.

⁴ AAIJ 12O reports $(1.83 \pm 0.21 \pm 0.10 \pm 0.14 \pm 0.07) \times 10^{-5}$ from a measurement of $[\Gamma(B_s^0 \rightarrow J/\psi(1S) K_S^0)/\Gamma_{total}] / [B(B^0 \rightarrow J/\psi(1S) K^0)] \times [\Gamma(\bar{B} \rightarrow B^0)/\Gamma(\bar{B} \rightarrow B^0)]$ assuming $B(B^0 \rightarrow J/\psi(1S) K^0) = (8.71 \pm 0.32) \times 10^{-4}$, $\Gamma(\bar{B} \rightarrow B^0)/\Gamma(\bar{B} \rightarrow B^0) = 0.267_{-0.021}^{+0.021}$, which we rescale to our best values $B(B^0 \rightarrow J/\psi(1S) K^0) = (8.91 \pm 0.21) \times 10^{-4}$, $\Gamma(\bar{B} \rightarrow B^0)/\Gamma(\bar{B} \rightarrow B^0) = 0.246 \pm 0.023$. Our first error is their experiment's error and our second error is the systematic error from using our best values.

$\Gamma(J/\psi(1S) \bar{K}^*(892)^0)/\Gamma_{total}$ Γ_{61}/Γ			
VALUE (units 10^{-5})	DOCUMENT ID	TECN	COMMENT
4.14 ± 0.18 ± 0.35	¹ AAIJ	15AV LHCb	pp at 7, 8 TeV
• • • We do not use the following data for averages, fits, limits, etc. • • •			
4.4 $_{-0.4}^{+0.5} \pm 0.8$	² AAIJ	12AP LHCb	Repl. by AAIJ 15AV
9 ± 4 ± 1	³ AALTONEN	11A CDF	$p\bar{p}$ at 1.96 TeV

¹ AAIJ 15AV result combines two measurements with different normalizing modes of $B^0 \rightarrow J/\psi K^*(892)^0$ and $B_s^0 \rightarrow J/\psi \phi$.

² AAIJ 12AP reports $B(B_s^0 \rightarrow J/\psi(1S) \bar{K}^*(892)^0)/B(B^0 \rightarrow J/\psi(1S) K^*(892)^0) = (3.43_{-0.36}^{+0.34} \pm 0.50) \times 10^{-2}$ and $B(B^0 \rightarrow J/\psi(1S) K^*(892)^0) = (1.29 \pm 0.05 \pm 0.13) \times 10^{-3}$ after correcting for the contribution from $K\pi$ S-wave beneath the K^* peak.

³ AALTONEN 11A reports $[\Gamma(B_s^0 \rightarrow J/\psi(1S) \bar{K}^*(892)^0)/\Gamma_{total}] \times [B(\bar{B} \rightarrow B^0)] / [B(\bar{B} \rightarrow B^0)] / [B(B^0 \rightarrow J/\psi(1S) K^*(892)^0)] = 0.0168 \pm 0.0024 \pm 0.0068$ which we multiply or divide by our best values $B(\bar{B} \rightarrow B^0) = (10.0 \pm 0.8) \times 10^{-2}$, $B(\bar{B} \rightarrow B^0) = (40.8 \pm 0.7) \times 10^{-2}$, $B(B^0 \rightarrow J/\psi(1S) K^*(892)^0) = (1.27 \pm 0.05) \times 10^{-3}$. Our first error is their experiment's error and our second error is the systematic error from using our best values.

$\Gamma(J/\psi(1S) \eta')/\Gamma_{total}$ Γ_{62}/Γ			
VALUE (units 10^{-4})	DOCUMENT ID	TECN	COMMENT
3.3 ± 0.4 OUR AVERAGE			
3.2 $_{-0.5}^{+0.4} \pm 0.2$	¹ AAIJ	13A LHCb	pp at 7 TeV
3.71 ± 0.61 $_{-0.60}^{+0.85}$	² LI	12 BELL	$e^+e^- \rightarrow \Upsilon(4S)$

¹ AAIJ 13A reports $[\Gamma(B_s^0 \rightarrow J/\psi(1S) \eta')/\Gamma_{total}] / [B(B^0 \rightarrow J/\psi(1S) \rho^0)] = 12.7 \pm 1.1_{-1.3}^{+0.5} \pm 1.0_{-0.9}$ which we multiply by our best value $B(B^0 \rightarrow J/\psi(1S) \rho^0) = (2.55_{-0.16}^{+0.18}) \times 10^{-5}$. Our first error is their experiment's error and our second error is the systematic error from using our best value.

² Observed for the first time with significances over 10σ . The second error are total systematic uncertainties including the error on $N(B_s^{(*)} \bar{B}_s^{(*)})$.

$\Gamma(J/\psi(1S) \eta')/\Gamma(J/\psi(1S) \eta)$ Γ_{62}/Γ_{59}			
VALUE	DOCUMENT ID	TECN	COMMENT
0.87 ± 0.06 OUR AVERAGE			
0.902 ± 0.072 ± 0.045	¹ AAIJ	15D LHCb	pp at 7, 8 TeV
0.90 ± 0.09 $_{-0.02}^{+0.06}$	² AAIJ	13A LHCb	pp at 7 TeV
0.73 ± 0.14 ± 0.02	² LI	12 BELL	$e^+e^- \rightarrow \Upsilon(4S)$

¹ Uses $J/\psi \rightarrow \mu^+ \mu^-$, $\eta' \rightarrow \rho^0 \gamma$, and $\eta' \rightarrow \eta \pi^+ \pi^-$ decays.

² Strongly correlated with measurements of $\Gamma(J/\psi(1S) \eta)/\Gamma$ and $\Gamma(J/\psi(1S) \eta')/\Gamma$ reported in the same reference.

$\Gamma(J/\psi(1S) \pi^+ \pi^-)/\Gamma(J/\psi(1S) \phi)$ Γ_{63}/Γ_{56}			
VALUE (units 10^{-2})	DOCUMENT ID	TECN	COMMENT
19.4 ± 1.5 OUR FIT Error includes scale factor of 2.2.			
19.9 ± 0.7 ± 0.2	¹ AAIJ	12A0 LHCb	pp at 7 TeV

¹ AAIJ 12A0 reports $(19.79 \pm 0.47 \pm 0.52) \times 10^{-2}$ from a measurement of $[\Gamma(B_s^0 \rightarrow J/\psi(1S) \pi^+ \pi^-)/\Gamma(B_s^0 \rightarrow J/\psi(1S) \phi)] / [B(\phi(1020) \rightarrow K^+ K^-)]$ assuming $B(\phi(1020) \rightarrow K^+ K^-) = (48.9 \pm 0.5) \times 10^{-2}$, which we rescale to our best value $B(\phi(1020) \rightarrow K^+ K^-) = (49.1 \pm 0.5) \times 10^{-2}$. Our first error is their experiment's error and our second error is the systematic error from using our best value.

$\Gamma(J/\psi(1S) f_0(500), f_0 \rightarrow \pi^+ \pi^-)/\Gamma(J/\psi(1S) f_0(980), f_0 \rightarrow \pi^+ \pi^-)$ Γ_{64}/Γ_{66}				
VALUE	CL%	DOCUMENT ID	TECN	COMMENT
<0.034	90	¹ AAIJ	14BR LHCb	pp at 7, 8 TeV

¹ Reported first of two solutions using the full Dalitz analysis.

$\Gamma(J/\psi(1S) \rho, \rho \rightarrow \pi^+ \pi^-)/\Gamma(J/\psi(1S) \pi^+ \pi^-)$ Γ_{65}/Γ_{63}				
VALUE	CL%	DOCUMENT ID	TECN	COMMENT
<0.017	90	¹ AAIJ	14BR LHCb	pp at 7, 8 TeV

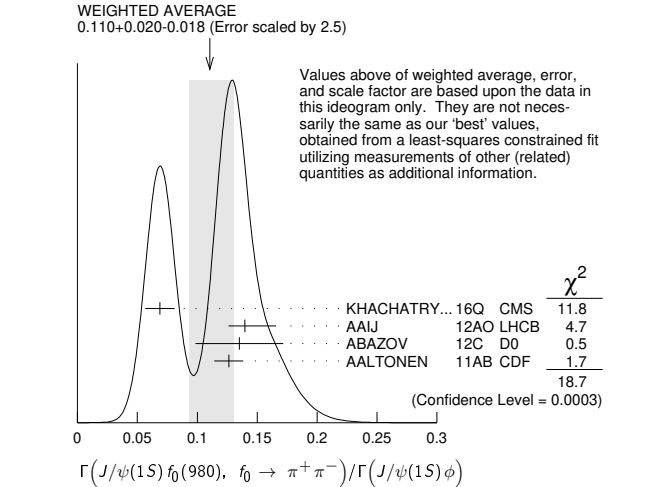
¹ Reported first of two solutions using the full Dalitz analysis.

$\Gamma(J/\psi(1S) f_0(980), f_0 \rightarrow \pi^+ \pi^-)/\Gamma_{total}$ Γ_{66}/Γ			
VALUE (units 10^{-4})	DOCUMENT ID	TECN	COMMENT
1.24 ± 0.15 OUR FIT Error includes scale factor of 2.1.			
1.16 $_{-0.19}^{+0.31} \pm 0.30$	¹ LI	11 BELL	$e^+e^- \rightarrow \Upsilon(5S)$

¹ The second error includes both the detector systematic and the uncertainty in the number of produced $\Upsilon(5S) \rightarrow B_s^{(*)} \bar{B}_s^{(*)}$ pairs.

$\Gamma(J/\psi(1S) f_0(980), f_0 \rightarrow \pi^+ \pi^-)/\Gamma(J/\psi(1S) \phi)$ Γ_{66}/Γ_{56}			
VALUE	DOCUMENT ID	TECN	COMMENT
0.119 ± 0.013 OUR FIT Error includes scale factor of 2.4.			
0.110 $_{-0.018}^{+0.020}$ OUR AVERAGE Error includes scale factor of 2.5. See the ideogram below.			

0.069 ± 0.012 ± 0.001	¹ KHACHATRYAN..16Q	CMS	pp at 7 TeV
0.140 $_{-0.013}^{+0.026} \pm 0.002$	^{2,3} AAIJ	12A0 LHCb	pp at 7 TeV
0.135 ± 0.036 ± 0.001	⁴ ABAZOV	12C D0	$p\bar{p}$ at 1.96 TeV
0.126 ± 0.012 ± 0.001	⁵ AALTONEN	11AB CDF	$p\bar{p}$ at 1.96 TeV
• • • We do not use the following data for averages, fits, limits, etc. • • •			
0.124 $_{-0.023}^{+0.026} \pm 0.001$	⁶ AAIJ	11 LHCb	Repl. by AAIJ 12A0



¹ KHACHATRYAN 16Q reports $[\Gamma(B_s^0 \rightarrow J/\psi(1S) f_0(980), f_0 \rightarrow \pi^+ \pi^-)/\Gamma(B_s^0 \rightarrow J/\psi(1S) \phi)] / [B(\phi(1020) \rightarrow K^+ K^-)] = 0.140 \pm 0.008 \pm 0.023$ which we multiply by our best value $B(\phi(1020) \rightarrow K^+ K^-) = (49.1 \pm 0.5) \times 10^{-2}$. Our first error is their experiment's error and our second error is the systematic error from using our best value.

² AAIJ 12A0 reports $(13.9 \pm 0.6_{-1.2}^{+2.5}) \times 10^{-2}$ from a measurement of $[\Gamma(B_s^0 \rightarrow J/\psi(1S) f_0(980), f_0 \rightarrow \pi^+ \pi^-)/\Gamma(B_s^0 \rightarrow J/\psi(1S) \phi)] / [B(\phi(1020) \rightarrow K^+ K^-)]$ assuming $B(\phi(1020) \rightarrow K^+ K^-) = (48.9 \pm 0.5) \times 10^{-2}$, which we rescale to our best value $B(\phi(1020) \rightarrow K^+ K^-) = (49.1 \pm 0.5) \times 10^{-2}$. Our first error is their experiment's error and our second error is the systematic error from using our best value.

³ Measured in Dalitz plot like analysis of $B_s \rightarrow J/\psi \pi^+ \pi^-$ decays.

⁴ ABAZOV 12C reports $[\Gamma(B_s^0 \rightarrow J/\psi(1S) f_0(980), f_0 \rightarrow \pi^+ \pi^-)/\Gamma(B_s^0 \rightarrow J/\psi(1S) \phi)] / [B(\phi(1020) \rightarrow K^+ K^-)] = 0.275 \pm 0.041 \pm 0.061$ which we multiply by our best value $B(\phi(1020) \rightarrow K^+ K^-) = (49.1 \pm 0.5) \times 10^{-2}$. Our first error is their experiment's error and our second error is the systematic error from using our best value.

⁵ AALTONEN 11AB reports $[\Gamma(B_s^0 \rightarrow J/\psi(1S) f_0(980), f_0 \rightarrow \pi^+ \pi^-)/\Gamma(B_s^0 \rightarrow J/\psi(1S) \phi)] / [B(\phi(1020) \rightarrow K^+ K^-)] = 0.257 \pm 0.020 \pm 0.014$ which we multiply by our best value $B(\phi(1020) \rightarrow K^+ K^-) = (49.1 \pm 0.5) \times 10^{-2}$. Our first error is their experiment's error and our second error is the systematic error from using our best value.

⁶ AAIJ 11 reports $[\Gamma(B_s^0 \rightarrow J/\psi(1S) f_0(980), f_0 \rightarrow \pi^+ \pi^-)/\Gamma(B_s^0 \rightarrow J/\psi(1S) \phi)] / [B(\phi(1020) \rightarrow K^+ K^-)] = 0.252_{-0.032-0.033}^{+0.046+0.027}$ which we multiply by our best value $B(\phi(1020) \rightarrow K^+ K^-) = (49.1 \pm 0.5) \times 10^{-2}$. Our first error is their experiment's error and our second error is the systematic error from using our best value.

$\Gamma(J/\psi(1S) f_0(980), f_0 \rightarrow \pi^+ \pi^-)/\Gamma(J/\psi(1S) \pi^+ \pi^-)$ Γ_{66}/Γ_{63}			
VALUE	DOCUMENT ID	TECN	COMMENT
0.61 ± 0.06 OUR FIT Error includes scale factor of 2.1.			
0.703 ± 0.015 $_{-0.051}^{+0.004}$	¹ AAIJ	14BR LHCb	pp at 7, 8 TeV

¹ Reported first of two solutions using the full Dalitz analysis.

Meson Particle Listings

 B_S^0 $\Gamma(J/\psi(1S) f_2(1270), f_2 \rightarrow \pi^+ \pi^-) / \Gamma(J/\psi(1S) \phi)$ $\Gamma_{67} / \Gamma_{56}$

VALUE (units 10^{-4})	DOCUMENT ID	TECN	COMMENT
$9.8^{+3.4}_{-3.6} \pm 0.1$	1,2 AAIJ	12A0 LHCB	pp at 7 TeV

¹ AAIJ 12A0 reports $(0.098 \pm 0.033^{+0.006}_{-0.015}) \times 10^{-2}$ from a measurement of $[\Gamma(B_S^0 \rightarrow J/\psi(1S) f_2(1270), f_2 \rightarrow \pi^+ \pi^-) / \Gamma(B_S^0 \rightarrow J/\psi(1S) \phi)] / [B(\phi(1020) \rightarrow K^+ K^-)]$ assuming $B(\phi(1020) \rightarrow K^+ K^-) = (48.9 \pm 0.5) \times 10^{-2}$, which we rescale to our best value $B(\phi(1020) \rightarrow K^+ K^-) = (49.1 \pm 0.5) \times 10^{-2}$. Our first error is their experiment's error and our second error is the systematic error from using our best value.

² Measured in Dalitz plot like analysis of $B_S \rightarrow J/\psi \pi^+ \pi^-$ decays for the f_2 helicity state $\lambda = 0$.

 $\Gamma(J/\psi(1S) f_2(1270)_0, f_2 \rightarrow \pi^+ \pi^-) / \Gamma(J/\psi(1S) \pi^+ \pi^-)$ $\Gamma_{68} / \Gamma_{63}$

VALUE (%)	DOCUMENT ID	TECN	COMMENT
$0.36 \pm 0.07 \pm 0.03$	1 AAIJ	14BR LHCB	pp at 7, 8 TeV

¹ Reported first of two solutions using the full Dalitz analysis.

 $\Gamma(J/\psi(1S) f_2(1270)_{||}, f_2 \rightarrow \pi^+ \pi^-) / \Gamma(J/\psi(1S) \pi^+ \pi^-)$ $\Gamma_{69} / \Gamma_{63}$

VALUE (%)	DOCUMENT ID	TECN	COMMENT
$0.52 \pm 0.15^{+0.05}_{-0.02}$	1 AAIJ	14BR LHCB	pp at 7, 8 TeV

¹ Reported first of two solutions using the full Dalitz analysis.

 $\Gamma(J/\psi(1S) f_2(1270)_{\perp}, f_2 \rightarrow \pi^+ \pi^-) / \Gamma(J/\psi(1S) \pi^+ \pi^-)$ $\Gamma_{70} / \Gamma_{63}$

VALUE (%)	DOCUMENT ID	TECN	COMMENT
$0.63 \pm 0.34^{+0.16}_{-0.08}$	1 AAIJ	14BR LHCB	pp at 7, 8 TeV

¹ Reported first of two solutions using the full Dalitz analysis.

 $\Gamma(J/\psi(1S) f_0(1370), f_0 \rightarrow \pi^+ \pi^-) / \Gamma_{total}$ Γ_{71} / Γ

VALUE (units 10^{-4})	DOCUMENT ID	TECN	COMMENT
$0.34^{+0.11+0.085}_{-0.14-0.054}$	1 LI	11 BELL	$e^+ e^- \rightarrow \Upsilon(5S)$

• • • We do not use the following data for averages, fits, limits, etc. • • •
¹ The second error includes both the detector systematic and the uncertainty in the number of produced $\Upsilon(5S) \rightarrow B_S^{(*)} \bar{B}_S^{(*)}$ pairs.

 $\Gamma(J/\psi(1S) f_0(1370), f_0 \rightarrow \pi^+ \pi^-) / \Gamma(J/\psi(1S) \phi)$ $\Gamma_{71} / \Gamma_{56}$

VALUE (units 10^{-2})	DOCUMENT ID	TECN	COMMENT
$4.21^{+0.54}_{-3.76} \pm 0.05$	1,2 AAIJ	12A0 LHCB	pp at 7 TeV

¹ AAIJ 12A0 reports $(4.19 \pm 0.53^{+0.12}_{-3.7}) \times 10^{-2}$ from a measurement of $[\Gamma(B_S^0 \rightarrow J/\psi(1S) f_0(1370), f_0 \rightarrow \pi^+ \pi^-) / \Gamma(B_S^0 \rightarrow J/\psi(1S) \phi)] / [B(\phi(1020) \rightarrow K^+ K^-)]$ assuming $B(\phi(1020) \rightarrow K^+ K^-) = (48.9 \pm 0.5) \times 10^{-2}$, which we rescale to our best value $B(\phi(1020) \rightarrow K^+ K^-) = (49.1 \pm 0.5) \times 10^{-2}$. Our first error is their experiment's error and our second error is the systematic error from using our best value.

² Measured in Dalitz plot like analysis of $B_S \rightarrow J/\psi \pi^+ \pi^-$ decays.

 $\Gamma(J/\psi(1S) f_0(1500), f_0 \rightarrow \pi^+ \pi^-) / \Gamma(J/\psi(1S) \pi^+ \pi^-)$ $\Gamma_{72} / \Gamma_{63}$

VALUE	DOCUMENT ID	TECN	COMMENT
$0.101 \pm 0.008^{+0.011}_{-0.003}$	1 AAIJ	14BR LHCB	pp at 7, 8 TeV

¹ Reported first of two solutions using the full Dalitz analysis.

 $\Gamma(J/\psi(1S) f_2'(1525)_0, f_2' \rightarrow \pi^+ \pi^-) / \Gamma(J/\psi(1S) \pi^+ \pi^-)$ $\Gamma_{73} / \Gamma_{63}$

VALUE (%)	DOCUMENT ID	TECN	COMMENT
$0.51 \pm 0.09^{+0.05}_{-0.04}$	1 AAIJ	14BR LHCB	pp at 7, 8 TeV

¹ Reported first of two solutions using the full Dalitz analysis.

 $\Gamma(J/\psi(1S) f_2'(1525)_{||}, f_2' \rightarrow \pi^+ \pi^-) / \Gamma(J/\psi(1S) \pi^+ \pi^-)$ $\Gamma_{74} / \Gamma_{63}$

VALUE (%)	DOCUMENT ID	TECN	COMMENT
$0.06^{+0.13}_{-0.04} \pm 0.01$	1 AAIJ	14BR LHCB	pp at 7, 8 TeV

¹ Reported first of two solutions using the full Dalitz analysis.

 $\Gamma(J/\psi(1S) f_2'(1525)_{\perp}, f_2' \rightarrow \pi^+ \pi^-) / \Gamma(J/\psi(1S) \pi^+ \pi^-)$ $\Gamma_{75} / \Gamma_{63}$

VALUE (%)	DOCUMENT ID	TECN	COMMENT
$0.26 \pm 0.18^{+0.06}_{-0.04}$	1 AAIJ	14BR LHCB	pp at 7, 8 TeV

¹ Reported first of two solutions using the full Dalitz analysis.

 $\Gamma(J/\psi(1S) f_0(1790), f_0 \rightarrow \pi^+ \pi^-) / \Gamma(J/\psi(1S) \pi^+ \pi^-)$ $\Gamma_{76} / \Gamma_{63}$

VALUE	DOCUMENT ID	TECN	COMMENT
$0.024 \pm 0.004^{+0.050}_{-0.002}$	1 AAIJ	14BR LHCB	pp at 7, 8 TeV

¹ Reported first of two solutions using the full Dalitz analysis.

 $\Gamma(J/\psi(1S) \pi^+ \pi^- (\text{nonresonant})) / \Gamma(J/\psi(1S) \phi)$ $\Gamma_{77} / \Gamma_{56}$

VALUE (units 10^{-2})	DOCUMENT ID	TECN	COMMENT
$1.67^{+1.01}_{-0.32} \pm 0.02$	1,2 AAIJ	12A0 LHCB	pp at 7 TeV

¹ AAIJ 12A0 reports $(1.66 \pm 0.31^{+0.96}_{-0.08}) \times 10^{-2}$ from a measurement of $[\Gamma(B_S^0 \rightarrow J/\psi(1S) \pi^+ \pi^- (\text{nonresonant})) / \Gamma(B_S^0 \rightarrow J/\psi(1S) \phi)] / [B(\phi(1020) \rightarrow K^+ K^-)]$ assuming $B(\phi(1020) \rightarrow K^+ K^-) = (48.9 \pm 0.5) \times 10^{-2}$, which we rescale to our best value $B(\phi(1020) \rightarrow K^+ K^-) = (49.1 \pm 0.5) \times 10^{-2}$. Our first error is their experiment's error and our second error is the systematic error from using our best value.

² Measured in Dalitz plot like analysis of $B_S \rightarrow J/\psi \pi^+ \pi^-$ decays.

 $\Gamma(J/\psi(1S) \bar{K}^0 \pi^+ \pi^-) / \Gamma_{total}$ Γ_{78} / Γ

VALUE	CL%	DOCUMENT ID	TECN	COMMENT
$< 4.4 \times 10^{-5}$	90	1 AAIJ	14L LHCB	pp at 7 TeV

¹ Measured with $B(B_S^0 \rightarrow J/\psi K_S^0 \pi^+ \pi^-) / B(B^0 \rightarrow J/\psi K_S^0 \pi^+ \pi^-)$ using PDG 12 values for the involved branching fractions.

 $\Gamma(J/\psi(1S) K^+ K^-) / \Gamma_{total}$ Γ_{79} / Γ

VALUE (units 10^{-4})	DOCUMENT ID	TECN	COMMENT
7.9 ± 0.7 OUR AVERAGE			
$7.70 \pm 0.08 \pm 0.72$	1 AAIJ	13AN LHCB	pp at 7 TeV
$10.1 \pm 0.9 \pm 2.1$	2 THORNE	13 BELL	$e^+ e^- \rightarrow \Upsilon(5S)$

¹ Uses $f_s/f_d = 0.256 \pm 0.020$ and $B(B^+ \rightarrow J/\psi K^+) = (10.18 \pm 0.42) \times 10^{-4}$.

² Uses $f_s = (17.2 \pm 3.0)\%$ as the fraction of $\Upsilon(5S)$ decaying to $B_S^{(*)} \bar{B}_S^{(*)}$.

 $\Gamma(J/\psi(1S) K^0 K^- \pi^+ + c.c.) / \Gamma_{total}$ Γ_{80} / Γ

VALUE (units 10^{-4})	DOCUMENT ID	TECN	COMMENT
$9.5 \pm 1.0 \pm 0.8$	1 AAIJ	14L LHCB	pp at 7 TeV

¹ AAIJ 14L reports $[\Gamma(B_S^0 \rightarrow J/\psi(1S) K^0 K^- \pi^+ + c.c.) / \Gamma_{total}] / [B(B^0 \rightarrow J/\psi(1S) K^0 \pi^+ \pi^-)] = 2.12 \pm 0.15 \pm 0.18$ which we multiply by our best value $B(B^0 \rightarrow J/\psi(1S) K^0 \pi^+ \pi^-) = (4.5 \pm 0.4) \times 10^{-4}$. Our first error is their experiment's error and our second error is the systematic error from using our best value. This is an observation of $B_S^0 \rightarrow J/\psi K_S^0 K^{\pm} \pi^{\mp}$ with more than 10 standard deviations.

 $\Gamma(J/\psi(1S) \bar{K}^0 K^+ K^-) / \Gamma_{total}$ Γ_{81} / Γ

VALUE	CL%	DOCUMENT ID	TECN	COMMENT
$< 12 \times 10^{-6}$	90	1 AAIJ	14L LHCB	pp at 7 TeV

¹ Measured with $B(B_S^0 \rightarrow J/\psi K_S^0 K^+ K^-) / B(B^0 \rightarrow J/\psi K_S^0 \pi^+ \pi^-)$ using PDG 12 values for the involved branching fractions.

 $\Gamma(J/\psi(1S) f_2'(1525)) / \Gamma_{total}$ Γ_{83} / Γ

VALUE (units 10^{-4})	DOCUMENT ID	TECN	COMMENT
$2.61 \pm 0.20^{+0.56}_{-0.50}$	1 AAIJ	13AN LHCB	pp at 7 TeV

¹ Uses $f_s/f_d = 0.256 \pm 0.020$ and $B(B^+ \rightarrow J/\psi K^+) = (10.18 \pm 0.42) \times 10^{-4}$.

 $\Gamma(J/\psi(1S) f_2'(1525)) / \Gamma(J/\psi(1S) \phi)$ $\Gamma_{83} / \Gamma_{56}$

VALUE (units 10^{-2})	DOCUMENT ID	TECN	COMMENT
21 ± 4 OUR AVERAGE			
$21.5 \pm 4.9 \pm 2.6$	1 THORNE	13 BELL	$e^+ e^- \rightarrow \Upsilon(5S)$
$21 \pm 7 \pm 1$	2,3 ABZOV	12AF D0	$p\bar{p}$ at 1.96 TeV

• • • We do not use the following data for averages, fits, limits, etc. • • •

VALUE	DOCUMENT ID	TECN	COMMENT
$27 \pm 4 \pm 1$	4 AAIJ	12S LHCB	Repl. by AAIJ 13AN

¹ Uses $B(f_2'(1525) \rightarrow K^+ K^-) = (44.4 \pm 1.1)\%$.

² ABZOV 12AF reports $[\Gamma(B_S^0 \rightarrow J/\psi(1S) f_2'(1525)) / \Gamma(B_S^0 \rightarrow J/\psi(1S) \phi)] \times B(f_2'(1525) \rightarrow K^+ K^-) / B(\phi(1020) \rightarrow K^+ K^-) = 0.19 \pm 0.05 \pm 0.04$ which we divide and multiply by our best values $B(f_2'(1525) \rightarrow K^+ K^-) = \frac{1}{2} (87.6 \pm 2.2) \times 10^{-2}$, $B(\phi(1020) \rightarrow K^+ K^-) = (49.1 \pm 0.5) \times 10^{-2}$. Our first error is their experiment's error and our second error is the systematic error from using our best values.

³ ABZOV 12AF fits the invariant masses of the $K^+ K^-$ pair in the range $1.35 < M(K^+ K^-) < 2$ GeV.

⁴ AAIJ 12S reports $[(26.4 \pm 2.7 \pm 2.4) \times 10^{-2}]$ from a measurement of $\Gamma(B_S^0 \rightarrow J/\psi(1S) f_2'(1525)) / \Gamma(B_S^0 \rightarrow J/\psi(1S) \phi) \times B(f_2'(1525) \rightarrow K^+ K^-) / B(\phi(1020) \rightarrow K^+ K^-)$ assuming $B(f_2'(1525) \rightarrow K^+ K^-) = (44.4 \pm 1.1) \times 10^{-2}$, $B(\phi(1020) \rightarrow K^+ K^-) = (48.9 \pm 0.5) \times 10^{-2}$, which we rescale to our best values $B(f_2'(1525) \rightarrow K^+ K^-) = \frac{1}{2} (87.6 \pm 2.2) \times 10^{-2}$, $B(\phi(1020) \rightarrow K^+ K^-) = (49.1 \pm 0.5) \times 10^{-2}$. Our first error is their experiment's error and our second error is the systematic error from using our best values.

 $\Gamma(J/\psi(1S) p\bar{p}) / \Gamma_{total}$ Γ_{84} / Γ

VALUE (units 10^{-6})	CL%	DOCUMENT ID	TECN	COMMENT
$3.58 \pm 0.19 \pm 0.39$		1 AAIJ	19U LHCB	pp at 7, 8, 13 TeV
< 4.8	90	2 AAIJ	13Z LHCB	Repl. by AAIJ 19U

• • • We do not use the following data for averages, fits, limits, etc. • • •

¹ Measured relative to $B_S^0 \rightarrow J/\psi \phi$ assuming $B(B_S^0 \rightarrow J/\psi \phi) = (10.5 \pm 0.13 \pm 0.64) \times 10^{-4}$ and taking into account small $K^+ K^- S$ -wave contribution.

² Uses $B(B_S^0 \rightarrow J/\psi(1S) \pi^+ \pi^-) = (1.98 \pm 0.20) \times 10^{-4}$.

$\Gamma(J/\psi(1S)\gamma)/\Gamma_{\text{total}}$ Γ_{85}/Γ

VALUE	CL%	DOCUMENT ID	TECN	COMMENT
$<7.3 \times 10^{-6}$	90	¹ AAIJ	15BB LHCB	pp at 7, 8 TeV

¹ Branching fractions of normalization modes $B_s^0 \rightarrow J/\psi\gamma X$ taken from PDG 14. Uses $f_s/f_d = 0.259 \pm 0.015$.

 $\Gamma(J/\psi(1S)\pi^+\pi^-\pi^+\pi^-)/\Gamma(J/\psi(1S)\pi^+\pi^-)$ Γ_{86}/Γ_{63}

VALUE	DOCUMENT ID	TECN	COMMENT
$0.371 \pm 0.015 \pm 0.022$	¹ AAIJ	14Y LHCB	pp at 7, 8 TeV

¹ Excludes contributions from $\psi(2S)$ and $\chi_{c1}(3872)$ decaying to $J/\psi(1S)\pi^+\pi^-$.

 $\Gamma(J/\psi(1S)f_1(1285))/\Gamma_{\text{total}}$ Γ_{87}/Γ

VALUE (units 10^{-5})	DOCUMENT ID	TECN	COMMENT
$7.2 \pm 1.3 \pm 0.4$	¹ AAIJ	14Y LHCB	pp at 7, 8 TeV

¹ AAIJ 14Y reports $(7.14 \pm 0.99 \pm 0.83 \pm 0.41) \times 10^{-5}$ from a measurement of $[\Gamma(B_s^0 \rightarrow J/\psi(1S)f_1(1285))/\Gamma_{\text{total}}] \times [B(f_1(1285) \rightarrow 2\pi^+2\pi^-) / B(f_1(1285) \rightarrow 2\pi^+2\pi^-)] = 0.11 \pm 0.007$, which we rescale to our best value $B(f_1(1285) \rightarrow 2\pi^+2\pi^-) = (10.9 \pm 0.6) \times 10^{-2}$. Our first error is their experiment's error and our second error is the systematic error from using our best value.

 $\Gamma(\psi(2S)\eta)/\Gamma(J/\psi(1S)\eta)$ Γ_{88}/Γ_{59}

VALUE	DOCUMENT ID	TECN	COMMENT
$0.83 \pm 0.14 \pm 0.12$	¹ AAIJ	13AA LHCB	pp at 7 TeV

¹ Assuming lepton universality for dimuon decay modes of J/ψ and $\psi(2S)$ mesons, the ratio $B(J/\psi \rightarrow \mu^+\mu^-)/B(\psi(2S) \rightarrow \mu^+\mu^-) = B(J/\psi \rightarrow e^+e^-)/B(\psi(2S) \rightarrow e^+e^-) = 7.69 \pm 0.19$ was used.

 $\Gamma(\psi(2S)\eta')/\Gamma(J/\psi(1S)\eta')$ Γ_{89}/Γ_{62}

VALUE (units 10^{-2})	DOCUMENT ID	TECN	COMMENT
$38.7 \pm 9.0 \pm 1.6$	¹ AAIJ	15D LHCB	pp at 7, 8 TeV

¹ Uses $J/\psi \rightarrow \mu^+\mu^-$, $\eta' \rightarrow \rho^0\gamma$, and $\eta' \rightarrow \eta\pi^+\pi^-$ decays.

 $\Gamma(\psi(2S)\pi^+\pi^-)/\Gamma(J/\psi(1S)\pi^+\pi^-)$ Γ_{90}/Γ_{63}

VALUE	DOCUMENT ID	TECN	COMMENT
$0.34 \pm 0.04 \pm 0.03$	¹ AAIJ	13AA LHCB	pp at 7 TeV

¹ Assuming lepton universality for dimuon decay modes of J/ψ and $\psi(2S)$ mesons, the ratio $B(J/\psi \rightarrow \mu^+\mu^-)/B(\psi(2S) \rightarrow \mu^+\mu^-) = B(J/\psi \rightarrow e^+e^-)/B(\psi(2S) \rightarrow e^+e^-) = 7.69 \pm 0.19$ was used.

 $\Gamma(\psi(2S)\phi)/\Gamma_{\text{total}}$ Γ_{91}/Γ

VALUE (units 10^{-4})	EVTS	DOCUMENT ID	TECN	COMMENT
• • • We do not use the following data for averages, fits, limits, etc. • • •				
seen	1	BUSKULIC	93G ALEP	$e^+e^- \rightarrow Z$

 $\Gamma(\psi(2S)\phi)/\Gamma(J/\psi(1S)\phi)$ Γ_{91}/Γ_{56}

VALUE	DOCUMENT ID	TECN	COMMENT
0.503 ± 0.034 OUR AVERAGE			
$0.500 \pm 0.034 \pm 0.011$	^{1,2} AAIJ	12L LHCB	pp at 7 TeV
$0.53 \pm 0.10 \pm 0.09$	ABAZOV	09Y D0	$p\bar{p}$ at 1.96 TeV
$0.52 \pm 0.13 \pm 0.07$	ABULENCIA	06N CDF	$p\bar{p}$ at 1.96 TeV

¹ AAIJ 12L reports $0.489 \pm 0.026 \pm 0.021 \pm 0.012$ from a measurement of $[\Gamma(B_s^0 \rightarrow \psi(2S)\phi)/\Gamma(B_s^0 \rightarrow J/\psi(1S)\phi)] \times [B(J/\psi(1S) \rightarrow e^+e^-)] / [B(\psi(2S) \rightarrow e^+e^-)]$ assuming $B(J/\psi(1S) \rightarrow e^+e^-) = (5.94 \pm 0.06) \times 10^{-2}$, $B(\psi(2S) \rightarrow e^+e^-) = (7.72 \pm 0.17) \times 10^{-3}$, which we rescale to our best values $B(J/\psi(1S) \rightarrow e^+e^-) = (5.971 \pm 0.032) \times 10^{-2}$, $B(\psi(2S) \rightarrow e^+e^-) = (7.93 \pm 0.17) \times 10^{-3}$. Our first error is their experiment's error and our second error is the systematic error from using our best values.

² Assumes $B(J/\psi \rightarrow \mu^+\mu^-) / B(\psi(2S) \rightarrow \mu^+\mu^-) = B(J/\psi \rightarrow e^+e^-) / B(\psi(2S) \rightarrow e^+e^-) = 7.69 \pm 0.19$.

 $\Gamma(\psi(2S)K^-\pi^+)/\Gamma_{\text{total}}$ Γ_{92}/Γ

VALUE (units 10^{-5})	DOCUMENT ID	TECN	COMMENT
$3.12 \pm 0.30 \pm 0.21$	¹ AAIJ	15U LHCB	pp at 7, 8 TeV

¹ AAIJ 15U reports $[\Gamma(B_s^0 \rightarrow \psi(2S)K^-\pi^+)/\Gamma_{\text{total}}] / [B(B^0 \rightarrow \psi(2S)K^+\pi^-)] = (5.38 \pm 0.36 \pm 0.22 \pm 0.31) \times 10^{-2}$ which we multiply by our best value $B(B^0 \rightarrow \psi(2S)K^+\pi^-) = (5.8 \pm 0.4) \times 10^{-4}$. Our first error is their experiment's error and our second error is the systematic error from using our best value.

 $\Gamma(\psi(2S)\bar{K}^*(892)^0)/\Gamma_{\text{total}}$ Γ_{93}/Γ

VALUE (units 10^{-5})	DOCUMENT ID	TECN	COMMENT
$3.3 \pm 0.5 \pm 0.3$	¹ AAIJ	15U LHCB	pp at 7, 8 TeV

¹ AAIJ 15U reports $[\Gamma(B_s^0 \rightarrow \psi(2S)\bar{K}^*(892)^0)/\Gamma_{\text{total}}] / [B(B^0 \rightarrow \psi(2S)K^*(892)^0)] = (5.58 \pm 0.57 \pm 0.40 \pm 0.32) \times 10^{-2}$ which we multiply by our best value $B(B^0 \rightarrow \psi(2S)K^*(892)^0) = (5.9 \pm 0.4) \times 10^{-4}$. Our first error is their experiment's error and our second error is the systematic error from using our best value.

 $\Gamma(\chi_{c1}\phi)/\Gamma(J/\psi(1S)\phi)$ Γ_{94}/Γ_{56}

VALUE (units 10^{-2})	DOCUMENT ID	TECN	COMMENT
$18.9 \pm 1.8 \pm 1.5$	¹ AAIJ	13AC LHCB	pp at 7 TeV

¹ Uses $B(\chi_{c1} \rightarrow J/\psi\gamma) = (34.4 \pm 1.5)\%$.

 $\Gamma(\chi_{c2}K^+K^-)/\Gamma(\chi_{c1}K^+K^-)$ Γ_{96}/Γ_{95}

VALUE (units 10^{-2})	DOCUMENT ID	TECN	COMMENT
$17.1 \pm 3.1 \pm 1.0$	¹ AAIJ	18AC LHCB	pp at 7, 8, 13 TeV

¹ Measures the ratio for ± 15 MeV window around ϕ mass.

 $\Gamma(\chi_{c1}(3872)\phi)/\Gamma(\psi(2S)\phi)$ Γ_{97}/Γ_{91}

VALUE	DOCUMENT ID	TECN	COMMENT
0.21 ± 0.07 OUR AVERAGE			
$0.22 \pm 0.02 \pm 0.07$	¹ AAIJ	21C LHCB	pp at 7, 8, 13 TeV
$0.20 \pm 0.03 \pm 0.07$	² SIRUNYAN	20BB CMS	pp at 13 TeV

¹ AAIJ 21C reports $[\Gamma(B_s^0 \rightarrow \chi_{c1}(3872)\phi)/\Gamma(B_s^0 \rightarrow \psi(2S)\phi)] \times [B(\chi_{c1}(3872) \rightarrow \pi^+\pi^-J/\psi(1S))] / [B(\psi(2S) \rightarrow J/\psi(1S)\pi^+\pi^-)] = (2.42 \pm 0.23 \pm 0.07) \times 10^{-2}$ which we multiply or divide by our best values $B(\chi_{c1}(3872) \rightarrow \pi^+\pi^-J/\psi(1S)) = (3.8 \pm 1.2) \times 10^{-2}$, $B(\psi(2S) \rightarrow J/\psi(1S)\pi^+\pi^-) = (34.68 \pm 0.30) \times 10^{-2}$. Our first error is their experiment's error and our second error is the systematic error from using our best values.

² SIRUNYAN 20BB reports $[\Gamma(B_s^0 \rightarrow \chi_{c1}(3872)\phi)/\Gamma(B_s^0 \rightarrow \psi(2S)\phi)] \times [B(\chi_{c1}(3872) \rightarrow \pi^+\pi^-J/\psi(1S))] / [B(\psi(2S) \rightarrow J/\psi(1S)\pi^+\pi^-)] = (2.21 \pm 0.29 \pm 0.17) \times 10^{-2}$ which we multiply or divide by our best values $B(\chi_{c1}(3872) \rightarrow \pi^+\pi^-J/\psi(1S)) = (3.8 \pm 1.2) \times 10^{-2}$, $B(\psi(2S) \rightarrow J/\psi(1S)\pi^+\pi^-) = (34.68 \pm 0.30) \times 10^{-2}$. Our first error is their experiment's error and our second error is the systematic error from using our best values.

 $\Gamma(J/\psi K^*(892)^0\bar{K}^*(892)^0)/\Gamma(\psi(2S)\phi)$ Γ_{82}/Γ_{91}

VALUE	DOCUMENT ID	TECN	COMMENT
$0.209 \pm 0.006 \pm 0.003$	¹ AAIJ	21C LHCB	pp at 7, 8, 13 TeV

¹ AAIJ 21C reports $\Gamma(B_s^0 \rightarrow J/\psi K^*(892)^0\bar{K}^*(892)^0)/\Gamma(B_s^0 \rightarrow \psi(2S)\phi) B^2(K^{*0} \rightarrow K^+\pi^-)/B(\psi(2S) \rightarrow J/\psi\pi^+\pi^-)/B(\phi \rightarrow K^+K^-) = 1.22 \pm 0.03 \pm 0.04$ which we adjust with PDG 20 values of $B(K^{*0} \rightarrow K^+\pi^-) = (99.902 \pm 0.009) \times 10^{-2}$, $B(\psi(2S) \rightarrow J/\psi\pi^+\pi^-) = (34.68 \pm 0.30) \times 10^{-2}$, and $B(\phi \rightarrow K^+K^-) = (49.2 \pm 0.5) \times 10^{-2}$. The first uncertainty is the total experiment's one and the second is due to the adjustment branching fractions.

 $\Gamma(\chi_{c1}(3872)(K^+K^-)_{\text{non-}\phi})/\Gamma(\chi_{c1}(3872)\phi)$ Γ_{98}/Γ_{97}

VALUE	DOCUMENT ID	TECN	COMMENT
$0.77 \pm 0.17 \pm 0.01$	¹ AAIJ	21C LHCB	pp at 7, 8, 13 TeV

¹ AAIJ 21C reports $[\Gamma(B_s^0 \rightarrow \chi_{c1}(3872)(K^+K^-)_{\text{non-}\phi})/\Gamma(B_s^0 \rightarrow \chi_{c1}(3872)\phi)] / [B(\phi(1020) \rightarrow K^+K^-)] = 1.57 \pm 0.32 \pm 0.12$ which we multiply by our best value $B(\phi(1020) \rightarrow K^+K^-) = (49.1 \pm 0.5) \times 10^{-2}$. Our first error is their experiment's error and our second error is the systematic error from using our best value.

 $\Gamma(\pi^+\pi^-)/\Gamma_{\text{total}}$ Γ_{99}/Γ

VALUE (units 10^{-7})	CL%	DOCUMENT ID	TECN	COMMENT
7.0 ± 1.0 OUR AVERAGE				
$7.3 \pm 0.9 \pm 0.7$		¹ AAIJ	17G LHCB	pp at 7 and 8 TeV
$6.4 \pm 1.8 \pm 0.6$		² AALTONEN	12L CDF	$p\bar{p}$ at 1.96 TeV
• • • We do not use the following data for averages, fits, limits, etc. • • •				
$10.4 \pm 2.4 \pm 1.0$		³ AAIJ	12AR LHCB	Repl. by AAIJ 17G
< 120	90	⁴ PENG	10 BELL	$e^+e^- \rightarrow \Upsilon(5S)$
< 12	90	⁵ AALTONEN	09C CDF	Repl. by AALTONEN 12L
< 17	90	⁶ ABULENCIA,A	06D CDF	Repl. by AALTONEN 09c
< 2320	90	⁷ ABE	00C SLD	$e^+e^- \rightarrow Z$
< 1700	90	⁸ BUSKULIC	96V ALEP	$e^+e^- \rightarrow Z$

¹ AAIJ 17G reports $[\Gamma(B_s^0 \rightarrow \pi^+\pi^-)/\Gamma_{\text{total}}] / [B(B^0 \rightarrow K^+\pi^-)] \times [\Gamma(\bar{B} \rightarrow B_s^0)/\Gamma(\bar{B} \rightarrow B^0)] = (9.15 \pm 0.71 \pm 0.83) \times 10^{-3}$ which we multiply or divide by our best values $B(B^0 \rightarrow K^+\pi^-) = (1.96 \pm 0.05) \times 10^{-5}$, $\Gamma(\bar{B} \rightarrow B_s^0)/\Gamma(\bar{B} \rightarrow B^0) = 0.246 \pm 0.023$. Our first error is their experiment's error and our second error is the systematic error from using our best values.

² AALTONEN 12L reports $[\Gamma(B_s^0 \rightarrow \pi^+\pi^-)/\Gamma_{\text{total}}] / [B(B^0 \rightarrow K^+\pi^-)] \times [\Gamma(\bar{B} \rightarrow B_s^0)/\Gamma(\bar{B} \rightarrow B^0)] = 0.008 \pm 0.002 \pm 0.001$ which we multiply or divide by our best values $B(B^0 \rightarrow K^+\pi^-) = (1.96 \pm 0.05) \times 10^{-5}$, $\Gamma(\bar{B} \rightarrow B_s^0)/\Gamma(\bar{B} \rightarrow B^0) = 0.246 \pm 0.023$. Our first error is their experiment's error and our second error is the systematic error from using our best values.

³ AAIJ 12AR reports $[\Gamma(B_s^0 \rightarrow \pi^+\pi^-)/\Gamma_{\text{total}}] / [B(B^0 \rightarrow \pi^+\pi^-)] \times [\Gamma(\bar{B} \rightarrow B_s^0)/\Gamma(\bar{B} \rightarrow B^0)] = 0.050 \pm 0.011 \pm 0.009 \pm 0.004$ which we multiply or divide by our best values $B(B^0 \rightarrow \pi^+\pi^-) = (5.12 \pm 0.19) \times 10^{-6}$, $\Gamma(\bar{B} \rightarrow B_s^0)/\Gamma(\bar{B} \rightarrow B^0) = 0.246 \pm 0.023$. Our first error is their experiment's error and our second error is the systematic error from using our best values.

⁴ Uses $\Upsilon(10860) \rightarrow B_s^* \bar{B}_s^*$ and assumes $B(\Upsilon(10860) \rightarrow B_s^* \bar{B}_s^*) = (19.3 \pm 2.9)\%$ and $\Gamma(\Upsilon(10860) \rightarrow B_s^* \bar{B}_s^*) / \Gamma(\Upsilon(10860) \rightarrow B_s^* \bar{B}_s^*) = (90.1 \pm 3.8) \pm 4.0\%$.

⁵ Obtains this result from $(f_s/f_d) \cdot B(B_s \rightarrow \pi^+\pi^-)/B(B^0 \rightarrow K^+\pi^-) = 0.007 \pm 0.004 \pm 0.005$, assuming $f_s/f_d = 0.276 \pm 0.034$ and $B(B^0 \rightarrow K^+\pi^-) = (19.4 \pm 0.6) \times 10^{-6}$.

⁶ ABULENCIA,A 06D obtains this from $B(B_s \rightarrow \pi^+\pi^-)/B(B_s \rightarrow K^+K^-) < 0.05$ at 90% CL, assuming $B(B_s \rightarrow K^+K^-) = (33 \pm 6 \pm 7) \times 10^{-6}$.

⁷ ABE 00c assumes $B(Z \rightarrow b\bar{b}) = (21.7 \pm 0.1)\%$ and the B fractions $f_{B^0} = f_{B^+} = (39.7 \pm 1.8) \pm 2.2\%$ and $f_{B_s} = (10.5 \pm 1.8) \pm 2.2\%$.

⁸ BUSKULIC 96v assumes PDG 96 production fractions for B^0, B^+, B_s, b baryons.

Meson Particle Listings

 B_S^0

$\Gamma(\pi^0\pi^0)/\Gamma_{\text{total}}$					Γ_{100}/Γ
VALUE	CL%	DOCUMENT ID	TECN	COMMENT	
$<2.1 \times 10^{-4}$	90	¹ ACCIARRI 95H L3		$e^+e^- \rightarrow Z$	
¹ ACCIARRI 95H assumes $f_{B^0} = 39.5 \pm 4.0$ and $f_{B_S} = 12.0 \pm 3.0\%$.					

$\Gamma(\eta\pi^0)/\Gamma_{\text{total}}$					Γ_{101}/Γ
VALUE	CL%	DOCUMENT ID	TECN	COMMENT	
$<1.0 \times 10^{-3}$	90	¹ ACCIARRI 95H L3		$e^+e^- \rightarrow Z$	
¹ ACCIARRI 95H assumes $f_{B^0} = 39.5 \pm 4.0$ and $f_{B_S} = 12.0 \pm 3.0\%$.					

$\Gamma(\eta\eta)/\Gamma_{\text{total}}$					Γ_{102}/Γ
VALUE	CL%	DOCUMENT ID	TECN	COMMENT	
$<1.43 \times 10^{-4}$	90	BHUYAN 22 BELL		$e^+e^- \rightarrow \Upsilon(5S)$	
• • • We do not use the following data for averages, fits, limits, etc. • • •					
$<1.5 \times 10^{-3}$	90	¹ ACCIARRI 95H L3		$e^+e^- \rightarrow Z$	
¹ ACCIARRI 95H assumes $f_{B^0} = 39.5 \pm 4.0$ and $f_{B_S} = 12.0 \pm 3.0\%$.					

$\Gamma(\rho^0\rho^0)/\Gamma_{\text{total}}$					Γ_{103}/Γ
VALUE	CL%	DOCUMENT ID	TECN	COMMENT	
$<3.20 \times 10^{-4}$	90	¹ ABE 00c SLD		$e^+e^- \rightarrow Z$	
¹ ABE 00c assumes $B(Z \rightarrow b\bar{b}) = (21.7 \pm 0.1)\%$ and the B fractions $f_{B^0} = f_{B^+} = (39.7 \pm 1.8, 2.2)\%$ and $f_{B_S} = (10.5 \pm 1.8, 2.2)\%$.					

$\Gamma(\eta'\eta)/\Gamma_{\text{total}}$					Γ_{104}/Γ
VALUE	CL%	DOCUMENT ID	TECN	COMMENT	
$<6.5 \times 10^{-5}$	90	¹ NISAR 21 BELL		$e^+e^- \rightarrow \Upsilon(5S)$	
¹ Uses $\Upsilon(10860) \rightarrow B_S^* \bar{B}_S^*$ decays and assumes $B(\Upsilon(10860) \rightarrow B_S^{(*)} \bar{B}_S^{(*)}) = (20.1 \pm 3.1)\%$.					

$\Gamma(\eta'\eta')/\Gamma_{\text{total}}$					Γ_{105}/Γ
VALUE (units 10^{-5})		DOCUMENT ID	TECN	COMMENT	
$3.3 \pm 0.7 \pm 0.1$		¹ AAIJ 15o LHCb		pp at 7, 8 TeV	
¹ AAIJ 15o reports $[\Gamma(B_S^0 \rightarrow \eta'\eta')/\Gamma_{\text{total}}] / [B(B^+ \rightarrow \eta'K^+)] = 0.47 \pm 0.09 \pm 0.04$ which we multiply by our best value $B(B^+ \rightarrow \eta'K^+) = (7.04 \pm 0.25) \times 10^{-5}$. Our first error is their experiment's error and our second error is the systematic error from using our best value.					

$\Gamma(\eta'\phi)/\Gamma_{\text{total}}$					Γ_{106}/Γ
VALUE	CL%	DOCUMENT ID	TECN	COMMENT	
$<0.82 \times 10^{-6}$	90	¹ AAIJ 17Ba LHCb		pp at 7, 8 TeV	
¹ Corresponds to the 95% CL upper limit 1.01×10^{-6} . Uses the normalization mode $B^+ \rightarrow \eta'K^+$ with branching fraction $(70.6 \pm 2.5) \times 10^{-6}$ and the ratio of hadronisation fractions $f_s/f_d = 0.259 \pm 0.015$, which is assumed equal to f_s/f_u .					

$\Gamma(\eta'X_{S3})/\Gamma_{\text{total}}$					Γ_{54}/Γ
VALUE (units 10^{-3})	CL%	DOCUMENT ID	TECN	COMMENT	
<1.4	90	¹ DUBEY 21 BELL		$e^+e^- \rightarrow \Upsilon(4S)$	
¹ DUBEY 21 result is for $m(X_{S3}) < 2.85 \text{ GeV}/c^2$.					

$\Gamma(\phi\eta_0(980), \eta_0(980) \rightarrow \pi^+\pi^-)/\Gamma_{\text{total}}$					Γ_{107}/Γ
VALUE (units 10^{-6})		DOCUMENT ID	TECN	COMMENT	
$1.12 \pm 0.16 \pm 0.14$		¹ AAIJ 17A LHCb		pp at 7, 8 TeV	
¹ Signal is observed with 8 standard deviations significance.					

$\Gamma(\phi f_2(1270), f_2(1270) \rightarrow \pi^+\pi^-)/\Gamma_{\text{total}}$					Γ_{108}/Γ
VALUE (units 10^{-6})		DOCUMENT ID	TECN	COMMENT	
$0.61 \pm 0.13 \pm 0.13$ 0.08		¹ AAIJ 17A LHCb		pp at 7, 8 TeV	
¹ Signal is observed with 5 standard deviations significance.					

$\Gamma(\phi\rho^0)/\Gamma_{\text{total}}$					Γ_{109}/Γ
VALUE (units 10^{-7})	CL%	DOCUMENT ID	TECN	COMMENT	
$2.7 \pm 0.7 \pm 0.3$		¹ AAIJ 17A LHCb		pp at 7, 8 TeV	
• • • We do not use the following data for averages, fits, limits, etc. • • •					
<6170	90	² ABE 00c SLD		$e^+e^- \rightarrow Z$	
¹ Signal evidence is 4 standard deviations.					
² ABE 00c assumes $B(Z \rightarrow b\bar{b}) = (21.7 \pm 0.1)\%$ and the B fractions $f_{B^0} = f_{B^+} = (39.7 \pm 1.8, 2.2)\%$ and $f_{B_S} = (10.5 \pm 1.8, 2.2)\%$.					

$\Gamma(\phi\pi^+\pi^-)/\Gamma_{\text{total}}$					Γ_{110}/Γ
VALUE (units 10^{-6})		DOCUMENT ID	TECN	COMMENT	
$3.48 \pm 0.23 \pm 0.39$		¹ AAIJ 17A LHCb		pp at 7, 8 TeV	
¹ Inclusive decays in mass range $400 < m(\pi^+\pi^-) < 1600 \text{ MeV}/c^2$.					

$\Gamma(\phi\phi)/\Gamma_{\text{total}}$					Γ_{111}/Γ
VALUE (units 10^{-6})	CL%	DOCUMENT ID	TECN	COMMENT	
$18.5 \pm 1.4 \pm 1.0$		¹ AAIJ 15As LHCb		pp at 7, 8 TeV	
• • • We do not use the following data for averages, fits, limits, etc. • • •					
14 ± 6		² ACOSTA 05J CDF		Repl. by AALTONEN 11AN	
<1183	90	³ ABE 00c SLD		$e^+e^- \rightarrow Z$	

¹ AAIJ 15As reports $[\Gamma(B_S^0 \rightarrow \phi\phi)/\Gamma_{\text{total}}] / [B(B^0 \rightarrow K^*(892)^0\phi)] = 1.84 \pm 0.05 \pm 0.13$ which we multiply by our best value $B(B^0 \rightarrow K^*(892)^0\phi) = (1.00 \pm 0.05) \times 10^{-5}$. Our first error is their experiment's error and our second error is the systematic error from using our best value.

² Uses $B(B^0 \rightarrow J/\psi\phi) = (1.38 \pm 0.49) \times 10^{-3}$ and production cross-section ratio of $\sigma(B_S)/\sigma(B^0) = 0.26 \pm 0.04$.

³ ABE 00c assumes $B(Z \rightarrow b\bar{b}) = (21.7 \pm 0.1)\%$ and the B fractions $f_{B^0} = f_{B^+} = (39.7 \pm 1.8, 2.2)\%$ and $f_{B_S} = (10.5 \pm 1.8, 2.2)\%$.

$\Gamma(\phi\phi)/\Gamma(J/\psi(1S)\phi)$					Γ_{111}/Γ_{56}
VALUE (units 10^{-2})		DOCUMENT ID	TECN	COMMENT	
1.77 ± 0.14		¹ OUR FIT			
$1.78 \pm 0.14 \pm 0.20$		AALTONEN 11AN CDF		$p\bar{p}$ at 1.96 TeV	

$\Gamma(\phi\phi\phi)/\Gamma(\phi\phi)$					$\Gamma_{112}/\Gamma_{111}$
VALUE		DOCUMENT ID	TECN	COMMENT	
$0.117 \pm 0.030 \pm 0.015$		AAIJ 17Bb LHCb		pp at 7, 8 TeV	

$\Gamma(\pi^+K^-)/\Gamma_{\text{total}}$					Γ_{113}/Γ
VALUE (units 10^{-6})	CL%	DOCUMENT ID	TECN	COMMENT	
5.8 ± 0.7		¹ OUR AVERAGE			
$5.9 \pm 0.7 \pm 0.6$		¹ AAIJ 12AR LHCb		pp at 7 TeV	
$5.7 \pm 1.0 \pm 0.5$		² AALTONEN 09c CDF		$p\bar{p}$ at 1.96 TeV	

• • • We do not use the following data for averages, fits, limits, etc. • • •

<26	90	³ PENG 10 BELL		$e^+e^- \rightarrow \Upsilon(5S)$	
<5.6	90	⁴ ABULENCIA, A 06D CDF		Repl. by AALTONEN 09c	
<261	90	⁵ ABE 00c SLD		$e^+e^- \rightarrow Z$	
<210	90	⁶ BUSKULIC 96V ALEP		$e^+e^- \rightarrow Z$	
<260	90	⁷ AKERS 94L OPAL		$e^+e^- \rightarrow Z$	

¹ AAIJ 12AR reports $[\Gamma(B_S^0 \rightarrow \pi^+K^-)/\Gamma_{\text{total}}] / [B(B^0 \rightarrow K^+\pi^-)] \times [\Gamma(\bar{B} \rightarrow B_S^0) / \Gamma(\bar{B} \rightarrow B^0)] = 0.074 \pm 0.006 \pm 0.006$ which we multiply or divide by our best values $B(B^0 \rightarrow K^+\pi^-) = (1.96 \pm 0.05) \times 10^{-5}$, $\Gamma(\bar{B} \rightarrow B_S^0) / \Gamma(\bar{B} \rightarrow B^0) = 0.246 \pm 0.023$. Our first error is their experiment's error and our second error is the systematic error from using our best values.

² AALTONEN 09c reports $[\Gamma(B_S^0 \rightarrow \pi^+K^-)/\Gamma_{\text{total}}] / [B(B^0 \rightarrow K^+\pi^-)] \times [B(\bar{B} \rightarrow B_S^0) / [B(\bar{B} \rightarrow B^0)]] = 0.071 \pm 0.010 \pm 0.007$ which we multiply or divide by our best values $B(B^0 \rightarrow K^+\pi^-) = (1.96 \pm 0.05) \times 10^{-5}$, $B(\bar{B} \rightarrow B_S^0) = (10.0 \pm 0.8) \times 10^{-2}$, $B(\bar{B} \rightarrow B^0) = (40.8 \pm 0.7) \times 10^{-2}$. Our first error is their experiment's error and our second error is the systematic error from using our best values.

³ Uses $\Upsilon(10860) \rightarrow B_S^* \bar{B}_S^*$ and assumes $B(\Upsilon(10860) \rightarrow B_S^{(*)} \bar{B}_S^{(*)}) = (19.3 \pm 2.9)\%$ and $\Gamma(\Upsilon(10860) \rightarrow B_S^* \bar{B}_S^*) / \Gamma(\Upsilon(10860) \rightarrow B_S^{(*)} \bar{B}_S^{(*)}) = (90.1 \pm 3.8, 4.0)\%$.

⁴ ABULENCIA, A 06D obtains this from $(f_s/f_d) (B(B_S \rightarrow \pi^+K^-) / B(B^0 \rightarrow K^+\pi^-)) < 0.08$ at 90% CL, assuming $f_s/f_d = 0.260 \pm 0.039$ and $B(B^0 \rightarrow K^+\pi^-) = (18.9 \pm 0.7) \times 10^{-6}$.

⁵ ABE 00c assumes $B(Z \rightarrow b\bar{b}) = (21.7 \pm 0.1)\%$ and the B fractions $f_{B^0} = f_{B^+} = (39.7 \pm 1.8, 2.2)\%$ and $f_{B_S} = (10.5 \pm 1.8, 2.2)\%$.

⁶ BUSKULIC 96V assumes PDG 96 production fractions for B^0, B^+, B_S, b baryons.

⁷ Assumes $B(Z \rightarrow b\bar{b}) = 0.217$ and $B_D^0(B_S^0)$ fraction 39.5% (12%).

$\Gamma(K^+K^-)/\Gamma_{\text{total}}$					Γ_{114}/Γ
VALUE (units 10^{-6})	CL%	DOCUMENT ID	TECN	COMMENT	
26.6 ± 2.2		¹ OUR AVERAGE			
$25.2 \pm 1.7 \pm 2.4$		¹ AAIJ 12AR LHCb		pp at 7 TeV	
$27.6 \pm 2.3 \pm 2.7$		² AALTONEN 11N CDF		$p\bar{p}$ at 1.96 TeV	
38 ± 9		³ PENG 10 BELL		$e^+e^- \rightarrow \Upsilon(5S)$	

• • • We do not use the following data for averages, fits, limits, etc. • • •

<310	90	DRUTSKOY 07A BELL		$e^+e^- \rightarrow \Upsilon(5S)$	
$33 \pm 6 \pm 7$		⁴ ABULENCIA, A 06D CDF		Repl. by AALTONEN 11N	
<283	90	⁵ ABE 00c SLD		$e^+e^- \rightarrow Z$	
<59	90	⁶ BUSKULIC 96V ALEP		$e^+e^- \rightarrow Z$	
<140	90	⁷ AKERS 94L OPAL		$e^+e^- \rightarrow Z$	

¹ AAIJ 12AR reports $[\Gamma(B_S^0 \rightarrow K^+K^-)/\Gamma_{\text{total}}] / [B(B^0 \rightarrow K^+\pi^-)] \times [\Gamma(\bar{B} \rightarrow B_S^0) / \Gamma(\bar{B} \rightarrow B^0)] = 0.316 \pm 0.009 \pm 0.019$ which we multiply or divide by our best values $B(B^0 \rightarrow K^+\pi^-) = (1.96 \pm 0.05) \times 10^{-5}$, $\Gamma(\bar{B} \rightarrow B_S^0) / \Gamma(\bar{B} \rightarrow B^0) = 0.246 \pm 0.023$. Our first error is their experiment's error and our second error is the systematic error from using our best values.

² AALTONEN 11N reports $(f_s/f_d) (B(B_S^0 \rightarrow K^+K^-) / B(B^0 \rightarrow K^+\pi^-)) = 0.347 \pm 0.020 \pm 0.021$. We multiply this result by our best value of $B(B^0 \rightarrow K^+\pi^-) = (1.96 \pm 0.05) \times 10^{-5}$ and divide by our best value of f_s/f_d , where $1/2 f_s/f_d = 0.1230 \pm 0.0115$. Our first quoted uncertainty is the combined experiment's uncertainty and our second is the systematic uncertainty from using our best values.

³ Uses $\Upsilon(10860) \rightarrow B_S^* \bar{B}_S^*$ and assumes $B(\Upsilon(10860) \rightarrow B_S^{(*)} \bar{B}_S^{(*)}) = (19.3 \pm 2.9)\%$ and $\Gamma(\Upsilon(10860) \rightarrow B_S^* \bar{B}_S^*) / \Gamma(\Upsilon(10860) \rightarrow B_S^{(*)} \bar{B}_S^{(*)}) = (90.1^{+3.8}_{-4.0})\%$.

⁴ ABULENCIA,A 06d obtains this from $(f_s/f_d) (B(B_S \rightarrow K^+ K^-) / B(B^0 \rightarrow K^+ \pi^-)) = 0.46 \pm 0.08 \pm 0.07$, assuming $f_s/f_d = 0.260 \pm 0.039$ and $B(B^0 \rightarrow K^+ \pi^-) = (18.9 \pm 0.7) \times 10^{-6}$.

⁵ ABE 00c assumes $B(Z \rightarrow b \bar{b}) = (21.7 \pm 0.1)\%$ and the B fractions $f_{B^0} = f_{B^+} = (39.7^{+1.8}_{-2.2})\%$ and $f_{B_S} = (10.5^{+1.8}_{-2.2})\%$.

⁶ BUSKULIC 96v assumes PDG 96 production fractions for B^0, B^+, B_S, b baryons.

⁷ Assumes $B(Z \rightarrow b \bar{b}) = 0.217$ and $B_d^0(B_S^0)$ fraction 39.5% (12%).

$\Gamma(K^0 \bar{K}^0) / \Gamma_{total}$ Γ_{115} / Γ

VALUE (units 10^{-5})	DOCUMENT ID	TECN	COMMENT
1.76 ± 0.31 OUR AVERAGE			
1.68 ± 0.34 ± 0.16 / 0.15	1 AAIJ	20F LHCb	pp at 7, 8, 13 TeV
1.96 ± 0.58 ± 0.10 ± 0.20 / 0.51	2 PAL	16 BELL	e ⁺ e ⁻ → $\Upsilon(5S)$

• • • We do not use the following data for averages, fits, limits, etc. • • •

<6.6	90	3 PENG	10 BELL Repl. by PAL 16
------	----	--------	-------------------------

¹ AAIJ 20F reports $[\Gamma(B_S^0 \rightarrow K^0 \bar{K}^0) / \Gamma_{total}] / [B(B^0 \rightarrow K^0 \phi)] = 2.3 \pm 0.4 \pm 0.2 \pm 0.1$ which we multiply by our best value $B(B^0 \rightarrow K^0 \phi) = (7.3 \pm 0.7) \times 10^{-6}$. Our first error is their experiment's error and our second error is the systematic error from using our best value.

² Observed in $B_S^0 \rightarrow K_S^0 K_S^0$ with significance of 5.1 σ . The last uncertainty is due to the uncertainty of the total number of $B_S^0 \bar{B}_S^0$ pairs.

³ Uses $\Upsilon(10860) \rightarrow B_S^* \bar{B}_S^*$ and assumes $B(\Upsilon(10860) \rightarrow B_S^{(*)} \bar{B}_S^{(*)}) = (19.3 \pm 2.9)\%$ and $\Gamma(\Upsilon(10860) \rightarrow B_S^* \bar{B}_S^*) / \Gamma(\Upsilon(10860) \rightarrow B_S^{(*)} \bar{B}_S^{(*)}) = (90.1^{+3.8}_{-4.0})\%$.

$\Gamma(K^0 \pi^+ \pi^-) / \Gamma_{total}$ Γ_{116} / Γ

VALUE (units 10^{-6})	DOCUMENT ID	TECN	COMMENT
9.5 ± 2.1 ± 0.3	1,2 AAIJ	17BP LHCb	pp at 7, 8 TeV

• • • We do not use the following data for averages, fits, limits, etc. • • •

14 ± 4 ± 1	3 AAIJ	13BP LHCb	Repl. by AAIJ 17BP
------------	--------	-----------	--------------------

¹ AAIJ 17BP reports $[\Gamma(B_S^0 \rightarrow K^0 \pi^+ \pi^-) / \Gamma_{total}] / [B(B^0 \rightarrow K^0 \pi^+ \pi^-)] = 0.191 \pm 0.027 \pm 0.033$ which we multiply by our best value $B(B^0 \rightarrow K^0 \pi^+ \pi^-) = (4.97 \pm 0.18) \times 10^{-5}$. Our first error is their experiment's error and our second error is the systematic error from using our best value.

² Used $f_s/f_d = 0.259 \pm 0.015$.

³ AAIJ 13BP reports $[\Gamma(B_S^0 \rightarrow K^0 \pi^+ \pi^-) / \Gamma_{total}] / [B(B^0 \rightarrow K^0 \pi^+ \pi^-)] = 0.29 \pm 0.06 \pm 0.04$ which we multiply by our best value $B(B^0 \rightarrow K^0 \pi^+ \pi^-) = (4.97 \pm 0.18) \times 10^{-5}$. Our first error is their experiment's error and our second error is the systematic error from using our best value.

$\Gamma(K^0 K^\pm \pi^\mp) / \Gamma_{total}$ Γ_{117} / Γ

VALUE (units 10^{-5})	DOCUMENT ID	TECN	COMMENT
8.4 ± 0.8 ± 0.3	1,2 AAIJ	17BP LHCb	pp at 7, 8 TeV

• • • We do not use the following data for averages, fits, limits, etc. • • •

7.4 ± 0.9 ± 0.3	3 AAIJ	13BP LHCb	Repl. by AAIJ 17BP
-----------------	--------	-----------	--------------------

¹ AAIJ 17BP reports $[\Gamma(B_S^0 \rightarrow K^0 K^\pm \pi^\mp) / \Gamma_{total}] / [B(B^0 \rightarrow K^0 \pi^+ \pi^-)] = 1.70 \pm 0.07 \pm 0.15$ which we multiply by our best value $B(B^0 \rightarrow K^0 \pi^+ \pi^-) = (4.97 \pm 0.18) \times 10^{-5}$. Our first error is their experiment's error and our second error is the systematic error from using our best value.

² Used $f_s/f_d = 0.259 \pm 0.015$.

³ AAIJ 13BP reports $[\Gamma(B_S^0 \rightarrow K^0 K^\pm \pi^\mp) / \Gamma_{total}] / [B(B^0 \rightarrow K^0 \pi^+ \pi^-)] = 1.48 \pm 0.12 \pm 0.14$ which we multiply by our best value $B(B^0 \rightarrow K^0 \pi^+ \pi^-) = (4.97 \pm 0.18) \times 10^{-5}$. Our first error is their experiment's error and our second error is the systematic error from using our best value.

$\Gamma(K^*(892)^- \pi^+) / \Gamma_{total}$ Γ_{118} / Γ

VALUE (units 10^{-6})	DOCUMENT ID	TECN	COMMENT
2.9 ± 1.0 ± 0.2	1,2 AAIJ	14BMLHCb	pp at 7 TeV

¹ AAIJ 14BM reports $[\Gamma(B^0 \rightarrow K^*(892)^- \pi^+) / \Gamma_{total}] / [B(B^0 \rightarrow K^*(892)^+ \pi^-)] = 0.39 \pm 0.13 \pm 0.05$ which we multiply by our best value $B(B^0 \rightarrow K^*(892)^+ \pi^-) = (7.5 \pm 0.4) \times 10^{-6}$. Our first error is their experiment's error and our second error is the systematic error from using our best value.

² Uses $f_s/f_d = 0.259 \pm 0.015$.

$\Gamma(K^*(892)^\pm K^\mp) / \Gamma_{total}$ Γ_{119} / Γ

VALUE (units 10^{-5})	DOCUMENT ID	TECN	COMMENT
1.86 ± 0.12 ± 0.45	1,2 AAIJ	19K LHCb	pp at 7, 8 TeV

• • • We do not use the following data for averages, fits, limits, etc. • • •

1.12 ± 0.21 ± 0.07 / 0.06	3,4 AAIJ	14BMLHCb	Repl. by AAIJ 19K
---------------------------	----------	----------	-------------------

¹ AAIJ 19K reports $(18.6 \pm 1.2 \pm 0.8 \pm 4.0 \pm 2.0) \times 10^{-6}$ as the measured value. We have combined in quadrature all systematic uncertainties into a single one.

² Measured in Dalitz plot analysis of $B_S^0 \rightarrow K_S^0 K^\pm \pi^\mp$ decays.

³ AAIJ 14BM reports $[\Gamma(B_S^0 \rightarrow K^*(892)^\pm K^\mp) / \Gamma_{total}] / [B(B^0 \rightarrow K^*(892)^+ \pi^-)] = 1.49 \pm 0.22 \pm 0.18$ which we multiply by our best value $B(B^0 \rightarrow K^*(892)^+ \pi^-) = (7.5 \pm 0.4) \times 10^{-6}$. Our first error is their experiment's error and our second error is the systematic error from using our best value.

⁴ Uses $f_s/f_d = 0.259 \pm 0.015$.

$\Gamma(K_S^0(1430)^\pm K^\mp) / \Gamma_{total}$ Γ_{120} / Γ

VALUE (units 10^{-5})	DOCUMENT ID	TECN	COMMENT
3.13 ± 0.23 ± 2.53	1,2 AAIJ	19K LHCb	pp at 7, 8 TeV

¹ AAIJ 19K reports $(31.3 \pm 2.3 \pm 0.7 \pm 25.1 \pm 3.3) \times 10^{-6}$ as the measured value. We have combined in quadrature all systematic uncertainties into a single one.

² Measured in Dalitz plot analysis of $B_S^0 \rightarrow K_S^0 K^\pm \pi^\mp$ decays.

$\Gamma(K_S^0(1430)^\pm K^\mp) / \Gamma_{total}$ Γ_{121} / Γ

VALUE (units 10^{-5})	DOCUMENT ID	TECN	COMMENT
1.03 ± 0.25 ± 1.64	1,2 AAIJ	19K LHCb	pp at 7, 8 TeV

¹ AAIJ 19K reports $(10.3 \pm 2.5 \pm 1.1 \pm 16.3 \pm 1.1) \times 10^{-6}$ as the measured value. We have combined in quadrature all systematic uncertainties into a single one.

² Measured in Dalitz plot analysis of $B_S^0 \rightarrow K_S^0 K^\pm \pi^\mp$ decays.

$\Gamma(K^*(892)^0 K^0 + c.c.) / \Gamma_{total}$ Γ_{122} / Γ

VALUE (units 10^{-5})	DOCUMENT ID	TECN	COMMENT
1.98 ± 0.28 ± 0.50	1,2 AAIJ	19K LHCb	pp at 7, 8 TeV

¹ AAIJ 19K reports $(19.8 \pm 2.8 \pm 1.2 \pm 4.4 \pm 2.1) \times 10^{-6}$ as the measured value. We have combined in quadrature all systematic uncertainties into a single one.

² Measured in Dalitz plot analysis of $B_S^0 \rightarrow K_S^0 K^\pm \pi^\mp$ decays.

$\Gamma(K_S^0(1430) K^0 + c.c.) / \Gamma_{total}$ Γ_{123} / Γ

VALUE (units 10^{-5})	DOCUMENT ID	TECN	COMMENT
3.30 ± 0.25 ± 0.98	1,2 AAIJ	19K LHCb	pp at 7, 8 TeV

¹ AAIJ 19K reports $(33.0 \pm 2.5 \pm 0.9 \pm 9.1 \pm 3.5) \times 10^{-6}$ as the measured value. We have combined in quadrature all systematic uncertainties into a single one.

² Measured in Dalitz plot analysis of $B_S^0 \rightarrow K_S^0 K^\pm \pi^\mp$ decays.

$\Gamma(K_S^0(1430)^0 K^0 + c.c.) / \Gamma_{total}$ Γ_{124} / Γ

VALUE (units 10^{-5})	DOCUMENT ID	TECN	COMMENT
1.68 ± 0.45 ± 2.13	1,2 AAIJ	19K LHCb	pp at 7, 8 TeV

¹ AAIJ 19K reports $(16.8 \pm 4.5 \pm 1.7 \pm 21.2 \pm 1.8) \times 10^{-6}$ as the measured value. We have combined in quadrature all systematic uncertainties into a single one.

² Measured in Dalitz plot analysis of $B_S^0 \rightarrow K_S^0 K^\pm \pi^\mp$ decays.

$\Gamma(K_S^0 K^*(892)^0 + c.c.) / \Gamma_{total}$ Γ_{125} / Γ

VALUE (units 10^{-6})	DOCUMENT ID	TECN	COMMENT
16.4 ± 3.4 ± 2.3	1 AAIJ	16 LHCb	pp at 7 TeV

¹ Measured relative to $B^0 \rightarrow K_S^0 \pi^+ \pi^-$ using the value of $B(B^0 \rightarrow K^0 \pi^+ \pi^-) = (4.96 \pm 0.2) \times 10^{-5}$.

$\Gamma(K^0 K^+ K^-) / \Gamma_{total}$ Γ_{126} / Γ

VALUE (units 10^{-7})	CL%	DOCUMENT ID	TECN	COMMENT
12.9 ± 6.5 ± 0.5		1,2,3 AAIJ	17BP LHCb	pp at 7, 8 TeV

• • • We do not use the following data for averages, fits, limits, etc. • • •

<34 90 4 AAIJ 13BP LHCb Repl. by AAIJ 17BP

¹ AAIJ 17BP reports $[\Gamma(B_S^0 \rightarrow K^0 K^+ K^-) / \Gamma_{total}] / [B(B^0 \rightarrow K^0 \pi^+ \pi^-)] = 0.026 \pm 0.011 \pm 0.007$ which we multiply by our best value $B(B^0 \rightarrow K^0 \pi^+ \pi^-) = (4.97 \pm 0.18) \times 10^{-5}$. Our first error is their experiment's error and our second error is the systematic error from using our best value.

² AAIJ 17BP also set the limit range $4-25 \times 10^{-7}$ at 90% CL using the world average value $B(B^0 \rightarrow K^0 \pi^+ \pi^-) = (4.96 \pm 0.20) \times 10^{-5}$.

³ Used $f_s/f_d = 0.259 \pm 0.015$.

⁴ AAIJ 13BP reports $[\Gamma(B_S^0 \rightarrow K^0 K^+ K^-) / \Gamma_{total}] / [B(B^0 \rightarrow K^0 \pi^+ \pi^-)] < 0.068$ which we multiply by our best value $B(B^0 \rightarrow K^0 \pi^+ \pi^-) = 4.97 \times 10^{-5}$.

$\Gamma(\bar{K}^*(892)^0 \rho^0) / \Gamma_{total}$ Γ_{127} / Γ

VALUE	CL%	DOCUMENT ID	TECN	COMMENT
<7.67 × 10⁻⁴	90	1 ABE	00c SLD	e ⁺ e ⁻ → Z

¹ ABE 00c assumes $B(Z \rightarrow b \bar{b}) = (21.7 \pm 0.1)\%$ and the B fractions $f_{B^0} = f_{B^+} = (39.7^{+1.8}_{-2.2})\%$ and $f_{B_S} = (10.5^{+1.8}_{-2.2})\%$.

$\Gamma(\bar{K}^*(892)^0 K^*(892)^0) / \Gamma_{total}$ Γ_{128} / Γ

VALUE (units 10^{-5})	CL%	DOCUMENT ID	TECN	COMMENT
1.11 ± 0.26 ± 0.06		1 AAIJ	15AF LHCb	pp at 7 TeV

• • • We do not use the following data for averages, fits, limits, etc. • • •

2.81 ± 0.46 ± 0.56 2 AAIJ 12F LHCb Repl. by AAIJ 15AF

<168.1 90 3 ABE 00c SLD e⁺e⁻ → Z

¹ AAIJ 15AF reports $[\Gamma(B_S^0 \rightarrow \bar{K}^*(892)^0 K^*(892)^0) / \Gamma_{total}] / [B(B^0 \rightarrow K^*(892)^0 \phi)] = 1.11 \pm 0.22 \pm 0.12 \pm 0.06$ which we multiply by our best value $B(B^0 \rightarrow K^*(892)^0 \phi) = (1.00 \pm 0.05) \times 10^{-5}$. Our first error is their experiment's error and our second error is the systematic error from using our best value.

² Uses $B^0 \rightarrow J/\psi K^{*0}$ for normalization and assumes $B(B^0 \rightarrow J/\psi K^{*0}) B(J/\psi \rightarrow \mu^+ \mu^-) B(K^{*0} \rightarrow K^+ \pi^-) = (1.33 \pm 0.06) \times 10^{-3}$ and $f_s/f_d = 0.253 \pm 0.031$. The second quoted error is total uncertainty including the error of 0.34 on f_s/f_d .

³ ABE 00c assumes $B(Z \rightarrow b \bar{b}) = (21.7 \pm 0.1)\%$ and the B fractions $f_{B^0} = f_{B^+} = (39.7^{+1.8}_{-2.2})\%$ and $f_{B_S} = (10.5^{+1.8}_{-2.2})\%$.

Meson Particle Listings

 B_s^0 $\Gamma(\phi K^*(892)^0)/\Gamma_{\text{total}}$ Γ_{132}/Γ

VALUE (units 10^{-6})	CL%	DOCUMENT ID	TECN	COMMENT
1.14 ± 0.29 ± 0.06		¹ AAIJ	13BW LHCB	pp at 7 TeV
• • • We do not use the following data for averages, fits, limits, etc. • • •				
<1013	90	² ABE	00c SLD	$e^+e^- \rightarrow Z$
¹ AAIJ 13BW reports $[\Gamma(B_s^0 \rightarrow \phi K^*(892)^0)/\Gamma_{\text{total}}] / [B(B^0 \rightarrow K^*(892)^0 \phi)] = 0.113 \pm 0.024 \pm 0.016$ which we multiply by our best value $B(B^0 \rightarrow K^*(892)^0 \phi) = (1.00 \pm 0.05) \times 10^{-5}$. Our first error is their experiment's error and our second error is the systematic error from using our best value.				
² ABE 00c assumes $B(Z \rightarrow b\bar{b}) = (21.7 \pm 0.1)\%$ and the B fractions $f_{B^0} = f_{B^+} = (39.7_{-2.2}^{+1.8})\%$ and $f_{B_s} = (10.5_{-2.2}^{+1.8})\%$.				

 $\Gamma(\rho\bar{\rho})/\Gamma_{\text{total}}$ Γ_{133}/Γ

VALUE (units 10^{-8})	CL%	DOCUMENT ID	TECN	COMMENT
< 1.5	90	¹ AAIJ	17BJ LHCB	pp at 7 and 8 TeV
• • • We do not use the following data for averages, fits, limits, etc. • • •				
$2.84_{-1.68}^{+2.03+0.85}$		² AAIJ	13BQ LHCB	Repl. by AAIJ 17BJ
<5900	90	³ BUSKULIC	96v ALEP	$e^+e^- \rightarrow Z$
¹ Uses normalization mode $B(B^0 \rightarrow K^+\pi^-) = (19.6 \pm 0.5) \times 10^{-6}$ and B production ratio $f(\bar{b} \rightarrow B_s^0)/f(\bar{b} \rightarrow B_d^0) = 0.259 \pm 0.015$.				
² Uses normalization mode $B(B^0 \rightarrow K^+\pi^-) = (19.55 \pm 0.54) \times 10^{-6}$ and B production ratio $f(\bar{b} \rightarrow B_s^0)/f(\bar{b} \rightarrow B_d^0) = 0.256 \pm 0.020$.				
³ BUSKULIC 96v assumes PDG 96 production fractions for B^0, B^+, B_s, b baryons.				

 $\Gamma(\rho\bar{\rho}K^+K^-)/\Gamma_{\text{total}}$ Γ_{134}/Γ

VALUE (units 10^{-6})	DOCUMENT ID	TECN	COMMENT
4.5 ± 0.4 ± 0.2	^{1,2} AAIJ	17BD LHCB	pp at 7, 8 TeV
¹ AAIJ 17BD reports $[\Gamma(B_s^0 \rightarrow \rho\bar{\rho}K^+K^-)/\Gamma_{\text{total}}] / [B(B^0 \rightarrow J/\psi(1S) K^*(892)^0)] / [B(J/\psi(1S) \rightarrow \rho\bar{\rho})] / [B(K^*(892) \rightarrow (K\pi)^\pm)] = 1.67 \pm 0.12 \pm 0.11$ which we multiply by our best values $B(B^0 \rightarrow J/\psi(1S) K^*(892)^0) = (1.27 \pm 0.05) \times 10^{-3}$, $B(J/\psi(1S) \rightarrow \rho\bar{\rho}) = (2.120 \pm 0.029) \times 10^{-3}$, $B(K^*(892) \rightarrow (K\pi)^\pm) = (99.902 \pm 0.009) \times 10^{-2}$. Our first error is their experiment's error and our second error is the systematic error from using our best values. Reported value assumes $f_s/f_d = 0.259 \pm 0.015$.			
² The branching ratio is given for $m_{\rho\bar{\rho}} < 2.85$ GeV.			

 $\Gamma(\rho\bar{\rho}K^+\pi^-)/\Gamma_{\text{total}}$ Γ_{135}/Γ

VALUE (units 10^{-7})	DOCUMENT ID	TECN	COMMENT
13.9 ± 2.5 ± 0.5	^{1,2} AAIJ	17BD LHCB	pp at 7, 8 TeV
¹ AAIJ 17BD reports $[\Gamma(B_s^0 \rightarrow \rho\bar{\rho}K^+\pi^-)/\Gamma_{\text{total}}] / [B(B^0 \rightarrow J/\psi(1S) K^*(892)^0)] / [B(J/\psi(1S) \rightarrow \rho\bar{\rho})] / [B(K^*(892) \rightarrow (K\pi)^\pm)] = 0.52 \pm 0.08 \pm 0.05$ which we multiply by our best values $B(B^0 \rightarrow J/\psi(1S) K^*(892)^0) = (1.27 \pm 0.05) \times 10^{-3}$, $B(J/\psi(1S) \rightarrow \rho\bar{\rho}) = (2.120 \pm 0.029) \times 10^{-3}$, $B(K^*(892) \rightarrow (K\pi)^\pm) = (99.902 \pm 0.009) \times 10^{-2}$. Our first error is their experiment's error and our second error is the systematic error from using our best values. Reported value assumes $f_s/f_d = 0.259 \pm 0.015$.			
² The branching ratio is given for $m_{\rho\bar{\rho}} < 2.85$ GeV.			

 $\Gamma(\rho\bar{\rho}K^+\pi^-)/\Gamma(\rho\bar{\rho}K^+K^-)$ $\Gamma_{135}/\Gamma_{134}$

VALUE	DOCUMENT ID	TECN	COMMENT
0.31 ± 0.05 ± 0.02	^{1,2} AAIJ	17BD LHCB	pp at 7, 8 TeV
¹ Reports $B(B_s^0 \rightarrow \rho\bar{\rho}K^+\pi^-) / B(B^0 \rightarrow \rho\bar{\rho}K^+K^-) = 0.22 \pm 0.04 \pm 0.02 \pm 0.01$, where the third error is due to f_s/f_d .			
² The ratio is given for $m_{\rho\bar{\rho}} < 2.85$ GeV and assuming $f_s/f_d = 0.259 \pm 0.015$.			

 $\Gamma(\rho\bar{\rho}\pi^+\pi^-)/\Gamma_{\text{total}}$ Γ_{136}/Γ

VALUE (units 10^{-7})	DOCUMENT ID	TECN	COMMENT
4.3 ± 2.0 ± 0.2	^{1,2} AAIJ	17BD LHCB	pp at 7, 8 TeV
¹ AAIJ 17BD reports $[\Gamma(B_s^0 \rightarrow \rho\bar{\rho}\pi^+\pi^-)/\Gamma_{\text{total}}] / [B(B^0 \rightarrow J/\psi(1S) K^*(892)^0)] / [B(J/\psi(1S) \rightarrow \rho\bar{\rho})] / [B(K^*(892) \rightarrow (K\pi)^\pm)] = 0.16 \pm 0.07 \pm 0.02$ which we multiply by our best values $B(B^0 \rightarrow J/\psi(1S) K^*(892)^0) = (1.27 \pm 0.05) \times 10^{-3}$, $B(J/\psi(1S) \rightarrow \rho\bar{\rho}) = (2.120 \pm 0.029) \times 10^{-3}$, $B(K^*(892) \rightarrow (K\pi)^\pm) = (99.902 \pm 0.009) \times 10^{-2}$. Our first error is their experiment's error and our second error is the systematic error from using our best values. Reported value assumes $f_s/f_d = 0.259 \pm 0.015$.			
² The branching ratio is given for $m_{\rho\bar{\rho}} < 2.85$ GeV.			

 $\Gamma(\rho\bar{\rho}K^+ + \text{c.c.})/\Gamma_{\text{total}}$ Γ_{137}/Γ

VALUE (units 10^{-6})	DOCUMENT ID	TECN	COMMENT
5.5 ± 0.6 ± 0.8	^{1,2} AAIJ	17AL LHCB	pp at 7, 8 TeV
¹ AAIJ 17AL reports $(5.46 \pm 0.61 \pm 0.82) \times 10^{-6}$ from a measurement of $[\Gamma(B_s^0 \rightarrow \rho\bar{\rho}K^+ + \text{c.c.})/\Gamma_{\text{total}}] / [B(B^0 \rightarrow \rho\bar{\rho}\pi^-)]$ assuming $B(B^0 \rightarrow \rho\bar{\rho}\pi^-) = (3.14 \pm 0.29) \times 10^{-6}$.			
² AAIJ 17AL value represents the sum of $B_s^0 \rightarrow \rho\bar{\rho}K^+$ and $B_s^0 \rightarrow \bar{\rho}K^+$ and assumes the fraction $f_s/f_d = 0.259 \pm 0.015$.			

 $\Gamma(\Lambda_c^- \Lambda\pi^+)/\Gamma_{\text{total}}$ Γ_{138}/Γ

VALUE (units 10^{-4})	DOCUMENT ID	TECN	COMMENT
3.6 ± 1.1 ± 1.2	¹ SOLOVIEVA	13 BELL	$e^+e^- \rightarrow \Upsilon(4S)$
¹ The second error is the total systematic uncertainty including the Λ_c absolute branching fractions and the normalization number of B_s events.			

 $\Gamma(\Lambda_c^- \Lambda_c^+)/\Gamma_{\text{total}}$ Γ_{139}/Γ

VALUE	CL%	DOCUMENT ID	TECN	COMMENT
< 8.0 × 10⁻⁵	95	¹ AAIJ	14AA LHCB	pp at 7 TeV
¹ Uses $B(\bar{B}^0 \rightarrow D^+ D_s^-) = (7.2 \pm 0.8) \times 10^{-3}$.				

 $\Gamma(\gamma\gamma)/\Gamma_{\text{total}}$ Γ_{140}/Γ

VALUE (units 10^{-6})	CL%	DOCUMENT ID	TECN	COMMENT
< 3.1	90	¹ DUTTA	15 BELL	$e^+e^- \rightarrow \Upsilon(5S)$
• • • We do not use the following data for averages, fits, limits, etc. • • •				
< 8.7	90	² WICHT	08A BELL	Repl. by DUTTA 15
< 53	90	² DRUTSKOY	07A BELL	Repl. by WICHT 08A
<148	90	³ ACCIARRI	95I L3	$e^+e^- \rightarrow Z$
¹ Assumes the fraction of $B_s^{(*)}\bar{B}_s^{(*)}$ in $b\bar{b}$ events is $f_s = (17.2 \pm 3.0)\%$.				
² Assumes $\Upsilon(5S) \rightarrow B_s^* \bar{B}_s^* = (19.5_{-3.0}^{+3.3})\%$.				
³ ACCIARRI 95I assumes $f_{B^0} = 39.5 \pm 4.0$ and $f_{B_s} = (12.0 \pm 3.0)\%$.				

 $\Gamma(\phi\gamma)/\Gamma_{\text{total}}$ Γ_{141}/Γ

VALUE (units 10^{-6})	CL%	DOCUMENT ID	TECN	COMMENT
34 ± 4 OUR AVERAGE				
$36 \pm 5 \pm 7$		¹ DUTTA	15 BELL	$e^+e^- \rightarrow \Upsilon(5S)$
$33.8 \pm 3.4 \pm 2.0$		² AAIJ	13 LHCB	pp at 7 TeV
• • • We do not use the following data for averages, fits, limits, etc. • • •				
39 ± 5		³ AAIJ	12AE LHCB	Repl. by AAIJ 13
57_{-15}^{+18}		⁴ WICHT	08A BELL	Repl. by DUTTA 15
<390	90	² DRUTSKOY	07A BELL	$e^+e^- \rightarrow \Upsilon(5S)$
<120	90	² ACOSTA	02G CDF	$p\bar{p}$ at 1.8 TeV
<700	90	⁵ ADAM	96D DLPH	$e^+e^- \rightarrow Z$

¹ Assumes the fraction of $B_s^{(*)}\bar{B}_s^{(*)}$ in $b\bar{b}$ events is $f_s = (17.2 \pm 3.0)\%$. The systematic uncertainty from f_s is 0.6×10^{-5} .				
² AAIJ 13 reports $[\Gamma(B_s^0 \rightarrow \phi\gamma)/\Gamma_{\text{total}}] / [B(B^0 \rightarrow K^*(892)^0 \gamma)] = 0.81 \pm 0.04 \pm 0.07$ which we multiply by our best value $B(B^0 \rightarrow K^*(892)^0 \gamma) = (4.18 \pm 0.25) \times 10^{-5}$. Our first error is their experiment's error and our second error is the systematic error from using our best value.				
³ Measures $B(B^0 \rightarrow K^* \gamma) / B(B_s \rightarrow \phi\gamma) = 1.12 \pm 0.08(\text{stat})_{-0.04}^{+0.06}(\text{sys})_{-0.08}^{+0.09}(f_s/f_d)$ and uses current world-average value of $B(B^0 \rightarrow K^* \gamma) = (4.33 \pm 0.15) \times 10^{-5}$.				
⁴ Assumes $\Upsilon(5S) \rightarrow B_s^* \bar{B}_s^* = (19.5_{-2.3}^{+3.0})\%$.				
⁵ ADAM 96D assumes $f_{B^0} = f_{B^-} = 0.39$ and $f_{B_s} = 0.12$.				

 $\Gamma(\mu^+\mu^-)/\Gamma_{\text{total}}$ Γ_{142}/Γ

VALUE (units 10^{-3})	CL%	DOCUMENT ID	TECN	COMMENT
3.01 ± 0.35 OUR AVERAGE				
$3.09_{-0.43}^{+0.46+0.15}$		AAIJ	22 LHCB	pp at 7, 8, 13 TeV
$2.9 \pm 0.6 \pm 0.4$		¹ SIRUNYAN	20AG CMS	pp at 7, 8, 13 TeV
$2.8_{-0.7}^{+0.8}$		² AABOUD	19L ATLS	pp at 7, 8, 13 TeV
13_{-7}^{+9}		³ AALTONEN	13F CDF	$p\bar{p}$ at 1.96 TeV
• • • We do not use the following data for averages, fits, limits, etc. • • •				
$3.0 \pm 0.6_{-0.2}^{+0.3}$		AAIJ	17AI LHCB	Repl. by AAIJ 22
$0.9_{-0.8}^{+1.1}$		⁴ AABOUD	16L ATLS	Repl. by AABOUD 19L
$2.8_{-0.6}^{+0.7}$		⁵ KHACHATRY...15BE	LHC	pp at 7, 8 TeV
$3.2_{-1.2}^{+1.4+0.5}$		⁶ AAIJ	13B LHCB	Repl. by AAIJ 13BA
$2.9_{-1.0}^{+1.1+0.3}$		⁷ AAIJ	13BA LHCB	Repl. by KHACHA- TRYAN 15BE
<12	90	⁸ ABAZOV	13C D0	$p\bar{p}$ at 1.96 TeV
$3.0_{-0.9}^{+1.0}$		⁹ CHATRCHYAN13AW	CMS	Repl. by SIRUNYAN 20AG
<19	90	¹⁰ AAD	12AE ATLS	pp at 7 TeV
<12	90	¹¹ AAIJ	12A LHCB	Repl. by AAIJ 12W
< 3.8	90	¹² AAIJ	12W LHCB	Repl. by AAIJ 13B
< 6.4	90	¹³ CHATRCHYAN12A	CMS	pp at 7 TeV
<43	90	¹⁴ AAIJ	11B LHCB	Repl. by AAIJ 12A
<35	90	¹⁵ AALTONEN	11AG CDF	$p\bar{p}$ at 1.96 TeV
<16	90	¹⁶ CHATRCHYAN11T	CMS	Repl. by CHATRCHYAN 12A
<42	90	¹⁷ ABAZOV	10S D0	$p\bar{p}$ at 1.96 TeV

¹ Uses normalization mode $B(B^+ \rightarrow J/\psi K^+) = (1.01 \pm 0.03) \times 10^{-3}$ and B production ratio $f(b \rightarrow B_s^0)/f(b \rightarrow B^+) = 0.252 \pm 0.012 \pm 0.015$.				
² Uses normalization mode $B(B^+ \rightarrow J/\psi K^+) = (1.010 \pm 0.029) \times 10^{-3}$ and B production ratio $f(b \rightarrow B_s^0)/f(b \rightarrow B^+) = 0.256 \pm 0.013$.				
³ Uses normalization mode $B(B^+ \rightarrow J/\psi K^+) = (10.22 \pm 0.35) \times 10^{-4}$ and B production ratio $f(\bar{b} \rightarrow B_s^0)/f(\bar{b} \rightarrow B_d^0) = 0.28 \pm 0.04$.				
⁴ This value corresponds to an upper limit of $< 3.0 \times 10^{-9}$ at 95% C.L. It uses $f_s/f_d = 0.24 \pm 0.02$.				
⁵ Determined from the joint fit to CMS and LHCb data. Uncertainty includes both statistical and systematic component.				

- ⁶ Uses B production ratio $f(\bar{B} \rightarrow B_s^0)/f(\bar{B} \rightarrow B_d^0) = 0.256 \pm 0.020$ and two normalization modes: $B(B^+ \rightarrow J/\psi K^+ \rightarrow \mu^+ \mu^- K^+) = (6.01 \pm 0.21) \times 10^{-5}$ and $B(B^0 \rightarrow K^+ \pi^-) = (1.94 \pm 0.06) \times 10^{-5}$.
- ⁷ Uses B production ratio $f(\bar{B} \rightarrow B_s^0)/f(\bar{B} \rightarrow B_d^0) = 0.259 \pm 0.015$ and normalization modes $B^+ \rightarrow J/\psi K^+ \rightarrow \mu^+ \mu^- K^+$ and $B^0 \rightarrow K^+ \pi^-$.
- ⁸ Uses normalization mode $B(B^+ \rightarrow J/\psi K^+ \rightarrow \mu^+ \mu^- K^+) = (6.01 \pm 0.21) \times 10^{-5}$ and B production ratio $f(\bar{B} \rightarrow B_s^0)/f(\bar{B} \rightarrow B_d^0) = 0.263 \pm 0.017$.
- ⁹ Uses B production ratio $f(\bar{B} \rightarrow B_s^0)/f(\bar{B} \rightarrow B_d^0) = 0.256 \pm 0.020$ and $B(B^+ \rightarrow J/\psi K^+ \rightarrow \mu^+ \mu^- K^+) = (6.0 \pm 0.2) \times 10^{-5}$ for normalization.
- ¹⁰ Uses B production ratio $f(\bar{B} \rightarrow B^+)/f(\bar{B} \rightarrow B_s^0) = 3.75 \pm 0.29$ and $B(B^+ \rightarrow J/\psi K^+ \rightarrow \mu^+ \mu^- K^+) = (6.0 \pm 0.2) \times 10^{-5}$.
- ¹¹ Uses B production ratio $f(\bar{B} \rightarrow B_s^0)/f(\bar{B} \rightarrow B_d^0) = 0.267^{+0.021}_{-0.020}$ and three normalization modes $B(B^+ \rightarrow J/\psi K^+ \rightarrow \mu^+ \mu^- K^+) = (6.01 \pm 0.21) \times 10^{-5}$, $B(B^0 \rightarrow K^+ \pi^-) = (1.94 \pm 0.06) \times 10^{-5}$, and $B(B_s^0 \rightarrow J/\psi \phi \rightarrow \mu^+ \mu^- K^+ K^-) = (3.4 \pm 0.9) \times 10^{-5}$.
- ¹² Uses B production ratio $f(\bar{B} \rightarrow B_s^0)/f(\bar{B} \rightarrow B_d^0) = 0.267^{+0.021}_{-0.020}$ and three normalization modes of $B^+ \rightarrow J/\psi K^+$, $B^0 \rightarrow K^+ \pi^-$, and $B_s^0 \rightarrow J/\psi \phi$.
- ¹³ Uses $f_s/f_u = 0.267 \pm 0.021$ and $B(B^+ \rightarrow J/\psi K^+ \rightarrow \mu^+ \mu^- K^+) = (6.0 \pm 0.2) \times 10^{-5}$.
- ¹⁴ Uses B production ratio $f(\bar{B} \rightarrow B^+)/f(\bar{B} \rightarrow B_s^0) = 3.71 \pm 0.47$ and three normalization modes.
- ¹⁵ Uses B production ratio $f(\bar{B} \rightarrow B^+)/f(\bar{B} \rightarrow B_s^0) = 3.55 \pm 0.47$ and $B(B^+ \rightarrow J/\psi K^+ \rightarrow \mu^+ \mu^- K^+) = (6.01 \pm 0.21) \times 10^{-5}$.
- ¹⁶ Uses B production ratio $f(\bar{B} \rightarrow B^+)/f(\bar{B} \rightarrow B_s^0) = 3.55 \pm 0.42$ and $B(B^+ \rightarrow J/\psi K^+ \rightarrow \mu^+ \mu^- K^+) = (6.0 \pm 0.2) \times 10^{-5}$.
- ¹⁷ Uses B production ratio $f(\bar{B} \rightarrow B^+)/f(\bar{B} \rightarrow B_s^0) = 3.86 \pm 0.59$, and the number of $B^+ \rightarrow J/\psi K^+$ decays.

$\Gamma(e^+ e^-)/\Gamma_{\text{total}}$ Γ_{143}/Γ
 Test for $\Delta B = 1$ weak neutral current.

VALUE	CL%	DOCUMENT ID	TECN	COMMENT
$<9.4 \times 10^{-9}$	90	¹ AAIJ	20W LHCb	pp at 7, 8, 13 TeV
• • • We do not use the following data for averages, fits, limits, etc. • • •				
$<2.8 \times 10^{-7}$	90	AALTONEN	09P CDF	$p\bar{p}$ at 1.96 TeV
$<5.4 \times 10^{-5}$	90	² ACCIARRI	97B L3	$e^+ e^- \rightarrow Z$

¹ Assumes no contribution from $B^0 \rightarrow e^+ e^-$ decays.
² ACCIARRI 97B assume PDG 96 production fractions for B^+ , B^0 , B_s , and Λ_b .

$\Gamma(\tau^+ \tau^-)/\Gamma_{\text{total}}$ Γ_{144}/Γ

VALUE	CL%	DOCUMENT ID	TECN	COMMENT
$<6.8 \times 10^{-3}$	95	¹ AAIJ	17Aj LHCb	pp at 7, 8 TeV

¹ Assuming no contribution from $B^0 \rightarrow \tau^+ \tau^-$.

$\Gamma(\mu^+ \mu^- \mu^+ \mu^-)/\Gamma_{\text{total}}$ Γ_{145}/Γ

VALUE	CL%	DOCUMENT ID	TECN	COMMENT
$<2.5 \times 10^{-9}$	95	AAIJ	17N LHCb	pp at 7, 8 TeV
• • • We do not use the following data for averages, fits, limits, etc. • • •				
$<1.2 \times 10^{-8}$	90	¹ AAIJ	13AW LHCb	Repl. by AAIJ 17N

¹ Also reports a limit of $<1.6 \times 10^{-8}$ at 95% CL.

$\Gamma(S, P, S \rightarrow \mu^+ \mu^-, P \rightarrow \mu^+ \mu^-)/\Gamma_{\text{total}}$ Γ_{146}/Γ
 Here S and P are the hypothetical scalar and pseudoscalar particles with masses of 2.5 GeV/ c^2 and 214.3 MeV/ c^2 , respectively.

VALUE	CL%	DOCUMENT ID	TECN	COMMENT
$<2.2 \times 10^{-9}$	95	AAIJ	17N LHCb	pp at 7, 8 TeV
• • • We do not use the following data for averages, fits, limits, etc. • • •				
$<1.2 \times 10^{-8}$	90	¹ AAIJ	13AW LHCb	Repl. by AAIJ 17N

¹ Also reports a limit of $<1.6 \times 10^{-8}$ at 95% CL.

$\Gamma(\phi(1020)\mu^+ \mu^-)/\Gamma_{\text{total}}$ Γ_{147}/Γ
 Test for $\Delta B = 1$ weak neutral current.

VALUE (units 10^{-7})	CL%	DOCUMENT ID	TECN	COMMENT
• • • We do not use the following data for averages, fits, limits, etc. • • •				
<32	90	¹ ABAZOV	06G D0	$p\bar{p}$ at 1.96 TeV
$<4.7 \times 10^2$	90	ACOSTA	02D CDF	$p\bar{p}$ at 1.8 TeV

¹ Uses $B(B_s^0 \rightarrow J/\psi \phi) = 9.3 \times 10^{-4}$.

$\Gamma(\phi(1020)\mu^+ \mu^-)/\Gamma(J/\psi(1S)\phi)$ Γ_{147}/Γ_{56}

VALUE (units 10^{-3})	CL%	DOCUMENT ID	TECN	COMMENT
0.806 ± 0.026 OUR AVERAGE				
$0.800 \pm 0.021 \pm 0.016$		AAIJ	21Ag LHCb	pp at 7, 8, 13 TeV
$1.13 \pm 0.19 \pm 0.07$		AALTONEN	11Ai CDF	$p\bar{p}$ at 1.96 TeV
• • • We do not use the following data for averages, fits, limits, etc. • • •				
$0.741^{+0.042}_{-0.040} \pm 0.029$		AAIJ	15Aq LHCb	Repl. by AAIJ 21Ag
$0.674^{+0.061}_{-0.056} \pm 0.016$		AAIJ	13X LHCb	Repl. by AAIJ 15Aq
$1.11 \pm 0.25 \pm 0.09$		AALTONEN	11L CDF	Repl. by AALTONEN 11Ai
<2.3	90	AALTONEN	09B CDF	Repl. by AALTONEN 11L

$\Gamma(K^*(892)^0 \mu^+ \mu^-)/\Gamma_{\text{total}}$ Γ_{149}/Γ

VALUE (units 10^{-8})	DOCUMENT ID	TECN	COMMENT
$2.9 \pm 1.0 \pm 0.4$	¹ AAIJ	18AB LHCb	pp at 7, 8, 13 TeV

¹ Normalizes to $B(B^0 \rightarrow J/\psi K^{*0}) = 1.19 \pm 0.01 \pm 0.08\%$ and $B(J/\psi \rightarrow \mu^+ \mu^-) = 5.96 \pm 0.03\%$, and uses $f_s/f_d = 0.259 \pm 0.015$.

$\Gamma(f_2'(1525)\mu^+ \mu^-)/\Gamma(J/\psi(1S)\phi)$ Γ_{148}/Γ_{56}

VALUE (units 10^{-4})	DOCUMENT ID	TECN	COMMENT
$1.55 \pm 0.19 \pm 0.08$	¹ AAIJ	21Ag LHCb	pp at 7, 8, 13 TeV

¹ Measured by combining the q^2 regions [0.1, 0.98], [1.1, 8.0], and [11.0, 12.5] GeV²/ c^4 .

$\Gamma(\pi^+ \pi^- \mu^+ \mu^-)/\Gamma_{\text{total}}$ Γ_{150}/Γ

VALUE (units 10^{-8})	DOCUMENT ID	TECN	COMMENT
$8.4 \pm 1.6 \pm 0.3$	¹ AAIJ	15s LHCb	pp at 7, 8 TeV

¹ AAIJ 15s reports $(8.6 \pm 1.5 \pm 0.7 \pm 0.7) \times 10^{-8}$ from a measurement of $[\Gamma(B_s^0 \rightarrow \pi^+ \pi^- \mu^+ \mu^-)/\Gamma_{\text{total}}] / [B(B^0 \rightarrow J/\psi(1S) K^*(892)^0)]$ assuming $B(B^0 \rightarrow J/\psi(1S) K^*(892)^0) = (1.3 \pm 0.1) \times 10^{-3}$, which we rescale to our best value $B(B^0 \rightarrow J/\psi(1S) K^*(892)^0) = (1.27 \pm 0.05) \times 10^{-3}$. Our first error is their experiment's error and our second error is the systematic error from using our best value.

$\Gamma(\phi\nu\bar{\nu})/\Gamma_{\text{total}}$ Γ_{151}/Γ
 Test for $\Delta B = 1$ weak neutral current.

VALUE	CL%	DOCUMENT ID	TECN	COMMENT
$<5.4 \times 10^{-3}$	90	¹ ADAM	96D DLPH	$e^+ e^- \rightarrow Z$

¹ ADAM 96D assumes $f_{B^0} = f_{B^-} = 0.39$ and $f_{B_s} = 0.12$.

$\Gamma(e^\pm \mu^\mp)/\Gamma_{\text{total}}$ Γ_{152}/Γ
 Test of lepton family number conservation.

VALUE	CL%	DOCUMENT ID	TECN	COMMENT
$<5.4 \times 10^{-9}$	90	¹ AAIJ	18T LHCb	pp at 7, 8 TeV
• • • We do not use the following data for averages, fits, limits, etc. • • •				
$<1.1 \times 10^{-8}$	90	² AAIJ	13Bm LHCb	Repl. by AAIJ 18T
$<2.0 \times 10^{-7}$	90	AALTONEN	09P CDF	$p\bar{p}$ at 1.96 TeV
$<6.1 \times 10^{-6}$	90	ABE	98V CDF	Repl. by AALTONEN 09P
$<4.1 \times 10^{-5}$	90	³ ACCIARRI	97B L3	$e^+ e^- \rightarrow Z$

¹ AAIJ 18T uses normalization modes $B(B^0 \rightarrow K^+ \pi^-) = (19.6 \pm 0.5) \times 10^{-6}$ and $B(B^+ \rightarrow J/\psi K^+) = (1.026 \pm 0.031) \times 10^{-3}$ with B production ratio $f(\bar{B} \rightarrow B_s^0)/f(\bar{B} \rightarrow B_d^0) = 0.259 \pm 0.015$. The upper limit increases to 6×10^{-9} with the assumption of B_L -dominated decay amplitude.
² Uses normalization mode $B(B^0 \rightarrow K^+ \pi^-) = (19.4 \pm 0.6) \times 10^{-6}$ and B production ratio $f(\bar{B} \rightarrow B_s^0)/f(\bar{B} \rightarrow B_d^0) = 0.256 \pm 0.020$.
³ ACCIARRI 97B assume PDG 96 production fractions for B^+ , B^0 , B_s , and Λ_b .

$\Gamma(\mu^\pm \tau^\mp)/\Gamma_{\text{total}}$ Γ_{153}/Γ

VALUE	CL%	DOCUMENT ID	TECN	COMMENT
$<4.2 \times 10^{-5}$	95	¹ AAIJ	19AK LHCb	pp at 7, 8 TeV

¹ Assuming no contribution from $B^0 \rightarrow \mu^\pm \tau^\mp$.

POLARIZATION IN B_s^0 DECAY

In decays involving two vector mesons, one can distinguish among the states in which meson polarizations are both longitudinal (L), or both are transverse and parallel (\parallel), or perpendicular (\perp) to each other with the parameters Γ_L/Γ , Γ_\parallel/Γ , and the relative phases ϕ_\parallel and ϕ_\perp . In decays involving two tensor mesons, the transverse polarization states are described by parameters $\Gamma_{\parallel 1}$, $\Gamma_{\parallel 2}$, $\Gamma_{\perp 1}$, $\Gamma_{\perp 2}$ and their relative phases $\phi_{\parallel 1}$, $\phi_{\parallel 2}$, $\phi_{\perp 1}$, $\phi_{\perp 2}$. See also the review on "Polarization in B Decays."

Γ_L/Γ in $B_s^0 \rightarrow D_s^* \rho^+$

VALUE	DOCUMENT ID	TECN	COMMENT
$1.05^{+0.08+0.03}_{-0.10-0.04}$	LOUVOT	10 BELL	$e^+ e^- \rightarrow \Upsilon(5S)$

Γ_L/Γ in $B_s^0 \rightarrow J/\psi(1S)\phi$

VALUE	DOCUMENT ID	TECN	COMMENT
0.5196 ± 0.0034 OUR AVERAGE	Error includes scale factor of 1.5. See the ideogram below.		
$0.5152 \pm 0.0012 \pm 0.0034$	¹ AAD	21AE ATLAS	pp at 7, 8, 13 TeV
$0.5289 \pm 0.0038 \pm 0.0041$	² SIRUNYAN	21E CMS	pp at 8, 13 TeV
$0.5186 \pm 0.0029 \pm 0.0023$	AAIJ	19Q LHCb	pp at 13 TeV
$0.524 \pm 0.013 \pm 0.015$	² AALTONEN	12D CDF	$p\bar{p}$ at 1.96 TeV
$0.558^{+0.017}_{-0.019}$	^{2,3} ABAZOV	12D D0	$p\bar{p}$ at 1.96 TeV
$0.61 \pm 0.14 \pm 0.02$	⁴ AFFOLDER	00N CDF	$p\bar{p}$ at 1.8 TeV
$0.56 \pm 0.21^{+0.02}_{-0.04}$	ABE	95Z CDF	$p\bar{p}$ at 1.8 TeV

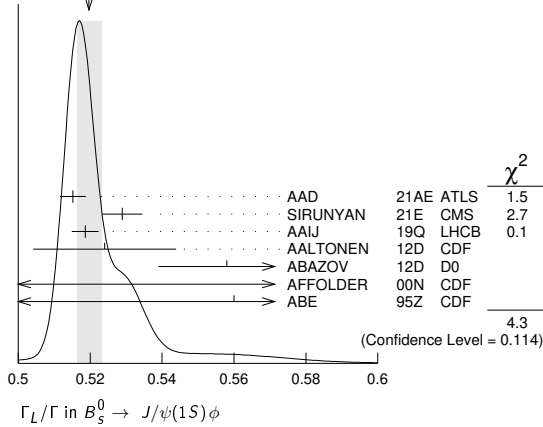
Meson Particle Listings

B_s^0

• • • We do not use the following data for averages, fits, limits, etc. • • •

$0.5350 \pm 0.0047 \pm 0.0049$	² SIRUNYAN	21E	CMS	pp at 13 TeV
$0.522 \pm 0.003 \pm 0.007$	¹ AAD	16AP	ATLS	Repl. by AAD 21AE
$0.510 \pm 0.005 \pm 0.011$	² KHACHATRY...	16S	CMS	pp at 8 TeV
$0.5241 \pm 0.0034 \pm 0.0067$	AAIJ	15I	LHCB	Repl. by AAIJ 19Q
$0.529 \pm 0.006 \pm 0.012$	¹ AAD	14U	ATLS	Repl. by AAD 16AP
$0.539 \pm 0.014 \pm 0.016$	² AAD	12CV	ATLS	Repl. by AAD 14U
$0.555 \pm 0.027 \pm 0.006$	⁵ ABAZOV	09E	D0	Repl. by ABAZOV 12D
$0.531 \pm 0.020 \pm 0.007$	² AALTONEN	08J	CDF	Repl. by AALTONEN 12D
$0.62 \pm 0.06 \pm 0.01$	ACOSTA	05	CDF	Repl. by AALTONEN 08J

WEIGHTED AVERAGE
 0.5196 ± 0.0034 (Error scaled by 1.5)



- Measured using the flavor tagged, time-dependent angular analysis of $B_s^0 \rightarrow J/\psi \phi$ decays.
- Measured using the time-dependent angular analysis of $B_s^0 \rightarrow J/\psi \phi$ decays.
- The error includes both statistical and systematic uncertainties.
- AFFOLDER 00N measurements are based on 40 B_s^0 candidates obtained from a data sample of 89 pb^{-1} . The P -wave fraction is found to be $0.23 \pm 0.19 \pm 0.04$.
- Measured the angular and lifetime parameters for the time-dependent angular untagged decays $B_d^0 \rightarrow J/\psi K^{*0}$ and $B_s^0 \rightarrow J/\psi \phi$.

Γ_L/Γ in $B_s^0 \rightarrow D_s^{*+} D_s^{*-}$

VALUE	DOCUMENT ID	TECN	COMMENT
$0.06^{+0.19}_{-0.17} \pm 0.03$	ESEN	13	BELL $e^+ e^- \rightarrow \Upsilon(5S)$

$\Gamma_{\parallel}/\Gamma$ in $B_s^0 \rightarrow J/\psi(1S)\phi$

VALUE	DOCUMENT ID	TECN	COMMENT
0.2222 ± 0.0027 OUR AVERAGE			
$0.2220 \pm 0.0017 \pm 0.0021$	¹ AAD	21AE	ATLS pp at 7, 8, 13 TeV
$0.231 \pm 0.014 \pm 0.015$	² AALTONEN	12D	CDF $p\bar{p}$ at 1.96 TeV
$0.231^{+0.024}_{-0.030}$	^{2,3} ABAZOV	12D	D0 $p\bar{p}$ at 1.96 TeV

• • • We do not use the following data for averages, fits, limits, etc. • • •

$0.227 \pm 0.004 \pm 0.006$	¹ AAD	16AP	ATLS	Repl. by AAD 21AE
$0.220 \pm 0.008 \pm 0.009$	¹ AAD	14U	ATLS	Repl. by AAD 16AP
$0.224 \pm 0.010 \pm 0.009$	² AAD	12CV	ATLS	Repl. by AAD 14U
$0.244 \pm 0.032 \pm 0.014$	⁴ ABAZOV	09E	D0	Repl. by ABAZOV 12D
$0.230 \pm 0.029 \pm 0.011$	² AALTONEN	08J	CDF	Repl. by AALTONEN 12D
$0.260 \pm 0.084 \pm 0.013$	ACOSTA	05	CDF	Repl. by AALTONEN 08J

- Measured using a tagged, time-dependent angular analysis of $B_s^0 \rightarrow J/\psi \phi$ decays.
- Measured using the time-dependent angular analysis of $B_s^0 \rightarrow J/\psi \phi$ decays.
- The error includes both statistical and systematic uncertainties.
- Measured the angular and lifetime parameters for the time-dependent angular untagged decays $B_d^0 \rightarrow J/\psi K^{*0}$ and $B_s^0 \rightarrow J/\psi \phi$.

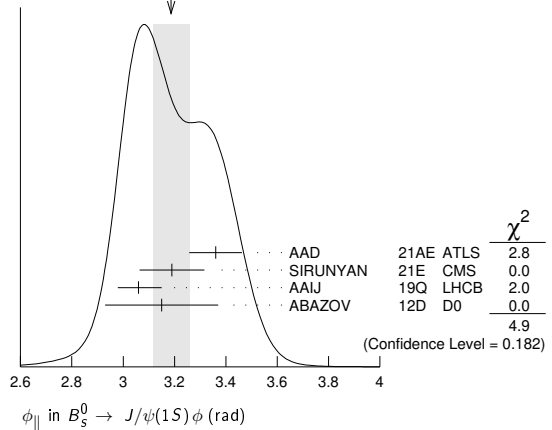
Γ_{\perp}/Γ in $B_s^0 \rightarrow J/\psi(1S)\phi$

VALUE	DOCUMENT ID	TECN	COMMENT	
0.243 ± 0.004 OUR AVERAGE				
$0.2393 \pm 0.0050 \pm 0.0037$	SIRUNYAN	21E	CMS pp at 8, 13 TeV	
$0.2456 \pm 0.0040 \pm 0.0019$	AAIJ	19Q	LHCB pp at 13 TeV	
• • • We do not use the following data for averages, fits, limits, etc. • • •				
$0.2337 \pm 0.0063 \pm 0.0045$	SIRUNYAN	21E	CMS pp at 13 TeV	
$0.243 \pm 0.008 \pm 0.012$	KHACHATRY...	16S	CMS pp at 8 TeV	
$0.2504 \pm 0.0049 \pm 0.0036$	AAIJ	15I	LHCB	Repl. by AAIJ 19Q

ϕ_{\parallel} in $B_s^0 \rightarrow J/\psi(1S)\phi$

VALUE (rad)	DOCUMENT ID	TECN	COMMENT	
3.19 ± 0.07 OUR AVERAGE	Error includes scale factor of 1.3. See the ideogram below.			
$3.36 \pm 0.05 \pm 0.09$	¹ AAD	21AE	ATLS pp at 7, 8, 13 TeV	
$3.19 \pm 0.12 \pm 0.04$	SIRUNYAN	21E	CMS pp at 8, 13 TeV	
$3.06^{+0.08}_{-0.07} \pm 0.04$	AAIJ	19Q	LHCB pp at 13 TeV	
3.15 ± 0.22	² ABAZOV	12D	D0 $p\bar{p}$ at 1.96 TeV	
• • • We do not use the following data for averages, fits, limits, etc. • • •				
$3.18 \pm 0.12 \pm 0.003$	SIRUNYAN	21E	CMS pp at 13 TeV	
$3.15 \pm 0.10 \pm 0.05$	AAID	16AP	ATLS	Repl. by AAD 21AE
$3.48^{+0.07}_{-0.09} \pm 0.68$	KHACHATRY...	16S	CMS pp at 8 TeV	
$3.26^{+0.10+0.06}_{-0.17-0.07}$	AAIJ	15I	LHCB	Repl. by AAIJ 19Q
$2.72^{+1.12}_{-0.27} \pm 0.26$	ABAZOV	09E	D0	Repl. by ABAZOV 12D

WEIGHTED AVERAGE
 3.19 ± 0.07 (Error scaled by 1.3)

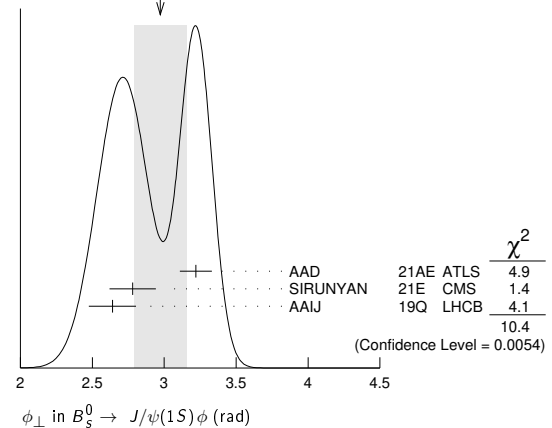


- The fit found another solution with $\phi_{\parallel} = 2.95 \pm 0.05 \pm 0.09$ rad.
- The error includes both statistical and systematic uncertainties.

ϕ_{\perp} in $B_s^0 \rightarrow J/\psi(1S)\phi$

VALUE (rad)	DOCUMENT ID	TECN	COMMENT	
2.97 ± 0.18 OUR AVERAGE	Error includes scale factor of 2.3. See the ideogram below.			
$3.22 \pm 0.10 \pm 0.05$	¹ AAD	21AE	ATLS pp at 7, 8, 13 TeV	
$2.78 \pm 0.15 \pm 0.06$	² SIRUNYAN	21E	CMS pp at 8, 13 TeV	
$2.64 \pm 0.13 \pm 0.10$	AAIJ	19Q	LHCB pp at 13 TeV	
• • • We do not use the following data for averages, fits, limits, etc. • • •				
$2.77 \pm 0.16 \pm 0.05$	² SIRUNYAN	21E	CMS pp at 13 TeV	
$4.15 \pm 0.32 \pm 0.16$	² AAD	16AP	ATLS	Repl. by AAD 21AE
$2.98 \pm 0.36 \pm 0.66$	² KHACHATRY...	16S	CMS	pp at 8 TeV
$3.08^{+0.14}_{-0.15} \pm 0.06$	AAIJ	15I	LHCB	Repl. by AAIJ 19Q
$3.89 \pm 0.47 \pm 0.11$	² AAD	14U	ATLS	Repl. by AAD 16AP

WEIGHTED AVERAGE
 2.97 ± 0.18 (Error scaled by 2.3)



- The fit found another solution with $\phi_{\perp} = 3.03 \pm 0.05 \pm 0.09$ rad.
- Measured using a tagged, time-dependent angular analysis of $B_s^0 \rightarrow J/\psi \phi$ decays.

Γ_{\perp}/Γ in $B_s^0 \rightarrow \psi(2S)\phi$	DOCUMENT ID	TECN	COMMENT
---	-------------	------	---------

0.264 $^{+0.024}_{-0.023}$ ± 0.002 ¹ AAIJ 16AK LHCb pp at 7, 8 TeV

¹ Measured using time-dependent angular analysis of $B_s^0 \rightarrow \psi(2S)\phi$ decays.

ϕ_{\parallel} in $B_s^0 \rightarrow \psi(2S)\phi$	DOCUMENT ID	TECN	COMMENT
--	-------------	------	---------

3.67 $^{+0.13}_{-0.18}$ ± 0.03 ¹ AAIJ 16AK LHCb pp at 7, 8 TeV

¹ Measured using time-dependent angular analysis of $B_s^0 \rightarrow \psi(2S)\phi$ decays.

ϕ_{\perp} in $B_s^0 \rightarrow \psi(2S)\phi$	DOCUMENT ID	TECN	COMMENT
--	-------------	------	---------

3.29 $^{+0.43}_{-0.39}$ ± 0.04 ¹ AAIJ 16AK LHCb pp at 7, 8 TeV

¹ Measured using time-dependent angular analysis of $B_s^0 \rightarrow \psi(2S)\phi$ decays.

Γ_L/Γ for $B_s^0 \rightarrow J/\psi(1S)\bar{K}^*(892)^0$	DOCUMENT ID	TECN	COMMENT
--	-------------	------	---------

Longitudinal polarization fraction, equals to f_L using notation of "Polarization in B decays" review.

0.497 ± 0.025 ± 0.025 AAIJ 15AV LHCb pp at 7, 8 TeV

••• We do not use the following data for averages, fits, limits, etc. •••

0.50 ± 0.08 ± 0.02 ¹ AAIJ 12AP LHCb Repl. by AAIJ 15AV

¹ The non-resonant $K\pi$ background contributions are subtracted. Also reports an S -wave amplitude $|A_S|^2 = 0.07^{+0.15}_{-0.07}$.

$\Gamma_{\parallel}/\Gamma$ for $B_s^0 \rightarrow J/\psi(1S)\bar{K}^*(892)^0$	DOCUMENT ID	TECN	COMMENT
--	-------------	------	---------

Parallel polarization fraction, equals to $1 - f_L - f_{\perp}$ using notation of "Polarization in B decays" review.

0.179 ± 0.027 ± 0.013 AAIJ 15AV LHCb pp at 7, 8 TeV

••• We do not use the following data for averages, fits, limits, etc. •••

0.19 $^{+0.10}_{-0.08}$ ± 0.02 ¹ AAIJ 12AP LHCb Repl. by AAIJ 15AV

¹ The non-resonant $K\pi$ background contributions are subtracted. Also reports an S -wave amplitude $|A_S|^2 = 0.07^{+0.15}_{-0.07}$.

$\Gamma_{\parallel}/\Gamma$ of $K^*(892)^0$ in $B_s^0 \rightarrow \psi(2S)\bar{K}^*(892)^0$	DOCUMENT ID	TECN	COMMENT
---	-------------	------	---------

0.524 ± 0.056 ± 0.029 AAIJ 15U LHCb pp at 7, 8 TeV

Γ_L/Γ in $B_s^0 \rightarrow \phi\phi$	DOCUMENT ID	TECN	COMMENT
---	-------------	------	---------

0.378 ± 0.013 OUR AVERAGE

0.381 ± 0.007 ± 0.012 AAIJ 19AP LHCb pp at 7, 8 and 13 TeV

0.348 ± 0.041 ± 0.021 AALTONEN 11AN CDF $p\bar{p}$ at 1.96 TeV

••• We do not use the following data for averages, fits, limits, etc. •••

0.364 ± 0.012 ± 0.009 AAIJ 14AE LHCb Repl. by AAIJ 19AP

0.365 ± 0.022 ± 0.012 AAIJ 12P LHCb Repl. by AAIJ 14AE

Γ_{\perp}/Γ in $B_s^0 \rightarrow \phi\phi$	DOCUMENT ID	TECN	COMMENT
---	-------------	------	---------

0.290 ± 0.008 ± 0.005 ¹ AAIJ 19AP LHCb pp at 7, 8 and 13 TeV

0.365 ± 0.044 ± 0.027 AALTONEN 11AN CDF $p\bar{p}$ at 1.96 TeV

••• We do not use the following data for averages, fits, limits, etc. •••

0.305 ± 0.013 ± 0.005 AAIJ 14AE LHCb Repl. by AAIJ 19AP

0.291 ± 0.024 ± 0.010 AAIJ 12P LHCb Repl. by AAIJ 14AE

¹ Note: in the summary of AAIJ 19AP the systematic uncertainty is 0.007. We take the systematic uncertainty as given in Table 5 in the paper.

ϕ_{\parallel} in $B_s^0 \rightarrow \phi\phi$	DOCUMENT ID	TECN	COMMENT
--	-------------	------	---------

2.56 ± 0.06 OUR AVERAGE

2.559 ± 0.045 ± 0.033 AAIJ 19AP LHCb pp at 7, 8 and 13 TeV

2.71 $^{+0.31}_{-0.36}$ ± 0.22 ¹ AALTONEN 11AN CDF $p\bar{p}$ at 1.96 TeV

••• We do not use the following data for averages, fits, limits, etc. •••

2.54 ± 0.07 ± 0.09 ² AAIJ 14AE LHCb Repl. by AAIJ 19AP

2.57 ± 0.15 ± 0.06 ³ AAIJ 12P LHCb Repl. by AAIJ 14AE

¹ AALTONEN 11AN quotes $\cos\phi_{\parallel} = -0.91^{+0.15}_{-0.13} \pm 0.09$ which we convert to ϕ_{\parallel} taking the smaller solution.

² AAIJ 14AE reports measurement of ϕ_{\perp} and $\phi_{\perp} - \phi_{\parallel}$, which we convert into ϕ_{\parallel} . Statistical uncertainty includes correlation between measured parameters, while systematic uncertainties are assumed uncorrelated.

³ AAIJ 12P quotes $\cos\phi_{\parallel} = -0.844 \pm 0.068 \pm 0.029$ which we convert to ϕ_{\parallel} , taking the smaller solution.

ϕ_{\perp} in $B_s^0 \rightarrow \phi\phi$	DOCUMENT ID	TECN	COMMENT
--	-------------	------	---------

2.818 ± 0.178 ± 0.073 AAIJ 19AP LHCb pp at 7, 8 and 13 TeV

••• We do not use the following data for averages, fits, limits, etc. •••

2.67 ± 0.23 ± 0.07 AAIJ 14AE LHCb Repl. by AAIJ 19AP

Γ_L/Γ in $B_s^0 \rightarrow K^{*0}\bar{K}^{*0}$	DOCUMENT ID	TECN	COMMENT
---	-------------	------	---------

0.240 ± 0.031 ± 0.025 ¹ AAIJ 19L LHCb pp at 7 and 8 TeV

••• We do not use the following data for averages, fits, limits, etc. •••

0.208 ± 0.032 ± 0.046 ² AAIJ 18S LHCb Repl. by AAIJ 19L

0.201 ± 0.057 ± 0.040 ³ AAIJ 15AF LHCb Repl. by AAIJ 18S

0.31 ± 0.12 ± 0.04 AAIJ 12F LHCb Repl. by AAIJ 15AF

¹ Untagged and time-integrated analysis within 150 MeV of the K^{*0} mass.

² Measured in angular analysis, which takes into account S -, P - and D -wave contributions.

³ Measured in angular analysis, which takes into account S -wave contributions.

Γ_{\perp}/Γ in $B_s^0 \rightarrow K^{*0}\bar{K}^{*0}$	DOCUMENT ID	TECN	COMMENT
---	-------------	------	---------

0.38 ± 0.11 ± 0.04 AAIJ 12F LHCb pp at 7 TeV

$\Gamma_{\parallel}/\Gamma$ in $B_s^0 \rightarrow K^*(892)^0\bar{K}^*(892)^0$	DOCUMENT ID	TECN	COMMENT
---	-------------	------	---------

0.297 ± 0.029 ± 0.042 ¹ AAIJ 18S LHCb pp at 7, 8 TeV

••• We do not use the following data for averages, fits, limits, etc. •••

0.215 ± 0.046 ± 0.015 AAIJ 15AF LHCb Repl. by AAIJ 18S

¹ Measured in angular analysis, which takes into account S -, P - and D -wave contributions.

ϕ_{\parallel} in $B_s^0 \rightarrow K^*(892)^0\bar{K}^*(892)^0$	DOCUMENT ID	TECN	COMMENT
--	-------------	------	---------

2.40 ± 0.11 ± 0.33 ¹ AAIJ 18S LHCb pp at 7, 8 TeV

••• We do not use the following data for averages, fits, limits, etc. •••

5.31 ± 0.24 ± 0.14 AAIJ 15AF LHCb Repl. by AAIJ 18S

¹ Measured in angular analysis, which takes into account S -, P - and D -wave contributions.

ϕ_{\perp} in $B_s^0 \rightarrow K^*(892)^0\bar{K}^*(892)^0$	DOCUMENT ID	TECN	COMMENT
--	-------------	------	---------

2.62 ± 0.26 ± 0.64 ¹ AAIJ 18S LHCb pp at 7, 8 TeV

¹ Measured in angular analysis, which takes into account S -, P - and D -wave contributions.

Γ_L/Γ in $B_s^0 \rightarrow \phi\bar{K}^{*0}$	DOCUMENT ID	TECN	COMMENT
---	-------------	------	---------

0.51 ± 0.15 ± 0.07 AAIJ 13BW LHCb pp at 7 TeV

$\Gamma_{\parallel}/\Gamma$ in $B_s^0 \rightarrow \phi\bar{K}^{*0}$	DOCUMENT ID	TECN	COMMENT
---	-------------	------	---------

0.21 ± 0.11 ± 0.02 AAIJ 13BW LHCb pp at 7 TeV

ϕ_{\parallel} in $B_s^0 \rightarrow \phi\bar{K}^{*0}$	DOCUMENT ID	TECN	COMMENT
--	-------------	------	---------

1.75 ± 0.53 ± 0.29 ¹ AAIJ 13BW LHCb pp at 7 TeV

¹ Measures $\cos(\phi_{\parallel}) = -0.18 \pm 0.52 \pm 0.29$, which we convert to ϕ_{\parallel} by taking the smaller solution.

Γ_L/Γ in $B_s^0 \rightarrow \bar{D}^{*0}\phi$	DOCUMENT ID	TECN	COMMENT
---	-------------	------	---------

0.73 ± 0.15 ± 0.04 AAIJ 18AY LHCb pp at 7 and 8 TeV

Γ_L/Γ in $B_s^0 \rightarrow K^*(892)^0\bar{K}_2^*(1430)^0$	DOCUMENT ID	TECN	COMMENT
--	-------------	------	---------

0.911 ± 0.020 ± 0.165 ¹ AAIJ 18S LHCb pp at 7, 8 TeV

¹ Measured in angular analysis, which takes into account S -, P - and D -wave contributions.

$\Gamma_{\parallel}/\Gamma$ in $B_s^0 \rightarrow K^*(892)^0\bar{K}_2^*(1430)^0$	DOCUMENT ID	TECN	COMMENT
--	-------------	------	---------

0.012 ± 0.008 ± 0.053 ¹ AAIJ 18S LHCb pp at 7, 8 TeV

¹ Measured in angular analysis, which takes into account S -, P - and D -wave contributions.

Γ_L/Γ in $B_s^0 \rightarrow K_2^*(1430)^0\bar{K}^*(892)^0$	DOCUMENT ID	TECN	COMMENT
--	-------------	------	---------

0.62 ± 0.16 ± 0.25 ¹ AAIJ 18S LHCb pp at 7, 8 TeV

¹ Measured in angular analysis, which takes into account S -, P - and D -wave contributions.

$\Gamma_{\parallel}/\Gamma$ in $B_s^0 \rightarrow K_2^*(1430)^0\bar{K}^*(892)^0$	DOCUMENT ID	TECN	COMMENT
--	-------------	------	---------

0.24 ± 0.10 ± 0.14 ¹ AAIJ 18S LHCb pp at 7, 8 TeV

¹ Measured in angular analysis, which takes into account S -, P - and D -wave contributions.

Γ_L/Γ in $B_s^0 \rightarrow K_2^*(1430)^0\bar{K}_2^*(1430)^0$	DOCUMENT ID	TECN	COMMENT
---	-------------	------	---------

0.25 ± 0.14 ± 0.18 ¹ AAIJ 18S LHCb pp at 7, 8 TeV

¹ Measured in angular analysis, which takes into account S -, P - and D -wave contributions.

Γ_{\perp}/Γ in $B_s^0 \rightarrow K_2^*(1430)^0\bar{K}_2^*(1430)^0$	DOCUMENT ID	TECN	COMMENT
---	-------------	------	---------

0.17 ± 0.11 ± 0.14 ¹ AAIJ 18S LHCb pp at 7, 8 TeV

¹ Measured in angular analysis, which takes into account S -, P - and D -wave contributions.

Meson Particle Listings

 B_s^0 $\Gamma_{\perp 1}/\Gamma$ in $B_s^0 \rightarrow K_2^*(1430)^0 \bar{K}_2^*(1430)^0$

VALUE	DOCUMENT ID	TECN	COMMENT
$0.30 \pm 0.18 \pm 0.21$	¹ AAIJ	18s LHCb	pp at 7, 8 TeV

¹ Measured in angular analysis, which takes into account S -, P - and D -wave. contributions. $\Gamma_{\parallel 2}/\Gamma$ in $B_s^0 \rightarrow K_2^*(1430)^0 \bar{K}_2^*(1430)^0$

VALUE	DOCUMENT ID	TECN	COMMENT
$0.015 \pm 0.033 \pm 0.107$	¹ AAIJ	18s LHCb	pp at 7, 8 TeV

¹ Measured in angular analysis, which takes into account S -, P - and D -wave. contributions. $F_L(B_s^0 \rightarrow \phi \mu^+ \mu^-)$ ($0.10 < q^2 < 2.00 \text{ GeV}^2/c^4$)

VALUE	DOCUMENT ID	TECN	COMMENT
$0.20_{-0.09}^{+0.08} \pm 0.02$	AAIJ	15AQ LHCb	pp at 7, 8 TeV

• • • We do not use the following data for averages, fits, limits, etc. • • •

$0.37_{-0.17}^{+0.19} \pm 0.07$	AAIJ	13x LHCb	Repl. by AAIJ 15AQ
---------------------------------	------	----------	--------------------

 $F_L(B_s^0 \rightarrow \phi \mu^+ \mu^-)$ ($2.00 < q^2 < 5.0 \text{ GeV}^2/c^4$)

VALUE	DOCUMENT ID	TECN	COMMENT
$0.68_{-0.13}^{+0.16} \pm 0.03$	AAIJ	15AQ LHCb	pp at 7, 8 TeV

• • • We do not use the following data for averages, fits, limits, etc. • • •

$0.53_{-0.23}^{+0.25} \pm 0.10$	¹ AAIJ	13x LHCb	Repl. by AAIJ 15AQ
---------------------------------	-------------------	----------	--------------------

¹ Measured in $2.0 < q^2 < 4.3 \text{ GeV}^2/c^4$. $F_L(B_s^0 \rightarrow \phi \mu^+ \mu^-)$ ($5.0 < q^2 < 8.0 \text{ GeV}^2/c^4$)

VALUE	DOCUMENT ID	TECN	COMMENT
$0.54_{-0.09}^{+0.10} \pm 0.02$	AAIJ	15AQ LHCb	pp at 7, 8 TeV

• • • We do not use the following data for averages, fits, limits, etc. • • •

$0.81_{-0.13}^{+0.11} \pm 0.05$	¹ AAIJ	13x LHCb	Repl. by AAIJ 15AQ
---------------------------------	-------------------	----------	--------------------

¹ Measured in $4.3 < q^2 < 8.68 \text{ GeV}^2/c^4$. $F_L(B_s^0 \rightarrow \phi \mu^+ \mu^-)$ ($11.0 < q^2 < 12.5 \text{ GeV}^2/c^4$)

VALUE	DOCUMENT ID	TECN	COMMENT
$0.29 \pm 0.11 \pm 0.04$	AAIJ	15AQ LHCb	pp at 7, 8 TeV

• • • We do not use the following data for averages, fits, limits, etc. • • •

$0.33_{-0.12}^{+0.14} \pm 0.06$	¹ AAIJ	13x LHCb	Repl. by AAIJ 15AQ
---------------------------------	-------------------	----------	--------------------

¹ Measured in $10.09 < q^2 < 12.90 \text{ GeV}^2/c^4$. $F_L(B_s^0 \rightarrow \phi \mu^+ \mu^-)$ ($15.0 < q^2 < 17.0 \text{ GeV}^2/c^4$)

VALUE	DOCUMENT ID	TECN	COMMENT
$0.23_{-0.08}^{+0.09} \pm 0.02$	AAIJ	15AQ LHCb	pp at 7, 8 TeV

• • • We do not use the following data for averages, fits, limits, etc. • • •

$0.34_{-0.17}^{+0.18} \pm 0.07$	¹ AAIJ	13x LHCb	Repl. by AAIJ 15AQ
---------------------------------	-------------------	----------	--------------------

¹ Measured in $14.18 < q^2 < 16 \text{ GeV}^2/c^4$. $F_L(B_s^0 \rightarrow \phi \mu^+ \mu^-)$ ($17.0 < q^2 < 19.0 \text{ GeV}^2/c^4$)

VALUE	DOCUMENT ID	TECN	COMMENT
$0.40_{-0.15}^{+0.13} \pm 0.02$	AAIJ	15AQ LHCb	pp at 7, 8 TeV

• • • We do not use the following data for averages, fits, limits, etc. • • •

$0.16_{-0.10}^{+0.17} \pm 0.07$	¹ AAIJ	13x LHCb	Repl. by AAIJ 15AQ
---------------------------------	-------------------	----------	--------------------

¹ Measured in $16.0 < q^2 < 19.0 \text{ GeV}^2/c^4$. $F_L(B_s^0 \rightarrow \phi \mu^+ \mu^-)$ ($15.0 < q^2 < 18.9 \text{ GeV}^2/c^4$)

VALUE	DOCUMENT ID	TECN	COMMENT
$0.359 \pm 0.031 \pm 0.019$	AAIJ	21AK LHCb	pp at 7, 8, 13 TeV

 $F_L(B_s^0 \rightarrow \phi \mu^+ \mu^-)$ ($1.00 < q^2 < 6.00 \text{ GeV}^2/c^4$)

VALUE	DOCUMENT ID	TECN	COMMENT
$0.715 \pm 0.036 \pm 0.013$	AAIJ	21AK LHCb	pp at 7, 8, 13 TeV

• • • We do not use the following data for averages, fits, limits, etc. • • •

$0.63_{-0.09}^{+0.09} \pm 0.03$	AAIJ	15AQ LHCb	Repl. by AAIJ 21AK
---------------------------------	------	-----------	--------------------

$0.56_{-0.16}^{+0.17} \pm 0.09$	AAIJ	13x LHCb	Repl. by AAIJ 15AQ
---------------------------------	------	----------	--------------------

 B_s^0 - \bar{B}_s^0 MIXING

For a discussion of B_s^0 - \bar{B}_s^0 mixing see the note on " B^0 - \bar{B}^0 Mixing" in the B^0 Particle Listings above.

x_s is a measure of the time-integrated B_s^0 - \bar{B}_s^0 mixing probability that produced B_s^0 (\bar{B}_s^0) decays as a \bar{B}_s^0 (B_s^0). Mixing violates $\Delta B \neq 2$ rule.

$$x_s = \frac{x_s^2}{2(1+x_s^2)}$$

$$x_s = \frac{\Delta m_{B_s^0}}{\Gamma_{B_s^0}} = (m_{B_{sH}^0} - m_{B_{sL}^0}) \tau_{B_s^0},$$

where H , L stand for heavy and light states of two B_s^0 CP eigenstates and

$$\tau_{B_s^0} = \frac{1}{0.5(\Gamma_{B_{sH}^0} + \Gamma_{B_{sL}^0})}.$$

$$\Delta m_{B_s^0} = m_{B_{sH}^0} - m_{B_{sL}^0}$$

$\Delta m_{B_s^0}$ is a measure of 2π times the B_s^0 - \bar{B}_s^0 oscillation frequency in time-dependent mixing experiments.

"OUR EVALUATION" is provided by the Heavy Flavor Averaging Group (HFLAV, <https://hflav.web.cern.ch/>) by taking into account correlations between measurements.

VALUE (10^{12} h s^{-1})	CL%	DOCUMENT ID	TECN	COMMENT
17.765 ± 0.006	OUR EVALUATION			
17.765 ± 0.005	OUR AVERAGE			
17.7683 ± 0.0051 ± 0.0032		¹ AAIJ	22B LHCb	pp at 13 TeV
17.757 ± 0.007 ± 0.008		² AAIJ	21M LHCb	pp at 7, 8, 13 TeV
17.51 $_{-0.09}^{+0.10}$ ± 0.03		³ SIRUNYAN	21E CMS	pp at 13 TeV
17.703 ± 0.059 ± 0.018		⁴ AAIJ	19Q LHCb	pp at 13 TeV
17.768 ± 0.023 ± 0.006		¹ AAIJ	13BI LHCb	pp at 7 TeV
17.93 ± 0.22 ± 0.15		⁵ AAIJ	13CF LHCb	pp at 7 TeV
17.77 ± 0.10 ± 0.07		⁶ ABULENCIA,A	06G CDF	$p\bar{p}$ at 1.96 TeV
• • • We do not use the following data for averages, fits, limits, etc. • • •				
17.711 $_{-0.057}^{+0.055}$ ± 0.011		⁴ AAIJ	15I LHCb	Repl. by AAIJ 19Q
17.63 ± 0.11 ± 0.02		⁷ AAIJ	12I LHCb	Repl. by AAIJ 21M
17–21	90	⁸ ABAZOV	06B D0	$p\bar{p}$ at 1.96 TeV
17.31 $_{-0.18}^{+0.33}$ ± 0.07		⁹ ABULENCIA	06Q CDF	Repl. by ABULENCIA,A 06G
> 8.0	95	¹⁰ ABDALLAH	04J DLPH	$e^+ e^- \rightarrow Z^0$
> 4.9	95	¹¹ ABDALLAH	04J DLPH	$e^+ e^- \rightarrow Z^0$
> 8.5	95	¹² ABDALLAH	04J DLPH	$e^+ e^- \rightarrow Z^0$
> 5.0	95	¹³ ABDALLAH	03B DLPH	$e^+ e^- \rightarrow Z$
> 10.3	95	¹⁴ ABE	03 SLD	$e^+ e^- \rightarrow Z$
> 10.9	95	¹⁵ HEISTER	03E ALEP	$e^+ e^- \rightarrow Z$
> 5.3	95	¹⁶ ABE	02V SLD	$e^+ e^- \rightarrow Z$
> 1.0	95	¹⁷ ABBIENDI	01D OPAL	$e^+ e^- \rightarrow Z$
> 7.4	95	¹⁸ ABREU	00Y DLPH	Repl. by ABDALLAH 04J
> 4.0	95	¹⁹ ABREU,P	00G DLPH	$e^+ e^- \rightarrow Z$
> 5.2	95	²⁰ ABBIENDI	99S OPAL	$e^+ e^- \rightarrow Z$
< 96	95	²¹ ABE	99D CDF	$p\bar{p}$ at 1.8 TeV
> 5.8	95	²² ABE	99J CDF	$p\bar{p}$ at 1.8 TeV
> 9.6	95	²³ BARATE	99J ALEP	$e^+ e^- \rightarrow Z$
> 7.9	95	²⁴ BARATE	98C ALEP	Repl. by BARATE 99J
> 3.1	95	²⁵ ACKERSTAFF	97U OPAL	Repl. by ABBIENDI 99S
> 2.2	95	²⁶ ACKERSTAFF	97V OPAL	Repl. by ABBIENDI 99S
> 6.5	95	²⁷ ADAM	97 DLPH	Repl. by ABREU 00Y
> 6.6	95	²⁸ BUSKULIC	96M ALEP	Repl. by BARATE 98C
> 2.2	95	²⁶ AKERS	95J OPAL	Sup. by ACKERSTAFF 97V
> 5.7	95	²⁹ BUSKULIC	95J ALEP	$e^+ e^- \rightarrow Z$
> 1.8	95	²⁸ BUSKULIC	94B ALEP	$e^+ e^- \rightarrow Z$

¹ Measured using $B_s^0 \rightarrow D_s^- \pi^+$ decays.² Measured using $B_s^0 \rightarrow D_s^- \pi^+ \pi^- \pi^+$ decays.³ Measured using time-dependent angular analysis of $B_s^0 \rightarrow J/\psi \phi$ decays.⁴ Measured using time-dependent angular analysis of $B_s^0 \rightarrow J/\psi K^+ K^-$ decays.⁵ Measured using $B_s^0 \rightarrow D_s^- \mu^+ \nu_\mu X$ decays.⁶ Significance of oscillation signal is 5.4σ . Also reports $|V_{td} / V_{ts}| = 0.2060 \pm 0.0007^{+0.0081}_{-0.0060}$.⁷ Measured using $B_s^0 \rightarrow D_s^- \pi^+$ and $D_s^- \pi^+ \pi^- \pi^+$ decays.⁸ A likelihood scan over the oscillation frequency, Δm_s , gives a most probable value of 19 ps^{-1} and a range of $17 < \Delta m_s < 21 \text{ (ps}^{-1})$ at 90% C.L. assuming Gaussian uncertainties. Also excludes $\Delta m_s < 14.8 \text{ ps}^{-1}$ at 95% C.L.⁹ Significance of oscillation signal is 0.2%. Also reported the value $|V_{td} / V_{ts}| = 0.208^{+0.001+0.008}_{-0.002-0.006}$.¹⁰ Uses leptons emitted with large momentum transverse to a jet and improved techniques for vertexing and flavor-tagging.¹¹ Updates of D_s -lepton analysis.¹² Combined results from all Delphi analyses.

- 13 Events with a high transverse momentum lepton were removed and an inclusively reconstructed vertex was required.
- 14 ABE 03 uses the novel "charge dipole" technique to reconstruct separate secondary and tertiary vertices originating from the $B \rightarrow D$ decay chain. The analysis excludes $\Delta m_S < 4.9 \text{ ps}^{-1}$ and $7.9 < \Delta m_S < 10.3 \text{ ps}^{-1}$.
- 15 Three analyses based on complementary event selections: (1) fully-reconstructed hadronic decays; (2) semileptonic decays with D_S exclusively reconstructed; (3) inclusive semileptonic decays.
- 16 ABE 02V uses exclusively reconstructed D_S^- mesons and excludes $\Delta m_S < 1.4 \text{ ps}^{-1}$ and $2.4 < \Delta m_S < 5.3 \text{ ps}^{-1}$ at 95% CL.
- 17 Uses fully or partially reconstructed $D_S \ell$ vertices and a mixing tag as a flavor tagging.
- 18 Replaced by ABDALLAH 04A. Uses $D_S^- \ell^+$, and $\phi \ell^+$ vertices, and a multi-variable discriminant as a flavor tagging.
- 19 Uses inclusive D_S vertices and fully reconstructed B_S decays and a multi-variable discriminant as a flavor tagging.
- 20 Uses ℓ - Q_{hem} and ℓ - ℓ .
- 21 ABE 99D assumes $\tau_{B_S^0} = 1.55 \pm 0.05 \text{ ps}$ and $\Delta\Gamma/\Delta m = (5.6 \pm 2.6) \times 10^{-3}$.
- 22 ABE 99J uses ϕ ℓ - ℓ correlation.
- 23 BARATE 99J uses combination of an inclusive lepton and D_S^- -based analyses.
- 24 BARATE 98c combines results from $D_S h$ - ℓ/Q_{hem} , $D_S h$ - K in the same side, $D_S \ell$ - ℓ/Q_{hem} and $D_S \ell$ - K in the same side.
- 25 Uses ℓ - Q_{hem} .
- 26 Uses ℓ - ℓ .
- 27 ADAM 97 combines results from $D_S \ell$ - Q_{hem} , ℓ - Q_{hem} , and ℓ - ℓ .
- 28 BUSKULIC 96M uses D_S lepton correlations and lepton, kaon, and jet charge tags.
- 29 BUSKULIC 95J uses ℓ - Q_{hem} . They find $\Delta m_S > 5.6$ [> 6.1] for $f_S = 10\%$ [12%]. We interpolate to our central value $f_S = 10.5\%$.

$x_S = \Delta m_{B_S^0} / \Gamma_{B_S^0}$
 This is derived by the Heavy Flavor Averaging Group (HFLAV, <https://hflav.web.cern.ch/>) from the results on $\Delta m_{B_S^0}$ and "OUR EVALUATION" of the B_S^0 mean lifetime.

VALUE	DOCUMENT ID
27.01 ± 0.10 OUR EVALUATION	

χ_S
 This is a $B_S^0 \bar{B}_S^0$ integrated mixing parameter derived from x_S above and OUR EVALUATION of $\Delta\Gamma_{B_S^0} / \Gamma_{B_S^0}$.

VALUE	DOCUMENT ID
0.499318 ± 0.000005 OUR EVALUATION	

CP VIOLATION PARAMETERS in B_S^0

$\text{Re}(\epsilon_{B_S^0}) / (1 + |\epsilon_{B_S^0}|^2)$
 CP impurity in B_S^0 system.

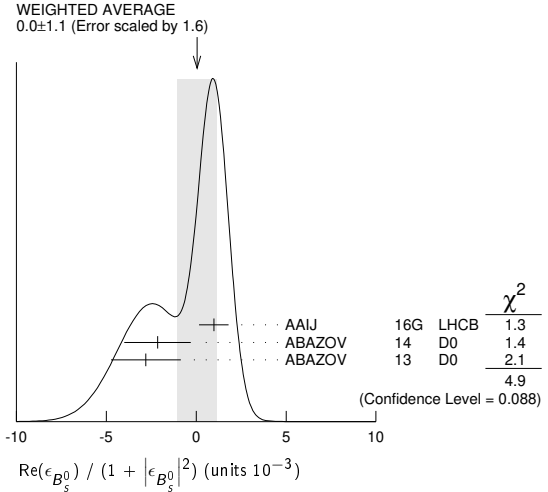
"OUR EVALUATION" is an average obtained by the Heavy Flavor Averaging Group (HFLAV, <https://hflav.web.cern.ch/>) and described at <https://hflav.web.cern.ch/>. It is the result of a fit to B_d and B_s CP asymmetries, which includes the B_s measurements listed below and the B_d measurements listed in the B_d section, and takes into account correlations between those measurements.

VALUE (units 10^{-3})	DOCUMENT ID	TECN	COMMENT
-0.15 ± 0.70 OUR EVALUATION			

VALUE	DOCUMENT ID	TECN	COMMENT
0.0 ± 1.1 OUR AVERAGE	Error includes scale factor of 1.6. See the ideogram below.		
0.98 ± 0.65 ± 0.5	1 AAIJ	16G LHCb	pp at 7, 8 TeV
-2.15 ± 1.85	2 ABAZOV	14 D0	$p\bar{p}$ at 1.96 TeV
-2.8 ± 1.9 ± 0.4	3 ABAZOV	13 D0	$p\bar{p}$ at 1.96 TeV
• • • We do not use the following data for averages, fits, limits, etc. • • •			
-0.15 ± 1.25 ± 0.90	4 AAIJ	14D LHCb	Repl. by AAIJ 16G
-4.5 ± 2.7	5 ABAZOV	11U D0	Repl. by ABAZOV 14
-0.4 ± 2.3 ± 0.4	6 ABAZOV	10E D0	Repl. by ABAZOV 13
-3.6 ± 1.9	7 ABAZOV	10H D0	Repl. by ABAZOV 11U
6.1 ± 4.8 ± 0.9	8 ABAZOV	07A D0	Repl. by ABAZOV 10E

- 1 AAIJ 16G reports a measurement of time-integrated flavor-specific asymmetry in $B_S^0 \rightarrow \mu^+ D_S^- X$ decays, $A_{SL}^S = (0.39 \pm 0.26 \pm 0.20)\%$, which is approximately equal to $4 \times \text{Re}(\epsilon_{B_S^0}) / (1 + |\epsilon_{B_S^0}|^2)$.
- 2 ABAZOV 14 uses the dimuon charge asymmetry with different impact parameters from which it reports $A_{SL}^S = (-0.86 \pm 0.74) \times 10^{-2}$.
- 3 ABAZOV 13 reports a measurement of time-integrated flavor-specific asymmetry in mixed semileptonic $B_S^0 \rightarrow \mu^+ D_S^- X$ decays $A_{SL}^S = (-1.12 \pm 0.74 \pm 0.17)\%$ which is approximately equal to $4 \times \text{Re}(\epsilon_{B_S^0}) / (1 + |\epsilon_{B_S^0}|^2)$.
- 4 AAIJ 14D reports a measurement of time-integrated flavor-specific asymmetry in $B_S^0 \rightarrow \mu^+ D_S^- X$ decays, $A_{SL}^S = (-0.06 \pm 0.50 \pm 0.36)\%$, which is approximately equal to $4 \times \text{Re}(\epsilon_{B_S^0}) / (1 + |\epsilon_{B_S^0}|^2)$.
- 5 ABAZOV 11U uses the dimuon charge asymmetry with different impact parameters from which it reports $A_{SL}^S = (-18.1 \pm 10.6) \times 10^{-3}$.

- 6 ABAZOV 10E reports a measurement of flavor-specific asymmetry in $B_{(s)}^0 \rightarrow \mu^+ D_{(s)}^{*-} X$ decays with a decay-time analysis including initial-state flavor tagging, $A_{SL}^S = (-1.7 \pm 9.1_{-1.5}^{+1.4}) \times 10^{-3}$ which is approximately equal to $4 \times \text{Re}(\epsilon_{B_S^0}) / (1 + |\epsilon_{B_S^0}|^2)$.
- 7 ABAZOV 10H reports a measurement of like-sign dimuon charge asymmetry of $A_{SL}^S = (-9.57 \pm 2.51 \pm 1.46) \times 10^{-3}$ in semileptonic b -hadron decays. Using the measured production ratio of B_d^0 and B_s^0 , and the asymmetry of B_d^0 , $A_{SL}^S = (-4.7 \pm 4.6) \times 10^{-3}$ measured from B -factories, they obtain the asymmetry for B_S^0 .
- 8 The first direct measurement of the time integrated flavor untagged charge asymmetry in semileptonic B_S^0 decays is reported as $2 \times A_{SL}^S(\text{untagged}) = A_{SL}^S = (2.45 \pm 1.93 \pm 0.35) \times 10^{-2}$.



$\mathcal{K}K(B_S^0 \rightarrow K^+ K^-)$

VALUE	DOCUMENT ID	TECN	COMMENT
0.162 ± 0.035 OUR AVERAGE			
0.164 ± 0.034 ± 0.014	AAIJ	21o LHCb	pp at 13 TeV
0.14 ± 0.11 ± 0.03	AAIJ	13Bo LHCb	pp at 7 TeV

$S_{KK}(B_S^0 \rightarrow K^+ K^-)$

VALUE	DOCUMENT ID	TECN	COMMENT
0.14 ± 0.05 OUR AVERAGE	Error includes scale factor of 1.3.		
0.123 ± 0.034 ± 0.015	AAIJ	21o LHCb	pp at 13 TeV
0.30 ± 0.12 ± 0.04	AAIJ	13Bo LHCb	pp at 7 TeV

$r_B(B_S^0 \rightarrow D_S^\mp K^\pm)$
 r_B and δ_B are the amplitude ratio and relative strong phase between the amplitudes of $A(B_S^0 \rightarrow D_S^+ K^-)$ and $A(B_S^0 \rightarrow D_S^- K^+)$,

VALUE	DOCUMENT ID	TECN	COMMENT
0.37 ± 0.10 ± 0.09	1 AAIJ	18U LHCb	pp at 7, 8 TeV
• • • We do not use the following data for averages, fits, limits, etc. • • •			
0.53 ± 0.17 ± 0.16	2 AAIJ	14BF LHCb	Repl. by AAIJ 18U

- 1 Measured in $B_S^0 \rightarrow D_S^\mp K^\pm$ decays, constraining $-2\beta_S$ by the measurement of $\phi_S = -0.030 \pm 0.033$ from HFLAV.
- 2 Measured in $B_S^0 \rightarrow D_S^\mp K^\pm$ decays, constraining $-2\beta_S$ by the measurement of $\phi_S = 0.01 \pm 0.07 \pm 0.0$ from AAIJ 13AR. At 68% CL.

$r_B(B_S^0 \rightarrow D_S^\mp K^\pm \pi^\pm \pi^\mp)$

VALUE	DOCUMENT ID	TECN	COMMENT
0.47 ± 0.08 ± 0.02 ± 0.03	1,2 AAIJ	21M LHCb	pp at 7, 8, 13 TeV

- 1 Measured in restricted phase space with $m(K^+ \pi^+ \pi^-) < 1950 \text{ MeV}$, $m(K^+ \pi^-) < 1200 \text{ MeV}$ and $m(\pi^+ \pi^-) < 1200 \text{ MeV}$.
- 2 A model-independent coherence factor for the decay $B_S \rightarrow D_S K \pi \pi$ (in the restricted phase space region) is also reported.

$\delta_B(B_S^0 \rightarrow D_S^\pm K^\mp)$

VALUE (°)	DOCUMENT ID	TECN	COMMENT
358 ± 13 ± 14	1 AAIJ	18U LHCb	pp at 7, 8 TeV
• • • We do not use the following data for averages, fits, limits, etc. • • •			
3 ± 19 ± 20	2 AAIJ	14BF LHCb	Repl. by AAIJ 18U
1 Measured in $B_S^0 \rightarrow D_S^\mp K^\pm$ decays, constraining $-2\beta_S$ by the measurement of $\phi_S = 0.030 \pm 0.033$ from HFLAV. The value is modulo 180°.			
2 Measured in $B_S^0 \rightarrow D_S^\mp K^\pm$ decays, constraining $-2\beta_S$ by the measurement of $\phi_S = 0.01 \pm 0.07 \pm 0.0$ from AAIJ 13AR. The value is modulo 180° at 68% CL.			

Meson Particle Listings

 B_S^0 $\delta_B(B_S^0 \rightarrow D_S^\pm K^\mp \pi^\pm \pi^\mp)$

VALUE (°)	DOCUMENT ID	TECN	COMMENT
-6^{+10+2}_{-12-4}	1,2 AAIJ	21M LHCB	pp at 7, 8, 13 TeV

¹ Measured in restricted phase space with $m(K^+\pi^+\pi^-) < 1950$ MeV, $m(K^+\pi^-)$ < 1200 MeV and $m(\pi^+\pi^-) < 1200$ MeV. The value is modulo 180°.

² A model-independent coherence factor for the decay $B_S \rightarrow D_S K \pi \pi$ (in the restricted phase space region) is also reported.

CP Violation phase β_s

$-2\beta_s$ is the weak phase difference between B_S^0 mixing amplitude and the $B_S^0 \rightarrow J/\psi \phi$ decay amplitude driven by the $b \rightarrow c\bar{c}s$ transition (such as $B_S \rightarrow J/\psi \phi, J/\psi K^+ K^-$,

$J/\psi \pi^+ \pi^-$, and $D_S^+ D_S^-$). The Standard Model value of β_s is $\arg(-\frac{V_{ts}V_{tb}^*}{V_{cs}V_{cb}^*})$ if penguin contributions are neglected.

“OUR EVALUATION” is an average using rescaled values of the data listed below. The average and rescaling were performed by the Heavy Flavor Averaging Group (HFLAV, <https://hflav.web.cern.ch/>) and are described at <https://hflav.web.cern.ch/>. The averaging/scaling procedure takes into account correlation between the measurements.

VALUE (10 ⁻² rad)	DOCUMENT ID	TECN	COMMENT
2.5 ± 1.0 OUR EVALUATION			
2.3 ± 1.0 OUR AVERAGE			
4.35 ± 1.80 ± 1.05	1 AAD	21AE ATLS	pp at 7, 8, 13 TeV
0 ± 14 ± 4	2 AAIJ	21AN LHCB	pp at 7, 8 TeV
1.05 ± 2.20 ± 0.50	3 SIRUNYAN	21E CMS	pp at 8, 13 TeV
-0.1 ± 2.2 ± 0.6	4 AAIJ	19AF LHCB	pp at 7, 8, 13 TeV
4.15 ± 2.05 ± 0.30	5 AAIJ	19Q LHCB	pp at 13 TeV
-5.95 ± 5.35 ± 1.70	6 AAIJ	17V LHCB	pp at 7, 8 TeV
-11.5 ⁺¹⁴ _{-14.5} ± 1	7 AAIJ	16AK LHCB	pp at 7, 8 TeV
2.9 ± 2.5 ± 0.3	8 AAIJ	15I LHCB	pp at 7, 8 TeV
-1 ± 9 ± 1	9 AAIJ	14AY LHCB	pp at 7, 8 TeV
	10 AALTONEN	12AJ CDF	$p\bar{p}$ at 1.96 TeV
	11 ABAZOV	12D D0	$p\bar{p}$ at 1.96 TeV
• • • We do not use the following data for averages, fits, limits, etc. • • •			
3.7 ± 5.8 ± 1.4	12,13 AAIJ	19AP LHCB	pp at 7, 8, 13 TeV
5.0 ± 6.5 ± 7.0	14 AAIJ	18S LHCB	pp at 7, 8 TeV
4.5 ± 3.9 ± 2.1	15 AAD	16AP ATLS	Repl. by AAD 21AE
3.75 ± 4.85 ± 1.55	16 KHACHATRYAN	16S CMS	Repl. by SIRUNYAN 21E
6 ⁺⁸ ₋₇	17,18 AAIJ	15K LHCB	pp at 7, 8 TeV
-6 ± 13 ± 3	19 AAD	14U ATLS	Repl. by AAD 21AE
8.5 ± 7.5 ± 1.5	20 AAIJ	14AE LHCB	Repl. by AAIJ 19AP
-3.5 ± 3.4 ± 0.4	21 AAIJ	14S LHCB	Repl. by AAIJ 19AF
-0.5 ± 3.5 ± 0.5	22 AAIJ	13AR LHCB	Repl. by AAIJ 15I
	23 AAIJ	13AY LHCB	pp at 7 TeV
-11.0 ± 20.5 ± 5.0	24 AAD	12CV ATLS	Repl. by AAD 14U
22 ± 22 ± 1	25 AAIJ	12B LHCB	Repl. by AAIJ 12Q
-8 ± 9 ± 3	26 AAIJ	12D LHCB	Repl. by AAIJ 13AR
0.95 ^{+8.70+0.15} _{-8.65-0.20}	27 AAIJ	12Q LHCB	Repl. by AAIJ 13AR
	28 AALTONEN	12D CDF	Repl. by AALTONEN 12AJ
	29 AALTONEN	08G CDF	Repl. by AALTONEN 12D
28 ⁺¹² ₋₁₅ ⁺⁴ ₋₁	11,30 ABAZOV	08AM D0	Repl. by ABAZOV 12D
39.5 ± 28.0 ^{+0.5} _{-7.0}	31,32 ABAZOV	07 D0	Repl. by ABAZOV 07N
35 ⁺²⁰ ₋₂₄	32,33 ABAZOV	07N D0	Repl. by ABAZOV 08AM

¹ AAD 21AE measured $\phi_s = -2\beta_s = -0.087 \pm 0.036 \pm 0.021$ rad. using a time-dependent angular analysis of $B_S^0 \rightarrow J/\psi \phi$ decays.

² AAIJ 21AN measured $\phi_s = -2\beta_s = 0.00 \pm 0.28 \pm 0.07$ rad, using a time-dependent angular analysis of $B_S^0 \rightarrow J/\psi \phi$ decays with $J/\psi \rightarrow e^+e^-$.

³ SIRUNYAN 21E measured $\phi_s = -2\beta_s = -0.021 \pm 0.044 \pm 0.010$ rad. using a time-dependent angular analysis of $B_S^0 \rightarrow J/\psi \phi$ decays.

⁴ AAIJ 19AF reports $\phi_s = -2\beta_s = 0.002 \pm 0.044 \pm 0.012$ rad. and $|\lambda| = 0.949 \pm 0.036 \pm 0.019$, when direct CP violation is allowed. Measured using a time-dependent fit to $B_S^0 \rightarrow J/\psi \pi^+ \pi^-$ decays, which is sensitive to $\phi_s(s\bar{s}s)$, not $\phi_s(c\bar{c}s)$.

⁵ AAIJ 19Q reports $\phi_s = -2\beta_s = -0.083 \pm 0.041 \pm 0.006$ rad. that was measured using a time-dependent angular analysis of $B_S^0 \rightarrow J/\psi K^+ K^-$ decays.

⁶ Measured $\phi_s = -2\beta_s = 0.119 \pm 0.107 \pm 0.034$ rad using time-dependent angular analysis of $B_S^0 \rightarrow J/\psi K^+ K^-$ in the region $m(KK) > 1.05$ GeV.

⁷ AAIJ 16AK reports $\phi_s = -2\beta_s = 0.23^{+0.29}_{-0.28} \pm 0.02$ rad. that was measured using a time-dependent angular analysis of $B_S^0 \rightarrow \psi(2S) \phi$ decays.

⁸ AAIJ 15I reports $\phi_s = -2\beta_s = -0.058 \pm 0.049 \pm 0.006$ rad. that was measured using a time-dependent angular analysis of $B_S^0 \rightarrow J/\psi K^+ K^-$ decays. It also combines this result with that of AAIJ 14S and quotes $\phi_s = -2\beta_s = -0.010 \pm 0.039$ rad.

⁹ AAIJ 14AY reports $\phi_s = -2\beta_s = 0.02 \pm 0.17 \pm 0.02$ rad. in a time-dependent fit to $B_S^0 \rightarrow D_S^+ D_S^-$, while allowing CP violation in decay.

¹⁰ AALTONEN 12AJ reports $-\pi/2 < \beta_s < -1.51$ or $-0.06 < \beta_s < 0.30$, or $1.26 < \beta_s < \pi/2$ rad. at 68% CL. Measured using the time-dependent angular analysis of $B_S^0 \rightarrow J/\psi \phi$ decays.

¹¹ ABAZOV 12D reports $\phi_s = -2\beta_s = -0.55^{+0.38}_{-0.36}$ rad. that was measured using a time-dependent angular analysis of $B_S^0 \rightarrow J/\psi \phi$ decays. A single error includes both statistical and systematic uncertainties.

¹² AAIJ 19AP reports $\phi_s^{s\bar{s}s} = -0.073 \pm 0.115 \pm 0.027$ rad and $|\lambda| = 0.99 \pm 0.05 \pm 0.01$. Measured using a time-dependent fit to $B_S^0 \rightarrow \phi \phi$ decays, assuming independence of the helicity of the $\phi \phi$ decay.

¹³ AAIJ 19AP reports also polarisation-dependent results assuming that the longitudinal weak phase is CP-conserving and that there is no direct CP violation, giving $\phi_{s,\parallel} = 0.014 \pm 0.055 \pm 0.011$ rad and $\phi_{s,\perp} = 0.044 \pm 0.059 \pm 0.019$ rad.

¹⁴ AAIJ 18S reports $\phi_s = -2\beta_s = -0.10 \pm 0.13 \pm 0.14$ rad measured in $B_S^0 \rightarrow (K^+\pi^-)(K^-\pi^+)$ in the region $0.75 < m(K^\pm \pi^\mp) < 1.6$ GeV. This is a $b \rightarrow d\bar{d}s$ transition with a decay amplitude phase different from that of $b \rightarrow c\bar{c}s$ transition.

¹⁵ AAD 16AP reports $\phi_s = -2\beta_s = -0.090 \pm 0.078 \pm 0.041$ rad. that was measured using a time-dependent angular analysis of $B_S^0 \rightarrow J/\psi \phi$ decays.

¹⁶ KHACHATRYAN 16S reports $\phi_s = -2\beta_s = -0.075 \pm 0.097 \pm 0.031$ rad. that was measured using a time-dependent angular analysis of $B_S^0 \rightarrow J/\psi \phi$ decays.

¹⁷ AAIJ 15K reports $-2\beta_s = -0.12^{+0.14}_{-0.16}$ rad. The value was obtained by measuring time-dependent CP asymmetry in $B_S^0 \rightarrow K^+ K^-$ and using a U-spin relation between $B_S^0 \rightarrow K^+ K^-$ and $B^0 \rightarrow \pi^+ \pi^-$.

¹⁸ Results are also presented using additional inputs on $B^0 \rightarrow \pi^0 \pi^0$ and $B^+ \rightarrow \pi^+ \pi^0$ decays from other experiments and isospin symmetry assumptions. The dependence of the results on the maximum allowed amount of U-spin breaking up to 50% is also included.

¹⁹ AAD 14U reports $\phi_s = -2\beta_s = 0.12 \pm 0.25 \pm 0.05$ rad. that was measured using a time-dependent angular analysis of $B_S^0 \rightarrow J/\psi \phi$ decays.

²⁰ AAIJ 14AE value measured in $B_S^0 \rightarrow \phi \phi$ decays. This is a $b \rightarrow s\bar{s}s$ transition with a decay amplitude phase different from that of $b \rightarrow c\bar{c}s$ transition. Also reports $\phi_s = -0.17 \pm 0.15 \pm 0.03$ rad.

²¹ AAIJ 14S reports $\phi_s = -2\beta_s = 0.070 \pm 0.068 \pm 0.008$ rad. and $|\lambda| = 0.89 \pm 0.05 \pm 0.01$, when direct CP violation is allowed. Measured using a time-dependent fit to $B_S^0 \rightarrow J/\psi \pi^+ \pi^-$ decays.

²² AAIJ 13AR reports $\phi_s = -2\beta_s = 0.01 \pm 0.07 \pm 0.01$ rad. obtained from combined fit to $B_S^0 \rightarrow J/\psi K^+ K^-$ and $B_S^0 \rightarrow J/\psi \pi^+ \pi^-$ data sets. Also reports separate results of $\phi_s = 0.07 \pm 0.09 \pm 0.01$ rad. from $B_S^0 \rightarrow J/\psi K^+ K^-$ decays and $\phi_s = -0.14^{+0.17}_{-0.16} \pm 0.01$ rad. from $B_S^0 \rightarrow J/\psi \pi^+ \pi^-$ decays.

²³ AAIJ 13AY uses $B_S^0 \rightarrow \phi \phi$ mode, and reports the 68% CL interval of $\phi_s = -2\beta_s$ as $[-2.46, -0.76]$ rad.

²⁴ AAD 12CV reports $\phi_s = -2\beta_s = 0.22 \pm 0.41 \pm 0.10$ rad. that was measured using a time-dependent angular analysis of $B_S^0 \rightarrow J/\psi \phi$ decays.

²⁵ Reports $\phi_s = -2\beta_s = -0.44 \pm 0.44 \pm 0.02$ rad. that was measured using a time-dependent fit to $B_S^0 \rightarrow J/\psi f_0(980)$ decays.

²⁶ Reports $\phi_s = -2\beta_s = 0.15 \pm 0.18 \pm 0.06$ rad. that was measured using a time-dependent angular analysis of $B_S^0 \rightarrow J/\psi \phi$ decays.

²⁷ Reports $\phi_s = -2\beta_s = -0.019^{+0.173+0.004}_{-0.174-0.003}$ rad. which was measured using a time-dependent fit to $B_S^0 \rightarrow J/\psi \pi^+ \pi^-$ decays, with the $\pi^+ \pi^-$ mass within 775–1550 MeV. Searches for, but finds no evidence, for direct CP violation in $B_S^0 \rightarrow J/\psi \pi \pi$ decays.

²⁸ Reports $0.02 < \phi_s < 0.52$ or $1.08 < \phi_s < 1.55$ rad. at 68% C.L. confidence regions in the two-dimensional space of ϕ_s and $\Delta\Gamma_{B_S^0}$ from $B_S^0 \rightarrow J/\psi \phi$ decays.

²⁹ Reports $0.32 < 2\beta_s < 2.82$ rad. at 68% C.L. and confidence regions in the two-dimensional space of $2\beta_s$ and $\Delta\Gamma$ from the first measurement of $B_S^0 \rightarrow J/\psi \phi$ decays using flavor tagging. The probability of a deviation from SM prediction as large as the level of observed data is 15%.

³⁰ Reports $\phi_s = -2\beta_s$ and obtains 90% CL interval $-0.03 < \beta_s < 0.60$ rad.

³¹ The first direct measurement of the CP-violating mixing phase is reported from the time-dependent analysis of flavor untagged $B_S^0 \rightarrow J/\psi \phi$ decays.

³² Reports ϕ_s which equals to $-2\beta_s$.

³³ Combines D0 collaboration measurements of time-dependent angular distributions in $B_S^0 \rightarrow J/\psi \phi$ and charge asymmetry in semileptonic decays. There is a 4-fold ambiguity in the solution.

 $|\lambda| (B_S^0 \rightarrow J/\psi(1S)\phi)$

VALUE	DOCUMENT ID	TECN	COMMENT
1.001 ± 0.018 OUR AVERAGE			Error includes scale factor of 1.2.
0.972 ± 0.026 ± 0.008	1 SIRUNYAN	21E CMS	pp at 13 TeV
1.012 ± 0.016 ± 0.006	AAIJ	19Q LHCB	pp at 13 TeV
• • • We do not use the following data for averages, fits, limits, etc. • • •			
0.964 ± 0.019 ± 0.007	AAIJ	15I LHCB	Repl. by AAIJ 19Q

¹ Measured using time-dependent angular analysis of $B_S^0 \rightarrow J/\psi \phi$ decays.

 $|\lambda|$

VALUE	DOCUMENT ID	TECN	COMMENT
0.999 ± 0.017 OUR AVERAGE			
0.99 ± 0.05 ± 0.01	1 AAIJ	19AP LHCB	pp at 7, 8, 13 TeV
1.035 ± 0.034 ± 0.089	2 AAIJ	18S LHCB	pp at 7, 8 TeV
0.994 ± 0.018 ± 0.006	3 AAIJ	17V LHCB	pp at 7, 8 TeV
1.045 ^{+0.069} _{-0.050} ± 0.007	4 AAIJ	16AK LHCB	pp at 7, 8 TeV
0.91 ^{+0.18} _{-0.15} ± 0.02	5 AAIJ	14AY LHCB	pp at 7, 8 TeV

- • • We do not use the following data for averages, fits, limits, etc. • • •
- 0.949 ± 0.036 ± 0.019 ⁶ AAIJ 19AF LHCB pp at 7, 8, 13 TeV
- 1.04 ± 0.07 ± 0.03 ⁷ AAIJ 14AE LHCB Repl. by AAIJ 19AP
- ¹ Measured in $B_s^0 \rightarrow \phi \phi$ decays.
- ² Measured in $B_s^0 \rightarrow (K^+ \pi^-)(K^- \pi^+)$ in the region $0.75 < m(K^\pm \pi^\mp) < 1.6$ GeV.
- ³ Measured using time-dependent angular analysis of $B_s^0 \rightarrow J/\psi K^+ K^-$ in the region $m(KK) > 1.05$ GeV.
- ⁴ Measured using time-dependent angular analysis of $B_s^0 \rightarrow \psi(2S) \phi$ decays.
- ⁵ Measured in $B_s^0 \rightarrow D_s^+ D_s^-$ decays.
- ⁶ Measured using time-dependent analysis of $B_s^0 \rightarrow J/\psi \pi^+ \pi^-$ decays.
- ⁷ Measured in $B_s^0 \rightarrow \phi \phi$ decays.

A, CP violation parameter

$$A = -2 \operatorname{Re}(\lambda) / (1 + |\lambda|^2)$$

VALUE	DOCUMENT ID	TECN	COMMENT
-0.79 ± 0.08 OUR AVERAGE			
-0.83 ± 0.05 ± 0.09	¹ AAIJ	21o LHCB	pp at 13 TeV
-0.79 ± 0.07 ± 0.10	¹ AAIJ	18o LHCB	pp at 7, 8 TeV
$0.49^{+0.77}_{-0.65} \pm 0.06$	² AAIJ	15AL LHCB	pp at 7, 8 TeV

- ¹ Measured in $B_s^0 \rightarrow K^+ K^-$ decays.
- ² Measured in $B_s^0 \rightarrow J/\psi K_S^0$ decays.

C, CP violation parameter

$$C = (1 - |\lambda|^2) / (1 + |\lambda|^2)$$

VALUE	DOCUMENT ID	TECN	COMMENT
0.19 ± 0.06 OUR AVERAGE			
0.20 ± 0.06 ± 0.02	¹ AAIJ	18o LHCB	pp at 7, 8 TeV
-0.28 ± 0.41 ± 0.08	² AAIJ	15AL LHCB	pp at 7, 8 TeV

- ¹ Measured in $B_s^0 \rightarrow K^+ K^-$ decays.
- ² Measured in $B_s^0 \rightarrow J/\psi K_S^0$ decays.

S, CP violation parameter

$$S = -2 \operatorname{Im}(\lambda) / (1 + |\lambda|^2)$$

VALUE	DOCUMENT ID	TECN	COMMENT
0.17 ± 0.06 OUR AVERAGE			
0.18 ± 0.06 ± 0.02	¹ AAIJ	18o LHCB	pp at 7, 8 TeV
-0.08 ± 0.40 ± 0.08	² AAIJ	15AL LHCB	pp at 7, 8 TeV

- ¹ Measured in $B_s^0 \rightarrow K^+ K^-$ decays.
- ² Measured in $B_s^0 \rightarrow J/\psi K_S^0$ decays.

$A_{CP}^{\perp}(B_s \rightarrow J/\psi \bar{K}^*(892)^0)$

VALUE	DOCUMENT ID	TECN	COMMENT
-0.048 ± 0.057 ± 0.020	AAIJ	15AV LHCB	pp at 7, 8 TeV

$A_{CP}^{\parallel}(B_s \rightarrow J/\psi \bar{K}^*(892)^0)$

VALUE	DOCUMENT ID	TECN	COMMENT
0.171 ± 0.152 ± 0.028	AAIJ	15AV LHCB	pp at 7, 8 TeV

$A_{CP}^{\perp}(B_s \rightarrow J/\psi \bar{K}^*(892)^0)$

VALUE	DOCUMENT ID	TECN	COMMENT
-0.049 ± 0.096 ± 0.025	AAIJ	15AV LHCB	pp at 7, 8 TeV

$A_{CP}(B_s \rightarrow \pi^+ K^-)$

A_{CP} is defined as

$$\frac{B(\bar{B}_s^0 \rightarrow f) - B(B_s^0 \rightarrow \bar{f})}{B(\bar{B}_s^0 \rightarrow f) + B(B_s^0 \rightarrow \bar{f})}$$

the CP-violation asymmetry of exclusive B_s^0 and \bar{B}_s^0 decay.

VALUE	DOCUMENT ID	TECN	COMMENT
0.224 ± 0.012 OUR AVERAGE			
0.236 ± 0.013 ± 0.011	AAIJ	21o LHCB	pp at 13 TeV
0.213 ± 0.015 ± 0.007	AAIJ	18o LHCB	pp at 7, 8 TeV
0.22 ± 0.07 ± 0.02	AALTONEN	14P CDF	$p\bar{p}$ at 1.96 TeV

- • • We do not use the following data for averages, fits, limits, etc. • • •
- 0.27 ± 0.04 ± 0.01 AAIJ 13AX LHCB Repl. by AAIJ 18o
- 0.27 ± 0.08 ± 0.02 AAIJ 12V LHCB Repl. by AAIJ 13AX
- 0.39 ± 0.15 ± 0.08 AALTONEN 11N CDF Repl. by AALTONEN 14P

$A_{CP}(B_s^0 \rightarrow [K^+ K^-]_D \bar{K}^*(892)^0)$

VALUE	DOCUMENT ID	TECN	COMMENT
-0.04 ± 0.07 ± 0.02	AAIJ	14BN LHCB	pp at 7, 8 TeV

- • • We do not use the following data for averages, fits, limits, etc. • • •
- 0.04 ± 0.16 ± 0.01 AAIJ 13L LHCB Repl. by AAIJ 14BN

$A_{CP}(B_s^0 \rightarrow [\pi^+ K^-]_D K^*(892)^0)$

VALUE	DOCUMENT ID	TECN	COMMENT
-0.01 ± 0.03 ± 0.02	AAIJ	14BN LHCB	pp at 7, 8 TeV

$A_{CP}(B_s^0 \rightarrow [\pi^+ \pi^-]_D K^*(892)^0)$

VALUE	DOCUMENT ID	TECN	COMMENT
0.06 ± 0.13 ± 0.02	AAIJ	14BN LHCB	pp at 7, 8 TeV

$S(B_s^0 \rightarrow \phi \gamma)$

VALUE	DOCUMENT ID	TECN	COMMENT
0.43 ± 0.30 ± 0.11	¹ AAIJ	19AE LHCB	pp at 7, 8 TeV

- ¹ Measured in flavor tagged time dependent analysis.

$C(B_s^0 \rightarrow \phi \gamma)$

VALUE	DOCUMENT ID	TECN	COMMENT
0.11 ± 0.29 ± 0.11	¹ AAIJ	19AE LHCB	pp at 7, 8 TeV

- ¹ Measured in flavor tagged time dependent analysis.

$A^{\Delta}(B_s^0 \rightarrow \phi \gamma)$

$A^{\Delta}(B_s^0 \rightarrow \phi \gamma)$ is the multiplicative coefficient of the $\sinh(\Delta\Gamma t/2)$ term in the $B_s^0 \rightarrow \phi \gamma$ decay rate time dependence.

VALUE	DOCUMENT ID	TECN	COMMENT
-0.67 ± 0.37 ± 0.41 ± 0.17	¹ AAIJ	19AE LHCB	pp at 7, 8 TeV

- • • We do not use the following data for averages, fits, limits, etc. • • •
- 0.98 ± 0.46 + 0.23 - 0.52 - 0.20 ² AAIJ 17B LHCB Repl. by AAIJ 19AE

- ¹ Measured in flavor tagged time dependent analysis, using tagged and un-tagged events. This result updates AAIJ 17B with better selection efficiency and other analysis improvements.
- ² Measured in time dependent analysis without initial flavor tagging.

CPT VIOLATION PARAMETERS

In the B_s^0 mixing, propagating mass eigenstates can be written as

$$\begin{aligned} |B_{sL}\rangle &\propto p \sqrt{1-\xi} |B_s^0\rangle + q \sqrt{1+\xi} |\bar{B}_s^0\rangle \\ |B_{sH}\rangle &\propto p \sqrt{1+\xi} |B_s^0\rangle - q \sqrt{1-\xi} |\bar{B}_s^0\rangle \end{aligned}$$

where parameter ξ controls CPT violation. If ξ is zero, then CPT is conserved. The parameter ξ can be written as

$$\xi = \frac{2(M_{11}-M_{22})-i(\Gamma_{11}-\Gamma_{22})}{-2\Delta m_s+i\Delta\Gamma_s} \approx \frac{-2\beta^\mu \Delta a_\mu}{2\Delta m_s-i\Delta\Gamma_s}$$

where M_{ii} , Γ_{ii} , Δm_s , and $\Delta\Gamma_s$ are parameters of Hamiltonian governing B_s^0 oscillations, β^μ is the B_s^0 meson velocity and Δa_μ characterizes Lorentz-invariance violation.

Δa_{\perp}

VALUE (10^{-12} GeV)	CL%	DOCUMENT ID	TECN	COMMENT
-0.47 ± 0.39 ± 0.08		¹ AAIJ	16E LHCB	pp at 7, 8 TeV
< 1.2	95	² ABAZOV	15L D0	$p\bar{p}$ at 1.96 TeV

- ¹ Uses $B_s^0 \rightarrow J/\psi K^+ K^-$ decays.
- ² Measured in semileptonic $B_s^0 \rightarrow D_s^- \mu^+ X$ decays. Also extracts limit on time and longitudinal components ($-0.8 < \Delta a_T - 0.396 \Delta a_Z < 3.9$) 10^{-13} GeV.

Δa_{\parallel}

VALUE (10^{-14} GeV)	DOCUMENT ID	TECN	COMMENT
-0.89 ± 1.41 ± 0.36	¹ AAIJ	16E LHCB	pp at 7, 8 TeV

- ¹ Uses $B_s^0 \rightarrow J/\psi K^+ K^-$ decays.

Δa_X

VALUE (10^{-14} GeV)	DOCUMENT ID	TECN	COMMENT
+1.01 ± 2.08 ± 0.71	¹ AAIJ	16E LHCB	pp at 7, 8 TeV

- ¹ Uses $B_s^0 \rightarrow J/\psi K^+ K^-$ decays.

Δa_Y

VALUE (10^{-14} GeV)	DOCUMENT ID	TECN	COMMENT
-3.83 ± 2.09 ± 0.71	¹ AAIJ	16E LHCB	pp at 7, 8 TeV

- ¹ Uses $B_s^0 \rightarrow J/\psi K^+ K^-$ decays.

$\operatorname{Re}(\xi)$

VALUE	DOCUMENT ID	TECN	COMMENT
-0.022 ± 0.033 ± 0.003	¹ AAIJ	16E LHCB	pp at 7, 8 TeV

- ¹ Uses $B_s^0 \rightarrow J/\psi K^+ K^-$ decays.

$\operatorname{Im}(\xi)$

VALUE	DOCUMENT ID	TECN	COMMENT
0.004 ± 0.011 ± 0.002	¹ AAIJ	16E LHCB	pp at 7, 8 TeV

- ¹ Uses $B_s^0 \rightarrow J/\psi K^+ K^-$ decays.

PARTIAL BRANCHING FRACTIONS IN $B_s \rightarrow \phi \ell^+ \ell^-$

$B(B_s \rightarrow \phi \ell^+ \ell^-)$ ($0.1 < q^2 < 2.0$ GeV²/c⁴)

VALUE (units 10^{-7})	DOCUMENT ID	TECN	COMMENT
1.14 ± 0.16 OUR AVERAGE			

- 1.11 $^{+0.14}_{-0.13} \pm 0.09$ ¹ AAIJ 15AQ LHCB pp at 7, 8 TeV
- 2.78 ± 0.95 ± 0.89 AALTONEN 11AI CDF $p\bar{p}$ at 1.96 TeV

- • • We do not use the following data for averages, fits, limits, etc. • • •
- 0.897 ± 0.207 ± 0.097 ¹ AAIJ 13X LHCB Repl. by AAIJ 15AQ

- ¹ Measured in $B_s^0 \rightarrow \phi \mu^+ \mu^-$ decays.

Meson Particle Listings

 B_s^0 $B(B_s^0 \rightarrow \phi \ell^+ \ell^-) (0.1 < q^2 < 0.98 \text{ GeV}^2/c^4)$

VALUE (units 10^{-8})	DOCUMENT ID	TECN	COMMENT
$6.81 \pm 0.47 \pm 0.34$	¹ AAIJ	21AG LHCb	pp at 7, 8, 13 TeV
¹ Measured in $B_s^0 \rightarrow \phi \mu^+ \mu^-$ decays			

 $B(B_s^0 \rightarrow \phi \ell^+ \ell^-) (1.1 < q^2 < 2.5 \text{ GeV}^2/c^4)$

VALUE (units 10^{-8})	DOCUMENT ID	TECN	COMMENT
$4.41 \pm 0.41 \pm 0.24$	¹ AAIJ	21AG LHCb	pp at 7, 8, 13 TeV
¹ Measured in $B_s^0 \rightarrow \phi \mu^+ \mu^-$ decays			

 $B(B_s \rightarrow \phi \ell^+ \ell^-) (2.0 < q^2 < 5.0 \text{ GeV}^2/c^4)$

VALUE (units 10^{-7})	DOCUMENT ID	TECN	COMMENT
$0.77 \pm 0.12 \pm 0.06$	¹ AAIJ	15AQ LHCb	pp at 7, 8 TeV
• • • We do not use the following data for averages, fits, limits, etc. • • •			
$0.529^{+0.182}_{-0.159} \pm 0.057$	^{1,2} AAIJ	13X LHCb	Repl. by AAIJ 15AQ
$0.58 \pm 0.55 \pm 0.19$	² AALTONEN	11AI CDF	$p\bar{p}$ at 1.96 TeV
¹ Measured in $B_s^0 \rightarrow \phi \mu^+ \mu^-$ decays.			
² Measured in $2 < q^2 < 4.3 \text{ GeV}^2/c^4$.			

 $B(B_s^0 \rightarrow \phi \ell^+ \ell^-) (2.5 < q^2 < 4.0 \text{ GeV}^2/c^4)$

VALUE (units 10^{-8})	DOCUMENT ID	TECN	COMMENT
$3.51 \pm 0.39 \pm 0.18$	¹ AAIJ	21AG LHCb	pp at 7, 8, 13 TeV
¹ Measured in $B_s^0 \rightarrow \phi \mu^+ \mu^-$ decays			

 $B(B_s^0 \rightarrow \phi \ell^+ \ell^-) (4.0 < q^2 < 6.0 \text{ GeV}^2/c^4)$

VALUE (units 10^{-8})	DOCUMENT ID	TECN	COMMENT
$6.22 \pm 0.48 \pm 0.32$	¹ AAIJ	21AG LHCb	pp at 7, 8, 13 TeV
¹ Measured in $B_s^0 \rightarrow \phi \mu^+ \mu^-$ decays			

 $B(B_s \rightarrow \phi \ell^+ \ell^-) (5.0 < q^2 < 8.0 \text{ GeV}^2/c^4)$

VALUE (units 10^{-7})	DOCUMENT ID	TECN	COMMENT
$0.96 \pm 0.13 \pm 0.08$	¹ AAIJ	15AQ LHCb	pp at 7, 8 TeV
• • • We do not use the following data for averages, fits, limits, etc. • • •			
$1.38^{+0.25}_{-0.23} \pm 0.14$	^{1,2} AAIJ	13X LHCb	Repl. by AAIJ 15AQ
$1.34 \pm 0.83 \pm 0.43$	² AALTONEN	11AI CDF	$p\bar{p}$ at 1.96 TeV
¹ Measured in $B_s^0 \rightarrow \phi \mu^+ \mu^-$ decays.			
² Measured in $4.3 < q^2 < 8.68 \text{ GeV}^2/c^4$.			

 $B(B_s^0 \rightarrow \phi \ell^+ \ell^-) (6.0 < q^2 < 8.0 \text{ GeV}^2/c^4)$

VALUE (units 10^{-8})	DOCUMENT ID	TECN	COMMENT
$6.30 \pm 0.48 \pm 0.32$	¹ AAIJ	21AG LHCb	pp at 7, 8, 13 TeV
¹ Measured in $B_s^0 \rightarrow \phi \mu^+ \mu^-$ decays			

 $B(B_s \rightarrow \phi \ell^+ \ell^-) (11.0 < q^2 < 12.5 \text{ GeV}^2/c^4)$

VALUE (units 10^{-7})	DOCUMENT ID	TECN	COMMENT
$0.717 \pm 0.045 \pm 0.036$	¹ AAIJ	21AG LHCb	pp at 7, 8, 13 TeV
• • • We do not use the following data for averages, fits, limits, etc. • • •			
$0.71 \pm 0.10 \pm 0.06$	¹ AAIJ	15AQ LHCb	Repl. by AAIJ 21AG
$1.18^{+0.22}_{-0.21} \pm 0.14$	^{1,2} AAIJ	13X LHCb	Repl. by AAIJ 15AQ
$2.98 \pm 0.95 \pm 0.95$	² AALTONEN	11AI CDF	$p\bar{p}$ at 1.96 TeV
¹ Measured in $B_s^0 \rightarrow \phi \mu^+ \mu^-$ decays.			
² Measured in $10.9 < q^2 < 12.86 \text{ GeV}^2/c^4$.			

 $B(B_s^0 \rightarrow \phi \ell^+ \ell^-) (15.0 < q^2 < 19.0 \text{ GeV}^2/c^4)$

VALUE (units 10^{-8})	DOCUMENT ID	TECN	COMMENT
$18.52 \pm 0.80 \pm 1.00$	¹ AAIJ	21AG LHCb	pp at 7, 8, 13 TeV
¹ Measured in $B_s^0 \rightarrow \phi \mu^+ \mu^-$ decays			

 $B(B_s \rightarrow \phi \ell^+ \ell^-) (15.0 < q^2 < 17.0 \text{ GeV}^2/c^4)$

VALUE (units 10^{-7})	DOCUMENT ID	TECN	COMMENT
$1.050 \pm 0.058 \pm 0.054$	¹ AAIJ	21AG LHCb	pp at 7, 8, 13 TeV
• • • We do not use the following data for averages, fits, limits, etc. • • •			
$0.90 \pm 0.11 \pm 0.07$	¹ AAIJ	15AQ LHCb	Repl. by AAIJ 21AG
$0.760^{+0.189}_{-0.169} \pm 0.087$	^{1,2} AAIJ	13X LHCb	Repl. by AAIJ 15AQ
$1.86 \pm 0.66 \pm 0.59$	² AALTONEN	11AI CDF	$p\bar{p}$ at 1.96 TeV
¹ Measured in $B_s^0 \rightarrow \phi \mu^+ \mu^-$ decays.			
² Measured in $14.18 < q^2 < 16 \text{ GeV}^2/c^4$.			

 $B(B_s \rightarrow \phi \ell^+ \ell^-) (17.0 < q^2 < 19.0 \text{ GeV}^2/c^4)$

VALUE (units 10^{-7})	DOCUMENT ID	TECN	COMMENT
$0.838 \pm 0.058 \pm 0.046$	¹ AAIJ	21AG LHCb	pp at 7, 8, 13 TeV
• • • We do not use the following data for averages, fits, limits, etc. • • •			
$0.79 \pm 0.11 \pm 0.07$	¹ AAIJ	15AQ LHCb	Repl. by AAIJ 21AG
$1.06^{+0.23}_{-0.21} \pm 0.12$	^{1,2} AAIJ	13X LHCb	Repl. by AAIJ 15AQ
$2.32 \pm 0.76 \pm 0.74$	² AALTONEN	11AI CDF	$p\bar{p}$ at 1.96 TeV
¹ Measured in $B_s^0 \rightarrow \phi \mu^+ \mu^-$ decays.			
² Measured in $16 < q^2 < 19 \text{ GeV}^2/c^4$.			

 $B(B_s \rightarrow \phi \ell^+ \ell^-) (1.0 < q^2 < 6.0 \text{ GeV}^2/c^4)$

VALUE (units 10^{-7})	DOCUMENT ID	TECN	COMMENT
1.44 ± 0.11 OUR AVERAGE			
$1.440 \pm 0.075 \pm 0.075$	¹ AAIJ	21AG LHCb	pp at 7, 8, 13 TeV
$1.14 \pm 0.79 \pm 0.36$	AALTONEN	11AI CDF	$p\bar{p}$ at 1.96 TeV
• • • We do not use the following data for averages, fits, limits, etc. • • •			
$1.29 \pm 0.16 \pm 0.10$	¹ AAIJ	15AQ LHCb	Repl. by AAIJ 21AG
$1.14^{+0.25}_{-0.23} \pm 0.13$	¹ AAIJ	13X LHCb	Repl. by AAIJ 15AQ
¹ Measured in $B_s^0 \rightarrow \phi \mu^+ \mu^-$ decays.			

 $B(B_s \rightarrow \phi \ell^+ \ell^-) (0.0 < q^2 < 4.3 \text{ GeV}^2/c^4)$

VALUE (units 10^{-7})	DOCUMENT ID	TECN	COMMENT
$3.30 \pm 1.09 \pm 1.05$	AALTONEN	11AI CDF	$p\bar{p}$ at 1.96 TeV

PRODUCTION ASYMMETRIES

 $A_P(B_s^0)$

$$A_P(B_s^0) = [\sigma(\bar{B}_s^0) - \sigma(B_s^0)] / [\sigma(\bar{B}_s^0) + \sigma(B_s^0)]$$

VALUE (units 10^{-2})	DOCUMENT ID	TECN	COMMENT
1.2 ± 1.6 OUR AVERAGE			
$-0.65 \pm 2.88 \pm 0.59$	¹ AAIJ	17BF LHCb	pp at 7 TeV
$1.98 \pm 1.90 \pm 0.59$	¹ AAIJ	17BF LHCb	pp at 8 TeV
• • • We do not use the following data for averages, fits, limits, etc. • • •			
$1.09 \pm 2.61 \pm 0.66$	² AAIJ	14BP LHCb	Repl. by AAIJ 17BF, pp at 7 TeV
¹ Based on time-dependent analysis of $B_s^0 \rightarrow D_s^- \pi^+$ in kinematic range $2 < p_T < 30 \text{ GeV}/c$ and $2.1 < \eta < 4.5$.			
² Based on time-dependent analysis of $B_s^0 \rightarrow D_s^- \pi^+$ in kinematic range $4 < p_T < 30 \text{ GeV}/c$ and $2.5 < \eta < 4.5$.			

 $B_s^0 \rightarrow D_s^{*-} \ell^+ \nu_\ell$ FORM FACTORS ρ^2 (form factor slope)

VALUE	DOCUMENT ID	TECN	COMMENT
1.17 ± 0.08 OUR AVERAGE			
$1.16 \pm 0.05 \pm 0.07$	¹ AAIJ	20AW LHCb	pp at 13 TeV
$1.23 \pm 0.17 \pm 0.05$	² AAIJ	20E LHCb	pp at 7, 8 TeV
¹ The $B_s^0 \rightarrow D_s^{*-} \mu^+ \nu_\mu$ decay is reconstructed through the decays of $D_s^{*-} \rightarrow D_s^- \gamma$, $D_s^- \rightarrow K^- K^+ \pi^-$.			
² The $B_s^0 \rightarrow D_s^{*-} \mu^+ \nu_\mu$ decay is reconstructed inclusively without γ from the decays of $D_s^{*-} \rightarrow D_s^- \gamma$, $D_s^- \rightarrow K^- K^+ \pi^-$.			

 B_s^0 REFERENCES

AAIJ	22	PRL 128 041801	R. Aaij et al.	(LHCb Collab.)
AAIJ	Also	PR D105 012010	R. Aaij et al.	(LHCb Collab.)
AAIJ	22B	NATP 18 1	R. Aaij et al.	(LHCb Collab.)
BHUYAN	22	PR D105 012007	B. Bhuyan et al.	(Belle Collab.)
WANG	22	PR D105 012004	B. Wang et al.	(Belle Collab.)
AAD	21AE	EPJ C81 342	G. Aad et al.	(ATLAS Collab.)
AAIJ	21AG	PRL 127 151801	R. Aaij et al.	(LHCb Collab.)
AAIJ	21AK	JHEP 2111 043	R. Aaij et al.	(LHCb Collab.)
AAIJ	21AN	EPJ C81 1026	R. Aaij et al.	(LHCb Collab.)
AAIJ	21C	JHEP 2102 024	R. Aaij et al.	(LHCb Collab.)
AAIJ	21G	PRL 126 081804	R. Aaij et al.	(LHCb Collab.)
AAIJ	21M	JHEP 2103 137	R. Aaij et al.	(LHCb Collab.)
AAIJ	21N	JHEP 2103 099	R. Aaij et al.	(LHCb Collab.)
AAIJ	21O	JHEP 2103 075	R. Aaij et al.	(LHCb Collab.)
AAIJ	21S	JHEP 2106 177	R. Aaij et al.	(LHCb Collab.)
AAIJ	21Y	PR D104 032005	R. Aaij et al.	(LHCb Collab.)
DUBEY	21	PR D104 012007	S. Dubey et al.	(Belle Collab.)
NISAR	21	PR D104 L031101	N. K. Nisar et al.	(Belle Collab.)
SIRUNYAN	21E	PL B816 136188	A.M. Sirunyan et al.	(CMS Collab.)
AAIJ	20AW	JHEP 2012 144	R. Aaij et al.	(LHCb Collab.)
AAIJ	20E	PR D101 072004	R. Aaij et al.	(LHCb Collab.)
AAIJ	20F	PR D102 012011	R. Aaij et al.	(LHCb Collab.)
AAIJ	20W	PRL 124 211802	R. Aaij et al.	(LHCb Collab.)
PDG	20	PTEP 2020 083C01	P.A. Zyla et al.	(PDG Collab.)
SIRUNYAN	20AG	JHEP 2004 182	A.M. Sirunyan et al.	(CMS Collab.)
SIRUNYAN	20BB	PRL 125 152001	A.M. Sirunyan et al.	(CMS Collab.)
ABOUD	19L	JHEP 1904 098	M. Aaboud et al.	(ATLAS Collab.)
AAIJ	19AE	PRL 123 081802	R. Aaij et al.	(LHCb Collab.)
AAIJ	19AF	PL B797 134789	R. Aaij et al.	(LHCb Collab.)
AAIJ	19AK	PRL 123 211801	R. Aaij et al.	(LHCb Collab.)
AAIJ	19AP	JHEP 1912 155	R. Aaij et al.	(LHCb Collab.)
AAIJ	19K	JHEP 1906 114	R. Aaij et al.	(LHCb Collab.)
AAIJ	19L	JHEP 1907 032	R. Aaij et al.	(LHCb Collab.)
AAIJ	19Q	EPJ C79 706	R. Aaij et al.	(LHCb Collab.)
Also		EPJ C80 601 (errata.)	R. Aaij et al.	(LHCb Collab.)
AAIJ	19U	PRL 122 191804	R. Aaij et al.	(LHCb Collab.)

Meson Particle Listings

$B_s^0, B_s^*, X(5568)^\pm$

ABE	96N	PRL 77 1945	F. Abe <i>et al.</i>	(CDF Collab.)
ABE	96Q	PR D54 6596	F. Abe <i>et al.</i>	(CDF Collab.)
ABREU	96F	ZPHY C71 11	P. Abreu <i>et al.</i>	(DELPHI Collab.)
ADAM	96D	ZPHY C72 207	W. Adam <i>et al.</i>	(DELPHI Collab.)
BUSKULIC	96E	ZPHY C69 585	D. Buskulic <i>et al.</i>	(ALEPH Collab.)
BUSKULIC	96M	PL B377 205	D. Buskulic <i>et al.</i>	(ALEPH Collab.)
BUSKULIC	96V	PL B384 471	D. Buskulic <i>et al.</i>	(ALEPH Collab.)
PDG	96	PR D54 1	R. M. Barnett <i>et al.</i>	(PDG Collab.)
ABE	95R	PRL 74 4988	F. Abe <i>et al.</i>	(CDF Collab.)
ABE	95Z	PRL 75 3068	F. Abe <i>et al.</i>	(CDF Collab.)
ACCIARRI	95H	PL B363 127	M. Acciarri <i>et al.</i>	(L3 Collab.)
ACCIARRI	95I	PL B363 137	M. Acciarri <i>et al.</i>	(L3 Collab.)
AKERS	95G	PL B350 273	R. Akers <i>et al.</i>	(OPAL Collab.)
AKERS	95J	ZPHY C66 555	R. Akers <i>et al.</i>	(OPAL Collab.)
BUSKULIC	95J	PL B356 409	D. Buskulic <i>et al.</i>	(ALEPH Collab.)
BUSKULIC	95O	PL B361 221	D. Buskulic <i>et al.</i>	(ALEPH Collab.)
ABREU	94D	PL B324 500	P. Abreu <i>et al.</i>	(DELPHI Collab.)
ABREU	94E	ZPHY C61 407	P. Abreu <i>et al.</i>	(DELPHI Collab.)
Also		PL B289 199	P. Abreu <i>et al.</i>	(DELPHI Collab.)
AKERS	94J	PL B337 196	R. Akers <i>et al.</i>	(OPAL Collab.)
AKERS	94L	PL B337 393	R. Akers <i>et al.</i>	(OPAL Collab.)
BUSKULIC	94B	PL B322 441	D. Buskulic <i>et al.</i>	(ALEPH Collab.)
BUSKULIC	94C	PL B322 275	D. Buskulic <i>et al.</i>	(ALEPH Collab.)
ABE	93F	PRL 71 1685	F. Abe <i>et al.</i>	(CDF Collab.)
ACTON	93H	PL B312 501	P.D. Acton <i>et al.</i>	(OPAL Collab.)
BUSKULIC	93G	PL B311 425	D. Buskulic <i>et al.</i>	(ALEPH Collab.)
ABREU	92M	PL B289 199	P. Abreu <i>et al.</i>	(DELPHI Collab.)
ACTON	92N	PL B295 357	P.D. Acton <i>et al.</i>	(OPAL Collab.)
BUSKULIC	92E	PL B294 145	D. Buskulic <i>et al.</i>	(ALEPH Collab.)
LEE-FRANZINI	90	PRL 65 2947	J. Lee-Franzini <i>et al.</i>	(CUSB II Collab.)

B_s^*

$$I(J^P) = 0(1^-)$$

I, J, P need confirmation. Quantum numbers shown are quark-model predictions.

B_s^* MASS

From mass difference below and the B_s^0 mass.

VALUE (MeV)	DOCUMENT ID	TECN	COMMENT
5415.4$^{+1.8}_{-1.5}$ OUR FIT	Error includes scale factor of 2.9.		
5415.8± 1.5 OUR AVERAGE	Error includes scale factor of 2.6.		
5416.4 $\pm 0.4 \pm 0.5$	LOUVOT 09	BELL	$e^+e^- \rightarrow \Upsilon(5S)$
5411.7 $\pm 1.6 \pm 0.6$	¹ AQUINES 06	CLEO	$e^+e^- \rightarrow \Upsilon(5S)$
••• We do not use the following data for averages, fits, limits, etc. •••			
5418 $\pm 1 \pm 3$	DRUTSKOY 07A	BELL	Repl. by LOUVOT 09
5414 $\pm 1 \pm 3$	² BONVICINI 06	CLEO	$e^+e^- \rightarrow \Upsilon(5S)$

¹ Utilized the beam constrained invariant mass peak positions for B^* and B_s^* to extract the measurement.
² Uses 14 candidates consistent with B_s decays into final states with a J/ψ and a $D_s^{(*)-}$.

$$m_{B_s^*} - m_{B_s}$$

VALUE (MeV)	DOCUMENT ID	TECN	COMMENT
48.5$^{+1.8}_{-1.5}$ OUR FIT	Error includes scale factor of 2.9.		
46.1± 1.5 OUR AVERAGE			
45.7 $\pm 1.7 \pm 0.7$	³ AQUINES 06	CLEO	$e^+e^- \rightarrow \Upsilon(5S)$
47.0 ± 2.6	⁴ LEE-FRANZINI 90	CSB2	$e^+e^- \rightarrow \Upsilon(5S)$
••• We do not use the following data for averages, fits, limits, etc. •••			
48 $\pm 1 \pm 3$	⁵ BONVICINI 06	CLEO	Repl. by AQUINES 06

³ Utilized the beam constrained invariant mass peak positions for B^* and B_s^* to extract the measurement.
⁴ LEE-FRANZINI 90 measure 46.7 $\pm 0.4 \pm 0.2$ MeV for an admixture of $B^0, B^+,$ and B_s . They use the shape of the photon line to separate the above value for B_s .
⁵ Uses 14 candidates consistent with B_s decays into final states with a J/ψ and a $D_s^{(*)-}$.

$$|(m_{B_s^*} - m_{B_s}) - (m_{B^*} - m_B)|$$

VALUE (MeV)	CL%	DOCUMENT ID	TECN	COMMENT
<6	95	ABREU 95R	DLPH	$E_{cm}^{\ell\ell} = 88-94$ GeV

B_s^* DECAY MODES

Mode	Fraction (Γ_i/Γ)
$\Gamma_1 B_s \gamma$	seen

B_s^* REFERENCES

LOUVOT 09	PRL 102 021801	R. Louvot <i>et al.</i>	(BELLE Collab.)
DRUTSKOY 07A	PR D76 012002	A. Drutskoy <i>et al.</i>	(BELLE Collab.)
AQUINES 06	PRL 96 152001	O. Aquines <i>et al.</i>	(CLEO Collab.)
BONVICINI 06	PRL 96 022002	G. Bonvicini <i>et al.</i>	(CLEO Collab.)
ABREU 95R	ZPHY C68 353	P. Abreu <i>et al.</i>	(DELPHI Collab.)
LEE-FRANZINI 90	PRL 65 2947	J. Lee-Franzini <i>et al.</i>	(CUSB II Collab.)

$X(5568)^\pm$

$$I(J^P) = ?(??)$$

OMITTED FROM SUMMARY TABLE

Seen as a peak in the $B_s \pi^\pm$ mass spectrum with a significance of more than 3σ by ABAZOV 16E and ABAZOV 18A in inclusive $p\bar{p}$ collisions at 1.96 TeV. Not seen by AAIJ 16AI, AABOUD 18L, AALTONEN 18A, and SIRUNYAN 18J. Needs confirmation.

$X(5568)^\pm$ MASS

VALUE (MeV)	EVTS	DOCUMENT ID	TECN	COMMENT
5566.9$^{+3.2+0.6}_{-3.1-1.2}$	278	¹ ABAZOV 18A	D0	$p\bar{p} \rightarrow B_s^0 \pi^\pm X$
••• We do not use the following data for averages, fits, limits, etc. •••				
5567.8 $\pm 2.9^{+0.9}_{-1.9}$	133	² ABAZOV 16E	D0	$p\bar{p} \rightarrow B_s^0 \pi^\pm X$
¹ From the combined analysis of $B_s^0 \rightarrow J/\psi \phi$ and $B_s^0 \rightarrow D_s^\pm \mu^\mp X$ decays.				
² Assumes $X(5568)^\pm \rightarrow B_s \pi^\pm$ decay. If $X(5568)^\pm \rightarrow B_s^* \pi^\pm$ decay is assumed, the mass shifts upward by 49 MeV.				

$X(5568)^\pm$ WIDTH

VALUE (MeV)	EVTS	DOCUMENT ID	TECN	COMMENT
18.6$^{+7.9+3.5}_{-6.1-3.8}$	278	¹ ABAZOV 18A	D0	$p\bar{p} \rightarrow B_s \pi^\pm X$
••• We do not use the following data for averages, fits, limits, etc. •••				
21.9 $\pm 6.4^{+5.0}_{-2.5}$	133	ABAZOV 16E	D0	$p\bar{p} \rightarrow B_s \pi^\pm X$
¹ From the combined analysis of $B_s^0 \rightarrow J/\psi \phi$ and $B_s^0 \rightarrow D_s^\pm \mu^\mp X$ decays.				

$X(5568)^\pm$ DECAY MODES

Mode	Fraction (Γ_i/Γ)
$\Gamma_1 B_s \pi^\pm$	seen

$\Gamma(B_s \pi^\pm)/\Gamma_{total}$	VALUE	EVTS	DOCUMENT ID	TECN	COMMENT	Γ_1/Γ
seen	145	¹ ABAZOV 18A	D0	$p\bar{p} \rightarrow B_s^0 \pi^\pm X$		
seen	133	² ABAZOV 16E	D0	$p\bar{p} \rightarrow B_s^0 \pi^\pm X$		
••• We do not use the following data for averages, fits, limits, etc. •••						
not seen		³ AABOUD 18L	ATLS	$pp \rightarrow B_s^0 \pi^\pm X$		
not seen		⁴ AALTONEN 18A	CDF	$p\bar{p} \rightarrow B_s^0 \pi^\pm X$		
not seen		⁵ SIRUNYAN 18J	CMS	$pp \rightarrow B_s^0 \pi^\pm X$		
not seen		⁶ AAIJ 16AI	LHCb	$pp \rightarrow B_s^0 \pi^\pm X$		

¹ With B_s mesons reconstructed in decays to $D_s^\pm \mu^\mp X$.
² Seen in $p\bar{p}$ collisions at 1.96 TeV at a rate of (8.6 $\pm 1.9 \pm 1.4$)% relative to inclusive B_s production in the kinematic region $10 < p_{\mathcal{T}}(B_s) < 30$ GeV/c, with B_s mesons reconstructed in decays to $J/\psi \phi$. An alternative possibility, $X(5568)^\pm \rightarrow B_s^* \pi^\pm$ with a missing γ , could not be ruled out.
³ Not seen in 24.4 fb $^{-1}$ of pp collision data at $\sqrt{s} = 7$ and 8 TeV with B_s mesons reconstructed in decays to $J/\psi \phi$. An upper limit on the production rate times branching fraction for $X(5568)^\pm \rightarrow B_s \pi^\pm$ relative to inclusive B_s production is less than 1.5% at $p_{\mathcal{T}}(B_s) > 10$ GeV/c and less than 1.6% at $p_{\mathcal{T}}(B_s) > 15$ GeV/c at 95% CL.
⁴ Not seen in 9.6 fb $^{-1}$ of $p\bar{p}$ collision data at $\sqrt{s} = 1.96$ TeV with B_s mesons reconstructed in decays to $J/\psi \phi$. An upper limit on the production rate times branching fraction for $X(5568)^\pm \rightarrow B_s \pi^\pm$ relative to inclusive B_s production is less than 6.7% at 95% CL.
⁵ Not seen in 19.7 fb $^{-1}$ of pp collisions data at $\sqrt{s} = 8$ TeV with B_s mesons reconstructed in decays to $J/\psi \phi$. An upper limit on the production rate times branching fraction for $X(5568)^\pm \rightarrow B_s \pi^\pm$ relative to inclusive B_s production is less than 1.1% at $p_{\mathcal{T}}(B_s) > 10$ GeV/c and less than 1.0% at $p_{\mathcal{T}}(B_s) > 15$ GeV/c at 95% CL.
⁶ Not seen in 3 fb $^{-1}$ of pp collision data at $\sqrt{s} = 7$ and 8 TeV in a scan over the $X(5568)$ mass and width, with B_s mesons reconstructed in decays to $D_s^\pm \pi^\pm$ or $J/\psi \phi$. An upper limit on the production rate times branching fraction for $X(5568)^\pm \rightarrow B_s \pi^\pm$ relative to inclusive B_s production is less than 2.1% at $p_{\mathcal{T}}(B_s) > 10$ GeV/c at 90% CL.

$X(5568)^\pm$ REFERENCES

AABOUD 18L	PRL 120 202007	M. Aaboud <i>et al.</i>	(ATLAS Collab.)
AALTONEN 18A	PRL 120 202006	T. Aaltonen <i>et al.</i>	(CDF Collab.)
ABAZOV 18A	PR D97 092004	V.M. Abazov <i>et al.</i>	(D0 Collab.)
SIRUNYAN 18J	PRL 120 202005	A.M. Sirunyan <i>et al.</i>	(CMS Collab.)
AAIJ 16AI	PRL 117 152003	R. Aaij <i>et al.</i>	(LHCb Collab.)
ABAZOV 16E	PRL 117 022003	V.M. Abazov <i>et al.</i>	(D0 Collab.)

See key on page 1127

Meson Particle Listings

$B_{s1}(5830)^0, B_{s2}^*(5840)^0, B_{sJ}^*(5850)$

$B_{s1}(5830)^0$ $I(J^P) = 0(1^+)$
I, J, P need confirmation.
 Quantum numbers shown are quark-model predictions.

$B_{s1}(5830)^0$ MASS

VALUE (MeV)	DOCUMENT ID	TECN	COMMENT
5828.70 ± 0.20 OUR FIT			
5828.65 ± 0.24 OUR AVERAGE			
5828.78 ± 0.09 ± 0.29	SIRUNYAN	18DF CMS	<i>pp</i> at 8 TeV
5828.40 ± 0.04 ± 0.41	¹ AAIJ	13o LHCB	<i>pp</i> at 7 TeV
• • • We do not use the following data for averages, fits, limits, etc. • • •			
5829.4 ± 0.7	² AALTONEN	08k CDF	Repl. by AALTONEN 14i
¹ Uses $B_{s1}(5830)^0 \rightarrow B^{*+} K^-$ decay.			
² Uses two-body decays into K^- and B^+ mesons reconstructed as $B^+ \rightarrow J/\psi K^+$, $J/\psi \rightarrow \mu^+ \mu^-$ or $B^+ \rightarrow \bar{D}^0 \pi^+$, $\bar{D}^0 \rightarrow K^+ \pi^-$.			

$m_{B_{s1}^0} - m_{B^{*+}}$

VALUE (MeV)	DOCUMENT ID	TECN	COMMENT
503.99 ± 0.17 OUR FIT			
504.03 ± 0.12 ± 0.15			
• • • We do not use the following data for averages, fits, limits, etc. • • •			
504.41 ± 0.21 ± 0.14	² AALTONEN	08k CDF	Repl. by AALTONEN 14i
¹ AALTONEN 14i reports $m_{B_{s1}(5830)^0} - m_{B^{*+}} - m_{K^-} = 10.35 \pm 0.12 \pm 0.15$ MeV which we adjusted by the K^- mass.			
² Uses two-body decays into K^- and B^+ mesons reconstructed as $B^+ \rightarrow J/\psi K^+$, $J/\psi \rightarrow \mu^+ \mu^-$ or $B^+ \rightarrow \bar{D}^0 \pi^+$, $\bar{D}^0 \rightarrow K^+ \pi^-$.			

$B_{s1}(5830)^0$ WIDTH

VALUE (MeV)	DOCUMENT ID	TECN	COMMENT
0.5 ± 0.3 ± 0.3	AALTONEN	14i CDF	<i>p\bar{p}</i> at 1.96 TeV

$B_{s1}(5830)^0$ DECAY MODES

Mode	Fraction (Γ_i/Γ)
Γ_1 $B^{*+} K^-$	seen
Γ_2 $B^{*0} K_S^0$	

$B_{s1}(5830)^0$ BRANCHING RATIOS

$\Gamma(B^{*+} K^-)/\Gamma_{total}$	Γ_1/Γ		
VALUE	DOCUMENT ID	TECN	COMMENT
seen	AALTONEN	08k CDF	<i>p\bar{p}</i> at 1.96 TeV
$\Gamma(B^{*0} K_S^0)/\Gamma(B^{*+} K^-)$	Γ_2/Γ_1		
VALUE	DOCUMENT ID	TECN	COMMENT
0.49 ± 0.12 ± 0.07	¹ SIRUNYAN	18DF CMS	<i>pp</i> at 8 TeV
¹ With the branching fractions $B(B^+ \rightarrow J/\psi K^+) = (1.026 \pm 0.031) \times 10^{-3}$ and $B(B^0 \rightarrow J/\psi K^{*0}) = (1.28 \pm 0.05) \times 10^{-3}$.			

$B_{s1}(5830)^0$ REFERENCES

SIRUNYAN	18DF EPJ C78 939	A.M. Sirunyan et al.	(CMS Collab.)
AALTONEN	14i PR D90 012013	T. Aaltonen et al.	(CDF Collab.)
AAIJ	13o PRL 110 151803	R. Aaij et al.	(LHCb Collab.)
AALTONEN	08k PRL 100 082001	T. Aaltonen et al.	(CDF Collab.)

$B_{s2}^*(5840)^0$ $I(J^P) = 0(2^+)$
I, J, P need confirmation.
 Quantum numbers shown are quark-model predictions.

$B_{s2}^*(5840)^0$ MASS

VALUE (MeV)	DOCUMENT ID	TECN	COMMENT
5839.86 ± 0.12 OUR FIT			
5839.92 ± 0.14 OUR AVERAGE			
5839.86 ± 0.09 ± 0.17	SIRUNYAN	18DF CMS	<i>pp</i> at 8 TeV
5839.99 ± 0.05 ± 0.20	AAIJ	13o LHCB	<i>pp</i> at 7 TeV
5839.6 ± 1.1 ± 0.7	¹ ABAZOV	08E D0	<i>p\bar{p}</i> at 1.96 TeV
• • • We do not use the following data for averages, fits, limits, etc. • • •			
5839.7 ± 0.7	² AALTONEN	08k CDF	Repl. by AALTONEN 14i
¹ Observed in $B_{s2}^0 \rightarrow B^+ K^-$. Measured production rate of B_{s2}^0 relative to B^+ to be $(1.15 \pm 0.23 \pm 0.13)\%$.			
² Uses two-body decays into K^- and B^+ mesons reconstructed as $B^+ \rightarrow J/\psi K^+$, $J/\psi \rightarrow \mu^+ \mu^-$ or $B^+ \rightarrow \bar{D}^0 \pi^+$, $\bar{D}^0 \rightarrow K^+ \pi^-$.			

$m_{B_{s2}^0} - m_{B_{s1}^0}$

VALUE (MeV)	DOCUMENT ID	TECN	COMMENT
• • • We do not use the following data for averages, fits, limits, etc. • • •			
10.5 ± 0.6	¹ AALTONEN	08k CDF	Repl. by AALTONEN 14i
¹ Uses two-body decays into K^- and B^+ mesons reconstructed as $B^+ \rightarrow J/\psi K^+$, $J/\psi \rightarrow \mu^+ \mu^-$ or $B^+ \rightarrow \bar{D}^0 \pi^+$, $\bar{D}^0 \rightarrow K^+ \pi^-$.			

$m_{B_{s2}^0} - m_{B^{*+}}$

VALUE (MeV)	DOCUMENT ID	TECN	COMMENT
560.52 ± 0.14 OUR FIT			
560.41 ± 0.13 ± 0.14			
¹ AALTONEN 14i reports $m_{B_{s2}(5840)^0} - m_{B^{*+}} - m_{K^-} = 66.73 \pm 0.13 \pm 0.14$ MeV which we adjusted by the K^- mass.			

$B_{s2}^*(5840)^0$ WIDTH

VALUE (MeV)	DOCUMENT ID	TECN	COMMENT
1.49 ± 0.27 OUR AVERAGE			
1.52 ± 0.34 ± 0.30	SIRUNYAN	18DF CMS	<i>pp</i> at 8 TeV
1.4 ± 0.4 ± 0.2	AALTONEN	14i CDF	<i>p\bar{p}</i> at 1.96 TeV
1.56 ± 0.13 ± 0.47	¹ AAIJ	13o LHCB	<i>pp</i> at 7 TeV
¹ Uses $B_{s2}^*(5840)^0 \rightarrow B^{*+} K^-$ decays.			

$B_{s2}^*(5840)^0$ DECAY MODES

Branching fractions are given relative to the one DEFINED AS 1.

Mode	Fraction (Γ_i/Γ)
Γ_1 $B^{*+} K^-$	DEFINED AS 1
Γ_2 $B^{*0} K^-$	0.093 ± 0.018
Γ_3 $B^0 K_S^0$	0.43 ± 0.11
Γ_4 $B^{*0} K_S^0$	0.04 ± 0.04

$B_{s2}^*(5840)^0$ BRANCHING RATIOS

$\Gamma(B^+ K^-)/\Gamma_{total}$	Γ_1/Γ		
VALUE	DOCUMENT ID	TECN	COMMENT
seen	AALTONEN	08k CDF	<i>p\bar{p}</i> at 1.96 TeV
seen	¹ ABAZOV	08E D0	<i>p\bar{p}</i> at 1.96 TeV
¹ Measured production rate of B_{s2}^0 relative to B^+ to be $(1.15 \pm 0.23 \pm 0.13)\%$.			
$\Gamma(B^{*+} K^-)/\Gamma(B^+ K^-)$	Γ_2/Γ_1		
VALUE	DOCUMENT ID	TECN	COMMENT
0.093 ± 0.013 ± 0.012	AAIJ	13o LHCB	<i>pp</i> at 7 TeV
$\Gamma(B^{*0} K_S^0)/\Gamma(B^0 K_S^0)$	Γ_4/Γ_3		
VALUE	DOCUMENT ID	TECN	COMMENT
0.093 ± 0.086 ± 0.014	¹ SIRUNYAN	18DF CMS	<i>pp</i> at 8 TeV
¹ With the branching fraction $B(B^0 \rightarrow J/\psi K^{*0}) = (1.28 \pm 0.05) \times 10^{-3}$.			
$\Gamma(B^0 K_S^0)/\Gamma(B^+ K^-)$	Γ_3/Γ_1		
VALUE	DOCUMENT ID	TECN	COMMENT
0.432 ± 0.077 ± 0.078	¹ SIRUNYAN	18DF CMS	<i>pp</i> at 8 TeV
¹ With the branching fractions $B(B^+ \rightarrow J/\psi K^+) = (1.026 \pm 0.031) \times 10^{-3}$ and $B(B^0 \rightarrow J/\psi K^{*0}) = (1.28 \pm 0.05) \times 10^{-3}$.			
$\Gamma(B^{*+} K^-)/\Gamma(B^+ K^-)$	Γ_2/Γ_1		
VALUE	DOCUMENT ID	TECN	COMMENT
0.081 ± 0.021 ± 0.015	¹ SIRUNYAN	18DF CMS	<i>pp</i> at 8 TeV
¹ With the branching fraction $B(B^+ \rightarrow J/\psi K^+) = (1.026 \pm 0.031) \times 10^{-3}$.			

$B_{s2}^*(5840)^0$ REFERENCES

SIRUNYAN	18DF EPJ C78 939	A.M. Sirunyan et al.	(CMS Collab.)
AALTONEN	14i PR D90 012013	T. Aaltonen et al.	(CDF Collab.)
AAIJ	13o PRL 110 151803	R. Aaij et al.	(LHCb Collab.)
AALTONEN	08k PRL 100 082001	T. Aaltonen et al.	(CDF Collab.)
ABAZOV	08E PRL 100 082002	V.M. Abazov et al.	(D0 Collab.)

$B_{sJ}^*(5850)$

$I(J^P) = ?(?)$

OMITTED FROM SUMMARY TABLE
 Signal can be interpreted as coming from $\bar{b}s$ states. Needs confirmation.

$B_{sJ}^*(5850)$ MASS

VALUE (MeV)	EVTS	DOCUMENT ID	TECN	COMMENT
5853 ± 15	141	AKERS	95E OPAL	$E_{cm}^{ce} = 88-94$ GeV

Meson Particle Listings

 $B_{sJ}^*(5850)$, $B_{sJ}(6063)^0$, $B_{sJ}(6114)^0$ $B_{sJ}^*(5850)$ WIDTH

VALUE (MeV)	EVTS	DOCUMENT ID	TECN	COMMENT
47 ± 22	141	AKERS	95E OPAL	$E_{cm}^e = 88-94$ GeV

 $B_{sJ}^*(5850)$ REFERENCES

AKERS 95E ZPHY C66 19 R. Akers et al. (OPAL Collab.)

 $B_{sJ}(6063)^0$

$I(J^P) = 0(?)^?$

OMITTED FROM SUMMARY TABLE

 $B_{sJ}(6063)^0$ MASS

VALUE (MeV)	DOCUMENT ID	TECN	COMMENT
$6063.5 \pm 1.2 \pm 0.8$	¹ AAIJ	21D LHCB	pp at 7, 8, 13 TeV
¹ Seen in the decay channel $B^\pm K^\mp$. Integrated luminosity = 9 fb ⁻¹ .			

 $B_{sJ}(6063)^0$ WIDTH

VALUE (MeV)	DOCUMENT ID	TECN	COMMENT
$26 \pm 4 \pm 4$	¹ AAIJ	21D LHCB	pp at 7, 8, 13 TeV
¹ Seen in the decay channel $B^\pm K^\mp$. Integrated luminosity = 9 fb ⁻¹ .			

 $B_{sJ}(6063)^0$ DECAY MODES

Mode	Fraction (Γ_i/Γ)
$\Gamma_1 B^+ K^-$	seen

 $\Gamma(B^+ K^-)/\Gamma_{total}$ Γ_1/Γ

VALUE	DOCUMENT ID	TECN	COMMENT
seen	AAIJ	21D LHCB	$B^\pm K^\mp$ mass spectrum

 $B_{sJ}(6063)^0$ REFERENCES

AAIJ 21D EPJ C81 601 R. Aaij et al. (LHCb Collab.)

 $B_{sJ}(6114)^0$

$I(J^P) = 0(?)^?$

OMITTED FROM SUMMARY TABLE

 $B_{sJ}(6114)^0$ MASS

VALUE (MeV)	DOCUMENT ID	TECN	COMMENT
$6114 \pm 3 \pm 5$	¹ AAIJ	21D LHCB	pp at 7, 8, 13 TeV
¹ Seen in the decay channel $B^\pm K^\mp$. Integrated luminosity = 9 fb ⁻¹ .			

 $B_{sJ}(6114)^0$ WIDTH

VALUE (MeV)	DOCUMENT ID	TECN	COMMENT
$66 \pm 18 \pm 21$	¹ AAIJ	21D LHCB	pp at 7, 8, 13 TeV
¹ Seen in the decay channel $B^\pm K^\mp$. Integrated luminosity = 9 fb ⁻¹ .			

 $B_{sJ}(6114)^0$ DECAY MODES

Mode	Fraction (Γ_i/Γ)
$\Gamma_1 B^+ K^-$	seen

 $\Gamma(B^+ K^-)/\Gamma_{total}$ Γ_1/Γ

VALUE	DOCUMENT ID	TECN	COMMENT
seen	AAIJ	21D LHCB	$B^\pm K^\mp$ mass spectrum

 $B_{sJ}(6114)^0$ REFERENCES

AAIJ 21D EPJ C81 601 R. Aaij et al. (LHCb Collab.)

BOTTOM, CHARMED MESONS ($B = C = \pm 1$)

$B_c^+ = c\bar{b}, B_c^- = \bar{c}b$, similarly for B_c^* 's

B_c^+

$I(J^P) = 0(0^-)$
I, J, P need confirmation.

Quantum numbers shown are quark-model predictions.

B_c^+ MASS

VALUE (MeV)	DOCUMENT ID	TECN	COMMENT
6274.47 ± 0.27 ± 0.17	¹ AAIJ	20R LHCb	pp at 7, 8, 13 TeV
6274.28 ± 1.40 ± 0.32	² AAIJ	17L LHCb	Repl. by AAIJ 20R
6274.0 ± 1.8 ± 0.4	³ AAIJ	14AQ LHCb	Repl. by AAIJ 20R
6276.28 ± 1.44 ± 0.36	⁴ AAIJ	13AS LHCb	Repl. by AAIJ 20R
6273.7 ± 1.3 ± 1.6	⁵ AAIJ	12AV LHCb	Repl. by AAIJ 20R
6275.6 ± 2.9 ± 2.5	⁶ AALTONEN	08M CDF	$p\bar{p}$ at 1.96 TeV
6300 ± 14 ± 5	⁶ ABAZOV	08T D0	$p\bar{p}$ at 1.96 TeV
6285.7 ± 5.3 ± 1.2	⁶ ABULENCIA	06C CDF	Repl. by AALTONEN 08M
6400 ± 390 ± 130	⁷ ABE	98M CDF	$p\bar{p}$ at 1.8 TeV
6320 ± 60	⁸ ACKERSTAFF	98O OPAL	$e^+e^- \rightarrow Z$

- ¹ AAIJ 20R uses the $B_c^+ \rightarrow J/\psi\pi^+, J/\psi\pi^+\pi^-\pi^+, J/\psi p\bar{p}\pi^+, J/\psi D_s^+, J/\psi D^0 K^+$ and $B_s^0\pi^+$ modes.
- ² Measured using $B_c^+ \rightarrow J/\psi D^0 K^+$ decays.
- ³ Uses $B_c^+ \rightarrow J/\psi p\bar{p}\pi^+$ decays.
- ⁴ AAIJ 13AS uses the $B_c^+ \rightarrow J/\psi D_s^+$.
- ⁵ AAIJ 12AV uses the $B_c^+ \rightarrow J/\psi\pi^+$ mode and also measures the mass difference $M(B_c^+) - M(B^+) = 994.6 \pm 1.3 \pm 0.6 \text{ MeV}/c^2$.
- ⁶ Measured using a fully reconstructed decay mode of $B_c \rightarrow J/\psi\pi$.
- ⁷ ABE 98M observed $20.4^{+6.2}_{-5.5}$ events in the $B_c^+ \rightarrow J/\psi(1S)\ell\nu\ell$ with a significance of > 4.8 standard deviations. The mass value is estimated from $m(J/\psi(1S)\ell)$.
- ⁸ ACKERSTAFF 98O observed 2 candidate events in the $B_c^+ \rightarrow J/\psi(1S)\pi^+$ channel with an estimated background of 0.63 ± 0.20 events.

$m_{B_c^+} - m_{B_s^0}$

VALUE (MeV)	DOCUMENT ID	TECN	COMMENT
907.75 ± 0.37 ± 0.27	¹ AAIJ	20R LHCb	pp at 7, 8, 13 TeV

- ¹ AAIJ 20R uses the $B_c^+ \rightarrow J/\psi\pi^+, J/\psi\pi^+\pi^-\pi^+, J/\psi p\bar{p}\pi^+, J/\psi D_s^+, J/\psi D^0 K^+$ and $B_s^0\pi^+$ modes.

B_c^+ MEAN LIFE

"OUR EVALUATION" is an average using rescaled values of the data listed below. The average and rescaling were performed by the Heavy Flavor Averaging Group (HFLAV) and are described at <https://hflav.web.cern.ch/>. The averaging/rescaling procedure takes into account correlations between the measurements.

VALUE (10^{-12} s)	DOCUMENT ID	TECN	COMMENT
0.510 ± 0.009 OUR EVALUATION			
0.510 ± 0.009 OUR AVERAGE			
0.541 ± 0.026 ± 0.014	¹ SIRUNYAN	18BY CMS	pp at 8 TeV
0.5134 ± 0.0110 ± 0.0057	^{2,3} AAIJ	15G LHCb	pp at 7, 8 TeV
0.509 ± 0.008 ± 0.012	⁴ AAIJ	14G LHCb	pp at 8 TeV
0.452 ± 0.048 ± 0.027	³ AALTONEN	13 CDF	$p\bar{p}$ at 1.96 TeV
0.448 $^{+0.038}_{-0.036}$ ± 0.032	⁵ ABAZOV	09H D0	$p\bar{p}$ at 1.96 TeV
0.463 $^{+0.073}_{-0.065}$ ± 0.036	⁵ ABULENCIA	06O CDF	$p\bar{p}$ at 1.96 TeV
0.46 $^{+0.18}_{-0.16}$ ± 0.03	⁵ ABE	98M CDF	$p\bar{p}$ 1.8 TeV

- ¹ The lifetime is measured using the decays $B_c^+ \rightarrow J/\psi\pi^+$ and $B^+ \rightarrow J/\psi K^+$.
- ² Also measures the width difference $\Delta\Gamma = \Gamma_{B_c^+} - \Gamma_{B^+} = 4.46 \pm 0.14 \pm 0.07 \text{ mm}^{-1} \text{ c}$.
- ³ Uses fully reconstructed $B_c^+ \rightarrow J/\psi\pi^+$ decays.
- ⁴ Measured using $B_c^+ \rightarrow J/\psi\mu^+\nu_\mu X$ decays.
- ⁵ The lifetime is measured from the $J/\psi e$ decay vertices.

B_c^+ DECAY MODES $\times B(\bar{b} \rightarrow B_c)$

B_c^- modes are charge conjugates of the modes below.

Mode	Fraction (Γ_i/Γ)	Confidence level
Γ_1 $J/\psi(1S)\ell^+\nu_\ell$ anything	seen	
Γ_2 $J/\psi(1S)\mu^+\nu_\mu$	seen	
Γ_3 $J/\psi(1S)\tau^+\nu_\tau$	seen	

Γ_4 $J/\psi(1S)\pi^+$	seen
Γ_5 $J/\psi(1S)K^+$	seen
Γ_6 $J/\psi(1S)\pi^+\pi^+\pi^-$	seen
Γ_7 $J/\psi(1S)a_1(1260)$	not seen
Γ_8 $J/\psi(1S)K^+K^-\pi^+$	seen
Γ_9 $J/\psi(1S)\pi^+\pi^+\pi^+\pi^-\pi^-$	seen
Γ_{10} $\psi(2S)\pi^+$	seen
Γ_{11} $J/\psi(1S)D^0 K^+$	seen
Γ_{12} $J/\psi(1S)D^*(2007)^0 K^+$	seen
Γ_{13} $J/\psi(1S)D^*(2010)^+ K^{*0}$	seen
Γ_{14} $J/\psi(1S)D^+ K^{*0}$	seen
Γ_{15} $J/\psi(1S)D_s^+$	seen
Γ_{16} $J/\psi(1S)D_s^{*+}$	seen
Γ_{17} $J/\psi(1S)\rho\bar{p}\pi^+$	seen
Γ_{18} $\chi_c^0\pi^+$	$(2.4^{+0.9}_{-0.8}) \times 10^{-5}$
Γ_{19} $p\bar{p}\pi^+$	not seen
Γ_{20} $D^0 K^+$	seen
Γ_{21} $D^0\pi^+$	not seen
Γ_{22} $D^{*0}\pi^+$	not seen
Γ_{23} $D^{*0}K^+$	not seen
Γ_{24} $D_s^+\bar{D}^0$	$< 7.2 \times 10^{-4}$ 90%
Γ_{25} $D_s^+D^0$	$< 3.0 \times 10^{-4}$ 90%
Γ_{26} $D^+\bar{D}^0$	$< 1.9 \times 10^{-4}$ 90%
Γ_{27} D^+D^0	$< 1.4 \times 10^{-4}$ 90%
Γ_{28} $D_s^{*+}\bar{D}^0$	$< 5.3 \times 10^{-4}$ 90%
Γ_{29} $D_s^+\bar{D}^*(2007)^0$	$< 4.6 \times 10^{-4}$ 90%
Γ_{30} $D_s^{*+}D^0$	$< 9 \times 10^{-4}$ 90%
Γ_{31} $D_s^+D^*(2007)^0$	$< 6.6 \times 10^{-4}$ 90%
Γ_{32} $D^*(2010)^+\bar{D}^0$	$< 3.8 \times 10^{-4}$ 90%
Γ_{33} $D^*(2010)^+\bar{D}^0, D^{*+} \rightarrow D^+\pi^0/\gamma$	not seen
Γ_{34} $D^+\bar{D}^*(2007)^0$	$< 6.5 \times 10^{-4}$ 90%
Γ_{35} $D^*(2007)^+\bar{D}^0$	$< 2.0 \times 10^{-4}$ 90%
Γ_{36} $D^*(2010)^+D^0, D^{*+} \rightarrow D^+\pi^0/\gamma$	not seen
Γ_{37} $D^+D^*(2007)^0$	$< 3.7 \times 10^{-4}$ 90%
Γ_{38} $D_s^{*+}\bar{D}^*(2007)^0$	$< 1.3 \times 10^{-3}$ 90%
Γ_{39} $D_s^+D^*(2007)^0$	$< 1.3 \times 10^{-3}$ 90%
Γ_{40} $D^*(2010)^+\bar{D}^*(2007)^0$	$< 1.0 \times 10^{-3}$ 90%
Γ_{41} $D^*(2010)^+D^*(2007)^0$	$< 7.7 \times 10^{-4}$ 90%
Γ_{42} D^+K^{*0}	not seen
Γ_{43} $D^+\bar{K}^{*0}$	not seen
Γ_{44} $D_s^+K^{*0}$	not seen
Γ_{45} $D_s^+\bar{K}^{*0}$	not seen
Γ_{46} $D_s^+\phi$	not seen
Γ_{47} K^+K^0	not seen
Γ_{48} $B_s^0\pi^+ / B(\bar{b} \rightarrow B_s)$	seen

B_c^+ BRANCHING RATIOS

VALUE (units 10^{-5})	CL%	DOCUMENT ID	TECN	COMMENT	$\Gamma_1/\Gamma \times B$
8.2 ± 1.3 OUR AVERAGE		Error includes scale factor of 1.4.			
$8.8 \pm 1.0 \pm 0.2$		^{1,2} AALTONEN	16A CDF	$p\bar{p}$ at 1.96 TeV	
$5.2^{+2.4}_{-2.1}$		³ ABE	98M CDF	$p\bar{p}$ 1.8 TeV	
< 16	90	⁴ ACKERSTAFF	98O OPAL	$e^+e^- \rightarrow Z$	
< 19	90	⁵ ABREU	97E DLPH	$e^+e^- \rightarrow Z$	
< 12	90	⁶ BARATE	97H ALEP	$e^+e^- \rightarrow Z$	

- We do not use the following data for averages, fits, limits, etc. •••**
- ¹ AALTONEN 16A reports $[\Gamma(B_c^+ \rightarrow J/\psi(1S)\ell^+\nu_\ell \text{ anything})/\Gamma_{\text{total}} \times B(\bar{b} \rightarrow B_c)] / [B(\bar{b} \rightarrow B^+)] / [B(B^+ \rightarrow J/\psi(1S)K^+)] = 0.211 \pm 0.012^{+0.021}_{-0.020}$ which we multiply by our best values $B(\bar{b} \rightarrow B^+) = (40.8 \pm 0.7) \times 10^{-2}$, $B(B^+ \rightarrow J/\psi(1S)K^+) = (1.020 \pm 0.019) \times 10^{-3}$. Our first error is their experiment's error and our second error is the systematic error from using our best values.
- ² AALTONEN 16A also measures the cross-section $\sigma(B_c) \times B(B_c \rightarrow J/\psi\mu\nu_\mu) = 0.60 \pm 0.09 \text{ nb}$ and estimates the total cross-section $\sigma(B_c)$ to be in the range 25 ± 4 to $52 \pm 8 \text{ nb}$ for $p_T(B_c) > 6 \text{ GeV}/c$ and $|y(B_c)| < 1$.
- ³ ABE 98M result is derived from the measurement of $[\sigma(B_c) \times B(B_c \rightarrow J/\psi(1S)\ell\nu_\ell)] / [\sigma(B^+) \times B(B^+ \rightarrow J/\psi(1S)K^+)] = 0.132^{+0.041}_{-0.037}(\text{stat}) \pm 0.031(\text{sys})^{+0.032}_{-0.020}(\text{lifetime})$ by using PDG 98 values of $B(b \rightarrow B^+)$ and $B(B^+ \rightarrow J/\psi(1S)K^+)$.
- ⁴ ACKERSTAFF 98O reports $B(Z \rightarrow B_c X)/B(Z \rightarrow qq) \times B(B_c \rightarrow J/\psi(1S)\ell\nu_\ell) < 6.95 \times 10^{-5}$ at 90%CL. We rescale to our PDG 98 values of $B(Z \rightarrow b\bar{b})$.
- ⁵ ABREU 97E value listed is for an assumed $\tau_{B_c} = 0.4 \text{ ps}$ and improves to 1.6×10^{-4} for $\tau_{B_c} = 1.4 \text{ ps}$.

Meson Particle Listings

 B_C^+

⁶ BARATE 97H reports $B(Z \rightarrow B_C X)/B(Z \rightarrow qq) \cdot B(B_C \rightarrow J/\psi(1S) \ell \nu_\ell) < 5.2 \times 10^{-5}$ at 90%CL. We rescale to our PDG 96 values of $B(Z \rightarrow b\bar{b})$. A $B_C^+ \rightarrow J/\psi(1S) \mu^+ \nu_\mu$ candidate event is found, compared to all the known background sources 2×10^{-3} , which gives $m_{B_C} = 5.96^{+0.25}_{-0.19}$ GeV and $\tau_{B_C} = 1.77 \pm 0.17$ ps.

VALUE	DOCUMENT ID	TECN	COMMENT	Γ_3/Γ_2
0.71 ± 0.17 ± 0.18	¹ AAIJ	18c	LHCB	pp at 7, 8 TeV

¹ AAIJ 18c uses $\tau^+ \rightarrow \mu^+ \nu_\mu \bar{\nu}_\tau$ mode to obtain the ratio value.

VALUE	CL%	DOCUMENT ID	TECN	COMMENT	$\Gamma_4/\Gamma \times B$
seen		¹ AABOUD	21	ATLS	pp at 8 TeV
seen		² AAIJ	15M	LHCB	pp at 8 TeV
seen		³ KHACHATRYAN...15AA	CMS		pp at 7 TeV
seen		⁴ AALTONEN	13	CDF	$p\bar{p}$ at 1.96 TeV
seen		⁴ AAIJ	12AV	LHCB	pp at 7 TeV
seen		AALTONEN	08M	CDF	$p\bar{p}$ at 1.96 TeV
seen		ABAZOV	08T	D0	$p\bar{p}$ at 1.96 TeV

• • • We do not use the following data for averages, fits, limits, etc. • • •

$< 2.4 \times 10^{-4}$	90	⁵ ACKERSTAFF	98o	OPAL	$e^+ e^- \rightarrow Z$
$< 3.4 \times 10^{-4}$	90	⁶ ABREU	97E	DLPH	$e^+ e^- \rightarrow Z$
$< 8.2 \times 10^{-5}$	90	⁷ BARATE	97H	ALEP	$e^+ e^- \rightarrow Z$
$< 2.0 \times 10^{-5}$	95	⁸ ABE	96R	CDF	$p\bar{p}$ 1.8 TeV

¹ AABOUD 21 reports a measurement of $B(B_C^+ \rightarrow J/\psi \pi^+) / B(B^+ \rightarrow J/\psi K^+)$ $\cdot f_c/f_u = (0.34 \pm 0.04^{+0.06}_{-0.02} \pm 0.01)$ %, at $p_T > 13$ GeV and $|y| < 2.3$.

² AAIJ 15M reports a measurement of $B(B_C^+ \rightarrow J/\psi \pi^+) / B(B^+ \rightarrow J/\psi K^+) \cdot f_c/f_u = (0.683 \pm 0.018 \pm 0.009)$ % at $p_T(B) < 20$ GeV and $2.0 < y(B) < 4.5$.

³ KHACHATRYAN 15AA reports a measurement of $B(B_C^+ \rightarrow J/\psi \pi^+) / B(B^+ \rightarrow J/\psi K^+) \cdot f_c/f_u = (0.48 \pm 0.05 \pm 0.03 \pm 0.05)$ %, at $p_T > 15$ GeV and $|\eta(B)| < 1.6$.

⁴ AAIJ 12AV reports a measurement of $B(B_C^+ \rightarrow J/\psi \pi^+) / B(B^+ \rightarrow J/\psi K^+) \cdot f_c/f_u = (0.68 \pm 0.10 \pm 0.03 \pm 0.05)$ % at $p_T(B) > 4$ GeV and $2.5 < \eta(B) < 4.5$.

⁵ ACKERSTAFF 98o reports $B(Z \rightarrow B_C X)/B(Z \rightarrow qq) \times B(B_C \rightarrow J/\psi(1S) \pi^+) < 1.06 \times 10^{-4}$ at 90%CL. We rescale to our PDG 98 values of $B(Z \rightarrow b\bar{b})$.

⁶ ABREU 97E value listed is for an assumed $\tau_{B_C} = 0.4$ ps and improves to 2.7×10^{-4} for $\tau_{B_C} = 1.4$ ps.

⁷ BARATE 97H reports $B(Z \rightarrow B_C X)/B(Z \rightarrow qq) \cdot B(B_C \rightarrow J/\psi(1S) \pi) < 3.6 \times 10^{-5}$ at 90%CL. We rescale to our PDG 96 values of $B(Z \rightarrow b\bar{b})$.

⁸ ABE 96R reports $B(b \rightarrow B_C X)/B(b \rightarrow B^+ X) \cdot B(B_C^+ \rightarrow J/\psi(1S) \pi^+) / B(B^+ \rightarrow J/\psi(1S) K^+) < 0.053$ at 95%CL for $\tau_{B_C} = 0.8$ ps. It changes from 0.15 to 0.04 for $0.17 \text{ ps} < \tau_{B_C} < 1.6$ ps. We rescale to our PDG 96 values of $B(b \rightarrow B^+) = 0.378 \pm 0.022$ and $B(B^+ \rightarrow J/\psi(1S) K^+) = 0.00101 \pm 0.00014$.

VALUE (units 10^{-2})	DOCUMENT ID	TECN	COMMENT	Γ_4/Γ_2
4.69 ± 0.28 ± 0.46	¹ AAIJ	14W	LHCB	pp at 7 TeV

¹ AAIJ 14W reports also a measurement $B(B_C^+ \rightarrow J/\psi \pi^+) / B(B^+ \rightarrow J/\psi \mu^+ \nu_\mu) = 0.271 \pm 0.016 \pm 0.016$ in the region $m_{J/\psi \mu^+} > 5.3$ GeV.

VALUE	EVTS	DOCUMENT ID	TECN	COMMENT	Γ_5/Γ_4
0.079 ± 0.007 ± 0.003		AAIJ	16AF	LHCB	pp at 7, 8 TeV
0.069 ± 0.019 ± 0.005	50	AAIJ	13BY	LHCB	Repl. by AAIJ 16AF

VALUE	CL%	DOCUMENT ID	TECN	COMMENT	$\Gamma_6/\Gamma \times B$
seen		AAIJ	12Y	LHCB	pp at 7 TeV

• • • We do not use the following data for averages, fits, limits, etc. • • •

$< 5.7 \times 10^{-4}$	90	¹ ABREU	97E	DLPH	$e^+ e^- \rightarrow Z$
------------------------	----	--------------------	-----	------	-------------------------

¹ ABREU 97E value listed is independent of $0.4 \text{ ps} < \tau_{B_C} < 1.4$ ps.

VALUE	DOCUMENT ID	TECN	COMMENT	Γ_6/Γ_4
2.4 ± 0.4 OUR AVERAGE				
$2.55 \pm 0.80 \pm 0.33^{+0.04}_{-0.01}$	KHACHATRY...15AA	CMS		pp at 7 TeV
$2.41 \pm 0.30 \pm 0.33$	AAIJ	12Y	LHCB	pp at 7 TeV

VALUE	CL%	DOCUMENT ID	TECN	COMMENT	$\Gamma_7/\Gamma \times B$
$< 1.2 \times 10^{-3}$	90	¹ ACKERSTAFF	98o	OPAL	$e^+ e^- \rightarrow Z$

¹ ACKERSTAFF 98o reports $B(Z \rightarrow B_C X)/B(Z \rightarrow qq) \times B(B_C \rightarrow J/\psi(1S) a_1(1260)) < 5.29 \times 10^{-4}$ at 90%CL. We rescale to our PDG 98 values of $B(Z \rightarrow b\bar{b})$.

VALUE	DOCUMENT ID	TECN	COMMENT	$\Gamma_8/\Gamma \times B$
seen	¹ AAIJ	13CA	LHCB	pp at 7, 8 TeV

¹ A signal yield of 78 ± 14 decays is reported with a significance of 6.2 standard deviations using an integrated luminosity of 3 fb^{-1} data.

VALUE	DOCUMENT ID	TECN	COMMENT	Γ_8/Γ_4
0.53 ± 0.10 ± 0.05	¹ AAIJ	13CA	LHCB	pp at 7, 8 TeV

¹ A signal yield of 78 ± 14 decays is reported with a significance of 6.2 standard deviations using an integrated luminosity of 3 fb^{-1} data.

VALUE	DOCUMENT ID	TECN	COMMENT	Γ_9/Γ_4
1.74 ± 0.44 ± 0.24	¹ AAIJ	14P	LHCB	pp at 7, 8 TeV

¹ A signal yield of 32 ± 8 decays is reported with a significance of 4.5 standard deviations.

VALUE	DOCUMENT ID	TECN	COMMENT	Γ_{10}/Γ_4
0.268 ± 0.032 ± 0.007 ± 0.006	¹ AAIJ	15AY	LHCB	pp at 7, 8 TeV
$0.250 \pm 0.068 \pm 0.014 \pm 0.006$	¹ AAIJ	13AM	LHCB	Repl. by AAIJ 15AY

¹ The last uncertainty is due to the uncertainty of the $B(\psi(2S) \rightarrow \mu^+ \mu^-) / B(J/\psi \rightarrow \mu^+ \mu^-)$ ratio measurement.

VALUE	DOCUMENT ID	TECN	COMMENT	Γ_{11}/Γ_4
0.432 ± 0.136 ± 0.028	AAIJ	17L	LHCB	pp at 7, 8 TeV

VALUE	DOCUMENT ID	TECN	COMMENT	Γ_{12}/Γ_{11}
5.1 ± 1.8 ± 0.4	AAIJ	17L	LHCB	pp at 7, 8 TeV

VALUE	DOCUMENT ID	TECN	COMMENT	Γ_{13}/Γ_{11}
2.10 ± 1.08 ± 0.34	AAIJ	17L	LHCB	pp at 7, 8 TeV

VALUE	DOCUMENT ID	TECN	COMMENT	Γ_{14}/Γ_{11}
0.63 ± 0.39 ± 0.08	AAIJ	17L	LHCB	pp at 7, 8 TeV

VALUE	DOCUMENT ID	TECN	COMMENT	Γ_{15}/Γ_4
3.1 ± 0.5 OUR AVERAGE				
$3.8 \pm 1.1 \pm 0.4$	AAD	16H	ATLS	pp at 7, 8 TeV
$2.90 \pm 0.57 \pm 0.24$	AAIJ	13AS	LHCB	pp at 7, 8 TeV

VALUE	DOCUMENT ID	TECN	COMMENT	Γ_{16}/Γ_4
10.4 ± 3.1 ± 1.6	AAD	16H	ATLS	pp at 7, 8 TeV

VALUE	DOCUMENT ID	TECN	COMMENT	Γ_{16}/Γ_{15}
2.5 ± 0.5 OUR AVERAGE				
$2.8^{+1.2}_{-0.8} \pm 0.3$	AAD	16H	ATLS	pp at 7, 8 TeV
$2.37 \pm 0.56 \pm 0.10$	AAIJ	13AS	LHCB	pp at 7, 8 TeV

VALUE	DOCUMENT ID	TECN	COMMENT	Γ_{17}/Γ_4
0.143 ± 0.041 -0.036	AAIJ	14AQ	LHCB	pp at 7, 8 TeV

VALUE (units 10^{-6})	DOCUMENT ID	TECN	COMMENT	Γ_{18}/Γ
24.0 ± 8.6 ± 0.4	^{1,2} AAIJ	16AT	LHCB	pp at 7 and 8 TeV

¹ AAIJ 16AT reports $[\Gamma(B_C^+ \rightarrow \chi_c^0 \pi^+)/\Gamma_{\text{total}}] \times [\Gamma(\bar{b} \rightarrow B^+)/\Gamma_{\text{total}}] = (9.8^{+3.4}_{-3.0} \pm 0.8) \times 10^{-6}$ which we divide by our best value $\Gamma(\bar{b} \rightarrow B^+)/\Gamma_{\text{total}} = 0.408 \pm 0.007$. Our first error is their experiment's error and our second error is the systematic error from using our best value.

² The significance of the observed signal is 4.0 standard deviations.

VALUE	DOCUMENT ID	TECN	COMMENT	Γ_{19}/Γ
not seen	¹ AAIJ	16K	LHCB	pp at 7, 8 TeV

¹ Measures the ratio $(f_c/f_u) \times B(B_C^+ \rightarrow p\bar{p}\pi^+) < 3.6 \times 10^{-8}$ at 95% CL, in the region $m(p\bar{p}) < 2.85 \text{ GeV}/c^2$, where f_c (f_u) represents the fragmentation fraction of the b -quark into the B_C^+ (B_u^+) meson.

See key on page 1127

Meson Particle Listings

B_c⁺

Γ(D⁰K⁺)/Γ_{total} × B(B⁻ → B_c) Γ₂₀/Γ × B

Table with columns: VALUE (units 10⁻⁷), DOCUMENT ID, TECN, COMMENT. Row 1: 3.8 ± 1.2 ± 0.1, 1 AAIJ, 17AG LHCB, pp at 7, 8 TeV

1 AAIJ 17AG reports [Γ(B_c⁺ → D⁰K⁺)/Γ_{total} × B(B⁻ → B_c)] / [B(B⁻ → B⁺)] = (9.3 ± 2.8 ± 0.6) × 10⁻⁷ which we multiply by our best value B(B⁻ → B⁺) = (40.8 ± 0.7) × 10⁻². Our first error is their experiment's error and our second error is the systematic error from using our best value.

Γ(D⁰π⁺)/Γ_{total} × B(B⁻ → B_c) Γ₂₁/Γ × B

Table with columns: VALUE, CL%, DOCUMENT ID, TECN, COMMENT. Row 1: <1.6 × 10⁻⁷, 95, 1 AAIJ, 17AG LHCB, pp at 7, 8 TeV

1 AAIJ 17AG reports [Γ(B_c⁺ → D⁰π⁺)/Γ_{total} × B(B⁻ → B_c)] / [B(B⁻ → B⁺)] < 3.9 × 10⁻⁷ which we multiply by our best value B(B⁻ → B⁺) = 40.8 × 10⁻².

Γ(D⁰*π⁺)/Γ_{total} × B(B⁻ → B_c) Γ₂₂/Γ × B

Table with columns: VALUE, CL%, DOCUMENT ID, TECN, COMMENT. Row 1: <4 × 10⁻⁷, 95, 1 AAIJ, 17AG LHCB, pp at 7, 8 TeV

1 AAIJ 17AG reports [Γ(B_c⁺ → D⁰*π⁺)/Γ_{total} × B(B⁻ → B_c)] / [B(B⁻ → B⁺)] < 1.1 × 10⁻⁶ which we multiply by our best value B(B⁻ → B⁺) = 40.8 × 10⁻².

Γ(D⁰*K⁺)/Γ_{total} × B(B⁻ → B_c) Γ₂₃/Γ × B

Table with columns: VALUE, CL%, DOCUMENT ID, TECN, COMMENT. Row 1: <4 × 10⁻⁷, 95, 1 AAIJ, 17AG LHCB, pp at 7, 8 TeV

1 AAIJ 17AG reports [Γ(B_c⁺ → D⁰*K⁺)/Γ_{total} × B(B⁻ → B_c)] / [B(B⁻ → B⁺)] < 1.1 × 10⁻⁶ which we multiply by our best value B(B⁻ → B⁺) = 40.8 × 10⁻².

Γ(D_s⁺D⁰)/Γ_{total} × B(B⁻ → B_c) Γ₂₄/Γ × B

Table with columns: VALUE, CL%, DOCUMENT ID, TECN, COMMENT. Row 1: <1.4 × 10⁻⁷, 90, 1 AAIJ, 18P LHCB, pp at 7, 8 TeV

1 AAIJ 18P reports [Γ(B_c⁺ → D_s⁺D⁰)/Γ_{total} × B(B⁻ → B_c)] / [B(B⁻ → B⁺)] / [B(B⁺ → D⁰D⁺)] < 0.9 × 10⁻³ which we multiply by our best values B(B⁻ → B⁺) = 40.8 × 10⁻², B(B⁺ → D⁰D⁺) = 3.8 × 10⁻⁴.

Γ(D_s⁺D⁰)/Γ_{total} × B(B⁻ → B_c) Γ₂₅/Γ × B

Table with columns: VALUE, CL%, DOCUMENT ID, TECN, COMMENT. Row 1: <6 × 10⁻⁸, 90, 1 AAIJ, 18P LHCB, pp at 7, 8 TeV

1 AAIJ 18P reports [Γ(B_c⁺ → D_s⁺D⁰)/Γ_{total} × B(B⁻ → B_c)] / [B(B⁻ → B⁺)] / [B(B⁺ → D⁰D⁺)] < 3.7 × 10⁻⁴ which we multiply by our best values B(B⁻ → B⁺) = 40.8 × 10⁻², B(B⁺ → D⁰D⁺) = 3.8 × 10⁻⁴.

Γ(D⁺D⁰)/Γ_{total} × B(B⁻ → B_c) Γ₂₆/Γ × B

Table with columns: VALUE, CL%, DOCUMENT ID, TECN, COMMENT. Row 1: <3.0 × 10⁻⁶, 90, 1 AAIJ, 18P LHCB, pp at 7, 8 TeV

1 AAIJ 18P reports [Γ(B_c⁺ → D⁺D⁰)/Γ_{total} × B(B⁻ → B_c)] / [B(B⁻ → B⁺)] / [B(B⁺ → D⁰D⁺)] < 1.9 × 10⁻² which we multiply by our best values B(B⁻ → B⁺) = 40.8 × 10⁻², B(B⁺ → D⁰D⁺) = 3.8 × 10⁻⁴.

Γ(D⁺D⁰)/Γ_{total} × B(B⁻ → B_c) Γ₂₇/Γ × B

Table with columns: VALUE, CL%, DOCUMENT ID, TECN, COMMENT. Row 1: <1.9 × 10⁻⁶, 90, 1 AAIJ, 18P LHCB, Repl. by AAIJ 21AF

1 AAIJ 18P reports [Γ(B_c⁺ → D⁺D⁰)/Γ_{total} × B(B⁻ → B_c)] / [B(B⁻ → B⁺)] / [B(B⁺ → D⁰D⁺)] < 1.2 × 10⁻² which we multiply by our best values B(B⁻ → B⁺) = 40.8 × 10⁻², B(B⁺ → D⁰D⁺) = 3.8 × 10⁻⁴.

[Γ(D_s⁺D⁰) + Γ(D_s⁺D⁰*)]/Γ_{total} × B(B⁻ → B_c) (Γ₂₈+Γ₂₉)/Γ × B

Table with columns: VALUE, CL%, DOCUMENT ID, TECN, COMMENT. Row 1: <4 × 10⁻⁷, 90, 1 AAIJ, 18P LHCB, Repl. by AAIJ 21AF

1 AAIJ 18P reports [Γ(B_c⁺ → D_s⁺D⁰) + Γ(B_c⁺ → D_s⁺D⁰*)]/Γ_{total} × B(B⁻ → B_c)] / [B(B⁻ → B⁺)] / [B(B⁺ → D⁰D⁺)] < 2.8 × 10⁻³ which we multiply by our best values B(B⁻ → B⁺) = 40.8 × 10⁻², B(B⁺ → D⁰D⁺) = 3.8 × 10⁻⁴.

[Γ(D_s⁺D⁰) + Γ(D_s⁺D⁰*)]/Γ_{total} × B(B⁻ → B_c) (Γ₃₀+Γ₃₁)/Γ × B

Table with columns: VALUE, CL%, DOCUMENT ID, TECN, COMMENT. Row 1: <5 × 10⁻⁷, 90, 1 AAIJ, 18P LHCB, Repl. by AAIJ 21AF

1 AAIJ 18P reports [Γ(B_c⁺ → D_s⁺D⁰) + Γ(B_c⁺ → D_s⁺D⁰*)]/Γ_{total} × B(B⁻ → B_c)] / [B(B⁻ → B⁺)] / [B(B⁺ → D⁰D⁺)] < 3.0 × 10⁻³ which we multiply by our best values B(B⁻ → B⁺) = 40.8 × 10⁻², B(B⁺ → D⁰D⁺) = 3.8 × 10⁻⁴.

Γ(D⁺(2010)+D⁰)/Γ_{total} × B(B⁻ → B_c) Γ₃₂/Γ × B

Table with columns: VALUE, CL%, DOCUMENT ID, TECN, COMMENT. Row 1: <6.2 × 10⁻³, 90, 1 BARATE, 98Q ALEP, e⁺e⁻ → Z

1 BARATE 98Q reports B(Z → B_cX) × B(B_c → D⁺(2010)+D⁰) < 1.9 × 10⁻³ at 90%CL. We rescale to our PDG 98 values of B(Z → bD⁻).

[Γ(D⁺(2010)+D⁰, D⁺* → D⁺π⁰/γ) + Γ(D⁺D⁰*(2007⁰))]/Γ_{total} × B(B⁻ → B_c) (Γ₃₃+Γ₃₄)/Γ × B

Table with columns: VALUE, CL%, DOCUMENT ID, TECN, COMMENT. Row 1: <9 × 10⁻⁶, 90, 1 AAIJ, 18P LHCB, Repl. by AAIJ 21AF

1 AAIJ 18P reports [Γ(B_c⁺ → D⁺(2010)+D⁰, D⁺* → D⁺π⁰/γ) + Γ(B_c⁺ → D⁺D⁰*(2007⁰))]/Γ_{total} × B(B⁻ → B_c)] / [B(B⁻ → B⁺)] / [B(B⁺ → D⁰D⁺)] < 5.5 × 10⁻² which we multiply by our best values B(B⁻ → B⁺) = 40.8 × 10⁻², B(B⁺ → D⁰D⁺) = 3.8 × 10⁻⁴.

[Γ(D⁺(2010)+D⁰, D⁺* → D⁺π⁰/γ) + Γ(D⁺D⁰*(2007⁰))]/Γ_{total} × B(B⁻ → B_c) (Γ₃₆+Γ₃₇)/Γ × B

Table with columns: VALUE, CL%, DOCUMENT ID, TECN, COMMENT. Row 1: <3.4 × 10⁻⁶, 90, 1 AAIJ, 18P LHCB, Repl. by AAIJ 21AF

1 AAIJ 18P reports [Γ(B_c⁺ → D⁺(2010)+D⁰, D⁺* → D⁺π⁰/γ) + Γ(B_c⁺ → D⁺D⁰*(2007⁰))]/Γ_{total} × B(B⁻ → B_c)] / [B(B⁻ → B⁺)] / [B(B⁺ → D⁰D⁺)] < 2.2 × 10⁻² which we multiply by our best values B(B⁻ → B⁺) = 40.8 × 10⁻², B(B⁺ → D⁰D⁺) = 3.8 × 10⁻⁴.

Γ(D_s⁺D⁰*(2007⁰))/Γ_{total} × B(B⁻ → B_c) Γ₃₈/Γ × B

Table with columns: VALUE, CL%, DOCUMENT ID, TECN, COMMENT. Row 1: <1.7 × 10⁻⁶, 90, 1 AAIJ, 18P LHCB, Repl. by AAIJ 21AF

1 AAIJ 18P reports [Γ(B_c⁺ → D_s⁺D⁰*(2007⁰))/Γ_{total} × B(B⁻ → B_c)] / [B(B⁻ → B⁺)] / [B(B⁺ → D⁰D⁺)] < 1.1 × 10⁻² which we multiply by our best values B(B⁻ → B⁺) = 40.8 × 10⁻², B(B⁺ → D⁰D⁺) = 3.8 × 10⁻⁴.

Γ(D_s⁺D⁰*(2007⁰))/Γ_{total} × B(B⁻ → B_c) Γ₃₉/Γ × B

Table with columns: VALUE, CL%, DOCUMENT ID, TECN, COMMENT. Row 1: <3.1 × 10⁻⁶, 90, 1 AAIJ, 18P LHCB, Repl. by AAIJ 21AF

1 AAIJ 18P reports [Γ(B_c⁺ → D_s⁺D⁰*(2007⁰))/Γ_{total} × B(B⁻ → B_c)] / [B(B⁻ → B⁺)] / [B(B⁺ → D⁰D⁺)] < 2.0 × 10⁻² which we multiply by our best values B(B⁻ → B⁺) = 40.8 × 10⁻², B(B⁺ → D⁰D⁺) = 3.8 × 10⁻⁴.

Γ(D⁺(2010)+D⁰*(2007⁰))/Γ_{total} × B(B⁻ → B_c) Γ₄₀/Γ × B

Table with columns: VALUE, CL%, DOCUMENT ID, TECN, COMMENT. Row 1: <1.0 × 10⁻⁴, 90, 1 AAIJ, 18P LHCB, Repl. by AAIJ 21AF

1 AAIJ 18P reports [Γ(B_c⁺ → D⁺(2010)+D⁰*(2007⁰))/Γ_{total} × B(B⁻ → B_c)] / [B(B⁻ → B⁺)] / [B(B⁺ → D⁰D⁺)] < 6.5 × 10⁻¹ which we multiply by our best values B(B⁻ → B⁺) = 40.8 × 10⁻², B(B⁺ → D⁰D⁺) = 3.8 × 10⁻⁴.

Γ(D⁺(2010)+D⁰*(2007⁰))/Γ_{total} × B(B⁻ → B_c) Γ₄₁/Γ × B

Table with columns: VALUE, CL%, DOCUMENT ID, TECN, COMMENT. Row 1: <2.0 × 10⁻⁵, 90, 1 AAIJ, 18P LHCB, Repl. by AAIJ 21AF

1 AAIJ 18P reports [Γ(B_c⁺ → D⁺(2010)+D⁰*(2007⁰))/Γ_{total} × B(B⁻ → B_c)] / [B(B⁻ → B⁺)] / [B(B⁺ → D⁰D⁺)] < 1.3 × 10⁻¹ which we multiply by our best values B(B⁻ → B⁺) = 40.8 × 10⁻², B(B⁺ → D⁰D⁺) = 3.8 × 10⁻⁴.

Γ(D⁺K⁰)/Γ_{total} × B(B⁻ → B_c) Γ₄₂/Γ × B

Table with columns: VALUE, CL%, DOCUMENT ID, TECN, COMMENT. Row 1: <2.0 × 10⁻⁷, 90, 1 AAIJ, 13R LHCB, pp at 7 TeV

1 AAIJ 13R reports [Γ(B_c⁺ → D⁺K⁰)/Γ_{total} × B(B⁻ → B_c)] / [B(B⁻ → B⁺)] < 0.5 × 10⁻⁶ which we multiply by our best value B(B⁻ → B⁺) = 40.8 × 10⁻².

Γ(D⁺K⁰*)/Γ_{total} × B(B⁻ → B_c) Γ₄₃/Γ × B

Table with columns: VALUE, CL%, DOCUMENT ID, TECN, COMMENT. Row 1: <1.6 × 10⁻⁷, 90, 1 AAIJ, 13R LHCB, pp at 7 TeV

1 AAIJ 13R reports [Γ(B_c⁺ → D⁺K⁰*)/Γ_{total} × B(B⁻ → B_c)] / [B(B⁻ → B⁺)] < 0.4 × 10⁻⁶ which we multiply by our best value B(B⁻ → B⁺) = 40.8 × 10⁻².

Γ(D_s⁺K⁰)/Γ_{total} × B(B⁻ → B_c) Γ₄₄/Γ × B

Table with columns: VALUE, CL%, DOCUMENT ID, TECN, COMMENT. Row 1: <2.9 × 10⁻⁷, 90, 1 AAIJ, 13R LHCB, pp at 7 TeV

1 AAIJ 13R reports [Γ(B_c⁺ → D_s⁺K⁰)/Γ_{total} × B(B⁻ → B_c)] / [B(B⁻ → B⁺)] < 0.7 × 10⁻⁶ which we multiply by our best value B(B⁻ → B⁺) = 40.8 × 10⁻².

Γ(D_s⁺K⁰*)/Γ_{total} × B(B⁻ → B_c) Γ₄₅/Γ × B

Table with columns: VALUE, CL%, DOCUMENT ID, TECN, COMMENT. Row 1: <4 × 10⁻⁷, 90, 1 AAIJ, 13R LHCB, pp at 7 TeV

1 AAIJ 13R reports [Γ(B_c⁺ → D_s⁺K⁰*)/Γ_{total} × B(B⁻ → B_c)] / [B(B⁻ → B⁺)] < 1.1 × 10⁻⁶ which we multiply by our best value B(B⁻ → B⁺) = 40.8 × 10⁻².

Meson Particle Listings

B_c^+

$\Gamma(D_s^+ \phi)/\Gamma_{\text{total}} \times B(\bar{b} \rightarrow B_c)$		$\Gamma_{46}/\Gamma \times B$	
VALUE	CL%	DOCUMENT ID	TECN COMMENT

$<3.3 \times 10^{-7}$ 90 1 AAIJ 13R LHCB *pp* at 7 TeV
 1 AAIJ 13R reports $[\Gamma(B_c^+ \rightarrow D_s^+ \phi)/\Gamma_{\text{total}} \times B(\bar{b} \rightarrow B_c)] / [B(\bar{b} \rightarrow B^+)] < 0.8 \times 10^{-6}$ which we multiply by our best value $B(\bar{b} \rightarrow B^+) = 40.8 \times 10^{-2}$.

$\Gamma(K^+ K^0)/\Gamma_{\text{total}} \times B(\bar{b} \rightarrow B_c)$		$\Gamma_{47}/\Gamma \times B$	
VALUE	CL%	DOCUMENT ID	TECN COMMENT

$<4.6 \times 10^{-7}$ 90 1 AAIJ 13Bs LHCB *pp* at 7 TeV
 1 Derived from $\Gamma(K^+ K^0)/\Gamma \times B(\bar{b} \rightarrow B_c) / (B(B^+ \rightarrow K^0 \pi^+) B(\bar{b} \rightarrow B^+)) < 5.8\%$ at 90% CL using normalization mode $B(B^+ \rightarrow K^0 \pi^+) = (23.97 \pm 0.53 \pm 0.71) \times 10^{-6}$ and assuming a B production ratio $f(\bar{b} \rightarrow B_c^+) = 0.33$.

$\Gamma(B_s^0 \pi^+ / B(\bar{b} \rightarrow B_s)) / \Gamma_{\text{total}} \times B(\bar{b} \rightarrow B_c)$		$\Gamma_{48}/\Gamma \times B$	
VALUE (units 10^{-3})	CL%	DOCUMENT ID	TECN COMMENT

$2.37 \pm 0.31 \pm 0.11 \pm 0.17 \pm 0.13$ 1 AAIJ 13Bu LHCB *pp* at 7, 8 TeV
 1 The last uncertainty is due to the uncertainty of the B_c^+ lifetime measurement.

$\Gamma(D_s^+ \bar{D}^0)/\Gamma_{\text{total}}$		Γ_{24}/Γ	
VALUE	CL%	DOCUMENT ID	TECN COMMENT

$<7.2 \times 10^{-4}$ 90 1 AAIJ 21AF LHCB *pp* at 13 TeV
 1 Uses $B(\bar{b} \rightarrow B_c)/B(\bar{b} \rightarrow B^+) = 0.76\%$ determined by AAIJ 19A1.

$\Gamma(D_s^+ D^0)/\Gamma_{\text{total}}$		Γ_{25}/Γ	
VALUE	CL%	DOCUMENT ID	TECN COMMENT

$<3.0 \times 10^{-4}$ 90 1 AAIJ 21AF LHCB *pp* at 13 TeV
 1 Uses $B(\bar{b} \rightarrow B_c)/B(\bar{b} \rightarrow B^+) = 0.76\%$ determined by AAIJ 19A1.

$\Gamma(D^+ \bar{D}^0)/\Gamma_{\text{total}}$		Γ_{26}/Γ	
VALUE	CL%	DOCUMENT ID	TECN COMMENT

$<1.9 \times 10^{-4}$ 90 1 AAIJ 21AF LHCB *pp* at 13 TeV
 1 Uses $B(\bar{b} \rightarrow B_c)/B(\bar{b} \rightarrow B^+) = 0.76\%$ determined by AAIJ 19A1.

$\Gamma(D^+ D^0)/\Gamma_{\text{total}}$		Γ_{27}/Γ	
VALUE	CL%	DOCUMENT ID	TECN COMMENT

$<1.4 \times 10^{-4}$ 90 1 AAIJ 21AF LHCB *pp* at 13 TeV
 1 Uses $B(\bar{b} \rightarrow B_c)/B(\bar{b} \rightarrow B^+) = 0.76\%$ determined by AAIJ 19A1.

$\Gamma(D_s^+ \bar{D}^0)/\Gamma_{\text{total}}$		Γ_{28}/Γ	
VALUE	CL%	DOCUMENT ID	TECN COMMENT

$<5.3 \times 10^{-4}$ 90 1 AAIJ 21AF LHCB *pp* at 13 TeV
 1 Uses $B(\bar{b} \rightarrow B_c)/B(\bar{b} \rightarrow B^+) = 0.76\%$ determined by AAIJ 19A1.

$\Gamma(D_s^+ \bar{D}^*(2007)^0)/\Gamma_{\text{total}}$		Γ_{29}/Γ	
VALUE	CL%	DOCUMENT ID	TECN COMMENT

$<4.6 \times 10^{-4}$ 90 1 AAIJ 21AF LHCB *pp* at 13 TeV
 1 Uses $B(\bar{b} \rightarrow B_c)/B(\bar{b} \rightarrow B^+) = 0.76\%$ determined by AAIJ 19A1.

$\Gamma(D_s^+ D^0)/\Gamma_{\text{total}}$		Γ_{30}/Γ	
VALUE	CL%	DOCUMENT ID	TECN COMMENT

$<0.9 \times 10^{-3}$ 90 1 AAIJ 21AF LHCB *pp* at 13 TeV
 1 Uses $B(\bar{b} \rightarrow B_c)/B(\bar{b} \rightarrow B^+) = 0.76\%$ determined by AAIJ 19A1.

$\Gamma(D_s^+ D^*(2007)^0)/\Gamma_{\text{total}}$		Γ_{31}/Γ	
VALUE	CL%	DOCUMENT ID	TECN COMMENT

$<6.6 \times 10^{-4}$ 90 1 AAIJ 21AF LHCB *pp* at 13 TeV
 1 Uses $B(\bar{b} \rightarrow B_c)/B(\bar{b} \rightarrow B^+) = 0.76\%$ determined by AAIJ 19A1.

$\Gamma(D^*(2010)^+ \bar{D}^0)/\Gamma_{\text{total}}$		Γ_{32}/Γ	
VALUE	CL%	DOCUMENT ID	TECN COMMENT

$<3.8 \times 10^{-4}$ 90 1 AAIJ 21AF LHCB *pp* at 13 TeV
 1 Uses $B(\bar{b} \rightarrow B_c)/B(\bar{b} \rightarrow B^+) = 0.76\%$ determined by AAIJ 19A1.

$\Gamma(D^*(2007)^+ D^0)/\Gamma_{\text{total}}$		Γ_{35}/Γ	
VALUE	CL%	DOCUMENT ID	TECN COMMENT

$<2.0 \times 10^{-4}$ 90 1 AAIJ 21AF LHCB *pp* at 13 TeV
 1 Uses $B(\bar{b} \rightarrow B_c)/B(\bar{b} \rightarrow B^+) = 0.76\%$ determined by AAIJ 19A1.

$\Gamma(D^+ \bar{D}^*(2007)^0)/\Gamma_{\text{total}}$		Γ_{34}/Γ	
VALUE	CL%	DOCUMENT ID	TECN COMMENT

$<6.5 \times 10^{-4}$ 90 1 AAIJ 21AF LHCB *pp* at 13 TeV
 1 Uses $B(\bar{b} \rightarrow B_c)/B(\bar{b} \rightarrow B^+) = 0.76\%$ determined by AAIJ 19A1.

$\Gamma(D^+ D^*(2007)^0)/\Gamma_{\text{total}}$		Γ_{37}/Γ	
VALUE	CL%	DOCUMENT ID	TECN COMMENT

$<3.7 \times 10^{-4}$ 90 1 AAIJ 21AF LHCB *pp* at 13 TeV
 1 Uses $B(\bar{b} \rightarrow B_c)/B(\bar{b} \rightarrow B^+) = 0.76\%$ determined by AAIJ 19A1.

$\Gamma(D_s^+ \bar{D}^*(2007)^0)/\Gamma_{\text{total}}$		Γ_{38}/Γ	
VALUE	CL%	DOCUMENT ID	TECN COMMENT

$<1.3 \times 10^{-3}$ 90 1 AAIJ 21AF LHCB *pp* at 13 TeV
 1 Uses $B(\bar{b} \rightarrow B_c)/B(\bar{b} \rightarrow B^+) = 0.76\%$ determined by AAIJ 19A1.

$\Gamma(D_s^+ D^*(2007)^0)/\Gamma_{\text{total}}$		Γ_{39}/Γ	
VALUE	CL%	DOCUMENT ID	TECN COMMENT

$<1.3 \times 10^{-3}$ 90 1 AAIJ 21AF LHCB *pp* at 13 TeV
 1 Uses $B(\bar{b} \rightarrow B_c)/B(\bar{b} \rightarrow B^+) = 0.76\%$ determined by AAIJ 19A1.

$\Gamma(D^*(2010)^+ \bar{D}^*(2007)^0)/\Gamma_{\text{total}}$		Γ_{40}/Γ	
VALUE	CL%	DOCUMENT ID	TECN COMMENT

$<1.0 \times 10^{-3}$ 90 1 AAIJ 21AF LHCB *pp* at 13 TeV
 1 Uses $B(\bar{b} \rightarrow B_c)/B(\bar{b} \rightarrow B^+) = 0.76\%$ determined by AAIJ 19A1.

$\Gamma(D^*(2010)^+ D^*(2007)^0)/\Gamma_{\text{total}}$		Γ_{41}/Γ	
VALUE	CL%	DOCUMENT ID	TECN COMMENT

$<7.7 \times 10^{-4}$ 90 1 AAIJ 21AF LHCB *pp* at 13 TeV
 1 Uses $B(\bar{b} \rightarrow B_c)/B(\bar{b} \rightarrow B^+) = 0.76\%$ determined by AAIJ 19A1.

POLARIZATION IN B_c^+ DECAY

In decays involving two vector mesons, one can distinguish among the states in which meson polarizations are both longitudinal (L) or both are transverse and parallel (\parallel) or perpendicular (\perp) to each other with the parameters Γ_L/Γ , $\Gamma_{\parallel}/\Gamma$, and the relative phases ϕ_{\parallel} and ϕ_{\perp} . See the definitions in the note on "Polarization in B Decays" review in the B^0 Particle Listings.

Γ_L/Γ in $B_c^+ \rightarrow J/\psi D_s^{*+}$			
VALUE	CL%	DOCUMENT ID	TECN COMMENT

0.54 ± 0.15 OUR AVERAGE
 0.62 ± 0.24 1 AAD 16H ATLS *pp* at 7, 8 TeV
 0.48 ± 0.20 2 AAIJ 13AS LHCB *pp* at 7, 8 TeV
 1 AAD 16H measures $1 - \Gamma_L/\Gamma = 0.38 \pm 0.24$.
 2 AAIJ 13AS measures $1 - \Gamma_L/\Gamma = 0.52 \pm 0.20$.

$A_P(B_c^+)$			
VALUE (units 10^{-2})	CL%	DOCUMENT ID	TECN COMMENT

-1.0 ± 1.0 OUR AVERAGE
 $A_P(B_c^+) = [\sigma(B_c^-) - \sigma(B_c^+)] / [\sigma(B_c^-) + \sigma(B_c^+)]$
 $-2.5 \pm 2.1 \pm 0.5$ 1 AAIJ 19A1 LHCB *pp* at 7 TeV
 $-0.5 \pm 1.1 \pm 0.4$ 1 AAIJ 19A1 LHCB *pp* at 13 TeV
 1 Measured using B_c^+ semileptonic decays.

B_c^+ REFERENCES

AABOUD	21	PR D104 012010	M. Aaboud <i>et al.</i>	(ATLAS Collab.)
AAIJ	21AF	JHEP 2112 117	R. Aaij <i>et al.</i>	(LHCb Collab.)
AAIJ	20R	JHEP 2007 123	R. Aaij <i>et al.</i>	(LHCb Collab.)
AAIJ	19A1	PR D100 112006	R. Aaij <i>et al.</i>	(LHCb Collab.)
AAIJ	18C	PRL 120 121801	R. Aaij <i>et al.</i>	(LHCb Collab.)
AAIJ	18P	NP B930 563	R. Aaij <i>et al.</i>	(LHCb Collab.)
SIRUNYAN	18BY	EPJ C78 457	A.M. Sirunyan <i>et al.</i>	(CMS Collab.)
AAIJ	17AG	PRL 118 111803	R. Aaij <i>et al.</i>	(LHCb Collab.)
AAIJ	17L	PR D95 032005	R. Aaij <i>et al.</i>	(LHCb Collab.)
AAD	16H	EPJ C76 4	G. Aad <i>et al.</i>	(ATLAS Collab.)
AAIJ	16AF	JHEP 1609 153	R. Aaij <i>et al.</i>	(LHCb Collab.)
AAIJ	16AT	PR D94 091102	R. Aaij <i>et al.</i>	(LHCb Collab.)
AAIJ	16K	PL B759 313	R. Aaij <i>et al.</i>	(LHCb Collab.)
AALTONEN	16A	PR D93 052001	T. Aaltonen <i>et al.</i>	(CDF Collab.)
AAIJ	15AY	PR D92 072007	R. Aaij <i>et al.</i>	(LHCb Collab.)
AAIJ	15G	PL B742 29	R. Aaij <i>et al.</i>	(LHCb Collab.)
AAIJ	15M	PRL 114 132001	R. Aaij <i>et al.</i>	(LHCb Collab.)
KHACHATRYAN...	15AA	JHEP 1501 063	V. Khachatryan <i>et al.</i>	(CMS Collab.)
AAIJ	14AQ	PRL 113 152003	R. Aaij <i>et al.</i>	(LHCb Collab.)
AAIJ	14G	EPJ C74 2839	R. Aaij <i>et al.</i>	(LHCb Collab.)
AAIJ	14P	JHEP 1405 148	R. Aaij <i>et al.</i>	(LHCb Collab.)
AAIJ	14W	PR D90 032009	R. Aaij <i>et al.</i>	(LHCb Collab.)
AAIJ	13AM	PR D87 071103	R. Aaij <i>et al.</i>	(LHCb Collab.)
AAIJ	13AS	PR D87 112012	R. Aaij <i>et al.</i>	(LHCb Collab.)
Also		PR D89 019901 (err.)	R. Aaij <i>et al.</i>	(LHCb Collab.)
AAIJ	13BS	PL B726 646	R. Aaij <i>et al.</i>	(LHCb Collab.)
AAIJ	13BU	PRL 111 181801	R. Aaij <i>et al.</i>	(LHCb Collab.)
AAIJ	13BY	JHEP 1309 075	R. Aaij <i>et al.</i>	(LHCb Collab.)
AAIJ	13CA	JHEP 1311 094	R. Aaij <i>et al.</i>	(LHCb Collab.)
AAIJ	13R	JHEP 1302 043	R. Aaij <i>et al.</i>	(LHCb Collab.)
AALTONEN	13	PR D87 011101	T. Aaltonen <i>et al.</i>	(CDF Collab.)
AAIJ	12AV	PRL 109 232001	R. Aaij <i>et al.</i>	(LHCb Collab.)
AAIJ	12Y	PRL 108 251802	R. Aaij <i>et al.</i>	(LHCb Collab.)
ABAZOV	09H	PRL 102 092001	V.M. Abazov <i>et al.</i>	(D0 Collab.)
AALTONEN	08M	PRL 100 182002	T. Aaltonen <i>et al.</i>	(CDF Collab.)
ABAZOV	08T	PRL 101 012001	V.M. Abazov <i>et al.</i>	(D0 Collab.)
ABULENCIA	06C	PRL 96 082002	A. Abulencia <i>et al.</i>	(CDF Collab.)
ABULENCIA	06O	PRL 97 012002	A. Abulencia <i>et al.</i>	(CDF Collab.)
ABE	98M	PRL 81 2432	F. Abe <i>et al.</i>	(CDF Collab.)
Also		PR D58 112004	F. Abe <i>et al.</i>	(CDF Collab.)
ACKERSTAFF	98O	PL B420 157	K. Ackersstaff <i>et al.</i>	(OPAL Collab.)
BARATE	98	EPJ C4 387	R. Barate <i>et al.</i>	(ALEPH Collab.)
PDG	98	EPJ C3 1	C. Caso <i>et al.</i>	(PDG Collab.)
ABREU	97E	PL B398 207	P. Abreu <i>et al.</i>	(DELPHI Collab.)
BARATE	97H	PL B402 213	R. Barate <i>et al.</i>	(ALEPH Collab.)
ABE	96R	PRL 77 5176	F. Abe <i>et al.</i>	(CDF Collab.)
PDG	96	PR D54 1	R. M. Barnett <i>et al.</i>	(PDG Collab.)

See key on page 1127

Meson Particle Listings

 $B_c(2S)^\pm$, Heavy Quarkonium Spectroscopy $B_c(2S)^\pm$

$$I(J^P) = 0(0^-)$$

Quantum numbers neither measured nor confirmed.

 $B_c(2S)^\pm$ MASS

VALUE (MeV)	EVTS	DOCUMENT ID	TECN	COMMENT
6871.2 ± 1.0 OUR AVERAGE				
6871.7 ± 1.3 ± 0.3	24	^{1,2} AAIJ	19Y LHCb	pp at 7, 8, 13 TeV
6870.6 ± 1.4 ± 0.3	51	^{3,4} SIRUNYAN	19M CMS	pp at 13 TeV
not seen		⁵ AAIJ	18AL LHCb	pp at 8 TeV
6842 ± 4 ± 5	57	^{6,7} AAD	14AQ ATLAS	pp at 7, 8 TeV

• • • We do not use the following data for averages, fits, limits, etc. • • •

- ¹ AAIJ 19Y observed $B_c(2S)^+$ in the decay mode $B_c(2S)^+ \rightarrow B_c^+ \pi^+ \pi^-$ ($B_c^+ \rightarrow J/\psi \pi^+$) with 2.2 (3.2) global (local) standard deviations significance.
- ² AAIJ 19Y reports mass difference measurement of $M(B_c(2S)^+) - M(B_c^+) = 597.2 \pm 1.3 \pm 0.1$ MeV. We have adjusted this measurement with our best value of $M(B_c^+) = 6274.47 \pm 0.32$ MeV. The first uncertainty of the $M(B_c(2S)^+)$ value is a total of uncertainties reported by the experiment and the second one comes from our best value of $M(B_c^+)$.
- ³ SIRUNYAN 19M observed $B_c(2S)^+$ in the decay mode $B_c(2S)^+ \rightarrow B_c^+ \pi^+ \pi^-$ ($B_c^+ \rightarrow J/\psi \pi^+$) with 6.5 standard deviations significance.
- ⁴ SIRUNYAN 19M reports mass difference measurement of $M(B_c(2S)^+) - M(B_c^+) = 596.1 \pm 1.2 \pm 0.8$ MeV. We have adjusted this measurement with our best value of $M(B_c^+) = 6274.47 \pm 0.32$ MeV. The first uncertainty of the $M(B_c(2S)^+)$ value is a total of uncertainties reported by the experiment and the second one comes from our best value of $M(B_c^+)$.
- ⁵ AAIJ 18AL reports an upper limit on the ratio of production cross sections for $[\sigma(B_c(2S)^+)/\sigma(B_c^+)] \cdot B(B_c(2S)^+ \rightarrow B_c^+ \pi^+ \pi^-) < 0.04-0.09$ at 95% CL for the mass value reported by AAD 14AQ.

⁶ Observed in the decay mode $B_c(2S)^+ \rightarrow B_c^+ \pi^+ \pi^-$ ($B_c^+ \rightarrow J/\psi \pi^+$) with 5.2 standard deviations significance.

⁷ Might be the $B_c^*(2S)$.

 $B_c(2S)^\pm$ DECAY MODES

Mode	Fraction (Γ_i/Γ)
Γ_1 $B_c^+ \pi^+ \pi^-$	seen

 $B_c(2S)^\pm$ BRANCHING RATIOS

$\Gamma(B_c^+ \pi^+ \pi^-)/\Gamma_{\text{total}}$	VALUE	EVTS	DOCUMENT ID	TECN	COMMENT	Γ_1/Γ
seen		57	¹ AAD	14AQ ATLAS	pp at 7, 8 TeV	
not seen			² AAIJ	18AL LHCb	pp at 8 TeV	

• • • We do not use the following data for averages, fits, limits, etc. • • •

- ¹ Observed with 5.2 standard deviations significance.
- ² AAIJ 18AL reports an upper limit on the ratio of production cross sections for $[\sigma(B_c(2S)^+)/\sigma(B_c^+)] \cdot B(B_c(2S)^+ \rightarrow B_c^+ \pi^+ \pi^-) < 0.04-0.09$ at 95% CL for the mass value reported by AAD 14AQ.

 $B_c(2S)^\pm$ REFERENCES

AAIJ	19Y	PRL 122 232001	R. Aaij <i>et al.</i>	(LHCb Collab.)
SIRUNYAN	19M	PRL 122 132001	A.M. Sirunyan <i>et al.</i>	(CMS Collab.)
AAIJ	18AL	JHEP 1801 138	R. Aaij <i>et al.</i>	(LHCb Collab.)
AAD	14AQ	PRL 113 212004	G. Aad <i>et al.</i>	(ATLAS Collab.)

See the related review(s):

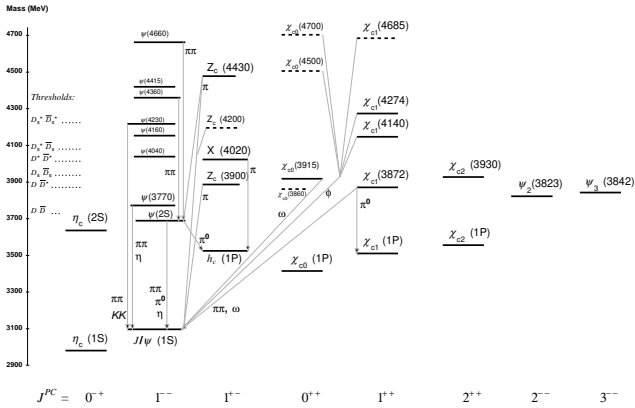
Spectroscopy of Mesons Containing Two Heavy Quarks

Meson Particle Listings

Charmonium, $\eta_c(1S)$

$c\bar{c}$ MESONS (including possibly non- $q\bar{q}$ states)

Updated March 2022.



The level scheme of meson states containing a minimal quark content of $c\bar{c}$. The name of a state is determined by its quantum numbers $I^G J^{PC}$ (see the review “Naming Scheme for Hadrons”). States with unestablished quantum numbers are called X and are drawn according to our best estimate of their likely J^{PC} . States included in the Summary Tables are shown with solid lines; selected states not in the Summary Tables, but with assigned quantum numbers, are shown with dotted lines. The arrows indicate the most dominant hadronic transitions. Single photon transitions, including $\psi(nS) \rightarrow \gamma\eta_c(mS)$, $\psi(nS) \rightarrow \gamma\chi_{cJ}(1P)$, and $\chi_{cJ}(1P) \rightarrow \gamma J/\psi$, are omitted for clarity. For orientation, the location of the thresholds related to a pair of ground state open charm mesons is indicated in the figure.

$\eta_c(1S)$

 $I^G(J^{PC}) = 0^+(0^-)$

$\eta_c(1S)$ MASS					
VALUE (MeV)	EVTS	DOCUMENT ID	TECN	COMMENT	
2983.9 ± 0.4 OUR AVERAGE		Error includes scale factor of 1.2.			
2983.9 ± 0.7 ± 0.1		1 AAIJ	20H LHCB	$pp \rightarrow bX \rightarrow p\bar{p}X$	
2985.9 ± 0.7 ± 2.1	1705	ABLIKIM	19AV BES3	$J/\psi \rightarrow \gamma\omega$	
2984.6 ± 0.7 ± 2.2	2673	XU	18 BELL	$e^+e^- \rightarrow e^+e^-\eta'\pi^+\pi^-$	
2986.7 ± 0.5 ± 0.9	11k	2 AAIJ	17AD LHCB	$pp \rightarrow B^+X \rightarrow p\bar{p}K^+X$	
2982.8 ± 1.0 ± 0.5	6.4k	3 AAIJ	17BB LHCB	$pp \rightarrow b\bar{b}X \rightarrow 2(K^+K^-)X$	
2982.2 ± 1.5 ± 0.1	2.0k	4 AAIJ	15BI LHCB	$pp \rightarrow \eta_c(1S)X$	
2983.5 ± 1.4 ± 1.6		5 ANASHIN	14 KEDR	$J/\psi \rightarrow \gamma\eta_c$	
2979.8 ± 0.8 ± 3.5	4.5k	6,7 LEES	14E BABR	$\gamma\gamma \rightarrow K^+K^-\pi^0$	
2984.1 ± 1.1 ± 2.1	900	6,7,8 LEES	14E BABR	$\gamma\gamma \rightarrow K^+K^-\eta$	
2984.3 ± 0.6 ± 0.6		9,10 ABLIKIM	12F BES3	$\psi(2S) \rightarrow \gamma\eta_c$	
2984.49 ± 1.16 ± 0.52	832	6 ABLIKIM	12N BES3	$\psi(2S) \rightarrow \pi^0\gamma$ hadrons	
2982.7 ± 1.8 ± 2.2	486	ZHANG	12A BELL	$e^+e^- \rightarrow e^+e^-\eta'\pi^+\pi^-$	
2984.5 ± 0.8 ± 3.1	11k	DEL-AMO-SA...	11M BABR	$\gamma\gamma \rightarrow K^+K^-\pi^+\pi^-\pi^0$	
2985.4 ± 1.5 ± 0.5	920	10 VINOKUROVA	11 BELL	$B^{\pm} \rightarrow K^{\pm}(K_S^0 K^{\pm}\pi^{\mp})$	
2982.2 ± 0.4 ± 1.6	14k	11 LEES	10 BABR	$10.6 e^+e^- \rightarrow e^+e^-K_S^0 K^{\pm}\pi^{\mp}$	

2985.8 ± 1.5 ± 3.1	0.9k	AUBERT	08AB BABR	$B \rightarrow \eta_c(1S) K^{(*)} \rightarrow K\bar{K}\pi K^{(*)}$	
2986.1 ± 1.0 ± 2.5	7.5k	UEHARA	08 BELL	$\gamma\gamma \rightarrow \eta_c \rightarrow$ hadrons	
2970 ± 5 ± 6	501	12 ABE	07 BELL	$e^+e^- \rightarrow J/\psi(c\bar{c})$	
2971 ± 3 ± 2	195	WU	06 BELL	$B^+ \rightarrow p\bar{p}K^+$	
2974 ± 7 ± 2	20	WU	06 BELL	$B^+ \rightarrow \Lambda\bar{\Lambda}K^+$	
2981.8 ± 1.3 ± 1.5	592	ASNER	04 CLEO	$\gamma\gamma \rightarrow \eta_c \rightarrow K_S^0 K^{\pm}\pi^{\mp}$	
2984.1 ± 2.1 ± 1.0	190	13 AMBROGIANI	03 E835	$\bar{p}p \rightarrow \eta_c \rightarrow \gamma\gamma$	
••• We do not use the following data for averages, fits, limits, etc. •••					
2982.5 ± 0.4 ± 1.4	12k	14 DEL-AMO-SA...	11M BABR	$\gamma\gamma \rightarrow K_S^0 K^{\pm}\pi^{\mp}$	
2982.2 ± 0.6	15	MITCHELL	09 CLEO	$e^+e^- \rightarrow \gamma X$	
2982 ± 5	270	16 AUBERT	06E BABR	$B^{\pm} \rightarrow K^{\pm} X_C \bar{c}$	
2982.5 ± 1.1 ± 0.9	2.5k	17 AUBERT	04D BABR	$\gamma\gamma \rightarrow \eta_c(1S) \rightarrow K\bar{K}\pi$	
2977.5 ± 1.0 ± 1.2	15,18	BAI	03 BES	$J/\psi \rightarrow \gamma\eta_c$	
2979.6 ± 2.3 ± 1.6	180	19 FANG	03 BELL	$B \rightarrow \eta_c K$	
2976.3 ± 2.3 ± 1.2	15,20	BAI	00F BES	$J/\psi, \psi(2S) \rightarrow \gamma\eta_c$	
2976.6 ± 2.9 ± 1.3	140	15,21 BAI	00F BES	$J/\psi \rightarrow \gamma\eta_c$	
2980.4 ± 2.3 ± 0.6	22	BRANDENB...	00B CLE2	$\gamma\gamma \rightarrow \eta_c \rightarrow K^{\pm} K_S^0 \pi^{\mp}$	
2975.8 ± 3.9 ± 1.2	21	BAI	99B BES	Sup. by BAI 00F	
2999 ± 8	25	ABREU	98O DLPH	$e^+e^- \rightarrow e^+e^- +$ hadrons	
2988.3 ± 3.3 ± 3.1		ARMSTRONG	95F E760	$\bar{p}p \rightarrow \gamma\gamma$	
2974.4 ± 1.9	15,23	BISELLO	91 DM2	$J/\psi \rightarrow \eta_c\gamma$	
2969 ± 4 ± 4	80	15 BAI	90B MRK3	$J/\psi \rightarrow \gamma X, \psi(2S) \rightarrow \gamma X$	
2956 ± 12 ± 12	15	BAI	90B MRK3	$J/\psi \rightarrow \gamma K^+K^- K^+K^-$	
2982.6 ± 2.7 ± 2.3	12	BAGLIN	87B SPEC	$\bar{p}p \rightarrow \gamma\gamma$	
2980.2 ± 1.6	15,23	BALTRUSAIT...	86 MRK3	$J/\psi \rightarrow \eta_c\gamma$	
2984 ± 2.3 ± 4.0	15	GAISER	86 CBAL	$J/\psi \rightarrow \gamma X, \psi(2S) \rightarrow \gamma X$	
2976 ± 8	15,24	BALTRUSAIT...	84 MRK3	$J/\psi \rightarrow 2\phi\gamma$	
2982 ± 8	18	25 HIMEL	80B MRK2	e^+e^-	
2980 ± 9	25	PARTRIDGE	80B CBAL	e^+e^-	

1 AAIJ 20H report $m_{J/\psi} - m_{\eta_c(1S)} = 113.0 \pm 0.7 \pm 0.1$ MeV. We use the current value $m_{J/\psi} = 3096.900 \pm 0.006$ MeV to obtain the quoted mass.

2 AAIJ 17AD report $m_{J/\psi} - m_{\eta_c(1S)} = 110.2 \pm 0.5 \pm 0.9$ MeV. We use the current value $m_{J/\psi} = 3096.900 \pm 0.006$ MeV to obtain the quoted mass.

3 From a fit of the $\phi\phi$ invariant mass with the mass and width of $\eta_c(1S)$ as free parameters.

4 AAIJ 15BI reports $m_{J/\psi} - m_{\eta_c(1S)} = 114.7 \pm 1.5 \pm 0.1$ MeV from a sample of $\eta_c(1S)$ and J/ψ produced in b -hadron decays. We have used current value of $m_{J/\psi} = 3096.900 \pm 0.006$ MeV to arrive at the quoted $m_{\eta_c(1S)}$ result.

5 Taking into account an asymmetric photon lineshape.

6 With floating width.

7 Ignoring possible interference with the non-resonant 0^- amplitude.

8 Using both, $\eta \rightarrow \gamma\gamma$ and $\eta \rightarrow \pi^+\pi^-\pi^0$ decays.

9 From a simultaneous fit to six decay modes of the η_c .

10 Accounts for interference with non-resonant continuum.

11 Taking into account interference with the non-resonant $J^P = 0^-$ amplitude.

12 From a fit of the J/ψ recoil mass spectrum. Supersedes ABE,K 02 and ABE 04G.

13 Using mass of $\psi(2S) = 3686.00$ MeV.

14 Not independent from the measurements reported by LEES 10.

15 MITCHELL 09 observes a significant asymmetry in the lineshapes of $\psi(2S) \rightarrow \gamma\eta_c$ and $J/\psi \rightarrow \gamma\eta_c$ transitions. If ignored, this asymmetry could lead to significant bias whenever the mass and width are measured in $\psi(2S)$ or J/ψ radiative decays.

16 From the fit of the kaon momentum spectrum. Systematic errors not evaluated.

17 Superseded by LEES 10.

18 From a simultaneous fit of five decay modes of the η_c .

19 Superseded by VINOKUROVA 11.

20 Weighted average of the $\psi(2S)$ and $J/\psi(1S)$ samples. Using an η_c width of 13.2 MeV.

21 Average of several decay modes. Using an η_c width of 13.2 MeV.

22 Superseded by ASNER 04.

23 Average of several decay modes.

24 $\eta_c \rightarrow \phi\phi$.

25 Mass adjusted by us to correspond to $J/\psi(1S)$ mass = 3097 MeV.

$\eta_c(1S)$ WIDTH					
VALUE (MeV)	EVTS	DOCUMENT ID	TECN	COMMENT	
32.0 ± 0.7 OUR FIT		Error includes scale factor of 1.1.			
32.1 ± 0.8 OUR AVERAGE					
33.8 ± 1.6 ± 4.1	1705	ABLIKIM	19AV BES3	$J/\psi \rightarrow \gamma\omega$	
30.8 ± 2.2 ± 2.9	2673	XU	18 BELL	$e^+e^- \rightarrow e^+e^-\eta'\pi^+\pi^-$	
34.0 ± 1.9 ± 1.3	11k	AAIJ	17AD LHCB	$pp \rightarrow B^+X \rightarrow p\bar{p}K^+X$	
31.4 ± 3.5 ± 2.0	6.4k	1 AAIJ	17BB LHCB	$pp \rightarrow b\bar{b}X \rightarrow 2(K^+K^-)X$	
27.2 ± 3.1 ± 5.4		2 ANASHIN	14 KEDR	$J/\psi \rightarrow \gamma\eta_c$	

See key on page 1127

Meson Particle Listings
 $\eta_c(1S)$

25.2 ± 2.6 ± 2.4	4.5k	3,4	LEES	14E	BABR	$\gamma\gamma \rightarrow K^+ K^- \pi^0$
34.8 ± 3.1 ± 4.0	900	3,4,5	LEES	14E	BABR	$\gamma\gamma \rightarrow K^+ K^- \eta$
32.0 ± 1.2 ± 1.0		6,7	ABLIKIM	12F	BES3	$\psi(2S) \rightarrow \gamma \eta_c$
36.4 ± 3.2 ± 1.7	832	3	ABLIKIM	12N	BES3	$\psi(2S) \rightarrow \pi^0 \gamma$ hadrons
37.8 ± 5.8 ± 3.1	486		ZHANG	12A	BELL	$e^+ e^- \rightarrow e^+ e^- \eta' \pi^+ \pi^-$
36.2 ± 2.8 ± 3.0	11k		DEL-AMO-SA...	11M	BABR	$\gamma\gamma \rightarrow K^+ K^- \pi^+ \pi^- \pi^0$
35.1 ± 3.1 ± 1.0	920	7	VINOKUROVA	11	BELL	$B^\pm \rightarrow K^\pm (K_S^0 K^\pm \pi^\mp)$
31.7 ± 1.2 ± 0.8	14k	8	LEES	10	BABR	$10.6 e^+ e^- \rightarrow e^+ e^- K_S^0 K^\pm \pi^\mp$
36.3 ± 3.7 ± 4.4	0.9k		AUBERT	08AB	BABR	$B \rightarrow \eta_c(1S) K^*(*) \rightarrow K \bar{K} \pi K^*(*)$
28.1 ± 3.2 ± 2.2	7.5k		UEHARA	08	BELL	$\gamma\gamma \rightarrow \eta_c \rightarrow$ hadrons
48 ± 8 ± 5	195		WU	06	BELL	$B^+ \rightarrow \rho \bar{p} K^+$
40 ± 19 ± 5	20		WU	06	BELL	$B^+ \rightarrow \Lambda \bar{\Lambda} K^+$
24.8 ± 3.4 ± 3.5	592		ASNER	04	CLEO	$\gamma\gamma \rightarrow \eta_c \rightarrow K_S^0 K^\pm \pi^\mp$
20.4 ± 7.7 ± 2.0	190		AMBROGIANI	03	E835	$\bar{p} p \rightarrow \eta_c \rightarrow \gamma\gamma$
23.9 ± 12.6 ± 7.1			ARMSTRONG	95F	E760	$\bar{p} p \rightarrow \gamma\gamma$

- • • We do not use the following data for averages, fits, limits, etc. • • •
 - 32.1 ± 1.1 ± 1.3 12k 9 DEL-AMO-SA...11M BABR $\gamma\gamma \rightarrow K_S^0 K^\pm \pi^\mp$
 - 34.3 ± 2.3 ± 0.9 2.5k 10 AUBERT 04D BABR $\gamma\gamma \rightarrow \eta_c(1S) \rightarrow K \bar{K} \pi$
 - 17.0 ± 3.7 ± 7.4 11 BAI 03 BES $J/\psi \rightarrow \gamma \eta_c$
 - 29 ± 8 ± 6 180 12 FANG 03 BELL $B \rightarrow \eta_c K$
 - 11.0 ± 8.1 ± 4.1 13 BAI 00F BES $J/\psi \rightarrow \gamma \eta_c$ and $\psi(2S) \rightarrow \gamma \eta_c$
 - 27.0 ± 5.8 ± 1.4 14 BRANDENB... 00B CLE2 $\gamma\gamma \rightarrow \eta_c \rightarrow K^\pm K_S^0 \pi^\mp$
 - 7.0 ± 7.5 ± 7.0 12 BAGLIN 87B SPEC $\bar{p} p \rightarrow \gamma\gamma$
 - 10.1 ± 33.0 ± 8.2 23 15 BALTRUSAIT...86 MRK3 $J/\psi \rightarrow \gamma \rho \bar{p}$
 - 11.5 ± 4.5 GAISER 86 CBAL $J/\psi \rightarrow \gamma X, \psi(2S) \rightarrow \gamma X$
 - < 40 90% CL 18 HIMEL 80B MRK2 $e^+ e^-$
 - < 20 90% CL PARTRIDGE 80B CBAL $e^+ e^-$
- 1 From a fit of the $\phi\phi$ invariant mass with the mass and width of $\eta_c(1S)$ as free parameters.
 2 Taking into account an asymmetric photon lineshape.
 3 With floating mass.
 4 Ignoring possible interference with the non-resonant 0^- amplitude.
 5 Using both, $\eta \rightarrow \gamma\gamma$ and $\eta \rightarrow \pi^+ \pi^- \pi^0$ decays.
 6 From a simultaneous fit to six decay modes of the η_c .
 7 Accounts for interference with non-resonant continuum.
 8 Taking into account interference with the non-resonant $J^P = 0^-$ amplitude.
 9 Not independent from the measurements reported by LEES 10.
 10 Superseded by LEES 10.
 11 From a simultaneous fit of five decay modes of the η_c .
 12 Superseded by VINOKUROVA 11.
 13 From a fit to the 4-prong invariant mass in $\psi(2S) \rightarrow \gamma \eta_c$ and $J/\psi(1S) \rightarrow \gamma \eta_c$ decays.
 14 Superseded by ASNER 04.
 15 Positive and negative errors correspond to 90% confidence level.

$\eta_c(1S)$ DECAY MODES

Mode	Fraction (Γ_i/Γ)	Confidence level
Decays involving hadronic resonances		
$\Gamma_1 \eta'(958) \pi \pi$	(4.1 ± 1.7) %	
$\Gamma_2 \eta'(958) K \bar{K}$	(3.5 ± 1.5) %	
$\Gamma_3 \rho \rho$	(1.8 ± 0.5) %	
$\Gamma_4 K^*(892)^0 K^- \pi^+ + c.c.$	(2.0 ± 0.7) %	
$\Gamma_5 K^*(892) \bar{K}^*(892)$	(6.9 ± 1.3) × 10 ⁻³	
$\Gamma_6 K^*(892)^0 \bar{K}^*(892)^0 \pi^+ \pi^-$	(1.1 ± 0.5) %	
$\Gamma_7 \phi K^+ K^-$	(2.9 ± 1.4) × 10 ⁻³	
$\Gamma_8 \phi \phi$	(1.74 ± 0.19) × 10 ⁻³	
$\Gamma_9 \phi 2(\pi^+ \pi^-)$	< 4 × 10 ⁻³	90%
$\Gamma_{10} a_0(980) \pi$	seen	
$\Gamma_{11} a_2(1320) \pi$	< 2 %	90%
$\Gamma_{12} K^*(892) \bar{K} + c.c.$	< 1.28 %	90%
$\Gamma_{13} f_2(1270) \eta$	< 1.1 %	90%
$\Gamma_{14} f_2(1270) \eta'$	seen	
$\Gamma_{15} \omega \omega$	(2.9 ± 0.8) × 10 ⁻³	
$\Gamma_{16} \omega \phi$	< 2.5 × 10 ⁻⁴	90%
$\Gamma_{17} f_2(1270) f_2(1270)$	(9.8 ± 2.5) × 10 ⁻³	
$\Gamma_{18} f_2(1270) f_2'(1525)$	(9.5 ± 3.2) × 10 ⁻³	
$\Gamma_{19} f_0(500) \eta$	seen	
$\Gamma_{20} f_0(500) \eta'$	seen	
$\Gamma_{21} f_0(980) \eta$	seen	
$\Gamma_{22} f_0(980) \eta'$	seen	
$\Gamma_{23} f_0(1500) \eta$	seen	

$\Gamma_{24} f_0(1710) \eta'$	seen
$\Gamma_{25} f_0(2100) \eta'$	seen
$\Gamma_{26} f_0(2200) \eta$	seen
$\Gamma_{27} a_0(1320) \pi$	seen
$\Gamma_{28} a_0(1450) \pi$	seen
$\Gamma_{29} a_0(1700) \pi$	seen
$\Gamma_{30} a_0(1950) \pi$	seen
$\Gamma_{31} K_0^*(1430) \bar{K}$	seen
$\Gamma_{32} K_2^*(1430) \bar{K}$	seen
$\Gamma_{33} K_0^*(1950) \bar{K}$	seen

Decays into stable hadrons

$\Gamma_{34} K \bar{K} \pi$	(7.3 ± 0.4) %	
$\Gamma_{35} K \bar{K} \eta$	(1.36 ± 0.15) %	
$\Gamma_{36} \eta \pi^+ \pi^-$	(1.7 ± 0.6) %	
$\Gamma_{37} \eta 2(\pi^+ \pi^-)$	(4.4 ± 1.6) %	
$\Gamma_{38} K^+ K^- \pi^+ \pi^-$	(6.6 ± 1.1) × 10 ⁻³	
$\Gamma_{39} K^+ K^- \pi^+ \pi^- \pi^0$	(3.5 ± 0.6) %	
$\Gamma_{40} K^0 K^- \pi^+ \pi^- \pi^+ + c.c.$	(5.6 ± 1.9) %	
$\Gamma_{41} K^+ K^- 2(\pi^+ \pi^-)$	(7.5 ± 2.4) × 10 ⁻³	
$\Gamma_{42} 2(K^+ K^-)$	(1.43 ± 0.30) × 10 ⁻³	
$\Gamma_{43} \pi^+ \pi^- \pi^0$	< 5 × 10 ⁻⁴	90%
$\Gamma_{44} \pi^+ \pi^- \pi^0 \pi^0$	(4.7 ± 1.4) %	
$\Gamma_{45} 2(\pi^+ \pi^-)$	(9.1 ± 1.2) × 10 ⁻³	
$\Gamma_{46} 2(\pi^+ \pi^- \pi^0)$	(15.8 ± 2.3) %	
$\Gamma_{47} 3(\pi^+ \pi^-)$	(1.7 ± 0.4) %	
$\Gamma_{48} \rho \bar{p}$	(1.44 ± 0.14) × 10 ⁻³	
$\Gamma_{49} \rho \bar{p} \pi^0$	(3.6 ± 1.5) × 10 ⁻³	
$\Gamma_{50} \Lambda \bar{\Lambda}$	(1.06 ± 0.23) × 10 ⁻³	
$\Gamma_{51} K^+ \bar{p} \Lambda + c.c.$	(2.5 ± 0.4) × 10 ⁻³	
$\Gamma_{52} \bar{\Lambda}(1520) \Lambda + c.c.$	(3.1 ± 1.3) × 10 ⁻³	
$\Gamma_{53} \Sigma^+ \bar{\Sigma}^-$	(2.1 ± 0.6) × 10 ⁻³	
$\Gamma_{54} \Xi^- \bar{\Xi}^+$	(9.0 ± 2.6) × 10 ⁻⁴	
$\Gamma_{55} \pi^+ \pi^- \rho \bar{p}$	(5.3 ± 2.1) × 10 ⁻³	

Radiative decays

$\Gamma_{56} \gamma\gamma$	(1.61 ± 0.12) × 10 ⁻⁴
----------------------------	------------------------------------

Charge conjugation (C), Parity (P),
Lepton family number (LF) violating modes

$\Gamma_{57} \pi^+ \pi^-$	$P, CP < 1.1$	× 10 ⁻⁴	90%
$\Gamma_{58} \pi^0 \pi^0$	$P, CP < 4$	× 10 ⁻⁵	90%
$\Gamma_{59} K^+ K^-$	$P, CP < 6$	× 10 ⁻⁴	90%
$\Gamma_{60} K_S^0 K_S^0$	$P, CP < 3.1$	× 10 ⁻⁴	90%

CONSTRAINED FIT INFORMATION

An overall fit to the total width, 8 combinations of partial widths obtained from integrated cross section, and 19 branching ratios uses 93 measurements and one constraint to determine 13 parameters. The overall fit has a $\chi^2 = 117.8$ for 81 degrees of freedom.

The following *off-diagonal* array elements are the correlation coefficients $\langle \delta p_i \delta p_j \rangle / (\delta p_i \delta p_j)$, in percent, from the fit to parameters p_i , including the branching fractions, $x_i \equiv \Gamma_i / \Gamma_{total}$. The fit constrains the x_i whose labels appear in this array to sum to one.

x_8	16									
x_{17}	3	5								
x_{34}	18	35	6							
x_{35}	9	17	3	47						
x_{38}	10	18	3	21	10					
x_{42}	7	13	2	21	10	8				
x_{45}	12	22	4	25	12	14	10			
x_{48}	11	20	4	27	13	12	10	15		
x_{50}	3	5	1	6	3	3	2	4	23	
x_{56}	-27	-51	-9	-59	-28	-32	-23	-38	-38	-9
Γ	-1	-3	0	-3	-1	-2	-1	-2	6	1
	x_5	x_8	x_{17}	x_{34}	x_{35}	x_{38}	x_{42}	x_{45}	x_{48}	x_{50}
Γ	-27									
	x_{56}									

Meson Particle Listings

 $\eta_c(1S)$

Mode	Rate (MeV)
Γ_5 $K^*(892)\bar{K}^*(892)$	0.22 ± 0.04
Γ_8 $\phi\phi$	0.056 ± 0.006
Γ_{17} $f_2(1270)f_2(1270)$	0.31 ± 0.08
Γ_{34} $K\bar{K}\pi$	2.32 ± 0.14
Γ_{35} $K\bar{K}\eta$	0.43 ± 0.05
Γ_{38} $K^+K^-\pi^+\pi^-$	0.210 ± 0.035
Γ_{42} $2(K^+K^-)$	0.046 ± 0.010
Γ_{45} $2(\pi^+\pi^-)$	0.29 ± 0.04
Γ_{48} $\rho\bar{\rho}$	0.046 ± 0.005
Γ_{50} $\Lambda\bar{\Lambda}$	0.034 ± 0.008
Γ_{56} $\gamma\gamma$	0.00515 ± 0.00035

 $\eta_c(1S)$ PARTIAL WIDTHS

$\Gamma(\gamma\gamma)$					Γ_{56}
VALUE (keV)	EVTS	DOCUMENT ID	TECN	COMMENT	
5.15 ± 0.35 OUR FIT					
• • • We do not use the following data for averages, fits, limits, etc. • • •					
5.8 ± 1.1	486	¹ ZHANG	12A BELL	$e^+e^- \rightarrow e^+\eta'\pi^+\pi^-$	
5.2 ± 1.2	273 ± 43	^{2,3} AUBERT	06E BABR	$B^\pm \rightarrow K^\pm X_{c\bar{c}}$	
5.5 ± 1.2 ± 1.8	57 ± 33	⁴ KUO	05 BELL	$\gamma\gamma \rightarrow \rho\bar{\rho}$	
7.4 ± 0.4 ± 2.3		⁵ ASNER	04 CLEO	$\gamma\gamma \rightarrow \eta_c \rightarrow K_S^0 K^\pm \pi^\mp$	
13.9 ± 2.0 ± 3.0	41	⁶ ABDALLAH	03J DLPH	$\gamma\gamma \rightarrow \eta_c$	
3.8 + 1.1 + 1.9 - 1.0 - 1.0	190	⁷ AMBROGIANI	03 E835	$\bar{p}p \rightarrow \eta_c \rightarrow \gamma\gamma$	
7.6 ± 0.8 ± 2.3		^{5,8} BRANDENB...	00B CLE2	$\gamma\gamma \rightarrow \eta_c \rightarrow K^\pm K_S^0 \pi^\mp$	
6.9 ± 1.7 ± 2.1	76	⁹ ACCIARRI	99T L3	$e^+e^- \rightarrow e^+e^-\eta_c$	
27 ± 16 ± 10	5	⁵ SHIRAI	98 AMY	58 e^+e^-	
6.7 + 2.4 - 1.7 ± 2.3		⁴ ARMSTRONG	95F E760	$\bar{p}p \rightarrow \gamma\gamma$	
11.3 ± 4.2		¹⁰ ALBRECHT	94H ARG	$e^+e^- \rightarrow e^+e^-\eta_c$	
8.0 ± 2.3 ± 2.4	17	¹¹ ADRIANI	93N L3	$e^+e^- \rightarrow e^+e^-\eta_c$	
5.9 + 2.1 + 1.9 - 1.8 - 1.8		⁷ CHEN	90B CLEO	$e^+e^- \rightarrow e^+e^-\eta_c$	
6.4 + 5.0 - 3.4		¹² AIHARA	88D TPC	$e^+e^- \rightarrow e^+e^-X$	
4.3 + 3.4 - 3.7 ± 2.4		⁴ BAGLIN	87B SPEC	$\bar{p}p \rightarrow \gamma\gamma$	
28 ± 15		^{5,13} BERGER	86 PLUT	$\gamma\gamma \rightarrow K\bar{K}\pi$	

- ¹ Assuming there is no interference with the non-resonant background.
² Calculated by us using $\Gamma(\eta_c \rightarrow K\bar{K}\pi) \times \Gamma(\eta_c \rightarrow \gamma\gamma) / \Gamma = 0.44 \pm 0.05$ keV from PDG 06 and $B(\eta_c \rightarrow K\bar{K}\pi) = (8.5 \pm 1.8)\%$ from AUBERT 06E.
³ Systematic errors not evaluated.
⁴ Normalized to $B(\eta_c \rightarrow \rho\bar{\rho}) = (1.3 \pm 0.4) \times 10^{-3}$.
⁵ Normalized to $B(\eta_c \rightarrow K^\pm K_S^0 \pi^\mp)$.
⁶ Average of $K_S^0 K^\pm \pi^\mp$, $\pi^+ \pi^- K^+ K^-$, and $2(K^+ K^-)$ decay modes.
⁷ Normalized to the sum of $B(\eta_c \rightarrow K^\pm K_S^0 \pi^\mp)$, $B(\eta_c \rightarrow K^+ K^- \pi^+ \pi^-)$, and $B(\eta_c \rightarrow 2\pi^+ 2\pi^-)$.
⁸ Superseded by ASNER 04.
⁹ Normalized to the sum of 9 branching ratios.
¹⁰ Normalized to the sum of $B(\eta_c \rightarrow K^\pm K_S^0 \pi^\mp)$, $B(\eta_c \rightarrow \phi\phi)$, $B(\eta_c \rightarrow K^+ K^- \pi^+ \pi^-)$, and $B(\eta_c \rightarrow 2\pi^+ 2\pi^-)$.
¹¹ Superseded by ACCIARRI 99T.
¹² Normalized to the sum of $B(\eta_c \rightarrow K^\pm K_S^0 \pi^\mp)$, $B(\eta_c \rightarrow 2K^+ 2K^-)$, $B(\eta_c \rightarrow K^+ K^- \pi^+ \pi^-)$, and $B(\eta_c \rightarrow 2\pi^+ 2\pi^-)$.
¹³ Re-evaluated by AIHARA 88D.

 $\eta_c(1S)$ $\Gamma(l)\Gamma(\gamma\gamma)/\Gamma(\text{total})$

$\Gamma(\eta'(958)\pi\pi) \times \Gamma(\gamma\gamma)/\Gamma(\text{total})$					Γ_{156}/Γ
VALUE (eV)	EVTS	DOCUMENT ID	TECN	COMMENT	
98.1 ± 3.9 ± 11.7	2673	XU	18 BELL	$e^+e^- \rightarrow e^+\eta'\pi^+\pi^-$	
• • • We do not use the following data for averages, fits, limits, etc. • • •					
75.8 + 6.3 - 6.2 ± 8.4	486	¹ ZHANG	12A BELL	$e^+e^- \rightarrow e^+\eta'\pi^+\pi^-$	
¹ Superseded by XU 18.					

$\Gamma(\rho\rho) \times \Gamma(\gamma\gamma)/\Gamma(\text{total})$					Γ_{356}/Γ
VALUE (eV)	CL%	EVTS	DOCUMENT ID	TECN	COMMENT
<39	90	< 1556	UEHARA	08 BELL	$\gamma\gamma \rightarrow 2(\pi^+ \pi^-)$

$\Gamma(K^*(892)\bar{K}^*(892)) \times \Gamma(\gamma\gamma)/\Gamma(\text{total})$					Γ_{556}/Γ
VALUE (eV)	EVTS	DOCUMENT ID	TECN	COMMENT	
36 ± 6 OUR FIT					
32.4 ± 4.2 ± 5.8	882 ± 115	UEHARA	08 BELL	$\gamma\gamma \rightarrow \pi^+ \pi^- K^+ K^-$	

$\Gamma(\phi\phi) \times \Gamma(\gamma\gamma)/\Gamma(\text{total})$					Γ_{856}/Γ
VALUE (eV)	EVTS	DOCUMENT ID	TECN	COMMENT	

9.0 ± 0.8 OUR FIT
7.75 ± 0.66 ± 0.62 386 ± 31 ¹ LIU 12B BELL $\gamma\gamma \rightarrow 2(K^+ K^-)$
• • • We do not use the following data for averages, fits, limits, etc. • • •
6.8 ± 1.2 ± 1.3 132 ± 23 UEHARA 08 BELL $\gamma\gamma \rightarrow 2(K^+ K^-)$
¹ Supersedes UEHARA 08. Using $B(\phi \rightarrow K^+ K^-) = (48.9 \pm 0.5)\%$.

$\Gamma(\omega\omega) \times \Gamma(\gamma\gamma)/\Gamma(\text{total})$					Γ_{1556}/Γ
VALUE (eV)	EVTS	DOCUMENT ID	TECN	COMMENT	

8.67 ± 2.86 ± 0.96 85 ± 29 ¹ LIU 12B BELL $\gamma\gamma \rightarrow 2(\pi^+ \pi^- \pi^0)$
¹ Using $B(\omega \rightarrow \pi^+ \pi^- \pi^0) = (89.2 \pm 0.7)\%$.

$\Gamma(\phi\phi) \times \Gamma(\gamma\gamma)/\Gamma(\text{total})$					Γ_{1656}/Γ
VALUE (eV)	CL%	EVTS	DOCUMENT ID	TECN	COMMENT

• • • We do not use the following data for averages, fits, limits, etc. • • •
<0.49 90 ¹ LIU 12B BELL $\gamma\gamma \rightarrow K^+ K^- \pi^+ \pi^- \pi^0$
¹ Using $B(\phi \rightarrow K^+ K^-) = (48.9 \pm 0.5)\%$ and $B(\omega \rightarrow \pi^+ \pi^- \pi^0) = (89.2 \pm 0.7)\%$.

$\Gamma(f_2(1270)f_2(1270)) \times \Gamma(\gamma\gamma)/\Gamma(\text{total})$					Γ_{1756}/Γ
VALUE (eV)	EVTS	DOCUMENT ID	TECN	COMMENT	

50 ± 13 OUR FIT
69 ± 17 ± 12 3182 ± 766 UEHARA 08 BELL $\gamma\gamma \rightarrow 2(\pi^+ \pi^-)$

$\Gamma(f_2(1270)f_2'(1525)) \times \Gamma(\gamma\gamma)/\Gamma(\text{total})$					Γ_{1856}/Γ
VALUE (eV)	EVTS	DOCUMENT ID	TECN	COMMENT	

49 ± 9 ± 13 1128 ± 206 UEHARA 08 BELL $\gamma\gamma \rightarrow \pi^+ \pi^- K^+ K^-$

$\Gamma(K\bar{K}\pi) \times \Gamma(\gamma\gamma)/\Gamma(\text{total})$					Γ_{3456}/Γ
VALUE (keV)	CL%	EVTS	DOCUMENT ID	TECN	COMMENT

0.374 ± 0.021 OUR FIT
0.407 ± 0.027 OUR AVERAGE Error includes scale factor of 1.2.
0.374 ± 0.009 ± 0.031 14k ¹ LEES 10 BABR $10.6 e^+e^- \rightarrow e^+e^- K_S^0 K^\pm \pi^\mp$
0.407 ± 0.022 ± 0.028 ^{2,3} ASNER 04 CLEO $\gamma\gamma \rightarrow \eta_c \rightarrow K_S^0 K^\pm \pi^\mp$
0.60 ± 0.12 ± 0.09 41 ^{3,4} ABDALLAH 03J DLPH $\gamma\gamma \rightarrow K^\pm K_S^0 \pi^\mp$
1.47 ± 0.87 ± 0.27 ³ SHIRAI 98 AMY $\gamma\gamma \rightarrow \eta_c \rightarrow K^\pm K_S^0 \pi^\mp$
0.84 ± 0.21 ³ ALBRECHT 94H ARG $\gamma\gamma \rightarrow K^\pm K_S^0 \pi^\mp$
0.60 + 0.23
- 0.20 ³ CHEN 90B CLEO $\gamma\gamma \rightarrow \eta_c K^\pm K_S^0 \pi^\mp$
1.06 ± 0.41 ± 0.27 11 ³ BRAUNSC... 89 TASS $\gamma\gamma \rightarrow K\bar{K}\pi$
1.5 + 0.60
- 0.45 ± 0.3 7 ³ BERGER 86 PLUT $\gamma\gamma \rightarrow K\bar{K}\pi$

• • • We do not use the following data for averages, fits, limits, etc. • • •
0.386 ± 0.008 ± 0.021 12k ⁵ DEL-AMO-SA..11M BABR $\gamma\gamma \rightarrow K_S^0 K^\pm \pi^\mp$
0.418 ± 0.044 ± 0.022 ^{3,6} BRANDENB... 00B CLE2 $\gamma\gamma \rightarrow \eta_c \rightarrow K^\pm K_S^0 \pi^\mp$
<0.63 95 ³ BEHREND 89 CELL $\gamma\gamma \rightarrow K_S^0 K^\pm \pi^\mp$
<4.4 95 ALTHOFF 85B TASS $\gamma\gamma \rightarrow K\bar{K}\pi$

- ¹ From the corrected and unfolded mass spectrum.
² Calculated by us from the value reported in ASNER 04 that assumes $B(\eta_c \rightarrow K\bar{K}\pi) = 5.5 \pm 1.7\%$.
³ We have multiplied $K^\pm K_S^0 \pi^\mp$ measurement by 3 to obtain $K\bar{K}\pi$.
⁴ Calculated by us from the value reported in ABDALLAH 03J, which uses $B(\eta_c \rightarrow K_S^0 K^\pm \pi^\mp) = (1.5 \pm 0.4)\%$.
⁵ Not independent from the measurements reported by LEES 10.
⁶ Superseded by ASNER 04.

$\Gamma(K^+ K^- \pi^+ \pi^-) \times \Gamma(\gamma\gamma)/\Gamma(\text{total})$					Γ_{3856}/Γ
VALUE (eV)	EVTS	DOCUMENT ID	TECN	COMMENT	

34 ± 5 OUR FIT
27 ± 6 OUR AVERAGE
25.7 ± 3.2 ± 4.9 2019 ± 248 UEHARA 08 BELL $\gamma\gamma \rightarrow \pi^+ \pi^- K^+ K^-$
280 ± 100 ± 60 42 ¹ ABDALLAH 03J DLPH $\gamma\gamma \rightarrow \pi^+ \pi^- K^+ K^-$
170 ± 80 ± 20 13.9 ± 6.6 ALBRECHT 94H ARG $\gamma\gamma \rightarrow \pi^+ \pi^- K^+ K^-$
¹ Calculated by us from the value reported in ABDALLAH 03J, which uses $B(\eta_c \rightarrow \pi^+ \pi^- K^+ K^-) = (2.0 \pm 0.7)\%$.

$\Gamma(K^+ K^- \pi^+ \pi^- \pi^0) \times \Gamma(\gamma\gamma)/\Gamma(\text{total})$					Γ_{3956}/Γ
VALUE (keV)	EVTS	DOCUMENT ID	TECN	COMMENT	

• • • We do not use the following data for averages, fits, limits, etc. • • •
0.190 ± 0.006 ± 0.028 11k ¹ DEL-AMO-SA..11M BABR $\gamma\gamma \rightarrow K^+ K^- \pi^+ \pi^- \pi^0$
¹ Not independent from other measurements reported in DEL-AMO-SANCHEZ 11M.

$\Gamma(2(K^+K^-)) \times \Gamma(\gamma\gamma)/\Gamma_{\text{total}}$ $\Gamma_{42}\Gamma_{56}/\Gamma$

VALUE (eV)	EVTS	DOCUMENT ID	TECN	COMMENT
7.3 ± 1.5 OUR FIT				
5.8 ± 1.9 OUR AVERAGE				
5.6 ± 1.1 ± 1.6	216 ± 42	UEHARA	08 BELL	$\gamma\gamma \rightarrow 2(K^+K^-)$
350 ± 90 ± 60	46	¹ ABDALLAH	03J DLPH	$\gamma\gamma \rightarrow 2(K^+K^-)$
231 ± 90 ± 23	9.1 ± 3.3	² ALBRECHT	94H ARG	$\gamma\gamma \rightarrow 2(K^+K^-)$

¹ Calculated by us from the value reported in ABDALLAH 03J, which uses $B(\eta_c \rightarrow 2(K^+K^-)) = (2.1 \pm 1.2)\%$.

² Includes all topological modes except $\eta_c \rightarrow \phi\phi$.

 $\Gamma(2(\pi^+\pi^-)) \times \Gamma(\gamma\gamma)/\Gamma_{\text{total}}$ $\Gamma_{45}\Gamma_{56}/\Gamma$

VALUE (eV)	EVTS	DOCUMENT ID	TECN	COMMENT
47 ± 6 OUR FIT				
42 ± 6 OUR AVERAGE				
40.7 ± 3.7 ± 5.3	5381 ± 492	UEHARA	08 BELL	$\gamma\gamma \rightarrow 2(\pi^+\pi^-)$
180 ± 70 ± 20	21.4 ± 8.6	ALBRECHT	94H ARG	$\gamma\gamma \rightarrow 2(\pi^+\pi^-)$

 $\Gamma(\rho\bar{\rho}) \times \Gamma(\gamma\gamma)/\Gamma_{\text{total}}$ $\Gamma_{48}\Gamma_{56}/\Gamma$

VALUE (eV)	EVTS	DOCUMENT ID	TECN	COMMENT
7.4 ± 0.7 OUR FIT				
7.20 ± 1.53 ± 0.67 - 0.75	157 ± 33	¹ KUO	05 BELL	$\gamma\gamma \rightarrow \rho\bar{\rho}$

• • • We do not use the following data for averages, fits, limits, etc. • • •

4.6 +1.3 ± 0.4 -1.1 ± 0.4 190 ¹AMBROGIANI 03 E835 $\bar{p}p \rightarrow \gamma\gamma$

8.1 +2.9 -2.0 ¹ARMSTRONG 95F E760 $\bar{p}p \rightarrow \gamma\gamma$

¹ Not independent from the $\Gamma_{\gamma\gamma}$ reported by the same experiment.

 $\Gamma(K_S^0 K_S^0) \times \Gamma(\gamma\gamma)/\Gamma_{\text{total}}$ $\Gamma_{60}\Gamma_{56}/\Gamma$

VALUE (eV)	CL%	DOCUMENT ID	TECN	COMMENT
<1.6	90	¹ UEHARA	13 BELL	$\gamma\gamma \rightarrow K_S^0 K_S^0$

• • • We do not use the following data for averages, fits, limits, etc. • • •

<0.29 90 ²UEHARA 13 BELL $\gamma\gamma \rightarrow K_S^0 K_S^0$

¹ Taking into account interference with the non-resonant continuum.

² Neglecting interference with the non-resonant continuum.

 $\eta_c(1S)$ BRANCHING RATIOS

HADRONIC DECAYS

 $\Gamma(\eta'(958)\pi\pi)/\Gamma_{\text{total}}$ Γ_1/Γ

VALUE	EVTS	DOCUMENT ID	TECN	COMMENT
0.041 ± 0.017	14	¹ BALTRUSAIT...86	MRK3	$J/\psi \rightarrow \eta_c \gamma$

¹ The quoted branching ratios use $B(J/\psi(1S) \rightarrow \gamma\eta_c(1S)) = 0.0127 \pm 0.0036$.

 $\Gamma(\rho\rho)/\Gamma_{\text{total}}$ Γ_3/Γ

VALUE (units 10^{-3})	CL%	EVTS	DOCUMENT ID	TECN	COMMENT
18 ± 5 OUR AVERAGE					
12.6 ± 3.8 ± 5.1	72	¹ ABLIKIM	05L BES2	$J/\psi \rightarrow \pi^+\pi^-\pi^+\pi^-\gamma$	
26.0 ± 2.4 ± 8.8	113	¹ BISELLO	91 DM2	$J/\psi \rightarrow \gamma\rho^0\rho^0$	
23.6 ± 10.6 ± 8.2	32	¹ BISELLO	91 DM2	$J/\psi \rightarrow \gamma\rho^+\rho^-$	

• • • We do not use the following data for averages, fits, limits, etc. • • •

<14 90 ¹BALTRUSAIT...86 MRK3 $J/\psi \rightarrow \eta_c \gamma$

¹ The quoted branching ratios use $B(J/\psi(1S) \rightarrow \gamma\eta_c(1S)) = 0.0127 \pm 0.0036$. Where relevant, the error in this branching ratio is treated as a common systematic in computing averages.

 $\Gamma(K^*(892)^0 K^- \pi^+ + c.c.)/\Gamma_{\text{total}}$ Γ_4/Γ

VALUE	EVTS	DOCUMENT ID	TECN	COMMENT
0.02 ± 0.007	63	^{1,2} BALTRUSAIT...86	MRK3	$J/\psi \rightarrow \eta_c \gamma$

¹ BALTRUSAITIS 86 has an error according to Partridge.

² The quoted branching ratios use $B(J/\psi(1S) \rightarrow \gamma\eta_c(1S)) = 0.0127 \pm 0.0036$.

 $\Gamma(K^*(892)\bar{K}^*(892))/\Gamma_{\text{total}}$ Γ_5/Γ

VALUE (units 10^{-4})	EVTS	DOCUMENT ID	TECN	COMMENT
69 ± 13 OUR FIT				
91 ± 26 OUR AVERAGE				
108 ± 25 ± 44	60	¹ ABLIKIM	05L BES2	$J/\psi \rightarrow K^+K^-\pi^+\pi^-\gamma$
82 ± 28 ± 27	14	¹ BISELLO	91 DM2	$e^+e^- \rightarrow \gamma K^+K^-\pi^+\pi^-$
90 ± 50	9	¹ BALTRUSAIT...86	MRK3	$J/\psi \rightarrow \eta_c \gamma$

¹ The quoted branching ratios use $B(J/\psi(1S) \rightarrow \gamma\eta_c(1S)) = 0.0127 \pm 0.0036$. Where relevant, the error in this branching ratio is treated as a common systematic in computing averages.

 $\Gamma(K^*(892)^0 \bar{K}^*(892)^0 \pi^+ \pi^-)/\Gamma_{\text{total}}$ Γ_6/Γ

VALUE (units 10^{-4})	EVTS	DOCUMENT ID	TECN	COMMENT
113 ± 47 ± 24	45	¹ ABLIKIM	06A BES2	$J/\psi \rightarrow K^{*0}\bar{K}^{*0}\pi^+\pi^-\gamma$

¹ ABLIKIM 06A reports $[\Gamma(\eta_c(1S) \rightarrow K^*(892)^0 \bar{K}^*(892)^0 \pi^+ \pi^-)/\Gamma_{\text{total}}] \times [B(J/\psi(1S) \rightarrow \gamma\eta_c(1S))] = (1.91 \pm 0.64 \pm 0.48) \times 10^{-4}$ which we divide by our best value $B(J/\psi(1S) \rightarrow \gamma\eta_c(1S)) = (1.7 \pm 0.4) \times 10^{-2}$. Our first error is their experiment's error and our second error is the systematic error from using our best value.

 $\Gamma(\phi K^+ K^-)/\Gamma_{\text{total}}$ Γ_7/Γ

VALUE (units 10^{-3})	EVTS	DOCUMENT ID	TECN	COMMENT
2.9 ± 0.9 ± 1.1	14.1 ± 4.4 - 3.7	¹ HUANG	03 BELL	$B^+ \rightarrow (\phi K^+ K^-) K^+$

¹ Using $B(B^+ \rightarrow \eta_c K^+) = (1.25 \pm 0.12 \pm 0.10) \times 10^{-3}$ from FANG 03 and $B(\eta_c \rightarrow K\bar{K}\pi) = (5.5 \pm 1.7) \times 10^{-2}$.

 $\Gamma(\phi\phi)/\Gamma_{\text{total}}$ Γ_8/Γ

VALUE (units 10^{-4})	EVTS	DOCUMENT ID	TECN	COMMENT
17.4 ± 1.9 OUR FIT				
28 ± 4 OUR AVERAGE				
26 ± 4 ± 5	1.2k	¹ ABLIKIM	17P BES3	$J/\psi \rightarrow K^+K^-K^+K^-\gamma$
25.3 ± 5.1 ± 9.1	72	² ABLIKIM	05L BES2	$J/\psi \rightarrow K^+K^-K^+K^-\gamma$
26 ± 9	357	² BAI	04 BES	$J/\psi \rightarrow \gamma K^+K^-K^+K^-$
31 ± 7 ± 10	19	² BISELLO	91 DM2	$J/\psi \rightarrow \gamma K^+K^-K^+K^-$
30 ± 18 - 12 ± 10	5	² BISELLO	91 DM2	$J/\psi \rightarrow \gamma K^+K^-K_S^0 K_L^0$
74 ± 18 ± 24	80	² BAI	90B MRK3	$J/\psi \rightarrow \gamma K^+K^-K^+K^-$
67 ± 21 ± 24		² BAI	90B MRK3	$J/\psi \rightarrow \gamma K^+K^-K_S^0 K_L^0$

• • • We do not use the following data for averages, fits, limits, etc. • • •

18 ± 8 ± 7 7 ³HUANG 03 BELL $B^+ \rightarrow (\phi\phi) K^+$

¹ ABLIKIM 17P reports $[\Gamma(\eta_c(1S) \rightarrow \phi\phi)/\Gamma_{\text{total}}] \times [B(J/\psi(1S) \rightarrow \gamma\eta_c(1S))] = (4.3 \pm 0.5 \pm 0.5) \times 10^{-5}$ which we divide by our best value $B(J/\psi(1S) \rightarrow \gamma\eta_c(1S)) = (1.7 \pm 0.4) \times 10^{-2}$. Our first error is their experiment's error and our second error is the systematic error from using our best value.

² The quoted branching ratios use $B(J/\psi(1S) \rightarrow \gamma\eta_c(1S)) = 0.0127 \pm 0.0036$. Where relevant, the error in this branching ratio is treated as a common systematic in computing averages.

³ Using $B(B^+ \rightarrow \eta_c K^+) = (1.25 \pm 0.12 \pm 0.10) \times 10^{-3}$ from FANG 03 and $B(\eta_c \rightarrow K\bar{K}\pi) = (5.5 \pm 1.7) \times 10^{-2}$.

 $\Gamma(\phi\phi)/\Gamma(K\bar{K}\pi)$ Γ_8/Γ_{34}

VALUE	EVTS	DOCUMENT ID	TECN	COMMENT
0.0240 ± 0.0025 OUR FIT				
0.044 ± 0.012 - 0.010 OUR AVERAGE				

0.055 ± 0.014 ± 0.005		AUBERT,B	04B BABR	$B^\pm \rightarrow K^\pm \eta_c$
0.032 ± 0.014 - 0.010 ± 0.009	7	¹ HUANG	03 BELL	$B^\pm \rightarrow K^\pm \phi\phi$

¹ Using $B(B^+ \rightarrow \eta_c K^+) = (1.25 \pm 0.12 \pm 0.10) \times 10^{-3}$ from FANG 03 and $B(\eta_c \rightarrow K\bar{K}\pi) = (5.5 \pm 1.7) \times 10^{-2}$.

 $\Gamma(\phi\phi)/\Gamma(\rho\bar{\rho})$ Γ_8/Γ_{48}

VALUE	EVTS	DOCUMENT ID	TECN	COMMENT
1.79 ± 0.14 ± 0.32	6.4k	¹ AAIJ	17BB LHCB	$\rho\rho \rightarrow b\bar{b}X \rightarrow 2(K^+K^-)X$

¹ Using inputs from AAJ 15As and AAJ 15B1 and $\Gamma(b \rightarrow J/\psi(1S) \text{ anything})/\Gamma_{\text{total}} = (1.16 \pm 0.10)\%$ and $\Gamma(J/\psi(1S) \rightarrow \rho\bar{\rho})/\Gamma_{\text{total}} = (2.120 \pm 0.029) \times 10^{-3}$ from PDG 16.

 $\Gamma(\phi(2\pi^+\pi^-))/\Gamma_{\text{total}}$ Γ_9/Γ

VALUE (units 10^{-4})	CL%	EVTS	DOCUMENT ID	TECN	COMMENT
<40	90	¹ ABLIKIM	06A BES2	$J/\psi \rightarrow \phi(2\pi^+\pi^-)\gamma$	

¹ ABLIKIM 06A reports $[\Gamma(\eta_c(1S) \rightarrow \phi(2\pi^+\pi^-))/\Gamma_{\text{total}}] \times [B(J/\psi(1S) \rightarrow \gamma\eta_c(1S))] < 0.603 \times 10^{-4}$ which we divide by our best value $B(J/\psi(1S) \rightarrow \gamma\eta_c(1S)) = 1.7 \times 10^{-2}$.

 $\Gamma(a_0(980)\pi)/\Gamma_{\text{total}}$ Γ_{10}/Γ

VALUE	CL%	DOCUMENT ID	TECN	COMMENT
seen		LEES	21A BABR	Dalitz anal. of $\eta_c \rightarrow \pi^+\pi^-\eta$
seen		LEES	14E BABR	Dalitz anal. of $\eta_c \rightarrow K^+K^-\pi^0$

• • • We do not use the following data for averages, fits, limits, etc. • • •

<0.02 90 ^{1,2}BALTRUSAIT...86 MRK3 $J/\psi \rightarrow \eta_c \gamma$

¹ The quoted branching ratios use $B(J/\psi(1S) \rightarrow \gamma\eta_c(1S)) = 0.0127 \pm 0.0036$.

² We are assuming $B(a_0(980) \rightarrow \eta\pi) > 0.5$.

 $\Gamma(a_2(1320)\pi)/\Gamma_{\text{total}}$ Γ_{11}/Γ

VALUE	CL%	DOCUMENT ID	TECN	COMMENT
seen		LEES	21A BABR	Dalitz anal. of $\eta_c \rightarrow \pi^+\pi^-\eta$
<0.02	90	¹ BALTRUSAIT...86	MRK3	$J/\psi \rightarrow \eta_c \gamma$

¹ The quoted branching ratios use $B(J/\psi(1S) \rightarrow \gamma\eta_c(1S)) = 0.0127 \pm 0.0036$.

 $\Gamma(K^*(892)\bar{K}^+ + c.c.)/\Gamma_{\text{total}}$ Γ_{12}/Γ

VALUE	CL%	DOCUMENT ID	TECN	COMMENT
<0.0128	90	BISELLO	91 DM2	$J/\psi \rightarrow \gamma K_S^0 K^\pm \pi^\mp$
<0.0132	90	¹ BISELLO	91 DM2	$J/\psi \rightarrow \gamma K^+ K^- \pi^0$

¹ The quoted branching ratios use $B(J/\psi(1S) \rightarrow \gamma\eta_c(1S)) = 0.0127 \pm 0.0036$.

Meson Particle Listings

 $\eta_c(1S)$

$\Gamma(f_2(1270)\eta)/\Gamma_{\text{total}}$		Γ_{13}/Γ	
VALUE	CL%	DOCUMENT ID	TECN COMMENT

seen LEES 21A BABR Dalitz anal. of $\eta_c \rightarrow \pi^+\pi^-\eta$

<0.011 90 ¹BALTRUSAIT...86 MRK3 $J/\psi \rightarrow \eta_c \gamma$

¹The quoted branching ratios use $B(J/\psi(1S) \rightarrow \gamma\eta_c(1S)) = 0.0127 \pm 0.0036$.

$\Gamma(f_2(1270)\eta')/\Gamma_{\text{total}}$		Γ_{14}/Γ	
VALUE	DOCUMENT ID	TECN	COMMENT

seen LEES 21A BABR Dalitz anal. of $\eta_c \rightarrow \pi^+\pi^-\eta'$; $K^+K^-\eta'$

$\Gamma(\omega\omega)/\Gamma_{\text{total}}$		Γ_{15}/Γ			
VALUE (units 10^{-3})	CL%	EVTs	DOCUMENT ID	TECN	COMMENT

2.9 ± 0.5 ± 0.6 1705 ¹ABLIKIM 19AV BES3 $J/\psi \rightarrow \gamma\omega\omega$

• • • We do not use the following data for averages, fits, limits, etc. • • •

<6.3 90 ²ABLIKIM 05L BES2 $J/\psi \rightarrow 2(\pi^+\pi^-\pi^0)\gamma$

<6.3 90 ²BISELLO 91 DM2 $J/\psi \rightarrow \gamma\omega\omega$

<3.1 90 ²BALTRUSAIT...86 MRK3 $J/\psi \rightarrow \eta_c\gamma$

¹ABLIKIM 19AV reports $[\Gamma(\eta_c(1S) \rightarrow \omega\omega)/\Gamma_{\text{total}}] \times [B(J/\psi(1S) \rightarrow \gamma\eta_c(1S))] = (4.90 \pm 0.17 \pm 0.77) \times 10^{-5}$ which we divide by our best value $B(J/\psi(1S) \rightarrow \gamma\eta_c(1S)) = (1.7 \pm 0.4) \times 10^{-2}$. Our first error is their experiment's error and our second error is the systematic error from using our best value.,

²The quoted branching ratios use $B(J/\psi(1S) \rightarrow \gamma\eta_c(1S)) = 0.0127 \pm 0.0036$. Where relevant, the error in this branching ratio is treated as a common systematic in computing averages.

$\Gamma(\omega\phi)/\Gamma_{\text{total}}$		Γ_{16}/Γ	
VALUE	CL%	DOCUMENT ID	TECN COMMENT

< **2.5 × 10⁻⁴** 90 ¹ABLIKIM 17P BES3 $J/\psi \rightarrow \pi^+\pi^-\pi^0 K^+K^-\gamma$

• • • We do not use the following data for averages, fits, limits, etc. • • •

<17 × 10⁻⁴ 90 ²ABLIKIM 05L BES2 $J/\psi \rightarrow \pi^+\pi^-\pi^0 K^+K^-\gamma$

¹Using $B(J/\psi \rightarrow \gamma\eta_c) = 0.017 \pm 0.004$.

²The quoted branching ratios use $B(J/\psi(1S) \rightarrow \gamma\eta_c(1S)) = 0.0127 \pm 0.0036$.

$\Gamma(f_2(1270)f_2(1270))/\Gamma_{\text{total}}$		Γ_{17}/Γ	
VALUE (units 10^{-2})	EVTs	DOCUMENT ID	TECN COMMENT

0.98 ± 0.25 OUR FIT

0.77 ± 0.25 ± 0.17 91.2 ± 19.8 ¹ABLIKIM 04M BES $J/\psi \rightarrow \gamma 2\pi^+ 2\pi^-$

¹ABLIKIM 04M reports $[\Gamma(\eta_c(1S) \rightarrow f_2(1270)f_2(1270))/\Gamma_{\text{total}}] \times [B(J/\psi(1S) \rightarrow \gamma\eta_c(1S))] = (1.3 \pm 0.3 \pm 0.3) \times 10^{-4}$ which we divide by our best value $B(J/\psi(1S) \rightarrow \gamma\eta_c(1S)) = (1.7 \pm 0.4) \times 10^{-2}$. Our first error is their experiment's error and our second error is the systematic error from using our best value.

$\Gamma(f_0(500)\eta)/\Gamma_{\text{total}}$		Γ_{19}/Γ	
VALUE	DOCUMENT ID	TECN	COMMENT

seen LEES 21A BABR Dalitz anal. of $\eta_c \rightarrow \pi^+\pi^-\eta$

$\Gamma(f_0(500)\eta')/\Gamma_{\text{total}}$		Γ_{20}/Γ	
VALUE	DOCUMENT ID	TECN	COMMENT

seen LEES 21A BABR Dalitz anal. of $\eta_c(1S) \rightarrow \pi^+\pi^-\eta'$

$\Gamma(f_0(980)\eta)/\Gamma_{\text{total}}$		Γ_{21}/Γ	
VALUE	DOCUMENT ID	TECN	COMMENT

seen LEES 21A BABR Dalitz anal. of $\eta_c \rightarrow \pi^+\pi^-\eta$

seen LEES 14E BABR Dalitz anal. of $\eta_c \rightarrow K^+K^-\eta$

$\Gamma(f_0(980)\eta')/\Gamma_{\text{total}}$		Γ_{22}/Γ	
VALUE	DOCUMENT ID	TECN	COMMENT

seen LEES 21A BABR Dalitz anal. of $\eta_c \rightarrow \pi^+\pi^-\eta'$

$\eta_c \rightarrow \pi^+\pi^-\eta'$, $K^+K^-\eta'$

$\Gamma(f_0(1500)\eta)/\Gamma_{\text{total}}$		Γ_{23}/Γ	
VALUE	DOCUMENT ID	TECN	COMMENT

seen LEES 21A BABR Dalitz anal. of $\eta_c \rightarrow \pi^+\pi^-\eta$

seen LEES 14E BABR Dalitz anal. of $\eta_c \rightarrow K^+K^-\eta$

$\Gamma(f_0(1710)\eta')/\Gamma_{\text{total}}$		Γ_{24}/Γ	
VALUE	DOCUMENT ID	TECN	COMMENT

seen LEES 21A BABR Dalitz anal. of $\eta_c \rightarrow K^+K^-\eta'$

$\Gamma(f_0(2100)\eta')/\Gamma_{\text{total}}$		Γ_{25}/Γ	
VALUE	DOCUMENT ID	TECN	COMMENT

seen LEES 21A BABR Dalitz anal. of $\eta_c \rightarrow \pi^+\pi^-\eta'$

$\Gamma(f_0(2200)\eta)/\Gamma_{\text{total}}$		Γ_{26}/Γ	
VALUE	DOCUMENT ID	TECN	COMMENT

seen LEES 14E BABR Dalitz anal. of $\eta_c \rightarrow K^+K^-\eta$

$\Gamma(a_0(1320)\pi)/\Gamma_{\text{total}}$		Γ_{27}/Γ	
VALUE	DOCUMENT ID	TECN	COMMENT

seen LEES 14E BABR Dalitz anal. of $\eta_c \rightarrow K^+K^-\pi^0$

$\Gamma(a_0(1450)\pi)/\Gamma_{\text{total}}$		Γ_{28}/Γ	
VALUE	DOCUMENT ID	TECN	COMMENT

seen LEES 21A BABR Dalitz anal. of $\eta_c \rightarrow \pi^+\pi^-\eta$

seen LEES 14E BABR Dalitz anal. of $\eta_c \rightarrow K^+K^-\pi^0$

$\Gamma(a_0(1700)\pi)/\Gamma_{\text{total}}$		Γ_{29}/Γ	
VALUE	DOCUMENT ID	TECN	COMMENT

seen LEES 21A BABR Dalitz anal. of $\eta_c \rightarrow \pi^+\pi^-\eta'$

$\Gamma(a_0(1950)\pi)/\Gamma_{\text{total}}$		Γ_{30}/Γ	
VALUE	EVTs	DOCUMENT ID	TECN COMMENT

seen LEES 21A BABR Dalitz anal. of $\eta_c(1S) \rightarrow \pi^+\pi^-\eta'$

seen 12k ¹LEES 16A BABR $\gamma\gamma \rightarrow \eta_c(1S) \rightarrow K\bar{K}\pi$

¹From a model-independent partial wave analysis.

$\Gamma(K_S^0(1430)\bar{K})/\Gamma_{\text{total}}$		Γ_{31}/Γ	
VALUE	EVTs	DOCUMENT ID	TECN COMMENT

seen 12k ¹LEES 16A BABR $\gamma\gamma \rightarrow \eta_c(1S) \rightarrow K\bar{K}\pi$

seen LEES 14E BABR Dalitz anal. of $\eta_c \rightarrow K^+K^-\eta/\pi^0$

¹From a model-independent partial wave analysis.

$\Gamma(K_S^0(1430)\bar{K})/\Gamma_{\text{total}}$		Γ_{32}/Γ	
VALUE	DOCUMENT ID	TECN	COMMENT

seen LEES 21A BABR Dalitz anal. of $\eta_c \rightarrow K^+K^-\eta'$

seen LEES 14E BABR Dalitz anal. of $\eta_c \rightarrow K^+K^-\pi^0$

$\Gamma(K_S^0(1950)\bar{K})/\Gamma_{\text{total}}$		Γ_{33}/Γ	
VALUE	EVTs	DOCUMENT ID	TECN COMMENT

seen LEES 21A BABR Dalitz anal. of $\eta_c \rightarrow K^+K^-\eta'$

seen 12k ¹LEES 16A BABR $\gamma\gamma \rightarrow \eta_c(1S) \rightarrow K\bar{K}\pi$

seen LEES 14E BABR Dalitz anal. of $\eta_c \rightarrow K^+K^-\eta/\pi^0$

¹From a Dalitz plot analysis using an isobar model.

$\Gamma(K\bar{K}\pi)/\Gamma_{\text{total}}$		Γ_{34}/Γ	
VALUE (units 10^{-2})	EVTs	DOCUMENT ID	TECN COMMENT

7.3 ± 0.4 OUR FIT

6.9 ± 0.5 OUR AVERAGE

6.9 ± 0.7 ± 0.6 146 ¹ABLIKIM 19AP BES3 $h_c \rightarrow \gamma\eta_c$

7.8 ± 0.6 ± 0.6 267 ²ABLIKIM 19AP BES3 $h_c \rightarrow \gamma\eta_c$

6.3 ± 1.3 ± 1.4 55 ^{3,4}ABLIKIM 12N BES3 $\psi(2S) \rightarrow \pi^0\gamma K^+K^-\pi^0$

7.9 ± 1.4 ± 1.8 107 ^{5,6}ABLIKIM 12N BES3 $\psi(2S) \rightarrow \pi^0\gamma K_S^0 K^{\mp}\pi^{\pm}$

8.5 ± 1.8 ⁷AUBERT 06E BABR $B^{\pm} \rightarrow K^{\pm} X_{c\bar{c}}$

5.1 ± 2.1 0.6k ⁸BAI 04 BES $J/\psi \rightarrow \gamma K^{\pm}\pi^{\mp} K_S^0$

6.90 ± 1.42 ± 1.32 33 ⁸BISELLO 91 DM2 $J/\psi \rightarrow \gamma K^+K^-\pi^0$

5.43 ± 0.94 ± 0.94 68 ⁸BISELLO 91 DM2 $J/\psi \rightarrow \gamma K^{\pm}\pi^{\mp} K_S^0$

4.8 ± 1.7 95 ^{8,9}BALTRUSAIT...86 MRK3 $J/\psi \rightarrow \eta_c\gamma$

16.1 +9.2 -7.3 10,11 HIMEL 80B MRK2 $\psi(2S) \rightarrow \eta_c\gamma$

• • • We do not use the following data for averages, fits, limits, etc. • • •

< 10.7 90% CL ^{8,12}PARTRIDGE 80B CBAL $J/\psi \rightarrow \eta_c\gamma$

¹ABLIKIM 19AP quotes $B(\eta_c \rightarrow K^+K^-\pi^0) = (1.15 \pm 0.12 \pm 0.10) \times 10^{-2}$ which we multiply by 6 to account for isospin symmetry.

²ABLIKIM 19AP quotes $B(\eta_c \rightarrow K_S^0 K^{\pm}\pi^{\mp}) = (2.60 \pm 0.21 \pm 0.20) \times 10^{-2}$ which we multiply by 3 to account for isospin symmetry.

³ABLIKIM 12N quotes $B(\psi(2S) \rightarrow \pi^0 h_c) \cdot B(h_c \rightarrow \gamma\eta_c) \cdot B(\eta_c \rightarrow K^+K^-\pi^0) = (4.54 \pm 0.76 \pm 0.48) \times 10^{-6}$ which we multiply by 6 to account for isospin symmetry.

⁴ABLIKIM 12N reports $[\Gamma(\eta_c(1S) \rightarrow K\bar{K}\pi)/\Gamma_{\text{total}}] \times [B(\psi(2S) \rightarrow h_c(1P)\pi^0)] \times [B(h_c(1P) \rightarrow \gamma\eta_c(1S))] = (27.24 \pm 4.56 \pm 2.88) \times 10^{-6}$ which we divide by our best values $B(\psi(2S) \rightarrow h_c(1P)\pi^0) = (8.6 \pm 1.3) \times 10^{-4}$, $B(h_c(1P) \rightarrow \gamma\eta_c(1S)) = (50 \pm 9) \times 10^{-2}$. Our first error is their experiment's error and our second error is the systematic error from using our best values.

⁵ABLIKIM 12N quotes $B(\psi(2S) \rightarrow \pi^0 h_c) \cdot B(h_c \rightarrow \gamma\eta_c) \cdot B(\eta_c \rightarrow K_S^0 K^{\pm}\pi^{\mp}) = (11.35 \pm 1.25 \pm 1.50) \times 10^{-6}$ which we multiply by 3 to account for isospin symmetry.

⁶ABLIKIM 12N reports $[\Gamma(\eta_c(1S) \rightarrow K\bar{K}\pi)/\Gamma_{\text{total}}] \times [B(\psi(2S) \rightarrow h_c(1P)\pi^0)] \times [B(h_c(1P) \rightarrow \gamma\eta_c(1S))] = (34.05 \pm 3.75 \pm 4.50) \times 10^{-6}$ which we divide by our best values $B(\psi(2S) \rightarrow h_c(1P)\pi^0) = (8.6 \pm 1.3) \times 10^{-4}$, $B(h_c(1P) \rightarrow \gamma\eta_c(1S)) = (50 \pm 9) \times 10^{-2}$. Our first error is their experiment's error and our second error is the systematic error from using our best values.

⁷Determined from the ratio of $B(B^{\pm} \rightarrow K^{\pm}\eta_c) B(\eta_c \rightarrow K\bar{K}\pi) = (7.4 \pm 0.5 \pm 0.7) \times 10^{-5}$ reported in AUBERT, B 04B and $B(B^{\pm} \rightarrow K^{\pm}\eta_c) = (8.7 \pm 1.5) \times 10^{-3}$ reported in AUBERT 06E.

⁸The quoted branching ratios use $B(J/\psi(1S) \rightarrow \gamma\eta_c(1S)) = 0.0127 \pm 0.0036$. Where relevant, the error in this branching ratio is treated as a common systematic in computing averages.

⁹Average from $K^+K^-\pi^0$ and $K^{\pm}K_S^0\pi^{\mp}$ decay channels.

¹⁰ $K^{\pm}K_S^0\pi^{\mp}$ corrected to $K\bar{K}\pi$ by factor 3. KS, MR.

¹¹Estimated using $B(\psi(2S) \rightarrow \gamma\eta_c(1S)) = 0.0028 \pm 0.0006$.

¹² $K^+K^-\pi^0$ corrected to $K\bar{K}\pi$ by factor 6. KS, MR

$\Gamma(\phi K^+ K^-)/\Gamma(K\bar{K}\pi)$ Γ_7/Γ_{34}

VALUE	EVTS	DOCUMENT ID	TECN	COMMENT
$0.052 \pm 0.016 \pm 0.014$	7	¹ HUANG	03	BELL $B^\pm \rightarrow K^\pm \phi$

¹ Using $B(B^+ \rightarrow \eta_c K^+) = (1.25 \pm 0.12 \pm 0.10) \times 10^{-3}$ from FANG 03 and $B(\eta_c \rightarrow K\bar{K}\pi) = (5.5 \pm 1.7) \times 10^{-2}$.

 $\Gamma(K\bar{K}\eta)/\Gamma_{total}$ Γ_{35}/Γ

VALUE (units 10^{-2})	CL%	EVTS	DOCUMENT ID	TECN	COMMENT
1.36 ± 0.15 OUR FIT					
$1.0 \pm 0.5 \pm 0.2$		7	^{1,2} ABLIKIM	12N	BES3 $\psi(2S) \rightarrow \pi^0 \gamma \eta K^+ K^-$

• • • We do not use the following data for averages, fits, limits, etc. • • •
 <3.1 90 ³ BALTRUSAIT...86 MRK3 $J/\psi \rightarrow \eta_c \gamma$

¹ ABLIKIM 12N quotes $B(\psi(2S) \rightarrow \pi^0 h_c) \cdot B(h_c \rightarrow \gamma \eta_c) \cdot B(\eta_c \rightarrow K^+ K^- \eta) = (2.11 \pm 1.01 \pm 0.32) \times 10^{-6}$ which we multiply by 2 to account for isospin symmetry.

² ABLIKIM 12N reports $[\Gamma(\eta_c(1S) \rightarrow K\bar{K}\eta)/\Gamma_{total}] \times [B(\psi(2S) \rightarrow h_c(1P)\pi^0)] \times [B(h_c(1P) \rightarrow \gamma \eta_c(1S))] = (4.22 \pm 2.02 \pm 0.64) \times 10^{-6}$ which we divide by our best values $B(\psi(2S) \rightarrow h_c(1P)\pi^0) = (8.6 \pm 1.3) \times 10^{-4}$, $B(h_c(1P) \rightarrow \gamma \eta_c(1S)) = (50 \pm 9) \times 10^{-2}$. Our first error is their experiment's error and our second error is the systematic error from using our best values.

³ The quoted branching ratios use $B(J/\psi(1S) \rightarrow \eta_c \gamma) = 0.0127 \pm 0.0036$.

 $\Gamma(K\bar{K}\eta)/\Gamma(K\bar{K}\pi)$ Γ_{35}/Γ_{34}

VALUE	EVTS	DOCUMENT ID	TECN	COMMENT
0.187 ± 0.018 OUR FIT				
$0.190 \pm 0.008 \pm 0.017$	5.4k	¹ LEES	14E	BABR $\gamma \gamma \rightarrow K^+ K^- \eta/\pi^0$

¹ LEES 14E reports $B(\eta_c(1S) \rightarrow K^+ K^- \eta)/B(\eta_c(1S) \rightarrow K^+ K^- \pi^0) = 0.571 \pm 0.025 \pm 0.051$, which we divide by 3 to account for isospin symmetry. It uses both $\eta \rightarrow \gamma \gamma$ and $\eta \rightarrow \pi^+ \pi^- \pi^0$ decays.

 $\Gamma(\eta \pi^+ \pi^-)/\Gamma_{total}$ Γ_{36}/Γ

VALUE (units 10^{-2})	EVTS	DOCUMENT ID	TECN	COMMENT
$1.7 \pm 0.4 \pm 0.4$	33	¹ ABLIKIM	12N	BES3 $\psi(2S) \rightarrow \pi^0 \gamma \eta \pi^+ \pi^-$

• • • We do not use the following data for averages, fits, limits, etc. • • •

5.4 ± 2.0 75 ² BALTRUSAIT...86 MRK3 $J/\psi \rightarrow \eta_c \gamma$
 $3.7 \pm 1.3 \pm 2.0$ 18 ² PARTRIDGE 80B CBAL $J/\psi \rightarrow \eta \pi^+ \pi^- \gamma$

¹ ABLIKIM 12N reports $[\Gamma(\eta_c(1S) \rightarrow \eta \pi^+ \pi^-)/\Gamma_{total}] \times [B(\psi(2S) \rightarrow h_c(1P)\pi^0)] \times [B(h_c(1P) \rightarrow \gamma \eta_c(1S))] = (7.22 \pm 1.47 \pm 1.11) \times 10^{-6}$ which we divide by our best values $B(\psi(2S) \rightarrow h_c(1P)\pi^0) = (8.6 \pm 1.3) \times 10^{-4}$, $B(h_c(1P) \rightarrow \gamma \eta_c(1S)) = (50 \pm 9) \times 10^{-2}$. Our first error is their experiment's error and our second error is the systematic error from using our best values.

² The quoted branching ratios use $B(J/\psi(1S) \rightarrow \eta_c \gamma) = 0.0127 \pm 0.0036$. Where relevant, the error in this branching ratio is treated as a common systematic in computing averages.

 $\Gamma(\eta 2(\pi^+ \pi^-))/\Gamma_{total}$ Γ_{37}/Γ

VALUE (units 10^{-2})	EVTS	DOCUMENT ID	TECN	COMMENT
$4.4 \pm 1.2 \pm 1.0$	39	¹ ABLIKIM	12N	BES3 $\psi(2S) \rightarrow \pi^0 \gamma \eta 2(\pi^+ \pi^-)$

¹ ABLIKIM 12N reports $[\Gamma(\eta_c(1S) \rightarrow \eta 2(\pi^+ \pi^-))/\Gamma_{total}] \times [B(\psi(2S) \rightarrow h_c(1P)\pi^0)] \times [B(h_c(1P) \rightarrow \gamma \eta_c(1S))] = (19.17 \pm 3.77 \pm 3.72) \times 10^{-6}$ which we divide by our best values $B(\psi(2S) \rightarrow h_c(1P)\pi^0) = (8.6 \pm 1.3) \times 10^{-4}$, $B(h_c(1P) \rightarrow \gamma \eta_c(1S)) = (50 \pm 9) \times 10^{-2}$. Our first error is their experiment's error and our second error is the systematic error from using our best values.

 $\Gamma(K^+ K^- \pi^+ \pi^-)/\Gamma_{total}$ Γ_{38}/Γ

VALUE (units 10^{-3})	EVTS	DOCUMENT ID	TECN	COMMENT
6.6 ± 1.1 OUR FIT				
11.8 ± 2.3 OUR AVERAGE				

$9.7 \pm 2.2 \pm 2.2$ 38 ¹ ABLIKIM 12N BES3 $\psi(2S) \rightarrow \pi^0 \gamma K^+ K^- \pi^+ \pi^-$
 12 ± 4 0.4k ² BAI 04 BES $J/\psi \rightarrow \gamma K^+ K^- \pi^+ \pi^-$
 21 ± 7 110 ² BALTRUSAIT...86 MRK3 $J/\psi \rightarrow \eta_c \gamma$
 14 ± 2.2 ³ HIMEL 80B MRK2 $\psi(2S) \rightarrow \eta_c \gamma$

¹ ABLIKIM 12N reports $[\Gamma(\eta_c(1S) \rightarrow K^+ K^- \pi^+ \pi^-)/\Gamma_{total}] \times [B(\psi(2S) \rightarrow h_c(1P)\pi^0)] \times [B(h_c(1P) \rightarrow \gamma \eta_c(1S))] = (4.16 \pm 0.76 \pm 0.59) \times 10^{-6}$ which we divide by our best values $B(\psi(2S) \rightarrow h_c(1P)\pi^0) = (8.6 \pm 1.3) \times 10^{-4}$, $B(h_c(1P) \rightarrow \gamma \eta_c(1S)) = (50 \pm 9) \times 10^{-2}$. Our first error is their experiment's error and our second error is the systematic error from using our best values.

² The quoted branching ratios use $B(J/\psi(1S) \rightarrow \eta_c \gamma) = 0.0127 \pm 0.0036$. Where relevant, the error in this branching ratio is treated as a common systematic in computing averages.

³ Estimated using $B(\psi(2S) \rightarrow \eta_c \gamma) = 0.0028 \pm 0.0006$.

 $\Gamma(K^+ K^- \pi^+ \pi^- \pi^0)/\Gamma(K\bar{K}\pi)$ Γ_{39}/Γ_{34}

VALUE	EVTS	DOCUMENT ID	TECN	COMMENT
$0.477 \pm 0.017 \pm 0.070$	11k	¹ DEL-AMO-SA...11M	BABR	$\gamma \gamma \rightarrow K^+ K^- \pi^+ \pi^- \pi^0$

¹ We have multiplied the value of $\Gamma(K^+ K^- \pi^+ \pi^- \pi^0)/\Gamma(K_S^0 K^\pm \pi^\mp)$ reported in DEL-AMO-SANCHEZ 11M by a factor 1/3 to obtain $\Gamma(K^+ K^- \pi^+ \pi^- \pi^0)/\Gamma(K\bar{K}\pi)$. Not independent from other measurements reported in DEL-AMO-SANCHEZ 11M.

 $\Gamma(K^0 K^- \pi^+ \pi^- \pi^+ + c.c.)/\Gamma_{total}$ Γ_{40}/Γ

VALUE (units 10^{-2})	EVTS	DOCUMENT ID	TECN	COMMENT
$5.6 \pm 1.4 \pm 1.3$	43	^{1,2} ABLIKIM	12N	BES3 $\psi(2S) \rightarrow \pi^0 \gamma K_S^0 K^\mp \pi^\mp 2\pi^\pm$

¹ ABLIKIM 12N quotes $B(\psi(2S) \rightarrow \pi^0 h_c) \cdot B(h_c \rightarrow \gamma \eta_c) \cdot B(\eta_c \rightarrow K_S^0 K^- \pi^- 2\pi^+) = (12.01 \pm 2.22 \pm 2.04) \times 10^{-6}$ which we multiply by 2 to take c.c. into account.

² ABLIKIM 12N reports $[\Gamma(\eta_c(1S) \rightarrow K^0 K^- \pi^+ \pi^- \pi^+ + c.c.)/\Gamma_{total}] \times [B(\psi(2S) \rightarrow h_c(1P)\pi^0)] \times [B(h_c(1P) \rightarrow \gamma \eta_c(1S))] = (24.02 \pm 4.44 \pm 4.08) \times 10^{-6}$ which we divide by our best values $B(\psi(2S) \rightarrow h_c(1P)\pi^0) = (8.6 \pm 1.3) \times 10^{-4}$, $B(h_c(1P) \rightarrow \gamma \eta_c(1S)) = (50 \pm 9) \times 10^{-2}$. Our first error is their experiment's error and our second error is the systematic error from using our best values.

 $\Gamma(K^+ K^- 2(\pi^+ \pi^-))/\Gamma_{total}$ Γ_{41}/Γ

VALUE (units 10^{-3})	EVTS	DOCUMENT ID	TECN	COMMENT
7.5 ± 2.4 OUR AVERAGE				
$8 \pm 4 \pm 2$	10	¹ ABLIKIM	12N	BES3 $\psi(2S) \rightarrow \pi^0 \gamma K^+ K^- 2(\pi^+ \pi^-)$

$7.2 \pm 2.4 \pm 1.5$ 100 ² ABLIKIM 06A BES2 $J/\psi \rightarrow K^+ K^- 2(\pi^+ \pi^-) \gamma$

¹ ABLIKIM 12N reports $[\Gamma(\eta_c(1S) \rightarrow K^+ K^- 2(\pi^+ \pi^-))/\Gamma_{total}] \times [B(\psi(2S) \rightarrow h_c(1P)\pi^0)] \times [B(h_c(1P) \rightarrow \gamma \eta_c(1S))] = (3.60 \pm 1.71 \pm 0.64) \times 10^{-6}$ which we divide by our best values $B(\psi(2S) \rightarrow h_c(1P)\pi^0) = (8.6 \pm 1.3) \times 10^{-4}$, $B(h_c(1P) \rightarrow \gamma \eta_c(1S)) = (50 \pm 9) \times 10^{-2}$. Our first error is their experiment's error and our second error is the systematic error from using our best values.

² ABLIKIM 06A reports $[\Gamma(\eta_c(1S) \rightarrow K^+ K^- 2(\pi^+ \pi^-))/\Gamma_{total}] \times [B(J/\psi(1S) \rightarrow \gamma \eta_c(1S))] = (1.21 \pm 0.32 \pm 0.24) \times 10^{-4}$ which we divide by our best value $B(J/\psi(1S) \rightarrow \gamma \eta_c(1S)) = (1.7 \pm 0.4) \times 10^{-2}$. Our first error is their experiment's error and our second error is the systematic error from using our best values.

 $\Gamma(2(K^+ K^-))/\Gamma_{total}$ Γ_{42}/Γ

VALUE (units 10^{-3})	EVTS	DOCUMENT ID	TECN	COMMENT
1.43 ± 0.30 OUR FIT				
$2.2 \pm 0.9 \pm 0.5$	7	¹ ABLIKIM	12N	BES3 $\psi(2S) \rightarrow \pi^0 \gamma 2(K^+ K^-)$

• • • We do not use the following data for averages, fits, limits, etc. • • •

$1.4 \pm 0.5 \pm 0.6$ 14.5 ± 4.6 ² HUANG 03 BELL $B^+ \rightarrow 2(K^+ K^-) K^+$

$21 \pm 10 \pm 6$ ³ ALBRECHT 94H ARG $\gamma \gamma \rightarrow K^+ K^- K^+ K^-$

¹ ABLIKIM 12N reports $[\Gamma(2(K^+ K^-))/\Gamma_{total}] \times [B(\psi(2S) \rightarrow h_c(1P)\pi^0)] \times [B(h_c(1P) \rightarrow \gamma \eta_c(1S))] = (0.94 \pm 0.37 \pm 0.14) \times 10^{-6}$ which we divide by our best values $B(\psi(2S) \rightarrow h_c(1P)\pi^0) = (8.6 \pm 1.3) \times 10^{-4}$, $B(h_c(1P) \rightarrow \gamma \eta_c(1S)) = (50 \pm 9) \times 10^{-2}$. Our first error is their experiment's error and our second error is the systematic error from using our best values.

² Using $B(B^+ \rightarrow \eta_c K^+) = (1.25 \pm 0.12 \pm 0.10) \times 10^{-3}$ from FANG 03 and $B(\eta_c \rightarrow K\bar{K}\pi) = (5.5 \pm 1.7) \times 10^{-2}$.

³ Normalized to the sum of $B(\eta_c \rightarrow K^\pm K_S^0 \pi^\mp)$, $B(\eta_c \rightarrow \phi \phi)$, $B(\eta_c \rightarrow K^+ K^- \pi^+ \pi^-)$, and $B(\eta_c \rightarrow 2\pi^+ 2\pi^-)$.

 $\Gamma(2(K^+ K^-))/\Gamma(K\bar{K}\pi)$ Γ_{42}/Γ_{34}

VALUE	EVTS	DOCUMENT ID	TECN	COMMENT
0.020 ± 0.004 OUR FIT				
0.024 ± 0.007 OUR AVERAGE				

$0.023 \pm 0.007 \pm 0.006$ AUBERT,B 04B BABR $B^\pm \rightarrow K^\pm \eta_c$

$0.026 \pm 0.009 \pm 0.007$ 15 ¹ HUANG 03 BELL $B^\pm \rightarrow K^\pm (2K^+ 2K^-)$

¹ Using $B(B^+ \rightarrow \eta_c K^+) = (1.25 \pm 0.12 \pm 0.10) \times 10^{-3}$ from FANG 03 and $B(\eta_c \rightarrow K\bar{K}\pi) = (5.5 \pm 1.7) \times 10^{-2}$.

 $\Gamma(\eta'(958) K\bar{K})/\Gamma(\eta'(958) \pi\pi)$ Γ_2/Γ_1

VALUE	DOCUMENT ID	TECN	COMMENT
$0.859 \pm 0.052 \pm 0.043$	¹ LEES	21A	BABR $\gamma \gamma \rightarrow \eta' K^+ K^-$, $\eta' \pi^+ \pi^-$

¹ Based on Dalitz-plot analysis of the $\eta_c \rightarrow \eta' K^+ K^-$, $\eta' \pi^+ \pi^-$ final states where the fit fractions and relative phases are determined for numerous two-body intermediate states.

 $\Gamma(\pi^+ \pi^- \pi^0)/\Gamma_{total}$ Γ_{43}/Γ

VALUE	CL%	DOCUMENT ID	TECN	COMMENT
$<5 \times 10^{-4}$	90	¹ ABLIKIM	17AJ	BES3 $\psi(2S) \rightarrow \gamma \pi^+ \pi^- \pi^0$

¹ ABLIKIM 17AJ reports $[\Gamma(\eta_c(1S) \rightarrow \pi^+ \pi^- \pi^0)/\Gamma_{total}] \times [B(\psi(2S) \rightarrow \gamma \eta_c(1S))] < 1.6 \times 10^{-6}$ which we divide by our best value $B(\psi(2S) \rightarrow \gamma \eta_c(1S)) = 3.4 \times 10^{-3}$.

 $\Gamma(\pi^+ \pi^- \pi^0 \pi^0)/\Gamma_{total}$ Γ_{44}/Γ

VALUE (units 10^{-2})	EVTS	DOCUMENT ID	TECN	COMMENT
$4.7 \pm 0.9 \pm 1.1$	118	¹ ABLIKIM	12N	BES3 $\psi(2S) \rightarrow \pi^0 \gamma \pi^+ \pi^- 2\pi^0$

¹ ABLIKIM 12N reports $[\Gamma(\eta_c(1S) \rightarrow \pi^+ \pi^- \pi^0 \pi^0)/\Gamma_{total}] \times [B(\psi(2S) \rightarrow h_c(1P)\pi^0)] \times [B(h_c(1P) \rightarrow \gamma \eta_c(1S))] = (20.31 \pm 2.20 \pm 3.33) \times 10^{-6}$ which we divide by our best values $B(\psi(2S) \rightarrow h_c(1P)\pi^0) = (8.6 \pm 1.3) \times 10^{-4}$, $B(h_c(1P) \rightarrow \gamma \eta_c(1S)) = (50 \pm 9) \times 10^{-2}$. Our first error is their experiment's error and our second error is the systematic error from using our best values.

Meson Particle Listings

 $\eta_c(1S)$ $\Gamma(2(\pi^+\pi^-))/\Gamma_{\text{total}}$ Γ_{45}/Γ

VALUE (units 10^{-2})	EVTS	DOCUMENT ID	TECN	COMMENT
0.91 ± 0.12 OUR FIT				
1.27 ± 0.23 OUR AVERAGE				
1.7 ± 0.3 ± 0.4	100	1 ABLIKIM	12N BES3	$\psi(2S) \rightarrow \pi^0 \gamma 2(\pi^+\pi^-)$
1.0 ± 0.5	542 ± 75	2 BAI	04 BES	$J/\psi \rightarrow \gamma 2(\pi^+\pi^-)$
1.05 ± 0.17 ± 0.34	137	2 BISELLO	91 DM2	$J/\psi \rightarrow \gamma 2\pi^+ 2\pi^-$
1.3 ± 0.6	25	2 BALTRUSAIT..86	MRK3	$J/\psi \rightarrow \eta_c \gamma$
2.0 $^{+1.5}_{-1.0}$		3 HIMEL	80B MRK2	$\psi(2S) \rightarrow \eta_c \gamma$

¹ ABLIKIM 12N reports $[\Gamma(\eta_c(1S) \rightarrow 2(\pi^+\pi^-))/\Gamma_{\text{total}}] \times [B(\psi(2S) \rightarrow h_c(1P)\pi^0)] \times [B(h_c(1P) \rightarrow \gamma\eta_c(1S))] = (7.51 \pm 0.85 \pm 1.11) \times 10^{-6}$ which we divide by our best values $B(\psi(2S) \rightarrow h_c(1P)\pi^0) = (8.6 \pm 1.3) \times 10^{-4}$, $B(h_c(1P) \rightarrow \gamma\eta_c(1S)) = (50 \pm 9) \times 10^{-2}$. Our first error is their experiment's error and our second error is the systematic error from using our best values.

² The quoted branching ratios use $B(J/\psi(1S) \rightarrow \gamma\eta_c(1S)) = 0.0127 \pm 0.0036$. Where relevant, the error in this branching ratio is treated as a common systematic in computing averages.

³ Estimated using $B(\psi(2S) \rightarrow \gamma\eta_c(1S)) = 0.0028 \pm 0.0006$.

 $\Gamma(2(\pi^+\pi^-\pi^0))/\Gamma_{\text{total}}$ Γ_{46}/Γ

VALUE (units 10^{-2})	EVTS	DOCUMENT ID	TECN	COMMENT
15.8 ± 2.3 OUR AVERAGE				
15.3 ± 1.8 ± 1.8	333	ABLIKIM	19AP BES3	$h_c \rightarrow \gamma\eta_c$
17 ± 3 ± 4	175	1 ABLIKIM	12N BES3	$\psi(2S) \rightarrow \pi^0 \gamma 2(\pi^+\pi^-\pi^0)$

¹ ABLIKIM 12N reports $[\Gamma(\eta_c(1S) \rightarrow 2(\pi^+\pi^-\pi^0))/\Gamma_{\text{total}}] \times [B(\psi(2S) \rightarrow h_c(1P)\pi^0)] \times [B(h_c(1P) \rightarrow \gamma\eta_c(1S))] = (75.13 \pm 7.42 \pm 9.99) \times 10^{-6}$ which we divide by our best values $B(\psi(2S) \rightarrow h_c(1P)\pi^0) = (8.6 \pm 1.3) \times 10^{-4}$, $B(h_c(1P) \rightarrow \gamma\eta_c(1S)) = (50 \pm 9) \times 10^{-2}$. Our first error is their experiment's error and our second error is the systematic error from using our best values.

 $\Gamma(3(\pi^+\pi^-))/\Gamma_{\text{total}}$ Γ_{47}/Γ

VALUE (units 10^{-3})	EVTS	DOCUMENT ID	TECN	COMMENT
17 ± 4 OUR AVERAGE				
20 ± 5 ± 5	51	1 ABLIKIM	12N BES3	$\psi(2S) \rightarrow \pi^0 \gamma 3(\pi^+\pi^-)$
15.4 ± 3.4 ± 3.3	479	2 ABLIKIM	06A BES2	$J/\psi \rightarrow 3(\pi^+\pi^-) \gamma$

¹ ABLIKIM 12N reports $[\Gamma(\eta_c(1S) \rightarrow 3(\pi^+\pi^-))/\Gamma_{\text{total}}] \times [B(\psi(2S) \rightarrow h_c(1P)\pi^0)] \times [B(h_c(1P) \rightarrow \gamma\eta_c(1S))] = (8.82 \pm 1.57 \pm 1.59) \times 10^{-6}$ which we divide by our best values $B(\psi(2S) \rightarrow h_c(1P)\pi^0) = (8.6 \pm 1.3) \times 10^{-4}$, $B(h_c(1P) \rightarrow \gamma\eta_c(1S)) = (50 \pm 9) \times 10^{-2}$. Our first error is their experiment's error and our second error is the systematic error from using our best values.

² ABLIKIM 06A reports $[\Gamma(\eta_c(1S) \rightarrow 3(\pi^+\pi^-))/\Gamma_{\text{total}}] \times [B(J/\psi(1S) \rightarrow \gamma\eta_c(1S))] = (2.59 \pm 0.32 \pm 0.47) \times 10^{-4}$ which we divide by our best value $B(J/\psi(1S) \rightarrow \gamma\eta_c(1S)) = (1.7 \pm 0.4) \times 10^{-2}$. Our first error is their experiment's error and our second error is the systematic error from using our best value.

 $\Gamma(p\bar{p})/\Gamma_{\text{total}}$ Γ_{48}/Γ

VALUE (units 10^{-4})	EVTS	DOCUMENT ID	TECN	COMMENT
14.4 ± 1.4 OUR FIT				
12.6 ± 2.1 OUR AVERAGE				
12.0 ± 2.6 ± 1.5	34	ABLIKIM	19APBES3	$h_c \rightarrow \gamma\eta_c$
15 ± 5 ± 3	15	1 ABLIKIM	12N BES3	$\psi(2S) \rightarrow \pi^0 \gamma p\bar{p}$
15 ± 6	213 ± 33	2 BAI	04 BES	$J/\psi \rightarrow \gamma p\bar{p}$
10 ± 3 ± 4	18	2 BISELLO	91 DM2	$J/\psi \rightarrow \gamma p\bar{p}$
11 ± 6	23	2 BALTRUSAIT..86	MRK3	$J/\psi \rightarrow \eta_c \gamma$
29 $^{+29}_{-15}$		3 HIMEL	80B MRK2	$\psi(2S) \rightarrow \eta_c \gamma$

• • • We do not use the following data for averages, fits, limits, etc. • • •

13.1 $^{+1.8}_{-2.1}$ ± 0.9	195	4 WU	06 BELL	$B^+ \rightarrow p\bar{p}K^+$
-----------------------------	-----	------	---------	-------------------------------

¹ ABLIKIM 12N reports $[\Gamma(\eta_c(1S) \rightarrow p\bar{p})/\Gamma_{\text{total}}] \times [B(\psi(2S) \rightarrow h_c(1P)\pi^0)] \times [B(h_c(1P) \rightarrow \gamma\eta_c(1S))] = (0.65 \pm 0.19 \pm 0.10) \times 10^{-6}$ which we divide by our best values $B(\psi(2S) \rightarrow h_c(1P)\pi^0) = (8.6 \pm 1.3) \times 10^{-4}$, $B(h_c(1P) \rightarrow \gamma\eta_c(1S)) = (50 \pm 9) \times 10^{-2}$. Our first error is their experiment's error and our second error is the systematic error from using our best values.

² The quoted branching ratios use $B(J/\psi(1S) \rightarrow \gamma\eta_c(1S)) = 0.0127 \pm 0.0036$. Where relevant, the error in this branching ratio is treated as a common systematic in computing averages.

³ Estimated using $B(\psi(2S) \rightarrow \gamma\eta_c(1S)) = 0.0028 \pm 0.0006$.

⁴ WU 06 reports $[\Gamma(\eta_c(1S) \rightarrow p\bar{p})/\Gamma_{\text{total}}] \times [B(B^+ \rightarrow \eta_c K^+)] = (1.42 \pm 0.11 $^{+0.16}_{-0.20}$) \times 10^{-6}$ which we divide by our best value $B(B^+ \rightarrow \eta_c K^+) = (1.09 \pm 0.08) \times 10^{-3}$. Our first error is their experiment's error and our second error is the systematic error from using our best value.

 $\Gamma(p\bar{p})/\Gamma(K^+K^-)$ Γ_{48}/Γ_{34}

VALUE	EVTS	DOCUMENT ID	TECN	COMMENT
0.0198 ± 0.0019 OUR FIT				
0.021 ± 0.002 $^{+0.004}_{-0.006}$	195	1 WU	06 BELL	$B^\pm \rightarrow K^\pm p\bar{p}$

¹ Using $B(B^+ \rightarrow \eta_c K^+) = (1.25 \pm 0.12 $^{+0.10}_{-0.12}$) \times 10^{-3}$ from FANG 03 and $B(\eta_c \rightarrow K^+K^-) = (5.5 \pm 1.7) \times 10^{-2}$.

 $\Gamma(p\bar{p})/\Gamma_{\text{total}} \times \Gamma(\phi\phi)/\Gamma_{\text{total}}$ $\Gamma_{48}/\Gamma \times \Gamma_8/\Gamma$

VALUE (units 10^{-9})	DOCUMENT ID	TECN	COMMENT
0.25 ± 0.04 OUR FIT			
4.0 $^{+3.5}_{-3.2}$	BAGLIN	89	SPEC $\bar{p}p \rightarrow K^+K^-K^+K^-$

 $\Gamma(p\bar{p}\pi^0)/\Gamma_{\text{total}}$ Γ_{49}/Γ

VALUE (units 10^{-2})	EVTS	DOCUMENT ID	TECN	COMMENT
0.36 ± 0.13 ± 0.08	14	1 ABLIKIM	12N BES3	$\psi(2S) \rightarrow \pi^0 \gamma p\bar{p}\pi^0$

¹ ABLIKIM 12N reports $[\Gamma(\eta_c(1S) \rightarrow p\bar{p}\pi^0)/\Gamma_{\text{total}}] \times [B(\psi(2S) \rightarrow h_c(1P)\pi^0)] \times [B(h_c(1P) \rightarrow \gamma\eta_c(1S))] = (1.53 \pm 0.49 \pm 0.23) \times 10^{-6}$ which we divide by our best values $B(\psi(2S) \rightarrow h_c(1P)\pi^0) = (8.6 \pm 1.3) \times 10^{-4}$, $B(h_c(1P) \rightarrow \gamma\eta_c(1S)) = (50 \pm 9) \times 10^{-2}$. Our first error is their experiment's error and our second error is the systematic error from using our best values.

 $\Gamma(\Lambda\bar{\Lambda})/\Gamma_{\text{total}}$ Γ_{50}/Γ

VALUE (units 10^{-4})	CL%	EVTS	DOCUMENT ID	TECN	COMMENT
10.6 ± 2.3 OUR FIT					
11.8 ± 2.3 ± 2.5			1 ABLIKIM	12B BES3	

• • • We do not use the following data for averages, fits, limits, etc. • • •

8.7 $^{+2.4}_{-2.3}$ ± 0.6	20	2 WU	06 BELL	$B^+ \rightarrow \Lambda\bar{\Lambda}K^+$
<20	90	3 BISELLO	91 DM2	$e^+e^- \rightarrow \gamma\Lambda\bar{\Lambda}$

¹ ABLIKIM 12B reports $[\Gamma(\eta_c(1S) \rightarrow \Lambda\bar{\Lambda})/\Gamma_{\text{total}}] \times [B(J/\psi(1S) \rightarrow \gamma\eta_c(1S))] = (0.198 \pm 0.021 \pm 0.032) \times 10^{-4}$ which we divide by our best value $B(J/\psi(1S) \rightarrow \gamma\eta_c(1S)) = (1.7 \pm 0.4) \times 10^{-2}$. Our first error is their experiment's error and our second error is the systematic error from using our best value.

² WU 06 reports $[\Gamma(\eta_c(1S) \rightarrow \Lambda\bar{\Lambda})/\Gamma_{\text{total}}] \times [B(B^+ \rightarrow \eta_c K^+)] = (0.95 $^{+0.25}_{-0.22}$ $^{+0.08}_{-0.11}$) \times 10^{-6}$ which we divide by our best value $B(B^+ \rightarrow \eta_c K^+) = (1.09 \pm 0.08) \times 10^{-3}$. Our first error is their experiment's error and our second error is the systematic error from using our best value.

³ The quoted branching ratios use $B(J/\psi(1S) \rightarrow \gamma\eta_c(1S)) = 0.0127 \pm 0.0036$.

 $\Gamma(\Lambda\bar{\Lambda})/\Gamma(p\bar{p})$ Γ_{50}/Γ_{48}

VALUE	DOCUMENT ID	TECN	COMMENT
0.74 ± 0.16 OUR FIT			
0.67 $^{+0.19}_{-0.16}$ ± 0.12	1 WU	06 BELL	$B^+ \rightarrow p\bar{p}K^+, \Lambda\bar{\Lambda}K^+$

¹ Not independent from other $\eta_c \rightarrow \Lambda\bar{\Lambda}, p\bar{p}$ branching ratios reported by WU 06.

 $\Gamma(K^+\bar{p}\Lambda + \text{c.c.})/\Gamma_{\text{total}}$ Γ_{51}/Γ

VALUE (units 10^{-3})	EVTS	DOCUMENT ID	TECN	COMMENT
2.50 $^{+0.34}_{-0.32}$ ± 0.17	157	1 LU	19 BELL	$B^+ \rightarrow \bar{p}\Lambda K^+ K^+$

¹ LU 19 reports $(2.83 $^{+0.36}_{-0.34}$ ± 0.35) \times 10^{-3}$ from a measurement of $[\Gamma(\eta_c(1S) \rightarrow K^+\bar{p}\Lambda + \text{c.c.})/\Gamma_{\text{total}}] \times [B(B^+ \rightarrow \eta_c K^+)]$ assuming $B(B^+ \rightarrow \eta_c K^+) = (9.6 \pm 1.1) \times 10^{-4}$, which we rescale to our best value $B(B^+ \rightarrow \eta_c K^+) = (1.09 \pm 0.08) \times 10^{-3}$. Our first error is their experiment's error and our second error is the systematic error from using our best value.

 $\Gamma(\bar{\Lambda}(1520)\Lambda + \text{c.c.})/\Gamma_{\text{total}}$ Γ_{52}/Γ

VALUE (units 10^{-3})	EVTS	DOCUMENT ID	TECN	COMMENT
3.1 ± 1.3 ± 0.2	43	1 LU	19 BELL	$B^+ \rightarrow \bar{p}\Lambda K^+ K^+$

¹ LU 19 reports $(3.48 \pm 1.48 \pm 0.46) \times 10^{-3}$ from a measurement of $[\Gamma(\eta_c(1S) \rightarrow \bar{\Lambda}(1520)\Lambda + \text{c.c.})/\Gamma_{\text{total}}] \times [B(B^+ \rightarrow \eta_c K^+)]$ assuming $B(B^+ \rightarrow \eta_c K^+) = (9.6 \pm 1.1) \times 10^{-4}$, which we rescale to our best value $B(B^+ \rightarrow \eta_c K^+) = (1.09 \pm 0.08) \times 10^{-3}$. Our first error is their experiment's error and our second error is the systematic error from using our best value.

 $\Gamma(\Sigma^+\bar{\Sigma}^-)/\Gamma_{\text{total}}$ Γ_{53}/Γ

VALUE (units 10^{-3})	EVTS	DOCUMENT ID	TECN	COMMENT
2.1 ± 0.3 ± 0.5	112	1 ABLIKIM	13C BES3	$J/\psi \rightarrow \gamma p\bar{p}\pi^0\pi^0$

¹ ABLIKIM 13C reports $[\Gamma(\eta_c(1S) \rightarrow \Sigma^+\bar{\Sigma}^-)/\Gamma_{\text{total}}] \times [B(J/\psi(1S) \rightarrow \gamma\eta_c(1S))] = (3.60 \pm 0.48 \pm 0.31) \times 10^{-5}$ which we divide by our best value $B(J/\psi(1S) \rightarrow \gamma\eta_c(1S)) = (1.7 \pm 0.4) \times 10^{-2}$. Our first error is their experiment's error and our second error is the systematic error from using our best value.

 $\Gamma(\Xi^-\bar{\Xi}^+)/\Gamma_{\text{total}}$ Γ_{54}/Γ

VALUE (units 10^{-3})	EVTS	DOCUMENT ID	TECN	COMMENT
0.90 ± 0.18 ± 0.19	78	1 ABLIKIM	13C BES3	$J/\psi \rightarrow \gamma\Lambda\bar{\Lambda}\pi^+\pi^-$

¹ ABLIKIM 13C reports $[\Gamma(\eta_c(1S) \rightarrow \Xi^-\bar{\Xi}^+)/\Gamma_{\text{total}}] \times [B(J/\psi(1S) \rightarrow \gamma\eta_c(1S))] = (1.51 \pm 0.27 \pm 0.14) \times 10^{-5}$ which we divide by our best value $B(J/\psi(1S) \rightarrow \gamma\eta_c(1S)) = (1.7 \pm 0.4) \times 10^{-2}$. Our first error is their experiment's error and our second error is the systematic error from using our best value.

 $\Gamma(\pi^+\pi^-\rho\bar{\rho})/\Gamma_{\text{total}}$ Γ_{55}/Γ

VALUE (units 10^{-3})	CL%	EVTS	DOCUMENT ID	TECN	COMMENT
5.3 ± 1.7 ± 1.2			1 ABLIKIM	12N BES3	$\psi(2S) \rightarrow \pi^0 \gamma p\bar{p}\pi^+\pi^-$
<12	90		HIMEL	80B MRK2	$\psi(2S) \rightarrow \eta_c \gamma$

• • • We do not use the following data for averages, fits, limits, etc. • • •

$\eta_c(1S)$

¹ ABLIKIM 12N reports $[\Gamma(\eta_c(1S) \rightarrow \pi^+ \pi^- p \bar{p})/\Gamma_{total}] \times [B(\psi(2S) \rightarrow h_c(1P)\pi^0)] \times [B(h_c(1P) \rightarrow \gamma\eta_c(1S))] = (2.30 \pm 0.65 \pm 0.36) \times 10^{-6}$ which we divide by our best values $B(\psi(2S) \rightarrow h_c(1P)\pi^0) = (8.6 \pm 1.3) \times 10^{-4}$, $B(h_c(1P) \rightarrow \gamma\eta_c(1S)) = (50 \pm 9) \times 10^{-2}$. Our first error is their experiment's error and our second error is the systematic error from using our best values.

RADIATIVE DECAYS

Table with 6 columns: $\Gamma(\gamma\gamma)/\Gamma_{total}$, VALUE (units 10^{-4}), CL%, EVTS, DOCUMENT ID, TECN, COMMENT, Γ_{56}/Γ . Row 1: 1.61 ± 0.12 OUR FIT

1.9 +0.7 -0.6 OUR AVERAGE

Table with 6 columns: VALUE (units 10^{-4}), CL%, EVTS, DOCUMENT ID, TECN, COMMENT, Γ_{56}/Γ . Row 1: 2.7 ± 0.8 ± 0.6, 1 ABLIKIM, 13i, BES3

• • • We do not use the following data for averages, fits, limits, etc. • • •

Table with 6 columns: VALUE (units 10^{-4}), CL%, EVTS, DOCUMENT ID, TECN, COMMENT, Γ_{56}/Γ . Row 1: 2.0 +0.9 -0.7 ± 0.1, 13, 3 WICHT, 08, BELL, $B^\pm \rightarrow K^\pm \gamma\gamma$

Table with 6 columns: VALUE (units 10^{-4}), CL%, EVTS, DOCUMENT ID, TECN, COMMENT, Γ_{56}/Γ . Row 1: 2.80 +0.67 -0.58 ± 1.0, 5 ARMSTRONG, 95F, E760, $\bar{p}p \rightarrow \gamma\gamma$

Table with 6 columns: VALUE (units 10^{-4}), CL%, EVTS, DOCUMENT ID, TECN, COMMENT, Γ_{56}/Γ . Row 1: < 9, 90, 5 BISELLO, 91, DM2, $J/\psi \rightarrow \gamma\gamma\gamma$

Table with 6 columns: VALUE (units 10^{-4}), CL%, EVTS, DOCUMENT ID, TECN, COMMENT, Γ_{56}/Γ . Row 1: 6 +4 -3 ± 4, 4 BAGLIN, 87B, SPEC, $\bar{p}p \rightarrow \gamma\gamma$

Table with 6 columns: VALUE (units 10^{-4}), CL%, EVTS, DOCUMENT ID, TECN, COMMENT, Γ_{56}/Γ . Row 1: < 18, 90, 6 BLOOM, 83, CBAL, $J/\psi \rightarrow \eta_c\gamma$

¹ ABLIKIM 13i reports $[\Gamma(\eta_c(1S) \rightarrow \gamma\gamma)/\Gamma_{total}] \times [B(J/\psi(1S) \rightarrow \gamma\eta_c(1S))] = (4.5 \pm 1.2 \pm 0.6) \times 10^{-6}$ which we divide by our best value $B(J/\psi(1S) \rightarrow \gamma\eta_c(1S)) = (1.7 \pm 0.4) \times 10^{-2}$. Our first error is their experiment's error and our second error is the systematic error from using our best value.

² ADAMS 08 reports $[\Gamma(\eta_c(1S) \rightarrow \gamma\gamma)/\Gamma_{total}] \times [B(J/\psi(1S) \rightarrow \gamma\eta_c(1S))] = (2.4 +1.1 -0.8 \pm 0.3) \times 10^{-6}$ which we divide by our best value $B(J/\psi(1S) \rightarrow \gamma\eta_c(1S)) = (1.7 \pm 0.4) \times 10^{-2}$. Our first error is their experiment's error and our second error is the systematic error from using our best value.

³ WICHT 08 reports $[\Gamma(\eta_c(1S) \rightarrow \gamma\gamma)/\Gamma_{total}] \times [B(B^+ \rightarrow \eta_c K^+)] = (2.2 +0.9 -0.4 \pm 0.4) \times 10^{-7}$ which we divide by our best value $B(B^+ \rightarrow \eta_c K^+) = (1.09 \pm 0.08) \times 10^{-3}$. Our first error is their experiment's error and our second error is the systematic error from using our best value.

⁴ Not independent from the values of the total and two-photon width quoted by the same experiment.

⁵ The quoted branching ratios use $B(J/\psi(1S) \rightarrow \gamma\eta_c(1S)) = 0.0127 \pm 0.0036$.

⁶ Using $B(J/\psi(1S) \rightarrow \gamma\eta_c(1S)) = 0.0127 \pm 0.0036$.

Table with 6 columns: $\Gamma(\gamma\gamma)/\Gamma(K\bar{K}\pi)$, VALUE (units 10^{-3}), EVTS, DOCUMENT ID, TECN, COMMENT, Γ_{56}/Γ_{34} . Row 1: 2.22 ± 0.25 OUR FIT

3.2 +1.3 -1.0 ± 0.8 -0.6, 13, 1 WICHT, 08, BELL, $B^\pm \rightarrow K^\pm \gamma\gamma$

¹ Using $B(B^+ \rightarrow \eta_c K^+) = (1.25 \pm 0.12 \pm 0.10 -0.12) \times 10^{-3}$ from FANG 03 and $B(\eta_c \rightarrow K\bar{K}\pi) = (5.5 \pm 1.7) \times 10^{-2}$.

Table with 6 columns: $\Gamma(p\bar{p})/\Gamma_{total} \times \Gamma(\gamma\gamma)/\Gamma_{total}$, VALUE (units 10^{-6}), EVTS, DOCUMENT ID, TECN, COMMENT, $\Gamma_{48}/\Gamma \times \Gamma_{56}/\Gamma$. Row 1: 0.232 ± 0.022 OUR FIT

0.26 ± 0.05 OUR AVERAGE Error includes scale factor of 1.4.

Table with 6 columns: VALUE (units 10^{-6}), EVTS, DOCUMENT ID, TECN, COMMENT, $\Gamma_{48}/\Gamma \times \Gamma_{56}/\Gamma$. Row 1: 0.224 +0.038 -0.037 ± 0.020, 190, AMBROGIANI, 03, E835, $\bar{p}p \rightarrow \eta_c \rightarrow \gamma\gamma$

Table with 6 columns: VALUE (units 10^{-6}), EVTS, DOCUMENT ID, TECN, COMMENT, $\Gamma_{48}/\Gamma \times \Gamma_{56}/\Gamma$. Row 1: 0.336 +0.080 -0.070, ARMSTRONG, 95F, E760, $\bar{p}p \rightarrow \gamma\gamma$

Table with 6 columns: VALUE (units 10^{-6}), EVTS, DOCUMENT ID, TECN, COMMENT, $\Gamma_{48}/\Gamma \times \Gamma_{56}/\Gamma$. Row 1: 0.68 +0.42 -0.31, 12, BAGLIN, 87B, SPEC, $\bar{p}p \rightarrow \gamma\gamma$

Charge conjugation (C), Parity (P), Lepton family number (LF) violating modes

Table with 6 columns: $\Gamma(\pi^+ \pi^-)/\Gamma_{total}$, VALUE (units 10^{-5}), CL%, DOCUMENT ID, TECN, COMMENT, Γ_{57}/Γ . Row 1: < 11, 90, 1 ABLIKIM, 11G, BES3, $J/\psi \rightarrow \gamma\pi^+ \pi^-$

• • • We do not use the following data for averages, fits, limits, etc. • • •

Table with 6 columns: VALUE (units 10^{-5}), CL%, DOCUMENT ID, TECN, COMMENT, Γ_{57}/Γ . Row 1: < 70, 90, 2 ABLIKIM, 06B, BES2, $J/\psi \rightarrow \pi^+ \pi^- \gamma$

¹ ABLIKIM 11G reports $[\Gamma(\eta_c(1S) \rightarrow \pi^+ \pi^-)/\Gamma_{total}] \times [B(J/\psi(1S) \rightarrow \gamma\eta_c(1S))] < 1.82 \times 10^{-6}$ which we divide by our best value $B(J/\psi(1S) \rightarrow \gamma\eta_c(1S)) = 1.7 \times 10^{-2}$.

² ABLIKIM 06B reports $[\Gamma(\eta_c(1S) \rightarrow \pi^+ \pi^-)/\Gamma_{total}] \times [B(J/\psi(1S) \rightarrow \gamma\eta_c(1S))] < 1.1 \times 10^{-5}$ which we divide by our best value $B(J/\psi(1S) \rightarrow \gamma\eta_c(1S)) = 1.7 \times 10^{-2}$.

Table with 6 columns: $\Gamma(\pi^0 \pi^0)/\Gamma_{total}$, VALUE (units 10^{-5}), CL%, DOCUMENT ID, TECN, COMMENT, Γ_{58}/Γ . Row 1: < 4, 90, 1 ABLIKIM, 11G, BES3, $J/\psi \rightarrow \gamma\pi^0 \pi^0$

• • • We do not use the following data for averages, fits, limits, etc. • • •

Table with 6 columns: VALUE (units 10^{-5}), CL%, DOCUMENT ID, TECN, COMMENT, Γ_{58}/Γ . Row 1: < 40, 90, 2 ABLIKIM, 06B, BES2, $J/\psi \rightarrow \pi^0 \pi^0 \gamma$

¹ ABLIKIM 11G reports $[\Gamma(\eta_c(1S) \rightarrow \pi^0 \pi^0)/\Gamma_{total}] \times [B(J/\psi(1S) \rightarrow \gamma\eta_c(1S))] < 6.0 \times 10^{-7}$ which we divide by our best value $B(J/\psi(1S) \rightarrow \gamma\eta_c(1S)) = 1.7 \times 10^{-2}$.

² ABLIKIM 06B reports $[\Gamma(\eta_c(1S) \rightarrow \pi^0 \pi^0)/\Gamma_{total}] \times [B(J/\psi(1S) \rightarrow \gamma\eta_c(1S))] < 0.71 \times 10^{-5}$ which we divide by our best value $B(J/\psi(1S) \rightarrow \gamma\eta_c(1S)) = 1.7 \times 10^{-2}$.

Table with 6 columns: $\Gamma(K^+ K^-)/\Gamma_{total}$, VALUE (units 10^{-5}), CL%, DOCUMENT ID, TECN, COMMENT, Γ_{59}/Γ . Row 1: < 60, 90, 1 ABLIKIM, 06B, BES2, $J/\psi \rightarrow K^+ K^- \gamma$

¹ ABLIKIM 06B reports $[\Gamma(\eta_c(1S) \rightarrow K^+ K^-)/\Gamma_{total}] \times [B(J/\psi(1S) \rightarrow \gamma\eta_c(1S))] < 0.96 \times 10^{-5}$ which we divide by our best value $B(J/\psi(1S) \rightarrow \gamma\eta_c(1S)) = 1.7 \times 10^{-2}$.

Table with 6 columns: $\Gamma(K_S^0 K_S^0)/\Gamma_{total}$, VALUE (units 10^{-5}), CL%, DOCUMENT ID, TECN, COMMENT, Γ_{60}/Γ . Row 1: < 31, 90, 1 ABLIKIM, 06B, BES2, $J/\psi \rightarrow K_S^0 K_S^0 \gamma$

• • • We do not use the following data for averages, fits, limits, etc. • • •

Table with 6 columns: VALUE (units 10^{-5}), CL%, DOCUMENT ID, TECN, COMMENT, Γ_{60}/Γ . Row 1: < 32, 90, 2 UEHARA, 13, BELL, $\gamma\gamma \rightarrow K_S^0 K_S^0$

Table with 6 columns: VALUE (units 10^{-5}), CL%, DOCUMENT ID, TECN, COMMENT, Γ_{60}/Γ . Row 1: < 5.6, 90, 3 UEHARA, 13, BELL, $\gamma\gamma \rightarrow K_S^0 K_S^0$

¹ ABLIKIM 06B reports $[\Gamma(\eta_c(1S) \rightarrow K_S^0 K_S^0)/\Gamma_{total}] \times [B(J/\psi(1S) \rightarrow \gamma\eta_c(1S))] < 0.53 \times 10^{-5}$ which we divide by our best value $B(J/\psi(1S) \rightarrow \gamma\eta_c(1S)) = 1.7 \times 10^{-2}$.

² Taking into account interference with the non-resonant continuum.

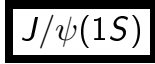
³ Neglecting interference with the non-resonant continuum.

$\eta_c(1S)$ REFERENCES

Table of references with columns: AUTHOR, YEAR, JOURNAL, DOCUMENT ID, TECN, COMMENT. Includes entries for LEES, AAIJ, ABLIKIM, LU, XU, etc.

Meson Particle Listings

$J/\psi(1S)$



$$I^G(J^{PC}) = 0^-(1^{--})$$

$J/\psi(1S)$ MASS

VALUE (MeV)	EVTs	DOCUMENT ID	TECN	COMMENT
3096.900 ± 0.006 OUR AVERAGE				
3096.900 ± 0.002 ± 0.006		1 ANASHIN 15	KEDR	$e^+e^- \rightarrow$ hadrons
3096.89 ± 0.09	502	2 ARTAMONOV 00	OLYA	$e^+e^- \rightarrow$ hadrons
3096.91 ± 0.03 ± 0.01		3 ARMSTRONG 93B	E760	$\bar{p}p \rightarrow e^+e^-$
3096.95 ± 0.1 ± 0.3	193	BAGLIN 87	SPEC	$\bar{p}p \rightarrow e^+e^-X$
••• We do not use the following data for averages, fits, limits, etc. •••				
3096.66 ± 0.19 ± 0.02	6.1k	4 AAIJ 15B1	LHCB	$pp \rightarrow J/\psi X$
3096.917 ± 0.010 ± 0.007		AULCHENKO 03	KEDR	$e^+e^- \rightarrow$ hadrons
3097.5 ± 0.3		GRIBUSHIN 96	FMP5	$515 \pi^- Be \rightarrow 2\mu X$
3098.4 ± 2.0	38k	LEMOIGNE 82	GOLI	$185 \pi^- Be \rightarrow \gamma \mu^+ \mu^- A$
3096.93 ± 0.09	502	5 ZHOLENTZ 80	REDE	e^+e^-
3097.0 ± 1		6 BRANDELIK 79c	DASP	e^+e^-

- Supersedes AULCHENKO 03.
- Reanalysis of ZHOLENTZ 80 using new electron mass (COHEN 87) and radiative corrections (KURAEV 85).
- Mass central value and systematic error recalculated by us according to Eq. (16) in ARMSTRONG 93B, using the value for the $\psi(2S)$ mass from AULCHENKO 03.
- From a sample of $\eta_c(1S)$ and J/ψ produced in b -hadron decays. Systematic uncertainties not estimated.
- Superseded by ARTAMONOV 00.
- From a simultaneous fit to e^+e^- , $\mu^+\mu^-$ and hadronic channels assuming $\Gamma(e^+e^-) = \Gamma(\mu^+\mu^-)$.

$J/\psi(1S)$ WIDTH

VALUE (keV)	EVTs	DOCUMENT ID	TECN	COMMENT
92.6 ± 1.7 OUR AVERAGE				Error includes scale factor of 1.1.
92.45 ± 1.40 ± 1.48		1 ANASHIN 20	KEDR	e^+e^-
96.1 ± 3.2	13k	2 ADAMS 06A	CLEO	$e^+e^- \rightarrow \mu^+\mu^- \gamma$
84.4 ± 8.9		BAI 95B	BES	e^+e^-
91 ± 11 ± 6		3 ARMSTRONG 93B	E760	$\bar{p}p \rightarrow e^+e^-$
85.5 ± 6.1		4 HSUEH 92	RVUE	See Υ mini-review
85.5 ± 5.8				
••• We do not use the following data for averages, fits, limits, etc. •••				
92.94 ± 1.83		5,6 ANASHIN 18A	KEDR	e^+e^-
94.1 ± 2.7		7 ANASHIN 10	KEDR	$3.097 e^+e^- \rightarrow e^+e^- \mu^+\mu^-$
93.7 ± 3.5	7.8k	2 AUBERT 04	BABR	$e^+e^- \rightarrow \mu^+\mu^- \gamma$

- Based on the same dataset as ANASHIN 18A and correlated to the values reported there
- Calculated by us from the reported values of $\Gamma(e^+e^-) \times B(\mu^+\mu^-)$ using $B(e^+e^-) = (5.94 \pm 0.06)\%$ and $B(\mu^+\mu^-) = (5.93 \pm 0.06)\%$.
- The initial-state radiation correction reevaluated by ANDREOTTI 07 in its Ref. [4].
- Using data from COFFMAN 92, BALDINI-CELIO 75, BOYARSKI 75, ESPOSITO 75B, BRANDELIK 79c.
- Using $\Gamma(e^+e^-)$ from ANASHIN 18A and $B(J/\psi(1S) \rightarrow e^+e^-) = (5.971 \pm 0.032)\%$ from PDG 16.
- Superseded by ANASHIN 20 that is based on the same dataset.
- Assuming $\Gamma(e^+e^-) = \Gamma(\mu^+\mu^-)$ and using $\Gamma(e^+e^-)/\Gamma_{\text{total}} = (5.94 \pm 0.06)\%$.

$J/\psi(1S)$ DECAY MODES

Mode	Fraction (Γ_i/Γ)	Scale factor/ Confidence level
Γ_1 hadrons	(87.7 ± 0.5) %	
Γ_2 virtual $\gamma \rightarrow$ hadrons	(13.50 ± 0.30) %	
Γ_3 ggg	(64.1 ± 1.0) %	
Γ_4 γgg	(8.8 ± 1.1) %	
Γ_5 e^+e^-	(5.971 ± 0.032) %	
Γ_6 $e^+e^- \gamma$	[a] (8.8 ± 1.4) × 10 ⁻³	
Γ_7 $\mu^+\mu^-$	(5.961 ± 0.033) %	

Decays involving hadronic resonances

Γ_8 $\rho\pi$	(1.69 ± 0.15) %	S=2.4
Γ_9 $\rho^0\pi^0$	(5.6 ± 0.7) × 10 ⁻³	
Γ_{10} $a_2(1320)\rho$	(1.09 ± 0.22) %	
Γ_{11} $\eta\pi^+\pi^-$	(3.8 ± 0.7) × 10 ⁻⁴	
Γ_{12} $\eta\pi^+\pi^-\pi^0$	(1.17 ± 0.20) %	
Γ_{13} $\eta\pi^+\pi^-3\pi^0$	(4.9 ± 1.0) × 10 ⁻³	
Γ_{14} $\eta\rho$	(1.93 ± 0.23) × 10 ⁻⁴	
Γ_{15} $\eta\phi(2170) \rightarrow \eta\phi f_0(980) \rightarrow \eta\phi\pi^+\pi^-$	(1.2 ± 0.4) × 10 ⁻⁴	
Γ_{16} $\eta\phi(2170) \rightarrow \eta K^*(892)^0 \bar{K}^*(892)^0$	< 2.52 × 10 ⁻⁴	CL=90%
Γ_{17} $\eta K^\pm K_S^0 \pi^\mp$	[b] (2.2 ± 0.4) × 10 ⁻³	

Γ_{18} $\eta K^*(892)^0 \bar{K}^*(892)^0$	(1.15 ± 0.26) × 10 ⁻³	
Γ_{19} $\rho\eta'(958)$	(8.1 ± 0.8) × 10 ⁻⁵	S=1.6
Γ_{20} $\rho^\pm \pi^\mp \pi^+ \pi^- 2\pi^0$	(2.8 ± 0.8) %	
Γ_{21} $\rho^\pm \rho^- \pi^+ \pi^- \pi^0$	(6 ± 4) × 10 ⁻³	
Γ_{22} $\rho^\mp K^\pm K_S^0$	(1.9 ± 0.4) × 10 ⁻³	
Γ_{23} $\rho(1450)\pi$		
Γ_{24} $\rho(1450)\pi \rightarrow \pi^+\pi^-\pi^0$	(2.3 ± 0.7) × 10 ⁻³	
Γ_{25} $\rho(1450)^\pm \pi^\mp \rightarrow K_S^0 K^\pm \pi^\mp$	(3.5 ± 0.6) × 10 ⁻⁴	
Γ_{26} $\rho(1450)^0 \pi^0 \rightarrow K^+ K^- \pi^0$	(2.7 ± 0.6) × 10 ⁻⁴	
Γ_{27} $\rho(1450)\eta'(958) \rightarrow \pi^+\pi^-\eta'(958)$	(3.3 ± 0.7) × 10 ⁻⁶	
Γ_{28} $\rho(1700)\pi$		
Γ_{29} $\rho(1700)\pi \rightarrow \pi^+\pi^-\pi^0$	(1.7 ± 1.1) × 10 ⁻⁴	
Γ_{30} $\rho(2150)\pi$		
Γ_{31} $\rho(2150)\pi \rightarrow \pi^+\pi^-\pi^0$	(8 ± 40) × 10 ⁻⁶	
Γ_{32} $\rho_3(1690)\pi \rightarrow \pi^+\pi^-\pi^0$		
Γ_{33} $\omega\pi^0$	(4.5 ± 0.5) × 10 ⁻⁴	S=1.4
Γ_{34} $\omega\pi^0 \rightarrow \pi^+\pi^-\pi^0$	(1.7 ± 0.8) × 10 ⁻⁵	
Γ_{35} $\omega\pi^+\pi^-$	(7.2 ± 1.0) × 10 ⁻³	
Γ_{36} $\omega\pi^0\pi^0$	(3.4 ± 0.8) × 10 ⁻³	
Γ_{37} $\omega 3\pi^0$	(1.9 ± 0.6) × 10 ⁻³	
Γ_{38} $\omega f_2(1270)$	(4.3 ± 0.6) × 10 ⁻³	
Γ_{39} $\omega\eta$	(1.74 ± 0.20) × 10 ⁻³	S=1.6
Γ_{40} $\omega\pi^+\pi^-\pi^0$	(4.0 ± 0.7) × 10 ⁻³	
Γ_{41} $\omega\pi^0\eta$	(3.4 ± 1.7) × 10 ⁻⁴	
Γ_{42} $\omega\pi^+\pi^+\pi^-\pi^-$	(8.5 ± 3.4) × 10 ⁻³	
Γ_{43} $\omega\pi^+\pi^-\pi^0$	(3.3 ± 0.5) %	
Γ_{44} $\omega\eta'\pi^+\pi^-$	(1.12 ± 0.13) × 10 ⁻³	
Γ_{45} $\omega\eta'(958)$	(1.89 ± 0.18) × 10 ⁻⁴	
Γ_{46} $\omega f_0(980)$	(1.4 ± 0.5) × 10 ⁻⁴	
Γ_{47} $\omega f_0(1710) \rightarrow \omega K \bar{K}$	(4.8 ± 1.1) × 10 ⁻⁴	
Γ_{48} $\omega f_1(1420)$	(6.8 ± 2.4) × 10 ⁻⁴	
Γ_{49} $\omega f_2'(1525)$	< 2.2 × 10 ⁻⁴	CL=90%
Γ_{50} $\omega X(1835) \rightarrow \omega p \bar{p}$	< 3.9 × 10 ⁻⁶	CL=95%
Γ_{51} $\omega X(1835), X \rightarrow \eta'\pi^+\pi^-$	< 6.2 × 10 ⁻⁵	
Γ_{52} $\omega K^\pm K_S^0 \pi^\mp$	[b] (3.4 ± 0.5) × 10 ⁻³	
Γ_{53} $\omega K \bar{K}$	(1.9 ± 0.4) × 10 ⁻³	
Γ_{54} $\omega K^*(892) \bar{K} + c.c.$	(6.1 ± 0.9) × 10 ⁻³	
Γ_{55} $\eta' K^* \pm K^\mp$	(1.48 ± 0.13) × 10 ⁻³	
Γ_{56} $\eta' K^* 0 \bar{K}^0 + c.c.$	(1.66 ± 0.21) × 10 ⁻³	
Γ_{57} $\eta' h_1(1415) \rightarrow \eta' K^* \bar{K} + c.c.$	(2.16 ± 0.31) × 10 ⁻⁴	
Γ_{58} $\eta' h_1(1415) \rightarrow \eta' K^* \pm K^\mp$	(1.51 ± 0.23) × 10 ⁻⁴	
Γ_{59} $\bar{K} K^*(892) + c.c.$		
Γ_{60} $\bar{K} K^*(892) + c.c. \rightarrow K_S^0 K^\pm \pi^\mp$	(5.0 ± 0.5) × 10 ⁻³	
Γ_{61} $K^+ K^*(892)^- + c.c.$	(6.0 ± 0.8 - 1.0) × 10 ⁻³	S=2.9
Γ_{62} $K^+ K^*(892)^- + c.c. \rightarrow K^+ K^- \pi^0$	(2.69 ± 0.13 - 0.20) × 10 ⁻³	
Γ_{63} $K^+ K^*(892)^- + c.c. \rightarrow K^0 K^\pm \pi^\mp + c.c.$	(3.0 ± 0.4) × 10 ⁻³	
Γ_{64} $K^0 \bar{K}^*(892)^0 + c.c.$	(4.2 ± 0.4) × 10 ⁻³	
Γ_{65} $K^0 \bar{K}^*(892)^0 + c.c. \rightarrow K^0 K^\pm \pi^\mp + c.c.$	(3.2 ± 0.4) × 10 ⁻³	
Γ_{66} $\bar{K}^*(892)^0 K^+ \pi^- + c.c.$	(7.7 ± 1.6) × 10 ⁻³	
Γ_{67} $K^*(892)^\pm K^\mp \pi^0$	(4.1 ± 1.3) × 10 ⁻³	
Γ_{68} $K^*(892)^+ K_S^0 \pi^- + c.c.$	(2.0 ± 0.5) × 10 ⁻³	
Γ_{69} $K^*(892)^+ K_S^0 \pi^- + c.c. \rightarrow K_S^0 K_S^0 \pi^+ \pi^-$	(6.7 ± 2.2) × 10 ⁻⁴	
Γ_{70} $K^*(892)^0 K_S^0 \rightarrow \gamma K_S^0 K_S^0$	(6.3 ± 0.6 - 0.5) × 10 ⁻⁶	
Γ_{71} $K^*(892)^0 K_S^0 \pi^0$	(7 ± 4) × 10 ⁻⁴	
Γ_{72} $K^*(892)^\pm K^*(700)^\mp$	(1.1 ± 1.0 - 0.6) × 10 ⁻³	
Γ_{73} $K^*(892)^0 \bar{K}^*(892)^0$	(2.3 ± 0.6) × 10 ⁻⁴	
Γ_{74} $K^*(892)^\pm K^*(892)^\mp$	(1.00 ± 0.22 - 0.40) × 10 ⁻³	
Γ_{75} $K_1(1400)^\pm K^\mp$	(3.8 ± 1.4) × 10 ⁻³	
Γ_{76} $K^*(1410) \bar{K} + c.c.$		
Γ_{77} $K^*(1410) \bar{K} + c.c. \rightarrow K^\pm K^\mp \pi^0$	(7 ± 4) × 10 ⁻⁵	
Γ_{78} $K^*(1410) \bar{K} + c.c. \rightarrow K_S^0 K^\pm \pi^\mp$	(8 ± 6) × 10 ⁻⁵	
Γ_{79} $K_2^*(1430) \bar{K} + c.c.$		
Γ_{80} $K_2^*(1430) \bar{K} + c.c. \rightarrow K^\pm K^\mp \pi^0$	(1.0 ± 0.5) × 10 ⁻⁴	

Γ_{81}	$K_2^*(1430)\bar{K} + c.c. \rightarrow K_S^0 K^\pm \pi^\mp$	$(4.0 \pm 1.0) \times 10^{-4}$		Γ_{143}	$\bar{\Theta}(1540)K^+n \rightarrow K_S^0 \bar{p}K^+n$	$[c] < 5.6$	$\times 10^{-5}$	CL=90%	
Γ_{82}	$\bar{K}_2^*(1430)K + c.c.$	< 4.0	$\times 10^{-3}$	CL=90%	Γ_{144}	$\bar{\Theta}(1540)K_S^0 p \rightarrow K_S^0 pK^-\bar{\pi}$	$[c] < 1.1$	$\times 10^{-5}$	CL=90%
Γ_{83}	$K_2^*(1430)^+K^- + c.c. \rightarrow K^+K^-\pi^0$	$(2.69 \pm 0.25) \times 10^{-4}$		Decays into stable hadrons					
Γ_{84}	$K_2^*(1430)^+K_S^0\pi^- + c.c.$	$(3.6 \pm 1.8) \times 10^{-3}$		Γ_{145}	$2(\pi^+\pi^-)\pi^0$	$(3.71 \pm 0.28) \%$		S=1.3	
Γ_{85}	$\bar{K}_2^*(1430)^0K_S^*(892)^0 + c.c.$	$(4.67 \pm 0.29) \times 10^{-3}$		Γ_{146}	$3(\pi^+\pi^-)\pi^0$	$(2.9 \pm 0.6) \%$			
Γ_{86}	$K_2^*(1430)^-K^*(892)^+ + c.c.$	$(3.4 \pm 2.9) \times 10^{-3}$		Γ_{147}	$\pi^+\pi^-3\pi^0$	$(1.9 \pm 0.9) \%$			
Γ_{87}	$K_2^*(1430)^-K^*(892)^++ c.c. \rightarrow K^*(892)^+K_S^0\pi^- + c.c.$	$(4 \pm 4) \times 10^{-4}$		Γ_{148}	$\pi^+\pi^-4\pi^0$	$(6.5 \pm 1.3) \times 10^{-3}$			
Γ_{88}	$K_2^*(1430)^0\bar{K}_2^*(1430)^0$	< 2.9	$\times 10^{-3}$	CL=90%	Γ_{149}	$\rho^\pm\pi^\mp\pi^0\pi^0$	$(1.41 \pm 0.22) \%$		
Γ_{89}	$\bar{K}_2(1770)^0K^*(892)^0 + c.c. \rightarrow K^*(892)^0K^-\pi^+ + c.c.$	$(6.9 \pm 0.9) \times 10^{-4}$		Γ_{150}	$\rho^+\rho^-\pi^0$	$(6.0 \pm 1.1) \times 10^{-3}$			
Γ_{90}	$K_2^*(1980)^+K^- + c.c. \rightarrow K^+K^-\pi^0$	$(1.10 \pm 0.60) \times 10^{-5}$		Γ_{151}	$\pi^+\pi^-\pi^0$	$(2.10 \pm 0.08) \%$		S=1.6	
Γ_{91}	$K_2^*(2045)^+K^- + c.c. \rightarrow K^+K^-\pi^0$	$(6.2 \pm 2.9) \times 10^{-6}$		Γ_{152}	$2(\pi^+\pi^-\pi^0)$	$(1.61 \pm 0.20) \%$			
Γ_{92}	$K_1(1270)^\pm K^\mp$	< 3.0	$\times 10^{-3}$	CL=90%	Γ_{153}	$\pi^+\pi^-\pi^0K^+K^-$	$(1.20 \pm 0.30) \%$		
Γ_{93}	$K_1(1270)K_S^0 \rightarrow \gamma K_S^0 K_S^0$	$(8.5 \pm 2.5) \times 10^{-7}$		Γ_{154}	$\pi^+\pi^-$	$(1.47 \pm 0.14) \times 10^{-4}$			
Γ_{94}	$a_2(1320)^\pm\pi^\mp$	$[b] < 4.3$	$\times 10^{-3}$	CL=90%	Γ_{155}	$2(\pi^+\pi^-)$	$(3.57 \pm 0.30) \times 10^{-3}$		
Γ_{95}	$\phi\pi^0$	3×10^{-6} or 1×10^{-7}		Γ_{156}	$3(\pi^+\pi^-)$	$(4.3 \pm 0.4) \times 10^{-3}$			
Γ_{96}	$\phi\pi^+\pi^-$	$(9.4 \pm 1.5) \times 10^{-4}$		S=1.7	Γ_{157}	$2(\pi^+\pi^-)3\pi^0$	$(6.2 \pm 0.9) \%$		
Γ_{97}	$\phi\pi^0\pi^0$	$(5.0 \pm 1.0) \times 10^{-4}$		Γ_{158}	$4(\pi^+\pi^-)\pi^0$	$(9.0 \pm 3.0) \times 10^{-3}$			
Γ_{98}	$\phi 2(\pi^+\pi^-)$	$(1.60 \pm 0.32) \times 10^{-3}$		Γ_{159}	$2(\pi^+\pi^-)\eta$	$(2.29 \pm 0.28) \times 10^{-3}$			
Γ_{99}	$\phi\eta$	$(7.4 \pm 0.8) \times 10^{-4}$		S=1.5	Γ_{160}	$3(\pi^+\pi^-)\eta$	$(7.2 \pm 1.5) \times 10^{-4}$		
Γ_{100}	$\phi\eta'(958)$	$(4.6 \pm 0.5) \times 10^{-4}$		S=2.2	Γ_{161}	$2(\pi^+\pi^-\pi^0)\eta$	$(1.6 \pm 0.5) \times 10^{-3}$		
Γ_{101}	$\phi\eta\eta'$	$(2.32 \pm 0.17) \times 10^{-4}$		Γ_{162}	$\pi^+\pi^-\pi^0\pi^0\eta$	$(2.4 \pm 0.5) \times 10^{-3}$			
Γ_{102}	$\phi f_0(980)$	$(3.2 \pm 0.9) \times 10^{-4}$		S=1.9	Γ_{163}	$\rho^\pm\pi^\mp\pi^0\eta$	$(1.9 \pm 0.8) \times 10^{-3}$		
Γ_{103}	$\phi f_0(980) \rightarrow \phi\pi^+\pi^-$	$(2.60 \pm 0.34) \times 10^{-4}$		Γ_{164}	K^+K^-	$(2.86 \pm 0.21) \times 10^{-4}$			
Γ_{104}	$\phi f_0(980) \rightarrow \phi\pi^0\pi^0$	$(1.8 \pm 0.5) \times 10^{-4}$		Γ_{165}	$K_S^0 K_L^0$	$(1.95 \pm 0.11) \times 10^{-4}$		S=2.4	
Γ_{105}	$\phi\pi^0 f_0(980) \rightarrow \phi\pi^0\pi^+\pi^-$	$(4.5 \pm 1.0) \times 10^{-6}$		Γ_{166}	$K_S^0 K_S^0$	< 1.4	$\times 10^{-8}$	CL=95%	
Γ_{106}	$\phi\pi^0 f_0(980) \rightarrow \phi\pi^0\rho^0\pi^0$	$(1.7 \pm 0.6) \times 10^{-6}$		Γ_{167}	$K\bar{K}\pi$	$(6.1 \pm 1.0) \times 10^{-3}$			
Γ_{107}	$\phi f_0(980)\eta \rightarrow \eta\phi\pi^+\pi^-$	$(3.2 \pm 1.0) \times 10^{-4}$		Γ_{168}	$K^+K^-\pi^0$	$(2.88 \pm 0.12) \times 10^{-3}$			
Γ_{108}	$\phi a_0(980)^0 \rightarrow \phi\eta\pi^0$	$(4.4 \pm 1.4) \times 10^{-6}$		Γ_{169}	$K_S^0 K^\pm\pi^\mp$	$(5.6 \pm 0.5) \times 10^{-3}$			
Γ_{109}	$\phi f_2(1270)$	$(3.2 \pm 0.6) \times 10^{-4}$		Γ_{170}	$K_S^0 K_L^0\pi^0$	$(2.06 \pm 0.26) \times 10^{-3}$			
Γ_{110}	$\phi f_1(1285)$	$(2.6 \pm 0.5) \times 10^{-4}$		Γ_{171}	$K^*(892)^0\bar{K}^0 + c.c. \rightarrow K_S^0 K_L^0\pi^0$	$(1.21 \pm 0.18) \times 10^{-3}$			
Γ_{111}	$\phi f_1(1285) \rightarrow \phi\pi^0 f_0(980) \rightarrow \phi\pi^0\pi^+\pi^-$	$(9.4 \pm 2.8) \times 10^{-7}$		Γ_{172}	$K_2^*(1430)^0\bar{K}^0 + c.c. \rightarrow K_S^0 K_L^0\pi^0$	$(4.3 \pm 1.3) \times 10^{-4}$			
Γ_{112}	$\phi f_1(1285) \rightarrow \phi\pi^0 f_0(980) \rightarrow \phi 3\pi^0$	$(2.1 \pm 2.2) \times 10^{-7}$		Γ_{173}	$K^+K^-\pi^+\pi^-$	$(6.86 \pm 0.28) \times 10^{-3}$			
Γ_{113}	$\phi\eta(1405) \rightarrow \phi\eta\pi^+\pi^-$	$(2.0 \pm 1.0) \times 10^{-5}$		Γ_{174}	$K^+K^-\pi^0\pi^0$	$(2.13 \pm 0.22) \times 10^{-3}$			
Γ_{114}	$\phi f_2(1525)$	$(8 \pm 4) \times 10^{-4}$		S=2.7	Γ_{175}	$K_S^0 K_L^0\pi^+\pi^-$	$(3.8 \pm 0.6) \times 10^{-3}$		
Γ_{115}	$\phi X(1835) \rightarrow \phi p\bar{p}$	< 2.1	$\times 10^{-7}$	CL=90%	Γ_{176}	$K_S^0 K_L^0\pi^0\pi^0$	$(1.9 \pm 0.4) \times 10^{-3}$		
Γ_{116}	$\phi X(1835) \rightarrow \phi\eta\pi^+\pi^-$	< 2.8	$\times 10^{-4}$	CL=90%	Γ_{177}	$K_S^0 K_L^0\eta$	$(1.45 \pm 0.33) \times 10^{-3}$		
Γ_{117}	$\phi X(1870) \rightarrow \phi\eta\pi^+\pi^-$	< 6.13	$\times 10^{-5}$	CL=90%	Γ_{178}	$K_S^0 K_S^0\pi^+\pi^-$	$(1.68 \pm 0.19) \times 10^{-3}$		
Γ_{118}	$\phi K\bar{K}$	$(1.77 \pm 0.16) \times 10^{-3}$		S=1.3	Γ_{179}	$K^\mp K_S^0\pi^\pm\pi^0$	$(5.7 \pm 0.5) \times 10^{-3}$		
Γ_{119}	$\phi f_0(1710) \rightarrow \phi K\bar{K}$	$(3.6 \pm 0.6) \times 10^{-4}$		Γ_{180}	$K^+K^-2(\pi^+\pi^-)$	$(3.1 \pm 1.3) \times 10^{-3}$			
Γ_{120}	ϕK^+K^-	$(8.3 \pm 1.1) \times 10^{-4}$		Γ_{181}	$K^+K^-\pi^+\pi^-\eta$	$(4.7 \pm 0.7) \times 10^{-3}$			
Γ_{121}	$\phi K_S^0 K_S^0$	$(5.9 \pm 1.5) \times 10^{-4}$		Γ_{182}	$2(K^+K^-)$	$(7.2 \pm 0.8) \times 10^{-4}$			
Γ_{122}	$\phi K^\pm K_S^0\pi^\mp$	$[b] (7.2 \pm 0.8) \times 10^{-4}$		Γ_{183}	$K^+K^-K_S^0 K_S^0$	$(4.2 \pm 0.7) \times 10^{-4}$			
Γ_{123}	$\phi K^*(892)\bar{K} + c.c.$	$(2.18 \pm 0.23) \times 10^{-3}$		Γ_{184}	$p\bar{p}$	$(2.120 \pm 0.029) \times 10^{-3}$			
Γ_{124}	$b_1(1235)^\pm\pi^\mp$	$[b] (3.0 \pm 0.5) \times 10^{-3}$		Γ_{185}	$p\bar{p}\pi^0$	$(1.19 \pm 0.08) \times 10^{-3}$		S=1.1	
Γ_{125}	$b_1(1235)^0\pi^0$	$(2.3 \pm 0.6) \times 10^{-3}$		Γ_{186}	$p\bar{p}\pi^+\pi^-$	$(6.0 \pm 0.5) \times 10^{-3}$		S=1.3	
Γ_{126}	$f_2'(1525)K^+K^-$	$(1.06 \pm 0.35) \times 10^{-3}$		Γ_{187}	$p\bar{p}\pi^+\pi^-\pi^0$	$[d] (2.3 \pm 0.9) \times 10^{-3}$		S=1.9	
Γ_{127}	$\Delta(1232)^+\bar{p}$	< 1	$\times 10^{-4}$	CL=90%	Γ_{188}	$p\bar{p}\eta$	$(2.00 \pm 0.12) \times 10^{-3}$		
Γ_{128}	$\Delta(1232)^{++}\bar{p}\pi^-$	$(1.6 \pm 0.5) \times 10^{-3}$		Γ_{189}	$p\bar{p}\rho$	< 3.1	$\times 10^{-4}$	CL=90%	
Γ_{129}	$\Delta(1232)^{++}\bar{\Delta}(1232)^{--}$	$(1.10 \pm 0.29) \times 10^{-3}$		Γ_{190}	$p\bar{p}\omega$	$(9.8 \pm 1.0) \times 10^{-4}$		S=1.3	
Γ_{130}	$\Sigma(1385)^0 pK^-$	$(5.1 \pm 3.2) \times 10^{-4}$		Γ_{191}	$p\bar{p}\eta'(958)$	$(1.29 \pm 0.14) \times 10^{-4}$		S=2.0	
Γ_{131}	$\Sigma(1385)^0\bar{\Lambda} + c.c.$	< 8.2	$\times 10^{-6}$	CL=90%	Γ_{192}	$p\bar{p}a_0(980) \rightarrow p\bar{p}\pi^0\eta$	$(6.8 \pm 1.8) \times 10^{-5}$		
Γ_{132}	$\Sigma(1385)^-\bar{\Sigma}^+(or c.c.)$	$[b] (3.1 \pm 0.5) \times 10^{-4}$		Γ_{193}	$p\bar{p}\phi$	$(5.19 \pm 0.33) \times 10^{-5}$			
Γ_{133}	$\Sigma(1385)^-\bar{\Sigma}(1385)^+(or c.c.)$	$[b] (1.16 \pm 0.05) \times 10^{-3}$		Γ_{194}	$p\bar{p}\pi^-$	$(2.12 \pm 0.09) \times 10^{-3}$			
Γ_{134}	$\Sigma(1385)^0\bar{\Sigma}(1385)^0$	$(1.07 \pm 0.08) \times 10^{-3}$		Γ_{195}	$n\bar{n}$	$(2.09 \pm 0.16) \times 10^{-3}$			
Γ_{135}	$\Lambda(1520)\bar{\Lambda} + c.c. \rightarrow \gamma\Lambda\bar{\Lambda}$	< 4.1	$\times 10^{-6}$	CL=90%	Γ_{196}	$n\bar{n}\pi^+\pi^-$	$(4 \pm 4) \times 10^{-3}$		
Γ_{136}	$\bar{\Lambda}(1520)\Lambda + c.c. \equiv^0\Xi^0$	< 1.80	$\times 10^{-3}$	CL=90%	Γ_{197}	$nN(1440)$	seen		
Γ_{137}	$\Xi(1530)^-\Xi^+ + c.c.$	$(1.17 \pm 0.04) \times 10^{-3}$		Γ_{198}	$nN(1520)$	seen			
Γ_{138}	$\Xi(1530)^-\Xi^+ + c.c.$	$(3.18 \pm 0.08) \times 10^{-4}$		Γ_{199}	$nN(1535)$	seen			
Γ_{139}	$\Xi(1530)^0\Xi^0$	$(3.2 \pm 1.4) \times 10^{-4}$		Γ_{200}	$\Lambda\bar{\Lambda}$	$(1.89 \pm 0.09) \times 10^{-3}$		S=2.8	
Γ_{140}	$\Theta(1540)\bar{\Theta}(1540) \rightarrow K_S^0 pK^-\bar{\pi} + c.c.$	$[c] < 1.1$	$\times 10^{-5}$	CL=90%	Γ_{201}	$\Lambda\bar{\Lambda}\pi^0$	$(3.8 \pm 0.4) \times 10^{-5}$		
Γ_{141}	$\Theta(1540)K^-\bar{\pi} \rightarrow K_S^0 pK^-\bar{\pi}$	$[c] < 2.1$	$\times 10^{-5}$	CL=90%	Γ_{202}	$\Lambda\bar{\Lambda}\pi^+\pi^-$	$(4.3 \pm 1.0) \times 10^{-3}$		
Γ_{142}	$\Theta(1540)K_S^0\bar{p} \rightarrow K_S^0\bar{p}K^+n$	$[c] < 1.6$	$\times 10^{-5}$	CL=90%	Γ_{203}	$\Lambda\bar{\Lambda}\eta$	$(1.62 \pm 0.17) \times 10^{-4}$		
				Γ_{204}	$\Lambda\bar{\Sigma}^-\pi^+(or c.c.)$	$[b] (8.3 \pm 0.7) \times 10^{-4}$		S=1.2	
				Γ_{205}	$\rho K^-\bar{\Lambda} + c.c.$	$(8.6 \pm 1.1) \times 10^{-4}$			
				Γ_{206}	$\rho K^-\bar{\Sigma}^0$	$(2.9 \pm 0.8) \times 10^{-4}$			
				Γ_{207}	$\bar{\Lambda}nK_S^0 + c.c.$	$(6.5 \pm 1.1) \times 10^{-4}$			
				Γ_{208}	$\Lambda\Sigma^+ + c.c.$	$(2.83 \pm 0.23) \times 10^{-5}$			
				Γ_{209}	$\Sigma^+\bar{\Sigma}^-$	$(1.07 \pm 0.04) \times 10^{-3}$			
				Γ_{210}	$\Sigma^0\bar{\Sigma}^0$	$(1.172 \pm 0.032) \times 10^{-3}$		S=1.4	
				Γ_{211}	$\Xi^-\bar{\Xi}^+$	$(9.7 \pm 0.8) \times 10^{-4}$		S=1.4	

Meson Particle Listings

 $J/\psi(1S)$

Radiative decays																																																							
Γ_{212}	$\gamma\eta_c(1S)$	$(1.7 \pm 0.4) \%$	S=1.5																																																				
Γ_{213}	$\gamma\eta_c(1S) \rightarrow 3\gamma$	$(3.8 \pm 1.3) \times 10^{-6}$	S=1.1																																																				
Γ_{214}	$\gamma\eta_c(1S) \rightarrow \gamma\eta\eta\eta'$	$(4.9 \pm 0.8) \times 10^{-5}$																																																					
Γ_{215}	3γ	$(1.16 \pm 0.22) \times 10^{-5}$																																																					
Γ_{216}	4γ	$< 9 \times 10^{-6}$	CL=90%																																																				
Γ_{217}	5γ	$< 1.5 \times 10^{-5}$	CL=90%																																																				
Γ_{218}	$\gamma\pi^0$	$(3.56 \pm 0.17) \times 10^{-5}$																																																					
Γ_{219}	$\gamma\pi^0\pi^0$	$(1.15 \pm 0.05) \times 10^{-3}$																																																					
Γ_{220}	$\gamma 2\pi^+\pi^-$	$(2.8 \pm 0.5) \times 10^{-3}$	S=1.9																																																				
Γ_{221}	$\gamma f_2(1270) f_2(1270)$	$(9.5 \pm 1.7) \times 10^{-4}$																																																					
Γ_{222}	$\gamma f_2(1270) f_2(1270)$ (non resonant)	$(8.2 \pm 1.9) \times 10^{-4}$																																																					
Γ_{223}	$\gamma\pi^+\pi^-2\pi^0$	$(8.3 \pm 3.1) \times 10^{-3}$																																																					
Γ_{224}	$\gamma K_S^0 K_S^0$	$(8.1 \pm 0.4) \times 10^{-4}$																																																					
Γ_{225}	$\gamma(K\bar{K}\pi) [PC = 0^{-+}]$	$(7 \pm 4) \times 10^{-4}$	S=2.1																																																				
Γ_{226}	$\gamma K^+ K^- \pi^+ \pi^-$	$(2.1 \pm 0.6) \times 10^{-3}$																																																					
Γ_{227}	$\gamma K^*(892) \bar{K}^*(892)$	$(4.0 \pm 1.3) \times 10^{-3}$																																																					
Γ_{228}	$\gamma\eta$	$(1.085 \pm 0.018) \times 10^{-3}$																																																					
Γ_{229}	$\gamma\eta\pi^0$	$(2.14 \pm 0.31) \times 10^{-5}$																																																					
Γ_{230}	$\gamma f_0(500) \rightarrow \gamma\pi\pi$																																																						
Γ_{231}	$\gamma f_0(500) \rightarrow \gamma K\bar{K}$																																																						
Γ_{232}	$\gamma f_0(500) \rightarrow \gamma\eta\eta$																																																						
Γ_{233}	$\gamma a_0(980)^0 \rightarrow \gamma\eta\pi^0$	$< 2.5 \times 10^{-6}$	CL=95%																																																				
Γ_{234}	$\gamma a_2(1320)^0 \rightarrow \gamma\eta\pi^0$	$< 6.6 \times 10^{-6}$	CL=95%																																																				
Γ_{235}	$\gamma\eta\pi\pi$	$(6.1 \pm 1.0) \times 10^{-3}$																																																					
Γ_{236}	$\gamma\eta_2(1870) \rightarrow \gamma\eta\pi^+\pi^-$	$(6.2 \pm 2.4) \times 10^{-4}$																																																					
Γ_{237}	$\gamma\eta'(958)$	$(5.25 \pm 0.07) \times 10^{-3}$	S=1.3																																																				
Γ_{238}	$\gamma f_0(980) \rightarrow \gamma\pi\pi$																																																						
Γ_{239}	$\gamma f_0(980) \rightarrow \gamma K\bar{K}$																																																						
Γ_{240}	$\gamma\rho\rho$	$(4.5 \pm 0.8) \times 10^{-3}$																																																					
Γ_{241}	$\gamma\rho\omega$	$< 5.4 \times 10^{-4}$	CL=90%																																																				
Γ_{242}	$\gamma\rho\phi$	$< 8.8 \times 10^{-5}$	CL=90%																																																				
Γ_{243}	$\gamma\omega\omega$	$(1.61 \pm 0.33) \times 10^{-3}$																																																					
Γ_{244}	$\gamma\phi\phi$	$(4.0 \pm 1.2) \times 10^{-4}$	S=2.1																																																				
Γ_{245}	$\gamma\eta(1405/1475) \rightarrow \gamma K\bar{K}\pi$	$(2.8 \pm 0.6) \times 10^{-3}$	S=1.6																																																				
Γ_{246}	$\gamma\eta(1405/1475) \rightarrow \gamma\gamma\rho^0$	$(7.8 \pm 2.0) \times 10^{-5}$	S=1.8																																																				
Γ_{247}	$\gamma\eta(1405/1475) \rightarrow \gamma\eta\pi^+\pi^-$	$(3.0 \pm 0.5) \times 10^{-4}$																																																					
Γ_{248}	$\gamma\eta(1405/1475) \rightarrow \gamma\rho^0\rho^0$	$(1.7 \pm 0.4) \times 10^{-3}$	S=1.3																																																				
Γ_{249}	$\gamma\eta(1405/1475) \rightarrow \gamma\gamma\phi$	$< 8.2 \times 10^{-5}$	CL=95%																																																				
Γ_{250}	$\gamma\eta(1405) \rightarrow \gamma\gamma\gamma$	$< 2.63 \times 10^{-6}$	CL=90%																																																				
Γ_{251}	$\gamma\eta(1475) \rightarrow \gamma\gamma\gamma$	$< 1.86 \times 10^{-6}$	CL=90%																																																				
Γ_{252}	$\gamma\eta(1760) \rightarrow \gamma\rho^0\rho^0$	$(1.3 \pm 0.9) \times 10^{-4}$																																																					
Γ_{253}	$\gamma\eta(1760) \rightarrow \gamma\omega\omega$	$(1.98 \pm 0.33) \times 10^{-3}$																																																					
Γ_{254}	$\gamma\eta(1760) \rightarrow \gamma\gamma\gamma$	$< 4.80 \times 10^{-6}$	CL=90%																																																				
Γ_{255}	$\gamma\eta(2225)$	$(3.14 \pm 0.50) \times 10^{-4}$																																																					
Γ_{256}	$\gamma f_2(1270)$	$(1.64 \pm 0.12) \times 10^{-3}$	S=1.3																																																				
Γ_{257}	$\gamma f_2(1270) \rightarrow \gamma K_S^0 K_S^0$	$(2.58 \pm 0.60) \times 10^{-5}$																																																					
Γ_{258}	$\gamma f_1(1285)$	$(6.1 \pm 0.8) \times 10^{-4}$																																																					
Γ_{259}	$\gamma f_0(1370) \rightarrow \gamma\pi\pi$																																																						
Γ_{260}	$\gamma f_0(1370) \rightarrow \gamma K\bar{K}$	$(4.2 \pm 1.5) \times 10^{-4}$																																																					
Γ_{261}	$\gamma f_0(1370) \rightarrow \gamma K_S^0 K_S^0$	$(1.1 \pm 0.4) \times 10^{-5}$																																																					
Γ_{262}	$\gamma f_0(1370) \rightarrow \gamma\eta\eta$																																																						
Γ_{263}	$\gamma f_0(1370) \rightarrow \gamma\eta\eta'$																																																						
Γ_{264}	$\gamma f_1(1420) \rightarrow \gamma K\bar{K}\pi$	$(7.9 \pm 1.3) \times 10^{-4}$																																																					
Γ_{265}	$\gamma f_0(1500) \rightarrow \gamma\pi\pi$	$(1.09 \pm 0.24) \times 10^{-4}$																																																					
Γ_{266}	$\gamma f_0(1500) \rightarrow \gamma\eta\eta$	$(1.7 \pm 0.6) \times 10^{-5}$																																																					
Γ_{267}	$\gamma f_0(1500) \rightarrow \gamma K_S^0 K_S^0$	$(1.59 \pm 0.24) \times 10^{-5}$																																																					
Γ_{268}	$\gamma f_0(1500) \rightarrow \gamma\eta\eta'$																																																						
Γ_{269}	$\gamma f_1(1510) \rightarrow \gamma\eta\pi^+\pi^-$	$(4.5 \pm 1.2) \times 10^{-4}$																																																					
Γ_{270}	$\gamma f_2'(1525)$	$(5.7 \pm 0.8) \times 10^{-4}$	S=1.5																																																				
Γ_{271}	$\gamma f_2'(1525) \rightarrow \gamma K_S^0 K_S^0$	$(8.0 \pm 0.7) \times 10^{-5}$																																																					
Γ_{272}	$\gamma f_2'(1525) \rightarrow \gamma\eta\eta$	$(3.4 \pm 1.4) \times 10^{-5}$																																																					
Γ_{273}	$\gamma f_2(1640) \rightarrow \gamma\omega\omega$	$(2.8 \pm 1.8) \times 10^{-4}$																																																					
Γ_{274}	$\gamma f_0(1710) \rightarrow \gamma\pi\pi$	$(3.8 \pm 0.5) \times 10^{-4}$																																																					
Γ_{275}	$\gamma f_0(1710) \rightarrow \gamma K\bar{K}$	$(9.5 \pm 1.0) \times 10^{-4}$	S=1.5																																																				
Γ_{276}	$\gamma f_0(1710) \rightarrow \gamma\omega\omega$	$(3.1 \pm 1.0) \times 10^{-4}$																																																					
Γ_{277}	$\gamma f_0(1710) \rightarrow \gamma\eta\eta$	$(2.4 \pm 1.2) \times 10^{-4}$																																																					
Γ_{278}	$\gamma f_0(1710) \rightarrow \gamma\eta\eta'$																																																						
Γ_{279}	$\gamma f_0(1710) \rightarrow \gamma\omega\phi$	$(2.5 \pm 0.6) \times 10^{-4}$																																																					
Γ_{280}	$\gamma f_0(1750) \rightarrow \gamma K_S^0 K_S^0$	$(1.11 \pm 0.20) \times 10^{-5}$																																																					
Γ_{281}	$\gamma f_2(1810) \rightarrow \gamma\eta\eta$	$(5.4 \pm 3.5) \times 10^{-5}$																																																					
Γ_{282}	$\gamma f_2(1910) \rightarrow \gamma\omega\omega$	$(2.0 \pm 1.4) \times 10^{-4}$																																																					
Γ_{283}	$\gamma f_2(1950) \rightarrow \gamma K^*(892) \bar{K}^*(892)$	$(7.0 \pm 2.2) \times 10^{-4}$																																																					
Γ_{284}	$\gamma f_0(2020) \rightarrow \gamma\pi\pi$																																																						
Γ_{285}	$\gamma f_0(2020) \rightarrow \gamma K\bar{K}$																																																						
Γ_{286}	$\gamma f_0(2020) \rightarrow \gamma\eta\eta$																																																						
Γ_{287}	$\gamma f_4(2050)$	$(2.7 \pm 0.7) \times 10^{-3}$																																																					
Γ_{288}	$\gamma f_0(2100) \rightarrow \gamma\eta\eta$	$(1.13 \pm 0.60) \times 10^{-4}$																																																					
Γ_{289}	$\gamma f_0(2100) \rightarrow \gamma K\bar{K}$																																																						
Γ_{290}	$\gamma f_0(2100) \rightarrow \gamma\pi\pi$	$(6.2 \pm 1.0) \times 10^{-4}$																																																					
Γ_{291}	$\gamma f_0(2200)$																																																						
Γ_{292}	$\gamma f_0(2200) \rightarrow \gamma K\bar{K}$	$(5.9 \pm 1.3) \times 10^{-4}$																																																					
Γ_{293}	$\gamma f_0(2200) \rightarrow \gamma K_S^0 K_S^0$	$(2.72 \pm 0.19) \times 10^{-4}$																																																					
Γ_{294}	$\gamma f_0(2200) \rightarrow \gamma\pi\pi$																																																						
Γ_{295}	$\gamma f_0(2200) \rightarrow \gamma\eta\eta$																																																						
Γ_{296}	$\gamma f_J(2220)$																																																						
Γ_{297}	$\gamma f_J(2220) \rightarrow \gamma\pi\pi$	$< 3.9 \times 10^{-5}$	CL=90%																																																				
Γ_{298}	$\gamma f_J(2220) \rightarrow \gamma K\bar{K}$	$< 4.1 \times 10^{-5}$	CL=90%																																																				
Γ_{299}	$\gamma f_J(2220) \rightarrow \gamma\rho\bar{\rho}$	$(1.5 \pm 0.8) \times 10^{-5}$																																																					
Γ_{300}	$\gamma f_0(2330) \rightarrow \gamma K_S^0 K_S^0$	$(4.9 \pm 0.7) \times 10^{-5}$																																																					
Γ_{301}	$\gamma f_0(2330) \rightarrow \gamma\pi\pi$																																																						
Γ_{302}	$\gamma f_0(2330) \rightarrow \gamma\eta\eta$																																																						
Γ_{303}	$\gamma f_2(2340) \rightarrow \gamma\eta\eta$	$(5.6 \pm 2.4) \times 10^{-5}$																																																					
Γ_{304}	$\gamma f_2(2340) \rightarrow \gamma K_S^0 K_S^0$	$(5.5 \pm 4.0) \times 10^{-5}$																																																					
Γ_{305}	$\gamma X(1835) \rightarrow \gamma\pi^+\pi^-\eta'$	$(2.7 \pm 0.6) \times 10^{-4}$	S=1.6																																																				
Γ_{306}	$\gamma X(1835) \rightarrow \gamma\rho\bar{\rho}$	$(7.7 \pm 1.5) \times 10^{-5}$																																																					
Γ_{307}	$\gamma X(1835) \rightarrow \gamma K_S^0 K_S^0 \eta$	$(3.3 \pm 2.0) \times 10^{-5}$																																																					
Γ_{308}	$\gamma X(1835) \rightarrow \gamma\gamma\phi(1020)$																																																						
Γ_{309}	$\gamma X(1835) \rightarrow \gamma\gamma\gamma$	$< 3.56 \times 10^{-6}$	CL=90%																																																				
Γ_{310}	$\gamma X(1835) \rightarrow \gamma 3(\pi^+\pi^-)$	$(2.4 \pm 0.7) \times 10^{-5}$																																																					
Γ_{311}	$\gamma X(2370) \rightarrow \gamma K^+ K^- \eta'$	$(1.8 \pm 0.7) \times 10^{-5}$																																																					
Γ_{312}	$\gamma X(2370) \rightarrow \gamma K_S^0 K_S^0 \eta'$	$(1.2 \pm 0.5) \times 10^{-5}$																																																					
Γ_{313}	$\gamma X(2370) \rightarrow \gamma\eta\eta\eta'$	$< 9.2 \times 10^{-6}$	CL=90%																																																				
Γ_{314}	$\gamma\rho\bar{\rho}$	$(3.8 \pm 1.0) \times 10^{-4}$																																																					
Γ_{315}	$\gamma\rho\bar{\rho}\pi^+\pi^-$	$< 7.9 \times 10^{-4}$	CL=90%																																																				
Γ_{316}	$\gamma\Lambda\bar{\Lambda}$	$< 1.3 \times 10^{-4}$	CL=90%																																																				
Γ_{317}	$\gamma A \rightarrow \gamma$ invisible	$[e] < 1.7 \times 10^{-6}$	CL=90%																																																				
Γ_{318}	$\gamma A^0 \rightarrow \gamma\mu^+\mu^-$	$[f] < 5 \times 10^{-6}$	CL=90%																																																				
Dalitz decays																																																							
Γ_{319}	$\pi^0 e^+ e^-$	$(7.6 \pm 1.4) \times 10^{-7}$																																																					
Γ_{320}	$\eta e^+ e^-$	$(1.42 \pm 0.08) \times 10^{-5}$																																																					
Γ_{321}	$\eta'(958) e^+ e^-$	$(6.59 \pm 0.18) \times 10^{-5}$																																																					
Γ_{322}	$\eta U \rightarrow \eta e^+ e^-$	$[g] < 9.11 \times 10^{-7}$	CL=90%																																																				
Γ_{323}	$\eta'(958) U \rightarrow \eta'(958) e^+ e^-$	$[g] < 2.0 \times 10^{-7}$	CL=90%																																																				
Γ_{324}	$\phi e^+ e^-$	$< 1.2 \times 10^{-7}$	CL=90%																																																				
Weak decays																																																							
Γ_{325}	$D^- e^+ \nu_e + c.c.$	$< 7.1 \times 10^{-8}$	CL=90%																																																				
Γ_{326}	$\bar{D}^0 e^+ e^- + c.c.$	$< 8.5 \times 10^{-8}$	CL=90%																																																				
Γ_{327}	$D_S^- e^+ \nu_e + c.c.$	$< 1.3 \times 10^{-6}$	CL=90%	Γ_{328}	$D_S^{*-} e^+ \nu_e + c.c.$	$< 1.8 \times 10^{-6}$	CL=90%	Γ_{329}	$D^- \pi^+ + c.c.$	$< 7.5 \times 10^{-5}$	CL=90%	Γ_{330}	$\bar{D}^0 \bar{K}^0 + c.c.$	$< 1.7 \times 10^{-4}$	CL=90%	Γ_{331}	$\bar{D}^0 \bar{K}^{*0} + c.c.$	$< 2.5 \times 10^{-6}$	CL=90%	Γ_{332}	$D_S^- \pi^+ + c.c.$	$< 1.3 \times 10^{-4}$	CL=90%	Γ_{333}	$D_S^- \rho^+ + c.c.$	$< 1.3 \times 10^{-5}$	CL=90%	Charge conjugation (C), Parity (P), Lepton Family number (LF) violating modes				Γ_{334}	$\gamma\gamma$	C	$< 2.7 \times 10^{-7}$ CL=90%	Γ_{335}	$\gamma\phi$	C	$< 1.4 \times 10^{-6}$ CL=90%	Γ_{336}	$e^\pm \mu^\mp$	LF	$< 1.6 \times 10^{-7}$ CL=90%	Γ_{337}	$e^\pm \tau^\mp$	LF	$< 7.5 \times 10^{-8}$ CL=90%	Γ_{338}	$\mu^\pm \tau^\mp$	LF	$< 2.0 \times 10^{-6}$ CL=90%	Γ_{339}	$A_c^\pm + c.c.$		$< 6.9 \times 10^{-8}$ CL=90%
Γ_{328}	$D_S^{*-} e^+ \nu_e + c.c.$	$< 1.8 \times 10^{-6}$	CL=90%																																																				
Γ_{329}	$D^- \pi^+ + c.c.$	$< 7.5 \times 10^{-5}$	CL=90%																																																				
Γ_{330}	$\bar{D}^0 \bar{K}^0 + c.c.$	$< 1.7 \times 10^{-4}$	CL=90%																																																				
Γ_{331}	$\bar{D}^0 \bar{K}^{*0} + c.c.$	$< 2.5 \times 10^{-6}$	CL=90%																																																				
Γ_{332}	$D_S^- \pi^+ + c.c.$	$< 1.3 \times 10^{-4}$	CL=90%																																																				
Γ_{333}	$D_S^- \rho^+ + c.c.$	$< 1.3 \times 10^{-5}$	CL=90%																																																				
Charge conjugation (C), Parity (P), Lepton Family number (LF) violating modes																																																							
Γ_{334}	$\gamma\gamma$	C	$< 2.7 \times 10^{-7}$ CL=90%																																																				
Γ_{335}	$\gamma\phi$	C	$< 1.4 \times 10^{-6}$ CL=90%																																																				
Γ_{336}	$e^\pm \mu^\mp$	LF	$< 1.6 \times 10^{-7}$ CL=90%																																																				
Γ_{337}	$e^\pm \tau^\mp$	LF	$< 7.5 \times 10^{-8}$ CL=90%																																																				
Γ_{338}	$\mu^\pm \tau^\mp$	LF	$< 2.0 \times 10^{-6}$ CL=90%																																																				
Γ_{339}	$A_c^\pm + c.c.$		$< 6.9 \times 10^{-8}$ CL=90%																																																				

Other decays

Γ_{340} invisible $< 7 \times 10^{-4}$ CL=90%

- [a] For $E_\gamma > 100$ MeV.
- [b] The value is for the sum of the charge states or particle/antiparticle states indicated.
- [c] $\Theta(1540)$ is a hypothetical pentaquark state of 1.54 GeV/c² mass and a width of less than 25 MeV/c².
- [d] Includes $p\bar{p}\pi^+\pi^-\gamma$ and excludes $p\bar{p}\eta, p\bar{p}\omega, p\bar{p}\eta'$.
- [e] For a narrow state A with mass less than 960 MeV.
- [f] For a narrow scalar or pseudoscalar A^0 with mass 0.21–3.0 GeV.
- [g] For a dark photon U with mass between 100 and 2100 MeV.

$J/\psi(1S)$ PARTIAL WIDTHS

$\Gamma(\text{hadrons})$

Γ_1

VALUE (keV)	DOCUMENT ID	TECN	COMMENT
81.37 ± 1.36 ± 1.30	¹ ANASHIN 20	KEDR	e^+e^-
••• We do not use the following data for averages, fits, limits, etc. •••			
74.1 ± 8.1	BAI	95B	BES e^+e^-
59 ± 24	BALDINI...	75	FRAG e^+e^-
59 ± 14	BOYARSKI	75	MRK1 e^+e^-
50 ± 25	ESPOSITO	75B	FRAM e^+e^-

¹ Based on the same dataset as ANASHIN 18A and correlated to the values reported there

$\Gamma(e^+e^-)$

Γ_5

VALUE (keV)	EVTS	DOCUMENT ID	TECN	COMMENT
5.53 ± 0.10 OUR AVERAGE				
5.550 ± 0.056 ± 0.089		^{1,2} ANASHIN 18A	KEDR	e^+e^-
5.36 $^{+0.29}_{-0.28}$		³ HSUEH 92	RVUE	See \mathcal{T} mini-review
••• We do not use the following data for averages, fits, limits, etc. •••				
5.58 ± 0.05 ± 0.08		⁴ ABLIKIM 16Q	BES3	3.773 $e^+e^- \rightarrow \mu^+\mu^-\gamma$
5.71 ± 0.16	13k	⁵ ADAMS 06A	CLEO	$e^+e^- \rightarrow \mu^+\mu^-\gamma$
5.57 ± 0.19	7.8k	⁵ AUBERT 04	BABR	$e^+e^- \rightarrow \mu^+\mu^-\gamma$
5.14 ± 0.39		BAI	95B	BES e^+e^-
4.72 ± 0.35		ALEXANDER 89	RVUE	See \mathcal{T} mini-review
4.4 ± 0.6		³ BRANDELIK 79c	DASP	e^+e^-
4.6 ± 0.8		⁶ BALDINI... 75	FRAG	e^+e^-
4.8 ± 0.6		BOYARSKI 75	MRK1	e^+e^-
4.6 ± 1.0		ESPOSITO 75b	FRAM	e^+e^-

- ¹ From the cross sections of $e^+e^- \rightarrow e^+e^-$ and $e^+e^- \rightarrow \text{hadrons}$ near the $J/\psi(1S)$ peak.
- ² Based on the same dataset as ANASHIN 20 and correlated to the values reported there.
- ³ From a simultaneous fit to e^+e^- , $\mu^+\mu^-$, and hadronic channels assuming $\Gamma(e^+e^-) = \Gamma(\mu^+\mu^-)$.
- ⁴ Using $B(J/\psi \rightarrow \mu^+\mu^-) = (5.973 \pm 0.007 \pm 0.037)\%$ from ABLIKIM 13R.
- ⁵ Calculated by us from the reported values of $\Gamma(e^+e^-) \times B(\mu^+\mu^-)$ using $B(\mu^+\mu^-) = (5.93 \pm 0.06)\%$.
- ⁶ Assuming equal partial widths for e^+e^- and $\mu^+\mu^-$.

$\Gamma(\mu^+\mu^-)$

Γ_7

VALUE (keV)	DOCUMENT ID	TECN	COMMENT
••• We do not use the following data for averages, fits, limits, etc. •••			
5.13 ± 0.52	BAI	95B	BES e^+e^-
4.8 ± 0.6	BOYARSKI	75	MRK1 e^+e^-
5 ± 1	ESPOSITO	75B	FRAM e^+e^-

$\Gamma(\gamma\gamma)$

Γ_{334}

VALUE (eV)	CL%	DOCUMENT ID	TECN	COMMENT
< 5.4	90	BRANDELIK 79c	DASP	e^+e^-

$J/\psi(1S) \Gamma(l)\Gamma(e^+e^-)/\Gamma(\text{total})$

This combination of a partial width with the partial width into e^+e^- and with the total width is obtained from the integrated cross section into channel(l) in the e^+e^- annihilation.

$\Gamma(\text{hadrons}) \times \Gamma(e^+e^-)/\Gamma_{\text{total}}$

$\Gamma_1\Gamma_5/\Gamma$

VALUE (keV)	DOCUMENT ID	TECN	COMMENT
••• We do not use the following data for averages, fits, limits, etc. •••			
4.884 ± 0.048 ± 0.078	^{1,2} ANASHIN 18A	KEDR	e^+e^-
4 ± 0.8	³ BALDINI... 75	FRAG	e^+e^-
3.9 ± 0.8	³ ESPOSITO 75B	FRAM	e^+e^-

- ¹ From the cross sections of $e^+e^- \rightarrow e^+e^-$ and $e^+e^- \rightarrow \text{hadrons}$ near the $J/\psi(1S)$ peak.
- ² Based on the same dataset as ANASHIN 20 and correlated to the values reported there.
- ³ Data redundant with branching ratios or partial widths above.

$\Gamma(e^+e^-) \times \Gamma(e^+e^-)/\Gamma_{\text{total}}$

$\Gamma_5\Gamma_5/\Gamma$

VALUE (eV)	DOCUMENT ID	TECN	COMMENT
••• We do not use the following data for averages, fits, limits, etc. •••			
333.1 ± 6.6 ± 4.0	^{1,2} ANASHIN 18A	KEDR	e^+e^-
332.3 ± 6.4 ± 4.8	ANASHIN 10	KEDR	3.097 $e^+e^- \rightarrow e^+e^-$
350 ± 20	BRANDELIK 79c	DASP	e^+e^-
320 ± 70	³ BALDINI... 75	FRAG	e^+e^-
340 ± 90	³ ESPOSITO 75B	FRAM	e^+e^-
360 ± 100	³ FORD 75	SPEC	e^+e^-

- ¹ From the cross sections of $e^+e^- \rightarrow e^+e^-$ and $e^+e^- \rightarrow \text{hadrons}$ near the $J/\psi(1S)$ peak.
- ² Based on the same dataset as ANASHIN 20 and correlated to the values reported there.
- ³ Data redundant with branching ratios or partial widths above.

$\Gamma(\mu^+\mu^-) \times \Gamma(e^+e^-)/\Gamma_{\text{total}}$

$\Gamma_7\Gamma_5/\Gamma$

VALUE (eV)	EVTS	DOCUMENT ID	TECN	COMMENT
333 ± 4 OUR AVERAGE				
333.4 ± 2.5 ± 4.4		ABLIKIM 16Q	BES3	3.773 $e^+e^- \rightarrow \mu^+\mu^-\gamma$
331.8 ± 5.2 ± 6.3		ANASHIN 10	KEDR	3.097 $e^+e^- \rightarrow \mu^+\mu^-$
338.4 ± 5.8 ± 7.1	13k	ADAMS 06A	CLEO	$e^+e^- \rightarrow \mu^+\mu^-\gamma$
330.1 ± 7.7 ± 7.3	7.8k	AUBERT 04	BABR	$e^+e^- \rightarrow \mu^+\mu^-\gamma$
••• We do not use the following data for averages, fits, limits, etc. •••				
510 ± 90		DASP 75	DASP	e^+e^-
380 ± 50		¹ ESPOSITO 75B	FRAM	e^+e^-

¹ Data redundant with branching ratios or partial widths above.

$\Gamma(\eta\pi^+\pi^-) \times \Gamma(e^+e^-)/\Gamma_{\text{total}}$

$\Gamma_{11}\Gamma_5/\Gamma$

VALUE (eV)	EVTS	DOCUMENT ID	TECN	COMMENT
2.3 ± 0.4 OUR AVERAGE				
2.34 ± 0.43 ± 0.16	49	LEES 18	BABR	$e^+e^- \rightarrow \eta\pi^+\pi^-\gamma$
2.22 ± 0.96 ± 0.02	9	¹ AUBERT 07AU	BABR	10.6 $e^+e^- \rightarrow \eta\pi^+\pi^-\gamma$

¹ AUBERT 07AU reports $[\Gamma(J/\psi(1S) \rightarrow \eta\pi^+\pi^-) \times \Gamma(J/\psi(1S) \rightarrow e^+e^-)]/\Gamma_{\text{total}} \times [B(\eta \rightarrow \pi^+\pi^-\pi^0)] = 0.51 \pm 0.22 \pm 0.03$ eV which we divide by our best value $B(\eta \rightarrow \pi^+\pi^-\pi^0) = (23.02 \pm 0.25) \times 10^{-2}$. Our first error is their experiment's error and our second error is the systematic error from using our best value.

$\Gamma(\eta\pi^+\pi^-\pi^0) \times \Gamma(e^+e^-)/\Gamma_{\text{total}}$

$\Gamma_{12}\Gamma_5/\Gamma$

VALUE (eV)	EVTS	DOCUMENT ID	TECN	COMMENT
64.8 ± 11.1 ± 0.4	200	¹ LEES 21c	BABR	$e^+e^- \rightarrow \gamma_{ISR}(\pi^+\pi^-\pi^0)$
••• We do not use the following data for averages, fits, limits, etc. •••				
¹ LEES 21c reports $[\Gamma(J/\psi(1S) \rightarrow \eta\pi^+\pi^-\pi^0) \times \Gamma(J/\psi(1S) \rightarrow e^+e^-)]/\Gamma_{\text{total}} \times [B(\eta \rightarrow 3\pi^0)] = 21.1 \pm 1.7 \pm 3.2$ eV which we divide by our best value $B(\eta \rightarrow 3\pi^0) = (32.57 \pm 0.21) \times 10^{-2}$. Our first error is their experiment's error and our second error is the systematic error from using our best value.				

$\Gamma(\eta\pi^+\pi^-3\pi^0) \times \Gamma(e^+e^-)/\Gamma_{\text{total}}$

$\Gamma_{13}\Gamma_5/\Gamma$

VALUE (eV)	EVTS	DOCUMENT ID	TECN	COMMENT
26.9 ± 5.7 ± 0.1	101	¹ LEES 21c	BABR	$e^+e^- \rightarrow \gamma_{ISR}(\pi^+\pi^-3\pi^0\gamma)$
••• We do not use the following data for averages, fits, limits, etc. •••				
¹ LEES 21c reports $[\Gamma(J/\psi(1S) \rightarrow \eta\pi^+\pi^-3\pi^0) \times \Gamma(J/\psi(1S) \rightarrow e^+e^-)]/\Gamma_{\text{total}} \times [B(\eta \rightarrow 2\gamma)] = 10.6 \pm 1.6 \pm 1.6$ eV which we divide by our best value $B(\eta \rightarrow 2\gamma) = (39.36 \pm 0.18) \times 10^{-2}$. Our first error is their experiment's error and our second error is the systematic error from using our best value.				

$\Gamma(\eta K^{\pm} K_S^0 \pi^{\mp}) \times \Gamma(e^+e^-)/\Gamma_{\text{total}}$

$\Gamma_{17}\Gamma_5/\Gamma$

VALUE (eV)	EVTS	DOCUMENT ID	TECN	COMMENT
7.3 ± 1.4 ± 0.4	44	LEES 17D	BABR	$e^+e^- \rightarrow K_S^0 K^{\pm} \pi^{\mp} \pi^0 \gamma$

$\Gamma(\rho^{\pm} \pi^{\mp} \pi^{\pm} \pi^0) \times \Gamma(e^+e^-)/\Gamma_{\text{total}}$

$\Gamma_{20}\Gamma_5/\Gamma$

VALUE (eV)	EVTS	DOCUMENT ID	TECN	COMMENT
155 ± 26 ± 36	14k	LEES 21	BABR	10.6 $e^+e^- \rightarrow 2(\pi^+\pi^-)3\pi^0\gamma$

$\Gamma(\rho^{\pm} \rho^{\mp} \pi^{\pm} \pi^0) \times \Gamma(e^+e^-)/\Gamma_{\text{total}}$

$\Gamma_{21}\Gamma_5/\Gamma$

VALUE (eV)	EVTS	DOCUMENT ID	TECN	COMMENT
32 ± 13 ± 15	14k	LEES 21	BABR	10.6 $e^+e^- \rightarrow 2(\pi^+\pi^-)3\pi^0\gamma$

$\Gamma(\rho^{\mp} K^{\pm} K_S^0) \times \Gamma(e^+e^-)/\Gamma_{\text{total}}$

$\Gamma_{22}\Gamma_5/\Gamma$

VALUE (eV)	EVTS	DOCUMENT ID	TECN	COMMENT
10.4 ± 1.0 ± 1.9	130	LEES 17D	BABR	$e^+e^- \rightarrow K_S^0 K^{\pm} \pi^{\mp} \pi^0 \gamma$

$\Gamma(\omega\pi^+\pi^-) \times \Gamma(e^+e^-)/\Gamma_{\text{total}}$

$\Gamma_{35}\Gamma_5/\Gamma$

VALUE (eV)	EVTS	DOCUMENT ID	TECN	COMMENT
53.6 ± 5.0 ± 0.4	788	¹ AUBERT 07AU	BABR	10.6 $e^+e^- \rightarrow \omega\pi^+\pi^-\gamma$
••• We do not use the following data for averages, fits, limits, etc. •••				
¹ AUBERT 07AU reports $[\Gamma(J/\psi(1S) \rightarrow \omega\pi^+\pi^-) \times \Gamma(J/\psi(1S) \rightarrow e^+e^-)]/\Gamma_{\text{total}} \times [B(\omega(782) \rightarrow \pi^+\pi^-\pi^0)] = 47.8 \pm 3.1 \pm 3.2$ eV which we divide by our best value $B(\omega(782) \rightarrow \pi^+\pi^-\pi^0) = (89.2 \pm 0.7) \times 10^{-2}$. Our first error is their experiment's error and our second error is the systematic error from using our best value.				

$\Gamma(\omega\pi^0\pi^0) \times \Gamma(e^+e^-)/\Gamma_{\text{total}}$

$\Gamma_{36}\Gamma_5/\Gamma$

VALUE (eV)	EVTS	DOCUMENT ID	TECN	COMMENT
27.8 ± 3.5 ± 0.2	398	¹ LEES 18E	BABR	10.6 $e^+e^- \rightarrow \pi^+\pi^-\pi^0\gamma$
••• We do not use the following data for averages, fits, limits, etc. •••				
¹ LEES 18E reports $[\Gamma(J/\psi(1S) \rightarrow \omega\pi^0\pi^0) \times \Gamma(J/\psi(1S) \rightarrow e^+e^-)]/\Gamma_{\text{total}} \times [B(\omega(782) \rightarrow \pi^+\pi^-\pi^0)] = 24.8 \pm 1.8 \pm 2.5$ eV which we divide by our best value $B(\omega(782) \rightarrow \pi^+\pi^-\pi^0) = (89.2 \pm 0.7) \times 10^{-2}$. Our first error is their experiment's error and our second error is the systematic error from using our best value.				

Meson Particle Listings

 $J/\psi(1S)$

$\Gamma(\omega 3\pi^0) \times \Gamma(e^+e^-)/\Gamma_{\text{total}}$					$\Gamma_{37}\Gamma_5/\Gamma$
VALUE (eV)	EVTs	DOCUMENT ID	TECN	COMMENT	

10.5 ± 3.1 ± 0.1 89 1 LEES 21c BABR $e^+e^- \rightarrow \gamma ISR(\pi^+\pi^-4\pi^0)$
 1 LEES 21c reports $[\Gamma(J/\psi(1S) \rightarrow \omega 3\pi^0) \times \Gamma(J/\psi(1S) \rightarrow e^+e^-)/\Gamma_{\text{total}}] \times [B(\omega(782) \rightarrow \pi^+\pi^-\pi^0)] = 9.4 \pm 2.3 \pm 1.5$ eV which we divide by our best value $B(\omega(782) \rightarrow \pi^+\pi^-\pi^0) = (89.2 \pm 0.7) \times 10^{-2}$. Our first error is their experiment's error and our second error is the systematic error from using our best value.

$\Gamma(\omega\pi^+\pi^-\pi^0) \times \Gamma(e^+e^-)/\Gamma_{\text{total}}$					$\Gamma_{40}\Gamma_5/\Gamma$
VALUE (10^{-2} keV)	EVTs	DOCUMENT ID	TECN	COMMENT	

2.2 ± 0.3 ± 0.2 170 AUBERT 06D BABR $10.6 e^+e^- \rightarrow \omega\pi^+\pi^-\pi^0\gamma$

$\Gamma(\omega\eta) \times \Gamma(e^+e^-)/\Gamma_{\text{total}}$					$\Gamma_{39}\Gamma_5/\Gamma$
VALUE (eV)	EVTs	DOCUMENT ID	TECN	COMMENT	

16.9 ± 7.6 ± 0.2 1 LEES 21c BABR $e^+e^- \rightarrow \gamma ISR(\pi^+\pi^-4\pi^0)$
 1 Different final state as in AUBERT 06. LEES 21c reports $[\Gamma(J/\psi(1S) \rightarrow \omega\eta) \times \Gamma(J/\psi(1S) \rightarrow e^+e^-)/\Gamma_{\text{total}}] \times [B(\eta \rightarrow 3\pi^0)] \times [B(\omega(782) \rightarrow \pi^+\pi^-\pi^0)] = 4.9 \pm 2.1 \pm 0.7$ eV which we divide by our best values $B(\eta \rightarrow 3\pi^0) = (32.57 \pm 0.21) \times 10^{-2}$, $B(\omega(782) \rightarrow \pi^+\pi^-\pi^0) = (89.2 \pm 0.7) \times 10^{-2}$. Our first error is their experiment's error and our second error is the systematic error from using our best values.

$\Gamma(\omega\pi^0\eta) \times \Gamma(e^+e^-)/\Gamma_{\text{total}}$					$\Gamma_{41}\Gamma_5/\Gamma$
VALUE (eV)	EVTs	DOCUMENT ID	TECN	COMMENT	

1.90 ± 0.96 ± 0.01 27 1 LEES 18E BABR $10.6 e^+e^- \rightarrow \pi^+\pi^-\pi^0\eta\gamma$
 1 LEES 18E reports $[\Gamma(J/\psi(1S) \rightarrow \omega\pi^0\eta) \times \Gamma(J/\psi(1S) \rightarrow e^+e^-)/\Gamma_{\text{total}}] \times [B(\omega(782) \rightarrow \pi^+\pi^-\pi^0)] = 1.7 \pm 0.8 \pm 0.3$ eV which we divide by our best value $B(\omega(782) \rightarrow \pi^+\pi^-\pi^0) = (89.2 \pm 0.7) \times 10^{-2}$. Our first error is their experiment's error and our second error is the systematic error from using our best value.

$\Gamma(\omega\pi^+\pi^-2\pi^0) \times \Gamma(e^+e^-)/\Gamma_{\text{total}}$					$\Gamma_{43}\Gamma_5/\Gamma$
VALUE (eV)	EVTs	DOCUMENT ID	TECN	COMMENT	

185 ± 30 ± 1 14k 1 LEES 21 BABR $10.6 e^+e^- \rightarrow 2(\pi^+\pi^-)3\pi^0\gamma$
 1 LEES 21 reports $[\Gamma(J/\psi(1S) \rightarrow \omega\pi^+\pi^-2\pi^0) \times \Gamma(J/\psi(1S) \rightarrow e^+e^-)/\Gamma_{\text{total}}] \times [B(\omega(782) \rightarrow \pi^+\pi^-\pi^0)] = 165 \pm 9 \pm 25$ eV which we divide by our best value $B(\omega(782) \rightarrow \pi^+\pi^-\pi^0) = (89.2 \pm 0.7) \times 10^{-2}$. Our first error is their experiment's error and our second error is the systematic error from using our best value.

$\Gamma(\omega K\bar{K}) \times \Gamma(e^+e^-)/\Gamma_{\text{total}}$					$\Gamma_{53}\Gamma_5/\Gamma$
VALUE (eV)	EVTs	DOCUMENT ID	TECN	COMMENT	

3.70 ± 1.98 ± 0.03 24 1 AUBERT 07AU BABR $10.6 e^+e^- \rightarrow \omega K^+ K^- \gamma$
 1 AUBERT 07AU reports $[\Gamma(J/\psi(1S) \rightarrow \omega K\bar{K}) \times \Gamma(J/\psi(1S) \rightarrow e^+e^-)/\Gamma_{\text{total}}] \times [B(\omega(782) \rightarrow \pi^+\pi^-\pi^0)] = 3.3 \pm 1.3 \pm 1.2$ eV which we divide by our best value $B(\omega(782) \rightarrow \pi^+\pi^-\pi^0) = (89.2 \pm 0.7) \times 10^{-2}$. Our first error is their experiment's error and our second error is the systematic error from using our best value.

$\Gamma(K^+ K^*(892)^- + c.c.) \times \Gamma(e^+e^-)/\Gamma_{\text{total}}$					$\Gamma_{61}\Gamma_5/\Gamma$
VALUE (eV)	EVTs	DOCUMENT ID	TECN	COMMENT	

29.0 ± 1.7 ± 1.3 AUBERT 08s BABR $10.6 e^+e^- \rightarrow K^+ K^*(892)^- \gamma$

$\Gamma(K^+ K^*(892)^- + c.c. \rightarrow K^+ K^- \pi^0) \times \Gamma(e^+e^-)/\Gamma_{\text{total}}$					$\Gamma_{62}\Gamma_5/\Gamma$
VALUE (eV)	EVTs	DOCUMENT ID	TECN	COMMENT	

10.96 ± 0.85 ± 0.70 155 AUBERT 08s BABR $10.6 e^+e^- \rightarrow K^+ K^- \pi^0 \gamma$

$\Gamma(K^+ K^*(892)^- + c.c. \rightarrow K^0 K^\pm \pi^\mp + c.c.) \times \Gamma(e^+e^-)/\Gamma_{\text{total}}$					$\Gamma_{63}\Gamma_5/\Gamma$
VALUE (eV)	EVTs	DOCUMENT ID	TECN	COMMENT	

16.76 ± 1.70 ± 1.00 89 AUBERT 08s BABR $10.6 e^+e^- \rightarrow K_S^0 K^\pm \pi^\mp \gamma$

$\Gamma(K^0 \bar{K}^*(892)^0 + c.c.) \times \Gamma(e^+e^-)/\Gamma_{\text{total}}$					$\Gamma_{64}\Gamma_5/\Gamma$
VALUE (eV)	EVTs	DOCUMENT ID	TECN	COMMENT	

26.6 ± 2.5 ± 1.5 AUBERT 08s BABR $10.6 e^+e^- \rightarrow K^0 \bar{K}^*(892)^0 \gamma$

$\Gamma(K^0 \bar{K}^*(892)^0 + c.c. \rightarrow K^0 K^\pm \pi^\mp + c.c.) \times \Gamma(e^+e^-)/\Gamma_{\text{total}}$					$\Gamma_{65}\Gamma_5/\Gamma$
VALUE (eV)	EVTs	DOCUMENT ID	TECN	COMMENT	

17.70 ± 1.70 ± 1.00 94 AUBERT 08s BABR $10.6 e^+e^- \rightarrow K_S^0 K^\pm \pi^\mp \gamma$

$\Gamma(\bar{K}^*(892)^0 K^+ \pi^- + c.c.) \times \Gamma(e^+e^-)/\Gamma_{\text{total}}$					$\Gamma_{66}\Gamma_5/\Gamma$
VALUE (eV)	EVTs	DOCUMENT ID	TECN	COMMENT	

42.6 ± 4.8 ± 7.2 99 1 LEES 17D BABR $e^+e^- \rightarrow K_S^0 K^\pm \pi^\mp \pi^0 \gamma$

1 Dividing by 1/6 to account for $B(K^*(892)^0 \rightarrow K_S^0 \pi^0) = 1/6$.

$\Gamma(K^*(892)^\pm K^\mp \pi^0) \times \Gamma(e^+e^-)/\Gamma_{\text{total}}$					$\Gamma_{67}\Gamma_5/\Gamma$
VALUE (eV)	EVTs	DOCUMENT ID	TECN	COMMENT	

22.6 ± 2.8 ± 6.8 80 1 LEES 17D BABR $e^+e^- \rightarrow K_S^0 K^\pm \pi^\mp \pi^0 \gamma$

1 Dividing by 1/4 to account for $B(K^*(892)^\pm \rightarrow K_S^0 \pi^\pm) = 1/4$.

$\Gamma(K^*(892)^+ K_S^0 \pi^- + c.c.) \times \Gamma(e^+e^-)/\Gamma_{\text{total}}$					$\Gamma_{68}\Gamma_5/\Gamma$
VALUE (eV)	EVTs	DOCUMENT ID	TECN	COMMENT	

11.0 ± 2.8 OUR AVERAGE

9.2 ± 1.2 ± 3.2 64 1 LEES 17D BABR $e^+e^- \rightarrow K_S^0 K^\pm \pi^\mp \pi^0 \gamma$

14.8 ± 4.8 ± 1.2 53 2 LEES 14H BABR $e^+e^- \rightarrow \pi^+\pi^- K_S^0 K_S^0 \gamma$

1 Dividing by 1/2 to take into account $B(K^*(892)^\pm \rightarrow K^\pm \pi^\mp) = 1/2$.
 2 Dividing by 1/4 to take into account $B(K^*(892) \rightarrow K_S^0 \pi) = 1/4$.

$\Gamma(K^*(892)^+ K_S^0 \pi^- + c.c. \rightarrow K_S^0 K_S^0 \pi^+ \pi^-) \times \Gamma(e^+e^-)/\Gamma_{\text{total}}$					$\Gamma_{69}\Gamma_5/\Gamma$
VALUE (eV)	EVTs	DOCUMENT ID	TECN	COMMENT	

3.7 ± 1.2 ± 0.3 53 LEES 14H BABR $e^+e^- \rightarrow \pi^+\pi^- K_S^0 K_S^0 \gamma$

$\Gamma(K^*(892)^0 K_S^0 \pi^0) \times \Gamma(e^+e^-)/\Gamma_{\text{total}}$					$\Gamma_{71}\Gamma_5/\Gamma$
VALUE (eV)	EVTs	DOCUMENT ID	TECN	COMMENT	

3.60 ± 0.75 ± 2.25 34 1 LEES 17D BABR $e^+e^- \rightarrow K_S^0 K^\pm \pi^\mp \pi^0 \gamma$

1 Dividing by 2/3 to account for $B(K^*(892)^0 \rightarrow K^+ \pi^-) = 2/3$.

$\Gamma(K^*(892)^0 \bar{K}^*(892)^0) \times \Gamma(e^+e^-)/\Gamma_{\text{total}}$					$\Gamma_{73}\Gamma_5/\Gamma$
VALUE (eV)	EVTs	DOCUMENT ID	TECN	COMMENT	

1.28 ± 0.34 ± 0.07 47 ± 12 1 LEES 12F BABR $10.6 e^+e^- \rightarrow \pi^+\pi^- K^+ K^- \gamma$

• • • We do not use the following data for averages, fits, limits, etc. • • •

1.28 ± 0.40 ± 0.11 25 ± 8 1,2 AUBERT 07AK BABR $10.6 e^+e^- \rightarrow \pi^+\pi^- K^+ K^- \gamma$

1 Dividing by $(2/3)^2$ to take twice into account that $B(K^* \rightarrow K^+ \pi^-) = 2/3$ $B(K^* \rightarrow K^- \pi^+) = 2/3$.

2 Superseded by LEES 12F.

$\Gamma(K^*(892)^\pm K^*(892)^\mp) \times \Gamma(e^+e^-)/\Gamma_{\text{total}}$					$\Gamma_{74}\Gamma_5/\Gamma$
VALUE (eV)	EVTs	DOCUMENT ID	TECN	COMMENT	

0.80 ± 0.48 ± 0.32 1 ± 5 1 LEES 14H BABR $e^+e^- \rightarrow \pi^+\pi^- K_S^0 K_S^0 \gamma$

1 Dividing by $(1/4)^2$ to take twice into account $B(K^*(892) \rightarrow K_S^0 \pi) = 1/4$.

$\Gamma(K_S^0(1430)^+ K_S^0 \pi^- + c.c.) \times \Gamma(e^+e^-)/\Gamma_{\text{total}}$					$\Gamma_{84}\Gamma_5/\Gamma$
VALUE (eV)	EVTs	DOCUMENT ID	TECN	COMMENT	

20.1 ± 9.8 ± 0.5 35 1,2 LEES 14H BABR $e^+e^- \rightarrow \pi^+\pi^- K_S^0 K_S^0 \gamma$

1 Dividing by 1/4 to take into account $B(K^*(1430) \rightarrow K_S^0 \pi) = 1/4$ $B(K^*(1430) \rightarrow K \pi)$.

2 LEES 14H reports $[\Gamma(J/\psi(1S) \rightarrow K_S^0(1430)^+ K_S^0 \pi^- + c.c.) \times \Gamma(J/\psi(1S) \rightarrow e^+e^-)/\Gamma_{\text{total}}] \times [B(K_S^0(1430)^+ \rightarrow K \pi)] = 10.0 \pm 4.8 \pm 0.8$ eV which we divide by our best value $B(K_S^0(1430)^+ \rightarrow K \pi) = (49.9 \pm 1.2) \times 10^{-2}$. Our first error is their experiment's error and our second error is the systematic error from using our best value.

$\Gamma(\bar{K}_S^0(1430)^0 K^*(892)^0 + c.c.) \times \Gamma(e^+e^-)/\Gamma_{\text{total}}$					$\Gamma_{85}\Gamma_5/\Gamma$
VALUE (eV)	EVTs	DOCUMENT ID	TECN	COMMENT	

25.8 ± 1.4 ± 0.6 710 1,2,3 LEES 12F BABR $10.6 e^+e^- \rightarrow \pi^+\pi^- K^+ K^- \gamma$

• • • We do not use the following data for averages, fits, limits, etc. • • •

33 ± 4 ± 1 317 2,4 AUBERT 07AK BABR $10.6 e^+e^- \rightarrow \pi^+\pi^- K^+ K^- \gamma$

1 LEES 12F reports $[\Gamma(J/\psi(1S) \rightarrow \bar{K}_S^0(1430)^0 K^*(892)^0 + c.c.) \times \Gamma(J/\psi(1S) \rightarrow e^+e^-)/\Gamma_{\text{total}}] \times [B(K_S^0(1430)^0 \rightarrow K \pi)] = 12.89 \pm 0.54 \pm 0.41$ eV which we divide by our best value $B(K_S^0(1430)^0 \rightarrow K \pi) = (49.9 \pm 1.2) \times 10^{-2}$. Our first error is their experiment's error and our second error is the systematic error from using our best value.

2 Dividing by 2/3 to take into account that $B(K^* \rightarrow K^+ \pi^-) = 2/3$ $B(K^* \rightarrow K^- \pi^+) = 2/3$.

3 The $K_S^0(1430)$ cannot be distinguished from the $K_0^0(1430)$.

4 Superseded by LEES 12F. AUBERT 07AK reports $[\Gamma(J/\psi(1S) \rightarrow \bar{K}_S^0(1430)^0 K^*(892)^0 + c.c.) \times \Gamma(J/\psi(1S) \rightarrow e^+e^-)/\Gamma_{\text{total}}] \times [B(K_S^0(1430)^0 \rightarrow K \pi)] = 16.4 \pm 1.1 \pm 1.4$ eV which we divide by our best value $B(K_S^0(1430)^0 \rightarrow K \pi) = (49.9 \pm 1.2) \times 10^{-2}$. Our first error is their experiment's error and our second error is the systematic error from using our best value.

$\Gamma(K_S^0(1430)^- K^*(892)^+ + c.c.) \times \Gamma(e^+e^-)/\Gamma_{\text{total}}$					$\Gamma_{86}\Gamma_5/\Gamma$
VALUE (eV)	EVTs	DOCUMENT ID	TECN	COMMENT	

18.6 ± 16.1 ± 0.4 8 ± 8 1,2 LEES 14H BABR $e^+e^- \rightarrow \pi^+\pi^- K_S^0 K_S^0 \gamma$

1 Dividing by $(1/4)^2$ to take into account $B(K^*(892) \rightarrow K_S^0 \pi) = 1/4$ and $B(K^*(1430) \rightarrow K_S^0 \pi) = 1/4$ $B(K^*(1430) \rightarrow K \pi)$.

2 LEES 14H reports $[\Gamma(J/\psi(1S) \rightarrow K_S^0(1430)^- K^*(892)^+ + c.c.) \times \Gamma(J/\psi(1S) \rightarrow e^+e^-)/\Gamma_{\text{total}}] \times [B(K_S^0(1430)^- \rightarrow K \pi)] = 9.28 \pm 8.0 \pm 0.32$ eV which we divide by our best value $B(K_S^0(1430)^- \rightarrow K \pi) = (49.9 \pm 1.2) \times 10^{-2}$. Our first error is their experiment's error and our second error is the systematic error from using our best value.

$\Gamma(K_S^0(1430)^- K^*(892)^+ + c.c. \rightarrow K^*(892)^+ K_S^0 \pi^- + c.c.) \times \Gamma(e^+e^-)/\Gamma_{\text{total}}$					$\Gamma_{87}\Gamma_5/\Gamma$
VALUE (eV)	EVTs	DOCUMENT ID	TECN	COMMENT	

2.32 ± 2.00 ± 0.08 8 ± 8 1 LEES 14H BABR $e^+e^- \rightarrow \pi^+\pi^- K_S^0 K_S^0 \gamma$

1 Dividing by 1/4 to take into account $B(K^*(892) \rightarrow K_S^0 \pi) = 1/4$.

See key on page 1127

Meson Particle Listings

$J/\psi(1S)$

$$\Gamma(\bar{K}_2(1770)^0 K^*(892)^0 + c.c. \rightarrow K^*(892)^0 K^- \pi^+ + c.c.) \times \Gamma(e^+ e^-) / \Gamma_{\text{total}} \quad \Gamma_{89} \Gamma_5 / \Gamma$$

VALUE (eV)	EVTs	DOCUMENT ID	TECN	COMMENT
3.8 ± 0.4 ± 0.3	110 ± 14	¹ AUBERT 07AK BABR		10.6 e ⁺ e ⁻ → π ⁺ π ⁻ K ⁺ K ⁻ γ

¹ Dividing by 2/3 to take into account that B(K*⁰ → K⁺π⁻) = 2/3.

$$\Gamma(\phi \pi^+ \pi^-) \times \Gamma(e^+ e^-) / \Gamma_{\text{total}} \quad \Gamma_{96} \Gamma_5 / \Gamma$$

VALUE (eV)	EVTs	DOCUMENT ID	TECN	COMMENT
4.48 ± 0.35 OUR AVERAGE				
4.46 ± 0.49 ± 0.05	181	¹ LEES 12F BABR		10.6 e ⁺ e ⁻ → K ⁺ K ⁻ π ⁺ π ⁻ γ
4.51 ± 0.48 ± 0.05	254 ± 23	² SHEN 09 BELL		10.6 e ⁺ e ⁻ → K ⁺ K ⁻ π ⁺ π ⁻ γ

• • • We do not use the following data for averages, fits, limits, etc. • • •

5.3 ± 0.7 ± 0.1	103	³ AUBERT, BE 06D BABR		10.6 e ⁺ e ⁻ → K ⁺ K ⁻ π ⁺ π ⁻ γ
-----------------	-----	----------------------------------	--	--

¹ LEES 12F reports [Γ(J/ψ(1S) → φπ⁺π⁻) × Γ(J/ψ(1S) → e⁺e⁻)/Γ_{total}] × [B(φ(1020) → K⁺K⁻)] = 2.19 ± 0.23 ± 0.07 eV which we divide by our best value B(φ(1020) → K⁺K⁻) = (49.1 ± 0.5) × 10⁻². Our first error is their experiment's error and our second error is the systematic error from using our best value.

² SHEN 09 reports 4.50 ± 0.41 ± 0.26 eV from a measurement of [Γ(J/ψ(1S) → φπ⁺π⁻) × Γ(J/ψ(1S) → e⁺e⁻)/Γ_{total}] × [B(φ(1020) → K⁺K⁻)] assuming B(φ(1020) → K⁺K⁻) = (49.2 ± 0.6) × 10⁻², which we rescale to our best value B(φ(1020) → K⁺K⁻) = (49.1 ± 0.5) × 10⁻². Our first error is their experiment's error and our second error is the systematic error from using our best value.

³ Superseded by LEES 12F. AUBERT, BE 06D reports [Γ(J/ψ(1S) → φπ⁺π⁻) × Γ(J/ψ(1S) → e⁺e⁻)/Γ_{total}] × [B(φ(1020) → K⁺K⁻)] = 2.61 ± 0.30 ± 0.18 eV which we divide by our best value B(φ(1020) → K⁺K⁻) = (49.1 ± 0.5) × 10⁻². Our first error is their experiment's error and our second error is the systematic error from using our best value.

$$\Gamma(\phi \pi^0 \pi^0) \times \Gamma(e^+ e^-) / \Gamma_{\text{total}} \quad \Gamma_{97} \Gamma_5 / \Gamma$$

VALUE (eV)	EVTs	DOCUMENT ID	TECN	COMMENT
2.77 ± 0.57 ± 0.03	45	¹ LEES 12F BABR		10.6 e ⁺ e ⁻ → K ⁺ K ⁻ π ⁰ π ⁰ γ

• • • We do not use the following data for averages, fits, limits, etc. • • •

3.13 ± 0.88 ± 0.03	23	² AUBERT, BE 06D BABR		10.6 e ⁺ e ⁻ → K ⁺ K ⁻ π ⁰ π ⁰ γ
--------------------	----	----------------------------------	--	--

¹ LEES 12F reports [Γ(J/ψ(1S) → φπ⁰π⁰) × Γ(J/ψ(1S) → e⁺e⁻)/Γ_{total}] × [B(φ(1020) → K⁺K⁻)] = 1.36 ± 0.27 ± 0.07 eV which we divide by our best value B(φ(1020) → K⁺K⁻) = (49.1 ± 0.5) × 10⁻². Our first error is their experiment's error and our second error is the systematic error from using our best value.

² Superseded by LEES 12F. AUBERT, BE 06D reports [Γ(J/ψ(1S) → φπ⁰π⁰) × Γ(J/ψ(1S) → e⁺e⁻)/Γ_{total}] × [B(φ(1020) → K⁺K⁻)] = 1.54 ± 0.40 ± 0.16 eV which we divide by our best value B(φ(1020) → K⁺K⁻) = (49.1 ± 0.5) × 10⁻². Our first error is their experiment's error and our second error is the systematic error from using our best value.

$$\Gamma(\phi(2\pi^+ \pi^-)) \times \Gamma(e^+ e^-) / \Gamma_{\text{total}} \quad \Gamma_{98} \Gamma_5 / \Gamma$$

VALUE (10 ⁻² keV)	EVTs	DOCUMENT ID	TECN	COMMENT
0.96 ± 0.19 ± 0.01	35	¹ AUBERT 06D BABR		10.6 e ⁺ e ⁻ → φ(2π ⁺ π ⁻)γ

¹ AUBERT 06D reports [Γ(J/ψ(1S) → φ(2π⁺π⁻)) × Γ(J/ψ(1S) → e⁺e⁻)/Γ_{total}] × [B(φ(1020) → K⁺K⁻)] = (0.47 ± 0.09 ± 0.03) × 10⁻² keV which we divide by our best value B(φ(1020) → K⁺K⁻) = (49.1 ± 0.5) × 10⁻². Our first error is their experiment's error and our second error is the systematic error from using our best value.

$$\Gamma(\phi \eta) \times \Gamma(e^+ e^-) / \Gamma_{\text{total}} \quad \Gamma_{99} \Gamma_5 / \Gamma$$

VALUE (eV)	EVTs	DOCUMENT ID	TECN	COMMENT
6.1 ± 2.7 ± 0.4	6	¹ AUBERT 07AU BABR		10.6 e ⁺ e ⁻ → φηγ

¹ AUBERT 07AU quotes Γ_{ee}^{J/ψ} · B(J/ψ → φη) · B(φ → K⁺K⁻) · B(η → 3π) = 0.84 ± 0.37 ± 0.05 eV.

$$\Gamma(\phi_0(980) \rightarrow \phi \pi^+ \pi^-) \times \Gamma(e^+ e^-) / \Gamma_{\text{total}} \quad \Gamma_{103} \Gamma_5 / \Gamma$$

VALUE (eV)	EVTs	DOCUMENT ID	TECN	COMMENT
1.44 ± 0.19 OUR AVERAGE				
1.40 ± 0.25 ± 0.02	57 ± 9	¹ LEES 12F BABR		10.6 e ⁺ e ⁻ → π ⁺ π ⁻ K ⁺ K ⁻ γ
1.48 ± 0.27 ± 0.09	60 ± 11	² SHEN 09 BELL		10.6 e ⁺ e ⁻ → K ⁺ K ⁻ π ⁺ π ⁻ γ

• • • We do not use the following data for averages, fits, limits, etc. • • •

1.02 ± 0.24 ± 0.01	20 ± 5	³ AUBERT 07AK BABR		10.6 e ⁺ e ⁻ → π ⁺ π ⁻ K ⁺ K ⁻ γ
--------------------	--------	-------------------------------	--	--

¹ LEES 12F reports [Γ(J/ψ(1S) → φ₀(980) → φπ⁺π⁻) × Γ(J/ψ(1S) → e⁺e⁻)/Γ_{total}] × [B(φ(1020) → K⁺K⁻)] = 0.69 ± 0.11 ± 0.05 eV which we divide by our best value B(φ(1020) → K⁺K⁻) = (49.1 ± 0.5) × 10⁻². Our first error is their experiment's error and our second error is the systematic error from using our best value.

² Multiplied by 2/3 to take into account the φπ⁺π⁻ mode only. Using B(φ → K⁺K⁻) = (49.2 ± 0.6)%.

³ Superseded by LEES 12F. AUBERT 07AK reports [Γ(J/ψ(1S) → φ₀(980) → φπ⁺π⁻) × Γ(J/ψ(1S) → e⁺e⁻)/Γ_{total}] × [B(φ(1020) → K⁺K⁻)] = 0.50 ± 0.11 ± 0.04 eV which we divide by our best value B(φ(1020) → K⁺K⁻) = (49.1 ± 0.5) × 10⁻². Our first error is their experiment's error and our second error is the systematic error from using our best value.

$$\Gamma(\phi_0(980) \rightarrow \phi \pi^0 \pi^0) \times \Gamma(e^+ e^-) / \Gamma_{\text{total}} \quad \Gamma_{104} \Gamma_5 / \Gamma$$

VALUE (eV)	EVTs	DOCUMENT ID	TECN	COMMENT
0.98 ± 0.26 ± 0.01	16 ± 4	¹ LEES 12F BABR		10.6 e ⁺ e ⁻ → π ⁰ π ⁰ K ⁺ K ⁻ γ

• • • We do not use the following data for averages, fits, limits, etc. • • •

0.96 ± 0.40 ± 0.01

² AUBERT 07AK BABR 10.6 e⁺e⁻ → π⁰π⁰K⁺K⁻γ

¹ LEES 12F reports [Γ(J/ψ(1S) → φ₀(980) → φπ⁰π⁰) × Γ(J/ψ(1S) → e⁺e⁻)/Γ_{total}] × [B(φ(1020) → K⁺K⁻)] = 0.48 ± 0.12 ± 0.05 eV which we divide by our best value B(φ(1020) → K⁺K⁻) = (49.1 ± 0.5) × 10⁻². Our first error is their experiment's error and our second error is the systematic error from using our best value.

² Superseded by LEES 12F. AUBERT 07AK reports [Γ(J/ψ(1S) → φ₀(980) → φπ⁰π⁰) × Γ(J/ψ(1S) → e⁺e⁻)/Γ_{total}] × [B(φ(1020) → K⁺K⁻)] = 0.47 ± 0.19 ± 0.05 eV which we divide by our best value B(φ(1020) → K⁺K⁻) = (49.1 ± 0.5) × 10⁻². Our first error is their experiment's error and our second error is the systematic error from using our best value.

$$\Gamma(\phi_2(1270)) \times \Gamma(e^+ e^-) / \Gamma_{\text{total}} \quad \Gamma_{109} \Gamma_5 / \Gamma$$

VALUE (eV)	EVTs	DOCUMENT ID	TECN	COMMENT
1.79 ± 0.32 ± 0.02_0.06	61	^{1,2,3} LEES 12F BABR		10.6 e ⁺ e ⁻ → π ⁺ π ⁻ K ⁺ K ⁻ γ

• • • We do not use the following data for averages, fits, limits, etc. • • •

4.08 ± 0.73 ± 0.04_0.14	44	^{2,4} AUBERT 07AK BABR		10.6 e ⁺ e ⁻ → π ⁺ π ⁻ K ⁺ K ⁻ γ
-------------------------	----	---------------------------------	--	--

¹ LEES 12F reports [Γ(J/ψ(1S) → φ₂(1270)) × Γ(J/ψ(1S) → e⁺e⁻)/Γ_{total}] × [B(φ₂(1270) → ππ)] = 1.51 ± 0.25 ± 0.10 eV which we divide by our best value B(φ₂(1270) → ππ) = (84.2 ± 2.9) × 10⁻². Our first error is their experiment's error and our second error is the systematic error from using our best value.

² Using B(φ → K⁺K⁻) = (48.9 ± 0.5)%.

³ Using π⁺π⁻ invariant mass between 1.1 and 1.5 GeV. May include other sources such as f₀(1370).

⁴ Superseded by LEES 12F. AUBERT 07AK reports [Γ(J/ψ(1S) → φ₂(1270)) × Γ(J/ψ(1S) → e⁺e⁻)/Γ_{total}] × [B(φ₂(1270) → ππ)] = 3.44 ± 0.55 ± 0.28 eV which we divide by our best value B(φ₂(1270) → ππ) = (84.2 ± 2.9) × 10⁻². Our first error is their experiment's error and our second error is the systematic error from using our best value.

$$\Gamma(\phi f_2'(1525)) \times \Gamma(e^+ e^-) / \Gamma_{\text{total}} \quad \Gamma_{114} \Gamma_5 / \Gamma$$

VALUE (eV)	EVTs	DOCUMENT ID	TECN	COMMENT
8.2 ± 3.2 ± 0.2	11	^{1,2} LEES 14H BABR		e ⁺ e ⁻ → K _S ⁰ K _S ⁰ K ⁺ K ⁻ γ

¹ Dividing by 1/4 to take into account B(f₂'(1525) → K_S⁰K_S⁰) = 1/4 B(f₂'(1525) → K_L⁰K_L⁰) and using B(φ → K⁺K⁻) = (48.9 ± 0.5)%.

² LEES 14H reports [Γ(J/ψ(1S) → φ f₂'(1525)) × Γ(J/ψ(1S) → e⁺e⁻)/Γ_{total}] × [B(f₂'(1525) → K_L⁰K_L⁰)] = 7.2 ± 2.8 ± 0.3 eV which we divide by our best value B(f₂'(1525) → K_L⁰K_L⁰) = (87.6 ± 2.2) × 10⁻². Our first error is their experiment's error and our second error is the systematic error from using our best value.

$$\Gamma(\phi K^+ K^-) \times \Gamma(e^+ e^-) / \Gamma_{\text{total}} \quad \Gamma_{120} \Gamma_5 / \Gamma$$

VALUE (eV)	EVTs	DOCUMENT ID	TECN	COMMENT
4.60 ± 0.62 ± 0.05	163	¹ LEES 12F BABR		10.6 e ⁺ e ⁻ → K ⁺ K ⁻ K ⁺ K ⁻ γ

¹ LEES 12F reports [Γ(J/ψ(1S) → φK⁺K⁻) × Γ(J/ψ(1S) → e⁺e⁻)/Γ_{total}] × [B(φ(1020) → K⁺K⁻)] = 2.26 ± 0.26 ± 0.16 eV which we divide by our best value B(φ(1020) → K⁺K⁻) = (49.1 ± 0.5) × 10⁻². Our first error is their experiment's error and our second error is the systematic error from using our best value.

$$\Gamma(\phi K_S^0 K_S^0) \times \Gamma(e^+ e^-) / \Gamma_{\text{total}} \quad \Gamma_{121} \Gamma_5 / \Gamma$$

VALUE (eV)	EVTs	DOCUMENT ID	TECN	COMMENT
3.26 ± 0.84 ± 0.04	29	¹ LEES 14H BABR		e ⁺ e ⁻ → K _S ⁰ K _S ⁰ K ⁺ K ⁻ γ

¹ LEES 14H reports [Γ(J/ψ(1S) → φK_S⁰K_S⁰) × Γ(J/ψ(1S) → e⁺e⁻)/Γ_{total}] × [B(φ(1020) → K⁺K⁻)] = 1.6 ± 0.4 ± 0.1 eV which we divide by our best value B(φ(1020) → K⁺K⁻) = (49.1 ± 0.5) × 10⁻². Our first error is their experiment's error and our second error is the systematic error from using our best value.

$$\Gamma(f_2'(1525) K^+ K^-) \times \Gamma(e^+ e^-) / \Gamma_{\text{total}} \quad \Gamma_{126} \Gamma_5 / \Gamma$$

VALUE (eV)	EVTs	DOCUMENT ID	TECN	COMMENT
5.8 ± 1.9 ± 0.1	16	^{1,2} LEES 14H BABR		e ⁺ e ⁻ → K _S ⁰ K _S ⁰ K ⁺ K ⁻ γ

¹ Dividing by 1/4 to take into account B(f₂'(1525) → K_S⁰K_S⁰) = 1/4 B(f₂'(1525) → K_L⁰K_L⁰).

² LEES 14H reports [Γ(J/ψ(1S) → f₂'(1525)K⁺K⁻) × Γ(J/ψ(1S) → e⁺e⁻)/Γ_{total}] × [B(f₂'(1525) → K_L⁰K_L⁰)] = 5.12 ± 1.68 ± 0.20 eV which we divide by our best value B(f₂'(1525) → K_L⁰K_L⁰) = (87.6 ± 2.2) × 10⁻². Our first error is their experiment's error and our second error is the systematic error from using our best value.

$$\Gamma(2(\pi^+ \pi^-) \pi^0) \times \Gamma(e^+ e^-) / \Gamma_{\text{total}} \quad \Gamma_{145} \Gamma_5 / \Gamma$$

VALUE (eV)	EVTs	DOCUMENT ID	TECN	COMMENT
303 ± 5 ± 18	4990	AUBERT 07AU BABR		10.6 e ⁺ e ⁻ → 2(π ⁺ π ⁻)π ⁰ γ

Meson Particle Listings

 $J/\psi(1S)$ $\Gamma(\pi^+\pi^-3\pi^0) \times \Gamma(e^+e^-)/\Gamma_{total}$ $\Gamma_{147}\Gamma_5/\Gamma$

VALUE (eV)	EVTs	DOCUMENT ID	TECN	COMMENT
104 ± 5.0	OUR AVERAGE	Error includes scale factor of 4.3.		
55.4 ± 15.9 ± 0.5	14k	1 LEES	21	BABR 10.6 e ⁺ e ⁻ → 2(π ⁺ π ⁻)3π ⁰ γ
150.0 ± 4.0 ± 15.0	2.3k	LEES	18E	BABR 10.6 e ⁺ e ⁻ → π ⁺ π ⁻ 3π ⁰ γ

¹ LEES 21 reports $[\Gamma(J/\psi(1S) \rightarrow \pi^+\pi^-3\pi^0) \times \Gamma(J/\psi(1S) \rightarrow e^+e^-)/\Gamma_{total}] \times [\Gamma(\psi(2S) \rightarrow J/\psi(1S)\pi^+\pi^-)/\Gamma_{total}] = 19.2 \pm 4.5 \pm 3.2$ eV which we divide by our best value $\Gamma(\psi(2S) \rightarrow J/\psi(1S)\pi^+\pi^-)/\Gamma_{total} = 0.3468 \pm 0.0030$. Our first error is their experiment's error and our second error is the systematic error from using our best value.

 $\Gamma(\pi^+\pi^-4\pi^0) \times \Gamma(e^+e^-)/\Gamma_{total}$ $\Gamma_{148}\Gamma_5/\Gamma$

VALUE (eV)	EVTs	DOCUMENT ID	TECN	COMMENT
35.8 ± 4.4 ± 5.4	340	LEES	21c	BABR e ⁺ e ⁻ → γISR(π ⁺ π ⁻ 4π ⁰)

 $\Gamma(\rho^\pm\pi^\mp\pi^0\pi^0) \times \Gamma(e^+e^-)/\Gamma_{total}$ $\Gamma_{149}\Gamma_5/\Gamma$

VALUE (eV)	EVTs	DOCUMENT ID	TECN	COMMENT
78.0 ± 9.0 ± 8.0	1.2k	LEES	18E	BABR 10.6 e ⁺ e ⁻ → π ⁺ π ⁻ 3π ⁰ γ

 $\Gamma(\rho^+\rho^-\pi^0) \times \Gamma(e^+e^-)/\Gamma_{total}$ $\Gamma_{150}\Gamma_5/\Gamma$

VALUE (eV)	EVTs	DOCUMENT ID	TECN	COMMENT
33.0 ± 5.0 ± 3.3	529	LEES	18E	BABR 10.6 e ⁺ e ⁻ → π ⁺ π ⁻ 3π ⁰ γ

 $\Gamma(\pi^+\pi^-\pi^0) \times \Gamma(e^+e^-)/\Gamma_{total}$ $\Gamma_{151}\Gamma_5/\Gamma$

VALUE (keV)	DOCUMENT ID	TECN	COMMENT
0.1248 ± 0.0019 ± 0.0026	LEES	21B	BABR 10.5 e ⁺ e ⁻ → π ⁺ π ⁻ π ⁰ γ

• • • We do not use the following data for averages, fits, limits, etc. • • •
0.122 ± 0.005 ± 0.008 AUBERT,B 04N BABR 10.6 e⁺e⁻ → π⁺π⁻π⁰γ

 $\Gamma(2(\pi^+\pi^-\pi^0)) \times \Gamma(e^+e^-)/\Gamma_{total}$ $\Gamma_{152}\Gamma_5/\Gamma$

VALUE (10 ⁻² keV)	EVTs	DOCUMENT ID	TECN	COMMENT
8.9 ± 0.5 ± 1.0	761	AUBERT	06D	BABR 10.6 e ⁺ e ⁻ → 2(π ⁺ π ⁻ π ⁰)γ

 $\Gamma(\pi^+\pi^-\pi^0 K^+K^-) \times \Gamma(e^+e^-)/\Gamma_{total}$ $\Gamma_{153}\Gamma_5/\Gamma$

VALUE (eV)	EVTs	DOCUMENT ID	TECN	COMMENT
107.0 ± 4.3 ± 6.4	768	AUBERT	07AU	BABR 10.6 e ⁺ e ⁻ → K ⁺ K ⁻ π ⁺ π ⁻ π ⁰ γ

 $\Gamma(2(\pi^+\pi^-)) \times \Gamma(e^+e^-)/\Gamma_{total}$ $\Gamma_{155}\Gamma_5/\Gamma$

VALUE (eV)	EVTs	DOCUMENT ID	TECN	COMMENT
20.4 ± 0.9 ± 0.4		LEES	12E	BABR 10.6 e ⁺ e ⁻ → 2π ⁺ 2π ⁻ γ

• • • We do not use the following data for averages, fits, limits, etc. • • •
19.5 ± 1.4 ± 1.3 270 ¹ AUBERT 05D BABR 10.6 e⁺e⁻ → 2(π⁺π⁻)γ

¹ Superseded by LEES 12E.

 $\Gamma(3(\pi^+\pi^-)) \times \Gamma(e^+e^-)/\Gamma_{total}$ $\Gamma_{156}\Gamma_5/\Gamma$

VALUE (10 ⁻² keV)	EVTs	DOCUMENT ID	TECN	COMMENT
2.37 ± 0.16 ± 0.14	496	AUBERT	06D	BABR 10.6 e ⁺ e ⁻ → 3(π ⁺ π ⁻)γ

 $\Gamma(2(\pi^+\pi^-)3\pi^0) \times \Gamma(e^+e^-)/\Gamma_{total}$ $\Gamma_{157}\Gamma_5/\Gamma$

VALUE (eV)	EVTs	DOCUMENT ID	TECN	COMMENT
345 ± 10 ± 50	14k	LEES	21	BABR 10.6 e ⁺ e ⁻ → 2(π ⁺ π ⁻)3π ⁰ γ

 $\Gamma(2(\pi^+\pi^-)\eta) \times \Gamma(e^+e^-)/\Gamma_{total}$ $\Gamma_{159}\Gamma_5/\Gamma$

VALUE (eV)	EVTs	DOCUMENT ID	TECN	COMMENT
13.1 ± 2.4 ± 0.1	85	¹ AUBERT	07AU	BABR 10.6 e ⁺ e ⁻ → 2(π ⁺ π ⁻)ηγ

¹ AUBERT 07AU reports $[\Gamma(J/\psi(1S) \rightarrow 2(\pi^+\pi^-)\eta) \times \Gamma(J/\psi(1S) \rightarrow e^+e^-)/\Gamma_{total}] \times [B(\eta \rightarrow 2\gamma)] = 5.16 \pm 0.85 \pm 0.39$ eV which we divide by our best value $B(\eta \rightarrow 2\gamma) = (39.36 \pm 0.18) \times 10^{-2}$. Our first error is their experiment's error and our second error is the systematic error from using our best value.

 $\Gamma(2(\pi^+\pi^-\pi^0)\eta) \times \Gamma(e^+e^-)/\Gamma_{total}$ $\Gamma_{161}\Gamma_5/\Gamma$

VALUE (eV)	EVTs	DOCUMENT ID	TECN	COMMENT
9.1 ± 2.6 ± 1.4	14k	LEES	21	BABR 10.6 e ⁺ e ⁻ → 2(π ⁺ π ⁻)3π ⁰ γ

 $\Gamma(\pi^+\pi^-\pi^0\pi^0\eta) \times \Gamma(e^+e^-)/\Gamma_{total}$ $\Gamma_{162}\Gamma_5/\Gamma$

VALUE (eV)	EVTs	DOCUMENT ID	TECN	COMMENT
13.1 ± 2.7 OUR AVERAGE				
26.1 ± 17.9 ± 0.3	14k	¹ LEES	21	BABR 10.6 e ⁺ e ⁻ → 2(π ⁺ π ⁻)3π ⁰ γ
12.8 ± 1.8 ± 2.0	203	LEES	18E	BABR 10.6 e ⁺ e ⁻ → π ⁺ π ⁻ π ⁰ π ⁰ ηγ

¹ LEES 21 reports $[\Gamma(J/\psi(1S) \rightarrow \pi^+\pi^-\pi^0\pi^0\eta) \times \Gamma(J/\psi(1S) \rightarrow e^+e^-)/\Gamma_{total}] \times [B(\eta \rightarrow \pi^+\pi^-\pi^0)] = 6 \pm 4 \pm 1$ eV which we divide by our best value $B(\eta \rightarrow \pi^+\pi^-\pi^0) = (23.02 \pm 0.25) \times 10^{-2}$. Our first error is their experiment's error and our second error is the systematic error from using our best value.

 $\Gamma(\rho^\pm\pi^\mp\pi^0\eta) \times \Gamma(e^+e^-)/\Gamma_{total}$ $\Gamma_{163}\Gamma_5/\Gamma$

VALUE (eV)	EVTs	DOCUMENT ID	TECN	COMMENT
10.5 ± 4.1 ± 1.6	168	LEES	18E	BABR 10.6 e ⁺ e ⁻ → π ⁺ π ⁻ π ⁰ π ⁰ ηγ

 $\Gamma(K^+K^-) \times \Gamma(e^+e^-)/\Gamma_{total}$ $\Gamma_{164}\Gamma_5/\Gamma$

VALUE (eV)	EVTs	DOCUMENT ID	TECN	COMMENT
• • •		We do not use the following data for averages, fits, limits, etc. • • •		
1.78 ± 0.11 ± 0.05	462	¹ LEES	15J	BABR e ⁺ e ⁻ → K ⁺ K ⁻ γ
1.94 ± 0.11 ± 0.05	462	² LEES	15J	BABR e ⁺ e ⁻ → K ⁺ K ⁻ γ
1.42 ± 0.23 ± 0.08	51	³ LEES	13Q	BABR e ⁺ e ⁻ → K ⁺ K ⁻ γ

¹ sin φ > 0.
² sin φ < 0.
³ Interference with non-resonant K⁺K⁻ production not taken into account.

 $\Gamma(K_S^0 K_L^0 \pi^0) \times \Gamma(e^+e^-)/\Gamma_{total}$ $\Gamma_{170}\Gamma_5/\Gamma$

VALUE (eV)	EVTs	DOCUMENT ID	TECN	COMMENT
11.4 ± 1.3 ± 0.6	182	LEES	17A	BABR e ⁺ e ⁻ → K _S ⁰ K _L ⁰ π ⁰ γ

 $\Gamma(K^*(892)^0 \bar{K}^0 + c.c. \rightarrow K_S^0 K_L^0 \pi^0) \times \Gamma(e^+e^-)/\Gamma_{total}$ $\Gamma_{171}\Gamma_5/\Gamma$

VALUE (eV)	EVTs	DOCUMENT ID	TECN	COMMENT
6.7 ± 0.9 ± 0.4	106	LEES	17A	BABR e ⁺ e ⁻ → K _S ⁰ K _L ⁰ π ⁰ γ

 $\Gamma(K_S^0(1430)^0 \bar{K}^0 + c.c. \rightarrow K_S^0 K_L^0 \pi^0) \times \Gamma(e^+e^-)/\Gamma_{total}$ $\Gamma_{172}\Gamma_5/\Gamma$

VALUE (eV)	EVTs	DOCUMENT ID	TECN	COMMENT
2.4 ± 0.7 ± 0.1	37	LEES	17A	BABR e ⁺ e ⁻ → K _S ⁰ K _L ⁰ π ⁰ γ

 $\Gamma(K^+K^-\pi^+\pi^-) \times \Gamma(e^+e^-)/\Gamma_{total}$ $\Gamma_{173}\Gamma_5/\Gamma$

VALUE (keV)	EVTs	DOCUMENT ID	TECN	COMMENT
37.94 ± 0.81 ± 1.10	3.1k	LEES	12F	BABR 10.6 e ⁺ e ⁻ → π ⁺ π ⁻ K ⁺ K ⁻ γ

• • • We do not use the following data for averages, fits, limits, etc. • • •
36.3 ± 1.3 ± 2.1 1.5k ¹ AUBERT 07AK BABR 10.6 e⁺e⁻ → π⁺π⁻K⁺K⁻γ

33.6 ± 2.7 ± 2.7 233 ² AUBERT 05D BABR 10.6 e⁺e⁻ → K⁺K⁻π⁺π⁻γ

¹ Superseded by LEES 12F.
² Superseded by AUBERT 07AK.

 $\Gamma(K^+K^-\pi^0\pi^0) \times \Gamma(e^+e^-)/\Gamma_{total}$ $\Gamma_{174}\Gamma_5/\Gamma$

VALUE (eV)	EVTs	DOCUMENT ID	TECN	COMMENT
11.75 ± 0.81 ± 0.90	388	LEES	12F	BABR 10.6 e ⁺ e ⁻ → π ⁰ π ⁰ K ⁺ K ⁻ γ

• • • We do not use the following data for averages, fits, limits, etc. • • •
13.6 ± 1.1 ± 1.3 203 ¹ AUBERT 07AK BABR 10.6 e⁺e⁻ → π⁰π⁰K⁺K⁻γ

¹ Superseded by LEES 12F.

 $\Gamma(K_S^0 K_L^0 \pi^+\pi^-) \times \Gamma(e^+e^-)/\Gamma_{total}$ $\Gamma_{175}\Gamma_5/\Gamma$

VALUE (eV)	EVTs	DOCUMENT ID	TECN	COMMENT
20.8 ± 2.3 ± 2.1	248	LEES	14H	BABR e ⁺ e ⁻ → π ⁺ π ⁻ K _S ⁰ K _L ⁰ γ

 $\Gamma(K_S^0 K_L^0 \pi^0\pi^0) \times \Gamma(e^+e^-)/\Gamma_{total}$ $\Gamma_{176}\Gamma_5/\Gamma$

VALUE (eV)	EVTs	DOCUMENT ID	TECN	COMMENT
10.3 ± 2.3 ± 0.5	47	LEES	17A	BABR e ⁺ e ⁻ → K _S ⁰ K _L ⁰ π ⁰ π ⁰ γ

 $\Gamma(K_S^0 K_L^0 \eta) \times \Gamma(e^+e^-)/\Gamma_{total}$ $\Gamma_{177}\Gamma_5/\Gamma$

VALUE (eV)	EVTs	DOCUMENT ID	TECN	COMMENT
8.0 ± 1.8 ± 0.4	45	LEES	17A	BABR e ⁺ e ⁻ → K _S ⁰ K _L ⁰ ηγ

 $\Gamma(K_S^0 K_S^0 \pi^+\pi^-) \times \Gamma(e^+e^-)/\Gamma_{total}$ $\Gamma_{178}\Gamma_5/\Gamma$

VALUE (eV)	EVTs	DOCUMENT ID	TECN	COMMENT
9.3 ± 0.9 ± 0.5	133	LEES	14H	BABR e ⁺ e ⁻ → π ⁺ π ⁻ K _S ⁰ K _S ⁰ γ

 $\Gamma(K^\mp K_S^0 \pi^\pm \pi^0) \times \Gamma(e^+e^-)/\Gamma_{total}$ $\Gamma_{179}\Gamma_5/\Gamma$

VALUE (eV)	EVTs	DOCUMENT ID	TECN	COMMENT
31.7 ± 1.9 ± 1.8	393	LEES	17D	BABR e ⁺ e ⁻ → K _S ⁰ K _S ⁰ π [±] π ⁰ γ

 $\Gamma(K^+K^-2(\pi^+\pi^-)) \times \Gamma(e^+e^-)/\Gamma_{total}$ $\Gamma_{180}\Gamma_5/\Gamma$

VALUE (10 ⁻² keV)	EVTs	DOCUMENT ID	TECN	COMMENT
2.75 ± 0.23 ± 0.17	205	AUBERT	06D	BABR 10.6 e ⁺ e ⁻ → K ⁺ K ⁻ 2(π ⁺ π ⁻)γ

 $\Gamma(K^+K^-\pi^+\pi^-\eta) \times \Gamma(e^+e^-)/\Gamma_{total}$ $\Gamma_{181}\Gamma_5/\Gamma$

VALUE (eV)	EVTs	DOCUMENT ID	TECN	COMMENT
25.9 ± 3.9 ± 0.1	73	¹ AUBERT	07AU	BABR 10.6 e ⁺ e ⁻ → K ⁺ K ⁻ π ⁺ π ⁻ ηγ

¹ AUBERT 07AU reports $[\Gamma(J/\psi(1S) \rightarrow K^+K^-\pi^+\pi^-\eta) \times \Gamma(J/\psi(1S) \rightarrow e^+e^-)/\Gamma_{total}] \times [B(\eta \rightarrow 2\gamma)] = 10.2 \pm 1.3 \pm 0.8$ eV which we divide by our best value $B(\eta \rightarrow 2\gamma) = (39.36 \pm 0.18) \times 10^{-2}$. Our first error is their experiment's error and our second error is the systematic error from using our best value.

 $\Gamma(2(K^+K^-)) \times \Gamma(e^+e^-)/\Gamma_{total}$ $\Gamma_{182}\Gamma_5/\Gamma$

VALUE (eV)	EVTs	DOCUMENT ID	TECN	COMMENT
4.00 ± 0.33 ± 0.29	287 ± 24	LEES	12F	BABR 10.6 e ⁺ e ⁻ → 2(K ⁺ K ⁻)γ

• • • We do not use the following data for averages, fits, limits, etc. • • •
4.11 ± 0.39 ± 0.30 156 ± 15 ¹ AUBERT 07AK BABR 10.6 e⁺e⁻ → 2(K⁺K⁻)γ

4.0 ± 0.7 ± 0.6 38 ² AUBERT 05D BABR 10.6 e⁺e⁻ → 2(K⁺K⁻)γ

¹ Superseded by LEES 12F.
² Superseded by AUBERT 07AK.

See key on page 1127

Meson Particle Listings

$J/\psi(1S)$

$\Gamma(K^+K^-K_S^0K_S^0) \times \Gamma(e^+e^-)/\Gamma_{total}$					$\Gamma_{183}\Gamma_5/\Gamma$
VALUE (eV)	EVTS	DOCUMENT ID	TECN	COMMENT	
2.3 ± 0.4 ± 0.1	29	LEES	14H	BABR $e^+e^- \rightarrow K_S^0K_S^0K^+K^- \gamma$	

$\Gamma(p\bar{p}) \times \Gamma(e^+e^-)/\Gamma_{total}$					$\Gamma_{184}\Gamma_5/\Gamma$
VALUE (eV)	EVTS	DOCUMENT ID	TECN	COMMENT	
11.9 ± 0.6 OUR AVERAGE	Error includes scale factor of 1.8. See the ideogram below.				
11.3 ± 0.4 ± 0.3	821	1 LEES	13O	BABR $e^+e^- \rightarrow p\bar{p}\gamma$	
12.9 ± 0.4 ± 0.4	918	2 LEES	13Y	BABR $e^+e^- \rightarrow p\bar{p}\gamma$	
9.7 ± 1.7		3 ARMSTRONG	93B	E760 $\bar{p}p \rightarrow e^+e^-$	
••• We do not use the following data for averages, fits, limits, etc. •••					
12.0 ± 0.6 ± 0.5	438	4 AUBERT	06B	BABR $e^+e^- \rightarrow p\bar{p}\gamma$	

WEIGHTED AVERAGE
11.9 ± 0.6 (Error scaled by 1.8)

Values above of weighted average, error, and scale factor are based upon the data in this ideogram only. They are not necessarily the same as our 'best' values, obtained from a least-squares constrained fit utilizing measurements of other (related) quantities as additional information.

	χ^2
LEES 13O BABR	1.4
LEES 13Y BABR	3.2
ARMSTRONG 93B E760	1.7
	6.2
	6.2

(Confidence Level = 0.044)

$\Gamma(p\bar{p}) \times \Gamma(e^+e^-)/\Gamma_{total}$ (eV)

- 1 ISR photon reconstructed in the detector
- 2 ISR photon undetected
- 3 Using $\Gamma_{total} = 85.5^{+6.1}_{-5.8}$ MeV.
- 4 Superseded by LEES 13O

$\Gamma(\Lambda\bar{\Lambda}) \times \Gamma(e^+e^-)/\Gamma_{total}$					$\Gamma_{200}\Gamma_5/\Gamma$
VALUE (eV)	DOCUMENT ID	TECN	COMMENT		
10.7 ± 0.9 ± 0.7	AUBERT	07BD	BABR	10.6 $e^+e^- \rightarrow \Lambda\bar{\Lambda}\gamma$	

$\Gamma(\Sigma^0\Sigma^0) \times \Gamma(e^+e^-)/\Gamma_{total}$					$\Gamma_{210}\Gamma_5/\Gamma$
VALUE (eV)	DOCUMENT ID	TECN	COMMENT		
6.4 ± 1.2 ± 0.6	AUBERT	07BD	BABR	10.6 $e^+e^- \rightarrow \Sigma^0\Sigma^0\gamma$	

$J/\psi(1S)$ BRANCHING RATIOS

For the first four branching ratios, see also the partial widths, and (partial widths) $\times \Gamma(e^+e^-)/\Gamma_{total}$ above.

$\Gamma(\text{hadrons})/\Gamma_{total}$					Γ_1/Γ
VALUE	DOCUMENT ID	TECN	COMMENT		
0.877 ± 0.005 OUR AVERAGE					
0.878 ± 0.005	BAI	95B	BES	e^+e^-	
0.86 ± 0.02	BOYARSKI	75	MRK1	e^+e^-	

$\Gamma(\text{virtual } \gamma \rightarrow \text{hadrons})/\Gamma_{total}$					Γ_2/Γ
VALUE	DOCUMENT ID	TECN	COMMENT		
0.135 ± 0.003	1,2	SETH	04	RVUE e^+e^-	
••• We do not use the following data for averages, fits, limits, etc. •••					
0.17 ± 0.02	1	BOYARSKI	75	MRK1 e^+e^-	

- 1 Included in $\Gamma(\text{hadrons})/\Gamma_{total}$.
- 2 Using $B(J/\psi \rightarrow \ell^+\ell^-) = (5.90 \pm 0.09)\%$ from RPP-2002 and $R = 2.28 \pm 0.04$ determined by a fit to data from BAI 00 and BAI 02c.

$\Gamma(ggg)/\Gamma_{total}$					Γ_3/Γ
VALUE (units 10^{-2})	EVTS	DOCUMENT ID	TECN	COMMENT	
64.1 ± 1.0	6 M	1 BESSON	08	CLEO $\psi(2S) \rightarrow \pi^+\pi^-\text{hadrons}$	
1 Calculated using the value $\Gamma(\gamma gg)/\Gamma(ggg) = 0.137 \pm 0.001 \pm 0.016 \pm 0.004$ from BESSON 08 and the PDG 08 values of $B(\ell^+\ell^-)$, $B(\text{virtual } \gamma \rightarrow \text{hadrons})$, and $B(\gamma\eta_c)$. The statistical error is negligible and the systematic error is partially correlated with that of $\Gamma(\gamma gg)/\Gamma_{total}$ measurement of BESSON 08.					

$\Gamma(\gamma gg)/\Gamma_{total}$					Γ_4/Γ
VALUE (units 10^{-2})	EVTS	DOCUMENT ID	TECN	COMMENT	
8.79 ± 1.05	200 k	1 BESSON	08	CLEO $\psi(2S) \rightarrow \pi^+\pi^-\gamma + \text{hadrons}$	
1 Calculated using the value $\Gamma(\gamma gg)/\Gamma(ggg) = 0.137 \pm 0.001 \pm 0.016 \pm 0.004$ from BESSON 08 and the value of $\Gamma(ggg)/\Gamma_{total}$. The statistical error is negligible and the systematic error is partially correlated with that of $\Gamma(ggg)/\Gamma_{total}$ measurement of BESSON 08.					

$\Gamma(\gamma gg)/\Gamma(ggg)$					Γ_4/Γ_3
VALUE (units 10^{-2})	EVTS	DOCUMENT ID	TECN	COMMENT	
13.7 ± 0.1 ± 0.7	6 M	BESSON	08	CLEO $\psi(2S) \rightarrow \pi^+\pi^-J/\psi$	

$\Gamma(e^+e^-)/\Gamma_{total}$					Γ_5/Γ
VALUE (units 10^{-2})	EVTS	DOCUMENT ID	TECN	COMMENT	
5.971 ± 0.032 OUR AVERAGE					
5.983 ± 0.007 ± 0.037	720k				
5.945 ± 0.067 ± 0.042	15k				
5.90 ± 0.05 ± 0.10					
6.09 ± 0.33					
5.92 ± 0.15 ± 0.20					
6.9 ± 0.9					

$\Gamma(e^+e^-\gamma)/\Gamma_{total}$					Γ_6/Γ
VALUE (units 10^{-3})	DOCUMENT ID	TECN	COMMENT		
8.8 ± 1.3 ± 0.4	1	ARMSTRONG	96	E760 $\bar{p}p \rightarrow e^+e^-\gamma$	
1 For $E_\gamma > 100$ MeV.					

$\Gamma(\mu^+\mu^-)/\Gamma_{total}$					Γ_7/Γ
VALUE (units 10^{-2})	EVTS	DOCUMENT ID	TECN	COMMENT	
5.961 ± 0.033 OUR AVERAGE					
5.973 ± 0.007 ± 0.038	770k				
5.960 ± 0.065 ± 0.050	17k				
5.84 ± 0.06 ± 0.10					
6.08 ± 0.33					
5.90 ± 0.15 ± 0.19					
6.9 ± 0.9					

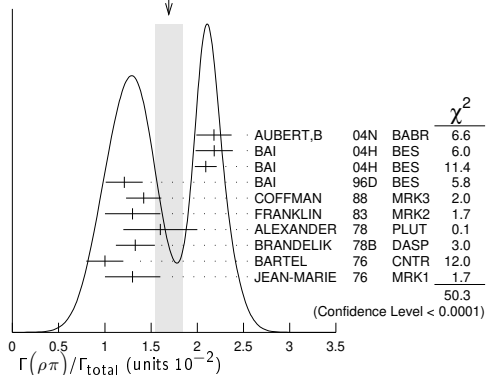
$\Gamma(e^+e^-)/\Gamma(\mu^+\mu^-)$					Γ_5/Γ_7
VALUE	DOCUMENT ID	TECN	COMMENT		
1.0016 ± 0.0031 OUR AVERAGE					
1.0022 ± 0.0044 ± 0.0048	1	AULCHENKO	14	KEDR $e^+e^- \rightarrow e^+e^-, \mu^+\mu^-$	
1.0017 ± 0.0017 ± 0.0033	2	ABLIKIM	13R	BES3 $\psi(2S) \rightarrow J/\psi\pi^+\pi^-$	
1.002 ± 0.021 ± 0.013	3	ANASHIN	10	KEDR $e^+e^- \rightarrow e^+e^-, \mu^+\mu^-$	
0.997 ± 0.012 ± 0.006		LI	05c	CLEO $\psi(2S) \rightarrow J/\psi\pi^+\pi^-$	
••• We do not use the following data for averages, fits, limits, etc. •••					
1.011 ± 0.013 ± 0.016		BAI	98D	BES $\psi(2S) \rightarrow J/\psi\pi^+\pi^-$	
1.00 ± 0.07		BAI	95B	BES e^+e^-	
1.00 ± 0.05		BOYARSKI	75	MRK1 e^+e^-	
0.91 ± 0.15		ESPOSITO	75B	FRAM e^+e^-	
0.93 ± 0.10		FORD	75	SPEC e^+e^-	

- 1 From 235.3k $J/\psi \rightarrow e^+e^-$ and 156.6k $J/\psi \rightarrow \mu^+\mu^-$ observed events.
- 2 Not independent of the corresponding measurements of $\Gamma(e^+e^-)/\Gamma_{total}$ and $\Gamma(\mu^+\mu^-)/\Gamma_{total}$.
- 3 Not independent of the corresponding measurements of $\Gamma(e^+e^-) \times \Gamma(e^+e^-)/\Gamma_{total}$ and $\Gamma(\mu^+\mu^-) \times \Gamma(e^+e^-)/\Gamma_{total}$.

HADRONIC DECAYS

$\Gamma(\rho\pi)/\Gamma_{total}$					Γ_8/Γ
VALUE (units 10^{-2})	EVTS	DOCUMENT ID	TECN	COMMENT	
1.69 ± 0.15 OUR AVERAGE					
2.18 ± 0.19		1,2	AUBERT,B	04N	BABR $10.6 e^+e^- \rightarrow \pi^+\pi^-\pi^0\gamma$
2.184 ± 0.005 ± 0.201	220k	2,3	BAI	04H	BES $e^+e^- \rightarrow J/\psi \rightarrow \pi^+\pi^-\pi^0$
2.091 ± 0.021 ± 0.116		2,4	BAI	04H	BES $\psi(2S) \rightarrow \pi^+\pi^-J/\psi$
1.21 ± 0.20			BAI	96D	BES $e^+e^- \rightarrow \rho\pi$
1.42 ± 0.01 ± 0.19			COFFMAN	88	MRK3 e^+e^-
1.3 ± 0.3	150		FRANKLIN	83	MRK2 e^+e^-
1.6 ± 0.4	183		ALEXANDER	78	PLUT e^+e^-
1.33 ± 0.21			BRANDELIC	78B	DASP e^+e^-
1.0 ± 0.2	543		BARTEL	76	CNTR e^+e^-
1.3 ± 0.3	153		JEAN-MARIE	76	MRK1 e^+e^-

WEIGHTED AVERAGE
1.69 ± 0.15 (Error scaled by 2.4)



Meson Particle Listings

J/ψ(1S)

- ¹ From the ratio of $\Gamma(e^+e^-)B(\pi^+\pi^-\pi^0)$ and $\Gamma(e^+e^-)B(\mu^+\mu^-)$ (AUBERT 04).
- ² Not independent of their $B(\pi^+\pi^-\pi^0)$.
- ³ From $J/\psi \rightarrow \pi^+\pi^-\pi^0$ events directly.
- ⁴ Obtained comparing the rates for $\pi^+\pi^-\pi^0$ and $\mu^+\mu^-$, using J/ψ events produced via $\psi(2S) \rightarrow \pi^+\pi^-J/\psi$ and with $B(J/\psi \rightarrow \mu^+\mu^-) = 5.88 \pm 0.10\%$.

$\Gamma(\rho\pi)/\Gamma(\pi^+\pi^-\pi^0)$		Γ_8/Γ_{151}		
VALUE	EVTS	DOCUMENT ID	TECN	COMMENT
1.142±0.011±0.026	20k	¹ LEES	17c BABR	$J/\psi \rightarrow \pi^+\pi^-\pi^0$
••• We do not use the following data for averages, fits, limits, etc. •••				
1.331±0.033	20k	² LEES	17c BABR	$J/\psi \rightarrow \pi^+\pi^-\pi^0$
¹ From a Dalitz plot analysis in an isobar model.				
² From a Dalitz plot analysis in a Veneziano model.				

$\Gamma(\rho^0\pi^0)/\Gamma(\rho\pi)$		Γ_9/Γ_8		
VALUE	DOCUMENT ID	TECN	COMMENT	
0.328±0.005±0.027	COFFMAN	88 MRK3	e^+e^-	
••• We do not use the following data for averages, fits, limits, etc. •••				
0.35 ± 0.08	ALEXANDER	78 PLUT	e^+e^-	
0.32 ± 0.08	BRANDELIK	78B DASP	e^+e^-	
0.39 ± 0.11	BARTEL	76 CNTR	e^+e^-	
0.37 ± 0.09	JEAN-MARIE	76 MRK1	e^+e^-	

$\Gamma(a_2(1320)\rho)/\Gamma_{total}$		Γ_{10}/Γ		
VALUE (units 10 ⁻³)	EVTS	DOCUMENT ID	TECN	COMMENT
10.9±2.2 OUR AVERAGE				
11.7±0.7±2.5	7584	AUGUSTIN	89 DM2	$J/\psi \rightarrow \rho^0\rho^\pm\pi^\mp$
8.4±4.5	36	VANNUCCI	77 MRK1	$e^+e^- \rightarrow 2(\pi^+\pi^-)\pi^0$

$\Gamma(\eta\pi^+\pi^-)/\Gamma_{total}$		Γ_{11}/Γ		
VALUE (units 10 ⁻⁴)	EVTS	DOCUMENT ID	TECN	COMMENT
3.78±0.68	471	¹ ABLIKIM	19q BES3	$e^+e^- \rightarrow J/\psi \rightarrow \eta\pi^+\pi^-$
¹ From an energy scan of $e^+e^- \rightarrow J/\psi \rightarrow \eta\pi^+\pi^-$ assuming PDG 16 values for $\Gamma(e^+e^-)$, $\Gamma(\mu^+\mu^-)$, and Γ_{total} .				

$\Gamma(\eta\rho)/\Gamma_{total}$		Γ_{14}/Γ		
VALUE (units 10 ⁻³)	EVTS	DOCUMENT ID	TECN	COMMENT
0.193±0.023 OUR AVERAGE				
0.194±0.017±0.029	299	JOUSSET	90 DM2	$J/\psi \rightarrow \text{hadrons}$
0.193±0.013±0.029		COFFMAN	88 MRK3	$e^+e^- \rightarrow \pi^+\pi^-\eta$

$\Gamma(\eta\phi(2170) \rightarrow \eta\phi f_0(980) \rightarrow \eta\phi\pi^+\pi^-)/\Gamma_{total}$		Γ_{15}/Γ		
VALUE (units 10 ⁻⁴)	EVTS	DOCUMENT ID	TECN	COMMENT
1.20±0.14±0.37	471	ABLIKIM	15H BES3	$e^+e^- \rightarrow J/\psi \rightarrow \phi\eta\pi^+\pi^-$

$\Gamma(\eta\phi(2170) \rightarrow \eta K^*(892)^0 \bar{K}^*(892)^0)/\Gamma_{total}$		Γ_{16}/Γ		
VALUE	CL%	DOCUMENT ID	TECN	COMMENT
<2.52 × 10⁻⁴	90	ABLIKIM	10c BES2	$J/\psi \rightarrow \eta K^+\pi^- K^-\pi^+$

$\Gamma(\eta K^\pm K_S^0 \pi^\mp)/\Gamma_{total}$		Γ_{17}/Γ		
VALUE (units 10 ⁻⁴)	EVTS	DOCUMENT ID	TECN	COMMENT
21.8±2.2±3.4	232 ± 23	ABLIKIM	08E BES2	$e^+e^- \rightarrow J/\psi$

$\Gamma(\eta K^*(892)^0 \bar{K}^*(892)^0)/\Gamma_{total}$		Γ_{18}/Γ		
VALUE (units 10 ⁻³)	EVTS	DOCUMENT ID	TECN	COMMENT
1.15±0.13±0.22	209	ABLIKIM	10c BES2	$J/\psi \rightarrow \eta K^+\pi^- K^-\pi^+$

$\Gamma(\rho\eta(958))/\Gamma_{total}$		Γ_{19}/Γ		
VALUE (units 10 ⁻³)	EVTS	DOCUMENT ID	TECN	COMMENT
8.1 ± 0.8 OUR AVERAGE				Error includes scale factor of 1.6.
7.90±0.19±0.49	3476	¹ ABLIKIM	17AK BES3	$J/\psi \rightarrow \pi^+\pi^-\eta'$
8.3 ± 3.0 ± 1.2	19	JOUSSET	90 DM2	$J/\psi \rightarrow \text{hadrons}$
11.4 ± 1.4 ± 1.6		COFFMAN	88 MRK3	$J/\psi \rightarrow \pi^+\pi^-\eta'$
¹ From a partial wave analysis of the decay $J/\psi \rightarrow \pi^+\pi^-\eta'$.				

$\Gamma(\rho(1450)\pi \rightarrow \pi^+\pi^-\pi^0)/\Gamma(\pi^+\pi^-\pi^0)$		Γ_{24}/Γ_{151}		
VALUE (%)	EVTS	DOCUMENT ID	TECN	COMMENT
10.9 ± 1.7 ± 2.7	20k	¹ LEES	17c BABR	$J/\psi \rightarrow \pi^+\pi^-\pi^0$
••• We do not use the following data for averages, fits, limits, etc. •••				
0.80±0.27	20k	² LEES	17c BABR	$J/\psi \rightarrow \pi^+\pi^-\pi^0$
¹ From a Dalitz plot analysis in an isobar model.				
² From a Dalitz plot analysis in a Veneziano model.				

$\Gamma(\rho(1450)\pi^\pm \pi^\mp \rightarrow K_S^0 K^\pm \pi^\mp)/\Gamma(K_S^0 K^\pm \pi^\mp)$		Γ_{25}/Γ_{169}		
VALUE (%)	EVTS	DOCUMENT ID	TECN	COMMENT
6.3±0.8±0.6	4k	¹ LEES	17c BABR	$J/\psi \rightarrow K_S^0 K^\pm \pi^\mp$
¹ From a Dalitz plot analysis in an isobar model.				

$\Gamma(\rho(1450)^0\pi^0 \rightarrow K^+K^-\pi^0)/\Gamma(K^+K^-\pi^0)$		Γ_{26}/Γ_{168}		
VALUE (%)	EVTS	DOCUMENT ID	TECN	COMMENT
9.3±2.0±0.6	2k	¹ LEES	17c BABR	$J/\psi \rightarrow K^+K^-\pi^0$
¹ From a Dalitz plot analysis in an isobar model.				

$\Gamma(\rho(1450)\eta'(958) \rightarrow \pi^+\pi^-\eta'(958))/\Gamma_{total}$		Γ_{27}/Γ		
VALUE (units 10 ⁻⁶)	EVTS	DOCUMENT ID	TECN	COMMENT
3.28±0.55±0.44	119	¹ ABLIKIM	17AK BES3	$J/\psi \rightarrow \pi^+\pi^-\eta'$
¹ From a partial wave analysis of the decay $J/\psi \rightarrow \pi^+\pi^-\eta'$.				

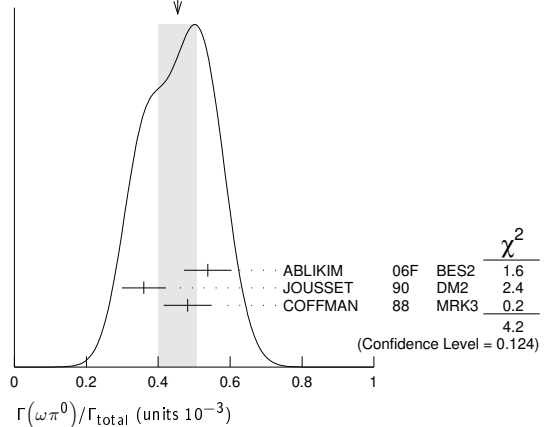
$\Gamma(\rho(1700)\pi \rightarrow \pi^+\pi^-\pi^0)/\Gamma(\pi^+\pi^-\pi^0)$		Γ_{29}/Γ_{151}		
VALUE (units 10 ⁻³)	EVTS	DOCUMENT ID	TECN	COMMENT
8±2±5	20k	¹ LEES	17c BABR	$J/\psi \rightarrow \pi^+\pi^-\pi^0$
••• We do not use the following data for averages, fits, limits, etc. •••				
22±6	20k	² LEES	17c BABR	$J/\psi \rightarrow \pi^+\pi^-\pi^0$
¹ From a Dalitz plot analysis in an isobar model.				
² From a Dalitz plot analysis in a Veneziano model.				

$\Gamma(\rho(2150)\pi \rightarrow \pi^+\pi^-\pi^0)/\Gamma(\pi^+\pi^-\pi^0)$		Γ_{31}/Γ_{151}		
VALUE (units 10 ⁻⁴)	EVTS	DOCUMENT ID	TECN	COMMENT
4 ± 1 ± 20	20k	¹ LEES	17c BABR	$J/\psi \rightarrow \pi^+\pi^-\pi^0$
••• We do not use the following data for averages, fits, limits, etc. •••				
600±250	20k	² LEES	17c BABR	$J/\psi \rightarrow \pi^+\pi^-\pi^0$
¹ From a Dalitz plot analysis in an isobar model.				
² From a Dalitz plot analysis in a Veneziano model.				

$\Gamma(\rho_3(1690)\pi \rightarrow \pi^+\pi^-\pi^0)/\Gamma(\pi^+\pi^-\pi^0)$		Γ_{32}/Γ_{151}		
VALUE (units 10 ⁻³)	EVTS	DOCUMENT ID	TECN	COMMENT
••• We do not use the following data for averages, fits, limits, etc. •••				
4.0±0.8	20k	¹ LEES	17c BABR	$J/\psi \rightarrow \pi^+\pi^-\pi^0$
¹ From a Dalitz plot analysis in a Veneziano model.				

$\Gamma(\omega\pi^0)/\Gamma_{total}$		Γ_{33}/Γ		
VALUE (units 10 ⁻³)	EVTS	DOCUMENT ID	TECN	COMMENT
0.45 ± 0.05 OUR AVERAGE				Error includes scale factor of 1.4. See the ideogram below.
0.538±0.012±0.065	2090	¹ ABLIKIM	06F BES2	$J/\psi \rightarrow \omega\pi^0$
0.360±0.028±0.054	222	JOUSSET	90 DM2	$J/\psi \rightarrow \text{hadrons}$
0.482±0.019±0.064		COFFMAN	88 MRK3	$e^+e^- \rightarrow \pi^0\pi^+\pi^-\pi^0$

WEIGHTED AVERAGE
0.45±0.05 (Error scaled by 1.4)



$\Gamma(\omega\pi^0 \rightarrow \pi^+\pi^-\pi^0)/\Gamma(\pi^+\pi^-\pi^0)$		Γ_{34}/Γ_{151}		
VALUE (units 10 ⁻⁴)	EVTS	DOCUMENT ID	TECN	COMMENT
8±3±2	20k	¹ LEES	17c BABR	$J/\psi \rightarrow \pi^+\pi^-\pi^0$
¹ From a Dalitz plot analysis in an isobar model and significance 4.9 σ.				

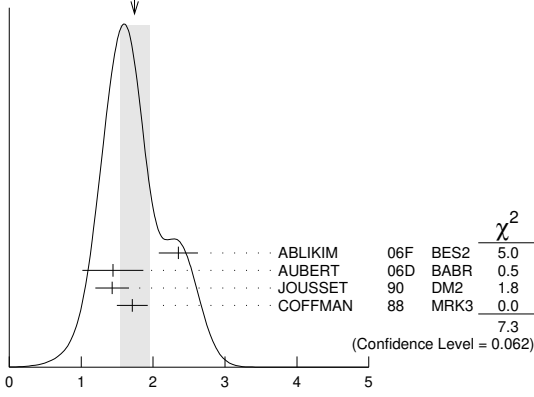
$\Gamma(\omega\pi^+\pi^-)/\Gamma_{total}$		Γ_{35}/Γ		
VALUE (units 10 ⁻³)	EVTS	DOCUMENT ID	TECN	COMMENT
7.2±1.0 OUR AVERAGE				
7.0±1.6	18058	AUGUSTIN	89 DM2	$J/\psi \rightarrow 2(\pi^+\pi^-)\pi^0$
7.8±1.6	215	BURMESTER	77D PLUT	e^+e^-
6.8±1.9	348	VANNUCCI	77 MRK1	$e^+e^- \rightarrow 2(\pi^+\pi^-)\pi^0$

$\Gamma(\omega\pi^0\pi^0)/\Gamma_{total}$		Γ_{36}/Γ		
VALUE (units 10 ⁻³)	EVTS	DOCUMENT ID	TECN	COMMENT
3.4±0.3±0.7	509	AUGUSTIN	89 DM2	$J/\psi \rightarrow \pi^+\pi^-\pi^0$

$\Gamma(\omega f_2(1270))/\Gamma_{total}$		Γ_{38}/Γ		
VALUE (units 10 ⁻³)	EVTS	DOCUMENT ID	TECN	COMMENT
4.3±0.6 OUR AVERAGE				
4.3±0.2±0.6	5860	AUGUSTIN	89 DM2	e^+e^-
4.0±1.6	70	BURMESTER	77D PLUT	e^+e^-
••• We do not use the following data for averages, fits, limits, etc. •••				
1.9±0.8	81	VANNUCCI	77 MRK1	$e^+e^- \rightarrow 2(\pi^+\pi^-)\pi^0$

$\Gamma(\omega\eta)/\Gamma_{\text{total}}$		Γ_{39}/Γ		
VALUE (units 10^{-3})	EVTS	DOCUMENT ID	TECN	COMMENT
1.74 ± 0.20 OUR AVERAGE		Error includes scale factor of 1.6. See the ideogram below.		
2.352 ± 0.273	5k	¹ ABLIKIM	06F BES2	J/ψ → ωη
1.44 ± 0.40 ± 0.14	13	² AUBERT	06D BABR	10.6 e ⁺ e ⁻ → ωηγ
1.43 ± 0.10 ± 0.21	378	JOUSSET	90 DM2	J/ψ → hadrons
1.71 ± 0.08 ± 0.20		COFFMAN	88 MRK3	e ⁺ e ⁻ → 3πη

WEIGHTED AVERAGE
1.74±0.20 (Error scaled by 1.6)



¹ Using $B(\eta \rightarrow 2\gamma) = (39.43 \pm 0.26)\%$, $B(\eta \rightarrow \pi^+\pi^-\pi^0) = 22.6 \pm 0.4\%$, $B(\eta \rightarrow \pi^+\pi^-\gamma) = 4.68 \pm 0.11\%$, and $B(\omega \rightarrow \pi^+\pi^-\pi^0) = (89.1 \pm 0.7)\%$.
² Using $\Gamma(J/\psi \rightarrow e^+e^-) = 5.52 \pm 0.14 \pm 0.04$ keV.

$\Gamma(\omega\pi^+\pi^-\pi^0)/\Gamma_{\text{total}}$		Γ_{42}/Γ		
VALUE (units 10^{-4})	EVTS	DOCUMENT ID	TECN	COMMENT
85 ± 34	140	VANNUCCI	77 MRK1	e ⁺ e ⁻ → 3(π ⁺ π ⁻)π ⁰

$\Gamma(\omega\eta'\pi^+\pi^-)/\Gamma_{\text{total}}$		Γ_{44}/Γ		
VALUE (units 10^{-3})	EVTS	DOCUMENT ID	TECN	COMMENT
1.12 ± 0.02 ± 0.13	14k	¹ ABLIKIM	19AC BES3	J/ψ → ωη'π ⁺ π ⁻
¹ Using the decays ω → π ⁺ π ⁻ π ⁰ and η' → ηπ ⁺ π ⁻ .				

$\Gamma(\omega\eta'(958))/\Gamma_{\text{total}}$		Γ_{45}/Γ		
VALUE (units 10^{-4})	EVTS	DOCUMENT ID	TECN	COMMENT
1.89 ± 0.18 OUR AVERAGE				
2.08 ± 0.30 ± 0.14	137	¹ ABLIKIM	17AK BES3	J/ψ → π ⁺ π ⁻ η'
2.26 ± 0.43	218	² ABLIKIM	06F BES2	J/ψ → ωη'
1.8 ^{+1.0} _{-0.8} ± 0.3	6	JOUSSET	90 DM2	J/ψ → hadrons
1.66 ± 0.17 ± 0.19		COFFMAN	88 MRK3	e ⁺ e ⁻ → 3πη'

¹ From a partial wave analysis of the decay J/ψ → π⁺π⁻η'.
² Using $B(\eta' \rightarrow \pi^+\pi^-\eta) = (44.3 \pm 1.5)\%$, $B(\eta' \rightarrow \pi^+\pi^-\gamma) = 29.5 \pm 1.0\%$, $B(\eta \rightarrow 2\gamma) = 39.43 \pm 0.26\%$, and $B(\omega \rightarrow \pi^+\pi^-\pi^0) = (89.1 \pm 0.7)\%$.

$\Gamma(\omega f_0(980))/\Gamma_{\text{total}}$		Γ_{46}/Γ		
VALUE (units 10^{-4})	EVTS	DOCUMENT ID	TECN	COMMENT
1.41 ± 0.27 ± 0.47		¹ AUGUSTIN	89 DM2	J/ψ → 2(π ⁺ π ⁻)π ⁰
¹ Assuming $B(f_0(980) \rightarrow \pi\pi) = 0.78$.				

$\Gamma(\omega f_0(1710) \rightarrow \omega K\bar{K})/\Gamma_{\text{total}}$		Γ_{47}/Γ		
VALUE (units 10^{-4})	EVTS	DOCUMENT ID	TECN	COMMENT
4.8 ± 1.1 ± 0.3		^{1,2} FALVARD	88 DM2	J/ψ → hadrons
¹ Includes unknown branching fraction $f_0(1710) \rightarrow K\bar{K}$. ² Addition of $f_0(1710) \rightarrow K^+K^-$ and $f_0(1710) \rightarrow K^0\bar{K}^0$ branching ratios.				

$\Gamma(\omega f_1(1420))/\Gamma_{\text{total}}$		Γ_{48}/Γ		
VALUE (units 10^{-4})	EVTS	DOCUMENT ID	TECN	COMMENT
6.8 ± 1.9 ⁺³¹_{-1.6} ± 1.7	111	BECKER	87 MRK3	e ⁺ e ⁻ → hadrons

$\Gamma(\omega f'_2(1525))/\Gamma_{\text{total}}$		Γ_{49}/Γ		
VALUE	CL%	DOCUMENT ID	TECN	COMMENT
< 2.2 × 10⁻⁴	90	¹ VANNUCCI	77 MRK1	e ⁺ e ⁻ → π ⁺ π ⁻ π ⁰ K ⁺ K ⁻
••• We do not use the following data for averages, fits, limits, etc. •••				
< 2.8 × 10 ⁻⁴	90	¹ FALVARD	88 DM2	J/ψ → hadrons
¹ Re-evaluated assuming $B(f'_2(1525) \rightarrow K\bar{K}) = 0.713$.				

$\Gamma(\omega X(1835) \rightarrow \omega p\bar{p})/\Gamma_{\text{total}}$		Γ_{50}/Γ		
VALUE	CL%	DOCUMENT ID	TECN	COMMENT
< 3.9 × 10⁻⁶	95	ABLIKIM	13P BES3	J/ψ → γπ ⁰ p \bar{p}

$\Gamma(\omega X(1835), X \rightarrow \eta'\pi^+\pi^-)/\Gamma_{\text{total}}$		Γ_{51}/Γ		
VALUE	EVTS	DOCUMENT ID	TECN	COMMENT
< 6.2 × 10⁻⁵		¹ ABLIKIM	19AC BES3	J/ψ → ωη'π ⁺ π ⁻
¹ Using the decays ω → π ⁺ π ⁻ π ⁰ and η' → ηπ ⁺ π ⁻ .				

$\Gamma(\omega K^\pm K_S^0 \pi^\mp)/\Gamma_{\text{total}}$		Γ_{52}/Γ		
VALUE (units 10^{-4})	EVTS	DOCUMENT ID	TECN	COMMENT
34 ± 5 OUR AVERAGE				
37.7 ± 0.8 ± 5.8	1972 ± 41	ABLIKIM	08E BES2	e ⁺ e ⁻ → J/ψ
29.5 ± 1.4 ± 7.0	879 ± 41	BECKER	87 MRK3	e ⁺ e ⁻ → hadrons

$\Gamma(\omega K\bar{K})/\Gamma_{\text{total}}$		Γ_{53}/Γ		
VALUE (units 10^{-4})	EVTS	DOCUMENT ID	TECN	COMMENT
19 ± 4 OUR AVERAGE				
19.8 ± 2.1 ± 3.9		¹ FALVARD	88 DM2	J/ψ → hadrons
16 ± 10	22	FELDMAN	77 MRK1	e ⁺ e ⁻
¹ Addition of ωK ⁺ K ⁻ and ωK ⁰ \bar{K}^0 branching ratios.				

$\Gamma(\omega K^*(892)\bar{K} + c.c.)/\Gamma_{\text{total}}$		Γ_{54}/Γ		
VALUE (units 10^{-4})	EVTS	DOCUMENT ID	TECN	COMMENT
61 ± 9 OUR AVERAGE				
62.0 ± 6.8 ± 10.6	899 ± 98	ABLIKIM	08E BES2	J/ψ → ωK ⁰ K [±] π [∓]
65.3 ± 10.2 ± 13.5	176 ± 28	ABLIKIM	08E BES2	J/ψ → ωK ⁺ K ⁻ π ⁰
53 ± 14 ± 14	530 ± 140	BECKER	87 MRK3	e ⁺ e ⁻ → hadrons

$\Gamma(\eta' K^{*\pm} K^\mp)/\Gamma_{\text{total}}$		Γ_{55}/Γ		
VALUE (units 10^{-3})	EVTS	DOCUMENT ID	TECN	COMMENT
1.48 ± 0.13 OUR AVERAGE				
1.50 ± 0.02 ± 0.19		¹ ABLIKIM	18AB BES3	J/ψ → η'K* \bar{K}
1.47 ± 0.03 ± 0.17		² ABLIKIM	18AB BES3	J/ψ → η'K* \bar{K}
¹ From η'K ⁺ K ⁻ π ⁰ . ² From η'K ⁰ \bar{K}^0 K [±] π [∓] .				

$\Gamma(\eta' K^{*0} \bar{K}^0 + c.c.)/\Gamma_{\text{total}}$		Γ_{56}/Γ		
VALUE (units 10^{-3})	EVTS	DOCUMENT ID	TECN	COMMENT
1.66 ± 0.03 ± 0.21		¹ ABLIKIM	18AB BES3	J/ψ → η'K* \bar{K}
¹ From η'K ⁰ \bar{K}^0 K [±] π [∓] .				

$\Gamma(\eta' h_1(1415) \rightarrow \eta' K^* \bar{K} + c.c.)/\Gamma_{\text{total}}$		Γ_{57}/Γ		
VALUE (units 10^{-4})	EVTS	DOCUMENT ID	TECN	COMMENT
2.16 ± 0.12 ± 0.29	1.1k	¹ ABLIKIM	18AB BES3	J/ψ → η'h ₁ → η'K* \bar{K}
¹ From η'K ⁰ \bar{K}^0 K [±] π [∓] .				

$\Gamma(\eta' h_1(1415) \rightarrow \eta' K^{*\pm} K^\mp)/\Gamma_{\text{total}}$		Γ_{58}/Γ		
VALUE (units 10^{-4})	EVTS	DOCUMENT ID	TECN	COMMENT
1.51 ± 0.09 ± 0.21	1.0k	¹ ABLIKIM	18AB BES3	J/ψ → η'h ₁ → η'K* \bar{K}
¹ From η'K ⁺ K ⁻ π ⁰ .				

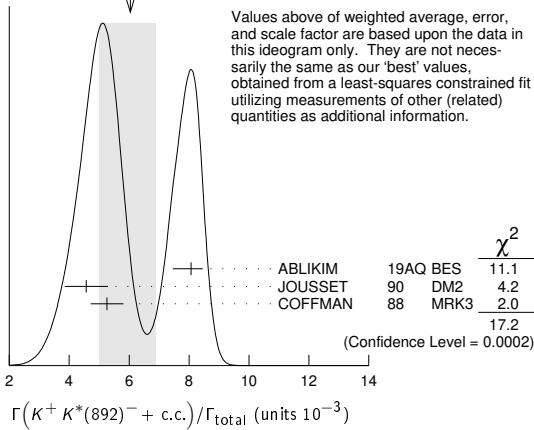
$\Gamma(K^* K^*(892) + c.c. \rightarrow K_S^0 K^\pm \pi^\mp)/\Gamma(K_S^0 K^\pm \pi^\mp)$		Γ_{60}/Γ_{69}		
VALUE (%)	EVTS	DOCUMENT ID	TECN	COMMENT
90.5 ± 0.9 ± 3.8	4k	¹ LEES	17C BABR	J/ψ → K ⁰ \bar{K}^0 K [±] π [∓]
¹ From a Dalitz plot analysis in an isobar model.				

$\Gamma(K^+ K^*(892)^- + c.c.)/\Gamma_{\text{total}}$		Γ_{61}/Γ		
VALUE (units 10^{-3})	EVTS	DOCUMENT ID	TECN	COMMENT
6.0 ^{+0.8}_{-1.0} OUR AVERAGE		Error includes scale factor of 2.9. See the ideogram below.		
8.07 ± 0.04 ^{+0.38} _{-0.61}	183k	ABLIKIM	19AQ BES	J/ψ → K ⁺ K ⁻ π ⁰
4.57 ± 0.17 ± 0.70	2285	JOUSSET	90 DM2	J/ψ → hadrons
5.26 ± 0.13 ± 0.53		COFFMAN	88 MRK3	J/ψ → K [±] K ⁰ \bar{K}^0 π [∓] , K ⁺ K ⁻ π ⁰
••• We do not use the following data for averages, fits, limits, etc. •••				
2.6 ± 0.6	24	FRANKLIN	83 MRK2	J/ψ → K ⁺ K ⁻ π ⁰
3.2 ± 0.6	48	VANNUCCI	77 MRK1	J/ψ → K [±] K ⁰ \bar{K}^0 π [∓]
4.1 ± 1.2	39	BRAUNSCH...	76 DASP	J/ψ → K [±] X

Meson Particle Listings

$J/\psi(1S)$

WEIGHTED AVERAGE
6.0±0.8-1.0 (Error scaled by 2.9)



$\Gamma(K^+K^*(892)^- + c.c. \rightarrow K^+K^-\pi^0)/\Gamma_{total}$ Γ_{62}/Γ

VALUE (units 10^{-3})	EVTS	DOCUMENT ID	TECN	COMMENT
$2.69 \pm 0.01 \pm_{-0.20}^{+0.13}$	183k	ABLIKIM	19AQ BES	$J/\psi \rightarrow K^+K^-\pi^0$

$\Gamma(K^+K^*(892)^- + c.c. \rightarrow K^+K^-\pi^0)/\Gamma(K^+K^-\pi^0)$ Γ_{62}/Γ_{168}

VALUE (%)	EVTS	DOCUMENT ID	TECN	COMMENT
$92.4 \pm 1.5 \pm 3.4$	2k	¹ LEES	17c BABR	$J/\psi \rightarrow K^+K^-\pi^0$

¹ From a Dalitz plot analysis in an isobar model.

$\Gamma(K^0\bar{K}^*(892)^0 + c.c.)/\Gamma_{total}$ Γ_{64}/Γ

VALUE (units 10^{-3})	EVTS	DOCUMENT ID	TECN	COMMENT
4.2 ± 0.4 OUR AVERAGE				
$3.96 \pm 0.15 \pm 0.60$	1192	JOUSSET	90 DM2	$J/\psi \rightarrow$ hadrons
$4.33 \pm 0.12 \pm 0.45$		COFFMAN	88 MRK3	$J/\psi \rightarrow K^\pm K_S^0 \pi^\mp$
••• We do not use the following data for averages, fits, limits, etc. •••				
2.7 ± 0.6	45	VANNUCCI	77 MRK1	$J/\psi \rightarrow K^\pm K_S^0 \pi^\mp$

$\Gamma(\bar{K}^*(892)^0 K^+ \pi^- + c.c.)/\Gamma_{total}$ Γ_{66}/Γ

VALUE	DOCUMENT ID	TECN	COMMENT
••• We do not use the following data for averages, fits, limits, etc. •••			
seen	¹ ABLIKIM	06c BES2	$J/\psi \rightarrow \bar{K}^*(892)^0 K^+ \pi^-$

¹ A $K_0^*(700)$ is observed by ABLIKIM 06c in the $K^+ \pi^-$ mass spectrum of the $\bar{K}^*(892)^0 K^+ \pi^-$ final state against the $\bar{K}^*(892)$. A corresponding branching fraction of the $J/\psi(1S)$ is not presented.

$\Gamma(K^*(892)^0 K_S^0 \rightarrow \gamma K_S^0 K_S^0)/\Gamma_{total}$ Γ_{70}/Γ

VALUE (units 10^{-6})	DOCUMENT ID	TECN	COMMENT
$6.28 \pm_{-0.17}^{+0.16} \pm_{-0.52}^{+0.59}$	ABLIKIM	18AA BES3	$J/\psi \rightarrow \gamma K_S^0 K_S^0$

$\Gamma(K^*(892)^\pm K^*(700)^\mp)/\Gamma_{total}$ Γ_{72}/Γ

VALUE (units 10^{-3})	EVTS	DOCUMENT ID	TECN	COMMENT
$1.09 \pm 0.18 \pm_{-0.54}^{+0.94}$	655	ABLIKIM	10E BES2	$J/\psi \rightarrow K^\pm K_S^0 \pi^\mp \pi^0$

$\Gamma(K^*(892)^0 \bar{K}^*(892)^0)/\Gamma_{total}$ Γ_{73}/Γ

VALUE (units 10^{-4})	CL%	DOCUMENT ID	TECN	COMMENT
<5	90	VANNUCCI	77 MRK1	$e^+e^- \rightarrow \pi^+ \pi^- K^+ K^-$

$\Gamma(K^*(892)^\pm K^*(892)^\mp)/\Gamma_{total}$ Γ_{74}/Γ

VALUE (units 10^{-3})	EVTS	DOCUMENT ID	TECN	COMMENT
$1.00 \pm 0.19 \pm_{-0.32}^{+0.11}$	323	ABLIKIM	10E BES2	$J/\psi \rightarrow K^\pm K_S^0 \pi^\mp \pi^0$

$\Gamma(K_1(1400)^\pm K^\mp)/\Gamma_{total}$ Γ_{75}/Γ

VALUE (units 10^{-3})	DOCUMENT ID	TECN	COMMENT
$3.8 \pm 0.8 \pm 1.2$	¹ BAI	99c BES	e^+e^-

¹ Assuming $B(K_1(1400) \rightarrow K^* \pi) = 0.94 \pm 0.06$

$\Gamma(K^*(1410)\bar{K} + c.c. \rightarrow K^\pm K^\mp \pi^0)/\Gamma(K^+K^-\pi^0)$ Γ_{77}/Γ_{168}

VALUE (%)	EVTS	DOCUMENT ID	TECN	COMMENT
$2.3 \pm 1.1 \pm 0.7$	2k	¹ LEES	17c BABR	$J/\psi \rightarrow K^+K^-\pi^0$

¹ From a Dalitz plot analysis in an isobar model.

$\Gamma(K^*(1410)\bar{K} + c.c. \rightarrow K_S^0 K^\pm \pi^\mp)/\Gamma(K_S^0 K^\pm \pi^\mp)$ Γ_{78}/Γ_{169}

VALUE (%)	EVTS	DOCUMENT ID	TECN	COMMENT
$1.5 \pm 0.5 \pm 0.9$	4k	¹ LEES	17c BABR	$J/\psi \rightarrow K_S^0 K^\pm \pi^\mp$

¹ From a Dalitz plot analysis in an isobar model.

$\Gamma(K_S^2(1430)\bar{K} + c.c. \rightarrow K^\pm K^\mp \pi^0)/\Gamma(K^+K^-\pi^0)$ Γ_{80}/Γ_{168}

VALUE (%)	EVTS	DOCUMENT ID	TECN	COMMENT
$3.5 \pm 1.3 \pm 0.9$	2k	¹ LEES	17c BABR	$J/\psi \rightarrow K^+K^-\pi^0$

¹ From a Dalitz plot analysis in an isobar model.

$\Gamma(K_S^2(1430)\bar{K} + c.c. \rightarrow K_S^0 K^\pm \pi^\mp)/\Gamma(K_S^0 K^\pm \pi^\mp)$ Γ_{81}/Γ_{169}

VALUE (%)	EVTS	DOCUMENT ID	TECN	COMMENT
$7.1 \pm 1.3 \pm 1.2$	4k	¹ LEES	17c BABR	$J/\psi \rightarrow K_S^0 K^\pm \pi^\mp$

¹ From a Dalitz plot analysis in an isobar model.

$\Gamma(\bar{K}_2^2(1430)K + c.c.)/\Gamma_{total}$ Γ_{82}/Γ

VALUE	CL%	DOCUMENT ID	TECN	COMMENT
< 40×10^{-4}	90	VANNUCCI	77 MRK1	$e^+e^- \rightarrow K^0 \bar{K}_2^{*0}$
••• We do not use the following data for averages, fits, limits, etc. •••				
< 66×10^{-4}	90	BRAUNSCH...	76 DASP	$e^+e^- \rightarrow K^\pm \bar{K}_2^{*\mp}$

$\Gamma(K_S^2(1430)^+ K^- + c.c. \rightarrow K^+ K^- \pi^0)/\Gamma_{total}$ Γ_{83}/Γ

VALUE (units 10^{-4})	EVTS	DOCUMENT ID	TECN	COMMENT
$2.69 \pm 0.04 \pm_{-0.19}^{+0.25}$	183k	ABLIKIM	19AQ BES	$J/\psi \rightarrow K^+K^-\pi^0$

$\Gamma(\bar{K}_2^2(1430)^0 K^*(892)^0 + c.c.)/\Gamma_{total}$ Γ_{85}/Γ

VALUE (units 10^{-3})	EVTS	DOCUMENT ID	TECN	COMMENT
••• We do not use the following data for averages, fits, limits, etc. •••				
6.7 ± 2.6	40	VANNUCCI	77 MRK1	$e^+e^- \rightarrow \pi^+ \pi^- K^+ K^-$

$\Gamma(K_S^2(1430)^0 \bar{K}_2^2(1430)^0)/\Gamma_{total}$ Γ_{88}/Γ

VALUE	CL%	DOCUMENT ID	TECN	COMMENT
< 29×10^{-4}	90	VANNUCCI	77 MRK1	$e^+e^- \rightarrow \pi^+ \pi^- K^+ K^-$

$\Gamma(K_S^2(1980)^+ K^- + c.c. \rightarrow K^+ K^- \pi^0)/\Gamma_{total}$ Γ_{90}/Γ

VALUE (units 10^{-5})	EVTS	DOCUMENT ID	TECN	COMMENT
$1.1 \pm 0.1 \pm_{-0.1}^{+0.6}$	183k	ABLIKIM	19AQ BES	$J/\psi \rightarrow K^+K^-\pi^0$

$\Gamma(K_S^2(2045)^+ K^- + c.c. \rightarrow K^+ K^- \pi^0)/\Gamma_{total}$ Γ_{91}/Γ

VALUE (units 10^{-6})	EVTS	DOCUMENT ID	TECN	COMMENT
$6.2 \pm 0.7 \pm_{-1.4}^{+2.8}$	183k	ABLIKIM	19AQ BES	$J/\psi \rightarrow K^+K^-\pi^0$

$\Gamma(K_1(1270)^\pm K^\mp)/\Gamma_{total}$ Γ_{92}/Γ

VALUE	CL%	DOCUMENT ID	TECN	COMMENT
< 3.0×10^{-3}	90	¹ BAI	99c BES	e^+e^-

¹ Assuming $B(K_1(1270) \rightarrow K \rho) = 0.42 \pm 0.06$

$\Gamma(K_1(1270)K_S^0 \rightarrow \gamma K_S^0 K_S^0)/\Gamma_{total}$ Γ_{93}/Γ

VALUE (units 10^{-7})	DOCUMENT ID	TECN	COMMENT
$8.54 \pm_{-2.13}^{+1.07} \pm_{-2.13}^{+2.35}$	ABLIKIM	18AA BES3	$J/\psi \rightarrow \gamma K_S^0 K_S^0$

$\Gamma(a_2(1320)^\pm \pi^\mp)/\Gamma_{total}$ Γ_{94}/Γ

VALUE	CL%	DOCUMENT ID	TECN	COMMENT
< 43×10^{-4}	90	BRAUNSCH...	76 DASP	e^+e^-

$\Gamma(\phi \pi^0)/\Gamma_{total}$ Γ_{95}/Γ

The two different fit values of ABLIKIM 15k below have the same statistical significance of 6.4 σ and cannot be distinguished at this moment.

VALUE (units 10^{-6})	CL%	EVTS	DOCUMENT ID	TECN	COMMENT
$2.94 \pm 0.16 \pm 0.16$		0.8k	¹ ABLIKIM	15k BES3	$e^+e^- \rightarrow J/\psi \rightarrow K^+K^-\gamma\gamma$
$0.124 \pm 0.033 \pm 0.030$		35 ± 9	² ABLIKIM	15k BES3	$e^+e^- \rightarrow J/\psi \rightarrow K^+K^-\gamma\gamma$

••• We do not use the following data for averages, fits, limits, etc. •••

VALUE	CL%	DOCUMENT ID	TECN	COMMENT
<6.4	90	³ ABLIKIM	05B BES2	$e^+e^- \rightarrow J/\psi \rightarrow \phi \gamma \gamma$
<6.8	90	COFFMAN	88 MRK3	$e^+e^- \rightarrow K^+K^-\pi^0$

¹ Corresponding to one of the two fit solutions with $\delta = (-95.9 \pm 1.5)^\circ$ for the phase angle between the resonant $J/\psi \rightarrow \phi \pi^0$ and non-phi $J/\psi \rightarrow K^+K^-\pi^0$ contributions.

² Corresponding to one of the two fit solutions with $\delta = (-152.1 \pm 7.7)^\circ$ for the phase angle between the resonant $J/\psi \rightarrow \phi \pi^0$ and non-phi $J/\psi \rightarrow K^+K^-\pi^0$ contributions.

³ Superseded by ABLIKIM 15k.

$\Gamma(\phi\pi^+\pi^-)/\Gamma_{total}$ Γ_{96}/Γ

VALUE (units 10^{-3})	EVTS	DOCUMENT ID	TECN	COMMENT
0.94 ± 0.15 OUR AVERAGE		Error includes scale factor of 1.7.		
1.09 ± 0.02 ± 0.13		ABLIKIM	05 BES2	$J/\psi \rightarrow \phi\pi^+\pi^-$
0.78 ± 0.03 ± 0.12		FALVARD	88 DM2	$J/\psi \rightarrow$ hadrons
2.1 ± 0.9	23	FELDMAN	77 MRK1	e^+e^-

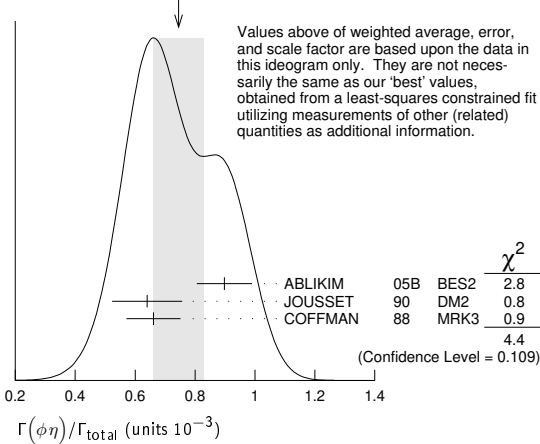
$\Gamma(\phi 2(\pi^+\pi^-))/\Gamma_{total}$ Γ_{98}/Γ

VALUE (units 10^{-4})	DOCUMENT ID	TECN	COMMENT
16.0 ± 1.0 ± 3.0	FALVARD	88 DM2	$J/\psi \rightarrow$ hadrons

$\Gamma(\phi\eta)/\Gamma_{total}$ Γ_{99}/Γ

VALUE (units 10^{-3})	EVTS	DOCUMENT ID	TECN	COMMENT
0.74 ± 0.08 OUR AVERAGE		Error includes scale factor of 1.5. See the ideogram below.		
0.898 ± 0.024 ± 0.089		ABLIKIM	05B BES2	$e^+e^- \rightarrow J/\psi \rightarrow$ hadr
0.64 ± 0.04 ± 0.11	346	JOUSSET	90 DM2	$J/\psi \rightarrow$ hadrons
0.661 ± 0.045 ± 0.078		COFFMAN	88 MRK3	$e^+e^- \rightarrow K^+K^-\eta$

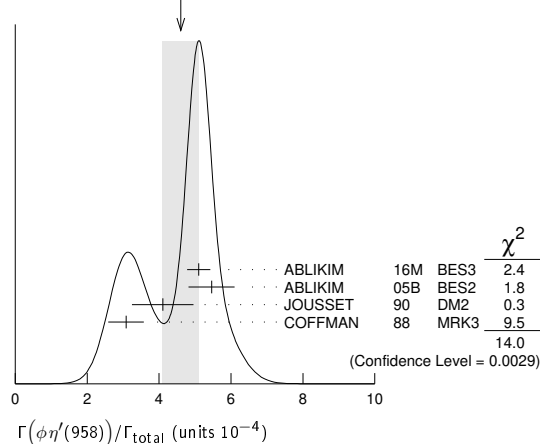
WEIGHTED AVERAGE
0.74 ± 0.08 (Error scaled by 1.5)



$\Gamma(\phi\eta'(958))/\Gamma_{total}$ Γ_{100}/Γ

VALUE (units 10^{-4})	CL%	EVTS	DOCUMENT ID	TECN	COMMENT
4.6 ± 0.5 OUR AVERAGE			Error includes scale factor of 2.2. See the ideogram below.		
5.10 ± 0.03 ± 0.32		31k	ABLIKIM	16M BES3	$e^+e^- \rightarrow J/\psi \rightarrow$ hadrons
5.46 ± 0.31 ± 0.56			ABLIKIM	05B BES2	$e^+e^- \rightarrow J/\psi \rightarrow$ hadrons
4.1 ± 0.3 ± 0.8		167	JOUSSET	90 DM2	$J/\psi \rightarrow$ hadrons
3.08 ± 0.34 ± 0.36			COFFMAN	88 MRK3	$e^+e^- \rightarrow K^+K^-\eta'$
••• We do not use the following data for averages, fits, limits, etc. •••					
< 13		90	VANNUCCI	77 MRK1	e^+e^-

WEIGHTED AVERAGE
4.6 ± 0.5 (Error scaled by 2.2)



$\Gamma(\phi\eta\eta')/\Gamma_{total}$ Γ_{101}/Γ

VALUE (units 10^{-4})	EVTS	DOCUMENT ID	TECN	COMMENT
2.32 ± 0.06 ± 0.16	2.2k	1 ABLIKIM	19AN BES3	$e^+e^- \rightarrow J/\psi \rightarrow$ hadrons
1 Including contributions from intermediate resonances. Evidence for an intermediate resonance at $M \approx 2$ GeV and $\Gamma \approx 150$ MeV decaying to $\phi\eta'$ with $J^P = 1^+$ or $J^P = 1^-$, and $B(J/\psi \rightarrow \eta X) \times B(X \rightarrow \phi\eta') \approx 10^{-4}$.				

$\Gamma(\phi f_0(980))/\Gamma_{total}$ Γ_{102}/Γ

VALUE (units 10^{-4})	EVTS	DOCUMENT ID	TECN	COMMENT
3.2 ± 0.9 OUR AVERAGE		Error includes scale factor of 1.9.		
4.6 ± 0.4 ± 0.8		1 FALVARD	88 DM2	$J/\psi \rightarrow$ hadrons
2.6 ± 0.6	50	1 GIDAL	81 MRK2	$J/\psi \rightarrow K^+K^-K^+K^-$
1 Assuming $B(f_0(980) \rightarrow \pi\pi) = 0.78$.				

$\Gamma(\phi\pi^0 f_0(980) \rightarrow \phi\pi^0\pi^+\pi^-)/\Gamma_{total}$ Γ_{105}/Γ

VALUE (units 10^{-6})	EVTS	DOCUMENT ID	TECN	COMMENT
4.50 ± 0.80 ± 0.61	355	ABLIKIM	15P BES3	$J/\psi \rightarrow K^+K^-3\pi$

$\Gamma(\phi\pi^0 f_0(980) \rightarrow \phi\pi^0\rho^0\pi^0)/\Gamma_{total}$ Γ_{106}/Γ

VALUE (units 10^{-6})	EVTS	DOCUMENT ID	TECN	COMMENT
1.67 ± 0.50 ± 0.24	70	ABLIKIM	15P BES3	$J/\psi \rightarrow K^+K^-3\pi$

$\Gamma(\phi f_0(980)\eta \rightarrow \eta\phi\pi^+\pi^-)/\Gamma_{total}$ Γ_{107}/Γ

VALUE (units 10^{-4})	EVTS	DOCUMENT ID	TECN	COMMENT
3.23 ± 0.75 ± 0.73	52	ABLIKIM	08F BES	$J/\psi \rightarrow \eta\phi f_0(980)$

$\Gamma(\phi a_0(980)^0 \rightarrow \phi\eta\pi^0)/\Gamma_{total}$ Γ_{108}/Γ

VALUE (units 10^{-6})	DOCUMENT ID	TECN	COMMENT
4.37 ± 1.35	1 ABLIKIM	18D BES3	$J/\psi \rightarrow \phi\eta\pi^0$
••• We do not use the following data for averages, fits, limits, etc. •••			
5.0 ± 2.7 ± 2.5	2 ABLIKIM	11D BES3	$J/\psi \rightarrow \phi\eta\pi^0$
1 Assuming constructive interference between $a_0(980) - f_0(980)$ mixing and electromagnetic decay. Destructive interference gives a value of $(4.93 \pm 1.77) \times 10^{-6}$ for this branching fraction.			
2 Assuming $a_0(980) - f_0(980)$ mixing and isospin breaking via γ^* and K^*K loops.			

$\Gamma(\phi f_2(1270))/\Gamma_{total}$ Γ_{109}/Γ

VALUE (units 10^{-3})	CL%	DOCUMENT ID	TECN	COMMENT
••• We do not use the following data for averages, fits, limits, etc. •••				
< 0.45	90	FALVARD	88 DM2	$J/\psi \rightarrow$ hadrons
< 0.37	90	VANNUCCI	77 MRK1	$e^+e^- \rightarrow \pi^+\pi^-K^+K^-$

$\Gamma(\phi f_1(1285))/\Gamma_{total}$ Γ_{110}/Γ

VALUE (units 10^{-4})	EVTS	DOCUMENT ID	TECN	COMMENT
2.6 ± 0.5 OUR AVERAGE				
3.4 ± 1.8 ± 1.5	1.1k	1 ABLIKIM	15H BES3	$e^+e^- \rightarrow J/\psi \rightarrow \phi\eta\pi^+\pi^-$
3.2 ± 0.6 ± 0.4		JOUSSET	90 DM2	$J/\psi \rightarrow \phi 2(\pi^+\pi^-)$
2.1 ± 0.5 ± 0.4	25	2 JOUSSET	90 DM2	$J/\psi \rightarrow \phi\eta\pi^+\pi^-$
••• We do not use the following data for averages, fits, limits, etc. •••				
0.6 ± 0.2 ± 0.1	16	BECKER	87 MRK3	$J/\psi \rightarrow \phi K\bar{K}\pi$
1 ABLIKIM 15H reports $[\Gamma(J/\psi(1S) \rightarrow \phi f_1(1285))/\Gamma_{total}] \times [B(f_1(1285) \rightarrow \eta\pi^+\pi^-)] = (1.20 \pm 0.6 \pm 0.14) \times 10^{-4}$ which we divide by our best value $B(f_1(1285) \rightarrow \eta\pi^+\pi^-) = (35 \pm 15) \times 10^{-2}$. Our first error is their experiment's error and our second error is the systematic error from using our best value.				
2 We attribute to the $f_1(1285)$ the signal observed in the $\pi^+\pi^-\eta$ invariant mass distribution at 1297 MeV.				

$\Gamma(\phi f_1(1285) \rightarrow \phi\pi^0 f_0(980) \rightarrow \phi\pi^0\pi^+\pi^-)/\Gamma_{total}$ Γ_{111}/Γ

VALUE (units 10^{-7})	EVTS	DOCUMENT ID	TECN	COMMENT
9.36 ± 2.31 ± 1.54	78	ABLIKIM	15P BES3	$J/\psi \rightarrow K^+K^-3\pi$

$\Gamma(\phi f_1(1285) \rightarrow \phi\pi^0 f_0(980) \rightarrow \phi 3\pi^0)/\Gamma_{total}$ Γ_{112}/Γ

VALUE (units 10^{-7})	EVTS	DOCUMENT ID	TECN	COMMENT
2.08 ± 1.63 ± 1.47	9	ABLIKIM	15P BES3	$J/\psi \rightarrow K^+K^-3\pi$

$\Gamma(\phi\eta(1405) \rightarrow \phi\eta\pi^+\pi^-)/\Gamma_{total}$ Γ_{113}/Γ

VALUE (units 10^{-5})	CL%	EVTS	DOCUMENT ID	TECN	COMMENT
2.01 ± 0.58 ± 0.82		172	1 ABLIKIM	15H BES3	$e^+e^- \rightarrow J/\psi \rightarrow \phi\eta\pi^+\pi^-$
••• We do not use the following data for averages, fits, limits, etc. •••					
< 17	90	2 FALVARD	88 DM2	$J/\psi \rightarrow$ hadrons	
1 With 3.6 σ significance.					
2 Includes unknown branching fraction $\eta(1405) \rightarrow \eta\pi\pi$.					

$\Gamma(\phi f_2'(1525))/\Gamma_{total}$ Γ_{114}/Γ

VALUE (units 10^{-4})	EVTS	DOCUMENT ID	TECN	COMMENT
8 ± 4 OUR AVERAGE		Error includes scale factor of 2.7.		
12.3 ± 0.6 ± 2.0		1,2 FALVARD	88 DM2	$J/\psi \rightarrow$ hadrons
4.8 ± 1.8	46	1 GIDAL	81 MRK2	$J/\psi \rightarrow K^+K^-K^+K^-$
1 Re-evaluated using $B(f_2'(1525) \rightarrow K\bar{K}) = 0.713$.				
2 Including interference with $f_0(1710)$.				

$\Gamma(\phi X(1835) \rightarrow \phi\rho\bar{\rho})/\Gamma_{total}$ Γ_{115}/Γ

VALUE	CL%	DOCUMENT ID	TECN	COMMENT
< 2.1 × 10⁻⁷	90	1 ABLIKIM	16K BES3	$J/\psi \rightarrow \rho\bar{\rho}K_S^0 K_L^0, \rho\bar{\rho}K^+K^-$
1 Upper limit applies to any $\rho\bar{\rho}$ mass enhancement near threshold.				

Meson Particle Listings

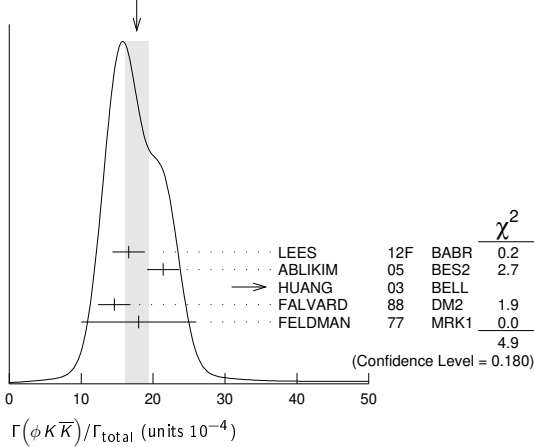
$J/\psi(1S)$

$\Gamma(\phi X(1835) \rightarrow \phi \eta \pi^+ \pi^-) / \Gamma_{\text{total}}$					Γ_{116} / Γ
VALUE	CL%	DOCUMENT ID	TECN	COMMENT	
$< 2.8 \times 10^{-4}$	90	ABLIKIM	15H BES3	$e^+ e^- \rightarrow J/\psi \rightarrow \phi \eta \pi^+ \pi^-$	

$\Gamma(\phi X(1870) \rightarrow \phi \eta \pi^+ \pi^-) / \Gamma_{\text{total}}$					Γ_{117} / Γ
VALUE	CL%	DOCUMENT ID	TECN	COMMENT	
$< 6.13 \times 10^{-5}$	90	ABLIKIM	15H BES3	$e^+ e^- \rightarrow J/\psi \rightarrow \phi \eta \pi^+ \pi^-$	

$\Gamma(\phi K \bar{K}) / \Gamma_{\text{total}}$					Γ_{118} / Γ
VALUE (units 10^{-4})	EVTS	DOCUMENT ID	TECN	COMMENT	
17.7 ± 1.6 OUR AVERAGE	Error includes scale factor of 1.3. See the ideogram below.				
$16.6 \pm 1.9 \pm 1.2$	163 ± 19	LEES	12F BABR	$10.6 e^+ e^- \rightarrow 2(K^+ K^-) \gamma$	
$21.4 \pm 0.4 \pm 2.2$		ABLIKIM	05 BES2	$J/\psi \rightarrow \phi \pi^+ \pi^-$	
$48 \begin{smallmatrix} +20 \\ -16 \end{smallmatrix} \pm 6$	$9.0 \begin{smallmatrix} +3.7 \\ -3.0 \end{smallmatrix}$	^{1,2} HUANG	03 BELL	$B^+ \rightarrow (\phi K^+ K^-) K^+$	
$14.6 \pm 0.8 \pm 2.1$		³ FALVARD	88 DM2	$J/\psi \rightarrow \text{hadrons}$	
18 ± 8	14	FELDMAN	77 MRK1	$e^+ e^-$	

WEIGHTED AVERAGE
 17.7 ± 1.6 (Error scaled by 1.3)



¹ We have multiplied $K^+ K^-$ measurement by 2 to obtain $K \bar{K}$.
² Using $B(B^+ \rightarrow J/\psi K^+) = (1.01 \pm 0.05) \times 10^{-3}$.
³ Addition of $\phi K^+ K^-$ and $\phi K^0 \bar{K}^0$ branching ratios.

$\Gamma(\phi f_0(1710) \rightarrow \phi K \bar{K}) / \Gamma_{\text{total}}$					Γ_{119} / Γ
VALUE (units 10^{-4})	EVTS	DOCUMENT ID	TECN	COMMENT	
$3.6 \pm 0.2 \pm 0.6$		^{1,2} FALVARD	88 DM2	$J/\psi \rightarrow \text{hadrons}$	

¹ Including interference with $f_2'(1525)$.
² Includes unknown branching fraction $f_0(1710) \rightarrow K \bar{K}$.

$\Gamma(\phi K^\pm K_S^0 \pi^\mp) / \Gamma_{\text{total}}$					Γ_{122} / Γ
VALUE (units 10^{-4})	EVTS	DOCUMENT ID	TECN	COMMENT	
7.2 ± 0.8 OUR AVERAGE					
$7.4 \pm 0.6 \pm 1.4$	227 ± 19	ABLIKIM	08E BES2	$e^+ e^- \rightarrow J/\psi$	
$7.4 \pm 0.9 \pm 1.1$		FALVARD	88 DM2	$J/\psi \rightarrow \text{hadrons}$	
$7 \pm 0.6 \pm 1.0$	163 ± 15	BECKER	87 MRK3	$e^+ e^- \rightarrow \text{hadrons}$	

$\Gamma(\phi K^*(892) \bar{K} + \text{c.c.}) / \Gamma_{\text{total}}$					Γ_{123} / Γ
VALUE (units 10^{-4})	EVTS	DOCUMENT ID	TECN	COMMENT	
21.8 ± 2.3 OUR AVERAGE					
$20.8 \pm 2.7 \pm 3.9$	195 ± 25	ABLIKIM	08E BES2	$J/\psi \rightarrow \phi K_S^0 K^\pm \pi^\mp$	
$29.6 \pm 3.7 \pm 4.7$	238 ± 30	ABLIKIM	08E BES2	$J/\psi \rightarrow \phi K^+ K^- \pi^0$	
$20.7 \pm 2.4 \pm 3.0$		FALVARD	88 DM2	$J/\psi \rightarrow \text{hadrons}$	
$20 \pm 3 \pm 3$	155 ± 20	BECKER	87 MRK3	$e^+ e^- \rightarrow \text{hadrons}$	

$\Gamma(b_1(1235)^\pm \pi^\mp) / \Gamma_{\text{total}}$					Γ_{124} / Γ
VALUE (units 10^{-4})	EVTS	DOCUMENT ID	TECN	COMMENT	
30 ± 5 OUR AVERAGE					
31 ± 6	4600	AUGUSTIN	89 DM2	$J/\psi \rightarrow 2(\pi^+ \pi^-) \pi^0$	
29 ± 7	87	BURMESTER	77D PLUT	$e^+ e^-$	

$\Gamma(b_1(1235)^0 \pi^0) / \Gamma_{\text{total}}$					Γ_{125} / Γ
VALUE (units 10^{-4})	EVTS	DOCUMENT ID	TECN	COMMENT	
$23 \pm 3 \pm 5$	229	AUGUSTIN	89 DM2	$e^+ e^-$	

$\Gamma(\Delta(1232) \bar{p}) / \Gamma_{\text{total}}$					Γ_{127} / Γ
VALUE	CL%	DOCUMENT ID	TECN	COMMENT	
$< 0.1 \times 10^{-3}$	90	HENRARD	87 DM2	$e^+ e^-$	

$\Gamma(\Delta(1232)^{++} \bar{p} \pi^-) / \Gamma_{\text{total}}$					Γ_{128} / Γ
VALUE (units 10^{-3})	EVTS	DOCUMENT ID	TECN	COMMENT	
$1.58 \pm 0.23 \pm 0.40$	332	EATON	84 MRK2	$e^+ e^-$	

$\Gamma(\Delta(1232)^{++} \bar{\Delta}(1232)^{-}) / \Gamma_{\text{total}}$					Γ_{129} / Γ
VALUE (units 10^{-3})	EVTS	DOCUMENT ID	TECN	COMMENT	
$1.10 \pm 0.09 \pm 0.28$	233	EATON	84 MRK2	$e^+ e^-$	

$\Gamma(\Sigma(1385)^0 \rho K^-) / \Gamma_{\text{total}}$					Γ_{130} / Γ
VALUE (units 10^{-3})	EVTS	DOCUMENT ID	TECN	COMMENT	
$0.51 \pm 0.26 \pm 0.18$	89	EATON	84 MRK2	$e^+ e^-$	

$\Gamma(\Sigma(1385)^0 \bar{\Lambda} + \text{c.c.}) / \Gamma_{\text{total}}$					Γ_{131} / Γ
VALUE	CL%	DOCUMENT ID	TECN	COMMENT	
$< 0.82 \times 10^{-5}$	90	ABLIKIM	13F BES3	$J/\psi \rightarrow \rho \bar{p} \pi^+ \pi^- \gamma \gamma$	
• • • We do not use the following data for averages, fits, limits, etc. • • •					
$< 0.2 \times 10^{-3}$	90	HENRARD	87 DM2	$e^+ e^-$	

$\Gamma(\Sigma(1385)^- \bar{\Sigma}^+ (\text{or c.c.})) / \Gamma_{\text{total}}$					Γ_{132} / Γ
VALUE (units 10^{-3})	EVTS	DOCUMENT ID	TECN	COMMENT	
0.31 ± 0.05 OUR AVERAGE					
$0.30 \pm 0.03 \pm 0.07$	74 ± 8	HENRARD	87 DM2	$e^+ e^- \rightarrow \Sigma^{*-}$	
$0.34 \pm 0.04 \pm 0.07$	77 ± 9	HENRARD	87 DM2	$e^+ e^- \rightarrow \Sigma^{*+}$	
$0.29 \pm 0.11 \pm 0.10$	26	EATON	84 MRK2	$e^+ e^- \rightarrow \Sigma^{*-}$	
$0.31 \pm 0.11 \pm 0.11$	28	EATON	84 MRK2	$e^+ e^- \rightarrow \Sigma^{*+}$	

$\Gamma(\Sigma(1385)^- \bar{\Sigma}(1385)^+ (\text{or c.c.})) / \Gamma_{\text{total}}$					Γ_{133} / Γ
VALUE (units 10^{-3})	EVTS	DOCUMENT ID	TECN	COMMENT	
1.16 ± 0.05 OUR AVERAGE					
$1.096 \pm 0.012 \pm 0.071$	43k	ABLIKIM	16L BES3	$J/\psi \rightarrow \Sigma(1385)^- \bar{\Sigma}(1385)^+$	
$1.258 \pm 0.014 \pm 0.078$	53k	ABLIKIM	16L BES3	$J/\psi \rightarrow \Sigma(1385)^+ \bar{\Sigma}(1385)^-$	
$1.23 \pm 0.07 \pm 0.30$	0.8k	ABLIKIM	12P BES2	$J/\psi \rightarrow \Sigma(1385)^- \bar{\Sigma}(1385)^+$	
$1.50 \pm 0.08 \pm 0.38$	1k	ABLIKIM	12P BES2	$J/\psi \rightarrow \Sigma(1385)^+ \bar{\Sigma}(1385)^-$	
$1.00 \pm 0.04 \pm 0.21$	0.6k	HENRARD	87 DM2	$e^+ e^- \rightarrow \Sigma^{*-}$	
$1.19 \pm 0.04 \pm 0.25$	0.7k	HENRARD	87 DM2	$e^+ e^- \rightarrow \Sigma^{*+}$	
$0.86 \pm 0.18 \pm 0.22$	56	EATON	84 MRK2	$e^+ e^- \rightarrow \Sigma^{*-}$	
$1.03 \pm 0.24 \pm 0.25$	68	EATON	84 MRK2	$e^+ e^- \rightarrow \Sigma^{*+}$	

$\Gamma(\Sigma(1385)^0 \bar{\Sigma}(1385)^0) / \Gamma_{\text{total}}$					Γ_{134} / Γ
VALUE (units 10^{-3})	EVTS	DOCUMENT ID	TECN	COMMENT	
$1.071 \pm 0.009 \pm 0.082$	103k	ABLIKIM	17E BES3	$e^+ e^- \rightarrow J/\psi \rightarrow \text{hadrons}$	

$\Gamma(\Lambda(1520) \bar{\Lambda} + \text{c.c.} \rightarrow \gamma \Lambda \bar{\Lambda}) / \Gamma_{\text{total}}$					Γ_{135} / Γ
VALUE	CL%	DOCUMENT ID	TECN	COMMENT	
$< 4.1 \times 10^{-6}$	90	ABLIKIM	12B BES3	$J/\psi \rightarrow \Lambda \bar{\Lambda} \gamma$	

$\Gamma(\bar{\Lambda}(1520) \Lambda + \text{c.c.}) / \Gamma_{\text{total}}$					Γ_{136} / Γ
VALUE	CL%	DOCUMENT ID	TECN	COMMENT	
$< 1.80 \times 10^{-3}$	90	LU	19 BELL	$B^+ \rightarrow \bar{p} \Lambda K^+ K^+$	

$\Gamma(\Xi^0 \Xi^0) / \Gamma_{\text{total}}$					Γ_{137} / Γ
VALUE (units 10^{-3})	EVTS	DOCUMENT ID	TECN	COMMENT	
1.17 ± 0.04 OUR AVERAGE					
$1.165 \pm 0.004 \pm 0.043$	135k	ABLIKIM	17E BES3	$e^+ e^- \rightarrow J/\psi \rightarrow \text{hadrons}$	
$1.20 \pm 0.12 \pm 0.21$	206	ABLIKIM	080 BES2	$e^+ e^- \rightarrow J/\psi$	

$\Gamma(\Xi(1530) \bar{\Xi}^+ + \text{c.c.}) / \Gamma_{\text{total}}$					Γ_{138} / Γ
VALUE (units 10^{-3})	EVTS	DOCUMENT ID	TECN	COMMENT	
0.318 ± 0.008 OUR AVERAGE					
$0.317 \pm 0.002 \pm 0.008$	70k	ABLIKIM	20 BES3	$e^+ e^- \rightarrow J/\psi$	
$0.59 \pm 0.09 \pm 0.12$	75	HENRARD	87 DM2	$e^+ e^-$	

$\Gamma(\Xi(1530)^0 \Xi^0) / \Gamma_{\text{total}}$					Γ_{139} / Γ
VALUE (units 10^{-3})	EVTS	DOCUMENT ID	TECN	COMMENT	
$0.32 \pm 0.12 \pm 0.07$	24 ± 9	HENRARD	87 DM2	$e^+ e^-$	

$\Gamma(\Theta(1540) \bar{\Theta}(1540) \rightarrow K_S^0 \rho K^- \pi + \text{c.c.}) / \Gamma_{\text{total}}$					Γ_{140} / Γ
VALUE	CL%	DOCUMENT ID	TECN	COMMENT	
$< 1.1 \times 10^{-5}$	90	BAI	04G BES2	$e^+ e^-$	

$\Gamma(\Theta(1540) K^- \pi \rightarrow K_S^0 \rho K^- \pi) / \Gamma_{\text{total}}$					Γ_{141} / Γ
VALUE	CL%	DOCUMENT ID	TECN	COMMENT	
$< 2.1 \times 10^{-5}$	90	BAI	04G BES2	$e^+ e^-$	

$\Gamma(\Theta(1540) K_S^0 \bar{p} \rightarrow K_S^0 \bar{p} K^+ n) / \Gamma_{\text{total}}$					Γ_{142} / Γ
VALUE	CL%	DOCUMENT ID	TECN	COMMENT	
$< 1.6 \times 10^{-5}$	90	BAI	04G BES2	$e^+ e^-$	

$\Gamma(\bar{\Theta}(1540) K^+ n \rightarrow K_S^0 \bar{p} K^+ n) / \Gamma_{\text{total}}$					Γ_{143} / Γ
VALUE	CL%	DOCUMENT ID	TECN	COMMENT	
$< 5.6 \times 10^{-5}$	90	BAI	04G BES2	$e^+ e^-$	

$\Gamma(\bar{\Theta}(1540) K_S^0 p \rightarrow K_S^0 \bar{p} K^- n) / \Gamma_{\text{total}}$					Γ_{144} / Γ
VALUE	CL%	DOCUMENT ID	TECN	COMMENT	
$< 1.1 \times 10^{-5}$	90	BAI	04G BES2	$e^+ e^-$	

See key on page 1127

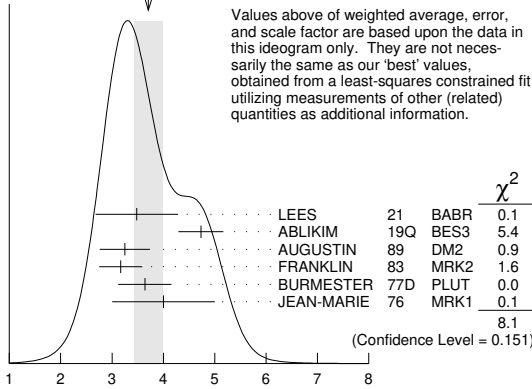
Meson Particle Listings

$J/\psi(1S)$

STABLE HADRONS

$\Gamma(2(\pi^+\pi^-\pi^0))/\Gamma_{total}$				Γ_{145}/Γ	
VALUE (units 10^{-2})	EVTS	DOCUMENT ID	TECN	COMMENT	
3.71 ± 0.28 OUR AVERAGE	Error	includes scale factor of 1.3. See the ideogram below.			
3.5 ± 0.8 ± 0.1	14k	¹ LEES	21	BABR	10.6 $e^+e^- \rightarrow 2(\pi^+\pi^-)\pi^0\gamma$
4.73 ± 0.44	228k	² ABLIKIM	19Q	BES3	$J/\psi \rightarrow 2(\pi^+\pi^-)\pi^0$
3.25 ± 0.49	46055	AUGUSTIN	89	DM2	$J/\psi \rightarrow 2(\pi^+\pi^-)\pi^0$
3.17 ± 0.42	147	FRANKLIN	83	MRK2	$e^+e^- \rightarrow$ hadrons
3.64 ± 0.52	1500	BURMESTER	77D	PLUT	e^+e^-
4 ± 1	675	JEAN-MARIE	76	MRK1	e^+e^-

WEIGHTED AVERAGE
3.71 ± 0.28 (Error scaled by 1.3)



Values above of weighted average, error, and scale factor are based upon the data in this ideogram only. They are not necessarily the same as our 'best' values, obtained from a least-squares constrained fit utilizing measurements of other (related) quantities as additional information.

			χ^2	
.....	LEES	21	BABR	0.1
.....	ABLIKIM	19Q	BES3	5.4
.....	AUGUSTIN	89	DM2	0.9
.....	FRANKLIN	83	MRK2	1.6
.....	BURMESTER	77D	PLUT	0.0
.....	JEAN-MARIE	76	MRK1	0.1
				8.1

(Confidence Level = 0.151)

$\Gamma(2(\pi^+\pi^-\pi^0))/\Gamma_{total}$ (units 10^{-2})

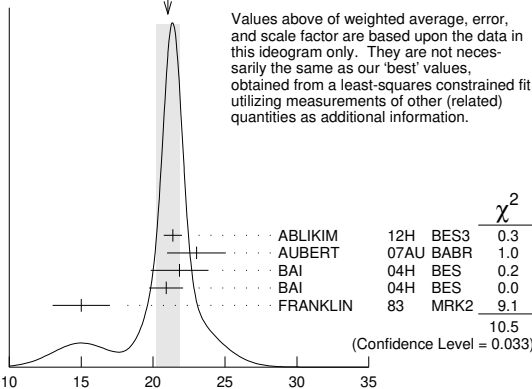
¹ LEES 21 reports $[\Gamma(J/\psi(1S) \rightarrow 2(\pi^+\pi^-\pi^0))/\Gamma_{total}] \times [\Gamma(\psi(2S) \rightarrow e^+e^-)] \times [B(\psi(2S) \rightarrow J/\psi(1S)\pi^0\pi^0)] = (14.8 \pm 2.6 \pm 2.2) \times 10^{-3}$ keV which we divide by our best values $\Gamma(\psi(2S) \rightarrow e^+e^-) = 2.33 \pm 0.04$ keV, $B(\psi(2S) \rightarrow J/\psi(1S)\pi^0\pi^0) = (18.24 \pm 0.31) \times 10^{-2}$. Our first error is their experiment's error and our second error is the systematic error from using our best values.

² From an energy scan of $e^+e^- \rightarrow J/\psi \rightarrow 2(\pi^+\pi^-)\pi^0$, assuming PDG 16 values for $\Gamma(e^+e^-)$, $\Gamma(\mu^+\mu^-)$, and Γ_{total} , and for a phase difference between strong and electromagnetic amplitudes of $(84.9 \pm 3.6)^\circ$. An alternative solution is $(4.85 \pm 0.45)^\circ$ with a phase of $(-84.7 \pm 3.1)^\circ$.

$\Gamma(3(\pi^+\pi^-\pi^0))/\Gamma_{total}$				Γ_{146}/Γ	
VALUE	EVTS	DOCUMENT ID	TECN	COMMENT	
0.029 ± 0.006 OUR AVERAGE					
0.028 ± 0.009	11	FRANKLIN	83	MRK2	$e^+e^- \rightarrow$ hadrons
0.029 ± 0.007	181	JEAN-MARIE	76	MRK1	e^+e^-

$\Gamma(\pi^+\pi^-\pi^0)/\Gamma_{total}$				Γ_{151}/Γ	
VALUE (units 10^{-3})	EVTS	DOCUMENT ID	TECN	COMMENT	
21.0 ± 0.8 OUR AVERAGE	Error	includes scale factor of 1.6. See the ideogram below.			
21.37 ± 0.04 ± 0.64 ± 0.62	1.8M	^{1,2} ABLIKIM	12H	BES3	$e^+e^- \rightarrow J/\psi$
23.0 ± 2.0 ± 0.4	256	³ AUBERT	07AU	BABR	10.6 $e^+e^- \rightarrow J/\psi\pi^+\pi^-\gamma$
21.84 ± 0.05 ± 2.01	220k	^{1,4} BAI	04H	BES	e^+e^-
20.91 ± 0.21 ± 1.16		^{4,5} BAI	04H	BES	e^+e^-
15 ± 2	168	FRANKLIN	83	MRK2	e^+e^-

WEIGHTED AVERAGE
21.0 ± 0.8 (Error scaled by 1.6)



Values above of weighted average, error, and scale factor are based upon the data in this ideogram only. They are not necessarily the same as our 'best' values, obtained from a least-squares constrained fit utilizing measurements of other (related) quantities as additional information.

			χ^2	
.....	ABLIKIM	12H	BES3	0.3
.....	AUBERT	07AU	BABR	1.0
.....	BAI	04H	BES	0.2
.....	BAI	04H	BES	0.0
.....	FRANKLIN	83	MRK2	9.1
				10.5

(Confidence Level = 0.033)

$\Gamma(\pi^+\pi^-\pi^0)/\Gamma_{total}$ (units 10^{-3})

¹ From $J/\psi \rightarrow \pi^+\pi^-\pi^0$ events directly.

² The quoted systematic error includes a contribution of 1.23% (added in quadrature) from the uncertainty on the number of J/ψ events.

³ AUBERT 07AU reports $[\Gamma(J/\psi(1S) \rightarrow \pi^+\pi^-\pi^0)/\Gamma_{total}] \times [\Gamma(\psi(2S) \rightarrow J/\psi(1S)\pi^+\pi^-) \times \Gamma(\psi(2S) \rightarrow e^+e^-)/\Gamma_{total}] = (18.6 \pm 1.2 \pm 1.1) \times 10^{-3}$ keV which we divide by our best value $\Gamma(\psi(2S) \rightarrow J/\psi(1S)\pi^+\pi^-) \times \Gamma(\psi(2S) \rightarrow e^+e^-)/\Gamma_{total} = 0.808 \pm 0.013$ keV. Our first error is their experiment's error and our second error is the systematic error from using our best value.

⁴ Mostly $\rho\pi$, see also $\rho\pi$ subsection.

⁵ Obtained comparing the rates for $\pi^+\pi^-\pi^0$ and $\mu^+\mu^-$, using J/ψ events produced via $\psi(2S) \rightarrow \pi^+\pi^-J/\psi$ and with $B(J/\psi \rightarrow \mu^+\mu^-) = 5.88 \pm 0.10\%$.

$\Gamma(\pi^+\pi^-\pi^0 K^+K^-)/\Gamma_{total}$				Γ_{153}/Γ	
VALUE (units 10^{-2})	EVTS	DOCUMENT ID	TECN	COMMENT	
1.2 ± 0.3	309	VANNUCCI	77	MRK1	e^+e^-

$\Gamma(\pi^+\pi^-)/\Gamma_{total}$				Γ_{154}/Γ	
VALUE (units 10^{-4})	EVTS	DOCUMENT ID	TECN	COMMENT	
1.47 ± 0.14 OUR AVERAGE					
1.47 ± 0.13 ± 0.13	140	¹ METREVELI	12		$\psi(2S) \rightarrow 2(\pi^+\pi^-)$
1.58 ± 0.20 ± 0.15	84	BALTRUSAIT..85D	MRK3		e^+e^-
1.0 ± 0.5	5	BRANDELIK	78B	DASP	e^+e^-
1.6 ± 1.6	1	VANNUCCI	77	MRK1	e^+e^-

¹ Obtained by analyzing CLEO-c data but not authored by the CLEO Collaboration.

$\Gamma(2(\pi^+\pi^-))/\Gamma_{total}$				Γ_{155}/Γ	
VALUE (units 10^{-3})	EVTS	DOCUMENT ID	TECN	COMMENT	
3.57 ± 0.30 OUR AVERAGE					
3.53 ± 0.12 ± 0.29	1107	¹ ABLIKIM	05H	BES2	$e^+e^- \rightarrow \psi(2S) \rightarrow J/\psi\pi^+\pi^-\pi^0, J/\psi \rightarrow 2(\pi^+\pi^-)$
4.0 ± 1.0	76	JEAN-MARIE	76	MRK1	e^+e^-

¹ Computed using $B(J/\psi \rightarrow \mu^+\mu^-) = 0.0588 \pm 0.0010$.

$\Gamma(3(\pi^+\pi^-))/\Gamma_{total}$				Γ_{156}/Γ	
VALUE (units 10^{-4})	EVTS	DOCUMENT ID	TECN	COMMENT	
40 ± 20	32	JEAN-MARIE	76	MRK1	e^+e^-

• • • We do not use the following data for averages, fits, limits, etc. • • •

$\Gamma(4(\pi^+\pi^-)\pi^0)/\Gamma_{total}$				Γ_{158}/Γ	
VALUE (units 10^{-4})	EVTS	DOCUMENT ID	TECN	COMMENT	
90 ± 30	13	JEAN-MARIE	76	MRK1	e^+e^-

$\Gamma(2(\pi^+\pi^-\eta))/\Gamma_{total}$				Γ_{159}/Γ	
VALUE (units 10^{-3})	EVTS	DOCUMENT ID	TECN	COMMENT	
2.29 ± 0.28 OUR AVERAGE					
3.1 ± 1.5 ± 0.1	14k	¹ LEES	21	BABR	10.6 $e^+e^- \rightarrow 2(\pi^+\pi^-)\pi^0\gamma$
2.26 ± 0.08 ± 0.27	4.8k	ABLIKIM	05c	BES2	$e^+e^- \rightarrow 2(\pi^+\pi^-)\eta$

¹ LEES 21 reports $[\Gamma(J/\psi(1S) \rightarrow 2(\pi^+\pi^-)\eta)/\Gamma_{total}] \times [\Gamma(J/\psi(1S) \rightarrow e^+e^-)] \times [B(\eta \rightarrow 3\pi^0)] = (5.6 \pm 2.6 \pm 0.8) \times 10^{-3}$ keV which we divide by our best values $\Gamma(J/\psi(1S) \rightarrow e^+e^-) = 5.53 \pm 0.10$ keV, $B(\eta \rightarrow 3\pi^0) = (32.57 \pm 0.21) \times 10^{-2}$. Our first error is their experiment's error and our second error is the systematic error from using our best values.

$\Gamma(3(\pi^+\pi^-\eta))/\Gamma_{total}$				Γ_{160}/Γ	
VALUE (units 10^{-4})	EVTS	DOCUMENT ID	TECN	COMMENT	
7.24 ± 0.96 ± 1.11	616	ABLIKIM	05c	BES2	$e^+e^- \rightarrow 3(\pi^+\pi^-)\eta$

$\Gamma(K^+K^-)/\Gamma_{total}$				Γ_{164}/Γ	
VALUE (units 10^{-4})	EVTS	DOCUMENT ID	TECN	COMMENT	
2.86 ± 0.09 ± 0.19	1k	¹ METREVELI	12		$\psi(2S) \rightarrow \pi^+\pi^-K^+K^-$
2.39 ± 0.24 ± 0.22	107	² BALTRUSAIT..85D	MRK3		e^+e^-
2.2 ± 0.9	6	² BRANDELIK	79c	DASP	e^+e^-

¹ Obtained by analyzing CLEO-c data but not authored by the CLEO Collaboration.

² Interference with non-resonant K^+K^- production not taken into account.

$\Gamma(K_S^0 K_L^0)/\Gamma_{total}$				Γ_{165}/Γ	
VALUE (units 10^{-4})	EVTS	DOCUMENT ID	TECN	COMMENT	
1.95 ± 0.11 OUR AVERAGE	Error	includes scale factor of 2.4. See the ideogram below.			
1.93 ± 0.01 ± 0.05	110k	ABLIKIM	17AH	BES3	$J/\psi \rightarrow K_S^0 K_L^0 \rightarrow \pi^+\pi^-X$
2.62 ± 0.15 ± 0.14	0.3k	¹ METREVELI	12		$\psi(2S) \rightarrow \pi^+\pi^-K_S^0 K_L^0$
1.82 ± 0.04 ± 0.13	2.1k	² BAI	04A	BES2	$J/\psi \rightarrow K_S^0 K_L^0 \rightarrow \pi^+\pi^-X$

• • • We do not use the following data for averages, fits, limits, etc. • • •

1.18 ± 0.12 ± 0.18 JOUSSET 90 DM2 $J/\psi \rightarrow$ hadrons

1.01 ± 0.16 ± 0.09 74 BALTRUSAIT..85D MRK3 e^+e^-

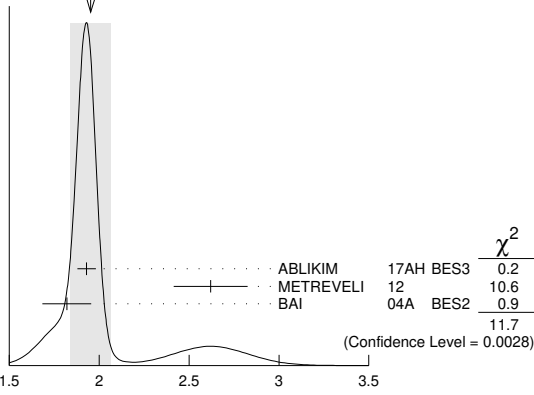
¹ Obtained by analyzing CLEO-c data but not authored by the CLEO Collaboration.

² Using $B(K_S^0 \rightarrow \pi^+\pi^-) = 0.6868 \pm 0.0027$.

Meson Particle Listings

$J/\psi(1S)$

WEIGHTED AVERAGE
1.95±0.11 (Error scaled by 2.4)



$\Gamma(K_S^0 K_S^0)/\Gamma_{total}$

VALUE	CL%	DOCUMENT ID	TECN	COMMENT
<1.4 × 10⁻⁸	95	1 ABLIKIM 17AH BES3		$J/\psi \rightarrow K_S^0 K_S^0 \rightarrow \pi^+ \pi^- \pi^+ \pi^-$

- • • We do not use the following data for averages, fits, limits, etc. • • •
 - <1 × 10⁻⁶ 95 1 BAI 04D BES e⁺e⁻
 - <5.2 × 10⁻⁶ 90 1 BALTRUSAIT...85c MRK3 e⁺e⁻
- ¹ Forbidden by CP.

$\Gamma(K^+ K^- \pi)/\Gamma_{total}$

VALUE (units 10 ⁻⁴)	EVTS	DOCUMENT ID	TECN	COMMENT
61 ± 10 OUR AVERAGE				
55.2 ± 12.0	25	FRANKLIN 83	MRK2	e ⁺ e ⁻ → K ⁺ K ⁻ π ⁰
78.0 ± 21.0	126	VANNUCCI 77	MRK1	e ⁺ e ⁻ → K _S ⁰ K _S ⁰ π [±]

$\Gamma(K^+ K^- \pi^0)/\Gamma_{total}$

VALUE (units 10 ⁻³)	EVTS	DOCUMENT ID	TECN	COMMENT
2.88 ± 0.01 ± 0.12	183k	ABLIKIM 19AQ BES		$J/\psi \rightarrow K^+ K^- \pi^0$

$\Gamma(K^+ K^- \pi^0)/\Gamma(\pi^+ \pi^- \pi^0)$

VALUE (%)	EVTS	DOCUMENT ID	TECN	COMMENT
12.0 ± 0.3 ± 0.9	23k	LEES 17C BABR		$J/\psi \rightarrow h^+ h^- \pi^0$

$\Gamma(K_S^0 K^\pm \pi^\mp)/\Gamma(\pi^+ \pi^- \pi^0)$

VALUE (%)	EVTS	DOCUMENT ID	TECN	COMMENT
26.5 ± 0.5 ± 2.1	24k	LEES 17C BABR		$J/\psi \rightarrow h^0 h^\pm \pi^\mp$

$\Gamma(K^+ K^- \pi^+ \pi^-)/\Gamma_{total}$

VALUE (units 10 ⁻³)	EVTS	DOCUMENT ID	TECN	COMMENT
7.2 ± 2.3	205	VANNUCCI 77	MRK1	e ⁺ e ⁻

$\Gamma(K^+ K^- 2(\pi^+ \pi^-))/\Gamma_{total}$

VALUE (units 10 ⁻⁴)	EVTS	DOCUMENT ID	TECN	COMMENT
31 ± 13	30	VANNUCCI 77	MRK1	e ⁺ e ⁻

$\Gamma(2(K^+ K^-))/\Gamma_{total}$

VALUE (units 10 ⁻³)	EVTS	DOCUMENT ID	TECN	COMMENT
1.4^{+0.5}_{-0.4} ± 0.2	11.0^{+4.3}_{-3.5}	1 HUANG 03	BELL	B ⁺ → 2(K ⁺ K ⁻) K ⁺
0.7 ± 0.3		VANNUCCI 77	MRK1	e ⁺ e ⁻

¹ Using B(B⁺ → J/ψ K⁺) = (1.01 ± 0.05) × 10⁻³.

$\Gamma(p\bar{p})/\Gamma_{total}$

VALUE (units 10 ⁻³)	EVTS	DOCUMENT ID	TECN	COMMENT
2.120 ± 0.029 OUR AVERAGE				
2.112 ± 0.004 ± 0.031	314k	ABLIKIM 12c	BES3	e ⁺ e ⁻
2.17 ± 0.16 ± 0.04	317	1 WU 06	BELL	B ⁺ → p \bar{p} K ⁺
2.26 ± 0.01 ± 0.14	63316	BAI 04E	BES2	e ⁺ e ⁻ → J/ψ
1.97 ± 0.22	99	BALDINI 98	FENI	e ⁺ e ⁻
1.91 ± 0.04 ± 0.30		PALLIN 87	DM2	e ⁺ e ⁻
2.16 ± 0.07 ± 0.15	1420	EATON 84	MRK2	e ⁺ e ⁻

2.5 ± 0.4	133	BRANDELIK 79c	DASP	e ⁺ e ⁻
2.0 ± 0.5		BESCH 78	BONA	e ⁺ e ⁻
2.2 ± 0.2	331	2 PERUZZI 78	MRK1	e ⁺ e ⁻

• • • We do not use the following data for averages, fits, limits, etc. • • •

2.0 ± 0.3	48	ANTONELLI 93	SPEC	e ⁺ e ⁻
-----------	----	--------------	------	-------------------------------

¹ WU 06 reports [Γ(J/ψ(1S) → p \bar{p})/Γ_{total}] × [B(B⁺ → J/ψ(1S) K⁺)] = (2.21 ± 0.13 ± 0.10) × 10⁻⁶ which we divide by our best value B(B⁺ → J/ψ(1S) K⁺) = (1.020 ± 0.019) × 10⁻³. Our first error is their experiment's error and our second error is the systematic error from using our best value.

² Assuming angular distribution (1+cos²θ).

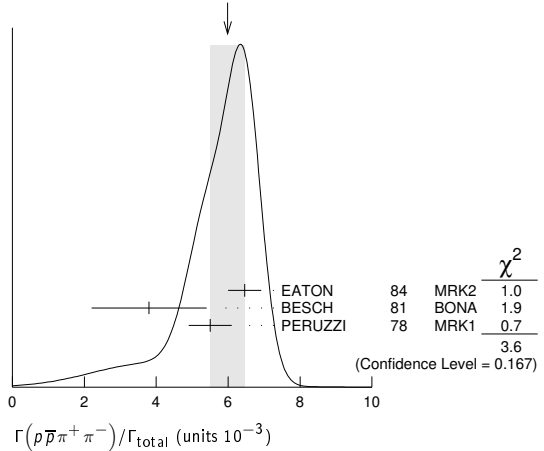
$\Gamma(p\bar{p}\pi^0)/\Gamma_{total}$

VALUE (units 10 ⁻³)	EVTS	DOCUMENT ID	TECN	COMMENT
1.19 ± 0.08 OUR AVERAGE				Error includes scale factor of 1.1.
1.33 ± 0.02 ± 0.11	11k	ABLIKIM 09b	BES2	e ⁺ e ⁻
1.13 ± 0.09 ± 0.09	685	EATON 84	MRK2	e ⁺ e ⁻
1.4 ± 0.4		BRANDELIK 79c	DASP	e ⁺ e ⁻
1.00 ± 0.15	109	PERUZZI 78	MRK1	e ⁺ e ⁻

$\Gamma(p\bar{p}\pi^+\pi^-)/\Gamma_{total}$

VALUE (units 10 ⁻³)	EVTS	DOCUMENT ID	TECN	COMMENT
6.0 ± 0.5 OUR AVERAGE				Error includes scale factor of 1.3. See the ideogram below.
6.46 ± 0.17 ± 0.43	1435	EATON 84	MRK2	e ⁺ e ⁻
3.8 ± 1.6	48	BESCH 81	BONA	e ⁺ e ⁻
5.5 ± 0.6	533	PERUZZI 78	MRK1	e ⁺ e ⁻

WEIGHTED AVERAGE
6.0±0.5 (Error scaled by 1.3)



$\Gamma(p\bar{p}\pi^+\pi^-\pi^0)/\Gamma_{total}$

VALUE (units 10 ⁻³)	EVTS	DOCUMENT ID	TECN	COMMENT
2.3 ± 0.9 OUR AVERAGE				Error includes scale factor of 1.9.
3.36 ± 0.65 ± 0.28	364	EATON 84	MRK2	e ⁺ e ⁻
1.6 ± 0.6	39	PERUZZI 78	MRK1	e ⁺ e ⁻

$\Gamma(p\bar{p}\eta)/\Gamma_{total}$

VALUE (units 10 ⁻³)	EVTS	DOCUMENT ID	TECN	COMMENT
2.00 ± 0.12 OUR AVERAGE				
1.91 ± 0.02 ± 0.17	13k	1 ABLIKIM 09	BES2	e ⁺ e ⁻
2.03 ± 0.13 ± 0.15	826	EATON 84	MRK2	e ⁺ e ⁻
2.5 ± 1.2		BRANDELIK 79c	DASP	e ⁺ e ⁻
2.3 ± 0.4	197	PERUZZI 78	MRK1	e ⁺ e ⁻

¹ From the combination of p \bar{p} η → p \bar{p} γγ and p \bar{p} η → p \bar{p} π⁺π⁻π⁰ channels.

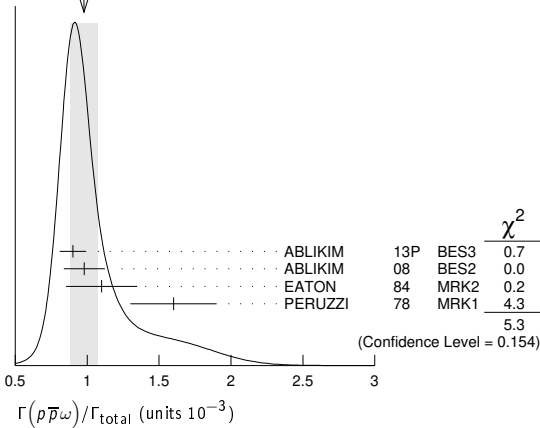
$\Gamma(p\bar{p}\rho)/\Gamma_{total}$

VALUE	CL%	DOCUMENT ID	TECN	COMMENT
<0.31 × 10⁻³	90	EATON 84	MRK2	e ⁺ e ⁻ → hadronsγ

$\Gamma(p\bar{p}\omega)/\Gamma_{total}$

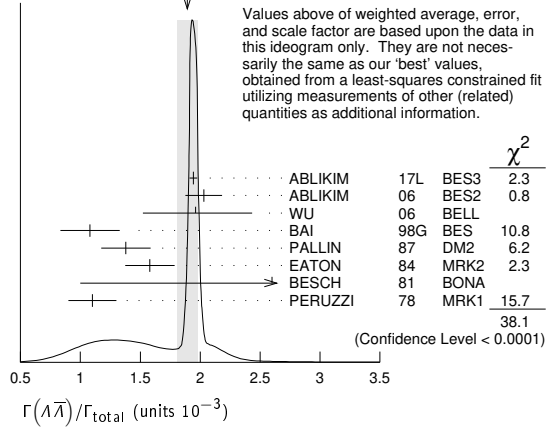
VALUE (units 10 ⁻³)	EVTS	DOCUMENT ID	TECN	COMMENT
0.98 ± 0.10 OUR AVERAGE				Error includes scale factor of 1.3. See the ideogram below.
0.90 ± 0.02 ± 0.09	2670	ABLIKIM 13p	BES3	e ⁺ e ⁻
0.98 ± 0.03 ± 0.14	2449	ABLIKIM 08	BES2	e ⁺ e ⁻
1.10 ± 0.17 ± 0.18	486	EATON 84	MRK2	e ⁺ e ⁻
1.6 ± 0.3	77	PERUZZI 78	MRK1	e ⁺ e ⁻

WEIGHTED AVERAGE
0.98±0.10 (Error scaled by 1.3)



$= (1.020 \pm 0.019) \times 10^{-3}$. Our first error is their experiment's error and our second error is the systematic error from using our best value.

WEIGHTED AVERAGE
1.89±0.09 (Error scaled by 2.8)



Values above of weighted average, error, and scale factor are based upon the data in this ideogram only. They are not necessarily the same as our 'best' values, obtained from a least-squares constrained fit utilizing measurements of other (related) quantities as additional information.

$\Gamma(p\bar{p}\eta'(958))/\Gamma_{total}$ Γ_{191}/Γ

VALUE (units 10 ⁻³)	EVTS	DOCUMENT ID	TECN	COMMENT
0.129±0.014 OUR AVERAGE		Error includes scale factor of 2.0.		
0.126±0.002±0.007	16k	1 ABLIKIM	19N	BES3 e⁺e⁻
0.200±0.023±0.028	265 ± 31	2 ABLIKIM	09	BES2 e⁺e⁻
0.68 ± 0.23 ± 0.17	19	EATON	84	MRK2 e⁺e⁻
1.8 ± 0.6	19	PERUZZI	78	MRK1 e⁺e⁻

¹ From the combination of $p\bar{p}\eta' \rightarrow p\bar{p}\pi^+\pi^-\eta$ and $p\bar{p}\eta' \rightarrow p\bar{p}\pi^+\pi^-\gamma$ channels.
² From the combination of $p\bar{p}\eta' \rightarrow p\bar{p}\pi^+\pi^-\eta$ and $p\bar{p}\eta' \rightarrow p\bar{p}\gamma\rho^0$ channels.

$\Gamma(p\bar{p}\pi_0(980) \rightarrow p\bar{p}\pi^0\eta)/\Gamma_{total}$ Γ_{192}/Γ

VALUE (units 10 ⁻⁵)	DOCUMENT ID	TECN	COMMENT
6.8±1.2±1.3	ABLIKIM	14N	BES3 e⁺e⁻ → J/ψ

$\Gamma(p\bar{p}\phi)/\Gamma_{total}$ Γ_{193}/Γ

VALUE (units 10 ⁻⁴)	EVTS	DOCUMENT ID	TECN	COMMENT
0.519±0.033 OUR AVERAGE				
0.523±0.006±0.033	14k	ABLIKIM	16K	BES3 J/ψ → p̄πK _S ⁰ K _L ⁰ , p̄πK ⁺ K ⁻
0.45 ± 0.13 ± 0.07		FALVARD	88	DM2 J/ψ → hadrons

$\Gamma(p\bar{p}\pi^-)/\Gamma_{total}$ Γ_{194}/Γ

VALUE (units 10 ⁻³)	EVTS	DOCUMENT ID	TECN	COMMENT
2.12±0.09 OUR AVERAGE				
2.36±0.02±0.21	59k	ABLIKIM	06K	BES2 J/ψ → pπ ⁻ π̄
2.47±0.02±0.24	55k	ABLIKIM	06K	BES2 J/ψ → p̄π ⁺ n
2.02±0.07±0.16	1288	EATON	84	MRK2 e⁺e⁻ → pπ ⁻
1.93±0.07±0.16	1191	EATON	84	MRK2 e⁺e⁻ → p̄π ⁺
1.7 ± 0.7	32	BESCH	81	BONA e⁺e⁻ → pπ ⁻
1.6 ± 1.2	5	BESCH	81	BONA e⁺e⁻ → p̄π ⁺
2.16±0.29	194	PERUZZI	78	MRK1 e⁺e⁻ → pπ ⁻
2.04±0.27	204	PERUZZI	78	MRK1 e⁺e⁻ → p̄π ⁺

$\Gamma(n\bar{n})/\Gamma_{total}$ Γ_{195}/Γ

VALUE (units 10 ⁻³)	EVTS	DOCUMENT ID	TECN	COMMENT
2.09±0.16 OUR AVERAGE				
2.07±0.01±0.17	36k	ABLIKIM	12c	BES3 e⁺e⁻
2.31±0.49	79	BALDINI	98	FENI e⁺e⁻
1.8 ± 0.9		BESCH	78	BONA e⁺e⁻
• • • We do not use the following data for averages, fits, limits, etc. • • •				
1.90±0.55	40	ANTONELLI	93	SPEC e⁺e⁻

$\Gamma(n\bar{n}\pi^+\pi^-)/\Gamma_{total}$ Γ_{196}/Γ

VALUE (units 10 ⁻³)	EVTS	DOCUMENT ID	TECN	COMMENT
3.8±3.6	5	BESCH	81	BONA e⁺e⁻

$\Gamma(\Lambda\bar{\Lambda})/\Gamma_{total}$ Γ_{200}/Γ

VALUE (units 10 ⁻³)	EVTS	DOCUMENT ID	TECN	COMMENT
1.89±0.09 OUR AVERAGE		Error includes scale factor of 2.8. See the ideogram below.		
1.943±0.003±0.033	441k	ABLIKIM	17L	BES3 e⁺e⁻
2.03±0.03±0.15	8887	ABLIKIM	06	BES2 J/ψ → ΛΛ̄
1.96 ^{+0.47} / _{-0.44}	46	1 WU	06	BELL B⁺ → ΛΛ̄K⁺
1.08 ± 0.06 ± 0.24	631	BAI	98G	BES e⁺e⁻
1.38 ± 0.05 ± 0.20	1847	PALLIN	87	DM2 e⁺e⁻
1.58 ± 0.08 ± 0.19	365	EATON	84	MRK2 e⁺e⁻
2.6 ± 1.6	5	BESCH	81	BONA e⁺e⁻
1.1 ± 0.2	196	PERUZZI	78	MRK1 e⁺e⁻

¹ WU 06 reports $[\Gamma(J/\psi(1S) \rightarrow \Lambda\bar{\Lambda})/\Gamma_{total}] \times [B(B^+ \rightarrow J/\psi(1S)K^+)] = (2.00^{+0.34}_{-0.29} \pm 0.34) \times 10^{-6}$ which we divide by our best value $B(B^+ \rightarrow J/\psi(1S)K^+)$

$\Gamma(\Lambda\bar{\Lambda}\pi^0)/\Gamma_{total}$ Γ_{201}/Γ

VALUE (units 10 ⁻⁵)	CL%	EVTS	DOCUMENT ID	TECN	COMMENT
3.78±0.27±0.30		323	1 ABLIKIM	13F	BES3 J/ψ → p̄ππ⁺π⁻γγ
• • • We do not use the following data for averages, fits, limits, etc. • • •					
< 6.4		90	2 ABLIKIM	07H	BES2 e⁺e⁻ → ψ(2S)
23 ± 7 ± 8		11	BAI	98G	BES e⁺e⁻
22 ± 5 ± 5		19	HENRRARD	87	DM2 e⁺e⁻
¹ Using B(Λ → π ⁻ p) = 63.9% and B(π ⁰ → γγ) = 98.8%. ² Using B(Λ → π ⁻ p) = 63.9%.					

$\Gamma(\Lambda\bar{\Lambda}\pi^+\pi^-)/\Gamma_{total}$ Γ_{202}/Γ

VALUE (units 10 ⁻³)	EVTS	DOCUMENT ID	TECN	COMMENT
4.30±0.13±0.99	2.4k	ABLIKIM	12P	BES2 J/ψ

$\Gamma(\Lambda\bar{\Lambda}\eta)/\Gamma_{total}$ Γ_{203}/Γ

VALUE (units 10 ⁻⁵)	EVTS	DOCUMENT ID	TECN	COMMENT
16.2±1.7 OUR AVERAGE				
15.7±0.80±1.54	454	1 ABLIKIM	13F	BES3 J/ψ → p̄ππ⁺π⁻γγ
26.2±6.0 ± 4.4	44	2 ABLIKIM	07H	BES2 e⁺e⁻ → ψ(2S)
¹ Using B(Λ → π ⁻ p) = 63.9% and B(η → γγ) = 39.31%. ² Using B(Λ → π ⁻ p) = 63.9% and B(η → γγ) = 39.4%.				

$\Gamma(\Lambda\bar{\Sigma}^-\pi^+ \text{ (or c.c.)})/\Gamma_{total}$ Γ_{204}/Γ

VALUE (units 10 ⁻³)	EVTS	DOCUMENT ID	TECN	COMMENT
0.83 ± 0.07 OUR AVERAGE		Error includes scale factor of 1.2.		
0.770±0.051±0.083	335	1 ABLIKIM	07H	BES2 e⁺e⁻ → ΛΣ ⁺ π ⁻
0.747±0.056±0.076	254	1 ABLIKIM	07H	BES2 e⁺e⁻ → ΛΣ ⁻ π ⁺
0.90 ± 0.06 ± 0.16	225 ± 15	HENRRARD	87	DM2 e⁺e⁻ → ΛΣ ⁺ π ⁻
1.11 ± 0.06 ± 0.20	342 ± 18	HENRRARD	87	DM2 e⁺e⁻ → ΛΣ ⁻ π ⁺
1.53 ± 0.17 ± 0.38	135	EATON	84	MRK2 e⁺e⁻ → ΛΣ ⁺ π ⁻
1.38 ± 0.21 ± 0.35	118	EATON	84	MRK2 e⁺e⁻ → ΛΣ ⁻ π ⁺
¹ Using B(Λ → π ⁻ p) = 63.9% and B(Σ ⁺ → π ⁰ p) = 51.6%.				

$\Gamma(pK^-\bar{\Lambda}+c.c.)/\Gamma_{total}$ Γ_{205}/Γ

VALUE (units 10 ⁻³)	EVTS	DOCUMENT ID	TECN	COMMENT
0.86±0.11 OUR AVERAGE				
0.84 ^{+0.17} / _{-0.15} ± 0.02	45	1 LU	19	BELL B⁺ → p̄ΛK⁺K⁺
0.89±0.07±0.14	307	EATON	84	MRK2 e⁺e⁻
¹ LU 19 reports $(8.32^{+1.63}_{-1.45} \pm 0.49) \times 10^{-4}$ from a measurement of $[\Gamma(J/\psi(1S) \rightarrow pK^-\bar{\Lambda}+c.c.)/\Gamma_{total}] \times [B(B^+ \rightarrow J/\psi(1S)K^+)]$ assuming $B(B^+ \rightarrow J/\psi(1S)K^+) = (1.026 \pm 0.031) \times 10^{-3}$, which we rescale to our best value $B(B^+ \rightarrow J/\psi(1S)K^+) = (1.020 \pm 0.019) \times 10^{-3}$. Our first error is their experiment's error and our second error is the systematic error from using our best value.				

$\Gamma(pK^-\Sigma^0)/\Gamma_{total}$ Γ_{206}/Γ

VALUE (units 10 ⁻³)	EVTS	DOCUMENT ID	TECN	COMMENT
0.29±0.06±0.05	90	EATON	84	MRK2 e⁺e⁻

$\Gamma(\bar{\Lambda}nK_S^0 + c.c.)/\Gamma_{total}$ Γ_{207}/Γ

VALUE (units 10 ⁻⁴)	EVTS	DOCUMENT ID	TECN	COMMENT
6.46±0.20±1.07	1058	1 ABLIKIM	08c	BES2 e⁺e⁻ → J/ψ
¹ Using B(Λ̄ → p̄π ⁺) = 63.9% and B(K _S ⁰ → π ⁺ π ⁻) = 69.2%.				

Meson Particle Listings

$J/\psi(1S)$

$\Gamma(\Lambda\bar{\Sigma} + c.c.)/\Gamma_{total}$			Γ_{208}/Γ		
VALUE (units 10^{-3})	CL%	EVTS	DOCUMENT ID	TECN	COMMENT
2.83 ± 0.23 OUR AVERAGE					
2.74 ± 0.24 ± 0.22		234 ± 21	1 ABLIKIM	12B BES3	$J/\psi \rightarrow \Lambda\bar{\Sigma}^0$
2.92 ± 0.22 ± 0.24		308 ± 24	2 ABLIKIM	12B BES3	$J/\psi \rightarrow \bar{\Lambda}\Sigma^0$

• • • We do not use the following data for averages, fits, limits, etc. • • •

VALUE (units 10^{-3})	CL%	EVTS	DOCUMENT ID	TECN	COMMENT
<18			2 HENRARD	87 DM2	$J/\psi \rightarrow \bar{\Lambda}\Sigma^0$
<15	90	90	PERUZZI	78 MRK1	$e^+e^- \rightarrow \Lambda X$

1 ABLIKIM 12B quotes $B(J/\psi \rightarrow \Lambda\bar{\Sigma}^0)$ which we multiply by 2.
 2 ABLIKIM 12B and HENRARD 87 quote results for $B(J/\psi \rightarrow \bar{\Lambda}\Sigma^0)$ which we multiply by 2.

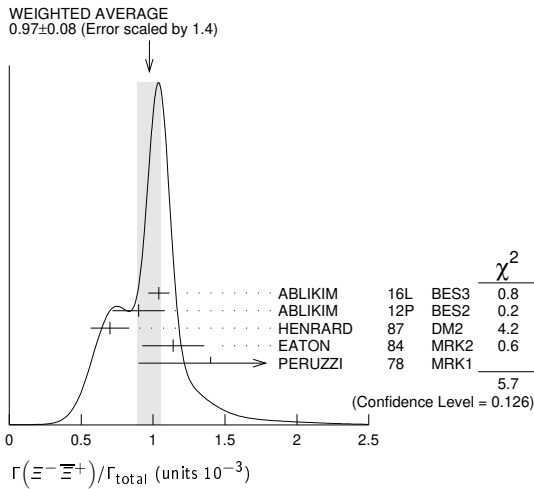
$\Gamma(\Sigma^+ \bar{\Sigma}^-)/\Gamma_{total}$			Γ_{209}/Γ		
VALUE (units 10^{-3})	CL%	EVTS	DOCUMENT ID	TECN	COMMENT
1.07 ± 0.04 OUR AVERAGE					
1.061 ± 0.004 ± 0.036		87k	ABLIKIM	21AT BES3	$J/\psi \rightarrow p\pi^0\bar{p}\pi^0$
1.50 ± 0.10 ± 0.22		399	ABLIKIM	08o BES2	$e^+e^- \rightarrow J/\psi$

$\Gamma(\Sigma^0 \bar{\Sigma}^0)/\Gamma_{total}$			Γ_{210}/Γ		
VALUE (units 10^{-3})	CL%	EVTS	DOCUMENT ID	TECN	COMMENT
1.172 ± 0.032 OUR AVERAGE					
1.164 ± 0.004 ± 0.023		111k	ABLIKIM	17L BES3	$J/\psi \rightarrow \Sigma^0 \bar{\Sigma}^0$
1.33 ± 0.04 ± 0.11		1.7k	ABLIKIM	06 BES2	$J/\psi \rightarrow \Sigma^0 \bar{\Sigma}^0$
1.06 ± 0.04 ± 0.23		884	PALLIN	87 DM2	$e^+e^- \rightarrow \Sigma^0 \bar{\Sigma}^0$
1.58 ± 0.16 ± 0.25		90	EATON	84 MRK2	$e^+e^- \rightarrow \Sigma^0 \bar{\Sigma}^0$
1.3 ± 0.4		52	PERUZZI	78 MRK1	$e^+e^- \rightarrow \Sigma^0 \bar{\Sigma}^0$
2.4 ± 2.6		3	BESCH	81 BONA	$e^+e^- \rightarrow \Sigma^+ \bar{\Sigma}^-$

• • • We do not use the following data for averages, fits, limits, etc. • • •

$\Gamma(\Xi^- \bar{\Xi}^+)/\Gamma_{total}$			Γ_{211}/Γ		
VALUE (units 10^{-3})	CL%	EVTS	DOCUMENT ID	TECN	COMMENT
0.97 ± 0.08 OUR AVERAGE					
1.040 ± 0.006 ± 0.074		43k	ABLIKIM	16L BES3	$J/\psi \rightarrow \Xi^- \bar{\Xi}^+$
0.90 ± 0.03 ± 0.18		961	ABLIKIM	12P BES2	$J/\psi \rightarrow \Xi^- \bar{\Xi}^+$
0.70 ± 0.06 ± 0.12		132	HENRARD	87 DM2	$e^+e^- \rightarrow \Xi^- \bar{\Xi}^+$
1.14 ± 0.08 ± 0.20		194	EATON	84 MRK2	$e^+e^- \rightarrow \Xi^- \bar{\Xi}^+$
1.4 ± 0.5		51	PERUZZI	78 MRK1	$e^+e^- \rightarrow \Xi^- \bar{\Xi}^+$

Error includes scale factor of 1.4. See the ideogram below.



RADIATIVE DECAYS

$\Gamma(\gamma\eta_c(1S))/\Gamma_{total}$			Γ_{212}/Γ		
VALUE (units 10^{-2})	CL%	EVTS	DOCUMENT ID	TECN	COMMENT
1.7 ± 0.4 OUR AVERAGE					
2.00 ± 0.31 ± 0.02			1 MITCHELL	09 CLEO	$e^+e^- \rightarrow \gamma X$
1.27 ± 0.36			GAISER	86 CBAL	$J/\psi \rightarrow \gamma X$

• • • We do not use the following data for averages, fits, limits, etc. • • •

VALUE (units 10^{-2})	CL%	EVTS	DOCUMENT ID	TECN	COMMENT
0.79 ± 0.20		273 ± 43	2 AUBERT	06E BABR	$B^\pm \rightarrow K^\pm X_c \bar{\tau}$
seen		16	BALTRUSAITIS...	84 MRK3	$J/\psi \rightarrow 2\phi\gamma$

1 MITCHELL 09 reports $(1.98 \pm 0.09 \pm 0.30) \times 10^{-2}$ from a measurement of $[\Gamma(J/\psi(1S) \rightarrow \gamma\eta_c(1S))/\Gamma_{total}] \times [B(\psi(2S) \rightarrow J/\psi(1S)\pi^+\pi^-)]$ assuming $B(\psi(2S) \rightarrow J/\psi(1S)\pi^+\pi^-) = (35.04 \pm 0.07 \pm 0.77) \times 10^{-2}$, which we rescale to our best value $B(\psi(2S) \rightarrow J/\psi(1S)\pi^+\pi^-) = (34.68 \pm 0.30) \times 10^{-2}$. Our first error is their experiment's error and our second error is the systematic error from using our best value.
 2 Calculated by the authors using an average of $B(J/\psi \rightarrow \gamma\eta_c) \times B(\eta_c \rightarrow K\bar{K}\pi)$ from BALTRUSAITIS 86, BISELLO 91, BAL 04 and $B(\eta_c \rightarrow K\bar{K}\pi) = (8.5 \pm 1.8)\%$ from AUBERT 06E.

$\Gamma(\gamma\eta_c(1S) \rightarrow 3\gamma)/\Gamma_{total}$			Γ_{213}/Γ		
VALUE (units 10^{-6})	CL%	EVTS	DOCUMENT ID	TECN	COMMENT
3.8 ± 1.3 OUR AVERAGE					
4.5 ± 1.2 ± 0.6		33 ± 9	ABLIKIM	13i BES3	$\psi(2S) \rightarrow \pi^+\pi^-J/\psi$
1.2 ± 2.7 ± 0.3		1.2 ± 2.8 ± 1.1	ADAMS	08 CLEO	$\psi(2S) \rightarrow \pi^+\pi^-J/\psi$

Error includes scale factor of 1.1.

$\Gamma(\gamma\eta_c(1S) \rightarrow \gamma\eta\eta')/\Gamma_{total}$			Γ_{214}/Γ		
VALUE (units 10^{-5})	CL%	EVTS	DOCUMENT ID	TECN	COMMENT
4.86 ± 0.62 ± 0.45					
		137	ABLIKIM	21c BES3	$J/\psi(1S) \rightarrow \gamma\eta\eta'$

$\Gamma(3\gamma)/\Gamma_{total}$			Γ_{215}/Γ		
VALUE (units 10^{-6})	CL%	EVTS	DOCUMENT ID	TECN	COMMENT
11.6 ± 2.2 OUR AVERAGE					
11.3 ± 1.8 ± 2.0		113 ± 18	ABLIKIM	13i BES3	$\psi(2S) \rightarrow \pi^+\pi^-J/\psi$
12 ± 3 ± 2		24.2 ± 7.2 ± 6.0	ADAMS	08 CLEO	$\psi(2S) \rightarrow \pi^+\pi^-J/\psi$

• • • We do not use the following data for averages, fits, limits, etc. • • •

VALUE (units 10^{-6})	CL%	EVTS	DOCUMENT ID	TECN	COMMENT
<55		90	PARTRIDGE	80 CBAL	e^+e^-

$\Gamma(4\gamma)/\Gamma_{total}$			Γ_{216}/Γ		
VALUE	CL%	EVTS	DOCUMENT ID	TECN	COMMENT
<9 × 10⁻⁶					
	90		ADAMS	08 CLEO	$\psi(2S) \rightarrow \pi^+\pi^-J/\psi$

$\Gamma(5\gamma)/\Gamma_{total}$			Γ_{217}/Γ		
VALUE	CL%	EVTS	DOCUMENT ID	TECN	COMMENT
<15 × 10⁻⁶					
	90		ADAMS	08 CLEO	$\psi(2S) \rightarrow \pi^+\pi^-J/\psi$

$\Gamma(\gamma\pi^0)/\Gamma_{total}$			Γ_{218}/Γ		
VALUE (units 10^{-5})	CL%	EVTS	DOCUMENT ID	TECN	COMMENT
3.56 ± 0.17 OUR AVERAGE					
3.59 ± 0.20 ± 0.03		1.6k	1 ABLIKIM	18o BES3	$\psi(2S) \rightarrow \pi^+\pi^-\gamma\gamma$
3.63 ± 0.36 ± 0.13			PEDLAR	09 CLE3	$J/\psi \rightarrow \pi^0\gamma$
3.13 ± 0.65 ± 0.47		586	ABLIKIM	06E BES2	$J/\psi \rightarrow \pi^0\gamma$
3.6 ± 1.1 ± 0.7			BLOOM	83 CBAL	e^+e^-
7.3 ± 4.7		10	BRANDELIK	79c DASP	e^+e^-

• • • We do not use the following data for averages, fits, limits, etc. • • •

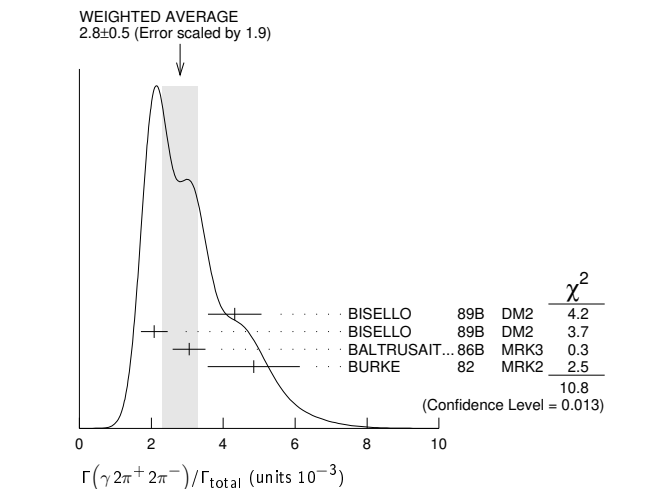
1 ABLIKIM 18o reports $[\Gamma(J/\psi(1S) \rightarrow \gamma\pi^0)/\Gamma_{total}] \times [B(\pi^0 \rightarrow 2\gamma)] = (3.57 \pm 0.12 \pm 0.16) \times 10^{-5}$ from a measurement of $[\Gamma(J/\psi(1S) \rightarrow \gamma\pi^0)/\Gamma_{total}] \times [B(\pi^0 \rightarrow 2\gamma)] \times [B(\psi(2S) \rightarrow J/\psi(1S)\pi^+\pi^-)]$ assuming $B(\psi(2S) \rightarrow J/\psi(1S)\pi^+\pi^-) = (34.49 \pm 0.30) \times 10^{-2}$, which we rescale to our best values $B(\pi^0 \rightarrow 2\gamma) = (98.823 \pm 0.034) \times 10^{-2}$, $B(\psi(2S) \rightarrow J/\psi(1S)\pi^+\pi^-) = (34.68 \pm 0.30) \times 10^{-2}$. Our first error is their experiment's error and our second error is the systematic error from using our best values.

$\Gamma(\gamma\pi^0\pi^0)/\Gamma_{total}$			Γ_{219}/Γ		
VALUE (units 10^{-3})	CL%	EVTS	DOCUMENT ID	TECN	COMMENT
1.15 ± 0.05					
			1 ABLIKIM	15AE BES3	$J/\psi \rightarrow \gamma\pi^0\pi^0$

1 The uncertainty is systematic as statistical is negligible.

$\Gamma(\gamma 2\pi^+ 2\pi^-)/\Gamma_{total}$			Γ_{220}/Γ		
VALUE (units 10^{-3})	CL%	EVTS	DOCUMENT ID	TECN	COMMENT
2.8 ± 0.5 OUR AVERAGE					
4.32 ± 0.14 ± 0.73			1 BISELLO	89B DM2	$J/\psi \rightarrow 4\pi\gamma$
2.08 ± 0.13 ± 0.35			2 BISELLO	89B DM2	$J/\psi \rightarrow 4\pi\gamma$
3.05 ± 0.08 ± 0.45			2 BALTRUSAITIS...	86B MRK3	$J/\psi \rightarrow 4\pi\gamma$
4.85 ± 0.45 ± 1.20			3 BURKE	82 MRK2	e^+e^-

Error includes scale factor of 1.9. See the ideogram below.



1 4π mass less than 3.0 GeV.

² 4π mass less than 2.0 GeV.
³ 4π mass less than 2.5 GeV.

Γ(γ f₂(1270) f₂(1270))/Γ_{total} Γ₂₂₁/Γ

Γ(γ f₂(1270) f₂(1270) (non resonant))/Γ_{total} Γ₂₂₂/Γ

Γ(γ π⁺ π⁻ 2π⁰)/Γ_{total} Γ₂₂₃/Γ

Γ(γ K_S⁰ K_S⁰)/Γ_{total} Γ₂₂₄/Γ

Γ(γ (K⁺ K⁻ π⁺ π⁻))/Γ_{total} Γ₂₂₅/Γ

Γ(γ K⁺ K⁻ π⁺ π⁻)/Γ_{total} Γ₂₂₆/Γ

Γ(γ K⁺(892) K⁻(892))/Γ_{total} Γ₂₂₇/Γ

Γ(γγ)/Γ_{total} Γ₂₂₈/Γ

¹ ABLIKIM 180 reports [Γ(J/ψ(1S) → γη)/Γ_{total}] × [B(η → 2γ)] = (4.42 ± 0.04 ± 0.18) × 10⁻⁴ from a measurement of [Γ(J/ψ(1S) → γη)/Γ_{total}] × [B(η → 2γ)] × [B(ψ(2S) → J/ψ(1S) π⁺ π⁻)] assuming B(ψ(2S) → J/ψ(1S) π⁺ π⁻) = (34.49 ± 0.30) × 10⁻², which we rescale to our best values B(η → 2γ) = (39.36 ± 0.18) × 10⁻², B(ψ(2S) → J/ψ(1S) π⁺ π⁻) = (34.68 ± 0.30) × 10⁻². Our first error is their experiment's error and our second error is the systematic error from using our best values.

Γ(γγπ⁰)/Γ_{total} Γ₂₂₉/Γ

Γ(γ a₀(980)⁰ → γηπ⁰)/Γ_{total} Γ₂₃₃/Γ

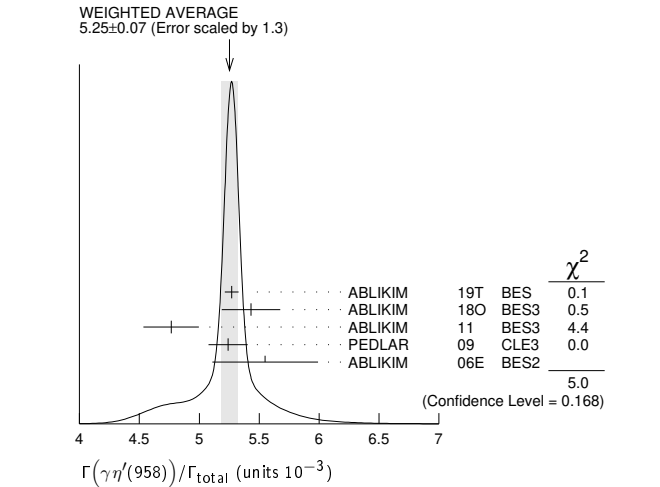
Γ(γ a₂(1320)⁰ → γηπ⁰)/Γ_{total} Γ₂₃₄/Γ

Γ(γγππ)/Γ_{total} Γ₂₃₅/Γ

Γ(γγ₂(1870) → γηπ⁺ π⁻)/Γ_{total} Γ₂₃₆/Γ

Γ(γγ(958))/Γ_{total} Γ₂₃₇/Γ

¹ ABLIKIM 180 reports [Γ(J/ψ(1S) → γη'(958))/Γ_{total}] × [B(η'(958) → γγ)] = (1.26 ± 0.02 ± 0.05) × 10⁻⁴ from a measurement of [Γ(J/ψ(1S) → γη'(958))/Γ_{total}] × [B(η'(958) → γγ)] × [B(ψ(2S) → J/ψ(1S) π⁺ π⁻)] assuming B(ψ(2S) → J/ψ(1S) π⁺ π⁻) = (34.49 ± 0.30) × 10⁻², which we rescale to our best values B(η'(958) → γγ) = (2.307 ± 0.033) × 10⁻², B(ψ(2S) → J/ψ(1S) π⁺ π⁻) = (34.68 ± 0.30) × 10⁻². Our first error is their experiment's error and our second error is the systematic error from using our best values.
² ABLIKIM 11 reports (4.84 ± 0.03 ± 0.24) × 10⁻³ from a measurement of [Γ(J/ψ(1S) → γη'(958))/Γ_{total}] / [B(η'(958) → π⁺ π⁻ η)] / [B(η → 2γ)] assuming B(η'(958) → π⁺ π⁻ η) = (43.2 ± 0.7) × 10⁻², B(η → 2γ) = (39.31 ± 0.20) × 10⁻², which we rescale to our best values B(η'(958) → π⁺ π⁻ η) = (42.5 ± 0.5) × 10⁻², B(η → 2γ) = (39.36 ± 0.18) × 10⁻². Our first error is their experiment's error and our second error is the systematic error from using our best values.



Γ(γ f₀(500) → γππ)/Γ_{total} Γ₂₃₀/Γ

Γ(γ f₀(500) → γK⁺ K⁻)/Γ_{total} Γ₂₃₁/Γ

Γ(γ f₀(500) → γηη)/Γ_{total} Γ₂₃₂/Γ

Γ(γ f₀(980) → γππ)/Γ_{total} Γ₂₃₈/Γ

Γ(γ f₀(980) → γK⁺ K⁻)/Γ_{total} Γ₂₃₉/Γ

Meson Particle Listings

$J/\psi(1S)$

$\Gamma(\gamma\rho\rho)/\Gamma_{total}$ Γ_{240}/Γ

VALUE (units 10^{-3})	CL%	DOCUMENT ID	TECN	COMMENT
4.5 ± 0.8 OUR AVERAGE				
4.7 ± 0.3 ± 0.9		1 BALTRUSAIT..86B	MRK3	$J/\psi \rightarrow 4\pi\gamma$
3.75 ± 1.05 ± 1.20		2 BURKE	82 MRK2	$J/\psi \rightarrow 4\pi\gamma$
• • • We do not use the following data for averages, fits, limits, etc. • • •				
<0.09	90	3 BISELLO	89B	$J/\psi \rightarrow 4\pi\gamma$
1 4π mass less than 2.0 GeV. 2 4π mass less than 2.0 GeV. We have multiplied $2\rho^0$ measurement by 3 to obtain 2ρ . 3 4π mass in the range 2.0–25 GeV.				

$\Gamma(\gamma\rho\omega)/\Gamma_{total}$ Γ_{241}/Γ

VALUE	CL%	DOCUMENT ID	TECN	COMMENT
<5.4 × 10⁻⁴	90	ABLIKIM	08A	BES2 $e^+e^- \rightarrow J/\psi$

$\Gamma(\gamma\rho\phi)/\Gamma_{total}$ Γ_{242}/Γ

VALUE	CL%	DOCUMENT ID	TECN	COMMENT
<8.8 × 10⁻⁵	90	ABLIKIM	08A	BES2 $e^+e^- \rightarrow J/\psi$

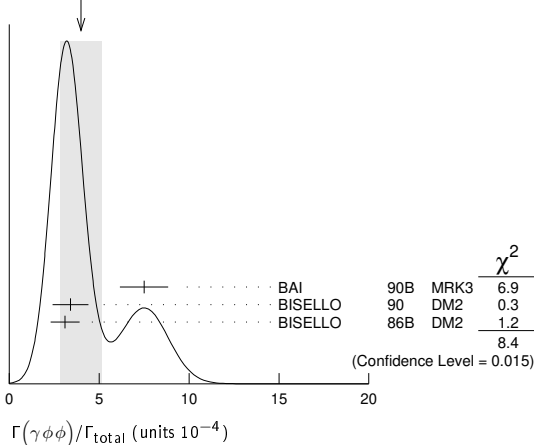
$\Gamma(\gamma\omega\omega)/\Gamma_{total}$ Γ_{243}/Γ

VALUE (units 10^{-3})	EVTS	DOCUMENT ID	TECN	COMMENT
1.61 ± 0.33 OUR AVERAGE				
6.0 ± 4.8 ± 1.8		ABLIKIM	08A	BES2 $J/\psi \rightarrow \gamma\omega\pi^+\pi^-$
1.41 ± 0.2 ± 0.42	120 ± 17	BISELLO	87	SPEC e^+e^- , hadrons γ
1.76 ± 0.09 ± 0.45		BALTRUSAIT..85c	MRK3	$e^+e^- \rightarrow$ hadrons γ

$\Gamma(\gamma\phi\phi)/\Gamma_{total}$ Γ_{244}/Γ

VALUE (units 10^{-4})	EVTS	DOCUMENT ID	TECN	COMMENT
4.0 ± 1.2 OUR AVERAGE				Error includes scale factor of 2.1. See the ideogram below.
7.5 ± 0.6 ± 1.2	168	BAI	90B	MRK3 $J/\psi \rightarrow \gamma 4K$
3.4 ± 0.8 ± 0.6	33 ± 7	1 BISELLO	90	DM2 $J/\psi \rightarrow \gamma K^+ K^- K_S^0 K_L^0$
3.1 ± 0.7 ± 0.4		1 BISELLO	86B	DM2 $J/\psi \rightarrow \gamma K^+ K^- K^+ K^-$

WEIGHTED AVERAGE
4.0 ± 1.2 (Error scaled by 2.1)



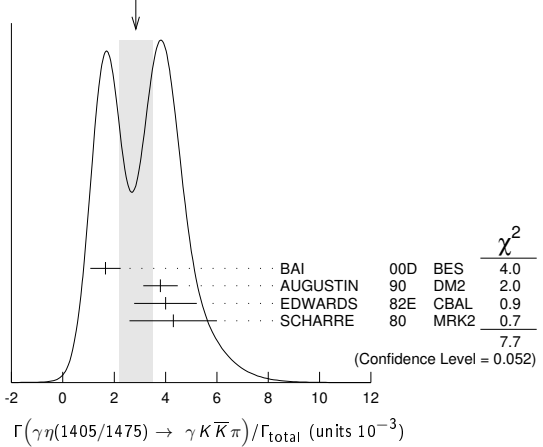
1 $\phi\phi$ mass less than 2.9 GeV, η_c excluded.

$\Gamma(\gamma\eta(1405/1475) \rightarrow \gamma K\bar{K}\pi)/\Gamma_{total}$ Γ_{245}/Γ

VALUE (units 10^{-3})	DOCUMENT ID	TECN	COMMENT
2.8 ± 0.6 OUR AVERAGE			Error includes scale factor of 1.6. See the ideogram below.
1.66 ± 0.1 ± 0.58	1,2 BAI	00D	BES $J/\psi \rightarrow \gamma K^\pm K_S^0 \pi^\mp$
3.8 ± 0.3 ± 0.6	3 AUGUSTIN	90	DM2 $J/\psi \rightarrow \gamma K\bar{K}\pi$
4.0 ± 0.7 ± 1.0	3 EDWARDS	82E	CBAL $J/\psi \rightarrow K^+ K^- \pi^0 \gamma$
4.3 ± 1.7	3,4 SCHARRE	80	MRK2 e^+e^-
• • • We do not use the following data for averages, fits, limits, etc. • • •			
1.78 ± 0.21 ± 0.33	3,5,6 AUGUSTIN	92	DM2 $J/\psi \rightarrow \gamma K\bar{K}\pi$
0.83 ± 0.13 ± 0.18	3,7,8 AUGUSTIN	92	DM2 $J/\psi \rightarrow \gamma K\bar{K}\pi$
0.66 ± 0.17 ± 0.24	3,6,9 BAI	90c	MRK3 $J/\psi \rightarrow \gamma K_S^0 K^\pm \pi^\mp$
1.03 ± 0.21 ± 0.26	3,8,10 BAI	90c	MRK3 $J/\psi \rightarrow \gamma K_S^0 K^\pm \pi^\mp$
1.03 ± 0.18 ± 0.19			

- Interference with the $J/\psi(1S)$ radiative transition to the broad $K\bar{K}\pi$ pseudoscalar state around 1800 is $(0.15 \pm 0.01 \pm 0.05) \times 10^{-3}$.
- Interference with $J/\psi \rightarrow \gamma f_1(1420)$ is $(-0.03 \pm 0.01 \pm 0.01) \times 10^{-3}$.
- Includes unknown branching fraction $\eta(1405) \rightarrow K\bar{K}\pi$.
- Corrected for spin-zero hypothesis for $\eta(1405)$.
- From fit to the $a_0(980)\pi^0$ partial wave.
- $a_0(980)\pi$ mode.
- From fit to the $K^*(892)K^0$ partial wave.
- K^*K mode.
- From $a_0(980)\pi$ final state.
- From $K^*(890)K$ final state.

WEIGHTED AVERAGE
2.8 ± 0.6 (Error scaled by 1.6)



$\Gamma(\gamma\eta(1405/1475) \rightarrow \gamma\rho\rho^0)/\Gamma_{total}$ Γ_{246}/Γ

VALUE (units 10^{-4})	DOCUMENT ID	TECN	COMMENT
0.78 ± 0.20 OUR AVERAGE			Error includes scale factor of 1.8.
1.07 ± 0.17 ± 0.11	1 BAI	04J	BES2 $J/\psi \rightarrow \gamma\eta\pi^+\pi^-$
0.64 ± 0.12 ± 0.07	1 COFFMAN	90	MRK3 $J/\psi \rightarrow \gamma\eta\pi^+\pi^-$
1 Includes unknown branching fraction $\eta(1405) \rightarrow \gamma\rho^0$.			

$\Gamma(\gamma\eta(1405/1475) \rightarrow \gamma\eta\pi^+\pi^-)/\Gamma_{total}$ Γ_{247}/Γ

VALUE (units 10^{-4})	EVTS	DOCUMENT ID	TECN	COMMENT
3.0 ± 0.5 OUR AVERAGE				
2.6 ± 0.7 ± 0.4		BAI	99	BES $J/\psi \rightarrow \gamma\eta\pi^+\pi^-$
3.38 ± 0.33 ± 0.64		1 BOLTON	92B	MRK3 $J/\psi \rightarrow \gamma\eta\pi^+\pi^-$
• • • We do not use the following data for averages, fits, limits, etc. • • •				
7.0 ± 0.6 ± 1.1	261	2 AUGUSTIN	90	DM2 $J/\psi \rightarrow \gamma\eta\pi^+\pi^-$
1 Via $a_0(980)\pi$. 2 Includes unknown branching fraction to $\eta\pi^+\pi^-$.				

$\Gamma(\gamma\eta(1405/1475) \rightarrow \gamma\rho^0\rho^0)/\Gamma_{total}$ Γ_{248}/Γ

VALUE (units 10^{-3})	DOCUMENT ID	TECN	COMMENT
1.7 ± 0.4 OUR AVERAGE			Error includes scale factor of 1.3.
2.1 ± 0.4	BUGG	95	MRK3 $J/\psi \rightarrow \gamma\pi^+\pi^-\pi^+\pi^-$
1.36 ± 0.38	1,2 BISELLO	89B	DM2 $J/\psi \rightarrow 4\pi\gamma$
1 Estimated by us from various fits. 2 Includes unknown branching fraction to $\rho^0\rho^0$.			

$\Gamma(\gamma\eta(1405/1475) \rightarrow \gamma\phi\phi)/\Gamma_{total}$ Γ_{249}/Γ

VALUE (units 10^{-6})	CL%	EVTS	DOCUMENT ID	TECN	COMMENT
<82	95		BAI	04J	BES2 $J/\psi \rightarrow \gamma\gamma K^+ K^-$
• • • We do not use the following data for averages, fits, limits, etc. • • •					
7.03 ± 0.92 ± 0.91	1.3k		1 ABLIKIM	18i	BES3 $J/\psi \rightarrow \gamma\gamma\phi(1020)$
10.36 ± 1.51 ± 1.54	1.9k		2 ABLIKIM	18i	BES3 $J/\psi \rightarrow \gamma\gamma\phi(1020)$
1 Constructive interference between the $X(1835)$ and $\eta(1405)/\eta(1475)$ is assumed in a fit to the $\gamma\phi$ invariant mass. 2 Destructive interference between the $X(1835)$ and $\eta(1405)/\eta(1475)$ is assumed in a fit to the $\gamma\phi$ invariant mass.					

$\Gamma(\gamma\eta(1405) \rightarrow \gamma\gamma\gamma)/\Gamma_{total}$ Γ_{250}/Γ

VALUE	CL%	DOCUMENT ID	TECN	COMMENT
<2.63 × 10⁻⁶	90	ABLIKIM	18o	BES3 $\psi(2S) \rightarrow \pi^+\pi^-\gamma\gamma\gamma$

$\Gamma(\gamma\eta(1475) \rightarrow \gamma\gamma\gamma)/\Gamma_{total}$ Γ_{251}/Γ

VALUE	CL%	DOCUMENT ID	TECN	COMMENT
<1.86 × 10⁻⁶	90	ABLIKIM	18o	BES3 $\psi(2S) \rightarrow \pi^+\pi^-\gamma\gamma\gamma$

$\Gamma(\gamma\eta(1760) \rightarrow \gamma\rho^0\rho^0)/\Gamma_{total}$ Γ_{252}/Γ

VALUE (units 10^{-3})	DOCUMENT ID	TECN	COMMENT
0.13 ± 0.09	1,2 BISELLO	89B	DM2 $J/\psi \rightarrow 4\pi\gamma$
1 Estimated by us from various fits. 2 Includes unknown branching fraction to $\rho^0\rho^0$.			

$\Gamma(\gamma\eta(1760) \rightarrow \gamma\omega\omega)/\Gamma_{total}$ Γ_{253}/Γ

VALUE (units 10^{-3})	EVTS	DOCUMENT ID	TECN	COMMENT
1.98 ± 0.08 ± 0.32	1045	ABLIKIM	06H	BES $J/\psi \rightarrow \gamma\omega\omega$

$\Gamma(\gamma\eta(1760) \rightarrow \gamma\gamma\gamma)/\Gamma_{total}$ Γ_{254}/Γ

VALUE	CL%	DOCUMENT ID	TECN	COMMENT
<4.80 × 10⁻⁶	90	ABLIKIM	18o	BES3 $\psi(2S) \rightarrow \pi^+\pi^-\gamma\gamma\gamma$

Γ(γη(2225))/Γ_{total} Γ₂₅₅/Γ

Table with columns: VALUE (units 10^-4), EVTS, DOCUMENT ID, TECN, COMMENT. Includes 'OUR AVERAGE' and data from ABLIKIM, BAI, BISELLO.

1 From a partial wave analysis of J/ψ → γφφ that also finds significant signals for η(2100), 0-+ phase space, f0(2100), f2(2010), f2(2300), f2(2340), and a previously unseen 0-+ state X(2500) (M = 2470 ± 15 + 101 - 23 MeV, Γ = 230 ± 64 + 56 - 33 MeV).

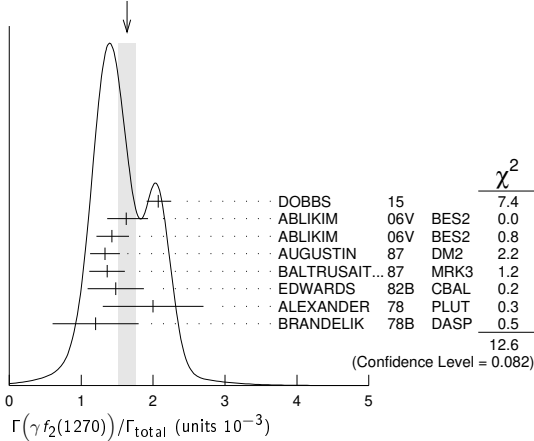
2 Includes unknown branching fraction to φφ.
3 Estimated by us from various fits.
4 Includes unknown branching fraction to ρ0ρ0.

Γ(γf2(1270))/Γ_{total} Γ₂₅₆/Γ

Table with columns: VALUE (units 10^-3), EVTS, DOCUMENT ID, TECN, COMMENT. Includes 'OUR AVERAGE' and data from DOBBS, ABLIKIM, AUGUSTIN, BALTRUSAIT., EDWARDS, ALEXANDER, BRANDELIK.

1 Using CLEO-c data but not authored by the CLEO Collaboration.
2 DOBBS 15 reports [Γ(J/ψ(1S) → γf2(1270))/Γ_{total}] × [B(f2(1270) → ππ)] = (1.744 ± 0.052 ± 0.122) × 10^-3 which we divide by our best value B(f2(1270) → ππ) = (84.2 ± 2.9 / 0.9) × 10^-2. Our first error is their experiment's error and our second error is the systematic error from using our best value.
3 ABLIKIM 06v reports [Γ(J/ψ(1S) → γf2(1270))/Γ_{total}] × [B(f2(1270) → ππ)] = (1.371 ± 0.010 ± 0.222) × 10^-3 which we divide by our best value B(f2(1270) → ππ) = (84.2 ± 2.9 / 0.9) × 10^-2. Our first error is their experiment's error and our second error is the systematic error from using our best value.
4 ABLIKIM 06v reports [Γ(J/ψ(1S) → γf2(1270))/Γ_{total}] × [B(f2(1270) → ππ)] = (1.200 ± 0.027 ± 0.174) × 10^-3 which we divide by our best value B(f2(1270) → ππ) = (84.2 ± 2.9 / 0.9) × 10^-2. Our first error is their experiment's error and our second error is the systematic error from using our best value.
5 Estimated using B(f2(1270) → ππ) = 0.843 ± 0.012. The errors do not contain the uncertainty in the f2(1270) decay.
6 Restated by us to take account of spread of E1, M2, E3 transitions.

WEIGHTED AVERAGE
1.64 ± 0.12 (Error scaled by 1.3)



Γ(γf2(1270) → γK_S^0 K_S^0)/Γ_{total} Γ₂₅₇/Γ

Table with columns: VALUE (units 10^-5), DOCUMENT ID, TECN, COMMENT. Includes 'OUR AVERAGE' and data from ABLIKIM.

Γ(γf1(1285))/Γ_{total} Γ₂₅₈/Γ

Table with columns: VALUE (units 10^-3), DOCUMENT ID, TECN, COMMENT. Includes 'OUR AVERAGE' and data from BAI.

Table with columns: VALUE, DOCUMENT ID, TECN, COMMENT. Includes data from BOLTON.

4 BOLTON 92 MRK3 J/ψ → γf1(1285)
5 BOLTON 92B MRK3 J/ψ → γηπ+π-
1 Assuming B(f1(1285) → ρ0γ) = 0.055 ± 0.013.
2 Assuming Γ(f1(1285) → K K π)/Γ_{total} = 0.090 ± 0.004.
3 Assuming Γ(f1(1285) → ηππ)/Γ_{total} = 0.5 ± 0.18.
4 Obtained summing the sequential decay channels
B(J/ψ → γf1(1285), f1(1285) → ππππ) = (1.44 ± 0.39 ± 0.27) × 10^-4;
B(J/ψ → γf1(1285), f1(1285) → a0(980)π, a0(980) → ηπ) = (3.90 ± 0.42 ± 0.87) × 10^-4;
B(J/ψ → γf1(1285), f1(1285) → a0(980)π, a0(980) → K K) = (0.66 ± 0.26 ± 0.29) × 10^-4;
B(J/ψ → γf1(1285), f1(1285) → γρ0) = (0.25 ± 0.07 ± 0.03) × 10^-4.
5 Using B(f1(1285) → a0(980)π) = 0.37, and including unknown branching ratio for a0(980) → ηπ.

Γ(γf0(1370) → γππ)/Γ_{total} Γ₂₅₉/Γ

Table with columns: VALUE (units 10^-5), DOCUMENT ID, TECN, COMMENT. Includes 'OUR AVERAGE' and data from SARANTSEV.

Γ(γf0(1370) → γK K)/Γ_{total} Γ₂₆₀/Γ

Table with columns: VALUE (units 10^-4), EVTS, DOCUMENT ID, TECN, COMMENT. Includes 'OUR AVERAGE' and data from DOBBS, SARANTSEV.

1 Using CLEO-c data but not authored by the CLEO Collaboration.

Γ(γf0(1370) → γK_S^0 K_S^0)/Γ_{total} Γ₂₆₁/Γ

Table with columns: VALUE (units 10^-5), DOCUMENT ID, TECN, COMMENT. Includes 'OUR AVERAGE' and data from ABLIKIM.

Γ(γf0(1370) → γηη)/Γ_{total} Γ₂₆₂/Γ

Table with columns: VALUE (units 10^-5), DOCUMENT ID, TECN, COMMENT. Includes 'OUR AVERAGE' and data from SARANTSEV.

Γ(γf0(1370) → γηη')/Γ_{total} Γ₂₆₃/Γ

Table with columns: VALUE (units 10^-5), DOCUMENT ID, TECN, COMMENT. Includes 'OUR AVERAGE' and data from SARANTSEV.

Γ(γf1(1420) → γK K π)/Γ_{total} Γ₂₆₄/Γ

Table with columns: VALUE (units 10^-3), DOCUMENT ID, TECN, COMMENT. Includes 'OUR AVERAGE' and data from BAI, AUGUSTIN.

1 Included unknown branching fraction f1(1420) → K K π.
2 From fit to the K*(892) K 1 + + partial wave.

Γ(γf0(1500) → γππ)/Γ_{total} Γ₂₆₅/Γ

Table with columns: VALUE (units 10^-4), EVTS, DOCUMENT ID, TECN, COMMENT. Includes 'OUR AVERAGE' and data from DOBBS, ABLIKIM, SARANTSEV, BUGG.

1 Using CLEO-c data but not authored by the CLEO Collaboration.
2 Including unknown branching fraction to ππ.
3 Including unknown branching ratio for f0(1500) → π+π-π+π-.

4 Assuming that f0(1500) decays only to two S-wave dipions.

Γ(γf0(1500) → γηη)/Γ_{total} Γ₂₆₆/Γ

Table with columns: VALUE (units 10^-5), EVTS, DOCUMENT ID, TECN, COMMENT. Includes 'OUR AVERAGE' and data from ABLIKIM, SARANTSEV.

1 From partial wave analysis including all possible combinations of 0+, 2+, and 4+ resonances.

Γ(γf0(1500) → γK_S^0 K_S^0)/Γ_{total} Γ₂₆₇/Γ

Table with columns: VALUE (units 10^-5), DOCUMENT ID, TECN, COMMENT. Includes 'OUR AVERAGE' and data from ABLIKIM, SARANTSEV.

Meson Particle Listings

$J/\psi(1S)$

$\Gamma(\gamma f_0(1500) \rightarrow \gamma \eta \eta')/\Gamma_{\text{total}}$ Γ_{268}/Γ

VALUE (units 10^{-5})	DOCUMENT ID	TECN	COMMENT
1.2 ± 0.5	SARANTSEV 21	RVUE	$J/\psi(1S) \rightarrow \gamma(\pi\pi, K\bar{K}, \eta\eta, \omega\phi)$

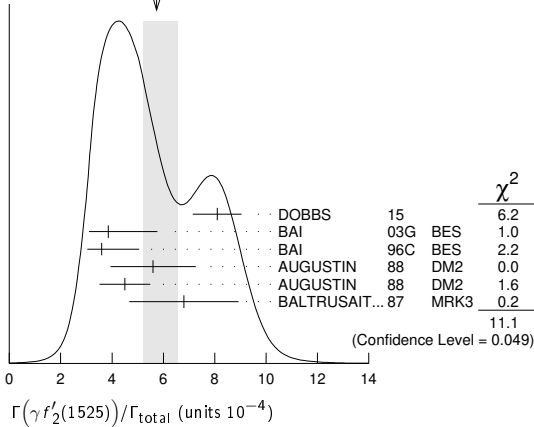
$\Gamma(\gamma f_1(1510) \rightarrow \gamma \eta \pi^+ \pi^-)/\Gamma_{\text{total}}$ Γ_{269}/Γ

VALUE (units 10^{-4})	DOCUMENT ID	TECN	COMMENT
$4.5 \pm 1.0 \pm 0.7$	BAI	99	BES $J/\psi \rightarrow \gamma \eta \pi^+ \pi^-$

$\Gamma(\gamma f_2'(1525))/\Gamma_{\text{total}}$ Γ_{270}/Γ

VALUE (units 10^{-4})	CL%	EVTS	DOCUMENT ID	TECN	COMMENT
5.7 ± 0.8					OUR AVERAGE Error includes scale factor of 1.5. See the ideogram below.
$8.1 \pm 0.9 \pm 0.2$		750	1,2 DOBBS 15		$J/\psi \rightarrow \gamma K\bar{K}$
$3.85 \pm 0.17 + 1.91$			3 BAI 03G	BES	$J/\psi \rightarrow \gamma K\bar{K}$
$3.6 \pm 0.4 + 1.4$			3 BAI 96C	BES	$J/\psi \rightarrow \gamma K^+ K^-$
$5.6 \pm 1.4 \pm 0.9$			3 AUGUSTIN 88	DM2	$J/\psi \rightarrow \gamma K^+ K^-$
$4.5 \pm 0.4 \pm 0.9$			3 AUGUSTIN 88	DM2	$J/\psi \rightarrow \gamma K_S^0 K_S^0$
$6.8 \pm 1.6 \pm 1.4$			3 BALTRUSAIT...87	MRK3	$J/\psi \rightarrow \gamma K^+ K^-$
< 3.4	90	4	4 BRANDELIK 79C	DASP	$e^+ e^- \rightarrow \pi^+ \pi^- \gamma$
< 2.3	90	3	ALEXANDER 78	PLUT	$e^+ e^- \rightarrow K^+ K^- \gamma$

WEIGHTED AVERAGE
5.7+0.8-0.5 (Error scaled by 1.5)



1 Using CLEO-c data but not authored by the CLEO Collaboration.
 2 DOBBS 15 reports $[\Gamma(J/\psi(1S) \rightarrow \gamma f_2'(1525))/\Gamma_{\text{total}}] \times [B(f_2'(1525) \rightarrow K\bar{K})] = (7.09 \pm 0.46 \pm 0.67) \times 10^{-4}$ which we divide by our best value $B(f_2'(1525) \rightarrow K\bar{K}) = (87.6 \pm 2.2) \times 10^{-2}$. Our first error is their experiment's error and our second error is the systematic error from using our best value.
 3 Using $B(f_2'(1525) \rightarrow K\bar{K}) = 0.888$.
 4 Assuming isotropic production and decay of the $f_2'(1525)$ and isospin.

$\Gamma(\gamma f_2'(1525) \rightarrow \gamma K_S^0 K_S^0)/\Gamma_{\text{total}}$ Γ_{271}/Γ

VALUE (units 10^{-5})	DOCUMENT ID	TECN	COMMENT
$7.99 \pm 0.03 + 0.69$	ABLIKIM 18AA	BES3	$J/\psi \rightarrow \gamma K_S^0 K_S^0$
$-0.04 - 0.50$			

$\Gamma(\gamma f_2'(1525) \rightarrow \gamma \eta \eta)/\Gamma_{\text{total}}$ Γ_{272}/Γ

VALUE (units 10^{-5})	EVTS	DOCUMENT ID	TECN	COMMENT
$3.42 \pm 0.43 + 1.37$	5.5k	1 ABLIKIM 13N	BES3	$J/\psi \rightarrow \gamma \eta \eta$
$-0.51 - 1.30$				

1 From partial wave analysis including all possible combinations of 0^{++} , 2^{++} , and 4^{++} resonances.

$\Gamma(\gamma f_2(1640) \rightarrow \gamma \omega \omega)/\Gamma_{\text{total}}$ Γ_{273}/Γ

VALUE (units 10^{-3})	EVTS	DOCUMENT ID	TECN	COMMENT
$0.28 \pm 0.05 \pm 0.17$	141	ABLIKIM 06H	BES	$J/\psi \rightarrow \gamma \omega \omega$

$\Gamma(\gamma f_0(1710) \rightarrow \gamma \pi \pi)/\Gamma_{\text{total}}$ Γ_{274}/Γ

VALUE (units 10^{-4})	EVTS	DOCUMENT ID	TECN	COMMENT
3.8 ± 0.5				OUR AVERAGE
$3.72 \pm 0.30 \pm 0.43$	483	1 DOBBS 15		$J/\psi \rightarrow \gamma \pi \pi$
$3.96 \pm 0.06 \pm 1.12$		2 ABLIKIM 06v	BES2	$e^+ e^- \rightarrow J/\psi \rightarrow \gamma \pi^+ \pi^-$
$3.99 \pm 0.15 \pm 2.64$		2 ABLIKIM 06v	BES2	$e^+ e^- \rightarrow J/\psi \rightarrow \gamma \pi^0 \pi^0$
0.6 ± 0.2		3 SARANTSEV 21	RVUE	$J/\psi(1S) \rightarrow \gamma(\pi\pi, K\bar{K}, \eta\eta, \omega\phi)$
$2.5 \pm 1.6 \pm 0.8$		BAI 98H	BES	$J/\psi \rightarrow \gamma \pi^0 \pi^0$

1 Using CLEO-c data but not authored by the CLEO Collaboration.

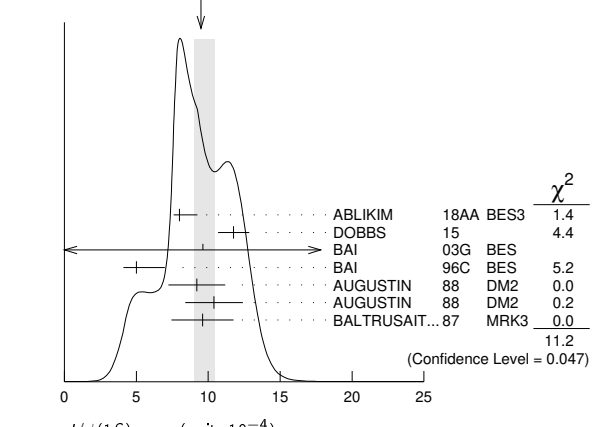
2 Including unknown branching fraction to $\pi\pi$.

3 There is a further $(2.4 \pm 0.8) \times 10^{-4}$ scalar contribution at 1765 MeV.

$\Gamma(\gamma f_0(1710) \rightarrow \gamma K\bar{K})/\Gamma_{\text{total}}$ Γ_{275}/Γ

VALUE (units 10^{-4})	CL%	EVTS	DOCUMENT ID	TECN	COMMENT
9.5 ± 1.0					OUR AVERAGE Error includes scale factor of 1.5. See the ideogram below.
$8.00 \pm 0.12 + 1.24$			1 ABLIKIM 18AA	BES3	$J/\psi \rightarrow \gamma K_S^0 K_S^0$
$0.08 - 0.40$			2 DOBBS 15		$J/\psi \rightarrow \gamma K\bar{K}$
$11.76 \pm 0.54 \pm 0.94$		1.2k	3 BAI 03G	BES	$J/\psi \rightarrow \gamma K\bar{K}$
$9.62 \pm 0.29 + 3.51$			1,4 BAI 96C	BES	$J/\psi \rightarrow \gamma K^+ K^-$
$-1.86 - 0.4$					
$5.0 \pm 0.8 + 1.8$			1 AUGUSTIN 88	DM2	$J/\psi \rightarrow \gamma K^+ K^-$
-0.4			1 AUGUSTIN 88	DM2	$J/\psi \rightarrow \gamma K_S^0 K_S^0$
$9.2 \pm 1.4 \pm 1.4$			1 BALTRUSAIT...87	MRK3	$J/\psi \rightarrow \gamma K^+ K^-$
$10.4 \pm 1.2 \pm 1.6$			5 SARANTSEV 21	RVUE	$J/\psi(1S) \rightarrow \gamma(\pi\pi, K\bar{K}, \eta\eta, \omega\phi)$
$9.6 \pm 1.2 \pm 1.8$			1,6 BAI 96C	BES	$J/\psi \rightarrow \gamma K^+ K^-$
2.3 ± 0.8			7 BISELLO 89B		$J/\psi \rightarrow 4\pi\gamma$
$1.6 \pm 0.2 + 0.6$		90	8 BALTRUSAIT...87	MRK3	$J/\psi \rightarrow \gamma \pi^+ \pi^-$
-0.2			9 EDWARDS 82D	CBAL	$e^+ e^- \rightarrow \eta \eta \gamma$
< 0.8					
$1.6 \pm 0.4 \pm 0.3$					
3.8 ± 1.6					

WEIGHTED AVERAGE
9.5+1.0-0.5 (Error scaled by 1.5)



1 Includes unknown branching fraction to $K^+ K^-$ or $K_S^0 K_S^0$. We have multiplied $K^+ K^-$ measurement by 2, and $K_S^0 K_S^0$ by 4 to obtain $K\bar{K}$ result.
 2 Using CLEO-c data but not authored by the CLEO Collaboration.
 3 Includes unknown branching ratio to $K^+ K^-$ or $K_S^0 K_S^0$.
 4 Assuming $J^P = 2^+$ for $f_0(1710)$.
 5 There is a further $(6 \pm 2) \times 10^{-4}$ scalar contribution at 1765 MeV.
 6 Assuming $J^P = 0^+$ for $f_0(1710)$.
 7 Includes unknown branching fraction to $\rho^0 \rho^0$.
 8 Includes unknown branching fraction to $\pi^+ \pi^-$.
 9 Includes unknown branching fraction to $\eta \eta$.

$\Gamma(\gamma f_0(1710) \rightarrow \gamma \omega \omega)/\Gamma_{\text{total}}$ Γ_{276}/Γ

VALUE (units 10^{-3})	EVTS	DOCUMENT ID	TECN	COMMENT
$0.31 \pm 0.06 \pm 0.08$	180	ABLIKIM 06H	BES	$J/\psi \rightarrow \gamma \omega \omega$

$\Gamma(\gamma f_0(1710) \rightarrow \gamma \eta \eta)/\Gamma_{\text{total}}$ Γ_{277}/Γ

VALUE (units 10^{-4})	EVTS	DOCUMENT ID	TECN	COMMENT
$2.35 \pm 0.13 + 1.24$	5.5k	1 ABLIKIM 13N	BES3	$J/\psi \rightarrow \gamma \eta \eta$
$-0.11 - 0.74$				

••• We do not use the following data for averages, fits, limits, etc. •••

1,2 From partial wave analysis including all possible combinations of 0^{++} , 2^{++} , and 4^{++} resonances.
 2 There is a further $(0.7 \pm 0.1) \times 10^{-4}$ scalar contribution at 1765 MeV.

$\Gamma(\gamma f_0(1710) \rightarrow \gamma \eta \eta')/\Gamma_{\text{total}}$ Γ_{278}/Γ

VALUE (units 10^{-5})	DOCUMENT ID	TECN	COMMENT
6.5 ± 2.5	1 SARANTSEV 21	RVUE	$J/\psi(1S) \rightarrow \gamma(\pi\pi, K\bar{K}, \eta\eta, \omega\phi)$

••• We do not use the following data for averages, fits, limits, etc. •••

1 There is a further $(2.5 \pm 1.1) \times 10^{-5}$ scalar contribution at 1765 MeV.

See key on page 1127

Meson Particle Listings

$J/\psi(1S)$

$\Gamma(\gamma f_0(1710) \rightarrow \gamma \omega \phi) / \Gamma_{total}$ Γ_{279}/Γ
 VALUE (units 10^{-4}) EVTS DOCUMENT ID TECN COMMENT
2.5 ± 0.6 OUR AVERAGE

2.00 ± 0.08 ± $\frac{1.38}{1.64}$ 1.3k ABLIKIM 13J BES3 $J/\psi \rightarrow \gamma \omega \phi$

2.61 ± 0.27 ± 0.65 95 ABLIKIM 06J BES2 $J/\psi \rightarrow \gamma \omega \phi$

• • • We do not use the following data for averages, fits, limits, etc. • • •

0.1 ± 0.1 ¹SARANTSEV 21 RVUE $J/\psi(1S) \rightarrow \gamma(\pi\pi, K\bar{K}, \eta\eta, \omega\phi)$

¹There is a further $(2.2 \pm 0.4) \times 10^{-4}$ scalar contribution at 1765 MeV.

$\Gamma(\gamma f_0(1750) \rightarrow \gamma K_S^0 K_S^0) / \Gamma_{total}$ Γ_{280}/Γ

VALUE (units 10^{-5}) DOCUMENT ID TECN COMMENT
1.11 ± 0.06 ± $\frac{0.19}{0.32}$ ABLIKIM 18AA BES3 $J/\psi \rightarrow \gamma K_S^0 K_S^0$

$\Gamma(\gamma f_2(1810) \rightarrow \gamma \eta \eta) / \Gamma_{total}$ Γ_{281}/Γ

VALUE (units 10^{-5}) EVTS DOCUMENT ID COMMENT
5.40 ± $\frac{0.60 + 3.42}{0.67 - 2.35}$ 5.5k ¹ABLIKIM 13N $J/\psi \rightarrow \gamma \eta \eta$

¹From partial wave analysis including all possible combinations of 0^{++} , 2^{++} , and 4^{++} resonances.

$\Gamma(\gamma f_2(1910) \rightarrow \gamma \omega \omega) / \Gamma_{total}$ Γ_{282}/Γ

VALUE (units 10^{-3}) EVTS DOCUMENT ID TECN COMMENT
0.20 ± 0.04 ± 0.13 151 ABLIKIM 06H BES $J/\psi \rightarrow \gamma \omega \omega$

$\Gamma(\gamma f_2(1950) \rightarrow \gamma K^*(892) \bar{K}^*(892)) / \Gamma_{total}$ Γ_{283}/Γ

VALUE (units 10^{-3}) DOCUMENT ID TECN COMMENT
0.7 ± 0.1 ± 0.2 BAI 00B BES $J/\psi \rightarrow \gamma K^+ K^0 \pi^+ \pi^-$

$\Gamma(\gamma f_0(2020) \rightarrow \gamma \pi \pi) / \Gamma_{total}$ Γ_{284}/Γ

VALUE (units 10^{-5}) DOCUMENT ID TECN COMMENT
 • • • We do not use the following data for averages, fits, limits, etc. • • •
 42 ± 10 SARANTSEV 21 RVUE $J/\psi(1S) \rightarrow \gamma(\pi\pi, K\bar{K}, \eta\eta, \omega\phi)$

$\Gamma(\gamma f_0(2020) \rightarrow \gamma K \bar{K}) / \Gamma_{total}$ Γ_{285}/Γ

VALUE (units 10^{-5}) DOCUMENT ID TECN COMMENT
 • • • We do not use the following data for averages, fits, limits, etc. • • •
 55 ± 25 SARANTSEV 21 RVUE $J/\psi(1S) \rightarrow \gamma(\pi\pi, K\bar{K}, \eta\eta, \omega\phi)$

$\Gamma(\gamma f_0(2020) \rightarrow \gamma \eta \eta) / \Gamma_{total}$ Γ_{286}/Γ

VALUE (units 10^{-5}) DOCUMENT ID TECN COMMENT
 • • • We do not use the following data for averages, fits, limits, etc. • • •
 10 ± 10 SARANTSEV 21 RVUE $J/\psi(1S) \rightarrow \gamma(\pi\pi, K\bar{K}, \eta\eta, \omega\phi)$

$\Gamma(\gamma f_4(2050) / \Gamma_{total}$ Γ_{287}/Γ

VALUE (units 10^{-3}) DOCUMENT ID TECN COMMENT
2.7 ± 0.5 ± 0.5 ¹BALTRUSAIT...87 MRK3 $J/\psi \rightarrow \gamma \pi^+ \pi^-$

¹Assuming branching fraction $f_4(2050) \rightarrow \pi \pi / total = 0.167$.

$\Gamma(\gamma f_0(2100) \rightarrow \gamma \eta \eta) / \Gamma_{total}$ Γ_{288}/Γ

VALUE (units 10^{-4}) EVTS DOCUMENT ID TECN COMMENT
1.13 ± $\frac{0.09 + 0.64}{0.10 - 0.28}$ 5.5k ¹ABLIKIM 13N BES3 $J/\psi \rightarrow \gamma \eta \eta$

• • • We do not use the following data for averages, fits, limits, etc. • • •

1.8 ± 1.5 SARANTSEV 21 RVUE $J/\psi(1S) \rightarrow \gamma(\pi\pi, K\bar{K}, \eta\eta, \omega\phi)$

¹From partial wave analysis including all possible combinations of 0^{++} , 2^{++} , and 4^{++} resonances.

$\Gamma(\gamma f_0(2100) \rightarrow \gamma \pi \pi) / \Gamma_{total}$ Γ_{290}/Γ

VALUE (units 10^{-4}) EVTS DOCUMENT ID TECN COMMENT
6.24 ± 0.48 ± 0.87 744 ¹DOBBS 15 $J/\psi \rightarrow \gamma \pi \pi$

• • • We do not use the following data for averages, fits, limits, etc. • • •

2.0 ± 0.8 SARANTSEV 21 RVUE $J/\psi(1S) \rightarrow \gamma(\pi\pi, K\bar{K}, \eta\eta, \omega\phi)$

¹Using CLEO-c data but not authored by the CLEO Collaboration.

$\Gamma(\gamma f_0(2100) \rightarrow \gamma K \bar{K}) / \Gamma_{total}$ Γ_{289}/Γ

VALUE (units 10^{-5}) DOCUMENT ID TECN COMMENT
 • • • We do not use the following data for averages, fits, limits, etc. • • •
 32 ± 20 SARANTSEV 21 RVUE $J/\psi(1S) \rightarrow \gamma(\pi\pi, K\bar{K}, \eta\eta, \omega\phi)$

$\Gamma(\gamma f_0(2200) / \Gamma_{total}$ Γ_{291}/Γ

VALUE (units 10^{-4}) DOCUMENT ID TECN COMMENT
 • • • We do not use the following data for averages, fits, limits, etc. • • •
 1.5 ¹AUGUSTIN 88 DM2 $J/\psi \rightarrow \gamma K_S^0 K_S^0$

¹Includes unknown branching fraction to $K_S^0 K_S^0$.

$\Gamma(\gamma f_0(2200) \rightarrow \gamma \pi \pi) / \Gamma_{total}$ Γ_{294}/Γ

VALUE (units 10^{-5}) DOCUMENT ID TECN COMMENT
 • • • We do not use the following data for averages, fits, limits, etc. • • •
 5 ± 2 SARANTSEV 21 RVUE $J/\psi(1S) \rightarrow \gamma(\pi\pi, K\bar{K}, \eta\eta, \omega\phi)$

$\Gamma(\gamma f_0(2200) \rightarrow \gamma K \bar{K}) / \Gamma_{total}$ Γ_{292}/Γ

VALUE (units 10^{-4}) EVTS DOCUMENT ID TECN COMMENT
5.86 ± 0.49 ± 1.20 490 ¹DOBBS 15 $J/\psi \rightarrow \gamma K \bar{K}$

• • • We do not use the following data for averages, fits, limits, etc. • • •

0.5 ± 0.5 SARANTSEV 21 RVUE $J/\psi(1S) \rightarrow \gamma(\pi\pi, K\bar{K}, \eta\eta, \omega\phi)$

¹Using CLEO-c data but not authored by the CLEO Collaboration.

$\Gamma(\gamma f_0(2200) \rightarrow \gamma K_S^0 K_S^0) / \Gamma_{total}$ Γ_{293}/Γ

VALUE (units 10^{-4}) DOCUMENT ID TECN COMMENT
2.72 ± $\frac{0.08 + 0.17}{0.06 - 0.47}$ ABLIKIM 18AA BES3 $J/\psi \rightarrow \gamma K_S^0 K_S^0$

$\Gamma(\gamma f_0(2200) \rightarrow \gamma \eta \eta) / \Gamma_{total}$ Γ_{295}/Γ

VALUE (units 10^{-5}) DOCUMENT ID TECN COMMENT
 • • • We do not use the following data for averages, fits, limits, etc. • • •
 0.7 ± 0.4 SARANTSEV 21 RVUE $J/\psi(1S) \rightarrow \gamma(\pi\pi, K\bar{K}, \eta\eta, \omega\phi)$

$\Gamma(\gamma f_J(2220) / \Gamma_{total}$ Γ_{296}/Γ

VALUE (units 10^{-5}) CL% EVTS DOCUMENT ID TECN COMMENT
 • • • We do not use the following data for averages, fits, limits, etc. • • •
 >300 ¹BAI 96B BES $e^+ e^- \rightarrow \gamma \bar{p} p, K \bar{K}$

>250 ²HASAN 96 SPEC $\bar{p} p \rightarrow \pi^+ \pi^-$

< 2.3 95 ³AUGUSTIN 88 DM2 $J/\psi \rightarrow \gamma K^+ K^-$

< 1.6 95 ³AUGUSTIN 88 DM2 $J/\psi \rightarrow \gamma K_S^0 K_S^0$

12.4 ± $\frac{6.4}{-5.2} \pm 2.8$ 23 ³BALTRUSAIT...86D MRK3 $J/\psi \rightarrow \gamma K_S^0 K_S^0$

8.4 ± $\frac{3.4}{-2.8} \pm 1.6$ 93 ³BALTRUSAIT...86D MRK3 $J/\psi \rightarrow \gamma K^+ K^-$

¹Using BARNES 93.

²Using BAI 96B.

³Includes unknown branching fraction to $K^+ K^-$ or $K_S^0 K_S^0$.

$\Gamma(\gamma f_J(2220) \rightarrow \gamma \pi \pi) / \Gamma_{total}$ Γ_{297}/Γ

VALUE (units 10^{-5}) CL% EVTS DOCUMENT ID TECN COMMENT
< 3.9 90 ^{1,2}DOBBS 15 $J/\psi \rightarrow \gamma \pi \pi$

• • • We do not use the following data for averages, fits, limits, etc. • • •
 14 ± 8 ± 4 BAI 98H BES $J/\psi \rightarrow \gamma \pi^0 \pi^0$

8.4 ± 2.6 ± 3.0 BAI 96B BES $e^+ e^- \rightarrow J/\psi \rightarrow \gamma \pi^+ \pi^-$

¹Using CLEO-c data but not authored by the CLEO Collaboration.

²For $\Gamma = 20/50$ MeV, the 90% CL upper limits for $\pi^+ \pi^-$ and $\pi^0 \pi^0$ are 2.6/5.2 × 10⁻⁵ and 1.3/1.9 × 10⁻⁵, respectively.

$\Gamma(\gamma f_J(2220) \rightarrow \gamma K \bar{K}) / \Gamma_{total}$ Γ_{298}/Γ

VALUE (units 10^{-5}) CL% EVTS DOCUMENT ID TECN COMMENT
< 4.1 90 ^{1,2}DOBBS 15 $J/\psi \rightarrow \gamma K \bar{K}$

• • • We do not use the following data for averages, fits, limits, etc. • • •
 < 3.6 ³DEL-AMO-SA...10o BABR $e^+ e^- \rightarrow J/\psi \rightarrow \gamma K^+ K^-$

< 2.9 ³DEL-AMO-SA...10o BABR $e^+ e^- \rightarrow J/\psi \rightarrow \gamma K_S^0 K_S^0$

6.6 ± 2.9 ± 2.4 BAI 96B BES $e^+ e^- \rightarrow J/\psi \rightarrow \gamma K^+ K^-$

10.8 ± 4.0 ± 3.2 BAI 96B BES $e^+ e^- \rightarrow J/\psi \rightarrow \gamma K_S^0 K_S^0$

¹Using CLEO-c data but not authored by the CLEO Collaboration.

²For $\Gamma = 20/50$ MeV, the 90% CL upper limits for $K^+ K^-$ and $K_S^0 K_S^0$ are 1.7/3.1 × 10⁻⁵ and 1.2/2.0 × 10⁻⁵, respectively.

³For spin 2 and helicity 0; other combinations lead to more stringent upper limits.

$\Gamma(\gamma f_J(2220) \rightarrow \gamma \bar{p} \bar{p}) / \Gamma_{total}$ Γ_{299}/Γ

VALUE (units 10^{-5}) DOCUMENT ID TECN COMMENT
1.5 ± 0.6 ± 0.5 BAI 96B BES $e^+ e^- \rightarrow J/\psi \rightarrow \gamma \bar{p} \bar{p}$

$\Gamma(\gamma f_0(2330) \rightarrow \gamma K_S^0 K_S^0) / \Gamma_{total}$ Γ_{300}/Γ

VALUE (units 10^{-5}) DOCUMENT ID TECN COMMENT
4.95 ± 0.21 ± $\frac{0.66}{0.72}$ ABLIKIM 18AA BES3 $J/\psi \rightarrow \gamma K_S^0 K_S^0$

• • • We do not use the following data for averages, fits, limits, etc. • • •

0.6 ± 0.1 SARANTSEV 21 RVUE $J/\psi(1S) \rightarrow \gamma(\pi\pi, K\bar{K}, \eta\eta, \omega\phi)$

$\Gamma(\gamma f_0(2330) \rightarrow \gamma \pi \pi) / \Gamma_{total}$ Γ_{301}/Γ

VALUE (units 10^{-5}) DOCUMENT ID TECN COMMENT
 • • • We do not use the following data for averages, fits, limits, etc. • • •
 4 ± 2 SARANTSEV 21 RVUE $J/\psi(1S) \rightarrow \gamma(\pi\pi, K\bar{K}, \eta\eta, \omega\phi)$

Meson Particle Listings

$J/\psi(1S)$

$\Gamma(\gamma f_0(2330) \rightarrow \gamma \eta \eta) / \Gamma_{total}$ Γ_{302} / Γ

VALUE (units 10^{-5})	DOCUMENT ID	TECN	COMMENT
1.5 ± 0.4	SARANTSEV 21	RVUE	$J/\psi(1S) \rightarrow \gamma(\pi\pi, K\bar{K}, \eta\eta, \omega\phi)$

• • • We do not use the following data for averages, fits, limits, etc. • • •

$\Gamma(\gamma f_2(2340) \rightarrow \gamma \eta \eta) / \Gamma_{total}$ Γ_{303} / Γ

VALUE (units 10^{-5})	EVTs	DOCUMENT ID	TECN	COMMENT
$5.60^{+0.62+2.37}_{-0.65-2.07}$	5.5k	¹ ABLIKIM	13N BES3	$J/\psi \rightarrow \gamma \eta \eta$

¹ From partial wave analysis including all possible combinations of 0^{++} , 2^{++} , and 4^{++} resonances.

$\Gamma(\gamma f_2(2340) \rightarrow \gamma K_S^0 K_S^0) / \Gamma_{total}$ Γ_{304} / Γ

VALUE (units 10^{-5})	DOCUMENT ID	TECN	COMMENT
$5.54^{+0.34+3.82}_{-0.40-1.49}$	ABLIKIM	18AA BES3	$J/\psi \rightarrow \gamma K_S^0 K_S^0$

$\Gamma(\gamma X(1835) \rightarrow \gamma \pi^+ \pi^- \eta') / \Gamma_{total}$ Γ_{305} / Γ

VALUE (units 10^{-4})	EVTs	DOCUMENT ID	TECN	COMMENT
$2.7^{+0.6}_{-0.8}$	OUR AVERAGE	Error includes scale factor of 1.6.		

$3.93 \pm 0.38^{+0.31}_{-0.84}$	¹ ABLIKIM	16J BES3	$J/\psi \rightarrow \gamma \pi^+ \pi^- \eta'$
$2.2 \pm 0.4 \pm 0.4$	264	ABLIKIM 05R BES2	$J/\psi \rightarrow \gamma \pi^+ \pi^- \eta'$

• • • We do not use the following data for averages, fits, limits, etc. • • •

$2.87 \pm 0.09^{+0.49}_{-0.52}$	4265	² ABLIKIM	11c BES3	$J/\psi \rightarrow \gamma \pi^+ \pi^- \eta'$
---------------------------------	------	----------------------	----------	---

¹ From a fit of the measured $\pi^+ \pi^- \eta'$ lineshape that accounts for the abrupt distortion observed at the $p\bar{p}$ threshold with a Flatté formula in addition to known backgrounds and contributors, as well as an *ad hoc* Breit-Wigner ($M \approx 1919$ MeV; $\Gamma \approx 51$ MeV) that is required for a good fit. Another explanation for the distortion provided by ABLIKIM 16J is that a second resonance near 1870 MeV interferes with the $X(1835)$; fits to this possibility yield product branching fraction values compatible with that shown within the respective systematic uncertainties.

² From a fit of the $\pi^+ \pi^- \eta'$ mass distribution to a combination of $\gamma f_1(1510)$, $\gamma X(1835)$, and two states $\gamma X(2120)$ and $\gamma X(2370)$, for $M(\pi^+ \pi^- \eta') < 2.8$ GeV, and accounting for backgrounds from non- η' events and $J/\psi \rightarrow \pi^0 \pi^+ \pi^- \eta'$.

$\Gamma(\gamma X(1835) \rightarrow \gamma \rho \bar{p}) / \Gamma_{total}$ Γ_{306} / Γ

VALUE (units 10^{-4})	EVTs	DOCUMENT ID	TECN	COMMENT
$0.77^{+0.15}_{-0.09}$	OUR AVERAGE			

$0.90^{+0.04+0.27}_{-0.11-0.55}$	¹ ABLIKIM	12D BES3	$J/\psi \rightarrow \gamma \rho \bar{p}$
----------------------------------	----------------------	----------	--

$1.14^{+0.43+0.42}_{-0.30-0.26}$	231	² ALEXANDER	10 CLEO	$J/\psi \rightarrow \gamma \rho \bar{p}$
----------------------------------	-----	------------------------	---------	--

$0.70 \pm 0.04^{+0.19}_{-0.08}$	BAI	03F BES2	$J/\psi \rightarrow \gamma \rho \bar{p}$
---------------------------------	-----	----------	--

¹ From the fit including final state interaction effects in isospin 0 S-wave according to SIBIRTSEV 05A.

² From a fit of the $p\bar{p}$ mass distribution to a combination of $\gamma X(1835)$, γR with $M(R) = 2100$ MeV and $\Gamma(R) = 160$ MeV, and $\gamma \rho \bar{p}$ phase space, for $M(p\bar{p}) < 2.85$ GeV.

$\Gamma(\gamma X(1835) \rightarrow \gamma K_S^0 K_S^0 \eta) / \Gamma_{total}$ Γ_{307} / Γ

VALUE (units 10^{-5})	DOCUMENT ID	TECN	COMMENT
$3.31^{+0.33+1.96}_{-0.30-1.29}$	ABLIKIM	15T BES3	$J/\psi \rightarrow \gamma K_S^0 K_S^0 \eta$

$\Gamma(\gamma X(1835) \rightarrow \gamma \gamma \phi(1020)) / \Gamma_{total}$ Γ_{308} / Γ

VALUE (units 10^{-6})	EVTs	DOCUMENT ID	TECN	COMMENT
$1.77 \pm 0.35 \pm 0.25$	305	¹ ABLIKIM	18i BES3	$J/\psi \rightarrow \gamma \gamma \phi(1020)$
$8.09 \pm 1.99 \pm 1.36$	1.3k	² ABLIKIM	18i BES3	$J/\psi \rightarrow \gamma \gamma \phi(1020)$

• • • We do not use the following data for averages, fits, limits, etc. • • •

¹ Constructive interference between the $X(1835)$ and $\eta(1405)/\eta(1475)$ is assumed in a fit to the $\gamma \phi$ invariant mass.

² Destructive interference between the $X(1835)$ and $\eta(1405)/\eta(1475)$ is assumed in a fit to the $\gamma \phi$ invariant mass.

$\Gamma(\gamma X(1835) \rightarrow \gamma \gamma \gamma) / \Gamma_{total}$ Γ_{309} / Γ

VALUE	CL%	DOCUMENT ID	TECN	COMMENT
$< 3.56 \times 10^{-6}$	90	ABLIKIM	18o BES3	$\psi(2S) \rightarrow \pi^+ \pi^- \gamma \gamma \gamma$

$\Gamma(\gamma X(1835) \rightarrow \gamma 3(\pi^+ \pi^-)) / \Gamma_{total}$ Γ_{310} / Γ

VALUE (units 10^{-5})	EVTs	DOCUMENT ID	TECN	COMMENT
$2.44 \pm 0.36^{+0.60}_{-0.74}$	0.6k	ABLIKIM	13u BES3	$J/\psi \rightarrow \gamma 3(\pi^+ \pi^-)$

$\Gamma(\gamma X(2370) \rightarrow \gamma K^+ K^- \eta') / \Gamma_{total}$ Γ_{311} / Γ

VALUE (units 10^{-5})	DOCUMENT ID	TECN	COMMENT
$1.79 \pm 0.23 \pm 0.65$	ABLIKIM	20q BES3	$J/\psi \rightarrow \gamma K^+ K^- \eta'$

$\Gamma(\gamma X(2370) \rightarrow \gamma K_S^0 K_S^0 \eta') / \Gamma_{total}$ Γ_{312} / Γ

VALUE (units 10^{-5})	DOCUMENT ID	TECN	COMMENT
$1.18 \pm 0.32 \pm 0.39$	ABLIKIM	20q BES3	$J/\psi \rightarrow \gamma K_S^0 K_S^0 \eta'$

$\Gamma(\gamma X(2370) \rightarrow \gamma \eta \eta \eta') / \Gamma_{total}$ Γ_{313} / Γ

VALUE (units 10^{-6})	CL%	DOCUMENT ID	TECN	COMMENT
< 9.2	90	ABLIKIM	21c BES3	$J/\psi(1S) \rightarrow \gamma \eta \eta \eta'$

$\Gamma(\gamma \rho \bar{p}) / \Gamma_{total}$ Γ_{314} / Γ

VALUE (units 10^{-3})	CL%	EVTs	DOCUMENT ID	TECN	COMMENT
$0.38 \pm 0.07 \pm 0.07$		49	EATON	84	MRK2 $e^+ e^-$

• • • We do not use the following data for averages, fits, limits, etc. • • •

< 0.11	90	PERUZZI	78	MRK1	$e^+ e^-$
----------	----	---------	----	------	-----------

$\Gamma(\gamma \rho \bar{p} \pi^+ \pi^-) / \Gamma_{total}$ Γ_{315} / Γ

VALUE	CL%	DOCUMENT ID	TECN	COMMENT
$< 0.79 \times 10^{-3}$	90	EATON	84	MRK2 $e^+ e^-$

$\Gamma(\gamma A \bar{A}) / \Gamma_{total}$ Γ_{316} / Γ

VALUE	CL%	DOCUMENT ID	TECN	COMMENT
$< 0.13 \times 10^{-3}$	90	HENRARD	87	DM2 $e^+ e^-$

• • • We do not use the following data for averages, fits, limits, etc. • • •

$< 0.16 \times 10^{-3}$	90	BAI	98g BES	$e^+ e^-$
-------------------------	----	-----	---------	-----------

$\Gamma(\gamma A \rightarrow \gamma \text{invisible}) / \Gamma_{total}$ Γ_{317} / Γ

VALUE	CL%	EVTs	DOCUMENT ID	TECN	COMMENT
$< 1.7 \times 10^{-6}$	90	88M	¹ ABLIKIM	20k BES3	$\psi(2S) \rightarrow J/\psi \pi^+ \pi^-$

• • • We do not use the following data for averages, fits, limits, etc. • • •

$< 6.3 \times 10^{-6}$	90	3.7M	² INSLER	10 CLEO	$\psi(2S) \rightarrow J/\psi \pi^+ \pi^-$
------------------------	----	------	---------------------	---------	---

¹ For a narrow state A with mass $m_A < 1.2$ GeV. The limit varies with m_A , reaching its largest value of 1.7×10^{-6} at 1.2 GeV and being 7.0×10^{-7} for $m_A = 0$.

² The limit varies with mass m_A of a narrow state A and is 4.3×10^{-6} for $m_A = 0$, reaches its largest value of 6.3×10^{-6} at $m_A = 500$ MeV, and is 3.6×10^{-6} at $m_A = 960$ MeV.

$\Gamma(\gamma A^0 \rightarrow \gamma \mu^+ \mu^-) / \Gamma_{total}$ Γ_{318} / Γ

VALUE	CL%	DOCUMENT ID	TECN	COMMENT
$< 0.5 \times 10^{-5}$	90	¹ ABLIKIM	16E BES3	$J/\psi \rightarrow \gamma \mu^+ \mu^-$

• • • We do not use the following data for averages, fits, limits, etc. • • •

$< 2.1 \times 10^{-5}$	90	² ABLIKIM	12 BES3	$J/\psi \rightarrow \gamma \mu^+ \mu^-$
------------------------	----	----------------------	---------	---

¹ For a narrow scalar or pseudoscalar, A^0 , with a mass in the range 0.21–3 GeV. The measured 90% CL limit as a function of m_{A^0} is in the range $(2.8-495.3) \times 10^{-8}$.

² For a narrow scalar or pseudoscalar, A^0 , with a mass in the range 0.21–3.00 GeV. The measured 90% CL limit as a function of m_{A^0} ranges from 4×10^{-7} to 2.1×10^{-5} .

————— DALITZ DECAYS —————

$\Gamma(\pi^0 e^+ e^-) / \Gamma_{total}$ Γ_{319} / Γ

VALUE (units 10^{-7})	EVTs	DOCUMENT ID	TECN	COMMENT
$7.56 \pm 1.32 \pm 0.50$	39	ABLIKIM	14i BES3	$J/\psi \rightarrow \pi^0 e^+ e^-$

$\Gamma(\eta e^+ e^-) / \Gamma_{total}$ Γ_{320} / Γ

VALUE (units 10^{-5})	EVTs	DOCUMENT ID	TECN	COMMENT
$1.42 \pm 0.04 \pm 0.07$	2.47k	^{1,2} ABLIKIM	19A BES3	$J/\psi \rightarrow \eta e^+ e^-$

• • • We do not use the following data for averages, fits, limits, etc. • • •

$1.16 \pm 0.07 \pm 0.06$	320	¹ ABLIKIM	14i BES3	$J/\psi \rightarrow \eta e^+ e^-$
--------------------------	-----	----------------------	----------	-----------------------------------

¹ Using both $\eta \rightarrow \gamma \gamma$ and $\eta \rightarrow \pi^+ \pi^- \pi^0$ decays.

² Approximation of the transition form factor squared as an incoherent sum of the ρ -meson and one-pole non-resonant amplitudes gives the pole mass $m(A) = 2.56 \pm 0.04 \pm 0.03$ GeV. Supersedes ABLIKIM 14i.

$\Gamma(\eta'(958) e^+ e^-) / \Gamma_{total}$ Γ_{321} / Γ

VALUE (units 10^{-9})	EVTs	DOCUMENT ID	TECN	COMMENT
$6.59 \pm 0.07 \pm 0.17$	8.9k	¹ ABLIKIM	19H BES3	$J/\psi \rightarrow \eta'(958) e^+ e^-$

• • • We do not use the following data for averages, fits, limits, etc. • • •

$5.81 \pm 0.16 \pm 0.31$	1.4k	^{1,2} ABLIKIM	14i BES3	$J/\psi \rightarrow \eta'(958) e^+ e^-$
--------------------------	------	------------------------	----------	---

¹ Using both $\eta' \rightarrow \gamma \pi^+ \pi^-$ and $\eta' \rightarrow \pi^+ \pi^- \eta$ decays.

² Superseded by ABLIKIM 19H.

$\Gamma(\eta U \rightarrow \eta e^+ e^-) / \Gamma_{total}$ Γ_{322} / Γ

VALUE	CL%	DOCUMENT ID	TECN	COMMENT
$< 9.11 \times 10^{-7}$	90	¹ ABLIKIM	19A BES3	$J/\psi \rightarrow \eta e^+ e^-$

¹ For a dark photon U with mass between 10 and 2400 MeV. Obtained 90% C.L. limits as a function of m_U range from 1.9×10^{-8} to 91.1×10^{-8} .

$\Gamma(\eta'(958) U \rightarrow \eta'(958) e^+ e^-) / \Gamma_{total}$ Γ_{323} / Γ

VALUE	CL%	DOCUMENT ID	TECN	COMMENT
$< 2.0 \times 10^{-7}$	90	¹ ABLIKIM	19H BES3	$J/\psi \rightarrow \eta'(958) e^+ e^-$

¹ For a dark photon U with mass between 100 and 2100 MeV. Obtained 90% C.L. limits as a function of m_U range from 1.8×10^{-8} to 2.0×10^{-7} . The corresponding limits on the branching fraction $J/\psi \rightarrow \eta' U$ range from 5.7×10^{-8} to 7.4×10^{-7} .

See key on page 1127

Meson Particle Listings

$J/\psi(1S)$

$\Gamma(\phi e^+ e^-)/\Gamma_{total}$		Γ_{324}/Γ		
VALUE (units 10^{-7})	CL%	DOCUMENT ID	TECN	COMMENT
<1.2	90	1 ABLIKIM	19AB BES3	$J/\psi \rightarrow \phi e^+ e^-$
¹ Using $B(\phi \rightarrow K^+ K^-) = (48.9 \pm 0.5)\%$ and $B(\psi(2S) \rightarrow \pi^+ \pi^- J/\psi) = (34.49 \pm 0.30)\%$.				

WEAK DECAYS

$\Gamma(D^- e^+ \nu_e + c.c.)/\Gamma_{total}$		Γ_{325}/Γ		
VALUE	CL%	DOCUMENT ID	TECN	COMMENT
<7.1 $\times 10^{-8}$	90	ABLIKIM	21Q BES3	$e^+ e^- \rightarrow J/\psi$
••• We do not use the following data for averages, fits, limits, etc. •••				
<1.2 $\times 10^{-5}$	90	ABLIKIM	06M BES2	$e^+ e^- \rightarrow J/\psi$

$\Gamma(D^0 e^+ e^- + c.c.)/\Gamma_{total}$		Γ_{326}/Γ		
VALUE	CL%	DOCUMENT ID	TECN	COMMENT
<8.5 $\times 10^{-8}$	90	1 ABLIKIM	17AF BES3	$e^+ e^- \rightarrow J/\psi$
••• We do not use the following data for averages, fits, limits, etc. •••				
<1.1 $\times 10^{-5}$	90	ABLIKIM	06M BES2	$e^+ e^- \rightarrow J/\psi$
¹ Using D^0 decays to $K^- \pi^+$, $K^- \pi^+ \pi^0$, and $K^- \pi^+ \pi^+ \pi^-$.				

$\Gamma(D_s^- e^+ \nu_e + c.c.)/\Gamma_{total}$		Γ_{327}/Γ		
VALUE	CL%	DOCUMENT ID	TECN	COMMENT
<1.3 $\times 10^{-6}$	90	ABLIKIM	14R BES3	$e^+ e^- \rightarrow J/\psi$
••• We do not use the following data for averages, fits, limits, etc. •••				
<3.6 $\times 10^{-5}$	90	1 ABLIKIM	06M BES2	$e^+ e^- \rightarrow J/\psi$
¹ Using $B(D_s^- \rightarrow \phi \pi^-) = 4.4 \pm 0.5\%$.				

$\Gamma(D_s^{*-} e^+ \nu_e + c.c.)/\Gamma_{total}$		Γ_{328}/Γ		
VALUE	CL%	DOCUMENT ID	TECN	COMMENT
<1.8 $\times 10^{-6}$	90	ABLIKIM	14R BES3	$e^+ e^- \rightarrow J/\psi$

$\Gamma(D^- \pi^+ + c.c.)/\Gamma_{total}$		Γ_{329}/Γ		
VALUE	CL%	DOCUMENT ID	TECN	COMMENT
<7.5 $\times 10^{-5}$	90	ABLIKIM	08J BES2	$e^+ e^- \rightarrow J/\psi$

$\Gamma(D^0 \bar{K}^0 + c.c.)/\Gamma_{total}$		Γ_{330}/Γ		
VALUE	CL%	DOCUMENT ID	TECN	COMMENT
<1.7 $\times 10^{-4}$	90	ABLIKIM	08J BES2	$e^+ e^- \rightarrow J/\psi$

$\Gamma(D^0 \bar{K}^{*0} + c.c.)/\Gamma_{total}$		Γ_{331}/Γ		
VALUE	CL%	DOCUMENT ID	TECN	COMMENT
<2.5 $\times 10^{-6}$	90	ABLIKIM	14K BES3	$e^+ e^- \rightarrow J/\psi$

$\Gamma(D_s^- \pi^+ + c.c.)/\Gamma_{total}$		Γ_{332}/Γ		
VALUE	CL%	DOCUMENT ID	TECN	COMMENT
<1.3 $\times 10^{-4}$	90	ABLIKIM	08J BES2	$e^+ e^- \rightarrow J/\psi$

$\Gamma(D_s^- \rho^+ + c.c.)/\Gamma_{total}$		Γ_{333}/Γ		
VALUE	CL%	DOCUMENT ID	TECN	COMMENT
<1.3 $\times 10^{-5}$	90	ABLIKIM	14K BES3	$e^+ e^- \rightarrow J/\psi$

CHARGE CONJUGATION (C), PARITY (P), LEPTON FAMILY NUMBER (LF) VIOLATING MODES

$\Gamma(\gamma\gamma)/\Gamma_{total}$		Γ_{334}/Γ		
VALUE	CL%	DOCUMENT ID	TECN	COMMENT
< 2.7 $\times 10^{-7}$	90	ABLIKIM	14Q BES3	$\psi(2S) \rightarrow \pi^+ \pi^- J/\psi$
••• We do not use the following data for averages, fits, limits, etc. •••				
< 0.5 $\times 10^{-5}$	90	ADAMS	08 CLEO	$\psi(2S) \rightarrow \pi^+ \pi^- J/\psi$
< 1.6 $\times 10^{-4}$	90	1 WICHT	08 BELL	$B^{\pm} \rightarrow K^{\pm} \gamma\gamma$
< 2.2 $\times 10^{-5}$	90	ABLIKIM	07J BES2	$\psi(2S) \rightarrow J/\psi \pi^+ \pi^-$
<50 $\times 10^{-5}$	90	BARTEL	77 CNTR	$e^+ e^-$

¹ WICHT 08 reports $[\Gamma(J/\psi(1S) \rightarrow \gamma\gamma)/\Gamma_{total}] \times [B(B^+ \rightarrow J/\psi(1S) K^+)] < 0.16 \times 10^{-6}$ which we divide by our best value $B(B^+ \rightarrow J/\psi(1S) K^+) = 1.020 \times 10^{-3}$.

$\Gamma(\gamma\phi)/\Gamma_{total}$		Γ_{335}/Γ		
VALUE	CL%	DOCUMENT ID	TECN	COMMENT
<1.4 $\times 10^{-6}$	90	ABLIKIM	14Q BES3	$\psi(2S) \rightarrow \pi^+ \pi^- J/\psi$

$\Gamma(e^{\pm} \mu^{\mp})/\Gamma_{total}$		Γ_{336}/Γ		
VALUE	CL%	DOCUMENT ID	TECN	COMMENT
<1.6 $\times 10^{-7}$	90	ABLIKIM	13L BES3	$e^+ e^- \rightarrow J/\psi$
••• We do not use the following data for averages, fits, limits, etc. •••				
<1.1 $\times 10^{-6}$	90	BAI	03D BES	$e^+ e^- \rightarrow J/\psi$

$\Gamma(e^{\pm} \tau^{\mp})/\Gamma_{total}$		Γ_{337}/Γ		
VALUE	CL%	DOCUMENT ID	TECN	COMMENT
<7.5 $\times 10^{-8}$	90	ABLIKIM	21M BES3	$e^+ e^- \rightarrow J/\psi$
••• We do not use the following data for averages, fits, limits, etc. •••				
<8.3 $\times 10^{-6}$	90	1 ABLIKIM	04 BES	$e^+ e^- \rightarrow J/\psi$
¹ Superseded by ABLIKIM 21M.				

$\Gamma(\mu^{\pm} \tau^{\mp})/\Gamma_{total}$		Γ_{338}/Γ		
VALUE	CL%	DOCUMENT ID	TECN	COMMENT
<2.0 $\times 10^{-6}$	90	ABLIKIM	04 BES	$e^+ e^- \rightarrow J/\psi$

$\Gamma(A_C^{\pm} e^- + c.c.)/\Gamma_{total}$		Γ_{339}/Γ		
VALUE	CL%	DOCUMENT ID	TECN	COMMENT
<6.9 $\times 10^{-8}$	90	ABLIKIM	19AF BES3	$e^+ e^- \rightarrow J/\psi \rightarrow p K^- \pi^+ e^- (+ c.c.)$

OTHER DECAYS

$\Gamma(\text{invisible})/\Gamma(e^+ e^-)$		Γ_{340}/Γ_5		
VALUE	CL%	DOCUMENT ID	TECN	COMMENT
<6.6 $\times 10^{-2}$	90	LEES	13I BABR	$B \rightarrow K^{(*)} J/\psi$

$\Gamma(\text{invisible})/\Gamma(\mu^+ \mu^-)$		Γ_{340}/Γ_7		
VALUE	CL%	DOCUMENT ID	TECN	COMMENT
<1.2 $\times 10^{-2}$	90	ABLIKIM	08G BES2	$\psi(2S) \rightarrow \pi^+ \pi^- J/\psi$

J/ψ(1S) REFERENCES

ABLIKIM	21AM	PR D104 092004	M. Ablikim et al.	(BESIII Collab.)
ABLIKIM	21AT	JHEP 2111 226	M. Ablikim et al.	(BESIII Collab.)
ABLIKIM	21C	PR D103 012009	M. Ablikim et al.	(BESIII Collab.)
ABLIKIM	21M	PR D103 112007	M. Ablikim et al.	(BESIII Collab.)
ABLIKIM	21Q	JHEP 2106 157	M. Ablikim et al.	(BESIII Collab.)
LEES	21	PR D103 092001	J.P. Lees et al.	(BABAR Collab.)
LEES	21B	PR D104 112003	J.P. Lees et al.	(BABAR Collab.)
LEES	21C	PR D104 112004	J.P. Lees et al.	(BABAR Collab.)
SARANTSEV	21	PL B816 136227	A.V. Sarantsev et al.	(BONN, PHPI)
ABLIKIM	20	PR D101 012004	M. Ablikim et al.	(BESIII Collab.)
ABLIKIM	20K	PR D101 112005	M. Ablikim et al.	(BESIII Collab.)
ABLIKIM	20Q	EPJ C80 746	M. Ablikim et al.	(BESIII Collab.)
ANASHIN	20	JHEP 2007 112	V. V. Anashin et al.	(KEDR Collab.)
ABLIKIM	19A	PR D99 012006	M. Ablikim et al.	(BESIII Collab.)
	Also	PR D104 099001	(errat.) M. Ablikim et al.	(BESIII Collab.)
ABLIKIM	19AB	PR D99 052010	M. Ablikim et al.	(BESIII Collab.)
ABLIKIM	19AC	PR D99 071101	M. Ablikim et al.	(BESIII Collab.)
ABLIKIM	19AF	PR D99 072006	M. Ablikim et al.	(BESIII Collab.)
ABLIKIM	19AQ	PR D99 112008	M. Ablikim et al.	(BESIII Collab.)
ABLIKIM	19AN	PR D100 032004	M. Ablikim et al.	(BESIII Collab.)
ABLIKIM	19H	PR D99 012013	M. Ablikim et al.	(BESIII Collab.)
ABLIKIM	19N	PR D99 032006	M. Ablikim et al.	(BESIII Collab.)
ABLIKIM	19Q	PL B791 375	M. Ablikim et al.	(BESIII Collab.)
ABLIKIM	19T	PRL 122 142002	M. Ablikim et al.	(BESIII Collab.)
LU	19	PR D99 032003	P.-C. Lu et al.	(BELLE Collab.)
ABLIKIM	18AA	PR D98 072003	M. Ablikim et al.	(BESIII Collab.)
ABLIKIM	18AB	PR D98 072005	M. Ablikim et al.	(BESIII Collab.)
ABLIKIM	18D	PRL 121 022001	M. Ablikim et al.	(BESIII Collab.)
ABLIKIM	18I	PR D97 051101	M. Ablikim et al.	(BESIII Collab.)
ABLIKIM	18O	PR D97 072014	M. Ablikim et al.	(BESIII Collab.)
ANASHIN	18A	JHEP 1805 119	V.V. Anashin et al.	(KEDR Collab.)
LEES	18	PR D97 052007	J.P. Lees et al.	(BABAR Collab.)
LEES	18E	PR D98 112015	J.P. Lees et al.	(BABAR Collab.)
ABLIKIM	17AF	PR D96 111101	M. Ablikim et al.	(BESIII Collab.)
ABLIKIM	17AH	PR D96 112001	M. Ablikim et al.	(BESIII Collab.)
ABLIKIM	17AK	PR D96 112012	M. Ablikim et al.	(BESIII Collab.)
ABLIKIM	17E	PL B770 217	M. Ablikim et al.	(BESIII Collab.)
ABLIKIM	17L	PR D95 052003	M. Ablikim et al.	(BESIII Collab.)
LEES	17C	PR D95 052001	J.P. Lees et al.	(BABAR Collab.)
LEES	17A	PR D95 072007	J.P. Lees et al.	(BABAR Collab.)
LEES	17D	PR D95 092005	J.P. Lees et al.	(BABAR Collab.)
ABLIKIM	16E	PR D93 052005	M. Ablikim et al.	(BESIII Collab.)
ABLIKIM	16J	PRL 117 042001	M. Ablikim et al.	(BESIII Collab.)
ABLIKIM	16K	PR D93 052010	M. Ablikim et al.	(BESIII Collab.)
ABLIKIM	16L	PR D93 072003	M. Ablikim et al.	(BESIII Collab.)
ABLIKIM	16M	PR D93 072008	M. Ablikim et al.	(BESIII Collab.)
ABLIKIM	16N	PR D93 112011	M. Ablikim et al.	(BESIII Collab.)
ABLIKIM	16P	PR D94 072005	M. Ablikim et al.	(BESIII Collab.)
ABLIKIM	16Q	PL B761 98	M. Ablikim et al.	(BESIII Collab.)
PDG	16	CP C40 100001	C. Patrignani et al.	(PDG Collab.)
AAIJ	15B1	EPJ C75 311	R. Aaij et al.	(LHCb Collab.)
ABLIKIM	15AE	PR D92 052003	M. Ablikim et al.	(BESIII Collab.)
ABLIKIM	15H	PR D91 052017	M. Ablikim et al.	(BESIII Collab.)
ABLIKIM	15K	PR D91 112001	M. Ablikim et al.	(BESIII Collab.)
ABLIKIM	15P	PR D92 012007	M. Ablikim et al.	(BESIII Collab.)
ABLIKIM	15T	PRL 115 091803	M. Ablikim et al.	(BESIII Collab.)
ANASHIN	15	PL B749 50	V.V. Anashin et al.	(KEDR Collab.)
DOBBS	15	PR D91 052006	S. Dobbs et al.	(NWES)
LEES	15J	PR D92 072008	J.P. Lees et al.	(BABAR Collab.)
ABLIKIM	14J	PR D89 092008	M. Ablikim et al.	(BESIII Collab.)
ABLIKIM	14K	PR D89 071101	M. Ablikim et al.	(BESIII Collab.)
ABLIKIM	14N	PR D90 052009	M. Ablikim et al.	(BESIII Collab.)
ABLIKIM	14R	PR D90 092002	M. Ablikim et al.	(BESIII Collab.)
ABLIKIM	14Q	PR D90 112014	M. Ablikim et al.	(BESIII Collab.)
ANASHIN	14	PL B738 391	V.V. Anashin et al.	(KEDR Collab.)
AULCHENKO	14	PL B731 227	V.M. Aulchenko et al.	(KEDR Collab.)
LEES	14H	PR D89 092002	J.P. Lees et al.	(BABAR Collab.)
ABLIKIM	13F	PR D87 052007	M. Ablikim et al.	(BESIII Collab.)
ABLIKIM	13I	PR D87 032003	M. Ablikim et al.	(BESIII Collab.)
ABLIKIM	13J	PR D87 032008	M. Ablikim et al.	(BESIII Collab.)
ABLIKIM	13L	PR D87 112007	M. Ablikim et al.	(BESIII Collab.)
ABLIKIM	13N	PR D87 092009	M. Ablikim et al.	(BESIII Collab.)
ABLIKIM	13P	PR D87 112004	M. Ablikim et al.	(BESIII Collab.)
ABLIKIM	13R	PR D88 032007	M. Ablikim et al.	(BESIII Collab.)
ABLIKIM	13U	PR D88 091502	M. Ablikim et al.	(BESIII Collab.)
LEES	13I	PR D87 112005	J.P. Lees et al.	(BABAR Collab.)
LEES	13O	PR D87 092005	J.P. Lees et al.	(BABAR Collab.)
LEES	13Q	PR D88 032013	J.P. Lees et al.	(BABAR Collab.)
LEES	13Y	PR D88 072009	J.P. Lees et al.	(BABAR Collab.)
ABLIKIM	12	PR D85 092012	M. Ablikim et al.	(BESIII Collab.)
ABLIKIM	12B	PR D86 032008	M. Ablikim et al.	(BESIII Collab.)
ABLIKIM	12C	PR D86 032014	M. Ablikim et al.	(BESIII Collab.)
ABLIKIM	12D	PRL 108 112003	M. Ablikim et al.	(BESIII Collab.)
ABLIKIM	12H	PL B710 594	M. Ablikim et al.	(BESIII Collab.)
ABLIKIM	12P	CP C36 1031	M. Ablikim et al.	(BES II Collab.)
LEES	12E	PR D85 112009	J.P. Lees et al.	(BABAR Collab.)
LEES	12F	PR D86 022008	J.P. Lees et al.	(BABAR Collab.)
METREVELLI	12	PR D85 092007	Z. Metreveli et al.	(NWES, FLOR, WAYN+)
ABLIKIM	11	PR D83 012003	M. Ablikim et al.	(BESIII Collab.)
ABLIKIM	11C	PRL 106 072002	M. Ablikim et al.	(BESIII Collab.)
ABLIKIM	11D	PR D83 032003	M. Ablikim et al.	(BESIII Collab.)

Meson Particle Listings

Branching Ratios of ψ 's and χ 's, $\chi_{c0}(1P)$

given by the collaborations, or rescaling back the published results. The information was sometimes spread over several articles, and some articles referred to papers still unpublished, which in turn contained the relevant numbers in footnotes.

Even though the experimental collaborations are entitled to extract whatever branching ratios they consider appropriate by using other published results, we would like to encourage them to also quote explicitly in their articles the actual quantities measured, so that they can be used directly in averages and fits of different experimental determinations.

To inform the reader how we computed some of the values used in this edition of RPP, we use footnotes to indicate the branching ratios actually given by the experiments and the quantities they use to derive them from the true combination of branching ratios actually measured.

None of the branching ratios of the $\chi_{c0,1,2}$ are measured independently of the $\psi(2S)$ radiative decays. We tried to identify those branching ratios which can be correlated in a non-trivial way, and although we cannot preclude the existence of other cases, we are confident that the most relevant correlations have already been removed. Nevertheless, correlations in the errors of different quantities measured by the same experiment have not been taken into account.

Fit information

This is an overall fit to 4 total widths, 1 partial width, 26 combinations of partial widths, 24 branching ratios, and 108 combinations of branching ratios. Of the latter 62 involve decays of more than one particle.

The overall fit uses 248 measurements to determine 49 parameters and has a χ^2 of 379.8 for 199 degrees of freedom.

The relatively high χ^2 of the fit, 1.9 per d.o.f., can be traced back to a few specific discrepancies in the data. No scaling factors to fit uncertainties have been applied.

In the listing we provide the inter-particle correlation coefficients $\langle \delta x_i \delta x_j \rangle / (\delta x_i \cdot \delta x_j)$, in percent, from the fit to the corresponding parameter x_i .

References

1. Y.F. Gu and X.H. Li, Phys. Lett. **B449**, 361 (1999).
2. C. Patrignani, Phys. Rev. **D64**, 034017 (2001).
3. K. Hagiwara *et al.* (Particle Data Group), Phys. Rev. **D68**, 010001 (2002).

$\chi_{c0}(1P)$

$$J^{PC} = 0^+(0^{++})$$

$\chi_{c0}(1P)$ MASS				
VALUE (MeV)	EVTS	DOCUMENT ID	TECN	COMMENT
3414.71 ± 0.30 OUR AVERAGE				
3413.0 ± 1.9 ± 0.6	933	1 AAIJ	17BB LHCB	$pp \rightarrow b\bar{b}X \rightarrow 2(K^+K^-)X$
3414.2 ± 0.5 ± 2.3	5.4k	UEHARA	08 BELL	$\gamma\gamma \rightarrow \chi_{c0} \rightarrow \text{hadrons}$
3406 ± 7 ± 6	230	2 ABE	07 BELL	$e^+e^- \rightarrow J/\psi(c\bar{c})$
3414.21 ± 0.39 ± 0.27		ABLIKIM	05G BES2	$\psi(2S) \rightarrow \gamma\chi_{c0}$
3414.7 ± 0.7 ± 0.2		3 ANDREOTTI	03 E835	$\bar{p}p \rightarrow \chi_{c0} \rightarrow \pi^0\pi^0$
3415.5 ± 0.4 ± 0.4	392	4 BAGNASCO	02 E835	$\bar{p}p \rightarrow \chi_{c0} \rightarrow J/\psi\gamma$

3417.4 +1.8 -1.9 ± 0.2		3 AMBROGIANI	99B E835	$\bar{p}p \rightarrow e^+e^-\gamma$
3414.1 ± 0.6 ± 0.8		BAI	99B BES	$\psi(2S) \rightarrow \gamma X$
3417.8 ± 0.4 ± 4		3 GAISER	86 CBAL	$\psi(2S) \rightarrow \gamma X$
3416 ± 3 ± 4		5 TANENBAUM	78 MRK1	e^+e^-
• • • We do not use the following data for averages, fits, limits, etc. • • •				
3414.6 ± 1.1	266	UEHARA	13 BELL	$\gamma\gamma \rightarrow K_S^0 K_S^0$
3416.5 ± 3.0		EISENSTEIN	01 CLE2	$e^+e^- \rightarrow e^+e^-\chi_{c0}$
3422 ± 10		5 BARTEL	78B CNTR	$e^+e^- \rightarrow J/\psi 2\gamma$
3415 ± 9		5 BIDDICK	77 CNTR	$e^+e^- \rightarrow \gamma X$

¹ From a fit of the $\phi\phi$ invariant mass with the width of $\chi_{c0}(1P)$ fixed to the PDG 16 value.
² From a fit of the J/ψ recoil mass spectrum. Supersedes ABE,K 02 and ABE 04G.
³ Using mass of $\psi(2S) = 3686.0$ MeV.
⁴ Recalculated by ANDREOTTI 05A, using the value of $\psi(2S)$ mass from AULCHENKO 03.
⁵ Mass value shifted by us by amount appropriate for $\psi(2S)$ mass = 3686 MeV and $J/\psi(1S)$ mass = 3097 MeV.

$\chi_{c0}(1P)$ WIDTH				
VALUE (MeV)	EVTS	DOCUMENT ID	TECN	COMMENT
10.8 ± 0.6 OUR FIT				
10.5 ± 0.8 OUR AVERAGE	Error includes scale factor of 1.1.			
10.6 ± 1.9 ± 2.6	5.4k	UEHARA	08 BELL	$\gamma\gamma \rightarrow \chi_{c0} \rightarrow \text{hadrons}$
12.6 +1.5 +0.9 -1.6 -1.1		ABLIKIM	05G BES2	$\psi(2S) \rightarrow \gamma\chi_{c0}$
8.6 +1.7 -1.3 ± 0.1		ANDREOTTI	03 E835	$\bar{p}p \rightarrow \chi_{c0} \rightarrow \pi^0\pi^0$
9.7 ± 1.0	392	1 BAGNASCO	02 E835	$\bar{p}p \rightarrow \chi_{c0} \rightarrow J/\psi\gamma$
16.6 +5.2 -3.7 ± 0.1		AMBROGIANI	99B E835	$\bar{p}p \rightarrow e^+e^-\gamma$
14.3 ± 2.0 ± 3.0		BAI	98I BES	$\psi(2S) \rightarrow \gamma\pi^+\pi^-$
13.5 ± 3.3 ± 4.2		GAISER	86 CBAL	$\psi(2S) \rightarrow \gamma X, \gamma\pi^0\pi^0$
• • • We do not use the following data for averages, fits, limits, etc. • • •				
13.2 ± 2.1	266	UEHARA	13 BELL	$\gamma\gamma \rightarrow K_S^0 K_S^0$

¹ Recalculated by ANDREOTTI 05A.

$\chi_{c0}(1P)$ DECAY MODES				Scale factor/ Confidence level
Mode	Fraction (Γ_i/Γ)			
Hadronic decays				
Γ_1	$2(\pi^+\pi^-)$	(2.34 ± 0.18) %		
Γ_2	$\rho^0\pi^+\pi^-$	(9.1 ± 2.9) × 10 ⁻³		
Γ_3	$\rho^0\rho^0$			
Γ_4	$f_0(980)f_0(980)$	(6.6 ± 2.1) × 10 ⁻⁴		
Γ_5	$\pi^+\pi^-\pi^0\pi^0$	(3.3 ± 0.4) %		
Γ_6	$\rho^+\pi^-\pi^0 + \text{c.c.}$	(2.9 ± 0.4) %		
Γ_7	$4\pi^0$	(3.3 ± 0.4) × 10 ⁻³		
Γ_8	$\pi^+\pi^-K^+K^-$	(1.81 ± 0.14) %		
Γ_9	$K_0^*(1430)^0\bar{K}_0^*(1430)^0 \rightarrow \pi^+\pi^-K^+K^-$	(9.8 +4.0 -2.8) × 10 ⁻⁴		
Γ_{10}	$K_0^*(1430)^0\bar{K}_2^*(1430)^0 + \text{c.c.} \rightarrow \pi^+\pi^-K^+K^-$	(8.0 +2.0 -2.4) × 10 ⁻⁴		
Γ_{11}	$K_1(1270)^+K^- + \text{c.c.} \rightarrow \pi^+\pi^-K^+K^-$	(6.3 ± 1.9) × 10 ⁻³		
Γ_{12}	$K_1(1400)^+K^- + \text{c.c.} \rightarrow \pi^+\pi^-K^+K^-$	< 2.7 × 10 ⁻³		CL=90%
Γ_{13}	$f_0(980)f_0(980)$	(1.6 +1.0 -0.9) × 10 ⁻⁴		
Γ_{14}	$f_0(980)f_0(2200)$	(7.9 +2.0 -2.5) × 10 ⁻⁴		
Γ_{15}	$f_0(1370)f_0(1370)$	< 2.7 × 10 ⁻⁴		CL=90%
Γ_{16}	$f_0(1370)f_0(1500)$	< 1.7 × 10 ⁻⁴		CL=90%
Γ_{17}	$f_0(1370)f_0(1710)$	(6.7 +3.5 -2.3) × 10 ⁻⁴		
Γ_{18}	$f_0(1500)f_0(1370)$	< 1.3 × 10 ⁻⁴		CL=90%
Γ_{19}	$f_0(1500)f_0(1500)$	< 5 × 10 ⁻⁵		CL=90%
Γ_{20}	$f_0(1500)f_0(1710)$	< 7 × 10 ⁻⁵		CL=90%
Γ_{21}	$K^+K^-\pi^+\pi^-\pi^0$	(8.6 ± 0.9) × 10 ⁻³		
Γ_{22}	$K_S^0 K^\pm\pi^\mp\pi^+\pi^-$	(4.2 ± 0.4) × 10 ⁻³		
Γ_{23}	$K^+K^-\pi^0\pi^0$	(5.6 ± 0.9) × 10 ⁻³		
Γ_{24}	$K^+\pi^-\bar{K}^0\pi^0 + \text{c.c.}$	(2.49 ± 0.33) %		
Γ_{25}	$\rho^+K^-K^0 + \text{c.c.}$	(1.21 ± 0.21) %		
Γ_{26}	$K^*(892)^-K^+\pi^0 \rightarrow K^+\pi^-\bar{K}^0\pi^0 + \text{c.c.}$	(4.6 ± 1.2) × 10 ⁻³		
Γ_{27}	$K_S^0 K_S^0\pi^+\pi^-$	(5.7 ± 1.1) × 10 ⁻³		
Γ_{28}	$K^+K^-\eta\pi^0$	(3.0 ± 0.7) × 10 ⁻³		
Γ_{29}	$3(\pi^+\pi^-)$	(1.20 ± 0.18) %		
Γ_{30}	$K^+\bar{K}^*(892)^0\pi^- + \text{c.c.}$	(7.5 ± 1.6) × 10 ⁻³		
Γ_{31}	$K^*(892)^0\bar{K}^*(892)^0$	(1.7 ± 0.6) × 10 ⁻³		

Meson Particle Listings

 $\chi_{c0}(1P)$

Γ_{32}	$\pi\pi$	$(8.51 \pm 0.33) \times 10^{-3}$	
Γ_{33}	$\pi^0\eta$	$< 1.8 \times 10^{-4}$	
Γ_{34}	$\pi^0\eta'$	$< 1.1 \times 10^{-3}$	
Γ_{35}	$\pi^0\eta_c$	$< 1.6 \times 10^{-3}$	CL=90%
Γ_{36}	$\eta\eta$	$(3.01 \pm 0.19) \times 10^{-3}$	
Γ_{37}	$\eta\eta'$	$(9.1 \pm 1.1) \times 10^{-5}$	
Γ_{38}	$\eta'\eta'$	$(2.17 \pm 0.12) \times 10^{-3}$	
Γ_{39}	$\omega\omega$	$(9.7 \pm 1.1) \times 10^{-4}$	
Γ_{40}	$\omega\phi$	$(1.41 \pm 0.13) \times 10^{-4}$	
Γ_{41}	$\omega K^+ K^-$	$(1.94 \pm 0.21) \times 10^{-3}$	
Γ_{42}	$K^+ K^-$	$(6.05 \pm 0.31) \times 10^{-3}$	
Γ_{43}	$K_S^0 K_S^0$	$(3.16 \pm 0.17) \times 10^{-3}$	
Γ_{44}	$\pi^+ \pi^- \eta$	$< 2.0 \times 10^{-4}$	CL=90%
Γ_{45}	$\pi^+ \pi^- \eta'$	$< 4 \times 10^{-4}$	CL=90%
Γ_{46}	$\bar{K}^0 K^+ \pi^- + c.c.$	$< 9 \times 10^{-5}$	CL=90%
Γ_{47}	$K^+ K^- \pi^0$	$< 6 \times 10^{-5}$	CL=90%
Γ_{48}	$K^+ K^- \eta$	$< 2.3 \times 10^{-4}$	CL=90%
Γ_{49}	$K^+ K^- K_S^0 K_S^0$	$(1.4 \pm 0.5) \times 10^{-3}$	
Γ_{50}	$K_S^0 K_S^0 K_S^0 K_S^0$	$(5.8 \pm 0.5) \times 10^{-4}$	
Γ_{51}	$K^+ K^- K^+ K^-$	$(2.82 \pm 0.29) \times 10^{-3}$	
Γ_{52}	$K^+ K^- \phi$	$(9.7 \pm 2.5) \times 10^{-4}$	
Γ_{53}	$\bar{K}^0 K^+ \pi^- \phi + c.c.$	$(3.7 \pm 0.6) \times 10^{-3}$	
Γ_{54}	$K^+ K^- \pi^0 \phi$	$(1.90 \pm 0.35) \times 10^{-3}$	
Γ_{55}	$\phi \pi^+ \pi^- \pi^0$	$(1.18 \pm 0.15) \times 10^{-3}$	
Γ_{56}	$\phi\phi$	$(8.0 \pm 0.7) \times 10^{-4}$	
Γ_{57}	$\phi\phi\eta$	$(8.4 \pm 1.0) \times 10^{-4}$	
Γ_{58}	$\rho\bar{\rho}$	$(2.21 \pm 0.08) \times 10^{-4}$	
Γ_{59}	$\rho\bar{\rho}\pi^0$	$(7.0 \pm 0.7) \times 10^{-4}$	S=1.3
Γ_{60}	$\rho\bar{\rho}\eta$	$(3.5 \pm 0.4) \times 10^{-4}$	
Γ_{61}	$\rho\bar{\rho}\omega$	$(5.2 \pm 0.6) \times 10^{-4}$	
Γ_{62}	$\rho\bar{\rho}\phi$	$(6.0 \pm 1.4) \times 10^{-5}$	
Γ_{63}	$\rho\bar{\rho}\pi^+ \pi^-$	$(2.1 \pm 0.7) \times 10^{-3}$	S=1.4
Γ_{64}	$\rho\bar{\rho}\pi^0 \pi^0$	$(1.04 \pm 0.28) \times 10^{-3}$	
Γ_{65}	$\rho\bar{\rho} K^+ K^-$ (non-resonant)	$(1.22 \pm 0.26) \times 10^{-4}$	
Γ_{66}	$\rho\bar{\rho} K_S^0 K_S^0$	$< 8.8 \times 10^{-4}$	CL=90%
Γ_{67}	$\rho\bar{\rho}\pi^-$	$(1.27 \pm 0.11) \times 10^{-3}$	
Γ_{68}	$\bar{\rho}\eta\pi^+$	$(1.37 \pm 0.12) \times 10^{-3}$	
Γ_{69}	$\rho\bar{\rho}\pi^- \pi^0$	$(2.34 \pm 0.21) \times 10^{-3}$	
Γ_{70}	$\bar{\rho}\eta\pi^+ \pi^0$	$(2.21 \pm 0.18) \times 10^{-3}$	
Γ_{71}	$\Lambda\bar{\Lambda}$	$(3.59 \pm 0.15) \times 10^{-4}$	
Γ_{72}	$\Lambda\bar{\Lambda}\pi^+ \pi^-$	$(1.18 \pm 0.13) \times 10^{-3}$	
Γ_{73}	$\Lambda\bar{\Lambda}\pi^+ \pi^-$ (non-resonant)	$< 5 \times 10^{-4}$	CL=90%
Γ_{74}	$\Sigma(1385)^+ \bar{\Lambda}\pi^- + c.c.$	$< 5 \times 10^{-4}$	CL=90%
Γ_{75}	$\Sigma(1385)^- \bar{\Lambda}\pi^+ + c.c.$	$< 5 \times 10^{-4}$	CL=90%
Γ_{76}	$K^+ \bar{\rho}\Lambda + c.c.$	$(1.25 \pm 0.12) \times 10^{-3}$	S=1.3
Γ_{77}	$n K_S^0 \bar{\Lambda} + c.c.$	$(6.6 \pm 0.5) \times 10^{-4}$	
Γ_{78}	$K^*(892)^+ \bar{\rho}\Lambda + c.c.$	$(4.8 \pm 0.9) \times 10^{-4}$	
Γ_{79}	$K^+ \bar{\rho}\Lambda(1520) + c.c.$	$(2.9 \pm 0.7) \times 10^{-4}$	
Γ_{80}	$\Lambda(1520) \bar{\Lambda}(1520)$	$(3.1 \pm 1.2) \times 10^{-4}$	
Γ_{81}	$\Sigma^0 \bar{\Sigma}^0$	$(4.68 \pm 0.32) \times 10^{-4}$	
Γ_{82}	$\Sigma^+ \bar{\rho} K_S^0 + c.c.$	$(3.52 \pm 0.27) \times 10^{-4}$	
Γ_{83}	$\Sigma^0 \bar{\rho} K^+ + c.c.$	$(3.03 \pm 0.20) \times 10^{-4}$	
Γ_{84}	$\Sigma^+ \bar{\Sigma}^-$	$(4.6 \pm 0.8) \times 10^{-4}$	S=2.6
Γ_{85}	$\Sigma^- \bar{\Sigma}^+$	$(5.1 \pm 0.5) \times 10^{-4}$	
Γ_{86}	$\Sigma(1385)^+ \bar{\Sigma}(1385)^-$	$(1.6 \pm 0.6) \times 10^{-4}$	
Γ_{87}	$\Sigma(1385)^- \bar{\Sigma}(1385)^+$	$(2.3 \pm 0.7) \times 10^{-4}$	
Γ_{88}	$K^- \bar{\Lambda}\Xi^+ + c.c.$	$(1.94 \pm 0.35) \times 10^{-4}$	
Γ_{89}	$\Xi^0 \bar{\Xi}^0$	$(3.1 \pm 0.8) \times 10^{-4}$	
Γ_{90}	$\Xi^- \bar{\Xi}^+$	$(4.8 \pm 0.7) \times 10^{-4}$	
Γ_{91}	$\eta_c \pi^+ \pi^-$	$< 7 \times 10^{-4}$	CL=90%

Radiative decays

Γ_{92}	$\gamma J/\psi(1S)$	$(1.40 \pm 0.05) \%$	
Γ_{93}	$\gamma\rho^0$	$< 9 \times 10^{-6}$	CL=90%
Γ_{94}	$\gamma\omega$	$< 8 \times 10^{-6}$	CL=90%
Γ_{95}	$\gamma\phi$	$< 6 \times 10^{-6}$	CL=90%
Γ_{96}	$\gamma\gamma$	$(2.04 \pm 0.09) \times 10^{-4}$	
Γ_{97}	$e^+ e^- J/\psi(1S)$	$(1.33 \pm 0.29) \times 10^{-4}$	
Γ_{98}	$\mu^+ \mu^- J/\psi(1S)$	$< 1.9 \times 10^{-5}$	CL=90%

CONSTRAINED FIT INFORMATION

A multiparticle fit to $\chi_{c1}(1P)$, $\chi_{c0}(1P)$, $\chi_{c2}(1P)$, and $\psi(2S)$ with 4 total widths, a partial width, 25 combinations of partial widths obtained from integrated cross section, and 84 branching ratios uses 248 measurements to determine 49 parameters. The overall fit has a $\chi^2 = 379.8$ for 199 degrees of freedom.

The following *off-diagonal* array elements are the correlation coefficients $\langle \delta p_i \delta p_j \rangle / (\delta p_i \delta p_j)$, in percent, from the fit to parameters p_i , including the branching fractions, $x_i \equiv \Gamma_i / \Gamma_{\text{total}}$.

x_2	24										
x_8	9	2									
x_{30}	5	1	28								
x_{32}	8	2	10	3							
x_{36}	4	1	5	1	14						
x_{42}	8	2	8	3	18	11					
x_{43}	7	2	8	2	18	10	14				
x_{51}	5	1	5	2	9	5	7	7			
x_{56}	7	2	6	2	9	5	7	7	4		
x_{58}	3	1	4	1	3	-1	7	7	3	3	
x_{71}	7	2	9	2	23	13	18	18	8	9	
x_{92}	5	1	6	2	17	11	13	12	6	6	
x_{96}	-8	-2	-2	-3	14	9	10	10	3	1	
Γ	-26	-6	-19	-10	-15	-7	-14	-12	-10	-13	

x_{71}	9										
x_{92}	-19	16									
x_{96}	6	15	13								
Γ	-4	-13	-9	-38							

 $\chi_{c0}(1P)$ PARTIAL WIDTHS $\chi_{c0}(1P) \Gamma(i) \Gamma(\gamma J/\psi(1S)) / \Gamma(\text{total})$

$\Gamma(\rho\bar{\rho}) \times \Gamma(\gamma J/\psi(1S)) / \Gamma_{\text{total}}$	$\Gamma_{58} \Gamma_{92} / \Gamma$			
VALUE (eV)	EVTS	DOCUMENT ID	TECN	COMMENT
33.6 ± 2.3 OUR FIT				
• • • We do not use the following data for averages, fits, limits, etc. • • •				
26.6 ± 2.6 ± 1.4	392	1,2 BAGNASCO 02 E835	$\bar{p}p \rightarrow \chi_{c0} \rightarrow J/\psi\gamma$	
48.7 ± 11.3 ± 8.9 ± 2.4		1,2 AMBROGIANI 99B E835	$\bar{p}p \rightarrow \gamma J/\psi$	
1 Calculated by us using $B(J/\psi(1S) \rightarrow e^+ e^-) = 0.0593 \pm 0.0010$.				
2 Values in $(\Gamma(\rho\bar{\rho}) \times \Gamma(\gamma J/\psi(1S)) / \Gamma_{\text{total}})$ and $(\Gamma(\rho\bar{\rho}) / \Gamma_{\text{total}}) \times \Gamma(\gamma J/\psi(1S)) / \Gamma_{\text{total}}$ are not independent. The latter is used in the fit since it is less correlated to the total width.				

 $\chi_{c0}(1P) \Gamma(i) \Gamma(\gamma\gamma) / \Gamma(\text{total})$

$\Gamma(2\pi^+ \pi^-) \times \Gamma(\gamma\gamma) / \Gamma_{\text{total}}$	$\Gamma_1 \Gamma_{96} / \Gamma$			
VALUE (eV)	EVTS	DOCUMENT ID	TECN	COMMENT
52 ± 4 OUR FIT				
49 ± 10 OUR AVERAGE				Error includes scale factor of 1.8.
44.7 ± 3.6 ± 4.9	3.6k	UEHARA 08 BELL	$\gamma\gamma \rightarrow \chi_{c0} \rightarrow 2(\pi^+ \pi^-)$	
75 ± 13 ± 8		EISENSTEIN 01 CLE2	$e^+ e^- \rightarrow e^+ e^- \chi_{c0}$	
$\Gamma(\rho^0 \rho^0) \times \Gamma(\gamma\gamma) / \Gamma_{\text{total}}$	$\Gamma_3 \Gamma_{96} / \Gamma$			
VALUE (eV)	CL% EVTS	DOCUMENT ID	TECN	COMMENT
• • • We do not use the following data for averages, fits, limits, etc. • • •				
<12	90	<252	UEHARA 08 BELL	$\gamma\gamma \rightarrow \chi_{c0} \rightarrow 2(\pi^+ \pi^-)$

$\Gamma(\pi^+ \pi^- K^+ K^-) \times \Gamma(\gamma\gamma) / \Gamma_{\text{total}}$	$\Gamma_8 \Gamma_{96} / \Gamma$			
VALUE (eV)	EVTS	DOCUMENT ID	TECN	COMMENT
40.0 ± 3.5 OUR FIT				
38.8 ± 3.7 ± 4.7	1.7k	UEHARA 08 BELL	$\gamma\gamma \rightarrow \chi_{c0} \rightarrow K^+ K^- \pi^+ \pi^-$	

$\Gamma(K^+ K^- \pi^+ \pi^- \pi^0) \times \Gamma(\gamma\gamma) / \Gamma_{\text{total}}$	$\Gamma_{21} \Gamma_{96} / \Gamma$			
VALUE (eV)	EVTS	DOCUMENT ID	TECN	COMMENT
26 ± 4 ± 4	1094	DEL-AMO-SA...11M BABR	$\gamma\gamma \rightarrow K^+ K^- \pi^+ \pi^- \pi^0$	

$\Gamma(K^+ \bar{K}^*(892)^0 \pi^- + c.c.) \times \Gamma(\gamma\gamma) / \Gamma_{\text{total}}$	$\Gamma_{30} \Gamma_{96} / \Gamma$			
VALUE (eV)	EVTS	DOCUMENT ID	TECN	COMMENT
16 ± 4 OUR FIT				
16.7 ± 6.1 ± 3.0	495 ± 182	UEHARA 08 BELL	$\gamma\gamma \rightarrow \chi_{c0} \rightarrow K^+ K^- \pi^+ \pi^-$	

See key on page 1127

Meson Particle Listings

$\chi_{c0}(1P)$

$\Gamma(K^*(892)^0 \bar{K}^*(892)^0) \times \Gamma(\gamma\gamma)/\Gamma_{total}$					$\Gamma_{31} \Gamma_{96}/\Gamma$
VALUE (eV)	CL%	EVTS	DOCUMENT ID	TECN	COMMENT

• • • We do not use the following data for averages, fits, limits, etc. • • •
 <6 90 <148 UEHARA 08 BELL $\gamma\gamma \rightarrow \chi_{c0} \rightarrow K^+ K^- \pi^+ \pi^-$

$\Gamma(\pi\pi) \times \Gamma(\gamma\gamma)/\Gamma_{total}$					$\Gamma_{32} \Gamma_{96}/\Gamma$
VALUE (eV)	CL%	EVTS	DOCUMENT ID	TECN	COMMENT

18.8 ± 1.3 OUR FIT
23 ± 5 OUR AVERAGE
 29.7^{+17.4}_{-12.0} ± 4.8 103⁺⁶⁰₋₄₂ ¹UEHARA 09 BELL 10.6 e⁺e⁻ → e⁺e⁻π⁰π⁰
 22.7 ± 3.2 ± 3.5 129 ± 18 ²NAKAZAWA 05 BELL 10.6 e⁺e⁻ → e⁺e⁻π⁺π⁻
¹We multiplied the measurement by 3 to convert from π⁰π⁰ to ππ. Interference with the continuum included.
²We have multiplied π⁺π⁻ measurement by 3/2 to obtain ππ.

$\Gamma(\eta\eta) \times \Gamma(\gamma\gamma)/\Gamma_{total}$					$\Gamma_{36} \Gamma_{96}/\Gamma$
VALUE (eV)	CL%	EVTS	DOCUMENT ID	TECN	COMMENT

9.4 ± 2.3 ± 1.2 22 ¹UEHARA 10A BELL 10.6 e⁺e⁻ → e⁺e⁻ηη
¹Interference with the continuum not included.

$\Gamma(\omega\omega) \times \Gamma(\gamma\gamma)/\Gamma_{total}$					$\Gamma_{39} \Gamma_{96}/\Gamma$
VALUE (eV)	CL%	EVTS	DOCUMENT ID	TECN	COMMENT

• • • We do not use the following data for averages, fits, limits, etc. • • •
 <3.9 90 ¹LIU 12B BELL $\gamma\gamma \rightarrow 2(\pi^+ \pi^- \pi^0)$
¹Using B(ω → π⁺π⁻π⁰) = (89.2 ± 0.7)%.

$\Gamma(\omega\phi) \times \Gamma(\gamma\gamma)/\Gamma_{total}$					$\Gamma_{40} \Gamma_{96}/\Gamma$
VALUE (eV)	CL%	EVTS	DOCUMENT ID	TECN	COMMENT

• • • We do not use the following data for averages, fits, limits, etc. • • •
 <0.34 90 ¹LIU 12B BELL $\gamma\gamma \rightarrow K^+ K^- \pi^+ \pi^- \pi^0$
¹Using B(φ → K⁺K⁻) = (48.9 ± 0.5)% and B(ω → π⁺π⁻π⁰) = (89.2 ± 0.7)%.

$\Gamma(K^+ K^-) \times \Gamma(\gamma\gamma)/\Gamma_{total}$					$\Gamma_{42} \Gamma_{96}/\Gamma$
VALUE (eV)	CL%	EVTS	DOCUMENT ID	TECN	COMMENT

13.4 ± 1.0 OUR FIT
14.3 ± 1.6 ± 2.3 153 ± 17 NAKAZAWA 05 BELL 10.6 e⁺e⁻ → e⁺e⁻K⁺K⁻

$\Gamma(K_S^0 K_S^0) \times \Gamma(\gamma\gamma)/\Gamma_{total}$					$\Gamma_{43} \Gamma_{96}/\Gamma$
VALUE (eV)	CL%	EVTS	DOCUMENT ID	TECN	COMMENT

7.0 ± 0.5 OUR FIT
8.7 ± 1.7 ± 0.9 266 ¹UEHARA 13 BELL $\gamma\gamma \rightarrow K_S^0 K_S^0$
 • • • We do not use the following data for averages, fits, limits, etc. • • •
 7.00 ± 0.65 ± 0.71 134 ± 12 CHEN 07B BELL e⁺e⁻ → e⁺e⁻χ_{c0}
¹Supersedes CHEN 07B.

$\Gamma(K^+ K^- K^+ K^-) \times \Gamma(\gamma\gamma)/\Gamma_{total}$					$\Gamma_{51} \Gamma_{96}/\Gamma$
VALUE (eV)	CL%	EVTS	DOCUMENT ID	TECN	COMMENT

6.2 ± 0.7 OUR FIT
7.9 ± 1.3 ± 1.1 215 ± 36 UEHARA 08 BELL $\gamma\gamma \rightarrow \chi_{c0} \rightarrow 2(K^+ K^-)$

$\Gamma(\phi\phi) \times \Gamma(\gamma\gamma)/\Gamma_{total}$					$\Gamma_{56} \Gamma_{96}/\Gamma$
VALUE (eV)	CL%	EVTS	DOCUMENT ID	TECN	COMMENT

1.76 ± 0.18 OUR FIT
1.72 ± 0.33 ± 0.14 56 ± 11 ¹LIU 12B BELL $\gamma\gamma \rightarrow 2(K^+ K^-)$
 • • • We do not use the following data for averages, fits, limits, etc. • • •
 2.3 ± 0.9 ± 0.4 23.6 ± 9.6 UEHARA 08 BELL $\gamma\gamma \rightarrow \chi_{c0} \rightarrow 2(K^+ K^-)$
¹Supersedes UEHARA 08. Using B(φ → K⁺K⁻) = (48.9 ± 0.5)%.

$\chi_{c0}(1P)$ BRANCHING RATIOS

HADRONIC DECAYS

$\Gamma(2(\pi^+ \pi^-))/\Gamma_{total}$		Γ_1/Γ
VALUE	DOCUMENT ID	

0.0234 ± 0.0018 OUR FIT

$\Gamma(\rho^0 \pi^+ \pi^-)/\Gamma(2(\pi^+ \pi^-))$		Γ_2/Γ_1	
VALUE	DOCUMENT ID	TECN	COMMENT

0.39 ± 0.12 OUR FIT
0.39 ± 0.12 TANENBAUM 78 MRK1 $\psi(2S) \rightarrow \gamma\chi_{c0}$

$\Gamma(\rho^0 \pi^+ \pi^-)/\Gamma_{total}$		Γ_2/Γ
VALUE	DOCUMENT ID	

0.0091 ± 0.0029 OUR FIT

$\Gamma(f_0(980) f_0(980))/\Gamma_{total}$		Γ_4/Γ		
VALUE (units 10 ⁻⁴)	EVTS	DOCUMENT ID	TECN	COMMENT

6.6 ± 2.1 ± 0.1 36 ± 9 ¹ABLIKIM 04G BES $\psi(2S) \rightarrow \gamma 2\pi^+ 2\pi^-$
¹ABLIKIM 04G reports [$\Gamma(\chi_{c0}(1P) \rightarrow f_0(980)f_0(980))/\Gamma_{total}$] × [B(ψ(2S) → γχ_{c0}(1P))] = (6.5 ± 1.6 ± 1.3) × 10⁻⁵ which we divide by our best value B(ψ(2S) → γχ_{c0}(1P)) = (9.79 ± 0.20) × 10⁻². Our first error is their experiment's error and our second error is the systematic error from using our best value.

$\Gamma(\pi^+ \pi^- \pi^0 \pi^0)/\Gamma_{total}$					Γ_5/Γ
VALUE (%)	CL%	EVTS	DOCUMENT ID	TECN	COMMENT

3.3 ± 0.4 ± 0.1 1751.4 ¹HE 08B CLEO e⁺e⁻ → γh⁺h⁻h⁰h⁰
¹HE 08B reports 3.54 ± 0.10 ± 0.43 ± 0.18 % from a measurement of [$\Gamma(\chi_{c0}(1P) \rightarrow \pi^+ \pi^- \pi^0 \pi^0)/\Gamma_{total}$] × [B(ψ(2S) → γχ_{c0}(1P))] assuming B(ψ(2S) → γχ_{c0}(1P)) = (9.22 ± 0.11 ± 0.46) × 10⁻², which we rescale to our best value B(ψ(2S) → γχ_{c0}(1P)) = (9.79 ± 0.20) × 10⁻². Our first error is their experiment's error and our second error is the systematic error from using our best value.

$\Gamma(\rho^+ \pi^- \pi^0 + c.c.)/\Gamma_{total}$					Γ_6/Γ
VALUE (%)	CL%	EVTS	DOCUMENT ID	TECN	COMMENT

2.9 ± 0.4 ± 0.1 1358.5 ^{1,2}HE 08B CLEO e⁺e⁻ → γh⁺h⁻h⁰h⁰
¹HE 08B reports 3.04 ± 0.18 ± 0.42 ± 0.16 % from a measurement of [$\Gamma(\chi_{c0}(1P) \rightarrow \rho^+ \pi^- \pi^0 + c.c.)/\Gamma_{total}$] × [B(ψ(2S) → γχ_{c0}(1P))] assuming B(ψ(2S) → γχ_{c0}(1P)) = (9.22 ± 0.11 ± 0.46) × 10⁻², which we rescale to our best value B(ψ(2S) → γχ_{c0}(1P)) = (9.79 ± 0.20) × 10⁻². Our first error is their experiment's error and our second error is the systematic error from using our best value.
²Calculated by us. We have added the values from HE 08B for ρ⁺π⁻π⁰ and ρ⁻π⁺π⁰ decays assuming uncorrelated statistical and fully correlated systematic uncertainties.

$\Gamma(4\pi^0)/\Gamma_{total}$					Γ_7/Γ
VALUE (units 10 ⁻³)	CL%	EVTS	DOCUMENT ID	TECN	COMMENT

3.3 ± 0.4 ± 0.1 3296 ¹ABLIKIM 11A BES3 e⁺e⁻ → ψ(2S) → γχ_{c0}
¹ABLIKIM 11A reports (3.34 ± 0.06 ± 0.44) × 10⁻³ from a measurement of [$\Gamma(\chi_{c0}(1P) \rightarrow 4\pi^0)/\Gamma_{total}$] × [B(ψ(2S) → γχ_{c0}(1P))] assuming B(ψ(2S) → γχ_{c0}(1P)) = (9.62 ± 0.31) × 10⁻², which we rescale to our best value B(ψ(2S) → γχ_{c0}(1P)) = (9.79 ± 0.20) × 10⁻². Our first error is their experiment's error and our second error is the systematic error from using our best value.

$\Gamma(\pi^+ \pi^- K^+ K^-)/\Gamma_{total}$		Γ_8/Γ
VALUE (units 10 ⁻³)	DOCUMENT ID	

18.1 ± 1.4 OUR FIT

$\Gamma(K^+ \bar{K}^*(892)^0 \pi^- + c.c.)/\Gamma(\pi^+ \pi^- K^+ K^-)$					Γ_{30}/Γ_8
VALUE	CL%	EVTS	DOCUMENT ID	TECN	COMMENT

0.41 ± 0.09 OUR FIT
0.41 ± 0.10 TANENBAUM 78 MRK1 $\psi(2S) \rightarrow \gamma\chi_{c0}$

$\Gamma(K_S^0(1430)^0 \bar{K}_S^0(1430)^0 \rightarrow \pi^+ \pi^- K^+ K^-)/\Gamma_{total}$					Γ_9/Γ
VALUE (units 10 ⁻⁴)	CL%	EVTS	DOCUMENT ID	TECN	COMMENT

9.8 ± 3.6 ± 0.2 83 ¹ABLIKIM 05Q BES2 $\psi(2S) \rightarrow \gamma\pi^+ \pi^- K^+ K^-$
¹ABLIKIM 05Q reports (10.44 ± 2.37^{+3.05}_{-1.90}) × 10⁻⁴ from a measurement of [$\Gamma(\chi_{c0}(1P) \rightarrow K_S^0(1430)^0 \bar{K}_S^0(1430)^0 \rightarrow \pi^+ \pi^- K^+ K^-)/\Gamma_{total}$] × [B(ψ(2S) → γχ_{c0}(1P))] assuming B(ψ(2S) → γχ_{c0}(1P)) = (9.22 ± 0.11 ± 0.46) × 10⁻², which we rescale to our best value B(ψ(2S) → γχ_{c0}(1P)) = (9.79 ± 0.20) × 10⁻². Our first error is their experiment's error and our second error is the systematic error from using our best value.

$\Gamma(K_S^0(1430)^0 \bar{K}_S^0(1430)^0 + c.c. \rightarrow \pi^+ \pi^- K^+ K^-)/\Gamma_{total}$					Γ_{10}/Γ
VALUE (units 10 ⁻⁴)	CL%	EVTS	DOCUMENT ID	TECN	COMMENT

8.0 ± 2.0 ± 0.2 62 ¹ABLIKIM 05Q BES2 $\psi(2S) \rightarrow \gamma\pi^+ \pi^- K^+ K^-$
¹ABLIKIM 05Q reports (8.49 ± 1.66^{+1.32}_{-1.99}) × 10⁻⁴ from a measurement of [$\Gamma(\chi_{c0}(1P) \rightarrow K_S^0(1430)^0 \bar{K}_S^0(1430)^0 + c.c. \rightarrow \pi^+ \pi^- K^+ K^-)/\Gamma_{total}$] × [B(ψ(2S) → γχ_{c0}(1P))] assuming B(ψ(2S) → γχ_{c0}(1P)) = (9.22 ± 0.11 ± 0.46) × 10⁻², which we rescale to our best value B(ψ(2S) → γχ_{c0}(1P)) = (9.79 ± 0.20) × 10⁻². Our first error is their experiment's error and our second error is the systematic error from using our best value.

$\Gamma(K_1(1270)^+ K^- + c.c. \rightarrow \pi^+ \pi^- K^+ K^-)/\Gamma_{total}$					Γ_{11}/Γ
VALUE (units 10 ⁻³)	CL%	EVTS	DOCUMENT ID	TECN	COMMENT

6.3 ± 1.9 ± 0.1 68 ¹ABLIKIM 05Q BES2 $\psi(2S) \rightarrow \gamma\pi^+ \pi^- K^+ K^-$
¹ABLIKIM 05Q reports (6.66 ± 1.31^{+1.60}_{-1.51}) × 10⁻³ from a measurement of [$\Gamma(\chi_{c0}(1P) \rightarrow K_1(1270)^+ K^- + c.c. \rightarrow \pi^+ \pi^- K^+ K^-)/\Gamma_{total}$] × [B(ψ(2S) → γχ_{c0}(1P))] assuming B(ψ(2S) → γχ_{c0}(1P)) = (9.22 ± 0.11 ± 0.46) × 10⁻², which we rescale to our best value B(ψ(2S) → γχ_{c0}(1P)) = (9.79 ± 0.20) × 10⁻². Our first error is their experiment's error and our second error is the systematic error from using our best value. The measurement assumes B(K₁(1270) → Kρ(770)) = 42 ± 6%.

$\Gamma(K_1(1400)^+ K^- + c.c. \rightarrow \pi^+ \pi^- K^+ K^-)/\Gamma_{total}$					Γ_{12}/Γ
VALUE (units 10 ⁻³)	CL%	EVTS	DOCUMENT ID	TECN	COMMENT

<2.7 90 ¹ABLIKIM 05Q BES2 $\psi(2S) \rightarrow \gamma\pi^+ \pi^- K^+ K^-$
¹ABLIKIM 05Q reports < 2.85 × 10⁻³ from a measurement of [$\Gamma(\chi_{c0}(1P) \rightarrow K_1(1400)^+ K^- + c.c. \rightarrow \pi^+ \pi^- K^+ K^-)/\Gamma_{total}$] × [B(ψ(2S) → γχ_{c0}(1P))] assuming B(ψ(2S) → γχ_{c0}(1P)) = (9.22 ± 0.11 ± 0.46) × 10⁻², which we rescale to our best value B(ψ(2S) → γχ_{c0}(1P)) = 9.79 × 10⁻². The measurement assumes B(K₁(1400) → K*(892)π) = 94 ± 6%.

Meson Particle Listings

 $\chi_{c0}(1P)$

$\Gamma(f_0(980) f_0(980))/\Gamma_{\text{total}}$		Γ_{13}/Γ	
VALUE (units 10^{-5})	EVTS	DOCUMENT ID	TECN COMMENT

16.2^{+10.4}_{-9.0} ± 0.3 28 ¹ ABLIKIM 05Q BES2 $\psi(2S) \rightarrow \gamma \pi^+ \pi^- K^+ K^-$
¹ ABLIKIM 05Q reports $[\Gamma(\chi_{c0}(1P) \rightarrow f_0(980) f_0(980))/\Gamma_{\text{total}}] \times [\text{B}(\psi(2S) \rightarrow \gamma \chi_{c0}(1P))] = (1.59 \pm 0.50^{+0.89}_{-0.72}) \times 10^{-5}$ which we divide by our best value $\text{B}(\psi(2S) \rightarrow \gamma \chi_{c0}(1P)) = (9.79 \pm 0.20) \times 10^{-2}$. Our first error is their experiment's error and our second error is the systematic error from using our best value. One of the $f_0(980)$ mesons is identified via decay to $\pi^+ \pi^-$ while the other via $K^+ K^-$ decay.

$\Gamma(f_0(980) f_0(2200))/\Gamma_{\text{total}}$		Γ_{14}/Γ	
VALUE (units 10^{-4})	EVTS	DOCUMENT ID	TECN COMMENT

7.9^{+2.9}_{-2.5} ± 0.2 77 ¹ ABLIKIM 05Q BES2 $\psi(2S) \rightarrow \gamma \pi^+ \pi^- K^+ K^-$
¹ ABLIKIM 05Q reports $(8.42 \pm 1.42^{+1.65}_{-2.29}) \times 10^{-4}$ from a measurement of $[\Gamma(\chi_{c0}(1P) \rightarrow f_0(980) f_0(2200))/\Gamma_{\text{total}}] \times [\text{B}(\psi(2S) \rightarrow \gamma \chi_{c0}(1P))]$ assuming $\text{B}(\psi(2S) \rightarrow \gamma \chi_{c0}(1P)) = (9.22 \pm 0.11 \pm 0.46) \times 10^{-2}$, which we rescale to our best value $\text{B}(\psi(2S) \rightarrow \gamma \chi_{c0}(1P)) = (9.79 \pm 0.20) \times 10^{-2}$. Our first error is their experiment's error and our second error is the systematic error from using our best value. The f_0 mesons are identified via $f_0(980) \rightarrow \pi^+ \pi^-$ and $f_0(2200) \rightarrow K^+ K^-$ decays.

$\Gamma(f_0(1370) f_0(1370))/\Gamma_{\text{total}}$		Γ_{15}/Γ	
VALUE (units 10^{-4})	CL%	DOCUMENT ID	TECN COMMENT

<2.7 90 ¹ ABLIKIM 05Q BES2 $\psi(2S) \rightarrow \gamma \pi^+ \pi^- K^+ K^-$
¹ ABLIKIM 05Q reports $< 2.9 \times 10^{-4}$ from a measurement of $[\Gamma(\chi_{c0}(1P) \rightarrow f_0(1370) f_0(1370))/\Gamma_{\text{total}}] \times [\text{B}(\psi(2S) \rightarrow \gamma \chi_{c0}(1P))]$ assuming $\text{B}(\psi(2S) \rightarrow \gamma \chi_{c0}(1P)) = (9.22 \pm 0.11 \pm 0.46) \times 10^{-2}$, which we rescale to our best value $\text{B}(\psi(2S) \rightarrow \gamma \chi_{c0}(1P)) = 9.79 \times 10^{-2}$. One of the $f_0(1370)$ mesons is identified via decay to $\pi^+ \pi^-$ while the other via $K^+ K^-$ decay. Both branching fractions for these f_0 decays are implicitly included in the quoted result.

$\Gamma(f_0(1370) f_0(1500))/\Gamma_{\text{total}}$		Γ_{16}/Γ	
VALUE (units 10^{-4})	CL%	DOCUMENT ID	TECN COMMENT

<1.7 90 ¹ ABLIKIM 05Q BES2 $\psi(2S) \rightarrow \gamma \pi^+ \pi^- K^+ K^-$
¹ ABLIKIM 05Q reports $< 1.8 \times 10^{-4}$ from a measurement of $[\Gamma(\chi_{c0}(1P) \rightarrow f_0(1370) f_0(1500))/\Gamma_{\text{total}}] \times [\text{B}(\psi(2S) \rightarrow \gamma \chi_{c0}(1P))]$ assuming $\text{B}(\psi(2S) \rightarrow \gamma \chi_{c0}(1P)) = (9.22 \pm 0.11 \pm 0.46) \times 10^{-2}$, which we rescale to our best value $\text{B}(\psi(2S) \rightarrow \gamma \chi_{c0}(1P)) = 9.79 \times 10^{-2}$. The f_0 mesons are identified via $f_0(1370) \rightarrow \pi^+ \pi^-$ and $f_0(1500) \rightarrow K^+ K^-$ decays. Both branching fractions for these f_0 decays are implicitly included in the quoted result.

$\Gamma(f_0(1370) f_0(1710))/\Gamma_{\text{total}}$		Γ_{17}/Γ	
VALUE (units 10^{-4})	EVTS	DOCUMENT ID	TECN COMMENT

6.7^{+3.5}_{-2.5} ± 0.1 61 ¹ ABLIKIM 05Q BES2 $\psi(2S) \rightarrow \gamma \pi^+ \pi^- K^+ K^-$
¹ ABLIKIM 05Q reports $(7.12 \pm 1.85^{+3.28}_{-1.68}) \times 10^{-4}$ from a measurement of $[\Gamma(\chi_{c0}(1P) \rightarrow f_0(1370) f_0(1710))/\Gamma_{\text{total}}] \times [\text{B}(\psi(2S) \rightarrow \gamma \chi_{c0}(1P))]$ assuming $\text{B}(\psi(2S) \rightarrow \gamma \chi_{c0}(1P)) = (9.22 \pm 0.11 \pm 0.46) \times 10^{-2}$, which we rescale to our best value $\text{B}(\psi(2S) \rightarrow \gamma \chi_{c0}(1P)) = (9.79 \pm 0.20) \times 10^{-2}$. Our first error is their experiment's error and our second error is the systematic error from using our best value. The f_0 mesons are identified via $f_0(1370) \rightarrow \pi^+ \pi^-$ and $f_0(1710) \rightarrow K^+ K^-$ decays. Both branching fractions for these f_0 decays are implicitly included in the quoted result.

$\Gamma(f_0(1500) f_0(1370))/\Gamma_{\text{total}}$		Γ_{18}/Γ	
VALUE (units 10^{-4})	CL%	DOCUMENT ID	TECN COMMENT

<1.3 90 ¹ ABLIKIM 05Q BES2 $\psi(2S) \rightarrow \gamma \pi^+ \pi^- K^+ K^-$
¹ ABLIKIM 05Q reports $< 1.4 \times 10^{-4}$ from a measurement of $[\Gamma(\chi_{c0}(1P) \rightarrow f_0(1500) f_0(1370))/\Gamma_{\text{total}}] \times [\text{B}(\psi(2S) \rightarrow \gamma \chi_{c0}(1P))]$ assuming $\text{B}(\psi(2S) \rightarrow \gamma \chi_{c0}(1P)) = (9.22 \pm 0.11 \pm 0.46) \times 10^{-2}$, which we rescale to our best value $\text{B}(\psi(2S) \rightarrow \gamma \chi_{c0}(1P)) = 9.79 \times 10^{-2}$. The f_0 mesons are identified via $f_0(1500) \rightarrow \pi^+ \pi^-$ and $f_0(1370) \rightarrow K^+ K^-$ decays. Both branching fractions for these f_0 decays are implicitly included in the quoted result.

$\Gamma(f_0(1500) f_0(1500))/\Gamma_{\text{total}}$		Γ_{19}/Γ	
VALUE (units 10^{-4})	CL%	DOCUMENT ID	TECN COMMENT

<0.5 90 ¹ ABLIKIM 05Q BES2 $\psi(2S) \rightarrow \gamma \pi^+ \pi^- K^+ K^-$
¹ ABLIKIM 05Q reports $< 0.55 \times 10^{-4}$ from a measurement of $[\Gamma(\chi_{c0}(1P) \rightarrow f_0(1500) f_0(1500))/\Gamma_{\text{total}}] \times [\text{B}(\psi(2S) \rightarrow \gamma \chi_{c0}(1P))]$ assuming $\text{B}(\psi(2S) \rightarrow \gamma \chi_{c0}(1P)) = (9.22 \pm 0.11 \pm 0.46) \times 10^{-2}$, which we rescale to our best value $\text{B}(\psi(2S) \rightarrow \gamma \chi_{c0}(1P)) = 9.79 \times 10^{-2}$. One of the $f_0(1500)$ is identified via decay to $\pi^+ \pi^-$ while the other via $K^+ K^-$ decay. Both branching fractions for these f_0 decays are implicitly included in the quoted result.

$\Gamma(f_0(1500) f_0(1710))/\Gamma_{\text{total}}$		Γ_{20}/Γ	
VALUE (units 10^{-4})	CL%	DOCUMENT ID	TECN COMMENT

<0.7 90 ¹ ABLIKIM 05Q BES2 $\psi(2S) \rightarrow \gamma \pi^+ \pi^- K^+ K^-$
¹ ABLIKIM 05Q reports $< 0.73 \times 10^{-4}$ from a measurement of $[\Gamma(\chi_{c0}(1P) \rightarrow f_0(1500) f_0(1710))/\Gamma_{\text{total}}] \times [\text{B}(\psi(2S) \rightarrow \gamma \chi_{c0}(1P))]$ assuming $\text{B}(\psi(2S) \rightarrow \gamma \chi_{c0}(1P)) = (9.22 \pm 0.11 \pm 0.46) \times 10^{-2}$, which we rescale to our best value $\text{B}(\psi(2S) \rightarrow \gamma \chi_{c0}(1P)) = 9.79 \times 10^{-2}$. The f_0 mesons are identified via $f_0(1500) \rightarrow \pi^+ \pi^-$ and $f_0(1710) \rightarrow K^+ K^-$ decays. Both branching fractions for these f_0 decays are implicitly included in the quoted result.

$\Gamma(K^+ K^- \pi^+ \pi^- \pi^0)/\Gamma_{\text{total}}$		Γ_{21}/Γ	
VALUE (units 10^{-3})	EVTS	DOCUMENT ID	TECN COMMENT

8.61 ± 0.13 ± 0.94 9.0k ¹ ABLIKIM 13B BES3 $e^+ e^- \rightarrow \psi(2S) \rightarrow \gamma \chi_{c0}$
¹ Using 1.06×10^8 $\psi(2S)$ mesons and $\text{B}(\psi(2S) \rightarrow \chi_{c0} \gamma) = (9.68 \pm 0.31)\%$.

$\Gamma(K_S^0 K_S^0 \pi^+ \pi^-)/\Gamma_{\text{total}}$		Γ_{22}/Γ	
VALUE (units 10^{-3})	EVTS	DOCUMENT ID	TECN COMMENT

4.22 ± 0.10 ± 0.43 2.7k ¹ ABLIKIM 13B BES3 $e^+ e^- \rightarrow \psi(2S) \rightarrow \gamma \chi_{c0}$
¹ Using 1.06×10^8 $\psi(2S)$ mesons and $\text{B}(\psi(2S) \rightarrow \chi_{c0} \gamma) = (9.68 \pm 0.31)\%$.

$\Gamma(K^+ K^- \pi^0 \pi^0)/\Gamma_{\text{total}}$		Γ_{23}/Γ	
VALUE (%)	EVTS	DOCUMENT ID	TECN COMMENT

0.56 ± 0.09 ± 0.01 213.5 ¹ HE 08B CLEO $e^+ e^- \rightarrow \gamma h^+ h^- h^0 h^0$
¹ HE 08B reports $0.59 \pm 0.05 \pm 0.08 \pm 0.03\%$ from a measurement of $[\Gamma(\chi_{c0}(1P) \rightarrow K^+ K^- \pi^0 \pi^0)/\Gamma_{\text{total}}] \times [\text{B}(\psi(2S) \rightarrow \gamma \chi_{c0}(1P))]$ assuming $\text{B}(\psi(2S) \rightarrow \gamma \chi_{c0}(1P)) = (9.22 \pm 0.11 \pm 0.46) \times 10^{-2}$, which we rescale to our best value $\text{B}(\psi(2S) \rightarrow \gamma \chi_{c0}(1P)) = (9.79 \pm 0.20) \times 10^{-2}$. Our first error is their experiment's error and our second error is the systematic error from using our best value.

$\Gamma(K^+ \pi^- \bar{K}^0 \pi^0 + \text{c.c.})/\Gamma_{\text{total}}$		Γ_{24}/Γ	
VALUE (%)	EVTS	DOCUMENT ID	TECN COMMENT

2.49 ± 0.33 ± 0.05 401.7 ¹ HE 08B CLEO $e^+ e^- \rightarrow \gamma h^+ h^- h^0 h^0$
¹ HE 08B reports $2.64 \pm 0.15 \pm 0.31 \pm 0.14\%$ from a measurement of $[\Gamma(\chi_{c0}(1P) \rightarrow K^+ \pi^- \bar{K}^0 \pi^0 + \text{c.c.})/\Gamma_{\text{total}}] \times [\text{B}(\psi(2S) \rightarrow \gamma \chi_{c0}(1P))]$ assuming $\text{B}(\psi(2S) \rightarrow \gamma \chi_{c0}(1P)) = (9.22 \pm 0.11 \pm 0.46) \times 10^{-2}$, which we rescale to our best value $\text{B}(\psi(2S) \rightarrow \gamma \chi_{c0}(1P)) = (9.79 \pm 0.20) \times 10^{-2}$. Our first error is their experiment's error and our second error is the systematic error from using our best value.

$\Gamma(\rho^+ K^- K^0 + \text{c.c.})/\Gamma_{\text{total}}$		Γ_{25}/Γ	
VALUE (%)	EVTS	DOCUMENT ID	TECN COMMENT

1.21 ± 0.21 ± 0.02 179.7 ¹ HE 08B CLEO $e^+ e^- \rightarrow \gamma h^+ h^- h^0 h^0$
¹ HE 08B reports $1.28 \pm 0.16 \pm 0.15 \pm 0.07\%$ from a measurement of $[\Gamma(\chi_{c0}(1P) \rightarrow \rho^+ K^- K^0 + \text{c.c.})/\Gamma_{\text{total}}] \times [\text{B}(\psi(2S) \rightarrow \gamma \chi_{c0}(1P))]$ assuming $\text{B}(\psi(2S) \rightarrow \gamma \chi_{c0}(1P)) = (9.22 \pm 0.11 \pm 0.46) \times 10^{-2}$, which we rescale to our best value $\text{B}(\psi(2S) \rightarrow \gamma \chi_{c0}(1P)) = (9.79 \pm 0.20) \times 10^{-2}$. Our first error is their experiment's error and our second error is the systematic error from using our best value.

$\Gamma(K^*(892)^- K^+ \pi^0 \rightarrow K^+ \pi^- \bar{K}^0 \pi^0 + \text{c.c.})/\Gamma_{\text{total}}$		Γ_{26}/Γ	
VALUE (%)	EVTS	DOCUMENT ID	TECN COMMENT

0.46 ± 0.12 ± 0.01 64.1 ¹ HE 08B CLEO $e^+ e^- \rightarrow \gamma h^+ h^- h^0 h^0$
¹ HE 08B reports $0.49 \pm 0.10 \pm 0.07 \pm 0.03\%$ from a measurement of $[\Gamma(\chi_{c0}(1P) \rightarrow K^*(892)^- K^+ \pi^0 \rightarrow K^+ \pi^- \bar{K}^0 \pi^0 + \text{c.c.})/\Gamma_{\text{total}}] \times [\text{B}(\psi(2S) \rightarrow \gamma \chi_{c0}(1P))]$ assuming $\text{B}(\psi(2S) \rightarrow \gamma \chi_{c0}(1P)) = (9.22 \pm 0.11 \pm 0.46) \times 10^{-2}$, which we rescale to our best value $\text{B}(\psi(2S) \rightarrow \gamma \chi_{c0}(1P)) = (9.79 \pm 0.20) \times 10^{-2}$. Our first error is their experiment's error and our second error is the systematic error from using our best value.

$\Gamma(K_S^0 K_S^0 \pi^+ \pi^-)/\Gamma_{\text{total}}$		Γ_{27}/Γ	
VALUE (units 10^{-3})	EVTS	DOCUMENT ID	TECN COMMENT

5.7 ± 1.0 ± 0.1 152 ± 14 ¹ ABLIKIM 05Q BES2 $\psi(2S) \rightarrow \gamma \chi_{c0}$
¹ ABLIKIM 05Q reports $[\Gamma(\chi_{c0}(1P) \rightarrow K_S^0 K_S^0 \pi^+ \pi^-)/\Gamma_{\text{total}}] \times [\text{B}(\psi(2S) \rightarrow \gamma \chi_{c0}(1P))] = (0.558 \pm 0.051 \pm 0.089) \times 10^{-3}$ which we divide by our best value $\text{B}(\psi(2S) \rightarrow \gamma \chi_{c0}(1P)) = (9.79 \pm 0.20) \times 10^{-2}$. Our first error is their experiment's error and our second error is the systematic error from using our best value.

$\Gamma(K^+ K^- \eta \pi^0)/\Gamma_{\text{total}}$		Γ_{28}/Γ	
VALUE (%)	EVTS	DOCUMENT ID	TECN COMMENT

0.30 ± 0.07 ± 0.01 56.4 ¹ HE 08B CLEO $e^+ e^- \rightarrow \gamma h^+ h^- h^0 h^0$
¹ HE 08B reports $0.32 \pm 0.05 \pm 0.05 \pm 0.02\%$ from a measurement of $[\Gamma(\chi_{c0}(1P) \rightarrow K^+ K^- \eta \pi^0)/\Gamma_{\text{total}}] \times [\text{B}(\psi(2S) \rightarrow \gamma \chi_{c0}(1P))]$ assuming $\text{B}(\psi(2S) \rightarrow \gamma \chi_{c0}(1P)) = (9.22 \pm 0.11 \pm 0.46) \times 10^{-2}$, which we rescale to our best value $\text{B}(\psi(2S) \rightarrow \gamma \chi_{c0}(1P)) = (9.79 \pm 0.20) \times 10^{-2}$. Our first error is their experiment's error and our second error is the systematic error from using our best value.

$\Gamma(3(\pi^+ \pi^-))/\Gamma_{\text{total}}$		Γ_{29}/Γ	
VALUE (units 10^{-3})	DOCUMENT ID	TECN COMMENT	

12.0 ± 1.8 OUR EVALUATION Treating systematic error as correlated.
12.0 ± 1.7 OUR AVERAGE
 11.7 ± 1.0 ± 1.9 ¹ BAI 99B BES $\psi(2S) \rightarrow \gamma \chi_{c0}$
 12.5 ± 2.9 ± 0.5 ¹ TANENBAUM 78 MRK1 $\psi(2S) \rightarrow \gamma \chi_{c0}$
¹ Rescaled by us using $\text{B}(\psi(2S) \rightarrow \gamma \chi_{c0}) = (9.4 \pm 0.4)\%$ and $\text{B}(\psi(2S) \rightarrow J/\psi(1S) \pi^+ \pi^-) = (32.6 \pm 0.5)\%$.

$\Gamma(K^+ \bar{K}^*(892)^0 \pi^- + \text{c.c.})/\Gamma_{\text{total}}$		Γ_{30}/Γ	
VALUE	DOCUMENT ID		

0.0075 ± 0.0016 OUR FIT

$\Gamma(K^*(892)^0 \bar{K}^*(892)^0)/\Gamma_{\text{total}}$		Γ_{31}/Γ	
VALUE (units 10^{-3})	EVTS	DOCUMENT ID	TECN COMMENT

1.72^{+0.60}_{-0.54} ± 0.04 64 ¹ ABLIKIM 05Q BES2 $\psi(2S) \rightarrow \gamma \pi^+ \pi^- K^+ K^-$

See key on page 1127

Meson Particle Listings

$\chi_{c0}(1P)$

• • • We do not use the following data for averages, fits, limits, etc. • • •
 1.56 ± 0.40 ± 0.03 30 ± 6 ^{2,3} ABLIKIM 04H BES Repl. by ABLIKIM 05Q
¹ ABLIKIM 05Q reports $[\Gamma(\chi_{c0}(1P) \rightarrow K^*(892)^0 \bar{K}^*(892)^0)/\Gamma_{\text{total}}] \times [B(\psi(2S) \rightarrow \gamma \chi_{c0}(1P))] = (0.168 \pm 0.035^{+0.047}_{-0.040}) \times 10^{-3}$ which we divide by our best value $B(\psi(2S) \rightarrow \gamma \chi_{c0}(1P)) = (9.79 \pm 0.20) \times 10^{-2}$. Our first error is their experiment's error and our second error is the systematic error from using our best value.
² Assumes $B(K^*(892)^0 \rightarrow K^- \pi^+) = 2/3$.
³ ABLIKIM 04H reports $[\Gamma(\chi_{c0}(1P) \rightarrow K^*(892)^0 \bar{K}^*(892)^0)/\Gamma_{\text{total}}] \times [B(\psi(2S) \rightarrow \gamma \chi_{c0}(1P))] = (1.53 \pm 0.29 \pm 0.26) \times 10^{-4}$ which we divide by our best value $B(\psi(2S) \rightarrow \gamma \chi_{c0}(1P)) = (9.79 \pm 0.20) \times 10^{-2}$. Our first error is their experiment's error and our second error is the systematic error from using our best value.

$\Gamma(\pi\pi)/\Gamma_{\text{total}}$ **Γ_{32}/Γ**

VALUE (units 10^{-3})	CL%	EVTS	DOCUMENT ID	TECN	COMMENT
8.51 ± 0.33 OUR FIT					

$\Gamma(\pi^0 \eta_c)/\Gamma_{\text{total}}$ **Γ_{35}/Γ**

VALUE	CL%	EVTS	DOCUMENT ID	TECN	COMMENT
< 1.6 × 10⁻³	90		¹ ABLIKIM	15N BES3	$\psi(2S) e^+ e^- \rightarrow \gamma \pi^0 \eta_c$
¹ Using $B(\eta_c \rightarrow K_S^0 K^\pm \pi^\mp) \times B(K_S^0 \rightarrow \pi^+ \pi^-) \times B(\pi^0 \rightarrow \gamma\gamma) = (1.66 \pm 0.11) \times 10^{-2}$.					

$\Gamma(\eta\eta)/\Gamma_{\text{total}}$ **Γ_{36}/Γ**

VALUE (units 10^{-3})	CL%	EVTS	DOCUMENT ID	TECN	COMMENT
3.01 ± 0.19 OUR FIT					

$\Gamma(\eta\pi)/\Gamma(\pi\pi)$ **Γ_{36}/Γ_{32}**

VALUE	CL%	EVTS	DOCUMENT ID	TECN	COMMENT
0.353 ± 0.025 OUR FIT					
• • • We do not use the following data for averages, fits, limits, etc. • • •					
0.26 ± 0.09 ^{+0.03} / _{-0.02}			¹ ANDREOTTI	05c E835	$\bar{p}p \rightarrow 2$ mesons
0.24 ± 0.10 ± 0.08			¹ BAI	03c BES	$\psi(2S) \rightarrow 5\gamma$
¹ We have multiplied $\pi^0 \pi^0$ measurement by 3 to obtain $\pi\pi$.					

$\Gamma(\eta\eta')/\Gamma_{\text{total}}$ **Γ_{37}/Γ**

VALUE (units 10^{-5})	CL%	EVTS	DOCUMENT ID	TECN	COMMENT
9.1 ± 1.1 ± 0.2		85	¹ ABLIKIM	17A1 BES3	$\psi(2S) \rightarrow \gamma \eta' \eta$
• • • We do not use the following data for averages, fits, limits, etc. • • •					
< 24	90	35 ± 13	² ASNER	09 CLEO	$\psi(2S) \rightarrow \gamma \eta' \eta$
< 50	90		³ ADAMS	07 CLEO	$\psi(2S) \rightarrow \gamma \chi_{c0}$

¹ ABLIKIM 17A1 reports $(8.92 \pm 0.84 \pm 0.65) \times 10^{-5}$ from a measurement of $[\Gamma(\chi_{c0}(1P) \rightarrow \eta\eta')/\Gamma_{\text{total}}] \times [B(\psi(2S) \rightarrow \gamma \chi_{c0}(1P))]$ assuming $B(\psi(2S) \rightarrow \gamma \chi_{c0}(1P)) = (9.99 \pm 0.27) \times 10^{-2}$, which we rescale to our best value $B(\psi(2S) \rightarrow \gamma \chi_{c0}(1P)) = (9.79 \pm 0.20) \times 10^{-2}$. Our first error is their experiment's error and our second error is the systematic error from using our best value.
² ASNER 09 reports $< 0.25 \times 10^{-3}$ from a measurement of $[\Gamma(\chi_{c0}(1P) \rightarrow \eta\eta')/\Gamma_{\text{total}}] \times [B(\psi(2S) \rightarrow \gamma \chi_{c0}(1P))]$ assuming $B(\psi(2S) \rightarrow \gamma \chi_{c0}(1P)) = (9.22 \pm 0.11 \pm 0.46) \times 10^{-2}$, which we rescale to our best value $B(\psi(2S) \rightarrow \gamma \chi_{c0}(1P)) = 9.79 \times 10^{-2}$.
³ Superseded by ASNER 09. ADAMS 07 reports $< 0.5 \times 10^{-3}$ from a measurement of $[\Gamma(\chi_{c0}(1P) \rightarrow \eta\eta')/\Gamma_{\text{total}}] \times [B(\psi(2S) \rightarrow \gamma \chi_{c0}(1P))]$ assuming $B(\psi(2S) \rightarrow \gamma \chi_{c0}(1P)) = (9.22 \pm 0.11 \pm 0.46) \times 10^{-2}$, which we rescale to our best value $B(\psi(2S) \rightarrow \gamma \chi_{c0}(1P)) = 9.79 \times 10^{-2}$.

$\Gamma(\eta'\eta')/\Gamma_{\text{total}}$ **Γ_{38}/Γ**

VALUE (units 10^{-3})	CL%	EVTS	DOCUMENT ID	TECN	COMMENT
2.17 ± 0.12 OUR AVERAGE					
2.23 ± 0.13 ± 0.05		2.5k	¹ ABLIKIM	17A1 BES3	$\psi(2S) \rightarrow \gamma \eta' \eta'$
2.00 ± 0.21 ± 0.04		0.4k	² ASNER	09 CLEO	$\psi(2S) \rightarrow \gamma \eta' \eta'$
• • • We do not use the following data for averages, fits, limits, etc. • • •					
1.60 ± 0.41 ± 0.03		23	³ ADAMS	07 CLEO	$\psi(2S) \rightarrow \gamma \chi_{c0}$

¹ ABLIKIM 17A1 reports $(2.19 \pm 0.03 \pm 0.14) \times 10^{-3}$ from a measurement of $[\Gamma(\chi_{c0}(1P) \rightarrow \eta' \eta')/\Gamma_{\text{total}}] \times [B(\psi(2S) \rightarrow \gamma \chi_{c0}(1P))]$ assuming $B(\psi(2S) \rightarrow \gamma \chi_{c0}(1P)) = (9.99 \pm 0.27) \times 10^{-2}$, which we rescale to our best value $B(\psi(2S) \rightarrow \gamma \chi_{c0}(1P)) = (9.79 \pm 0.20) \times 10^{-2}$. Our first error is their experiment's error and our second error is the systematic error from using our best value.
² ASNER 09 reports $(2.12 \pm 0.13 \pm 0.21) \times 10^{-3}$ from a measurement of $[\Gamma(\chi_{c0}(1P) \rightarrow \eta' \eta')/\Gamma_{\text{total}}] \times [B(\psi(2S) \rightarrow \gamma \chi_{c0}(1P))]$ assuming $B(\psi(2S) \rightarrow \gamma \chi_{c0}(1P)) = (9.22 \pm 0.11 \pm 0.46) \times 10^{-2}$, which we rescale to our best value $B(\psi(2S) \rightarrow \gamma \chi_{c0}(1P)) = (9.79 \pm 0.20) \times 10^{-2}$. Our first error is their experiment's error and our second error is the systematic error from using our best value.
³ Superseded by ASNER 09. ADAMS 07 reports $(1.7 \pm 0.4 \pm 0.2) \times 10^{-3}$ from a measurement of $[\Gamma(\chi_{c0}(1P) \rightarrow \eta' \eta')/\Gamma_{\text{total}}] \times [B(\psi(2S) \rightarrow \gamma \chi_{c0}(1P))]$ assuming $B(\psi(2S) \rightarrow \gamma \chi_{c0}(1P)) = 0.0922 \pm 0.0011 \pm 0.0046$, which we rescale to our best value $B(\psi(2S) \rightarrow \gamma \chi_{c0}(1P)) = (9.79 \pm 0.20) \times 10^{-2}$. Our first error is their experiment's error and our second error is the systematic error from using our best value.

$\Gamma(\omega\omega)/\Gamma_{\text{total}}$ **Γ_{39}/Γ**

VALUE (units 10^{-3})	CL%	EVTS	DOCUMENT ID	TECN	COMMENT
0.97 ± 0.11 OUR AVERAGE					
0.93 ± 0.11 ± 0.02		991	¹ ABLIKIM	11k BES3	$\psi(2S) \rightarrow \gamma$ hadrons

2.16 ± 0.66 ± 0.04 38.1 ± 9.6 ² ABLIKIM 05N BES2 $\psi(2S) \rightarrow \gamma \chi_{c0} \rightarrow \gamma 6\pi$
¹ ABLIKIM 11k reports $(0.95 \pm 0.03 \pm 0.11) \times 10^{-3}$ from a measurement of $[\Gamma(\chi_{c0}(1P) \rightarrow \omega\omega)/\Gamma_{\text{total}}] \times [B(\psi(2S) \rightarrow \gamma \chi_{c0}(1P))]$ assuming $B(\psi(2S) \rightarrow \gamma \chi_{c0}(1P)) = (9.62 \pm 0.31) \times 10^{-2}$, which we rescale to our best value $B(\psi(2S) \rightarrow \gamma \chi_{c0}(1P)) = (9.79 \pm 0.20) \times 10^{-2}$. Our first error is their experiment's error and our second error is the systematic error from using our best value.
² ABLIKIM 05N reports $[\Gamma(\chi_{c0}(1P) \rightarrow \omega\omega)/\Gamma_{\text{total}}] \times [B(\psi(2S) \rightarrow \gamma \chi_{c0}(1P))] = (0.212 \pm 0.053 \pm 0.037) \times 10^{-3}$ which we divide by our best value $B(\psi(2S) \rightarrow \gamma \chi_{c0}(1P)) = (9.79 \pm 0.20) \times 10^{-2}$. Our first error is their experiment's error and our second error is the systematic error from using our best value.

$\Gamma(\omega\phi)/\Gamma_{\text{total}}$ **Γ_{40}/Γ**

VALUE (units 10^{-4})	CL%	EVTS	DOCUMENT ID	TECN	COMMENT
1.41 ± 0.13 ± 0.03		486	¹ ABLIKIM	19J BES3	$\psi(2S) \rightarrow \gamma$ hadrons

• • • We do not use the following data for averages, fits, limits, etc. • • •
 1.18 ± 0.22 ± 0.02 76 ^{2,3} ABLIKIM 11k BES3 $\psi(2S) \rightarrow \gamma$ hadrons
¹ ABLIKIM 19J reports $[\Gamma(\chi_{c0}(1P) \rightarrow \omega\phi)/\Gamma_{\text{total}}] \times [B(\psi(2S) \rightarrow \gamma \chi_{c0}(1P))] = (13.83 \pm 0.70 \pm 1.01) \times 10^{-6}$ which we divide by our best value $B(\psi(2S) \rightarrow \gamma \chi_{c0}(1P)) = (9.79 \pm 0.20) \times 10^{-2}$. Our first error is their experiment's error and our second error is the systematic error from using our best value.
² ABLIKIM 11k reports $(1.2 \pm 0.1 \pm 0.2) \times 10^{-4}$ from a measurement of $[\Gamma(\chi_{c0}(1P) \rightarrow \omega\phi)/\Gamma_{\text{total}}] \times [B(\psi(2S) \rightarrow \gamma \chi_{c0}(1P))]$ assuming $B(\psi(2S) \rightarrow \gamma \chi_{c0}(1P)) = (9.62 \pm 0.31) \times 10^{-2}$, which we rescale to our best value $B(\psi(2S) \rightarrow \gamma \chi_{c0}(1P)) = (9.79 \pm 0.20) \times 10^{-2}$. Our first error is their experiment's error and our second error is the systematic error from using our best value.
³ Superseded by ABLIKIM 19J.

$\Gamma(\omega K^+ K^-)/\Gamma_{\text{total}}$ **Γ_{41}/Γ**

VALUE (units 10^{-3})	CL%	EVTS	DOCUMENT ID	TECN	COMMENT
1.94 ± 0.06 ± 0.20		1.4k	¹ ABLIKIM	13B BES3	$e^+ e^- \rightarrow \psi(2S) \rightarrow \gamma \chi_{c0}$
¹ Using $1.06 \times 10^8 \psi(2S)$ mesons and $B(\psi(2S) \rightarrow \chi_{c0} \gamma) = (9.68 \pm 0.31)\%$.					

$\Gamma(K^+ K^-)/\Gamma_{\text{total}}$ **Γ_{42}/Γ**

VALUE (units 10^{-3})	CL%	EVTS	DOCUMENT ID	TECN	COMMENT
6.05 ± 0.31 OUR FIT					

$\Gamma(K_S^0 K_S^0)/\Gamma_{\text{total}}$ **Γ_{43}/Γ**

VALUE (units 10^{-3})	CL%	EVTS	DOCUMENT ID	TECN	COMMENT
3.16 ± 0.17 OUR FIT					

$\Gamma(K_S^0 K_S^0)/\Gamma(\pi\pi)$ **Γ_{43}/Γ_{32}**

VALUE	CL%	EVTS	DOCUMENT ID	TECN	COMMENT
0.371 ± 0.023 OUR FIT					
• • • We do not use the following data for averages, fits, limits, etc. • • •					
0.31 ± 0.05 ± 0.05			^{1,2} CHEN	07B BELL	$e^+ e^- \rightarrow e^+ e^- \chi_{c0}$
¹ Using $\Gamma(\pi\pi \times \Gamma(\gamma\gamma))/\Gamma_{\text{total}}$ from the $\pi^+ \pi^-$ measurement of NAKAZAWA 05 rescaled by 3/2 to convert to $\pi\pi$.					
² Not independent from other measurements.					

$\Gamma(K_S^0 K_S^0)/\Gamma(K^+ K^-)$ **Γ_{43}/Γ_{42}**

VALUE	CL%	EVTS	DOCUMENT ID	TECN	COMMENT
0.52 ± 0.04 OUR FIT					
• • • We do not use the following data for averages, fits, limits, etc. • • •					
0.49 ± 0.07 ± 0.08			^{1,2} CHEN	07B BELL	$e^+ e^- \rightarrow e^+ e^- \chi_{c0}$
¹ Using $\Gamma(K^+ K^-) \times \Gamma(\gamma\gamma)/\Gamma_{\text{total}}$ from NAKAZAWA 05.					
² Not independent from other measurements.					

$\Gamma(\pi^+ \pi^- \eta)/\Gamma_{\text{total}}$ **Γ_{44}/Γ**

VALUE (units 10^{-3})	CL%	EVTS	DOCUMENT ID	TECN	COMMENT
< 0.20	90		¹ ATHAR	07 CLEO	$\psi(2S) \rightarrow \gamma h^+ h^- h^0$
• • • We do not use the following data for averages, fits, limits, etc. • • •					
< 1.0	90		² ABLIKIM	06R BES2	$\psi(2S) \rightarrow \gamma \chi_{c0}$

¹ ATHAR 07 reports $< 0.21 \times 10^{-3}$ from a measurement of $[\Gamma(\chi_{c0}(1P) \rightarrow \pi^+ \pi^- \eta)/\Gamma_{\text{total}}] \times [B(\psi(2S) \rightarrow \gamma \chi_{c0}(1P))]$ assuming $B(\psi(2S) \rightarrow \gamma \chi_{c0}(1P)) = (9.22 \pm 0.11 \pm 0.46) \times 10^{-2}$, which we rescale to our best value $B(\psi(2S) \rightarrow \gamma \chi_{c0}(1P)) = 9.79 \times 10^{-2}$.
² ABLIKIM 06R reports $< 1.1 \times 10^{-3}$ from a measurement of $[\Gamma(\chi_{c0}(1P) \rightarrow \pi^+ \pi^- \eta)/\Gamma_{\text{total}}] \times [B(\psi(2S) \rightarrow \gamma \chi_{c0}(1P))]$ assuming $B(\psi(2S) \rightarrow \gamma \chi_{c0}(1P)) = (9.2 \pm 0.4) \times 10^{-2}$, which we rescale to our best value $B(\psi(2S) \rightarrow \gamma \chi_{c0}(1P)) = 9.79 \times 10^{-2}$.

$\Gamma(\pi^+ \pi^- \eta')/\Gamma_{\text{total}}$ **Γ_{45}/Γ**

VALUE (units 10^{-3})	CL%	EVTS	DOCUMENT ID	TECN	COMMENT
< 0.4	90		¹ ATHAR	07 CLEO	$\psi(2S) \rightarrow \gamma h^+ h^- h^0$
¹ ATHAR 07 reports $< 0.38 \times 10^{-3}$ from a measurement of $[\Gamma(\chi_{c0}(1P) \rightarrow \pi^+ \pi^- \eta')/\Gamma_{\text{total}}] \times [B(\psi(2S) \rightarrow \gamma \chi_{c0}(1P))]$ assuming $B(\psi(2S) \rightarrow \gamma \chi_{c0}(1P)) = (9.22 \pm 0.11 \pm 0.46) \times 10^{-2}$, which we rescale to our best value $B(\psi(2S) \rightarrow \gamma \chi_{c0}(1P)) = 9.79 \times 10^{-2}$.					

Meson Particle Listings

 $\chi_{c0}(1P)$ $\Gamma(\bar{K}^0 K^+ \pi^- + \text{c.c.})/\Gamma_{\text{total}}$ Γ_{46}/Γ

VALUE (units 10^{-3})	CL%	DOCUMENT ID	TECN	COMMENT
<0.09	90	¹ ATHAR	07 CLEO	$\psi(2S) \rightarrow \gamma h^+ h^- h^0$
<0.7	90	^{2,3} ABLIKIM	06R BES2	$\psi(2S) \rightarrow \gamma \chi_{c0}$
<0.7	90	^{3,4} BAI	99B BES	$\psi(2S) \rightarrow \gamma \chi_{c0}$

¹ ATHAR 07 reports $<0.10 \times 10^{-3}$ from a measurement of $[\Gamma(\chi_{c0}(1P) \rightarrow \bar{K}^0 K^+ \pi^- + \text{c.c.})/\Gamma_{\text{total}}] \times [B(\psi(2S) \rightarrow \gamma \chi_{c0}(1P))]$ assuming $B(\psi(2S) \rightarrow \gamma \chi_{c0}(1P)) = (9.22 \pm 0.11 \pm 0.46) \times 10^{-2}$, which we rescale to our best value $B(\psi(2S) \rightarrow \gamma \chi_{c0}(1P)) = 9.79 \times 10^{-2}$.

² ABLIKIM 06R reports $<0.70 \times 10^{-3}$ from a measurement of $[\Gamma(\chi_{c0}(1P) \rightarrow \bar{K}^0 K^+ \pi^- + \text{c.c.})/\Gamma_{\text{total}}] \times [B(\psi(2S) \rightarrow \gamma \chi_{c0}(1P))]$ assuming $B(\psi(2S) \rightarrow \gamma \chi_{c0}(1P)) = (9.2 \pm 0.4) \times 10^{-2}$, which we rescale to our best value $B(\psi(2S) \rightarrow \gamma \chi_{c0}(1P)) = 9.79 \times 10^{-2}$.

³ We have multiplied the $K_S^0 K^+ \pi^-$ measurement by a factor of 2 to convert to $K^0 K^+ \pi^-$.

⁴ Rescaled by us using $B(\psi(2S) \rightarrow \gamma \chi_{c0}) = (9.4 \pm 0.4)\%$ and $B(\psi(2S) \rightarrow J/\psi(1S) \pi^+ \pi^-) = (32.6 \pm 0.5)\%$.

 $\Gamma(K^+ K^- \pi^0)/\Gamma_{\text{total}}$ Γ_{47}/Γ

VALUE (units 10^{-3})	CL%	DOCUMENT ID	TECN	COMMENT
<0.06	90	¹ ATHAR	07 CLEO	$\psi(2S) \rightarrow \gamma h^+ h^- h^0$

¹ ATHAR 07 reports $<0.06 \times 10^{-3}$ from a measurement of $[\Gamma(\chi_{c0}(1P) \rightarrow K^+ K^- \pi^0)/\Gamma_{\text{total}}] \times [B(\psi(2S) \rightarrow \gamma \chi_{c0}(1P))]$ assuming $B(\psi(2S) \rightarrow \gamma \chi_{c0}(1P)) = (9.22 \pm 0.11 \pm 0.46) \times 10^{-2}$, which we rescale to our best value $B(\psi(2S) \rightarrow \gamma \chi_{c0}(1P)) = 9.79 \times 10^{-2}$.

 $\Gamma(K^+ K^- \eta)/\Gamma_{\text{total}}$ Γ_{48}/Γ

VALUE (units 10^{-3})	CL%	DOCUMENT ID	TECN	COMMENT
<0.23	90	¹ ATHAR	07 CLEO	$\psi(2S) \rightarrow \gamma h^+ h^- h^0$

¹ ATHAR 07 reports $<0.24 \times 10^{-3}$ from a measurement of $[\Gamma(\chi_{c0}(1P) \rightarrow K^+ K^- \eta)/\Gamma_{\text{total}}] \times [B(\psi(2S) \rightarrow \gamma \chi_{c0}(1P))]$ assuming $B(\psi(2S) \rightarrow \gamma \chi_{c0}(1P)) = (9.22 \pm 0.11 \pm 0.46) \times 10^{-2}$, which we rescale to our best value $B(\psi(2S) \rightarrow \gamma \chi_{c0}(1P)) = 9.79 \times 10^{-2}$.

 $\Gamma(K^+ K^- K_S^0 K_S^0)/\Gamma_{\text{total}}$ Γ_{49}/Γ

VALUE (units 10^{-3})	EVTS	DOCUMENT ID	TECN	COMMENT
1.41 ± 0.47 ± 0.03	16.8 ± 4.8	¹ ABLIKIM	05o BES2	$\psi(2S) \rightarrow \gamma \chi_{c0}$

¹ ABLIKIM 05o reports $[\Gamma(\chi_{c0}(1P) \rightarrow K^+ K^- K_S^0 K_S^0)/\Gamma_{\text{total}}] \times [B(\psi(2S) \rightarrow \gamma \chi_{c0}(1P))]$ = $(0.138 \pm 0.039 \pm 0.025) \times 10^{-3}$ which we divide by our best value $B(\psi(2S) \rightarrow \gamma \chi_{c0}(1P)) = (9.79 \pm 0.20) \times 10^{-2}$. Our first error is their experiment's error and our second error is the systematic error from using our best value.

 $\Gamma(K_S^0 K_S^0 K_S^0 K_S^0)/\Gamma_{\text{total}}$ Γ_{50}/Γ

VALUE (units 10^{-4})	EVTS	DOCUMENT ID	TECN	COMMENT
5.8 ± 0.5 ± 0.1	319	¹ ABLIKIM	19AA BES3	$\psi(2S) \rightarrow \gamma 4K_S^0$

¹ Using $B(K_S^0 \rightarrow \pi^+ \pi^-) = (69.20 \pm 0.05)\%$. ABLIKIM 19AA reports $[\Gamma(\chi_{c0}(1P) \rightarrow K_S^0 K_S^0 K_S^0 K_S^0)/\Gamma_{\text{total}}] \times [B(\psi(2S) \rightarrow \gamma \chi_{c0}(1P))]$ = $(5.64 \pm 0.33 \pm 0.37) \times 10^{-5}$ which we divide by our best value $B(\psi(2S) \rightarrow \gamma \chi_{c0}(1P)) = (9.79 \pm 0.20) \times 10^{-2}$. Our first error is their experiment's error and our second error is the systematic error from using our best value..

 $\Gamma(K^+ K^- K^+ K^-)/\Gamma_{\text{total}}$ Γ_{51}/Γ

VALUE (units 10^{-3})	DOCUMENT ID
2.82 ± 0.29 OUR FIT	

 $\Gamma(K^+ K^- \phi)/\Gamma_{\text{total}}$ Γ_{52}/Γ

VALUE (units 10^{-3})	EVTS	DOCUMENT ID	TECN	COMMENT
0.97 ± 0.25 ± 0.02	38	¹ ABLIKIM	06T BES2	$\psi(2S) \rightarrow \gamma 2K^+ 2K^-$

¹ ABLIKIM 06T reports $(1.03 \pm 0.22 \pm 0.15) \times 10^{-3}$ from a measurement of $[\Gamma(\chi_{c0}(1P) \rightarrow K^+ K^- \phi)/\Gamma_{\text{total}}] \times [B(\psi(2S) \rightarrow \gamma \chi_{c0}(1P))]$ assuming $B(\psi(2S) \rightarrow \gamma \chi_{c0}(1P)) = (9.2 \pm 0.4) \times 10^{-2}$, which we rescale to our best value $B(\psi(2S) \rightarrow \gamma \chi_{c0}(1P)) = (9.79 \pm 0.20) \times 10^{-2}$. Our first error is their experiment's error and our second error is the systematic error from using our best value.

 $\Gamma(\bar{K}^0 K^+ \pi^- \phi + \text{c.c.})/\Gamma_{\text{total}}$ Γ_{53}/Γ

VALUE (units 10^{-3})	DOCUMENT ID	TECN	COMMENT
3.68 ± 0.30 ± 0.50	ABLIKIM	15M BES3	$\psi(2S) \rightarrow \gamma \chi_{c0}$

 $\Gamma(K^+ K^- \pi^0 \phi)/\Gamma_{\text{total}}$ Γ_{54}/Γ

VALUE (units 10^{-3})	DOCUMENT ID	TECN	COMMENT
1.90 ± 0.14 ± 0.32	ABLIKIM	15M BES3	$\psi(2S) \rightarrow \gamma \chi_{c0}$

 $\Gamma(\phi \pi^+ \pi^- \pi^0)/\Gamma_{\text{total}}$ Γ_{55}/Γ

VALUE (units 10^{-3})	EVTS	DOCUMENT ID	TECN	COMMENT
1.18 ± 0.07 ± 0.13	538	¹ ABLIKIM	13B BES3	$e^+ e^- \rightarrow \psi(2S) \rightarrow \gamma \chi_{c0}$

¹ Using $1.06 \times 10^8 \psi(2S)$ mesons and $B(\psi(2S) \rightarrow \chi_{c0} \gamma) = (9.68 \pm 0.31)\%$.

 $\Gamma(\phi \phi)/\Gamma_{\text{total}}$ Γ_{56}/Γ

VALUE (units 10^{-3})	DOCUMENT ID
0.80 ± 0.07 OUR FIT	

 $\Gamma(\phi \phi \eta)/\Gamma_{\text{total}}$ Γ_{57}/Γ

VALUE (units 10^{-4})	EVTS	DOCUMENT ID	TECN	COMMENT
8.4 ± 0.7 ± 0.6	186.6	¹ ABLIKIM	20B BES3	$\psi(2S) \rightarrow \gamma \phi \phi \eta$

¹ ABLIKIM 20B reports $(8.41 \pm 0.74 \pm 0.62) \times 10^{-4}$ from a measurement of $[\Gamma(\chi_{c0}(1P) \rightarrow \phi \phi \eta)/\Gamma_{\text{total}}] \times [B(\psi(2S) \rightarrow \gamma \chi_{c0}(1P))]$ assuming $B(\psi(2S) \rightarrow \gamma \chi_{c0}(1P)) = (9.79 \pm 0.20) \times 10^{-2}$.

 $\Gamma(\rho \bar{\rho})/\Gamma_{\text{total}}$ Γ_{58}/Γ

VALUE (units 10^{-4})	DOCUMENT ID
2.21 ± 0.08 OUR FIT	

 $\Gamma(\rho \bar{\rho} \pi^0)/\Gamma_{\text{total}}$ Γ_{59}/Γ

VALUE (units 10^{-3})	DOCUMENT ID	TECN	COMMENT
0.70 ± 0.07 OUR AVERAGE	Error includes scale factor of 1.3.		
0.73 ± 0.06 ± 0.01	¹ ONYISI	10 CLE3	$\psi(2S) \rightarrow \gamma \rho \bar{\rho} X$
0.56 ± 0.12 ± 0.01	² ATHAR	07 CLEO	$\psi(2S) \rightarrow \gamma h^+ h^- h^0$

¹ ONYISI 10 reports $(7.76 \pm 0.37 \pm 0.51 \pm 0.39) \times 10^{-4}$ from a measurement of $[\Gamma(\chi_{c0}(1P) \rightarrow \rho \bar{\rho} \pi^0)/\Gamma_{\text{total}}] \times [B(\psi(2S) \rightarrow \gamma \chi_{c0}(1P))]$ assuming $B(\psi(2S) \rightarrow \gamma \chi_{c0}(1P)) = (9.22 \pm 0.11 \pm 0.46) \times 10^{-2}$, which we rescale to our best value $B(\psi(2S) \rightarrow \gamma \chi_{c0}(1P)) = (9.79 \pm 0.20) \times 10^{-2}$. Our first error is their experiment's error and our second error is the systematic error from using our best value.

² ATHAR 07 reports $(0.59 \pm 0.10 \pm 0.08) \times 10^{-3}$ from a measurement of $[\Gamma(\chi_{c0}(1P) \rightarrow \rho \bar{\rho} \pi^0)/\Gamma_{\text{total}}] \times [B(\psi(2S) \rightarrow \gamma \chi_{c0}(1P))]$ assuming $B(\psi(2S) \rightarrow \gamma \chi_{c0}(1P)) = (9.22 \pm 0.11 \pm 0.46) \times 10^{-2}$, which we rescale to our best value $B(\psi(2S) \rightarrow \gamma \chi_{c0}(1P)) = (9.79 \pm 0.20) \times 10^{-2}$. Our first error is their experiment's error and our second error is the systematic error from using our best value.

 $\Gamma(\rho \bar{\rho} \eta)/\Gamma_{\text{total}}$ Γ_{60}/Γ

VALUE (units 10^{-3})	DOCUMENT ID	TECN	COMMENT
0.35 ± 0.04 OUR AVERAGE			
0.35 ± 0.04 ± 0.01	¹ ONYISI	10 CLE3	$\psi(2S) \rightarrow \gamma \rho \bar{\rho} X$
0.37 ± 0.11 ± 0.01	² ATHAR	07 CLEO	$\psi(2S) \rightarrow \gamma h^+ h^- h^0$

¹ ONYISI 10 reports $(3.73 \pm 0.38 \pm 0.28 \pm 0.19) \times 10^{-4}$ from a measurement of $[\Gamma(\chi_{c0}(1P) \rightarrow \rho \bar{\rho} \eta)/\Gamma_{\text{total}}] \times [B(\psi(2S) \rightarrow \gamma \chi_{c0}(1P))]$ assuming $B(\psi(2S) \rightarrow \gamma \chi_{c0}(1P)) = (9.22 \pm 0.11 \pm 0.46) \times 10^{-2}$, which we rescale to our best value $B(\psi(2S) \rightarrow \gamma \chi_{c0}(1P)) = (9.79 \pm 0.20) \times 10^{-2}$. Our first error is their experiment's error and our second error is the systematic error from using our best value.

² ATHAR 07 reports $(0.39 \pm 0.11 \pm 0.04) \times 10^{-3}$ from a measurement of $[\Gamma(\chi_{c0}(1P) \rightarrow \rho \bar{\rho} \eta)/\Gamma_{\text{total}}] \times [B(\psi(2S) \rightarrow \gamma \chi_{c0}(1P))]$ assuming $B(\psi(2S) \rightarrow \gamma \chi_{c0}(1P)) = (9.22 \pm 0.11 \pm 0.46) \times 10^{-2}$, which we rescale to our best value $B(\psi(2S) \rightarrow \gamma \chi_{c0}(1P)) = (9.79 \pm 0.20) \times 10^{-2}$. Our first error is their experiment's error and our second error is the systematic error from using our best value.

 $\Gamma(\rho \bar{\rho} \omega)/\Gamma_{\text{total}}$ Γ_{61}/Γ

VALUE (units 10^{-3})	DOCUMENT ID	TECN	COMMENT
0.52 ± 0.06 ± 0.01	¹ ONYISI	10 CLE3	$\psi(2S) \rightarrow \gamma \rho \bar{\rho} X$

¹ ONYISI 10 reports $(5.57 \pm 0.48 \pm 0.42 \pm 0.14) \times 10^{-4}$ from a measurement of $[\Gamma(\chi_{c0}(1P) \rightarrow \rho \bar{\rho} \omega)/\Gamma_{\text{total}}] \times [B(\psi(2S) \rightarrow \gamma \chi_{c0}(1P))]$ assuming $B(\psi(2S) \rightarrow \gamma \chi_{c0}(1P)) = (9.22 \pm 0.11 \pm 0.46) \times 10^{-2}$, which we rescale to our best value $B(\psi(2S) \rightarrow \gamma \chi_{c0}(1P)) = (9.79 \pm 0.20) \times 10^{-2}$. Our first error is their experiment's error and our second error is the systematic error from using our best value.

 $\Gamma(\rho \bar{\rho} \phi)/\Gamma_{\text{total}}$ Γ_{62}/Γ

VALUE (units 10^{-5})	EVTS	DOCUMENT ID	TECN	COMMENT
6.0 ± 1.4 ± 0.1	42 ± 8	¹ ABLIKIM	11F BES3	$\psi(2S) \rightarrow \gamma \rho \bar{\rho} K^+ K^-$

¹ ABLIKIM 11F reports $(6.12 \pm 1.18 \pm 0.86) \times 10^{-5}$ from a measurement of $[\Gamma(\chi_{c0}(1P) \rightarrow \rho \bar{\rho} \phi)/\Gamma_{\text{total}}] \times [B(\psi(2S) \rightarrow \gamma \chi_{c0}(1P))]$ assuming $B(\psi(2S) \rightarrow \gamma \chi_{c0}(1P)) = (9.62 \pm 0.31) \times 10^{-2}$, which we rescale to our best value $B(\psi(2S) \rightarrow \gamma \chi_{c0}(1P)) = (9.79 \pm 0.20) \times 10^{-2}$. Our first error is their experiment's error and our second error is the systematic error from using our best value.

 $\Gamma(\rho \bar{\rho} \pi^+ \pi^-)/\Gamma_{\text{total}}$ Γ_{63}/Γ

VALUE (units 10^{-3})	DOCUMENT ID	TECN	COMMENT
2.1 ± 0.7 OUR EVALUATION	Error includes scale factor of 1.4. Treating systematic error as correlated.		
2.1 ± 1.0 OUR AVERAGE	Error includes scale factor of 2.0.		
1.57 ± 0.21 ± 0.53	¹ BAI	99B BES	$\psi(2S) \rightarrow \gamma \chi_{c0}$
4.20 ± 1.15 ± 0.18	¹ TANENBAUM	78 MRK1	$\psi(2S) \rightarrow \gamma \chi_{c0}$

¹ Rescaled by us using $B(\psi(2S) \rightarrow \gamma \chi_{c0}) = (9.4 \pm 0.4)\%$ and $B(\psi(2S) \rightarrow J/\psi(1S) \pi^+ \pi^-) = (32.6 \pm 0.5)\%$.

 $\Gamma(\rho \bar{\rho} \pi^0 \pi^0)/\Gamma_{\text{total}}$ Γ_{64}/Γ

VALUE (%)	EVTS	DOCUMENT ID	TECN	COMMENT
0.104 ± 0.028 ± 0.002	39.5	¹ HE	08B CLEO	$e^+ e^- \rightarrow \gamma h^+ h^- h^0 h^0$

¹ HE 08B reports $0.11 \pm 0.02 \pm 0.02 \pm 0.01\%$ from a measurement of $[\Gamma(\chi_{c0}(1P) \rightarrow \rho \bar{\rho} \pi^0 \pi^0)/\Gamma_{\text{total}}] \times [B(\psi(2S) \rightarrow \gamma \chi_{c0}(1P))]$ assuming $B(\psi(2S) \rightarrow \gamma \chi_{c0}(1P)) = (9.22 \pm 0.11 \pm 0.46) \times 10^{-2}$, which we rescale to our best value $B(\psi(2S) \rightarrow \gamma \chi_{c0}(1P)) = (9.79 \pm 0.20) \times 10^{-2}$. Our first error is their experiment's error and our second error is the systematic error from using our best value.

See key on page 1127

Meson Particle Listings

 $\chi_{c0}(1P)$ $\Gamma(p\bar{p}K^+K^- \text{ (non-resonant)})/\Gamma_{\text{total}}$ Γ_{65}/Γ

VALUE (units 10^{-4})	EVTS	DOCUMENT ID	TECN	COMMENT
1.22±0.26±0.02	48 ± 8	¹ ABLIKIM	11F BES3	$\psi(2S) \rightarrow \gamma p\bar{p}K^+K^-$
¹ ABLIKIM 11F reports $(1.24 \pm 0.20 \pm 0.18) \times 10^{-4}$ from a measurement of $[\Gamma(\chi_{c0}(1P) \rightarrow p\bar{p}K^+K^- \text{ (non-resonant)})/\Gamma_{\text{total}}] \times [B(\psi(2S) \rightarrow \gamma\chi_{c0}(1P))]$ assuming $B(\psi(2S) \rightarrow \gamma\chi_{c0}(1P)) = (9.62 \pm 0.31) \times 10^{-2}$, which we rescale to our best value $B(\psi(2S) \rightarrow \gamma\chi_{c0}(1P)) = (9.79 \pm 0.20) \times 10^{-2}$. Our first error is their experiment's error and our second error is the systematic error from using our best value.				

 $\Gamma(p\bar{p}K_S^0K_S^0)/\Gamma_{\text{total}}$ Γ_{66}/Γ

VALUE (units 10^{-4})	CL%	DOCUMENT ID	TECN	COMMENT
<8.8	90	¹ ABLIKIM	06D BES2	$\psi(2S) \rightarrow \chi_{c0}\gamma$
¹ Using $B(\psi(2S) \rightarrow \chi_{c0}\gamma) = (9.2 \pm 0.5)\%$				

 $\Gamma(p\bar{p}\pi^-)/\Gamma_{\text{total}}$ Γ_{67}/Γ

VALUE (units 10^{-4})	EVTS	DOCUMENT ID	TECN	COMMENT
12.7±1.1 OUR AVERAGE				
12.9±1.1±0.3	5150	¹ ABLIKIM	12J BES3	$\psi(2S) \rightarrow \gamma p\bar{p}\pi^-$
11.2±3.1±0.2		² ABLIKIM	06I BES2	$\psi(2S) \rightarrow \gamma p\pi^-X$
¹ ABLIKIM 12J reports $[\Gamma(\chi_{c0}(1P) \rightarrow p\bar{p}\pi^-)/\Gamma_{\text{total}}] \times [B(\psi(2S) \rightarrow \gamma\chi_{c0}(1P))] = (1.26 \pm 0.02 \pm 0.11) \times 10^{-4}$ which we divide by our best value $B(\psi(2S) \rightarrow \gamma\chi_{c0}(1P)) = (9.79 \pm 0.20) \times 10^{-2}$. Our first error is their experiment's error and our second error is the systematic error from using our best value.				
² ABLIKIM 06I reports $[\Gamma(\chi_{c0}(1P) \rightarrow p\bar{p}\pi^-)/\Gamma_{\text{total}}] \times [B(\psi(2S) \rightarrow \gamma\chi_{c0}(1P))] = (1.10 \pm 0.24 \pm 0.18) \times 10^{-4}$ which we divide by our best value $B(\psi(2S) \rightarrow \gamma\chi_{c0}(1P)) = (9.79 \pm 0.20) \times 10^{-2}$. Our first error is their experiment's error and our second error is the systematic error from using our best value.				

 $\Gamma(p\bar{p}\pi^+)/\Gamma_{\text{total}}$ Γ_{68}/Γ

VALUE (units 10^{-4})	EVTS	DOCUMENT ID	TECN	COMMENT
13.7±1.2±0.3	5808	¹ ABLIKIM	12J BES3	$\psi(2S) \rightarrow \gamma p\bar{p}\pi^+$
¹ ABLIKIM 12J reports $[\Gamma(\chi_{c0}(1P) \rightarrow p\bar{p}\pi^+)/\Gamma_{\text{total}}] \times [B(\psi(2S) \rightarrow \gamma\chi_{c0}(1P))] = (1.34 \pm 0.03 \pm 0.11) \times 10^{-4}$ which we divide by our best value $B(\psi(2S) \rightarrow \gamma\chi_{c0}(1P)) = (9.79 \pm 0.20) \times 10^{-2}$. Our first error is their experiment's error and our second error is the systematic error from using our best value.				

 $\Gamma(p\bar{p}\pi^-\pi^0)/\Gamma_{\text{total}}$ Γ_{69}/Γ

VALUE (units 10^{-4})	EVTS	DOCUMENT ID	TECN	COMMENT
23.4±2.0±0.5	2480	¹ ABLIKIM	12J BES3	$\psi(2S) \rightarrow \gamma p\bar{p}\pi^-\pi^0$
¹ ABLIKIM 12J reports $[\Gamma(\chi_{c0}(1P) \rightarrow p\bar{p}\pi^-\pi^0)/\Gamma_{\text{total}}] \times [B(\psi(2S) \rightarrow \gamma\chi_{c0}(1P))] = (2.29 \pm 0.08 \pm 0.18) \times 10^{-4}$ which we divide by our best value $B(\psi(2S) \rightarrow \gamma\chi_{c0}(1P)) = (9.79 \pm 0.20) \times 10^{-2}$. Our first error is their experiment's error and our second error is the systematic error from using our best value.				

 $\Gamma(p\bar{p}\pi^+\pi^0)/\Gamma_{\text{total}}$ Γ_{70}/Γ

VALUE (units 10^{-4})	EVTS	DOCUMENT ID	TECN	COMMENT
22.1±1.8±0.5	2757	¹ ABLIKIM	12J BES3	$\psi(2S) \rightarrow \gamma p\bar{p}\pi^+\pi^0$
¹ ABLIKIM 12J reports $[\Gamma(\chi_{c0}(1P) \rightarrow p\bar{p}\pi^+\pi^0)/\Gamma_{\text{total}}] \times [B(\psi(2S) \rightarrow \gamma\chi_{c0}(1P))] = (2.16 \pm 0.07 \pm 0.16) \times 10^{-4}$ which we divide by our best value $B(\psi(2S) \rightarrow \gamma\chi_{c0}(1P)) = (9.79 \pm 0.20) \times 10^{-2}$. Our first error is their experiment's error and our second error is the systematic error from using our best value.				

 $\Gamma(\Lambda\bar{\Lambda})/\Gamma_{\text{total}}$ Γ_{71}/Γ

VALUE (units 10^{-4})	DOCUMENT ID	TECN	COMMENT
3.59±0.15 OUR FIT			

 $\Gamma(\Lambda\bar{\Lambda}\pi^+\pi^-)/\Gamma_{\text{total}}$ Γ_{72}/Γ

VALUE (units 10^{-5})	CL%	EVTS	DOCUMENT ID	TECN	COMMENT
118±12±2		426	¹ ABLIKIM	12I BES3	$\psi(2S) \rightarrow \gamma\Lambda\bar{\Lambda}\pi^+\pi^-$
• • • We do not use the following data for averages, fits, limits, etc. • • •					
<400		90	² ABLIKIM	06D BES2	$\psi(2S) \rightarrow \chi_{c0}\gamma$
¹ ABLIKIM 12I reports $(119.0 \pm 6.4 \pm 11.4) \times 10^{-5}$ from a measurement of $[\Gamma(\chi_{c0}(1P) \rightarrow \Lambda\bar{\Lambda}\pi^+\pi^-)/\Gamma_{\text{total}}] \times [B(\psi(2S) \rightarrow \gamma\chi_{c0}(1P))]$ assuming $B(\psi(2S) \rightarrow \gamma\chi_{c0}(1P)) = (9.68 \pm 0.31) \times 10^{-2}$, which we rescale to our best value $B(\psi(2S) \rightarrow \gamma\chi_{c0}(1P)) = (9.79 \pm 0.20) \times 10^{-2}$. Our first error is their experiment's error and our second error is the systematic error from using our best value.					
² Using $B(\psi(2S) \rightarrow \chi_{c0}\gamma) = (9.2 \pm 0.5)\%$					

 $\Gamma(\Lambda\bar{\Lambda}\pi^+\pi^- \text{ (non-resonant)})/\Gamma_{\text{total}}$ Γ_{73}/Γ

VALUE (units 10^{-5})	CL%	DOCUMENT ID	TECN	COMMENT
<50	90	¹ ABLIKIM	12I BES3	$\psi(2S) \rightarrow \gamma\Lambda\bar{\Lambda}\pi^+\pi^-$
¹ ABLIKIM 12I reports $< 54 \times 10^{-5}$ from a measurement of $[\Gamma(\chi_{c0}(1P) \rightarrow \Lambda\bar{\Lambda}\pi^+\pi^- \text{ (non-resonant)})/\Gamma_{\text{total}}] \times [B(\psi(2S) \rightarrow \gamma\chi_{c0}(1P))]$ assuming $B(\psi(2S) \rightarrow \gamma\chi_{c0}(1P)) = (9.68 \pm 0.31) \times 10^{-2}$, which we rescale to our best value $B(\psi(2S) \rightarrow \gamma\chi_{c0}(1P)) = 9.79 \times 10^{-2}$.				

 $\Gamma(\Sigma(1385)^+\bar{\Lambda}\pi^- + \text{c.c.})/\Gamma_{\text{total}}$ Γ_{74}/Γ

VALUE (units 10^{-5})	CL%	DOCUMENT ID	TECN	COMMENT
<50	90	¹ ABLIKIM	12I BES3	$\psi(2S) \rightarrow \gamma\Sigma(1385)^+\bar{\Lambda}\pi^-$
¹ ABLIKIM 12I reports $< 55 \times 10^{-5}$ from a measurement of $[\Gamma(\chi_{c0}(1P) \rightarrow \Sigma(1385)^+\bar{\Lambda}\pi^- + \text{c.c.})/\Gamma_{\text{total}}] \times [B(\psi(2S) \rightarrow \gamma\chi_{c0}(1P))]$ assuming $B(\psi(2S) \rightarrow \gamma\chi_{c0}(1P)) = (9.68 \pm 0.31) \times 10^{-2}$, which we rescale to our best value $B(\psi(2S) \rightarrow \gamma\chi_{c0}(1P)) = 9.79 \times 10^{-2}$.				

 $\Gamma(\Sigma(1385)^-\bar{\Lambda}\pi^+ + \text{c.c.})/\Gamma_{\text{total}}$ Γ_{75}/Γ

VALUE (units 10^{-5})	CL%	DOCUMENT ID	TECN	COMMENT
<50	90	¹ ABLIKIM	12I BES3	$\psi(2S) \rightarrow \gamma\Sigma(1385)^-\bar{\Lambda}\pi^+$
¹ ABLIKIM 12I reports $< 50 \times 10^{-5}$ from a measurement of $[\Gamma(\chi_{c0}(1P) \rightarrow \Sigma(1385)^-\bar{\Lambda}\pi^+ + \text{c.c.})/\Gamma_{\text{total}}] \times [B(\psi(2S) \rightarrow \gamma\chi_{c0}(1P))]$ assuming $B(\psi(2S) \rightarrow \gamma\chi_{c0}(1P)) = (9.68 \pm 0.31) \times 10^{-2}$, which we rescale to our best value $B(\psi(2S) \rightarrow \gamma\chi_{c0}(1P)) = 9.79 \times 10^{-2}$.				

 $\Gamma(K^+\bar{p}\Lambda + \text{c.c.})/\Gamma_{\text{total}}$ Γ_{76}/Γ

VALUE (units 10^{-3})	EVTS	DOCUMENT ID	TECN	COMMENT
1.25±0.12 OUR AVERAGE				Error includes scale factor of 1.3.
1.30±0.09±0.03	9k	^{1,2} ABLIKIM	13D BES3	$\psi(2S) \rightarrow \gamma\Lambda\bar{p}K^+$
1.01±0.19±0.02		³ ATHAR	07 CLEO	$\psi(2S) \rightarrow \gamma h^+h^-h^0$
¹ ABLIKIM 13D reports $(1.32 \pm 0.03 \pm 0.10) \times 10^{-3}$ from a measurement of $[\Gamma(\chi_{c0}(1P) \rightarrow K^+\bar{p}\Lambda + \text{c.c.})/\Gamma_{\text{total}}] \times [B(\psi(2S) \rightarrow \gamma\chi_{c0}(1P))]$ assuming $B(\psi(2S) \rightarrow \gamma\chi_{c0}(1P)) = (9.68 \pm 0.31) \times 10^{-2}$, which we rescale to our best value $B(\psi(2S) \rightarrow \gamma\chi_{c0}(1P)) = (9.79 \pm 0.20) \times 10^{-2}$. Our first error is their experiment's error and our second error is the systematic error from using our best value.				
² Using $B(\Lambda \rightarrow p\pi^-) = 63.9\%$.				
³ ATHAR 07 reports $(1.07 \pm 0.17 \pm 0.12) \times 10^{-3}$ from a measurement of $[\Gamma(\chi_{c0}(1P) \rightarrow K^+\bar{p}\Lambda + \text{c.c.})/\Gamma_{\text{total}}] \times [B(\psi(2S) \rightarrow \gamma\chi_{c0}(1P))]$ assuming $B(\psi(2S) \rightarrow \gamma\chi_{c0}(1P)) = (9.22 \pm 0.11 \pm 0.46) \times 10^{-2}$, which we rescale to our best value $B(\psi(2S) \rightarrow \gamma\chi_{c0}(1P)) = (9.79 \pm 0.20) \times 10^{-2}$. Our first error is their experiment's error and our second error is the systematic error from using our best value.				

 $\Gamma(K^*(892)^+\bar{p}\Lambda + \text{c.c.})/\Gamma_{\text{total}}$ Γ_{78}/Γ

VALUE (units 10^{-4})	EVTS	DOCUMENT ID	TECN	COMMENT
4.8±0.9±0.1	254	¹ ABLIKIM	19AU BES3	$\psi(2S) \rightarrow \gamma K^*\bar{p}\Lambda$
¹ ABLIKIM 19AU reports $[\Gamma(\chi_{c0}(1P) \rightarrow K^*(892)^+\bar{p}\Lambda + \text{c.c.})/\Gamma_{\text{total}}] \times [B(\psi(2S) \rightarrow \gamma\chi_{c0}(1P))] = (4.7 \pm 0.7 \pm 0.5) \times 10^{-5}$ which we divide by our best value $B(\psi(2S) \rightarrow \gamma\chi_{c0}(1P)) = (9.79 \pm 0.20) \times 10^{-2}$. Our first error is their experiment's error and our second error is the systematic error from using our best value.				

 $\Gamma(K^+\bar{p}\Lambda(1520) + \text{c.c.})/\Gamma_{\text{total}}$ Γ_{79}/Γ

VALUE (units 10^{-4})	EVTS	DOCUMENT ID	TECN	COMMENT
2.9±0.7±0.1	62 ± 12	¹ ABLIKIM	11F BES3	$\psi(2S) \rightarrow \gamma p\bar{p}K^+K^-$
¹ ABLIKIM 11F reports $(3.00 \pm 0.58 \pm 0.50) \times 10^{-4}$ from a measurement of $[\Gamma(\chi_{c0}(1P) \rightarrow K^+\bar{p}\Lambda(1520) + \text{c.c.})/\Gamma_{\text{total}}] \times [B(\psi(2S) \rightarrow \gamma\chi_{c0}(1P))]$ assuming $B(\psi(2S) \rightarrow \gamma\chi_{c0}(1P)) = (9.62 \pm 0.31) \times 10^{-2}$, which we rescale to our best value $B(\psi(2S) \rightarrow \gamma\chi_{c0}(1P)) = (9.79 \pm 0.20) \times 10^{-2}$. Our first error is their experiment's error and our second error is the systematic error from using our best value.				

 $\Gamma(nK_S^0\bar{\Lambda} + \text{c.c.})/\Gamma_{\text{total}}$ Γ_{77}/Γ

VALUE (units 10^{-4})	EVTS	DOCUMENT ID	TECN	COMMENT
6.7±0.3±0.4	1284	¹ ABLIKIM	21AV BES3	$\psi(2S) \rightarrow \gamma nK_S^0\bar{\Lambda} + \text{c.c.}$
¹ ABLIKIM 21AV reports $(6.65 \pm 0.26 \pm 0.41) \times 10^{-4}$ from a measurement of $[\Gamma(\chi_{c0}(1P) \rightarrow nK_S^0\bar{\Lambda} + \text{c.c.})/\Gamma_{\text{total}}] \times [B(\psi(2S) \rightarrow \gamma\chi_{c0}(1P))]$ assuming $B(\psi(2S) \rightarrow \gamma\chi_{c0}(1P)) = 0.0979 \pm 0.0020$. Also uses $B(\bar{\Lambda} \rightarrow \bar{p}\pi^+) = (63.9 \pm 0.5)\%$ and $B(K_S^0 \rightarrow \pi^+\pi^-) = (69.20 \pm 0.05)\%$.				

 $\Gamma(\Lambda(1520)\bar{\Lambda}(1520))/\Gamma_{\text{total}}$ Γ_{80}/Γ

VALUE (units 10^{-4})	EVTS	DOCUMENT ID	TECN	COMMENT
3.1±1.2±0.1	28 ± 10	¹ ABLIKIM	11F BES3	$\psi(2S) \rightarrow \gamma p\bar{p}K^+K^-$
¹ ABLIKIM 11F reports $(3.18 \pm 1.11 \pm 0.53) \times 10^{-4}$ from a measurement of $[\Gamma(\chi_{c0}(1P) \rightarrow \Lambda(1520)\bar{\Lambda}(1520))/\Gamma_{\text{total}}] \times [B(\psi(2S) \rightarrow \gamma\chi_{c0}(1P))]$ assuming $B(\psi(2S) \rightarrow \gamma\chi_{c0}(1P)) = (9.62 \pm 0.31) \times 10^{-2}$, which we rescale to our best value $B(\psi(2S) \rightarrow \gamma\chi_{c0}(1P)) = (9.79 \pm 0.20) \times 10^{-2}$. Our first error is their experiment's error and our second error is the systematic error from using our best value.				

 $\Gamma(\Sigma^0\bar{\Sigma}^0)/\Gamma_{\text{total}}$ Γ_{81}/Γ

VALUE (units 10^{-4})	EVTS	DOCUMENT ID	TECN	COMMENT
4.68±0.32 OUR AVERAGE				
4.82±0.34±0.10	1046	¹ ABLIKIM	18V BES3	$\psi(2S) \rightarrow \gamma\Sigma^0\bar{\Sigma}^0$
4.2 ± 0.7 ± 0.1	78 ± 10	² NAIK	08 CLEO	$\psi(2S) \rightarrow \gamma\Sigma^0\bar{\Sigma}^0$
• • • We do not use the following data for averages, fits, limits, etc. • • •				
4.7 ± 0.5 ± 0.1	243	^{3,4} ABLIKIM	13H BES3	$\psi(2S) \rightarrow \gamma\Sigma^0\bar{\Sigma}^0$

Meson Particle Listings

$\chi_{c0}(1P)$

- ¹ ABLIKIM 18v reports $[\Gamma(\chi_{c0}(1P) \rightarrow \Sigma^0 \bar{\Sigma}^0)/\Gamma_{\text{total}}] \times [B(\psi(2S) \rightarrow \gamma \chi_{c0}(1P))] = (4.72 \pm 0.18 \pm 0.28) \times 10^{-5}$ which we divide by our best value $B(\psi(2S) \rightarrow \gamma \chi_{c0}(1P)) = (9.79 \pm 0.20) \times 10^{-2}$. Our first error is their experiment's error and our second error is the systematic error from using our best value.
- ² NAIK 08 reports $(4.41 \pm 0.56 \pm 0.47) \times 10^{-4}$ from a measurement of $[\Gamma(\chi_{c0}(1P) \rightarrow \Sigma^0 \bar{\Sigma}^0)/\Gamma_{\text{total}}] \times [B(\psi(2S) \rightarrow \gamma \chi_{c0}(1P))]$ assuming $B(\psi(2S) \rightarrow \gamma \chi_{c0}(1P)) = (9.22 \pm 0.11 \pm 0.46) \times 10^{-2}$, which we rescale to our best value $B(\psi(2S) \rightarrow \gamma \chi_{c0}(1P)) = (9.79 \pm 0.20) \times 10^{-2}$. Our first error is their experiment's error and our second error is the systematic error from using our best value.
- ³ ABLIKIM 13H reports $(4.78 \pm 0.34 \pm 0.39) \times 10^{-4}$ from a measurement of $[\Gamma(\chi_{c0}(1P) \rightarrow \Sigma^0 \bar{\Sigma}^0)/\Gamma_{\text{total}}] \times [B(\psi(2S) \rightarrow \gamma \chi_{c0}(1P))]$ assuming $B(\psi(2S) \rightarrow \gamma \chi_{c0}(1P)) = (9.62 \pm 0.31) \times 10^{-2}$, which we rescale to our best value $B(\psi(2S) \rightarrow \gamma \chi_{c0}(1P)) = (9.79 \pm 0.20) \times 10^{-2}$. Our first error is their experiment's error and our second error is the systematic error from using our best value.
- ⁴ Superseded by ABLIKIM 18v

$\Gamma(\Sigma^+ \bar{\Sigma}^-)/\Gamma_{\text{total}}$ Γ_{84}/Γ

VALUE (units 10^{-4})	EVTS	DOCUMENT ID	TECN	COMMENT
4.6 ± 0.8 OUR AVERAGE				Error includes scale factor of 2.6.
5.10 ± 0.35 ± 0.10	747	¹ ABLIKIM	18v BES3	$\psi(2S) \rightarrow \gamma \Sigma^+ \bar{\Sigma}^-$
3.1 ± 0.7 ± 0.1	39 ± 7	² NAIK	08 CLEO	$\psi(2S) \rightarrow \gamma \Sigma^+ \bar{\Sigma}^-$

• • • We do not use the following data for averages, fits, limits, etc. • • •

4.5 ± 0.5 ± 0.1 148 ^{3,4} ABLIKIM 13H BES3 $\psi(2S) \rightarrow \gamma \Sigma^+ \bar{\Sigma}^-$

- ¹ ABLIKIM 18v reports $[\Gamma(\chi_{c0}(1P) \rightarrow \Sigma^+ \bar{\Sigma}^-)/\Gamma_{\text{total}}] \times [B(\psi(2S) \rightarrow \gamma \chi_{c0}(1P))] = (4.99 \pm 0.24 \pm 0.24) \times 10^{-5}$ which we divide by our best value $B(\psi(2S) \rightarrow \gamma \chi_{c0}(1P)) = (9.79 \pm 0.20) \times 10^{-2}$. Our first error is their experiment's error and our second error is the systematic error from using our best value.
- ² NAIK 08 reports $(3.25 \pm 0.57 \pm 0.43) \times 10^{-4}$ from a measurement of $[\Gamma(\chi_{c0}(1P) \rightarrow \Sigma^+ \bar{\Sigma}^-)/\Gamma_{\text{total}}] \times [B(\psi(2S) \rightarrow \gamma \chi_{c0}(1P))]$ assuming $B(\psi(2S) \rightarrow \gamma \chi_{c0}(1P)) = (9.22 \pm 0.11 \pm 0.46) \times 10^{-2}$, which we rescale to our best value $B(\psi(2S) \rightarrow \gamma \chi_{c0}(1P)) = (9.79 \pm 0.20) \times 10^{-2}$. Our first error is their experiment's error and our second error is the systematic error from using our best value.
- ³ ABLIKIM 13H reports $(4.54 \pm 0.42 \pm 0.30) \times 10^{-4}$ from a measurement of $[\Gamma(\chi_{c0}(1P) \rightarrow \Sigma^+ \bar{\Sigma}^-)/\Gamma_{\text{total}}] \times [B(\psi(2S) \rightarrow \gamma \chi_{c0}(1P))]$ assuming $B(\psi(2S) \rightarrow \gamma \chi_{c0}(1P)) = (9.62 \pm 0.31) \times 10^{-2}$, which we rescale to our best value $B(\psi(2S) \rightarrow \gamma \chi_{c0}(1P)) = (9.79 \pm 0.20) \times 10^{-2}$. Our first error is their experiment's error and our second error is the systematic error from using our best value.
- ⁴ Superseded by ABLIKIM 18v

$\Gamma(\Sigma^- \bar{\Sigma}^+)/\Gamma_{\text{total}}$ Γ_{85}/Γ

VALUE (units 10^{-4})	EVTS	DOCUMENT ID	TECN	COMMENT
5.1 ± 0.2 ± 0.4	2143	¹ ABLIKIM	20i BES3	$\psi(2S) \rightarrow \gamma \Sigma^- \bar{\Sigma}^+$

¹ ABLIKIM 20i reports $(5.13 \pm 0.24 \pm 0.41) \times 10^{-4}$ from a measurement of $[\Gamma(\chi_{c0}(1P) \rightarrow \Sigma^- \bar{\Sigma}^+)/\Gamma_{\text{total}}] \times [B(\psi(2S) \rightarrow \gamma \chi_{c0}(1P))]$ assuming $B(\psi(2S) \rightarrow \gamma \chi_{c0}(1P)) = (9.79 \pm 0.20) \times 10^{-2}$.

$\Gamma(\Sigma(1385)^+ \bar{\Sigma}(1385)^-)/\Gamma_{\text{total}}$ Γ_{86}/Γ

VALUE (units 10^{-5})	EVTS	DOCUMENT ID	TECN	COMMENT
16.2 ± 5.8 ± 0.3	27	¹ ABLIKIM	12i BES3	$\psi(2S) \rightarrow \gamma \Lambda \bar{\Lambda} \pi^+ \pi^-$

¹ ABLIKIM 12i reports $(16.4 \pm 5.7 \pm 1.6) \times 10^{-5}$ from a measurement of $[\Gamma(\chi_{c0}(1P) \rightarrow \Sigma(1385)^+ \bar{\Sigma}(1385)^-)/\Gamma_{\text{total}}] \times [B(\psi(2S) \rightarrow \gamma \chi_{c0}(1P))]$ assuming $B(\psi(2S) \rightarrow \gamma \chi_{c0}(1P)) = (9.68 \pm 0.31) \times 10^{-2}$, which we rescale to our best value $B(\psi(2S) \rightarrow \gamma \chi_{c0}(1P)) = (9.79 \pm 0.20) \times 10^{-2}$. Our first error is their experiment's error and our second error is the systematic error from using our best value.

$\Gamma(\Sigma(1385)^- \bar{\Sigma}(1385)^+)/\Gamma_{\text{total}}$ Γ_{87}/Γ

VALUE (units 10^{-5})	EVTS	DOCUMENT ID	TECN	COMMENT
23.2 ± 6.5 ± 0.5	33	¹ ABLIKIM	12i BES3	$\psi(2S) \rightarrow \gamma \Lambda \bar{\Lambda} \pi^+ \pi^-$

¹ ABLIKIM 12i reports $(23.5 \pm 6.2 \pm 2.3) \times 10^{-5}$ from a measurement of $[\Gamma(\chi_{c0}(1P) \rightarrow \Sigma(1385)^- \bar{\Sigma}(1385)^+)/\Gamma_{\text{total}}] \times [B(\psi(2S) \rightarrow \gamma \chi_{c0}(1P))]$ assuming $B(\psi(2S) \rightarrow \gamma \chi_{c0}(1P)) = (9.68 \pm 0.31) \times 10^{-2}$, which we rescale to our best value $B(\psi(2S) \rightarrow \gamma \chi_{c0}(1P)) = (9.79 \pm 0.20) \times 10^{-2}$. Our first error is their experiment's error and our second error is the systematic error from using our best value.

$\Gamma(K^- \Lambda \bar{\Sigma}^+ + \text{c.c.})/\Gamma_{\text{total}}$ Γ_{88}/Γ

VALUE (units 10^{-4})	EVTS	DOCUMENT ID	TECN	COMMENT
1.94 ± 0.35 ± 0.04	57	¹ ABLIKIM	15i BES3	$\psi(2S) \rightarrow \gamma K^- \Lambda \bar{\Sigma}^+ + \text{c.c.}$

¹ ABLIKIM 15i reports $[\Gamma(\chi_{c0}(1P) \rightarrow K^- \Lambda \bar{\Sigma}^+ + \text{c.c.})/\Gamma_{\text{total}}] \times [B(\psi(2S) \rightarrow \gamma \chi_{c0}(1P))] = (1.90 \pm 0.30 \pm 0.16) \times 10^{-5}$ which we divide by our best value $B(\psi(2S) \rightarrow \gamma \chi_{c0}(1P)) = (9.79 \pm 0.20) \times 10^{-2}$. Our first error is their experiment's error and our second error is the systematic error from using our best value.

$\Gamma(\Xi^0 \Xi^0)/\Gamma_{\text{total}}$ Γ_{89}/Γ

VALUE (units 10^{-4})	EVTS	DOCUMENT ID	TECN	COMMENT
3.1 ± 0.8 ± 0.1	23.3 ± 4.9	¹ NAIK	08 CLEO	$\psi(2S) \rightarrow \gamma \Xi^0 \Xi^0$

¹ NAIK 08 reports $(3.34 \pm 0.70 \pm 0.48) \times 10^{-4}$ from a measurement of $[\Gamma(\chi_{c0}(1P) \rightarrow \Xi^0 \Xi^0)/\Gamma_{\text{total}}] \times [B(\psi(2S) \rightarrow \gamma \chi_{c0}(1P))]$ assuming $B(\psi(2S) \rightarrow \gamma \chi_{c0}(1P)) = (9.22 \pm 0.11 \pm 0.46) \times 10^{-2}$, which we rescale to our best value $B(\psi(2S) \rightarrow \gamma \chi_{c0}(1P)) = (9.79 \pm 0.20) \times 10^{-2}$. Our first error is their experiment's error and our second error is the systematic error from using our best value.

$\Gamma(\Xi^- \bar{\Xi}^+)/\Gamma_{\text{total}}$ Γ_{90}/Γ

VALUE (units 10^{-4})	CL%	EVTS	DOCUMENT ID	TECN	COMMENT
4.8 ± 0.7 ± 0.1		95 ± 11	¹ NAIK	08 CLEO	$\psi(2S) \rightarrow \gamma \Xi^- \bar{\Xi}^+$

• • • We do not use the following data for averages, fits, limits, etc. • • •

<10.3 90 ² ABLIKIM 06D BES2 $\psi(2S) \rightarrow \chi_{c0} \gamma$

¹ NAIK 08 reports $(5.14 \pm 0.60 \pm 0.47) \times 10^{-4}$ from a measurement of $[\Gamma(\chi_{c0}(1P) \rightarrow \Xi^- \bar{\Xi}^+)/\Gamma_{\text{total}}] \times [B(\psi(2S) \rightarrow \gamma \chi_{c0}(1P))]$ assuming $B(\psi(2S) \rightarrow \gamma \chi_{c0}(1P)) = (9.22 \pm 0.11 \pm 0.46) \times 10^{-2}$, which we rescale to our best value $B(\psi(2S) \rightarrow \gamma \chi_{c0}(1P)) = (9.79 \pm 0.20) \times 10^{-2}$. Our first error is their experiment's error and our second error is the systematic error from using our best value.

² Using $B(\psi(2S) \rightarrow \chi_{c0} \gamma) = (9.2 \pm 0.5)\%$

$\Gamma(\eta_c \pi^+ \pi^-)/\Gamma_{\text{total}}$ Γ_{91}/Γ

VALUE	CL%	DOCUMENT ID	TECN	COMMENT
< 7 × 10⁻⁴	90	^{1,2} ABLIKIM	13B BES3	$e^+ e^- \rightarrow \psi(2S) \rightarrow \gamma \chi_{c0}$

• • • We do not use the following data for averages, fits, limits, etc. • • •

<1 × 10⁻⁴ 90 ^{1,3} ABLIKIM 13B BES3 $e^+ e^- \rightarrow \psi(2S) \rightarrow \gamma \chi_{c0}$

¹ Using $1.06 \times 10^8 \psi(2S)$ mesons and $B(\psi(2S) \rightarrow \chi_{c0} \gamma) = (9.68 \pm 0.31)\%$.

² From the $\eta_c \rightarrow K_S^0 K^\pm \pi^\mp$ decays.

³ From the $\eta_c \rightarrow K^\pm K^\mp \pi^0$ decays.

$\Gamma(\rho \bar{\rho})/\Gamma_{\text{total}} \times \Gamma(\pi \pi)/\Gamma_{\text{total}}$ $\Gamma_{58}/\Gamma \times \Gamma_{32}/\Gamma$

VALUE (units 10^{-7})	DOCUMENT ID	TECN	COMMENT
18.8 ± 1.0 OUR FIT			
15.3 ± 2.4 ± 0.8	¹ ANDREOTTI	03 E835	$\bar{p} p \rightarrow \chi_{c0} \rightarrow \pi^0 \pi^0$

¹ We have multiplied $B(\rho \bar{\rho}) \cdot B(\pi^0 \pi^0)$ measurement by 3 to obtain $B(\rho \bar{\rho}) \cdot B(\pi \pi)$.

$\Gamma(\rho \bar{\rho})/\Gamma_{\text{total}} \times \Gamma(\pi^0 \eta)/\Gamma_{\text{total}}$ $\Gamma_{58}/\Gamma \times \Gamma_{33}/\Gamma$

VALUE (units 10^{-7})	DOCUMENT ID	TECN	COMMENT
< 0.4	ANDREOTTI	05c E835	$\bar{p} p \rightarrow \pi^0 \eta$

$\Gamma(\rho \bar{\rho})/\Gamma_{\text{total}} \times \Gamma(\pi^0 \eta')/\Gamma_{\text{total}}$ $\Gamma_{58}/\Gamma \times \Gamma_{34}/\Gamma$

VALUE (units 10^{-7})	DOCUMENT ID	TECN	COMMENT
< 2.5	ANDREOTTI	05c E835	$\bar{p} p \rightarrow \pi^0 \eta'$

$\Gamma(\rho \bar{\rho})/\Gamma_{\text{total}} \times \Gamma(\eta \eta)/\Gamma_{\text{total}}$ $\Gamma_{58}/\Gamma \times \Gamma_{36}/\Gamma$

VALUE (units 10^{-7})	DOCUMENT ID	TECN	COMMENT
6.7 ± 0.5 OUR FIT			
4.0 ± 1.2 ± 0.5	ANDREOTTI	05c E835	$\bar{p} p \rightarrow \eta \eta$

$\Gamma(\rho \bar{\rho})/\Gamma_{\text{total}} \times \Gamma(\eta \eta')/\Gamma_{\text{total}}$ $\Gamma_{58}/\Gamma \times \Gamma_{37}/\Gamma$

VALUE (units 10^{-6})	DOCUMENT ID	TECN	COMMENT
2.1 ± 2.3	ANDREOTTI	05c E835	$\bar{p} p \rightarrow \pi^0 \eta'$

RADIATIVE DECAYS

$\Gamma(\gamma J/\psi(1S))/\Gamma_{\text{total}}$ Γ_{92}/Γ

VALUE (units 10^{-2})	EVTS	DOCUMENT ID	TECN	COMMENT
1.40 ± 0.05 OUR FIT				
0.25 ± 0.16 ± 2.15	12k	¹ ABLIKIM	17U BES3	$e^+ e^- \rightarrow \gamma X$
2.0 ± 0.2 ± 0.2		² ADAM	05A CLEO	$e^+ e^- \rightarrow \psi(2S) \rightarrow \gamma \chi_{c0}$

• • • We do not use the following data for averages, fits, limits, etc. • • •

¹ Not independent from $B(\psi(2S) \rightarrow \gamma \chi_{c0}(1P))$ and the product $B(\psi(2S) \rightarrow \gamma \chi_{c0}(1P)) \times B(\chi_{c0}(1P) \rightarrow \gamma J/\psi(1S))$ also measured in ABLIKIM 17U.

² Uses $B(\psi(2S) \rightarrow \gamma \chi_{c0}) \rightarrow \gamma J/\psi$ from ADAM 05A and $B(\psi(2S) \rightarrow \gamma \chi_{c0})$ from ATHAR 04.

$\Gamma(\gamma \rho^0)/\Gamma_{\text{total}}$ Γ_{93}/Γ

VALUE (units 10^{-6})	CL%	EVTS	DOCUMENT ID	TECN	COMMENT
< 9	90	1.2 ± 4.5	¹ BENNETT	08A CLEO	$\psi(2S) \rightarrow \gamma \gamma \rho^0$

• • • We do not use the following data for averages, fits, limits, etc. • • •

<10 90 6 ± 12 ² ABLIKIM 11E BES3 $\psi(2S) \rightarrow \gamma \gamma \rho^0$

¹ BENNETT 08A reports $< 9.6 \times 10^{-6}$ from a measurement of $[\Gamma(\chi_{c0}(1P) \rightarrow \gamma \rho^0)/\Gamma_{\text{total}}] \times [B(\psi(2S) \rightarrow \gamma \chi_{c0}(1P))]$ assuming $B(\psi(2S) \rightarrow \gamma \chi_{c0}(1P)) = (9.2 \pm 0.4) \times 10^{-2}$, which we rescale to our best value $B(\psi(2S) \rightarrow \gamma \chi_{c0}(1P)) = 9.79 \times 10^{-2}$.

² ABLIKIM 11E reports $< 10.5 \times 10^{-6}$ from a measurement of $[\Gamma(\chi_{c0}(1P) \rightarrow \gamma \rho^0)/\Gamma_{\text{total}}] \times [B(\psi(2S) \rightarrow \gamma \chi_{c0}(1P))]$ assuming $B(\psi(2S) \rightarrow \gamma \chi_{c0}(1P)) = (9.62 \pm 0.31) \times 10^{-2}$, which we rescale to our best value $B(\psi(2S) \rightarrow \gamma \chi_{c0}(1P)) = 9.79 \times 10^{-2}$.

$\Gamma(\gamma \omega)/\Gamma_{\text{total}}$ Γ_{94}/Γ

VALUE (units 10^{-6})	CL%	EVTS	DOCUMENT ID	TECN	COMMENT
< 8	90	0.0 ± 2.8	¹ BENNETT	08A CLEO	$\psi(2S) \rightarrow \gamma \gamma \omega$

• • • We do not use the following data for averages, fits, limits, etc. • • •

<13 90 5 ± 11 ² ABLIKIM 11E BES3 $\psi(2S) \rightarrow \gamma \gamma \omega$

¹ BENNETT 08A reports $< 8.8 \times 10^{-6}$ from a measurement of $[\Gamma(\chi_{c0}(1P) \rightarrow \gamma \omega)/\Gamma_{\text{total}}] \times [B(\psi(2S) \rightarrow \gamma \chi_{c0}(1P))]$ assuming $B(\psi(2S) \rightarrow \gamma \chi_{c0}(1P)) = (9.2 \pm 0.4) \times 10^{-2}$, which we rescale to our best value $B(\psi(2S) \rightarrow \gamma \chi_{c0}(1P)) = 9.79 \times 10^{-2}$.

² ABLIKIM 11E reports $< 12.9 \times 10^{-6}$ from a measurement of $[\Gamma(\chi_{c0}(1P) \rightarrow \gamma \omega)/\Gamma_{\text{total}}] \times [B(\psi(2S) \rightarrow \gamma \chi_{c0}(1P))]$ assuming $B(\psi(2S) \rightarrow \gamma \chi_{c0}(1P)) = (9.62 \pm 0.31) \times 10^{-2}$, which we rescale to our best value $B(\psi(2S) \rightarrow \gamma \chi_{c0}(1P)) = 9.79 \times 10^{-2}$.

$\Gamma(\gamma\phi)/\Gamma_{\text{total}}$ Γ_{95}/Γ

VALUE (units 10^{-6})	CL%	EVTS	DOCUMENT ID	TECN	COMMENT
< 6	90	0.1 ± 1.6	¹ BENNETT 08A	CLEO	$\psi(2S) \rightarrow \gamma\gamma\phi$

• • • We do not use the following data for averages, fits, limits, etc. • • •

VALUE (units 10^{-6})	CL%	EVTS	DOCUMENT ID	TECN	COMMENT
< 16	90	15 ± 7	² ABLIKIM 11E	BES3	$\psi(2S) \rightarrow \gamma\gamma\phi$

¹ BENNETT 08A reports $< 6.4 \times 10^{-6}$ from a measurement of $[\Gamma(\chi_{c0}(1P) \rightarrow \gamma\phi)/\Gamma_{\text{total}}] \times [B(\psi(2S) \rightarrow \gamma\chi_{c0}(1P))]$ assuming $B(\psi(2S) \rightarrow \gamma\chi_{c0}(1P)) = (9.2 \pm 0.4) \times 10^{-2}$, which we rescale to our best value $B(\psi(2S) \rightarrow \gamma\chi_{c0}(1P)) = 9.79 \times 10^{-2}$.

² ABLIKIM 11E reports $< 16.2 \times 10^{-6}$ from a measurement of $[\Gamma(\chi_{c0}(1P) \rightarrow \gamma\phi)/\Gamma_{\text{total}}] \times [B(\psi(2S) \rightarrow \gamma\chi_{c0}(1P))]$ assuming $B(\psi(2S) \rightarrow \gamma\chi_{c0}(1P)) = (9.62 \pm 0.31) \times 10^{-2}$, which we rescale to our best value $B(\psi(2S) \rightarrow \gamma\chi_{c0}(1P)) = 9.79 \times 10^{-2}$.

 $\Gamma(\gamma\gamma)/\Gamma_{\text{total}}$ Γ_{96}/Γ

VALUE (units 10^{-4})	CL%	DOCUMENT ID	TECN	COMMENT
2.04 ± 0.09 OUR FIT				

• • • We do not use the following data for averages, fits, limits, etc. • • •

VALUE (units 10^{-4})	CL%	DOCUMENT ID	TECN	COMMENT
< 7	90	¹ WICHT 08	BELL	$B^{\pm} \rightarrow K^{\pm}\gamma\gamma$

¹ WICHT 08 reports $[\Gamma(\chi_{c0}(1P) \rightarrow \gamma\gamma)/\Gamma_{\text{total}}] \times [B(B^{\pm} \rightarrow \chi_{c0} K^{\pm})] < 0.11 \times 10^{-6}$ which we divide by our best value $B(B^{\pm} \rightarrow \chi_{c0} K^{\pm}) = 1.51 \times 10^{-4}$.

 $\Gamma(e^{+}e^{-}J/\psi(1S))/\Gamma_{\text{total}}$ Γ_{97}/Γ

VALUE (units 10^{-4})	EVTS	DOCUMENT ID	TECN	COMMENT
1.54 ± 0.33 ± 0.03	56	^{1,2} ABLIKIM 17I	BES3	$\psi(2S) \rightarrow \gamma e^{+}e^{-}J/\psi$

• • • We do not use the following data for averages, fits, limits, etc. • • •

¹ ABLIKIM 17I reports $(1.51 \pm 0.30 \pm 0.13) \times 10^{-4}$ from a measurement of $[\Gamma(\chi_{c0}(1P) \rightarrow e^{+}e^{-}J/\psi(1S))/\Gamma_{\text{total}}] \times [B(\psi(2S) \rightarrow \gamma\chi_{c0}(1P))]$ assuming $B(\psi(2S) \rightarrow \gamma\chi_{c0}(1P)) = (9.99 \pm 0.27) \times 10^{-2}$, which we rescale to our best value $B(\psi(2S) \rightarrow \gamma\chi_{c0}(1P)) = (9.79 \pm 0.20) \times 10^{-2}$. Our first error is their experiment's error and our second error is the systematic error from using our best value.

² Not independent from other measurements reported by ABLIKIM 17I

 $\Gamma(e^{+}e^{-}J/\psi(1S))/\Gamma(\gamma J/\psi(1S))$ Γ_{97}/Γ_{92}

VALUE (units 10^{-3})	EVTS	DOCUMENT ID	TECN	COMMENT
9.5 ± 1.9 ± 0.7	56	¹ ABLIKIM 17I	BES3	$\psi(2S) \rightarrow e^{+}e^{-}\gamma J/\psi$

¹ Uses $B(\psi(2S) \rightarrow \gamma\chi_{c0}(1P)) \times B(\chi_{c0}(1P) \rightarrow \gamma J/\psi(1S)) = (15.8 \pm 0.3 \pm 0.6) \times 10^{-4}$ from ABLIKIM 17I and accounts for common systematic errors.

 $\Gamma(\mu^{+}\mu^{-}J/\psi(1S))/\Gamma(e^{+}e^{-}J/\psi(1S))$ Γ_{98}/Γ_{97}

VALUE	CL%	EVTS	DOCUMENT ID	TECN	COMMENT
< 0.14	90	< 9.5	ABLIKIM 19Z	BES3	$\psi(2S) \rightarrow \gamma\chi_{c0} \rightarrow \gamma(\mu^{+}\mu^{-}J/\psi)$

• • • We do not use the following data for averages, fits, limits, etc. • • •

 $\Gamma(\gamma\gamma)/\Gamma(\gamma J/\psi(1S))$ Γ_{96}/Γ_{92}

VALUE (units 10^{-2})	DOCUMENT ID	TECN	COMMENT
1.45 ± 0.08 OUR FIT			
2.0 ± 0.4 OUR AVERAGE			

2.2 ± 0.4 ± 0.1	¹ ANDREOTTI 04	E835	$p\bar{p} \rightarrow \chi_{c0} \rightarrow \gamma\gamma$
1.45 ± 0.74	² AMBROGIANI 00B	E835	$p\bar{p} \rightarrow \chi_{c2} \rightarrow \gamma\gamma, \gamma J/\psi$

¹ The values of $B(p\bar{p})B(\gamma\gamma)$ and $B(\gamma\gamma)B(\gamma J/\psi)$ measured by ANDREOTTI 04 are not independent. The latter is used in the fit because of smaller systematics.

² Calculated by us using $B(J/\psi(1S) \rightarrow e^{+}e^{-}) = 0.0593 \pm 0.0010$.

 $\Gamma(p\bar{p})/\Gamma_{\text{total}} \times \Gamma(\gamma J/\psi(1S))/\Gamma_{\text{total}}$ $\Gamma_{58}/\Gamma \times \Gamma_{92}/\Gamma$

VALUE (units 10^{-7})	EVTS	DOCUMENT ID	TECN	COMMENT
31.1 ± 1.5 OUR FIT				
28.2 ± 2.1 OUR AVERAGE				

28.0 ± 1.9 ± 1.3	392	^{1,2,3} BAGNASCO 02	E835	$p\bar{p} \rightarrow \chi_{c0} \rightarrow J/\psi\gamma$
29.3 ^{+5.7} _{-4.7} ± 1.5	89	^{1,2} AMBROGIANI 99B		$p\bar{p} \rightarrow \chi_{c0} \rightarrow J/\psi\gamma$

¹ Values in $(\Gamma(p\bar{p}) \times \Gamma(\gamma J/\psi(1S))/\Gamma_{\text{total}})$ and $(\Gamma(p\bar{p})/\Gamma_{\text{total}} \times \Gamma(\gamma J/\psi(1S))/\Gamma_{\text{total}})$ are not independent. The latter is used in the fit since it is less correlated to the total width.

² Calculated by us using $B(J/\psi(1S) \rightarrow e^{+}e^{-}) = 0.0593 \pm 0.0010$.

³ Recalculated by ANDREOTTI 05A.

 $\Gamma(p\bar{p})/\Gamma_{\text{total}} \times \Gamma(\gamma\gamma)/\Gamma_{\text{total}}$ $\Gamma_{58}/\Gamma \times \Gamma_{96}/\Gamma$

VALUE (units 10^{-8})	DOCUMENT ID	TECN	COMMENT
4.52 ± 0.27 OUR FIT			

• • • We do not use the following data for averages, fits, limits, etc. • • •

6.52 ± 1.18 ^{+0.48} _{-0.72}	¹ ANDREOTTI 04	E835	$p\bar{p} \rightarrow \chi_{c0} \rightarrow \gamma\gamma$
---	---------------------------	------	---

¹ The values of $B(p\bar{p})B(\gamma\gamma)$ and $B(\gamma\gamma)B(\gamma J/\psi)$ measured by ANDREOTTI 04 are not independent. The latter is used in the fit because of smaller systematics.

 $\chi_{c0}(1P)$ CROSS-PARTICLE BRANCHING RATIOS
 $\Gamma(\chi_{c0}(1P) \rightarrow p\bar{p})/\Gamma_{\text{total}} \times \Gamma(\psi(2S) \rightarrow \gamma\chi_{c0}(1P))/\Gamma_{\text{total}}$

VALUE (units 10^{-6})	EVTS	DOCUMENT ID	TECN	COMMENT
21.7 ± 0.9 OUR FIT				
23.7 ± 1.0 OUR AVERAGE				

23.7 ± 0.8 ± 0.9	1222	ABLIKIM 13V	BES3	$\psi(2S) \rightarrow \gamma p\bar{p}$
23.7 ± 1.4 ± 1.4	383 ± 22	¹ NAIK 08	CLEO	$\psi(2S) \rightarrow \gamma p\bar{p}$
23.6 ^{+3.7} _{-3.4} ± 3.4	89.5 ⁺¹⁴ ₋₁₃	BAI 04F	BES	$\psi(2S) \rightarrow \gamma\chi_{c0}(1P) \rightarrow \gamma p\bar{p}$

¹ Calculated by us. NAIK 08 reports $B(\chi_{c0} \rightarrow p\bar{p}) = (25.7 \pm 1.5 \pm 1.5 \pm 1.3) \times 10^{-5}$ using $B(\psi(2S) \rightarrow \gamma\chi_{c0}) = (9.22 \pm 0.11 \pm 0.46)\%$.

$\Gamma(\chi_{c0}(1P) \rightarrow p\bar{p})/\Gamma_{\text{total}} \times \Gamma(\psi(2S) \rightarrow \gamma\chi_{c0}(1P))/\Gamma(\psi(2S) \rightarrow J/\psi(1S)\pi^{+}\pi^{-})$

VALUE (units 10^{-5})	DOCUMENT ID	TECN	COMMENT
6.25 ± 0.26 OUR FIT			
4.6 ± 1.9	¹ BAI 98I	BES	$\psi(2S) \rightarrow \gamma\chi_{c0} \rightarrow \gamma p\bar{p}$

¹ Calculated by us. The value for $B(\chi_{c0} \rightarrow p\bar{p})$ reported in BAI 98I is derived using $B(\psi(2S) \rightarrow \gamma\chi_{c0}) = (9.3 \pm 0.8)\%$ and $B(\psi(2S) \rightarrow J/\psi(1S)\pi^{+}\pi^{-}) = (32.4 \pm 2.6)\%$ [BAI 98D].

$\Gamma(\chi_{c0}(1P) \rightarrow \Lambda\bar{\Lambda})/\Gamma_{\text{total}} \times \Gamma(\psi(2S) \rightarrow \gamma\chi_{c0}(1P))/\Gamma_{\text{total}}$

VALUE (units 10^{-6})	EVTS	DOCUMENT ID	TECN	COMMENT
35.2 ± 1.3 OUR FIT				
35.1 ± 1.4 OUR AVERAGE				Error includes scale factor of 1.1.

35.6 ± 1.0 ± 1.0	1486	ABLIKIM 21L	BES3	$\psi(2S) \rightarrow \gamma p\pi^{-}\bar{p}\pi^{+}$
31.2 ± 3.3 ± 2.0	131	¹ NAIK 08	CLEO	$\psi(2S) \rightarrow \gamma\Lambda\bar{\Lambda}$

• • • We do not use the following data for averages, fits, limits, etc. • • •

32.0 ± 1.9 ± 2.2	369	^{2,3} ABLIKIM 13H	BES3	$\psi(2S) \rightarrow \gamma\Lambda\bar{\Lambda}$
------------------	-----	----------------------------	------	---

¹ Calculated by us. NAIK 08 reports $B(\chi_{c0} \rightarrow \Lambda\bar{\Lambda}) = (33.8 \pm 3.6 \pm 2.2 \pm 1.7) \times 10^{-5}$ using $B(\psi(2S) \rightarrow \gamma\chi_{c0}) = (9.22 \pm 0.11 \pm 0.46)\%$.

² Superseded by ABLIKIM 21L

³ Calculated by us. ABLIKIM 13H reports $B(\chi_{c0} \rightarrow \Lambda\bar{\Lambda}) = (33.3 \pm 2.0 \pm 2.6) \times 10^{-5}$ from a measurement of $B(\chi_{c0} \rightarrow \Lambda\bar{\Lambda}) \times B(\psi(2S) \rightarrow \gamma\chi_{c0})$ assuming $B(\psi(2S) \rightarrow \gamma\chi_{c0}) = (9.62 \pm 0.31)\%$.

$\Gamma(\chi_{c0}(1P) \rightarrow \Lambda\bar{\Lambda})/\Gamma_{\text{total}} \times \Gamma(\psi(2S) \rightarrow \gamma\chi_{c0}(1P))/\Gamma(\psi(2S) \rightarrow J/\psi(1S)\pi^{+}\pi^{-})$

VALUE (units 10^{-5})	EVTS	DOCUMENT ID	TECN	COMMENT
10.1 ± 0.4 OUR FIT				
13.0^{+3.6}_{-3.5} ± 2.5	15.2 ^{+4.2} _{-4.0}	¹ BAI 03E	BES	$\psi(2S) \rightarrow \gamma\Lambda\bar{\Lambda}$

¹ BAI 03E reports $[B(\chi_{c0} \rightarrow \Lambda\bar{\Lambda})B(\psi(2S) \rightarrow \gamma\chi_{c0})/B(\psi(2S) \rightarrow J/\psi\pi^{+}\pi^{-})] \times [B^{2}(\Lambda \rightarrow \pi^{-}p)/B(J/\psi \rightarrow p\bar{p})] = (2.45^{+0.68}_{-0.65} ± 0.46)\%$. We calculate from this measurement the presented value using $B(\Lambda \rightarrow \pi^{-}p) = (63.9 \pm 0.5)\%$ and $B(J/\psi \rightarrow p\bar{p}) = (2.17 \pm 0.07) \times 10^{-3}$.

$\Gamma(\chi_{c0}(1P) \rightarrow \Lambda\bar{\Lambda})/\Gamma_{\text{total}} \times \Gamma(\psi(2S) \rightarrow \gamma\chi_{c0}(1P))/\Gamma(\psi(2S) \rightarrow J/\psi(1S)\pi^{+}\pi^{-})$

VALUE (units 10^{-5})	EVTS	DOCUMENT ID	TECN	COMMENT
10.1 ± 0.4 OUR FIT				

• • • We do not use the following data for averages, fits, limits, etc. • • •

10.1 ± 0.4 ± 0.4				
------------------	--	--	--	--

¹ BAI 03E reports $[B(\chi_{c0} \rightarrow \Lambda\bar{\Lambda})B(\psi(2S) \rightarrow \gamma\chi_{c0})/B(\psi(2S) \rightarrow J/\psi\pi^{+}\pi^{-})] \times [B^{2}(\Lambda \rightarrow \pi^{-}p)/B(J/\psi \rightarrow p\bar{p})] = (2.45^{+0.68}_{-0.65} ± 0.46)\%$. We calculate from this measurement the presented value using $B(\Lambda \rightarrow \pi^{-}p) = (63.9 \pm 0.5)\%$ and $B(J/\psi \rightarrow p\bar{p}) = (2.17 \pm 0.07) \times 10^{-3}$.

$\Gamma(\chi_{c0}(1P) \rightarrow \gamma J/\psi(1S))/\Gamma_{\text{total}} \times \Gamma(\psi(2S) \rightarrow \gamma\chi_{c0}(1P))/\Gamma_{\text{total}}$

VALUE (units 10^{-2})	EVTS	DOCUMENT ID	TECN	COMMENT
0.138 ± 0.005 OUR FIT				
0.147 ± 0.029 OUR AVERAGE				Error includes scale factor of 4.6.

0.158 ± 0.003 ± 0.006	4.8k	¹ ABLIKIM 17N	BES3	$\psi(2S) \rightarrow \gamma\gamma J/\psi$
0.024 ± 0.015 ± 0.205	12k	ABLIKIM 17U	BES3	$e^{+}e^{-} \rightarrow \gamma X$
0.069 ± 0.018		² OREGLIA 82	CBAL	$\psi(2S) \rightarrow \gamma\chi_{c0}$
0.4 ± 0.3		³ BRANDELIK 79B	DASP	$\psi(2S) \rightarrow \gamma\chi_{c0}$
0.16 ± 0.11		³ BARTEL 78B	CNTR	$\psi(2S) \rightarrow \gamma\chi_{c0}$
3.3 ± 1.7		⁴ BIDDICK 77	CNTR	$e^{+}e^{-} \rightarrow \gamma X$

• • • We do not use the following data for averages, fits, limits, etc. • • •

0.151 ± 0.003 ± 0.010	4.3k	⁵ ABLIKIM 12O	BES3	$\psi(2S) \rightarrow \gamma\chi_{c0}$
0.125 ± 0.007 ± 0.013	560	⁶ MENDEZ 08	CLEO	$\psi(2S) \rightarrow \gamma\chi_{c0}$
0.18 ± 0.01 ± 0.02	172	⁷ ADAM 05A	CLEO	Repl. by MENDEZ 08

¹ Uses $B(J/\psi \rightarrow e^{+}e^{-}) = (5.971 \pm 0.032)\%$ and $B(J/\psi \rightarrow \mu^{+}\mu^{-}) = (5.961 \pm 0.033)\%$.

² Recalculated by us using $B(J/\psi(1S) \rightarrow e^{+}e^{-}) = 0.1181 \pm 0.0020$.

³ Recalculated by us using $B(J/\psi(1S) \rightarrow \mu^{+}\mu^{-}) = 0.0588 \pm 0.0010$.

⁴ Assumes isotropic gamma distribution.

⁵ Superseded by ABLIKIM 17N.

⁶ Not independent from other measurements of MENDEZ 08.

⁷ Not independent from other values reported by ADAM 05A.

Meson Particle Listings

 $\chi_{c0}(1P)$

$$\Gamma(\chi_{c0}(1P) \rightarrow \gamma J/\psi(1S))/\Gamma_{\text{total}} \times \Gamma(\psi(2S) \rightarrow \gamma \chi_{c0}(1P))/\Gamma(\psi(2S) \rightarrow J/\psi(1S) \text{ anything})$$

$$\frac{\Gamma_{92}/\Gamma \times \Gamma_{162}^{\psi(2S)}/\Gamma_{10}^{\psi(2S)}}{\Gamma_{92}/\Gamma \times \Gamma_{162}^{\psi(2S)}/\Gamma_{10}^{\psi(2S)} + \Gamma_{12}^{\psi(2S)}/\Gamma_{12}^{\psi(2S)} + \Gamma_{13}^{\psi(2S)}/\Gamma_{13}^{\psi(2S)} + \Gamma_{14}^{\psi(2S)}/\Gamma_{14}^{\psi(2S)} + 0.343\Gamma_{163}^{\psi(2S)} + 0.190\Gamma_{164}^{\psi(2S)}}$$

VALUE (units 10^{-2}) EVTS DOCUMENT ID TECN COMMENT
0.224 ± 0.009 OUR FIT

• • • We do not use the following data for averages, fits, limits, etc. • • •

0.201 ± 0.011 ± 0.021 560 ¹ MENDEZ 08 CLEO $\psi(2S) \rightarrow \gamma \chi_{c0}$
 0.31 ± 0.02 ± 0.03 172 ADAM 05A CLEO Repl. by MENDEZ 08

¹ Not independent from other measurements of MENDEZ 08.

$$\Gamma(\chi_{c0}(1P) \rightarrow \gamma J/\psi(1S))/\Gamma_{\text{total}} \times \Gamma(\psi(2S) \rightarrow \gamma \chi_{c0}(1P))/\Gamma(\psi(2S) \rightarrow J/\psi(1S) \pi^+ \pi^-)$$

$$\frac{\Gamma_{92}/\Gamma \times \Gamma_{162}^{\psi(2S)}/\Gamma_{12}^{\psi(2S)}}{\Gamma_{92}/\Gamma \times \Gamma_{162}^{\psi(2S)}/\Gamma_{12}^{\psi(2S)} + \Gamma_{13}^{\psi(2S)}/\Gamma_{13}^{\psi(2S)} + \Gamma_{14}^{\psi(2S)}/\Gamma_{14}^{\psi(2S)} + 0.343\Gamma_{163}^{\psi(2S)} + 0.190\Gamma_{164}^{\psi(2S)}}$$

VALUE (units 10^{-2}) EVTS DOCUMENT ID TECN COMMENT
0.397 ± 0.015 OUR FIT
0.358 ± 0.020 ± 0.037

• • • We do not use the following data for averages, fits, limits, etc. • • •

0.55 ± 0.04 ± 0.06 172 ¹ ADAM 05A CLEO Repl. by MENDEZ 08

¹ Not independent from other values reported by ADAM 05A.

$$\Gamma(\chi_{c0}(1P) \rightarrow \gamma \gamma)/\Gamma_{\text{total}} \times \Gamma(\psi(2S) \rightarrow \gamma \chi_{c0}(1P))/\Gamma_{\text{total}}$$

$$\frac{\Gamma_{96}/\Gamma \times \Gamma_{162}^{\psi(2S)}/\Gamma_{\psi(2S)}}{\Gamma_{96}/\Gamma \times \Gamma_{162}^{\psi(2S)}/\Gamma_{\psi(2S)} + \Gamma_{13}^{\psi(2S)}/\Gamma_{13}^{\psi(2S)} + \Gamma_{14}^{\psi(2S)}/\Gamma_{14}^{\psi(2S)} + 0.343\Gamma_{163}^{\psi(2S)} + 0.190\Gamma_{164}^{\psi(2S)}}$$

VALUE (units 10^{-5}) EVTS DOCUMENT ID TECN COMMENT
2.00 ± 0.08 OUR FIT
1.95 ± 0.09 OUR AVERAGE

1.93 ± 0.08 ± 0.05 3.5k ABLIKIM 17A BES3 $\psi(2S) \rightarrow \gamma \chi_{c0} \rightarrow 3\gamma$
 2.17 ± 0.32 ± 0.10 0.2k ECKLUND 08A CLEO $\psi(2S) \rightarrow \gamma \chi_{c0} \rightarrow 3\gamma$
 3.7 ± 1.8 ± 1.0 LEE 85 CBAL $\psi(2S) \rightarrow \gamma \chi_{c0}$

• • • We do not use the following data for averages, fits, limits, etc. • • •

2.17 ± 0.17 ± 0.12 0.8k ¹ ABLIKIM 12A BES3 $\psi(2S) \rightarrow \gamma \chi_{c0} \rightarrow 3\gamma$

¹ Superseded by ABLIKIM 17A.

$$\Gamma(\chi_{c0}(1P) \rightarrow \pi \pi)/\Gamma_{\text{total}} \times \Gamma(\psi(2S) \rightarrow \gamma \chi_{c0}(1P))/\Gamma_{\text{total}}$$

$$\frac{\Gamma_{32}/\Gamma \times \Gamma_{162}^{\psi(2S)}/\Gamma_{\psi(2S)}}{\Gamma_{32}/\Gamma \times \Gamma_{162}^{\psi(2S)}/\Gamma_{\psi(2S)} + \Gamma_{13}^{\psi(2S)}/\Gamma_{13}^{\psi(2S)} + \Gamma_{14}^{\psi(2S)}/\Gamma_{14}^{\psi(2S)} + 0.343\Gamma_{163}^{\psi(2S)} + 0.190\Gamma_{164}^{\psi(2S)}}$$

VALUE (units 10^{-4}) EVTS DOCUMENT ID TECN COMMENT
8.34 ± 0.29 OUR FIT
8.80 ± 0.34 OUR AVERAGE

9.11 ± 0.08 ± 0.65 17k ¹ ABLIKIM 10A BES3 $e^+e^- \rightarrow \psi(2S) \rightarrow \gamma \chi_{c0}$
 8.81 ± 0.11 ± 0.43 8.9k ² ASNER 09 CLEO $\psi(2S) \rightarrow \gamma \pi^+ \pi^-$
 8.13 ± 0.19 ± 0.89 2.8k ³ ASNER 09 CLEO $\psi(2S) \rightarrow \gamma \pi^0 \pi^0$

¹ Calculated by us. ABLIKIM 10A reports $B(\chi_{c0} \rightarrow \pi^0 \pi^0) = (3.23 \pm 0.03 \pm 0.23 \pm 0.14) \times 10^{-3}$ using $B(\psi(2S) \rightarrow \gamma \chi_{c0}) = (9.4 \pm 0.4)\%$. We have multiplied the $\pi^0 \pi^0$ measurement by 3 to obtain $\pi \pi$.

² Calculated by us. ASNER 09 reports $B(\chi_{c0} \rightarrow \pi^+ \pi^-) = (6.37 \pm 0.08 \pm 0.31 \pm 0.32) \times 10^{-3}$ using $B(\psi(2S) \rightarrow \gamma \chi_{c0}) = (9.22 \pm 0.11 \pm 0.46)\%$. We have multiplied the $\pi^+ \pi^-$ measurement by 3/2 to obtain $\pi \pi$.

³ Calculated by us. ASNER 09 reports $B(\chi_{c0} \rightarrow \pi^0 \pi^0) = (2.94 \pm 0.07 \pm 0.32 \pm 0.15) \times 10^{-3}$ using $B(\psi(2S) \rightarrow \gamma \chi_{c0}) = (9.22 \pm 0.11 \pm 0.46)\%$. We have multiplied the $\pi^0 \pi^0$ measurement by 3 to obtain $\pi \pi$.

$$\Gamma(\chi_{c0}(1P) \rightarrow \pi \pi)/\Gamma_{\text{total}} \times \Gamma(\psi(2S) \rightarrow \gamma \chi_{c0}(1P))/\Gamma(\psi(2S) \rightarrow J/\psi(1S) \pi^+ \pi^-)$$

$$\frac{\Gamma_{32}/\Gamma \times \Gamma_{162}^{\psi(2S)}/\Gamma_{12}^{\psi(2S)}}{\Gamma_{32}/\Gamma \times \Gamma_{162}^{\psi(2S)}/\Gamma_{12}^{\psi(2S)} + \Gamma_{13}^{\psi(2S)}/\Gamma_{13}^{\psi(2S)} + \Gamma_{14}^{\psi(2S)}/\Gamma_{14}^{\psi(2S)} + 0.343\Gamma_{163}^{\psi(2S)} + 0.190\Gamma_{164}^{\psi(2S)}}$$

VALUE (units 10^{-4}) EVTS DOCUMENT ID TECN COMMENT
24.0 ± 0.8 OUR FIT
20.7 ± 1.7 OUR AVERAGE

23.9 ± 2.7 ± 4.1 97 ± 11 ¹ BAI 03c BES $\psi(2S) \rightarrow \gamma \chi_{c0} \rightarrow \gamma \pi^0 \pi^0$
 20.2 ± 1.1 ± 1.5 720 ± 32 ² BAI 98i BES $\psi(2S) \rightarrow \gamma \chi_{c0} \rightarrow \gamma \pi^+ \pi^-$

¹ We have multiplied $\pi^0 \pi^0$ measurement by 3 to obtain $\pi \pi$.

² Calculated by us. The value for $B(\chi_{c0} \rightarrow \pi^+ \pi^-)$ reported in BAI 98i is derived using $B(\psi' \rightarrow \gamma \chi_{c0}) = (9.3 \pm 0.8)\%$ and $B(\psi' \rightarrow J/\psi \pi^+ \pi^-) = (32.4 \pm 2.6)\%$ [BAI 98b]. We have multiplied $\pi^+ \pi^-$ measurement by 3/2 to obtain $\pi \pi$.

$$\Gamma(\chi_{c0}(1P) \rightarrow \eta \eta)/\Gamma_{\text{total}} \times \Gamma(\psi(2S) \rightarrow \gamma \chi_{c0}(1P))/\Gamma_{\text{total}}$$

$$\frac{\Gamma_{36}/\Gamma \times \Gamma_{162}^{\psi(2S)}/\Gamma_{\psi(2S)}}{\Gamma_{36}/\Gamma \times \Gamma_{162}^{\psi(2S)}/\Gamma_{\psi(2S)} + \Gamma_{13}^{\psi(2S)}/\Gamma_{13}^{\psi(2S)} + \Gamma_{14}^{\psi(2S)}/\Gamma_{14}^{\psi(2S)} + 0.343\Gamma_{163}^{\psi(2S)} + 0.190\Gamma_{164}^{\psi(2S)}}$$

VALUE (units 10^{-4}) EVTS DOCUMENT ID TECN COMMENT
2.95 ± 0.18 OUR FIT
3.12 ± 0.19 OUR AVERAGE

3.23 ± 0.09 ± 0.23 2132 ¹ ABLIKIM 10A BES3 $e^+e^- \rightarrow \psi(2S) \rightarrow \gamma \chi_{c0}$
 2.93 ± 0.12 ± 0.29 0.9k ² ASNER 09 CLEO $\psi(2S) \rightarrow \gamma \eta \eta$

• • • We do not use the following data for averages, fits, limits, etc. • • •

2.86 ± 0.46 ± 0.37 48 ³ ADAMS 07 CLEO $\psi(2S) \rightarrow \gamma \chi_{c0}$

¹ Calculated by us. ABLIKIM 10A reports $B(\chi_{c0} \rightarrow \eta \eta) = (3.44 \pm 0.10 \pm 0.24 \pm 0.13) \times 10^{-3}$ using $B(\psi(2S) \rightarrow \gamma \chi_{c0}) = (9.4 \pm 0.4)\%$.

² Calculated by us. ASNER 09 reports $B(\chi_{c0} \rightarrow \eta \eta) = (3.18 \pm 0.13 \pm 0.31 \pm 0.16) \times 10^{-3}$ using $B(\psi(2S) \rightarrow \gamma \chi_{c0}) = (9.22 \pm 0.11 \pm 0.46)\%$.

³ Superseded by ASNER 09. Calculated by us. The value of $B(\chi_{c0}(1P) \rightarrow \eta \eta)$ reported by ADAMS 07 was derived using $B(\psi(2S) \rightarrow \gamma \chi_{c0}(1P)) = (9.22 \pm 0.11 \pm 0.46)\%$ (ATHAR 04).

$$\Gamma(\chi_{c0}(1P) \rightarrow \eta \eta)/\Gamma_{\text{total}} \times \Gamma(\psi(2S) \rightarrow \gamma \chi_{c0}(1P))/\Gamma(\psi(2S) \rightarrow J/\psi(1S) \pi^+ \pi^-)$$

$$\frac{\Gamma_{36}/\Gamma \times \Gamma_{162}^{\psi(2S)}/\Gamma_{12}^{\psi(2S)}}{\Gamma_{36}/\Gamma \times \Gamma_{162}^{\psi(2S)}/\Gamma_{12}^{\psi(2S)} + \Gamma_{13}^{\psi(2S)}/\Gamma_{13}^{\psi(2S)} + \Gamma_{14}^{\psi(2S)}/\Gamma_{14}^{\psi(2S)} + 0.343\Gamma_{163}^{\psi(2S)} + 0.190\Gamma_{164}^{\psi(2S)}}$$

VALUE (units 10^{-3}) DOCUMENT ID TECN COMMENT
0.85 ± 0.05 OUR FIT
0.578 ± 0.241 ± 0.158

BAI 03c BES $\psi(2S) \rightarrow \gamma \eta \eta$

$$\Gamma(\chi_{c0}(1P) \rightarrow K^+ K^-)/\Gamma_{\text{total}} \times \Gamma(\psi(2S) \rightarrow \gamma \chi_{c0}(1P))/\Gamma_{\text{total}}$$

$$\frac{\Gamma_{42}/\Gamma \times \Gamma_{162}^{\psi(2S)}/\Gamma_{\psi(2S)}}{\Gamma_{42}/\Gamma \times \Gamma_{162}^{\psi(2S)}/\Gamma_{\psi(2S)} + \Gamma_{13}^{\psi(2S)}/\Gamma_{13}^{\psi(2S)} + \Gamma_{14}^{\psi(2S)}/\Gamma_{14}^{\psi(2S)} + 0.343\Gamma_{163}^{\psi(2S)} + 0.190\Gamma_{164}^{\psi(2S)}}$$

VALUE (units 10^{-4}) EVTS DOCUMENT ID TECN COMMENT
5.92 ± 0.28 OUR FIT
5.97 ± 0.07 ± 0.32

8.1k ¹ ASNER 09 CLEO $\psi(2S) \rightarrow \gamma K^+ K^-$

¹ Calculated by us. ASNER 09 reports $B(\chi_{c0} \rightarrow K^+ K^-) = (6.47 \pm 0.08 \pm 0.35 \pm 0.32) \times 10^{-3}$ using $B(\psi(2S) \rightarrow \gamma \chi_{c0}) = (9.22 \pm 0.11 \pm 0.46)\%$.

$$\Gamma(\chi_{c0}(1P) \rightarrow K^+ K^-)/\Gamma_{\text{total}} \times \Gamma(\psi(2S) \rightarrow \gamma \chi_{c0}(1P))/\Gamma(\psi(2S) \rightarrow J/\psi(1S) \pi^+ \pi^-)$$

$$\frac{\Gamma_{42}/\Gamma \times \Gamma_{162}^{\psi(2S)}/\Gamma_{12}^{\psi(2S)}}{\Gamma_{42}/\Gamma \times \Gamma_{162}^{\psi(2S)}/\Gamma_{12}^{\psi(2S)} + \Gamma_{13}^{\psi(2S)}/\Gamma_{13}^{\psi(2S)} + \Gamma_{14}^{\psi(2S)}/\Gamma_{14}^{\psi(2S)} + 0.343\Gamma_{163}^{\psi(2S)} + 0.190\Gamma_{164}^{\psi(2S)}}$$

VALUE (units 10^{-3}) EVTS DOCUMENT ID TECN COMMENT
1.71 ± 0.08 OUR FIT
1.63 ± 0.10 ± 0.15

774 ± 38 ¹ BAI 98i BES $\psi(2S) \rightarrow \gamma K^+ K^-$

¹ Calculated by us. The value for $B(\chi_{c0} \rightarrow K^+ K^-)$ reported by BAI 98i is derived using $B(\psi(2S) \rightarrow \gamma \chi_{c0}) = (9.3 \pm 0.8)\%$ and $B(\psi(2S) \rightarrow J/\psi \pi^+ \pi^-) = (32.4 \pm 2.6)\%$ [BAI 98b].

$$\Gamma(\chi_{c0}(1P) \rightarrow K_S^0 K_S^0)/\Gamma_{\text{total}} \times \Gamma(\psi(2S) \rightarrow \gamma \chi_{c0}(1P))/\Gamma_{\text{total}}$$

$$\frac{\Gamma_{43}/\Gamma \times \Gamma_{162}^{\psi(2S)}/\Gamma_{\psi(2S)}}{\Gamma_{43}/\Gamma \times \Gamma_{162}^{\psi(2S)}/\Gamma_{\psi(2S)} + \Gamma_{13}^{\psi(2S)}/\Gamma_{13}^{\psi(2S)} + \Gamma_{14}^{\psi(2S)}/\Gamma_{14}^{\psi(2S)} + 0.343\Gamma_{163}^{\psi(2S)} + 0.190\Gamma_{164}^{\psi(2S)}}$$

VALUE (units 10^{-4}) EVTS DOCUMENT ID TECN COMMENT
3.10 ± 0.16 OUR FIT
3.18 ± 0.17 OUR AVERAGE

3.22 ± 0.07 ± 0.17 2.1k ¹ ASNER 09 CLEO $\psi(2S) \rightarrow \gamma K_S^0 K_S^0$

3.02 ± 0.19 ± 0.33 322 ABLIKIM 05o BES2 $\psi(2S) \rightarrow \gamma K_S^0 K_S^0$

¹ Calculated by us. ASNER 09 reports $B(\chi_{c0} \rightarrow K_S^0 K_S^0) = (3.49 \pm 0.08 \pm 0.18 \pm 0.17) \times 10^{-3}$ using $B(\psi(2S) \rightarrow \gamma \chi_{c0}) = (9.22 \pm 0.11 \pm 0.46)\%$.

$$\Gamma(\chi_{c0}(1P) \rightarrow K_S^0 K_S^0)/\Gamma_{\text{total}} \times \Gamma(\psi(2S) \rightarrow \gamma \chi_{c0}(1P))/\Gamma(\psi(2S) \rightarrow J/\psi(1S) \pi^+ \pi^-)$$

$$\frac{\Gamma_{43}/\Gamma \times \Gamma_{162}^{\psi(2S)}/\Gamma_{12}^{\psi(2S)}}{\Gamma_{43}/\Gamma \times \Gamma_{162}^{\psi(2S)}/\Gamma_{12}^{\psi(2S)} + \Gamma_{13}^{\psi(2S)}/\Gamma_{13}^{\psi(2S)} + \Gamma_{14}^{\psi(2S)}/\Gamma_{14}^{\psi(2S)} + 0.343\Gamma_{163}^{\psi(2S)} + 0.190\Gamma_{164}^{\psi(2S)}}$$

VALUE (units 10^{-3}) DOCUMENT ID TECN COMMENT
8.9 ± 0.5 OUR FIT
5.6 ± 0.8 ± 1.3

¹ BAI 99b BES $\psi(2S) \rightarrow \gamma K_S^0 K_S^0$

¹ Calculated by us. The value of $B(\chi_{c0} \rightarrow K_S^0 K_S^0)$ reported by BAI 99b was derived using $B(\psi(2S) \rightarrow \gamma \chi_{c0}(1P)) = (9.3 \pm 0.8)\%$ and $B(\psi(2S) \rightarrow J/\psi \pi^+ \pi^-) = (32.4 \pm 2.6)\%$ [BAI 98b].

$$\Gamma(\chi_{c0}(1P) \rightarrow 2(\pi^+ \pi^-))/\Gamma_{\text{total}} \times \Gamma(\psi(2S) \rightarrow \gamma \chi_{c0}(1P))/\Gamma(\psi(2S) \rightarrow J/\psi(1S) \pi^+ \pi^-)$$

$$\frac{\Gamma_{11}/\Gamma \times \Gamma_{162}^{\psi(2S)}/\Gamma_{12}^{\psi(2S)}}{\Gamma_{11}/\Gamma \times \Gamma_{162}^{\psi(2S)}/\Gamma_{12}^{\psi(2S)} + \Gamma_{13}^{\psi(2S)}/\Gamma_{13}^{\psi(2S)} + \Gamma_{14}^{\psi(2S)}/\Gamma_{14}^{\psi(2S)} + 0.343\Gamma_{163}^{\psi(2S)} + 0.190\Gamma_{164}^{\psi(2S)}}$$

VALUE (units 10^{-3}) DOCUMENT ID TECN COMMENT
6.6 ± 0.5 OUR FIT
6.9 ± 2.4 OUR AVERAGE

Error includes scale factor of 3.8.

4.4 ± 0.1 ± 0.9 ¹ BAI 99b BES $\psi(2S) \rightarrow \gamma \chi_{c0}$

9.3 ± 0.9 ² TANENBAUM 78 MRK1 $\psi(2S) \rightarrow \gamma \chi_{c0}$

¹ Calculated by us. The value for $B(\chi_{c0} \rightarrow 2\pi^+ 2\pi^-)$ reported in BAI 99b is derived using $B(\psi(2S) \rightarrow \gamma \chi_{c0}) = (9.3 \pm 0.8)\%$ and $B(\psi(2S) \rightarrow J/\psi(1S) \pi^+ \pi^-) = (32.4 \pm 2.6)\%$ [BAI 98b].

² The value $B(\psi(1S) \rightarrow \gamma \chi_{c0}) \times B(\chi_{c0} \rightarrow 2\pi^+ 2\pi^-)$ reported in TANENBAUM 78 is derived using $B(\psi(2S) \rightarrow J/\psi(1S) \pi^+ \pi^-) \times B(J/\psi(1S) \rightarrow \ell^+ \ell^-) = (4.6 \pm 0.7)\%$. Calculated by us using $B(J/\psi(1S) \rightarrow \ell^+ \ell^-) = 0.1181 \pm 0.0020$.

$$\Gamma(\chi_{c0}(1P) \rightarrow \pi^+ \pi^- K^+ K^-)/\Gamma_{\text{total}} \times \Gamma(\psi(2S) \rightarrow \gamma \chi_{c0}(1P))/\Gamma_{\text{total}}$$

$$\frac{\Gamma_{8}/\Gamma \times \Gamma_{162}^{\psi(2S)}/\Gamma_{\psi(2S)}}{\Gamma_{8}/\Gamma \times \Gamma_{162}^{\psi(2S)}/\Gamma_{\psi(2S)} + \Gamma_{13}^{\psi(2S)}/\Gamma_{13}^{\psi(2S)} + \Gamma_{14}^{\psi(2S)}/\Gamma_{14}^{\psi(2S)} + 0.343\Gamma_{163}^{\psi(2S)} + 0.190\Gamma_{164}^{\psi(2S)}}$$

VALUE (units 10^{-3}) DOCUMENT ID TECN COMMENT
1.78 ± 0.14 OUR FIT
1.64 ± 0.05 ± 0.2

ABLIKIM 05q BES2 $\psi(2S) \rightarrow \gamma \chi_{c0}$

$$\Gamma(\chi_{c0}(1P) \rightarrow \pi^+ \pi^- K^+ K^-)/\Gamma_{\text{total}} \times \Gamma(\psi(2S) \rightarrow \gamma \chi_{c0}(1P))/\Gamma(\psi(2S) \rightarrow J/\psi(1S) \pi^+ \pi^-)$$

$$\frac{\Gamma_{8}/\Gamma \times \Gamma_{162}^{\psi(2S)}/\Gamma_{12}^{\psi(2S)}}{\Gamma_{8}/\Gamma \times \Gamma_{162}^{\psi(2S)}/\Gamma_{12}^{\psi(2S)} + \Gamma_{13}^{\psi(2S)}/\Gamma_{13}^{\psi(2S)} + \Gamma_{14}^{\psi(2S)}/\Gamma_{14}^{\psi(2S)} + 0.343\Gamma_{163}^{\psi(2S)} + 0.190\Gamma_{164}^{\psi(2S)}}$$

VALUE (units 10^{-3}) DOCUMENT ID TECN COMMENT
5.1 ± 0.4 OUR FIT
5.8 ± 1.6 OUR AVERAGE

Error includes scale factor of 2.3.

4.22 ± 0.20 ± 0.97 BAI 99b BES $\psi(2S) \rightarrow \gamma \chi_{c0}$

7.4 ± 1.0 ¹ TANENBAUM 78 MRK1 $\psi(2S) \rightarrow \gamma \chi_{c0}$

¹ The reported value is derived using $B(\psi(2S) \rightarrow \pi^+ \pi^- J/\psi) \times B(J/\psi \rightarrow \ell^+ \ell^-) = (4.6 \pm 0.7)\%$. Calculated by us using $B(J/\psi \rightarrow \ell^+ \ell^-) = 0.1181 \pm 0.0020$.

$$\Gamma(\chi_{c0}(1P) \rightarrow K^+ K^- K^+ K^-)/\Gamma_{\text{total}} \times \Gamma(\psi(2S) \rightarrow \gamma \chi_{c0}(1P))/\Gamma_{\text{total}}$$

$$\frac{\Gamma_{51}/\Gamma \times \Gamma_{162}^{\psi(2S)}/\Gamma_{\psi(2S)}}{\Gamma_{51}/\Gamma \times \Gamma_{162}^{\psi(2S)}/\Gamma_{\psi(2S)} + \Gamma_{13}^{\psi(2S)}/\Gamma_{13}^{\psi(2S)} + \Gamma_{14}^{\psi(2S)}/\Gamma_{14}^{\psi(2S)} + 0.343\Gamma_{163}^{\psi(2S)} + 0.190\Gamma_{164}^{\psi(2S)}}$$

VALUE (units 10^{-4}) EVTS DOCUMENT ID TECN COMMENT
2.76 ± 0.28 OUR FIT
3.20 ± 0.11 ± 0.41

278 ¹ ABLIKIM 06t BES2 $\psi(2S) \rightarrow \gamma 2K^+ 2K^-$

¹ Calculated by us. The value of $B(\chi_{c0} \rightarrow 2K^+ 2K^-)$ reported by ABLIKIM 06t was derived using $B(\psi(2S) \rightarrow \gamma \chi_{c0}(1P)) = (9.2 \pm 0.4)\%$.

See key on page 1127

Meson Particle Listings

$\chi_{c0}(1P), \chi_{c1}(1P)$

$\Gamma(\chi_{c0}(1P) \rightarrow K^+K^-K^+K^-)/\Gamma_{total} \times \Gamma(\psi(2S) \rightarrow \gamma\chi_{c0}(1P))/\Gamma(\psi(2S) \rightarrow J/\psi(1S)\pi^+\pi^-)$

Table with columns: VALUE (units 10^-4), DOCUMENT ID, TECN, COMMENT. Row 1: 8.0 ± 0.8 OUR FIT. Row 2: 6.1 ± 0.8 ± 0.9. Row 3: 1 BAI 99B BES ψ(2S) → γ2K+2K-

1 Calculated by us. The value of B(χc0 → 2K+2K-) reported by BAI 99B was derived using B(ψ(2S) → γχc0(1P)) = (9.3 ± 0.8)% and B(ψ(2S) → J/ψπ+π-) = (32.4 ± 2.6)% [BAI 98d].

$\Gamma(\chi_{c0}(1P) \rightarrow \phi\phi)/\Gamma_{total} \times \Gamma(\psi(2S) \rightarrow \gamma\chi_{c0}(1P))/\Gamma_{total}$

Table with columns: VALUE (units 10^-4), EVTS, DOCUMENT ID, TECN, COMMENT. Row 1: 0.78 ± 0.07 OUR FIT. Row 2: 0.78 ± 0.08 OUR AVERAGE. Row 3: 0.77 ± 0.03 ± 0.08. Row 4: 0.86 ± 0.19 ± 0.12

1 Calculated by us. The value of B(χc0 → φφ) reported by ABLIKIM 11K was derived using B(ψ(2S) → γχc0(1P)) = (9.62 ± 0.31)%.

2 Calculated by us. The value of B(χc0 → φφ) reported by ABLIKIM 06T was derived using B(ψ(2S) → γχc0(1P)) = (9.2 ± 0.4)%.

$\Gamma(\chi_{c0}(1P) \rightarrow \phi\phi)/\Gamma_{total} \times \Gamma(\psi(2S) \rightarrow \gamma\chi_{c0}(1P))/\Gamma(\psi(2S) \rightarrow J/\psi(1S)\pi^+\pi^-)$

Table with columns: VALUE (units 10^-4), DOCUMENT ID, TECN, COMMENT. Row 1: 2.25 ± 0.21 OUR FIT. Row 2: 2.6 ± 0.10 ± 1.1

1 Calculated by us. The value of B(χc0 → φφ) reported by BAI 99B was derived using B(ψ(2S) → γχc0(1P)) = (9.3 ± 0.8)% and B(ψ(2S) → J/ψπ+π-) = (32.4 ± 2.6)% [BAI 98d].

$\Gamma(\chi_{c0}(1P) \rightarrow \Sigma^+\bar{p}K_S^0 + c.c.)/\Gamma_{total} \times \Gamma(\psi(2S) \rightarrow \gamma\chi_{c0}(1P))/\Gamma_{total}$

Table with columns: VALUE (units 10^-5), EVTS, DOCUMENT ID, TECN, COMMENT. Row 1: 3.45 ± 0.17 ± 0.19

1 Calculated by us. ABLIKIM 19BB reports B(χc0 → Σ+ p-bar KS0 + c.c.) = (3.52 ± 0.19 ± 0.21) × 10^-4 using B(ψ(2S) → γχc0) = (9.79 ± 0.20)% and other branching fractions from PDG 18.

$\Gamma(\chi_{c0}(1P) \rightarrow \Sigma^0\bar{p}K^+ + c.c.)/\Gamma_{total} \times \Gamma(\psi(2S) \rightarrow \gamma\chi_{c0}(1P))/\Gamma_{total}$

Table with columns: VALUE (units 10^-5), EVTS, DOCUMENT ID, TECN, COMMENT. Row 1: 2.97 ± 0.12 ± 0.14

1 Calculated by us. ABLIKIM 20AE reports B(χc0 → Σ0 p-bar K+ + c.c.) = (3.03 ± 0.12 ± 0.15) × 10^-4 using B(ψ(2S) → γχc0) = (9.79 ± 0.20)% and other branching fractions from PDG 20.

χc0(1P) REFERENCES

Table with columns: ABLIKIM, JHEP, PR, PTEP, etc. and corresponding document IDs and comments for χc0(1P) references.

Table listing various experiments (HE, MENDEZ, NAIK, etc.) and their associated document IDs and comments for χc0(1P) and χc1(1P) listings.

χc1(1P) J^PC = 0+(1+ +) See the Review on "ψ(2S) and χc branching ratios" before the χc0(1P) Listings.

χc1(1P) MASS

Table with columns: VALUE (MeV), EVTS, DOCUMENT ID, TECN, COMMENT. Row 1: 3510.67 ± 0.05 OUR AVERAGE. Row 2: 3508.4 ± 1.9 ± 0.7. Row 3: 3510.71 ± 0.04 ± 0.09. Row 4: 3510.30 ± 0.14 ± 0.16. Row 5: 3510.719 ± 0.051 ± 0.019. Row 6: 3509.4 ± 0.9. Row 7: 3510.60 ± 0.087 ± 0.019. Row 8: 3511.3 ± 0.4 ± 0.4. Row 9: 3512.3 ± 0.3 ± 4.0. Row 10: 3507.4 ± 1.7. Row 11: 3510.4 ± 0.6. Row 12: 3510.1 ± 1.1. Row 13: 3509 ± 11. Row 14: 3507 ± 3. Row 15: 3505.0 ± 4 ± 4. Row 16: 3513 ± 7. Row 17: 3500 ± 10. Row 18: 3508.4 ± 1.9 ± 0.7.

1 From a fit of the φφ invariant mass with the width of χc1(1P) fixed to the PDG 16 value. 2 AAIJ 17BI reports also m(χc2) - m(χc1) = 45.39 ± 0.07 ± 0.03 MeV. 3 Recalculated by ANDREOTTI 05A, using the value of ψ(2S) mass from AULCHENKO 03. 4 Using mass of ψ(2S) = 3686.0 MeV. 5 J/ψ(1S) mass constrained to 3097 MeV. 6 Mass value shifted by us by amount appropriate for ψ(2S) mass = 3686 MeV and J/ψ(1S) mass = 3097 MeV. 7 From a simultaneous fit to radiative and hadronic decay channels.

χc1(1P) WIDTH

Table with columns: VALUE (MeV), CL%, EVTS, DOCUMENT ID, TECN, COMMENT. Row 1: 0.84 ± 0.04 OUR FIT. Row 2: 0.88 ± 0.05 OUR AVERAGE. Row 3: 1.39 +0.40 +0.26 -0.38 -0.77. Row 4: 0.876 ± 0.045 ± 0.026. Row 5: 0.87 ± 0.11 ± 0.08. Row 6: <1.3. Row 7: <3.8. Row 8: 0.87 ± 0.11 ± 0.08. Row 9: <1.3. Row 10: <3.8. Row 11: 0.87 ± 0.11 ± 0.08.

Downloaded from https://academic.oup.com/ptep/article/2022/8/083C01/6651666 by CERN Library user on 11 October 2022

Meson Particle Listings

$\chi_{c1}(1P)$

$\chi_{c1}(1P)$ DECAY MODES

Mode	Fraction (Γ_i/Γ)	Scale factor/ Confidence level
Hadronic decays		
Γ_1 $3(\pi^+\pi^-)$	$(5.8 \pm 1.4) \times 10^{-3}$	S=1.2
Γ_2 $2(\pi^+\pi^-)$	$(7.6 \pm 2.6) \times 10^{-3}$	
Γ_3 $\pi^+\pi^-\pi^0\pi^0$	$(1.19 \pm 0.15) \%$	
Γ_4 $\rho^+\pi^-\pi^0 + c.c.$	$(1.45 \pm 0.24) \%$	
Γ_5 $\rho^0\pi^+\pi^-$	$(3.9 \pm 3.5) \times 10^{-3}$	
Γ_6 $4\pi^0$	$(5.4 \pm 0.8) \times 10^{-4}$	
Γ_7 $\pi^+\pi^-K^+K^-$	$(4.5 \pm 1.0) \times 10^{-3}$	
Γ_8 $K^+K^-\pi^0\pi^0$	$(1.12 \pm 0.27) \times 10^{-3}$	
Γ_9 $K^+K^-\pi^+\pi^-$	$(1.15 \pm 0.13) \%$	
Γ_{10} $K_S^0 K^\pm \pi^\mp \pi^+ \pi^-$	$(7.5 \pm 0.8) \times 10^{-3}$	
Γ_{11} $K^+\pi^-\bar{K}^0\pi^0 + c.c.$	$(8.6 \pm 1.4) \times 10^{-3}$	
Γ_{12} $\rho^-K^+\bar{K}^0 + c.c.$	$(5.0 \pm 1.2) \times 10^{-3}$	
Γ_{13} $K^*(892)^0\bar{K}^0\pi^0 \rightarrow K^+\pi^-\bar{K}^0\pi^0 + c.c.$	$(2.3 \pm 0.6) \times 10^{-3}$	
Γ_{14} $K^+K^-\eta\pi^0$	$(1.12 \pm 0.34) \times 10^{-3}$	
Γ_{15} $\pi^+\pi^-K_S^0K_S^0$	$(6.9 \pm 2.9) \times 10^{-4}$	
Γ_{16} $K^+K^-\eta$	$(3.2 \pm 1.0) \times 10^{-4}$	
Γ_{17} $\bar{K}^0K^+\pi^- + c.c.$	$(7.0 \pm 0.6) \times 10^{-3}$	
Γ_{18} $K^*(892)^0\bar{K}^0 + c.c.$	$(10 \pm 4) \times 10^{-4}$	
Γ_{19} $K^*(892)^+K^- + c.c.$	$(1.4 \pm 0.6) \times 10^{-3}$	
Γ_{20} $K_J^*(1430)^0\bar{K}^0 + c.c. \rightarrow K_S^0K^+\pi^- + c.c.$	$< 8 \times 10^{-4}$	CL=90%
Γ_{21} $K_J^*(1430)^+K^- + c.c. \rightarrow K_S^0K^+\pi^- + c.c.$	$< 2.1 \times 10^{-3}$	CL=90%
Γ_{22} $K^+K^-\pi^0$	$(1.81 \pm 0.24) \times 10^{-3}$	
Γ_{23} $\eta\pi^+\pi^-$	$(4.62 \pm 0.23) \times 10^{-3}$	
Γ_{24} $a_0(980)^+\pi^- + c.c. \rightarrow \eta\pi^+\pi^-$	$(3.2 \pm 0.4) \times 10^{-3}$	S=2.2
Γ_{25} $\partial_2(1320)^+\pi^- + c.c. \rightarrow \eta\pi^+\pi^-$	$(1.76 \pm 0.24) \times 10^{-4}$	
Γ_{26} $\partial_2(1700)^+\pi^- + c.c. \rightarrow \eta\pi^+\pi^-$	$(4.6 \pm 0.7) \times 10^{-5}$	
Γ_{27} $f_2(1270)\eta \rightarrow \eta\pi^+\pi^-$	$(3.5 \pm 0.6) \times 10^{-4}$	
Γ_{28} $f_4(2050)\eta \rightarrow \eta\pi^+\pi^-$	$(2.5 \pm 0.9) \times 10^{-5}$	
Γ_{29} $\pi_1(1400)^+\pi^- + c.c. \rightarrow \eta\pi^+\pi^-$	$< 5 \times 10^{-5}$	CL=90%
Γ_{30} $\pi_1(1600)^+\pi^- + c.c. \rightarrow \eta\pi^+\pi^-$	$< 1.5 \times 10^{-5}$	CL=90%
Γ_{31} $\pi_1(2015)^+\pi^- + c.c. \rightarrow \eta\pi^+\pi^-$	$< 8 \times 10^{-6}$	CL=90%
Γ_{32} $f_2(1270)\eta$	$(6.7 \pm 1.1) \times 10^{-4}$	
Γ_{33} $\pi^+\pi^-\eta'$	$(2.2 \pm 0.4) \times 10^{-3}$	
Γ_{34} $K^+K^-\eta'(958)$	$(8.8 \pm 0.9) \times 10^{-4}$	
Γ_{35} $K_0^*(1430)^+K^- + c.c.$	$(6.4 \pm_{-2.8}^{2.2}) \times 10^{-4}$	
Γ_{36} $f_0(980)\eta'(958)$	$(1.6 \pm_{-0.7}^{1.4}) \times 10^{-4}$	
Γ_{37} $f_0(1710)\eta'(958)$	$(7 \pm_{-5}^7) \times 10^{-5}$	
Γ_{38} $f_2'(1525)\eta'(958)$	$(9 \pm 6) \times 10^{-5}$	
Γ_{39} $\pi^0 f_0(980) \rightarrow \pi^0\pi^+\pi^-$	$(3.5 \pm 0.9) \times 10^{-7}$	
Γ_{40} $K^+K^*(892)^0\pi^- + c.c.$	$(3.2 \pm 2.1) \times 10^{-3}$	
Γ_{41} $K^*(892)^0\bar{K}^*(892)^0$	$(1.4 \pm 0.4) \times 10^{-3}$	
Γ_{42} $K^+K^-K_S^0K_S^0$	$< 4 \times 10^{-4}$	CL=90%
Γ_{43} $K_S^0K_S^0K_S^0K_S^0$	$(3.5 \pm 1.0) \times 10^{-5}$	
Γ_{44} $K^+K^-K^+K^-$	$(5.4 \pm 1.1) \times 10^{-4}$	
Γ_{45} $K^+K^-\phi$	$(4.1 \pm 1.5) \times 10^{-4}$	
Γ_{46} $\bar{K}^0K^+\pi^-\phi + c.c.$	$(3.3 \pm 0.5) \times 10^{-3}$	
Γ_{47} $K^+K^-\pi^0\phi$	$(1.62 \pm 0.30) \times 10^{-3}$	
Γ_{48} $\phi\pi^+\pi^-\pi^0$	$(7.5 \pm 1.0) \times 10^{-4}$	
Γ_{49} $\omega\omega$	$(5.7 \pm 0.7) \times 10^{-4}$	
Γ_{50} ωK^+K^-	$(7.8 \pm 0.9) \times 10^{-4}$	
Γ_{51} $\omega\phi$	$(2.7 \pm 0.4) \times 10^{-5}$	
Γ_{52} $\phi\phi$	$(4.2 \pm 0.5) \times 10^{-4}$	
Γ_{53} $\phi\phi\eta$	$(3.0 \pm 0.5) \times 10^{-4}$	
Γ_{54} $\rho\bar{\rho}$	$(7.60 \pm 0.34) \times 10^{-5}$	
Γ_{55} $\rho\bar{\rho}\pi^0$	$(1.55 \pm 0.18) \times 10^{-4}$	
Γ_{56} $\rho\bar{\rho}\eta$	$(1.45 \pm 0.25) \times 10^{-4}$	
Γ_{57} $\rho\bar{\rho}\omega$	$(2.12 \pm 0.31) \times 10^{-4}$	
Γ_{58} $\rho\bar{\rho}\phi$	$< 1.7 \times 10^{-5}$	CL=90%
Γ_{59} $\rho\bar{\rho}\pi^+\pi^-$	$(5.0 \pm 1.9) \times 10^{-4}$	
Γ_{60} $\rho\bar{\rho}\pi^0\pi^0$	$< 5 \times 10^{-4}$	CL=90%
Γ_{61} $\rho\bar{\rho}K^+K^-$ (non-resonant)	$(1.27 \pm 0.22) \times 10^{-4}$	
Γ_{62} $\rho\bar{\rho}K_S^0K_S^0$	$< 4.5 \times 10^{-4}$	CL=90%
Γ_{63} $\rho\bar{\rho}\pi^-$	$(3.8 \pm 0.5) \times 10^{-4}$	
Γ_{64} $\rho\bar{\rho}\pi^+$	$(3.9 \pm 0.5) \times 10^{-4}$	
Γ_{65} $\rho\bar{\rho}\pi^-\pi^0$	$(1.03 \pm 0.12) \times 10^{-3}$	

Γ_{66} $\bar{\rho}\eta\pi^+\pi^0$	$(1.01 \pm 0.12) \times 10^{-3}$	
Γ_{67} $\Lambda\bar{\Lambda}$	$(1.27 \pm 0.08) \times 10^{-4}$	
Γ_{68} $\Lambda\bar{\Lambda}\pi^+\pi^-$	$(2.9 \pm 0.5) \times 10^{-4}$	
Γ_{69} $\Lambda\bar{\Lambda}\pi^+\pi^-$ (non-resonant)	$(2.5 \pm 0.6) \times 10^{-4}$	
Γ_{70} $\Sigma(1385)^+\bar{\Lambda}\pi^- + c.c.$	$< 1.3 \times 10^{-4}$	CL=90%
Γ_{71} $\Sigma(1385)^-\bar{\Lambda}\pi^+ + c.c.$	$< 1.3 \times 10^{-4}$	CL=90%
Γ_{72} $K^+\bar{\rho}\Lambda + c.c.$	$(4.2 \pm 0.4) \times 10^{-4}$	S=1.2
Γ_{73} $nK_S^0\bar{\Lambda} + c.c.$	$(1.66 \pm 0.17) \times 10^{-4}$	
Γ_{74} $K^*(892)^+\bar{\rho}\Lambda + c.c.$	$(4.9 \pm 0.7) \times 10^{-4}$	
Γ_{75} $K^+\bar{\rho}\Lambda(1520) + c.c.$	$(1.7 \pm 0.4) \times 10^{-4}$	
Γ_{76} $\Lambda(1520)\bar{\Lambda}(1520)$	$< 9 \times 10^{-5}$	CL=90%
Γ_{77} $\Sigma^0\bar{\Sigma}^0$	$(4.2 \pm 0.6) \times 10^{-5}$	
Γ_{78} $\Sigma^+\bar{\rho}K_S^0 + c.c.$	$(1.53 \pm 0.12) \times 10^{-4}$	
Γ_{79} $\Sigma^0\bar{\rho}K^+ + c.c.$	$(1.46 \pm 0.10) \times 10^{-4}$	
Γ_{80} $\Sigma^+\bar{\Sigma}^-$	$(3.6 \pm 0.7) \times 10^{-5}$	
Γ_{81} $\Sigma^-\bar{\Sigma}^+$	$(5.7 \pm 1.5) \times 10^{-5}$	
Γ_{82} $\Sigma(1385)^+\bar{\Sigma}(1385)^-$	$< 9 \times 10^{-5}$	CL=90%
Γ_{83} $\Sigma(1385)^-\bar{\Sigma}(1385)^+$	$< 5 \times 10^{-5}$	CL=90%
Γ_{84} $K^-\Lambda\bar{\Xi}^+ + c.c.$	$(1.35 \pm 0.24) \times 10^{-4}$	
Γ_{85} $\Xi^0\bar{\Xi}^0$	$< 6 \times 10^{-5}$	CL=90%
Γ_{86} $\Xi^-\bar{\Xi}^+$	$(8.0 \pm 2.1) \times 10^{-5}$	
Γ_{87} $\pi^+\pi^- + K^+K^-$	$< 2.1 \times 10^{-3}$	
Γ_{88} $K_S^0K_S^0$	$< 6 \times 10^{-5}$	CL=90%
Γ_{89} $\eta_c\pi^+\pi^-$	$< 3.2 \times 10^{-3}$	CL=90%

Radiative decays

Γ_{90} $\gamma J/\psi(1S)$	$(34.3 \pm 1.0) \%$	
Γ_{91} $\gamma\rho^0$	$(2.16 \pm 0.17) \times 10^{-4}$	
Γ_{92} $\gamma\omega$	$(6.8 \pm 0.8) \times 10^{-5}$	
Γ_{93} $\gamma\phi$	$(2.4 \pm 0.5) \times 10^{-5}$	
Γ_{94} $\gamma\gamma$	$< 6.3 \times 10^{-6}$	CL=90%
Γ_{95} $e^+e^- J/\psi(1S)$	$(3.46 \pm 0.22) \times 10^{-3}$	
Γ_{96} $\mu^+\mu^- J/\psi(1S)$	$(2.33 \pm 0.29) \times 10^{-4}$	

CONSTRAINED FIT INFORMATION

A multiparticle fit to $\chi_{c1}(1P)$, $\chi_{c0}(1P)$, $\chi_{c2}(1P)$, and $\psi(2S)$ with 4 total widths, a partial width, 25 combinations of partial widths obtained from integrated cross section, and 84 branching ratios uses 248 measurements to determine 49 parameters. The overall fit has a $\chi^2 = 379.8$ for 199 degrees of freedom.

The following *off-diagonal* array elements are the correlation coefficients $\langle \delta p_i \delta p_j \rangle / (\delta p_i \delta p_j)$, in percent, from the fit to parameters p_i , including the branching fractions, $x_i \equiv \Gamma_i / \Gamma_{\text{total}}$.

x_{44}	3				
x_{54}	4	2			
x_{67}	11	4	5		
x_{90}	23	9	2	29	
Γ	-12	-5	-63	-15	-41
	x_{17}	x_{44}	x_{54}	x_{67}	x_{90}

$\chi_{c1}(1P)$ PARTIAL WIDTHS

$\Gamma(\rho\bar{\rho}) \times \Gamma(\gamma J/\psi(1S)) / \Gamma_{\text{total}}$	DOCUMENT ID	TECN	COMMENT
21.9 ± 0.8 OUR FIT			
21.4 ± 0.9 OUR AVERAGE			
21.5 ± 0.5 ± 0.8	¹ ANDREOTTI 05A	E835	$\rho\bar{\rho} \rightarrow e^+e^-\gamma$
21.4 ± 1.5 ± 2.2	^{1,2} ARMSTRONG 92	E760	$\bar{p}p \rightarrow e^+e^-\gamma$
19.9 ^{+4.4} _{-4.0}	¹ BAGLIN	86B SPEC	$\bar{p}p \rightarrow e^+e^-\gamma$
¹ Calculated by us using $B(J/\psi(1S) \rightarrow e^+e^-) = 0.0593 \pm 0.0010$.			
² Recalculated by ANDREOTTI 05A.			

$\chi_{c1}(1P)$ BRANCHING RATIOS

HADRONIC DECAYS

$\Gamma(3(\pi^+\pi^-)) / \Gamma_{\text{total}}$	DOCUMENT ID	TECN	COMMENT
5.8 ± 1.4 OUR EVALUATION			Error includes scale factor of 1.2. Treating systematic error as correlated.
5.8 ± 1.1 OUR AVERAGE			
5.4 ± 0.7 ± 0.9	¹ BAI	99B BES	$\psi(2S) \rightarrow \gamma\chi_{c1}$
16.0 ± 5.9 ± 0.8	¹ TANENBAUM 78	MRK1	$\psi(2S) \rightarrow \gamma\chi_{c1}$
¹ Rescaled by us using $B(\psi(2S) \rightarrow \gamma\chi_{c1}) = (8.8 \pm 0.4)\%$ and $B(\psi(2S) \rightarrow J/\psi(1S)\pi^+\pi^-) = (32.6 \pm 0.5)\%$.			

$\Gamma(2(\pi^+\pi^-))/\Gamma_{\text{total}}$ Γ_2/Γ

VALUE (units 10^{-3})	DOCUMENT ID	TECN	COMMENT
7.6±2.6 OUR EVALUATION	Treating systematic error as correlated.		
8 ±4 OUR AVERAGE	Error includes scale factor of 1.5.		
4.6±2.1±2.6	1 BAI	99B BES	$\psi(2S) \rightarrow \gamma\chi_{c1}$
12.5±4.2±0.6	1 TANENBAUM	78 MRK1	$\psi(2S) \rightarrow \gamma\chi_{c1}$
1 Rescaled by us using $B(\psi(2S) \rightarrow \gamma\chi_{c1}) = (8.8 \pm 0.4)\%$ and $B(\psi(2S) \rightarrow J/\psi(1S)\pi^+\pi^-) = (32.6 \pm 0.5)\%$.			

 $\Gamma(\pi^+\pi^-\pi^0\pi^0)/\Gamma_{\text{total}}$ Γ_3/Γ

VALUE (%)	EVTS	DOCUMENT ID	TECN	COMMENT
1.19±0.15±0.03	604.7	1 HE	08B CLEO	$e^+e^- \rightarrow \gamma h^+ h^- h^0 h^0$
1 HE 08B reports $1.28 \pm 0.06 \pm 0.15 \pm 0.08\%$ from a measurement of $[\Gamma(\chi_{c1}(1P) \rightarrow \pi^+\pi^-\pi^0\pi^0)/\Gamma_{\text{total}}] \times [B(\psi(2S) \rightarrow \gamma\chi_{c1}(1P))]$ assuming $B(\psi(2S) \rightarrow \gamma\chi_{c1}(1P)) = (9.07 \pm 0.11 \pm 0.54) \times 10^{-2}$, which we rescale to our best value $B(\psi(2S) \rightarrow \gamma\chi_{c1}(1P)) = (9.75 \pm 0.24) \times 10^{-2}$. Our first error is their experiment's error and our second error is the systematic error from using our best value.				

 $\Gamma(\rho^+\pi^-\pi^0 + \text{c.c.})/\Gamma_{\text{total}}$ Γ_4/Γ

VALUE (%)	EVTS	DOCUMENT ID	TECN	COMMENT
1.45±0.24±0.04	712.3	1,2 HE	08B CLEO	$e^+e^- \rightarrow \gamma h^+ h^- h^0 h^0$
1 HE 08B reports $1.56 \pm 0.13 \pm 0.22 \pm 0.10\%$ from a measurement of $[\Gamma(\chi_{c1}(1P) \rightarrow \rho^+\pi^-\pi^0 + \text{c.c.})/\Gamma_{\text{total}}] \times [B(\psi(2S) \rightarrow \gamma\chi_{c1}(1P))]$ assuming $B(\psi(2S) \rightarrow \gamma\chi_{c1}(1P)) = (9.07 \pm 0.11 \pm 0.54) \times 10^{-2}$, which we rescale to our best value $B(\psi(2S) \rightarrow \gamma\chi_{c1}(1P)) = (9.75 \pm 0.24) \times 10^{-2}$. Our first error is their experiment's error and our second error is the systematic error from using our best value.				
2 Calculated by us. We have added the values from HE 08B for $\rho^+\pi^-\pi^0$ and $\rho^-\pi^+\pi^0$ decays assuming uncorrelated statistical and fully correlated systematic uncertainties.				

 $\Gamma(\rho^0\pi^+\pi^-)/\Gamma_{\text{total}}$ Γ_5/Γ

VALUE (units 10^{-3})	DOCUMENT ID	TECN	COMMENT
3.9±3.5	1 TANENBAUM	78 MRK1	$\psi(2S) \rightarrow \gamma\chi_{c1}$
1 Estimated using $B(\psi(2S) \rightarrow \gamma\chi_{c1}(1P)) = 0.087$. The errors do not contain the uncertainty in the $\psi(2S)$ decay.			

 $\Gamma(4\pi^0)/\Gamma_{\text{total}}$ Γ_6/Γ

VALUE (units 10^{-4})	EVTS	DOCUMENT ID	TECN	COMMENT
5.4±0.8±0.1	608	1 ABLIKIM	11A BES3	$e^+e^- \rightarrow \psi(2S) \rightarrow \gamma\chi_{c1}$
1 ABLIKIM 11A reports $(0.57 \pm 0.03 \pm 0.08) \times 10^{-3}$ from a measurement of $[\Gamma(\chi_{c1}(1P) \rightarrow 4\pi^0)/\Gamma_{\text{total}}] \times [B(\psi(2S) \rightarrow \gamma\chi_{c1}(1P))]$ assuming $B(\psi(2S) \rightarrow \gamma\chi_{c1}(1P)) = (9.2 \pm 0.4) \times 10^{-2}$, which we rescale to our best value $B(\psi(2S) \rightarrow \gamma\chi_{c1}(1P)) = (9.75 \pm 0.24) \times 10^{-2}$. Our first error is their experiment's error and our second error is the systematic error from using our best value.				

 $\Gamma(\pi^+\pi^-K^+K^-)/\Gamma_{\text{total}}$ Γ_7/Γ

VALUE (units 10^{-3})	DOCUMENT ID	TECN	COMMENT
4.5±1.0 OUR EVALUATION	Treating systematic error as correlated.		
4.5±0.9 OUR AVERAGE			
4.2±0.4±0.9	1 BAI	99B BES	$\psi(2S) \rightarrow \gamma\chi_{c1}$
7.3±3.0±0.4	1 TANENBAUM	78 MRK1	$\psi(2S) \rightarrow \gamma\chi_{c1}$
1 Rescaled by us using $B(\psi(2S) \rightarrow \gamma\chi_{c1}) = (8.8 \pm 0.4)\%$ and $B(\psi(2S) \rightarrow J/\psi(1S)\pi^+\pi^-) = (32.6 \pm 0.5)\%$.			

 $\Gamma(K^+K^-\pi^0\pi^0)/\Gamma_{\text{total}}$ Γ_8/Γ

VALUE (units 10^{-3})	EVTS	DOCUMENT ID	TECN	COMMENT
1.12±0.27±0.03	45.1	1 HE	08B CLEO	$e^+e^- \rightarrow \gamma h^+ h^- h^0 h^0$
1 HE 08B reports $(0.12 \pm 0.02 \pm 0.02 \pm 0.01) \times 10^{-2}$ from a measurement of $[\Gamma(\chi_{c1}(1P) \rightarrow K^+K^-\pi^0\pi^0)/\Gamma_{\text{total}}] \times [B(\psi(2S) \rightarrow \gamma\chi_{c1}(1P))]$ assuming $B(\psi(2S) \rightarrow \gamma\chi_{c1}(1P)) = (9.07 \pm 0.11 \pm 0.54) \times 10^{-2}$, which we rescale to our best value $B(\psi(2S) \rightarrow \gamma\chi_{c1}(1P)) = (9.75 \pm 0.24) \times 10^{-2}$. Our first error is their experiment's error and our second error is the systematic error from using our best value.				

 $\Gamma(K^+K^-\pi^+\pi^-)/\Gamma_{\text{total}}$ Γ_9/Γ

VALUE (units 10^{-3})	EVTS	DOCUMENT ID	TECN	COMMENT
11.46±0.12±1.29	12k	1 ABLIKIM	13B BES3	$e^+e^- \rightarrow \psi(2S) \rightarrow \gamma\chi_{c1}$
1 Using 1.06×10^8 $\psi(2S)$ mesons and $B(\psi(2S) \rightarrow \chi_{c1}\gamma) = (9.2 \pm 0.4)\%$.				

 $\Gamma(K_S^0 K^{\pm}\pi^{\mp}\pi^{\pm}\pi^-)/\Gamma_{\text{total}}$ Γ_{10}/Γ

VALUE (units 10^{-3})	EVTS	DOCUMENT ID	TECN	COMMENT
7.52±0.11±0.79	5.1k	1 ABLIKIM	13B BES3	$e^+e^- \rightarrow \psi(2S) \rightarrow \gamma\chi_{c1}$
1 Using 1.06×10^8 $\psi(2S)$ mesons and $B(\psi(2S) \rightarrow \chi_{c1}\gamma) = (9.2 \pm 0.4)\%$.				

 $\Gamma(K^+\pi^-\bar{K}^0\pi^0 + \text{c.c.})/\Gamma_{\text{total}}$ Γ_{11}/Γ

VALUE (%)	EVTS	DOCUMENT ID	TECN	COMMENT
0.86±0.13±0.02	141.3	1 HE	08B CLEO	$e^+e^- \rightarrow \gamma h^+ h^- h^0 h^0$
1 HE 08B reports $0.92 \pm 0.09 \pm 0.11 \pm 0.06\%$ from a measurement of $[\Gamma(\chi_{c1}(1P) \rightarrow K^+\pi^-\bar{K}^0\pi^0 + \text{c.c.})/\Gamma_{\text{total}}] \times [B(\psi(2S) \rightarrow \gamma\chi_{c1}(1P))]$ assuming $B(\psi(2S) \rightarrow \gamma\chi_{c1}(1P)) = (9.07 \pm 0.11 \pm 0.54) \times 10^{-2}$, which we rescale to our best value $B(\psi(2S) \rightarrow \gamma\chi_{c1}(1P)) = (9.75 \pm 0.24) \times 10^{-2}$. Our first error is their experiment's error and our second error is the systematic error from using our best value.				

 $\Gamma(\rho^-K^+\bar{K}^0 + \text{c.c.})/\Gamma_{\text{total}}$ Γ_{12}/Γ

VALUE (%)	EVTS	DOCUMENT ID	TECN	COMMENT
0.50±0.12±0.01	141.3	1 HE	08B CLEO	$e^+e^- \rightarrow \gamma h^+ h^- h^0 h^0$
1 HE 08B reports $0.54 \pm 0.11 \pm 0.07 \pm 0.03\%$ from a measurement of $[\Gamma(\chi_{c1}(1P) \rightarrow \rho^-K^+\bar{K}^0 + \text{c.c.})/\Gamma_{\text{total}}] \times [B(\psi(2S) \rightarrow \gamma\chi_{c1}(1P))]$ assuming $B(\psi(2S) \rightarrow \gamma\chi_{c1}(1P)) = (9.07 \pm 0.11 \pm 0.54) \times 10^{-2}$, which we rescale to our best value $B(\psi(2S) \rightarrow \gamma\chi_{c1}(1P)) = (9.75 \pm 0.24) \times 10^{-2}$. Our first error is their experiment's error and our second error is the systematic error from using our best value.				

 $\Gamma(K^*(892)^0\bar{K}^0\pi^0 \rightarrow K^+\pi^-\bar{K}^0\pi^0 + \text{c.c.})/\Gamma_{\text{total}}$ Γ_{13}/Γ

VALUE (%)	EVTS	DOCUMENT ID	TECN	COMMENT
0.23±0.06±0.01	141.3	1 HE	08B CLEO	$e^+e^- \rightarrow \gamma h^+ h^- h^0 h^0$
1 HE 08B reports $0.25 \pm 0.06 \pm 0.03 \pm 0.02\%$ from a measurement of $[\Gamma(\chi_{c1}(1P) \rightarrow K^*(892)^0\bar{K}^0\pi^0 \rightarrow K^+\pi^-\bar{K}^0\pi^0 + \text{c.c.})/\Gamma_{\text{total}}] \times [B(\psi(2S) \rightarrow \gamma\chi_{c1}(1P))]$ assuming $B(\psi(2S) \rightarrow \gamma\chi_{c1}(1P)) = (9.07 \pm 0.11 \pm 0.54) \times 10^{-2}$, which we rescale to our best value $B(\psi(2S) \rightarrow \gamma\chi_{c1}(1P)) = (9.75 \pm 0.24) \times 10^{-2}$. Our first error is their experiment's error and our second error is the systematic error from using our best value.				

 $\Gamma(K^+K^-\eta\pi^0)/\Gamma_{\text{total}}$ Γ_{14}/Γ

VALUE (%)	EVTS	DOCUMENT ID	TECN	COMMENT
0.112±0.034±0.003	141.3	1 HE	08B CLEO	$e^+e^- \rightarrow \gamma h^+ h^- h^0 h^0$
1 HE 08B reports $0.12 \pm 0.03 \pm 0.02 \pm 0.01\%$ from a measurement of $[\Gamma(\chi_{c1}(1P) \rightarrow K^+K^-\eta\pi^0)/\Gamma_{\text{total}}] \times [B(\psi(2S) \rightarrow \gamma\chi_{c1}(1P))]$ assuming $B(\psi(2S) \rightarrow \gamma\chi_{c1}(1P)) = (9.07 \pm 0.11 \pm 0.54) \times 10^{-2}$, which we rescale to our best value $B(\psi(2S) \rightarrow \gamma\chi_{c1}(1P)) = (9.75 \pm 0.24) \times 10^{-2}$. Our first error is their experiment's error and our second error is the systematic error from using our best value.				

 $\Gamma(\pi^+\pi^-K_S^0K_S^0)/\Gamma_{\text{total}}$ Γ_{15}/Γ

VALUE (units 10^{-4})	EVTS	DOCUMENT ID	TECN	COMMENT
6.9±2.9±0.2	19.8±7.7	1 ABLIKIM	05o BES2	$\psi(2S) \rightarrow \chi_{c1}\gamma$
1 ABLIKIM 05o reports $[\Gamma(\chi_{c1}(1P) \rightarrow \pi^+\pi^-K_S^0K_S^0)/\Gamma_{\text{total}}] \times [B(\psi(2S) \rightarrow \gamma\chi_{c1}(1P))]$ $= (0.67 \pm 0.26 \pm 0.11) \times 10^{-4}$ which we divide by our best value $B(\psi(2S) \rightarrow \gamma\chi_{c1}(1P)) = (9.75 \pm 0.24) \times 10^{-2}$. Our first error is their experiment's error and our second error is the systematic error from using our best value.				

 $\Gamma(K^+K^-\eta)/\Gamma_{\text{total}}$ Γ_{16}/Γ

VALUE (units 10^{-4})	DOCUMENT ID	TECN	COMMENT
3.2±1.0±0.1	1 ATHAR	07 CLEO	$\psi(2S) \rightarrow \gamma h^+ h^- h^0$
1 ATHAR 07 reports $(0.34 \pm 0.10 \pm 0.04) \times 10^{-3}$ from a measurement of $[\Gamma(\chi_{c1}(1P) \rightarrow K^+K^-\eta)/\Gamma_{\text{total}}] \times [B(\psi(2S) \rightarrow \gamma\chi_{c1}(1P))]$ assuming $B(\psi(2S) \rightarrow \gamma\chi_{c1}(1P)) = 0.0907 \pm 0.0011 \pm 0.0054$, which we rescale to our best value $B(\psi(2S) \rightarrow \gamma\chi_{c1}(1P)) = (9.75 \pm 0.24) \times 10^{-2}$. Our first error is their experiment's error and our second error is the systematic error from using our best value.			

 $\Gamma(\bar{K}^0K^+\pi^- + \text{c.c.})/\Gamma_{\text{total}}$ Γ_{17}/Γ

VALUE (units 10^{-3})	DOCUMENT ID
7.0±0.6 OUR FIT	

 $\Gamma(K^*(892)^0\bar{K}^0 + \text{c.c.})/\Gamma_{\text{total}}$ Γ_{18}/Γ

VALUE (units 10^{-3})	EVTS	DOCUMENT ID	TECN	COMMENT
0.98±0.37±0.02	22	1 ABLIKIM	06R BES2	$\psi(2S) \rightarrow \gamma\chi_{c1}$
1 ABLIKIM 06R reports $(1.1 \pm 0.4 \pm 0.1) \times 10^{-3}$ from a measurement of $[\Gamma(\chi_{c1}(1P) \rightarrow K^*(892)^0\bar{K}^0 + \text{c.c.})/\Gamma_{\text{total}}] \times [B(\psi(2S) \rightarrow \gamma\chi_{c1}(1P))]$ assuming $B(\psi(2S) \rightarrow \gamma\chi_{c1}(1P)) = (8.7 \pm 0.4) \times 10^{-2}$, which we rescale to our best value $B(\psi(2S) \rightarrow \gamma\chi_{c1}(1P)) = (9.75 \pm 0.24) \times 10^{-2}$. Our first error is their experiment's error and our second error is the systematic error from using our best value.				

 $\Gamma(K^*(892)^+K^- + \text{c.c.})/\Gamma_{\text{total}}$ Γ_{19}/Γ

VALUE (units 10^{-3})	EVTS	DOCUMENT ID	TECN	COMMENT
1.43±0.65±0.03	27	1 ABLIKIM	06R BES2	$\psi(2S) \rightarrow \gamma\chi_{c1}$
1 ABLIKIM 06R reports $(1.6 \pm 0.7 \pm 0.2) \times 10^{-3}$ from a measurement of $[\Gamma(\chi_{c1}(1P) \rightarrow K^*(892)^+K^- + \text{c.c.})/\Gamma_{\text{total}}] \times [B(\psi(2S) \rightarrow \gamma\chi_{c1}(1P))]$ assuming $B(\psi(2S) \rightarrow \gamma\chi_{c1}(1P)) = (8.7 \pm 0.4) \times 10^{-2}$, which we rescale to our best value $B(\psi(2S) \rightarrow \gamma\chi_{c1}(1P)) = (9.75 \pm 0.24) \times 10^{-2}$. Our first error is their experiment's error and our second error is the systematic error from using our best value.				

 $\Gamma(K_S^*(1430)^0\bar{K}^0 + \text{c.c.} \rightarrow K_S^0K^+\pi^- + \text{c.c.})/\Gamma_{\text{total}}$ Γ_{20}/Γ

VALUE	CL%	DOCUMENT ID	TECN	COMMENT
<8 × 10⁻⁴	90	1 ABLIKIM	06R BES2	$\psi(2S) \rightarrow \gamma\chi_{c1}$
1 ABLIKIM 06R reports $< 0.9 \times 10^{-3}$ from a measurement of $[\Gamma(\chi_{c1}(1P) \rightarrow K_S^*(1430)^0\bar{K}^0 + \text{c.c.} \rightarrow K_S^0K^+\pi^- + \text{c.c.})/\Gamma_{\text{total}}] \times [B(\psi(2S) \rightarrow \gamma\chi_{c1}(1P))]$ assuming $B(\psi(2S) \rightarrow \gamma\chi_{c1}(1P)) = (8.7 \pm 0.4) \times 10^{-2}$, which we rescale to our best value $B(\psi(2S) \rightarrow \gamma\chi_{c1}(1P)) = 9.75 \times 10^{-2}$.				

 $\Gamma(K_S^*(1430)^+K^- + \text{c.c.} \rightarrow K_S^0K^+\pi^- + \text{c.c.})/\Gamma_{\text{total}}$ Γ_{21}/Γ

VALUE	CL%	DOCUMENT ID	TECN	COMMENT
<2.1 × 10⁻³	90	1 ABLIKIM	06R BES2	$\psi(2S) \rightarrow \gamma\chi_{c1}$
1 ABLIKIM 06R reports $< 2.4 \times 10^{-3}$ from a measurement of $[\Gamma(\chi_{c1}(1P) \rightarrow K_S^*(1430)^+K^- + \text{c.c.} \rightarrow K_S^0K^+\pi^- + \text{c.c.})/\Gamma_{\text{total}}] \times [B(\psi(2S) \rightarrow \gamma\chi_{c1}(1P))]$ assuming $B(\psi(2S) \rightarrow \gamma\chi_{c1}(1P)) = (8.7 \pm 0.4) \times 10^{-2}$, which we rescale to our best value $B(\psi(2S) \rightarrow \gamma\chi_{c1}(1P)) = 9.75 \times 10^{-2}$.				

Meson Particle Listings

 $\chi_{c1}(1P)$ $\Gamma(K^+ K^- \pi^0)/\Gamma_{\text{total}}$ Γ_{22}/Γ

VALUE (units 10^{-3})	DOCUMENT ID	TECN	COMMENT
1.81 ± 0.24 ± 0.04	1 ATHAR	07	CLEO $\psi(2S) \rightarrow \gamma h^+ h^- h^0$

¹ ATHAR 07 reports $(1.95 \pm 0.16 \pm 0.23) \times 10^{-3}$ from a measurement of $[\Gamma(\chi_{c1}(1P) \rightarrow K^+ K^- \pi^0)/\Gamma_{\text{total}}] \times [B(\psi(2S) \rightarrow \gamma \chi_{c1}(1P))]$ assuming $B(\psi(2S) \rightarrow \gamma \chi_{c1}(1P)) = 0.0907 \pm 0.0011 \pm 0.0054$, which we rescale to our best value $B(\psi(2S) \rightarrow \gamma \chi_{c1}(1P)) = (9.75 \pm 0.24) \times 10^{-2}$. Our first error is their experiment's error and our second error is the systematic error from using our best value.

 $\Gamma(\eta \pi^+ \pi^-)/\Gamma_{\text{total}}$ Γ_{23}/Γ

VALUE (units 10^{-3})	EVTS	DOCUMENT ID	TECN	COMMENT
4.62 ± 0.23 OUR AVERAGE				
4.58 ± 0.23 ± 0.11		1,2 ABLIKIM	17k	BES3 $\psi(2S) \rightarrow \gamma \eta \pi^+ \pi^-$
4.7 ± 0.5 ± 0.1		3 ATHAR	07	CLEO $\psi(2S) \rightarrow \gamma h^+ h^- h^0$
5.3 ± 0.9 ± 0.1	222	4 ABLIKIM	06R	BES2 $\psi(2S) \rightarrow \gamma \chi_{c1}$

¹ From an amplitude analysis using an isobar model.
² ABLIKIM 17k reports $(4.67 \pm 0.03 \pm 0.23 \pm 0.16) \times 10^{-3}$ from a measurement of $[\Gamma(\chi_{c1}(1P) \rightarrow \eta \pi^+ \pi^-)/\Gamma_{\text{total}}] \times [B(\psi(2S) \rightarrow \gamma \chi_{c1}(1P))]$ assuming $B(\psi(2S) \rightarrow \gamma \chi_{c1}(1P)) = (9.55 \pm 0.31) \times 10^{-2}$, which we rescale to our best value $B(\psi(2S) \rightarrow \gamma \chi_{c1}(1P)) = (9.75 \pm 0.24) \times 10^{-2}$. Our first error is their experiment's error and our second error is the systematic error from using our best value.
³ ATHAR 07 reports $(5.0 \pm 0.3 \pm 0.5) \times 10^{-3}$ from a measurement of $[\Gamma(\chi_{c1}(1P) \rightarrow \eta \pi^+ \pi^-)/\Gamma_{\text{total}}] \times [B(\psi(2S) \rightarrow \gamma \chi_{c1}(1P))]$ assuming $B(\psi(2S) \rightarrow \gamma \chi_{c1}(1P)) = 0.0907 \pm 0.0011 \pm 0.0054$, which we rescale to our best value $B(\psi(2S) \rightarrow \gamma \chi_{c1}(1P)) = (9.75 \pm 0.24) \times 10^{-2}$. Our first error is their experiment's error and our second error is the systematic error from using our best value.
⁴ ABLIKIM 06R reports $(5.9 \pm 0.7 \pm 0.8) \times 10^{-3}$ from a measurement of $[\Gamma(\chi_{c1}(1P) \rightarrow \eta \pi^+ \pi^-)/\Gamma_{\text{total}}] \times [B(\psi(2S) \rightarrow \gamma \chi_{c1}(1P))]$ assuming $B(\psi(2S) \rightarrow \gamma \chi_{c1}(1P)) = (8.7 \pm 0.4) \times 10^{-2}$, which we rescale to our best value $B(\psi(2S) \rightarrow \gamma \chi_{c1}(1P)) = (9.75 \pm 0.24) \times 10^{-2}$. Our first error is their experiment's error and our second error is the systematic error from using our best value.

 $\Gamma(a_0(980)^+ \pi^- + \text{c.c.} \rightarrow \eta \pi^+ \pi^-)/\Gamma_{\text{total}}$ Γ_{24}/Γ

VALUE (units 10^{-3})	EVTS	DOCUMENT ID	TECN	COMMENT
3.2 ± 0.4 OUR AVERAGE				Error includes scale factor of 2.2.
3.33 ± 0.19 ± 0.08		1,2 ABLIKIM	17k	BES3 $\psi(2S) \rightarrow \gamma \eta \pi^+ \pi^-$
1.79 ± 0.63 ± 0.04	58	3 ABLIKIM	06R	BES2 $\psi(2S) \rightarrow \gamma \chi_{c1}$

¹ From an amplitude analysis using an isobar model.
² ABLIKIM 17k reports $(3.40 \pm 0.03 \pm 0.19 \pm 0.11) \times 10^{-3}$ from a measurement of $[\Gamma(\chi_{c1}(1P) \rightarrow a_0(980)^+ \pi^- + \text{c.c.} \rightarrow \eta \pi^+ \pi^-)/\Gamma_{\text{total}}] \times [B(\psi(2S) \rightarrow \gamma \chi_{c1}(1P))]$ assuming $B(\psi(2S) \rightarrow \gamma \chi_{c1}(1P)) = (9.55 \pm 0.31) \times 10^{-2}$, which we rescale to our best value $B(\psi(2S) \rightarrow \gamma \chi_{c1}(1P)) = (9.75 \pm 0.24) \times 10^{-2}$. Our first error is their experiment's error and our second error is the systematic error from using our best value.
³ ABLIKIM 06R reports $(2.0 \pm 0.5 \pm 0.5) \times 10^{-3}$ from a measurement of $[\Gamma(\chi_{c1}(1P) \rightarrow a_0(980)^+ \pi^- + \text{c.c.} \rightarrow \eta \pi^+ \pi^-)/\Gamma_{\text{total}}] \times [B(\psi(2S) \rightarrow \gamma \chi_{c1}(1P))]$ assuming $B(\psi(2S) \rightarrow \gamma \chi_{c1}(1P)) = (8.7 \pm 0.4) \times 10^{-2}$, which we rescale to our best value $B(\psi(2S) \rightarrow \gamma \chi_{c1}(1P)) = (9.75 \pm 0.24) \times 10^{-2}$. Our first error is their experiment's error and our second error is the systematic error from using our best value.

 $\Gamma(a_2(1320)^+ \pi^- + \text{c.c.} \rightarrow \eta \pi^+ \pi^-)/\Gamma_{\text{total}}$ Γ_{25}/Γ

VALUE (units 10^{-3})	DOCUMENT ID	TECN	COMMENT
0.176 ± 0.023 ± 0.004	1,2 ABLIKIM	17k	BES3 $\psi(2S) \rightarrow \gamma \eta \pi^+ \pi^-$

¹ From an amplitude analysis using an isobar model.
² ABLIKIM 17k reports $(0.18 \pm 0.01 \pm 0.02 \pm 0.01) \times 10^{-3}$ from a measurement of $[\Gamma(\chi_{c1}(1P) \rightarrow a_2(1320)^+ \pi^- + \text{c.c.} \rightarrow \eta \pi^+ \pi^-)/\Gamma_{\text{total}}] \times [B(\psi(2S) \rightarrow \gamma \chi_{c1}(1P))]$ assuming $B(\psi(2S) \rightarrow \gamma \chi_{c1}(1P)) = (9.55 \pm 0.31) \times 10^{-2}$, which we rescale to our best value $B(\psi(2S) \rightarrow \gamma \chi_{c1}(1P)) = (9.75 \pm 0.24) \times 10^{-2}$. Our first error is their experiment's error and our second error is the systematic error from using our best value.

 $\Gamma(a_2(1700)^+ \pi^- + \text{c.c.} \rightarrow \eta \pi^+ \pi^-)/\Gamma_{\text{total}}$ Γ_{26}/Γ

VALUE (units 10^{-5})	DOCUMENT ID	TECN	COMMENT
4.6 ± 0.7 ± 0.1	1,2 ABLIKIM	17k	BES3 $\psi(2S) \rightarrow \gamma \eta \pi^+ \pi^-$

¹ From an amplitude analysis using an isobar model.
² ABLIKIM 17k reports $(4.7 \pm 0.4 \pm 0.6 \pm 0.2) \times 10^{-5}$ from a measurement of $[\Gamma(\chi_{c1}(1P) \rightarrow a_2(1700)^+ \pi^- + \text{c.c.} \rightarrow \eta \pi^+ \pi^-)/\Gamma_{\text{total}}] \times [B(\psi(2S) \rightarrow \gamma \chi_{c1}(1P))]$ assuming $B(\psi(2S) \rightarrow \gamma \chi_{c1}(1P)) = (9.55 \pm 0.31) \times 10^{-2}$, which we rescale to our best value $B(\psi(2S) \rightarrow \gamma \chi_{c1}(1P)) = (9.75 \pm 0.24) \times 10^{-2}$. Our first error is their experiment's error and our second error is the systematic error from using our best value.

 $\Gamma(f_2(1270) \eta \rightarrow \eta \pi^+ \pi^-)/\Gamma_{\text{total}}$ Γ_{27}/Γ

VALUE (units 10^{-4})	DOCUMENT ID	TECN	COMMENT
3.5 ± 0.6 ± 0.1	1,2 ABLIKIM	17k	BES3 $\psi(2S) \rightarrow \gamma \eta \pi^+ \pi^-$

¹ From an amplitude analysis using an isobar model.
² ABLIKIM 17k reports $(0.36 \pm 0.01 \pm 0.06 \pm 0.01) \times 10^{-3}$ from a measurement of $[\Gamma(\chi_{c1}(1P) \rightarrow f_2(1270) \eta \rightarrow \eta \pi^+ \pi^-)/\Gamma_{\text{total}}] \times [B(\psi(2S) \rightarrow \gamma \chi_{c1}(1P))]$ assuming $B(\psi(2S) \rightarrow \gamma \chi_{c1}(1P)) = (9.55 \pm 0.31) \times 10^{-2}$, which we rescale to our best value $B(\psi(2S) \rightarrow \gamma \chi_{c1}(1P)) = (9.75 \pm 0.24) \times 10^{-2}$. Our first error is their experiment's error and our second error is the systematic error from using our best value.

 $\Gamma(f_4(2050) \eta \rightarrow \eta \pi^+ \pi^-)/\Gamma_{\text{total}}$ Γ_{28}/Γ

VALUE (units 10^{-5})	DOCUMENT ID	TECN	COMMENT
2.5 ± 0.9 ± 0.1	1,2 ABLIKIM	17k	BES3 $\psi(2S) \rightarrow \gamma \eta \pi^+ \pi^-$

¹ From an amplitude analysis using an isobar model.
² ABLIKIM 17k reports $(2.6 \pm 0.4 \pm 0.8 \pm 0.1) \times 10^{-5}$ from a measurement of $[\Gamma(\chi_{c1}(1P) \rightarrow f_4(2050) \eta \rightarrow \eta \pi^+ \pi^-)/\Gamma_{\text{total}}] \times [B(\psi(2S) \rightarrow \gamma \chi_{c1}(1P))]$ assuming $B(\psi(2S) \rightarrow \gamma \chi_{c1}(1P)) = (9.55 \pm 0.31) \times 10^{-2}$, which we rescale to our best value $B(\psi(2S) \rightarrow \gamma \chi_{c1}(1P)) = (9.75 \pm 0.24) \times 10^{-2}$. Our first error is their experiment's error and our second error is the systematic error from using our best value.

 $\Gamma(\pi_1(1400)^+ \pi^- + \text{c.c.} \rightarrow \eta \pi^+ \pi^-)/\Gamma_{\text{total}}$ Γ_{29}/Γ

VALUE	CL%	DOCUMENT ID	TECN	COMMENT
< 5 × 10⁻⁵	90	1,2 ABLIKIM	17k	BES3 $\psi(2S) \rightarrow \gamma \eta \pi^+ \pi^-$

¹ From an amplitude analysis using an isobar model.
² ABLIKIM 17k reports $< 4.6 \times 10^{-5}$ from a measurement of $[\Gamma(\chi_{c1}(1P) \rightarrow \pi_1(1400)^+ \pi^- + \text{c.c.} \rightarrow \eta \pi^+ \pi^-)/\Gamma_{\text{total}}] \times [B(\psi(2S) \rightarrow \gamma \chi_{c1}(1P))]$ assuming $B(\psi(2S) \rightarrow \gamma \chi_{c1}(1P)) = (9.55 \pm 0.31) \times 10^{-2}$, which we rescale to our best value $B(\psi(2S) \rightarrow \gamma \chi_{c1}(1P)) = 9.75 \times 10^{-2}$.

 $\Gamma(\pi_1(1600)^+ \pi^- + \text{c.c.} \rightarrow \eta \pi^+ \pi^-)/\Gamma_{\text{total}}$ Γ_{30}/Γ

VALUE	CL%	DOCUMENT ID	TECN	COMMENT
< 1.5 × 10⁻⁵	90	1,2 ABLIKIM	17k	BES3 $\psi(2S) \rightarrow \gamma \eta \pi^+ \pi^-$

¹ From an amplitude analysis using an isobar model.
² ABLIKIM 17k reports $< 1.5 \times 10^{-5}$ from a measurement of $[\Gamma(\chi_{c1}(1P) \rightarrow \pi_1(1600)^+ \pi^- + \text{c.c.} \rightarrow \eta \pi^+ \pi^-)/\Gamma_{\text{total}}] \times [B(\psi(2S) \rightarrow \gamma \chi_{c1}(1P))]$ assuming $B(\psi(2S) \rightarrow \gamma \chi_{c1}(1P)) = (9.55 \pm 0.31) \times 10^{-2}$, which we rescale to our best value $B(\psi(2S) \rightarrow \gamma \chi_{c1}(1P)) = 9.75 \times 10^{-2}$.

 $\Gamma(\pi_1(2015)^+ \pi^- + \text{c.c.} \rightarrow \eta \pi^+ \pi^-)/\Gamma_{\text{total}}$ Γ_{31}/Γ

VALUE	CL%	DOCUMENT ID	TECN	COMMENT
< 8 × 10⁻⁶	90	1,2 ABLIKIM	17k	BES3 $\psi(2S) \rightarrow \gamma \eta \pi^+ \pi^-$

¹ From an amplitude analysis using an isobar model.
² ABLIKIM 17k reports $< 8 \times 10^{-6}$ from a measurement of $[\Gamma(\chi_{c1}(1P) \rightarrow \pi_1(2015)^+ \pi^- + \text{c.c.} \rightarrow \eta \pi^+ \pi^-)/\Gamma_{\text{total}}] \times [B(\psi(2S) \rightarrow \gamma \chi_{c1}(1P))]$ assuming $B(\psi(2S) \rightarrow \gamma \chi_{c1}(1P)) = (9.55 \pm 0.31) \times 10^{-2}$, which we rescale to our best value $B(\psi(2S) \rightarrow \gamma \chi_{c1}(1P)) = 9.75 \times 10^{-2}$.

 $\Gamma(f_2(1270) \eta)/\Gamma_{\text{total}}$ Γ_{32}/Γ

VALUE (units 10^{-3})	EVTS	DOCUMENT ID	TECN	COMMENT
0.67 ± 0.11 OUR AVERAGE				
0.63 ± 0.11 ± 0.02		1,2 ABLIKIM	17k	BES3 $\psi(2S) \rightarrow \gamma \eta \pi^+ \pi^-$
2.7 ± 0.8 ± 0.1	53	3 ABLIKIM	06R	BES2 $\psi(2S) \rightarrow \gamma \chi_{c1}$

¹ ABLIKIM 17k reports $(6.4 \pm 1.1) \times 10^{-4}$ from a measurement of $[\Gamma(\chi_{c1}(1P) \rightarrow f_2(1270) \eta)/\Gamma_{\text{total}}] \times [B(\psi(2S) \rightarrow \gamma \chi_{c1}(1P))]$ assuming $B(\psi(2S) \rightarrow \gamma \chi_{c1}(1P)) = (9.55 \pm 0.31) \times 10^{-2}$, which we rescale to our best value $B(\psi(2S) \rightarrow \gamma \chi_{c1}(1P)) = (9.75 \pm 0.24) \times 10^{-2}$. Our first error is their experiment's error and our second error is the systematic error from using our best value.
² From an amplitude analysis using an isobar model.
³ ABLIKIM 06R reports $(3.0 \pm 0.7 \pm 0.5) \times 10^{-3}$ from a measurement of $[\Gamma(\chi_{c1}(1P) \rightarrow f_2(1270) \eta)/\Gamma_{\text{total}}] \times [B(\psi(2S) \rightarrow \gamma \chi_{c1}(1P))]$ assuming $B(\psi(2S) \rightarrow \gamma \chi_{c1}(1P)) = (8.7 \pm 0.4) \times 10^{-2}$, which we rescale to our best value $B(\psi(2S) \rightarrow \gamma \chi_{c1}(1P)) = (9.75 \pm 0.24) \times 10^{-2}$. Our first error is their experiment's error and our second error is the systematic error from using our best value.

 $\Gamma(\pi^+ \pi^- \eta)/\Gamma_{\text{total}}$ Γ_{33}/Γ

VALUE (units 10^{-3})	DOCUMENT ID	TECN	COMMENT
2.2 ± 0.4 ± 0.1	1 ATHAR	07	CLEO $\psi(2S) \rightarrow \gamma h^+ h^- h^0$

¹ ATHAR 07 reports $(2.4 \pm 0.4 \pm 0.3) \times 10^{-3}$ from a measurement of $[\Gamma(\chi_{c1}(1P) \rightarrow \pi^+ \pi^- \eta)/\Gamma_{\text{total}}] \times [B(\psi(2S) \rightarrow \gamma \chi_{c1}(1P))]$ assuming $B(\psi(2S) \rightarrow \gamma \chi_{c1}(1P)) = 0.0907 \pm 0.0011 \pm 0.0054$, which we rescale to our best value $B(\psi(2S) \rightarrow \gamma \chi_{c1}(1P)) = (9.75 \pm 0.24) \times 10^{-2}$. Our first error is their experiment's error and our second error is the systematic error from using our best value.

 $\Gamma(K^+ K^- \eta'(958))/\Gamma_{\text{total}}$ Γ_{34}/Γ

VALUE (units 10^{-4})	EVTS	DOCUMENT ID	TECN	COMMENT
8.75 ± 0.87	310	1 ABLIKIM	14J	BES3 $\psi(2S) \rightarrow \gamma K^+ K^- \eta'(958)$

¹ Derived using $B(\psi(2S) \rightarrow \gamma \chi_{c1}) = (9.2 \pm 0.4)\%$. Uncertainty includes both statistical and systematic contributions combined in quadrature.

 $\Gamma(K_0^*(1430)^+ K^- + \text{c.c.})/\Gamma_{\text{total}}$ Γ_{35}/Γ

VALUE (units 10^{-4})	DOCUMENT ID	TECN	COMMENT
6.41 ± 0.57 ± 2.09 - 2.71	1 ABLIKIM	14J	BES3 $\psi(2S) \rightarrow \gamma K^+ K^- \eta'(958)$

¹ Normalized to $B(\chi_{c1} \rightarrow K^+ K^- \eta'(958))$ branching fraction.

 $\Gamma(f_0(980) \eta'(958))/\Gamma_{\text{total}}$ Γ_{36}/Γ

VALUE (units 10^{-4})	DOCUMENT ID	TECN	COMMENT
1.65 ± 0.47 ± 1.32 - 0.56	1 ABLIKIM	14J	BES3 $\psi(2S) \rightarrow \gamma K^+ K^- \eta'(958)$

¹ Normalized to $B(\chi_{c1} \rightarrow K^+ K^- \eta'(958))$ branching fraction.

See key on page 1127

Meson Particle Listings

$\chi_{c1}(1P)$

$\Gamma(f_0(1710)\eta'(958))/\Gamma_{total}$	Γ_{37}/Γ
VALUE (units 10^{-4})	DOCUMENT ID TECN COMMENT

0.71 ± 0.22 ± 0.68
 -0.48 ¹ ABLIKIM 14J BES3 $\psi(2S) \rightarrow \gamma K^+ K^- \eta'(958)$
¹ Normalized to $B(\chi_{c1} \rightarrow K^+ K^- \eta'(958))$ branching fraction.

$\Gamma(f_2'(1525)\eta'(958))/\Gamma_{total}$	Γ_{38}/Γ
VALUE (units 10^{-4})	DOCUMENT ID TECN COMMENT

0.92 ± 0.23 ± 0.55
 -0.51 ¹ ABLIKIM 14J BES3 $\psi(2S) \rightarrow \gamma K^+ K^- \eta'(958)$
¹ Normalized to $B(\chi_{c1} \rightarrow K^+ K^- \eta'(958))$ branching fraction.

$\Gamma(\pi^0 f_0(980) \rightarrow \pi^0 \pi^+ \pi^-)/\Gamma_{total}$	Γ_{39}/Γ
VALUE (units 10^{-6}) CL%	DOCUMENT ID TECN COMMENT

0.35 ± 0.09
 ••• We do not use the following data for averages, fits, limits, etc. •••
 <6 90 ¹ ABLIKIM 11D BES3 $\psi(2S) \rightarrow \gamma \pi^0 \pi^+ \pi^-$
¹ ABLIKIM 11D reports $[\Gamma(\chi_{c1}(1P) \rightarrow \pi^0 f_0(980) \rightarrow \pi^0 \pi^+ \pi^-)/\Gamma_{total}] \times [B(\psi(2S) \rightarrow \gamma \chi_{c1}(1P))] < 6.0 \times 10^{-7}$ which we divide by our best value $B(\psi(2S) \rightarrow \gamma \chi_{c1}(1P)) = 9.75 \times 10^{-2}$.

$\Gamma(K^+ \bar{K}^*(892)^0 \pi^- + c.c.)/\Gamma_{total}$	Γ_{40}/Γ
VALUE (units 10^{-4})	DOCUMENT ID TECN COMMENT

32 ± 21 ¹ TANENBAUM 78 MRK1 $\psi(2S) \rightarrow \gamma \chi_{c1}$
¹ Estimated using $B(\psi(2S) \rightarrow \gamma \chi_{c1}(1P)) = 0.087$. The errors do not contain the uncertainty in the $\psi(2S)$ decay.

$\Gamma(K^*(892)^0 \bar{K}^*(892)^0)/\Gamma_{total}$	Γ_{41}/Γ
VALUE (units 10^{-3}) EVTS	DOCUMENT ID TECN COMMENT

1.44 ± 0.36 ± 0.03 28.4 ± 5.5 ^{1,2} ABLIKIM 04H BES $\psi(2S) \rightarrow \gamma K^+ K^- \pi^+ \pi^-$
¹ ABLIKIM 04H reports $[\Gamma(\chi_{c1}(1P) \rightarrow K^*(892)^0 \bar{K}^*(892)^0)/\Gamma_{total}] \times [B(\psi(2S) \rightarrow \gamma \chi_{c1}(1P))] = (1.40 \pm 0.27 \pm 0.22) \times 10^{-4}$ which we divide by our best value $B(\psi(2S) \rightarrow \gamma \chi_{c1}(1P)) = (9.75 \pm 0.24) \times 10^{-2}$. Our first error is their experiment's error and our second error is the systematic error from using our best value.
² Assumes $B(K^*(892)^0 \rightarrow K^- \pi^+) = 2/3$.

$\Gamma(K^+ K^- K_S^0 K_S^0)/\Gamma_{total}$	Γ_{42}/Γ
VALUE CL% EVTS	DOCUMENT ID TECN COMMENT

<4 × 10⁻⁴ 90 3.2 ± 2.4 ¹ ABLIKIM 05o BES2 $\psi(2S) \rightarrow \chi_{c1} \gamma$
¹ ABLIKIM 05o reports $[\Gamma(\chi_{c1}(1P) \rightarrow K^+ K^- K_S^0 K_S^0)/\Gamma_{total}] \times [B(\psi(2S) \rightarrow \gamma \chi_{c1}(1P))] < 4.2 \times 10^{-5}$ which we divide by our best value $B(\psi(2S) \rightarrow \gamma \chi_{c1}(1P)) = 9.75 \times 10^{-2}$.

$\Gamma(K_S^0 K_S^0 K_S^0 K_S^0)/\Gamma_{total}$	Γ_{43}/Γ
VALUE (units 10^{-4}) EVTS	DOCUMENT ID TECN COMMENT

0.35 ± 0.10 ± 0.01 22 ¹ ABLIKIM 19AA BES3 $\psi(2S) \rightarrow \gamma 4K_S^0$
¹ Using $B(K_S^0 \rightarrow \pi^+ \pi^-) = (69.20 \pm 0.05)\%$. ABLIKIM 19AA reports $[\Gamma(\chi_{c1}(1P) \rightarrow K_S^0 K_S^0 K_S^0 K_S^0)/\Gamma_{total}] \times [B(\psi(2S) \rightarrow \gamma \chi_{c1}(1P))] = (3.4 \pm 0.9 \pm 0.3) \times 10^{-6}$ which we divide by our best value $B(\psi(2S) \rightarrow \gamma \chi_{c1}(1P)) = (9.75 \pm 0.24) \times 10^{-2}$. Our first error is their experiment's error and our second error is the systematic error from using our best value..

$\Gamma(K^+ K^- K^+ K^-)/\Gamma_{total}$	Γ_{44}/Γ
VALUE (units 10^{-3})	DOCUMENT ID

0.54 ± 0.11 OUR FIT

$\Gamma(K^+ K^- \phi)/\Gamma_{total}$	Γ_{45}/Γ
VALUE (units 10^{-3}) EVTS	DOCUMENT ID TECN COMMENT

0.41 ± 0.15 ± 0.01 17 ¹ ABLIKIM 06T BES2 $\psi(2S) \rightarrow \gamma 2K^+ 2K^-$
¹ ABLIKIM 06T reports $(0.46 \pm 0.16 \pm 0.06) \times 10^{-3}$ from a measurement of $[\Gamma(\chi_{c1}(1P) \rightarrow K^+ K^- \phi)/\Gamma_{total}] \times [B(\psi(2S) \rightarrow \gamma \chi_{c1}(1P))]$ assuming $B(\psi(2S) \rightarrow \gamma \chi_{c1}(1P)) = (8.7 \pm 0.4) \times 10^{-2}$, which we rescale to our best value $B(\psi(2S) \rightarrow \gamma \chi_{c1}(1P)) = (9.75 \pm 0.24) \times 10^{-2}$. Our first error is their experiment's error and our second error is the systematic error from using our best value.

$\Gamma(\bar{K}^0 K^+ \pi^- \phi + c.c.)/\Gamma_{total}$	Γ_{46}/Γ
VALUE (units 10^{-3})	DOCUMENT ID TECN COMMENT

3.27 ± 0.28 ± 0.46 ABLIKIM 15M BES3 $\psi(2S) \rightarrow \gamma \chi_{c1}$

$\Gamma(K^+ K^- \pi^0 \phi)/\Gamma_{total}$	Γ_{47}/Γ
VALUE (units 10^{-3})	DOCUMENT ID TECN COMMENT

1.62 ± 0.12 ± 0.28 ABLIKIM 15M BES3 $\psi(2S) \rightarrow \gamma \chi_{c1}$

$\Gamma(\phi \pi^+ \pi^- \pi^0)/\Gamma_{total}$	Γ_{48}/Γ
VALUE (units 10^{-3}) EVTS	DOCUMENT ID TECN COMMENT

0.75 ± 0.06 ± 0.08 373 ¹ ABLIKIM 13B BES3 $e^+ e^- \rightarrow \psi(2S) \rightarrow \gamma \chi_{c1}$
¹ Using $1.06 \times 10^8 \psi(2S)$ mesons and $B(\psi(2S) \rightarrow \chi_{c1} \gamma) = (9.2 \pm 0.4)\%$.

$\Gamma(\omega\omega)/\Gamma_{total}$	Γ_{49}/Γ
VALUE (units 10^{-4}) EVTS	DOCUMENT ID TECN COMMENT

5.7 ± 0.7 ± 0.1 597 ¹ ABLIKIM 11K BES3 $\psi(2S) \rightarrow \gamma$ hadrons
¹ ABLIKIM 11K reports $(6.0 \pm 0.3 \pm 0.7) \times 10^{-4}$ from a measurement of $[\Gamma(\chi_{c1}(1P) \rightarrow \omega\omega)/\Gamma_{total}] \times [B(\psi(2S) \rightarrow \gamma \chi_{c1}(1P))]$ assuming $B(\psi(2S) \rightarrow \gamma \chi_{c1}(1P)) = (9.2 \pm 0.4) \times 10^{-2}$, which we rescale to our best value $B(\psi(2S) \rightarrow \gamma \chi_{c1}(1P)) = (9.75 \pm 0.24) \times 10^{-2}$. Our first error is their experiment's error and our second error is the systematic error from using our best value.

$\Gamma(\omega K^+ K^-)/\Gamma_{total}$	Γ_{50}/Γ
VALUE (units 10^{-3}) EVTS	DOCUMENT ID TECN COMMENT

0.78 ± 0.04 ± 0.08 628 ¹ ABLIKIM 13B BES3 $e^+ e^- \rightarrow \psi(2S) \rightarrow \gamma \chi_{c1}$
¹ Using $1.06 \times 10^8 \psi(2S)$ mesons and $B(\psi(2S) \rightarrow \chi_{c1} \gamma) = (9.2 \pm 0.4)\%$.

$\Gamma(\omega\phi)/\Gamma_{total}$	Γ_{51}/Γ
VALUE (units 10^{-4}) EVTS	DOCUMENT ID TECN COMMENT

0.27 ± 0.04 ± 0.01 105 ¹ ABLIKIM 19J BES3 $\psi(2S) \rightarrow \gamma$ hadrons
 ••• We do not use the following data for averages, fits, limits, etc. •••
 0.21 ± 0.06 ± 0.01 15 ^{2,3} ABLIKIM 11K BES3 $\psi(2S) \rightarrow \gamma$ hadrons

¹ ABLIKIM 19J reports $[\Gamma(\chi_{c1}(1P) \rightarrow \omega\phi)/\Gamma_{total}] \times [B(\psi(2S) \rightarrow \gamma \chi_{c1}(1P))] = (2.67 \pm 0.31 \pm 0.27) \times 10^{-6}$ which we divide by our best value $B(\psi(2S) \rightarrow \gamma \chi_{c1}(1P)) = (9.75 \pm 0.24) \times 10^{-2}$. Our first error is their experiment's error and our second error is the systematic error from using our best value.
² ABLIKIM 11K reports $(0.22 \pm 0.06 \pm 0.02) \times 10^{-4}$ from a measurement of $[\Gamma(\chi_{c1}(1P) \rightarrow \omega\phi)/\Gamma_{total}] \times [B(\psi(2S) \rightarrow \gamma \chi_{c1}(1P))]$ assuming $B(\psi(2S) \rightarrow \gamma \chi_{c1}(1P)) = (9.2 \pm 0.4) \times 10^{-2}$, which we rescale to our best value $B(\psi(2S) \rightarrow \gamma \chi_{c1}(1P)) = (9.75 \pm 0.24) \times 10^{-2}$. Our first error is their experiment's error and our second error is the systematic error from using our best value.
³ Superseded by ABLIKIM 19J.

$\Gamma(\phi\phi)/\Gamma_{total}$	Γ_{52}/Γ
VALUE (units 10^{-4}) EVTS	DOCUMENT ID TECN COMMENT

4.2 ± 0.5 ± 0.1 366 ¹ ABLIKIM 11K BES3 $\psi(2S) \rightarrow \gamma$ hadrons
¹ ABLIKIM 11K reports $(4.4 \pm 0.3 \pm 0.5) \times 10^{-4}$ from a measurement of $[\Gamma(\chi_{c1}(1P) \rightarrow \phi\phi)/\Gamma_{total}] \times [B(\psi(2S) \rightarrow \gamma \chi_{c1}(1P))]$ assuming $B(\psi(2S) \rightarrow \gamma \chi_{c1}(1P)) = (9.2 \pm 0.4) \times 10^{-2}$, which we rescale to our best value $B(\psi(2S) \rightarrow \gamma \chi_{c1}(1P)) = (9.75 \pm 0.24) \times 10^{-2}$. Our first error is their experiment's error and our second error is the systematic error from using our best value.

$\Gamma(\phi\phi\eta)/\Gamma_{total}$	Γ_{53}/Γ
VALUE (units 10^{-4}) EVTS	DOCUMENT ID TECN COMMENT

3.0 ± 0.4 ± 0.2 83.6 ¹ ABLIKIM 20B BES3 $\psi(2S) \rightarrow \gamma \phi\phi\eta$
¹ ABLIKIM 20B reports $(2.96 \pm 0.43 \pm 0.22) \times 10^{-4}$ from a measurement of $[\Gamma(\chi_{c1}(1P) \rightarrow \phi\phi\eta)/\Gamma_{total}] \times [B(\psi(2S) \rightarrow \gamma \chi_{c1}(1P))]$ assuming $B(\psi(2S) \rightarrow \gamma \chi_{c1}(1P)) = (9.75 \pm 0.24) \times 10^{-2}$.

$\Gamma(\rho\bar{\rho})/\Gamma_{total}$	Γ_{54}/Γ
VALUE (units 10^{-4})	DOCUMENT ID

0.760 ± 0.034 OUR FIT

$\Gamma(\rho\bar{\rho}\pi^0)/\Gamma_{total}$	Γ_{55}/Γ
VALUE (units 10^{-3})	DOCUMENT ID TECN COMMENT

0.155 ± 0.018 OUR AVERAGE
 0.163 ± 0.019 ± 0.004 ¹ ONYISI 10 CLE3 $\psi(2S) \rightarrow \gamma \rho\bar{\rho} X$
 0.112 ± 0.047 ± 0.003 ² ATHAR 07 CLEO $\psi(2S) \rightarrow \gamma h^+ h^- h^0$

¹ ONYISI 10 reports $(1.75 \pm 0.16 \pm 0.13 \pm 0.11) \times 10^{-4}$ from a measurement of $[\Gamma(\chi_{c1}(1P) \rightarrow \rho\bar{\rho}\pi^0)/\Gamma_{total}] \times [B(\psi(2S) \rightarrow \gamma \chi_{c1}(1P))]$ assuming $B(\psi(2S) \rightarrow \gamma \chi_{c1}(1P)) = (9.07 \pm 0.11 \pm 0.54) \times 10^{-2}$, which we rescale to our best value $B(\psi(2S) \rightarrow \gamma \chi_{c1}(1P)) = (9.75 \pm 0.24) \times 10^{-2}$. Our first error is their experiment's error and our second error is the systematic error from using our best value.
² ATHAR 07 reports $(1.2 \pm 0.5 \pm 0.1) \times 10^{-4}$ from a measurement of $[\Gamma(\chi_{c1}(1P) \rightarrow \rho\bar{\rho}\pi^0)/\Gamma_{total}] \times [B(\psi(2S) \rightarrow \gamma \chi_{c1}(1P))]$ assuming $B(\psi(2S) \rightarrow \gamma \chi_{c1}(1P)) = (9.07 \pm 0.11 \pm 0.54) \times 10^{-2}$, which we rescale to our best value $B(\psi(2S) \rightarrow \gamma \chi_{c1}(1P)) = (9.75 \pm 0.24) \times 10^{-2}$. Our first error is their experiment's error and our second error is the systematic error from using our best value.

$\Gamma(\rho\bar{\rho}\eta)/\Gamma_{total}$	Γ_{56}/Γ
VALUE (units 10^{-3}) CL%	DOCUMENT ID TECN COMMENT

0.145 ± 0.024 ± 0.004 ¹ ONYISI 10 CLE3 $\psi(2S) \rightarrow \gamma \rho\bar{\rho} X$
 ••• We do not use the following data for averages, fits, limits, etc. •••
 <0.15 90 ² ATHAR 07 CLEO $\psi(2S) \rightarrow \gamma h^+ h^- h^0$

¹ ONYISI 10 reports $(1.56 \pm 0.22 \pm 0.14 \pm 0.10) \times 10^{-4}$ from a measurement of $[\Gamma(\chi_{c1}(1P) \rightarrow \rho\bar{\rho}\eta)/\Gamma_{total}] \times [B(\psi(2S) \rightarrow \gamma \chi_{c1}(1P))]$ assuming $B(\psi(2S) \rightarrow \gamma \chi_{c1}(1P)) = (9.07 \pm 0.11 \pm 0.54) \times 10^{-2}$, which we rescale to our best value $B(\psi(2S) \rightarrow \gamma \chi_{c1}(1P)) = (9.75 \pm 0.24) \times 10^{-2}$. Our first error is their experiment's error and our second error is the systematic error from using our best value.
² ATHAR 07 reports $< 0.16 \times 10^{-3}$ from a measurement of $[\Gamma(\chi_{c1}(1P) \rightarrow \rho\bar{\rho}\eta)/\Gamma_{total}] \times [B(\psi(2S) \rightarrow \gamma \chi_{c1}(1P))]$ assuming $B(\psi(2S) \rightarrow \gamma \chi_{c1}(1P)) = (9.07 \pm 0.11 \pm 0.54) \times 10^{-2}$, which we rescale to our best value $B(\psi(2S) \rightarrow \gamma \chi_{c1}(1P)) = 9.75 \times 10^{-2}$.

Meson Particle Listings

 $\chi_{c1}(1P)$

$\Gamma(p\bar{p}\omega)/\Gamma_{\text{total}}$	Γ_{57}/Γ			
VALUE (units 10^{-3})	DOCUMENT ID	TECN	COMMENT	
0.212 ± 0.030 ± 0.005	¹ ONYISI	10	CLE3	$\psi(2S) \rightarrow \gamma p\bar{p}\chi$

¹ ONYISI 10 reports $(2.28 \pm 0.28 \pm 0.16 \pm 0.14) \times 10^{-4}$ from a measurement of $[\Gamma(\chi_{c1}(1P) \rightarrow p\bar{p}\omega)/\Gamma_{\text{total}}] \times [B(\psi(2S) \rightarrow \gamma\chi_{c1}(1P))]$ assuming $B(\psi(2S) \rightarrow \gamma\chi_{c1}(1P)) = (9.07 \pm 0.11 \pm 0.54) \times 10^{-2}$, which we rescale to our best value $B(\psi(2S) \rightarrow \gamma\chi_{c1}(1P)) = (9.75 \pm 0.24) \times 10^{-2}$. Our first error is their experiment's error and our second error is the systematic error from using our best value.

$\Gamma(p\bar{p}\phi)/\Gamma_{\text{total}}$	Γ_{58}/Γ			
VALUE	CL%	DOCUMENT ID	TECN	COMMENT
<1.7 × 10⁻⁵	90	¹ ABLIKIM	11F	BES3 $\psi(2S) \rightarrow \gamma p\bar{p}K + K^-$

¹ ABLIKIM 11F reports $< 1.82 \times 10^{-5}$ from a measurement of $[\Gamma(\chi_{c1}(1P) \rightarrow p\bar{p}\phi)/\Gamma_{\text{total}}] \times [B(\psi(2S) \rightarrow \gamma\chi_{c1}(1P))]$ assuming $B(\psi(2S) \rightarrow \gamma\chi_{c1}(1P)) = (9.2 \pm 0.4) \times 10^{-2}$, which we rescale to our best value $B(\psi(2S) \rightarrow \gamma\chi_{c1}(1P)) = 9.75 \times 10^{-2}$.

$\Gamma(p\bar{p}\pi^+\pi^-)/\Gamma_{\text{total}}$	Γ_{59}/Γ			
VALUE (units 10^{-3})	DOCUMENT ID	TECN	COMMENT	
0.50 ± 0.19 OUR EVALUATION	Treating systematic error as correlated.			
0.50 ± 0.19 OUR AVERAGE				
0.46 ± 0.12 ± 0.15	¹ BAI	99B	BES	$\psi(2S) \rightarrow \gamma\chi_{c1}$
1.08 ± 0.77 ± 0.05	¹ TANENBAUM	78	MRK1	$\psi(2S) \rightarrow \gamma\chi_{c1}$

¹ Rescaled by us using $B(\psi(2S) \rightarrow \gamma\chi_{c1}) = (8.8 \pm 0.4)\%$ and $B(\psi(2S) \rightarrow J/\psi(1S)\pi^+\pi^-) = (32.6 \pm 0.5)\%$.

$\Gamma(p\bar{p}\pi^0\pi^0)/\Gamma_{\text{total}}$	Γ_{60}/Γ			
VALUE	CL%	DOCUMENT ID	TECN	COMMENT
<5 × 10⁻⁴	90	¹ HE	08B	CLEO $e^+e^- \rightarrow \gamma h^+ h^- h^0 h^0$

¹ HE 08B reports $< 0.05 \times 10^{-2}$ from a measurement of $[\Gamma(\chi_{c1}(1P) \rightarrow p\bar{p}\pi^0\pi^0)/\Gamma_{\text{total}}] \times [B(\psi(2S) \rightarrow \gamma\chi_{c1}(1P))]$ assuming $B(\psi(2S) \rightarrow \gamma\chi_{c1}(1P)) = (9.07 \pm 0.11 \pm 0.54) \times 10^{-2}$, which we rescale to our best value $B(\psi(2S) \rightarrow \gamma\chi_{c1}(1P)) = 9.75 \times 10^{-2}$.

$\Gamma(p\bar{p}K^+K^- \text{ (non-resonant)})/\Gamma_{\text{total}}$	Γ_{61}/Γ			
VALUE (units 10^{-4})	EVTS	DOCUMENT ID	TECN	COMMENT
1.27 ± 0.22 ± 0.03	82 ± 9	¹ ABLIKIM	11F	BES3 $\psi(2S) \rightarrow \gamma p\bar{p}K^+K^-$

¹ ABLIKIM 11F reports $(1.35 \pm 0.15 \pm 0.19) \times 10^{-4}$ from a measurement of $[\Gamma(\chi_{c1}(1P) \rightarrow p\bar{p}K^+K^- \text{ (non-resonant)})/\Gamma_{\text{total}}] \times [B(\psi(2S) \rightarrow \gamma\chi_{c1}(1P))]$ assuming $B(\psi(2S) \rightarrow \gamma\chi_{c1}(1P)) = (9.2 \pm 0.4) \times 10^{-2}$, which we rescale to our best value $B(\psi(2S) \rightarrow \gamma\chi_{c1}(1P)) = (9.75 \pm 0.24) \times 10^{-2}$. Our first error is their experiment's error and our second error is the systematic error from using our best value.

$\Gamma(p\bar{p}K_S^0 K_S^0)/\Gamma_{\text{total}}$	Γ_{62}/Γ			
VALUE (units 10^{-4})	CL%	DOCUMENT ID	TECN	COMMENT
<4.5	90	¹ ABLIKIM	06D	BES2 $\psi(2S) \rightarrow \gamma\chi_{c1}$

¹ Using $B(\psi(2S) \rightarrow \chi_{c1}\gamma) (9.1 \pm 0.6)\%$.

$\Gamma(p\bar{p}\pi^-)/\Gamma_{\text{total}}$	Γ_{63}/Γ			
VALUE (units 10^{-4})	EVTS	DOCUMENT ID	TECN	COMMENT
3.8 ± 0.5 ± 0.1	1412	¹ ABLIKIM	12J	BES3 $\psi(2S) \rightarrow \gamma p\bar{p}\pi^-$

¹ ABLIKIM 12J reports $[\Gamma(\chi_{c1}(1P) \rightarrow p\bar{p}\pi^-)/\Gamma_{\text{total}}] \times [B(\psi(2S) \rightarrow \gamma\chi_{c1}(1P))] = (0.37 \pm 0.02 \pm 0.04) \times 10^{-4}$ which we divide by our best value $B(\psi(2S) \rightarrow \gamma\chi_{c1}(1P)) = (9.75 \pm 0.24) \times 10^{-2}$. Our first error is their experiment's error and our second error is the systematic error from using our best value.

$\Gamma(p\bar{p}n\pi^+)/\Gamma_{\text{total}}$	Γ_{64}/Γ			
VALUE (units 10^{-4})	EVTS	DOCUMENT ID	TECN	COMMENT
3.9 ± 0.5 ± 0.1	1625	¹ ABLIKIM	12J	BES3 $\psi(2S) \rightarrow \gamma p\bar{p}n\pi^+$

¹ ABLIKIM 12J reports $[\Gamma(\chi_{c1}(1P) \rightarrow p\bar{p}n\pi^+)/\Gamma_{\text{total}}] \times [B(\psi(2S) \rightarrow \gamma\chi_{c1}(1P))] = (0.38 \pm 0.02 \pm 0.04) \times 10^{-4}$ which we divide by our best value $B(\psi(2S) \rightarrow \gamma\chi_{c1}(1P)) = (9.75 \pm 0.24) \times 10^{-2}$. Our first error is their experiment's error and our second error is the systematic error from using our best value.

$\Gamma(p\bar{p}\pi^-\pi^0)/\Gamma_{\text{total}}$	Γ_{65}/Γ			
VALUE (units 10^{-4})	EVTS	DOCUMENT ID	TECN	COMMENT
10.3 ± 1.1 ± 0.2	1082	¹ ABLIKIM	12J	BES3 $\psi(2S) \rightarrow \gamma p\bar{p}\pi^-\pi^0$

¹ ABLIKIM 12J reports $[\Gamma(\chi_{c1}(1P) \rightarrow p\bar{p}\pi^-\pi^0)/\Gamma_{\text{total}}] \times [B(\psi(2S) \rightarrow \gamma\chi_{c1}(1P))] = (1.00 \pm 0.05 \pm 0.10) \times 10^{-4}$ which we divide by our best value $B(\psi(2S) \rightarrow \gamma\chi_{c1}(1P)) = (9.75 \pm 0.24) \times 10^{-2}$. Our first error is their experiment's error and our second error is the systematic error from using our best value.

$\Gamma(p\bar{p}n\pi^+\pi^0)/\Gamma_{\text{total}}$	Γ_{66}/Γ			
VALUE (units 10^{-4})	EVTS	DOCUMENT ID	TECN	COMMENT
10.1 ± 1.1 ± 0.2	1261	¹ ABLIKIM	12J	BES3 $\psi(2S) \rightarrow \gamma p\bar{p}n\pi^+\pi^0$

¹ ABLIKIM 12J reports $[\Gamma(\chi_{c1}(1P) \rightarrow p\bar{p}n\pi^+\pi^0)/\Gamma_{\text{total}}] \times [B(\psi(2S) \rightarrow \gamma\chi_{c1}(1P))] = (0.98 \pm 0.05 \pm 0.10) \times 10^{-4}$ which we divide by our best value $B(\psi(2S) \rightarrow \gamma\chi_{c1}(1P)) = (9.75 \pm 0.24) \times 10^{-2}$. Our first error is their experiment's error and our second error is the systematic error from using our best value.

$\Gamma(\Lambda\bar{\Lambda})/\Gamma_{\text{total}}$	Γ_{67}/Γ			
VALUE (units 10^{-4})	DOCUMENT ID	TECN	COMMENT	
1.27 ± 0.08 OUR FIT				

$\Gamma(\Lambda\bar{\Lambda}\pi^+\pi^-)/\Gamma_{\text{total}}$	Γ_{68}/Γ				
VALUE (units 10^{-5})	CL%	EVTS	DOCUMENT ID	TECN	COMMENT
29 ± 5 ± 1		105	¹ ABLIKIM	12I	BES3 $\psi(2S) \rightarrow \gamma\Lambda\bar{\Lambda}\pi^+\pi^-$

• • • We do not use the following data for averages, fits, limits, etc. • • •
<150 90 ² ABLIKIM 06D BES2 $\psi(2S) \rightarrow \gamma\chi_{c1}$

¹ ABLIKIM 12I reports $(31.1 \pm 3.4 \pm 3.9) \times 10^{-5}$ from a measurement of $[\Gamma(\chi_{c1}(1P) \rightarrow \Lambda\bar{\Lambda}\pi^+\pi^-)/\Gamma_{\text{total}}] \times [B(\psi(2S) \rightarrow \gamma\chi_{c1}(1P))]$ assuming $B(\psi(2S) \rightarrow \gamma\chi_{c1}(1P)) = (9.2 \pm 0.4) \times 10^{-2}$, which we rescale to our best value $B(\psi(2S) \rightarrow \gamma\chi_{c1}(1P)) = (9.75 \pm 0.24) \times 10^{-2}$. Our first error is their experiment's error and our second error is the systematic error from using our best value.

$\Gamma(\Lambda\bar{\Lambda}\pi^+\pi^- \text{ (non-resonant)})/\Gamma_{\text{total}}$	Γ_{69}/Γ			
VALUE (units 10^{-5})	EVTS	DOCUMENT ID	TECN	COMMENT
25 ± 6 ± 1	13	¹ ABLIKIM	12I	BES3 $\psi(2S) \rightarrow \gamma\Lambda\bar{\Lambda}\pi^+\pi^-$

¹ ABLIKIM 12I reports $(26.2 \pm 5.5 \pm 3.3) \times 10^{-5}$ from a measurement of $[\Gamma(\chi_{c1}(1P) \rightarrow \Lambda\bar{\Lambda}\pi^+\pi^- \text{ (non-resonant)})/\Gamma_{\text{total}}] \times [B(\psi(2S) \rightarrow \gamma\chi_{c1}(1P))]$ assuming $B(\psi(2S) \rightarrow \gamma\chi_{c1}(1P)) = (9.2 \pm 0.4) \times 10^{-2}$, which we rescale to our best value $B(\psi(2S) \rightarrow \gamma\chi_{c1}(1P)) = (9.75 \pm 0.24) \times 10^{-2}$. Our first error is their experiment's error and our second error is the systematic error from using our best value.

$\Gamma(\Sigma(1385)^+\bar{\Lambda}\pi^- + \text{c.c.})/\Gamma_{\text{total}}$	Γ_{70}/Γ			
VALUE	CL%	DOCUMENT ID	TECN	COMMENT
<1.3 × 10⁻⁴	90	¹ ABLIKIM	12I	BES3 $\psi(2S) \rightarrow \gamma\Sigma(1385)^+\bar{\Lambda}\pi^-$

¹ ABLIKIM 12I reports $< 14 \times 10^{-5}$ from a measurement of $[\Gamma(\chi_{c1}(1P) \rightarrow \Sigma(1385)^+\bar{\Lambda}\pi^- + \text{c.c.})/\Gamma_{\text{total}}] \times [B(\psi(2S) \rightarrow \gamma\chi_{c1}(1P))]$ assuming $B(\psi(2S) \rightarrow \gamma\chi_{c1}(1P)) = (9.2 \pm 0.4) \times 10^{-2}$, which we rescale to our best value $B(\psi(2S) \rightarrow \gamma\chi_{c1}(1P)) = 9.75 \times 10^{-2}$.

$\Gamma(\Sigma(1385)^-\bar{\Lambda}\pi^+ + \text{c.c.})/\Gamma_{\text{total}}$	Γ_{71}/Γ			
VALUE (units 10^{-5})	CL%	DOCUMENT ID	TECN	COMMENT
<13	90	¹ ABLIKIM	12I	BES3 $\psi(2S) \rightarrow \gamma\Sigma(1385)^-\bar{\Lambda}\pi^+$

¹ ABLIKIM 12I reports $< 14 \times 10^{-5}$ from a measurement of $[\Gamma(\chi_{c1}(1P) \rightarrow \Sigma(1385)^-\bar{\Lambda}\pi^+ + \text{c.c.})/\Gamma_{\text{total}}] \times [B(\psi(2S) \rightarrow \gamma\chi_{c1}(1P))]$ assuming $B(\psi(2S) \rightarrow \gamma\chi_{c1}(1P)) = (9.2 \pm 0.4) \times 10^{-2}$, which we rescale to our best value $B(\psi(2S) \rightarrow \gamma\chi_{c1}(1P)) = 9.75 \times 10^{-2}$.

$\Gamma(K^+\bar{p}\Lambda + \text{c.c.})/\Gamma_{\text{total}}$	Γ_{72}/Γ			
VALUE (units 10^{-4})	EVTS	DOCUMENT ID	TECN	COMMENT
4.2 ± 0.4 OUR AVERAGE	Error includes scale factor of 1.2.			
9.2 ± 2.8 ± 0.4	24	¹ LU	19	BELL $B^+ \rightarrow \bar{p}\Lambda K^+ K^+$
4.2 ± 0.4 ± 0.1	3k	^{2,3} ABLIKIM	13D	BES3 $\psi(2S) \rightarrow \gamma\Lambda\bar{p}K^+$
3.1 ± 0.9 ± 0.1		⁴ ATHAR	07	CLEO $\psi(2S) \rightarrow \gamma h^+ h^- h^0$

¹ LU 19 reports $(9.15 \pm 2.63 \pm 0.86) \times 10^{-4}$ from a measurement of $[\Gamma(\chi_{c1}(1P) \rightarrow K^+\bar{p}\Lambda + \text{c.c.})/\Gamma_{\text{total}}] \times [B(B^+ \rightarrow \chi_{c1}(1P)K^+)]$ assuming $B(B^+ \rightarrow \chi_{c1}(1P)K^+) = (4.79 \pm 0.23) \times 10^{-4}$, which we rescale to our best value $B(B^+ \rightarrow \chi_{c1}(1P)K^+) = (4.74 \pm 0.22) \times 10^{-4}$. Our first error is their experiment's error and our second error is the systematic error from using our best value.

² ABLIKIM 13D reports $(4.5 \pm 0.2 \pm 0.4) \times 10^{-4}$ from a measurement of $[\Gamma(\chi_{c1}(1P) \rightarrow K^+\bar{p}\Lambda + \text{c.c.})/\Gamma_{\text{total}}] \times [B(\psi(2S) \rightarrow \gamma\chi_{c1}(1P))]$ assuming $B(\psi(2S) \rightarrow \gamma\chi_{c1}(1P)) = (9.2 \pm 0.4) \times 10^{-2}$, which we rescale to our best value $B(\psi(2S) \rightarrow \gamma\chi_{c1}(1P)) = (9.75 \pm 0.24) \times 10^{-2}$. Our first error is their experiment's error and our second error is the systematic error from using our best value.

³ Using $B(\Lambda \rightarrow p\pi^-) = 63.9\%$.

⁴ ATHAR 07 reports $(3.3 \pm 0.9 \pm 0.4) \times 10^{-4}$ from a measurement of $[\Gamma(\chi_{c1}(1P) \rightarrow K^+\bar{p}\Lambda + \text{c.c.})/\Gamma_{\text{total}}] \times [B(\psi(2S) \rightarrow \gamma\chi_{c1}(1P))]$ assuming $B(\psi(2S) \rightarrow \gamma\chi_{c1}(1P)) = (9.07 \pm 0.11 \pm 0.54) \times 10^{-2}$, which we rescale to our best value $B(\psi(2S) \rightarrow \gamma\chi_{c1}(1P)) = (9.75 \pm 0.24) \times 10^{-2}$. Our first error is their experiment's error and our second error is the systematic error from using our best value.

$\Gamma(nK_S^0\bar{\Lambda} + \text{c.c.})/\Gamma_{\text{total}}$	Γ_{73}/Γ			
VALUE (units 10^{-4})	EVTS	DOCUMENT ID	TECN	COMMENT
1.66 ± 0.12 ± 0.12	399	¹ ABLIKIM	21AV	BES3 $\psi(2S) \rightarrow \gamma nK_S^0\bar{\Lambda} + \text{c.c.}$

¹ ABLIKIM 21AV reports $(1.66 \pm 0.12 \pm 0.12) \times 10^{-4}$ from a measurement of $[\Gamma(\chi_{c1}(1P) \rightarrow nK_S^0\bar{\Lambda} + \text{c.c.})/\Gamma_{\text{total}}] \times [B(\psi(2S) \rightarrow \gamma\chi_{c1}(1P))]$ assuming $B(\psi(2S) \rightarrow \gamma\chi_{c1}(1P)) = 0.0975 \pm 0.0024$. Also uses $B(\bar{\Lambda} \rightarrow \bar{p}\pi^+) = (63.9 \pm 0.5)\%$ and $B(K_S^0 \rightarrow \pi^+\pi^-) = (69.20 \pm 0.05)\%$.

$\Gamma(K^*(892)^+\bar{p}\Lambda + \text{c.c.})/\Gamma_{\text{total}}$	Γ_{74}/Γ			
VALUE (units 10^{-4})	EVTS	DOCUMENT ID	TECN	COMMENT
4.9 ± 0.7 ± 0.1	328	¹ ABLIKIM	19AU	BES3 $\psi(2S) \rightarrow \gamma K^*\bar{p}\Lambda$

¹ ABLIKIM 19AU reports $[\Gamma(\chi_{c1}(1P) \rightarrow K^*(892)^+\bar{p}\Lambda + \text{c.c.})/\Gamma_{\text{total}}] \times [B(\psi(2S) \rightarrow \gamma\chi_{c1}(1P))] = (4.8 \pm 0.5 \pm 0.4) \times 10^{-5}$ which we divide by our best value $B(\psi(2S) \rightarrow \gamma\chi_{c1}(1P)) = (9.75 \pm 0.24) \times 10^{-2}$. Our first error is their experiment's error and our second error is the systematic error from using our best value.

See key on page 1127

Meson Particle Listings

 $\chi_{c1}(1P)$ $\Gamma(K^+ \bar{p} \Lambda(1520) + c.c.) / \Gamma_{\text{total}}$ Γ_{75} / Γ

VALUE (units 10^{-4})	EVTS	DOCUMENT ID	TECN	COMMENT
$1.71 \pm 0.44 \pm 0.04$	48 ± 10	¹ ABLIKIM	11F BES3	$\psi(2S) \rightarrow \gamma \bar{p} K^+ K^-$
¹ ABLIKIM 11F reports $(1.81 \pm 0.38 \pm 0.28) \times 10^{-4}$ from a measurement of $[\Gamma(\chi_{c1}(1P) \rightarrow K^+ \bar{p} \Lambda(1520) + c.c.) / \Gamma_{\text{total}}] \times [B(\psi(2S) \rightarrow \gamma \chi_{c1}(1P))]$ assuming $B(\psi(2S) \rightarrow \gamma \chi_{c1}(1P)) = (9.2 \pm 0.4) \times 10^{-2}$, which we rescale to our best value $B(\psi(2S) \rightarrow \gamma \chi_{c1}(1P)) = (9.75 \pm 0.24) \times 10^{-2}$. Our first error is their experiment's error and our second error is the systematic error from using our best value.				

 $\Gamma(\Lambda(1520) \bar{\Lambda}(1520)) / \Gamma_{\text{total}}$ Γ_{76} / Γ

VALUE	CL%	EVTS	DOCUMENT ID	TECN	COMMENT
$< 9 \times 10^{-5}$	90	¹ ABLIKIM	11F BES3	$\psi(2S) \rightarrow \gamma \bar{p} K^+ K^-$	
¹ ABLIKIM 11F reports $< 1.00 \times 10^{-4}$ from a measurement of $[\Gamma(\chi_{c1}(1P) \rightarrow \Lambda(1520) \bar{\Lambda}(1520)) / \Gamma_{\text{total}}] \times [B(\psi(2S) \rightarrow \gamma \chi_{c1}(1P))]$ assuming $B(\psi(2S) \rightarrow \gamma \chi_{c1}(1P)) = (9.2 \pm 0.4) \times 10^{-2}$, which we rescale to our best value $B(\psi(2S) \rightarrow \gamma \chi_{c1}(1P)) = 9.75 \times 10^{-2}$.					

 $\Gamma(\Sigma^0 \bar{\Sigma}^0) / \Gamma_{\text{total}}$ Γ_{77} / Γ

VALUE (units 10^{-5})	CL%	EVTS	DOCUMENT ID	TECN	COMMENT
$4.2 \pm 0.6 \pm 0.1$	103	¹ ABLIKIM	18v BES3	$\psi(2S) \rightarrow \gamma \Sigma^0 \bar{\Sigma}^0$	
• • • We do not use the following data for averages, fits, limits, etc. • • •					
<6	90	² ABLIKIM	13H BES3	$\psi(2S) \rightarrow \gamma \Sigma^0 \bar{\Sigma}^0$	
<4	90	3.8 ± 2.5	³ NAIK	08 CLEO	$\psi(2S) \rightarrow \gamma \Sigma^0 \bar{\Sigma}^0$
¹ ABLIKIM 18v reports $[\Gamma(\chi_{c1}(1P) \rightarrow \Sigma^0 \bar{\Sigma}^0) / \Gamma_{\text{total}}] \times [B(\psi(2S) \rightarrow \gamma \chi_{c1}(1P))] = (0.41 \pm 0.05 \pm 0.03) \times 10^{-5}$ which we divide by our best value $B(\psi(2S) \rightarrow \gamma \chi_{c1}(1P)) = (9.75 \pm 0.24) \times 10^{-2}$. Our first error is their experiment's error and our second error is the systematic error from using our best value.					
² ABLIKIM 13H reports $< 0.62 \times 10^{-4}$ from a measurement of $[\Gamma(\chi_{c1}(1P) \rightarrow \Sigma^0 \bar{\Sigma}^0) / \Gamma_{\text{total}}] \times [B(\psi(2S) \rightarrow \gamma \chi_{c1}(1P))]$ assuming $B(\psi(2S) \rightarrow \gamma \chi_{c1}(1P)) = (9.2 \pm 0.4) \times 10^{-2}$, which we rescale to our best value $B(\psi(2S) \rightarrow \gamma \chi_{c1}(1P)) = 9.75 \times 10^{-2}$.					
³ NAIK 08 reports $< 0.44 \times 10^{-4}$ from a measurement of $[\Gamma(\chi_{c1}(1P) \rightarrow \Sigma^0 \bar{\Sigma}^0) / \Gamma_{\text{total}}] \times [B(\psi(2S) \rightarrow \gamma \chi_{c1}(1P))]$ assuming $B(\psi(2S) \rightarrow \gamma \chi_{c1}(1P)) = (9.07 \pm 0.11 \pm 0.54) \times 10^{-2}$, which we rescale to our best value $B(\psi(2S) \rightarrow \gamma \chi_{c1}(1P)) = 9.75 \times 10^{-2}$.					

 $\Gamma(\Sigma^+ \bar{\Sigma}^-) / \Gamma_{\text{total}}$ Γ_{80} / Γ

VALUE (units 10^{-5})	CL%	EVTS	DOCUMENT ID	TECN	COMMENT
$3.6 \pm 0.6 \pm 0.1$	59	¹ ABLIKIM	18v BES3	$\psi(2S) \rightarrow \gamma \Sigma^+ \bar{\Sigma}^-$	
• • • We do not use the following data for averages, fits, limits, etc. • • •					
<8	90	² ABLIKIM	13H BES3	$\psi(2S) \rightarrow \gamma \Sigma^+ \bar{\Sigma}^-$	
<6	90	4.3 ± 2.3	³ NAIK	08 CLEO	$\psi(2S) \rightarrow \gamma \Sigma^+ \bar{\Sigma}^-$
¹ ABLIKIM 18v reports $[\Gamma(\chi_{c1}(1P) \rightarrow \Sigma^+ \bar{\Sigma}^-) / \Gamma_{\text{total}}] \times [B(\psi(2S) \rightarrow \gamma \chi_{c1}(1P))] = (0.35 \pm 0.06 \pm 0.02) \times 10^{-5}$ which we divide by our best value $B(\psi(2S) \rightarrow \gamma \chi_{c1}(1P)) = (9.75 \pm 0.24) \times 10^{-2}$. Our first error is their experiment's error and our second error is the systematic error from using our best value.					
² ABLIKIM 13H reports $< 0.87 \times 10^{-4}$ from a measurement of $[\Gamma(\chi_{c1}(1P) \rightarrow \Sigma^+ \bar{\Sigma}^-) / \Gamma_{\text{total}}] \times [B(\psi(2S) \rightarrow \gamma \chi_{c1}(1P))]$ assuming $B(\psi(2S) \rightarrow \gamma \chi_{c1}(1P)) = (9.2 \pm 0.4) \times 10^{-2}$, which we rescale to our best value $B(\psi(2S) \rightarrow \gamma \chi_{c1}(1P)) = 9.75 \times 10^{-2}$.					
³ NAIK 08 reports $< 0.65 \times 10^{-4}$ from a measurement of $[\Gamma(\chi_{c1}(1P) \rightarrow \Sigma^+ \bar{\Sigma}^-) / \Gamma_{\text{total}}] \times [B(\psi(2S) \rightarrow \gamma \chi_{c1}(1P))]$ assuming $B(\psi(2S) \rightarrow \gamma \chi_{c1}(1P)) = (9.07 \pm 0.11 \pm 0.54) \times 10^{-2}$, which we rescale to our best value $B(\psi(2S) \rightarrow \gamma \chi_{c1}(1P)) = 9.75 \times 10^{-2}$.					

 $\Gamma(\Sigma^- \bar{\Sigma}^+) / \Gamma_{\text{total}}$ Γ_{81} / Γ

VALUE (units 10^{-5})	EVTS	DOCUMENT ID	TECN	COMMENT
$5.7 \pm 1.4 \pm 0.6$	214	¹ ABLIKIM	20i BES3	$\psi(2S) \rightarrow \gamma \Sigma^- \bar{\Sigma}^+$
¹ ABLIKIM 20i reports $(5.7 \pm 1.4 \pm 0.6) \times 10^{-5}$ from a measurement of $[\Gamma(\chi_{c1}(1P) \rightarrow \Sigma^- \bar{\Sigma}^+) / \Gamma_{\text{total}}] \times [B(\psi(2S) \rightarrow \gamma \chi_{c1}(1P))]$ assuming $B(\psi(2S) \rightarrow \gamma \chi_{c1}(1P)) = (9.75 \pm 0.24) \times 10^{-2}$.				

 $\Gamma(\Sigma(1385)^+ \bar{\Sigma}(1385)^-) / \Gamma_{\text{total}}$ Γ_{82} / Γ

VALUE	CL%	EVTS	DOCUMENT ID	TECN	COMMENT
$< 9 \times 10^{-5}$	90	¹ ABLIKIM	12i BES3	$\psi(2S) \rightarrow \gamma \Lambda \bar{\Lambda} \pi^+ \pi^-$	
¹ ABLIKIM 12i reports $< 10 \times 10^{-5}$ from a measurement of $[\Gamma(\chi_{c1}(1P) \rightarrow \Sigma(1385)^+ \bar{\Sigma}(1385)^-) / \Gamma_{\text{total}}] \times [B(\psi(2S) \rightarrow \gamma \chi_{c1}(1P))]$ assuming $B(\psi(2S) \rightarrow \gamma \chi_{c1}(1P)) = (9.2 \pm 0.4) \times 10^{-2}$, which we rescale to our best value $B(\psi(2S) \rightarrow \gamma \chi_{c1}(1P)) = 9.75 \times 10^{-2}$.					

 $\Gamma(\Sigma(1385)^- \bar{\Sigma}(1385)^+) / \Gamma_{\text{total}}$ Γ_{83} / Γ

VALUE	CL%	EVTS	DOCUMENT ID	TECN	COMMENT
$< 5 \times 10^{-5}$	90	¹ ABLIKIM	12i BES3	$\psi(2S) \rightarrow \gamma \Lambda \bar{\Lambda} \pi^+ \pi^-$	
¹ ABLIKIM 12i reports $< 5.7 \times 10^{-5}$ from a measurement of $[\Gamma(\chi_{c1}(1P) \rightarrow \Sigma(1385)^- \bar{\Sigma}(1385)^+) / \Gamma_{\text{total}}] \times [B(\psi(2S) \rightarrow \gamma \chi_{c1}(1P))]$ assuming $B(\psi(2S) \rightarrow \gamma \chi_{c1}(1P)) = (9.2 \pm 0.4) \times 10^{-2}$, which we rescale to our best value $B(\psi(2S) \rightarrow \gamma \chi_{c1}(1P)) = 9.75 \times 10^{-2}$.					

 $\Gamma(K^- \Lambda \bar{\Sigma}^+ + c.c.) / \Gamma_{\text{total}}$ Γ_{84} / Γ

VALUE (units 10^{-4})	EVTS	DOCUMENT ID	TECN	COMMENT
$1.35 \pm 0.24 \pm 0.03$	49	¹ ABLIKIM	15i BES3	$\psi(2S) \rightarrow \gamma K^- \Lambda \bar{\Sigma}^+ + c.c.$
¹ ABLIKIM 15i reports $[\Gamma(\chi_{c1}(1P) \rightarrow K^- \Lambda \bar{\Sigma}^+ + c.c.) / \Gamma_{\text{total}}] \times [B(\psi(2S) \rightarrow \gamma \chi_{c1}(1P))] = (1.32 \pm 0.20 \pm 0.12) \times 10^{-5}$ which we divide by our best value $B(\psi(2S) \rightarrow \gamma \chi_{c1}(1P)) = (9.75 \pm 0.24) \times 10^{-2}$. Our first error is their experiment's error and our second error is the systematic error from using our best value.				

 $\Gamma(\Xi^0 \bar{\Xi}^0) / \Gamma_{\text{total}}$ Γ_{85} / Γ

VALUE	CL%	EVTS	DOCUMENT ID	TECN	COMMENT
$< 6 \times 10^{-5}$	90	1.7 ± 2.4	¹ NAIK	08 CLEO	$\psi(2S) \rightarrow \gamma \Xi^0 \bar{\Xi}^0$
¹ NAIK 08 reports $< 0.60 \times 10^{-4}$ from a measurement of $[\Gamma(\chi_{c1}(1P) \rightarrow \Xi^0 \bar{\Xi}^0) / \Gamma_{\text{total}}] \times [B(\psi(2S) \rightarrow \gamma \chi_{c1}(1P))]$ assuming $B(\psi(2S) \rightarrow \gamma \chi_{c1}(1P)) = (9.07 \pm 0.11 \pm 0.54) \times 10^{-2}$, which we rescale to our best value $B(\psi(2S) \rightarrow \gamma \chi_{c1}(1P)) = 9.75 \times 10^{-2}$.					

 $\Gamma(\Xi^- \bar{\Xi}^+) / \Gamma_{\text{total}}$ Γ_{86} / Γ

VALUE (units 10^{-4})	CL%	EVTS	DOCUMENT ID	TECN	COMMENT
$0.80 \pm 0.21 \pm 0.02$	16.4 ± 4.3	¹ NAIK	08 CLEO	$\psi(2S) \rightarrow \gamma \Xi^+ \bar{\Xi}^-$	
• • • We do not use the following data for averages, fits, limits, etc. • • •					
< 3.4	90		² ABLIKIM	06D BES2	$\psi(2S) \rightarrow \gamma \chi_{c1}$

¹ NAIK 08 reports $(0.86 \pm 0.22 \pm 0.08) \times 10^{-4}$ from a measurement of $[\Gamma(\chi_{c1}(1P) \rightarrow \Xi^- \bar{\Xi}^+) / \Gamma_{\text{total}}] \times [B(\psi(2S) \rightarrow \gamma \chi_{c1}(1P))]$ assuming $B(\psi(2S) \rightarrow \gamma \chi_{c1}(1P)) = (9.07 \pm 0.11 \pm 0.54) \times 10^{-2}$, which we rescale to our best value $B(\psi(2S) \rightarrow \gamma \chi_{c1}(1P)) = (9.75 \pm 0.24) \times 10^{-2}$. Our first error is their experiment's error and our second error is the systematic error from using our best value.

² Using $B(\psi(2S) \rightarrow \chi_{c1} \gamma) = (9.1 \pm 0.6)\%$.

 $[\Gamma(\pi^+ \pi^-) + \Gamma(K^+ K^-)] / \Gamma_{\text{total}}$ Γ_{87} / Γ

VALUE	CL%	DOCUMENT ID	TECN	COMMENT
$< 21 \times 10^{-4}$		¹ FELDMAN	77 MRK1	$\psi(2S) \rightarrow \gamma \chi_{c1}$
• • • We do not use the following data for averages, fits, limits, etc. • • •				
<38 × 10 ⁻⁴	90	¹ BRANDELIK	79B DASP	$\psi(2S) \rightarrow \gamma \chi_{c1}$
¹ Estimated using $B(\psi(2S) \rightarrow \gamma \chi_{c1}(1P)) = 0.087$. The errors do not contain the uncertainty in the $\psi(2S)$ decay.				

 $\Gamma(K_S^0 K_S^0) / \Gamma_{\text{total}}$ Γ_{88} / Γ

VALUE	CL%	DOCUMENT ID	TECN	COMMENT
$< 6 \times 10^{-5}$	90	¹ ABLIKIM	05o BES2	$\psi(2S) \rightarrow \chi_{c1} \gamma$
¹ ABLIKIM 05o reports $[\Gamma(\chi_{c1}(1P) \rightarrow K_S^0 K_S^0) / \Gamma_{\text{total}}] \times [B(\psi(2S) \rightarrow \gamma \chi_{c1}(1P))] < 0.6 \times 10^{-5}$ which we divide by our best value $B(\psi(2S) \rightarrow \gamma \chi_{c1}(1P)) = 9.75 \times 10^{-2}$.				

 $\Gamma(\eta_c \pi^+ \pi^-) / \Gamma_{\text{total}}$ Γ_{89} / Γ

VALUE	CL%	DOCUMENT ID	TECN	COMMENT
$< 3.2 \times 10^{-3}$	90	^{1,2} ABLIKIM	13B BES3	$e^+ e^- \rightarrow \psi(2S) \rightarrow \gamma \chi_{c1}$
• • • We do not use the following data for averages, fits, limits, etc. • • •				
<4.4 × 10 ⁻³	90	^{1,3} ABLIKIM	13B BES3	$e^+ e^- \rightarrow \psi(2S) \rightarrow \gamma \chi_{c1}$
¹ Using $1.06 \times 10^8 \psi(2S)$ mesons and $B(\psi(2S) \rightarrow \chi_{c1} \gamma) = (9.2 \pm 0.4)\%$.				
² Using the $\eta_c \rightarrow K_S^0 K_S^0 \pi^+ \pi^-$ decays.				
³ Using the $\eta_c \rightarrow K^+ K^- \pi^0$ decays.				

RADIATIVE DECAYS

 $\Gamma(\gamma J / \psi(1S)) / \Gamma_{\text{total}}$ Γ_{90} / Γ

VALUE (units 10^{-2})	EVTS	DOCUMENT ID	TECN	COMMENT
34.3 ± 1.0 OUR FIT				
• • • We do not use the following data for averages, fits, limits, etc. • • •				
34.75 ± 0.11 ± 1.70	1.9M	¹ ABLIKIM	17u BES3	$e^+ e^- \rightarrow \gamma X$
37.9 ± 0.8 ± 2.1		² ADAM	05A CLEO	$e^+ e^- \rightarrow \psi(2S) \rightarrow \gamma \chi_{c1}$
¹ Not independent from $B(\psi(2S) \rightarrow \gamma \chi_{c1}(1P))$ and the product $B(\psi(2S) \rightarrow \gamma \chi_{c1}(1P)) \times B(\chi_{c1}(1P) \rightarrow \gamma J / \psi(1S))$ also measured in ABLIKIM 17u.				
² Uses $B(\psi(2S) \rightarrow \gamma \chi_{c1} \rightarrow \gamma J / \psi)$ from ADAM 05A and $B(\psi(2S) \rightarrow \gamma \chi_{c1})$ from ATHAR 04.				

 $\Gamma(\gamma \rho^0) / \Gamma_{\text{total}}$ Γ_{91} / Γ

VALUE (units 10^{-6})	EVTS	DOCUMENT ID	TECN	COMMENT
216 ± 17 OUR AVERAGE				
215 ± 22 ± 5	432 ± 25	¹ ABLIKIM	11E BES3	$\psi(2S) \rightarrow \gamma \gamma \rho^0$
217 ± 24 ± 5	186 ± 15	² BENNETT	08A CLEO	$\psi(2S) \rightarrow \gamma \gamma \rho^0$
¹ ABLIKIM 11E reports $(228 \pm 13 \pm 22) \times 10^{-6}$ from a measurement of $[\Gamma(\chi_{c1}(1P) \rightarrow \gamma \rho^0) / \Gamma_{\text{total}}] \times [B(\psi(2S) \rightarrow \gamma \chi_{c1}(1P))]$ assuming $B(\psi(2S) \rightarrow \gamma \chi_{c1}(1P)) = (9.2 \pm 0.4) \times 10^{-2}$, which we rescale to our best value $B(\psi(2S) \rightarrow \gamma \chi_{c1}(1P)) = (9.75 \pm 0.24) \times 10^{-2}$. Our first error is their experiment's error and our second error is the systematic error from using our best value.				
² BENNETT 08A reports $(243 \pm 19 \pm 22) \times 10^{-6}$ from a measurement of $[\Gamma(\chi_{c1}(1P) \rightarrow \gamma \rho^0) / \Gamma_{\text{total}}] \times [B(\psi(2S) \rightarrow \gamma \chi_{c1}(1P))]$ assuming $B(\psi(2S) \rightarrow \gamma \chi_{c1}(1P)) = (8.7 \pm 0.4) \times 10^{-2}$, which we rescale to our best value $B(\psi(2S) \rightarrow \gamma \chi_{c1}(1P)) = (9.75 \pm 0.24) \times 10^{-2}$. Our first error is their experiment's error and our second error is the systematic error from using our best value.				

Meson Particle Listings

$\chi_{c1}(1P)$

$\Gamma(\gamma\omega)/\Gamma_{total}$		Γ_{92}/Γ		
VALUE (units 10^{-6})	EVTS	DOCUMENT ID	TECN	COMMENT
68 ± 8 OUR AVERAGE				
66 ± 9 ± 2	136 ± 14	¹ ABLIKIM	11E BES3	$\psi(2S) \rightarrow \gamma\gamma\omega$
74 ± 17 ± 2	39 ± 7	² BENNETT	08A CLEO	$\psi(2S) \rightarrow \gamma\gamma\omega$

¹ ABLIKIM 11E reports $(69.7 \pm 7.2 \pm 6.6) \times 10^{-6}$ from a measurement of $[\Gamma(\chi_{c1}(1P) \rightarrow \gamma\omega)/\Gamma_{total}] \times [B(\psi(2S) \rightarrow \gamma\chi_{c1}(1P))]$ assuming $B(\psi(2S) \rightarrow \gamma\chi_{c1}(1P)) = (9.2 \pm 0.4) \times 10^{-2}$, which we rescale to our best value $B(\psi(2S) \rightarrow \gamma\chi_{c1}(1P)) = (9.75 \pm 0.24) \times 10^{-2}$. Our first error is their experiment's error and our second error is the systematic error from using our best value.

² BENNETT 08A reports $(83 \pm 15 \pm 12) \times 10^{-6}$ from a measurement of $[\Gamma(\chi_{c1}(1P) \rightarrow \gamma\omega)/\Gamma_{total}] \times [B(\psi(2S) \rightarrow \gamma\chi_{c1}(1P))]$ assuming $B(\psi(2S) \rightarrow \gamma\chi_{c1}(1P)) = (8.7 \pm 0.4) \times 10^{-2}$, which we rescale to our best value $B(\psi(2S) \rightarrow \gamma\chi_{c1}(1P)) = (9.75 \pm 0.24) \times 10^{-2}$. Our first error is their experiment's error and our second error is the systematic error from using our best value.

$\Gamma(\gamma\phi)/\Gamma_{total}$		Γ_{93}/Γ			
VALUE (units 10^{-6})	CL%	EVTS	DOCUMENT ID	TECN	COMMENT
24 ± 5 ± 1		43 ± 9	¹ ABLIKIM	11E BES3	$\psi(2S) \rightarrow \gamma\gamma\phi$
< 23	90	5.2 ± 3.1	² BENNETT	08A CLEO	$\psi(2S) \rightarrow \gamma\gamma\phi$

¹ ABLIKIM 11E reports $(25.8 \pm 5.2 \pm 2.3) \times 10^{-6}$ from a measurement of $[\Gamma(\chi_{c1}(1P) \rightarrow \gamma\phi)/\Gamma_{total}] \times [B(\psi(2S) \rightarrow \gamma\chi_{c1}(1P))]$ assuming $B(\psi(2S) \rightarrow \gamma\chi_{c1}(1P)) = (9.2 \pm 0.4) \times 10^{-2}$, which we rescale to our best value $B(\psi(2S) \rightarrow \gamma\chi_{c1}(1P)) = (9.75 \pm 0.24) \times 10^{-2}$. Our first error is their experiment's error and our second error is the systematic error from using our best value.

² BENNETT 08A reports $< 26 \times 10^{-6}$ from a measurement of $[\Gamma(\chi_{c1}(1P) \rightarrow \gamma\phi)/\Gamma_{total}] \times [B(\psi(2S) \rightarrow \gamma\chi_{c1}(1P))]$ assuming $B(\psi(2S) \rightarrow \gamma\chi_{c1}(1P)) = (8.7 \pm 0.4) \times 10^{-2}$, which we rescale to our best value $B(\psi(2S) \rightarrow \gamma\chi_{c1}(1P)) = 9.75 \times 10^{-2}$.

$\Gamma(\gamma\gamma)/\Gamma_{total}$		Γ_{94}/Γ			
VALUE	CL%	EVTS	DOCUMENT ID	TECN	COMMENT
< 6.3 × 10⁻⁶	90		ABLIKIM	17A BES3	$\psi(2S) \rightarrow \gamma\chi_{c1} \rightarrow 3\gamma$
< 3.5 × 10 ⁻⁵	90		ECKLUND	08A CLEO	$\psi(2S) \rightarrow \gamma\chi_{c1} \rightarrow 3\gamma$
< 150 × 10 ⁻⁵	90		¹ YAMADA	77 DASP	$e^+e^- \rightarrow 3\gamma$

$\Gamma(e^+e^- J/\psi(1S))/\Gamma_{total}$		Γ_{95}/Γ		
VALUE (units 10^{-3})	EVTS	DOCUMENT ID	TECN	COMMENT
3.65 ± 0.23 ± 0.09	1.9k	^{1,2} ABLIKIM	17I BES3	$\psi(2S) \rightarrow \gamma e^+e^- J/\psi$

¹ ABLIKIM 17I reports $(3.73 \pm 0.09 \pm 0.25) \times 10^{-3}$ from a measurement of $[\Gamma(\chi_{c1}(1P) \rightarrow e^+e^- J/\psi(1S))/\Gamma_{total}] \times [B(\psi(2S) \rightarrow \gamma\chi_{c1}(1P))]$ assuming $B(\psi(2S) \rightarrow \gamma\chi_{c1}(1P)) = (9.55 \pm 0.31) \times 10^{-2}$, which we rescale to our best value $B(\psi(2S) \rightarrow \gamma\chi_{c1}(1P)) = (9.75 \pm 0.24) \times 10^{-2}$. Our first error is their experiment's error and our second error is the systematic error from using our best value.

² Not independent from other measurements reported by ABLIKIM 17I.

$\Gamma(e^+e^- J/\psi(1S))/\Gamma(\gamma J/\psi(1S))$		Γ_{95}/Γ_{90}		
VALUE (units 10^{-3})	EVTS	DOCUMENT ID	TECN	COMMENT
10.1 ± 0.3 ± 0.5	1.9k	¹ ABLIKIM	17I BES3	$\psi(2S) \rightarrow e^+e^- \gamma J/\psi$

¹ Uses $B(\psi(2S) \rightarrow \gamma\chi_{c1}(1P)) \times B(\chi_{c1}(1P) \rightarrow \gamma J/\psi(1S)) = (351.8 \pm 1.0 \pm 12.0) \times 10^{-4}$ from ABLIKIM 17N and accounts for common systematic errors.

$\Gamma(\mu^+\mu^- J/\psi(1S))/\Gamma(e^+e^- J/\psi(1S))$		Γ_{96}/Γ_{95}		
VALUE (units 10^{-2})	EVTS	DOCUMENT ID	TECN	COMMENT
6.73 ± 0.51 ± 0.50	222	ABLIKIM	19Z BES3	$\psi(2S) \rightarrow \gamma\chi_{c1} \rightarrow \gamma(\mu^+\mu^- J/\psi)$

$\chi_{c1}(1P)$ CROSS-PARTICLE BRANCHING RATIOS

$\Gamma(\chi_{c1}(1P) \rightarrow \rho\bar{\rho})/\Gamma_{total} \times \Gamma(\psi(2S) \rightarrow \gamma\chi_{c1}(1P))/\Gamma(\psi(2S) \rightarrow J/\psi(1S)\pi^+\pi^-)$		$\Gamma_{54}/\Gamma \times \Gamma_{163}^{\psi(2S)}/\Gamma_{12}^{\psi(2S)}$		
VALUE (units 10^{-5})	EVTS	DOCUMENT ID	TECN	COMMENT
2.14 ± 0.10 OUR FIT				
1.1 ± 1.0		¹ BAI	98I BES	$\psi(2S) \rightarrow \gamma\chi_{c1} \rightarrow \gamma\rho\bar{\rho}$

¹ Calculated by us. The value for $B(\chi_{c1} \rightarrow \rho\bar{\rho})$ reported in BAI 98I is derived using $B(\psi(2S) \rightarrow \gamma\chi_{c1}) = (8.7 \pm 0.8)\%$ and $B(\psi(2S) \rightarrow J/\psi(1S)\pi^+\pi^-) = (32.4 \pm 2.6)\%$ [BAI 98d].

$\Gamma(\chi_{c1}(1P) \rightarrow \Lambda\bar{\Lambda})/\Gamma_{total} \times \Gamma(\psi(2S) \rightarrow \gamma\chi_{c1}(1P))/\Gamma_{total}$		$\Gamma_{67}/\Gamma \times \Gamma_{163}^{\psi(2S)}/\Gamma_{12}^{\psi(2S)}$		
VALUE (units 10^{-6})	EVTS	DOCUMENT ID	TECN	COMMENT
12.4 ± 0.8 OUR FIT				
12.3 ± 0.9 OUR AVERAGE				Error includes scale factor of 1.2.
12.8 ± 0.6 ± 0.6	528	ABLIKIM	21L BES3	$\psi(2S) \rightarrow \gamma\rho\pi^-\bar{\rho}\pi^+$
10.5 ± 1.6 ± 0.6	46	¹ NAIK	08 CLEO	$\psi(2S) \rightarrow \gamma\Lambda\bar{\Lambda}$

• • • We do not use the following data for averages, fits, limits, etc. • • •

11.2 ± 1.0 ± 0.9 136 ^{2,3} ABLIKIM 13H BES3 $\psi(2S) \rightarrow \gamma\Lambda\bar{\Lambda}$

¹ Calculated by us. NAIK 08 reports $B(\chi_{c1} \rightarrow \Lambda\bar{\Lambda}) = (11.6 \pm 1.8 \pm 0.7 \pm 0.7) \times 10^{-5}$ using $B(\psi(2S) \rightarrow \gamma\chi_{c1}) = (9.07 \pm 0.11 \pm 0.54)\%$.

² Superseded by ABLIKIM 21L

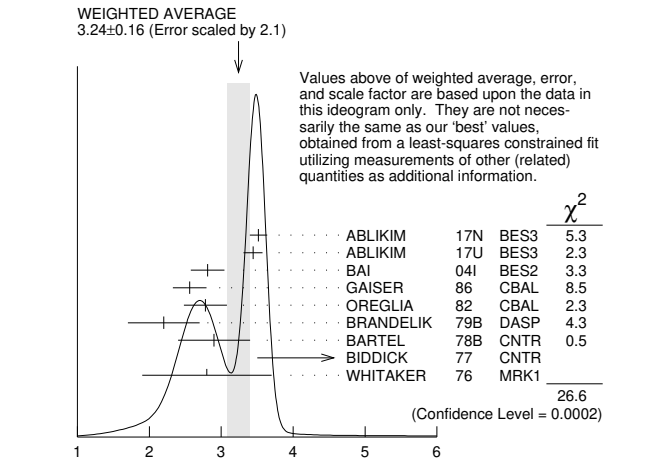
³ Calculated by us. ABLIKIM 13H reports $B(\chi_{c1} \rightarrow \Lambda\bar{\Lambda}) = (12.2 \pm 1.1 \pm 1.1) \times 10^{-5}$ from a measurement of $B(\chi_{c1} \rightarrow \Lambda\bar{\Lambda}) \times B(\psi(2S) \rightarrow \gamma\chi_{c1})$ assuming $B(\psi(2S) \rightarrow \gamma\chi_{c1}) = (9.2 \pm 0.4)\%$.

$\Gamma(\chi_{c1}(1P) \rightarrow \Lambda\bar{\Lambda})/\Gamma_{total} \times \Gamma(\psi(2S) \rightarrow \gamma\chi_{c1}(1P))/\Gamma(\psi(2S) \rightarrow J/\psi(1S)\pi^+\pi^-)$		$\Gamma_{67}/\Gamma \times \Gamma_{163}^{\psi(2S)}/\Gamma_{12}^{\psi(2S)}$		
VALUE (units 10^{-5})	EVTS	DOCUMENT ID	TECN	COMMENT
3.58 ± 0.22 OUR FIT				
7.1 ^{+2.8} _{-2.4} ± 1.3	9.0 ^{+3.5} _{-3.1}	¹ BAI	03E BES	$\psi(2S) \rightarrow \gamma\Lambda\bar{\Lambda}$

¹ BAI 03E reports $[B(\chi_{c1} \rightarrow \Lambda\bar{\Lambda}) B(\psi(2S) \rightarrow \gamma\chi_{c1}) / B(\psi(2S) \rightarrow J/\psi\pi^+\pi^-)] \times [B^2(\Lambda \rightarrow \pi^-\rho) / B(J/\psi \rightarrow \rho\bar{\rho})] = (1.33 ^{+0.52} _{-0.46} ± 0.25)\%$. We calculate from this measurement the presented value using $B(\Lambda \rightarrow \pi^-\rho) = (63.9 \pm 0.5)\%$ and $B(J/\psi \rightarrow \rho\bar{\rho}) = (2.17 \pm 0.07) \times 10^{-3}$.

$\Gamma(\chi_{c1}(1P) \rightarrow \gamma J/\psi(1S))/\Gamma_{total} \times \Gamma(\psi(2S) \rightarrow \gamma\chi_{c1}(1P))/\Gamma_{total}$		$\Gamma_{90}/\Gamma \times \Gamma_{163}^{\psi(2S)}/\Gamma_{12}^{\psi(2S)}$		
VALUE (units 10^{-2})	EVTS	DOCUMENT ID	TECN	COMMENT
3.34 ± 0.06 OUR FIT				
3.24 ± 0.16 OUR AVERAGE				Error includes scale factor of 2.1. See the ideogram below.

3.518 ± 0.010 ± 0.120	143k	¹ ABLIKIM	17N BES3	$\psi(2S) \rightarrow \gamma\gamma J/\psi$
3.442 ± 0.010 ± 0.132	1.9M	ABLIKIM	17U BES3	$e^+e^- \rightarrow \gamma X$
2.81 ± 0.05 ± 0.23	13k	BAI	04I BES2	$\psi(2S) \rightarrow J/\psi\gamma\gamma$
2.56 ± 0.12 ± 0.20		GAISER	86 CBAL	$\psi(2S) \rightarrow \gamma X$
2.78 ± 0.30		² OREGLIA	82 CBAL	$\psi(2S) \rightarrow \gamma\chi_{c1}$
2.2 ± 0.5		³ BRANDELIK	79B DASP	$\psi(2S) \rightarrow \gamma\chi_{c1}$
2.9 ± 0.5		³ BARTEL	78B CNTR	$\psi(2S) \rightarrow \gamma\chi_{c1}$
5.0 ± 1.5		⁴ BIDDICK	77 CNTR	$e^+e^- \rightarrow \gamma X$
2.8 ± 0.9		² WHITAKER	76 MRK1	e^+e^-
3.377 ± 0.009 ± 0.183	142k	⁵ ABLIKIM	12O BES3	$\psi(2S) \rightarrow \gamma\chi_{c1}$
3.56 ± 0.03 ± 0.12	24.9k	⁶ MENDEZ	08 CLEO	$\psi(2S) \rightarrow \gamma\chi_{c1}$
3.44 ± 0.06 ± 0.13	3.7k	⁷ ADAM	05A CLEO	Repl. by MENDEZ 08



$\Gamma(\chi_{c1}(1P) \rightarrow \gamma J/\psi(1S))/\Gamma_{total} \times \Gamma(\psi(2S) \rightarrow \gamma\chi_{c1}(1P))/\Gamma_{total}$ (units 10^{-2})

¹ Uses $B(J/\psi \rightarrow e^+e^-) = (5.971 \pm 0.032)\%$ and $B(J/\psi \rightarrow \mu^+\mu^-) = (5.961 \pm 0.033)\%$.

² Recalculated by us using $B(J/\psi(1S) \rightarrow \ell^+\ell^-) = 0.1181 \pm 0.0020$.

³ Recalculated by us using $B(J/\psi(1S) \rightarrow \mu^+\mu^-) = 0.0588 \pm 0.0010$.

⁴ Assumes isotropic gamma distribution.

⁵ Superseded by ABLIKIM 17N.

⁶ Not independent from other measurements of MENDEZ 08.

⁷ Not independent from other values reported by ADAM 05A.

$\Gamma(\chi_{c1}(1P) \rightarrow \gamma J/\psi(1S))/\Gamma_{total} \times \Gamma(\psi(2S) \rightarrow \gamma\chi_{c1}(1P))/\Gamma(\psi(2S) \rightarrow J/\psi(1S)\text{anything})$		$\Gamma_{90}/\Gamma \times \Gamma_{163}^{\psi(2S)}/\Gamma_{12}^{\psi(2S)}$		
VALUE (units 10^{-2})	EVTS	DOCUMENT ID	TECN	COMMENT
5.43 ± 0.10 OUR FIT				
5.70 ± 0.04 ± 0.15	24.9k	¹ MENDEZ	08 CLEO	$\psi(2S) \rightarrow \gamma\chi_{c1}$
5.77 ± 0.10 ± 0.12	3.7k	ADAM	05A CLEO	Repl. by MENDEZ 08

• • • We do not use the following data for averages, fits, limits, etc. • • •

5.70 ± 0.04 ± 0.15 24.9k ¹ MENDEZ 08 CLEO $\psi(2S) \rightarrow \gamma\chi_{c1}$

5.77 ± 0.10 ± 0.12 3.7k ADAM 05A CLEO Repl. by MENDEZ 08

¹ Not independent from other measurements of MENDEZ 08.

$$\Gamma(\chi_{c1}(1P) \rightarrow \gamma J/\psi(1S))/\Gamma_{\text{total}} \times \Gamma(\psi(2S) \rightarrow \gamma \chi_{c1}(1P))/\Gamma(\psi(2S) \rightarrow J/\psi(1S)\pi^+\pi^-)$$

$$\Gamma_{90}/\Gamma \times \Gamma_{163}^{\psi(2S)}/\Gamma_{12}^{\psi(2S)}$$

VALUE (units 10^{-2})	EVTS	DOCUMENT ID	TECN	COMMENT
9.63 ± 0.17 OUR FIT				
10.15 ± 0.28 OUR AVERAGE				
10.17 ± 0.07 ± 0.27	24.9k	MENDEZ	08 CLEO	$\psi(2S) \rightarrow \gamma \chi_{c1}$
12.6 ± 0.3 ± 3.8	3k	¹ ABLIKIM	04B BES	$\psi(2S) \rightarrow J/\psi X$
8.5 ± 2.1		² HIMEL	80 MRK2	$\psi(2S) \rightarrow \gamma \chi_{c1}$
• • • We do not use the following data for averages, fits, limits, etc. • • •				
10.24 ± 0.17 ± 0.23	3.7k	³ ADAM	05A CLEO	Repl. by MENDEZ 08

¹ From a fit to the J/ψ recoil mass spectra.
² The value for $B(\psi(2S) \rightarrow \gamma \chi_{c1}) \times B(\chi_{c1} \rightarrow \gamma J/\psi(1S))$ quoted in HIMEL 80 is derived using $B(\psi(2S) \rightarrow J/\psi(1S)\pi^+\pi^-) = (33 \pm 3)\%$ and $B(J/\psi(1S) \rightarrow \ell^+\ell^-) = 0.138 \pm 0.018$. Calculated by us using $B(J/\psi(1S) \rightarrow \ell^+\ell^-) = 0.1181 \pm 0.0020$.
³ Not independent from other values reported by ADAM 05A.

$$\Gamma(\chi_{c1}(1P) \rightarrow \bar{K}^0 K^+ \pi^- + \text{c.c.})/\Gamma_{\text{total}} \times \Gamma(\psi(2S) \rightarrow \gamma \chi_{c1}(1P))/\Gamma_{\text{total}}$$

$$\Gamma_{17}/\Gamma \times \Gamma_{163}^{\psi(2S)}/\Gamma_{12}^{\psi(2S)}$$

VALUE (units 10^{-4})	DOCUMENT ID	TECN	COMMENT
6.8 ± 0.5 OUR FIT			
7.2 ± 0.6 OUR AVERAGE			
7.3 ± 0.5 ± 0.5	¹ ATHAR	07 CLEO	$\psi(2S) \rightarrow \gamma K_S^0 K^+ \pi^-$
7.0 ± 0.5 ± 0.9	² ABLIKIM	06R BES2	$\psi(2S) \rightarrow \gamma \chi_{c1}$

¹ Calculated by us. The value of $B(\chi_{c1} \rightarrow K^0 K^+ \pi^- + \text{c.c.})$ reported by ATHAR 07 was derived using $B(\psi(2S) \rightarrow \gamma \chi_{c1}(1P)) = (9.07 \pm 0.11 \pm 0.54)\%$.
² Calculated by us. ABLIKIM 06R reports $B(\chi_{c1} \rightarrow K_S^0 K^+ \pi^-) = (4.0 \pm 0.3 \pm 0.5) \times 10^{-3}$. We use $B(\psi(2S) \rightarrow \gamma \chi_{c1}) = (8.7 \pm 0.4) \times 10^{-2}$.

$$\Gamma(\chi_{c1}(1P) \rightarrow \bar{K}^0 K^+ \pi^- + \text{c.c.})/\Gamma_{\text{total}} \times \Gamma(\psi(2S) \rightarrow \gamma \chi_{c1}(1P))/\Gamma(\psi(2S) \rightarrow J/\psi(1S)\pi^+\pi^-)$$

$$\Gamma_{17}/\Gamma \times \Gamma_{163}^{\psi(2S)}/\Gamma_{12}^{\psi(2S)}$$

VALUE (units 10^{-4})	DOCUMENT ID	TECN	COMMENT
19.6 ± 1.6 OUR FIT			
13.2 ± 2.4 ± 3.2	¹ BAI	99B BES	$\psi(2S) \rightarrow \gamma K_S^0 K^+ \pi^-$

¹ Calculated by us. The value of $B(\chi_{c1} \rightarrow K_S^0 K^+ \pi^-)$ reported by BAI 99B was derived using $B(\psi(2S) \rightarrow \gamma \chi_{c1}(1P)) = (8.7 \pm 0.8)\%$ and $B(\psi(2S) \rightarrow J/\psi\pi^+\pi^-) = (32.4 \pm 2.6)\%$ [BAI 98d].

$$\Gamma(\chi_{c1}(1P) \rightarrow K^+ K^- K^+ K^-)/\Gamma_{\text{total}} \times \Gamma(\psi(2S) \rightarrow \gamma \chi_{c1}(1P))/\Gamma_{\text{total}}$$

$$\Gamma_{44}/\Gamma \times \Gamma_{163}^{\psi(2S)}/\Gamma_{12}^{\psi(2S)}$$

VALUE (units 10^{-4})	EVTS	DOCUMENT ID	TECN	COMMENT
0.53 ± 0.11 OUR FIT				
0.61 ± 0.11 ± 0.08	54	¹ ABLIKIM	06T BES2	$\psi(2S) \rightarrow \gamma K^+ K^+ K^- K^-$

¹ Calculated by us. The value of $B(\chi_{c1} \rightarrow 2K^+ 2K^-)$ reported by ABLIKIM 06T was derived using $B(\psi(2S) \rightarrow \gamma \chi_{c1}(1P)) = (8.7 \pm 0.8)\%$.

$$\Gamma(\chi_{c1}(1P) \rightarrow K^+ K^- K^+ K^-)/\Gamma_{\text{total}} \times \Gamma(\psi(2S) \rightarrow \gamma \chi_{c1}(1P))/\Gamma(\psi(2S) \rightarrow J/\psi(1S)\pi^+\pi^-)$$

$$\Gamma_{44}/\Gamma \times \Gamma_{163}^{\psi(2S)}/\Gamma_{12}^{\psi(2S)}$$

VALUE (units 10^{-4})	DOCUMENT ID	TECN	COMMENT
1.52 ± 0.31 OUR FIT			
1.13 ± 0.40 ± 0.29	¹ BAI	99B BES	$\psi(2S) \rightarrow \gamma K^+ K^+ K^- K^-$

¹ Calculated by us. The value of $B(\chi_{c1} \rightarrow 2K^+ 2K^-)$ reported by BAI 99B was derived using $B(\psi(2S) \rightarrow \gamma \chi_{c1}(1P)) = (8.7 \pm 0.8)\%$ and $B(\psi(2S) \rightarrow J/\psi\pi^+\pi^-) = (32.4 \pm 2.6)\%$ [BAI 98d].

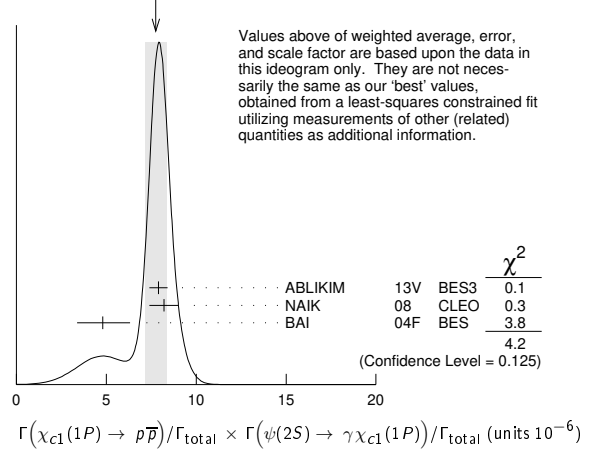
$$\Gamma(\chi_{c1}(1P) \rightarrow p\bar{p})/\Gamma_{\text{total}} \times \Gamma(\psi(2S) \rightarrow \gamma \chi_{c1}(1P))/\Gamma_{\text{total}}$$

$$\Gamma_{54}/\Gamma \times \Gamma_{163}^{\psi(2S)}/\Gamma_{12}^{\psi(2S)}$$

VALUE (units 10^{-6})	EVTS	DOCUMENT ID	TECN	COMMENT
7.41 ± 0.35 OUR FIT				
7.8 ± 0.6 OUR AVERAGE				Error includes scale factor of 1.4. See the ideogram below.
7.9 ± 0.4 ± 0.3	453	ABLIKIM	13V BES3	$\psi(2S) \rightarrow \gamma p\bar{p}$
8.2 ± 0.7 ± 0.4	141 ± 13	¹ NAIK	08 CLEO	$\psi(2S) \rightarrow \gamma p\bar{p}$
4.8 ^{+1.4} _{-1.3} ± 0.6	18.2 ^{+5.5} _{-4.9}	BAI	04F BES	$\psi(2S) \rightarrow \gamma \chi_{c1}(1P) \rightarrow \gamma p\bar{p}$

¹ Calculated by us. NAIK 08 reports $B(\chi_{c1} \rightarrow p\bar{p}) = (9.0 \pm 0.8 \pm 0.4 \pm 0.5) \times 10^{-5}$ using $B(\psi(2S) \rightarrow \gamma \chi_{c1}) = (9.07 \pm 0.11 \pm 0.54)\%$.

WEIGHTED AVERAGE
7.8 ± 0.6 (Error scaled by 1.4)



$$\Gamma(\chi_{c1}(1P) \rightarrow \Sigma^+ \bar{p} K_S^0 + \text{c.c.})/\Gamma_{\text{total}} \times \Gamma(\psi(2S) \rightarrow \gamma \chi_{c1}(1P))/\Gamma_{\text{total}}$$

$$\Gamma_{78}/\Gamma \times \Gamma_{163}^{\psi(2S)}/\Gamma_{12}^{\psi(2S)}$$

VALUE (units 10^{-5})	EVTS	DOCUMENT ID	TECN	COMMENT
1.49 ± 0.09 ± 0.07	258	¹ ABLIKIM	19BB BES3	$\psi(2S) \rightarrow \gamma \Sigma^+ \bar{p} K_S^0 + \text{c.c.}$

¹ Calculated by us. ABLIKIM 19BB reports $B(\chi_{c1} \rightarrow \Sigma^+ \bar{p} K_S^0 + \text{c.c.}) = (1.53 \pm 0.10 \pm 0.08) \times 10^{-4}$ using $B(\psi(2S) \rightarrow \gamma \chi_{c1}) = (9.75 \pm 0.24)\%$ and other branching fractions from PDG 18.

$$\Gamma(\chi_{c1}(1P) \rightarrow \Sigma^0 \bar{p} K^+ + \text{c.c.})/\Gamma_{\text{total}} \times \Gamma(\psi(2S) \rightarrow \gamma \chi_{c1}(1P))/\Gamma_{\text{total}}$$

$$\Gamma_{79}/\Gamma \times \Gamma_{163}^{\psi(2S)}/\Gamma_{12}^{\psi(2S)}$$

VALUE (units 10^{-5})	EVTS	DOCUMENT ID	TECN	COMMENT
1.42 ± 0.07 ± 0.06	493	¹ ABLIKIM	20AE BES3	$\psi(2S) \rightarrow \gamma \Sigma^0 \bar{p} K^+ + \text{c.c.}$

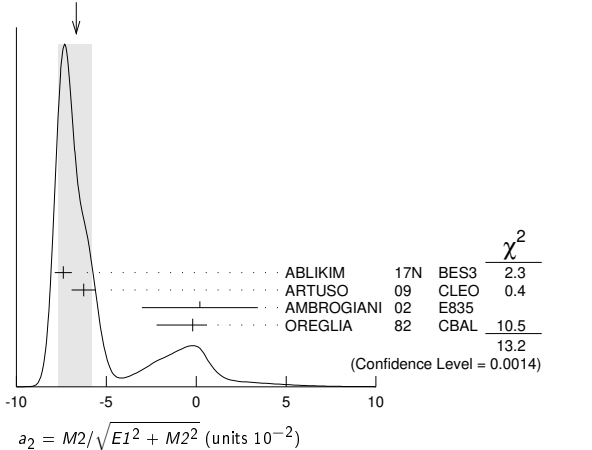
¹ Calculated by us. ABLIKIM 20AE reports $B(\chi_{c1} \rightarrow \Sigma^0 \bar{p} K^+ + \text{c.c.}) = (1.46 \pm 0.07 \pm 0.07) \times 10^{-4}$ using $B(\psi(2S) \rightarrow \gamma \chi_{c1}) = (9.75 \pm 0.24)\%$ and other branching fractions from PDG 20.

MULTIPOLE AMPLITUDES IN $\chi_{c1}(1P) \rightarrow \gamma J/\psi(1S)$

$a_2 = M2/\sqrt{E1^2 + M2^2}$ Magnetic quadrupole fractional transition amplitude

VALUE (units 10^{-2})	EVTS	DOCUMENT ID	TECN	COMMENT
-6.7 ± 0.9 OUR AVERAGE				Error includes scale factor of 2.6. See the ideogram below.
-7.40 ± 0.33 ± 0.34	164k	¹ ABLIKIM	17N BES3	$\psi(2S) \rightarrow \gamma \gamma \ell^+ \ell^-$
-6.26 ± 0.63 ± 0.24	39k	ARTUSO	09 CLEO	$\psi(2S) \rightarrow \gamma \gamma \ell^+ \ell^-$
0.2 ± 3.2 ± 0.4	2090	AMBROGIANI	02 E835	$p\bar{p} \rightarrow \chi_{c1} \rightarrow J/\psi \gamma$
-0.2 ^{+0.8} _{-2.0}	921	OREGLIA	82 CBAL	$\psi(2S) \rightarrow \chi_{c1} \gamma \rightarrow J/\psi \gamma \gamma$

WEIGHTED AVERAGE
-6.7 ± 0.9 (Error scaled by 2.6)



¹ Correlated with b_2 with correlation coefficient $\rho_{a_2 b_2} = 0.133$.

Meson Particle Listings

$\chi_{c1}(1P), h_c(1P)$

MULTIPOLE AMPLITUDES IN $\psi(2S) \rightarrow \gamma\chi_{c1}(1S)$ RADIATIVE DECAY

$b_2 = M_2/\sqrt{E_1^2 + M^2}$ Magnetic quadrupole fractional transition amplitude

VALUE (units 10^{-2})	EVTS	DOCUMENT ID	TECN	COMMENT
2.5 ± 0.4 OUR AVERAGE				
2.29 ± 0.39 ± 0.27	164k	¹ ABLIKIM	17N BES3	$\psi(2S) \rightarrow \gamma\gamma\ell^+\ell^-$
2.76 ± 0.73 ± 0.23	39k	ARTUSO	09 CLEO	$\psi(2S) \rightarrow \gamma\gamma\ell^+\ell^-$
7.7 ^{+5.0} / _{-4.5}	921	OREGLIA	82 CBAL	$\psi(2S) \rightarrow \gamma\gamma\ell^+\ell^-$

¹ Correlated with a_2 with correlation coefficient $\rho_{a_2 b_2} = 0.133$.

MULTIPOLE AMPLITUDE RATIOS IN RADIATIVE DECAYS $\psi(2S) \rightarrow \gamma\chi_{c1}(1S)$ and $\chi_{c1} \rightarrow \gamma J/\psi(1S)$

a_2/b_2 Magnetic quadrupole transition amplitude ratio

VALUE	EVTS	DOCUMENT ID	TECN	COMMENT
-2.27 ^{+0.57}/_{-0.99}	39k	¹ ARTUSO	09 CLEO	$\psi(2S) \rightarrow \gamma\gamma\ell^+\ell^-$

¹ Statistical and systematic errors combined. Not independent of $a_2(\chi_{c1})$ and $b_2(\chi_{c1})$ values from ARTUSO 09.

$\chi_{c1}(1P)$ REFERENCES

ABLIKIM	21AV	JHEP 2111 217	M. Ablikim et al.	(BESIII Collab.)
ABLIKIM	21L	PR D103 112004	M. Ablikim et al.	(BESIII Collab.)
ABLIKIM	20AE	PR D102 092006	M. Ablikim et al.	(BESIII Collab.)
ABLIKIM	20B	PR D101 012012	M. Ablikim et al.	(BESIII Collab.)
ABLIKIM	20I	PR D101 092002	M. Ablikim et al.	(BESIII Collab.)
PDG	20	PTEP 2020 083C01	P.A. Zyla et al.	(PDG Collab.)
ABLIKIM	19AA	PR D99 052008	M. Ablikim et al.	(BESIII Collab.)
ABLIKIM	19AU	PR D100 052010	M. Ablikim et al.	(BESIII Collab.)
ABLIKIM	19BB	PR D100 092006	M. Ablikim et al.	(BESIII Collab.)
ABLIKIM	19J	PR D99 012015	M. Ablikim et al.	(BESIII Collab.)
ABLIKIM	19Z	PR D99 051101	M. Ablikim et al.	(BESIII Collab.)
LU	19	PR D99 032003	P.-C. Lu et al.	(BELLE Collab.)
ABLIKIM	18D	PRL 121 022001	M. Ablikim et al.	(BESIII Collab.)
ABLIKIM	18V	PR D97 052011	M. Ablikim et al.	(BESIII Collab.)
PDG	18	PR D98 030001	M. Tanabashi et al.	(PDG Collab.)
AALJ	17BB	EPJ C77 609	R. Aaij et al.	(LHCb Collab.)
AALJ	17BI	PRL 119 221801	R. Aaij et al.	(LHCb Collab.)
ABLIKIM	17AE	PR D96 092007	M. Ablikim et al.	(BESIII Collab.)
ABLIKIM	17I	PRL 118 221802	M. Ablikim et al.	(BESIII Collab.)
ABLIKIM	17K	PR D95 032002	M. Ablikim et al.	(BESIII Collab.)
ABLIKIM	17N	PR D95 072004	M. Ablikim et al.	(BESIII Collab.)
ABLIKIM	17U	PR D96 032001	M. Ablikim et al.	(BESIII Collab.)
PDG	16	CP C40 100001	C. Patrignani et al.	(PDG Collab.)
ABLIKIM	15I	PR D91 092006	M. Ablikim et al.	(BESIII Collab.)
ABLIKIM	15M	PR D91 112008	M. Ablikim et al.	(BESIII Collab.)
ABLIKIM	14J	PR D89 074030	M. Ablikim et al.	(BESIII Collab.)
ABLIKIM	13B	PR D87 012002	M. Ablikim et al.	(BESIII Collab.)
ABLIKIM	13D	PR D87 012007	M. Ablikim et al.	(BESIII Collab.)
ABLIKIM	13H	PR D87 032007	M. Ablikim et al.	(BESIII Collab.)
ABLIKIM	13V	PR D88 112001	M. Ablikim et al.	(BESIII Collab.)
ABLIKIM	12I	PR D86 052004	M. Ablikim et al.	(BESIII Collab.)
ABLIKIM	12J	PR D86 052011	M. Ablikim et al.	(BESIII Collab.)
ABLIKIM	12O	PRL 109 172002	M. Ablikim et al.	(BESIII Collab.)
ABLIKIM	11A	PR D83 012006	M. Ablikim et al.	(BESIII Collab.)
ABLIKIM	11D	PR D83 032003	M. Ablikim et al.	(BESIII Collab.)
ABLIKIM	11E	PR D83 112005	M. Ablikim et al.	(BESIII Collab.)
ABLIKIM	11F	PR D83 112009	M. Ablikim et al.	(BESIII Collab.)
ABLIKIM	11K	PRL 107 092001	M. Ablikim et al.	(BESIII Collab.)
ONYISI	10	PR D82 011103	P.U.E. Onyisi et al.	(CLEO Collab.)
ARTUSO	09	PR D80 112003	M. Artuso et al.	(CLEO Collab.)
BENNETT	08A	PRL 101 151801	J.V. Bennett et al.	(CLEO Collab.)
ECKLUND	08A	PR D78 091501	K.M. Ecklund et al.	(CLEO Collab.)
HE	08B	PR D78 092004	Q. He et al.	(CLEO Collab.)
MENDEZ	08	PR D78 011102	H. Mendez et al.	(CLEO Collab.)
NAIK	08	PR D78 031101	P. Naik et al.	(CLEO Collab.)
ATHAR	07	PR D75 032002	S.B. Athar et al.	(CLEO Collab.)
ABLIKIM	06D	PR D73 052006	M. Ablikim et al.	(BES Collab.)
ABLIKIM	06R	PR D74 072001	M. Ablikim et al.	(BES Collab.)
ABLIKIM	06T	PL B642 197	M. Ablikim et al.	(BES Collab.)
ABLIKIM	05G	PR D71 092002	M. Ablikim et al.	(BES Collab.)
ABLIKIM	05O	PL B630 21	M. Ablikim et al.	(BES Collab.)
ADAM	05A	PRL 94 232002	N.E. Adam et al.	(CLEO Collab.)
ANDREOTTI	05A	NP B717 34	M. Andreotti et al.	(FNAL E835 Collab.)
ABLIKIM	04B	PR D70 012003	M. Ablikim et al.	(BES Collab.)
ABLIKIM	04H	PR D70 092003	M. Ablikim et al.	(BES Collab.)
ATHAR	04	PR D70 112002	S.B. Athar et al.	(CLEO Collab.)
BAI	04F	PR D69 092001	J.Z. Bai et al.	(BES Collab.)
BAI	04I	PR D70 012006	J.Z. Bai et al.	(BES Collab.)
AULCHENKO	03	PL B573 63	V.M. Aulchenko et al.	(KEDR Collab.)
BAI	03E	PR D67 112001	J.Z. Bai et al.	(BES Collab.)
AMBROGIANI	02	PR D65 052002	M. Ambrogiani et al.	(FNAL E835 Collab.)
BAI	99B	PR D60 072001	J.Z. Bai et al.	(BES Collab.)
BAI	98D	PR D58 092006	J.Z. Bai et al.	(BES Collab.)
BAI	98I	PRL 81 3091	J.Z. Bai et al.	(BES Collab.)
ARMSTRONG	92	NP B373 35	T.A. Armstrong et al.	(FNAL, FERR, GENO+)
Also		PRL 68 1468	T.A. Armstrong et al.	(FNAL, FERR, GENO+)
BAGLIN	86B	PL B172 455	C. Baglin	(LAPP, CERN, GENO, LYON, OSLO+)
GAISER	86	PR D34 711	J. Gaiser et al.	(Crystal Ball Collab.)
LEMOIGNE	82	PL 113B 509	Y. Lemoigne et al.	(SACL, LOIC, SHMP+)
OREGLIA	82	PR D25 2259	M.J. Oreglia et al.	(SLAC, CIT, HARV+)
Also		Private comm.	M.J. Oreglia	(EFI)
HIMEL	80	PRL 44 920	T. Himel et al.	(LBL, SLAC)
Also		Private Comm.	G. Trilling	(LBL, UCB)
BRANDELIK	79B	NP B160 426	R. Brandelik et al.	(DASP Collab.)
BARTEL	78B	PL 79B 492	W. Bartel et al.	(DESY, HEIDP)
TANENBAUM	78	PR D17 1731	W.M. Tanenbaum et al.	(SLAC, LBL)
Also		Private Comm.	G. Trilling	(LBL, UCB)
BIDDICK	77	PRL 38 1324	C.J. Biddick et al.	(UCSD, UMD, PAVI+)
FELDMAN	77	PRPL 33C 285	G.J. Feldman, M.L. Perl	(LBL, SLAC)
YAMADA	77	Hamburg Conf. 69	S. Yamada	(DASP Collab.)
WHITAKER	76	PRL 37 1596	J.S. Whitaker et al.	(SLAC, LBL)
TANENBAUM	75	PRL 35 1323	W.M. Tanenbaum et al.	(LBL, SLAC)

$h_c(1P)$

$$I^G(J^{PC}) = 0^-(1^{+-})$$

Quantum numbers are quark model prediction, C = - established by $\eta_c\gamma$ decay.

$h_c(1P)$ MASS

VALUE (MeV)	EVTS	DOCUMENT ID	TECN	COMMENT
3525.38 ± 0.11 OUR AVERAGE				
3525.31 ± 0.11 ± 0.14	832	¹ ABLIKIM	12N BES3	$\psi(2S) \rightarrow \pi^0\gamma$ hadrons
3525.40 ± 0.13 ± 0.18	3679	ABLIKIM	10B BES3	$\psi(2S) \rightarrow \pi^0\gamma\eta_c$
3525.20 ± 0.18 ± 0.12	1282	² DOBBS	08A CLEO	$\psi(2S) \rightarrow \pi^0\eta_c\gamma$
3525.8 ± 0.2 ± 0.2	13	ANDREOTTI	05B E835	$\bar{p}p \rightarrow \eta_c\gamma$
• • • We do not use the following data for averages, fits, limits, etc. • • •				
3525.6 ± 0.5	92 ⁺²³ / ₋₂₂	ADAMS	09 CLEO	$\psi(2S) \rightarrow 2(\pi^+\pi^-\pi^0)$
3524.4 ± 0.6 ± 0.4	168 ± 40	³ ROSNER	05 CLEO	$\psi(2S) \rightarrow \pi^0\eta_c\gamma$
3527 ± 0.8	42	ANTONIAZZI	94 E705	300 $\pi^\pm, \rho Li \rightarrow J/\psi\pi^0 X$
3526.28 ± 0.18 ± 0.19	59	⁴ ARMSTRONG	92D E760	$\bar{p}p \rightarrow J/\psi\pi^0$
3525.4 ± 0.8 ± 0.4	5	BAGLIN	86 SPEC	$\bar{p}p \rightarrow J/\psi X$

¹ With floating width.

² Combination of exclusive and inclusive analyses for the reaction $\psi(2S) \rightarrow \pi^0 h_c \rightarrow \pi^0 \eta_c \gamma$. This result is the average of DOBBS 08A and ROSNER 05.

³ Superseded by DOBBS 08A.

⁴ Mass central value and systematic error recalculated by us according to Eq. (16) in ARMSTRONG 93B, using the value for the $\psi(2S)$ mass from AULCHENKO 03.

$h_c(1P)$ WIDTH

VALUE (MeV)	CL%	EVTS	DOCUMENT ID	TECN	COMMENT
0.70 ± 0.28 ± 0.22		832	¹ ABLIKIM	12N BES3	$\psi(2S) \rightarrow \pi^0\gamma$ hadrons
• • • We do not use the following data for averages, fits, limits, etc. • • •					
< 1.44	90	3679	² ABLIKIM	10B BES3	$\psi(2S) \rightarrow \pi^0\gamma\eta_c$
< 1		13	ANDREOTTI	05B E835	$\bar{p}p \rightarrow \eta_c\gamma$
< 1.1	90	59	ARMSTRONG	92D E760	$\bar{p}p \rightarrow J/\psi\pi^0$

¹ With floating mass.

² The central value is $\Gamma = 0.73 \pm 0.45 \pm 0.28$ MeV.

$h_c(1P)$ DECAY MODES

Mode	Fraction (Γ_i/Γ)	Confidence level
Γ_1	$J/\psi(1S)\pi^0$	
Γ_2	$J/\psi(1S)\pi\pi$	not seen
Γ_3	$J/\psi(1S)\pi^+\pi^-$	< 2.3 × 10 ⁻³ 90%
Γ_4	$\rho\bar{\rho}$	< 1.5 × 10 ⁻⁴ 90%
Γ_5	$\rho\bar{\rho}\pi^+\pi^-$	(2.9 ± 0.6) × 10 ⁻³
Γ_6	$\rho\bar{\rho}\pi^0\pi^0$	< 5 × 10 ⁻⁴
Γ_7	$\pi^+\pi^-\pi^0$	(1.6 ± 0.5) × 10 ⁻³
Γ_8	$\pi^+\pi^-\pi^0\eta$	(7.2 ± 2.3) × 10 ⁻³
Γ_9	$2\pi^+2\pi^-\pi^0$	(8.1 ± 1.8) × 10 ⁻³
Γ_{10}	$3\pi^+3\pi^-\pi^0$	< 9 × 10 ⁻³ 90%
Γ_{11}	$K^+K^-\pi^+\pi^-$	< 6 × 10 ⁻⁴ 90%
Γ_{12}	$K^+K^-\pi^+\pi^-\pi^0$	(3.2 ± 0.8) × 10 ⁻³
Γ_{13}	$K^+K^-\pi^+\pi^-\eta$	< 2.3 × 10 ⁻³ 90%
Γ_{14}	$K^+K^-\pi^0$	< 6 × 10 ⁻⁴ 90%
Γ_{15}	$K^+K^-\pi^0\eta$	< 2.1 × 10 ⁻³ 90%
Γ_{16}	$K^+K^-\eta$	< 9 × 10 ⁻⁴ 90%
Γ_{17}	$2K^+2K^-\pi^0$	< 2.4 × 10 ⁻⁴ 90%
Γ_{18}	$K_S^0 K^\pm\pi^\mp$	< 6 × 10 ⁻⁴ 90%
Γ_{19}	$K_S^0 K^\pm\pi^\mp\pi^+\pi^-$	(2.8 ± 1.0) × 10 ⁻³

Radiative decays

Γ_{20}	$\gamma\eta$	(4.7 ± 2.1) × 10 ⁻⁴
Γ_{21}	$\gamma\eta'(958)$	(1.5 ± 0.4) × 10 ⁻³
Γ_{22}	$\gamma\eta_c(1S)$	(50 ± 9) %

$h_c(1P)$ PARTIAL WIDTHS

$h_c(1P) \Gamma(i)/\Gamma(\bar{p}p)/\Gamma(\text{total})$

$\Gamma(\gamma\eta_c(1S)) \times \Gamma(\bar{p}p)/\Gamma(\text{total})$	VALUE (eV)	EVTS	DOCUMENT ID	TECN	COMMENT
$\Gamma_{22}\Gamma_4/\Gamma$					
• • • We do not use the following data for averages, fits, limits, etc. • • •					
12.0 ± 4.5	13	¹ ANDREOTTI	05B E835	$\bar{p}p \rightarrow \eta_c\gamma$	

¹ Assuming $\Gamma = 1$ MeV.

See key on page 1127

Meson Particle Listings
 $h_c(1P)$ $h_c(1P)$ BRANCHING RATIOS

$\Gamma(J/\psi(1S)\pi\pi)/\Gamma(J/\psi(1S)\pi^0)$					Γ_2/Γ_1
VALUE	CL%	DOCUMENT ID	TECN	COMMENT	
<0.18	90	ARMSTRONG 92D	E760	$\bar{p}p \rightarrow J/\psi\pi^0$	

$\Gamma(J/\psi(1S)\pi^+\pi^-)/\Gamma_{total}$					Γ_3/Γ
VALUE	CL%	DOCUMENT ID	TECN	COMMENT	
$2.3 \pm 0.5 \times 10^{-3}$	90	¹ ABLIKIM	18M BES3	$\psi(2S) \rightarrow \pi^0\pi^+\pi^- J/\psi$	
¹ ABLIKIM 18M reports $[\Gamma(h_c(1P) \rightarrow J/\psi(1S)\pi^+\pi^-)/\Gamma_{total}] \times [B(\psi(2S) \rightarrow h_c(1P)\pi^0)] < 2.0 \times 10^{-6}$ which we divide by our best value $B(\psi(2S) \rightarrow h_c(1P)\pi^0) = 8.6 \times 10^{-4}$.					

$\Gamma(p\bar{p})/\Gamma_{total}$					Γ_4/Γ
VALUE	CL%	DOCUMENT ID	TECN	COMMENT	
$<1.5 \times 10^{-4}$	90	¹ ABLIKIM	13V BES3	$\psi(2S) \rightarrow \gamma p\bar{p}$	
¹ ABLIKIM 13V reports $[\Gamma(h_c(1P) \rightarrow p\bar{p})/\Gamma_{total}] \times [B(\psi(2S) \rightarrow h_c(1P)\pi^0)] < 1.3 \times 10^{-7}$ which we divide by our best value $B(\psi(2S) \rightarrow h_c(1P)\pi^0) = 8.6 \times 10^{-4}$.					

$\Gamma(\pi^+\pi^-\pi^0)/\Gamma_{total}$					Γ_7/Γ
VALUE (units 10^{-3})	CL%	EVTS	DOCUMENT ID	TECN	COMMENT
$1.6 \pm 0.5 \pm 0.2$	101		¹ ABLIKIM	19AG BES3	$\psi(2S) \rightarrow \pi^0 h_c(1P)$
••• We do not use the following data for averages, fits, limits, etc. •••					
<2.2	90		² ADAMS	09 CLEO	$\psi(2S) \rightarrow \pi^0\gamma\eta_C$
¹ ABLIKIM 19AG reports $[\Gamma(h_c(1P) \rightarrow \pi^+\pi^-\pi^0)/\Gamma_{total}] \times [B(\psi(2S) \rightarrow h_c(1P)\pi^0)] = (1.38 \pm 0.35 \pm 0.17) \times 10^{-6}$ which we divide by our best value $B(\psi(2S) \rightarrow h_c(1P)\pi^0) = (8.6 \pm 1.3) \times 10^{-4}$. Our first error is their experiment's error and our second error is the systematic error from using our best value.					
² ADAMS 09 reports $[\Gamma(h_c(1P) \rightarrow \pi^+\pi^-\pi^0)/\Gamma_{total}] \times [B(\psi(2S) \rightarrow h_c(1P)\pi^0)] < 0.19 \times 10^{-5}$ which we divide by our best value $B(\psi(2S) \rightarrow h_c(1P)\pi^0) = 8.6 \times 10^{-4}$.					

$\Gamma(\pi^+\pi^-\pi^0\eta)/\Gamma_{total}$					Γ_8/Γ
VALUE (units 10^{-3})	EVTS	DOCUMENT ID	TECN	COMMENT	
$7.2 \pm 2.0 \pm 1.0$	35	¹ ABLIKIM	20AH BES3	$\psi(2S) \rightarrow \pi^0 h_c(1P)$	
¹ ABLIKIM 20AH reports $[\Gamma(h_c(1P) \rightarrow \pi^+\pi^-\pi^0\eta)/\Gamma_{total}] \times [B(\psi(2S) \rightarrow h_c(1P)\pi^0)] = (6.2 \pm 1.6 \pm 0.7) \times 10^{-6}$ which we divide by our best value $B(\psi(2S) \rightarrow h_c(1P)\pi^0) = (8.6 \pm 1.3) \times 10^{-4}$. Our first error is their experiment's error and our second error is the systematic error from using our best value.					

$\Gamma(2\pi^+2\pi^-\pi^0)/\Gamma_{total}$					Γ_9/Γ
VALUE (units 10^{-2})	EVTS	DOCUMENT ID	TECN	COMMENT	
0.81 ± 0.18 OUR AVERAGE					
$0.74 \pm 0.14 \pm 0.11$	254	¹ ABLIKIM	19AG BES3	$\psi(2S) \rightarrow \pi^0 h_c(1P)$	
$2.2 \pm 0.8 \pm 0.3$	92	² ADAMS	09 CLEO	$\psi(2S) \rightarrow \pi^0\gamma\eta_C$	
¹ ABLIKIM 19AG reports $[\Gamma(h_c(1P) \rightarrow 2\pi^+2\pi^-\pi^0)/\Gamma_{total}] \times [B(\psi(2S) \rightarrow h_c(1P)\pi^0)] = (6.40 \pm 0.81 \pm 0.87) \times 10^{-6}$ which we divide by our best value $B(\psi(2S) \rightarrow h_c(1P)\pi^0) = (8.6 \pm 1.3) \times 10^{-4}$. Our first error is their experiment's error and our second error is the systematic error from using our best value.					
² ADAMS 09 reports $[\Gamma(h_c(1P) \rightarrow 2\pi^+2\pi^-\pi^0)/\Gamma_{total}] \times [B(\psi(2S) \rightarrow h_c(1P)\pi^0)] = (1.88 \pm 0.48 \pm 0.47) \times 10^{-5}$ which we divide by our best value $B(\psi(2S) \rightarrow h_c(1P)\pi^0) = (8.6 \pm 1.3) \times 10^{-4}$. Our first error is their experiment's error and our second error is the systematic error from using our best value.					

$\Gamma(3\pi^+3\pi^-\pi^0)/\Gamma_{total}$					Γ_{10}/Γ
VALUE	CL%	DOCUMENT ID	TECN	COMMENT	
<9 $\times 10^{-3}$	90	¹ ABLIKIM	19AG BES3	$\psi(2S) \rightarrow \pi^0 h_c(1P)$	
••• We do not use the following data for averages, fits, limits, etc. •••					
<0.029	90	² ADAMS	09 CLEO	$\psi(2S) \rightarrow \pi^0\gamma\eta_C$	
¹ ABLIKIM 19AG reports $[\Gamma(h_c(1P) \rightarrow 3\pi^+3\pi^-\pi^0)/\Gamma_{total}] \times [B(\psi(2S) \rightarrow h_c(1P)\pi^0)] < 7.5 \times 10^{-6}$ which we divide by our best value $B(\psi(2S) \rightarrow h_c(1P)\pi^0) = 8.6 \times 10^{-4}$.					
² ADAMS 09 reports $[\Gamma(h_c(1P) \rightarrow 3\pi^+3\pi^-\pi^0)/\Gamma_{total}] \times [B(\psi(2S) \rightarrow h_c(1P)\pi^0)] < 2.5 \times 10^{-5}$ which we divide by our best value $B(\psi(2S) \rightarrow h_c(1P)\pi^0) = 8.6 \times 10^{-4}$.					

$\Gamma(p\bar{p}\pi^+\pi^-)/\Gamma_{total}$					Γ_5/Γ
VALUE (units 10^{-3})	EVTS	DOCUMENT ID	TECN	COMMENT	
$2.9 \pm 0.5 \pm 0.4$	230	¹ ABLIKIM	19AG BES3	$\psi(2S) \rightarrow \pi^0 h_c(1P)$	
¹ ABLIKIM 19AG reports $[\Gamma(h_c(1P) \rightarrow p\bar{p}\pi^+\pi^-)/\Gamma_{total}] \times [B(\psi(2S) \rightarrow h_c(1P)\pi^0)] = (2.49 \pm 0.27 \pm 0.28) \times 10^{-6}$ which we divide by our best value $B(\psi(2S) \rightarrow h_c(1P)\pi^0) = (8.6 \pm 1.3) \times 10^{-4}$. Our first error is their experiment's error and our second error is the systematic error from using our best value.					

$\Gamma(p\bar{p}\pi^0\pi^0)/\Gamma_{total}$					Γ_6/Γ
VALUE	CL%	EVTS	DOCUMENT ID	TECN	COMMENT
<5 $\times 10^{-4}$	90	12	¹ ABLIKIM	20AH BES3	$\psi(2S) \rightarrow \pi^0 h_c(1P)$
¹ ABLIKIM 20AH reports $[\Gamma(h_c(1P) \rightarrow p\bar{p}\pi^0\pi^0)/\Gamma_{total}] \times [B(\psi(2S) \rightarrow h_c(1P)\pi^0)] < 4.4 \times 10^{-7}$ which we divide by our best value $B(\psi(2S) \rightarrow h_c(1P)\pi^0) = 8.6 \times 10^{-4}$.					

$\Gamma(K^+K^-\pi^+\pi^-)/\Gamma_{total}$					Γ_{11}/Γ
VALUE	CL%	DOCUMENT ID	TECN	COMMENT	
<6 $\times 10^{-4}$	90	¹ ABLIKIM	19AG BES3	$\psi(2S) \rightarrow \pi^0 h_c(1P)$	
¹ ABLIKIM 19AG reports $[\Gamma(h_c(1P) \rightarrow K^+K^-\pi^+\pi^-)/\Gamma_{total}] \times [B(\psi(2S) \rightarrow h_c(1P)\pi^0)] < 0.5 \times 10^{-6}$ which we divide by our best value $B(\psi(2S) \rightarrow h_c(1P)\pi^0) = 8.6 \times 10^{-4}$.					

$\Gamma(K^+K^-\pi^+\pi^-\pi^0)/\Gamma_{total}$					Γ_{12}/Γ
VALUE (units 10^{-3})	EVTS	DOCUMENT ID	TECN	COMMENT	
$3.2 \pm 0.7 \pm 0.5$	80	¹ ABLIKIM	20AH BES3	$\psi(2S) \rightarrow \pi^0 h_c(1P)$	
¹ ABLIKIM 20AH reports $[\Gamma(h_c(1P) \rightarrow K^+K^-\pi^+\pi^-\pi^0)/\Gamma_{total}] \times [B(\psi(2S) \rightarrow h_c(1P)\pi^0)] = (2.8 \pm 0.5 \pm 0.3) \times 10^{-6}$ which we divide by our best value $B(\psi(2S) \rightarrow h_c(1P)\pi^0) = (8.6 \pm 1.3) \times 10^{-4}$. Our first error is their experiment's error and our second error is the systematic error from using our best value.					

$\Gamma(K^+K^-\pi^+\pi^-\eta)/\Gamma_{total}$					Γ_{13}/Γ
VALUE	CL%	EVTS	DOCUMENT ID	TECN	COMMENT
<2.3 $\times 10^{-3}$	90	24	¹ ABLIKIM	20AH BES3	$\psi(2S) \rightarrow \pi^0 h_c(1P)$
¹ ABLIKIM 20AH reports $[\Gamma(h_c(1P) \rightarrow K^+K^-\pi^+\pi^-\eta)/\Gamma_{total}] \times [B(\psi(2S) \rightarrow h_c(1P)\pi^0)] < 2.0 \times 10^{-6}$ which we divide by our best value $B(\psi(2S) \rightarrow h_c(1P)\pi^0) = 8.6 \times 10^{-4}$.					

$\Gamma(K^+K^-\pi^0)/\Gamma_{total}$					Γ_{14}/Γ
VALUE	CL%	EVTS	DOCUMENT ID	TECN	COMMENT
<6 $\times 10^{-4}$	90	20	¹ ABLIKIM	20AH BES3	$\psi(2S) \rightarrow \pi^0 h_c(1P)$
¹ ABLIKIM 20AH reports $[\Gamma(h_c(1P) \rightarrow K^+K^-\pi^0)/\Gamma_{total}] \times [B(\psi(2S) \rightarrow h_c(1P)\pi^0)] < 4.8 \times 10^{-7}$ which we divide by our best value $B(\psi(2S) \rightarrow h_c(1P)\pi^0) = 8.6 \times 10^{-4}$.					

$\Gamma(2K^+2K^-\pi^0)/\Gamma_{total}$					Γ_{17}/Γ
VALUE	CL%	EVTS	DOCUMENT ID	TECN	COMMENT
<2.4 $\times 10^{-4}$	90	11	¹ ABLIKIM	20AH BES3	$\psi(2S) \rightarrow \pi^0 h_c(1P)$
¹ ABLIKIM 20AH reports $[\Gamma(h_c(1P) \rightarrow 2K^+2K^-\pi^0)/\Gamma_{total}] \times [B(\psi(2S) \rightarrow h_c(1P)\pi^0)] < 2.1 \times 10^{-7}$ which we divide by our best value $B(\psi(2S) \rightarrow h_c(1P)\pi^0) = 8.6 \times 10^{-4}$.					

$\Gamma(K^+K^-\pi^0\eta)/\Gamma_{total}$					Γ_{15}/Γ
VALUE	CL%	EVTS	DOCUMENT ID	TECN	COMMENT
<2.1 $\times 10^{-3}$	90	20	¹ ABLIKIM	20AH BES3	$\psi(2S) \rightarrow \pi^0 h_c(1P)$
¹ ABLIKIM 20AH reports $[\Gamma(h_c(1P) \rightarrow K^+K^-\pi^0\eta)/\Gamma_{total}] \times [B(\psi(2S) \rightarrow h_c(1P)\pi^0)] < 1.8 \times 10^{-6}$ which we divide by our best value $B(\psi(2S) \rightarrow h_c(1P)\pi^0) = 8.6 \times 10^{-4}$.					

$\Gamma(K^+K^-\eta)/\Gamma_{total}$					Γ_{16}/Γ
VALUE	CL%	EVTS	DOCUMENT ID	TECN	COMMENT
<9 $\times 10^{-4}$	90	18	¹ ABLIKIM	20AH BES3	$\psi(2S) \rightarrow \pi^0 h_c(1P)$
¹ ABLIKIM 20AH reports $[\Gamma(h_c(1P) \rightarrow K^+K^-\eta)/\Gamma_{total}] \times [B(\psi(2S) \rightarrow h_c(1P)\pi^0)] < 7.5 \times 10^{-7}$ which we divide by our best value $B(\psi(2S) \rightarrow h_c(1P)\pi^0) = 8.6 \times 10^{-4}$.					

$\Gamma(K_S^0 K^{\pm} \pi^{\mp})/\Gamma_{total}$					Γ_{18}/Γ
VALUE	CL%	EVTS	DOCUMENT ID	TECN	COMMENT
<6 $\times 10^{-4}$	90	17	¹ ABLIKIM	20AH BES3	$\psi(2S) \rightarrow \pi^0 h_c(1P)$
¹ ABLIKIM 20AH reports $[\Gamma(h_c(1P) \rightarrow K_S^0 K^{\pm} \pi^{\mp})/\Gamma_{total}] \times [B(\psi(2S) \rightarrow h_c(1P)\pi^0)] < 4.8 \times 10^{-7}$ which we divide by our best value $B(\psi(2S) \rightarrow h_c(1P)\pi^0) = 8.6 \times 10^{-4}$.					

$\Gamma(K_S^0 K^{\pm} \pi^{\mp} \pi^{\pm} \pi^{\mp})/\Gamma_{total}$					Γ_{19}/Γ
VALUE (units 10^{-3})	EVTS	DOCUMENT ID	TECN	COMMENT	
$2.8 \pm 0.9 \pm 0.4$	41	¹ ABLIKIM	20AH BES3	$\psi(2S) \rightarrow \pi^0 h_c(1P)$	
¹ ABLIKIM 20AH reports $[\Gamma(h_c(1P) \rightarrow K_S^0 K^{\pm} \pi^{\mp} \pi^{\pm} \pi^{\mp})/\Gamma_{total}] \times [B(\psi(2S) \rightarrow h_c(1P)\pi^0)] = (2.4 \pm 0.7 \pm 0.3) \times 10^{-6}$ which we divide by our best value $B(\psi(2S) \rightarrow h_c(1P)\pi^0) = (8.6 \pm 1.3) \times 10^{-4}$. Our first error is their experiment's error and our second error is the systematic error from using our best value.					

RADIATIVE DECAYS

$\Gamma(\gamma\eta)/\Gamma_{total}$					Γ_{20}/Γ
VALUE (units 10^{-4})	EVTS	DOCUMENT ID	TECN	COMMENT	
$4.7 \pm 1.5 \pm 1.4$	18	ABL IKIM	16I BES3	$\psi(2S) \rightarrow \pi^0\gamma\eta$	

$\Gamma(\gamma\eta'(958))/\Gamma_{total}$					Γ_{21}/Γ
VALUE (units 10^{-3})	EVTS	DOCUMENT ID	TECN	COMMENT	
$1.52 \pm 0.27 \pm 0.29$	44	ABL IKIM	16I BES3	$\psi(2S) \rightarrow \pi^0\gamma\eta'(958)$	

$\Gamma(\gamma\eta_C(1S))/\Gamma_{total}$					Γ_{22}/Γ
VALUE (units 10^{-2})	EVTS	DOCUMENT ID	TECN	COMMENT	
50 ± 9 OUR AVERAGE					
$53 \pm 7 \pm 8$	3679	¹ ABLIKIM	10B BES3	$\psi(2S) \rightarrow \pi^0\eta_C\gamma$	
$48 \pm 6 \pm 7$		² DOBBS	08A CLEO	$\psi(2S) \rightarrow \pi^0\eta_C\gamma$	

Meson Particle Listings

$h_c(1P), \chi_{c2}(1P)$

••• We do not use the following data for averages, fits, limits, etc. •••

- 48 ± 6 ± 7 1282 ³ DOBBS 08A CLEO $\psi(2S) \rightarrow \pi^0 \eta_C \gamma$
 46 ± 12 ± 7 168 ⁴ ROSNER 05 CLEO $\psi(2S) \rightarrow \pi^0 \eta_C \gamma$
- ¹ ABLIKIM 10B reports $[\Gamma(h_c(1P) \rightarrow \gamma \eta_C(1S))/\Gamma_{\text{total}}] \times [B(\psi(2S) \rightarrow h_c(1P)\pi^0)] = (4.58 \pm 0.40 \pm 0.50) \times 10^{-4}$ which we divide by our best value $B(\psi(2S) \rightarrow h_c(1P)\pi^0) = (8.6 \pm 1.3) \times 10^{-4}$. Our first error is their experiment's error and our second error is the systematic error from using our best value.
 - ² Average of DOBBS 08A and ROSNER 05. DOBBS 08A reports $[\Gamma(h_c(1P) \rightarrow \gamma \eta_C(1S))/\Gamma_{\text{total}}] \times [B(\psi(2S) \rightarrow h_c(1P)\pi^0)] = (4.16 \pm 0.30 \pm 0.37) \times 10^{-4}$ which we divide by our best value $B(\psi(2S) \rightarrow h_c(1P)\pi^0) = (8.6 \pm 1.3) \times 10^{-4}$. Our first error is their experiment's error and our second error is the systematic error from using our best value.
 - ³ DOBBS 08A reports $[\Gamma(h_c(1P) \rightarrow \gamma \eta_C(1S))/\Gamma_{\text{total}}] \times [B(\psi(2S) \rightarrow h_c(1P)\pi^0)] = (4.19 \pm 0.32 \pm 0.45) \times 10^{-4}$ which we divide by our best value $B(\psi(2S) \rightarrow h_c(1P)\pi^0) = (8.6 \pm 1.3) \times 10^{-4}$. Our first error is their experiment's error and our second error is the systematic error from using our best value.
 - ⁴ ROSNER 05 reports $[\Gamma(h_c(1P) \rightarrow \gamma \eta_C(1S))/\Gamma_{\text{total}}] \times [B(\psi(2S) \rightarrow h_c(1P)\pi^0)] = (4.0 \pm 0.8 \pm 0.7) \times 10^{-4}$ which we divide by our best value $B(\psi(2S) \rightarrow h_c(1P)\pi^0) = (8.6 \pm 1.3) \times 10^{-4}$. Our first error is their experiment's error and our second error is the systematic error from using our best value.

$h_c(1P)$ REFERENCES

ABLIKIM 20AH PR D102 112007	M. Ablikim et al.	(BESIII Collab.)
ABLIKIM 19AG PR D99 072008	M. Ablikim et al.	(BESIII Collab.)
ABLIKIM 18M PR D97 052008	M. Ablikim et al.	(BESIII Collab.)
ABLIKIM 16I PRL 116 251802	M. Ablikim et al.	(BESIII Collab.)
ABLIKIM 13V PR D88 112001	M. Ablikim et al.	(BESIII Collab.)
ABLIKIM 12N PR D86 092009	M. Ablikim et al.	(BESIII Collab.)
ABLIKIM 10B PRL 104 132002	M. Ablikim et al.	(BESIII Collab.)
ADAMS 09 PR D80 051106	G.S. Adams et al.	(CLEO Collab.)
DOBBS 08A PRL 101 102003	S. Dobbs et al.	(CLEO Collab.)
ANDREOTTI 05B PR D72 032001	M. Andreotti et al.	(FNAL E835 Collab.)
ROSNER 05 PRL 95 102003	J.L. Rosner et al.	(CLEO Collab.)
AULCHENKO 03 PL B573 63	V.M. Aulchenko et al.	(KEDR Collab.)
ANTONIAZZI 94 PR D50 4258	L. Antoniazzi et al.	(E705 Collab.)
ARMSTRONG 93B PR D47 772	T.A. Armstrong et al.	(FNAL E760 Collab.)
ARMSTRONG 92D PRL 69 2337	T.A. Armstrong et al.	(FNAL, FERR, GENO+)
BAGLIN 86 PL B171 135	C. Baglin et al.	(LAPP, CERN, TORI, STRB+)

$\chi_{c2}(1P)$

See the Review on " $\psi(2S)$ and χ_c branching ratios" before the $\chi_{c0}(1P)$ Listings.

$\chi_{c2}(1P)$ MASS

VALUE (MeV)	EVTS	DOCUMENT ID	TECN	COMMENT
3556.17 ± 0.07 OUR AVERAGE				
3557.3 ± 1.7 ± 0.7	611	¹ AAIJ	17Bb LHCB	$pp \rightarrow b\bar{b}X \rightarrow 2(K^+ K^-)X$
3556.10 ± 0.06 ± 0.11	4.0k	² AAIJ	17Bi LHCB	$\chi_{c2} \rightarrow J/\psi \mu^+ \mu^-$
3555.3 ± 0.6 ± 2.2	2.5k	UEHARA	08 BELL	$\gamma\gamma \rightarrow \text{hadrons}$
3555.70 ± 0.59 ± 0.39		ABLIKIM	05G BES2	$\psi(2S) \rightarrow \gamma \chi_{c2}$
3556.173 ± 0.123 ± 0.020		ANDREOTTI	05A E835	$p\bar{p} \rightarrow e^+ e^- \gamma$
3559.9 ± 2.9		EISENSTEIN	01 CLE2	$e^+ e^- \rightarrow \chi_{c2}$
3556.4 ± 0.7		BAI	99B BES	$\psi(2S) \rightarrow \gamma X$
3556.22 ± 0.131 ± 0.020	585	³ ARMSTRONG	92 E760	$p\bar{p} \rightarrow e^+ e^- \gamma$
3556.9 ± 0.4 ± 0.5	50	BAGLIN	86B SPEC	$p\bar{p} \rightarrow e^+ e^- X$
3557.8 ± 0.2 ± 4		⁴ GAISER	86 CBAL	$\psi(2S) \rightarrow \gamma X$
3553.4 ± 2.2	66	⁵ LEMOIGNE	82 GOLI	$185 \pi^- \text{Be} \rightarrow \gamma \mu^+ \mu^- A$
3555.9 ± 0.7		⁶ OREGLIA	82 CBAL	$e^+ e^- \rightarrow J/\psi 2\gamma$
3557 ± 1.5	69	⁷ HIMEL	80 MRK2	$e^+ e^- \rightarrow J/\psi 2\gamma$
3551 ± 11	15	BRANDELIK	79B DASP	$e^+ e^- \rightarrow J/\psi 2\gamma$
3553 ± 4		⁷ BARTEL	78B CNTR	$e^+ e^- \rightarrow J/\psi 2\gamma$
3553 ± 4 ± 4		^{7,8} TANENBAUM	78 MRK1	$e^+ e^-$
3563 ± 7	360	⁷ BIDDICK	77 CNTR	$e^+ e^- \rightarrow \gamma X$
••• We do not use the following data for averages, fits, limits, etc. •••				
3555.4 ± 1.3	53	UEHARA	13 BELL	$\gamma\gamma \rightarrow K_S^0 K_S^0$
3543 ± 10	4	WHITAKER	76 MRK1	$e^+ e^- \rightarrow J/\psi 2\gamma$

- ¹ From a fit of the $\phi\phi$ invariant mass with the width of $\chi_{c2}(1P)$ fixed to the PDG 16 value.
- ² AAIJ 17Bi reports also $m(\chi_{c2}) - m(\chi_{c1}) = 45.39 \pm 0.07 \pm 0.03$ MeV.
- ³ Recalculated by ANDREOTTI 05A, using the value of $\psi(2S)$ mass from AULCHENKO 03.
- ⁴ Using mass of $\psi(2S) = 3686.0$ MeV.
- ⁵ $J/\psi(1S)$ mass constrained to 3097 MeV.
- ⁶ Assuming $\psi(2S)$ mass = 3686 MeV and $J/\psi(1S)$ mass = 3097 MeV.
- ⁷ Mass value shifted by us by amount appropriate for $\psi(2S)$ mass = 3686 MeV and $J/\psi(1S)$ mass = 3097 MeV.
- ⁸ From a simultaneous fit to radiative and hadronic decay channels.

$\chi_{c2}(1P)$ WIDTH

VALUE (MeV)	EVTS	DOCUMENT ID	TECN	COMMENT
1.97 ± 0.09 OUR FIT				
2.00 ± 0.11 OUR AVERAGE				
2.10 ± 0.20 ± 0.02	4.0k	AAIJ	17Bi LHCB	$\chi_{c2} \rightarrow J/\psi \mu^+ \mu^-$
1.915 ± 0.188 ± 0.013		ANDREOTTI	05A E835	$p\bar{p} \rightarrow e^+ e^- \gamma$
1.96 ± 0.17 ± 0.07	585	¹ ARMSTRONG	92 E760	$p\bar{p} \rightarrow e^+ e^- \gamma$
2.6 ^{+1.4} _{-1.0}	50	BAGLIN	86B SPEC	$p\bar{p} \rightarrow e^+ e^- X$
2.8 ^{+2.1} _{-2.0}		² GAISER	86 CBAL	$\psi(2S) \rightarrow \gamma X$

- ¹ Recalculated by ANDREOTTI 05A.
- ² Errors correspond to 90% confidence level; authors give only width range.

$\chi_{c2}(1P)$ DECAY MODES

Mode	Fraction (Γ_i/Γ)	Confidence level
Hadronic decays		
Γ_1 $2(\pi^+ \pi^-)$	(1.02 ± 0.09) %	
Γ_2 $\rho\rho$		
Γ_3 $\pi^+ \pi^- \pi^0 \pi^0$	(1.83 ± 0.23) %	
Γ_4 $\rho^+ \pi^- \pi^0 + \text{c.c.}$	(2.19 ± 0.34) %	
Γ_5 $4\pi^0$	(1.11 ± 0.15) × 10 ⁻³	
Γ_6 $K^+ K^- \pi^0 \pi^0$	(2.1 ± 0.4) × 10 ⁻³	
Γ_7 $K^+ \pi^- \bar{K}^0 \pi^0 + \text{c.c.}$	(1.38 ± 0.20) %	
Γ_8 $\rho^- K^+ \bar{K}^0 + \text{c.c.}$	(4.1 ± 1.2) × 10 ⁻³	
Γ_9 $K^*(892)^0 K^- \pi^+ \rightarrow K^- \pi^+ K^0 \pi^0 + \text{c.c.}$	(2.9 ± 0.8) × 10 ⁻³	
Γ_{10} $K^*(892)^0 \bar{K}^0 \pi^0 \rightarrow K^+ \pi^- \bar{K}^0 \pi^0 + \text{c.c.}$	(3.8 ± 0.9) × 10 ⁻³	
Γ_{11} $K^*(892)^- K^+ \pi^0 \rightarrow K^+ \pi^- \bar{K}^0 \pi^0 + \text{c.c.}$	(3.7 ± 0.8) × 10 ⁻³	
Γ_{12} $K^*(892)^+ \bar{K}^0 \pi^- \rightarrow K^+ \pi^- \bar{K}^0 \pi^0 + \text{c.c.}$	(2.9 ± 0.8) × 10 ⁻³	
Γ_{13} $K^+ K^- \eta \pi^0$	(1.3 ± 0.4) × 10 ⁻³	
Γ_{14} $K^+ K^- \pi^+ \pi^-$	(8.4 ± 0.9) × 10 ⁻³	
Γ_{15} $K^+ K^- \pi^+ \pi^- \pi^0$	(1.17 ± 0.13) %	
Γ_{16} $K_S^0 K^\pm \pi^\mp \pi^+ \pi^-$	(7.3 ± 0.8) × 10 ⁻³	
Γ_{17} $K^+ \bar{K}^*(892)^0 \pi^- + \text{c.c.}$	(2.1 ± 1.1) × 10 ⁻³	
Γ_{18} $K^*(892)^0 \bar{K}^*(892)^0$	(2.3 ± 0.4) × 10 ⁻³	
Γ_{19} $3(\pi^+ \pi^-)$	(8.6 ± 1.8) × 10 ⁻³	
Γ_{20} $\phi\phi$	(1.06 ± 0.09) × 10 ⁻³	
Γ_{21} $\phi\phi\eta$	(5.3 ± 0.6) × 10 ⁻⁴	
Γ_{22} $\omega\omega$	(8.4 ± 1.0) × 10 ⁻⁴	
Γ_{23} $\omega K^+ K^-$	(7.3 ± 0.9) × 10 ⁻⁴	
Γ_{24} $\omega\phi$	(9.6 ± 2.7) × 10 ⁻⁶	
Γ_{25} $\pi\pi$	(2.23 ± 0.09) × 10 ⁻³	
Γ_{26} $\rho^0 \pi^+ \pi^-$	(3.7 ± 1.6) × 10 ⁻³	
Γ_{27} $\pi^+ \pi^- \pi^0$ (non-resonant)	(2.0 ± 0.4) × 10 ⁻⁵	
Γ_{28} $\rho(770)^\pm \pi^\mp$	(6 ± 4) × 10 ⁻⁶	
Γ_{29} $\pi^+ \pi^- \eta$	(4.8 ± 1.3) × 10 ⁻⁴	
Γ_{30} $\pi^+ \pi^- \eta'$	(5.0 ± 1.8) × 10 ⁻⁴	
Γ_{31} $\eta\eta$	(5.4 ± 0.4) × 10 ⁻⁴	
Γ_{32} $K^+ K^-$	(1.01 ± 0.06) × 10 ⁻³	
Γ_{33} $K_S^0 K_S^0$	(5.2 ± 0.4) × 10 ⁻⁴	
Γ_{34} $K^*(892)^\pm K^\mp$	(1.44 ± 0.21) × 10 ⁻⁴	
Γ_{35} $K^*(892)^0 \bar{K}^0 + \text{c.c.}$	(1.24 ± 0.27) × 10 ⁻⁴	
Γ_{36} $K_S^*(1430)^\pm K^\mp$	(1.48 ± 0.12) × 10 ⁻³	
Γ_{37} $K_S^*(1430)^0 \bar{K}^0 + \text{c.c.}$	(1.24 ± 0.17) × 10 ⁻³	
Γ_{38} $K_S^*(1780)^\pm K^\mp$	(5.2 ± 0.8) × 10 ⁻⁴	
Γ_{39} $K_S^*(1780)^0 \bar{K}^0 + \text{c.c.}$	(5.6 ± 2.1) × 10 ⁻⁴	
Γ_{40} $a_2(1320)^0 \pi^0$	(1.29 ± 0.34) × 10 ⁻³	
Γ_{41} $a_2(1320)^\pm \pi^\mp$	(1.8 ± 0.6) × 10 ⁻³	
Γ_{42} $\bar{K}^0 K^+ \pi^- + \text{c.c.}$	(1.28 ± 0.18) × 10 ⁻³	
Γ_{43} $K^+ K^- \pi^0$	(3.0 ± 0.8) × 10 ⁻⁴	
Γ_{44} $K^+ K^- \eta$	< 3.2 × 10 ⁻⁴	90%
Γ_{45} $K^+ K^- \eta'(958)$	(1.94 ± 0.34) × 10 ⁻⁴	
Γ_{46} $\eta\eta'$	(2.2 ± 0.5) × 10 ⁻⁵	
Γ_{47} $\eta'\eta'$	(4.6 ± 0.6) × 10 ⁻⁵	
Γ_{48} $\pi^+ \pi^- K_S^0 K_S^0$	(2.2 ± 0.5) × 10 ⁻³	
Γ_{49} $K^+ K^- K_S^0 K_S^0$	< 4 × 10 ⁻⁴	90%
Γ_{50} $K_S^0 K_S^0 K_S^0 K_S^0$	(1.13 ± 0.18) × 10 ⁻⁴	
Γ_{51} $K^+ K^- K^+ K^-$	(1.65 ± 0.20) × 10 ⁻³	
Γ_{52} $K^+ K^- \phi$	(1.42 ± 0.29) × 10 ⁻³	
Γ_{53} $\bar{K}^0 K^+ \pi^- \phi + \text{c.c.}$	(4.8 ± 0.7) × 10 ⁻³	
Γ_{54} $K^+ K^- \pi^0 \phi$	(2.7 ± 0.5) × 10 ⁻³	

See key on page 1127

Meson Particle Listings

$\chi_{c2}(1P)$

Table of particle properties for chi_c2(1P), including decay channels like phi pi+ pi- pi0, rho pi pi0, and various K and eta decays, with associated branching ratios and widths.

Radiative decays

Table of radiative decay properties for chi_c2(1P), including gamma J/psi(1S), gamma rho0, gamma omega, gamma phi, gamma eta, e+ e- J/psi(1S), and mu+ mu- J/psi(1S).

CONSTRAINED FIT INFORMATION

A multiparticle fit to chi_c1(1P), chi_c0(1P), chi_c2(1P), and psi(2S) with 4 total widths, a partial width, 25 combinations of partial widths obtained from integrated cross section, and 84 branching ratios uses 248 measurements to determine 49 parameters.

The following off-diagonal array elements are the correlation coefficients <delta p_i delta p_j> / (delta p_i delta p_j), in percent, from the fit to parameters p_i, including the branching fractions, x_i = Gamma_i / Gamma_total.

Correlation coefficient matrix showing the relationship between various parameters x14, x17, x18, x20, x25, x26, x31, x32, x33.

Correlation matrix for parameters x51, x56, x69, x92, x96, and Gamma.

chi_c2(1P) PARTIAL WIDTHS

chi_c2(1P) Gamma(i)Gamma(gamma J/psi(1S))/Gamma(total)

Table for Gamma(rho pi) x Gamma(gamma J/psi(1S))/Gamma(total) with columns for VALUE (eV), DOCUMENT ID, TECN, COMMENT, and Gamma_56 Gamma_92 / Gamma.

Table for Gamma(gamma gamma) x Gamma(gamma J/psi(1S))/Gamma(total) with columns for VALUE (eV), EVTS, DOCUMENT ID, TECN, COMMENT, and Gamma_96 Gamma_92 / Gamma.

Footnotes for the radiative decay tables, including calculations for B(J/psi -> l+ l-) and systematic error handling.

chi_c2(1P) Gamma(i)Gamma(gamma gamma)/Gamma(total)

Table for Gamma(2 pi+ pi-) x Gamma(gamma gamma)/Gamma(total) with columns for VALUE (eV), EVTS, DOCUMENT ID, TECN, COMMENT, and Gamma_1 Gamma_96 / Gamma.

Table for Gamma(rho rho) x Gamma(gamma gamma)/Gamma(total) with columns for VALUE (eV), CL%, EVTS, DOCUMENT ID, TECN, COMMENT, and Gamma_2 Gamma_96 / Gamma.

Table for Gamma(K+ K- pi+ pi-) x Gamma(gamma gamma)/Gamma(total) with columns for VALUE (eV), EVTS, DOCUMENT ID, TECN, COMMENT, and Gamma_14 Gamma_96 / Gamma.

Table for Gamma(K+ K- pi+ pi- pi0) x Gamma(gamma gamma)/Gamma(total) with columns for VALUE (eV), EVTS, DOCUMENT ID, TECN, COMMENT, and Gamma_15 Gamma_96 / Gamma.

Table for Gamma(K*(892)0 K*(892)0) x Gamma(gamma gamma)/Gamma(total) with columns for VALUE (eV), EVTS, DOCUMENT ID, TECN, COMMENT, and Gamma_18 Gamma_96 / Gamma.

Table for Gamma(phi phi) x Gamma(gamma gamma)/Gamma(total) with columns for VALUE (eV), EVTS, DOCUMENT ID, TECN, COMMENT, and Gamma_20 Gamma_96 / Gamma.

Footnote for the phi phi table: Supersedes UEHARA 08. Using B(phi -> K+ K-) = (48.9 +/- 0.5)%.

Meson Particle Listings

 $\chi_{c2}(1P)$

$\Gamma(\omega) \times \Gamma(\gamma\gamma)/\Gamma_{\text{total}}$		$\Gamma_{22} \Gamma_{96}/\Gamma$		
VALUE (eV)	CL%	DOCUMENT ID	TECN	COMMENT

• • • We do not use the following data for averages, fits, limits, etc. • • •

<0.64 90 ¹LIU 12B BELL $\gamma\gamma \rightarrow 2(\pi^+\pi^-\pi^0)$

¹ Using $B(\omega \rightarrow \pi^+\pi^-\pi^0) = (89.2 \pm 0.7)\%$.

$\Gamma(\omega\phi) \times \Gamma(\gamma\gamma)/\Gamma_{\text{total}}$		$\Gamma_{24} \Gamma_{96}/\Gamma$		
VALUE (eV)	CL%	DOCUMENT ID	TECN	COMMENT

• • • We do not use the following data for averages, fits, limits, etc. • • •

<0.04 90 ¹LIU 12B BELL $\gamma\gamma \rightarrow K^+K^-\pi^+\pi^-\pi^0$

¹ Using $B(\phi \rightarrow K^+K^-) = (48.9 \pm 0.5)\%$ and $B(\omega \rightarrow \pi^+\pi^-\pi^0) = (89.2 \pm 0.7)\%$.

$\Gamma(\pi\pi) \times \Gamma(\gamma\gamma)/\Gamma_{\text{total}}$		$\Gamma_{25} \Gamma_{96}/\Gamma$		
VALUE (eV)	EVTS	DOCUMENT ID	TECN	COMMENT

1.25 ± 0.07 OUR FIT

1.18 ± 0.25 OUR AVERAGE

1.44 ± 0.54 ± 0.47 34 ± 13 ¹UEHARA 09 BELL 10.6 e⁺e⁻ → e⁺e⁻π⁰π⁰

1.14 ± 0.21 ± 0.17 54 ± 10 ²NAKAZAWA 05 BELL 10.6 e⁺e⁻ → e⁺e⁻π⁺π⁻

¹ We multiplied the measurement by 3 to convert from π⁰π⁰ to ππ. Interference with the continuum included.

² We have multiplied π⁺π⁻ measurement by 3/2 to obtain ππ.

$\Gamma(\rho^0\pi^+\pi^-) \times \Gamma(\gamma\gamma)/\Gamma_{\text{total}}$		$\Gamma_{26} \Gamma_{96}/\Gamma$		
VALUE (eV)	EVTS	DOCUMENT ID	TECN	COMMENT

2.1 ± 0.9 OUR FIT

3.2 ± 1.9 ± 0.5

986 ± 578 UEHARA 08 BELL $\gamma\gamma \rightarrow \chi_{c2} \rightarrow 2(\pi^+\pi^-)$

$\Gamma(\eta) \times \Gamma(\gamma\gamma)/\Gamma_{\text{total}}$		$\Gamma_{31} \Gamma_{96}/\Gamma$		
VALUE (eV)	EVTS	DOCUMENT ID	TECN	COMMENT

0.53 ± 0.22 ± 0.09

8 ¹UEHARA 10A BELL 10.6 e⁺e⁻ → e⁺e⁻ηη

¹ Interference with the continuum not included.

$\Gamma(K^+K^-) \times \Gamma(\gamma\gamma)/\Gamma_{\text{total}}$		$\Gamma_{32} \Gamma_{96}/\Gamma$		
VALUE (eV)	EVTS	DOCUMENT ID	TECN	COMMENT

0.56 ± 0.04 OUR FIT

0.44 ± 0.11 ± 0.07 33 ± 8 NAKAZAWA 05 BELL 10.6 e⁺e⁻ → e⁺e⁻K⁺K⁻

$\Gamma(K_S^0 K_L^0) \times \Gamma(\gamma\gamma)/\Gamma_{\text{total}}$		$\Gamma_{33} \Gamma_{96}/\Gamma$		
VALUE (eV)	EVTS	DOCUMENT ID	TECN	COMMENT

0.294 ± 0.025 OUR FIT

0.27 ± 0.07 ± 0.03 53 ¹UEHARA 13 BELL $\gamma\gamma \rightarrow K_S^0 K_L^0$

• • • We do not use the following data for averages, fits, limits, etc. • • •

0.31 ± 0.05 ± 0.03 38 ± 7 CHEN 07B BELL e⁺e⁻ → e⁺e⁻χ_{c2}

¹ Supersedes CHEN 07b.

$\Gamma(\bar{K}^0 K^+ \pi^- + \text{c.c.}) \times \Gamma(\gamma\gamma)/\Gamma_{\text{total}}$		$\Gamma_{42} \Gamma_{96}/\Gamma$		
VALUE (eV)	EVTS	DOCUMENT ID	TECN	COMMENT

0.72 ± 0.11 OUR FIT

1.20 ± 0.33 ± 0.13 126 ¹DEL-AMO-SA...11M BABR $\gamma\gamma \rightarrow K_S^0 K^\pm \pi^\mp$

¹ We have multiplied $\bar{K}K\pi$ by 2/3 to obtain $\bar{K}^0 K^+ \pi^- + \text{c.c.}$

$\Gamma(K^+ K^- K^+ K^-) \times \Gamma(\gamma\gamma)/\Gamma_{\text{total}}$		$\Gamma_{51} \Gamma_{96}/\Gamma$		
VALUE (eV)	EVTS	DOCUMENT ID	TECN	COMMENT

0.93 ± 0.11 OUR FIT

1.10 ± 0.21 ± 0.15 126 ± 24 UEHARA 08 BELL $\gamma\gamma \rightarrow \chi_{c2} \rightarrow 2(K^+K^-)$

$\Gamma(\eta_c(1S)\pi^+\pi^-) \times \Gamma(\gamma\gamma)/\Gamma_{\text{total}}$		$\Gamma_{91} \Gamma_{96}/\Gamma$		
VALUE (eV)	CL%	DOCUMENT ID	TECN	COMMENT

<15.7

90 LEES 12AE BABR e⁺e⁻ → e⁺e⁻π⁺π⁻η_c

 $\chi_{c2}(1P)$ BRANCHING RATIOS

HADRONIC DECAYS

$\Gamma(2(\pi^+\pi^-))/\Gamma_{\text{total}}$		Γ_1/Γ
VALUE	DOCUMENT ID	

0.0102 ± 0.0009 OUR FIT

$\Gamma(\rho^0\pi^+\pi^-)/\Gamma(2(\pi^+\pi^-))$		Γ_{26}/Γ_1	
VALUE	DOCUMENT ID	TECN	COMMENT

0.36 ± 0.15 OUR FIT

0.31 ± 0.17 TANENBAUM 78 MRK1 $\psi(2S) \rightarrow \gamma\chi_{c2}$

$\Gamma(\pi^+\pi^-\pi^0\pi^0)/\Gamma_{\text{total}}$		Γ_3/Γ		
VALUE (%)	EVTS	DOCUMENT ID	TECN	COMMENT

1.83 ± 0.23 ± 0.04 903.5 ¹HE 08B CLEO e⁺e⁻ → γh⁺h⁻h⁰h⁰

¹ HE 08B reports 1.87 ± 0.07 ± 0.22 ± 0.13 % from a measurement of $[\Gamma(\chi_{c2}(1P) \rightarrow \pi^+\pi^-\pi^0\pi^0)/\Gamma_{\text{total}}] \times [B(\psi(2S) \rightarrow \gamma\chi_{c2}(1P))]$ assuming $B(\psi(2S) \rightarrow \gamma\chi_{c2}(1P)) = (9.33 \pm 0.14 \pm 0.61) \times 10^{-2}$, which we rescale to our best value $B(\psi(2S) \rightarrow \gamma\chi_{c2}(1P)) = (9.52 \pm 0.20) \times 10^{-2}$. Our first error is their experiment's error and our second error is the systematic error from using our best value.

$\Gamma(\rho^+\pi^-\pi^0 + \text{c.c.})/\Gamma_{\text{total}}$		Γ_4/Γ		
VALUE (%)	EVTS	DOCUMENT ID	TECN	COMMENT

2.19 ± 0.34 ± 0.05 1031.9 ^{1,2}HE 08B CLEO e⁺e⁻ → γh⁺h⁻h⁰h⁰

¹ HE 08B reports 2.23 ± 0.11 ± 0.32 ± 0.16 % from a measurement of $[\Gamma(\chi_{c2}(1P) \rightarrow \rho^+\pi^-\pi^0 + \text{c.c.})/\Gamma_{\text{total}}] \times [B(\psi(2S) \rightarrow \gamma\chi_{c2}(1P))]$ assuming $B(\psi(2S) \rightarrow \gamma\chi_{c2}(1P)) = (9.33 \pm 0.14 \pm 0.61) \times 10^{-2}$, which we rescale to our best value $B(\psi(2S) \rightarrow \gamma\chi_{c2}(1P)) = (9.52 \pm 0.20) \times 10^{-2}$. Our first error is their experiment's error and our second error is the systematic error from using our best value.

² Calculated by us. We have added the values from HE 08B for $\rho^+\pi^-\pi^0$ and $\rho^-\pi^+\pi^0$ decays assuming uncorrelated statistical and fully correlated systematic uncertainties.

$\Gamma(4\pi^0)/\Gamma_{\text{total}}$		Γ_5/Γ		
VALUE (units 10 ⁻³)	EVTS	DOCUMENT ID	TECN	COMMENT

1.11 ± 0.15 ± 0.02 1164 ¹ABLKIM 11A BES3 e⁺e⁻ → ψ(2S) → γχ_{c2}

¹ ABLKIM 11A reports $(1.21 \pm 0.05 \pm 0.16) \times 10^{-3}$ from a measurement of $[\Gamma(\chi_{c2}(1P) \rightarrow 4\pi^0)/\Gamma_{\text{total}}] \times [B(\psi(2S) \rightarrow \gamma\chi_{c2}(1P))]$ assuming $B(\psi(2S) \rightarrow \gamma\chi_{c2}(1P)) = (8.74 \pm 0.35) \times 10^{-2}$, which we rescale to our best value $B(\psi(2S) \rightarrow \gamma\chi_{c2}(1P)) = (9.52 \pm 0.20) \times 10^{-2}$. Our first error is their experiment's error and our second error is the systematic error from using our best value.

$\Gamma(K^+K^-\pi^0\pi^0)/\Gamma_{\text{total}}$		Γ_6/Γ		
VALUE (%)	EVTS	DOCUMENT ID	TECN	COMMENT

0.206 ± 0.040 ± 0.004 76.9 ¹HE 08B CLEO e⁺e⁻ → γh⁺h⁻h⁰h⁰

¹ HE 08B reports 0.21 ± 0.03 ± 0.03 ± 0.01 % from a measurement of $[\Gamma(\chi_{c2}(1P) \rightarrow K^+K^-\pi^0\pi^0)/\Gamma_{\text{total}}] \times [B(\psi(2S) \rightarrow \gamma\chi_{c2}(1P))]$ assuming $B(\psi(2S) \rightarrow \gamma\chi_{c2}(1P)) = (9.33 \pm 0.14 \pm 0.61) \times 10^{-2}$, which we rescale to our best value $B(\psi(2S) \rightarrow \gamma\chi_{c2}(1P)) = (9.52 \pm 0.20) \times 10^{-2}$. Our first error is their experiment's error and our second error is the systematic error from using our best value.

$\Gamma(K^+\pi^-\bar{K}^0\pi^0 + \text{c.c.})/\Gamma_{\text{total}}$		Γ_7/Γ		
VALUE (%)	EVTS	DOCUMENT ID	TECN	COMMENT

1.38 ± 0.19 ± 0.03 211.6 ¹HE 08B CLEO e⁺e⁻ → γh⁺h⁻h⁰h⁰

¹ HE 08B reports 1.41 ± 0.11 ± 0.16 ± 0.10 % from a measurement of $[\Gamma(\chi_{c2}(1P) \rightarrow K^+\pi^-\bar{K}^0\pi^0 + \text{c.c.})/\Gamma_{\text{total}}] \times [B(\psi(2S) \rightarrow \gamma\chi_{c2}(1P))]$ assuming $B(\psi(2S) \rightarrow \gamma\chi_{c2}(1P)) = (9.33 \pm 0.14 \pm 0.61) \times 10^{-2}$, which we rescale to our best value $B(\psi(2S) \rightarrow \gamma\chi_{c2}(1P)) = (9.52 \pm 0.20) \times 10^{-2}$. Our first error is their experiment's error and our second error is the systematic error from using our best value.

$\Gamma(\rho^-K^+\bar{K}^0 + \text{c.c.})/\Gamma_{\text{total}}$		Γ_8/Γ		
VALUE (%)	EVTS	DOCUMENT ID	TECN	COMMENT

0.41 ± 0.12 ± 0.01 62.9 ¹HE 08B CLEO e⁺e⁻ → γh⁺h⁻h⁰h⁰

¹ HE 08B reports 0.42 ± 0.11 ± 0.06 ± 0.03 % from a measurement of $[\Gamma(\chi_{c2}(1P) \rightarrow \rho^-K^+\bar{K}^0 + \text{c.c.})/\Gamma_{\text{total}}] \times [B(\psi(2S) \rightarrow \gamma\chi_{c2}(1P))]$ assuming $B(\psi(2S) \rightarrow \gamma\chi_{c2}(1P)) = (9.33 \pm 0.14 \pm 0.61) \times 10^{-2}$, which we rescale to our best value $B(\psi(2S) \rightarrow \gamma\chi_{c2}(1P)) = (9.52 \pm 0.20) \times 10^{-2}$. Our first error is their experiment's error and our second error is the systematic error from using our best value.

$\Gamma(K^*(892)^0 K^- \pi^+ \rightarrow K^- \pi^+ K^0 \pi^0 + \text{c.c.})/\Gamma_{\text{total}}$		Γ_9/Γ		
VALUE (%)	EVTS	DOCUMENT ID	TECN	COMMENT

0.29 ± 0.08 ± 0.01 38.7 ¹HE 08B CLEO e⁺e⁻ → γh⁺h⁻h⁰h⁰

¹ HE 08B reports 0.30 ± 0.07 ± 0.04 ± 0.02 % from a measurement of $[\Gamma(\chi_{c2}(1P) \rightarrow K^*(892)^0 K^- \pi^+ \rightarrow K^- \pi^+ K^0 \pi^0 + \text{c.c.})/\Gamma_{\text{total}}] \times [B(\psi(2S) \rightarrow \gamma\chi_{c2}(1P))]$ assuming $B(\psi(2S) \rightarrow \gamma\chi_{c2}(1P)) = (9.33 \pm 0.14 \pm 0.61) \times 10^{-2}$, which we rescale to our best value $B(\psi(2S) \rightarrow \gamma\chi_{c2}(1P)) = (9.52 \pm 0.20) \times 10^{-2}$. Our first error is their experiment's error and our second error is the systematic error from using our best value.

$\Gamma(K^*(892)^0 \bar{K}^0 \pi^0 \rightarrow K^+\pi^-\bar{K}^0\pi^0 + \text{c.c.})/\Gamma_{\text{total}}$		Γ_{10}/Γ		
VALUE (%)	EVTS	DOCUMENT ID	TECN	COMMENT

0.38 ± 0.09 ± 0.01 63.0 ¹HE 08B CLEO e⁺e⁻ → γh⁺h⁻h⁰h⁰

¹ HE 08B reports 0.39 ± 0.07 ± 0.05 ± 0.03 % from a measurement of $[\Gamma(\chi_{c2}(1P) \rightarrow K^*(892)^0 \bar{K}^0 \pi^0 \rightarrow K^+\pi^-\bar{K}^0\pi^0 + \text{c.c.})/\Gamma_{\text{total}}] \times [B(\psi(2S) \rightarrow \gamma\chi_{c2}(1P))]$ assuming $B(\psi(2S) \rightarrow \gamma\chi_{c2}(1P)) = (9.33 \pm 0.14 \pm 0.61) \times 10^{-2}$, which we rescale to our best value $B(\psi(2S) \rightarrow \gamma\chi_{c2}(1P)) = (9.52 \pm 0.20) \times 10^{-2}$. Our first error is their experiment's error and our second error is the systematic error from using our best value.

$\Gamma(K^*(892)^- K^+ \pi^0 \rightarrow K^+\pi^-\bar{K}^0\pi^0 + \text{c.c.})/\Gamma_{\text{total}}$		Γ_{11}/Γ		
VALUE (%)	EVTS	DOCUMENT ID	TECN	COMMENT

0.37 ± 0.08 ± 0.01 51.1 ¹HE 08B CLEO e⁺e⁻ → γh⁺h⁻h⁰h⁰

¹ HE 08B reports 0.38 ± 0.07 ± 0.04 ± 0.03 % from a measurement of $[\Gamma(\chi_{c2}(1P) \rightarrow K^*(892)^- K^+ \pi^0 \rightarrow K^+\pi^-\bar{K}^0\pi^0 + \text{c.c.})/\Gamma_{\text{total}}] \times [B(\psi(2S) \rightarrow \gamma\chi_{c2}(1P))]$ assuming $B(\psi(2S) \rightarrow \gamma\chi_{c2}(1P)) = (9.33 \pm 0.14 \pm 0.61) \times 10^{-2}$, which we rescale to our best value $B(\psi(2S) \rightarrow \gamma\chi_{c2}(1P)) = (9.52 \pm 0.20) \times 10^{-2}$. Our first error is their experiment's error and our second error is the systematic error from using our best value.

$\Gamma(K^*(892)^+ \bar{K}^0 \pi^- \rightarrow K^+\pi^-\bar{K}^0\pi^0 + \text{c.c.})/\Gamma_{\text{total}}$		Γ_{12}/Γ		
VALUE (%)	EVTS	DOCUMENT ID	TECN	COMMENT

0.29 ± 0.08 ± 0.01 39.3 ¹HE 08B CLEO e⁺e⁻ → γh⁺h⁻h⁰h⁰

¹ HE 08B reports 0.30 ± 0.07 ± 0.04 ± 0.02 % from a measurement of $[\Gamma(\chi_{c2}(1P) \rightarrow K^*(892)^+ \bar{K}^0 \pi^- \rightarrow K^+\pi^-\bar{K}^0\pi^0 + \text{c.c.})/\Gamma_{\text{total}}] \times [B(\psi(2S) \rightarrow \gamma\chi_{c2}(1P))]$ assuming $B(\psi(2S) \rightarrow \gamma\chi_{c2}(1P)) = (9.33 \pm 0.14 \pm 0.61) \times 10^{-2}$, which we rescale to our best value $B(\psi(2S) \rightarrow \gamma\chi_{c2}(1P)) = (9.52 \pm 0.20) \times 10^{-2}$. Our first error is their experiment's error and our second error is the systematic error from using our best value.

$\Gamma(K^+ K^- \eta \pi^0)/\Gamma_{\text{total}}$	Γ_{13}/Γ			
VALUE (%)	EVTS	DOCUMENT ID	TECN	COMMENT
0.127 ± 0.044 ± 0.003	22.9	¹ HE	08B	CLEO $e^+e^- \rightarrow \gamma h^+ h^- h^0 h^0$

¹HE 08B reports $0.13 \pm 0.04 \pm 0.02 \pm 0.01$ % from a measurement of $[\Gamma(\chi_{c2}(1P) \rightarrow K^+ K^- \eta \pi^0)/\Gamma_{\text{total}}] \times [B(\psi(2S) \rightarrow \gamma \chi_{c2}(1P))]$ assuming $B(\psi(2S) \rightarrow \gamma \chi_{c2}(1P)) = (9.33 \pm 0.14 \pm 0.61) \times 10^{-2}$, which we rescale to our best value $B(\psi(2S) \rightarrow \gamma \chi_{c2}(1P)) = (9.52 \pm 0.20) \times 10^{-2}$. Our first error is their experiment's error and our second error is the systematic error from using our best value.

$\Gamma(K^+ K^- \pi^+ \pi^-)/\Gamma_{\text{total}}$	Γ_{14}/Γ
VALUE (units 10^{-3})	DOCUMENT ID
8.4 ± 0.9 OUR FIT	

$\Gamma(K^+ K^- \pi^+ \pi^- \pi^0)/\Gamma_{\text{total}}$	Γ_{15}/Γ			
VALUE (units 10^{-3})	EVTS	DOCUMENT ID	TECN	COMMENT
11.69 ± 0.13 ± 1.31	11k	¹ ABLIKIM	13B	BES3 $e^+e^- \rightarrow \psi(2S) \rightarrow \gamma \chi_{c2}$

¹Using 1.06×10^8 $\psi(2S)$ mesons and $B(\psi(2S) \rightarrow \chi_{c2} \gamma) = (8.72 \pm 0.34)\%$.

$\Gamma(K_S^0 K^{\pm} \pi^{\mp} \pi^+ \pi^-)/\Gamma_{\text{total}}$	Γ_{16}/Γ			
VALUE (units 10^{-3})	EVTS	DOCUMENT ID	TECN	COMMENT
7.30 ± 0.11 ± 0.75	4.5k	¹ ABLIKIM	13B	BES3 $e^+e^- \rightarrow \psi(2S) \rightarrow \gamma \chi_{c2}$

¹Using 1.06×10^8 $\psi(2S)$ mesons and $B(\psi(2S) \rightarrow \chi_{c2} \gamma) = (8.72 \pm 0.34)\%$.

$\Gamma(K^+ \bar{K}^*(892)^0 \pi^- + \text{c.c.})/\Gamma(K^+ K^- \pi^+ \pi^-)$	Γ_{17}/Γ_{14}		
VALUE	DOCUMENT ID	TECN	COMMENT
0.25 ± 0.13 OUR FIT			
0.25 ± 0.13	TANENBAUM 78	MRK1	$\psi(2S) \rightarrow \gamma \chi_{c2}$

$\Gamma(K^+ \bar{K}^*(892)^0 \pi^- + \text{c.c.})/\Gamma_{\text{total}}$	Γ_{17}/Γ
VALUE (units 10^{-4})	DOCUMENT ID
21 ± 11 OUR FIT	

$\Gamma(K^*(892)^0 \bar{K}^*(892)^0)/\Gamma_{\text{total}}$	Γ_{18}/Γ
VALUE (units 10^{-3})	DOCUMENT ID
2.3 ± 0.4 OUR FIT	

$\Gamma(3(\pi^+ \pi^-))/\Gamma_{\text{total}}$	Γ_{19}/Γ		
VALUE (units 10^{-3})	DOCUMENT ID	TECN	COMMENT
8.6 ± 1.8 OUR EVALUATION			Treating systematic error as correlated.
8.6 ± 1.8 OUR AVERAGE			

¹BAI 99B BES $\psi(2S) \rightarrow \gamma \chi_{c2}$
²TANENBAUM 78 MRK1 $\psi(2S) \rightarrow \gamma \chi_{c2}$

¹Rescaled by us using $B(\psi(2S) \rightarrow \gamma \chi_{c2}) = (8.3 \pm 0.4)\%$ and $B(\psi(2S) \rightarrow J/\psi(1S) \pi^+ \pi^-) = (32.6 \pm 0.5)\%$. Multiplied by a factor of 2 to convert from $K_S^0 K^+ \pi^-$ to $K^0 K^+ \pi^-$ decay.

$\Gamma(\phi \phi)/\Gamma_{\text{total}}$	Γ_{20}/Γ
VALUE (units 10^{-3})	DOCUMENT ID
1.06 ± 0.09 OUR FIT	

$\Gamma(\phi \phi \eta)/\Gamma_{\text{total}}$	Γ_{21}/Γ			
VALUE (units 10^{-4})	EVTS	DOCUMENT ID	TECN	COMMENT
5.3 ± 0.5 ± 0.4	143.6	¹ ABLIKIM	20B	BES3 $\psi(2S) \rightarrow \gamma \phi \phi \eta$

¹ABLIKIM 20B reports $(5.33 \pm 0.52 \pm 0.39) \times 10^{-4}$ from a measurement of $[\Gamma(\chi_{c2}(1P) \rightarrow \phi \phi \eta)/\Gamma_{\text{total}}] \times [B(\psi(2S) \rightarrow \gamma \chi_{c2}(1P))]$ assuming $B(\psi(2S) \rightarrow \gamma \chi_{c2}(1P)) = (9.52 \pm 0.20) \times 10^{-2}$.

$\Gamma(\omega \omega)/\Gamma_{\text{total}}$	Γ_{22}/Γ			
VALUE (units 10^{-3})	EVTS	DOCUMENT ID	TECN	COMMENT
0.84 ± 0.10 OUR AVERAGE				
0.82 ± 0.10 ± 0.02	762	¹ ABLIKIM	11k	BES3 $\psi(2S) \rightarrow \gamma$ hadrons
1.73 ± 0.57 ± 0.04	27.7 ± 7.4	² ABLIKIM	05N	BES2 $\psi(2S) \rightarrow \gamma \chi_{c2} \rightarrow \gamma 6\pi$

¹ABLIKIM 11k reports $(8.9 \pm 0.3 \pm 1.1) \times 10^{-4}$ from a measurement of $[\Gamma(\chi_{c2}(1P) \rightarrow \omega \omega)/\Gamma_{\text{total}}] \times [B(\psi(2S) \rightarrow \gamma \chi_{c2}(1P))]$ assuming $B(\psi(2S) \rightarrow \gamma \chi_{c2}(1P)) = (8.74 \pm 0.35) \times 10^{-2}$, which we rescale to our best value $B(\psi(2S) \rightarrow \gamma \chi_{c2}(1P)) = (9.52 \pm 0.20) \times 10^{-2}$. Our first error is their experiment's error and our second error is the systematic error from using our best value.

²ABLIKIM 05N reports $[\Gamma(\chi_{c2}(1P) \rightarrow \omega \omega)/\Gamma_{\text{total}}] \times [B(\psi(2S) \rightarrow \gamma \chi_{c2}(1P))] = (0.165 \pm 0.044 \pm 0.032) \times 10^{-3}$ which we divide by our best value $B(\psi(2S) \rightarrow \gamma \chi_{c2}(1P)) = (9.52 \pm 0.20) \times 10^{-2}$. Our first error is their experiment's error and our second error is the systematic error from using our best value.

$\Gamma(\omega K^+ K^-)/\Gamma_{\text{total}}$	Γ_{23}/Γ			
VALUE (units 10^{-3})	EVTS	DOCUMENT ID	TECN	COMMENT
0.73 ± 0.04 ± 0.08	512	¹ ABLIKIM	13B	BES3 $e^+e^- \rightarrow \psi(2S) \rightarrow \gamma \chi_{c2}$

¹Using 1.06×10^8 $\psi(2S)$ mesons and $B(\psi(2S) \rightarrow \chi_{c2} \gamma) = (8.72 \pm 0.34)\%$.

$\Gamma(\omega \phi)/\Gamma_{\text{total}}$	Γ_{24}/Γ				
VALUE (units 10^{-6})	CL%	EVTS	DOCUMENT ID	TECN	COMMENT
9.6 ± 2.7 ± 0.2		33	¹ ABLIKIM	19J	BES3 $\psi(2S) \rightarrow \gamma$ hadrons

• • • We do not use the following data for averages, fits, limits, etc. • • •

<18 90 ^{2,3}ABLIKIM 11k BES3 $\psi(2S) \rightarrow \gamma$ hadrons
¹ABLIKIM 19J reports $[\Gamma(\chi_{c2}(1P) \rightarrow \omega \phi)/\Gamma_{\text{total}}] \times [B(\psi(2S) \rightarrow \gamma \chi_{c2}(1P))] = (0.91 \pm 0.23 \pm 0.12) \times 10^{-6}$ which we divide by our best value $B(\psi(2S) \rightarrow \gamma \chi_{c2}(1P)) = (9.52 \pm 0.20) \times 10^{-2}$. Our first error is their experiment's error and our second error is the systematic error from using our best value.
²ABLIKIM 11k reports $< 2 \times 10^{-5}$ from a measurement of $[\Gamma(\chi_{c2}(1P) \rightarrow \omega \phi)/\Gamma_{\text{total}}] \times [B(\psi(2S) \rightarrow \gamma \chi_{c2}(1P))]$ assuming $B(\psi(2S) \rightarrow \gamma \chi_{c2}(1P)) = (8.74 \pm 0.35) \times 10^{-2}$, which we rescale to our best value $B(\psi(2S) \rightarrow \gamma \chi_{c2}(1P)) = 9.52 \times 10^{-2}$.
³Superseded by ABLIKIM 19J.

$\Gamma(\pi \pi)/\Gamma_{\text{total}}$	Γ_{25}/Γ
VALUE (units 10^{-3})	DOCUMENT ID
2.23 ± 0.09 OUR FIT	

$\Gamma(\rho^0 \pi^+ \pi^-)/\Gamma_{\text{total}}$	Γ_{26}/Γ
VALUE (units 10^{-4})	DOCUMENT ID
37 ± 16 OUR FIT	

$\Gamma(\pi^+ \pi^- \pi^0 (\text{non-resonant}))/\Gamma_{\text{total}}$	Γ_{27}/Γ			
VALUE (units 10^{-5})	EVTS	DOCUMENT ID	TECN	COMMENT
2.01 ± 0.42 ± 0.04	64	¹ ABLIKIM	17AG	BES3 $\psi(2S) \rightarrow \gamma \pi^+ \pi^- \pi^0$

¹ABLIKIM 17AG reports $(2.1 \pm 0.4 \pm 0.2) \times 10^{-5}$ from a measurement of $[\Gamma(\chi_{c2}(1P) \rightarrow \pi^+ \pi^- \pi^0 (\text{non-resonant}))/\Gamma_{\text{total}}] \times [B(\psi(2S) \rightarrow \gamma \chi_{c2}(1P))]$ assuming $B(\psi(2S) \rightarrow \gamma \chi_{c2}(1P)) = (9.11 \pm 0.31) \times 10^{-2}$, which we rescale to our best value $B(\psi(2S) \rightarrow \gamma \chi_{c2}(1P)) = (9.52 \pm 0.20) \times 10^{-2}$. Our first error is their experiment's error and our second error is the systematic error from using our best value.

$\Gamma(\rho(770)^\pm \pi^\mp)/\Gamma_{\text{total}}$	Γ_{28}/Γ			
VALUE (units 10^{-5})	EVTS	DOCUMENT ID	TECN	COMMENT
0.61 ± 0.38 ± 0.01	15	¹ ABLIKIM	17AG	BES3 $\psi(2S) \rightarrow \gamma \pi^+ \pi^- \pi^0$

¹ABLIKIM 17AG reports $(0.64 \pm 0.39 \pm 0.07) \times 10^{-5}$ from a measurement of $[\Gamma(\chi_{c2}(1P) \rightarrow \rho(770)^\pm \pi^\mp)/\Gamma_{\text{total}}] \times [B(\psi(2S) \rightarrow \gamma \chi_{c2}(1P))]$ assuming $B(\psi(2S) \rightarrow \gamma \chi_{c2}(1P)) = (9.11 \pm 0.31) \times 10^{-2}$, which we rescale to our best value $B(\psi(2S) \rightarrow \gamma \chi_{c2}(1P)) = (9.52 \pm 0.20) \times 10^{-2}$. Our first error is their experiment's error and our second error is the systematic error from using our best value.

$\Gamma(\pi^+ \pi^- \eta)/\Gamma_{\text{total}}$	Γ_{29}/Γ			
VALUE (units 10^{-3})	CL%	DOCUMENT ID	TECN	COMMENT
0.48 ± 0.13 ± 0.01		¹ ATHAR	07	CLEO $\psi(2S) \rightarrow \gamma h^+ h^- h^0$

• • • We do not use the following data for averages, fits, limits, etc. • • •

<1.4 90 ²ABLIKIM 06R BES2 $\psi(2S) \rightarrow \gamma \chi_{c2}$
¹ATHAR 07 reports $(0.49 \pm 0.12 \pm 0.06) \times 10^{-3}$ from a measurement of $[\Gamma(\chi_{c2}(1P) \rightarrow \pi^+ \pi^- \eta)/\Gamma_{\text{total}}] \times [B(\psi(2S) \rightarrow \gamma \chi_{c2}(1P))]$ assuming $B(\psi(2S) \rightarrow \gamma \chi_{c2}(1P)) = (9.33 \pm 0.14 \pm 0.61) \times 10^{-2}$, which we rescale to our best value $B(\psi(2S) \rightarrow \gamma \chi_{c2}(1P)) = (9.52 \pm 0.20) \times 10^{-2}$. Our first error is their experiment's error and our second error is the systematic error from using our best value.
²ABLIKIM 06R reports $< 1.7 \times 10^{-3}$ from a measurement of $[\Gamma(\chi_{c2}(1P) \rightarrow \pi^+ \pi^- \eta)/\Gamma_{\text{total}}] \times [B(\psi(2S) \rightarrow \gamma \chi_{c2}(1P))]$ assuming $B(\psi(2S) \rightarrow \gamma \chi_{c2}(1P)) = (8.1 \pm 0.4) \times 10^{-2}$, which we rescale to our best value $B(\psi(2S) \rightarrow \gamma \chi_{c2}(1P)) = 9.52 \times 10^{-2}$.

$\Gamma(\pi^+ \pi^- \eta')/\Gamma_{\text{total}}$	Γ_{30}/Γ		
VALUE (units 10^{-3})	DOCUMENT ID	TECN	COMMENT
0.50 ± 0.18 ± 0.01		¹ ATHAR	07 CLEO $\psi(2S) \rightarrow \gamma h^+ h^- h^0$

¹ATHAR 07 reports $(0.51 \pm 0.18 \pm 0.06) \times 10^{-3}$ from a measurement of $[\Gamma(\chi_{c2}(1P) \rightarrow \pi^+ \pi^- \eta')/\Gamma_{\text{total}}] \times [B(\psi(2S) \rightarrow \gamma \chi_{c2}(1P))]$ assuming $B(\psi(2S) \rightarrow \gamma \chi_{c2}(1P)) = (9.33 \pm 0.14 \pm 0.61) \times 10^{-2}$, which we rescale to our best value $B(\psi(2S) \rightarrow \gamma \chi_{c2}(1P)) = (9.52 \pm 0.20) \times 10^{-2}$. Our first error is their experiment's error and our second error is the systematic error from using our best value.

$\Gamma(\eta \eta)/\Gamma_{\text{total}}$	Γ_{31}/Γ
VALUE (units 10^{-4})	DOCUMENT ID
5.4 ± 0.4 OUR FIT	

$\Gamma(K^+ K^-)/\Gamma_{\text{total}}$	Γ_{32}/Γ
VALUE (units 10^{-3})	DOCUMENT ID
1.01 ± 0.06 OUR FIT	

$\Gamma(K_S^0 K_S^0)/\Gamma_{\text{total}}$	Γ_{33}/Γ
VALUE (units 10^{-3})	DOCUMENT ID
0.52 ± 0.04 OUR FIT	

Meson Particle Listings

 $\chi_{c2}(1P)$ $\Gamma(K_S^0 K_S^0)/\Gamma(\pi\pi)$ Γ_{33}/Γ_{25}

VALUE	DOCUMENT ID	TECN	COMMENT
0.235 ± 0.019 OUR FIT			
$0.27 \pm 0.07 \pm 0.04$	^{1,2} CHEN	07B	BELL $e^+ e^- \rightarrow e^+ e^- \chi_{c2}$

¹ Using $\Gamma(\pi\pi) \times \Gamma(\gamma\gamma)/\Gamma_{\text{total}}$ from the $\pi^+ \pi^-$ measurement of NAKAZAWA 05 rescaled by 3/2 to convert to $\pi\pi$.
² Not independent from other measurements.

 $\Gamma(K_S^0 K_S^0)/\Gamma(K^+ K^-)$ Γ_{33}/Γ_{32}

VALUE	DOCUMENT ID	TECN	COMMENT
0.52 ± 0.05 OUR FIT			
$0.70 \pm 0.21 \pm 0.12$	^{1,2} CHEN	07B	BELL $e^+ e^- \rightarrow e^+ e^- \chi_{c2}$

¹ Using $\Gamma(K^+ K^-) \times \Gamma(\gamma\gamma)/\Gamma_{\text{total}}$ from NAKAZAWA 05.
² Not independent from other measurements.

 $\Gamma(K^*(892)^\pm K^\mp)/\Gamma_{\text{total}}$ Γ_{34}/Γ

VALUE (units 10^{-4})	DOCUMENT ID	TECN	COMMENT
$1.44 \pm 0.21 \pm 0.03$	¹ ABLIKIM	17AG BES3	$\psi(2S) \rightarrow \gamma K \bar{K} \pi$
$1.72 \pm 0.26 \pm 0.04$	² ABLIKIM	17AG BES3	$\psi(2S) \rightarrow \gamma K^+ K^- \pi^0$
$1.34 \pm 0.27 \pm 0.03$	³ ABLIKIM	17AG BES3	$\psi(2S) \rightarrow \gamma K_S^0 K^\pm \pi^\mp$

¹ ABLIKIM 17AG reports $(1.5 \pm 0.1 \pm 0.2) \times 10^{-4}$ from a measurement of $[\Gamma(\chi_{c2}(1P) \rightarrow K^*(892)^\pm K^\mp)/\Gamma_{\text{total}}] \times [B(\psi(2S) \rightarrow \gamma \chi_{c2}(1P))]$ assuming $B(\psi(2S) \rightarrow \gamma \chi_{c2}(1P)) = (9.11 \pm 0.31) \times 10^{-2}$, which we rescale to our best value $B(\psi(2S) \rightarrow \gamma \chi_{c2}(1P)) = (9.52 \pm 0.20) \times 10^{-2}$. Our first error is their experiment's error and our second error is the systematic error from using our best value.
² ABLIKIM 17AG reports $(1.8 \pm 0.2 \pm 0.2) \times 10^{-4}$ from a measurement of $[\Gamma(\chi_{c2}(1P) \rightarrow K^*(892)^\pm K^\mp)/\Gamma_{\text{total}}] \times [B(\psi(2S) \rightarrow \gamma \chi_{c2}(1P))]$ assuming $B(\psi(2S) \rightarrow \gamma \chi_{c2}(1P)) = (9.11 \pm 0.31) \times 10^{-2}$, which we rescale to our best value $B(\psi(2S) \rightarrow \gamma \chi_{c2}(1P)) = (9.52 \pm 0.20) \times 10^{-2}$. Our first error is their experiment's error and our second error is the systematic error from using our best value.
³ ABLIKIM 17AG reports $(1.4 \pm 0.2 \pm 0.2) \times 10^{-4}$ from a measurement of $[\Gamma(\chi_{c2}(1P) \rightarrow K^*(892)^\pm K^\mp)/\Gamma_{\text{total}}] \times [B(\psi(2S) \rightarrow \gamma \chi_{c2}(1P))]$ assuming $B(\psi(2S) \rightarrow \gamma \chi_{c2}(1P)) = (9.11 \pm 0.31) \times 10^{-2}$, which we rescale to our best value $B(\psi(2S) \rightarrow \gamma \chi_{c2}(1P)) = (9.52 \pm 0.20) \times 10^{-2}$. Our first error is their experiment's error and our second error is the systematic error from using our best value.

 $\Gamma(K^*(892)^0 \bar{K}^0 + \text{c.c.})/\Gamma_{\text{total}}$ Γ_{35}/Γ

VALUE (units 10^{-4})	DOCUMENT ID	TECN	COMMENT
$1.24 \pm 0.27 \pm 0.03$	¹ ABLIKIM	17AG BES3	$\psi(2S) \rightarrow \gamma K_S^0 K^\pm \pi^\mp$

¹ ABLIKIM 17AG reports $(1.3 \pm 0.2 \pm 0.2) \times 10^{-4}$ from a measurement of $[\Gamma(\chi_{c2}(1P) \rightarrow K^*(892)^0 \bar{K}^0 + \text{c.c.})/\Gamma_{\text{total}}] \times [B(\psi(2S) \rightarrow \gamma \chi_{c2}(1P))]$ assuming $B(\psi(2S) \rightarrow \gamma \chi_{c2}(1P)) = (9.11 \pm 0.31) \times 10^{-2}$, which we rescale to our best value $B(\psi(2S) \rightarrow \gamma \chi_{c2}(1P)) = (9.52 \pm 0.20) \times 10^{-2}$. Our first error is their experiment's error and our second error is the systematic error from using our best value.

 $\Gamma(K_S^0(1430)^\pm K^\mp)/\Gamma_{\text{total}}$ Γ_{36}/Γ

VALUE (units 10^{-4})	DOCUMENT ID	TECN	COMMENT
$14.8 \pm 1.2 \pm 0.3$	¹ ABLIKIM	17AG BES3	$\psi(2S) \rightarrow \gamma K \bar{K} \pi$
$17.4 \pm 1.6 \pm 0.4$	² ABLIKIM	17AG BES3	$\psi(2S) \rightarrow \gamma K^+ K^- \pi^0$
$13.0 \pm 1.5 \pm 0.3$	³ ABLIKIM	17AG BES3	$\psi(2S) \rightarrow \gamma K_S^0 K^\pm \pi^\mp$

¹ ABLIKIM 17AG reports $(15.5 \pm 0.6 \pm 1.2) \times 10^{-4}$ from a measurement of $[\Gamma(\chi_{c2}(1P) \rightarrow K_S^0(1430)^\pm K^\mp)/\Gamma_{\text{total}}] \times [B(\psi(2S) \rightarrow \gamma \chi_{c2}(1P))]$ assuming $B(\psi(2S) \rightarrow \gamma \chi_{c2}(1P)) = (9.11 \pm 0.31) \times 10^{-2}$, which we rescale to our best value $B(\psi(2S) \rightarrow \gamma \chi_{c2}(1P)) = (9.52 \pm 0.20) \times 10^{-2}$. Our first error is their experiment's error and our second error is the systematic error from using our best value.
² ABLIKIM 17AG reports $(18.2 \pm 0.8 \pm 1.6) \times 10^{-4}$ from a measurement of $[\Gamma(\chi_{c2}(1P) \rightarrow K_S^0(1430)^\pm K^\mp)/\Gamma_{\text{total}}] \times [B(\psi(2S) \rightarrow \gamma \chi_{c2}(1P))]$ assuming $B(\psi(2S) \rightarrow \gamma \chi_{c2}(1P)) = (9.11 \pm 0.31) \times 10^{-2}$, which we rescale to our best value $B(\psi(2S) \rightarrow \gamma \chi_{c2}(1P)) = (9.52 \pm 0.20) \times 10^{-2}$. Our first error is their experiment's error and our second error is the systematic error from using our best value.
³ ABLIKIM 17AG reports $(13.6 \pm 0.8 \pm 1.4) \times 10^{-4}$ from a measurement of $[\Gamma(\chi_{c2}(1P) \rightarrow K_S^0(1430)^\pm K^\mp)/\Gamma_{\text{total}}] \times [B(\psi(2S) \rightarrow \gamma \chi_{c2}(1P))]$ assuming $B(\psi(2S) \rightarrow \gamma \chi_{c2}(1P)) = (9.11 \pm 0.31) \times 10^{-2}$, which we rescale to our best value $B(\psi(2S) \rightarrow \gamma \chi_{c2}(1P)) = (9.52 \pm 0.20) \times 10^{-2}$. Our first error is their experiment's error and our second error is the systematic error from using our best value.

 $\Gamma(K_S^0(1430)^0 \bar{K}^0 + \text{c.c.})/\Gamma_{\text{total}}$ Γ_{37}/Γ

VALUE (units 10^{-4})	DOCUMENT ID	TECN	COMMENT
$12.4 \pm 1.7 \pm 0.3$	¹ ABLIKIM	17AG BES3	$\psi(2S) \rightarrow \gamma K_S^0 K^\pm \pi^\mp$

¹ ABLIKIM 17AG reports $(13.0 \pm 1.0 \pm 1.5) \times 10^{-4}$ from a measurement of $[\Gamma(\chi_{c2}(1P) \rightarrow K_S^0(1430)^0 \bar{K}^0 + \text{c.c.})/\Gamma_{\text{total}}] \times [B(\psi(2S) \rightarrow \gamma \chi_{c2}(1P))]$ assuming $B(\psi(2S) \rightarrow \gamma \chi_{c2}(1P)) = (9.11 \pm 0.31) \times 10^{-2}$, which we rescale to our best value $B(\psi(2S) \rightarrow \gamma \chi_{c2}(1P)) = (9.52 \pm 0.20) \times 10^{-2}$. Our first error is their experiment's error and our second error is the systematic error from using our best value.

 $\Gamma(K_S^0(1780)^\pm K^\mp)/\Gamma_{\text{total}}$ Γ_{38}/Γ

VALUE (units 10^{-4})	DOCUMENT ID	TECN	COMMENT
$5.2 \pm 0.8 \pm 0.1$	¹ ABLIKIM	17AG BES3	$\psi(2S) \rightarrow \gamma K \bar{K} \pi$
$5.1 \pm 1.0 \pm 0.1$	² ABLIKIM	17AG BES3	$\psi(2S) \rightarrow \gamma K^+ K^- \pi^0$
$5.6 \pm 1.8 \pm 0.1$	³ ABLIKIM	17AG BES3	$\psi(2S) \rightarrow \gamma K_S^0 K^\pm \pi^\mp$

¹ ABLIKIM 17AG reports $(5.4 \pm 0.5 \pm 0.7) \times 10^{-4}$ from a measurement of $[\Gamma(\chi_{c2}(1P) \rightarrow K_S^0(1780)^\pm K^\mp)/\Gamma_{\text{total}}] \times [B(\psi(2S) \rightarrow \gamma \chi_{c2}(1P))]$ assuming $B(\psi(2S) \rightarrow \gamma \chi_{c2}(1P)) = (9.11 \pm 0.31) \times 10^{-2}$, which we rescale to our best value $B(\psi(2S) \rightarrow \gamma \chi_{c2}(1P)) = (9.52 \pm 0.20) \times 10^{-2}$. Our first error is their experiment's error and our second error is the systematic error from using our best value.
² ABLIKIM 17AG reports $(5.3 \pm 0.5 \pm 0.9) \times 10^{-4}$ from a measurement of $[\Gamma(\chi_{c2}(1P) \rightarrow K_S^0(1780)^\pm K^\mp)/\Gamma_{\text{total}}] \times [B(\psi(2S) \rightarrow \gamma \chi_{c2}(1P))]$ assuming $B(\psi(2S) \rightarrow \gamma \chi_{c2}(1P)) = (9.11 \pm 0.31) \times 10^{-2}$, which we rescale to our best value $B(\psi(2S) \rightarrow \gamma \chi_{c2}(1P)) = (9.52 \pm 0.20) \times 10^{-2}$. Our first error is their experiment's error and our second error is the systematic error from using our best value.
³ ABLIKIM 17AG reports $(5.9 \pm 1.1 \pm 1.5) \times 10^{-4}$ from a measurement of $[\Gamma(\chi_{c2}(1P) \rightarrow K_S^0(1780)^\pm K^\mp)/\Gamma_{\text{total}}] \times [B(\psi(2S) \rightarrow \gamma \chi_{c2}(1P))]$ assuming $B(\psi(2S) \rightarrow \gamma \chi_{c2}(1P)) = (9.11 \pm 0.31) \times 10^{-2}$. Our first error is their experiment's error and our second error is the systematic error from using our best value.

 $\Gamma(K_S^0(1780)^0 \bar{K}^0 + \text{c.c.})/\Gamma_{\text{total}}$ Γ_{39}/Γ

VALUE (units 10^{-4})	DOCUMENT ID	TECN	COMMENT
$5.6 \pm 2.1 \pm 0.1$	¹ ABLIKIM	17AG BES3	$\psi(2S) \rightarrow \gamma K_S^0 K^\pm \pi^\mp$

¹ ABLIKIM 17AG reports $(5.9 \pm 1.6 \pm 1.5) \times 10^{-4}$ from a measurement of $[\Gamma(\chi_{c2}(1P) \rightarrow K_S^0(1780)^0 \bar{K}^0 + \text{c.c.})/\Gamma_{\text{total}}] \times [B(\psi(2S) \rightarrow \gamma \chi_{c2}(1P))]$ assuming $B(\psi(2S) \rightarrow \gamma \chi_{c2}(1P)) = (9.11 \pm 0.31) \times 10^{-2}$, which we rescale to our best value $B(\psi(2S) \rightarrow \gamma \chi_{c2}(1P)) = (9.52 \pm 0.20) \times 10^{-2}$. Our first error is their experiment's error and our second error is the systematic error from using our best value.

 $\Gamma(a_2(1320)^0 \pi^0)/\Gamma_{\text{total}}$ Γ_{40}/Γ

VALUE (units 10^{-4})	DOCUMENT ID	TECN	COMMENT
$12.9 \pm 3.4 \pm 0.3$	¹ ABLIKIM	17AG BES3	$\psi(2S) \rightarrow \gamma K^+ K^- \pi^0$

¹ ABLIKIM 17AG reports $(13.5 \pm 1.6 \pm 3.2) \times 10^{-4}$ from a measurement of $[\Gamma(\chi_{c2}(1P) \rightarrow a_2(1320)^0 \pi^0)/\Gamma_{\text{total}}] \times [B(\psi(2S) \rightarrow \gamma \chi_{c2}(1P))]$ assuming $B(\psi(2S) \rightarrow \gamma \chi_{c2}(1P)) = (9.11 \pm 0.31) \times 10^{-2}$, which we rescale to our best value $B(\psi(2S) \rightarrow \gamma \chi_{c2}(1P)) = (9.52 \pm 0.20) \times 10^{-2}$. Our first error is their experiment's error and our second error is the systematic error from using our best value.

 $\Gamma(a_2(1320)^\pm \pi^\mp)/\Gamma_{\text{total}}$ Γ_{41}/Γ

VALUE (units 10^{-4})	DOCUMENT ID	TECN	COMMENT
$17.6 \pm 6.1 \pm 0.4$	¹ ABLIKIM	17AG BES3	$\psi(2S) \rightarrow \gamma K_S^0 K^\pm \pi^\mp$

¹ ABLIKIM 17AG reports $(18.4 \pm 3.3 \pm 5.5) \times 10^{-4}$ from a measurement of $[\Gamma(\chi_{c2}(1P) \rightarrow a_2(1320)^\pm \pi^\mp)/\Gamma_{\text{total}}] \times [B(\psi(2S) \rightarrow \gamma \chi_{c2}(1P))]$ assuming $B(\psi(2S) \rightarrow \gamma \chi_{c2}(1P)) = (9.11 \pm 0.31) \times 10^{-2}$, which we rescale to our best value $B(\psi(2S) \rightarrow \gamma \chi_{c2}(1P)) = (9.52 \pm 0.20) \times 10^{-2}$. Our first error is their experiment's error and our second error is the systematic error from using our best value.

 $\Gamma(K^+ K^- \pi^0)/\Gamma_{\text{total}}$ Γ_{43}/Γ

VALUE (units 10^{-3})	DOCUMENT ID	TECN	COMMENT
$0.30 \pm 0.08 \pm 0.01$	¹ ATHAR	07 CLEO	$\psi(2S) \rightarrow \gamma h^+ h^- h^0$

¹ ATHAR 07 reports $(0.31 \pm 0.07 \pm 0.04) \times 10^{-3}$ from a measurement of $[\Gamma(\chi_{c2}(1P) \rightarrow K^+ K^- \pi^0)/\Gamma_{\text{total}}] \times [B(\psi(2S) \rightarrow \gamma \chi_{c2}(1P))]$ assuming $B(\psi(2S) \rightarrow \gamma \chi_{c2}(1P)) = (9.33 \pm 0.14 \pm 0.61) \times 10^{-2}$, which we rescale to our best value $B(\psi(2S) \rightarrow \gamma \chi_{c2}(1P)) = (9.52 \pm 0.20) \times 10^{-2}$. Our first error is their experiment's error and our second error is the systematic error from using our best value.

 $\Gamma(K^+ K^- \eta)/\Gamma_{\text{total}}$ Γ_{44}/Γ

VALUE (units 10^{-3})	CL%	DOCUMENT ID	TECN	COMMENT
< 0.32	90	¹ ATHAR	07 CLEO	$\psi(2S) \rightarrow \gamma h^+ h^- h^0$

¹ ATHAR 07 reports $< 0.33 \times 10^{-3}$ from a measurement of $[\Gamma(\chi_{c2}(1P) \rightarrow K^+ K^- \eta)/\Gamma_{\text{total}}] \times [B(\psi(2S) \rightarrow \gamma \chi_{c2}(1P))]$ assuming $B(\psi(2S) \rightarrow \gamma \chi_{c2}(1P)) = (9.33 \pm 0.14 \pm 0.61) \times 10^{-2}$, which we rescale to our best value $B(\psi(2S) \rightarrow \gamma \chi_{c2}(1P)) = 9.52 \times 10^{-2}$.

 $\Gamma(K^+ K^- \eta'(958))/\Gamma_{\text{total}}$ Γ_{45}/Γ

VALUE (units 10^{-4})	EVTS	DOCUMENT ID	TECN	COMMENT
1.94 ± 0.34	107	¹ ABLIKIM	14J BES3	$\psi(2S) \rightarrow \gamma K^+ K^- \eta'(958)$

¹ Derived using $B(\psi(2S) \rightarrow \gamma \chi_{c2}) = (8.72 \pm 0.34)\%$. Uncertainty includes both statistical and systematic contributions combined in quadrature.

 $\Gamma(\eta\eta')/\Gamma_{\text{total}}$ Γ_{46}/Γ

VALUE (units 10^{-5})	CL%	EVTS	DOCUMENT ID	TECN	COMMENT
$2.17 \pm 0.47 \pm 0.05$		20	¹ ABLIKIM	17AI BES3	$\psi(2S) \rightarrow \gamma \eta \eta'$

See key on page 1127

Meson Particle Listings

$\chi_{c2}(1P)$

••• We do not use the following data for averages, fits, limits, etc. •••
< 6 90 3.3 ± 0.0 2 ASNER 09 CLEO $\psi(2S) \rightarrow \gamma\eta'$
<23 90 3 ADAMS 07 CLEO $\psi(2S) \rightarrow \gamma\chi_{c2}$

1 ABLIKIM 17Al reports $(2.27 \pm 0.43 \pm 0.25) \times 10^{-5}$ from a measurement of $[\Gamma(\chi_{c2}(1P) \rightarrow \eta\eta')/\Gamma_{total}] \times [B(\psi(2S) \rightarrow \gamma\chi_{c2}(1P))]$ assuming $B(\psi(2S) \rightarrow \gamma\chi_{c2}(1P)) = (9.11 \pm 0.31) \times 10^{-2}$, which we rescale to our best value $B(\psi(2S) \rightarrow \gamma\chi_{c2}(1P)) = (9.52 \pm 0.20) \times 10^{-2}$. Our first error is their experiment's error and our second error is the systematic error from using our best value.
2 ASNER 09 reports $< 0.6 \times 10^{-4}$ from a measurement of $[\Gamma(\chi_{c2}(1P) \rightarrow \eta\eta')/\Gamma_{total}] \times [B(\psi(2S) \rightarrow \gamma\chi_{c2}(1P))]$ assuming $B(\psi(2S) \rightarrow \gamma\chi_{c2}(1P)) = (9.33 \pm 0.14 \pm 0.61) \times 10^{-2}$, which we rescale to our best value $B(\psi(2S) \rightarrow \gamma\chi_{c2}(1P)) = 9.52 \times 10^{-2}$.
3 Superseded by ASNER 09. ADAMS 07 reports $< 2.3 \times 10^{-4}$ from a measurement of $[\Gamma(\chi_{c2}(1P) \rightarrow \eta\eta')/\Gamma_{total}] \times [B(\psi(2S) \rightarrow \gamma\chi_{c2}(1P))]$ assuming $B(\psi(2S) \rightarrow \gamma\chi_{c2}(1P)) = 0.0933 \pm 0.0014 \pm 0.0061$, which we rescale to our best value $B(\psi(2S) \rightarrow \gamma\chi_{c2}(1P)) = 9.52 \times 10^{-2}$.

$\Gamma(\eta'\eta')/\Gamma_{total}$ Γ_{47}/Γ
VALUE (units 10^{-5}) CL% EVTS DOCUMENT ID TECN COMMENT
4.6 ± 0.6 ± 0.1 60 1 ABLIKIM 17Al BES3 $\psi(2S) \rightarrow \gamma\eta'\eta'$

••• We do not use the following data for averages, fits, limits, etc. •••
<10 90 12 ± 7 2 ASNER 09 CLEO $\psi(2S) \rightarrow \eta'\eta'$
<30 90 3 ADAMS 07 CLEO $\psi(2S) \rightarrow \gamma\chi_{c2}$
1 ABLIKIM 17Al reports $(4.76 \pm 0.56 \pm 0.38) \times 10^{-5}$ from a measurement of $[\Gamma(\chi_{c2}(1P) \rightarrow \eta'\eta')/\Gamma_{total}] \times [B(\psi(2S) \rightarrow \gamma\chi_{c2}(1P))]$ assuming $B(\psi(2S) \rightarrow \gamma\chi_{c2}(1P)) = (9.11 \pm 0.31) \times 10^{-2}$, which we rescale to our best value $B(\psi(2S) \rightarrow \gamma\chi_{c2}(1P)) = (9.52 \pm 0.20) \times 10^{-2}$. Our first error is their experiment's error and our second error is the systematic error from using our best value.
2 ASNER 09 reports $< 1.0 \times 10^{-4}$ from a measurement of $[\Gamma(\chi_{c2}(1P) \rightarrow \eta'\eta')/\Gamma_{total}] \times [B(\psi(2S) \rightarrow \gamma\chi_{c2}(1P))]$ assuming $B(\psi(2S) \rightarrow \gamma\chi_{c2}(1P)) = (9.33 \pm 0.14 \pm 0.61) \times 10^{-2}$, which we rescale to our best value $B(\psi(2S) \rightarrow \gamma\chi_{c2}(1P)) = 9.52 \times 10^{-2}$.
3 Superseded by ASNER 09. ADAMS 07 reports $< 3.1 \times 10^{-4}$ from a measurement of $[\Gamma(\chi_{c2}(1P) \rightarrow \eta'\eta')/\Gamma_{total}] \times [B(\psi(2S) \rightarrow \gamma\chi_{c2}(1P))]$ assuming $B(\psi(2S) \rightarrow \gamma\chi_{c2}(1P)) = 0.0933 \pm 0.0014 \pm 0.0061$, which we rescale to our best value $B(\psi(2S) \rightarrow \gamma\chi_{c2}(1P)) = 9.52 \times 10^{-2}$.

$\Gamma(\pi^+\pi^-K_S^0K_S^0)/\Gamma_{total}$ Γ_{48}/Γ
VALUE (units 10^{-3}) EVTS DOCUMENT ID TECN COMMENT
2.17 ± 0.54 ± 0.05 57 ± 11 1 ABLIKIM 05o BES2 $\psi(2S) \rightarrow \gamma\chi_{c2}$

1 ABLIKIM 05o reports $[\Gamma(\chi_{c2}(1P) \rightarrow \pi^+\pi^-K_S^0K_S^0)/\Gamma_{total}] \times [B(\psi(2S) \rightarrow \gamma\chi_{c2}(1P))] = (0.207 \pm 0.039 \pm 0.033) \times 10^{-3}$ which we divide by our best value $B(\psi(2S) \rightarrow \gamma\chi_{c2}(1P)) = (9.52 \pm 0.20) \times 10^{-2}$. Our first error is their experiment's error and our second error is the systematic error from using our best value.

$\Gamma(K^+K^-K_S^0K_S^0)/\Gamma_{total}$ Γ_{49}/Γ
VALUE (units 10^{-4}) CL% EVTS DOCUMENT ID TECN COMMENT
<4 90 2.3 ± 2.2 1 ABLIKIM 05o BES2 $e^+e^- \rightarrow \chi_{c2}\gamma$

1 ABLIKIM 05o reports $[\Gamma(\chi_{c2}(1P) \rightarrow K^+K^-K_S^0K_S^0)/\Gamma_{total}] \times [B(\psi(2S) \rightarrow \gamma\chi_{c2}(1P))] < 3.5 \times 10^{-5}$ which we divide by our best value $B(\psi(2S) \rightarrow \gamma\chi_{c2}(1P)) = 9.52 \times 10^{-2}$.

$\Gamma(K_S^0K_S^0K_S^0K_S^0)/\Gamma_{total}$ Γ_{50}/Γ
VALUE (units 10^{-4}) EVTS DOCUMENT ID TECN COMMENT
1.13 ± 0.18 ± 0.02 68 1 ABLIKIM 19AA BES3 $\psi(2S) \rightarrow \gamma 4K_S^0$

1 Using $B(K_S^0 \rightarrow \pi^+\pi^-) = (69.20 \pm 0.05)\%$. ABLIKIM 19AA reports $[\Gamma(\chi_{c2}(1P) \rightarrow K_S^0K_S^0K_S^0K_S^0)/\Gamma_{total}] \times [B(\psi(2S) \rightarrow \gamma\chi_{c2}(1P))] = (10.8 \pm 1.5 \pm 0.8) \times 10^{-6}$ which we divide by our best value $B(\psi(2S) \rightarrow \gamma\chi_{c2}(1P)) = (9.52 \pm 0.20) \times 10^{-2}$. Our first error is their experiment's error and our second error is the systematic error from using our best value.

$\Gamma(K^+K^-K^+K^-)/\Gamma_{total}$ Γ_{51}/Γ
VALUE (units 10^{-3}) DOCUMENT ID TECN COMMENT
1.65 ± 0.20 OUR FIT

$\Gamma(K^+K^-\phi)/\Gamma_{total}$ Γ_{52}/Γ
VALUE (units 10^{-3}) EVTS DOCUMENT ID TECN COMMENT
1.42 ± 0.29 ± 0.03 52 1 ABLIKIM 06T BES2 $\psi(2S) \rightarrow \gamma 2K^+ 2K^-$

1 ABLIKIM 06T reports $(1.67 \pm 0.26 \pm 0.24) \times 10^{-3}$ from a measurement of $[\Gamma(\chi_{c2}(1P) \rightarrow K^+K^-\phi)/\Gamma_{total}] \times [B(\psi(2S) \rightarrow \gamma\chi_{c2}(1P))]$ assuming $B(\psi(2S) \rightarrow \gamma\chi_{c2}(1P)) = (8.1 \pm 0.4) \times 10^{-2}$, which we rescale to our best value $B(\psi(2S) \rightarrow \gamma\chi_{c2}(1P)) = (9.52 \pm 0.20) \times 10^{-2}$. Our first error is their experiment's error and our second error is the systematic error from using our best value.

$\Gamma(K^0K^+\pi^-\phi + c.c.)/\Gamma_{total}$ Γ_{53}/Γ
VALUE (units 10^{-3}) DOCUMENT ID TECN COMMENT
4.83 ± 0.32 ± 0.66 ABLIKIM 15M BES3 $\psi(2S) \rightarrow \gamma\chi_{c2}$

$\Gamma(K^+K^-\pi^0\phi)/\Gamma_{total}$ Γ_{54}/Γ
VALUE (units 10^{-3}) DOCUMENT ID TECN COMMENT
2.74 ± 0.16 ± 0.44 ABLIKIM 15M BES3 $\psi(2S) \rightarrow \gamma\chi_{c2}$

$\Gamma(\phi\pi^+\pi^-\pi^0)/\Gamma_{total}$ Γ_{55}/Γ
VALUE (units 10^{-3}) EVTS DOCUMENT ID TECN COMMENT
0.93 ± 0.06 ± 0.10 408 1 ABLIKIM 13B BES3 $e^+e^- \rightarrow \psi(2S) \rightarrow \gamma\chi_{c2}$

1 Using 1.06×10^8 $\psi(2S)$ mesons and $B(\psi(2S) \rightarrow \chi_{c2}\gamma) = (8.72 \pm 0.34)\%$.

$\Gamma(p\bar{p})/\Gamma_{total}$ Γ_{56}/Γ
VALUE (units 10^{-4}) DOCUMENT ID TECN COMMENT
0.733 ± 0.033 OUR FIT

$\Gamma(p\bar{p}\pi^0)/\Gamma_{total}$ Γ_{57}/Γ
VALUE (units 10^{-3}) DOCUMENT ID TECN COMMENT
0.47 ± 0.04 ± 0.01 1 ONYISI 10 CLE3 $\psi(2S) \rightarrow \gamma p\bar{p}\chi$
0.43 ± 0.09 ± 0.01 2 ATHAR 07 CLEO $\psi(2S) \rightarrow \gamma h^+ h^- h^0$

1 ONYISI 10 reports $(4.83 \pm 0.25 \pm 0.35 \pm 0.31) \times 10^{-4}$ from a measurement of $[\Gamma(\chi_{c2}(1P) \rightarrow p\bar{p}\pi^0)/\Gamma_{total}] \times [B(\psi(2S) \rightarrow \gamma\chi_{c2}(1P))]$ assuming $B(\psi(2S) \rightarrow \gamma\chi_{c2}(1P)) = (9.33 \pm 0.14 \pm 0.61) \times 10^{-2}$, which we rescale to our best value $B(\psi(2S) \rightarrow \gamma\chi_{c2}(1P)) = (9.52 \pm 0.20) \times 10^{-2}$. Our first error is their experiment's error and our second error is the systematic error from using our best value.
2 ATHAR 07 reports $(0.44 \pm 0.08 \pm 0.05) \times 10^{-3}$ from a measurement of $[\Gamma(\chi_{c2}(1P) \rightarrow p\bar{p}\pi^0)/\Gamma_{total}] \times [B(\psi(2S) \rightarrow \gamma\chi_{c2}(1P))]$ assuming $B(\psi(2S) \rightarrow \gamma\chi_{c2}(1P)) = (9.33 \pm 0.14 \pm 0.61) \times 10^{-2}$, which we rescale to our best value $B(\psi(2S) \rightarrow \gamma\chi_{c2}(1P)) = (9.52 \pm 0.20) \times 10^{-2}$. Our first error is their experiment's error and our second error is the systematic error from using our best value.

$\Gamma(p\bar{p}\eta)/\Gamma_{total}$ Γ_{58}/Γ
VALUE (units 10^{-3}) DOCUMENT ID TECN COMMENT
0.174 ± 0.025 OUR AVERAGE
0.172 ± 0.026 ± 0.004 1 ONYISI 10 CLE3 $\psi(2S) \rightarrow \gamma p\bar{p}\chi$
0.186 ± 0.070 ± 0.004 2 ATHAR 07 CLEO $\psi(2S) \rightarrow \gamma h^+ h^- h^0$

1 ONYISI 10 reports $(1.76 \pm 0.23 \pm 0.14 \pm 0.11) \times 10^{-4}$ from a measurement of $[\Gamma(\chi_{c2}(1P) \rightarrow p\bar{p}\eta)/\Gamma_{total}] \times [B(\psi(2S) \rightarrow \gamma\chi_{c2}(1P))]$ assuming $B(\psi(2S) \rightarrow \gamma\chi_{c2}(1P)) = (9.33 \pm 0.14 \pm 0.61) \times 10^{-2}$, which we rescale to our best value $B(\psi(2S) \rightarrow \gamma\chi_{c2}(1P)) = (9.52 \pm 0.20) \times 10^{-2}$. Our first error is their experiment's error and our second error is the systematic error from using our best value.
2 ATHAR 07 reports $(0.19 \pm 0.07 \pm 0.02) \times 10^{-3}$ from a measurement of $[\Gamma(\chi_{c2}(1P) \rightarrow p\bar{p}\eta)/\Gamma_{total}] \times [B(\psi(2S) \rightarrow \gamma\chi_{c2}(1P))]$ assuming $B(\psi(2S) \rightarrow \gamma\chi_{c2}(1P)) = (9.33 \pm 0.14 \pm 0.61) \times 10^{-2}$, which we rescale to our best value $B(\psi(2S) \rightarrow \gamma\chi_{c2}(1P)) = (9.52 \pm 0.20) \times 10^{-2}$. Our first error is their experiment's error and our second error is the systematic error from using our best value.

$\Gamma(p\bar{p}\omega)/\Gamma_{total}$ Γ_{59}/Γ
VALUE (units 10^{-3}) DOCUMENT ID TECN COMMENT
0.36 ± 0.04 ± 0.01 1 ONYISI 10 CLE3 $\psi(2S) \rightarrow \gamma p\bar{p}\chi$

1 ONYISI 10 reports $(3.68 \pm 0.35 \pm 0.26 \pm 0.24) \times 10^{-4}$ from a measurement of $[\Gamma(\chi_{c2}(1P) \rightarrow p\bar{p}\omega)/\Gamma_{total}] \times [B(\psi(2S) \rightarrow \gamma\chi_{c2}(1P))]$ assuming $B(\psi(2S) \rightarrow \gamma\chi_{c2}(1P)) = (9.33 \pm 0.14 \pm 0.61) \times 10^{-2}$, which we rescale to our best value $B(\psi(2S) \rightarrow \gamma\chi_{c2}(1P)) = (9.52 \pm 0.20) \times 10^{-2}$. Our first error is their experiment's error and our second error is the systematic error from using our best value.

$\Gamma(p\bar{p}\phi)/\Gamma_{total}$ Γ_{60}/Γ
VALUE (units 10^{-3}) EVTS DOCUMENT ID TECN COMMENT
2.8 ± 0.9 ± 0.1 24 ± 7 1 ABLIKIM 11F BES3 $\psi(2S) \rightarrow \gamma p\bar{p}K^+K^-$

1 ABLIKIM 11F reports $(3.04 \pm 0.85 \pm 0.43) \times 10^{-3}$ from a measurement of $[\Gamma(\chi_{c2}(1P) \rightarrow p\bar{p}\phi)/\Gamma_{total}] \times [B(\psi(2S) \rightarrow \gamma\chi_{c2}(1P))]$ assuming $B(\psi(2S) \rightarrow \gamma\chi_{c2}(1P)) = (8.74 \pm 0.35) \times 10^{-2}$, which we rescale to our best value $B(\psi(2S) \rightarrow \gamma\chi_{c2}(1P)) = (9.52 \pm 0.20) \times 10^{-2}$. Our first error is their experiment's error and our second error is the systematic error from using our best value.

$\Gamma(p\bar{p}\pi^+\pi^-)/\Gamma_{total}$ Γ_{61}/Γ
VALUE (units 10^{-3}) DOCUMENT ID TECN COMMENT
1.32 ± 0.34 OUR EVALUATION Treating systematic error as correlated.
1.3 ± 0.4 OUR AVERAGE Error includes scale factor of 1.3.
1.17 ± 0.19 ± 0.30 1 BAI 99B BES $\psi(2S) \rightarrow \gamma\chi_{c2}$
2.64 ± 1.03 ± 0.14 1 TANENBAUM 78 MRK1 $\psi(2S) \rightarrow \gamma\chi_{c2}$

1 Rescaled by us using $B(\psi(2S) \rightarrow \gamma\chi_{c2}) = (8.3 \pm 0.4)\%$ and $B(\psi(2S) \rightarrow J/\psi(1S)\pi^+\pi^-) = (32.6 \pm 0.5)\%$. Multiplied by a factor of 2 to convert from $K_S^0 K^+\pi^-$ to $K^0 K^+\pi^-$ decay.

$\Gamma(p\bar{p}\pi^0\pi^0)/\Gamma_{total}$ Γ_{62}/Γ
VALUE (%) EVTS DOCUMENT ID TECN COMMENT
0.078 ± 0.023 ± 0.002 29.2 1 HE 08B CLEO $e^+e^- \rightarrow \gamma h^+ h^- h^0 h^0$

1 HE 08B reports $0.08 \pm 0.02 \pm 0.01 \pm 0.01\%$ from a measurement of $[\Gamma(\chi_{c2}(1P) \rightarrow p\bar{p}\pi^0\pi^0)/\Gamma_{total}] \times [B(\psi(2S) \rightarrow \gamma\chi_{c2}(1P))]$ assuming $B(\psi(2S) \rightarrow \gamma\chi_{c2}(1P)) = (9.33 \pm 0.14 \pm 0.61) \times 10^{-2}$, which we rescale to our best value $B(\psi(2S) \rightarrow \gamma\chi_{c2}(1P)) = (9.52 \pm 0.20) \times 10^{-2}$. Our first error is their experiment's error and our second error is the systematic error from using our best value.

Meson Particle Listings

 $\chi_{c2}(1P)$ $\Gamma(p\bar{p}K^+K^- \text{ (non-resonant)})/\Gamma_{\text{total}}$ Γ_{63}/Γ

VALUE (units 10^{-4})	EVTS	DOCUMENT ID	TECN	COMMENT
1.91±0.32±0.04	131 ± 12	¹ ABLIKIM	11F BES3	$\psi(2S) \rightarrow \gamma p\bar{p}K^+K^-$
¹ ABLIKIM 11F reports $(2.08 \pm 0.19 \pm 0.30) \times 10^{-4}$ from a measurement of $[\Gamma(\chi_{c2}(1P) \rightarrow p\bar{p}K^+K^- \text{ (non-resonant)})/\Gamma_{\text{total}}] \times [B(\psi(2S) \rightarrow \gamma\chi_{c2}(1P))]$ assuming $B(\psi(2S) \rightarrow \gamma\chi_{c2}(1P)) = (8.74 \pm 0.35) \times 10^{-2}$, which we rescale to our best value $B(\psi(2S) \rightarrow \gamma\chi_{c2}(1P)) = (9.52 \pm 0.20) \times 10^{-2}$. Our first error is their experiment's error and our second error is the systematic error from using our best value.				

 $\Gamma(p\bar{p}K_S^0K_S^0)/\Gamma_{\text{total}}$ Γ_{64}/Γ

VALUE (units 10^{-4})	CL%	DOCUMENT ID	TECN	COMMENT
<7.9	90	¹ ABLIKIM	06D BES2	$\psi(2S) \rightarrow \chi_{c2}\gamma$
¹ Using $B(\psi(2S) \rightarrow \chi_{c2}\gamma) = (9.3 \pm 0.6)\%$.				

 $\Gamma(p\bar{p}\pi^-)/\Gamma_{\text{total}}$ Γ_{65}/Γ

VALUE (units 10^{-4})	EVTS	DOCUMENT ID	TECN	COMMENT
8.5±0.9 OUR AVERAGE				
8.4±1.0±0.2	3309	¹ ABLIKIM	12J BES3	$\psi(2S) \rightarrow \gamma p\bar{p}\pi^-$
10.2±3.4±0.2		² ABLIKIM	06I BES2	$\psi(2S) \rightarrow \gamma p\pi^- X$
¹ ABLIKIM 12J reports $[\Gamma(\chi_{c2}(1P) \rightarrow p\bar{p}\pi^-)/\Gamma_{\text{total}}] \times [B(\psi(2S) \rightarrow \gamma\chi_{c2}(1P))] = (0.80 \pm 0.02 \pm 0.09) \times 10^{-4}$ which we divide by our best value $B(\psi(2S) \rightarrow \gamma\chi_{c2}(1P)) = (9.52 \pm 0.20) \times 10^{-2}$. Our first error is their experiment's error and our second error is the systematic error from using our best value.				
² ABLIKIM 06I reports $[\Gamma(\chi_{c2}(1P) \rightarrow p\bar{p}\pi^-)/\Gamma_{\text{total}}] \times [B(\psi(2S) \rightarrow \gamma\chi_{c2}(1P))] = (0.97 \pm 0.20 \pm 0.26) \times 10^{-4}$ which we divide by our best value $B(\psi(2S) \rightarrow \gamma\chi_{c2}(1P)) = (9.52 \pm 0.20) \times 10^{-2}$. Our first error is their experiment's error and our second error is the systematic error from using our best value.				

 $\Gamma(p\bar{p}\pi^+)/\Gamma_{\text{total}}$ Γ_{66}/Γ

VALUE (units 10^{-4})	EVTS	DOCUMENT ID	TECN	COMMENT
8.9±0.8±0.2	3732	¹ ABLIKIM	12J BES3	$\psi(2S) \rightarrow \gamma p\bar{p}\pi^+$
¹ ABLIKIM 12J reports $[\Gamma(\chi_{c2}(1P) \rightarrow p\bar{p}\pi^+)/\Gamma_{\text{total}}] \times [B(\psi(2S) \rightarrow \gamma\chi_{c2}(1P))] = (0.85 \pm 0.02 \pm 0.07) \times 10^{-4}$ which we divide by our best value $B(\psi(2S) \rightarrow \gamma\chi_{c2}(1P)) = (9.52 \pm 0.20) \times 10^{-2}$. Our first error is their experiment's error and our second error is the systematic error from using our best value.				

 $\Gamma(p\bar{p}\pi^-\pi^0)/\Gamma_{\text{total}}$ Γ_{67}/Γ

VALUE (units 10^{-4})	EVTS	DOCUMENT ID	TECN	COMMENT
21.7±1.7±0.5	2128	¹ ABLIKIM	12J BES3	$\psi(2S) \rightarrow \gamma p\bar{p}\pi^-\pi^0$
¹ ABLIKIM 12J reports $[\Gamma(\chi_{c2}(1P) \rightarrow p\bar{p}\pi^-\pi^0)/\Gamma_{\text{total}}] \times [B(\psi(2S) \rightarrow \gamma\chi_{c2}(1P))] = (2.07 \pm 0.06 \pm 0.15) \times 10^{-4}$ which we divide by our best value $B(\psi(2S) \rightarrow \gamma\chi_{c2}(1P)) = (9.52 \pm 0.20) \times 10^{-2}$. Our first error is their experiment's error and our second error is the systematic error from using our best value.				

 $\Gamma(p\bar{p}\pi^+\pi^0)/\Gamma_{\text{total}}$ Γ_{68}/Γ

VALUE (units 10^{-4})	EVTS	DOCUMENT ID	TECN	COMMENT
21.1±1.8±0.4	2352	¹ ABLIKIM	12J BES3	$\psi(2S) \rightarrow \gamma p\bar{p}\pi^+\pi^0$
¹ ABLIKIM 12J reports $[\Gamma(\chi_{c2}(1P) \rightarrow p\bar{p}\pi^+\pi^0)/\Gamma_{\text{total}}] \times [B(\psi(2S) \rightarrow \gamma\chi_{c2}(1P))] = (2.01 \pm 0.06 \pm 0.16) \times 10^{-4}$ which we divide by our best value $B(\psi(2S) \rightarrow \gamma\chi_{c2}(1P)) = (9.52 \pm 0.20) \times 10^{-2}$. Our first error is their experiment's error and our second error is the systematic error from using our best value.				

 $\Gamma(\Lambda\bar{\Lambda})/\Gamma_{\text{total}}$ Γ_{69}/Γ

VALUE (units 10^{-4})	DOCUMENT ID
1.83±0.16 OUR FIT	

 $\Gamma(\Lambda\bar{\Lambda}\pi^+\pi^-)/\Gamma_{\text{total}}$ Γ_{70}/Γ

VALUE (units 10^{-5})	CL%	EVTS	DOCUMENT ID	TECN	COMMENT
125±15±3		371	¹ ABLIKIM	12I BES3	$\psi(2S) \rightarrow \gamma\Lambda\bar{\Lambda}\pi^+\pi^-$
•••					We do not use the following data for averages, fits, limits, etc. •••
<350	90		² ABLIKIM	06D BES2	$\psi(2S) \rightarrow \chi_{c2}\gamma$
¹ ABLIKIM 12I reports $(137.0 \pm 7.6 \pm 15.7) \times 10^{-5}$ from a measurement of $[\Gamma(\chi_{c2}(1P) \rightarrow \Lambda\bar{\Lambda}\pi^+\pi^-)/\Gamma_{\text{total}}] \times [B(\psi(2S) \rightarrow \gamma\chi_{c2}(1P))]$ assuming $B(\psi(2S) \rightarrow \gamma\chi_{c2}(1P)) = (8.72 \pm 0.34) \times 10^{-2}$, which we rescale to our best value $B(\psi(2S) \rightarrow \gamma\chi_{c2}(1P)) = (9.52 \pm 0.20) \times 10^{-2}$. Our first error is their experiment's error and our second error is the systematic error from using our best value.					
² Using $B(\psi(2S) \rightarrow \chi_{c2}\gamma) = (9.3 \pm 0.6)\%$.					

 $\Gamma(\Lambda\bar{\Lambda}\pi^+\pi^- \text{ (non-resonant)})/\Gamma_{\text{total}}$ Γ_{71}/Γ

VALUE (units 10^{-5})	EVTS	DOCUMENT ID	TECN	COMMENT
66±15±1	36	¹ ABLIKIM	12I BES3	$\psi(2S) \rightarrow \gamma\Lambda\bar{\Lambda}\pi^+\pi^-$
¹ ABLIKIM 12I reports $(71.8 \pm 14.5 \pm 8.2) \times 10^{-5}$ from a measurement of $[\Gamma(\chi_{c2}(1P) \rightarrow \Lambda\bar{\Lambda}\pi^+\pi^- \text{ (non-resonant)})/\Gamma_{\text{total}}] \times [B(\psi(2S) \rightarrow \gamma\chi_{c2}(1P))]$ assuming $B(\psi(2S) \rightarrow \gamma\chi_{c2}(1P)) = (8.72 \pm 0.34) \times 10^{-2}$, which we rescale to our best value $B(\psi(2S) \rightarrow \gamma\chi_{c2}(1P)) = (9.52 \pm 0.20) \times 10^{-2}$. Our first error is their experiment's error and our second error is the systematic error from using our best value.				

 $\Gamma(\Sigma(1385)^+\bar{\Lambda}\pi^- + \text{c.c.})/\Gamma_{\text{total}}$ Γ_{72}/Γ

VALUE (units 10^{-5})	CL%	DOCUMENT ID	TECN	COMMENT
<40	90	¹ ABLIKIM	12I BES3	$\psi(2S) \rightarrow \gamma\Sigma(1385)^+\bar{\Lambda}\pi^-$
¹ ABLIKIM 12I reports $< 42 \times 10^{-5}$ from a measurement of $[\Gamma(\chi_{c2}(1P) \rightarrow \Sigma(1385)^+\bar{\Lambda}\pi^- + \text{c.c.})/\Gamma_{\text{total}}] \times [B(\psi(2S) \rightarrow \gamma\chi_{c2}(1P))]$ assuming $B(\psi(2S) \rightarrow \gamma\chi_{c2}(1P)) = (8.72 \pm 0.34) \times 10^{-2}$, which we rescale to our best value $B(\psi(2S) \rightarrow \gamma\chi_{c2}(1P)) = 9.52 \times 10^{-2}$.				

 $\Gamma(\Sigma(1385)^-\bar{\Lambda}\pi^+ + \text{c.c.})/\Gamma_{\text{total}}$ Γ_{73}/Γ

VALUE (units 10^{-5})	CL%	DOCUMENT ID	TECN	COMMENT
<60	90	¹ ABLIKIM	12I BES3	$\psi(2S) \rightarrow \gamma\Sigma(1385)^-\bar{\Lambda}\pi^+$
¹ ABLIKIM 12I reports $< 61 \times 10^{-5}$ from a measurement of $[\Gamma(\chi_{c2}(1P) \rightarrow \Sigma(1385)^-\bar{\Lambda}\pi^+ + \text{c.c.})/\Gamma_{\text{total}}] \times [B(\psi(2S) \rightarrow \gamma\chi_{c2}(1P))]$ assuming $B(\psi(2S) \rightarrow \gamma\chi_{c2}(1P)) = (8.72 \pm 0.34) \times 10^{-2}$, which we rescale to our best value $B(\psi(2S) \rightarrow \gamma\chi_{c2}(1P)) = 9.52 \times 10^{-2}$.				

 $\Gamma(K^+\bar{p}\Lambda + \text{c.c.})/\Gamma_{\text{total}}$ Γ_{74}/Γ

VALUE (units 10^{-4})	EVTS	DOCUMENT ID	TECN	COMMENT
7.8±0.5 OUR AVERAGE				
7.7±0.5±0.2	5k	^{1,2} ABLIKIM	13D BES3	$\psi(2S) \rightarrow \gamma\Lambda\bar{p}K^+$
8.3±1.6±0.2		³ ATHAR	07 CLEO	$\psi(2S) \rightarrow \gamma h^+ h^- h^0$
¹ ABLIKIM 13D reports $(8.4 \pm 0.3 \pm 0.6) \times 10^{-4}$ from a measurement of $[\Gamma(\chi_{c2}(1P) \rightarrow K^+\bar{p}\Lambda + \text{c.c.})/\Gamma_{\text{total}}] \times [B(\psi(2S) \rightarrow \gamma\chi_{c2}(1P))]$ assuming $B(\psi(2S) \rightarrow \gamma\chi_{c2}(1P)) = (8.72 \pm 0.34) \times 10^{-2}$, which we rescale to our best value $B(\psi(2S) \rightarrow \gamma\chi_{c2}(1P)) = (9.52 \pm 0.20) \times 10^{-2}$. Our first error is their experiment's error and our second error is the systematic error from using our best value.				
² Using $B(\Lambda \rightarrow p\pi^-) = 63.9\%$.				
³ ATHAR 07 reports $(8.5 \pm 1.4 \pm 1.0) \times 10^{-4}$ from a measurement of $[\Gamma(\chi_{c2}(1P) \rightarrow K^+\bar{p}\Lambda + \text{c.c.})/\Gamma_{\text{total}}] \times [B(\psi(2S) \rightarrow \gamma\chi_{c2}(1P))]$ assuming $B(\psi(2S) \rightarrow \gamma\chi_{c2}(1P)) = (9.33 \pm 0.14 \pm 0.61) \times 10^{-2}$, which we rescale to our best value $B(\psi(2S) \rightarrow \gamma\chi_{c2}(1P)) = (9.52 \pm 0.20) \times 10^{-2}$. Our first error is their experiment's error and our second error is the systematic error from using our best value.				

 $\Gamma(nK_S^0\bar{\Lambda} + \text{c.c.})/\Gamma_{\text{total}}$ Γ_{75}/Γ

VALUE (units 10^{-4})	EVTS	DOCUMENT ID	TECN	COMMENT
3.58±0.16±0.23	879	¹ ABLIKIM	21AV BES3	$\psi(2S) \rightarrow \gamma nK_S^0\bar{\Lambda} + \text{c.c.}$
¹ ABLIKIM 21AV reports $(3.58 \pm 0.16 \pm 0.23) \times 10^{-4}$ from a measurement of $[\Gamma(\chi_{c2}(1P) \rightarrow nK_S^0\bar{\Lambda} + \text{c.c.})/\Gamma_{\text{total}}] \times [B(\psi(2S) \rightarrow \gamma\chi_{c2}(1P))]$ assuming $B(\psi(2S) \rightarrow \gamma\chi_{c2}(1P)) = 0.0952 \pm 0.0020$. Also uses $B(\bar{\Lambda} \rightarrow \bar{p}\pi^+) = (63.9 \pm 0.5)\%$ and $B(K_S^0 \rightarrow \pi^+\pi^-) = (69.20 \pm 0.05)\%$.				

 $\Gamma(K^*(892)^+\bar{p}\Lambda + \text{c.c.})/\Gamma_{\text{total}}$ Γ_{76}/Γ

VALUE (units 10^{-4})	EVTS	DOCUMENT ID	TECN	COMMENT
8.2±1.1±0.2	476	¹ ABLIKIM	19AU BES3	$\psi(2S) \rightarrow \gamma K^*\bar{p}\Lambda$
¹ ABLIKIM 19AU reports $[\Gamma(\chi_{c2}(1P) \rightarrow K^*(892)^+\bar{p}\Lambda + \text{c.c.})/\Gamma_{\text{total}}] \times [B(\psi(2S) \rightarrow \gamma\chi_{c2}(1P))] = (7.8 \pm 0.9 \pm 0.6) \times 10^{-5}$ which we divide by our best value $B(\psi(2S) \rightarrow \gamma\chi_{c2}(1P)) = (9.52 \pm 0.20) \times 10^{-2}$. Our first error is their experiment's error and our second error is the systematic error from using our best value.				

 $\Gamma(K^+\bar{p}\Lambda(1520) + \text{c.c.})/\Gamma_{\text{total}}$ Γ_{77}/Γ

VALUE (units 10^{-4})	EVTS	DOCUMENT ID	TECN	COMMENT
2.8±0.7±0.1	79 ± 13	¹ ABLIKIM	11F BES3	$\psi(2S) \rightarrow \gamma p\bar{p}K^+K^-$
¹ ABLIKIM 11F reports $(3.06 \pm 0.50 \pm 0.54) \times 10^{-4}$ from a measurement of $[\Gamma(\chi_{c2}(1P) \rightarrow K^+\bar{p}\Lambda(1520) + \text{c.c.})/\Gamma_{\text{total}}] \times [B(\psi(2S) \rightarrow \gamma\chi_{c2}(1P))]$ assuming $B(\psi(2S) \rightarrow \gamma\chi_{c2}(1P)) = (8.74 \pm 0.35) \times 10^{-2}$, which we rescale to our best value $B(\psi(2S) \rightarrow \gamma\chi_{c2}(1P)) = (9.52 \pm 0.20) \times 10^{-2}$. Our first error is their experiment's error and our second error is the systematic error from using our best value.				

 $\Gamma(\Lambda(1520)\bar{\Lambda}(1520))/\Gamma_{\text{total}}$ Γ_{78}/Γ

VALUE (units 10^{-4})	EVTS	DOCUMENT ID	TECN	COMMENT
4.6±1.4±0.1	29 ± 7	¹ ABLIKIM	11F BES3	$\psi(2S) \rightarrow \gamma p\bar{p}K^+K^-$
¹ ABLIKIM 11F reports $(5.05 \pm 1.29 \pm 0.93) \times 10^{-4}$ from a measurement of $[\Gamma(\chi_{c2}(1P) \rightarrow \Lambda(1520)\bar{\Lambda}(1520))/\Gamma_{\text{total}}] \times [B(\psi(2S) \rightarrow \gamma\chi_{c2}(1P))]$ assuming $B(\psi(2S) \rightarrow \gamma\chi_{c2}(1P)) = (8.74 \pm 0.35) \times 10^{-2}$, which we rescale to our best value $B(\psi(2S) \rightarrow \gamma\chi_{c2}(1P)) = (9.52 \pm 0.20) \times 10^{-2}$. Our first error is their experiment's error and our second error is the systematic error from using our best value.				

 $\Gamma(\Sigma^0\bar{\Sigma}^0)/\Gamma_{\text{total}}$ Γ_{79}/Γ

VALUE (units 10^{-5})	CL%	EVTS	DOCUMENT ID	TECN	COMMENT
3.7±0.6±0.1		91	¹ ABLIKIM	18V BES3	$\psi(2S) \rightarrow \gamma\Sigma^0\bar{\Sigma}^0$
•••					We do not use the following data for averages, fits, limits, etc. •••
<6	90		² ABLIKIM	13H BES3	$\psi(2S) \rightarrow \gamma\Sigma^0\bar{\Sigma}^0$
<7	90	7.5 ± 3.4	³ NAIK	08 CLEO	$\psi(2S) \rightarrow \gamma\Sigma^0\bar{\Sigma}^0$

See key on page 1127

Meson Particle Listings

$\chi_{c2}(1P)$

¹ ABLIKIM 18v reports $[\Gamma(\chi_{c2}(1P) \rightarrow \Sigma^0 \bar{\Sigma}^0)/\Gamma_{total}] \times [B(\psi(2S) \rightarrow \gamma \chi_{c2}(1P))] = (0.35 \pm 0.05 \pm 0.02) \times 10^{-5}$ which we divide by our best value $B(\psi(2S) \rightarrow \gamma \chi_{c2}(1P)) = (9.52 \pm 0.20) \times 10^{-2}$. Our first error is their experiment's error and our second error is the systematic error from using our best value.

² ABLIKIM 13H reports $< 0.65 \times 10^{-4}$ from a measurement of $[\Gamma(\chi_{c2}(1P) \rightarrow \Sigma^0 \bar{\Sigma}^0)/\Gamma_{total}] \times [B(\psi(2S) \rightarrow \gamma \chi_{c2}(1P))]$ assuming $B(\psi(2S) \rightarrow \gamma \chi_{c2}(1P)) = (8.74 \pm 0.35) \times 10^{-2}$, which we rescale to our best value $B(\psi(2S) \rightarrow \gamma \chi_{c2}(1P)) = 9.52 \times 10^{-2}$.

³ NAIK 08 reports $< 0.75 \times 10^{-4}$ from a measurement of $[\Gamma(\chi_{c2}(1P) \rightarrow \Sigma^0 \bar{\Sigma}^0)/\Gamma_{total}] \times [B(\psi(2S) \rightarrow \gamma \chi_{c2}(1P))]$ assuming $B(\psi(2S) \rightarrow \gamma \chi_{c2}(1P)) = (9.33 \pm 0.14 \pm 0.61) \times 10^{-2}$, which we rescale to our best value $B(\psi(2S) \rightarrow \gamma \chi_{c2}(1P)) = 9.52 \times 10^{-2}$.

$\Gamma(\Sigma^+ \bar{\Sigma}^-)/\Gamma_{total}$ Γ_{82}/Γ

Table with 5 columns: VALUE (units 10^-5), CL%, EVTS, DOCUMENT ID, TECN, COMMENT. Row 1: 3.4 ± 0.7 ± 0.1, 55, 1 ABLIKIM 18v BES3 ψ(2S) → γ Σ+ Σ-.

• • • We do not use the following data for averages, fits, limits, etc. • • •

Table with 5 columns: VALUE (units 10^-5), CL%, EVTS, DOCUMENT ID, TECN, COMMENT. Row 1: <8, 90, 2 ABLIKIM 13H BES3 ψ(2S) → γ Σ+ Σ-.

¹ ABLIKIM 18v reports $[\Gamma(\chi_{c2}(1P) \rightarrow \Sigma^+ \bar{\Sigma}^-)/\Gamma_{total}] \times [B(\psi(2S) \rightarrow \gamma \chi_{c2}(1P))] = (0.32 \pm 0.06 \pm 0.03) \times 10^{-5}$ which we divide by our best value $B(\psi(2S) \rightarrow \gamma \chi_{c2}(1P)) = (9.52 \pm 0.20) \times 10^{-2}$. Our first error is their experiment's error and our second error is the systematic error from using our best value.

² ABLIKIM 13H reports $< 0.88 \times 10^{-4}$ from a measurement of $[\Gamma(\chi_{c2}(1P) \rightarrow \Sigma^+ \bar{\Sigma}^-)/\Gamma_{total}] \times [B(\psi(2S) \rightarrow \gamma \chi_{c2}(1P))]$ assuming $B(\psi(2S) \rightarrow \gamma \chi_{c2}(1P)) = (8.74 \pm 0.35) \times 10^{-2}$, which we rescale to our best value $B(\psi(2S) \rightarrow \gamma \chi_{c2}(1P)) = 9.52 \times 10^{-2}$.

³ NAIK 08 reports $< 0.67 \times 10^{-4}$ from a measurement of $[\Gamma(\chi_{c2}(1P) \rightarrow \Sigma^+ \bar{\Sigma}^-)/\Gamma_{total}] \times [B(\psi(2S) \rightarrow \gamma \chi_{c2}(1P))]$ assuming $B(\psi(2S) \rightarrow \gamma \chi_{c2}(1P)) = (9.33 \pm 0.14 \pm 0.61) \times 10^{-2}$, which we rescale to our best value $B(\psi(2S) \rightarrow \gamma \chi_{c2}(1P)) = 9.52 \times 10^{-2}$.

$\Gamma(\Sigma^- \bar{\Sigma}^+)/\Gamma_{total}$ Γ_{83}/Γ

Table with 5 columns: VALUE (units 10^-5), CL%, EVTS, DOCUMENT ID, TECN, COMMENT. Row 1: 4.4 ± 1.7 ± 0.5, 131, 1 ABLIKIM 20i BES3 ψ(2S) → γ Σ- Σ+.

¹ ABLIKIM 20i reports $(4.4 \pm 1.7 \pm 0.5) \times 10^{-5}$ from a measurement of $[\Gamma(\chi_{c2}(1P) \rightarrow \Sigma^- \bar{\Sigma}^+)/\Gamma_{total}] \times [B(\psi(2S) \rightarrow \gamma \chi_{c2}(1P))]$ assuming $B(\psi(2S) \rightarrow \gamma \chi_{c2}(1P)) = (9.52 \pm 0.20) \times 10^{-2}$.

$\Gamma(\Sigma(1385)^+ \bar{\Sigma}(1385)^-)/\Gamma_{total}$ Γ_{84}/Γ

Table with 5 columns: VALUE (units 10^-5), CL%, DOCUMENT ID, TECN, COMMENT. Row 1: <16, 90, 1 ABLIKIM 12i BES3 ψ(2S) → γ Σ(1385)+ Σ(1385)-.

¹ ABLIKIM 12i reports $< 17 \times 10^{-5}$ from a measurement of $[\Gamma(\chi_{c2}(1P) \rightarrow \Sigma(1385)^+ \bar{\Sigma}(1385)^-)/\Gamma_{total}] \times [B(\psi(2S) \rightarrow \gamma \chi_{c2}(1P))]$ assuming $B(\psi(2S) \rightarrow \gamma \chi_{c2}(1P)) = (8.72 \pm 0.34) \times 10^{-2}$, which we rescale to our best value $B(\psi(2S) \rightarrow \gamma \chi_{c2}(1P)) = 9.52 \times 10^{-2}$.

$\Gamma(\Sigma(1385)^- \bar{\Sigma}(1385)^+)/\Gamma_{total}$ Γ_{85}/Γ

Table with 5 columns: VALUE (units 10^-5), CL%, DOCUMENT ID, TECN, COMMENT. Row 1: <8, 90, 1 ABLIKIM 12i BES3 ψ(2S) → γ Σ(1385)- Σ(1385)+.

¹ ABLIKIM 12i reports $< 8.5 \times 10^{-5}$ from a measurement of $[\Gamma(\chi_{c2}(1P) \rightarrow \Sigma(1385)^- \bar{\Sigma}(1385)^+)/\Gamma_{total}] \times [B(\psi(2S) \rightarrow \gamma \chi_{c2}(1P))]$ assuming $B(\psi(2S) \rightarrow \gamma \chi_{c2}(1P)) = (8.72 \pm 0.34) \times 10^{-2}$, which we rescale to our best value $B(\psi(2S) \rightarrow \gamma \chi_{c2}(1P)) = 9.52 \times 10^{-2}$.

$\Gamma(K^- \Lambda \bar{\Xi}^+ + c.c.)/\Gamma_{total}$ Γ_{86}/Γ

Table with 5 columns: VALUE (units 10^-4), EVTS, DOCUMENT ID, TECN, COMMENT. Row 1: 1.76 ± 0.32 ± 0.04, 51, 1 ABLIKIM 15i BES3 ψ(2S) → γ K- ΛΞ+ + c.c.

¹ ABLIKIM 15i reports $[\Gamma(\chi_{c2}(1P) \rightarrow K^- \Lambda \bar{\Xi}^+ + c.c.)/\Gamma_{total}] \times [B(\psi(2S) \rightarrow \gamma \chi_{c2}(1P))] = (1.68 \pm 0.26 \pm 0.15) \times 10^{-5}$ which we divide by our best value $B(\psi(2S) \rightarrow \gamma \chi_{c2}(1P)) = (9.52 \pm 0.20) \times 10^{-2}$. Our first error is their experiment's error and our second error is the systematic error from using our best value.

$\Gamma(\Xi^0 \bar{\Xi}^0)/\Gamma_{total}$ Γ_{87}/Γ

Table with 5 columns: VALUE (units 10^-4), CL%, EVTS, DOCUMENT ID, TECN, COMMENT. Row 1: <1.0, 90, 2.9 ± 1.7, 1 NAIK 08 CLEO ψ(2S) → γ Ξ0 Ξ0.

¹ NAIK 08 reports $< 1.06 \times 10^{-4}$ from a measurement of $[\Gamma(\chi_{c2}(1P) \rightarrow \Xi^0 \bar{\Xi}^0)/\Gamma_{total}] \times [B(\psi(2S) \rightarrow \gamma \chi_{c2}(1P))]$ assuming $B(\psi(2S) \rightarrow \gamma \chi_{c2}(1P)) = (9.33 \pm 0.14 \pm 0.61) \times 10^{-2}$, which we rescale to our best value $B(\psi(2S) \rightarrow \gamma \chi_{c2}(1P)) = 9.52 \times 10^{-2}$.

$\Gamma(\Xi^- \bar{\Xi}^+)/\Gamma_{total}$ Γ_{88}/Γ

Table with 5 columns: VALUE (units 10^-4), CL%, EVTS, DOCUMENT ID, TECN, COMMENT. Row 1: 1.42 ± 0.31 ± 0.03, 29 ± 5, 1 NAIK 08 CLEO ψ(2S) → γ Ξ- Ξ+.

• • • We do not use the following data for averages, fits, limits, etc. • • •

Table with 5 columns: VALUE (units 10^-4), CL%, EVTS, DOCUMENT ID, TECN, COMMENT. Row 1: < 3.7, 90, 2 ABLIKIM 06D BES2 ψ(2S) → χc2 γ.

¹ NAIK 08 reports $(1.45 \pm 0.30 \pm 0.15) \times 10^{-4}$ from a measurement of $[\Gamma(\chi_{c2}(1P) \rightarrow \Xi^- \bar{\Xi}^+)/\Gamma_{total}] \times [B(\psi(2S) \rightarrow \gamma \chi_{c2}(1P))]$ assuming $B(\psi(2S) \rightarrow \gamma \chi_{c2}(1P)) = (9.33 \pm 0.14 \pm 0.61) \times 10^{-2}$, which we rescale to our best value $B(\psi(2S) \rightarrow \gamma \chi_{c2}(1P)) = (9.52 \pm 0.20) \times 10^{-2}$. Our first error is their experiment's error and our second error is the systematic error from using our best value.

² Using $B(\psi(2S) \rightarrow \chi_{c2} \gamma) = (9.3 \pm 0.6)\%$.

$\Gamma(J/\psi(1S) \pi^+ \pi^- \pi^0)/\Gamma_{total}$ Γ_{89}/Γ

Table with 5 columns: VALUE, CL%, DOCUMENT ID, TECN, COMMENT. Row 1: <0.015, 90, BARATE 81 SPEC 190 GeV π- Be → 2π 2μ.

$\Gamma(\pi^0 \eta_c)/\Gamma_{total}$ Γ_{90}/Γ

Table with 5 columns: VALUE, CL%, DOCUMENT ID, TECN, COMMENT. Row 1: <3.2 × 10^-3, 90, 1 ABLIKIM 15N BES3 ψ(2S) e+ e- → γ π0 ηc.

¹ Using $B(\eta_c \rightarrow K_S^0 K^\pm \pi^\mp) \times B(K_S^0 \rightarrow \pi^+ \pi^-) \times B(\pi^0 \rightarrow \gamma \gamma) = (1.66 \pm 0.11) \times 10^{-2}$.

$\Gamma(\eta_c(1S) \pi^+ \pi^-)/\Gamma_{total}$ Γ_{91}/Γ

Table with 5 columns: VALUE, CL%, DOCUMENT ID, TECN, COMMENT. Row 1: <0.54 × 10^-2, 90, 1,2 ABLIKIM 13B BES3 e+ e- → ψ(2S) → γ χc2.

• • • We do not use the following data for averages, fits, limits, etc. • • •

Table with 5 columns: VALUE, CL%, DOCUMENT ID, TECN, COMMENT. Row 1: <1.2 × 10^-2, 90, 1,3 ABLIKIM 13B BES3 e+ e- → ψ(2S) → γ χc2.

¹ Using 1.06×10^8 $\psi(2S)$ mesons and $B(\psi(2S) \rightarrow \chi_{c2} \gamma) = (8.72 \pm 0.34)\%$.

² From the $\eta_c \rightarrow K_S^0 K^\pm \pi^\mp$ decays.

³ From the $\eta_c \rightarrow K^+ K^- \pi^0$ decays.

$\Gamma(\eta_c(1S) \pi^+ \pi^-)/\Gamma(K^0 K^+ \pi^- + c.c.)$ Γ_{91}/Γ_{42}

Table with 5 columns: VALUE, CL%, DOCUMENT ID, TECN, COMMENT. Row 1: <16.4, 90, 1 LEES 12AE BABR e+ e- → e+ e- π+ π- ηc.

¹ We divided the reported limit by 2 to take into account the $K_L^0 K^+ \pi^-$ mode.

RADIATIVE DECAYS

$\Gamma(\gamma J/\psi(1S))/\Gamma_{total}$ Γ_{92}/Γ

Table with 5 columns: VALUE (units 10^-2), CL%, EVTS, DOCUMENT ID, TECN, COMMENT. Row 1: 19.0 ± 0.5 OUR FIT.

• • • We do not use the following data for averages, fits, limits, etc. • • •

Table with 5 columns: VALUE, CL%, EVTS, DOCUMENT ID, TECN, COMMENT. Row 1: 18.64 ± 0.08 ± 1.69 1.0M, 1 ABLIKIM 17U BES3 e+ e- → γ X.

¹ Not independent from $B(\psi(2S) \rightarrow \gamma \chi_{c2}(1P))$ and the product $B(\psi(2S) \rightarrow \gamma \chi_{c2}(1P)) \times B(\chi_{c2}(1P) \rightarrow \gamma J/\psi(1S))$ also measured in ABLIKIM 17U.

² Uses $B(\psi(2S) \rightarrow \gamma \chi_{c2} \rightarrow \gamma J/\psi)$ from ADAM 05A and $B(\psi(2S) \rightarrow \gamma \chi_{c2})$ from ATHAR 04.

$\Gamma(\gamma \rho^0)/\Gamma_{total}$ Γ_{93}/Γ

Table with 5 columns: VALUE (units 10^-6), CL%, EVTS, DOCUMENT ID, TECN, COMMENT. Row 1: <19, 90, 13 ± 11, 1 ABLIKIM 11E BES3 ψ(2S) → γ γ ρ0.

• • • We do not use the following data for averages, fits, limits, etc. • • •

Table with 5 columns: VALUE, CL%, EVTS, DOCUMENT ID, TECN, COMMENT. Row 1: <40, 90, 17.2 ± 6.8, 2 BENNETT 08A CLEO ψ(2S) → γ γ ρ0.

¹ ABLIKIM 11E reports $< 20.8 \times 10^{-6}$ from a measurement of $[\Gamma(\chi_{c2}(1P) \rightarrow \gamma \rho^0)/\Gamma_{total}] \times [B(\psi(2S) \rightarrow \gamma \chi_{c2}(1P))]$ assuming $B(\psi(2S) \rightarrow \gamma \chi_{c2}(1P)) = (8.74 \pm 0.35) \times 10^{-2}$, which we rescale to our best value $B(\psi(2S) \rightarrow \gamma \chi_{c2}(1P)) = 9.52 \times 10^{-2}$.

² BENNETT 08A reports $< 50 \times 10^{-6}$ from a measurement of $[\Gamma(\chi_{c2}(1P) \rightarrow \gamma \rho^0)/\Gamma_{total}] \times [B(\psi(2S) \rightarrow \gamma \chi_{c2}(1P))]$ assuming $B(\psi(2S) \rightarrow \gamma \chi_{c2}(1P)) = (8.1 \pm 0.4) \times 10^{-2}$, which we rescale to our best value $B(\psi(2S) \rightarrow \gamma \chi_{c2}(1P)) = 9.52 \times 10^{-2}$.

$\Gamma(\gamma \omega)/\Gamma_{total}$ Γ_{94}/Γ

Table with 5 columns: VALUE (units 10^-6), CL%, EVTS, DOCUMENT ID, TECN, COMMENT. Row 1: <6, 90, 1 ± 6, 1 ABLIKIM 11E BES3 ψ(2S) → γ γ ω.

• • • We do not use the following data for averages, fits, limits, etc. • • •

Table with 5 columns: VALUE, CL%, EVTS, DOCUMENT ID, TECN, COMMENT. Row 1: <6, 90, 0.0 ± 1.8, 2 BENNETT 08A CLEO ψ(2S) → γ γ ω.

¹ ABLIKIM 11E reports $< 6.1 \times 10^{-6}$ from a measurement of $[\Gamma(\chi_{c2}(1P) \rightarrow \gamma \omega)/\Gamma_{total}] \times [B(\psi(2S) \rightarrow \gamma \chi_{c2}(1P))]$ assuming $B(\psi(2S) \rightarrow \gamma \chi_{c2}(1P)) = (8.74 \pm 0.35) \times 10^{-2}$, which we rescale to our best value $B(\psi(2S) \rightarrow \gamma \chi_{c2}(1P)) = 9.52 \times 10^{-2}$.

² BENNETT 08A reports $< 7.0 \times 10^{-6}$ from a measurement of $[\Gamma(\chi_{c2}(1P) \rightarrow \gamma \omega)/\Gamma_{total}] \times [B(\psi(2S) \rightarrow \gamma \chi_{c2}(1P))]$ assuming $B(\psi(2S) \rightarrow \gamma \chi_{c2}(1P)) = (8.1 \pm 0.4) \times 10^{-2}$, which we rescale to our best value $B(\psi(2S) \rightarrow \gamma \chi_{c2}(1P)) = 9.52 \times 10^{-2}$.

$\Gamma(\gamma \phi)/\Gamma_{total}$ Γ_{95}/Γ

Table with 5 columns: VALUE (units 10^-6), CL%, EVTS, DOCUMENT ID, TECN, COMMENT. Row 1: < 7, 90, 5 ± 5, 1 ABLIKIM 11E BES3 ψ(2S) → γ γ φ.

• • • We do not use the following data for averages, fits, limits, etc. • • •

Table with 5 columns: VALUE, CL%, EVTS, DOCUMENT ID, TECN, COMMENT. Row 1: <11, 90, 1.3 ± 2.5, 2 BENNETT 08A CLEO ψ(2S) → γ γ φ.

¹ ABLIKIM 11E reports $< 8.1 \times 10^{-6}$ from a measurement of $[\Gamma(\chi_{c2}(1P) \rightarrow \gamma \phi)/\Gamma_{total}] \times [B(\psi(2S) \rightarrow \gamma \chi_{c2}(1P))]$ assuming $B(\psi(2S) \rightarrow \gamma \chi_{c2}(1P)) = (8.74 \pm 0.35) \times 10^{-2}$, which we rescale to our best value $B(\psi(2S) \rightarrow \gamma \chi_{c2}(1P)) = 9.52 \times 10^{-2}$.

² BENNETT 08A reports $< 13 \times 10^{-6}$ from a measurement of $[\Gamma(\chi_{c2}(1P) \rightarrow \gamma \phi)/\Gamma_{total}] \times [B(\psi(2S) \rightarrow \gamma \chi_{c2}(1P))]$ assuming $B(\psi(2S) \rightarrow \gamma \chi_{c2}(1P)) = (8.1 \pm 0.4) \times 10^{-2}$, which we rescale to our best value $B(\psi(2S) \rightarrow \gamma \chi_{c2}(1P)) = 9.52 \times 10^{-2}$.

$\Gamma(\gamma \gamma)/\Gamma_{total}$ Γ_{96}/Γ

Table with 5 columns: VALUE (units 10^-4), CL%, DOCUMENT ID. Row 1: 2.85 ± 0.10 OUR FIT.

Meson Particle Listings

$\chi_{c2}(1P)$

$\Gamma(e^+e^- J/\psi(1S))/\Gamma_{total}$ Γ_{97}/Γ

VALUE (units 10^{-3})	EVTS	DOCUMENT ID	TECN	COMMENT
--------------------------	------	-------------	------	---------

••• We do not use the following data for averages, fits, limits, etc. •••

2.37±0.15±0.05 1.3k 1,2 ABLIKIM 17i BES3 $\psi(2S) \rightarrow \gamma e^+e^- J/\psi$

¹ ABLIKIM 17i reports $(2.48 \pm 0.08 \pm 0.16) \times 10^{-3}$ from a measurement of $[\Gamma(\chi_{c2}(1P) \rightarrow e^+e^- J/\psi(1S))/\Gamma_{total}] \times [B(\psi(2S) \rightarrow \gamma \chi_{c2}(1P))]$ assuming $B(\psi(2S) \rightarrow \gamma \chi_{c2}(1P)) = (9.11 \pm 0.31) \times 10^{-2}$, which we rescale to our best value $B(\psi(2S) \rightarrow \gamma \chi_{c2}(1P)) = (9.52 \pm 0.20) \times 10^{-2}$. Our first error is their experiment's error and our second error is the systematic error from using our best value.

² Not independent from other measurements reported by ABLIKIM 17i

$\Gamma(e^+e^- J/\psi(1S))/\Gamma(\gamma J/\psi(1S))$ Γ_{97}/Γ_{92}

VALUE (units 10^{-3})	EVTS	DOCUMENT ID	TECN	COMMENT
--------------------------	------	-------------	------	---------

11.3±0.4±0.5 1.3k 1 ABLIKIM 17i BES3 $\psi(2S) \rightarrow e^+e^- \gamma J/\psi$

¹ Uses $B(\psi(2S) \rightarrow \gamma \chi_{c2}(1P)) \times B(\chi_{c2}(1P) \rightarrow \gamma J/\psi(1S)) = (199.6 \pm 0.8 \pm 7.0) \times 10^{-4}$ from ABLIKIM 17N and accounts for common systematic errors.

$\Gamma(\mu^+\mu^- J/\psi(1S))/\Gamma(e^+e^- J/\psi(1S))$ Γ_{98}/Γ_{97}

VALUE (units 10^{-2})	EVTS	DOCUMENT ID	TECN	COMMENT
--------------------------	------	-------------	------	---------

9.40±0.79±1.15 219 ABLIKIM 19z BES3 $\psi(2S) \rightarrow \gamma \chi_{c2} \rightarrow \gamma(\mu^+\mu^- J/\psi)$

$\Gamma(\gamma\gamma)/\Gamma(\gamma J/\psi(1S))$ Γ_{96}/Γ_{92}

VALUE (units 10^{-3})	DOCUMENT ID	TECN	COMMENT
--------------------------	-------------	------	---------

1.50±0.05 OUR FIT
0.99±0.18 1 AMBROGIANI 00b E835 $\bar{p}p \rightarrow \chi_{c2} \rightarrow \gamma\gamma, \gamma J/\psi$

¹ Calculated by us using $B(J/\psi(1S) \rightarrow e^+e^-) = 0.0593 \pm 0.0010$.

$\Gamma(\gamma\gamma)/\Gamma_{total} \times \Gamma(\bar{p}p)/\Gamma_{total}$ $\Gamma_{96}/\Gamma \times \Gamma_{56}/\Gamma$

VALUE (units 10^{-8})	DOCUMENT ID	TECN	COMMENT
--------------------------	-------------	------	---------

2.09±0.13 OUR FIT
1.7 ± 0.4 OUR AVERAGE

1.60±0.42 ARMSTRONG 93 E760 $\bar{p}p \rightarrow \gamma\gamma X$
9.9 ± 4.5 BAGLIN 87b SPEC $\bar{p}p \rightarrow \gamma\gamma X$

$\chi_{c2}(1P)$ CROSS-PARTICLE BRANCHING RATIOS

$\Gamma(\chi_{c2}(1P) \rightarrow K^+K^-\pi^+\pi^-)/\Gamma_{total} \times \Gamma(\psi(2S) \rightarrow \gamma \chi_{c2}(1P))/\Gamma(\psi(2S) \rightarrow J/\psi(1S)\pi^+\pi^-)$ $\Gamma_{14}/\Gamma \times \Gamma_{164}^{\psi(2S)}/\Gamma_{12}^{\psi(2S)}$

VALUE (units 10^{-3})	DOCUMENT ID	TECN	COMMENT
--------------------------	-------------	------	---------

2.31±0.26 OUR FIT
2.5 ± 0.9 OUR AVERAGE Error includes scale factor of 2.3.

1.90±0.14±0.44 BAI 99b BES $\psi(2S) \rightarrow \gamma \chi_{c2}$
3.8 ± 0.67 1 TANENBAUM 78 MRK1 $\psi(2S) \rightarrow \gamma \chi_{c2}$

¹ The reported value is derived using $B(\psi(2S) \rightarrow \pi^+\pi^- J/\psi) \times B(J/\psi \rightarrow \ell^+\ell^-) = (4.6 \pm 0.7)\%$. Calculated by us using $B(J/\psi \rightarrow \ell^+\ell^-) = 0.1181 \pm 0.0020$.

$\Gamma(\chi_{c2}(1P) \rightarrow K^*(892)^0 \bar{K}^*(892)^0)/\Gamma_{total} \times \Gamma(\psi(2S) \rightarrow \gamma \chi_{c2}(1P))/\Gamma_{total}$ $\Gamma_{18}/\Gamma \times \Gamma_{164}^{\psi(2S)}/\Gamma_{12}^{\psi(2S)}$

VALUE (units 10^{-4})	DOCUMENT ID	TECN	COMMENT
--------------------------	-------------	------	---------

2.1 ± 0.4 OUR FIT
3.11±0.36±0.48 ABLIKIM 04H BES2 $\psi(2S) \rightarrow \gamma \chi_{c2}$

$\Gamma(\chi_{c2}(1P) \rightarrow \rho\bar{\rho})/\Gamma_{total} \times \Gamma(\psi(2S) \rightarrow \gamma \chi_{c2}(1P))/\Gamma(\psi(2S) \rightarrow J/\psi(1S)\pi^+\pi^-)$ $\Gamma_{56}/\Gamma \times \Gamma_{164}^{\psi(2S)}/\Gamma_{12}^{\psi(2S)}$

VALUE (units 10^{-5})	DOCUMENT ID	TECN	COMMENT
--------------------------	-------------	------	---------

2.01±0.09 OUR FIT
1.4 ± 1.1 1 BAI 98i BES $\psi(2S) \rightarrow \gamma \chi_{c2} \rightarrow \gamma \bar{\rho}\rho$

¹ Calculated by us. The value for $B(\chi_{c2} \rightarrow \rho\bar{\rho})$ reported in BAI 98i is derived using $B(\psi(2S) \rightarrow \gamma \chi_{c2}) = (7.8 \pm 0.8)\%$ and $B(\psi(2S) \rightarrow J/\psi(1S)\pi^+\pi^-) = (32.4 \pm 2.6)\%$ [BAI 98b].

$\Gamma(\chi_{c2}(1P) \rightarrow \rho\bar{\rho})/\Gamma_{total} \times \Gamma(\psi(2S) \rightarrow \gamma \chi_{c2}(1P))/\Gamma_{total}$ $\Gamma_{56}/\Gamma \times \Gamma_{164}^{\psi(2S)}/\Gamma_{12}^{\psi(2S)}$

VALUE (units 10^{-6})	EVTS	DOCUMENT ID	TECN	COMMENT
--------------------------	------	-------------	------	---------

6.98±0.32 OUR FIT
7.1 ± 0.5 OUR AVERAGE Error includes scale factor of 1.2.

7.3 ± 0.4 ± 0.3 405 ABLIKIM 13v BES3 $\psi(2S) \rightarrow \gamma \rho\bar{\rho}$
7.2 ± 0.7 ± 0.4 121 ± 12 1 NAIK 08 CLEO $\psi(2S) \rightarrow \gamma \rho\bar{\rho}$
4.4 +1.6 ± 0.6 14.3 +5.2 -4.7 BAI 04f BES $\psi(2S) \rightarrow \gamma \chi_{c2}(1P) \rightarrow \gamma \bar{\rho}\rho$

¹ Calculated by us. NAIK 08 reports $B(\chi_{c2} \rightarrow \rho\bar{\rho}) = (7.7 \pm 0.8 \pm 0.4 \pm 0.5) \times 10^{-5}$ using $B(\psi(2S) \rightarrow \gamma \chi_{c2}) = (9.33 \pm 0.14 \pm 0.61)\%$.

$\Gamma(\chi_{c2}(1P) \rightarrow \Lambda\bar{\Lambda})/\Gamma_{total} \times \Gamma(\psi(2S) \rightarrow \gamma \chi_{c2}(1P))/\Gamma_{total}$ $\Gamma_{69}/\Gamma \times \Gamma_{164}^{\psi(2S)}/\Gamma_{12}^{\psi(2S)}$

VALUE (units 10^{-6})	EVTS	DOCUMENT ID	TECN	COMMENT
--------------------------	------	-------------	------	---------

17.4±1.4 OUR FIT
17.3±1.5 OUR AVERAGE

18.2±0.8±1.7 670 ABLIKIM 21L BES3 $\psi(2S) \rightarrow \gamma \rho\pi^-\bar{\rho}\pi^+$
15.9±2.1±1.0 71 1 NAIK 08 CLEO $\psi(2S) \rightarrow \gamma \Lambda\bar{\Lambda}$

••• We do not use the following data for averages, fits, limits, etc. •••

18.2±1.4±0.9 207 2,3 ABLIKIM 13H BES3 $\psi(2S) \rightarrow \gamma \Lambda\bar{\Lambda}$

¹ Calculated by us. NAIK 08 reports $B(\chi_{c2} \rightarrow \Lambda\bar{\Lambda}) = (17.0 \pm 2.2 \pm 1.1 \pm 1.1) \times 10^{-5}$ using $B(\psi(2S) \rightarrow \gamma \chi_{c2}) = (9.33 \pm 0.14 \pm 0.61)\%$.

² Superseded by ABLIKIM 21L

³ Calculated by us. ABLIKIM 13H reports $B(\chi_{c2} \rightarrow \Lambda\bar{\Lambda}) = (20.8 \pm 1.6 \pm 2.3) \times 10^{-5}$ from a measurement of $B(\chi_{c2} \rightarrow \Lambda\bar{\Lambda}) \times B(\psi(2S) \rightarrow \gamma \chi_{c2})$ assuming $B(\psi(2S) \rightarrow \gamma \chi_{c2}) = (8.74 \pm 0.35)\%$.

$\Gamma(\chi_{c2}(1P) \rightarrow \Lambda\bar{\Lambda})/\Gamma_{total} \times \Gamma(\psi(2S) \rightarrow \gamma \chi_{c2}(1P))/\Gamma(\psi(2S) \rightarrow J/\psi(1S)\pi^+\pi^-)$ $\Gamma_{69}/\Gamma \times \Gamma_{164}^{\psi(2S)}/\Gamma_{12}^{\psi(2S)}$

VALUE (units 10^{-5})	EVTS	DOCUMENT ID	TECN	COMMENT
--------------------------	------	-------------	------	---------

5.0±0.4 OUR FIT
7.1 +3.1 -2.9 ± 1.3 8.3 +3.7 -3.4 1 BAI 03E BES $\psi(2S) \rightarrow \gamma \Lambda\bar{\Lambda}$

¹ BAI 03E reports $[B(\chi_{c2} \rightarrow \Lambda\bar{\Lambda}) B(\psi(2S) \rightarrow \gamma \chi_{c2}) / B(\psi(2S) \rightarrow J/\psi\pi^+\pi^-)] \times [B^2(\Lambda \rightarrow \pi^-p) / B(J/\psi \rightarrow \rho\bar{\rho})] = (1.33 +0.59 -0.55 \pm 0.25)\%$. We calculate from this measurement the presented value using $B(\Lambda \rightarrow \pi^-p) = (63.9 \pm 0.5)\%$ and $B(J/\psi \rightarrow \rho\bar{\rho}) = (2.17 \pm 0.07) \times 10^{-3}$.

$\Gamma(\chi_{c2}(1P) \rightarrow \pi\pi)/\Gamma_{total} \times \Gamma(\psi(2S) \rightarrow \gamma \chi_{c2}(1P))/\Gamma_{total}$ $\Gamma_{25}/\Gamma \times \Gamma_{164}^{\psi(2S)}/\Gamma_{12}^{\psi(2S)}$

VALUE (units 10^{-4})	EVTS	DOCUMENT ID	TECN	COMMENT
--------------------------	------	-------------	------	---------

2.12±0.08 OUR FIT
2.17±0.09 OUR AVERAGE

2.19±0.05±0.15 4.5k 1 ABLIKIM 10A BES3 $e^+e^- \rightarrow \psi(2S) \rightarrow \gamma \chi_{c2}$
2.23±0.06±0.10 2.5k 2 ASNER 09 CLEO $\psi(2S) \rightarrow \gamma\pi^+\pi^-$
1.90±0.08±0.20 0.8k 3 ASNER 09 CLEO $\psi(2S) \rightarrow \gamma\pi^0\pi^0$

¹ Calculated by us. ABLIKIM 10A reports $B(\chi_{c2} \rightarrow \pi^0\pi^0) = (0.88 \pm 0.02 \pm 0.06 \pm 0.04) \times 10^{-3}$ using $B(\psi(2S) \rightarrow \gamma \chi_{c2}) = (8.3 \pm 0.4)\%$. We have multiplied the $\pi^0\pi^0$ measurement by 3 to obtain $\pi\pi$.

² Calculated by us. ASNER 09 reports $B(\chi_{c2} \rightarrow \pi^+\pi^-) = (1.59 \pm 0.04 \pm 0.07 \pm 0.10) \times 10^{-3}$ using $B(\psi(2S) \rightarrow \gamma \chi_{c2}) = (9.33 \pm 0.14 \pm 0.61)\%$. We have multiplied the $\pi^+\pi^-$ measurement by 3/2 to obtain $\pi\pi$.

³ Calculated by us. ASNER 09 reports $B(\chi_{c2} \rightarrow \pi^0\pi^0) = (0.68 \pm 0.03 \pm 0.07 \pm 0.04) \times 10^{-3}$ using $B(\psi(2S) \rightarrow \gamma \chi_{c2}) = (9.33 \pm 0.14 \pm 0.61)\%$. We have multiplied the $\pi^0\pi^0$ measurement by 3 to obtain $\pi\pi$.

$\Gamma(\chi_{c2}(1P) \rightarrow \pi\pi)/\Gamma_{total} \times \Gamma(\psi(2S) \rightarrow \gamma \chi_{c2}(1P))/\Gamma(\psi(2S) \rightarrow J/\psi(1S)\pi^+\pi^-)$ $\Gamma_{25}/\Gamma \times \Gamma_{164}^{\psi(2S)}/\Gamma_{12}^{\psi(2S)}$

VALUE (units 10^{-3})	EVTS	DOCUMENT ID	TECN	COMMENT
--------------------------	------	-------------	------	---------

0.612±0.023 OUR FIT
0.54 ± 0.06 OUR AVERAGE

0.66 ± 0.18 ± 0.37 21 ± 6 1 BAI 03c BES $\psi(2S) \rightarrow \gamma\pi^0\pi^0$
0.54 ± 0.05 ± 0.04 185 ± 16 2 BAI 98i BES $\psi(2S) \rightarrow \gamma\pi^+\pi^-$

¹ We have multiplied $\pi^0\pi^0$ measurement by 3 to obtain $\pi\pi$.

² Calculated by us. The value for $B(\chi_{c2} \rightarrow \pi^+\pi^-)$ reported by BAI 98i is derived using $B(\psi(2S) \rightarrow \gamma \chi_{c2}) = (7.8 \pm 0.8)\%$ and $B(\psi(2S) \rightarrow J/\psi\pi^+\pi^-) = (32.4 \pm 2.6)\%$ [BAI 98d]. We have multiplied $\pi^+\pi^-$ measurement by 3/2 to obtain $\pi\pi$.

$\Gamma(\chi_{c2}(1P) \rightarrow \eta\eta)/\Gamma_{total} \times \Gamma(\psi(2S) \rightarrow \gamma \chi_{c2}(1P))/\Gamma_{total}$ $\Gamma_{31}/\Gamma \times \Gamma_{164}^{\psi(2S)}/\Gamma_{12}^{\psi(2S)}$

VALUE (units 10^{-4})	CL%	EVTS	DOCUMENT ID	TECN	COMMENT
--------------------------	-----	------	-------------	------	---------

0.52±0.04 OUR FIT
0.52±0.04 OUR AVERAGE

0.54±0.03±0.04 386 1 ABLIKIM 10A BES3 $e^+e^- \rightarrow \psi(2S) \rightarrow \gamma \chi_{c2}$
0.47±0.05±0.05 156 ASNER 09 CLEO $\psi(2S) \rightarrow \gamma\eta\eta$

••• We do not use the following data for averages, fits, limits, etc. •••

< 0.44 90 2 ADAMS 07 CLEO $\psi(2S) \rightarrow \gamma \chi_{c2}$
< 3 90 BAI 03c BES $\psi(2S) \rightarrow \gamma\eta\eta \rightarrow 5\gamma$
0.62±0.31±0.19 LEE 85 CBAL $\psi(2S) \rightarrow$ photons

¹ Calculated by us. ABLIKIM 10A reports $B(\chi_{c2} \rightarrow \eta\eta) = (0.65 \pm 0.04 \pm 0.05 \pm 0.03) \times 10^{-3}$ using $B(\psi(2S) \rightarrow \gamma \chi_{c2}) = (8.3 \pm 0.4)\%$.

² Superseded by ASNER 09.

$\Gamma(\chi_{c2}(1P) \rightarrow K^+K^-)/\Gamma_{total} \times \Gamma(\psi(2S) \rightarrow \gamma \chi_{c2}(1P))/\Gamma_{total}$ $\Gamma_{32}/\Gamma \times \Gamma_{164}^{\psi(2S)}/\Gamma_{12}^{\psi(2S)}$

VALUE (units 10^{-5})	EVTS	DOCUMENT ID	TECN	COMMENT
--------------------------	------	-------------	------	---------

9.6±0.6 OUR FIT
10.5±0.3±0.6 1.6k 1 ASNER 09 CLEO $\psi(2S) \rightarrow \gamma K^+K^-$

¹ Calculated by us. ASNER 09 reports $B(\chi_{c2} \rightarrow K^+K^-) = (1.13 \pm 0.03 \pm 0.06 \pm 0.07) \times 10^{-3}$ using $B(\psi(2S) \rightarrow \gamma \chi_{c2}) = (9.33 \pm 0.14 \pm 0.61)\%$.

$\Gamma(\chi_{c2}(1P) \rightarrow K^+K^-)/\Gamma_{total} \times \Gamma(\psi(2S) \rightarrow \gamma \chi_{c2}(1P))/\Gamma(\psi(2S) \rightarrow J/\psi(1S)\pi^+\pi^-)$ $\Gamma_{32}/\Gamma \times \Gamma_{164}^{\psi(2S)}/\Gamma_{12}^{\psi(2S)}$

VALUE (units 10^{-3})	EVTS	DOCUMENT ID	TECN	COMMENT
--------------------------	------	-------------	------	---------

0.276±0.017 OUR FIT
0.190±0.034±0.019 115 ± 13 1 BAI 98i BES $\psi(2S) \rightarrow \gamma K^+K^-$

¹ Calculated by us. The value for $B(\chi_{c2} \rightarrow K^+K^-)$ reported by BAI 98i is derived using $B(\psi(2S) \rightarrow \gamma \chi_{c2}) = (7.8 \pm 0.8)\%$ and $B(\psi(2S) \rightarrow J/\psi\pi^+\pi^-) = (32.4 \pm 2.6)\%$ [BAI 98d].

$$\Gamma(\chi_{c2}(1P) \rightarrow K_S^0 K_S^0) / \Gamma_{\text{total}} \times \Gamma(\psi(2S) \rightarrow \gamma \chi_{c2}(1P)) / \Gamma_{\text{total}}$$

$$\Gamma_{33} / \Gamma \times \Gamma_{164}^{\psi(2S)} / \Gamma_{12}^{\psi(2S)}$$

VALUE (units 10 ⁻⁵)	EVTS	DOCUMENT ID	TECN	COMMENT
5.0 ± 0.4 OUR FIT				
5.0 ± 0.4 OUR AVERAGE				
4.9 ± 0.3 ± 0.3	373 ± 20	¹ ASNER 09	CLEO	$\psi(2S) \rightarrow \gamma K_S^0 K_S^0$
5.72 ± 0.76 ± 0.63	65	ABLIKIM 05o	BES2	$\psi(2S) \rightarrow \gamma K_S^0 K_S^0$
¹ Calculated by us. ASNER 09 reports $B(\chi_{c2} \rightarrow K_S^0 K_S^0) = (0.53 \pm 0.03 \pm 0.03 \pm 0.03) \times 10^{-3}$ using $B(\psi(2S) \rightarrow \gamma \chi_{c2}) = (9.33 \pm 0.14 \pm 0.61)\%$.				

$$\Gamma(\chi_{c2}(1P) \rightarrow K_S^0 K_S^0) / \Gamma_{\text{total}} \times \Gamma(\psi(2S) \rightarrow \gamma \chi_{c2}(1P)) / \Gamma_{\text{total}}$$

$$J/\psi(1S) \pi^+ \pi^- \Gamma_{33} / \Gamma \times \Gamma_{164}^{\psi(2S)} / \Gamma_{12}^{\psi(2S)}$$

VALUE (units 10 ⁻⁵)	EVTS	DOCUMENT ID	TECN	COMMENT
14.4 ± 1.1 OUR FIT				
14.7 ± 4.1 ± 3.3				
		¹ BAI 99b	BES	$\psi(2S) \rightarrow \gamma K_S^0 K_S^0$
¹ Calculated by us. The value of $B(\chi_{c2} \rightarrow K_S^0 K_S^0)$ reported by BAI 99b was derived using $B(\psi(2S) \rightarrow \gamma \chi_{c2}(1P)) = (7.8 \pm 0.8)\%$ and $B(\psi(2S) \rightarrow J/\psi \pi^+ \pi^-) = (32.4 \pm 2.6)\%$ [BAI 98d].				

$$\Gamma(\chi_{c2}(1P) \rightarrow \bar{K}^0 K^+ \pi^- + \text{c.c.}) / \Gamma_{\text{total}} \times \Gamma(\psi(2S) \rightarrow \gamma \chi_{c2}(1P)) / \Gamma_{\text{total}}$$

$$\Gamma_{42} / \Gamma \times \Gamma_{164}^{\psi(2S)} / \Gamma_{12}^{\psi(2S)}$$

VALUE (units 10 ⁻⁴)	EVTS	DOCUMENT ID	TECN	COMMENT
1.22 ± 0.17 OUR FIT				
1.15 ± 0.18 OUR AVERAGE				
1.21 ± 0.19 ± 0.09	37	¹ ATHAR 07	CLEO	$\psi(2S) \rightarrow \gamma K^0 K^\pm \pi^\mp$
0.97 ± 0.32 ± 0.13	28	² ABLIKIM 06R	BES2	$\psi(2S) \rightarrow \gamma K_S^0 K^\pm \pi^\mp$
¹ Calculated by us. ATHAR 07 reports $B(\chi_{c2} \rightarrow \bar{K}^0 K^+ \pi^- + \text{c.c.}) = (1.3 \pm 0.2 \pm 0.1 \pm 0.1) \times 10^{-3}$ using $B(\psi(2S) \rightarrow \gamma \chi_{c2}) = (9.33 \pm 0.14 \pm 0.61)\%$.				
² Calculated by us. ABLIKIM 06R reports $B(\chi_{c2} \rightarrow K_S^0 K^\pm \pi^\mp) = (0.6 \pm 0.2 \pm 0.1) \times 10^{-3}$ using $B(\psi(2S) \rightarrow \gamma \chi_{c2}) = (8.1 \pm 0.6)\%$. We have multiplied by 2 to obtain $\bar{K}^0 K^+ \pi^- + \text{c.c.}$ from $K_S^0 K^\pm \pi^\mp$.				

$$\Gamma(\chi_{c2}(1P) \rightarrow 2(\pi^+ \pi^-)) / \Gamma_{\text{total}} \times \Gamma(\psi(2S) \rightarrow \gamma \chi_{c2}(1P)) / \Gamma_{\text{total}}$$

$$J/\psi(1S) \pi^+ \pi^- \Gamma_1 / \Gamma \times \Gamma_{164}^{\psi(2S)} / \Gamma_{12}^{\psi(2S)}$$

VALUE (units 10 ⁻³)	EVTS	DOCUMENT ID	TECN	COMMENT
2.79 ± 0.26 OUR FIT				
3.1 ± 1.0 OUR AVERAGE				Error includes scale factor of 2.5.
2.3 ± 0.1 ± 0.5		¹ BAI 99b	BES	$\psi(2S) \rightarrow \gamma \chi_{c2}$
4.3 ± 0.6		² TANENBAUM 78	MRK1	$\psi(2S) \rightarrow \gamma \chi_{c2}$
¹ Calculated by us. The value for $B(\chi_{c2} \rightarrow 2\pi^+ 2\pi^-)$ reported in BAI 99b is derived using $B(\psi(2S) \rightarrow \gamma \chi_{c2}) = (7.8 \pm 0.8)\%$ and $B(\psi(2S) \rightarrow J/\psi(1S) \pi^+ \pi^-) = (32.4 \pm 2.6)\%$ [BAI 98d].				
² The value for $B(\psi(2S) \rightarrow \gamma \chi_{c2}) \times B(\chi_{c2} \rightarrow 2\pi^+ 2\pi^-)$ reported in TANENBAUM 78 is derived using $B(\psi(2S) \rightarrow J/\psi(1S) \pi^+ \pi^-) \times B(J/\psi(1S) \ell^+ \ell^-) = (4.6 \pm 0.7)\%$. Calculated by us using $B(J/\psi(1S) \rightarrow \ell^+ \ell^-) = 0.1181 \pm 0.0020$.				

$$\Gamma(\chi_{c2}(1P) \rightarrow K^+ K^- K^+ K^-) / \Gamma_{\text{total}} \times \Gamma(\psi(2S) \rightarrow \gamma \chi_{c2}(1P)) / \Gamma_{\text{total}}$$

$$\Gamma_{51} / \Gamma \times \Gamma_{164}^{\psi(2S)} / \Gamma_{12}^{\psi(2S)}$$

VALUE (units 10 ⁻⁴)	EVTS	DOCUMENT ID	TECN	COMMENT
1.57 ± 0.19 OUR FIT				
1.76 ± 0.16 ± 0.24	160	¹ ABLIKIM 06T	BES2	$\psi(2S) \rightarrow \gamma 2K^+ 2K^-$
¹ Calculated by us. The value of $B(\chi_{c2} \rightarrow 2K^+ 2K^-)$ reported by ABLIKIM 06T was derived using $B(\psi(2S) \rightarrow \gamma \chi_{c2}(1P)) = (8.1 \pm 0.4)\%$.				

$$\Gamma(\chi_{c2}(1P) \rightarrow K^+ K^- K^+ K^-) / \Gamma_{\text{total}} \times \Gamma(\psi(2S) \rightarrow \gamma \chi_{c2}(1P)) / \Gamma_{\text{total}}$$

$$\Gamma(\psi(2S) \rightarrow J/\psi(1S) \pi^+ \pi^-) \Gamma_{51} / \Gamma \times \Gamma_{164}^{\psi(2S)} / \Gamma_{12}^{\psi(2S)}$$

VALUE (units 10 ⁻⁴)	EVTS	DOCUMENT ID	TECN	COMMENT
4.5 ± 0.5 OUR FIT				
3.6 ± 0.6 ± 0.6				
		¹ BAI 99b	BES	$\psi(2S) \rightarrow \gamma 2K^+ 2K^-$
¹ Calculated by us. The value of $B(\chi_{c2} \rightarrow 2K^+ 2K^-)$ reported by BAI 99b was derived using $B(\psi(2S) \rightarrow \gamma \chi_{c2}(1P)) = (7.8 \pm 0.8)\%$ and $B(\psi(2S) \rightarrow J/\psi \pi^+ \pi^-) = (32.4 \pm 2.6)\%$ [BAI 98d].				

$$\Gamma(\chi_{c2}(1P) \rightarrow \phi \phi) / \Gamma_{\text{total}} \times \Gamma(\psi(2S) \rightarrow \gamma \chi_{c2}(1P)) / \Gamma_{\text{total}}$$

$$\Gamma_{20} / \Gamma \times \Gamma_{164}^{\psi(2S)} / \Gamma_{12}^{\psi(2S)}$$

VALUE (units 10 ⁻⁴)	EVTS	DOCUMENT ID	TECN	COMMENT
1.01 ± 0.08 OUR FIT				
0.98 ± 0.13 OUR AVERAGE				Error includes scale factor of 1.3.
0.94 ± 0.03 ± 0.10	849	¹ ABLIKIM 11k	BES3	$\psi(2S) \rightarrow \gamma$ hadrons
1.38 ± 0.24 ± 0.23	41	² ABLIKIM 06T	BES2	$\psi(2S) \rightarrow \gamma 2K^+ 2K^-$
¹ Calculated by us. The value of $B(\chi_{c2} \rightarrow \phi \phi)$ reported by ABLIKIM 11k was derived using $B(\psi(2S) \rightarrow \gamma \chi_{c2}(1P)) = (8.74 \pm 0.35)\%$.				
² Calculated by us. The value of $B(\chi_{c2} \rightarrow \phi \phi)$ reported by ABLIKIM 06T was derived using $B(\psi(2S) \rightarrow \gamma \chi_{c2}(1P)) = (8.1 \pm 0.4)\%$.				

$$\Gamma(\chi_{c2}(1P) \rightarrow \phi \phi) / \Gamma_{\text{total}} \times \Gamma(\psi(2S) \rightarrow \gamma \chi_{c2}(1P)) / \Gamma_{\text{total}}$$

$$J/\psi(1S) \pi^+ \pi^- \Gamma_{20} / \Gamma \times \Gamma_{164}^{\psi(2S)} / \Gamma_{12}^{\psi(2S)}$$

VALUE (units 10 ⁻⁴)	EVTS	DOCUMENT ID	TECN	COMMENT
2.92 ± 0.24 OUR FIT				
4.8 ± 1.3 ± 1.3				
		¹ BAI 99b	BES	$\psi(2S) \rightarrow \gamma 2K^+ 2K^-$
¹ Calculated by us. The value of $B(\chi_{c2} \rightarrow \phi \phi)$ reported by BAI 99b was derived using $B(\psi(2S) \rightarrow \gamma \chi_{c2}(1P)) = (7.8 \pm 0.8)\%$ and $B(\psi(2S) \rightarrow J/\psi \pi^+ \pi^-) = (32.4 \pm 2.6)\%$ [BAI 98d].				

$$\Gamma(\chi_{c2}(1P) \rightarrow \Sigma^+ \bar{p} K_S^0 + \text{c.c.}) / \Gamma_{\text{total}} \times \Gamma(\psi(2S) \rightarrow \gamma \chi_{c2}(1P)) / \Gamma_{\text{total}}$$

$$\Gamma_{80} / \Gamma \times \Gamma_{164}^{\psi(2S)} / \Gamma_{12}^{\psi(2S)}$$

VALUE (units 10 ⁻⁶)	EVTS	DOCUMENT ID	TECN	COMMENT
7.85 ± 0.77 ± 0.44	129	¹ ABLIKIM 19bB	BES3	$\psi(2S) \rightarrow \gamma \Sigma^+ \bar{p} K_S^0 + \text{c.c.}$
¹ Calculated by us. ABLIKIM 19bB reports $B(\chi_{c2} \rightarrow \Sigma^+ \bar{p} K_S^0 + \text{c.c.}) = (8.25 \pm 0.83 \pm 0.49) \times 10^{-5}$ using $B(\psi(2S) \rightarrow \gamma \chi_{c2}) = (9.52 \pm 0.20)\%$ and other branching fractions from PDG 18.				

$$\Gamma(\chi_{c2}(1P) \rightarrow \Sigma^0 \bar{p} K^+ + \text{c.c.}) / \Gamma_{\text{total}} \times \Gamma(\psi(2S) \rightarrow \gamma \chi_{c2}(1P)) / \Gamma_{\text{total}}$$

$$\Gamma_{81} / \Gamma \times \Gamma_{164}^{\psi(2S)} / \Gamma_{12}^{\psi(2S)}$$

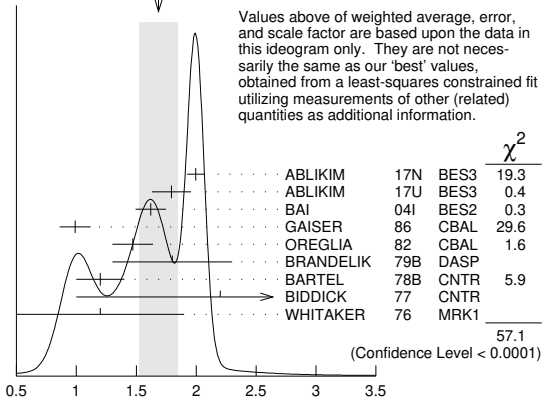
VALUE (units 10 ⁻⁵)	EVTS	DOCUMENT ID	TECN	COMMENT
0.87 ± 0.06 ± 0.04	271	¹ ABLIKIM 20AE	BES3	$\psi(2S) \rightarrow \gamma \Sigma^0 \bar{p} K^+ + \text{c.c.}$
¹ Calculated by us. ABLIKIM 20AE reports $B(\chi_{c2} \rightarrow \Sigma^0 \bar{p} K^+ + \text{c.c.}) = (0.91 \pm 0.06 \pm 0.05) \times 10^{-4}$ using $B(\psi(2S) \rightarrow \gamma \chi_{c2}) = (9.52 \pm 0.20)\%$ and other branching fractions from PDG 20.				

$$\Gamma(\chi_{c2}(1P) \rightarrow \gamma J/\psi(1S)) / \Gamma_{\text{total}} \times \Gamma(\psi(2S) \rightarrow \gamma \chi_{c2}(1P)) / \Gamma_{\text{total}}$$

$$\Gamma_{92} / \Gamma \times \Gamma_{164}^{\psi(2S)} / \Gamma_{12}^{\psi(2S)}$$

VALUE (units 10 ⁻²)	EVTS	DOCUMENT ID	TECN	COMMENT
1.81 ± 0.04 OUR FIT				
1.69 ± 0.16 OUR AVERAGE				Error includes scale factor of 3.4. See the ideogram below.
1.996 ± 0.008 ± 0.070	81k	¹ ABLIKIM 17N	BES3	$\psi(2S) \rightarrow \gamma \gamma J/\psi$
1.793 ± 0.008 ± 0.163	1.0M	ABLIKIM 17U	BES3	$e^+ e^- \rightarrow \gamma X$
1.62 ± 0.04 ± 0.12	5.8k	BAI 04I	BES2	$\psi(2S) \rightarrow J/\psi \gamma \gamma$
0.99 ± 0.10 ± 0.08		GAISER 86	CBAL	$\psi(2S) \rightarrow \gamma X$
1.47 ± 0.17		² OREGLIA 82	CBAL	$\psi(2S) \rightarrow \gamma \chi_{c2}$
1.8 ± 0.5		³ BRANDELIK 79B	DASP	$\psi(2S) \rightarrow \gamma \chi_{c2}$
1.2 ± 0.2		³ BARTEL 78B	CNTR	$\psi(2S) \rightarrow \gamma \chi_{c2}$
2.2 ± 1.2		⁴ BIDDICK 77	CNTR	$e^+ e^- \rightarrow \gamma X$
1.2 ± 0.7		² WHITAKER 76	MRK1	$e^+ e^-$
••• We do not use the following data for averages, fits, limits, etc. •••				
1.874 ± 0.007 ± 0.102	76k	⁵ ABLIKIM 12O	BES3	$\psi(2S) \rightarrow \gamma \chi_{c2}$
1.95 ± 0.02 ± 0.07	12.4k	⁶ MENDEZ 08	CLEO	$\psi(2S) \rightarrow \gamma \chi_{c2}$
1.85 ± 0.04 ± 0.07	1.9k	⁷ ADAM 05A	CLEO	Repl. by MENDEZ 08

WEIGHTED AVERAGE
1.69 ± 0.16 (Error scaled by 3.4)



$$\Gamma(\chi_{c2}(1P) \rightarrow \gamma J/\psi(1S)) / \Gamma_{\text{total}} \times \Gamma(\psi(2S) \rightarrow \gamma \chi_{c2}(1P)) / \Gamma_{\text{total}}$$

(units 10⁻²)

- ¹ Uses $B(J/\psi \rightarrow e^+ e^-) = (5.971 \pm 0.032)\%$ and $B(J/\psi \rightarrow \mu^+ \mu^-) = (5.961 \pm 0.033)\%$.
- ² Recalculated by us using $B(J/\psi(1S) \rightarrow \ell^+ \ell^-) = 0.1181 \pm 0.0020$.
- ³ Recalculated by us using $B(J/\psi(1S) \rightarrow \mu^+ \mu^-) = 0.0588 \pm 0.0010$.
- ⁴ Assumes isotropic gamma distribution.
- ⁵ Superseded by ABLIKIM 17N.
- ⁶ Not independent from other measurements of MENDEZ 08.
- ⁷ Not independent from other values reported by ADAM 05A.

Meson Particle Listings

$\chi_{c2}(1P)$

$$\Gamma(\chi_{c2}(1P) \rightarrow \gamma J/\psi(1S))/\Gamma_{\text{total}} \times \Gamma(\psi(2S) \rightarrow \gamma \chi_{c2}(1P))/\Gamma(\psi(2S) \rightarrow J/\psi(1S) \text{ anything})$$

$$\frac{\Gamma_{92}/\Gamma \times \Gamma_{164}^{\psi(2S)}/\Gamma_{10}^{\psi(2S)}}{\Gamma_{92}/\Gamma \times \Gamma_{164}^{\psi(2S)}/\Gamma_{10}^{\psi(2S)} + \Gamma_{12}^{\psi(2S)} + \Gamma_{13}^{\psi(2S)} + \Gamma_{14}^{\psi(2S)} + 0.343\Gamma_{163}^{\psi(2S)} + 0.190\Gamma_{164}^{\psi(2S)}}$$

VALUE (units 10^{-2})	EVTS	DOCUMENT ID	TECN	COMMENT
2.95 ± 0.06 OUR FIT				
3.12 ± 0.03 ± 0.09	12.4k	¹ MENDEZ	08 CLEO	$\psi(2S) \rightarrow \gamma \chi_{c2}$
3.11 ± 0.07 ± 0.07	1.9k	ADAM	05A CLEO	Repl. by MENDEZ 08

¹ Not independent from other measurements of MENDEZ 08.

$$\Gamma(\chi_{c2}(1P) \rightarrow \gamma J/\psi(1S))/\Gamma_{\text{total}} \times \Gamma(\psi(2S) \rightarrow \gamma \chi_{c2}(1P))/\Gamma(\psi(2S) \rightarrow J/\psi(1S) \pi^+ \pi^-)$$

$$\frac{\Gamma_{92}/\Gamma \times \Gamma_{164}^{\psi(2S)}/\Gamma_{12}^{\psi(2S)}}{\Gamma_{92}/\Gamma \times \Gamma_{164}^{\psi(2S)}/\Gamma_{12}^{\psi(2S)} + \Gamma_{13}^{\psi(2S)} + \Gamma_{14}^{\psi(2S)} + 0.343\Gamma_{163}^{\psi(2S)} + 0.190\Gamma_{164}^{\psi(2S)}}$$

VALUE (units 10^{-2})	EVTS	DOCUMENT ID	TECN	COMMENT
5.22 ± 0.11 OUR FIT				
5.53 ± 0.17 OUR AVERAGE				
5.56 ± 0.05 ± 0.16	12.4k	MENDEZ	08 CLEO	$\psi(2S) \rightarrow \gamma \chi_{c2}$
6.0 ± 2.8	1.3k	¹ ABLIKIM	04B BES	$\psi(2S) \rightarrow J/\psi X$
3.9 ± 1.2		² HIMEL	80 MRK2	$\psi(2S) \rightarrow \gamma \chi_{c2}$
5.52 ± 0.13 ± 0.13	1.9k	³ ADAM	05A CLEO	Repl. by MENDEZ 08

¹ From a fit to the J/ψ recoil mass spectra.

² The value for $B(\psi(2S) \rightarrow \gamma \chi_{c2}) \times B(\chi_{c2} \rightarrow \gamma J/\psi(1S))$ reported in HIMEL 80 is derived using $B(\psi(2S) \rightarrow J/\psi(1S) \pi^+ \pi^-) = (33 \pm 3)\%$ and $B(J/\psi(1S) \rightarrow \ell^+ \ell^-) = 0.138 \pm 0.018$. Calculated by us using $B(J/\psi(1S) \rightarrow \ell^+ \ell^-) = (0.1181 \pm 0.0020)$.

³ Not independent from other values reported by ADAM 05A.

$$\Gamma(\chi_{c2}(1P) \rightarrow \gamma\gamma)/\Gamma_{\text{total}} \times \Gamma(\psi(2S) \rightarrow \gamma \chi_{c2}(1P))/\Gamma_{\text{total}}$$

$$\frac{\Gamma_{96}/\Gamma \times \Gamma_{164}^{\psi(2S)}/\Gamma_{12}^{\psi(2S)}}{\Gamma_{96}/\Gamma \times \Gamma_{164}^{\psi(2S)}/\Gamma_{12}^{\psi(2S)} + \Gamma_{13}^{\psi(2S)} + \Gamma_{14}^{\psi(2S)} + 0.343\Gamma_{163}^{\psi(2S)} + 0.190\Gamma_{164}^{\psi(2S)}}$$

VALUE (units 10^{-5})	EVTS	DOCUMENT ID	TECN	COMMENT
2.71 ± 0.08 OUR FIT				
2.82 ± 0.10 OUR AVERAGE				
2.83 ± 0.08 ± 0.06	5k	¹ ABLIKIM	17AE BES3	$\psi(2S) \rightarrow \gamma \chi_{c2} \rightarrow 3\gamma$
2.68 ± 0.28 ± 0.15	0.3k	ECKLUND	08A CLEO	$\psi(2S) \rightarrow \gamma \chi_{c2} \rightarrow 3\gamma$
7.0 ± 2.1 ± 2.0		LEE	85 CBAL	$\psi(2S) \rightarrow \gamma \chi_{c2}$
2.81 ± 0.17 ± 0.15	1.1k	² ABLIKIM	12A BES3	$\psi(2S) \rightarrow \gamma \chi_{c2} \rightarrow 3\gamma$

¹ ABLIKIM 17AE measures the ratio of two-photon partial widths for the helicity $\lambda = 0$ and helicity $\lambda = 2$ components to be $f_{0/2} = \Gamma_{\gamma\gamma}^{\lambda=0} / \Gamma_{\gamma\gamma}^{\lambda=2} = 0.000 \pm 0.006 \pm 0.012$.

² ABLIKIM 12A measures the ratio of two-photon partial widths for the helicity $\lambda = 0$ and helicity $\lambda = 2$ components to be $f_{0/2} = \Gamma_{\gamma\gamma}^{\lambda=0} / \Gamma_{\gamma\gamma}^{\lambda=2} = 0.00 \pm 0.02 \pm 0.02$. Superseded by ABLIKIM 17AE.

$$\Gamma(\chi_{c2}(1P) \rightarrow \gamma\gamma)/\Gamma(\chi_{c0}(1P) \rightarrow \gamma\gamma)$$

$$\frac{\Gamma_{96}/\Gamma_{96}^{\chi_{c0}(1P)}}{\Gamma_{96}/\Gamma_{96}^{\chi_{c0}(1P)}}$$

VALUE	EVTS	DOCUMENT ID	TECN	COMMENT
0.292 ± 0.028 OUR AVERAGE				
0.295 ± 0.014 ± 0.028	8k	¹ ABLIKIM	17AE BES3	$\psi(2S) \rightarrow \gamma \chi_{cJ} \rightarrow 3\gamma$
0.278 ± 0.050 ± 0.036	0.5k	¹ ECKLUND	08A CLEO	$\psi(2S) \rightarrow \gamma \chi_{cJ} \rightarrow 3\gamma$
0.271 ± 0.029 ± 0.030	1.9k	^{1,2} ABLIKIM	12A BES3	$\psi(2S) \rightarrow \gamma \chi_{cJ} \rightarrow 3\gamma$

¹ Not independent from the values of $\Gamma(\chi_{c0}, \chi_{c2})$ and $B(\psi(2S) \rightarrow \chi_{c0}, \chi_{c2})$.

² Superseded by ABLIKIM 17AE.

MULTIPOLE AMPLITUDES IN $\chi_{c2}(1P) \rightarrow \gamma J/\psi(1S)$ RADIATIVE DECAY

$a_2 = M_2/\sqrt{E_1^2 + M_2^2 + E_3^2}$ Magnetic quadrupole fractional transition amplitude

VALUE (units 10^{-2})	EVTS	DOCUMENT ID	TECN	COMMENT
-11.0 ± 1.0 OUR AVERAGE				
-12.0 ± 1.3 ± 0.4	89k	¹ ABLIKIM	17N BES3	$\psi(2S) \rightarrow \gamma\gamma \ell^+ \ell^-$
-9.3 ± 1.6 ± 0.3	19.8k	² ARTUSO	09 CLEO	$\psi(2S) \rightarrow \gamma\gamma \ell^+ \ell^-$
-9.3 ± 3.9 ± 0.6	5.9k	³ AMBROGIANI	02 E835	$p\bar{p} \rightarrow \chi_{c2} \rightarrow J/\psi\gamma$
-14 ± 6	1.9k	³ ARMSTRONG	93E E760	$p\bar{p} \rightarrow \chi_{c2} \rightarrow J/\psi\gamma$
-33.3 ± 11.6 ± 29.2	441	³ OREGLIA	82 CBAL	$\psi(2S) \rightarrow \chi_{c1}\gamma \rightarrow J/\psi\gamma\gamma$
-7.9 ± 1.9 ± 0.3	19.8k	⁴ ARTUSO	09 CLEO	$\psi(2S) \rightarrow \gamma\gamma \ell^+ \ell^-$

¹ Correlated with $a_3, b_2,$ and b_3 with correlation coefficients $\rho_{a_2 a_3} = 0.733, \rho_{a_2 b_2} = -0.605,$ and $\rho_{a_2 b_3} = -0.095$.

² From a fit with floating M_2 amplitudes a_2 and $b_2,$ and fixed E_3 amplitudes $a_3 = b_3 = 0$.

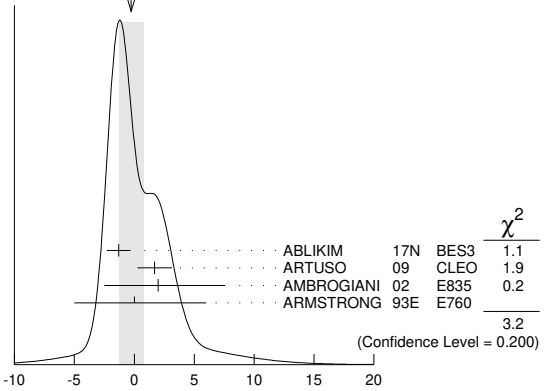
³ Assuming $a_3 = 0$.

⁴ From a fit with floating M_2 and E_3 amplitudes $a_2, b_2,$ and $a_3,$ and b_3 .

$a_3 = E_3/\sqrt{E_1^2 + M_2^2 + E_3^2}$ Electric octupole fractional transition amplitude

VALUE (units 10^{-2})	EVTS	DOCUMENT ID	TECN	COMMENT
-0.3 ± 1.0 OUR AVERAGE				Error includes scale factor of 1.3. See the ideogram below.
-1.3 ± 0.9 ± 0.4	89k	¹ ABLIKIM	17N BES3	$\psi(2S) \rightarrow \gamma\gamma \ell^+ \ell^-$
1.7 ± 1.4 ± 0.3	19.8k	² ARTUSO	09 CLEO	$\psi(2S) \rightarrow \gamma\gamma \ell^+ \ell^-$
2.0 ± 5.5 ± 4.4	5908	AMBROGIANI	02 E835	$p\bar{p} \rightarrow \chi_{c2} \rightarrow J/\psi\gamma$
0 ± 6 ± 5	1904	ARMSTRONG	93E E760	$p\bar{p} \rightarrow \chi_{c2} \rightarrow J/\psi\gamma$

WEIGHTED AVERAGE
-0.3 ± 1.0 (Error scaled by 1.3)



$a_3 = E_3/\sqrt{E_1^2 + M_2^2 + E_3^2}$ Electric octupole fractional transition amplitude (units 10^{-2})

¹ Correlated with $a_2, b_2,$ and b_3 with correlation coefficients $\rho_{a_2 a_3} = 0.733, \rho_{a_3 b_2} = -0.422,$ and $\rho_{a_3 b_3} = -0.024$.

² From a fit with floating M_2 and E_3 amplitudes $a_2, b_2,$ and $a_3,$ and b_3 .

MULTIPOLE AMPLITUDES IN $\psi(2S) \rightarrow \gamma \chi_{c2}(1P)$ RADIATIVE DECAY

$b_2 = M_2/\sqrt{E_1^2 + M_2^2 + E_3^2}$ Magnetic quadrupole fractional transition amplitude

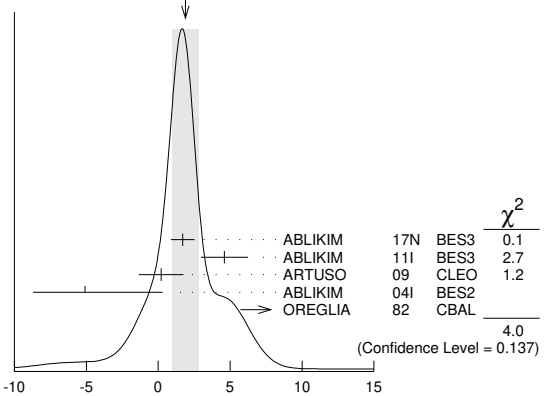
VALUE (units 10^{-2})	EVTS	DOCUMENT ID	TECN	COMMENT
1.9 ± 0.9 OUR AVERAGE				Error includes scale factor of 1.4. See the ideogram below.
1.7 ± 0.8 ± 0.2	89k	¹ ABLIKIM	17N BES3	$\psi(2S) \rightarrow \gamma\gamma \ell^+ \ell^-$
4.6 ± 1.0 ± 1.3	13.8k	² ABLIKIM	11I BES3	$\psi(2S) \rightarrow \gamma\pi^+ \pi^-, \gamma K^+ K^-$
0.2 ± 1.5 ± 0.4	19.8k	³ ARTUSO	09 CLEO	$\psi(2S) \rightarrow \gamma\gamma \ell^+ \ell^-$
-5.1 ± 5.4 ± 3.6	721	² ABLIKIM	04I BES2	$\psi(2S) \rightarrow \gamma\pi^+ \pi^-, \gamma K^+ K^-$
13.2 ± 9.8 ± 7.5	441	⁴ OREGLIA	82 CBAL	$\psi(2S) \rightarrow \gamma\gamma \ell^+ \ell^-$
1.0 ± 1.3 ± 0.3	19.8k	⁴ ARTUSO	09 CLEO	$\psi(2S) \rightarrow \gamma\gamma \ell^+ \ell^-$

¹ Correlated with $a_2, a_3,$ and b_3 with correlation coefficients $\rho_{a_2 b_2} = -0.605, \rho_{a_3 b_2} = -0.422,$ and $\rho_{b_2 b_3} = 0.384$.

² From a fit with floating M_2 and E_3 amplitudes b_2 and b_3 .

³ From a fit with floating M_2 and E_3 amplitudes $a_2, b_2,$ and $a_3,$ and b_3 .

WEIGHTED AVERAGE
1.9 ± 0.9 (Error scaled by 1.4)



$b_2 = M_2/\sqrt{E_1^2 + M_2^2 + E_3^2}$ Magnetic quadrupole fractional transition amplitude (units 10^{-2})

¹ Correlated with $a_2, a_3,$ and b_3 with correlation coefficients $\rho_{a_2 b_2} = -0.605, \rho_{a_3 b_2} = -0.422,$ and $\rho_{b_2 b_3} = 0.384$.

² From a fit with floating M_2 and E_3 amplitudes b_2 and b_3 .

³ From a fit with floating M_2 and E_3 amplitudes $a_2, b_2,$ and $a_3,$ and b_3 .

See key on page 1127

Meson Particle Listings

$\chi_{c2}(1P), \eta_c(2S)$

⁴ From a fit with floating $M2$ amplitudes a_2 and b_2 , and fixed $E3$ amplitudes $a_3=b_3=0$.

$b_3 = E3/\sqrt{E2^2 + M2^2 + E3^2}$ Electric octupole fractional transition amplitude

Table with columns: VALUE (units 10^-2), EVTS, DOCUMENT ID, TECN, COMMENT. Rows include OUR AVERAGE and data points from ABLIKIM, ARTUSO, etc.

¹ Correlated with $a_2, a_3,$ and b_2 with correlation coefficients $\rho_{a_2 b_3} = -0.095, \rho_{a_3 b_3} = -0.024,$ and $\rho_{b_2 b_3} = 0.384$.

² From a fit with floating $M2$ and $E3$ amplitudes b_2 and b_3 .

MULTIPOLE AMPLITUDE RATIOS IN RADIATIVE DECAYS
 $\psi(2S) \rightarrow \gamma\chi_{c2}(1P)$ and $\chi_{c2} \rightarrow \gamma J/\psi(1S)$

b_2/a_2 Magnetic quadrupole transition amplitude ratio

Table with columns: VALUE (units 10^-2), EVTS, DOCUMENT ID, TECN, COMMENT. Row includes ARTUSO 09 CLEO.

¹ Statistical and systematic errors combined. From a fit with floating $M2$ amplitudes a_2 and b_2 , and fixed $E3$ amplitudes $a_3=b_3=0$. Not independent of values for $a_2(\chi_{c2}(1P))$ and $b_2(\chi_{c2}(1P))$ from ARTUSO 09.

$\chi_{c2}(1P)$ REFERENCES

Large table listing references for chi_c2(1P) with columns: ABLIKIM, VALUE, DOCUMENT ID, TECN, COMMENT.

Table listing references for chi_c2(1P) with columns: EISENSTEIN, AMBROGIANI, ACCIARRI, BAI, ACKER...K..., BAI, DOMINICK, ARMSTRONG, ARMSTRONG, BAUER, ARMSTRONG, BAGLIN, BAGLIN, GAISER, LEE, LEMOIGNE, OREGLIA, BARATE, HIMEL, BRANDELIK, BARTEL, TANENBAUM, BIDDICK, WHITAKER, and various collaboration names.

$\eta_c(2S)$

$I^G(J^{PC}) = 0^+(0^-)$

Quantum numbers are quark model predictions.

$\eta_c(2S)$ MASS

Table with columns: VALUE (MeV), EVTS, DOCUMENT ID, TECN, COMMENT. Rows include OUR AVERAGE and data points from XU, AAIJ, LEES, ABLIKIM, DEL-AMO-SA., BELL, AUBERT, CHOI, EDWARDS, etc.

¹ AAIJ 17AD report $m_{\psi(2S)} - m_{\eta_c(2S)} = 52.5 \pm 1.7 \pm 0.6$ MeV. We use the current value $m_{\psi(2S)} = 3686.097 \pm 0.025$ MeV to obtain the quoted mass.
² From a fit of the $\phi\phi$ invariant mass with the width of $\eta_c(2S)$ fixed to the PDG 16 value.
³ Ignoring possible interference with continuum.
⁴ With a width fixed to 11.3 MeV.
⁵ With a width fixed to 11.3 MeV. Using both $\eta \rightarrow \gamma\gamma$ and $\eta \rightarrow \pi^+\pi^-\pi^0$ decays.
⁶ From a simultaneous fit to $K_S^0 K^\pm \pi^\mp$ and $K^+ K^- \pi^0$ decay modes.
⁷ Accounts for interference with non-resonant continuum.
⁸ From a fit of the J/ψ recoil mass spectrum. Supersedes ABE,K 02 and ABE 04c.
⁹ From the fit of the kaon momentum spectrum. Systematic errors not evaluated.
¹⁰ Superseded by DEL-AMO-SANCHEZ 11M.
¹¹ Superseded by VINO KUROVA 11.
¹² Assuming mass of $\psi(2S) = 3686$ MeV.

$\eta_c(2S)$ WIDTH

Table with columns: VALUE (MeV), CL%, EVTS, DOCUMENT ID, TECN, COMMENT. Rows include OUR AVERAGE and data points from ABLIKIM, DEL-AMO-SA., BELL, ASNER, etc.

Meson Particle Listings

$\eta_c(2S)$

••• We do not use the following data for averages, fits, limits, etc. •••

< 23	90	98 ± 52	16 AUBERT	06E BABR	$B^{\pm} \rightarrow K^{\pm} X_{c1} \bar{c}$
22 ± 14		121 ± 27	AUBERT	05c BABR	$e^+ e^- \rightarrow J/\psi c \bar{c}$
17.0 ± 8.3 ± 2.5		112 ± 24	17 AUBERT	04D BABR	$\gamma \gamma \rightarrow \eta_c(2S) \rightarrow K_S^0 K^{\pm} \pi^{\mp}$
< 55	90	39 ± 11	18 CHOI	02 BELL	$B \rightarrow K K_S^0 K^{\mp} \pi^{\pm}$
< 8.0	95		19 EDWARDS	82c CBAL	$e^+ e^- \rightarrow \gamma X$

- ¹³ From a simultaneous fit to $K_S^0 K^{\pm} \pi^{\mp}$ and $K^+ K^- \pi^0$ decay modes.
- ¹⁴ Ignoring possible interference with continuum.
- ¹⁵ Accounts for interference with non-resonant continuum.
- ¹⁶ From the fit of the kaon momentum spectrum. Systematic errors not evaluated.
- ¹⁷ Superseded by DEL-AMO-SANCHEZ 11M.
- ¹⁸ For a mass value of 3654 ± 6 MeV. Superseded by VINOKUROVA 11.
- ¹⁹ For a mass value of 3594 ± 5 MeV

$\eta_c(2S)$ DECAY MODES

Mode	Fraction (Γ_i/Γ)	Confidence level
Γ_1 hadrons	not seen	
Γ_2 $K \bar{K} \pi$	(1.9 ± 1.2) %	
Γ_3 $K \bar{K} \eta$	(5 ± 4) × 10 ⁻³	
Γ_4 $2\pi^+ 2\pi^-$	not seen	
Γ_5 $\rho^0 \rho^0$	not seen	
Γ_6 $3\pi^+ 3\pi^-$	not seen	
Γ_7 $K^+ K^- \pi^+ \pi^-$	not seen	
Γ_8 $K^{*0} \bar{K}^{*0}$	not seen	
Γ_9 $K^+ K^- \pi^+ \pi^- \pi^0$	(1.4 ± 1.0) %	
Γ_{10} $K^+ K^- 2\pi^+ 2\pi^-$	not seen	
Γ_{11} $K_S^0 K^- 2\pi^+ \pi^- + c.c.$	seen	
Γ_{12} $2K^+ 2K^-$	not seen	
Γ_{13} $\phi \phi$	not seen	
Γ_{14} $p \bar{p}$	seen	
Γ_{15} $p \bar{p} \pi^+ \pi^-$	seen	
Γ_{16} $\gamma \gamma$	(1.9 ± 1.3) × 10 ⁻⁴	
Γ_{17} $\gamma J/\psi(1S)$	< 1.4 %	90%
Γ_{18} $\pi^+ \pi^- \eta'$	not seen	
Γ_{19} $\pi^+ \pi^- \eta$	not seen	
Γ_{20} $\pi^+ \pi^- \eta_c(1S)$	< 25 %	90%

$\eta_c(2S)$ PARTIAL WIDTHS

$\Gamma(\gamma\gamma)$	VALUE (keV)	EVTS	DOCUMENT ID	TECN	COMMENT	Γ_{16}
••• We do not use the following data for averages, fits, limits, etc. •••						
	0.44 ± 0.14	106	20 XU	18 BELL	$e^+ e^- \rightarrow e^+ e^- \eta' / \pi^+ \pi^-$	
	1.3 ± 0.6		21 ASNER	04 CLEO	$\gamma \gamma \rightarrow \eta_c \rightarrow K_S^0 K^{\pm} \pi^{\mp}$	

²⁰ Assuming that the branching fraction into $\eta' \pi^+ \pi^-$ is the same as for $\eta_c(1S)$.

²¹ They measure $\Gamma(\eta_c(2S) \gamma \gamma) B(\eta_c(2S) \rightarrow K \bar{K} \pi) = (0.18 \pm 0.05 \pm 0.02) \Gamma(\eta_c(1S) \gamma \gamma) B(\eta_c(1S) \rightarrow K \bar{K} \pi)$. The value for $\Gamma(\eta_c(2S) \rightarrow \gamma \gamma)$ is derived assuming that the branching fractions for $\eta_c(2S)$ and $\eta_c(1S)$ decays to $K_S^0 K \pi$ are equal and using $\Gamma(\eta_c(1S) \rightarrow \gamma \gamma) = 7.4 \pm 0.4 \pm 2.3$ keV.

$\Gamma(\gamma\gamma) \times \Gamma(\pi^+ \pi^- \eta')/\Gamma_{total}$	VALUE (eV)	EVTS	DOCUMENT ID	TECN	COMMENT	$\Gamma_{16} \Gamma_{19}/\Gamma$
••• We do not use the following data for averages, fits, limits, etc. •••						
	5.6 ± 1.2 ± 1.1	106	XU	18 BELL	$e^+ e^- \rightarrow e^+ e^- \eta' / \pi^+ \pi^-$	

$\eta_c(2S) \Gamma(i)\Gamma(\gamma\gamma)/\Gamma_{total}$

$\Gamma(2\pi^+ 2\pi^-) \times \Gamma(\gamma\gamma)/\Gamma_{total}$	VALUE (eV)	CL%	DOCUMENT ID	TECN	COMMENT	$\Gamma_4 \Gamma_{16}/\Gamma$
••• We do not use the following data for averages, fits, limits, etc. •••						
	< 6.5		90 UEHARA	08 BELL	$\gamma \gamma \rightarrow \eta_c(2S) \rightarrow 2(\pi^+ \pi^-)$	

$\Gamma(K \bar{K} \pi) \times \Gamma(\gamma\gamma)/\Gamma_{total}$	VALUE (eV)	EVTS	DOCUMENT ID	TECN	COMMENT	$\Gamma_2 \Gamma_{16}/\Gamma$
••• We do not use the following data for averages, fits, limits, etc. •••						
	41 ± 4 ± 6	624	22 DEL-AMO-SA..11M	BABR	$\gamma \gamma \rightarrow K_S^0 K^{\pm} \pi^{\mp}$	

²² Not independent from other measurements reported in DEL-AMO-SANCHEZ 11M.

$\Gamma(K^+ K^- \pi^+ \pi^-) \times \Gamma(\gamma\gamma)/\Gamma_{total}$	VALUE (eV)	CL%	DOCUMENT ID	TECN	COMMENT	$\Gamma_7 \Gamma_{16}/\Gamma$
••• We do not use the following data for averages, fits, limits, etc. •••						
	< 5.0		90 UEHARA	08 BELL	$\gamma \gamma \rightarrow \eta_c(2S) \rightarrow K^+ K^- \pi^+ \pi^-$	

$\Gamma(K^+ K^- \pi^+ \pi^- \pi^0) \times \Gamma(\gamma\gamma)/\Gamma_{total}$	VALUE (eV)	EVTS	DOCUMENT ID	TECN	COMMENT	$\Gamma_9 \Gamma_{16}/\Gamma$
••• We do not use the following data for averages, fits, limits, etc. •••						
	30 ± 6 ± 5	1201	23 DEL-AMO-SA..11M	BABR	$\gamma \gamma \rightarrow K^+ K^- \pi^+ \pi^- \pi^0$	

²³ Not independent from other measurements reported in DEL-AMO-SANCHEZ 11M.

$\Gamma(2K^+ 2K^-) \times \Gamma(\gamma\gamma)/\Gamma_{total}$	VALUE (eV)	CL%	DOCUMENT ID	TECN	COMMENT	$\Gamma_{12} \Gamma_{16}/\Gamma$
••• We do not use the following data for averages, fits, limits, etc. •••						
	< 2.9		90 UEHARA	08 BELL	$\gamma \gamma \rightarrow \eta_c(2S) \rightarrow 2(K^+ K^-)$	

$\Gamma(\pi^+ \pi^- \eta_c(1S)) \times \Gamma(\gamma\gamma)/\Gamma_{total}$	VALUE (eV)	CL%	DOCUMENT ID	TECN	COMMENT	$\Gamma_{20} \Gamma_{16}/\Gamma$
••• We do not use the following data for averages, fits, limits, etc. •••						
	< 133		90 LEES	12AE BABR	$e^+ e^- \rightarrow e^+ e^- \pi^+ \pi^- \eta_c$	

$\eta_c(2S) \Gamma(i)\Gamma(\gamma\gamma)/\Gamma^2_{total}$

$\Gamma(p \bar{p})/\Gamma_{total} \times \Gamma(\gamma\gamma)/\Gamma_{total}$	VALUE (units 10 ⁻⁸)	CL%	DOCUMENT ID	TECN	COMMENT	$\Gamma_{14}/\Gamma \times \Gamma_{16}/\Gamma$
••• We do not use the following data for averages, fits, limits, etc. •••						
	< 5.6		90 ^{24,25,26} AMBROGIANI	01 E835	$\bar{p} p \rightarrow \gamma \gamma$	
••• We do not use the following data for averages, fits, limits, etc. •••						
	< 8.0		90 ^{24,25,27} AMBROGIANI	01 E835	$\bar{p} p \rightarrow \gamma \gamma$	
	< 12.0		90 ^{25,27} AMBROGIANI	01 E835	$\bar{p} p \rightarrow \gamma \gamma$	

- ²⁴ Including the measurements of ARMSTRONG 95F in the AMBROGIANI 01 analysis.
- ²⁵ For a total width $\Gamma=5$ MeV.
- ²⁶ For the resonance mass region 3589–3599 MeV/c².
- ²⁷ For the resonance mass region 3575–3660 MeV/c².

$\eta_c(2S)$ BRANCHING RATIOS

$\Gamma(\text{hadrons})/\Gamma_{total}$	VALUE	DOCUMENT ID	TECN	COMMENT	Γ_1/Γ
••• We do not use the following data for averages, fits, limits, etc. •••					
not seen		ABREU	98o DLPH	$e^+ e^- \rightarrow e^+ e^- + \text{hadrons}$	
••• We do not use the following data for averages, fits, limits, etc. •••					
seen		28 EDWARDS	82c CBAL	$e^+ e^- \rightarrow \gamma X$	

²⁸ For a mass value of 3594 ± 5 MeV

$\Gamma(K \bar{K} \pi)/\Gamma_{total}$	VALUE (units 10 ⁻²)	EVTS	DOCUMENT ID	TECN	COMMENT	Γ_2/Γ
••• We do not use the following data for averages, fits, limits, etc. •••						
	1.9 ± 0.4 ± 1.1	59 ± 12	29 AUBERT	08AB BABR	$B \rightarrow \eta_c(2S) K \rightarrow K \bar{K} \pi K$	
••• We do not use the following data for averages, fits, limits, etc. •••						
seen		127 ± 18	ABLIKIM	13k BES3	$\psi(2S) \rightarrow \gamma K \bar{K} \pi$	
seen		39 ± 11	30 CHOI	02 BELL	$B \rightarrow K K_S^0 K^{\mp} \pi^{\pm}$	

²⁹ Derived from a measurement of $[B(B^+ \rightarrow \eta_c(2S) K^+) \times B(\eta_c(2S) \rightarrow K \bar{K} \pi)] / [B(B^+ \rightarrow \eta_c K^+) \times B(\eta_c \rightarrow K \bar{K} \pi)] = (9.6^{+2.0}_{-1.9} \pm 2.5)\%$ and using $B(B^+ \rightarrow \eta_c(2S) K^+) = (3.4 \pm 1.8) \times 10^{-4}$, and $[B(B^+ \rightarrow \eta_c K^+) \times B(\eta_c \rightarrow K \bar{K} \pi)] = (6.88 \pm 0.77^{+0.55}_{-0.66}) \times 10^{-5}$.

³⁰ For a mass value of 3654 ± 6 MeV

$\Gamma(K \bar{K} \eta)/\Gamma(K \bar{K} \pi)$	VALUE	DOCUMENT ID	TECN	COMMENT	Γ_3/Γ_2
••• We do not use the following data for averages, fits, limits, etc. •••					
	27.3 ± 7.0 ± 9.0	225	31 LEES	14E BABR	$\gamma \gamma \rightarrow K^+ K^- \gamma \gamma$

³¹ LEES 14E reports $B(\eta_c(2S) \rightarrow K^+ K^- \eta)/B(\eta_c(2S) \rightarrow K^+ K^- \pi^0) = 0.82 \pm 0.21 \pm 0.27$, which we divide by 3 to account for isospin symmetry.

$\Gamma(2\pi^+ 2\pi^-)/\Gamma_{total}$	VALUE	DOCUMENT ID	TECN	COMMENT	Γ_4/Γ
••• We do not use the following data for averages, fits, limits, etc. •••					
not seen		UEHARA	08 BELL	$\gamma \gamma \rightarrow \eta_c(2S)$	

$\Gamma(\rho^0 \rho^0)/\Gamma_{total}$	VALUE	DOCUMENT ID	TECN	COMMENT	Γ_5/Γ
••• We do not use the following data for averages, fits, limits, etc. •••					
not seen		ABLIKIM	11H BES3	$\psi(2S) \rightarrow \gamma 2\pi^+ 2\pi^-$	

$\Gamma(K^+ K^- \pi^+ \pi^-)/\Gamma_{total}$	VALUE	DOCUMENT ID	TECN	COMMENT	Γ_7/Γ
••• We do not use the following data for averages, fits, limits, etc. •••					
not seen		UEHARA	08 BELL	$\gamma \gamma \rightarrow \eta_c(2S)$	

$\Gamma(K^+ K^- \pi^+ \pi^- \pi^0)/\Gamma(K \bar{K} \pi)$	VALUE	EVTS	DOCUMENT ID	TECN	COMMENT	Γ_9/Γ_2
••• We do not use the following data for averages, fits, limits, etc. •••						
	0.73 ± 0.17 ± 0.17	1201	32 DEL-AMO-SA..11M	BABR	$\gamma \gamma \rightarrow K^+ K^- \pi^+ \pi^- \pi^0$	

³² We have multiplied the value of $\Gamma(K^+ K^- \pi^+ \pi^- \pi^0)/\Gamma(K_S^0 K^{\pm} \pi^{\mp})$ reported in DEL-AMO-SANCHEZ 11M by a factor 1/3 to obtain $\Gamma(K^+ K^- \pi^+ \pi^- \pi^0)/\Gamma(K \bar{K} \pi)$. Not independent from other measurements reported in DEL-AMO-SANCHEZ 11M.

$\Gamma(K^{*0} \bar{K}^{*0})/\Gamma_{total}$	VALUE	DOCUMENT ID	TECN	COMMENT	Γ_8/Γ
••• We do not use the following data for averages, fits, limits, etc. •••					
not seen		ABLIKIM	11H BES3	$\psi(2S) \rightarrow \gamma K^+ K^- \pi^+ \pi^-$	

$\Gamma(K_S^0 K^- 2\pi^+ \pi^- + c.c.)/\Gamma_{total}$	VALUE	EVTS	DOCUMENT ID	TECN	COMMENT	Γ_{11}/Γ
••• We do not use the following data for averages, fits, limits, etc. •••						
seen		57 ± 17	ABLIKIM	13k BES3	$\psi(2S) \rightarrow \gamma K_S^0 K^{\pm} \pi^{\mp} \pi^{\pm} \pi^{\mp}$	

$\Gamma(2K^+ 2K^-)/\Gamma_{total}$	VALUE	DOCUMENT ID	TECN	COMMENT	Γ_{12}/Γ
••• We do not use the following data for averages, fits, limits, etc. •••					
not seen		UEHARA	08 BELL	$\gamma \gamma \rightarrow \eta_c(2S)$	

See key on page 1127

Meson Particle Listings

$\eta_c(2S)$

$\Gamma(\phi\phi)/\Gamma_{\text{total}}$	DOCUMENT ID	TECN	COMMENT	Γ_{13}/Γ
VALUE				
not seen	ABLIKIM	11H	BES3 $\psi(2S) \rightarrow \gamma K^+ K^- K^+ K^-$	

$\Gamma(p\bar{p})/\Gamma_{\text{total}}$	DOCUMENT ID	TECN	COMMENT	Γ_{14}/Γ
VALUE				
seen	106	33	AAIJ 17AD LHCB $p\bar{p} \rightarrow B^+ X \rightarrow p\bar{p} K^+ X$	
³³ AAIJ 17AD report a 6.4 standard deviation signal, with $B(B^+ \rightarrow \eta_c(2S) K^+ \rightarrow p\bar{p} K^+)/B(B^+ \rightarrow J/\psi K^+ \rightarrow p\bar{p} K^+) = (1.58 \pm 0.33 \pm 0.09) \times 10^{-2}$.				

$\Gamma(p\bar{p}\pi^+\pi^-)/\Gamma_{\text{total}}$	DOCUMENT ID	TECN	COMMENT	Γ_{15}/Γ
VALUE				
seen	110	34	CHILIKIN 19 BELL $e^+e^- \rightarrow \Upsilon(4S)$	
³⁴ CHILIKIN 19 reports signals in $B^+ \rightarrow \eta_c(2S) K^+$ and $B^0 \rightarrow \eta_c(2S) K_S^0$ with 12.3 and 5.9 standard deviations, respectively.				

$\Gamma(\gamma\gamma)/\Gamma_{\text{total}}$	DOCUMENT ID	TECN	COMMENT	Γ_{16}/Γ
VALUE				
<ul style="list-style-type: none"> • • • We do not use the following data for averages, fits, limits, etc. • • • 				
<4 × 10 ⁻⁴	90	35	WICHT 08 BELL $B^\pm \rightarrow K^\pm \gamma\gamma$	
not seen			AMBROGIANI 01 E835 $\bar{p}p \rightarrow \gamma\gamma$	
<0.01	90		LEE 85 CBAL $\psi' \rightarrow \text{photons}$	
³⁵ WICHT 08 reports $[\Gamma(\eta_c(2S) \rightarrow \gamma\gamma)/\Gamma_{\text{total}}] \times [B(B^+ \rightarrow \eta_c(2S) K^+)] < 0.18 \times 10^{-6}$ which we divide by our best value $B(B^+ \rightarrow \eta_c(2S) K^+) = 4.4 \times 10^{-4}$.				

$\Gamma(\pi^+\pi^-\eta_c(1S))/\Gamma(K\bar{K}\pi)$	DOCUMENT ID	TECN	COMMENT	Γ_{20}/Γ_2
VALUE				
<3.33	90	36	LEES 12AE BABR $e^+e^- \rightarrow e^+e^-\pi^+\pi^-\eta_c$	

³⁶We divided the reported limit by 3 to take into account isospin relations.

$\eta_c(2S)$ CROSS-PARTICLE BRANCHING RATIOS

$\Gamma(\eta_c(2S) \rightarrow K\bar{K}\eta)/\Gamma_{\text{total}} \times \Gamma(\psi(2S) \rightarrow \gamma\eta_c(2S))/\Gamma_{\text{total}}$	DOCUMENT ID	TECN	COMMENT	$\Gamma_3/\Gamma \times \Gamma_{166}^{\psi(2S)}/\Gamma_{\psi(2S)}$
VALUE				
<11.8 × 10 ⁻⁶	90	37	CRONIN-HEN.10 CLEO $\psi(2S) \rightarrow \gamma K^+ K^- \eta$	

³⁷CRONIN-HENNESSY 10 reports a limit of < 5.9 × 10⁻⁶ for the decay $\eta_c(2S) \rightarrow K^+ K^- \eta$ which we multiply by 2 account for isospin symmetry. It assumes $\Gamma(\eta_c(2S)) = 14$ MeV. It also gives the analytic dependence of limits on width.

$\Gamma(\eta_c(2S) \rightarrow 2\pi^+ 2\pi^-)/\Gamma_{\text{total}} \times \Gamma(\psi(2S) \rightarrow \gamma\eta_c(2S))/\Gamma_{\text{total}}$	DOCUMENT ID	TECN	COMMENT	$\Gamma_4/\Gamma \times \Gamma_{166}^{\psi(2S)}/\Gamma_{\psi(2S)}$
VALUE				
<14.6 × 10 ⁻⁶	90	38	CRONIN-HEN.10 CLEO $\psi(2S) \rightarrow \gamma 2\pi^+ 2\pi^-$	

³⁸Assuming $\Gamma(\eta_c(2S)) = 14$ MeV. CRONIN-HENNESSY 10 gives the analytic dependence of limits on width.

$\Gamma(\eta_c(2S) \rightarrow \rho^0 \rho^0)/\Gamma_{\text{total}} \times \Gamma(\psi(2S) \rightarrow \gamma\eta_c(2S))/\Gamma_{\text{total}}$	DOCUMENT ID	TECN	COMMENT	$\Gamma_5/\Gamma \times \Gamma_{166}^{\psi(2S)}/\Gamma_{\psi(2S)}$
VALUE				
<12.7 × 10 ⁻⁷	90		ABLIKIM 11H BES3 $\psi(2S) \rightarrow \gamma 2\pi^+ 2\pi^-$	

$\Gamma(\eta_c(2S) \rightarrow 3\pi^+ 3\pi^-)/\Gamma_{\text{total}} \times \Gamma(\psi(2S) \rightarrow \gamma\eta_c(2S))/\Gamma_{\text{total}}$	DOCUMENT ID	TECN	COMMENT	$\Gamma_6/\Gamma \times \Gamma_{166}^{\psi(2S)}/\Gamma_{\psi(2S)}$
VALUE				
<13.2 × 10 ⁻⁶	90	39	CRONIN-HEN.10 CLEO $\psi(2S) \rightarrow \gamma 3\pi^+ 3\pi^-$	

³⁹Assuming $\Gamma(\eta_c(2S)) = 14$ MeV. CRONIN-HENNESSY 10 gives the analytic dependence of limits on width.

$\Gamma(\eta_c(2S) \rightarrow K^+ K^- \pi^+ \pi^-)/\Gamma_{\text{total}} \times \Gamma(\psi(2S) \rightarrow \gamma\eta_c(2S))/\Gamma_{\text{total}}$	DOCUMENT ID	TECN	COMMENT	$\Gamma_7/\Gamma \times \Gamma_{166}^{\psi(2S)}/\Gamma_{\psi(2S)}$
VALUE				
<9.6 × 10 ⁻⁶	90	40	CRONIN-HEN.10 CLEO $\psi(2S) \rightarrow \gamma K^+ K^- \pi^+ \pi^-$	

⁴⁰Assuming $\Gamma(\eta_c(2S)) = 14$ MeV. CRONIN-HENNESSY 10 gives the analytic dependence of limits on width.

$\Gamma(\eta_c(2S) \rightarrow K^* 0 \bar{K}^* 0)/\Gamma_{\text{total}} \times \Gamma(\psi(2S) \rightarrow \gamma\eta_c(2S))/\Gamma_{\text{total}}$	DOCUMENT ID	TECN	COMMENT	$\Gamma_8/\Gamma \times \Gamma_{166}^{\psi(2S)}/\Gamma_{\psi(2S)}$
VALUE				
<19.6 × 10 ⁻⁷	90		ABLIKIM 11H BES3 $\psi(2S) \rightarrow \gamma K^+ K^- \pi^+ \pi^-$	

$\Gamma(\eta_c(2S) \rightarrow K^+ K^- \pi^+ \pi^- \pi^0)/\Gamma_{\text{total}} \times \Gamma(\psi(2S) \rightarrow \gamma\eta_c(2S))/\Gamma_{\text{total}}$	DOCUMENT ID	TECN	COMMENT	$\Gamma_9/\Gamma \times \Gamma_{166}^{\psi(2S)}/\Gamma_{\psi(2S)}$
VALUE				
<43.0 × 10 ⁻⁶	90	41	CRONIN-HEN.10 CLEO $\psi(2S) \rightarrow \gamma K^+ K^- \pi^+ \pi^- \pi^0$	

⁴¹Assuming $\Gamma(\eta_c(2S)) = 14$ MeV. CRONIN-HENNESSY 10 gives the analytic dependence of limits on width.

$\Gamma(\eta_c(2S) \rightarrow K^+ K^- 2\pi^+ 2\pi^-)/\Gamma_{\text{total}} \times \Gamma(\psi(2S) \rightarrow \gamma\eta_c(2S))/\Gamma_{\text{total}}$	DOCUMENT ID	TECN	COMMENT	$\Gamma_{10}/\Gamma \times \Gamma_{166}^{\psi(2S)}/\Gamma_{\psi(2S)}$
VALUE				
<9.7 × 10 ⁻⁶	90	42	CRONIN-HEN.10 CLEO $\psi(2S) \rightarrow \gamma K^+ K^- 2\pi^+ 2\pi^-$	

⁴²Assuming $\Gamma(\eta_c(2S)) = 14$ MeV. CRONIN-HENNESSY 10 gives the analytic dependence of limits on width.

$\Gamma(\eta_c(2S) \rightarrow K_S^0 K^- 2\pi^+ \pi^- + \text{c.c.})/\Gamma_{\text{total}} \times \Gamma(\psi(2S) \rightarrow \gamma\eta_c(2S))/\Gamma_{\text{total}}$	DOCUMENT ID	TECN	COMMENT	$\Gamma_{11}/\Gamma \times \Gamma_{166}^{\psi(2S)}/\Gamma_{\psi(2S)}$
VALUE (units 10 ⁻⁶)				
7.03 ± 2.10 ± 0.7	60		ABLIKIM 13K BES3 $\psi(2S) \rightarrow \gamma K_S^0 K^- 2\pi^+ \pi^- + \text{c.c.}$	

- • • We do not use the following data for averages, fits, limits, etc. • • •

< 15.2 90 ⁴³CRONIN-HEN.10 CLEO $\psi(2S) \rightarrow \gamma K_S^0 K^- 2\pi^+ \pi^- + \text{c.c.}$

⁴³Assuming $\Gamma(\eta_c(2S)) = 14$ MeV. CRONIN-HENNESSY 10 gives the analytic dependence of limits on width.

$\Gamma(\eta_c(2S) \rightarrow \phi\phi)/\Gamma_{\text{total}} \times \Gamma(\psi(2S) \rightarrow \gamma\eta_c(2S))/\Gamma_{\text{total}}$	DOCUMENT ID	TECN	COMMENT	$\Gamma_{13}/\Gamma \times \Gamma_{166}^{\psi(2S)}/\Gamma_{\psi(2S)}$
VALUE				
<7.8 × 10 ⁻⁷	90		ABLIKIM 11H BES3 $\psi(2S) \rightarrow \gamma K^+ K^- K^+ K^-$	

$\Gamma(\eta_c(2S) \rightarrow \rho\bar{\rho})/\Gamma_{\text{total}} \times \Gamma(\psi(2S) \rightarrow \gamma\eta_c(2S))/\Gamma_{\text{total}}$	DOCUMENT ID	TECN	COMMENT	$\Gamma_{14}/\Gamma \times \Gamma_{166}^{\psi(2S)}/\Gamma_{\psi(2S)}$
VALUE				
<1.4 × 10 ⁻⁶	90		ABLIKIM 13V BES3 $\psi(2S) \rightarrow \gamma \rho\bar{\rho}$	

$\Gamma(\eta_c(2S) \rightarrow \gamma J/\psi(1S))/\Gamma_{\text{total}} \times \Gamma(\psi(2S) \rightarrow \gamma\eta_c(2S))/\Gamma_{\text{total}}$	DOCUMENT ID	TECN	COMMENT	$\Gamma_{17}/\Gamma \times \Gamma_{166}^{\psi(2S)}/\Gamma_{\psi(2S)}$
VALUE				
<9.7 × 10 ⁻⁶	90	33	44	ABLIKIM 17N BES3 $\psi(2S) \rightarrow \gamma\gamma J/\psi$

⁴⁴Uses $B(J/\psi \rightarrow e^+e^-) = (5.971 \pm 0.032)\%$ and $B(J/\psi \rightarrow \mu^+\mu^-) = (5.961 \pm 0.033)\%$.

$\Gamma(\eta_c(2S) \rightarrow \pi^+ \pi^- \eta)/\Gamma_{\text{total}} \times \Gamma(\psi(2S) \rightarrow \gamma\eta_c(2S))/\Gamma_{\text{total}}$	DOCUMENT ID	TECN	COMMENT	$\Gamma_{18}/\Gamma \times \Gamma_{166}^{\psi(2S)}/\Gamma_{\psi(2S)}$
VALUE				
<4.3 × 10 ⁻⁶	90	45	CRONIN-HEN.10 CLEO $\psi(2S) \rightarrow \gamma \pi^+ \pi^- \eta$	

⁴⁵Assuming $\Gamma(\eta_c(2S)) = 14$ MeV. CRONIN-HENNESSY 10 gives the analytic dependence of limits on width.

$\Gamma(\eta_c(2S) \rightarrow \pi^+ \pi^- \eta')/\Gamma_{\text{total}} \times \Gamma(\psi(2S) \rightarrow \gamma\eta_c(2S))/\Gamma_{\text{total}}$	DOCUMENT ID	TECN	COMMENT	$\Gamma_{19}/\Gamma \times \Gamma_{166}^{\psi(2S)}/\Gamma_{\psi(2S)}$
VALUE				
<14.2 × 10 ⁻⁶	90	46	CRONIN-HEN.10 CLEO $\psi(2S) \rightarrow \gamma \pi^+ \pi^- \eta'$	

⁴⁶Assuming $\Gamma(\eta_c(2S)) = 14$ MeV. CRONIN-HENNESSY 10 gives the analytic dependence of limits on width.

$\Gamma(\eta_c(2S) \rightarrow \pi^+ \pi^- \eta_c(1S))/\Gamma_{\text{total}} \times \Gamma(\psi(2S) \rightarrow \gamma\eta_c(2S))/\Gamma_{\text{total}}$	DOCUMENT ID	TECN	COMMENT	$\Gamma_{20}/\Gamma \times \Gamma_{166}^{\psi(2S)}/\Gamma_{\psi(2S)}$
VALUE				
<1.7 × 10 ⁻⁴	90	47	CRONIN-HEN.10 CLEO $\psi(2S) \rightarrow \gamma \pi^+ \pi^- \eta_c(1S)$	

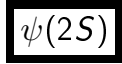
⁴⁷Assuming $\Gamma(\eta_c(2S)) = 14$ MeV. CRONIN-HENNESSY 10 gives the analytic dependence of limits on width.

$\eta_c(2S)$ REFERENCES

CHILIKIN 19	PR D100 012001	K. Chilikin et al.	(BELLE Collab.)
XU 18	PR D98 072001	Q.N. Xu et al.	(BELLE Collab.)
AAIJ 17AD	PL B769 305	R. Aaij et al.	(LHCb Collab.)
AAIJ 17BB	EPJ C77 609	R. Aaij et al.	(LHCb Collab.)
ABLIKIM 17N	PR D95 072004	M. Ablikim et al.	(BESIII Collab.)
PDC 16	CP C40 100001	C. Patrignani et al.	(PDG Collab.)
LEES 14E	PR D89 112004	J.P. Lees et al.	(BABAR Collab.)
ABLIKIM 13K	PR D87 052005	M. Ablikim et al.	(BESIII Collab.)
ABLIKIM 13V	PR D88 112001	M. Ablikim et al.	(BESIII Collab.)
ABLIKIM 12G	PRL 109 042003	M. Ablikim et al.	(BESIII Collab.)
LEES 12AE	PR D86 092005	J.P. Lees et al.	(BABAR Collab.)
ABLIKIM 11H	PR D84 091102	M. Ablikim et al.	(BESIII Collab.)
DEL-AMO-SA... 11M	PR D84 012004	P. del Amo Sanchez et al.	(BABAR Collab.)
VINOKUROVA 11	PL B706 139	A. Vinokurova et al.	(BELLE Collab.)
CRONIN-HEN.10	PR D81 052002	D. Cronin-Hennessey et al.	(CLEO Collab.)
AUBERT 08AB	PR D78 012006	B. Aubert et al.	(BABAR Collab.)
UEHARA 08	EPJ C53 1	S. Uehara et al.	(BELLE Collab.)
WICHT 07	PL B662 323	J. Wicht et al.	(BELLE Collab.)
ABE 07	PRL 98 082001	K. Abe et al.	(BELLE Collab.)
AUBERT 06E	PRL 96 052002	B. Aubert et al.	(BABAR Collab.)
AUBERT 05C	PR D72 031101	B. Aubert et al.	(BABAR Collab.)
ABE 04G	PR D70 071102	K. Abe et al.	(BELLE Collab.)
ASNER 04	PRL 92 142001	D.M. Asner et al.	(CLEO Collab.)
AUBERT 04D	PRL 92 142002	B. Aubert et al.	(BABAR Collab.)
ABE,K 02	PRL 89 142001	K. Abe et al.	(BELLE Collab.)
CHOI 02	PRL 89 102001	S.-K. Choi et al.	(BELLE Collab.)
AMBROGIANI 01	PR D64 052003	M. Ambrogiani et al.	(FNAL E835 Collab.)
ABREU 98O	PL B441 479	P. Abreu et al.	(DELPHI Collab.)
ARMSTRONG 95F	PR D52 4839	T.A. Armstrong et al.	(FNAL, FERMI, GENO+)
LEE 85	SLAC 282	R.A. Lee	(SLAC)
EDWARDS 82C	PRL 48 70	C. Edwards et al.	(CIT, HARV, PRIN+)

Meson Particle Listings

$\psi(2S)$



$$I^G(J^{PC}) = 0^-(1^{--})$$

See the Review on " $\psi(2S)$ and χ_c branching ratios" before the $\chi_{c0}(1P)$ Listings.

$\psi(2S)$ MASS

OUR FIT includes measurements of $m_{\psi(2S)}$, $m_{\psi(3770)}$, and $m_{\psi(3770)} - m_{\psi(2S)}$.

VALUE (MeV)	EVTS	DOCUMENT ID	TECN	COMMENT
3686.10 ± 0.06 OUR FIT				Error includes scale factor of 5.9.
3686.097 ± 0.010 OUR AVERAGE				
3686.099 ± 0.004 ± 0.009		¹ ANASHIN 15	KEDR	$e^+e^- \rightarrow$ hadrons
3686.12 ± 0.06 ± 0.10	4k	AAIJ 12H	LHCB	$pp \rightarrow J/\psi \pi^+ \pi^- X$
3685.95 ± 0.10	413	² ARTAMONOV 00	OLYA	$e^+e^- \rightarrow$ hadrons
3685.98 ± 0.09 ± 0.04		³ ARMSTRONG 93B	E760	$\bar{p}p \rightarrow e^+e^-$
3686.114 ± 0.007 ± 0.011 -0.016		⁴ ANASHIN 12	KEDR	$e^+e^- \rightarrow$ hadrons
3686.111 ± 0.025 ± 0.009		AULCHENKO 03	KEDR	$e^+e^- \rightarrow$ hadrons
3686.00 ± 0.10	413	⁵ ZHOLENTZ 80	OLYA	e^+e^-

- ¹ Supersedes AULCHENKO 03 and ANASHIN 12.
- ² Reanalysis of ZHOLENTZ 80 using new electron mass (COHEN 87) and radiative corrections (KURAEV 85).
- ³ Mass central value and systematic error recalculated by us according to Eq. (16) in ARMSTRONG 93B, using the value for the $J/\psi(1S)$ mass from AULCHENKO 03.
- ⁴ From the scans in 2004 and 2006. ANASHIN 12 reports the value $3686.114 \pm 0.007 \pm 0.011 \pm 0.002$ MeV, where the third uncertainty is due to assumptions on the interference between the resonance and hadronic continuum. We combined the two systematic uncertainties.
- ⁵ Superseded by ARTA MONOV 00.

$m_{\psi(2S)} - m_{J/\psi(1S)}$

VALUE (MeV)	DOCUMENT ID	TECN	COMMENT
589.188 ± 0.028 OUR AVERAGE			
589.194 ± 0.027 ± 0.011	¹ AULCHENKO 03	KEDR	$e^+e^- \rightarrow$ hadrons
589.7 ± 1.2	LEMOIGNE 82	GOLI	$185 \pi^- \text{Be} \rightarrow \gamma \mu^+ \mu^- A$
589.07 ± 0.13	¹ ZHOLENTZ 80	OLYA	e^+e^-
588.7 ± 0.8	LUTH 75	MRK1	
588 ± 1	² BAI 98E	BES	e^+e^-

- ¹ Redundant with data in mass above.
- ² Systematic errors not evaluated.

$\psi(2S)$ WIDTH

VALUE (keV)	EVTS	DOCUMENT ID	TECN	COMMENT
294 ± 8 OUR FIT				
286 ± 16 OUR AVERAGE				
358 ± 88 ± 4		ABLIIKIM 08B	BES2	$e^+e^- \rightarrow$ hadrons
290 ± 25 ± 4	2.7k	ANDREOTTI 07	E835	$p\bar{p} \rightarrow e^+e^-, J/\psi X$
331 ± 58 ± 2		ABLIIKIM 06L	BES2	$e^+e^- \rightarrow$ hadrons
264 ± 27		¹ BAI 02B	BES2	e^+e^-
287 ± 37 ± 16		² ARMSTRONG 93B	E760	$\bar{p}p \rightarrow e^+e^-$

- ¹ From a simultaneous fit to the hadronic and $\mu^+ \mu^-$ cross section, assuming $\Gamma = \Gamma_h + \Gamma_e + \Gamma_\mu + \Gamma_\tau$ and lepton universality. Does not include vacuum polarization correction.
- ² The initial-state radiation correction reevaluated by ANDREOTTI 07 in its Ref. [4].

$\psi(2S)$ DECAY MODES

Mode	Fraction (Γ_i/Γ)	Scale factor/ Confidence level
Γ_1 hadrons	(97.85 ± 0.13) %	S=1.5
Γ_2 virtual $\gamma \rightarrow$ hadrons	(1.73 ± 0.14) %	
Γ_3 ggg	(10.6 ± 1.6) %	
Γ_4 γgg	(1.03 ± 0.29) %	
Γ_5 light hadrons	(15.4 ± 1.5) %	
Γ_6 K_S^0 anything	(16.0 ± 1.1) %	
Γ_7 e^+e^-	(7.93 ± 0.17) × 10 ⁻³	
Γ_8 $\mu^+\mu^-$	(8.0 ± 0.6) × 10 ⁻³	
Γ_9 $\tau^+\tau^-$	(3.1 ± 0.4) × 10 ⁻³	

Decays into $J/\psi(1S)$ and anything

Γ_{10} $J/\psi(1S)$ anything	(61.4 ± 0.6) %
Γ_{11} $J/\psi(1S)$ neutrals	(25.38 ± 0.32) %
Γ_{12} $J/\psi(1S) \pi^+ \pi^-$	(34.68 ± 0.30) %
Γ_{13} $J/\psi(1S) \pi^0 \pi^0$	(18.24 ± 0.31) %
Γ_{14} $J/\psi(1S) \eta$	(3.37 ± 0.05) %
Γ_{15} $J/\psi(1S) \pi^0$	(1.268 ± 0.032) × 10 ⁻³

Hadronic decays

Γ_{16} $\pi^+ \pi^-$	(7.8 ± 2.6) × 10 ⁻⁶	
Γ_{17} $\pi^+ \pi^- \pi^0$	(2.01 ± 0.17) × 10 ⁻⁴	S=1.7
Γ_{18} $\rho(770) \pi \rightarrow \pi^+ \pi^- \pi^0$	(3.2 ± 1.2) × 10 ⁻⁵	S=1.8
Γ_{19} $\rho(2150) \pi \rightarrow \pi^+ \pi^- \pi^0$	(1.9 ± 1.2 -0.4) × 10 ⁻⁴	
Γ_{20} $2(\pi^+ \pi^-)$	(2.4 ± 0.6) × 10 ⁻⁴	S=2.2
Γ_{21} $\rho^0 \pi^+ \pi^-$	(2.2 ± 0.6) × 10 ⁻⁴	S=1.4
Γ_{22} $2(\pi^+ \pi^-) \pi^0$	(2.9 ± 1.0) × 10 ⁻³	S=4.7
Γ_{23} $\rho \rho_2(1320)$	(2.6 ± 0.9) × 10 ⁻⁴	
Γ_{24} $\pi^+ \pi^- \pi^0 \pi^0 \pi^0$	(5.3 ± 0.9) × 10 ⁻³	
Γ_{25} $\pi^+ \pi^- 4\pi^0$	(1.4 ± 1.0) × 10 ⁻³	
Γ_{26} $\rho^\pm \pi^\mp \pi^0 \pi^0$	< 2.7 × 10 ⁻³	CL=90%
Γ_{27} $3(\pi^+ \pi^-)$	(3.5 ± 2.0) × 10 ⁻⁴	S=2.8
Γ_{28} $2(\pi^+ \pi^-) \pi^0$	(4.8 ± 1.5) × 10 ⁻³	
Γ_{29} $3(\pi^+ \pi^-) \pi^0$	(3.5 ± 1.6) × 10 ⁻³	
Γ_{30} $2(\pi^+ \pi^-) 3\pi^0$	(1.42 ± 0.31) %	
Γ_{31} $\eta \pi^+ \pi^-$	< 1.6 × 10 ⁻⁴	CL=90%
Γ_{32} $\eta \pi^+ \pi^- \pi^0$	(9.5 ± 1.7) × 10 ⁻⁴	
Γ_{33} $\eta 2(\pi^+ \pi^-)$	(1.2 ± 0.6) × 10 ⁻³	
Γ_{34} $\eta \pi^+ \pi^- \pi^0 \pi^0$	< 4 × 10 ⁻⁴	CL=90%
Γ_{35} $\eta \pi^+ \pi^- 3\pi^0$	< 2.1 × 10 ⁻³	CL=90%
Γ_{36} $\eta 2(\pi^+ \pi^-) \pi^0$	< 2.1 × 10 ⁻³	CL=90%
Γ_{37} $\rho \eta$	(2.2 ± 0.6) × 10 ⁻⁵	S=1.1
Γ_{38} $\eta' \pi^+ \pi^- \pi^0$	(4.5 ± 2.1) × 10 ⁻⁴	
Γ_{39} $\eta' \rho$	(1.9 ± 1.7 -1.2) × 10 ⁻⁵	
Γ_{40} $\omega \pi^0$	(2.1 ± 0.6) × 10 ⁻⁵	
Γ_{41} $\omega \pi^+ \pi^-$	(7.3 ± 1.2) × 10 ⁻⁴	S=2.1
Γ_{42} $\omega \pi^+ \pi^- 2\pi^0$	(8.7 ± 2.4) × 10 ⁻³	
Γ_{43} $b_1^\pm \pi^\mp$	(4.0 ± 0.6) × 10 ⁻⁴	S=1.1
Γ_{44} $\omega f_2(1270)$	(2.2 ± 0.4) × 10 ⁻⁴	
Γ_{45} $\omega \pi^0 \pi^0$	(1.11 ± 0.35) × 10 ⁻³	
Γ_{46} $\omega 3\pi^0$	< 8 × 10 ⁻⁴	CL=90%
Γ_{47} $b_1^0 \pi^0$	(2.4 ± 0.6) × 10 ⁻⁴	
Γ_{48} $\omega \eta$	< 1.1 × 10 ⁻⁵	CL=90%
Γ_{49} $\omega \eta'$	(3.2 ± 2.5 -2.1) × 10 ⁻⁵	
Γ_{50} $\phi \pi^0$	< 4 × 10 ⁻⁷	CL=90%
Γ_{51} $\phi \pi^+ \pi^-$	(1.18 ± 0.26) × 10 ⁻⁴	S=1.5
Γ_{52} $\phi f_0(980) \rightarrow \pi^+ \pi^-$	(7.5 ± 3.3) × 10 ⁻⁵	S=1.6
Γ_{53} $\phi \eta$	(3.10 ± 0.31) × 10 ⁻⁵	
Γ_{54} $\eta \phi(2170), \phi(2170) \rightarrow \phi f_0(980), f_0 \rightarrow \pi^+ \pi^-$	< 2.2 × 10 ⁻⁶	CL=90%
Γ_{55} $\phi \eta'$	(1.54 ± 0.20) × 10 ⁻⁵	
Γ_{56} $\phi f_1(1285)$	(3.0 ± 1.3) × 10 ⁻⁵	
Γ_{57} $\phi \eta(1405) \rightarrow \phi \pi^+ \pi^- \eta$	(8.5 ± 1.7) × 10 ⁻⁶	
Γ_{58} $\phi f_2'(1525)$	(4.4 ± 1.6) × 10 ⁻⁵	
Γ_{59} $K^+ K^-$	(7.5 ± 0.5) × 10 ⁻⁵	
Γ_{60} $K^+ K^- \pi^+$	(7.3 ± 0.5) × 10 ⁻⁴	
Γ_{61} $K^+ K^- \pi^0$	(4.07 ± 0.31) × 10 ⁻⁵	
Γ_{62} $K_S^0 K_S^0$	< 4.6 × 10 ⁻⁶	
Γ_{63} $K_S^0 K_L^0$	(5.34 ± 0.33) × 10 ⁻⁵	
Γ_{64} $K_S^0 K_L^0 \pi^0$	< 3.0 × 10 ⁻⁴	CL=90%
Γ_{65} $K^+ K^- \pi^0 \pi^0$	(2.6 ± 1.3) × 10 ⁻⁴	
Γ_{66} $K^+ K^- \pi^+ \pi^- \pi^0$	(1.26 ± 0.09) × 10 ⁻³	
Γ_{67} $\omega f_0(1710) \rightarrow \omega K^+ K^-$	(5.9 ± 2.2) × 10 ⁻⁵	
Γ_{68} $K^*(892)^0 K^- \pi^+ \pi^0 + \text{c.c.}$	(8.6 ± 2.2) × 10 ⁻⁴	
Γ_{69} $K^*(892)^+ K^- \pi^+ \pi^- + \text{c.c.}$	(9.6 ± 2.8) × 10 ⁻⁴	
Γ_{70} $K^*(892)^+ K^- \rho^0 + \text{c.c.}$	(7.3 ± 2.6) × 10 ⁻⁴	
Γ_{71} $K^*(892)^0 K^- \rho^+ + \text{c.c.}$	(6.1 ± 1.8) × 10 ⁻⁴	
Γ_{72} $K_S^0 K_S^0 \pi^+ \pi^-$	(2.2 ± 0.4) × 10 ⁻⁴	
Γ_{73} $K_S^0 K_L^0 \pi^0 \pi^0$	(1.3 ± 0.6) × 10 ⁻³	
Γ_{74} $K_S^0 K_L^0 \eta$	(1.3 ± 0.5) × 10 ⁻³	
Γ_{75} $K^+ K^- \rho^0$	(2.2 ± 0.4) × 10 ⁻⁴	
Γ_{76} $K^*(892)^0 \bar{K}_2^*(1430)^0$	(1.9 ± 0.5) × 10 ⁻⁴	
Γ_{77} $K^+ K^- \pi^+ \pi^- \eta$	(1.3 ± 0.7) × 10 ⁻³	
Γ_{78} $K^+ K^- 2(\pi^+ \pi^-)$	(1.9 ± 0.9) × 10 ⁻³	
Γ_{79} $K^+ K^- 2(\pi^+ \pi^-) \pi^0$	(1.00 ± 0.31) × 10 ⁻³	
Γ_{80} $K^+ K^*(892)^- + \text{c.c.}$	(2.9 ± 0.4) × 10 ⁻⁵	S=1.2
Γ_{81} $2(K^+ K^-)$	(6.3 ± 1.3) × 10 ⁻⁵	
Γ_{82} $2(K^+ K^-) \pi^0$	(1.10 ± 0.28) × 10 ⁻⁴	
Γ_{83} $K^+ K^- \phi$	(7.0 ± 1.6) × 10 ⁻⁵	
Γ_{84} $K_1^*(1270)^\pm K^\mp$	(1.00 ± 0.28) × 10 ⁻³	
Γ_{85} $K^+ \bar{K}^*(892)^0 \pi^- + \text{c.c.}$	(6.7 ± 2.5) × 10 ⁻⁴	
Γ_{86} $\eta K^+ K^-$, no $\eta \phi$	(3.49 ± 0.17) × 10 ⁻⁵	

See key on page 1127

Meson Particle Listings

$\psi(2S)$

$\Gamma(J/\psi(1S)\eta) \times \Gamma(e^+e^-)/\Gamma_{total}$ $\Gamma_{14}\Gamma_7/\Gamma$

VALUE (eV)	EVTs	DOCUMENT ID	TECN	COMMENT
78.6 ± 1.6 OUR FIT				
87 ± 9 OUR AVERAGE				
83 ± 25 ± 5	14	¹ AUBERT	07AU BABR	10.6 e ⁺ e ⁻ → J/ψπ ⁺ π ⁻ π ⁰ γ
88 ± 6 ± 7	291 ± 24	ADAM	06 CLEO	3.773 e ⁺ e ⁻ → γψ(2S)
¹ AUBERT 07AU quotes Γ _{ee} ^{ψ(2S)} · B(ψ(2S) → J/ψη) · B(J/ψ → μ ⁺ μ ⁻) · B(η → π ⁺ π ⁻ π ⁰) = 1.11 ± 0.33 ± 0.07 eV.				

$\Gamma(J/\psi(1S)\pi^0) \times \Gamma(e^+e^-)/\Gamma_{total}$ $\Gamma_{15}\Gamma_7/\Gamma$

VALUE (eV)	CL%	EVTs	DOCUMENT ID	TECN	COMMENT
<8	90	<37	ADAM	06 CLEO	3.773 e ⁺ e ⁻ → γψ(2S)

$\Gamma(2(\pi^+\pi^-)\pi^0) \times \Gamma(e^+e^-)/\Gamma_{total}$ $\Gamma_{22}\Gamma_7/\Gamma$

VALUE (eV)	EVTs	DOCUMENT ID	TECN	COMMENT
29.7 ± 2.2 ± 1.8	410	AUBERT	07AU BABR	10.6 e ⁺ e ⁻ → 2(π ⁺ π ⁻)π ⁰ γ

$\Gamma(\pi^+\pi^-\pi^0\pi^0) \times \Gamma(e^+e^-)/\Gamma_{total}$ $\Gamma_{24}\Gamma_7/\Gamma$

VALUE (eV)	EVTs	DOCUMENT ID	TECN	COMMENT
12.4 ± 1.8 ± 1.2	177	LEES	18E BABR	10.6 e ⁺ e ⁻ → π ⁺ π ⁻ 3π ⁰ γ

$\Gamma(\pi^+\pi^-4\pi^0) \times \Gamma(e^+e^-)/\Gamma_{total}$ $\Gamma_{25}\Gamma_7/\Gamma$

VALUE (eV)	EVTs	DOCUMENT ID	TECN	COMMENT
3.3 ± 2.3 ± 0.5	18	LEES	21C BABR	e ⁺ e ⁻ → γISR(π ⁺ π ⁻ 4π ⁰)

$\Gamma(\rho^+\pi^-\pi^0\pi^0) \times \Gamma(e^+e^-)/\Gamma_{total}$ $\Gamma_{26}\Gamma_7/\Gamma$

VALUE (eV)	CL%	DOCUMENT ID	TECN	COMMENT
<6.2	90	LEES	18E BABR	10.6 e ⁺ e ⁻ → π ⁺ π ⁻ 3π ⁰ γ

$\Gamma(2(\pi^+\pi^-\pi^0)) \times \Gamma(e^+e^-)/\Gamma_{total}$ $\Gamma_{28}\Gamma_7/\Gamma$

VALUE (eV)	EVTs	DOCUMENT ID	TECN	COMMENT
11.2 ± 3.3 ± 1.3	43	AUBERT	06D BABR	10.6 e ⁺ e ⁻ → 2(π ⁺ π ⁻ π ⁰)γ

$\Gamma(2(\pi^+\pi^-)3\pi^0) \times \Gamma(e^+e^-)/\Gamma_{total}$ $\Gamma_{30}\Gamma_7/\Gamma$

VALUE (eV)	EVTs	DOCUMENT ID	TECN	COMMENT
33 ± 5 ± 5	14k	LEES	21 BABR	10.6 e ⁺ e ⁻ → 2(π ⁺ π ⁻)3π ⁰ γ

$\Gamma(\eta 2(\pi^+\pi^-)) \times \Gamma(e^+e^-)/\Gamma_{total}$ $\Gamma_{33}\Gamma_7/\Gamma$

VALUE (eV)	CL%	EVTs	DOCUMENT ID	TECN	COMMENT
2.87 ± 1.41 ± 0.01		16	¹ AUBERT	07AU BABR	10.6 e ⁺ e ⁻ → 2(π ⁺ π ⁻)ηγ

• • • We do not use the following data for averages, fits, limits, etc. • • •
 <7 90 14k ²LEES 21 BABR 10.6 e⁺e⁻ → 2(π⁺π⁻)3π⁰γ

¹AUBERT 07AU reports [Γ(ψ(2S) → η2(π⁺π⁻)) × Γ(ψ(2S) → e⁺e⁻)/Γ_{total}] × [B(η → 2γ)] = 1.13 ± 0.55 ± 0.08 eV which we divide by our best value B(η → 2γ) = (39.36 ± 0.18) × 10⁻². Our first error is their experiment's error and our second error is the systematic error from using our best value.

²LEES 21 reports [Γ(ψ(2S) → η2(π⁺π⁻)) × Γ(ψ(2S) → e⁺e⁻)/Γ_{total}] × [B(η → 3π⁰)] < 2.3 eV which we divide by our best value B(η → 3π⁰) = 32.57 × 10⁻².

$\Gamma(\eta\pi^+\pi^-\pi^0) \times \Gamma(e^+e^-)/\Gamma_{total}$ $\Gamma_{34}\Gamma_7/\Gamma$

VALUE (eV)	CL%	DOCUMENT ID	TECN	COMMENT
<0.85	90	LEES	18E BABR	10.6 e ⁺ e ⁻ → π ⁺ π ⁻ π ⁰ ηγ

$\Gamma(\eta\pi^+\pi^-3\pi^0) \times \Gamma(e^+e^-)/\Gamma_{total}$ $\Gamma_{35}\Gamma_7/\Gamma$

VALUE (eV)	CL%	DOCUMENT ID	TECN	COMMENT
<5	90	¹ LEES	21C BABR	e ⁺ e ⁻ → γISR(π ⁺ π ⁻ 3π ⁰ γ)

¹LEES 21C reports [Γ(ψ(2S) → ηπ⁺π⁻3π⁰) × Γ(ψ(2S) → e⁺e⁻)/Γ_{total}] × [B(η → 2γ)] < 1.9 eV which we divide by our best value B(η → 2γ) = 39.36 × 10⁻².

$\Gamma(\eta 2(\pi^+\pi^-\pi^0)) \times \Gamma(e^+e^-)/\Gamma_{total}$ $\Gamma_{36}\Gamma_7/\Gamma$

VALUE (eV)	CL%	EVTs	DOCUMENT ID	TECN	COMMENT
<5	90	14k	¹ LEES	21 BABR	10.6 e ⁺ e ⁻ → 2(π ⁺ π ⁻)3π ⁰ γ

¹LEES 21 reports [Γ(ψ(2S) → η2(π⁺π⁻π⁰)) × Γ(ψ(2S) → e⁺e⁻)/Γ_{total}] × [B(η → 2γ)] < 1.9 eV which we divide by our best value B(η → 2γ) = 39.36 × 10⁻².

$\Gamma(\omega\pi^+\pi^-) \times \Gamma(e^+e^-)/\Gamma_{total}$ $\Gamma_{41}\Gamma_7/\Gamma$

VALUE (eV)	EVTs	DOCUMENT ID	TECN	COMMENT
3.01 ± 0.84 ± 0.02	37	¹ AUBERT	07AU BABR	10.6 e ⁺ e ⁻ → ωπ ⁺ π ⁻ γ

¹AUBERT 07AU reports [Γ(ψ(2S) → ωπ⁺π⁻) × Γ(ψ(2S) → e⁺e⁻)/Γ_{total}] × [B(ω(782) → π⁺π⁻π⁰)] = 2.69 ± 0.73 ± 0.16 eV which we divide by our best value B(ω(782) → π⁺π⁻π⁰) = (89.2 ± 0.7) × 10⁻². Our first error is their experiment's error and our second error is the systematic error from using our best value.

$\Gamma(\omega\pi^+\pi^-2\pi^0) \times \Gamma(e^+e^-)/\Gamma_{total}$ $\Gamma_{42}\Gamma_7/\Gamma$

VALUE (eV)	EVTs	DOCUMENT ID	TECN	COMMENT
20.2 ± 5.6 ± 0.1	14k	¹ LEES	21 BABR	10.6 e ⁺ e ⁻ → 2(π ⁺ π ⁻)3π ⁰ γ

¹LEES 21 reports [Γ(ψ(2S) → ωπ⁺π⁻2π⁰) × Γ(ψ(2S) → e⁺e⁻)/Γ_{total}] × [B(ω(782) → π⁺π⁻π⁰)] = 18 ± 4 ± 3 eV which we divide by our best value B(ω(782) → π⁺π⁻π⁰) = (89.2 ± 0.7) × 10⁻². Our first error is their experiment's error and our second error is the systematic error from using our best value.

$\Gamma(\omega\pi^0\pi^0) \times \Gamma(e^+e^-)/\Gamma_{total}$ $\Gamma_{45}\Gamma_7/\Gamma$

VALUE (eV)	EVTs	DOCUMENT ID	TECN	COMMENT
2.58 ± 0.82 ± 0.02	33	¹ LEES	18E BABR	10.6 e ⁺ e ⁻ → π ⁺ π ⁻ 3π ⁰ γ

¹LEES 18E reports [Γ(ψ(2S) → ωπ⁰π⁰) × Γ(ψ(2S) → e⁺e⁻)/Γ_{total}] × [B(ω(782) → π⁺π⁻π⁰)] = 2.3 ± 0.7 ± 0.2 eV which we divide by our best value B(ω(782) → π⁺π⁻π⁰) = (89.2 ± 0.7) × 10⁻². Our first error is their experiment's error and our second error is the systematic error from using our best value.

$\Gamma(\omega 3\pi^0) \times \Gamma(e^+e^-)/\Gamma_{total}$ $\Gamma_{46}\Gamma_7/\Gamma$

VALUE (eV)	CL%	DOCUMENT ID	TECN	COMMENT
<1.8	90	¹ LEES	21C BABR	e ⁺ e ⁻ → γISR(π ⁺ π ⁻ 4π ⁰)

¹LEES 21C reports [Γ(ψ(2S) → ω3π⁰) × Γ(ψ(2S) → e⁺e⁻)/Γ_{total}] × [B(ω(782) → π⁺π⁻π⁰)] < 1.6 eV which we divide by our best value B(ω(782) → π⁺π⁻π⁰) = 89.2 × 10⁻².

$\Gamma(\phi\pi^+\pi^-) \times \Gamma(e^+e^-)/\Gamma_{total}$ $\Gamma_{51}\Gamma_7/\Gamma$

VALUE (eV)	EVTs	DOCUMENT ID	TECN	COMMENT
0.55 ± 0.19 ± 0.01	19	¹ LEES	12F BABR	10.6 e ⁺ e ⁻ → K ⁺ K ⁻ π ⁺ π ⁻ γ

• • • We do not use the following data for averages, fits, limits, etc. • • •
 0.57 ± 0.23 ± 0.01 10 ²AUBERT, BE 06D BABR 10.6 e⁺e⁻ → K⁺K⁻π⁺π⁻γ

¹LEES 12F reports [Γ(ψ(2S) → φπ⁺π⁻) × Γ(ψ(2S) → e⁺e⁻)/Γ_{total}] × [B(φ(1020) → K⁺K⁻)] = 0.27 ± 0.09 ± 0.02 eV which we divide by our best value B(φ(1020) → K⁺K⁻) = (49.1 ± 0.5) × 10⁻². Our first error is their experiment's error and our second error is the systematic error from using our best value.

²Superseded by LEES 12F. AUBERT, BE 06D reports [Γ(ψ(2S) → φπ⁺π⁻) × Γ(ψ(2S) → e⁺e⁻)/Γ_{total}] × [B(φ(1020) → K⁺K⁻)] = 0.28 ± 0.11 ± 0.02 eV which we divide by our best value B(φ(1020) → K⁺K⁻) = (49.1 ± 0.5) × 10⁻². Our first error is their experiment's error and our second error is the systematic error from using our best value.

$\Gamma(\phi_0(980) \rightarrow \pi^+\pi^-) \times \Gamma(e^+e^-)/\Gamma_{total}$ $\Gamma_{52}\Gamma_7/\Gamma$

VALUE (eV)	EVTs	DOCUMENT ID	TECN	COMMENT
0.346 ± 0.129 ± 0.004	12	¹ LEES	12F BABR	10.6 e ⁺ e ⁻ → π ⁺ π ⁻ K ⁺ K ⁻ γ

• • • We do not use the following data for averages, fits, limits, etc. • • •
 0.346 ± 0.168 ± 0.004 6 ± 3 ²AUBERT 07AK BABR 10.6 e⁺e⁻ → π⁺π⁻K⁺K⁻γ

¹LEES 12F reports [Γ(ψ(2S) → φ₀(980) → π⁺π⁻) × Γ(ψ(2S) → e⁺e⁻)/Γ_{total}] × [B(φ(1020) → K⁺K⁻)] = 0.17 ± 0.06 ± 0.02 eV which we divide by our best value B(φ(1020) → K⁺K⁻) = (49.1 ± 0.5) × 10⁻². Our first error is their experiment's error and our second error is the systematic error from using our best value.

²Superseded by LEES 12F. AUBERT 07AK reports [Γ(ψ(2S) → φ₀(980) → π⁺π⁻) × Γ(ψ(2S) → e⁺e⁻)/Γ_{total}] × [B(φ(1020) → K⁺K⁻)] = 0.17 ± 0.08 ± 0.02 eV which we divide by our best value B(φ(1020) → K⁺K⁻) = (49.1 ± 0.5) × 10⁻². Our first error is their experiment's error and our second error is the systematic error from using our best value.

$\Gamma(K^+K^-) \times \Gamma(e^+e^-)/\Gamma_{total}$ $\Gamma_{59}\Gamma_7/\Gamma$

VALUE (eV)	EVTs	DOCUMENT ID	TECN	COMMENT
0.147 ± 0.035 ± 0.005	66	¹ LEES	15J BABR	e ⁺ e ⁻ → K ⁺ K ⁻ γ
0.197 ± 0.035 ± 0.005	66	² LEES	15J BABR	e ⁺ e ⁻ → K ⁺ K ⁻ γ
0.35 ± 0.14 ± 0.03	11	³ LEES	13Q BABR	e ⁺ e ⁻ → K ⁺ K ⁻ γ

• • • We do not use the following data for averages, fits, limits, etc. • • •
 0.17 ± 0.035 ± 0.005 66 ¹LEES 15J BABR e⁺e⁻ → K⁺K⁻γ
 0.197 ± 0.035 ± 0.005 66 ²LEES 15J BABR e⁺e⁻ → K⁺K⁻γ
 0.35 ± 0.14 ± 0.03 11 ³LEES 13Q BABR e⁺e⁻ → K⁺K⁻γ

¹sin φ > 0.
²sin φ < 0.
³Interference with non-resonant K⁺K⁻ production not taken into account.

$\Gamma(K^+K^-\pi^+) \times \Gamma(e^+e^-)/\Gamma_{total}$ $\Gamma_{60}\Gamma_7/\Gamma$

VALUE (eV)	EVTs	DOCUMENT ID	TECN	COMMENT
1.92 ± 0.30 ± 0.06	133	LEES	12F BABR	10.6 e ⁺ e ⁻ → π ⁺ π ⁻ K ⁺ K ⁻ γ

• • • We do not use the following data for averages, fits, limits, etc. • • •
 2.56 ± 0.42 ± 0.16 85 ¹AUBERT 07AK BABR 10.6 e⁺e⁻ → π⁺π⁻K⁺K⁻γ

¹Superseded by LEES 12F.

$\Gamma(K_S^0 K_L^0 \pi^0) \times \Gamma(e^+e^-)/\Gamma_{total}$ $\Gamma_{64}\Gamma_7/\Gamma$

VALUE (eV)	CL%	EVTs	DOCUMENT ID	TECN	COMMENT
<0.7	90	8	LEES	17A BABR	e ⁺ e ⁻ → K _S ⁰ K _L ⁰ π ⁰ γ

$\Gamma(K^+K^-\pi^0\pi^0) \times \Gamma(e^+e^-)/\Gamma_{total}$ $\Gamma_{65}\Gamma_7/\Gamma$

VALUE (eV)	EVTs	DOCUMENT ID	TECN	COMMENT
0.60 ± 0.31 ± 0.03	17	LEES	12F BABR	10.6 e ⁺ e ⁻ → π ⁰ π ⁰ K ⁺ K ⁻ γ

Meson Particle Listings

$\psi(2S)$

$\Gamma(K^+K^-\pi^+\pi^-\pi^0) \times \Gamma(e^+e^-)/\Gamma_{total}$					$\Gamma_{66}\Gamma_7/\Gamma$
VALUE (eV)	EVTS	DOCUMENT ID	TECN	COMMENT	
4.4 ± 1.3 ± 0.3	32	AUBERT	07AU	BABR	10.6 $e^+e^- \rightarrow K^+K^-\pi^+\pi^-\pi^0\gamma$

$\Gamma(K_S^0 K_L^0 \pi^0 \pi^0) \times \Gamma(e^+e^-)/\Gamma_{total}$					$\Gamma_{73}\Gamma_7/\Gamma$
VALUE (eV)	EVTS	DOCUMENT ID	TECN	COMMENT	
2.92 ± 1.27 ± 0.15	14	LEES	17A	BABR	$e^+e^- \rightarrow K_S^0 K_L^0 \pi^0 \pi^0 \gamma$

$\Gamma(K_S^0 K_L^0 \eta) \times \Gamma(e^+e^-)/\Gamma_{total}$					$\Gamma_{74}\Gamma_7/\Gamma$
VALUE (eV)	EVTS	DOCUMENT ID	TECN	COMMENT	
3.14 ± 1.08 ± 0.16	16	LEES	17A	BABR	$e^+e^- \rightarrow K_S^0 K_L^0 \eta \gamma$

$\Gamma(K^+K^-\pi^+\pi^-\eta) \times \Gamma(e^+e^-)/\Gamma_{total}$					$\Gamma_{77}\Gamma_7/\Gamma$
VALUE (eV)	EVTS	DOCUMENT ID	TECN	COMMENT	
3.05 ± 1.80 ± 0.01	7	AUBERT	07AU	BABR	10.6 $e^+e^- \rightarrow K^+K^-\pi^+\pi^-\eta\gamma$

¹ AUBERT 07AU reports $[\Gamma(\psi(2S) \rightarrow K^+K^-\pi^+\pi^-\eta) \times \Gamma(\psi(2S) \rightarrow e^+e^-)]/\Gamma_{total} \times [B(\eta \rightarrow 2\gamma)] = 1.2 \pm 0.7 \pm 0.1$ eV which we divide by our best value $B(\eta \rightarrow 2\gamma) = (39.36 \pm 0.18) \times 10^{-2}$. Our first error is their experiment's error and our second error is the systematic error from using our best value.

$\Gamma(K^+K^-2(\pi^+\pi^-)) \times \Gamma(e^+e^-)/\Gamma_{total}$					$\Gamma_{78}\Gamma_7/\Gamma$
VALUE (eV)	EVTS	DOCUMENT ID	TECN	COMMENT	
4.4 ± 2.1 ± 0.3	26	AUBERT	06D	BABR	10.6 $e^+e^- \rightarrow K^+K^-2(\pi^+\pi^-)\gamma$

$\Gamma(2(K^+K^-)) \times \Gamma(e^+e^-)/\Gamma_{total}$					$\Gamma_{81}\Gamma_7/\Gamma$
VALUE (eV)	EVTS	DOCUMENT ID	TECN	COMMENT	
0.22 ± 0.10 ± 0.02	13	LEES	12F	BABR	10.6 $e^+e^- \rightarrow K^+K^-K^+K^-\gamma$

$\Gamma(\rho\bar{\rho}) \times \Gamma(e^+e^-)/\Gamma_{total}$					$\Gamma_{101}\Gamma_7/\Gamma$
VALUE (eV)	EVTS	DOCUMENT ID	TECN	COMMENT	
0.686 ± 0.019 OUR FIT					

0.63 ± 0.05 OUR AVERAGE Error includes scale factor of 1.2.
 0.67 ± 0.12 ± 0.02 43 ¹ LEES 130 BABR $e^+e^- \rightarrow \rho\bar{\rho}\gamma$
 0.74 ± 0.07 ± 0.04 142 ² LEES 13V BABR $e^+e^- \rightarrow \rho\bar{\rho}\gamma$
 0.579 ± 0.038 ± 0.036 2.7k ANDREOTTI 07 E835 $\rho\bar{\rho} \rightarrow e^+e^-, J/\psi X$
 ••• We do not use the following data for averages, fits, limits, etc. •••
 0.70 ± 0.17 ± 0.03 22 ³ AUBERT 06B BABR $e^+e^- \rightarrow \rho\bar{\rho}\gamma$

¹ ISR photon reconstructed in the detector
² ISR photon undetected
³ Superseded by LEES 130

$\Gamma(\Lambda\bar{\Lambda}) \times \Gamma(e^+e^-)/\Gamma_{total}$					$\Gamma_{124}\Gamma_7/\Gamma$
VALUE (eV)	EVTS	DOCUMENT ID	TECN	COMMENT	
1.5 ± 0.4 ± 0.1		AUBERT	07BD	BABR	10.6 $e^+e^- \rightarrow \Lambda\bar{\Lambda}\gamma$

$\psi(2S)$ BRANCHING RATIOS

$\Gamma(\text{hadrons})/\Gamma_{total}$					Γ_1/Γ
VALUE	EVTS	DOCUMENT ID	TECN	COMMENT	
0.9785 ± 0.0013 OUR AVERAGE					
0.9779 ± 0.0015		¹ BAI	02B	BES2	e^+e^-
0.981 ± 0.003		¹ LUTH	75	MRK1	e^+e^-

¹ Includes cascade decay into $J/\psi(1S)$.

$\Gamma(\text{virtual } \gamma \rightarrow \text{hadrons})/\Gamma_{total}$					Γ_2/Γ
VALUE	EVTS	DOCUMENT ID	TECN	COMMENT	
0.0173 ± 0.0014 OUR AVERAGE					
0.0166 ± 0.0010		^{1,2} SETH	04	RVUE	e^+e^-
0.0199 ± 0.0019		¹ BAI	02B	BES2	e^+e^-

••• We do not use the following data for averages, fits, limits, etc. •••
 0.029 ± 0.004 ¹ LUTH 75 MRK1 e^+e^-
¹ Included in $\Gamma(\text{hadrons})/\Gamma_{total}$.
² Using $B(\psi(2S) \rightarrow \ell^+\ell^-) = (0.73 \pm 0.04)\%$ from RPP-2002 and $R = 2.28 \pm 0.04$ determined by a fit to data from BAI 00 and BAI 02c.

$\Gamma(gg)/\Gamma_{total}$					Γ_3/Γ
VALUE (units 10^{-2})	EVTS	DOCUMENT ID	TECN	COMMENT	
10.58 ± 1.62	2.9 M	¹ LIBBY	09	CLEO	$\psi(2S) \rightarrow \text{hadrons}$

¹ Calculated using $\Gamma(\gamma gg)/\Gamma(gg) = 0.097 \pm 0.026 \pm 0.016$ from LIBBY 09, $B(\psi(2S) \rightarrow X J/\psi)$ relative and absolute branching fractions from MENDEZ 08, $B(\psi(2S) \rightarrow \gamma \eta_c)$ from MITCHELL 09, and $B(\psi(2S) \rightarrow \text{virtual } \gamma \rightarrow \text{hadrons})$, $B(\psi(2S) \rightarrow \gamma \chi_{cJ})$, and $B(\psi(2S) \rightarrow \ell^+\ell^-)$ from PDG 08. The statistical error is negligible and the systematic error is largely uncorrelated with that of $\Gamma(\gamma gg)/\Gamma_{total}$ LIBBY 09 measurement.

$\Gamma(\gamma gg)/\Gamma_{total}$					Γ_4/Γ
VALUE (units 10^{-2})	EVTS	DOCUMENT ID	TECN	COMMENT	
1.025 ± 0.288	200 k	¹ LIBBY	09	CLEO	$\psi(2S) \rightarrow \gamma + \text{hadrons}$

¹ Calculated using $\Gamma(\gamma gg)/\Gamma(gg) = 0.097 \pm 0.026 \pm 0.016$ from LIBBY 09. The statistical error is negligible and the systematic error is largely uncorrelated with that of $\Gamma(gg)/\Gamma_{total}$ LIBBY 09 measurement.

$\Gamma(\gamma gg)/\Gamma(gg)$					Γ_4/Γ_3
VALUE (units 10^{-2})	EVTS	DOCUMENT ID	TECN	COMMENT	
9.7 ± 2.6 ± 1.6	2.9 M	LIBBY	09	CLEO	$\psi(2S) \rightarrow (\gamma +) \text{hadrons}$

$\Gamma(\text{light hadrons})/\Gamma_{total}$					Γ_5/Γ
VALUE	EVTS	DOCUMENT ID	TECN	COMMENT	
0.154 ± 0.015		¹ MENDEZ	08	CLEO	$e^+e^- \rightarrow \psi(2S)$

••• We do not use the following data for averages, fits, limits, etc. •••
 0.169 ± 0.026 ² ADAM 05A CLEO $e^+e^- \rightarrow \psi(2S)$
¹ Uses $B(\psi(2S) \rightarrow J/\psi X)$ from MENDEZ 08 and other branching fractions from PDG 07.
² Uses $B(J/\psi X)$ from ADAM 05A, $B(\chi_{cJ}\gamma)$, $B(\eta_c\gamma)$ from ATHAR 04 and $B(\ell^+\ell^-)$ from PDG 04. Superseded by MENDEZ 08.

$\Gamma(e^+e^-)/\Gamma_{total}$					Γ_7/Γ
VALUE (units 10^{-4})	EVTS	DOCUMENT ID	TECN	COMMENT	
79.3 ± 1.7 OUR FIT					

••• We do not use the following data for averages, fits, limits, etc. •••
 88 ± 13 ¹ FELDMAN 77 RVUE e^+e^-
¹ From an overall fit assuming equal partial widths for e^+e^- and $\mu^+\mu^-$. For a measurement of the ratio see the entry $\Gamma(\mu^+\mu^-)/\Gamma(e^+e^-)$ below. Includes LUTH 75, HILGER 75, BURMESTER 77.

$\Gamma(\mu^+\mu^-)/\Gamma_{total}$					Γ_8/Γ
VALUE (units 10^{-4})	EVTS	DOCUMENT ID	TECN	COMMENT	
80 ± 6 OUR FIT					

$\Gamma(\mu^+\mu^-)/\Gamma(e^+e^-)$					Γ_8/Γ_7
VALUE	EVTS	DOCUMENT ID	TECN	COMMENT	
1.00 ± 0.08 OUR FIT					

$\Gamma(\tau^+\tau^-)/\Gamma_{total}$					Γ_9/Γ
VALUE (units 10^{-4})	EVTS	DOCUMENT ID	TECN	COMMENT	
31 ± 4 OUR FIT					

30.8 ± 2.1 ± 3.8 ¹ ABLIKIM 06w BES $e^+e^- \rightarrow \psi(2S)$
¹ Computed using PDG 02 value of $B(\psi(2S) \rightarrow \text{hadrons}) = 0.9810 \pm 0.0030$ to estimate the total number of $\psi(2S)$ events.

DECAYS INTO $J/\psi(1S)$ AND ANYTHING

$\Gamma(J/\psi(1S) \text{ anything})/\Gamma_{total}$					$\Gamma_{10}/\Gamma = (\Gamma_{12} + \Gamma_{13} + \Gamma_{14} + 0.343\Gamma_{163} + 0.190\Gamma_{164})/\Gamma$
VALUE	EVTS	DOCUMENT ID	TECN	COMMENT	
0.614 ± 0.006 OUR FIT					

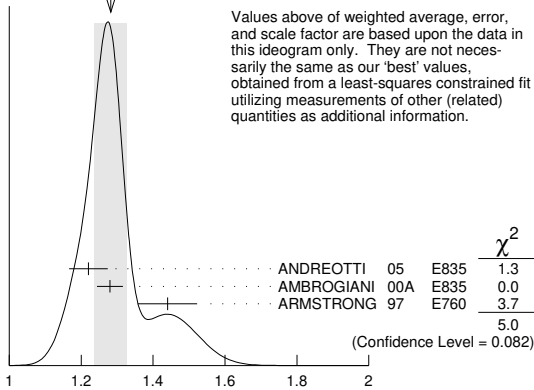
0.55 ± 0.07 OUR AVERAGE
 0.51 ± 0.12 BRANDELIK 79c DASP $e^+e^- \rightarrow \mu^+\mu^-X$
 0.57 ± 0.08 ABRAMS 75B MRK1 $e^+e^- \rightarrow \mu^+\mu^-X$
 ••• We do not use the following data for averages, fits, limits, etc. •••
 0.644 ± 0.006 ± 0.016 ¹ ABLIKIM 21z BES3 $e^+e^- \rightarrow \ell^+\ell^-X$
 0.6254 ± 0.0016 ± 0.0155 1.1M ² MENDEZ 08 CLEO $\psi(2S) \rightarrow \ell^+\ell^-X$
 0.5950 ± 0.0015 ± 0.0190 151k ADAM 05A CLEO Repl. by MENDEZ 08

¹ From a fit to the $e^+e^- \rightarrow J/\psi X$ cross section between 3.645 and 3.891 GeV, with $\Gamma(\text{ee})$ and Γ fixed to the PDG 20 values of the cross particle fit which are correlated to "OUR FIT" value for $B(\psi(2S) \rightarrow J/\psi X)$.
² Not independent from other measurements of MENDEZ 08.

$\Gamma(e^+e^-)/\Gamma(J/\psi(1S) \text{ anything})$					Γ_7/Γ_{10}
VALUE (units 10^{-2})	EVTS	DOCUMENT ID	TECN	COMMENT	
1.291 ± 0.026 OUR FIT					

1.28 ± 0.04 OUR AVERAGE Error includes scale factor of 1.6. See the ideogram below.
 1.22 ± 0.02 ± 0.05 5097 ± 73 ¹ ANDREOTTI 05 E835 $\rho\bar{\rho} \rightarrow \psi(2S) \rightarrow e^+e^-$
 1.28 ± 0.03 ± 0.02 ¹ AMBROGIANI 00a E835 $\rho\bar{\rho} \rightarrow \psi(2S)$
 1.44 ± 0.08 ± 0.02 ¹ ARMSTRONG 97 E760 $\bar{p}p \rightarrow \psi(2S)$

WEIGHTED AVERAGE
 1.28±0.04 (Error scaled by 1.6)



Values above of weighted average, error, and scale factor are based upon the data in this ideogram only. They are not necessarily the same as our 'best' values, obtained from a least-squares constrained fit utilizing measurements of other (related) quantities as additional information.

$\Gamma(e^+e^-)/\Gamma(J/\psi(1S) \text{ anything})$ Γ_7/Γ_{10}
 (units 10^{-2})

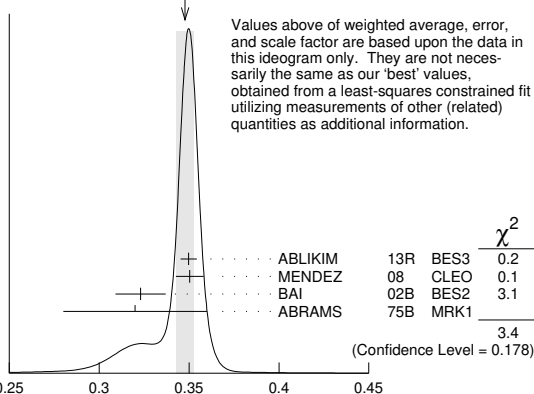
¹ Using $B(J/\psi(1S) \rightarrow e^+e^-) = 0.0593 \pm 0.0010$.

VALUE	DOCUMENT ID	TECN	COMMENT	Γ_8/Γ_{10}
0.0130 ± 0.0010 OUR FIT				
0.014 ± 0.003	HILGER	75	SPEC e^+e^-	

VALUE	DOCUMENT ID	Γ_{11}/Γ
0.2538 ± 0.0032 OUR FIT		

VALUE	DOCUMENT ID	TECN	COMMENT	Γ_{12}/Γ
0.3468 ± 0.0030 OUR FIT				
0.348 ± 0.005 OUR AVERAGE			Error includes scale factor of 1.3. See the ideogram below.	
0.3498 ± 0.0002 ± 0.0045	20M	ABLIKIM	13R BES3 $\psi(2S) \rightarrow J/\psi \pi^+ \pi^-$	
0.3504 ± 0.0007 ± 0.0077	565k	MENDEZ	08 CLEO $\psi(2S) \rightarrow \ell^+ \ell^- \pi^+ \pi^-$	
0.323 ± 0.014		BAI	02B BES2 e^+e^-	
0.32 ± 0.04		ABRAMS	75B MRK1 $e^+e^- \rightarrow J/\psi \pi^+ \pi^-$	
0.3354 ± 0.0014 ± 0.0110	60k	¹ ADAM	05A CLEO Repl. by MENDEZ 08	

WEIGHTED AVERAGE
 0.348±0.005 (Error scaled by 1.3)



Values above of weighted average, error, and scale factor are based upon the data in this ideogram only. They are not necessarily the same as our 'best' values, obtained from a least-squares constrained fit utilizing measurements of other (related) quantities as additional information.

$\Gamma(J/\psi(1S) \pi^+ \pi^-)/\Gamma_{total}$

¹ Not independent from other values reported by ADAM 05A.

VALUE	DOCUMENT ID	TECN	COMMENT	Γ_7/Γ_{12}
0.0229 ± 0.0005 OUR FIT				
0.0252 ± 0.0028 ± 0.0011	¹ AUBERT	02B	BABR e^+e^-	

¹ Using $B(J/\psi(1S) \rightarrow e^+e^-) = 0.0593 \pm 0.0010$.

VALUE	DOCUMENT ID	TECN	COMMENT	Γ_8/Γ_{12}
0.0230 ± 0.0017 OUR FIT				
0.0228 ± 0.0018 OUR AVERAGE				
0.0230 ± 0.0020 ± 0.0012	¹ AAIJ	16Y	LHCB $\Lambda_b^0 \rightarrow \psi(2S) X$	
0.0216 ± 0.0026 ± 0.0014	² AUBERT	02B	BABR e^+e^-	
0.0327 ± 0.0077 ± 0.0072	² GRIBUSHIN	96	FMPS 515 $\pi^- \text{Be} \rightarrow 2\mu X$	

¹ Using $B(J/\psi(1S) \rightarrow \mu^+ \mu^-) = (5.961 \pm 0.033) \times 10^{-2}$.

² Using $B(J/\psi(1S) \rightarrow \mu^+ \mu^-) = (5.88 \pm 0.10) \times 10^{-2}$.

$\Gamma(\tau^+ \tau^-)/\Gamma(J/\psi(1S) \pi^+ \pi^-)$ Γ_9/Γ_{12}

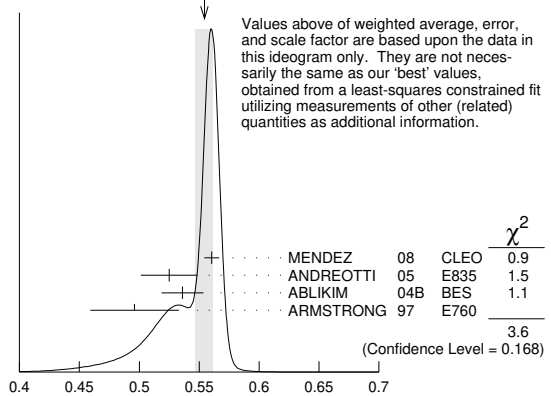
VALUE (units 10^{-3})	DOCUMENT ID	TECN	COMMENT
8.8 ± 1.1 OUR FIT			
8.73 ± 1.39 ± 1.57	BAI	02	BES e^+e^-

$\Gamma(J/\psi(1S) \pi^+ \pi^-)/\Gamma(J/\psi(1S) \text{ anything})$ Γ_{12}/Γ_{10}

VALUE	EVTs	DOCUMENT ID	TECN	COMMENT
0.5645 ± 0.0026 OUR FIT				
0.554 ± 0.008 OUR AVERAGE				Error includes scale factor of 1.3. See the ideogram below.
0.5604 ± 0.0009 ± 0.0062	565k	MENDEZ	08	CLEO $\psi(2S) \rightarrow \ell^+ \ell^- \pi^+ \pi^-$
0.525 ± 0.009 ± 0.022	4k	ANDREOTTI	05	E835 $\psi(2S) \rightarrow J/\psi X$
0.536 ± 0.007 ± 0.016	20k	^{1,2} ABLIKIM	04B	BES $\psi(2S) \rightarrow J/\psi X$
0.496 ± 0.037		ARMSTRONG	97	E760 $\bar{p}p \rightarrow \psi(2S)$
0.5637 ± 0.0027 ± 0.0046	60k	ADAM	05A	CLEO Repl. by MENDEZ 08

• • • We do not use the following data for averages, fits, limits, etc. • • •

WEIGHTED AVERAGE
 0.554±0.008 (Error scaled by 1.3)



Values above of weighted average, error, and scale factor are based upon the data in this ideogram only. They are not necessarily the same as our 'best' values, obtained from a least-squares constrained fit utilizing measurements of other (related) quantities as additional information.

$\Gamma(J/\psi(1S) \pi^+ \pi^-)/\Gamma(J/\psi(1S) \text{ anything})$

¹ From a fit to the J/ψ recoil mass spectra.

² ABLIKIM 04B quotes $B(\psi(2S) \rightarrow J/\psi X) / B(\psi(2S) \rightarrow J/\psi \pi^+ \pi^-)$.

$\Gamma(J/\psi(1S) \text{ neutrals})/\Gamma(J/\psi(1S) \pi^+ \pi^-)$ $\Gamma_{11}/\Gamma_{12} = (0.9761\Gamma_{13} + 0.719\Gamma_{14} + 0.343\Gamma_{163} + 0.190\Gamma_{164})/\Gamma_{12}$

VALUE	DOCUMENT ID	TECN	COMMENT
0.732 ± 0.008 OUR FIT			
0.73 ± 0.09	TANENBAUM	76	MRK1 e^+e^-

$\Gamma(J/\psi(1S) \pi^0 \pi^0)/\Gamma_{total}$ Γ_{13}/Γ

VALUE	EVTs	DOCUMENT ID	TECN	COMMENT
0.1824 ± 0.0031 OUR FIT				
0.1769 ± 0.0008 ± 0.0053	61k	¹ MENDEZ	08	CLEO $\psi(2S) \rightarrow \ell^+ \ell^- 2\pi^0$
0.1652 ± 0.0014 ± 0.0058	13.4k	² ADAM	05A	CLEO Repl. by MENDEZ 08

¹ Not independent from other measurements of MENDEZ 08.

² Not independent from other values reported by ADAM 05A.

$\Gamma(J/\psi(1S) \pi^0 \pi^0)/\Gamma(J/\psi(1S) \text{ anything})$ Γ_{13}/Γ_{10}

VALUE	EVTs	DOCUMENT ID	TECN	COMMENT
0.2968 ± 0.0031 OUR FIT				
0.320 ± 0.012 OUR AVERAGE				
0.300 ± 0.008 ± 0.022	1655 ± 44	ANDREOTTI	05	E835 $\psi(2S) \rightarrow J/\psi X$
0.328 ± 0.013 ± 0.008		AMBROGIANI	00A	E835 $p\bar{p} \rightarrow \psi(2S)$
0.323 ± 0.033		ARMSTRONG	97	E760 $\bar{p}p \rightarrow \psi(2S)$
0.2829 ± 0.0012 ± 0.0056	61k	MENDEZ	08	CLEO $\psi(2S) \rightarrow \ell^+ \ell^- 2\pi^0$
0.2776 ± 0.0025 ± 0.0043	13.4k	ADAM	05A	CLEO Repl. by MENDEZ 08

$\Gamma(J/\psi(1S) \pi^0 \pi^0)/\Gamma(J/\psi(1S) \pi^+ \pi^-)$ Γ_{13}/Γ_{12}

VALUE	EVTs	DOCUMENT ID	TECN	COMMENT
0.526 ± 0.008 OUR FIT				
0.513 ± 0.022 OUR AVERAGE				Error includes scale factor of 2.2.
0.5047 ± 0.0022 ± 0.0102	61k	MENDEZ	08	CLEO $\psi(2S) \rightarrow \ell^+ \ell^- 2\pi^0$
0.570 ± 0.009 ± 0.026	14k	¹ ABLIKIM	04B	BES $\psi(2S) \rightarrow J/\psi X$
0.4924 ± 0.0047 ± 0.0086	73k	^{2,3} ADAM	05A	CLEO Repl. by MENDEZ 08
0.571 ± 0.018 ± 0.044		⁴ ANDREOTTI	05	E835 $\psi(2S) \rightarrow J/\psi X$
0.53 ± 0.06		TANENBAUM	76	MRK1 e^+e^-
0.64 ± 0.15		⁵ HILGER	75	SPEC e^+e^-

¹ From a fit to the J/ψ recoil mass spectra.

² Not independent from other values reported by ADAM 05A.

³ Using 13,217 $J/\psi \pi^0 \pi^0$ and 60,010 $J/\psi \pi^+ \pi^-$ events.

⁴ Not independent from other values reported by ANDREOTTI 05.

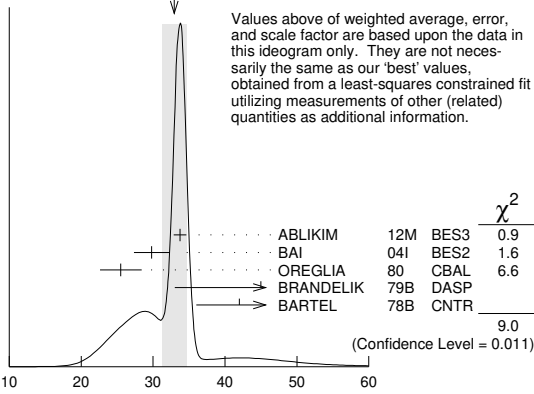
⁵ Ignoring the $J/\psi(1S) \eta$ and $J/\psi(1S) \gamma\gamma$ decays.

Meson Particle Listings

$\psi(2S)$

$\Gamma(J/\psi(1S)\eta)/\Gamma_{total}$			Γ_{14}/Γ		
VALUE (units 10^{-3})	EVTs	DOCUMENT ID	TECN	COMMENT	
33.7 ± 0.5 OUR FIT					
32.9 ± 1.7 OUR AVERAGE				Error includes scale factor of 2.1. See the ideogram below.	
33.75 ± 0.17 ± 0.86	68.2k	ABLIKIM 12M	BES3	$e^+e^- \rightarrow \ell^+\ell^-2\gamma$	
29.8 ± 0.9 ± 2.3	5.7k	BAI 04I	BES2	$\psi(2S) \rightarrow J/\psi\gamma\gamma$	
25.5 ± 2.9	386	¹ OREGLIA 80	CBAL	$e^+e^- \rightarrow J/\psi2\gamma$	
45 ± 12	17	² BRANDELIK 79B	DASP	$e^+e^- \rightarrow J/\psi2\gamma$	
42 ± 6	164	² BARTEL 78B	CNTR	e^+e^-	
••• We do not use the following data for averages, fits, limits, etc. •••					
34.3 ± 0.4 ± 0.9	18.4k	³ MENDEZ 08	CLEO	$\psi(2S) \rightarrow \ell^+\ell^-\eta$	
32.5 ± 0.6 ± 1.1	2.8k	⁴ ADAM 05A	CLEO	Repl. by MENDEZ 08	
43 ± 8	44	TANENBAUM 76	MRK1	e^+e^-	

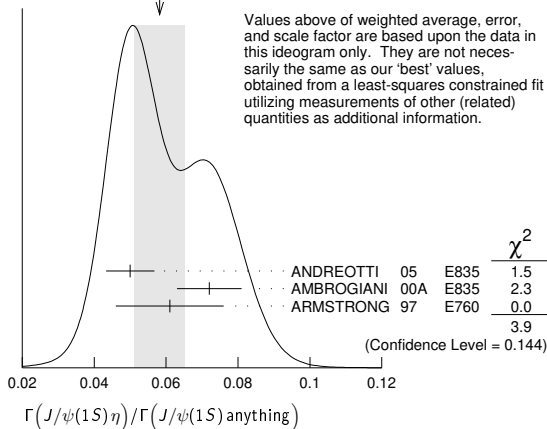
WEIGHTED AVERAGE
32.9±1.7 (Error scaled by 2.1)



- ¹ Recalculated by us using $B(J/\psi(1S) \rightarrow \ell^+\ell^-) = 0.1181 \pm 0.0020$.
- ² Recalculated by us using $B(J/\psi(1S) \rightarrow \mu^+\mu^-) = 0.0588 \pm 0.0010$.
- ³ Not independent from other measurements of MENDEZ 08.
- ⁴ Not independent from other values reported by ADAM 05A.

$\Gamma(J/\psi(1S)\eta)/\Gamma(J/\psi(1S)\text{anything})$			Γ_{14}/Γ_{10}		
VALUE	EVTs	DOCUMENT ID	TECN	COMMENT	
0.0549 ± 0.0008 OUR FIT					
0.058 ± 0.007 OUR AVERAGE				Error includes scale factor of 1.4. See the ideogram below.	
0.050 ± 0.006 ± 0.003	298 ± 20	ANDREOTTI 05	E835	$\psi(2S) \rightarrow J/\psi X$	
0.072 ± 0.009		AMBROGIANI 00A	E835	$p\bar{p} \rightarrow \psi(2S)$	
0.061 ± 0.015		ARMSTRONG 97	E760	$p\bar{p} \rightarrow \psi(2S)$	
••• We do not use the following data for averages, fits, limits, etc. •••					
0.0549 ± 0.0006 ± 0.0009	18.4k	¹ MENDEZ 08	CLEO	$\psi(2S) \rightarrow \ell^+\ell^-\eta$	
0.0546 ± 0.0010 ± 0.0007	2.8k	ADAM 05A	CLEO	Repl. by MENDEZ 08	

WEIGHTED AVERAGE
0.058±0.007 (Error scaled by 1.4)



- ¹ Not independent from other measurements of MENDEZ 08.

$\Gamma(J/\psi(1S)\eta)/\Gamma(J/\psi(1S)\pi^+\pi^-)$			Γ_{14}/Γ_{12}		
VALUE	EVTs	DOCUMENT ID	TECN	COMMENT	
0.0972 ± 0.0014 OUR FIT					
0.0979 ± 0.0018 OUR AVERAGE					
0.0979 ± 0.0010 ± 0.0015	18.4k	MENDEZ 08	CLEO	$\psi(2S) \rightarrow \ell^+\ell^-\eta$	
0.098 ± 0.005 ± 0.010	2k	¹ ABLIKIM 04B	BES	$\psi(2S) \rightarrow J/\psi X$	

0.091 ± 0.021		² HIMEL 80	MRK2	$e^+e^- \rightarrow \psi(2S) X$	
••• We do not use the following data for averages, fits, limits, etc. •••					
0.0968 ± 0.0019 ± 0.0013	2.8k	³ ADAM 05A	CLEO	Repl. by MENDEZ 08	
0.095 ± 0.007 ± 0.007		⁴ ANDREOTTI 05	E835	$\psi(2S) \rightarrow J/\psi X$	

- ¹ From a fit to the J/ψ recoil mass spectra.
- ² The value for $B(\psi(2S) \rightarrow J/\psi(1S)\eta)$ reported in HIMEL 80 is derived using $B(\psi(2S) \rightarrow J/\psi(1S)\pi^+\pi^-) = (33 \pm 3)\%$ and $B(J/\psi(1S) \rightarrow \ell^+\ell^-) = 0.138 \pm 0.018$. Calculated by us using $B(J/\psi(1S) \rightarrow \ell^+\ell^-) = (0.1181 \pm 0.0020)$.
- ³ Not independent from other values reported by ADAM 05A.
- ⁴ Not independent from other values reported by ANDREOTTI 05.

$\Gamma(J/\psi(1S)\pi^0)/\Gamma_{total}$			Γ_{15}/Γ		
VALUE (units 10^{-4})	EVTs	DOCUMENT ID	TECN	COMMENT	
12.68 ± 0.32 OUR AVERAGE					
12.6 ± 0.2 ± 0.3	4.1k	ABLIKIM 12M	BES3	$e^+e^- \rightarrow \ell^+\ell^-2\gamma$	
13.3 ± 0.8 ± 0.3	530	MENDEZ 08	CLEO	$\psi(2S) \rightarrow \ell^+\ell^-2\gamma$	
14.3 ± 1.4 ± 1.2	280	BAI 04I	BES2	$\psi(2S) \rightarrow J/\psi\gamma\gamma$	
14 ± 6	7	HIMEL 80	MRK2	e^+e^-	
9 ± 2 ± 1	23	¹ OREGLIA 80	CBAL	$\psi(2S) \rightarrow J/\psi2\gamma$	
••• We do not use the following data for averages, fits, limits, etc. •••					
13 ± 1 ± 1	88	ADAM 05A	CLEO	Repl. by MENDEZ 08	

- ¹ Recalculated by us using $B(J/\psi(1S) \rightarrow \ell^+\ell^-) = 0.1181 \pm 0.0020$.

$\Gamma(J/\psi(1S)\pi^0)/\Gamma(J/\psi(1S)\text{anything})$			$\Gamma_{15}/\Gamma_{10} = \Gamma_{15}/(\Gamma_{12} + \Gamma_{13} + \Gamma_{14} + 0.343\Gamma_{163} + 0.190\Gamma_{164})$		
VALUE (units 10^{-2})	EVTs	DOCUMENT ID	TECN	COMMENT	
0.213 ± 0.012 ± 0.003	527	¹ MENDEZ 08	CLEO	$e^+e^- \rightarrow J/\psi\gamma\gamma$	
0.22 ± 0.02 ± 0.01		² ADAM 05A	CLEO	$e^+e^- \rightarrow \psi(2S) \rightarrow J/\psi\gamma\gamma$	

- ¹ Not independent from other values reported by MENDEZ 08. Supersedes ADAM 05A.
- ² Not independent from other values reported by ADAM 05A.

$\Gamma(J/\psi(1S)\pi^0)/\Gamma(J/\psi(1S)\pi^+\pi^-)$			Γ_{15}/Γ_{12}		
VALUE (units 10^{-2})	EVTs	DOCUMENT ID	TECN	COMMENT	
0.380 ± 0.022 ± 0.005	527	¹ MENDEZ 08	CLEO	$e^+e^- \rightarrow J/\psi\gamma\gamma$	
0.39 ± 0.04 ± 0.01		² ADAM 05A	CLEO	$e^+e^- \rightarrow \psi(2S) \rightarrow J/\psi\gamma\gamma$	

- ¹ Not independent from other values reported by MENDEZ 08. Supersedes ADAM 05A.
- ² Not independent from other values reported by ADAM 05A.

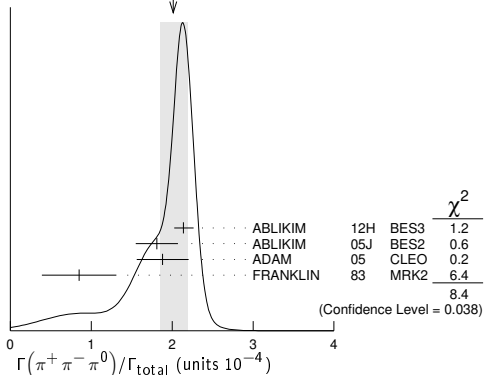
HADRONIC DECAYS

$\Gamma(\pi^+\pi^-)/\Gamma_{total}$			Γ_{16}/Γ		
VALUE (units 10^{-5})	CL%	EVTs	DOCUMENT ID	TECN	COMMENT
0.78 ± 0.26 OUR AVERAGE					
0.76 ± 0.25 ± 0.06		30	¹ METREVELI 12		$\psi(2S) \rightarrow \pi^+\pi^-$
8 ± 5			BRANDELIK 79c	DASP	e^+e^-
••• We do not use the following data for averages, fits, limits, etc. •••					
<2.1		90	DOBBS 06A	CLEO	$e^+e^- \rightarrow \psi(2S)$
<5		90	FELDMAN 77	MRK1	e^+e^-

- ¹ Obtained by analyzing CLEO-c data but not authored by the CLEO Collaboration. Using $\psi(3770) \rightarrow \pi^+\pi^-$ for continuum subtraction.

$\Gamma(\pi^+\pi^-\pi^0)/\Gamma_{total}$			Γ_{17}/Γ		
VALUE (units 10^{-4})	EVTs	DOCUMENT ID	TECN	COMMENT	
2.01 ± 0.17 OUR AVERAGE				Error includes scale factor of 1.7. See the ideogram below.	
2.14 ± 0.03 ± 0.12	7k	¹ ABLIKIM 12H	BES3	$e^+e^- \rightarrow \psi(2S)$	
1.81 ± 0.18 ± 0.19	260 ± 19	² ABLIKIM 05J	BES2	$e^+e^- \rightarrow \psi(2S)$	
1.88 ^{+0.16} _{-0.15} ± 0.28	194	ADAM 05	CLEO	$e^+e^- \rightarrow \psi(2S)$	
0.85 ± 0.46	4	FRANKLIN 83	MRK2	$e^+e^- \rightarrow \text{hadrons}$	

WEIGHTED AVERAGE
2.01±0.17 (Error scaled by 1.7)



See key on page 1127

Meson Particle Listings

$\psi(2S)$

¹ From $\psi(2S) \rightarrow \pi^+\pi^-\pi^0$ events directly. The quoted systematic error includes a contribution of 4% (added in quadrature) from the uncertainty on the number of $\psi(2S)$ events.

² From a PW analysis of $\psi(2S) \rightarrow \pi^+\pi^-\pi^0$.

$\Gamma(\rho(770)\pi \rightarrow \pi^+\pi^-\pi^0)/\Gamma_{total}$						Γ_{18}/Γ
VALUE (units 10^{-4})	CL%	EVTS	DOCUMENT ID	TECN	COMMENT	
0.32 ± 0.12 OUR AVERAGE			Error includes scale factor of 1.8.			
0.51 ± 0.07 ± 0.11			¹ ABLIKIM	05J BES2	$\psi(2S) \rightarrow \rho(770)\pi \rightarrow \pi^+\pi^-\pi^0$	
0.24 ^{+0.08} _{-0.07} ± 0.02	22		ADAM	05 CLEO	$e^+e^- \rightarrow \psi(2S)$	
• • • We do not use the following data for averages, fits, limits, etc. • • •						
<0.83	90	1	FRANKLIN	83 MRK2	e^+e^-	
<10	90		BARTEL	76 CNTR	e^+e^-	
<10	90		² ABRAMS	75 MRK1	e^+e^-	

¹ From a PW analysis of $\psi(2S) \rightarrow \pi^+\pi^-\pi^0$.

² Final state $\rho^0\pi^0$.

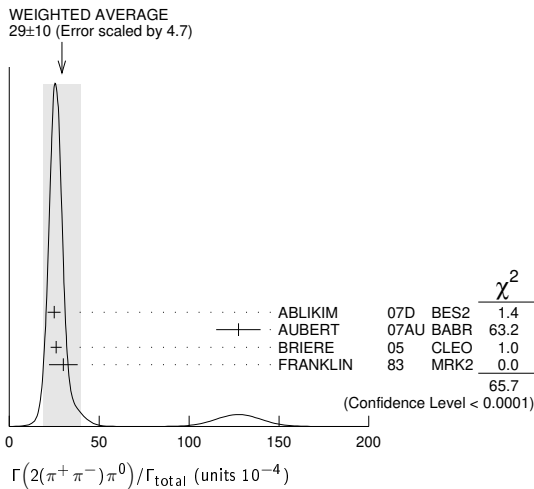
$\Gamma(\rho(2150)\pi \rightarrow \pi^+\pi^-\pi^0)/\Gamma_{total}$						Γ_{19}/Γ
VALUE (units 10^{-4})	DOCUMENT ID	TECN	COMMENT			
1.94 ± 0.25 ± 1.15	¹ ABLIKIM	05J BES2	$\psi(2S) \rightarrow \rho(2150)\pi \rightarrow \pi^+\pi^-\pi^0$			
1.74 ± 0.34						

¹ From a PW analysis of $\psi(2S) \rightarrow \pi^+\pi^-\pi^0$.

$\Gamma(2(\pi^+\pi^-))/\Gamma_{total}$						Γ_{20}/Γ
VALUE (units 10^{-4})	EVTS	DOCUMENT ID	TECN	COMMENT		
2.4 ± 0.6 OUR AVERAGE		Error includes scale factor of 2.2.				
2.2 ± 0.2 ± 0.2	308	BRIERE	05 CLEO	$e^+e^- \rightarrow \psi(2S) \rightarrow 2(\pi^+\pi^-)$		
4.5 ± 1.0		TANENBAUM	78 MRK1	e^+e^-		

$\Gamma(\rho^0\pi^+\pi^-)/\Gamma_{total}$						Γ_{21}/Γ
VALUE (units 10^{-4})	EVTS	DOCUMENT ID	TECN	COMMENT		
2.2 ± 0.6 OUR AVERAGE		Error includes scale factor of 1.4.				
2.0 ± 0.2 ± 0.4	285.5	BRIERE	05 CLEO	$e^+e^- \rightarrow \psi(2S) \rightarrow 2(\pi^+\pi^-)$		
4.2 ± 1.5		TANENBAUM	78 MRK1	e^+e^-		

$\Gamma(2(\pi^+\pi^-\pi^0))/\Gamma_{total}$						Γ_{22}/Γ
VALUE (units 10^{-4})	EVTS	DOCUMENT ID	TECN	COMMENT		
29 ± 10 OUR AVERAGE		Error includes scale factor of 4.7. See the ideogram below.				
24.9 ± 0.7 ± 3.6	2173	ABLIKIM	07D BES2	$e^+e^- \rightarrow \psi(2S)$		
127 ± 12 ± 2	410	¹ AUBERT	07AU BABR	10.6 $e^+e^- \rightarrow 2(\pi^+\pi^-)\pi^0\gamma$		
26.1 ± 0.7 ± 3.0	1703	BRIERE	05 CLEO	$e^+e^- \rightarrow \psi(2S) \rightarrow 2(\pi^+\pi^-)\pi^0$		
30 ± 8	42	FRANKLIN	83 MRK2	e^+e^-		



¹ AUBERT 07AU reports $[\Gamma(\psi(2S) \rightarrow 2(\pi^+\pi^-\pi^0))/\Gamma_{total}] \times [\Gamma(\psi(2S) \rightarrow e^+e^-)] = (297 \pm 22 \pm 18) \times 10^{-4}$ keV which we divide by our best value $\Gamma(\psi(2S) \rightarrow e^+e^-) = 2.33 \pm 0.04$ keV. Our first error is their experiment's error and our second error is the systematic error from using our best value.

$\Gamma(\rho_2(1320))/\Gamma_{total}$						Γ_{23}/Γ
VALUE (units 10^{-4})	CL%	EVTS	DOCUMENT ID	TECN	COMMENT	
2.55 ± 0.73 ± 0.47		112 ± 31	BAI	04C BES2	$\psi(2S) \rightarrow 2(\pi^+\pi^-)\pi^0$	
• • • We do not use the following data for averages, fits, limits, etc. • • •						
<2.3	90		BAI	98J BES	e^+e^-	

$\Gamma(3(\pi^+\pi^-))/\Gamma_{total}$						Γ_{27}/Γ
VALUE (units 10^{-4})	EVTS	DOCUMENT ID	TECN	COMMENT		
3.5 ± 2.0 OUR AVERAGE		Error includes scale factor of 2.8.				
5.45 ± 0.42 ± 0.87	671	ABLIKIM	05H BES2	$e^+e^- \rightarrow \psi(2S) \rightarrow 3(\pi^+\pi^-)$		

1.5 ± 1.0
¹ TANENBAUM 78 MRK1 e^+e^-
¹ Assuming entirely strong decay.

$\Gamma(3(\pi^+\pi^-\pi^0))/\Gamma_{total}$						Γ_{29}/Γ
VALUE (units 10^{-4})	EVTS	DOCUMENT ID	TECN	COMMENT		
35 ± 16	6	FRANKLIN	83 MRK2	$e^+e^- \rightarrow$ hadrons		

$\Gamma(\eta\pi^+\pi^-)/\Gamma_{total}$						Γ_{31}/Γ
VALUE (units 10^{-4})	CL%	DOCUMENT ID	TECN	COMMENT		
<1.6	90	BRIERE	05 CLEO	$e^+e^- \rightarrow \psi(2S) \rightarrow 2(\pi^+\pi^-)\pi^0$		

$\Gamma(\eta\pi^+\pi^-\pi^0)/\Gamma_{total}$						Γ_{32}/Γ
VALUE (units 10^{-4})	EVTS	DOCUMENT ID	TECN	COMMENT		
9.5 ± 0.7 ± 1.5		¹ BRIERE	05 CLEO	$e^+e^- \rightarrow \psi(2S) \rightarrow$ hadr		

• • • We do not use the following data for averages, fits, limits, etc. • • •
10.3 ± 0.8 ± 1.4 201.7 ² BRIERE 05 CLEO $e^+e^- \rightarrow \psi(2S) \rightarrow \eta 3\pi(\eta \rightarrow \gamma\gamma)$
8.1 ± 1.4 ± 1.6 50.0 ² BRIERE 05 CLEO $e^+e^- \rightarrow \psi(2S) \rightarrow \eta 3\pi(\eta \rightarrow 3\pi)$

¹ Average of $\eta \rightarrow \gamma\gamma$ and $\eta \rightarrow 3\pi$.
² Not independent from other values reported by BRIERE 05.

$\Gamma(\rho\eta)/\Gamma_{total}$						Γ_{37}/Γ
VALUE (units 10^{-5})	EVTS	DOCUMENT ID	TECN	COMMENT		
2.2 ± 0.6 OUR AVERAGE		Error includes scale factor of 1.1.				
3.0 ^{+1.1} _{-0.9} ± 0.2	18	ADAM	05 CLEO	$e^+e^- \rightarrow \psi(2S)$		
1.78 ^{+0.67} _{-0.62} ± 0.17	13	ABLIKIM	04L BES	$e^+e^- \rightarrow \psi(2S)$		

$\Gamma(\eta'\pi^+\pi^-\pi^0)/\Gamma_{total}$						Γ_{38}/Γ
VALUE (units 10^{-4})	EVTS	DOCUMENT ID	TECN	COMMENT		
4.5 ± 1.6 ± 1.3	12.8	BRIERE	05 CLEO	$e^+e^- \rightarrow \psi(2S) \rightarrow$ hadr		

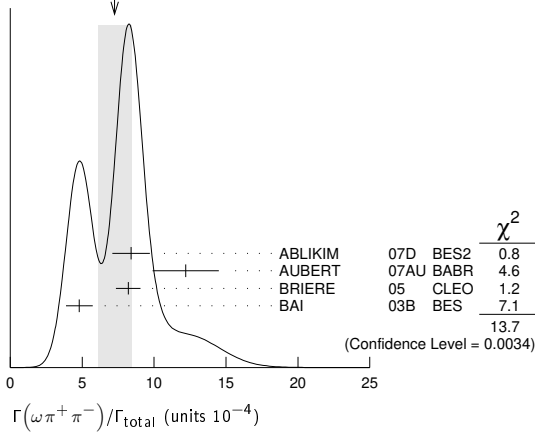
$\Gamma(\eta'\rho)/\Gamma_{total}$						Γ_{39}/Γ
VALUE (units 10^{-5})	EVTS	DOCUMENT ID	TECN	COMMENT		
1.87^{+1.64}_{-1.11} ± 0.33	2	ABLIKIM	04L BES	$e^+e^- \rightarrow \psi(2S)$		
• • • We do not use the following data for averages, fits, limits, etc. • • •						
1.02 ± 0.11 ± 0.24	143	¹ ABLIKIM	17AK BES3	$e^+e^- \rightarrow \psi(2S)$		
0.569 ± 0.128 ± 0.236	80	² ABLIKIM	17AK BES3	$e^+e^- \rightarrow \psi(2S)$		

¹ Destructive-interference solution of a partial wave analysis of the decay $\psi(2S) \rightarrow \pi^+\pi^-\eta'$.
² Constructive-interference solution of a partial wave analysis of the decay $\psi(2S) \rightarrow \pi^+\pi^-\eta'$.

$\Gamma(\omega\pi^0)/\Gamma_{total}$						Γ_{40}/Γ
VALUE (units 10^{-5})	EVTS	DOCUMENT ID	TECN	COMMENT		
2.1 ± 0.6 OUR AVERAGE						
2.5 ^{+1.2} _{-1.0} ± 0.2	14	ADAM	05 CLEO	$e^+e^- \rightarrow \psi(2S)$		
1.87 ^{+0.68} _{-0.62} ± 0.28	14	ABLIKIM	04L BES	$e^+e^- \rightarrow \psi(2S)$		

$\Gamma(\omega\pi^+\pi^-)/\Gamma_{total}$						Γ_{41}/Γ
VALUE (units 10^{-4})	EVTS	DOCUMENT ID	TECN	COMMENT		
7.3 ± 1.2 OUR AVERAGE		Error includes scale factor of 2.1. See the ideogram below.				
8.4 ± 0.5 ± 1.2	386	ABLIKIM	07D BES2	$e^+e^- \rightarrow \psi(2S)$		
12.2 ± 2.2 ± 0.7	37	¹ AUBERT	07AU BABR	10.6 $e^+e^- \rightarrow \omega\pi^+\pi^-\gamma$		
8.2 ± 0.5 ± 0.7	391	BRIERE	05 CLEO	$e^+e^- \rightarrow \psi(2S) \rightarrow 2(\pi^+\pi^-)\pi^0$		
4.8 ± 0.6 ± 0.7	100 ± 22	² BAI	03B BES	$\psi(2S) \rightarrow 2(\pi^+\pi^-)\pi^0$		
¹ AUBERT 07AU quotes $\Gamma_{ee}^{\psi(2S)} \cdot B(\psi(2S) \rightarrow \omega\pi^+\pi^-) \cdot B(\omega \rightarrow 3\pi) = 2.69 \pm 0.73 \pm 0.16$ eV.						
² Normalized to $B(\psi(2S) \rightarrow J/\psi\pi^+\pi^-) = 0.305 \pm 0.016$.						

Meson Particle Listings

 $\psi(2S)$ WEIGHTED AVERAGE
7.3±1.2 (Error scaled by 2.1) $\Gamma(b_1^\pm \pi^\mp)/\Gamma_{total}$ Γ_{43}/Γ

VALUE (units 10^{-4})	EVTS	DOCUMENT ID	TECN	COMMENT
4.0 ± 0.6 OUR AVERAGE		Error includes scale factor of 1.1.		
5.1 ± 0.6 ± 0.8	202	ABLIKIM 07D	BES2	$e^+e^- \rightarrow \psi(2S)$
4.18 ^{+0.43} _{-0.42} ± 0.92	170	ADAM 05	CLEO	$e^+e^- \rightarrow \psi(2S)$
3.2 ± 0.6 ± 0.5	61 ± 11	1,2 BAI 03B	BES	$\psi(2S) \rightarrow 2(\pi^+\pi^-)\pi^0$
• • • We do not use the following data for averages, fits, limits, etc. • • •				
5.2 ± 0.8 ± 1.0		1 BAI 99c	BES	Repl. by BAI 03B

¹ Assuming $B(b_1 \rightarrow \omega\pi) = 1$.
² Normalized to $B(\psi(2S) \rightarrow J/\psi\pi^+\pi^-) = 0.305 \pm 0.016$.

 $\Gamma(\omega f_2(1270))/\Gamma_{total}$ Γ_{44}/Γ

VALUE (units 10^{-4})	CL%	EVTS	DOCUMENT ID	TECN	COMMENT
2.2 ± 0.4 OUR AVERAGE					
2.3 ± 0.5 ± 0.4		57	ABLIKIM 07D	BES2	$e^+e^- \rightarrow \psi(2S)$
2.05 ± 0.41 ± 0.38		62 ± 12	BAI 04c	BES2	$\psi(2S) \rightarrow 2(\pi^+\pi^-)\pi^0$
• • • We do not use the following data for averages, fits, limits, etc. • • •					
<1.5		90	1 BAI 03B	BES	$\psi(2S) \rightarrow 2(\pi^+\pi^-)\pi^0$
<1.7		90	BAI 98J	BES	Repl. by BAI 03B

¹ Normalized to $B(\psi(2S) \rightarrow J/\psi\pi^+\pi^-) = 0.305 \pm 0.016$.

 $\Gamma(b_1^0 \pi^0)/\Gamma_{total}$ Γ_{47}/Γ

VALUE (units 10^{-4})	EVTS	DOCUMENT ID	TECN	COMMENT
2.35^{+0.47}_{-0.42} ± 0.40	45	ADAM 05	CLEO	$e^+e^- \rightarrow \psi(2S)$

 $\Gamma(\omega\eta)/\Gamma_{total}$ Γ_{48}/Γ

VALUE (units 10^{-5})	CL%	DOCUMENT ID	TECN	COMMENT
<1.1	90	ADAM 05	CLEO	$e^+e^- \rightarrow \psi(2S)$
• • • We do not use the following data for averages, fits, limits, etc. • • •				
<3.1	90	ABLIKIM 04K	BES	$e^+e^- \rightarrow \psi(2S)$

 $\Gamma(\omega\eta')/\Gamma_{total}$ Γ_{49}/Γ

VALUE (units 10^{-5})	EVTS	DOCUMENT ID	TECN	COMMENT
3.2^{+2.4}_{-2.0} ± 0.7	4	1 ABLIKIM 04K	BES	$e^+e^- \rightarrow \psi(2S)$

¹ Calculated combining $\eta' \rightarrow \gamma\rho$ and $\eta\pi^+\pi^-$ channels.

 $\Gamma(\phi\pi^0)/\Gamma_{total}$ Γ_{50}/Γ

VALUE (units 10^{-5})	CL%	DOCUMENT ID	TECN	COMMENT
<0.04	90	ABLIKIM 12L	BES3	$e^+e^- \rightarrow \psi(2S)$
• • • We do not use the following data for averages, fits, limits, etc. • • •				
<0.7	90	ADAM 05	CLEO	$e^+e^- \rightarrow \psi(2S)$
<0.4	90	ABLIKIM 04K	BES	$e^+e^- \rightarrow \psi(2S)$

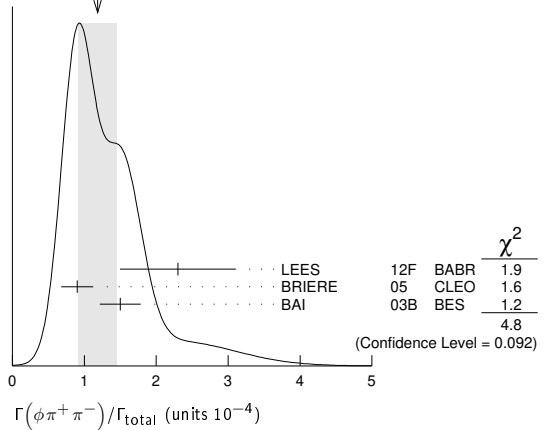
 $\Gamma(\phi\pi^+\pi^-)/\Gamma_{total}$ Γ_{51}/Γ

VALUE (units 10^{-4})	EVTS	DOCUMENT ID	TECN	COMMENT
1.18 ± 0.26 OUR AVERAGE		Error includes scale factor of 1.5. See the ideogram below.		
2.3 ± 0.8 ± 0.1	19 ± 6	LEES 12F	BABR	10.6 $e^+e^- \rightarrow \pi^+\pi^-\pi^+\pi^- K^+K^-\gamma$
0.9 ± 0.2 ± 0.1	47.6	BRIERE 05	CLEO	$e^+e^- \rightarrow \psi(2S) \rightarrow K^+K^-\pi^+\pi^-$
1.5 ± 0.2 ± 0.2	51.5 ± 8.3	1 BAI 03B	BES	$\psi(2S) \rightarrow K^+K^-\pi^+\pi^-$
• • • We do not use the following data for averages, fits, limits, etc. • • •				
2.45 ± 0.96 ± 0.04	10 ± 4	2,3 AUBERT 07AK	BABR	10.6 $e^+e^- \rightarrow \pi^+\pi^-\pi^+\pi^- K^+K^-\gamma$

¹ Normalized to $B(\psi(2S) \rightarrow J/\psi\pi^+\pi^-) = 0.305 \pm 0.016$.

² Superseded by LEES 12F. AUBERT 07AK reports $[\Gamma(\psi(2S) \rightarrow \phi\pi^+\pi^-)/\Gamma_{total}] \times [\Gamma(\psi(2S) \rightarrow e^+e^-)] = (0.57 \pm 0.22 \pm 0.04) \times 10^{-3}$ keV which we divide by our best value $\Gamma(\psi(2S) \rightarrow e^+e^-) = 2.33 \pm 0.04$ keV. Our first error is their experiment's error and our second error is the systematic error from using our best value.

³ Using $B(\phi \rightarrow K^+K^-) = (49.3 \pm 0.6)\%$.

WEIGHTED AVERAGE
1.18±0.26 (Error scaled by 1.5) $\Gamma(\phi f_0(980) \rightarrow \pi^+\pi^-)/\Gamma_{total}$ Γ_{52}/Γ

VALUE (units 10^{-4})	EVTS	DOCUMENT ID	TECN	COMMENT
0.75 ± 0.33 OUR AVERAGE		Error includes scale factor of 1.6.		
1.5 ± 0.5 ± 0.1	12 ± 4	LEES 12F	BABR	10.6 $e^+e^- \rightarrow \pi^+\pi^-\pi^+\pi^- K^+K^-\gamma$
0.6 ± 0.2 ± 0.1	18.4 ± 6.4	1 BAI 03B	BES	$\psi(2S) \rightarrow K^+K^-\pi^+\pi^-$
• • • We do not use the following data for averages, fits, limits, etc. • • •				
1.46 ± 0.71 ± 0.02	6 ± 3	2,3 AUBERT 07AK	BABR	10.6 $e^+e^- \rightarrow \pi^+\pi^-\pi^+\pi^- K^+K^-\gamma$

¹ Normalized to $B(\psi(2S) \rightarrow J/\psi\pi^+\pi^-) = 0.305 \pm 0.016$.

² Superseded by LEES 12F. AUBERT 07AK reports $[\Gamma(\psi(2S) \rightarrow \phi f_0(980) \rightarrow \pi^+\pi^-)/\Gamma_{total}] \times [\Gamma(\psi(2S) \rightarrow e^+e^-)] = (0.34 \pm 0.16 \pm 0.04) \times 10^{-3}$ keV which we divide by our best value $\Gamma(\psi(2S) \rightarrow e^+e^-) = 2.33 \pm 0.04$ keV. Our first error is their experiment's error and our second error is the systematic error from using our best value.

³ Using $B(\phi \rightarrow K^+K^-) = (49.3 \pm 0.6)\%$.

 $\Gamma(\phi\eta)/\Gamma_{total}$ Γ_{53}/Γ

VALUE (units 10^{-5})	EVTS	DOCUMENT ID	TECN	COMMENT
3.10 ± 0.31 OUR AVERAGE				
3.14 ± 0.23 ± 0.23	0.2k	ABLIKIM 12L	BES3	$e^+e^- \rightarrow \psi(2S)$
2.0 ^{+1.5} _{-1.1} ± 0.4	6	ADAM 05	CLEO	$e^+e^- \rightarrow \psi(2S)$
3.3 ± 1.1 ± 0.5	17	ABLIKIM 04K	BES	$e^+e^- \rightarrow \psi(2S)$

 $\Gamma(\eta\phi(2170), \phi(2170) \rightarrow \phi f_0(980), f_0 \rightarrow \pi^+\pi^-)/\Gamma_{total}$ Γ_{54}/Γ

VALUE	CL%	DOCUMENT ID	TECN	COMMENT
<2.2 × 10⁻⁶	90	ABLIKIM 19I	BES3	$e^+e^- \rightarrow \eta\phi f_0(980)$

 $\Gamma(\phi\eta')/\Gamma_{total}$ Γ_{55}/Γ

VALUE (units 10^{-5})	EVTS	DOCUMENT ID	TECN	COMMENT
1.54 ± 0.20 OUR AVERAGE				
1.51 ± 0.16 ± 0.12	201	ABLIKIM 19BA	BES3	$e^+e^- \rightarrow \psi(2S)$
3.1 ± 1.4 ± 0.7	8	1 ABLIKIM 04K	BES	$e^+e^- \rightarrow \psi(2S)$

¹ Calculated combining $\eta' \rightarrow \gamma\rho$ and $\eta\pi^+\pi^-$ channels.

 $\Gamma(\phi f_1(1285))/\Gamma_{total}$ Γ_{56}/Γ

VALUE (units 10^{-5})	EVTS	DOCUMENT ID	TECN	COMMENT
3.0 ± 0.4 ± 1.3	234	1 ABLIKIM 19BA	BES3	$e^+e^- \rightarrow \psi(2S)$

¹ ABLIKIM 19BA reports $[\Gamma(\psi(2S) \rightarrow \phi f_1(1285))/\Gamma_{total}] \times [B(f_1(1285) \rightarrow \eta\pi^+\pi^-)] = (1.03 \pm 0.10 \pm 0.09) \times 10^{-5}$ which we divide by our best value $B(f_1(1285) \rightarrow \eta\pi^+\pi^-) = (35 \pm 15) \times 10^{-2}$. Our first error is their experiment's error and our second error is the systematic error from using our best value.

 $\Gamma(\phi\eta(1405) \rightarrow \phi\pi^+\pi^-)/\Gamma_{total}$ Γ_{57}/Γ

VALUE (units 10^{-6})	EVTS	DOCUMENT ID	TECN	COMMENT
8.46 ± 1.37 ± 0.92	195	ABLIKIM 19BA	BES3	$e^+e^- \rightarrow \psi(2S)$

 $\Gamma(\phi f_2'(1525))/\Gamma_{total}$ Γ_{58}/Γ

VALUE (units 10^{-4})	CL%	EVTS	DOCUMENT ID	TECN	COMMENT
0.44 ± 0.12 ± 0.11		20 ± 6	BAI 04c	BES	$\psi(2S) \rightarrow 2(K^+K^-)$
• • • We do not use the following data for averages, fits, limits, etc. • • •					
<0.45	90	BAI 98J	BES	$e^+e^- \rightarrow 2(K^+K^-)$	

See key on page 1127

Meson Particle Listings

$\psi(2S)$

$\Gamma(K^+K^-)/\Gamma_{total}$ Γ_{59}/Γ

VALUE (units 10^{-5})	CL%	EVTS	DOCUMENT ID	TECN	COMMENT
7.48 ± 0.23 ± 0.39		1.3k	¹ METREVELI 12		$\psi(2S) \rightarrow K^+K^-$
• • • We do not use the following data for averages, fits, limits, etc. • • •					
6.2 ± 1.5 ± 0.2		66	^{2,3} LEES 15J	BABR	$e^+e^- \rightarrow K^+K^-\gamma$
8.3 ± 1.5 ± 0.2		66	^{3,4} LEES 15J	BABR	$e^+e^- \rightarrow K^+K^-\gamma$
6.3 ± 0.6 ± 0.3			⁵ DOBBS 06A	CLEO	e^+e^-
10 ± 7			⁵ BRANDELIK 79C	DASP	e^+e^-
< 5	90		FELDMAN 77	MRK1	e^+e^-

¹ Obtained by analyzing CLEO-c data but not authored by the CLEO Collaboration.
² $\sin\phi > 0$.
³ Using $\Gamma(\psi(2S) \rightarrow e^+e^-) = (2.37 \pm 0.04)$ keV.
⁴ $\sin\phi < 0$.
⁵ Interference with non-resonant K^+K^- production not taken into account.

$\Gamma(K^+K^-\pi^+)/\Gamma_{total}$ Γ_{60}/Γ

VALUE (units 10^{-4})	EVTS	DOCUMENT ID	TECN	COMMENT
7.3 ± 0.5 OUR AVERAGE				
8.1 ± 1.3 ± 0.3	133	LEES 12F	BABR	$10.6 e^+e^- \rightarrow \pi^+\pi^-K^+K^-\gamma$
7.1 ± 0.3 ± 0.4	817.2	BRIERE 05	CLEO	$e^+e^- \rightarrow \psi(2S) \rightarrow K^+K^-\pi^+\pi^-$
16 ± 4		¹ TANENBAUM 78	MRK1	e^+e^-
• • • We do not use the following data for averages, fits, limits, etc. • • •				
11.0 ± 1.9 ± 0.2	85	² AUBERT 07AK	BABR	$10.6 e^+e^- \rightarrow \pi^+\pi^-K^+K^-\gamma$

¹ Assuming entirely strong decay.
² Superseded by LEES 12F. AUBERT 07AK reports $[\Gamma(\psi(2S) \rightarrow K^+K^-\pi^+)/\Gamma_{total}] \times [\Gamma(\psi(2S) \rightarrow e^+e^-)] = (2.56 \pm 0.42 \pm 0.16) \times 10^{-3}$ keV which we divide by our best value $\Gamma(\psi(2S) \rightarrow e^+e^-) = 2.33 \pm 0.04$ keV. Our first error is their experiment's error and our second error is the systematic error from using our best value.

$\Gamma(K^+K^-\pi^0)/\Gamma_{total}$ Γ_{61}/Γ

VALUE (units 10^{-5})	CL%	EVTS	DOCUMENT ID	TECN	COMMENT
4.07 ± 0.16 ± 0.26		0.9k	ABLIKIM 12L	BES3	$e^+e^- \rightarrow \psi(2S)$
• • • We do not use the following data for averages, fits, limits, etc. • • •					
< 8.9	90	1	FRANKLIN 83	MRK2	$e^+e^- \rightarrow$ hadrons

$\Gamma(K_S^0 K_S^0)/\Gamma_{total}$ Γ_{62}/Γ

VALUE (units 10^{-4})	DOCUMENT ID	TECN	COMMENT
< 0.046	¹ BAI 04D	BES	e^+e^-

¹ Forbidden by CP.

$\Gamma(K_S^0 K_L^0)/\Gamma_{total}$ Γ_{63}/Γ

VALUE (units 10^{-5})	EVTS	DOCUMENT ID	TECN	COMMENT
5.34 ± 0.33 OUR AVERAGE				
5.28 ± 0.25 ± 0.34	478 ± 23	¹ METREVELI 12		$\psi(2S) \rightarrow K_S^0 K_L^0$
5.8 ± 0.8 ± 0.4		DOBBS 06A	CLEO	e^+e^-
5.24 ± 0.47 ± 0.48	156 ± 14	² BAI 04B	BES2	$\psi(2S) \rightarrow K_S^0 K_L^0 \rightarrow \pi^+\pi^-X$

¹ Obtained by analyzing CLEO-c data but not authored by the CLEO Collaboration.
² Using $B(K_S^0 \rightarrow \pi^+\pi^-) = 0.6860 \pm 0.0027$.

$\Gamma(K^+K^-\pi^+\pi^0)/\Gamma_{total}$ Γ_{66}/Γ

VALUE (units 10^{-4})	EVTS	DOCUMENT ID	TECN	COMMENT
12.6 ± 0.9 OUR AVERAGE				
18.9 ± 5.7 ± 0.3	32	¹ AUBERT 07AU	BABR	$10.6 e^+e^- \rightarrow K^+K^-\pi^+\pi^0\gamma$
11.7 ± 1.0 ± 1.5	597	ABLIKIM 06G	BES2	$\psi(2S) \rightarrow K^+K^-\pi^+\pi^0$
12.7 ± 0.5 ± 1.0	711.6	BRIERE 05	CLEO	$e^+e^- \rightarrow \psi(2S) \rightarrow K^+K^-\pi^+\pi^0$

¹ AUBERT 07AU reports $[\Gamma(\psi(2S) \rightarrow K^+K^-\pi^+\pi^0)/\Gamma_{total}] \times [\Gamma(\psi(2S) \rightarrow e^+e^-)] = (44 \pm 13 \pm 3) \times 10^{-4}$ keV which we divide by our best value $\Gamma(\psi(2S) \rightarrow e^+e^-) = 2.33 \pm 0.04$ keV. Our first error is their experiment's error and our second error is the systematic error from using our best value.

$\Gamma(\omega f_0(1710) \rightarrow \omega K^+K^-)/\Gamma_{total}$ Γ_{67}/Γ

VALUE (units 10^{-5})	EVTS	DOCUMENT ID	TECN	COMMENT
5.9 ± 2.0 ± 0.9	19	ABLIKIM 06G	BES2	$\psi(2S) \rightarrow K^+K^-\pi^+\pi^0$

$\Gamma(K^*(892)^0 K^-\pi^+\pi^0 + c.c.)/\Gamma_{total}$ Γ_{68}/Γ

VALUE (units 10^{-4})	EVTS	DOCUMENT ID	TECN	COMMENT
8.6 ± 1.3 ± 1.8	238	ABLIKIM 06G	BES2	$\psi(2S) \rightarrow K^+K^-\pi^+\pi^0$

$\Gamma(K^*(892)^+ K^-\pi^+\pi^- + c.c.)/\Gamma_{total}$ Γ_{69}/Γ

VALUE (units 10^{-4})	EVTS	DOCUMENT ID	TECN	COMMENT
9.6 ± 2.2 ± 1.7	133	ABLIKIM 06G	BES2	$\psi(2S) \rightarrow K^+K^-\pi^+\pi^0$

$\Gamma(K^*(892)^+ K^-\rho^0 + c.c.)/\Gamma_{total}$ Γ_{70}/Γ

VALUE (units 10^{-4})	EVTS	DOCUMENT ID	TECN	COMMENT
7.3 ± 2.2 ± 1.4	78	ABLIKIM 06G	BES2	$\psi(2S) \rightarrow K^+K^-\pi^+\pi^0$

$\Gamma(K^*(892)^0 K^-\rho^+ + c.c.)/\Gamma_{total}$ Γ_{71}/Γ

VALUE (units 10^{-4})	EVTS	DOCUMENT ID	TECN	COMMENT
6.1 ± 1.3 ± 1.2	125	ABLIKIM 06G	BES2	$\psi(2S) \rightarrow K^+K^-\pi^+\pi^0$

$\Gamma(K_S^0 K_S^0 \pi^+\pi^-)/\Gamma_{total}$ Γ_{72}/Γ

VALUE (units 10^{-4})	EVTS	DOCUMENT ID	TECN	COMMENT
2.20 ± 0.25 ± 0.37	83 ± 9	ABLIKIM 05o	BES2	$e^+e^- \rightarrow \psi(2S)$

$\Gamma(K^+K^-\rho^0)/\Gamma_{total}$ Γ_{75}/Γ

VALUE (units 10^{-4})	EVTS	DOCUMENT ID	TECN	COMMENT
2.2 ± 0.2 ± 0.4	223.8	BRIERE 05	CLEO	$e^+e^- \rightarrow \psi(2S) \rightarrow K^+K^-\pi^+\pi^-$

$\Gamma(K^*(892)^0 K_S^0 \pi^0)/\Gamma_{total}$ Γ_{76}/Γ

VALUE (units 10^{-4})	CL%	EVTS	DOCUMENT ID	TECN	COMMENT
1.86 ± 0.32 ± 0.43		93 ± 16	BAI 04c		$\psi(2S) \rightarrow K^+K^-\pi^+\pi^-$
• • • We do not use the following data for averages, fits, limits, etc. • • •					
< 1.2	90		BAI 98J	BES	e^+e^-

$\Gamma(K^+K^-\pi^+\pi^-\eta)/\Gamma_{total}$ Γ_{77}/Γ

VALUE (units 10^{-5})	EVTS	DOCUMENT ID	TECN	COMMENT
1.3 ± 0.7 ± 0.1	7	¹ AUBERT 07AU	BABR	$10.6 e^+e^- \rightarrow K^+K^-\pi^+\pi^-\eta$
¹ AUBERT 07AU quotes $\Gamma_{ee}^{\psi(2S)} \cdot B(\psi(2S) \rightarrow 2(\pi^+\pi^-\eta)) \cdot B(\eta \rightarrow \gamma\gamma) = 1.2 \pm 0.7 \pm 0.1$ eV.				

$\Gamma(K^+K^-\pi^+\pi^-\pi^0)/\Gamma_{total}$ Γ_{79}/Γ

VALUE (units 10^{-4})	EVTS	DOCUMENT ID	TECN	COMMENT
10.0 ± 2.5 ± 1.8	65	ABLIKIM 07D	BES2	$e^+e^- \rightarrow \psi(2S)$

$\Gamma(K^+K^*(892)^- + c.c.)/\Gamma_{total}$ Γ_{80}/Γ

VALUE (units 10^{-5})	CL%	EVTS	DOCUMENT ID	TECN	COMMENT
2.9 ± 0.4 OUR AVERAGE					Error includes scale factor of 1.2.
3.18 ± 0.30 ± 0.26		0.2k	ABLIKIM 12L	BES3	$e^+e^- \rightarrow \psi(2S)$
2.9 ± 1.3 ± 0.4		9.6 ± 4.2	ABLIKIM 05i	BES2	$e^+e^- \rightarrow \psi(2S)$
1.3 ± 1.0 ± 0.7		7	ADAM 05	CLEO	$e^+e^- \rightarrow \psi(2S)$
• • • We do not use the following data for averages, fits, limits, etc. • • •					
< 5.4	90		FRANKLIN 83	MRK2	$e^+e^- \rightarrow$ hadrons

$\Gamma(2(K^+K^-))/\Gamma_{total}$ Γ_{81}/Γ

VALUE (units 10^{-4})	EVTS	DOCUMENT ID	TECN	COMMENT
0.63 ± 0.13 OUR AVERAGE				
0.9 ± 0.4 ± 0.1	13	LEES 12F	BABR	$10.6 e^+e^- \rightarrow 2(K^+K^-)\gamma$
0.6 ± 0.1 ± 0.1	59.2	BRIERE 05	CLEO	$e^+e^- \rightarrow \psi(2S) \rightarrow 2(K^+K^-)$

$\Gamma(2(K^+K^-)\pi^0)/\Gamma_{total}$ Γ_{82}/Γ

VALUE (units 10^{-4})	EVTS	DOCUMENT ID	TECN	COMMENT
1.1 ± 0.2 ± 0.2	44.7	BRIERE 05	CLEO	$e^+e^- \rightarrow \psi(2S) \rightarrow 2(K^+K^-)\pi^0$

$\Gamma(K^+K^-\phi)/\Gamma_{total}$ Γ_{83}/Γ

VALUE (units 10^{-4})	EVTS	DOCUMENT ID	TECN	COMMENT
0.70 ± 0.16 OUR AVERAGE				
0.8 ± 0.2 ± 0.1	36.8	BRIERE 05	CLEO	$e^+e^- \rightarrow \psi(2S) \rightarrow 2(K^+K^-)$
0.6 ± 0.2 ± 0.1	16.1 ± 5.0	¹ BAI 03B	BES	$\psi(2S) \rightarrow 2(K^+K^-)$
¹ Normalized to $B(\psi(2S) \rightarrow J/\psi\pi^+\pi^-) = 0.305 \pm 0.016$.				

$\Gamma(K_1(1270)^\pm K^\mp)/\Gamma_{total}$ Γ_{84}/Γ

VALUE (units 10^{-4})	DOCUMENT ID	TECN	COMMENT
10.0 ± 1.8 ± 2.1	¹ BAI 99c	BES	e^+e^-
¹ Assuming $B(K_1(1270) \rightarrow K\rho) = 0.42 \pm 0.06$			

$\Gamma(K^+K^*(892)^0 \pi^- + c.c.)/\Gamma_{total}$ Γ_{85}/Γ

VALUE (units 10^{-4})	DOCUMENT ID	TECN	COMMENT
6.7 ± 2.5	TANENBAUM 78	MRK1	e^+e^-

Meson Particle Listings

 $\psi(2S)$ $\Gamma(\eta K^+ K^-, \text{no } \eta\phi)/\Gamma_{\text{total}}$ Γ_{86}/Γ

VALUE (units 10^{-5})	CL%	EVTS	DOCUMENT ID	TECN	COMMENT
$3.49 \pm 0.09 \pm 0.15$		1.8k	¹ ABLIKIM	20F BES3	$\psi(2S) \rightarrow K^+ K^- \gamma \gamma$

• • • We do not use the following data for averages, fits, limits, etc. • • •

$3.08 \pm 0.29 \pm 0.25$	0.3k	^{1,2} ABLIKIM	12L BES3	$\psi(2S) \rightarrow K^+ K^- \gamma \gamma$
<13	90	BRIERE	05 CLEO	$e^+ e^- \rightarrow \psi(2S) \rightarrow K^+ K^- \pi^+ \pi^- \pi^0$

¹ Excluding $\eta\phi$.

² Superseded by ABLIKIM 20F.

 $\Gamma(X(1750)\eta \rightarrow K^+ K^- \eta)/\Gamma_{\text{total}}$ Γ_{87}/Γ

VALUE (units 10^{-6})	DOCUMENT ID	TECN	COMMENT
$4.8 \pm 1.0 \pm 2.6$	ABLIKIM	20F BES3	$\psi(2S) \rightarrow K^+ K^- \eta$

 $\Gamma(K_1(1400)^\pm K^\mp)/\Gamma_{\text{total}}$ Γ_{88}/Γ

VALUE (units 10^{-4})	CL%	DOCUMENT ID	TECN	COMMENT
<3.1	90	¹ BAI	99c BES	$e^+ e^-$

¹ Assuming $B(K_1(1400) \rightarrow K^* \pi) = 0.94 \pm 0.06$

 $\Gamma(K_2^*(1430)^\pm K^\mp)/\Gamma_{\text{total}}$ Γ_{89}/Γ

VALUE (units 10^{-5})	EVTS	DOCUMENT ID	TECN	COMMENT
$7.12 \pm 0.62 \pm 1.13$	251 ± 22	ABLIKIM	12L BES3	$e^+ e^- \rightarrow \psi(2S)$

 $\Gamma(K^*(892)^0 K^0 + \text{c.c.})/\Gamma_{\text{total}}$ Γ_{90}/Γ

VALUE (units 10^{-5})	EVTS	DOCUMENT ID	TECN	COMMENT
10.9 ± 2.0 OUR AVERAGE				
$13.3 \pm 2.4 \pm 1.7$	65.6 ± 9.0	ABLIKIM	05i BES2	$e^+ e^- \rightarrow \psi(2S)$
$9.2 \pm 2.7 \pm 0.9$	25	ADAM	05 CLEO	$e^+ e^- \rightarrow \psi(2S)$

 $\Gamma(K^+ K^*(892)^- + \text{c.c.})/\Gamma(K^*(892)^0 K^0 + \text{c.c.})$ Γ_{80}/Γ_{90}

VALUE	DOCUMENT ID	TECN	COMMENT
0.16 ± 0.06 OUR AVERAGE			
$0.22 \pm 0.10 \pm 0.14$	ABLIKIM	05i BES2	$e^+ e^- \rightarrow \psi(2S)$
$0.14 \pm 0.08 \pm 0.06$	ADAM	05 CLEO	$e^+ e^- \rightarrow \psi(2S)$

 $\Gamma(\omega K^+ K^-)/\Gamma_{\text{total}}$ Γ_{91}/Γ

VALUE (units 10^{-4})	EVTS	DOCUMENT ID	TECN	COMMENT
1.62 ± 0.11 OUR AVERAGE				Error includes scale factor of 1.1.
$1.56 \pm 0.04 \pm 0.11$	2.8k	ABLIKIM	14G BES3	$\psi(2S) \rightarrow K^+ K^- \pi^+ \pi^- \pi^0$
$2.38 \pm 0.37 \pm 0.29$	78	ABLIKIM	06G BES2	$\psi(2S) \rightarrow K^+ K^- \pi^+ \pi^- \pi^0$
$1.9 \pm 0.3 \pm 0.3$	76.8	BRIERE	05 CLEO	$e^+ e^- \rightarrow \psi(2S) \rightarrow K^+ K^- \pi^+ \pi^- \pi^0$
$1.5 \pm 0.3 \pm 0.2$	23	¹ BAI	03B BES	$\psi(2S) \rightarrow K^+ K^- \pi^+ \pi^- \pi^0$

¹ Normalized to $B(\psi(2S) \rightarrow J/\psi \pi^+ \pi^-) = 0.305 \pm 0.016$.

 $\Gamma(\omega K_S^0 K_S^0)/\Gamma_{\text{total}}$ Γ_{92}/Γ

VALUE (units 10^{-5})	EVTS	DOCUMENT ID	TECN	COMMENT
$7.04 \pm 0.39 \pm 0.36$	1.5k	ABLIKIM	21AL BES3	$\psi(2S) \rightarrow \pi^+ \pi^- \pi^0 K_S^0 K_S^0$

 $\Gamma(\omega K^*(892)^+ K^- + \text{c.c.})/\Gamma_{\text{total}}$ Γ_{93}/Γ

VALUE (units 10^{-5})	EVTS	DOCUMENT ID	TECN	COMMENT
20.7 ± 2.6 OUR AVERAGE				
$18.9 \pm 2.9 \pm 2.2$	396	ABLIKIM	13M BES3	$\psi(2S) \rightarrow \omega K_S^0 K^- \pi^+$
$22.6 \pm 3.0 \pm 2.4$	535	ABLIKIM	13M BES3	$\psi(2S) \rightarrow \omega K^+ K^- \pi^0$

 $\Gamma(\omega K_2^*(1430)^+ K^- + \text{c.c.})/\Gamma_{\text{total}}$ Γ_{94}/Γ

VALUE (units 10^{-5})	EVTS	DOCUMENT ID	TECN	COMMENT
6.1 ± 1.2 OUR AVERAGE				
$6.39 \pm 1.50 \pm 0.78$	128	ABLIKIM	13M BES3	$\psi(2S) \rightarrow \omega K_S^0 K^- \pi^+$
$5.86 \pm 1.61 \pm 0.83$	143	ABLIKIM	13M BES3	$\psi(2S) \rightarrow \omega K^+ K^- \pi^0$

 $\Gamma(\omega \bar{K}^*(892)^0 K^0)/\Gamma_{\text{total}}$ Γ_{95}/Γ

VALUE (units 10^{-5})	EVTS	DOCUMENT ID	TECN	COMMENT
$16.8 \pm 2.5 \pm 1.6$	356	ABLIKIM	13M BES3	$\psi(2S) \rightarrow \omega K_S^0 K^- \pi^+$

 $\Gamma(\omega \bar{K}_2^*(1430)^0 K^0)/\Gamma_{\text{total}}$ Γ_{96}/Γ

VALUE (units 10^{-5})	EVTS	DOCUMENT ID	TECN	COMMENT
$5.82 \pm 2.08 \pm 0.72$	116	ABLIKIM	13M BES3	$\psi(2S) \rightarrow \omega K_S^0 K^- \pi^+$

 $\Gamma(\omega X(1440) \rightarrow \omega K_S^0 K^- \pi^+ + \text{c.c.})/\Gamma_{\text{total}}$ Γ_{97}/Γ

VALUE (units 10^{-5})	EVTS	DOCUMENT ID	TECN	COMMENT
$1.60 \pm 0.27 \pm 0.24$	109	¹ ABLIKIM	13M BES3	$\psi(2S) \rightarrow \omega K_S^0 K^- \pi^+$

¹ $X(1440)$ compatible with $\eta(1405)$ and $\eta(1475)$. A $f_1(1420)$ is also possible.

 $\Gamma(\omega X(1440) \rightarrow \omega K^+ K^- \pi^0)/\Gamma_{\text{total}}$ Γ_{98}/Γ

VALUE (units 10^{-5})	EVTS	DOCUMENT ID	TECN	COMMENT
$1.09 \pm 0.20 \pm 0.16$	82	¹ ABLIKIM	13M BES3	$\psi(2S) \rightarrow \omega K^+ K^- \pi^0$

¹ $X(1440)$ compatible with $\eta(1405)$ and $\eta(1475)$. A $f_1(1420)$ is also possible.

 $\Gamma(\omega f_1(1285) \rightarrow \omega K_S^0 K^- \pi^+ + \text{c.c.})/\Gamma_{\text{total}}$ Γ_{99}/Γ

VALUE (units 10^{-5})	EVTS	DOCUMENT ID	TECN	COMMENT
$0.302 \pm 0.098 \pm 0.027$	22	¹ ABLIKIM	13M BES3	$\psi(2S) \rightarrow \omega K_S^0 K^- \pi^+$

¹ Statistical significance 4.5 σ . This measurement is equivalent to a limit of $< 0.478 \times 10^{-5}$ at 90% C.L.

 $\Gamma(\omega f_1(1285) \rightarrow \omega K^+ K^- \pi^0)/\Gamma_{\text{total}}$ Γ_{100}/Γ

VALUE (units 10^{-5})	EVTS	DOCUMENT ID	TECN	COMMENT
$0.125 \pm 0.070 \pm 0.013$	10	¹ ABLIKIM	13M BES3	$\psi(2S) \rightarrow \omega K^+ K^- \pi^0$

¹ Statistical significance 3.2 σ . This measurement is equivalent to a limit of $< 0.221 \times 10^{-5}$ at 90% C.L.

 $\Gamma(p\bar{p})/\Gamma_{\text{total}}$ Γ_{101}/Γ

VALUE (units 10^{-4})	EVTS	DOCUMENT ID	TECN	COMMENT
2.94 ± 0.08 OUR FIT				
3.02 ± 0.08 OUR AVERAGE				
$3.05 \pm 0.02 \pm 0.12$	19k	ABLIKIM	18T BES3	$e^+ e^- \rightarrow \psi(2S) \rightarrow p\bar{p}$
$3.08 \pm 0.05 \pm 0.18$	4.5k	¹ DOBBS	14	$e^+ e^- \rightarrow \psi(2S) \rightarrow p\bar{p}$
$3.36 \pm 0.09 \pm 0.25$	1.6k	ABLIKIM	07c BES	$e^+ e^- \rightarrow \psi(2S) \rightarrow p\bar{p}$
$2.87 \pm 0.12 \pm 0.15$	557	PEDLAR	05 CLEO	$e^+ e^- \rightarrow \psi(2S) \rightarrow p\bar{p}$
1.4 ± 0.8	4	BRANDELIK	79c DASP	$e^+ e^- \rightarrow \psi(2S) \rightarrow p\bar{p}$
2.3 ± 0.7		FELDMAN	77 MRK1	$e^+ e^- \rightarrow \psi(2S) \rightarrow p\bar{p}$

¹ Using CLEO-c data but not authored by the CLEO Collaboration.

 $\Gamma(p\bar{p})/\Gamma(J/\psi(1S)\pi^+\pi^-)$ Γ_{101}/Γ_{12}

VALUE (units 10^{-4})	DOCUMENT ID	TECN	COMMENT
8.49 ± 0.23 OUR FIT			
$6.98 \pm 0.49 \pm 0.97$	BAI	01 BES	$e^+ e^- \rightarrow \psi(2S) \rightarrow p\bar{p}$

 $\Gamma(n\bar{n})/\Gamma_{\text{total}}$ Γ_{102}/Γ

VALUE (units 10^{-4})	EVTS	DOCUMENT ID	TECN	COMMENT
$3.06 \pm 0.06 \pm 0.14$	6k	ABLIKIM	18T BES3	$e^+ e^- \rightarrow \psi(2S) \rightarrow n\bar{n}$

 $\Gamma(p\bar{p}\pi^0)/\Gamma_{\text{total}}$ Γ_{103}/Γ

VALUE (units 10^{-4})	EVTS	DOCUMENT ID	TECN	COMMENT
1.53 ± 0.07 OUR AVERAGE				
$1.65 \pm 0.03 \pm 0.15$	4.5k	ABLIKIM	13A BES3	$\psi(2S) \rightarrow p\bar{p}\pi^0$
$1.54 \pm 0.06 \pm 0.06$	948	ALEXANDER	10 CLEO	$\psi(2S) \rightarrow \pi^0 p\bar{p}$
$1.32 \pm 0.10 \pm 0.15$	256	¹ ABLIKIM	05E BES2	$e^+ e^- \rightarrow \psi(2S) \rightarrow p\bar{p}\gamma\gamma$
1.4 ± 0.5	9	FRANKLIN	83 MRK2	$e^+ e^-$

¹ Computed using $B(\pi^0 \rightarrow \gamma\gamma) = (98.80 \pm 0.03)\%$.

 $\Gamma(N(940)\bar{p} + \text{c.c.} \rightarrow p\bar{p}\pi^0)/\Gamma_{\text{total}}$ Γ_{104}/Γ

VALUE (units 10^{-5})	EVTS	DOCUMENT ID	TECN	COMMENT
$6.42 \pm 0.20 \pm 1.78$	1.9k	¹ ABLIKIM	13A BES3	$\psi(2S) \rightarrow p\bar{p}\pi^0$

¹ From a fit of $\pi^0 p\bar{p}$ data to eight distinct intermediate $N\bar{p}$ resonant states.

 $\Gamma(N(1440)\bar{p} + \text{c.c.} \rightarrow p\bar{p}\pi^0)/\Gamma_{\text{total}}$ Γ_{105}/Γ

VALUE (units 10^{-5})	EVTS	DOCUMENT ID	TECN	COMMENT
7.3 ± 1.7 OUR AVERAGE				Error includes scale factor of 2.5.
$3.58 \pm 0.25 \pm 1.59 \pm 0.84$	1.1k	¹ ABLIKIM	13A BES3	$\psi(2S) \rightarrow p\bar{p}\pi^0$
$8.1 \pm 0.7 \pm 0.3$	474	² ALEXANDER	10 CLEO	$\psi(2S) \rightarrow \pi^0 p\bar{p}$

¹ From a fit of $\pi^0 p\bar{p}$ data to eight distinct intermediate $N\bar{p}$ resonant states.

² From a fit of the $p\bar{p}$ and $p\pi^0$ mass distributions to a combination of $N(1440)\bar{p}$, a broad $p\bar{p}$ enhancement around 2100 MeV, and two other broad, unestablished resonances.

 $\Gamma(N(1520)\bar{p} + \text{c.c.} \rightarrow p\bar{p}\pi^0)/\Gamma_{\text{total}}$ Γ_{106}/Γ

VALUE (units 10^{-5})	EVTS	DOCUMENT ID	TECN	COMMENT
$0.64 \pm 0.05 \pm 0.22$	0.2k	¹ ABLIKIM	13A BES3	$\psi(2S) \rightarrow p\bar{p}\pi^0$

¹ From a fit of $\pi^0 p\bar{p}$ data to eight distinct intermediate $N\bar{p}$ resonant states.

 $\Gamma(N(1535)\bar{p} + \text{c.c.} \rightarrow p\bar{p}\pi^0)/\Gamma_{\text{total}}$ Γ_{107}/Γ

VALUE (units 10^{-5})	EVTS	DOCUMENT ID	TECN	COMMENT
$2.47 \pm 0.28 \pm 0.99$	0.7k	¹ ABLIKIM	13A BES3	$\psi(2S) \rightarrow p\bar{p}\pi^0$

¹ From a fit of $\pi^0 p\bar{p}$ data to eight distinct intermediate $N\bar{p}$ resonant states.

 $\Gamma(N(1650)\bar{p} + \text{c.c.} \rightarrow p\bar{p}\pi^0)/\Gamma_{\text{total}}$ Γ_{108}/Γ

VALUE (units 10^{-5})	EVTS	DOCUMENT ID	TECN	COMMENT
$3.76 \pm 0.28 \pm 1.37$	1.1k	¹ ABLIKIM	13A BES3	$\psi(2S) \rightarrow p\bar{p}\pi^0$

¹ From a fit of $\pi^0 p\bar{p}$ data to eight distinct intermediate $N\bar{p}$ resonant states.

$\Gamma(N(1720)\bar{p} + c.c. \rightarrow p\bar{p}\pi^0)/\Gamma_{total}$					Γ_{109}/Γ
VALUE (units 10^{-5})	EVTS	DOCUMENT ID	TECN	COMMENT	
$1.79 \pm 0.10 \pm 0.24$ -0.71	0.5k	¹ ABLIKIM	13A BES3	$\psi(2S) \rightarrow p\bar{p}\pi^0$	

¹ From a fit of $\pi^0 p\bar{p}$ data to eight distinct intermediate $N\bar{p}$ resonant states.

$\Gamma(N(2300)\bar{p} + c.c. \rightarrow p\bar{p}\pi^0)/\Gamma_{total}$					Γ_{110}/Γ
VALUE (units 10^{-5})	EVTS	DOCUMENT ID	TECN	COMMENT	
$2.62 \pm 0.28 \pm 1.12$ -0.64	0.9k	¹ ABLIKIM	13A BES3	$\psi(2S) \rightarrow p\bar{p}\pi^0$	

¹ From a fit of $\pi^0 p\bar{p}$ data to eight distinct intermediate $N\bar{p}$ resonant states.

$\Gamma(N(2570)\bar{p} + c.c. \rightarrow p\bar{p}\pi^0)/\Gamma_{total}$					Γ_{111}/Γ
VALUE (units 10^{-5})	EVTS	DOCUMENT ID	TECN	COMMENT	
$2.13 \pm 0.08 \pm 0.40$ -0.30	0.8k	¹ ABLIKIM	13A BES3	$\psi(2S) \rightarrow p\bar{p}\pi^0$	

¹ From a fit of $\pi^0 p\bar{p}$ data to eight distinct intermediate $N\bar{p}$ resonant states.

$\Gamma(p\bar{p}\pi^+\pi^-)/\Gamma_{total}$					Γ_{112}/Γ
VALUE (units 10^{-4})	EVTS	DOCUMENT ID	TECN	COMMENT	
6.0 ± 0.4 OUR AVERAGE					
$5.9 \pm 0.2 \pm 0.4$	904.5	BRIERE	05 CLEO	$e^+e^- \rightarrow \psi(2S) \rightarrow p\bar{p}\pi^+\pi^-$	
8 ± 2		¹ TANENBAUM	78 MRK1	e^+e^-	

¹ Assuming entirely strong decay.

$\Gamma(p\bar{p}K^+K^-)/\Gamma_{total}$					Γ_{113}/Γ
VALUE (units 10^{-5})	EVTS	DOCUMENT ID	TECN	COMMENT	
$2.7 \pm 0.6 \pm 0.4$	30.1	BRIERE	05 CLEO	$e^+e^- \rightarrow \psi(2S) \rightarrow p\bar{p}K^+K^-$	

$\Gamma(p\bar{p}\eta)/\Gamma_{total}$					Γ_{114}/Γ
VALUE (units 10^{-5})	EVTS	DOCUMENT ID	TECN	COMMENT	
6.0 ± 0.4 OUR AVERAGE					
$6.4 \pm 0.2 \pm 0.6$	679	¹ ABLIKIM	13s BES3	$\psi(2S) \rightarrow \eta p\bar{p}$	
$5.6 \pm 0.6 \pm 0.3$	154	¹ ALEXANDER	10 CLEO	$\psi(2S) \rightarrow \eta p\bar{p}$	
$5.8 \pm 1.1 \pm 0.7$	44.8 ± 8.5	² ABLIKIM	05E BES2	$e^+e^- \rightarrow \psi(2S) \rightarrow p\bar{p}\eta\gamma$	
$8 \pm 3 \pm 3$	9.8	BRIERE	05 CLEO	$e^+e^- \rightarrow \psi(2S) \rightarrow p\bar{p}\pi^+\pi^-\pi^0$	

¹ With $N(1535)$ decaying to $p\eta$.

² Computed using $B(\eta \rightarrow \gamma\gamma) = (39.43 \pm 0.26)\%$.

$\Gamma(N(1535)\bar{p} + c.c. \rightarrow p\bar{p}\eta)/\Gamma_{total}$					Γ_{115}/Γ
VALUE (units 10^{-5})	EVTS	DOCUMENT ID	TECN	COMMENT	
4.5 ± 0.7 OUR AVERAGE -0.6					
$5.2 \pm 0.3 \pm 3.2$ -1.2	527	¹ ABLIKIM	13s BES3	$\psi(2S) \rightarrow \eta p\bar{p}$	
$4.4 \pm 0.6 \pm 0.3$	123	² ALEXANDER	10 CLEO	$\psi(2S) \rightarrow \eta p\bar{p}$	

¹ With $N(1535)$ decaying to $p\eta$.

² From a fit of the $p\bar{p}$ and $p\eta$ distributions to a combination of $N^*(1535)\bar{p}$ and a broad $p\bar{p}$ enhancement around 2100 MeV.

$\Gamma(p\bar{p}\pi^+\pi^-\pi^0)/\Gamma_{total}$					Γ_{116}/Γ
VALUE (units 10^{-4})	EVTS	DOCUMENT ID	TECN	COMMENT	
$7.3 \pm 0.4 \pm 0.6$	434.9	BRIERE	05 CLEO	$e^+e^- \rightarrow \psi(2S) \rightarrow p\bar{p}\pi^+\pi^-\pi^0$	

$\Gamma(p\bar{p}\rho^0)/\Gamma_{total}$					Γ_{117}/Γ
VALUE (units 10^{-4})	EVTS	DOCUMENT ID	TECN	COMMENT	
$0.5 \pm 0.1 \pm 0.2$	61.1	BRIERE	05 CLEO	$e^+e^- \rightarrow \psi(2S) \rightarrow p\bar{p}\pi^+\pi^-$	

$\Gamma(p\bar{p}\omega)/\Gamma_{total}$					Γ_{118}/Γ
VALUE (units 10^{-4})	EVTS	DOCUMENT ID	TECN	COMMENT	
0.69 ± 0.21 OUR AVERAGE					
$0.6 \pm 0.2 \pm 0.2$	21.2	BRIERE	05 CLEO	$e^+e^- \rightarrow \psi(2S) \rightarrow p\bar{p}\pi^+\pi^-\pi^0$	
$0.8 \pm 0.3 \pm 0.1$	14.9 ± 0.1	¹ BAI	03B BES	$\psi(2S) \rightarrow p\bar{p}\pi^+\pi^-\pi^0$	

¹ Normalized to $B(\psi(2S) \rightarrow J/\psi\pi^+\pi^-) = 0.305 \pm 0.016$.

$\Gamma(p\bar{p}\eta')/\Gamma_{total}$					Γ_{119}/Γ
VALUE (units 10^{-5})	EVTS	DOCUMENT ID	TECN	COMMENT	
$1.10 \pm 0.10 \pm 0.08$	491	¹ ABLIKIM	19N BES3	$\psi(2S) \rightarrow \eta' p\bar{p}$	

¹ From the combination of $p\bar{p}\eta' \rightarrow p\bar{p}\pi^+\pi^-\eta$ and $p\bar{p}\eta' \rightarrow p\bar{p}\pi^+\pi^-\gamma$ channels.

$\Gamma(p\bar{p}\phi)/\Gamma_{total}$					Γ_{120}/Γ
VALUE (units 10^{-6})	CL%	EVTS	DOCUMENT ID	TECN	COMMENT
$6.06 \pm 0.38 \pm 0.48$		753	ABLIKIM	19A0 BES3	$e^+e^- \rightarrow \psi(2S) \rightarrow p\bar{p}K^+K^-$

• • • We do not use the following data for averages, fits, limits, etc. • • •

<24	90	BRIERE	05 CLEO	$e^+e^- \rightarrow \psi(2S) \rightarrow p\bar{p}K^+K^-$
<26	90	¹ BAI	03B BES	$\psi(2S) \rightarrow K^+K^-\rho\bar{p}$

¹ Normalized to $B(\psi(2S) \rightarrow J/\psi\pi^+\pi^-) = 0.305 \pm 0.016$.

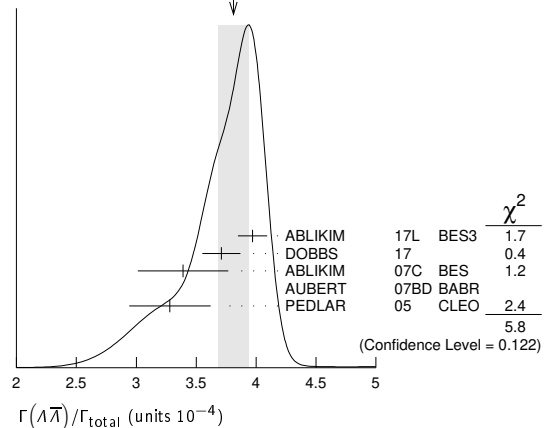
$\Gamma(\phi X(1835) \rightarrow p\bar{p}\phi)/\Gamma_{total}$					Γ_{121}/Γ
VALUE	CL%	DOCUMENT ID	TECN	COMMENT	
<1.82 $\times 10^{-7}$	90	ABLIKIM	19A0 BES3	$e^+e^- \rightarrow \psi(2S) \rightarrow p\bar{p}K^+K^-$	

$\Gamma(p\bar{p}\pi^-\pi^0 \text{ or c.c.})/\Gamma_{total}$					Γ_{122}/Γ
VALUE (units 10^{-4})	EVTS	DOCUMENT ID	TECN	COMMENT	
2.48 ± 0.17 OUR AVERAGE					
$2.45 \pm 0.11 \pm 0.21$	851	ABLIKIM	06i BES2	$e^+e^- \rightarrow p\pi^-X$	
$2.52 \pm 0.12 \pm 0.22$	849	ABLIKIM	06i BES2	$e^+e^- \rightarrow \bar{p}\pi^+X$	

$\Gamma(p\bar{p}\pi^-\pi^0)/\Gamma_{total}$					Γ_{123}/Γ
VALUE (units 10^{-4})	EVTS	DOCUMENT ID	TECN	COMMENT	
$3.18 \pm 0.50 \pm 0.50$	135 ± 21	ABLIKIM	06i BES2	$e^+e^- \rightarrow p\pi^-\pi^0 X$	

$\Gamma(\Lambda\bar{\Lambda})/\Gamma_{total}$					Γ_{124}/Γ
VALUE (units 10^{-4})	CL%	EVTS	DOCUMENT ID	TECN	COMMENT
3.81 ± 0.13 OUR AVERAGE					Error includes scale factor of 1.4. See the ideogram below.
$3.97 \pm 0.02 \pm 0.12$	31k	ABLIKIM	17L BES3	$e^+e^- \rightarrow \Lambda\bar{\Lambda}$	
$3.71 \pm 0.05 \pm 0.15$	6.5k	¹ DOBBS	17	$e^+e^- \rightarrow \Lambda\bar{\Lambda}$	
$3.39 \pm 0.20 \pm 0.32$	337	ABLIKIM	07c BES	$e^+e^- \rightarrow \psi(2S) \rightarrow \text{hadrons}$	
$6.4 \pm 1.8 \pm 0.1$		² AUBERT	07BD BABR	$10.6 e^+e^- \rightarrow \Lambda\bar{\Lambda}\gamma$	
$3.28 \pm 0.23 \pm 0.25$	208	PEDLAR	05 CLEO	$e^+e^- \rightarrow \psi(2S) \rightarrow \text{hadrons}$	
• • • We do not use the following data for averages, fits, limits, etc. • • •					
$3.75 \pm 0.09 \pm 0.23$	1.9k	^{1,3} DOBBS	14	$e^+e^- \rightarrow \Lambda\bar{\Lambda}$	
$1.81 \pm 0.20 \pm 0.27$	80	⁴ BAI	01 BES	$e^+e^- \rightarrow \psi(2S) \rightarrow \text{hadrons}$	
< 4	90	FELDMAN	77 MRK1	$e^+e^- \rightarrow \psi(2S) \rightarrow \text{hadrons}$	

WEIGHTED AVERAGE
 3.81 ± 0.13 (Error scaled by 1.4)



¹ Using CLEO-c data but not authored by the CLEO Collaboration.

² AUBERT 07BD reports $[\Gamma(\psi(2S) \rightarrow \Lambda\bar{\Lambda})/\Gamma_{total}] \times [\Gamma(\psi(2S) \rightarrow e^+e^-)] = (15 \pm 4 \pm 1) \times 10^{-4}$ keV which we divide by our best value $\Gamma(\psi(2S) \rightarrow e^+e^-) = 2.33 \pm 0.04$ keV. Our first error is their experiment's error and our second error is the systematic error from using our best value.

³ Superseded by DOBBS 17.

⁴ Estimated using $B(\psi(2S) \rightarrow J/\psi\pi^+\pi^-) = 0.310 \pm 0.028$.

$\Gamma(\Lambda\bar{\Lambda}\pi^0)/\Gamma_{total}$					Γ_{125}/Γ
VALUE (units 10^{-5})	CL%	DOCUMENT ID	TECN	COMMENT	
< 0.29	90	¹ ABLIKIM	13F BES3	$\psi(2S) \rightarrow p\bar{p}\pi^+\pi^-\gamma\gamma$	
• • • We do not use the following data for averages, fits, limits, etc. • • •					
<12	90	² ABLIKIM	07H BES2	$e^+e^- \rightarrow \psi(2S)$	

¹ Using $B(\Lambda \rightarrow \pi^-p) = 63.9\%$ and $B(\pi^0 \rightarrow \gamma\gamma) = 98.8\%$.

² Using $B(\Lambda \rightarrow \pi^-p) = 63.9\%$ and $B(\eta \rightarrow \gamma\gamma) = 39.4\%$.

Meson Particle Listings

 $\psi(2S)$ $\Gamma(\Lambda\bar{\Lambda}\eta)/\Gamma_{\text{total}}$ Γ_{126}/Γ

VALUE (units 10^{-5})	CL% EVTS	DOCUMENT ID	TECN	COMMENT
2.46 ± 0.34 ± 0.19	60	¹ ABLIKIM	13F BES3	$\psi(2S) \rightarrow p\bar{p}\pi^+\pi^-\gamma\gamma$

• • • We do not use the following data for averages, fits, limits, etc. • • •

<4.9 90 ² ABLIKIM 07H BES2 $e^+e^- \rightarrow \psi(2S)$

¹ Using $B(\Lambda \rightarrow \pi^-p) = 63.9\%$ and $B(\eta \rightarrow \gamma\gamma) = 39.31\%$.

² Using $B(\Lambda \rightarrow \pi^-p) = 63.9\%$.

 $\Gamma(\Lambda\bar{\Lambda}\pi^+\pi^-)/\Gamma_{\text{total}}$ Γ_{127}/Γ

VALUE (units 10^{-4})	EVTS	DOCUMENT ID	TECN	COMMENT
2.8 ± 0.4 ± 0.5	73.4	BRIERE	05 CLEO	$e^+e^- \rightarrow \psi(2S) \rightarrow p\bar{p}2(\pi^+\pi^-)$

 $\Gamma(\Lambda\bar{p}K^+)/\Gamma_{\text{total}}$ Γ_{128}/Γ

VALUE (units 10^{-4})	EVTS	DOCUMENT ID	TECN	COMMENT
1.0 ± 0.1 ± 0.1	74.0	BRIERE	05 CLEO	$e^+e^- \rightarrow \psi(2S) \rightarrow p\bar{p}K^+\pi^-$

 $\Gamma(\Lambda\bar{p}K^*(892)^+ + \text{c.c.})/\Gamma_{\text{total}}$ Γ_{129}/Γ

VALUE (units 10^{-5})	EVTS	DOCUMENT ID	TECN	COMMENT
6.3 ± 0.5 ± 0.5	1011	ABLIKIM	19AU BES3	$e^+e^- \rightarrow \psi(2S)$

 $\Gamma(\Lambda\bar{p}K^+\pi^+\pi^-)/\Gamma_{\text{total}}$ Γ_{130}/Γ

VALUE (units 10^{-4})	EVTS	DOCUMENT ID	TECN	COMMENT
1.8 ± 0.3 ± 0.3	45.8	BRIERE	05 CLEO	$e^+e^- \rightarrow \psi(2S) \rightarrow p\bar{p}K^+\pi^+\pi^-$

 $\Gamma(\Lambda n K_S^0 + \text{c.c.})/\Gamma_{\text{total}}$ Γ_{131}/Γ

VALUE (units 10^{-4})	EVTS	DOCUMENT ID	TECN	COMMENT
0.81 ± 0.11 ± 0.14	50	¹ ABLIKIM	08c BES2	$e^+e^- \rightarrow J/\psi$

¹ Using $B(\bar{\Lambda} \rightarrow \bar{p}\pi^+) = 63.9\%$ and $B(K_S^0 \rightarrow \pi^+\pi^-) = 69.2\%$.

 $\Gamma(\Delta^{++}\bar{\Delta}^{--})/\Gamma_{\text{total}}$ Γ_{132}/Γ

VALUE (units 10^{-5})	EVTS	DOCUMENT ID	TECN	COMMENT
12.0 ± 1.0 ± 3.4	157	¹ BAI	01 BES	$e^+e^- \rightarrow \psi(2S) \rightarrow$ hadrons

¹ Estimated using $B(\psi(2S) \rightarrow J/\psi\pi^+\pi^-) = 0.310 \pm 0.028$.

 $\Gamma(\Lambda\bar{\Sigma}^+\pi^- + \text{c.c.})/\Gamma_{\text{total}}$ Γ_{133}/Γ

VALUE (units 10^{-4})	EVTS	DOCUMENT ID	TECN	COMMENT
1.40 ± 0.03 ± 0.13	2.8k	ABLIKIM	13W BES3	$\psi(2S) \rightarrow$ hadrons

 $\Gamma(\Lambda\bar{\Sigma}^-\pi^+ + \text{c.c.})/\Gamma_{\text{total}}$ Γ_{134}/Γ

VALUE (units 10^{-4})	EVTS	DOCUMENT ID	TECN	COMMENT
1.54 ± 0.04 ± 0.13	2.8k	ABLIKIM	13W BES3	$\psi(2S) \rightarrow$ hadrons

 $\Gamma(\Lambda\bar{\Sigma}^0 + \text{c.c.})/\Gamma_{\text{total}}$ Γ_{135}/Γ

VALUE (units 10^{-6})	EVTS	DOCUMENT ID	TECN	COMMENT
1.60 ± 0.31 ± 0.59	60	ABLIKIM	21L BES3	$e^+e^- \rightarrow \psi(2S) \rightarrow$ hadrons

 $\Gamma(\Lambda\bar{\Sigma}^0)/\Gamma_{\text{total}}$ Γ_{136}/Γ

VALUE (units 10^{-5})	EVTS	DOCUMENT ID	TECN	COMMENT
--------------------------	------	-------------	------	---------

• • • We do not use the following data for averages, fits, limits, etc. • • •

1.23 ± 0.23 ± 0.08 30 ¹ DOBBS 17 $e^+e^- \rightarrow \psi(2S) \rightarrow$ hadrons

¹ Using CLEO-c data but not authored by the CLEO Collaboration.

 $\Gamma(\Sigma^0\bar{p}K^+ + \text{c.c.})/\Gamma_{\text{total}}$ Γ_{137}/Γ

VALUE (units 10^{-5})	EVTS	DOCUMENT ID	TECN	COMMENT
1.67 ± 0.13 ± 0.12	276	¹ ABLIKIM	13D BES3	$\psi(2S) \rightarrow \gamma\Lambda\bar{p}K^+$

¹ Using $B(\Lambda \rightarrow p\pi^-) = 63.9\%$, and $B(\Sigma^0 \rightarrow \Lambda\gamma) = 100\%$.

 $\Gamma(\Sigma^+\bar{\Sigma}^-)/\Gamma_{\text{total}}$ Γ_{138}/Γ

VALUE (units 10^{-4})	EVTS	DOCUMENT ID	TECN	COMMENT
2.43 ± 0.10 OUR AVERAGE	Error includes scale factor of 1.4.			

2.52 ± 0.04 ± 0.09 5.4k ABLIKIM 21AT BES3 $\psi(2S) \rightarrow p\pi^0\bar{p}\pi^0$

2.31 ± 0.06 ± 0.10 1.9k ¹ DOBBS 17 $e^+e^- \rightarrow \psi(2S) \rightarrow$ hadrons

2.57 ± 0.44 ± 0.68 35 PEDLAR 05 CLEO $e^+e^- \rightarrow \psi(2S) \rightarrow$ hadrons

• • • We do not use the following data for averages, fits, limits, etc. • • •

2.51 ± 0.15 ± 0.16 281 ^{1,2} DOBBS 14 $e^+e^- \rightarrow \psi(2S) \rightarrow$ hadrons

¹ Using CLEO-c data but not authored by the CLEO Collaboration.

² Superseded by DOBBS 17.

 $\Gamma(\Sigma^0\bar{\Sigma}^0)/\Gamma_{\text{total}}$ Γ_{139}/Γ

VALUE (units 10^{-4})	EVTS	DOCUMENT ID	TECN	COMMENT
2.35 ± 0.09 OUR AVERAGE	Error includes scale factor of 1.1.			

2.44 ± 0.03 ± 0.11 7k ABLIKIM 17L BES3 $e^+e^- \rightarrow \psi(2S) \rightarrow$ hadrons

2.22 ± 0.05 ± 0.11 2.6k ¹ DOBBS 17 $e^+e^- \rightarrow \psi(2S) \rightarrow$ hadrons

2.35 ± 0.36 ± 0.32 59 ABLIKIM 07c BES $e^+e^- \rightarrow \psi(2S) \rightarrow$ hadrons

2.63 ± 0.35 ± 0.21 58 PEDLAR 05 CLEO $e^+e^- \rightarrow \psi(2S) \rightarrow$ hadrons

• • • We do not use the following data for averages, fits, limits, etc. • • •

2.25 ± 0.11 ± 0.16 439 ^{1,2} DOBBS 14 $e^+e^- \rightarrow \psi(2S) \rightarrow$ hadrons

1.2 ± 0.4 ± 0.4 8 ³ BAI 01 BES $e^+e^- \rightarrow \psi(2S) \rightarrow$ hadrons

¹ Using CLEO-c data but not authored by the CLEO Collaboration.

² Superseded by DOBBS 17.

³ Estimated using $B(\psi(2S) \rightarrow J/\psi\pi^+\pi^-) = 0.310 \pm 0.028$.

 $\Gamma(\Sigma(1385)^+\bar{\Sigma}(1385)^-)/\Gamma_{\text{total}}$ Γ_{140}/Γ

VALUE (units 10^{-5})	EVTS	DOCUMENT ID	TECN	COMMENT
--------------------------	------	-------------	------	---------

8.5 ± 0.7 OUR AVERAGE

8.4 ± 0.5 ± 0.5 1.5k ABLIKIM 16L BES3 $\psi(2S) \rightarrow \Sigma(1385)^+\bar{\Sigma}(1385)^-$

11 ± 3 ± 3 14 ¹ BAI 01 BES $e^+e^- \rightarrow \psi(2S) \rightarrow$ hadrons

¹ Estimated using $B(\psi(2S) \rightarrow J/\psi\pi^+\pi^-) = 0.310 \pm 0.028$.

 $\Gamma(\Sigma(1385)^-\bar{\Sigma}(1385)^+)/\Gamma_{\text{total}}$ Γ_{141}/Γ

VALUE (units 10^{-5})	EVTS	DOCUMENT ID	TECN	COMMENT
--------------------------	------	-------------	------	---------

8.5 ± 0.6 ± 0.6 1.4k ABLIKIM 16L BES3 $\psi(2S) \rightarrow \Sigma(1385)^-\bar{\Sigma}(1385)^+$

0.69 ± 0.05 ± 0.05 2.2k ABLIKIM 17E BES3 $e^+e^- \rightarrow \psi(2S) \rightarrow$
hadrons

 $\Gamma(\Sigma(1385)^0\bar{\Sigma}(1385)^0)/\Gamma_{\text{total}}$ Γ_{142}/Γ

VALUE (units 10^{-4})	EVTS	DOCUMENT ID	TECN	COMMENT
--------------------------	------	-------------	------	---------

2.87 ± 0.11 OUR AVERAGE

3.03 ± 0.05 ± 0.14 3.6k Error includes scale factor of 1.1.

2.78 ± 0.05 ± 0.14 5k ABLIKIM 16L BES3 $\psi(2S) \rightarrow \Xi^-\bar{\Xi}^+$

3.03 ± 0.40 ± 0.32 67 ABLIKIM 07c BES $e^+e^- \rightarrow \psi(2S) \rightarrow$ hadrons

2.38 ± 0.30 ± 0.21 63 PEDLAR 05 CLEO $e^+e^- \rightarrow \psi(2S) \rightarrow$ hadrons

• • • We do not use the following data for averages, fits, limits, etc. • • •

2.66 ± 0.12 ± 0.20 548 ^{1,2} DOBBS 14 $e^+e^- \rightarrow \psi(2S) \rightarrow$ hadrons

0.94 ± 0.27 ± 0.15 12 ³ BAI 01 BES $e^+e^- \rightarrow \psi(2S) \rightarrow$ hadrons

<2 90 FELDMAN 77 MRK1 $e^+e^- \rightarrow \psi(2S) \rightarrow$ hadrons

¹ Using CLEO-c data but not authored by the CLEO Collaboration.

² Superseded by DOBBS 17.

³ Estimated using $B(\psi(2S) \rightarrow J/\psi\pi^+\pi^-) = 0.310 \pm 0.028$.

 $\Gamma(\Xi^0\bar{\Xi}^0)/\Gamma_{\text{total}}$ Γ_{144}/Γ

VALUE (units 10^{-4})	EVTS	DOCUMENT ID	TECN	COMMENT
--------------------------	------	-------------	------	---------

2.3 ± 0.4 OUR AVERAGE Error includes scale factor of 4.2.

2.73 ± 0.03 ± 0.13 11k ABLIKIM 17E BES3 $e^+e^- \rightarrow \psi(2S) \rightarrow$ hadrons

1.97 ± 0.06 ± 0.11 1.2k ¹ DOBBS 17 $e^+e^- \rightarrow \psi(2S) \rightarrow$ hadrons

2.75 ± 0.64 ± 0.61 19 PEDLAR 05 CLEO $e^+e^- \rightarrow \psi(2S) \rightarrow$ hadrons

• • • We do not use the following data for averages, fits, limits, etc. • • •

2.02 ± 0.19 ± 0.15 112 ^{1,2} DOBBS 14 $e^+e^- \rightarrow \psi(2S) \rightarrow$ hadrons

¹ Using CLEO-c data but not authored by the CLEO Collaboration.

² Superseded by DOBBS 17.

 $\Gamma(\Xi(1530)^0\bar{\Xi}(1530)^0)/\Gamma_{\text{total}}$ Γ_{145}/Γ

VALUE (units 10^{-5})	CL% EVTS	DOCUMENT ID	TECN	COMMENT
--------------------------	----------	-------------	------	---------

6.77 ± 0.14 ± 0.39 2951 ABLIKIM 21A0 BES3 $e^+e^- \rightarrow \psi(2S) \rightarrow$
hadrons

• • • We do not use the following data for averages, fits, limits, etc. • • •

<32 90 PEDLAR 05 CLEO $e^+e^- \rightarrow \psi(2S) \rightarrow$ hadrons

< 8.1 90 ¹ BAI 01 BES $e^+e^- \rightarrow \psi(2S) \rightarrow$ hadrons

¹ Estimated using $B(\psi(2S) \rightarrow J/\psi\pi^+\pi^-) = 0.310 \pm 0.028$.

 $\Gamma(\Lambda\bar{\Xi}^+K^- + \text{c.c.})/\Gamma_{\text{total}}$ Γ_{146}/Γ

VALUE (units 10^{-5})	EVTS	DOCUMENT ID	TECN	COMMENT
--------------------------	------	-------------	------	---------

3.86 ± 0.27 ± 0.32 236 ABLIKIM 15I BES3 $e^+e^- \rightarrow \psi(2S) \rightarrow$
 $K^-\Lambda\bar{\Xi}^+ + \text{c.c.}$

 $\Gamma(\Xi(1530)^-\bar{\Xi}(1530)^+)/\Gamma_{\text{total}}$ Γ_{147}/Γ

VALUE (units 10^{-5})	EVTS	DOCUMENT ID	TECN	COMMENT
--------------------------	------	-------------	------	---------

11.45 ± 0.40 ± 0.59 5k ABLIKIM 19AT BES3 $e^+e^- \rightarrow \psi(2S) \rightarrow$
hadrons

 $\Gamma(\Xi(1530)^-\bar{\Xi}^+)/\Gamma_{\text{total}}$ Γ_{148}/Γ

VALUE (units 10^{-6})	EVTS	DOCUMENT ID	TECN	COMMENT
--------------------------	------	-------------	------	---------

7.0 ± 1.1 ± 0.4 399 ABLIKIM 19AT BES3 $e^+e^- \rightarrow \psi(2S) \rightarrow$ hadrons

 $\Gamma(\Xi(1530)^0\bar{\Xi}^0)/\Gamma_{\text{total}}$ Γ_{149}/Γ

VALUE (units 10^{-5})	EVTS	DOCUMENT ID	TECN	COMMENT
--------------------------	------	-------------	------	---------

0.53 ± 0.04 ± 0.03 278 ABLIKIM 21A0 BES3 $e^+e^- \rightarrow \psi(2S) \rightarrow$ hadrons

 $\Gamma(\Xi(1690)^-\bar{\Xi}^+ \rightarrow K^-\Lambda\bar{\Xi}^+ + \text{c.c.})/\Gamma_{\text{total}}$ Γ_{150}/Γ

VALUE (units 10^{-6})	EVTS	DOCUMENT ID	TECN	COMMENT
--------------------------	------	-------------	------	---------

5.21 ± 1.48 ± 0.57 74 ABLIKIM 15I BES3 $e^+e^- \rightarrow \psi(2S) \rightarrow$
 $K^-\Lambda\bar{\Xi}^+ + \text{c.c.}$

$\Gamma(\Xi(1820)^-\Xi^+ \rightarrow K^-\Lambda\Xi^+ + \text{c.c.})/\Gamma_{\text{total}}$					Γ_{151}/Γ
VALUE (units 10^{-6})	EVTS	DOCUMENT ID	TECN	COMMENT	
12.03 ± 2.94 ± 1.22	136	ABLIKIM	15i BES3	$e^+e^- \rightarrow \psi(2S) \rightarrow K^-\Lambda\Xi^+ + \text{c.c.}$	

$\Gamma(\Sigma^0\Xi^+ K^- + \text{c.c.})/\Gamma_{\text{total}}$					Γ_{152}/Γ
VALUE (units 10^{-5})	EVTS	DOCUMENT ID	TECN	COMMENT	
3.67 ± 0.33 ± 0.28	142	ABLIKIM	15i BES3	$e^+e^- \rightarrow \psi(2S) \rightarrow K^-\Sigma^0\Xi^+ + \text{c.c.}$	

$\Gamma(\Omega^-\bar{\Omega}^+)/\Gamma_{\text{total}}$					Γ_{153}/Γ
VALUE (units 10^{-5})	CL%	EVTS	DOCUMENT ID	TECN	COMMENT
5.66 ± 0.30 OUR AVERAGE			Error includes scale factor of 1.3.		
5.85 ± 0.12 ± 0.25		4k	¹ ABLIKIM	21E BES3	$\psi(2S) \rightarrow \Omega^-\bar{\Omega}^+ \rightarrow \Lambda K^-\bar{\Lambda} K^+$
5.2 ± 0.3 ± 0.3		326	^{1,2} DOBBS	17	$e^+e^- \rightarrow \psi(2S) \rightarrow \text{hadrons}$

• • • We do not use the following data for averages, fits, limits, etc. • • •

4.7 ± 0.9 ± 0.5		27	^{1,2,3} DOBBS	14	$e^+e^- \rightarrow \psi(2S) \rightarrow \text{hadrons}$
<15		90	ABLIKIM	12Q BES2	$e^+e^- \rightarrow \psi(2S) \rightarrow \text{hadrons}$
<16		90	PEDLAR	05 CLEO	$e^+e^- \rightarrow \psi(2S) \rightarrow \text{hadrons}$
< 7.3		90	⁴ BAI	01 BES	$e^+e^- \rightarrow \psi(2S) \rightarrow \text{hadrons}$

¹ Using $B(\Omega^- \rightarrow \Lambda K^-) = (67.8 \pm 0.7)\%$ and $B(\Lambda \rightarrow p\pi^-) = (63.9 \pm 0.5)\%$.
² Using CLEO-c data but not authored by the CLEO Collaboration.
³ Superseded by DOBBS 17.
⁴ Estimated using $B(\psi(2S) \rightarrow J/\psi\pi^+\pi^-) = 0.310 \pm 0.028$.

$\Gamma(\eta_c\pi^+\pi^-\pi^0)/\Gamma_{\text{total}}$					Γ_{154}/Γ
VALUE (units 10^{-3})	CL%	DOCUMENT ID	TECN	COMMENT	
<1.0		90	PEDLAR	07 CLEO	$e^+e^- \rightarrow \psi(2S)$

$\Gamma(h_c(1P)\pi^0)/\Gamma_{\text{total}}$					Γ_{155}/Γ
VALUE (units 10^{-4})	CL%	EVTS	DOCUMENT ID	TECN	COMMENT
8.6 ± 1.3 OUR AVERAGE					
9.0 ± 1.5 ± 1.3		3k	¹ GE	11 CLEO	$\psi(2S) \rightarrow \pi^0 \text{ anything}$
8.4 ± 1.3 ± 1.0		11k	ABLIKIM	10B BES3	$\psi(2S) \rightarrow \pi^0 h_c$
seen		92^{+23}_{-22}	ADAMS	09 CLEO	$\psi(2S) \rightarrow 2\pi^+ 2\pi^- 2\pi^0$
seen		1282	DOBBS	08A CLEO	$\psi(2S) \rightarrow \pi^0 \eta_c \gamma$
seen		168 ± 40	ROSNER	05 CLEO	$\psi(2S) \rightarrow \pi^0 \eta_c \gamma$

• • • We do not use the following data for averages, fits, limits, etc. • • •

¹ Assuming a width $\Gamma(h_c(1P)) = 0.86 \text{ MeV} \equiv \Gamma_0$, a measured dependence of the central value of $B = (7.6 + 1.4 \times \Gamma(h_c(1P))/\Gamma_0) \times 10^{-4}$, and with a systematic error that accounts for the width variation range 0.43–1.29 MeV.

$\Gamma(\Lambda_c^+ \bar{p} e^+ e^- + \text{c.c.})/\Gamma_{\text{total}}$					Γ_{156}/Γ
VALUE	CL%	EVTS	DOCUMENT ID	TECN	COMMENT
<1.7 × 10⁻⁶		90 450M	ABLIKIM	18Q BES3	$e^+e^- \rightarrow \psi(2S)$

$\Gamma(\Theta(1540)\bar{\Theta}(1540) \rightarrow K_S^0 p K^- \bar{n} + \text{c.c.})/\Gamma_{\text{total}}$					Γ_{157}/Γ
VALUE (units 10^{-5})	CL%	DOCUMENT ID	TECN	COMMENT	
<0.88		90	BAI	04G BES2	e^+e^-

$\Gamma(\Theta(1540)K^-\bar{n} \rightarrow K_S^0 p K^-\bar{n})/\Gamma_{\text{total}}$					Γ_{158}/Γ
VALUE (units 10^{-5})	CL%	DOCUMENT ID	TECN	COMMENT	
<1.0		90	BAI	04G BES2	e^+e^-

$\Gamma(\Theta(1540)K_S^0 \bar{p} \rightarrow K_S^0 \bar{p} K^+ n)/\Gamma_{\text{total}}$					Γ_{159}/Γ
VALUE (units 10^{-5})	CL%	DOCUMENT ID	TECN	COMMENT	
<0.70		90	BAI	04G BES2	e^+e^-

$\Gamma(\bar{\Theta}(1540)K^+ n \rightarrow K_S^0 \bar{p} K^+ n)/\Gamma_{\text{total}}$					Γ_{160}/Γ
VALUE (units 10^{-5})	CL%	DOCUMENT ID	TECN	COMMENT	
<2.6		90	BAI	04G BES2	e^+e^-

$\Gamma(\bar{\Theta}(1540)K_S^0 p \rightarrow K_S^0 p K^-\bar{n})/\Gamma_{\text{total}}$					Γ_{161}/Γ
VALUE (units 10^{-5})	CL%	DOCUMENT ID	TECN	COMMENT	
<0.60		90	BAI	04G BES2	e^+e^-

RADIATIVE DECAYS

$\Gamma(\gamma\chi_{c0}(1P))/\Gamma_{\text{total}}$					Γ_{162}/Γ
VALUE (units 10^{-2})	CL%	EVTS	DOCUMENT ID	TECN	COMMENT
9.79 ± 0.20 OUR FIT					
9.33 ± 0.26 OUR AVERAGE					
9.389 ± 0.014 ± 0.332		4.7M	ABLIKIM	17U BES3	$e^+e^- \rightarrow \gamma X$
9.22 ± 0.11 ± 0.46		72k	ATHAR	04 CLEO	$e^+e^- \rightarrow \gamma X$
9.9 ± 0.5 ± 0.8			¹ GAISER	86 CBAL	$e^+e^- \rightarrow \gamma X$
7.2 ± 2.3			¹ BIDDICK	77 CNTR	$e^+e^- \rightarrow \gamma X$
7.5 ± 2.6			¹ WHITAKER	76 MRK1	e^+e^-

¹ Angular distribution $(1+\cos^2\theta)$ assumed.

$\Gamma(\gamma\chi_{c1}(1P))/\Gamma_{\text{total}}$					Γ_{163}/Γ
VALUE (units 10^{-2})	CL%	EVTS	DOCUMENT ID	TECN	COMMENT
9.75 ± 0.24 OUR FIT					
9.54 ± 0.29 OUR AVERAGE					
9.905 ± 0.011 ± 0.353		5.0M	ABLIKIM	17U BES3	$e^+e^- \rightarrow \gamma X$
9.07 ± 0.11 ± 0.54		76k	ATHAR	04 CLEO	$e^+e^- \rightarrow \gamma X$
9.0 ± 0.5 ± 0.7			¹ GAISER	86 CBAL	$e^+e^- \rightarrow \gamma X$
7.1 ± 1.9			² BIDDICK	77 CNTR	$e^+e^- \rightarrow \gamma X$

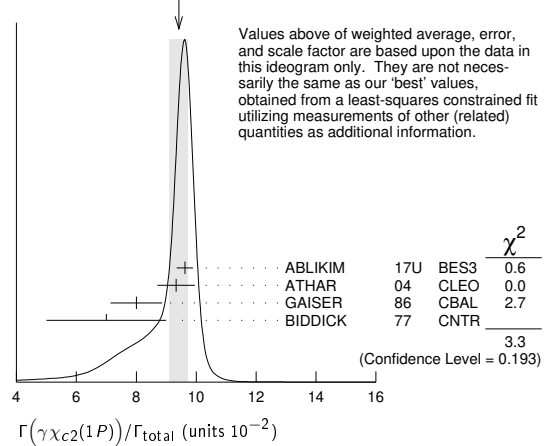
¹ Angular distribution $(1-0.189 \cos^2\theta)$ assumed.
² Valid for isotropic distribution of the photon.

$\Gamma(\gamma\chi_{c0}(1P))/\Gamma(\gamma\chi_{c1}(1P))$					$\Gamma_{162}/\Gamma_{163}$
VALUE	CL%	EVTS	DOCUMENT ID	TECN	COMMENT
• • •					We do not use the following data for averages, fits, limits, etc. • • •
1.02 ± 0.01 ± 0.07			¹ ATHAR	04 CLEO	$e^+e^- \rightarrow \gamma X$

¹ Not independent from ATHAR 04 measurements of $B(\gamma\chi_{cJ})$.

$\Gamma(\gamma\chi_{c2}(1P))/\Gamma_{\text{total}}$					Γ_{164}/Γ
VALUE (units 10^{-2})	CL%	EVTS	DOCUMENT ID	TECN	COMMENT
9.52 ± 0.20 OUR FIT					
9.42 ± 0.31 OUR AVERAGE					Error includes scale factor of 1.3. See the ideogram below.
9.621 ± 0.013 ± 0.272		4.2M	ABLIKIM	17U BES3	$e^+e^- \rightarrow \gamma X$
9.33 ± 0.14 ± 0.61		79k	ATHAR	04 CLEO	$e^+e^- \rightarrow \gamma X$
8.0 ± 0.5 ± 0.7			¹ GAISER	86 CBAL	$e^+e^- \rightarrow \gamma X$
7.0 ± 2.0			² BIDDICK	77 CNTR	$e^+e^- \rightarrow \gamma X$

WEIGHTED AVERAGE
 9.42 ± 0.31 (Error scaled by 1.3)



$[\Gamma(\gamma\chi_{c0}(1P)) + \Gamma(\gamma\chi_{c1}(1P)) + \Gamma(\gamma\chi_{c2}(1P))]/\Gamma_{\text{total}}$					$(\Gamma_{162} + \Gamma_{163} + \Gamma_{164})/\Gamma$
VALUE	CL%	EVTS	DOCUMENT ID	TECN	COMMENT
• • •					We do not use the following data for averages, fits, limits, etc. • • •
27.6 ± 0.3 ± 2.0			¹ ATHAR	04 CLEO	$e^+e^- \rightarrow \gamma X$

¹ Not independent from ATHAR 04 measurements of $B(\gamma\chi_{cJ})$.

$\Gamma(\gamma\chi_{c0}(1P))/\Gamma(\gamma\chi_{c2}(1P))$					$\Gamma_{162}/\Gamma_{164}$
VALUE	CL%	EVTS	DOCUMENT ID	TECN	COMMENT
• • •					We do not use the following data for averages, fits, limits, etc. • • •
0.99 ± 0.02 ± 0.08			¹ ATHAR	04 CLEO	$e^+e^- \rightarrow \gamma X$

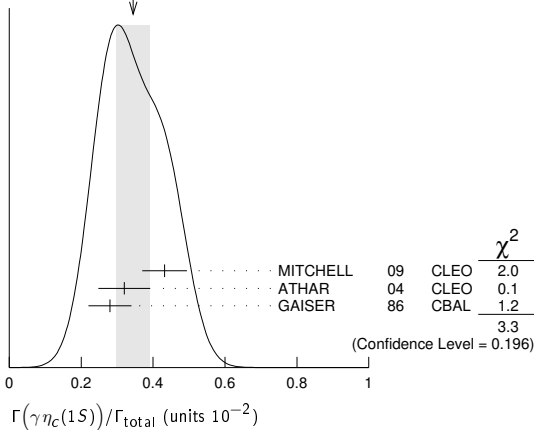
¹ Not independent from ATHAR 04 measurements of $B(\gamma\chi_{cJ})$.

$\Gamma(\gamma\chi_{c2}(1P))/\Gamma(\gamma\chi_{c1}(1P))$					$\Gamma_{164}/\Gamma_{163}$
VALUE	CL%	EVTS	DOCUMENT ID	TECN	COMMENT
• • •					We do not use the following data for averages, fits, limits, etc. • • •
1.03 ± 0.02 ± 0.03			¹ ATHAR	04 CLEO	$e^+e^- \rightarrow \gamma X$

¹ Not independent from ATHAR 04 measurements of $B(\gamma\chi_{cJ})$.

$\Gamma(\gamma\eta_c(1S))/\Gamma_{\text{total}}$					Γ_{165}/Γ
VALUE (units 10^{-2})	CL%	EVTS	DOCUMENT ID	TECN	COMMENT
0.34 ± 0.05 OUR AVERAGE					Error includes scale factor of 1.3. See the ideogram below.
0.432 ± 0.016 ± 0.060			MITCHELL	09 CLEO	$e^+e^- \rightarrow \gamma X$
0.32 ± 0.04 ± 0.06		2.5k	¹ ATHAR	04 CLEO	$e^+e^- \rightarrow \gamma X$
0.28 ± 0.06			² GAISER	86 CBAL	$e^+e^- \rightarrow \gamma X$

Meson Particle Listings

 $\psi(2S)$ WEIGHTED AVERAGE
0.34±0.05 (Error scaled by 1.3)

¹ ATHAR 04 used $\Gamma_{\eta_c(1S)} = 24.8 \pm 4.9$ MeV to obtain this result.

² GAISER 86 used $\Gamma_{\eta_c(1S)} = 11.5 \pm 4.5$ MeV to obtain this result.

 $\Gamma(\gamma\eta_c(2S))/\Gamma_{total}$ Γ_{166}/Γ

VALUE (units 10^{-4})	CL%	DOCUMENT ID	TECN	COMMENT
7±2±4		¹ ABLIKIM	12G	BES3 $\psi(2S) \rightarrow \gamma K^0 K\pi, K\bar{K}\pi$
•••		We do not use the following data for averages, fits, limits, etc. •••		
< 8	90	² CRONIN-HEN..10	CLEO	$\psi(2S) \rightarrow \gamma K\bar{K}\pi$
< 20	90	ATHAR	04	CLEO $e^+e^- \rightarrow \gamma X$
20-130	95	EDWARDS	82c	CBAL $e^+e^- \rightarrow \gamma X$

¹ ABLIKIM 12G reports $[\Gamma(\psi(2S) \rightarrow \gamma\eta_c(2S))/\Gamma_{total}] \times [B(\eta_c(2S) \rightarrow K\bar{K}\pi)] = (1.30 \pm 0.20 \pm 0.30) \times 10^{-5}$ which we divide by our best value $B(\eta_c(2S) \rightarrow K\bar{K}\pi) = (1.9 \pm 1.2) \times 10^{-2}$. Our first error is their experiment's error and our second error is the systematic error from using our best value.

² CRONIN-HENNESSY 10 reports $[\Gamma(\psi(2S) \rightarrow \gamma\eta_c(2S))/\Gamma_{total}] \times [B(\eta_c(2S) \rightarrow K\bar{K}\pi)] < 14.5 \times 10^{-6}$ which we divide by our best value $B(\eta_c(2S) \rightarrow K\bar{K}\pi) = 1.9 \times 10^{-2}$. This measurement assumes $\Gamma(\eta_c(2S)) = 14$ MeV. CRONIN-HENNESSY 10 gives the analytic dependence of limits on width.

 $\Gamma(\gamma\pi^0)/\Gamma_{total}$ Γ_{167}/Γ

VALUE (units 10^{-6})	CL%	EVTS	DOCUMENT ID	TECN	COMMENT
1.04±0.22 OUR AVERAGE					Error includes scale factor of 1.4.
0.95±0.16±0.05		423	ABLIKIM	17X	BES3 $\psi(2S) \rightarrow \gamma\pi^0$
1.58±0.40±0.13		37	ABLIKIM	10F	BES3 $\psi(2S) \rightarrow \gamma\pi^0$
•••		We do not use the following data for averages, fits, limits, etc. •••			
< 5	90		PEDLAR	09	CLE3 $\psi(2S) \rightarrow \gamma X$
< 5400	95		¹ LIBERMAN	75	SPEC e^+e^-
< 1×10^4	90		WIJK	75	DASP e^+e^-

¹ Restated by us using $B(\psi(2S) \rightarrow \mu^+\mu^-) = 0.0077$.

 $\Gamma(\gamma 2(\pi^+\pi^-))/\Gamma_{total}$ Γ_{168}/Γ

VALUE (units 10^{-5})	EVTS	DOCUMENT ID	TECN	COMMENT
39.6±2.8±5.0	583	ABLIKIM	07D	BES2 $e^+e^- \rightarrow \psi(2S)$

 $\Gamma(\gamma 3(\pi^+\pi^-))/\Gamma_{total}$ Γ_{169}/Γ

VALUE (units 10^{-5})	CL%	DOCUMENT ID	TECN	COMMENT
< 17	90	ABLIKIM	07D	BES2 $e^+e^- \rightarrow \psi(2S)$

 $\Gamma(\gamma\eta'(958))/\Gamma_{total}$ Γ_{170}/Γ

VALUE (units 10^{-4})	CL%	EVTS	DOCUMENT ID	TECN	COMMENT
1.24 ± 0.04 OUR AVERAGE					
1.251 ± 0.022 ± 0.062		56k	ABLIKIM	17X	BES3 $\psi(2S) \rightarrow \gamma\pi^+\pi^-\eta, \gamma\pi^0\pi^0\eta$
1.26 ± 0.03 ± 0.08		2226	¹ ABLIKIM	10F	BES3 $\psi(2S) \rightarrow 3\gamma\pi^+\pi^-, 2\gamma\pi^+\pi^-$
1.19 ± 0.08 ± 0.03			PEDLAR	09	CLE3 $\psi(2S) \rightarrow \gamma X$
1.24 ± 0.27 ± 0.15		23	ABLIKIM	06R	BES2 $e^+e^- \rightarrow \psi(2S)$
1.54 ± 0.31 ± 0.20		~ 43	BAI	98F	BES $\psi(2S) \rightarrow \pi^+\pi^- 2\gamma, \pi^+\pi^-\pi^-\pi^-\gamma$

••• We do not use the following data for averages, fits, limits, etc. •••

< 60 90 ² BRAUNSCH... 77 DASP e^+e^-

< 11 90 ³ BARTEL 76 CNTR e^+e^-

¹ Combining the results from $\eta' \rightarrow \pi^+\pi^-\eta$ and $\eta' \rightarrow \pi^+\pi^-\gamma$ decay modes.

² Restated by us using total decay width 228 keV.

³ The value is normalized to the branching ratio for $\Gamma(J/\psi(1S)\eta)/\Gamma_{total}$.

 $\Gamma(\gamma f_2(1270))/\Gamma_{total}$ Γ_{171}/Γ

VALUE (units 10^{-4})	EVTS	DOCUMENT ID	TECN	COMMENT
2.73±0.29 OUR AVERAGE				Error includes scale factor of 1.8.
2.84±0.15±0.03	1.9k	^{1,2} DOBBS	15	$\psi(2S) \rightarrow \gamma\pi\pi$
2.12±0.19±0.32		^{3,4} BAI	03c	BES $\psi(2S) \rightarrow \gamma\pi\pi$
•••		We do not use the following data for averages, fits, limits, etc. •••		
2.08±0.19±0.33	200.6 ± 18.8	³ BAI	03c	BES $\psi(2S) \rightarrow \gamma\pi^+\pi^-$
2.90±1.08±1.07	29.9 ± 11.1	³ BAI	03c	BES $\psi(2S) \rightarrow \gamma\pi^0\pi^0$

¹ Using CLEO-c data but not authored by the CLEO Collaboration.

² DOBBS 15 reports $[\Gamma(\psi(2S) \rightarrow \gamma f_2(1270))/\Gamma_{total}] \times [B(f_2(1270) \rightarrow \pi\pi)] = (2.39 \pm 0.09 \pm 0.09) \times 10^{-4}$ which we divide by our best value $B(f_2(1270) \rightarrow \pi\pi) = (84.2 \pm 2.9) \times 10^{-2}$. Our first error is their experiment's error and our second error is the systematic error from using our best value.

³ Normalized to $B(\psi(2S) \rightarrow J/\psi\pi^+\pi^-) = 0.305 \pm 0.016$.

⁴ Combining the results from $\pi^+\pi^-$ and $\pi^0\pi^0$ decay modes.

 $\Gamma(\gamma f_0(1370) \rightarrow \gamma K\bar{K})/\Gamma_{total}$ Γ_{172}/Γ

VALUE (units 10^{-5})	EVTS	DOCUMENT ID	COMMENT
3.1±1.0±1.4	175	¹ DOBBS	15 $\psi(2S) \rightarrow \gamma K\bar{K}$

¹ Using CLEO-c data but not authored by the CLEO Collaboration.

 $\Gamma(\gamma f_0(1500))/\Gamma_{total}$ Γ_{173}/Γ

VALUE (units 10^{-5})	EVTS	DOCUMENT ID	COMMENT
9.3±1.8±0.6	274	^{1,2} DOBBS	15 $\psi(2S) \rightarrow \gamma\pi\pi$

¹ DOBBS 15 reports $[\Gamma(\psi(2S) \rightarrow \gamma f_0(1500))/\Gamma_{total}] \times [B(f_0(1500) \rightarrow \pi\pi)] = (3.2 \pm 0.6 \pm 0.2) \times 10^{-5}$ which we divide by our best value $B(f_0(1500) \rightarrow \pi\pi) = (34.5 \pm 2.2) \times 10^{-2}$. Our first error is their experiment's error and our second error is the systematic error from using our best value.

² Using CLEO-c data but not authored by the CLEO Collaboration.

 $\Gamma(\gamma f_2'(1525))/\Gamma_{total}$ Γ_{174}/Γ

VALUE (units 10^{-5})	EVTS	DOCUMENT ID	COMMENT
3.3±0.8±0.1	136	^{1,2} DOBBS	15 $\psi(2S) \rightarrow \gamma K\bar{K}$

¹ DOBBS 15 reports $[\Gamma(\psi(2S) \rightarrow \gamma f_2'(1525))/\Gamma_{total}] \times [B(f_2'(1525) \rightarrow K\bar{K})] = (2.9 \pm 0.6 \pm 0.3) \times 10^{-5}$ which we divide by our best value $B(f_2'(1525) \rightarrow K\bar{K}) = (87.6 \pm 2.2) \times 10^{-2}$. Our first error is their experiment's error and our second error is the systematic error from using our best value.

² Using CLEO-c data but not authored by the CLEO Collaboration.

 $\Gamma(\gamma f_0(1710) \rightarrow \gamma\pi\pi)/\Gamma_{total}$ Γ_{176}/Γ

VALUE (units 10^{-5})	EVTS	DOCUMENT ID	TECN	COMMENT
3.5 ± 0.6 OUR AVERAGE				
3.6 ± 0.4 ± 0.5	290	¹ DOBBS	15	$\psi(2S) \rightarrow \gamma\pi\pi$
3.01±0.41±1.24	35.6 ± 4.8	² BAI	03c	BES $\psi(2S) \rightarrow \gamma\pi^+\pi^-$

¹ Using CLEO-c data but not authored by the CLEO Collaboration.

² Normalized to $B(\psi(2S) \rightarrow J/\psi\pi^+\pi^-) = 0.305 \pm 0.016$.

 $\Gamma(\gamma f_0(1710) \rightarrow \gamma K\bar{K})/\Gamma_{total}$ Γ_{177}/Γ

VALUE (units 10^{-5})	CL%	EVTS	DOCUMENT ID	TECN	COMMENT
6.6 ± 0.7 OUR AVERAGE					
6.7 ± 0.6 ± 0.6		375	¹ DOBBS	15	$\psi(2S) \rightarrow \gamma K\bar{K}$
6.04±0.90±1.32		39.6 ± 5.9	^{2,3} BAI	03c	BES $\psi(2S) \rightarrow \gamma K^+K^-$

••• We do not use the following data for averages, fits, limits, etc. •••

< 15.6 90 6.8 ± 3.1 ^{2,3} BAI 03c BES $\psi(2S) \rightarrow \gamma K_S^0 K_S^0$

¹ Using CLEO-c data but not authored by the CLEO Collaboration.

² Includes unknown branching fractions to K^+K^- or $K_S^0 K_S^0$. We have multiplied the K^+K^- result by a factor of 2 and the $K_S^0 K_S^0$ result by a factor of 4 to obtain the $K\bar{K}$ result.

³ Normalized to $B(\psi(2S) \rightarrow J/\psi\pi^+\pi^-) = 0.305 \pm 0.016$.

 $\Gamma(\gamma f_0(2100) \rightarrow \gamma\pi\pi)/\Gamma_{total}$ Γ_{178}/Γ

VALUE (units 10^{-6})	EVTS	DOCUMENT ID	COMMENT
4.8±0.5±0.9	373	¹ DOBBS	15 $\psi(2S) \rightarrow \gamma\pi\pi$

¹ Using CLEO-c data but not authored by the CLEO Collaboration.

 $\Gamma(\gamma f_0(2200) \rightarrow \gamma K\bar{K})/\Gamma_{total}$ Γ_{179}/Γ

VALUE (units 10^{-6})	EVTS	DOCUMENT ID	COMMENT
3.2±0.6±0.8	207	¹ DOBBS	15 $\psi(2S) \rightarrow \gamma K\bar{K}$

¹ Using CLEO-c data but not authored by the CLEO Collaboration.

 $\Gamma(\gamma f_J(2220) \rightarrow \gamma\pi\pi)/\Gamma_{total}$ Γ_{180}/Γ

VALUE	CL%	DOCUMENT ID	COMMENT
< 5.8 × 10⁻⁶	90	^{1,2} DOBBS	15 $\psi(2S) \rightarrow \gamma\pi\pi$

¹ Using CLEO-c data but not authored by the CLEO Collaboration.

² For $\Gamma = 20/50$ MeV, the 90% CL upper limits for $\pi^+\pi^-$ and $\pi^0\pi^0$ are $3.2/4.3 \times 10^{-6}$ and $2.6/4.0 \times 10^{-6}$, respectively.

See key on page 1127

Meson Particle Listings

$\psi(2S)$

$\Gamma(\gamma f_J(2220) \rightarrow \gamma K \bar{K})/\Gamma_{\text{total}}$					Γ_{181}/Γ
VALUE	CL%	DOCUMENT ID	TECN	COMMENT	
$<9.5 \times 10^{-6}$	90	^{1,2} DOBBS	15	$\psi(2S) \rightarrow \gamma K \bar{K}$	

¹ Using CLEO-c data but not authored by the CLEO Collaboration.
² For $\Gamma = 20/50$ MeV, the 90% CL upper limits for $K^+ K^-$ and $K_S^0 K_S^0$ are $2.1/4.3 \times 10^{-6}$ and $3.7/5.5 \times 10^{-6}$, respectively.

$\Gamma(\gamma \eta)/\Gamma_{\text{total}}$					Γ_{182}/Γ
VALUE (units 10^{-6})	CL%	EVTs	DOCUMENT ID	TECN	COMMENT
0.92 ± 0.18 OUR AVERAGE					
$0.85 \pm 0.18 \pm 0.04$		382	¹ ABLIKIM	17X BES3	$\psi(2S) \rightarrow \gamma \pi^+ \pi^- \pi^0$, $\gamma 3\pi^0$
$1.38 \pm 0.48 \pm 0.09$		13	¹ ABLIKIM	10F BES3	$\psi(2S) \rightarrow \gamma \pi^+ \pi^- \pi^0$, $\gamma 3\pi^0$

• • • We do not use the following data for averages, fits, limits, etc. • • •

< 2	90	PEDLAR	09	CLE3	$\psi(2S) \rightarrow \gamma X$
< 90	90	BAI	98F	BES	$\psi(2S) \rightarrow \pi^+ \pi^- 3\gamma$
< 200	90	YAMADA	77	DASP	$e^+ e^- \rightarrow 3\gamma$

¹ Combining the results from $\eta \rightarrow \pi^+ \pi^- \pi^0$ and $\eta \rightarrow 3\pi^0$ decay modes.

$\Gamma(\gamma \eta \pi^+ \pi^-)/\Gamma_{\text{total}}$					Γ_{183}/Γ
VALUE (units 10^{-4})	EVTs	DOCUMENT ID	TECN	COMMENT	
$8.71 \pm 1.25 \pm 1.64$	418	ABLIKIM	06R BES2	$\psi(2S) \rightarrow \gamma \eta \pi^+ \pi^-$	

$\Gamma(\gamma \eta(1405) \rightarrow \gamma K \bar{K} \pi)/\Gamma_{\text{total}}$					Γ_{185}/Γ
VALUE (units 10^{-4})	CL%	DOCUMENT ID	TECN	COMMENT	
<0.9	90	ABLIKIM	06R BES2	$\psi(2S) \rightarrow \gamma K_S^0 K^+ \pi^- + \text{c.c.}$	

• • • We do not use the following data for averages, fits, limits, etc. • • •

< 1.3	90	ABLIKIM	06R BES2	$\psi(2S) \rightarrow \gamma K^+ K^- \pi^0$
< 1.2	90	¹ SCHARRE	80 MRK1	$e^+ e^-$

¹ Includes unknown branching fraction $\eta(1405) \rightarrow K \bar{K} \pi$.

$\Gamma(\gamma \eta(1405) \rightarrow \gamma \eta \pi^+ \pi^-)/\Gamma_{\text{total}}$					Γ_{186}/Γ
VALUE (units 10^{-4})	EVTs	DOCUMENT ID	TECN	COMMENT	
$0.36 \pm 0.25 \pm 0.05$	10	ABLIKIM	06R BES2	$\psi(2S) \rightarrow \gamma \eta \pi^+ \pi^-$	

$\Gamma(\gamma \eta(1405) \rightarrow \gamma f_0(980) \pi^0 \rightarrow \gamma \pi^+ \pi^- \pi^0)/\Gamma_{\text{total}}$					Γ_{187}/Γ
VALUE	CL%	DOCUMENT ID	TECN	COMMENT	
$<5.0 \times 10^{-7}$	90	ABLIKIM	17AJ BES3	$\psi(2S) \rightarrow \gamma \pi^+ \pi^- \pi^0$	

$\Gamma(\gamma \eta(1475) \rightarrow \gamma K \bar{K} \pi)/\Gamma_{\text{total}}$					Γ_{189}/Γ
VALUE (units 10^{-4})	CL%	DOCUMENT ID	TECN	COMMENT	
<1.4	90	ABLIKIM	06R BES2	$\psi(2S) \rightarrow \gamma K^+ K^- \pi^0$	

• • • We do not use the following data for averages, fits, limits, etc. • • •

< 1.5	90	ABLIKIM	06R BES2	$\psi(2S) \rightarrow \gamma K_S^0 K^+ \pi^- + \text{c.c.}$
---------	----	---------	----------	---

$\Gamma(\gamma \eta(1475) \rightarrow \gamma \eta \pi^+ \pi^-)/\Gamma_{\text{total}}$					Γ_{190}/Γ
VALUE (units 10^{-4})	CL%	DOCUMENT ID	TECN	COMMENT	
<0.88	90	ABLIKIM	06R BES2	$\psi(2S) \rightarrow \gamma \eta \pi^+ \pi^-$	

$\Gamma(\gamma K^* K^+ \pi^- + \text{c.c.})/\Gamma_{\text{total}}$					Γ_{191}/Γ
VALUE (units 10^{-5})	EVTs	DOCUMENT ID	TECN	COMMENT	
$37.0 \pm 6.1 \pm 7.2$	237	ABLIKIM	07D BES2	$e^+ e^- \rightarrow \psi(2S)$	

$\Gamma(\gamma K^* K^0 \bar{K}^0)/\Gamma_{\text{total}}$					Γ_{192}/Γ
VALUE (units 10^{-5})	EVTs	DOCUMENT ID	TECN	COMMENT	
$24.0 \pm 4.5 \pm 5.0$	41	ABLIKIM	07D BES2	$e^+ e^- \rightarrow \psi(2S)$	

$\Gamma(\gamma K_S^0 K^+ \pi^- + \text{c.c.})/\Gamma_{\text{total}}$					Γ_{193}/Γ
VALUE (units 10^{-5})	EVTs	DOCUMENT ID	TECN	COMMENT	
$25.6 \pm 3.6 \pm 3.6$	115	ABLIKIM	07D BES2	$e^+ e^- \rightarrow \psi(2S)$	

$\Gamma(\gamma K^+ K^- \pi^+ \pi^-)/\Gamma_{\text{total}}$					Γ_{194}/Γ
VALUE (units 10^{-5})	EVTs	DOCUMENT ID	TECN	COMMENT	
$19.1 \pm 2.7 \pm 4.3$	132	ABLIKIM	07D BES2	$e^+ e^- \rightarrow \psi(2S)$	

$\Gamma(\gamma K^+ K^- 2(\pi^+ \pi^-))/\Gamma_{\text{total}}$					Γ_{195}/Γ
VALUE (units 10^{-5})	CL%	DOCUMENT ID	TECN	COMMENT	
<22	90	ABLIKIM	07D BES2	$e^+ e^- \rightarrow \psi(2S)$	

$\Gamma(\gamma 2(K^+ K^-))/\Gamma_{\text{total}}$					Γ_{196}/Γ
VALUE (units 10^{-5})	CL%	DOCUMENT ID	TECN	COMMENT	
<4	90	ABLIKIM	07D BES2	$e^+ e^- \rightarrow \psi(2S)$	

$\Gamma(\gamma \rho \bar{\rho})/\Gamma_{\text{total}}$					Γ_{197}/Γ
VALUE (units 10^{-5})	EVTs	DOCUMENT ID	TECN	COMMENT	
3.9 ± 0.5 OUR AVERAGE				Error includes scale factor of 2.0.	
$4.18 \pm 0.26 \pm 0.18$	348	¹ ALEXANDER	10 CLEO	$\psi(2S) \rightarrow \gamma \rho \bar{\rho}$	
$2.9 \pm 0.4 \pm 0.4$	142	ABLIKIM	07D BES2	$e^+ e^- \rightarrow \psi(2S)$	

¹ From a fit of the $\rho \bar{\rho}$ mass distribution to a combination of $\gamma f_2(1950)$, $\gamma f_2(2150)$, and $\gamma \rho \bar{\rho}$ phase space, for $M(\rho \bar{\rho}) < 2.85$ GeV, and accounting for backgrounds from $\psi(2S) \rightarrow \pi^0 \rho \bar{\rho}$ and continuum.

$\Gamma(\gamma f_2(1950) \rightarrow \gamma \rho \bar{\rho})/\Gamma_{\text{total}}$					Γ_{198}/Γ
VALUE (units 10^{-5})	EVTs	DOCUMENT ID	TECN	COMMENT	
$1.2 \pm 0.2 \pm 0.1$	111	¹ ALEXANDER	10 CLEO	$\psi(2S) \rightarrow \gamma \rho \bar{\rho}$	

¹ From a fit of the $\rho \bar{\rho}$ mass distribution to a combination of $\gamma f_2(1950)$, $\gamma f_2(2150)$, and $\gamma \rho \bar{\rho}$ phase space, for $M(\rho \bar{\rho}) < 2.85$ GeV, and accounting for backgrounds from $\psi(2S) \rightarrow \pi^0 \rho \bar{\rho}$ and continuum.

$\Gamma(\gamma f_2(2150) \rightarrow \gamma \rho \bar{\rho})/\Gamma_{\text{total}}$					Γ_{199}/Γ
VALUE (units 10^{-5})	EVTs	DOCUMENT ID	TECN	COMMENT	
$0.72 \pm 0.18 \pm 0.03$	73	¹ ALEXANDER	10 CLEO	$\psi(2S) \rightarrow \gamma \rho \bar{\rho}$	

¹ From a fit of the $\rho \bar{\rho}$ mass distribution to a combination of $\gamma f_2(1950)$, $\gamma f_2(2150)$, and $\gamma \rho \bar{\rho}$ phase space, for $M(\rho \bar{\rho}) < 2.85$ GeV, and accounting for backgrounds from $\psi(2S) \rightarrow \pi^0 \rho \bar{\rho}$ and continuum.

$\Gamma(\gamma X(1835) \rightarrow \gamma \rho \bar{\rho})/\Gamma_{\text{total}}$					Γ_{200}/Γ
VALUE (units 10^{-6})	CL%	DOCUMENT ID	TECN	COMMENT	
$4.57 \pm 0.36 \pm 1.77$				$J/\psi \rightarrow \gamma \rho \bar{\rho}$	
4.26		ABLIKIM	12D BES3		

• • • We do not use the following data for averages, fits, limits, etc. • • •

< 1.6	90	ALEXANDER	10 CLEO	$\psi(2S) \rightarrow \gamma \rho \bar{\rho}$
< 5.4	90	ABLIKIM	07D BES	$\psi(2S) \rightarrow \gamma \rho \bar{\rho}$

$\Gamma(\gamma X \rightarrow \gamma \rho \bar{\rho})/\Gamma_{\text{total}}$					Γ_{201}/Γ
VALUE (units 10^{-6})	CL%	DOCUMENT ID	TECN	COMMENT	
<2	90	ALEXANDER	10 CLEO	$\psi(2S) \rightarrow \gamma \rho \bar{\rho}$	

For a narrow resonance in the range $2.2 < M(X) < 2.8$ GeV.

$\Gamma(\gamma \rho \bar{\rho} \pi^+ \pi^-)/\Gamma_{\text{total}}$					Γ_{202}/Γ
VALUE (units 10^{-5})	EVTs	DOCUMENT ID	TECN	COMMENT	
$2.8 \pm 1.2 \pm 0.7$	17	ABLIKIM	07D BES2	$e^+ e^- \rightarrow \psi(2S)$	

$\Gamma(\gamma \gamma J/\psi)/\Gamma_{\text{total}}$					Γ_{204}/Γ
VALUE (units 10^{-4})	EVTs	DOCUMENT ID	TECN	COMMENT	
$3.1 \pm 0.6 \pm 1.0$	1.1k	ABLIKIM	12o BES3	$e^+ e^- \rightarrow \psi(2S)$	

• • • We do not use the following data for averages, fits, limits, etc. • • •

3.2 ± 0.6	1.1k	¹ ABLIKIM	17N BES3	$\psi(2S) \rightarrow \gamma \gamma J/\psi$
---------------	------	----------------------	----------	---

¹ Uses $B(J/\psi \rightarrow e^+ e^-) = (5.971 \pm 0.032)\%$ and $B(J/\psi \rightarrow \mu^+ \mu^-) = (5.961 \pm 0.033)\%$. No systematic error estimation.

$\Gamma(e^+ e^- \eta)/\Gamma_{\text{total}}$					Γ_{205}/Γ
VALUE (units 10^{-6})	EVTs	DOCUMENT ID	TECN	COMMENT	
1.90 ± 0.26 OUR AVERAGE					
$1.99 \pm 0.33 \pm 0.12$	57	ABLIKIM	18Z BES3	$\psi(2S) \rightarrow \eta' e^+ e^-$, $\eta' \rightarrow \gamma \pi^+ \pi^-$	
$1.79 \pm 0.38 \pm 0.11$	20	ABLIKIM	18Z BES3	$\psi(2S) \rightarrow \eta' e^+ e^-$, $\eta' \rightarrow \eta \pi^+ \pi^-$	

$\Gamma(e^+ e^- \chi_{c0}(1P))/\Gamma_{\text{total}}$					Γ_{206}/Γ
VALUE (units 10^{-4})	EVTs	DOCUMENT ID	TECN	COMMENT	
$10.6 \pm 2.4 \pm 0.4$	48	¹ ABLIKIM	17i BES3	$\psi(2S) \rightarrow e^+ e^- \gamma J/\psi$	

¹ ABLIKIM 17i reports $(11.7 \pm 2.5 \pm 1.0) \times 10^{-4}$ from a measurement of $[\Gamma(\psi(2S) \rightarrow e^+ e^- \chi_{c0}(1P))/\Gamma_{\text{total}}] \times [B(\chi_{c0}(1P) \rightarrow \gamma J/\psi(1S))]$ assuming $B(\chi_{c0}(1P) \rightarrow \gamma J/\psi(1S)) = (1.27 \pm 0.06) \times 10^{-2}$, which we rescale to our best value $B(\chi_{c0}(1P) \rightarrow \gamma J/\psi(1S)) = (1.40 \pm 0.05) \times 10^{-2}$. Our first error is their experiment's error and our second error is the systematic error from using our best value.

$\Gamma(e^+ e^- \chi_{c0}(1P))/\Gamma(\gamma \chi_{c0}(1P))$					$\Gamma_{206}/\Gamma_{162}$
VALUE (units 10^{-3})	EVTs	DOCUMENT ID	TECN	COMMENT	
$9.4 \pm 1.9 \pm 0.6$	48	¹ ABLIKIM	17i BES3	$\psi(2S) \rightarrow e^+ e^- \gamma J/\psi$	

¹ Uses $B(\psi(2S) \rightarrow \gamma \chi_{c0}(1P)) \times B(\chi_{c0}(1P) \rightarrow \gamma J/\psi(1S)) = (15.8 \pm 0.3 \pm 0.6) \times 10^{-4}$ from ABLIKIM 17N and accounts for common systematic errors.

$\Gamma(e^+ e^- \chi_{c1}(1P))/\Gamma_{\text{total}}$					Γ_{207}/Γ
VALUE (units 10^{-4})	EVTs	DOCUMENT ID	TECN	COMMENT	
$8.5 \pm 0.6 \pm 0.2$	873	¹ ABLIKIM	17i BES3	$\psi(2S) \rightarrow e^+ e^- \gamma J/\psi$	

¹ ABLIKIM 17i reports $(8.6 \pm 0.3 \pm 0.6) \times 10^{-4}$ from a measurement of $[\Gamma(\psi(2S) \rightarrow e^+ e^- \chi_{c1}(1P))/\Gamma_{\text{total}}] \times [B(\chi_{c1}(1P) \rightarrow \gamma J/\psi(1S))]$ assuming $B(\chi_{c1}(1P) \rightarrow \gamma J/\psi(1S)) = (33.9 \pm 1.2) \times 10^{-2}$, which we rescale to our best value $B(\chi_{c1}(1P) \rightarrow \gamma J/\psi(1S)) = (34.3 \pm 1.0) \times 10^{-2}$. Our first error is their experiment's error and our second error is the systematic error from using our best value.

Meson Particle Listings

$\psi(2S)$

$\Gamma(e^+e^-\chi_{c1}(1P))/\Gamma(\gamma\chi_{c1}(1P))$ $\Gamma_{207}/\Gamma_{163}$

VALUE (units 10^{-3})	EVTS	DOCUMENT ID	TECN	COMMENT
$8.3 \pm 0.3 \pm 0.4$	873	¹ ABLIKIM	17I BES3	$\psi(2S) \rightarrow e^+e^-\gamma J/\psi$

¹ Uses $B(\psi(2S) \rightarrow \gamma\chi_{c1}(1P)) \times B(\chi_{c1}(1P) \rightarrow \gamma J/\psi(1S)) = (351.8 \pm 1.0 \pm 12.0) \times 10^{-4}$ from ABLIKIM 17N and accounts for common systematic errors.

$\Gamma(e^+e^-\chi_{c2}(1P))/\Gamma_{total}$ Γ_{208}/Γ

VALUE (units 10^{-4})	EVTS	DOCUMENT ID	TECN	COMMENT
$7.0 \pm 0.7 \pm 0.2$	227	¹ ABLIKIM	17I BES3	$\psi(2S) \rightarrow e^+e^-\gamma J/\psi$

¹ ABLIKIM 17I reports $(6.9 \pm 0.5 \pm 0.6) \times 10^{-4}$ from a measurement of $[\Gamma(\psi(2S) \rightarrow e^+e^-\chi_{c2}(1P))/\Gamma_{total}] \times [B(\chi_{c2}(1P) \rightarrow \gamma J/\psi(1S))]$ assuming $B(\chi_{c2}(1P) \rightarrow \gamma J/\psi(1S)) = (19.2 \pm 0.7) \times 10^{-2}$, which we rescale to our best value $B(\chi_{c2}(1P) \rightarrow \gamma J/\psi(1S)) = (19.0 \pm 0.5) \times 10^{-2}$. Our first error is their experiment's error and our second error is the systematic error from using our best value.

$\Gamma(e^+e^-\chi_{c2}(1P))/\Gamma(\gamma\chi_{c2}(1P))$ $\Gamma_{208}/\Gamma_{164}$

VALUE (units 10^{-3})	EVTS	DOCUMENT ID	TECN	COMMENT
$6.6 \pm 0.5 \pm 0.4$	227	¹ ABLIKIM	17I BES3	$\psi(2S) \rightarrow e^+e^-\gamma J/\psi$

¹ Uses $B(\psi(2S) \rightarrow \gamma\chi_{c2}(1P)) \times B(\chi_{c2}(1P) \rightarrow \gamma J/\psi(1S)) = (199.6 \pm 0.8 \pm 7.0) \times 10^{-4}$ from ABLIKIM 17N and accounts for common systematic errors.

WEAK DECAYS

$\Gamma(D^0 e^+e^- + c.c.)/\Gamma_{total}$ Γ_{209}/Γ

VALUE	CL%	DOCUMENT ID	TECN	COMMENT
$< 1.4 \times 10^{-7}$	90	¹ ABLIKIM	17AF BES3	$e^+e^- \rightarrow \psi(2S)$

¹ Using D^0 decays to $K^-\pi^+$, $K^-\pi^+\pi^0$, and $K^-\pi^+\pi^+\pi^-$.

OTHER DECAYS

$\Gamma(\text{invisible})/\Gamma(e^+e^-)$ Γ_{210}/Γ_7

VALUE	CL%	DOCUMENT ID	TECN	COMMENT
< 2.0	90	LEES	13I BABR	$B \rightarrow K(*)\psi(2S)$

$\psi(2S)$ CROSS-PARTICLE BRANCHING RATIOS

For measurements involving $B(\psi(2S) \rightarrow \gamma\chi_{cJ}(1P)) \times B(\chi_{cJ}(1P) \rightarrow X)$ see the corresponding entries in the $\chi_{cJ}(1P)$ sections.

MULTIPOLE AMPLITUDE RATIOS IN RADIATIVE DECAYS

$\psi(2S) \rightarrow \gamma\chi_{cJ}(1P)$ and $\chi_{cJ} \rightarrow \gamma J/\psi(1S)$

$a_2(\chi_{c1})/a_2(\chi_{c2})$ Magnetic quadrupole transition amplitude ratio

VALUE (units 10^{-2})	EVTS	DOCUMENT ID	TECN	COMMENT
63 ± 7 OUR AVERAGE				
61.7 ± 8.3	253k	¹ ABLIKIM	17N BES3	$\psi(2S) \rightarrow \gamma\gamma\ell^+\ell^-$
67^{+19}_{-13}	59k	² ARTUSO	09 CLEO	$\psi(2S) \rightarrow \gamma\gamma\ell^+\ell^-$

- ¹ Statistical and systematic errors combined.
² Statistical and systematic errors combined. Using values from fits with floating $M2$ amplitudes $a_2(\chi_{c1})$, $a_2(\chi_{c2})$, $b_2(\chi_{c1})$, $b_2(\chi_{c2})$ and fixed $E3$ amplitudes of $a_3(\chi_{c2}) = b_3(\chi_{c2}) = 0$. Not independent of values for $a_2(\chi_{c1}(1P))$ and $a_2(\chi_{c2}(1P))$ from ARTUSO 09.

$b_2(\chi_{c2})/b_2(\chi_{c1})$ Magnetic quadrupole transition amplitude ratio

VALUE (units 10^{-2})	EVTS	DOCUMENT ID	TECN	COMMENT
60 ± 31 OUR AVERAGE				
74 ± 40	253k	¹ ABLIKIM	17N BES3	$\psi(2S) \rightarrow \gamma\gamma\ell^+\ell^-$
37^{+53}_{-47}	59k	² ARTUSO	09 CLEO	$\psi(2S) \rightarrow \gamma\gamma\ell^+\ell^-$

- ¹ Statistical and systematic errors combined. Derived from the reported measurement of $b_2(\chi_{c1})/b_2(\chi_{c2}) = 1.35 \pm 0.72$.
² Statistical and systematic errors combined. Using values from fits with floating $M2$ amplitudes $a_2(\chi_{c1})$, $a_2(\chi_{c2})$, $b_2(\chi_{c1})$, $b_2(\chi_{c2})$ and fixed $E3$ amplitudes of $a_3(\chi_{c2}) = b_3(\chi_{c2}) = 0$. Not independent of values for $b_2(\chi_{c1}(1P))$ and $b_2(\chi_{c2}(1P))$ from ARTUSO 09.

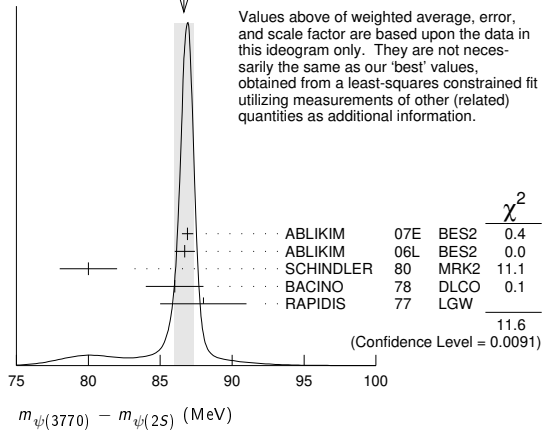
$\psi(2S)$ REFERENCES

ABLIKIM 21AL PR D104 092003 M. Ablikim et al. (BESIII Collab.)
 ABLIKIM 21AO PR D104 092012 M. Ablikim et al. (BESIII Collab.)
 ABLIKIM 21AT JHEP 2111 226 M. Ablikim et al. (BESIII Collab.)
 ABLIKIM 21E PRL 126 092002 M. Ablikim et al. (BESIII Collab.)
 ABLIKIM 21L PR D103 112004 M. Ablikim et al. (BESIII Collab.)
 ABLIKIM 21S PL B820 136576 M. Ablikim et al. (BESIII Collab.)
 ABLIKIM 21Z PRL 127 082002 M. Ablikim et al. (BESIII Collab.)
 LEES 21 PR D103 092001 J.P. Lees et al. (BABAR Collab.)
 LEES 21C PR D104 112004 J.P. Lees et al. (BABAR Collab.)
 ABLIKIM 20F PR D101 032008 M. Ablikim et al. (BESIII Collab.)
 PDG 20 PTEP 2020 083C01 P.A. Zyla et al. (PDG Collab.)
 ABLIKIM 19AO PR D99 112010 M. Ablikim et al. (BESIII Collab.)
 ABLIKIM 19AT PR D100 051101 M. Ablikim et al. (BESIII Collab.)
 ABLIKIM 19AU PR D100 052010 M. Ablikim et al. (BESIII Collab.)
 ABLIKIM 19BA PR D100 092003 M. Ablikim et al. (BESIII Collab.)
 ABLIKIM 19I PR D99 012014 M. Ablikim et al. (BESIII Collab.)
 ABLIKIM 19N PR D99 032006 M. Ablikim et al. (BESIII Collab.)
 ABLIKIM 18Q PR D97 091102 M. Ablikim et al. (BESIII Collab.)
 ABLIKIM 18T PR D98 032006 M. Ablikim et al. (BESIII Collab.)
 ABLIKIM 18Z PL B783 452 M. Ablikim et al. (BESIII Collab.)
 ANASHIN 18 PL B781 174 V.V. Anashin et al. (KEDR Collab.)
 LEES 18E PR D98 112015 J.P. Lees et al. (BABAR Collab.)

ABLIKIM 17AF PR D96 111101 M. Ablikim et al. (BESIII Collab.)
 ABLIKIM 17AJ PR D96 112008 M. Ablikim et al. (BESIII Collab.)
 ABLIKIM 17AK PR D96 112012 M. Ablikim et al. (BESIII Collab.)
 ABLIKIM 17E PL B770 217 M. Ablikim et al. (BESIII Collab.)
 ABLIKIM 17I PRL 118 221802 M. Ablikim et al. (BESIII Collab.)
 ABLIKIM 17L PR D95 052003 M. Ablikim et al. (BESIII Collab.)
 ABLIKIM 17N PR D95 072004 M. Ablikim et al. (BESIII Collab.)
 ABLIKIM 17O PR D96 032001 M. Ablikim et al. (BESIII Collab.)
 ABLIKIM 17X PR D96 052003 M. Ablikim et al. (BESIII Collab.)
 DOBBS 17 PR D96 092004 S. Dobbs et al. (NWES WAYN)
 LEES 17A PR D95 052001 J.P. Lees et al. (BABAR Collab.)
 ANJ 16Y JHEP 1605 132 R. Aaij et al. (LHCb Collab.)
 ABLIKIM 16L PR D93 072003 M. Ablikim et al. (BESIII Collab.)
 ABLIKIM 15I PR D91 092006 M. Ablikim et al. (BESIII Collab.)
 ABLIKIM 15V PL B749 414 M. Ablikim et al. (BESIII Collab.)
 ANASHIN 15 PL B749 50 V.V. Anashin et al. (KEDR Collab.)
 DOBBS 15 PR D91 052006 S. Dobbs et al. (NWES)
 LEES 15J PR D92 072008 J.P. Lees et al. (BABAR Collab.)
 ABLIKIM 14G PR D89 112006 M. Ablikim et al. (BESIII Collab.)
 DOBBS 14 PL B739 30 S. Dobbs et al. (NWES WAYN)
 ABLIKIM 13A PRL 110 022001 M. Ablikim et al. (BESIII Collab.)
 ABLIKIM 13D PR D87 012007 M. Ablikim et al. (BESIII Collab.)
 ABLIKIM 13F PR D87 052007 M. Ablikim et al. (BESIII Collab.)
 ABLIKIM 13M PR D87 092006 M. Ablikim et al. (BESIII Collab.)
 ABLIKIM 13R PR D88 032007 M. Ablikim et al. (BESIII Collab.)
 ABLIKIM 13S PR D88 032010 M. Ablikim et al. (BESIII Collab.)
 ABLIKIM 13W PR D88 112007 M. Ablikim et al. (BESIII Collab.)
 LEES 13I PR D87 112005 J.P. Lees et al. (BABAR Collab.)
 LEES 13O PR D87 092005 J.P. Lees et al. (BABAR Collab.)
 LEES 13Y PR D88 032013 J.P. Lees et al. (BABAR Collab.)
 ABLIKIM 12H EPJ C72 1972 R. Aaij et al. (LHC Collab.)
 ABLIKIM 12G PRL 108 112003 M. Ablikim et al. (BESIII Collab.)
 ABLIKIM 12D PRL 109 042003 M. Ablikim et al. (BESIII Collab.)
 ABLIKIM 12H PL B710 594 M. Ablikim et al. (BESIII Collab.)
 ABLIKIM 12L PR D86 072011 M. Ablikim et al. (BESIII Collab.)
 ABLIKIM 12M PR D86 092008 M. Ablikim et al. (BESIII Collab.)
 ABLIKIM 12O PRL 109 172002 M. Ablikim et al. (BESIII Collab.)
 ABLIKIM 12Q CP C36 1040 M. Ablikim et al. (BES II Collab.)
 ANASHIN 12 PL B711 280 V.V. Anashin et al. (KEDR Collab.)
 LEES 12E PR D85 112009 J.P. Lees et al. (BABAR Collab.)
 LEES 12F PR D86 012008 J.P. Lees et al. (BABAR Collab.)
 METREVELLI 12 PR D85 092007 Z. Metreveli et al. (NWES, FLOW WAYN+)
 GE 11 PR D84 032008 J.Y. Ge et al. (CLEO Collab.)
 ABLIKIM 10B PRL 104 132002 M. Ablikim et al. (BESIII Collab.)
 ABLIKIM 10F PRL 105 261801 M. Ablikim et al. (BESIII Collab.)
 ALEXANDER 10 PR D82 092002 J.P. Alexander et al. (CLEO Collab.)
 CRONIN-HENNESSY... 10 PR D81 052002 D. Cronin-Hennessey et al. (CLEO Collab.)
 ADAMS 09 PR D80 051106 G.S. Adams et al. (CLEO Collab.)
 ARTUSO 09 PR D80 112003 M. Artuso et al. (CLEO Collab.)
 LIBBY 09 PR D80 072002 J. Libby et al. (CLEO Collab.)
 MITCHELL 09 PRL 102 011801 R.E. Mitchell et al. (CLEO Collab.)
 PEDLAR 09 PR D79 111101 T.K. Pedlar et al. (CLEO Collab.)
 ABLIKIM 08B PR B659 74 M. Ablikim et al. (BES Collab.)
 ABLIKIM 08C PL B659 789 M. Ablikim et al. (BES Collab.)
 DOBBS 08A PRL 101 182003 S. Dobbs et al. (CLEO Collab.)
 MENDEZ 08 PR D78 011102 H. Mendez et al. (CLEO Collab.)
 PDG 08 PL B667 1 C. Amstler et al. (PDG Collab.)
 ABLIKIM 07C PL B648 149 M. Ablikim et al. (BES Collab.)
 ABLIKIM 07D PRL 99 011802 M. Ablikim et al. (BES II Collab.)
 ABLIKIM 07H PR D76 092003 M. Ablikim et al. (BES Collab.)
 ANASHIN 07 JETPL 85 347 V.V. Anashin et al. (KEDR Collab.)
 Translated from ZETFP 85 429.
 ANDREOTTI 07 PL B64 74 M. Andreotti et al. (Femlab E835 Collab.)
 AUBERT 07AK PR D76 012008 B. Aubert et al. (BABAR Collab.)
 AUBERT 07AU PR D76 092005 B. Aubert et al. (BABAR Collab.)
 Also PR D77 119902E (err.) B. Aubert et al. (BABAR Collab.)
 AUBERT 07BD PR D76 092006 B. Aubert et al. (BABAR Collab.)
 PDG 07 Unofficial 2007 WWW edition (PDG Collab.)
 PEDLAR 07 PR D75 011102 T.K. Pedlar et al. (CLEO Collab.)
 ABLIKIM 06G PR D73 052004 M. Ablikim et al. (BES Collab.)
 ABLIKIM 06L PR D74 012004 M. Ablikim et al. (BES Collab.)
 ABLIKIM 06I PRL 97 121801 M. Ablikim et al. (BES Collab.)
 ABLIKIM 06R PR D74 072001 M. Ablikim et al. (BES Collab.)
 ABLIKIM 06W PR D74 012003 M. Ablikim et al. (BES Collab.)
 ADAM 06 PRL 96 082004 N.E. Adam et al. (CLEO Collab.)
 AUBERT 06B PR D73 012005 B. Aubert et al. (BABAR Collab.)
 AUBERT 06D PR D73 052003 B. Aubert et al. (BABAR Collab.)
 AUBERT.BE 06A PR D74 091103 B. Aubert et al. (BABAR Collab.)
 DOBBS 06D PR D74 011105 S. Dobbs et al. (CLEO Collab.)
 ABLIKIM 05E PR D71 072006 M. Ablikim et al. (BES Collab.)
 ABLIKIM 05H PR D72 012002 M. Ablikim et al. (BES Collab.)
 ABLIKIM 05J PL B614 37 M. Ablikim et al. (BES Collab.)
 ABLIKIM 05I PL B619 247 M. Ablikim et al. (BES Collab.)
 ABLIKIM 05O PL B630 21 M. Ablikim et al. (BES Collab.)
 ADAM 05 PR 94 012005 N.E. Adam et al. (CLEO Collab.)
 ADAM 05A PRL 94 232002 N.E. Adam et al. (CLEO Collab.)
 ANDREOTTI 05 PR D71 032006 M. Andreotti et al. (FNAL E835 Collab.)
 AUBERT 05D PR D71 052001 B. Aubert et al. (BABAR Collab.)
 BRIERE 05 PRL 95 062001 R.A. Briere et al. (CLEO Collab.)
 PEDLAR 05 PR D72 051108 T.K. Pedlar et al. (CLEO Collab.)
 ROSNER 05 PRL 95 102003 J.L. Rosner et al. (CLEO Collab.)
 ABLIKIM 04B PR D70 012003 M. Ablikim et al. (BES Collab.)
 ABLIKIM 04K PR D70 112003 M. Ablikim et al. (BES Collab.)
 ABLIKIM 04L PR D70 112007 M. Ablikim et al. (BES Collab.)
 ATHAR 04 PR D70 112002 S.B. Athar et al. (CLEO Collab.)
 BAI 04B PRL 92 052001 J.Z. Bai et al. (BES Collab.)
 BAI 04C PR D69 072001 J.Z. Bai et al. (BES Collab.)
 BAI 04D PL B589 7 J.Z. Bai et al. (BES Collab.)
 BAI 04G PR D70 012004 J.Z. Bai et al. (BES Collab.)
 BAI 04I PR D70 012006 J.Z. Bai et al. (BES Collab.)
 PDG 04 PL B592 1 S. Eidelman et al. (PDG Collab.)
 SETH 04 PR D69 097503 K.K. Seth
 AULCHENKO 03 PL B573 63 V.M. Aulchenko et al. (KEDR Collab.)
 BAI 03B PR D67 052002 J.Z. Bai et al. (BES Collab.)
 BAI 03C PR D67 032004 J.Z. Bai et al. (BES Collab.)
 AUBERT 02B PR D65 031101 B. Aubert et al. (BABAR Collab.)
 BAI 02 PR D65 052004 J.Z. Bai et al. (BES Collab.)
 BAI 02C PL B550 24 J.Z. Bai et al. (BES Collab.)
 BAI 02C PRL 88 101802 J.Z. Bai et al. (BES Collab.)
 PDG 02 PR D66 010001 K. Hagihara et al. (PDG Collab.)
 BAI 01 PR D63 032002 J.Z. Bai et al. (BES Collab.)
 AMBROGIANI 00A PR D62 032004 M. Ambrogiani et al. (FNAL E835 Collab.)
 ARTAMONOV 00 PL B474 427 A.S. Artamonov et al.
 BAI 00 PRL 84 594 J.Z. Bai et al. (BES Collab.)
 BAI 99C PRL 83 1918 J.Z. Bai et al. (BES Collab.)
 BAI 98E PR D57 3854 J.Z. Bai et al. (BES Collab.)
 BAI 98F PR D58 097101 J.Z. Bai et al. (BES Collab.)
 BAI 98J PRL 81 5080 J.Z. Bai et al. (BES Collab.)
 ARMSTRONG 97 PR D55 1153 T.A. Armstrong et al. (E760 Collab.)
 GRIBUSHIN 96 PR D53 4723 A. Gribushin et al. (E672 and E706 Collab.)
 ARMSTRONG 93B PR D47 772 T.A. Armstrong et al. (FNAL E760 Collab.)

ALEXANDER	89	NP B320 45	J.P. Alexander et al.	(LBL, MICH, SLAC)
COHEN	87	RMP 59 1121	E.R. Cohen, B.N. Taylor	(RISC, NBS)
GAISER	86	PR D34 711	J. Gaiser et al.	(Crystal Ball Collab.)
KURAEV	85	SJNP 41 466	E.A. Kurayev, V.S. Fadin	(NOVO)
Translated from YAF 41 733.				
FRANKLIN	83	PRL 51 963	M.E.B. Franklin et al.	(LBL, SLAC)
EDWARDS	82C	PRL 49 70	C. Edwards et al.	(CIT, HARV, PRIN+)
LEMOIGNE	82	PL 113B 509	Y. Lemoigne et al.	(SACL, LOIC, SHMP+)
HIMEL	80	PRL 44 920	T. Himel et al.	(LBL, SLAC)
OREGLIA	80	PRL 45 959	M.J. Oreglia et al.	(SLAC, CIT, HARV+)
SCHARRE	80	PL 97B 329	D.L. Scharre et al.	(SLAC, LBL)
ZHOLENTZ	80	PL 96B 214	A.A. Zholents et al.	(NOVO)
Also		SJNP 34 814	A.A. Zholents et al.	(NOVO)
Translated from YAF 34 1471.				
BRANDELIK	79B	NP B160 426	R. Brandelik et al.	(DASP Collab.)
BRANDELIK	79C	ZPHY C1 233	R. Brandelik et al.	(DASP Collab.)
BARTEL	78B	PL 79B 492	W. Bartel et al.	(DESY, HEIDP)
TANENBAUM	78	PR D17 1731	W.M. Tanenbaum et al.	(SLAC, LBL)
BIDDICK	77	PRL 38 1324	C.J. Biddick et al.	(UCSD, UMD, PAVI+)
BRAUNSCHEWIG	77	PL 67B 249	W. Braunschweig et al.	(DASP Collab.)
BURMESTER	77	PL 66B 395	J. Burmester et al.	(DESY, HAMB, SIEG+)
FELDMAN	77	PRPL 33C 285	G.J. Feldman, M.L. Perl	(LBL, SLAC)
YAMADA	77	Hamburg Conf. 69	S. Yamada	(DASP Collab.)
BARTEL	76	PL 64B 483	W. Bartel et al.	(DESY, HEIDP)
TANENBAUM	76	PRL 36 402	W.M. Tanenbaum et al.	(SLAC, LBL) IG
WHITAKER	76	PRL 37 1596	J.S. Whitaker et al.	(SLAC, LBL)
ABRAMS	75	Stanford Symp. 25	G.S. Abrams	(LBL)
ABRAMS	75B	PRL 34 1181	G.S. Abrams et al.	(LBL, SLAC)
BOYARSKI	75C	Palermo Conf. 54	A.M. Boyarski et al.	(SLAC, LBL)
HILGER	75	PRL 35 625	E. Hilger et al.	(STAN, PENN)
LIBERMAN	75	Stanford Symp. 55	A.D. Liberman	(STAN)
LUTH	75	PRL 35 1124	V. Luth et al.	(SLAC, LBL) JPC
WIIK	75	Stanford Symp. 69	B.H. Wiik	(DESY)

WEIGHTED AVERAGE
86.6±0.7 (Error scaled by 2.0)



$\psi(3770)$

$J^{PC} = 0^{-}(1^{-}-)$

$\psi(3770)$ MASS (MeV)

OUR FIT includes measurements of $m_{\psi(2S)}$, $m_{\psi(3770)}$, and $m_{\psi(3770)} - m_{\psi(2S)}$.

VALUE (MeV)	EVTs	DOCUMENT ID	TECN	COMMENT
3773.7±0.4 OUR FIT				Error includes scale factor of 1.4.
3778.1±0.7 OUR AVERAGE				
3778.1±0.7±0.6		1 AAJ	19M LHCB	$pp \rightarrow D\bar{D} + \text{anything}$
3779.2+1.8+0.6 -1.7-0.8		2 ANASHIN	12A KEDR	$e^+e^- \rightarrow D\bar{D}$
3775.5±2.4±0.5	57	AUBERT	08B BABR	$B \rightarrow D\bar{D}K$
3776 ±5 ±4	68	BRODZICKA	08 BELL	$B^+ \rightarrow D^0\bar{D}^0K^+$
3778.8±1.9±0.9		AUBERT	07BE BABR	$e^+e^- \rightarrow D\bar{D}\gamma$
••• We do not use the following data for averages, fits, limits, etc. •••				
3779.8±0.6		3 SHAMOV	17 RVUE	$e^+e^- \rightarrow D\bar{D}$, hadrons
3772.0±1.9		4,5 ABLIKIM	08D BES2	$e^+e^- \rightarrow \text{hadrons}$
3778.4±3.0±1.3	34	CHISTOV	04 BELL	Sup. by BRODZICKA 08

- Measured in prompt hadroproduction.
- Taking into account interference between the resonant and non-resonant $D\bar{D}$ production.
- From the joint analysis of the data on the $D\bar{D}$ and inclusive hadronic cross sections in the $\psi(3770)$ region from BaBar, Belle, BES-II, CLEO and KEDR.
- Reanalysis of data presented in BAI 02c. From a global fit over the center-of-mass energy region 3.7–5.0 GeV covering the $\psi(3770)$, $\psi(4040)$, $\psi(4160)$, and $\psi(4415)$ resonances. Phase angle fixed in the fit to $\delta = 0^\circ$.
- Interference between the resonant and non-resonant $D\bar{D}$ production not taken into account.

$m_{\psi(3770)} - m_{\psi(2S)}$

OUR FIT includes measurements of $m_{\psi(2S)}$, $m_{\psi(3770)}$, and $m_{\psi(3770)} - m_{\psi(2S)}$.

VALUE (MeV)	DOCUMENT ID	TECN	COMMENT
87.6±0.4 OUR FIT			Error includes scale factor of 1.4.
86.6±0.7 OUR AVERAGE			Error includes scale factor of 2.0. See the ideogram below.
86.9±0.4	1 ABLIKIM 07E BES2		$e^+e^- \rightarrow \text{hadrons}$
86.7±0.7	ABLIKIM 06L BES2		$e^+e^- \rightarrow \text{hadrons}$
80 ±2	SCHINDLER 80 MRK2		e^+e^-
86 ±2	2 BACINO 78 DLCO		e^+e^-
88 ±3	RAPIDIS 77 LGW		e^+e^-

- BES-II $\psi(2S)$ mass subtracted (see ABLIKIM 06L).
- SPEAR $\psi(2S)$ mass subtracted (see SCHINDLER 80).

$\psi(3770)$ WIDTH

VALUE (MeV)	EVTs	DOCUMENT ID	TECN	COMMENT
27.2± 1.0 OUR FIT				
27.5± 0.9 OUR AVERAGE				
24.9± 4.6+0.5 -4.0-1.1		1 ANASHIN	12A KEDR	$e^+e^- \rightarrow D\bar{D}$
30.4± 8.5		2,3 ABLIKIM	08D BES2	$e^+e^- \rightarrow \text{hadrons}$
27 ±10 ±5	68	BRODZICKA	08 BELL	$B^+ \rightarrow D^0\bar{D}^0K^+$
28.5± 1.2±0.2		3 ABLIKIM	07E BES2	$e^+e^- \rightarrow \text{hadrons}$
23.5± 3.7±0.9		AUBERT	07BE BABR	$e^+e^- \rightarrow D\bar{D}\gamma$
26.9± 2.4±0.3		3 ABLIKIM	06L BES2	$e^+e^- \rightarrow \text{hadrons}$
24 ± 5		3 SCHINDLER	80 MRK2	e^+e^-
24 ± 5		3 BACINO	78 DLCO	e^+e^-
28 ± 5		3 RAPIDIS	77 LGW	e^+e^-
••• We do not use the following data for averages, fits, limits, etc. •••				
25.8± 1.3		4 SHAMOV	17 RVUE	$e^+e^- \rightarrow D\bar{D}$, hadrons

- Taking into account interference between the resonant and non-resonant $D\bar{D}$ production.
- Reanalysis of data presented in BAI 02c. From a global fit over the center-of-mass energy region 3.7–5.0 GeV covering the $\psi(3770)$, $\psi(4040)$, $\psi(4160)$, and $\psi(4415)$ resonances. Phase angle fixed in the fit to $\delta = 0^\circ$.
- Interference between the resonant and non-resonant $D\bar{D}$ production not taken into account.
- From the joint analysis of the data on the $D\bar{D}$ and inclusive hadronic cross sections in the $\psi(3770)$ region from BaBar, Belle, BES-II, CLEO and KEDR.

$\psi(3770)$ DECAY MODES

Mode	Fraction (Γ_i/Γ)	Scale factor/ Confidence level
$\Gamma_1 D\bar{D}$	(93 ± 8 / -5) %	S=2.0
$\Gamma_2 D^0\bar{D}^0$	(52 ± 4 / -5) %	S=2.0
$\Gamma_3 D^+D^-$	(41 ± 4 /) %	S=2.0
$\Gamma_4 J/\psi X$	(5.0 ± 2.2 /) $\times 10^{-3}$	
$\Gamma_5 J/\psi \pi^+\pi^-$	(1.93 ± 0.28 /) $\times 10^{-3}$	
$\Gamma_6 J/\psi \pi^0\pi^0$	(8.0 ± 3.0 /) $\times 10^{-4}$	
$\Gamma_7 J/\psi \eta$	(9 ± 4 /) $\times 10^{-4}$	
$\Gamma_8 J/\psi \pi^0$	< 2.8	CL=90%
$\Gamma_9 e^+e^-$	(9.6 ± 0.7 /) $\times 10^{-6}$	S=1.3

Decays to light hadrons

$\Gamma_{10} b_1(1235)\pi$	< 1.4	$\times 10^{-5}$	CL=90%
$\Gamma_{11} \phi\eta'$	< 7	$\times 10^{-4}$	CL=90%
$\Gamma_{12} \omega\eta'$	< 4	$\times 10^{-4}$	CL=90%
$\Gamma_{13} \rho^0\eta'$	< 6	$\times 10^{-4}$	CL=90%
$\Gamma_{14} \phi\eta$	(3.1 ± 0.7 /) $\times 10^{-4}$		
$\Gamma_{15} \omega\eta$	< 1.4	$\times 10^{-5}$	CL=90%
$\Gamma_{16} \rho^0\eta$	< 5	$\times 10^{-4}$	CL=90%
$\Gamma_{17} \phi\pi^0$	< 3	$\times 10^{-5}$	CL=90%
$\Gamma_{18} \omega\pi^0$	< 6	$\times 10^{-4}$	CL=90%
$\Gamma_{19} \pi^+\pi^-\pi^0$	< 5	$\times 10^{-6}$	CL=90%
$\Gamma_{20} \rho\pi$	< 5	$\times 10^{-6}$	CL=90%
$\Gamma_{21} K^+K^-$			
$\Gamma_{22} K^*(892)^+K^- + c.c.$	< 1.4	$\times 10^{-5}$	CL=90%
$\Gamma_{23} K^*(892)^0\bar{K}^0 + c.c.$	< 1.2	$\times 10^{-3}$	CL=90%
$\Gamma_{24} K_S^0 K_L^0$	< 1.2	$\times 10^{-5}$	CL=90%
$\Gamma_{25} 2(\pi^+\pi^-)$	< 1.12	$\times 10^{-3}$	CL=90%

Meson Particle Listings

$\psi(3770)$

Γ_{26}	$2(\pi^+\pi^-)\pi^0$	< 1.06	$\times 10^{-3}$	CL=90%
Γ_{27}	$2(\pi^+\pi^-\pi^0)$	< 5.85	%	CL=90%
Γ_{28}	$\omega\pi^+\pi^-$	< 6.0	$\times 10^{-4}$	CL=90%
Γ_{29}	$3(\pi^+\pi^-)$	< 9.1	$\times 10^{-3}$	CL=90%
Γ_{30}	$3(\pi^+\pi^-\pi^0)$	< 1.37	%	CL=90%
Γ_{31}	$3(\pi^+\pi^-)2\pi^0$	< 11.74	%	CL=90%
Γ_{32}	$\eta\pi^+\pi^-$	< 1.24	$\times 10^{-3}$	CL=90%
Γ_{33}	$\pi^+\pi^-2\pi^0$	< 8.9	$\times 10^{-3}$	CL=90%
Γ_{34}	$\rho^0\pi^+\pi^-$	< 6.9	$\times 10^{-3}$	CL=90%
Γ_{35}	$\eta3\pi$	< 1.34	$\times 10^{-3}$	CL=90%
Γ_{36}	$\eta2(\pi^+\pi^-)$	< 2.43	%	CL=90%
Γ_{37}	$\eta\rho^0\pi^+\pi^-$	< 1.45	%	CL=90%
Γ_{38}	$\eta'3\pi$	< 2.44	$\times 10^{-3}$	CL=90%
Γ_{39}	$K^+K^-\pi^+\pi^-$	< 9.0	$\times 10^{-4}$	CL=90%
Γ_{40}	$\phi\pi^+\pi^-$	< 4.1	$\times 10^{-4}$	CL=90%
Γ_{41}	$K^+K^-2\pi^0$	< 4.2	$\times 10^{-3}$	CL=90%
Γ_{42}	$4(\pi^+\pi^-)$	< 1.67	%	CL=90%
Γ_{43}	$4(\pi^+\pi^-\pi^0)$	< 3.06	%	CL=90%
Γ_{44}	$\phi f_0(980)$	< 4.5	$\times 10^{-4}$	CL=90%
Γ_{45}	$K^+K^-\pi^+\pi^-\pi^0$	< 2.36	$\times 10^{-3}$	CL=90%
Γ_{46}	$K^+K^-\rho^0\pi^0$	< 8	$\times 10^{-4}$	CL=90%
Γ_{47}	$K^+K^-\rho^+\pi^-$	< 1.46	%	CL=90%
Γ_{48}	ωK^+K^-	< 3.4	$\times 10^{-4}$	CL=90%
Γ_{49}	$\phi\pi^+\pi^-\pi^0$	< 3.8	$\times 10^{-3}$	CL=90%
Γ_{50}	$K^{*0}K^-\pi^+\pi^0 + c.c.$	< 1.62	%	CL=90%
Γ_{51}	$K^{*+}K^-\pi^+\pi^- + c.c.$	< 3.23	%	CL=90%
Γ_{52}	$K^+K^-\pi^+\pi^-2\pi^0$	< 2.67	%	CL=90%
Γ_{53}	$K^+K^-2(\pi^+\pi^-)$	< 1.03	%	CL=90%
Γ_{54}	$K^+K^-2(\pi^+\pi^-\pi^0)$	< 3.60	%	CL=90%
Γ_{55}	ηK^+K^-	< 4.1	$\times 10^{-4}$	CL=90%
Γ_{56}	$\eta K^+K^-\pi^+\pi^-$	< 1.24	%	CL=90%
Γ_{57}	$\rho^0 K^+K^-$	< 5.0	$\times 10^{-3}$	CL=90%
Γ_{58}	$2(K^+K^-)$	< 6.0	$\times 10^{-4}$	CL=90%
Γ_{59}	ϕK^+K^-	< 7.5	$\times 10^{-4}$	CL=90%
Γ_{60}	$2(K^+K^-)\pi^0$	< 2.9	$\times 10^{-4}$	CL=90%
Γ_{61}	$2(K^+K^-)\pi^+\pi^-$	< 3.2	$\times 10^{-3}$	CL=90%
Γ_{62}	$K_S^0 K^-\pi^+$	< 3.2	$\times 10^{-3}$	CL=90%
Γ_{63}	$K_S^0 K^-\pi^+\pi^0$	< 1.33	%	CL=90%
Γ_{64}	$K_S^0 K^-\rho^+$	< 6.6	$\times 10^{-3}$	CL=90%
Γ_{65}	$K_S^0 K^-\pi^+\pi^-$	< 8.7	$\times 10^{-3}$	CL=90%
Γ_{66}	$K_S^0 K^-\pi^+\rho^0$	< 1.6	%	CL=90%
Γ_{67}	$K_S^0 K^-\pi^+\eta$	< 1.3	%	CL=90%
Γ_{68}	$K_S^0 K^-\pi^+\pi^-\pi^0$	< 4.18	%	CL=90%
Γ_{69}	$K_S^0 K^-\pi^+\pi^-\eta$	< 4.8	%	CL=90%
Γ_{70}	$K_S^0 K^-\pi^+2(\pi^+\pi^-)$	< 1.22	%	CL=90%
Γ_{71}	$K_S^0 K^-\pi^+2\pi^0$	< 2.65	%	CL=90%
Γ_{72}	$K_S^0 K^-\pi^+K^-\pi^+$	< 4.9	$\times 10^{-3}$	CL=90%
Γ_{73}	$K_S^0 K^-\pi^+K^-\pi^+\pi^0$	< 3.0	%	CL=90%
Γ_{74}	$K_S^0 K^-\pi^+K^-\pi^+\eta$	< 2.2	%	CL=90%
Γ_{75}	$K^{*0}K^-\pi^+ + c.c.$	< 9.7	$\times 10^{-3}$	CL=90%
Γ_{76}	$\rho\bar{\rho}$			
Γ_{77}	$\rho\bar{\rho}\pi^0$	< 4	$\times 10^{-5}$	CL=90%
Γ_{78}	$\rho\bar{\rho}\pi^+\pi^-$	< 5.8	$\times 10^{-4}$	CL=90%
Γ_{79}	$\Lambda\bar{\Lambda}$	< 1.2	$\times 10^{-4}$	CL=90%
Γ_{80}	$\rho\bar{\rho}\pi^+\pi^-\pi^0$	< 1.85	$\times 10^{-3}$	CL=90%
Γ_{81}	$\omega\rho\bar{\rho}$	< 2.9	$\times 10^{-4}$	CL=90%
Γ_{82}	$\Lambda\bar{\Lambda}\pi^0$	< 7	$\times 10^{-5}$	CL=90%
Γ_{83}	$\rho\bar{\rho}2(\pi^+\pi^-)$	< 2.6	$\times 10^{-3}$	CL=90%
Γ_{84}	$\eta\rho\bar{\rho}$	< 5.4	$\times 10^{-4}$	CL=90%
Γ_{85}	$\eta\rho\bar{\rho}\pi^+\pi^-$	< 3.3	$\times 10^{-3}$	CL=90%
Γ_{86}	$\rho^0\rho\bar{\rho}$	< 1.7	$\times 10^{-3}$	CL=90%
Γ_{87}	$\rho\bar{\rho}K^+K^-$	< 3.2	$\times 10^{-4}$	CL=90%
Γ_{88}	$\eta\rho\bar{\rho}K^+K^-$	< 6.9	$\times 10^{-3}$	CL=90%
Γ_{89}	$\pi^0\rho\bar{\rho}K^+K^-$	< 1.2	$\times 10^{-3}$	CL=90%
Γ_{90}	$\phi\rho\bar{\rho}$	< 1.3	$\times 10^{-4}$	CL=90%
Γ_{91}	$\Lambda\bar{\Lambda}\pi^+\pi^-$	< 2.5	$\times 10^{-4}$	CL=90%
Γ_{92}	$\Lambda\bar{\rho}K^+$	< 2.8	$\times 10^{-4}$	CL=90%
Γ_{93}	$\Lambda\bar{\rho}K^+\pi^+\pi^-$	< 6.3	$\times 10^{-4}$	CL=90%
Γ_{94}	$\Lambda\bar{\Lambda}\eta$	< 1.9	$\times 10^{-4}$	CL=90%
Γ_{95}	$\Sigma^+\Sigma^-$	< 1.0	$\times 10^{-4}$	CL=90%
Γ_{96}	$\Sigma^0\Sigma^0$	< 4	$\times 10^{-5}$	CL=90%
Γ_{97}	$\Xi^+\Xi^-$	< 1.5	$\times 10^{-4}$	CL=90%
Γ_{98}	$\Xi^0\Xi^0$	< 1.4	$\times 10^{-4}$	CL=90%

Radiative decays

Γ_{99}	$\gamma\chi_{c2}$	< 6.4	$\times 10^{-4}$	CL=90%
Γ_{100}	$\gamma\chi_{c1}$	(2.49±0.23)	$\times 10^{-3}$	
Γ_{101}	$\gamma\chi_{c0}$	(6.9 ± 0.6)	$\times 10^{-3}$	
Γ_{102}	$\gamma\eta_c$	< 7	$\times 10^{-4}$	CL=90%
Γ_{103}	$\gamma\eta_c(2S)$	< 9	$\times 10^{-4}$	CL=90%
Γ_{104}	$\gamma\eta'$	< 1.8	$\times 10^{-4}$	CL=90%
Γ_{105}	$\gamma\eta$	< 1.5	$\times 10^{-4}$	CL=90%
Γ_{106}	$\gamma\pi^0$	< 2	$\times 10^{-4}$	CL=90%

CONSTRAINED FIT INFORMATION

An overall fit to the total width, a partial width, and 3 branching ratios uses 23 measurements and one constraint to determine 5 parameters. The overall fit has a $\chi^2 = 20.1$ for 19 degrees of freedom.

The following *off-diagonal* array elements are the correlation coefficients $\langle \delta p_i \delta p_j \rangle / (\delta p_i \delta p_j)$, in percent, from the fit to parameters p_i , including the branching fractions, $x_i \equiv \Gamma_i / \Gamma_{\text{total}}$. The fit constrains the x_i whose labels appear in this array to sum to one.

x_3	99		
x_9	0	0	
Γ	0	0	-44
	x_2	x_3	x_9

Mode	Rate (MeV)	Scale factor		
Γ_2	$D^0\bar{D}^0$	14.0 ± 1.4	1.8	
Γ_3	D^+D^-	11.2 ± 1.1	1.7	
Γ_9	e^+e^-	(2.62±0.18)	$\times 10^{-4}$	1.4

$\psi(3770)$ PARTIAL WIDTHS

$\Gamma(e^+e^-)$	Γ_9			
VALUE (keV)	EVTs	DOCUMENT ID	TECN	COMMENT
0.262±0.018 OUR FIT	Error includes scale factor of 1.4.			
0.256±0.016 OUR AVERAGE	Error includes scale factor of 1.2.			
0.154+0.079+0.021 -0.058-0.027	1,2	ANASHIN	12A	KEDR $e^+e^- \rightarrow D\bar{D}$
0.22 ± 0.05	3,4	ABLIKIM	08D	BES2 $e^+e^- \rightarrow$ hadrons
0.277±0.011±0.013	4	ABLIKIM	07E	BES2 $e^+e^- \rightarrow$ hadrons
0.203±0.003+0.041 -0.027	1,4M	4,5	BESSION	06 CLEO $e^+e^- \rightarrow$ hadrons
0.276±0.050	4	SCHINDLER	80	MRK2 e^+e^-
0.18 ± 0.06	4	BACINO	78	DLCO e^+e^-
••• We do not use the following data for averages, fits, limits, etc. •••				
0.196±0.018	6	SHAMOV	17	RVUE $e^+e^- \rightarrow D\bar{D}$, hadrons
0.414+0.072+0.093 -0.080-0.028	2,7	ANASHIN	12A	KEDR $e^+e^- \rightarrow D\bar{D}$
0.37 ± 0.09	8	RAPIDIS	77	LGW e^+e^-

- Solution I of the two solutions.
- Taking into account interference between the resonant and non-resonant $D\bar{D}$ production.
- Reanalysis of data presented in BAI 02C. From a global fit over the center-of-mass energy region 3.7–5.0 GeV covering the $\psi(3770)$, $\psi(4040)$, $\psi(4160)$, and $\psi(4415)$ resonances. Phase angle fixed in the fit to $\delta = 0^\circ$.
- Interference between the resonant and non-resonant $D\bar{D}$ production not taken into account.
- BESSION 06 (as corrected in BESSION 10) measure $\sigma(e^+e^- \rightarrow \psi(3770) \rightarrow \text{hadrons}) = 6.36 \pm 0.08^{+0.41}_{-0.30}$ nb at $\sqrt{s} = 3773 \pm 1$ MeV, and obtain Γ_{ee} from the Born-level cross section calculated using $\psi(3770)$ mass and width from our 2004 edition, PDG 04.
- From the joint analysis of the data on the $D\bar{D}$ and inclusive hadronic cross sections in the $\psi(3770)$ region from BaBar, Belle, BES-II, CLEO and KEDR.
- Solution II of the two solutions.
- See also $\Gamma(e^+e^-) / \Gamma_{\text{total}}$ below.

$\psi(3770)$ BRANCHING RATIOS

$\Gamma(D\bar{D}) / \Gamma_{\text{total}}$	$\Gamma_1 / \Gamma = (\Gamma_2 + \Gamma_3) / \Gamma$			
VALUE	EVTs	DOCUMENT ID	TECN	COMMENT
0.93 +0.08 -0.09 OUR FIT	Error includes scale factor of 2.0.			
0.93 +0.08 -0.09 OUR AVERAGE	Error includes scale factor of 2.1.			
0.849±0.056±0.018	1	ABLIKIM	08B	BES2 $e^+e^- \rightarrow$ non- $D\bar{D}$
1.033±0.014+0.048 -0.066	1,427M	2	BESSION	06 CLEO $e^+e^- \rightarrow$ hadrons
••• We do not use the following data for averages, fits, limits, etc. •••				
0.836±0.049	3	SHAMOV	17	RVUE $e^+e^- \rightarrow D\bar{D}$, hadrons
0.866±0.050±0.036	4,5	ABLIKIM	07K	BES2 $e^+e^- \rightarrow$ non- $D\bar{D}$
0.836±0.073±0.042	5	ABLIKIM	06L	BES2 $e^+e^- \rightarrow D\bar{D}$
0.855±0.017±0.058	5,6	ABLIKIM	06N	BES2 $e^+e^- \rightarrow D\bar{D}$

¹ Neglecting interference.

² Obtained by comparing a measurement of the total cross section (corrected in BESSON 10) with that of $D\bar{D}$ reported by CLEO in DOBBS 07.

³ From the joint analysis of the data on the $D\bar{D}$ and inclusive hadronic cross sections in the $\psi(3770)$ region from BaBar, Belle, BES-II, CLEO and KEDR.

⁴ Using $\sigma^{obs} = 7.07 \pm 0.58$ nb and neglecting interference.

⁵ Not independent of ABLIKIM 08b.

⁶ From a measurement of $\sigma(e^+e^- \rightarrow D\bar{D})$ at $\sqrt{s} = 3773$ MeV, using the $\psi(3770)$ resonance parameters measured by ABLIKIM 06L.

$\Gamma(D^0\bar{D}^0)/\Gamma_{total}$		Γ_2/Γ	
VALUE	DOCUMENT ID	TECN	COMMENT
0.52 \pm 0.04 \pm 0.05	OUR FIT		Error includes scale factor of 2.0.

VALUE	DOCUMENT ID	TECN	COMMENT
0.467 \pm 0.047 \pm 0.023	ABLIKIM 06L	BES2	$e^+e^- \rightarrow D^0\bar{D}^0$
0.499 \pm 0.013 \pm 0.038	¹ ABLIKIM 06N	BES2	$e^+e^- \rightarrow D^0\bar{D}^0$

¹ From a measurement of $\sigma(e^+e^- \rightarrow D\bar{D})$ at $\sqrt{s} = 3773$ MeV, using the $\psi(3770)$ resonance parameters measured by ABLIKIM 06L.

$\Gamma(D^+D^-)/\Gamma_{total}$		Γ_3/Γ	
VALUE	DOCUMENT ID	TECN	COMMENT
0.41 \pm 0.04	OUR FIT		Error includes scale factor of 2.0.

VALUE	DOCUMENT ID	TECN	COMMENT
0.369 \pm 0.037 \pm 0.028	ABLIKIM 06L	BES2	$e^+e^- \rightarrow D^+D^-$
0.357 \pm 0.011 \pm 0.034	¹ ABLIKIM 06N	BES2	$e^+e^- \rightarrow D^+D^-$

¹ From a measurement of $\sigma(e^+e^- \rightarrow D\bar{D})$ at $\sqrt{s} = 3773$ MeV, using the $\psi(3770)$ resonance parameters measured by ABLIKIM 06L.

$\Gamma(D^0\bar{D}^0)/\Gamma(D^+D^-)$		Γ_2/Γ_3		
VALUE	EVTS	DOCUMENT ID	TECN	COMMENT
1.253 \pm 0.016	OUR FIT			
1.253 \pm 0.016	OUR AVERAGE			

VALUE	EVTS	DOCUMENT ID	TECN	COMMENT
1.252 \pm 0.009 \pm 0.013	5.3M	BONVICINI 14	CLEO	$e^+e^- \rightarrow D\bar{D}$
1.39 \pm 0.31 \pm 0.12		PAKHLOVA 08	BELL	10.6 $e^+e^- \rightarrow D\bar{D}\gamma$
1.78 \pm 0.33 \pm 0.24		AUBERT 07BE	BABR	$e^+e^- \rightarrow D\bar{D}\gamma$
1.27 \pm 0.12 \pm 0.08		ABLIKIM 06L	BES2	$e^+e^- \rightarrow D\bar{D}$
2.43 \pm 1.50 \pm 0.43	34	¹ CHISTOV 04	BELL	$B \rightarrow \psi(3770) K^+$

• • • We do not use the following data for averages, fits, limits, etc. • • •

1.258 \pm 0.016 \pm 0.014 ² DOBBS 07 CLEO $e^+e^- \rightarrow D\bar{D}$

¹ See ADLER 88c for older measurements of this quantity.

² Superseded by BONVICINI 14.

$\Gamma(J/\psi X)/\Gamma_{total}$		Γ_4/Γ	
VALUE (%)	DOCUMENT ID	TECN	COMMENT
0.5 \pm 0.2 \pm 0.1	¹ ABLIKIM 21z	BES3	$e^+e^- \rightarrow \ell^+ \ell^- X$

¹ From a fit to the $e^+e^- \rightarrow J/\psi X$ cross section between 3.645 and 3.891 GeV, with $\psi(2S)$ and $\psi(3770)$ masses, total widths and leptonic widths fixed to the values from the PDG 20. An alternative fit with an improved χ^2 , corresponding to a significance of 5.3 σ , uses an additional resonance with a mass of $3766.2 \pm 3.8 \pm 0.4$ MeV/ c^2 , a total width of $22.2 \pm 5.9 \pm 1.4$ MeV, and $\Gamma(e^-e^-B)/\Gamma(J/\psi X) = 79.4 \pm 85.5 \pm 11.7$ eV, possibly compatible with the results of ABLIKIM 08h.

$\Gamma(J/\psi\pi^+\pi^-)/\Gamma_{total}$		Γ_5/Γ		
VALUE (units 10^{-3})	EVTS	DOCUMENT ID	TECN	COMMENT
1.93 \pm 0.28	OUR AVERAGE			

VALUE	EVTS	DOCUMENT ID	TECN	COMMENT
1.89 \pm 0.20 \pm 0.20	231 \pm 33	ADAM 06	CLEO	$e^+e^- \rightarrow \psi(3770)$
3.4 \pm 1.4 \pm 0.9	17.8 \pm 4.8	BAI 05	BES2	$e^+e^- \rightarrow \psi(3770)$

$\Gamma(J/\psi\pi^0\pi^0)/\Gamma_{total}$		Γ_6/Γ		
VALUE (units 10^{-2})	EVTS	DOCUMENT ID	TECN	COMMENT
0.080 \pm 0.025 \pm 0.016	39 \pm 14	ADAM 06	CLEO	$e^+e^- \rightarrow \psi(3770)$

$\Gamma(J/\psi\eta)/\Gamma_{total}$		Γ_7/Γ		
VALUE (units 10^{-5})	EVTS	DOCUMENT ID	TECN	COMMENT
87 \pm 33 \pm 22	22 \pm 10	ADAM 06	CLEO	$e^+e^- \rightarrow \psi(3770)$

$\Gamma(J/\psi\pi^0)/\Gamma_{total}$		Γ_8/Γ			
VALUE (units 10^{-5})	CL%	EVTS	DOCUMENT ID	TECN	COMMENT
<28	90	<10	ADAM 06	CLEO	$e^+e^- \rightarrow \psi(3770)$

$\Gamma(e^+e^-)/\Gamma_{total}$		Γ_9/Γ	
VALUE (units 10^{-5})	DOCUMENT ID	TECN	COMMENT
0.96 \pm 0.07	OUR FIT		Error includes scale factor of 1.3.
1.3 \pm 0.2	RAPIDIS 77	LGW	e^+e^-

DECAYS TO LIGHT HADRONS

$\Gamma(b_1(1235)\pi)/\Gamma_{total}$		Γ_{10}/Γ		
VALUE (units 10^{-5})	CL%	DOCUMENT ID	TECN	COMMENT
<1.4	90	¹ ADAMS 06	CLEO	$e^+e^- \rightarrow \psi(3770)$

¹ Comparing cross sections at $\sqrt{s} = 3.773$ GeV and $\sqrt{s} = 3.671$ GeV, neglecting interference, and using $\sigma(\psi(3770) \rightarrow D\bar{D}) = 6.39 \pm 0.20$ nb.

$\Gamma(\phi\eta')/\Gamma_{total}$		Γ_{11}/Γ		
VALUE (units 10^{-4})	CL%	DOCUMENT ID	TECN	COMMENT
<7	90	¹ ADAMS 06	CLEO	$e^+e^- \rightarrow \psi(3770)$

¹ Comparing cross sections at $\sqrt{s} = 3.773$ GeV and $\sqrt{s} = 3.671$ GeV, neglecting interference, and using $\sigma(\psi(3770) \rightarrow D\bar{D}) = 6.39 \pm 0.20$ nb.

$\Gamma(\omega\eta')/\Gamma_{total}$		Γ_{12}/Γ		
VALUE (units 10^{-4})	CL%	DOCUMENT ID	TECN	COMMENT
<4	90	¹ ADAMS 06	CLEO	$e^+e^- \rightarrow \psi(3770)$

¹ Comparing cross sections at $\sqrt{s} = 3.773$ GeV and $\sqrt{s} = 3.671$ GeV, neglecting interference, and using $\sigma(\psi(3770) \rightarrow D\bar{D}) = 6.39 \pm 0.20$ nb.

$\Gamma(\rho^0\eta)/\Gamma_{total}$		Γ_{13}/Γ		
VALUE (units 10^{-4})	CL%	DOCUMENT ID	TECN	COMMENT
<6	90	¹ ADAMS 06	CLEO	$e^+e^- \rightarrow \psi(3770)$

¹ Comparing cross sections at $\sqrt{s} = 3.773$ GeV and $\sqrt{s} = 3.671$ GeV, neglecting interference, and using $\sigma(\psi(3770) \rightarrow D\bar{D}) = 6.39 \pm 0.20$ nb.

$\Gamma(\phi\eta)/\Gamma_{total}$		Γ_{14}/Γ		
VALUE (units 10^{-4})	CL%	DOCUMENT ID	TECN	COMMENT
3.1 \pm 0.6 \pm 0.3		¹ ADAMS 06	CLEO	3.773 $e^+e^- \rightarrow \phi\eta$

• • • We do not use the following data for averages, fits, limits, etc. • • •

VALUE	DOCUMENT ID	TECN	COMMENT	
<19	90	² ABLIKIM 07B	BES2	$e^+e^- \rightarrow \psi(3770)$

¹ Comparing cross sections at $\sqrt{s} = 3.773$ GeV and $\sqrt{s} = 3.671$ GeV, neglecting interference, and using $\sigma(\psi(3770) \rightarrow D\bar{D}) = 6.39 \pm 0.20$ nb.

² Assuming that interference effects between resonance and continuum can be neglected and using $\sigma^{obs}(e^+e^- \rightarrow \psi(3770)) = 7.15 \pm 0.38$ nb.

$\Gamma(\omega\eta)/\Gamma_{total}$		Γ_{15}/Γ		
VALUE (units 10^{-5})	CL%	DOCUMENT ID	TECN	COMMENT
<1.4	90	¹ ADAMS 06	CLEO	$e^+e^- \rightarrow \psi(3770)$

¹ Comparing cross sections at $\sqrt{s} = 3.773$ GeV and $\sqrt{s} = 3.671$ GeV, neglecting interference, and using $\sigma(\psi(3770) \rightarrow D\bar{D}) = 6.39 \pm 0.20$ nb.

$\Gamma(\rho^0\eta)/\Gamma_{total}$		Γ_{16}/Γ		
VALUE (units 10^{-4})	CL%	DOCUMENT ID	TECN	COMMENT
<5	90	¹ ADAMS 06	CLEO	$e^+e^- \rightarrow \psi(3770)$

¹ Comparing cross sections at $\sqrt{s} = 3.773$ GeV and $\sqrt{s} = 3.671$ GeV, neglecting interference, and using $\sigma(\psi(3770) \rightarrow D\bar{D}) = 6.39 \pm 0.20$ nb.

$\Gamma(\phi\pi^0)/\Gamma_{total}$		Γ_{17}/Γ		
VALUE (units 10^{-5})	CL%	DOCUMENT ID	TECN	COMMENT
<3	90	¹ ADAMS 06	CLEO	$e^+e^- \rightarrow \psi(3770)$

• • • We do not use the following data for averages, fits, limits, etc. • • •

VALUE	DOCUMENT ID	TECN	COMMENT	
<50	90	² ABLIKIM 07B	BES2	$e^+e^- \rightarrow \psi(3770)$

¹ Comparing cross sections at $\sqrt{s} = 3.773$ GeV and $\sqrt{s} = 3.671$ GeV, neglecting interference, and using $\sigma(\psi(3770) \rightarrow D\bar{D}) = 6.39 \pm 0.20$ nb.

² Assuming that interference effects between resonance and continuum can be neglected and using $\sigma^{obs}(e^+e^- \rightarrow \psi(3770)) = 7.15 \pm 0.38$ nb.

$\Gamma(\omega\pi^0)/\Gamma_{total}$		Γ_{18}/Γ		
VALUE (units 10^{-4})	CL%	DOCUMENT ID	TECN	COMMENT
<6	90	¹ ADAMS 06	CLEO	$e^+e^- \rightarrow \psi(3770)$

¹ Comparing cross sections at $\sqrt{s} = 3.773$ GeV and $\sqrt{s} = 3.671$ GeV, neglecting interference, and using $\sigma(\psi(3770) \rightarrow D\bar{D}) = 6.39 \pm 0.20$ nb.

$\Gamma(\pi^+\pi^-\pi^0)/\Gamma_{total}$		Γ_{19}/Γ		
VALUE (units 10^{-6})	CL%	DOCUMENT ID	TECN	COMMENT
<5	90	^{1,2} ADAMS 06	CLEO	$e^+e^- \rightarrow \psi(3770)$

¹ Data suggest possible destructive interference with continuum.

² Comparing cross sections at $\sqrt{s} = 3.773$ GeV and $\sqrt{s} = 3.671$ GeV, neglecting interference, and using $\sigma(\psi(3770) \rightarrow D\bar{D}) = 6.39 \pm 0.20$ nb.

$\Gamma(\rho\pi)/\Gamma_{total}$		Γ_{20}/Γ		
VALUE (units 10^{-6})	CL%	DOCUMENT ID	TECN	COMMENT
<5	90	^{1,2} ADAMS 06	CLEO	$e^+e^- \rightarrow \psi(3770)$

¹ Comparing cross sections at $\sqrt{s} = 3.773$ GeV and $\sqrt{s} = 3.671$ GeV, neglecting interference, and using $\sigma(\psi(3770) \rightarrow D\bar{D}) = 6.39 \pm 0.20$ nb.

² Data suggest possible destructive interference with continuum.

$\Gamma(K^+K^-)/\Gamma_{total}$		Γ_{21}/Γ	
VALUE	DOCUMENT ID	TECN	COMMENT
$\sim 10^{-5}$	¹ DRUZHININ 15	RVUE	$e^+e^- \rightarrow \psi(3770)$

¹ DRUZHININ 15 uses BABAR and CLEO data taking into account interference of the processes $e^+e^- \rightarrow K^+K^-$ and $e^+e^- \rightarrow K_S^0 K_L^0$.

Meson Particle Listings

 $\psi(3770)$ $\Gamma(K^*(892)^+ K^- + c.c.)/\Gamma_{\text{total}}$ Γ_{22}/Γ

VALUE (units 10^{-5})	CL%	DOCUMENT ID	TECN	COMMENT
<1.4	90	¹ ADAMS	06 CLEO	$e^+ e^- \rightarrow \psi(3770)$

¹ Comparing cross sections at $\sqrt{s} = 3.773$ GeV and $\sqrt{s} = 3.671$ GeV, neglecting interference, and using $\sigma(\psi(3770) \rightarrow D\bar{D}) = 6.39 \pm 0.20$ nb.

 $\Gamma(K^*(892)^0 \bar{K}^0 + c.c.)/\Gamma_{\text{total}}$ Γ_{23}/Γ

VALUE (units 10^{-3})	CL%	DOCUMENT ID	TECN	COMMENT
<1.2	90	¹ ADAMS	06 CLEO	$e^+ e^- \rightarrow \psi(3770)$

¹ Comparing cross sections at $\sqrt{s} = 3.773$ GeV and $\sqrt{s} = 3.671$ GeV, neglecting interference, and using $\sigma(\psi(3770) \rightarrow D\bar{D}) = 6.39 \pm 0.20$ nb.

 $\Gamma(K_S^0 K_L^0)/\Gamma_{\text{total}}$ Γ_{24}/Γ

VALUE (units 10^{-5})	CL%	DOCUMENT ID	TECN	COMMENT
< 1.2	90	¹ CRONIN-HEN.06	CLEO	$e^+ e^- \rightarrow \psi(3770)$

• • • We do not use the following data for averages, fits, limits, etc. • • •

VALUE (units 10^{-5})	CL%	DOCUMENT ID	TECN	COMMENT
<21	90	² ABLIKIM	04F BES	$e^+ e^- \rightarrow \psi(3770)$

¹ Using $\sigma(e^+ e^- \rightarrow \psi(3770) \rightarrow \text{hadrons}) = (6.38 \pm 0.08^{+0.41}_{-0.30})$ nb from BESSON 06 and $B(K_S^0 \rightarrow \pi^+ \pi^-) = 0.6895 \pm 0.0014$.

² Using $B(K_S^0 \rightarrow \pi^+ \pi^-) = 0.6860 \pm 0.0027$.

 $\Gamma(2(\pi^+ \pi^-))/\Gamma_{\text{total}}$ Γ_{25}/Γ

VALUE (units 10^{-4})	CL%	DOCUMENT ID	TECN	COMMENT
<11.2	90	¹ HUANG	06A CLEO	$e^+ e^- \rightarrow \psi(3770)$

• • • We do not use the following data for averages, fits, limits, etc. • • •

VALUE (units 10^{-4})	CL%	DOCUMENT ID	TECN	COMMENT
<48	90	² ABLIKIM	07B BES2	$e^+ e^- \rightarrow \psi(3770)$

¹ Using $\sigma_{\text{tot}}(e^+ e^- \rightarrow \psi(3770)) = 7.9 \pm 0.6$ nb at the resonance.

² Assuming that interference effects between resonance and continuum can be neglected and using $\sigma^{\text{obs}}(e^+ e^- \rightarrow \psi(3770)) = 7.15 \pm 0.38$ nb.

 $\Gamma(2(\pi^+ \pi^- \pi^0))/\Gamma_{\text{total}}$ Γ_{26}/Γ

VALUE (units 10^{-4})	CL%	DOCUMENT ID	TECN	COMMENT
<10.6	90	¹ HUANG	06A CLEO	$e^+ e^- \rightarrow \psi(3770)$

• • • We do not use the following data for averages, fits, limits, etc. • • •

VALUE (units 10^{-4})	CL%	DOCUMENT ID	TECN	COMMENT
<62	90	² ABLIKIM	07B BES2	$e^+ e^- \rightarrow \psi(3770)$

¹ Using $\sigma_{\text{tot}}(e^+ e^- \rightarrow \psi(3770)) = 7.9 \pm 0.6$ nb at the resonance.

² Assuming that interference effects between resonance and continuum can be neglected and using $\sigma^{\text{obs}}(e^+ e^- \rightarrow \psi(3770)) = 7.15 \pm 0.38$ nb.

 $\Gamma(2(\pi^+ \pi^- \pi^0))/\Gamma_{\text{total}}$ Γ_{27}/Γ

VALUE (units 10^{-3})	CL%	EVTS	DOCUMENT ID	TECN	COMMENT
<58.5	90	305	ABLIKIM	08N BES2	$e^+ e^- \rightarrow \psi(3770)$

 $\Gamma(\omega \pi^+ \pi^-)/\Gamma_{\text{total}}$ Γ_{28}/Γ

VALUE (units 10^{-4})	CL%	DOCUMENT ID	TECN	COMMENT
< 6.0	90	¹ HUANG	06A CLEO	$e^+ e^- \rightarrow \psi(3770)$

• • • We do not use the following data for averages, fits, limits, etc. • • •

VALUE (units 10^{-4})	CL%	DOCUMENT ID	TECN	COMMENT
<55	90	² ABLIKIM	07I BES2	$3.77 e^+ e^-$

¹ Using $\sigma_{\text{tot}}(e^+ e^- \rightarrow \psi(3770)) = 7.9 \pm 0.6$ nb at the resonance.

² Assuming that interference effects between resonance and continuum can be neglected and using $\sigma^{\text{obs}}(e^+ e^- \rightarrow \psi(3770)) = 7.15 \pm 0.38$ nb.

 $\Gamma(3(\pi^+ \pi^-))/\Gamma_{\text{total}}$ Γ_{29}/Γ

VALUE (units 10^{-4})	CL%	DOCUMENT ID	TECN	COMMENT
<91	90	¹ ABLIKIM	07B BES2	$e^+ e^- \rightarrow \psi(3770)$

¹ Assuming that interference effects between resonance and continuum can be neglected and using $\sigma^{\text{obs}}(e^+ e^- \rightarrow \psi(3770)) = 7.15 \pm 0.38$ nb.

 $\Gamma(3(\pi^+ \pi^- \pi^0))/\Gamma_{\text{total}}$ Γ_{30}/Γ

VALUE (units 10^{-4})	CL%	DOCUMENT ID	TECN	COMMENT
<137	90	¹ ABLIKIM	07B BES2	$e^+ e^- \rightarrow \psi(3770)$

¹ Assuming that interference effects between resonance and continuum can be neglected and using $\sigma^{\text{obs}}(e^+ e^- \rightarrow \psi(3770)) = 7.15 \pm 0.38$ nb.

 $\Gamma(3(\pi^+ \pi^- 2\pi^0))/\Gamma_{\text{total}}$ Γ_{31}/Γ

VALUE (units 10^{-3})	CL%	EVTS	DOCUMENT ID	TECN	COMMENT
<117.4	90	59	ABLIKIM	08N BES2	$e^+ e^- \rightarrow \psi(3770)$

 $\Gamma(\eta \pi^+ \pi^-)/\Gamma_{\text{total}}$ Γ_{32}/Γ

VALUE (units 10^{-3})	CL%	DOCUMENT ID	TECN	COMMENT
<1.24	90	¹ HUANG	06A CLEO	$e^+ e^- \rightarrow \psi(3770)$

• • • We do not use the following data for averages, fits, limits, etc. • • •

VALUE (units 10^{-3})	CL%	DOCUMENT ID	TECN	COMMENT
<2.3	90	² ABLIKIM	10D BES2	$e^+ e^- \rightarrow \psi(3770)$

¹ Using $\sigma_{\text{tot}}(e^+ e^- \rightarrow \psi(3770)) = 7.9 \pm 0.6$ nb at the resonance.

² Assuming that interference effects between resonance and continuum can be neglected and using $\sigma^{\text{obs}}(e^+ e^- \rightarrow \psi(3770)) = 7.15 \pm 0.38$ nb.

 $\Gamma(\pi^+ \pi^- 2\pi^0)/\Gamma_{\text{total}}$ Γ_{33}/Γ

VALUE (units 10^{-3})	CL%	EVTS	DOCUMENT ID	TECN	COMMENT
<8.9	90	218	ABLIKIM	08N BES2	$e^+ e^- \rightarrow \psi(3770)$

 $\Gamma(\rho^0 \pi^+ \pi^-)/\Gamma_{\text{total}}$ Γ_{34}/Γ

VALUE (units 10^{-3})	CL%	DOCUMENT ID	TECN	COMMENT
<6.9	90	¹ ABLIKIM	07F BES2	$e^+ e^- \rightarrow \psi(3770)$

¹ Assuming that interference effects between resonance and continuum can be neglected and using $\sigma^{\text{obs}}(e^+ e^- \rightarrow \psi(3770)) = 7.15 \pm 0.38$ nb.

 $\Gamma(\eta 3\pi)/\Gamma_{\text{total}}$ Γ_{35}/Γ

VALUE (units 10^{-4})	CL%	DOCUMENT ID	TECN	COMMENT
<13.4	90	¹ HUANG	06A CLEO	$e^+ e^- \rightarrow \psi(3770)$

¹ Using $\sigma_{\text{tot}}(e^+ e^- \rightarrow \psi(3770)) = 7.9 \pm 0.6$ nb at the resonance.

 $\Gamma(\eta 2(\pi^+ \pi^-))/\Gamma_{\text{total}}$ Γ_{36}/Γ

VALUE (units 10^{-4})	CL%	DOCUMENT ID	TECN	COMMENT
<24.3	90	¹ ABLIKIM	07B BES2	$e^+ e^- \rightarrow \psi(3770)$

¹ Assuming that interference effects between resonance and continuum can be neglected and using $\sigma^{\text{obs}}(e^+ e^- \rightarrow \psi(3770)) = 7.15 \pm 0.38$ nb.

 $\Gamma(\eta \rho^0 \pi^+ \pi^-)/\Gamma_{\text{total}}$ Γ_{37}/Γ

VALUE (units 10^{-2})	CL%	DOCUMENT ID	TECN	COMMENT
<1.45	90	¹ ABLIKIM	10D BES2	$e^+ e^- \rightarrow \psi(3770)$

¹ Assuming that interference effects between resonance and continuum can be neglected and using $\sigma^{\text{obs}}(e^+ e^- \rightarrow \psi(3770)) = 7.15 \pm 0.38$ nb.

 $\Gamma(\eta' 3\pi)/\Gamma_{\text{total}}$ Γ_{38}/Γ

VALUE (units 10^{-4})	CL%	DOCUMENT ID	TECN	COMMENT
<24.4	90	¹ HUANG	06A CLEO	$e^+ e^- \rightarrow \psi(3770)$

¹ Using $\sigma_{\text{tot}}(e^+ e^- \rightarrow \psi(3770)) = 7.9 \pm 0.6$ nb at the resonance.

 $\Gamma(K^+ K^- \pi^+ \pi^-)/\Gamma_{\text{total}}$ Γ_{39}/Γ

VALUE (units 10^{-4})	CL%	DOCUMENT ID	TECN	COMMENT
< 9.0	90	¹ HUANG	06A CLEO	$e^+ e^- \rightarrow \psi(3770)$

• • • We do not use the following data for averages, fits, limits, etc. • • •

VALUE (units 10^{-4})	CL%	DOCUMENT ID	TECN	COMMENT
<48	90	² ABLIKIM	07B BES2	$e^+ e^- \rightarrow \psi(3770)$

¹ Using $\sigma_{\text{tot}}(e^+ e^- \rightarrow \psi(3770)) = 7.9 \pm 0.6$ nb at the resonance.

² Assuming that interference effects between resonance and continuum can be neglected and using $\sigma^{\text{obs}}(e^+ e^- \rightarrow \psi(3770)) = 7.15 \pm 0.38$ nb.

 $\Gamma(\phi \pi^+ \pi^-)/\Gamma_{\text{total}}$ Γ_{40}/Γ

VALUE (units 10^{-4})	CL%	DOCUMENT ID	TECN	COMMENT
< 4.1	90	¹ HUANG	06A CLEO	$e^+ e^- \rightarrow \psi(3770)$

• • • We do not use the following data for averages, fits, limits, etc. • • •

VALUE (units 10^{-4})	CL%	DOCUMENT ID	TECN	COMMENT
<16	90	² ABLIKIM	07B BES2	$e^+ e^- \rightarrow \psi(3770)$

¹ Using $\sigma_{\text{tot}}(e^+ e^- \rightarrow \psi(3770)) = 7.9 \pm 0.6$ nb at the resonance.

² Assuming that interference effects between resonance and continuum can be neglected and using $\sigma^{\text{obs}}(e^+ e^- \rightarrow \psi(3770)) = 7.15 \pm 0.38$ nb.

 $\Gamma(K^+ K^- 2\pi^0)/\Gamma_{\text{total}}$ Γ_{41}/Γ

VALUE (units 10^{-3})	CL%	EVTS	DOCUMENT ID	TECN	COMMENT
<4.2	90	14	ABLIKIM	08N BES2	$e^+ e^- \rightarrow \psi(3770)$

 $\Gamma(4(\pi^+ \pi^-))/\Gamma_{\text{total}}$ Γ_{42}/Γ

VALUE (units 10^{-3})	CL%	DOCUMENT ID	TECN	COMMENT
<16.7	90	¹ ABLIKIM	07F BES2	$e^+ e^- \rightarrow \psi(3770)$

¹ Assuming that interference effects between resonance and continuum can be neglected and using $\sigma^{\text{obs}}(e^+ e^- \rightarrow \psi(3770)) = 7.15 \pm 0.38$ nb.

 $\Gamma(4(\pi^+ \pi^- \pi^0))/\Gamma_{\text{total}}$ Γ_{43}/Γ

VALUE (units 10^{-3})	CL%	DOCUMENT ID	TECN	COMMENT
<30.6	90	¹ ABLIKIM	07F BES2	$e^+ e^- \rightarrow \psi(3770)$

¹ Assuming that interference effects between resonance and continuum can be neglected and using $\sigma^{\text{obs}}(e^+ e^- \rightarrow \psi(3770)) = 7.15 \pm 0.38$ nb.

 $\Gamma(\phi f_0(980))/\Gamma_{\text{total}}$ Γ_{44}/Γ

VALUE (units 10^{-4})	CL%	DOCUMENT ID	TECN	COMMENT
<4.5	90	¹ HUANG	06A CLEO	$e^+ e^- \rightarrow \psi(3770)$

¹ Using $\sigma_{\text{tot}}(e^+ e^- \rightarrow \psi(3770)) = 7.9 \pm 0.6$ nb at the resonance.

 $\Gamma(K^+ K^- \pi^+ \pi^- \pi^0)/\Gamma_{\text{total}}$ Γ_{45}/Γ

VALUE (units 10^{-4})	CL%	DOCUMENT ID	TECN	COMMENT
< 23.6	90	¹ HUANG	06A CLEO	$e^+ e^- \rightarrow \psi(3770)$

• • • We do not use the following data for averages, fits, limits, etc. • • •

VALUE (units 10^{-4})	CL%	DOCUMENT ID	TECN	COMMENT
<111	90	² ABLIKIM	07B BES2	$e^+ e^- \rightarrow \psi(3770)$

¹ Using $\sigma_{\text{tot}}(e^+ e^- \rightarrow \psi(3770)) = 7.9 \pm 0.6$ nb at the resonance.

² Assuming that interference effects between resonance and continuum can be neglected and using $\sigma^{\text{obs}}(e^+ e^- \rightarrow \psi(3770)) = 7.15 \pm 0.38$ nb.

$\Gamma(K^+ K^- \rho^0 \pi^0) / \Gamma_{total}$ Γ_{46} / Γ

VALUE (units 10^{-4})	CL%	DOCUMENT ID	TECN	COMMENT
<8	90	¹ ABLIKIM 07i	BES2	$3.77 e^+ e^-$

¹ Assuming that interference effects between resonance and continuum can be neglected and using $\sigma^{obs}(e^+ e^- \rightarrow \psi(3770)) = 7.15 \pm 0.38$ nb.

$\Gamma(K^+ K^- \rho^+ \pi^-) / \Gamma_{total}$ Γ_{47} / Γ

VALUE (units 10^{-4})	CL%	DOCUMENT ID	TECN	COMMENT
<146	90	¹ ABLIKIM 07i	BES2	$3.77 e^+ e^-$

¹ Assuming that interference effects between resonance and continuum can be neglected and using $\sigma^{obs}(e^+ e^- \rightarrow \psi(3770)) = 7.15 \pm 0.38$ nb.

$\Gamma(\omega K^+ K^-) / \Gamma_{total}$ Γ_{48} / Γ

VALUE (units 10^{-4})	CL%	DOCUMENT ID	TECN	COMMENT
< 3.4	90	¹ HUANG 06A	CLEO	$e^+ e^- \rightarrow \psi(3770)$
•••		We do not use the following data for averages, fits, limits, etc. •••		
<66	90	² ABLIKIM 07i	BES2	$3.77 e^+ e^-$

¹ Using $\sigma_{tot}(e^+ e^- \rightarrow \psi(3770)) = 7.9 \pm 0.6$ nb at the resonance.
² Assuming that interference effects between resonance and continuum can be neglected and using $\sigma^{obs}(e^+ e^- \rightarrow \psi(3770)) = 7.15 \pm 0.38$ nb.

$\Gamma(\phi \pi^+ \pi^- \pi^0) / \Gamma_{total}$ Γ_{49} / Γ

VALUE (units 10^{-4})	CL%	DOCUMENT ID	TECN	COMMENT
<38	90	¹ ABLIKIM 07i	BES2	$3.77 e^+ e^-$

¹ Assuming that interference effects between resonance and continuum can be neglected and using $\sigma^{obs}(e^+ e^- \rightarrow \psi(3770)) = 7.15 \pm 0.38$ nb.

$\Gamma(K^{*0} K^- \pi^+ \pi^0 + c.c.) / \Gamma_{total}$ Γ_{50} / Γ

VALUE (units 10^{-4})	CL%	DOCUMENT ID	TECN	COMMENT
<162	90	¹ ABLIKIM 07i	BES2	$3.77 e^+ e^-$

¹ Assuming that interference effects between resonance and continuum can be neglected and using $\sigma^{obs}(e^+ e^- \rightarrow \psi(3770)) = 7.15 \pm 0.38$ nb.

$\Gamma(K^{*+} K^- \pi^+ \pi^- + c.c.) / \Gamma_{total}$ Γ_{51} / Γ

VALUE (units 10^{-4})	CL%	DOCUMENT ID	TECN	COMMENT
<323	90	¹ ABLIKIM 07i	BES2	$3.77 e^+ e^-$

¹ Assuming that interference effects between resonance and continuum can be neglected and using $\sigma^{obs}(e^+ e^- \rightarrow \psi(3770)) = 7.15 \pm 0.38$ nb.

$\Gamma(K^+ K^- \pi^+ \pi^- 2\pi^0) / \Gamma_{total}$ Γ_{52} / Γ

VALUE (units 10^{-3})	CL%	EVTS	DOCUMENT ID	TECN	COMMENT
<26.7	90	24	ABLIKIM 08N	BES2	$e^+ e^- \rightarrow \psi(3770)$

$\Gamma(K^+ K^- 2(\pi^+ \pi^-)) / \Gamma_{total}$ Γ_{53} / Γ

VALUE (units 10^{-3})	CL%	DOCUMENT ID	TECN	COMMENT
<10.3	90	¹ ABLIKIM 07F	BES2	$e^+ e^- \rightarrow \psi(3770)$

¹ Assuming that interference effects between resonance and continuum can be neglected and using $\sigma^{obs}(e^+ e^- \rightarrow \psi(3770)) = 7.15 \pm 0.38$ nb.

$\Gamma(K^+ K^- 2(\pi^+ \pi^-) \pi^0) / \Gamma_{total}$ Γ_{54} / Γ

VALUE (units 10^{-3})	CL%	DOCUMENT ID	TECN	COMMENT
<36.0	90	¹ ABLIKIM 07F	BES2	$e^+ e^- \rightarrow \psi(3770)$

¹ Assuming that interference effects between resonance and continuum can be neglected and using $\sigma^{obs}(e^+ e^- \rightarrow \psi(3770)) = 7.15 \pm 0.38$ nb.

$\Gamma(\eta K^+ K^-) / \Gamma_{total}$ Γ_{55} / Γ

VALUE (units 10^{-4})	CL%	DOCUMENT ID	TECN	COMMENT
< 4.1	90	¹ HUANG 06A	CLEO	$e^+ e^- \rightarrow \psi(3770)$
•••		We do not use the following data for averages, fits, limits, etc. •••		
<31	90	² ABLIKIM 10d	BES2	$e^+ e^- \rightarrow \psi(3770)$

¹ Using $\sigma_{tot}(e^+ e^- \rightarrow \psi(3770)) = 7.9 \pm 0.6$ nb at the resonance.
² Assuming that interference effects between resonance and continuum can be neglected and using $\sigma^{obs}(e^+ e^- \rightarrow \psi(3770)) = 7.15 \pm 0.38$ nb.

$\Gamma(\eta K^+ K^- \pi^+ \pi^-) / \Gamma_{total}$ Γ_{56} / Γ

VALUE (units 10^{-2})	CL%	DOCUMENT ID	TECN	COMMENT
<1.24	90	¹ ABLIKIM 10d	BES2	$e^+ e^- \rightarrow \psi(3770)$

¹ Assuming that interference effects between resonance and continuum can be neglected and using $\sigma^{obs}(e^+ e^- \rightarrow \psi(3770)) = 7.15 \pm 0.38$ nb.

$\Gamma(\rho^0 K^+ K^-) / \Gamma_{total}$ Γ_{57} / Γ

VALUE (units 10^{-3})	CL%	DOCUMENT ID	TECN	COMMENT
<5.0	90	¹ ABLIKIM 07F	BES2	$e^+ e^- \rightarrow \psi(3770)$

¹ Assuming that interference effects between resonance and continuum can be neglected and using $\sigma^{obs}(e^+ e^- \rightarrow \psi(3770)) = 7.15 \pm 0.38$ nb.

$\Gamma(2(K^+ K^-)) / \Gamma_{total}$ Γ_{58} / Γ

VALUE (units 10^{-4})	CL%	DOCUMENT ID	TECN	COMMENT
< 6.0	90	¹ HUANG 06A	CLEO	$e^+ e^- \rightarrow \psi(3770)$
•••		We do not use the following data for averages, fits, limits, etc. •••		
<17	90	² ABLIKIM 07B	BES2	$e^+ e^- \rightarrow \psi(3770)$

¹ Using $\sigma_{tot}(e^+ e^- \rightarrow \psi(3770)) = 7.9 \pm 0.6$ nb at the resonance.
² Assuming that interference effects between resonance and continuum can be neglected and using $\sigma^{obs}(e^+ e^- \rightarrow \psi(3770)) = 7.15 \pm 0.38$ nb.

$\Gamma(\phi K^+ K^-) / \Gamma_{total}$ Γ_{59} / Γ

VALUE (units 10^{-4})	CL%	DOCUMENT ID	TECN	COMMENT
< 7.5	90	¹ HUANG 06A	CLEO	$e^+ e^- \rightarrow \psi(3770)$
•••		We do not use the following data for averages, fits, limits, etc. •••		
<24	90	² ABLIKIM 07B	BES2	$e^+ e^- \rightarrow \psi(3770)$

¹ Using $\sigma_{tot}(e^+ e^- \rightarrow \psi(3770)) = 7.9 \pm 0.6$ nb at the resonance.
² Assuming that interference effects between resonance and continuum can be neglected and using $\sigma^{obs}(e^+ e^- \rightarrow \psi(3770)) = 7.15 \pm 0.38$ nb.

$\Gamma(2(K^+ K^-) \pi^0) / \Gamma_{total}$ Γ_{60} / Γ

VALUE (units 10^{-4})	CL%	DOCUMENT ID	TECN	COMMENT
< 2.9	90	¹ HUANG 06A	CLEO	$e^+ e^- \rightarrow \psi(3770)$
•••		We do not use the following data for averages, fits, limits, etc. •••		
<46	90	² ABLIKIM 07B	BES2	$e^+ e^- \rightarrow \psi(3770)$

¹ Using $\sigma_{tot}(e^+ e^- \rightarrow \psi(3770)) = 7.9 \pm 0.6$ nb at the resonance.
² Assuming that interference effects between resonance and continuum can be neglected and using $\sigma^{obs}(e^+ e^- \rightarrow \psi(3770)) = 7.15 \pm 0.38$ nb.

$\Gamma(2(K^+ K^-) \pi^+ \pi^-) / \Gamma_{total}$ Γ_{61} / Γ

VALUE (units 10^{-3})	CL%	DOCUMENT ID	TECN	COMMENT
<3.2	90	¹ ABLIKIM 07F	BES2	$e^+ e^- \rightarrow \psi(3770)$

¹ Assuming that interference effects between resonance and continuum can be neglected and using $\sigma^{obs}(e^+ e^- \rightarrow \psi(3770)) = 7.15 \pm 0.38$ nb.

$\Gamma(K_S^0 K^- \pi^+) / \Gamma_{total}$ Γ_{62} / Γ

VALUE (units 10^{-3})	CL%	EVTS	DOCUMENT ID	TECN	COMMENT
<3.2	90	18	ABLIKIM 08M	BES2	$e^+ e^- \rightarrow \psi(3770)$

$\Gamma(K_S^0 K^- \pi^+ \pi^0) / \Gamma_{total}$ Γ_{63} / Γ

VALUE (units 10^{-3})	CL%	EVTS	DOCUMENT ID	TECN	COMMENT
<13.3	90	40	ABLIKIM 08M	BES2	$e^+ e^- \rightarrow \psi(3770)$

$\Gamma(K_S^0 K^- \rho^+) / \Gamma_{total}$ Γ_{64} / Γ

VALUE (units 10^{-3})	CL%	DOCUMENT ID	TECN	COMMENT
<6.6	90	ABLIKIM 09C	BES2	$e^+ e^- \rightarrow \psi(3770)$

$\Gamma(K_S^0 K^- 2\pi^+ \pi^-) / \Gamma_{total}$ Γ_{65} / Γ

VALUE (units 10^{-3})	CL%	EVTS	DOCUMENT ID	TECN	COMMENT
<8.7	90	39	ABLIKIM 08M	BES2	$e^+ e^- \rightarrow \psi(3770)$

$\Gamma(K_S^0 K^- \pi^+ \rho^0) / \Gamma_{total}$ Γ_{66} / Γ

VALUE (units 10^{-2})	CL%	DOCUMENT ID	TECN	COMMENT
<1.6	90	ABLIKIM 09C	BES2	$e^+ e^- \rightarrow \psi(3770)$

$\Gamma(K_S^0 K^- \pi^+ \eta) / \Gamma_{total}$ Γ_{67} / Γ

VALUE (units 10^{-2})	CL%	DOCUMENT ID	TECN	COMMENT
<1.3	90	ABLIKIM 09C	BES2	$e^+ e^- \rightarrow \psi(3770)$

$\Gamma(K_S^0 K^- 2\pi^+ \pi^- \pi^0) / \Gamma_{total}$ Γ_{68} / Γ

VALUE (units 10^{-3})	CL%	EVTS	DOCUMENT ID	TECN	COMMENT
<41.8	90	23	ABLIKIM 08M	BES2	$e^+ e^- \rightarrow \psi(3770)$

$\Gamma(K_S^0 K^- 2\pi^+ \pi^- \eta) / \Gamma_{total}$ Γ_{69} / Γ

VALUE (units 10^{-2})	CL%	DOCUMENT ID	TECN	COMMENT
<4.8	90	ABLIKIM 09C	BES2	$e^+ e^- \rightarrow \psi(3770)$

$\Gamma(K_S^0 K^- \pi^+ 2(\pi^+ \pi^-)) / \Gamma_{total}$ Γ_{70} / Γ

VALUE (units 10^{-3})	CL%	EVTS	DOCUMENT ID	TECN	COMMENT
<12.2	90	4	ABLIKIM 08M	BES2	$e^+ e^- \rightarrow \psi(3770)$

$\Gamma(K_S^0 K^- \pi^+ 2\pi^0) / \Gamma_{total}$ Γ_{71} / Γ

VALUE (units 10^{-3})	CL%	EVTS	DOCUMENT ID	TECN	COMMENT
<26.5	90	17	ABLIKIM 08M	BES2	$e^+ e^- \rightarrow \psi(3770)$

$\Gamma(K_S^0 K^- K^+ K^- \pi^+) / \Gamma_{total}$ Γ_{72} / Γ

VALUE (units 10^{-3})	CL%	DOCUMENT ID	TECN	COMMENT
<4.9	90	ABLIKIM 09C	BES2	$e^+ e^- \rightarrow \psi(3770)$

Meson Particle Listings

 $\psi(3770)$

$\Gamma(K_S^0 K^- K^+ K^- \pi^+ \pi^0)/\Gamma_{\text{total}}$					Γ_{73}/Γ
VALUE (units 10^{-2})	CL%	DOCUMENT ID	TECN	COMMENT	
<3.0	90	ABLIKIM	09C	BES2 $e^+ e^- \rightarrow \psi(3770)$	

$\Gamma(K_S^0 K^- K^+ K^- \pi^+ \eta)/\Gamma_{\text{total}}$					Γ_{74}/Γ
VALUE (units 10^{-2})	CL%	DOCUMENT ID	TECN	COMMENT	
<2.2	90	ABLIKIM	09C	BES2 $e^+ e^- \rightarrow \psi(3770)$	

$\Gamma(K^{*0} K^- \pi^+ + \text{c.c.})/\Gamma_{\text{total}}$					Γ_{75}/Γ
VALUE (units 10^{-3})	CL%	DOCUMENT ID	TECN	COMMENT	
<9.7	90	¹ ABLIKIM	07F	BES2 $e^+ e^- \rightarrow \psi(3770)$	

¹ Assuming that interference effects between resonance and continuum can be neglected and using $\sigma^{\text{obs}}(e^+ e^- \rightarrow \psi(3770)) = 7.15 \pm 0.38$ nb.

$\Gamma(p\bar{p})/\Gamma_{\text{total}}$					Γ_{76}/Γ
VALUE (units 10^{-6})	EVTs	DOCUMENT ID	TECN	COMMENT	
not seen		¹ AAIJ	17AD	LHCB $p\bar{p} \rightarrow B^+ X \rightarrow p\bar{p} K^+ X$	
$7.1^{+8.6}_{-2.9}$	684	² ABLIKIM	14L	BES3 $e^+ e^- \rightarrow \psi(3770)$	
310 ± 30	684	³ ABLIKIM	14L	BES3 $e^+ e^- \rightarrow \psi(3770)$	

¹ AAIJ 17AD reports $B(B^+ \rightarrow \psi(3770) K^+ \rightarrow p\bar{p} K^+)/B(B^+ \rightarrow J/\psi K^+ \rightarrow p\bar{p} K^+) < 0.09$ (0.10) at 90% (95%) CL.
² Solution I of two equivalent solutions in a fit with a resonance interfering with continuum.
³ Solution II of two equivalent solutions in a fit with a resonance interfering with continuum.

$\Gamma(p\bar{p}\pi^0)/\Gamma_{\text{total}}$					Γ_{77}/Γ
VALUE (units 10^{-4})	CL%	DOCUMENT ID	TECN	COMMENT	
<0.4	90	^{1,2} ABLIKIM	14O	BES3 $e^+ e^- \rightarrow \psi(3770)$	

^{1,2} We do not use the following data for averages, fits, limits, etc. ● ● ●
 $59^{+3}_{-2} \pm 5$ ^{1,3}ABLIKIM 14O BES3 $e^+ e^- \rightarrow \psi(3770)$
 <12 90 ⁴ABLIKIM 07B BES2 $e^+ e^- \rightarrow \psi(3770)$

¹ Calculated by the authors using $\sigma(e^+ e^- \rightarrow \psi(3770) \rightarrow \text{hadrons}) = 6.36 \pm 0.08^{+0.41}_{-0.30}$ nb from BESSON 10.
² Solution I of two equivalent solutions in a fit with a resonance interfering with continuum.
³ Solution II of two equivalent solutions in a fit with a resonance interfering with continuum.
⁴ Assuming that interference effects between resonance and continuum can be neglected and using $\sigma^{\text{obs}}(e^+ e^- \rightarrow \psi(3770)) = 7.15 \pm 0.38$ nb.

$\Gamma(p\bar{p}\pi^+\pi^-)/\Gamma_{\text{total}}$					Γ_{78}/Γ
VALUE (units 10^{-4})	CL%	DOCUMENT ID	TECN	COMMENT	
<5.8	90	¹ HUANG	06A	CLEO $e^+ e^- \rightarrow \psi(3770)$	

¹ We do not use the following data for averages, fits, limits, etc. ● ● ●
 <16 90 ²ABLIKIM 07B BES2 $e^+ e^- \rightarrow \psi(3770)$
¹ Using $\sigma_{\text{tot}}(e^+ e^- \rightarrow \psi(3770)) = 7.9 \pm 0.6$ nb at the resonance.
² Assuming that interference effects between resonance and continuum can be neglected and using $\sigma^{\text{obs}}(e^+ e^- \rightarrow \psi(3770)) = 7.15 \pm 0.38$ nb.

$\Gamma(\Lambda\bar{\Lambda})/\Gamma_{\text{total}}$					Γ_{79}/Γ
VALUE	CL%	DOCUMENT ID	TECN	COMMENT	
<1.2 $\times 10^{-4}$	90	¹ HUANG	06A	CLEO $e^+ e^- \rightarrow \psi(3770)$	

¹ We do not use the following data for averages, fits, limits, etc. ● ● ●
 <1.8 $\times 10^{-4}$ 90 ²ABLIKIM 21AS BES3 $e^+ e^- \rightarrow \psi(3770)$
 <4 $\times 10^{-4}$ 90 ³ABLIKIM 07F BES2 $e^+ e^- \rightarrow \psi(3770)$
¹ Using $\sigma_{\text{tot}}(e^+ e^- \rightarrow \psi(3770)) = 7.9 \pm 0.6$ nb at the resonance.
² From a measurement of the $e^+ e^- \rightarrow \Lambda\bar{\Lambda}$ cross section between 3.5 and 4.6 GeV. At a 90% CL the lower bound is $> 2.4 \times 10^{-6}$.
³ Assuming that interference effects between resonance and continuum can be neglected and using $\sigma^{\text{obs}}(e^+ e^- \rightarrow \psi(3770)) = 7.15 \pm 0.38$ nb.

$\Gamma(p\bar{p}\pi^+\pi^-\pi^0)/\Gamma_{\text{total}}$					Γ_{80}/Γ
VALUE (units 10^{-4})	CL%	DOCUMENT ID	TECN	COMMENT	
<18.5	90	¹ HUANG	06A	CLEO $e^+ e^- \rightarrow \psi(3770)$	

¹ We do not use the following data for averages, fits, limits, etc. ● ● ●
 <73 90 ²ABLIKIM 07B BES2 $e^+ e^- \rightarrow \psi(3770)$
¹ Using $\sigma_{\text{tot}}(e^+ e^- \rightarrow \psi(3770)) = 7.9 \pm 0.6$ nb at the resonance.
² Assuming that interference effects between resonance and continuum can be neglected and using $\sigma^{\text{obs}}(e^+ e^- \rightarrow \psi(3770)) = 7.15 \pm 0.38$ nb.

$\Gamma(\omega p\bar{p})/\Gamma_{\text{total}}$					Γ_{81}/Γ
VALUE (units 10^{-4})	CL%	DOCUMENT ID	TECN	COMMENT	
<2.9	90	¹ HUANG	06A	CLEO $e^+ e^- \rightarrow \psi(3770)$	

¹ We do not use the following data for averages, fits, limits, etc. ● ● ●
 <30 90 ²ABLIKIM 07I BES2 $3.77 e^+ e^-$
¹ Using $\sigma_{\text{tot}}(e^+ e^- \rightarrow \psi(3770)) = 7.9 \pm 0.6$ nb at the resonance.
² Using $\sigma^{\text{obs}} = 7.15 \pm 0.27 \pm 0.27$ nb and neglecting interference.

$\Gamma(\Lambda\bar{\Lambda}\pi^0)/\Gamma_{\text{total}}$					Γ_{82}/Γ
VALUE (units 10^{-4})	CL%	DOCUMENT ID	TECN	COMMENT	
<0.7	90	¹ ABLIKIM	13Q	BES3 $e^+ e^- \rightarrow \psi(3770)$	

● ● ● We do not use the following data for averages, fits, limits, etc. ● ● ●
 <12 90 ²ABLIKIM 07I BES2 $3.77 e^+ e^-$
¹ Assuming that interference effects between resonance and continuum can be neglected.
² Assuming that interference effects between resonance and continuum can be neglected and using $\sigma^{\text{obs}}(e^+ e^- \rightarrow \psi(3770)) = 7.15 \pm 0.38$ nb.

$\Gamma(p\bar{p}2(\pi^+\pi^-))/\Gamma_{\text{total}}$					Γ_{83}/Γ
VALUE (units 10^{-3})	CL%	DOCUMENT ID	TECN	COMMENT	
<2.6	90	¹ ABLIKIM	07F	BES2 $e^+ e^- \rightarrow \psi(3770)$	

¹ Assuming that interference effects between resonance and continuum can be neglected and using $\sigma^{\text{obs}}(e^+ e^- \rightarrow \psi(3770)) = 7.15 \pm 0.38$ nb.

$\Gamma(\eta p\bar{p})/\Gamma_{\text{total}}$					Γ_{84}/Γ
VALUE (units 10^{-4})	CL%	DOCUMENT ID	TECN	COMMENT	
<5.4	90	¹ HUANG	06A	CLEO $e^+ e^- \rightarrow \psi(3770)$	

● ● ● We do not use the following data for averages, fits, limits, etc. ● ● ●
 <11 90 ²ABLIKIM 10D BES2 $e^+ e^- \rightarrow \psi(3770)$
¹ Using $\sigma_{\text{tot}}(e^+ e^- \rightarrow \psi(3770)) = 7.9 \pm 0.6$ nb at the resonance.
² Assuming that interference effects between resonance and continuum can be neglected and using $\sigma^{\text{obs}}(e^+ e^- \rightarrow \psi(3770)) = 7.15 \pm 0.38$ nb.

$\Gamma(\eta p\bar{p}\pi^+\pi^-)/\Gamma_{\text{total}}$					Γ_{85}/Γ
VALUE (units 10^{-3})	CL%	DOCUMENT ID	TECN	COMMENT	
<3.3	90	¹ ABLIKIM	10D	BES2 $e^+ e^- \rightarrow \psi(3770)$	

¹ Assuming that interference effects between resonance and continuum can be neglected and using $\sigma^{\text{obs}}(e^+ e^- \rightarrow \psi(3770)) = 7.15 \pm 0.38$ nb.

$\Gamma(\rho^0 p\bar{p})/\Gamma_{\text{total}}$					Γ_{86}/Γ
VALUE (units 10^{-3})	CL%	DOCUMENT ID	TECN	COMMENT	
<1.7	90	¹ ABLIKIM	07F	BES2 $e^+ e^- \rightarrow \psi(3770)$	

¹ Assuming that interference effects between resonance and continuum can be neglected and using $\sigma^{\text{obs}}(e^+ e^- \rightarrow \psi(3770)) = 7.15 \pm 0.38$ nb.

$\Gamma(p\bar{p}K^+K^-)/\Gamma_{\text{total}}$					Γ_{87}/Γ
VALUE (units 10^{-4})	CL%	DOCUMENT ID	TECN	COMMENT	
<3.2	90	¹ HUANG	06A	CLEO $e^+ e^- \rightarrow \psi(3770)$	

● ● ● We do not use the following data for averages, fits, limits, etc. ● ● ●
 <11 90 ²ABLIKIM 07B BES2 $e^+ e^- \rightarrow \psi(3770)$
¹ Using $\sigma_{\text{tot}}(e^+ e^- \rightarrow \psi(3770)) = 7.9 \pm 0.6$ nb at the resonance.
² Assuming that interference effects between resonance and continuum can be neglected and using $\sigma^{\text{obs}}(e^+ e^- \rightarrow \psi(3770)) = 7.15 \pm 0.38$ nb.

$\Gamma(\eta p\bar{p}K^+K^-)/\Gamma_{\text{total}}$					Γ_{88}/Γ
VALUE (units 10^{-3})	CL%	DOCUMENT ID	TECN	COMMENT	
<6.9	90	¹ ABLIKIM	10D	BES2 $e^+ e^- \rightarrow \psi(3770)$	

¹ Assuming that interference effects between resonance and continuum can be neglected and using $\sigma^{\text{obs}}(e^+ e^- \rightarrow \psi(3770)) = 7.15 \pm 0.38$ nb.

$\Gamma(\pi^0 p\bar{p}K^+K^-)/\Gamma_{\text{total}}$					Γ_{89}/Γ
VALUE (units 10^{-3})	CL%	DOCUMENT ID	TECN	COMMENT	
<1.2	90	¹ ABLIKIM	10D	BES2 $e^+ e^- \rightarrow \psi(3770)$	

¹ Assuming that interference effects between resonance and continuum can be neglected and using $\sigma^{\text{obs}}(e^+ e^- \rightarrow \psi(3770)) = 7.15 \pm 0.38$ nb.

$\Gamma(\phi p\bar{p})/\Gamma_{\text{total}}$					Γ_{90}/Γ
VALUE (units 10^{-4})	CL%	DOCUMENT ID	TECN	COMMENT	
<1.3	90	¹ HUANG	06A	CLEO $e^+ e^- \rightarrow \psi(3770)$	

● ● ● We do not use the following data for averages, fits, limits, etc. ● ● ●
 <9 90 ²ABLIKIM 07B BES2 $e^+ e^- \rightarrow \psi(3770)$
¹ Using $\sigma_{\text{tot}}(e^+ e^- \rightarrow \psi(3770)) = 7.9 \pm 0.6$ nb at the resonance.
² Assuming that interference effects between resonance and continuum can be neglected and using $\sigma^{\text{obs}}(e^+ e^- \rightarrow \psi(3770)) = 7.15 \pm 0.38$ nb.

$\Gamma(\Lambda\bar{\Lambda}\pi^+\pi^-)/\Gamma_{\text{total}}$					Γ_{91}/Γ
VALUE (units 10^{-4})	CL%	DOCUMENT ID	TECN	COMMENT	
<2.5	90	¹ HUANG	06A	CLEO $e^+ e^- \rightarrow \psi(3770)$	

● ● ● We do not use the following data for averages, fits, limits, etc. ● ● ●
 <4.7 90 ²ABLIKIM 13Q BES3 $e^+ e^- \rightarrow \psi(3770)$
 <39 90 ³ABLIKIM 07F BES2 $e^+ e^- \rightarrow \psi(3770)$
¹ Using $\sigma_{\text{tot}}(e^+ e^- \rightarrow \psi(3770)) = 7.9 \pm 0.6$ nb at the resonance.
² Assuming that interference effects between resonance and continuum can be neglected.
³ Assuming that interference effects between resonance and continuum can be neglected and using $\sigma^{\text{obs}}(e^+ e^- \rightarrow \psi(3770)) = 7.15 \pm 0.38$ nb.

$\Gamma(\Lambda\bar{P}K^+)/\Gamma_{total}$		Γ_{92}/Γ	
VALUE (units 10^{-4})	CL%	DOCUMENT ID	TECN COMMENT
<2.8	90	1 HUANG 06A CLEO	$e^+e^- \rightarrow \psi(3770)$

¹ Using $\sigma_{tot}(e^+e^- \rightarrow \psi(3770)) = 7.9 \pm 0.6$ nb at the resonance.

$\Gamma(\Lambda\bar{P}K^+\pi^-\pi^-)/\Gamma_{total}$		Γ_{93}/Γ	
VALUE (units 10^{-4})	CL%	DOCUMENT ID	TECN COMMENT
<6.3	90	1 HUANG 06A CLEO	$e^+e^- \rightarrow \psi(3770)$

¹ Using $\sigma_{tot}(e^+e^- \rightarrow \psi(3770)) = 7.9 \pm 0.6$ nb at the resonance.

$\Gamma(\Lambda\bar{K}\eta)/\Gamma_{total}$		Γ_{94}/Γ	
VALUE (units 10^{-4})	CL%	DOCUMENT ID	TECN COMMENT
<1.9	90	1 ABLIKIM 13Q BES3	$e^+e^- \rightarrow \psi(3770)$

¹ Assuming that interference effects between resonance and continuum can be neglected.

$\Gamma(\Sigma^+\Sigma^-)/\Gamma_{total}$		Γ_{95}/Γ	
VALUE (units 10^{-4})	CL%	DOCUMENT ID	TECN COMMENT
<1.0	90	1 ABLIKIM 13Q BES3	$e^+e^- \rightarrow \psi(3770)$

¹ Assuming that interference effects between resonance and continuum can be neglected.

$\Gamma(\Sigma^0\Sigma^0)/\Gamma_{total}$		Γ_{96}/Γ	
VALUE (units 10^{-4})	CL%	DOCUMENT ID	TECN COMMENT
<0.4	90	1 ABLIKIM 13Q BES3	$e^+e^- \rightarrow \psi(3770)$

¹ Assuming that interference effects between resonance and continuum can be neglected.

$\Gamma(\Xi^+\Xi^-)/\Gamma_{total}$		Γ_{97}/Γ	
VALUE (units 10^{-4})	CL%	DOCUMENT ID	TECN COMMENT
<1.5	90	1 ABLIKIM 13Q BES3	$e^+e^- \rightarrow \psi(3770)$

¹ Assuming that interference effects between resonance and continuum can be neglected.

$\Gamma(\Xi^0\Xi^0)/\Gamma_{total}$		Γ_{98}/Γ	
VALUE (units 10^{-4})	CL%	DOCUMENT ID	TECN COMMENT
<1.4	90	1 ABLIKIM 13Q BES3	$e^+e^- \rightarrow \psi(3770)$

¹ Assuming that interference effects between resonance and continuum can be neglected.

RADIATIVE DECAYS

$\Gamma(\gamma\chi_{c2})/\Gamma_{total}$		Γ_{99}/Γ	
VALUE (units 10^{-3})	CL%	DOCUMENT ID	TECN COMMENT
<0.64	90	1 ABLIKIM 15J BES3	$e^+e^- \rightarrow \psi(3770) \rightarrow \gamma\gamma J/\psi$

• • • We do not use the following data for averages, fits, limits, etc. • • •

<2.0	90	2 BRIERE 06 CLEO	$e^+e^- \rightarrow \psi(3770) \rightarrow \gamma + \text{hadrons}$
<0.9	90	3 COAN 06A CLEO	$e^+e^- \rightarrow \psi(3770) \rightarrow \gamma\gamma J/\psi$

¹ This limit is equivalent to $(0.25 \pm 0.21 \pm 0.18) \times 10^{-3}$ branching fraction value.

² Uses $B(\psi(2S) \rightarrow \gamma\chi_{c2}) = 9.22 \pm 0.11 \pm 0.46\%$ from ATHAR 04, $\psi(2S)$ mass and width from PDG 04, and $\Gamma_{ee}(\psi(2S)) = 2.54 \pm 0.03 \pm 0.11$ keV from ADAM 06.

³ Using $\Gamma_{ee}(\psi(2S)) = (2.54 \pm 0.03 \pm 0.11)$ keV from ADAM 06 and taking $\sigma(e^+e^- \rightarrow D\bar{D})$ from HE 05 for $\sigma(e^+e^- \rightarrow \psi(3770))$.

$\Gamma(\gamma\chi_{c1})/\Gamma_{total}$		Γ_{100}/Γ	
VALUE (units 10^{-3})	EVTS	DOCUMENT ID	TECN COMMENT
2.49 ± 0.23 OUR AVERAGE			
1.98 ± 0.78 ± 0.05	202	1 ABLIKIM 16B BES3	$e^+e^- \rightarrow \psi(3770) \rightarrow \gamma + \text{hadrons}$

2.48 ± 0.15 ± 0.23 0.6k ABLIKIM 15J BES3 $e^+e^- \rightarrow \psi(3770) \rightarrow \gamma\gamma J/\psi$

2.4 ± 0.8 ± 0.2 2 ABLIKIM 14H BES3 $e^+e^- \rightarrow \psi(3770) \rightarrow K_S^0 K^\pm \pi^\mp$

2.9 ± 0.5 ± 0.4 3 BRIERE 06 CLEO $e^+e^- \rightarrow \psi(3770) \rightarrow \gamma + \text{hadrons}, \gamma\gamma J/\psi$

• • • We do not use the following data for averages, fits, limits, etc. • • •

3.9 ± 1.4 ± 0.6 54 4 BRIERE 06 CLEO $e^+e^- \rightarrow \psi(3770) \rightarrow \gamma + \text{hadrons}$

2.8 ± 0.5 ± 0.4 53 5 COAN 06A CLEO $e^+e^- \rightarrow \psi(3770) \rightarrow \gamma\gamma J/\psi$

¹ ABLIKIM 16B reports $(1.94 \pm 0.42 \pm 0.64) \times 10^{-3}$ from a measurement of $[\Gamma(\psi(3770) \rightarrow \gamma\chi_{c1})/\Gamma_{total}] / [B(\psi(2S) \rightarrow \gamma\chi_{c1}(1P))]$ assuming $B(\psi(2S) \rightarrow \gamma\chi_{c1}(1P)) = (9.55 \pm 0.31) \times 10^{-2}$, which we rescale to our best value $B(\psi(2S) \rightarrow \gamma\chi_{c1}(1P)) = (9.75 \pm 0.24) \times 10^{-2}$. Our first error is their experiment's error and our second error is the systematic error from using our best value.

² ABLIKIM 14H reports $[\Gamma(\psi(3770) \rightarrow \gamma\chi_{c1})/\Gamma_{total}] \times [B(\chi_{c1}(1P) \rightarrow K_S^0 K^\pm \pi^\mp)] = (8.51 \pm 2.39 \pm 1.42) \times 10^{-6}$ which we divide by our best value $B(\chi_{c1}(1P) \rightarrow K_S^0 K^\pm \pi^\mp) = 0.00349 \pm 0.00029$. Our first error is their experiment's error and our second error is the systematic error from using our best value. We have calculated the best value of $B(\chi_{c1}(1P) \rightarrow K_S^0 K^\pm \pi^\mp)$ as 1/2 of $B(\chi_{c1}(1P) \rightarrow \bar{K}^0 K^+ \pi^- + c.c.) = (7.0 \pm 0.6) \times 10^{-3}$.

³ Averages the two measurements from COAN 06A and BRIERE 06.

⁴ Uses $B(\psi(2S) \rightarrow \gamma\chi_{c1}) = 9.07 \pm 0.11 \pm 0.54\%$ from ATHAR 04, $\psi(2S)$ mass and width from PDG 04, and $\Gamma_{ee}(\psi(2S)) = 2.54 \pm 0.03 \pm 0.11$ keV from ADAM 06.

⁵ Using $\Gamma_{ee}(\psi(2S)) = (2.54 \pm 0.03 \pm 0.11)$ keV from ADAM 06 and taking $\sigma(e^+e^- \rightarrow D\bar{D})$ from HE 05 for $\sigma(e^+e^- \rightarrow \psi(3770))$.

$\Gamma(\gamma\chi_{c1})/\Gamma(J/\psi\pi^+\pi^-)$		Γ_{100}/Γ_5	
VALUE	EVTS	DOCUMENT ID	TECN COMMENT
1.49 ± 0.31 ± 0.26	53 ± 10	1 COAN 06A CLEO	$e^+e^- \rightarrow \psi(3770) \rightarrow \gamma\gamma J/\psi$

¹ Using $B(\psi(3770) \rightarrow J/\psi\pi^+\pi^-) = (1.89 \pm 0.20 \pm 0.20) \times 10^{-3}$ from ADAM 06.

$\Gamma(\gamma\chi_{c0})/\Gamma_{total}$		Γ_{101}/Γ	
VALUE (units 10^{-3})	CL% EVTS	DOCUMENT ID	TECN COMMENT
6.9 ± 0.6 OUR AVERAGE			
6.7 ± 0.7 ± 0.1	2.2k	1 ABLIKIM 16B BES3	$e^+e^- \rightarrow \psi(3770) \rightarrow \gamma + \text{hadrons}$

7.3 ± 0.7 ± 0.6 274 BRIERE 06 CLEO $e^+e^- \rightarrow \psi(3770) \rightarrow \gamma + \text{hadrons}$

• • • We do not use the following data for averages, fits, limits, etc. • • •

< 44 90 2 COAN 06A CLEO $e^+e^- \rightarrow \psi(3770) \rightarrow \gamma\gamma J/\psi$

¹ ABLIKIM 16B reports $(6.88 \pm 0.28 \pm 0.67) \times 10^{-3}$ from a measurement of $[\Gamma(\psi(3770) \rightarrow \gamma\chi_{c0})/\Gamma_{total}] / [B(\psi(2S) \rightarrow \gamma\chi_{c0}(1P))]$ assuming $B(\psi(2S) \rightarrow \gamma\chi_{c0}(1P)) = (9.99 \pm 0.27) \times 10^{-2}$, which we rescale to our best value $B(\psi(2S) \rightarrow \gamma\chi_{c0}(1P)) = (9.79 \pm 0.20) \times 10^{-2}$. Our first error is their experiment's error and our second error is the systematic error from using our best value.

² Using $\Gamma_{ee}(\psi(2S)) = (2.54 \pm 0.03 \pm 0.11)$ keV from ADAM 06 and taking $\sigma(e^+e^- \rightarrow D\bar{D})$ from HE 05 for $\sigma(e^+e^- \rightarrow \psi(3770))$.

$\Gamma(\gamma\chi_{c0})/\Gamma(\gamma\chi_{c2})$		Γ_{101}/Γ_{99}	
VALUE	CL%	DOCUMENT ID	TECN COMMENT
> 8	90	1 BRIERE 06 CLEO	$e^+e^- \rightarrow \psi(3770)$

¹ Not independent of other results in BRIERE 06.

$\Gamma(\gamma\chi_{c0})/\Gamma(\gamma\chi_{c1})$		$\Gamma_{101}/\Gamma_{100}$	
VALUE	CL%	DOCUMENT ID	TECN COMMENT
2.5 ± 0.6	90	1 BRIERE 06 CLEO	$e^+e^- \rightarrow \psi(3770)$

¹ Not independent of other results in BRIERE 06.

$\Gamma(\gamma\eta_c)/\Gamma_{total}$		Γ_{102}/Γ	
VALUE	CL%	DOCUMENT ID	TECN COMMENT
< 7 × 10 ⁻⁴	90	1 ABLIKIM 14H BES3	

¹ ABLIKIM 14H reports $[\Gamma(\psi(3770) \rightarrow \gamma\eta_c)/\Gamma_{total}] \times [B(\eta_c(1S) \rightarrow K_S^0 K^\pm \pi^\mp)] < 1.6 \times 10^{-6}$ which we divide by our best value $B(\eta_c(1S) \rightarrow K_S^0 K^\pm \pi^\mp) = 2.42 \times 10^{-2}$. We have calculated the best value of $B(\eta_c(1S) \rightarrow K_S^0 K^\pm \pi^\mp)$ as 1/3 of $B(\eta_c(1S) \rightarrow K\bar{K}\pi) = 7.3 \times 10^{-2}$.

$\Gamma(\gamma\eta_c(2S))/\Gamma_{total}$		Γ_{103}/Γ	
VALUE	CL%	DOCUMENT ID	TECN COMMENT
< 9 × 10 ⁻⁴	90	1 ABLIKIM 14H BES3	

¹ ABLIKIM 14H reports $[\Gamma(\psi(3770) \rightarrow \gamma\eta_c(2S))/\Gamma_{total}] \times [B(\eta_c(2S) \rightarrow K_S^0 K^\pm \pi^\mp)] < 5.6 \times 10^{-6}$ which we divide by our best value $B(\eta_c(2S) \rightarrow K_S^0 K^\pm \pi^\mp) = 6 \times 10^{-3}$. We have calculated the best value of $B(\eta_c(2S) \rightarrow K_S^0 K^\pm \pi^\mp)$ as 1/3 of $B(\eta_c(2S) \rightarrow K\bar{K}\pi) = 1.9 \times 10^{-2}$.

$\Gamma(\gamma\eta)/\Gamma_{total}$		Γ_{104}/Γ	
VALUE (units 10^{-4})	CL%	DOCUMENT ID	TECN COMMENT
< 1.8	90	1 PEDLAR 09 CLE3	$\psi(2S) \rightarrow \gamma X$

¹ Assuming maximal destructive interference between $\psi(3770)$ and continuum sources.

$\Gamma(\gamma\eta)/\Gamma_{total}$		Γ_{105}/Γ	
VALUE (units 10^{-4})	CL%	DOCUMENT ID	TECN COMMENT
< 1.5	90	1 PEDLAR 09 CLE3	$\psi(2S) \rightarrow \gamma X$

¹ Assuming maximal destructive interference between $\psi(3770)$ and continuum sources.

$\Gamma(\gamma\pi^0)/\Gamma_{total}$		Γ_{106}/Γ	
VALUE (units 10^{-4})	CL%	DOCUMENT ID	TECN COMMENT
< 2	90	PEDLAR 09 CLE3	$\psi(2S) \rightarrow \gamma X$

$\psi(3770)$ REFERENCES

ABLIKIM 21AS	PR D104 L091104	M. Ablikim <i>et al.</i>	(BESIII Collab.)
ABLIKIM 21Z	PRL 127 082002	M. Ablikim <i>et al.</i>	(BESIII Collab.)
PDG 20	PTEP 2020 083C01	P.A. Zyla <i>et al.</i>	(PDG Collab.)
AAJ 19M	JHEP 1907 035	R. Aaij <i>et al.</i>	(LHCb Collab.)
AAJ 17AD	PL B769 305	R. Aaij <i>et al.</i>	(LHCb Collab.)
SHAMOV 17	PL B769 187	A.G. Shamov, K.Yu. Todyshev	
ABLIKIM 16B	PL B753 103	M. Ablikim <i>et al.</i>	(BESIII Collab.)
ABLIKIM 15J	PR D91 092009	M. Ablikim <i>et al.</i>	(BESIII Collab.)
DRUZHININ 15	PR D92 054024	V.P. Druzhinin	(IYUVO)
ABLIKIM 14H	PR D89 112005	M. Ablikim <i>et al.</i>	(BESIII Collab.)
ABLIKIM 14L	PL B735 101	M. Ablikim <i>et al.</i>	(BESIII Collab.)
ABLIKIM 14O	PR D90 032007	M. Ablikim <i>et al.</i>	(BESIII Collab.)
BONVICINI 14	PR D89 072002	G. Bonvicini <i>et al.</i>	(CLEO Collab.)
ABLIKIM 13Q	PR D87 112011	M. Ablikim <i>et al.</i>	(BESIII Collab.)
ANASHIN 12A	PL B711 292	V.V. Anashin <i>et al.</i>	(KEDR Collab.)
ABLIKIM 10D	EPJ C66 11	M. Ablikim <i>et al.</i>	(BES II Collab.)
BESSON 10	PRL 104 159901 (err.)	D. Besson <i>et al.</i>	(CLEO Collab.)
ABLIKIM 09C	EPJ C64 243	M. Ablikim <i>et al.</i>	(BES Collab.)
PEDLAR 09	PR D79 111101	T.K. Pedlar <i>et al.</i>	(CLEO Collab.)

Meson Particle Listings

$\psi(3770)$, $\psi_2(3823)$

ABLIKIM	08B	PL B659 74	M. Ablikim et al.	(BES Collab.)
ABLIKIM	08D	PL B660 315	M. Ablikim et al.	(BES Collab.)
ABLIKIM	08H	PRL 101 102004	M. Ablikim et al.	(BES Collab.)
ABLIKIM	08M	PL B670 179	M. Ablikim et al.	(BES Collab.)
ABLIKIM	08N	PL B670 184	M. Ablikim et al.	(BES Collab.)
AUBERT	08B	PR D77 011102	B. Aubert et al.	(BABAR Collab.)
BRODZICKA	08	PRL 100 092001	J. Brodzicka et al.	(BELLE Collab.)
PAKHOVA	08	PR D77 011103	G. Pakhlova et al.	(BELLE Collab.)
ABLIKIM	07B	PL B650 111	M. Ablikim et al.	(BES Collab.)
ABLIKIM	07E	PL B652 238	M. Ablikim et al.	(BES Collab.)
ABLIKIM	07F	PL B656 30	M. Ablikim et al.	(BES Collab.)
ABLIKIM	07I	EPJ C52 805	M. Ablikim et al.	(BES Collab.)
ABLIKIM	07K	PR D76 122002	M. Ablikim et al.	(BES Collab.)
AUBERT	07BE	PR D76 111105	B. Aubert et al.	(BABAR Collab.)
DOBBS	07	PR D76 112001	S. Dobbs et al.	(CLEO Collab.)
ABLIKIM	06L	PRL 97 121801	M. Ablikim et al.	(BES Collab.)
ABLIKIM	06N	PL B641 145	M. Ablikim et al.	(BES Collab.)
ADAM	06	PRL 96 082004	N.E. Adam et al.	(CLEO Collab.)
ADAMS	06	PR D73 012002	G.S. Adams et al.	(CLEO Collab.)
BESSION	06	PRL 96 092002	D. Besson et al.	(CLEO Collab.)
Also		PRL 104 159901 (errata.)	D. Besson et al.	(CLEO Collab.)
BRIERE	06	PR D74 031106	R.A. Briere et al.	(CLEO Collab.)
COAN	06A	PRL 96 182002	T.E. Coan et al.	(CLEO Collab.)
CRONIN-HEN.	06	PR D74 012005	D. Cronin-Hennessy et al.	(CLEO Collab.)
HUANG	06A	PRL 96 032003	G.S. Huang et al.	(CLEO Collab.)
BAI	05	PL B605 63	J.Z. Bai et al.	(BES Collab.)
HE	05	PRL 95 121801	Q. He et al.	(CLEO Collab.)
Also		PRL 96 199903 (errata.)	Q. He et al.	(CLEO Collab.)
ABLIKIM	04F	PR D70 077101	M. Ablikim et al.	(BES Collab.)
ATHAR	04	PR D70 112002	S.B. Athar et al.	(CLEO Collab.)
CHISTOV	04	PRL 93 051803	R. Chistov et al.	(BELLE Collab.)
PDG	04	PL B592 1	J.Z. Bai et al.	(PDG Collab.)
BAI	02C	PRL 88 101802	J.Z. Bai et al.	(BES Collab.)
ADLER	85C	PRL 60 89	J. Adler et al.	(Mark III Collab.)
SCHINDLER	80	PR D21 2716	R.H. Schindler et al.	(Mark II Collab.)
BACINO	78	PRL 40 671	W.J. Bacino et al.	(SLAC, UCLA, UCI)
RAPIDIS	77	PRL 39 526	P.A. Rapidis et al.	(LGW Collab.)

$\psi_2(3823)$

was $\psi(3823)$, $X(3823)$

Seen by BHARDWAJ 13 in $B \rightarrow \chi_{c1} \gamma K$ and ABLIKIM 15S in $e^+e^- \rightarrow \pi^+\pi^-\gamma\chi_{c1}$ decays as a narrow peak in the invariant mass distribution of the $\chi_{c1} \gamma$ system. Properties consistent with the $\psi_2(1^3D_2) c\bar{c}$ state.

$$I^G(J^{PC}) = 0^-(2^{--})$$

I, J, P need confirmation.

$\psi_2(3823)$ MASS

VALUE (MeV)	EVTS	DOCUMENT ID	TECN	COMMENT
3823.7 ± 0.5	OUR AVERAGE	Error includes scale factor of 1.1.		
3824.08 ± 0.53 ± 0.14	137	¹ AAIJ	20s LHCb	$B^+ \rightarrow J/\psi \pi^+ \pi^- K^+$
3821.7 ± 1.3 ± 0.7	19 ± 5	² ABLIKIM	15s BES3	$e^+e^- \rightarrow \pi^+\pi^-\chi_{c1}\gamma$
3823.1 ± 1.8 ± 0.7	33 ± 10	³ BHARDWAJ	13 BELL	$B^\pm \rightarrow \chi_{c1} \gamma K^\pm$

- ¹ Using the measured $m_{\psi_2(3823)} - m_{\psi(2S)} = 137.98 \pm 0.53 \pm 0.14$ MeV.
- ² From a simultaneous unbinned maximum likelihood fit of $e^+e^- \rightarrow \pi^+\pi^-\chi_{c1}\gamma$ data (the $\pi^+\pi^-$ recoil mass) taken at \sqrt{s} values of 4.23, 4.26, 4.36, 4.42, and 4.60 GeV to simulated events including both $\psi(2S) \rightarrow \chi_{c1}\gamma$ and $\psi_2(3823) \rightarrow \chi_{c1}\gamma$ together, with floating mass scale offset for $\psi(2S)$, floating $\psi_2(3823)$ mass, and zero $\psi_2(3823)$ width, resulting in a significance of 5.9 σ when including systematic uncertainties.
- ³ From a simultaneous fit to $B^\pm \rightarrow (\chi_{c1}\gamma)K^\pm$ and $B^0 \rightarrow (\chi_{c1}\gamma)K_S^0$ with significance 4.0 σ including systematics. Corrected for the measured $\psi(2S)$ mass using $B \rightarrow \psi(2S)K \rightarrow (\gamma\chi_{c1})K$ decays.

$m_{\psi_2(3823)} - m_{\psi(2S)}$

VALUE (MeV)	EVTS	DOCUMENT ID	TECN	COMMENT
137.98 ± 0.53 ± 0.14	137	¹ AAIJ	20s LHCb	$B^+ \rightarrow J/\psi \pi^+ \pi^- K^+$

¹ AAIJ 20s also reports $m_{\chi_{c1}(3872)} - m_{\psi_2(3823)} = 47.50 \pm 0.53 \pm 0.13$ MeV.

$\psi_2(3823)$ WIDTH

VALUE (MeV)	CL%	DOCUMENT ID	TECN	COMMENT
< 5.2	90	¹ AAIJ	20s LHCb	$B^+ \rightarrow J/\psi \pi^+ \pi^- K^+$
<16	90	² ABLIKIM	15s BES3	$e^+e^- \rightarrow \pi^+\pi^-\chi_{c1}\gamma$
<24	90	³ BHARDWAJ	13 BELL	$B^\pm \rightarrow \chi_{c1} \gamma K^\pm$

- ¹ AAIJ 20s also provides a limit of < 6.6 MeV with 95% CL.
- ² From a fit of $e^+e^- \rightarrow \pi^+\pi^-\chi_{c1}\gamma$ data (the $\pi^+\pi^-$ recoil mass) taken at \sqrt{s} values of 4.23, 4.26, 4.36, 4.42, and 4.60 GeV to a Breit-Wigner function with the mass fixed from the likelihood fit above, Gaussian resolution smearing, and floating width.
- ³ From a simultaneous fit to $B^\pm \rightarrow (\chi_{c1}\gamma)K^\pm$ and $B^0 \rightarrow (\chi_{c1}\gamma)K_S^0$ with significance 4.0 σ including systematics.

$\psi_2(3823)$ DECAY MODES

Branching fractions are given relative to the one **DEFINED AS 1**.

Mode	Fraction (Γ_i/Γ)	Confidence level	
Γ_1	$J/\psi(1S)\pi^+\pi^-$	<0.06	90%
Γ_2	$J/\psi(1S)\pi^0\pi^0$	<0.11	90%
Γ_3	$J/\psi(1S)\pi^0\pi^0$	<0.030	90%

Γ_4	$J/\psi(1S)\eta$	<0.14	90%
Γ_5	$\chi_{c0}\gamma$	<0.24	90%
Γ_6	$\chi_{c1}\gamma$	DEFINED AS 1	
Γ_7	$\chi_{c2}\gamma$	$0.28^{+0.14}_{-0.11}$	

$\psi_2(3823)$ BRANCHING RATIOS

$\Gamma(J/\psi(1S)\pi^+\pi^-)/\Gamma_{total}$	VALUE	EVTS	DOCUMENT ID	TECN	COMMENT	Γ_1/Γ
---	-------	------	-------------	------	---------	-------------------

- We do not use the following data for averages, fits, limits, etc. **•••**
- not seen ¹ABLIKIM 21o BES3 $e^+e^- \rightarrow \pi^+\pi^-X$
- seen 137 ± 26 AAJJ 20s LHCb $B^+ \rightarrow J/\psi \pi^+ \pi^- K^+$
- ¹ From a simultaneous unbinned maximum likelihood fit of the $\pi^+\pi^-$ recoil mass distributions of seven decay channels in the process $e^+e^- \rightarrow \pi^+\pi^-X$.

$\Gamma(J/\psi(1S)\pi^+\pi^-)/\Gamma(\chi_{c1}\gamma)$	VALUE	CL%	DOCUMENT ID	TECN	COMMENT	Γ_1/Γ_6
--	-------	-----	-------------	------	---------	---------------------

- <0.06** 90 ¹ABLIKIM 21o BES3 $e^+e^- \rightarrow \pi^+\pi^-X$
- ¹ From a simultaneous unbinned maximum likelihood fit of the $\pi^+\pi^-$ recoil mass distributions of seven decay channels in the process $e^+e^- \rightarrow \pi^+\pi^-X$.

$\Gamma(J/\psi(1S)\pi^0\pi^0)/\Gamma(\chi_{c1}\gamma)$	VALUE	CL%	DOCUMENT ID	TECN	COMMENT	Γ_2/Γ_6
--	-------	-----	-------------	------	---------	---------------------

- <0.11** 90 ¹ABLIKIM 21o BES3 $e^+e^- \rightarrow \pi^+\pi^-X$
- ¹ From a simultaneous unbinned maximum likelihood fit of the $\pi^+\pi^-$ recoil mass distributions of seven decay channels in the process $e^+e^- \rightarrow \pi^+\pi^-X$.

$\Gamma(J/\psi(1S)\pi^0)/\Gamma(\chi_{c1}\gamma)$	VALUE	CL%	DOCUMENT ID	TECN	COMMENT	Γ_3/Γ_6
---	-------	-----	-------------	------	---------	---------------------

- <0.03** 90 ¹ABLIKIM 21o BES3 $e^+e^- \rightarrow \pi^+\pi^-X$
- ¹ From a simultaneous unbinned maximum likelihood fit of the $\pi^+\pi^-$ recoil mass distributions of seven decay channels in the process $e^+e^- \rightarrow \pi^+\pi^-X$.

$\Gamma(J/\psi(1S)\eta)/\Gamma(\chi_{c1}\gamma)$	VALUE	CL%	DOCUMENT ID	TECN	COMMENT	Γ_4/Γ_6
--	-------	-----	-------------	------	---------	---------------------

- <0.14** 90 ¹ABLIKIM 21o BES3 $e^+e^- \rightarrow \pi^+\pi^-X$
- ¹ From a simultaneous unbinned maximum likelihood fit of the $\pi^+\pi^-$ recoil mass distributions of seven decay channels in the process $e^+e^- \rightarrow \pi^+\pi^-X$.

$\Gamma(\chi_{c0}\gamma)/\Gamma_{total}$	VALUE	DOCUMENT ID	TECN	COMMENT	Γ_5/Γ
--	-------	-------------	------	---------	-------------------

- We do not use the following data for averages, fits, limits, etc. **•••**
- not seen ¹ABLIKIM 21o BES3 $e^+e^- \rightarrow \pi^+\pi^-X$
- ¹ From a simultaneous unbinned maximum likelihood fit of the $\pi^+\pi^-$ recoil mass distributions of seven decay channels in the process $e^+e^- \rightarrow \pi^+\pi^-X$.

$\Gamma(\chi_{c1}\gamma)/\Gamma_{total}$	VALUE	EVTS	DOCUMENT ID	TECN	COMMENT	Γ_6/Γ
--	-------	------	-------------	------	---------	-------------------

- seen 33 ± 10 ¹BHARDWAJ 13 BELL $B^\pm \rightarrow \chi_{c1} \gamma K^\pm$
- We do not use the following data for averages, fits, limits, etc. **•••**
- seen 63 ± 9 ²ABLIKIM 21o BES3 $e^+e^- \rightarrow \pi^+\pi^-X$
- seen 16 ± 5 ³ABLIKIM 21o BES3 $e^+e^- \rightarrow \pi^0\pi^0X$
- ¹ BHARDWAJ 13 reports $B(B^\pm \rightarrow \psi_2(3823)K^\pm) \times B(\psi_2(3823) \rightarrow \gamma\chi_{c1}) = (9.7 \pm 2.8 \pm 1.1) \times 10^{-6}$ with statistical significance 3.8 σ .
- ² From a simultaneous unbinned maximum likelihood fit of the $\pi^+\pi^-$ recoil mass distributions of seven decay channels in the process $e^+e^- \rightarrow \pi^+\pi^-X$. Signal has a 11.8 σ significance.
- ³ From a fit of the invariant $\pi^0\pi^0$ recoil-mass distribution. Signal has a 4.3 σ significance.

$\Gamma(\chi_{c0}\gamma)/\Gamma(\chi_{c1}\gamma)$	VALUE	CL%	DOCUMENT ID	TECN	COMMENT	Γ_5/Γ_6
---	-------	-----	-------------	------	---------	---------------------

- <0.24** 90 ¹ABLIKIM 21o BES3 $e^+e^- \rightarrow \pi^+\pi^-X$
- ¹ From a simultaneous unbinned maximum likelihood fit of the $\pi^+\pi^-$ recoil mass distributions of seven decay channels in the process $e^+e^- \rightarrow \pi^+\pi^-X$.

$\Gamma(\chi_{c2}\gamma)/\Gamma_{total}$	VALUE	DOCUMENT ID	TECN	COMMENT	Γ_7/Γ
--	-------	-------------	------	---------	-------------------

- We do not use the following data for averages, fits, limits, etc. **•••**
- seen ¹ABLIKIM 21o BES3 $e^+e^- \rightarrow \pi^+\pi^-X$
- not seen ²ABLIKIM 15s BES3 $e^+e^- \rightarrow \pi^+\pi^-\chi_{c2}\gamma$
- not seen ³BHARDWAJ 13 BELL $B^\pm \rightarrow \chi_{c2} \gamma K^\pm$
- ¹ From a simultaneous unbinned maximum likelihood fit of the $\pi^+\pi^-$ recoil mass distributions of seven decay channels in the process $e^+e^- \rightarrow \pi^+\pi^-X$. Signal has a 3.2 σ significance.
- ² From a simultaneous unbinned maximum likelihood fit of $e^+e^- \rightarrow \pi^+\pi^-\chi_{c2}\gamma$ data (the $\pi^+\pi^-$ recoil mass) taken at \sqrt{s} values of 4.23, 4.26, 4.36, 4.42, and 4.60 GeV to simulated events including both $\psi(2S) \rightarrow \chi_{c2}\gamma$ and $\psi_2(3823) \rightarrow \chi_{c2}\gamma$ together, with floating mass scale offset for $\psi(2S)$, $\psi_2(3823)$ mass floating (fixed to that above), and zero $\psi_2(3823)$ width.
- ³ BHARDWAJ 13 reports $B(B^\pm \rightarrow \psi_2(3823)K^\pm) \times B(\psi_2(3823) \rightarrow \gamma\chi_{c2}) < 3.6 \times 10^{-6}$ at 90% CL.

See key on page 1127

Meson Particle Listings

$\psi_2(3823)$, $\psi_3(3842)$, $\chi_{c0}(3860)$, $\chi_{c1}(3872)$

$\Gamma(\chi_{c2}\gamma)/\Gamma(\chi_{c1}\gamma)$	CL%	EVTs	DOCUMENT ID	TECN	COMMENT	Γ_1/Γ_6
0.28 ± 0.14 0.11 ± 0.02		9 ± 4	1 ABLIKIM	21o	BES3 $e^+e^- \rightarrow \pi^+\pi^-\chi_{c2}\gamma$	
<0.42	90		2 ABLIKIM	15s	BES3 $e^+e^- \rightarrow \pi^+\pi^-\chi_{c2}\gamma$	
<0.41	90		BHARDWAJ	13	BELL $B^\pm \rightarrow \chi_{c1/c2}\gamma K^\pm$	

• • • We do not use the following data for averages, fits, limits, etc. • • •
 1 From a simultaneous unbinned maximum likelihood fit of the $\pi^+\pi^-$ recoil mass distributions of seven decay channels in the process $e^+e^- \rightarrow \pi^+\pi^-X$.
 2 From a simultaneous unbinned maximum likelihood fit of $e^+e^- \rightarrow \pi^+\pi^-\chi_{c1(2)}\gamma$ data (the $\pi^+\pi^-$ recoil mass) taken at \sqrt{s} values of 4.23, 4.26, 4.36, 4.42, and 4.60 GeV to simulated events including both $\psi(2S) \rightarrow \chi_{c1(2)}\gamma$ and $\psi_2(3823) \rightarrow \chi_{c1(2)}\gamma$ together, with floating mass scale offset for $\psi(2S)$, $\psi_2(3823)$ mass floating (fixed to that above), and zero $\psi_2(3823)$ width.

$\psi_2(3823)$ REFERENCES

ABLIKIM	21O	PR D103 L091102	M. Ablikim et al.	(BESIII Collab.)
AAIJ	20S	JHEP 2008 123	R. Aaij et al.	(LHCb Collab.)
ABLIKIM	15S	PRL 115 011803	M. Ablikim et al.	(BESIII Collab.)
BHARDWAJ	13	PRL 111 032001	V. Bhardwaj et al.	(BELLE Collab.)

$\psi_3(3842)$

$I^G(J^{PC}) = 0^-(3^{--})$
 J, P need confirmation.

J^P has not been measured, 3^- is the quark model prediction.

$\psi_3(3842)$ MASS

VALUE (MeV)	DOCUMENT ID	TECN	COMMENT
$3842.71 \pm 0.16 \pm 0.12$	AAIJ	19M	LHCB $pp \rightarrow D\bar{D} + \text{anything}$

$\psi_3(3842)$ WIDTH

VALUE (MeV)	DOCUMENT ID	TECN	COMMENT
$2.79 \pm 0.51 \pm 0.35$	AAIJ	19M	LHCB $pp \rightarrow D\bar{D} + \text{anything}$

$\psi_3(3842)$ DECAY MODES

Mode	Fraction (Γ_i/Γ)
Γ_1 D^+D^-	seen
Γ_2 $D^0\bar{D}^0$	seen

$\psi_3(3842)$ BRANCHING RATIOS

$\Gamma(D^+D^-)/\Gamma_{\text{total}}$	DOCUMENT ID	TECN	COMMENT	Γ_1/Γ
seen	AAIJ	19M	LHCB $pp \rightarrow D\bar{D} + \text{anything}$	

$\Gamma(D^0\bar{D}^0)/\Gamma_{\text{total}}$	DOCUMENT ID	TECN	COMMENT	Γ_2/Γ
seen	AAIJ	19M	LHCB $pp \rightarrow D\bar{D} + \text{anything}$	

$\psi_3(3842)$ REFERENCES

AAIJ	19M	JHEP 1907 035	R. Aaij et al.	(LHCb Collab.)
------	-----	---------------	----------------	----------------

$\chi_{c0}(3860)$

$I^G(J^{PC}) = 0^+(0^{++})$

OMITTED FROM SUMMARY TABLE

The assignment $J^P = 0^+$ is preferred over 2^+ by 2.5 sigma.

Observed by CHILIKIN 17 using full amplitude analysis of the process $e^+e^- \rightarrow J/\psi D\bar{D}$, where $D = D^0, D^+$. Not seen by AAIJ 20A1 in the decay $B^+ \rightarrow D^+D^-K^+$.

$\chi_{c0}(3860)$ MASS

VALUE (MeV)	DOCUMENT ID	TECN	COMMENT
$3862 \pm 26 + 40$ $32 - 13$	CHILIKIN	17	BELL $e^+e^- \rightarrow J/\psi D\bar{D}$

$\chi_{c0}(3860)$ WIDTH

VALUE (MeV)	DOCUMENT ID	TECN	COMMENT
$201 \pm 154 + 88$ $67 - 82$	CHILIKIN	17	BELL $e^+e^- \rightarrow J/\psi D\bar{D}$

$\chi_{c0}(3860)$ DECAY MODES

Mode	Fraction (Γ_i/Γ)
Γ_1 $D^0\bar{D}^0$	seen
Γ_2 D^+D^-	seen

$\chi_{c0}(3860)$ BRANCHING RATIOS

$\Gamma(D^0\bar{D}^0)/\Gamma_{\text{total}}$	DOCUMENT ID	TECN	COMMENT	Γ_1/Γ
seen	CHILIKIN	17	BELL $e^+e^- \rightarrow J/\psi D^0\bar{D}^0$	

$\Gamma(D^+D^-)/\Gamma_{\text{total}}$	DOCUMENT ID	TECN	COMMENT	Γ_2/Γ
seen	CHILIKIN	17	BELL $e^+e^- \rightarrow J/\psi D^+D^-$	

$\chi_{c0}(3860)$ REFERENCES

AAIJ	20A1	PR D102 112003	R. Aaij et al.	(LHCb Collab.)
CHILIKIN	17	PR D95 112003	K. Chilikin et al.	(BELLE Collab.) JPC

$\chi_{c1}(3872)$

$I^G(J^{PC}) = 0^+(1^{++})$

also known as X(3872)

This state shows properties different from a conventional $q\bar{q}$ state. A candidate for an exotic structure. See the review on non- $q\bar{q}$ states.

First observed by CHOI 03 in $B \rightarrow K\pi^+\pi^-J/\psi(1S)$ decays as a narrow peak in the invariant mass distribution of the $\pi^+\pi^-J/\psi(1S)$ final state. Isovector hypothesis excluded by AUBERT 05B and CHOI 11.

AAIJ 13Q perform a full five-dimensional amplitude analysis of the angular correlations between the decay products in $B^+ \rightarrow \chi_{c1}(3872)K^+$ decays, where $\chi_{c1}(3872) \rightarrow J/\psi\pi^+\pi^-$ and $J/\psi \rightarrow \mu^+\mu^-$, which unambiguously gives the $J^{PC} = 1^{++}$ assignment under the assumption that the $\pi^+\pi^-$ and J/ψ are in an S-wave. AAIJ 15AO extend this analysis with more data to limit D-wave contributions to < 4% at 95% CL.

See the review on "Spectroscopy of Mesons Containing Two Heavy Quarks."

$\chi_{c1}(3872)$ MASS FROM $J/\psi X$ MODE

VALUE (MeV)	EVTs	DOCUMENT ID	TECN	COMMENT
3871.65 ± 0.06	OUR AVERAGE			
$3871.64 \pm 0.06 \pm 0.01$	19.8k	1 AAIJ	20s	LHCB $B^+ \rightarrow J/\psi\pi^+\pi^-K^+$
$3871.9 \pm 0.7 \pm 0.2$	20	ABLIKIM	14	BES3 $e^+e^- \rightarrow J/\psi\pi^+\pi^-\gamma$
$3871.95 \pm 0.48 \pm 0.12$	0.6k	AAIJ	12H	LHCB $pp \rightarrow J/\psi\pi^+\pi^-X$
$3871.85 \pm 0.27 \pm 0.19$	170	2 CHOI	11	BELL $B \rightarrow K\pi^+\pi^-J/\psi$
3873 ± 1.8 -1.6	± 1.3 27	3 DEL-AMO-SA.	10B	BABR $B \rightarrow \omega J/\psi K$
$3871.61 \pm 0.16 \pm 0.19$	6k	3,4 AALTONEN	09AU	CDF2 $p\bar{p} \rightarrow J/\psi\pi^+\pi^-X$
$3871.4 \pm 0.6 \pm 0.1$	93.4	AUBERT	08Y	BABR $B^+ \rightarrow K^+J/\psi\pi^+\pi^-$
$3868.7 \pm 1.5 \pm 0.4$	9.4	AUBERT	08Y	BABR $B^0 \rightarrow K_S^0 J/\psi\pi^+\pi^-$
$3871.8 \pm 3.1 \pm 3.0$	522	3,5 ABAZOV	04F	D0 $p\bar{p} \rightarrow J/\psi\pi^+\pi^-X$
$3871.695 \pm 0.067 \pm 0.068$	15.6k	6 AAIJ	20AD	LHCB $pp \rightarrow J/\psi\pi^+\pi^-X$
$3871.59 \pm 0.06 \pm 0.03$	4.2k	7 AAIJ	20s	LHCB $B^+ \rightarrow J/\psi\pi^+\pi^-K^+$
$3873.3 \pm 1.1 \pm 1.0$	45	8 ABLIKIM	19V	BES $e^+e^- \rightarrow \gamma\omega J/\psi$
3860.0 ± 10.4	13.6	3,9 AGHASYAN	18A	COMP $\gamma^*N \rightarrow X\pi^\pm N'$
$3868.6 \pm 1.2 \pm 0.2$	8	10 AUBERT	06	BABR $B^0 \rightarrow K_S^0 J/\psi\pi^+\pi^-$
$3871.3 \pm 0.6 \pm 0.1$	61	10 AUBERT	06	BABR $B^- \rightarrow K^- J/\psi\pi^+\pi^-$
3873.4 ± 1.4	25	11 AUBERT	05R	BABR $B^+ \rightarrow K^+ J/\psi\pi^+\pi^-$
$3871.3 \pm 0.7 \pm 0.4$	730	3,12 ACOSTA	04	CDF2 $p\bar{p} \rightarrow J/\psi\pi^+\pi^-X$
$3872.0 \pm 0.6 \pm 0.5$	36	13 CHOI	03	BELL $B \rightarrow K\pi^+\pi^-J/\psi$
3836 ± 13	58	3,14 ANTONIAZZI	94	E705 $300\pi^\pm L_1 \rightarrow J/\psi\pi^+\pi^-X$

1 Calculated from $m_{\chi_{c1}(3872)} - m_{\psi(2S)} = 185.54 \pm 0.06$ MeV obtained by combining the data with $\chi_{c1}(3872)$ produced in B^+ decays from AAIJ 20s and inclusive b-hadron decays from AAIJ 20AD and using $m_{\psi(2S)} = 3686.097$ MeV. Breit-Wigner parametrization.
 2 The mass difference for the $\chi_{c1}(3872)$ produced in B^+ and B^0 decays is $(-0.71 \pm 0.96 \pm 0.19)$ MeV.

Meson Particle Listings

$\chi_{c1}(3872)$

- ³Width consistent with detector resolution.
- ⁴A possible equal mixture of two states with a mass difference greater than 3.6 MeV/ c^2 is excluded at 95% CL.
- ⁵Calculated from the corresponding $m_{\chi_{c1}(3872)} - m_{J/\psi}$ using $m_{J/\psi} = 3096.916$ MeV.
- ⁶Using $\chi_{c1}(3872)$ produced in inclusive b -hadron decays and $m_{\psi(2S)} = 3686.097 \pm 0.010$ MeV. Breit-Wigner parametrization. Superseded by the combined value in AAIJ 20s.
- ⁷Using Breit-Wigner parametrization. Superseded by the combined value in AAIJ 20s.
- ⁸Fit with fixed width and including two resonances, $\chi_{c0}(3915)$ and $X(3960)$.
- ⁹Could be a different state.
- ¹⁰Calculated from the corresponding $m_{\chi_{c1}(3872)} - m_{\psi(2S)}$ using $m_{\psi(2S)} = 3686.093$ MeV. Superseded by AUBERT 08y.
- ¹¹Calculated from the corresponding $m_{\chi_{c1}(3872)} - m_{\psi(2S)}$ using $m_{\psi(2S)} = 3685.96$ MeV. Superseded by AUBERT 06.
- ¹²Superseded by AALTONEN 09Au.
- ¹³Superseded by CHOI 11.
- ¹⁴A lower mass value can be due to an incorrect momentum scale for soft pions.

$\chi_{c1}(3872)$ MASS FROM $\bar{D}^{*0} D^0$ MODE

VALUE (MeV)	EVTS	DOCUMENT ID	TECN	COMMENT
••• We do not use the following data for averages, fits, limits, etc. •••				
$3872.9^{+0.6+0.4}_{-0.4-0.5}$	50	^{1,2} AUSHEV	10 BELL	$B \rightarrow \bar{D}^{*0} D^0 K$
$3875.1^{+0.7+0.5}_{-0.5+0.5}$	33 ± 6	² AUBERT	08B BABR	$B \rightarrow \bar{D}^{*0} D^0 K$
$3875.2 \pm 0.7^{+0.9}_{-1.8}$	24 ± 6	^{2,3} GOKHROO	06 BELL	$B \rightarrow D^0 \bar{D}^0 \pi^0 K$

¹ Calculated from the measured $m_{\chi_{c1}(3872)} - m_{D^{*0}} - m_{\bar{D}^0} = 1.1^{+0.6+0.1}_{-0.4-0.3}$ MeV.
² Experiments report $D^{*0} \bar{D}^0$ invariant mass above $D^{*0} \bar{D}^0$ threshold because D^{*0} decay products are kinematically constrained to the D^{*0} mass, even though the D^{*0} may decay off-shell.
³ Superseded by AUSHEV 10.

$m_{\chi_{c1}(3872)} - m_{J/\psi}$

VALUE (MeV)	EVTS	DOCUMENT ID	TECN	COMMENT
$774.9 \pm 3.1 \pm 3.0$	522	ABAZOV	04F D0	$p\bar{p} \rightarrow J/\psi \pi^+ \pi^- X$

$m_{\chi_{c1}(3872)} - m_{\psi(2S)}$

VALUE (MeV)	EVTS	DOCUMENT ID	TECN	COMMENT
••• We do not use the following data for averages, fits, limits, etc. •••				
$185.598 \pm 0.067 \pm 0.068$	15.6k	¹ AAIJ	20AD LHCb	$pp \rightarrow J/\psi \pi^+ \pi^- X$
185.54 ± 0.06	19.8k	² AAIJ	20s LHCb	$pp \rightarrow J/\psi \pi^+ \pi^- X$
187.4 ± 1.4	25	³ AUBERT	05R BABR	$B^+ \rightarrow K^+ J/\psi \pi^+ \pi^-$

¹ Using $\chi_{c1}(3872)$ produced in inclusive b -hadron decays. Breit-Wigner parametrization. Superseded by the combined value in AAIJ 20s.
² Combining $m_{\chi_{c1}(3872)} - m_{\psi(2S)} = 185.49 \pm 0.06 \pm 0.03$ MeV from AAIJ 20s and the measured mass difference from AAIJ 20AD. Breit-Wigner parametrization.
³ Superseded by AUBERT 06.

$\chi_{c1}(3872)$ WIDTH

VALUE (MeV)	CL%	EVTS	DOCUMENT ID	TECN	COMMENT
1.19 ± 0.21 OUR AVERAGE Error includes scale factor of 1.1.					
$1.39 \pm 0.24 \pm 0.10$		15.6k	¹ AAIJ	20AD LHCb	$pp \rightarrow J/\psi \pi^+ \pi^- X$
$0.96^{+0.19}_{-0.18} \pm 0.21$		4.2k	² AAIJ	20s LHCb	$B^+ \rightarrow J/\psi \pi^+ \pi^- K^+$

••• We do not use the following data for averages, fits, limits, etc. •••

<2.4	90	1	ABL IKIM	14 BES3	$e^+ e^- \rightarrow J/\psi \pi^+ \pi^- \gamma$
<1.2	90		CHOI	11 BELL	$B \rightarrow K \pi^+ \pi^- J/\psi$
<3.3	90		AUBERT	08y BABR	$B^+ \rightarrow K^+ J/\psi \pi^+ \pi^-$
<4.1	90	69	AUBERT	06 BABR	$B \rightarrow K \pi^+ \pi^- J/\psi$
<2.3	90	36	³ CHOI	03 BELL	$B \rightarrow K \pi^+ \pi^- J/\psi$

¹ Using $\chi_{c1}(3872)$ produced in inclusive b -hadron decays. Breit-Wigner parametrization.
² Using Breit-Wigner parametrization. Partially overlapping dataset with that of AAIJ 20AD.
³ Superseded by CHOI 11.

$\chi_{c1}(3872)$ WIDTH FROM $\bar{D}^{*0} D^0$ MODE

VALUE (MeV)	EVTS	DOCUMENT ID	TECN	COMMENT
••• We do not use the following data for averages, fits, limits, etc. •••				
$3.9^{+2.8+0.2}_{-1.4-1.1}$	50	¹ AUSHEV	10 BELL	$B \rightarrow \bar{D}^{*0} D^0 K$
$3.0^{+1.9}_{-1.4} \pm 0.9$	33 ± 6	AUBERT	08B BABR	$B \rightarrow \bar{D}^{*0} D^0 K$

¹ With a measured value of $B(B \rightarrow \chi_{c1}(3872) K) \times B(\chi_{c1}(3872) \rightarrow D^{*0} \bar{D}^0) = (0.80 \pm 0.20 \pm 0.10) \times 10^{-4}$, assumed to be equal for both charged and neutral modes.

$\chi_{c1}(3872)$ DECAY MODES

Mode	Fraction (Γ_i/Γ)	Confidence level
Γ_1 $e^+ e^-$	< 2.8 $\times 10^{-6}$	90%
Γ_2 $\pi^+ \pi^- J/\psi(1S)$	(3.8 ± 1.2) %	
Γ_3 $\pi^+ \pi^- \pi^0 J/\psi(1S)$	not seen	
Γ_4 $\omega \eta_c(1S)$	< 33 %	90%
Γ_5 $\omega J/\psi(1S)$	(4.3 ± 2.1) %	
Γ_6 $\phi \phi$	not seen	
Γ_7 $D^0 \bar{D}^0 \pi^0$	(49 \pm $^{18}_{-20}$) %	
Γ_8 $\bar{D}^{*0} D^0$	(37 ± 9) %	
Γ_9 $\gamma \gamma$	< 11 %	90%
Γ_{10} $D^0 \bar{D}^0$	< 29 %	90%
Γ_{11} $D^+ D^-$	< 19 %	90%
Γ_{12} $\pi^0 \chi_{c2}$	< 4 %	90%
Γ_{13} $\pi^0 \chi_{c1}$	(3.4 ± 1.6) %	
Γ_{14} $\pi^0 \chi_{c0}$	< 70 %	90%
Γ_{15} $\pi^+ \pi^- \eta_c(1S)$	< 14 %	90%
Γ_{16} $\pi^+ \pi^- \chi_{c1}$	< 7 $\times 10^{-3}$	90%
Γ_{17} $p\bar{p}$	< 2.4 $\times 10^{-5}$	95%

Radiative decays

Γ_{18} $\gamma D^+ D^-$	< 4 %	90%
Γ_{19} $\gamma \bar{D}^0 D^0$	< 6 %	90%
Γ_{20} $\gamma J/\psi$	(8 ± 4) $\times 10^{-3}$	
Γ_{21} $\gamma \chi_{c1}$	< 9 $\times 10^{-3}$	90%
Γ_{22} $\gamma \chi_{c2}$	< 3.2 %	90%
Γ_{23} $\gamma \psi(2S)$	(4.5 ± 2.0) %	

C-violating decays

Γ_{24} $\eta J/\psi$	< 1.8 %	90%
-----------------------------	---------	-----

$\chi_{c1}(3872)$ PARTIAL WIDTHS

$\Gamma(e^+ e^-)$	Γ_1			
VALUE (eV)	CL%	DOCUMENT ID	TECN	COMMENT
••• We do not use the following data for averages, fits, limits, etc. •••				
< 4.3	90	¹ ABLIKIM	15v BES3	$4.0-4.4 e^+ e^- \rightarrow \pi^+ \pi^- J/\psi$
<280	90	² YUAN	04 RVUE	$e^+ e^- \rightarrow \pi^+ \pi^- J/\psi$

¹ ABLIKIM 15v reports this limit from the measurement of $\Gamma(\chi_{c1}(3872) \rightarrow \pi^+ \pi^- J/\psi(1S)) \times \Gamma(\chi_{c1}(3872) \rightarrow e^+ e^-) / \Gamma < 0.13$ eV using $\Gamma(\chi_{c1}(3872) \rightarrow \pi^+ \pi^- J/\psi(1S)) / \Gamma = 3\%$.
² Using BAI 98E data on $e^+ e^- \rightarrow \pi^+ \pi^- \ell^+ \ell^-$. Assuming that $\Gamma(\pi^+ \pi^- J/\psi)$ of $\chi_{c1}(3872)$ is the same as that of $\psi(2S)$ (85.4 keV).

$\Gamma(\gamma\gamma) \times \Gamma(\pi^+ \pi^- J/\psi(1S)) / \Gamma_{total}$ $\Gamma_9 \Gamma_2 / \Gamma$

$\chi_{c1}(3872) \Gamma(i)\Gamma(e^+ e^-) / \Gamma_{total}$

$\Gamma(\pi^+ \pi^- J/\psi(1S)) \times \Gamma(e^+ e^-) / \Gamma_{total}$	$\Gamma_2 \Gamma_1 / \Gamma$			
VALUE (eV)	CL%	DOCUMENT ID	TECN	COMMENT
••• We do not use the following data for averages, fits, limits, etc. •••				
< 0.13	90	ABL IKIM	15v BES3	$4.0-4.4 e^+ e^- \rightarrow \pi^+ \pi^- J/\psi$
< 6.2	90	^{1,2} AUBERT	05D BABR	$10.6 e^+ e^- \rightarrow K^+ K^- \pi^+ \pi^- \gamma$
< 8.3	90	² DOBBS	05 CLE3	$e^+ e^- \rightarrow \pi^+ \pi^- J/\psi$
<10	90	³ YUAN	04 RVUE	$e^+ e^- \rightarrow \pi^+ \pi^- J/\psi$

¹ Using $B(\chi_{c1}(3872) \rightarrow J/\psi \pi^+ \pi^-) \cdot B(J/\psi \rightarrow \mu^+ \mu^-) \cdot \Gamma(\chi_{c1}(3872) \rightarrow e^+ e^-) < 0.37$ eV from AUBERT 05D and $B(J/\psi \rightarrow \mu^+ \mu^-) = 0.0588 \pm 0.0010$ from the PDG 04.
² Assuming $\chi_{c1}(3872)$ has $J^{PC} = 1^{---}$.
³ Using BAI 98E data on $e^+ e^- \rightarrow \pi^+ \pi^- \ell^+ \ell^-$. From theoretical calculation of the production cross section and using $B(J/\psi \rightarrow \mu^+ \mu^-) = (5.88 \pm 0.10)\%$.

$\chi_{c1}(3872) \Gamma(i)\Gamma(\gamma\gamma) / \Gamma_{total}$

$\Gamma(\pi^+ \pi^- J/\psi(1S)) \times \Gamma(\gamma\gamma) / \Gamma_{total}$	$\Gamma_2 \Gamma_9 / \Gamma$				
VALUE (eV)	CL%	EVTS	DOCUMENT ID	TECN	COMMENT
••• We do not use the following data for averages, fits, limits, etc. •••					
$5.5^{+4.1}_{-3.8} \pm 0.7$		3	¹ TERAMOTO	21 BELL	$e^+ e^- \rightarrow \gamma^* \gamma$ at $\Upsilon(ns)$
<12.9	90		² DOBBS	05 CLE3	$e^+ e^- \rightarrow \pi^+ \pi^- J/\psi \gamma$

¹ Measured in single-tag two-photon production assuming Q^2 dependence of a $c\bar{c}$ meson model. Here, $\Gamma(\chi_{c1}(3872) \rightarrow \gamma\gamma)$ is the reduced two-photon decay width, $\bar{\Gamma}_{\gamma\gamma}$.
² Assuming $\chi_{c1}(3872)$ has positive C parity and spin 0.

$\Gamma(\omega J/\psi(1S)) \times \Gamma(\gamma\gamma)/\Gamma_{total}$					$\Gamma_5\Gamma_9/\Gamma$
VALUE (eV)	CL%	DOCUMENT ID	TECN	COMMENT	

• • • We do not use the following data for averages, fits, limits, etc. • • •
 <1.7 90 ¹LEES 12Ad BABR $e^+e^- \rightarrow e^+e^-\omega J/\psi$
¹ Assuming $\chi_{c1}(3872)$ has spin 2.

$\Gamma(\pi^+\pi^-\eta_c(1S)) \times \Gamma(\gamma\gamma)/\Gamma_{total}$					$\Gamma_{15}\Gamma_9/\Gamma$
VALUE (eV)	CL%	DOCUMENT ID	TECN	COMMENT	

<11.1 90 LEES 12AE BABR $e^+e^- \rightarrow e^+e^-\pi^+\pi^-\eta_c$

$\chi_{c1}(3872)$ BRANCHING RATIOS

$\Gamma(\pi^+\pi^-J/\psi(1S))/\Gamma_{total}$					Γ_2/Γ
VALUE	EVTS	DOCUMENT ID	TECN	COMMENT	

0.038±0.012 OUR AVERAGE
 0.038±0.002±0.012 ¹AALJ 20s LHCb $B^+ \rightarrow J/\psi\pi^+\pi^-K^+$
 0.041±0.005±0.013 ²CHOI 11 BELL $B^+ \rightarrow \pi^+\pi^-J/\psi K^+$
 0.040±0.008±0.013 93 ^{3,4}AUBERT 08Y BABR $B \rightarrow \chi_{c1}(3872)K$
 • • • We do not use the following data for averages, fits, limits, etc. • • •
 seen 151 ⁵BALA 15 BELL $B \rightarrow \chi_{c1}(3872)K\pi$
 0.061±0.020±0.020 30 ⁶AUBERT 05R BABR $B^+ \rightarrow K^+\pi^+\pi^-J/\psi$
 0.065±0.014±0.021 36 ⁷CHOI 03 BELL $B^+ \rightarrow K^+\pi^+\pi^-J/\psi$

¹ AALJ 20s reports $[\Gamma(\chi_{c1}(3872) \rightarrow \pi^+\pi^-J/\psi(1S))/\Gamma_{total}] \times [B(B^+ \rightarrow \chi_{c1}(3872)K^+)] = (7.95 \pm 0.15 \pm 0.33) \times 10^{-6}$ which we divide by our best value $B(B^+ \rightarrow \chi_{c1}(3872)K^+) = (2.1 \pm 0.7) \times 10^{-4}$. Our first error is their experiment's error and our second error is the systematic error from using our best value.
² CHOI 11 reports $[\Gamma(\chi_{c1}(3872) \rightarrow \pi^+\pi^-J/\psi(1S))/\Gamma_{total}] \times [B(B^+ \rightarrow \chi_{c1}(3872)K^+)] = (8.63 \pm 0.82 \pm 0.52) \times 10^{-6}$ which we divide by our best value $B(B^+ \rightarrow \chi_{c1}(3872)K^+) = (2.1 \pm 0.7) \times 10^{-4}$. Our first error is their experiment's error and our second error is the systematic error from using our best value.
³ AUBERT 08Y reports $[\Gamma(\chi_{c1}(3872) \rightarrow \pi^+\pi^-J/\psi(1S))/\Gamma_{total}] \times [B(B^+ \rightarrow \chi_{c1}(3872)K^+)] = (8.4 \pm 1.5 \pm 0.7) \times 10^{-6}$ which we divide by our best value $B(B^+ \rightarrow \chi_{c1}(3872)K^+) = (2.1 \pm 0.7) \times 10^{-4}$. Our first error is their experiment's error and our second error is the systematic error from using our best value.
⁴ superseded by LEES 20c
⁵ BALA 15 reports $B(\chi_{c1}(3872) \rightarrow \pi^+\pi^-J/\psi) \times B(B^0 \rightarrow \chi_{c1}(3872)K^+\pi^-) = (7.9 \pm 1.3 \pm 0.4) \times 10^{-6}$ and $B(\chi_{c1}(3872) \rightarrow \pi^+\pi^-J/\psi) \times B(B^+ \rightarrow \chi_{c1}(3872)K^0\pi^+) = (10.6 \pm 3.0 \pm 0.9) \times 10^{-6}$.
⁶ Superseded by AUBERT 08Y. AUBERT 05R reports $[\Gamma(\chi_{c1}(3872) \rightarrow \pi^+\pi^-J/\psi(1S))/\Gamma_{total}] \times [B(B^+ \rightarrow \chi_{c1}(3872)K^+)] = (1.28 \pm 0.41) \times 10^{-5}$ which we divide by our best value $B(B^+ \rightarrow \chi_{c1}(3872)K^+) = (2.1 \pm 0.7) \times 10^{-4}$. Our first error is their experiment's error and our second error is the systematic error from using our best value.
⁷ CHOI 03 reports $[\Gamma(\chi_{c1}(3872) \rightarrow \pi^+\pi^-J/\psi(1S))/\Gamma_{total}] \times [B(B^+ \rightarrow \chi_{c1}(3872)K^+)] / [B(B^+ \rightarrow \psi(2S)K^+)] / [B(\psi(2S) \rightarrow J/\psi(1S)\pi^+\pi^-)] = 0.063 \pm 0.012 \pm 0.007$ which we multiply or divide by our best values $B(B^+ \rightarrow \chi_{c1}(3872)K^+) = (2.1 \pm 0.7) \times 10^{-4}$, $B(B^+ \rightarrow \psi(2S)K^+) = (6.24 \pm 0.20) \times 10^{-4}$, $B(\psi(2S) \rightarrow J/\psi(1S)\pi^+\pi^-) = (34.68 \pm 0.30) \times 10^{-2}$. Our first error is their experiment's error and our second error is the systematic error from using our best values.

$\Gamma(\pi^+\pi^-\pi^0 J/\psi(1S))/\Gamma_{total}$					Γ_3/Γ
VALUE	DOCUMENT ID	TECN	COMMENT		

not seen ¹WANG 11B BELL $\Upsilon(2S) \rightarrow \gamma X$
 not seen ²SHEN 10A BELL $\Upsilon(1S) \rightarrow \gamma X$
¹ WANG 11B reports $B(\Upsilon(2S) \rightarrow \gamma\chi_{c1}(3872)) \times B(\chi_{c1} \rightarrow \pi^+\pi^-\pi^0 J/\psi) < 2.4 \times 10^{-6}$ at 95% CL.
² SHEN 10A reports $B(\Upsilon(1S) \rightarrow \gamma\chi_{c1}(3872)) \times B(\chi_{c1} \rightarrow \pi^+\pi^-\pi^0 J/\psi) < 2.8 \times 10^{-6}$ at 95% CL.

$\Gamma(\omega\eta_c(1S))/\Gamma_{total}$					Γ_4/Γ
VALUE	CL%	DOCUMENT ID	TECN	COMMENT	

<0.33 90 ¹VINOKUROVA 15 BELL $B^+ \rightarrow \omega\eta_c K^+$
¹ VINOKUROVA 15 reports $[\Gamma(\chi_{c1}(3872) \rightarrow \omega\eta_c(1S))/\Gamma_{total}] \times [B(B^+ \rightarrow \chi_{c1}(3872)K^+)] < 6.9 \times 10^{-5}$ which we divide by our best value $B(B^+ \rightarrow \chi_{c1}(3872)K^+) = 2.1 \times 10^{-4}$.

$\Gamma(\omega J/\psi(1S))/\Gamma_{total}$					Γ_5/Γ
VALUE	EVTS	DOCUMENT ID	TECN	COMMENT	

• • • We do not use the following data for averages, fits, limits, etc. • • •
 0.029±0.011±0.009 21±7 ¹DEL-AMO-SA...10B BABR $B^+ \rightarrow \omega J/\psi K^+$
¹ DEL-AMO-SANCHEZ 10B reports $[\Gamma(\chi_{c1}(3872) \rightarrow \omega J/\psi(1S))/\Gamma_{total}] \times [B(B^+ \rightarrow \chi_{c1}(3872)K^+)] = (6 \pm 2 \pm 1) \times 10^{-6}$ which we divide by our best value $B(B^+ \rightarrow \chi_{c1}(3872)K^+) = (2.1 \pm 0.7) \times 10^{-4}$. Our first error is their experiment's error and our second error is the systematic error from using our best value. DEL-AMO-SANCHEZ 10B also reports $B(B^0 \rightarrow \chi_{c1}(3872)K^0) \times B(\chi_{c1}(3872) \rightarrow J/\psi\omega) = (6 \pm 3 \pm 1) \times 10^{-6}$.

$\Gamma(\omega J/\psi(1S))/\Gamma(\pi^+\pi^-J/\psi(1S))$					Γ_5/Γ_2
VALUE	DOCUMENT ID	TECN	COMMENT		

1.1±0.4 OUR AVERAGE Error includes scale factor of 1.7.
 1.6^{+0.4}_{-0.3}±0.2 ¹ABLIKIM 19v BES $e^+e^- \rightarrow \gamma\omega J/\psi$
 0.8±0.3 ²DEL-AMO-SA...10B BABR $B \rightarrow \omega J/\psi K$
¹ Fit with fixed width and including two resonances, $\chi_{c0}(3915)$ and $X(3960)$.
² Statistical and systematic errors added in quadrature. Uses the values of $B(B \rightarrow \chi_{c1}(3872)K) \times B(\chi_{c1}(3872) \rightarrow J/\psi\pi^+\pi^-)$ reported in AUBERT 08Y, taking into account the common systematics.

$\Gamma(\phi\phi)/\Gamma_{total}$					Γ_6/Γ
VALUE	DOCUMENT ID	TECN	COMMENT		

not seen ¹AALJ 17Bb LHCb pp at 7, 8 TeV
¹ AALJ 17Bb reports $B(b \rightarrow \chi_{c1}(3872) \text{ anything}) \times B(\chi_{c1}(3872) \rightarrow \phi\phi) < 4.5 \times 10^{-7}$ at 95% CL.

$\Gamma(D^0\bar{D}^0\pi^0)/\Gamma_{total}$					Γ_7/Γ
VALUE	CL%	EVTS	DOCUMENT ID	TECN	COMMENT

0.49^{+0.18}_{-0.20}±0.16 17 ¹GOKHROO 06 BELL $B^+ \rightarrow D^0\bar{D}^0\pi^0 K^+$
 • • • We do not use the following data for averages, fits, limits, etc. • • •
 <0.29 90 ²CHISTOV 04 BELL Sup. by GOKHROO 06
¹ GOKHROO 06 reports $[\Gamma(\chi_{c1}(3872) \rightarrow D^0\bar{D}^0\pi^0)/\Gamma_{total}] \times [B(B^+ \rightarrow \chi_{c1}(3872)K^+)] = (1.02 \pm 0.31^{+0.21}_{-0.29}) \times 10^{-4}$ which we divide by our best value $B(B^+ \rightarrow \chi_{c1}(3872)K^+) = (2.1 \pm 0.7) \times 10^{-4}$. Our first error is their experiment's error and our second error is the systematic error from using our best value.
² CHISTOV 04 reports $[\Gamma(\chi_{c1}(3872) \rightarrow D^0\bar{D}^0\pi^0)/\Gamma_{total}] \times [B(B^+ \rightarrow \chi_{c1}(3872)K^+)] < 0.6 \times 10^{-4}$ which we divide by our best value $B(B^+ \rightarrow \chi_{c1}(3872)K^+) = 2.1 \times 10^{-4}$.

$\Gamma(D^0\bar{D}^0\pi^0)/\Gamma(\pi^+\pi^-J/\psi(1S))$					Γ_7/Γ_2
VALUE	CL%	DOCUMENT ID	TECN	COMMENT	

• • • We do not use the following data for averages, fits, limits, etc. • • •
 <1.16 90 ABLIKIM 20W BES3 $e^+e^- \rightarrow \gamma\chi_{c1}(3872)$

$\Gamma(\bar{D}^{*0}D^0)/\Gamma_{total}$					Γ_8/Γ
VALUE	EVTS	DOCUMENT ID	TECN	COMMENT	

0.37±0.09±0.12 41⁺⁹₋₈ ¹AUSHEV 10 BELL $B^+ \rightarrow D^{*0}\bar{D}^0 K^+$
 • • • We do not use the following data for averages, fits, limits, etc. • • •
 0.80±0.28±0.26 27±6 ²AUBERT 08B BABR $B^+ \rightarrow \bar{D}^{*0}D^0 K^+$
¹ AUSHEV 10 reports $[\Gamma(\chi_{c1}(3872) \rightarrow \bar{D}^{*0}D^0)/\Gamma_{total}] \times [B(B^+ \rightarrow \chi_{c1}(3872)K^+)] = (0.77 \pm 0.16 \pm 0.10) \times 10^{-4}$ which we divide by our best value $B(B^+ \rightarrow \chi_{c1}(3872)K^+) = (2.1 \pm 0.7) \times 10^{-4}$. Our first error is their experiment's error and our second error is the systematic error from using our best value.
² AUBERT 08B reports $[\Gamma(\chi_{c1}(3872) \rightarrow \bar{D}^{*0}D^0)/\Gamma_{total}] \times [B(B^+ \rightarrow \chi_{c1}(3872)K^+)] = (1.67 \pm 0.36 \pm 0.47) \times 10^{-4}$ which we divide by our best value $B(B^+ \rightarrow \chi_{c1}(3872)K^+) = (2.1 \pm 0.7) \times 10^{-4}$. Our first error is their experiment's error and our second error is the systematic error from using our best value.

$\Gamma(\bar{D}^{*0}D^0)/\Gamma(\pi^+\pi^-J/\psi(1S))$					Γ_8/Γ_2
VALUE	EVTS	DOCUMENT ID	TECN	COMMENT	

11.77±3.09 50 ABLIKIM 20W BES3 $e^+e^- \rightarrow \gamma\chi_{c1}(3872)$

$\Gamma(\gamma\gamma)/\Gamma_{total}$					Γ_9/Γ
VALUE	CL%	DOCUMENT ID	TECN	COMMENT	

<0.11 90 ¹WICHT 08 BELL $e^+e^- \rightarrow \Upsilon(4S)$
¹ WICHT 08 reports $[\Gamma(\chi_{c1}(3872) \rightarrow \gamma\gamma)/\Gamma_{total}] \times [B(B^+ \rightarrow \chi_{c1}(3872)K^+)] < 2.4 \times 10^{-5}$ which we divide by our best value $B(B^+ \rightarrow \chi_{c1}(3872)K^+) = 2.1 \times 10^{-4}$.

$\Gamma(D^0\bar{D}^0)/\Gamma_{total}$					Γ_{10}/Γ
VALUE	CL%	DOCUMENT ID	TECN	COMMENT	

<0.29 90 ¹CHISTOV 04 BELL $B \rightarrow K D^0\bar{D}^0$
¹ CHISTOV 04 reports $[\Gamma(\chi_{c1}(3872) \rightarrow D^0\bar{D}^0)/\Gamma_{total}] \times [B(B^+ \rightarrow \chi_{c1}(3872)K^+)] < 6 \times 10^{-5}$ which we divide by our best value $B(B^+ \rightarrow \chi_{c1}(3872)K^+) = 2.1 \times 10^{-4}$.

$\Gamma(D^+D^-)/\Gamma_{total}$					Γ_{11}/Γ
VALUE	CL%	DOCUMENT ID	TECN	COMMENT	

<0.19 90 ¹CHISTOV 04 BELL $B \rightarrow K D^+D^-$
¹ CHISTOV 04 reports $[\Gamma(\chi_{c1}(3872) \rightarrow D^+D^-)/\Gamma_{total}] \times [B(B^+ \rightarrow \chi_{c1}(3872)K^+)] < 4 \times 10^{-5}$ which we divide by our best value $B(B^+ \rightarrow \chi_{c1}(3872)K^+) = 2.1 \times 10^{-4}$.

$\Gamma(\pi^0\chi_{c2})/\Gamma(\pi^+\pi^-J/\psi(1S))$					Γ_{12}/Γ_2
VALUE	CL%	DOCUMENT ID	TECN	COMMENT	

<1.1 90 ABLIKIM 19U BES3 $e^+e^- \rightarrow \gamma\chi_{c1}(3872)$

Meson Particle Listings

 $\chi_{c1}(3872)$ $\Gamma(\pi^0 \chi_{c1})/\Gamma_{\text{total}}$ Γ_{13}/Γ

VALUE	CL%	DOCUMENT ID	TECN	COMMENT
<0.04	90	¹ BHARDWAJ 19	BELL	$B^{\pm} \rightarrow \pi^0 \chi_{c1} K^{\pm}$
<p>¹BHARDWAJ 19 reports $[\Gamma(\chi_{c1}(3872) \rightarrow \pi^0 \chi_{c1})/\Gamma_{\text{total}}] \times [B(B^+ \rightarrow \chi_{c1}(3872) K^+) < 8.1 \times 10^{-6}$ which we divide by our best value $B(B^+ \rightarrow \chi_{c1}(3872) K^+) = 2.1 \times 10^{-4}$.</p>				

 $\Gamma(\pi^0 \chi_{c1})/\Gamma(\pi^+ \pi^- J/\psi(1S))$ Γ_{13}/Γ_2

VALUE (units 10^{-2})	EVTS	DOCUMENT ID	TECN	COMMENT
$88^{+33}_{-27} \pm 10$	10.8	ABLIKIM 19U	BES3	$e^+ e^- \rightarrow \gamma \chi_{c1}(3872)$

 $\Gamma(\pi^0 \chi_{c0})/\Gamma(\pi^+ \pi^- J/\psi(1S))$ Γ_{14}/Γ_2

VALUE	CL%	DOCUMENT ID	TECN	COMMENT
<19	90	ABLIKIM 19U	BES3	$e^+ e^- \rightarrow \gamma \chi_{c1}(3872)$

 $\Gamma(\pi^+ \pi^- \eta_c(1S))/\Gamma_{\text{total}}$ Γ_{15}/Γ

VALUE	CL%	DOCUMENT ID	TECN	COMMENT
<0.14	90	¹ VINOKUROVA 15	BELL	$B^+ \rightarrow \pi^+ \pi^- \eta_c K^+$
<p>¹VINOKUROVA 15 reports $[\Gamma(\chi_{c1}(3872) \rightarrow \pi^+ \pi^- \eta_c(1S))/\Gamma_{\text{total}}] \times [B(B^+ \rightarrow \chi_{c1}(3872) K^+) < 3.0 \times 10^{-5}$ which we divide by our best value $B(B^+ \rightarrow \chi_{c1}(3872) K^+) = 2.1 \times 10^{-4}$.</p>				

 $\Gamma(\pi^+ \pi^- \chi_{c1})/\Gamma_{\text{total}}$ Γ_{16}/Γ

VALUE	CL%	DOCUMENT ID	TECN	COMMENT
$<7 \times 10^{-3}$	90	¹ BHARDWAJ 16	BELL	$B^+ \rightarrow \pi^+ \pi^- \chi_{c1} K^+$
<p>¹BHARDWAJ 16 reports $[\Gamma(\chi_{c1}(3872) \rightarrow \pi^+ \pi^- \chi_{c1})/\Gamma_{\text{total}}] \times [B(B^+ \rightarrow \chi_{c1}(3872) K^+) < 1.5 \times 10^{-6}$ which we divide by our best value $B(B^+ \rightarrow \chi_{c1}(3872) K^+) = 2.1 \times 10^{-4}$.</p>				

 $\Gamma(p\bar{p})/\Gamma_{\text{total}}$ Γ_{17}/Γ

VALUE	CL%	DOCUMENT ID	TECN	COMMENT
$<2.4 \times 10^{-5}$	95	¹ AAIJ 17AD	LHCB	$B^+ \rightarrow p\bar{p} K^+$
<p>••• We do not use the following data for averages, fits, limits, etc. ••••</p>				
$<8 \times 10^{-5}$	95	² AAIJ 13s	LHCB	$B^+ \rightarrow p\bar{p} K^+$
<p>¹AAIJ 17AD reports $[\Gamma(\chi_{c1}(3872) \rightarrow p\bar{p})/\Gamma_{\text{total}}] \times [B(B^+ \rightarrow \chi_{c1}(3872) K^+) < 0.5 \times 10^{-8}$ which we divide by our best value $B(B^+ \rightarrow \chi_{c1}(3872) K^+) = 2.1 \times 10^{-4}$.</p> <p>²AAIJ 13s reports $[\Gamma(\chi_{c1}(3872) \rightarrow p\bar{p})/\Gamma_{\text{total}}] \times [B(B^+ \rightarrow \chi_{c1}(3872) K^+) < 1.7 \times 10^{-8}$ which we divide by our best value $B(B^+ \rightarrow \chi_{c1}(3872) K^+) = 2.1 \times 10^{-4}$.</p>				

Radiative decays

 $\Gamma(\gamma D^+ D^-)/\Gamma(\pi^+ \pi^- J/\psi(1S))$ Γ_{18}/Γ_2

VALUE	CL%	DOCUMENT ID	TECN	COMMENT
<0.99	90	ABLIKIM 20W	BES3	$e^+ e^- \rightarrow \gamma \chi_{c1}(3872)$

 $\Gamma(\gamma \bar{D}^0 D^0)/\Gamma(\pi^+ \pi^- J/\psi(1S))$ Γ_{19}/Γ_2

VALUE	CL%	DOCUMENT ID	TECN	COMMENT
<1.58	90	ABLIKIM 20W	BES3	$e^+ e^- \rightarrow \gamma \chi_{c1}(3872)$

 $\Gamma(\gamma J/\psi)/\Gamma_{\text{total}}$ Γ_{20}/Γ

VALUE	EVTS	DOCUMENT ID	TECN	COMMENT
$0.0085^{+0.0024}_{-0.0022} \pm 0.0027$		¹ BHARDWAJ 11	BELL	$B^{\pm} \rightarrow \gamma J/\psi K^{\pm}$
<p>••• We do not use the following data for averages, fits, limits, etc. ••••</p>				
$0.013 \pm 0.004 \pm 0.004$	20	² AUBERT 09B	BABR	$B^+ \rightarrow \gamma J/\psi K^+$
$0.016 \pm 0.005 \pm 0.005$	19	³ AUBERT,BE	06M BABR	$B^+ \rightarrow \gamma J/\psi K^+$

¹BHARDWAJ 11 reports $[\Gamma(\chi_{c1}(3872) \rightarrow \gamma J/\psi)/\Gamma_{\text{total}}] \times [B(B^+ \rightarrow \chi_{c1}(3872) K^+) < (1.78^{+0.48}_{-0.44} \pm 0.12) \times 10^{-6}$ which we divide by our best value $B(B^+ \rightarrow \chi_{c1}(3872) K^+) = (2.1 \pm 0.7) \times 10^{-4}$. Our first error is their experiment's error and our second error is the systematic error from using our best value.

²AUBERT 09B reports $[\Gamma(\chi_{c1}(3872) \rightarrow \gamma J/\psi)/\Gamma_{\text{total}}] \times [B(B^+ \rightarrow \chi_{c1}(3872) K^+) < (2.8 \pm 0.8 \pm 0.1) \times 10^{-6}$ which we divide by our best value $B(B^+ \rightarrow \chi_{c1}(3872) K^+) = (2.1 \pm 0.7) \times 10^{-4}$. Our first error is their experiment's error and our second error is the systematic error from using our best value.

³Superseded by AUBERT 09B. AUBERT,BE 06M reports $[\Gamma(\chi_{c1}(3872) \rightarrow \gamma J/\psi)/\Gamma_{\text{total}}] \times [B(B^+ \rightarrow \chi_{c1}(3872) K^+) < (3.3 \pm 1.0 \pm 0.3) \times 10^{-6}$ which we divide by our best value $B(B^+ \rightarrow \chi_{c1}(3872) K^+) = (2.1 \pm 0.7) \times 10^{-4}$. Our first error is their experiment's error and our second error is the systematic error from using our best value.

 $\Gamma(\gamma J/\psi)/\Gamma(\pi^+ \pi^- J/\psi(1S))$ Γ_{20}/Γ_2

VALUE	CL%	DOCUMENT ID	TECN	COMMENT
0.79 ± 0.28		ABLIKIM 20W	BES3	$e^+ e^- \rightarrow \gamma \chi_{c1}(3872)$

 $\Gamma(\gamma \chi_{c1})/\Gamma_{\text{total}}$ Γ_{21}/Γ

VALUE	CL%	DOCUMENT ID	TECN	COMMENT
$<9 \times 10^{-3}$	90	¹ BHARDWAJ 13	BELL	$B^{\pm} \rightarrow \chi_{c1} \gamma K^{\pm}$
<p>¹BHARDWAJ 13 reports $[\Gamma(\chi_{c1}(3872) \rightarrow \gamma \chi_{c1})/\Gamma_{\text{total}}] \times [B(B^+ \rightarrow \chi_{c1}(3872) K^+) < 1.9 \times 10^{-6}$ which we divide by our best value $B(B^+ \rightarrow \chi_{c1}(3872) K^+) = 2.1 \times 10^{-4}$.</p>				

 $\Gamma(\gamma \chi_{c1})/\Gamma(\pi^+ \pi^- J/\psi(1S))$ Γ_{21}/Γ_2

VALUE	CL%	DOCUMENT ID	TECN	COMMENT
<0.89	90	CHOI 03	BELL	$B \rightarrow K \pi^+ \pi^- J/\psi$

 $\Gamma(\gamma \chi_{c2})/\Gamma_{\text{total}}$ Γ_{22}/Γ

VALUE	CL%	DOCUMENT ID	TECN	COMMENT
<0.032	90	¹ BHARDWAJ 13	BELL	$B^{\pm} \rightarrow \chi_{c2} \gamma K^{\pm}$
<p>¹BHARDWAJ 13 reports $[\Gamma(\chi_{c1}(3872) \rightarrow \gamma \chi_{c2})/\Gamma_{\text{total}}] \times [B(B^+ \rightarrow \chi_{c1}(3872) K^+) < 6.7 \times 10^{-6}$ which we divide by our best value $B(B^+ \rightarrow \chi_{c1}(3872) K^+) = 2.1 \times 10^{-4}$.</p>				

 $\Gamma(\gamma \psi(2S))/\Gamma_{\text{total}}$ Γ_{23}/Γ

VALUE	EVTS	DOCUMENT ID	TECN	COMMENT
$0.045 \pm 0.013 \pm 0.015$	25 \pm 7	¹ AUBERT 09B	BABR	$B^+ \rightarrow \gamma \psi(2S) K^+$
<p>••• We do not use the following data for averages, fits, limits, etc. ••••</p>				
seen	36 \pm 9	² AAIJ 14AH	LHCB	$B^+ \rightarrow \gamma \psi(2S) K^+$
not seen		³ BHARDWAJ 11	BELL	$B^+ \rightarrow \gamma \psi(2S) K^+$

¹AUBERT 09B reports $[\Gamma(\chi_{c1}(3872) \rightarrow \gamma \psi(2S))/\Gamma_{\text{total}}] \times [B(B^+ \rightarrow \chi_{c1}(3872) K^+) < (9.5 \pm 2.7 \pm 0.6) \times 10^{-6}$ which we divide by our best value $B(B^+ \rightarrow \chi_{c1}(3872) K^+) < (2.1 \pm 0.7) \times 10^{-4}$. Our first error is their experiment's error and our second error is the systematic error from using our best value.

²From 36.4 \pm 9.0 events of $\chi_{c1}(3872) \rightarrow J/\psi \gamma$ decays with a statistical significance of 4.4 σ .

³BHARDWAJ 11 reports $B(B^+ \rightarrow K^+ \chi_{c1}(3872)) \times B(\chi_{c1}(3872) \rightarrow \gamma \psi(2S)) < 3.45 \times 10^{-6}$ at 90% CL.

 $\Gamma(\gamma \psi(2S))/\Gamma(\pi^+ \pi^- J/\psi(1S))$ Γ_{23}/Γ_2

VALUE	CL%	DOCUMENT ID	TECN	COMMENT
<0.42	90	ABLIKIM 20W	BES3	$e^+ e^- \rightarrow \gamma \chi_{c1}(3872)$

 $\Gamma(\gamma \psi(2S))/\Gamma(\gamma J/\psi)$ Γ_{23}/Γ_{20}

VALUE	CL%	EVTS	DOCUMENT ID	TECN	COMMENT
2.6 ± 0.6		OUR AVERAGE			
$2.46 \pm 0.64 \pm 0.29$		36 \pm 9	¹ AAIJ 14AH	LHCB	$B^+ \rightarrow \gamma \psi(2S) K^+$
3.4 ± 1.4			AUBERT 09B	BABR	$B^+ \rightarrow \gamma c\bar{c} K'$

••• We do not use the following data for averages, fits, limits, etc. **••••**

<2.1 90 BHARDWAJ 11 BELL $B^+ \rightarrow \gamma \psi(2S) K^+$

¹From 36.4 \pm 9.0 events of $\chi_{c1}(3872) \rightarrow J/\psi \gamma$ decays with a statistical significance of 4.4 σ .

C-violating decays

 $\Gamma(\eta J/\psi)/\Gamma_{\text{total}}$ Γ_{24}/Γ

VALUE	CL%	DOCUMENT ID	TECN	COMMENT
<0.018	90	^{1,2} IWASHITA 14	BELL	$B \rightarrow K \eta J/\psi$
<p>••• We do not use the following data for averages, fits, limits, etc. ••••</p>				
<0.04	90	³ AUBERT 04Y	BABR	$B \rightarrow K \eta J/\psi$

¹IWASHITA 14 reports $[\Gamma(\chi_{c1}(3872) \rightarrow \eta J/\psi)/\Gamma_{\text{total}}] \times [B(B^+ \rightarrow \chi_{c1}(3872) K^+) < 3.8 \times 10^{-6}$ which we divide by our best value $B(B^+ \rightarrow \chi_{c1}(3872) K^+) = 2.1 \times 10^{-4}$.

²IWASHITA 14 also scans the $\eta J/\psi$ mass range 3.8–4.75 GeV and sets upper limits for $B(B^{\pm} \rightarrow \chi_{c1}(3872) K^{\pm}) \times B(\chi_{c1}(3872) \rightarrow \eta J/\psi)$ in 5 MeV intervals.

³AUBERT 04Y reports $[\Gamma(\chi_{c1}(3872) \rightarrow \eta J/\psi)/\Gamma_{\text{total}}] \times [B(B^+ \rightarrow \chi_{c1}(3872) K^+) < 7.7 \times 10^{-6}$ which we divide by our best value $B(B^+ \rightarrow \chi_{c1}(3872) K^+) = 2.1 \times 10^{-4}$.

 $\chi_{c1}(3872)$ REFERENCES

TERAMOTO 21	PRL 126 122001	Y. Teramoto <i>et al.</i>	(BELLE Collab.)
AAIJ 20AD	PR D102 092005	R. Aaij <i>et al.</i>	(LHCb Collab.)
AAIJ 20S	JHEP 2008 123	R. Aaij <i>et al.</i>	(LHCb Collab.)
ABLIKIM 20W	PRL 124 242001	M. Ablikim <i>et al.</i>	(BESIII Collab.)
LEES 20C	PRL 124 152001	J.P. Lees <i>et al.</i>	(BABAR Collab.)
ABLIKIM 19U	PRL 122 202001	M. Ablikim <i>et al.</i>	(BESIII Collab.)
ABLIKIM 19V	PRL 122 220002	M. Ablikim <i>et al.</i>	(BESIII Collab.)
BHARDWAJ 19	PR D99 111101	V. Bhardwaj <i>et al.</i>	(BELLE Collab.)
AGHASYAN 18A	PL B783 334	M. Aghasyan <i>et al.</i>	(COMPASS Collab.)
AAIJ 17AD	PL B769 305	R. Aaij <i>et al.</i>	(LHCb Collab.)
AAIJ 17BB	EPJ C77 609	R. Aaij <i>et al.</i>	(LHCb Collab.)
BHARDWAJ 16	PR D93 052016	V. Bhardwaj <i>et al.</i>	(BELLE Collab.)
AAIJ 15AO	PR D92 011102	R. Aaij <i>et al.</i>	(LHCb Collab.)
ABLIKIM 15V	PL B749 414	M. Ablikim <i>et al.</i>	(BESIII Collab.)
BALA 15	PR D91 051101	A. Bala <i>et al.</i>	(BELLE Collab.)
VINOKUROVA 15	JHEP 1506 132	A. Vinokurova <i>et al.</i>	(BELLE Collab.)
AAIJ Also	JHEP 1702 088 (errata.)	A. Vinokurova <i>et al.</i>	(BELLE Collab.)
AAIJ 14AH	NP B866 665	R. Aaij <i>et al.</i>	(LHCb Collab.)
ABLIKIM 14	PRL 112 092001	M. Ablikim <i>et al.</i>	(BESIII Collab.)
IWASHITA 14	PTEP 2014 043C01	T. Iwashita <i>et al.</i>	(BELLE Collab.)
AAIJ 13Q	PRL 110 222001	R. Aaij <i>et al.</i>	(LHCb Collab.)
AAIJ 13S	EPJ C73 2462	R. Aaij <i>et al.</i>	(LHCb Collab.)
BHARDWAJ 13	PRL 111 032001	V. Bhardwaj <i>et al.</i>	(BELLE Collab.)
AAIJ 12H	EPJ C72 1972	R. Aaij <i>et al.</i>	(LHCb Collab.)
LEES 12AD	PR D86 072002	J.P. Lees <i>et al.</i>	(BABAR Collab.)
LEES 12AE	PR D86 092005	J.P. Lees <i>et al.</i>	(BABAR Collab.)
BHARDWAJ 11	PRL 107 091803	V. Bhardwaj <i>et al.</i>	(BELLE Collab.)
CHOI 11	PR D84 052004	S.-K. Choi <i>et al.</i>	(BELLE Collab.)
WANG 11B	PR D84 071107	X.L. Wang <i>et al.</i>	(BELLE Collab.)
AUSHEV 10	PR D81 031103	T. Aushev <i>et al.</i>	(BELLE Collab.)
DEL-AMO-SA... 10B	PR D82 011101	P. del Amo Sanchez <i>et al.</i>	(BABAR Collab.)
SHEN 10A	PR D82 051504	C.P. Shen <i>et al.</i>	(BELLE Collab.)
AALTONEN 09AU	PRL 103 152001	T. Aaltonen <i>et al.</i>	(CDF Collab.)
AUBERT 09B	PRL 102 132001	B. Aubert <i>et al.</i>	(BABAR Collab.)
AUBERT 08B	PR D77 011102	B. Aubert <i>et al.</i>	(BABAR Collab.)
AUBERT 08Y	PR D77 111101	B. Aubert <i>et al.</i>	(BABAR Collab.)
WICHT 08	PL B662 323	J. Wicht <i>et al.</i>	(BELLE Collab.)
AUBERT 06	PR D73 011101	B. Aubert <i>et al.</i>	(BABAR Collab.)
AUBERT,BE 06M	PR D74 071101	B. Aubert <i>et al.</i>	(BABAR Collab.)
GOKHROO 06	PRL 97 162002	G. Gokhroo <i>et al.</i>	(BELLE Collab.)

AUBERT	05B	PR D71 031501	B. Aubert <i>et al.</i>	(BABAR Collab.)
AUBERT	05D	PR D71 052001	B. Aubert <i>et al.</i>	(BABAR Collab.)
AUBERT	05R	PR D71 071103	B. Aubert <i>et al.</i>	(BABAR Collab.)
DOBBS	05	PRL 94 032004	S. Dobbs <i>et al.</i>	(CLEO Collab.)
ABAZOV	04F	PRL 93 162002	V.M. Abazov <i>et al.</i>	(DO Collab.)
ACOSTA	04	PRL 93 072001	D. Acosta <i>et al.</i>	(CDF Collab.)
AUBERT	04Y	PRL 93 041801	B. Aubert <i>et al.</i>	(BABAR Collab.)
CHISTOV	04	PRL 93 051803	R. Chistov <i>et al.</i>	(BELLE Collab.)
PDG	04	PL B592 1	S. Eidelman <i>et al.</i>	(PDG Collab.)
YUAN	04	PL B579 74	C.Z. Yuan <i>et al.</i>	(PDG Collab.)
CHOI	03	PRL 91 262001	S.-K. Choi <i>et al.</i>	(BELLE Collab.)
BAI	95E	PR D57 3854	J.Z. Bai <i>et al.</i>	(BES Collab.)
ANTONIAZZI	94	PR D50 4258	L. Antoniazzi <i>et al.</i>	(E705 Collab.)

$Z_c(3900)$ $J^G(J^{PC}) = 1^+(1^{+-})$

was $X(3900)$
 Properties incompatible with a $q\bar{q}$ structure (exotic state). See the review on non- $q\bar{q}$ states.

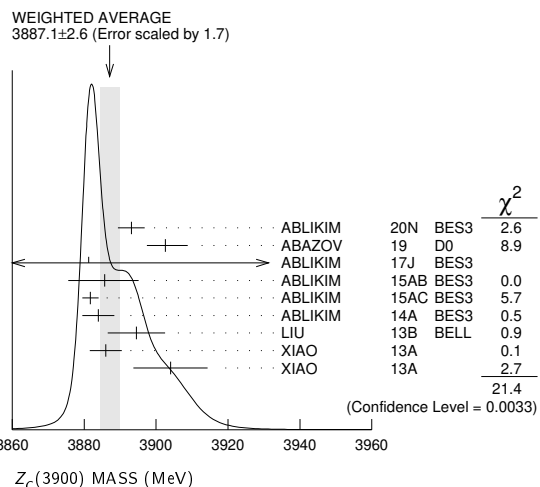
Charged $Z_c(3900)$ seen as a peak in the invariant mass distribution of the $J/\psi\pi^\pm$ system by BES III (ABLIKIM 13T) in $e^+e^- \rightarrow \pi^+\pi^-J/\psi$ at c.m. energy of 4.26 GeV and by radiative return from e^+e^- collisions at \sqrt{s} from 9.46 to 10.86 GeV at Belle (LIU 13B). Partial wave analysis of ABLIKIM 17J determines $J^P = 1^+$ with more than 7σ significance. Neutral $Z_c(3900)$ seen in the $J/\psi\pi^0$ invariant mass distribution in $e^+e^- \rightarrow \pi^0\pi^0J/\psi$ at c.m. energies of 4.23, 4.26, and 4.36 GeV by BES III (ABLIKIM 15U) and at 4.17 GeV by XIAO 13A. Peaks in $(D\bar{D}^*)^\pm$ reported by BES III (ABLIKIM 14A, ABLIKIM 15AB) are assumed to be related.

$Z_c(3900)$ MASS

VALUE (MeV)	EVTS	DOCUMENT ID	TECN	CHG	COMMENT
3887.1 ± 2.6 OUR AVERAGE		Error includes scale factor of 1.7. See the ideogram below.			
3893.1 ± 2.2 ± 3.0	3	¹ ABLIKIM	20N	BES3	0 $e^+e^- \rightarrow \pi^0\pi^0J/\psi$
3902.6 ^{+5.2+3.3} _{-5.0-1.4}	2,3	ABAZOV	19	D0	± 1.96 TeV $p\bar{p} \rightarrow J/\psi\pi^+\pi^-X$
3881.2 ± 4.2 ± 52.7	6k	⁴ ABLIKIM	17J	BES3	± $e^+e^- \rightarrow \pi^+\pi^-J/\psi$
3885.7 ^{+4.3} _{-5.7} ± 8.4	2,4	ABLIKIM	15AB	BES3	0 $e^+e^- \rightarrow \pi^0(D\bar{D}^*)^0$
3881.7 ± 1.6 ± 1.6	1.2k	^{2,4} ABLIKIM	15AC	BES3	± $e^+e^- \rightarrow \pi^\pm(D\bar{D}^*)^\mp$
3883.9 ± 1.5 ± 4.2	1.2k	^{2,4} ABLIKIM	14A	BES3	± $e^+e^- \rightarrow \pi^\pm(D\bar{D}^*)^\mp$
3894.5 ± 6.6 ± 4.5	159	² LIU	13B	BELL	± $e^+e^- \rightarrow \gamma\pi^+\pi^-J/\psi$
3886 ± 4 ± 2	81	^{2,5} XIAO	13A		± 4.17 $e^+e^- \rightarrow \pi^+\pi^-J/\psi$
3904 ± 9 ± 5	25	^{2,5} XIAO	13A	0	4.17 $e^+e^- \rightarrow \pi^0\pi^0J/\psi$

• • • We do not use the following data for averages, fits, limits, etc. • • •

3895.0 ± 5.2 ^{+4.0} _{-2.7}	502	^{2,6} ABAZOV	18B	D0	± 1.96 TeV $p\bar{p} \rightarrow J/\psi\pi^+\pi^-X$
3894.8 ± 2.3 ± 3.2	356	^{2,7} ABLIKIM	15U	BES3	0 $e^+e^- \rightarrow \pi^0\pi^0J/\psi$
3899.0 ± 3.6 ± 4.9	307	^{2,8} ABLIKIM	13T	BES3	± $e^+e^- \rightarrow \pi^+\pi^-J/\psi$



¹ Pole mass obtained from a fit to a relativistic Breit-Wigner.
² Neglecting interference between the $Z_c(3900)$ and other processes.
³ Measured in weak decays of b -flavored hadrons (nonprompt).
⁴ Pole mass obtained from a fit to a Flatte-like formula.
⁵ For $M^2(\pi^+\pi^-) < 0.65 \text{ GeV}^2$. Obtained by analyzing CLEO-c data but not authored by the CLEO Collaboration.
⁶ The signal of the $Z_c(3900)$ is correlated with a parent $J/\psi\pi^+\pi^-$ system in the invariant mass range 4.2–4.7 GeV. Superseded by ABAZOV 19.
⁷ Superseded by ABLIKIM 20N.

⁸ Superseded by ABLIKIM 17J.

$Z_c(3900)$ WIDTH

VALUE (MeV)	EVTS	DOCUMENT ID	TECN	CHG	COMMENT
28.4 ± 2.6 OUR AVERAGE					
44.4 ± 5.2 ± 14.0	1	ABLIKIM	20N	BES3	0 $e^+e^- \rightarrow \pi^0\pi^0J/\psi$
32 ⁺²⁸⁺²⁶ ₋₂₁₋₇	2,3	ABAZOV	19	D0	± 1.96 TeV $p\bar{p} \rightarrow \pi^+\pi^-J/\psi X$ (non-prompt)
51.8 ± 4.6 ± 36.0	6 k	⁴ ABLIKIM	17J	BES3	± $e^+e^- \rightarrow \pi^+\pi^-J/\psi$
35 ⁺¹¹ ₋₁₂ ± 15	2,4	ABLIKIM	15AB	BES3	0 $e^+e^- \rightarrow \pi^0(D\bar{D}^*)^0$
26.6 ± 2.0 ± 2.1	1248	^{2,4} ABLIKIM	15AC	BES3	± $e^+e^- \rightarrow \pi^\pm(D\bar{D}^*)^\mp$
24.8 ± 3.3 ± 11.0	1212	^{2,4} ABLIKIM	14A	BES3	± $e^+e^- \rightarrow \pi^\pm(D\bar{D}^*)^\mp$
63 ± 24 ± 26	159	² LIU	13B	BELL	± $e^+e^- \rightarrow \gamma\pi^+\pi^-J/\psi$
37 ± 4 ± 8	81	^{2,5} XIAO	13A		± 4.17 $e^+e^- \rightarrow \pi^+\pi^-J/\psi$

• • • We do not use the following data for averages, fits, limits, etc. • • •

29.6 ± 8.2 ± 8.2	356	^{2,6} ABLIKIM	15U	BES3	0 $e^+e^- \rightarrow \pi^0\pi^0J/\psi$
46 ± 10 ± 20	307	^{2,7} ABLIKIM	13T	BES3	± $e^+e^- \rightarrow \pi^+\pi^-J/\psi$

¹ Pole width obtained from a fit to a relativistic Breit-Wigner.
² Neglecting interference between the $Z_c(3900)$ and other processes.
³ Measured in weak decays of b -flavored hadrons (nonprompt).
⁴ Pole width obtained from a fit to a Flatte-like formula.
⁵ For $M^2(\pi^+\pi^-) < 0.65 \text{ GeV}^2$. Obtained by analyzing CLEO-c data but not authored by the CLEO Collaboration.
⁶ Superseded by ABLIKIM 20N.
⁷ Superseded by ABLIKIM 17J.

$Z_c(3900)$ DECAY MODES

Mode	Fraction (Γ_i/Γ)
Γ_1 $J/\psi\pi$	seen
Γ_2 $h_c\pi^\pm$	not seen
Γ_3 $\eta_c\pi^+\pi^-$	not seen
Γ_4 $\eta_c(1S)\rho(770)^\pm$	
Γ_5 $(D\bar{D}^*)^\pm$	seen
Γ_6 $D^0D^{*-} + \text{c.c.}$	seen
Γ_7 $D^-D^{*0} + \text{c.c.}$	seen
Γ_8 $\omega\pi^\pm$	not seen
Γ_9 $J/\psi\eta$	not seen
Γ_{10} $D^+D^{*-} + \text{c.c.}$	seen
Γ_{11} $D^0\bar{D}^{*0} + \text{c.c.}$	seen

$Z_c(3900)$ BRANCHING RATIOS

$\Gamma(J/\psi\pi)/\Gamma_{\text{total}}$	Γ_1/Γ				
VALUE	EVTS	DOCUMENT ID	TECN	CHG	COMMENT
seen		ABLIKIM	20N	BES3	0 $e^+e^- \rightarrow \pi^0\pi^0J/\psi$
seen		¹ ABAZOV	19	D0	± 1.96 TeV $p\bar{p} \rightarrow \pi^+\pi^-J/\psi X$ (prompt)
seen	356	ABLIKIM	17J	BES3	± $e^+e^- \rightarrow \pi^+\pi^-J/\psi$
seen		ABLIKIM	15U	BES3	0 $e^+e^- \rightarrow \pi^0\pi^0J/\psi$
not seen		² ADOLPH	15D	COMP	± $\gamma N \rightarrow J/\psi\pi^\pm N$
seen	307	ABLIKIM	13T	BES3	± $e^+e^- \rightarrow \pi^+\pi^-J/\psi$
seen	25	³ XIAO	13A	0	4.17 $e^+e^- \rightarrow \pi^0\pi^0J/\psi$

¹ But not seen in the "prompt" sample (no b -hadron enhancement).
² ADOLPH 15D measure $B(Z_c(3900)^\pm \rightarrow J/\psi\pi^\pm)\sigma(\gamma N \rightarrow Z_c(3900)^\pm N)/\sigma(\gamma N \rightarrow J/\psi N) < 3.7 \times 10^{-3}$ at 90% CL.
³ Obtained by analyzing CLEO-c data but not authored by the CLEO Collaboration.

$\Gamma(h_c\pi^\pm)/\Gamma_{\text{total}}$	Γ_2/Γ			
VALUE	DOCUMENT ID	TECN	CHG	COMMENT
not seen	ABLIKIM	13X	BES3	± $e^+e^- \rightarrow h_c\pi^+\pi^-$

$\Gamma(\eta_c\pi^+\pi^-)/\Gamma_{\text{total}}$	Γ_3/Γ			
VALUE	DOCUMENT ID	TECN	CHG	COMMENT
not seen	¹ VINOKUROVA	15	BELL	0 $B^+ \rightarrow K^+\eta_c\pi^+\pi^-$
	VINOKUROVA	15		reports $B(B^+ \rightarrow K^+Z_c(3900)^0) \times B(X \rightarrow \eta_c\pi^+\pi^-) < 4.7 \times 10^{-5}$ at 90% CL.

$\Gamma((D\bar{D}^*)^\pm)/\Gamma(J/\psi\pi)$	Γ_5/Γ_1			
VALUE	DOCUMENT ID	TECN	CHG	COMMENT
6.2 ± 1.1 ± 2.7	¹ ABLIKIM	14A	BES3	± $e^+e^- \rightarrow \pi^\pm(D\bar{D}^*)^\mp$
				¹ Assuming the same origin of the $(D\bar{D}^*)^\pm$ and $\pi^\pm J/\psi$ decay modes.

$\Gamma(D^0D^{*-} + \text{c.c.})/\Gamma_{\text{total}}$	Γ_6/Γ			
VALUE	DOCUMENT ID	TECN	CHG	COMMENT
seen	ABLIKIM	15AC	BES3	± $e^+e^- \rightarrow \pi^+D^0D^{*-} + \text{c.c.}$
seen	ABLIKIM	14A	BES3	± $e^+e^- \rightarrow \pi^+D^0D^{*-} + \text{c.c.}$

Meson Particle Listings

$Z_c(3900)$, $\chi_{c0}(3915)$

$\Gamma(D^- D^{*0} + c.c.)/\Gamma_{total}$					Γ_7/Γ
VALUE	DOCUMENT ID	TECN	CHG	COMMENT	
seen	ABLIKIM	15AC	BES3	\pm	$e^+e^- \rightarrow \pi^+ D^- D^{*0} + c.c.$
seen	ABLIKIM	14A	BES3	\pm	$e^+e^- \rightarrow \pi^+ D^- D^{*0} + c.c.$

$\Gamma(\omega\pi^\pm)/\Gamma_{total}$					Γ_8/Γ
VALUE	DOCUMENT ID	TECN	CHG	COMMENT	
not seen	ABLIKIM	15R	BES3	\pm	$e^+e^- \rightarrow \omega\pi^+\pi^-$

$\Gamma(J/\psi\eta)/\Gamma_{total}$					Γ_9/Γ
VALUE	DOCUMENT ID	TECN	CHG	COMMENT	
not seen	ABLIKIM	15Q	BES3	0	$4.0\text{--}4.6 e^+e^- \rightarrow J/\psi\eta\pi^0$

$\Gamma(J/\psi\eta)/\Gamma(J/\psi\pi)$					Γ_9/Γ_1	
VALUE	CL%	DOCUMENT ID	TECN	CHG	COMMENT	
<0.15	90	ABLIKIM	15Q	BES3	0	$4.226 e^+e^- \rightarrow J/\psi\eta\pi^0$
••• We do not use the following data for averages, fits, limits, etc. •••						
<0.65	90	ABLIKIM	15Q	BES3	0	$4.257 e^+e^- \rightarrow J/\psi\eta\pi^0$

$\Gamma(\eta_c(1S)\rho(770)^\pm)/\Gamma(J/\psi\pi)$					Γ_4/Γ_1
VALUE	EVTs	DOCUMENT ID	TECN	COMMENT	
2.3 ± 0.8	332	¹ ABLIKIM	19BC	BES3	$e^+e^- \rightarrow \pi^+\pi^-\pi^0\eta_c(1S)$
¹ Using $e^+e^- \rightarrow \pi^\mp(Z_c(3900)^\pm \rightarrow J/\psi\pi^\pm)$ cross section at 4.23 and 4.26 GeV from ABLIKIM 171.					

$\Gamma(D^+ D^{*-} + c.c.)/\Gamma_{total}$					Γ_{10}/Γ
VALUE	DOCUMENT ID	TECN	CHG	COMMENT	
seen	ABLIKIM	15AB	BES3	0	$e^+e^- \rightarrow \pi^0(D\bar{D}^*)^0$

$\Gamma(D^0\bar{D}^{*0} + c.c.)/\Gamma_{total}$					Γ_{11}/Γ
VALUE	DOCUMENT ID	TECN	CHG	COMMENT	
seen	ABLIKIM	15AB	BES3	0	$e^+e^- \rightarrow \pi^0(D\bar{D}^*)^0$

$\Gamma(D^+ D^{*+} + c.c.)/\Gamma(D^0\bar{D}^{*0} + c.c.)$					Γ_{10}/Γ_{11}
VALUE	DOCUMENT ID	TECN	CHG	COMMENT	
0.96 ± 0.18 ± 0.12	ABLIKIM	15AB	BES3	0	$e^+e^- \rightarrow \pi^0(D\bar{D}^*)^0$

$Z_c(3900)$ REFERENCES

ABLIKIM	20N	PR D102 012009	M. ABLIKIM <i>et al.</i>	(BESIII Collab.) JP
ABAZOV	19	PR D100 012005	V.M. Abazov <i>et al.</i>	(DO Collab.)
ABLIKIM	19BC	PR D100 111102	M. ABLIKIM <i>et al.</i>	(BESIII Collab.)
ABAZOV	18B	PR D98 052010	V.M. Abazov <i>et al.</i>	(DO Collab.)
ABLIKIM	17J	PRL 119 072001	M. ABLIKIM <i>et al.</i>	(BESIII Collab.) JP
ABLIKIM	15AB	PRL 115 222002	M. ABLIKIM <i>et al.</i>	(BESIII Collab.)
ABLIKIM	15AC	PR D92 092006	M. ABLIKIM <i>et al.</i>	(BESIII Collab.) JP
ABLIKIM	15Q	PR D92 012008	M. ABLIKIM <i>et al.</i>	(BESIII Collab.)
ABLIKIM	15R	PR D92 032009	M. ABLIKIM <i>et al.</i>	(BESIII Collab.)
ABLIKIM	15U	PRL 115 112003	M. ABLIKIM <i>et al.</i>	(BESIII Collab.)
ADOLPH	15D	PL B742 330	C. Adolph <i>et al.</i>	(COMPASS Collab.)
VINOKUROVA	15	JHEP 1506 132	A. Vinokurova <i>et al.</i>	(BELLE Collab.)
Also	JHEP	1702 088 (errata)	A. Vinokurava <i>et al.</i>	(BELLE Collab.)
ABLIKIM	14A	PRL 112 022001	M. ABLIKIM <i>et al.</i>	(BESIII Collab.) JP
ABLIKIM	13T	PRL 110 252001	M. ABLIKIM <i>et al.</i>	(BESIII Collab.)
ABLIKIM	13X	PRL 111 242001	M. ABLIKIM <i>et al.</i>	(BESIII Collab.)
LIU	13B	PRL 110 252002	Z.Q. Liu <i>et al.</i>	(BELLE Collab.)
XIAO	13A	PL B727 366	T. Xiao <i>et al.</i>	(NWES)

$\chi_{c0}(3915)$

$$I^G(J^{PC}) = 0^+(0^{++})$$

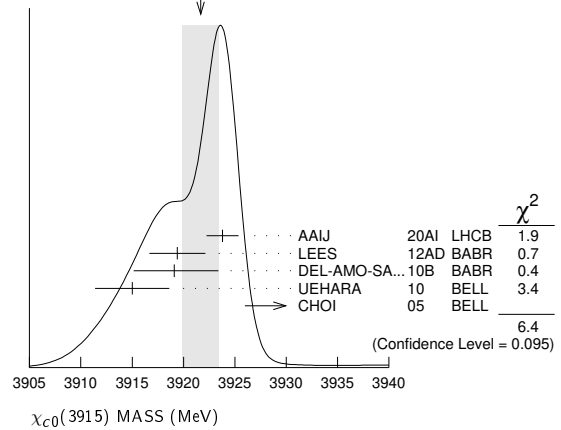
was $X(3915)$

The $\chi_{c0}(3915)$ was originally seen by BELLE in its $\omega J/\psi$ decay mode and was produced in both B decays in CHOI 05 and $\gamma\gamma$ collisions in UEHARA 10. The J^{PC} was determined to be 0^{++} by BABAR in LEES 12AD but this assignment was questioned by ZHOU 15C. In AAIJ 20AI LHCb found the $D^+ D^-$ decay mode of the $\chi_{c0}(3915)$ using B decays and determined its J^{PC} to be 0^{++} . Based on their compatible mass, width, and J^{PC} , we assume the state decaying to $\omega J/\psi$ and the state decaying to $D^+ D^-$ are both the $\chi_{c0}(3915)$. See also the $\chi_{c2}(3930)$.

$\chi_{c0}(3915)$ MASS

VALUE (MeV)	EVTs	DOCUMENT ID	TECN	COMMENT
3921.7 ± 1.8 OUR AVERAGE				Error includes scale factor of 1.5. See the ideogram below.
3923.8 ± 1.5 ± 0.4	1.2k	¹ AAIJ	20AI	LHCb $B^+ \rightarrow D^+ D^- K^+$
3919.4 ± 2.2 ± 1.6	59 ± 10	LEES	12AD	BABR $e^+e^- \rightarrow e^+e^- \omega J/\psi$
3919.1 ± 3.8 ± 2.0		DEL-AMO-SA..10B	BABR	$B \rightarrow \omega J/\psi K$
3915 ± 3 ± 2	49 ± 15	UEHARA	10	BELL $10.6 e^+e^- \rightarrow e^+e^- \omega J/\psi$
3943 ± 11 ± 13	58 ± 11	² CHOI	05	BELL $B \rightarrow \omega J/\psi K$
••• We do not use the following data for averages, fits, limits, etc. •••				
3926.4 ± 2.2 ± 1.2		³ ABLIKIM	19V	BES $e^+e^- \rightarrow \gamma\omega J/\psi$
3914.6 ± 3.8 ± 2.0		² AUBERT	08W	BABR Superseded by DEL-AMO-SANCHEZ 10B

WEIGHTED AVERAGE
3921.7 ± 1.8 (Error scaled by 1.5)



- Obtained from the full amplitude analysis. Parameterized with the relativistic Breit-Wigner line shape.
- $\omega J/\psi$ threshold enhancement fitted as an S-wave Breit-Wigner resonance.
- Could also be $X(3940)$. Significance 3.1σ . Fit with additional resonance at 3963.7 ± 5.7 MeV, significance 3.4σ .

$\chi_{c0}(3915)$ WIDTH

VALUE (MeV)	EVTs	DOCUMENT ID	TECN	COMMENT
18.8 ± 3.5 OUR AVERAGE				
17.4 ± 5.1 ± 0.8	1.2k	¹ AAIJ	20AI	LHCb $B^+ \rightarrow D^+ D^- K^+$
13 ± 6 ± 3	59	LEES	12AD	BABR $e^+e^- \rightarrow e^+e^- \omega J/\psi$
31 ± 10 ± 5		DEL-AMO-SA..10B	BABR	$B \rightarrow \omega J/\psi K$
17 ± 10 ± 3	49	UEHARA	10	BELL $10.6 e^+e^- \rightarrow e^+e^- \omega J/\psi$
87 ± 22 ± 26	58	² CHOI	05	BELL $B \rightarrow \omega J/\psi K$
••• We do not use the following data for averages, fits, limits, etc. •••				
3.8 ± 7.5 ± 2.6		³ ABLIKIM	19V	BES $e^+e^- \rightarrow \gamma\omega J/\psi$
34 ± 12 ± 5		² AUBERT	08W	BABR Superseded by DEL-AMO-SANCHEZ 10B

- Obtained from the full amplitude analysis. Parameterized with the relativistic Breit-Wigner line shape.
- $\omega J/\psi$ threshold enhancement fitted as an S-wave Breit-Wigner resonance.
- Could also be $X(3940)$. Significance 3.1σ . Fit with additional resonance at 3963.7 ± 5.7 MeV, significance 3.4σ .

$\chi_{c0}(3915)$ DECAY MODES

Mode	Fraction (Γ_i/Γ)
Γ_1 $\omega J/\psi$	seen
Γ_2 $\bar{D}^{*0} D^0$	not seen
Γ_3 $D^+ D^-$	seen
Γ_4 $\pi^+ \pi^- \eta_c(1S)$	not seen
Γ_5 $\eta_c \eta$	not seen
Γ_6 $\eta_c \pi^0$	not seen
Γ_7 $K \bar{K}$	not seen
Γ_8 $\gamma\gamma$	seen
Γ_9 $\pi^0 \chi_{c1}$	not seen

$\chi_{c0}(3915)$ $\Gamma(i)\Gamma(\gamma\gamma)/\Gamma_{total}$

VALUE (eV)	EVTs	DOCUMENT ID	TECN	COMMENT
54 ± 9 OUR AVERAGE				
52 ± 10 ± 3	59 ± 10	¹ LEES	12AD	BABR $e^+e^- \rightarrow e^+e^- \omega J/\psi$
61 ± 17 ± 8	49 ± 15	¹ UEHARA	10	BELL $10.6 e^+e^- \rightarrow e^+e^- \omega J/\psi$
••• We do not use the following data for averages, fits, limits, etc. •••				
18 ± 5 ± 2	49 ± 15	² UEHARA	10	BELL $10.6 e^+e^- \rightarrow e^+e^- \omega J/\psi$
¹ For $J^P = 0^+$.				
² For $J^P = 2^+$, helicity-2.				

$\Gamma(\pi^+ \pi^- \eta_c(1S)) \times \Gamma(\gamma\gamma)/\Gamma_{total}$					$\Gamma_4/\Gamma_8/\Gamma$
VALUE (eV)	CL%	DOCUMENT ID	TECN	COMMENT	
<16	90	LEES	12AE	BABR $e^+e^- \rightarrow e^+e^- \pi^+ \pi^- \eta_c$	

$\Gamma(K\bar{K}) \times \Gamma(\gamma\gamma)/\Gamma_{total}$					$\Gamma_7/\Gamma_8/\Gamma$
VALUE (eV)	CL%	DOCUMENT ID	TECN	COMMENT	
<1.96	90	UEHARA	13	BELL $\gamma\gamma \rightarrow K_S^0 K_S^0$	

$\chi_{c0}(3915)$ BRANCHING RATIOS

$\Gamma(\omega J/\psi)/\Gamma_{total}$ Γ_1/Γ

VALUE	DOCUMENT ID	TECN	COMMENT
seen	¹ DEL-AMO-SA...10B	BABR	$B \rightarrow \omega J/\psi K$
seen	² CHOI 05	BELL	$B \rightarrow \omega J/\psi K$

¹ DEL-AMO-SANCHEZ 10B reports $B(B^{\pm} \rightarrow \chi_{c0}(3915) K^{\pm}) \times B(\chi_{c0}(3915) \rightarrow J/\psi \omega) = (3.0^{+0.7+0.5}_{-0.6-0.3}) \times 10^{-5}$ and $B(B^0 \rightarrow \chi_{c0}(3915) K^0) \times B(\chi_{c0}(3915) \rightarrow J/\psi \omega) = (2.1 \pm 0.9 \pm 0.3) \times 10^{-5}$.
² CHOI 05 reports $B(B \rightarrow \chi_{c0}(3915) K) \times B(\chi_{c0}(3915) \rightarrow J/\psi \omega) = (7.1 \pm 1.3 \pm 3.1) \times 10^{-5}$.

$\Gamma(\omega J/\psi)/\Gamma(D^{*0} D^0)$ Γ_1/Γ_2

VALUE	CL%	DOCUMENT ID	TECN	COMMENT
>0.71	90	¹ AUSHEV 10	BELL	$B \rightarrow D^{*0} D^0 K$

¹ By combining the upper limit $B(B \rightarrow \chi_{c0}(3915) K) \times B(\chi_{c0}(3915) \rightarrow D^{*0} D^0) < 0.67 \times 10^{-4}$ from AUSHEV 10 with the average of CHOI 05 and AUBERT 08W measurements $B(B \rightarrow \chi_{c0}(3915) K) \times B(\chi_{c0}(3915) \rightarrow \omega J/\psi) = (0.51 \pm 0.11) \times 10^{-4}$.

$\Gamma(D^+ D^-)/\Gamma_{total}$ Γ_3/Γ

VALUE	DOCUMENT ID	TECN	COMMENT
seen	AAIJ 20A1	LHCB	$B^+ \rightarrow D^+ D^- K^+$

$\Gamma(\eta_c \eta)/\Gamma_{total}$ Γ_5/Γ

VALUE	CL%	DOCUMENT ID	TECN	COMMENT
not seen	90	¹ VINOKUROVA 15	BELL	$B^+ \rightarrow K^+ \eta_c \eta$

¹ VINOKUROVA 15 reports $B(B^+ \rightarrow K^+ \chi_{c0}(3915)) \times B(\chi_{c0}(3915) \rightarrow \eta_c \eta) < 4.7 \times 10^{-5}$ at 90% CL.

$\Gamma(\eta_c \pi^0)/\Gamma_{total}$ Γ_6/Γ

VALUE	CL%	DOCUMENT ID	TECN	COMMENT
not seen	90	¹ VINOKUROVA 15	BELL	$B^+ \rightarrow K^+ \eta_c \pi^0$

¹ VINOKUROVA 15 reports $B(B^+ \rightarrow K^+ \chi_{c0}(3915)^0) \times B(\chi_{c0}(3915) \rightarrow \eta_c \pi^0) < 1.7 \times 10^{-5}$ at 90% CL.

$\Gamma(\gamma\gamma)/\Gamma_{total}$ Γ_8/Γ

VALUE	EVTS	DOCUMENT ID	TECN	COMMENT
seen	59 ± 10	LEES 12AD	BABR	$e^+ e^- \rightarrow e^+ e^- \omega J/\psi$
seen		UEHARA 10	BELL	10.6 $e^+ e^- \rightarrow e^+ e^- \omega J/\psi$

$\Gamma(\pi^0 \chi_{c1})/\Gamma_{total}$ Γ_9/Γ

VALUE	EVTS	DOCUMENT ID	TECN	COMMENT
not seen	42 ± 14	¹ BHARDWAJ 19	BELL	$B^+ \rightarrow \chi_{c1} \pi^0 K^{\pm}$

¹ BHARDWAJ 19 reports $B(B^+ \rightarrow K^+ \chi_{c0}(3915)) \times B(\chi_{c0}(3915) \rightarrow \chi_{c1} \pi^0) < 3.8 \times 10^{-5}$ at 90% CL. A signal significance 2.3 standard deviations.

$\chi_{c0}(3915)$ REFERENCES

AAIJ	20A1	PR D102 112003	R. Aaij et al.	(LHCb Collab.) JPC
ABLIKIM	19V	PRL 122 232002	M. Ablikim et al.	(BESIII Collab.)
BHARDWAJ	19	PR D99 111101	V. Bhardwaj et al.	(BESIII Collab.)
VINOKUROVA	15	JHEP 1506 132	A. Vinokurova et al.	(BELLE Collab.)
	Also	JHEP 1702 088 (errata.)	A. Vinokurava et al.	(BELLE Collab.)
ZHOU	15C	PRL 115 022001	Z.-Y. Zhou, Z. Xiao, H.-Q. Zhou	(BEIJT, NANJ)
UEHARA	13	PTEP 2013 123C01	S. Uehara et al.	(BELLE Collab.)
LEES	12AD	PR D86 072002	J.P. Lees et al.	(BABAR Collab.)
LEES	12AE	PR D86 092005	J.P. Lees et al.	(BABAR Collab.)
AUSHEV	10	PR D81 031103	T. Aushev et al.	(BELLE Collab.)
DEL-AMO-SA...	10B	PR D82 011101	P. del Amo Sanchez et al.	(BABAR Collab.)
UEHARA	10	PRL 104 092001	S. Uehara et al.	(BELLE Collab.)
AUBERT	08W	PRL 101 082001	B. Aubert et al.	(BABAR Collab.)
CHOI	05	PRL 94 182002	S.-K. Choi et al.	(BELLE Collab.)

$\chi_{c2}(3930)$

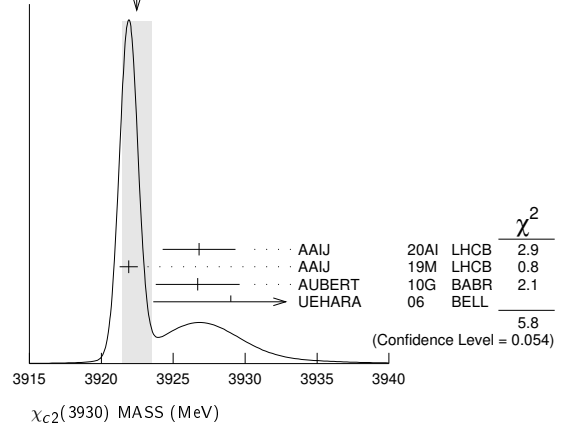
$I^G(J^{PC}) = 0^+(2^{++})$

$\chi_{c2}(3930)$ MASS

VALUE (MeV)	EVTS	DOCUMENT ID	TECN	COMMENT
3922.5 ± 1.0 OUR AVERAGE				Error includes scale factor of 1.7. See the ideogram below.
3926.8 ± 2.4 ± 0.8	1.2k	¹ AAIJ	20A1	LHCB $B^+ \rightarrow D^+ D^- K^+$
3921.9 ± 0.6 ± 0.2		² AAIJ	19M	LHCB $pp \rightarrow D \bar{D} + \text{anything}$
3926.7 ± 2.7 ± 1.1	76 ± 17	AUBERT	10G	BABR 10.6 $e^+ e^- \rightarrow e^+ e^- D \bar{D}$
3929 ± 5 ± 2	64	UEHARA	06	BELL 10.6 $e^+ e^- \rightarrow e^+ e^- D \bar{D}$

¹ Obtained from the full amplitude analysis. Parameterized with the relativistic Breit-Wigner line shape. Previous measurements assumed a single state in this region. This analysis revealed the presence of $\chi_{c0}(3930)$ with the same mass.
² Measured in prompt hadroproduction.

WEIGHTED AVERAGE
3922.5±1.0 (Error scaled by 1.7)



$\chi_{c2}(3930)$ WIDTH

VALUE (MeV)	EVTS	DOCUMENT ID	TECN	COMMENT
35.2 ± 2.2 OUR AVERAGE				Error includes scale factor of 1.2.
34.2 ± 6.6 ± 1.1	1.2k	¹ AAIJ	20A1	LHCB $B^+ \rightarrow D^+ D^- K^+$
36.6 ± 1.9 ± 0.9		² AAIJ	19M	LHCB $pp \rightarrow D \bar{D} + \text{anything}$
21.3 ± 6.8 ± 3.6	76 ± 17	AUBERT	10G	BABR 10.6 $e^+ e^- \rightarrow e^+ e^- D \bar{D}$
29 ± 10 ± 2	64	UEHARA	06	BELL 10.6 $e^+ e^- \rightarrow e^+ e^- D \bar{D}$

¹ Obtained from the full amplitude analysis. Parameterized with the relativistic Breit-Wigner line shape. Previous measurements assumed a single state in this region. This analysis revealed the presence of $\chi_{c0}(3930)$ with the same mass.
² Measured in prompt hadroproduction.

$\chi_{c2}(3930)$ DECAY MODES

Mode	Fraction (Γ_i/Γ)
Γ_1 $\gamma\gamma$	seen
Γ_2 $K \bar{K} \pi$	
Γ_3 $K^+ K^- \pi^+ \pi^- \pi^0$	
Γ_4 $D \bar{D}$	seen
Γ_5 $D^+ D^-$	seen
Γ_6 $D^0 \bar{D}^0$	seen
Γ_7 $\pi^+ \pi^- \eta_c(1S)$	not seen
Γ_8 $K \bar{K}$	not seen

$\chi_{c2}(3930)$ PARTIAL WIDTHS

$\chi_{c2}(3930)$ $\Gamma(i)\Gamma(\gamma\gamma)/\Gamma_{total}$

MODE	VALUE (eV)	CL%	DOCUMENT ID	TECN	COMMENT
$\Gamma(K \bar{K} \pi) \times \Gamma(\gamma\gamma)/\Gamma_{total}$ $\Gamma_2 \Gamma_1/\Gamma$	<2.1	90	DEL-AMO-SA...11M	BABR	$\gamma\gamma \rightarrow K_S^0 K^{\pm} \bar{K}^{\mp}$

MODE	VALUE (eV)	CL%	DOCUMENT ID	TECN	COMMENT
$\Gamma(K^+ K^- \pi^+ \pi^- \pi^0) \times \Gamma(\gamma\gamma)/\Gamma_{total}$ $\Gamma_3 \Gamma_1/\Gamma$	<3.4	90	DEL-AMO-SA...11M	BABR	$\gamma\gamma \rightarrow K^+ K^- \pi^+ \pi^- \pi^0$

MODE	VALUE (keV)	EVTS	DOCUMENT ID	TECN	COMMENT
$\Gamma(D \bar{D}) \times \Gamma(\gamma\gamma)/\Gamma_{total}$ $\Gamma_4 \Gamma_1/\Gamma$	0.21 ± 0.04 OUR AVERAGE				
	0.24 ± 0.05 ± 0.04	76 ± 17	AUBERT	10G	BABR 10.6 $e^+ e^- \rightarrow e^+ e^- D \bar{D}$
	0.18 ± 0.05 ± 0.03	64	¹ UEHARA	06	BELL 10.6 $e^+ e^- \rightarrow e^+ e^- D \bar{D}$

¹ Assuming $B(D^+ D^-) = 0.89 B(D^0 \bar{D}^0)$.

MODE	VALUE (eV)	CL%	DOCUMENT ID	TECN	COMMENT
$\Gamma(\pi^+ \pi^- \eta_c(1S)) \times \Gamma(\gamma\gamma)/\Gamma_{total}$ $\Gamma_7 \Gamma_1/\Gamma$	<18	90	LEES	12AE	BABR $e^+ e^- \rightarrow e^+ e^- \pi^+ \pi^- \eta_c$

MODE	VALUE (eV)	CL%	DOCUMENT ID	TECN	COMMENT
$\Gamma(K \bar{K}) \times \Gamma(\gamma\gamma)/\Gamma_{total}$ $\Gamma_8 \Gamma_1/\Gamma$	<0.256	90	UEHARA	13	BELL $\gamma\gamma \rightarrow K_S^0 K_S^0$

Meson Particle Listings

$\chi_{c2}(3930), X(3940), X(4020)^\pm$

$\chi_{c2}(3930)$ BRANCHING RATIOS

$\Gamma(D^+ D^-)/\Gamma(D^0 \bar{D}^0)$					Γ_5/Γ_6
VALUE	EVTS	DOCUMENT ID	TECN	COMMENT	
$0.74 \pm 0.43 \pm 0.16$	64	UEHARA	06	BELL	$10.6 e^+ e^- \rightarrow e^+ e^- D \bar{D}$

$\chi_{c2}(3930)$ REFERENCES

AAIJ	20AI	PR D102 112003	R. Aaij <i>et al.</i>	(LHCb Collab.)
AAIJ	19M	JHEP 1907 035	R. Aaij <i>et al.</i>	(LHCb Collab.)
UEHARA	13	PTEP 2013 123 C01	S. Uehara <i>et al.</i>	(BELLE Collab.)
LEES	12AE	PR D86 092005	J.P. Lees <i>et al.</i>	(BABAR Collab.)
DEL-AMO-SA...	11M	PR D84 012004	P. del Amo Sanchez <i>et al.</i>	(BABAR Collab.)
AUBERT	10G	PR D81 092003	B. Aubert <i>et al.</i>	(BABAR Collab.)
UEHARA	06	PRL 96 082003	S. Uehara <i>et al.</i>	(BELLE Collab.)

$X(3940)$

$$J^G(JPC) = ?^?(?^{??})$$

OMITTED FROM SUMMARY TABLE

Reported by ABE 07, observed in $e^+ e^- \rightarrow J/\psi X$.

$X(3940)$ MASS

VALUE (MeV)	EVTS	DOCUMENT ID	TECN	COMMENT
$3942 \pm \frac{7}{6} \pm 6$	52	PAKHLOV	08	BELL $e^+ e^- \rightarrow J/\psi X$
● ● ● We do not use the following data for averages, fits, limits, etc. ● ● ●				
$3943 \pm 6 \pm 6$	25	¹ ABE	07	BELL $e^+ e^- \rightarrow J/\psi X$
3936 ± 14	266	² ABE	07	BELL $e^+ e^- \rightarrow J/\psi(c\bar{c})$
¹ From a fit to $D^{*+} D^-$ and $D^{*0} \bar{D}^0$ events.				
² From the inclusive fit. Not independent of the exclusive measurement by ABE 07.				

$X(3940)$ WIDTH

VALUE (MeV)	CL%	EVTS	DOCUMENT ID	TECN	COMMENT
$37 \pm \frac{26}{15} \pm 8$		52	PAKHLOV	08	BELL $e^+ e^- \rightarrow J/\psi X$
● ● ● We do not use the following data for averages, fits, limits, etc. ● ● ●					
<52	90	25	ABE	07	BELL $e^+ e^- \rightarrow J/\psi X$

$X(3940)$ DECAY MODES

Mode	Fraction (Γ_i/Γ)
Γ_1 $D \bar{D}^* + c.c.$	seen
Γ_2 $D \bar{D}$	not seen
Γ_3 $J/\psi \omega$	not seen

$X(3940)$ BRANCHING RATIOS

$\Gamma(D \bar{D}^* + c.c.)/\Gamma_{\text{total}}$					$\Gamma_1/\Gamma_{\text{total}}$
VALUE	CL%	EVTS	DOCUMENT ID	TECN	COMMENT
● ● ● We do not use the following data for averages, fits, limits, etc. ● ● ●					
>0.45	90	25	^{1,2} ABE	07	BELL $e^+ e^- \rightarrow J/\psi X$
¹ For $X(3940)$ decaying to final states with more than two tracks.					
² PAKHLOV 08 finds that the inclusive peak near 3940 MeV/c ² may consist of several states.					

$\Gamma(D \bar{D})/\Gamma_{\text{total}}$					$\Gamma_2/\Gamma_{\text{total}}$
VALUE	CL%	DOCUMENT ID	TECN	COMMENT	
● ● ● We do not use the following data for averages, fits, limits, etc. ● ● ●					
<0.41	90	^{1,2} ABE	07	BELL $e^+ e^- \rightarrow J/\psi X$	
¹ For $X(3940)$ decaying to final states with more than two tracks.					
² PAKHLOV 08 finds that the inclusive peak near 3940 MeV/c ² may consist of several states.					

$\Gamma(J/\psi \omega)/\Gamma_{\text{total}}$					$\Gamma_3/\Gamma_{\text{total}}$
VALUE	CL%	DOCUMENT ID	TECN	COMMENT	
● ● ● We do not use the following data for averages, fits, limits, etc. ● ● ●					
<0.26	90	^{1,2} ABE	07	BELL $e^+ e^- \rightarrow J/\psi X$	
¹ For $X(3940)$ decaying to final states with more than two tracks.					
² PAKHLOV 08 finds that the inclusive peak near 3940 MeV/c ² may consist of several states.					

$X(3940)$ REFERENCES

PAKHLOV	08	PRL 100 202001	P. Pakhlov <i>et al.</i>	(BELLE Collab.)
ABE	07	PRL 98 082001	K. Abe <i>et al.</i>	(BELLE Collab.)

$X(4020)^\pm$

$$J^G(JPC) = 1^+(?^{?^-})$$

Properties incompatible with a $q\bar{q}$ structure (exotic state). See the review on non- $q\bar{q}$ states.

Charged $X(4020)$ seen by ABLIKIM 13X from $e^+ e^- \rightarrow \pi^+ \pi^- h_c(1P)$ at c.m. energy from 3.90 to 4.42 GeV as a peak in the invariant mass distribution of the $\pi^\pm h_c(1P)$ system, and by ABLIKIM 14B from $e^+ e^- \rightarrow (D^* \bar{D}^*)^\pm \pi^\mp$ events in $(D^* \bar{D}^*)^\pm$ mass. A neutral $X(4020)$ seen by ABLIKIM 14P at three c.m. energies in the same range in $e^+ e^- \rightarrow \pi^0 \pi^0 h_c(1P)$ as a peak in the larger of the two masses recoiling against a π^0 . ABLIKIM 15AA observes a 5.9σ signal in $(D^* \bar{D}^*)^0$ in $e^+ e^- \rightarrow (D^* \bar{D}^*)^0 \pi^0$ events using collisions at two c.m. energies. Production rates and mass values support grouping neutral and charged $X(4020)$ together as manifestations of a single $I = 1$ particle.

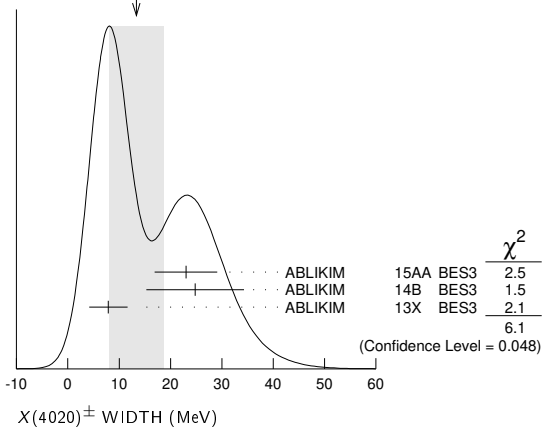
$X(4020)^\pm$ MASS

VALUE (MeV)	EVTS	DOCUMENT ID	TECN	CHG	COMMENT
4024.1 ± 1.9 OUR AVERAGE					
$4025.5 \pm \frac{2.0}{4.7} \pm 3.1$	116	¹ ABLIKIM	15AA	BES3	0 $e^+ e^- \rightarrow (D^* \bar{D}^*)^0 \pi^0$
$4026.3 \pm 2.6 \pm 3.7$	401	¹ ABLIKIM	14B	BES3	± $e^+ e^- \rightarrow (D^* \bar{D}^*)^\pm \pi^\mp$
$4023.9 \pm 2.2 \pm 3.8$	61	^{1,2} ABLIKIM	14P	BES3	0 $e^+ e^- \rightarrow \pi^0 \pi^0 h_c$
$4022.9 \pm 0.8 \pm 2.7$	253	¹ ABLIKIM	13X	BES3	± $e^+ e^- \rightarrow \pi^\pm \pi^\mp h_c$
¹ Neglecting interference between the $X(4020)$ and non-resonant continuum.					
² Assuming $J^P = 1^+$ and width of 7.9 ± 2.6 MeV.					

$X(4020)^\pm$ WIDTH

VALUE (MeV)	EVTS	DOCUMENT ID	TECN	CHG	COMMENT
13 ± 5 OUR AVERAGE Error includes scale factor of 1.7. See the ideogram below.					
$23.0 \pm 6.0 \pm 1.0$	116	¹ ABLIKIM	15AA	BES3	0 $e^+ e^- \rightarrow (D^* \bar{D}^*)^0 \pi^0$
$24.8 \pm 5.6 \pm 7.7$	401	¹ ABLIKIM	14B	BES3	± $e^+ e^- \rightarrow (D^* \bar{D}^*)^\pm \pi^\mp$
$7.9 \pm 2.7 \pm 2.6$	253	¹ ABLIKIM	13X	BES3	± $e^+ e^- \rightarrow \pi^\pm \pi^\mp h_c$
¹ Neglecting interference between the $X(4020)$ and non-resonant continuum.					

WEIGHTED AVERAGE
13±5 (Error scaled by 1.7)



$X(4020)^\pm$ DECAY MODES

Mode	Fraction (Γ_i/Γ)
Γ_1 $h_c(1P)\pi$	seen
Γ_2 $D^* \bar{D}^*$	seen
Γ_3 $D \bar{D}^* + c.c.$	not seen
Γ_4 $\eta_c \pi^+ \pi^-$	not seen
Γ_5 $\eta_c(1S)\rho(770)^\pm$	
Γ_6 $J/\psi(1S)\pi^\pm$	not seen

$X(4020)^\pm$ BRANCHING RATIOS

$\Gamma(h_c(1P)\pi)/\Gamma_{\text{total}}$					$\Gamma_1/\Gamma_{\text{total}}$
VALUE	EVTS	DOCUMENT ID	TECN	CHG	COMMENT
seen	61	ABLIKIM	14P	BES3	0 $e^+ e^- \rightarrow \pi^0 \pi^0 h_c$
seen	253	ABLIKIM	13X	BES3	± $e^+ e^- \rightarrow \pi^\pm \pi^\mp h_c$

$\Gamma(D^*\bar{D}^*)/\Gamma_{total}$						Γ_2/Γ
VALUE	EVTs	DOCUMENT ID	TECN	CHG	COMMENT	
seen	116	¹ ABLIKIM	15AA	BES3	0	$e^+e^- \rightarrow (D^*\bar{D}^*)^0 \pi^0$
seen	401	¹ ABLIKIM	14B	BES3	\pm	$e^+e^- \rightarrow (D^*\bar{D}^*)^\pm \pi^\mp$

¹ Neglecting interference between the $X(4020)$ and non-resonant continuum.

$\Gamma(D\bar{D}^* + c.c.)/\Gamma_{total}$						Γ_3/Γ
VALUE		DOCUMENT ID	TECN	CHG	COMMENT	
not seen		ABLIKIM	15AC	BES3	\pm	$e^+e^- \rightarrow \pi^\pm(D\bar{D}^*)^\mp$

$\Gamma(\eta_c \pi^+ \pi^-)/\Gamma_{total}$						Γ_4/Γ
VALUE		DOCUMENT ID	TECN	CHG	COMMENT	
not seen		¹ VINOKUROVA	15	BELL		$B^+ \rightarrow K^+ \eta_c \pi^+ \pi^-$

¹ VINOKUROVA 15 reports $B(B^+ \rightarrow K^+ X(4020)^0) \times B(X \rightarrow \eta_c \pi^+ \pi^-) < 1.6 \times 10^{-5}$ at 90% CL.

$\Gamma(\eta_c(1S)\rho(770)^\pm)/\Gamma(\eta_c(1P)\pi)$						Γ_5/Γ_1
VALUE	CL%	DOCUMENT ID	TECN	CHG	COMMENT	
< 1.2	90	¹ ABLIKIM	19bC	BES3	$e^+e^- \rightarrow \pi^+ \pi^- \pi^0 \eta_c(1S)$	

¹ Using $e^+e^- \rightarrow \pi^\mp(Z_c(4020)^\pm \rightarrow \eta_c(1P)\pi^\pm)$ cross section at 4.23, 4.26 and 4.36 GeV from ABLIKIM 13x.

$\Gamma(J/\psi(1S)\pi^\pm)/\Gamma_{total}$						Γ_6/Γ
VALUE		DOCUMENT ID	TECN	CHG	COMMENT	
not seen		¹ ABLIKIM	17J	BES3	$e^+e^- \rightarrow \pi^+ \pi^- J/\psi$	

¹ From Partial Wave Analysis assuming $J^P = 1^+$.

$X(4020)^\pm$ REFERENCES

ABLIKIM	19bC	PR D100 111102	M. Ablikim et al.	(BESIII Collab.)
ABLIKIM	17J	PRL 119 072001	M. Ablikim et al.	(BESIII Collab.)
ABLIKIM	15AA	PRL 115 182002	M. Ablikim et al.	(BESIII Collab.)
ABLIKIM	15AC	PR D92 092006	M. Ablikim et al.	(BESIII Collab.)
VINOKUROVA	15	JHEP 1506 132	A. Vinokurova et al.	(BELLE Collab.)
Also		JHEP 1702 088 (errata.)	A. Vinokurova et al.	(BELLE Collab.)
ABLIKIM	14B	PRL 112 132001	M. Ablikim et al.	(BESIII Collab.)
ABLIKIM	14P	PRL 113 212002	M. Ablikim et al.	(BESIII Collab.)
ABLIKIM	13X	PRL 111 242001	M. Ablikim et al.	(BESIII Collab.)

$\psi(4040)$

$$I^G(J^{PC}) = 0^-(1^{--})$$

$\psi(4040)$ MASS

VALUE (MeV)		DOCUMENT ID	TECN	COMMENT
4039 ± 1 OUR ESTIMATE				
4039.6 ± 4.3		¹ ABLIKIM	08D	BES2 $e^+e^- \rightarrow$ hadrons
• • • We do not use the following data for averages, fits, limits, etc. • • •				
4034 ± 6		² MO	10	RVUE $e^+e^- \rightarrow$ hadrons
4037 ± 2		³ SETH	05A	RVUE $e^+e^- \rightarrow$ hadrons
4040 ± 1		⁴ SETH	05A	RVUE $e^+e^- \rightarrow$ hadrons
4040 ± 10		BRANDELIK	78c	DASP e^+e^-

¹ Reanalysis of data presented in BAI 02c. From a global fit over the center-of-mass energy region 3.7–5.0 GeV covering the $\psi(3770)$, $\psi(4040)$, $\psi(4160)$, and $\psi(4415)$ resonances. Phase angle fixed in the fit to $\delta = (130 \pm 46)^\circ$.

² Reanalysis of data presented in BAI 00 and BAI 02c. From a global fit over the center-of-mass energy 3.8–4.8 GeV covering the $\psi(4040)$, $\psi(4160)$ and $\psi(4415)$ resonances and including interference effects.

³ From a fit to Crystal Ball (OSTERHELD 86) data.

⁴ From a fit to BES (BAI 02c) data.

$\psi(4040)$ WIDTH

VALUE (MeV)		DOCUMENT ID	TECN	COMMENT
80 ± 10 OUR ESTIMATE				
84.5 ± 12.3		⁵ ABLIKIM	08D	BES2 $e^+e^- \rightarrow$ hadrons
• • • We do not use the following data for averages, fits, limits, etc. • • •				
87 ± 11		⁶ MO	10	RVUE $e^+e^- \rightarrow$ hadrons
85 ± 10		⁷ SETH	05A	RVUE $e^+e^- \rightarrow$ hadrons
89 ± 6		⁸ SETH	05A	RVUE $e^+e^- \rightarrow$ hadrons
52 ± 10		BRANDELIK	78c	DASP e^+e^-

⁵ Reanalysis of data presented in BAI 02c. From a global fit over the center-of-mass energy region 3.7–5.0 GeV covering the $\psi(3770)$, $\psi(4040)$, $\psi(4160)$, and $\psi(4415)$ resonances. Phase angle fixed in the fit to $\delta = (130 \pm 46)^\circ$.

⁶ Reanalysis of data presented in BAI 00 and BAI 02c. From a global fit over the center-of-mass energy 3.8–4.8 GeV covering the $\psi(4040)$, $\psi(4160)$ and $\psi(4415)$ resonances and including interference effects.

⁷ From a fit to Crystal Ball (OSTERHELD 86) data.

⁸ From a fit to BES (BAI 02c) data.

$\psi(4040)$ DECAY MODES

Due to the complexity of the $c\bar{c}$ threshold region, in this listing, “seen” (“not seen”) means that a cross section for the mode in question has been measured at effective \sqrt{s} near this particle’s central mass value, more (less) than 2σ above zero, without regard to any peaking behavior in \sqrt{s} or absence thereof. See mode listing(s) for details and references.

Mode	Fraction (Γ_i/Γ)	Confidence level
Γ_1 e^+e^-	$(1.07 \pm 0.16) \times 10^{-5}$	
Γ_2 $D\bar{D}$	seen	
Γ_3 $D^0\bar{D}^0$	seen	
Γ_4 D^+D^-	seen	
Γ_5 $D^*\bar{D} + c.c.$	seen	
Γ_6 $D^*(2007)^0\bar{D}^0 + c.c.$	seen	
Γ_7 $D^*(2010)^+D^- + c.c.$	seen	
Γ_8 $D^*\bar{D}^*$	seen	
Γ_9 $D^*(2007)^0\bar{D}^*(2007)^0$	seen	
Γ_{10} $D^*(2010)^+D^*(2010)^-$	seen	
Γ_{11} $D\bar{D}\pi$ (excl. $D^*\bar{D}$)		
Γ_{12} $D^0D^-\pi^+ + c.c.$ (excl. $D^*(2007)^0\bar{D}^0 + c.c., D^*(2010)^+D^- + c.c.$)	not seen	
Γ_{13} $D\bar{D}^*\pi$ (excl. $D^*\bar{D}^*$)	not seen	
Γ_{14} $D^0\bar{D}^*\pi^+ + c.c.$ (excl. $D^*(2010)^+D^*(2010)^-$)	seen	
Γ_{15} $D_s^+D_s^-$	seen	
Γ_{16} $\pi^+\pi^+\pi^-\pi^-\pi^0$		
Γ_{17} $J/\psi(1S)$ hadrons		
Γ_{18} $J/\psi\pi^+\pi^-$	< 4	$\times 10^{-3}$ 90%
Γ_{19} $J/\psi\pi^0\pi^0$	< 2	$\times 10^{-3}$ 90%
Γ_{20} $J/\psi\eta$	$(5.2 \pm 0.7) \times 10^{-3}$	
Γ_{21} $J/\psi\pi^0$	< 2.8	$\times 10^{-4}$ 90%
Γ_{22} $J/\psi\pi^+\pi^-\pi^0$	< 2	$\times 10^{-3}$ 90%
Γ_{23} $\chi_{c1}\gamma$	< 3.4	$\times 10^{-3}$ 90%
Γ_{24} $\chi_{c2}\gamma$	< 5	$\times 10^{-3}$ 90%
Γ_{25} $\chi_{c1}\pi^+\pi^-\pi^0$	< 1.1	% 90%
Γ_{26} $\chi_{c2}\pi^+\pi^-\pi^0$	< 3.2	% 90%
Γ_{27} $h_c(1P)\pi^+\pi^-$	< 3	$\times 10^{-3}$ 90%
Γ_{28} $\phi\pi^+\pi^-$	< 3	$\times 10^{-3}$ 90%
Γ_{29} $\Lambda\bar{\Lambda}\pi^+\pi^-$	< 2.9	$\times 10^{-4}$ 90%
Γ_{30} $\Lambda\bar{\Lambda}\pi^0$	< 9	$\times 10^{-5}$ 90%
Γ_{31} $\Lambda\bar{\Lambda}\eta$	< 3.0	$\times 10^{-4}$ 90%
Γ_{32} $\Lambda\bar{\Lambda}$	< 6	$\times 10^{-6}$ 90%
Γ_{33} $\Sigma^+\bar{\Sigma}^-$	< 1.3	$\times 10^{-4}$ 90%
Γ_{34} $\Sigma^0\bar{\Sigma}^0$	< 7	$\times 10^{-5}$ 90%
Γ_{35} $\Xi^+\bar{\Xi}^-$	< 1.6	$\times 10^{-4}$ 90%
Γ_{36} $\Xi^0\bar{\Xi}^0$	< 1.8	$\times 10^{-4}$ 90%
Γ_{37} $\mu^+\mu^-$	$(9 \pm 6) \times 10^{-6}$	

$\psi(4040)$ PARTIAL WIDTHS

$\Gamma(e^+e^-)$	DOCUMENT ID	TECN	COMMENT	Γ_1
0.86 ± 0.07 OUR ESTIMATE				
0.83 ± 0.20	⁹ ABLIKIM	08D	BES2 $e^+e^- \rightarrow$ hadrons	
• • • We do not use the following data for averages, fits, limits, etc. • • •				
0.6 to 1.4	¹⁰ MO	10	RVUE $e^+e^- \rightarrow$ hadrons	
0.88 ± 0.11	¹¹ SETH	05A	RVUE $e^+e^- \rightarrow$ hadrons	
0.91 ± 0.13	¹² SETH	05A	RVUE $e^+e^- \rightarrow$ hadrons	
0.75 ± 0.15	BRANDELIK	78c	DASP e^+e^-	

⁹ Reanalysis of data presented in BAI 02c. From a global fit over the center-of-mass energy region 3.7–5.0 GeV covering the $\psi(3770)$, $\psi(4040)$, $\psi(4160)$, and $\psi(4415)$ resonances. Phase angle fixed in the fit to $\delta = (130 \pm 46)^\circ$.

¹⁰ Reanalysis of data presented in BAI 00 and BAI 02c. From a global fit over the center-of-mass energy 3.8–4.8 GeV covering the $\psi(4040)$, $\psi(4160)$ and $\psi(4415)$ resonances and including interference effects. Four sets of solutions are obtained with the same fit quality, mass and total width, but with different e^+e^- partial widths. We quote only the range of values.

¹¹ From a fit to Crystal Ball (OSTERHELD 86) data.

¹² From a fit to BES (BAI 02c) data.

$\Gamma(\mu^+\mu^-)$	DOCUMENT ID	TECN	COMMENT	Γ_{37}
0.73 ± 0.48 ± 0.12	^{13,14} ABLIKIM	20AG	BES3 $e^+e^- \rightarrow \mu^+\mu^-$	

¹³ From a fit to the $e^+e^- \rightarrow \mu^+\mu^-$ cross section between 3.8 and 4.6 GeV to the coherent sum of four resonant amplitudes assuming $\Gamma(\mu^+\mu^-) = \Gamma(e^+e^-)$.

¹⁴ From solution 1 of 8 with equal fit quality. Other solutions range from $0.58 \pm 0.52 \pm 0.10$ to $0.80 \pm 0.48 \pm 0.13$ keV.

Meson Particle Listings

 $\psi(4040)$ $\psi(4040) \Gamma(i) \times \Gamma(e^+ e^-) / \Gamma(\text{total})$

$\Gamma(\chi_{c1}\gamma) \times \Gamma(e^+ e^-) / \Gamma_{\text{total}}$					$\Gamma_{23} \Gamma_1 / \Gamma$
VALUE (eV)	CL%	DOCUMENT ID	TECN	COMMENT	
<2.9	90	15 HAN	15	BELL	10.58 $e^+ e^- \rightarrow \chi_{c1} \gamma$
15 Using $B(\eta \rightarrow \gamma\gamma) = (39.41 \pm 0.21)\%$.					

$\Gamma(\chi_{c2}\gamma) \times \Gamma(e^+ e^-) / \Gamma_{\text{total}}$					$\Gamma_{24} \Gamma_1 / \Gamma$
VALUE (eV)	CL%	DOCUMENT ID	TECN	COMMENT	
<4.6	90	16 HAN	15	BELL	10.58 $e^+ e^- \rightarrow \chi_{c2} \gamma$
16 Using $B(\eta \rightarrow \gamma\gamma) = (39.41 \pm 0.21)\%$.					

$\Gamma(J/\psi\eta) \times \Gamma(e^+ e^-) / \Gamma_{\text{total}}$					$\Gamma_{20} \Gamma_1 / \Gamma$
VALUE (eV)	CL%	DOCUMENT ID	TECN	COMMENT	
• • • We do not use the following data for averages, fits, limits, etc. • • •					
1.5 ± 0.3		17 ABLIKIM	20o	BES3	$e^+ e^- \rightarrow \eta J/\psi$
1.4 ± 0.3		18 ABLIKIM	20o	BES3	$e^+ e^- \rightarrow \eta J/\psi$
7.0 ± 0.6		19 ABLIKIM	20o	BES3	$e^+ e^- \rightarrow \eta J/\psi$

17 Solution 1 of three equivalent fit solutions using three resonant structures.
 18 Solution 2 of three equivalent fit solutions using three resonant structures.
 19 Solution 3 of three equivalent fit solutions using three resonant structures.

 $\psi(4040) \Gamma(i) \times \Gamma(e^+ e^-) / \Gamma^2(\text{total})$

$\Gamma(J/\psi\eta) / \Gamma_{\text{total}} \times \Gamma(e^+ e^-) / \Gamma_{\text{total}}$					$\Gamma_{20} \Gamma / \Gamma_1 / \Gamma$
VALUE (units 10^{-8})	CL%	DOCUMENT ID	TECN	COMMENT	
• • • We do not use the following data for averages, fits, limits, etc. • • •					
5.1 ± 1.4 ± 1.5		20 WANG	13B	BELL	$e^+ e^- \rightarrow J/\psi \eta \gamma$
12.8 ± 2.1 ± 1.9		21 WANG	13B	BELL	$e^+ e^- \rightarrow J/\psi \eta \gamma$

20 Solution I of two equivalent solutions in a fit using two interfering resonances. Mass and width fixed at 4039 MeV and 80 MeV, respectively.
 21 Solution II of two equivalent solutions in a fit using two interfering resonances. Mass and width fixed at 4039 MeV and 80 MeV, respectively.

$\Gamma(\Lambda\bar{\Lambda}) \times \Gamma(e^+ e^-) / \Gamma_{\text{total}}$					$\Gamma_{32} \Gamma_1 / \Gamma$
VALUE (eV)	CL%	DOCUMENT ID	TECN	COMMENT	
<5.5 × 10⁻³	90	22 ABLIKIM	21As	BES3	$e^+ e^- \rightarrow \psi(4040)$
22 From a measurement of the $e^+ e^- \rightarrow \Lambda\bar{\Lambda}$ cross section between 3.5 and 4.6 GeV.					

 $\psi(4040)$ BRANCHING RATIOS

$\Gamma(e^+ e^-) / \Gamma_{\text{total}}$					Γ_1 / Γ
VALUE (units 10^{-5})	CL%	DOCUMENT ID	TECN	COMMENT	
• • • We do not use the following data for averages, fits, limits, etc. • • •					
~ 1.0		FELDMAN	77	MRK1	$e^+ e^-$

$\Gamma(D^0 \bar{D}^0) / \Gamma_{\text{total}}$					Γ_3 / Γ
VALUE	CL%	DOCUMENT ID	TECN	COMMENT	
seen		AUBERT	09M	BABR	$e^+ e^- \rightarrow D^0 \bar{D}^0 \gamma$
seen		CRONIN-HEN..09	CLEO		$e^+ e^- \rightarrow D^0 \bar{D}^0$
seen		PAKHLOVA	08	BELL	$e^+ e^- \rightarrow D^0 \bar{D}^0 \gamma$

$\Gamma(D^+ D^-) / \Gamma_{\text{total}}$					Γ_4 / Γ
VALUE	CL%	DOCUMENT ID	TECN	COMMENT	
seen		AUBERT	09M	BABR	$e^+ e^- \rightarrow D^+ D^- \gamma$
seen		CRONIN-HEN..09	CLEO		$e^+ e^- \rightarrow D^+ D^-$
seen		PAKHLOVA	08	BELL	$e^+ e^- \rightarrow D^+ D^- \gamma$

$\Gamma(D \bar{D}) / \Gamma(D^* \bar{D}^* + \text{c.c.})$					Γ_2 / Γ_5
VALUE	CL%	DOCUMENT ID	TECN	COMMENT	
0.24 ± 0.05 ± 0.12		AUBERT	09M	BABR	$e^+ e^- \rightarrow \gamma D^{(*)} \bar{D}$

$\Gamma(D^0 \bar{D}^0) / \Gamma(D^*(2007)^0 \bar{D}^0 + \text{c.c.})$					Γ_3 / Γ_6
VALUE	CL%	DOCUMENT ID	TECN	COMMENT	
0.05 ± 0.03		23 GOLDHABER	77	MRK1	$e^+ e^-$
23 Phase-space factor (p^3) explicitly removed.					

$\Gamma(D^*(2007)^0 \bar{D}^0 + \text{c.c.}) / \Gamma_{\text{total}}$					Γ_6 / Γ
VALUE	CL%	DOCUMENT ID	TECN	COMMENT	
seen		AUBERT	09M	BABR	$e^+ e^- \rightarrow D^{*0} \bar{D}^0 \gamma$
seen		CRONIN-HEN..09	CLEO		$e^+ e^- \rightarrow D^{*0} \bar{D}^0$

$\Gamma(D^*(2010)^+ D^- + \text{c.c.}) / \Gamma_{\text{total}}$					Γ_7 / Γ
VALUE	CL%	DOCUMENT ID	TECN	COMMENT	
seen		24 ZHUKOVA	18	BELL	$e^+ e^- \rightarrow D^{*+} D^- \gamma$
seen		AUBERT	09M	BABR	$e^+ e^- \rightarrow D^{*+} D^- \gamma$
seen		CRONIN-HEN..09	CLEO		$e^+ e^- \rightarrow D^{*+} D^-$
• • • We do not use the following data for averages, fits, limits, etc. • • •					
seen		PAKHLOVA	07	BELL	$e^+ e^- \rightarrow D^{*+} D^- \gamma$

24 Supersedes PAKHLOVA 07.

$\Gamma(D^*(2010)^+ D^- + \text{c.c.}) / \Gamma(D^*(2007)^0 \bar{D}^0 + \text{c.c.})$					Γ_7 / Γ_6
VALUE	CL%	DOCUMENT ID	TECN	COMMENT	
0.95 ± 0.09 ± 0.10		AUBERT	09M	BABR	$e^+ e^- \rightarrow \gamma D^* \bar{D}$

$\Gamma(D^* \bar{D}^*) / \Gamma(D^* \bar{D}^* + \text{c.c.})$					Γ_8 / Γ_5
VALUE	CL%	DOCUMENT ID	TECN	COMMENT	
0.18 ± 0.14 ± 0.03		AUBERT	09M	BABR	$e^+ e^- \rightarrow \gamma D^{(*)} \bar{D}^{(*)}$

$\Gamma(D^*(2007)^0 \bar{D}^*(2007)^0) / \Gamma_{\text{total}}$					Γ_9 / Γ
VALUE	CL%	DOCUMENT ID	TECN	COMMENT	
seen		AUBERT	09M	BABR	$e^+ e^- \rightarrow D^{*0} \bar{D}^{*0} \gamma$
seen		CRONIN-HEN..09	CLEO		$e^+ e^- \rightarrow D^{*0} \bar{D}^{*0}$

$\Gamma(D^*(2007)^0 \bar{D}^*(2007)^0) / \Gamma(D^*(2007)^0 \bar{D}^0 + \text{c.c.})$					Γ_9 / Γ_6
VALUE	CL%	DOCUMENT ID	TECN	COMMENT	
32.0 ± 12.0		25 GOLDHABER	77	MRK1	$e^+ e^-$
25 Phase-space factor (p^3) explicitly removed.					

$\Gamma(D^*(2010)^+ D^*(2010)^-) / \Gamma_{\text{total}}$					Γ_{10} / Γ
VALUE	CL%	DOCUMENT ID	TECN	COMMENT	
seen		26 ZHUKOVA	18	BELL	$e^+ e^- \rightarrow D^{*+} D^{*-} \gamma$
seen		AUBERT	09M	BABR	$e^+ e^- \rightarrow D^{*+} D^{*-} \gamma$
seen		CRONIN-HEN..09	CLEO		$e^+ e^- \rightarrow D^{*+} D^{*-}$
• • • We do not use the following data for averages, fits, limits, etc. • • •					
seen		PAKHLOVA	07	BELL	$e^+ e^- \rightarrow D^{*+} D^{*-} \gamma$

26 Supersedes PAKHLOVA 07.

$\Gamma(D^0 D^- \pi^+ + \text{c.c. (excl. } D^*(2007)^0 \bar{D}^0 + \text{c.c., } D^*(2010)^+ D^- + \text{c.c.})) / \Gamma_{\text{total}}$					Γ_{12} / Γ
VALUE	CL%	DOCUMENT ID	TECN	COMMENT	
not seen		PAKHLOVA	08A	BELL	$e^+ e^- \rightarrow D^0 D^- \pi^+ \gamma$

$\Gamma(D \bar{D}^* \pi \text{ (excl. } D^* \bar{D}^*)) / \Gamma_{\text{total}}$					Γ_{13} / Γ
VALUE	CL%	DOCUMENT ID	TECN	COMMENT	
not seen		CRONIN-HEN..09	CLEO		$e^+ e^- \rightarrow D \bar{D}^* \pi$

$\Gamma(D^0 \bar{D}^{*-} \pi^+ + \text{c.c. (excl. } D^*(2010)^+ D^*(2010)^-) / \Gamma_{\text{total}}$					Γ_{14} / Γ
VALUE	CL%	DOCUMENT ID	TECN	COMMENT	
seen		PAKHLOVA	09	BELL	$e^+ e^- \rightarrow D^0 D^{*-} \pi^+ \gamma$

$\Gamma(D_s^+ D_s^-) / \Gamma_{\text{total}}$					Γ_{15} / Γ
VALUE	CL%	DOCUMENT ID	TECN	COMMENT	
seen		PAKHLOVA	11	BELL	$e^+ e^- \rightarrow D_s^+ D_s^- \gamma$
seen		DEL-AMO-SA..10N	BABR		$e^+ e^- \rightarrow D_s^+ D_s^- \gamma$
seen		CRONIN-HEN..09	CLEO		$e^+ e^- \rightarrow D_s^+ D_s^-$

$\Gamma(\pi^+ \pi^+ \pi^- \pi^0) / \Gamma_{\text{total}}$					Γ_{16} / Γ
VALUE	CL%	DOCUMENT ID	TECN	COMMENT	
• • • We do not use the following data for averages, fits, limits, etc. • • •					
(3.51 ± 1.89 ± 1.24) × 10 ⁻⁵		27 ABLIKIM	21AW	BES3	$e^+ e^- \rightarrow 2\pi^+ 2\pi^- \pi^0$
(2.41 ± 0.05 ± 0.79) × 10 ⁻²		28 ABLIKIM	21AW	BES3	$e^+ e^- \rightarrow 2\pi^+ 2\pi^- \pi^0$

27 Solution 1 of two solutions with equal fit quality. The significance of the $\psi(4040)$ signal is 3.6 σ .
 28 Solution 2 of two solutions with equal fit quality. The significance of the $\psi(4040)$ signal is 3.6 σ .

$\Gamma(J/\psi \pi^+ \pi^-) / \Gamma_{\text{total}}$					Γ_{18} / Γ
VALUE (units 10^{-3})	CL%	DOCUMENT ID	TECN	COMMENT	
<4	90	COAN	06	CLEO	3.97–4.06 $e^+ e^- \rightarrow$ hadrons

$\Gamma(J/\psi \pi^0 \pi^0) / \Gamma_{\text{total}}$					Γ_{19} / Γ
VALUE (units 10^{-3})	CL%	DOCUMENT ID	TECN	COMMENT	
<2	90	COAN	06	CLEO	3.97–4.06 $e^+ e^- \rightarrow$ hadrons

$\Gamma(J/\psi\eta) / \Gamma_{\text{total}}$					Γ_{20} / Γ
VALUE (units 10^{-3})	CL%	DOCUMENT ID	TECN	COMMENT	
5.2 ± 0.5 ± 0.5		29 ABLIKIM	12k	BES3	$e^+ e^- \rightarrow \ell^+ \ell^- 2\gamma$

• • • We do not use the following data for averages, fits, limits, etc. • • •
 <7 90 COAN 06 CLEO 3.97–4.06 $e^+ e^- \rightarrow$ hadrons
 29 ABLIKIM 12k measure $\sigma(e^+ e^- \rightarrow J/\psi\eta) = 32.1 \pm 2.8 \pm 1.3$ pb. They assume the $\eta/J/\psi$ fully originates from $\psi(4040)$ decays.

$\Gamma(J/\psi \pi^0) / \Gamma_{\text{total}}$					Γ_{21} / Γ
VALUE (units 10^{-3})	CL%	DOCUMENT ID	TECN	COMMENT	
<0.28	90	30 ABLIKIM	12k	BES3	$e^+ e^- \rightarrow \ell^+ \ell^- 2\gamma$
• • • We do not use the following data for averages, fits, limits, etc. • • •					
<2	90	COAN	06	CLEO	3.97–4.06 $e^+ e^- \rightarrow$ hadrons
30 ABLIKIM 12k measure $\sigma(e^+ e^- \rightarrow J/\psi \pi^0) < 1.6$ pb. They assume the $\eta/J/\psi$ fully originates from $\psi(4040)$ decays.					

See key on page 1127

Meson Particle Listings

$\psi(4040), X(4050)^\pm$

$\Gamma(J/\psi\pi^+\pi^-\pi^0)/\Gamma_{total}$					Γ_{22}/Γ
VALUE (units 10^{-3})	CL%	DOCUMENT ID	TECN	COMMENT	
<2	90	COAN 06	CLEO	3.97-4.06 $e^+e^- \rightarrow$ hadrons	

$\Gamma(\chi_{c1}\gamma)/\Gamma_{total}$					Γ_{23}/Γ
VALUE (units 10^{-3})	CL%	DOCUMENT ID	TECN	COMMENT	
<11	90	COAN 06	CLEO	3.97-4.06 $e^+e^- \rightarrow$ hadrons	

$\Gamma(\chi_{c2}\gamma)/\Gamma_{total}$					Γ_{24}/Γ
VALUE (units 10^{-3})	CL%	DOCUMENT ID	TECN	COMMENT	
<17	90	COAN 06	CLEO	3.97-4.06 $e^+e^- \rightarrow$ hadrons	

$\Gamma(\chi_{c1}\pi^+\pi^-\pi^0)/\Gamma_{total}$					Γ_{25}/Γ
VALUE (units 10^{-3})	CL%	DOCUMENT ID	TECN	COMMENT	
<11	90	COAN 06	CLEO	3.97-4.06 $e^+e^- \rightarrow$ hadrons	

$\Gamma(\chi_{c2}\pi^+\pi^-\pi^0)/\Gamma_{total}$					Γ_{26}/Γ
VALUE (units 10^{-3})	CL%	DOCUMENT ID	TECN	COMMENT	
<32	90	COAN 06	CLEO	3.97-4.06 $e^+e^- \rightarrow$ hadrons	

$\Gamma(h_c(1P)\pi^+\pi^-)/\Gamma_{total}$					Γ_{27}/Γ
VALUE (units 10^{-3})	CL%	DOCUMENT ID	TECN	COMMENT	
<3	90	31 PEDLAR 11	CLEO	$e^+e^- \rightarrow h_c(1P)\pi^+\pi^-$	

31 From several values of \sqrt{s} near the peak of the $\psi(4040)$, PEDLAR 11 measures $\sigma(e^+e^- \rightarrow h_c(1P)\pi^+\pi^-) = 1.0 \pm 8.0 \pm 5.4 \pm 0.2$ pb, where the errors are statistical, systematic, and due to uncertainty in $B(\psi(2S) \rightarrow \pi^0 h_c(1P))$, respectively.

$\Gamma(\phi\pi^+\pi^-)/\Gamma_{total}$					Γ_{28}/Γ
VALUE (units 10^{-3})	CL%	DOCUMENT ID	TECN	COMMENT	
<3	90	COAN 06	CLEO	3.97-4.06 $e^+e^- \rightarrow$ hadrons	

$\Gamma(\Lambda\bar{\Lambda}\pi^+\pi^-)/\Gamma_{total}$					Γ_{29}/Γ
VALUE (units 10^{-4})	CL%	DOCUMENT ID	TECN	COMMENT	
<2.9	90	32 ABLIKIM 13q	BES3	$e^+e^- \rightarrow \psi(4040)$	

32 Assuming that interference effects between resonance and continuum can be neglected.

$\Gamma(\Lambda\bar{\Lambda}\pi^0)/\Gamma_{total}$					Γ_{30}/Γ
VALUE (units 10^{-4})	CL%	DOCUMENT ID	TECN	COMMENT	
<0.9	90	33 ABLIKIM 13q	BES3	$e^+e^- \rightarrow \psi(4040)$	

33 Assuming that interference effects between resonance and continuum can be neglected.

$\Gamma(\Lambda\bar{\Lambda}\eta)/\Gamma_{total}$					Γ_{31}/Γ
VALUE (units 10^{-4})	CL%	DOCUMENT ID	TECN	COMMENT	
<3.0	90	34 ABLIKIM 13q	BES3	$e^+e^- \rightarrow \psi(4040)$	

34 Assuming that interference effects between resonance and continuum can be neglected.

$\Gamma(\Sigma^+\Sigma^-)/\Gamma_{total}$					Γ_{33}/Γ
VALUE (units 10^{-4})	CL%	DOCUMENT ID	TECN	COMMENT	
<1.3	90	35 ABLIKIM 13q	BES3	$e^+e^- \rightarrow \psi(4040)$	

35 Assuming that interference effects between resonance and continuum can be neglected.

$\Gamma(\Sigma^0\Sigma^0)/\Gamma_{total}$					Γ_{34}/Γ
VALUE (units 10^{-4})	CL%	DOCUMENT ID	TECN	COMMENT	
<0.7	90	36 ABLIKIM 13q	BES3	$e^+e^- \rightarrow \psi(4040)$	

36 Assuming that interference effects between resonance and continuum can be neglected.

$\Gamma(\Xi^+\Xi^-)/\Gamma_{total}$					Γ_{35}/Γ
VALUE (units 10^{-4})	CL%	DOCUMENT ID	TECN	COMMENT	
<1.6	90	37 ABLIKIM 13q	BES3	$e^+e^- \rightarrow \psi(4040)$	

37 Assuming that interference effects between resonance and continuum can be neglected.

$\Gamma(\Xi^0\Xi^0)/\Gamma_{total}$					Γ_{36}/Γ
VALUE (units 10^{-4})	CL%	DOCUMENT ID	TECN	COMMENT	
<1.8	90	38 ABLIKIM 13q	BES3	$e^+e^- \rightarrow \psi(4040)$	

38 Assuming that interference effects between resonance and continuum can be neglected.

$\psi(4040)$ REFERENCES

ABLIKIM 21AS	PR D104 L091104	M. Ablikim et al.	(BESIII Collab.)
ABLIKIM 21AW	PR D104 112009	M. Ablikim et al.	(BESIII Collab.)
ABLIKIM 20AG	P D102 112009	M. Ablikim et al.	(BESIII Collab.)
ABLIKIM 20O	PR D102 031101	M. Ablikim et al.	(BESIII Collab.)
ZHUKOVA 18	PR D97 012002	V. Zhukova et al.	(BELLE Collab.)
HAN 15	PR D92 012011	Y.L. Han et al.	(BELLE Collab.)
ABLIKIM 13Q	PR D87 112011	M. Ablikim et al.	(BESIII Collab.)
WANG 13B	PR D87 051101	X.L. Wang et al.	(BELLE Collab.)
ABLIKIM 12K	PR D86 071101	M. Ablikim et al.	(BESIII Collab.)
PAKHOVA 11	PR D83 011101	G. Pakhlova et al.	(BELLE Collab.)
PEDLAR 11	PRL 107 041803	T. Pedlar et al.	(CLEO Collab.)
DEL-AMO-SA...10N	PR D82 052004	P. del Amo Sanchez et al.	(BABAR Collab.)
MO 10	PR D82 077501	X.H. Mo, C.Z. Yuan, P. Wang	(BHEP)

AUBERT 09M	PR D79 092001	B. Aubert et al.	(BABAR Collab.)
CRONIN-HEN...09	PR D80 072001	D. Cronin-Hennessy et al.	(CLEO Collab.)
PAKHOVA 09	PR D80 091101	G. Pakhlova et al.	(BELLE Collab.)
ABLIKIM 08D	PL B660 315	M. Ablikim et al.	(BES Collab.)
PAKHOVA 08	PR D77 011103	G. Pakhlova et al.	(BELLE Collab.)
PAKHOVA 08A	PRL 100 062001	G. Pakhlova et al.	(BELLE Collab.)
PAKHOVA 07	PRL 98 092001	G. Pakhlova et al.	(BELLE Collab.)
COAN 06	PRL 96 162003	T.E. Coan et al.	(CLEO Collab.)
SETH 05A	PR D72 017501	K.K. Seth	(BES Collab.)
BAI 02C	PRL 88 101802	J.Z. Bai et al.	(BES Collab.)
BAI 00	PRL 84 594	J.Z. Bai et al.	(BES Collab.)
OSTERHELD 86	SLAC-PUB-4160	A. Osterheld et al.	(SLAC Crystal Ball Collab.)
BRANDELIC 78C	PL 76B 361	R. Brandelik et al.	(DASP Collab.)
DEL	ZPHY C1 233	R. Brandelik et al.	(DASP Collab.)
FELDMAN 77	PRPL 33C 285	G.J. Feldman, M.L. Perl	(LBL, SLAC)
GOLDBABER 77	PL 69B 503	G. Goldhaber et al.	(Mark I Collab.)

$X(4050)^\pm$

$I^G(J^{PC}) = 1^-(?^{?+})$
I, G, C need confirmation.

OMITTED FROM SUMMARY TABLE
Properties incompatible with a $q\bar{q}$ structure (exotic state). See the review on non- $q\bar{q}$ states.

Observed by MIZUK 08 in the $\pi^+\chi_{c1}(1P)$ invariant mass distribution in $\bar{B}^0 \rightarrow K^-\pi^+\chi_{c1}(1P)$ decays. Not seen by LEES 12B in this same mode after accounting for $K\pi$ resonant mass and angular structure.

$X(4050)^\pm$ MASS

VALUE (MeV)	DOCUMENT ID	TECN	COMMENT
$4051 \pm 14 + 20 - 41$	1 MIZUK 08	BELL	$\bar{B}^0 \rightarrow K^-\pi^+\chi_{c1}(1P)$

1 From a Dalitz plot analysis with two Breit-Wigner amplitudes.

$X(4050)^\pm$ WIDTH

VALUE (MeV)	DOCUMENT ID	TECN	COMMENT
$82 + 21 + 47 - 17 - 22$	1 MIZUK 08	BELL	$\bar{B}^0 \rightarrow K^-\pi^+\chi_{c1}(1P)$

1 From a Dalitz plot analysis with two Breit-Wigner amplitudes.

$X(4050)^\pm$ DECAY MODES

Mode	Fraction (Γ_i/Γ)
$\Gamma_1 \pi^+\chi_{c1}(1P)$	seen
$\Gamma_2 \pi^+\psi(3770)$	not seen
$\Gamma_3 \pi^+\chi_{c0}(1P)$	not seen
$\Gamma_4 \pi^+\chi_{c2}(1P)$	not seen

$X(4050)^\pm$ BRANCHING RATIOS

$\Gamma(\pi^+\chi_{c1}(1P))/\Gamma_{total}$					Γ_1/Γ
VALUE	EVTS	DOCUMENT ID	TECN	COMMENT	
seen	1	MIZUK 08	BELL	$\bar{B}^0 \rightarrow K^-\pi^+\chi_{c1}(1P)$	
not seen	16	2 ABLIKIM 21W	BES3	$e^+e^- \rightarrow \chi_{cJ}\pi^+\pi^+$	
not seen	3	LEES 12B	BABR	$B \rightarrow K\pi\chi_{c1}(1P)$	

1 With a product branching fraction measurement of $B(\bar{B}^0 \rightarrow K^-\pi^+\chi_{c1}(1P)) \times B(X(4050)^+ \rightarrow \pi^+\chi_{c1}(1P)) = (3.0 + 1.5 + 3.7 - 0.8 - 1.6) \times 10^{-5}$.
2 ABLIKIM 21W measurement is limited by statistics.
3 With a product branching fraction limit of $B(\bar{B}^0 \rightarrow X(4050)^+K^-) \times B(X(4050)^+ \rightarrow \chi_{c1}\pi^+) < 1.8 \times 10^{-5}$ at 90% CL.

$\Gamma(\pi^+\chi_{c0}(1P))/\Gamma_{total}$					Γ_3/Γ
VALUE	EVTS	DOCUMENT ID	TECN	COMMENT	
not seen	18	1 ABLIKIM 21W	BES3	$e^+e^- \rightarrow \chi_{cJ}\pi^+\pi^+$	

1 ABLIKIM 21W measurement is limited by statistics.

$\Gamma(\pi^+\chi_{c2}(1P))/\Gamma_{total}$					Γ_4/Γ
VALUE	EVTS	DOCUMENT ID	TECN	COMMENT	
not seen	14	1 ABLIKIM 21W	BES3	$e^+e^- \rightarrow \chi_{cJ}\pi^+\pi^+$	

1 ABLIKIM 21W measurement is limited by statistics.

$\Gamma(\pi^+\psi(3770))/\Gamma_{total}$					Γ_2/Γ
VALUE	DOCUMENT ID	TECN	COMMENT		
not seen	1 ABLIKIM 19AR	BES3	$e^+e^- \rightarrow \pi^+\pi^-D\bar{D}$		

1 From a measurement of $\sigma(e^+e^- \rightarrow \pi^+\pi^-D\bar{D})$ between $\sqrt{s} = 4.08$ and 4.6 GeV.

$X(4050)^\pm$ REFERENCES

ABLIKIM 21W	PR D103 052010	M. Ablikim et al.	(BESIII Collab.)
ABLIKIM 19AR	PR D100 032005	M. Ablikim et al.	(BESIII Collab.)
LEES 12B	PR D85 052003	J.P. Lees et al.	(BABAR Collab.)
MIZUK 08	PR D78 072004	R. Mizuk et al.	(BELLE Collab.)

Meson Particle Listings

 $X(4055)^\pm, X(4100)^\pm, \chi_{c1}(4140)$ **$X(4055)^\pm$**

$$I^G(J^{PC}) = 1^+(?^{?^-})$$

I, G, C need confirmation.

OMITTED FROM SUMMARY TABLE

Properties incompatible with a $q\bar{q}$ structure (exotic state). See the review on non- $q\bar{q}$ states.

Needs confirmation. Seen by WANG 15A in the $\psi(2S)\pi^+$ invariant mass distribution in $\psi(4360) \rightarrow \psi(2S)\pi^+\pi^-$ decay.

 $X(4055)^\pm$ MASS

VALUE (MeV)	DOCUMENT ID	TECN	COMMENT
4054 ± 3 ± 1	¹ WANG	15A	BELL 10.58 $e^+e^- \rightarrow \gamma\pi^+\pi^-\psi(2S)$
4039.3 ± 6.0	² ABLIKIM	18K	BES3 $e^+e^- \rightarrow \pi^0\pi^0\psi(2S)$
4032.1 ± 2.4	³ ABLIKIM	17V	BES3 $e^+e^- \rightarrow \pi^+\pi^-\psi(2S)$

- • • We do not use the following data for averages, fits, limits, etc. • • •
- ¹ Statistical significance of 3.5 σ .
- ² Statistical error only, with significance of 5.9 σ (from a fit with a 19% CL). Identified as the same structure observed in ABLIKIM 17V in $e^+e^- \rightarrow \pi^+\pi^-\psi(2S)$ decays.
- ³ Statistical error only, with significance of 9.2 σ . From an unbinned maximum likelihood fit of the $\pi^+\pi^-\psi(2S)$ Dalitz plot from data collected at $\sqrt{s} = 4.416$ GeV for a $J^C = 1^+$ state. The fit does not match the detailed structure of the data, having a C.L. of only 8%.

 $X(4055)^\pm$ WIDTH

VALUE (MeV)	DOCUMENT ID	TECN	COMMENT
45 ± 11 ± 6	¹ WANG	15A	BELL 10.58 $e^+e^- \rightarrow \gamma\pi^+\pi^-\psi(2S)$
31.9 ± 14.8	² ABLIKIM	18K	BES3 $e^+e^- \rightarrow \pi^0\pi^0\psi(2S)$
26.1 ± 5.3	³ ABLIKIM	17V	BES3 $e^+e^- \rightarrow \pi^+\pi^-\psi(2S)$

- • • We do not use the following data for averages, fits, limits, etc. • • •
- ¹ Statistical significance of 3.5 σ .
- ² Statistical error only, with significance of 5.9 σ (from a fit with a 19% CL). Identified as the same structure observed in ABLIKIM 17V in $e^+e^- \rightarrow \pi^+\pi^-\psi(2S)$ decays.
- ³ Statistical error only, with significance of 9.2 σ . From an unbinned maximum likelihood fit of the $\pi^+\pi^-\psi(2S)$ Dalitz plot from data collected at $\sqrt{s} = 4.416$ GeV for a $J^C = 1^+$ state. The fit does not match the detailed structure of the data, having a C.L. of only 8%.

 $X(4055)^\pm$ DECAY MODES

Mode	Fraction (Γ_i/Γ)
Γ_1 $\pi^+\psi(2S)$	seen
Γ_2 $\pi^\pm\psi(3770)$	not seen

 $X(4055)^\pm$ BRANCHING RATIOS

$\Gamma(\pi^+\psi(2S))/\Gamma_{\text{total}}$	Γ_1/Γ		
VALUE	DOCUMENT ID	TECN	COMMENT
seen	¹ WANG	15A	BELL 10.58 $e^+e^- \rightarrow \gamma\pi^+\pi^-\psi(2S)$

- ¹ Statistical significance of 3.5 σ .

$\Gamma(\pi^\pm\psi(3770))/\Gamma_{\text{total}}$	Γ_2/Γ		
VALUE	DOCUMENT ID	TECN	COMMENT
not seen	¹ ABLIKIM	19AR	BES3 $e^+e^- \rightarrow \pi^+\pi^-D\bar{D}$

- ¹ From a measurement of $\sigma(e^+e^- \rightarrow \pi^+\pi^-D\bar{D})$ between $\sqrt{s} = 4.08$ and 4.6 GeV.

 $X(4055)^\pm$ REFERENCES

ABLIKIM	19AR	PR D100 032005	M. Ablikim <i>et al.</i>	(BESIII Collab.)
ABLIKIM	18K	PR D97 052001	M. Ablikim <i>et al.</i>	(BESIII Collab.)
ABLIKIM	17V	PR D96 032004	M. Ablikim <i>et al.</i>	(BESIII Collab.)
Also	PR D99 019903 (errata)	M. Ablikim <i>et al.</i>	(BESIII Collab.)	
WANG	15A	PR D91 112007	X.L. Wang <i>et al.</i>	(BELLE Collab.)

 $X(4100)^\pm$

$$I^G(J^{PC}) = 1^-(?^{??})$$

OMITTED FROM SUMMARY TABLE

Properties incompatible with a $q\bar{q}$ structure (exotic state). See the review on non- $q\bar{q}$ states.

Reported by AAIJ 18AN in the $\eta_c(1S)\pi^-$ invariant mass distribution in $B^0 \rightarrow \eta_c(1S)K^+\pi^-$ decays with a significance of 3.4 σ . $J^P = 0^+$ or 1^- assignment consistent with data.

 $X(4100)^\pm$ MASS

VALUE (MeV)	DOCUMENT ID	TECN	COMMENT
4096 ± 20 ⁺¹⁸ ₋₂₂	AAIJ	18AN	LHCB $B^0 \rightarrow \eta_c(1S)K^+\pi^-$

 $X(4100)^\pm$ WIDTH

VALUE (MeV)	DOCUMENT ID	TECN	COMMENT
152 ± 58 ⁺⁶⁰ ₋₃₅	AAIJ	18AN	LHCB $B^0 \rightarrow \eta_c(1S)K^+\pi^-$

 $X(4100)^\pm$ DECAY MODES

Mode	Fraction (Γ_i/Γ)
Γ_1 $\eta_c(1S)\pi^-$	seen
Γ_2 $\pi^\pm\psi(3770)$	not seen

 $X(4100)^\pm$ BRANCHING RATIOS

$\Gamma(\eta_c(1S)\pi^-)/\Gamma_{\text{total}}$	Γ_1/Γ		
VALUE	DOCUMENT ID	TECN	COMMENT
seen	¹ AAIJ	18AN	LHCB $B^0 \rightarrow \eta_c(1S)K^+\pi^-$
¹ AAIJ 18AN quotes a fit fraction for $B^0 \rightarrow X(4100)^-K^+ \rightarrow \eta_c(1S)\pi^-K^+$ of $(3.3 \pm 1.1 \pm 1.2 \pm 1.1)\%$ from an amplitude analysis.			

$\Gamma(\pi^\pm\psi(3770))/\Gamma_{\text{total}}$	Γ_2/Γ		
VALUE	DOCUMENT ID	TECN	COMMENT
not seen	¹ ABLIKIM	19AR	BES3 $e^+e^- \rightarrow \pi^+\pi^-D\bar{D}$
¹ From a measurement of $\sigma(e^+e^- \rightarrow \pi^+\pi^-D\bar{D})$ between $\sqrt{s} = 4.08$ and 4.6 GeV.			

 $X(4100)^\pm$ REFERENCES

ABLIKIM	19AR	PR D100 032005	M. Ablikim <i>et al.</i>	(BESIII Collab.)
AAIJ	18AN	EPJ C78 1019	R. Aaij <i>et al.</i>	(LHCB Collab.)

 $\chi_{c1}(4140)$

$$I^G(J^{PC}) = 0^+(1^{++})$$

was $X(4140)$

This state shows properties different from a conventional $q\bar{q}$ state. A candidate for an exotic structure. See the review on non- $q\bar{q}$ states.

Seen by AALTONEN 09AH, ABZOV 14A, CHATRCHYAN 14M, AAIJ 17C in $B^+ \rightarrow \chi_{c1}K^+, \chi_{c1} \rightarrow J/\psi\phi$, and by ABZOV 15M separately in both prompt (4.7 σ) and non-prompt (5.6 σ) production in $p\bar{p} \rightarrow J/\psi\phi + \text{anything}$. Not seen by SHEN 10 in $\gamma\gamma \rightarrow J/\psi\phi$ and ABLIKIM 15 in $e^+e^- \rightarrow \gamma J/\psi\phi$ at $\sqrt{s} = 4.23, 4.26, 4.36$ GeV.

 $\chi_{c1}(4140)$ MASS

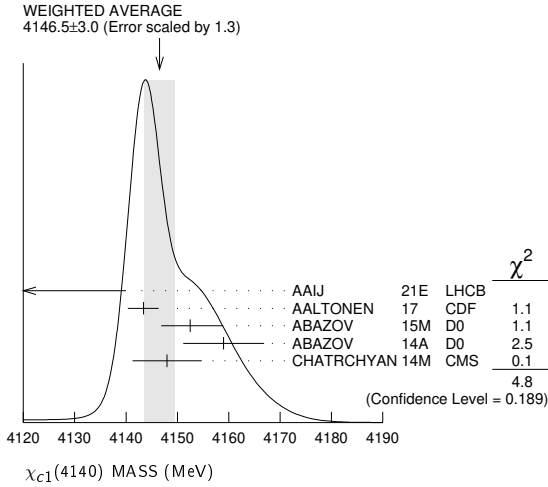
VALUE (MeV)	EVTS	DOCUMENT ID	TECN	COMMENT
4146.5 ± 3.0 OUR AVERAGE		Error includes scale factor of 1.3. See the ideogram below.		
4118 ± 11 ⁺¹⁹ ₋₃₆	24k	¹ AAIJ	21E	LHCB $B^+ \rightarrow J/\psi\phi K^+$
4143.4 ^{+2.9} _{-3.0} ± 0.6	19	² AALTONEN	17	CDF $B^+ \rightarrow J/\psi\phi K^+$
4152.5 ± 1.7 ^{+6.2} _{-5.4}	616	³ ABZOV	15M	D0 $p\bar{p} \rightarrow J/\psi\phi + \text{anything}$
4159.0 ± 4.3 ± 5.6	52	⁴ ABZOV	14A	D0 $B^+ \rightarrow J/\psi\phi K^+$
4148.0 ± 2.4 ± 6.3	0.3k	⁵ CHATRCHYAN14M	CMS	$B^+ \rightarrow J/\psi\phi K^+$
• • • We do not use the following data for averages, fits, limits, etc. • • •				
4146.5 ± 4.5 ^{+4.6} _{-2.8}	4289	^{6,7} AAIJ	17C	LHCB $B^+ \rightarrow J/\psi\phi K^+$
4143.0 ± 2.9 ± 1.2	14	^{8,9} AALTONEN	09AH	CDF $B^+ \rightarrow J/\psi\phi K^+$

- ¹ From an amplitude analysis of the decay $B^+ \rightarrow J/\psi\phi K^+$ with a significance of 13 σ .
- ² Statistical significance of more than 5 σ .
- ³ Statistical significance of more than 6 σ .
- ⁴ Statistical significance of 3.1 σ .
- ⁵ From a fit assuming an S-wave relativistic Breit-Wigner shape above a three-body phase-space non-resonant component with statistical significance of more than 5 σ .
- ⁶ From an amplitude analysis of the decay $B^+ \rightarrow J/\psi\phi K^+$ with a significance of 8.4 σ .
- ⁷ Superseded by AAIJ 21E.
- ⁸ Statistical significance of 3.8 σ .
- ⁹ Superseded by AALTONEN 17.

See key on page 1127

Meson Particle Listings

$\chi_{c1}(4140), \psi(4160)$



$\chi_{c1}(4140)$ WIDTH

VALUE (MeV)	EVTS	DOCUMENT ID	TECN	COMMENT
19 \pm 7	OUR AVERAGE			
162 \pm 21	24k	1 AAIJ	21E LHCB	$B^+ \rightarrow J/\psi \phi K^+$
15.3 \pm 10.4	19	2 AALTONEN	17 CDF	$B^+ \rightarrow J/\psi \phi K^+$
16.3 \pm 5.6	616	3 ABAZOV	15M D0	$p\bar{p} \rightarrow J/\psi \phi + \text{anything}$
20 \pm 13	52	4 ABAZOV	14A D0	$B^+ \rightarrow J/\psi \phi K^+$
28 \pm 15	0.3k	5 CHATRCHYAN	14M CMS	$B^+ \rightarrow J/\psi \phi K^+$

- • • We do not use the following data for averages, fits, limits, etc. • • •
- 83 \pm 21 \pm 21
- 11.7 \pm 8.3 \pm 5.0 \pm 3.7
- 14 8,9 AALTONEN 09AH CDF $B^+ \rightarrow J/\psi \phi K^+$
- 1 From an amplitude analysis of the decay $B^+ \rightarrow J/\psi \phi K^+$ with a significance of 13 σ .
- 2 Statistical significance of more than 5 σ .
- 3 Statistical significance of more than 6 σ .
- 4 Statistical significance of 3.1 σ .
- 5 From a fit assuming an S-wave relativistic Breit-Wigner shape above a three-body phase-space non-resonant component with statistical significance of more than 5 σ .
- 6 From an amplitude analysis of the decay $B^+ \rightarrow J/\psi \phi K^+$ with a significance of 8.4 σ .
- 7 Superseded by AAIJ 21E.
- 8 Statistical significance of 3.8 σ .
- 9 Superseded by AALTONEN 17.

$\chi_{c1}(4140)$ DECAY MODES

Mode	Fraction (Γ_i/Γ)
Γ_1 $J/\psi \phi$	seen
Γ_2 $\gamma \gamma$	not seen

$\chi_{c1}(4140)$ $\Gamma(i)\Gamma(\gamma\gamma)/\Gamma(\text{total})$

VALUE (eV)	CL%	DOCUMENT ID	TECN	COMMENT	$\Gamma_2\Gamma_1/\Gamma$
<41	90	1 SHEN	10 BELL	10.6 $e^+e^- \rightarrow e^+e^- J/\psi \phi$	
< 6	90	2 SHEN	10 BELL	10.6 $e^+e^- \rightarrow e^+e^- J/\psi \phi$	

1 For $J^P = 0^+$.
2 For $J^P = 2^+$.

$\chi_{c1}(4140)$ BRANCHING RATIOS

VALUE	EVTS	DOCUMENT ID	TECN	COMMENT	Γ_1/Γ
seen	24k	1 AAIJ	21E LHCB	$B^+ \rightarrow J/\psi \phi K^+$	
seen	616	2 ABAZOV	15M D0	$p\bar{p} \rightarrow J/\psi \phi + \text{anything}$	
seen	52	3 ABAZOV	14A D0	$B^+ \rightarrow J/\psi \phi K^+$	
seen	0.3k	4 CHATRCHYAN	14M CMS	$B^+ \rightarrow J/\psi \phi K^+$	
seen	14	5 AALTONEN	09AH CDF	$B^+ \rightarrow J/\psi \phi K^+$	

- • • We do not use the following data for averages, fits, limits, etc. • • •
- seen 4289 6,7 AAIJ 17c LHCB $B^+ \rightarrow J/\psi \phi K^+$
- not seen 8 ABLIKIM 15 BES3 $e^+e^- \rightarrow \gamma \phi J/\psi$
- not seen 9 AAIJ 12AA LHCB $p\bar{p} \rightarrow B^+ X$ at 7 TeV
- 1 From an amplitude analysis of the decay $B^+ \rightarrow J/\psi \phi K^+$ with a significance of 13 σ .
- 2 Statistical significance of more than 6 σ .
- 3 ABAZOV 14A reports $B(B^+ \rightarrow \chi_{c1}(4140) K^+ \rightarrow J/\psi \phi K^+)/B(B^+ \rightarrow J/\psi \phi K^+) = (19 \pm 7 \pm 4)\%$ with 3.1 σ significance.
- 4 From a fit assuming an S-wave relativistic Breit-Wigner shape above a three-body phase-space non-resonant component with statistical significance of more than 5 σ .
- 5 Statistical significance of 3.8 σ .
- 6 From an amplitude analysis of the decay $B^+ \rightarrow J/\psi \phi K^+$ with a significance of 8.4 σ .
- 7 Superseded by AAIJ 21E.
- 8 Reported $\sigma(e^+e^- \rightarrow \gamma \chi_{c1}(4140)) \cdot B(\chi_{c1}(4140) \rightarrow J/\psi \phi) < 0.35, 0.28,$ and 0.33 pb at 4.23, 4.26, and 4.36 GeV, respectively, at 90% CL.
- 9 Reported $B(B^+ \rightarrow \chi_{c1}(4140) K^+) \cdot B(\chi_{c1}(4140) \rightarrow J/\psi \phi)/B(B^+ \rightarrow J/\psi \phi K^+) < 0.07$ at 90% CL.

$\Gamma(\gamma\gamma)/\Gamma_{\text{total}}$	DOCUMENT ID	TECN	COMMENT	Γ_2/Γ
not seen	SHEN	10 BELL	10.6 $e^+e^- \rightarrow e^+e^- J/\psi \phi$	

$\chi_{c1}(4140)$ REFERENCES

AAIJ	21E	PRL 127 082001	R. Aaij et al.	(LHCb Collab.)
AAIJ	17C	PRL 118 022003	R. Aaij et al.	(LHCb Collab.) JP
Abso		PR D95 012002	R. Aaij et al.	(LHCb Collab.)
AALTONEN	17	MPL A32 1750139	T. Aaltonen et al.	(CDF Collab.)
ABAZOV	15M	PRL 115 232001	V.M. Abazov et al.	(D0 Collab.)
ABLIKIM	15	PR D91 032001	M. Ablikim et al.	(BESIII Collab.)
ABAZOV	14A	PR D89 012004	V.M. Abazov et al.	(D0 Collab.)
CHATRCHYAN	14M	PL B734 261	S. Chatrchyan et al.	(CMS Collab.)
AAIJ	12AA	PR D85 091103	R. Aaij et al.	(LHCb Collab.)
SHEN	10	PRL 104 112004	C.P. Shen et al.	(BELLE Collab.)
AALTONEN	09AH	PRL 102 242002	T. Aaltonen et al.	(CDF Collab.)

$\psi(4160)$

$I^G(J^{PC}) = 0^-(1^{--})$

$\psi(4160)$ MASS

VALUE (MeV)	DOCUMENT ID	TECN	COMMENT
4191 \pm 5	OUR AVERAGE		
4191 \pm 9	AAIJ	13bc LHCB	$B^+ \rightarrow K^+ \mu^+ \mu^-$
4191.7 \pm 6.5	1 ABLIKIM	08b BES2	$e^+e^- \rightarrow \text{hadrons}$
4193 \pm 7	2 MO	10 RVUE	$e^+e^- \rightarrow \text{hadrons}$
4151 \pm 4	3 SETH	05A RVUE	$e^+e^- \rightarrow \text{hadrons}$
4155 \pm 5	4 SETH	05A RVUE	$e^+e^- \rightarrow \text{hadrons}$
4159 \pm 20	BRANDELIK	78c DASP	e^+e^-

- • • We do not use the following data for averages, fits, limits, etc. • • •
- 1 Reanalysis of data presented in BAI 02c. From a global fit over the center-of-mass energy region 3.7–5.0 GeV covering the $\psi(3770), \psi(4040), \psi(4160),$ and $\psi(4415)$ resonances. Phase angle fixed in the fit to $\delta = (293 \pm 57)^\circ$.
- 2 Reanalysis of data presented in BAI 00 and BAI 02c. From a global fit over the center-of-mass energy 3.8–4.8 GeV covering the $\psi(4040), \psi(4160)$ and $\psi(4415)$ resonances and including interference effects.
- 3 From a fit to Crystal Ball (OSTERHELD 86) data.
- 4 From a fit to BES (BAI 02c) data.

$\psi(4160)$ WIDTH

VALUE (MeV)	DOCUMENT ID	TECN	COMMENT
70 \pm 10	OUR AVERAGE		
65 \pm 22	AAIJ	13bc LHCB	$B^+ \rightarrow K^+ \mu^+ \mu^-$
71.8 \pm 12.3	1 ABLIKIM	08b BES2	$e^+e^- \rightarrow \text{hadrons}$
79 \pm 14	2 MO	10 RVUE	$e^+e^- \rightarrow \text{hadrons}$
107 \pm 10	3 SETH	05A RVUE	$e^+e^- \rightarrow \text{hadrons}$
107 \pm 16	4 SETH	05A RVUE	$e^+e^- \rightarrow \text{hadrons}$
78 \pm 20	BRANDELIK	78c DASP	e^+e^-

- • • We do not use the following data for averages, fits, limits, etc. • • •
- 1 Reanalysis of data presented in BAI 02c. From a global fit over the center-of-mass energy region 3.7–5.0 GeV covering the $\psi(3770), \psi(4040), \psi(4160),$ and $\psi(4415)$ resonances. Phase angle fixed in the fit to $\delta = (293 \pm 57)^\circ$.
- 2 Reanalysis of data presented in BAI 00 and BAI 02c. From a global fit over the center-of-mass energy 3.8–4.8 GeV covering the $\psi(4040), \psi(4160)$ and $\psi(4415)$ resonances and including interference effects.
- 3 From a fit to Crystal Ball (OSTERHELD 86) data.
- 4 From a fit to BES (BAI 02c) data.

Meson Particle Listings

$\psi(4160)$

$\psi(4160)$ DECAY MODES

Due to the complexity of the $c\bar{c}$ threshold region, in this listing, "seen" ("not seen") means that a cross section for the mode in question has been measured at effective \sqrt{s} near this particle's central mass value, more (less) than 2σ above zero, without regard to any peaking behavior in \sqrt{s} or absence thereof. See mode listing(s) for details and references.

Mode	Fraction (Γ_i/Γ)	Confidence level
Γ_1 e^+e^-	$(6.9 \pm 3.3) \times 10^{-6}$	
Γ_2 $\mu^+\mu^-$	seen	
Γ_3 $D\bar{D}$	seen	
Γ_4 $D^0\bar{D}^0$	seen	
Γ_5 D^+D^-	seen	
Γ_6 $D^*\bar{D}^+ + c.c.$	seen	
Γ_7 $D^*(2007)^0\bar{D}^0 + c.c.$	seen	
Γ_8 $D^*(2010)^+D^- + c.c.$	seen	
Γ_9 $D^*\bar{D}^*$	seen	
Γ_{10} $D^*(2007)^0\bar{D}^*(2007)^0$	seen	
Γ_{11} $D^*(2010)^+D^*(2010)^-$	seen	
Γ_{12} $D^0D^-\pi^+ + c.c. (excl. D^*(2007)^0\bar{D}^0 + c.c., D^*(2010)^+D^- + c.c.)$	not seen	
Γ_{13} $D\bar{D}^*\pi + c.c. (excl. D^*\bar{D}^*)$	seen	
Γ_{14} $D^0D^-\pi^+ + c.c. (excl. D^*(2010)^+D^*(2010)^-)$	not seen	
Γ_{15} $D_s^+D_s^-$	not seen	
Γ_{16} $D_s^*D_s^* + c.c.$	seen	
Γ_{17} $J/\psi\pi^+\pi^-$	$< 3 \times 10^{-3}$	90%
Γ_{18} $J/\psi\pi^0\pi^0$	$< 3 \times 10^{-3}$	90%
Γ_{19} $J/\psi K^+K^-$	$< 2 \times 10^{-3}$	90%
Γ_{20} $J/\psi\eta$	$< 8 \times 10^{-3}$	90%
Γ_{21} $J/\psi\pi^0$	$< 1 \times 10^{-3}$	90%
Γ_{22} $J/\psi\eta'$	$< 5 \times 10^{-3}$	90%
Γ_{23} $J/\psi\pi^+\pi^-\pi^0$	$< 1 \times 10^{-3}$	90%
Γ_{24} $\psi(2S)\pi^+\pi^-$	$< 4 \times 10^{-3}$	90%
Γ_{25} $\chi_{c1}\gamma$	$< 5 \times 10^{-3}$	90%
Γ_{26} $\chi_{c2}\gamma$	$< 1.3\%$	90%
Γ_{27} $\chi_{c1}\pi^+\pi^-\pi^0$	$< 2 \times 10^{-3}$	90%
Γ_{28} $\chi_{c2}\pi^+\pi^-\pi^0$	$< 8 \times 10^{-3}$	90%
Γ_{29} $h_c(1P)\pi^+\pi^-$	$< 5 \times 10^{-3}$	90%
Γ_{30} $h_c(1P)\pi^0\pi^0$	$< 2 \times 10^{-3}$	90%
Γ_{31} $h_c(1P)\eta$	$< 2 \times 10^{-3}$	90%
Γ_{32} $h_c(1P)\pi^0$	$< 4 \times 10^{-4}$	90%
Γ_{33} $\phi\pi^+\pi^-$	$< 2 \times 10^{-3}$	90%
Γ_{34} $\gamma\chi_{c1}(3872)$	$< 1.8 \times 10^{-3}$	90%
Γ_{35} $\gamma\chi_{c0}(3915) \rightarrow \gamma J/\psi\pi^+\pi^-$	$< 1.36 \times 10^{-4}$	90%
Γ_{36} $\gamma X(3930) \rightarrow \gamma J/\psi\pi^+\pi^-$	$< 1.18 \times 10^{-4}$	90%
Γ_{37} $\gamma X(3940) \rightarrow \gamma J/\psi\pi^+\pi^-$	$< 1.47 \times 10^{-4}$	90%
Γ_{38} $\gamma\chi_{c0}(3915) \rightarrow \gamma\gamma J/\psi$	$< 1.26 \times 10^{-4}$	90%
Γ_{39} $\gamma X(3930) \rightarrow \gamma\gamma J/\psi$	$< 8.8 \times 10^{-5}$	90%
Γ_{40} $\gamma X(3940) \rightarrow \gamma\gamma J/\psi$	$< 1.79 \times 10^{-4}$	90%
Γ_{41} K^+K^-		
Γ_{42} $K_S^0 K^\pm\pi^\mp$		
Γ_{43} $\rho\bar{\rho}\rho\bar{\rho}$	not seen	
Γ_{44} $\Lambda\bar{\Lambda}$	$< 1.5 \times 10^{-6}$	90%

$\psi(4160)$ PARTIAL WIDTHS

$\Gamma(e^+e^-)$	DOCUMENT ID	TECN	COMMENT
0.49 ± 0.22	1 ABLIKIM	08D BES2	$e^+e^- \rightarrow$ hadrons
••• We do not use the following data for averages, fits, limits, etc. •••			
0.4 to 1.1	2 MO	10 RVUE	$e^+e^- \rightarrow$ hadrons
0.83 \pm 0.08	3 SETH	05A RVUE	$e^+e^- \rightarrow$ hadrons
0.84 \pm 0.13	4 SETH	05A RVUE	$e^+e^- \rightarrow$ hadrons
0.77 \pm 0.23	BRANDELIK	78C DASP	e^+e^-

¹ Reanalysis of data presented in BAI 02c. From a global fit over the center-of-mass energy region 3.7–5.0 GeV covering the $\psi(3770)$, $\psi(4040)$, $\psi(4160)$, and $\psi(4415)$ resonances. Phase angle fixed in the fit to $\delta = (293 \pm 57)^\circ$.
² Reanalysis of data presented in BAI 00 and BAI 02c. From a global fit over the center-of-mass energy 3.8–4.8 GeV covering the $\psi(4040)$, $\psi(4160)$ and $\psi(4415)$ resonances and including interference effects. Four sets of solutions are obtained with the same fit quality, mass and total width, but with different e^+e^- partial widths. We quote only the range of values.
³ From a fit to Crystal Ball (OSTERHELD 86) data.
⁴ From a fit to BES (BAI 02c) data.

$\Gamma(\mu^+\mu^-)$	DOCUMENT ID	TECN	COMMENT
$2.45 \pm 1.24 \pm 0.94$	1,2 ABLIKIM	20A BES3	$e^+e^- \rightarrow \mu^+\mu^-$
••• We do not use the following data for averages, fits, limits, etc. •••			
	1		From a fit to the $e^+e^- \rightarrow \mu^+\mu^-$ cross section between 3.8 and 4.6 GeV to the coherent sum of four resonant amplitudes assuming $\Gamma(\mu^+\mu^-) = \Gamma(e^+e^-)$.
	2		From solution I of 8 with equal fit quality. Other solutions range from $2.08 \pm 0.99 \pm 0.80$ to $2.45 \pm 1.24 \pm 0.94$ keV.

$\psi(4160)$ $\Gamma(i) \times \Gamma(e^+e^-)/\Gamma(\text{total})$

$\Gamma(J/\psi\eta) \times \Gamma(e^+e^-)/\Gamma_{\text{total}}$	DOCUMENT ID	TECN	COMMENT
0.17 ± 0.04	86	1,2 ABLIKIM	20A BES3 $e^+e^- \rightarrow \eta' J/\psi$
1.07 ± 0.09	86	1,3 ABLIKIM	20A BES3 $e^+e^- \rightarrow \eta' J/\psi$
••• We do not use the following data for averages, fits, limits, etc. •••			
	1		Based on a fit to $\sigma(e^+e^- \rightarrow \eta' J/\psi)$ from $\sqrt{s} = 4.18$ to 4.60 GeV assuming interfering $\psi(4160)$ and $\psi(4260)$ contributions. At $\sqrt{s} = 4.18$ GeV, $\sigma(e^+e^- \rightarrow \eta' J/\psi) = 2.4 \pm 0.3 \pm 0.2$ pb.
	2		Solution I of the fit, corresponding to a phase of -0.03 ± 0.44 rad.
	3		Solution II of the fit, corresponding to a phase of 2.54 ± 0.04 rad.

$\Gamma(\chi_{c1}\gamma) \times \Gamma(e^+e^-)/\Gamma_{\text{total}}$	DOCUMENT ID	TECN	COMMENT
< 2.2	90	1 HAN	15 BELL $10.58 e^+e^- \rightarrow \chi_{c1}\gamma$
••• We do not use the following data for averages, fits, limits, etc. •••			
	1		Using $B(\eta \rightarrow \gamma\gamma) = (39.41 \pm 0.21)\%$.

$\Gamma(\chi_{c2}\gamma) \times \Gamma(e^+e^-)/\Gamma_{\text{total}}$	DOCUMENT ID	TECN	COMMENT
< 6.1	90	1 HAN	15 BELL $10.58 e^+e^- \rightarrow \chi_{c2}\gamma$
••• We do not use the following data for averages, fits, limits, etc. •••			
	1		Using $B(\eta \rightarrow \gamma\gamma) = (39.41 \pm 0.21)\%$.

$\Gamma(K_S^0 K^\pm\pi^\mp) \times \Gamma(e^+e^-)/\Gamma_{\text{total}}$	DOCUMENT ID	TECN	COMMENT
$2.71 \pm 0.13 \pm 0.12$	1	ABLIKIM	19AE BES3 $e^+e^- \rightarrow K_S^0 K^\pm\pi^\mp$
$0.0095 \pm 0.0088 \pm 0.0004$	2	ABLIKIM	19AE BES3 $e^+e^- \rightarrow K_S^0 K^\pm\pi^\mp$
••• We do not use the following data for averages, fits, limits, etc. •••			
	1		Solution I of the fit including the $\psi(4160)$ with mass 4191 ± 5 MeV and width 70 ± 10 MeV from PDG 16 and the $\psi(4230)$ with mass $4219.6 \pm 3.3 \pm 5.1$ MeV and width $56.0 \pm 3.6 \pm 6.9$ MeV from GAO 17.
	2		Solution II of the fit including the $\psi(4160)$ with mass 4191 ± 5 MeV and width 70 ± 10 MeV from PDG 16 and the $\psi(4230)$ with mass $4219.6 \pm 3.3 \pm 5.1$ MeV and width $56.0 \pm 3.6 \pm 6.9$ MeV from GAO 17.

$\psi(4160)$ $\Gamma(i) \times \Gamma(e^+e^-)/\Gamma^2(\text{total})$

$\Gamma(J/\psi\eta)/\Gamma_{\text{total}} \times \Gamma(e^+e^-)/\Gamma_{\text{total}}$	DOCUMENT ID	TECN	COMMENT
$2.8 \pm 0.9 \pm 0.9$	1	WANG	13B BELL $e^+e^- \rightarrow J/\psi\eta\gamma$
$12.8 \pm 1.7 \pm 2.0$	2	WANG	13B BELL $e^+e^- \rightarrow J/\psi\eta\gamma$
••• We do not use the following data for averages, fits, limits, etc. •••			
	1		Solution I of two equivalent solutions in a fit using two interfering resonances. Mass and width fixed at 4153 MeV and 103 MeV, respectively.
	2		Solution II of two equivalent solutions in a fit using two interfering resonances. Mass and width fixed at 4153 MeV and 103 MeV, respectively.

$\psi(4160)$ BRANCHING RATIOS

$\Gamma(\mu^+\mu^-)/\Gamma_{\text{total}}$	DOCUMENT ID	TECN	COMMENT
seen	1	AAIJ	13Bc LHCB $B^+ \rightarrow K^+\mu^+\mu^-$
••• We do not use the following data for averages, fits, limits, etc. •••			
	1		AAIJ 13Bc report $B(B^+ \rightarrow K^+\psi(4160))B(\psi(4160) \rightarrow \mu^+\mu^-) = (3.5_{-0.8}^{+0.9}) \times 10^{-9}$.

$\Gamma(D\bar{D})/\Gamma(D^*\bar{D}^*)$	DOCUMENT ID	TECN	COMMENT
$0.02 \pm 0.03 \pm 0.02$	AUBERT	09M BABR	$e^+e^- \rightarrow \gamma D^*(*)\bar{D}^*(*)$

$\Gamma(D^0\bar{D}^0)/\Gamma_{\text{total}}$	DOCUMENT ID	TECN	COMMENT
seen	CRONIN-HEN..09	CLEO	$e^+e^- \rightarrow D^0\bar{D}^0$
seen	PAKHOVA	08 BELL	$e^+e^- \rightarrow D^0\bar{D}^0\gamma$
••• We do not use the following data for averages, fits, limits, etc. •••			
not seen	AUBERT	09M BABR	$e^+e^- \rightarrow D^0\bar{D}^0\gamma$

$\Gamma(D^+D^-)/\Gamma_{\text{total}}$	DOCUMENT ID	TECN	COMMENT
seen	CRONIN-HEN..09	CLEO	$e^+e^- \rightarrow D^+D^-$
seen	PAKHOVA	08 BELL	$e^+e^- \rightarrow D^+D^-\gamma$
••• We do not use the following data for averages, fits, limits, etc. •••			
not seen	AUBERT	09M BABR	$e^+e^- \rightarrow D^+D^-\gamma$

$\Gamma(D^*(2007)^0 \bar{D}^0 + c.c.)/\Gamma_{total}$				Γ_7/Γ
VALUE	DOCUMENT ID	TECN	COMMENT	
seen	AUBERT 09M	BABR	$e^+ e^- \rightarrow D^{*0} \bar{D}^0 \gamma$	
seen	CRONIN-HEN..09	CLEO	$e^+ e^- \rightarrow D^{*0} \bar{D}^0$	

$\Gamma(D^*(2010)^+ D^- + c.c.)/\Gamma_{total}$				Γ_8/Γ
VALUE	DOCUMENT ID	TECN	COMMENT	
seen	1 ZHU KOVA 18	BELL	$e^+ e^- \rightarrow D^{*+} D^- \gamma$	
seen	AUBERT 09M	BABR	$e^+ e^- \rightarrow D^{*+} D^- \gamma$	
seen	CRONIN-HEN..09	CLEO	$e^+ e^- \rightarrow D^{*+} D^-$	
•••	We do not use the following data for averages, fits, limits, etc. •••			
seen	PAKHLOVA 07	BELL	$e^+ e^- \rightarrow D^{*+} D^- \gamma$	

¹ Supersedes PAKHLOVA 07.

$\Gamma(D^* \bar{D} + c.c.)/\Gamma(D^* \bar{D}^*)$				Γ_6/Γ_9
VALUE	DOCUMENT ID	TECN	COMMENT	
$0.34 \pm 0.14 \pm 0.05$	AUBERT 09M	BABR	$e^+ e^- \rightarrow \gamma D^{(*)} \bar{D}^{(*)}$	

$\Gamma(D^*(2007)^0 \bar{D}^*(2007)^0)/\Gamma_{total}$				Γ_{10}/Γ
VALUE	DOCUMENT ID	TECN	COMMENT	
seen	AUBERT 09M	BABR	$e^+ e^- \rightarrow D^{*0} \bar{D}^{*0} \gamma$	
seen	CRONIN-HEN..09	CLEO	$e^+ e^- \rightarrow D^{*0} \bar{D}^{*0}$	

$\Gamma(D^*(2010)^+ D^*(2010)^-)/\Gamma_{total}$				Γ_{11}/Γ
VALUE	DOCUMENT ID	TECN	COMMENT	
seen	1 ZHU KOVA 18	BELL	$e^+ e^- \rightarrow D^{*+} D^{*-} \gamma$	
seen	AUBERT 09M	BABR	$e^+ e^- \rightarrow D^{*+} D^{*-} \gamma$	
seen	CRONIN-HEN..09	CLEO	$e^+ e^- \rightarrow D^{*+} D^{*-}$	
•••	We do not use the following data for averages, fits, limits, etc. •••			
seen	PAKHLOVA 07	BELL	$e^+ e^- \rightarrow D^{*+} D^{*-} \gamma$	

¹ Supersedes PAKHLOVA 07.

$\Gamma(D^0 D^- \pi^+ + c.c. (excl. D^*(2007)^0 \bar{D}^0 + c.c., D^*(2010)^+ D^- + c.c.))/\Gamma_{total}$				Γ_{12}/Γ
VALUE	DOCUMENT ID	TECN	COMMENT	
not seen	PAKHLOVA 08A	BELL	$e^+ e^- \rightarrow D^0 D^- \pi^+ \gamma$	

$\Gamma(D \bar{D}^* \pi + c.c. (excl. D^* \bar{D}^*))/\Gamma_{total}$				Γ_{13}/Γ
VALUE	DOCUMENT ID	TECN	COMMENT	
seen	CRONIN-HEN..09	CLEO	$e^+ e^- \rightarrow D \bar{D}^* \pi$	

$\Gamma(D^0 D^{*-} \pi^+ + c.c. (excl. D^*(2010)^+ D^*(2010)^-))/\Gamma_{total}$				Γ_{14}/Γ
VALUE	DOCUMENT ID	TECN	COMMENT	
not seen	PAKHLOVA 09	BELL	$e^+ e^- \rightarrow D^0 D^{*-} \pi^+ \gamma$	

$\Gamma(D_s^+ D_s^-)/\Gamma_{total}$				Γ_{15}/Γ
VALUE	DOCUMENT ID	TECN	COMMENT	
not seen	PAKHLOVA 11	BELL	$e^+ e^- \rightarrow D_s^+ D_s^- \gamma$	
not seen	DEL-AMO-SA..10N	BABR	$e^+ e^- \rightarrow D_s^+ D_s^- \gamma$	
not seen	CRONIN-HEN..09	CLEO	$e^+ e^- \rightarrow D_s^+ D_s^-$	

$\Gamma(D_s^{*+} D_s^- + c.c.)/\Gamma_{total}$				Γ_{16}/Γ
VALUE	DOCUMENT ID	TECN	COMMENT	
seen	PAKHLOVA 11	BELL	$e^+ e^- \rightarrow D_s^{*+} D_s^- \gamma$	
seen	DEL-AMO-SA..10N	BABR	$e^+ e^- \rightarrow D_s^{*+} D_s^- \gamma$	
seen	CRONIN-HEN..09	CLEO	$e^+ e^- \rightarrow D_s^{*+} D_s^-$	

$\Gamma(J/\psi \pi^+ \pi^-)/\Gamma_{total}$				Γ_{17}/Γ
VALUE (units 10^{-3})	CL%	DOCUMENT ID	TECN	COMMENT
<3	90	COAN 06	CLEO	4.12-4.2 $e^+ e^- \rightarrow$ hadrons

$\Gamma(J/\psi \pi^0 \pi^0)/\Gamma_{total}$				Γ_{18}/Γ
VALUE (units 10^{-3})	CL%	DOCUMENT ID	TECN	COMMENT
<3	90	COAN 06	CLEO	4.12-4.2 $e^+ e^- \rightarrow$ hadrons

$\Gamma(J/\psi K^+ K^-)/\Gamma_{total}$				Γ_{19}/Γ
VALUE (units 10^{-3})	CL%	DOCUMENT ID	TECN	COMMENT
<2	90	COAN 06	CLEO	4.12-4.2 $e^+ e^- \rightarrow$ hadrons

$\Gamma(J/\psi \eta)/\Gamma_{total}$				Γ_{20}/Γ
VALUE (units 10^{-3})	CL%	DOCUMENT ID	TECN	COMMENT
<8	90	COAN 06	CLEO	4.12-4.2 $e^+ e^- \rightarrow$ hadrons
•••	We do not use the following data for averages, fits, limits, etc. •••			
possibly seen	1	ABLIKIM 15L	BES3	$e^+ e^- \rightarrow J/\psi \eta$
seen		WA NG 13B	BELL	$e^+ e^- \rightarrow J/\psi \eta \gamma$

¹ An enhancement around 4.2 GeV is observed.

$\Gamma(J/\psi \pi^0)/\Gamma_{total}$				Γ_{21}/Γ
VALUE (units 10^{-3})	CL%	DOCUMENT ID	TECN	COMMENT
<1	90	COAN 06	CLEO	4.12-4.2 $e^+ e^- \rightarrow$ hadrons

$\Gamma(J/\psi \eta')/\Gamma_{total}$				Γ_{22}/Γ
VALUE (units 10^{-3})	CL%	DOCUMENT ID	TECN	COMMENT
<5	90	COAN 06	CLEO	4.12-4.2 $e^+ e^- \rightarrow$ hadrons

$\Gamma(J/\psi \pi^+ \pi^- \pi^0)/\Gamma_{total}$				Γ_{23}/Γ
VALUE (units 10^{-3})	CL%	DOCUMENT ID	TECN	COMMENT
<1	90	COAN 06	CLEO	4.12-4.2 $e^+ e^- \rightarrow$ hadrons

$\Gamma(\psi(2S) \pi^+ \pi^-)/\Gamma_{total}$				Γ_{24}/Γ
VALUE (units 10^{-3})	CL%	DOCUMENT ID	TECN	COMMENT
<4	90	COAN 06	CLEO	4.12-4.2 $e^+ e^- \rightarrow$ hadrons

$\Gamma(\chi_{c1} \gamma)/\Gamma_{total}$				Γ_{25}/Γ
VALUE (units 10^{-3})	CL%	DOCUMENT ID	TECN	COMMENT
<7	90	COAN 06	CLEO	4.12-4.2 $e^+ e^- \rightarrow$ hadrons
•••	We do not use the following data for averages, fits, limits, etc. •••			

$\Gamma(\chi_{c2} \gamma)/\Gamma_{total}$				Γ_{26}/Γ
VALUE (units 10^{-3})	CL%	DOCUMENT ID	TECN	COMMENT
<13	90	COAN 06	CLEO	4.12-4.2 $e^+ e^- \rightarrow$ hadrons

$\Gamma(\chi_{c1} \pi^+ \pi^- \pi^0)/\Gamma_{total}$				Γ_{27}/Γ
VALUE (units 10^{-3})	CL%	DOCUMENT ID	TECN	COMMENT
<2	90	COAN 06	CLEO	4.12-4.2 $e^+ e^- \rightarrow$ hadrons

$\Gamma(\chi_{c2} \pi^+ \pi^- \pi^0)/\Gamma_{total}$				Γ_{28}/Γ
VALUE (units 10^{-3})	CL%	DOCUMENT ID	TECN	COMMENT
<8	90	COAN 06	CLEO	4.12-4.2 $e^+ e^- \rightarrow$ hadrons

$\Gamma(h_c(1P) \pi^+ \pi^-)/\Gamma_{total}$				Γ_{29}/Γ
VALUE (units 10^{-3})	CL%	DOCUMENT ID	TECN	COMMENT
<5	90	1 PEDLAR 11	CLEO	$e^+ e^- \rightarrow h_c(1P) \pi^+ \pi^-$
				¹ At $\sqrt{s} = 4170$ MeV, PEDLAR 11 measures $\sigma(e^+ e^- \rightarrow h_c(1P) \pi^+ \pi^-) = 15.6 \pm 2.3 \pm 1.9 \pm 3.0$ pb, where the errors are statistical, systematic, and due to uncertainty in $B(\psi(2S) \rightarrow \pi^0 h_c(1P))$, respectively.

$\Gamma(h_c(1P) \pi^0 \pi^0)/\Gamma_{total}$				Γ_{30}/Γ
VALUE (units 10^{-3})	CL%	DOCUMENT ID	TECN	COMMENT
<2	90	1 PEDLAR 11	CLEO	$e^+ e^- \rightarrow h_c(1P) \pi^0 \pi^0$
				¹ At $\sqrt{s} = 4170$ MeV, PEDLAR 11 measures $\sigma(e^+ e^- \rightarrow h_c(1P) \pi^0 \pi^0) = 3.0 \pm 3.3 \pm 1.1 \pm 0.6$ pb, where the errors are statistical, systematic, and due to uncertainty in $B(\psi(2S) \rightarrow \pi^0 h_c(1P))$, respectively.

$\Gamma(h_c(1P) \eta)/\Gamma_{total}$				Γ_{31}/Γ	
VALUE (units 10^{-3})	CL%	EVTS	DOCUMENT ID	TECN	COMMENT
<2	90		1 PEDLAR 11	CLEO	$e^+ e^- \rightarrow h_c(1P) \eta$
•••	We do not use the following data for averages, fits, limits, etc. •••				
possibly seen		41	2 ABLIKIM 17R	BES3	$e^+ e^- \rightarrow h_c(1P) \eta$
					¹ At $\sqrt{s} = 4170$ MeV, PEDLAR 11 measures $\sigma(e^+ e^- \rightarrow h_c(1P) \eta) = 4.7 \pm 1.7 \pm 1.0 \pm 0.9$ pb, where the errors are statistical, systematic, and due to uncertainty in $B(\psi(2S) \rightarrow \pi^0 h_c(1P))$, respectively.
					² An enhancement around 4.2 GeV is observed.

$\Gamma(h_c(1P) \pi^0)/\Gamma_{total}$				Γ_{32}/Γ
VALUE (units 10^{-3})	CL%	DOCUMENT ID	TECN	COMMENT
<0.4	90	1 PEDLAR 11	CLEO	$e^+ e^- \rightarrow h_c(1P) \pi^0$
				¹ At $\sqrt{s} = 4170$ MeV, PEDLAR 11 measures $\sigma(e^+ e^- \rightarrow h_c(1P) \pi^0) = -0.7 \pm 1.8 \pm 0.7 \pm 0.1$ pb, where the errors are statistical, systematic, and due to uncertainty in $B(\psi(2S) \rightarrow \pi^0 h_c(1P))$, respectively.

$\Gamma(\phi \pi^+ \pi^-)/\Gamma_{total}$				Γ_{33}/Γ
VALUE (units 10^{-3})	CL%	DOCUMENT ID	TECN	COMMENT
<2	90	COAN 06	CLEO	4.12-4.2 $e^+ e^- \rightarrow$ hadrons

$\Gamma(\gamma \chi_{c1}(3872))/\Gamma_{total}$				Γ_{34}/Γ
VALUE	CL%	DOCUMENT ID	COMMENT	
<1.8 $\times 10^{-3}$	90	1,2 XIAO 13	$\psi(4160) \rightarrow \gamma J/\psi \pi^+ \pi^-$	
<0.012	90	1,3 XIAO 13	$\psi(4160) \rightarrow \gamma J/\psi \pi^+ \pi^-$	

¹ Obtained by analyzing CLEO data but not authored by the CLEO Collaboration.
² XIAO 13 reports $[\Gamma(\psi(4160) \rightarrow \gamma \chi_{c1}(3872))/\Gamma_{total}] \times [B(\chi_{c1}(3872) \rightarrow \pi^+ \pi^- J/\psi(1S))] < 0.68 \times 10^{-4}$ which we divide by our best value $B(\chi_{c1}(3872) \rightarrow \pi^+ \pi^- J/\psi(1S)) = 3.8 \times 10^{-2}$.
³ XIAO 13 reports $[\Gamma(\psi(4160) \rightarrow \gamma \chi_{c1}(3872))/\Gamma_{total}] \times [B(\chi_{c1}(3872) \rightarrow \gamma J/\psi)] < 1.05 \times 10^{-4}$ which we divide by our best value $B(\chi_{c1}(3872) \rightarrow \gamma J/\psi) = 8 \times 10^{-3}$.

$\Gamma(\gamma \chi_{c0}(3915) \rightarrow \gamma J/\psi \pi^+ \pi^-)/\Gamma_{total}$				Γ_{35}/Γ
VALUE	CL%	DOCUMENT ID	COMMENT	
<1.36 $\times 10^{-4}$	90	1 XIAO 13	$\psi(4160) \rightarrow \gamma J/\psi \pi^+ \pi^-$	
				¹ Obtained by analyzing CLEO data but not authored by the CLEO Collaboration.

Meson Particle Listings

$\psi(4160)$, $X(4160)$, $Z_c(4200)$

$\Gamma(\gamma X(3930) \rightarrow \gamma J/\psi \pi^+ \pi^-) / \Gamma_{\text{total}}$				Γ_{36} / Γ
VALUE	CL%	DOCUMENT ID	COMMENT	
$<1.18 \times 10^{-4}$	90	¹ XIAO 13	$\psi(4160) \rightarrow \gamma J/\psi \pi^+ \pi^-$	

¹ Obtained by analyzing CLEO data but not authored by the CLEO Collaboration.

$\Gamma(\gamma X(3940) \rightarrow \gamma J/\psi \pi^+ \pi^-) / \Gamma_{\text{total}}$				Γ_{37} / Γ
VALUE	CL%	DOCUMENT ID	COMMENT	
$<1.47 \times 10^{-4}$	90	¹ XIAO 13	$\psi(4160) \rightarrow \gamma J/\psi \pi^+ \pi^-$	

¹ Obtained by analyzing CLEO data but not authored by the CLEO Collaboration.

$\Gamma(\gamma X_{c0}(3915) \rightarrow \gamma \gamma J/\psi) / \Gamma_{\text{total}}$				Γ_{38} / Γ
VALUE	CL%	DOCUMENT ID	COMMENT	
$<1.26 \times 10^{-4}$	90	¹ XIAO 13	$\psi(4160) \rightarrow \gamma \gamma J/\psi$	

¹ Obtained by analyzing CLEO data but not authored by the CLEO Collaboration.

$\Gamma(\gamma X(3930) \rightarrow \gamma \gamma J/\psi) / \Gamma_{\text{total}}$				Γ_{39} / Γ
VALUE	CL%	DOCUMENT ID	COMMENT	
$<0.88 \times 10^{-4}$	90	¹ XIAO 13	$\psi(4160) \rightarrow \gamma \gamma J/\psi$	

¹ Obtained by analyzing CLEO data but not authored by the CLEO Collaboration.

$\Gamma(\gamma X(3940) \rightarrow \gamma \gamma J/\psi) / \Gamma_{\text{total}}$				Γ_{40} / Γ
VALUE	CL%	DOCUMENT ID	COMMENT	
$<1.79 \times 10^{-4}$	90	¹ XIAO 13	$\psi(4160) \rightarrow \gamma \gamma J/\psi$	

¹ Obtained by analyzing CLEO data but not authored by the CLEO Collaboration.

$\Gamma(K^+ K^-) / \Gamma_{\text{total}}$					Γ_{41} / Γ
VALUE	CL%	DOCUMENT ID	TECN	COMMENT	
$<2 \times 10^{-5}$	90	¹ DRUZHININ 15	RVUE	$e^+ e^- \rightarrow \psi(3770)$	

• • • We do not use the following data for averages, fits, limits, etc. • • •
¹ DRUZHININ 15 uses BABAR and CLEO data taking into account interference of the processes $e^+ e^- \rightarrow K^+ K^-$ and $e^+ e^- \rightarrow K_S^0 K_L^0$.

$\Gamma(p\bar{p}p\bar{p}) / \Gamma_{\text{total}}$					Γ_{43} / Γ
VALUE	CL%	DOCUMENT ID	TECN	COMMENT	
not seen		ABLIKIM 21D	BES3	$4.0\text{--}4.6 e^+ e^- \rightarrow p\bar{p}p\bar{p}$	

$\Gamma(\Lambda\bar{\Lambda}) \times \Gamma(e^+ e^-) / \Gamma_{\text{total}}$					$\Gamma_{44} \Gamma_1 / \Gamma$
VALUE (eV)	CL%	DOCUMENT ID	TECN	COMMENT	
$<0.7 \times 10^{-3}$	90	¹ ABLIKIM 21AS	BES3	$e^+ e^- \rightarrow \psi(4160)$	

¹ From a measurement of the $e^+ e^- \rightarrow \Lambda\bar{\Lambda}$ cross section between 3.5 and 4.6 GeV.

$\psi(4160)$ REFERENCES

ABLIKIM 21AS	PR D104 L091104	M. Ablikim et al.	(BESIII Collab.)
ABLIKIM 21D	PR D103 052003	M. Ablikim et al.	(BESIII Collab.)
ABLIKIM 20A	PR D101 012008	M. Ablikim et al.	(BESIII Collab.)
ABLIKIM 20AG	PR D102 112009	M. Ablikim et al.	(BESIII Collab.)
ABLIKIM 19AE	PR D99 072005	M. Ablikim et al.	(BESIII Collab.)
ZHUKOVA 18	PR D97 012002	V. Zhukova et al.	(BELLE Collab.)
ABLIKIM 17R	PR D96 012001	M. Ablikim et al.	(BESIII Collab.)
GAO 17	PR D95 092007	X.Y. Gao, C.P. Shen, C.Z. Yuan	(PDG Collab.)
PDG 16	CP C40 100001	C. Patrignani et al.	(BESIII Collab.)
ABLIKIM 15L	PR D91 112005	M. Ablikim et al.	(BESIII Collab.)
DRUZHININ 15	PR D92 054024	V.P. Druzhinin	(NOVO)
HAN 15	PR D92 012011	Y.L. Han et al.	(BELLE Collab.)
AAIJ 13BC	PRL 111 112003	R. Aaij et al.	(LHCb Collab.)
WANG 13B	PR D87 051101	X.L. Wang et al.	(BELLE Collab.)
XIAO 13	PR D87 057501	T. Xiao et al.	(NWES, WAYN)
PAKHLOVA 11	PR D83 011101	G. Pakhlova et al.	(BELLE Collab.)
PEDLAR 11	PRL 107 041803	T. Pedlar et al.	(CLEO Collab.)
DEL-AMO-SA... 10N	PR D82 052004	P. del Amo Sanchez et al.	(BABAR Collab.)
MO 10	PR D82 077501	X.H. Mo, C.Z. Yuan, P. Wang	(BHEP)
AUBERT 09M	PR D79 092001	B. Aubert et al.	(BABAR Collab.)
CRONIN-HEN... 09	PR D80 072001	D. Cronin-Hennessy et al.	(CLEO Collab.)
PAKHLOVA 09	PR D80 091101	G. Pakhlova et al.	(BELLE Collab.)
ABLIKIM 08D	PL B660 315	M. Ablikim et al.	(BES Collab.)
PAKHLOVA 08	PR D77 011103	G. Pakhlova et al.	(BELLE Collab.)
PAKHLOVA 08A	PRL 100 062001	G. Pakhlova et al.	(BELLE Collab.)
PAKHLOVA 07	PRL 98 092001	G. Pakhlova et al.	(BELLE Collab.)
COAN 06	PRL 96 162003	T.E. Coan et al.	(CLEO Collab.)
SETH 05A	PR D72 017501	K.K. Seth	
BAI 02C	PRL 88 101802	J.Z. Bai et al.	(BES Collab.)
BAI 00	PRL 84 594	J.Z. Bai et al.	(BES Collab.)
OSTERHELD 86	SLAC-PUB-4160	A. Osterheld et al.	(SLAC Crystal Ball Collab.)
BRANDELK 78C	PL 76B 361	R. Brandelik et al.	(DASP Collab.)

$X(4160)$

$$J^G(J^{PC}) = ?^?(???)$$

OMITTED FROM SUMMARY TABLE

Seen by PAKHLOV 08 in $e^+ e^- \rightarrow J/\psi X$, $X \rightarrow D^* \bar{D}^*$

A state with consistent mass and width is seen by AAIJ 21E in $B^+ \rightarrow X(4160) K^+$ with $X(4160) \rightarrow J/\psi \phi$ using an amplitude analysis of $B^+ \rightarrow J/\psi \phi K^+$ with a significance (accounting for systematic uncertainties) of 4.8σ . The $J^{PC} = 2^- 1^+$ assignment is favored over other assignments with a significance of more than 4σ .

$X(4160)$ MASS

VALUE (MeV)	EVTS	DOCUMENT ID	TECN	COMMENT
-------------	------	-------------	------	---------

4153⁺²³₋₂₁ OUR AVERAGE

4146 ± 18 ± 33	24k	¹ AAIJ	21E	LHCb $B^+ \rightarrow J/\psi \phi K^+$
4156 ⁺²⁵ ₋₂₀ ± 15	24	PAKHLOV	08	BELL $e^+ e^- \rightarrow J/\psi X$

¹ From an amplitude analysis of the decay $B^+ \rightarrow J/\psi \phi K^+$ with a significance of 4.8σ .

$X(4160)$ WIDTH

VALUE (MeV)	EVTS	DOCUMENT ID	TECN	COMMENT
-------------	------	-------------	------	---------

136⁺⁶⁰₋₃₅ OUR AVERAGE

135 ± 28 ⁺⁵⁹ ₋₃₀	24k	¹ AAIJ	21E	LHCb $B^+ \rightarrow J/\psi \phi K^+$
139 ⁺¹¹¹ ₋₆₁ ± 21	24	PAKHLOV	08	BELL $e^+ e^- \rightarrow J/\psi X$

¹ From an amplitude analysis of the decay $B^+ \rightarrow J/\psi \phi K^+$ with a significance of 4.8σ .

$X(4160)$ DECAY MODES

Mode	Fraction (Γ_i / Γ)
Γ_1 $D \bar{D}$	not seen
Γ_2 $D^* \bar{D}^+$ + c.c.	not seen
Γ_3 $D^* \bar{D}^*$	seen
Γ_4 $J/\psi \phi$	seen

$X(4160)$ BRANCHING RATIOS

$\Gamma(D \bar{D}) / \Gamma(D^* \bar{D}^*)$				Γ_1 / Γ_3
VALUE	CL%	DOCUMENT ID	TECN	COMMENT
<0.09	90	PAKHLOV 08	BELL	$e^+ e^- \rightarrow J/\psi X$

$\Gamma(D^* \bar{D}^+ \text{ c.c.}) / \Gamma(D^* \bar{D}^*)$				Γ_2 / Γ_3
VALUE	CL%	DOCUMENT ID	TECN	COMMENT
<0.22	90	PAKHLOV 08	BELL	$e^+ e^- \rightarrow J/\psi X$

$\Gamma(J/\psi \phi) / \Gamma_{\text{total}}$				Γ_4 / Γ
VALUE	EVTS	DOCUMENT ID	TECN	COMMENT
seen	24k	¹ AAIJ	21E	LHCb $B^+ \rightarrow J/\psi \phi K^+$

¹ From an amplitude analysis of the decay $B^+ \rightarrow J/\psi \phi K^+$ with a significance of 4.8σ .

$X(4160)$ REFERENCES

AAIJ 21E	PRL 127 082001	R. Aaij et al.	(LHCb Collab.)
PAKHLOV 08	PRL 100 202001	P. Pakhlov et al.	(BELLE Collab.)

$Z_c(4200)$

$$J^G(J^{PC}) = 1^+(1^+ -)$$

I, G, C need confirmation.

OMITTED FROM SUMMARY TABLE

was $X(4200)^{\pm}$

This state shows properties different from a conventional $q\bar{q}$ state. A candidate for an exotic structure. See the review on non- $q\bar{q}$ states.

Reported by CHILIKIN 14 in $J/\psi \pi^+$ at a significance of 6.2σ . Assignments of 0^- , 1^- , 2^- , and 2^+ excluded at 6.1σ , 7.4σ , 4.4σ , and 7.0σ level, respectively. Needs confirmation.

$Z_c(4200)$ MASS

VALUE (MeV)	DOCUMENT ID	TECN	COMMENT
-------------	-------------	------	---------

4196⁺³¹₋₂₉ ± 17₋₁₃ CHILIKIN 14 BELL $\bar{B}^0 \rightarrow J/\psi K^- \pi^+$

$Z_c(4200)$ WIDTH

VALUE (MeV)	DOCUMENT ID	TECN	COMMENT
-------------	-------------	------	---------

370 ± 70⁺⁷⁰₋₁₃₂ CHILIKIN 14 BELL $\bar{B}^0 \rightarrow J/\psi K^- \pi^+$

$Z_c(4200)$ DECAY MODES

Mode	Fraction (Γ_i / Γ)
Γ_1 $J/\psi \pi^+$	seen

See key on page 1127

Meson Particle Listings

Z_c(4200), ψ(4230)

Z_c(4200) BRANCHING RATIOS

Γ(J/ψπ ⁺)/Γ _{total}	DOCUMENT ID	TECN	COMMENT	Γ ₁ /Γ
seen	CHILIKIN	14	BELL $\bar{B}^0 \rightarrow J/\psi K^- \pi^+$	
possibly seen	¹ AALJ	19R	LHCb $B^0 \rightarrow K^+ \pi^- J/\psi + c.c.$	

• • • We do not use the following data for averages, fits, limits, etc. • • •

¹ From a model-independent analysis.

Z_c(4200) REFERENCES

AALJ	19R	PRL 122 152002	R. Aaij <i>et al.</i>	(LHCb Collab.)
CHILIKIN	14	PR D90 112009	K. Chilikin <i>et al.</i>	(BELLE Collab.)

ψ(4230)

$$J^G(J^{PC}) = 0^-(1^{--})$$

also known as Y(4230); was ψ(4260)

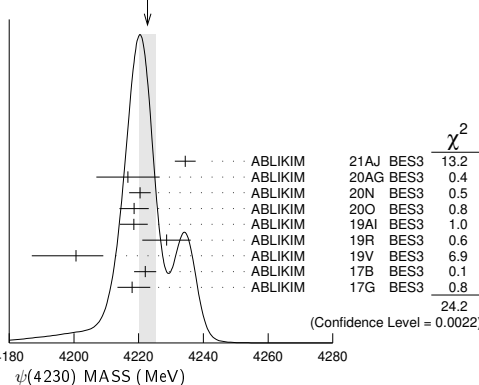
The original ψ(4260) (also known as Y(4260)) was observed by AUBERT, B 051 as a peak in the energy dependence of the e⁺e⁻ → π⁺π⁻J/ψ cross section and was confirmed by HE 06B, YUAN 07, LEES 12AC, and LIU 13B in the same process. A higher-statistics analysis by ABLIKIM 17B revealed an asymmetry in the cross section and resulted in a shift of the peak position to a lower mass. The ψ(4260) was therefore renamed ψ(4230). The energy-dependent cross sections for e⁺e⁻ to other channels also exhibit peaks in the same mass region. The parameters corresponding to those peaks are also listed here, but the number of states in this region remains to be determined.

For details see the review on "Spectroscopy of mesons containing two heavy quarks."

ψ(4230) MASS

VALUE (MeV)	EVTS	DOCUMENT ID	TECN	COMMENT
4222.7 ± 2.6 OUR AVERAGE				Error includes scale factor of 1.7. See the ideogram below.
4234.4 ± 3.2 ± 0.2		¹ ABLIKIM	21AJ BES3	e ⁺ e ⁻ → π ⁺ π ⁻ ψ(2S)
4216.7 ± 8.9 ± 4.1		² ABLIKIM	20AG BES3	e ⁺ e ⁻ → μ ⁺ μ ⁻
4220.4 ± 2.4 ± 2.3		³ ABLIKIM	20N BES3	e ⁺ e ⁻ → π ⁰ π ⁰ J/ψ
4218.6 ± 3.8 ± 2.5		³ ABLIKIM	20O BES3	e ⁺ e ⁻ → ηJ/ψ
4218.5 ± 1.6 ± 4.0		⁴ ABLIKIM	19AI BES3	e ⁺ e ⁻ → ωχ _{c0}
4228.6 ± 4.1 ± 6.3		ABLIKIM	19R BES3	e ⁺ e ⁻ → π ⁺ D ⁰ D ^{0*} + c.c.
4200.6 ^{+7.9} _{-13.3} ± 3.0		⁵ ABLIKIM	19V BES3	e ⁺ e ⁻ → γχ _{c1} (3872)
4222.0 ± 3.1 ± 1.4		⁶ ABLIKIM	17B BES3	e ⁺ e ⁻ → π ⁺ π ⁻ J/ψ
4218 ± 5.5 ± 0.9		ABLIKIM	17G BES3	e ⁺ e ⁻ → π ⁺ π ⁻ h _c
• • • We do not use the following data for averages, fits, limits, etc. • • •				
4231.9 ± 5.3 ± 4.9		ABLIKIM	20N BES3	e ⁺ e ⁻ → π ⁰ Z _c (3900) ⁰ , Z _c ⁰ → π ⁰ J/ψ
4209.5 ± 7.4 ± 1.4		⁷ ABLIKIM	17V BES3	e ⁺ e ⁻ → π ⁺ π ⁻ ψ(2S)
4209.1 ± 6.8 ± 7.0		⁶ ZHANG	17B RVUE	e ⁺ e ⁻ → π ⁺ π ⁻ ψ(2S)
4223.3 ± 1.6 ± 2.5		⁸ ZHANG	17C RVUE	e ⁺ e ⁻ → π ⁺ π ⁻ J/ψ or ψ(2S)
4230 ± 8 ± 6180		⁹ ABLIKIM	15C BES3	e ⁺ e ⁻ → ωχ _{c0}
4258.6 ± 8.3 ± 12.1		¹⁰ LIU	13B BELL	e ⁺ e ⁻ → γπ ⁺ π ⁻ J/ψ
4245 ± 5 ± 4		¹¹ LEES	12AC BABR	10.58 e ⁺ e ⁻ → γπ ⁺ π ⁻ J/ψ
4247 ± 12 ± 17		^{10,12} YUAN	07 BELL	10.58 e ⁺ e ⁻ → γπ ⁺ π ⁻ J/ψ
4284 ± 17		HE	06B CLEO	9.4-10.6 e ⁺ e ⁻ → γπ ⁺ π ⁻ J/ψ
4259 ± 8 ± 2		¹³ AUBERT, B	05I BABR	10.58 e ⁺ e ⁻ → γπ ⁺ π ⁻ J/ψ

WEIGHTED AVERAGE
4222.7 ± 2.6 (Error scaled by 1.7)



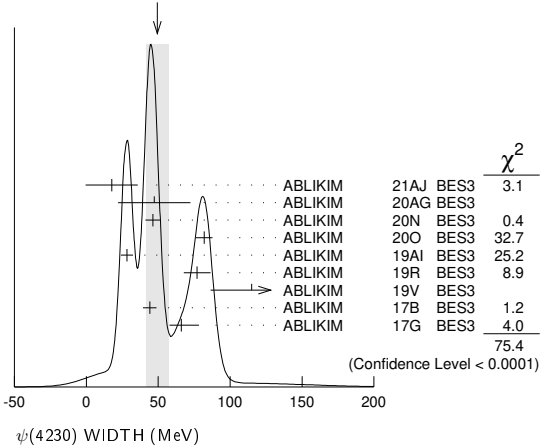
¹ From a three-resonance fit to the Born cross section in the range √s = 4.008–4.698 GeV.

- Solution 1 of 8 with equal fit quality to the e⁺e⁻ → μ⁺μ⁻ cross section between 3.8 and 4.6 GeV to the coherent sum of four resonant amplitudes. Other solutions range from 4212.8 ± 7.2 ± 4.0 to 4219.4 ± 11.2 ± 4.1 MeV.
- From a fit of the measured cross section in the range √s = 3.808–4.600 GeV.
- From a fit of the measured cross section from √s = 4.178–4.278 GeV. Supersedes ABLIKIM 15C.
- Simultaneous fit to χ_{c1} → ωJ/ψ and χ_{c1} → π⁺π⁻J/ψ.
- From a three-resonance fit.
- From a fit to the cross section for e⁺e⁻ → π⁺π⁻ψ(2S) → 2(π⁺π⁻)ℓ⁺ℓ⁻ obtained from 16 center-of-mass energies between 4.008 and 4.600 GeV and comprising 5.1 fb⁻¹. Superseded by ABLIKIM 21A.
- From a combined fit of BELLE, BABAR and BES3 e⁺e⁻ → π⁺π⁻J/ψ and e⁺e⁻ → π⁺π⁻ψ(2S) data.
- From a 3-parameter fit of measured cross sections from √s = 4.21–4.42 GeV to a phase-space modified Breit-Wigner function, using the decays χ_{c0} → π⁺π⁻, χ_{c0} → K⁺K⁻, and ω → π⁺π⁻π⁰.
- From a two-resonance fit.
- From a single-resonance fit. Supersedes AUBERT, B 051.
- Superseded by LIU 13B.
- From a single-resonance fit. Two interfering resonances are not excluded. Superseded by LEES 12AC.

ψ(4230) WIDTH

VALUE (MeV)	EVTS	DOCUMENT ID	TECN	COMMENT
49 ± 8 OUR AVERAGE				Error includes scale factor of 3.5. See the ideogram below.
17.6 ± 18.1 ± 0.9		¹ ABLIKIM	21AJ BES3	e ⁺ e ⁻ → π ⁺ π ⁻ ψ(2S)
47.2 ± 22.8 ± 10.5		² ABLIKIM	20AG BES3	e ⁺ e ⁻ → μ ⁺ μ ⁻
46.2 ± 4.7 ± 2.1		³ ABLIKIM	20N BES3	e ⁺ e ⁻ → π ⁰ π ⁰ J/ψ
82.0 ± 5.7 ± 0.4		³ ABLIKIM	20O BES3	e ⁺ e ⁻ → ηJ/ψ
28.2 ± 3.9 ± 1.6		⁴ ABLIKIM	19AI BES3	e ⁺ e ⁻ → ωχ _{c0}
77.0 ± 6.8 ± 6.3		ABLIKIM	19R BES3	e ⁺ e ⁻ → π ⁺ D ⁰ D ^{0*} + c.c.
115 ⁺³⁸ ₋₂₆ ± 12		⁵ ABLIKIM	19V BES3	e ⁺ e ⁻ → γχ _{c1} (3872)
44.1 ± 4.3 ± 2.0		⁶ ABLIKIM	17B BES3	e ⁺ e ⁻ → π ⁺ π ⁻ J/ψ
66.0 ^{+12.3} _{-8.3} ± 0.4		ABLIKIM	17G BES3	e ⁺ e ⁻ → π ⁺ π ⁻ h _c
• • • We do not use the following data for averages, fits, limits, etc. • • •				
41.2 ± 16.0 ± 16.4		ABLIKIM	20N BES3	e ⁺ e ⁻ → π ⁰ Z _c (3900) ⁰ , Z _c ⁰ → π ⁰ J/ψ
80.1 ± 24.6 ± 2.9		⁷ ABLIKIM	17V BES3	e ⁺ e ⁻ → π ⁺ π ⁻ ψ(2S)
76.6 ± 14.2 ± 2.4		⁶ ZHANG	17B RVUE	e ⁺ e ⁻ → π ⁺ π ⁻ ψ(2S)
54.2 ± 2.6 ± 1.0		⁸ ZHANG	17C RVUE	e ⁺ e ⁻ → π ⁺ π ⁻ J/ψ or ψ(2S)
38 ± 12 ± 2 180		⁹ ABLIKIM	15C BES3	e ⁺ e ⁻ → ωχ _{c0}
134.1 ± 16.4 ± 5.5		¹⁰ LIU	13B BELL	e ⁺ e ⁻ → γπ ⁺ π ⁻ J/ψ
114 ⁺¹⁶ ₋₁₅ ± 7		¹¹ LEES	12AC BABR	10.58 e ⁺ e ⁻ → γπ ⁺ π ⁻ J/ψ
108 ± 19 ± 10		^{10,12} YUAN	07 BELL	10.58 e ⁺ e ⁻ → γπ ⁺ π ⁻ J/ψ
73 ± 39		HE	06B CLEO	9.4-10.6 e ⁺ e ⁻ → γπ ⁺ π ⁻ J/ψ
88 ± 23 ± 6		¹²⁵ AUBERT, B	05I BABR	10.58 e ⁺ e ⁻ → γπ ⁺ π ⁻ J/ψ

WEIGHTED AVERAGE
49 ± 8 (Error scaled by 3.5)



- From a three-resonance fit to the Born cross section in the range √s = 4.008–4.698 GeV.
- Solution 1 of 8 with equal fit quality to the e⁺e⁻ → μ⁺μ⁻ cross section between 3.8 and 4.6 GeV to the coherent sum of four resonant amplitudes. Other solutions range from 36.4 ± 16.8 ± 8.1 to 49.6 ± 22.6 ± 11.0 MeV.
- From a fit of the measured cross section in the range √s = 3.808–4.600 GeV.
- From a fit of the measured cross section from √s = 4.178–4.278 GeV. Supersedes ABLIKIM 15C.
- Simultaneous fit to χ_{c1} → ωJ/ψ and χ_{c1} → π⁺π⁻J/ψ.
- From a three-resonance fit.
- From a fit to the cross section for e⁺e⁻ → π⁺π⁻ψ(2S) → 2(π⁺π⁻)ℓ⁺ℓ⁻ obtained from 16 center-of-mass energies between 4.008 and 4.600 GeV and comprising 5.1 fb⁻¹. Superseded by ABLIKIM 21A.

Meson Particle Listings

$\psi(4230)$

- ⁸From a combined fit of BELLE, BABAR and BES3 $e^+e^- \rightarrow \pi^+\pi^- J/\psi$ and $e^+e^- \rightarrow \pi^+\pi^-\psi(2S)$ data.
- ⁹From a 3-parameter fit of measured cross sections from $\sqrt{s} = 4.21\text{--}4.42$ GeV to a phase-space modified Breit-Wigner function, using the decays $\chi_{c0} \rightarrow \pi^+\pi^-$, $\chi_{c0} \rightarrow K^+K^-$, and $\omega \rightarrow \pi^+\pi^-\pi^0$.
- ¹⁰From a two-resonance fit.
- ¹¹From a single-resonance fit. Supersedes AUBERT,B 05i.
- ¹²Superseded by LIU 13b.
- ¹³From a single-resonance fit. Two interfering resonances are not excluded. Superseded by LEES 12Ac.

$\psi(4230)$ DECAY MODES

Mode	Fraction (Γ_i/Γ)
Γ_1 e^+e^-	
Γ_2 $\mu^+\mu^-$	$(3.1 \pm 2.8) \times 10^{-5}$
Γ_3 $\eta_c(1S)\pi^+\pi^-$	not seen
Γ_4 $\eta_c(1S)\pi^+\pi^-\pi^0$	seen
Γ_5 $J/\psi\pi^+\pi^-$	seen
Γ_6 $J/\psi f_0(980)$, $f_0(980) \rightarrow \pi^+\pi^-$	seen
Γ_7 $Z_c(3900)^\pm \pi^\mp$, $Z_c^\pm \rightarrow J/\psi\pi^\pm$	seen
Γ_8 $J/\psi\pi^0\pi^0$	seen
Γ_9 $J/\psi K^+K^-$	seen
Γ_{10} $J/\psi K_S^0 K_S^0$	not seen
Γ_{11} $J/\psi\eta$	seen
Γ_{12} $J/\psi\pi^0$	not seen
Γ_{13} $J/\psi\eta'$	seen
Γ_{14} $J/\psi\pi^+\pi^-\pi^0$	not seen
Γ_{15} $J/\psi\eta\pi^0$	not seen
Γ_{16} $J/\psi\eta\eta$	not seen
Γ_{17} $\psi(2S)\pi^+\pi^-$	seen
Γ_{18} $\psi(2S)\eta$	not seen
Γ_{19} $\chi_{c0}\omega$	seen
Γ_{20} $\chi_{c1}\pi^+\pi^-\pi^0$	not seen
Γ_{21} $\chi_{c2}\pi^+\pi^-\pi^0$	not seen
Γ_{22} $h_c(1P)\pi^+\pi^-$	seen
Γ_{23} $\phi\pi^+\pi^-$	not seen
Γ_{24} $\phi f_0(980) \rightarrow \phi\pi^+\pi^-$	not seen
Γ_{25} $D\bar{D}^0$	not seen
Γ_{26} $D^0\bar{D}^0$	not seen
Γ_{27} D^+D^-	not seen
Γ_{28} $D^*\bar{D}^0 + c.c.$	not seen
Γ_{29} $D^*(2007)^0\bar{D}^0 + c.c.$	not seen
Γ_{30} $D^*(2010)^+D^- + c.c.$	not seen
Γ_{31} $D^*\bar{D}^*$	
Γ_{32} $D^*(2007)^0\bar{D}^*(2007)^0$	not seen
Γ_{33} $D^*(2010)^+D^*(2010)^-$	not seen
Γ_{34} $D\bar{D}\pi + c.c.$	
Γ_{35} $D^0D^-\pi^+ + c.c.$ (excl. $D^*(2007)^0\bar{D}^{*0} + c.c.$, $D^*(2010)^+D^- + c.c.$)	not seen
Γ_{36} $D\bar{D}^*\pi + c.c.$ (excl. $D^*\bar{D}^*$)	not seen
Γ_{37} $D^0D^-\pi^+ + c.c.$ (excl. $D^*(2010)^+D^*(2010)^-$)	not seen
Γ_{38} $D^0D^*(2010)^-\pi^+ + c.c.$	seen
Γ_{39} $D_1(2420)\bar{D} + c.c.$	not seen
Γ_{40} $D^*\bar{D}^*\pi$	not seen
Γ_{41} $D_s^+D_s^-$	not seen
Γ_{42} $D_s^{*+}D_s^- + c.c.$	not seen
Γ_{43} $D_s^{*+}D_s^{*-}$	not seen
Γ_{44} $\rho\bar{\rho}$	not seen
Γ_{45} $\rho\bar{\rho}\pi^0$	not seen
Γ_{46} $\rho\bar{\rho}\eta$	not seen
Γ_{47} $\rho\bar{\rho}\omega$	not seen
Γ_{48} $\Xi^- \Xi^+$	not seen
Γ_{49} $\pi^+\pi^+\pi^-\pi^-$	not seen
Γ_{50} $\pi^+\pi^+\pi^-\pi^-\pi^0$	not seen
Γ_{51} $K_S^0 K^\pm\pi^\mp$	not seen
Γ_{52} $K_S^0 K^\pm\pi^\mp\pi^0$	not seen
Γ_{53} $K_S^0 K^\pm\pi^\mp\eta$	not seen
Γ_{54} $K^+K^-\pi^0$	not seen
Γ_{55} $K^+K^-\pi^+\pi^-$	not seen
Γ_{56} $K^+K^-\pi^+\pi^-\pi^0$	not seen
Γ_{57} $K^+K^+K^-K^-$	not seen
Γ_{58} $K^+K^+K^-K^-\pi^0$	not seen

Γ_{59} $\rho\bar{\rho}\pi^+\pi^-$	not seen
Γ_{60} $\rho\bar{\rho}\pi^+\pi^-\pi^0$	not seen
Γ_{61} $\rho\bar{\rho}\rho\bar{\rho}$	not seen
Γ_{62} $\Lambda\bar{\Lambda}$	not seen

Radiative decays

Γ_{63} $\eta_c(1S)\gamma$	possibly seen
Γ_{64} $\eta_c(1S)\pi^0\gamma$	not seen
Γ_{65} $\chi_{c1}\gamma$	not seen
Γ_{66} $\chi_{c2}\gamma$	not seen
Γ_{67} $\chi_{c1}(3872)\gamma$	seen

$\psi(4230)$ PARTIAL WIDTHS

$\Gamma(\mu^+\mu^-)$	VALUE (keV)	DOCUMENT ID	TECN	COMMENT
$1.53 \pm 1.26 \pm 0.54$		1,2 ABLIKIM	20A BES3	$e^+e^- \rightarrow \mu^+\mu^-$

¹ From a fit to the $e^+e^- \rightarrow \mu^+\mu^-$ cross section between 3.8 and 4.6 GeV to the coherent sum of four resonant amplitudes assuming $\Gamma(\mu^+\mu^-) = \Gamma(e^+e^-)$.
² From solution I of 8 with equal fit quality. Other solutions range from $1.09 \pm 0.84 \pm 0.39$ to $1.53 \pm 1.26 \pm 0.54$ keV.

$\psi(4230)$ $\Gamma(i) \times \Gamma(e^+e^-)/\Gamma(\text{total})$

$\Gamma(J/\psi\pi^+\pi^-) \times \Gamma(e^+e^-)/\Gamma_{\text{total}}$	VALUE (eV)	EVTS	DOCUMENT ID	TECN	COMMENT
9.2 ± 1.0 OUR AVERAGE					
	$9.2 \pm 0.8 \pm 0.7$		¹ LEES	12Ac BABR	$10.58 e^+e^- \rightarrow \gamma\pi^+\pi^- J/\psi$
	$8.9^{+3.9}_{-3.1} \pm 1.8$	8.1	HE	06B CLEO	$9.4\text{--}10.6 e^+e^- \rightarrow \gamma\pi^+\pi^- J/\psi$
	$6.4 \pm 0.8 \pm 0.6$		² LIU	13B BELL	$9.4\text{--}10.9 e^+e^- \rightarrow \gamma\pi^+\pi^- J/\psi$
	$20.5 \pm 1.4 \pm 2.0$		³ LIU	13B BELL	$e^+e^- \rightarrow \gamma\pi^+\pi^- J/\psi$
	$6.0 \pm 1.2^{+4.7}_{-0.5}$		^{2,4} YUAN	07 BELL	$10.58 e^+e^- \rightarrow \gamma\pi^+\pi^- J/\psi$
	$20.6 \pm 2.3^{+9.1}_{-1.7}$		^{3,4} YUAN	07 BELL	$10.58 e^+e^- \rightarrow \gamma\pi^+\pi^- J/\psi$
	$5.5 \pm 1.0^{+0.8}_{-0.7}$	125	⁵ AUBERT,B	05i BABR	$10.58 e^+e^- \rightarrow \gamma\pi^+\pi^- J/\psi$

- ¹ From a single-resonance fit. Supersedes AUBERT,B 05i.
- ² Solution I of two equivalent solutions in a fit using two interfering resonances.
- ³ Solution II of two equivalent solutions in a fit using two interfering resonances.
- ⁴ Superseded by LIU 13b.
- ⁵ From a single-resonance fit. Two interfering resonances are not excluded. Superseded by LEES 12Ac.

$\Gamma(J/\psi K^+K^-) \times \Gamma(e^+e^-)/\Gamma_{\text{total}}$	VALUE (eV)	CL%	DOCUMENT ID	TECN	COMMENT
<1.7	90		¹ SHEN	14 BELL	$9.4\text{--}10.9 e^+e^- \rightarrow \gamma K^+K^- J/\psi$
<1.2	90		² YUAN	08 BELL	$e^+e^- \rightarrow \gamma K^+K^- J/\psi$

- ¹ From a fit of the broad $K^+K^- J/\psi$ enhancement including a coherent $\psi(4260)$ amplitude with mass and width from LIU 13b. Supersedes YUAN 08. The shape of the cross section observed by ABLIKIM 18N between 2.2 and 2.3 GeV is incompatible with that of $e^+e^- \rightarrow \pi^+\pi^- J/\psi$ in ABLIKIM 13T and ABLIKIM 17b. They also observe a broad enhancement around 2.5 GeV.
- ² From a fit of the broad $K^+K^- J/\psi$ enhancement including a coherent $\psi(4260)$ amplitude with mass and width from YUAN 07.

$\Gamma(J/\psi K_S^0 K_S^0) \times \Gamma(e^+e^-)/\Gamma_{\text{total}}$	VALUE (eV)	CL%	DOCUMENT ID	TECN	COMMENT
<0.85	90		¹ SHEN	14 BELL	$9.4\text{--}10.9 e^+e^- \rightarrow \gamma K_S^0 K_S^0 J/\psi$

- ¹ From a fit of the $K_S^0 K_S^0 J/\psi$ mass range from 4.4 to 5.5 GeV including a coherent $\psi(4260)$ amplitude with mass and width from LIU 13b.

$\Gamma(J/\psi\eta) \times \Gamma(e^+e^-)/\Gamma_{\text{total}}$	VALUE (eV)	CL%	DOCUMENT ID	TECN	COMMENT
	8.0 ± 1.7		¹ ABLIKIM	20a BES3	$e^+e^- \rightarrow \eta J/\psi$
	4.8 ± 1.0		² ABLIKIM	20a BES3	$e^+e^- \rightarrow \eta J/\psi$
	7.0 ± 1.5		³ ABLIKIM	20a BES3	$e^+e^- \rightarrow \eta J/\psi$
	<14.2	90	WANG	13B BELL	$e^+e^- \rightarrow J/\psi\eta\gamma$

- ¹ Solution 1 of three equivalent fit solutions using three resonant structures.
- ² Solution 2 of three equivalent fit solutions using three resonant structures.
- ³ Solution 3 of three equivalent fit solutions using three resonant structures.

$\Gamma(J/\psi\eta') \times \Gamma(e^+e^-)/\Gamma_{\text{total}}$	VALUE (eV)	EVTS	DOCUMENT ID	TECN	COMMENT
	0.06 ± 0.03	46	^{1,2} ABLIKIM	20A BES3	$e^+e^- \rightarrow \eta' J/\psi$
	1.38 ± 0.11	46	^{1,3} ABLIKIM	20A BES3	$e^+e^- \rightarrow \eta' J/\psi$

¹ Based on a fit to $\sigma(e^+e^- \rightarrow \eta' J/\psi)$ from $\sqrt{s} = 4.18$ to 4.60 GeV assuming interfering $\psi(4160)$ and $\psi(4260)$ contributions. At $\sqrt{s} = 4.23$ GeV, $\sigma(e^+e^- \rightarrow \eta' J/\psi) = 3.6 \pm 0.6 \pm 0.3$ pb.
² Solution I of the fit, corresponding to a phase of -0.03 ± 0.44 rad.
³ Solution II of the fit, corresponding to a phase of 2.54 ± 0.04 rad.

$\Gamma(\psi(2S)\pi^+\pi^-) \times \Gamma(e^+e^-)/\Gamma_{total}$ $\Gamma_{17}\Gamma_1/\Gamma$

VALUE (eV)	CL%	DOCUMENT ID	TECN	COMMENT
1.59±0.75		¹ ABLIKIM	21AJ BES3	$e^+e^- \rightarrow \pi^+\pi^-\psi(2S)$
1.63±0.78		² ABLIKIM	21AJ BES3	$e^+e^- \rightarrow \pi^+\pi^-\psi(2S)$
0.02±0.01		³ ABLIKIM	21AJ BES3	$e^+e^- \rightarrow \pi^+\pi^-\psi(2S)$
1.6 ±1.3		⁴ ABLIKIM	19K BES3	$e^+e^- \rightarrow \pi^+\pi^-\psi(2S)$
1.8 ±1.4		⁵ ABLIKIM	19K BES3	$e^+e^- \rightarrow \pi^+\pi^-\psi(2S)$
<4.3	90	⁶ LIU	08H RVUE	10.58 $e^+e^- \rightarrow \psi(2S)\pi^+\pi^-\gamma$
7.4 ^{+2.1} _{-1.7}		⁷ LIU	08H RVUE	10.58 $e^+e^- \rightarrow \psi(2S)\pi^+\pi^-\gamma$

- • • We do not use the following data for averages, fits, limits, etc. • • •
- ¹ Solution I of four equivalent solutions in a fit using three interfering resonances.
- ² Solution II of four equivalent solutions in a fit using three interfering resonances.
- ³ Solutions III and IV of four equivalent solutions in a fit using three interfering resonances.
- ⁴ Solution I of two equivalent solutions in a fit using two interfering resonances.
- ⁵ Solution II of two equivalent solutions in a fit using two interfering resonances.
- ⁶ For constructive interference with the $\psi(4360)$ in a combined fit of AUBERT 07s and WANG 07b data with three resonances.
- ⁷ For destructive interference with the $\psi(4360)$ in a combined fit of AUBERT 07s and WANG 07b data with three resonances.

$\Gamma(\chi_{c0}\omega) \times \Gamma(e^+e^-)/\Gamma_{total}$ $\Gamma_{19}\Gamma_1/\Gamma$

VALUE (eV)	CL%	DOCUMENT ID	TECN	COMMENT
2.5 ± 0.2 ± 0.3		¹ ABLIKIM	19Ai BES3	$e^+e^- \rightarrow \omega\chi_{c0}$
2.7 ± 0.5 ± 0.4	180	² ABLIKIM	15c BES3	$e^+e^- \rightarrow \omega\chi_{c0}$

• • • We do not use the following data for averages, fits, limits, etc. • • •

¹ From a fit of the measured cross section from $\sqrt{s} = 4.178-4.278$ GeV. Supersedes ABLIKIM 15c.
² From a 3-parameter fit of measured cross sections from $\sqrt{s} = 4.21-4.42$ GeV to a phase-space modified Breit-Wigner function, using the decays $\chi_{c0} \rightarrow \pi^+\pi^-$, $\chi_{c0} \rightarrow K^+K^-$, and $\omega \rightarrow \pi^+\pi^-\pi^0$.

$\Gamma(h_c(1P)\pi^+\pi^-) \times \Gamma(e^+e^-)/\Gamma_{total}$ $\Gamma_{22}\Gamma_1/\Gamma$

VALUE (eV)	CL%	DOCUMENT ID	TECN	COMMENT
4.6 ^{+2.9}_{-1.4} ± 0.8		ABLIKIM	17G BES3	$e^+e^- \rightarrow \pi^+\pi^-h_c$

$\Gamma(\phi\pi^+\pi^-) \times \Gamma(e^+e^-)/\Gamma_{total}$ $\Gamma_{23}\Gamma_1/\Gamma$

VALUE (eV)	CL%	DOCUMENT ID	TECN	COMMENT
<0.4	90	AUBERT, BE	06D BABR	10.6 $e^+e^- \rightarrow K^+K^-\pi^+\pi^-\gamma$

$\Gamma(\phi f_0(980) \rightarrow \phi\pi^+\pi^-) \times \Gamma(e^+e^-)/\Gamma_{total}$ $\Gamma_{24}\Gamma_1/\Gamma$

VALUE (eV)	CL%	DOCUMENT ID	TECN	COMMENT
<0.28	90	¹ AUBERT	07AK BABR	10.6 $e^+e^- \rightarrow \pi^+\pi^-K^+K^-\gamma$

¹ AUBERT 07AK reports $\Gamma(\psi(4230) \rightarrow \phi f_0(980) \rightarrow \phi\pi^+\pi^-) \times \Gamma(\psi(4230) \rightarrow e^+e^-)/\Gamma_{total} \times [B(\phi(1020) \rightarrow K^+K^-)] < 0.14$ eV which we divide by our best value $B(\phi(1020) \rightarrow K^+K^-) = 49.1 \times 10^{-2}$.

$\Gamma(\Xi^-\Xi^+) \times \Gamma(e^+e^-)/\Gamma_{total}$ $\Gamma_{48}\Gamma_1/\Gamma$

VALUE (eV)	CL%	DOCUMENT ID	TECN	COMMENT
<2.7 × 10 ⁻⁴	90	ABLIKIM	20c BES3	$e^+e^- \rightarrow \Xi^-\Xi^+$

$\Gamma(\pi^+\pi^+\pi^-\pi^-) \times \Gamma(e^+e^-)/\Gamma_{total}$ $\Gamma_{49}\Gamma_1/\Gamma$

VALUE (eV)	CL%	DOCUMENT ID	TECN	COMMENT
<32	90	ABLIKIM	21AW BES3	$e^+e^- \rightarrow 2\pi^+2\pi^-$

$\Gamma(\pi^+\pi^+\pi^-\pi^-\pi^0) \times \Gamma(e^+e^-)/\Gamma_{total}$ $\Gamma_{50}\Gamma_1/\Gamma$

VALUE (eV)	CL%	DOCUMENT ID	TECN	COMMENT
<16	90	ABLIKIM	21AW BES3	$e^+e^- \rightarrow 2\pi^+2\pi^-\pi^0$

$\Gamma(K_S^0 K^\pm \pi^\mp) \times \Gamma(e^+e^-)/\Gamma_{total}$ $\Gamma_{51}\Gamma_1/\Gamma$

VALUE (eV)	CL%	DOCUMENT ID	TECN	COMMENT
2.04 ± 0.19 ± 0.09		¹ ABLIKIM	19AE BES3	$e^+e^- \rightarrow K_S^0 K^\pm \pi^\mp$
0.0027 ± 0.0023 ± 0.0001		² ABLIKIM	19AE BES3	$e^+e^- \rightarrow K_S^0 K^\pm \pi^\mp$
< 0.5 at 90% CL		AUBERT	08s BABR	10.6 $e^+e^- \rightarrow K_S^0 K^\pm \pi^\mp \gamma$

- • • We do not use the following data for averages, fits, limits, etc. • • •
- ¹ Solution I of the fit including the $\psi(4160)$ with mass 4191 ± 5 MeV and width 70 ± 10 MeV from PDG 16 and the $\psi(4230)$ with mass $4219.6 \pm 3.3 \pm 5.1$ MeV and width $56.0 \pm 3.6 \pm 6.9$ MeV from GAO 17.
- ² Solution II of the fit including the $\psi(4160)$ with mass 4191 ± 5 MeV and width 70 ± 10 MeV from PDG 16 and the $\psi(4230)$ with mass $4219.6 \pm 3.3 \pm 5.1$ MeV and width $56.0 \pm 3.6 \pm 6.9$ MeV from GAO 17.

$\Gamma(K_S^0 K^\pm \pi^\mp \pi^0) \times \Gamma(e^+e^-)/\Gamma_{total}$ $\Gamma_{52}\Gamma_1/\Gamma$

VALUE (eV)	CL%	DOCUMENT ID	TECN	COMMENT
<0.05	90	ABLIKIM	19 BES3	$e^+e^- \rightarrow K_S^0 K^\pm \pi^\mp \pi^0$

$\Gamma(K_S^0 K^\pm \pi^\mp \eta) \times \Gamma(e^+e^-)/\Gamma_{total}$ $\Gamma_{53}\Gamma_1/\Gamma$

VALUE (eV)	CL%	DOCUMENT ID	TECN	COMMENT
<0.19	90	ABLIKIM	19 BES3	$e^+e^- \rightarrow K_S^0 K^\pm \pi^\mp \eta$

$\Gamma(K^+K^-\pi^0) \times \Gamma(e^+e^-)/\Gamma_{total}$ $\Gamma_{54}\Gamma_1/\Gamma$

VALUE (eV)	CL%	DOCUMENT ID	TECN	COMMENT
<0.6	90	AUBERT	08s BABR	10.6 $e^+e^- \rightarrow K^+K^-\pi^0\gamma$

$\Gamma(K^+K^-\pi^+\pi^-) \times \Gamma(e^+e^-)/\Gamma_{total}$ $\Gamma_{55}\Gamma_1/\Gamma$

VALUE (eV)	CL%	DOCUMENT ID	TECN	COMMENT
<20		ABLIKIM	21AW BES3	$e^+e^- \rightarrow K^+K^-\pi^+\pi^-$

$\Gamma(K^+K^-\pi^+\pi^-\pi^0) \times \Gamma(e^+e^-)/\Gamma_{total}$ $\Gamma_{56}\Gamma_1/\Gamma$

VALUE (eV)	CL%	DOCUMENT ID	TECN	COMMENT
<43	90	ABLIKIM	21AW BES3	$e^+e^- \rightarrow K^+K^-\pi^+\pi^-\pi^0$

$\Gamma(K^+K^+K^-K^-) \times \Gamma(e^+e^-)/\Gamma_{total}$ $\Gamma_{57}\Gamma_1/\Gamma$

VALUE (eV)	CL%	DOCUMENT ID	TECN	COMMENT
<3.8	90	ABLIKIM	21AW BES3	$e^+e^- \rightarrow 2K^+2K^-$

$\Gamma(K^+K^+K^-K^-\pi^0) \times \Gamma(e^+e^-)/\Gamma_{total}$ $\Gamma_{58}\Gamma_1/\Gamma$

VALUE (eV)	CL%	DOCUMENT ID	TECN	COMMENT
<2.1	90	ABLIKIM	21AW BES3	$e^+e^- \rightarrow 2K^+2K^-\pi^0$

$\Gamma(\rho\pi^+\pi^-) \times \Gamma(e^+e^-)/\Gamma_{total}$ $\Gamma_{59}\Gamma_1/\Gamma$

VALUE (eV)	CL%	DOCUMENT ID	TECN	COMMENT
<7.2	90	ABLIKIM	21AW BES3	$e^+e^- \rightarrow \rho\pi^+\pi^-$

$\Gamma(\rho\pi^+\pi^-\pi^0) \times \Gamma(e^+e^-)/\Gamma_{total}$ $\Gamma_{60}\Gamma_1/\Gamma$

VALUE (eV)	CL%	DOCUMENT ID	TECN	COMMENT
<15	90	ABLIKIM	21AW BES3	$e^+e^- \rightarrow \rho\pi^+\pi^-\pi^0$

$\Gamma(\Lambda\bar{\Lambda}) \times \Gamma(e^+e^-)/\Gamma_{total}$ $\Gamma_{62}\Gamma_1/\Gamma$

VALUE (eV)	CL%	DOCUMENT ID	TECN	COMMENT
<0.8 × 10 ⁻³	90	¹ ABLIKIM	21As BES3	$e^+e^- \rightarrow \psi(4260)$

¹ From a measurement of the $e^+e^- \rightarrow \Lambda\bar{\Lambda}$ cross section between 3.5 and 4.6 GeV.

$\Gamma(\chi_{c1}\gamma) \times \Gamma(e^+e^-)/\Gamma_{total}$ $\Gamma_{65}\Gamma_1/\Gamma$

VALUE (eV)	CL%	DOCUMENT ID	TECN	COMMENT
<1.4	90	¹ HAN	15 BELL	10.58 $e^+e^- \rightarrow \chi_{c1}\gamma$

¹ Using $B(\eta \rightarrow \gamma\gamma) = (39.41 \pm 0.21)\%$.

$\Gamma(\chi_{c2}\gamma) \times \Gamma(e^+e^-)/\Gamma_{total}$ $\Gamma_{66}\Gamma_1/\Gamma$

VALUE (eV)	CL%	DOCUMENT ID	TECN	COMMENT
<4.0	90	¹ HAN	15 BELL	10.58 $e^+e^- \rightarrow \chi_{c2}\gamma$

¹ Using $B(\eta \rightarrow \gamma\gamma) = (39.41 \pm 0.21)\%$.

$\psi(4230)$ BRANCHING RATIOS

$\Gamma(\eta_c(1S)\pi^+\pi^-)/\Gamma_{total}$ Γ_3/Γ

VALUE	CL%	DOCUMENT ID	TECN	COMMENT
not seen		¹ ABLIKIM	21B BES3	$e^+e^- \rightarrow \pi^+\pi^-\eta_c$

¹ Not seen in $e^+e^- \rightarrow \pi^+\pi^-\eta_c$ at $\sqrt{s} = 4.226$ GeV with a 90% C.L. upper limit on the cross section of 16.8 pb.

$\Gamma(\eta_c(1S)\pi^+\pi^-\pi^0)/\Gamma_{total}$ Γ_4/Γ

VALUE	CL%	DOCUMENT ID	TECN	COMMENT
seen		¹ ABLIKIM	21B BES3	$e^+e^- \rightarrow \pi^+\pi^-\pi^0\eta_c$

¹ Seen as a peak in the $e^+e^- \rightarrow \pi^+\pi^-\pi^0\eta_c$ cross section with a peak value of $46.1^{+9.5}_{-9.4} \pm 6.6$ pb at $\sqrt{s} = 4.226$ GeV.

$\Gamma(J/\psi\pi^+\pi^-)/\Gamma_{total}$ Γ_5/Γ

VALUE	CL%	DOCUMENT ID	TECN	COMMENT
seen		ABLIKIM	17B BES3	$e^+e^- \rightarrow \pi^+\pi^-J/\psi$

$\Gamma(J/\psi f_0(980), f_0(980) \rightarrow \pi^+\pi^-)/\Gamma(J/\psi\pi^+\pi^-)$ Γ_6/Γ_5

VALUE	CL%	DOCUMENT ID	TECN	COMMENT
0.17 ± 0.13		¹ LEES	12Ac BABR	10.58 $e^+e^- \rightarrow \gamma\pi^+\pi^-J/\psi$

• • • We do not use the following data for averages, fits, limits, etc. • • •

¹ Systematic uncertainties not estimated.

$\Gamma(Z_c(3900)^\pm \pi^\mp, Z_c^\pm \rightarrow J/\psi\pi^\pm)/\Gamma(J/\psi\pi^+\pi^-)$ Γ_7/Γ_5

VALUE	CL%	DOCUMENT ID	TECN	COMMENT
0.215 ± 0.033 ± 0.075		¹ ABLIKIM	13T BES3	$e^+e^- \rightarrow \pi^+\pi^-J/\psi$
0.29 ± 0.08		² LIU	13B BELL	$e^+e^- \rightarrow \gamma\pi^+\pi^-J/\psi$

• • • We do not use the following data for averages, fits, limits, etc. • • •

¹ Assuming that the cross section of $e^+e^- \rightarrow \pi^+\pi^-J/\psi$ is fully due to the $\psi(4260)$.
² Systematic error not evaluated.

$\Gamma(J/\psi\pi^0\pi^0)/\Gamma_{total}$ Γ_8/Γ

VALUE	CL%	DOCUMENT ID	TECN	COMMENT
seen		¹ ABLIKIM	20N BES3	$e^+e^- \rightarrow \pi^0\pi^0J/\psi$

¹ From a fit to the cross section $e^+e^- \rightarrow \pi^0\pi^0J/\psi$ at center-of-mass energies between 3.808 and 4.600 GeV.

Meson Particle Listings

 $\psi(4230)$

$\Gamma(J/\psi K_S^0 K_S^0)/\Gamma_{\text{total}}$	VALUE	DOCUMENT ID	TECN	COMMENT	Γ_{10}/Γ
not seen		SHEN	14	BELL 9.4-10.9 $e^+e^- \rightarrow \gamma K_S^0 K_S^0 J/\psi$	

$\Gamma(J/\psi\eta)/\Gamma_{\text{total}}$	VALUE	DOCUMENT ID	TECN	COMMENT	Γ_{11}/Γ
seen		ABLIKIM	20a	BES3 $e^+e^- \rightarrow \eta J/\psi$	

$\Gamma(J/\psi\eta\pi^0)/\Gamma_{\text{total}}$	VALUE	DOCUMENT ID	TECN	COMMENT	Γ_{15}/Γ
not seen		ABLIKIM	15Q	BES3 4.0-4.6 $e^+e^- \rightarrow J/\psi\eta\pi^0$	

$\Gamma(\psi(2S)\pi^+\pi^-)/\Gamma_{\text{total}}$	VALUE	DOCUMENT ID	TECN	COMMENT	Γ_{17}/Γ
seen		1 ABLIKIM	17V	BES3 $e^+e^- \rightarrow \pi^+\pi^-\psi(2S)$	

¹ From a fit to the cross section for $e^+e^- \rightarrow \pi^+\pi^-\psi(2S) \rightarrow 2(\pi^+\pi^-)\ell^+\ell^-$ obtained from 16 center-of-mass energies between 4.008 and 4.600 GeV and comprising 5.1 fb⁻¹.

$\Gamma(\psi(2S)\pi^+\pi^-)/\Gamma(J/\psi\pi^+\pi^-)$	VALUE	DOCUMENT ID	TECN	COMMENT	Γ_{17}/Γ_5
••• We do not use the following data for averages, fits, limits, etc. •••					
(0.11 ± 0.03 ± 0.03) to (0.55 ± 0.18 ± 0.19)		1 ZHANG	17c	RVUE $e^+e^- \rightarrow \pi^+\pi^- J/\psi$ or $\psi(2S)$	

¹ From a combined fit of BELLE, BABAR and BES3 $e^+e^- \rightarrow \pi^+\pi^- J/\psi$ and $e^+e^- \rightarrow \pi^+\pi^-\psi(2S)$ data.

$\Gamma(\chi_{c0}\omega)/\Gamma_{\text{total}}$	VALUE	EVTS	DOCUMENT ID	TECN	COMMENT	Γ_{19}/Γ
seen		180	1 ABLIKIM	15c	BES3 $e^+e^- \rightarrow \omega\chi_{c0}$	

¹ From a 3-parameter fit of measured cross sections from $\sqrt{s} = 4.21-4.42$ GeV to a phase-space modified Breit-Wigner function, using the decays $\chi_{c0} \rightarrow \pi^+\pi^-, \chi_{c0} \rightarrow K^+K^-,$ and $\omega \rightarrow \pi^+\pi^-\pi^0$.

$\Gamma(h_c(1P)\pi^+\pi^-)/\Gamma_{\text{total}}$	VALUE	DOCUMENT ID	TECN	COMMENT	Γ_{22}/Γ
seen		ABLIKIM	17G	BES3 $e^+e^- \rightarrow \pi^+\pi^- h_c$	

$\Gamma(h_c(1P)\pi^+\pi^-)/\Gamma(J/\psi\pi^+\pi^-)$	VALUE	CL%	DOCUMENT ID	TECN	COMMENT	Γ_{22}/Γ_5
<1.0		90	1 PEDLAR	11	CLEO $e^+e^- \rightarrow h_c(1P)\pi^+\pi^-$	

¹ At $\sqrt{s} = 4260$ MeV, PEDLAR 11 measures $\sigma(e^+e^- \rightarrow h_c(1P)\pi^+\pi^-) = 32 \pm 17 \pm 6$ pb, where the errors are statistical, systematic, and due to uncertainty in $B(\psi(2S) \rightarrow \pi^0 h_c(1P))$, respectively.

$\Gamma(D\bar{D})/\Gamma(J/\psi\pi^+\pi^-)$	VALUE	CL%	DOCUMENT ID	TECN	COMMENT	Γ_{25}/Γ_5
<1.0		90	1 AUBERT	07BE	BABR $e^+e^- \rightarrow D\bar{D}\gamma$	

••• We do not use the following data for averages, fits, limits, etc. •••

$\Gamma(D\bar{D})/\Gamma(J/\psi\pi^+\pi^-)$	VALUE	DOCUMENT ID	TECN	COMMENT	Γ_{25}/Γ_5
<4.0		90	CRONIN-HEN..09	CLEO e^+e^-	

¹ Using 4259 ± 10 MeV for the mass and 88 ± 24 MeV for the width of $\psi(4260)$.

$\Gamma(D^0\bar{D}^0)/\Gamma_{\text{total}}$	VALUE	DOCUMENT ID	TECN	COMMENT	Γ_{26}/Γ
not seen		CRONIN-HEN..09	CLEO	$e^+e^- \rightarrow D^0\bar{D}^0$	

••• We do not use the following data for averages, fits, limits, etc. •••

not seen		AUBERT	09M	BABR $e^+e^- \rightarrow D^0\bar{D}^0\gamma$	
not seen		PAKHLOVA	08	BELL $e^+e^- \rightarrow D^0\bar{D}^0\gamma$	

$\Gamma(D^+D^-)/\Gamma_{\text{total}}$	VALUE	DOCUMENT ID	TECN	COMMENT	Γ_{27}/Γ
not seen		CRONIN-HEN..09	CLEO	$e^+e^- \rightarrow D^+D^-$	

••• We do not use the following data for averages, fits, limits, etc. •••

not seen		AUBERT	09M	BABR $e^+e^- \rightarrow D^+D^-\gamma$	
not seen		PAKHLOVA	08	BELL $e^+e^- \rightarrow D^+D^-\gamma$	

$\Gamma(D^*\bar{D}^*+c.c.)/\Gamma(J/\psi\pi^+\pi^-)$	VALUE	CL%	DOCUMENT ID	TECN	COMMENT	Γ_{28}/Γ_5
<34		90	AUBERT	09M	BABR $e^+e^- \rightarrow \gamma D^*\bar{D}^*$	

••• We do not use the following data for averages, fits, limits, etc. •••

$\Gamma(D^*\bar{D}^*+c.c.)/\Gamma(J/\psi\pi^+\pi^-)$	VALUE	DOCUMENT ID	TECN	COMMENT	Γ_{28}/Γ_5
<45		90	CRONIN-HEN..09	CLEO e^+e^-	

$\Gamma(D^*(2007)^0\bar{D}^0+c.c.)/\Gamma_{\text{total}}$	VALUE	DOCUMENT ID	TECN	COMMENT	Γ_{29}/Γ
not seen		CRONIN-HEN..09	CLEO	$e^+e^- \rightarrow D^{*0}\bar{D}^0$	

••• We do not use the following data for averages, fits, limits, etc. •••

not seen		AUBERT	09M	BABR $e^+e^- \rightarrow D^{*0}\bar{D}^0\gamma$	
----------	--	--------	-----	---	--

$\Gamma(D^*(2010)^+D^-+c.c.)/\Gamma_{\text{total}}$	VALUE	DOCUMENT ID	TECN	COMMENT	Γ_{30}/Γ
not seen		CRONIN-HEN..09	CLEO	$e^+e^- \rightarrow D^{*+}D^-$	

not seen

••• We do not use the following data for averages, fits, limits, etc. •••

not seen		PAKHLOVA	07	BELL $e^+e^- \rightarrow D^{*+}D^-\gamma$	
----------	--	----------	----	---	--

not seen

not seen		AUBERT	09M	BABR $e^+e^- \rightarrow D^{*+}D^-\gamma$	
----------	--	--------	-----	---	--

$\Gamma(D^*\bar{D}^*)/\Gamma(J/\psi\pi^+\pi^-)$	VALUE	CL%	DOCUMENT ID	TECN	COMMENT	Γ_{31}/Γ_5
<11		90	CRONIN-HEN..09	CLEO	e^+e^-	

••• We do not use the following data for averages, fits, limits, etc. •••

$\Gamma(D^*(2007)^0\bar{D}^*(2007)^0)/\Gamma_{\text{total}}$	VALUE	DOCUMENT ID	TECN	COMMENT	Γ_{32}/Γ	
<40		90	AUBERT	09M	BABR $e^+e^- \rightarrow \gamma D^*\bar{D}^*$	

not seen

••• We do not use the following data for averages, fits, limits, etc. •••

not seen		AUBERT	09M	BABR $e^+e^- \rightarrow D^{*0}\bar{D}^{*0}\gamma$	
----------	--	--------	-----	--	--

$\Gamma(D^*(2010)^+D^*(2010)^-)/\Gamma_{\text{total}}$	VALUE	DOCUMENT ID	TECN	COMMENT	Γ_{33}/Γ
not seen		CRONIN-HEN..09	CLEO	$e^+e^- \rightarrow D^{*+}D^{*-}$	

not seen

••• We do not use the following data for averages, fits, limits, etc. •••

not seen		PAKHLOVA	07	BELL $e^+e^- \rightarrow D^{*+}D^{*-}\gamma$	
----------	--	----------	----	--	--

not seen

not seen		AUBERT	09M	BABR $e^+e^- \rightarrow D^{*+}D^{*-}\gamma$	
----------	--	--------	-----	--	--

$\Gamma(D^0D^-\pi^++c.c. \text{ (excl. } D^*(2007)^0\bar{D}^{*0}+c.c., D^*(2010)^+D^-+c.c.)/\Gamma_{\text{total}}$	VALUE	DOCUMENT ID	TECN	COMMENT	Γ_{35}/Γ
not seen		PAKHLOVA	08A	BELL 10.6 $e^+e^- \rightarrow D^0D^-\pi^+\gamma$	

not seen

$\Gamma(D\bar{D}^*\pi+c.c. \text{ (excl. } D^*\bar{D}^*)/\Gamma_{\text{total}}$	VALUE	DOCUMENT ID	TECN	COMMENT	Γ_{36}/Γ
not seen		CRONIN-HEN..09	CLEO	$e^+e^- \rightarrow D^*\bar{D}^*\pi$	

not seen

$\Gamma(D\bar{D}^*\pi+c.c. \text{ (excl. } D^*\bar{D}^*)/\Gamma(J/\psi\pi^+\pi^-)$	VALUE	CL%	DOCUMENT ID	TECN	COMMENT	Γ_{36}/Γ_5
<15		90	CRONIN-HEN..09	CLEO	e^+e^-	

not seen

$\Gamma(D^0D^{*-}\pi^++c.c. \text{ (excl. } D^*(2010)^+D^*(2010)^-)/\Gamma_{\text{total}}$	VALUE	DOCUMENT ID	TECN	COMMENT	Γ_{37}/Γ
not seen		PAKHLOVA	09	BELL $e^+e^- \rightarrow D^0D^{*-}\pi^+\gamma$	

not seen

$\Gamma(D^0D^*(2010)^-\pi^++c.c.)/\Gamma_{\text{total}}$	VALUE	DOCUMENT ID	TECN	COMMENT	Γ_{38}/Γ
seen		ABLIKIM	19R	BES3 $e^+e^- \rightarrow \pi^+D^0D^{*-}+c.c.$	

not seen

$\Gamma(D^0D^*(2010)^-\pi^++c.c.)/\Gamma(J/\psi\pi^+\pi^-)$	VALUE	CL%	DOCUMENT ID	TECN	COMMENT	Γ_{38}/Γ_5
<9		90	PAKHLOVA	09	BELL $e^+e^- \rightarrow D^0D^{*-}\pi^+$	

not seen

$\Gamma(D^0D^*(2010)^-\pi^++c.c.)/\Gamma_{\text{total}} \times \Gamma(e^+e^-)/\Gamma_{\text{total}}$	VALUE	CL%	DOCUMENT ID	TECN	COMMENT	$\Gamma_{38}/\Gamma \times \Gamma_1/\Gamma$
<0.42 × 10 ⁻⁶		90	1 PAKHLOVA	09	BELL $e^+e^- \rightarrow D^0D^{*-}\pi^+$	

¹ Using 4263⁺⁸/₋₉ MeV for the mass of $\psi(4260)$.

$\Gamma(D_1(2420)\bar{D}+c.c.)/\Gamma_{\text{total}}$	VALUE	DOCUMENT ID	TECN	COMMENT	Γ_{39}/Γ
not seen		1 ABLIKIM	19AR	BES3 $e^+e^- \rightarrow \pi^+\pi^-D\bar{D}$	

not seen

¹ Results from a measurement of $\sigma(e^+e^- \rightarrow D_1(2420)\bar{D}+c.c.)$ between $\sqrt{s} = 4.3$ and 4.6 GeV.

$\Gamma(D^*\bar{D}^*\pi)/\Gamma_{\text{total}}$	VALUE	DOCUMENT ID	TECN	COMMENT	Γ_{40}/Γ
not seen		CRONIN-HEN..09	CLEO	$e^+e^- \rightarrow D^*\bar{D}^*\pi$	

not seen

$\Gamma(D^*\bar{D}^*\pi)/\Gamma(J/\psi\pi^+\pi^-)$	VALUE	CL%	DOCUMENT ID	TECN	COMMENT	Γ_{40}/Γ_5
<8.2		90	CRONIN-HEN..09	CLEO	e^+e^-	

not seen

$\Gamma(D_s^+D_s^-)/\Gamma_{\text{total}}$	VALUE	DOCUMENT ID	TECN	COMMENT	Γ_{41}/Γ
not seen		DEL-AMO-SA..10N	BABR	$e^+e^- \rightarrow D_s^+D_s^-\gamma$	

not seen

••• We do not use the following data for averages, fits, limits, etc. •••

not seen		CRONIN-HEN..09	CLEO	$e^+e^- \rightarrow D_s^+D_s^-$	
----------	--	----------------	------	---------------------------------	--

not seen

not seen		PAKHLOVA	11	BELL $e^+e^- \rightarrow D_s^+D_s^-\gamma$	
----------	--	----------	----	--	--

See key on page 1127

Meson Particle Listings

$\psi(4230)$, $R_{c0}(4240)$

$\Gamma(D_s^+ D_s^-)/\Gamma(J/\psi\pi^+\pi^-)$ Γ_{41}/Γ_5

Table with columns: VALUE, CL%, DOCUMENT ID, TECN, COMMENT. Includes data for DEL-AMO-SA..10N BABR and CRONIN-HEN..09 CLEO.

$\Gamma(D_s^{*+} D_s^- + c.c.)/\Gamma_{total}$ Γ_{42}/Γ

Table with columns: VALUE, DOCUMENT ID, TECN, COMMENT. Includes data for DEL-AMO-SA..10N BABR and CRONIN-HEN..09 CLEO.

$\Gamma(D_s^{*+} D_s^- + c.c.)/\Gamma(J/\psi\pi^+\pi^-)$ Γ_{42}/Γ_5

Table with columns: VALUE, CL%, DOCUMENT ID, TECN, COMMENT. Includes data for CRONIN-HEN..09 CLEO and DEL-AMO-SA..10N BABR.

$\Gamma(D_s^{*+} D_s^{*-})/\Gamma_{total}$ Γ_{43}/Γ

Table with columns: VALUE, DOCUMENT ID, TECN, COMMENT. Includes data for CRONIN-HEN..09 CLEO and PAKHLOVA 11 BELL.

$\Gamma(D_s^{*+} D_s^{*-})/\Gamma(J/\psi\pi^+\pi^-)$ Γ_{43}/Γ_5

Table with columns: VALUE, CL%, DOCUMENT ID, TECN, COMMENT. Includes data for CRONIN-HEN..09 CLEO and DEL-AMO-SA..10N BABR.

$\Gamma(p\bar{p})/\Gamma(J/\psi\pi^+\pi^-)$ Γ_{44}/Γ_5

Table with columns: VALUE, CL%, DOCUMENT ID, TECN, COMMENT. Includes data for AUBERT 06B BABR.

$\Gamma(p\bar{p}\pi^0)/\Gamma(J/\psi\pi^+\pi^-)$ Γ_{45}/Γ_5

Table with columns: VALUE, CL%, DOCUMENT ID, TECN, COMMENT. Includes data for ABLIKIM 17F BES3.

$\Gamma(p\bar{p}\eta)/\Gamma_{total}$ Γ_{46}/Γ

Table with columns: VALUE, DOCUMENT ID, TECN, COMMENT. Includes data for ABLIKIM 21AN BES3.

$\Gamma(p\bar{p}\omega)/\Gamma_{total}$ Γ_{47}/Γ

Table with columns: VALUE, DOCUMENT ID, TECN, COMMENT. Includes data for ABLIKIM 21AN BES3.

$\Gamma(p\bar{p}p\bar{p})/\Gamma_{total}$ Γ_{61}/Γ

Table with columns: VALUE, DOCUMENT ID, TECN, COMMENT. Includes data for ABLIKIM 21D BES3.

Radiative decays

$\Gamma(\eta_c(1S)\gamma)/\Gamma_{total}$ Γ_{63}/Γ

Table with columns: VALUE, DOCUMENT ID, TECN, COMMENT. Includes data for ABLIKIM 17W.

$\Gamma(\eta_c(1S)\pi^0\gamma)/\Gamma_{total}$ Γ_{64}/Γ

Table with columns: VALUE, DOCUMENT ID, TECN, COMMENT. Includes data for ABLIKIM 21B BES3.

$\Gamma(\chi_{c1}(3872)\gamma)/\Gamma_{total}$ Γ_{67}/Γ

Table with columns: VALUE, EVTS, DOCUMENT ID, TECN, COMMENT. Includes data for ABLIKIM 19v BES3.

$\psi(4230)$ REFERENCES

Reference list for $\psi(4230)$ with columns: ABLIKIM, PR, P, D, TECN, COMMENT.

Main reference list for $\psi(4230)$ and $R_{c0}(4240)$ with columns: ABLIKIM, PR, P, D, TECN, COMMENT.

$R_{c0}(4240)$

$I^G(J^{PC}) = 1^+(0^{--})$
I, G, C need confirmation.

OMITTED FROM SUMMARY TABLE
was $X(4240)^\pm$

Properties incompatible with a $q\bar{q}$ structure (exotic state). See the review on non- $q\bar{q}$ states.

Spin and parity assignment $J^P = 0^-$ is favored over 1^- , 2^- , and 2^+ by 8 σ and over 1^+ by 1 σ , according to the four-dimensional amplitude analysis of AAIJ 14AG.

$R_{c0}(4240)$ MASS

Table with columns: VALUE (MeV), DOCUMENT ID, TECN, COMMENT. Includes data for AAIJ 14AG LHCB.

¹ From a 4-dimensional analysis when a second, lower mass resonance is allowed in the $Z_c(4430)$ fit, with significance 6 σ including systematic variations.

$R_{c0}(4240)$ WIDTH

Table with columns: VALUE (MeV), DOCUMENT ID, TECN, COMMENT. Includes data for AAIJ 14AG LHCB.

¹ From a 4-dimensional analysis when a second, lower mass resonance is allowed in the $Z_c(4430)$ fit, with significance 6 σ including systematic variations.

$R_{c0}(4240)$ DECAY MODES

Table with columns: Mode, Fraction (Γ_i/Γ). Includes $\pi^- \psi(2S)$ seen.

$R_{c0}(4240)$ BRANCHING RATIOS

Table with columns: VALUE, DOCUMENT ID, TECN, COMMENT. Includes data for AAIJ 14AG LHCB.

¹ From a 4-dimensional analysis when a second, lower mass resonance is allowed in the $Z_c(4430)$ fit. No partial branching fraction quoted.

$R_{c0}(4240)$ REFERENCES

Reference list for $R_{c0}(4240)$ with columns: AAIJ, P, D, TECN, COMMENT.

Meson Particle Listings

 $X(4250)^\pm$, $\chi_{c1}(4274)$, $X(4350)$ **$X(4250)^\pm$**

$$I^G(J^{PC}) = 1^-(?^?+)$$

I, G, C need confirmation.

OMITTED FROM SUMMARY TABLE

Properties incompatible with a $q\bar{q}$ structure (exotic state). See the review on non- $q\bar{q}$ states.

Observed by MIZUK 08 in the $\pi^+\chi_{c1}(1P)$ invariant mass distribution in $\bar{B}^0 \rightarrow K^-\pi^+\chi_{c1}(1P)$ decays. Not seen by LEES 12B in this same mode after accounting for $K\pi$ resonant mass and angular structure.

 $X(4250)^\pm$ MASS

VALUE (MeV)	DOCUMENT ID	TECN	COMMENT
$4248_{-29}^{+44+180}$ -35	¹ MIZUK	08	BELL $\bar{B}^0 \rightarrow K^-\pi^+\chi_{c1}(1P)$

¹ From a Dalitz plot analysis with two Breit-Wigner amplitudes.

 $X(4250)^\pm$ WIDTH

VALUE (MeV)	DOCUMENT ID	TECN	COMMENT
$177_{-39}^{+54+316}$ -61	¹ MIZUK	08	BELL $\bar{B}^0 \rightarrow K^-\pi^+\chi_{c1}(1P)$

¹ From a Dalitz plot analysis with two Breit-Wigner amplitudes.

 $X(4250)^\pm$ DECAY MODES

Mode	Fraction (Γ_i/Γ)
$\Gamma_1 \pi^+\chi_{c1}(1P)$	seen

 $X(4250)^\pm$ BRANCHING RATIOS

$\Gamma(\pi^+\chi_{c1}(1P))/\Gamma_{\text{total}}$	DOCUMENT ID	TECN	COMMENT	Γ_1/Γ
seen	¹ MIZUK	08	BELL $\bar{B}^0 \rightarrow K^-\pi^+\chi_{c1}(1P)$	
not seen	² LEES	12b	BABR $B \rightarrow K\pi\chi_{c1}(1P)$	

¹ With a product branching fraction measurement of $B(\bar{B}^0 \rightarrow K^-\chi_{c1}(1P)) \times B(\chi_{c1}(1P) \rightarrow \pi^+\chi_{c1}(1P)) = (4.0 \pm 2.3 + 19.7_{-0.9}^{+0.5}) \times 10^{-5}$.

² With a product branching fraction limit of $B(\bar{B}^0 \rightarrow X(4250)^+K^-) \times B(X(4250)^+ \rightarrow \chi_{c1}\pi^+) < 4.0 \times 10^{-5}$ at 90% CL.

 $X(4250)^\pm$ REFERENCES

LEES	12B	PR D85 052003	J.P. Lees et al.	(BABAR Collab.)
MIZUK	08	PR D78 072004	R. Mizuk et al.	(BELLE Collab.)

 $\chi_{c1}(4274)$

$$I^G(J^{PC}) = 0^+(1^{++})$$

was $X(4274)$

This state shows properties different from a conventional $q\bar{q}$ state. A candidate for an exotic structure. See the review on non- $q\bar{q}$ states.

Seen by AAIJ 17C in $B^+ \rightarrow \chi_{c1}K^+$, $\chi_{c1} \rightarrow J/\psi\phi$ using an amplitude analysis of $B^+ \rightarrow J/\psi\phi K^+$ with a significance (accounting for systematic uncertainties) of 6.0 σ .

 $\chi_{c1}(4274)$ MASS

VALUE (MeV)	EVTS	DOCUMENT ID	TECN	COMMENT
4286_{-9}^{+8} OUR AVERAGE				Error includes scale factor of 1.7.

$4294 \pm 4 \pm 3$ -6	24k	¹ AAIJ	21E	LHCB $B^+ \rightarrow J/\psi\phi K^+$
----------------------------	-----	-------------------	-----	---------------------------------------

$4274.4_{-6.7}^{+8.4} \pm 1.9$	22	² AALTONEN	17	CDF $B^+ \rightarrow J/\psi\phi K^+$
--------------------------------	----	-----------------------	----	--------------------------------------

• • • We do not use the following data for averages, fits, limits, etc. • • •

$4273.3 \pm 8.3 \pm 17.2$ -3.6	4289	^{3,4} AAIJ	17c	LHCB $B^+ \rightarrow J/\psi\phi K^+$
-------------------------------------	------	---------------------	-----	---------------------------------------

¹ From an amplitude analysis of the decay $B^+ \rightarrow J/\psi\phi K^+$ with a significance of 18 σ .

² From a fit to the invariant mass spectrum with a significance of 3.1 σ .

³ From an amplitude analysis of the decay $B^+ \rightarrow J/\psi\phi K^+$ with a significance of 6.0 σ .

⁴ Superseded by AAIJ 21E.

 $\chi_{c1}(4274)$ WIDTH

VALUE (MeV)	EVTS	DOCUMENT ID	TECN	COMMENT
51 ± 7 OUR AVERAGE				

$53 \pm 5 \pm 5$	24k	¹ AAIJ	21E	LHCB $B^+ \rightarrow J/\psi\phi K^+$
------------------	-----	-------------------	-----	---------------------------------------

$32.3_{-15.3}^{+21.9} \pm 7.6$	22	² AALTONEN	17	CDF $B^+ \rightarrow J/\psi\phi K^+$
--------------------------------	----	-----------------------	----	--------------------------------------

• • • We do not use the following data for averages, fits, limits, etc. • • •

$56 \pm 11 \pm 8$ -11	4289	^{3,4} AAIJ	17c	LHCB $B^+ \rightarrow J/\psi\phi K^+$
----------------------------	------	---------------------	-----	---------------------------------------

¹ From an amplitude analysis of the decay $B^+ \rightarrow J/\psi\phi K^+$ with a significance of 18 σ .

² From a fit to the invariant mass spectrum with a significance of 3.1 σ .

³ From an amplitude analysis of the decay $B^+ \rightarrow J/\psi\phi K^+$ with a significance of 6.0 σ .

⁴ Superseded by AAIJ 21E.

 $\chi_{c1}(4274)$ DECAY MODES

Mode	Fraction (Γ_i/Γ)
$\Gamma_1 J/\psi\phi$	seen

 $\chi_{c1}(4274)$ BRANCHING RATIOS

$\Gamma(J/\psi\phi)/\Gamma_{\text{total}}$	EVTS	DOCUMENT ID	TECN	COMMENT	Γ_1/Γ
seen	24k	¹ AAIJ	21E	LHCB $B^+ \rightarrow J/\psi\phi K^+$	
seen	4289	^{2,3} AAIJ	17c	LHCB $B^+ \rightarrow J/\psi\phi K^+$	

¹ From an amplitude analysis of the decay $B^+ \rightarrow J/\psi\phi K^+$ with a significance of 18 σ .

² From an amplitude analysis of the decay $B^+ \rightarrow J/\psi\phi K^+$ with a significance of 6.0 σ .

³ Superseded by AAIJ 21E.

 $\chi_{c1}(4274)$ REFERENCES

AAIJ	21E	PRL 127 082001	R. Aaij et al.	(LHCb Collab.)
AAIJ	17C	PRL 118 022003	R. Aaij et al.	(LHCb Collab.)JP
		PR D95 012002	R. Aaij et al.	(LHCb Collab.)
AALTONEN	17	MPL A32 1750139	T. Altonen et al.	(CDF Collab.)

 $X(4350)$

$$I^G(J^{PC}) = 0^+(?^?+)$$

OMITTED FROM SUMMARY TABLE

Seen by SHEN 10 in the $\gamma\gamma \rightarrow J/\psi\phi$. Needs confirmation.

 $X(4350)$ MASS

VALUE (MeV)	EVTS	DOCUMENT ID	TECN	COMMENT
$4350.6_{-5.1}^{+4.6} \pm 0.7$	$8.8_{-3.2}^{+4.2}$	¹ SHEN	10	BELL $10.6 e^+e^- \rightarrow e^+e^- J/\psi\phi$

¹ Statistical significance of 3.2 σ .

 $X(4350)$ WIDTH

VALUE (MeV)	EVTS	DOCUMENT ID	TECN	COMMENT
$13_{-9}^{+18} \pm 4$	$8.8_{-3.2}^{+4.2}$	¹ SHEN	10	BELL $10.6 e^+e^- \rightarrow e^+e^- J/\psi\phi$

¹ Statistical significance of 3.2 σ .

 $X(4350)$ DECAY MODES

Mode	Fraction (Γ_i/Γ)
$\Gamma_1 J/\psi\phi$	seen
$\Gamma_2 \gamma\gamma$	seen

 $X(4350)$ $\Gamma(i)\Gamma(\gamma\gamma)/\Gamma(\text{total})$

$\Gamma(\gamma\gamma) \times \Gamma(J/\psi\phi)/\Gamma_{\text{total}}$	EVTS	DOCUMENT ID	TECN	COMMENT	$\Gamma_2\Gamma_1/\Gamma$
$6.7_{-2.4}^{+3.2} \pm 1.1$	$8.8_{-3.2}^{+4.2}$	¹ SHEN	10	BELL $10.6 e^+e^- \rightarrow e^+e^- J/\psi\phi$	
$1.5_{-0.6}^{+0.7} \pm 0.3$	$8.8_{-3.2}^{+4.2}$	² SHEN	10	BELL $10.6 e^+e^- \rightarrow e^+e^- J/\psi\phi$	

¹ For $J^P = 0^+$. Statistical significance of 3.2 σ .

² For $J^P = 2^+$. Statistical significance of 3.2 σ .

 $X(4350)$ BRANCHING RATIOS

$\Gamma(J/\psi\phi)/\Gamma_{\text{total}}$	DOCUMENT ID	TECN	COMMENT	Γ_1/Γ
seen	¹ SHEN	10	BELL $10.6 e^+e^- \rightarrow e^+e^- J/\psi\phi$	

¹ Statistical significance of 3.2 σ .

$\Gamma(\gamma\gamma)/\Gamma_{\text{total}}$	DOCUMENT ID	TECN	COMMENT	Γ_2/Γ
seen	¹ SHEN	10	BELL $10.6 e^+e^- \rightarrow e^+e^- J/\psi\phi$	

¹ Statistical significance of 3.2 σ .

 $X(4350)$ REFERENCES

SHEN	10	PRL 104 112004	C.P. Shen et al.	(BELLE Collab.)
------	----	----------------	------------------	-----------------

$\psi(4360)$

$$J^G(J^{PC}) = 0^-(1^{--})$$

also known as $Y(4360)$; was $X(4360)$

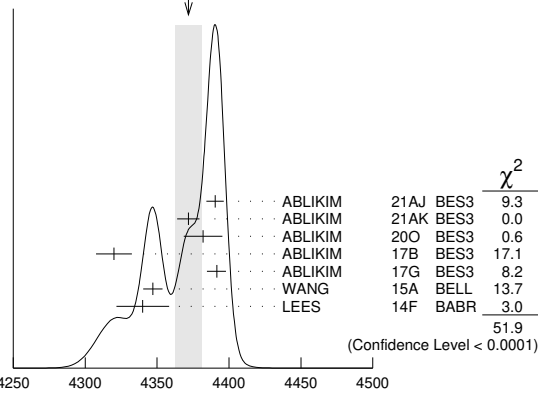
This state shows properties different from a conventional $q\bar{q}$ state. A candidate for an exotic structure. See the review on non- $q\bar{q}$ states.

Seen in radiative return from e^+e^- collisions at $\sqrt{s} = 9.54\text{--}10.58$ GeV by AUBERT 07S, WANG 07D, and LEES 14F. See also the review on "Spectroscopy of mesons containing two heavy quarks."

$\psi(4360)$ MASS

VALUE (MeV)	EVTS	DOCUMENT ID	TECN	COMMENT
4372 ± 9	OUR AVERAGE	Error includes scale factor of 2.9. See the ideogram below.		
4390.3 ± 6.0 ± 0.7		¹ ABLIKIM	21AJ BES3	$e^+e^- \rightarrow \pi^+\pi^-\psi(2S)$
4371.7 ± 7.5 ± 1.8		² ABLIKIM	21AK BES3	$e^+e^- \rightarrow \gamma\chi_{C2} \rightarrow \gamma\gamma J/\psi$
4382.0 ± 13.3 ± 1.7		³ ABLIKIM	20O BES3	$e^+e^- \rightarrow \eta J/\psi$
4320.0 ± 10.4 ± 7.0		⁴ ABLIKIM	17B BES3	$e^+e^- \rightarrow \pi^+\pi^- J/\psi$
4391.5 ± 6.3 ± 6.8 ± 1.0		ABLIKIM	17G BES3	$e^+e^- \rightarrow \pi^+\pi^- h_c$
4347 ± 6 ± 3	279	⁵ WANG	15A BELL	10.58 $e^+e^- \rightarrow \gamma\pi^+\pi^-\psi(2S)$
4340 ± 16 ± 9	37	⁶ LEES	14F BABR	10.58 $e^+e^- \rightarrow \gamma\pi^+\pi^-\psi(2S)$
• • • We do not use the following data for averages, fits, limits, etc. • • •				
4383.8 ± 4.2 ± 0.8		⁷ ABLIKIM	17V BES3	$e^+e^- \rightarrow \pi^+\pi^-\psi(2S)$
4383.7 ± 2.9 ± 6.2		⁸ ZHANG	17B RVUE	$e^+e^- \rightarrow \pi^+\pi^-\psi(2S)$
4386.4 ± 2.1 ± 6.4		⁹ ZHANG	17C RVUE	$e^+e^- \rightarrow \pi^+\pi^- J/\psi$ or $\psi(2S)$
4355 ± 9 ± 10	74	¹⁰ LIU	08H RVUE	10.58 $e^+e^- \rightarrow \gamma\pi^+\pi^-\psi(2S)$
4324 ± 24		¹¹ AUBERT	07S BABR	10.58 $e^+e^- \rightarrow \gamma\pi^+\pi^-\psi(2S)$
4361 ± 9 ± 9	47	⁶ WANG	07D BELL	10.58 $e^+e^- \rightarrow \gamma\pi^+\pi^-\psi(2S)$

WEIGHTED AVERAGE
4372±9 (Error scaled by 2.9)



$\psi(4360)$ MASS (MeV)

- From a three-resonance fit to the Born cross section in the range $\sqrt{s} = 4.008\text{--}4.698$ GeV.
- From a five-resonance fit to the cross section for $e^+e^- \rightarrow \gamma\gamma J/\psi \rightarrow \gamma\gamma\ell^+\ell^-$.
- From a fit of the measured cross section in the range $\sqrt{s} = 3.808\text{--}4.600$ GeV.
- From a three-resonance fit.
- From a two-resonance fit. Supersedes WANG 07D.
- From a two-resonance fit.
- From a fit to the cross section for $e^+e^- \rightarrow \pi^+\pi^-\psi(2S) \rightarrow 2(\pi^+\pi^-)\ell^+\ell^-$ obtained from 16 center-of-mass energies between 4.008 and 4.600 GeV and comprising 5.1 fb^{-1} . Superseded by ABLIKIM 21AJ.
- From a three-resonance fit.
- From a combined fit of BELLE, BABAR and BES3 $e^+e^- \rightarrow \pi^+\pi^- J/\psi$ and $e^+e^- \rightarrow \pi^+\pi^-\psi(2S)$ data.
- From a combined fit of AUBERT 07s and WANG 07D data with two resonances.
- From a single-resonance fit. Systematic errors not estimated.

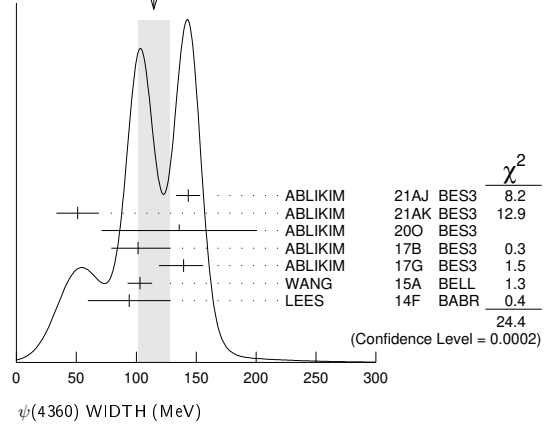
$\psi(4360)$ WIDTH

VALUE (MeV)	EVTS	DOCUMENT ID	TECN	COMMENT
115 ± 13	OUR AVERAGE	Error includes scale factor of 2.2. See the ideogram below.		
143.3 ± 10.0 ± 0.5		¹ ABLIKIM	21AJ BES3	$e^+e^- \rightarrow \pi^+\pi^-\psi(2S)$
51.1 ± 17.6 ± 1.9		² ABLIKIM	21AK BES3	$e^+e^- \rightarrow \gamma\chi_{C2} \rightarrow \gamma\gamma J/\psi$
135.8 ± 60.8 ± 22.5		³ ABLIKIM	20O BES3	$e^+e^- \rightarrow \eta J/\psi$
101.4 ± 25.3 ± 19.7 ± 10.2		⁴ ABLIKIM	17B BES3	$e^+e^- \rightarrow \pi^+\pi^- J/\psi$
139.5 ± 16.2 ± 20.6 ± 19.7		ABLIKIM	17G BES3	$e^+e^- \rightarrow \pi^+\pi^- h_c$
103 ± 9 ± 5	279	⁵ WANG	15A BELL	10.58 $e^+e^- \rightarrow \gamma\pi^+\pi^-\psi(2S)$
94 ± 32 ± 13	37	⁶ LEES	14F BABR	10.58 $e^+e^- \rightarrow \gamma\pi^+\pi^-\psi(2S)$

• • • We do not use the following data for averages, fits, limits, etc. • • •

84.2 ± 12.5 ± 2.1		⁷ ABLIKIM	17V BES3	$e^+e^- \rightarrow \pi^+\pi^-\psi(2S)$
94.2 ± 7.3 ± 2.0		⁸ ZHANG	17B RVUE	$e^+e^- \rightarrow \pi^+\pi^-\psi(2S)$
96.0 ± 6.7 ± 2.7		⁹ ZHANG	17C RVUE	$e^+e^- \rightarrow \pi^+\pi^- J/\psi$ or $\psi(2S)$
103 ± 17 ± 15 ± 11	74	¹⁰ LIU	08H RVUE	10.58 $e^+e^- \rightarrow \gamma\pi^+\pi^-\psi(2S)$
172 ± 33		¹¹ AUBERT	07S BABR	10.58 $e^+e^- \rightarrow \gamma\pi^+\pi^-\psi(2S)$
74 ± 15 ± 10	47	⁶ WANG	07D BELL	10.58 $e^+e^- \rightarrow \gamma\pi^+\pi^-\psi(2S)$

WEIGHTED AVERAGE
115±13 (Error scaled by 2.2)



$\psi(4360)$ WIDTH (MeV)

- From a three-resonance fit to the Born cross section in the range $\sqrt{s} = 4.008\text{--}4.698$ GeV.
- From a five-resonance fit to the cross section for $e^+e^- \rightarrow \gamma\gamma J/\psi \rightarrow \gamma\gamma\ell^+\ell^-$.
- From a fit of the measured cross section in the range $\sqrt{s} = 3.808\text{--}4.600$ GeV.
- From a three-resonance fit.
- From a two-resonance fit. Supersedes WANG 07D.
- From a two-resonance fit.
- From a fit to the cross section for $e^+e^- \rightarrow \pi^+\pi^-\psi(2S) \rightarrow 2(\pi^+\pi^-)\ell^+\ell^-$ obtained from 16 center-of-mass energies between 4.008 and 4.600 GeV and comprising 5.1 fb^{-1} . Superseded by ABLIKIM 21AJ.
- From a three-resonance fit.
- From a combined fit of BELLE, BABAR and BES3 $e^+e^- \rightarrow \pi^+\pi^- J/\psi$ and $e^+e^- \rightarrow \pi^+\pi^-\psi(2S)$ data.
- From a combined fit of AUBERT 07s and WANG 07D data with two resonances.
- From a single-resonance fit. Systematic errors not estimated.

$\psi(4360)$ DECAY MODES

Mode	Fraction (Γ_i/Γ)
Γ_1 e^+e^-	
Γ_2 $h_c\pi^+\pi^-$	seen
Γ_3 $J/\psi\pi^+\pi^-$	
Γ_4 $\psi(2S)\pi^+\pi^-$	seen
Γ_5 $\psi(3770)\pi^+\pi^-$	possibly seen
Γ_6 $\psi_2(3823)\pi^+\pi^-$	possibly seen
Γ_7 $J/\psi\eta$	seen
Γ_8 $D^0 D^{*-}\pi^+$	
Γ_9 $D_1(2420)\bar{D} + c.c.$	possibly seen
Γ_{10} $p\bar{p}\eta$	not seen
Γ_{11} $p\bar{p}\omega$	not seen
Γ_{12} $\chi_{c1}\gamma$	
Γ_{13} $\chi_{c2}\gamma$	

$\psi(4360)$ $\Gamma(i) \times \Gamma(e^+e^-)/\Gamma(\text{total})$

VALUE (eV)	DOCUMENT ID	TECN	COMMENT
11.6 ± 5.0 ± 4.4 ± 1.9	ABLIKIM	17G BES3	$e^+e^- \rightarrow \pi^+\pi^- h_c$

VALUE (eV)	EVTS	DOCUMENT ID	TECN	COMMENT
11.6 ± 5.0 ± 4.4 ± 1.9		ABLIKIM	17G BES3	$e^+e^- \rightarrow \pi^+\pi^- h_c$

• • • We do not use the following data for averages, fits, limits, etc. • • •

10.7 ± 4.1		¹ ABLIKIM	21AJ BES3	$e^+e^- \rightarrow \pi^+\pi^-\psi(2S)$
20.7 ± 2.5		² ABLIKIM	21AJ BES3	$e^+e^- \rightarrow \pi^+\pi^-\psi(2S)$
9.9 ± 4.1		³ ABLIKIM	21AJ BES3	$e^+e^- \rightarrow \pi^+\pi^-\psi(2S)$
19.4 ± 2.0		⁴ ABLIKIM	21AJ BES3	$e^+e^- \rightarrow \pi^+\pi^-\psi(2S)$
7.3 ± 2.8		⁵ ABLIKIM	19K BES3	$e^+e^- \rightarrow \pi^+\pi^-\psi(2S)$

Meson Particle Listings

$\psi(4360), \psi(4415)$

11.0±3.8	6	ABLIKIM	19K	BES3	$e^+e^- \rightarrow \pi^+\pi^-\psi(2S)$
9.2±0.6±0.6	279	7	WANG	15A	BELL 10.58 $e^+e^- \rightarrow \gamma\pi^+\pi^-\psi(2S)$
10.9±0.6±0.7	279	8	WANG	15A	BELL 10.58 $e^+e^- \rightarrow \gamma\pi^+\pi^-\psi(2S)$
6.0±1.0±0.5	37	5	LEES	14F	BABR 10.58 $e^+e^- \rightarrow \gamma\pi^+\pi^-\psi(2S)$
7.2±1.0±0.6	37	6	LEES	14F	BABR 10.58 $e^+e^- \rightarrow \gamma\pi^+\pi^-\psi(2S)$
11.1 ^{+1.3} _{-1.2}	74	9	LIU	08H	RVUE 10.58 $e^+e^- \rightarrow \gamma\pi^+\pi^-\psi(2S)$
12.3±1.2	74	10	LIU	08H	RVUE 10.58 $e^+e^- \rightarrow \gamma\pi^+\pi^-\psi(2S)$
10.4±1.7±1.5	47	5	WANG	07D	BELL 10.58 $e^+e^- \rightarrow \gamma\pi^+\pi^-\psi(2S)$
11.8±1.8±1.4	47	6	WANG	07D	BELL 10.58 $e^+e^- \rightarrow \gamma\pi^+\pi^-\psi(2S)$

- Solution I of four equivalent solutions in a fit using three interfering resonances. Supersedes ABLIKIM 19K.
- Solution II of four equivalent solutions in a fit using three interfering resonances. Supersedes ABLIKIM 19K.
- Solution III of four equivalent solutions in a fit using three interfering resonances. Supersedes ABLIKIM 19K.
- Solution IV of four equivalent solutions in a fit using three interfering resonances. Supersedes ABLIKIM 19K.
- Solution I of two equivalent solutions in a fit using two interfering resonances.
- Solution II of two equivalent solutions in a fit using two interfering resonances.
- Solution I of two equivalent solutions from a fit using two interfering resonances. Supersedes WANG 07D.
- Solution II of two equivalent solutions from a fit using two interfering resonances. Supersedes WANG 07D.
- Solution I in a combined fit of AUBERT 07s and WANG 07D data with two resonances.
- Solution II in a combined fit of AUBERT 07s and WANG 07D data with two resonances.

$\Gamma(J/\psi\eta) \times \Gamma(e^+e^-)/\Gamma_{total}$		Γ_{71}/Γ			
VALUE (eV)	CL%	DOCUMENT ID	TECN	COMMENT	
•••	•••	••• We do not use the following data for averages, fits, limits, etc. •••			
3.4±2.2		1	ABLIKIM	200	BES3 $e^+e^- \rightarrow \eta J/\psi$
1.5±1.0		2	ABLIKIM	200	BES3 $e^+e^- \rightarrow \eta J/\psi$
1.7±1.1		3	ABLIKIM	200	BES3 $e^+e^- \rightarrow \eta J/\psi$
<6.8	90	WANG	13B	BELL $e^+e^- \rightarrow J/\psi\eta\gamma$	

- Solution 1 of three equivalent fit solutions using three resonant structures.
- Solution 2 of three equivalent fit solutions using three resonant structures.
- Solution 3 of three equivalent fit solutions using three resonant structures.

$\Gamma(\chi_{c1}\gamma) \times \Gamma(e^+e^-)/\Gamma_{total}$		$\Gamma_{12}\Gamma_1/\Gamma$			
VALUE (eV)	CL%	DOCUMENT ID	TECN	COMMENT	
<0.57	90	1	HAN	15	BELL 10.58 $e^+e^- \rightarrow \chi_{c1}\gamma$

¹ Using $B(\eta \rightarrow \gamma\gamma) = (39.41 \pm 0.21)\%$.

$\Gamma(\chi_{c2}\gamma) \times \Gamma(e^+e^-)/\Gamma_{total}$		$\Gamma_{13}\Gamma_1/\Gamma$			
VALUE (eV)	CL%	DOCUMENT ID	TECN	COMMENT	
<1.9	90	1	HAN	15	BELL 10.58 $e^+e^- \rightarrow \chi_{c2}\gamma$

¹ Using $B(\eta \rightarrow \gamma\gamma) = (39.41 \pm 0.21)\%$.

$\psi(4360)$ BRANCHING RATIOS

$\Gamma(h_c\pi^+\pi^-)/\Gamma_{total}$		Γ_2/Γ		
VALUE	DOCUMENT ID	TECN	COMMENT	
seen	ABLIKIM	17G	BES3	$e^+e^- \rightarrow \pi^+\pi^-h_c$

$\Gamma(\psi(2S)\pi^+\pi^-)/\Gamma_{total}$		Γ_4/Γ		
VALUE	DOCUMENT ID	TECN	COMMENT	
seen	1	ABLIKIM	17V	BES3 $e^+e^- \rightarrow \pi^+\pi^-\psi(2S)$

¹ From a fit to the cross section for $e^+e^- \rightarrow \pi^+\pi^-\psi(2S) \rightarrow 2(\pi^+\pi^-)\ell^+\ell^-$ obtained from 16 center-of-mass energies between 4.008 and 4.600 GeV and comprising 5.1 fb⁻¹.

$\Gamma(\psi(2S)\pi^+\pi^-)/\Gamma(J/\psi\pi^+\pi^-)$		Γ_4/Γ_3		
VALUE	DOCUMENT ID	TECN	COMMENT	
(0.81 ± 0.12 ± 0.13) to (42 ± 15 ± 15)	1	ZHANG	17C	RVUE $e^+e^- \rightarrow \pi^+\pi^- J/\psi$ or $\psi(2S)$

¹ From a combined fit of BELLE, BABAR and BES3 $e^+e^- \rightarrow \pi^+\pi^- J/\psi$ and $e^+e^- \rightarrow \pi^+\pi^-\psi(2S)$ data.

$\Gamma(\psi(3770)\pi^+\pi^-)/\Gamma_{total}$		Γ_5/Γ		
VALUE	DOCUMENT ID	TECN	COMMENT	
possibly seen	1	ABLIKIM	19AR	BES3 $e^+e^- \rightarrow \pi^+\pi^-D\bar{D}$

¹ Observe $e^+e^- \rightarrow \pi^+\pi^-\psi(3770)$ at $\sqrt{s} = 4.26, 4.36, \text{ and } 4.42$ GeV but cannot establish if continuum or resonant.

$\Gamma(\psi_2(3823)\pi^+\pi^-)/\Gamma_{total}$		Γ_6/Γ			
VALUE	EVTS	DOCUMENT ID	TECN	COMMENT	
possibly seen	19	1	ABLIKIM	15S	BES3 $e^+e^- \rightarrow \pi^+\pi^-\chi_{c1}\gamma$

¹ From a fit of $e^+e^- \rightarrow \pi^+\pi^-\psi_2(3823), \psi_2(3823) \rightarrow \chi_{c1}\gamma$ cross sections taken at \sqrt{s} values of 4.23, 4.26, 4.36, 4.42, and 4.60 GeV to the $\psi(4360)$ line shape.

$\Gamma(J/\psi\eta)/\Gamma_{total}$		Γ_7/Γ		
VALUE	DOCUMENT ID	TECN	COMMENT	
seen	1	ABLIKIM	200	BES3 $e^+e^- \rightarrow \eta J/\psi$

¹ With a significance of 6.0 σ .

$\Gamma(D^0D^{*-}\pi^+)/\Gamma_{total} \times \Gamma(e^+e^-)/\Gamma_{total}$		$\Gamma_8/\Gamma \times \Gamma_1/\Gamma$			
VALUE	CL%	DOCUMENT ID	TECN	COMMENT	
<0.72 × 10 ⁻⁶	90	1	PAKHLOVA	09	BELL $e^+e^- \rightarrow \psi(4360) \rightarrow D^0D^{*-}\pi^+$

¹ Using $4355^{+9}_{-10} \pm 9$ MeV for the mass of $\psi(4360)$.

$\Gamma(D^0D^{*-}\pi^+)/\Gamma(\psi(2S)\pi^+\pi^-)$		Γ_8/Γ_4		
VALUE	CL%	DOCUMENT ID	TECN	COMMENT
<8	90	PAKHLOVA	09	BELL $e^+e^- \rightarrow \psi(4360) \rightarrow D^0D^{*-}\pi^+$

$\Gamma(D_1(2420)\bar{D} + c.c.)/\Gamma_{total}$		Γ_9/Γ		
VALUE	DOCUMENT ID	TECN	COMMENT	
possibly seen	1	ABLIKIM	19AR	BES3 $e^+e^- \rightarrow \pi^+\pi^-D\bar{D}$

¹ Evidence for $e^+e^- \rightarrow D_1(2420)\bar{D} + c.c.$ between $\sqrt{s} = 4.3$ and 4.6 GeV, not necessarily resonant.

$\Gamma(\rho\bar{\rho}\eta)/\Gamma_{total}$		Γ_{10}/Γ		
VALUE	DOCUMENT ID	TECN	COMMENT	
not seen	ABLIKIM	21AN	BES3	$e^+e^- \rightarrow \rho\bar{\rho}\eta$

$\Gamma(\rho\bar{\rho}\omega)/\Gamma_{total}$		Γ_{11}/Γ		
VALUE	DOCUMENT ID	TECN	COMMENT	
not seen	ABLIKIM	21AN	BES3	$e^+e^- \rightarrow \rho\bar{\rho}\omega$

$\psi(4360)$ REFERENCES

ABLIKIM	21AJ	PR	D104	052012	M. Ablikim <i>et al.</i>	(BESIII Collab.)
ABLIKIM	21AK	PR	D104	092001	M. Ablikim <i>et al.</i>	(BESIII Collab.)
ABLIKIM	21AN	PR	D104	092008	M. Ablikim <i>et al.</i>	(BESIII Collab.)
ABLIKIM	200	PR	D102	031101	M. Ablikim <i>et al.</i>	(BESIII Collab.)
ABLIKIM	19AR	PR	D100	032005	M. Ablikim <i>et al.</i>	(BESIII Collab.)
ABLIKIM	19K	PR	D99	019903 (errata.)	M. Ablikim <i>et al.</i>	(BESIII Collab.)
ABLIKIM	17B	PRL	118	092001	M. Ablikim <i>et al.</i>	(BESIII Collab.)
ABLIKIM	17G	PRL	118	092002	M. Ablikim <i>et al.</i>	(BESIII Collab.)
ABLIKIM	17V	PR	D96	032004	M. Ablikim <i>et al.</i>	(BESIII Collab.)
Also	PR	D99	019903 (errata.)	M. Ablikim <i>et al.</i>	(BESIII Collab.)	
ZHANG	17B	PR	D96	054008	J. Zhang, J. Zhang	
ZHANG	17C	EPJ	C77	727	J. Zhang, L. Yuan	
ABLIKIM	15S	PRL	115	011803	M. Ablikim <i>et al.</i>	(BESIII Collab.)
HAN	15	PR	D92	012011	Y.L. Han <i>et al.</i>	(BELLE Collab.)
WANG	15A	PR	D91	112007	X.L. Wang <i>et al.</i>	(BELLE Collab.)
LEES	14F	PR	D89	111103	J.P. Lees <i>et al.</i>	(BABAR Collab.)
WANG	13B	PR	D87	051101	X.L. Wang <i>et al.</i>	(BELLE Collab.)
PAKHLOVA	09	PR	D80	091101	G. Pakhlova <i>et al.</i>	(BELLE Collab.)
LIU	08H	PR	D78	014032	Z.Q. Liu, X.S. Qin, C.Z. Yuan	
AUBERT	07S	PRL	98	212001	B. Aubert <i>et al.</i>	(BABAR Collab.)
WANG	07D	PRL	99	142002	X.L. Wang <i>et al.</i>	(BELLE Collab.)

$\psi(4415)$

$$J^{PC} = 0^-(1^--)$$

$\psi(4415)$ MASS

VALUE (MeV)	DOCUMENT ID	TECN	COMMENT	
4421 ± 4 OUR ESTIMATE				
4415.1 ± 7.9	1	ABLIKIM	08D	BES2 $e^+e^- \rightarrow$ hadrons

••• We do not use the following data for averages, fits, limits, etc. •••

4412 ± 15	2	MO	10	RVUE $e^+e^- \rightarrow$ hadrons
4411 ± 7	3	PAKHLOVA	08A	BELL 10.6 $e^+e^- \rightarrow D^0D^-\pi^+\gamma$
4425 ± 6	4	SETH	05A	RVUE $e^+e^- \rightarrow$ hadrons
4429 ± 9	5	SETH	05A	RVUE $e^+e^- \rightarrow$ hadrons
4417 ± 10		BRANDELIK	78C	DASP e^+e^-
4414 ± 7		SIEGRIST	76	MRK1 e^+e^-

¹ Reanalysis of data presented in BAI 02c. From a global fit over the center-of-mass energy region 3.7–5.0 GeV covering the $\psi(3770), \psi(4040), \psi(4160), \text{ and } \psi(4415)$ resonances. Phase angle fixed in the fit to $\delta = (234 \pm 88)^\circ$.

² Reanalysis of data presented in BAI 00 and BAI 02c. From a global fit over the center-of-mass energy 3.8–4.8 GeV covering the $\psi(4040), \psi(4160)$ and $\psi(4415)$ resonances and including interference effects.

³ Systematic uncertainties not estimated.

⁴ From a fit to Crystal Ball (OSTERHELD 86) data.

⁵ From a fit to BES (BAI 02c) data.

$\psi(4415)$ WIDTH

VALUE (MeV)	DOCUMENT ID	TECN	COMMENT	
62 ± 20 OUR ESTIMATE				
71.5 ± 19.0	6	ABLIKIM	08D	BES2 $e^+e^- \rightarrow$ hadrons

••• We do not use the following data for averages, fits, limits, etc. •••

118 ± 32	7	MO	10	RVUE $e^+e^- \rightarrow$ hadrons
77 ± 20	8	PAKHLOVA	08A	BELL 10.6 $e^+e^- \rightarrow D^0D^-\pi^+\gamma$
119 ± 16	9	SETH	05A	RVUE $e^+e^- \rightarrow$ hadrons
118 ± 35	10	SETH	05A	RVUE $e^+e^- \rightarrow$ hadrons

66 ±15	BRANDELIK	78c	DASP	e^+e^-
33 ±10	SIEGRIST	76	MRK1	e^+e^-

⁶ Reanalysis of data presented in BAI 02c. From a global fit over the center-of-mass energy region 3.7–5.0 GeV covering the $\psi(3770)$, $\psi(4040)$, $\psi(4160)$, and $\psi(4415)$ resonances. Phase angle fixed in the fit to $\delta = (234 \pm 88)^\circ$.

⁷ Reanalysis of data presented in BAI 00 and BAI 02c. From a global fit over the center-of-mass energy 3.8–4.8 GeV covering the $\psi(4040)$, $\psi(4160)$ and $\psi(4415)$ resonances and including interference effects.

⁸ Systematic uncertainties not estimated.

⁹ From a fit to Crystal Ball (OSTERHELD 86) data.

¹⁰ From a fit to BES (BAI 02c) data.

$\psi(4415)$ DECAY MODES

Due to the complexity of the $c\bar{c}$ threshold region, in this listing, “seen” (“not seen”) means that a cross section for the mode in question has been measured at effective \sqrt{s} near this particle’s central mass value, more (less) than 2σ above zero, without regard to any peaking behavior in \sqrt{s} or absence thereof. See mode listing(s) for details and references.

Mode	Fraction (Γ_i/Γ)	Confidence level
Γ_1 $D\bar{D}$	seen	
Γ_2 $D^0\bar{D}^0$	seen	
Γ_3 D^+D^-	seen	
Γ_4 $D^*\bar{D}^+$ + c.c.	seen	
Γ_5 $D^*(2007)^0\bar{D}^0$ + c.c.	seen	
Γ_6 $D^*(2010)^+D^-$ + c.c.	seen	
Γ_7 $D^*\bar{D}^*$	seen	
Γ_8 $D^*(2007)^0\bar{D}^*(2007)^0$ + c.c.	seen	
Γ_9 $D^*(2010)^+D^*(2010)^-$ + c.c.	seen	
Γ_{10} $D^0D^-\pi^+$ (excl. $D^*(2007)^0\bar{D}^0$ + c.c., $D^*(2010)^+D^-$ + c.c.)	< 2.3 %	90%
Γ_{11} $D\bar{D}_2^*(2460) \rightarrow D^0D^-\pi^+$ + c.c.	(10 ± 4) %	
Γ_{12} $D^0D^*\pi^+$ + c.c.	< 11 %	90%
Γ_{13} $D_1(2420)\bar{D}^+$ + c.c.	possibly seen	
Γ_{14} $D_s^+D_s^-$	not seen	
Γ_{15} $\omega\chi_{c2}$	possibly seen	
Γ_{16} $D_s^{*+}D_s^-$ + c.c.	seen	
Γ_{17} $D_s^{*+}D_s^{*-}$	not seen	
Γ_{18} $\psi_2(3823)\pi^+\pi^-$	possibly seen	
Γ_{19} $\psi(3770)\pi^+\pi^-$	possibly seen	
Γ_{20} $J/\psi\eta$	< 6 × 10 ⁻³	90%
Γ_{21} $\chi_{c1}\gamma$	< 8 × 10 ⁻⁴	90%
Γ_{22} $\chi_{c2}\gamma$	< 4 × 10 ⁻³	90%
Γ_{23} $\Lambda\bar{\Lambda}$	< 3.1 × 10 ⁻⁶	90%
Γ_{24} e^+e^-	(9.4 ± 3.2) × 10 ⁻⁶	
Γ_{25} $\mu^+\mu^-$	(2.0 ± 1.0) × 10 ⁻⁵	

$\psi(4415)$ PARTIAL WIDTHS

$\Gamma(e^+e^-)$	DOCUMENT ID	TECN	COMMENT	Γ_{24}
0.58 ± 0.07 OUR ESTIMATE				
0.35 ± 0.12	11 ABLIKIM	08d	BES2 $e^+e^- \rightarrow$ hadrons	
• • • We do not use the following data for averages, fits, limits, etc. • • •				
0.4 to 0.8	12 MO	10	RVUE $e^+e^- \rightarrow$ hadrons	
0.72 ± 0.11	13 SETH	05A	RVUE $e^+e^- \rightarrow$ hadrons	
0.64 ± 0.23	14 SETH	05A	RVUE $e^+e^- \rightarrow$ hadrons	
0.49 ± 0.13	BRANDELIK	78c	DASP e^+e^-	
0.44 ± 0.14	SIEGRIST	76	MRK1 e^+e^-	

¹¹ Reanalysis of data presented in BAI 02c. From a global fit over the center-of-mass energy region 3.7–5.0 GeV covering the $\psi(3770)$, $\psi(4040)$, $\psi(4160)$, and $\psi(4415)$ resonances. Phase angle fixed in the fit to $\delta = (234 \pm 88)^\circ$.

¹² Reanalysis of data presented in BAI 00 and BAI 02c. From a global fit over the center-of-mass energy 3.8–4.8 GeV covering the $\psi(4040)$, $\psi(4160)$ and $\psi(4415)$ resonances and including interference effects. Four sets of solutions are obtained with the same fit quality, mass and total width, but with different e^+e^- partial widths. We quote only the range of values.

¹³ From a fit to Crystal Ball (OSTERHELD 86) data.

¹⁴ From a fit to BES (BAI 02c) data.

$\Gamma(\mu^+\mu^-)$	DOCUMENT ID	TECN	COMMENT	Γ_{25}
1.25 ± 0.28 ± 0.35	15,16 ABLIKIM	20Ag	BES3 $e^+e^- \rightarrow \mu^+\mu^-$	
From a fit to the $e^+e^- \rightarrow \mu^+\mu^-$ cross section between 3.8 and 4.6 GeV to the coherent sum of four resonant amplitudes assuming $\Gamma(\mu^+\mu^-) = \Gamma(e^+e^-)$.				
From solution 1 of 8 with equal fit quality. Other solutions range from 1.24 ± 0.28 ± 0.35 to 1.27 ± 0.41 ± 0.36 keV.				

$\psi(4415)$ $\Gamma(i) \times \Gamma(e^+e^-)/\Gamma(\text{total})$

$\Gamma(J/\psi\eta) \times \Gamma(e^+e^-)/\Gamma_{\text{total}}$	VALUE (eV)	CL%	DOCUMENT ID	TECN	COMMENT	$\Gamma_{20}\Gamma_{24}/\Gamma$
< 3.6	90		WANG	13B	BELL $e^+e^- \rightarrow J/\psi\eta\gamma$	
$\Gamma(\chi_{c1}\gamma) \times \Gamma(e^+e^-)/\Gamma_{\text{total}}$	VALUE (eV)	CL%	DOCUMENT ID	TECN	COMMENT	$\Gamma_{21}\Gamma_{24}/\Gamma$
< 0.47	90	17	HAN	15	BELL 10.58 $e^+e^- \rightarrow \chi_{c1}\gamma$	
17 Using $B(\eta \rightarrow \gamma\gamma) = (39.41 \pm 0.21)\%$.						
$\Gamma(\chi_{c2}\gamma) \times \Gamma(e^+e^-)/\Gamma_{\text{total}}$	VALUE (eV)	CL%	DOCUMENT ID	TECN	COMMENT	$\Gamma_{22}\Gamma_{24}/\Gamma$
< 2.3	90	18	HAN	15	BELL 10.58 $e^+e^- \rightarrow \chi_{c2}\gamma$	
18 Using $B(\eta \rightarrow \gamma\gamma) = (39.41 \pm 0.21)\%$.						
$\Gamma(\Lambda\bar{\Lambda}) \times \Gamma(e^+e^-)/\Gamma_{\text{total}}$	VALUE (eV)	CL%	DOCUMENT ID	TECN	COMMENT	$\Gamma_{23}\Gamma_{24}/\Gamma$
< 1.8 × 10 ⁻³	90	19	ABLIKIM	21As	BES3 $e^+e^- \rightarrow \psi(4415)$	
19 From a measurement of the $e^+e^- \rightarrow \Lambda\bar{\Lambda}$ cross section between 3.5 and 4.6 GeV.						

$\psi(4415)$ BRANCHING RATIOS

$\Gamma(D^0\bar{D}^0)/\Gamma_{\text{total}}$	VALUE	DOCUMENT ID	TECN	COMMENT	Γ_2/Γ	
seen		PAKHOVA	08	BELL $e^+e^- \rightarrow D^0\bar{D}^0\gamma$		
• • • We do not use the following data for averages, fits, limits, etc. • • •						
not seen		AUBERT	09M	BABR $e^+e^- \rightarrow D^0\bar{D}^0\gamma$		
$\Gamma(D^+D^-)/\Gamma_{\text{total}}$	VALUE	DOCUMENT ID	TECN	COMMENT	Γ_3/Γ	
seen		PAKHOVA	08	BELL $e^+e^- \rightarrow D^+D^-\gamma$		
• • • We do not use the following data for averages, fits, limits, etc. • • •						
not seen		AUBERT	09M	BABR $e^+e^- \rightarrow D^+D^-\gamma$		
$\Gamma(D\bar{D})/\Gamma(D^*\bar{D}^*)$	VALUE	DOCUMENT ID	TECN	COMMENT	Γ_1/Γ_7	
0.14 ± 0.12 ± 0.03		AUBERT	09M	BABR $e^+e^- \rightarrow \gamma D^{(*)}\bar{D}^{(*)}$		
$\Gamma(D^*(2007)^0\bar{D}^0 + \text{c.c.})/\Gamma_{\text{total}}$	VALUE	DOCUMENT ID	TECN	COMMENT	Γ_5/Γ	
seen		AUBERT	09M	BABR $e^+e^- \rightarrow D^{*0}\bar{D}^0\gamma$		
$\Gamma(D^*(2010)^+D^- + \text{c.c.})/\Gamma_{\text{total}}$	VALUE	DOCUMENT ID	TECN	COMMENT	Γ_6/Γ	
seen		20 ZHUKOVA	18	BELL $e^+e^- \rightarrow D^{*+}D^-\gamma$		
seen		AUBERT	09M	BABR $e^+e^- \rightarrow D^{*+}D^-\gamma$		
• • • We do not use the following data for averages, fits, limits, etc. • • •						
seen		PAKHOVA	07	BELL $e^+e^- \rightarrow D^{*+}D^-\gamma$		
20 Supersedes PAKHOVA 07.						
$\Gamma(D^*\bar{D}^+ + \text{c.c.})/\Gamma(D^*\bar{D}^*)$	VALUE	DOCUMENT ID	TECN	COMMENT	Γ_4/Γ_7	
0.17 ± 0.25 ± 0.03		AUBERT	09M	BABR $e^+e^- \rightarrow \gamma D^{(*)}\bar{D}^{(*)}$		
$\Gamma(D^*(2007)^0\bar{D}^*(2007)^0 + \text{c.c.})/\Gamma_{\text{total}}$	VALUE	DOCUMENT ID	TECN	COMMENT	Γ_8/Γ	
seen		AUBERT	09M	BABR $e^+e^- \rightarrow D^{*0}\bar{D}^{*0}\gamma$		
$\Gamma(D^*(2010)^+D^*(2010)^- + \text{c.c.})/\Gamma_{\text{total}}$	VALUE	DOCUMENT ID	TECN	COMMENT	Γ_9/Γ	
seen		21 ZHUKOVA	18	BELL $e^+e^- \rightarrow D^{*+}D^{*-}\gamma$		
seen		AUBERT	09M	BABR $e^+e^- \rightarrow D^{*+}D^{*-}\gamma$		
• • • We do not use the following data for averages, fits, limits, etc. • • •						
seen		PAKHOVA	07	BELL $e^+e^- \rightarrow D^{*+}D^{*-}\gamma$		
21 Supersedes PAKHOVA 07.						
$\Gamma(D\bar{D}_2^*(2460) \rightarrow D^0D^-\pi^+ + \text{c.c.})/\Gamma_{\text{total}}$	VALUE (units 10 ⁻²)	DOCUMENT ID	TECN	COMMENT	Γ_{11}/Γ	
10.5 ± 2.4 ± 3.8		22 PAKHOVA	08A	BELL 10.6 $e^+e^- \rightarrow D^0D^-\pi^+\gamma$		
22 Using 4421 ± 4 MeV for the mass and 62 ± 20 MeV for the width of $\psi(4415)$.						
$\Gamma(D^0D^-\pi^+ \text{ (excl. } D^*(2007)^0\bar{D}^0 + \text{c.c., } D^*(2010)^+D^- + \text{c.c.})/\Gamma_{\text{total}}$	VALUE	CL%	DOCUMENT ID	TECN	COMMENT	Γ_{10}/Γ_{11}
< 0.22	90	23	PAKHOVA	08A	BELL 10.6 $e^+e^- \rightarrow D^0D^-\pi^+\gamma$	
23 Using 4421 ± 4 MeV for the mass and 62 ± 20 MeV for the width of $\psi(4415)$.						

Meson Particle Listings

$\psi(4415)$, $Z_c(4430)$, $\chi_{c0}(4500)$

$\Gamma(D^0 D^{*-} \pi^+ + c.c.) / \Gamma_{\text{total}} \times \Gamma(e^+ e^-) / \Gamma_{\text{total}}$		$\Gamma_{12} / \Gamma \times \Gamma_{24} / \Gamma$	
VALUE	CL%	DOCUMENT ID	TECN COMMENT
$<0.99 \times 10^{-6}$	90	24 PAKHLOVA	09 BELL $e^+ e^- \rightarrow D^0 D^{*-} \pi^+$
24 Using 4421 ± 4 MeV for the mass of $\psi(4415)$.			

$\Gamma(D_1(2420) \bar{D}^+ + c.c.) / \Gamma_{\text{total}}$		Γ_{13} / Γ	
VALUE	CL%	DOCUMENT ID	TECN COMMENT
possibly seen		25 ABLIKIM	19AR BES3 $e^+ e^- \rightarrow \pi^+ \pi^- D \bar{D}$
25 Evidence for $e^+ e^- \rightarrow D_1(2420) \bar{D}^+ + c.c.$ between $\sqrt{s} = 4.3$ and 4.6 GeV, not necessarily resonant.			

$\Gamma(D_s^+ D_s^-) / \Gamma_{\text{total}}$		Γ_{14} / Γ	
VALUE	CL%	DOCUMENT ID	TECN COMMENT
not seen		PAKHLOVA	11 BELL $e^+ e^- \rightarrow D_s^+ D_s^- \gamma$
not seen		DEL-AMO-SA...10N	BABR $e^+ e^- \rightarrow D_s^+ D_s^- \gamma$

$\Gamma(\omega \chi_{c2}) / \Gamma_{\text{total}}$		Γ_{15} / Γ	
VALUE	CL%	DOCUMENT ID	TECN COMMENT
possibly seen		ABLIKIM	16A BES3 $e^+ e^- \rightarrow \gamma \pi^+ \pi^- \pi^0 \ell^+ \ell^-$

$\Gamma(D_s^{*+} D_s^- + c.c.) / \Gamma_{\text{total}}$		Γ_{16} / Γ	
VALUE	CL%	DOCUMENT ID	TECN COMMENT
seen		PAKHLOVA	11 BELL $e^+ e^- \rightarrow D_s^{*+} D_s^- \gamma$
seen		DEL-AMO-SA...10N	BABR $e^+ e^- \rightarrow D_s^{*+} D_s^- \gamma$

$\Gamma(D_s^{*+} D_s^{*-}) / \Gamma_{\text{total}}$		Γ_{17} / Γ	
VALUE	CL%	DOCUMENT ID	TECN COMMENT
not seen		PAKHLOVA	11 BELL $e^+ e^- \rightarrow D_s^{*+} D_s^{*-} \gamma$
not seen		DEL-AMO-SA...10N	BABR $e^+ e^- \rightarrow D_s^{*+} D_s^{*-} \gamma$

$\Gamma(\psi(3770) \pi^+ \pi^-) / \Gamma_{\text{total}}$		Γ_{19} / Γ	
VALUE	CL%	DOCUMENT ID	TECN COMMENT
possibly seen		26 ABLIKIM	19AR BES3 $e^+ e^- \rightarrow \pi^+ \pi^- D \bar{D}$
26 Observe $e^+ e^- \rightarrow \pi^+ \pi^- \psi(3770)$ at $\sqrt{s} = 4.26, 4.36, \text{ and } 4.42$ GeV but cannot establish if continuum or resonant.			

$\Gamma(\psi_2(3823) \pi^+ \pi^-) / \Gamma_{\text{total}}$		Γ_{18} / Γ	
VALUE	EVTS	DOCUMENT ID	TECN COMMENT
possibly seen	19	27 ABLIKIM	15s BES3 $e^+ e^- \rightarrow \pi^+ \pi^- \chi_{c1} \gamma$
27 From a fit of $e^+ e^- \rightarrow \pi^+ \pi^- \psi_2(3823)$, $\psi_2(3823) \rightarrow \chi_{c1} \gamma$ cross sections taken at \sqrt{s} values of 4.23, 4.26, 4.36, 4.42, and 4.60 GeV to the $\psi(4415)$ line shape.			

$\psi(4415)$ REFERENCES

ABLIKIM	21AS	PR D104 L091104	M. Ablikim et al.	(BESIII Collab.)
ABLIKIM	20AG	PR D102 112009	M. Ablikim et al.	(BESIII Collab.)
ABLIKIM	19AR	PR D100 032005	M. Ablikim et al.	(BESIII Collab.)
ZHUKOVA	18	PR D97 012002	V. Zhukova et al.	(BELLE Collab.)
ABLIKIM	16A	PR D93 011102	M. Ablikim et al.	(BESIII Collab.)
ABLIKIM	15S	PRL 115 011803	M. Ablikim et al.	(BESIII Collab.)
HAN	15	PR D92 012011	Y.L. Han et al.	(BELLE Collab.)
WANG	13B	PR D87 051101	X.L. Wang et al.	(BELLE Collab.)
PAKHLOVA	11	PR D83 011101	G. Pakhlova et al.	(BELLE Collab.)
DEL-AMO-SA...10N	PR	D82 052004	P. del Amo Sanchez et al.	(BABAR Collab.)
MO	10	PR D82 077501	X.H. Mo, C.Z. Yuan, P. Wang	(BHEP)
AUBERT	09M	PR D79 092001	B. Aubert et al.	(BABAR Collab.)
PAKHLOVA	09	PR D80 091101	G. Pakhlova et al.	(BELLE Collab.)
ABLIKIM	08D	PL B660 315	M. Ablikim et al.	(BES Collab.)
PAKHLOVA	08	PR D77 011103	G. Pakhlova et al.	(BELLE Collab.)
PAKHLOVA	08A	PRL 100 062001	G. Pakhlova et al.	(BELLE Collab.)
PAKHLOVA	07	PRL 98 092001	G. Pakhlova et al.	(BELLE Collab.)
SETH	05A	PR D72 017501	K.K. Seth	
BAI	02C	PRL 88 101802	J.Z. Bai et al.	(BES Collab.)
BAI	00	PRL 84 594	J.Z. Bai et al.	(BES Collab.)
OSTERHELD	86	SLAC-PUB-4160	A. Osterheld et al.	(SLAC Crystal Ball Collab.)
BRANDELIK	78C	PL 76B 361	R. Brandelik et al.	(DASP Collab.)
SIEGRIST	76	PRL 36 700	J.L. Siegrist et al.	(LBL, SLAC)

$Z_c(4430)$

$$I^G(J^{PC}) = 1^+(1^{+-})$$

G, C need confirmation.

was $X(4430)^{\pm}$

Properties incompatible with a $q\bar{q}$ structure (exotic state). See the review on non- $q\bar{q}$ states.

First seen by CHOI 08 in $B \rightarrow K \pi^+ \psi(2S)$ decays, confirmed by AAIJ 14AG, and confirmed in a model-independent way by AAIJ 15BH. Also seen by CHILIKIN 14 in $B \rightarrow K^+ \pi J/\psi$ decays. J^P was determined by CHILIKIN 13 and AAIJ 14AG.

$Z_c(4430)$ MASS

VALUE (MeV)	DOCUMENT ID	TECN	COMMENT
4478⁺¹⁵₋₁₈ OUR AVERAGE			
4475 \pm 7 ⁺¹⁵ ₋₂₅	1 AAIJ	14AG LHCB	$B^0 \rightarrow K^+ \pi^- \psi(2S)$
4485 \pm 22 ⁺²⁸ ₋₁₁	1 CHILIKIN	13 BELL	$B^0 \rightarrow K^+ \pi^- \psi(2S)$

- • • We do not use the following data for averages, fits, limits, etc. • • •
- 4443⁺¹⁵₋₁₂ 19 MIZUK 09 BELL $B \rightarrow K \pi^+ \psi(2S)$
- 4433 \pm 4 \pm 2 3 CHOI 08 BELL $B \rightarrow K \pi^+ \psi(2S)$
- 1 From a four-dimensional amplitude analysis.
- 2 From a Dalitz plot analysis. Superseded by CHILIKIN 13.
- 3 Superseded by MIZUK 09 and CHILIKIN 13.

$Z_c(4430)$ WIDTH

VALUE (MeV)	DOCUMENT ID	TECN	COMMENT
181\pm31 OUR AVERAGE			
172 \pm 13 ⁺³⁷ ₋₃₄	1 AAIJ	14AG LHCB	$B^0 \rightarrow K^+ \pi^- \psi(2S)$
200 \pm 41 ⁺²⁶ ₋₄₆ 35	1 CHILIKIN	13 BELL	$B^0 \rightarrow K^+ \pi^- \psi(2S)$
107 \pm 86 ⁺⁷⁴ ₋₄₃ 56	2 MIZUK	09 BELL	$B \rightarrow K \pi^+ \psi(2S)$
45 \pm 18 ⁺³⁰ ₋₁₃ 13	3 CHOI	08 BELL	$B \rightarrow K \pi^+ \psi(2S)$

$Z_c(4430)$ DECAY MODES

Mode	Fraction (Γ_i / Γ)
$\Gamma_1 \pi^+ \psi(2S)$	seen
$\Gamma_2 \pi^+ J/\psi$	seen

$Z_c(4430)$ BRANCHING RATIOS

$\Gamma(\pi^+ \psi(2S)) / \Gamma_{\text{total}}$	Γ_1 / Γ		
VALUE	DOCUMENT ID	TECN	COMMENT
seen	1 AAIJ	14AG LHCB	$B^0 \rightarrow K^+ \pi^- \psi(2S)$
seen	2 CHILIKIN	13 BELL	$B^0 \rightarrow K^+ \pi^- \psi(2S)$
not seen	3 AUBERT	09AA BABR	$B \rightarrow K \pi^+ \psi(2S)$
not seen	4 MIZUK	09 BELL	$B \rightarrow K \pi^+ \psi(2S)$

$\Gamma(\pi^+ J/\psi) / \Gamma_{\text{total}}$	Γ_2 / Γ		
VALUE	DOCUMENT ID	TECN	COMMENT
seen	1,2 CHILIKIN	14 BELL	$\bar{B}^0 \rightarrow K^- \pi^+ J/\psi$
not seen	3 AUBERT	09AA BABR	$B \rightarrow K \pi^+ J/\psi$

$Z_c(4430)$ REFERENCES

AAIJ	19R	PRL 122 152002	R. Aaij et al.	(LHCb Collab.)
AAIJ	15BH	PR D92 112009	R. Aaij et al.	(LHCb Collab.)
AAIJ	14AG	PRL 112 222002	R. Aaij et al.	(LHCb Collab.)
CHILIKIN	14	PR D90 112009	K. Chilikin et al.	(BELLE Collab.)
CHILIKIN	13	PR D88 074026	K. Chilikin et al.	(BELLE Collab.)
AUBERT	09AA	PR D79 112001	B. Aubert et al.	(BABAR Collab.)
MIZUK	09	PR D80 031104	R. Mizuk et al.	(BELLE Collab.)
CHOI	08	PRL 100 142001	S.-K. Choi et al.	(BELLE Collab.)

$\chi_{c0}(4500)$

$$I^G(J^{PC}) = 0^+(0^{++})$$

OMITTED FROM SUMMARY TABLE

was $X(4500)$

This state shows properties different from a conventional $q\bar{q}$ state. A candidate for an exotic structure. See the review on non- $q\bar{q}$ states.

Seen by AAIJ 17C in $B^+ \rightarrow \chi_{c0} K^+$, $\chi_{c0} \rightarrow J/\psi \phi$ using an amplitude analysis of $B^+ \rightarrow J/\psi \phi K^+$ with a significance (accounting for systematic uncertainties) of 6.1 σ .

See key on page 1127

Meson Particle Listings

$\chi_{c0}(4500)$, $X(4630)$, $\psi(4660)$

$\chi_{c0}(4500)$ MASS

VALUE (MeV)	EVTS	DOCUMENT ID	TECN	COMMENT
$4474 \pm 3 \pm 3$	24k	¹ AAIJ	21E LHCb	$B^+ \rightarrow J/\psi \phi K^+$
• • • We do not use the following data for averages, fits, limits, etc. • • •				
$4506 \pm 11 \pm 12$	4289	^{2,3} AAIJ	17c LHCb	$B^+ \rightarrow J/\psi \phi K^+$

- ¹ From an amplitude analysis of the decay $B^+ \rightarrow J/\psi \phi K^+$ with a significance of 20 σ .
- ² From an amplitude analysis of the decay $B^+ \rightarrow J/\psi \phi K^+$ with a significance of 6.1 σ .
- ³ Superseded by AAIJ 21E.

$\chi_{c0}(4500)$ WIDTH

VALUE (MeV)	EVTS	DOCUMENT ID	TECN	COMMENT
$77 \pm 6 \pm 10$	24k	¹ AAIJ	21E LHCb	$B^+ \rightarrow J/\psi \phi K^+$
• • • We do not use the following data for averages, fits, limits, etc. • • •				
$92 \pm 21 \pm 21$	4289	^{2,3} AAIJ	17c LHCb	$B^+ \rightarrow J/\psi \phi K^+$

- ¹ From an amplitude analysis of the decay $B^+ \rightarrow J/\psi \phi K^+$ with a significance of 20 σ .
- ² From an amplitude analysis of the decay $B^+ \rightarrow J/\psi \phi K^+$ with a significance of 6.1 σ .
- ³ Superseded by AAIJ 21E.

$\chi_{c0}(4500)$ DECAY MODES

Mode	Fraction (Γ_i/Γ)
Γ_1 $J/\psi \phi$	seen

$\chi_{c0}(4500)$ BRANCHING RATIOS

$\Gamma(J/\psi \phi)/\Gamma_{total}$	VALUE	EVTS	DOCUMENT ID	TECN	COMMENT	Γ_1/Γ
seen		24k	¹ AAIJ	21E LHCb	$B^+ \rightarrow J/\psi \phi K^+$	
• • • We do not use the following data for averages, fits, limits, etc. • • •						
seen		4289	^{2,3} AAIJ	17c LHCb	$B^+ \rightarrow J/\psi \phi K^+$	

- ¹ From an amplitude analysis of the decay $B^+ \rightarrow J/\psi \phi K^+$ with a significance of 20 σ .
- ² From an amplitude analysis of the decay $B^+ \rightarrow J/\psi \phi K^+$ with a significance of 6.1 σ .
- ³ Superseded by AAIJ 21E.

$\chi_{c0}(4500)$ REFERENCES

AAIJ	21E	PRL 127 082001	R. Aaij et al.	(LHCb Collab.)
AAIJ	17C	PRL 118 022003	R. Aaij et al.	(LHCb Collab.) JIP
Also		PR D95 012002	R. Aaij et al.	(LHCb Collab.)

$X(4630)$

$I^G(J^{PC}) = 0^+(?^?+)$

OMITTED FROM SUMMARY TABLE

This state shows properties different from a conventional $q\bar{q}$ state. A candidate for an exotic structure. See the review on "Heavy Non- $q\bar{q}$ Mesons."

Seen by AAIJ 21E in $B^+ \rightarrow X(4630) K^+$ with $X(4630) \rightarrow J/\psi \phi$ using an amplitude analysis of $B^+ \rightarrow J/\psi \phi K^+$ with a significance (accounting for systematic uncertainties) of 5.5 σ . The $J^P = 1^-$ assignment is favored over 2^- with a significance of 3 σ and other assignments are disfavored by more than 5 σ .

$X(4630)$ MASS

VALUE (MeV)	EVTS	DOCUMENT ID	TECN	COMMENT
$4626 \pm 16 \pm 18$	24k	¹ AAIJ	21E LHCb	$B^+ \rightarrow J/\psi \phi K^+$

- ¹ From an amplitude analysis of the decay $B^+ \rightarrow J/\psi \phi K^+$ with a significance of 5.5 σ .

$X(4630)$ WIDTH

VALUE (MeV)	EVTS	DOCUMENT ID	TECN	COMMENT
$174 \pm 27 \pm 134$	24k	¹ AAIJ	21E LHCb	$B^+ \rightarrow J/\psi \phi K^+$

- ¹ From an amplitude analysis of the decay $B^+ \rightarrow J/\psi \phi K^+$ with a significance of 5.5 σ .

$X(4630)$ DECAY MODES

Mode	Fraction (Γ_i/Γ)
Γ_1 $J/\psi \phi$	seen

$\Gamma(J/\psi \phi)/\Gamma_{total}$	VALUE	EVTS	DOCUMENT ID	TECN	COMMENT	Γ_1/Γ
seen		24k	¹ AAIJ	21E LHCb	$B^+ \rightarrow J/\psi \phi K^+$	

- ¹ From an amplitude analysis of the decay $B^+ \rightarrow J/\psi \phi K^+$ with a significance of 5.5 σ .

$X(4630)$ REFERENCES

AAIJ	21E	PRL 127 082001	R. Aaij et al.	(LHCb Collab.)
------	-----	----------------	----------------	----------------

$\psi(4660)$

$I^G(J^{PC}) = 0^-(1^{--})$

also known as $Y(4660)$; was $X(4660)$

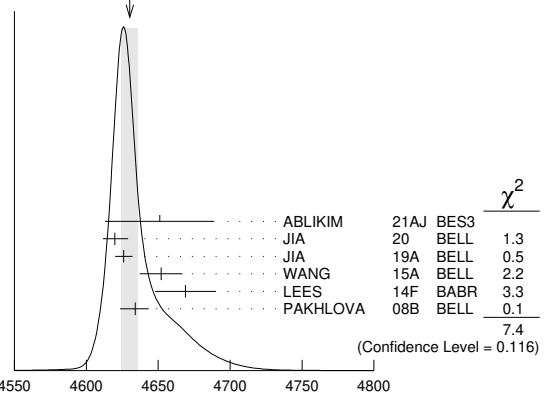
This state shows properties different from a conventional $q\bar{q}$ state. A candidate for an exotic structure. See the review on non- $q\bar{q}$ states.

Seen in radiative return from e^+e^- collisions at $\sqrt{s} = 9.54\text{--}10.58$ GeV by WANG 07D. Also obtained in a combined fit of WANG 07D, AUBERT 07S, and LEES 14F. See also the review on "Spectroscopy of mesons containing two heavy quarks."

$\psi(4660)$ MASS

VALUE (MeV)	EVTS	DOCUMENT ID	TECN	COMMENT
4630 ± 6	OUR AVERAGE	Error includes scale factor of 1.4. See the ideogram below.		
$4651.0 \pm 37.8 \pm 2.1$		¹ ABLIKIM	21AJ BES3	$e^+e^- \rightarrow \pi^+\pi^-\psi(2S)$
$4619.8 \pm 8.9 \pm 8.0$	66	² JIA	20 BELL	$e^+e^- \rightarrow \gamma D_s^* D_{s2}^*(2573)^-$
$4625.9 \pm 6.2 \pm 6.0$	89	³ JIA	19A BELL	$e^+e^- \rightarrow \gamma D_s^* D_{s1}(2536)^-$
$4652 \pm 10 \pm 11$	279	⁴ WANG	15A BELL	$10.58 e^+e^- \rightarrow \gamma \pi^+\pi^-\psi(2S)$
$4669 \pm 21 \pm 3$	37	⁵ LEES	14F BABR	$10.58 e^+e^- \rightarrow \gamma \pi^+\pi^-\psi(2S)$
$4634 \pm 8 \pm 5$	142	⁶ PAKHLOVA	08B BELL	$e^+e^- \rightarrow \Lambda_c^+ \Lambda_c^-$
• • • We do not use the following data for averages, fits, limits, etc. • • •				
$4652.5 \pm 3.4 \pm 1.1$		⁷ DAI	17 RVUE	$e^+e^- \rightarrow \Lambda_c^+ \Lambda_c^-$
$4645.2 \pm 9.5 \pm 6.0$		⁸ ZHANG	17B RVUE	$e^+e^- \rightarrow \pi^+\pi^-\psi(2S)$
$4646.4 \pm 9.7 \pm 4.8$		⁹ ZHANG	17C RVUE	$e^+e^- \rightarrow \pi^+\pi^-\psi(2S)$
$4661 \pm 9 \pm 8$	44	¹⁰ LIU	08H RVUE	$10.58 e^+e^- \rightarrow \gamma \pi^+\pi^-\psi(2S)$
$4664 \pm 11 \pm 5$	44	WANG	07D BELL	$10.58 e^+e^- \rightarrow \gamma \pi^+\pi^-\psi(2S)$

WEIGHTED AVERAGE
4630±6 (Error scaled by 1.4)



- ¹ From a three-resonance fit to the Born cross section in the range $\sqrt{s} = 4.008\text{--}4.698$ GeV.
- ² Using $D_{s2}^*(2573)^- \rightarrow \bar{D}^0 K^-$ decays.
- ³ From a fit of a Breit-Wigner convolved with a Gaussian.
- ⁴ From a two-resonance fit. Supersedes WANG 07D.
- ⁵ From a two-resonance fit.
- ⁶ The $\pi^+\pi^-\psi(2S)$ and $\Lambda_c^+\Lambda_c^-$ states are not necessarily the same.
- ⁷ The pole parameters are extracted from the speed plot.
- ⁸ From a three-resonance fit.
- ⁹ From a combined fit of BELLE, BABAR and BES3 $e^+e^- \rightarrow \pi^+\pi^-\psi(2S)$ and $e^+e^- \rightarrow \pi^+\pi^-\psi(2S)$ data.
- ¹⁰ From a combined fit of AUBERT 07S and WANG 07D data with two resonances.

$\psi(4660)$ WIDTH

VALUE (MeV)	EVTS	DOCUMENT ID	TECN	COMMENT
72 ± 14	OUR AVERAGE	Error includes scale factor of 1.7. See the ideogram below.		
$155.4 \pm 24.8 \pm 0.8$		¹ ABLIKIM	21AJ BES3	$e^+e^- \rightarrow \pi^+\pi^-\psi(2S)$
$47.0 \pm 31.3 \pm 14.8$	66	² JIA	20 BELL	$e^+e^- \rightarrow \gamma D_s^* D_{s2}^*(2573)^-$
$49.8 \pm 13.9 \pm 11.5$	89	³ JIA	19A BELL	$e^+e^- \rightarrow \gamma D_s^* D_{s1}(2536)^-$

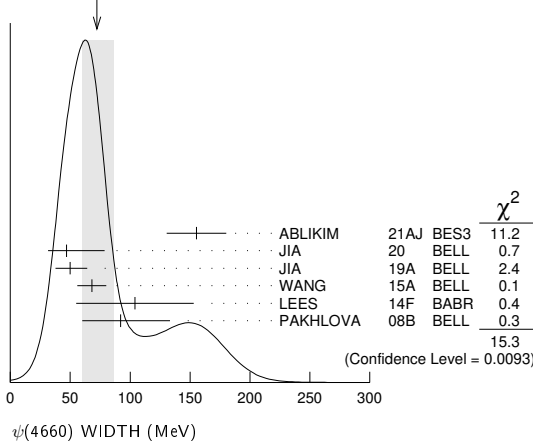
Meson Particle Listings

$\psi(4660)$

68 ±11 ± 5	279	⁴ WANG	15A BELL	10.58 e ⁺ e ⁻ → $\gamma\pi^+\pi^-\psi(2S)$
104 ±48 ±10	37	⁵ LEES	14F BABR	10.58 e ⁺ e ⁻ → $\gamma\pi^+\pi^-\psi(2S)$
92 ⁺⁴⁰ ₋₂₄ ⁺¹⁰ ₋₂₁	142	⁶ PAKHLOVA	08B BELL	e ⁺ e ⁻ → $\Lambda_C^+ \Lambda_C^-$
62.6 ± 5.6 ± 4.3		⁷ DAI	17 RVUE	e ⁺ e ⁻ → $\Lambda_C^+ \Lambda_C^-$
113.8 ± 18.1 ± 3.4		⁸ ZHANG	17B RVUE	e ⁺ e ⁻ → $\pi^+\pi^-\psi(2S)$
103.5 ± 15.6 ± 4.0		⁹ ZHANG	17c RVUE	e ⁺ e ⁻ → $\pi^+\pi^- J/\psi$ or $\psi(2S)$
42 ⁺¹⁷ ₋₁₂ ± 6	44	¹⁰ LIU	08H RVUE	10.58 e ⁺ e ⁻ → $\gamma\pi^+\pi^-\psi(2S)$
48 ± 15 ± 3	44	WANG	07D BELL	10.58 e ⁺ e ⁻ → $\gamma\pi^+\pi^-\psi(2S)$

- • • We do not use the following data for averages, fits, limits, etc. • • •
- 1 From a three-resonance fit to the Born cross section in the range $\sqrt{s} = 4.008\text{--}4.698$ GeV.
- 2 Using $D_s^*(2573)^- \rightarrow \bar{D}^0 K^-$ decays.
- 3 From a fit of a Breit-Wigner convolved with a Gaussian.
- 4 From a two-resonance fit. Supersedes WANG 07D.
- 5 From a two-resonance fit.
- 6 The $\pi^+\pi^-\psi(2S)$ and $\Lambda_C^+ \Lambda_C^-$ states are not necessarily the same.
- 7 The pole parameters are extracted from the speed plot.
- 8 From a three-resonance fit.
- 9 From a combined fit of BELLE, BABAR and BES3 e⁺e⁻ → $\pi^+\pi^- J/\psi$ and e⁺e⁻ → $\pi^+\pi^-\psi(2S)$ data.
- 10 From a combined fit of AUBERT 07s and WANG 07D data with two resonances.

WEIGHTED AVERAGE
72+14-12 (Error scaled by 1.7)



$\psi(4660)$ DECAY MODES

Mode	Fraction (Γ_i/Γ)
Γ_1 e ⁺ e ⁻	not seen
Γ_2 $\psi(2S)\pi^+\pi^-$	seen
Γ_3 $J/\psi\eta$	not seen
Γ_4 $D^0 D^{*-}\pi^+$	not seen
Γ_5 $\chi_{c1}\gamma$	not seen
Γ_6 $\chi_{c2}\gamma$	not seen
Γ_7 $\Lambda_C^+ \Lambda_C^-$	seen
Γ_8 $D_s^+ D_{s1}^-(2536)^-$	seen
Γ_9 $D_s^+ D_{s2}^*(2573)^-$	

$\psi(4660) \Gamma(i) \times \Gamma(e^+e^-)/\Gamma(\text{total})$

VALUE (eV)	EVTS	DOCUMENT ID	TECN	COMMENT	$\Gamma_2\Gamma_1/\Gamma$
4.7 ± 3.8		¹ ABLIKIM	21AJ BES3	e ⁺ e ⁻ → $\pi^+\pi^-\psi(2S)$	
11.2 ± 3.2		² ABLIKIM	21AJ BES3	e ⁺ e ⁻ → $\pi^+\pi^-\psi(2S)$	
4.7 ± 4.2		³ ABLIKIM	21AJ BES3	e ⁺ e ⁻ → $\pi^+\pi^-\psi(2S)$	
11.3 ± 3.3		⁴ ABLIKIM	21AJ BES3	e ⁺ e ⁻ → $\pi^+\pi^-\psi(2S)$	
2.0 ± 0.3 ± 0.2	279	⁵ WANG	15A BELL	10.58 e ⁺ e ⁻ → $\gamma\pi^+\pi^-\psi(2S)$	
8.1 ± 1.1 ± 1.0	279	⁶ WANG	15A BELL	10.58 e ⁺ e ⁻ → $\gamma\pi^+\pi^-\psi(2S)$	
2.7 ± 1.3 ± 0.5	37	⁷ LEES	14F BABR	10.58 e ⁺ e ⁻ → $\gamma\pi^+\pi^-\psi(2S)$	

7.5 ± 1.7 ± 0.7	37	⁸ LEES	14F BABR	10.58 e ⁺ e ⁻ → $\gamma\pi^+\pi^-\psi(2S)$
2.2 ^{+0.7} _{-0.6}	44	⁹ LIU	08H RVUE	10.58 e ⁺ e ⁻ → $\gamma\pi^+\pi^-\psi(2S)$
5.9 ± 1.6	44	¹⁰ LIU	08H RVUE	10.58 e ⁺ e ⁻ → $\gamma\pi^+\pi^-\psi(2S)$
3.0 ± 0.9 ± 0.3	44	⁷ WANG	07D BELL	10.58 e ⁺ e ⁻ → $\gamma\pi^+\pi^-\psi(2S)$
7.6 ± 1.8 ± 0.8	44	⁸ WANG	07D BELL	10.58 e ⁺ e ⁻ → $\gamma\pi^+\pi^-\psi(2S)$

- 1 Solution I of four equivalent solutions in a fit using three interfering resonances.
- 2 Solution II of four equivalent solutions in a fit using three interfering resonances.
- 3 Solution III of four equivalent solutions in a fit using three interfering resonances.
- 4 Solution IV of four equivalent solutions in a fit using three interfering resonances.
- 5 Solution I of two equivalent solutions from a fit using two interfering resonances. Supersedes WANG 07D.
- 6 Solution II of two equivalent solutions from a fit using two interfering resonances. Supersedes WANG 07D.
- 7 Solution I of two equivalent solutions in a fit using two interfering resonances.
- 8 Solution II of two equivalent solutions in a fit using two interfering resonances.
- 9 Solution I in a combined fit of AUBERT 07s and WANG 07D data with two resonances.
- 10 Solution II in a combined fit of AUBERT 07s and WANG 07D data with two resonances.

$\Gamma(J/\psi\eta) \times \Gamma(e^+e^-)/\Gamma_{\text{total}}$ $\Gamma_3\Gamma_1/\Gamma$

VALUE (eV)	CL%	DOCUMENT ID	TECN	COMMENT
<0.94	90	WANG	13B BELL	e ⁺ e ⁻ → $J/\psi\eta\gamma$

$\Gamma(\chi_{c1}\gamma) \times \Gamma(e^+e^-)/\Gamma_{\text{total}}$ $\Gamma_5\Gamma_1/\Gamma$

VALUE (eV)	CL%	DOCUMENT ID	TECN	COMMENT
<0.45	90	¹ HAN	15 BELL	10.58 e ⁺ e ⁻ → $\chi_{c1}\gamma$

¹ Using $B(\eta \rightarrow \gamma\gamma) = (39.41 \pm 0.21)\%$.

$\Gamma(\chi_{c2}\gamma) \times \Gamma(e^+e^-)/\Gamma_{\text{total}}$ $\Gamma_6\Gamma_1/\Gamma$

VALUE (eV)	CL%	DOCUMENT ID	TECN	COMMENT
<2.1	90	¹ HAN	15 BELL	10.58 e ⁺ e ⁻ → $\chi_{c2}\gamma$

¹ Using $B(\eta \rightarrow \gamma\gamma) = (39.41 \pm 0.21)\%$.

$\Gamma(D_s^+ D_{s1}^-(2536)^-) \times \Gamma(e^+e^-)/\Gamma_{\text{total}}$ $\Gamma_8\Gamma_1/\Gamma$

VALUE (eV)	EVTS	DOCUMENT ID	TECN	COMMENT
14.3 ^{+2.8} _{-2.6} ± 1.5	89	¹ JIA	19A BELL	e ⁺ e ⁻ → $\gamma D_s^+ D_{s1}^-(2536)^-$

¹ Assuming $B(D_{s1}^-(2536)^- \rightarrow \bar{D}^0 K^-) = 1$.

$\Gamma(D_s^+ D_{s2}^*(2573)^-) \times \Gamma(e^+e^-)/\Gamma_{\text{total}}$ $\Gamma_9\Gamma_1/\Gamma$

VALUE (eV)	EVTS	DOCUMENT ID	TECN	COMMENT
14.7 ^{+5.9} _{-4.5} ± 3.6	66	¹ JIA	20 BELL	e ⁺ e ⁻ → $\gamma D_s^+ D_{s2}^*(2573)^-$

¹ Assuming $B(D_{s2}^*(2573)^- \rightarrow \bar{D}^0 K^-) = 1$.

$\psi(4660)$ BRANCHING RATIOS

$\Gamma(D^0 D^{*-}\pi^+)/\Gamma(\psi(2S)\pi^+\pi^-)$ Γ_4/Γ_2

VALUE	CL%	DOCUMENT ID	TECN	COMMENT
<10	90	PAKHLOVA	09 BELL	e ⁺ e ⁻ → $D^0 D^{*-}\pi^+$

$\Gamma(D^0 D^{*-}\pi^+)/\Gamma_{\text{total}} \times \Gamma(e^+e^-)/\Gamma_{\text{total}}$ $\Gamma_4/\Gamma \times \Gamma_1/\Gamma$

VALUE	CL%	DOCUMENT ID	TECN	COMMENT
<0.37 × 10 ⁻⁶	90	¹ PAKHLOVA	09 BELL	e ⁺ e ⁻ → $D^0 D^{*-}\pi^+$

¹ Using 4664 ± 11 ± 5 MeV for the mass of $\psi(4660)$.

$\Gamma(\Lambda_C^+ \Lambda_C^-)/\Gamma_{\text{total}} \times \Gamma(e^+e^-)/\Gamma_{\text{total}}$ $\Gamma_7/\Gamma \times \Gamma_1/\Gamma$

VALUE (units 10 ⁻⁶)	EVTS	DOCUMENT ID	TECN	COMMENT
0.68 ^{+0.16 + 0.29} _{-0.15 - 0.30}	142	¹ PAKHLOVA	08B BELL	e ⁺ e ⁻ → $\Lambda_C^+ \Lambda_C^-$

¹ The $\pi^+\pi^-\psi(2S)$ and $\Lambda_C^+ \Lambda_C^-$ states are not necessarily the same.

$\psi(4660)$ REFERENCES

ABLIKIM	21AJ	PR D104 052012	M. Ablikim et al.	(BESIII Collab.)
JIA	20	PR D101 091101	S. Jia et al.	(BELLE Collab.)
JIA	19A	PR D100 111103	S. Jia et al.	(BELLE Collab.)
DAI	17	PR D96 116001	L.-Y. Dai, J. Haidenbauer, U.-G. Meissner	(JUL)
ZHANG	17B	PR D96 054008	J. Zhang, J. Zhang	
ZHANG	17C	EPI C77 727	J. Zhang, L. Yuan	
HAN	15	PR D92 012011	Y.L. Han et al.	(BELLE Collab.)
WANG	15A	PR D91 112007	X.L. Wang et al.	(BELLE Collab.)
LEES	14F	PR D89 111103	J.P. Lees et al.	(BABAR Collab.)
WANG	13B	PR D87 051101	X.L. Wang et al.	(BELLE Collab.)
PAKHLOVA	09	PR D80 091101	G. Pakhlova et al.	(BELLE Collab.)
LIU	08H	PR D78 014032	Z.Q. Liu, X.S. Qin, C.Z. Yuan	
PAKHLOVA	08B	PRL 101 172001	C. Pakhlova et al.	(BELLE Collab.)
AUBERT	07S	PRL 98 212001	B. Aubert et al.	(BABAR Collab.)
WANG	07D	PRL 99 142002	X.L. Wang et al.	(BELLE Collab.)

See key on page 1127

Meson Particle Listings

$\chi_{c1}(4685), \chi_{c0}(4700)$

$\chi_{c1}(4685)$

$$I^G(J^{PC}) = 0^+(1^{++})$$

OMITTED FROM SUMMARY TABLE

This state shows properties different from a conventional $q\bar{q}$ state. A candidate for an exotic structure. See the review on "Heavy Non- $q\bar{q}$ Mesons."

Seen by AAIJ 21E in $B^+ \rightarrow \chi_{c1}(4685)K^+$ with $\chi_{c1}(4685) \rightarrow J/\psi\phi$ using an amplitude analysis of $B^+ \rightarrow J/\psi\phi K^+$ with a significance (accounting for systematic uncertainties) of 15σ . The $J^P = 1^+$ assignment is favored with high significance.

$\chi_{c1}(4685)$ MASS

VALUE (MeV)	EVTS	DOCUMENT ID	TECN	COMMENT
$4684 \pm 7^{+13}_{-16}$	24k	¹ AAIJ	21E LHCb	$B^+ \rightarrow J/\psi\phi K^+$

¹ From an amplitude analysis of the decay $B^+ \rightarrow J/\psi\phi K^+$ with a significance of 15σ .

$\chi_{c1}(4685)$ WIDTH

VALUE (MeV)	EVTS	DOCUMENT ID	TECN	COMMENT
$126 \pm 15^{+37}_{-41}$	24k	¹ AAIJ	21E LHCb	$B^+ \rightarrow J/\psi\phi K^+$

¹ From an amplitude analysis of the decay $B^+ \rightarrow J/\psi\phi K^+$ with a significance of 15σ .

$\chi_{c1}(4685)$ DECAY MODES

Mode	Fraction (Γ_i/Γ)
$\Gamma_1 J/\psi\phi$	seen

$\Gamma(J/\psi\phi)/\Gamma_{total}$	Γ_1/Γ
seen	seen

VALUE	EVTS	DOCUMENT ID	TECN	COMMENT
seen	24k	¹ AAIJ	21E LHCb	$B^+ \rightarrow J/\psi\phi K^+$

¹ From an amplitude analysis of the decay $B^+ \rightarrow J/\psi\phi K^+$ with a significance of 15σ .

$\chi_{c1}(4685)$ REFERENCES

AAIJ	21E	PRL 127 082001	R. Aaij <i>et al.</i>	(LHCb Collab.) JP
------	-----	----------------	-----------------------	-------------------

$\chi_{c0}(4700)$

$$I^G(J^{PC}) = 0^+(0^{++})$$

OMITTED FROM SUMMARY TABLE

was $X(4700)$

This state shows properties different from a conventional $q\bar{q}$ state. A candidate for an exotic structure. See the review on non- $q\bar{q}$ states.

Seen by AAIJ 17C in $B^+ \rightarrow \chi_{c0}K^+, \chi_{c0} \rightarrow J/\psi\phi$ using an amplitude analysis of $B^+ \rightarrow J/\psi\phi K^+$ with a significance (accounting for systematic uncertainties) of 5.6σ .

$\chi_{c0}(4700)$ MASS

VALUE (MeV)	EVTS	DOCUMENT ID	TECN	COMMENT
$4694 \pm 4^{+16}_{-3}$	24k	¹ AAIJ	21E LHCb	$B^+ \rightarrow J/\psi\phi K^+$
$4741 \pm 6 \pm 6$	175	² AAIJ	21C LHCb	$B_S^0 \rightarrow J/\psi\phi\pi^+\pi^-$
$4704 \pm 10^{+14}_{-24}$	4289	^{3,4} AAIJ	17C LHCb	$B^+ \rightarrow J/\psi\phi K^+$

¹ From an amplitude analysis of the decay $B^+ \rightarrow J/\psi\phi K^+$ with a significance of 17σ .

² From a 1D fit to the $J/\psi\phi$ mass distribution with a significance of 5.3σ . The identification of this structure as the $\chi_{c0}(4700)$ needs confirmation.

³ From an amplitude analysis of the decay $B^+ \rightarrow J/\psi\phi K^+$ with a significance of 5.6σ .

⁴ Superseded by AAIJ 21E.

$\chi_{c0}(4700)$ WIDTH

VALUE (MeV)	EVTS	DOCUMENT ID	TECN	COMMENT
$87 \pm 8^{+16}_{-6}$	24k	¹ AAIJ	21E LHCb	$B^+ \rightarrow J/\psi\phi K^+$
$53 \pm 15 \pm 11$	175	² AAIJ	21C LHCb	$B_S^0 \rightarrow J/\psi\phi\pi^+\pi^-$
$120 \pm 31^{+42}_{-33}$	4289	^{3,4} AAIJ	17C LHCb	$B^+ \rightarrow J/\psi\phi K^+$

¹ From an amplitude analysis of the decay $B^+ \rightarrow J/\psi\phi K^+$ with a significance of 17σ .

² From a 1D fit to the $J/\psi\phi$ mass distribution with a significance of 5.3σ . The identification of this structure as the $\chi_{c0}(4700)$ needs confirmation.

³ From an amplitude analysis of the decay $B^+ \rightarrow J/\psi\phi K^+$ with a significance of 5.6σ .

⁴ Superseded by AAIJ 21E.

$\chi_{c0}(4700)$ DECAY MODES

Mode	Fraction (Γ_i/Γ)
$\Gamma_1 J/\psi\phi$	seen

$\chi_{c0}(4700)$ BRANCHING RATIOS

$\Gamma(J/\psi\phi)/\Gamma_{total}$	Γ_1/Γ
seen	seen

VALUE	EVTS	DOCUMENT ID	TECN	COMMENT
seen	24k	¹ AAIJ	21E LHCb	$B^+ \rightarrow J/\psi\phi K^+$

¹ From an amplitude analysis of the decay $B^+ \rightarrow J/\psi\phi K^+$ with a significance of 17σ .

² From a 1D fit to the $J/\psi\phi$ mass distribution with a significance of 5.3σ . The identification of this structure as the $\chi_{c0}(4700)$ needs confirmation.

³ From an amplitude analysis of the decay $B^+ \rightarrow J/\psi\phi K^+$ with a significance of 5.6σ .

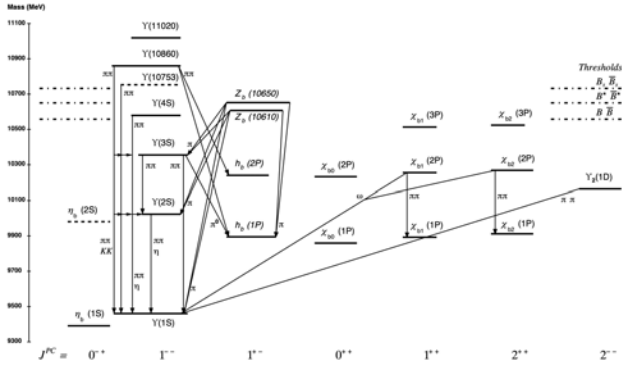
⁴ Superseded by AAIJ 21E.

$\chi_{c0}(4700)$ REFERENCES

AAIJ	21C	JHEP 2102 024	R. Aaij <i>et al.</i>	(LHCb Collab.)
AAIJ	21E	PRL 127 082001	R. Aaij <i>et al.</i>	(LHCb Collab.)
AAIJ	17C	PRL 118 022003	R. Aaij <i>et al.</i>	(LHCb Collab.) JP
Also		PR D95 012002	R. Aaij <i>et al.</i>	(LHCb Collab.)

$b\bar{b}$ MESONS
(including possibly non- $q\bar{q}$ states)

Updated July 2021.



The level scheme of meson states containing a minimal quark content of $b\bar{b}$. The name of a state is determined by its quantum numbers $I^G J^{PC}$ (see the review “Naming Scheme for Hadrons”). States included in the Summary Tables are shown with solid lines; those requiring confirmation are shown with dotted lines. The arrows indicate the most dominant hadronic transitions. Single photon transitions, including $\Upsilon(nS) \rightarrow \gamma\eta_b(mS)$, $\Upsilon(nS) \rightarrow \gamma\chi_{bJ}(mP)$, and $\chi_{bJ}(nP) \rightarrow \gamma\Upsilon(mS)$, are omitted for clarity. For orientation, the location of the thresholds related to a pair of ground state open bottom mesons is indicated in the figure.

WIDTH DETERMINATIONS OF THE Υ STATES

As is the case for the $J/\psi(1S)$ and $\psi(2S)$, the full widths of the $b\bar{b}$ states $\Upsilon(1S)$, $\Upsilon(2S)$, and $\Upsilon(3S)$ are not directly measurable, since they are much narrower than the energy resolution of the e^+e^- storage rings where these states are produced. The common indirect method to determine Γ starts from

$$\Gamma = \Gamma_{\ell\ell}/B_{\ell\ell} \tag{1}$$

where $\Gamma_{\ell\ell}$ is one leptonic partial width and $B_{\ell\ell}$ is the corresponding branching fraction ($\ell = e, \mu, \text{ or } \tau$). One then assumes $e-\mu-\tau$ universality and uses

$$\Gamma_{\ell\ell} = \Gamma_{ee}$$

$$B_{\ell\ell} = \text{average of } B_{ee}, B_{\mu\mu}, \text{ and } B_{\tau\tau} \tag{2}$$

The electronic partial width Γ_{ee} is also not directly measurable at e^+e^- storage rings, only in the combination $\Gamma_{ee}\Gamma_{\text{had}}/\Gamma$, where Γ_{had} is the hadronic partial width and

$$\Gamma_{\text{had}} + 3\Gamma_{ee} = \Gamma \tag{3}$$

This combination is obtained experimentally from the energy-integrated hadronic cross section

$$\int_{\text{resonance}} \sigma(e^+e^- \rightarrow \Upsilon \rightarrow \text{hadrons})dE$$

$$= \frac{6\pi^2 \Gamma_{ee}\Gamma_{\text{had}}}{M^2 \Gamma} C_r = \frac{6\pi^2 \Gamma_{ee}^{(0)}\Gamma_{\text{had}}}{M^2 \Gamma} C_r^{(0)} \tag{4}$$

where M is the Υ mass, and C_r and $C_r^{(0)}$ are radiative correction factors. C_r is used for obtaining Γ_{ee} as defined in Eq. (1), and contains corrections from all orders of QED for describing $(b\bar{b}) \rightarrow e^+e^-$. The lowest order QED value $\Gamma_{ee}^{(0)}$, relevant for comparison with potential-model calculations, is defined by the lowest order QED graph (Born term) alone, and is about 7% lower than Γ_{ee} .

The Listings give experimental results on B_{ee} , $B_{\mu\mu}$, $B_{\tau\tau}$, and $\Gamma_{ee}\Gamma_{\text{had}}/\Gamma$. The entries of the last quantity have been re-evaluated consistently using the correction procedure of KURAEV 85 [1]. The partial width Γ_{ee} is obtained from the average values for $\Gamma_{ee}\Gamma_{\text{had}}/\Gamma$ and $B_{\ell\ell}$ using

$$\Gamma_{ee} = \frac{\Gamma_{ee}\Gamma_{\text{had}}}{\Gamma(1 - 3B_{\ell\ell})} \tag{5}$$

The total width Γ is then obtained from Eq. (1). We do not list Γ_{ee} and Γ values of individual experiments. The Γ_{ee} values in the Meson Summary Table are also those defined in Eq. (1).

References

- E.A. Kuraev, V.S. Fadin, Sov. J. Nucl. Phys. **41**, 466 (1985).

$\eta_b(1S)$

$$I^G(J^{PC}) = 0^+(0^{-+})$$

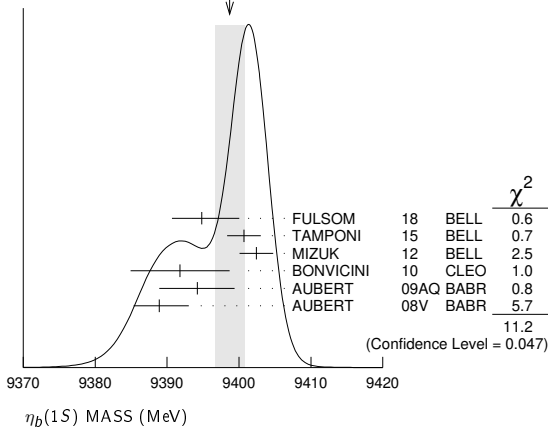
Quantum numbers shown are quark-model predictions. Observed in radiative decay of the $\Upsilon(3S)$, therefore $C = +$.

$\eta_b(1S)$ MASS

VALUE (MeV)	EVTS	DOCUMENT ID	TECN	COMMENT
9398.7 ± 2.0 OUR AVERAGE				Error includes scale factor of 1.5. See the ideogram below.
9394.8 ⁺ _{-2.7} ± 2.7 + 4.5	29k	FULSOM	18	BELL $\Upsilon(2S) \rightarrow \gamma X$
9400.7 ± 1.7 ± 1.6	33.1k	TAMPONI	15	BELL $e^+e^- \rightarrow \gamma\eta + \text{hadrons}$
9402.4 ± 1.5 ± 1.8	34k	¹ MIZUK	12	BELL $e^+e^- \rightarrow \gamma\pi^+\pi^- + \text{hadrons}$
9391.8 ± 6.6 ± 2.0	2.3k	² BONVICINI	10	CLEO $\Upsilon(3S) \rightarrow \gamma X$
9394.2 ⁺ _{-4.9} ± 4.9 ± 2.0	13k	² AUBERT	09AQ	BABR $\Upsilon(2S) \rightarrow \gamma X$
9388.9 ⁺ _{-2.3} ± 3.1 ± 2.7	19k	² AUBERT	08V	BABR $\Upsilon(3S) \rightarrow \gamma X$
•••				We do not use the following data for averages, fits, limits, etc. •••
9393.2 ± 3.4 ± 2.3	10	^{2,3} DOBBS	12	$\Upsilon(2S) \rightarrow \gamma \text{hadrons}$
9300 ± 20 ± 20		HEISTER	02D	ALEP 181-209 e^+e^-

¹ With floating width. Not independent of the corresponding mass difference measurement.
² Assuming $\Gamma_{\eta_b(1S)} = 10$ MeV. Not independent of the corresponding γ energy or mass difference measurements.
³ Obtained by analyzing CLEO III data but not authored by the CLEO Collaboration.

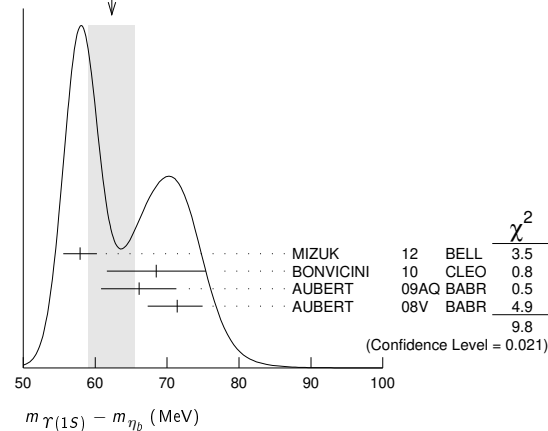
WEIGHTED AVERAGE
9398.7±2.0 (Error scaled by 1.5)



$m_{\Upsilon(1S)} - m_{\eta_b}$

VALUE (MeV)	EVTS	DOCUMENT ID	TECN	COMMENT
62.3±3.2 OUR AVERAGE	Error includes scale factor of 1.8. See the ideogram below.			
57.9±1.5±1.8	34k	¹ MIZUK	12 BELL	$e^+e^- \rightarrow \gamma\pi^+\pi^-$
68.5±6.6±2.0	2.3±0.5k	² BONVICINI	10 CLEO	$\Upsilon(3S) \rightarrow \gamma X$ + hadrons
66.1 ^{+4.8} _{-4.9} ±2.0	13±5k	² AUBERT	09AQ BABR	$\Upsilon(2S) \rightarrow \gamma X$
71.4 ^{+2.3} _{-3.1} ±2.7	19±3k	² AUBERT	08V BABR	$\Upsilon(3S) \rightarrow \gamma X$
67.1±3.4±2.3	10 ⁺⁵ ₋₄	^{2,3} DOBBS	12	$\Upsilon(2S) \rightarrow \gamma$ hadrons

WEIGHTED AVERAGE
62.3±3.2 (Error scaled by 1.8)



¹ With floating width. Not independent of the corresponding mass measurement.
² Assuming $\Gamma_{\eta_b(1S)} = 10$ MeV. Not independent of the corresponding γ energy or mass measurements.
³ Obtained by analyzing CLEO III data but not authored by the CLEO Collaboration.

γ ENERGY IN $\Upsilon(3S)$ DECAY

VALUE (MeV)	EVTS	DOCUMENT ID	TECN	COMMENT
920.6^{+2.8}_{-3.2} OUR AVERAGE				
918.6±6.0±1.9	2.3±0.5k	¹ BONVICINI	10 CLEO	$\Upsilon(3S) \rightarrow \gamma X$
921.2 ^{+2.1} _{-2.8} ±2.4	19±3k	¹ AUBERT	08V BABR	$\Upsilon(3S) \rightarrow \gamma X$

¹ Assuming $\Gamma_{\eta_b(1S)} = 10$ MeV. Not independent of the corresponding mass or mass difference measurements.

γ ENERGY IN $\Upsilon(2S)$ DECAY

VALUE (MeV)	EVTS	DOCUMENT ID	TECN	COMMENT
609.3^{+4.6}_{-4.5}±1.9	13±5k	¹ AUBERT	09AQ BABR	$\Upsilon(2S) \rightarrow \gamma X$

¹ Assuming $\Gamma_{\eta_b(1S)} = 10$ MeV. Not independent of the corresponding mass or mass difference measurements.

$\eta_b(1S)$ WIDTH

VALUE (MeV)	EVTS	DOCUMENT ID	TECN	COMMENT
10⁺⁵₋₄ OUR AVERAGE				
8 ⁺⁶ ₋₅ ±5	33.1k	¹ TAMPONI	15 BELL	$e^+e^- \rightarrow \gamma\eta$ hadrons
10.8 ^{+4.0+4.5} _{-3.7-2.0}	34k	¹ MIZUK	12 BELL	$e^+e^- \rightarrow \gamma\pi^+\pi^-$ + hadrons

¹ With floating mass.

$\eta_b(1S)$ DECAY MODES

Mode	Fraction (Γ_i/Γ)	Confidence level
Γ_1 hadrons	seen	
Γ_2 $3h^+3h^-$	not seen	
Γ_3 $2h^+2h^-$	not seen	
Γ_4 $4h^+4h^-$	not seen	
Γ_5 $\gamma\gamma$	not seen	
Γ_6 $\mu^+\mu^-$	$<9 \times 10^{-3}$	90%
Γ_7 $\tau^+\tau^-$	$<8\%$	90%

$\eta_b(1S)$ $\Gamma(i)\Gamma(\gamma\gamma)/\Gamma(\text{total})$

VALUE (eV)	CL%	DOCUMENT ID	TECN	COMMENT
$\Gamma(3h^+3h^-) \times \Gamma(\gamma\gamma)/\Gamma_{\text{total}}$				$\Gamma_2\Gamma_5/\Gamma$
<470	95	ABDALLAH	06 DLPH	161-209 e^+e^-
<132	95	HEISTER	02D ALEP	181-209 e^+e^-

VALUE (eV)	CL%	DOCUMENT ID	TECN	COMMENT
$\Gamma(2h^+2h^-) \times \Gamma(\gamma\gamma)/\Gamma_{\text{total}}$				$\Gamma_3\Gamma_5/\Gamma$
<190	95	ABDALLAH	06 DLPH	161-209 e^+e^-
<48	95	HEISTER	02D ALEP	181-209 e^+e^-

VALUE (eV)	CL%	DOCUMENT ID	TECN	COMMENT
$\Gamma(4h^+4h^-) \times \Gamma(\gamma\gamma)/\Gamma_{\text{total}}$				$\Gamma_4\Gamma_5/\Gamma$
<660	95	ABDALLAH	06 DLPH	161-209 e^+e^-

$\eta_b(1S)$ BRANCHING RATIOS

$\Gamma(\text{hadrons})/\Gamma_{\text{total}}$	EVTS	DOCUMENT ID	TECN	COMMENT
seen	34k	MIZUK	12 BELL	$e^+e^- \rightarrow \gamma\pi^+\pi^-$ + hadrons

VALUE	CL%	DOCUMENT ID	TECN	COMMENT
$\Gamma(\mu^+\mu^-)/\Gamma_{\text{total}}$				Γ_6/Γ
$<9 \times 10^{-3}$	90	¹ AUBERT	09Z BABR	$e^+e^- \rightarrow \Upsilon(2S, 3S) \rightarrow \gamma\eta_b$

¹ Obtained using $B(\Upsilon(2S) \rightarrow \gamma\eta_b) = (4.2^{+1.1}_{-1.0} \pm 0.9) \times 10^{-4}$ and $B(\Upsilon(3S) \rightarrow \gamma\eta_b) = (4.8 \pm 0.5 \pm 0.6) \times 10^{-4}$. This limit is equivalent to $B(\eta_b \rightarrow \mu^+\mu^-) = (-0.25 \pm 0.51 \pm 0.33)\%$ measurement.

VALUE	CL%	DOCUMENT ID	TECN	COMMENT
$\Gamma(\tau^+\tau^-)/\Gamma_{\text{total}}$				Γ_7/Γ
$<8 \times 10^{-2}$	90	AUBERT	09P BABR	$e^+e^- \rightarrow \gamma\tau^+\tau^-$

$\eta_b(1S)$ REFERENCES

FULSOM	18	PRL 121 232001	B. G. Fulsom <i>et al.</i>	(BELLE Collab.)
TAMPONI	15	PRL 115 142001	U. Tamponi <i>et al.</i>	(BELLE Collab.)
DOBBS	12	PRL 109 082001	S. Dobbs <i>et al.</i>	
MIZUK	12	PRL 109 232002	R. Mizuk <i>et al.</i>	(BELLE Collab.)
BONVICINI	10	PR D81 031104	G. Bonvicini <i>et al.</i>	(CLEO Collab.)
AUBERT	09AQ	PRL 103 161801	B. Aubert <i>et al.</i>	(BABAR Collab.)
AUBERT	09P	PRL 103 181801	B. Aubert <i>et al.</i>	(BABAR Collab.)
AUBERT	09Z	PRL 103 081803	B. Aubert <i>et al.</i>	(BABAR Collab.)
AUBERT	08V	PRL 101 071801	B. Aubert <i>et al.</i>	(BABAR Collab.)
ABDALLAH	06	PL B634 340	J.M. Abdallah <i>et al.</i>	(DELPHI Collab.)
HEISTER	02D	PL B530 56	A. Heister <i>et al.</i>	(ALEPH Collab.)

Meson Particle Listings

$\Upsilon(1S)$

$\Upsilon(1S)$

$$I^G(J^{PC}) = 0^-(1^{--})$$

$\Upsilon(1S)$ MASS

VALUE (MeV)	DOCUMENT ID	TECN	COMMENT
9460.30 ± 0.26 OUR AVERAGE	Error includes scale factor of 3.3.		
9460.51 ± 0.09 ± 0.05	¹ ARTAMONOV 00	MD1	$e^+e^- \rightarrow$ hadrons
9459.97 ± 0.11 ± 0.07	MACKAY 84	REDE	$e^+e^- \rightarrow$ hadrons
••• We do not use the following data for averages, fits, limits, etc. •••			
9460.60 ± 0.09 ± 0.05	^{2,3} BARU	92B REDE	$e^+e^- \rightarrow$ hadrons
9460.59 ± 0.12	BARU	86 REDE	$e^+e^- \rightarrow$ hadrons
9460.6 ± 0.4	^{3,4} ARTAMONOV 84	REDE	$e^+e^- \rightarrow$ hadrons
¹ Reanalysis of BARU 92B and ARTAMONOV 84 using new electron mass (COHEN 87).			
² Superseding BARU 86.			
³ Superseded by ARTAMONOV 00.			
⁴ Value includes data of ARTAMONOV 82.			

$\Upsilon(1S)$ WIDTH

VALUE (keV)	DOCUMENT ID
54.02 ± 1.25 OUR EVALUATION	See the Note on "Width Determinations of the Υ States"

$\Upsilon(1S)$ DECAY MODES

Mode	Fraction (Γ_i/Γ)	Scale factor/ Confidence level
$\Gamma_1 \tau^+ \tau^-$	(2.60 ± 0.10) %	
$\Gamma_2 e^+ e^-$	(2.38 ± 0.11) %	
$\Gamma_3 \mu^+ \mu^-$	(2.48 ± 0.05) %	
Hadronic decays		
$\Gamma_4 g\bar{g}g$	(81.7 ± 0.7) %	
$\Gamma_5 \gamma\bar{g}g$	(2.2 ± 0.6) %	
$\Gamma_6 \eta(958)$ anything	(2.94 ± 0.24) %	
$\Gamma_7 J/\psi(1S)$ anything	(5.4 ± 0.4) × 10 ⁻⁴	S=1.4
$\Gamma_8 J/\psi(1S)\eta_c$	< 2.2	× 10 ⁻⁶ CL=90%
$\Gamma_9 J/\psi(1S)\chi_{c0}$	< 3.4	× 10 ⁻⁶ CL=90%
$\Gamma_{10} J/\psi(1S)\chi_{c1}$	(3.9 ± 1.2) × 10 ⁻⁶	
$\Gamma_{11} J/\psi(1S)\chi_{c2}$	< 1.4	× 10 ⁻⁶ CL=90%
$\Gamma_{12} J/\psi(1S)\eta_c(2S)$	< 2.2	× 10 ⁻⁶ CL=90%
$\Gamma_{13} J/\psi(1S)X(3940)$	< 5.4	× 10 ⁻⁶ CL=90%
$\Gamma_{14} J/\psi(1S)X(4160)$	< 5.4	× 10 ⁻⁶ CL=90%
$\Gamma_{15} X(4350)$ anything, $X \rightarrow J/\psi(1S)\phi$	< 8.1	× 10 ⁻⁶ CL=90%
$\Gamma_{16} Z_c(3900)^\pm$ anything, $Z_c \rightarrow J/\psi(1S)\pi^\pm$	< 1.3	× 10 ⁻⁵ CL=90%
$\Gamma_{17} Z_c(4200)^\pm$ anything, $Z_c \rightarrow J/\psi(1S)\pi^\pm$	< 6.0	× 10 ⁻⁵ CL=90%
$\Gamma_{18} Z_c(4430)^\pm$ anything, $Z_c \rightarrow J/\psi(1S)\pi^\pm$	< 4.9	× 10 ⁻⁵ CL=90%
$\Gamma_{19} X_{cs}^\pm$ anything, $X \rightarrow J/\psi K^\pm$	< 5.7	× 10 ⁻⁶ CL=90%
$\Gamma_{20} \psi(4230)$ anything, $\psi \rightarrow J/\psi(1S)\pi^+\pi^-$	< 3.8	× 10 ⁻⁵ CL=90%
$\Gamma_{21} \psi(4230)$ anything, $\psi \rightarrow J/\psi(1S)K^+K^-$	< 7.5	× 10 ⁻⁶ CL=90%
$\Gamma_{22} \chi_{c1}(4140)$ anything, $\chi_{c1} \rightarrow J/\psi(1S)\phi$	< 5.2	× 10 ⁻⁶ CL=90%
$\Gamma_{23} \chi_{c0}$ anything	< 4	× 10 ⁻³ CL=90%
$\Gamma_{24} \chi_{c1}$ anything	(1.90 ± 0.35) × 10 ⁻⁴	
$\Gamma_{25} \chi_{c1}(1P)X_{tetra}$	< 3.78	× 10 ⁻⁵ CL=90%
$\Gamma_{26} \chi_{c2}$ anything	(2.8 ± 0.8) × 10 ⁻⁴	
$\Gamma_{27} \psi(2S)$ anything	(1.23 ± 0.20) × 10 ⁻⁴	
$\Gamma_{28} \psi(2S)\eta_c$	< 3.6	× 10 ⁻⁶ CL=90%
$\Gamma_{29} \psi(2S)\chi_{c0}$	< 6.5	× 10 ⁻⁶ CL=90%
$\Gamma_{30} \psi(2S)\chi_{c1}$	< 4.5	× 10 ⁻⁶ CL=90%
$\Gamma_{31} \psi(2S)\chi_{c2}$	< 2.1	× 10 ⁻⁶ CL=90%
$\Gamma_{32} \psi(2S)\eta_c(2S)$	< 3.2	× 10 ⁻⁶ CL=90%
$\Gamma_{33} \psi(2S)X(3940)$	< 2.9	× 10 ⁻⁶ CL=90%
$\Gamma_{34} \psi(2S)X(4160)$	< 2.9	× 10 ⁻⁶ CL=90%
$\Gamma_{35} \psi(4230)$ anything, $\psi \rightarrow \psi(2S)\pi^+\pi^-$	< 7.9	× 10 ⁻⁵ CL=90%
$\Gamma_{36} \psi(4360)$ anything, $\psi \rightarrow \psi(2S)\pi^+\pi^-$	< 5.2	× 10 ⁻⁵ CL=90%
$\Gamma_{37} \psi(4660)$ anything, $\psi \rightarrow \psi(2S)\pi^+\pi^-$	< 2.2	× 10 ⁻⁵ CL=90%

$\Gamma_{38} X(4050)^\pm$ anything, $X \rightarrow \psi(2S)\pi^\pm$	< 8.8	× 10 ⁻⁵ CL=90%
$\Gamma_{39} Z_c(4430)^\pm$ anything, $Z_c \rightarrow \psi(2S)\pi^\pm$	< 6.7	× 10 ⁻⁵ CL=90%
$\Gamma_{40} \chi_{c1}(3872)$ anything	< 2.5	× 10 ⁻⁴ CL=90%
$\Gamma_{41} Z_c(4200)+Z_c(4200)^-$	< 2.23	× 10 ⁻⁵ CL=90%
$\Gamma_{42} Z_c(3900)^\pm Z_c(4200)^\mp$	< 8.1	× 10 ⁻⁶ CL=90%
$\Gamma_{43} Z_c(3900)+Z_c(3900)^-$	< 1.8	× 10 ⁻⁶ CL=90%
$\Gamma_{44} X(4050)+X(4050)^-$	< 15.8	× 10 ⁻⁵ CL=90%
$\Gamma_{45} X(4250)+X(4250)^-$	< 2.66	× 10 ⁻⁵ CL=90%
$\Gamma_{46} X(4050)^\pm X(4250)^\mp$	< 4.42	× 10 ⁻⁵ CL=90%
$\Gamma_{47} Z_c(4430)+Z_c(4430)^-$	< 2.03	× 10 ⁻⁵ CL=90%
$\Gamma_{48} X(4055)^\pm X(4055)^\mp$	< 2.33	× 10 ⁻⁵ CL=90%
$\Gamma_{49} X(4055)^\pm Z_c(4430)^\mp$	< 4.55	× 10 ⁻⁵ CL=90%
$\Gamma_{50} \rho\pi$	< 3.68	× 10 ⁻⁶ CL=90%
$\Gamma_{51} \omega\pi^0$	< 3.90	× 10 ⁻⁶ CL=90%
$\Gamma_{52} \pi^+\pi^-$	< 5	× 10 ⁻⁴ CL=90%
$\Gamma_{53} K^+K^-$	< 5	× 10 ⁻⁴ CL=90%
$\Gamma_{54} p\bar{p}$	< 5	× 10 ⁻⁴ CL=90%
$\Gamma_{55} \pi^+\pi^-\pi^0$	(2.1 ± 0.8) × 10 ⁻⁶	
$\Gamma_{56} \phi K^+K^-$	(2.4 ± 0.5) × 10 ⁻⁶	
$\Gamma_{57} \omega\pi^+\pi^-$	(4.5 ± 1.0) × 10 ⁻⁶	
$\Gamma_{58} K^*(892)^0 K^-\pi^+ + c.c.$	(4.4 ± 0.8) × 10 ⁻⁶	
$\Gamma_{59} \phi f_2'(1525)$	< 1.63	× 10 ⁻⁶ CL=90%
$\Gamma_{60} \omega f_2'(1270)$	< 1.79	× 10 ⁻⁶ CL=90%
$\Gamma_{61} \rho(770)\omega_2(1320)$	< 2.24	× 10 ⁻⁶ CL=90%
$\Gamma_{62} K^*(892)^0 K_2^*(1430)^0 + c.c.$	(3.0 ± 0.8) × 10 ⁻⁶	
$\Gamma_{63} K_1(1270)^\pm K^\mp$	< 2.41	× 10 ⁻⁶ CL=90%
$\Gamma_{64} K_1(1400)^\pm K^\mp$	(1.0 ± 0.4) × 10 ⁻⁶	
$\Gamma_{65} b_1(1235)^\pm \pi^\mp$	< 1.25	× 10 ⁻⁶ CL=90%
$\Gamma_{66} \pi^+\pi^-\pi^0\pi^0$	(1.28 ± 0.30) × 10 ⁻⁵	
$\Gamma_{67} K_S^0 K^+\pi^- + c.c.$	(1.6 ± 0.4) × 10 ⁻⁶	
$\Gamma_{68} K^*(892)^0 \bar{K}^0 + c.c.$	(2.9 ± 0.9) × 10 ⁻⁶	
$\Gamma_{69} K^*(892)^- K^+ + c.c.$	< 1.11	× 10 ⁻⁶ CL=90%
$\Gamma_{70} f_1(1285)$ anything	(4.6 ± 3.1) × 10 ⁻³	
$\Gamma_{71} D^*(2010)^\pm$ anything	(2.52 ± 0.20) %	
$\Gamma_{72} f_1(1285)X_{tetra}$	< 6.24	× 10 ⁻⁵ CL=90%
$\Gamma_{73} {}^2H$ anything	(2.85 ± 0.25) × 10 ⁻⁵	
Γ_{74} Sum of 100 exclusive modes	(1.200 ± 0.017) %	
Radiative decays		
$\Gamma_{75} \gamma\pi^+\pi^-$	(6.3 ± 1.8) × 10 ⁻⁵	
$\Gamma_{76} \gamma\pi^0\pi^0$	(1.7 ± 0.7) × 10 ⁻⁵	
$\Gamma_{77} \gamma\pi\pi$ (S-wave)	(4.6 ± 0.7) × 10 ⁻⁵	
$\Gamma_{78} \gamma\pi^0\eta$	< 2.4	× 10 ⁻⁶ CL=90%
$\Gamma_{79} \gamma K^+K^-$	[a] (1.14 ± 0.13) × 10 ⁻⁵	
$\Gamma_{80} \gamma\rho\bar{\rho}$	[b] < 6	× 10 ⁻⁶ CL=90%
$\Gamma_{81} \gamma 2h^+ 2h^-$	(7.0 ± 1.5) × 10 ⁻⁴	
$\Gamma_{82} \gamma 3h^+ 3h^-$	(5.4 ± 2.0) × 10 ⁻⁴	
$\Gamma_{83} \gamma 4h^+ 4h^-$	(7.4 ± 3.5) × 10 ⁻⁴	
$\Gamma_{84} \gamma\pi^+\pi^- K^+K^-$	(2.9 ± 0.9) × 10 ⁻⁴	
$\Gamma_{85} \gamma 2\pi^+ 2\pi^-$	(2.5 ± 0.9) × 10 ⁻⁴	
$\Gamma_{86} \gamma 3\pi^+ 3\pi^-$	(2.5 ± 1.2) × 10 ⁻⁴	
$\Gamma_{87} \gamma 2\pi^+ 2\pi^- K^+K^-$	(2.4 ± 1.2) × 10 ⁻⁴	
$\Gamma_{88} \gamma\pi^+\pi^- p\bar{p}$	(1.5 ± 0.6) × 10 ⁻⁴	
$\Gamma_{89} \gamma 2\pi^+ 2\pi^- p\bar{p}$	(4 ± 6) × 10 ⁻⁵	
$\Gamma_{90} \gamma 2K^+ 2K^-$	(2.0 ± 2.0) × 10 ⁻⁵	
$\Gamma_{91} \gamma\eta(958)$	< 1.9	× 10 ⁻⁶ CL=90%
$\Gamma_{92} \gamma\eta$	< 1.0	× 10 ⁻⁶ CL=90%
$\Gamma_{93} \gamma f_0(980)$	< 3	× 10 ⁻⁵ CL=90%
$\Gamma_{94} \gamma f_2'(1525)$	(2.9 ± 0.6) × 10 ⁻⁵	
$\Gamma_{95} \gamma f_2'(1270)$	(1.01 ± 0.06) × 10 ⁻⁴	
$\Gamma_{96} \gamma\eta(1405)$	< 8.2	× 10 ⁻⁵ CL=90%
$\Gamma_{97} \gamma f_0(1500)$	< 1.5	× 10 ⁻⁵ CL=90%
$\Gamma_{98} \gamma f_0(1500) \rightarrow \gamma K^+ K^-$	(1.0 ± 0.4) × 10 ⁻⁵	
$\Gamma_{99} \gamma f_0(1710)$	< 2.6	× 10 ⁻⁴ CL=90%
$\Gamma_{100} \gamma f_0(1710) \rightarrow \gamma K^+ K^-$	(1.01 ± 0.32) × 10 ⁻⁵	
$\Gamma_{101} \gamma f_0(1710) \rightarrow \gamma\pi^+\pi^-$	(5.3 ± 2.0) × 10 ⁻⁶	
$\Gamma_{102} \gamma f_0(1710) \rightarrow \gamma\pi^0\pi^0$	< 1.4	× 10 ⁻⁶ CL=90%
$\Gamma_{103} \gamma f_0(1710) \rightarrow \gamma\eta\eta$	< 1.8	× 10 ⁻⁶ CL=90%
$\Gamma_{104} \gamma f_4(2050)$	< 5.3	× 10 ⁻⁵ CL=90%
$\Gamma_{105} \gamma f_0(2200) \rightarrow \gamma K^+ K^-$	< 2	× 10 ⁻⁴ CL=90%
$\Gamma_{106} \gamma f_j(2220) \rightarrow \gamma K^+ K^-$	< 8	× 10 ⁻⁷ CL=90%
$\Gamma_{107} \gamma f_j(2220) \rightarrow \gamma\pi^+\pi^-$	< 6	× 10 ⁻⁷ CL=90%
$\Gamma_{108} \gamma f_j(2220) \rightarrow \gamma p\bar{p}$	< 1.1	× 10 ⁻⁶ CL=90%

Γ_{109}	$\gamma\eta(2225) \rightarrow \gamma\phi\phi$	< 3	$\times 10^{-3}$	CL=90%
Γ_{110}	$\gamma\eta_c(1S)$	< 2.9	$\times 10^{-5}$	CL=90%
Γ_{111}	$\gamma\eta_c(2S)$	< 4	$\times 10^{-4}$	CL=90%
Γ_{112}	$\gamma\chi_{c0}$	< 6.6	$\times 10^{-5}$	CL=90%
Γ_{113}	$\gamma\chi_{c1}$	(4.7 -1.9)	$\times 10^{-5}$	
Γ_{114}	$\gamma\chi_{c2}$	< 7.6	$\times 10^{-6}$	CL=90%
Γ_{115}	$\gamma\chi_{c1}(3872)$	< 4	$\times 10^{-5}$	CL=90%
Γ_{116}	$\gamma\chi_{c1}(3872), \chi_{c1} \rightarrow \pi^+\pi^-\pi^0 J/\psi$	< 2.8	$\times 10^{-6}$	CL=90%
Γ_{117}	$\gamma\chi_{c0}(3915) \rightarrow \omega J/\psi$	< 3.0	$\times 10^{-6}$	CL=90%
Γ_{118}	$\gamma\chi_{c1}(4140) \rightarrow \phi J/\psi$	< 2.2	$\times 10^{-6}$	CL=90%
Γ_{119}	γX	[c] < 4.5	$\times 10^{-6}$	CL=90%
Γ_{120}	$\gamma X \bar{X} (m_X < 3.1 \text{ GeV})$	[d] < 1	$\times 10^{-3}$	CL=90%
Γ_{121}	$\gamma X \bar{X} (m_X < 4.5 \text{ GeV})$	[e] < 2.4	$\times 10^{-4}$	CL=90%
Γ_{122}	$\gamma X \rightarrow \gamma + \geq 4 \text{ prongs}$	[f] < 1.78	$\times 10^{-4}$	CL=95%
Γ_{123}	$\gamma a_0^0 \rightarrow \gamma \mu^+ \mu^-$	[g] < 9	$\times 10^{-6}$	CL=90%
Γ_{124}	$\gamma a_1^0 \rightarrow \gamma \tau^+ \tau^-$	[a] < 1.30	$\times 10^{-4}$	CL=90%
Γ_{125}	$\gamma a_1^0 \rightarrow \gamma g g$	[h] < 1	%	CL=90%
Γ_{126}	$\gamma a_1^0 \rightarrow \gamma S \bar{S}$	[h] < 1	$\times 10^{-3}$	CL=90%

Lepton Family number (LF) violating modes

Γ_{127}	$\mu^\pm \tau^\mp$	LF < 6.0	$\times 10^{-6}$	CL=95%
----------------	--------------------	----------	------------------	--------

Other decays

Γ_{128}	invisible	< 3.0	$\times 10^{-4}$	CL=90%
Γ_{129}	hadrons	(97 \pm 5) %		

- [a] $2m_\tau < M(\tau^+ \tau^-) < 9.2 \text{ GeV}$
- [b] $2 \text{ GeV} < m_{K^+ K^-} < 3 \text{ GeV}$
- [c] $X = \text{scalar with } m < 8.0 \text{ GeV}$
- [d] $X \bar{X} = \text{vectors with } m < 3.1 \text{ GeV}$
- [e] $X \text{ and } \bar{X} = \text{zero spin with } m < 4.5 \text{ GeV}$
- [f] $1.5 \text{ GeV} < m_X < 5.0 \text{ GeV}$
- [g] $201 \text{ MeV} < M(\mu^+ \mu^-) < 3565 \text{ MeV}$
- [h] $0.5 \text{ GeV} < m_X < 9.0 \text{ GeV}$, where m_X is the invariant mass of the hadronic final state.

$\Upsilon(1S) \Gamma(\text{anything})/\Gamma(\text{total})$

$\Gamma(\mu^+ \mu^-) \times \Gamma(e^+ e^-)/\Gamma(\text{total})$				Γ_{32}/Γ
VALUE (eV)	DOCUMENT ID	TECN	COMMENT	
31.2 \pm 1.6 \pm 1.7	KOBEL	92	CBAL $e^+ e^- \rightarrow \mu^+ \mu^-$	

$\Gamma(\text{hadrons}) \times \Gamma(e^+ e^-)/\Gamma(\text{total})$				$\Gamma_{129}\Gamma_2/\Gamma$
VALUE (keV)	DOCUMENT ID	TECN	COMMENT	
1.240 \pm 0.016 OUR AVERAGE				
1.252 \pm 0.004 \pm 0.019	1 ROSNER	06	CLEO 9.5 $e^+ e^- \rightarrow \text{hadrons}$	
1.187 \pm 0.023 \pm 0.031	1 BARU	92B	MD1 $e^+ e^- \rightarrow \text{hadrons}$	
1.23 \pm 0.02 \pm 0.05	1 JAKUBOWSKI	88	CBAL $e^+ e^- \rightarrow \text{hadrons}$	
1.37 \pm 0.06 \pm 0.09	2 GILES	84B	CLEO $e^+ e^- \rightarrow \text{hadrons}$	
1.23 \pm 0.08 \pm 0.04	2 ALBRECHT	82	DASP $e^+ e^- \rightarrow \text{hadrons}$	
1.13 \pm 0.07 \pm 0.11	2 NICZYPORUK	82	LENA $e^+ e^- \rightarrow \text{hadrons}$	
1.09 \pm 0.25	2 BOCK	80	CNTR $e^+ e^- \rightarrow \text{hadrons}$	
1.35 \pm 0.14	3 BERGER	79	PLUT $e^+ e^- \rightarrow \text{hadrons}$	

¹ Radiative corrections evaluated following KURAEV 85.
² Radiative corrections reevaluated by BUCHMUELLER 88 following KURAEV 85.
³ Radiative corrections reevaluated by ALEXANDER 89 using $B(\mu\mu) = 0.026$.

$\Upsilon(1S)$ PARTIAL WIDTHS

$\Gamma(e^+ e^-)$			Γ_2
VALUE (keV)	DOCUMENT ID		
1.340 \pm 0.018 OUR EVALUATION			

$\Upsilon(1S)$ BRANCHING RATIOS

$\Gamma(\tau^+ \tau^-)/\Gamma(\text{total})$				Γ_1/Γ
VALUE (units 10^{-2})	EVTS	DOCUMENT ID	TECN	COMMENT
2.60 \pm 0.10 OUR AVERAGE				
2.53 \pm 0.13 \pm 0.05	60k	1 BESSON	07	CLEO $e^+ e^- \rightarrow \Upsilon(1S) \rightarrow \tau^+ \tau^-$
2.61 \pm 0.12 \pm 0.09	25k	2 CINABRO	94B	CLE2 $e^+ e^- \rightarrow \tau^+ \tau^-$
2.7 \pm 0.4 \pm 0.2		2 ALBRECHT	85c	ARG $\Upsilon(2S) \rightarrow \pi^+ \pi^- \tau^+ \tau^-$
3.4 \pm 0.4 \pm 0.4		3 GILES	83	CLEO $e^+ e^- \rightarrow \tau^+ \tau^-$

¹ BESSON 07 reports $[\Gamma(\Upsilon(1S) \rightarrow \tau^+ \tau^-)/\Gamma(\text{total})] / [B(\Upsilon(1S) \rightarrow \mu^+ \mu^-)] = 1.02 \pm 0.02 \pm 0.05$ which we multiply by our best value $B(\Upsilon(1S) \rightarrow \mu^+ \mu^-) = (2.48 \pm 0.05) \times 10^{-2}$. Our first error is their experiment's error and our second error is the systematic error from using our best value.
² Using $B(\Upsilon(1S) \rightarrow ee) = B(\Upsilon(1S) \rightarrow \mu\mu) = 0.0256$; not used for width evaluations.

$\Gamma(e^+ e^-)/\Gamma(\text{total})$				Γ_2/Γ
VALUE (units 10^{-2})	EVTS	DOCUMENT ID	TECN	COMMENT
2.38 \pm 0.11 OUR AVERAGE				
2.29 \pm 0.08 \pm 0.11		ALEXANDER	98	CLE2 $\Upsilon(2S) \rightarrow \pi^+ \pi^- e^+ e^-$
2.42 \pm 0.14 \pm 0.14	307	ALBRECHT	87	ARG $\Upsilon(2S) \rightarrow \pi^+ \pi^- e^+ e^-$
2.8 \pm 0.3 \pm 0.2	826	BESSON	84	CLEO $\Upsilon(2S) \rightarrow \pi^+ \pi^- e^+ e^-$
5.1 \pm 3.0		BERGER	80c	PLUT $e^+ e^- \rightarrow e^+ e^-$

$\Gamma(\mu^+ \mu^-)/\Gamma(\text{total})$				Γ_3/Γ
VALUE	EVTS	DOCUMENT ID	TECN	COMMENT
0.0248 \pm 0.0005 OUR AVERAGE				
0.0249 \pm 0.0002 \pm 0.0007	345k	ADAMS	05	CLEO $e^+ e^- \rightarrow \mu^+ \mu^-$
0.0249 \pm 0.0008 \pm 0.0013		ALEXANDER	98	CLE2 $\Upsilon(2S) \rightarrow \mu^+ \mu^-$
0.0212 \pm 0.0020 \pm 0.0010		1 BARU	92	MD1 $\pi^+ \pi^- \mu^+ \mu^-$
0.0231 \pm 0.0012 \pm 0.0010		1 KOBEL	92	CBAL $e^+ e^- \rightarrow \mu^+ \mu^-$
0.0252 \pm 0.0007 \pm 0.0007		CHEN	89B	CLEO $e^+ e^- \rightarrow \mu^+ \mu^-$
0.0261 \pm 0.0009 \pm 0.0011		KAARSBERG	89	CSB2 $e^+ e^- \rightarrow \mu^+ \mu^-$
0.0230 \pm 0.0025 \pm 0.0013	86	ALBRECHT	87	ARG $\Upsilon(2S) \rightarrow \mu^+ \mu^-$
0.029 \pm 0.003 \pm 0.002	864	BESSON	84	CLEO $\Upsilon(2S) \rightarrow \mu^+ \mu^-$
0.027 \pm 0.003 \pm 0.003		ANDREWS	83	CLEO $e^+ e^- \rightarrow \mu^+ \mu^-$
0.032 \pm 0.013 \pm 0.003		ALBRECHT	82	DASP $e^+ e^- \rightarrow \mu^+ \mu^-$
0.038 \pm 0.015 \pm 0.002		NICZYPORUK	82	LENA $e^+ e^- \rightarrow \mu^+ \mu^-$
0.014 \pm 0.034		BOCK	80	CNTR $e^+ e^- \rightarrow \mu^+ \mu^-$
-0.014				
0.022 \pm 0.020		BERGER	79	PLUT $e^+ e^- \rightarrow \mu^+ \mu^-$

¹ Taking into account interference between the resonance and continuum.

$\Gamma(\tau^+ \tau^-)/\Gamma(\mu^+ \mu^-)$				Γ_1/Γ_3
VALUE	EVTS	DOCUMENT ID	TECN	COMMENT
1.008 \pm 0.023 OUR AVERAGE				
1.005 \pm 0.013 \pm 0.022	0.7M	1 DEL-AMO-SA...	10c	BABR $\Upsilon(3S) \rightarrow \pi^+ \pi^- \Upsilon(1S)$
1.02 \pm 0.02 \pm 0.05	60k	BESSON	07	CLEO $e^+ e^- \rightarrow \Upsilon(1S)$

¹ Allows any number of extra photons with total energy < 500 MeV.

$\Gamma(g g g)/\Gamma(\text{total})$				Γ_4/Γ
VALUE (units 10^{-2})	EVTS	DOCUMENT ID	TECN	COMMENT
81.7 \pm 0.7	20M	1 BESSON	06A	CLEO $\Upsilon(1S) \rightarrow \text{hadrons}$

¹ Calculated using the value $\Gamma(\gamma g g)/\Gamma(g g g) = (2.70 \pm 0.01 \pm 0.13 \pm 0.24)\%$ from BESSON 06A and PDG 08 values of $B(\mu^+ \mu^-) = (2.48 \pm 0.05)\%$ and $R_{\text{hadrons}} = 3.51$. The statistical error is negligible and the systematic error is partially correlated with that of $\Gamma(\gamma g g)/\Gamma(\text{total})$ measurement of BESSON 06A.

$\Gamma(\gamma g g)/\Gamma(\text{total})$				Γ_5/Γ
VALUE (units 10^{-2})	EVTS	DOCUMENT ID	TECN	COMMENT
2.20 \pm 0.60	400k	1 BESSON	06A	CLEO $\Upsilon(1S) \rightarrow \gamma + \text{hadrons}$

¹ Calculated using BESSON 06A values of $\Gamma(\gamma g g)/\Gamma(g g g) = (2.70 \pm 0.01 \pm 0.13 \pm 0.24)\%$ and $\Gamma(g g g)/\Gamma(\text{total})$. The statistical error is negligible and the systematic error is partially correlated with that of $\Gamma(g g g)/\Gamma(\text{total})$ measurement of BESSON 06A.

$\Gamma(\gamma g g)/\Gamma(g g g)$				Γ_5/Γ_4
VALUE (units 10^{-2})	EVTS	DOCUMENT ID	TECN	COMMENT
2.70 \pm 0.01 \pm 0.27	20M	BESSON	06A	CLEO $\Upsilon(1S) \rightarrow (\gamma +) \text{hadrons}$

$\Gamma(\eta'(958) \text{ anything})/\Gamma(\text{total})$				Γ_6/Γ
VALUE	DOCUMENT ID	TECN	COMMENT	
0.0294 \pm 0.0024 OUR AVERAGE				
0.030 \pm 0.002 \pm 0.002		AQUINES	06A	CLE3 $\Upsilon(1S) \rightarrow \eta' \text{ anything}$
0.028 \pm 0.004 \pm 0.002		ARTUSO	03	CLE2 $\Upsilon(1S) \rightarrow \eta' \text{ anything}$

$\Gamma(J/\psi(1S) \text{ anything})/\Gamma(\text{total})$				Γ_7/Γ
VALUE (units 10^{-4})	CL% EVTS	DOCUMENT ID	TECN	COMMENT
5.4 \pm 0.4 OUR FIT	Error includes scale factor of 1.4.			
5.4 \pm 0.4 OUR AVERAGE	Error includes scale factor of 1.5.			
5.25 \pm 0.13 \pm 0.25	3k	SHEN	16	BELL $e^+ e^- \rightarrow J/\psi X$
6.4 \pm 0.4 \pm 0.6	730	BRIERE	04	CLEO $e^+ e^- \rightarrow J/\psi X$
11 \pm 4 \pm 2		1 FULTON	89	CLEO $e^+ e^- \rightarrow \mu^+ \mu^- X$

••• We do not use the following data for averages, fits, limits, etc. •••
 <6.8 90 ALBRECHT 92j ARG $e^+ e^- \rightarrow e^+ e^- X, \mu^+ \mu^- X$
 <17 90 MASCHMANN 90 CBAL $e^+ e^- \rightarrow \text{hadrons}$
 <200 90 NICZYPORUK 83 LENA
¹ Using $B(J/\psi) \rightarrow \mu^+ \mu^- = (6.9 \pm 0.9)\%$.

$\Gamma(J/\psi(1S) \eta_c)/\Gamma(\text{total})$				Γ_8/Γ
VALUE	CL%	DOCUMENT ID	TECN	COMMENT
<2.2 $\times 10^{-6}$	90	YANG	14	BELL $e^+ e^- \rightarrow J/\psi X$

$\Gamma(J/\psi(1S) \chi_{c0})/\Gamma(\text{total})$				Γ_9/Γ
VALUE	CL%	DOCUMENT ID	TECN	COMMENT
<3.4 $\times 10^{-6}$	90	YANG	14	BELL $e^+ e^- \rightarrow J/\psi X$

Meson Particle Listings

$\Upsilon(1S)$

$\Gamma(J/\psi(1S)\chi_{c1})/\Gamma_{total}$		Γ_{10}/Γ	
VALUE (units 10^{-6})	EVTS	DOCUMENT ID	TECN COMMENT
$3.90 \pm 1.21 \pm 0.23$	20	YANG	14 BELL $e^+e^- \rightarrow J/\psi X$

$\Gamma(J/\psi(1S)\chi_{c2})/\Gamma_{total}$		Γ_{11}/Γ	
VALUE	CL%	DOCUMENT ID	TECN COMMENT
$<1.4 \times 10^{-6}$	90	YANG	14 BELL $e^+e^- \rightarrow J/\psi X$

$\Gamma(J/\psi(1S)\eta_c(2S))/\Gamma_{total}$		Γ_{12}/Γ	
VALUE	CL%	DOCUMENT ID	TECN COMMENT
$<2.2 \times 10^{-6}$	90	YANG	14 BELL $e^+e^- \rightarrow J/\psi X$

$\Gamma(J/\psi(1S)X(3940))/\Gamma_{total}$		Γ_{13}/Γ	
VALUE	CL%	DOCUMENT ID	TECN COMMENT
$<5.4 \times 10^{-6}$	90	YANG	14 BELL $e^+e^- \rightarrow J/\psi X$

$\Gamma(J/\psi(1S)X(4160))/\Gamma_{total}$		Γ_{14}/Γ	
VALUE	CL%	DOCUMENT ID	TECN COMMENT
$<5.4 \times 10^{-6}$	90	YANG	14 BELL $e^+e^- \rightarrow J/\psi X$

$\Gamma(X(4350) \text{ anything, } X \rightarrow J/\psi(1S)\phi)/\Gamma_{total}$		Γ_{15}/Γ	
VALUE	CL%	DOCUMENT ID	TECN COMMENT
$<8.1 \times 10^{-6}$	90	SHEN	16 BELL $\Upsilon(1S) \rightarrow J/\psi K^+ K^- X$

$\Gamma(Z_c(3900)^\pm \text{ anything, } Z_c \rightarrow J/\psi(1S)\pi^\pm)/\Gamma_{total}$		Γ_{16}/Γ	
VALUE	CL%	DOCUMENT ID	TECN COMMENT
$<1.3 \times 10^{-5}$	90	SHEN	16 BELL $\Upsilon(1S) \rightarrow J/\psi \pi^\pm X$

$\Gamma(Z_c(4200)^\pm \text{ anything, } Z_c \rightarrow J/\psi(1S)\pi^\pm)/\Gamma_{total}$		Γ_{17}/Γ	
VALUE	CL%	DOCUMENT ID	TECN COMMENT
$<6.0 \times 10^{-5}$	90	SHEN	16 BELL $\Upsilon(1S) \rightarrow J/\psi \pi^\pm X$

$\Gamma(Z_c(4430)^\pm \text{ anything, } Z_c \rightarrow J/\psi(1S)\pi^\pm)/\Gamma_{total}$		Γ_{18}/Γ	
VALUE	CL%	DOCUMENT ID	TECN COMMENT
$<4.9 \times 10^{-5}$	90	SHEN	16 BELL $\Upsilon(1S) \rightarrow J/\psi \pi^\pm X$

$\Gamma(X_{cs}^\pm \text{ anything, } X \rightarrow J/\psi K^\pm)/\Gamma_{total}$		Γ_{19}/Γ	
VALUE	CL%	DOCUMENT ID	TECN COMMENT
$<5.7 \times 10^{-6}$	90	SHEN	16 BELL $\Upsilon(1S) \rightarrow J/\psi K^- X$

$\Gamma(\psi(4230) \text{ anything, } \psi \rightarrow J/\psi(1S)\pi^+\pi^-)/\Gamma_{total}$		Γ_{20}/Γ	
VALUE	CL%	DOCUMENT ID	TECN COMMENT
$<3.8 \times 10^{-5}$	90	SHEN	16 BELL $\Upsilon(1S) \rightarrow J/\psi \pi^+\pi^- X$

$\Gamma(\psi(4230) \text{ anything, } \psi \rightarrow J/\psi(1S)K^+K^-)/\Gamma_{total}$		Γ_{21}/Γ	
VALUE	CL%	DOCUMENT ID	TECN COMMENT
$<7.5 \times 10^{-6}$	90	SHEN	16 BELL $\Upsilon(1S) \rightarrow J/\psi K^+ K^- X$

$\Gamma(\chi_{c1}(4140) \text{ anything, } \chi_{c1} \rightarrow J/\psi(1S)\phi)/\Gamma_{total}$		Γ_{22}/Γ	
VALUE	CL%	DOCUMENT ID	TECN COMMENT
$<5.2 \times 10^{-6}$	90	SHEN	16 BELL $\Upsilon(1S) \rightarrow J/\psi K^+ K^- X$

$\Gamma(\chi_{c0} \text{ anything})/\Gamma(J/\psi(1S) \text{ anything})$		Γ_{23}/Γ_7	
VALUE	CL%	DOCUMENT ID	TECN COMMENT
<7.4	90	BRIERE	04 CLEO $e^+e^- \rightarrow J/\psi X$

$\Gamma(\chi_{c1} \text{ anything})/\Gamma_{total}$		Γ_{24}/Γ	
VALUE (units 10^{-4})	EVTS	DOCUMENT ID	TECN COMMENT
1.90 ± 0.35 OUR FIT		JIA	17 BELL $\Upsilon(1S) \rightarrow \gamma J/\psi(1S)$
$1.90 \pm 0.43 \pm 0.14$	215		

$\Gamma(\chi_{c1} \text{ anything})/\Gamma(J/\psi(1S) \text{ anything})$		Γ_{24}/Γ_7	
VALUE	EVTS	DOCUMENT ID	TECN COMMENT
0.35 ± 0.07 OUR FIT		BRIERE	04 CLEO $e^+e^- \rightarrow J/\psi X$
$0.35 \pm 0.08 \pm 0.06$	52 ± 12		

$\Gamma(\chi_{c1}(1P)X_{tetra})/\Gamma_{total}$		Γ_{25}/Γ	
VALUE	CL%	DOCUMENT ID	TECN COMMENT
$<37.8 \times 10^{-6}$	90	¹ JIA	17A BELL $e^+e^- \rightarrow \text{hadrons}$

¹ For a tetraquark state X_{tetra} , with mass in the range 1.16–2.46 GeV and width in the range 0–0.3 GeV. Measured 90% CL limits as a function of X_{tetra} mass and width range from 4.4×10^{-6} to 37.8×10^{-6} .

$\Gamma(\chi_{c2} \text{ anything})/\Gamma(J/\psi(1S) \text{ anything})$		Γ_{26}/Γ_7	
VALUE	EVTS	DOCUMENT ID	TECN COMMENT
$0.52 \pm 0.12 \pm 0.09$	47 ± 11	BRIERE	04 CLEO $e^+e^- \rightarrow J/\psi X$

$\Gamma(\psi(2S) \text{ anything})/\Gamma_{total}$		Γ_{27}/Γ	
VALUE (units 10^{-4})	EVTS	DOCUMENT ID	TECN COMMENT
$1.23 \pm 0.17 \pm 0.11$	215	SHEN	16 BELL $e^+e^- \rightarrow \psi(2S) X$

$\Gamma(\psi(2S) \text{ anything})/\Gamma(J/\psi(1S) \text{ anything})$		Γ_{27}/Γ_7	
VALUE	EVTS	DOCUMENT ID	TECN COMMENT
$0.41 \pm 0.11 \pm 0.08$	42 ± 11	BRIERE	04 CLEO $e^+e^- \rightarrow J/\psi \pi^+ \pi^- X$

$\Gamma(\psi(2S)\eta_c)/\Gamma_{total}$		Γ_{28}/Γ	
VALUE	CL%	DOCUMENT ID	TECN COMMENT
$<3.6 \times 10^{-6}$	90	YANG	14 BELL $e^+e^- \rightarrow \psi(2S) X$

$\Gamma(\psi(2S)\chi_{c0})/\Gamma_{total}$		Γ_{29}/Γ	
VALUE	CL%	DOCUMENT ID	TECN COMMENT
$<6.5 \times 10^{-6}$	90	YANG	14 BELL $e^+e^- \rightarrow \psi(2S) X$

$\Gamma(\psi(2S)\chi_{c1})/\Gamma_{total}$		Γ_{30}/Γ	
VALUE	CL%	DOCUMENT ID	TECN COMMENT
$<4.5 \times 10^{-6}$	90	YANG	14 BELL $e^+e^- \rightarrow \psi(2S) X$

$\Gamma(\psi(2S)\chi_{c2})/\Gamma_{total}$		Γ_{31}/Γ	
VALUE	CL%	DOCUMENT ID	TECN COMMENT
$<2.1 \times 10^{-6}$	90	YANG	14 BELL $e^+e^- \rightarrow \psi(2S) X$

$\Gamma(\psi(2S)\eta_c(2S))/\Gamma_{total}$		Γ_{32}/Γ	
VALUE	CL%	DOCUMENT ID	TECN COMMENT
$<3.2 \times 10^{-6}$	90	YANG	14 BELL $e^+e^- \rightarrow \psi(2S) X$

$\Gamma(\psi(2S)X(3940))/\Gamma_{total}$		Γ_{33}/Γ	
VALUE	CL%	DOCUMENT ID	TECN COMMENT
$<2.9 \times 10^{-6}$	90	YANG	14 BELL $e^+e^- \rightarrow \psi(2S) X$

$\Gamma(\psi(2S)X(4160))/\Gamma_{total}$		Γ_{34}/Γ	
VALUE	CL%	DOCUMENT ID	TECN COMMENT
$<2.9 \times 10^{-6}$	90	YANG	14 BELL $e^+e^- \rightarrow \psi(2S) X$

$\Gamma(\psi(4230) \text{ anything, } \psi \rightarrow \psi(2S)\pi^+\pi^-)/\Gamma_{total}$		Γ_{35}/Γ	
VALUE	CL%	DOCUMENT ID	TECN COMMENT
$<7.9 \times 10^{-5}$	90	SHEN	16 BELL $\Upsilon(1S) \rightarrow \psi(2S)\pi^+\pi^- X$

$\Gamma(\psi(4360) \text{ anything, } \psi \rightarrow \psi(2S)\pi^+\pi^-)/\Gamma_{total}$		Γ_{36}/Γ	
VALUE	CL%	DOCUMENT ID	TECN COMMENT
$<5.2 \times 10^{-5}$	90	SHEN	16 BELL $\Upsilon(1S) \rightarrow \psi(2S)\pi^+\pi^- X$

$\Gamma(\psi(4660) \text{ anything, } \psi \rightarrow \psi(2S)\pi^+\pi^-)/\Gamma_{total}$		Γ_{37}/Γ	
VALUE	CL%	DOCUMENT ID	TECN COMMENT
$<2.2 \times 10^{-5}$	90	SHEN	16 BELL $\Upsilon(1S) \rightarrow \psi(2S)\pi^+\pi^- X$

$\Gamma(X(4050)^\pm \text{ anything, } X \rightarrow \psi(2S)\pi^\pm)/\Gamma_{total}$		Γ_{38}/Γ	
VALUE	CL%	DOCUMENT ID	TECN COMMENT
$<8.8 \times 10^{-5}$	90	SHEN	16 BELL $\Upsilon(1S) \rightarrow \psi(2S)\pi^\pm X$

$\Gamma(Z_c(4430)^\pm \text{ anything, } Z_c \rightarrow \psi(2S)\pi^\pm)/\Gamma_{total}$		Γ_{39}/Γ	
VALUE	CL%	DOCUMENT ID	TECN COMMENT
$<6.7 \times 10^{-5}$	90	SHEN	16 BELL $\Upsilon(1S) \rightarrow \psi(2S)\pi^\pm X$

$\Gamma(\chi_{c1}(3872) \text{ anything})/\Gamma_{total}$		Γ_{40}/Γ	
VALUE	CL%	DOCUMENT ID	TECN COMMENT
$<2.5 \times 10^{-4}$	90	¹ SHEN	16 BELL $\Upsilon(1S) \rightarrow J/\psi \pi^+ \pi^- X$

¹ SHEN 16 reports $[\Gamma(\Upsilon(1S) \rightarrow \chi_{c1}(3872) \text{ anything})/\Gamma_{total}] \times [B(\chi_{c1}(3872) \rightarrow \pi^+\pi^- J/\psi(1S))] < 9.5 \times 10^{-6}$ which we divide by our best value $B(\chi_{c1}(3872) \rightarrow \pi^+\pi^- J/\psi(1S)) = 3.8 \times 10^{-2}$.

$\Gamma(Z_c(4200)^+ Z_c(4200)^-)/\Gamma_{total}$		Γ_{41}/Γ	
VALUE	CL%	DOCUMENT ID	TECN COMMENT
$<22.3 \times 10^{-6}$	90	¹ JIA	18 BELL $\Upsilon(1S) \rightarrow J/\psi \pi^\pm X$

¹ Assuming $B(Z_c(4200)^\pm \rightarrow J/\psi \pi^\pm) = 1$.

$\Gamma(Z_c(3900)^\pm Z_c(4200)^\mp)/\Gamma_{total}$		Γ_{42}/Γ	
VALUE	CL%	DOCUMENT ID	TECN COMMENT
$<8.1 \times 10^{-6}$	90	¹ JIA	18 BELL $\Upsilon(1S) \rightarrow J/\psi \pi^\pm X$

¹ Assuming $B(Z_c(4200)^\pm \rightarrow J/\psi \pi^\pm) = 1 = B(Z_c(3900)^\pm \rightarrow J/\psi \pi^\pm)$.

$\Gamma(Z_c(3900)^+ Z_c(3900)^-)/\Gamma_{total}$		Γ_{43}/Γ	
VALUE	CL%	DOCUMENT ID	TECN COMMENT
$<1.8 \times 10^{-6}$	90	¹ JIA	18 BELL $\Upsilon(1S) \rightarrow J/\psi \pi^\pm X$

¹ Assuming $B(Z_c(3900)^\pm \rightarrow J/\psi \pi^\pm) = 1$.

$\Gamma(X(4050)^+ X(4050)^-)/\Gamma_{total}$		Γ_{44}/Γ	
VALUE	CL%	DOCUMENT ID	TECN COMMENT
$<15.8 \times 10^{-6}$	90	¹ JIA	18 BELL $\Upsilon(1S) \rightarrow \chi_{c1}(1P)\pi^\pm X$

¹ Assuming $B(X(4050)^\pm \rightarrow \chi_{c1}(1P)\pi^\pm) = 1$.

See key on page 1127

Meson Particle Listings
 $\Upsilon(1S)$ $\Gamma(X(4250)^+ X(4250)^-)/\Gamma_{\text{total}}$ Γ_{45}/Γ

VALUE	CL%	DOCUMENT ID	TECN	COMMENT
$<26.6 \times 10^{-6}$	90	¹ JIA	18	BELL $\Upsilon(1S) \rightarrow \chi_{c1}(1P)\pi^\pm X$

¹ Assuming $B(X(4250)^\pm \rightarrow \chi_{c1}(1P)\pi^\pm) = 1$ $\Gamma(X(4050)^\pm X(4250)^\mp)/\Gamma_{\text{total}}$ Γ_{46}/Γ

VALUE	CL%	DOCUMENT ID	TECN	COMMENT
$<44.2 \times 10^{-6}$	90	¹ JIA	18	BELL $\Upsilon(1S) \rightarrow \chi_{c1}(1P)\pi^\pm X$

¹ Assuming $B(X(4050)^\pm \rightarrow \chi_{c1}(1P)\pi^\pm) = 1 = B(X(4250)^\pm \rightarrow \chi_{c1}(1P)\pi^\pm)$ $\Gamma(Z_c(4430)^+ Z_c(4430)^-)/\Gamma_{\text{total}}$ Γ_{47}/Γ

VALUE	CL%	DOCUMENT ID	TECN	COMMENT
$<20.3 \times 10^{-6}$	90	¹ JIA	18	BELL $\Upsilon(2S) \rightarrow \psi(2S)\pi^\pm X$

¹ Assuming $B(Z_c(4430)^\pm \rightarrow \psi(2S)\pi^\pm) = 1$ $\Gamma(X(4055)^\pm X(4055)^\mp)/\Gamma_{\text{total}}$ Γ_{48}/Γ

VALUE	CL%	DOCUMENT ID	TECN	COMMENT
$<23.3 \times 10^{-6}$	90	¹ JIA	18	BELL $\Upsilon(1S) \rightarrow \psi(2S)\pi^\pm X$

¹ Assuming $B(X(4055)^\pm \rightarrow \psi(2S)\pi^\pm) = 1$ $\Gamma(X(4055)^\pm Z_c(4430)^\mp)/\Gamma_{\text{total}}$ Γ_{49}/Γ

VALUE	CL%	DOCUMENT ID	TECN	COMMENT
$<45.5 \times 10^{-6}$	90	¹ JIA	18	BELL $\Upsilon(1S) \rightarrow \psi(2S)\pi^\pm X$

¹ Assuming $B(X(4055)^\pm \rightarrow \psi(2S)\pi^\pm) = 1 = B(Z_c(4430)^\pm \rightarrow \psi(2S)\pi^\pm)$ $\Gamma(\rho\pi)/\Gamma_{\text{total}}$ Γ_{50}/Γ

VALUE (units 10^{-6})	CL%	DOCUMENT ID	TECN	COMMENT
<3.68	90	SHEN	13	BELL $\Upsilon(1S) \rightarrow \pi^+ \pi^- \pi^0$
••• We do not use the following data for averages, fits, limits, etc. •••				
$<1 \times 10^3$	90	BLINOV	90	MD1 $\Upsilon(1S) \rightarrow \rho^0 \pi^0$
$<2 \times 10^2$	90	FULTON	90B	$\Upsilon(1S) \rightarrow \rho^0 \pi^0$
$<2.1 \times 10^3$	90	NICZYPORUK	83	LENA $\Upsilon(1S) \rightarrow \rho^0 \pi^0$

 $\Gamma(\omega\pi^0)/\Gamma_{\text{total}}$ Γ_{51}/Γ

VALUE (units 10^{-6})	CL%	DOCUMENT ID	TECN	COMMENT
<3.90	90	SHEN	13	BELL $\Upsilon(1S) \rightarrow \pi^+ \pi^- \pi^0 \pi^0$

 $\Gamma(\pi^+ \pi^-)/\Gamma_{\text{total}}$ Γ_{52}/Γ

VALUE (units 10^{-4})	CL%	DOCUMENT ID	TECN	COMMENT
<5	90	BARU	92	MD1 $\Upsilon(1S) \rightarrow \pi^+ \pi^-$

 $\Gamma(K^+ K^-)/\Gamma_{\text{total}}$ Γ_{53}/Γ

VALUE (units 10^{-4})	CL%	DOCUMENT ID	TECN	COMMENT
<5	90	BARU	92	MD1 $\Upsilon(1S) \rightarrow K^+ K^-$

 $\Gamma(p\bar{p})/\Gamma_{\text{total}}$ Γ_{54}/Γ

VALUE (units 10^{-4})	CL%	DOCUMENT ID	TECN	COMMENT
<5	90	¹ BARU	96	MD1 $\Upsilon(1S) \rightarrow p\bar{p}$

¹ Supersedes BARU 92 in this node. $\Gamma(\pi^+ \pi^- \pi^0)/\Gamma_{\text{total}}$ Γ_{55}/Γ

VALUE (units 10^{-6})	CL%	EVTS	DOCUMENT ID	TECN	COMMENT
$2.14 \pm 0.72 \pm 0.34$	26 ± 9	SHEN	13	BELL	$\Upsilon(1S) \rightarrow \pi^+ \pi^- \pi^0$
••• We do not use the following data for averages, fits, limits, etc. •••					
<18.4	90		ANASTASSOV	99	CLE2 $e^+ e^- \rightarrow \text{hadrons}$

 $\Gamma(\phi K^+ K^-)/\Gamma_{\text{total}}$ Γ_{56}/Γ

VALUE (units 10^{-6})	EVTS	DOCUMENT ID	TECN	COMMENT
$2.36 \pm 0.37 \pm 0.29$	56	SHEN	12A	BELL $\Upsilon(1S) \rightarrow 2(K^+ K^-)$

 $\Gamma(\omega\pi^+ \pi^-)/\Gamma_{\text{total}}$ Γ_{57}/Γ

VALUE (units 10^{-6})	EVTS	DOCUMENT ID	TECN	COMMENT
$4.46 \pm 0.67 \pm 0.72$	64	SHEN	12A	BELL $\Upsilon(1S) \rightarrow 2(\pi^+ \pi^-)\pi^0$

 $\Gamma(K^*(892)^0 K^- \pi^+ + \text{c.c.})/\Gamma_{\text{total}}$ Γ_{58}/Γ

VALUE (units 10^{-6})	EVTS	DOCUMENT ID	TECN	COMMENT
$4.42 \pm 0.50 \pm 0.58$	173	SHEN	12A	BELL $\Upsilon(1S) \rightarrow K^+ K^- \pi^+ \pi^-$

 $\Gamma(\phi f_2(1525))/\Gamma_{\text{total}}$ Γ_{59}/Γ

VALUE (units 10^{-6})	CL%	DOCUMENT ID	TECN	COMMENT
<1.63	90	SHEN	12A	BELL $\Upsilon(1S) \rightarrow 2(K^+ K^-)$

 $\Gamma(\omega f_2(1270))/\Gamma_{\text{total}}$ Γ_{60}/Γ

VALUE (units 10^{-6})	CL%	DOCUMENT ID	TECN	COMMENT
<1.79	90	SHEN	12A	BELL $\Upsilon(1S) \rightarrow 2(\pi^+ \pi^-)\pi^0$

 $\Gamma(\rho(770) a_2(1320))/\Gamma_{\text{total}}$ Γ_{61}/Γ

VALUE (units 10^{-6})	CL%	DOCUMENT ID	TECN	COMMENT
<2.24	90	SHEN	12A	BELL $\Upsilon(1S) \rightarrow 2(\pi^+ \pi^-)\pi^0$

 $\Gamma(K^*(892)^0 \bar{K}_2^0(1430)^0 + \text{c.c.})/\Gamma_{\text{total}}$ Γ_{62}/Γ

VALUE (units 10^{-6})	EVTS	DOCUMENT ID	TECN	COMMENT
$3.02 \pm 0.68 \pm 0.34$	42	SHEN	12A	BELL $\Upsilon(1S) \rightarrow K^+ K^- \pi^+ \pi^-$

 $\Gamma(K_1(1270)^\pm K^\mp)/\Gamma_{\text{total}}$ Γ_{63}/Γ

VALUE (units 10^{-6})	CL%	DOCUMENT ID	TECN	COMMENT
<2.41	90	SHEN	12A	BELL $\Upsilon(1S) \rightarrow K^+ K^- \pi^+ \pi^-$

 $\Gamma(K_1(1400)^\pm K^\mp)/\Gamma_{\text{total}}$ Γ_{64}/Γ

VALUE (units 10^{-6})	EVTS	DOCUMENT ID	TECN	COMMENT
$1.02 \pm 0.35 \pm 0.22$	24	SHEN	12A	BELL $\Upsilon(1S) \rightarrow K^+ K^- \pi^+ \pi^-$

 $\Gamma(b_1(1235)^\pm \pi^\mp)/\Gamma_{\text{total}}$ Γ_{65}/Γ

VALUE (units 10^{-6})	CL%	DOCUMENT ID	TECN	COMMENT
<1.25	90	SHEN	12A	BELL $\Upsilon(1S) \rightarrow 2(\pi^+ \pi^-)\pi^0$

 $\Gamma(\pi^+ \pi^- \pi^0 \pi^0)/\Gamma_{\text{total}}$ Γ_{66}/Γ

VALUE (units 10^{-6})	EVTS	DOCUMENT ID	TECN	COMMENT
$12.8 \pm 2.0 \pm 2.3$	143 ± 22	SHEN	13	BELL $\Upsilon(1S) \rightarrow \pi^+ \pi^- \pi^0 \pi^0$

 $\Gamma(K_S^0 K^+ \pi^- + \text{c.c.})/\Gamma_{\text{total}}$ Γ_{67}/Γ

VALUE (units 10^{-6})	CL%	EVTS	DOCUMENT ID	TECN	COMMENT
$1.59 \pm 0.33 \pm 0.18$	37 ± 8	SHEN	13	BELL	$\Upsilon(1S) \rightarrow K_S^0 K^- \pi^+$
••• We do not use the following data for averages, fits, limits, etc. •••					
<3.4	90	¹ DOBBS	12A		$\Upsilon(1S) \rightarrow K_S^0 K^- \pi^+$

¹ Obtained by analyzing CLEO III data but not authored by the CLEO Collaboration. $\Gamma(K^*(892)^0 \bar{K}^0 + \text{c.c.})/\Gamma_{\text{total}}$ Γ_{68}/Γ

VALUE (units 10^{-6})	EVTS	DOCUMENT ID	TECN	COMMENT
$2.92 \pm 0.85 \pm 0.37$	16 ± 5	SHEN	13	BELL $\Upsilon(1S) \rightarrow K_S^0 K^- \pi^+$

 $\Gamma(K^*(892)^- K^+ + \text{c.c.})/\Gamma_{\text{total}}$ Γ_{69}/Γ

VALUE (units 10^{-6})	CL%	DOCUMENT ID	TECN	COMMENT
<1.11	90	SHEN	13	BELL $\Upsilon(1S) \rightarrow K_S^0 K^- \pi^+$

 $\Gamma(f_1(1285) \text{ anything})/\Gamma_{\text{total}}$ Γ_{70}/Γ

VALUE (units 10^{-3})	EVTS	DOCUMENT ID	TECN	COMMENT
$4.6 \pm 2.8 \pm 1.3$	3.1k	JIA	17A	BELL $e^+ e^- \rightarrow \text{hadrons}$

 $\Gamma(D^*(2010)^\pm \text{ anything})/\Gamma_{\text{total}}$ Γ_{71}/Γ

VALUE (units 10^{-3})	CL%	EVTS	DOCUMENT ID	TECN	COMMENT
$25.2 \pm 1.3 \pm 1.5$	≈ 2k	¹ AUBERT	10c	BABR	$\Upsilon(2S) \rightarrow \pi^+ \pi^- \Upsilon(1S)$
••• We do not use the following data for averages, fits, limits, etc. •••					
<19	90	² ALBRECHT	92j	ARG	$e^+ e^- \rightarrow D^0 \pi^\pm X$

¹ For $x_p > 0.1$.² For $x_p > 0.2$. $\Gamma(f_1(1285) X_{\text{tetra}})/\Gamma_{\text{total}}$ Γ_{72}/Γ

VALUE	CL%	DOCUMENT ID	TECN	COMMENT
$<62.4 \times 10^{-6}$	90	¹ JIA	17A	BELL $e^+ e^- \rightarrow \text{hadrons}$

¹ For a tetraquark state X_{tetra} , with mass in the range 1.16–2.46 GeV and width in the range 0–0.3 GeV. Measured 90% CL limits as a function of X_{tetra} mass and width range from 4.6×10^{-6} to 62.4×10^{-6} . $\Gamma(\bar{2}H \text{ anything})/\Gamma_{\text{total}}$ Γ_{73}/Γ

VALUE (units 10^{-5})	EVTS	DOCUMENT ID	TECN	COMMENT
2.85 ± 0.25 OUR AVERAGE				
$2.81 \pm 0.49 \pm 0.20$ -0.24		LEES	14G	BABR $e^+ e^- \rightarrow \bar{2}H X$
$2.86 \pm 0.19 \pm 0.21$	455	ASNER	07	CLEO $e^+ e^- \rightarrow \bar{2}H X$

 $\Gamma(\text{Sum of 100 exclusive modes})/\Gamma_{\text{total}}$ Γ_{74}/Γ

VALUE (units 10^{-2})	DOCUMENT ID	TECN	COMMENT
1.200 ± 0.017	^{1,2} DOBBS	12A	$\Upsilon(1S) \rightarrow \text{hadrons}$

¹ DOBBS 12A presents individual exclusive branching fractions or upper limits for 100 modes of four to ten pions, kaons, or protons.² Obtained by analyzing CLEO III data but not authored by the CLEO Collaboration. $\Gamma(ggg, \gamma g g \rightarrow \bar{d} \text{ anything})/\Gamma(ggg, \gamma g g \rightarrow \text{anything})$

VALUE (units 10^{-5})	EVTS	DOCUMENT ID	TECN	COMMENT
$3.36 \pm 0.23 \pm 0.25$	455	ASNER	07	CLEO $e^+ e^- \rightarrow \bar{d} X$

 $\Gamma(\gamma\pi^+ \pi^-)/\Gamma_{\text{total}}$ Γ_{75}/Γ

VALUE (units 10^{-5})	DOCUMENT ID	TECN	COMMENT
$6.3 \pm 1.2 \pm 1.3$	¹ ANASTASSOV	99	CLE2 $e^+ e^- \rightarrow \text{hadrons}$

¹ For $m_{\pi\pi} > 1$ GeV.

Meson Particle Listings

 $\Upsilon(1S)$

$\Gamma(\gamma\pi^0\pi^0)/\Gamma_{total}$	Γ_{76}/Γ
VALUE (units 10^{-5})	DOCUMENT ID TECN COMMENT
$1.7 \pm 0.6 \pm 0.3$	¹ ANASTASSOV 99 CLE2 $e^+e^- \rightarrow \text{hadrons}$

¹ For $m_{\pi\pi} > 1$ GeV.

$\Gamma(\gamma\pi\pi(\text{S-wave}))/\Gamma_{total}$	Γ_{77}/Γ
VALUE (units 10^{-5})	DOCUMENT ID TECN COMMENT
$4.63 \pm 0.56 \pm 0.48$	LEES 18A BABR $\Upsilon(1S) \rightarrow \gamma\pi^+\pi^-$

$\Gamma(\gamma\pi^0\eta)/\Gamma_{total}$	Γ_{78}/Γ
VALUE (units 10^{-6})	DOCUMENT ID TECN COMMENT
< 2.4	90 ¹ BESSON 07A CLEO $e^+e^- \rightarrow \Upsilon(1S)$

¹ BESSON 07A obtained this limit for $0.7 < m_{\pi^0\eta} < 3$ GeV.

$\Gamma(\gamma K^+ K^-)/\Gamma_{total}$	Γ_{79}/Γ
($2 < m_{K^+K^-} < 3$ GeV)	DOCUMENT ID TECN COMMENT
VALUE (units 10^{-5})	CL%
$1.14 \pm 0.08 \pm 0.10$	90
	ATHAR 06 CLE3 $\Upsilon(1S) \rightarrow \gamma K^+ K^-$

$\Gamma(\gamma\rho\bar{\rho})/\Gamma_{total}$	Γ_{80}/Γ
($2 < m_{\rho\bar{\rho}} < 3$ GeV)	DOCUMENT ID TECN COMMENT
VALUE (units 10^{-5})	CL%
< 0.6	90
	ATHAR 06 CLE3 $\Upsilon(1S) \rightarrow \gamma\rho\bar{\rho}$

$\Gamma(\gamma 2h^+ 2h^-)/\Gamma_{total}$	Γ_{81}/Γ
VALUE (units 10^{-4})	EVTS
$7.0 \pm 1.1 \pm 1.0$	80 ± 12
	FULTON 90B CLEO $e^+e^- \rightarrow \text{hadrons}$

$\Gamma(\gamma 3h^+ 3h^-)/\Gamma_{total}$	Γ_{82}/Γ
VALUE (units 10^{-4})	EVTS
$5.4 \pm 1.5 \pm 1.3$	39 ± 11
	FULTON 90B CLEO $e^+e^- \rightarrow \text{hadrons}$

$\Gamma(\gamma 4h^+ 4h^-)/\Gamma_{total}$	Γ_{83}/Γ
VALUE (units 10^{-4})	EVTS
$7.4 \pm 2.5 \pm 2.5$	36 ± 12
	FULTON 90B CLEO $e^+e^- \rightarrow \text{hadrons}$

$\Gamma(\gamma\pi^+\pi^-K^+K^-)/\Gamma_{total}$	Γ_{84}/Γ
VALUE (units 10^{-4})	EVTS
$2.9 \pm 0.7 \pm 0.6$	29 ± 8
	FULTON 90B CLEO $e^+e^- \rightarrow \text{hadrons}$

$\Gamma(\gamma 2\pi^+ 2\pi^-)/\Gamma_{total}$	Γ_{85}/Γ
VALUE (units 10^{-4})	EVTS
$2.5 \pm 0.7 \pm 0.5$	26 ± 7
	FULTON 90B CLEO $e^+e^- \rightarrow \text{hadrons}$

$\Gamma(\gamma 3\pi^+ 3\pi^-)/\Gamma_{total}$	Γ_{86}/Γ
VALUE (units 10^{-4})	EVTS
$2.5 \pm 0.9 \pm 0.8$	17 ± 5
	FULTON 90B CLEO $e^+e^- \rightarrow \text{hadrons}$

$\Gamma(\gamma 2\pi^+ 2\pi^- K^+ K^-)/\Gamma_{total}$	Γ_{87}/Γ
VALUE (units 10^{-4})	EVTS
$2.4 \pm 0.9 \pm 0.8$	18 ± 7
	FULTON 90B CLEO $e^+e^- \rightarrow \text{hadrons}$

$\Gamma(\gamma\pi^+\pi^-\rho\bar{\rho})/\Gamma_{total}$	Γ_{88}/Γ
VALUE (units 10^{-4})	EVTS
$1.5 \pm 0.5 \pm 0.3$	22 ± 6
	FULTON 90B CLEO $e^+e^- \rightarrow \text{hadrons}$

$\Gamma(\gamma 2\pi^+ 2\pi^-\rho\bar{\rho})/\Gamma_{total}$	Γ_{89}/Γ
VALUE (units 10^{-4})	EVTS
$0.4 \pm 0.4 \pm 0.4$	7 ± 6
	FULTON 90B CLEO $e^+e^- \rightarrow \text{hadrons}$

$\Gamma(\gamma 2K^+ 2K^-)/\Gamma_{total}$	Γ_{90}/Γ
VALUE (units 10^{-4})	EVTS
0.2 ± 0.2	2 ± 2
	FULTON 90B CLEO $e^+e^- \rightarrow \text{hadrons}$

$\Gamma(\gamma\eta(958))/\Gamma_{total}$	Γ_{91}/Γ
VALUE (units 10^{-6})	CL%
< 1.9	90
	ATHAR 07A CLEO $\Upsilon(1S) \rightarrow \gamma\eta' \rightarrow \gamma\pi^+\pi^-\eta, \gamma\rho$

• • • We do not use the following data for averages, fits, limits, etc. • • •

< 16 90 RICHICHI 01B CLE2 $\Upsilon(1S) \rightarrow \gamma\eta' \rightarrow \gamma\eta\pi^+\pi^-$

$\Gamma(\gamma\eta)/\Gamma_{total}$	Γ_{92}/Γ
VALUE (units 10^{-6})	CL%
< 1.0	90
	ATHAR 07A CLEO $\Upsilon(1S) \rightarrow \gamma\eta \rightarrow \gamma\gamma\gamma, \gamma\pi^+\pi^-\pi^0, \gamma 3\pi^0$

• • • We do not use the following data for averages, fits, limits, etc. • • •

< 21 90 MASEK 02 CLEO $\Upsilon(1S) \rightarrow \gamma\eta$

$\Gamma(\gamma f_0(980))/\Gamma_{total}$	Γ_{93}/Γ
VALUE (units 10^{-5})	CL%
< 3	90
	¹ ATHAR 06 CLE3 $\Upsilon(1S) \rightarrow \gamma\pi^+\pi^-$

¹ Assuming $B(f_0(980) \rightarrow \pi\pi) = 1$.

$\Gamma(\gamma f'_2(1525))/\Gamma_{total}$	Γ_{94}/Γ
VALUE (units 10^{-5})	CL% EVTS
2.9 ± 0.6	OUR AVERAGE
$2.13 \pm 0.28 \pm 0.72$	¹ LEES 18A BABR $\Upsilon(1S) \rightarrow \gamma K^+ K^-$
$4.1 \pm 1.4 \pm 0.1$	² BESSON 11 CLEO $\Upsilon(1S) \rightarrow K_S^0 K_S^0$
$3.7 \pm 0.9 \pm 0.8$	ATHAR 06 CLE3 $\Upsilon(1S) \rightarrow \gamma K^+ K^-$

• • • We do not use the following data for averages, fits, limits, etc. • • •

< 14 90 ³ FULTON 90B CLEO $\Upsilon(1S) \rightarrow \gamma K^+ K^-$

< 19.4 90 ³ ALBRECHT 89 ARG $\Upsilon(1S) \rightarrow \gamma K^+ K^-$

¹ Using $B(f'_2(1525) \rightarrow K\bar{K}) = 0.887 \pm 0.022$ and $B(K^0\bar{K}^0) = 1/2 B(K\bar{K})$.

² BESSON 11 reports $(4.0 \pm 1.3 \pm 0.6) \times 10^{-5}$ from a measurement of $[\Gamma(\Upsilon(1S) \rightarrow \gamma f'_2(1525))/\Gamma_{total}] \times [B(f'_2(1525) \rightarrow K\bar{K})]$ assuming $B(f'_2(1525) \rightarrow K\bar{K}) = (88.8 \pm 3.1) \times 10^{-2}$, which we rescale to our best value $B(f'_2(1525) \rightarrow K\bar{K}) = (87.6 \pm 2.2) \times 10^{-2}$. Our first error is their experiment's error and our second error is the systematic error from using our best value. The result also assumes $B(K_S^0 \rightarrow \pi^+\pi^-) = (69.20 \pm 0.05)\%$ and $B(f'_2(1525) \rightarrow K\bar{K}) = 4 B(f'_2(1525) \rightarrow K_S^0 K_S^0)$.

³ Assuming $B(f'_2(1525) \rightarrow K\bar{K}) = 0.71$.

$\Gamma(\gamma f_2(1270))/\Gamma_{total}$	Γ_{95}/Γ
VALUE (units 10^{-5})	CL%
10.1 ± 0.6	OUR AVERAGE
$10.15 \pm 0.59 \pm 0.54$	¹ LEES 18A BABR $\Upsilon(1S) \rightarrow \gamma\pi^+\pi^-$
$10.5 \pm 1.6 \pm 1.9$	² BESSON 07A CLE3 $\Upsilon(1S) \rightarrow \gamma\pi^0\pi^0$
$10.2 \pm 0.8 \pm 0.7$	ATHAR 06 CLE3 $\Upsilon(1S) \rightarrow \gamma\pi^+\pi^-$
$8.1 \pm 2.3 \pm 2.9$	³ ANASTASSOV 99 CLE2 $e^+e^- \rightarrow \text{hadrons}$

• • • We do not use the following data for averages, fits, limits, etc. • • •

< 21 90 ³ FULTON 90B CLEO $\Upsilon(1S) \rightarrow \gamma\pi^+\pi^-$

< 13 90 ³ ALBRECHT 89 ARG $\Upsilon(1S) \rightarrow \gamma\pi^+\pi^-$

< 81 90 SCHMITT 88 CBAL $\Upsilon(1S) \rightarrow \gamma X$

¹ Using $B(f_2(1270) \rightarrow \pi^0\pi^0) = 1/3 B(f_2(1270) \rightarrow \pi\pi)$ and $B(f_2(1270) \rightarrow \pi\pi) = (84.2 \pm 2.9 \pm 0.9)\%$.

² Using $B(f_2(1270) \rightarrow \pi^0\pi^0) = B(f_2(1270) \rightarrow \pi\pi)/3$ and $B(f_2(1270) \rightarrow \pi\pi) = (84.7 \pm 2.5 \pm 1.2)\%$.

³ Using $B(f_2(1270) \rightarrow \pi\pi) = 0.84$.

$\Gamma(\gamma\eta(1405))/\Gamma_{total}$	Γ_{96}/Γ
VALUE (units 10^{-5})	CL%
< 8.2	90
	¹ FULTON 90B CLEO $\Upsilon(1S) \rightarrow \gamma K^\pm\pi^\mp K_S^0$

¹ Includes unknown branching ratio of $\eta(1405) \rightarrow K^\pm\pi^\mp K_S^0$.

$\Gamma(\gamma f_0(1500))/\Gamma_{total}$	Γ_{97}/Γ
VALUE (units 10^{-5})	CL%
< 1.5	90
	¹ BESSON 07A CLEO $e^+e^- \rightarrow \Upsilon(1S) \rightarrow \gamma\pi^0\pi^0$

• • • We do not use the following data for averages, fits, limits, etc. • • •

< 6.1 90 ² BESSON 07A CLEO $e^+e^- \rightarrow \Upsilon(1S) \rightarrow \gamma\eta\eta$

¹ Using $B(f_0(1500) \rightarrow \pi^0\pi^0) = B(f_0(1500) \rightarrow \pi\pi)/3$ and $B(f_0(1500) \rightarrow \pi\pi) = (0.349 \pm 0.023)\%$.

² Calculated by us using $B(f_0(1500) \rightarrow \eta\eta) = (5.1 \pm 0.9)\%$.

$\Gamma(\gamma f_0(1500) \rightarrow \gamma K^+ K^-)/\Gamma_{total}$	Γ_{98}/Γ
VALUE (units 10^{-5})	DOCUMENT ID TECN COMMENT
$1.04 \pm 0.14 \pm 0.33$	¹ LEES 18A BABR $e^+e^- \rightarrow \Upsilon(1S) \rightarrow \gamma K^+ K^-$

¹ LEES 18A quotes $B(\Upsilon(1S) \rightarrow \gamma f_0(1500) \rightarrow \gamma K\bar{K}) = (2.08 \pm 0.27 \pm 0.65) \times 10^{-5}$ assuming $B(K^0\bar{K}^0) = 1/2 B(K\bar{K})$.

$\Gamma(\gamma f_0(1710))/\Gamma_{total}$	Γ_{99}/Γ
VALUE (units 10^{-4})	CL%
< 2.6	90
	¹ ALBRECHT 89 ARG $\Upsilon(1S) \rightarrow \gamma K^+ K^-$

• • • We do not use the following data for averages, fits, limits, etc. • • •

< 6.3 90 ¹ FULTON 90B CLEO $\Upsilon(1S) \rightarrow \gamma K^+ K^-$

< 19 90 ¹ FULTON 90B CLEO $\Upsilon(1S) \rightarrow \gamma K_S^0 K_S^0$

< 8 90 ² ALBRECHT 89 ARG $\Upsilon(1S) \rightarrow \gamma\pi^+\pi^-$

< 24 90 ³ SCHMITT 88 CBAL $\Upsilon(1S) \rightarrow \gamma X$

¹ Assuming $B(f_0(1710) \rightarrow K\bar{K}) = 0.38$.

² Assuming $B(f_0(1710) \rightarrow \pi\pi) = 0.04$.

³ Assuming $B(f_0(1710) \rightarrow \eta\eta) = 0.18$.

See key on page 1127

Meson Particle Listings
 $\Upsilon(1S)$

$\Gamma(\gamma f_0(1710) \rightarrow \gamma K^+ K^-) / \Gamma_{\text{total}}$ Γ_{100} / Γ

VALUE (units 10^{-5})	CL%	DOCUMENT ID	TECN	COMMENT
$1.01 \pm 0.26 \pm 0.18$		¹ LEES	18A BABR	$e^+ e^- \rightarrow \Upsilon(1S) \rightarrow \gamma K^+ K^-$
••• We do not use the following data for averages, fits, limits, etc. •••				
<0.7	90	ATHAR	06 CLEO	$e^+ e^- \rightarrow \Upsilon(1S) \rightarrow \gamma K^+ K^-$
¹ LEES 18A quotes $B(\Upsilon(1S) \rightarrow \gamma f_0(1710) \rightarrow \gamma K \bar{K}) = (2.02 \pm 0.51 \pm 0.35) \times 10^{-5}$ assuming $B(K^0 \bar{K}^0) = 1/2 B(K \bar{K})$.				

$\Gamma(\gamma f_0(1710) \rightarrow \gamma \pi^+ \pi^-) / \Gamma_{\text{total}}$ Γ_{101} / Γ

VALUE (units 10^{-5})	DOCUMENT ID	TECN	COMMENT
$0.53 \pm 0.17 \pm 0.11$	¹ LEES	18A BABR	$\Upsilon(1S) \rightarrow \gamma \pi^+ \pi^-$
¹ LEES 18A quotes $B(\Upsilon(1S) \rightarrow \gamma f_0(1710) \rightarrow \gamma \pi \pi) = (0.79 \pm 0.26 \pm 0.17) \times 10^{-5}$ assuming $B(\pi^0 \pi^0) = 1/3 B(\pi \pi)$.			

$\Gamma(\gamma f_0(1710) \rightarrow \gamma \pi^0 \pi^0) / \Gamma_{\text{total}}$ Γ_{102} / Γ

VALUE (units 10^{-6})	CL%	DOCUMENT ID	TECN	COMMENT
< 1.4	90	BESSON	07A CLEO	$e^+ e^- \rightarrow \Upsilon(1S) \rightarrow \gamma \pi^0 \pi^0$

$\Gamma(\gamma f_0(1710) \rightarrow \gamma \eta \eta) / \Gamma_{\text{total}}$ Γ_{103} / Γ

VALUE (units 10^{-6})	CL%	DOCUMENT ID	TECN	COMMENT
< 1.8	90	BESSON	07A CLEO	$e^+ e^- \rightarrow \Upsilon(1S) \rightarrow \gamma \eta \eta$

$\Gamma(\gamma f_4(2050) / \Gamma_{\text{total}}$ Γ_{104} / Γ

VALUE (units 10^{-5})	CL%	DOCUMENT ID	TECN	COMMENT
< 5.3	90	¹ ATHAR	06 CLE3	$\Upsilon(1S) \rightarrow \gamma \pi^+ \pi^-$
¹ Assuming $B(f_4(2050) \rightarrow \pi \pi) = 0.17$.				

$\Gamma(\gamma f_0(2200) \rightarrow \gamma K^+ K^-) / \Gamma_{\text{total}}$ Γ_{105} / Γ

VALUE	CL%	DOCUMENT ID	TECN	COMMENT
< 0.0002	90	BARU	89 MD1	$\Upsilon(1S) \rightarrow \gamma K^+ K^-$

$\Gamma(\gamma f_J(2220) \rightarrow \gamma K^+ K^-) / \Gamma_{\text{total}}$ Γ_{106} / Γ

VALUE (units 10^{-7})	CL%	DOCUMENT ID	TECN	COMMENT
< 8	90	ATHAR	06 CLE3	$\Upsilon(1S) \rightarrow \gamma K^+ K^-$
••• We do not use the following data for averages, fits, limits, etc. •••				
< 160	90	MASEK	02 CLEO	$\Upsilon(1S) \rightarrow \gamma K^+ K^-$
< 150	90	FULTON	90B CLEO	$\Upsilon(1S) \rightarrow \gamma K^+ K^-$
< 290	90	ALBRECHT	89 ARG	$\Upsilon(1S) \rightarrow \gamma K^+ K^-$
<2000	90	BARU	89 MD1	$\Upsilon(1S) \rightarrow \gamma K^+ K^-$

$\Gamma(\gamma f_J(2220) \rightarrow \gamma \pi^+ \pi^-) / \Gamma_{\text{total}}$ Γ_{107} / Γ

VALUE (units 10^{-7})	CL%	DOCUMENT ID	TECN	COMMENT
< 6	90	ATHAR	06 CLE3	$\Upsilon(1S) \rightarrow \gamma \pi^+ \pi^-$
••• We do not use the following data for averages, fits, limits, etc. •••				
<120	90	MASEK	02 CLEO	$\Upsilon(1S) \rightarrow \gamma \pi^+ \pi^-$

$\Gamma(\gamma f_J(2220) \rightarrow \gamma \rho \bar{\rho}) / \Gamma_{\text{total}}$ Γ_{108} / Γ

VALUE (units 10^{-7})	CL%	DOCUMENT ID	TECN	COMMENT
< 11	90	ATHAR	06 CLE3	$\Upsilon(1S) \rightarrow \gamma \rho \bar{\rho}$
••• We do not use the following data for averages, fits, limits, etc. •••				
<160	90	MASEK	02 CLEO	$\Upsilon(1S) \rightarrow \gamma \rho \bar{\rho}$

$\Gamma(\gamma \eta(2225) \rightarrow \gamma \phi \phi) / \Gamma_{\text{total}}$ Γ_{109} / Γ

VALUE	CL%	DOCUMENT ID	TECN	COMMENT
< 0.003	90	BARU	89 MD1	$\Upsilon(1S) \rightarrow \gamma K^+ K^- K^+ K^-$

$\Gamma(\gamma \eta_c(1S)) / \Gamma_{\text{total}}$ Γ_{110} / Γ

VALUE	CL%	DOCUMENT ID	TECN	COMMENT
< 2.9×10^{-5}	90	¹ KATRENKO	20 BELL	$e^+ e^- \rightarrow \gamma + \text{hadrons}$
••• We do not use the following data for averages, fits, limits, etc. •••				
< 5.7×10^{-5}	90	SHEN	10A BELL	$\Upsilon(1S) \rightarrow \gamma X$
¹ Using $\Upsilon(2S) \rightarrow \Upsilon(1S) \pi^+ \pi^-$ decays.				

$\Gamma(\gamma \eta_c(2S)) / \Gamma_{\text{total}}$ Γ_{111} / Γ

VALUE	CL%	DOCUMENT ID	TECN	COMMENT
< 4×10^{-4}	90	¹ KATRENKO	20 BELL	$e^+ e^- \rightarrow \gamma + \text{hadrons}$
¹ Using $\Upsilon(2S) \rightarrow \Upsilon(1S) \pi^+ \pi^-$ decays.				

$\Gamma(\gamma \chi_{c0}) / \Gamma_{\text{total}}$ Γ_{112} / Γ

VALUE	CL%	DOCUMENT ID	TECN	COMMENT
< 6.6×10^{-5}	90	¹ KATRENKO	20 BELL	$\Upsilon(1S) \rightarrow \gamma + \text{hadrons}$
••• We do not use the following data for averages, fits, limits, etc. •••				
< 6.5×10^{-4}	90	SHEN	10A BELL	$\Upsilon(1S) \rightarrow \gamma X$
¹ Using $\Upsilon(2S) \rightarrow \Upsilon(1S) \pi^+ \pi^-$ decays.				

$\Gamma(\gamma \chi_{c1}) / \Gamma_{\text{total}}$ Γ_{113} / Γ

VALUE (units 10^{-9})	CL%	EVTS	DOCUMENT ID	TECN	COMMENT
$4.7 \pm 2.4 \pm 0.4$		5	¹ KATRENKO	20 BELL	$\Upsilon(1S) \rightarrow \gamma + \text{hadrons}$
••• We do not use the following data for averages, fits, limits, etc. •••					
<2.3	90		SHEN	10A BELL	$\Upsilon(1S) \rightarrow \gamma X$
¹ Using $\Upsilon(2S) \rightarrow \Upsilon(1S) \pi^+ \pi^-$ decays.					

$\Gamma(\gamma \chi_{c2}) / \Gamma_{\text{total}}$ Γ_{114} / Γ

VALUE	CL%	DOCUMENT ID	TECN	COMMENT
< 7.6×10^{-6}	90	SHEN	10A BELL	$\Upsilon(1S) \rightarrow \gamma X$
••• We do not use the following data for averages, fits, limits, etc. •••				
< 3.3×10^{-5}	90	¹ KATRENKO	20 BELL	$\Upsilon(1S) \rightarrow \gamma + \text{hadrons}$
¹ Using $\Upsilon(2S) \rightarrow \Upsilon(1S) \pi^+ \pi^-$ decays.				

$\Gamma(\gamma \chi_{c1}(3872)) / \Gamma_{\text{total}}$ Γ_{115} / Γ

VALUE	CL%	DOCUMENT ID	TECN	COMMENT
< 4×10^{-5}	90	¹ SHEN	10A BELL	$\Upsilon(1S) \rightarrow \gamma X$
¹ SHEN 10A reports $[\Gamma(\Upsilon(1S) \rightarrow \gamma \chi_{c1}(3872)) / \Gamma_{\text{total}}] \times [B(\chi_{c1}(3872) \rightarrow \pi^+ \pi^- J/\psi(1S))] < 1.6 \times 10^{-6}$ which we divide by our best value $B(\chi_{c1}(3872) \rightarrow \pi^+ \pi^- J/\psi(1S)) = 3.8 \times 10^{-2}$.				

$\Gamma(\gamma \chi_{c1}(3872), \chi_{c1} \rightarrow \pi^+ \pi^- \pi^0 J/\psi) / \Gamma_{\text{total}}$ Γ_{116} / Γ

VALUE	CL%	DOCUMENT ID	TECN	COMMENT
< 2.8×10^{-6}	90	SHEN	10A BELL	$\Upsilon(1S) \rightarrow \gamma X$

$\Gamma(\gamma \chi_{c0}(3915) \rightarrow \omega J/\psi) / \Gamma_{\text{total}}$ Γ_{117} / Γ

VALUE (units 10^{-6})	CL%	DOCUMENT ID	TECN	COMMENT
< 3.0	90	SHEN	10A BELL	$\Upsilon(1S) \rightarrow \gamma X$

$\Gamma(\gamma \chi_{c1}(4140) \rightarrow \phi J/\psi) / \Gamma_{\text{total}}$ Γ_{118} / Γ

VALUE (units 10^{-6})	CL%	DOCUMENT ID	TECN	COMMENT
< 2.2	90	SHEN	10A BELL	$\Upsilon(1S) \rightarrow \gamma X$

$\Gamma(\gamma X) / \Gamma_{\text{total}}$ Γ_{119} / Γ

VALUE (units 10^{-6})	CL%	DOCUMENT ID	TECN	COMMENT
< 4.5	90	¹ DEL-AMO-SA..11J	BABR	$e^+ e^- \rightarrow \gamma + X$
••• We do not use the following data for averages, fits, limits, etc. •••				
<30	90	² BALEST	95 CLEO	$e^+ e^- \rightarrow \gamma + X$
¹ For a noninteracting scalar X with mass $m < 8.0$ GeV.				
² For a noninteracting pseudoscalar X with mass < 7.2 GeV.				

$\Gamma(\gamma X \bar{X} (m_X < 3.1 \text{ GeV})) / \Gamma_{\text{total}}$ Γ_{120} / Γ

VALUE (units 10^{-3})	CL%	DOCUMENT ID	TECN	COMMENT
< 1	90	¹ BALEST	95 CLEO	$e^+ e^- \rightarrow \gamma + X \bar{X}$
¹ For a noninteracting vector X with mass < 3.1 GeV.				

$\Gamma(\gamma X \bar{X} (m_X < 4.5 \text{ GeV})) / \Gamma_{\text{total}}$ Γ_{121} / Γ

VALUE (units 10^{-5})	CL%	DOCUMENT ID	TECN	COMMENT
< 24	90	¹ DEL-AMO-SA..11J	BABR	$e^+ e^- \rightarrow \gamma + X \bar{X}$
¹ For a noninteracting scalar X with mass $m < 4.5$ GeV.				

$\Gamma(\gamma X \rightarrow \gamma + \geq 4 \text{ prongs}) / \Gamma_{\text{total}}$ Γ_{122} / Γ

VALUE (units 10^{-4})	CL%	DOCUMENT ID	TECN	COMMENT
< 1.78	95	ROSNER	07A CLEO	$e^+ e^- \rightarrow \gamma X$

$\Gamma(\gamma a_1^0 \rightarrow \gamma \mu^+ \mu^-) / \Gamma_{\text{total}}$ Γ_{123} / Γ

VALUE (units 10^{-6})	CL%	DOCUMENT ID	TECN	COMMENT
< 9	90	¹ LOVE	08 CLEO	$e^+ e^- \rightarrow \gamma a_1^0 \rightarrow \gamma \mu^+ \mu^-$
••• We do not use the following data for averages, fits, limits, etc. •••				
<9.7	90	² LEES	13c BABR	$e^+ e^- \rightarrow \gamma a_1^0 \rightarrow \gamma \mu^+ \mu^-$
¹ For a narrow scalar or pseudoscalar a_1^0 with $201 < M(\mu^+ \mu^-) < 3565$ MeV, excluding J/ψ . Measured 90% CL limits as a function of $M(\mu^+ \mu^-)$ range from $1-9 \times 10^{-6}$.				
² For a narrow scalar or pseudoscalar a_1^0 with mass in the range 212–9200 MeV, excluding J/ψ and $\psi(2S)$. Measured 90% CL limits as a function of $m_{a_1^0}$ range from 0.28–9.7 $\times 10^{-6}$.				

Meson Particle Listings

$\Upsilon(1S), \chi_{b0}(1P)$

$\Gamma(\gamma a_1^0 \to \gamma \tau^+ \tau^-) / \Gamma_{total}$
($2m_\tau < M(\tau^+ \tau^-) < 9.2 \text{ GeV}$) Γ_{124}/Γ

Table with columns: VALUE (units 10^-6), CL%, DOCUMENT ID, TECN, COMMENT. Row 1: <130, 90, 1 LEES, 13R BABR, \Upsilon(2S) \to \gamma \tau^+ \tau^- \pi^+ \pi^-

••• We do not use the following data for averages, fits, limits, etc. •••
1 For a narrow scalar a_1^0 with 2m_\tau < M(a_1^0) < 9.2 GeV, which result in a 90% CL upper limits of 0.9 \times 10^-5 at M(a_1^0) = 2m_\tau, \approx 1.5 \times 10^-5 at M(a_1^0) = 7.5 GeV, and 13 \times 10^-5 at M(a_1^0) = 9.2 GeV.

2 For a narrow scalar or pseudoscalar a_1^0 with 2m_\tau < M(a_1^0) < 7.5 GeV, which result in a 90% CL limits ranging from 1 \times 10^-5 at M(a_1^0) = 2m_\tau to 5 \times 10^-5 at M(a_1^0) = 7.5 GeV.

$\Gamma(\gamma a_1^0 \to \gamma \rho^0) / \Gamma_{total}$
($0.5 \text{ GeV} < m < 9.0 \text{ GeV}$) Γ_{125}/Γ

Table with columns: VALUE, CL%, DOCUMENT ID, TECN, COMMENT. Row 1: <1 \times 10^-2, 90, 1 LEES, 13L BABR, \Upsilon(1S) \to \gamma X

1 For a narrow, CP-odd pseudoscalar a_1^0 searched for in 26 hadronic decay modes with invariant mass 0.5 GeV < m_X < 9.0 GeV. Measured 90% CL limit as a function of m_X range from 10^-6 to 10^-2.

$\Gamma(\gamma a_1^0 \to \gamma \rho^0) / \Gamma_{total}$
($0.5 \text{ GeV} < m < 9.0 \text{ GeV}$) Γ_{126}/Γ

Table with columns: VALUE, CL%, DOCUMENT ID, TECN, COMMENT. Row 1: <1 \times 10^-3, 90, 1 LEES, 13L BABR, \Upsilon(1S) \to \gamma X

1 For a narrow, CP-odd pseudoscalar a_1^0 searched for in 14 hadronic decay modes with invariant mass 1.5 GeV < m_X < 9.0 GeV. Measured 90% CL limit as a function of m_X range from 10^-5 to 10^-3.

LEPTON FAMILY NUMBER (LF) VIOLATING MODES

$\Gamma(\mu^+ \tau^-) / \Gamma_{total}$ Γ_{127}/Γ

Table with columns: VALUE (units 10^-6), CL%, DOCUMENT ID, TECN, COMMENT. Row 1: <6.0, 95, LOVE, 08A CLEO, e^+ e^- \to \mu^+ \tau^-

OTHER DECAYS

$\Gamma(\text{invisible}) / \Gamma_{total}$ Γ_{128}/Γ

Table with columns: VALUE (units 10^-4), CL%, DOCUMENT ID, TECN, COMMENT. Row 1: < 3.0, 90, AUBERT, 09AX BABR, \Upsilon(3S) \to \pi^+ \pi^- \Upsilon(1S)

\Upsilon(1S) REFERENCES

Large table listing references for \Upsilon(1S) with columns: Author, Document ID, TECN, Comment. Includes entries like KATRENKO, JIA, LEES, etc.

Table listing references for \Upsilon(1S) and \chi_{b0}(1P) with columns: Author, Document ID, TECN, Comment. Includes entries like KOBEL, BLINOV, FULTON, etc.

\chi_{b0}(1P)

J^G(J^PC) = 0^+(0^+ +)
J needs confirmation.

Observed in radiative decay of the \Upsilon(2S), therefore C = +. Branching ratio requires E1 transition, M1 is strongly disfavored, therefore P = +.

\chi_{b0}(1P) MASS

Table with columns: VALUE (MeV), DOCUMENT ID. Row 1: 9859.44 \pm 0.42 \pm 0.31 OUR EVALUATION

m_{\chi_{b1}(1P)} - m_{\chi_{b0}(1P)}

Table with columns: VALUE (MeV), DOCUMENT ID, TECN, COMMENT. Row 1: 32.49 \pm 0.93, LEES, 14M BABR, \Upsilon(2S) \to \gamma \gamma \mu^+ \mu^-

\gamma ENERGY IN \Upsilon(2S) DECAY

Table with columns: VALUE (MeV), DOCUMENT ID, TECN, COMMENT. Row 1: 162.5 \pm 0.4 OUR AVERAGE

\chi_{b0}(1P) DECAY MODES

Table with columns: Mode, Fraction (\Gamma_i/\Gamma), Confidence level. Row 1: \Gamma_1 \gamma \Upsilon(1S) (1.94 \pm 0.27) %

$\chi_{b0}(1P)$

$\chi_{b0}(1P)$ BRANCHING RATIOS

$\Gamma(\gamma T(1S))/\Gamma_{\text{total}}$						Γ_1/Γ
VALUE (%)	CL%	EVTS	DOCUMENT ID	TECN	COMMENT	
1.94 ± 0.27 OUR AVERAGE						
2.07 ± 0.24 ± 0.21			1,2 LEES	14M BABR	$T(2S) \rightarrow \gamma\gamma\mu^+\mu^-$	
1.76 ± 0.30 ± 0.18	87		3,4 KORNICER	11 CLEO	$e^+e^- \rightarrow \gamma\gamma\ell^+\ell^-$	
••• We do not use the following data for averages, fits, limits, etc. •••						
< 4.6	90		5 LEES	11J BABR	$T(2S) \rightarrow X\gamma$	
< 6	90		WALK	86 CBAL	$T(2S) \rightarrow \gamma\gamma\ell^+\ell^-$	
< 11	90		PAUSS	83 CUSB	$T(2S) \rightarrow \gamma\gamma\ell^+\ell^-$	
1 LEES 14M quotes $\Gamma(\chi_{b0}(1P) \rightarrow \gamma T(1S))/\Gamma_{\text{total}} \times \Gamma(T(2S) \rightarrow \gamma\chi_{b0}(1P))/\Gamma_{\text{total}} = (7.75 \pm 0.91) \times 10^{-4}$ combining the results from samples of $T(2S) \rightarrow \gamma\gamma\mu^+\mu^-$ with and without converted photons. Assumes $B(T(1S) \rightarrow \mu^+\mu^-) = (2.48 \pm 0.05)\%$.						
2 LEES 14M reports $[\Gamma(\chi_{b0}(1P) \rightarrow \gamma T(1S))/\Gamma_{\text{total}}] \times [B(T(2S) \rightarrow \gamma\chi_{b0}(1P))] = (7.75 \pm 0.91) \times 10^{-4}$ which we divide by our best value $B(T(2S) \rightarrow \gamma\chi_{b0}(1P)) = (3.8 \pm 0.4) \times 10^{-2}$. Our first error is their experiment's error and our second error is the systematic error from using our best value.						
3 Assuming $B(T(1S) \rightarrow \ell^+\ell^-) = (2.48 \pm 0.05)\%$.						
4 KORNICER 11 reports $[\Gamma(\chi_{b0}(1P) \rightarrow \gamma T(1S))/\Gamma_{\text{total}}] \times [B(T(2S) \rightarrow \gamma\chi_{b0}(1P))] = (6.59 \pm 0.96 \pm 0.60) \times 10^{-4}$ which we divide by our best value $B(T(2S) \rightarrow \gamma\chi_{b0}(1P)) = (3.8 \pm 0.4) \times 10^{-2}$. Our first error is their experiment's error and our second error is the systematic error from using our best value.						
5 LEES 11J quotes a central value of $\Gamma(\chi_{b0}(1P) \rightarrow \gamma T(1S))/\Gamma_{\text{total}} \times \Gamma(T(2S) \rightarrow \gamma\chi_{b0}(1P))/\Gamma_{\text{total}} = (8.3 \pm 5.6^{+3.7}_{-2.6}) \times 10^{-4}$.						

$\Gamma(D^0 X)/\Gamma_{\text{total}}$						Γ_2/Γ
VALUE	CL%	DOCUMENT ID	TECN	COMMENT		
< 10.4 × 10⁻²	90	6,7 BRIERE	08	CLEO	$T(2S) \rightarrow \gamma D^0 X$	
6 For $p_{D^0} > 2.5 \text{ GeV}/c$.						
7 The authors also present their result as $(5.6 \pm 3.6 \pm 0.5) \times 10^{-2}$.						

$\Gamma(\pi^+\pi^-K^+K^-\pi^0)/\Gamma_{\text{total}}$						Γ_3/Γ
VALUE (units 10 ⁻⁴)	CL%	DOCUMENT ID	TECN	COMMENT		
< 1.6	90	8 ASNER	08A	CLEO	$T(2S) \rightarrow \gamma\pi^+\pi^-K^+K^-\pi^0$	
8 ASNER 08A reports $[\Gamma(\chi_{b0}(1P) \rightarrow \pi^+\pi^-K^+K^-\pi^0)/\Gamma_{\text{total}}] \times [B(T(2S) \rightarrow \gamma\chi_{b0}(1P))] < 6 \times 10^{-6}$ which we divide by our best value $B(T(2S) \rightarrow \gamma\chi_{b0}(1P)) = 3.8 \times 10^{-2}$.						

$\Gamma(2\pi^+\pi^-K^-K_S^0)/\Gamma_{\text{total}}$						Γ_4/Γ
VALUE (units 10 ⁻⁴)	CL%	DOCUMENT ID	TECN	COMMENT		
< 0.5	90	9 ASNER	08A	CLEO	$T(2S) \rightarrow \gamma 2\pi^+\pi^-K^-K_S^0$	
9 ASNER 08A reports $[\Gamma(\chi_{b0}(1P) \rightarrow 2\pi^+\pi^-K^-K_S^0)/\Gamma_{\text{total}}] \times [B(T(2S) \rightarrow \gamma\chi_{b0}(1P))] < 2 \times 10^{-6}$ which we divide by our best value $B(T(2S) \rightarrow \gamma\chi_{b0}(1P)) = 3.8 \times 10^{-2}$.						

$\Gamma(2\pi^+\pi^-K^-K_S^0 2\pi^0)/\Gamma_{\text{total}}$						Γ_5/Γ
VALUE (units 10 ⁻⁴)	CL%	DOCUMENT ID	TECN	COMMENT		
< 5	90	10 ASNER	08A	CLEO	$T(2S) \rightarrow \gamma 2\pi^+\pi^-K^-2\pi^0$	
10 ASNER 08A reports $[\Gamma(\chi_{b0}(1P) \rightarrow 2\pi^+\pi^-K^-K_S^0 2\pi^0)/\Gamma_{\text{total}}] \times [B(T(2S) \rightarrow \gamma\chi_{b0}(1P))] < 18 \times 10^{-6}$ which we divide by our best value $B(T(2S) \rightarrow \gamma\chi_{b0}(1P)) = 3.8 \times 10^{-2}$.						

$\Gamma(2\pi^+2\pi^-2\pi^0)/\Gamma_{\text{total}}$						Γ_6/Γ
VALUE (units 10 ⁻⁴)	CL%	DOCUMENT ID	TECN	COMMENT		
< 2.1	90	11 ASNER	08A	CLEO	$T(2S) \rightarrow \gamma 2\pi^+2\pi^-2\pi^0$	
11 ASNER 08A reports $[\Gamma(\chi_{b0}(1P) \rightarrow 2\pi^+2\pi^-2\pi^0)/\Gamma_{\text{total}}] \times [B(T(2S) \rightarrow \gamma\chi_{b0}(1P))] < 8 \times 10^{-6}$ which we divide by our best value $B(T(2S) \rightarrow \gamma\chi_{b0}(1P)) = 3.8 \times 10^{-2}$.						

$\Gamma(2\pi^+2\pi^-K^+K^-)/\Gamma_{\text{total}}$						Γ_7/Γ
VALUE (units 10 ⁻⁴)	EVTS	DOCUMENT ID	TECN	COMMENT		
1.1 ± 0.6 ± 0.1	7	12 ASNER	08A	CLEO	$T(2S) \rightarrow \gamma 2\pi^+2\pi^-K^+K^-$	
12 ASNER 08A reports $[\Gamma(\chi_{b0}(1P) \rightarrow 2\pi^+2\pi^-K^+K^-)/\Gamma_{\text{total}}] \times [B(T(2S) \rightarrow \gamma\chi_{b0}(1P))] = (4 \pm 2 \pm 1) \times 10^{-6}$ which we divide by our best value $B(T(2S) \rightarrow \gamma\chi_{b0}(1P)) = (3.8 \pm 0.4) \times 10^{-2}$. Our first error is their experiment's error and our second error is the systematic error from using our best value.						

$\Gamma(2\pi^+2\pi^-K^+K^-\pi^0)/\Gamma_{\text{total}}$						Γ_8/Γ
VALUE (units 10 ⁻⁴)	CL%	DOCUMENT ID	TECN	COMMENT		
< 2.7	90	13 ASNER	08A	CLEO	$T(2S) \rightarrow \gamma 2\pi^+2\pi^-K^+K^-\pi^0$	
13 ASNER 08A reports $[\Gamma(\chi_{b0}(1P) \rightarrow 2\pi^+2\pi^-K^+K^-\pi^0)/\Gamma_{\text{total}}] \times [B(T(2S) \rightarrow \gamma\chi_{b0}(1P))] < 10 \times 10^{-6}$ which we divide by our best value $B(T(2S) \rightarrow \gamma\chi_{b0}(1P)) = 3.8 \times 10^{-2}$.						

$\Gamma(2\pi^+2\pi^-K^+K^-2\pi^0)/\Gamma_{\text{total}}$						Γ_9/Γ
VALUE (units 10 ⁻⁴)	CL%	DOCUMENT ID	TECN	COMMENT		
< 5	90	14 ASNER	08A	CLEO	$T(2S) \rightarrow \gamma 2\pi^+2\pi^-K^+K^-2\pi^0$	
14 ASNER 08A reports $[\Gamma(\chi_{b0}(1P) \rightarrow 2\pi^+2\pi^-K^+K^-2\pi^0)/\Gamma_{\text{total}}] \times [B(T(2S) \rightarrow \gamma\chi_{b0}(1P))] < 20 \times 10^{-6}$ which we divide by our best value $B(T(2S) \rightarrow \gamma\chi_{b0}(1P)) = 3.8 \times 10^{-2}$.						

$\Gamma(3\pi^+2\pi^-K^-K_S^0\pi^0)/\Gamma_{\text{total}}$						Γ_{10}/Γ
VALUE (units 10 ⁻⁴)	CL%	DOCUMENT ID	TECN	COMMENT		
< 1.6	90	15 ASNER	08A	CLEO	$T(2S) \rightarrow \gamma 3\pi^+2\pi^-K^-K_S^0\pi^0$	
15 ASNER 08A reports $[\Gamma(\chi_{b0}(1P) \rightarrow 3\pi^+2\pi^-K^-K_S^0\pi^0)/\Gamma_{\text{total}}] \times [B(T(2S) \rightarrow \gamma\chi_{b0}(1P))] < 6 \times 10^{-6}$ which we divide by our best value $B(T(2S) \rightarrow \gamma\chi_{b0}(1P)) = 3.8 \times 10^{-2}$.						

$\Gamma(3\pi^+3\pi^-)/\Gamma_{\text{total}}$						Γ_{11}/Γ
VALUE (units 10 ⁻⁴)	CL%	DOCUMENT ID	TECN	COMMENT		
< 0.8	90	16 ASNER	08A	CLEO	$T(2S) \rightarrow \gamma 3\pi^+3\pi^-$	
16 ASNER 08A reports $[\Gamma(\chi_{b0}(1P) \rightarrow 3\pi^+3\pi^-)/\Gamma_{\text{total}}] \times [B(T(2S) \rightarrow \gamma\chi_{b0}(1P))] < 3 \times 10^{-6}$ which we divide by our best value $B(T(2S) \rightarrow \gamma\chi_{b0}(1P)) = 3.8 \times 10^{-2}$.						

$\Gamma(3\pi^+3\pi^-2\pi^0)/\Gamma_{\text{total}}$						Γ_{12}/Γ
VALUE (units 10 ⁻⁴)	CL%	DOCUMENT ID	TECN	COMMENT		
< 6	90	17 ASNER	08A	CLEO	$T(2S) \rightarrow \gamma 3\pi^+3\pi^-2\pi^0$	
17 ASNER 08A reports $[\Gamma(\chi_{b0}(1P) \rightarrow 3\pi^+3\pi^-2\pi^0)/\Gamma_{\text{total}}] \times [B(T(2S) \rightarrow \gamma\chi_{b0}(1P))] < 22 \times 10^{-6}$ which we divide by our best value $B(T(2S) \rightarrow \gamma\chi_{b0}(1P)) = 3.8 \times 10^{-2}$.						

$\Gamma(3\pi^+3\pi^-K^+K^-)/\Gamma_{\text{total}}$						Γ_{13}/Γ
VALUE (units 10 ⁻⁴)	EVTS	DOCUMENT ID	TECN	COMMENT		
2.4 ± 1.2 ± 0.2	9	18 ASNER	08A	CLEO	$T(2S) \rightarrow \gamma 3\pi^+3\pi^-K^+K^-$	
18 ASNER 08A reports $[\Gamma(\chi_{b0}(1P) \rightarrow 3\pi^+3\pi^-K^+K^-)/\Gamma_{\text{total}}] \times [B(T(2S) \rightarrow \gamma\chi_{b0}(1P))] = (9 \pm 4 \pm 2) \times 10^{-6}$ which we divide by our best value $B(T(2S) \rightarrow \gamma\chi_{b0}(1P)) = (3.8 \pm 0.4) \times 10^{-2}$. Our first error is their experiment's error and our second error is the systematic error from using our best value.						

$\Gamma(3\pi^+3\pi^-K^+K^-\pi^0)/\Gamma_{\text{total}}$						Γ_{14}/Γ
VALUE (units 10 ⁻⁴)	CL%	DOCUMENT ID	TECN	COMMENT		
< 10	90	19 ASNER	08A	CLEO	$T(2S) \rightarrow \gamma 3\pi^+3\pi^-K^+K^-\pi^0$	
19 ASNER 08A reports $[\Gamma(\chi_{b0}(1P) \rightarrow 3\pi^+3\pi^-K^+K^-\pi^0)/\Gamma_{\text{total}}] \times [B(T(2S) \rightarrow \gamma\chi_{b0}(1P))] < 37 \times 10^{-6}$ which we divide by our best value $B(T(2S) \rightarrow \gamma\chi_{b0}(1P)) = 3.8 \times 10^{-2}$.						

$\Gamma(4\pi^+4\pi^-)/\Gamma_{\text{total}}$						Γ_{15}/Γ
VALUE (units 10 ⁻⁴)	CL%	DOCUMENT ID	TECN	COMMENT		
< 0.8	90	20 ASNER	08A	CLEO	$T(2S) \rightarrow \gamma 4\pi^+4\pi^-$	
20 ASNER 08A reports $[\Gamma(\chi_{b0}(1P) \rightarrow 4\pi^+4\pi^-)/\Gamma_{\text{total}}] \times [B(T(2S) \rightarrow \gamma\chi_{b0}(1P))] < 3 \times 10^{-6}$ which we divide by our best value $B(T(2S) \rightarrow \gamma\chi_{b0}(1P)) = 3.8 \times 10^{-2}$.						

$\Gamma(4\pi^+4\pi^-2\pi^0)/\Gamma_{\text{total}}$						Γ_{16}/Γ
VALUE (units 10 ⁻⁴)	CL%	DOCUMENT ID	TECN	COMMENT		
< 21	90	21 ASNER	08A	CLEO	$T(2S) \rightarrow \gamma 4\pi^+4\pi^-2\pi^0$	
21 ASNER 08A reports $[\Gamma(\chi_{b0}(1P) \rightarrow 4\pi^+4\pi^-2\pi^0)/\Gamma_{\text{total}}] \times [B(T(2S) \rightarrow \gamma\chi_{b0}(1P))] < 77 \times 10^{-6}$ which we divide by our best value $B(T(2S) \rightarrow \gamma\chi_{b0}(1P)) = 3.8 \times 10^{-2}$.						

$\Gamma(J/\psi J/\psi)/\Gamma_{\text{total}}$						Γ_{17}/Γ
VALUE (units 10 ⁻⁵)	CL%	DOCUMENT ID	TECN	COMMENT		
< 7	90	22 SHEN	12	BELL	$T(2S) \rightarrow \gamma\psi X$	
22 SHEN 12 reports $< 7.1 \times 10^{-5}$ from a measurement of $[\Gamma(\chi_{b0}(1P) \rightarrow J/\psi J/\psi)/\Gamma_{\text{total}}] \times [B(T(2S) \rightarrow \gamma\chi_{b0}(1P))] \times [B(T(2S) \rightarrow \gamma\chi_{b0}(1P))] \times [B(T(2S) \rightarrow \gamma\chi_{b0}(1P))] = (3.8 \pm 0.4) \times 10^{-2}$.						

$\Gamma(J/\psi\psi(2S))/\Gamma_{\text{total}}$						Γ_{18}/Γ
VALUE (units 10 ⁻⁵)	CL%	DOCUMENT ID	TECN	COMMENT		
< 12	90	23 SHEN	12	BELL	$T(2S) \rightarrow \gamma\psi X$	
23 SHEN 12 reports $< 12 \times 10^{-5}$ from a measurement of $[\Gamma(\chi_{b0}(1P) \rightarrow J/\psi\psi(2S))/\Gamma_{\text{total}}] \times [B(T(2S) \rightarrow \gamma\chi_{b0}(1P))] \times [B(T(2S) \rightarrow \gamma\chi_{b0}(1P))] \times [B(T(2S) \rightarrow \gamma\chi_{b0}(1P))] = (3.8 \pm 0.4) \times 10^{-2}$.						

$\Gamma(\psi(2S)\psi(2S))/\Gamma_{\text{total}}$						Γ_{19}/Γ
VALUE (units 10 ⁻⁵)	CL%	DOCUMENT ID	TECN	COMMENT		
< 3.1	90	24 SHEN	12	BELL	$T(2S) \rightarrow \gamma\psi X$	
24 SHEN 12 reports $< 3.1 \times 10^{-5}$ from a measurement of $[\Gamma(\chi_{b0}(1P) \rightarrow \psi(2S)\psi(2S))/\Gamma_{\text{total}}] \times [B(T(2S) \rightarrow \gamma\chi_{b0}(1P))] \times [B(T(2S) \rightarrow \gamma\chi_{b0}(1P))] \times [B(T(2S) \rightarrow \gamma\chi_{b0}(1P))] = (3.8 \pm 0.4) \times 10^{-2}$.						

$\Gamma(J/\psi(1S) \text{ anything})/\Gamma_{\text{total}}$						Γ_{20}/Γ
VALUE	CL%	DOCUMENT ID	TECN	COMMENT		
< 2.3 × 10⁻³	90	JIA	17A	BELL	$e^+e^- \rightarrow \text{hadrons}$	

$\chi_{b0}(1P)$ CROSS-PARTICLE BRANCHING RATIOS

$\Gamma(\chi_{b0}(1P) \rightarrow \gamma T(1S))/\Gamma_{\text{total}} \times \Gamma(T(2S) \rightarrow \gamma\chi_{b0}(1P))/\Gamma_{\text{total}}$						$\Gamma_1/\Gamma \times \Gamma_{61}^{T(2S)}/\Gamma T(2S)$
VALUE	CL%	DOCUMENT ID	TECN	COMMENT		
< 1.7 × 10⁻³	90	25 LEES	11J	BABR	$T(2S) \rightarrow X\gamma$	
25 LEES 11J quotes a central value of $\Gamma(\chi_{b0}(1P) \rightarrow \gamma T(1S))/\Gamma_{\text{total}} \times \Gamma(T(2S) \rightarrow \gamma\chi_{b0}(1P))/\Gamma_{\text{total}} = (8.3 \pm 5.6^{+3.7}_{-2.6}) \times 10^{-4}$ and derives a 90% CL upper limit of $\Gamma(\gamma T(1S))/\Gamma_{\text{total}} < 4.6\%$ using $B(T(2S) \rightarrow \gamma\chi_{b0}(1P)) = (3.8 \pm 0.4)\%$.						

Meson Particle Listings

$\chi_{b0}(1P), \chi_{b1}(1P)$

$B(\chi_{b0}(1P) \rightarrow \gamma T(1S)) \times B(T(2S) \rightarrow \gamma \chi_{b0}(1P)) \times B(T(1S) \rightarrow \ell^+ \ell^-)$

VALUE (units 10^{-5})	EVTS	DOCUMENT ID	TECN	COMMENT
1.67 ± 0.28	OUR AVERAGE			

2.9	$\frac{+1.7}{-1.4} \frac{+0.1}{-0.8}$	²⁶ LEES	14M BABR	$T(2S) \rightarrow \gamma \gamma \mu^+ \mu^-$
1.63	$\pm 0.24 \pm 0.15$	87 KORNICER	11 CLEO	$e^+ e^- \rightarrow \gamma \gamma \ell^+ \ell^-$

²⁶ From a sample of $T(2S) \rightarrow \gamma \gamma \mu^+ \mu^-$ with one converted photon.

$[B(\chi_{b0}(1P) \rightarrow \gamma T(1S)) \times B(T(2S) \rightarrow \gamma \chi_{b0}(1P))] / [B(\chi_{b1}(1P) \rightarrow \gamma T(1S)) \times B(T(2S) \rightarrow \gamma \chi_{b1}(1P))]$

VALUE (%)	DOCUMENT ID	TECN	COMMENT
3.28 ± 0.37	²⁷ LEES	14M BABR	$T(2S) \rightarrow \gamma \gamma \mu^+ \mu^-$

²⁷ From a sample of $T(2S) \rightarrow \gamma \gamma \mu^+ \mu^-$ without converted photons.

$\chi_{b0}(1P)$ REFERENCES

JIA	17A	PR D96 112002	S. Jia et al.	(BELLE Collab.)
LEES	14M	PR D90 112010	J.P. Lees et al.	(BABAR Collab.)
SHEN	12	PR D85 071102	C.P. Shen et al.	(BELLE Collab.)
KORNICER	11	PR D83 054003	M. Kornicer et al.	(CLEO Collab.)
LEES	11J	PR D84 072002	J.P. Lees et al.	(BABAR Collab.)
ASNER	08A	PR D78 091103	D.M. Asner et al.	(CLEO Collab.)
BRIERE	08	PR D78 092007	R.A. Briere et al.	(CLEO Collab.)
ARTUSO	05	PRL 94 032001	M. Artuso et al.	(CLEO Collab.)
EDWARDS	99	PR D59 032003	K.W. Edwards et al.	(CLEO Collab.)
WALK	86	PR D34 2611	W.S. Walk et al.	(Crystal Ball Collab.)
ALBRECHT	85E	PL 160B 331	H. Albrecht et al.	(ARGUS Collab.)
NERNST	85	PRL 54 2195	R. Nernst et al.	(Crystal Ball Collab.)
HAAS	84	PRL 52 799	J. Haas et al.	(CLEO Collab.)
KLOPFEN...	83	PRL 51 160	C. Klopfenstein et al.	(CUSB Collab.)
PAUSS	83	PL 130B 439	F. Pauss et al.	(MPIM, COLU, CORN, LSU+)

$\chi_{b1}(1P)$

$$I^G(JPC) = 0^+(1^{++})$$

J needs confirmation.

Observed in radiative decay of the $T(2S)$, therefore $C = +$. Branching ratio requires E1 transition. M1 is strongly disfavored, therefore $P = +$. $J = 1$ from SKWARNICKI 87.

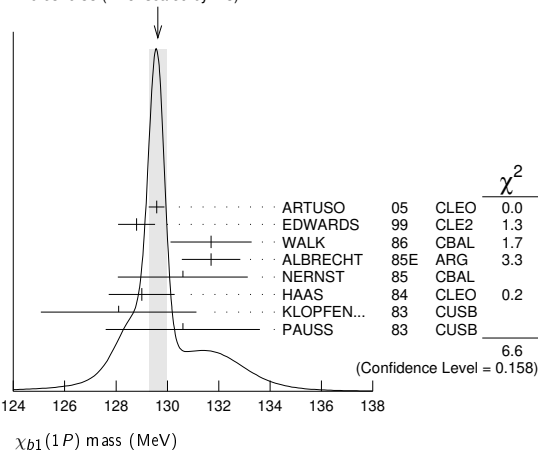
$\chi_{b1}(1P)$ MASS

VALUE (MeV)	DOCUMENT ID	COMMENT
$9892.78 \pm 0.26 \pm 0.31$	OUR EVALUATION	From average γ energy below, using $T(2S)$ mass = 10023.26 ± 0.31 MeV

γ ENERGY IN $T(2S)$ DECAY

VALUE (MeV)	DOCUMENT ID	TECN	COMMENT
129.63 ± 0.33	OUR AVERAGE		Error includes scale factor of 1.3. See the ideogram below.
129.58	$\pm 0.09 \pm 0.29$	ARTUSO 05	CLEO $T(2S) \rightarrow \gamma X$
128.8	$\pm 0.4 \pm 0.6$	EDWARDS 99	CLE2 $T(2S) \rightarrow \gamma \chi(1P)$
131.7	$\pm 0.9 \pm 1.3$	WALK 86	CBAL $T(2S) \rightarrow \gamma \gamma \ell^+ \ell^-$
131.7	$\pm 0.3 \pm 1.1$	ALBRECHT 85E	ARG $T(2S) \rightarrow \text{conv. } \gamma X$
130.6	$\pm 0.8 \pm 2.4$	NERNST 85	CBAL $T(2S) \rightarrow \gamma X$
129	$\pm 0.8 \pm 1$	HAAS 84	CLEO $T(2S) \rightarrow \text{conv. } \gamma X$
128.1	$\pm 0.4 \pm 3.0$	KLOPFEN... 83	CUSB $T(2S) \rightarrow \gamma X$
130.6	± 3.0	PAUSS 83	CUSB $T(2S) \rightarrow \gamma \gamma \ell^+ \ell^-$

WEIGHTED AVERAGE
 129.63 ± 0.33 (Error scaled by 1.3)



$\chi_{b1}(1P)$ DECAY MODES

Mode	Fraction (Γ_i/Γ)	Confidence level
Γ_1 $\gamma T(1S)$	$(35.2 \pm 2.0) \%$	
Γ_2 $D^0 X$	$(12.6 \pm 2.2) \%$	
Γ_3 $\pi^+ \pi^- K^+ K^- \pi^0$	$(2.0 \pm 0.6) \times 10^{-4}$	
Γ_4 $2\pi^+ \pi^- K^- K_S^0$	$(1.3 \pm 0.5) \times 10^{-4}$	
Γ_5 $2\pi^+ \pi^- K^- K_S^0 2\pi^0$	$< 6 \times 10^{-4}$	90%
Γ_6 $2\pi^+ 2\pi^- 2\pi^0$	$(8.0 \pm 2.5) \times 10^{-4}$	
Γ_7 $2\pi^+ 2\pi^- K^+ K^-$	$(1.5 \pm 0.5) \times 10^{-4}$	
Γ_8 $2\pi^+ 2\pi^- K^+ K^- \pi^0$	$(3.5 \pm 1.2) \times 10^{-4}$	
Γ_9 $2\pi^+ 2\pi^- K^+ K^- 2\pi^0$	$(8.6 \pm 3.2) \times 10^{-4}$	
Γ_{10} $3\pi^+ 2\pi^- K^- K_S^0 \pi^0$	$(9.3 \pm 3.3) \times 10^{-4}$	
Γ_{11} $3\pi^+ 3\pi^-$	$(1.9 \pm 0.6) \times 10^{-4}$	
Γ_{12} $3\pi^+ 3\pi^- 2\pi^0$	$(1.7 \pm 0.5) \times 10^{-3}$	
Γ_{13} $3\pi^+ 3\pi^- K^+ K^-$	$(2.6 \pm 0.8) \times 10^{-4}$	
Γ_{14} $3\pi^+ 3\pi^- K^+ K^- \pi^0$	$(7.5 \pm 2.6) \times 10^{-4}$	
Γ_{15} $4\pi^+ 4\pi^-$	$(2.6 \pm 0.9) \times 10^{-4}$	
Γ_{16} $4\pi^+ 4\pi^- 2\pi^0$	$(1.4 \pm 0.6) \times 10^{-3}$	
Γ_{17} ω anything	$(4.9 \pm 1.4) \%$	
Γ_{18} ωX_{tetra}	$< 4.44 \times 10^{-4}$	90%
Γ_{19} $J/\psi J/\psi$	$< 2.7 \times 10^{-5}$	90%
Γ_{20} $J/\psi \psi(2S)$	$< 1.7 \times 10^{-5}$	90%
Γ_{21} $\psi(2S) \psi(2S)$	$< 6 \times 10^{-5}$	90%
Γ_{22} $J/\psi(1S)$ anything	$< 1.1 \times 10^{-3}$	90%
Γ_{23} $J/\psi(1S) X_{tetra}$	$< 2.27 \times 10^{-4}$	90%

$\chi_{b1}(1P)$ BRANCHING RATIOS

VALUE	EVTS	DOCUMENT ID	TECN	COMMENT	Γ_i/Γ
0.352 ± 0.020	OUR AVERAGE				
0.356	$\frac{+0.016}{-0.022} \pm 0.019$	964k ¹ FULSOM	18 BELL	$T(2S) \rightarrow \gamma X$	
0.364	$\pm 0.017 \pm 0.019$	2,3,4 LEES	14M BABR	$T(2S) \rightarrow \gamma \gamma \mu^+ \mu^-$	
0.331	$\pm 0.018 \pm 0.017$	3222 ^{4,5} KORNICER	11 CLEO	$e^+ e^- \rightarrow \gamma \gamma \ell^+ \ell^-$	
0.350	$\pm 0.023 \pm 0.018$	13k ⁶ LEES	11J BABR	$T(2S) \rightarrow \gamma X$	
0.34	$\pm 0.07 \pm 0.02$	53 ^{4,7,8} WALK	86 CBAL	$T(2S) \rightarrow \gamma \gamma \ell^+ \ell^-$	
0.47	± 0.18	KLOPFEN... 83	CUSB	$T(2S) \rightarrow \gamma \gamma \ell^+ \ell^-$	

- ¹ FULSOM 18 reports $[\Gamma(\chi_{b1}(1P) \rightarrow \gamma T(1S))/\Gamma_{\text{total}}] \times [B(T(2S) \rightarrow \gamma \chi_{b1}(1P))]$ = $(2.45 \pm 0.02 \pm \frac{0.11}{0.15}) \times 10^{-2}$ which we divide by our best value $B(T(2S) \rightarrow \gamma \chi_{b1}(1P)) = (6.9 \pm 0.4) \times 10^{-2}$. Our first error is their experiment's error and our second error is the systematic error from using our best value.
- ² LEES 14M quotes $\Gamma(\chi_{b1}(1P) \rightarrow \gamma T(1S))/\Gamma_{\text{total}} \times \Gamma(T(2S) \rightarrow \gamma \chi_{b1}(1P))/\Gamma_{\text{total}} = (2.51 \pm 0.12) \%$ combining the results from samples of $T(2S) \rightarrow \gamma \gamma \mu^+ \mu^-$ with and without converted photons.
- ³ LEES 14M reports $[\Gamma(\chi_{b1}(1P) \rightarrow \gamma T(1S))/\Gamma_{\text{total}}] \times [B(T(2S) \rightarrow \gamma \chi_{b1}(1P))]$ = $(2.51 \pm 0.12) \times 10^{-2}$ which we divide by our best value $B(T(2S) \rightarrow \gamma \chi_{b1}(1P)) = (6.9 \pm 0.4) \times 10^{-2}$. Our first error is their experiment's error and our second error is the systematic error from using our best value.
- ⁴ Assuming $B(T(1S) \rightarrow \mu^+ \mu^-) = (2.48 \pm 0.05) \%$.
- ⁵ KORNICER 11 reports $[\Gamma(\chi_{b1}(1P) \rightarrow \gamma T(1S))/\Gamma_{\text{total}}] \times [B(T(2S) \rightarrow \gamma \chi_{b1}(1P))]$ = $(22.8 \pm 0.4 \pm 1.2) \times 10^{-3}$ which we divide by our best value $B(T(2S) \rightarrow \gamma \chi_{b1}(1P)) = (6.9 \pm 0.4) \times 10^{-2}$. Our first error is their experiment's error and our second error is the systematic error from using our best value.
- ⁶ LEES 11J reports $[\Gamma(\chi_{b1}(1P) \rightarrow \gamma T(1S))/\Gamma_{\text{total}}] \times [B(T(2S) \rightarrow \gamma \chi_{b1}(1P))]$ = $(24.1 \pm 0.6 \pm 1.5) \times 10^{-3}$ which we divide by our best value $B(T(2S) \rightarrow \gamma \chi_{b1}(1P)) = (6.9 \pm 0.4) \times 10^{-2}$. Our first error is their experiment's error and our second error is the systematic error from using our best value.
- ⁷ WALK 86 quotes $B(T(2S) \rightarrow \gamma \chi_{b1}(1P)) \times B(\chi_{b1}(1P) \rightarrow \gamma T(1S)) \times B(T(1S) \rightarrow \ell^+ \ell^-) = (5.8 \pm 0.9 \pm 0.7) \%$.
- ⁸ WALK 86 reports $[\Gamma(\chi_{b1}(1P) \rightarrow \gamma T(1S))/\Gamma_{\text{total}}] \times [B(T(2S) \rightarrow \gamma \chi_{b1}(1P))]$ = $(23.4 \pm 3.63 \pm 2.82) \times 10^{-3}$ which we divide by our best value $B(T(2S) \rightarrow \gamma \chi_{b1}(1P)) = (6.9 \pm 0.4) \times 10^{-2}$. Our first error is their experiment's error and our second error is the systematic error from using our best value.

VALUE (units 10^{-2})	EVTS	DOCUMENT ID	TECN	COMMENT	Γ_2/Γ
$12.6 \pm 1.9 \pm 1.1$	2310	¹ BRIERE 08	CLEO	$T(2S) \rightarrow \gamma D^0 X$	

¹ For $p_{D^0} > 2.5$ GeV/c.

VALUE (units 10^{-4})	EVTS	DOCUMENT ID	TECN	COMMENT	Γ_3/Γ
$2.0 \pm 0.6 \pm 0.1$	18	¹ ASNER 08A	CLEO	$T(2S) \rightarrow \gamma \pi^+ \pi^- K^+ K^- \pi^0$	

- ¹ ASNER 08A reports $[\Gamma(\chi_{b1}(1P) \rightarrow \pi^+ \pi^- K^+ K^- \pi^0)/\Gamma_{\text{total}}] \times [B(T(2S) \rightarrow \gamma \chi_{b1}(1P))]$ = $(14 \pm 3 \pm 3) \times 10^{-6}$ which we divide by our best value $B(T(2S) \rightarrow \gamma \chi_{b1}(1P)) = (6.9 \pm 0.4) \times 10^{-2}$. Our first error is their experiment's error and our second error is the systematic error from using our best value.

$\Gamma(2\pi^+\pi^-K^-K_S^0)/\Gamma_{total}$ Γ_4/Γ

VALUE (units 10^{-4})	EVTS	DOCUMENT ID	TECN	COMMENT
1.3±0.5±0.1	11	¹ ASNER	08A CLEO	$\Upsilon(2S) \rightarrow \gamma 2\pi^+\pi^-K^-K_S^0$
¹ ASNER 08A reports $[\Gamma(\chi_{b1}(1P) \rightarrow 2\pi^+\pi^-K^-K_S^0)/\Gamma_{total}] \times [B(\Upsilon(2S) \rightarrow \gamma\chi_{b1}(1P))]$ = $(9 \pm 3 \pm 2) \times 10^{-6}$ which we divide by our best value $B(\Upsilon(2S) \rightarrow \gamma\chi_{b1}(1P)) = (6.9 \pm 0.4) \times 10^{-2}$. Our first error is their experiment's error and our second error is the systematic error from using our best value.				

$\Gamma(2\pi^+\pi^-K^-K_S^0 2\pi^0)/\Gamma_{total}$ Γ_5/Γ

VALUE (units 10^{-4})	CL%	DOCUMENT ID	TECN	COMMENT
<6	90	¹ ASNER	08A CLEO	$\Upsilon(2S) \rightarrow \gamma 2\pi^+\pi^-K^-2\pi^0$
¹ ASNER 08A reports $[\Gamma(\chi_{b1}(1P) \rightarrow 2\pi^+\pi^-K^-K_S^0 2\pi^0)/\Gamma_{total}] \times [B(\Upsilon(2S) \rightarrow \gamma\chi_{b1}(1P))]$ < 42×10^{-6} which we divide by our best value $B(\Upsilon(2S) \rightarrow \gamma\chi_{b1}(1P)) = 6.9 \times 10^{-2}$.				

$\Gamma(2\pi^+2\pi^-2\pi^0)/\Gamma_{total}$ Γ_6/Γ

VALUE (units 10^{-4})	EVTS	DOCUMENT ID	TECN	COMMENT
8.0±2.4±0.4	46	¹ ASNER	08A CLEO	$\Upsilon(2S) \rightarrow \gamma 2\pi^+2\pi^-2\pi^0$
¹ ASNER 08A reports $[\Gamma(\chi_{b1}(1P) \rightarrow 2\pi^+2\pi^-2\pi^0)/\Gamma_{total}] \times [B(\Upsilon(2S) \rightarrow \gamma\chi_{b1}(1P))]$ = $(55 \pm 9 \pm 14) \times 10^{-6}$ which we divide by our best value $B(\Upsilon(2S) \rightarrow \gamma\chi_{b1}(1P)) = (6.9 \pm 0.4) \times 10^{-2}$. Our first error is their experiment's error and our second error is the systematic error from using our best value.				

$\Gamma(2\pi^+2\pi^-K^+K^-)/\Gamma_{total}$ Γ_7/Γ

VALUE (units 10^{-4})	EVTS	DOCUMENT ID	TECN	COMMENT
1.5±0.5±0.1	18	¹ ASNER	08A CLEO	$\Upsilon(2S) \rightarrow \gamma 2\pi^+2\pi^-K^+K^-$
¹ ASNER 08A reports $[\Gamma(\chi_{b1}(1P) \rightarrow 2\pi^+2\pi^-K^+K^-)/\Gamma_{total}] \times [B(\Upsilon(2S) \rightarrow \gamma\chi_{b1}(1P))]$ = $(10 \pm 3 \pm 2) \times 10^{-6}$ which we divide by our best value $B(\Upsilon(2S) \rightarrow \gamma\chi_{b1}(1P)) = (6.9 \pm 0.4) \times 10^{-2}$. Our first error is their experiment's error and our second error is the systematic error from using our best value.				

$\Gamma(2\pi^+2\pi^-K^+K^-\pi^0)/\Gamma_{total}$ Γ_8/Γ

VALUE (units 10^{-4})	EVTS	DOCUMENT ID	TECN	COMMENT
3.5±1.2±0.2	22	¹ ASNER	08A CLEO	$\Upsilon(2S) \rightarrow \gamma 2\pi^+2\pi^-K^+K^-\pi^0$
¹ ASNER 08A reports $[\Gamma(\chi_{b1}(1P) \rightarrow 2\pi^+2\pi^-K^+K^-\pi^0)/\Gamma_{total}] \times [B(\Upsilon(2S) \rightarrow \gamma\chi_{b1}(1P))]$ = $(24 \pm 6 \pm 6) \times 10^{-6}$ which we divide by our best value $B(\Upsilon(2S) \rightarrow \gamma\chi_{b1}(1P)) = (6.9 \pm 0.4) \times 10^{-2}$. Our first error is their experiment's error and our second error is the systematic error from using our best value.				

$\Gamma(2\pi^+2\pi^-K^+K^-2\pi^0)/\Gamma_{total}$ Γ_9/Γ

VALUE (units 10^{-4})	EVTS	DOCUMENT ID	TECN	COMMENT
8.6±3.2±0.4	26	¹ ASNER	08A CLEO	$\Upsilon(2S) \rightarrow \gamma 2\pi^+2\pi^-K^+K^-2\pi^0$
¹ ASNER 08A reports $[\Gamma(\chi_{b1}(1P) \rightarrow 2\pi^+2\pi^-K^+K^-2\pi^0)/\Gamma_{total}] \times [B(\Upsilon(2S) \rightarrow \gamma\chi_{b1}(1P))]$ = $(59 \pm 14 \pm 17) \times 10^{-6}$ which we divide by our best value $B(\Upsilon(2S) \rightarrow \gamma\chi_{b1}(1P)) = (6.9 \pm 0.4) \times 10^{-2}$. Our first error is their experiment's error and our second error is the systematic error from using our best value.				

$\Gamma(3\pi^+2\pi^-K^-K_S^0\pi^0)/\Gamma_{total}$ Γ_{10}/Γ

VALUE (units 10^{-4})	EVTS	DOCUMENT ID	TECN	COMMENT
9.3±3.3±0.5	21	¹ ASNER	08A CLEO	$\Upsilon(2S) \rightarrow \gamma 3\pi^+2\pi^-K^-K_S^0\pi^0$
¹ ASNER 08A reports $[\Gamma(\chi_{b1}(1P) \rightarrow 3\pi^+2\pi^-K^-K_S^0\pi^0)/\Gamma_{total}] \times [B(\Upsilon(2S) \rightarrow \gamma\chi_{b1}(1P))]$ = $(64 \pm 16 \pm 16) \times 10^{-6}$ which we divide by our best value $B(\Upsilon(2S) \rightarrow \gamma\chi_{b1}(1P)) = (6.9 \pm 0.4) \times 10^{-2}$. Our first error is their experiment's error and our second error is the systematic error from using our best value.				

$\Gamma(3\pi^+3\pi^-)/\Gamma_{total}$ Γ_{11}/Γ

VALUE (units 10^{-4})	EVTS	DOCUMENT ID	TECN	COMMENT
1.9±0.6±0.1	25	¹ ASNER	08A CLEO	$\Upsilon(2S) \rightarrow \gamma 3\pi^+3\pi^-$
¹ ASNER 08A reports $[\Gamma(\chi_{b1}(1P) \rightarrow 3\pi^+3\pi^-)/\Gamma_{total}] \times [B(\Upsilon(2S) \rightarrow \gamma\chi_{b1}(1P))]$ = $(13 \pm 3 \pm 3) \times 10^{-6}$ which we divide by our best value $B(\Upsilon(2S) \rightarrow \gamma\chi_{b1}(1P)) = (6.9 \pm 0.4) \times 10^{-2}$. Our first error is their experiment's error and our second error is the systematic error from using our best value.				

$\Gamma(3\pi^+3\pi^-2\pi^0)/\Gamma_{total}$ Γ_{12}/Γ

VALUE (units 10^{-4})	EVTS	DOCUMENT ID	TECN	COMMENT
17±5±1	56	¹ ASNER	08A CLEO	$\Upsilon(2S) \rightarrow \gamma 3\pi^+3\pi^-2\pi^0$
¹ ASNER 08A reports $[\Gamma(\chi_{b1}(1P) \rightarrow 3\pi^+3\pi^-2\pi^0)/\Gamma_{total}] \times [B(\Upsilon(2S) \rightarrow \gamma\chi_{b1}(1P))]$ = $(119 \pm 18 \pm 32) \times 10^{-6}$ which we divide by our best value $B(\Upsilon(2S) \rightarrow \gamma\chi_{b1}(1P)) = (6.9 \pm 0.4) \times 10^{-2}$. Our first error is their experiment's error and our second error is the systematic error from using our best value.				

$\Gamma(3\pi^+3\pi^-K^+K^-)/\Gamma_{total}$ Γ_{13}/Γ

VALUE (units 10^{-4})	EVTS	DOCUMENT ID	TECN	COMMENT
2.6±0.8±0.1	21	¹ ASNER	08A CLEO	$\Upsilon(2S) \rightarrow \gamma 3\pi^+3\pi^-K^+K^-$
¹ ASNER 08A reports $[\Gamma(\chi_{b1}(1P) \rightarrow 3\pi^+3\pi^-K^+K^-)/\Gamma_{total}] \times [B(\Upsilon(2S) \rightarrow \gamma\chi_{b1}(1P))]$ = $(18 \pm 4 \pm 4) \times 10^{-6}$ which we divide by our best value $B(\Upsilon(2S) \rightarrow \gamma\chi_{b1}(1P)) = (6.9 \pm 0.4) \times 10^{-2}$. Our first error is their experiment's error and our second error is the systematic error from using our best value.				

$\Gamma(3\pi^+3\pi^-K^+K^-\pi^0)/\Gamma_{total}$ Γ_{14}/Γ

VALUE (units 10^{-4})	EVTS	DOCUMENT ID	TECN	COMMENT
7.5±2.6±0.4	28	¹ ASNER	08A CLEO	$\Upsilon(2S) \rightarrow \gamma 3\pi^+3\pi^-K^+K^-\pi^0$
¹ ASNER 08A reports $[\Gamma(\chi_{b1}(1P) \rightarrow 3\pi^+3\pi^-K^+K^-\pi^0)/\Gamma_{total}] \times [B(\Upsilon(2S) \rightarrow \gamma\chi_{b1}(1P))]$ = $(52 \pm 11 \pm 14) \times 10^{-6}$ which we divide by our best value $B(\Upsilon(2S) \rightarrow \gamma\chi_{b1}(1P)) = (6.9 \pm 0.4) \times 10^{-2}$. Our first error is their experiment's error and our second error is the systematic error from using our best value.				

$\Gamma(4\pi^+4\pi^-)/\Gamma_{total}$ Γ_{15}/Γ

VALUE (units 10^{-4})	EVTS	DOCUMENT ID	TECN	COMMENT
2.6±0.9±0.1	24	¹ ASNER	08A CLEO	$\Upsilon(2S) \rightarrow \gamma 4\pi^+4\pi^-$
¹ ASNER 08A reports $[\Gamma(\chi_{b1}(1P) \rightarrow 4\pi^+4\pi^-)/\Gamma_{total}] \times [B(\Upsilon(2S) \rightarrow \gamma\chi_{b1}(1P))]$ = $(18 \pm 4 \pm 5) \times 10^{-6}$ which we divide by our best value $B(\Upsilon(2S) \rightarrow \gamma\chi_{b1}(1P)) = (6.9 \pm 0.4) \times 10^{-2}$. Our first error is their experiment's error and our second error is the systematic error from using our best value.				

$\Gamma(4\pi^+4\pi^-2\pi^0)/\Gamma_{total}$ Γ_{16}/Γ

VALUE (units 10^{-4})	EVTS	DOCUMENT ID	TECN	COMMENT
14±5±1	26	¹ ASNER	08A CLEO	$\Upsilon(2S) \rightarrow \gamma 4\pi^+4\pi^-2\pi^0$
¹ ASNER 08A reports $[\Gamma(\chi_{b1}(1P) \rightarrow 4\pi^+4\pi^-2\pi^0)/\Gamma_{total}] \times [B(\Upsilon(2S) \rightarrow \gamma\chi_{b1}(1P))]$ = $(96 \pm 24 \pm 29) \times 10^{-6}$ which we divide by our best value $B(\Upsilon(2S) \rightarrow \gamma\chi_{b1}(1P)) = (6.9 \pm 0.4) \times 10^{-2}$. Our first error is their experiment's error and our second error is the systematic error from using our best value.				

$\Gamma(\omega \text{ anything})/\Gamma_{total}$ Γ_{17}/Γ

VALUE (units 10^{-2})	EVTS	DOCUMENT ID	TECN	COMMENT
4.9±1.3±0.6	51k	JIA	17A BELL	$e^+e^- \rightarrow \text{hadrons}$

$\Gamma(\omega X_{tetra})/\Gamma_{total}$ Γ_{18}/Γ

VALUE	CL%	DOCUMENT ID	TECN	COMMENT
<44.4 × 10⁻⁵	90	¹ JIA	17A BELL	$e^+e^- \rightarrow \text{hadrons}$
¹ For a tetraquark state X_{tetra} , with mass in the range 1.16–2.46 GeV and width in the range 0–0.3 GeV. Measured 90% CL limits as a function of X_{tetra} mass and width range from 3.3×10^{-5} to 44.4×10^{-5} .				

$\Gamma(J/\psi J/\psi)/\Gamma_{total}$ Γ_{19}/Γ

VALUE (units 10^{-5})	CL%	DOCUMENT ID	TECN	COMMENT
<2.7	90	¹ SHEN	12 BELL	$\Upsilon(2S) \rightarrow \gamma\psi X$
¹ SHEN 12 reports < 2.7×10^{-5} from a measurement of $[\Gamma(\chi_{b1}(1P) \rightarrow J/\psi J/\psi)/\Gamma_{total}] \times [B(\Upsilon(2S) \rightarrow \gamma\chi_{b1}(1P))]$ assuming $B(\Upsilon(2S) \rightarrow \gamma\chi_{b1}(1P)) = (6.9 \pm 0.4) \times 10^{-2}$.				

$\Gamma(J/\psi\psi(2S))/\Gamma_{total}$ Γ_{20}/Γ

VALUE (units 10^{-5})	CL%	DOCUMENT ID	TECN	COMMENT
<1.7	90	¹ SHEN	12 BELL	$\Upsilon(2S) \rightarrow \gamma\psi X$
¹ SHEN 12 reports < 1.7×10^{-5} from a measurement of $[\Gamma(\chi_{b1}(1P) \rightarrow J/\psi\psi(2S))/\Gamma_{total}] \times [B(\Upsilon(2S) \rightarrow \gamma\chi_{b1}(1P))]$ assuming $B(\Upsilon(2S) \rightarrow \gamma\chi_{b1}(1P)) = (6.9 \pm 0.4) \times 10^{-2}$.				

$\Gamma(\psi(2S)\psi(2S))/\Gamma_{total}$ Γ_{21}/Γ

VALUE (units 10^{-5})	CL%	DOCUMENT ID	TECN	COMMENT
<6	90	¹ SHEN	12 BELL	$\Upsilon(2S) \rightarrow \gamma\psi X$
¹ SHEN 12 reports < 6.2×10^{-5} from a measurement of $[\Gamma(\chi_{b1}(1P) \rightarrow \psi(2S)\psi(2S))/\Gamma_{total}] \times [B(\Upsilon(2S) \rightarrow \gamma\chi_{b1}(1P))]$ assuming $B(\Upsilon(2S) \rightarrow \gamma\chi_{b1}(1P)) = (6.9 \pm 0.4) \times 10^{-2}$.				

$\Gamma(J/\psi(1S) \text{ anything})/\Gamma_{total}$ Γ_{22}/Γ

VALUE	CL%	DOCUMENT ID	TECN	COMMENT
<1.1 × 10⁻³	90	JIA	17A BELL	$e^+e^- \rightarrow \text{hadrons}$

$\Gamma(J/\psi(1S) X_{tetra})/\Gamma_{total}$ Γ_{23}/Γ

VALUE	CL%	DOCUMENT ID	TECN	COMMENT
<22.7 × 10⁻⁵	90	¹ JIA	17A BELL	$e^+e^- \rightarrow \text{hadrons}$
¹ For a tetraquark state X_{tetra} , with mass in the range 1.16–2.46 GeV and width in the range 0–0.3 GeV. Measured 90% CL limits as a function of X_{tetra} mass and width range from 1.8×10^{-5} to 22.7×10^{-5} .				

$\chi_{b1}(1P)$ Cross-Particle Branching Ratios

$\Gamma(\chi_{b1}(1P) \rightarrow \gamma \Upsilon(1S))/\Gamma_{total} \times \Gamma(\Upsilon(2S) \rightarrow \gamma \chi_{b1}(1P))/\Gamma_{total}$
 $\Gamma_1/\Gamma \times \Gamma_{59}^{T(2S)}/\Gamma T(2S)$

VALUE (units 10^{-3})	EVTS	DOCUMENT ID	TECN	COMMENT
24.1±0.6±1.5	13k	LEES	11J BABR	$\Upsilon(2S) \rightarrow X \gamma$

$B(\chi_{b1}(1P) \rightarrow \gamma \Upsilon(1S)) \times B(\Upsilon(2S) \rightarrow \gamma \chi_{b1}(1P)) \times B(\Upsilon(1S) \rightarrow \ell^+\ell^-)$

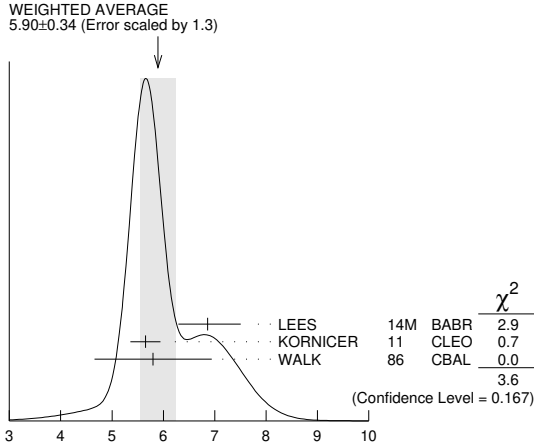
VALUE (units 10^{-4})	EVTS	DOCUMENT ID	TECN	COMMENT
5.90±0.34 OUR AVERAGE				Error includes scale factor of 1.3. See the ideogram below.
$6.86^{+0.47+0.44}_{-0.45-0.35}$		¹ LEES	14M BABR	$\Upsilon(2S) \rightarrow \gamma \gamma \mu^+\mu^-$

Meson Particle Listings

$\chi_{b1}(1P), h_b(1P), \chi_{b2}(1P)$

5.65 ± 0.11 ± 0.27 3222 KORNICER 11 CLEO $e^+e^- \rightarrow \gamma\gamma\ell^+\ell^-$
 5.8 ± 0.9 ± 0.7 53 WALK 86 CBAL $\Upsilon(2S) \rightarrow \gamma\gamma\ell^+\ell^-$

¹ From a sample of $\Upsilon(2S) \rightarrow \gamma\gamma\mu^+\mu^-$ with one converted photon.



$$B(\chi_{b1}(1P) \rightarrow \gamma \Upsilon(1S)) \times B(\Upsilon(2S) \rightarrow \gamma \chi_{b1}(1P)) \times B(\Upsilon(1S) \rightarrow \ell^+ \ell^-)$$

(units 10^{-4})

$B(\chi_{b1}(1P) \rightarrow \gamma \Upsilon(1S)) \times B(\Upsilon(3S) \rightarrow \gamma \chi_{b1}(1P)) \times B(\Upsilon(1S) \rightarrow \ell^+ \ell^-)$
 VALUE (units 10^{-5}) EVTS DOCUMENT ID TECN COMMENT
1.30 ± 0.34 OUR AVERAGE

1.16 ^{+0.78} _{-0.67} ± 0.14
 1.33 ± 0.30 ± 0.23 50 LEES 14M BABR $\Upsilon(3S) \rightarrow \gamma\gamma\mu^+\mu^-$
 KORNICER 11 CLEO $e^+e^- \rightarrow \gamma\gamma\ell^+\ell^-$

¹ From a sample of $\Upsilon(3S) \rightarrow \gamma\gamma\mu^+\mu^-$ with converted photons.

$B(\chi_{b2}(1P) \rightarrow \rho X + \bar{\rho} X) / B(\chi_{b1}(1P) \rightarrow \rho X + \bar{\rho} X)$
 VALUE DOCUMENT ID TECN COMMENT
1.068 ± 0.010 ± 0.040 BRIERE 07 CLEO $\Upsilon(2S) \rightarrow \gamma\chi_{bJ}(1P)$

$B(\chi_{b0}(1P) \rightarrow \rho X + \bar{\rho} X) / B(\chi_{b1}(1P) \rightarrow \rho X + \bar{\rho} X)$
 VALUE DOCUMENT ID TECN COMMENT
1.11 ± 0.15 ± 0.20 BRIERE 07 CLEO $\Upsilon(2S) \rightarrow \gamma\chi_{bJ}(1P)$

$\chi_{b1}(1P)$ REFERENCES

FULSOM 18 PRL 121 232001 B.G. Fulsom et al. (BELLE Collab.)
JIA 17A PR D96 112002 S. Jia et al. (BELLE Collab.)
LEES 14M PR D90 112010 J.P. Lees et al. (BABAR Collab.)
SHEN 12 PR D85 071102 C.P. Shen et al. (BELLE Collab.)
KORNICER 11 PR D83 054003 M. Koricner et al. (CLEO Collab.)
LEES 11J PR D84 072002 J.P. Lees et al. (BABAR Collab.)
ASNER 08A PR D78 091103 D.M. Asner et al. (CLEO Collab.)
BRIERE 08 PR D78 092007 R.A. Briere et al. (CLEO Collab.)
BRIERE 07 PR D76 012005 R.A. Briere et al. (CLEO Collab.)
ARTUSO 05 PRL 94 032001 M. Artuso et al. (CLEO Collab.)
EDWARDS 99 PR D59 032003 K.W. Edwards et al. (CLEO Collab.)
SKWARNICKI 87 PRL 58 972 T. Skwarnicki et al. (Crystal Ball Collab.)
WALK 86 PR D34 2611 W.S. Walk et al. (Crystal Ball Collab.)
ALBRECHT 85E PL 160B 331 H. Albrecht et al. (ARGUS Collab.)
NERNST 85 PRL 54 2195 R. Nernst et al. (Crystal Ball Collab.)
HAAS 84 PRL 52 799 J. Haas et al. (CLEO Collab.)
KLOPFEN... 83 PRL 51 160 C. Klopfenstein et al. (CUSP Collab.)
PAUSS 83 PL 130B 439 F. Pauss et al. (MPIM, COLU, CORN, LSU+)

$h_b(1P)$ $I^G(J^{PC}) = 0^-(1^{+-})$

Quantum numbers are quark model predictions, $C = -$ established by $\eta_b \gamma$ decay.

$h_b(1P)$ MASS

VALUE (MeV) EVTS DOCUMENT ID TECN COMMENT
9899.3 ± 0.8 OUR AVERAGE
 9899.3 ± 0.4 ± 1.0 112k TAMPONI 15 BELL $e^+e^- \rightarrow \gamma\eta + \text{hadrons}$
 9899.1 ± 0.4 ± 1.0 70k MIZUK 12 BELL $e^+e^- \rightarrow \pi^+\pi^- \text{hadrons}$
 9902 ± 4 ± 2 10.8k LEES 11K BABR $\Upsilon(3S) \rightarrow \eta_b \gamma \pi^0$

• • • We do not use the following data for averages, fits, limits, etc. • • •

9898.2 ^{+1.1} _{-1.0} ± 1.0 50.0k ¹ADACHI 12 BELL 10.86 $e^+e^- \rightarrow \pi^+\pi^- \text{MM}$

¹ Superseded by MIZUK 12.

$h_b(1P)$ DECAY MODES

Mode	Fraction (Γ_i/Γ)
$\Gamma_1 \eta_b(1S)\gamma$	(52 ± 6) %

$h_b(1P)$ BRANCHING RATIOS

$\Gamma(\eta_b(1S)\gamma)/\Gamma_{\text{total}}$ VALUE (units 10^{-2}) EVTS DOCUMENT ID TECN COMMENT Γ_1/Γ

52 ± 6 OUR AVERAGE

56 ± 8 ± 4 33.1k ¹TAMPONI 15 BELL $e^+e^- \rightarrow \gamma\eta + \text{hadrons}$
 49.2 ± 5.7 ^{+5.6} _{-3.3} 24k MIZUK 12 BELL $e^+e^- \rightarrow (\gamma)\pi^+\pi^- \text{hadrons}$

• • • We do not use the following data for averages, fits, limits, etc. • • •

seen 10.8k LEES 11K BABR $\Upsilon(3S) \rightarrow \eta_b \gamma \pi^0$

¹ Using $B(\eta \rightarrow 2\gamma) = (39.41 \pm 0.20)\%$.

$h_b(1P)$ REFERENCES

TAMPONI 15 PRL 115 142001 U. Tamponi et al. (BELLE Collab.)
ADACHI 12 PRL 108 032001 I. Adachi et al. (BELLE Collab.)
MIZUK 12 PRL 109 232002 R. Mizuk et al. (BELLE Collab.)
LEES 11K PR D84 091101 J.P. Lees et al. (BABAR Collab.)

$\chi_{b2}(1P)$ $I^G(J^{PC}) = 0^+(2^{++})$ J needs confirmation.

Observed in radiative decay of the $\Upsilon(2S)$, therefore $C = +$. Branching ratio requires E1 transition, M1 is strongly disfavored, therefore $P = +$, $J = 2$ from SKWARNICKI 87.

$\chi_{b2}(1P)$ MASS

VALUE (MeV) DOCUMENT ID
9912.21 ± 0.26 ± 0.31 OUR EVALUATION From average γ energy below, using $\Upsilon(2S)$ mass = 10023.26 ± 0.31 MeV

$m_{\chi_{b2}(1P)} - m_{\chi_{b1}(1P)}$

VALUE (MeV) DOCUMENT ID TECN COMMENT
19.10 ± 0.25 OUR AVERAGE Error includes scale factor of 1.1.
 19.81 ± 0.65 ± 0.20 ¹AALJ 14BG LHCb $pp \rightarrow \gamma\mu^+\mu^- X$
 19.01 ± 0.24 LEES 14M BABR $\Upsilon(2S) \rightarrow \gamma\gamma\mu^+\mu^-$

¹ From the $\chi_{bj}(1P) \rightarrow \Upsilon(1S)\gamma$ transition.

γ ENERGY IN $\Upsilon(2S)$ DECAY

VALUE (MeV) DOCUMENT ID TECN COMMENT
110.44 ± 0.29 OUR AVERAGE Error includes scale factor of 1.1.
 110.58 ± 0.08 ± 0.30 ARTUSO 05 CLEO $\Upsilon(2S) \rightarrow \gamma X$
 110.8 ± 0.3 ± 0.6 EDWARDS 99 CLE2 $\Upsilon(2S) \rightarrow \gamma\chi(1P)$
 107.0 ± 1.1 ± 1.3 WALK 86 CBAL $\Upsilon(2S) \rightarrow \gamma\gamma\ell^+\ell^-$
 110.6 ± 0.3 ± 0.9 ALBRECHT 85E ARG $\Upsilon(2S) \rightarrow \text{conv.}\gamma X$
 110.4 ± 0.8 ± 2.2 NERNST 85 CBAL $\Upsilon(2S) \rightarrow \gamma X$
 109.5 ± 0.7 ± 1.0 HAAS 84 CLEO $\Upsilon(2S) \rightarrow \text{conv.}\gamma X$
 108.2 ± 0.3 ± 2.0 KLOPFEN... 83 CUSB $\Upsilon(2S) \rightarrow \gamma X$
 108.8 ± 4.0 PAUSS 83 CUSB $\Upsilon(2S) \rightarrow \gamma\gamma\ell^+\ell^-$

$\chi_{b2}(1P)$ DECAY MODES

Mode	Fraction (Γ_i/Γ)	Confidence level
$\Gamma_1 \gamma \Upsilon(1S)$	(18.0 ± 1.0) %	
$\Gamma_2 D^0 X$	< 7.9 %	90%
$\Gamma_3 \pi^+\pi^- K^+ K^- \pi^0$	(8 ± 5) × 10 ⁻⁵	
$\Gamma_4 2\pi^+\pi^- K^- K_S^0$	< 1.0 × 10 ⁻⁴	90%
$\Gamma_5 2\pi^+\pi^- K^- K_S^0 2\pi^0$	(5.3 ± 2.4) × 10 ⁻⁴	
$\Gamma_6 2\pi^+ 2\pi^- 2\pi^0$	(3.5 ± 1.4) × 10 ⁻⁴	
$\Gamma_7 2\pi^+ 2\pi^- K^+ K^-$	(1.1 ± 0.4) × 10 ⁻⁴	
$\Gamma_8 2\pi^+ 2\pi^- K^+ K^- \pi^0$	(2.1 ± 0.9) × 10 ⁻⁴	
$\Gamma_9 2\pi^+ 2\pi^- K^+ K^- 2\pi^0$	(3.9 ± 1.8) × 10 ⁻⁴	
$\Gamma_{10} 3\pi^+ 2\pi^- K^- K_S^0 \pi^0$	< 5 × 10 ⁻⁴	90%
$\Gamma_{11} 3\pi^+ 3\pi^-$	(7.0 ± 3.1) × 10 ⁻⁵	
$\Gamma_{12} 3\pi^+ 3\pi^- 2\pi^0$	(1.0 ± 0.4) × 10 ⁻³	
$\Gamma_{13} 3\pi^+ 3\pi^- K^+ K^-$	< 8 × 10 ⁻⁵	90%
$\Gamma_{14} 3\pi^+ 3\pi^- K^+ K^- \pi^0$	(3.6 ± 1.5) × 10 ⁻⁴	
$\Gamma_{15} 4\pi^+ 4\pi^-$	(8 ± 4) × 10 ⁻⁵	
$\Gamma_{16} 4\pi^+ 4\pi^- 2\pi^0$	(1.8 ± 0.7) × 10 ⁻³	
$\Gamma_{17} J/\psi J/\psi$	< 4 × 10 ⁻⁵	90%
$\Gamma_{18} J/\psi \psi(2S)$	< 5 × 10 ⁻⁵	90%
$\Gamma_{19} \psi(2S) \psi(2S)$	< 1.6 × 10 ⁻⁵	90%
$\Gamma_{20} J/\psi(1S) \text{anything}$	(1.5 ± 0.4) × 10 ⁻³	

$\chi_{b2}(1P)$ BRANCHING RATIOS

$\Gamma(\gamma \mathcal{T}(1S))/\Gamma_{\text{total}}$					Γ_1/Γ
VALUE	EVTS	DOCUMENT ID	TECN	COMMENT	
0.180 ± 0.010 OUR AVERAGE					
0.164 ± 0.009 -0.016 ± 0.008	503k	¹ FULSOM	18	BELL $\mathcal{T}(2S) \rightarrow \gamma X$	
0.185 ± 0.008 ± 0.009	2,3,4	LEES	14M	BABR $\mathcal{T}(2S) \rightarrow \gamma \gamma \mu^+ \mu^-$	
0.186 ± 0.011 ± 0.009	1770	^{4,5} KORNICER	11	CLEO $e^+ e^- \rightarrow \gamma \gamma \ell^+ \ell^-$	
0.194 + 0.014 - 0.017 ± 0.009	8k	⁶ LEES	11J	BABR $\mathcal{T}(2S) \rightarrow X \gamma$	
0.25 ± 0.06 ± 0.01	35	^{4,7,8} WALK	86	CBAL $\mathcal{T}(2S) \rightarrow \gamma \gamma \ell^+ \ell^-$	
0.20 ± 0.05		KLOPFEN...	83	CUSB $\mathcal{T}(2S) \rightarrow \gamma \gamma \ell^+ \ell^-$	

¹ FULSOM 18 reports $[\Gamma(\chi_{b2}(1P) \rightarrow \gamma \mathcal{T}(1S))/\Gamma_{\text{total}}] \times [B(\mathcal{T}(2S) \rightarrow \gamma \chi_{b2}(1P))]$ = $(1.17 \pm 0.01 + 0.09_{-0.07}) \times 10^{-2}$ which we divide by our best value $B(\mathcal{T}(2S) \rightarrow \gamma \chi_{b2}(1P))$ = $(7.15 \pm 0.35) \times 10^{-2}$. Our first error is their experiment's error and our second error is the systematic error from using our best value.

² LEES 14M quotes $\Gamma(\chi_{b2}(1P) \rightarrow \gamma \mathcal{T}(1S))/\Gamma_{\text{total}} \times \Gamma(\mathcal{T}(2S) \rightarrow \gamma \chi_{b2}(1P))/\Gamma_{\text{total}}$ = $(1.32 \pm 0.06)\%$ combining the results from samples of $\mathcal{T}(2S) \rightarrow \gamma \gamma \mu^+ \mu^-$ with and without converted photons.

³ LEES 14M reports $[\Gamma(\chi_{b2}(1P) \rightarrow \gamma \mathcal{T}(1S))/\Gamma_{\text{total}}] \times [B(\mathcal{T}(2S) \rightarrow \gamma \chi_{b2}(1P))]$ = $(1.32 \pm 0.06) \times 10^{-2}$ which we divide by our best value $B(\mathcal{T}(2S) \rightarrow \gamma \chi_{b2}(1P))$ = $(7.15 \pm 0.35) \times 10^{-2}$. Our first error is their experiment's error and our second error is the systematic error from using our best value.

⁴ KORNICER 11 reports $B(\mathcal{T}(1S) \rightarrow \mu^+ \mu^-) = (2.48 \pm 0.05)\%$.

⁵ KORNICER 11 reports $[\Gamma(\chi_{b2}(1P) \rightarrow \gamma \mathcal{T}(1S))/\Gamma_{\text{total}}] \times [B(\mathcal{T}(2S) \rightarrow \gamma \chi_{b2}(1P))]$ = $(1.33 \pm 0.04 \pm 0.07) \times 10^{-2}$ which we divide by our best value $B(\mathcal{T}(2S) \rightarrow \gamma \chi_{b2}(1P))$ = $(7.15 \pm 0.35) \times 10^{-2}$. Our first error is their experiment's error and our second error is the systematic error from using our best value.

⁶ LEES 11J reports $[\Gamma(\chi_{b2}(1P) \rightarrow \gamma \mathcal{T}(1S))/\Gamma_{\text{total}}] \times [B(\mathcal{T}(2S) \rightarrow \gamma \chi_{b2}(1P))]$ = $(13.9 \pm 0.5_{-1.1}) \times 10^{-3}$ which we divide by our best value $B(\mathcal{T}(2S) \rightarrow \gamma \chi_{b2}(1P))$ = $(7.15 \pm 0.35) \times 10^{-2}$. Our first error is their experiment's error and our second error is the systematic error from using our best value.

⁷ WALK 86 quotes $B(\mathcal{T}(2S) \rightarrow \gamma \chi_{b2}(1P)) \times B(\chi_{b2}(1P) \rightarrow \gamma \mathcal{T}(1S)) \times B(\mathcal{T}(1S) \rightarrow \ell^+ \ell^-)$ = $(4.4 \pm 0.9 \pm 0.5)\%$.

⁸ WALK 86 reports $[\Gamma(\chi_{b2}(1P) \rightarrow \gamma \mathcal{T}(1S))/\Gamma_{\text{total}}] \times [B(\mathcal{T}(2S) \rightarrow \gamma \chi_{b2}(1P))]$ = $(17.7 \pm 3.6 \pm 2.0) \times 10^{-3}$ which we divide by our best value $B(\mathcal{T}(2S) \rightarrow \gamma \chi_{b2}(1P))$ = $(7.15 \pm 0.35) \times 10^{-2}$. Our first error is their experiment's error and our second error is the systematic error from using our best value.

$\Gamma(D^0 X)/\Gamma_{\text{total}}$					Γ_2/Γ
VALUE	CL%	DOCUMENT ID	TECN	COMMENT	
< 7.9 × 10⁻²	90	^{1,2} BRIERE	08	CLEO $\mathcal{T}(2S) \rightarrow \gamma D^0 X$	

¹ For $p_{D^0} > 2.5$ GeV/c.

² The authors also present their result as $(5.4 \pm 1.9 \pm 0.5) \times 10^{-2}$.

$\Gamma(\pi^+ \pi^- K^+ K^- \pi^0)/\Gamma_{\text{total}}$					Γ_3/Γ
VALUE (units 10 ⁻⁴)	EVTS	DOCUMENT ID	TECN	COMMENT	
0.84 ± 0.50 ± 0.04	8	¹ ASNER	08A	CLEO $\mathcal{T}(2S) \rightarrow \gamma \pi^+ \pi^- K^+ K^- \pi^0$	

¹ ASNER 08A reports $[\Gamma(\chi_{b2}(1P) \rightarrow \pi^+ \pi^- K^+ K^- \pi^0)/\Gamma_{\text{total}}] \times [B(\mathcal{T}(2S) \rightarrow \gamma \chi_{b2}(1P))]$ = $(6 \pm 3 \pm 2) \times 10^{-6}$ which we divide by our best value $B(\mathcal{T}(2S) \rightarrow \gamma \chi_{b2}(1P))$ = $(7.15 \pm 0.35) \times 10^{-2}$. Our first error is their experiment's error and our second error is the systematic error from using our best value.

$\Gamma(2\pi^+ \pi^- K^- K_S^0)/\Gamma_{\text{total}}$					Γ_4/Γ
VALUE (units 10 ⁻⁴)	CL%	DOCUMENT ID	TECN	COMMENT	
< 1.0	90	¹ ASNER	08A	CLEO $\mathcal{T}(2S) \rightarrow \gamma 2\pi^+ \pi^- K^- K_S^0$	

¹ ASNER 08A reports $[\Gamma(\chi_{b2}(1P) \rightarrow 2\pi^+ \pi^- K^- K_S^0)/\Gamma_{\text{total}}] \times [B(\mathcal{T}(2S) \rightarrow \gamma \chi_{b2}(1P))]$ < 7×10^{-6} which we divide by our best value $B(\mathcal{T}(2S) \rightarrow \gamma \chi_{b2}(1P))$ = 7.15×10^{-2} .

$\Gamma(2\pi^+ \pi^- K^- K_S^0 2\pi^0)/\Gamma_{\text{total}}$					Γ_5/Γ
VALUE (units 10 ⁻⁴)	EVTS	DOCUMENT ID	TECN	COMMENT	
5.3 ± 2.4 ± 0.3	11	¹ ASNER	08A	CLEO $\mathcal{T}(2S) \rightarrow \gamma 2\pi^+ \pi^- K^- 2\pi^0$	

¹ ASNER 08A reports $[\Gamma(\chi_{b2}(1P) \rightarrow 2\pi^+ \pi^- K^- K_S^0 2\pi^0)/\Gamma_{\text{total}}] \times [B(\mathcal{T}(2S) \rightarrow \gamma \chi_{b2}(1P))]$ = $(38 \pm 14 \pm 10) \times 10^{-6}$ which we divide by our best value $B(\mathcal{T}(2S) \rightarrow \gamma \chi_{b2}(1P))$ = $(7.15 \pm 0.35) \times 10^{-2}$. Our first error is their experiment's error and our second error is the systematic error from using our best value.

$\Gamma(2\pi^+ 2\pi^- 2\pi^0)/\Gamma_{\text{total}}$					Γ_6/Γ
VALUE (units 10 ⁻⁴)	EVTS	DOCUMENT ID	TECN	COMMENT	
3.5 ± 1.4 ± 0.2	19	¹ ASNER	08A	CLEO $\mathcal{T}(2S) \rightarrow \gamma 2\pi^+ 2\pi^- 2\pi^0$	

¹ ASNER 08A reports $[\Gamma(\chi_{b2}(1P) \rightarrow 2\pi^+ 2\pi^- 2\pi^0)/\Gamma_{\text{total}}] \times [B(\mathcal{T}(2S) \rightarrow \gamma \chi_{b2}(1P))]$ = $(25 \pm 8 \pm 6) \times 10^{-6}$ which we divide by our best value $B(\mathcal{T}(2S) \rightarrow \gamma \chi_{b2}(1P))$ = $(7.15 \pm 0.35) \times 10^{-2}$. Our first error is their experiment's error and our second error is the systematic error from using our best value.

$\Gamma(2\pi^+ 2\pi^- K^+ K^-)/\Gamma_{\text{total}}$					Γ_7/Γ
VALUE (units 10 ⁻⁴)	EVTS	DOCUMENT ID	TECN	COMMENT	
1.1 ± 0.4 ± 0.1	14	¹ ASNER	08A	CLEO $\mathcal{T}(2S) \rightarrow \gamma 2\pi^+ 2\pi^- K^+ K^-$	

¹ ASNER 08A reports $[\Gamma(\chi_{b2}(1P) \rightarrow 2\pi^+ 2\pi^- K^+ K^-)/\Gamma_{\text{total}}] \times [B(\mathcal{T}(2S) \rightarrow \gamma \chi_{b2}(1P))]$ = $(8 \pm 2 \pm 2) \times 10^{-6}$ which we divide by our best value $B(\mathcal{T}(2S) \rightarrow \gamma \chi_{b2}(1P))$ = $(7.15 \pm 0.35) \times 10^{-2}$. Our first error is their experiment's error and our second error is the systematic error from using our best value.

$\Gamma(2\pi^+ 2\pi^- K^+ K^- \pi^0)/\Gamma_{\text{total}}$					Γ_8/Γ
VALUE (units 10 ⁻⁴)	EVTS	DOCUMENT ID	TECN	COMMENT	
2.1 ± 0.9 ± 0.1	13	¹ ASNER	08A	CLEO $\mathcal{T}(2S) \rightarrow \gamma 2\pi^+ 2\pi^- K^+ K^- \pi^0$	

¹ ASNER 08A reports $[\Gamma(\chi_{b2}(1P) \rightarrow 2\pi^+ 2\pi^- K^+ K^- \pi^0)/\Gamma_{\text{total}}] \times [B(\mathcal{T}(2S) \rightarrow \gamma \chi_{b2}(1P))]$ = $(15 \pm 5 \pm 4) \times 10^{-6}$ which we divide by our best value $B(\mathcal{T}(2S) \rightarrow \gamma \chi_{b2}(1P))$ = $(7.15 \pm 0.35) \times 10^{-2}$. Our first error is their experiment's error and our second error is the systematic error from using our best value.

$\Gamma(2\pi^+ 2\pi^- K^+ K^- 2\pi^0)/\Gamma_{\text{total}}$					Γ_9/Γ
VALUE (units 10 ⁻⁴)	EVTS	DOCUMENT ID	TECN	COMMENT	
3.9 ± 1.8 ± 0.2	11	¹ ASNER	08A	CLEO $\mathcal{T}(2S) \rightarrow \gamma 2\pi^+ 2\pi^- K^+ K^- 2\pi^0$	

¹ ASNER 08A reports $[\Gamma(\chi_{b2}(1P) \rightarrow 2\pi^+ 2\pi^- K^+ K^- 2\pi^0)/\Gamma_{\text{total}}] \times [B(\mathcal{T}(2S) \rightarrow \gamma \chi_{b2}(1P))]$ = $(28 \pm 11 \pm 7) \times 10^{-6}$ which we divide by our best value $B(\mathcal{T}(2S) \rightarrow \gamma \chi_{b2}(1P))$ = $(7.15 \pm 0.35) \times 10^{-2}$. Our first error is their experiment's error and our second error is the systematic error from using our best value.

$\Gamma(3\pi^+ 2\pi^- K^- K_S^0 \pi^0)/\Gamma_{\text{total}}$					Γ_{10}/Γ
VALUE (units 10 ⁻⁴)	CL%	DOCUMENT ID	TECN	COMMENT	
< 5	90	¹ ASNER	08A	CLEO $\mathcal{T}(2S) \rightarrow \gamma 3\pi^+ 2\pi^- K^- K_S^0 \pi^0$	

¹ ASNER 08A reports $[\Gamma(\chi_{b2}(1P) \rightarrow 3\pi^+ 2\pi^- K^- K_S^0 \pi^0)/\Gamma_{\text{total}}] \times [B(\mathcal{T}(2S) \rightarrow \gamma \chi_{b2}(1P))]$ < 36×10^{-6} which we divide by our best value $B(\mathcal{T}(2S) \rightarrow \gamma \chi_{b2}(1P))$ = 7.15×10^{-2} .

$\Gamma(3\pi^+ 3\pi^-)/\Gamma_{\text{total}}$					Γ_{11}/Γ
VALUE (units 10 ⁻⁴)	EVTS	DOCUMENT ID	TECN	COMMENT	
0.70 ± 0.31 ± 0.03	9	¹ ASNER	08A	CLEO $\mathcal{T}(2S) \rightarrow \gamma 3\pi^+ 3\pi^-$	

¹ ASNER 08A reports $[\Gamma(\chi_{b2}(1P) \rightarrow 3\pi^+ 3\pi^-)/\Gamma_{\text{total}}] \times [B(\mathcal{T}(2S) \rightarrow \gamma \chi_{b2}(1P))]$ = $(5 \pm 2 \pm 1) \times 10^{-6}$ which we divide by our best value $B(\mathcal{T}(2S) \rightarrow \gamma \chi_{b2}(1P))$ = $(7.15 \pm 0.35) \times 10^{-2}$. Our first error is their experiment's error and our second error is the systematic error from using our best value.

$\Gamma(3\pi^+ 3\pi^- 2\pi^0)/\Gamma_{\text{total}}$					Γ_{12}/Γ
VALUE (units 10 ⁻⁴)	EVTS	DOCUMENT ID	TECN	COMMENT	
10.2 ± 3.6 ± 0.5	34	¹ ASNER	08A	CLEO $\mathcal{T}(2S) \rightarrow \gamma 3\pi^+ 3\pi^- 2\pi^0$	

¹ ASNER 08A reports $[\Gamma(\chi_{b2}(1P) \rightarrow 3\pi^+ 3\pi^- 2\pi^0)/\Gamma_{\text{total}}] \times [B(\mathcal{T}(2S) \rightarrow \gamma \chi_{b2}(1P))]$ = $(73 \pm 16 \pm 20) \times 10^{-6}$ which we divide by our best value $B(\mathcal{T}(2S) \rightarrow \gamma \chi_{b2}(1P))$ = $(7.15 \pm 0.35) \times 10^{-2}$. Our first error is their experiment's error and our second error is the systematic error from using our best value.

$\Gamma(3\pi^+ 3\pi^- K^+ K^-)/\Gamma_{\text{total}}$					Γ_{13}/Γ
VALUE (units 10 ⁻⁴)	CL%	DOCUMENT ID	TECN	COMMENT	
< 0.8	90	¹ ASNER	08A	CLEO $\mathcal{T}(2S) \rightarrow \gamma 3\pi^+ 3\pi^- K^+ K^-$	

¹ ASNER 08A reports $[\Gamma(\chi_{b2}(1P) \rightarrow 3\pi^+ 3\pi^- K^+ K^-)/\Gamma_{\text{total}}] \times [B(\mathcal{T}(2S) \rightarrow \gamma \chi_{b2}(1P))]$ < 6×10^{-6} which we divide by our best value $B(\mathcal{T}(2S) \rightarrow \gamma \chi_{b2}(1P))$ = 7.15×10^{-2} .

$\Gamma(3\pi^+ 3\pi^- K^+ K^- \pi^0)/\Gamma_{\text{total}}$					Γ_{14}/Γ
VALUE (units 10 ⁻⁴)	EVTS	DOCUMENT ID	TECN	COMMENT	
3.6 ± 1.5 ± 0.2	14	¹ ASNER	08A	CLEO $\mathcal{T}(2S) \rightarrow \gamma 3\pi^+ 3\pi^- K^+ K^- \pi^0$	

¹ ASNER 08A reports $[\Gamma(\chi_{b2}(1P) \rightarrow 3\pi^+ 3\pi^- K^+ K^- \pi^0)/\Gamma_{\text{total}}] \times [B(\mathcal{T}(2S) \rightarrow \gamma \chi_{b2}(1P))]$ = $(26 \pm 8 \pm 7) \times 10^{-6}$ which we divide by our best value $B(\mathcal{T}(2S) \rightarrow \gamma \chi_{b2}(1P))$ = $(7.15 \pm 0.35) \times 10^{-2}$. Our first error is their experiment's error and our second error is the systematic error from using our best value.

$\Gamma(4\pi^+ 4\pi^-)/\Gamma_{\text{total}}$					Γ_{15}/Γ
VALUE (units 10 ⁻⁴)	EVTS	DOCUMENT ID	TECN	COMMENT	
0.84 ± 0.40 ± 0.04	7	¹ ASNER	08A	CLEO $\mathcal{T}(2S) \rightarrow \gamma 4\pi^+ 4\pi^-$	

¹ ASNER 08A reports $[\Gamma(\chi_{b2}(1P) \rightarrow 4\pi^+ 4\pi^-)/\Gamma_{\text{total}}] \times [B(\mathcal{T}(2S) \rightarrow \gamma \chi_{b2}(1P))]$ = $(6 \pm 2 \pm 2) \times 10^{-6}$ which we divide by our best value $B(\mathcal{T}(2S) \rightarrow \gamma \chi_{b2}(1P))$ = $(7.15 \pm 0.35) \times 10^{-2}$. Our first error is their experiment's error and our second error is the systematic error from using our best value.

$\Gamma(4\pi^+ 4\pi^- 2\pi^0)/\Gamma_{\text{total}}$					Γ_{16}/Γ
VALUE (units 10 ⁻⁴)	EVTS	DOCUMENT ID	TECN	COMMENT	
18 ± 7 ± 1	29	¹ ASNER	08A	CLEO $\mathcal{T}(2S) \rightarrow \gamma 4\pi^+ 4\pi^- 2\pi^0$	

¹ ASNER 08A reports $[\Gamma(\chi_{b2}(1P) \rightarrow 4\pi^+ 4\pi^- 2\pi^0)/\Gamma_{\text{total}}] \times [B(\mathcal{T}(2S) \rightarrow \gamma \chi_{b2}(1P))]$ = $(132 \pm 31 \pm 40) \times 10^{-6}$ which we divide by our best value $B(\mathcal{T}(2S) \rightarrow \gamma \chi_{b2}(1P))$ = $(7.15 \pm 0.35) \times 10^{-2}$. Our first error is their experiment's error and our second error is the systematic error from using our best value.

Meson Particle Listings

$\chi_{b2}(1P), \eta_b(2S), \Upsilon(2S)$

$\Gamma(J/\psi J/\psi)/\Gamma_{\text{total}}$				Γ_{17}/Γ
VALUE (units 10^{-5})	CL%	DOCUMENT ID	TECN	COMMENT
<5	90	¹ SHEN 12	BELL	$\Upsilon(2S) \rightarrow \gamma\psi X$

¹ SHEN 12 reports $< 4.5 \times 10^{-5}$ from a measurement of $[\Gamma(\chi_{b2}(1P) \rightarrow J/\psi J/\psi)/\Gamma_{\text{total}}] \times [B(\Upsilon(2S) \rightarrow \gamma\chi_{b2}(1P))]$ assuming $B(\Upsilon(2S) \rightarrow \gamma\chi_{b2}(1P)) = (7.15 \pm 0.35) \times 10^{-2}$.

$\Gamma(J/\psi\psi(2S))/\Gamma_{\text{total}}$				Γ_{18}/Γ
VALUE (units 10^{-5})	CL%	DOCUMENT ID	TECN	COMMENT
<5	90	¹ SHEN 12	BELL	$\Upsilon(2S) \rightarrow \gamma\psi X$

¹ SHEN 12 reports $< 4.9 \times 10^{-5}$ from a measurement of $[\Gamma(\chi_{b2}(1P) \rightarrow J/\psi\psi(2S))/\Gamma_{\text{total}}] \times [B(\Upsilon(2S) \rightarrow \gamma\chi_{b2}(1P))]$ assuming $B(\Upsilon(2S) \rightarrow \gamma\chi_{b2}(1P)) = (7.15 \pm 0.35) \times 10^{-2}$.

$\Gamma(\psi(2S)\psi(2S))/\Gamma_{\text{total}}$				Γ_{19}/Γ
VALUE (units 10^{-5})	CL%	DOCUMENT ID	TECN	COMMENT
<1.6	90	¹ SHEN 12	BELL	$\Upsilon(2S) \rightarrow \gamma\psi X$

¹ SHEN 12 reports $< 1.6 \times 10^{-5}$ from a measurement of $[\Gamma(\chi_{b2}(1P) \rightarrow \psi(2S)\psi(2S))/\Gamma_{\text{total}}] \times [B(\Upsilon(2S) \rightarrow \gamma\chi_{b2}(1P))]$ assuming $B(\Upsilon(2S) \rightarrow \gamma\chi_{b2}(1P)) = (7.15 \pm 0.35) \times 10^{-2}$.

$\Gamma(J/\psi(1S) \text{ anything})/\Gamma_{\text{total}}$				Γ_{20}/Γ
VALUE (units 10^{-3})	EVTS	DOCUMENT ID	TECN	COMMENT
$1.50 \pm 0.34 \pm 0.22$	462	JIA	17A	BELL $e^+e^- \rightarrow \text{hadrons}$

$\chi_{b2}(1P)$ Cross-Particle Branching Ratios

$\Gamma(\chi_{b2}(1P) \rightarrow \gamma \Upsilon(1S))/\Gamma_{\text{total}} \times \Gamma(\Upsilon(2S) \rightarrow \gamma\chi_{b2}(1P))/\Gamma_{\text{total}}$				$\Gamma_{21}/\Gamma \times \Gamma_{60}^{\Upsilon(2S)}/\Gamma \Upsilon(2S)$
VALUE (units 10^{-3})	EVTS	DOCUMENT ID	TECN	COMMENT
$13.9 \pm 0.5 \pm 0.9$	8k	LEES	11J	BABR $\Upsilon(2S) \rightarrow X\gamma$

$B(\chi_{b2}(1P) \rightarrow \gamma \Upsilon(1S)) \times B(\Upsilon(2S) \rightarrow \gamma\chi_{b2}(1P)) \times B(\Upsilon(1S) \rightarrow \ell^+\ell^-)$				
VALUE (units 10^{-4})	EVTS	DOCUMENT ID	TECN	COMMENT
3.38 ± 0.16 OUR AVERAGE				
$3.63^{+0.36+0.18}_{-0.34-0.19}$		¹ LEES	14M	BABR $\Upsilon(2S) \rightarrow \gamma\gamma\mu^+\mu^-$
$3.29 \pm 0.09 \pm 0.16$	1770	KORNICER	11	CLEO $e^+e^- \rightarrow \gamma\gamma\ell^+\ell^-$
$4.4 \pm 0.9 \pm 0.5$	35	WALK	86	CBAL $\Upsilon(2S) \rightarrow \gamma\gamma\ell^+\ell^-$

¹ From a sample of $\Upsilon(2S) \rightarrow \gamma\gamma\mu^+\mu^-$ with converted photons.

$[B(\chi_{b2}(1P) \rightarrow \gamma \Upsilon(1S)) \times B(\Upsilon(2S) \rightarrow \gamma\chi_{b2}(1P))] / [B(\chi_{b1}(1P) \rightarrow \gamma \Upsilon(1S)) \times B(\Upsilon(2S) \rightarrow \gamma\chi_{b1}(1P))]$				
VALUE (%)	DOCUMENT ID	TECN	COMMENT	
55.6 ± 1.6	¹ LEES	14M	BABR	$\Upsilon(2S) \rightarrow \gamma\gamma\mu^+\mu^-$

¹ From a sample of $\Upsilon(2S) \rightarrow \gamma\gamma\mu^+\mu^-$ events without converted photons.

$B(\chi_{b2}(1P) \rightarrow \gamma \Upsilon(1S)) \times B(\Upsilon(3S) \rightarrow \gamma\chi_{b2}(1P)) \times B(\Upsilon(1S) \rightarrow \ell^+\ell^-)$				
VALUE (units 10^{-9})	EVTS	DOCUMENT ID	TECN	COMMENT
3.8 ± 0.5 OUR AVERAGE				
$4.68^{+0.99}_{-0.92} \pm 0.37$		¹ LEES	14M	BABR $\Upsilon(3S) \rightarrow \gamma\gamma\mu^+\mu^-$
$3.56 \pm 0.40 \pm 0.41$	126	KORNICER	11	CLEO $e^+e^- \rightarrow \gamma\gamma\ell^+\ell^-$

¹ From a sample of $\Upsilon(3S) \rightarrow \gamma\gamma\mu^+\mu^-$ with converted photons.

$\chi_{b2}(1P)$ REFERENCES

FULSOM	18	PRL 121 232001	B. G. Fulsom et al.	(BELLE Collab.)
JIA	17A	PR D96 112002	S. Jia et al.	(BELLE Collab.)
AAJ	14BG	JHEP 1410 088	R. Aaij et al.	(LHCb Collab.)
LEES	14M	PR D90 112010	J.P. Lees et al.	(BABAR Collab.)
SHEN	12	PR D85 071102	C.P. Shen et al.	(BELLE Collab.)
KORNICER	11	PR D83 054003	M. Kornicer et al.	(CLEO Collab.)
LEES	11J	PR D84 072002	J.P. Lees et al.	(BABAR Collab.)
ASNER	08A	PR D78 091103	D.M. Asner et al.	(CLEO Collab.)
BRIERE	08	PR D78 092007	R.A. Briere et al.	(CLEO Collab.)
ARTUSO	05	PRL 94 032001	M. Artuso et al.	(CLEO Collab.)
EDWARDS	99	PR D59 032003	K.W. Edwards et al.	(CLEO Collab.)
SKWARNICKI	87	PRL 58 972	T. Skwarnicki et al.	(Crystal Ball Collab.)
WALK	86	PR D34 2611	W.S. Walk et al.	(Crystal Ball Collab.)
ALBRECHT	85E	PL 160B 331	H. Albrecht et al.	(ARGUS Collab.)
NERNST	85	PL 54 2195	R. Nernst et al.	(Crystal Ball Collab.)
HAAS	84	PRL 52 799	J. Haas et al.	(CLEO Collab.)
KLOPFEN...	83	PRL 51 160	C. Klopfenstein et al.	(CUSB Collab.)
PAUSS	83	PL 130B 439	F. Pauss et al.	(MPIM, COLU, CORN, LSU+)

$\eta_b(2S)$ $J^{G(JPC)} = 0^+(0^-)$

OMITTED FROM SUMMARY TABLE
Quantum numbers shown are quark-model predictions.

$\eta_b(2S)$ MASS

VALUE (MeV)	EVTS	DOCUMENT ID	TECN	COMMENT
$9999.0 \pm 3.5 \pm 2.8$	26k	¹ MIZUK	12	BELL $e^+e^- \rightarrow \gamma\pi^+\pi^- + \text{hadrons}$

••• We do not use the following data for averages, fits, limits, etc. •••

$9974.6 \pm 2.3 \pm 2.1$	11 ± 4	^{2,3,4} DOBBS	12	$\Upsilon(2S) \rightarrow \gamma \text{ hadrons}$
--------------------------	------------	------------------------	----	---

¹ Assuming $\Gamma_{\eta_b(2S)} = 4.9$ MeV. Not independent of the corresponding mass difference measurement.
² SANDILYA 13 (Belle Collab.) search for such a state reconstructed in the same 26 exclusive hadronic final states as DOBBS 12 using a sample of $(157.8 \pm 3.6) \times 10^6$ $\Upsilon(2S)$ decays or about 17 times larger and find no evidence for a signal. Their 90% C.L. upper limit on the branching fraction $B(\Upsilon(2S) \rightarrow \eta_b(2S)\gamma) \times \sum_i B(\eta_b(2S) \rightarrow X_i) < 4.9 \times 10^{-6}$, summed over the exclusive hadronic final states X_i , is an order of magnitude smaller than that reported by DOBBS 12.
³ Obtained by analyzing CLEO III data but not authored by the CLEO Collaboration.
⁴ Assuming $\Gamma_{\eta_b(2S)} = 5$ MeV. Not independent of the corresponding mass difference measurement.

$m\Upsilon(2S) - m\eta_b(2S)$

VALUE (MeV)	EVTS	DOCUMENT ID	TECN	COMMENT
$24.3 \pm 3.5 \pm 1.9$	26k	⁵ MIZUK	12	BELL $e^+e^- \rightarrow \gamma\pi^+\pi^- + \text{hadrons}$

••• We do not use the following data for averages, fits, limits, etc. •••

$48.7 \pm 2.3 \pm 2.1$	11 ± 4	^{6,7,8} DOBBS	12	$\Upsilon(2S) \rightarrow \gamma \text{ hadrons}$
------------------------	------------	------------------------	----	---

⁵ Assuming $\Gamma_{\eta_b(2S)} = 4.9$ MeV. Not independent of the corresponding mass measurement.
⁶ SANDILYA 13 (Belle Collab.) search for such a state reconstructed in the same 26 exclusive hadronic final states as DOBBS 12 using a sample of $(157.8 \pm 3.6) \times 10^6$ $\Upsilon(2S)$ decays or about 17 times larger and find no evidence for a signal. Their 90% C.L. upper limit on the branching fraction $B(\Upsilon(2S) \rightarrow \eta_b(2S)\gamma) \times \sum_i B(\eta_b(2S) \rightarrow X_i) < 4.9 \times 10^{-6}$, summed over the exclusive hadronic final states X_i , is an order of magnitude smaller than that reported by DOBBS 12.
⁷ Obtained by analyzing CLEO III data but not authored by the CLEO Collaboration.
⁸ Assuming $\Gamma_{\eta_b(2S)} = 5$ MeV. Not independent of the corresponding mass measurement.

$\eta_b(2S)$ WIDTH

VALUE (MeV)	CL%	DOCUMENT ID	TECN	COMMENT
<24	90	MIZUK	12	BELL $e^+e^- \rightarrow \gamma\pi^+\pi^- \text{ hadrons}$

$\eta_b(2S)$ DECAY MODES

Mode	Fraction (Γ_i/Γ)
Γ_1 hadrons	seen

$\eta_b(2S)$ BRANCHING RATIOS

$\Gamma(\text{hadrons})/\Gamma_{\text{total}}$				Γ_1/Γ
VALUE	EVTS	DOCUMENT ID	TECN	COMMENT
seen	26k	MIZUK	12	BELL $e^+e^- \rightarrow \gamma\pi^+\pi^- \text{ hadrons}$

••• We do not use the following data for averages, fits, limits, etc. •••

seen	9.10	DOBBS	12	$\Upsilon(2S) \rightarrow \gamma \text{ hadrons}$
------	--------	-------	----	---

⁹ SANDILYA 13 (Belle Collab.) search for such a state reconstructed in the same 26 exclusive hadronic final states as DOBBS 12 using a sample of $(157.8 \pm 3.6) \times 10^6$ $\Upsilon(2S)$ decays or about 17 times larger and find no evidence for a signal. Their 90% C.L. upper limit on the branching fraction $B(\Upsilon(2S) \rightarrow \eta_b(2S)\gamma) \times \sum_i B(\eta_b(2S) \rightarrow X_i) < 4.9 \times 10^{-6}$, summed over the exclusive hadronic final states X_i , is an order of magnitude smaller than that reported by DOBBS 12.
¹⁰ Obtained by analyzing CLEO III data but not authored by the CLEO Collaboration.

$\eta_b(2S)$ REFERENCES

SANDILYA	13	PRL 111 112001	S. Sandilya et al.	(BELLE Collab.)
DOBBS	12	PRL 109 082001	S. Dobbs et al.	
MIZUK	12	PRL 109 232002	R. Mizuk et al.	(BELLE Collab.)

$\Upsilon(2S)$

$$J^{G(JPC)} = 0^-(1^{--})$$

$\Upsilon(2S)$ MASS

VALUE (MeV)	DOCUMENT ID	TECN	COMMENT
10023.26 ± 0.31 OUR AVERAGE			
10023.5 ± 0.5	¹ ARTAMONOV 00	MD1	$e^+e^- \rightarrow \text{hadrons}$
10023.1 ± 0.4	BARBER 84	REDE	$e^+e^- \rightarrow \text{hadrons}$

••• We do not use the following data for averages, fits, limits, etc. •••

10023.6 ± 0.5	^{2,3} BARU	86B	$e^+e^- \rightarrow \text{hadrons}$
-------------------	---------------------	-----	-------------------------------------

¹ Reanalysis of BARU 86B using new electron mass (COHEN 87).
² Reanalysis of ARTAMONOV 84.
³ Superseded by ARTAMONOV 00.

$m\Upsilon(3S) - m\Upsilon(2S)$

VALUE (MeV)	DOCUMENT ID	TECN	COMMENT
$331.50 \pm 0.02 \pm 0.13$	LEES	11c	BABR $e^+e^- \rightarrow \pi^+\pi^- X$

$\Upsilon(2S)$ WIDTH

VALUE (keV)	DOCUMENT ID
31.98 ± 2.63 OUR EVALUATION	See the Note on "Width Determinations of the Υ States"

Meson Particle Listings
 $\Upsilon(2S)$

$\Upsilon(2S)$ DECAY MODES

Mode	Fraction (Γ_i/Γ)	Scale factor/ Confidence level
Γ_1 $\Upsilon(1S)\pi^+\pi^-$	(17.85 ± 0.26) %	
Γ_2 $\Upsilon(1S)\pi^0\pi^0$	(8.6 ± 0.4) %	
Γ_3 $\tau^+\tau^-$	(2.00 ± 0.21) %	S=2.2
Γ_4 $\mu^+\mu^-$	(1.93 ± 0.17) %	
Γ_5 e^+e^-	(1.91 ± 0.16) %	
Γ_6 $\Upsilon(1S)\pi^0$	< 4 × 10 ⁻⁵	CL=90%
Γ_7 $\Upsilon(1S)\eta$	(2.9 ± 0.4) × 10 ⁻⁴	S=2.0
Γ_8 $J/\psi(1S)$ anything	< 6 × 10 ⁻³	CL=90%
Γ_9 $J/\psi(1S)\eta_c$	< 5.4 × 10 ⁻⁶	CL=90%
Γ_{10} $J/\psi(1S)\chi_{c0}$	< 3.4 × 10 ⁻⁶	CL=90%
Γ_{11} $J/\psi(1S)\chi_{c1}$	< 1.2 × 10 ⁻⁶	CL=90%
Γ_{12} $J/\psi(1S)\chi_{c2}$	< 2.0 × 10 ⁻⁶	CL=90%
Γ_{13} $J/\psi(1S)\eta_c(2S)$	< 2.5 × 10 ⁻⁶	CL=90%
Γ_{14} $J/\psi(1S)X(3940)$	< 2.0 × 10 ⁻⁶	CL=90%
Γ_{15} $J/\psi(1S)X(4160)$	< 2.0 × 10 ⁻⁶	CL=90%
Γ_{16} χ_{c1} anything	(2.2 ± 0.5) × 10 ⁻⁴	
Γ_{17} $\chi_{c1}(1P)^0 \chi_{tetra}$	< 3.67 × 10 ⁻⁵	CL=90%
Γ_{18} χ_{c2} anything	(2.3 ± 0.8) × 10 ⁻⁴	
Γ_{19} $\psi(2S)\eta_c$	< 5.1 × 10 ⁻⁶	CL=90%
Γ_{20} $\psi(2S)\chi_{c0}$	< 4.7 × 10 ⁻⁶	CL=90%
Γ_{21} $\psi(2S)\chi_{c1}$	< 2.5 × 10 ⁻⁶	CL=90%
Γ_{22} $\psi(2S)\chi_{c2}$	< 1.9 × 10 ⁻⁶	CL=90%
Γ_{23} $\psi(2S)\eta_c(2S)$	< 3.3 × 10 ⁻⁶	CL=90%
Γ_{24} $\psi(2S)X(3940)$	< 3.9 × 10 ⁻⁶	CL=90%
Γ_{25} $\psi(2S)X(4160)$	< 3.9 × 10 ⁻⁶	CL=90%
Γ_{26} $Z_c(3900)^+ Z_c(3900)^-$	< 1.0 × 10 ⁻⁶	CL=90%
Γ_{27} $Z_c(4200)^+ Z_c(4200)^-$	< 1.67 × 10 ⁻⁵	CL=90%
Γ_{28} $Z_c(3900)^\pm Z_c(4200)^\mp$	< 7.3 × 10 ⁻⁶	CL=90%
Γ_{29} $X(4050)^+ X(4050)^-$	< 1.35 × 10 ⁻⁵	CL=90%
Γ_{30} $X(4250)^+ X(4250)^-$	< 2.67 × 10 ⁻⁵	CL=90%
Γ_{31} $X(4050)^\pm X(4250)^\mp$	< 2.72 × 10 ⁻⁵	CL=90%
Γ_{32} $Z_c(4430)^+ Z_c(4430)^-$	< 2.03 × 10 ⁻⁵	CL=90%
Γ_{33} $X(4055)^\pm X(4055)^\mp$	< 1.11 × 10 ⁻⁵	CL=90%
Γ_{34} $X(4055)^\pm Z_c(4430)^\mp$	< 2.11 × 10 ⁻⁵	CL=90%
Γ_{35} 2H anything	(2.78 ± 0.30 / 0.26) × 10 ⁻⁵	S=1.2
Γ_{36} hadrons	(94 ± 11) %	
Γ_{37} ggg	(58.8 ± 1.2) %	
Γ_{38} γgg	(1.87 ± 0.28) %	
Γ_{39} $\phi K^+ K^-$	(1.6 ± 0.4) × 10 ⁻⁶	
Γ_{40} $\omega\pi^+\pi^-$	< 2.58 × 10 ⁻⁶	CL=90%
Γ_{41} $K^*(892)^0 K^- \pi^+ + c.c.$	(2.3 ± 0.7) × 10 ⁻⁶	
Γ_{42} $\phi f'_2(1525)$	< 1.33 × 10 ⁻⁶	CL=90%
Γ_{43} $\omega f_2(1270)$	< 5.7 × 10 ⁻⁷	CL=90%
Γ_{44} $\rho(770) a_2(1320)$	< 8.8 × 10 ⁻⁷	CL=90%
Γ_{45} $K^*(892)^0 \bar{K}_2^0(1430)^0 + c.c.$	(1.5 ± 0.6) × 10 ⁻⁶	
Γ_{46} $K_1(1270)^\pm K^\mp$	< 3.22 × 10 ⁻⁶	CL=90%
Γ_{47} $K_1(1400)^\pm K^\mp$	< 8.3 × 10 ⁻⁷	CL=90%
Γ_{48} $b_1(1235)^\pm \pi^\mp$	< 4.0 × 10 ⁻⁷	CL=90%
Γ_{49} $\rho\pi$	< 1.16 × 10 ⁻⁶	CL=90%
Γ_{50} $\pi^+\pi^-\pi^0$	< 8.0 × 10 ⁻⁷	CL=90%
Γ_{51} $\omega\pi^0$	< 1.63 × 10 ⁻⁶	CL=90%
Γ_{52} $\pi^+\pi^-\pi^0\pi^0$	(1.30 ± 0.28) × 10 ⁻⁵	
Γ_{53} $K_S^0 K^+ \pi^- + c.c.$	(1.14 ± 0.33) × 10 ⁻⁶	
Γ_{54} $K^*(892)^0 \bar{K}^0 + c.c.$	< 4.22 × 10 ⁻⁶	CL=90%
Γ_{55} $K^*(892)^- K^+ + c.c.$	< 1.45 × 10 ⁻⁶	CL=90%
Γ_{56} $f_1(1285)$ anything	(2.2 ± 1.6) × 10 ⁻³	
Γ_{57} $f_1(1285) \chi_{tetra}$	< 6.47 × 10 ⁻⁵	CL=90%
Γ_{58} Sum of 100 exclusive modes	(2.90 ± 0.30) × 10 ⁻³	

Radiative decays

Γ_{59} $\gamma\chi_{b1}(1P)$	(6.9 ± 0.4) %	
Γ_{60} $\gamma\chi_{b2}(1P)$	(7.15 ± 0.35) %	
Γ_{61} $\gamma\chi_{b0}(1P)$	(3.8 ± 0.4) %	
Γ_{62} $\gamma f_0(1710)$	< 5.9 × 10 ⁻⁴	CL=90%
Γ_{63} $\gamma f'_2(1525)$	< 5.3 × 10 ⁻⁴	CL=90%
Γ_{64} $\gamma f_2(1270)$	< 2.41 × 10 ⁻⁴	CL=90%
Γ_{65} $\gamma f_3(2220)$		
Γ_{66} $\gamma\eta_c(1S)$	< 2.7 × 10 ⁻⁵	CL=90%
Γ_{67} $\gamma\chi_{c0}$	< 3.0 × 10 ⁻⁴	CL=90%
Γ_{68} $\gamma\chi_{c1}$	< 3.6 × 10 ⁻⁶	CL=90%

Γ_{69} $\gamma\chi_{c2}$	< 1.5 × 10 ⁻⁵	CL=90%
Γ_{70} $\gamma\chi_{c1}(3872)$	< 2.1 × 10 ⁻⁵	CL=90%
Γ_{71} $\gamma\chi_{c1}(3872), \chi_{c1} \rightarrow \pi^+\pi^-\pi^0 J/\psi$	< 2.4 × 10 ⁻⁶	CL=90%
Γ_{72} $\gamma\chi_{c0}(3915) \rightarrow \omega J/\psi$	< 2.8 × 10 ⁻⁶	CL=90%
Γ_{73} $\gamma\chi_{c1}(4140) \rightarrow \phi J/\psi$	< 1.2 × 10 ⁻⁶	CL=90%
Γ_{74} $\gamma X(4350) \rightarrow \phi J/\psi$	< 1.3 × 10 ⁻⁶	CL=90%
Γ_{75} $\gamma\eta_b(1S)$	(5.5 ± 1.1 / 0.9) × 10 ⁻⁴	S=1.2
Γ_{76} $\gamma\eta_b(1S) \rightarrow \gamma$ Sum of 26 exclusive modes	< 3.7 × 10 ⁻⁶	CL=90%
Γ_{77} $\gamma X_{b\bar{b}} \rightarrow \gamma$ Sum of 26 exclusive modes	< 4.9 × 10 ⁻⁶	CL=90%
Γ_{78} $\gamma X \rightarrow \gamma + \geq 4$ prongs	[a] < 1.95 × 10 ⁻⁴	CL=95%
Γ_{79} $\gamma A^0 \rightarrow \gamma$ hadrons	< 8 × 10 ⁻⁵	CL=90%
Γ_{80} $\gamma a_1^0 \rightarrow \gamma\mu^+\mu^-$	< 8.3 × 10 ⁻⁶	CL=90%

Lepton Family number (LF) violating modes

Γ_{81} $e^\pm\tau^\mp$	LF	< 3.2 × 10 ⁻⁶	CL=90%
Γ_{82} $\mu^\pm\tau^\mp$	LF	< 3.3 × 10 ⁻⁶	CL=90%

[a] 1.5 GeV < m_X < 5.0 GeV

CONSTRAINED FIT INFORMATION

An overall fit to 3 branching ratios uses 13 measurements and one constraint to determine 3 parameters. The overall fit has a $\chi^2 = 11.8$ for 11 degrees of freedom.

The following off-diagonal array elements are the correlation coefficients $\langle \delta x_i \delta x_j \rangle / (\delta x_i \delta x_j)$, in percent, from the fit to the branching fractions, $x_i \equiv \Gamma_i/\Gamma_{total}$. The fit constrains the x_i whose labels appear in this array to sum to one.

$$x_7 \begin{matrix} \text{---} & \text{---} \\ | & | \\ \text{---} & \text{---} \\ & x_1 \end{matrix}$$

$\Upsilon(2S) \Gamma(i)\Gamma(e^+e^-)/\Gamma(total)$

$\Gamma(\mu^+\mu^-) \times \Gamma(e^+e^-)/\Gamma_{total}$	DOCUMENT ID	TECN	COMMENT
6.5 ± 1.5 ± 1.0	KOBEL	92	CBAL $e^+e^- \rightarrow \mu^+\mu^-$

$\Gamma(\Upsilon(1S)\pi^+\pi^-) \times \Gamma(e^+e^-)/\Gamma_{total}$	DOCUMENT ID	TECN	COMMENT
105.4 ± 1.0 ± 4.2	11.8k	1 AUBERT	08BP BABR 10.58 $e^+e^- \rightarrow \gamma\pi^+\pi^-\ell^+\ell^-$
			¹ Using B($\Upsilon(1S) \rightarrow e^+e^-$) = (2.38 ± 0.11)% and B($\Upsilon(1S) \rightarrow \mu^+\mu^-$) = (2.48 ± 0.05)%.

$\Gamma(hadrons) \times \Gamma(e^+e^-)/\Gamma_{total}$	DOCUMENT ID	TECN	COMMENT
0.581 ± 0.004 ± 0.009	1 ROSNER	06	CLEO 10.0 $e^+e^- \rightarrow hadrons$
0.552 ± 0.031 ± 0.017	1 BARU	96	MD1 $e^+e^- \rightarrow hadrons$
0.54 ± 0.04 ± 0.02	1 JAKUBOWSKI	88	CBAL $e^+e^- \rightarrow hadrons$
0.58 ± 0.03 ± 0.04	2 GILES	84B	CLEO $e^+e^- \rightarrow hadrons$
0.60 ± 0.12 ± 0.07	2 ALBRECHT	82	DASP $e^+e^- \rightarrow hadrons$
0.54 ± 0.07 ± 0.09 / -0.05	2 NICZYPORUK	81C	LENA $e^+e^- \rightarrow hadrons$
0.41 ± 0.18	2 BOCK	80	CNTR $e^+e^- \rightarrow hadrons$

¹Radiative corrections evaluated following KURAEV 85.
²Radiative corrections reevaluated by BUCHMUELLER 88 following KURAEV 85.

$\Upsilon(2S)$ PARTIAL WIDTHS

$\Gamma(e^+e^-)$	DOCUMENT ID
0.612 ± 0.011 OUR EVALUATION	

$\Upsilon(2S)$ BRANCHING RATIOS

$\Gamma(\Upsilon(1S)\pi^+\pi^-)/\Gamma_{total}$	DOCUMENT ID	TECN	COMMENT
17.85 ± 0.26 OUR FIT			
17.92 ± 0.26 OUR AVERAGE			
16.8 ± 1.1 ± 1.3	906k	1 LEES	11C BABR $e^+e^- \rightarrow \pi^+\pi^- X$
17.80 ± 0.05 ± 0.37	170k	2 LEES	11L BABR $\Upsilon(2S) \rightarrow \pi^+\pi^- \mu^+\mu^-$
18.02 ± 0.02 ± 0.61	851k	3 BHARI	09 CLEO $e^+e^- \rightarrow \pi^+\pi^- MM$
17.22 ± 0.17 ± 0.75	11.8k	4 AUBERT	08BP BABR $e^+e^- \rightarrow \gamma\pi^+\pi^-\ell^+\ell^-$
19.2 ± 0.2 ± 1.0	52.6k	5 ALEXANDER	98 CLE2 $\pi^+\pi^-\ell^+\ell^-, \pi^+\pi^- MM$

Meson Particle Listings

$\Upsilon(2S)$

18.1 ± 0.5 ± 1.0	11.6k	ALBRECHT	87	ARG	$e^+e^- \rightarrow \pi^+\pi^-MM$
16.9 ± 4.0		GELPHMAN	85	CBAL	$e^+e^- \rightarrow e^+e^-\pi^+\pi^-$
19.1 ± 1.2 ± 0.6		BESSON	84	CLEO	$\pi^+\pi^-MM$
18.9 ± 2.6		FONSECA	84	CUSB	$e^+e^- \rightarrow \ell^+\ell^-\pi^+\pi^-$
21 ± 7	7	NICZYPORUK	81B	LENA	$e^+e^- \rightarrow \ell^+\ell^-\pi^+\pi^-$

¹ LEES 11c reports $[\Gamma(\Upsilon(2S) \rightarrow \Upsilon(1S)\pi^+\pi^-)/\Gamma_{total}] \times [B(\Upsilon(3S) \rightarrow \Upsilon(2S)\text{anything})] = (1.78 \pm 0.02 \pm 0.11) \times 10^{-2}$ which we divide by our best value $B(\Upsilon(3S) \rightarrow \Upsilon(2S)\text{anything}) = (10.6 \pm 0.8) \times 10^{-2}$. Our first error is their experiment's error and our second error is the systematic error from using our best value.

- ² Using $B(\Upsilon(1S) \rightarrow \mu^+\mu^-) = (2.48 \pm 0.05)\%$.
- ³ A weighted average of the inclusive and exclusive results.
- ⁴ Using $B(\Upsilon(2S) \rightarrow e^+e^-) = (1.91 \pm 0.16)\%$, $B(\Upsilon(2S) \rightarrow \mu^+\mu^-) = (1.93 \pm 0.17)\%$ and, $\Gamma_{ee}(\Upsilon(2S)) = 0.612 \pm 0.011$ keV.
- ⁵ Using $B(\Upsilon(1S) \rightarrow e^+e^-) = (2.52 \pm 0.17)\%$ and $B(\Upsilon(1S) \rightarrow \mu^+\mu^-) = (2.48 \pm 0.07)\%$.

$\Gamma(\Upsilon(1S)\pi^0\pi^0)/\Gamma_{total}$		Γ_2/Γ			
VALUE (units 10^{-2})	EVTS	DOCUMENT ID	TECN	COMMENT	
8.6 ± 0.4 OUR AVERAGE				Error includes scale factor of 2.0.	
8.43 ± 0.16 ± 0.42	38k	¹ BHARI	09	CLEO	$e^+e^- \rightarrow \pi^0\pi^0\ell^+\ell^-$
9.2 ± 0.6 ± 0.8	275	² ALEXANDER	98	CLE2	$e^+e^- \rightarrow \pi^0\pi^0\ell^+\ell^-$
9.5 ± 1.9 ± 1.9	25	ALBRECHT	87	ARG	$e^+e^- \rightarrow \pi^0\pi^0\ell^+\ell^-$
8.0 ± 1.5		GELPHMAN	85	CBAL	$e^+e^- \rightarrow \pi^0\pi^0\ell^+\ell^-$
10.3 ± 2.3		FONSECA	84	CUSB	$e^+e^- \rightarrow \pi^0\pi^0\ell^+\ell^-$

- ¹ Authors assume $B(\Upsilon(1S) \rightarrow e^+e^-) + B(\Upsilon(1S) \rightarrow \mu^+\mu^-) = 4.96\%$.
- ² Using $B(\Upsilon(1S) \rightarrow e^+e^-) = (2.52 \pm 0.17)\%$ and $B(\Upsilon(1S) \rightarrow \mu^+\mu^-) = (2.48 \pm 0.07)\%$.

$\Gamma(\Upsilon(1S)\pi^0\pi^0)/\Gamma(\Upsilon(1S)\pi^+\pi^-)$		Γ_2/Γ_1			
VALUE	DOCUMENT ID	TECN	COMMENT		
0.462 ± 0.037	¹ BHARI	09	CLEO	$e^+e^- \rightarrow \Upsilon(2S)$	

- ¹ Not independent of other values reported by BHARI 09.

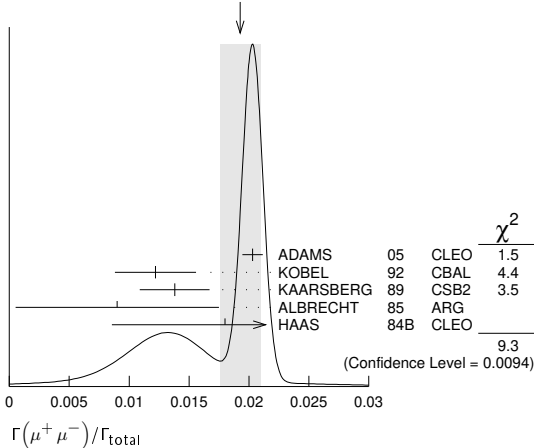
$\Gamma(\tau^+\tau^-)/\Gamma_{total}$		Γ_3/Γ			
VALUE (units 10^{-2})	EVTS	DOCUMENT ID	TECN	COMMENT	
2.00 ± 0.21 OUR AVERAGE				Error includes scale factor of 2.2. See the ideogram below.	
2.00 ± 0.12 ± 0.18	22k	¹ BESSON	07	CLEO	$e^+e^- \rightarrow \Upsilon(2S) \rightarrow \tau^+\tau^-$
1.7 ± 1.5 ± 0.6		HAAS	84B	CLEO	$e^+e^- \rightarrow \tau^+\tau^-$

¹ BESSON 07 reports $[\Gamma(\Upsilon(2S) \rightarrow \tau^+\tau^-)/\Gamma_{total}] / [B(\Upsilon(2S) \rightarrow \mu^+\mu^-)] = 1.04 \pm 0.04 \pm 0.05$ which we multiply by our best value $B(\Upsilon(2S) \rightarrow \mu^+\mu^-) = (1.93 \pm 0.17) \times 10^{-2}$. Our first error is their experiment's error and our second error is the systematic error from using our best value.

$\Gamma(\mu^+\mu^-)/\Gamma_{total}$		Γ_4/Γ			
VALUE	CL%	EVTS	DOCUMENT ID	TECN	COMMENT
0.0193 ± 0.0017 OUR AVERAGE					Error includes scale factor of 2.2. See the ideogram below.
0.0203 ± 0.0003 ± 0.0008		120k	ADAMS	05	CLEO $e^+e^- \rightarrow \mu^+\mu^-$
0.0122 ± 0.0028 ± 0.0019			¹ KOBEL	92	CBAL $e^+e^- \rightarrow \mu^+\mu^-$
0.0138 ± 0.0025 ± 0.0015			KAARSBERG	89	CSB2 $e^+e^- \rightarrow \mu^+\mu^-$
0.009 ± 0.006 ± 0.006			² ALBRECHT	85	ARG $e^+e^- \rightarrow \mu^+\mu^-$
0.018 ± 0.008 ± 0.005			HAAS	84B	CLEO $e^+e^- \rightarrow \mu^+\mu^-$
< 0.038		90	NICZYPORUK	81c	LENA $e^+e^- \rightarrow \mu^+\mu^-$

- ¹ We do not use the following data for averages, fits, limits, etc. ● ● ●

WEIGHTED AVERAGE
0.0193 ± 0.0017 (Error scaled by 2.2)



- ¹ Taking into account interference between the resonance and continuum.
- ² Re-evaluated using $B(\Upsilon(1S) \rightarrow \mu^+\mu^-) = 0.026$.

$\Gamma(\tau^+\tau^-)/\Gamma(\mu^+\mu^-)$		Γ_3/Γ_4			
VALUE	EVTS	DOCUMENT ID	TECN	COMMENT	
1.04 ± 0.04 ± 0.05	22k	BESSON	07	CLEO	$e^+e^- \rightarrow \Upsilon(2S)$

$\Gamma(\Upsilon(1S)\pi^0)/\Gamma_{total}$		Γ_6/Γ			
VALUE (units 10^{-5})	CL%	DOCUMENT ID	TECN	COMMENT	
< 4	90	¹ TAMPONI	13	BELL	$e^+e^- \rightarrow \Upsilon(1S)\pi^0$
< 18	90	² HE	08A	CLEO	$e^+e^- \rightarrow \ell^+\ell^-\gamma\gamma$
< 110	90	ALEXANDER	98	CLE2	$e^+e^- \rightarrow \ell^+\ell^-\gamma\gamma$
< 800	90	LURZ	87	CBAL	$e^+e^- \rightarrow \ell^+\ell^-\gamma\gamma$

¹ TAMPONI 13 reports $[\Gamma(\Upsilon(2S) \rightarrow \Upsilon(1S)\pi^0)/\Gamma_{total}] / [B(\Upsilon(2S) \rightarrow \Upsilon(1S)\pi^+\pi^-)] < 2.3 \times 10^{-4}$ which we multiply by our best value $B(\Upsilon(2S) \rightarrow \Upsilon(1S)\pi^+\pi^-) = 17.85 \times 10^{-2}$.

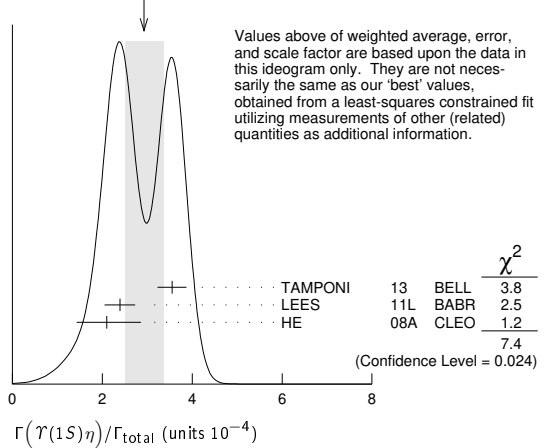
² Authors assume $B(\Upsilon(1S) \rightarrow e^+e^-) + B(\Upsilon(1S) \rightarrow \mu^+\mu^-) = 4.96\%$.

$\Gamma(\Upsilon(1S)\pi^0)/\Gamma(\Upsilon(1S)\pi^+\pi^-)$		Γ_6/Γ_1			
VALUE (units 10^{-4})	CL%	DOCUMENT ID	TECN	COMMENT	
< 2.3	90	TAMPONI	13	BELL	$e^+e^- \rightarrow \Upsilon(1S)\pi^0$

$\Gamma(\Upsilon(1S)\eta)/\Gamma_{total}$		Γ_7/Γ			
VALUE (units 10^{-4})	CL%	EVTS	DOCUMENT ID	TECN	COMMENT
2.9 ± 0.4 OUR FIT					Error includes scale factor of 2.0.
2.9 ± 0.4 OUR AVERAGE					Error includes scale factor of 1.9. See the ideogram below.
2.39 ± 0.31 ± 0.14		112	¹ LEES	11L	BABR $\Upsilon(2S) \rightarrow \ell^+\ell^-\eta$
2.1 ± 0.7 ± 0.3		14	² HE	08A	CLEO $e^+e^- \rightarrow \ell^+\ell^-\eta$

- ● ● We do not use the following data for averages but not for fits. ● ● ●
- 3.55 ± 0.32 ± 0.05 241 ³ TAMPONI 13 BELL $e^+e^- \rightarrow \Upsilon(1S)\eta$
- ● ● We do not use the following data for averages, fits, limits, etc. ● ● ●
- < 9 90 ^{1,4} AUBERT 08BP BABR $e^+e^- \rightarrow \gamma\pi^+\pi^-\pi^0\ell^+\ell^-$
- < 28 90 ALEXANDER 98 CLE2 $e^+e^- \rightarrow \ell^+\ell^-\eta$
- < 50 90 ALBRECHT 87 ARG $e^+e^- \rightarrow \pi^+\pi^-\ell^+\ell^-MM$
- < 70 90 LURZ 87 CBAL $e^+e^- \rightarrow \ell^+\ell^-(\gamma\gamma, 3\pi^0)$
- < 100 90 BESSON 84 CLEO $e^+e^- \rightarrow \pi^+\pi^-\ell^+\ell^-MM$
- < 20 90 FONSECA 84 CUSB $e^+e^- \rightarrow \ell^+\ell^-(\gamma\gamma, \pi^+\pi^-\pi^0)$

WEIGHTED AVERAGE
2.9 ± 0.4 (Error scaled by 1.9)



- ¹ Using $B(\Upsilon(1S) \rightarrow e^+e^-) = (2.38 \pm 0.11)\%$ and $B(\Upsilon(1S) \rightarrow \mu^+\mu^-) = (2.48 \pm 0.05)\%$.
- ² Authors assume $B(\Upsilon(1S) \rightarrow e^+e^-) + B(\Upsilon(1S) \rightarrow \mu^+\mu^-) = 4.96\%$.
- ³ TAMPONI 13 reports $[\Gamma(\Upsilon(2S) \rightarrow \Upsilon(1S)\eta)/\Gamma_{total}] / [B(\Upsilon(2S) \rightarrow \Upsilon(1S)\pi^+\pi^-)] = (1.99 \pm 0.14 \pm 0.11) \times 10^{-3}$ which we multiply by our best value $B(\Upsilon(2S) \rightarrow \Upsilon(1S)\pi^+\pi^-) = (17.85 \pm 0.26) \times 10^{-2}$. Our first error is their experiment's error and our second error is the systematic error from using our best value.
- ⁴ Using $\Gamma_{ee}(\Upsilon(2S)) = 0.612 \pm 0.011$ keV.

$\Gamma(\Upsilon(1S)\eta)/\Gamma(\Upsilon(1S)\pi^+\pi^-)$		Γ_7/Γ_1			
VALUE (units 10^{-3})	CL%	EVTS	DOCUMENT ID	TECN	COMMENT
1.64 ± 0.25 OUR FIT					Error includes scale factor of 2.0.
1.99 ± 0.14 ± 0.11		241	TAMPONI	13	BELL $e^+e^- \rightarrow \Upsilon(1S)\eta$

- ● ● We do not use the following data for averages, fits, limits, etc. ● ● ●
- 1.35 ± 0.17 ± 0.08 ¹ LEES 11L BABR $\Upsilon(2S) \rightarrow (\pi^+\pi^-)(\gamma\gamma)\mu^+\mu^-$
- < 5.2 90 ² AUBERT 08BP BABR $e^+e^- \rightarrow \gamma\pi^+\pi^-(\pi^0)\ell^+\ell^-$
- ¹ Not independent of other values reported by LEES 11L.
- ² Not independent of other values reported by AUBERT 08BP.

$\Gamma(\Upsilon(1S)\pi^0)/\Gamma(\Upsilon(1S)\eta)$		Γ_6/Γ_7			
VALUE	CL%	DOCUMENT ID	TECN	COMMENT	
< 0.13	90	TAMPONI	13	BELL	$e^+e^- \rightarrow \Upsilon(1S)\pi^0$

$\Gamma(J/\psi(1S) \text{ anything})/\Gamma_{\text{total}}$					Γ_8/Γ
VALUE	CL%	DOCUMENT ID	TECN	COMMENT	
<0.006	90	MASCHMANN 90	CBAL	$e^+ e^- \rightarrow \text{hadrons}$	

$\Gamma(J/\psi(1S) \eta_c)/\Gamma_{\text{total}}$					Γ_9/Γ
VALUE	CL%	DOCUMENT ID	TECN	COMMENT	
$<5.4 \times 10^{-6}$	90	YANG	14	BELL $e^+ e^- \rightarrow J/\psi X$	

$\Gamma(J/\psi(1S) \chi_{c0})/\Gamma_{\text{total}}$					Γ_{10}/Γ
VALUE	CL%	DOCUMENT ID	TECN	COMMENT	
$<3.4 \times 10^{-6}$	90	YANG	14	BELL $e^+ e^- \rightarrow J/\psi X$	

$\Gamma(J/\psi(1S) \chi_{c1})/\Gamma_{\text{total}}$					Γ_{11}/Γ
VALUE	CL%	DOCUMENT ID	TECN	COMMENT	
$<1.2 \times 10^{-6}$	90	YANG	14	BELL $e^+ e^- \rightarrow J/\psi X$	

$\Gamma(J/\psi(1S) \chi_{c2})/\Gamma_{\text{total}}$					Γ_{12}/Γ
VALUE	CL%	DOCUMENT ID	TECN	COMMENT	
$<2.0 \times 10^{-6}$	90	YANG	14	BELL $e^+ e^- \rightarrow J/\psi X$	

$\Gamma(J/\psi(1S) \eta_c(2S))/\Gamma_{\text{total}}$					Γ_{13}/Γ
VALUE	CL%	DOCUMENT ID	TECN	COMMENT	
$<2.5 \times 10^{-6}$	90	YANG	14	BELL $e^+ e^- \rightarrow J/\psi X$	

$\Gamma(J/\psi(1S) X(3940))/\Gamma_{\text{total}}$					Γ_{14}/Γ
VALUE	CL%	DOCUMENT ID	TECN	COMMENT	
$<2.0 \times 10^{-6}$	90	YANG	14	BELL $e^+ e^- \rightarrow J/\psi X$	

$\Gamma(J/\psi(1S) X(4160))/\Gamma_{\text{total}}$					Γ_{15}/Γ
VALUE	CL%	DOCUMENT ID	TECN	COMMENT	
$<2.0 \times 10^{-6}$	90	YANG	14	BELL $e^+ e^- \rightarrow J/\psi X$	

$\Gamma(\chi_{c1} \text{ anything})/\Gamma_{\text{total}}$					Γ_{16}/Γ
VALUE (units 10^{-4})	EVTS	DOCUMENT ID	TECN	COMMENT	
$2.24 \pm 0.44 \pm 0.20$	376	JIA	17	BELL $\Upsilon(2S) \rightarrow \gamma J/\psi(1S)$	

$\Gamma(\chi_{c1}(1P)^0 X_{tetra})/\Gamma_{\text{total}}$					Γ_{17}/Γ
VALUE	CL%	DOCUMENT ID	TECN	COMMENT	
$<36.7 \times 10^{-6}$	90	¹ JIA	17A	BELL $e^+ e^- \rightarrow \text{hadrons}$	

¹ For a tetraquark state X_{tetra} , with mass in the range 1.16–2.46 GeV and width in the range 0–0.3 GeV. Measured 90% CL limits as a function of X_{tetra} mass and width range from 4.4×10^{-6} to 36.7×10^{-6} .

$\Gamma(\chi_{c2} \text{ anything})/\Gamma_{\text{total}}$					Γ_{18}/Γ
VALUE (units 10^{-4})	EVTS	DOCUMENT ID	TECN	COMMENT	
$2.28 \pm 0.73 \pm 0.34$		JIA	17	BELL $\Upsilon(2S) \rightarrow \gamma J/\psi(1S)$	

$\Gamma(\psi(2S) \eta_c)/\Gamma_{\text{total}}$					Γ_{19}/Γ
VALUE	CL%	DOCUMENT ID	TECN	COMMENT	
$<5.1 \times 10^{-6}$	90	YANG	14	BELL $e^+ e^- \rightarrow \psi(2S) X$	

$\Gamma(\psi(2S) \chi_{c0})/\Gamma_{\text{total}}$					Γ_{20}/Γ
VALUE	CL%	DOCUMENT ID	TECN	COMMENT	
$<4.7 \times 10^{-6}$	90	YANG	14	BELL $e^+ e^- \rightarrow \psi(2S) X$	

$\Gamma(\psi(2S) \chi_{c1})/\Gamma_{\text{total}}$					Γ_{21}/Γ
VALUE	CL%	DOCUMENT ID	TECN	COMMENT	
$<2.5 \times 10^{-6}$	90	YANG	14	BELL $e^+ e^- \rightarrow \psi(2S) X$	

$\Gamma(\psi(2S) \chi_{c2})/\Gamma_{\text{total}}$					Γ_{22}/Γ
VALUE	CL%	DOCUMENT ID	TECN	COMMENT	
$<1.9 \times 10^{-6}$	90	YANG	14	BELL $e^+ e^- \rightarrow \psi(2S) X$	

$\Gamma(\psi(2S) \eta_c(2S))/\Gamma_{\text{total}}$					Γ_{23}/Γ
VALUE	CL%	DOCUMENT ID	TECN	COMMENT	
$<3.3 \times 10^{-6}$	90	YANG	14	BELL $e^+ e^- \rightarrow \psi(2S) X$	

$\Gamma(\psi(2S) X(3940))/\Gamma_{\text{total}}$					Γ_{24}/Γ
VALUE	CL%	DOCUMENT ID	TECN	COMMENT	
$<3.9 \times 10^{-6}$	90	YANG	14	BELL $e^+ e^- \rightarrow \psi(2S) X$	

$\Gamma(\psi(2S) X(4160))/\Gamma_{\text{total}}$					Γ_{25}/Γ
VALUE	CL%	DOCUMENT ID	TECN	COMMENT	
$<3.9 \times 10^{-6}$	90	YANG	14	BELL $e^+ e^- \rightarrow \psi(2S) X$	

$\Gamma(Z_c(3900)^+ Z_c(3900)^-)/\Gamma_{\text{total}}$					Γ_{26}/Γ
VALUE	CL%	DOCUMENT ID	TECN	COMMENT	
$<1.0 \times 10^{-6}$	90	¹ JIA	18	BELL $\Upsilon(2S) \rightarrow J/\psi \pi^\pm X$	

¹ Assuming $B(Z_c(3900)^\pm \rightarrow J/\psi \pi^\pm) = 1$.

$\Gamma(Z_c(4200)^+ Z_c(4200)^-)/\Gamma_{\text{total}}$					Γ_{27}/Γ
VALUE	CL%	DOCUMENT ID	TECN	COMMENT	
$<16.7 \times 10^{-6}$	90	¹ JIA	18	BELL $\Upsilon(1S) \rightarrow J/\psi \pi^\pm X$	

¹ Assuming $B(Z_c(4200)^\pm \rightarrow J/\psi \pi^\pm) = 1$.

$\Gamma(Z_c(3900)^\pm Z_c(4200)^\mp)/\Gamma_{\text{total}}$					Γ_{28}/Γ
VALUE	CL%	DOCUMENT ID	TECN	COMMENT	
$<7.3 \times 10^{-6}$	90	¹ JIA	18	BELL $\Upsilon(2S) \rightarrow J/\psi \pi^\pm X$	

¹ Assuming $B(Z_c(4200)^\pm \rightarrow J/\psi \pi^\pm) = 1 = B(Z_c(3900)^\pm \rightarrow J/\psi \pi^\pm)$.

$\Gamma(X(4050)^+ X(4050)^-)/\Gamma_{\text{total}}$					Γ_{29}/Γ
VALUE	CL%	DOCUMENT ID	TECN	COMMENT	
$<13.5 \times 10^{-6}$	90	¹ JIA	18	BELL $\Upsilon(2S) \rightarrow \chi_{c1}(1P) \pi^\pm X$	

¹ Assuming $B(X(4050)^\pm \rightarrow \chi_{c1}(1P) \pi^\pm)$

$\Gamma(X(4250)^+ X(4250)^-)/\Gamma_{\text{total}}$					Γ_{30}/Γ
VALUE	CL%	DOCUMENT ID	TECN	COMMENT	
$<26.7 \times 10^{-6}$	90	¹ JIA	18	BELL $\Upsilon(2S) \rightarrow \chi_{c1}(1P) \pi^\pm X$	

¹ Assuming $B(X(4250)^\pm \rightarrow \chi_{c1}(1P) \pi^\pm) = 1$

$\Gamma(X(4050)^\pm X(4250)^\mp)/\Gamma_{\text{total}}$					Γ_{31}/Γ
VALUE	CL%	DOCUMENT ID	TECN	COMMENT	
$<27.2 \times 10^{-6}$	90	¹ JIA	18	BELL $\Upsilon(2S) \rightarrow \chi_{c1}(1P) \pi^\pm X$	

¹ Assuming $B(X(4050)^\pm \rightarrow \chi_{c1}(1P) \pi^\pm) = 1 = B(X(4250)^\pm \rightarrow \chi_{c1}(1P) \pi^\pm)$

$\Gamma(Z_c(4430)^+ Z_c(4430)^-)/\Gamma_{\text{total}}$					Γ_{32}/Γ
VALUE	CL%	DOCUMENT ID	TECN	COMMENT	
$<20.3 \times 10^{-6}$	90	¹ JIA	18	BELL $\Upsilon(2S) \rightarrow \psi(2S) \pi^\pm X$	

¹ Assuming $B(Z_c(4430)^\pm \rightarrow \psi(2P) \pi^\pm) = 1$

$\Gamma(X(4055)^\pm X(4055)^\mp)/\Gamma_{\text{total}}$					Γ_{33}/Γ
VALUE	CL%	DOCUMENT ID	TECN	COMMENT	
$<11.1 \times 10^{-6}$	90	¹ JIA	18	BELL $\Upsilon(2S) \rightarrow \psi(2S) \pi^\pm X$	

¹ Assuming $B(X(4055)^\pm \rightarrow \psi(2S) \pi^\pm) = 1$

$\Gamma(X(4055)^\pm Z_c(4430)^\mp)/\Gamma_{\text{total}}$					Γ_{34}/Γ
VALUE	CL%	DOCUMENT ID	TECN	COMMENT	
$<21.1 \times 10^{-6}$	90	¹ JIA	18	BELL $\Upsilon(2S) \rightarrow \psi(2S) \pi^\pm X$	

¹ Assuming $B(X(4055)^\pm \rightarrow \psi(2S) \pi^\pm) = 1 = B(Z_c(4430)^\pm \rightarrow \psi(2S) \pi^\pm)$

$\Gamma(\overline{2}H \text{ anything})/\Gamma_{\text{total}}$					Γ_{35}/Γ
VALUE (units 10^{-5})	EVTS	DOCUMENT ID	TECN	COMMENT	
$2.78^{+0.30}_{-0.26}$	OUR AVERAGE			Error includes scale factor of 1.2.	

$2.64 \pm 0.11^{+0.26}_{-0.21}$		LEES	14G	BABR $e^+ e^- \rightarrow \overline{2}H X$	
$3.37 \pm 0.50 \pm 0.25$	58	ASNER	07	CLEO $e^+ e^- \rightarrow \overline{2}H X$	

$\Gamma(g g g)/\Gamma_{\text{total}}$					Γ_{37}/Γ
VALUE (units 10^{-2})	EVTS	DOCUMENT ID	TECN	COMMENT	
58.8 ± 1.2	6M	¹ BESSON	06A	CLEO $\Upsilon(2S) \rightarrow \text{hadrons}$	

¹ Calculated using the value $\Gamma(\gamma g g)/\Gamma(g g g) = (3.18 \pm 0.04 \pm 0.22 \pm 0.41)\%$ from BESSON 06A and PDG 08 values of $B(\pi^+ \pi^- \Upsilon(1S)) = (18.1 \pm 0.4)\%$, $B(\pi^0 \pi^0 \Upsilon(1S)) = (8.6 \pm 0.4)\%$, $B(\mu^+ \mu^-) = (1.93 \pm 0.17)\%$, and $R_{\text{hadrons}} = 3.51$. The statistical error is negligible and the systematic error is partially correlated with that of $\Gamma(\gamma g g)/\Gamma_{\text{total}}$ measurement of BESSON 06A.

$\Gamma(\gamma g g)/\Gamma(g g g)$					Γ_{38}/Γ_{37}
VALUE (units 10^{-2})	EVTS	DOCUMENT ID	TECN	COMMENT	
$3.18 \pm 0.04 \pm 0.47$	6M	BESSON	06A	CLEO $\Upsilon(2S) \rightarrow (\gamma + \gamma) \text{ hadrons}$	

$\Gamma(\phi K^+ K^-)/\Gamma_{\text{total}}$					Γ_{39}/Γ
VALUE (units 10^{-6})	EVTS	DOCUMENT ID	TECN	COMMENT	
$1.58 \pm 0.33 \pm 0.18$	58	SHEN	12A	BELL $\Upsilon(1S) \rightarrow 2(K^+ K^-)$	

$\Gamma(\omega \pi^+ \pi^-)/\Gamma_{\text{total}}$					Γ_{40}/Γ
VALUE (units 10^{-6})	CL%	DOCUMENT ID	TECN	COMMENT	
<2.58	90	SHEN	12A	BELL $\Upsilon(1S) \rightarrow 2(\pi^+ \pi^-) \pi^0$	

$\Gamma(K^*(892)^0 K^- \pi^+ + c.c.)/\Gamma_{\text{total}}$					Γ_{41}/Γ
VALUE (units 10^{-6})	EVTS	DOCUMENT ID	TECN	COMMENT	
$2.32 \pm 0.40 \pm 0.54$	135	SHEN	12A	BELL $\Upsilon(1S) \rightarrow K^+ K^- \pi^+ \pi^-$	

$\Gamma(\phi f_2'(1525))/\Gamma_{\text{total}}$					Γ_{42}/Γ
VALUE (units 10^{-6})	CL%	DOCUMENT ID	TECN	COMMENT	
<1.33	90	SHEN	12A	BELL $\Upsilon(1S) \rightarrow 2(K^+ K^-)$	

$\Gamma(\omega f_2(1270))/\Gamma_{\text{total}}$					Γ_{43}/Γ
VALUE (units 10^{-6})	CL%	DOCUMENT ID	TECN	COMMENT	
<0.57	90	SHEN	12A	BELL $\Upsilon(1S) \rightarrow 2(\pi^+ \pi^-) \pi^0$	

$\Gamma(\rho(770) a_2(1320))/\Gamma_{\text{total}}$					Γ_{44}/Γ
VALUE (units 10^{-6})	CL%	DOCUMENT ID	TECN	COMMENT	
<0.88	90	SHEN	12A	BELL $\Upsilon(1S) \rightarrow 2(\pi^+ \pi^-) \pi^0$	

Meson Particle Listings

$\Upsilon(2S)$

$\Gamma(K^*(892)^0 \overline{K}_S^0(1430)^0 + c.c.)/\Gamma_{total}$				Γ_{45}/Γ
VALUE (units 10^{-6})	EVTS	DOCUMENT ID	TECN	COMMENT
$1.53 \pm 0.52 \pm 0.19$	32	SHEN	12A	BELL $\Upsilon(1S) \rightarrow K^+ K^- \pi^+ \pi^-$

$\Gamma(K_1(1270)^\pm K^\mp)/\Gamma_{total}$				Γ_{46}/Γ
VALUE (units 10^{-6})	CL%	DOCUMENT ID	TECN	COMMENT
< 3.22	90	SHEN	12A	BELL $\Upsilon(1S) \rightarrow K^+ K^- \pi^+ \pi^-$

$\Gamma(K_1(1400)^\pm K^\mp)/\Gamma_{total}$				Γ_{47}/Γ
VALUE (units 10^{-6})	CL%	DOCUMENT ID	TECN	COMMENT
< 0.83	90	SHEN	12A	BELL $\Upsilon(1S) \rightarrow K^+ K^- \pi^+ \pi^-$

$\Gamma(b_1(1235)^\pm \pi^\mp)/\Gamma_{total}$				Γ_{48}/Γ
VALUE (units 10^{-6})	CL%	DOCUMENT ID	TECN	COMMENT
< 0.40	90	SHEN	12A	BELL $\Upsilon(1S) \rightarrow 2(\pi^+ \pi^-) \pi^0$

$\Gamma(\rho\pi)/\Gamma_{total}$				Γ_{49}/Γ
VALUE (units 10^{-6})	CL%	DOCUMENT ID	TECN	COMMENT
< 1.16	90	SHEN	13	BELL $\Upsilon(2S) \rightarrow \pi^+ \pi^- \pi^0$

$\Gamma(\pi^+ \pi^- \pi^0)/\Gamma_{total}$				Γ_{50}/Γ
VALUE (units 10^{-6})	CL%	DOCUMENT ID	TECN	COMMENT
< 0.80	90	SHEN	13	BELL $\Upsilon(2S) \rightarrow \pi^+ \pi^- \pi^0$

$\Gamma(\omega\pi^0)/\Gamma_{total}$				Γ_{51}/Γ
VALUE (units 10^{-6})	CL%	DOCUMENT ID	TECN	COMMENT
< 1.63	90	SHEN	13	BELL $\Upsilon(2S) \rightarrow \pi^+ \pi^- \pi^0 \pi^0$

$\Gamma(\pi^+ \pi^- \pi^0 \pi^0)/\Gamma_{total}$				Γ_{52}/Γ
VALUE (units 10^{-6})	EVTS	DOCUMENT ID	TECN	COMMENT
$13.0 \pm 1.9 \pm 2.1$	261 ± 37	SHEN	13	BELL $\Upsilon(2S) \rightarrow \pi^+ \pi^- \pi^0 \pi^0$

$\Gamma(K_S^0 K^+ \pi^- + c.c.)/\Gamma_{total}$				Γ_{53}/Γ	
VALUE (units 10^{-6})	CL%	EVTS	DOCUMENT ID	TECN	COMMENT
$1.14 \pm 0.30 \pm 0.13$		40 ± 10	SHEN	13	BELL $\Upsilon(2S) \rightarrow K_S^0 K^- \pi^+$
••• We do not use the following data for averages, fits, limits, etc. •••					
< 3.2	90		¹ DOBBS	12A	$\Upsilon(2S) \rightarrow K_S^0 K^- \pi^+$
¹ Obtained by analyzing CLEO III data but not authored by the CLEO Collaboration.					

$\Gamma(K^*(892)^0 \overline{K}^0 + c.c.)/\Gamma_{total}$				Γ_{54}/Γ
VALUE (units 10^{-6})	CL%	DOCUMENT ID	TECN	COMMENT
< 4.22	90	SHEN	13	BELL $\Upsilon(2S) \rightarrow K_S^0 K^- \pi^+$

$\Gamma(K^*(892)^- K^+ + c.c.)/\Gamma_{total}$				Γ_{55}/Γ
VALUE (units 10^{-6})	CL%	DOCUMENT ID	TECN	COMMENT
< 1.45	90	SHEN	13	BELL $\Upsilon(2S) \rightarrow K_S^0 K^- \pi^+$

$\Gamma(f_1(1285) \text{ anything})/\Gamma_{total}$				Γ_{56}/Γ
VALUE (units 10^{-3})	EVTS	DOCUMENT ID	TECN	COMMENT
$2.20 \pm 1.50 \pm 0.63$	2.9k	JIA	17A	BELL $e^+ e^- \rightarrow \text{hadrons}$

$\Gamma(f_1(1285) X_{tetra})/\Gamma_{total}$				Γ_{57}/Γ	
VALUE	CL%	DOCUMENT ID	TECN	COMMENT	
$< 64.7 \times 10^{-6}$		90	¹ JIA	17A	BELL $e^+ e^- \rightarrow \text{hadrons}$
¹ For a tetraquark state X_{tetra} , with mass in the range 1.16–2.46 GeV and width in the range 0–0.3 GeV. Measured 90% CL limits as a function of X_{tetra} mass and width range from 7.8×10^{-6} to 64.7×10^{-6} .					

$\Gamma(\text{Sum of 100 exclusive modes})/\Gamma_{total}$				Γ_{58}/Γ	
VALUE (units 10^{-2})		DOCUMENT ID	TECN	COMMENT	
0.29 ± 0.03		1,2	DOBBS	12A	$\Upsilon(2S) \rightarrow \text{hadrons}$
¹ DOBBS 12A presents individual exclusive branching fractions or upper limits for 100 modes of four to ten pions, kaons, or protons.					
² Obtained by analyzing CLEO III data but not authored by the CLEO Collaboration.					

$\Gamma(\gamma\chi_{b1}(1P))/\Gamma_{total}$				Γ_{59}/Γ
VALUE	EVTS	DOCUMENT ID	TECN	COMMENT
0.069 ± 0.004 OUR AVERAGE				
$0.0693 \pm 0.0012 \pm 0.0041$	407k	ARTUSO	05	CLEO $e^+ e^- \rightarrow \gamma X$
$0.069 \pm 0.005 \pm 0.009$		EDWARDS	99	CLE2 $\Upsilon(2S) \rightarrow \gamma\chi(1P)$
$0.091 \pm 0.018 \pm 0.022$		ALBRECHT	85E	ARG $e^+ e^- \rightarrow \gamma \text{conv. } X$
$0.065 \pm 0.007 \pm 0.012$		NERNST	85	CBAL $e^+ e^- \rightarrow \gamma X$
$0.080 \pm 0.017 \pm 0.016$		HAAS	84	CLEO $e^+ e^- \rightarrow \gamma \text{conv. } X$
0.059 ± 0.014		KLOPFEN...	83	CUSB $e^+ e^- \rightarrow \gamma X$

$\Gamma(\gamma\chi_{b2}(1P))/\Gamma_{total}$				Γ_{60}/Γ
VALUE	EVTS	DOCUMENT ID	TECN	COMMENT
0.0715 ± 0.0035 OUR AVERAGE				
$0.0724 \pm 0.0011 \pm 0.0040$	410k	ARTUSO	05	CLEO $e^+ e^- \rightarrow \gamma X$
$0.074 \pm 0.005 \pm 0.008$		EDWARDS	99	CLE2 $\Upsilon(2S) \rightarrow \gamma\chi(1P)$

$0.098 \pm 0.021 \pm 0.024$		ALBRECHT	85E	ARG $e^+ e^- \rightarrow \gamma \text{conv. } X$
$0.058 \pm 0.007 \pm 0.010$		NERNST	85	CBAL $e^+ e^- \rightarrow \gamma X$
$0.102 \pm 0.018 \pm 0.021$		HAAS	84	CLEO $e^+ e^- \rightarrow \gamma \text{conv. } X$
0.061 ± 0.014		KLOPFEN...	83	CUSB $e^+ e^- \rightarrow \gamma X$

$\Gamma(\gamma\chi_{b0}(1P))/\Gamma_{total}$				Γ_{61}/Γ
VALUE	EVTS	DOCUMENT ID	TECN	COMMENT
0.038 ± 0.004 OUR AVERAGE				
$0.0375 \pm 0.0012 \pm 0.0047$	198k	ARTUSO	05	CLEO $e^+ e^- \rightarrow \gamma X$
$0.034 \pm 0.005 \pm 0.006$		EDWARDS	99	CLE2 $\Upsilon(2S) \rightarrow \gamma\chi(1P)$
$0.064 \pm 0.014 \pm 0.016$		ALBRECHT	85E	ARG $e^+ e^- \rightarrow \gamma \text{conv. } X$
$0.036 \pm 0.008 \pm 0.009$		NERNST	85	CBAL $e^+ e^- \rightarrow \gamma X$
$0.044 \pm 0.023 \pm 0.009$		HAAS	84	CLEO $e^+ e^- \rightarrow \gamma \text{conv. } X$
••• We do not use the following data for averages, fits, limits, etc. •••				
0.035 ± 0.014		KLOPFEN...	83	CUSB $e^+ e^- \rightarrow \gamma X$

$\Gamma(\gamma f_0(1710))/\Gamma_{total}$				Γ_{62}/Γ
VALUE (units 10^{-5})	CL%	DOCUMENT ID	TECN	COMMENT
< 59	90	¹ ALBRECHT	89	ARG $\Upsilon(2S) \rightarrow \gamma K^+ K^-$
••• We do not use the following data for averages, fits, limits, etc. •••				
< 5.9	90	² ALBRECHT	89	ARG $\Upsilon(2S) \rightarrow \gamma \pi^+ \pi^-$
¹ Re-evaluated assuming $B(f_0(1710) \rightarrow K^+ K^-) = 0.19$.				
² Includes unknown branching ratio of $f_0(1710) \rightarrow \pi^+ \pi^-$.				

$\Gamma(\gamma f'_2(1525))/\Gamma_{total}$				Γ_{63}/Γ
VALUE (units 10^{-5})	CL%	DOCUMENT ID	TECN	COMMENT
< 53	90	¹ ALBRECHT	89	ARG $\Upsilon(2S) \rightarrow \gamma K^+ K^-$
¹ Re-evaluated assuming $B(f'_2(1525) \rightarrow K \overline{K}) = 0.71$.				

$\Gamma(\gamma f_2(1270))/\Gamma_{total}$				Γ_{64}/Γ
VALUE (units 10^{-5})	CL%	DOCUMENT ID	TECN	COMMENT
< 24.1	90	¹ ALBRECHT	89	ARG $\Upsilon(2S) \rightarrow \gamma \pi^+ \pi^-$
¹ Using $B(f_2(1270) \rightarrow \pi\pi) = 0.84$.				

$\Gamma(\gamma f_J(2220))/\Gamma_{total}$				Γ_{65}/Γ
VALUE (units 10^{-5})	CL%	DOCUMENT ID	TECN	COMMENT
< 6.8	90	¹ ALBRECHT	89	ARG $\Upsilon(2S) \rightarrow \gamma K^+ K^-$
••• We do not use the following data for averages, fits, limits, etc. •••				
¹ Includes unknown branching ratio of $f_J(2220) \rightarrow K^+ K^-$.				

$\Gamma(\gamma\eta_c(1S))/\Gamma_{total}$				Γ_{66}/Γ
VALUE	CL%	DOCUMENT ID	TECN	COMMENT
$< 2.7 \times 10^{-5}$	90	WANG	11B	BELL $\Upsilon(2S) \rightarrow \gamma X$

$\Gamma(\gamma\chi_{c0})/\Gamma_{total}$				Γ_{67}/Γ
VALUE	CL%	DOCUMENT ID	TECN	COMMENT
$< 1.0 \times 10^{-4}$	90	WANG	11B	BELL $\Upsilon(2S) \rightarrow \gamma X$

$\Gamma(\gamma\chi_{c1})/\Gamma_{total}$				Γ_{68}/Γ
VALUE	CL%	DOCUMENT ID	TECN	COMMENT
$< 3.6 \times 10^{-6}$	90	WANG	11B	BELL $\Upsilon(2S) \rightarrow \gamma X$

$\Gamma(\gamma\chi_{c2})/\Gamma_{total}$				Γ_{69}/Γ
VALUE	CL%	DOCUMENT ID	TECN	COMMENT
$< 1.5 \times 10^{-5}$	90	WANG	11B	BELL $\Upsilon(2S) \rightarrow \gamma X$

$\Gamma(\gamma\chi_{c1}(3872))/\Gamma_{total}$				Γ_{70}/Γ
VALUE	CL%	DOCUMENT ID	TECN	COMMENT
$< 2.1 \times 10^{-5}$	90	¹ WANG	11B	BELL $\Upsilon(2S) \rightarrow \gamma X$
¹ WANG 11B reports $[\Gamma(\Upsilon(2S) \rightarrow \gamma\chi_{c1}(3872))/\Gamma_{total}] \times [B(\chi_{c1}(3872) \rightarrow \pi^+ \pi^- J/\psi(1S))] < 0.8 \times 10^{-6}$ which we divide by our best value $B(\chi_{c1}(3872) \rightarrow \pi^+ \pi^- J/\psi(1S)) = 3.8 \times 10^{-2}$.				

$\Gamma(\gamma\chi_{c1}(3872), \chi_{c1} \rightarrow \pi^+ \pi^- \pi^0 J/\psi)/\Gamma_{total}$				Γ_{71}/Γ
VALUE	CL%	DOCUMENT ID	TECN	COMMENT
$< 2.4 \times 10^{-6}$	90	WANG	11B	BELL $\Upsilon(2S) \rightarrow \gamma X$

$\Gamma(\gamma\chi_{c0}(3915) \rightarrow \omega J/\psi)/\Gamma_{total}$				Γ_{72}/Γ
VALUE	CL%	DOCUMENT ID	TECN	COMMENT
$< 2.8 \times 10^{-6}$	90	WANG	11B	BELL $\Upsilon(2S) \rightarrow \gamma X$

$\Gamma(\gamma\chi_{c1}(4140) \rightarrow \phi J/\psi)/\Gamma_{total}$				Γ_{73}/Γ
VALUE	CL%	DOCUMENT ID	TECN	COMMENT
$< 1.2 \times 10^{-6}$	90	WANG	11B	BELL $\Upsilon(2S) \rightarrow \gamma X$

$\Gamma(\gamma X(4350) \rightarrow \phi J/\psi)/\Gamma_{total}$				Γ_{74}/Γ
VALUE	CL%	DOCUMENT ID	TECN	COMMENT
$< 1.3 \times 10^{-6}$	90	WANG	11B	BELL $\Upsilon(2S) \rightarrow \gamma X$

See key on page 1127

Meson Particle Listings

$\Upsilon(2S)$, $\Upsilon_2(1D)$

$\Gamma(\gamma\eta_b(1S))/\Gamma_{total}$				Γ_{75}/Γ	
VALUE (units 10^{-4})	CL%	EVTS	DOCUMENT ID	TECN	COMMENT
5.5 ± 0.9			OUR AVERAGE Error includes scale factor of 1.2.		
$6.1^{+0.6+0.9}_{-0.7-0.6}$		29k	FULSOM	18	BELL $\Upsilon(2S) \rightarrow \gamma X$
$3.9 \pm 1.1^{+1.1}_{-0.9}$		$13 \pm 5k$	¹ AUBERT	09Aq	BABR $\Upsilon(2S) \rightarrow \gamma X$
• • • We do not use the following data for averages, fits, limits, etc. • • •					
<21	90		LEES	11J	BABR $\Upsilon(2S) \rightarrow X \gamma$
< 8.4	90		¹ BONVICINI	10	CLEO $\Upsilon(2S) \rightarrow \gamma X$
< 5.1	90		² ARTUSO	05	CLEO $e^+e^- \rightarrow \gamma X$
¹ Assuming $\Gamma_{\eta_b(1S)} = 10$ MeV.					
² Superseded by BONVICINI 10.					

$\Gamma(\gamma\eta_b(1S) \rightarrow \gamma \text{Sum of 26 exclusive modes})/\Gamma_{total}$				Γ_{76}/Γ	
VALUE	CL%	DOCUMENT ID	TECN	COMMENT	
<3.7 x 10⁻⁶	90	SANDILYA	13	BELL	$\Upsilon(2S) \rightarrow \gamma$ hadrons
• • • We do not use the following data for averages, fits, limits, etc. • • •					
$46.2^{+29.7}_{-14.2} \pm 10.6$		10	¹ DOBBS	12	$\Upsilon(2S) \rightarrow \gamma$ hadrons
¹ Obtained by analyzing CLEO III data but not authored by the CLEO Collaboration.					

$\Gamma(\gamma X \text{ } b\bar{b} \rightarrow \gamma \text{Sum of 26 exclusive modes})/\Gamma_{total}$				Γ_{77}/Γ	
VALUE (units 10^{-6})	CL%	DOCUMENT ID	TECN	COMMENT	
< 4.9	90	SANDILYA	13	BELL	$\Upsilon(2S) \rightarrow \gamma$ hadrons
• • • We do not use the following data for averages, fits, limits, etc. • • •					
$46.2^{+29.7}_{-14.2} \pm 10.6$		10	¹ DOBBS	12	$\Upsilon(2S) \rightarrow \gamma$ hadrons
¹ Obtained by analyzing CLEO III data but not authored by the CLEO Collaboration.					

$\Gamma(\gamma A^0 \rightarrow \gamma + \geq 4 \text{ prongs})/\Gamma_{total}$				Γ_{78}/Γ	
(1.5 GeV < m_X < 5.0 GeV)					
VALUE (units 10^{-4})	CL%	DOCUMENT ID	TECN	COMMENT	
<1.95	95	ROSNER	07A	CLEO	$e^+e^- \rightarrow \gamma X$
• • • We do not use the following data for averages, fits, limits, etc. • • •					
$46.2^{+29.7}_{-14.2} \pm 10.6$		10	¹ DOBBS	12	$\Upsilon(2S) \rightarrow \gamma$ hadrons
¹ For a narrow scalar or pseudoscalar A^0 , excluding known resonances, with mass in the range 0.3–7 GeV. Measured 90% CL limits as a function of m_{A^0} range from 1×10^{-6} to 8×10^{-5} .					

$\Gamma(\gamma a_1^0 \rightarrow \gamma \mu^+ \mu^-)/\Gamma_{total}$				Γ_{80}/Γ	
VALUE (units 10^{-6})	CL%	DOCUMENT ID	TECN	COMMENT	
<8.3	90	¹ AUBERT	09Z	BABR	$e^+e^- \rightarrow \gamma a_1^0 \rightarrow \gamma \mu^+ \mu^-$
¹ For a narrow scalar or pseudoscalar a_1^0 with mass in the range 212–9300 MeV, excluding J/ψ and $\psi(2S)$. Measured 90% CL limits as a function of $m_{a_1^0}$ range from 0.26–8.3 x 10^{-6} .					

LEPTON FAMILY NUMBER (LF) VIOLATING MODES

$\Gamma(e^\pm \tau^\mp)/\Gamma_{total}$				Γ_{81}/Γ	
VALUE (units 10^{-6})	CL%	DOCUMENT ID	TECN	COMMENT	
<3.2	90	LEES	10B	BABR	$e^+e^- \rightarrow e^\pm \tau^\mp$
• • • We do not use the following data for averages, fits, limits, etc. • • •					
$46.2^{+29.7}_{-14.2} \pm 10.6$		10	¹ DOBBS	12	$\Upsilon(2S) \rightarrow \gamma$ hadrons
¹ For a narrow scalar or pseudoscalar A^0 , excluding known resonances, with mass in the range 0.3–7 GeV. Measured 90% CL limits as a function of m_{A^0} range from 1×10^{-6} to 8×10^{-5} .					

$\Upsilon(2S)$ Cross-Particle Branching Ratios

$B(\Upsilon(2S) \rightarrow \pi^+ \pi^-) \times B(\Upsilon(3S) \rightarrow \Upsilon(2S) X)$				
VALUE (units 10^{-2})	EVTS	DOCUMENT ID	TECN	COMMENT
$1.78 \pm 0.02 \pm 0.11$	906k	LEES	11c	BABR $e^+e^- \rightarrow \pi^+ \pi^- X$

$\Upsilon(2S)$ REFERENCES

NAME	YEAR	TECN	DOCUMENT ID	TECN	COMMENT
FULSOM	18	PRL	121 232001	B.G. Fulson et al.	(BELLE Collab.)
JIA	18	PR	D97 112004	S. Jia et al.	(BELLE Collab.)
JIA	17	PR	D95 012001	S. Jia et al.	(BELLE Collab.)
JIA	17A	PR	D96 112002	S. Jia et al.	(BELLE Collab.)
LEES	14G	PR	D89 111102	J.P. Lees et al.	(BABAR Collab.)
YANG	14	PR	D90 112008	S.D. Yang et al.	(BELLE Collab.)
SANDILYA	13	PRL	111 112001	S. Sandilya et al.	(BELLE Collab.)
SHEN	13	PR	D88 011102	C.P. Shen et al.	(BELLE Collab.)
TAMPONI	13	PR	D87 011104	U. Tamponi et al.	(BELLE Collab.)
DOBBS	12	PRL	109 082001	S. Dobbs et al.	(CLEO Collab.)
DOBBS	12A	PR	D86 052003	S. Dobbs et al.	(CLEO Collab.)
SHEN	12A	PR	D86 031102	C.P. Shen et al.	(BELLE Collab.)
LEES	11C	PR	D84 011104	J.P. Lees et al.	(BABAR Collab.)
LEES	11H	PRL	107 221803	J.P. Lees et al.	(BABAR Collab.)
LEES	11J	PR	D84 072002	J.P. Lees et al.	(BABAR Collab.)
LEES	11L	PR	D84 092003	J.P. Lees et al.	(BABAR Collab.)
WANG	11B	PR	D84 071107	X.L. Wang et al.	(BELLE Collab.)
BONVICINI	10	PR	D81 031104	G. Bonvicini et al.	(CLEO Collab.)

NAME	YEAR	TECN	DOCUMENT ID	TECN	COMMENT
LEES	10B	PRL	104 151802	J.P. Lees et al.	(BABAR Collab.)
AUBERT	09AQ	PRL	103 161801	B. Aubert et al.	(BABAR Collab.)
AUBERT	09Z	PRL	103 081803	B. Aubert et al.	(BABAR Collab.)
BHARI	09	PR	D79 011103	S.R. Bhari et al.	(CLEO Collab.)
AUBERT	08BP	PR	D78 112002	B. Aubert et al.	(BABAR Collab.)
HE	08A	PRL	101 192001	Q. He et al.	(CLEO Collab.)
LOVE	08A	PRL	101 201601	W. Love et al.	(CLEO Collab.)
PDG	08	PL	B667 1	C. Amsler et al.	(PDG Collab.)
ASNER	07	PR	D75 012009	D.M. Asner et al.	(CLEO Collab.)
BESSON	07	PRL	98 052002	D. Besson et al.	(CLEO Collab.)
ROSNER	07A	PR	D76 117102	J.L. Rosner et al.	(CLEO Collab.)
BESSON	06A	PR	D74 012003	D. Besson et al.	(CLEO Collab.)
ROSNER	06	PRL	96 092003	J.L. Rosner et al.	(CLEO Collab.)
ADAMS	05	PRL	94 012001	G.S. Adams et al.	(CLEO Collab.)
ARTUSO	05	PRL	94 032001	M. Artuso et al.	(CLEO Collab.)
ARTAMONOV	00	PL	B474 427	A.S. Artamonov et al.	(CLEO Collab.)
EDWARDS	99	PR	D59 032003	K.W. Edwards et al.	(CLEO Collab.)
ALEXANDER	98	PR	D58 052004	J.P. Alexander et al.	(CLEO Collab.)
BARU	96	PRPL	267 71	S.E. Baru et al.	(NOVO)
KOBEL	92	ZPHY	C53 193	M. Kobel et al.	(Crystal Ball Collab.)
MASCHMANN	90	ZPHY	C46 555	W.S. Maschmann et al.	(Crystal Ball Collab.)
ALBRECHT	89	ZPHY	C42 349	H. Albrecht et al.	(ARGUS Collab.)
KAAARSBERG	89	PRL	62 2077	T.M. Kaarsberg et al.	(CUSB Collab.)
BUCHMUELLER	88	HE	e ⁺ e ⁻ Physics 412	W. Buchmuller, S. Cooper	(HANN, DESY, MIT)
JAKUBOWSKI	88	ZPHY	C40 49	Z. Jakubowski et al.	(Crystal Ball Collab.)
ALBRECHT	87	ZPHY	C35 283	H. Albrecht et al.	(ARGUS Collab.)
COHEN	87	RMP	59 1121	E.R. Cohen, B.N. Taylor	(RIS, NBS)
LURZ	87	ZPHY	C36 383	B. Lurz et al.	(Crystal Ball Collab.)
BARU	86B	ZPHY	C32 622 (erratum)	S.E. Baru et al.	(NOVO)
ALBRECHT	85	ZPHY	C28 45	H. Albrecht et al.	(ARGUS Collab.)
ALBRECHT	85E	PL	160B 331	H. Albrecht et al.	(ARGUS Collab.)
GELPHMAN	85	PR	D32 2893	D. Gelfhman et al.	(Crystal Ball Collab.)
KURAEV	85	SJNP	41 466	E.A. Kuraev, V.S. Fadin	(NOVO)
Translated from YAF 41 733.					
NERNST	85	PRL	54 2195	R. Nernst et al.	(Crystal Ball Collab.)
ARTAMONOV	84	PL	137B 272	A.S. Artamonov et al.	(NOVO)
BARBER	84	PL	135B 498	D.P. Barber et al.	(CLEO Collab.)
BESSON	84	PR	D30 1433	D. Besson et al.	(CLEO Collab.)
FONSECA	84	NP	B242 31	V. Fonseca et al.	(CUSB Collab.)
GILES	84B	PR	D29 1285	R. Giles et al.	(CLEO Collab.)
HAAS	84	PRL	52 799	J. Haas et al.	(CLEO Collab.)
HAAS	84B	PR	D30 1996	J. Haas et al.	(CLEO Collab.)
KLOPFEN	83	PRL	51 160	C. Klopstein et al.	(CUSB Collab.)
ALBRECHT	82	PL	116B 383	H. Albrecht et al.	(DESY, DORT, HEIDH+)
NICZYPORUK	81C	PL	100B 95	B. Niczyporuk et al.	(LENA Collab.)
NICZYPORUK	81C	PL	99B 169	B. Niczyporuk et al.	(LENA Collab.)
BOCK	80	ZPHY	C6 125	P. Bock et al.	(HEIDP, MPIM, DESY, HAMB)

$\Upsilon_2(1D)$

was $\Upsilon(1D)$

First observed by BONVICINI 04 in the decay to $\gamma\gamma \Upsilon(1S)$ and confirmed by DEL-AMO-SANCHEZ 10R in the decay to $\pi^+\pi^- \Upsilon(1S)$. Data consistent with $J^P = 2^-$. The states with $J = 1$ and 3 also possibly seen, but need confirmation.

$$I^G(J^{PC}) = 0^-(2^{-})$$

$\Upsilon_2(1D)$ MASS

VALUE (MeV)	EVTS	DOCUMENT ID	TECN	COMMENT
10163.7 ± 1.4		OUR AVERAGE Error includes scale factor of 1.7.		
10164.5 $\pm 0.8 \pm 0.5$		DEL-AMO-SA...10R	BABR	$\Upsilon(3S) \rightarrow \gamma\gamma \pi^+ \pi^- \ell^+ \ell^-$
10161.1 $\pm 0.6 \pm 1.6$	38	BONVICINI	04	CLE3 $\Upsilon(3S) \rightarrow 4\gamma \ell^+ \ell^-$

$\Upsilon_2(1D)$ DECAY MODES

Mode	Fraction (Γ_i/Γ)
Γ_1 $\gamma\gamma \Upsilon(1S)$	seen
Γ_2 $\gamma\chi_{bJ}(1P)$	seen
Γ_3 $\eta \Upsilon(1S)$	not seen
Γ_4 $\pi^+ \pi^- \Upsilon(1S)$	$(6.6 \pm 1.6) \times 10^{-3}$

$\Upsilon_2(1D)$ BRANCHING RATIOS

$\Gamma(\eta \Upsilon(1S))/\Gamma(\gamma\gamma \Upsilon(1S))$				Γ_3/Γ_1	
VALUE	CL%	DOCUMENT ID	TECN	COMMENT	
<0.25	90	BONVICINI	04	CLE3	$\Upsilon(3S) \rightarrow 4\gamma \ell^+ \ell^-$

$\Gamma(\pi^+ \pi^- \Upsilon(1S))/\Gamma_{total}$				Γ_4/Γ	
VALUE (units 10^{-2})	CL%	DOCUMENT ID	TECN	COMMENT	
$0.66^{+0.15}_{-0.14} \pm 0.06$		¹ DEL-AMO-SA...10R	BABR	$\Upsilon(3S) \rightarrow \gamma\gamma \pi^+ \pi^- \ell^+ \ell^-$	
¹ Using theoretical predictions for $B(\chi_{bJ}(2P) \rightarrow \gamma \Upsilon_2(1D))$.					

$\Gamma(\pi^+ \pi^- \Upsilon(1S))/\Gamma(\gamma\gamma \Upsilon(1S))$				Γ_4/Γ_1	
VALUE	CL%	DOCUMENT ID	TECN	COMMENT	
<1.2	90	² BONVICINI	04	CLE3	$\Upsilon(3S) \rightarrow 4\gamma \ell^+ \ell^-$
² Assuming $J = 2$.					

$\Upsilon_2(1D)$ REFERENCES

NAME	YEAR	TECN	DOCUMENT ID	TECN	COMMENT
DEL-AMO-SA...10R	10R	PR	D82 111102	P. del Amo Sanchez et al.	(BABAR Collab.)
BONVICINI	04	PR	D70 032001	G. Bonvicini et al.	(CLEO Collab.)

Meson Particle Listings

$\chi_{b0}(2P)$

$\chi_{b0}(2P)$

$$I^G(J^{PC}) = 0^+(0^{++})$$

J needs confirmation.

Observed in radiative decay of the $\Upsilon(3S)$, therefore $C = +$. Branching ratio requires E1 transition, M1 is strongly disfavored, therefore $P = +$.

$\chi_{b0}(2P)$ MASS

VALUE (MeV)	DOCUMENT ID
10232.5 ± 0.4 ± 0.5 OUR EVALUATION	From γ energy below, using $\Upsilon(3S)$ mass = 10355.2 ± 0.5 MeV

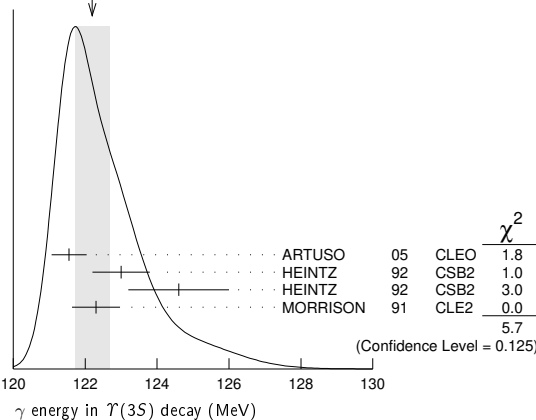
$m_{\chi_{b1}(2P)} - m_{\chi_{b0}(2P)}$

VALUE (MeV)	DOCUMENT ID	TECN	COMMENT
23.8 ± 1.7	LEES	14M BABR	$\Upsilon(3S) \rightarrow \gamma\gamma\mu^+\mu^-$

γ ENERGY IN $\Upsilon(3S)$ DECAY

VALUE (MeV)	EVTS	DOCUMENT ID	TECN	COMMENT
121.9 ± 0.4 OUR EVALUATION		Treating systematic errors as correlated		
122.2 ± 0.5 OUR AVERAGE	Error includes scale factor of 1.4.	See the ideogram below.		
121.55 ± 0.16 ± 0.46		ARTUSO 05	CLEO	$\Upsilon(3S) \rightarrow \gamma X$
123.0 ± 0.8	4959	1 HEINTZ 92	CSB2	$e^+e^- \rightarrow \gamma X$
124.6 ± 1.4	17	2 HEINTZ 92	CSB2	$e^+e^- \rightarrow \ell^+\ell^-\gamma\gamma$
122.3 ± 0.3 ± 0.6	9903	MORRISON 91	CLE2	$e^+e^- \rightarrow \gamma X$

WEIGHTED AVERAGE
122.2 ± 0.5 (Error scaled by 1.4)



1 A systematic uncertainty on the energy scale of 0.9% not included. Supersedes NARAIN 91.
 2 A systematic uncertainty on the energy scale of 0.9% not included. Supersedes HEINTZ 91.

$\chi_{b0}(2P)$ DECAY MODES

Mode	Fraction (Γ_i/Γ)	Confidence level
Γ_1 $\gamma \Upsilon(2S)$	(1.38 ± 0.30) %	
Γ_2 $\gamma \Upsilon(1S)$	(3.8 ± 1.7) × 10 ⁻³	
Γ_3 $D^0 X$	< 8.2 %	90%
Γ_4 $\pi^+ \pi^- K^+ K^- \pi^0$	< 3.4 × 10 ⁻⁵	90%
Γ_5 $2\pi^+ \pi^- K^- K_S^0$	< 5 × 10 ⁻⁵	90%
Γ_6 $2\pi^+ \pi^- K^- K_S^0 2\pi^0$	< 2.2 × 10 ⁻⁴	90%
Γ_7 $2\pi^+ 2\pi^- 2\pi^0$	< 2.4 × 10 ⁻⁴	90%
Γ_8 $2\pi^+ 2\pi^- K^+ K^-$	< 1.5 × 10 ⁻⁴	90%
Γ_9 $2\pi^+ 2\pi^- K^+ K^- \pi^0$	< 2.2 × 10 ⁻⁴	90%
Γ_{10} $2\pi^+ 2\pi^- K^+ K^- 2\pi^0$	< 1.1 × 10 ⁻³	90%
Γ_{11} $3\pi^+ 2\pi^- K^- K_S^0 \pi^0$	< 7 × 10 ⁻⁴	90%
Γ_{12} $3\pi^+ 3\pi^-$	< 7 × 10 ⁻⁵	90%
Γ_{13} $3\pi^+ 3\pi^- 2\pi^0$	< 1.2 × 10 ⁻³	90%
Γ_{14} $3\pi^+ 3\pi^- K^+ K^-$	< 1.5 × 10 ⁻⁴	90%
Γ_{15} $3\pi^+ 3\pi^- K^+ K^- \pi^0$	< 7 × 10 ⁻⁴	90%
Γ_{16} $4\pi^+ 4\pi^-$	< 1.7 × 10 ⁻⁴	90%
Γ_{17} $4\pi^+ 4\pi^- 2\pi^0$	< 6 × 10 ⁻⁴	90%

$\chi_{b0}(2P)$ BRANCHING RATIOS

$\Gamma(\gamma \Upsilon(2S))/\Gamma_{total}$	CL%	DOCUMENT ID	TECN	COMMENT	Γ_1/Γ
1.38 ± 0.30 OUR AVERAGE					
1.31 ± 0.27 ± 0.13 -0.12		3,4 LEES	14M BABR	$\Upsilon(3S) \rightarrow \gamma\gamma\mu^+\mu^-$	
3.6 ± 1.6 ± 0.3		3,5 HEINTZ	92 CSB2	$e^+e^- \rightarrow \ell^+\ell^-\gamma\gamma$	

••• We do not use the following data for averages, fits, limits, etc. •••

VALUE (%)	CL%	DOCUMENT ID	TECN	COMMENT
< 2.8	90	6 LEES	11J BABR	$\Upsilon(3S) \rightarrow X\gamma$
< 8.9	90	7 CRAWFORD	92B CLE2	$e^+e^- \rightarrow \ell^+\ell^-\gamma\gamma$

- 3 Assuming $B(\Upsilon(2S) \rightarrow \mu^+\mu^-) = (1.93 \pm 0.17)\%$.
- 4 LEES 14M reports $[\Gamma(\chi_{b0}(2P) \rightarrow \gamma \Upsilon(2S))/\Gamma_{total}] \times [B(\Upsilon(3S) \rightarrow \gamma \chi_{b0}(2P))] = (7.7 \pm 1.6) \times 10^{-4}$ which we divide by our best value $B(\Upsilon(3S) \rightarrow \gamma \chi_{b0}(2P)) = (5.9 \pm 0.6) \times 10^{-2}$. Our first error is their experiment's error and our second error is the systematic error from using our best value.
- 5 Recalculated by us. HEINTZ 92 quotes $B(\Upsilon(3S) \rightarrow \gamma \chi_{b0}(2P)) \times B(\chi_{b0}(2P) \rightarrow \gamma \Upsilon(2S)) = (0.28 \pm 0.12 \pm 0.03)\%$ using $B(\Upsilon(2S) \rightarrow \mu^+\mu^-) = (1.44 \pm 0.10)\%$. Supersedes HEINTZ 91.
- 6 LEES 11J quotes a central value of $\Gamma(\chi_{b0}(2P) \rightarrow \gamma \Upsilon(2S))/\Gamma_{total} \times \Gamma(\Upsilon(3S) \rightarrow \gamma \chi_{b0}(2P))/\Gamma_{total} = (-0.3 \pm 0.2 \pm 0.5) \times 10^{-4}\%$.
- 7 Using $B(\Upsilon(2S) \rightarrow \mu^+\mu^-) = (1.37 \pm 0.26)\%$, $B(\Upsilon(3S) \rightarrow \gamma \Upsilon(2S)) \times 2 B(\Upsilon(2S) \rightarrow \mu^+\mu^-) < 1.19 \times 10^{-4}$, and $B(\Upsilon(3S) \rightarrow \chi_{b0}(2P)\gamma) = 0.049$.

$\Gamma(\gamma \Upsilon(1S))/\Gamma_{total}$ Γ_2/Γ

VALUE (%)	CL%	DOCUMENT ID	TECN	COMMENT
0.38 ± 0.17 OUR AVERAGE				
0.36 ± 0.17 ± 0.03		8,9,10 LEES	14M BABR	$\Upsilon(3S) \rightarrow \gamma\gamma\mu^+\mu^-$
0.9 ± 0.7 ± 0.1		9,11 HEINTZ	92 CSB2	$e^+e^- \rightarrow \ell^+\ell^-\gamma\gamma$

••• We do not use the following data for averages, fits, limits, etc. •••

- < 1.2 90 12 LEES 11J BABR $\Upsilon(3S) \rightarrow X\gamma$
- < 2.5 90 13 CRAWFORD 92B CLE2 $e^+e^- \rightarrow \ell^+\ell^-\gamma\gamma$
- 8 LEES 14M quotes $\Gamma(\chi_{b0}(2P) \rightarrow \gamma \Upsilon(1S))/\Gamma_{total} \times \Gamma(\Upsilon(3S) \rightarrow \gamma \chi_{b0}(2P))/\Gamma_{total} = (2.1 \pm 1.0) \times 10^{-4}$ combining the results from $\Upsilon(3S) \rightarrow \gamma\gamma\mu^+\mu^-$ samples with and without photon conversions.
- 9 Assuming $B(\Upsilon(1S) \rightarrow \mu^+\mu^-) = (2.48 \pm 0.05)\%$.
- 10 LEES 14M reports $[\Gamma(\chi_{b0}(2P) \rightarrow \gamma \Upsilon(1S))/\Gamma_{total}] \times [B(\Upsilon(3S) \rightarrow \gamma \chi_{b0}(2P))] = (2.1 \pm 1.0) \times 10^{-4}$ which we divide by our best value $B(\Upsilon(3S) \rightarrow \gamma \chi_{b0}(2P)) = (5.9 \pm 0.6) \times 10^{-2}$. Our first error is their experiment's error and our second error is the systematic error from using our best value.
- 11 Recalculated by us. HEINTZ 92 quotes $B(\Upsilon(3S) \rightarrow \gamma \chi_{b0}(2P)) \times B(\chi_{b0}(2P) \rightarrow \gamma \Upsilon(1S)) = (0.05 \pm 0.04 \pm 0.01)\%$ using $B(\Upsilon(1S) \rightarrow \mu^+\mu^-) = (2.57 \pm 0.05)\%$. Supersedes HEINTZ 91.
- 12 LEES 11J quotes a central value of $\Gamma(\chi_{b0}(2P) \rightarrow \gamma \Upsilon(1S))/\Gamma_{total} \times \Gamma(\Upsilon(3S) \rightarrow \gamma \chi_{b0}(2P))/\Gamma_{total} = (3.9 \pm 2.2 \pm 1.2) \times 10^{-4}$.
- 13 Using $B(\Upsilon(1S) \rightarrow \mu^+\mu^-) = (2.57 \pm 0.07)\%$, $B(\Upsilon(3S) \rightarrow \gamma \Upsilon(1S)) \times 2 B(\Upsilon(1S) \rightarrow \mu^+\mu^-) < 0.63 \times 10^{-4}$, and $B(\Upsilon(3S) \rightarrow \chi_{b0}(2P)\gamma) = 0.049$.

$\Gamma(D^0 X)/\Gamma_{total}$ Γ_3/Γ

VALUE	CL%	DOCUMENT ID	TECN	COMMENT
< 8.2 × 10⁻²	90	14,15 BRIERE	08 CLEO	$\Upsilon(3S) \rightarrow \gamma D^0 X$

14 For $p_{D^0} > 2.5$ GeV/c.
 15 The authors also present their result as $(4.1 \pm 3.0 \pm 0.4) \times 10^{-2}$.

$\Gamma(\pi^+ \pi^- K^+ K^- \pi^0)/\Gamma_{total}$ Γ_4/Γ

VALUE (units 10 ⁻⁴)	CL%	DOCUMENT ID	TECN	COMMENT
< 0.34	90	16 ASNER	08A CLEO	$\Upsilon(3S) \rightarrow \gamma\pi^+\pi^-K^+K^- \pi^0$

16 ASNER 08A reports $[\Gamma(\chi_{b0}(2P) \rightarrow \pi^+\pi^-K^+K^- \pi^0)/\Gamma_{total}] \times [B(\Upsilon(3S) \rightarrow \gamma \chi_{b0}(2P))] < 2 \times 10^{-6}$ which we divide by our best value $B(\Upsilon(3S) \rightarrow \gamma \chi_{b0}(2P)) = 5.9 \times 10^{-2}$.

$\Gamma(2\pi^+ \pi^- K^- K_S^0)/\Gamma_{total}$ Γ_5/Γ

VALUE (units 10 ⁻⁴)	CL%	DOCUMENT ID	TECN	COMMENT
< 0.5	90	17 ASNER	08A CLEO	$\Upsilon(3S) \rightarrow \gamma 2\pi^+ \pi^- K^- K_S^0$

17 ASNER 08A reports $[\Gamma(\chi_{b0}(2P) \rightarrow 2\pi^+ \pi^- K^- K_S^0)/\Gamma_{total}] \times [B(\Upsilon(3S) \rightarrow \gamma \chi_{b0}(2P))] < 3 \times 10^{-6}$ which we divide by our best value $B(\Upsilon(3S) \rightarrow \gamma \chi_{b0}(2P)) = 5.9 \times 10^{-2}$.

$\Gamma(2\pi^+ \pi^- K^- K_S^0 2\pi^0)/\Gamma_{total}$ Γ_6/Γ

VALUE (units 10 ⁻⁴)	CL%	DOCUMENT ID	TECN	COMMENT
< 2.2	90	18 ASNER	08A CLEO	$\Upsilon(3S) \rightarrow \gamma 2\pi^+ \pi^- K^- 2\pi^0$

18 ASNER 08A reports $[\Gamma(\chi_{b0}(2P) \rightarrow 2\pi^+ \pi^- K^- K_S^0 2\pi^0)/\Gamma_{total}] \times [B(\Upsilon(3S) \rightarrow \gamma \chi_{b0}(2P))] < 13 \times 10^{-6}$ which we divide by our best value $B(\Upsilon(3S) \rightarrow \gamma \chi_{b0}(2P)) = 5.9 \times 10^{-2}$.

$\Gamma(2\pi^+ 2\pi^- 2\pi^0)/\Gamma_{total}$ Γ_7/Γ

VALUE (units 10 ⁻⁴)	CL%	DOCUMENT ID	TECN	COMMENT
< 2.4	90	19 ASNER	08A CLEO	$\Upsilon(3S) \rightarrow \gamma 2\pi^+ 2\pi^- 2\pi^0$

19 ASNER 08A reports $[\Gamma(\chi_{b0}(2P) \rightarrow 2\pi^+ 2\pi^- 2\pi^0)/\Gamma_{total}] \times [B(\Upsilon(3S) \rightarrow \gamma \chi_{b0}(2P))] < 14 \times 10^{-6}$ which we divide by our best value $B(\Upsilon(3S) \rightarrow \gamma \chi_{b0}(2P)) = 5.9 \times 10^{-2}$.

$\Gamma(2\pi^+ 2\pi^- K^+ K^-)/\Gamma_{total}$ Γ_8/Γ

VALUE (units 10 ⁻⁴)	CL%	DOCUMENT ID	TECN	COMMENT
< 1.5	90	20 ASNER	08A CLEO	$\Upsilon(3S) \rightarrow \gamma 2\pi^+ 2\pi^- K^+ K^-$

20 ASNER 08A reports $[\Gamma(\chi_{b0}(2P) \rightarrow 2\pi^+ 2\pi^- K^+ K^-)/\Gamma_{total}] \times [B(\Upsilon(3S) \rightarrow \gamma \chi_{b0}(2P))] < 9 \times 10^{-6}$ which we divide by our best value $B(\Upsilon(3S) \rightarrow \gamma \chi_{b0}(2P)) = 5.9 \times 10^{-2}$.

See key on page 1127

Meson Particle Listings

$\chi_{b0}(2P), \chi_{b1}(2P)$

$\Gamma(2\pi^+2\pi^-K^+K^-\pi^0)/\Gamma_{total}$ Γ_9/Γ

VALUE (units 10^{-4})	CL%	DOCUMENT ID	TECN	COMMENT
<2.2	90	21 ASNER	08A CLEO	$\Upsilon(3S) \rightarrow \gamma 2\pi^+2\pi^-K^+K^-\pi^0$
21 ASNER 08A reports $[\Gamma(\chi_{b0}(2P) \rightarrow 2\pi^+2\pi^-K^+K^-\pi^0)/\Gamma_{total}] \times [B(\Upsilon(3S) \rightarrow \gamma\chi_{b0}(2P))]$ < 13×10^{-6} which we divide by our best value $B(\Upsilon(3S) \rightarrow \gamma\chi_{b0}(2P)) = 5.9 \times 10^{-2}$.				

$\Gamma(2\pi^+2\pi^-K^+K^-2\pi^0)/\Gamma_{total}$ Γ_{10}/Γ

VALUE (units 10^{-4})	CL%	DOCUMENT ID	TECN	COMMENT
<11	90	22 ASNER	08A CLEO	$\Upsilon(3S) \rightarrow \gamma 2\pi^+2\pi^-K^+K^-2\pi^0$
22 ASNER 08A reports $[\Gamma(\chi_{b0}(2P) \rightarrow 2\pi^+2\pi^-K^+K^-2\pi^0)/\Gamma_{total}] \times [B(\Upsilon(3S) \rightarrow \gamma\chi_{b0}(2P))]$ < 63×10^{-6} which we divide by our best value $B(\Upsilon(3S) \rightarrow \gamma\chi_{b0}(2P)) = 5.9 \times 10^{-2}$.				

$\Gamma(3\pi^+2\pi^-K^-K_S^0\pi^0)/\Gamma_{total}$ Γ_{11}/Γ

VALUE (units 10^{-4})	CL%	DOCUMENT ID	TECN	COMMENT
<7	90	23 ASNER	08A CLEO	$\Upsilon(3S) \rightarrow \gamma 3\pi^+2\pi^-K^-K_S^0\pi^0$
23 ASNER 08A reports $[\Gamma(\chi_{b0}(2P) \rightarrow 3\pi^+2\pi^-K^-K_S^0\pi^0)/\Gamma_{total}] \times [B(\Upsilon(3S) \rightarrow \gamma\chi_{b0}(2P))]$ < 39×10^{-6} which we divide by our best value $B(\Upsilon(3S) \rightarrow \gamma\chi_{b0}(2P)) = 5.9 \times 10^{-2}$.				

$\Gamma(3\pi^+3\pi^-)/\Gamma_{total}$ Γ_{12}/Γ

VALUE (units 10^{-4})	CL%	DOCUMENT ID	TECN	COMMENT
<0.7	90	24 ASNER	08A CLEO	$\Upsilon(3S) \rightarrow \gamma 3\pi^+3\pi^-$
24 ASNER 08A reports $[\Gamma(\chi_{b0}(2P) \rightarrow 3\pi^+3\pi^-)/\Gamma_{total}] \times [B(\Upsilon(3S) \rightarrow \gamma\chi_{b0}(2P))]$ < 4×10^{-6} which we divide by our best value $B(\Upsilon(3S) \rightarrow \gamma\chi_{b0}(2P)) = 5.9 \times 10^{-2}$.				

$\Gamma(3\pi^+3\pi^-2\pi^0)/\Gamma_{total}$ Γ_{13}/Γ

VALUE (units 10^{-4})	CL%	DOCUMENT ID	TECN	COMMENT
<12	90	25 ASNER	08A CLEO	$\Upsilon(3S) \rightarrow \gamma 3\pi^+3\pi^-2\pi^0$
25 ASNER 08A reports $[\Gamma(\chi_{b0}(2P) \rightarrow 3\pi^+3\pi^-2\pi^0)/\Gamma_{total}] \times [B(\Upsilon(3S) \rightarrow \gamma\chi_{b0}(2P))]$ < 72×10^{-6} which we divide by our best value $B(\Upsilon(3S) \rightarrow \gamma\chi_{b0}(2P)) = 5.9 \times 10^{-2}$.				

$\Gamma(3\pi^+3\pi^-K^+K^-)/\Gamma_{total}$ Γ_{14}/Γ

VALUE (units 10^{-4})	CL%	DOCUMENT ID	TECN	COMMENT
<1.5	90	26 ASNER	08A CLEO	$\Upsilon(3S) \rightarrow \gamma 3\pi^+3\pi^-K^+K^-$
26 ASNER 08A reports $[\Gamma(\chi_{b0}(2P) \rightarrow 3\pi^+3\pi^-K^+K^-)/\Gamma_{total}] \times [B(\Upsilon(3S) \rightarrow \gamma\chi_{b0}(2P))]$ < 9×10^{-6} which we divide by our best value $B(\Upsilon(3S) \rightarrow \gamma\chi_{b0}(2P)) = 5.9 \times 10^{-2}$.				

$\Gamma(3\pi^+3\pi^-K^+K^-\pi^0)/\Gamma_{total}$ Γ_{15}/Γ

VALUE (units 10^{-4})	CL%	DOCUMENT ID	TECN	COMMENT
<7	90	27 ASNER	08A CLEO	$\Upsilon(3S) \rightarrow \gamma 3\pi^+3\pi^-K^+K^-\pi^0$
27 ASNER 08A reports $[\Gamma(\chi_{b0}(2P) \rightarrow 3\pi^+3\pi^-K^+K^-\pi^0)/\Gamma_{total}] \times [B(\Upsilon(3S) \rightarrow \gamma\chi_{b0}(2P))]$ < 43×10^{-6} which we divide by our best value $B(\Upsilon(3S) \rightarrow \gamma\chi_{b0}(2P)) = 5.9 \times 10^{-2}$.				

$\Gamma(4\pi^+4\pi^-)/\Gamma_{total}$ Γ_{16}/Γ

VALUE (units 10^{-4})	CL%	DOCUMENT ID	TECN	COMMENT
<1.7	90	28 ASNER	08A CLEO	$\Upsilon(3S) \rightarrow \gamma 4\pi^+4\pi^-$
28 ASNER 08A reports $[\Gamma(\chi_{b0}(2P) \rightarrow 4\pi^+4\pi^-)/\Gamma_{total}] \times [B(\Upsilon(3S) \rightarrow \gamma\chi_{b0}(2P))]$ < 10×10^{-6} which we divide by our best value $B(\Upsilon(3S) \rightarrow \gamma\chi_{b0}(2P)) = 5.9 \times 10^{-2}$.				

$\Gamma(4\pi^+4\pi^-2\pi^0)/\Gamma_{total}$ Γ_{17}/Γ

VALUE (units 10^{-4})	CL%	DOCUMENT ID	TECN	COMMENT
<6	90	29 ASNER	08A CLEO	$\Upsilon(3S) \rightarrow \gamma 4\pi^+4\pi^-2\pi^0$
29 ASNER 08A reports $[\Gamma(\chi_{b0}(2P) \rightarrow 4\pi^+4\pi^-2\pi^0)/\Gamma_{total}] \times [B(\Upsilon(3S) \rightarrow \gamma\chi_{b0}(2P))]$ < 38×10^{-6} which we divide by our best value $B(\Upsilon(3S) \rightarrow \gamma\chi_{b0}(2P)) = 5.9 \times 10^{-2}$.				

$\Gamma(\chi_{b0}(2P) \rightarrow \gamma \Upsilon(1S))/\Gamma_{total} \times \Gamma(\Upsilon(3S) \rightarrow \gamma\chi_{b0}(2P))/\Gamma_{total}$ $\Gamma_2/\Gamma \times \Gamma_{22}^{(3S)}/\Gamma \Upsilon(3S)$

VALUE (units 10^{-4})	CL%	DOCUMENT ID	TECN	COMMENT
<8.2	90	30 LEES	11J BABR	$\Upsilon(3S) \rightarrow X\gamma$
30 LEES 11J quotes a central value of $\Gamma(\chi_{b0}(2P) \rightarrow \gamma \Upsilon(1S))/\Gamma_{total} \times \Gamma(\Upsilon(3S) \rightarrow \gamma\chi_{b0}(2P))/\Gamma_{total} = (3.9 \pm 2.2 \pm 1.2) \times 10^{-4}$ and derives a 90% CL upper limit of $B(\chi_{b0}(2P) \rightarrow \gamma \Upsilon(1S)) < 1.2\%$ using $B(\Upsilon(3S) \rightarrow \gamma\chi_{b0}(2P)) = (5.9 \pm 0.6)\%$.				

$B(\chi_{b0}(2P) \rightarrow \gamma \Upsilon(1S)) \times B(\Upsilon(3S) \rightarrow \gamma\chi_{b0}(2P)) \times B(\Upsilon(1S) \rightarrow \ell^+\ell^-)$

VALUE (units 10^{-5})	DOCUMENT ID	TECN	COMMENT
1.4 ± 0.9 OUR AVERAGE			
1.7 +1.5 +0.1 -1.4 -1.2	31 LEES	14M BABR	$\Upsilon(3S) \rightarrow \gamma\gamma\mu^+\mu^-$
1.3 ± 1.0 ± 0.3	32 HEINTZ	92 CSB2	$\Upsilon(3S) \rightarrow \gamma\gamma\ell^+\ell^-$

31 From a sample of $\Upsilon(3S) \rightarrow \gamma\gamma\mu^+\mu^-$ with one converted photon.
32 Calculated by us. HEINTZ 92 quotes $B(\Upsilon(3S) \rightarrow \gamma\chi_{b0}(2P)) \times B(\chi_{b0}(2P) \rightarrow \gamma \Upsilon(1S)) = (0.05 \pm 0.04 \pm 0.01)\%$ using $B(\Upsilon(1S) \rightarrow \mu^+\mu^-) = (2.57 \pm 0.05)\%$.

$[B(\chi_{b0}(2P) \rightarrow \gamma \Upsilon(1S)) \times B(\Upsilon(3S) \rightarrow \gamma\chi_{b0}(2P))] / [B(\chi_{b1}(2P) \rightarrow \gamma \Upsilon(1S)) \times B(\Upsilon(3S) \rightarrow \gamma\chi_{b1}(2P))]$

VALUE (%)	DOCUMENT ID	TECN	COMMENT
1.71 ± 0.80	33 LEES	14M BABR	$\Upsilon(3S) \rightarrow \gamma\gamma\mu^+\mu^-$
33 From a sample of $\Upsilon(3S) \rightarrow \gamma\gamma\mu^+\mu^-$ without converted photons.			

$\Gamma(\chi_{b0}(2P) \rightarrow \gamma \Upsilon(2S))/\Gamma_{total} \times \Gamma(\Upsilon(3S) \rightarrow \gamma\chi_{b0}(2P))/\Gamma_{total}$ $\Gamma_1/\Gamma \times \Gamma_{22}^{(3S)}/\Gamma \Upsilon(3S)$

VALUE (units 10^{-3})	CL%	DOCUMENT ID	TECN	COMMENT
<1.6	90	34 LEES	11J BABR	$\Upsilon(3S) \rightarrow X\gamma$
34 LEES 11J quotes a central value of $\Gamma(\chi_{b0}(2P) \rightarrow \gamma \Upsilon(2S))/\Gamma_{total} \times \Gamma(\Upsilon(3S) \rightarrow \gamma\chi_{b0}(2P))/\Gamma_{total} = (-0.3 \pm 0.2 \pm 0.5) \times 10^{-3}$ and derives a 90% CL upper limit of $B(\chi_{b0}(2P) \rightarrow \gamma \Upsilon(2S)) < 2.8\%$ using $B(\Upsilon(3S) \rightarrow \gamma\chi_{b0}(2P)) = (5.9 \pm 0.6)\%$.				

$B(\chi_{b0}(2P) \rightarrow \gamma \Upsilon(2S)) \times B(\Upsilon(3S) \rightarrow \gamma\chi_{b0}(2P)) \times B(\Upsilon(2S) \rightarrow \ell^+\ell^-)$

VALUE (units 10^{-5})	DOCUMENT ID	TECN	COMMENT
4.4 ± 1.6 OUR AVERAGE			
6.6 +4.9 +2.0 -4.0 -0.3	35 LEES	14M BABR	$\Upsilon(3S) \rightarrow \gamma\gamma\mu^+\mu^-$
4.0 ± 1.7 ± 0.3	36 HEINTZ	92 CSB2	$\Upsilon(3S) \rightarrow \gamma\gamma\ell^+\ell^-$

35 From a sample of $\Upsilon(3S) \rightarrow \gamma\gamma\mu^+\mu^-$ with one converted photon.
36 Calculated by us. HEINTZ 92 quotes $B(\Upsilon(3S) \rightarrow \gamma\chi_{b0}(2P)) \times B(\chi_{b0}(2P) \rightarrow \gamma \Upsilon(2S)) = (0.28 \pm 0.12 \pm 0.03)\%$ using $B(\Upsilon(2S) \rightarrow \mu^+\mu^-) = (1.44 \pm 0.10)\%$.

$[B(\chi_{b0}(2P) \rightarrow \gamma \Upsilon(2S)) \times B(\Upsilon(3S) \rightarrow \gamma\chi_{b0}(2P))] / [B(\chi_{b1}(2P) \rightarrow \gamma \Upsilon(2S)) \times B(\Upsilon(3S) \rightarrow \gamma\chi_{b1}(2P))]$

VALUE (%)	DOCUMENT ID	TECN	COMMENT
3.31 ± 0.56	37 LEES	14M BABR	$\Upsilon(3S) \rightarrow \gamma\gamma\mu^+\mu^-$
37 From a sample of $\Upsilon(3S) \rightarrow \gamma\gamma\mu^+\mu^-$ without converted photons.			

$\chi_{b0}(2P)$ REFERENCES

LEES	14M	PR D90 112010	J.P. Lees et al.	(BABAR Collab.)
LEES	11J	PR D84 072002	J.P. Lees et al.	(BABAR Collab.)
ASNER	08A	PR D78 091103	D.M. Asner et al.	(CLEO Collab.)
BRIERE	08	PR D78 092007	R.A. Briere et al.	(CLEO Collab.)
ARTUSO	05	PRL 94 032001	M. Artuso et al.	(CLEO Collab.)
CRAWFORD	92B	PL B294 139	G. Crawford et al.	(CLEO Collab.)
HEINTZ	92	PR D46 1928	U. Heintz et al.	(CUSP II Collab.)
HEINTZ	91	PRL 66 1563	U. Heintz et al.	(CUSB Collab.)
MORRISON	91	PRL 67 1696	R.J. Morrison et al.	(CLEO Collab.)
NARAIN	91	PRL 66 3113	M. Narain et al.	(CUSB Collab.)

$\chi_{b1}(2P)$

$$J^G(J^{PC}) = 0^+(1^+ +)$$

J needs confirmation.

Observed in radiative decay of the $\Upsilon(3S)$, therefore $C = +$. Branching ratio requires E1 transition, M1 is strongly disfavored, therefore $P = +$.

$\chi_{b1}(2P)$ MASS

VALUE (MeV)	DOCUMENT ID
10255.46 ± 0.22 ± 0.50 OUR EVALUATION	From γ energy below, using $\Upsilon(3S)$ mass = 10355.2 ± 0.5 MeV

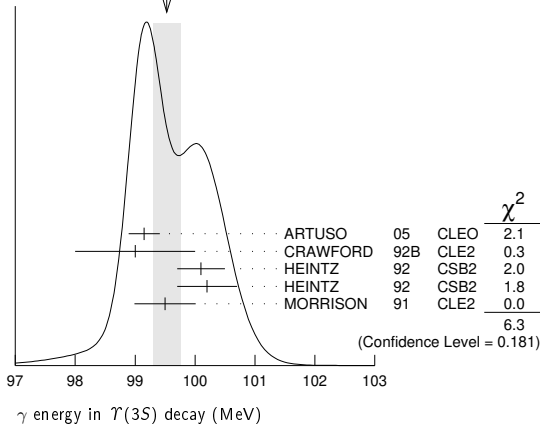
$m_{\chi_{b1}(2P)} - m_{\chi_{b0}(2P)}$

VALUE (MeV)	DOCUMENT ID	TECN	COMMENT
23.5 ± 0.7 ± 0.7	1 HEINTZ	92 CSB2	$e^+e^- \rightarrow \gamma X, \ell^+\ell^- \gamma\gamma$
1 From the average photon energy for inclusive and exclusive events. Supersedes NARAIN 91.			

γ ENERGY IN $\Upsilon(3S)$ DECAY

VALUE (MeV)	EVTs	DOCUMENT ID	TECN	COMMENT
99.26 ± 0.22 OUR EVALUATION		Treating systematic errors as correlated		
99.53 ± 0.23 OUR AVERAGE		Error includes scale factor of 1.3. See the ideogram below.		
99.15 ± 0.07 ± 0.25		ARTUSO 05	CLEO	$\Upsilon(3S) \rightarrow \gamma X$
99 ± 1	169	CRAWFORD 92B	CLE2	$e^+e^- \rightarrow \ell^+\ell^- \gamma\gamma$
100.1 ± 0.4	11147	2 HEINTZ 92	CSB2	$e^+e^- \rightarrow \gamma X$
100.2 ± 0.5	223	3 HEINTZ 92	CSB2	$e^+e^- \rightarrow \ell^+\ell^- \gamma\gamma$
99.5 ± 0.1 ± 0.5	25759	MORRISON 91	CLE2	$e^+e^- \rightarrow \gamma X$
2 A systematic uncertainty on the energy scale of 0.9% not included. Supersedes NARAIN 91.				
3 A systematic uncertainty on the energy scale of 0.9% not included. Supersedes HEINTZ 91.				

Meson Particle Listings

 $\chi_{b1}(2P)$ WEIGHTED AVERAGE
99.53±0.23 (Error scaled by 1.3) $\chi_{b1}(2P)$ DECAY MODES

Mode	Fraction (Γ_i/Γ)
Γ_1 $\omega T(1S)$	$(1.63^{+0.40}_{-0.34})\%$
Γ_2 $\gamma T(2S)$	$(18.1 \pm 1.9)\%$
Γ_3 $\gamma T(1S)$	$(9.9 \pm 1.0)\%$
Γ_4 $\pi\pi\chi_{b1}(1P)$	$(9.1 \pm 1.3) \times 10^{-3}$
Γ_5 $D^0 X$	$(8.8 \pm 1.7)\%$
Γ_6 $\pi^+\pi^-K^+K^-\pi^0$	$(3.1 \pm 1.0) \times 10^{-4}$
Γ_7 $2\pi^+\pi^-K^-K_S^0$	$(1.1 \pm 0.5) \times 10^{-4}$
Γ_8 $2\pi^+\pi^-K^-K_S^0 2\pi^0$	$(7.7 \pm 3.2) \times 10^{-4}$
Γ_9 $2\pi^+ 2\pi^- 2\pi^0$	$(5.9 \pm 2.0) \times 10^{-4}$
Γ_{10} $2\pi^+ 2\pi^- K^+ K^-$	$(10 \pm 4) \times 10^{-5}$
Γ_{11} $2\pi^+ 2\pi^- K^+ K^- \pi^0$	$(5.5 \pm 1.8) \times 10^{-4}$
Γ_{12} $2\pi^+ 2\pi^- K^+ K^- 2\pi^0$	$(10 \pm 4) \times 10^{-4}$
Γ_{13} $3\pi^+ 2\pi^- K^- K_S^0 \pi^0$	$(6.7 \pm 2.6) \times 10^{-4}$
Γ_{14} $3\pi^+ 3\pi^-$	$(1.2 \pm 0.4) \times 10^{-4}$
Γ_{15} $3\pi^+ 3\pi^- 2\pi^0$	$(1.2 \pm 0.4) \times 10^{-3}$
Γ_{16} $3\pi^+ 3\pi^- K^+ K^-$	$(2.0 \pm 0.8) \times 10^{-4}$
Γ_{17} $3\pi^+ 3\pi^- K^+ K^- \pi^0$	$(6.1 \pm 2.2) \times 10^{-4}$
Γ_{18} $4\pi^+ 4\pi^-$	$(1.7 \pm 0.6) \times 10^{-4}$
Γ_{19} $4\pi^+ 4\pi^- 2\pi^0$	$(1.9 \pm 0.7) \times 10^{-3}$

 $\chi_{b1}(2P)$ BRANCHING RATIOS

$\Gamma(\omega T(1S))/\Gamma_{total}$	VALUE (units 10^{-2})	EVTS	DOCUMENT ID	TECN	COMMENT
	$1.63^{+0.35}_{-0.31} \pm 0.16$	$32.6^{+6.9}_{-6.1}$	4 CRONIN-HEN.04	CLE3	$T(3S) \rightarrow \gamma\omega T(1S)$

⁴ Using $B(T(3S) \rightarrow \gamma\chi_{b1}(2P)) = (11.3 \pm 0.6)\%$ and $B(T(1S) \rightarrow \ell^+\ell^-) = 2 B(T(1S) \rightarrow \mu^+\mu^-) = 2(2.48 \pm 0.06)\%$.

$\Gamma(\gamma T(2S))/\Gamma_{total}$	VALUE	EVTS	DOCUMENT ID	TECN	COMMENT
	0.181 ± 0.019 OUR AVERAGE				

$0.211 \pm 0.017 \pm 0.019$	5,6,7	LEES	14M	BABR	$T(3S) \rightarrow \gamma\gamma\mu^+\mu^-$
$0.190 \pm 0.018 \pm 0.017$	4.3k	8	LEES	11J	BABR $T(3S) \rightarrow X\gamma$
$0.206 \pm 0.035 \pm 0.019$	5,9	CRAWFORD	92B	CLE2	$e^+e^- \rightarrow \ell^+\ell^- \gamma\gamma$
$0.132 \pm 0.018 \pm 0.012$	5,10	HEINTZ	92	CSB2	$e^+e^- \rightarrow \ell^+\ell^- \gamma\gamma$

⁵ Assuming $B(T(2S) \rightarrow \mu^+\mu^-) = (1.93 \pm 0.17)\%$.

⁶ LEES 14M quotes $\Gamma(\chi_{b1}(2P) \rightarrow \gamma T(2S))/\Gamma_{total} \times \Gamma(T(3S) \rightarrow \gamma\chi_{b1}(2P))/\Gamma_{total} = (2.66 \pm 0.22)\%$ combining the results from $T(3S) \rightarrow \gamma\gamma\mu^+\mu^-$ samples with and without photon conversions.

⁷ LEES 14M reports $[\Gamma(\chi_{b1}(2P) \rightarrow \gamma T(2S))/\Gamma_{total}] \times [B(T(3S) \rightarrow \gamma\chi_{b1}(2P))] = (2.66 \pm 0.22) \times 10^{-2}$ which we divide by our best value $B(T(3S) \rightarrow \gamma\chi_{b1}(2P)) = (12.6 \pm 1.2) \times 10^{-2}$. Our first error is their experiment's error and our second error is the systematic error from using our best value.

⁸ LEES 11J reports $[\Gamma(\chi_{b1}(2P) \rightarrow \gamma T(2S))/\Gamma_{total}] \times [B(T(3S) \rightarrow \gamma\chi_{b1}(2P))] = (2.4 \pm 0.1 \pm 0.2) \times 10^{-2}$ which we divide by our best value $B(T(3S) \rightarrow \gamma\chi_{b1}(2P)) = (12.6 \pm 1.2) \times 10^{-2}$. Our first error is their experiment's error and our second error is the systematic error from using our best value.

⁹ CRAWFORD 92B quotes $B(T(3S) \rightarrow \gamma\chi_{b1}(2P)) \times B(\chi_{b1}(2P) \rightarrow \gamma T(2S)) \times 2 B(T(2S) \rightarrow \ell^+\ell^-) = (10.23 \pm 1.20 \pm 1.26) 10^{-4}$.

¹⁰ Recalculated by us. HEINTZ 92 quotes $B(T(3S) \rightarrow \gamma\chi_{b1}(2P)) \times B(\chi_{b1}(2P) \rightarrow \gamma T(2S)) = (2.29 \pm 0.23 \pm 0.21)\%$ using $B(T(2S) \rightarrow \mu^+\mu^-) = (1.44 \pm 0.10)\%$. Supersedes HEINTZ 91.

 $\Gamma(\gamma T(1S))/\Gamma_{total}$

VALUE	EVTS	DOCUMENT ID	TECN	COMMENT	
0.099 ± 0.010 OUR AVERAGE					
$0.107 \pm 0.006 \pm 0.010$	11,12,13	LEES	14M	BABR $T(3S) \rightarrow \gamma\gamma\mu^+\mu^-$	
$0.098 \pm 0.005 \pm 0.009$	15k	14	LEES	11J	BABR $T(3S) \rightarrow X\gamma$
$0.103 \pm 0.023 \pm 0.009$	11,15	CRAWFORD	92B	CLE2	$e^+e^- \rightarrow \ell^+\ell^- \gamma\gamma$
$0.075 \pm 0.010 \pm 0.007$	11,16	HEINTZ	92	CSB2	$e^+e^- \rightarrow \ell^+\ell^- \gamma\gamma$

¹¹ Assuming $B(T(1S) \rightarrow \mu^+\mu^-) = (2.48 \pm 0.05)\%$.

¹² LEES 14M quotes $\Gamma(\chi_{b1}(2P) \rightarrow \gamma T(1S))/\Gamma_{total} \times \Gamma(T(3S) \rightarrow \gamma\chi_{b1}(2P))/\Gamma_{total} = (13.48 \pm 0.72) \times 10^{-3}$ combining the results from samples of $T(3S) \rightarrow \gamma\gamma\mu^+\mu^-$ with and without converted photons.

¹³ LEES 14M reports $[\Gamma(\chi_{b1}(2P) \rightarrow \gamma T(1S))/\Gamma_{total}] \times [B(T(3S) \rightarrow \gamma\chi_{b1}(2P))] = (13.48 \pm 0.72) \times 10^{-3}$ which we divide by our best value $B(T(3S) \rightarrow \gamma\chi_{b1}(2P)) = (12.6 \pm 1.2) \times 10^{-2}$. Our first error is their experiment's error and our second error is the systematic error from using our best value.

¹⁴ LEES 11J reports $[\Gamma(\chi_{b1}(2P) \rightarrow \gamma T(1S))/\Gamma_{total}] \times [B(T(3S) \rightarrow \gamma\chi_{b1}(2P))] = (12.4 \pm 0.3 \pm 0.6) \times 10^{-3}$ which we divide by our best value $B(T(3S) \rightarrow \gamma\chi_{b1}(2P)) = (12.6 \pm 1.2) \times 10^{-2}$. Our first error is their experiment's error and our second error is the systematic error from using our best value.

¹⁵ CRAWFORD 92B quotes $B(T(3S) \rightarrow \gamma\chi_{b1}(2P)) \times B(\chi_{b1}(2P) \rightarrow \gamma T(1S)) \times 2 B(T(1S) \rightarrow \ell^+\ell^-) = (6.47 \pm 1.12 \pm 0.82) 10^{-4}$.

¹⁶ Recalculated by us. HEINTZ 92 quotes $B(T(3S) \rightarrow \gamma\chi_{b1}(2P)) \times B(\chi_{b1}(2P) \rightarrow \gamma T(1S)) = (0.91 \pm 0.11 \pm 0.06)\%$ using $B(T(1S) \rightarrow \mu^+\mu^-) = (2.57 \pm 0.05)\%$. Supersedes HEINTZ 91.

 $\Gamma(\pi\pi\chi_{b1}(1P))/\Gamma_{total}$

VALUE (units 10^{-3})	EVTS	DOCUMENT ID	TECN	COMMENT	
9.1 ± 1.3 OUR AVERAGE					
$9.2 \pm 1.1 \pm 0.8$	31k	17	LEES	11C	BABR $e^+e^- \rightarrow \pi^+\pi^- X$
$8.6 \pm 2.3 \pm 2.1$		18	CAWLFIELD	06	CLE3 $T(3S) \rightarrow 2(\gamma\pi\ell)$

¹⁷ LEES 11C measures $B(T(3S) \rightarrow \chi_{b1}(2P) X) \times B(\chi_{b1}(2P) \rightarrow \chi_{b1}(1P)\pi^+\pi^-) = (1.16 \pm 0.07 \pm 0.12) \times 10^{-3}$. We derive the value assuming $B(T(3S) \rightarrow \chi_{b1}(2P) X) = B(T(3S) \rightarrow \chi_{b1}(2P)\gamma) = (12.6 \pm 1.2) \times 10^{-2}$.

¹⁸ CAWLFIELD 06 quote $\Gamma(\chi_b(2P) \rightarrow \pi\pi\chi_b(1P)) = 0.83 \pm 0.22 \pm 0.08 \pm 0.19$ keV assuming l-spin conservation, no D-wave contribution, $\Gamma(\chi_{b1}(2P)) = 96 \pm 16$ keV, and $\Gamma(\chi_{b2}(2P)) = 138 \pm 19$ keV.

 $\Gamma(D^0 X)/\Gamma_{total}$

VALUE (units 10^{-2})	EVTS	DOCUMENT ID	TECN	COMMENT	
$8.8 \pm 1.5 \pm 0.8$	2243	19	BRIERE	08	CLEO $T(3S) \rightarrow \gamma D^0 X$

¹⁹ For $p_{D^0} > 2.5$ GeV/c.

 $\Gamma(\pi^+\pi^-K^+K^-\pi^0)/\Gamma_{total}$

VALUE (units 10^{-4})	EVTS	DOCUMENT ID	TECN	COMMENT	
$3.1 \pm 1.0 \pm 0.3$	30	20	ASNER	08A	CLEO $T(3S) \rightarrow \gamma\pi^+\pi^-K^+K^-\pi^0$

²⁰ ASNER 08A reports $[\Gamma(\chi_{b1}(2P) \rightarrow \pi^+\pi^-K^+K^-\pi^0)/\Gamma_{total}] \times [B(T(3S) \rightarrow \gamma\chi_{b1}(2P))] = (39 \pm 8 \pm 9) \times 10^{-6}$ which we divide by our best value $B(T(3S) \rightarrow \gamma\chi_{b1}(2P)) = (12.6 \pm 1.2) \times 10^{-2}$. Our first error is their experiment's error and our second error is the systematic error from using our best value.

 $\Gamma(2\pi^+\pi^-K^-K_S^0)/\Gamma_{total}$

VALUE (units 10^{-4})	EVTS	DOCUMENT ID	TECN	COMMENT	
$1.1 \pm 0.5 \pm 0.1$	10	21	ASNER	08A	CLEO $T(3S) \rightarrow \gamma 2\pi^+\pi^-K^-K_S^0$

²¹ ASNER 08A reports $[\Gamma(\chi_{b1}(2P) \rightarrow 2\pi^+\pi^-K^-K_S^0)/\Gamma_{total}] \times [B(T(3S) \rightarrow \gamma\chi_{b1}(2P))] = (14 \pm 5 \pm 3) \times 10^{-6}$ which we divide by our best value $B(T(3S) \rightarrow \gamma\chi_{b1}(2P)) = (12.6 \pm 1.2) \times 10^{-2}$. Our first error is their experiment's error and our second error is the systematic error from using our best value.

 $\Gamma(2\pi^+\pi^-K^-K_S^0 2\pi^0)/\Gamma_{total}$

VALUE (units 10^{-4})	EVTS	DOCUMENT ID	TECN	COMMENT	
$7.7 \pm 3.1 \pm 0.7$	15	22	ASNER	08A	CLEO $T(3S) \rightarrow \gamma 2\pi^+\pi^-K^- 2\pi^0$

²² ASNER 08A reports $[\Gamma(\chi_{b1}(2P) \rightarrow 2\pi^+\pi^-K^-K_S^0 2\pi^0)/\Gamma_{total}] \times [B(T(3S) \rightarrow \gamma\chi_{b1}(2P))] = (97 \pm 30 \pm 26) \times 10^{-6}$ which we divide by our best value $B(T(3S) \rightarrow \gamma\chi_{b1}(2P)) = (12.6 \pm 1.2) \times 10^{-2}$. Our first error is their experiment's error and our second error is the systematic error from using our best value.

 $\Gamma(2\pi^+ 2\pi^- 2\pi^0)/\Gamma_{total}$

VALUE (units 10^{-4})	EVTS	DOCUMENT ID	TECN	COMMENT	
$5.9 \pm 2.0 \pm 0.5$	36	23	ASNER	08A	CLEO $T(3S) \rightarrow \gamma 2\pi^+ 2\pi^- 2\pi^0$

²³ ASNER 08A reports $[\Gamma(\chi_{b1}(2P) \rightarrow 2\pi^+ 2\pi^- 2\pi^0)/\Gamma_{total}] \times [B(T(3S) \rightarrow \gamma\chi_{b1}(2P))] = (74 \pm 16 \pm 19) \times 10^{-6}$ which we divide by our best value $B(T(3S) \rightarrow \gamma\chi_{b1}(2P)) = (12.6 \pm 1.2) \times 10^{-2}$. Our first error is their experiment's error and our second error is the systematic error from using our best value.

 $\Gamma(2\pi^+ 2\pi^- K^+ K^-)/\Gamma_{total}$

VALUE (units 10^{-4})	EVTS	DOCUMENT ID	TECN	COMMENT	
$1.0 \pm 0.4 \pm 0.1$	12	24	ASNER	08A	CLEO $T(3S) \rightarrow \gamma 2\pi^+ 2\pi^- K^+ K^-$

²⁴ ASNER 08A reports $[\Gamma(\chi_{b1}(2P) \rightarrow 2\pi^+ 2\pi^- K^+ K^-)/\Gamma_{total}] \times [B(T(3S) \rightarrow \gamma\chi_{b1}(2P))] = (12 \pm 4 \pm 3) \times 10^{-6}$ which we divide by our best value $B(T(3S) \rightarrow \gamma\chi_{b1}(2P)) = (12.6 \pm 1.2) \times 10^{-2}$. Our first error is their experiment's error and our second error is the systematic error from using our best value.

$\Gamma(2\pi^+2\pi^-K^+K^-\pi^0)/\Gamma_{total}$ Γ_{11}/Γ

VALUE (units 10^{-4})	EVTS	DOCUMENT ID	TECN	COMMENT
5.5 ± 1.7 ± 0.5	38	25 ASNER	08A CLEO	$\Upsilon(3S) \rightarrow \gamma 2\pi^+ 2\pi^- K^+ K^-\pi^0$
25 ASNER 08A reports $[\Gamma(\chi_{b1}(2P) \rightarrow 2\pi^+ 2\pi^- K^+ K^-\pi^0)/\Gamma_{total}] \times [B(\Upsilon(3S) \rightarrow \gamma \chi_{b1}(2P))]$ = $(69 \pm 13 \pm 17) \times 10^{-6}$ which we divide by our best value $B(\Upsilon(3S) \rightarrow \gamma \chi_{b1}(2P)) = (12.6 \pm 1.2) \times 10^{-2}$. Our first error is their experiment's error and our second error is the systematic error from using our best value.				

$\Gamma(2\pi^+2\pi^-K^+K^-\pi^0)/\Gamma_{total}$ Γ_{12}/Γ

VALUE (units 10^{-4})	EVTS	DOCUMENT ID	TECN	COMMENT
9.6 ± 3.5 ± 0.9	27	26 ASNER	08A CLEO	$\Upsilon(3S) \rightarrow \gamma 2\pi^+ 2\pi^- K^+ K^-\pi^0$
26 ASNER 08A reports $[\Gamma(\chi_{b1}(2P) \rightarrow 2\pi^+ 2\pi^- K^+ K^-\pi^0)/\Gamma_{total}] \times [B(\Upsilon(3S) \rightarrow \gamma \chi_{b1}(2P))]$ = $(121 \pm 29 \pm 33) \times 10^{-6}$ which we divide by our best value $B(\Upsilon(3S) \rightarrow \gamma \chi_{b1}(2P)) = (12.6 \pm 1.2) \times 10^{-2}$. Our first error is their experiment's error and our second error is the systematic error from using our best value.				

$\Gamma(3\pi^+2\pi^-K^0K_S^0\pi^0)/\Gamma_{total}$ Γ_{13}/Γ

VALUE (units 10^{-4})	EVTS	DOCUMENT ID	TECN	COMMENT
6.7 ± 2.5 ± 0.6	17	27 ASNER	08A CLEO	$\Upsilon(3S) \rightarrow \gamma 3\pi^+ 2\pi^- K^0 K_S^0 \pi^0$
27 ASNER 08A reports $[\Gamma(\chi_{b1}(2P) \rightarrow 3\pi^+ 2\pi^- K^0 K_S^0 \pi^0)/\Gamma_{total}] \times [B(\Upsilon(3S) \rightarrow \gamma \chi_{b1}(2P))]$ = $(85 \pm 23 \pm 22) \times 10^{-6}$ which we divide by our best value $B(\Upsilon(3S) \rightarrow \gamma \chi_{b1}(2P)) = (12.6 \pm 1.2) \times 10^{-2}$. Our first error is their experiment's error and our second error is the systematic error from using our best value.				

$\Gamma(3\pi^+3\pi^-)/\Gamma_{total}$ Γ_{14}/Γ

VALUE (units 10^{-4})	EVTS	DOCUMENT ID	TECN	COMMENT
1.2 ± 0.4 ± 0.1	18	28 ASNER	08A CLEO	$\Upsilon(3S) \rightarrow \gamma 3\pi^+ 3\pi^-$
28 ASNER 08A reports $[\Gamma(\chi_{b1}(2P) \rightarrow 3\pi^+ 3\pi^-)/\Gamma_{total}] \times [B(\Upsilon(3S) \rightarrow \gamma \chi_{b1}(2P))]$ = $(15 \pm 4 \pm 3) \times 10^{-6}$ which we divide by our best value $B(\Upsilon(3S) \rightarrow \gamma \chi_{b1}(2P)) = (12.6 \pm 1.2) \times 10^{-2}$. Our first error is their experiment's error and our second error is the systematic error from using our best value.				

$\Gamma(3\pi^+3\pi^-2\pi^0)/\Gamma_{total}$ Γ_{15}/Γ

VALUE (units 10^{-4})	EVTS	DOCUMENT ID	TECN	COMMENT
12 ± 4 ± 1	44	29 ASNER	08A CLEO	$\Upsilon(3S) \rightarrow \gamma 3\pi^+ 3\pi^- 2\pi^0$
29 ASNER 08A reports $[\Gamma(\chi_{b1}(2P) \rightarrow 3\pi^+ 3\pi^- 2\pi^0)/\Gamma_{total}] \times [B(\Upsilon(3S) \rightarrow \gamma \chi_{b1}(2P))]$ = $(150 \pm 30 \pm 40) \times 10^{-6}$ which we divide by our best value $B(\Upsilon(3S) \rightarrow \gamma \chi_{b1}(2P)) = (12.6 \pm 1.2) \times 10^{-2}$. Our first error is their experiment's error and our second error is the systematic error from using our best value.				

$\Gamma(3\pi^+3\pi^-K^+K^-)/\Gamma_{total}$ Γ_{16}/Γ

VALUE (units 10^{-4})	EVTS	DOCUMENT ID	TECN	COMMENT
2.0 ± 0.7 ± 0.2	16	30 ASNER	08A CLEO	$\Upsilon(3S) \rightarrow \gamma 3\pi^+ 3\pi^- K^+ K^-$
30 ASNER 08A reports $[\Gamma(\chi_{b1}(2P) \rightarrow 3\pi^+ 3\pi^- K^+ K^-)/\Gamma_{total}] \times [B(\Upsilon(3S) \rightarrow \gamma \chi_{b1}(2P))]$ = $(25 \pm 7 \pm 6) \times 10^{-6}$ which we divide by our best value $B(\Upsilon(3S) \rightarrow \gamma \chi_{b1}(2P)) = (12.6 \pm 1.2) \times 10^{-2}$. Our first error is their experiment's error and our second error is the systematic error from using our best value.				

$\Gamma(3\pi^+3\pi^-K^+K^-\pi^0)/\Gamma_{total}$ Γ_{17}/Γ

VALUE (units 10^{-4})	EVTS	DOCUMENT ID	TECN	COMMENT
6.1 ± 2.1 ± 0.6	25	31 ASNER	08A CLEO	$\Upsilon(3S) \rightarrow \gamma 3\pi^+ 3\pi^- K^+ K^-\pi^0$
31 ASNER 08A reports $[\Gamma(\chi_{b1}(2P) \rightarrow 3\pi^+ 3\pi^- K^+ K^-\pi^0)/\Gamma_{total}] \times [B(\Upsilon(3S) \rightarrow \gamma \chi_{b1}(2P))]$ = $(77 \pm 17 \pm 21) \times 10^{-6}$ which we divide by our best value $B(\Upsilon(3S) \rightarrow \gamma \chi_{b1}(2P)) = (12.6 \pm 1.2) \times 10^{-2}$. Our first error is their experiment's error and our second error is the systematic error from using our best value.				

$\Gamma(4\pi^+4\pi^-)/\Gamma_{total}$ Γ_{18}/Γ

VALUE (units 10^{-4})	EVTS	DOCUMENT ID	TECN	COMMENT
1.7 ± 0.6 ± 0.2	16	32 ASNER	08A CLEO	$\Upsilon(3S) \rightarrow \gamma 4\pi^+ 4\pi^-$
32 ASNER 08A reports $[\Gamma(\chi_{b1}(2P) \rightarrow 4\pi^+ 4\pi^-)/\Gamma_{total}] \times [B(\Upsilon(3S) \rightarrow \gamma \chi_{b1}(2P))]$ = $(22 \pm 6 \pm 5) \times 10^{-6}$ which we divide by our best value $B(\Upsilon(3S) \rightarrow \gamma \chi_{b1}(2P)) = (12.6 \pm 1.2) \times 10^{-2}$. Our first error is their experiment's error and our second error is the systematic error from using our best value.				

$\Gamma(4\pi^+4\pi^-2\pi^0)/\Gamma_{total}$ Γ_{19}/Γ

VALUE (units 10^{-4})	EVTS	DOCUMENT ID	TECN	COMMENT
19 ± 7 ± 2	41	33 ASNER	08A CLEO	$\Upsilon(3S) \rightarrow \gamma 4\pi^+ 4\pi^- 2\pi^0$
33 ASNER 08A reports $[\Gamma(\chi_{b1}(2P) \rightarrow 4\pi^+ 4\pi^- 2\pi^0)/\Gamma_{total}] \times [B(\Upsilon(3S) \rightarrow \gamma \chi_{b1}(2P))]$ = $(241 \pm 47 \pm 72) \times 10^{-6}$ which we divide by our best value $B(\Upsilon(3S) \rightarrow \gamma \chi_{b1}(2P)) = (12.6 \pm 1.2) \times 10^{-2}$. Our first error is their experiment's error and our second error is the systematic error from using our best value.				

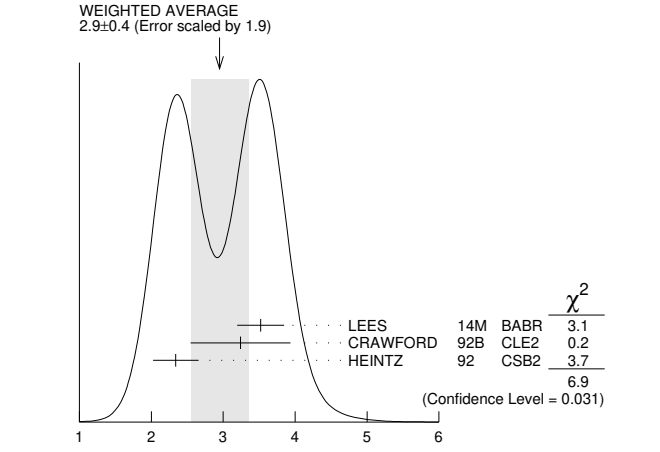
$\chi_{b1}(2P)$ Cross-Particle Branching Ratios

$\Gamma(\chi_{b1}(2P) \rightarrow \gamma \Upsilon(1S))/\Gamma_{total} \times \Gamma(\Upsilon(3S) \rightarrow \gamma \chi_{b1}(2P))/\Gamma_{total}$
 $\Gamma_3/\Gamma \times \Gamma_{21}^{\Upsilon(3S)}/\Gamma \Upsilon(3S)$

VALUE (units 10^{-3})	EVTS	DOCUMENT ID	TECN	COMMENT
12.4 ± 0.3 ± 0.6	15k	LEES	11J BABR	$\Upsilon(3S) \rightarrow X \gamma$

$B(\chi_{b1}(2P) \rightarrow \gamma \Upsilon(1S)) \times B(\Upsilon(3S) \rightarrow \gamma \chi_{b1}(2P)) \times B(\Upsilon(1S) \rightarrow \ell^+ \ell^-)$

VALUE (units 10^{-4})	EVTS	DOCUMENT ID	TECN	COMMENT
2.9 ± 0.4 OUR AVERAGE				Error includes scale factor of 1.9. See the ideogram below.
$3.52^{+0.28+0.17}_{-0.27-0.18}$		34 LEES	14M BABR	$\Upsilon(3S) \rightarrow \gamma \gamma \mu^+ \mu^-$
$3.24 \pm 0.56 \pm 0.41$	58	35 CRAWFORD	92B CLE2	$\Upsilon(3S) \rightarrow \gamma \gamma \ell^+ \ell^-$
$2.34 \pm 0.28 \pm 0.15$		36 HEINTZ	92 CSB2	$\Upsilon(3S) \rightarrow \gamma \gamma \ell^+ \ell^-$



$B(\chi_{b1}(2P) \rightarrow \gamma \Upsilon(1S)) \times B(\Upsilon(3S) \rightarrow \gamma \chi_{b1}(2P)) \times B(\Upsilon(1S) \rightarrow \ell^+ \ell^-)$ (units 10^{-4})

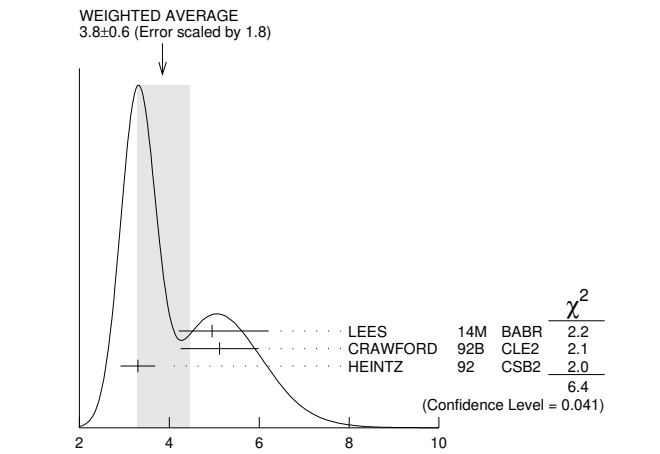
- 34 From a sample of $\Upsilon(3S) \rightarrow \gamma \gamma \mu^+ \mu^-$ with one converted photon.
- 35 CRAWFORD 92B quotes $2 \times B(\Upsilon(3S) \rightarrow \gamma \chi_{bJ}(2P)) B(\chi_{bJ}(2P) \rightarrow \gamma \Upsilon(nS)) B(\Upsilon(nS) \rightarrow \ell^+ \ell^-)$.
- 36 Calculated by us. HEINTZ 92 quotes $B(\Upsilon(3S) \rightarrow \gamma \chi_{b1}(2P)) \times B(\chi_{b1}(2P) \rightarrow \gamma \Upsilon(1S)) = (0.91 \pm 0.11 \pm 0.06)\%$ using $B(\Upsilon(1S) \rightarrow \mu^+ \mu^-) = (2.57 \pm 0.05)\%$.

$\Gamma(\chi_{b1}(2P) \rightarrow \gamma \Upsilon(2S))/\Gamma_{total} \times \Gamma(\Upsilon(3S) \rightarrow \gamma \chi_{b1}(2P))/\Gamma_{total}$
 $\Gamma_2/\Gamma \times \Gamma_{21}^{\Upsilon(3S)}/\Gamma \Upsilon(3S)$

VALUE (units 10^{-2})	EVTS	DOCUMENT ID	TECN	COMMENT
2.4 ± 0.1 ± 0.2	4.3k	LEES	11J BABR	$\Upsilon(3S) \rightarrow X \gamma$

$B(\chi_{b1}(2P) \rightarrow \gamma \Upsilon(2S)) \times B(\Upsilon(3S) \rightarrow \gamma \chi_{b1}(2P)) \times B(\Upsilon(2S) \rightarrow \ell^+ \ell^-)$

VALUE (units 10^{-4})	EVTS	DOCUMENT ID	TECN	COMMENT
3.8 ± 0.6 OUR AVERAGE				Error includes scale factor of 1.8. See the ideogram below.
$4.95^{+0.75+1.01}_{-0.70-0.24}$		37 LEES	14M BABR	$\Upsilon(3S) \rightarrow \gamma \gamma \mu^+ \mu^-$
$5.12 \pm 0.60 \pm 0.63$	111	38 CRAWFORD	92B CLE2	$\Upsilon(3S) \rightarrow \gamma \gamma \ell^+ \ell^-$
$3.30 \pm 0.33 \pm 0.20$		39 HEINTZ	92 CSB2	$\Upsilon(3S) \rightarrow \gamma \gamma \ell^+ \ell^-$



$B(\chi_{b1}(2P) \rightarrow \gamma \Upsilon(2S)) \times B(\Upsilon(3S) \rightarrow \gamma \chi_{b1}(2P)) \times B(\Upsilon(2S) \rightarrow \ell^+ \ell^-)$ (units 10^{-4})

- 37 From a sample of $\Upsilon(3S) \rightarrow \gamma \gamma \mu^+ \mu^-$ with one converted photon.
- 38 CRAWFORD 92B quotes $2 \times B(\Upsilon(3S) \rightarrow \gamma \chi_{bJ}(2P)) B(\chi_{bJ}(2P) \rightarrow \gamma \Upsilon(nS)) B(\Upsilon(nS) \rightarrow \ell^+ \ell^-)$.
- 39 Calculated by us. HEINTZ 92 quotes $B(\Upsilon(3S) \rightarrow \gamma \chi_{b1}(2P)) \times B(\chi_{b1}(2P) \rightarrow \gamma \Upsilon(2S)) = (2.29 \pm 0.23 \pm 0.21)\%$ using $B(\Upsilon(2S) \rightarrow \mu^+ \mu^-) = (1.44 \pm 0.10)\%$.

$B(\chi_{b1}(2P) \rightarrow \chi_{b1}(1P) \pi^+ \pi^-) \times B(\Upsilon(3S) \rightarrow \chi_{b1}(2P) X)$

VALUE (units 10^{-3})	EVTS	DOCUMENT ID	TECN	COMMENT
1.16 ± 0.07 ± 0.12	31k	LEES	11C BABR	$e^+ e^- \rightarrow \pi^+ \pi^- X$

Meson Particle Listings

$\chi_{b1}(2P)$, $h_b(2P)$, $\chi_{b2}(2P)$

$B(\chi_{b2}(2P) \rightarrow pX + \bar{p}X)/B(\chi_{b1}(2P) \rightarrow pX + \bar{p}X)$

VALUE	DOCUMENT ID	TECN	COMMENT
1.109 ± 0.007 ± 0.040	BRIERE	07	CLEO $\Upsilon(3S) \rightarrow \gamma \chi_{bJ}(2P)$

$B(\chi_{b0}(2P) \rightarrow pX + \bar{p}X)/B(\chi_{b1}(2P) \rightarrow pX + \bar{p}X)$

VALUE	DOCUMENT ID	TECN	COMMENT
1.082 ± 0.025 ± 0.060	BRIERE	07	CLEO $\Upsilon(3S) \rightarrow \gamma \chi_{bJ}(2P)$

$\chi_{b1}(2P)$ REFERENCES

LEES	14M	PR D90 112010	J.P. Lees <i>et al.</i>	(BABAR Collab.)
LEES	11C	PR D84 011104	J.P. Lees <i>et al.</i>	(BABAR Collab.)
LEES	11J	PR D84 072002	J.P. Lees <i>et al.</i>	(BABAR Collab.)
ASNER	08A	PR D78 091103	D.M. Asner <i>et al.</i>	(CLEO Collab.)
BRIERE	08	PR D78 092007	R.A. Briere <i>et al.</i>	(CLEO Collab.)
BRIERE	07	PR D76 012005	R.A. Briere <i>et al.</i>	(CLEO Collab.)
CRAWFIELD	06	PR D73 012003	C. Crawford <i>et al.</i>	(CLEO Collab.)
ARTUSO	05	PRL 94 032001	M. Artuso <i>et al.</i>	(CLEO Collab.)
CRONIN-HEN.	04	PRL 92 222002	D. Cronin-Hennessy <i>et al.</i>	(CLEO Collab.)
CRAWFORD	92B	PL B294 139	G. Crawford <i>et al.</i>	(CLEO Collab.)
HEINTZ	92	PR D46 1928	U. Heintz <i>et al.</i>	(CUSB II Collab.)
HEINTZ	91	PRL 66 1563	U. Heintz <i>et al.</i>	(CUSB Collab.)
MORRISON	91	PRL 67 1696	R.J. Morrison <i>et al.</i>	(CLEO Collab.)
NARAIN	91	PRL 66 3113	M. Narain <i>et al.</i>	(CUSB Collab.)

$h_b(2P)$

$$I^G(J^{PC}) = 0^-(1^{+-})$$

Quantum numbers are quark model predictions. $C = -$ established by $\eta_b \gamma$ decay.

$h_b(2P)$ MASS

VALUE (MeV)	EVTS	DOCUMENT ID	TECN	COMMENT
10259.8 ± 0.5 ± 1.1	90k	1 MIZUK	12	BELL $e^+e^- \rightarrow \pi^+\pi^-$ hadrons
• • • We do not use the following data for averages, fits, limits, etc. • • •				
10259.8 ± 0.6 ^{+1.4} _{-1.0}	83.9k	2 ADACHI	12	BELL 10.86 $e^+e^- \rightarrow \pi^+\pi^-$ MM

¹ Observed with 9 standard deviations significance.
² Superseded by MIZUK 12.

$h_b(2P)$ DECAY MODES

Mode	Fraction (Γ_i/Γ)
Γ_1 hadrons	not seen
Γ_2 $\eta_b(1S)\gamma$	(22 ± 5) %
Γ_3 $\eta_b(2S)\gamma$	(48 ± 13) %

$h_b(2P)$ BRANCHING RATIOS

$\Gamma(\text{hadrons})/\Gamma_{\text{total}}$	Γ_1/Γ
not seen	83.9k
ADACHI	12
BELL	10.86 $e^+e^- \rightarrow \pi^+\pi^-$ MM
$\Gamma(\eta_b(1S)\gamma)/\Gamma_{\text{total}}$	Γ_2/Γ
22.3 ± 3.8 ^{+3.1} _{-3.3}	10k
MIZUK	12
BELL	$e^+e^- \rightarrow (\gamma)\pi^+\pi^-$ hadrons
$\Gamma(\eta_b(2S)\gamma)/\Gamma_{\text{total}}$	Γ_3/Γ
47.5 ± 10.5 ^{+6.8} _{-7.7}	26k
MIZUK	12
BELL	$e^+e^- \rightarrow (\gamma)\pi^+\pi^-$ hadrons

$h_b(2P)$ REFERENCES

ADACHI	12	PRL 108 032001	I. Adachi <i>et al.</i>	(BELLE Collab.)
MIZUK	12	PRL 109 232002	R. Mizuk <i>et al.</i>	(BELLE Collab.)

$\chi_{b2}(2P)$

$$I^G(J^{PC}) = 0^+(2^{++})$$

J needs confirmation.

Observed in radiative decay of the $\Upsilon(3S)$, therefore $C = +$. Branching ratio requires E1 transition, M1 is strongly disfavored, therefore $P = +$.

$\chi_{b2}(2P)$ MASS

VALUE (MeV)	DOCUMENT ID
10268.65 ± 0.22 ± 0.50 OUR EVALUATION	From γ energy below, using $\Upsilon(3S)$ mass = 10355.2 ± 0.5 MeV

$m_{\chi_{b2}(2P)} - m_{\chi_{b1}(2P)}$

VALUE (MeV)	DOCUMENT ID	TECN	COMMENT
13.10 ± 0.24 OUR AVERAGE			
12.3 ± 2.6 ± 0.6	1 AAJ	14B	LHCb $pp \rightarrow \gamma \mu^+ \mu^- X$
13.04 ± 0.26	LEES	14M	BABR $\Upsilon(3S) \rightarrow \gamma \gamma \mu^+ \mu^-$
13.5 ± 0.4 ± 0.5	2 HEINTZ	92	CSB2 $e^+e^- \rightarrow \gamma X, \ell^+ \ell^- \gamma \gamma$

¹ From the $\chi_{bJ}(2P) \rightarrow \Upsilon(1S)\gamma$ transition.

² From the average photon energy for inclusive and exclusive events. Supersedes NARAIN 91.

γ ENERGY IN $\Upsilon(3S)$ DECAY

VALUE (MeV)	EVTS	DOCUMENT ID	TECN	COMMENT
86.19 ± 0.22 OUR EVALUATION				Treating systematic errors as correlated
86.40 ± 0.18 OUR AVERAGE				
86.04 ± 0.06 ± 0.27		ARTUSO	05	CLEO $\Upsilon(3S) \rightarrow \gamma X$
86 ± 1	101	CRAWFORD	92B	CLE2 $e^+e^- \rightarrow \ell^+\ell^- \gamma \gamma$
86.7 ± 0.4	10319	3 HEINTZ	92	CSB2 $e^+e^- \rightarrow \gamma X$
86.9 ± 0.4	157	4 HEINTZ	92	CSB2 $e^+e^- \rightarrow \ell^+\ell^- \gamma \gamma$
86.4 ± 0.1 ± 0.4	30741	MORRISON	91	CLE2 $e^+e^- \rightarrow \gamma X$

³ A systematic uncertainty on the energy scale of 0.9% not included. Supersedes NARAIN 91.
⁴ A systematic uncertainty on the energy scale of 0.9% not included. Supersedes HEINTZ 91.

$\chi_{b2}(2P)$ DECAY MODES

Mode	Fraction (Γ_i/Γ)	Confidence level
Γ_1 $\omega \Upsilon(1S)$	(1.10 ^{+0.34} _{-0.30}) %	
Γ_2 $\gamma \Upsilon(2S)$	(8.9 ± 1.2) %	
Γ_3 $\gamma \Upsilon(1S)$	(6.6 ± 0.8) %	
Γ_4 $\pi\pi \chi_{b2}(1P)$	(5.1 ± 0.9) × 10 ⁻³	
Γ_5 $D^0 X$	< 2.4 %	90%
Γ_6 $\pi^+ \pi^- K^+ K^- \pi^0$	< 1.1 × 10 ⁻⁴	90%
Γ_7 $2\pi^+ \pi^- K^- K_S^0$	< 9 × 10 ⁻⁵	90%
Γ_8 $2\pi^+ \pi^- K^- K_S^0 2\pi^0$	< 7 × 10 ⁻⁴	90%
Γ_9 $2\pi^+ 2\pi^- 2\pi^0$	(3.9 ± 1.6) × 10 ⁻⁴	
Γ_{10} $2\pi^+ 2\pi^- K^+ K^-$	(9 ± 4) × 10 ⁻⁵	
Γ_{11} $2\pi^+ 2\pi^- K^+ K^- \pi^0$	(2.4 ± 1.1) × 10 ⁻⁴	
Γ_{12} $2\pi^+ 2\pi^- K^+ K^- 2\pi^0$	(4.7 ± 2.3) × 10 ⁻⁴	
Γ_{13} $3\pi^+ 2\pi^- K^- K_S^0 \pi^0$	< 4 × 10 ⁻⁴	90%
Γ_{14} $3\pi^+ 3\pi^-$	(9 ± 4) × 10 ⁻⁵	
Γ_{15} $3\pi^+ 3\pi^- 2\pi^0$	(1.2 ± 0.4) × 10 ⁻³	
Γ_{16} $3\pi^+ 3\pi^- K^+ K^-$	(1.4 ± 0.7) × 10 ⁻⁴	
Γ_{17} $3\pi^+ 3\pi^- K^+ K^- \pi^0$	(4.2 ± 1.7) × 10 ⁻⁴	
Γ_{18} $4\pi^+ 4\pi^-$	(9 ± 5) × 10 ⁻⁵	
Γ_{19} $4\pi^+ 4\pi^- 2\pi^0$	(1.3 ± 0.5) × 10 ⁻³	

$\chi_{b2}(2P)$ BRANCHING RATIOS

$\Gamma(\omega \Upsilon(1S))/\Gamma_{\text{total}}$	Γ_1/Γ
1.10 ^{+0.32} _{-0.28} ± 0.11	20.1 ^{+5.8} _{-5.1}
5 CRONIN-HEN.04	CLE3 $\Upsilon(3S) \rightarrow \gamma \omega \Upsilon(1S)$

⁵ Using $B(\Upsilon(3S) \rightarrow \gamma \chi_{b2}(2P)) = (11.4 \pm 0.8)\%$ and $B(\Upsilon(1S) \rightarrow \ell^+\ell^-) = 2$
 $B(\Upsilon(1S) \rightarrow \mu^+\mu^-) = 2(2.48 \pm 0.06)\%$.

$\Gamma(\gamma \Upsilon(2S))/\Gamma_{\text{total}}$	Γ_2/Γ
0.089 ± 0.012 OUR AVERAGE	
0.085 ± 0.010 ± 0.010	6,7,8 LEES 14M BABR $\Upsilon(3S) \rightarrow \gamma \gamma \mu^+ \mu^-$
0.084 ± 0.011 ± 0.010	2.5k 9 LEES 11J BABR $\Upsilon(3S) \rightarrow X \gamma$
0.096 ± 0.022 ± 0.012	7,10 CRAWFORD 92B CLE2 $e^+e^- \rightarrow \ell^+\ell^- \gamma \gamma$
0.106 ± 0.016 ± 0.013	7,11 HEINTZ 92 CSB2 $e^+e^- \rightarrow \ell^+\ell^- \gamma \gamma$

⁶ LEES 14M quotes $\Gamma(\chi_{b2}(2P) \rightarrow \gamma \Upsilon(2S))/\Gamma_{\text{total}} \times \Gamma(\Upsilon(3S) \rightarrow \gamma \chi_{b2}(2P))/\Gamma_{\text{total}} = (1.12 \pm 0.13)\%$ combining the results from samples of $\Upsilon(3S) \rightarrow \gamma \gamma \mu^+ \mu^-$ with and without converted photons.

⁷ Assuming $B(\Upsilon(2S) \rightarrow \mu^+ \mu^-) = (1.93 \pm 0.17)\%$.

⁸ LEES 14M reports $[\Gamma(\chi_{b2}(2P) \rightarrow \gamma \Upsilon(2S))/\Gamma_{\text{total}}] \times [B(\Upsilon(3S) \rightarrow \gamma \chi_{b2}(2P))] = (1.12 \pm 0.13) \times 10^{-2}$ which we divide by our best value $B(\Upsilon(3S) \rightarrow \gamma \chi_{b2}(2P)) = (13.1 \pm 1.6) \times 10^{-2}$. Our first error is their experiment's error and our second error is the systematic error from using our best value.

⁹ LEES 11J reports $[\Gamma(\chi_{b2}(2P) \rightarrow \gamma \Upsilon(2S))/\Gamma_{\text{total}}] \times [B(\Upsilon(3S) \rightarrow \gamma \chi_{b2}(2P))] = (1.1 \pm 0.1 \pm 0.1) \times 10^{-2}$ which we divide by our best value $B(\Upsilon(3S) \rightarrow \gamma \chi_{b2}(2P)) = (13.1 \pm 1.6) \times 10^{-2}$. Our first error is their experiment's error and our second error is the systematic error from using our best value.

¹⁰ CRAWFORD 92B quotes $B(\Upsilon(3S) \rightarrow \gamma \chi_{b1}(2P)) \times B(\chi_{b2}(2P) \rightarrow \gamma \Upsilon(2S)) \times 2$
 $B(\Upsilon(2S) \rightarrow \ell^+ \ell^-) = (4.98 \pm 0.94 \pm 0.62) 10^{-4}$.

¹¹ Recalculated by us. HEINTZ 92 quotes $B(\Upsilon(3S) \rightarrow \gamma \chi_{b2}(2P)) \times B(\chi_{b2}(2P) \rightarrow \gamma \Upsilon(2S)) = (1.90 \pm 0.23 \pm 0.18) \%$ using $B(\Upsilon(2S) \rightarrow \mu^+ \mu^-) = (1.44 \pm 0.10)\%$. Supersedes HEINTZ 91.

$\Gamma(\gamma \Upsilon(1S))/\Gamma_{\text{total}}$	Γ_3/Γ
0.066 ± 0.008 OUR AVERAGE	
0.061 ± 0.004 ± 0.007	12,13,14 LEES 14M BABR $\Upsilon(3S) \rightarrow \gamma \gamma \mu^+ \mu^-$
0.070 ± 0.004 ± 0.008	11k 15 LEES 11J BABR $\Upsilon(3S) \rightarrow X \gamma$

See key on page 1127

Meson Particle Listings

$\chi_{b2}(2P)$

0.077±0.018±0.009	13.16	CRAWFORD	92b	CLE2	$e^+e^- \rightarrow \ell^+\ell^-\gamma\gamma$
0.061±0.009±0.007	13.17	HEINTZ	92	CSB2	$e^+e^- \rightarrow \ell^+\ell^-\gamma\gamma$
<p>¹² LEES 14M quotes $\Gamma(\chi_{b2}(2P) \rightarrow \gamma\gamma(1S))/\Gamma_{\text{total}} \times \Gamma(\Upsilon(3S) \rightarrow \gamma\chi_{b2}(2P))/\Gamma_{\text{total}} = (8.03 \pm 0.50) \times 10^{-3}$ combining the results from samples of $\Upsilon(3S) \rightarrow \gamma\gamma\mu^+\mu^-$ with and without converted photons.</p> <p>¹³ Assuming $B(\Upsilon(1S) \rightarrow \mu^+\mu^-) = (2.48 \pm 0.05)\%$.</p> <p>¹⁴ LEES 14M reports $[\Gamma(\chi_{b2}(2P) \rightarrow \gamma\gamma(1S))/\Gamma_{\text{total}}] \times [B(\Upsilon(3S) \rightarrow \gamma\chi_{b2}(2P))] = (8.03 \pm 0.50) \times 10^{-3}$ which we divide by our best value $B(\Upsilon(3S) \rightarrow \gamma\chi_{b2}(2P)) = (13.1 \pm 1.6) \times 10^{-2}$. Our first error is their experiment's error and our second error is the systematic error from using our best value.</p> <p>¹⁵ LEES 11J reports $[\Gamma(\chi_{b2}(2P) \rightarrow \gamma\gamma(1S))/\Gamma_{\text{total}}] \times [B(\Upsilon(3S) \rightarrow \gamma\chi_{b2}(2P))] = (9.2 \pm 0.3 \pm 0.4) \times 10^{-3}$ which we divide by our best value $B(\Upsilon(3S) \rightarrow \gamma\chi_{b2}(2P)) = (13.1 \pm 1.6) \times 10^{-2}$. Our first error is their experiment's error and our second error is the systematic error from using our best value.</p> <p>¹⁶ CRAWFORD 92b quotes $B(\Upsilon(3S) \rightarrow \gamma\chi_{b2}(2P)) \times B(\chi_{b2}(2P) \rightarrow \gamma\Upsilon(1S)) \times 2 B(\Upsilon(1S) \rightarrow \ell^+\ell^-) = (5.03 \pm 0.94 \pm 0.63) 10^{-4}$.</p> <p>¹⁷ Recalculated by us. HEINTZ 92 quotes $B(\Upsilon(3S) \rightarrow \gamma\chi_{b2}(2P)) \times B(\chi_{b2}(2P) \rightarrow \gamma\Upsilon(1S)) = (0.77 \pm 0.11 \pm 0.05)\%$ using $B(\Upsilon(1S) \rightarrow \mu^+\mu^-) = (2.57 \pm 0.05)\%$. Supersedes HEINTZ 91.</p>					

$\Gamma(\pi\pi\chi_{b2}(1P))/\Gamma_{\text{total}}$ Γ_4/Γ

VALUE (units 10 ⁻³)	CL%	DOCUMENT ID	TECN	COMMENT
5.1±0.9 OUR AVERAGE				
4.9±0.7±0.6	17k	18 LEES	11c	BABR $e^+e^- \rightarrow \pi^+\pi^-X$
6.0±1.6±1.4		19 CAWLFIELD	06	CLE3 $\Upsilon(3S) \rightarrow 2(\gamma\pi\ell)$
<p>¹⁸ $(0.64 \pm 0.05 \pm 0.08) \times 10^{-3}$. We derive the value assuming $B(\Upsilon(3S) \rightarrow \chi_{b2}(2P)X) = B(\Upsilon(3S) \rightarrow \chi_{b2}(2P)\gamma) = (13.1 \pm 1.6) \times 10^{-2}$.</p> <p>¹⁹ CAWLFIELD 06 quote $\Gamma(\chi_{b2}(2P) \rightarrow \pi\pi\chi_b(1P)) = 0.83 \pm 0.22 \pm 0.08 \pm 0.19$ keV assuming l-spin conservation, no D-wave contribution, $\Gamma(\chi_{b1}(2P)) = 96 \pm 16$ keV, and $\Gamma(\chi_{b2}(2P)) = 138 \pm 19$ keV.</p>				

$\Gamma(D^0X)/\Gamma_{\text{total}}$ Γ_5/Γ

VALUE	CL%	DOCUMENT ID	TECN	COMMENT
<2.4 × 10⁻²	90	20,21 BRIERE	08	CLEO $\Upsilon(3S) \rightarrow \gamma D^0 X$
<p>²⁰ For $p_{D^0} > 2.5$ GeV/c.</p> <p>²¹ The authors also present their result as $(0.2 \pm 1.4 \pm 0.1) \times 10^{-2}$.</p>				

$\Gamma(\pi^+\pi^-K^+K^-\pi^0)/\Gamma_{\text{total}}$ Γ_6/Γ

VALUE (units 10 ⁻⁴)	CL%	DOCUMENT ID	TECN	COMMENT
<1.1	90	22 ASNER	08a	CLEO $\Upsilon(3S) \rightarrow \gamma\pi^+\pi^-K^+K^-\pi^0$
<p>²² ASNER 08a reports $[\Gamma(\chi_{b2}(2P) \rightarrow \pi^+\pi^-K^+K^-\pi^0)/\Gamma_{\text{total}}] \times [B(\Upsilon(3S) \rightarrow \gamma\chi_{b2}(2P))] < 14 \times 10^{-6}$ which we divide by our best value $B(\Upsilon(3S) \rightarrow \gamma\chi_{b2}(2P)) = 13.1 \times 10^{-2}$.</p>				

$\Gamma(2\pi^+\pi^-K^-K_S^0)/\Gamma_{\text{total}}$ Γ_7/Γ

VALUE (units 10 ⁻⁴)	CL%	DOCUMENT ID	TECN	COMMENT
<0.9	90	23 ASNER	08a	CLEO $\Upsilon(3S) \rightarrow \gamma 2\pi^+\pi^-K^-K_S^0$
<p>²³ ASNER 08a reports $[\Gamma(\chi_{b2}(2P) \rightarrow 2\pi^+\pi^-K^-K_S^0)/\Gamma_{\text{total}}] \times [B(\Upsilon(3S) \rightarrow \gamma\chi_{b2}(2P))] < 12 \times 10^{-6}$ which we divide by our best value $B(\Upsilon(3S) \rightarrow \gamma\chi_{b2}(2P)) = 13.1 \times 10^{-2}$.</p>				

$\Gamma(2\pi^+\pi^-K^-K_S^0 2\pi^0)/\Gamma_{\text{total}}$ Γ_8/Γ

VALUE (units 10 ⁻⁴)	CL%	DOCUMENT ID	TECN	COMMENT
<7	90	24 ASNER	08a	CLEO $\Upsilon(3S) \rightarrow \gamma 2\pi^+\pi^-K^-2\pi^0$
<p>²⁴ ASNER 08a reports $[\Gamma(\chi_{b2}(2P) \rightarrow 2\pi^+\pi^-K^-K_S^0 2\pi^0)/\Gamma_{\text{total}}] \times [B(\Upsilon(3S) \rightarrow \gamma\chi_{b2}(2P))] < 87 \times 10^{-6}$ which we divide by our best value $B(\Upsilon(3S) \rightarrow \gamma\chi_{b2}(2P)) = 13.1 \times 10^{-2}$.</p>				

$\Gamma(2\pi^+2\pi^-2\pi^0)/\Gamma_{\text{total}}$ Γ_9/Γ

VALUE (units 10 ⁻⁴)	EVTS	DOCUMENT ID	TECN	COMMENT
3.9±1.6±0.5	23	25 ASNER	08a	CLEO $\Upsilon(3S) \rightarrow \gamma 2\pi^+2\pi^-2\pi^0$
<p>²⁵ ASNER 08a reports $[\Gamma(\chi_{b2}(2P) \rightarrow 2\pi^+2\pi^-2\pi^0)/\Gamma_{\text{total}}] \times [B(\Upsilon(3S) \rightarrow \gamma\chi_{b2}(2P))] = (51 \pm 16 \pm 13) \times 10^{-6}$ which we divide by our best value $B(\Upsilon(3S) \rightarrow \gamma\chi_{b2}(2P)) = (13.1 \pm 1.6) \times 10^{-2}$. Our first error is their experiment's error and our second error is the systematic error from using our best value.</p>				

$\Gamma(2\pi^+2\pi^-K^+K^-)/\Gamma_{\text{total}}$ Γ_{10}/Γ

VALUE (units 10 ⁻⁴)	EVTS	DOCUMENT ID	TECN	COMMENT
0.9±0.4±0.1	11	26 ASNER	08a	CLEO $\Upsilon(3S) \rightarrow \gamma 2\pi^+2\pi^-K^+K^-$
<p>²⁶ ASNER 08a reports $[\Gamma(\chi_{b2}(2P) \rightarrow 2\pi^+2\pi^-K^+K^-)/\Gamma_{\text{total}}] \times [B(\Upsilon(3S) \rightarrow \gamma\chi_{b2}(2P))] = (12 \pm 4 \pm 3) \times 10^{-6}$ which we divide by our best value $B(\Upsilon(3S) \rightarrow \gamma\chi_{b2}(2P)) = (13.1 \pm 1.6) \times 10^{-2}$. Our first error is their experiment's error and our second error is the systematic error from using our best value.</p>				

$\Gamma(2\pi^+2\pi^-K^+K^-\pi^0)/\Gamma_{\text{total}}$ Γ_{11}/Γ

VALUE (units 10 ⁻⁴)	EVTS	DOCUMENT ID	TECN	COMMENT
2.4±1.0±0.3	16	27 ASNER	08a	CLEO $\Upsilon(3S) \rightarrow \gamma 2\pi^+2\pi^-K^+K^-\pi^0$
<p>²⁷ ASNER 08a reports $[\Gamma(\chi_{b2}(2P) \rightarrow 2\pi^+2\pi^-K^+K^-\pi^0)/\Gamma_{\text{total}}] \times [B(\Upsilon(3S) \rightarrow \gamma\chi_{b2}(2P))] = (32 \pm 11 \pm 8) \times 10^{-6}$ which we divide by our best value $B(\Upsilon(3S) \rightarrow \gamma\chi_{b2}(2P)) = (13.1 \pm 1.6) \times 10^{-2}$. Our first error is their experiment's error and our second error is the systematic error from using our best value.</p>				

$\Gamma(2\pi^+2\pi^-K^+K^-2\pi^0)/\Gamma_{\text{total}}$ Γ_{12}/Γ

VALUE (units 10 ⁻⁴)	EVTS	DOCUMENT ID	TECN	COMMENT
4.7±2.2±0.6	14	28 ASNER	08a	CLEO $\Upsilon(3S) \rightarrow \gamma 2\pi^+2\pi^-K^+K^-2\pi^0$
<p>²⁸ ASNER 08a reports $[\Gamma(\chi_{b2}(2P) \rightarrow 2\pi^+2\pi^-K^+K^-2\pi^0)/\Gamma_{\text{total}}] \times [B(\Upsilon(3S) \rightarrow \gamma\chi_{b2}(2P))] = (62 \pm 23 \pm 17) \times 10^{-6}$ which we divide by our best value $B(\Upsilon(3S) \rightarrow \gamma\chi_{b2}(2P)) = (13.1 \pm 1.6) \times 10^{-2}$. Our first error is their experiment's error and our second error is the systematic error from using our best value.</p>				

$\Gamma(3\pi^+2\pi^-K^-K_S^0\pi^0)/\Gamma_{\text{total}}$ Γ_{13}/Γ

VALUE (units 10 ⁻⁴)	CL%	DOCUMENT ID	TECN	COMMENT
<4	90	29 ASNER	08a	CLEO $\Upsilon(3S) \rightarrow \gamma 3\pi^+2\pi^-K^-K_S^0\pi^0$
<p>²⁹ ASNER 08a reports $[\Gamma(\chi_{b2}(2P) \rightarrow 3\pi^+2\pi^-K^-K_S^0\pi^0)/\Gamma_{\text{total}}] \times [B(\Upsilon(3S) \rightarrow \gamma\chi_{b2}(2P))] < 58 \times 10^{-6}$ which we divide by our best value $B(\Upsilon(3S) \rightarrow \gamma\chi_{b2}(2P)) = 13.1 \times 10^{-2}$.</p>				

$\Gamma(3\pi^+3\pi^-)/\Gamma_{\text{total}}$ Γ_{14}/Γ

VALUE (units 10 ⁻⁴)	EVTS	DOCUMENT ID	TECN	COMMENT
0.9±0.4±0.1	14	30 ASNER	08a	CLEO $\Upsilon(3S) \rightarrow \gamma 3\pi^+3\pi^-$
<p>³⁰ ASNER 08a reports $[\Gamma(\chi_{b2}(2P) \rightarrow 3\pi^+3\pi^-)/\Gamma_{\text{total}}] \times [B(\Upsilon(3S) \rightarrow \gamma\chi_{b2}(2P))] = (12 \pm 4 \pm 3) \times 10^{-6}$ which we divide by our best value $B(\Upsilon(3S) \rightarrow \gamma\chi_{b2}(2P)) = (13.1 \pm 1.6) \times 10^{-2}$. Our first error is their experiment's error and our second error is the systematic error from using our best value.</p>				

$\Gamma(3\pi^+3\pi^-2\pi^0)/\Gamma_{\text{total}}$ Γ_{15}/Γ

VALUE (units 10 ⁻⁴)	EVTS	DOCUMENT ID	TECN	COMMENT
12±4±1	45	31 ASNER	08a	CLEO $\Upsilon(3S) \rightarrow \gamma 3\pi^+3\pi^-2\pi^0$
<p>³¹ ASNER 08a reports $[\Gamma(\chi_{b2}(2P) \rightarrow 3\pi^+3\pi^-2\pi^0)/\Gamma_{\text{total}}] \times [B(\Upsilon(3S) \rightarrow \gamma\chi_{b2}(2P))] = (159 \pm 33 \pm 43) \times 10^{-6}$ which we divide by our best value $B(\Upsilon(3S) \rightarrow \gamma\chi_{b2}(2P)) = (13.1 \pm 1.6) \times 10^{-2}$. Our first error is their experiment's error and our second error is the systematic error from using our best value.</p>				

$\Gamma(3\pi^+3\pi^-K^+K^-)/\Gamma_{\text{total}}$ Γ_{16}/Γ

VALUE (units 10 ⁻⁴)	EVTS	DOCUMENT ID	TECN	COMMENT
1.4±0.7±0.2	12	32 ASNER	08a	CLEO $\Upsilon(3S) \rightarrow \gamma 3\pi^+3\pi^-K^+K^-$
<p>³² ASNER 08a reports $[\Gamma(\chi_{b2}(2P) \rightarrow 3\pi^+3\pi^-K^+K^-)/\Gamma_{\text{total}}] \times [B(\Upsilon(3S) \rightarrow \gamma\chi_{b2}(2P))] = (19 \pm 7 \pm 5) \times 10^{-6}$ which we divide by our best value $B(\Upsilon(3S) \rightarrow \gamma\chi_{b2}(2P)) = (13.1 \pm 1.6) \times 10^{-2}$. Our first error is their experiment's error and our second error is the systematic error from using our best value.</p>				

$\Gamma(3\pi^+3\pi^-K^+K^-\pi^0)/\Gamma_{\text{total}}$ Γ_{17}/Γ

VALUE (units 10 ⁻⁴)	EVTS	DOCUMENT ID	TECN	COMMENT
4.2±1.7±0.5	16	33 ASNER	08a	CLEO $\Upsilon(3S) \rightarrow \gamma 3\pi^+3\pi^-K^+K^-\pi^0$
<p>³³ ASNER 08a reports $[\Gamma(\chi_{b2}(2P) \rightarrow 3\pi^+3\pi^-K^+K^-\pi^0)/\Gamma_{\text{total}}] \times [B(\Upsilon(3S) \rightarrow \gamma\chi_{b2}(2P))] = (55 \pm 16 \pm 15) \times 10^{-6}$ which we divide by our best value $B(\Upsilon(3S) \rightarrow \gamma\chi_{b2}(2P)) = (13.1 \pm 1.6) \times 10^{-2}$. Our first error is their experiment's error and our second error is the systematic error from using our best value.</p>				

$\Gamma(4\pi^+4\pi^-)/\Gamma_{\text{total}}$ Γ_{18}/Γ

VALUE (units 10 ⁻⁴)	EVTS	DOCUMENT ID	TECN	COMMENT
0.9±0.4±0.1	9	34 ASNER	08a	CLEO $\Upsilon(3S) \rightarrow \gamma 4\pi^+4\pi^-$
<p>³⁴ ASNER 08a reports $[\Gamma(\chi_{b2}(2P) \rightarrow 4\pi^+4\pi^-)/\Gamma_{\text{total}}] \times [B(\Upsilon(3S) \rightarrow \gamma\chi_{b2}(2P))] = (12 \pm 5 \pm 3) \times 10^{-6}$ which we divide by our best value $B(\Upsilon(3S) \rightarrow \gamma\chi_{b2}(2P)) = (13.1 \pm 1.6) \times 10^{-2}$. Our first error is their experiment's error and our second error is the systematic error from using our best value.</p>				

$\Gamma(4\pi^+4\pi^-2\pi^0)/\Gamma_{\text{total}}$ Γ_{19}/Γ

VALUE (units 10 ⁻⁴)	EVTS	DOCUMENT ID	TECN	COMMENT
13±5±2	27	35 ASNER	08a	CLEO $\Upsilon(3S) \rightarrow \gamma 4\pi^+4\pi^-2\pi^0$
<p>³⁵ ASNER 08a reports $[\Gamma(\chi_{b2}(2P) \rightarrow 4\pi^+4\pi^-2\pi^0)/\Gamma_{\text{total}}] \times [B(\Upsilon(3S) \rightarrow \gamma\chi_{b2}(2P))] = (165 \pm 46 \pm 50) \times 10^{-6}$ which we divide by our best value $B(\Upsilon(3S) \rightarrow \gamma\chi_{b2}(2P)) = (13.1 \pm 1.6) \times 10^{-2}$. Our first error is their experiment's error and our second error is the systematic error from using our best value.</p>				

$\chi_{b2}(2P)$ Cross-Particle Branching Ratios

$\Gamma(\chi_{b2}(2P) \rightarrow \gamma\Upsilon(1S))/\Gamma_{\text{total}} \times \Gamma(\Upsilon(3S) \rightarrow \gamma\chi_{b2}(2P))/\Gamma_{\text{total}}$ $\Gamma_3/\Gamma \times \Gamma_{20}^{(3S)}/\Gamma\Upsilon(3S)$

VALUE (units 10 ⁻³)	EVTS	DOCUMENT ID	TECN	COMMENT
9.2±0.3±0.4	11k	LEES	11j	BABR $\Upsilon(3S) \rightarrow X\gamma$

$\Gamma(\chi_{b2}(2P) \rightarrow \gamma\Upsilon(2S))/\Gamma_{\text{total}} \times \Gamma(\Upsilon(3S) \rightarrow \gamma\chi_{b2}(2P))/\Gamma_{\text{total}}$ $\Gamma_2/\Gamma \times \Gamma_{20}^{(3S)}/\Gamma\Upsilon(3S)$

VALUE (units 10 ⁻²)	EVTS	DOCUMENT ID	TECN	COMMENT
1.1±0.1±0.1	2.5k	LEES	11j	BABR $\Upsilon(3S) \rightarrow X\gamma$

$B(\chi_{b2}(2P) \rightarrow \chi_{b2}(1P)\pi^+\pi^-) \times B(\Upsilon(3S) \rightarrow \chi_{b2}(2P)X)$

VALUE (units 10 ⁻³)	EVTS	DOCUMENT ID	TECN	COMMENT
0.64±0.05±0.08	17k	LEES	11c	BABR $e^+e^- \rightarrow \pi^+\pi^-X$

Meson Particle Listings

$\chi_{b2}(2P), \Upsilon(3S)$

$B(\chi_{b2}(2P) \rightarrow \gamma \Upsilon(1S)) \times B(\Upsilon(3S) \rightarrow \gamma \chi_{b2}(2P)) \times B(\Upsilon(1S) \rightarrow \ell^+ \ell^-)$

VALUE (units 10^{-4})	EVTS	DOCUMENT ID	TECN	COMMENT
2.02±0.18 OUR AVERAGE				

1.95 ^{+0.22+0.10} _{-0.21-0.16}		36 LEES	14M BABR	$\Upsilon(3S) \rightarrow \gamma \mu^+ \mu^-$
2.52±0.47±0.32	48	37 CRAWFORD	92B CLE2	$\Upsilon(3S) \rightarrow \gamma \gamma \ell^+ \ell^-$
1.98±0.28±0.12		38 HEINTZ	92 CSB2	$\Upsilon(3S) \rightarrow \gamma \gamma \ell^+ \ell^-$

³⁶ From a sample of $\Upsilon(3S) \rightarrow \gamma \mu^+ \mu^-$ with converted photons.
³⁷ CRAWFORD 92b quotes $2 \times B(\Upsilon(3S) \rightarrow \gamma \chi_{bJ}(2P)) B(\chi_{bJ}(2P) \rightarrow \gamma \Upsilon(nS)) B(\Upsilon(nS) \rightarrow \ell^+ \ell^-)$.
³⁸ Calculated by us. HEINTZ 92 quotes $B(\Upsilon(3S) \rightarrow \gamma \chi_{b2}(2P)) \times B(\chi_{b2}(2P) \rightarrow \gamma \Upsilon(1S)) = (0.77 \pm 0.11 \pm 0.05)\%$ using $B(\Upsilon(1S) \rightarrow \mu^+ \mu^-) = (2.57 \pm 0.05)\%$.

$[B(\chi_{b2}(2P) \rightarrow \gamma \Upsilon(1S)) \times B(\Upsilon(3S) \rightarrow \gamma \chi_{b2}(2P))] / [B(\chi_{b1}(2P) \rightarrow \gamma \Upsilon(1S)) \times B(\Upsilon(3S) \rightarrow \gamma \chi_{b1}(2P))]$

VALUE (%)	DOCUMENT ID	TECN	COMMENT
66.6±3.0	39 LEES	14M BABR	$\Upsilon(3S) \rightarrow \gamma \mu^+ \mu^-$

³⁹ From a sample of $\Upsilon(3S) \rightarrow \gamma \mu^+ \mu^-$ events without converted photons.

$B(\chi_{b2}(2P) \rightarrow \gamma \Upsilon(2S)) \times B(\Upsilon(3S) \rightarrow \gamma \chi_{b2}(2P)) \times B(\Upsilon(2S) \rightarrow \ell^+ \ell^-)$

VALUE (units 10^{-4})	EVTS	DOCUMENT ID	TECN	COMMENT
2.74±0.29 OUR AVERAGE				

3.22 ^{+0.58+0.16} _{-0.53-0.71}		40 LEES	14M BABR	$\Upsilon(3S) \rightarrow \gamma \mu^+ \mu^-$
2.49±0.47±0.31	53	41 CRAWFORD	92B CLE2	$\Upsilon(3S) \rightarrow \gamma \gamma \ell^+ \ell^-$
2.74±0.33±0.18		42 HEINTZ	92 CSB2	$\Upsilon(3S) \rightarrow \gamma \gamma \ell^+ \ell^-$

⁴⁰ From a sample of $\Upsilon(3S) \rightarrow \gamma \mu^+ \mu^-$ with converted photons.
⁴¹ CRAWFORD 92b quotes $2 \times B(\Upsilon(3S) \rightarrow \gamma \chi_{bJ}(2P)) B(\chi_{bJ}(2P) \rightarrow \gamma \Upsilon(nS)) B(\Upsilon(nS) \rightarrow \ell^+ \ell^-)$.
⁴² Calculated by us. HEINTZ 92 quotes $B(\Upsilon(3S) \rightarrow \gamma \chi_{b2}(2P)) \times B(\chi_{b2}(2P) \rightarrow \gamma \Upsilon(2S)) = (1.90 \pm 0.23 \pm 0.18)\%$ using $B(\Upsilon(2S) \rightarrow \mu^+ \mu^-) = (1.44 \pm 0.10)\%$.

$[B(\chi_{b2}(2P) \rightarrow \gamma \Upsilon(2S)) \times B(\Upsilon(3S) \rightarrow \gamma \chi_{b2}(2P))] / [B(\chi_{b1}(2P) \rightarrow \gamma \Upsilon(2S)) \times B(\Upsilon(3S) \rightarrow \gamma \chi_{b1}(2P))]$

VALUE (%)	DOCUMENT ID	TECN	COMMENT
46.9±2.0	43 LEES	14M BABR	$\Upsilon(3S) \rightarrow \gamma \mu^+ \mu^-$

⁴³ From a sample of $\Upsilon(3S) \rightarrow \gamma \mu^+ \mu^-$ without converted photons.

$\chi_{b2}(2P)$ REFERENCES

AALI	14BG	JHEP 1410 088	R. Aaij et al.	(LHCb Collab.)
LEES	14M	PR D90 112010	J.P. Lees et al.	(BABAR Collab.)
LEES	11C	PR D84 011304	J.P. Lees et al.	(BABAR Collab.)
LEES	11J	PR D84 072002	J.P. Lees et al.	(BABAR Collab.)
ASNER	08A	PR D78 091103	D.M. Asner et al.	(CLEO Collab.)
BRIERE	08	PR D78 092007	R.A. Briere et al.	(CLEO Collab.)
CAWLFIELD	06	PR D73 012003	C. Cawfield et al.	(CLEO Collab.)
ARTUSO	05	PRL 94 032001	M. Artuso et al.	(CLEO Collab.)
CRONIN-HEIN...	04	PRL 92 222002	D. Cronin-Hennessy et al.	(CLEO Collab.)
CRAWFORD	92B	PL B294 139	G. Crawford et al.	(CLEO Collab.)
HEINTZ	92	PR D46 1928	U. Heintz et al.	(CSB II Collab.)
HEINTZ	91	PRL 66 1563	U. Heintz et al.	(CSB Collab.)
MORRISON	91	PRL 67 1696	R.J. Morrison et al.	(CLEO Collab.)
NARAIN	91	PRL 66 3113	M. Narain et al.	(CSB Collab.)

$\Upsilon(3S)$

$$J^{PC} = 0^{-}(1^{- -})$$

$\Upsilon(3S)$ MASS

VALUE (MeV)	DOCUMENT ID	TECN	COMMENT
10355.2±0.5	¹ ARTAMONOV 00	MD1	$e^+ e^- \rightarrow$ hadrons
••• We do not use the following data for averages, fits, limits, etc. •••			
10355.3±0.5	^{2,3} BARU	86B REDE	$e^+ e^- \rightarrow$ hadrons

¹ Reanalysis of BARU 86b using new electron mass (COHEN 87).
² Reanalysis of ARTAMONOV 84.
³ Superseded by ARTAMONOV 00.

$m \Upsilon(3S) - m \Upsilon(2S)$

VALUE (MeV)	DOCUMENT ID	TECN	COMMENT
331.50±0.02±0.13	LEES	11c	BABR $e^+ e^- \rightarrow \pi^+ \pi^- X$

$\Upsilon(3S)$ WIDTH

VALUE (keV)	DOCUMENT ID	COMMENT
20.32±1.85 OUR EVALUATION		See the Note on "Width Determinations of the Υ States"

$\Upsilon(3S)$ DECAY MODES

Mode	Fraction (Γ_i/Γ)	Scale factor/ Confidence level
Γ_1	$\Upsilon(2S)$ anything	(10.6 ± 0.8) %
Γ_2	$\Upsilon(2S) \pi^+ \pi^-$	(2.82 ± 0.18) % S=1.6
Γ_3	$\Upsilon(2S) \pi^0 \pi^0$	(1.85 ± 0.14) %

Γ_4	$\Upsilon(2S) \gamma \gamma$	(5.0 ± 0.7) %
Γ_5	$\Upsilon(2S) \pi^0$	< 5.1 × 10 ⁻⁴ CL=90%
Γ_6	$\Upsilon(1S) \pi^+ \pi^-$	(4.37 ± 0.08) %
Γ_7	$\Upsilon(1S) \pi^0 \pi^0$	(2.20 ± 0.13) %
Γ_8	$\Upsilon(1S) \eta$	< 1 × 10 ⁻⁴ CL=90%
Γ_9	$\Upsilon(1S) \pi^0$	< 7 × 10 ⁻⁵ CL=90%
Γ_{10}	$h_b(1P) \pi^0$	< 1.2 × 10 ⁻³ CL=90%
Γ_{11}	$h_b(1P) \pi^0 \rightarrow \gamma h_b(1S) \pi^0$	(4.3 ± 1.4) × 10 ⁻⁴
Γ_{12}	$h_b(1P) \pi^+ \pi^-$	< 1.2 × 10 ⁻⁴ CL=90%
Γ_{13}	$\tau^+ \tau^-$	(2.29 ± 0.30) %
Γ_{14}	$\mu^+ \mu^-$	(2.18 ± 0.21) % S=2.1
Γ_{15}	$e^+ e^-$	(2.18 ± 0.20) %
Γ_{16}	hadrons	(93 ± 12) %
Γ_{17}	ggg	(35.7 ± 2.6) %
Γ_{18}	γgg	(9.7 ± 1.8) × 10 ⁻³
Γ_{19}	2H anything	(2.33 ± 0.33) × 10 ⁻⁵

Radiative decays

Γ_{20}	$\gamma \chi_{b2}(2P)$	(13.1 ± 1.6) % S=3.4
Γ_{21}	$\gamma \chi_{b1}(2P)$	(12.6 ± 1.2) % S=2.4
Γ_{22}	$\gamma \chi_{b0}(2P)$	(5.9 ± 0.6) % S=1.4
Γ_{23}	$\gamma \chi_{b2}(1P)$	(10.0 ± 1.0) × 10 ⁻³ S=1.7
Γ_{24}	$\gamma \chi_{b1}(1P)$	(9 ± 5) × 10 ⁻⁴ S=1.8
Γ_{25}	$\gamma \chi_{b0}(1P)$	(2.7 ± 0.4) × 10 ⁻³
Γ_{26}	$\gamma h_b(2S)$	< 6.2 × 10 ⁻⁴ CL=90%
Γ_{27}	$\gamma h_b(1S)$	(5.1 ± 0.7) × 10 ⁻⁴
Γ_{28}	$\gamma A^0 \rightarrow \gamma$ hadrons	< 8 × 10 ⁻⁵ CL=90%
Γ_{29}	$\gamma X \rightarrow \gamma + \geq 4$ prongs	[a] < 2.2 × 10 ⁻⁴ CL=95%
Γ_{30}	$\gamma a_1^0 \rightarrow \gamma \mu^+ \mu^-$	< 5.5 × 10 ⁻⁶ CL=90%
Γ_{31}	$\gamma a_1^0 \rightarrow \gamma \tau^+ \tau^-$	[b] < 1.6 × 10 ⁻⁴ CL=90%

Lepton Family number (LF) violating modes

Γ_{32}	$e^\pm \tau^\mp$	LF	< 4.2 × 10 ⁻⁶ CL=90%
Γ_{33}	$\mu^\pm \tau^\mp$	LF	< 3.1 × 10 ⁻⁶ CL=90%

[a] 1.5 GeV < m_X < 5.0 GeV

[b] For $m_{\tau^+ \tau^-}$ in the ranges 4.03–9.52 and 9.61–10.10 GeV.

$\Upsilon(3S) \Gamma(\ell^+ \ell^-) / \Gamma(\text{total})$

$\Gamma(\text{hadrons}) \times \Gamma(e^+ e^-) / \Gamma_{\text{total}}$ $\Gamma_{16} \Gamma_{15} / \Gamma$

VALUE (keV)	DOCUMENT ID	TECN	COMMENT
0.414±0.007 OUR AVERAGE			
0.413 ± 0.004 ± 0.006	ROSNER 06	CLEO	10.4 $e^+ e^- \rightarrow$ hadrons
0.45 ± 0.03 ± 0.03	⁴ GILES	84B CLEO	$e^+ e^- \rightarrow$ hadrons

⁴ Radiative corrections reevaluated by BUCHMUELLER 88 following KURAEV 85.

$\Gamma(\Upsilon(1S) \pi^+ \pi^-) \times \Gamma(e^+ e^-) / \Gamma_{\text{total}}$ $\Gamma_6 \Gamma_{15} / \Gamma$

VALUE (eV)	EVTS	DOCUMENT ID	TECN	COMMENT
18.46±0.27±0.77	6.4k	⁵ AUBERT	08BP BABR	$e^+ e^- \rightarrow \gamma \pi^+ \pi^- \ell^+ \ell^-$

⁵ Using $B(\Upsilon(1S) \rightarrow e^+ e^-) = (2.38 \pm 0.11)\%$ and $B(\Upsilon(1S) \rightarrow \mu^+ \mu^-) = (2.48 \pm 0.05)\%$.

$\Upsilon(3S)$ PARTIAL WIDTHS

$\Gamma(e^+ e^-)$ Γ_{15}

VALUE (keV)	DOCUMENT ID
0.443±0.008 OUR EVALUATION	

$\Upsilon(3S)$ BRANCHING RATIOS

$\Gamma(\Upsilon(2S) \text{ anything}) / \Gamma_{\text{total}}$ Γ_1 / Γ

VALUE	EVTS	DOCUMENT ID	TECN	COMMENT
0.106 ± 0.008 OUR AVERAGE				
0.1023 ± 0.0105	4625	^{6,7,8} BUTLER	94B CLE2	$e^+ e^- \rightarrow \ell^+ \ell^- X$
0.111 ± 0.012	4891	^{7,8,9} BROCK	91 CLEO	$e^+ e^- \rightarrow \pi^+ \pi^- X$, $\pi^+ \pi^- \ell^+ \ell^-$

⁶ Using $B(\Upsilon(2S) \rightarrow \Upsilon(1S) \gamma \gamma) = (0.038 \pm 0.007)\%$, and $B(\Upsilon(2S) \rightarrow \Upsilon(1S) \pi^0 \pi^0) = (1/2)B(\Upsilon(2S) \rightarrow \Upsilon(1S) \pi^+ \pi^-)$.

⁷ Using $B(\Upsilon(1S) \rightarrow \mu^+ \mu^-) = (2.48 \pm 0.06)\%$. With the assumption of $e\mu$ universality.

⁸ Using $B(\Upsilon(2S) \rightarrow \Upsilon(1S) \pi^+ \pi^-) = (18.5 \pm 0.8)\%$.

⁹ Using $B(\Upsilon(2S) \rightarrow \mu^+ \mu^-) = (1.31 \pm 0.21)\%$, $B(\Upsilon(2S) \rightarrow \Upsilon(1S) \gamma \gamma) \times 2B(\Upsilon(1S) \rightarrow \mu^+ \mu^-) = (0.188 \pm 0.035)\%$, and $B(\Upsilon(2S) \rightarrow \Upsilon(1S) \pi^0 \pi^0) \times 2B(\Upsilon(1S) \rightarrow \mu^+ \mu^-) = (0.436 \pm 0.056)\%$. With the assumption of $e\mu$ universality.

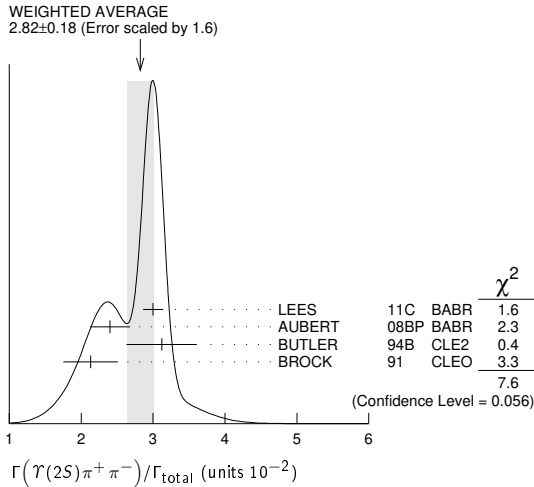
$\Gamma(\Upsilon(2S) \pi^+ \pi^-) / \Gamma_{\text{total}}$ Γ_2 / Γ

VALUE (units 10^{-2})	EVTS	DOCUMENT ID	TECN	COMMENT
2.82±0.18 OUR AVERAGE				Error includes scale factor of 1.6. See the ideogram below.
3.00 ± 0.02 ± 0.14	543k	LEES	11c BABR	$e^+ e^- \rightarrow \pi^+ \pi^- X$
2.40 ± 0.10 ± 0.26	800	¹⁰ AUBERT	08BP BABR	$e^+ e^- \rightarrow \gamma \pi^+ \pi^- e^+ e^-$

Meson Particle Listings

$\Upsilon(3S)$

3.12±0.49	980	^{11,12} BUTLER	94B	CLE2	$e^+e^- \rightarrow \pi^+\pi^-\ell^+\ell^-$
2.13±0.38	974	¹³ BROCK	91	CLEO	$e^+e^- \rightarrow \pi^+\pi^-X,$ $\pi^+\pi^-\ell^+\ell^-$
• • • We do not use the following data for averages, fits, limits, etc. • • •					
4.82±0.65±0.53	138	¹³ WU	93	CUSB	$\Upsilon(3S) \rightarrow \pi^+\pi^-\ell^+\ell^-$
3.1 ± 2.0	5	MAGERAS	82	CUSB	$\Upsilon(3S) \rightarrow \pi^+\pi^-\ell^+\ell^-$
¹⁰ Using B($\Upsilon(1S) \rightarrow e^+e^-$) = (2.38 ± 0.11)%, B($\Upsilon(1S) \rightarrow \mu^+\mu^-$) = (2.48 ± 0.05)%, and $\Gamma_{ee}(\Upsilon(3S)) = 0.443 \pm 0.008$ keV.					
¹¹ From the exclusive mode.					
¹² Using B($\Upsilon(2S) \rightarrow \Upsilon(1S)\gamma\gamma$) = (0.038 ± 0.007)%, and B($\Upsilon(2S) \rightarrow \Upsilon(1S)\pi^0\pi^0$) = (1/2)B($\Upsilon(2S) \rightarrow \Upsilon(1S)\pi^+\pi^-$).					
¹³ Using B($\Upsilon(2S) \rightarrow \mu^+\mu^-$) = (1.31 ± 0.21)%, B($\Upsilon(2S) \rightarrow \Upsilon(1S)\gamma\gamma$)×2B($\Upsilon(1S) \rightarrow \mu^+\mu^-$) = (0.188 ± 0.035)%, and B($\Upsilon(2S) \rightarrow \Upsilon(1S)\pi^0\pi^0$)×2B($\Upsilon(1S) \rightarrow \mu^+\mu^-$) = (0.436 ± 0.056)%. With the assumption of $e\mu$ universality.					



$\Gamma(\Upsilon(2S)\pi^0\pi^0)/\Gamma_{total}$						Γ_3/Γ
VALUE (units 10^{-2})	EVTS	DOCUMENT ID	TECN	COMMENT		
1.85±0.14 OUR AVERAGE						
1.82±0.09±0.12	4391	¹⁴ BHARI	09	CLEO	$e^+e^- \rightarrow \pi^0\pi^0\ell^+\ell^-$	
2.16±0.39		^{15,16} BUTLER	94B	CLE2	$e^+e^- \rightarrow \pi^0\pi^0\ell^+\ell^-$	
1.7 ± 0.5 ± 0.2	10	¹⁷ HEINTZ	92	CSB2	$e^+e^- \rightarrow \pi^0\pi^0\ell^+\ell^-$	
¹⁴ Authors assume B($\Upsilon(1S) \rightarrow e^+e^-$) + B($\Upsilon(1S) \rightarrow \mu^+\mu^-$) = 4.06%.						
¹⁵ B($\Upsilon(2S) \rightarrow \mu^+\mu^-$) = (1.31 ± 0.21)% and assuming $e\mu$ universality.						
¹⁶ From the exclusive mode.						
¹⁷ B($\Upsilon(2S) \rightarrow \mu^+\mu^-$) = (1.44 ± 0.10)% and assuming $e\mu$ universality. Supersedes HEINTZ 91.						

$\Gamma(\Upsilon(2S)\gamma\gamma)/\Gamma_{total}$						Γ_4/Γ
VALUE	DOCUMENT ID	TECN	COMMENT			
0.0502±0.0069	¹⁸ BUTLER	94B	CLE2	$e^+e^- \rightarrow \ell^+\ell^-\gamma$		
¹⁸ From the exclusive mode.						

$\Gamma(\Upsilon(2S)\pi^0)/\Gamma_{total}$						Γ_5/Γ
VALUE (units 10^{-3})	CL%	DOCUMENT ID	TECN	COMMENT		
<0.51	90	¹⁹ HE	08A	CLEO	$e^+e^- \rightarrow \ell^+\ell^-\gamma\gamma$	
¹⁹ Authors assume B($\Upsilon(2S) \rightarrow e^+e^-$) + B($\Upsilon(1S) \rightarrow \mu^+\mu^-$) = 4.06%.						

$\Gamma(\Upsilon(1S)\pi^+\pi^-)/\Gamma_{total}$						Γ_6/Γ
Abbreviation MM in the COMMENT field below stands for missing mass.						
VALUE (units 10^{-2})	EVTS	DOCUMENT ID	TECN	COMMENT		
4.37±0.08 OUR AVERAGE						
4.32±0.07±0.13	90k	²⁰ LEES	11L	BABR	$\Upsilon(3S) \rightarrow \pi^+\pi^-\ell^+\ell^-$	
4.46±0.01±0.13	190k	²¹ BHARI	09	CLEO	$e^+e^- \rightarrow \pi^+\pi^-MM$	
4.17±0.06±0.19	6.4k	²² AUBERT	08BP	BABR	10.58 $e^+e^- \rightarrow \gamma\pi^+\pi^-\ell^+\ell^-$	
4.52±0.35	11830	²³ BUTLER	94B	CLE2	$e^+e^- \rightarrow \pi^+\pi^-X,$ $\pi^+\pi^-\ell^+\ell^-$	
4.46±0.34±0.50	451	²³ WU	93	CUSB	$\Upsilon(3S) \rightarrow \pi^+\pi^-\ell^+\ell^-$	
4.46±0.30	11221	²³ BROCK	91	CLEO	$e^+e^- \rightarrow \pi^+\pi^-X,$ $\pi^+\pi^-\ell^+\ell^-$	
• • • We do not use the following data for averages, fits, limits, etc. • • •						
4.9 ± 1.0	22	GREEN	82	CLEO	$\Upsilon(3S) \rightarrow \pi^+\pi^-\ell^+\ell^-$	
3.9 ± 1.3	26	MAGERAS	82	CUSB	$\Upsilon(3S) \rightarrow \pi^+\pi^-\ell^+\ell^-$	
²⁰ Using B($\Upsilon(1S) \rightarrow e^+e^-$) = (2.38 ± 0.11)% and B($\Upsilon(1S) \rightarrow \mu^+\mu^-$) = (2.48 ± 0.05)%.						
²¹ A weighted average of the inclusive and exclusive results.						
²² Using B($\Upsilon(2S) \rightarrow e^+e^-$) = (1.91 ± 0.16)%, B($\Upsilon(2S) \rightarrow \mu^+\mu^-$) = (1.93 ± 0.17)%, and $\Gamma_{ee}(\Upsilon(3S)) = 0.443 \pm 0.008$ keV.						
²³ Using B($\Upsilon(1S) \rightarrow \mu^+\mu^-$) = (2.48 ± 0.06)%. With the assumption of $e\mu$ universality.						

$\Gamma(\Upsilon(2S)\pi^+\pi^-)/\Gamma(\Upsilon(1S)\pi^+\pi^-)$						Γ_2/Γ_6
VALUE	EVTS	DOCUMENT ID	TECN	COMMENT		
0.577±0.026±0.060	800	²⁴ AUBERT	08BP	BABR	$e^+e^- \rightarrow \gamma\pi^+\pi^-\ell^+\ell^-$	
²⁴ Using B($\Upsilon(1S) \rightarrow e^+e^-$) = (2.38 ± 0.11)%, B($\Upsilon(1S) \rightarrow \mu^+\mu^-$) = (2.48 ± 0.05)%, B($\Upsilon(2S) \rightarrow e^+e^-$) = (1.91 ± 0.16)%, and B($\Upsilon(2S) \rightarrow \mu^+\mu^-$) = (1.93 ± 0.17)%. Not independent of other values reported by AUBERT 08BP.						

$\Gamma(\Upsilon(1S)\pi^0\pi^0)/\Gamma_{total}$						Γ_7/Γ
VALUE (units 10^{-2})	EVTS	DOCUMENT ID	TECN	COMMENT		
2.20±0.13 OUR AVERAGE						
2.24±0.09±0.11	6584	²⁵ BHARI	09	CLEO	$e^+e^- \rightarrow \pi^0\pi^0\ell^+\ell^-$	
1.99±0.34	56	²⁶ BUTLER	94B	CLE2	$e^+e^- \rightarrow \pi^0\pi^0\ell^+\ell^-$	
2.2 ± 0.4 ± 0.3	33	²⁷ HEINTZ	92	CSB2	$e^+e^- \rightarrow \pi^0\pi^0\ell^+\ell^-$	
²⁵ Authors assume B($\Upsilon(1S) \rightarrow e^+e^-$) + B($\Upsilon(1S) \rightarrow \mu^+\mu^-$) = 4.96%.						
²⁶ Using B($\Upsilon(1S) \rightarrow \mu^+\mu^-$) = (2.48 ± 0.06)% and assuming $e\mu$ universality.						
²⁷ Using B($\Upsilon(1S) \rightarrow \mu^+\mu^-$) = (2.57 ± 0.07)% and assuming $e\mu$ universality. Supersedes HEINTZ 91.						

$\Gamma(\Upsilon(1S)\pi^0\pi^0)/\Gamma(\Upsilon(1S)\pi^+\pi^-)$						Γ_7/Γ_6
VALUE	DOCUMENT ID	TECN	COMMENT			
0.501±0.043	²⁸ BHARI	09	CLEO	$e^+e^- \rightarrow \Upsilon(3S)$		
²⁸ Not independent of other values reported by BHARI 09.						

$\Gamma(\Upsilon(1S)\eta)/\Gamma_{total}$						Γ_8/Γ
VALUE (units 10^{-3})	CL%	DOCUMENT ID	TECN	COMMENT		
<0.1	90	²⁹ LEES	11L	BABR	$\Upsilon(3S) \rightarrow (\pi^+\pi^-\gamma)\ell^+\ell^-$	
• • • We do not use the following data for averages, fits, limits, etc. • • •						
<0.8	90	^{29,30} AUBERT	08BP	BABR	$e^+e^- \rightarrow \gamma\pi^+\pi^-\pi^0\ell^+\ell^-$	
<0.18	90	³¹ HE	08A	CLEO	$e^+e^- \rightarrow \ell^+\ell^-\eta$	
<2.2	90	BROCK	91	CLEO	$e^+e^- \rightarrow \ell^+\ell^-\eta$	
²⁹ Using B($\Upsilon(1S) \rightarrow e^+e^-$) = (2.38 ± 0.11)%, B($\Upsilon(1S) \rightarrow \mu^+\mu^-$) = (2.48 ± 0.05)%.						
³⁰ Using $\Gamma_{ee}(\Upsilon(3S)) = 0.443 \pm 0.008$ keV.						
³¹ Authors assume B($\Upsilon(1S) \rightarrow e^+e^-$) + B($\Upsilon(1S) \rightarrow \mu^+\mu^-$) = 4.96%.						

$\Gamma(\Upsilon(1S)\eta)/\Gamma(\Upsilon(1S)\pi^+\pi^-)$						Γ_8/Γ_6
VALUE (units 10^{-2})	CL%	DOCUMENT ID	TECN	COMMENT		
<0.23	90	³² LEES	11L	BABR	$\Upsilon(3S) \rightarrow (\pi^+\pi^-\gamma)\ell^+\ell^-$	
• • • We do not use the following data for averages, fits, limits, etc. • • •						
<1.9	90	³³ AUBERT	08BP	BABR	$e^+e^- \rightarrow \gamma\pi^+\pi^-(\pi^0)\ell^+\ell^-$	
³² Not independent of other values reported by LEES 11L.						
³³ Not independent of other values reported by AUBERT 08BP.						

$\Gamma(\Upsilon(1S)\pi^0)/\Gamma_{total}$						Γ_9/Γ
VALUE (units 10^{-3})	CL%	DOCUMENT ID	TECN	COMMENT		
<0.07	90	³⁴ HE	08A	CLEO	$e^+e^- \rightarrow \ell^+\ell^-\gamma\gamma$	
³⁴ Authors assume B($\Upsilon(1S) \rightarrow e^+e^-$) + B($\Upsilon(1S) \rightarrow \mu^+\mu^-$) = 4.96%.						

$\Gamma(h_b(1P)\pi^0)/\Gamma_{total}$						Γ_{10}/Γ
VALUE	CL%	DOCUMENT ID	TECN	COMMENT		
<1.2 × 10⁻³	90	³⁵ GE	11	CLEO	$\Upsilon(3S) \rightarrow \pi^0$ anything $\gamma\eta_b(1S)$ to vary from 0–100%.	
³⁵ Assuming $M(h_b(1P)) = 9900$ MeV and $\Gamma(h_b(1P)) = 0$ MeV, and allowing B($h_b(1P) \rightarrow \gamma\eta_b(1S)$) to vary from 0–100%.						

$\Gamma(h_b(1P)\pi^0 \rightarrow \gamma\eta_b(1S)\pi^0)/\Gamma_{total}$						Γ_{11}/Γ
VALUE (units 10^{-4})	DOCUMENT ID	TECN	COMMENT			
4.3±1.1±0.9	LEES	11k	BABR	$\Upsilon(3S) \rightarrow \eta_b\gamma\pi^0$		

$\Gamma(h_b(1P)\pi^+\pi^-)/\Gamma_{total}$						Γ_{12}/Γ
VALUE (units 10^{-4})	CL%	DOCUMENT ID	TECN	COMMENT		
< 1.2	90	³⁶ LEES	11c	BABR	$e^+e^- \rightarrow \pi^+\pi^-X$	
• • • We do not use the following data for averages, fits, limits, etc. • • •						
<18		³⁶ BUTLER	94B	CLE2	$e^+e^- \rightarrow \pi^+\pi^-X$	
<15		³⁶ BROCK	91	CLEO	$e^+e^- \rightarrow \pi^+\pi^-X$	
³⁶ For $M(h_b(1P)) = 9900$ MeV.						

$\Gamma(\tau^+\tau^-)/\Gamma_{total}$						Γ_{13}/Γ
VALUE (units 10^{-2})	EVTS	DOCUMENT ID	TECN	COMMENT		
2.29±0.21±0.22	15k	³⁷ BESSON	07	CLEO	$e^+e^- \rightarrow \Upsilon(3S) \rightarrow \tau^+\tau^-$	
³⁷ BESSON 07 reports $[\Gamma(\Upsilon(3S) \rightarrow \tau^+\tau^-)/\Gamma_{total}] / [B(\Upsilon(3S) \rightarrow \mu^+\mu^-)] = 1.05 \pm 0.08 \pm 0.05$ which we multiply by our best value B($\Upsilon(3S) \rightarrow \mu^+\mu^-$) = (2.18 ± 0.21) × 10 ⁻² . Our first error is their experiment's error and our second error is the systematic error from using our best value.						

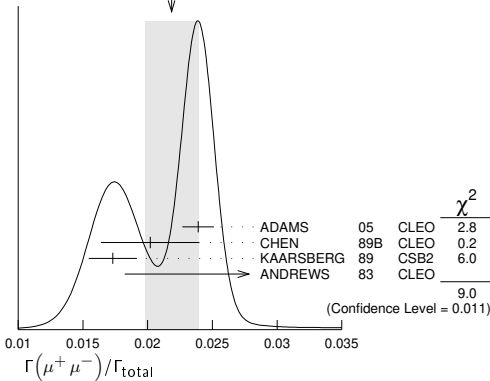
$\Gamma(\tau^+\tau^-)/\Gamma(\mu^+\mu^-)$						Γ_{13}/Γ_{14}
VALUE	EVTS	DOCUMENT ID	TECN	COMMENT		
0.968±0.016 OUR AVERAGE						
0.966±0.008±0.014	2.2M	LEES	20E	BABR	$e^+e^- \rightarrow \Upsilon(3S)$	
1.05 ± 0.08 ± 0.05	15k	BESSON	07	CLEO	$e^+e^- \rightarrow \Upsilon(3S)$	

Meson Particle Listings

$\Upsilon(3S)$

$\Gamma(\mu^+\mu^-)/\Gamma_{total}$		Γ_{14}/Γ				
VALUE	EVTS	DOCUMENT ID	TECN	COMMENT		
0.0218 ± 0.0021 OUR AVERAGE		Error includes scale factor of 2.1. See the ideogram below.				
0.0239 ± 0.0007 ± 0.0010	81k	ADAMS	05	CLEO	$e^+e^- \rightarrow \mu^+\mu^-$	
0.0202 ± 0.0019 ± 0.0033		CHEN	89b	CLEO	$e^+e^- \rightarrow \mu^+\mu^-$	
0.0173 ± 0.0015 ± 0.0011		KAARSBERG	89	CSB2	$e^+e^- \rightarrow \mu^+\mu^-$	
0.033 ± 0.013 ± 0.007	1096	ANDREWS	83	CLEO	$e^+e^- \rightarrow \mu^+\mu^-$	

WEIGHTED AVERAGE
0.0218 ± 0.0021 (Error scaled by 2.1)



$\Gamma(ggg)/\Gamma_{total}$		Γ_{17}/Γ				
VALUE (units 10^{-2})	EVTS	DOCUMENT ID	TECN	COMMENT		
35.7 ± 2.6	3M	38 BESSON	06A	CLEO	$\Upsilon(3S) \rightarrow \text{hadrons}$	

³⁸ Calculated using BESSON 06A value of $\Gamma(\gamma g g)/\Gamma(g g g) = (2.72 \pm 0.06 \pm 0.32 \pm 0.37)\%$ and the PDG 08 values of $B(\Upsilon(2S) + \text{anything}) = (10.6 \pm 0.8)\%$, $B(\pi^+\pi^-\Upsilon(1S)) = (4.40 \pm 0.10)\%$, $B(\pi^0\pi^0\Upsilon(1S)) = (2.20 \pm 0.13)\%$, $B(\gamma\chi_{b2}(2P)) = (13.1 \pm 1.6)\%$, $B(\gamma\chi_{b1}(2P)) = (12.6 \pm 1.2)\%$, $B(\gamma\chi_{b0}(2P)) = (5.9 \pm 0.6)\%$, $B(\gamma\chi_{b0}(1P)) = (0.30 \pm 0.11)\%$, $B(\mu^+\mu^-) = (2.18 \pm 0.21)\%$, and $R_{\text{hadrons}} = 3.51$. The statistical error is negligible and the systematic error is partially correlated with $\Gamma(\gamma g g)/\Gamma_{total}$ BESSON 06A value.

$\Gamma(\gamma g g)/\Gamma_{total}$		Γ_{18}/Γ				
VALUE (units 10^{-2})	EVTS	DOCUMENT ID	TECN	COMMENT		
0.97 ± 0.18	60k	39 BESSON	06A	CLEO	$\Upsilon(3S) \rightarrow \gamma + \text{hadrons}$	

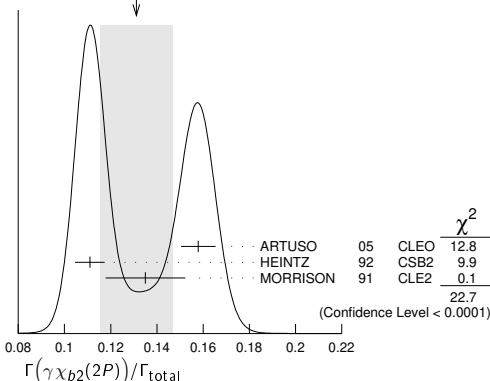
³⁹ Calculated using BESSON 06A values of $\Gamma(\gamma g g)/\Gamma(g g g) = (2.72 \pm 0.06 \pm 0.32 \pm 0.37)\%$ and $\Gamma(g g g)/\Gamma_{total}$. The statistical error is negligible and the systematic error is partially correlated with $\Gamma(g g g)/\Gamma_{total}$ BESSON 06A value.

$\Gamma(\gamma g g)/\Gamma(g g g)$		Γ_{18}/Γ_{17}				
VALUE (units 10^{-2})	EVTS	DOCUMENT ID	TECN	COMMENT		
2.72 ± 0.06 ± 0.49	3M	BESSON	06A	CLEO	$\Upsilon(3S) \rightarrow (\gamma +) \text{hadrons}$	

$\Gamma(2H \text{ anything})/\Gamma_{total}$		Γ_{19}/Γ				
VALUE (units 10^{-5})	EVTS	DOCUMENT ID	TECN	COMMENT		
2.33 ± 0.15 ± 0.31 ± 0.28		LEES	14G	BABR	$e^+e^- \rightarrow 2H X$	

$\Gamma(\gamma\chi_{b2}(2P))/\Gamma_{total}$		Γ_{20}/Γ				
VALUE	EVTS	DOCUMENT ID	TECN	COMMENT		
0.131 ± 0.016 OUR AVERAGE		Error includes scale factor of 3.4. See the ideogram below.				
0.1579 ± 0.0017 ± 0.0073	568k	ARTUSO	05	CLEO	$e^+e^- \rightarrow \gamma X$	
0.111 ± 0.005 ± 0.004	10319	40 HEINTZ	92	CSB2	$e^+e^- \rightarrow \gamma X$	
0.135 ± 0.003 ± 0.017	30741	MORRISON	91	CLE2	$e^+e^- \rightarrow \gamma X$	

WEIGHTED AVERAGE
0.131 ± 0.016 (Error scaled by 3.4)

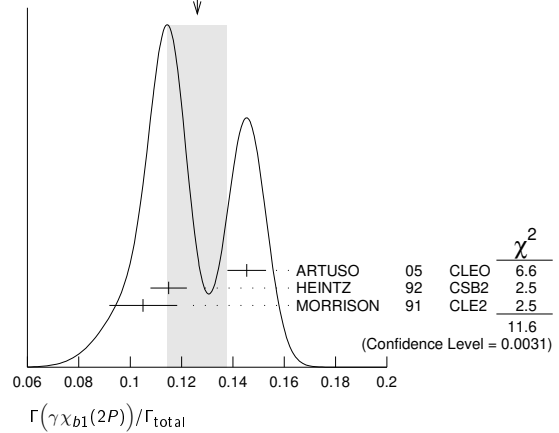


⁴⁰ Supersedes NARAIN 91.

$\Gamma(\gamma\chi_{b1}(2P))/\Gamma_{total}$		Γ_{21}/Γ				
VALUE	EVTS	DOCUMENT ID	TECN	COMMENT		
0.126 ± 0.012 OUR AVERAGE		Error includes scale factor of 2.4. See the ideogram below.				
0.1454 ± 0.0018 ± 0.0073	537k	ARTUSO	05	CLEO	$e^+e^- \rightarrow \gamma X$	
0.115 ± 0.005 ± 0.005	11147	41 HEINTZ	92	CSB2	$e^+e^- \rightarrow \gamma X$	
0.105 ± 0.003 ± 0.013	25759	MORRISON	91	CLE2	$e^+e^- \rightarrow \gamma X$	

⁴¹ Supersedes NARAIN 91.

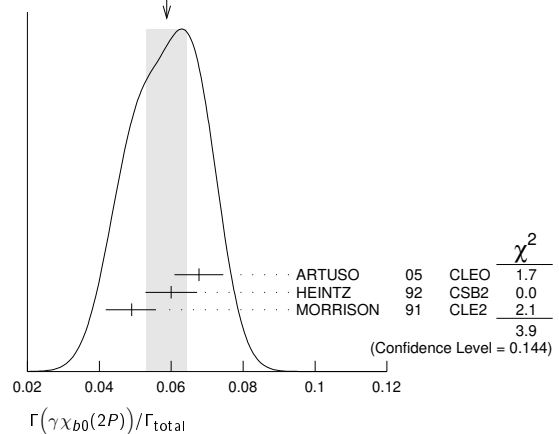
WEIGHTED AVERAGE
0.126 ± 0.012 (Error scaled by 2.4)



$\Gamma(\gamma\chi_{b0}(2P))/\Gamma_{total}$		Γ_{22}/Γ				
VALUE	EVTS	DOCUMENT ID	TECN	COMMENT		
0.059 ± 0.006 OUR AVERAGE		Error includes scale factor of 1.4. See the ideogram below.				
0.0677 ± 0.0020 ± 0.0065	225k	ARTUSO	05	CLEO	$e^+e^- \rightarrow \gamma X$	
0.060 ± 0.004 ± 0.006	4959	42 HEINTZ	92	CSB2	$e^+e^- \rightarrow \gamma X$	
0.049 ± 0.003 ± 0.006	9903	MORRISON	91	CLE2	$e^+e^- \rightarrow \gamma X$	

⁴² Supersedes NARAIN 91.

WEIGHTED AVERAGE
0.059 ± 0.006 (Error scaled by 1.4)



$\Gamma(\gamma\chi_{b2}(1P))/\Gamma_{total}$		Γ_{23}/Γ				
VALUE (units 10^{-3})	CL% EVTS	DOCUMENT ID	TECN	COMMENT		
10.0 ± 1.0 OUR AVERAGE		Error includes scale factor of 1.7.				
8.0 ± 1.3 ± 0.4	126	43,44 KORNICER	11	CLEO	$e^+e^- \rightarrow \gamma\gamma\ell^+\ell^-$	
10.5 ± 0.3 ± 0.7 ± 0.6	9.7k	LEES	11j	BABR	$\Upsilon(3S) \rightarrow X\gamma$	

• • • We do not use the following data for averages, fits, limits, etc. • • •

<19	90	45 ASNER	08A	CLEO	$\Upsilon(3S) \rightarrow \gamma + \text{hadrons}$	seen
		46 HEINTZ	92	CSB2	$e^+e^- \rightarrow \gamma\gamma\ell^+\ell^-$	

⁴³ Assuming $B(\Upsilon(1S) \rightarrow \ell^+\ell^-) = (2.48 \pm 0.05)\%$.

⁴⁴ KORNICER 11 reports $[\Gamma(\Upsilon(3S) \rightarrow \gamma\chi_{b2}(1P))/\Gamma_{total}] \times [B(\chi_{b2}(1P) \rightarrow \gamma\Upsilon(1S))] = (1.435 \pm 0.162 \pm 0.169) \times 10^{-3}$ which we divide by our best value $B(\chi_{b2}(1P) \rightarrow \gamma\Upsilon(1S)) = (18.0 \pm 1.0) \times 10^{-2}$. Our first error is their experiment's error and our second error is the systematic error from using our best value.

⁴⁵ ASNER 08A reports $[\Gamma(\Upsilon(3S) \rightarrow \gamma\chi_{b2}(1P))/\Gamma_{total}] / [B(\Upsilon(2S) \rightarrow \gamma\chi_{b2}(1P))] < 27.1 \times 10^{-2}$ which we multiply by our best value $B(\Upsilon(2S) \rightarrow \gamma\chi_{b2}(1P)) = 7.15 \times 10^{-2}$.

See key on page 1127

Meson Particle Listings

$\Upsilon(3S), \chi_{b1}(3P)$

⁴⁶ HEINTZ 92, while unable to distinguish between different J states, measures $\sum J B(\Upsilon(3S) \rightarrow \gamma \chi_{bJ}) \times B(\chi_{bJ} \rightarrow \gamma \Upsilon(1S)) = (1.7 \pm 0.4 \pm 0.6) \times 10^{-3}$ for $J = 0, 1, 2$ using inclusive $\Upsilon(1S)$ decays and $(1.2^{+0.4}_{-0.3} \pm 0.09) \times 10^{-3}$ for $J = 1, 2$ using $\Upsilon(1S) \rightarrow \ell^+ \ell^-$.

$\Gamma(\gamma \chi_{b1}(1P))/\Gamma_{total}$ Γ_{24}/Γ

VALUE (units 10^{-3})	CL%	EVTS	DOCUMENT ID	TECN	COMMENT
0.9 ± 0.5 OUR AVERAGE					Error includes scale factor of 1.8.
$1.5 \pm 0.4 \pm 0.1$	50	47,48	KORNICER	11	CLEO $e^+ e^- \rightarrow \gamma \gamma \ell^+ \ell^-$
$0.5 \pm 0.3^{+0.2}_{-0.1}$			LEES	11J	BABR $\Upsilon(3S) \rightarrow X \gamma$

• • • We do not use the following data for averages, fits, limits, etc. • • •

<1.7	90	49	ASNER	08A	CLEO $\Upsilon(3S) \rightarrow \gamma +$ hadrons seen
		50	HEINTZ	92	CSB2 $e^+ e^- \rightarrow \gamma \gamma \ell^+ \ell^-$

⁴⁷ Assuming $B(\Upsilon(1S) \rightarrow \ell^+ \ell^-) = (2.48 \pm 0.05)\%$.

⁴⁸ KORNICER 11 reports $[\Gamma(\Upsilon(3S) \rightarrow \gamma \chi_{b1}(1P))/\Gamma_{total}] \times [B(\chi_{b1}(1P) \rightarrow \gamma \Upsilon(1S))] = (5.38 \pm 1.20 \pm 0.95) \times 10^{-4}$ which we divide by our best value $B(\chi_{b1}(1P) \rightarrow \gamma \Upsilon(1S)) = (35.2 \pm 2.0) \times 10^{-2}$. Our first error is their experiment's error and our second error is the systematic error from using our best value.

⁴⁹ ASNER 08A reports $[\Gamma(\Upsilon(3S) \rightarrow \gamma \chi_{b1}(1P))/\Gamma_{total}] / [B(\Upsilon(2S) \rightarrow \gamma \chi_{b1}(1P))] < 2.5 \times 10^{-2}$ which we multiply by our best value $B(\Upsilon(2S) \rightarrow \gamma \chi_{b1}(1P)) = 6.9 \times 10^{-2}$.

⁵⁰ HEINTZ 92, while unable to distinguish between different J states, measures $\sum J B(\Upsilon(3S) \rightarrow \gamma \chi_{bJ}) \times B(\chi_{bJ} \rightarrow \gamma \Upsilon(1S)) = (1.7 \pm 0.4 \pm 0.6) \times 10^{-3}$ for $J = 0, 1, 2$ using inclusive $\Upsilon(1S)$ decays and $(1.2^{+0.4}_{-0.3} \pm 0.09) \times 10^{-3}$ for $J = 1, 2$ using $\Upsilon(1S) \rightarrow \ell^+ \ell^-$.

$\Gamma(\gamma \chi_{b0}(1P))/\Gamma_{total}$ Γ_{25}/Γ

VALUE (units 10^{-2})	CL%	EVTS	DOCUMENT ID	TECN	COMMENT
0.27 ± 0.04 OUR AVERAGE					
$0.27 \pm 0.04 \pm 0.02$	2.3k		LEES	11J	BABR $\Upsilon(3S) \rightarrow X \gamma$
$0.30 \pm 0.04 \pm 0.10$	8.7k		ARTUSO	05	CLEO $e^+ e^- \rightarrow \gamma X$

• • • We do not use the following data for averages, fits, limits, etc. • • •

<0.8 90 ⁵¹ ASNER 08A reports $[\Gamma(\Upsilon(3S) \rightarrow \gamma \chi_{b0}(1P))/\Gamma_{total}] / [B(\Upsilon(2S) \rightarrow \gamma \chi_{b0}(1P))] < 21.9 \times 10^{-2}$ which we multiply by our best value $B(\Upsilon(2S) \rightarrow \gamma \chi_{b0}(1P)) = 3.8 \times 10^{-2}$.

$\Gamma(\gamma \eta_b(2S))/\Gamma_{total}$ Γ_{26}/Γ

VALUE (units 10^{-4})	CL%	DOCUMENT ID	TECN	COMMENT
0.6 ± 0.2	90	ARTUSO 05	CLEO	$e^+ e^- \rightarrow \gamma X$
<19	90	LEES	11J	BABR $\Upsilon(3S) \rightarrow X \gamma$

$\Gamma(\gamma \eta_b(1S))/\Gamma_{total}$ Γ_{27}/Γ

VALUE (units 10^{-4})	CL%	EVTS	DOCUMENT ID	TECN	COMMENT
5.1 ± 0.7 OUR AVERAGE					
$7.1 \pm 1.8 \pm 1.3$	$2.3 \pm 0.5k$	52	BONVICINI	10	CLEO $\Upsilon(3S) \rightarrow \gamma X$
$4.8 \pm 0.5 \pm 0.6$	$19 \pm 3k$	52	AUBERT	09AQ	BABR $\Upsilon(3S) \rightarrow \gamma X$

• • • We do not use the following data for averages, fits, limits, etc. • • •

<8.5 90 LEES 11J BABR $\Upsilon(3S) \rightarrow X \gamma$

$4.8 \pm 0.5 \pm 1.2$ $19 \pm 3k$ ^{52,53} AUBERT 08V BABR $\Upsilon(3S) \rightarrow \gamma X$

<4.3 90 ⁵⁴ ARTUSO 05 CLEO $e^+ e^- \rightarrow \gamma X$

⁵² Assuming $\Gamma_{\eta_b(1S)} = 10$ MeV.

⁵³ Systematic error re-evaluated by AUBERT 09AQ.

⁵⁴ Superseded by BONVICINI 10.

$\Gamma(\gamma A^0 \rightarrow \gamma \text{hadrons})/\Gamma_{total}$ Γ_{28}/Γ

($0.3 \text{ GeV} < m_{A^0} < 7 \text{ GeV}$)

VALUE	CL%	DOCUMENT ID	TECN	COMMENT
$< 8 \times 10^{-5}$	90	⁵⁵ LEES	11H	BABR $\Upsilon(3S) \rightarrow \gamma$ hadrons

⁵⁵ For a narrow scalar or pseudoscalar A^0 , excluding known resonances, with mass in the range 0.3–7 GeV. Measured 90% CL limits as a function of m_{A^0} range from 1×10^{-6} to 8×10^{-5} .

$\Gamma(\gamma X \rightarrow \gamma + \geq 4 \text{ prongs})/\Gamma_{total}$ Γ_{29}/Γ

($1.5 \text{ GeV} < m_X < 5.0 \text{ GeV}$)

VALUE (units 10^{-4})	CL%	DOCUMENT ID	TECN	COMMENT
< 2.2	95	ROSNER	07A	CLEO $e^+ e^- \rightarrow \gamma X$

$\Gamma(\gamma a_1^0 \rightarrow \gamma \mu^+ \mu^-)/\Gamma_{total}$ Γ_{30}/Γ

VALUE (units 10^{-6})	CL%	DOCUMENT ID	TECN	COMMENT
< 5.5	90	⁵⁶ AUBERT	09Z	BABR $e^+ e^- \rightarrow \gamma a_1^0 \rightarrow \gamma \mu^+ \mu^-$

⁵⁶ For a narrow scalar or pseudoscalar a_1^0 with mass in the range 212–9300 MeV, excluding J/ψ and $\psi(2S)$. Measured 90% CL limits as a function of $m_{a_1^0}$ range from 0.27–5.5 $\times 10^{-6}$.

$\Gamma(\gamma a_1^0 \rightarrow \gamma \tau^+ \tau^-)/\Gamma_{total}$ Γ_{31}/Γ

VALUE	CL%	DOCUMENT ID	TECN	COMMENT
$< 1.6 \times 10^{-4}$	90	⁵⁷ AUBERT	09P	BABR $e^+ e^- \rightarrow \gamma a_1^0 \rightarrow \gamma \tau^+ \tau^-$

⁵⁷ For a narrow scalar or pseudoscalar a_1^0 with $M(\tau^+ \tau^-)$ in the ranges 4.03–9.52 and 9.61–10.10 GeV. Measured 90% CL limits as a function of $M(\tau^+ \tau^-)$ range from $1.5\text{--}16 \times 10^{-5}$.

LEPTON FAMILY NUMBER (LF) VIOLATING MODES

$\Gamma(e^\pm \tau^\mp)/\Gamma_{total}$ Γ_{32}/Γ

VALUE (units 10^{-6})	CL%	DOCUMENT ID	TECN	COMMENT
< 4.2	90	LEES	10B	BABR $e^+ e^- \rightarrow e^\pm \tau^\mp$

$\Gamma(\mu^\pm \tau^\mp)/\Gamma_{total}$ Γ_{33}/Γ

VALUE (units 10^{-6})	CL%	DOCUMENT ID	TECN	COMMENT
< 3.1	90	LEES	10B	BABR $e^+ e^- \rightarrow \mu^\pm \tau^\mp$

• • • We do not use the following data for averages, fits, limits, etc. • • •

<20.3	95	LOVE	08A	CLEO $e^+ e^- \rightarrow \mu^\pm \tau^\mp$
-------	----	------	-----	---

$\Upsilon(3S)$ REFERENCES

LEES	20E	PRL 125 241801	J.P. Lees et al.	(BABAR Collab.)
LEES	14G	PR D89 111102	J.P. Lees et al.	(BABAR Collab.)
GE	11	PR D84 032008	J.Y. Ge et al.	(CLEO Collab.)
KORNICER	11	PR D83 054003	M. Kornicer et al.	(CLEO Collab.)
LEES	11C	PR D84 011104	J.P. Lees et al.	(BABAR Collab.)
LEES	11H	PRL 107 221803	J.P. Lees et al.	(BABAR Collab.)
LEES	11J	PR D84 072002	J.P. Lees et al.	(BABAR Collab.)
LEES	11K	PR D84 091101	J.P. Lees et al.	(BABAR Collab.)
LEES	11L	PR D84 092003	J.P. Lees et al.	(BABAR Collab.)
BONVICINI	10	PR D81 031104	G. Bonvicini et al.	(CLEO Collab.)
LEES	10B	PRL 104 151802	J.P. Lees et al.	(BABAR Collab.)
AUBERT	09AQ	PRL 103 161801	B. Aubert et al.	(BABAR Collab.)
AUBERT	09P	PRL 103 181801	B. Aubert et al.	(BABAR Collab.)
AUBERT	09Z	PRL 103 081803	B. Aubert et al.	(BABAR Collab.)
BHARI	09	PR D79 011103	S.R. Bhatti et al.	(CLEO Collab.)
ASNER	08A	PR D78 091103	D.M. Asner et al.	(CLEO Collab.)
AUBERT	08BP	PR D78 112002	B. Aubert et al.	(BABAR Collab.)
AUBERT	08V	PRL 101 071801	B. Aubert et al.	(BABAR Collab.)
HE	08A	PRL 101 192001	Q. He et al.	(CLEO Collab.)
LOVE	08A	PRL 101 201601	W. Love et al.	(CLEO Collab.)
PDG	08	PL B667 1	C. Amsler et al.	(PDG Collab.)
BESSON	07	PRL 98 052002	D. Besson et al.	(CLEO Collab.)
ROSNER	07A	PR D76 117102	J.L. Rosner et al.	(CLEO Collab.)
BESSON	06A	PR D74 012003	D. Besson et al.	(CLEO Collab.)
ROSNER	06	PRL 96 092003	J.L. Rosner et al.	(CLEO Collab.)
ADAMS	05	PRL 94 012001	G.S. Adams et al.	(CLEO Collab.)
ARTUSO	05	PRL 94 032001	M. Artuso et al.	(CLEO Collab.)
ARTAMONOV	00	PL B474 427	A.S. Artamonov et al.	(CLEO Collab.)
BUTLER	94B	PR D49 40	F. Butler et al.	(CLEO Collab.)
WU	93	PL B301 307	Q.W. Wu et al.	(CLEO Collab.)
HEINTZ	92	PR D46 1928	U. Heintz et al.	(CUSB II Collab.)
BROCK	91	PR D43 1448	I.C. Brock et al.	(CLEO Collab.)
HEINTZ	91	PRL 66 1563	U. Heintz et al.	(CUSB Collab.)
MORRISON	91	PRL 67 1696	R.J. Morrison et al.	(CLEO Collab.)
NARAIN	91	PRL 66 3113	M. Narain et al.	(CLEO Collab.)
CHEN	89B	PR D39 3528	W.Y. Chen et al.	(CLEO Collab.)
KAARSBERG	89	PRL 62 2077	T.M. Kaarsberg et al.	(CLEO Collab.)
BUCHMUELLER	88	HE $e^+ e^-$ Physics 412	W. Buchmueller, S. Cooper	(HANN, DESY, MIT)
Editors: A. Ali and P. Soeding, World Scientific, Singapore				
COHEN	87	RMP 59 1121	E.R. Cohen, B.N. Taylor	(RIS, NBS)
BARU	86B	ZPHY C32 622	(erratum) S.E. Baru et al.	(NOVO)
KURAEV	85	SJNP 41 466	E.A. Kuraev, V.S. Fadin	(NOVO)
Translated from YAF 41 733.				
ARTAMONOV	84	PL 137B 272	A.S. Artamonov et al.	(NOVO)
GILES	84B	PR D29 1285	R. Giles et al.	(CLEO Collab.)
ANDREWS	83	PRL 50 807	D.E. Andrews et al.	(CLEO Collab.)
GREEN	82	PRL 49 617	J. Green et al.	(CLEO Collab.)
MAGERAS	82	PL 118B 453	G. Mageras et al.	(COLU, CORN, LSU+)

$$\chi_{b1}(3P)$$

$$I^G(J^{PC}) = 0^+(1^{++})$$

Observed in the radiative decay to $\Upsilon(1S, 2S, 3S)$, therefore $C = +$.
 J needs confirmation.

$\chi_{b1}(3P)$ MASS

VALUE (MeV)	EVTS	DOCUMENT ID	TECN	COMMENT
$10513.42 \pm 0.41 \pm 0.53$		¹ SIRUNYAN	18N	CMS $pp \rightarrow \gamma \mu^+ \mu^- X$
$10515.7 \pm 2.2 \pm 1.5$	169	² AAIJ	14B6	LHCB $pp \rightarrow \gamma \mu^+ \mu^- X$
$10512.1 \pm 2.1 \pm 0.9$	351	³ AAIJ	14B6	LHCB $pp \rightarrow \gamma \mu^+ \mu^- X$
$10511.3 \pm 1.7 \pm 2.5$	182	⁴ AAIJ	14B1	LHCB $pp \rightarrow \gamma \mu^+ \mu^- X$
$10530 \pm 5 \pm 9$		⁵ AAD	12A	ATLS $pp \rightarrow \gamma \mu^+ \mu^- X$
$10551 \pm 14 \pm 17$		⁵ ABAZOV	12Q	D0 $p\bar{p} \rightarrow \gamma \mu^+ \mu^- X$

¹ Systematic error includes an additional 0.5 MeV for the uncertainty on the $\Upsilon(3S)$ mass. Also measures $m_{\chi_{b2}(3P)} - m_{\chi_{b1}(3P)} = 10.60 \pm 0.64 \pm 0.17$ MeV. A total of 372 $\chi_{b1}(3P)$ and $\chi_{b2}(3P)$ events was observed.

² From $\chi_{b1}(3P) \rightarrow \Upsilon(1S, 2S) \gamma$ transitions assuming $m_{\chi_{b2}(3P)} - m_{\chi_{b1}(3P)} = 10.5 \pm 1.5$ MeV and allowing for $\pm 30\%$ variation in the $\chi_{b2}(3P)$ production rate relative to that of $\chi_{b1}(3P)$.

³ The mass of the $\chi_{b1}(3P)$ state obtained by combining the results of AAIJ 14B6 with that of AAIJ 14B1. The first uncertainty is experimental and the second attributable to the unknown mass splitting, assumed to be $m_{\chi_{b2}(3P)} - m_{\chi_{b1}(3P)} = 10.5 \pm 1.5$ MeV.

⁴ From $\chi_{b1}(3P) \rightarrow \Upsilon(3S) \gamma$ transition assuming $m_{\chi_{b2}(3P)} - m_{\chi_{b1}(3P)} = 10.5 \pm 1.5$ MeV.

⁵ The mass barycenter of the merged lineshapes from the $J = 1$ and 2 states.

Meson Particle Listings

$\chi_{b1}(3P)$, $\chi_{b2}(3P)$, $\Upsilon(4S)$

$\chi_{b1}(3P)$ DECAY MODES

Mode	Fraction (Γ_i/Γ)
Γ_1 $\Upsilon(1S)\gamma$	seen
Γ_2 $\Upsilon(2S)\gamma$	seen
Γ_3 $\Upsilon(3S)\gamma$	seen

$\chi_{b1}(3P)$ BRANCHING RATIOS

$\Gamma(\Upsilon(1S)\gamma)/\Gamma_{total}$					Γ_1/Γ
VALUE	EVTS	DOCUMENT ID	TECN	COMMENT	
seen	169	¹ AAIJ	148G LHCb	$pp \rightarrow \gamma\mu^+\mu^-X$	
••• We do not use the following data for averages, fits, limits, etc. •••					
seen		AAD	12A ATLAS	$pp \rightarrow \gamma\mu^+\mu^-X$	
seen		ABAZOV	12Q D0	$p\bar{p} \rightarrow \gamma\mu^+\mu^-X$	

¹ From $\chi_{b1}(3P) \rightarrow \Upsilon(1S, 2S)\gamma$ transitions assuming $m_{\chi_{b2}(3P)} - m_{\chi_{b1}(3P)} = 10.5 \pm 1.5$ MeV and allowing for $\pm 30\%$ variation in the $\chi_{b2}(3P)$ production rate relative to that of $\chi_{b1}(3P)$.

$\Gamma(\Upsilon(2S)\gamma)/\Gamma_{total}$					Γ_2/Γ
VALUE	EVTS	DOCUMENT ID	TECN	COMMENT	
seen	169	¹ AAIJ	148G LHCb	$pp \rightarrow \gamma\mu^+\mu^-X$	
••• We do not use the following data for averages, fits, limits, etc. •••					
seen		AAD	12A ATLAS	$pp \rightarrow \gamma\mu^+\mu^-X$	

¹ From $\chi_{b1}(3P) \rightarrow \Upsilon(1S, 2S)\gamma$ transitions assuming $m_{\chi_{b2}(3P)} - m_{\chi_{b1}(3P)} = 10.5 \pm 1.5$ MeV and allowing for $\pm 30\%$ variation in the $\chi_{b2}(3P)$ production rate relative to that of $\chi_{b1}(3P)$.

$\Gamma(\Upsilon(3S)\gamma)/\Gamma_{total}$					Γ_3/Γ
VALUE	EVTS	DOCUMENT ID	TECN	COMMENT	
seen		SIRUNYAN	18N CMS	$pp \rightarrow \gamma\mu^+\mu^-X$	
seen	182	AAIJ	148I LHCb	$pp \rightarrow \gamma\mu^+\mu^-X$	

$\chi_{b1}(3P)$ REFERENCES

SIRUNYAN	18N	PRL 121 092002	A.M. Sirunyan et al.	(CMS Collab.)
AAIJ	148G	JHEP 1410 088	R. Aaij et al.	(LHCb Collab.)
AAIJ	148I	EPJ C74 3092	R. Aaij et al.	(LHCb Collab.)
AAD	12A	PRL 108 152001	G. Aad et al.	(ATLAS Collab.)
ABAZOV	12Q	PR D86 031103	V.M. Abazov et al.	(D0 Collab.)

$\chi_{b2}(3P)$

$$I^G(J^{PC}) = 0^+(2^{++})$$

Observed in the radiative decay to $\Upsilon(3S)$, therefore $C = +$. J needs confirmation.

$\chi_{b2}(3P)$ MASS

VALUE (MeV)	DOCUMENT ID	TECN	COMMENT
$10524.02 \pm 0.57 \pm 0.53$	¹ SIRUNYAN	18N CMS	$pp \rightarrow \gamma\mu^+\mu^-X$
••• We do not use the following data for averages, fits, limits, etc. •••			
10530 ± 5 ± 9	² AAD	12A ATLAS	$pp \rightarrow \gamma\mu^+\mu^-X$

¹ Systematic error includes an additional 0.5 MeV for the uncertainty on the $\Upsilon(3S)$ mass. Also measures $m_{\chi_{b2}(3P)} - m_{\chi_{b1}(3P)} = 10.60 \pm 0.64 \pm 0.17$ MeV. A total of 372 $\chi_{b1}(3P)$ and $\chi_{b2}(3P)$ events was observed.

² The mass barycenter of the merged lineshapes from the $J = 1$ and 2 states.

$\chi_{b2}(3P)$ DECAY MODES

Mode	Fraction (Γ_i/Γ)
Γ_1 $\Upsilon(3S)\gamma$	seen

$\chi_{b2}(3P)$ BRANCHING RATIOS

$\Gamma(\Upsilon(3S)\gamma)/\Gamma_{total}$					Γ_1/Γ
VALUE	DOCUMENT ID	TECN	COMMENT		
seen	SIRUNYAN	18N CMS	$pp \rightarrow \gamma\mu^+\mu^-X$		

$\chi_{b2}(3P)$ REFERENCES

SIRUNYAN	18N	PRL 121 092002	A.M. Sirunyan et al.	(CMS Collab.)
AAD	12A	PRL 108 152001	G. Aad et al.	(ATLAS Collab.)

$\Upsilon(4S)$

$$I^G(J^{PC}) = 0^-(1^{--})$$

also known as $\Upsilon(10580)$

$\Upsilon(4S)$ MASS

VALUE (MeV)	DOCUMENT ID	TECN	COMMENT
10579.4 ± 1.2 OUR AVERAGE			
10579.3 $\pm 0.4 \pm 1.2$	AUBERT	05Q BABR	$e^+e^- \rightarrow$ hadrons
10580.0 ± 3.5	¹ BEBEK	87 CLEO	$e^+e^- \rightarrow$ hadrons
••• We do not use the following data for averages, fits, limits, etc. •••			
10577.4 ± 1.0	² LOVELOCK	85 CUSB	$e^+e^- \rightarrow$ hadrons
¹ Reanalysis of BESSON 85.			
² No systematic error given.			

$\Upsilon(4S)$ WIDTH

VALUE (MeV)	DOCUMENT ID	TECN	COMMENT
20.5 ± 2.5 OUR AVERAGE			
20.7 $\pm 1.6 \pm 2.5$	AUBERT	05Q BABR	$e^+e^- \rightarrow$ hadrons
20 ± 2 ± 4	BESSON	85 CLEO	$e^+e^- \rightarrow$ hadrons
••• We do not use the following data for averages, fits, limits, etc. •••			
25 ± 2.5	LOVELOCK	85 CUSB	$e^+e^- \rightarrow$ hadrons

$\Upsilon(4S)$ DECAY MODES

Mode	Fraction (Γ_i/Γ)	Confidence level
Γ_1 $B\bar{B}$	> 96 %	95%
Γ_2 B^+B^-	(51.4 ± 0.6) %	
Γ_3 D_s^+ anything + c.c.	(17.8 ± 2.6) %	
Γ_4 $B^0\bar{B}^0$	(48.6 ± 0.6) %	
Γ_5 $J/\psi K_S^0 + (J/\psi, \eta_c) K_S^0$	< 4 $\times 10^{-7}$	90%
Γ_6 non- $B\bar{B}$	< 4 %	95%
Γ_7 e^+e^-	(1.57 ± 0.08) $\times 10^{-5}$	
Γ_8 $\rho^+\rho^-$	< 5.7 $\times 10^{-6}$	90%
Γ_9 $K^*(892)^0\bar{K}^0$	< 2.0 $\times 10^{-6}$	90%
Γ_{10} $J/\psi(1S)$ anything	< 1.9 $\times 10^{-4}$	95%
Γ_{11} D^{*+} anything + c.c.	< 7.4 %	90%
Γ_{12} ϕ anything	(7.1 ± 0.6) %	
Γ_{13} $\phi\eta$	< 1.8 $\times 10^{-6}$	90%
Γ_{14} $\phi\eta'$	< 4.3 $\times 10^{-6}$	90%
Γ_{15} $\rho\eta$	< 1.3 $\times 10^{-6}$	90%
Γ_{16} $\rho\eta'$	< 2.5 $\times 10^{-6}$	90%
Γ_{17} $\Upsilon(1S)$ anything	< 4 $\times 10^{-3}$	90%
Γ_{18} $\Upsilon(1S)\pi^+\pi^-$	(8.2 ± 0.4) $\times 10^{-5}$	
Γ_{19} $\Upsilon(1S)\eta$	(1.81 ± 0.18) $\times 10^{-4}$	
Γ_{20} $\Upsilon(1S)\eta'$	(3.4 ± 0.9) $\times 10^{-5}$	
Γ_{21} $\Upsilon(2S)\pi^+\pi^-$	(8.2 ± 0.8) $\times 10^{-5}$	
Γ_{22} $h_b(1P)\pi^+\pi^-$	not seen	
Γ_{23} $h_b(1P)\eta$	(2.18 ± 0.21) $\times 10^{-3}$	
Γ_{24} $\eta_b(1S)\omega$	< 1.8 $\times 10^{-4}$	90%
Γ_{25} 2H anything	< 1.3 $\times 10^{-5}$	90%

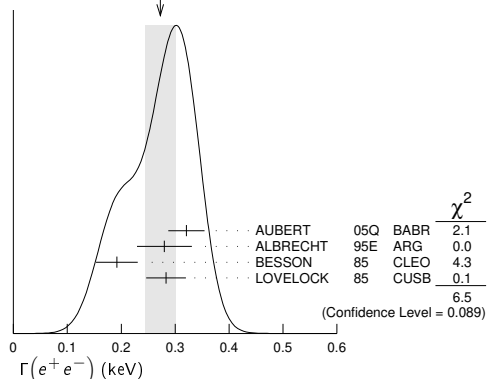
Double Radiative Decays

Γ_{26} $\gamma\gamma\Upsilon(D) \rightarrow \gamma\gamma\eta\Upsilon(1S)$	< 2.3 $\times 10^{-5}$	90%
--	--------------------------	-----

$\Upsilon(4S)$ PARTIAL WIDTHS

$\Gamma(e^+e^-)$		Γ_7	
VALUE (keV)	DOCUMENT ID	TECN	COMMENT
0.272 ± 0.029 OUR AVERAGE	Error includes scale factor of 1.5.		See the ideogram below.
0.321 $\pm 0.017 \pm 0.029$	AUBERT	05Q BABR	$e^+e^- \rightarrow$ hadrons
0.28 $\pm 0.05 \pm 0.01$	¹ ALBRECHT	95E ARG	$e^+e^- \rightarrow$ hadrons
0.192 $\pm 0.007 \pm 0.038$	BESSON	85 CLEO	$e^+e^- \rightarrow$ hadrons
0.283 ± 0.037	LOVELOCK	85 CUSB	$e^+e^- \rightarrow$ hadrons

WEIGHTED AVERAGE
0.272 ± 0.029 (Error scaled by 1.5)



¹ Using LEYAOUANC 77 parametrization of $\Gamma(s)$.

$\Upsilon(4S)$ BRANCHING RATIOS

$B\bar{B}$ DECAYS

The ratio of branching fraction to charged and neutral B mesons is often derived assuming isospin invariance in the decays, and relies on the knowledge of the B^+/B^0 lifetime ratio. "OUR EVALUATION" is obtained based on averages of rescaled data listed below. The average and rescaling were performed by the Heavy Flavor Averaging Group (HFLAV) and are described at <https://hflav.web.cern.ch/>. The averaging/rescaling procedure takes into account the common dependence of the measurement on the value of the lifetime ratio.

$\Gamma(B^+B^-)/\Gamma_{total}$		Γ_2/Γ	
VALUE	DOCUMENT ID	TECN	COMMENT
0.514 ± 0.006 OUR EVALUATION	Assuming $B(\Upsilon(4S) \rightarrow B\bar{B}) = 1$		

$\Gamma(D_s^+ \text{ anything} + c.c.)/\Gamma_{total}$		Γ_3/Γ	
VALUE	DOCUMENT ID	TECN	COMMENT
0.178 ± 0.021 ± 0.016	¹ ARTUSO 05B CLE3		$e^+e^- \rightarrow D_X K$

¹ ARTUSO 05B reports $[\Gamma(\Upsilon(4S) \rightarrow D_s^+ \text{ anything} + c.c.)/\Gamma_{total}] \times [B(D_s^+ \rightarrow \phi\pi^+)] = (8.0 \pm 0.2 \pm 0.9) \times 10^{-3}$ which we divide by our best value $B(D_s^+ \rightarrow \phi\pi^+) = (4.5 \pm 0.4) \times 10^{-2}$. Our first error is their experiment's error and our second error is the systematic error from using our best value.

$\Gamma(B^0\bar{B}^0)/\Gamma_{total}$		Γ_4/Γ	
VALUE	DOCUMENT ID	TECN	COMMENT
0.486 ± 0.006 OUR EVALUATION	Assuming $B(\Upsilon(4S) \rightarrow B\bar{B}) = 1$		

• • • We do not use the following data for averages, fits, limits, etc. • • •
0.487 ± 0.010 ± 0.008 ¹ AUBERT,B 05H BABR $\Upsilon(4S) \rightarrow \bar{B}B \rightarrow D^*\ell\nu_\ell$
¹ Direct measurement. This value is averaged with the value extracted from the $\Gamma(B^+B^-)/\Gamma(B^0\bar{B}^0)$ measurements.

$\Gamma(B^+B^-)/\Gamma(B^0\bar{B}^0)$		Γ_2/Γ_4	
VALUE	DOCUMENT ID	TECN	COMMENT
1.058 ± 0.024 OUR EVALUATION			

1.006 ± 0.036 ± 0.031 ¹ AUBERT 04F BABR $\Upsilon(4S) \rightarrow B\bar{B} \rightarrow J/\psi K$
1.01 ± 0.03 ± 0.09 ¹ HASTINGS 03 BELL $\Upsilon(4S) \rightarrow B\bar{B} \rightarrow$ dileptons
1.058 ± 0.084 ± 0.136 ² ATHAR 02 CLEO $\Upsilon(4S) \rightarrow B\bar{B} \rightarrow D^*\ell\nu$
1.10 ± 0.06 ± 0.05 ³ AUBERT 02 BABR $\Upsilon(4S) \rightarrow B\bar{B} \rightarrow (c\bar{c})K^*$
1.04 ± 0.07 ± 0.04 ⁴ ALEXANDER 01 CLEO $\Upsilon(4S) \rightarrow B\bar{B} \rightarrow J/\psi K^*$
¹ HASTINGS 03 and AUBERT 04F assume $\tau(B^+)/\tau(B^0) = 1.083 \pm 0.017$.
² ATHAR 02 assumes $\tau(B^+)/\tau(B^0) = 1.074 \pm 0.028$. Supersedes BARISH 95.
³ AUBERT 02 assumes $\tau(B^+)/\tau(B^0) = 1.062 \pm 0.029$.
⁴ ALEXANDER 01 assumes $\tau(B^+)/\tau(B^0) = 1.066 \pm 0.024$.

$[\Gamma(J/\psi K_S^0) + \Gamma((J/\psi, \eta_c) K_S^0)]/\Gamma_{total}$		Γ_5/Γ	
VALUE (units 10^{-7})	DOCUMENT ID	TECN	COMMENT
<4	¹ TAJIMA 07A BELL		$\Upsilon(4S) \rightarrow B^0\bar{B}^0$

Forbidden by CP invariance.
¹ $\Upsilon(4S)$ with CP = +1 decays to the final state with CP = -1.

non- $B\bar{B}$ DECAYS

$\Gamma(\text{non-}B\bar{B})/\Gamma_{total}$		Γ_6/Γ	
VALUE	DOCUMENT ID	TECN	COMMENT
<0.04	95 BARISH 96B CLEO		e^+e^-

$\Gamma(e^+e^-)/\Gamma_{total}$		Γ_7/Γ	
VALUE (units 10^{-5})	DOCUMENT ID	TECN	COMMENT
1.57 ± 0.08 OUR AVERAGE			

1.55 ± 0.04 ± 0.07 AUBERT 05Q BABR $e^+e^- \rightarrow$ hadrons
2.77 ± 0.50 ± 0.49 ¹ ALBRECHT 95E ARG $e^+e^- \rightarrow$ hadrons
¹ Using LEYAOUANNC 77 parametrization of $\Gamma(s)$.

$\Gamma(\rho^+\rho^-)/\Gamma_{total}$		Γ_8/Γ	
VALUE	DOCUMENT ID	TECN	COMMENT
<5.7 × 10⁻⁶	90 AUBERT 08B0 BABR		$e^+e^- \rightarrow \pi^+\pi^-2\pi^0$

$\Gamma(K^*(892)^0\bar{K}^0)/\Gamma_{total}$		Γ_9/Γ	
VALUE	DOCUMENT ID	TECN	COMMENT
<2.0 × 10⁻⁶	90 SHEN 13A BELL		$e^+e^- \rightarrow K^*(892)^0\bar{K}^0$

$\Gamma(J/\psi(1S) \text{ anything})/\Gamma_{total}$		Γ_{10}/Γ	
VALUE (units 10^{-4})	DOCUMENT ID	TECN	COMMENT
<1.9	95 ¹ ABE 02D BELL		$e^+e^- \rightarrow J/\psi X \rightarrow \ell^+\ell^-X$

• • • We do not use the following data for averages, fits, limits, etc. • • •
<4.7 90 ¹ AUBERT 01C BABR $e^+e^- \rightarrow J/\psi X \rightarrow \ell^+\ell^-X$
¹ Uses $B(J/\psi \rightarrow e^+e^-) = 0.0593 \pm 0.0010$ and $B(J/\psi \rightarrow \mu^+\mu^-) = 0.0588 \pm 0.0010$.

$\Gamma(D^{*+} \text{ anything} + c.c.)/\Gamma_{total}$		Γ_{11}/Γ	
VALUE	DOCUMENT ID	TECN	COMMENT
<0.074	90 ¹ ALEXANDER 90C CLEO		e^+e^-

¹ For $x > 0.473$.

$\Gamma(\phi \text{ anything})/\Gamma_{total}$		Γ_{12}/Γ	
VALUE (units 10^{-2})	DOCUMENT ID	TECN	COMMENT
7.1 ± 0.1 ± 0.6	07 HUANG CLEO		$\Upsilon(4S) \rightarrow \phi X$

• • • We do not use the following data for averages, fits, limits, etc. • • •
<0.23 90 ¹ ALEXANDER 90C CLEO e^+e^-
¹ For $x > 0.52$.

$\Gamma(\phi\eta)/\Gamma_{total}$		Γ_{13}/Γ	
VALUE (units 10^{-6})	DOCUMENT ID	TECN	COMMENT
<1.8	90 ¹ BELOUS 09 BELL		$e^+e^- \rightarrow \phi\eta$

• • • We do not use the following data for averages, fits, limits, etc. • • •
<2.5 90 AUBERT, BE 06F BABR $e^+e^- \rightarrow \phi\eta$
¹ Using all intermediate branching fraction values from PDG 08.

$\Gamma(\phi\eta')/\Gamma_{total}$		Γ_{14}/Γ	
VALUE (units 10^{-6})	DOCUMENT ID	TECN	COMMENT
<4.3	90 ¹ BELOUS 09 BELL		$e^+e^- \rightarrow \phi\eta'$

¹ Using all intermediate branching fraction values from PDG 08.

$\Gamma(\rho\eta)/\Gamma_{total}$		Γ_{15}/Γ	
VALUE (units 10^{-6})	DOCUMENT ID	TECN	COMMENT
<1.3	90 ¹ BELOUS 09 BELL		$e^+e^- \rightarrow \rho\eta$

¹ Using all intermediate branching fraction values from PDG 08.

$\Gamma(\rho\eta')/\Gamma_{total}$		Γ_{16}/Γ	
VALUE (units 10^{-6})	DOCUMENT ID	TECN	COMMENT
<2.5	90 ¹ BELOUS 09 BELL		$e^+e^- \rightarrow \rho\eta'$

¹ Using all intermediate branching fraction values from PDG 08.

$\Gamma(\Upsilon(1S) \text{ anything})/\Gamma_{total}$		Γ_{17}/Γ	
VALUE	DOCUMENT ID	TECN	COMMENT
<0.004	90 ALEXANDER 90C CLEO		e^+e^-

$\Gamma(\Upsilon(1S)\pi^+\pi^-)/\Gamma_{total}$		Γ_{18}/Γ	
VALUE (units 10^{-5})	CL% EVTS	DOCUMENT ID	TECN COMMENT
8.2 ± 0.4 OUR AVERAGE			

8.2 ± 0.5 ± 0.4 515 GUIDO 17 BELL $\Upsilon(4S) \rightarrow \pi^+\pi^-\mu^+\mu^-$
8.5 ± 1.3 ± 0.2 113 ± 16 ¹ SOKOLOV 09 BELL $e^+e^- \rightarrow \pi^+\pi^-\mu^+\mu^-$
8.00 ± 0.64 ± 0.27 430 ² AUBERT 08BP BABR $\Upsilon(4S) \rightarrow \pi^+\pi^-\ell^+\ell^-$
• • • We do not use the following data for averages, fits, limits, etc. • • •
17.8 ± 4.0 ± 0.3 ^{3,4} SOKOLOV 07 BELL $e^+e^- \rightarrow \pi^+\pi^-\mu^+\mu^-$
9.0 ± 1.5 ± 0.2 167 ± 19 ⁵ AUBERT 06R BABR $e^+e^- \rightarrow \pi^+\pi^-\mu^+\mu^-$
<12 90 GLENN 99 CLE2 e^+e^-

¹ SOKOLOV 09 reports $[\Gamma(\Upsilon(4S) \rightarrow \Upsilon(1S)\pi^+\pi^-)/\Gamma_{total}] \times [B(\Upsilon(1S) \rightarrow \mu^+\mu^-)] = (0.211 \pm 0.030 \pm 0.014) \times 10^{-5}$ which we divide by our best value $B(\Upsilon(1S) \rightarrow \mu^+\mu^-) = (2.48 \pm 0.05) \times 10^{-2}$. Our first error is their experiment's error and our second error is the systematic error from using our best value.

² Using $B(\Upsilon(1S) \rightarrow e^+e^-) = (2.38 \pm 0.11)\%$ and $B(\Upsilon(1S) \rightarrow \mu^+\mu^-) = (2.48 \pm 0.05)\%$.

³ SOKOLOV 07 reports $[\Gamma(\Upsilon(4S) \rightarrow \Upsilon(1S)\pi^+\pi^-)/\Gamma_{total}] \times [B(\Upsilon(1S) \rightarrow \mu^+\mu^-)] = (4.42 \pm 0.81 \pm 0.56) \times 10^{-6}$ which we divide by our best value $B(\Upsilon(1S) \rightarrow \mu^+\mu^-) = (2.48 \pm 0.05) \times 10^{-2}$. Our first error is their experiment's error and our second error is the systematic error from using our best value.

⁴ According to the authors, systematic errors were underestimated.

⁵ Superseded by AUBERT 08BP. AUBERT 06R reports $[\Gamma(\Upsilon(4S) \rightarrow \Upsilon(1S)\pi^+\pi^-)/\Gamma_{total}] \times [B(\Upsilon(1S) \rightarrow \mu^+\mu^-)] = (2.23 \pm 0.25 \pm 0.27) \times 10^{-6}$ which we divide by our best value $B(\Upsilon(1S) \rightarrow \mu^+\mu^-) = (2.48 \pm 0.05) \times 10^{-2}$. Our first error is their experiment's error and our second error is the systematic error from using our best value.

$\Gamma(\Upsilon(1S)\eta)/\Gamma_{total}$		Γ_{19}/Γ	
VALUE (units 10^{-4})	CL% EVTS	DOCUMENT ID	TECN COMMENT
1.81 ± 0.18 OUR AVERAGE			

1.70 ± 0.23 ± 0.08 49 GUIDO 17 BELL $\Upsilon(4S) \rightarrow \pi^+\pi^-\pi^0\mu^+\mu^-$
1.96 ± 0.26 ± 0.09 56 ¹ AUBERT 08BP BABR $\Upsilon(4S) \rightarrow \pi^+\pi^-\pi^0\ell^+\ell^-$

• • • We do not use the following data for averages, fits, limits, etc. • • •
<2.7 90 ² TAMPONI 15 BELL $e^+e^- \rightarrow \gamma\eta +$ hadrons
¹ Using $B(\Upsilon(1S) \rightarrow e^+e^-) = (2.38 \pm 0.11)\%$ and $B(\Upsilon(1S) \rightarrow \mu^+\mu^-) = (2.48 \pm 0.05)\%$.
² Using $B(\eta \rightarrow 2\gamma) = (39.41 \pm 0.20)\%$.

$\Gamma(\Upsilon(1S)\eta')/\Gamma_{total}$		Γ_{20}/Γ	
VALUE (units 10^{-5})	EVTS	DOCUMENT ID	TECN COMMENT
3.43 ± 0.88 ± 0.21	27	GUIDO 18 BELL	$\Upsilon(4S) \rightarrow (\rho^0\gamma, \pi^+\pi^-\eta)\mu^+\mu^-$

Meson Particle Listings

$\Upsilon(4S)$, $Z_b(10610)$

$\Gamma(\Upsilon(1S)\eta)/\Gamma(\Upsilon(1S)\pi^+\pi^-)$ Γ_{19}/Γ_{18}

VALUE	EVTS	DOCUMENT ID	TECN	COMMENT
$2.41 \pm 0.40 \pm 0.12$	56	¹ AUBERT	08BP BABR	$\Upsilon(4S) \rightarrow \pi^+\pi^-(\pi^0)\ell^+\ell^-$

••• We do not use the following data for averages, fits, limits, etc. •••

¹ Not independent of other values reported by AUBERT 08BP.

$\Gamma(\Upsilon(2S)\pi^+\pi^-)/\Gamma_{total}$ Γ_{21}/Γ

VALUE (units 10^{-5})	CL%	EVTS	DOCUMENT ID	TECN	COMMENT
8.2 ± 0.8 OUR AVERAGE					
$7.9 \pm 1.0 \pm 0.4$		181	GUIDO	17 BELL	$\Upsilon(4S) \rightarrow \pi^+\pi^-\mu^+\mu^-$
$8.6 \pm 1.1 \pm 0.7$		220	¹ AUBERT	08BP BABR	$\Upsilon(4S) \rightarrow \pi^+\pi^-\ell^+\ell^-$

••• We do not use the following data for averages, fits, limits, etc. •••

$8.8 \pm 1.7 \pm 0.8$		97 ± 15	² AUBERT	06R BABR	$e^+e^- \rightarrow \pi^+\pi^-\mu^+\mu^-$
<3.9		90	GLENN	99 CLE2	e^+e^-

¹ Using $B(\Upsilon(2S) \rightarrow e^+e^-) = (1.91 \pm 0.16)\%$ and $B(\Upsilon(2S) \rightarrow \mu^+\mu^-) = (1.93 \pm 0.17)\%$.

² Superseded by AUBERT 08BP. AUBERT 06R reports $[\Gamma(\Upsilon(4S) \rightarrow \Upsilon(2S)\pi^+\pi^-)/\Gamma_{total}] \times [B(\Upsilon(2S) \rightarrow \mu^+\mu^-)] = (1.69 \pm 0.26 \pm 0.20) \times 10^{-6}$ which we divide by our best value $B(\Upsilon(2S) \rightarrow \mu^+\mu^-) = (1.93 \pm 0.17) \times 10^{-2}$. Our first error is their experiment's error and our second error is the systematic error from using our best value.

Using $B(\Upsilon(2S) \rightarrow e^+e^-) = (1.91 \pm 0.16)\%$ and $B(\Upsilon(2S) \rightarrow \mu^+\mu^-) = (1.93 \pm 0.17)\%$.

Superseded by AUBERT 08BP. AUBERT 06R reports $[\Gamma(\Upsilon(4S) \rightarrow \Upsilon(2S)\pi^+\pi^-)/\Gamma_{total}] \times [B(\Upsilon(2S) \rightarrow \mu^+\mu^-)] = (1.69 \pm 0.26 \pm 0.20) \times 10^{-6}$ which we divide by our best value $B(\Upsilon(2S) \rightarrow \mu^+\mu^-) = (1.93 \pm 0.17) \times 10^{-2}$. Our first error is their experiment's error and our second error is the systematic error from using our best value.

$\Gamma(\Upsilon(2S)\pi^+\pi^-)/\Gamma(\Upsilon(1S)\pi^+\pi^-)$ Γ_{21}/Γ_{18}

VALUE	EVTS	DOCUMENT ID	TECN	COMMENT
$1.16 \pm 0.16 \pm 0.14$	220	¹ AUBERT	08BP BABR	$\Upsilon(4S) \rightarrow \pi^+\pi^-\ell^+\ell^-$

••• We do not use the following data for averages, fits, limits, etc. •••

¹ Using $B(\Upsilon(1S) \rightarrow e^+e^-) = (2.38 \pm 0.11)\%$, $B(\Upsilon(1S) \rightarrow \mu^+\mu^-) = (2.48 \pm 0.05)\%$, $B(\Upsilon(2S) \rightarrow e^+e^-) = (1.91 \pm 0.16)\%$, and $B(\Upsilon(2S) \rightarrow \mu^+\mu^-) = (1.93 \pm 0.17)\%$. Not independent of other values reported by AUBERT 08BP.

$\Gamma(h_b(1P)\pi^+\pi^-)/\Gamma_{total}$ Γ_{22}/Γ

VALUE	EVTS	DOCUMENT ID	TECN	COMMENT
not seen	$(35 \pm \frac{32}{26})k$	¹ ADACHI	12 BELL	$10.58 e^+e^- \rightarrow h_b(1P)\pi^+\pi^-$

¹ From the upper limit on the ratio of $\sigma(e^+e^- \rightarrow h_b(1P)\pi^+\pi^-)$ at the $\Upsilon(4S)$ to that at the $\Upsilon(5S)$ of 0.27.

$\Gamma(h_b(1P)\eta)/\Gamma_{total}$ Γ_{23}/Γ

VALUE (units 10^{-3})	EVTS	DOCUMENT ID	TECN	COMMENT
$2.18 \pm 0.11 \pm 0.18$	112k	¹ TAMPONI	15 BELL	$e^+e^- \rightarrow h_b(1P)\eta$

¹ Using $B(\eta \rightarrow 2\gamma) = (39.41 \pm 0.20)\%$.

$\Gamma(h_b(1S)\omega)/\Gamma_{total}$ Γ_{24}/Γ

VALUE	CL%	DOCUMENT ID	TECN	COMMENT
<1.8 × 10⁻⁴	90	OSKIN	20 BELL	$e^+e^- \rightarrow \omega X$

$\Gamma(h_b(1S)\omega)/\Gamma(h_b(1P)\eta)$ Γ_{24}/Γ_{23}

VALUE	CL%	DOCUMENT ID	TECN	COMMENT
<8.4 × 10⁻²	90	¹ OSKIN	20 BELL	$e^+e^- \rightarrow \omega X$

¹ Using $B(\Upsilon(4S) \rightarrow h_b(1P)\eta) = (2.18 \pm 0.11 \pm 0.18) \times 10^{-3}$ from TAMPONI 15.

$\Gamma(\Upsilon(2S) \rightarrow \text{anything})/\Gamma_{total}$ Γ_{25}/Γ

VALUE (units 10^{-5})	CL%	DOCUMENT ID	TECN	COMMENT
<1.3	90	ASNER	07 CLEO	$e^+e^- \rightarrow \overline{D}X$

Double Radiative Decays

$\Gamma(\gamma\gamma \Upsilon(D) \rightarrow \gamma\gamma \eta \Upsilon(1S))/\Gamma_{total}$ Γ_{26}/Γ

VALUE	CL%	DOCUMENT ID	TECN	COMMENT
<2.3 × 10⁻⁵	90	GUIDO	17 BELL	$\Upsilon(4S) \rightarrow \gamma\gamma \pi^+\pi^-\pi^0 \mu^+\mu^-$

$\Upsilon(4S)$ REFERENCES

OSKIN	20	PR D102 092011	P. Oskin <i>et al.</i>	(BELLE Collab.)
GUIDO	17	PRL 121 062001	E. Guido <i>et al.</i>	(BELLE Collab.)
GUIDO	17	PR D96 052005	E. Guido <i>et al.</i>	(BELLE Collab.)
TAMPONI	15	PRL 115 142001	U. Tamponi <i>et al.</i>	(BELLE Collab.)
SHEN	13A	PR D88 052019	C.P. Shen <i>et al.</i>	(BELLE Collab.)
ADACHI	12	PRL 108 032001	I. Adachi <i>et al.</i>	(BELLE Collab.)
BELOUS	09	PL B681 400	K. Belous <i>et al.</i>	(BELLE Collab.)
SOKOLOV	09	PR D79 051103	A. Sokolov <i>et al.</i>	(BELLE Collab.)
AUBERT	08BO	PR D78 071103	B. Aubert <i>et al.</i>	(BABAR Collab.)
AUBERT	08BP	PR D78 112002	B. Aubert <i>et al.</i>	(BABAR Collab.)
PDG	08	PL B667 1	C. Amisler <i>et al.</i>	(PDG Collab.)
ASNER	07	PR D75 012009	D.M. Asner <i>et al.</i>	(CLEO Collab.)
HUANG	07	PR D75 012002	G.S. Huang <i>et al.</i>	(CLEO Collab.)
SOKOLOV	07	PR D75 071303	A. Sokolov <i>et al.</i>	(BELLE Collab.)
TAJIMA	07A	PR L 99 211601	O. Tajima <i>et al.</i>	(BELLE Collab.)
AUBERT	06R	PRL 96 232001	B. Aubert <i>et al.</i>	(BABAR Collab.)
AUBERT, BE	06F	PR D74 111103	B. Aubert <i>et al.</i>	(BABAR Collab.)
ARTUSO	05B	PRL 95 261801	M. Artuso <i>et al.</i>	(CLEO Collab.)
AUBERT	05Q	PR D72 032005	B. Aubert <i>et al.</i>	(BABAR Collab.)
AUBERT, B	05H	PRL 95 042001	B. Aubert <i>et al.</i>	(BABAR Collab.)
AUBERT	04F	PR D69 071101	B. Aubert <i>et al.</i>	(BABAR Collab.)
HASTINGS	03	PR D67 052004	N.C. Hastings <i>et al.</i>	(BELLE Collab.)
ABE	02D	PRL 88 052001	K. Abe <i>et al.</i>	(BELLE Collab.)
ATHAR	02	PR D66 052003	S.B. Athar <i>et al.</i>	(CLEO Collab.)
AUBERT	02	PR D65 032001	B. Aubert <i>et al.</i>	(BABAR Collab.)

ALEXANDER	01	PRL 86 2737	J.P. Alexander <i>et al.</i>	(CLEO Collab.)
AUBERT	01C	PRL 87 162002	B. Aubert <i>et al.</i>	(BABAR Collab.)
GLENN	99	PR D59 052003	S. Glenn <i>et al.</i>	(CLEO Collab.)
BARISH	96B	PRL 76 1570	B.C. Barish <i>et al.</i>	(CLEO Collab.)
ALBRECHT	95E	ZPHY C65 619	H. Albrecht <i>et al.</i>	(ARGUS Collab.)
BARISH	95	PR D51 1014	B.C. Barish <i>et al.</i>	(CLEO Collab.)
ALEXANDER	90C	PRL 64 2226	J. Alexander <i>et al.</i>	(CLEO Collab.)
BEBEK	87	PR D36 1289	C. Bebek <i>et al.</i>	(CLEO Collab.)
BESSON	85	PRL 54 361	D. Besson <i>et al.</i>	(CLEO Collab.)
LOVELOCK	85	PRL 54 377	D.M.J. Lovelock <i>et al.</i>	(CUSP Collab.)
LEYAOUANC	77	PL B71 397	A. Le Yaouanc <i>et al.</i>	(ORSAY)

$Z_b(10610)$

$$J^{PC} = 1^+(1^+ -)$$

was $X(10610)$
Properties incompatible with a $q\bar{q}$ structure (exotic state). See the review on non- $q\bar{q}$ states.

Observed by BONDAR 12 in $\Upsilon(5S)$ decays to $\Upsilon(nS)\pi^+\pi^-$ ($n = 1, 2, 3$) and $h_b(mP)\pi^+\pi^-$ ($m = 1, 2$). $J^P = 1^+$ is favored from angular analyses.

$Z_b(10610)^\pm$ MASS

VALUE (MeV)	DOCUMENT ID	TECN	COMMENT
10607.2 ± 2.0	¹ BONDAR	12 BELL	$e^+e^- \rightarrow$ hadrons
$10608.5 \pm 3.4 \pm \frac{3.7}{-1.4}$	² GARMASH	15 BELL	$e^+e^- \rightarrow \Upsilon(1S)\pi^+\pi^-$
$10608.1 \pm 1.2 \pm \frac{1.5}{-0.2}$	² GARMASH	15 BELL	$e^+e^- \rightarrow \Upsilon(2S)\pi^+\pi^-$
$10607.4 \pm 1.5 \pm \frac{0.8}{-0.2}$	² GARMASH	15 BELL	$e^+e^- \rightarrow \Upsilon(3S)\pi^+\pi^-$
$10611 \pm 4 \pm 3$	³ BONDAR	12 BELL	$e^+e^- \rightarrow \Upsilon(1S)\pi^+\pi^-$
$10609 \pm 2 \pm 3$	³ BONDAR	12 BELL	$e^+e^- \rightarrow \Upsilon(2S)\pi^+\pi^-$
$10608 \pm 2 \pm 3$	³ BONDAR	12 BELL	$e^+e^- \rightarrow \Upsilon(3S)\pi^+\pi^-$
$10605 \pm 2 \pm \frac{3}{-1}$	³ BONDAR	12 BELL	$e^+e^- \rightarrow h_b(1P)\pi^+\pi^-$
$10599 \pm \frac{6}{-3} \pm \frac{5}{-4}$	³ BONDAR	12 BELL	$e^+e^- \rightarrow h_b(2P)\pi^+\pi^-$

••• We do not use the following data for averages, fits, limits, etc. •••

¹ Average of the BONDAR 12 measurements in separate channels.
² Correlated with the corresponding result from BONDAR 12.
³ Superseded by the average measurement of BONDAR 12.

$Z_b(10610)^0$ MASS

VALUE (MeV)	DOCUMENT ID	TECN	COMMENT
$10609 \pm 4 \pm 4$	¹ KROKOVNY	13 BELL	$e^+e^- \rightarrow \Upsilon(2S)/\Upsilon(3S)\pi^0\pi^0$

¹ From a simultaneous fit to the KROKOVNY 13 Dalitz analysis of $e^+e^- \rightarrow \Upsilon(2S)/\Upsilon(3S)\pi^0\pi^0$ decays with fixed width $\Gamma(Z_b(10610)^0) = 18.4$ MeV.

$Z_b(10610)^\pm$ WIDTH

VALUE (MeV)	DOCUMENT ID	TECN	COMMENT
18.4 ± 2.4	¹ BONDAR	12 BELL	$e^+e^- \rightarrow$ hadrons
$18.5 \pm 5.3 \pm \frac{6.1}{-2.3}$	² GARMASH	15 BELL	$e^+e^- \rightarrow \Upsilon(1S)\pi^+\pi^-$
$20.8 \pm 2.5 \pm \frac{0.3}{-2.1}$	² GARMASH	15 BELL	$e^+e^- \rightarrow \Upsilon(2S)\pi^+\pi^-$
$18.7 \pm 3.4 \pm \frac{2.5}{-1.3}$	² GARMASH	15 BELL	$e^+e^- \rightarrow \Upsilon(3S)\pi^+\pi^-$
$22.3 \pm 7.7 \pm \frac{3.0}{-4.0}$	³ BONDAR	12 BELL	$e^+e^- \rightarrow \Upsilon(1S)\pi^+\pi^-$
$24.2 \pm 3.1 \pm \frac{2.0}{-3.0}$	³ BONDAR	12 BELL	$e^+e^- \rightarrow \Upsilon(2S)\pi^+\pi^-$
$17.6 \pm 3.0 \pm 3.0$	³ BONDAR	12 BELL	$e^+e^- \rightarrow \Upsilon(3S)\pi^+\pi^-$
$11.4 \pm \frac{4.5 \pm 2.1}{3.9 - 1.2}$	³ BONDAR	12 BELL	$e^+e^- \rightarrow h_b(1P)\pi^+\pi^-$
$13 \pm \frac{10}{-8} \pm \frac{9}{-7}$	³ BONDAR	12 BELL	$e^+e^- \rightarrow h_b(2P)\pi^+\pi^-$

••• We do not use the following data for averages, fits, limits, etc. •••

¹ Average of the BONDAR 12 measurements in separate channels.
² Correlated with the corresponding result from BONDAR 12.
³ Superseded by the average measurement of BONDAR 12.

$Z_b(10610)$ DECAY MODES

Mode	Fraction (Γ_i/Γ)
Γ_1 $\Upsilon(1S)\pi^+$	$(5.4 \pm \frac{1.9}{-1.5}) \times 10^{-3}$
Γ_2 $\Upsilon(1S)\pi^0$	not seen
Γ_3 $\Upsilon(2S)\pi^+$	$(3.6 \pm \frac{1.1}{-0.8})\%$
Γ_4 $\Upsilon(2S)\pi^0$	seen
Γ_5 $\Upsilon(3S)\pi^+$	$(2.1 \pm \frac{0.8}{-0.6})\%$

See key on page 1127

Meson Particle Listings

$Z_b(10610)$, $Z_b(10650)$

Γ_6	$\Upsilon(3S)\pi^0$	seen
Γ_7	$h_b(1P)\pi^+$	$(3.5_{-0.9}^{+1.2})\%$
Γ_8	$h_b(2P)\pi^+$	$(4.7_{-1.3}^{+1.7})\%$
Γ_9	$B^+\bar{B}^0$	not seen
Γ_{10}	$B^+\bar{B}^{*0} + B^{*+}\bar{B}^0$	$(85.6_{-2.9}^{+2.1})\%$

$Z_b(10610)$ BRANCHING RATIOS

$\Gamma(\Upsilon(1S)\pi^+)/\Gamma_{total}$	Γ_1/Γ
VALUE (units 10^{-3})	DOCUMENT ID TECN COMMENT
$5.4_{-1.3}^{+1.6+1.1}$	¹ GARMASH 16 BELL $e^+e^- \rightarrow \pi^- B^+ \bar{B}^{*0}$, $\pi^- \bar{B}^0 B^{*+}$
• • • We do not use the following data for averages, fits, limits, etc. • • •	
seen	GARMASH 15 BELL $e^+e^- \rightarrow \Upsilon(1S)\pi^+\pi^-$
seen	BONDAR 12 BELL $e^+e^- \rightarrow \Upsilon(1S)\pi^+\pi^-$
¹ Assuming the $Z_b(10610)$ decay width is saturated by the channels $\pi^+\Upsilon(1S, 2S, 3S)$, $\pi^+h_b(1P, 2P)$, and $B^+\bar{B}^{*0} + \bar{B}^0 B^{*+}$, and using the results from BONDAR 12 and MIZUK 16.	

$\Gamma(\Upsilon(1S)\pi^0)/\Gamma_{total}$	Γ_2/Γ
VALUE	DOCUMENT ID TECN COMMENT
not seen	KROKOVNY 13 BELL $e^+e^- \rightarrow \Upsilon(1S)\pi^0\pi^0$

$\Gamma(\Upsilon(2S)\pi^+)/\Gamma_{total}$	Γ_3/Γ
VALUE (units 10^{-2})	DOCUMENT ID TECN COMMENT
$3.62_{-0.59}^{+0.76+0.79}$	¹ GARMASH 16 BELL $e^+e^- \rightarrow \pi^- B^+ \bar{B}^{*0}$, $\pi^- \bar{B}^0 B^{*+}$
• • • We do not use the following data for averages, fits, limits, etc. • • •	
seen	GARMASH 15 BELL $e^+e^- \rightarrow \Upsilon(2S)\pi^+\pi^-$
seen	BONDAR 12 BELL $e^+e^- \rightarrow \Upsilon(2S)\pi^+\pi^-$
¹ Assuming the $Z_b(10610)$ decay width is saturated by the channels $\pi^+\Upsilon(1S, 2S, 3S)$, $\pi^+h_b(1P, 2P)$, and $B^+\bar{B}^{*0} + \bar{B}^0 B^{*+}$, and using the results from BONDAR 12 and MIZUK 16.	

$\Gamma(\Upsilon(2S)\pi^0)/\Gamma_{total}$	Γ_4/Γ
VALUE	DOCUMENT ID TECN COMMENT
seen	¹ KROKOVNY 13 BELL $e^+e^- \rightarrow \Upsilon(2S)\pi^0\pi^0$
¹ Combined significance in $e^+e^- \rightarrow \Upsilon(2S)/\Upsilon(3S)\pi^0\pi^0$, including systematics, of 6.5 σ .	

$\Gamma(\Upsilon(3S)\pi^+)/\Gamma_{total}$	Γ_5/Γ
VALUE (units 10^{-2})	DOCUMENT ID TECN COMMENT
$2.15_{-0.42}^{+0.55+0.60}$	¹ GARMASH 16 BELL $e^+e^- \rightarrow \pi^- B^+ \bar{B}^{*0}$, $\pi^- \bar{B}^0 B^{*+}$
• • • We do not use the following data for averages, fits, limits, etc. • • •	
seen	GARMASH 15 BELL $e^+e^- \rightarrow \Upsilon(3S)\pi^+\pi^-$
seen	BONDAR 12 BELL $e^+e^- \rightarrow \Upsilon(3S)\pi^+\pi^-$
¹ Assuming the $Z_b(10610)$ decay width is saturated by the channels $\pi^+\Upsilon(1S, 2S, 3S)$, $\pi^+h_b(1P, 2P)$, and $B^+\bar{B}^{*0} + \bar{B}^0 B^{*+}$, and using the results from BONDAR 12 and MIZUK 16.	

$\Gamma(\Upsilon(3S)\pi^0)/\Gamma_{total}$	Γ_6/Γ
VALUE	DOCUMENT ID TECN COMMENT
seen	¹ KROKOVNY 13 BELL $e^+e^- \rightarrow \Upsilon(3S)\pi^0\pi^0$
¹ Combined significance in $e^+e^- \rightarrow \Upsilon(2S)/\Upsilon(3S)\pi^0\pi^0$, including systematics, of 6.5 σ .	

$\Gamma(h_b(1P)\pi^+)/\Gamma_{total}$	Γ_7/Γ
VALUE (units 10^{-2})	DOCUMENT ID TECN COMMENT
$3.45_{-0.71}^{+0.87+0.86}$	¹ GARMASH 16 BELL $e^+e^- \rightarrow \pi^- B^+ \bar{B}^{*0}$, $\pi^- \bar{B}^0 B^{*+}$
• • • We do not use the following data for averages, fits, limits, etc. • • •	
possibly seen	² MIZUK 16 BELL $e^+e^- \rightarrow h_b(1P)\pi^+\pi^-$
seen	³ BONDAR 12 BELL $e^+e^- \rightarrow h_b(1P)\pi^+\pi^-$
¹ Assuming the $Z_b(10610)$ decay width is saturated by the channels $\pi^+\Upsilon(1S, 2S, 3S)$, $\pi^+h_b(1P, 2P)$, and $B^+\bar{B}^{*0} + \bar{B}^0 B^{*+}$, and using the results from BONDAR 12 and MIZUK 16.	
² Using e^+e^- energies near the $\Upsilon(11020)$.	
³ Using e^+e^- energies near the $\Upsilon(10860)$.	

$\Gamma(h_b(2P)\pi^+)/\Gamma_{total}$	Γ_8/Γ
VALUE (units 10^{-2})	DOCUMENT ID TECN COMMENT
$4.67_{-1.00}^{+1.24+1.18}$	¹ GARMASH 16 BELL $e^+e^- \rightarrow \pi^- B^+ \bar{B}^{*0}$, $\pi^- \bar{B}^0 B^{*+}$
• • • We do not use the following data for averages, fits, limits, etc. • • •	
possibly seen	² MIZUK 16 BELL $e^+e^- \rightarrow h_b(2P)\pi^+\pi^-$
seen	³ BONDAR 12 BELL $e^+e^- \rightarrow h_b(2P)\pi^+\pi^-$
¹ Assuming the $Z_b(10610)$ decay width is saturated by the channels $\pi^+\Upsilon(1S, 2S, 3S)$, $\pi^+h_b(1P, 2P)$, and $B^+\bar{B}^{*0} + \bar{B}^0 B^{*+}$, and using the results from BONDAR 12 and MIZUK 16.	
² Using e^+e^- energies near the $\Upsilon(11020)$.	
³ Using e^+e^- energies near the $\Upsilon(10860)$.	

$\Gamma(B^+\bar{B}^0)/\Gamma_{total}$	Γ_9/Γ
VALUE	DOCUMENT ID TECN COMMENT
not seen	GARMASH 16 BELL $e^+e^- \rightarrow \pi^- B^+ \bar{B}^0$

$[\Gamma(B^+\bar{B}^{*0}) + \Gamma(B^{*+}\bar{B}^0)]/\Gamma_{total}$	Γ_{10}/Γ
VALUE (units 10^{-2})	EVTS DOCUMENT ID TECN COMMENT
$85.6_{-2.0}^{+1.5+1.5}$	357 ¹ GARMASH 16 BELL $e^+e^- \rightarrow \pi^- B^+ \bar{B}^{*0}$, $\pi^- B^{*+} \bar{B}^0$

¹ Assuming the $Z_b(10610)$ decay width is saturated by the channels $\pi^+\Upsilon(1S, 2S, 3S)$, $\pi^+h_b(1P, 2P)$, and $B^+\bar{B}^{*0} + B^{*+}\bar{B}^0$, and using the results from BONDAR 12 and MIZUK 16. Using the mass and width of the $Z_b(10610)$ from BONDAR 12.

$[\Gamma(B^+\bar{B}^{*0}) + \Gamma(B^{*+}\bar{B}^0)]/[\Gamma(\Upsilon(1S)\pi^+) + \Gamma(\Upsilon(2S)\pi^+) + \Gamma(\Upsilon(3S)\pi^+) + \Gamma(h_b(1P)\pi^+) + \Gamma(h_b(2P)\pi^+)]$	$\Gamma_{10}/(\Gamma_1+\Gamma_3+\Gamma_5+\Gamma_7+\Gamma_8)$
VALUE (units 10^{-2})	EVTS DOCUMENT ID TECN COMMENT
$5.93_{-0.69}^{+0.99+1.01}$	357 ¹ GARMASH 16 BELL $e^+e^- \rightarrow \pi^- B^+ \bar{B}^{*0}$, $\pi^- \bar{B}^0 B^{*+}$

¹ Combined with the results of BONDAR 12 and MIZUK 16. Not independent from $Z_b(10610)$ branching fractions to $\pi^+\Upsilon(1S, 2S, 3S)$, $\pi^+h_b(1P, 2P)$, and $B^+\bar{B}^{*0} + \bar{B}^0 B^{*+}$.

$Z_b(10610)$ REFERENCES

GARMASH 16	PRL 116 212001	A. Garmash et al.	(BELLE Collab.)
MIZUK 16	PRL 117 142001	R. Mizuk et al.	(BELLE Collab.)
GARMASH 15	PR D91 072003	A. Garmash et al.	(BELLE Collab.)
KROKOVNY 13	PR D88 052016	P. Krokovny et al.	(BELLE Collab.)
BONDAR 12	PRL 108 122001	A. Bondar et al.	(BELLE Collab.)

$Z_b(10650)$

$$J^G(J^{PC}) = 1^+(1^+ -)$$

I, G, C need confirmation.

was $X(10650)^\pm$

Properties incompatible with a $q\bar{q}$ structure (exotic state). See the review on non- $q\bar{q}$ states.

Observed by BONDAR 12 in $\Upsilon(5S)$ decays to $\Upsilon(nS)\pi^+\pi^-$ ($n = 1, 2, 3$) and $h_b(mP)\pi^+\pi^-$ ($m = 1, 2$). $J^P = 1^+$ is favored from angular analyses.

$Z_b(10650)$ MASS

VALUE (MeV)	DOCUMENT ID TECN COMMENT
10652.2 ± 1.5	¹ BONDAR 12 BELL $e^+e^- \rightarrow$ hadrons
• • • We do not use the following data for averages, fits, limits, etc. • • •	
$10656.7 \pm 5.0_{-3.1}^{+1.1}$	² GARMASH 15 BELL $e^+e^- \rightarrow \Upsilon(1S)\pi^+\pi^-$
$10650.7 \pm 1.5_{-0.2}^{+0.5}$	² GARMASH 15 BELL $e^+e^- \rightarrow \Upsilon(2S)\pi^+\pi^-$
$10651.2 \pm 1.0_{-0.3}^{+0.4}$	² GARMASH 15 BELL $e^+e^- \rightarrow \Upsilon(3S)\pi^+\pi^-$
$10657 \pm 6 \pm 3$	³ BONDAR 12 BELL $e^+e^- \rightarrow \Upsilon(1S)\pi^+\pi^-$
$10651 \pm 2 \pm 3$	³ BONDAR 12 BELL $e^+e^- \rightarrow \Upsilon(2S)\pi^+\pi^-$
$10652 \pm 1 \pm 2$	³ BONDAR 12 BELL $e^+e^- \rightarrow \Upsilon(3S)\pi^+\pi^-$
$10654 \pm 3 \pm 1_{-2}$	³ BONDAR 12 BELL $e^+e^- \rightarrow h_b(1P)\pi^+\pi^-$
$10651 \pm 2 \pm 3_{-2}$	³ BONDAR 12 BELL $e^+e^- \rightarrow h_b(2P)\pi^+\pi^-$

¹ Average of the BONDAR 12 measurements in separate channels.
² Correlated with the corresponding result from BONDAR 12.
³ Superseded by the average measurement of BONDAR 12.

$Z_b(10650)$ WIDTH

VALUE (MeV)	DOCUMENT ID TECN COMMENT
11.5 ± 2.2	⁴ BONDAR 12 BELL $e^+e^- \rightarrow$ hadrons
• • • We do not use the following data for averages, fits, limits, etc. • • •	
$12.1_{-4.8}^{+11.3+2.7}$	⁵ GARMASH 15 BELL $e^+e^- \rightarrow \Upsilon(1S)\pi^+\pi^-$
$14.2 \pm 3.7_{-0.4}^{+1.9}$	⁵ GARMASH 15 BELL $e^+e^- \rightarrow \Upsilon(2S)\pi^+\pi^-$
$9.3 \pm 2.2_{-0.5}^{+0.3}$	⁵ GARMASH 15 BELL $e^+e^- \rightarrow \Upsilon(3S)\pi^+\pi^-$
$16.3 \pm 9.8_{-2.0}^{+6.0}$	⁶ BONDAR 12 BELL $e^+e^- \rightarrow \Upsilon(1S)\pi^+\pi^-$
$13.3 \pm 3.3_{-3.0}^{+4.0}$	⁶ BONDAR 12 BELL $e^+e^- \rightarrow \Upsilon(2S)\pi^+\pi^-$
$8.4 \pm 2.0 \pm 2.0$	⁶ BONDAR 12 BELL $e^+e^- \rightarrow \Upsilon(3S)\pi^+\pi^-$
$20.9_{-4.7}^{+5.4+2.1}$	⁶ BONDAR 12 BELL $e^+e^- \rightarrow h_b(1P)\pi^+\pi^-$
$19 \pm 7_{-11}^{+1}$	⁶ BONDAR 12 BELL $e^+e^- \rightarrow h_b(2P)\pi^+\pi^-$

⁴ Average of the BONDAR 12 measurements in separate channels.
⁵ Correlated with the corresponding result from BONDAR 12.
⁶ Superseded by the average measurement of BONDAR 12.

Meson Particle Listings

 $Z_b(10650)$, $\Upsilon(10753)$ $Z_b(10650)^+$ DECAY MODES $Z_b(10650)^-$ decay modes are charge conjugates of the modes below.

Mode	Fraction (Γ_i/Γ)
Γ_1 $\Upsilon(1S)\pi^+$	$(1.7^{+0.8}_{-0.6}) \times 10^{-3}$
Γ_2 $\Upsilon(2S)\pi^+$	$(1.4^{+0.6}_{-0.4})\%$
Γ_3 $\Upsilon(3S)\pi^+$	$(1.6^{+0.7}_{-0.5})\%$
Γ_4 $h_b(1P)\pi^+$	$(8.4^{+2.9}_{-2.4})\%$
Γ_5 $h_b(2P)\pi^+$	$(15 \pm 4)\%$
Γ_6 $B^+\bar{B}^0$	not seen
Γ_7 $B^+\bar{B}^{*0} + B^{*+}\bar{B}^0$	not seen
Γ_8 $B^{*+}\bar{B}^{*0}$	$(74 \pm 4_{-6})\%$

 $Z_b(10650)$ BRANCHING RATIOS

$\Gamma(\Upsilon(1S)\pi^+)/\Gamma_{\text{total}}$	$\Gamma_1/\Gamma_{\text{total}}$		
VALUE (units 10^{-3})	DOCUMENT ID	TECN	COMMENT
$1.7^{+0.7+0.3}_{-0.6-0.2}$	⁷ GARMASH 16	BELL	$e^+e^- \rightarrow \pi^- B^{*+}\bar{B}^{*0}$

• • • We do not use the following data for averages, fits, limits, etc. • • •

seen	GARMASH 15	BELL	$e^+e^- \rightarrow \Upsilon(1S)\pi^+\pi^-$
seen	BONDAR 12	BELL	$e^+e^- \rightarrow \Upsilon(1S)\pi^+\pi^-$

⁷ Assuming the $Z_b(10650)$ decay width is saturated by the channels $\pi^+\Upsilon(1S, 2S, 3S)$, $\pi^+h_b(1P, 2P)$, and $B^{*+}\bar{B}^{*0}$, and using the results from BONDAR 12 and MIZUK 16.

$\Gamma(\Upsilon(2S)\pi^+)/\Gamma_{\text{total}}$	$\Gamma_2/\Gamma_{\text{total}}$		
VALUE (units 10^{-2})	DOCUMENT ID	TECN	COMMENT
$1.39^{+0.48+0.34}_{-0.38-0.23}$	⁸ GARMASH 16		$e^+e^- \rightarrow \pi^- B^{*+}\bar{B}^{*0}$

• • • We do not use the following data for averages, fits, limits, etc. • • •

seen	GARMASH 15	BELL	$e^+e^- \rightarrow \Upsilon(2S)\pi^+\pi^-$
seen	BONDAR 12	BELL	$e^+e^- \rightarrow \Upsilon(2S)\pi^+\pi^-$

⁸ Assuming the $Z_b(10650)$ decay width is saturated by the channels $\pi^+\Upsilon(1S, 2S, 3S)$, $\pi^+h_b(1P, 2P)$, and $B^{*+}\bar{B}^{*0}$, and using the results from BONDAR 12 and MIZUK 16.

$\Gamma(\Upsilon(3S)\pi^+)/\Gamma_{\text{total}}$	$\Gamma_3/\Gamma_{\text{total}}$		
VALUE (units 10^{-2})	DOCUMENT ID	TECN	COMMENT
$1.63^{+0.53+0.39}_{-0.42-0.28}$	⁹ GARMASH 16	BELL	$e^+e^- \rightarrow \pi^- B^{*+}\bar{B}^{*0}$

• • • We do not use the following data for averages, fits, limits, etc. • • •

seen	GARMASH 15	BELL	$e^+e^- \rightarrow \Upsilon(3S)\pi^+\pi^-$
seen	BONDAR 12	BELL	$e^+e^- \rightarrow \Upsilon(3S)\pi^+\pi^-$

⁹ Assuming the $Z_b(10650)$ decay width is saturated by the channels $\pi^+\Upsilon(1S, 2S, 3S)$, $\pi^+h_b(1P, 2P)$, and $B^{*+}\bar{B}^{*0}$, and using the results from BONDAR 12 and MIZUK 16.

$\Gamma(h_b(1P)\pi^+)/\Gamma_{\text{total}}$	$\Gamma_4/\Gamma_{\text{total}}$		
VALUE (units 10^{-2})	DOCUMENT ID	TECN	COMMENT
$8.41^{+2.43+1.49}_{-2.12-1.06}$	¹⁰ GARMASH 16	BELL	$e^+e^- \rightarrow \pi^- B^{*+}\bar{B}^{*0}$

• • • We do not use the following data for averages, fits, limits, etc. • • •

seen	¹¹ MIZUK 16	BELL	$e^+e^- \rightarrow h_b(1P)\pi^+\pi^-$
seen	¹² BONDAR 12	BELL	$e^+e^- \rightarrow h_b(1P)\pi^+\pi^-$

¹⁰ Assuming the $Z_b(10650)$ decay width is saturated by the channels $\pi^+\Upsilon(1S, 2S, 3S)$, $\pi^+h_b(1P, 2P)$, and $B^{*+}\bar{B}^{*0}$, and using the results from BONDAR 12 and MIZUK 16.

¹¹ Using e^+e^- energies near the $\Upsilon(11020)$.

¹² Using e^+e^- energies near the $\Upsilon(10860)$.

$\Gamma(h_b(2P)\pi^+)/\Gamma_{\text{total}}$	$\Gamma_5/\Gamma_{\text{total}}$		
VALUE (units 10^{-2})	DOCUMENT ID	TECN	COMMENT
$14.7^{+3.2+2.8}_{-2.8-2.3}$	¹³ GARMASH 16	BELL	$e^+e^- \rightarrow \pi^- B^{*+}\bar{B}^{*0}$

• • • We do not use the following data for averages, fits, limits, etc. • • •

possibly seen	¹⁴ MIZUK 16	BELL	$e^+e^- \rightarrow h_b(2P)\pi^+\pi^-$
seen	¹⁵ BONDAR 12	BELL	$e^+e^- \rightarrow h_b(2P)\pi^+\pi^-$

¹³ Assuming the $Z_b(10650)$ decay width is saturated by the channels $\pi^+\Upsilon(1S, 2S, 3S)$, $\pi^+h_b(1P, 2P)$, and $B^{*+}\bar{B}^{*0}$, and using the results from BONDAR 12 and MIZUK 16.

¹⁴ Using e^+e^- energies near the $\Upsilon(11020)$.

¹⁵ Using e^+e^- energies near the $\Upsilon(10860)$.

$\Gamma(B^+\bar{B}^0)/\Gamma_{\text{total}}$	$\Gamma_6/\Gamma_{\text{total}}$		
VALUE	DOCUMENT ID	TECN	COMMENT
not seen	GARMASH 16	BELL	$e^+e^- \rightarrow \pi^- B^+\bar{B}^0$

$[\Gamma(B^+\bar{B}^{*0}) + \Gamma(B^{*+}\bar{B}^0)]/\Gamma_{\text{total}}$	$\Gamma_7/\Gamma_{\text{total}}$		
VALUE	DOCUMENT ID	TECN	COMMENT
not seen	GARMASH 16	BELL	$e^+e^- \rightarrow \pi^- B^+\bar{B}^{*0}$, $\pi^- \bar{B}^0 B^{*+}$

$\Gamma(B^{*+}\bar{B}^{*0})/\Gamma_{\text{total}}$	$\Gamma_8/\Gamma_{\text{total}}$			
VALUE (units 10^{-2})	EVTS	DOCUMENT ID	TECN	COMMENT
$73.7^{+3.4+2.7}_{-4.4-3.5}$	161	¹⁶ GARMASH 16	BELL	$e^+e^- \rightarrow \pi^- B^{*+}\bar{B}^{*0}$

¹⁶ Assuming the $Z_b(10650)$ decay width is saturated by the channels $\pi^+\Upsilon(1S, 2S, 3S)$, $\pi^+h_b(1P, 2P)$, and $B^{*+}\bar{B}^{*0}$, and using the results from BONDAR 12 and MIZUK 16. Using the mass and width of the $Z_b(10650)$ from BONDAR 12.

$\Gamma(B^{*+}\bar{B}^{*0})/[\Gamma(\Upsilon(1S)\pi^+) + \Gamma(\Upsilon(2S)\pi^+) + \Gamma(\Upsilon(3S)\pi^+) + \Gamma(h_b(1P)\pi^+) + \Gamma(h_b(2P)\pi^+)]$	$\Gamma_8/(\Gamma_1+\Gamma_2+\Gamma_3+\Gamma_4+\Gamma_5)$			
VALUE (units 10^{-2})	EVTS	DOCUMENT ID	TECN	COMMENT
$2.80^{+0.69+0.54}_{-0.40-0.36}$	161	¹⁷ GARMASH 16	BELL	$e^+e^- \rightarrow \pi^- B^{*+}\bar{B}^{*0}$

• • • We do not use the following data for averages, fits, limits, etc. • • •

¹⁷ Combined with the results of BONDAR 12 and MIZUK 16. Not independent from $Z_b(10650)$ branching fractions to $\pi^+\Upsilon(1S, 2S, 3S)$, $\pi^+h_b(1P, 2P)$, and $B^{*+}\bar{B}^{*0}$.

 $Z_b(10650)$ REFERENCES

GARMASH 16	PRL 116 212001	A. Garmash et al.	(BELLE Collab.)
MIZUK 16	PRL 117 142001	R. Mizuk et al.	(BELLE Collab.)
GARMASH 15	PR D91 072003	A. Garmash et al.	(BELLE Collab.)
BONDAR 12	PRL 108 122001	A. Bondar et al.	(BELLE Collab.)

 $\Upsilon(10753)$

$$J^{PC} = ?(1^{--})$$

OMITTED FROM SUMMARY TABLE

A candidate for $\Upsilon(3D)$ state or an exotic structure.

Seen by MIZUK 19 in $e^+e^- \rightarrow \Upsilon(nS)\pi^+\pi^-$ ($n=1,2,3$) with a significance of 5.2σ .

 $\Upsilon(10753)$ MASS

VALUE (MeV)	DOCUMENT ID	TECN	COMMENT
$10752.7 \pm 5.9^{+0.7}_{-1.1}$	¹ MIZUK 19	BELL	$e^+e^- \rightarrow \Upsilon(nS)\pi^+\pi^-$
10761 ± 2	² DONG 20A		$e^+e^- \rightarrow b\bar{b}$

• • • We do not use the following data for averages, fits, limits, etc. • • •

¹ From a simultaneous fit to the $\Upsilon(nS)\pi^+\pi^-$, $n=1,2,3$, cross sections at 28 energy points within $\sqrt{s} = 10.63\text{--}11.02$ GeV, including the initial-state radiation at $\Upsilon(10860)$.
² From a fit to the dressed cross sections of AUBERT 09E by BaBar and SANTEL 16 by Belle above 10.68 GeV with a coherent sum of a continuum amplitude and three Breit-Wigner functions with constant widths.

 $\Upsilon(10753)$ WIDTH

VALUE (MeV)	DOCUMENT ID	TECN	COMMENT
$35.5^{+17.6+3.9}_{-11.3-3.3}$	¹ MIZUK 19	BELL	$e^+e^- \rightarrow \Upsilon(nS)\pi^+\pi^-$
48.5 ± 3.0	² DONG 20A		$e^+e^- \rightarrow b\bar{b}$

• • • We do not use the following data for averages, fits, limits, etc. • • •
¹ From a simultaneous fit to the $\Upsilon(nS)\pi^+\pi^-$, $n=1,2,3$, cross sections at 28 energy points within $\sqrt{s} = 10.63\text{--}11.02$ GeV, including the initial-state radiation at $\Upsilon(10860)$.
² From a fit to the dressed cross sections of AUBERT 09E by BaBar and SANTEL 16 by Belle above 10.68 GeV with a coherent sum of a continuum amplitude and three Breit-Wigner functions with constant widths.

 $\Upsilon(10753)$ DECAY MODES

Mode	$\Upsilon(i)\Gamma(j)\Gamma(k)/\Gamma(\text{total})$
Γ_1 $\Upsilon(1S)\pi^+\pi^-$	
Γ_2 $\Upsilon(2S)\pi^+\pi^-$	
Γ_3 $\Upsilon(3S)\pi^+\pi^-$	
Γ_4 e^+e^-	

 $\Upsilon(10753)$ $\Gamma(i)\Gamma(j)\Gamma(k)/\Gamma(\text{total})$

$\Gamma(\Upsilon(1S)\pi^+\pi^-) \times \Gamma(e^+e^-)/\Gamma_{\text{total}}$	$\Gamma_1\Gamma_4/\Gamma_{\text{total}}$		
VALUE (eV)	DOCUMENT ID	TECN	COMMENT
0.295 ± 0.175	^{1,2} MIZUK 19	BELL	$e^+e^- \rightarrow \Upsilon(nS)\pi^+\pi^-$

• • • We do not use the following data for averages, fits, limits, etc. • • •

¹ From a simultaneous fit to the $\Upsilon(nS)\pi^+\pi^-$, $n=1,2,3$, cross sections at 28 energy points within $\sqrt{s} = 10.63\text{--}11.02$ GeV, including the initial-state radiation at $\Upsilon(10860)$.

² Reported as the range 0.12–0.47 eV obtained from multiple solutions of an amplitude fit within a model composed as a sum of Breit-Wigner functions.

$\Gamma(\Upsilon(2S)\pi^+\pi^-) \times \Gamma(e^+e^-)/\Gamma_{total}$ $\Gamma_2\Gamma_4/\Gamma$

VALUE (eV) DOCUMENT ID TECN COMMENT

••• We do not use the following data for averages, fits, limits, etc. •••
 0.875 ± 0.345 1,2 MIZUK 19 BELL $e^+e^- \rightarrow \Upsilon(nS)\pi^+\pi^-$

¹ From a simultaneous fit to the $\Upsilon(nS)\pi^+\pi^-$, $n = 1, 2, 3$, cross sections at 28 energy points within $\sqrt{s} = 10.63\text{--}11.02$ GeV, including the initial-state radiation at $\Upsilon(10860)$.
² Reported as the range 0.53–1.22 eV obtained from multiple solutions of an amplitude fit within a model composed as a sum of Breit-Wigner functions.

$\Gamma(\Upsilon(3S)\pi^+\pi^-) \times \Gamma(e^+e^-)/\Gamma_{total}$ $\Gamma_3\Gamma_4/\Gamma$

VALUE (eV) DOCUMENT ID TECN COMMENT

••• We do not use the following data for averages, fits, limits, etc. •••
 0.235 ± 0.025 1,2 MIZUK 19 BELL $e^+e^- \rightarrow \Upsilon(nS)\pi^+\pi^-$

¹ From a simultaneous fit to the $\Upsilon(nS)\pi^+\pi^-$, $n = 1, 2, 3$, cross sections at 28 energy points within $\sqrt{s} = 10.63\text{--}11.02$ GeV, including the initial-state radiation at $\Upsilon(10860)$.
² Reported as the range 0.21–0.26 eV obtained from multiple solutions of an amplitude fit within a model composed as a sum of Breit-Wigner functions.

$\Upsilon(10753)$ REFERENCES

DONG 20A CP C44 083001 X.-K. Dong et al.	(BELLE Collab.)
MIZUK 19 JHEP 1910 220 R. Mizuk et al.	(BELLE Collab.)
SANTEL 16 PR D93 011101 D. Santel et al.	(BELLE Collab.)
AUBERT 09E PRL 102 012001 B. Aubert et al.	(BABAR Collab.)

$\Upsilon(10860)$

$$I^G(J^{PC}) = 0^-(1^{--})$$

$\Upsilon(10860)$ MASS

VALUE (MeV) DOCUMENT ID TECN COMMENT

10885.2 ± 2.6 OUR AVERAGE
 10885.3 ± 1.5 ± 2.2 1 MIZUK 19 BELL $e^+e^- \rightarrow \Upsilon(nS)\pi^+\pi^-$

10884.7 ± 3.6 ± 8.9 2 MIZUK 16 BELL $e^+e^- \rightarrow h_b(1P, 2P)\pi^+\pi^-$
 3.4 ± 1.0

••• We do not use the following data for averages, fits, limits, etc. •••
 10882 ± 1 3 DONG 20A $e^+e^- \rightarrow b\bar{b}$
 10881.8 ± 1.0 ± 1.2 4,5 SANTEL 16 BELL $e^+e^- \rightarrow$ hadrons
 10891.1 ± 3.2 ± 1.2 6,7 SANTEL 16 BELL $e^+e^- \rightarrow \Upsilon(1S, 2S, 3S)\pi^+\pi^-$
 10879 ± 3 8,9 CHEN 10 BELL $e^+e^- \rightarrow$ hadrons
 10888.4 ± 2.7 ± 1.2 10 CHEN 10 BELL $e^+e^- \rightarrow \Upsilon(1S, 2S, 3S)\pi^+\pi^-$
 10876 ± 2 8 AUBERT 09E BABR $e^+e^- \rightarrow$ hadrons
 10869 ± 2 11 AUBERT 09E BABR $e^+e^- \rightarrow$ hadrons
 10868 ± 6 ± 5 12 BESSON 85 CLEO $e^+e^- \rightarrow$ hadrons
 10845 ± 20 13 LOVELOCK 85 CUSB $e^+e^- \rightarrow$ hadrons

¹ From a simultaneous fit to the $\Upsilon(nS)\pi^+\pi^-$, $n = 1, 2, 3$, cross sections at 28 energy points within $\sqrt{s} = 10.6\text{--}11.05$ GeV, including the initial-state radiation at $\Upsilon(10860)$.
² From a simultaneous fit to the $h_b(nP)\pi^+\pi^-$, $n = 1, 2$ cross sections at 22 energy points within $\sqrt{s} = 10.77\text{--}11.02$ GeV to a pair of interfering Breit-Wigner amplitudes modified by phase space factors, with eight resonance parameters (a mass and width for each of $\Upsilon(10860)$ and $\Upsilon(11020)$, a single relative phase, a single relative amplitude, and two overall normalization factors, one for each n). The systematic error estimate is dominated by possible interference with a small nonresonant continuum amplitude.
³ From a fit to the dressed cross sections of AUBERT 09E by BaBar and SANTEL 16 by Belle above 10.68 GeV with a coherent sum of a continuum amplitude and three Breit-Wigner functions with constant widths.
⁴ From a fit to the total hadronic cross sections measured at 60 energy points within $\sqrt{s} = 10.82\text{--}11.05$ GeV to a pair of interfering Breit-Wigner amplitudes and two floating continuum amplitudes with $1/\sqrt{s}$ dependence, one coherent with the resonances and one incoherent, with six resonance parameters (a mass, width, and an amplitude for each of $\Upsilon(10860)$ and $\Upsilon(11020)$, one relative phase, and one decoherence coefficient).
⁵ Not including uncertain and potentially large systematic errors due to assumed continuum amplitude $1/\sqrt{s}$ dependence and related interference contributions.
⁶ From a simultaneous fit to the $\Upsilon(nS)\pi^+\pi^-$, $n = 1, 2, 3$, cross sections at 25 energy points within $\sqrt{s} = 10.6\text{--}11.05$ GeV to a pair of interfering Breit-Wigner amplitudes modified by phase space factors, with fourteen resonance parameters (a mass, width, and three amplitudes for each of $\Upsilon(10860)$ and $\Upsilon(11020)$, a single universal relative phase, and three decoherence coefficients, one for each n). Continuum contributions were measured (and therefore fixed) to be zero.
⁷ Superseded by MIZUK 19.
⁸ In a model where a flat non-resonant $b\bar{b}$ -continuum is incoherently added to a second flat component interfering with two Breit-Wigner resonances. Systematic uncertainties not estimated.
⁹ The parameters of the $\Upsilon(11020)$ are fixed to those in AUBERT 09E.
¹⁰ In a model where a flat nonresonant $\Upsilon(1S, 2S, 3S)\pi^+\pi^-$ continuum interferes with a single Breit-Wigner resonance.
¹¹ In a model where a non-resonant $b\bar{b}$ -continuum represented by a threshold function at $\sqrt{s}=2m_B$ is incoherently added to a flat component interfering with two Breit-Wigner resonances. Not independent of other AUBERT 09E results. Systematic uncertainties not estimated.
¹² Assuming four Gaussians with radiative tails and a single step in R .
¹³ In a coupled-channel model with three resonances and a smooth step in R .

$\Upsilon(10860)$ WIDTH

VALUE (MeV) DOCUMENT ID TECN COMMENT

37 ± 4 OUR AVERAGE

36.6 + 4.5 + 0.5 - 3.9 - 1.1 1 MIZUK 19 BELL $e^+e^- \rightarrow \Upsilon(nS)\pi^+\pi^-$
 40.6 + 12.7 + 1.1 - 8.0 - 19.1 2 MIZUK 16 BELL $e^+e^- \rightarrow h_b(1P, 2P)\pi^+\pi^-$
 ••• We do not use the following data for averages, fits, limits, etc. •••
 49.5 ± 1.5 3 DONG 20A $e^+e^- \rightarrow b\bar{b}$
 48.5 + 1.9 + 2.0 - 1.8 - 2.8 4,5 SANTEL 16 BELL $e^+e^- \rightarrow$ hadrons
 53.7 + 7.1 + 1.3 - 5.6 - 5.4 6,7 SANTEL 16 BELL $e^+e^- \rightarrow \Upsilon(1S, 2S, 3S)\pi^+\pi^-$
 46 + 9 8,9 CHEN 10 BELL $e^+e^- \rightarrow$ hadrons
 30.7 + 8.3 ± 3.1 10 CHEN 10 BELL $e^+e^- \rightarrow \Upsilon(1S, 2S, 3S)\pi^+\pi^-$
 43 ± 4 8 AUBERT 09E BABR $e^+e^- \rightarrow$ hadrons
 74 ± 4 11 AUBERT 09E BABR $e^+e^- \rightarrow$ hadrons
 112 ± 17 ± 23 12 BESSON 85 CLEO $e^+e^- \rightarrow$ hadrons
 110 ± 15 13 LOVELOCK 85 CUSB $e^+e^- \rightarrow$ hadrons

¹ From a simultaneous fit to the $\Upsilon(nS)\pi^+\pi^-$, $n = 1, 2, 3$, cross sections at 28 energy points within $\sqrt{s} = 10.6\text{--}11.05$ GeV, including the initial-state radiation at $\Upsilon(10860)$.
² From a simultaneous fit to the $h_b(nP)\pi^+\pi^-$, $n = 1, 2$ cross sections at 22 energy points within $\sqrt{s} = 10.77\text{--}11.02$ GeV to a pair of interfering Breit-Wigner amplitudes modified by phase space factors, with eight resonance parameters (a mass and width for each of $\Upsilon(10860)$ and $\Upsilon(11020)$, a single relative phase, a single relative amplitude, and two overall normalization factors, one for each n). The systematic error estimate is dominated by possible interference with a small nonresonant continuum amplitude.
³ From a fit to the dressed cross sections of AUBERT 09E by BaBar and SANTEL 16 by Belle above 10.68 GeV with a coherent sum of a continuum amplitude and three Breit-Wigner functions with constant widths.
⁴ From a fit to the total hadronic cross sections measured at 60 energy points within $\sqrt{s} = 10.82\text{--}11.05$ GeV to a pair of interfering Breit-Wigner amplitudes and two floating continuum amplitudes with $1/\sqrt{s}$ dependence, one coherent with the resonances and one incoherent, with six resonance parameters (a mass, width, and an amplitude for each of $\Upsilon(10860)$ and $\Upsilon(11020)$, one relative phase, and one decoherence coefficient).
⁵ Not including uncertain and potentially large systematic errors due to assumed continuum amplitude $1/\sqrt{s}$ dependence and related interference contributions.
⁶ From a simultaneous fit to the $\Upsilon(nS)\pi^+\pi^-$, $n = 1, 2, 3$, cross sections at 25 energy points within $\sqrt{s} = 10.6\text{--}11.05$ GeV to a pair of interfering Breit-Wigner amplitudes modified by phase space factors, with fourteen resonance parameters (a mass, width, and three amplitudes for each of $\Upsilon(10860)$ and $\Upsilon(11020)$, a single universal relative phase, and three decoherence coefficients, one for each n). Continuum contributions were measured (and therefore fixed) to be zero.
⁷ Superseded by MIZUK 19.
⁸ In a model where a flat non-resonant $b\bar{b}$ -continuum is incoherently added to a second flat component interfering with two Breit-Wigner resonances. Systematic uncertainties not estimated.
⁹ The parameters of the $\Upsilon(11020)$ are fixed to those in AUBERT 09E.
¹⁰ In a model where a flat nonresonant $\Upsilon(1S, 2S, 3S)\pi^+\pi^-$ continuum interferes with a single Breit-Wigner resonance.
¹¹ In a model where a non-resonant $b\bar{b}$ -continuum represented by a threshold function at $\sqrt{s}=2m_B$ is incoherently added to a flat component interfering with two Breit-Wigner resonances. Not independent of other AUBERT 09E results. Systematic uncertainties not estimated.
¹² Assuming four Gaussians with radiative tails and a single step in R .
¹³ In a coupled-channel model with three resonances and a smooth step in R .

$\Upsilon(10860)$ DECAY MODES

Mode	Fraction (Γ_i/Γ)	Confidence level
Γ_1 $B\bar{B}X$	(76.2 + 2.7 - 4.0) %	
Γ_2 $B\bar{B}$	(5.5 ± 1.0) %	
Γ_3 $B\bar{B}^* +$ c.c.	(13.7 ± 1.6) %	
Γ_4 $B^*\bar{B}^*$	(38.1 ± 3.4) %	
Γ_5 $B\bar{B}^*(*)\pi$	< 19.7 %	90%
Γ_6 $B\bar{B}\pi$	(0.0 ± 1.2) %	
Γ_7 $B^*\bar{B}\pi + B\bar{B}^*\pi$	(7.3 ± 2.3) %	
Γ_8 $B^*\bar{B}^*\pi$	(1.0 ± 1.4) %	
Γ_9 $B\bar{B}\pi\pi$	< 8.9 %	90%
Γ_{10} $B_s^{(*)}\bar{B}_s^{(*)}$	(20.1 ± 3.1) %	
Γ_{11} $B_s\bar{B}_s$	(5 ± 5) × 10 ⁻³	
Γ_{12} $B_s\bar{B}_s^* +$ c.c.	(1.35 ± 0.32) %	
Γ_{13} $B_s^*\bar{B}_s^*$	(17.6 ± 2.7) %	
Γ_{14} no open-bottom	(3.8 + 5.0 - 0.5) %	
Γ_{15} e^+e^-	(8.3 ± 2.1) × 10 ⁻⁶	
Γ_{16} $K^*(892)^0\bar{K}^0$	< 1.0 × 10 ⁻⁵	90%
Γ_{17} $\Upsilon(1S)\pi^+\pi^-$	(5.3 ± 0.6) × 10 ⁻³	
Γ_{18} $\Upsilon(1S)\eta$	(8.5 ± 1.7) × 10 ⁻⁴	
Γ_{19} $\Upsilon(1S)\eta'$	< 6.9 × 10 ⁻⁵	90%
Γ_{20} $\Upsilon(2S)\pi^+\pi^-$	(7.8 ± 1.3) × 10 ⁻³	
Γ_{21} $\Upsilon(2S)\eta$	(4.1 ± 0.6) × 10 ⁻³	

Meson Particle Listings

 $\Upsilon(10860)$

Γ_{22}	$\Upsilon(3S)\pi^+\pi^-$	$(4.8^{+1.9}_{-1.7}) \times 10^{-3}$	
Γ_{23}	$\Upsilon(1S)K^+K^-$	$(6.1 \pm 1.8) \times 10^{-4}$	
Γ_{24}	$\eta \Upsilon_J(1D)$	$(4.8 \pm 1.1) \times 10^{-3}$	
Γ_{25}	$h_b(1P)\pi^+\pi^-$	$(3.5^{+1.0}_{-1.3}) \times 10^{-3}$	
Γ_{26}	$h_b(2P)\pi^+\pi^-$	$(5.7^{+1.7}_{-2.1}) \times 10^{-3}$	
Γ_{27}	$\chi_{bJ}(1P)\pi^+\pi^-\pi^0$	$(2.5 \pm 2.3) \times 10^{-3}$	
Γ_{28}	$\chi_{b0}(1P)\pi^+\pi^-\pi^0$	$< 6.3 \times 10^{-3}$	90%
Γ_{29}	$\chi_{b0}(1P)\omega$	$< 3.9 \times 10^{-3}$	90%
Γ_{30}	$\chi_{b0}(1P)(\pi^+\pi^-\pi^0)_{\text{non-}\omega}$	$< 4.8 \times 10^{-3}$	90%
Γ_{31}	$\chi_{b1}(1P)\pi^+\pi^-\pi^0$	$(1.85 \pm 0.33) \times 10^{-3}$	
Γ_{32}	$\chi_{b1}(1P)\omega$	$(1.57 \pm 0.30) \times 10^{-3}$	
Γ_{33}	$\chi_{b1}(1P)(\pi^+\pi^-\pi^0)_{\text{non-}\omega}$	$(5.2 \pm 1.9) \times 10^{-4}$	
Γ_{34}	$\chi_{b2}(1P)\pi^+\pi^-\pi^0$	$(1.17 \pm 0.30) \times 10^{-3}$	
Γ_{35}	$\chi_{b2}(1P)\omega$	$(6.0 \pm 2.7) \times 10^{-4}$	
Γ_{36}	$\chi_{b2}(1P)(\pi^+\pi^-\pi^0)_{\text{non-}\omega}$	$(6 \pm 4) \times 10^{-4}$	
Γ_{37}	$\gamma \chi_b \rightarrow \gamma \Upsilon(1S)\omega$	$< 3.8 \times 10^{-5}$	90%
Γ_{38}	$\eta_b(1S)\omega$	$< 1.3 \times 10^{-3}$	90%
Γ_{39}	$\eta_b(2S)\omega$	$< 5.6 \times 10^{-3}$	90%

Inclusive Decays.

These decay modes are submodes of one or more of the decay modes above.

Γ_{40}	ϕ anything	$(13.8^{+2.4}_{-1.7})\%$
Γ_{41}	D^0 anything + c.c.	$(108 \pm 8)\%$
Γ_{42}	D_s anything + c.c.	$(46 \pm 6)\%$
Γ_{43}	J/ψ anything	$(2.06 \pm 0.21)\%$
Γ_{44}	B^0 anything + c.c.	$(77 \pm 8)\%$
Γ_{45}	B^+ anything + c.c.	$(72 \pm 6)\%$

 $\Upsilon(10860)$ PARTIAL WIDTHS

$\Gamma(e^+e^-)$				Γ_{15}
VALUE (keV)	DOCUMENT ID	TECN	COMMENT	
0.31 ± 0.07 OUR AVERAGE	Error includes scale factor of 1.3.			
$0.22 \pm 0.05 \pm 0.07$	BESSON	85	CLEO $e^+e^- \rightarrow$ hadrons	
0.365 ± 0.070	LOVELOCK	85	CUSB $e^+e^- \rightarrow$ hadrons	

$\Gamma(e^+e^-) \times \Gamma(\Upsilon(1S)\pi^+\pi^-)/\Gamma_{\text{total}}$				$\Gamma_{15}\Gamma_{17}/\Gamma$
VALUE (eV)	DOCUMENT ID	TECN	COMMENT	
1.09 ± 0.34	^{1,2} MIZUK	19	BELL $e^+e^- \rightarrow \Upsilon(nS)\pi^+\pi^-$	

¹ From a simultaneous fit to the $\Upsilon(nS)\pi^+\pi^-$, $n = 1, 2, 3$, cross sections at 28 energy points within $\sqrt{s} = 10.6\text{--}11.05$ GeV, including the initial-state radiation at $\Upsilon(10860)$.
² Reported as the range 0.75–1.43 eV obtained from multiple solutions of an amplitude fit within a model composed as a sum of Breit-Wigner functions.

$\Gamma(e^+e^-) \times \Gamma(\Upsilon(2S)\pi^+\pi^-)/\Gamma_{\text{total}}$				$\Gamma_{15}\Gamma_{20}/\Gamma$
VALUE (eV)	DOCUMENT ID	TECN	COMMENT	
2.58 ± 1.22	^{1,2} MIZUK	19	BELL $e^+e^- \rightarrow \Upsilon(nS)\pi^+\pi^-$	

¹ From a simultaneous fit to the $\Upsilon(nS)\pi^+\pi^-$, $n = 1, 2, 3$, cross sections at 28 energy points within $\sqrt{s} = 10.6\text{--}11.05$ GeV, including the initial-state radiation at $\Upsilon(10860)$.
² Reported as the range 1.35–3.80 eV obtained from multiple solutions of an amplitude fit within a model composed as a sum of Breit-Wigner functions.

$\Gamma(e^+e^-) \times \Gamma(\Upsilon(3S)\pi^+\pi^-)/\Gamma_{\text{total}}$				$\Gamma_{15}\Gamma_{22}/\Gamma$
VALUE (eV)	DOCUMENT ID	TECN	COMMENT	
0.73 ± 0.30	^{1,2} MIZUK	19	BELL $e^+e^- \rightarrow \Upsilon(nS)\pi^+\pi^-$	

¹ From a simultaneous fit to the $\Upsilon(nS)\pi^+\pi^-$, $n = 1, 2, 3$, cross sections at 28 energy points within $\sqrt{s} = 10.6\text{--}11.05$ GeV, including the initial-state radiation at $\Upsilon(10860)$.
² Reported as the range 0.43–1.03 eV obtained from multiple solutions of an amplitude fit within a model composed as a sum of Breit-Wigner functions.

 $\Upsilon(10860)$ BRANCHING RATIOS

"OUR EVALUATION" is obtained based on averages of rescaled data listed below. The averages and scaling were performed by the Heavy Flavor Averaging Group (HFLAV) and are described at <https://hflav.web.cern.ch/>.

$\Gamma(B\bar{B}X)/\Gamma_{\text{total}}$				Γ_1/Γ
VALUE	EVTS	DOCUMENT ID	TECN	COMMENT
$0.762^{+0.027}_{-0.043}$ OUR EVALUATION				
0.71 ± 0.06 OUR AVERAGE				
$0.737 \pm 0.032 \pm 0.051$	1063	¹ DRUTSKOY	10	BELL $\Upsilon(5S) \rightarrow B^+X, B^0X$
$0.589 \pm 0.100 \pm 0.092$		² HUANG	07	CLEO $\Upsilon(5S) \rightarrow$ hadrons

¹ Not independent of DRUTSKOY 10 values for $\Upsilon(5S) \rightarrow B^{\pm,0}$ anything.

² Using measurements or limits from AQUINES 06.

$\Gamma(B\bar{B})/\Gamma_{\text{total}}$				Γ_2/Γ
VALUE (units 10^{-2})	CL%	DOCUMENT ID	TECN	COMMENT
$5.5^{+1.0}_{-0.9} \pm 0.4$		¹ DRUTSKOY	10	BELL $\Upsilon(5S) \rightarrow B^+X, B^0X$

• • • We do not use the following data for averages, fits, limits, etc. • • •

<13.8 90 ²HUANG 07 CLEO $\Upsilon(5S) \rightarrow$ hadrons

¹ Assuming isospin conservation.

² Using measurements or limits from AQUINES 06.

$\Gamma(B\bar{B})/\Gamma(B\bar{B}X)$				Γ_2/Γ_1
VALUE	CL%	DOCUMENT ID	TECN	COMMENT
<0.22	90	AQUINES	06	CLE3 $\Upsilon(5S) \rightarrow$ hadrons

$\Gamma(B\bar{B}^* + \text{c.c.})/\Gamma_{\text{total}}$				Γ_3/Γ
VALUE	CL%	DOCUMENT ID	TECN	COMMENT
0.137 ± 0.016 OUR AVERAGE				
$0.137 \pm 0.013 \pm 0.011$		¹ DRUTSKOY	10	BELL $\Upsilon(5S) \rightarrow B^+X, B^0X$
$0.143 \pm 0.053 \pm 0.027$		² HUANG	07	CLEO $\Upsilon(5S) \rightarrow$ hadrons

¹ Assuming isospin conservation.

² Using measurements or limits from AQUINES 06.

$\Gamma(B\bar{B}^* + \text{c.c.})/\Gamma(B\bar{B}X)$				Γ_3/Γ_1
VALUE	EVTS	DOCUMENT ID	TECN	COMMENT
$0.24 \pm 0.09 \pm 0.03$	10	AQUINES	06	CLE3 $\Upsilon(5S) \rightarrow$ hadrons

$\Gamma(B^*\bar{B}^*)/\Gamma_{\text{total}}$				Γ_4/Γ
VALUE	CL%	DOCUMENT ID	TECN	COMMENT
0.381 ± 0.034 OUR AVERAGE				
$0.375^{+0.021}_{-0.019} \pm 0.030$		¹ DRUTSKOY	10	BELL $\Upsilon(5S) \rightarrow B^+X, B^0X$
$0.436 \pm 0.083 \pm 0.072$		² HUANG	07	CLEO $\Upsilon(5S) \rightarrow$ hadrons

¹ Assuming isospin conservation.

² Using measurements or limits from AQUINES 06.

$\Gamma(B^*\bar{B}^*)/\Gamma(B\bar{B}X)$				Γ_4/Γ_1
VALUE	EVTS	DOCUMENT ID	TECN	COMMENT
$0.74 \pm 0.15 \pm 0.08$	31	AQUINES	06	CLE3 $\Upsilon(5S) \rightarrow$ hadrons

$\Gamma(B\bar{B}^*(\pi))/\Gamma_{\text{total}}$				Γ_5/Γ
VALUE	CL%	DOCUMENT ID	TECN	COMMENT
<0.197	90	¹ HUANG	07	CLEO $\Upsilon(5S) \rightarrow$ hadrons

¹ Using measurements or limits from AQUINES 06.

$\Gamma(B\bar{B}^*(\pi))/\Gamma(B\bar{B}X)$				Γ_5/Γ_1
VALUE	CL%	DOCUMENT ID	TECN	COMMENT
<0.32	90	AQUINES	06	CLE3 $\Upsilon(5S) \rightarrow$ hadrons

¹ Assuming isospin conservation.

$\Gamma(B\bar{B}\pi)/\Gamma_{\text{total}}$				Γ_6/Γ
VALUE (units 10^{-2})	EVTS	DOCUMENT ID	TECN	COMMENT
$0.0 \pm 1.2 \pm 0.3$	0	¹ DRUTSKOY	10	BELL $\Upsilon(5S) \rightarrow B^+,^0\pi^-X$

¹ Assuming isospin conservation.

$[\Gamma(B^*\bar{B}\pi) + \Gamma(B\bar{B}^*\pi)]/\Gamma_{\text{total}}$				Γ_7/Γ
VALUE (units 10^{-2})	EVTS	DOCUMENT ID	TECN	COMMENT
$7.3^{+2.3}_{-2.1} \pm 0.8$	38	¹ DRUTSKOY	10	BELL $\Upsilon(5S) \rightarrow B^+,^0\pi^-X$

¹ Assuming isospin conservation.

$\Gamma(B^*\bar{B}^*\pi)/\Gamma_{\text{total}}$				Γ_8/Γ
VALUE (units 10^{-2})	EVTS	DOCUMENT ID	TECN	COMMENT
$1.0^{+1.4}_{-1.3} \pm 0.4$	5	¹ DRUTSKOY	10	BELL $\Upsilon(5S) \rightarrow B^+,^0\pi^-X$

¹ Assuming isospin conservation.

$\Gamma(B\bar{B}\pi\pi)/\Gamma_{\text{total}}$				Γ_9/Γ
VALUE	CL%	DOCUMENT ID	TECN	COMMENT
<0.089	90	¹ HUANG	07	CLEO $\Upsilon(5S) \rightarrow$ hadrons

¹ Using measurements or limits from AQUINES 06.

$\Gamma(B\bar{B}\pi\pi)/\Gamma(B\bar{B}X)$				Γ_9/Γ_1
VALUE	CL%	DOCUMENT ID	TECN	COMMENT
<0.14	90	AQUINES	06	CLE3 $\Upsilon(5S) \rightarrow$ hadrons

¹ Using measurements or limits from AQUINES 06.

$\Gamma(B\bar{B}\pi\pi)/\Gamma(B\bar{B}X)$				Γ_9/Γ_1
VALUE	CL%	DOCUMENT ID	TECN	COMMENT
<0.14	90	AQUINES	06	CLE3 $\Upsilon(5S) \rightarrow$ hadrons

$\Gamma(B_s^{(*)}\bar{B}_s^{(*)})/\Gamma_{\text{total}}$				$\Gamma_{10}/\Gamma = (\Gamma_{11} + \Gamma_{12} + \Gamma_{13})/\Gamma$
VALUE	CL%	DOCUMENT ID	TECN	COMMENT
$0.201^{+0.030}_{-0.031}$ OUR EVALUATION				
$0.189^{+0.027}_{-0.021}$ OUR AVERAGE				

¹ ESEN 13 BELL $\Upsilon(5S) \rightarrow D^0X, D_sX$

² HUANG 07 CLEO $\Upsilon(5S) \rightarrow D_sX$

• • • We do not use the following data for averages, fits, limits, etc. • • •

0.172 ± 0.030

$0.21^{+0.06}_{-0.03}$

$0.180 \pm 0.013 \pm 0.032$

$0.160 \pm 0.026 \pm 0.058$

³ DRUTSKOY 07 BELL $\Upsilon(5S) \rightarrow D^0X, D_sX$

⁴ ARTUSO 05B CLEO $e^+e^- \rightarrow D_X X$

Meson Particle Listings
 $\Upsilon(10860)$

¹Supersedes DRUTSKOY 07.

²Supersedes ARTUSO 05B. Combining inclusive ϕ , D_S , and B measurements. Using $B(D_S^+ \rightarrow \phi\pi^+) = 4.4 \pm 0.6\%$ from PDG 06.

³Using $B(D_S^+ \rightarrow \phi\pi^+) = (4.4 \pm 0.6)\%$ from PDG 06.

⁴Uses a model-dependent estimate $B(B_S \rightarrow D_S X) = (92 \pm 11)\%$.

$\Gamma(B_S^{(*)}\bar{B}_S^{(*)})/\Gamma(B\bar{B}X)$		Γ_{10}/Γ_1	
VALUE	DOCUMENT ID	TECN	COMMENT
0.264 ± 0.052			OUR EVALUATION
0.264 ± 0.052			OUR EVALUATION

$\Gamma(B_S^{(*)}\bar{B}_S^{(*)})/\Gamma(B_S^{(*)}\bar{B}_S^{(*)})$		$\Gamma_{13}/\Gamma_{10} = \Gamma_{13}/(\Gamma_{11}+\Gamma_{12}+\Gamma_{13})$	
VALUE (units 10^{-2})	EVTS	DOCUMENT ID	TECN COMMENT
87.8 ± 1.5	OUR AVERAGE		
87.0 ± 1.7	1,2	ESEN 13	BELL $B_S^0 \rightarrow D_S^- \pi^+$
90.5 ± 3.2 ± 0.1	227	2,3	LI 12 BELL $B_S^0 \rightarrow J/\psi \eta^{(\prime)}$
• • • We do not use the following data for averages, fits, limits, etc. • • •			
90.1 ± 3.8 ± 0.2	4	LOUVOT 09	BELL 10.86 $e^+e^- \rightarrow B_S^{(*)}\bar{B}_S^{(*)}$
93 ± 7 ± 1	4	DRUTSKOY 07A	BELL Superseded by LOUVOT 09

¹Supersedes LOUVOT 09.

²With $N(B_S^{(*)}\bar{B}_S^{(*)}) = (7.11 \pm 1.30) \times 10^6$.

³The ratios $N(B_S^{(*)}\bar{B}_S^{(*)})/N(B_S^{(*)}\bar{B}_S^{(*)})$ and $N(B_S^{(*)}\bar{B}_S^{(*)})/N(B_S^{(*)}\bar{B}_S^{(*)})$ are measured with a correlation coefficient of -0.72 .

⁴From a measurement of $\sigma(e^+e^- \rightarrow B_S^{(*)}\bar{B}_S^{(*)})/\sigma(e^+e^- \rightarrow B_S^{(*)}\bar{B}_S^{(*)})$ at $\sqrt{s} = 10.86$ GeV.

$\Gamma(B_S\bar{B}_S)/\Gamma(B_S^{(*)}\bar{B}_S^{(*)})$		$\Gamma_{11}/\Gamma_{10} = \Gamma_{11}/(\Gamma_{11}+\Gamma_{12}+\Gamma_{13})$	
VALUE (units 10^{-2})	DOCUMENT ID	TECN	COMMENT
2.6 ± 2.6	LOUVOT 09	BELL	10.86 $e^+e^- \rightarrow B_S^{(*)}\bar{B}_S^{(*)}$

$\Gamma(B_S\bar{B}_S)/\Gamma(B_S^{(*)}\bar{B}_S^{(*)})$		Γ_{11}/Γ_{13}	
VALUE	CL%	DOCUMENT ID	TECN COMMENT
<0.16	90	BONVICINI 06	CLE3 e^+e^-

$\Gamma(B_S\bar{B}_S + c.c.)/\Gamma(B_S^{(*)}\bar{B}_S^{(*)})$		$\Gamma_{12}/\Gamma_{10} = \Gamma_{12}/(\Gamma_{11}+\Gamma_{12}+\Gamma_{13})$	
VALUE (units 10^{-2})	EVTS	DOCUMENT ID	TECN COMMENT
6.7 ± 1.2	OUR AVERAGE		
7.3 ± 1.4	1,2	ESEN 13	BELL $B_S^0 \rightarrow D_S^- \pi^+$
4.9 ± 2.5 ± 0.0	227	2,3	LI 12 BELL $B_S^0 \rightarrow J/\psi \eta^{(\prime)}$
• • • We do not use the following data for averages, fits, limits, etc. • • •			
7.3 ± 3.3 ± 0.1		LOUVOT 09	BELL 10.86 $e^+e^- \rightarrow B_S^{(*)}\bar{B}_S^{(*)}$

¹Supersedes LOUVOT 09.

²With $N(B_S^{(*)}\bar{B}_S^{(*)}) = (7.11 \pm 1.30) \times 10^6$.

³The ratios $N(B_S^{(*)}\bar{B}_S^{(*)})/N(B_S^{(*)}\bar{B}_S^{(*)})$ and $N(B_S^{(*)}\bar{B}_S^{(*)})/N(B_S^{(*)}\bar{B}_S^{(*)})$ are measured with a correlation coefficient of -0.72 .

$\Gamma(B_S\bar{B}_S + c.c.)/\Gamma(B_S^{(*)}\bar{B}_S^{(*)})$		Γ_{12}/Γ_{13}	
VALUE	CL%	DOCUMENT ID	TECN COMMENT
<0.16	90	BONVICINI 06	CLE3 e^+e^-

$\Gamma(\text{no open-bottom})/\Gamma_{\text{total}}$		Γ_{14}/Γ	
VALUE	DOCUMENT ID	TECN	COMMENT
0.038 ± 0.051			OUR EVALUATION
0.038 ± 0.051			OUR EVALUATION

$\Gamma(K^*(892)^0\bar{K}^0)/\Gamma_{\text{total}}$		Γ_{16}/Γ	
VALUE	CL%	DOCUMENT ID	TECN COMMENT
$<1.0 \times 10^{-5}$	90	SHEN 13A	BELL $e^+e^- \rightarrow K^*(892)^0\bar{K}^0$

$\Gamma(\eta\tau_J(1D))/\Gamma_{\text{total}}$		Γ_{24}/Γ	
VALUE (units 10^{-3})	DOCUMENT ID	TECN	COMMENT
$4.82 \pm 0.92 \pm 0.67$	1	TAMPONI 18	BELL $e^+e^- \rightarrow \Upsilon(5S) \rightarrow \eta X$
¹ Mainly $J = 2$, assumes no continuum contribution under $\Upsilon(5S)$.			

$\Gamma(\Upsilon(1S)\pi^+\pi^-)/\Gamma_{\text{total}}$		Γ_{17}/Γ	
VALUE (units 10^{-3})	EVTS	DOCUMENT ID	TECN COMMENT
$5.3 \pm 0.3 \pm 0.5$	325	1	CHEN 08 BELL 10.87 $e^+e^- \rightarrow \Upsilon(1S)\pi^+\pi^-$
¹ Assuming that the observed events are solely due to the $\Upsilon(5S)$ resonance.			

$\Gamma(\Upsilon(1S)\eta)/\Gamma_{\text{total}}$		Γ_{18}/Γ	
VALUE (units 10^{-3})	DOCUMENT ID	TECN	COMMENT
$0.85 \pm 0.15 \pm 0.08$	1,2	KOVALENKO 21	BELL $e^+e^- \rightarrow \Upsilon(5S)$
¹ Assuming that the observed events are solely due to the $\Upsilon(5S)$ resonance.			
² Using a data sample of 118.3 fb^{-1} of e^+e^- collisions at $\sqrt{s} = 10.866$ GeV.			

$\Gamma(\Upsilon(1S)\eta')/\Gamma_{\text{total}}$		Γ_{19}/Γ	
VALUE	CL%	DOCUMENT ID	TECN COMMENT
$<6.9 \times 10^{-5}$	90	1,2	KOVALENKO 21 BELL $e^+e^- \rightarrow \Upsilon(5S)$

¹Assuming that the observed events are solely due to the $\Upsilon(5S)$ resonance.

²Using a data sample of 118.3 fb^{-1} of e^+e^- collisions at $\sqrt{s} = 10.866$ GeV.

$\Gamma(\Upsilon(2S)\pi^+\pi^-)/\Gamma_{\text{total}}$		Γ_{20}/Γ	
VALUE (units 10^{-3})	EVTS	DOCUMENT ID	TECN COMMENT
$7.8 \pm 0.6 \pm 1.1$	186	1	CHEN 08 BELL 10.87 $e^+e^- \rightarrow \Upsilon(2S)\pi^+\pi^-$
¹ Assuming that the observed events are solely due to the $\Upsilon(5S)$ resonance.			

$\Gamma(\Upsilon(2S)\eta)/\Gamma_{\text{total}}$		Γ_{21}/Γ	
VALUE (units 10^{-3})	DOCUMENT ID	TECN	COMMENT
$4.13 \pm 0.41 \pm 0.37$	1,2	KOVALENKO 21	BELL $e^+e^- \rightarrow \Upsilon(5S)$
¹ Assuming that the observed events are solely due to the $\Upsilon(5S)$ resonance.			
² Using a data sample of 118.3 fb^{-1} of e^+e^- collisions at $\sqrt{s} = 10.866$ GeV.			

$\Gamma(\Upsilon(3S)\pi^+\pi^-)/\Gamma_{\text{total}}$		Γ_{22}/Γ	
VALUE (units 10^{-3})	EVTS	DOCUMENT ID	TECN COMMENT
$4.8 \pm 1.8 \pm 0.7$	10	1	CHEN 08 BELL 10.87 $e^+e^- \rightarrow \Upsilon(3S)\pi^+\pi^-$
¹ Assuming that the observed events are solely due to the $\Upsilon(5S)$ resonance.			

$\Gamma(\Upsilon(1S)K^+K^-)/\Gamma_{\text{total}}$		Γ_{23}/Γ	
VALUE (units 10^{-4})	EVTS	DOCUMENT ID	TECN COMMENT
$6.1 \pm 1.6 \pm 1.0$	20	1	CHEN 08 BELL 10.87 $e^+e^- \rightarrow \Upsilon(1S)K^+K^-$
¹ Assuming that the observed events are solely due to the $\Upsilon(5S)$ resonance.			

$\Gamma(h_b(1P)\pi^+\pi^-)/\Gamma(\Upsilon(2S)\pi^+\pi^-)$		Γ_{25}/Γ_{20}	
VALUE	DOCUMENT ID	TECN	COMMENT
$0.45 \pm 0.08 \pm 0.07$	ADACHI 12	BELL	10.86 $e^+e^- \rightarrow$ hadrons

$\Gamma(h_b(2P)\pi^+\pi^-)/\Gamma(\Upsilon(2S)\pi^+\pi^-)$		Γ_{26}/Γ_{20}	
VALUE	DOCUMENT ID	TECN	COMMENT
$0.77 \pm 0.08 \pm 0.22$	ADACHI 12	BELL	10.86 $e^+e^- \rightarrow$ hadrons

$\Gamma(h_b(1P)\pi^+\pi^-)/\Gamma(h_b(2P)\pi^+\pi^-)$		Γ_{25}/Γ_{26}	
VALUE	DOCUMENT ID	TECN	COMMENT
$0.616 \pm 0.052 \pm 0.017$	MIZUK 16	BELL	$e^+e^- \rightarrow h_b(1P, 2P)\pi^+\pi^-$

$\Gamma(\chi_{bJ}(1P)\pi^+\pi^-\pi^0)/\Gamma_{\text{total}}$		Γ_{27}/Γ	
VALUE (units 10^{-3})	DOCUMENT ID	TECN	COMMENT
$2.5 \pm 0.6 \pm 2.2$	YIN 18	BELL	$e^+e^- \rightarrow$ hadrons

$\Gamma(\chi_{b0}(1P)\pi^+\pi^-\pi^0)/\Gamma_{\text{total}}$		Γ_{28}/Γ	
VALUE	CL%	DOCUMENT ID	TECN COMMENT
$<6.3 \times 10^{-3}$	90	1	HE 14 BELL $\Upsilon(5S) \rightarrow \pi^+\pi^-\pi^0\gamma \Upsilon(1S)$
¹ Assuming that all the $b\bar{b}$ events are from $\Upsilon(5S)$ resonance decays and using $\sigma(e^+e^- \rightarrow b\bar{b}) = 0.340 \pm 0.016$ nb from ESEN 13. Correlated with other results from HE 14.			

$\Gamma(\chi_{b0}(1P)\omega)/\Gamma_{\text{total}}$		Γ_{29}/Γ	
VALUE	CL%	DOCUMENT ID	TECN COMMENT
$<3.9 \times 10^{-3}$	90	1	HE 14 BELL $\Upsilon(5S) \rightarrow \pi^+\pi^-\pi^0\gamma \Upsilon(1S)$
¹ Assuming that all the $b\bar{b}$ events are from $\Upsilon(5S)$ resonance decays and using $\sigma(e^+e^- \rightarrow b\bar{b}) = 0.340 \pm 0.016$ nb from ESEN 13. Correlated with other results from HE 14.			

$\Gamma(\chi_{b0}(1P)(\pi^+\pi^-\pi^0)_{\text{non-}\omega})/\Gamma_{\text{total}}$		Γ_{30}/Γ	
VALUE	CL%	DOCUMENT ID	TECN COMMENT
$<4.8 \times 10^{-3}$	90	1	HE 14 BELL $\Upsilon(5S) \rightarrow \pi^+\pi^-\pi^0\gamma \Upsilon(1S)$
¹ Assuming that all the $b\bar{b}$ events are from $\Upsilon(5S)$ resonance decays and using $\sigma(e^+e^- \rightarrow b\bar{b}) = 0.340 \pm 0.016$ nb from ESEN 13. Correlated with other results from HE 14.			

$\Gamma(\chi_{b1}(1P)\pi^+\pi^-\pi^0)/\Gamma_{\text{total}}$		Γ_{31}/Γ	
VALUE (units 10^{-3})	EVTS	DOCUMENT ID	TECN COMMENT
$1.85 \pm 0.23 \pm 0.23$	80	1	HE 14 BELL $\Upsilon(5S) \rightarrow \pi^+\pi^-\pi^0\gamma \Upsilon(1S)$
¹ Assuming that all the $b\bar{b}$ events are from $\Upsilon(5S)$ resonance decays and using $\sigma(e^+e^- \rightarrow b\bar{b}) = 0.340 \pm 0.016$ nb from ESEN 13. Correlated with other results from HE 14.			

$\Gamma(\chi_{b1}(1P)\omega)/\Gamma_{\text{total}}$		Γ_{32}/Γ	
VALUE (units 10^{-3})	EVTS	DOCUMENT ID	TECN COMMENT
$1.57 \pm 0.22 \pm 0.21$	60	1	HE 14 BELL $\Upsilon(5S) \rightarrow \pi^+\pi^-\pi^0\gamma \Upsilon(1S)$
¹ Assuming that all the $b\bar{b}$ events are from $\Upsilon(5S)$ resonance decays and using $\sigma(e^+e^- \rightarrow b\bar{b}) = 0.340 \pm 0.016$ nb from ESEN 13. Correlated with other results from HE 14.			

Meson Particle Listings

$\Upsilon(10860), \Upsilon(11020)$

$\Gamma(\chi_{b1}(1P)(\pi^+\pi^-\pi^0)_{\text{non-}\omega})/\Gamma_{\text{total}}$ Γ_{33}/Γ

VALUE (units 10^{-3})	EVTS	DOCUMENT ID	TECN	COMMENT
$0.52 \pm 0.15 \pm 0.11$	24	¹ HE	14	BELL $\Upsilon(5S) \rightarrow \pi^+\pi^-\pi^0\gamma \Upsilon(1S)$

¹ Assuming that all the $b\bar{b}$ events are from $\Upsilon(5S)$ resonance decays and using $\sigma(e^+e^- \rightarrow b\bar{b}) = 0.340 \pm 0.016$ nb from ESEN 13. Correlated with other results from HE 14.

$\Gamma(\chi_{b2}(1P)\pi^+\pi^-\pi^0)/\Gamma_{\text{total}}$ Γ_{34}/Γ

VALUE (units 10^{-3})	EVTS	DOCUMENT ID	TECN	COMMENT
$1.17 \pm 0.27 \pm 0.14$	29	¹ HE	14	BELL $\Upsilon(5S) \rightarrow \pi^+\pi^-\pi^0\gamma \Upsilon(1S)$

¹ Assuming that all the $b\bar{b}$ events are from $\Upsilon(5S)$ resonance decays and using $\sigma(e^+e^- \rightarrow b\bar{b}) = 0.340 \pm 0.016$ nb from ESEN 13. Correlated with other results from HE 14.

$\Gamma(\chi_{b2}(1P)\omega)/\Gamma_{\text{total}}$ Γ_{35}/Γ

VALUE (units 10^{-3})	EVTS	DOCUMENT ID	TECN	COMMENT
$0.60 \pm 0.23 \pm 0.15$	13	¹ HE	14	BELL $\Upsilon(5S) \rightarrow \pi^+\pi^-\pi^0\gamma \Upsilon(1S)$

¹ Assuming that all the $b\bar{b}$ events are from $\Upsilon(5S)$ resonance decays and using $\sigma(e^+e^- \rightarrow b\bar{b}) = 0.340 \pm 0.016$ nb from ESEN 13. Correlated with other results from HE 14.

$\Gamma(\chi_{b2}(1P)\omega)/\Gamma(\chi_{b1}(1P)\omega)$ Γ_{35}/Γ_{32}

VALUE	DOCUMENT ID	TECN	COMMENT
-------	-------------	------	---------

••• We do not use the following data for averages, fits, limits, etc. •••

$0.38 \pm 0.16 \pm 0.09$	¹ HE	14	BELL $\Upsilon(5S) \rightarrow \pi^+\pi^-\pi^0\gamma \Upsilon(1S)$
--------------------------	-----------------	----	--

¹ Accounting for correlated systematics.

$\Gamma(\chi_{b2}(1P)(\pi^+\pi^-\pi^0)_{\text{non-}\omega})/\Gamma_{\text{total}}$ Γ_{36}/Γ

VALUE (units 10^{-3})	EVTS	DOCUMENT ID	TECN	COMMENT
$0.61 \pm 0.22 \pm 0.28$	16	¹ HE	14	BELL $\Upsilon(5S) \rightarrow \pi^+\pi^-\pi^0\gamma \Upsilon(1S)$

¹ Assuming that all the $b\bar{b}$ events are from $\Upsilon(5S)$ resonance decays and using $\sigma(e^+e^- \rightarrow b\bar{b}) = 0.340 \pm 0.016$ nb from ESEN 13. Correlated with other results from HE 14.

$\Gamma(\chi_{b2}(1P)(\pi^+\pi^-\pi^0)_{\text{non-}\omega})/\Gamma(\chi_{b1}(1P)(\pi^+\pi^-\pi^0)_{\text{non-}\omega})$ Γ_{36}/Γ_{33}

VALUE	DOCUMENT ID	TECN	COMMENT
-------	-------------	------	---------

••• We do not use the following data for averages, fits, limits, etc. •••

$1.20 \pm 0.55 \pm 0.65$	¹ HE	14	BELL $\Upsilon(5S) \rightarrow \pi^+\pi^-\pi^0\gamma \Upsilon(1S)$
--------------------------	-----------------	----	--

¹ Accounting for correlated systematics.

$\Gamma(\eta_b(1S)\omega)/\Gamma_{\text{total}}$ Γ_{38}/Γ

VALUE	CL%	DOCUMENT ID	TECN	COMMENT
$< 1.3 \times 10^{-3}$	90	¹ OSKIN	20	BELL $e^+e^- \rightarrow \omega X$

¹ Using $\sigma_{b\bar{b}} = 0.340 \pm 0.016$ nb from TAMPONI 15.

$\Gamma(\eta_b(2S)\omega)/\Gamma_{\text{total}}$ Γ_{39}/Γ

VALUE	CL%	DOCUMENT ID	TECN	COMMENT
$< 5.6 \times 10^{-3}$	90	¹ OSKIN	20	BELL $e^+e^- \rightarrow \omega X$

¹ Using $\sigma_{b\bar{b}} = 0.340 \pm 0.016$ nb from TAMPONI 15.

$\Gamma(\gamma X_b \rightarrow \gamma \Upsilon(1S)\omega)/\Gamma_{\text{total}}$ Γ_{37}/Γ

VALUE	CL%	DOCUMENT ID	TECN	COMMENT
$< 3.8 \times 10^{-5}$	90	¹ HE	14	BELL $\Upsilon(5S) \rightarrow \pi^+\pi^-\pi^0\gamma \Upsilon(1S)$

¹ Assuming that all the $b\bar{b}$ events are from $\Upsilon(5S)$ resonance decays and using $\sigma(e^+e^- \rightarrow b\bar{b}) = 0.340 \pm 0.016$ nb from ESEN 13. Correlated with other results from HE 14. For a state X_b with mass between 10.55 GeV/ c^2 and 10.65 GeV/ c^2 , the obtained 90% upper limit as a function of mX_b varies from 2.6×10^{-5} to 3.8×10^{-5} .

$\Gamma(\phi \text{ anything})/\Gamma_{\text{total}}$ Γ_{40}/Γ

VALUE	DOCUMENT ID	TECN	COMMENT
$0.138 \pm 0.007 \pm 0.023$ -0.015	HUANG 07	CLEO	$\Upsilon(5S) \rightarrow \phi X$

$\Gamma(D^0 \text{ anything} + \text{c.c.})/\Gamma_{\text{total}}$ Γ_{41}/Γ

VALUE	DOCUMENT ID	TECN	COMMENT
$1.076 \pm 0.040 \pm 0.068$	DRUTSKOY 07	BELL	$\Upsilon(5S) \rightarrow D^0 X$

$\Gamma(D_s \text{ anything} + \text{c.c.})/\Gamma_{\text{total}}$ Γ_{42}/Γ

VALUE	DOCUMENT ID	TECN	COMMENT
0.46 ± 0.06 OUR AVERAGE			

$0.472 \pm 0.024 \pm 0.072$	¹ DRUTSKOY 07	BELL	$\Upsilon(5S) \rightarrow D_s X$
$0.44 \pm 0.09 \pm 0.04$	² ARTUSO 05B	CLE3	$e^+e^- \rightarrow D_s X$

¹ Using $B(D_s^+ \rightarrow \phi\pi^+) = (4.4 \pm 0.6)\%$ from PDG 06.

² ARTUSO 05B reports $[\Gamma(\Upsilon(10860) \rightarrow D_s \text{ anything} + \text{c.c.})/\Gamma_{\text{total}}] \times [B(D_s^+ \rightarrow \phi\pi^+)] = 0.0198 \pm 0.0019 \pm 0.0038$ which we divide by our best value $B(D_s^+ \rightarrow \phi\pi^+) = (4.5 \pm 0.4) \times 10^{-2}$. Our first error is their experiment's error and our second error is the systematic error from using our best value.

$\Gamma(J/\psi \text{ anything})/\Gamma_{\text{total}}$ Γ_{43}/Γ

VALUE (units 10^{-2})	DOCUMENT ID	TECN	COMMENT
$2.060 \pm 0.160 \pm 0.134$	DRUTSKOY 07	BELL	$\Upsilon(5S) \rightarrow J/\psi X$

$\Gamma(B^0 \text{ anything} + \text{c.c.})/\Gamma_{\text{total}}$ Γ_{44}/Γ

VALUE	EVTS	DOCUMENT ID	TECN	COMMENT
$0.770 \pm 0.058 \pm 0.061$	352	DRUTSKOY 10	BELL	$\Upsilon(5S) \rightarrow B^0 X$

$\Gamma(B^+ \text{ anything} + \text{c.c.})/\Gamma_{\text{total}}$ Γ_{45}/Γ

VALUE	EVTS	DOCUMENT ID	TECN	COMMENT
$0.721 \pm 0.039 \pm 0.050$	711	DRUTSKOY 10	BELL	$\Upsilon(5S) \rightarrow B^+ X$

$\Upsilon(10860)$ REFERENCES

KOVALENKO 21	PR D104 112006	E. Kovalenko et al.	(BELLE Collab.)
DONG 20A	CP C44 083001	X.-K. Dong et al.	(BELLE Collab.)
OSKIN 20	PR D102 092011	P. Oskin et al.	(BELLE Collab.)
MIZUK 19	JHEP 1910 220	R. Mizuk et al.	(BELLE Collab.)
TAMPONI 18	EPJ C78 633	U. Tamponi et al.	(BELLE Collab.)
YIN 18	PR D98 091102	J.H. Yin et al.	(BELLE Collab.)
MIZUK 16	PRL 117 142001	R. Mizuk et al.	(BELLE Collab.)
SANTEL 16	PR D93 011101	D. Santel et al.	(BELLE Collab.)
TAMPONI 15	PRL 115 142001	U. Tamponi et al.	(BELLE Collab.)
HE 14	PRL 113 142001	X.H. He et al.	(BELLE Collab.)
ESEN 13	PR D87 031101	S. Esen et al.	(BELLE Collab.)
SHEN 13A	PR D88 052019	C.P. Shen et al.	(BELLE Collab.)
ADACHI 12	PRL 108 032001	I. Adachi et al.	(BELLE Collab.)
LI 12	PRL 108 181808	J. Li et al.	(BELLE Collab.)
CHEN 10	PR D82 091106	K.-F. Chen et al.	(BELLE Collab.)
DRUTSKOY 09E	PR D81 112003	A. Drutskoy et al.	(BELLE Collab.)
AUBERT 09E	PRL 102 012001	B. Aubert et al.	(BABAR Collab.)
LOUVOT 09	PRL 102 021801	R. Louvot et al.	(BELLE Collab.)
CHEN 08	PR 100 112001	K.-F. Chen et al.	(BELLE Collab.)
DRUTSKOY 07	PRL 98 052001	A. Drutskoy et al.	(BELLE Collab.)
DRUTSKOY 07A	PR D76 012002	A. Drutskoy et al.	(BELLE Collab.)
HUANG 07	PR D75 012002	G.S. Huang et al.	(CLEO Collab.)
AQUINES 06	PRL 96 152001	O. Aquines et al.	(CLEO Collab.)
BONVICINI 06	PRL 96 022002	G. Bonvicini et al.	(CLEO Collab.)
PDG 06	JP G33 1	W.-M. Yao et al.	(PDG Collab.)
ARTUSO 05B	PRL 95 261801	M. Artuso et al.	(CLEO Collab.)
BESSON 85	PRL 54 381	D. Besson et al.	(CLEO Collab.)
LOVELOCK 85	PRL 54 377	D.M.J. Lovelock et al.	(CUSP Collab.)

$\Upsilon(11020)$

$$J^{PC} = 0^{-}(1^{-}-)$$

$\Upsilon(11020)$ MASS

VALUE (MeV)	DOCUMENT ID	TECN	COMMENT
-------------	-------------	------	---------

11000 ± 4 OUR AVERAGE			
$11000.0 \pm 4.0 \pm 1.0$ $-4.5 - 1.3$	¹ MIZUK	19	BELL $e^+e^- \rightarrow \Upsilon(1S, 2S, 3S)\pi^+\pi^-$
$10999.0 \pm 7.3 \pm 16.9$ $-7.8 - 1.0$	² MIZUK	16	BELL $e^+e^- \rightarrow h_b(1P, 2P)\pi^+\pi^-$

••• We do not use the following data for averages, fits, limits, etc. •••

11001 ± 1	³ DONG	20A	$e^+e^- \rightarrow b\bar{b}$
$11003.0 \pm 1.1 \pm 0.9$ -1.0	^{4,5} SANTEL	16	BELL $e^+e^- \rightarrow$ hadrons
$10987.5 \pm 6.4 \pm 9.1$ $-2.5 - 2.3$	^{6,7} SANTEL	16	BELL $e^+e^- \rightarrow \Upsilon(1S, 2S, 3S)\pi^+\pi^-$
10996 ± 2	⁸ AUBERT	09E	BABR $e^+e^- \rightarrow$ hadrons
$11019 \pm 5 \pm 7$	BESSON	85	CLEO $e^+e^- \rightarrow$ hadrons
11020 ± 30	LOVELOCK	85	CUSB $e^+e^- \rightarrow$ hadrons

- From a simultaneous fit to the $\Upsilon(nS)\pi^+\pi^-$, $n = 1, 2, 3$, cross sections at 28 energy points within $\sqrt{s} = 10.6\text{--}11.05$ GeV, including the initial-state radiation at $\Upsilon(10860)$.
- From a simultaneous fit to the $h_b(nP)\pi^+\pi^-$, $n = 1, 2$ cross sections at 22 energy points within $\sqrt{s} = 10.77\text{--}11.02$ GeV to a pair of interfering Breit-Wigner amplitudes modified by phase space factors, with eight resonance parameters (a mass and width for each of $\Upsilon(10860)$ and $\Upsilon(11020)$, a single relative phase, a single relative amplitude, and two overall normalization factors, one for each n). The systematic error estimate is dominated by possible interference with a small nonresonant continuum amplitude.
- From a fit to the dressed cross sections of AUBERT 09E by BaBar and SANTEL 16 by Belle above 10.68 GeV with a coherent sum of a continuum amplitude and three Breit-Wigner functions with constant widths.
- From a fit to the total hadronic cross sections measured at 60 energy points within $\sqrt{s} = 10.82\text{--}11.05$ GeV to a pair of interfering Breit-Wigner amplitudes and two floating continuum amplitudes with $1/\sqrt{s}$ dependence, one coherent with the resonances and one incoherent, with six resonance parameters (a mass, width, and an amplitude for each of $\Upsilon(10860)$ and $\Upsilon(11020)$, one relative phase, and one decoherence coefficient).
- Not including uncertain and potentially large systematic errors due to assumed continuum amplitude $1/\sqrt{s}$ dependence and related interference contributions.
- From a simultaneous fit to the $\Upsilon(nS)\pi^+\pi^-$, $n = 1, 2, 3$, cross sections at 25energy points within $\sqrt{s} = 10.6\text{--}11.05$ GeV to a pair of interfering Breit-Wigner amplitudes modified by phase space factors, with fourteen resonance parameters (a mass, width, and three amplitudes for each of $\Upsilon(10860)$ and $\Upsilon(11020)$, a single universal relative phase, and three decoherence coefficients, one for each n). Continuum contributions were measured (and therefore fixed) to be zero.
- Superseded by MIZUK 19.
- In a model where a flat non-resonant $b\bar{b}$ -continuum is incoherently added to a second flat component interfering with two Breit-Wigner resonances. Systematic uncertainties not estimated.

$\Upsilon(11020)$ WIDTH

VALUE (MeV)	DOCUMENT ID	TECN	COMMENT
-------------	-------------	------	---------

24 ± 8 OUR AVERAGE			
------------------------	--	--	--

$23.8 \pm 8.0 \pm 0.7$ $-6.8 - 1.8$	¹ MIZUK	19	BELL $e^+e^- \rightarrow \Upsilon(nS)\pi^+\pi^-$
$27 \pm 27 \pm 5$ $-11 - 12$	² MIZUK	16	BELL $e^+e^- \rightarrow h_b(1P, 2P)\pi^+\pi^-$

Meson Particle Listings
 $\Upsilon(11020)$

• • • We do not use the following data for averages, fits, limits, etc. • • •

35.1 ± 1.2	³ DONG	20A		$e^+ e^- \rightarrow b\bar{b}$
39.3 ^{+1.7+1.3} _{-1.6-2.4}	4.5 SANTEL	16	BELL	$e^+ e^- \rightarrow$ hadrons
61 ⁺⁹ ₋₁₉ ⁺² ₋₂₀	6.7 SANTEL	16	BELL	$e^+ e^- \rightarrow \Upsilon(1S, 2S, 3S) \pi^+ \pi^-$
37 ± 3	⁸ AUBERT	09E	BABR	$e^+ e^- \rightarrow$ hadrons
61 ± 13 ± 22	BESSON	85	CLEO	$e^+ e^- \rightarrow$ hadrons
90 ± 20	LOVELOCK	85	CUSB	$e^+ e^- \rightarrow$ hadrons

- From a simultaneous fit to the $\Upsilon(nS) \pi^+ \pi^-$, $n = 1, 2, 3$, cross sections at 28 energy points within $\sqrt{s} = 10.6\text{--}11.05$ GeV, including the initial-state radiation at $\Upsilon(10860)$.
- From a simultaneous fit to the $h_b(nP) \pi^+ \pi^-$, $n = 1, 2$ cross sections at 22 energy points within $\sqrt{s} = 10.77\text{--}11.02$ GeV to a pair of interfering Breit-Wigner amplitudes modified by phase space factors, with eight resonance parameters (a mass and width for each of $\Upsilon(10860)$ and $\Upsilon(11020)$, a single relative phase, a single relative amplitude, and two overall normalization factors, one for each n). The systematic error estimate is dominated by possible interference with a small nonresonant continuum amplitude.
- From a fit to the dressed cross sections of AUBERT 09E by BaBar and SANTEL 16 by Belle above 10.68 GeV with a coherent sum of a continuum amplitude and three Breit-Wigner functions with constant widths.
- From a fit to the total hadronic cross sections measured at 60 energy points within $\sqrt{s} = 10.82\text{--}11.05$ GeV to a pair of interfering Breit-Wigner amplitudes and two floating continuum amplitudes with $1/\sqrt{s}$ dependence, one coherent with the resonances and one incoherent, with six resonance parameters (a mass, width, and an amplitude for each of $\Upsilon(10860)$ and $\Upsilon(11020)$, one relative phase, and one decoherence coefficient).
- Not including uncertain and potentially large systematic errors due to assumed continuum amplitude $1/\sqrt{s}$ dependence and related interference contributions.
- From a simultaneous fit to the $\Upsilon(nS) \pi^+ \pi^-$, $n = 1, 2, 3$, cross sections at 25 energy points within $\sqrt{s} = 10.6\text{--}11.05$ GeV to a pair of interfering Breit-Wigner amplitudes modified by phase space factors, with fourteen resonance parameters (a mass, width, and three amplitudes for each of $\Upsilon(10860)$ and $\Upsilon(11020)$, a single universal relative phase, and three decoherence coefficients, one for each n). Continuum contributions were measured (and therefore fixed) to be zero.
- Superseded by MIZUK 19.
- In a model where a flat non-resonant $b\bar{b}$ -continuum is incoherently added to a second flat component interfering with two Breit-Wigner resonances. Systematic uncertainties not estimated.

$\Upsilon(11020)$ DECAY MODES

Mode	Fraction (Γ_i/Γ)
Γ_1 $e^+ e^-$	$(5.4^{+1.9}_{-2.1}) \times 10^{-6}$
Γ_2 $\Upsilon(1S) \pi^+ \pi^-$	
Γ_3 $\Upsilon(2S) \pi^+ \pi^-$	
Γ_4 $\Upsilon(3S) \pi^+ \pi^-$	
Γ_5 $\chi_{bJ}(1P) \pi^+ \pi^- \pi^0$	$(9^{+9}_{-8}) \times 10^{-3}$
Γ_6 $\chi_{b1}(1P) \pi^+ \pi^- \pi^0$	seen
Γ_7 $\chi_{b2}(1P) \pi^+ \pi^- \pi^0$	seen

$\Upsilon(11020)$ PARTIAL WIDTHS

$\Gamma(e^+ e^-)$				Γ_1
VALUE (keV)	DOCUMENT ID	TECN	COMMENT	
0.130 ± 0.030 OUR AVERAGE				
0.095 ± 0.03 ± 0.035	BESSON	85	CLEO $e^+ e^- \rightarrow$ hadrons	
0.156 ± 0.040	LOVELOCK	85	CUSB $e^+ e^- \rightarrow$ hadrons	

$\Gamma(e^+ e^-) \times \Gamma(\Upsilon(1S) \pi^+ \pi^-) / \Gamma_{total}$ $\Gamma_1 \Gamma_2 / \Gamma$

VALUE (eV)	DOCUMENT ID	TECN	COMMENT
• • • We do not use the following data for averages, fits, limits, etc. • • •			
0.46 ± 0.08	1,2 MIZUK	19	BELL $e^+ e^- \rightarrow \Upsilon(nS) \pi^+ \pi^-$
¹ From a simultaneous fit to the $\Upsilon(nS) \pi^+ \pi^-$, $n = 1, 2, 3$, cross sections at 28 energy points within $\sqrt{s} = 10.6\text{--}11.05$ GeV, including the initial-state radiation at $\Upsilon(10860)$. ² Reported as the range 0.38–0.54 eV obtained from multiple solutions of an amplitude fit within a model composed as a sum of Breit-Wigner functions.			

$\Gamma(e^+ e^-) \times \Gamma(\Upsilon(2S) \pi^+ \pi^-) / \Gamma_{total}$ $\Gamma_1 \Gamma_3 / \Gamma$

VALUE (eV)	DOCUMENT ID	TECN	COMMENT
• • • We do not use the following data for averages, fits, limits, etc. • • •			
0.65 ± 0.52	1,2 MIZUK	19	BELL $e^+ e^- \rightarrow \Upsilon(nS) \pi^+ \pi^-$
¹ From a simultaneous fit to the $\Upsilon(nS) \pi^+ \pi^-$, $n = 1, 2, 3$, cross sections at 28 energy points within $\sqrt{s} = 10.6\text{--}11.05$ GeV, including the initial-state radiation at $\Upsilon(10860)$. ² Reported as the range 0.13–1.16 eV obtained from multiple solutions of an amplitude fit within a model composed as a sum of Breit-Wigner functions.			

$\Gamma(e^+ e^-) \times \Gamma(\Upsilon(3S) \pi^+ \pi^-) / \Gamma_{total}$ $\Gamma_1 \Gamma_4 / \Gamma$

VALUE (eV)	DOCUMENT ID	TECN	COMMENT
• • • We do not use the following data for averages, fits, limits, etc. • • •			
0.33 ± 0.16	1,2 MIZUK	19	BELL $e^+ e^- \rightarrow \Upsilon(nS) \pi^+ \pi^-$
¹ From a simultaneous fit to the $\Upsilon(nS) \pi^+ \pi^-$, $n = 1, 2, 3$, cross sections at 28 energy points within $\sqrt{s} = 10.6\text{--}11.05$ GeV, including the initial-state radiation at $\Upsilon(10860)$. ² Reported as the range 0.17–0.49 eV obtained from multiple solutions of an amplitude fit within a model composed as a sum of Breit-Wigner functions.			

$\Gamma(\chi_{bJ}(1P) \pi^+ \pi^- \pi^0) / \Gamma_{total}$ Γ_5 / Γ

VALUE (units 10^{-3})	DOCUMENT ID	TECN	COMMENT
8.7 ± 4.3^{+7.6}_{-6.6}	YIN	18	BELL $e^+ e^- \rightarrow$ hadrons

$\Gamma(\chi_{b1}(1P) \pi^+ \pi^- \pi^0) / \Gamma_{total}$ Γ_6 / Γ

VALUE	DOCUMENT ID	TECN	COMMENT
seen	YIN	18	BELL $e^+ e^- \rightarrow$ hadrons

$\Gamma(\chi_{b2}(1P) \pi^+ \pi^- \pi^0) / \Gamma_{total}$ Γ_7 / Γ

VALUE	DOCUMENT ID	TECN	COMMENT
seen	YIN	18	BELL $e^+ e^- \rightarrow$ hadrons

$\Gamma(\chi_{b2}(1P) \pi^+ \pi^- \pi^0) / \Gamma(\chi_{b1}(1P) \pi^+ \pi^- \pi^0)$ Γ_7 / Γ_6

VALUE	DOCUMENT ID	TECN	COMMENT
0.4 ± 0.2	YIN	18	BELL $e^+ e^- \rightarrow$ hadrons

$\Upsilon(11020)$ REFERENCES

DONG	20A	CP C44 083001	X.-K. Dong <i>et al.</i>	
MIZUK	19	JHEP 1910 220	R. Mizuk <i>et al.</i>	(BELLE Collab.)
YIN	18	PR D98 091102	J.H. Yin <i>et al.</i>	(BELLE Collab.)
MIZUK	16	PRL 117 142001	R. Mizuk <i>et al.</i>	(BELLE Collab.)
SANTEL	16	PR D93 011101	D. Santel <i>et al.</i>	(BELLE Collab.)
AUBERT	09E	PRL 102 012001	B. Aubert <i>et al.</i>	(BABAR Collab.)
BESSON	85	PRL 54 381	D. Besson <i>et al.</i>	(CLEO Collab.)
LOVELOCK	85	PRL 54 377	D.M.J. Lovelock <i>et al.</i>	(CUSB Collab.)

Meson Particle Listings

Further States

OTHER MESONS

Further States

OMITTED FROM SUMMARY TABLE

This section contains states observed by a single group or states poorly established that thus need confirmation.

QUANTUM NUMBERS, MASSES, WIDTHS, AND BRANCHING RATIOS

X(360) $I^G(J^{PC}) = ?^?(?^?+)$		DOCUMENT ID	TECN	COMMENT
MASS (MeV)	WIDTH (MeV)	EVTs		
360 ± 7 ± 9	64 ± 18	2.3k	1	ABRAAMYAN 09 CNTR 2.75 $dC \rightarrow \gamma\gamma X$

¹ Not seen in $pC \rightarrow \gamma\gamma X$ at 5.5 GeV/c.

X(1070) $I^G(J^{PC}) = ?^?(0^{++})$		DOCUMENT ID	TECN	COMMENT
MASS (MeV)	WIDTH (MeV)			
1072 ± 1	3.5 ± 0.5	1	VLADIMIRSK...08	40 $\pi^- p \rightarrow K_S^0 K_S^0 n + m\pi^0$

¹ Supersedes GRIGOR'EV 05.

X(1110) $I^G(J^{PC}) = 0^+(\text{even}^{++})$		DOCUMENT ID	TECN	COMMENT
MASS (MeV)	WIDTH (MeV)			
1107 ± 4	111 ± 8 ± 15		DAFTARI 87	DBC 0. $\bar{p}n \rightarrow \rho^- \pi^+ \pi^-$

f₀(1200-1600) $I^G(J^{PC}) = 0^+(0^{++})$		DOCUMENT ID	TECN	COMMENT
MASS (MeV)	WIDTH (MeV)			
1323 ± 8	237 ± 20		VLADIMIRSK...06	SPEC 40 $\pi^- p \rightarrow K_S^0 K_S^0 n$
1480 +100 -150	1030 + 80 -170	1	ANISOVICH 03	SPEC
1530 +90 -250	560 ± 40	2	ANISOVICH 03	SPEC

¹ K-matrix pole from combined analysis of $\pi^- p \rightarrow \pi^0 \pi^0 n$, $\pi^- p \rightarrow K \bar{K} n$, $\pi^+ \pi^- \rightarrow \pi^+ \pi^-$, $\bar{p}p \rightarrow \pi^0 \pi^0 \pi^0$, $\pi^0 \eta$, $\pi^0 \pi^0 \eta$, $\pi^+ \pi^- \pi^0$, $K^+ K^- \pi^0$, $K_S^0 K_S^0 \pi^0$, $K^+ K_S^0 \pi^-$ at rest, $\bar{p}n \rightarrow \pi^- \pi^- \pi^+$, $K_S^0 K^- \pi^0$, $K_S^0 K_S^0 \pi^-$ at rest.
² K-matrix pole from combined analysis of $\pi^- p \rightarrow \pi^0 \pi^0 n$, $\pi^- p \rightarrow K \bar{K} n$, $\bar{p}p \rightarrow \pi^0 \pi^0 \pi^0$, $\pi^0 \eta$, $\pi^0 \pi^0 \eta$ at rest.

X(1420) $I^G(J^{PC}) = 2^+(0^{++})$		DOCUMENT ID	TECN	COMMENT
MASS (MeV)	WIDTH (MeV)			
1420 ± 20	160 ± 10		FILIPPI 00	OBLX 0 $\bar{p}p \rightarrow \pi^+ \pi^+ \pi^-$

X(1545) $I^G(J^{PC}) = ?^?(?^{++})$		DOCUMENT ID	TECN	COMMENT
MASS (MeV)	WIDTH (MeV)			
1545 ± 3	6.0 ± 2.5	1	VLADIMIRSK...08	40 $\pi^- p \rightarrow K_S^0 K_S^0 n + m\pi^0$

¹ Supersedes VLADIMIRSKII 00.

X(1575) $I^G(J^{PC}) = ?^?(1^{--})$		DOCUMENT ID	TECN	COMMENT
MASS (MeV)	WIDTH (MeV)			
1576 +49+98 -55-91	818 +22+64 -23-133	1	ABLIKIM 06s	BES $J/\psi \rightarrow K^+ K^- \pi^0$

¹ A broad peak observed at $K^+ K^-$ invariant mass. Mass and width above are its pole position. The observed branching ratio is $B(J/\psi \rightarrow X \pi^0) B(X \rightarrow K^+ K^-) = (8.5 \pm 0.6 +2.7 -3.6) \times 10^{-4}$.

X(1600) $I^G(J^{PC}) = 2^+(2^{++})$		DOCUMENT ID	TECN	COMMENT
MASS (MeV)	WIDTH (MeV)			
1600 ± 100	400 ± 200	1	ALBRECHT 91F ARG	10.2 $e^+ e^- \rightarrow e^+ e^- 2(\pi^+ \pi^-)$

¹ Our estimate.

X(1650) $I^G(J^{PC}) = 0^-(?^{-})$		DOCUMENT ID	TECN	COMMENT
MASS (MeV)	WIDTH (MeV)	EVTs		
1652 ± 7	<50	100	PROKOSHKIN 96	GAM2 32,38 $\rho p \rightarrow \omega \eta n$

a₀(1700) $I^G(J^{PC}) = 1^-(0^{+-})$		DOCUMENT ID	TECN	COMMENT
MASS (MeV)	WIDTH (MeV)			
1704 ± 5 ± 2	110 ± 15 ± 11		LEES 21A	$\eta_c(1S) \rightarrow \pi^+ \pi^- \eta$

X(1730) $I^G(J^{PC}) = ?^?(?^?+)$		DOCUMENT ID	TECN	COMMENT
MASS (MeV)	WIDTH (MeV)	EVTs		
1731.0 ± 1.2 ± 2.0	3.2 ± 0.8 ± 1.3	58	VLADIMIRSK...07	SPEC 40 $\pi^- p \rightarrow K_S^0 K_S^0 X$

f₂(1750) $I^G(J^{PC}) = 0^+(2^{++})$		DOCUMENT ID	TECN	COMMENT
MASS (MeV)	WIDTH (MeV)	EVTs		
1755 ± 10	67 ± 12	870	1	SCHEGELSKY 06A RVUE $\gamma\gamma \rightarrow K_S^0 K_S^0$

Γ(K[±]K[±])		DOCUMENT ID	TECN	COMMENT
VALUE (MeV)	EVTs			
17 ± 5	870	2	SCHEGELSKY 06A RVUE	$\gamma\gamma \rightarrow K_S^0 K_S^0$

Γ(γγ)		DOCUMENT ID	TECN	COMMENT
VALUE (keV)	EVTs			
0.13 ± 0.04	870	2	SCHEGELSKY 06A RVUE	$\gamma\gamma \rightarrow K_S^0 K_S^0$

Γ(ππ)		DOCUMENT ID	TECN	COMMENT
VALUE (MeV)	EVTs			
1.3 ± 1.0	870	2	SCHEGELSKY 06A RVUE	$\gamma\gamma \rightarrow K_S^0 K_S^0$

Γ(ηη)		DOCUMENT ID	TECN	COMMENT
VALUE (MeV)	EVTs			
2.0 ± 0.5	870	2	SCHEGELSKY 06A RVUE	$\gamma\gamma \rightarrow K_S^0 K_S^0$

¹ From analysis of L3 data at 91 and 183-209 GeV.
² From analysis of L3 data at 91 and 183-209 GeV and using SU(3) relations.

X(1775) $I^G(J^{PC}) = 1^-(?^{-})$		DOCUMENT ID	TECN	COMMENT
MASS (MeV)	WIDTH (MeV)			
1763 ± 20	192 ± 60	CONDO 91	SHF	$\gamma p \rightarrow (p\pi^+) (\pi^+ \pi^- \pi^-)$
1787 ± 18	118 ± 60	CONDO 91	SHF	$\gamma p \rightarrow n\pi^+ \pi^+ \pi^-$

X(1850 - 3100) $I^G(J^{PC}) = ?^?(1^{--})$		DOCUMENT ID	TECN	COMMENT
$\Gamma(e^+e^-)B(X \rightarrow \text{hadrons})$ (eV)	CL%			
<120	90	1	ANASHIN 11	KEDR $e^+ e^- \rightarrow \text{hadrons}$

¹ This limit is center-of-mass energy dependent. We quote the most stringent one.

X(1855) $I^G(J^{PC}) = ?^?(?^{??})$		DOCUMENT ID	TECN	COMMENT
MASS (MeV)	WIDTH (MeV)			
1856.6 ± 5	20 ± 5	BRIDGES 86D	SPEC	0. $\bar{p}d \rightarrow \pi\pi N$

X(1870) $I^G(J^{PC}) = ?^?(2^{??})$		DOCUMENT ID	TECN	COMMENT
MASS (MeV)	WIDTH (MeV)			
1870 ± 40	250 ± 30	ALDE 86D	GAM4	100 $\pi^- p \rightarrow 2\eta X$

a₃(1875) $I^G(J^{PC}) = 1^-(3^{+-})$		DOCUMENT ID	TECN	COMMENT
MASS (MeV)	WIDTH (MeV)			
1874 ± 43 ± 96	385 ± 121 ± 114	CHUNG 02	B852	18.3 $\pi^- p \rightarrow \pi^+ \pi^- \pi^- p$

B(a₃(1875) → f₂(1270)π)/B(a₃(1875) → ρπ)		DOCUMENT ID	TECN	COMMENT
VALUE				
0.8 ± 0.2		1	CHUNG 02	B852 18.3 $\pi^- p \rightarrow \pi^+ \pi^- \pi^- p$

¹ Using the observable fractions of 50.0% $\rho\pi$, 56.5% $f_2\pi$, and 11.8% $\rho_3\pi$.

B(a₃(1875) → ρ₃(1690)π)/B(a₃(1875) → ρπ)		DOCUMENT ID	TECN	COMMENT
VALUE				
0.9 ± 0.3		1	CHUNG 02	B852 18.3 $\pi^- p \rightarrow \pi^+ \pi^- \pi^- p$

¹ Using the observable fractions of 50.0% $\rho\pi$, 56.5% $f_2\pi$, and 11.8% $\rho_3\pi$.

a₁(1930) $I^G(J^{PC}) = 1^-(1^{+-})$		DOCUMENT ID	TECN	COMMENT
MASS (MeV)	WIDTH (MeV)			
1930 +30 -20	155 ± 45	ANISOVICH 01F	SPEC	2.0 $\bar{p}p \rightarrow 3\pi^0, \pi^0 \eta, \pi^0 \eta'$

X(1935) $I^G(J^{PC}) = 1^+(1^{-?})$		DOCUMENT ID	TECN	COMMENT
MASS (MeV)	WIDTH (MeV)			
1935 ± 20	215 ± 30	EVANGELIS... 79	OMEG	10,16 $\pi^- p \rightarrow \bar{p} \rho n$

ρ₂(1940) $I^G(J^{PC}) = 1^+(2^{--})$		DOCUMENT ID	TECN	COMMENT
MASS (MeV)	WIDTH (MeV)			
1940 ± 40	155 ± 40	1	ANISOVICH 02	SPEC 0.6-1.9 $\rho\bar{p} \rightarrow \omega\pi^0, \omega\eta\pi^0, \pi^+ \pi^-$

¹ From the combined analysis of ANISOVICH 00J, ANISOVICH 01D, ANISOVICH 01E, and ANISOVICH 02.

See key on page 1127

Meson Particle Listings
Further States

$\omega_3(1945)$ $I^G(J^{PC}) = 0^-(3^{--})$

MASS (MeV)	WIDTH (MeV)	DOCUMENT ID	TECN	COMMENT
1945 ± 20	115 ± 22	¹ ANISOVICH	02B	SPEC 0.6-1.9 $p\bar{p} \rightarrow \omega\eta, \omega\pi^0\pi^0$

¹ From the combined analysis of ANISOVICH 00D, ANISOVICH 01C, and ANISOVICH 02B.

$a_2(1950)$ $I^G(J^{PC}) = 1^-(2^{+-})$

MASS (MeV)	WIDTH (MeV)	DOCUMENT ID	TECN	COMMENT
1950 ± $^{+30}_{-70}$	180 ± $^{+30}_{-70}$	¹ ANISOVICH	01F	SPEC 1.96-2.41 $p\bar{p}$

¹ From the combined analysis of ANISOVICH 99C, ANISOVICH 99E, and ANISOVICH 01F.

$\omega(1960)$ $I^G(J^{PC}) = 0^-(1^{--})$

MASS (MeV)	WIDTH (MeV)	DOCUMENT ID	TECN	COMMENT
1960 ± 25	195 ± 60	¹ ANISOVICH	02B	SPEC 0.6-1.9 $p\bar{p} \rightarrow \omega\eta, \omega\pi^0\pi^0$

¹ From the combined analysis of ANISOVICH 00D, ANISOVICH 01C, and ANISOVICH 02B.

$b_1(1960)$ $I^G(J^{PC}) = 1^+(1^{+-})$

MASS (MeV)	WIDTH (MeV)	DOCUMENT ID	TECN	COMMENT
1960 ± 35	230 ± 50	¹ ANISOVICH	02	SPEC 0.6-1.9 $p\bar{p} \rightarrow \omega\pi^0, \omega\eta\pi^0, \pi^+\pi^-$

¹ From the combined analysis of ANISOVICH 00J, ANISOVICH 01D, ANISOVICH 01E, and ANISOVICH 02.

$h_1(1965)$ $I^G(J^{PC}) = 0^-(1^{+-})$

MASS (MeV)	WIDTH (MeV)	DOCUMENT ID	TECN	COMMENT
1965 ± 45	345 ± 75	¹ ANISOVICH	02B	SPEC 0.6-1.9 $p\bar{p} \rightarrow \omega\eta, \omega\pi^0\pi^0$

¹ From the combined analysis of ANISOVICH 00D, ANISOVICH 01C, and ANISOVICH 02B.

$f_1(1970)$ $I^G(J^{PC}) = 0^+(1^{++})$

MASS (MeV)	WIDTH (MeV)	DOCUMENT ID	TECN	COMMENT
1971 ± 15	240 ± 45	ANISOVICH	00J	SPEC

$X(1970)$ $I^G(J^{PC}) = ?^?(?^{??})$

MASS (MeV)	WIDTH (MeV)	DOCUMENT ID	TECN	COMMENT
1970 ± 10	40 ± 20	CHLIAPNIK...	80	HBC 32 $K^+\rho \rightarrow 2K_S^0 2\pi X$

$X(1975)$ $I^G(J^{PC}) = ?^?(?^{??})$

MASS (MeV)	WIDTH (MeV)	EVTs	DOCUMENT ID	TECN	COMMENT
1973 ± 15	80	30	CASO	70	HBC 11.2 $\pi^-\rho \rightarrow \rho 2\pi$

$\omega_2(1975)$ $I^G(J^{PC}) = 0^-(2^{--})$

MASS (MeV)	WIDTH (MeV)	DOCUMENT ID	TECN	COMMENT
1975 ± 20	175 ± 25	¹ ANISOVICH	02B	SPEC 0.6-1.9 $p\bar{p} \rightarrow \omega\eta, \omega\pi^0\pi^0$

¹ From the combined analysis of ANISOVICH 00D, ANISOVICH 01C, and ANISOVICH 02B.

$a_2(1990)$ $I^G(J^{PC}) = 1^-(2^{+-})$

MASS (MeV)	WIDTH (MeV)	EVTs	DOCUMENT ID	TECN	COMMENT
2050 ± 10 ± 40	190 ± 22 ± 100	18k	¹ SCHEGELSKY	06	RVUE $\gamma\gamma \rightarrow \pi^+\pi^-\pi^0$
2003 ± 10 ± 19	249 ± 23 ± 32		LU	05	B852 18 $\pi^-\rho \rightarrow \omega\pi^-\pi^0\rho$

¹ From analysis of L3 data at 183-209 GeV.

$\Gamma(\gamma\gamma) \Gamma(\pi^+\pi^-\pi^0) / \Gamma(\text{total})$

VALUE (keV)	EVTs	DOCUMENT ID	TECN	COMMENT
0.11 ± 0.04 ± 0.05	18k	¹ SCHEGELSKY	06	RVUE $\gamma\gamma \rightarrow \pi^+\pi^-\pi^0$

¹ From analysis of L3 data at 183-209 GeV.

$\rho(2000)$ $I^G(J^{PC}) = 1^+(1^{--})$

MASS (MeV)	WIDTH (MeV)	DOCUMENT ID	TECN	COMMENT
2000 ± 30	260 ± 45	¹ BUGG	04C	RVUE Compilation
~ 1988	~ 244	HASAN	94	RVUE $p\bar{p} \rightarrow \pi\pi$

¹ From the combined analysis of ANISOVICH 00J, ANISOVICH 01D, ANISOVICH 01E, and ANISOVICH 02.

$f_2(2000)$ $I^G(J^{PC}) = 0^+(2^{++})$

MASS (MeV)	WIDTH (MeV)	DOCUMENT ID	TECN	COMMENT
2001 ± 10	312 ± 32	ANISOVICH	00J	SPEC
~ 1996	~ 134	HASAN	94	RVUE $p\bar{p} \rightarrow \pi\pi$

$X(2000)$ $I^G(J^{PC}) = 1^-(?^{?+})$

MASS (MeV)	WIDTH (MeV)	DOCUMENT ID	TECN	CHG	COMMENT
1964 ± 35	225 ± 50	¹ ARMSTRONG	93D	E760	$p\bar{p} \rightarrow 3\pi^0 \rightarrow 6\gamma$
~ 2100	~ 500	¹ ANTIPOV	77	CIBS -	25 $\pi^-\rho \rightarrow \rho\pi^-\rho_3$
2214 ± 15	355 ± 21	² BALTAY	77	HBC 0	15 $\pi^-\rho \rightarrow \Delta^{++} 3\pi$
2080 ± 40	340 ± 80	KALELKAR	75	HBC +	15 $\pi^+\rho \rightarrow \rho\pi^+\rho_3$

¹ Cannot determine spin to be 3.
² BALTAY 77 favors $J^P = ,3^+$.

$X(2000)$ $I^G(J^{PC}) = ?^?(4^{++})$

MASS (MeV)	WIDTH (MeV)	DOCUMENT ID	TECN	COMMENT
1998 ± 3 ± 5	< 15	VLADIMIRSK...03	SPEC	$\pi^-\rho \rightarrow K_S^0 K_S^0 MM$

$\eta(2010)$ $I^G(J^{PC}) = 0^+(0^{-+})$

MASS (MeV)	WIDTH (MeV)	DOCUMENT ID	TECN	COMMENT
2010 ± $^{+35}_{-60}$	270 ± 60	ANISOVICH	00J	SPEC

$\pi_1(2015)$ $I^G(J^{PC}) = 1^-(1^{+-})$

MASS (MeV)	WIDTH (MeV)	EVTs	DOCUMENT ID	TECN	COMMENT
2014 ± 20 ± 16	230 ± 32 ± 73	145k	LU	05	B852 18 $\pi^-\rho \rightarrow \omega\pi^-\pi^0\rho$
2001 ± 30 ± 92	333 ± 52 ± 49	69k	KUHN	04	B852 18 $\pi^-\rho \rightarrow \eta\pi^+\pi^-\pi^-\rho$

$a_0(2020)$ $I^G(J^{PC}) = 1^-(0^{++})$

MASS (MeV)	WIDTH (MeV)	DOCUMENT ID	TECN	COMMENT
2025 ± 30	330 ± 75	ANISOVICH	99C	SPEC

$X(2020)$ $I^G(J^{PC}) = ?^?(?^{??})$

MASS (MeV)	WIDTH (MeV)	DOCUMENT ID	TECN	COMMENT
2015 ± 3	10 ± 4	FERRER	99	RVUE $\pi\rho \rightarrow \rho\rho\pi\pi(\pi)$

$h_3(2025)$ $I^G(J^{PC}) = 0^-(3^{+-})$

MASS (MeV)	WIDTH (MeV)	DOCUMENT ID	TECN	COMMENT
2025 ± 20	145 ± 30	¹ ANISOVICH	02B	SPEC 0.6-1.9 $p\bar{p} \rightarrow \omega\eta, \omega\pi^0\pi^0$

¹ From the combined analysis of ANISOVICH 00D, ANISOVICH 01C, and ANISOVICH 02B.

$b_3(2030)$ $I^G(J^{PC}) = 1^+(3^{+-})$

MASS (MeV)	WIDTH (MeV)	DOCUMENT ID	TECN	COMMENT
2032 ± 12	117 ± 11	¹ ANISOVICH	02	SPEC 0.6-1.9 $p\bar{p} \rightarrow \omega\pi^0, \omega\eta\pi^0, \pi^+\pi^-$

¹ From the combined analysis of ANISOVICH 00J, ANISOVICH 01D, ANISOVICH 01E, and ANISOVICH 02.

$a_2(2030)$ $I^G(J^{PC}) = 1^-(2^{+-})$

MASS (MeV)	WIDTH (MeV)	DOCUMENT ID	TECN	COMMENT
2030 ± 20	205 ± 30	¹ ANISOVICH	01F	SPEC 1.96-2.41 $p\bar{p}$

¹ From the combined analysis of ANISOVICH 99C, ANISOVICH 99E, and ANISOVICH 01F.

$a_3(2030)$ $I^G(J^{PC}) = 1^-(3^{+-})$

MASS (MeV)	WIDTH (MeV)	DOCUMENT ID	TECN	COMMENT
2031 ± 12	150 ± 18	¹ ANISOVICH	01F	SPEC 1.96-2.41 $p\bar{p}$

¹ From the combined analysis of ANISOVICH 99C, ANISOVICH 99E, and ANISOVICH 01F.

$\eta_2(2030)$ $I^G(J^{PC}) = 0^+(2^{-+})$

MASS (MeV)	WIDTH (MeV)	DOCUMENT ID	TECN	COMMENT
2030 ± 5 ± 15	205 ± 10 ± 15	ANISOVICH	00E	SPEC

$B(a_2\pi)_L=0/B(a_2\pi)_L=2$

VALUE	DOCUMENT ID	TECN	COMMENT
0.05 ± 0.03	¹ ANISOVICH	11	SPEC 0.9-1.94 $p\bar{p}$

¹ Reanalysis of ADOMEIT 96 and ANISOVICH 00E.

$B(a_0\pi)/B(a_2\pi)_L=2$

VALUE	DOCUMENT ID	TECN	COMMENT
0.10 ± 0.08	¹ ANISOVICH	11	SPEC 0.9-1.94 $p\bar{p}$

¹ Reanalysis of ADOMEIT 96 and ANISOVICH 00E.

$B(f_2\eta)/B(a_2\pi)_L=2$

VALUE	DOCUMENT ID	TECN	COMMENT
0.13 ± 0.06	¹ ANISOVICH	11	SPEC 0.9-1.94 $p\bar{p}$

¹ Reanalysis of ADOMEIT 96 and ANISOVICH 00E.

Meson Particle Listings

Further States

$f_3(2050)$ $I^G(J^{PC}) = 0^+(3^+)$		DOCUMENT ID	TECN	COMMENT
MASS (MeV)	WIDTH (MeV)			
2048 ± 8	213 ± 34	ANISOVICH	00J	SPEC 2.0 $\bar{p}p \rightarrow \eta\pi^0\pi^0$

$f_0(2060)$ $I^G(J^{PC}) = 0^+(0^+)$		DOCUMENT ID	TECN	COMMENT
MASS (MeV)	WIDTH (MeV)			
~ 2050	~ 120	1 OAKDEN	94	RVUE 0.36-1.55 $\bar{p}p \rightarrow \pi\pi$
~ 2060	~ 50	1 OAKDEN	94	RVUE 0.36-1.55 $\bar{p}p \rightarrow \pi\pi$
1 See SEMENOV 99 and KLOET 96.				

$\pi(2070)$ $I^G(J^{PC}) = 1^-(0^+)$		DOCUMENT ID	TECN	COMMENT
MASS (MeV)	WIDTH (MeV)			
2070 ± 35	310 ⁺¹⁰⁰ ₋₅₀	ANISOVICH	01F	SPEC 2.0 $\bar{p}p \rightarrow 3\pi^0, \pi^0\eta, \pi^0\eta'$

$X(2075)$ $I^G(J^{PC}) = ??(???)$		DOCUMENT ID	TECN	COMMENT
MASS (MeV)	WIDTH (MeV)			
2075 ± 12 ± 5	90 ± 35 ± 9	1 ABLIKIM	04J	BES2 $J/\psi \rightarrow K^- \rho^+ \bar{K}$
1 From a fit in the region $M_{\rho\bar{K}} - M_{\rho^-} - M_{K^-} < 150$ MeV. S-wave in the $\rho\bar{K}$ system preferred.				
A similar near-threshold enhancement in the $\rho\bar{K}$ system is observed in $B^+ \rightarrow \rho^+ \bar{K}^0 D^0$ by CHEN 11F.				

$X(2080)$ $I^G(J^{PC}) = ??(???)$		DOCUMENT ID	TECN	COMMENT
MASS (MeV)	WIDTH (MeV)			
2080 ± 10	110 ± 20	KREYMER	80	STRC 13 $\pi^- d \rightarrow \rho^+ p n(n_S)$

$X(2080)$ $I^G(J^{PC}) = ??(3^-)$		DOCUMENT ID	TECN	COMMENT
MASS (MeV)	WIDTH (MeV)			
2080 ± 10	190 ± 15	ROZANSKA	80	SPRK 18 $\pi^- p \rightarrow \rho^+ \bar{p} n$

$a_1(2095)$ $I^G(J^{PC}) = 1^-(1^+)$		DOCUMENT ID	TECN	COMMENT
MASS (MeV)	WIDTH (MeV)	EPTS		
2096 ± 17 ± 121	451 ± 41 ± 81	69k	KUHN	04 B852 18 $\pi^- p \rightarrow \eta\pi^+ \pi^- \pi^- p$

$B(a_1(2095) \rightarrow f_1(1285)\pi) / B(a_1(2095) \rightarrow a_1(1260))$		DOCUMENT ID	TECN	COMMENT
VALUE	EPTS			
3.18 ± 0.64	69k	KUHN	04	B852 18 $\pi^- p \rightarrow \eta\pi^+ \pi^- \pi^- p$

$\eta(2100)$ $I^G(J^{PC}) = 0^+(0^+)$		DOCUMENT ID	TECN	COMMENT
MASS (MeV)	WIDTH (MeV)	EPTS		
2050 ⁺³⁰⁺⁷⁵ ₋₂₄₋₂₆	250 ⁺³⁶⁺¹⁸¹ ₋₃₀₋₁₆₄	1 ABLIKIM	16N	BES3 $J/\psi \rightarrow \gamma K^+ K^- K^+ K^-$
2103 ± 50	187 ± 75	586	2 BISELLO	89B DM2 $J/\psi \rightarrow 4\pi\gamma$

1 From a partial wave analysis of $J/\psi \rightarrow \gamma\phi\phi$, for which the primary signal is $\eta(2225) \rightarrow \phi\phi$, and that also finds significant signals for for 0^-+ phase space, $f_0(2100)$, $f_2(2101)$, $f_2(2300)$, $f_2(2340)$, and a previously unseen 0^-+ state $X(2500)$ ($M = 2470^{+15+101}$ ₋₁₉₋₂₃ MeV, $\Gamma = 230^{+64+56}$ ₋₃₅₋₃₃ MeV).

2 ASTON 81B sees no peak, has 850 events in Ajinenko+Barth bins. ARESTOV 80 sees no peak.

$X(2100)$ $I^G(J^{PC}) = ??(0^?)$		DOCUMENT ID	TECN	COMMENT
MASS (MeV)	WIDTH (MeV)			
2100 ± 40	250 ± 40	ALDE	86D	GAM4 100 $\pi^- p \rightarrow 2\eta X$

$X(2110)$ $I^G(J^{PC}) = 1^+(3^-)$		DOCUMENT ID	TECN	COMMENT
MASS (MeV)	WIDTH (MeV)			
2110 ± 10	330 ± 20	EVANGELIS...	79	OMEG 10,16 $\pi^- p \rightarrow \bar{p} p n$

$f_2(2140)$ $I^G(J^{PC}) = 0^+(2^+)$		DOCUMENT ID	TECN	COMMENT
MASS (MeV)	WIDTH (MeV)	EPTS		
2141 ± 12	49 ± 28	389	GREEN	86 MPFS 400 $\rho A \rightarrow 4KX$

$X(2150)$ $I^G(J^{PC}) = ??(2^+)$		DOCUMENT ID	TECN	COMMENT
MASS (MeV)	WIDTH (MeV)			
2150 ± 10	260 ± 10	ROZANSKA	80	SPRK 18 $\pi^- p \rightarrow \rho^+ \bar{p} n$

$a_2(2175)$ $I^G(J^{PC}) = 1^-(2^+)$		DOCUMENT ID	TECN	COMMENT
MASS (MeV)	WIDTH (MeV)			
2175 ± 40	310 ⁺⁹⁰ ₋₄₅	ANISOVICH	01F	SPEC 2.0 $\bar{p}p \rightarrow 3\pi^0, \pi^0\eta, \pi^0\eta'$

$\eta(2190)$ $I^G(J^{PC}) = 0^+(0^+)$		DOCUMENT ID	TECN	COMMENT
MASS (MeV)	WIDTH (MeV)			
2190 ± 50	850 ± 100	BUGG	99	BES

$\omega_2(2195)$ $I^G(J^{PC}) = 0^-(2^-)$		DOCUMENT ID	TECN	COMMENT
MASS (MeV)	WIDTH (MeV)			
2195 ± 30	225 ± 40	1 ANISOVICH	02B	SPEC 0.6-1.9 $\rho\bar{p} \rightarrow \omega\eta, \omega\pi^0\pi^0$
1 From the combined analysis of ANISOVICH 00D, ANISOVICH 01C, and ANISOVICH 02B.				

$\omega(2205)$ $I^G(J^{PC}) = 0^-(1^-)$		DOCUMENT ID	TECN	COMMENT
MASS (MeV)	WIDTH (MeV)			
2205 ± 30	350 ± 90	1 ANISOVICH	02B	SPEC 0.6-1.9 $\rho\bar{p} \rightarrow \omega\eta, \omega\pi^0\pi^0$
1 From the combined analysis of ANISOVICH 00D, ANISOVICH 01C, and ANISOVICH 02B.				

$X(2210)$ $I^G(J^{PC}) = ??(???)$		DOCUMENT ID	TECN	COMMENT
MASS (MeV)	WIDTH (MeV)			
2210 ⁺⁷⁹ ₋₂₁	203 ⁺⁴³⁷ ₋₈₇	EVANGELIS...	79B	OMEG 10 $\pi^- p \rightarrow K^+ K^- n$

$X(2210)$ $I^G(J^{PC}) = ??(???)$		DOCUMENT ID	TECN	COMMENT
MASS (MeV)	WIDTH (MeV)			
2207 ± 22	130	CASO	70	HBC 11.2 $\pi^- p$

$h_1(2215)$ $I^G(J^{PC}) = 0^-(1^+)$		DOCUMENT ID	TECN	COMMENT
MASS (MeV)	WIDTH (MeV)			
2215 ± 40	325 ± 55	1 ANISOVICH	02B	SPEC 0.6-1.9 $\rho\bar{p} \rightarrow \omega\eta, \omega\pi^0\pi^0$
1 From the combined analysis of ANISOVICH 00D, ANISOVICH 01C, and ANISOVICH 02B.				

$\rho_2(2225)$ $I^G(J^{PC}) = 1^+(2^-)$		DOCUMENT ID	TECN	COMMENT
MASS (MeV)	WIDTH (MeV)			
2225 ± 35	335 ⁺¹⁰⁰ ₋₅₀	1 ANISOVICH	02	SPEC 0.6-1.9 $\rho\bar{p} \rightarrow \omega\pi^0, \omega\eta\pi^0, \pi^+\pi^-$
1 From the combined analysis of ANISOVICH 00J, ANISOVICH 01D, ANISOVICH 01E, and ANISOVICH 02.				

$\rho_4(2230)$ $I^G(J^{PC}) = 1^+(4^-)$		DOCUMENT ID	TECN	COMMENT
MASS (MeV)	WIDTH (MeV)			
2230 ± 25	210 ± 30	1 ANISOVICH	02	SPEC 0.6-1.9 $\rho\bar{p} \rightarrow \omega\pi^0, \omega\eta\pi^0, \pi^+\pi^-$
1 From the combined analysis of ANISOVICH 00J, ANISOVICH 01D, ANISOVICH 01E, and ANISOVICH 02.				

$b_1(2240)$ $I^G(J^{PC}) = 1^+(1^+)$		DOCUMENT ID	TECN	COMMENT
MASS (MeV)	WIDTH (MeV)			
2240 ± 35	320 ± 85	1 ANISOVICH	02	SPEC 0.6-1.9 $\rho\bar{p} \rightarrow \omega\pi^0, \omega\eta\pi^0, \pi^+\pi^-$
1 From the combined analysis of ANISOVICH 00J, ANISOVICH 01D, ANISOVICH 01E, and ANISOVICH 02.				

$f_2(2240)$ $I^G(J^{PC}) = 0^+(2^+)$		DOCUMENT ID	TECN	COMMENT
MASS (MeV)	WIDTH (MeV)			
2240 ± 15	241 ± 30	1 ANISOVICH	00J	SPEC 1.92-2.41 $\rho\bar{p}$
• • • We do not use the following data for averages, fits, limits, etc. • • •				
~ 2226	~ 226	HASAN	94	RVUE $\rho\bar{p} \rightarrow \pi\pi$

1 From the combined analysis of ANISOVICH 99C, ANISOVICH 99F, ANISOVICH 99J, ANISOVICH 99K, and ANISOVICH 00B. See also ANISOVICH 12.

$b_3(2245)$ $I^G(J^{PC}) = 1^+(3^+)$		DOCUMENT ID	TECN	COMMENT
MASS (MeV)	WIDTH (MeV)			
2245 ± 50	320 ± 70	1 BUGG	04C	RVUE
1 From the combined analysis of ANISOVICH 00J, ANISOVICH 01D, ANISOVICH 01E, and ANISOVICH 02.				

$\eta_2(2250)$ $I^G(J^{PC}) = 0^+(2^+)$		DOCUMENT ID	TECN	COMMENT
MASS (MeV)	WIDTH (MeV)			
2248 ± 20	280 ± 20	ANISOVICH	00I	SPEC
2267 ± 14	290 ± 50	ANISOVICH	00J	SPEC

$\pi_4(2250)$ $I^G(J^{PC}) = 1^-(4^+)$		DOCUMENT ID	TECN	COMMENT
MASS (MeV)	WIDTH (MeV)			
2250 ± 15	215 ± 25	ANISOVICH	01F	SPEC 2.0 $\bar{p}p \rightarrow 3\pi^0, \pi^0\eta, \pi^0\eta'$

$\omega_4(2250) \quad I^G(J^{PC}) = 0^-(4^{--})$

MASS (MeV)	WIDTH (MeV)	DOCUMENT ID	TECN	COMMENT
2250 ± 30	150 ± 50	¹ ANISOVICH	02B	SPEC 0.6-1.9 $p\bar{p} \rightarrow \omega\eta, \omega\pi^0\pi^0$

¹ From the combined analysis of ANISOVICH 00d, ANISOVICH 01c, and ANISOVICH 02b.

$\omega_5(2250) \quad I^G(J^{PC}) = 0^-(5^{--})$

MASS (MeV)	WIDTH (MeV)	DOCUMENT ID	TECN	COMMENT
2250 ± 70	320 ± 95	¹ BUGG	04	RVUE

¹ From the combined analysis of ANISOVICH 00d, ANISOVICH 01c, and ANISOVICH 02b.

$\omega_3(2255) \quad I^G(J^{PC}) = 0^-(3^{--})$

MASS (MeV)	WIDTH (MeV)	DOCUMENT ID	TECN	COMMENT
2255 ± 15	175 ± 30	¹ ANISOVICH	02B	SPEC 0.6-1.9 $p\bar{p} \rightarrow \omega\eta, \omega\pi^0\pi^0$

¹ From the combined analysis of ANISOVICH 00d, ANISOVICH 01c, and ANISOVICH 02b.

$a_4(2255) \quad I^G(J^{PC}) = 1^-(4^{++})$

MASS (MeV)	WIDTH (MeV)	DOCUMENT ID	TECN	COMMENT
2237 ± 5	291 ± 12	UMAN	06	E835 5.2 $\bar{p}p \rightarrow \eta\eta\pi^0$
2255 ± 40	330^{+110}_{-50}	¹ ANISOVICH	01F	SPEC 1.96-2.41 $\bar{p}p$

¹ From the combined analysis of ANISOVICH 99c, ANISOVICH 99e, and ANISOVICH 01f.

$a_2(2255) \quad I^G(J^{PC}) = 1^-(2^{++})$

MASS (MeV)	WIDTH (MeV)	DOCUMENT ID	TECN	COMMENT
2255 ± 20	230 ± 15	¹ ANISOVICH	01G	SPEC 1.96-2.41 $\bar{p}p$

¹ From the combined analysis of ANISOVICH 99c, ANISOVICH 99e, ANISOVICH 01f, and ANISOVICH 01g.

$X(2260) \quad I^G(J^{PC}) = 0^+(4^{+?})$

MASS (MeV)	WIDTH (MeV)	DOCUMENT ID	TECN	COMMENT
2260 ± 20	400 ± 100	EVANGELIS...	79	OMEG 10,16 $\pi^-p \rightarrow \bar{p}pn$

$\rho(2270) \quad I^G(J^{PC}) = 1^+(1^{--})$

MASS (MeV)	WIDTH (MeV)	DOCUMENT ID	TECN	COMMENT
2265 ± 40	325 ± 80	¹ ANISOVICH	02	SPEC 0.6-1.9 $p\bar{p} \rightarrow \omega\pi^0, \omega\eta\pi^0, \pi^+\pi^-$
2280 ± 50	440 ± 110	ATKINSON	85	OMEG 20-70 $\gamma p \rightarrow \rho\omega\pi^+\pi^-\pi^0$

¹ From the combined analysis of ANISOVICH 00i, ANISOVICH 01d, ANISOVICH 01e, and ANISOVICH 02.

$a_1(2270) \quad I^G(J^{PC}) = 1^-(1^{++})$

MASS (MeV)	WIDTH (MeV)	DOCUMENT ID	TECN	COMMENT
2270^{+55}_{-40}	305^{+70}_{-40}	ANISOVICH	01F	SPEC 2.0 $\bar{p}p \rightarrow 3\pi^0, \pi^0\eta, \pi^0\eta'$

$h_3(2275) \quad I^G(J^{PC}) = 0^-(3^{+-})$

MASS (MeV)	WIDTH (MeV)	DOCUMENT ID	TECN	COMMENT
2275 ± 25	190 ± 45	¹ ANISOVICH	02B	SPEC 0.6-1.9 $p\bar{p} \rightarrow \omega\eta, \omega\pi^0\pi^0$

¹ From the combined analysis of ANISOVICH 00d, ANISOVICH 01c, and ANISOVICH 02b.

$a_3(2275) \quad I^G(J^{PC}) = 1^-(3^{++})$

MASS (MeV)	WIDTH (MeV)	DOCUMENT ID	TECN	COMMENT
2275 ± 35	350^{+100}_{-50}	¹ ANISOVICH	01G	SPEC 1.96-2.41 $\bar{p}p$

¹ From the combined analysis of ANISOVICH 99c, ANISOVICH 99e, ANISOVICH 01f, and ANISOVICH 01g.

$\pi_2(2285) \quad I^G(J^{PC}) = 1^-(2^{-+})$

MASS (MeV)	WIDTH (MeV)	DOCUMENT ID	TECN	COMMENT
$2285 \pm 20 \pm 25$	$250 \pm 20 \pm 25$	¹ ANISOVICH	11	SPEC 0.9-1.94 $p\bar{p}$

¹ Reanalysis of ADOEIT 96 and ANISOVICH 00e.

$\omega_3(2285) \quad I^G(J^{PC}) = 0^-(3^{--})$

MASS (MeV)	WIDTH (MeV)	DOCUMENT ID	TECN	COMMENT
2278 ± 28	224 ± 50	¹ BUGG	04A	RVUE
2285 ± 60	230 ± 40	² ANISOVICH	02B	SPEC 0.6-1.9 $p\bar{p} \rightarrow \omega\eta, \omega\pi^0\pi^0$

¹ Partial wave analysis of the data on $p\bar{p} \rightarrow \bar{\Lambda}\Lambda$ from BARNES 00.
² From the combined analysis of ANISOVICH 00d, ANISOVICH 01c, and ANISOVICH 02b.

$\omega(2290) \quad I^G(J^{PC}) = 0^-(1^{--})$

MASS (MeV)	WIDTH (MeV)	DOCUMENT ID	TECN	COMMENT
2290 ± 20	275 ± 35	¹ BUGG	04A	RVUE

¹ Partial wave analysis of the data on $p\bar{p} \rightarrow \bar{\Lambda}\Lambda$ from BARNES 00.

$f_2(2295) \quad I^G(J^{PC}) = 0^+(2^{++})$

MASS (MeV)	WIDTH (MeV)	DOCUMENT ID	TECN	COMMENT
2293 ± 13	216 ± 37	¹ ANISOVICH	00J	SPEC 1.92-2.41 $p\bar{p}$

¹ From the combined analysis of ANISOVICH 99c, ANISOVICH 99f, ANISOVICH 99j, ANISOVICH 99k, and ANISOVICH 00b. See also ANISOVICH 12.

$f_3(2300) \quad I^G(J^{PC}) = 0^+(3^{++})$

MASS (MeV)	WIDTH (MeV)	DOCUMENT ID	TECN	COMMENT
2334 ± 25	200 ± 20	¹ BUGG	04A	RVUE

¹ Partial wave analysis of the data on $p\bar{p} \rightarrow \bar{\Lambda}\Lambda$ from BARNES 00.

$f_1(2310) \quad I^G(J^{PC}) = 0^+(1^{++})$

MASS (MeV)	WIDTH (MeV)	DOCUMENT ID	TECN	COMMENT
2310 ± 60	255 ± 70	ANISOVICH	00J	SPEC

$\eta(2320) \quad I^G(J^{PC}) = 0^+(0^{-+})$

MASS (MeV)	WIDTH (MeV)	DOCUMENT ID	TECN	COMMENT
2320 ± 15	230 ± 35	¹ ANISOVICH	00M	SPEC

¹ From the combined analysis of $\bar{p}p \rightarrow \eta\eta\eta$ from ANISOVICH 00m and $\bar{p}p \rightarrow \eta\pi^0\pi^0$ from ANISOVICH 00j.

$\eta_4(2330) \quad I^G(J^{PC}) = 0^+(4^{-+})$

MASS (MeV)	WIDTH (MeV)	DOCUMENT ID	TECN	COMMENT
2328 ± 38	240 ± 90	ANISOVICH	00J	SPEC 2.0 $p\bar{p} \rightarrow \eta\pi^0\pi^0$

$\omega(2330) \quad I^G(J^{PC}) = 0^-(1^{--})$

MASS (MeV)	WIDTH (MeV)	DOCUMENT ID	TECN	COMMENT
2330 ± 30	435 ± 75	ATKINSON	88	OMEG 25-50 $\gamma p \rightarrow \rho^\pm\rho^0\pi^\mp$

$X(2340) \quad I^G(J^{PC}) = ??(???)$

MASS (MeV)	WIDTH (MeV)	EVTS	DOCUMENT ID	TECN	COMMENT
2340 ± 20	180 ± 60	126	¹ BALTAY	75	HBC 15 $\pi^+p \rightarrow p_5\pi$

¹ Dominant decay into $\rho^0\rho^0\pi^+$. BALTAY 78 finds confirmation in $2\pi^+\pi^-\pi^0$ events which contain $\rho^+\rho^0\pi^0$ and $2\rho^+\pi^-$.

$\pi(2360) \quad I^G(J^{PC}) = 1^-(0^{-+})$

MASS (MeV)	WIDTH (MeV)	DOCUMENT ID	TECN	COMMENT
2360 ± 25	300^{+100}_{-50}	ANISOVICH	01F	SPEC 2.0 $\bar{p}p \rightarrow 3\pi^0, \pi^0\eta, \pi^0\eta'$

$X(2360) \quad I^G(J^{PC}) = ??(4^{+?})$

MASS (MeV)	WIDTH (MeV)	DOCUMENT ID	TECN	COMMENT
2360 ± 10	430 ± 30	ROZANSKA	80	SPRK 18 $\pi^-p \rightarrow p\bar{p}n$

$X(2440) \quad I^G(J^{PC}) = ??(5^{-?})$

MASS (MeV)	WIDTH (MeV)	DOCUMENT ID	TECN	COMMENT
2440 ± 10	310 ± 20	ROZANSKA	80	SPRK 18 $\pi^-p \rightarrow p\bar{p}n$

$a_6(2450) \quad I^G(J^{PC}) = 1^-(6^{++})$

MASS (MeV)	WIDTH (MeV)	DOCUMENT ID	TECN	COMMENT
2450 ± 130	400 ± 250	CLELAND	82B	SPEC 5.0 $\pi p \rightarrow K_S^0 K^\pm p$

$X(2540) \quad I^G(J^{PC}) = 0^+(0^{++})$

MASS (MeV)	WIDTH (MeV)	DOCUMENT ID	TECN	COMMENT
$2539 \pm 14^{+38}_{-14}$	$274^{+77+126}_{-61-163}$	UEHARA	13	BELL $\gamma\gamma \rightarrow K_S^0 K_S^0$

$\Gamma(\gamma\gamma) \times B(K\bar{K})$

VALUE (eV)	DOCUMENT ID	TECN	COMMENT
40^{+9+17}_{-7-40}	UEHARA	13	BELL $\gamma\gamma \rightarrow K_S^0 K_S^0$

$X(2632) \quad I^G(J^{PC}) = ??(???)$

MASS (MeV)	WIDTH (MeV)	DOCUMENT ID	TECN	COMMENT
2635.2 ± 3.3		¹ EVDOKIMOV	04	SELX X(2632) $\rightarrow D_S^+\eta$
2631.6 ± 2.1	< 17	² EVDOKIMOV	04	SELX X(2632) $\rightarrow D_S^0 K^+$

¹ From a mass difference to D_S^+ of 666.9 ± 3.3 MeV.
² From a mass difference to D_S^0 of 767.0 ± 2.0 MeV.

Meson Particle Listings

Further States

$B(X(2632) \rightarrow D^0 K^+) / B(X(2632) \rightarrow D_s^+ \eta)$

VALUE	DOCUMENT ID	TECN
0.14 ± 0.06	¹ EVDOKIMOV 04	SELX

¹ Possible interpretation of this decay pattern is discussed by YASUI 07.

$X(2680) \quad I^G(J^{PC}) = ?(???)$

MASS (MeV)	WIDTH (MeV)	DOCUMENT ID	TECN	COMMENT
2676 ± 27	150	CASO	70 HBC	11.2 $\pi^- p \rightarrow \rho^- \pi^+ \pi^- p$

$X(2710) \quad I^G(J^{PC}) = ?(6^{+?})$

MASS (MeV)	WIDTH (MeV)	DOCUMENT ID	TECN	COMMENT
2710 ± 20	170 ± 40	ROZANSKA	80 SPRK	18 $\pi^- p \rightarrow p \bar{p} n$

$X(2750) \quad I^G(J^{PC}) = ?(7^{-?})$

MASS (MeV)	WIDTH (MeV)	DOCUMENT ID	TECN	COMMENT
2747 ± 32	195 ± 75	DENNEY	83 LASS	10 $\pi^+ p \rightarrow K^+ K^- \pi^+ p$

$f_6(3100) \quad I^G(J^{PC}) = 0^{+}(6^{++})$

MASS (MeV)	WIDTH (MeV)	DOCUMENT ID	TECN	COMMENT
3100 ± 100	700 ± 130	BINON	05 GAMS	33 $\pi^- p \rightarrow \eta \eta n$

$X(3250) \quad I^G(J^{PC}) = ?(???)$ 3-Body Decays

MASS (MeV)	WIDTH (MeV)	DOCUMENT ID	TECN	COMMENT
3250 ± 8 ± 20	45 ± 18	ALEEV	93 BIS2	$X(3250) \rightarrow \Lambda \bar{p} K^+$
3265 ± 7 ± 20	40 ± 18	ALEEV	93 BIS2	$X(3250) \rightarrow \bar{\Lambda} p K^-$

$X(3250) \quad I^G(J^{PC}) = ?(???)$ 4-Body Decays

MASS (MeV)	WIDTH (MeV)	DOCUMENT ID	TECN	COMMENT
3245 ± 8 ± 20	25 ± 11	ALEEV	93 BIS2	$X(3250) \rightarrow \Lambda \bar{p} K^+ \pi^\pm$
3250 ± 9 ± 20	50 ± 20	ALEEV	93 BIS2	$X(3250) \rightarrow \bar{\Lambda} p K^- \pi^\mp$
3270 ± 8 ± 20	25 ± 11	ALEEV	93 BIS2	$X(3250) \rightarrow K_S^0 \bar{p} p K^\pm$

$X(3350) \quad I^G(J^{PC}) = ?(???)$

MASS (MeV)	WIDTH (MeV)	EVTS	DOCUMENT ID	TECN	COMMENT
3350 $^{+10}_{-20}$ ± 20	70 $^{+40}_{-30}$ ± 40	50 ± 10	¹ GABYSHEV 06A	BELL	$B^- \rightarrow \Lambda_c^+ \bar{p} \pi^-$

¹ A similar enhancement in the $\Lambda_c^+ \bar{p} \pi^-$ final state is also reported by BABAR collaboration in AUBERT 10H.

$Z_{cs}(4000)^+ \quad I(J^P) = 1/2(1^+)$

MASS (MeV)	WIDTH (MeV)	DOCUMENT ID	TECN	COMMENT
4003 ± 6 $^{+4}_{-14}$	131 ± 15 ± 26	^{1,2} AAJ	21E LHCB	$B^+ \rightarrow J/\psi \phi K^+$
3982.5 $^{+1.8}_{-2.6}$ ± 2.1	12.8 $^{+5.3}_{-4.4}$ ± 3.0	^{2,3} ABLIKIM	21G BES3	$e^+ e^- \rightarrow K^+ (D_s^- D^{*0} + D_s^{*-} D^0)$

¹ From an amplitude analysis of the decay $B^+ \rightarrow J/\psi \phi K^+$ with a significance of 15 σ .
² Properties incompatible with a $q\bar{q}$ structure (exotic state). See the review on "Heavy Non- $q\bar{q}$ Mesons."
³ Pole mass, width for a mass-width-dependent Breit-Wigner fit to the mass, width spectrum recoiling against K^+ at center of mass energies between 4.628 and 4.698 GeV, with a significance of 5.3 σ .

$Z_{cs}(4220)^+ \quad I(J^P) = 1/2(1^+)$

MASS (MeV)	WIDTH (MeV)	DOCUMENT ID	TECN	COMMENT
4216 ± 24 $^{+43}_{-30}$	233 ± 52 $^{+97}_{-73}$	^{1,2} AAJ	21E LHCB	$B^+ \rightarrow J/\psi \phi K^+$

¹ From an amplitude analysis of the decay $B^+ \rightarrow J/\psi \phi K^+$ with a significance of 5.9 σ .
² Properties incompatible with a $q\bar{q}$ structure (exotic state). See the review on "Heavy Non- $q\bar{q}$ Mesons."

$X(6900) \quad I^G(J^{PC}) = ?(???)$

MASS (MeV)	WIDTH (MeV)	DOCUMENT ID	TECN	COMMENT
6886 ± 11 ± 11	168 ± 33 ± 69	¹ AAJ	20AY LHCB	$pp \rightarrow J/\psi J/\psi X$

¹ Assuming the interference of a Breit-Wigner shape with non-resonant single-parton scattering. Without interference, the mass and width are $6905 \pm 11 \pm 7$ and $80 \pm 19 \pm 33$ MeV. State incompatible with a $q\bar{q}$ structure. See the review on "Heavy Non- $q\bar{q}$ Mesons."

REFERENCES for Further States

AAJ	21E	PRL 127 082001	R. Aaij <i>et al.</i>	(LHCb Collab.)
ABLIKIM	21G	PRL 126 102001	M. Ablikim <i>et al.</i>	(BESIII Collab.)
LEES	21A	PR D104 072002	J.P. Lees <i>et al.</i>	(BABAR Collab.)
AAJ	20AY	SCIB 65 1933	R. Aaij <i>et al.</i>	(LHCb Collab.)
ABLIKIM	16N	PR D93 112011	M. Ablikim	(BESIII Collab.)
UEHARA	13	PTEP 2013 123C01	S. Uehara <i>et al.</i>	(BELLE Collab.)
ANISOVICH	12	PR D85 014001	A.V. Anisovich <i>et al.</i>	
ANASHIN	11	PL B703 543	V.V. Anashin <i>et al.</i>	(KEDR Collab.)
ANISOVICH	11	EPJ C71 1511	A.V. Anisovich <i>et al.</i>	(LOQM, RAL, PNPI)
CHEN	11F	PR D84 071501	P. Chen <i>et al.</i>	(BESII Collab.)
AUBERT	10H	PR D82 031102	B. Aubert <i>et al.</i>	(BABAR Collab.)
ABRAAMYAN	09	PR C80 034001	Kh.U. Abraamyan <i>et al.</i>	
VLADIMIRSK...	08	PAN 71 2129	V.V. Vladimirsky <i>et al.</i>	(ITEP)
VLADIMIRSK...	07	PAN 70 1706	V. Vladimirsky <i>et al.</i>	
YASUI	07	PR D76 034009	S. Yasui, M. Oka	
ABLIKIM	06S	PRL 97 142002	M. Ablikim <i>et al.</i>	(BES Collab.)
GABYSHEV	06A	PRL 97 242001	N. Gabyshev <i>et al.</i>	(BELLE Collab.)
SCHEGELSKY	06	EPJ A27 199	V.A. Schegelsky <i>et al.</i>	
SCHEGELSKY	06A	EPJ A27 207	V.A. Schegelsky <i>et al.</i>	
UMAN	06	PR D73 052009	I. Uman <i>et al.</i>	(FNAL E835)
VLADIMIRSK...	06	PAN 69 493	V.V. Vladimirsky <i>et al.</i>	(ITEP, Moscow)
BINON	05	PAN 68 960	F. Binon <i>et al.</i>	
GRIGOR'EV	05	PAN 68 1271	V.K. Grigor'ev <i>et al.</i>	(ITEP)
LU	05	PRL 94 032002	M. Lu <i>et al.</i>	(BNL E852 Collab.)
ABLIKIM	04J	PRL 93 112002	M. Ablikim <i>et al.</i>	(BES Collab.)
BUGG	04	PL B595 556 (err.)	D.V. Bugg	
BUGG	04A	EPJ C36 161	D.V. Bugg	
BUGG	04C	PRPL 397 257	D.V. Bugg	
EVDOKIMOV	04	PRL 93 242001	A.V. Evdokimov <i>et al.</i>	(SELEX Collab.)
KUHN	04	PL B595 109	J. Kuhn <i>et al.</i>	(BNL E852 Collab.)
ANISOVICH	03	EPJ A16 229	V.V. Anisovich <i>et al.</i>	
VLADIMIRSK...	03	PAN 66 700	V.V. Vladimirsky <i>et al.</i>	
ANISOVICH	02	PL B542 8	A.V. Anisovich <i>et al.</i>	
ANISOVICH	02B	PL B542 19	A.V. Anisovich <i>et al.</i>	
CHUNG	02	PR D65 072001	S.U. Chung <i>et al.</i>	(BNL E852 Collab.)
ANISOVICH	01C	PL B507 23	A.V. Anisovich <i>et al.</i>	
ANISOVICH	01D	PL B508 6	A.V. Anisovich <i>et al.</i>	
ANISOVICH	01E	PL B513 281	A.V. Anisovich <i>et al.</i>	
ANISOVICH	01F	PL B517 261	A.V. Anisovich <i>et al.</i>	
ANISOVICH	01G	PL B517 273	A.V. Anisovich <i>et al.</i>	
ANISOVICH	00B	NP A662 319	A.V. Anisovich <i>et al.</i>	
ANISOVICH	00D	PL B476 15	A.V. Anisovich <i>et al.</i>	
ANISOVICH	00E	PL B477 19	A.V. Anisovich <i>et al.</i>	
ANISOVICH	00I	PL B491 40	A.V. Anisovich <i>et al.</i>	
ANISOVICH	00J	PL B491 47	A.V. Anisovich <i>et al.</i>	(RAL, LOQM, PNPI+)
ANISOVICH	00M	PL B496 145	A.V. Anisovich <i>et al.</i>	
BARNES	00	PR C62 055203	P.D. Barnes <i>et al.</i>	
FILIPPI	00	PL B495 284	A. Filippi <i>et al.</i>	(OBELIX Experiment)
VLADIMIRSKII	00	JETPL 72 486	V.V. Vladimirskii <i>et al.</i>	
ANISOVICH	99C	PL B452 173	A.V. Anisovich <i>et al.</i>	
ANISOVICH	99E	PL B452 187	A.V. Anisovich <i>et al.</i>	
ANISOVICH	99F	NP A651 253	A.V. Anisovich <i>et al.</i>	
ANISOVICH	99J	PL B471 271	A.V. Anisovich <i>et al.</i>	
ANISOVICH	99K	PL B468 309	A.V. Anisovich <i>et al.</i>	
BUGG	99	PL B458 511	D.V. Bugg <i>et al.</i>	
FERRER	99	EPJ C10 249	A. Ferrer <i>et al.</i>	
SEME NOV	99	SPU 42 847	S.V. Semenov	
ADOMEIT	96	ZPHY C71 227	J. Adomeit <i>et al.</i>	(Crystal Barrel Collab.)
KLOET	96	PR D53 6120	W.M. Kloet, F. Myhrer	(RUTG, NORD)
PROKOSHKIN	96	PD 41 247	Y.D. Prokoshkin, V.D. Samoilenko	(SERP)
HASAN	94	PL B334 215	A. Hasan, D.V. Bugg	(LOQM)
OAKDEN	94	NP A574 731	M.N. Oakden, M.R. Pennington	(DURH)
ALEEV	93	PAN 56 1358	A.N. Aleev <i>et al.</i>	(BIS-2 Collab.)
ARMSTRONG	93D	PL B307 399	T.A. Armstrong <i>et al.</i>	(FNAL, FERR, GENO+)
ALBRECHT	91F	ZPHY C50 1	H. Albrecht <i>et al.</i>	(ARGUS Collab.)
CONDO	91	PR D43 2787	G.T. Condo <i>et al.</i>	(SLAC Hybrid Collab.)
BISELLO	89B	PR D39 701	G. Busetto <i>et al.</i>	(DM2 Collab.)
ATKINSON	88	ZPHY C38 535	M. Atkinson <i>et al.</i>	(BONN, CERN, GLAS+)
DAFTAR I	87	PRL 58 859	I.K. Daftari <i>et al.</i>	(SYRA)
ALDE	86D	NP B269 485	D.M. Alde <i>et al.</i>	(BELG, LAPP, SERP, CERN+)
BRIDGES	86D	PL B180 313	D.L. Bridges <i>et al.</i>	(SYRA, BNL, CASE+)
GREEN	86	PRL 56 1639	D.R. Green <i>et al.</i>	(FNAL, ARIZ, FSU+)
ATKINSON	85	ZPHY C29 333	M. Atkinson <i>et al.</i>	(BONN, CERN, GLAS+)
DENNEY	83	PR D28 2726	D.L. Denney <i>et al.</i>	(IOWA, MICH)
CLELAND	82B	NP B208 228	W.E. Cleland <i>et al.</i>	(DURH, GEVA, LAUS+)
ASTON	81B	NP B189 205	D. Aston <i>et al.</i>	(BONN, CERN, EPOL, GLAS+)
ARESTOV	80	IHEP 80-165	Y.I. Arestov <i>et al.</i>	(SERP)
CHLIAPNIK...	80	ZPHY C3 285	P.V. Chliapnikov <i>et al.</i>	(SERP, BRUX, MONS)
KREYMER	80	PR D22 36	A.E. Kreymer <i>et al.</i>	(IND, PURD, SLAC+)
ROZANSKA	80	NP B162 505	M. Rozanska <i>et al.</i>	(MPIM, CERN)
EVANGELIS...	79B	NP B153 253	C. Evangelista <i>et al.</i>	(BARI, BONN, CERN+)
EVANGELIS...	79B	NP B154 381	C. Evangelista <i>et al.</i>	(BARI, BONN, CERN+)
BALTAY	78	PR D17 52	C. Baltay <i>et al.</i>	(COLU, BING)
ANTIPOV	77	NP B119 45	Y.M. Antipov <i>et al.</i>	(SERP, GEVA)
BALTAY	77	PRL 39 591	C. Baltay, C.V. Cautis, M. Kalelkar	(COLU)
BALTAY	77	PRL 35 931	C. Baltay <i>et al.</i>	(COLU, BING)
KALELKAR	75	Thesis Nevis 207	M.S. Kalelkar	(COLU)
CASO	70	LN C 3 707	C. Caso <i>et al.</i>	(GENO, HAMB, MILA, SACL)

p	1987
n	1997
N resonances	2003
Δ resonances	2042
Λ	2065
Λ resonances	2068
Σ^+	2090
Σ^0	2092
Σ^-	2093
Σ resonances	2095
Ξ^0	2121
Ξ^-	2123
Ξ resonances	2126
Ω^-	2133
Ω resonances	2135
Λ_c^+	2136
$\Lambda_c(2595)^+$	2143
$\Lambda_c(2625)^+$	2143
$\Lambda_c(2765)^+$ aka $\Sigma_c(2765)$	2144
$\Lambda_c(2860)^+$	2144
$\Lambda_c(2880)^+$	2144
$\Lambda_c(2940)^+$	2145
$\Sigma_c(2455)$	2145
$\Sigma_c(2520)$	2146
$\Sigma_c(2800)$	2147
Ξ_c^+	2148
Ξ_c^0	2149
$\Xi_c^{\prime+}$	2151
$\Xi_c^{\prime0}$	2151
$\Xi_c(2645)$	2152
$\Xi_c(2790)$	2152
$\Xi_c(2815)$	2153
$\Xi_c(2923)$	2153
$\Xi_c(2930)$	2154
$\Xi_c(2970)$ was $\Xi_c(2980)$	2154
$\Xi_c(3055)$	2155
$\Xi_c(3080)$	2155
$\Xi_c(3123)$	2156
Ω_c^0	2156
$\Omega_c(2770)^0$	2157
$\Omega_c(3000)^0$	2157
$\Omega_c(3050)^0$	2158
$\Omega_c(3065)^0$	2158
$\Omega_c(3090)^0$	2158
$\Omega_c(3120)^0$	2159

Ξ_{cc}^+	2160
Ξ_{cc}^{++}	2160
Λ_b^0	2161
$\Lambda_b(5912)^0$	2169
$\Lambda_b(5920)^0$	2169
$\Lambda_b(6070)^0$	2170
$\Lambda_b(6146)^0$	2170
$\Lambda_b(6152)^0$	2170
Σ_b	2171
Σ_b^*	2171
$\Sigma_b(6097)^+$	2172
$\Sigma_b(6097)^-$	2172
Ξ_b^-	2172
Ξ_b^0	2174
$\Xi_b'(5935)^-$	2175
$\Xi_b(5945)^0$	2176
$\Xi_b(5955)^-$	2176
$\Xi_b(6227)^0$	2177
$\Xi_b(6100)^-$	2176
Ξ_{bc}^0	2177
Ω_b^-	2177
$\Omega_b(6316)^-$	2178
$\Omega_b(6330)^-$	2179
$\Omega_b(6340)^-$	2179
$\Omega_b(6350)^-$	2179
$\Xi_b(6227)^-$	2176
b -baryon ADMIXTURE (Λ_b , Ξ_b , Ω_b)	2179
$P_c(4312)^+$	2181
$P_c(4440)^+$	2181
$P_c(4380)^+$	2181
$P_c(4457)^+$ was $P_c(4450)$	2181

Notes in the Listings

Radiative hyperon decays	2122
Ξ resonances	2126

Related Reviews in Volume 1

80. Baryon decay parameters	964
81. N and Δ resonances	965
82. Λ and Σ resonances (rev.)	970
83. Pole structure of the $\Lambda(1405)$ region (rev.)	973
84. Pentaquarks (rev.)	975

N BARYONS

(S = 0, I = 1/2)

$$p, N^+ = uud; \quad n, N^0 = udd$$

p

$$I(J^P) = \frac{1}{2}(\frac{1}{2}^+)$$
 Status: * * * *

p MASS (atomic mass units u)

The mass is known more precisely in u (atomic mass units) than in MeV.
See the next data block.

VALUE (u)	DOCUMENT ID	TECN	COMMENT
1.007276466621 ± 0.000000000053	OUR EVALUATION	2018	CODATA
1.007276466574 ± 0.000000000010	¹ FINK 21	SPEC	Penning trap
1.007276466621 ± 0.000000000053	² TIESINGA 21	RVUE	2018 CODATA value
• • • We do not use the following data for averages, fits, limits, etc. • • •			
1.007276466598 ± 0.000000000033	³ HEISSE 19	SPEC	Penning Trap
1.007276466583 ± 0.000000000032	⁴ HEISSE 17	SPEC	See HEISSE 19
1.007276466879 ± 0.000000000091	MOHR 16	RVUE	2014 CODATA value
1.007276466812 ± 0.000000000090	MOHR 12	RVUE	2010 CODATA value
1.00727646677 ± 0.000000000010	MOHR 08	RVUE	2006 CODATA value
1.00727646688 ± 0.000000000013	MOHR 05	RVUE	2002 CODATA value
1.00727646688 ± 0.000000000013	MOHR 99	RVUE	1998 CODATA value
1.007276470 ± 0.0000000012	COHEN 87	RVUE	1986 CODATA value

¹FINK 21 simultaneously measure the cyclotron frequencies of an H_2^+ ion and a deuteron in a coupled magnetron orbit. The proton mass is extracted using the precise deuteron mass value.

²The 2018 CODATA combination in TIESINGA 21 includes data from HEISSE 17, but does not include updates in HEISSE 19, which superseded HEISSE 17. Consequently, we do not average HEISSE 19 and TIESINGA 21. Updating the 2018 CODATA combination to use HEISSE 19 would shift the central value for the proton mass upwards by less than half a standard deviation. Therefore, we take the 2018 CODATA result in TIESINGA 21 as the recommended value for the proton mass.

³The value is an update of HEISSE 17; the result is shifted by 1.5×10^{-11} u, corresponding to 0.45σ due to the corrected motional temperatures of the particles. The statistical and total systematic uncertainties are given as 16 and 29 in the last two digits.

⁴The statistical and systematic errors are 15 and 29 in the last two places of the value. Superseded by HEISSE 19.

p MASS (MeV)

The mass is known more precisely in u (atomic mass units) than in MeV.
The conversion is: $1 \text{ u} = 931.494 \text{ 102 42(28) MeV}/c^2$ (2018 CODATA value, TIESINGA 21).

VALUE (MeV)	DOCUMENT ID	TECN	COMMENT
938.27208816 ± 0.00000029	OUR EVALUATION	2018	CODATA
938.27208812 ± 0.00000029	¹ FINK 21	SPEC	Penning trap
938.27208816 ± 0.00000029	TIESINGA 21	RVUE	2018 CODATA value
• • • We do not use the following data for averages, fits, limits, etc. • • •			
938.2720813 ± 0.0000058	MOHR 16	RVUE	2014 CODATA value
938.272046 ± 0.0000021	MOHR 12	RVUE	2010 CODATA value
938.272013 ± 0.0000023	MOHR 08	RVUE	2006 CODATA value
938.272029 ± 0.0000080	MOHR 05	RVUE	2002 CODATA value
938.271998 ± 0.0000038	MOHR 99	RVUE	1998 CODATA value
938.27231 ± 0.000028	COHEN 87	RVUE	1986 CODATA value
938.2796 ± 0.0027	COHEN 73	RVUE	1973 CODATA value

¹FINK 21 quote the more precise mass in atomic mass units.

$$|m_p - m_{\bar{p}}|/m_p$$

A test of CPT invariance. Note that the comparison of the \bar{p} and p charge-to-mass ratio, given in the next data block, is much better determined.

VALUE	CL%	DOCUMENT ID	TECN	COMMENT
<7 × 10⁻¹⁰	90	¹ HORI 11	SPEC	$\bar{p}e^-$ He atom
• • • We do not use the following data for averages, fits, limits, etc. • • •				
<2 × 10 ⁻⁹	90	¹ HORI 06	SPEC	$\bar{p}e^-$ He atom
<1.0 × 10 ⁻⁸	90	¹ HORI 03	SPEC	$\bar{p}e^-$ ⁴ He, $\bar{p}e^-$ ³ He
<6 × 10 ⁻⁸	90	¹ HORI 01	SPEC	$\bar{p}e^-$ He atom
<5 × 10 ⁻⁷		² TORII 99	SPEC	$\bar{p}e^-$ He atom

¹HORI 01, HORI 03, HORI 06, and HORI 11 use the more-precisely-known constraint on the \bar{p} charge-to-mass ratio of GABRIELSE 99 (see below) to get their results. Their results are not independent of the HORI 01, HORI 03, HORI 06, and HORI 11 values for $|q_p + q_{\bar{p}}|/e$, below.

²TORII 99 uses the more-precisely-known constraint on the \bar{p} charge-to-mass ratio of GABRIELSE 95 (see below) to get this result. This is not independent of the TORII 99 value for $|q_p + q_{\bar{p}}|/e$, below.

\bar{p}/p CHARGE-TO-MASS RATIO, $|\frac{q_{\bar{p}}}{m_{\bar{p}}}|/(\frac{q_p}{m_p})$

A test of CPT invariance. Listed here are measurements involving the inertial masses. For a discussion of what may be inferred about the ratio of \bar{p} and p gravitational masses, see ERICSON 90; they obtain an upper bound of 10^{-6} – 10^{-7} for violation of the equivalence principle for \bar{p} s.

VALUE	DOCUMENT ID	TECN	COMMENT
1.000000000003 ± 0.000000000016	OUR AVERAGE		
1.000000000003 ± 0.000000000016	BORCHERT 22	TRAP	Penning trap
1.000000000001 ± 0.000000000069	ULMER 15	TRAP	Penning trap
• • • We do not use the following data for averages, fits, limits, etc. • • •			
0.99999999991 ± 0.00000000009	GABRIELSE 99	TRAP	Penning trap
1.0000000015 ± 0.0000000011	¹ GABRIELSE 95	TRAP	Penning trap
1.000000023 ± 0.0000000042	² GABRIELSE 90	TRAP	Penning trap

¹Equation (2) of GABRIELSE 95 should read $M(\bar{p})/M(p) = 0.999\ 999\ 9985$ (11) (G. Gabrielse, private communication).

²GABRIELSE 90 also measures $m_{\bar{p}}/m_{e^-} = 1836.152660 \pm 0.000083$ and $m_p/m_{e^-} = 1836.152680 \pm 0.000088$. Both are completely consistent with the 1986 CODATA (COHEN 87) value for m_p/m_{e^-} of 1836.152701 ± 0.000037 .

$$\left(\frac{q_{\bar{p}}}{m_{\bar{p}}} - \frac{q_p}{m_p}\right) / \frac{q_p}{m_p}$$

A test of CPT invariance. Taken from the \bar{p}/p charge-to-mass ratio, above.

VALUE	DOCUMENT ID
(0.1 ± 6.9) × 10⁻¹¹	OUR EVALUATION

$$|q_p + q_{\bar{p}}|/e$$

A test of CPT invariance. Note that the comparison of the \bar{p} and p charge-to-mass ratios given above is much better determined. See also a similar test involving the electron.

VALUE	CL%	DOCUMENT ID	TECN	COMMENT
<7 × 10⁻¹⁰	90	¹ HORI 11	SPEC	$\bar{p}e^-$ He atom
• • • We do not use the following data for averages, fits, limits, etc. • • •				
<2 × 10 ⁻⁹	90	¹ HORI 06	SPEC	$\bar{p}e^-$ He atom
<1.0 × 10 ⁻⁸	90	¹ HORI 03	SPEC	$\bar{p}e^-$ ⁴ He, $\bar{p}e^-$ ³ He
<6 × 10 ⁻⁸	90	¹ HORI 01	SPEC	$\bar{p}e^-$ He atom
<5 × 10 ⁻⁷		² TORII 99	SPEC	$\bar{p}e^-$ He atom
<2 × 10 ⁻⁵		³ HUGHES 92	RVUE	

¹HORI 01, HORI 03, HORI 06, and HORI 11 use the more-precisely-known constraint on the \bar{p} charge-to-mass ratio of GABRIELSE 99 (see above) to get their results. Their results are not independent of the HORI 01, HORI 03, HORI 06, and HORI 11 values for $|m_p - m_{\bar{p}}|/m_p$, above.

²TORII 99 uses the more-precisely-known constraint on the \bar{p} charge-to-mass ratio of GABRIELSE 95 (see above) to get this result. This is not independent of the TORII 99 value for $|m_p - m_{\bar{p}}|/m_p$, above.

³HUGHES 92 uses recent measurements of Rydberg-energy and cyclotron-frequency ratios.

$$|q_p + q_e|/e$$

See BRESSI 11 for a summary of experiments on the neutrality of matter. See also "n CHARGE" in the neutron Listings.

VALUE	DOCUMENT ID	COMMENT
<1 × 10⁻²¹	¹ BRESSI 11	Neutrality of SF ₆
• • • We do not use the following data for averages, fits, limits, etc. • • •		
<3.2 × 10 ⁻²⁰	² SENGUPTA 00	binary pulsar
<0.8 × 10 ⁻²¹	MARINELLI 84	Magnetic levitation
<1.0 × 10 ⁻²¹	¹ DYLLA 73	Neutrality of SF ₆

¹BRESSI 11 uses the method of DYLLA 73 but finds serious errors in that experiment that greatly reduce its accuracy. The BRESSI 11 limit assumes that $n \rightarrow p e^- \nu_e$ conserves charge. Thus the limit applies equally to the charge of the neutron.

²SENGUPTA 00 uses the difference between the observed rate of rotational energy loss by the binary pulsar PSR B1913+16 and the rate predicted by general relativity to set this limit. See the paper for assumptions.

p MAGNETIC MOMENT

See the "Quark Model" review.

VALUE (μ_N)	DOCUMENT ID	TECN	COMMENT
2.79284734463 ± 0.00000000082	TIESINGA 21	RVUE	2018 CODATA value
• • • We do not use the following data for averages, fits, limits, etc. • • •			
2.79284734462 ± 0.00000000082	SCHNEIDER 17	TRAP	Double Penning trap
2.7928473508 ± 0.00000000085	MOHR 16	RVUE	2014 CODATA value
2.792847356 ± 0.0000000023	MOHR 12	RVUE	2010 CODATA value
2.792847356 ± 0.0000000023	MOHR 08	RVUE	2006 CODATA value
2.792847351 ± 0.0000000028	MOHR 05	RVUE	2002 CODATA value
2.792847337 ± 0.0000000029	MOHR 99	RVUE	1998 CODATA value
2.792847386 ± 0.0000000063	COHEN 87	RVUE	1986 CODATA value

Baryon Particle Listings

 ρ \bar{p} MAGNETIC MOMENT

A few early results have been omitted.

VALUE (μ_N)	DOCUMENT ID	TECN	COMMENT
-2.7928473441 ± 0.0000000042	SMORRA	17	TRAP Hot/cold \bar{p} frequencies, Penning traps
• • • We do not use the following data for averages, fits, limits, etc. • • •			
-2.7928465 ± 0.000023	NAGAHAMA	17	TRAP Single \bar{p} , Penning trap
-2.792845 ± 0.000012	DISCIACCA	13	TRAP Single \bar{p} , Penning trap
-2.7862 ± 0.0083	PASK	09	CNTR \bar{p} He ⁺ hyperfine structure
-2.8005 ± 0.0090	KREISSL	88	CNTR \bar{p} ²⁰⁸ Pb 11→10 X-ray
-2.817 ± 0.048	ROBERTS	78	CNTR Exotic atoms
-2.791 ± 0.021	HU	75	CNTR Exotic atoms

$$(\mu_p + \mu_{\bar{p}}) / \mu_p$$

A test of CPT invariance.

VALUE (units 10^{-6})	DOCUMENT ID	TECN	COMMENT
0.002 ± 0.004	SMORRA	17	TRAP Hot/cold \bar{p} frequencies, Penning traps
• • • We do not use the following data for averages, fits, limits, etc. • • •			
0.3 ± 0.8	NAGAHAMA	17	TRAP Single \bar{p} , Penning trap
0 ± 5	DISCIACCA	13	TRAP Single \bar{p} , Penning trap

 ρ ELECTRIC DIPOLE MOMENT

A nonzero value is forbidden by both T invariance and P invariance.

VALUE (10^{-23} e cm)	DOCUMENT ID	TECN	COMMENT
< 0.021	¹ SAHOO	17	Theory plus ¹⁹⁹ Hg atom EDM
• • • We do not use the following data for averages, fits, limits, etc. • • •			
< 0.54	¹ DMITRIEV	03	Theory plus ¹⁹⁹ Hg atom EDM
- 3.7 ± 6.3	CHO	89	NMR TI F molecules
< 400	DZUBA	85	THEO Uses ¹²⁹ Xe moment
130 ± 200	² WILKENING	84	
900 ± 1400	³ WILKENING	84	
700 ± 900	HARRISON	69	MBR Molecular beam

¹ SAHOO 17 and DMITRIEV 03 are not direct measurements of the proton electric dipole moment. They use theory to calculate this limit from the limit on the electric dipole moment of the ¹⁹⁹Hg atom.

² This WILKENING 84 value includes a finite-size effect and a magnetic effect.

³ This WILKENING 84 value is more cautious than the other and excludes the finite-size effect, which relies on uncertain nuclear integrals.

 ρ ELECTRIC POLARIZABILITY α_p

For a very complete review of the "polarizability of the nucleon and Compton scattering," see SCHUMACHER 05, updated in SCHUMACHER 19.

VALUE (10^{-4} fm ³)	DOCUMENT ID	TECN	COMMENT
11.2 ± 0.4 OUR AVERAGE			
10.65 ± 0.35 ± 0.36	MCGOVERN	13	RVUE χ EFT + Compton scattering
12.1 ± 1.1 ± 0.5	¹ BEANE	03	EFT + γp
11.82 ± 0.98 \pm 0.52 \pm 0.98	² BLANPIED	01	LEGS $\rho(\vec{\gamma}, \gamma)$, $\rho(\vec{\gamma}, \pi^0)$, $\rho(\vec{\gamma}, \pi^+)$
11.9 ± 0.5 ± 1.3	³ OLMOSDEL...	01	CNTR γp Compton scattering
12.1 ± 0.8 ± 0.5	⁴ MACGIBBON	95	RVUE global average
• • • We do not use the following data for averages, fits, limits, etc. • • •			
12.03 \pm 0.48 \pm 0.54	⁵ PASQUINI	19	fit of RCS data sets
11.7 ± 0.8 ± 0.7	⁶ BARANOV	01	RVUE Global average
12.5 ± 0.6 ± 0.9	MACGIBBON	95	CNTR γp Compton scattering
9.8 ± 0.4 ± 1.1	HALLIN	93	CNTR γp Compton scattering
10.62 \pm 1.25 \pm 1.07 \pm 1.19 \pm 1.03	ZIEGER	92	CNTR γp Compton scattering
10.9 ± 2.2 ± 1.3	⁷ FEDERSPIEL	91	CNTR γp Compton scattering

¹ BEANE 03 uses effective field theory and low-energy γp and γd Compton-scattering data. It also gets for the isoscalar polarizabilities (see the erratum) $\alpha_N = (13.0 \pm 1.9 \pm 3.9) \times 10^{-4}$ fm³ and $\beta_N = (-1.8 \pm 1.9 \pm 2.1 \pm 0.9) \times 10^{-4}$ fm³.

² BLANPIED 01 gives $\alpha_p + \beta_p$ and $\alpha_p - \beta_p$. The separate α_p and β_p are provided to us by A. Sandorfi. The first error above is statistics plus systematics; the second is from the model.

³ This OLMOSDELEON 01 result uses the TAPS data alone, and does not use the (re-evaluated) sum-rule constraint that $\alpha + \beta = (13.8 \pm 0.4) \times 10^{-4}$ fm³. See the paper for a discussion.

⁴ MACGIBBON 95 combine the results of ZIEGER 92, FEDERSPIEL 91, and their own experiment to get a "global average" in which model errors and systematic errors are treated in a consistent way. See MACGIBBON 95 for a discussion.

⁵ PASQUINI 19 fit data sets for the unpolarized proton RCS cross section, using fixed-t subtracted dispersion relations and a bootstrap-based fitting technique.

⁶ BARANOV 01 combines the results of 10 experiments from 1958 through 1995 to get a global average that takes into account both systematic and model errors and does not use the theoretical constraint on the sum $\alpha_p + \beta_p$.

⁷ FEDERSPIEL 91 obtains for the (static) electric polarizability α_p , defined in terms of the induced electric dipole moment by $\mathbf{D} = 4\pi\epsilon_0\alpha_p\mathbf{E}$, the value $(7.0 \pm 2.2 \pm 1.3) \times 10^{-4}$ fm³.

 ρ MAGNETIC POLARIZABILITY β_p The electric and magnetic polarizabilities are subject to a dispersion sum-rule constraint $\bar{\alpha} + \bar{\beta} = (14.2 \pm 0.5) \times 10^{-4}$ fm³. Errors here are anticorrelated with those on $\bar{\alpha}_p$ due to this constraint.

VALUE (10^{-4} fm ³)	DOCUMENT ID	TECN	COMMENT
2.5 ± 0.4 OUR AVERAGE			Error includes scale factor of 1.2.
3.15 ± 0.35 ± 0.36	MCGOVERN	13	RVUE χ EFT + Compton scattering
3.4 ± 1.1 ± 0.1	¹ BEANE	03	EFT + γp
1.43 ± 0.98 \pm 0.52 \pm 0.98	² BLANPIED	01	LEGS $\rho(\vec{\gamma}, \gamma)$, $\rho(\vec{\gamma}, \pi^0)$, $\rho(\vec{\gamma}, \pi^+)$
1.2 ± 0.7 ± 0.5	³ OLMOSDEL...	01	CNTR γp Compton scattering
2.1 ± 0.8 ± 0.5	⁴ MACGIBBON	95	RVUE global average
• • • We do not use the following data for averages, fits, limits, etc. • • •			
1.77 \pm 0.52 \pm 0.54	⁵ PASQUINI	19	fit of RCS data sets
2.3 ± 0.9 ± 0.7	⁶ BARANOV	01	RVUE Global average
1.7 ± 0.6 ± 0.9	MACGIBBON	95	CNTR γp Compton scattering
4.4 ± 0.4 ± 1.1	HALLIN	93	CNTR γp Compton scattering
3.58 \pm 1.19 \pm 1.03 \pm 1.25 \pm 1.07	ZIEGER	92	CNTR γp Compton scattering
3.3 ± 2.2 ± 1.3	FEDERSPIEL	91	CNTR γp Compton scattering

¹ BEANE 03 uses effective field theory and low-energy γp and γd Compton-scattering data. It also gets for the isoscalar polarizabilities (see the erratum) $\alpha_N = (13.0 \pm 1.9 \pm 3.9) \times 10^{-4}$ fm³ and $\beta_N = (-1.8 \pm 1.9 \pm 2.1 \pm 0.9) \times 10^{-4}$ fm³.

² BLANPIED 01 gives $\alpha_p + \beta_p$ and $\alpha_p - \beta_p$. The separate α_p and β_p are provided to us by A. Sandorfi. The first error above is statistics plus systematics; the second is from the model.

³ This OLMOSDELEON 01 result uses the TAPS data alone, and does not use the (re-evaluated) sum-rule constraint that $\alpha + \beta = (13.8 \pm 0.4) \times 10^{-4}$ fm³. See the paper for a discussion.

⁴ MACGIBBON 95 combine the results of ZIEGER 92, FEDERSPIEL 91, and their own experiment to get a "global average" in which model errors and systematic errors are treated in a consistent way. See MACGIBBON 95 for a discussion.

⁵ PASQUINI 19 fit data sets for the unpolarized proton RCS cross section, using fixed-t subtracted dispersion relations and a bootstrap-based fitting technique.

⁶ BARANOV 01 combines the results of 10 experiments from 1958 through 1995 to get a global average that takes into account both systematic and model errors and does not use the theoretical constraint on the sum $\alpha_p + \beta_p$.

 ρ CHARGE RADIUSThis is the rms electric charge radius, $\sqrt{\langle r_E^2 \rangle}$.

There are three kinds of measurements of the proton radius: via transitions in atomic hydrogen; via electron scattering off hydrogen; and via muonic hydrogen Lamb shift. Most measurements of the radius of the proton involve electron-proton interactions, the most recent of which is the electron scattering measurement $r_p = 0.831(14)$ fm (XIONG 19), and the atomic-hydrogen value, $r_p = 0.833(10)$ fm (BEZGINOV 19). These agree well with another recent atomic-hydrogen value $r_p = 0.8335(95)$ fm (BEYER 17), and with the best measurement using muonic hydrogen $r_p = 0.84087(39)$ fm (ANTOGNINI 13), that is far more precise.

The MOHR 16 value (2014 CODATA), obtained from the electronic results available at the time, was 0.8751(61) fm. This differs by 5.6 standard deviations from the muonic hydrogen value, leading to the so-called proton charge radius puzzle. See our 2018 edition (Physical Review **D98** 030001 (2018)) for a further discussion of interpretations of this puzzle. However, reflecting the new electronic measurements, the 2018 CODATA, TIESINGA 21, recommended value is 0.8414(19) fm, and the puzzle appears to be resolved.

See our 2014 edition (Chinese Physics **C38** 070001 (2014)) for values published before 2003.

VALUE (fm)	DOCUMENT ID	TECN	COMMENT
0.8409 ± 0.0004 OUR AVERAGE			
0.833 ± 0.010	¹ BEZGINOV	19	LASR 2S-2P transition in H
0.831 ± 0.007 ± 0.012	² XIONG	19	SPEC $ep \rightarrow ep$ form factor
0.84087 ± 0.00026 ± 0.00029	ANTOGNINI	13	LASR μp -atom Lamb shift
• • • We do not use the following data for averages, fits, limits, etc. • • •			
0.847 ± 0.008	³ CUI	21	FIT use existing ep data
0.878 ± 0.011 ± 0.031	⁴ MIHOVLOVIC	21	ISR $ep \rightarrow ep$ reanalysis
0.877 ± 0.013	⁵ FLEURBAEY	18	LASR 1S-3S transition in H
0.8335 ± 0.0095	⁶ BEYER	17	LASR 2S-4P transition in H
0.8751 ± 0.0061	MOHR	16	RVUE 2014 CODATA value
0.895 ± 0.014 ± 0.014	⁷ LEE	15	SPEC Just 2010 Mainz data
0.916 ± 0.024	LEE	15	SPEC World data, no Mainz
0.8775 ± 0.0051	MOHR	12	RVUE 2010 CODATA, ep data
0.875 ± 0.008 ± 0.006	ZHAN	11	SPEC Recoil polarimetry

0.879 ± 0.005 ± 0.006	BERNAUER	10	SPEC	$ep \rightarrow ep$ form factor
0.912 ± 0.009 ± 0.007	BORISYUK	10		reanalyzes old ep data
0.871 ± 0.009 ± 0.003	HILL	10		z-expansion reanalysis
0.84184 ± 0.00036 ± 0.00056	POHL	10	LASR	See ANTOGNINI 13
0.8768 ± 0.0069	MOHR	08	RVUE	2006 CODATA value
0.844 ± 0.008 - 0.004	BELUSHKIN	07		Dispersion analysis
0.897 ± 0.018	BLUNDEN	05		SICK 03 + 2γ correction
0.8750 ± 0.0068	MOHR	05	RVUE	2002 CODATA value
0.895 ± 0.010 ± 0.013	SICK	03		$ep \rightarrow ep$ reanalysis

¹ BEZGINOV 19 measures the $2S_{1/2}$ to $2P_{1/2}$ transition frequency in atomic hydrogen using the frequency-offset separated oscillatory field (FOSOF) technique. The result agrees well with the muonic hydrogen Lamb shift value.

² The XIONG 19 value from $ep \rightarrow ep$ scattering and supports the muonic hydrogen Lamb shift value.

³ CUI 21 employ a new mathematical procedure (statistical SPM, Schlessinger point method) based on form-unbiased interpolations of existing ep scattering data.

⁴ MIHOVLOVIC 21 reports a value of $0.878 \pm 0.011 \pm 0.031 \pm 0.002$ fm where the last uncertainty comes from the dependence on the model form factor function.

⁵ FLEURBAEY 18 measures the 1S-3S transition frequency in hydrogen and in combination with the 1S-2S transition frequency deduces the proton radius and the Rydberg constant.

⁶ The BEYER 17 result is 3.3 combined standard deviations below the MOHR 16 (2014 CODATA) value. The experiment measures the 2S-4P transition in hydrogen and gets the proton radius and the Rydberg constant.

⁷ Authors also provide values for combinations of all available data.

ρ MAGNETIC RADIUS

This is the rms magnetic radius, $\sqrt{\langle r_M^2 \rangle}$.

VALUE (fm)	DOCUMENT ID	TECN	COMMENT
0.851 ± 0.026	¹ LEE	15	Combination of world and Mainz data

• • • We do not use the following data for averages, fits, limits, etc. • • •

0.817 ± 0.027	² CUI	21B	FIT use existing ep data
0.87 ± 0.02	EPSTEIN	14	Using $ep, en, \pi\pi$ data
0.867 ± 0.009 ± 0.018	ZHAN	11	SPEC Recoil polarimetry
0.777 ± 0.013 ± 0.010	BERNAUER	10	SPEC $ep \rightarrow ep$ form factor
0.876 ± 0.010 ± 0.016	BORISYUK	10	Reanalyzes old $ep \rightarrow ep$ data
0.854 ± 0.005	BELUSHKIN	07	Dispersion analysis

¹ In a consistent reanalysis LEE 2015 extract values separately for the Mainz 2010 data only ($0.776 \pm 0.034 \pm 0.017$) fm and for the world data without Mainz data (0.914 ± 0.035) fm. The quoted value is a simple combination of the two, which ignores possible discrepancies and unknown correlations and should be considered with caution.

² CUI 21B employ a new mathematical procedure (statistical SPM, Schlessinger point method) based on form-unbiased interpolations of existing ep scattering data.

ρ MEAN LIFE

A test of baryon conservation. See the " ρ Partial Mean Lives" section below for limits for identified final states. The limits here are to "anything" or are for "disappearance" modes of a bound proton (p) or (n). See also the 3ν modes in the "Partial Mean Lives" section. Table 1 of BACK 03 is a nice summary.

LIMIT (years)	PARTICLE	CL%	DOCUMENT ID	TECN	COMMENT
>3.6 × 10²⁹	p	90	¹ ANDERSON	19A	SNO+ $p \rightarrow$ invisible
>5.8 × 10²⁹	n	90	² ARAKI	06	KLND $n \rightarrow$ invisible
• • • We do not use the following data for averages, fits, limits, etc. • • •					
>2.5 × 10 ²⁹	n	90	¹ ANDERSON	19A	SNO+ $n \rightarrow$ invisible
>2.1 × 10 ²⁹	p	90	¹ AHMED	04	SNO $p \rightarrow$ invisible
>1.9 × 10 ²⁹	n	90	¹ AHMED	04	SNO $n \rightarrow$ invisible
>1.8 × 10 ²⁵	n	90	³ BACK	03	BORX
>1.1 × 10 ²⁶	p	90	³ BACK	03	BORX
>3.5 × 10 ²⁸	p	90	⁴ ZDESENKO	03	$p \rightarrow$ invisible
>1 × 10 ²⁸	p	90	⁵ AHMAD	02	SNO $p \rightarrow$ invisible
>4 × 10 ²³	p	95	⁶ TRET'YAK	01	$d \rightarrow n + ?$
>1.9 × 10 ²⁴	p	90	⁶ BERNABEI	00B	DAMA
>1.6 × 10 ²⁵	p, n		⁷ EVANS	77	
>3 × 10 ²³	p		⁸ DIX	70	CNTR
>3 × 10 ²³	p, n		^{8,9} FLEROV	58	

¹ AHMED 04 and ANDERSON 19A look for γ rays from the de-excitation of a residual $^{15}\text{O}^*$ or $^{15}\text{N}^*$ following the disappearance of a neutron or proton in ^{16}O .

² ARAKI 06 looks for signs of de-excitation of the residual nucleus after disappearance of a neutron from the s shell of ^{12}C .

³ BACK 03 looks for decays of unstable nuclides left after N decays of parent ^{12}C , ^{13}C , ^{16}O nuclei. These are "invisible channel" limits.

⁴ ZDESENKO 03 gets this limit on proton disappearance in deuterium by analyzing SNO data in AHMAD 02.

⁵ AHMAD 02 (see its footnote 7) looks for neutrons left behind after the disappearance of the proton in deuterons.

⁶ BERNABEI 00B looks for the decay of a $^{129}_{53}\text{Xe}$ nucleus following the disappearance of a proton in the otherwise-stable $^{129}_{54}\text{Xe}$ nucleus.

⁷ EVANS 77 looks for the daughter nuclide ^{129}Xe from possible ^{130}Te decays in ancient Te ore samples.

⁸ This mean-life limit has been obtained from a half-life limit by dividing the latter by $\ln(2) = 0.693$.

⁹ FLEROV 58 looks for the spontaneous fission of a ^{232}Th nucleus after the disappearance of one of its nucleons.

\bar{p} MEAN LIFE

Of the two astrophysical limits here, that of GEER 00D involves considerably more refinements in its modeling. The other limits come from direct observations of stored antiprotons. See also " \bar{p} Partial Mean Lives" after " ρ Partial Mean Lives," below, for exclusive-mode limits. The best (lifetime/branching fraction) limit there is 7×10^5 years, for $\bar{p} \rightarrow e^- \gamma$. We advance only the exclusive-mode limits to our Summary Tables.

LIMIT (years)	CL%	EVTS	DOCUMENT ID	TECN	COMMENT
• • • We do not use the following data for averages, fits, limits, etc. • • •					
>5.0	90		SELLNER	17	TRAP Penning trap
>8 × 10 ⁵	90		¹ GEER	00D	\bar{p}/p ratio, cosmic rays
>0.28			GABRIELSE	90	TRAP Penning trap
>0.08	90	1	BELL	79	CNTR Storage ring
>1 × 10 ⁷			GOLDEN	79	SPEC \bar{p}/p ratio, cosmic rays
>3.7 × 10 ⁻³			BREGMAN	78	CNTR Storage ring

¹ GEER 00D uses agreement between a model of galactic \bar{p} production and propagation and the observed \bar{p}/p cosmic-ray spectrum to set this limit.

ρ DECAY MODES

See the "Note on Nucleon Decay" in our 1994 edition (Phys. Rev. **D50**, 1173) for a short review.

The "partial mean life" limits tabulated here are the limits on τ/B_j , where τ is the total mean life and B_j is the branching fraction for the mode in question. For N decays, p and n indicate proton and neutron partial lifetimes.

Mode	Partial mean life (10 ³⁰ years)	Confidence level
Antilepton + meson		
τ_1 $N \rightarrow e^+ \pi$	> 5300 (n), > 16000 (p)	90%
τ_2 $N \rightarrow \mu^+ \pi$	> 3500 (n), > 7700 (p)	90%
τ_3 $N \rightarrow \nu \pi$	> 1100 (n), > 390 (p)	90%
τ_4 $p \rightarrow e^+ \eta$	> 10000	90%
τ_5 $p \rightarrow \mu^+ \eta$	> 4700	90%
τ_6 $n \rightarrow \nu \eta$	> 158	90%
τ_7 $N \rightarrow e^+ \rho$	> 217 (n), > 720 (p)	90%
τ_8 $N \rightarrow \mu^+ \rho$	> 228 (n), > 570 (p)	90%
τ_9 $N \rightarrow \nu \rho$	> 19 (n), > 162 (p)	90%
τ_{10} $p \rightarrow e^+ \omega$	> 1600	90%
τ_{11} $p \rightarrow \mu^+ \omega$	> 2800	90%
τ_{12} $n \rightarrow \nu \omega$	> 108	90%
τ_{13} $N \rightarrow e^+ K$	> 17 (n), > 1000 (p)	90%
τ_{14} $p \rightarrow e^+ K_S^0$		
τ_{15} $p \rightarrow e^+ K_L^0$		
τ_{16} $N \rightarrow \mu^+ K$	> 26 (n), > 1600 (p)	90%
τ_{17} $p \rightarrow \mu^+ K_S^0$		
τ_{18} $p \rightarrow \mu^+ K_L^0$		
τ_{19} $N \rightarrow \nu K$	> 86 (n), > 5900 (p)	90%
τ_{20} $n \rightarrow \nu K_S^0$	> 260	90%
τ_{21} $p \rightarrow e^+ K^*(892)^0$	> 84	90%
τ_{22} $N \rightarrow \nu K^*(892)$	> 78 (n), > 51 (p)	90%
Antilepton + mesons		
τ_{23} $p \rightarrow e^+ \pi^+ \pi^-$	> 82	90%
τ_{24} $p \rightarrow e^+ \pi^0 \pi^0$	> 147	90%
τ_{25} $n \rightarrow e^+ \pi^- \pi^0$	> 52	90%
τ_{26} $p \rightarrow \mu^+ \pi^+ \pi^-$	> 133	90%
τ_{27} $p \rightarrow \mu^+ \pi^0 \pi^0$	> 101	90%
τ_{28} $n \rightarrow \mu^+ \pi^- \pi^0$	> 74	90%
τ_{29} $n \rightarrow e^+ K^0 \pi^-$	> 18	90%
Lepton + meson		
τ_{30} $n \rightarrow e^- \pi^+$	> 65	90%
τ_{31} $n \rightarrow \mu^- \pi^+$	> 49	90%
τ_{32} $n \rightarrow e^- \rho^+$	> 62	90%
τ_{33} $n \rightarrow \mu^- \rho^+$	> 7	90%
τ_{34} $n \rightarrow e^- K^+$	> 32	90%
τ_{35} $n \rightarrow \mu^- K^+$	> 57	90%
Lepton + mesons		
τ_{36} $p \rightarrow e^- \pi^+ \pi^+$	> 30	90%
τ_{37} $n \rightarrow e^- \pi^+ \pi^0$	> 29	90%
τ_{38} $p \rightarrow \mu^- \pi^+ \pi^+$	> 17	90%

Baryon Particle Listings

p

τ_{39}	$n \rightarrow \mu^- \pi^+ \pi^0$	> 34	90%
τ_{40}	$p \rightarrow e^- \pi^+ K^+$	> 75	90%
τ_{41}	$p \rightarrow \mu^- \pi^+ K^+$	> 245	90%

Antilepton + photon(s)

τ_{42}	$p \rightarrow e^+ \gamma$	> 670	90%
τ_{43}	$p \rightarrow \mu^+ \gamma$	> 478	90%
τ_{44}	$n \rightarrow \nu \gamma$	> 550	90%
τ_{45}	$p \rightarrow e^+ \gamma \gamma$	> 100	90%
τ_{46}	$n \rightarrow \nu \gamma \gamma$	> 219	90%

Antilepton + single massless

τ_{47}	$p \rightarrow e^+ X$	> 790	90%
τ_{48}	$p \rightarrow \mu^+ X$	> 410	90%

Three (or more) leptons

τ_{49}	$p \rightarrow e^+ e^+ e^-$	> 793	90%
τ_{50}	$p \rightarrow e^+ \mu^+ \mu^-$	> 359	90%
τ_{51}	$p \rightarrow e^+ \nu \nu$	> 170	90%
τ_{52}	$n \rightarrow e^+ e^- \nu$	> 257	90%
τ_{53}	$n \rightarrow \mu^+ e^- \nu$	> 83	90%
τ_{54}	$n \rightarrow \mu^+ \mu^- \nu$	> 79	90%
τ_{55}	$p \rightarrow \mu^+ e^+ e^-$	> 529	90%
τ_{56}	$p \rightarrow \mu^- e^+ e^+$	> 1.90×10^{34}	90%
τ_{57}	$p \rightarrow \mu^+ \mu^+ \mu^-$	> 675	90%
τ_{58}	$p \rightarrow \mu^+ \nu \nu$	> 220	90%
τ_{59}	$p \rightarrow e^- \mu^+ \mu^+$	> 6	90%
τ_{60}	$n \rightarrow 3\nu$	> 5×10^{-4}	90%
τ_{61}	$n \rightarrow 5\nu$		

Inclusive modes

τ_{62}	$N \rightarrow e^+$ anything	> 0.6 (n, p)	90%
τ_{63}	$N \rightarrow \mu^+$ anything	> 12 (n, p)	90%
τ_{64}	$N \rightarrow \nu$ anything		
τ_{65}	$N \rightarrow e^+ \pi^0$ anything	> 0.6 (n, p)	90%
τ_{66}	$N \rightarrow 2$ bodies, ν -free		

$\Delta B = 2$ dinucleon modes

The following are lifetime limits per iron nucleus.

τ_{67}	$pp \rightarrow \pi^+ \pi^+$	> 72.2	90%
τ_{68}	$p n \rightarrow \pi^+ \pi^0$	> 170	90%
τ_{69}	$n n \rightarrow \pi^+ \pi^-$	> 0.7	90%
τ_{70}	$n n \rightarrow \pi^0 \pi^0$	> 404	90%
τ_{71}	$pp \rightarrow K^+ K^+$	> 170	90%
τ_{72}	$pp \rightarrow e^+ e^+$	> 5.8	90%
τ_{73}	$pp \rightarrow e^+ \mu^+$	> 3.6	90%
τ_{74}	$pp \rightarrow \mu^+ \mu^+$	> 1.7	90%
τ_{75}	$p n \rightarrow e^+ \bar{\nu}$	> 260	90%
τ_{76}	$p n \rightarrow \mu^+ \bar{\nu}$	> 200	90%
τ_{77}	$p n \rightarrow \tau^+ \bar{\nu}_\tau$	> 29	90%
τ_{78}	$n n \rightarrow \nu_e \bar{\nu}_e$	> 1.4	90%
τ_{79}	$n n \rightarrow \nu_\mu \bar{\nu}_\mu$	> 1.4	90%
τ_{80}	$p n \rightarrow$ invisible	> 2.1×10^{-5}	90%
τ_{81}	$pp \rightarrow$ invisible	> 5×10^{-5}	90%

\bar{p} DECAY MODES

Mode	Partial mean life (years)	Confidence level	
τ_{82}	$\bar{p} \rightarrow e^- \gamma$	> 7×10^5	90%
τ_{83}	$\bar{p} \rightarrow \mu^- \gamma$	> 5×10^4	90%
τ_{84}	$\bar{p} \rightarrow e^- \pi^0$	> 4×10^5	90%
τ_{85}	$\bar{p} \rightarrow \mu^- \pi^0$	> 5×10^4	90%
τ_{86}	$\bar{p} \rightarrow e^- \eta$	> 2×10^4	90%
τ_{87}	$\bar{p} \rightarrow \mu^- \eta$	> 8×10^3	90%
τ_{88}	$\bar{p} \rightarrow e^- K_S^0$	> 900	90%
τ_{89}	$\bar{p} \rightarrow \mu^- K_S^0$	> 4×10^3	90%
τ_{90}	$\bar{p} \rightarrow e^- K_L^0$	> 9×10^3	90%
τ_{91}	$\bar{p} \rightarrow \mu^- K_L^0$	> 7×10^3	90%
τ_{92}	$\bar{p} \rightarrow e^- \gamma \gamma$	> 2×10^4	90%
τ_{93}	$\bar{p} \rightarrow \mu^- \gamma \gamma$	> 2×10^4	90%
τ_{94}	$\bar{p} \rightarrow e^- \omega$	> 200	90%

p PARTIAL MEAN LIVES

The "partial mean life" limits tabulated here are the limits on τ/B_j , where τ is the total mean life for the proton and B_j is the branching fraction for the mode in question.

Decaying particle: p = proton, n = bound neutron. The same event may appear under more than one partial decay mode. Background estimates may be accurate to a factor of two.

Antilepton + meson

$\tau(N \rightarrow e^+ \pi)$

LIMIT (10^{30} years)	PARTICLE	CL%	EVTs	BKGD EST	DOCUMENT ID	TECN
> 24000	p	90	0	0.59	1 TAKENAKA	20 SKAM
> 5300	n	90	0	0.41	ABE	17D SKAM

• • • We do not use the following data for averages, fits, limits, etc. • • •

> 16000	p	90	0	0.61	ABE	17 SKAM
> 2000	n	90	0	0.27	NISHINO	12 SKAM
> 8200	p	90	0	0.3	NISHINO	09 SKAM
> 540	p	90	0	0.2	MCGREW	99 IMB3
> 158	n	90	3	5	MCGREW	99 IMB3
> 1600	p	90	0	0.1	SHIOZAWA	98 SKAM
> 70	p	90	0	0.5	BERGER	91 FREJ
> 70	n	90	0	≤ 0.1	BERGER	91 FREJ
> 550	p	90	0	0.7	2 BECKER-SZ...	90 IMB3
> 260	p	90	0	< 0.04	HIRATA	89C KAMI
> 130	n	90	0	< 0.2	HIRATA	89C KAMI
> 310	p	90	0	0.6	SEIDEL	88 IMB
> 100	n	90	0	1.6	SEIDEL	88 IMB
> 1.3	n	90	0		BARTELT	87 SOUD
> 1.3	p	90	0		BARTELT	87 SOUD
> 250	p	90	0	0.3	HAINES	86 IMB
> 31	n	90	8	9	HAINES	86 IMB
> 64	p	90	0	< 0.4	ARISAKA	85 KAMI
> 26	n	90	0	< 0.7	ARISAKA	85 KAMI
> 82	p (free)	90	0	0.2	BLEWITT	85 IMB
> 250	p	90	0	0.2	BLEWITT	85 IMB
> 25	n	90	4	4	PARK	85 IMB
> 15	p, n	90	0		BATTISTONI	84 NUSX
> 0.5	p	90	1	0.3	3 BARTELT	83 SOUD
> 0.5	n	90	1	0.3	3 BARTELT	83 SOUD
> 5.8	p	90	2		4 KRISHNA...	82 KOLR
> 5.8	n	90	2		4 KRISHNA...	82 KOLR
> 0.1	n	90	0		5 GURR	67 CNTR

¹ TAKENAKA 20 includes data of ABE 17, and thus supersedes ABE 17.

² This BECKER-SZENDY 90 result includes data from SEIDEL 88.

³ Limit based on zero events.

⁴ We have calculated 90% CL limit from 1 confined event.

⁵ We have converted half-life to 90% CL mean life.

$\tau(N \rightarrow \mu^+ \pi)$

LIMIT (10^{30} years)	PARTICLE	CL%	EVTs	BKGD EST	DOCUMENT ID	TECN
> 16000	p	90	1	0.94	1 TAKENAKA	20 SKAM
> 3500	n	90	1	0.77	ABE	17D SKAM

• • • We do not use the following data for averages, fits, limits, etc. • • •

> 7700	p	90	2	0.87	ABE	17 SKAM
> 1000	n	90	1	0.43	NISHINO	12 SKAM
> 6600	p	90	0	0.3	NISHINO	09 SKAM
> 473	p	90	0	0.6	MCGREW	99 IMB3
> 90	n	90	1	1.9	MCGREW	99 IMB3
> 81	p	90	0	0.2	BERGER	91 FREJ
> 35	n	90	1	1.0	BERGER	91 FREJ
> 230	p	90	0	< 0.07	HIRATA	89C KAMI
> 100	n	90	0	< 0.2	HIRATA	89C KAMI
> 270	p	90	0	0.5	SEIDEL	88 IMB
> 63	n	90	0	0.5	SEIDEL	88 IMB
> 76	p	90	2	1	HAINES	86 IMB
> 23	n	90	8	7	HAINES	86 IMB
> 46	p	90	0	< 0.7	ARISAKA	85 KAMI
> 20	n	90	0	< 0.4	ARISAKA	85 KAMI
> 59	p (free)	90	0	0.2	BLEWITT	85 IMB
> 100	p	90	1	0.4	BLEWITT	85 IMB
> 38	n	90	1	4	PARK	85 IMB
> 10	p, n	90	0		BATTISTONI	84 NUSX
> 1.3	p, n	90	0		ALEKSEEV	81 BAKS

¹ TAKENAKA 20 includes the data of ABE 17 and thus supersedes ABE 17.

$\tau(N \rightarrow \nu \pi)$

LIMIT (10^{30} years)	PARTICLE	CL%	EVTs	BKGD EST	DOCUMENT ID	TECN
> 390	p	90	52.8		ABE	14E SKAM
> 1100	n	90	19.1		ABE	14E SKAM

••• We do not use the following data for averages, fits, limits, etc. •••

Table with columns: > [value], p, [value], [value], [value], [value], [value], [value]. Rows include data for WALL, MCGREW, BERGER, HIRATA, HAINES, KAJITA, PARK, BATTISTONI, KRISHNA..., CHERRY, GURR.

1 In estimating the background, this HIRATA 89c limit (as opposed to the later limits of WALL 00b and MCGREW 99) does not take into account present understanding that the flux of nu_mu originating in the upper atmosphere is depleted. Doing so would reduce the background and thus also would reduce the limit here.

2 We have calculated 90% CL limit from 1 confined event.

3 We have converted 2 possible events to 90% CL limit.

4 We have converted half-life to 90% CL mean life.

tau(p -> e+ eta) T4

Table with columns: LIMIT (10^30 years), PARTICLE, CL%, EVTS, BKGD EST, DOCUMENT ID, TECN. Row: >10000 p, 90, 0, 0.78, ABE, 17d, SKAM.

••• We do not use the following data for averages, fits, limits, etc. •••

Table with columns: > [value], p, [value], [value], [value], [value], [value], [value]. Rows include data for NISHINO, WALL, MCGREW, BERGER, HIRATA, SEIDEL, HAINES, ARISAKA, BLEWITT, CHERRY.

1 We have converted 2 possible events to 90% CL limit.

tau(p -> mu+ eta) T5

Table with columns: LIMIT (10^30 years), PARTICLE, CL%, EVTS, BKGD EST, DOCUMENT ID, TECN. Row: >4700 p, 90, 2, 0.85, ABE, 17d, SKAM.

••• We do not use the following data for averages, fits, limits, etc. •••

Table with columns: > [value], p, [value], [value], [value], [value], [value], [value]. Rows include data for NISHINO, WALL, MCGREW, BERGER, HIRATA, PHILLIPS, SEIDEL, HAINES, ARISAKA, BLEWITT.

tau(n -> nu eta) T6

Table with columns: LIMIT (10^30 years), PARTICLE, CL%, EVTS, BKGD EST, DOCUMENT ID, TECN. Row: >158 n, 90, 0, 1.2, MCGREW, 99, IMB3.

••• We do not use the following data for averages, fits, limits, etc. •••

Table with columns: > [value], n, [value], [value], [value], [value], [value], [value]. Rows include data for WALL, BERGER, HIRATA, SEIDEL, HAINES, KAJITA, PARK, CHERRY.

1 We have converted 2 possible events to 90% CL limit.

tau(N -> e+ rho) T7

Table with columns: LIMIT (10^30 years), PARTICLE, CL%, EVTS, BKGD EST, DOCUMENT ID, TECN. Row: >720 p, 90, 2, 0.64, ABE, 17d, SKAM.

••• We do not use the following data for averages, fits, limits, etc. •••

Table with columns: > [value], n, [value], [value], [value], [value], [value], [value]. Rows include data for ABE, NISHINO, BERGER.

Table with columns: > [value], n, [value], [value], [value], [value], [value], [value]. Rows include data for BERGER, HIRATA, SEIDEL, BARTELT, HAINES, ARISAKA, BLEWITT, PARK, BARTELT, KRISHNA..., CHERRY.

1 Limit based on zero events.

2 We have calculated 90% CL limit from 0 confined events.

3 We have converted 2 possible events to 90% CL limit.

tau(N -> mu+ rho) T8

Table with columns: LIMIT (10^30 years), PARTICLE, CL%, EVTS, BKGD EST, DOCUMENT ID, TECN. Row: >570 p, 90, 1, 1.30, ABE, 17d, SKAM.

••• We do not use the following data for averages, fits, limits, etc. •••

Table with columns: > [value], n, [value], [value], [value], [value], [value], [value]. Rows include data for ABE, NISHINO, BERGER, HIRATA, PHILLIPS, SEIDEL, HAINES, ARISAKA, BLEWITT, PARK.

tau(N -> nu rho) T9

Table with columns: LIMIT (10^30 years), PARTICLE, CL%, EVTS, BKGD EST, DOCUMENT ID, TECN. Row: >162 p, 90, 18, 21.7, MCGREW, 99, IMB3.

••• We do not use the following data for averages, fits, limits, etc. •••

Table with columns: > [value], n, [value], [value], [value], [value], [value], [value]. Rows include data for BERGER, HIRATA, SEIDEL, HAINES, KAJITA, BLEWITT, PARK, CHERRY.

1 We have converted 2 possible events to 90% CL limit.

tau(p -> e+ omega) T10

Table with columns: LIMIT (10^30 years), PARTICLE, CL%, EVTS, BKGD EST, DOCUMENT ID, TECN. Row: >1600 p, 90, 1, 1.35, ABE, 17d, SKAM.

••• We do not use the following data for averages, fits, limits, etc. •••

Table with columns: > [value], p, [value], [value], [value], [value], [value], [value]. Rows include data for NISHINO, MCGREW, BERGER, HIRATA, SEIDEL, BARTELT, HAINES, ARISAKA, BLEWITT, BARTELT, KRISHNA..., CHERRY.

1 Limit based on zero events.

2 We have calculated 90% CL limit from 0 confined events.

3 We have converted 2 possible events to 90% CL limit.

Baryon Particle Listings

ρ

$\tau(\rho \rightarrow \mu^+ \omega)$ τ_{11}

LIMIT (10^{30} years)	PARTICLE	CL%	EVTS	BKGD	EST	DOCUMENT ID	TECN
>2800	ρ	90	0	1.09		ABE 17d	SKAM
... We do not use the following data for averages, fits, limits, etc. ...							
> 780	ρ	90	0	0.48		NISHINO 12	SKAM
> 117	ρ	90	11	12.1		MCGREW 99	IMB3
> 11	ρ	90	0	1.0		BERGER 91	FREJ
> 57	ρ	90	2	1.9		HIRATA 89c	KAMI
> 4.4	ρ	90	0	0.7		PHILLIPS 89	HPW
> 10	ρ	90	2	1.3		SEIDEL 88	IMB
> 23	ρ	90	2	1		HAINES 86	IMB
> 6.5	ρ (free)	90	9	8.7		BLEWITT 85	IMB
> 23	ρ	90	8	7		BLEWITT 85	IMB

$\tau(n \rightarrow \nu \omega)$ τ_{12}

LIMIT (10^{30} years)	PARTICLE	CL%	EVTS	BKGD	EST	DOCUMENT ID	TECN
>108	n	90	12	22.5		MCGREW 99	IMB3
... We do not use the following data for averages, fits, limits, etc. ...							
> 17	n	90	1	0.7		BERGER 89	FREJ
> 43	n	90	3	2.7		HIRATA 89c	KAMI
> 6	n	90	2	1.3		SEIDEL 88	IMB
> 12	n	90	6	6		HAINES 86	IMB
> 18	n	90	2	2		KAJITA 86	KAMI
> 16	n	90	1	2		PARK 85	IMB
> 2.0	n	90	2			1 CHERRY 81	HOME

¹ We have converted 2 possible events to 90% CL limit.

$\tau(N \rightarrow e^+ K)$ τ_{13}

LIMIT (10^{30} years)	PARTICLE	CL%	EVTS	BKGD	EST	DOCUMENT ID	TECN
>1000	p	90	6	4.7		KOBAYASHI 05	SKAM
> 17	n	90	35	29.4		MCGREW 99	IMB3
... We do not use the following data for averages, fits, limits, etc. ...							
> 85	p	90	3	4.9		WALL 00	SOU2
> 31	p	90	23	25.2		MCGREW 99	IMB3
> 60	p	90	0			BERGER 91	FREJ
> 150	p	90	0	<0.27		HIRATA 89c	KAMI
> 70	p	90	0	1.8		SEIDEL 88	IMB
> 77	p	90	5	4.5		HAINES 86	IMB
> 38	p	90	0	<0.8		ARISAKA 85	KAMI
> 24	p (free)	90	7	8.5		BLEWITT 85	IMB
> 77	p	90	5	4		BLEWITT 85	IMB
> 1.3	p	90	0			ALEKSEEV 81	BAKS
> 1.3	n	90	0			ALEKSEEV 81	BAKS

$\tau(\rho \rightarrow e^+ K_S^0)$ τ_{14}

LIMIT (10^{30} years)	PARTICLE	CL%	EVTS	BKGD	EST	DOCUMENT ID	TECN
>120	p	90	1	1.3		WALL 00	SOU2
> 76	p	90	0	0.5		BERGER 91	FREJ

$\tau(\rho \rightarrow e^+ K_L^0)$ τ_{15}

LIMIT (10^{30} years)	PARTICLE	CL%	EVTS	BKGD	EST	DOCUMENT ID	TECN
>51	p	90	2	3.5		WALL 00	SOU2
>44	p	90	0	≤ 0.1		BERGER 91	FREJ

$\tau(N \rightarrow \mu^+ K)$ τ_{16}

LIMIT (10^{30} years)	PARTICLE	CL%	EVTS	BKGD	EST	DOCUMENT ID	TECN
>1600	p	90	13	13.2		REGIS 12	SKAM
> 26	n	90	20	28.4		MCGREW 99	IMB3
... We do not use the following data for averages, fits, limits, etc. ...							
>1300	p	90	3	3.9		KOBAYASHI 05	SKAM
> 120	p	90	0	<1.2		WALL 00	SOU2
> 120	p	90	4	7.2		MCGREW 99	IMB3
> 54	p	90	0			BERGER 91	FREJ
> 120	p	90	1	0.4		HIRATA 89c	KAMI
> 3.0	p	90	0	0.7		PHILLIPS 89	HPW
> 19	p	90	3	2.5		SEIDEL 88	IMB
> 1.5	p	90	0			1 BARTELT 87	SOUND
> 1.1	n	90	0			BARTELT 87	SOUND
> 40	p	90	7	6		HAINES 86	IMB
> 19	p	90	1	<1.1		ARISAKA 85	KAMI
> 6.7	p (free)	90	11	13		BLEWITT 85	IMB
> 40	p	90	7	8		BLEWITT 85	IMB
> 6	p	90	1			BATTISTONI 84	NUSX
> 0.6	p	90	0			2 BARTELT 83	SOUND
> 0.4	n	90	0			2 BARTELT 83	SOUND
> 5.8	p	90	2			3 KRISHNA... 82	KOLR
> 2.0	p	90	0			CHERRY 81	HOME
> 0.2	n	90				4 GURR 67	CNTR

- ¹ BARTELT 87 limit applies to $\rho \rightarrow \mu^+ K_S^0$.
- ² Limit based on zero events.
- ³ We have calculated 90% CL limit from 1 confined event.
- ⁴ We have converted half-life to 90% CL mean life.

$\tau(\rho \rightarrow \mu^+ K_S^0)$ τ_{17}

LIMIT (10^{30} years)	PARTICLE	CL%	EVTS	BKGD	EST	DOCUMENT ID	TECN
>150	p	90	0	<0.8		WALL 00	SOU2
> 64	p	90	0	1.2		BERGER 91	FREJ

$\tau(\rho \rightarrow \mu^+ K_L^0)$ τ_{18}

LIMIT (10^{30} years)	PARTICLE	CL%	EVTS	BKGD	EST	DOCUMENT ID	TECN
>83	p	90	0	0.4		WALL 00	SOU2
>44	p	90	0	≤ 0.1		BERGER 91	FREJ

$\tau(N \rightarrow \nu K)$ τ_{19}

LIMIT (10^{30} years)	PARTICLE	CL%	EVTS	BKGD	EST	DOCUMENT ID	TECN
>5900	p	90	0	1.0		ABE 14g	SKAM
> 86	n	90	0	2.4		HIRATA 89c	KAMI
... We do not use the following data for averages, fits, limits, etc. ...							
> 540	p	90	0	0.9		ASAKURA 15	KLND
>2300	p	90	0	1.3		KOBAYASHI 05	SKAM
> 26	n	90	16	9.1		WALL 00	SOU2
> 670	p	90				HAYATO 99	SKAM
> 151	p	90	15	21.4		MCGREW 99	IMB3
> 30	n	90	34	34.1		MCGREW 99	IMB3
> 43	p	90	1	1.54		1 ALLISON 98	SOU2
> 15	n	90	1	1.8		BERGER 89	FREJ
> 15	p	90	1	1.8		BERGER 89	FREJ
> 100	p	90	9	7.3		HIRATA 89c	KAMI
> 0.28	p	90	0	0.7		PHILLIPS 89	HPW
> 0.3	p	90	0			BARTELT 87	SOUND
> 0.75	n	90	0			2 BARTELT 87	SOUND
> 10	p	90	6	5		HAINES 86	IMB
> 15	n	90	3	5		HAINES 86	IMB
> 28	p	90	3	3		KAJITA 86	KAMI
> 32	n	90	0	1.4		KAJITA 86	KAMI
> 1.8	p (free)	90	6	11		BLEWITT 85	IMB
> 9.6	p	90	6	5		BLEWITT 85	IMB
> 10	n	90	2	2		PARK 85	IMB
> 5	n	90	0			BATTISTONI 84	NUSX
> 2	p	90	0			BATTISTONI 84	NUSX
> 0.3	n	90	0			3 BARTELT 83	SOUND
> 0.1	p	90	0			3 BARTELT 83	SOUND
> 5.8	p	90	1			4 KRISHNA... 82	KOLR
> 0.3	n	90	2			5 CHERRY 81	HOME

- ¹ This ALLISON 98 limit is with no background subtraction; with subtraction the limit becomes $> 46 \times 10^{30}$ years.
- ² BARTELT 87 limit applies to $n \rightarrow \nu K_S^0$.
- ³ Limit based on zero events.
- ⁴ We have calculated 90% CL limit from 1 confined event.
- ⁵ We have converted 2 possible events to 90% CL limit.

$\tau(n \rightarrow \nu K_S^0)$ τ_{20}

LIMIT (10^{30} years)	PARTICLE	CL%	EVTS	BKGD	EST	DOCUMENT ID	TECN
>260	n	90	34	30		1 KOBAYASHI 05	SKAM
... We do not use the following data for averages, fits, limits, etc. ...							
> 51	n	90	16	9.1		WALL 00	SOU2

¹ We have doubled the $n \rightarrow \nu K^0$ limit given in KOBAYASHI 05 to obtain this $n \rightarrow \nu K_S^0$ limit.

$\tau(\rho \rightarrow e^+ K^*(892)^0)$ τ_{21}

LIMIT (10^{30} years)	PARTICLE	CL%	EVTS	BKGD	EST	DOCUMENT ID	TECN
>84	p	90	38	52.0		MCGREW 99	IMB3
... We do not use the following data for averages, fits, limits, etc. ...							
>10	p	90	0	0.8		BERGER 91	FREJ
>52	p	90	2	1.55		HIRATA 89c	KAMI
>10	p	90	1	<1		ARISAKA 85	KAMI

$\tau(N \rightarrow \nu K^*(892)^0)$ τ_{22}

LIMIT (10^{30} years)	PARTICLE	CL%	EVTS	BKGD	EST	DOCUMENT ID	TECN
>51	p	90	7	9.1		MCGREW 99	IMB3
>78	n	90	40	50		MCGREW 99	IMB3
... We do not use the following data for averages, fits, limits, etc. ...							
>22	n	90	0	2.1		BERGER 89	FREJ
>17	p	90	0	2.4		BERGER 89	FREJ
>20	p	90	5	2.1		HIRATA 89c	KAMI
>21	n	90	4	2.4		HIRATA 89c	KAMI

>	Particle	90	7	6	HAINES	86	IMB
>	<i>n</i>	90	8	7	HAINES	86	IMB
>	<i>p</i>	90	3	2	KAJITA	86	KAMI
>	<i>n</i>	90	2	1.6	KAJITA	86	KAMI
>	<i>p</i> (free)	90	10	16	BLEWITT	85	IMB
>	<i>p</i>	90	7	6	BLEWITT	85	IMB
>	<i>n</i>	90	1	4	PARK	85	IMB
>	<i>p</i>	90	1		¹ BATTISTONI	82	NUSX

¹ We have converted 1 possible event to 90% CL limit.

Antilepton + mesons

$\tau(p \rightarrow e^+ \pi^+ \pi^-)$ 723

LIMIT (10 ³⁰ years)	PARTICLE	CL%	EVTs	BKGD EST	DOCUMENT ID	TECN
>82	<i>p</i>	90	16	23.1	MCGREW	99 IMB3
... We do not use the following data for averages, fits, limits, etc. ...						
>21	<i>p</i>	90	0	2.2	BERGER	91 FREJ

$\tau(p \rightarrow e^+ \pi^0 \pi^0)$ 724

LIMIT (10 ³⁰ years)	PARTICLE	CL%	EVTs	BKGD EST	DOCUMENT ID	TECN
>147	<i>p</i>	90	2	0.8	MCGREW	99 IMB3
... We do not use the following data for averages, fits, limits, etc. ...						
>38	<i>p</i>	90	1	0.5	BERGER	91 FREJ

$\tau(n \rightarrow e^+ \pi^- \pi^0)$ 725

LIMIT (10 ³⁰ years)	PARTICLE	CL%	EVTs	BKGD EST	DOCUMENT ID	TECN
>52	<i>n</i>	90	38	34.2	MCGREW	99 IMB3
... We do not use the following data for averages, fits, limits, etc. ...						
>32	<i>n</i>	90	1	0.8	BERGER	91 FREJ

$\tau(p \rightarrow \mu^+ \pi^+ \pi^-)$ 726

LIMIT (10 ³⁰ years)	PARTICLE	CL%	EVTs	BKGD EST	DOCUMENT ID	TECN
>133	<i>p</i>	90	25	38.0	MCGREW	99 IMB3
... We do not use the following data for averages, fits, limits, etc. ...						
>17	<i>p</i>	90	1	2.6	BERGER	91 FREJ
>3.3	<i>p</i>	90	0	0.7	PHILLIPS	89 HPW

$\tau(p \rightarrow \mu^+ \pi^0 \pi^0)$ 727

LIMIT (10 ³⁰ years)	PARTICLE	CL%	EVTs	BKGD EST	DOCUMENT ID	TECN
>101	<i>p</i>	90	3	1.6	MCGREW	99 IMB3
... We do not use the following data for averages, fits, limits, etc. ...						
>33	<i>p</i>	90	1	0.9	BERGER	91 FREJ

$\tau(n \rightarrow \mu^+ \pi^- \pi^0)$ 728

LIMIT (10 ³⁰ years)	PARTICLE	CL%	EVTs	BKGD EST	DOCUMENT ID	TECN
>74	<i>n</i>	90	17	20.8	MCGREW	99 IMB3
... We do not use the following data for averages, fits, limits, etc. ...						
>33	<i>n</i>	90	0	1.1	BERGER	91 FREJ

$\tau(n \rightarrow e^+ K^0 \pi^-)$ 729

LIMIT (10 ³⁰ years)	PARTICLE	CL%	EVTs	BKGD EST	DOCUMENT ID	TECN
>18	<i>n</i>	90	1	0.2	BERGER	91 FREJ

Lepton + meson

$\tau(n \rightarrow e^- \pi^+)$ 730

LIMIT (10 ³⁰ years)	PARTICLE	CL%	EVTs	BKGD EST	DOCUMENT ID	TECN
>65	<i>n</i>	90	0	1.6	SEIDEL	88 IMB
... We do not use the following data for averages, fits, limits, etc. ...						
>55	<i>n</i>	90	0	1.09	BERGER	91B FREJ
>16	<i>n</i>	90	9	7	HAINES	86 IMB
>25	<i>n</i>	90	2	4	PARK	85 IMB

$\tau(n \rightarrow \mu^- \pi^+)$ 731

LIMIT (10 ³⁰ years)	PARTICLE	CL%	EVTs	BKGD EST	DOCUMENT ID	TECN
>49	<i>n</i>	90	0	0.5	SEIDEL	88 IMB
... We do not use the following data for averages, fits, limits, etc. ...						
>33	<i>n</i>	90	0	1.40	BERGER	91B FREJ
>2.7	<i>n</i>	90	0	0.7	PHILLIPS	89 HPW
>25	<i>n</i>	90	7	6	HAINES	86 IMB
>27	<i>n</i>	90	2	3	PARK	85 IMB

$\tau(n \rightarrow e^- \rho^+)$ 732

LIMIT (10 ³⁰ years)	PARTICLE	CL%	EVTs	BKGD EST	DOCUMENT ID	TECN
>62	<i>n</i>	90	2	4.1	SEIDEL	88 IMB
... We do not use the following data for averages, fits, limits, etc. ...						
>12	<i>n</i>	90	13	6	HAINES	86 IMB
>12	<i>n</i>	90	5	3	PARK	85 IMB

$\tau(n \rightarrow \mu^- \rho^+)$ 733

LIMIT (10 ³⁰ years)	PARTICLE	CL%	EVTs	BKGD EST	DOCUMENT ID	TECN
>7	<i>n</i>	90	1	1.1	SEIDEL	88 IMB
... We do not use the following data for averages, fits, limits, etc. ...						
>2.6	<i>n</i>	90	0	0.7	PHILLIPS	89 HPW
>9	<i>n</i>	90	7	5	HAINES	86 IMB
>9	<i>n</i>	90	2	2	PARK	85 IMB

$\tau(n \rightarrow e^- K^+)$ 734

LIMIT (10 ³⁰ years)	PARTICLE	CL%	EVTs	BKGD EST	DOCUMENT ID	TECN
>32	<i>n</i>	90	3	2.96	BERGER	91B FREJ
... We do not use the following data for averages, fits, limits, etc. ...						
>0.23	<i>n</i>	90	0	0.7	PHILLIPS	89 HPW

$\tau(n \rightarrow \mu^- K^+)$ 735

LIMIT (10 ³⁰ years)	PARTICLE	CL%	EVTs	BKGD EST	DOCUMENT ID	TECN
>57	<i>n</i>	90	0	2.18	BERGER	91B FREJ
... We do not use the following data for averages, fits, limits, etc. ...						
>4.7	<i>n</i>	90	0	0.7	PHILLIPS	89 HPW

Lepton + mesons

$\tau(p \rightarrow e^- \pi^+ \pi^+)$ 736

LIMIT (10 ³⁰ years)	PARTICLE	CL%	EVTs	BKGD EST	DOCUMENT ID	TECN
>30	<i>p</i>	90	1	2.50	BERGER	91B FREJ
... We do not use the following data for averages, fits, limits, etc. ...						
>2.0	<i>p</i>	90	0	0.7	PHILLIPS	89 HPW

$\tau(n \rightarrow e^- \pi^+ \pi^0)$ 737

LIMIT (10 ³⁰ years)	PARTICLE	CL%	EVTs	BKGD EST	DOCUMENT ID	TECN
>29	<i>n</i>	90	1	0.78	BERGER	91B FREJ

$\tau(p \rightarrow \mu^- \pi^+ \pi^+)$ 738

LIMIT (10 ³⁰ years)	PARTICLE	CL%	EVTs	BKGD EST	DOCUMENT ID	TECN
>17	<i>p</i>	90	1	1.72	BERGER	91B FREJ
... We do not use the following data for averages, fits, limits, etc. ...						
>7.8	<i>p</i>	90	0	0.7	PHILLIPS	89 HPW

$\tau(n \rightarrow \mu^- \pi^+ \pi^0)$ 739

LIMIT (10 ³⁰ years)	PARTICLE	CL%	EVTs	BKGD EST	DOCUMENT ID	TECN
>34	<i>n</i>	90	0	0.78	BERGER	91B FREJ

$\tau(p \rightarrow e^- \pi^+ K^+)$ 740

LIMIT (10 ³⁰ years)	PARTICLE	CL%	EVTs	BKGD EST	DOCUMENT ID	TECN
>75	<i>p</i>	90	81	127.2	MCGREW	99 IMB3
... We do not use the following data for averages, fits, limits, etc. ...						
>20	<i>p</i>	90	3	2.50	BERGER	91B FREJ

$\tau(p \rightarrow \mu^- \pi^+ K^+)$ 741

LIMIT (10 ³⁰ years)	PARTICLE	CL%	EVTs	BKGD EST	DOCUMENT ID	TECN
>245	<i>p</i>	90	3	4.0	MCGREW	99 IMB3
... We do not use the following data for averages, fits, limits, etc. ...						
>5	<i>p</i>	90	2	0.78	BERGER	91B FREJ

Antilepton + photon(s)

$\tau(p \rightarrow e^+ \gamma)$ 742

LIMIT (10 ³⁰ years)	PARTICLE	CL%	EVTs	BKGD EST	DOCUMENT ID	TECN
>670	<i>p</i>	90	0	0.1	MCGREW	99 IMB3
... We do not use the following data for averages, fits, limits, etc. ...						
>133	<i>p</i>	90	0	0.3	BERGER	91 FREJ
>460	<i>p</i>	90	0	0.6	SEIDEL	88 IMB
>360	<i>p</i>	90	0	0.3	HAINES	86 IMB
>87	<i>p</i> (free)	90	0	0.2	BLEWITT	85 IMB
>360	<i>p</i>	90	0	0.2	BLEWITT	85 IMB
>0.1	<i>p</i>	90			¹ GURR	67 CNTR

¹ We have converted half-life to 90% CL mean life.

$\tau(p \rightarrow \mu^+ \gamma)$ 743

LIMIT (10 ³⁰ years)	PARTICLE	CL%	EVTs	BKGD EST	DOCUMENT ID	TECN
>478	<i>p</i>	90	0	0.1	MCGREW	99 IMB3
... We do not use the following data for averages, fits, limits, etc. ...						
>155	<i>p</i>	90	0	0.1	BERGER	91 FREJ
>380	<i>p</i>	90	0	0.5	SEIDEL	88 IMB
>97	<i>p</i>	90	3	2	HAINES	86 IMB
>61	<i>p</i> (free)	90	0	0.2	BLEWITT	85 IMB
>280	<i>p</i>	90	0	0.6	BLEWITT	85 IMB
>0.3	<i>p</i>	90			¹ GURR	67 CNTR

¹ We have converted half-life to 90% CL mean life.

Baryon Particle Listings

 p $\tau(p \rightarrow n \nu \gamma)$ 744

LIMIT (10^{30} years)	PARTICLE	CL%	EVTs	BKGD EST	DOCUMENT ID	TECN
>550	p	90			TAKHISTOV 15	SKAM
••• We do not use the following data for averages, fits, limits, etc. •••						
> 28	n	90	163	144.7	MCGREW 99	IMB3
> 24	n	90	10	6.86	BERGER 91B	FREJ
> 9	n	90	73	60	HAINES 86	IMB
> 11	n	90	28	19	PARK 85	IMB

 $\tau(p \rightarrow e^+ \gamma \gamma)$ 745

LIMIT (10^{30} years)	PARTICLE	CL%	EVTs	BKGD EST	DOCUMENT ID	TECN
>100	p	90	1	0.8	BERGER 91	FREJ

 $\tau(n \rightarrow \nu \gamma \gamma)$ 746

LIMIT (10^{30} years)	PARTICLE	CL%	EVTs	BKGD EST	DOCUMENT ID	TECN
>219	n	90	5	7.5	MCGREW 99	IMB3

Antilepton + single massless

 $\tau(p \rightarrow e^+ X)$ 747

VALUE (10^{30} years)	CL%	DOCUMENT ID	TECN
>790	90	TAKHISTOV 15	SKAM

 $\tau(p \rightarrow \mu^+ X)$ 748

VALUE (10^{30} years)	CL%	DOCUMENT ID	TECN
>410	90	TAKHISTOV 15	SKAM

Three (or more) leptons

 $\tau(p \rightarrow e^+ e^+ e^-)$ 749

LIMIT (10^{30} years)	PARTICLE	CL%	EVTs	BKGD EST	DOCUMENT ID	TECN
>34000	p	90	0	0.58	TANAKA 20	SKAM
••• We do not use the following data for averages, fits, limits, etc. •••						
> 793	p	90	0	0.5	MCGREW 99	IMB3
> 147	p	90	0	0.1	BERGER 91	FREJ
> 510	p	90	0	0.3	HAINES 86	IMB
> 89	p (free)	90	0	0.5	BLEWITT 85	IMB
> 510	p	90	0	0.7	BLEWITT 85	IMB

 $\tau(p \rightarrow e^+ \mu^+ \mu^-)$ 750

LIMIT (10^{30} years)	PARTICLE	CL%	EVTs	BKGD EST	DOCUMENT ID	TECN
>9200	p	90	1	0.27	TANAKA 20	SKAM
••• We do not use the following data for averages, fits, limits, etc. •••						
> 359	p	90	1	0.9	MCGREW 99	IMB3
> 81	p	90	0	0.16	BERGER 91	FREJ
> 5.0	p	90	0	0.7	PHILLIPS 89	HPW

 $\tau(p \rightarrow e^+ \nu \nu)$ 751

LIMIT (10^{30} years)	PARTICLE	CL%	EVTs	BKGD EST	DOCUMENT ID	TECN
>170	p	90			1 TAKHISTOV 14	SKAM
••• We do not use the following data for averages, fits, limits, etc. •••						
> 17	p	90	152	153.7	MCGREW 99	IMB3
> 11	p	90	11	6.08	BERGER 91B	FREJ

¹ Allowed events at 90% CL are 459. $\tau(n \rightarrow e^+ e^- \nu)$ 752

LIMIT (10^{30} years)	PARTICLE	CL%	EVTs	BKGD EST	DOCUMENT ID	TECN
>257	n	90	5	7.5	MCGREW 99	IMB3
••• We do not use the following data for averages, fits, limits, etc. •••						
> 74	n	90	0	< 0.1	BERGER 91B	FREJ
> 45	n	90	5	5	HAINES 86	IMB
> 26	n	90	4	3	PARK 85	IMB

 $\tau(n \rightarrow \mu^+ e^- \nu)$ 753

LIMIT (10^{30} years)	PARTICLE	CL%	EVTs	BKGD EST	DOCUMENT ID	TECN
>83	n	90	25	29.4	MCGREW 99	IMB3
••• We do not use the following data for averages, fits, limits, etc. •••						
>47	n	90	0	< 0.1	BERGER 91B	FREJ

 $\tau(n \rightarrow \mu^+ \mu^- \nu)$ 754

LIMIT (10^{30} years)	PARTICLE	CL%	EVTs	BKGD EST	DOCUMENT ID	TECN
>79	n	90	100	145	MCGREW 99	IMB3
••• We do not use the following data for averages, fits, limits, etc. •••						
>42	n	90	0	1.4	BERGER 91B	FREJ
> 5.1	n	90	0	0.7	PHILLIPS 89	HPW
>16	n	90	14	7	HAINES 86	IMB
>19	n	90	4	7	PARK 85	IMB

 $\tau(p \rightarrow \mu^+ e^+ e^-)$ 755

LIMIT (10^{30} years)	PARTICLE	CL%	EVTs	BKGD EST	DOCUMENT ID	TECN
>23000	p	90	0	0.5	TANAKA 20	SKAM
••• We do not use the following data for averages, fits, limits, etc. •••						
> 529	p	90	0	1.0	MCGREW 99	IMB3
> 91	p	90	0	\leq 0.1	BERGER 91	FREJ

 $\tau(p \rightarrow \mu^- e^+ e^+)$ 756

LIMIT (10^{30} years)	PARTICLE	CL%	EVTs	BKGD EST	DOCUMENT ID	TECN
>19000	p	90	0	0.5	TANAKA 20	SKAM

 $\tau(p \rightarrow \mu^+ \mu^+ \mu^-)$ 757

LIMIT (10^{30} years)	PARTICLE	CL%	EVTs	BKGD EST	DOCUMENT ID	TECN
>10000	p	90	1	0.4	TANAKA 20	SKAM
••• We do not use the following data for averages, fits, limits, etc. •••						
> 675	p	90	0	0.3	MCGREW 99	IMB3
> 119	p	90	0	0.2	BERGER 91	FREJ
> 10.5	p	90	0	0.7	PHILLIPS 89	HPW
> 190	p	90	1	0.1	HAINES 86	IMB
> 44	p (free)	90	1	0.7	BLEWITT 85	IMB
> 190	p	90	1	0.9	BLEWITT 85	IMB
> 2.1	p	90	1		1 BATTISTONI 82	NUSX

¹ We have converted 1 possible event to 90% CL limit. $\tau(p \rightarrow \mu^+ \nu \nu)$ 758

LIMIT (10^{30} years)	PARTICLE	CL%	EVTs	BKGD EST	DOCUMENT ID	TECN
>220	p	90			1 TAKHISTOV 14	SKAM
••• We do not use the following data for averages, fits, limits, etc. •••						
> 21	p	90	7	11.23	BERGER 91B	FREJ

¹ Allowed events at 90% CL are 286. $\tau(p \rightarrow e^- \mu^+ \mu^+)$ 759

LIMIT (10^{30} years)	PARTICLE	CL%	EVTs	BKGD EST	DOCUMENT ID	TECN
>11000	p	90	1	0.27	TANAKA 20	SKAM
••• We do not use the following data for averages, fits, limits, etc. •••						
> 6.0	p	90	0	0.7	PHILLIPS 89	HPW

 $\tau(n \rightarrow 3\nu)$ 760

See also the “to anything” and “disappearance” limits for bound nucleons in the “p Mean Life” data block just in front of the list of possible p decay modes. Such modes could of course be to three (or five) neutrinos, and the limits are stronger, but we do not repeat them here.

LIMIT (10^{30} years)	PARTICLE	CL%	EVTs	BKGD EST	DOCUMENT ID	TECN
>0.00049	n	90	2	2	1 SUZUKI 93B	KAMI
••• We do not use the following data for averages, fits, limits, etc. •••						
>0.0023	n	90			2 GLICENSTEIN 97	KAMI
>0.00003	n	90	11	6.1	3 BERGER 91B	FREJ
>0.00012	n	90	7	11.2	3 BERGER 91B	FREJ
>0.0005	n	90	0		LEARNED 79	RVUE

¹ The SUZUKI 93B limit applies to any of $\nu_e \nu_e \bar{\nu}_e$, $\nu_\mu \nu_\mu \bar{\nu}_\mu$, or $\nu_\tau \nu_\tau \bar{\nu}_\tau$.² GLICENSTEIN 97 uses Kamioka data and the idea that the disappearance of the neutron’s magnetic moment should produce radiation.³ The first BERGER 91B limit is for $n \rightarrow \nu_e \nu_e \bar{\nu}_e$, the second is for $n \rightarrow \nu_\mu \nu_\mu \bar{\nu}_\mu$. $\tau(n \rightarrow 5\nu)$ 761

LIMIT (10^{30} years)	PARTICLE	CL%	EVTs	BKGD EST	DOCUMENT ID	TECN
>0.0017	n	90			1 GLICENSTEIN 97	KAMI
••• We do not use the following data for averages, fits, limits, etc. •••						
>0.0017	n	90			1 GLICENSTEIN 97	KAMI

¹ GLICENSTEIN 97 uses Kamioka data and the idea that the disappearance of the neutron’s magnetic moment should produce radiation.

Inclusive modes

 $\tau(N \rightarrow e^+ \text{ anything})$ 762

LIMIT (10^{30} years)	PARTICLE	CL%	EVTs	BKGD EST	DOCUMENT ID	TECN
>0.6	p, n	90			1 LEARNED 79	RVUE
••• We do not use the following data for averages, fits, limits, etc. •••						
¹ The electron may be primary or secondary.						

 $\tau(N \rightarrow \mu^+ \text{ anything})$ 763

LIMIT (10^{30} years)	PARTICLE	CL%	EVTs	BKGD EST	DOCUMENT ID	TECN
>12	p, n	90	2		1,2 CHERRY 81	HOME
••• We do not use the following data for averages, fits, limits, etc. •••						
> 1.8	p, n	90			2 COWSIK 80	CNTR
> 6	p, n	90			2 LEARNED 79	RVUE

¹ We have converted 2 possible events to 90% CL limit.² The muon may be primary or secondary.

$\tau(N \rightarrow \nu \text{anything})$ 764
Anything = $\pi, \rho, K, \text{etc.}$

Table with columns: LIMIT (10^30 years), PARTICLE, CL%, EVTS, BKGD EST, DOCUMENT ID, TECN. Row: >0.0002, p, n, 90, 0, LEARNED, 79, RVUE

$\tau(N \rightarrow e^+ \pi^0 \text{anything})$ 765

Table with columns: LIMIT (10^30 years), PARTICLE, CL%, EVTS, BKGD EST, DOCUMENT ID, TECN. Row: >0.6, p, n, 90, 0, LEARNED, 79, RVUE

$\tau(N \rightarrow 2 \text{ bodies, } \nu\text{-free})$ 766

Table with columns: LIMIT (10^30 years), PARTICLE, CL%, EVTS, BKGD EST, DOCUMENT ID, TECN. Row: >1.3, p, n, 90, 0, ALEKSEEV, 81, BAKS

ΔB = 2 dinucleon modes

$\tau(pp \rightarrow \pi^+ \pi^+)$ 767

Table with columns: LIMIT (10^30 years), CL%, EVTS, BKGD EST, DOCUMENT ID, TECN, COMMENT. Row: >72.2, 90, 2, 4.45, GUSTAFSON, 15, SKAM, per oxygen nucleus

$\tau(pn \rightarrow \pi^+ \pi^0)$ 768

Table with columns: LIMIT (10^30 years), CL%, EVTS, BKGD EST, DOCUMENT ID, TECN, COMMENT. Row: >170, 90, GUSTAFSON, 15, SKAM, per oxygen nucleus

$\tau(nn \rightarrow \pi^+ \pi^-)$ 769

Table with columns: LIMIT (10^30 years), CL%, EVTS, BKGD EST, DOCUMENT ID, TECN, COMMENT. Row: >0.7, 90, 4, 2.18, BERGER, 91B, FREJ, per iron nucleus

$\tau(nn \rightarrow \pi^0 \pi^0)$ 770

Table with columns: LIMIT (10^30 years), CL%, EVTS, BKGD EST, DOCUMENT ID, TECN, COMMENT. Row: >404, 90, GUSTAFSON, 15, SKAM, per oxygen nucleus

$\tau(pp \rightarrow K^+ K^+)$ 771

Table with columns: LIMIT (10^30 years), CL%, EVTS, BKGD EST, DOCUMENT ID, TECN, COMMENT. Row: >170, 90, 0, 0.28, LITOS, 14, SKAM, per oxygen nucleus

$\tau(pp \rightarrow e^+ e^+)$ 772

Table with columns: LIMIT (10^30 years), CL%, EVTS, BKGD EST, DOCUMENT ID, TECN, COMMENT. Row: >5.8, 90, 0, <0.1, BERGER, 91B, FREJ, per iron nucleus

$\tau(pp \rightarrow e^+ \mu^+)$ 773

Table with columns: LIMIT (10^30 years), CL%, EVTS, BKGD EST, DOCUMENT ID, TECN, COMMENT. Row: >3.6, 90, 0, <0.1, BERGER, 91B, FREJ, per iron nucleus

$\tau(pp \rightarrow \mu^+ \mu^+)$ 774

Table with columns: LIMIT (10^30 years), CL%, EVTS, BKGD EST, DOCUMENT ID, TECN, COMMENT. Row: >1.7, 90, 0, 0.62, BERGER, 91B, FREJ, per iron nucleus

$\tau(pn \rightarrow e^+ \pi)$ 775

Table with columns: LIMIT (10^30 years), CL%, EVTS, BKGD EST, DOCUMENT ID, TECN, COMMENT. Row: >260, 90, TAKHISTOV, 15, SKAM

$\tau(pn \rightarrow \mu^+ \pi)$ 776

Table with columns: LIMIT (10^30 years), CL%, EVTS, BKGD EST, DOCUMENT ID, TECN, COMMENT. Row: >200, 90, TAKHISTOV, 15, SKAM

$\tau(pn \rightarrow \tau^+ \nu_\tau)$ 777

Table with columns: LIMIT (10^30 years), CL%, EVTS, BKGD EST, DOCUMENT ID, TECN, COMMENT. Row: >29, 90, TAKHISTOV, 15, SKAM

1 BRYMAN 14 uses a MCGREW 99 limit on the $p \rightarrow e^+ \nu \nu$ lifetime to extract this value.

$\tau(nn \rightarrow \nu_e \bar{\nu}_e)$ 778
We include "invisible" modes here.

Table with columns: LIMIT (10^30 years), CL%, EVTS, BKGD EST, DOCUMENT ID, TECN, COMMENT. Row: >1.4, 90, ARAKI, 06, KLND, nn -> invisible

1 ARAKI 06 looks for signs of de-excitation of the residual nucleus after disappearance of two neutrons from the s shell of 12C. 2 ANDERSON 19A looks for gamma rays from the de-excitation of a residual 14O* following the disappearance of nn in 16O. 3 TRETAYAK 04 uses data from an old Homestake-mine radiochemical experiment on limits for invisible decays of 39K to 37Ar. 4 BACK 03 looks for decays of unstable nuclides left after NN decays of parent 12C, 13C, 16O nuclei. These are "invisible channel" limits. 5 BERNABEI 00b looks for the decay of a 127Xe nucleus following the disappearance of an nn pair in the otherwise-stable 129Xe nucleus. The limit here applies as well to nn -> nu_mu nu_mu, nn -> nu_tau nu_tau, or any "disappearance" mode.

$\tau(nn \rightarrow \nu_\mu \bar{\nu}_\mu)$ 779

Table with columns: LIMIT (10^30 years), CL%, EVTS, BKGD EST, DOCUMENT ID, TECN, COMMENT. Row: >1.4 (CL=90%) OUR LIMIT, BERGER, 91B, FREJ, per iron nucleus

$\tau(pn \rightarrow \text{invisible})$ 780

Table with columns: VALUE (10^30 years), CL%, DOCUMENT ID, TECN. Row: >0.026, 90, ANDERSON, 19A, SNO+; >0.000021, 90, TRETAYAK, 04, CNTR

$\tau(pp \rightarrow \text{invisible})$ 781

Table with columns: LIMIT (10^30 years), CL%, EVTS, BKGD EST, DOCUMENT ID, TECN, COMMENT. Row: >0.047, 90, ANDERSON, 19A, SNO+; >0.00005, 90, BACK, 03, BORX; >0.0000055, 90, BERNABEI, 00b, DAMA

p PARTIAL MEAN LIVES

The "partial mean life" limits tabulated here are the limits on p/Bj, where p is the total mean life for the antiproton and Bj is the branching fraction for the mode in question.

$\tau(p \rightarrow e^- \gamma)$ 782

Table with columns: VALUE (years), CL%, DOCUMENT ID, TECN, COMMENT. Row: > 7 x 10^5, 90, GEER, 00, APEX, 8.9 GeV/c p beam

$\tau(p \rightarrow \mu^- \gamma)$ 783

Table with columns: VALUE (years), CL%, DOCUMENT ID, TECN, COMMENT. Row: >5 x 10^4, 90, GEER, 00, APEX, 8.9 GeV/c p beam

$\tau(p \rightarrow e^- \pi^0)$ 784

Table with columns: VALUE (years), CL%, DOCUMENT ID, TECN, COMMENT. Row: > 4 x 10^5, 90, GEER, 00, APEX, 8.9 GeV/c p beam

$\tau(p \rightarrow \mu^- \pi^0)$ 785

Table with columns: VALUE (years), CL%, DOCUMENT ID, TECN, COMMENT. Row: >5 x 10^4, 90, GEER, 00, APEX, 8.9 GeV/c p beam

Baryon Particle Listings

p

$\tau(\bar{p} \rightarrow e^- \eta)$ 786

Table with 5 columns: VALUE (years), CL%, DOCUMENT ID, TECN, COMMENT. Includes data for GEER 00 APEX 8.9 GeV/c p beam.

$\tau(\bar{p} \rightarrow \mu^- \eta)$ 787

Table with 5 columns: VALUE (years), CL%, DOCUMENT ID, TECN, COMMENT. Includes data for GEER 00 APEX 8.9 GeV/c p beam.

$\tau(\bar{p} \rightarrow e^- K_S^0)$ 788

Table with 5 columns: VALUE (years), CL%, DOCUMENT ID, TECN, COMMENT. Includes data for GEER 00 APEX 8.9 GeV/c p beam.

$\tau(\bar{p} \rightarrow \mu^- K_S^0)$ 789

Table with 5 columns: VALUE (years), CL%, DOCUMENT ID, TECN, COMMENT. Includes data for GEER 00 APEX 8.9 GeV/c p beam.

$\tau(\bar{p} \rightarrow e^- K_L^0)$ 790

Table with 5 columns: VALUE (years), CL%, DOCUMENT ID, TECN, COMMENT. Includes data for GEER 00 APEX 8.9 GeV/c p beam.

$\tau(\bar{p} \rightarrow \mu^- K_L^0)$ 791

Table with 5 columns: VALUE (years), CL%, DOCUMENT ID, TECN, COMMENT. Includes data for GEER 00 APEX 8.9 GeV/c p beam.

$\tau(\bar{p} \rightarrow e^- \gamma \gamma)$ 792

Table with 5 columns: VALUE (years), CL%, DOCUMENT ID, TECN, COMMENT. Includes data for GEER 00 APEX 8.9 GeV/c p beam.

$\tau(\bar{p} \rightarrow \mu^- \gamma \gamma)$ 793

Table with 5 columns: VALUE (years), CL%, DOCUMENT ID, TECN, COMMENT. Includes data for GEER 00 APEX 8.9 GeV/c p beam.

$\tau(\bar{p} \rightarrow e^- \omega)$ 794

Table with 5 columns: VALUE (years), CL%, DOCUMENT ID, TECN, COMMENT. Includes data for GEER 00 APEX 8.9 GeV/c p beam.

p REFERENCES

Vertical list of references on the left side of the page, starting with BORCHERT 22 NAT 601 53 and ending with NISHINO 12 PR D85 112001.

Main vertical list of references on the right side of the page, starting with REGIS 12 PR D86 012006 and ending with FLEROV 58 DOKL 3 79.

n

I(J^P) = 1/2(1/2⁺) Status: ****

We have omitted some results that have been superseded by later experiments. See our earlier editions.

Anyone interested in the neutron should look at these two review articles: D. Dubbers and M.G. Schmidt, "The neutron and its role in cosmology and particle physics," Reviews of Modern Physics 83 1111 (2011); and F.E. Wietfeldt and G.L. Greene, "The neutron lifetime," Reviews of Modern Physics 83 1173 (2011).

n MASS (atomic mass units)

The mass is known much more precisely in u (atomic mass units) than in MeV. See the next data block.

Table with columns: VALUE (u), DOCUMENT ID, TECN, COMMENT. Includes CODATA values and experimental data from MOHR and COHEN.

n MASS (MeV)

The mass is known more precisely in u (atomic mass units) than in MeV. The conversion is: 1 u = 931.494 102 42(28) MeV/c^2 (2018 CODATA value, TIESINGA 21).

Table with columns: VALUE (MeV), DOCUMENT ID, TECN, COMMENT. Includes CODATA value and experimental data from MOHR, KESSLER, and COHEN.

1 We use the 1998 CODATA u-to-MeV conversion factor... 2 The mass is known much more precisely in u... 3 These determinations are not independent... 4 The mass is known much more precisely in u...

pi MASS

Table with columns: VALUE (MeV), EVTS, DOCUMENT ID, TECN, COMMENT. Includes CODATA value and CRESTI measurement.

1 This is a corrected result (see the erratum). The error is statistical. The maximum systematic error is 0.029 MeV.

(m_n - m_pi) / m_n

A test of CPT invariance. Calculated from the n and pi masses, above.

Table with columns: VALUE, DOCUMENT ID. Shows OUR EVALUATION for (9 +/- 6) x 10^-5.

m_n - m_p

Table with columns: VALUE (MeV), DOCUMENT ID, TECN, COMMENT. Lists various experimental measurements of the neutron-proton mass difference.

- 1 The 2018 CODATA mass difference in u is m_n - m_p = 1.388 449 33(49) x 10^-3 u.
2 The 2014 CODATA mass difference in u is m_n - m_p = 1.388 449 00(51) x 10^-3 u.
3 The 2010 CODATA mass difference in u is m_n - m_p = 1.388 449 19(45) x 10^-3 u.
4 Calculated by us from the MOHR 08 ratio m_n/m_p = 1.00137841918(46). In u, m_n - m_p = 1.38844920(46) x 10^-3 u.
5 Calculated by us from the MOHR 05 ratio m_n/m_p = 1.00137841870 +/- 0.00000000058. In u, m_n - m_p = (1.3884487 +/- 0.0000006) x 10^-3 u.
6 Calculated by us from the MOHR 99 ratio m_n/m_p = 1.00137841887 +/- 0.00000000058. In u, m_n - m_p = (1.3884489 +/- 0.0000006) x 10^-3 u.
7 Calculated by us from the COHEN 87 ratio m_n/m_p = 1.001378404 +/- 0.000000009. In u, m_n - m_p = 0.001388434 +/- 0.000000009 u.

n MEAN LIFE

Limits on lifetimes for bound neutrons are given in the section "p PARTIAL MEAN LIVES."

We average seven of the best eight measurements, those made with ultracold neutrons (UCN's). If we include the one in-beam measurement with a comparable error (YUE 13), we get 879.6 +/- 0.8 s, where the scale factor is now 2.0.

For a recent discussion of the long-standing disagreement between in-beam and UCN results, see CZARNECKI 18 (Physical Review Letters 120 202002 (2018)). For a full review of all matters concerning the neutron lifetime until about 2010, see WIETFELDT 11, F.E. Wietfeldt and G.L. Greene, "The neutron lifetime," Reviews of Modern Physics 83 1173 (2011).

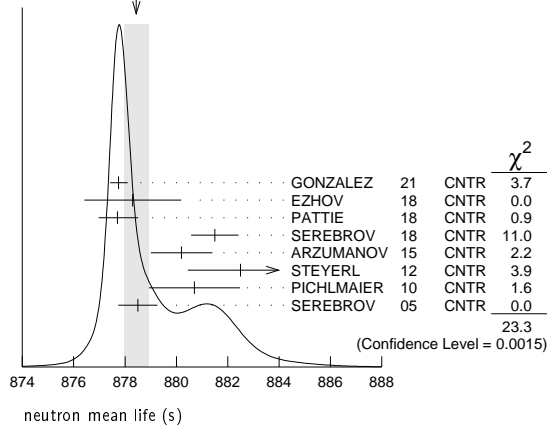
Table with columns: VALUE (s), DOCUMENT ID, TECN, COMMENT. Lists various experimental measurements of the neutron mean life.

- 1 PATTIE 18 uses a new technique, with a semi-toroidal magneto-gravitational asymmetric trap and a novel in situ n-detector.
2 ARZUMANOV 15 is a reanalysis of their 2008-2010 dataset, with improved systematic corrections of ARZUMANOV 00 and ARZUMANOV 12.
3 STEYERL 12 is a detailed reanalysis of neutron storage loss corrections to the raw data of MAMPE 89, and it replaces that value.
4 WILSON 21 extract the value from the flux of n escaping the moon using data from the Lunar Prospector Neutron Spectrometer.
5 YUE 13 differs from NICO 05 in that a different and better method was used to measure the neutron density in the fiducial volume. This shifted the lifetime by +1.4 seconds and reduced the previously largest source of systematic uncertainty by a factor of five.
6 ARZUMANOV 12 reanalyzes its systematic corrections in ARZUMANOV 00 and obtains this corrected value.
7 IGNATOVICH 95 calls into question some of the corrections and averaging procedures used by MAMPE 93. The response, BONDARENKO 96, denies the validity of the criticisms.
8 The NESVIZHEVSKII 92 measurement has been withdrawn by A. Serebrov.
9 The BYRNE 80 measurement has been withdrawn (J. Byrne, private communication, 1990).

Baryon Particle Listings

n

WEIGHTED AVERAGE
878.4±0.5 (Error scaled by 1.8)



the Bohr radius. Numerically, $\langle r_n^2 \rangle = 86.34 b_{ne}$, if we use a_0 for a nucleus with infinite mass.

VALUE (fm ²)	DOCUMENT ID	COMMENT
-0.1155 ± 0.0017 OUR AVERAGE		
-0.115 ± 0.002 ± 0.003	KOPECKY 97	<i>ne</i> scattering (Pb)
-0.124 ± 0.003 ± 0.005	KOPECKY 97	<i>ne</i> scattering (Bi)
-0.114 ± 0.003	KOESTER 95	<i>ne</i> scattering (Pb, Bi)
-0.115 ± 0.003	¹ KROHN 73	<i>ne</i> scattering (Ne, Ar, Kr, Xe)
● ● ● We do not use the following data for averages, fits, limits, etc. ● ● ●		
-0.1101 ± 0.0089	² HEACOCK 21	<i>n</i> interferometry
-0.106 + 0.007 - 0.005	³ FILIN 20	chiral EFT analysis
-0.117 + 0.007 - 0.011	BELUSHKIN 07	Dispersion analysis
-0.113 ± 0.003 ± 0.004	KOPECKY 95	<i>ne</i> scattering (Pb)
-0.134 ± 0.009	ALEKSANDR...86	<i>ne</i> scattering (Bi)
-0.114 ± 0.003	KOESTER 86	<i>ne</i> scattering (Pb, Bi)
-0.118 ± 0.002	KOESTER 76	<i>ne</i> scattering (Pb)
-0.120 ± 0.002	KOESTER 76	<i>ne</i> scattering (Bi)
-0.116 ± 0.003	KROHN 66	<i>ne</i> scattering (Ne, Ar, Kr, Xe)

¹ KROHN 73 measured $-0.112 \pm 0.003 \text{ fm}^2$. This value is as corrected by KOESTER 76.
² HEACOCK 21 extract the value from Pendeloesung interferometry to measure the neutron structure factors of silicon. This value is strongly anti-correlated with the mean-square thermal atomic displacement.
³ FILIN 20 extract the value based on their chiral-EFT calculation of the deuteron structure radius and use as input the atomic data for the difference of the deuteron and proton charge radii.

n MAGNETIC MOMENT

See the "Quark Model" review.

VALUE (μ _N)	DOCUMENT ID	TECN	COMMENT
-1.91304273 ± 0.00000045			
● ● ● We do not use the following data for averages, fits, limits, etc. ● ● ●			
-1.91304273 ± 0.00000045	MOHR 16	RVUE	2014 CODATA value
-1.91304272 ± 0.00000045	MOHR 12	RVUE	2010 CODATA value
-1.91304273 ± 0.00000045	MOHR 08	RVUE	2006 CODATA value
-1.91304273 ± 0.00000045	MOHR 05	RVUE	2002 CODATA value
-1.91304272 ± 0.00000045	MOHR 99	RVUE	1998 CODATA value
-1.91304275 ± 0.00000045	COHEN 87	RVUE	1986 CODATA value
-1.91304277 ± 0.00000048	¹ GREENE 82	MRS	

¹ GREENE 82 measures the moment to be $(1.04187564 \pm 0.00000026) \times 10^{-3}$ Bohr magnetons. The value above is obtained by multiplying this by $m_p/m_e = 1836.152701 \pm 0.000037$ (the 1986 CODATA value from COHEN 87).

n ELECTRIC DIPOLE MOMENT

A nonzero value is forbidden by both *T* invariance and *P* invariance. A number of early results have been omitted. See RAMSEY 90, GOLUB 94, and LAMOREAUX 09 for reviews.

The results are upper limits on $|d_n|$.

VALUE (10 ⁻²⁵ ecm)	CL%	DOCUMENT ID	TECN	COMMENT
< 0.18	90	¹ ABEL 20	MRS	UCN
● ● ● We do not use the following data for averages, fits, limits, etc. ● ● ●				
< 0.22	95	² SAHOO 17		¹⁹⁹ Hg atom EDM + theory
< 0.16	95	GRANER 16	MRS	¹⁹⁹ Hg atom EDM + theory
< 0.30	90	³ PENDLEBURY 15	MRS	Supersedes BAKER 06
< 0.55	90	SEREBROV 15	MRS	UCN's, $h\nu = 2\mu_n B \pm 2d_n E$
< 0.55	90	⁴ SEREBROV 14	MRS	See SEREBROV 15
< 0.29	90	⁵ BAKER 06	MRS	See PENDLEBURY 15
< 0.63	90	⁶ HARRIS 99	MRS	$d = (-0.1 \pm 0.36) \times 10^{-25}$
< 0.97	90	ALTAREV 96	MRS	See SEREBROV 14
< 1.1	95	ALTAREV 92	MRS	See ALTAREV 96
< 1.2	95	SMITH 90	MRS	See HARRIS 99
< 2.6	95	ALTAREV 86	MRS	$d = (-1.4 \pm 0.6) \times 10^{-25}$
0.3 ± 4.8		PENDLEBURY 84	MRS	Ultracold neutrons
< 6	90	ALTAREV 81	MRS	$d = (2.1 \pm 2.4) \times 10^{-25}$
< 16	90	ALTAREV 79	MRS	$d = (4.0 \pm 7.5) \times 10^{-25}$

¹ ABEL 20 reports $d = (0.0 \pm 1.1 \pm 0.2) \times 10^{-26}$ ecm value corresponding to the listed limit.
² SAHOO 17 develops theory to calculate this limit from the measured limit by GRANER 16 of the ¹⁹⁹Hg atom EDM.
³ PENDLEBURY 15 reports $d = (-0.21 \pm 1.82) \times 10^{-26}$ ecm value corresponding to the listed limit.
⁴ SEREBROV 14 includes the data of ALTAREV 96.
⁵ LAMOREAUX 07 faults BAKER 06 for not including in the estimate of systematic error an effect due to the Earth's rotation. BAKER 07 replies (1) that the effect was included implicitly in the analysis and (2) that further analysis confirms that the BAKER 06 limit is correct as is. See also SILENKO 07.
⁶ This HARRIS 99 result includes the result of SMITH 90. However, the averaging of the results of these two experiments has been criticized by LAMOREAUX 00.

n MEAN-SQUARE CHARGE RADIUS

The mean-square charge radius of the neutron, $\langle r_n^2 \rangle$, is related to the neutron-electron scattering length b_{ne} by $\langle r_n^2 \rangle = 3(m_e a_0 / m_n) b_{ne}$, where m_e and m_n are the masses of the electron and neutron, and a_0 is

n MAGNETIC RADIUS

This is the rms magnetic radius, $\sqrt{\langle r_{Mn}^2 \rangle}$.

VALUE (fm)	DOCUMENT ID	COMMENT
0.864 ± 0.009 OUR AVERAGE		
● ● ● We do not use the following data for averages, fits, limits, etc. ● ● ●		
0.89 ± 0.03	EPSTEIN 14	Using <i>e</i> <i>p</i> , <i>e</i> <i>n</i> , <i>ππ</i> data
0.862 ± 0.009 - 0.008	BELUSHKIN 07	Dispersion analysis

n ELECTRIC POLARIZABILITY α_n

Following is the electric polarizability α_n defined in terms of the induced electric dipole moment by $\mathbf{D} = 4\pi\epsilon_0\alpha_n\mathbf{E}$. For a review, see SCHMIED-MAYER 89.

For a very complete reviews of the polarizability of the nucleon and Compton scattering, see SCHUMACHER 05, updated in SCHUMACHER 19, and GRIESSHAMMER 12.

VALUE (10 ⁻⁴ fm ³)	DOCUMENT ID	TECN	COMMENT
11.8 ± 1.1 OUR AVERAGE			
11.55 ± 1.25 ± 0.8	MYERS 14	CNTR	$\gamma d \rightarrow \gamma d$
12.5 ± 1.8 + 1.6 - 1.3	¹ KOSSERT 03	CNTR	$\gamma d \rightarrow \gamma pn$
12.0 ± 1.5 ± 2.0	SCHMIEDM... 91	CNTR	<i>n</i> Pb transmission
10.7 + 3.3 - 10.7	ROSE 90b	CNTR	$\gamma d \rightarrow \gamma np$
● ● ● We do not use the following data for averages, fits, limits, etc. ● ● ●			
8.8 ± 2.4 ± 3.0	² LUNDIN 03	CNTR	$\gamma d \rightarrow \gamma d$
13.6	³ KOLB 00	CNTR	$\gamma d \rightarrow \gamma np$
0.0 ± 5.0	⁴ KOESTER 95	CNTR	<i>n</i> Pb, <i>n</i> Bi transmission
11.7 + 4.3 - 11.7	ROSE 90	CNTR	See ROSE 90b
8 ± 10	KOESTER 88	CNTR	<i>n</i> Pb, <i>n</i> Bi transmission
12 ± 10	SCHMIEDM... 88	CNTR	<i>n</i> Pb, <i>n</i> C transmission

¹ KOSSERT 03 gets $\alpha_n - \beta_n = (9.8 \pm 3.6 + 2.1 - 1.1 \pm 2.2) \times 10^{-4} \text{ fm}^3$, and uses $\alpha_n + \beta_n = (15.2 \pm 0.5) \times 10^{-4} \text{ fm}^3$ from LEVCHUK 00. Thus the errors on α_n and β_n are anti-correlated.
² LUNDIN 03 measures $\alpha_N - \beta_N = (6.4 \pm 2.4) \times 10^{-4} \text{ fm}^3$ and uses accurate values for α_p and α_p and a precise sum-rule result for $\alpha_n + \beta_n$. The second error is a model uncertainty, and errors on α_n and β_n are anticorrelated. The data from this paper aer included in the analysis of MYERS 14.
³ KOLB 00 obtains this value with a lower limit of $7.6 \times 10^{-4} \text{ fm}^3$ but no upper limit from this experiment alone. Combined with results of ROSE 90, the 1-σ range is $(7.6\text{-}14.0) \times 10^{-4} \text{ fm}^3$.
⁴ KOESTER 95 uses natural Pb and the isotopes 208, 207, and 206. See this paper for a discussion of methods used by various groups to extract α_n from data.

n MAGNETIC POLARIZABILITY β_n

VALUE (10 ⁻⁴ fm ³)	DOCUMENT ID	TECN	COMMENT
3.7 ± 1.2 OUR AVERAGE			
3.65 ± 1.25 ± 0.8	MYERS 14	CNTR	$\gamma d \rightarrow \gamma d$
2.7 ± 1.8 + 1.3 - 1.6	¹ KOSSERT 03	CNTR	$\gamma d \rightarrow \gamma pn$
6.5 ± 2.4 ± 3.0	² LUNDIN 03	CNTR	$\gamma d \rightarrow \gamma d$
● ● ● We do not use the following data for averages, fits, limits, etc. ● ● ●			
1.6	³ KOLB 00	CNTR	$\gamma d \rightarrow \gamma np$

¹ KOSSERT 03 gets $\alpha_n - \beta_n = (9.8 \pm 3.6^{+2.1}_{-1.1} \pm 2.2) \times 10^{-4} \text{ fm}^3$, and uses $\alpha_n + \beta_n = (15.2 \pm 0.5) \times 10^{-4} \text{ fm}^3$ from LEVCHUK 00. Thus the errors on α_n and β_n are anti-correlated.
² LUNDIN 03 measures $\alpha_n - \beta_n = (6.4 \pm 2.4) \times 10^{-4} \text{ fm}^3$ and uses accurate values for α_p and α_D and a precise sum-rule result for $\alpha_n + \beta_n$. The second error is a model uncertainty, and errors on α_n and β_n are anticorrelated.
³ KOLB 00 obtains this value with an upper limit of $7.6 \times 10^{-4} \text{ fm}^3$ but no lower limit from this experiment alone. Combined with results of ROSE 90, the 1- σ range is $(1.2\text{--}7.6) \times 10^{-4} \text{ fm}^3$.

n CHARGE

See also " $|q_p + q_e|/e$ " in the proton Listings.

VALUE ($10^{-21} e$)	DOCUMENT ID	TECN	COMMENT
-0.2 ± 0.8 OUR AVERAGE			
-0.1 ± 1.1	¹ BRESSI 11		Neutrality of SF ₆
-0.4 ± 1.1	² BAUMANN 88		Cold n deflection
• • • We do not use the following data for averages, fits, limits, etc. • • •			
-15 ± 22	³ GAEHLER 82	CNTR	Cold n deflection

¹ As a limit, this BRESSI 11 value is $< 1 \times 10^{-21} e$.
² The BAUMANN 88 error ± 1.1 gives the 68% CL limits about the value -0.4 .
³ The GAEHLER 82 error ± 22 gives the 90% CL limits about the value -15 .

LIMIT ON nπ OSCILLATIONS

Mean Time for nπ Transition

A test of $\Delta B=2$ baryon number nonconservation. MOHAPATRA 80 and MOHAPATRA 89 discuss the theoretical motivations for looking for $n\pi$ oscillations. DOVER 85 give phenomenological analyses. The best limits come from looking for the decay of neutrons bound in nuclei. However, these analyses require model-dependent corrections for nuclear effects. See KABIR 83, DOVER 89, ALBERICO 91, and GAL 00 for discussions. Direct searches for $n \rightarrow \pi$ transitions using reactor neutrons are cleaner but give somewhat poorer limits. We include limits for both free and bound neutrons in the Summary Table. See MOHAPATRA 09 and PHILLIPS 16 for recent reviews.

VALUE (s)	CL%	DOCUMENT ID	TECN	COMMENT
$>4.7 \times 10^8$	90	¹ ABE 21	CNTR	n bound in oxygen
$>8.6 \times 10^7$	90	BALDO...	94	CNTR Reactor (free) neutrons
• • • We do not use the following data for averages, fits, limits, etc. • • •				
$>1.37 \times 10^8$	90	² AHARMIM 17	SNO	n bound in deuteron
$>2.7 \times 10^8$	90	ABE 15c	CNTR	n bound in oxygen
$>1.3 \times 10^8$	90	CHUNG 02b	SOU2	n bound in iron
$>1 \times 10^7$	90	BALDO...	90	CNTR See BALDO-CEOLIN 94
$>1.2 \times 10^8$	90	BERGER 90	FREJ	n bound in iron
$>4.9 \times 10^5$	90	BRESSI 90	CNTR	Reactor neutrons
$>4.7 \times 10^5$	90	BRESSI 89	CNTR	See BRESSI 90
$>1.2 \times 10^8$	90	TAKITA 86	CNTR	n bound in oxygen
$>1 \times 10^6$	90	FIDECARO 85	CNTR	Reactor neutrons
$>8.8 \times 10^7$	90	PARK 85b	CNTR	
$>3 \times 10^7$		BATTISTONI 84	NUSX	
$>0.27\text{--}1.1 \times 10^8$		JONES 84	CNTR	
$>2 \times 10^7$		CHERRY 83	CNTR	

¹ ABE 21 supersedes ABE 15c.
² The AHARMIM 17 value is an unbounded limit (it does not assume a positive lifetime). The bounded limit is 1.23×10^8 sec.

LIMIT ON nn' OSCILLATIONS

Lee and Yang (LEE 56) proposed the existence of mirror world in an attempt to restore global parity symmetry. A possible candidate for dark matter. Limits depend on assumptions about fields B and B' . See the papers for details. See BEREZHIANI 18 for a recent discussion.

VALUE (s)	CL%	DOCUMENT ID	TECN	COMMENT
>352	95	¹ ABEL 21	CNTR	UCN, scan of B field
>448	90	SEREBROV 09a	CNTR	Assumes $B' < 100$ nT
• • • We do not use the following data for averages, fits, limits, etc. • • •				
> 17	95	² BEREZHIANI 18	CNTR	UCN, scan of B field
> 12	95	³ ALTAREV 09a	CNTR	UCN, scan $0 \leq B \leq 12.5 \mu\text{T}$
>414	90	SEREBROV 08	CNTR	UCN, B field on & off
>103	95	BAN 07	CNTR	UCN, B field on & off

¹ ABEL 21 determine several limits on the oscillation time as a function of the ratio mirror magnetic field B' to applied magnetic field B . The quoted limit of 352 s is for $B' = 0$. Lower limits on the oscillation time of 6 seconds are further obtained for any mirror field B' in the range $0.4\text{--}25.7 \mu\text{T}$.
² The B field was set to $(0.09, 0.12, 0.21)$ G. Limits on oscillation time are valid for any mirror field B' in $(0.08\text{--}0.17)$ G, and for aligned fields B and B' . For larger values of B' , the limits are significantly reduced.
³ Losses of neutrons due to oscillations to mirror neutrons would be maximal when the magnetic fields B and B' in the two worlds were equal. Hence the scan over B by ALTAREV 09a: the limit applies for any B' over the given range. At $B' = 0$, the limit is 141 s (95% CL).

n DECAY MODES

Mode	Fraction (Γ_i/Γ)	Confidence level
Γ_1 $p e^- \bar{\nu}_e$	100 %	
Γ_2 $p e^- \bar{\nu}_e \gamma$	[a] $(9.2 \pm 0.7) \times 10^{-3}$	
Γ_3 hydrogen-atom $\bar{\nu}_e$	$< 2.7 \times 10^{-3}$	95%

Charge conservation (Q) violating mode

Γ_4 $p \nu_e \bar{\nu}_e$	Q	$< 8 \times 10^{-27}$	68%
----------------------------------	---	-----------------------	-----

Baryon number violating decay

Γ_5 $e^+ e^-$ invisible			
--------------------------------	--	--	--

[a] This limit is for γ energies between 0.4 and 782 keV.

n BRANCHING RATIOS

$\Gamma(p e^- \bar{\nu}_e \gamma)/\Gamma_{\text{total}}$	CL%	DOCUMENT ID	TECN	COMMENT	Γ_2/Γ
$9.17 \pm 0.24 \pm 0.64$		¹ BALES 16	RDK2	Two different set-ups	
• • • We do not use the following data for averages, fits, limits, etc. • • •					
$3.09 \pm 0.11 \pm 0.30$		² COOPER 10	CNTR	See BALES 16	
$3.13 \pm 0.11 \pm 0.33$		NICO 06	CNTR	See COOPER 10	
< 6.9	90	³ BECK 02	CNTR	γ, p, e^- coincidence	

¹ BALES 16 gets a branching fraction of $(5.82 \pm 0.23 \pm 0.62) \times 10^{-3}$ for a photon energy range 0.4 to 14.0 keV, and with a different detector array, $(3.35 \pm 0.05 \pm 0.15) \times 10^{-3}$ for 14.1 to 782 keV. Our result above is the sum; the error on the sum is completely dominated by the error on the lower range.
² This COOPER 10 result is for γ energies between 15 and 340 keV.
³ This BECK 02 limit is for γ energies between 35 and 100 keV.

$\Gamma(\text{hydrogen-atom } \bar{\nu}_e)/\Gamma_{\text{total}}$

VALUE	CL%	DOCUMENT ID	TECN	COMMENT	Γ_3/Γ
$<0.27 \times 10^{-2}$	95	¹ CZARNECKI 18		Lifetime analysis	
• • • We do not use the following data for averages, fits, limits, etc. • • •					
$< 3 \times 10^{-2}$	95	² GREEN 90	RVUE		

¹ CZARNECKI 18 limit from an analysis of experimental discrepancies on the neutron lifetime and axial coupling applies as well to other possible exotic neutron decays.
² GREEN 90 infers that $\tau(\text{hydrogen-atom } \bar{\nu}_e) > 3 \times 10^4$ s by comparing neutron lifetime measurements made in storage experiments with those made in β -decay experiments. However, the result depends sensitively on the lifetime measurements, and does not of course take into account more recent measurements of same.

$\Gamma(p \nu_e \bar{\nu}_e)/\Gamma_{\text{total}}$
 Forbidden by charge conservation.

VALUE	CL%	DOCUMENT ID	TECN	COMMENT	Γ_4/Γ
$<8 \times 10^{-27}$	68	¹ NORMAN 96	RVUE	⁷¹ Ga \rightarrow ⁷¹ Ge neutrals	
• • • We do not use the following data for averages, fits, limits, etc. • • •					
$<9.7 \times 10^{-18}$	90	ROY 83	CNTR	¹¹³ Cd \rightarrow ^{113m} In neut.	
$<7.9 \times 10^{-21}$		VAIDYA 83	CNTR	⁸⁷ Rb \rightarrow ^{87m} Sr neut.	
$<9 \times 10^{-24}$	90	BARABANOV 80	CNTR	⁷¹ Ga \rightarrow ⁷¹ GeX	
$<3 \times 10^{-19}$		NORMAN 79	CNTR	⁸⁷ Rb \rightarrow ^{87m} Sr neut.	

¹ NORMAN 96 gets this limit by attributing SAGE and GALLEX counting rates to the charge-nonconserving transition ⁷¹Ga \rightarrow ⁷¹Ge+neutrals rather than to solar-neutrino reactions.

$\Gamma(e^+ e^- \text{ invisible})/\Gamma_{\text{total}}$
 Baryon number violating decay

VALUE	CL%	DOCUMENT ID	TECN	COMMENT	Γ_5/Γ
• • • We do not use the following data for averages, fits, limits, etc. • • •					
<0.01	90	¹ KLOPF 19	CNTR	re-interpretation of MUND 13	
$<1 \times 10^{-4}$	90	² SUN 18	SPEC	Ultracold n, polarized	

¹ KLOPF 19 value is for baryon number violating decay of neutron to electrons plus an invisible state, χ . The limit is valid for $\text{KE}(e^+ e^-)$ range between 32 keV and 664 keV, strengthening to few $\times 10^{-4}$ above approximately 100 keV.
² SUN 18 value is for baryon number violating decay of neutron to electrons plus an invisible state, χ . The limit is valid for $644 \text{ keV} > \text{KE}(e^+ e^-) > 100 \text{ keV}$. Assuming this decay $\chi e e$ is the only allowed χ decay channel, a 0.01 BR is ruled out for $644 \text{ keV} > \text{E}(e^+ e^-) > 100 \text{ keV}$ at over 5σ .

See the related review(s):
 Baryon Decay Parameters

Baryon Particle Listings

n

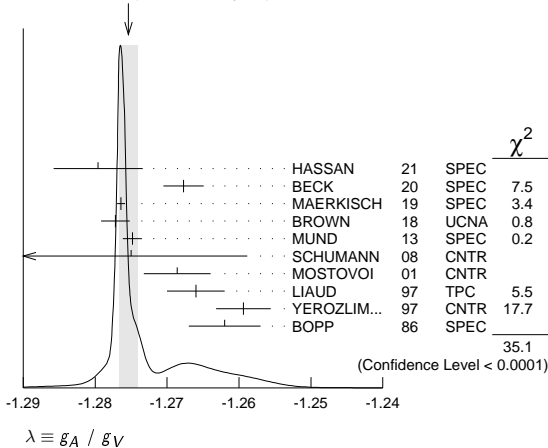
$n \rightarrow p e^- \bar{\nu}_e$ DECAY PARAMETERS

See the above "Note on Baryon Decay Parameters." For discussions of recent results, see the references cited at the beginning of the section on the neutron mean life. For discussions of the values of the weak coupling constants g_A and g_V obtained using the neutron lifetime and asymmetry parameter A , comparisons with other methods of obtaining these constants, and implications for particle physics and for astrophysics, see DUBBERS 91 and WOOLCOCK 91. For tests of the $V-A$ theory of neutron decay, see EROZOLIMSKII 91B, MOSTOVOI 96, NICO 05, SEVERIJNS 06, and ABELE 08.

$\lambda \equiv g_A / g_V$

VALUE	DOCUMENT ID	TECN	COMMENT
-1.2754 ± 0.0013 OUR AVERAGE	Error includes scale factor of 2.7. See the ideogram below.		
-1.2796 ± 0.0062	1 HASSAN 21	SPEC	Proton recoil spectrum
-1.2677 ± 0.0028	2 BECK 20	SPEC	Proton recoil spectrum
-1.27641 ± 0.00045 ± 0.00033	3 MAERKISCH 19	SPEC	pulsed cold n , polarized
-1.2772 ± 0.0020	4 BROWN 18	UCNA	Ultracold n , polarized
-1.2748 ± 0.0008 + 0.0010 - 0.0011	5 MUND 13	SPEC	Cold n , polarized
-1.2675 ± 0.006 ± 0.015	SCHUMANN 08	CNTR	Cold n , polarized
-1.2686 ± 0.0046 ± 0.0007	6 MOSTOVOI 01	CNTR	A and $B \times$ polarizations
-1.266 ± 0.004	LIAUD 97	TPC	Cold n , polarized, A
-1.2594 ± 0.0038	7 YEROZLIM... 97	CNTR	Cold n , polarized, A
-1.262 ± 0.005	BOPP 86	SPEC	Cold n , polarized, A
••• We do not use the following data for averages, fits, limits, etc. •••			
-1.27607 ± 0.00068	8 SAUL 20	SPEC	Cold n , polarized, A
-1.284 ± 0.014	9 DARIUS 17	SPEC	Cold n , unpolarized
-1.2755 ± 0.0030	10 MENDENHALL 13	UCNA	See BROWN 18
-1.27590 ± 0.00239 + 0.00331 - 0.00377	11 PLASTER 12	UCNA	See MENDENHALL 13
-1.27590 + 0.00409 - 0.00445	LIU 10	UCNA	See PLASTER 12
-1.2739 ± 0.0019	12 ABELE 02	SPEC	See MUND 13
-1.274 ± 0.003	ABELE 97D	SPEC	Cold n , polarized, A
-1.266 ± 0.004	SCHRECK... 95	TPC	See LIAUD 97
-1.2544 ± 0.0036	EROLZOLIM... 91	CNTR	See YEROZOLIMSKY 97
-1.226 ± 0.042	MOSTOVOY 83	RVUE	
-1.261 ± 0.012	EROLZOLIM... 79	CNTR	Cold n , polarized, A
-1.259 ± 0.017	13 STRATOWA 78	CNTR	p recoil spectrum, a
-1.263 ± 0.015	EROLZOLIM... 77	CNTR	See EROZOLIMSKII 79
-1.250 ± 0.036	13 DOBROZE... 75	CNTR	See STRATOWA 78
-1.258 ± 0.015	14 KROHN 75	CNTR	Cold n , polarized, A
-1.263 ± 0.016	15 KROPF 74	RVUE	n decay alone
-1.250 ± 0.009	15 KROPF 74	RVUE	n decay + nuclear ft

WEIGHTED AVERAGE
-1.2754 ± 0.0013 (Error scaled by 2.7)



- HASSAN 21 include earlier data of DARIUS 17. The value is extracted from the angular correlation coefficient a .
- BECK 20 calculates this value from the measurement of the β -decay $e^- \bar{\nu}_e$ angular correlation coefficient a .
- MAERKISCH 19 gets $A = -0.11985 \pm 0.00017 \pm 0.00012$.
- BROWN 18 gets $A = -0.12054 \pm 0.00044 \pm 0.00068$ and $\lambda = -1.2783 \pm 0.0022$. We quote the combined values that include the earlier UCNA measurements (MENDENHALL 13).
- This MUND 13 value includes earlier PERKEO II measurements (ABELE 02 and ABELE 97D).
- MOSTOVOI 01 measures the two P -odd correlations A and B , or rather SA and SB , where S is the n polarization, in free neutron decay.
- YEROZOLIMSKY 97 makes a correction to the EROZOLIMSKII 91 value.
- SAUL 20 quote this value of λ under the SM assumption of the Fierz term $b = 0$. In a combined fit authors extract a value of $\lambda = -1.2792 \pm 0.0060$.

- DARIUS 17 calculates this value from the measurement of the a parameter (see below). Data is included in HASSAN 21.
- MENDENHALL 13 gets $A = -0.11954 \pm 0.00055 \pm 0.00098$ and $\lambda = -1.2756 \pm 0.0030$. We quote the nearly identical values that include the earlier UCNA measurement (PLASTER 12), with a correction to that result.
- This PLASTER 12 value is identical with that given in LIU 10, but the experiment is now described in detail.
- This is the combined result of ABELE 02 and ABELE 97D.
- These experiments measure the absolute value of g_A/g_V only.
- KROHN 75 includes events of CHRISTENSEN 70.
- KROPF 74 reviews all data through 1972.

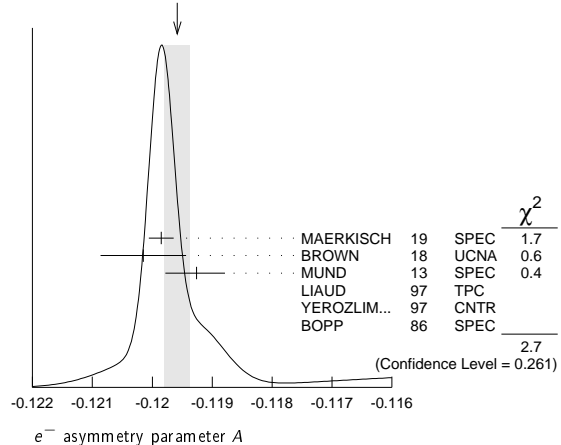
e^- ASYMMETRY PARAMETER A

This is the neutron-spin electron-momentum correlation coefficient. Unless otherwise noted, the values are corrected for radiative effects and weak magnetism. In the Standard Model, A is related to $\lambda \equiv g_A/g_V$ by $A = -2\lambda(\lambda + 1) / (1 + 3\lambda^2)$; this assumes that g_A and g_V are real.

VALUE	DOCUMENT ID	TECN	COMMENT
-0.11958 ± 0.00021 OUR AVERAGE	Error includes scale factor of 1.2. See the ideogram below.		
-0.11985 ± 0.00017 ± 0.00012	1 MAERKISCH 19	SPEC	pulsed cold n , polarized
-0.12015 ± 0.00034 ± 0.00063	2 BROWN 18	UCNA	Ultracold n , polarized
-0.11926 ± 0.00031 + 0.00036 - 0.00042	3 MUND 13	SPEC	Cold n , polarized
-0.1160 ± 0.0009 ± 0.0012	LIAUD 97	TPC	Cold n , polarized
-0.1135 ± 0.0014	4 YEROZLIM... 97	CNTR	Cold n , polarized
-0.1146 ± 0.0019	BOPP 86	SPEC	Cold n , polarized
••• We do not use the following data for averages, fits, limits, etc. •••			
-0.11972 ± 0.00025	5 SAUL 20	SPEC	Cold n , polarized
-0.11952 ± 0.00110	6 MENDENHALL 13	UCNA	See BROWN 18
-0.11966 ± 0.00089 + 0.00123 - 0.00140	7 PLASTER 12	UCNA	See MENDENHALL 13
-0.11966 ± 0.00089 + 0.00123 - 0.00140	LIU 10	UCNA	See PLASTER 12
-0.1138 ± 0.0046 ± 0.0021	PATTIE 09	SPEC	Ultracold n , polarized
-0.1189 ± 0.0007	8 ABELE 02	SPEC	See MUND 13
-0.1168 ± 0.0017	9 MOSTOVOI 01	CNTR	Inferred
-0.1189 ± 0.0012	ABELE 97D	SPEC	Cold n , polarized
-0.1160 ± 0.0009 ± 0.0011	SCHRECK... 95	TPC	See LIAUD 97
-0.1116 ± 0.0014	EROLZOLIM... 91	CNTR	See YEROZOLIMSKY 97
-0.114 ± 0.005	10 EROZOLIM... 79	CNTR	Cold n , polarized
-0.113 ± 0.006	10 KROHN 75	CNTR	Cold n , polarized

- MAERKISCH 19 further derive a value for the CKM-element $|V_{ud}| = 0.97351 \pm 0.00060$, using $\tau_n = 879.7(8)$ sec and the relation from CZARNECKI 18.
- BROWN 18 gets $A = -0.12054 \pm 0.00044 \pm 0.00068$ and $\lambda = -1.2783 \pm 0.0022$. We quote the combined values that include the earlier UCNA measurements (MENDENHALL 13).
- This MUND 13 value includes earlier PERKEO II measurements (ABELE 02 and ABELE 97D), with a correction to those results.
- YEROZOLIMSKY 97 makes a correction to the EROZOLIMSKII 91 value.
- Under the SM assumption that the Fierz term $b = 0$, SAUL 20 obtain the quoted asymmetry parameter A and $\lambda = -1.27607 \pm 0.00068$. In a combined fit authors extract the values $A = -0.1209 \pm 0.0015$, $\lambda = -1.2792 \pm 0.0060$, and $b = 0.017 \pm 0.021$.
- MENDENHALL 13 gets $A = -0.11954 \pm 0.00055 \pm 0.00098$ and $\lambda = -1.2756 \pm 0.0030$. We quote the nearly identical values that include the earlier UCNA measurement (PLASTER 12), with a correction to that result.
- This PLASTER 12 value is identical with that given in LIU 10, but the experiment is now described in detail.
- This is the combined result of ABELE 02 and ABELE 97D.
- MOSTOVOI 01 calculates this from its measurement of $\lambda = g_A/g_V$ above.
- These results are not corrected for radiative effects and weak magnetism, but the corrections are small compared to the errors.

WEIGHTED AVERAGE
-0.11958 ± 0.00021 (Error scaled by 1.2)

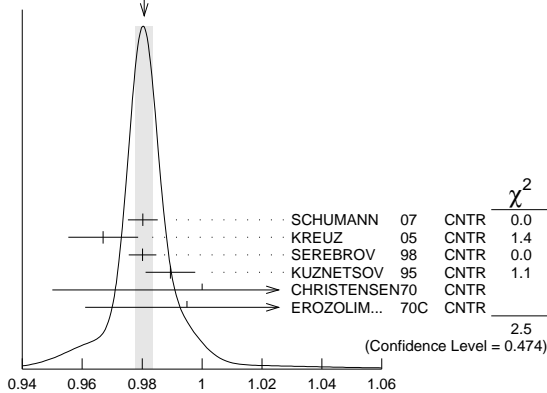


$\bar{\nu}_e$ ASYMMETRY PARAMETER *B*

This is the neutron-spin antineutrino-momentum correlation coefficient. In the Standard Model, *B* is related to $\lambda \equiv g_A/g_V$ by $B = 2\lambda(\lambda - 1) / (1 + 3\lambda^2)$; this assumes that g_A and g_V are real.

VALUE	DOCUMENT ID	TECN	COMMENT
0.9807 ± 0.0030 OUR AVERAGE	See the ideogram below.		
0.9802 ± 0.0034 ± 0.0036	SCHUMANN 07	CNTR	Cold <i>n</i> , polarized
0.967 ± 0.006 ± 0.010	KREUZ 05	CNTR	Cold <i>n</i> , polarized
0.9801 ± 0.0046	SEREBROV 98	CNTR	Cold <i>n</i> , polarized
0.9894 ± 0.0083	KUZNETSOV 95	CNTR	Cold <i>n</i> , polarized
1.00 ± 0.05	CHRISTENSEN70	CNTR	Cold <i>n</i> , polarized
0.995 ± 0.034	EROZOLIM... 70c	CNTR	Cold <i>n</i> , polarized
• • • We do not use the following data for averages, fits, limits, etc. • • •			
0.9876 ± 0.0004	¹ MOSTOVOI 01	CNTR	Inferred

WEIGHTED AVERAGE
0.9807 ± 0.0030 (Error scaled by 1.0)



$\bar{\nu}_e$ ASYMMETRY PARAMETER *B*

¹ MOSTOVOI 01 calculates this from its measurement of $\lambda = g_A/g_V$ above.

PROTON ASYMMETRY PARAMETER *C*

Describes the correlation between the neutron spin and the proton momentum. In the Standard Model, *C* is related to $\lambda \equiv g_A/g_V$ by $C = -x_c(A + B) = x_c 4\lambda/(1 + 3\lambda^2)$, where $x_c = 0.27484$ is a kinematic factor; this assumes that g_A and g_V are real.

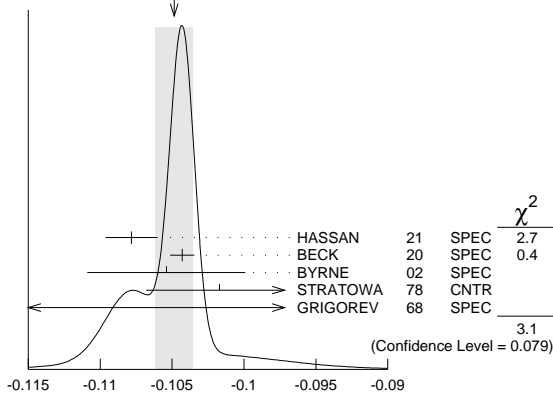
VALUE	DOCUMENT ID	TECN	COMMENT
-0.2377 ± 0.0010 ± 0.0024	SCHUMANN 08	CNTR	Cold <i>n</i> , polarized

e*- $\bar{\nu}_e$ ANGULAR CORRELATION COEFFICIENT *a

For a review of past experiments and plans for future measurements of the *a* parameter, see WIETFELDT 05. In the Standard Model, *a* is related to $\lambda \equiv g_A/g_V$ by $a = (1 - \lambda^2) / (1 + 3\lambda^2)$; this assumes that g_A and g_V are real.

VALUE	DOCUMENT ID	TECN	COMMENT
-0.1049 ± 0.0013 OUR AVERAGE	Error includes scale factor of 1.8. See the ideogram below.		
-0.10782 ± 0.00124 ± 0.00133	¹ HASSAN 21	SPEC	Proton recoil spectrum
-0.10430 ± 0.00084	BECK 20	SPEC	Proton recoil spectrum
-0.1054 ± 0.0055	BYRNE 02	SPEC	Proton recoil spectrum
-0.1017 ± 0.0051	STRATOWA 78	CNTR	Proton recoil spectrum
-0.091 ± 0.039	GRIGOREV 68	SPEC	Proton recoil spectrum
• • • We do not use the following data for averages, fits, limits, etc. • • •			
-0.1090 ± 0.0030 ± 0.0028	² DARIUS 17	SPEC	Cold <i>n</i> , unpolarized
-0.1045 ± 0.0014	³ MOSTOVOI 01	CNTR	Inferred

WEIGHTED AVERAGE
-0.1049 ± 0.0013 (Error scaled by 1.8)



e*- $\bar{\nu}_e$ Angular correlation coefficient *a

¹ The result of HASSAN 21 includes the data of DARIUS 17, and thus supersedes those entries. HASSAN 21 uses the asymmetry in time-of-flight between the beta electron and recoil proton in delayed coincidence.

² DARIUS 17 exploits a "wishbone" correlation, where the *p* time of flight is correlated with the momentum of the electron in delayed coincidence. Data is included in HASSAN 21.

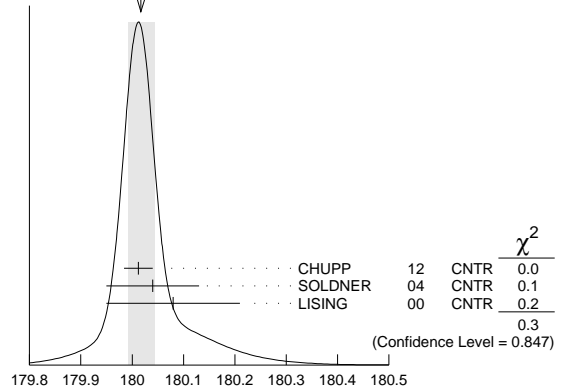
³ MOSTOVOI 01 calculates this from its measurement of $\lambda = g_A/g_V$ above.

ϕ_{AV} , PHASE OF g_A RELATIVE TO g_V

Time reversal invariance requires this to be 0 or 180°. This is related to *D* given in the next data block and $\lambda \equiv g_A/g_V$ by $\sin(\phi_{AV}) \equiv D(1+3\lambda^2)/2|\lambda|$; this assumes that g_A and g_V are real.

VALUE (°)	CL%	DOCUMENT ID	TECN	COMMENT
180.017 ± 0.026 OUR AVERAGE		See the ideogram below.		
180.012 ± 0.028	68	CHUPP 12	CNTR	Cold <i>n</i> , polarized > 91%
180.04 ± 0.09		SOLDNER 04	CNTR	Cold <i>n</i> , polarized
180.08 ± 0.13		LISING 00	CNTR	Polarized > 93%
• • • We do not use the following data for averages, fits, limits, etc. • • •				
180.013 ± 0.028		MUMM 11	CNTR	See CHUPP 12
179.71 ± 0.39		EROZOLIM... 78	CNTR	Cold <i>n</i> , polarized
180.35 ± 0.43		EROZOLIM... 74	CNTR	Cold <i>n</i> , polarized
181.1 ± 1.3		¹ KROPP 74	RVUE	<i>n</i> decay
180.14 ± 0.22		STEINBERG 74	CNTR	Cold <i>n</i> , polarized

WEIGHTED AVERAGE
180.017 ± 0.026 (Error scaled by 1.0)



ϕ_{AV} , PHASE OF g_A RELATIVE TO g_V (°)

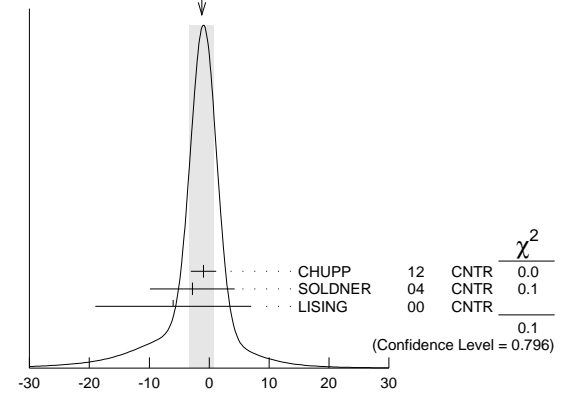
¹ KROPP 74 reviews all data through 1972.

TRIPLE CORRELATION COEFFICIENT *D*

These are measurements of the component of *n* spin perpendicular to the decay plane in β decay. Should be zero if *T* invariance is not violated.

VALUE (units 10 ⁻⁴)	DOCUMENT ID	TECN	COMMENT
-1.2 ± 2.0 OUR AVERAGE	See the ideogram below.		
-0.94 ± 1.89 ± 0.97	CHUPP 12	CNTR	Cold <i>n</i> , polarized > 91%
-2.8 ± 6.4 ± 3.0	SOLDNER 04	CNTR	Cold <i>n</i> , polarized
-6 ± 12 ± 5	LISING 00	CNTR	Polarized > 93%
• • • We do not use the following data for averages, fits, limits, etc. • • •			
-0.96 ± 1.89 ± 1.01	MUMM 11	CNTR	See CHUPP 12
+22 ± 30	EROZOLIM... 78	CNTR	Cold <i>n</i> , polarized
-27 ± 50	¹ EROZOLIM... 74	CNTR	Cold <i>n</i> , polarized
-11 ± 17	STEINBERG 74	CNTR	Cold <i>n</i> , polarized

WEIGHTED AVERAGE
-1.2 ± 2.0 (Error scaled by 1.0)



TRIPLE CORRELATION COEFFICIENT *D* (units 10⁻⁴)

See key on page 1127

Baryon Particle Listings

n , N 's and Δ 's, $N(1440)$

ROY	83	PR D28 1770	A. Roy et al.	(TATA)
VAIDYA	83	PR D27 486	S. C. Vaidya et al.	(TATA)
GAHLER	82	PR D25 2887	R. Gahler, J. Kalus, W. Mampe	(BAYR, ILLG)
GREENE	82	Metrologia 18 93	G.L. Greene et al.	(YALE, HARV, ILLG+)
ALTAREV	81	PL 102B 13	I.S. Altarev et al.	(PNPI)
BARABANOV	80	JETPL 32 359	I.R. Barabanov et al.	(PNPI)
Translated from ZETFP 32 384.				
BYRNE	80	PL 92B 274	J. Byrne et al.	(SUSS, RL)
KOSVINTSEV	80	JETPL 31 236	Y.Y. Kosvintsev et al.	(JINR)
Translated from ZETFP 31 257.				
MOHAPATRA	80	PRL 44 1316	R.N. Mohapatra, R.E. Marshak	(CUNY, VPI)
ALTAREV	79	JETPL 29 730	I.S. Altarev et al.	(PNPI)
Translated from ZETFP 29 794.				
EROZOLIM...	79	SJNP 30 356	B.G. Erokolimsky et al.	(KIAE)
Translated from YAF 30 692.				
NORMAN	79	PRL 43 1226	E.B. Norman, A.G. Seamster	(WASH)
BONDAREN...	78	JETPL 28 303	L.N. Bondarenko et al.	(KIAE)
Translated from ZETFP 28 328.				
Also Smolenice Conf.				
EROZOLIM...	78	SJNP 28 48	P.G. Bondarenko	(KIAE)
Translated from YAF 28 98.				
STRATOWA	78	PR D18 3970	C. Stratowa, R. Dobrozemsky, P. Weinzierl	(SEIB)
EROZOLIM...	77	JETPL 23 663	B.G. Erokolimsky et al.	(KIAE)
Translated from ZETFP 23 720.				
KOESTER	76	PRL 36 1021	L. Koester et al.	(YALE, ISNG)
STEINBERG	76	PR D13 2469	R.I. Steinberg et al.	(SEIB)
DOBROZE...	75	PR D11 510	R. Dobrozemsky et al.	(ANL)
KROHN	75	PL 55B 175	V.E. Krohn, G.R. Ringo	(ANL)
EROZOLIM...	74	JETPL 20 345	B.G. Erokolimsky et al.	(KIAE)
Translated from ZETFP 20 745.				
KROPF	74	ZPHY 267 129	H. Kropf, E. Paul	(LINZ)
Also NP A154 160				
STEINBERG	74	PRL 33 41	R.I. Steinberg et al.	(YALE, ISNG)
COHEN	73	JPCRD 2 664	E.R. Cohen, B.N. Taylor	(RISC, NBS)
KROHN	73	PR D8 1305	V.E. Krohn, G.R. Ringo	(RIS O)
CHRISTENSEN	72	PR D5 1628	C.J. Christensen et al.	(ANL)
CHRISTENSEN	70	PR C1 1693	C.J. Christensen, V.E. Krohn, G.R. Ringo	(KIAE)
EROZOLIM...	70C	PL 33B 351	B.G. Erokolimsky et al.	(ITEP)
GRIGOREV	68	SJNP 6 239	V.K. Grigoriev et al.	(ITEP)
Translated from YAF 6 329.				
KROHN	66	PR 148 1303	V.E. Krohn, G.R. Ringo	(COLU, BNL)
LEE	56	PR 104 254	T.D. Lee, C.N. Yang	

See the related review(s):
[N and \$\Delta\$ Resonances](#)

$$N(1440) \ 1/2^+$$

$$I(J^P) = \frac{1}{2}(\frac{1}{2}^+) \text{ Status: } ****$$

Older and obsolete values are listed and referenced in the 2014 edition, Chinese Physics C38 070001 (2014).

N(1440) POLE POSITION

REAL PART

VALUE (MeV)	DOCUMENT ID	TECN	COMMENT
1360 to 1380 (\approx 1370) OUR ESTIMATE			
1369 \pm 3	SOKHOYAN 15A	DPWA	Multichannel
1363 \pm 2 \pm 2	¹ SVARC 14	L+P	$\pi N \rightarrow \pi N$
1375 \pm 30	CUTKOSKY 80	IPWA	$\pi N \rightarrow \pi N$
••• We do not use the following data for averages, fits, limits, etc. •••			
1360	HUNT 19	DPWA	Multichannel
1355	ROENCHEN 15A	DPWA	Multichannel
1386	SHKLYAR 13	DPWA	Multichannel
1370 \pm 4	ANISOVICH 12A	DPWA	Multichannel
1363 \pm 11	BATINIC 10	DPWA	$\pi N \rightarrow N\pi, N\eta$
1359	ARNDT 06	DPWA	$\pi N \rightarrow \pi N, \eta N$
1383	VRANA 00	DPWA	Multichannel
1385	HOEHLER 93	SPED	$\pi N \rightarrow \pi N$

¹ Fit to the amplitudes of HOEHLER 79.

-2xIMAGINARY PART

VALUE (MeV)	DOCUMENT ID	TECN	COMMENT
160 to 190 (\approx 175) OUR ESTIMATE			
189 \pm 5	SOKHOYAN 15A	DPWA	Multichannel
180 \pm 4 \pm 5	¹ SVARC 14	L+P	$\pi N \rightarrow \pi N$
180 \pm 40	CUTKOSKY 80	IPWA	$\pi N \rightarrow \pi N$
••• We do not use the following data for averages, fits, limits, etc. •••			
186	HUNT 19	DPWA	Multichannel
215	ROENCHEN 15A	DPWA	Multichannel
277	SHKLYAR 13	DPWA	Multichannel
190 \pm 7	ANISOVICH 12A	DPWA	Multichannel
151 \pm 13	BATINIC 10	DPWA	$\pi N \rightarrow N\pi, N\eta$
162	ARNDT 06	DPWA	$\pi N \rightarrow \pi N, \eta N$
316	VRANA 00	DPWA	Multichannel
164	HOEHLER 93	SPED	$\pi N \rightarrow \pi N$

¹ Fit to the amplitudes of HOEHLER 79.

N(1440) ELASTIC POLE RESIDUE

MODULUS $|r|$

VALUE (MeV)	DOCUMENT ID	TECN	COMMENT
46 to 54 (\approx 50) OUR ESTIMATE			
49 \pm 3	SOKHOYAN 15A	DPWA	Multichannel
50 \pm 1 \pm 2	¹ SVARC 14	L+P	$\pi N \rightarrow \pi N$
52 \pm 5	CUTKOSKY 80	IPWA	$\pi N \rightarrow \pi N$

••• We do not use the following data for averages, fits, limits, etc. •••

62	ROENCHEN 15A	DPWA	Multichannel
126	SHKLYAR 13	DPWA	Multichannel
48 \pm 3	ANISOVICH 12A	DPWA	Multichannel
44	BATINIC 10	DPWA	$\pi N \rightarrow N\pi, N\eta$
38	ARNDT 06	DPWA	$\pi N \rightarrow \pi N, \eta N$
40	HOEHLER 93	SPED	$\pi N \rightarrow \pi N$

¹ Fit to the amplitudes of HOEHLER 79.

PHASE θ

VALUE ($^\circ$)	DOCUMENT ID	TECN	COMMENT
-100 to -80 (\approx -90) OUR ESTIMATE			
-82 \pm 5	SOKHOYAN 15A	DPWA	Multichannel
-88 \pm 1 \pm 2	¹ SVARC 14	L+P	$\pi N \rightarrow \pi N$
-100 \pm 35	CUTKOSKY 80	IPWA	$\pi N \rightarrow \pi N$

••• We do not use the following data for averages, fits, limits, etc. •••

-98	ROENCHEN 15A	DPWA	Multichannel
-60	SHKLYAR 13	DPWA	Multichannel
-78 \pm 4	ANISOVICH 12A	DPWA	Multichannel
-88	BATINIC 10	DPWA	$\pi N \rightarrow N\pi, N\eta$
-98	ARNDT 06	DPWA	$\pi N \rightarrow \pi N, \eta N$

¹ Fit to the amplitudes of HOEHLER 79.

N(1440) INELASTIC POLE RESIDUE

The "normalized residue" is the residue divided by $\Gamma_{pole}/2$.

Normalized residue in $N\pi \rightarrow N(1440) \rightarrow N\eta$

MODULUS	PHASE ($^\circ$)	DOCUMENT ID	TECN	COMMENT
••• We do not use the following data for averages, fits, limits, etc. •••				
0.078	-27	ROENCHEN 15A	DPWA	Multichannel

Normalized residue in $N\pi \rightarrow N(1440) \rightarrow \Delta\pi, P\text{-wave}$

MODULUS	PHASE ($^\circ$)	DOCUMENT ID	TECN	COMMENT
0.27 \pm 0.02	38 \pm 5	SOKHOYAN 15A	DPWA	Multichannel
••• We do not use the following data for averages, fits, limits, etc. •••				
0.27 \pm 0.02	40 \pm 5	ANISOVICH 12A	DPWA	Multichannel

Normalized residue in $N\pi \rightarrow N(1440) \rightarrow \Lambda K$

MODULUS	PHASE ($^\circ$)	DOCUMENT ID	TECN	COMMENT
••• We do not use the following data for averages, fits, limits, etc. •••				
0.016	145	ROENCHEN 15A	DPWA	Multichannel

Normalized residue in $N\pi \rightarrow N(1440) \rightarrow \Sigma K$

MODULUS	PHASE ($^\circ$)	DOCUMENT ID	TECN	COMMENT
••• We do not use the following data for averages, fits, limits, etc. •••				
0.027	113	ROENCHEN 15A	DPWA	Multichannel

Normalized residue in $N\pi \rightarrow N(1440) \rightarrow N(\pi\pi)_{S=0}^0\text{-wave}$

MODULUS	PHASE ($^\circ$)	DOCUMENT ID	TECN	COMMENT
0.21 \pm 0.04	-136 \pm 4	SOKHOYAN 15A	DPWA	Multichannel
••• We do not use the following data for averages, fits, limits, etc. •••				
0.21 \pm 0.05	-135 \pm 7	ANISOVICH 12A	DPWA	Multichannel

N(1440) BREIT-WIGNER MASS

VALUE (MeV)	DOCUMENT ID	TECN	COMMENT
1410 to 1470 (\approx 1440) OUR ESTIMATE			
1417 \pm 4	¹ HUNT 19	DPWA	Multichannel
1430 \pm 10	SOKHOYAN 15A	DPWA	Multichannel
1515 \pm 15	¹ SHKLYAR 13	DPWA	Multichannel
1485.0 \pm 1.2	¹ ARNDT 06	DPWA	$\pi N \rightarrow \pi N, \eta N$
1440 \pm 30	CUTKOSKY 80	IPWA	$\pi N \rightarrow \pi N$
1410 \pm 12	HOEHLER 79	IPWA	$\pi N \rightarrow \pi N$
••• We do not use the following data for averages, fits, limits, etc. •••			
1430 \pm 8	ANISOVICH 12A	DPWA	Multichannel
1412 \pm 2	¹ SHRESTHA 12A	DPWA	Multichannel
1439 \pm 19	BATINIC 10	DPWA	$\pi N \rightarrow N\pi, N\eta$
1518 \pm 5	PENNER 02C	DPWA	Multichannel
1479 \pm 80	VRANA 00	DPWA	Multichannel

¹ Statistical error only.

N(1440) BREIT-WIGNER WIDTH

VALUE (MeV)	DOCUMENT ID	TECN	COMMENT
250 to 450 (\approx 350) OUR ESTIMATE			
257 \pm 11	¹ HUNT 19	DPWA	Multichannel
360 \pm 30	SOKHOYAN 15A	DPWA	Multichannel
605 \pm 90	¹ SHKLYAR 13	DPWA	Multichannel
284 \pm 18	¹ ARNDT 06	DPWA	$\pi N \rightarrow \pi N, \eta N$
340 \pm 70	CUTKOSKY 80	IPWA	$\pi N \rightarrow \pi N$
135 \pm 10	HOEHLER 79	IPWA	$\pi N \rightarrow \pi N$

Baryon Particle Listings

$N(1440), N(1520)$

••• We do not use the following data for averages, fits, limits, etc. •••

365 ± 35	ANISOVICH	12A	DPWA	Multichannel
248 ± 5	¹ SHRESTHA	12A	DPWA	Multichannel
437 ± 141	BATINIC	10	DPWA	$\pi N \rightarrow N\pi, N\eta$
668 ± 41	PENNER	02C	DPWA	Multichannel
490 ± 120	VRANA	00	DPWA	Multichannel

¹ Statistical error only.

$N(1440)$ DECAY MODES

The following branching fractions are our estimates, not fits or averages.

Mode	Fraction (Γ_i/Γ)
Γ_1 $N\pi$	55–75 %
Γ_2 $N\eta$	<1 %
Γ_3 $N\pi\pi$	17–50 %
Γ_4 $\Delta(1232)\pi, P\text{-wave}$	6–27 %
Γ_5 $N\sigma$	11–23 %
Γ_6 $p\gamma, \text{ helicity}=1/2$	0.035–0.048 %
Γ_7 $n\gamma, \text{ helicity}=1/2$	0.02–0.04 %

$N(1440)$ BRANCHING RATIOS

$\Gamma(N\pi)/\Gamma_{\text{total}}$	DOCUMENT ID	TECN	COMMENT	Γ_1/Γ
55 to 75 (≈ 65) OUR ESTIMATE				
59 ± 2	¹ HUNT	19	DPWA	Multichannel
63 ± 2	SOKHOYAN	15A	DPWA	Multichannel
56 ± 2	¹ SHKLYAR	13	DPWA	Multichannel
78.7 ± 1.6	¹ ARNDT	06	DPWA	$\pi N \rightarrow \pi N, \eta N$
68 ± 4	CUTKOSKY	80	IPWA	$\pi N \rightarrow \pi N$
51 ± 5	HOEHLER	79	IPWA	$\pi N \rightarrow \pi N$
••• We do not use the following data for averages, fits, limits, etc. •••				
62 ± 3	ANISOVICH	12A	DPWA	Multichannel
64.8 ± 0.9	¹ SHRESTHA	12A	DPWA	Multichannel
62 ± 4	BATINIC	10	DPWA	$\pi N \rightarrow N\pi, N\eta$
57 ± 1	PENNER	02C	DPWA	Multichannel
72 ± 5	VRANA	00	DPWA	Multichannel

¹ Statistical error only.

$\Gamma(N\eta)/\Gamma_{\text{total}}$	DOCUMENT ID	TECN	COMMENT	Γ_2/Γ
0 ± 1				
0 ± 1	VRANA	00	DPWA	Multichannel

$\Gamma(\Delta(1232)\pi, P\text{-wave})/\Gamma_{\text{total}}$	DOCUMENT ID	TECN	COMMENT	Γ_4/Γ
6 to 27 (≈ 15) OUR ESTIMATE				
22 ± 4	¹ HUNT	19	DPWA	Multichannel
12 ± 3	SHKLYAR	16	DPWA	Multichannel
20 ± 7	SOKHOYAN	15A	DPWA	Multichannel

••• We do not use the following data for averages, fits, limits, etc. •••

21 ± 8	ANISOVICH	12A	DPWA	Multichannel
6.5 ± 0.8	¹ SHRESTHA	12A	DPWA	Multichannel
16 ± 1	VRANA	00	DPWA	Multichannel

¹ Statistical error only.

$\Gamma(N\sigma)/\Gamma_{\text{total}}$	DOCUMENT ID	TECN	COMMENT	Γ_5/Γ
16 ± 3	¹ HUNT	19	DPWA	Multichannel
27 ± 4	SHKLYAR	16	DPWA	Multichannel
17 ± 6	SOKHOYAN	15A	DPWA	Multichannel
••• We do not use the following data for averages, fits, limits, etc. •••				
17 ± 7	ANISOVICH	12A	DPWA	Multichannel
27 ± 1	¹ SHRESTHA	12A	DPWA	Multichannel
12 ± 1	VRANA	00	DPWA	Multichannel

¹ Statistical error only.

$N(1440)$ PHOTON DECAY AMPLITUDES AT THE POLE

$N(1440) \rightarrow p\gamma, \text{ helicity-1/2 amplitude } A_{1/2}$

MODULUS ($\text{GeV}^{-1/2}$)	PHASE ($^\circ$)	DOCUMENT ID	TECN	COMMENT
−0.044 ± 0.005	−40 ± 8	SOKHOYAN	15A	DPWA
−0.054 ± 0.004	5 ± 2	ROENCHEN	14	DPWA
−0.054 ± 0.003	−5	ROENCHEN	14	DPWA
••• We do not use the following data for averages, fits, limits, etc. •••				
−0.060	−23	ROENCHEN	15A	DPWA

$N(1440)$ BREIT-WIGNER PHOTON DECAY AMPLITUDES

$N(1440) \rightarrow p\gamma, \text{ helicity-1/2 amplitude } A_{1/2}$

VALUE ($\text{GeV}^{-1/2}$)	DOCUMENT ID	TECN	COMMENT
−0.080 to −0.050 (≈ −0.065) OUR ESTIMATE			
−0.091 ± 0.007	¹ HUNT	19	DPWA
−0.061 ± 0.006	SOKHOYAN	15A	DPWA
−0.085 ± 0.003	¹ SHKLYAR	13	DPWA
−0.056 ± 0.001	¹ WORKMAN	12A	DPWA
−0.051 ± 0.002	¹ DUGGER	07	DPWA
••• We do not use the following data for averages, fits, limits, etc. •••			
−0.061 ± 0.008	ANISOVICH	12A	DPWA
−0.084 ± 0.003	¹ SHRESTHA	12A	DPWA
−0.061	DRECHSEL	07	DPWA
−0.087	PENNER	02D	DPWA

¹ Statistical error only.

$N(1440) \rightarrow n\gamma, \text{ helicity-1/2 amplitude } A_{1/2}$

VALUE ($\text{GeV}^{-1/2}$)	DOCUMENT ID	TECN	COMMENT
0.035 to 0.055 (≈ 0.045) OUR ESTIMATE			
0.013 ± 0.012	¹ HUNT	19	DPWA
0.043 ± 0.012	ANISOVICH	13B	DPWA
0.048 ± 0.004	¹ CHEN	12A	DPWA
••• We do not use the following data for averages, fits, limits, etc. •••			
0.040 ± 0.005	¹ SHRESTHA	12A	DPWA
0.054	DRECHSEL	07	DPWA
0.121	PENNER	02D	DPWA

¹ Statistical error only.

$N(1440)$ REFERENCES

For early references, see Physics Letters **111B** 1 (1982).

HUNT	19	PR C99 055205	B.C. Hunt, D.M. Manley	
SHKLYAR	16	PR C93 045206	V. Shklyar, H. Lenske, U. Mosel	(GIES)
ROENCHEN	15A	EPJ A51 70	D. Roenchen et al.	
SOKHOYAN	15A	EPJ A51 95	V. Sokhoyan et al.	(CBELSA/TAPS Collab.)
PDG	14	CP C38 070001	K. Olive et al.	(PDG Collab.)
ROENCHEN	14	EPJ A50 101	D. Roenchen et al.	
		Also EPJ A51 63 (errata.)	D. Roenchen et al.	
SVARC	14	PR C89 045205	A. Svarc et al.	(RBI Zagreb, UNI Tuzla)
ANISOVICH	13B	EPJ A49 67	A.V. Anisovich et al.	
SHKLYAR	13	PR C87 015201	V. Shklyar, H. Lenske, U. Mosel	(GIES)
ANISOVICH	12A	EPJ A48 15	A.V. Anisovich et al.	(BONN, PNPI)
CHEN	12A	PR C86 015206	W. Chen et al.	(DUKE, GWU, MSST, ITP+)
SHRESTHA	12A	PR C86 055203	M. Shrestha, D.M. Manley	(KSU)
WORKMAN	12A	PR C86 015202	R. Workman et al.	(GWU)
BATINIC	10	PR C82 038203	M. Batinic et al.	(ZAGR)
DRECHSEL	07	EPJ A34 69	D. Drechsel, S.S. Kamalov, L. Tiator	(MAINZ, JINR)
DUGGER	07	PR C76 025211	M. Dugger et al.	(JLab CLAS Collab.)
ARNDT	06	PR C74 045205	R.A. Arndt et al.	(GWU)
PENNER	02C	PR C66 055211	G. Penner, U. Mosel	(GIES)
PENNER	02D	PR C66 055212	G. Penner, U. Mosel	(GIES)
VRANA	00	PRPL 328 181	T.P. Vrana, S.A. Dytman, T.-S.H. Lee	(PITT, ANL)
HOEHLER	93	πN Newsletter 9 1	G. Hohlner	(KARL)
CUTKOSKY	80	Toronto Conf. 19	R.E. Cutkosky et al.	(CMU, LBL) IJP
		Also PR D20 2839	R.E. Cutkosky et al.	(CMU, LBL) IJP
HOEHLER	79	PDAT 12-1	G. Hohlner et al.	(KARL) IJP
		Also Toronto Conf. 3	R. Koch	(KARL) IJP

$N(1520) \frac{3}{2}^-$

 $I(J^P) = \frac{1}{2}(\frac{3}{2}^-)$ Status: ***

Older and obsolete values are listed and referenced in the 2014 edition, Chinese Physics **C38** 070001 (2014).

$N(1520)$ POLE POSITION

REAL PART

VALUE (MeV)	DOCUMENT ID	TECN	COMMENT
1505 to 1515 (≈ 1510) OUR ESTIMATE			
1507 ± 2	SOKHOYAN	15A	DPWA
1506 ± 1 ± 1	¹ SVARC	14	L+P $\pi N \rightarrow \pi N$
1510 ± 5	CUTKOSKY	80	IPWA $\pi N \rightarrow \pi N$
••• We do not use the following data for averages, fits, limits, etc. •••			
1500	HUNT	19	DPWA
1512	ROENCHEN	15A	DPWA
1492	SHKLYAR	13	DPWA
1507 ± 3	ANISOVICH	12A	DPWA
1506 ± 9	BATINIC	10	DPWA
1515	ARNDT	06	DPWA
1504	VRANA	00	DPWA
1510	HOEHLER	93	ARGD $\pi N \rightarrow \pi N$

¹ Fit to the amplitudes of HOEHLER 79.

−2×IMAGINARY PART

VALUE (MeV)	DOCUMENT ID	TECN	COMMENT
105 to 120 (≈ 110) OUR ESTIMATE			
111 ± 3	SOKHOYAN	15A	DPWA
115 ± 2 ± 1	¹ SVARC	14	L+P $\pi N \rightarrow \pi N$
114 ± 10	CUTKOSKY	80	IPWA $\pi N \rightarrow \pi N$

• • • We do not use the following data for averages, fits, limits, etc. • • •

117	HUNT	19	DPWA	Multichannel
89	ROENCHEN	15A	DPWA	Multichannel
94	SHKLYAR	13	DPWA	Multichannel
111 ± 5	ANISOVICH	12A	DPWA	Multichannel
122 ± 9	BATINIC	10	DPWA	$\pi N \rightarrow N\pi, N\eta$
113	ARNDT	06	DPWA	$\pi N \rightarrow \pi N, \eta N$
112	VRANA	00	DPWA	Multichannel
120	HOEHLER	93	ARGD	$\pi N \rightarrow \pi N$

¹ Fit to the amplitudes of HOEHLER 79.

N(1520) ELASTIC POLE RESIDUE

MODULUS |r|

VALUE (MeV)	DOCUMENT ID	TECN	COMMENT
32 to 38 (≈ 35) OUR ESTIMATE			
36 ± 2	SOKHOYAN	15A	DPWA Multichannel
33 ± 1 ± 1	¹ SVARC	14	L+P $\pi N \rightarrow \pi N$
35 ± 2	CUTKOSKY	80	IPWA $\pi N \rightarrow \pi N$

• • • We do not use the following data for averages, fits, limits, etc. • • •

37	ROENCHEN	15A	DPWA	Multichannel
27	SHKLYAR	13	DPWA	Multichannel
36 ± 3	ANISOVICH	12A	DPWA	Multichannel
35	BATINIC	10	DPWA	$\pi N \rightarrow N\pi, N\eta$
38	ARNDT	06	DPWA	$\pi N \rightarrow \pi N, \eta N$
32	HOEHLER	93	ARGD	$\pi N \rightarrow \pi N$

¹ Fit to the amplitudes of HOEHLER 79.

PHASE θ

VALUE (°)	DOCUMENT ID	TECN	COMMENT
-15 to -5 (≈ -10) OUR ESTIMATE			
-14 ± 3	SOKHOYAN	15A	DPWA Multichannel
-15 ± 1 ± 1	¹ SVARC	14	L+P $\pi N \rightarrow \pi N$
-12 ± 5	CUTKOSKY	80	IPWA $\pi N \rightarrow \pi N$

• • • We do not use the following data for averages, fits, limits, etc. • • •

-6	ROENCHEN	15A	DPWA	Multichannel
-35	SHKLYAR	13	DPWA	Multichannel
-14 ± 3	ANISOVICH	12A	DPWA	Multichannel
-7	BATINIC	10	DPWA	$\pi N \rightarrow N\pi, N\eta$
-5	ARNDT	06	DPWA	$\pi N \rightarrow \pi N, \eta N$
-8	HOEHLER	93	ARGD	$\pi N \rightarrow \pi N$

¹ Fit to the amplitudes of HOEHLER 79.

N(1520) INELASTIC POLE RESIDUE

The "normalized residue" is the residue divided by $\Gamma_{pole}/2$.

Normalized residue in $N\pi \rightarrow N(1520) \rightarrow \Delta\pi, S\text{-wave}$

MODULUS	PHASE (°)	DOCUMENT ID	TECN	COMMENT
0.33 ± 0.04	155 ± 15	SOKHOYAN	15A	DPWA Multichannel
• • • We do not use the following data for averages, fits, limits, etc. • • •				
0.33 ± 0.05	150 ± 20	ANISOVICH	12A	DPWA Multichannel

Normalized residue in $N\pi \rightarrow N(1520) \rightarrow \Delta\pi, D\text{-wave}$

MODULUS	PHASE (°)	DOCUMENT ID	TECN	COMMENT
0.25 ± 0.03	105 ± 18	SOKHOYAN	15A	DPWA Multichannel
• • • We do not use the following data for averages, fits, limits, etc. • • •				
0.25 ± 0.03	100 ± 20	ANISOVICH	12A	DPWA Multichannel

Normalized residue in $N\pi \rightarrow N(1520) \rightarrow N\eta$

MODULUS	PHASE (°)	DOCUMENT ID	TECN	COMMENT
• • • We do not use the following data for averages, fits, limits, etc. • • •				
0.026	95	ROENCHEN	15A	DPWA Multichannel

Normalized residue in $N\pi \rightarrow N(1520) \rightarrow \Lambda K$

MODULUS	PHASE (°)	DOCUMENT ID	TECN	COMMENT
• • • We do not use the following data for averages, fits, limits, etc. • • •				
0.069	158	ROENCHEN	15A	DPWA Multichannel

Normalized residue in $N\pi \rightarrow N(1520) \rightarrow \Sigma K$

MODULUS	PHASE (°)	DOCUMENT ID	TECN	COMMENT
• • • We do not use the following data for averages, fits, limits, etc. • • •				
0.049	-41	ROENCHEN	15A	DPWA Multichannel

Normalized residue in $N\pi \rightarrow N(1520) \rightarrow N\sigma$

MODULUS	PHASE (°)	DOCUMENT ID	TECN	COMMENT
0.08 ± 0.03	-45 ± 25	SOKHOYAN	15A	DPWA Multichannel

N(1520) BREIT-WIGNER MASS

VALUE (MeV)	DOCUMENT ID	TECN	COMMENT
1510 to 1520 (≈ 1515) OUR ESTIMATE			
1512.0 ± 1.5	¹ HUNT	19	DPWA Multichannel
1516 ± 2	SOKHOYAN	15A	DPWA Multichannel
1505 ± 4	¹ SHKLYAR	13	DPWA Multichannel
1514.5 ± 0.2	¹ ARNDT	06	DPWA $\pi N \rightarrow \pi N, \eta N$
1525 ± 10	CUTKOSKY	80	IPWA $\pi N \rightarrow \pi N$
1519 ± 4	HOEHLER	79	IPWA $\pi N \rightarrow \pi N$
• • • We do not use the following data for averages, fits, limits, etc. • • •			
1517 ± 3	ANISOVICH	12A	DPWA Multichannel
1512.6 ± 0.5	¹ SHRESTHA	12A	DPWA Multichannel
1522 ± 8	BATINIC	10	DPWA $\pi N \rightarrow N\pi, N\eta$
1509 ± 1	PENNER	02C	DPWA Multichannel
1518 ± 3	VRANA	00	DPWA Multichannel

¹ Statistical error only.

N(1520) BREIT-WIGNER WIDTH

VALUE (MeV)	DOCUMENT ID	TECN	COMMENT
100 to 120 (≈ 110) OUR ESTIMATE			
121 ± 3	¹ HUNT	19	DPWA Multichannel
113 ± 4	SOKHOYAN	15A	DPWA Multichannel
100 ± 2	¹ SHKLYAR	13	DPWA Multichannel
103.6 ± 0.4	¹ ARNDT	06	DPWA $\pi N \rightarrow \pi N, \eta N$
120 ± 15	CUTKOSKY	80	IPWA $\pi N \rightarrow \pi N$
114 ± 7	HOEHLER	79	IPWA $\pi N \rightarrow \pi N$
• • • We do not use the following data for averages, fits, limits, etc. • • •			
114 ± 5	ANISOVICH	12A	DPWA Multichannel
117 ± 1	¹ SHRESTHA	12A	DPWA Multichannel
132 ± 11	BATINIC	10	DPWA $\pi N \rightarrow N\pi, N\eta$
100 ± 2	PENNER	02C	DPWA Multichannel
124 ± 4	VRANA	00	DPWA Multichannel

¹ Statistical error only.

N(1520) DECAY MODES

The following branching fractions are our estimates, not fits or averages.

Mode	Fraction (Γ_i/Γ)
Γ_1 $N\pi$	55-65 %
Γ_2 $N\eta$	0.07-0.09 %
Γ_3 $N\pi\pi$	25-35 %
Γ_4 $\Delta(1232)\pi$	22-34 %
Γ_5 $\Delta(1232)\pi, S\text{-wave}$	15-23 %
Γ_6 $\Delta(1232)\pi, D\text{-wave}$	7-11 %
Γ_7 $N\rho$	10-16 %
Γ_8 $N\rho, S=3/2, S\text{-wave}$	10-16 %
Γ_9 $N\rho, S=1/2, D\text{-wave}$	0.2-0.4 %
Γ_{10} $N\sigma$	<10 %
Γ_{11} $p\gamma$	0.31-0.52 %
Γ_{12} $p\gamma, \text{helicity}=1/2$	0.01-0.02 %
Γ_{13} $p\gamma, \text{helicity}=3/2$	0.30-0.50 %
Γ_{14} $n\gamma$	0.30-0.53 %
Γ_{15} $n\gamma, \text{helicity}=1/2$	0.04-0.10 %
Γ_{16} $n\gamma, \text{helicity}=3/2$	0.25-0.45 %

N(1520) BRANCHING RATIOS

$\Gamma(N\pi)/\Gamma_{\text{total}}$	DOCUMENT ID	TECN	COMMENT	Γ_1/Γ
55 to 65 (≈ 60) OUR ESTIMATE				
58.3 ± 1.5	¹ HUNT	19	DPWA Multichannel	
61 ± 2	SOKHOYAN	15A	DPWA Multichannel	
57 ± 2	¹ SHKLYAR	13	DPWA Multichannel	
63.2 ± 0.1	¹ ARNDT	06	DPWA $\pi N \rightarrow \pi N, \eta N$	
58 ± 3	CUTKOSKY	80	IPWA $\pi N \rightarrow \pi N$	
54 ± 3	HOEHLER	79	IPWA $\pi N \rightarrow \pi N$	
• • • We do not use the following data for averages, fits, limits, etc. • • •				
62 ± 3	ANISOVICH	12A	DPWA Multichannel	
62.7 ± 0.5	¹ SHRESTHA	12A	DPWA Multichannel	
55 ± 5	BATINIC	10	DPWA $\pi N \rightarrow N\pi, N\eta$	
56 ± 1	PENNER	02C	DPWA Multichannel	
63 ± 2	VRANA	00	DPWA Multichannel	

¹ Statistical error only.

Baryon Particle Listings

 $N(1520)$ $\Gamma(N\eta)/\Gamma_{\text{total}}$

VALUE (%)	DOCUMENT ID	TECN	COMMENT
<0.1	MUELLER 20	DPWA	Multichannel
0.03 ± 0.01	¹ HUNT 19	DPWA	Multichannel
0.08 ± 0.01	TIATOR 99	DPWA	$\gamma p \rightarrow p\eta$

• • • We do not use the following data for averages, fits, limits, etc. • • •

<1	SHKLYAR 13	DPWA	Multichannel
0.1 ± 0.1	BATINIC 10	DPWA	$\pi N \rightarrow N\pi, N\eta$
0.2 ± 0.1	THOMA 08	DPWA	Multichannel
0.08 to 0.12	ARNDT 05	DPWA	Multichannel
0.23 ± 0.04	PENNER 02c	DPWA	Multichannel
0 ± 1	VRANA 00	DPWA	Multichannel

¹ Statistical error only.

 $\Gamma(\Delta(1232)\pi, S\text{-wave})/\Gamma_{\text{total}}$

VALUE (%)	DOCUMENT ID	TECN	COMMENT
12.1 ± 2.1	ADAMCZEW... 20	DPWA	Multichannel
21 ± 2	¹ HUNT 19	DPWA	Multichannel
19 ± 4	SOKHOYAN 15A	DPWA	Multichannel

• • • We do not use the following data for averages, fits, limits, etc. • • •

19 ± 4	ANISOVICH 12A	DPWA	Multichannel
9.3 ± 0.7	¹ SHRESTHA 12A	DPWA	Multichannel
15 ± 2	VRANA 00	DPWA	Multichannel

¹ Statistical error only.

 $\Gamma(\Delta(1232)\pi, D\text{-wave})/\Gamma_{\text{total}}$

VALUE (%)	DOCUMENT ID	TECN	COMMENT
6 ± 2	ADAMCZEW... 20	DPWA	Multichannel
6 ± 1	¹ HUNT 19	DPWA	Multichannel
9 ± 2	SOKHOYAN 15A	DPWA	Multichannel

• • • We do not use the following data for averages, fits, limits, etc. • • •

9 ± 2	ANISOVICH 12A	DPWA	Multichannel
6.3 ± 0.5	¹ SHRESTHA 12A	DPWA	Multichannel
11 ± 2	VRANA 00	DPWA	Multichannel

¹ Statistical error only.

 $\Gamma(N\rho, S=3/2, S\text{-wave})/\Gamma_{\text{total}}$

VALUE (%)	DOCUMENT ID	TECN	COMMENT
10-16 % OUR EVALUATION			
11.8 ± 1.9	ADAMCZEW... 20	DPWA	Multichannel
14.1 ± 1.5	¹ HUNT 19	DPWA	Multichannel

¹ Statistical error only.

 $\Gamma(N\rho, S=1/2, D\text{-wave})/\Gamma_{\text{total}}$

VALUE (%)	DOCUMENT ID	TECN	COMMENT
0.2-0.4 % OUR EVALUATION			
0.4 ± 0.2	ADAMCZEW... 20	DPWA	Multichannel

 $\Gamma(N\sigma)/\Gamma_{\text{total}}$

VALUE (%)	DOCUMENT ID	TECN	COMMENT
<10 % OUR ESTIMATE			
7 ± 3	ADAMCZEW... 20	DPWA	Multichannel
<0.7	¹ HUNT 19	DPWA	Multichannel
<2	SOKHOYAN 15A	DPWA	Multichannel

• • • We do not use the following data for averages, fits, limits, etc. • • •

<1	¹ SHRESTHA 12A	DPWA	Multichannel
<4	THOMA 08	DPWA	Multichannel
1 ± 1	VRANA 00	DPWA	Multichannel

¹ Statistical error only.

 $N(1520)$ PHOTON DECAY AMPLITUDES AT THE POLE $N(1520) \rightarrow p\gamma$, helicity-1/2 amplitude $A_{1/2}$

MODULUS ($\text{GeV}^{-1/2}$)	PHASE ($^\circ$)	DOCUMENT ID	TECN	COMMENT
-0.023 ± 0.004	-6 ± 5	SOKHOYAN 15A	DPWA	Multichannel
-0.024 ± 0.008	-17 ± 16	ROENCHEN 14	DPWA	
-0.003	-6			

• • • We do not use the following data for averages, fits, limits, etc. • • •

-0.031	-17	ROENCHEN 15A	DPWA	Multichannel
--------	-----	--------------	------	--------------

 $N(1520) \rightarrow p\gamma$, helicity-3/2 amplitude $A_{3/2}$

MODULUS ($\text{GeV}^{-1/2}$)	PHASE ($^\circ$)	DOCUMENT ID	TECN	COMMENT
0.131 ± 0.006	4 ± 4	SOKHOYAN 15A	DPWA	Multichannel
0.117 ± 0.006	26 ± 2	ROENCHEN 14	DPWA	
-0.010				

• • • We do not use the following data for averages, fits, limits, etc. • • •

0.075	1.7	ROENCHEN 15A	DPWA	Multichannel
-------	-----	--------------	------	--------------

 $N(1520)$ BREIT-WIGNER PHOTON DECAY AMPLITUDES $N(1520) \rightarrow p\gamma$, helicity-1/2 amplitude $A_{1/2}$

VALUE ($\text{GeV}^{-1/2}$)	DOCUMENT ID	TECN	COMMENT
-0.030 to -0.015 (\approx -0.025) OUR ESTIMATE			
-0.034 ± 0.003	¹ HUNT 19	DPWA	Multichannel
-0.024 ± 0.004	SOKHOYAN 15A	DPWA	Multichannel
-0.015 ± 0.001	¹ SHKLYAR 13	DPWA	Multichannel
-0.019 ± 0.002	¹ WORKMAN 12A	DPWA	$\gamma N \rightarrow N\pi$
-0.028 ± 0.002	¹ DUGGER 07	DPWA	$\gamma N \rightarrow \pi N$
-0.038 ± 0.003	¹ AHRENS 02	DPWA	$\gamma N \rightarrow \pi N$

• • • We do not use the following data for averages, fits, limits, etc. • • •

-0.022 ± 0.004	ANISOVICH 12A	DPWA	Multichannel
-0.034 ± 0.001	¹ SHRESTHA 12A	DPWA	Multichannel
-0.027	DRECHSEL 07	DPWA	$\gamma N \rightarrow \pi N$
-0.003	PENNER 02D	DPWA	Multichannel
-0.052 ± 0.010 ± 0.007	¹ MUKHOPAD... 98		$\gamma p \rightarrow \eta p$

¹ Statistical error only.

 $N(1520) \rightarrow p\gamma$, helicity-3/2 amplitude $A_{3/2}$

VALUE ($\text{GeV}^{-1/2}$)	DOCUMENT ID	TECN	COMMENT
0.135 to 0.145 (\approx 0.140) OUR ESTIMATE			
0.142 ± 0.003	¹ HUNT 19	DPWA	Multichannel
0.130 ± 0.006	SOKHOYAN 15A	DPWA	Multichannel
0.146 ± 0.001	¹ SHKLYAR 13	DPWA	Multichannel
0.141 ± 0.002	¹ WORKMAN 12A	DPWA	$\gamma N \rightarrow N\pi$
0.143 ± 0.002	¹ DUGGER 07	DPWA	$\gamma N \rightarrow \pi N$
0.147 ± 0.010	¹ AHRENS 02	DPWA	$\gamma N \rightarrow \pi N$

• • • We do not use the following data for averages, fits, limits, etc. • • •

0.131 ± 0.010	ANISOVICH 12A	DPWA	Multichannel
0.127 ± 0.003	¹ SHRESTHA 12A	DPWA	Multichannel
0.161	DRECHSEL 07	DPWA	$\gamma N \rightarrow \pi N$
0.151	PENNER 02D	DPWA	Multichannel
0.130 ± 0.020 ± 0.015	¹ MUKHOPAD... 98		$\gamma p \rightarrow \eta p$

¹ Statistical error only.

 $N(1520) \rightarrow n\gamma$, helicity-1/2 amplitude $A_{1/2}$

VALUE ($\text{GeV}^{-1/2}$)	DOCUMENT ID	TECN	COMMENT
-0.055 to -0.040 (\approx -0.050) OUR ESTIMATE			
-0.072 ± 0.003	¹ HUNT 19	DPWA	Multichannel
-0.049 ± 0.008	ANISOVICH 13B	DPWA	Multichannel
-0.046 ± 0.006	¹ CHEN 12A	DPWA	$\gamma N \rightarrow \pi N$

• • • We do not use the following data for averages, fits, limits, etc. • • •

-0.038 ± 0.003	¹ SHRESTHA 12A	DPWA	Multichannel
-0.077	DRECHSEL 07	DPWA	$\gamma N \rightarrow \pi N$
-0.084	PENNER 02D	DPWA	Multichannel

¹ Statistical error only.

 $N(1520) \rightarrow n\gamma$, helicity-3/2 amplitude $A_{3/2}$

VALUE ($\text{GeV}^{-1/2}$)	DOCUMENT ID	TECN	COMMENT
-0.120 to -0.100 (\approx -0.115) OUR ESTIMATE			
-0.123 ± 0.006	¹ HUNT 19	DPWA	Multichannel
-0.113 ± 0.012	ANISOVICH 13B	DPWA	Multichannel
-0.115 ± 0.005	¹ CHEN 12A	DPWA	$\gamma N \rightarrow \pi N$

• • • We do not use the following data for averages, fits, limits, etc. • • •

-0.101 ± 0.004	¹ SHRESTHA 12A	DPWA	Multichannel
-0.154	DRECHSEL 07	DPWA	$\gamma N \rightarrow \pi N$
-0.159	PENNER 02D	DPWA	Multichannel

¹ Statistical error only.

 $N(1520)$ REFERENCES

For early references, see Physics Letters **111B** 1 (1982). For very early references, see Reviews of Modern Physics **37** 633 (1965).

ADAMCZEW... 20	PR C102 024001	J. Adamczewski-Musch et al.	(HADES Collab.)
MUELLER 20	PL B803 135323	J. Mueller et al.	(CBELSA/TAPS Collab.)
HUNT 19	PR C99 055205	B.C. Hunt, D.M. Manley	
ROENCHEN 15A	EPJ A51 70	D. Roenchen et al.	
SOKHOYAN 15A	EPJ A51 95	V. Sokhoyan et al.	(CBELSA/TAPS Collab.)
PDG 14	CP C38 070001	K. Olive et al.	(PDG Collab.)
ROENCHEN 14	EPJ A50 101	D. Roenchen et al.	
	Also	EPJ A51 63 (errata.)	
SVARC 14	PR C89 045205	A. Svarc et al.	(RBI Zagreb, UNI Tuzla)
ANISOVICH 13B	EPJ A49 67	A.V. Anisovich et al.	
SHKLYAR 13	PR C87 015201	V. Shklyar, H. Lenske, U. Mosel	(GIES)
ANISOVICH 12A	EPJ A48 15	A.V. Anisovich et al.	(BONN, PNPI)
CHEN 12A	PR C86 015206	W. Chen et al.	(DUKE, GWU, MSST, ITP+)
SHRESTHA 12A	PR C86 055203	M. Shrestha, D.M. Manley	(KSU)
WORKMAN 12A	PR C86 015202	R. Workman et al.	(GWU)
BATINIC 10	PR C82 038203	M. Batinic et al.	(ZAGR)
THOMA 08	PL B659 87	U. Thoma et al.	(CB-ELSA Collab.)
DRECHSEL 07	EPJ A34 69	D. Drechsel, S.S. Kamalov, L. Tiator	(MAINZ, JINR)
DUGGER 07	PR C76 025211	M. Dugger et al.	(JLab CLAS Collab.)
ARNDT 06	PR C74 045205	R.A. Arndt et al.	(GWU)
ARNDT 05	PR C72 045202	R.A. Arndt et al.	(GWU, PNPI)

See key on page 1127

Baryon Particle Listings

$N(1520)$, $N(1535)$

AHRENS	02	PRL 88 232002	J. Ahrens et al.	(Mainz MAMI GDH/A2 Collab.)
PENNER	02C	PR C66 055211	G. Penner, U. Mosel	(GIES)
PENNER	02D	PR C66 055212	G. Penner, U. Mosel	(GIES)
VRANA	00	PRPL 328 181	T.P. Vrana, S.A. Dytman, T.-S.H. Lee	(PITT, ANL)
TIATOR	99	PL C60 035210	L. Tiator et al.	
MUKHOPAD...	98	PL B444 7	N.C. Mukhopadhyay, N. Mathur	
HOEHLER	93	π N Newsletter 9 1	G. Höhler	(KARL)
CUTKOSKY	80	Toronto Conf. 19	R.E. Cutkosky et al.	(CMU, LBL) IJP
Albo		PR D20 2839	R.E. Cutkosky et al.	(CMU, LBL) IJP
HOEHLER	79	PDAT 12-1	G. Höhler et al.	(KARLT) IJP
Albo		Toronto Conf. 3	R. Koch	(KARLT) IJP

$N(1535) 1/2^-$

$$I(J^P) = \frac{1}{2}(\frac{1}{2}^-) \text{ Status: } * * * *$$

Older and obsolete values are listed and referenced in the 2014 edition, Chinese Physics C38 070001 (2014).

$N(1535)$ POLE POSITION

REAL PART

VALUE (MeV)	DOCUMENT ID	TECN	COMMENT
1500 to 1520 (≈ 1510) OUR ESTIMATE			
1496 \pm 4	AFZAL 20	DPWA	Multichannel
1500 \pm 4	SOKHOYAN 15A	DPWA	Multichannel
1509 \pm 4 \pm 2	¹ SVARC 14	L+P	$\pi N \rightarrow \pi N$
1510 \pm 50	CUTKOSKY 80	IPWA	$\pi N \rightarrow \pi N$
• • • We do not use the following data for averages, fits, limits, etc. • • •			
1496	HUNT 19	DPWA	Multichannel
1499	ROENCHEN 15A	DPWA	Multichannel
1490	SHKLYAR 13	DPWA	Multichannel
1501 \pm 4	ANISOVICH 12A	DPWA	Multichannel
1521 \pm 14	BATINIC 10	DPWA	$\pi N \rightarrow N\pi, N\eta$
1502	ARNDT 06	DPWA	$\pi N \rightarrow \pi N, \eta N$
1525	VRANA 00	DPWA	Multichannel
1487	HOEHLER 93	SPED	$\pi N \rightarrow \pi N$

¹ Fit to the amplitudes of HOEHLER 79.

-2xIMAGINARY PART

VALUE (MeV)	DOCUMENT ID	TECN	COMMENT
110 to 150 (≈ 130) OUR ESTIMATE			
125 \pm 6	AFZAL 20	DPWA	Multichannel
128 \pm 9	SOKHOYAN 15A	DPWA	Multichannel
118 \pm 9 \pm 2	² SVARC 14	L+P	$\pi N \rightarrow \pi N$
260 \pm 80	CUTKOSKY 80	IPWA	$\pi N \rightarrow \pi N$
• • • We do not use the following data for averages, fits, limits, etc. • • •			
119	HUNT 19	DPWA	Multichannel
104	ROENCHEN 15A	DPWA	Multichannel
100	SHKLYAR 13	DPWA	Multichannel
134 \pm 11	ANISOVICH 12A	DPWA	Multichannel
190 \pm 28	BATINIC 10	DPWA	$\pi N \rightarrow N\pi, N\eta$
95	ARNDT 06	DPWA	$\pi N \rightarrow \pi N, \eta N$
102	VRANA 00	DPWA	Multichannel

² Fit to the amplitudes of HOEHLER 79.

$N(1535)$ ELASTIC POLE RESIDUE

MODULUS $|r|$

VALUE (MeV)	DOCUMENT ID	TECN	COMMENT
15 to 35 (≈ 25) OUR ESTIMATE			
29 \pm 4	SOKHOYAN 15A	DPWA	Multichannel
22 \pm 2 \pm 0.4	³ SVARC 14	L+P	$\pi N \rightarrow \pi N$
120 \pm 40	CUTKOSKY 80	IPWA	$\pi N \rightarrow \pi N$
• • • We do not use the following data for averages, fits, limits, etc. • • •			
22	ROENCHEN 15A	DPWA	Multichannel
15	SHKLYAR 13	DPWA	Multichannel
31 \pm 4	ANISOVICH 12A	DPWA	Multichannel
68	BATINIC 10	DPWA	$\pi N \rightarrow N\pi, N\eta$
16	ARNDT 06	DPWA	$\pi N \rightarrow \pi N, \eta N$

³ Fit to the amplitudes of HOEHLER 79.

PHASE θ

VALUE ($^\circ$)	DOCUMENT ID	TECN	COMMENT
-30 to 0 (≈ -15) OUR ESTIMATE			
-20 \pm 10	SOKHOYAN 15A	DPWA	Multichannel
- 5 \pm 5 \pm 3	⁴ SVARC 14	L+P	$\pi N \rightarrow \pi N$
+15 \pm 45	CUTKOSKY 80	IPWA	$\pi N \rightarrow \pi N$
• • • We do not use the following data for averages, fits, limits, etc. • • •			
-46	ROENCHEN 15A	DPWA	Multichannel
-51	SHKLYAR 13	DPWA	Multichannel
-29 \pm 5	ANISOVICH 12A	DPWA	Multichannel
12	BATINIC 10	DPWA	$\pi N \rightarrow N\pi, N\eta$
-16	ARNDT 06	DPWA	$\pi N \rightarrow \pi N, \eta N$

⁴ Fit to the amplitudes of HOEHLER 79.

$N(1535)$ INELASTIC POLE RESIDUE

The "normalized residue" is the residue divided by $\Gamma_{pole}/2$.

Normalized residue in $N\pi \rightarrow N(1535) \rightarrow N\eta$

MODULUS	PHASE ($^\circ$)	DOCUMENT ID	TECN	COMMENT
0.43 \pm 0.03	-76 \pm 5	ANISOVICH 12A	DPWA	Multichannel
• • • We do not use the following data for averages, fits, limits, etc. • • •				
0.51	112	ROENCHEN 15A	DPWA	Multichannel

Normalized residue in $N\pi \rightarrow N(1535) \rightarrow \Lambda K$

MODULUS	PHASE ($^\circ$)	DOCUMENT ID	TECN	COMMENT
• • • We do not use the following data for averages, fits, limits, etc. • • •				
0.05	32	ROENCHEN 15A	DPWA	Multichannel

Normalized residue in $N\pi \rightarrow N(1535) \rightarrow \Sigma K$

MODULUS	PHASE ($^\circ$)	DOCUMENT ID	TECN	COMMENT
• • • We do not use the following data for averages, fits, limits, etc. • • •				
0.05	-69	ROENCHEN 15A	DPWA	Multichannel

Normalized residue in $N\pi \rightarrow N(1535) \rightarrow \Delta\pi, D\text{-wave}$

MODULUS	PHASE ($^\circ$)	DOCUMENT ID	TECN	COMMENT
0.11 \pm 0.02	160 \pm 20	SOKHOYAN 15A	DPWA	Multichannel
• • • We do not use the following data for averages, fits, limits, etc. • • •				
0.12 \pm 0.03	145 \pm 17	ANISOVICH 12A	DPWA	Multichannel

Normalized residue in $N\pi \rightarrow N(1535) \rightarrow N\sigma$

MODULUS	PHASE ($^\circ$)	DOCUMENT ID	TECN	COMMENT
0.16 \pm 0.07	25 \pm 40	SOKHOYAN 15A	DPWA	Multichannel

Normalized residue in $N\pi \rightarrow N(1535) \rightarrow N(1440)\pi$

MODULUS	PHASE ($^\circ$)	DOCUMENT ID	TECN	COMMENT
0.21 \pm 0.14	-45 \pm 50	SOKHOYAN 15A	DPWA	Multichannel

$N(1535)$ BREIT-WIGNER MASS

VALUE (MeV)	DOCUMENT ID	TECN	COMMENT
1515 to 1545 (≈ 1530) OUR ESTIMATE			
1525 \pm 2	⁵ HUNT 19	DPWA	Multichannel
1528 \pm 6	KASHEVAROV 17	DPWA	$\gamma p \rightarrow \eta p, \eta' p$
1517 \pm 4	SOKHOYAN 15A	DPWA	Multichannel
1526 \pm 2	⁵ SHKLYAR 13	DPWA	Multichannel
1547.0 \pm 0.7	⁵ ARNDT 06	DPWA	$\pi N \rightarrow \pi N, \eta N$
1550 \pm 40	CUTKOSKY 80	IPWA	$\pi N \rightarrow \pi N$
1526 \pm 7	HOEHLER 79	IPWA	$\pi N \rightarrow \pi N$
• • • We do not use the following data for averages, fits, limits, etc. • • •			
1519 \pm 5	ANISOVICH 12A	DPWA	Multichannel
1538 \pm 1	⁵ SHRESTHA 12A	DPWA	Multichannel
1553 \pm 8	BATINIC 10	DPWA	$\pi N \rightarrow N\pi, N\eta$
1546.7 \pm 2.2	ARNDT 04	DPWA	$\pi N \rightarrow \pi N, \eta N$
1526 \pm 2	PENNER 02C	DPWA	Multichannel
1530 \pm 10	BAI 01B	BES	$J/\psi \rightarrow p\bar{p}\eta$
1522 \pm 11	THOMPSON 01	CLAS	$\gamma^* p \rightarrow p\eta$
1542 \pm 3	VRANA 00	DPWA	Multichannel
1532 \pm 5	ARMSTRONG 99B	DPWA	$\gamma^* p \rightarrow p\eta$

⁵ Statistical error only.

$N(1535)$ BREIT-WIGNER WIDTH

VALUE (MeV)	DOCUMENT ID	TECN	COMMENT
125 to 175 (≈ 150) OUR ESTIMATE			
147 \pm 5	⁶ HUNT 19	DPWA	Multichannel
163 \pm 25	KASHEVAROV 17	DPWA	$\gamma p \rightarrow \eta p, \eta' p$
120 \pm 10	SOKHOYAN 15A	DPWA	Multichannel
131 \pm 12	⁶ SHKLYAR 13	DPWA	Multichannel
188.4 \pm 3.8	⁶ ARNDT 06	DPWA	$\pi N \rightarrow \pi N, \eta N$
240 \pm 80	CUTKOSKY 80	IPWA	$\pi N \rightarrow \pi N$
120 \pm 20	HOEHLER 79	IPWA	$\pi N \rightarrow \pi N$
• • • We do not use the following data for averages, fits, limits, etc. • • •			
128 \pm 14	ANISOVICH 12A	DPWA	Multichannel
141 \pm 4	⁶ SHRESTHA 12A	DPWA	Multichannel
182 \pm 25	BATINIC 10	DPWA	$\pi N \rightarrow N\pi, N\eta$
129 \pm 8	PENNER 02C	DPWA	Multichannel
95 \pm 25	BAI 01B	BES	$J/\psi \rightarrow p\bar{p}\eta$
143 \pm 18	THOMPSON 01	CLAS	$\gamma^* p \rightarrow p\eta$
112 \pm 19	VRANA 00	DPWA	Multichannel
154 \pm 20	ARMSTRONG 99B	DPWA	$\gamma^* p \rightarrow p\eta$

⁶ Statistical error only.

Baryon Particle Listings

 $N(1535)$ $N(1535)$ DECAY MODES

The following branching fractions are our estimates, not fits or averages.

Mode	Fraction (Γ_i/Γ)
Γ_1 $N\pi$	32–52 %
Γ_2 $N\eta$	30–55 %
Γ_3 $N\pi\pi$	4–31 %
Γ_4 $\Delta(1232)\pi$, D -wave	1–4 %
Γ_5 $N\rho$	2–17 %
Γ_6 $N\rho$, $S=1/2$, S -wave	2–16 %
Γ_7 $N\rho$, $S=3/2$, D -wave	<1 %
Γ_8 $N\sigma$	2–10 %
Γ_9 $N(1440)\pi$	5–12 %
Γ_{10} $\rho\gamma$, helicity=1/2	0.15–0.30 %
Γ_{11} $n\gamma$, helicity=1/2	0.01–0.25 %

 $N(1535)$ BRANCHING RATIOS

$\Gamma(N\pi)/\Gamma_{\text{total}}$	DOCUMENT ID	TECN	COMMENT	Γ_1/Γ
32–52 % OUR ESTIMATE				
42 ± 2	7 HUNT	19	DPWA Multichannel	
52 ± 5	SOKHOYAN	15A	DPWA Multichannel	
35 ± 3	7 SHKLYAR	13	DPWA Multichannel	
35.5 ± 0.2	7 ARNDT	06	DPWA $\pi N \rightarrow \pi N, \eta N$	
50 ± 10	CUTKOSKY	80	IPWA $\pi N \rightarrow \pi N$	
38 ± 4	HOEHLER	79	IPWA $\pi N \rightarrow \pi N$	
••• We do not use the following data for averages, fits, limits, etc. •••				
54 ± 5	ANISOVICH	12A	DPWA Multichannel	
37 ± 1	7 SHRESTHA	12A	DPWA Multichannel	
46 ± 7	BATINIC	10	DPWA $\pi N \rightarrow N\pi, N\eta$	
36 ± 1	PENNER	02c	DPWA Multichannel	
35 ± 8	VRANA	00	DPWA Multichannel	
7 Statistical error only.				

$\Gamma(N\eta)/\Gamma_{\text{total}}$	DOCUMENT ID	TECN	COMMENT	Γ_2/Γ
30–55 % OUR ESTIMATE				
41 ± 4	MUELLER	20	DPWA Multichannel	
43 ± 3	8 HUNT	19	DPWA Multichannel	
41 ± 4	9 KASHEVAROV	17	DPWA $\gamma\rho \rightarrow \eta\rho, \eta'\rho$	
58 ± 4	8 SHKLYAR	13	DPWA Multichannel	
33 ± 5	ANISOVICH	12A	DPWA Multichannel	
53 ± 1	PENNER	02c	DPWA Multichannel	
51 ± 5	VRANA	00	DPWA Multichannel	
••• We do not use the following data for averages, fits, limits, etc. •••				
41 ± 2	8 SHRESTHA	12A	DPWA Multichannel	
50 ± 7	BATINIC	10	DPWA $\pi N \rightarrow N\pi, N\eta$	
8 Statistical error only.				
9 Assuming $A_{1/2} = 0.115 \text{ GeV}^{-1/2}$.				

$\Gamma(N\eta)/\Gamma(N\pi)$	DOCUMENT ID	TECN	COMMENT	Γ_2/Γ_1
••• We do not use the following data for averages, fits, limits, etc. •••				
0.95 ± 0.03	AZNAURYAN	09	CLAS π, η electroproduction	

$\Gamma(\Delta(1232)\pi, D\text{-wave})/\Gamma_{\text{total}}$	DOCUMENT ID	TECN	COMMENT	Γ_4/Γ
1–4 % OUR ESTIMATE				
3 ± 1	ADAMCZEW... 20	DPWA	Multichannel	
<1.1	10 HUNT	19	DPWA Multichannel	
2.5 ± 1.5	SOKHOYAN	15A	DPWA Multichannel	
••• We do not use the following data for averages, fits, limits, etc. •••				
2.5 ± 1.5	ANISOVICH	12A	DPWA Multichannel	
1.8 ± 0.8	10 SHRESTHA	12A	DPWA Multichannel	
1 ± 1	VRANA	00	DPWA Multichannel	
10 Statistical error only.				

$\Gamma(N\rho, S=1/2, S\text{-wave})/\Gamma_{\text{total}}$	DOCUMENT ID	TECN	COMMENT	Γ_6/Γ
2–16 % OUR ESTIMATE				
2.7 ± 0.6	ADAMCZEW... 20	DPWA	Multichannel	
14 ± 2	11 HUNT	19	DPWA Multichannel	
11 Statistical error only.				

$\Gamma(N\rho, S=3/2, D\text{-wave})/\Gamma_{\text{total}}$	DOCUMENT ID	TECN	COMMENT	Γ_7/Γ
<1 % OUR ESTIMATE				
0.5 ± 0.5	ADAMCZEW... 20	DPWA	Multichannel	
<0.3	12 HUNT	19	DPWA Multichannel	
12 Statistical error only.				

$\Gamma(N\sigma)/\Gamma_{\text{total}}$	DOCUMENT ID	TECN	COMMENT	Γ_8/Γ
2–10 % OUR ESTIMATE				
<1	13 HUNT	19	DPWA Multichannel	
6 ± 4	SOKHOYAN	15A	DPWA Multichannel	
••• We do not use the following data for averages, fits, limits, etc. •••				
1.5 ± 0.5	13 SHRESTHA	12A	DPWA Multichannel	
2 ± 1	VRANA	00	DPWA Multichannel	
13 Statistical error only.				

$\Gamma(N(1440)\pi)/\Gamma_{\text{total}}$	DOCUMENT ID	TECN	COMMENT	Γ_9/Γ
5–12 % OUR ESTIMATE				
< 0.01	14 HUNT	19	DPWA Multichannel	
12 ± 8	SOKHOYAN	15A	DPWA Multichannel	
8 ± 2	14 STAROSTIN	03	$\pi^- p \rightarrow n3\pi^0$	
••• We do not use the following data for averages, fits, limits, etc. •••				
< 1	14 SHRESTHA	12A	DPWA Multichannel	
10 ± 9	VRANA	00	DPWA Multichannel	
14 This value is an estimate made using simplest assumptions.				

 $N(1535)$ PHOTON DECAY AMPLITUDES AT THE POLE

$N(1535) \rightarrow p\gamma$, helicity-1/2 amplitude $A_{1/2}$	MODULUS ($\text{GeV}^{-1/2}$)	PHASE ($^\circ$)	DOCUMENT ID	TECN	COMMENT
0.093 ± 0.009	8 ± 4		ANISOVICH	17D	DPWA Multichannel
0.050 ± 0.004	-14^{+12}_{-10}		15 ROENCHEN	14	DPWA
••• We do not use the following data for averages, fits, limits, etc. •••					
0.114 ± 0.008	10 ± 5		ANISOVICH	15A	DPWA Multichannel
0.106	5.2		ROENCHEN	15A	DPWA Multichannel
0.114 ± 0.008	10 ± 5		SOKHOYAN	15A	DPWA Multichannel
15 T-Matrix amplitude					

$N(1535) \rightarrow n\gamma$, helicity-1/2 amplitude $A_{1/2}$	MODULUS ($\text{GeV}^{-1/2}$)	PHASE ($^\circ$)	DOCUMENT ID	TECN	COMMENT
-0.088 ± 0.004	5 ± 4		ANISOVICH	17D	DPWA Multichannel
••• We do not use the following data for averages, fits, limits, etc. •••					
-0.095 ± 0.006	8 ± 5		ANISOVICH	15A	DPWA Multichannel

 $N(1535)$ BREIT-WIGNER PHOTON DECAY AMPLITUDES

$N(1535) \rightarrow p\gamma$, helicity-1/2 amplitude $A_{1/2}$	VALUE ($\text{GeV}^{-1/2}$)	DOCUMENT ID	TECN	COMMENT
0.090 to 0.120 (≈ 0.105) OUR ESTIMATE				
0.107 ± 0.003	16 HUNT	19	DPWA Multichannel	
0.101 ± 0.007	SOKHOYAN	15A	DPWA Multichannel	
0.091 ± 0.004	16 SHKLYAR	13	DPWA Multichannel	
0.128 ± 0.004	16 WORKMAN	12A	DPWA $\gamma N \rightarrow N\pi$	
0.091 ± 0.002	16 DUGGER	07	DPWA $\gamma N \rightarrow \pi N$	
••• We do not use the following data for averages, fits, limits, etc. •••				
0.105 ± 0.010	ANISOVICH	12A	DPWA Multichannel	
0.059 ± 0.003	16 SHRESTHA	12A	DPWA Multichannel	
0.066	DRECHSEL	07	DPWA $\gamma N \rightarrow \pi N$	
0.090	PENNER	02D	DPWA Multichannel	
16 Statistical error only.				

$N(1535) \rightarrow n\gamma$, helicity-1/2 amplitude $A_{1/2}$	VALUE ($\text{GeV}^{-1/2}$)	DOCUMENT ID	TECN	COMMENT
-0.095 to -0.055 (≈ -0.075) OUR ESTIMATE				
-0.055 ± 0.006	17 HUNT	19	DPWA Multichannel	
-0.093 ± 0.011	ANISOVICH	13B	DPWA Multichannel	
-0.058 ± 0.006	17 CHEN	12A	DPWA $\gamma N \rightarrow \pi N$	
••• We do not use the following data for averages, fits, limits, etc. •••				
-0.049 ± 0.003	17 SHRESTHA	12A	DPWA Multichannel	
-0.051	DRECHSEL	07	DPWA $\gamma N \rightarrow \pi N$	
-0.024	PENNER	02D	DPWA Multichannel	
17 Statistical error only.				

$N(1535) \rightarrow N\gamma$, ratio $A_{1/2}^n/A_{1/2}^p$	VALUE ($\text{GeV}^{-1/2}$)	DOCUMENT ID	TECN	COMMENT
••• We do not use the following data for averages, fits, limits, etc. •••				
-0.84 ± 0.15	MUKHOPAD... 95B	IPWA		

 $N(1535)$ REFERENCES

For early references, see Physics Letters **111B** 1 (1982).

ADAMCZEW... 20	PR C102 024001	J. Adamczewski-Musch et al.	(HADES Collab.)
AFZAL 20	PRL 125 152002	F. Afzal et al.	(CBELSA/TAPS Collab.)
MUELLER 20	PL B803 135323	J. Mueller et al.	(CBELSA/TAPS Collab.)
HUNT 19	PR C99 055205	B.C. Hunt, D.M. Manley	

Baryon Particle Listings
N(1535), N(1650)

Table listing various baryon particles and their properties, including ANISOVICH, KASHEVAROV, ROENCHEN, SOKHOYAN, PDG, etc.

Table listing baryon particles and their properties, including ROENCHEN, SHKLYAR, ANISOVICH, BATINIC, ARNDT, HOEHLER.

PHASE ̸

Table with columns: VALUE (°), DOCUMENT ID, TECN, COMMENT. Includes entries for SOKHOYAN, SVARC, CUTKOSKY, ROENCHEN, SHKLYAR, ANISOVICH, BATINIC, ARNDT, HOEHLER.

N(1650) 1/2-

I(J^P) = 1/2(1/2-) Status: * * * *

Older and obsolete values are listed and referenced in the 2014 edition, Chinese Physics C38 070001 (2014).

N(1650) POLE POSITION

REAL PART

Table with columns: VALUE (MeV), DOCUMENT ID, TECN, COMMENT. Includes entries for AFZAL, ANISOVICH, SVARC, CUTKOSKY, HUNT, ROENCHEN, SOKHOYAN, SHKLYAR, ANISOVICH, BATINIC, ARNDT, VRANA, HOEHLER.

1 Statistical error only. 2 Fit to the amplitudes of HOEHLER 79.

-2xIMAGINARY PART

Table with columns: VALUE (MeV), DOCUMENT ID, TECN, COMMENT. Includes entries for AFZAL, ANISOVICH, SVARC, CUTKOSKY, HUNT, ROENCHEN, SOKHOYAN, SHKLYAR, ANISOVICH, BATINIC, ARNDT, VRANA, HOEHLER.

1 Statistical error only. 2 Fit to the amplitudes of HOEHLER 79.

N(1650) ELASTIC POLE RESIDUE

MODULUS |r|

Table with columns: VALUE (MeV), DOCUMENT ID, TECN, COMMENT. Includes entries for SOKHOYAN, SVARC, CUTKOSKY.

N(1650) INELASTIC POLE RESIDUE

The "normalized residue" is the residue divided by Γ_pole/2.

Normalized residue in Nπ → N(1650) → Nη

Table with columns: MODULUS, PHASE (°), DOCUMENT ID, TECN, COMMENT. Includes entries for ANISOVICH, ROENCHEN.

Normalized residue in Nπ → N(1650) → ΛK

Table with columns: MODULUS, PHASE (°), DOCUMENT ID, TECN, COMMENT. Includes entries for ANISOVICH, ROENCHEN, ANISOVICH.

Normalized residue in Nπ → N(1650) → ΣK

Table with columns: MODULUS, PHASE (°), DOCUMENT ID, TECN, COMMENT. Includes entry for ROENCHEN.

Normalized residue in Nπ → N(1650) → Δπ, D-wave

Table with columns: MODULUS, PHASE (°), DOCUMENT ID, TECN, COMMENT. Includes entries for SOKHOYAN, ANISOVICH.

Normalized residue in Nπ → N(1650) → Nσ

Table with columns: MODULUS, PHASE (°), DOCUMENT ID, TECN, COMMENT. Includes entry for SOKHOYAN.

Normalized residue in Nπ → N(1650) → N(1440)π

Table with columns: MODULUS, PHASE (°), DOCUMENT ID, TECN, COMMENT. Includes entry for SOKHOYAN.

N(1650) BREIT-WIGNER MASS

Table with columns: VALUE (MeV), DOCUMENT ID, TECN, COMMENT. Includes entries for GOLOVATCH, HUNT, KASHEVAROV, SOKHOYAN, SHKLYAR, ARNDT, CUTKOSKY, HOEHLER, ANISOVICH, SHRESTHA, BATINIC, PENNER, BAI, VRANA.

$N(1650)$ BREIT-WIGNER WIDTH

VALUE (MeV)	DOCUMENT ID	TECN	COMMENT
100 to 150 (≈ 125) OUR ESTIMATE			
154 \pm 28	GOLOVATCH 19	DPWA	$\gamma p \rightarrow \pi^+ \pi^- p$
133 \pm 7	¹ HUNT 19	DPWA	Multichannel
128 \pm 16	KASHEVAROV 17	DPWA	$\gamma p \rightarrow \eta p, \eta' p$
102 \pm 8	SOKHOYAN 15A	DPWA	Multichannel
147 \pm 14	¹ SHKLYAR 13	DPWA	Multichannel
115.4 \pm 2.8	¹ ARNDT 06	DPWA	$\pi N \rightarrow \pi N, \eta N$
150 \pm 40	CUTKOSKY 80	IPWA	$\pi N \rightarrow \pi N$
180 \pm 20	HOEHLER 79	IPWA	$\pi N \rightarrow \pi N$
••• We do not use the following data for averages, fits, limits, etc. •••			
104 \pm 10	ANISOVICH 12A	DPWA	Multichannel
126 \pm 3	¹ SHRESTHA 12A	DPWA	Multichannel
202 \pm 16	BATINIC 10	DPWA	$\pi N \rightarrow N\pi, N\eta$
138 \pm 7	PENNER 02c	DPWA	Multichannel
145 \pm 80 -45	BAI 01B	BES	$J/\psi \rightarrow p\bar{p}\eta$
202 \pm 40	VRANA 00	DPWA	Multichannel
¹ Statistical error only.			

 $N(1650)$ DECAY MODES

The following branching fractions are our estimates, not fits or averages.

Mode	Fraction (Γ_i/Γ)
Γ_1 $N\pi$	50–70 %
Γ_2 $N\eta$	15–35 %
Γ_3 ΛK	5–15 %
Γ_4 $N\pi\pi$	20–58 %
Γ_5 $\Delta(1232)\pi, D$ -wave	6–18 %
Γ_6 $N\rho$	12–22 %
Γ_7 $N\rho, S=1/2, S$ -wave	<4 %
Γ_8 $N\rho, S=3/2, D$ -wave	12–18 %
Γ_9 $N\sigma$	2–18 %
Γ_{10} $N(1440)\pi$	6–26 %
Γ_{11} $p\gamma, \text{helicity}=1/2$	0.04–0.20 %
Γ_{12} $n\gamma, \text{helicity}=1/2$	0.003–0.17 %

 $N(1650)$ BRANCHING RATIOS

$\Gamma(N\pi)/\Gamma_{\text{total}}$	DOCUMENT ID	TECN	COMMENT	Γ_1/Γ
50 to 70 (≈ 60) OUR ESTIMATE				
64 \pm 4	¹ HUNT 19	DPWA	Multichannel	
51 \pm 4	SOKHOYAN 15A	DPWA	Multichannel	
74 \pm 3	¹ SHKLYAR 13	DPWA	Multichannel	
65 \pm 10	CUTKOSKY 80	IPWA	$\pi N \rightarrow \pi N$	
61 \pm 4	HOEHLER 79	IPWA	$\pi N \rightarrow \pi N$	
••• We do not use the following data for averages, fits, limits, etc. •••				
51 \pm 4	ANISOVICH 12A	DPWA	Multichannel	
57 \pm 2	¹ SHRESTHA 12A	DPWA	Multichannel	
79 \pm 6	BATINIC 10	DPWA	$\pi N \rightarrow N\pi, N\eta$	
100	ARNDT 06	DPWA	$\pi N \rightarrow \pi N, \eta N$	
65 \pm 4	PENNER 02c	DPWA	Multichannel	
74 \pm 2	VRANA 00	DPWA	Multichannel	
¹ Statistical error only.				

$\Gamma(N\eta)/\Gamma_{\text{total}}$	DOCUMENT ID	TECN	COMMENT	Γ_2/Γ
15 to 35 (≈ 25) OUR ESTIMATE				
33 \pm 4	MUELLER 20	DPWA	Multichannel	
0.8 \pm 0.6	¹ HUNT 19	DPWA	Multichannel	
28 \pm 11	² KASHEVAROV 17	DPWA	$\gamma p \rightarrow \eta p, \eta' p$	
< 3	SHKLYAR 13	DPWA	Multichannel	
18 \pm 4	ANISOVICH 12A	DPWA	Multichannel	
••• We do not use the following data for averages, fits, limits, etc. •••				
21 \pm 2	¹ SHRESTHA 12A	DPWA	Multichannel	
13 \pm 5	BATINIC 10	DPWA	$\pi N \rightarrow N\pi, N\eta$	
1.0 \pm 0.6	PENNER 02c	DPWA	Multichannel	
6 \pm 1	VRANA 00	DPWA	Multichannel	
¹ Statistical error only.				
² Assuming $A_{1/2} = 0.045 \text{ GeV}^{-1/2}$.				

$\Gamma(\Lambda K)/\Gamma_{\text{total}}$	DOCUMENT ID	TECN	COMMENT	Γ_3/Γ
5 to 15 (≈ 10) OUR ESTIMATE				
3.5 \pm 0.2	¹ HUNT 19	DPWA	Multichannel	
10 \pm 5	ANISOVICH 12A	DPWA	Multichannel	
4 \pm 1	¹ SHKLYAR 05	DPWA	Multichannel	
••• We do not use the following data for averages, fits, limits, etc. •••				
8 \pm 1	¹ SHRESTHA 12A	DPWA	Multichannel	
2.7 \pm 0.4	PENNER 02c	DPWA	Multichannel	
¹ Statistical error only.				

$\Gamma(N\pi\pi)/\Gamma_{\text{total}}$	DOCUMENT ID	TECN	COMMENT	Γ_4/Γ
0.12 \pm 0.02				
GOLOVATCH 19	DPWA	$\gamma p \rightarrow \pi^+ \pi^- p$		

$\Gamma(\Delta(1232)\pi, D$ -wave)/ Γ_{total}	DOCUMENT ID	TECN	COMMENT	Γ_5/Γ
VALUE (%)				
< 0.2	¹ HUNT 19	DPWA	Multichannel	
12 \pm 6	SOKHOYAN 15A	DPWA	Multichannel	
••• We do not use the following data for averages, fits, limits, etc. •••				
19 \pm 9	ANISOVICH 12A	DPWA	Multichannel	
7 \pm 2	¹ SHRESTHA 12A	DPWA	Multichannel	
2 \pm 1	VRANA 00	DPWA	Multichannel	
¹ Statistical error only.				

$\Gamma(N\rho, S=1/2, S$ -wave)/ Γ_{total}	DOCUMENT ID	TECN	COMMENT	Γ_7/Γ
VALUE (%)				
1.8 \pm 1.7	¹ HUNT 19	DPWA	Multichannel	
¹ Statistical error only.				

$\Gamma(N\rho, S=3/2, D$ -wave)/ Γ_{total}	DOCUMENT ID	TECN	COMMENT	Γ_8/Γ
VALUE (%)				
15 \pm 3	¹ HUNT 19	DPWA	Multichannel	
¹ Statistical error only.				

$\Gamma(N\sigma)/\Gamma_{\text{total}}$	DOCUMENT ID	TECN	COMMENT	Γ_9/Γ
VALUE (%)				
12 \pm 4	¹ HUNT 19	DPWA	Multichannel	
10 \pm 8	SOKHOYAN 15A	DPWA	Multichannel	
••• We do not use the following data for averages, fits, limits, etc. •••				
< 1	¹ SHRESTHA 12A	DPWA	Multichannel	
1 \pm 1	VRANA 00	DPWA	Multichannel	
¹ Statistical error only.				

$\Gamma(N(1440)\pi)/\Gamma_{\text{total}}$	DOCUMENT ID	TECN	COMMENT	Γ_{10}/Γ
VALUE (%)				
2 \pm 1	¹ HUNT 19	DPWA	Multichannel	
16 \pm 10	SOKHOYAN 15A	DPWA	Multichannel	
••• We do not use the following data for averages, fits, limits, etc. •••				
< 1	¹ SHRESTHA 12A	DPWA	Multichannel	
3 \pm 1	VRANA 00	DPWA	Multichannel	
¹ Statistical error only.				

 $N(1650)$ PHOTON DECAY AMPLITUDES AT THE POLE $N(1650) \rightarrow p\gamma, \text{helicity}-1/2$ amplitude $A_{1/2}$

MODULUS ($\text{GeV}^{-1/2}$)	PHASE ($^\circ$)	DOCUMENT ID	TECN	COMMENT
0.032 \pm 0.006	7 \pm 7	ANISOVICH 17D	DPWA	Multichannel
0.023 \pm 0.003 -0.008	6 \pm 28 -15	ROENCHEN 14	DPWA	
••• We do not use the following data for averages, fits, limits, etc. •••				
0.032 \pm 0.007	-2 \pm 11	ANISOVICH 15A	DPWA	Multichannel
0.059	-14	ROENCHEN 15A	DPWA	Multichannel
0.032 \pm 0.006	-2 \pm 11	SOKHOYAN 15A	DPWA	Multichannel

 $N(1650) \rightarrow n\gamma, \text{helicity}-1/2$ amplitude $A_{1/2}$

MODULUS ($\text{GeV}^{-1/2}$)	PHASE ($^\circ$)	DOCUMENT ID	TECN	COMMENT
0.016 \pm 0.004	-28 \pm 10	ANISOVICH 17D	DPWA	Multichannel
••• We do not use the following data for averages, fits, limits, etc. •••				
0.019 \pm 0.006	0 \pm 15	ANISOVICH 15A	DPWA	Multichannel

 $N(1650)$ BREIT-WIGNER PHOTON DECAY AMPLITUDES $N(1650) \rightarrow p\gamma, \text{helicity}-1/2$ amplitude $A_{1/2}$

VALUE ($\text{GeV}^{-1/2}$)	DOCUMENT ID	TECN	COMMENT
0.035 to 0.055 (≈ 0.045) OUR ESTIMATE			
0.0605 \pm 0.0077	GOLOVATCH 19	DPWA	$\gamma p \rightarrow \pi^+ \pi^- p$
0.048 \pm 0.003	¹ HUNT 19	DPWA	Multichannel
0.032 \pm 0.006	SOKHOYAN 15A	DPWA	Multichannel
0.063 \pm 0.006	¹ SHKLYAR 13	DPWA	Multichannel
0.055 \pm 0.030	¹ WORKMAN 12A	DPWA	$\gamma N \rightarrow N\pi$
0.022 \pm 0.007	¹ DUGGER 07	DPWA	$\gamma N \rightarrow \pi N$
••• We do not use the following data for averages, fits, limits, etc. •••			
0.033 \pm 0.007	ANISOVICH 12A	DPWA	Multichannel
0.030 \pm 0.003	¹ SHRESTHA 12A	DPWA	Multichannel
0.033	DRECHSEL 07	DPWA	$\gamma N \rightarrow \pi N$
0.049	PENNER 02D	DPWA	Multichannel
¹ Statistical error only.			

N(1650) → nγ, helicity-1/2 amplitude A_{1/2}

Table with columns: VALUE (GeV^{-1/2}), DOCUMENT ID, TECN, COMMENT. Includes 'OUR ESTIMATE' and a list of references with values ranging from -0.040 to 0.025.

N(1650) REFERENCES

For early references, see Physics Letters 111B 1 (1982).

Large reference table with columns: NAME, VALUE, DOCUMENT ID, TECN, COMMENT. Lists various authors and their contributions to the N(1650) data.

N(1675) 5/2⁻

I(J^P) = 1/2(5/2⁻) Status: * * * *

Older and obsolete values are listed and referenced in the 2014 edition, Chinese Physics C38 070001 (2014).

N(1675) POLE POSITION

REAL PART

Table with columns: VALUE (MeV), DOCUMENT ID, TECN, COMMENT. Lists real part pole positions for N(1675) with values like 1655 ± 4, 1654 ± 2, etc.

-2xIMAGINARY PART

Table with columns: VALUE (MeV), DOCUMENT ID, TECN, COMMENT. Lists imaginary part pole positions for N(1675) with values like 125 to 150, 147 ± 5, etc.

N(1675) ELASTIC POLE RESIDUE

MODULUS |r|

Table with columns: VALUE (MeV), DOCUMENT ID, TECN, COMMENT. Lists modulus values for N(1675) elastic pole residue, including 'OUR ESTIMATE' and references like SOKHOYAN, SVARC, etc.

PHASE θ

Table with columns: VALUE (°), DOCUMENT ID, TECN, COMMENT. Lists phase values for N(1675) elastic pole residue, including 'OUR ESTIMATE' and references like SOKHOYAN, SVARC, etc.

N(1675) INELASTIC POLE RESIDUE

The "normalized residue" is the residue divided by Γ_{pole}/2.

Normalized residue in Nπ → N(1675) → Δπ, D-wave

Table with columns: MODULUS, PHASE (°), DOCUMENT ID, TECN, COMMENT. Lists normalized residue values for N(1675) inelastic pole residue (D-wave).

Normalized residue in Nπ → N(1675) → Nη

Table with columns: MODULUS, PHASE (°), DOCUMENT ID, TECN, COMMENT. Lists normalized residue values for N(1675) inelastic pole residue (Nη).

Normalized residue in Nπ → N(1675) → ΛK

Table with columns: MODULUS, PHASE (°), DOCUMENT ID, TECN, COMMENT. Lists normalized residue values for N(1675) inelastic pole residue (ΛK).

Normalized residue in Nπ → N(1675) → ΣK

Table with columns: MODULUS, PHASE (°), DOCUMENT ID, TECN, COMMENT. Lists normalized residue values for N(1675) inelastic pole residue (ΣK).

Normalized residue in Nπ → N(1675) → Nσ

Table with columns: MODULUS, PHASE (°), DOCUMENT ID, TECN, COMMENT. Lists normalized residue values for N(1675) inelastic pole residue (Nσ).

N(1675) BREIT-WIGNER MASS

Table with columns: VALUE (MeV), DOCUMENT ID, TECN, COMMENT. Lists Breit-Wigner mass values for N(1675) with values like 1665 to 1680, 1669 ± 2, etc.

Baryon Particle Listings

 $N(1675)$ $N(1675)$ BREIT-WIGNER WIDTH

VALUE (MeV)	DOCUMENT ID	TECN	COMMENT
130 to 160 (≈ 145) OUR ESTIMATE			
161 \pm 8	¹ HUNT	19	DPWA Multichannel
146 \pm 6	SOKHOYAN	15A	DPWA Multichannel
148 \pm 1	¹ SHKLYAR	13	DPWA Multichannel
146.5 \pm 1.0	¹ ARNDT	06	DPWA $\pi N \rightarrow \pi N, \eta N$
160 \pm 20	CUTKOSKY	80	IPWA $\pi N \rightarrow \pi N$
120 \pm 15	HOEHLER	79	IPWA $\pi N \rightarrow \pi N$
••• We do not use the following data for averages, fits, limits, etc. •••			
152 \pm 7	ANISOVICH	12A	DPWA Multichannel
145 \pm 4	¹ SHRESTHA	12A	DPWA Multichannel
152 \pm 8	BATINIC	10	DPWA $\pi N \rightarrow N\pi, N\eta$
131 \pm 10	VRANA	00	DPWA Multichannel
¹ Statistical error only.			

 $N(1675)$ DECAY MODES

The following branching fractions are our estimates, not fits or averages.

Mode	Fraction (Γ_i/Γ)
Γ_1 $N\pi$	38–42 %
Γ_2 $N\eta$	< 1 %
Γ_3 ΛK	< 0.04 %
Γ_4 $N\pi\pi$	25–45 %
Γ_5 $\Delta(1232)\pi, D\text{-wave}$	23–37 %
Γ_6 $N\rho$	0.1–0.9 %
Γ_7 $N\rho, S=1/2$	< 0.2 %
Γ_8 $N\rho, S=3/2, D\text{-wave}$	0.1–0.7 %
Γ_9 $N\sigma$	3–7 %
Γ_{10} $p\gamma$	0–0.02 %
Γ_{11} $p\gamma, \text{ helicity}=1/2$	0–0.01 %
Γ_{12} $p\gamma, \text{ helicity}=3/2$	0–0.01 %
Γ_{13} $n\gamma$	0–0.15 %
Γ_{14} $n\gamma, \text{ helicity}=1/2$	0–0.05 %
Γ_{15} $n\gamma, \text{ helicity}=3/2$	0–0.10 %

 $N(1675)$ BRANCHING RATIOS

$\Gamma(N\pi)/\Gamma_{\text{total}}$	DOCUMENT ID	TECN	COMMENT	Γ_1/Γ
VALUE (%)				
38 to 42 (≈ 40) OUR ESTIMATE				
33 \pm 1	¹ HUNT	19	DPWA Multichannel	
41 \pm 2	SOKHOYAN	15A	DPWA Multichannel	
41 \pm 1	¹ SHKLYAR	13	DPWA Multichannel	
39.3 \pm 0.1	¹ ARNDT	06	DPWA $\pi N \rightarrow \pi N, \eta N$	
38 \pm 5	CUTKOSKY	80	IPWA $\pi N \rightarrow \pi N$	
38 \pm 3	HOEHLER	79	IPWA $\pi N \rightarrow \pi N$	
••• We do not use the following data for averages, fits, limits, etc. •••				
40 \pm 3	ANISOVICH	12A	DPWA Multichannel	
38.6 \pm 0.6	¹ SHRESTHA	12A	DPWA Multichannel	
35 \pm 4	BATINIC	10	DPWA $\pi N \rightarrow N\pi, N\eta$	
35 \pm 1	VRANA	00	DPWA Multichannel	
¹ Statistical error only.				

$\Gamma(N\eta)/\Gamma_{\text{total}}$	DOCUMENT ID	TECN	COMMENT	Γ_2/Γ
VALUE (%)				
0.5 \pm 0.5	MUELLER	20	DPWA Multichannel	
2.0 \pm 0.3	¹ HUNT	19	DPWA Multichannel	
< 1	SHKLYAR	13	DPWA Multichannel	
••• We do not use the following data for averages, fits, limits, etc. •••				
< 1	¹ SHRESTHA	12A	DPWA Multichannel	
0.1 \pm 0.1	BATINIC	10	DPWA $\pi N \rightarrow N\pi, N\eta$	
3 \pm 3	THOMA	08	DPWA Multichannel	
0 \pm 1	VRANA	00	DPWA Multichannel	
¹ Statistical error only.				

$\Gamma(\Lambda K)/\Gamma_{\text{total}}$	DOCUMENT ID	TECN	COMMENT	Γ_3/Γ
VALUE (%)				
< 0.04 % OUR ESTIMATE				
< 0.04	¹ HUNT	19	DPWA Multichannel	
¹ Statistical error only.				

$\Gamma(\Delta(1232)\pi, D\text{-wave})/\Gamma_{\text{total}}$	DOCUMENT ID	TECN	COMMENT	Γ_5/Γ
VALUE (%)				
58.3 \pm 0.2	¹ HUNT	19	DPWA Multichannel	
30 \pm 7	SOKHOYAN	15A	DPWA Multichannel	
••• We do not use the following data for averages, fits, limits, etc. •••				
33 \pm 8	ANISOVICH	12A	DPWA Multichannel	
46 \pm 1	¹ SHRESTHA	12A	DPWA Multichannel	
63 \pm 2	VRANA	00	DPWA Multichannel	
¹ Statistical error only.				

$\Gamma(N\rho, S=1/2)/\Gamma_{\text{total}}$	DOCUMENT ID	TECN	COMMENT	Γ_7/Γ
VALUE (%)				
< 0.2 % OUR ESTIMATE				
< 0.2	¹ HUNT	19	DPWA Multichannel	
¹ Statistical error only.				

$\Gamma(N\rho, S=3/2, D\text{-wave})/\Gamma_{\text{total}}$	DOCUMENT ID	TECN	COMMENT	Γ_8/Γ
VALUE (%)				
0.1–0.7 % OUR ESTIMATE				
0.4 \pm 0.3	¹ HUNT	19	DPWA Multichannel	
¹ Statistical error only.				

$\Gamma(N\sigma)/\Gamma_{\text{total}}$	DOCUMENT ID	TECN	COMMENT	Γ_9/Γ
VALUE (%)				
5 \pm 2	SOKHOYAN	15A	DPWA Multichannel	
••• We do not use the following data for averages, fits, limits, etc. •••				
7 \pm 3	ANISOVICH	12A	DPWA Multichannel	

 $N(1675)$ PHOTON DECAY AMPLITUDES AT THE POLE $N(1675) \rightarrow p\gamma, \text{ helicity-1/2 amplitude } A_{1/2}$

MODULUS ($\text{GeV}^{-1/2}$)	PHASE ($^\circ$)	DOCUMENT ID	TECN	COMMENT
0.022 \pm 0.003	–12 \pm 7	SOKHOYAN	15A	DPWA Multichannel
0.022 $^{+0.004}_{-0.007}$	49 $^{+5}_{-2}$	ROENCHEN	14	DPWA
••• We do not use the following data for averages, fits, limits, etc. •••				
0.032	36	ROENCHEN	15A	DPWA Multichannel

 $N(1675) \rightarrow p\gamma, \text{ helicity-3/2 amplitude } A_{3/2}$

MODULUS ($\text{GeV}^{-1/2}$)	PHASE ($^\circ$)	DOCUMENT ID	TECN	COMMENT
0.028 \pm 0.006	–17 \pm 6	SOKHOYAN	15A	DPWA Multichannel
0.036 $^{+0.004}_{-0.005}$	–30 \pm 4	ROENCHEN	14	DPWA
••• We do not use the following data for averages, fits, limits, etc. •••				
0.051	–9.3	ROENCHEN	15A	DPWA Multichannel

 $N(1675)$ BREIT-WIGNER PHOTON DECAY AMPLITUDES $N(1675) \rightarrow p\gamma, \text{ helicity-1/2 amplitude } A_{1/2}$

VALUE ($\text{GeV}^{-1/2}$)	DOCUMENT ID	TECN	COMMENT
0.010 to 0.025 (≈ 0.018) OUR ESTIMATE			
0.026 \pm 0.002	¹ HUNT	19	DPWA Multichannel
0.022 \pm 0.003	SOKHOYAN	15A	DPWA Multichannel
0.009 \pm 0.001	¹ SHKLYAR	13	DPWA Multichannel
0.013 \pm 0.001	¹ WORKMAN	12A	DPWA $\gamma N \rightarrow N\pi$
0.018 \pm 0.002	¹ DUGGER	07	DPWA $\gamma N \rightarrow \pi N$
••• We do not use the following data for averages, fits, limits, etc. •••			
0.024 \pm 0.003	ANISOVICH	12A	DPWA Multichannel
0.011 \pm 0.001	¹ SHRESTHA	12A	DPWA Multichannel
0.015	DRECHSEL	07	DPWA $\gamma N \rightarrow \pi N$
¹ Statistical error only.			

 $N(1675) \rightarrow p\gamma, \text{ helicity-3/2 amplitude } A_{3/2}$

VALUE ($\text{GeV}^{-1/2}$)	DOCUMENT ID	TECN	COMMENT
0.015 to 0.030 (≈ 0.022) OUR ESTIMATE			
0.005 \pm 0.002	¹ HUNT	19	DPWA Multichannel
0.027 \pm 0.006	SOKHOYAN	15A	DPWA Multichannel
0.021 \pm 0.001	¹ SHKLYAR	13	DPWA Multichannel
0.016 \pm 0.001	¹ WORKMAN	12A	DPWA $\gamma N \rightarrow N\pi$
0.021 \pm 0.001	¹ DUGGER	07	DPWA $\gamma N \rightarrow \pi N$
••• We do not use the following data for averages, fits, limits, etc. •••			
0.025 \pm 0.007	ANISOVICH	12A	DPWA Multichannel
0.020 \pm 0.001	¹ SHRESTHA	12A	DPWA Multichannel
0.022	DRECHSEL	07	DPWA $\gamma N \rightarrow \pi N$
¹ Statistical error only.			

 $N(1675) \rightarrow n\gamma, \text{ helicity-1/2 amplitude } A_{1/2}$

VALUE ($\text{GeV}^{-1/2}$)	DOCUMENT ID	TECN	COMMENT
–0.065 to –0.055 (≈ -0.060) OUR ESTIMATE			
–0.069 \pm 0.005	¹ HUNT	19	DPWA Multichannel
–0.060 \pm 0.007	ANISOVICH	13B	DPWA Multichannel
–0.058 \pm 0.002	¹ CHEN	12A	DPWA $\gamma N \rightarrow \pi N$
••• We do not use the following data for averages, fits, limits, etc. •••			
–0.040 \pm 0.004	¹ SHRESTHA	12A	DPWA Multichannel
–0.062	DRECHSEL	07	DPWA $\gamma N \rightarrow \pi N$
¹ Statistical error only.			

 $N(1675) \rightarrow n\gamma, \text{ helicity-3/2 amplitude } A_{3/2}$

VALUE ($\text{GeV}^{-1/2}$)	DOCUMENT ID	TECN	COMMENT
–0.095 to –0.075 (≈ -0.085) OUR ESTIMATE			
–0.031 \pm 0.005	¹ HUNT	19	DPWA Multichannel
–0.088 \pm 0.010	ANISOVICH	13B	DPWA Multichannel
–0.080 \pm 0.005	¹ CHEN	12A	DPWA $\gamma N \rightarrow \pi N$

See key on page 1127

Baryon Particle Listings

$N(1675)$, $N(1680)$

••• We do not use the following data for averages, fits, limits, etc. •••
 -0.068 ± 0.004 ¹ SHRESTHA 12A DPWA Multichannel
 -0.084 DRECHSEL 07 DPWA $\gamma N \rightarrow \pi N$
¹ Statistical error only.

$N(1675)$ REFERENCES

For early references, see Physics Letters **111B** 1 (1982).

MUELLER 20	PL B803 135323	J. Mueller <i>et al.</i>	(CBELSA/TAPS Collab.)
HUNT 19	PR C99 055205	B. C. Hunt, D.M. Manley	
ROENCHEN 15A	EPJ A51 70	D. Roenchen <i>et al.</i>	
SOKHOYAN 15A	EPJ A51 95	V. Sokhoyan <i>et al.</i>	(CBELSA/TAPS Collab.)
PDG 14	CP C38 070001	K. Olive <i>et al.</i>	(PDG Collab.)
ROENCHEN 14	EPJ A50 101	D. Roenchen <i>et al.</i>	
Also	EPJ A51 63 (errata.)	D. Roenchen <i>et al.</i>	
SVARC 14	PR C89 045205	A. Svarc <i>et al.</i>	(RBI Zagreb, UNI Tuzla)
ANISOVICH 13B	EPJ A49 67	A.V. Anisovich <i>et al.</i>	
SHKLYAR 13	PR C87 015201	V. Shklyar, H. Lenske, U. Mosel	(GIES)
ANISOVICH 12A	EPJ A48 15	A.V. Anisovich <i>et al.</i>	(BONN, PNPI)
CHEN 12A	PR C86 015206	W. Chen <i>et al.</i>	(DUKE, GWU, MSST, ITEP+)
SHRESTHA 12A	PR C86 055203	M. Shrestha, D.M. Manley	(KSU)
WORKMAN 12A	PR C86 015202	R. Workman <i>et al.</i>	(GWU)
BATINIC 10	PR C82 038203	M. Batinic <i>et al.</i>	(ZAGR)
THOMA 08	PL B65 9 87	U. Thoma <i>et al.</i>	(CB-ELSA Collab.)
DRECHSEL 07	EPJ A34 69	D. Drechsel, S.S. Kamalov, L. Tiator	(MAINZ, JINR)
DUGGER 07	PR C76 025211	M. Dugger <i>et al.</i>	(JLab CLAS Collab.)
ARNDT 06	PR C74 045205	R.A. Arndt <i>et al.</i>	(GWU)
VRANA 00	PRPL 328 181	T.P. Vrana, S.A. Dytman, T.-S.H. Lee	(PITT, ANL)
HOEHLER 93	πN Newsletter 9 1	G. Hohlner	(KARL)
CUTKOSKY 80	Toronto Conf. 19	R.E. Cutkosky <i>et al.</i>	(CMU, LBL) IJP
Also	PR D20 2839	R.E. Cutkosky <i>et al.</i>	(CMU, LBL) IJP
HOEHLER 79	PDAT 12-1	G. Hohlner <i>et al.</i>	(KARLT) IJP
Also	Toronto Conf. 3	R. Koch	(KARLT) IJP

$N(1680) 5/2^+$

$$J(P) = \frac{1}{2}(\frac{5}{2}^+)$$
 Status: * * * *

Older and obsolete values are listed and referenced in the 2014 edition, Chinese Physics **C38** 070001 (2014).

$N(1680)$ POLE POSITION

REAL PART

VALUE (MeV)	DOCUMENT ID	TECN	COMMENT
1665 to 1680 (≈ 1675) OUR ESTIMATE			
1678 ± 5	SOKHOYAN 15A	DPWA	Multichannel
1674 $\pm 2 \pm 1$	¹ SVARC 14	L+P	$\pi N \rightarrow \pi N$
1667 ± 5	CUTKOSKY 80	IPWA	$\pi N \rightarrow \pi N$
••• We do not use the following data for averages, fits, limits, etc. •••			
1668	HUNT 19	DPWA	Multichannel
1669	ROENCHEN 15A	DPWA	Multichannel
1660	SHKLYAR 13	DPWA	Multichannel
1676 ± 6	ANISOVICH 12A	DPWA	Multichannel
1666 ± 8	BATINIC 10	DPWA	$\pi N \rightarrow N\pi, N\eta$
1674	ARNDT 06	DPWA	$\pi N \rightarrow \pi N, \eta N$
1667	VRANA 00	DPWA	Multichannel
1673	HOEHLER 93	ARGD	$\pi N \rightarrow \pi N$

¹ Fit to the amplitudes of HOEHLER 79.

-2xIMAGINARY PART

VALUE (MeV)	DOCUMENT ID	TECN	COMMENT
110 to 135 (≈ 120) OUR ESTIMATE			
113 ± 4	SOKHOYAN 15A	DPWA	Multichannel
129 $\pm 3 \pm 1$	¹ SVARC 14	L+P	$\pi N \rightarrow \pi N$
110 ± 10	CUTKOSKY 80	IPWA	$\pi N \rightarrow \pi N$
••• We do not use the following data for averages, fits, limits, etc. •••			
118	HUNT 19	DPWA	Multichannel
100	ROENCHEN 15A	DPWA	Multichannel
98	SHKLYAR 13	DPWA	Multichannel
113 ± 4	ANISOVICH 12A	DPWA	Multichannel
135 ± 6	BATINIC 10	DPWA	$\pi N \rightarrow N\pi, N\eta$
115	ARNDT 06	DPWA	$\pi N \rightarrow \pi N, \eta N$
122	VRANA 00	DPWA	Multichannel
135	HOEHLER 93	ARGD	$\pi N \rightarrow \pi N$

¹ Fit to the amplitudes of HOEHLER 79.

$N(1680)$ ELASTIC POLE RESIDUE

MODULUS $|r|$

VALUE (MeV)	DOCUMENT ID	TECN	COMMENT
35 to 45 (≈ 40) OUR ESTIMATE			
45 ± 4	SOKHOYAN 15A	DPWA	Multichannel
44 $\pm 1 \pm 1$	¹ SVARC 14	L+P	$\pi N \rightarrow \pi N$
34 ± 2	CUTKOSKY 80	IPWA	$\pi N \rightarrow \pi N$
••• We do not use the following data for averages, fits, limits, etc. •••			
34	ROENCHEN 15A	DPWA	Multichannel
33	SHKLYAR 13	DPWA	Multichannel
43 ± 4	ANISOVICH 12A	DPWA	Multichannel
44	BATINIC 10	DPWA	$\pi N \rightarrow N\pi, N\eta$
42	ARNDT 06	DPWA	$\pi N \rightarrow \pi N, \eta N$
44	HOEHLER 93	ARGD	$\pi N \rightarrow \pi N$

¹ Fit to the amplitudes of HOEHLER 79.

PHASE θ

VALUE ($^\circ$)	DOCUMENT ID	TECN	COMMENT
-20 to 10 (≈ -5) OUR ESTIMATE			
5 ± 10	SOKHOYAN 15A	DPWA	Multichannel
-16 $\pm 1 \pm 1$	¹ SVARC 14	L+P	$\pi N \rightarrow \pi N$
-25 ± 5	CUTKOSKY 80	IPWA	$\pi N \rightarrow \pi N$
••• We do not use the following data for averages, fits, limits, etc. •••			
-19	ROENCHEN 15A	DPWA	Multichannel
-32	SHKLYAR 13	DPWA	Multichannel
-2 ± 10	ANISOVICH 12A	DPWA	Multichannel
-19	BATINIC 10	DPWA	$\pi N \rightarrow N\pi, N\eta$
-4	ARNDT 06	DPWA	$\pi N \rightarrow \pi N, \eta N$
-17	HOEHLER 93	ARGD	$\pi N \rightarrow \pi N$

¹ Fit to the amplitudes of HOEHLER 79.

$N(1680)$ INELASTIC POLE RESIDUE

The "normalized residue" is the residue divided by $\Gamma_{pole}/2$.

Normalized residue in $N\pi \rightarrow N(1680) \rightarrow \Delta\pi, P$ -wave

MODULUS	PHASE ($^\circ$)	DOCUMENT ID	TECN	COMMENT
0.15 ± 0.03	-60 ± 30	SOKHOYAN 15A	DPWA	Multichannel
••• We do not use the following data for averages, fits, limits, etc. •••				
0.15 ± 0.03	-70 ± 45	ANISOVICH 12A	DPWA	Multichannel

Normalized residue in $N\pi \rightarrow N(1680) \rightarrow \Delta\pi, F$ -wave

MODULUS	PHASE ($^\circ$)	DOCUMENT ID	TECN	COMMENT
0.23 ± 0.04	90 ± 12	SOKHOYAN 15A	DPWA	Multichannel
••• We do not use the following data for averages, fits, limits, etc. •••				
0.23 ± 0.04	85 ± 15	ANISOVICH 12A	DPWA	Multichannel

Normalized residue in $N\pi \rightarrow N(1680) \rightarrow N\eta$

MODULUS	PHASE ($^\circ$)	DOCUMENT ID	TECN	COMMENT
••• We do not use the following data for averages, fits, limits, etc. •••				
0.027	136	ROENCHEN 15A	DPWA	Multichannel

Normalized residue in $N\pi \rightarrow N(1680) \rightarrow \Lambda K$

MODULUS	PHASE ($^\circ$)	DOCUMENT ID	TECN	COMMENT
••• We do not use the following data for averages, fits, limits, etc. •••				
0.001	90	ROENCHEN 15A	DPWA	Multichannel

Normalized residue in $N\pi \rightarrow N(1680) \rightarrow \Sigma K$

MODULUS	PHASE ($^\circ$)	DOCUMENT ID	TECN	COMMENT
••• We do not use the following data for averages, fits, limits, etc. •••				
0.004	148	ROENCHEN 15A	DPWA	Multichannel

Normalized residue in $N\pi \rightarrow N(1680) \rightarrow N(\pi\pi)_{S\text{-wave}}^{J=0}$

MODULUS	PHASE ($^\circ$)	DOCUMENT ID	TECN	COMMENT
0.29 ± 0.06	-45 ± 15	SOKHOYAN 15A	DPWA	Multichannel
••• We do not use the following data for averages, fits, limits, etc. •••				
0.26 ± 0.04	-56 ± 15	ANISOVICH 12A	DPWA	Multichannel

$N(1680)$ BREIT-WIGNER MASS

VALUE (MeV)	DOCUMENT ID	TECN	COMMENT
1680 to 1690 (≈ 1685) OUR ESTIMATE			
1686 ± 5	GOLOVATCH 19	DPWA	$\gamma p \rightarrow \pi^+ \pi^- p$
1681.0 ± 0.1	¹ HUNT 19	DPWA	Multichannel
1690 ± 5	SOKHOYAN 15A	DPWA	Multichannel
1676 ± 2	¹ SHKLYAR 13	DPWA	Multichannel
1680.1 ± 0.2	¹ ARNDT 06	DPWA	$\pi N \rightarrow \pi N, \eta N$
1680 ± 10	CUTKOSKY 80	IPWA	$\pi N \rightarrow \pi N$
1684 ± 3	HOEHLER 79	IPWA	$\pi N \rightarrow \pi N$
••• We do not use the following data for averages, fits, limits, etc. •••			
1689 ± 6	ANISOVICH 12A	DPWA	Multichannel
1682.7 ± 0.5	¹ SHRESTHA 12A	DPWA	Multichannel
1680 ± 7	BATINIC 10	DPWA	$\pi N \rightarrow N\pi, N\eta$
1679 ± 3	VRANA 00	DPWA	Multichannel

¹ Statistical error only.

$N(1680)$ BREIT-WIGNER WIDTH

VALUE (MeV)	DOCUMENT ID	TECN	COMMENT
115 to 130 (≈ 120) OUR ESTIMATE			
118 ± 20	GOLOVATCH 19	DPWA	$\gamma p \rightarrow \pi^+ \pi^- p$
123 ± 3	¹ HUNT 19	DPWA	Multichannel
119 ± 4	SOKHOYAN 15A	DPWA	Multichannel
115 ± 1	¹ SHKLYAR 13	DPWA	Multichannel
128.0 ± 1.1	¹ ARNDT 06	DPWA	$\pi N \rightarrow \pi N, \eta N$
120 ± 10	CUTKOSKY 80	IPWA	$\pi N \rightarrow \pi N$
128 ± 8	HOEHLER 79	IPWA	$\pi N \rightarrow \pi N$

Baryon Particle Listings

 $N(1680)$

••• We do not use the following data for averages, fits, limits, etc. •••

118 ± 6	ANISOVICH	12A	DPWA	Multichannel
126 ± 1	¹ SHRESTHA	12A	DPWA	Multichannel
142 ± 7	BATINIC	10	DPWA	$\pi N \rightarrow N\pi, N\eta$
128 ± 9	VRANA	00	DPWA	Multichannel

¹ Statistical error only.

 $N(1680)$ DECAY MODES

The following branching fractions are our estimates, not fits or averages.

Mode	Fraction (Γ_i/Γ)
Γ_1 $N\pi$	60–70 %
Γ_2 $N\eta$	<1 %
Γ_3 $N\pi\pi$	28–53 %
Γ_4 $\Delta(1232)\pi$	11–23 %
Γ_5 $\Delta(1232)\pi, P\text{-wave}$	4–10 %
Γ_6 $\Delta(1232)\pi, F\text{-wave}$	1–13 %
Γ_7 $N\rho$	8–11 %
Γ_8 $N\rho, S=3/2, P\text{-wave}$	6–8 %
Γ_9 $N\rho, S=3/2, F\text{-wave}$	2–3 %
Γ_{10} $N\sigma$	9–19 %
Γ_{11} $p\gamma$	0.21–0.32 %
Γ_{12} $p\gamma, \text{helicity}=1/2$	0.001–0.011 %
Γ_{13} $p\gamma, \text{helicity}=3/2$	0.20–0.32 %
Γ_{14} $n\gamma$	0.021–0.046 %
Γ_{15} $n\gamma, \text{helicity}=1/2$	0.004–0.029 %
Γ_{16} $n\gamma, \text{helicity}=3/2$	0.01–0.024 %

 $N(1680)$ BRANCHING RATIOS

$\Gamma(N\pi)/\Gamma_{\text{total}}$	DOCUMENT ID	TECN	COMMENT	Γ_1/Γ
60 to 70 (≈ 65) OUR ESTIMATE				
68.0 ± 0.1	¹ HUNT	19	DPWA	Multichannel
62 ± 4	SOKHOYAN	15A	DPWA	Multichannel
68 ± 1	¹ SHKLYAR	13	DPWA	Multichannel
70.1 ± 0.1	¹ ARNDT	06	DPWA	$\pi N \rightarrow \pi N, \eta N$
62 ± 5	CUTKOSKY	80	IPWA	$\pi N \rightarrow \pi N$
65 ± 2	HOEHLER	79	IPWA	$\pi N \rightarrow \pi N$
••• We do not use the following data for averages, fits, limits, etc. •••				
64 ± 5	ANISOVICH	12A	DPWA	Multichannel
68.0 ± 0.5	¹ SHRESTHA	12A	DPWA	Multichannel
67 ± 3	BATINIC	10	DPWA	$\pi N \rightarrow N\pi, N\eta$
69 ± 2	VRANA	00	DPWA	Multichannel

¹ Statistical error only.

$\Gamma(N\eta)/\Gamma_{\text{total}}$	DOCUMENT ID	TECN	COMMENT	Γ_2/Γ
0.2 ± 0.1	MUELLER	20	DPWA	Multichannel
0.09 ± 0.02	¹ HUNT	19	DPWA	Multichannel
<1	SHKLYAR	13	DPWA	Multichannel
0.15 \pm $\frac{+0.35}{-0.10}$	TIATOR	99	DPWA	$\gamma p \rightarrow p\eta$
••• We do not use the following data for averages, fits, limits, etc. •••				
1.0 ± 0.3	¹ SHRESTHA	12A	DPWA	Multichannel
0.4 ± 0.2	BATINIC	10	DPWA	$\pi N \rightarrow N\pi, N\eta$
<1	THOMA	08	DPWA	Multichannel
0 ± 1	VRANA	00	DPWA	Multichannel

¹ Statistical error only.

$\Gamma(N\pi\pi)/\Gamma_{\text{total}}$	DOCUMENT ID	TECN	COMMENT	Γ_3/Γ
28–53 % OUR ESTIMATE				
24 ± 4	GOLOVATCH	19	DPWA	$\gamma p \rightarrow \pi^+\pi^-\rho$

$\Gamma(\Delta(1232)\pi, P\text{-wave})/\Gamma_{\text{total}}$	DOCUMENT ID	TECN	COMMENT	Γ_5/Γ
13 ± 1	¹ HUNT	19	DPWA	Multichannel
7 ± 3	SOKHOYAN	15A	DPWA	Multichannel
••• We do not use the following data for averages, fits, limits, etc. •••				
5 ± 3	ANISOVICH	12A	DPWA	Multichannel
10.5 ± 0.9	¹ SHRESTHA	12A	DPWA	Multichannel
14 ± 3	VRANA	00	DPWA	Multichannel

¹ Statistical error only.

$\Gamma(\Delta(1232)\pi, F\text{-wave})/\Gamma_{\text{total}}$	DOCUMENT ID	TECN	COMMENT	Γ_6/Γ
< 0.3	¹ HUNT	19	DPWA	Multichannel
10 ± 3	SOKHOYAN	15A	DPWA	Multichannel

••• We do not use the following data for averages, fits, limits, etc. •••

10 ± 3	ANISOVICH	12A	DPWA	Multichannel
1.0 ± 0.1	¹ SHRESTHA	12A	DPWA	Multichannel
1 ± 1	VRANA	00	DPWA	Multichannel

¹ Statistical error only.

$\Gamma(N\rho, S=3/2, P\text{-wave})/\Gamma_{\text{total}}$	DOCUMENT ID	TECN	COMMENT	Γ_8/Γ
6–8 % OUR ESTIMATE				
7 ± 1	¹ HUNT	19	DPWA	Multichannel

¹ Statistical error only.

$\Gamma(N\rho, S=3/2, F\text{-wave})/\Gamma_{\text{total}}$	DOCUMENT ID	TECN	COMMENT	Γ_9/Γ
2–3 % OUR ESTIMATE				
2.4 ± 0.4	¹ HUNT	19	DPWA	Multichannel

¹ Statistical error only.

$\Gamma(N\sigma)/\Gamma_{\text{total}}$	DOCUMENT ID	TECN	COMMENT	Γ_{10}/Γ
8.7 ± 1.5	¹ HUNT	19	DPWA	Multichannel
14 ± 5	SOKHOYAN	15A	DPWA	Multichannel

••• We do not use the following data for averages, fits, limits, etc. •••

14 ± 7	ANISOVICH	12A	DPWA	Multichannel
9.4 ± 0.8	¹ SHRESTHA	12A	DPWA	Multichannel
9 ± 1	VRANA	00	DPWA	Multichannel

¹ Statistical error only.

 $N(1680)$ PHOTON DECAY AMPLITUDES AT THE POLE **$N(1680) \rightarrow p\gamma, \text{helicity-1/2}$ amplitude $A_{1/2}$**

MODULUS ($\text{GeV}^{-1/2}$)	PHASE ($^\circ$)	DOCUMENT ID	TECN	COMMENT
-0.013 ± 0.003	-20 ± 17	SOKHOYAN	15A	DPWA
$-0.013 \pm \frac{+0.002}{-0.005}$	$-42 \pm \frac{9}{-18}$	ROENCHEN	14	DPWA
••• We do not use the following data for averages, fits, limits, etc. •••				
-0.022	-28	ROENCHEN	15A	DPWA

 $N(1680) \rightarrow p\gamma, \text{helicity-3/2}$ amplitude $A_{3/2}$

MODULUS ($\text{GeV}^{-1/2}$)	PHASE ($^\circ$)	DOCUMENT ID	TECN	COMMENT
0.135 ± 0.005	1 ± 3	SOKHOYAN	15A	DPWA
$0.126 \pm \frac{+0.001}{-0.002}$	$-7 \pm \frac{3}{-2}$	ROENCHEN	14	DPWA
••• We do not use the following data for averages, fits, limits, etc. •••				
0.102	-11	ROENCHEN	15A	DPWA

 $N(1680)$ BREIT-WIGNER PHOTON DECAY AMPLITUDES **$N(1680) \rightarrow p\gamma, \text{helicity-1/2}$ amplitude $A_{1/2}$**

VALUE ($\text{GeV}^{-1/2}$)	DOCUMENT ID	TECN	COMMENT
-0.018 to -0.005 (≈ -0.010) OUR ESTIMATE			
-0.0278 ± 0.0036	GOLOVATCH	19	DPWA
-0.026 ± 0.004	¹ HUNT	19	DPWA
-0.015 ± 0.002	SOKHOYAN	15A	DPWA
0.003 ± 0.001	¹ SHKLYAR	13	DPWA
-0.007 ± 0.002	¹ WORKMAN	12A	DPWA
-0.017 ± 0.001	¹ DUGGER	07	DPWA
••• We do not use the following data for averages, fits, limits, etc. •••			
-0.013 ± 0.003	ANISOVICH	12A	DPWA
-0.017 ± 0.001	¹ SHRESTHA	12A	DPWA
-0.025	DRECHSEL	07	DPWA

¹ Statistical error only.

 $N(1680) \rightarrow p\gamma, \text{helicity-3/2}$ amplitude $A_{3/2}$

VALUE ($\text{GeV}^{-1/2}$)	DOCUMENT ID	TECN	COMMENT
0.130 to 0.140 (≈ 0.135) OUR ESTIMATE			
0.128 ± 0.011	GOLOVATCH	19	DPWA
0.112 ± 0.005	¹ HUNT	19	DPWA
0.136 ± 0.005	SOKHOYAN	15A	DPWA
0.116 ± 0.001	¹ SHKLYAR	13	DPWA
0.140 ± 0.002	¹ WORKMAN	12A	DPWA
0.134 ± 0.002	¹ DUGGER	07	DPWA
••• We do not use the following data for averages, fits, limits, etc. •••			
0.135 ± 0.006	ANISOVICH	12A	DPWA
0.136 ± 0.001	¹ SHRESTHA	12A	DPWA
0.134	DRECHSEL	07	DPWA

¹ Statistical error only.

 $N(1680) \rightarrow n\gamma, \text{helicity-1/2}$ amplitude $A_{1/2}$

VALUE ($\text{GeV}^{-1/2}$)	DOCUMENT ID	TECN	COMMENT
0.020 to 0.040 (≈ 0.030) OUR ESTIMATE			
0.005 ± 0.004	¹ HUNT	19	DPWA
0.034 ± 0.006	ANISOVICH	13B	DPWA
0.026 ± 0.004	¹ CHEN	12A	DPWA

See key on page 1127

Baryon Particle Listings

$N(1680)$, $N(1700)$

••• We do not use the following data for averages, fits, limits, etc. •••
 0.029±0.002 ¹ SHRESTHA 12A DPWA Multichannel
 0.028 DRECHSEL 07 DPWA $\gamma N \rightarrow \pi N$
¹ Statistical error only.

$N(1680) \rightarrow n\gamma$, helicity-3/2 amplitude $A_{3/2}$

VALUE (GeV ^{-1/2})	DOCUMENT ID	TECN	COMMENT
-0.050 to -0.025 (≈ -0.035) OUR ESTIMATE			
-0.061±0.004	¹ HUNT 19	DPWA	Multichannel
-0.044±0.009	ANISOVICH 13B	DPWA	Multichannel
-0.029±0.002	¹ CHEN 12A	DPWA	$\gamma N \rightarrow \pi N$
••• We do not use the following data for averages, fits, limits, etc. •••			
-0.059±0.002	¹ SHRESTHA 12A	DPWA	Multichannel
-0.038	DRECHSEL 07	DPWA	$\gamma N \rightarrow \pi N$
¹ Statistical error only.			

N(1680) REFERENCES

For early references, see Physics Letters **111B** 1 (1982). For very early references, see Reviews of Modern Physics **37** 633 (1965).

MUELLER 20	PL B803 135323	J. Mueller et al.	(CBELSA/TAPS Collab.)
GOLOVATCH 19	PL B788 371	E. Golovatch et al.	(CLAS Collab.)
HUNT 19	PR C99 055205	B. C. Hunt, D. M. Manley	
ROENCHEN 15A	EPJ A51 70	D. Roenchen et al.	
SOKHOYAN 15A	EPJ A51 95	V. Sokhoyan et al.	(CBELSA/TAPS Collab.)
PDG 14	CP C38 070001	K. Olive et al.	(PDG Collab.)
ROENCHEN 14	EPJ A50 101	D. Roenchen et al.	
Also	EPJ A51 63 (errata.)	D. Roenchen et al.	
SVARC 14	PR C89 045205	A. Svarc et al.	(RBI Zagreb, UNI Tuzla)
ANISOVICH 13B	EPJ A49 67	A.V. Anisovich et al.	
SHKLYAR 13	PR C87 015201	V. Shklyar, H. Lenske, U. Mosel	(GIES)
ANISOVICH 12A	EPJ A48 15	A.V. Anisovich et al.	(BONN, PNPI)
CHEN 12A	PR C86 015206	W. Chen et al.	(DUKE, GWU, MSST, ITEP+)
SHRESTHA 12A	PR C86 055203	M. Shrestha, D.M. Manley	(KSU)
WORKMAN 12A	PR C86 015202	R. Workman et al.	(GWU)
BATINIC 10	PR C82 038203	M. Batinic et al.	(ZAGR)
THOMA 08	PL B65 9 87	U. Thoma et al.	(CB-ELSA Collab.)
DRECHSEL 07	EPJ A34 69	D. Drechsel, S.S. Kamalov, L. Tiator	(MAINZ, JINR)
DUGGER 07	PR C76 025211	M. Dugger et al.	(JLab CLAS Collab.)
ARNDT 06	PR C74 045205	R.A. Arndt et al.	(GWU)
VRANA 00	PRPL 328 181	T.P. Vrana, S.A. Dytman, T.-S.H. Lee	(PITT, ANL)
TIATOR 99	PR C60 035210	L. Tiator et al.	
HOEHLER 93	πN Newsletter 9 1	G. Hohlner	(KARL)
CUTKOSKY 80	Toronto Conf. 19	R.E. Cutkosky et al.	(CMU, LBL) IJP
Also	PR D20 2839	R.E. Cutkosky et al.	(CMU, LBL) IJP
HOEHLER 79	PDAT 12-1	G. Hohlner et al.	(KARLT) IJP
Also	Toronto Conf. 3	R. Koch	(KARLT) IJP

$N(1700) 3/2^-$

$I(J^P) = \frac{1}{2}(\frac{3}{2}^-)$ Status: ***

Older and obsolete values are listed and referenced in the 2014 edition, Chinese Physics **C38** 070001 (2014).

N(1700) POLE POSITION

REAL PART	DOCUMENT ID	TECN	COMMENT
1650 to 1750 (≈ 1700) OUR ESTIMATE			
1780±35	SOKHOYAN 15A	DPWA	Multichannel
1757± 4±1	¹ SVARC 14	L+P	$\pi N \rightarrow \pi N$
1660±30	CUTKOSKY 80	IPWA	$\pi N \rightarrow \pi N$
••• We do not use the following data for averages, fits, limits, etc. •••			
1647	HUNT 19	DPWA	Multichannel
1770±40	ANISOVICH 12A	DPWA	Multichannel
1806±23	BATINIC 10	DPWA	$\pi N \rightarrow N\pi, N\eta$
1704	VRANA 00	DPWA	Multichannel
1700	HOEHLER 93	SPED	$\pi N \rightarrow \pi N$
¹ Fit to the amplitudes of HOEHLER 79.			

-2xIMAGINARY PART

VALUE (MeV)	DOCUMENT ID	TECN	COMMENT
100 to 300 (≈ 200) OUR ESTIMATE			
420±140	SOKHOYAN 15A	DPWA	Multichannel
136± 7±4	¹ SVARC 14	L+P	$\pi N \rightarrow \pi N$
90± 40	CUTKOSKY 80	IPWA	$\pi N \rightarrow \pi N$
••• We do not use the following data for averages, fits, limits, etc. •••			
79	HUNT 19	DPWA	Multichannel
420±180	ANISOVICH 12A	DPWA	Multichannel
129± 33	BATINIC 10	DPWA	$\pi N \rightarrow N\pi, N\eta$
156	VRANA 00	DPWA	Multichannel
120	HOEHLER 93	SPED	$\pi N \rightarrow \pi N$
¹ Fit to the amplitudes of HOEHLER 79.			

N(1700) ELASTIC POLE RESIDUE

MODULUS r	DOCUMENT ID	TECN	COMMENT
5 to 50 (≈ 10) OUR ESTIMATE			
60±30	SOKHOYAN 15A	DPWA	Multichannel
7± 1±1	¹ SVARC 14	L+P	$\pi N \rightarrow \pi N$
6± 3	CUTKOSKY 80	IPWA	$\pi N \rightarrow \pi N$

••• We do not use the following data for averages, fits, limits, etc. •••
 50±40 ANISOVICH 12A DPWA Multichannel
 7 BATINIC 10 DPWA $\pi N \rightarrow N\pi, N\eta$
 5 HOEHLER 93 SPED $\pi N \rightarrow \pi N$
¹ Fit to the amplitudes of HOEHLER 79.

PHASE θ

VALUE (°)	DOCUMENT ID	TECN	COMMENT
-120 to 0 (≈ -90) OUR ESTIMATE			
-115±30	SOKHOYAN 15A	DPWA	Multichannel
-113± 4±2	¹ SVARC 14	L+P	$\pi N \rightarrow \pi N$
0±50	CUTKOSKY 80	IPWA	$\pi N \rightarrow \pi N$
••• We do not use the following data for averages, fits, limits, etc. •••			
-100±40	ANISOVICH 12A	DPWA	Multichannel
- 34	BATINIC 10	DPWA	$\pi N \rightarrow N\pi, N\eta$
¹ Fit to the amplitudes of HOEHLER 79.			

N(1700) INELASTIC POLE RESIDUE

The "normalized residue" is the residue divided by $\Gamma_{pole}/2$.

Normalized residue in $N\pi \rightarrow N(1700) \rightarrow \Delta\pi, S$ -wave

MODULUS	PHASE (°)	DOCUMENT ID	TECN	COMMENT
0.33±0.10	-70± 25	SOKHOYAN 15A	DPWA	Multichannel
••• We do not use the following data for averages, fits, limits, etc. •••				
0.34±0.21	-60± 40	ANISOVICH 12A	DPWA	Multichannel

Normalized residue in $N\pi \rightarrow N(1700) \rightarrow \Delta\pi, D$ -wave

MODULUS	PHASE (°)	DOCUMENT ID	TECN	COMMENT
0.10±0.06	75± 30	SOKHOYAN 15A	DPWA	Multichannel
••• We do not use the following data for averages, fits, limits, etc. •••				
0.08±0.06	90± 35	ANISOVICH 12A	DPWA	Multichannel

Normalized residue in $N\pi \rightarrow N(1700) \rightarrow N\sigma$

MODULUS	PHASE (°)	DOCUMENT ID	TECN	COMMENT
0.13±0.08	-100± 35	SOKHOYAN 15A	DPWA	Multichannel

Normalized residue in $N\pi \rightarrow N(1700) \rightarrow N(1440)\pi$

MODULUS	PHASE (°)	DOCUMENT ID	TECN	COMMENT
0.13±0.05	40± 35	SOKHOYAN 15A	DPWA	Multichannel

Normalized residue in $N\pi \rightarrow N(1700) \rightarrow N(1520)\pi, P$ -wave

MODULUS	PHASE (°)	DOCUMENT ID	TECN	COMMENT
0.07±0.03	160± 45	SOKHOYAN 15A	DPWA	Multichannel

N(1700) BREIT-WIGNER MASS

VALUE (MeV)	DOCUMENT ID	TECN	COMMENT
1650 to 1800 (≈ 1720) OUR ESTIMATE			
1653± 5	¹ HUNT 19	DPWA	Multichannel
1800±35	SOKHOYAN 15A	DPWA	Multichannel
1675±25	CUTKOSKY 80	IPWA	$\pi N \rightarrow \pi N$
1731±15	HOEHLER 79	IPWA	$\pi N \rightarrow \pi N$
••• We do not use the following data for averages, fits, limits, etc. •••			
1790±40	ANISOVICH 12A	DPWA	Multichannel
1665± 3	¹ SHRESTHA 12A	DPWA	Multichannel
1817±22	BATINIC 10	DPWA	$\pi N \rightarrow N\pi, N\eta$
1736±33	VRANA 00	DPWA	Multichannel
¹ Statistical error only.			

N(1700) BREIT-WIGNER WIDTH

VALUE (MeV)	DOCUMENT ID	TECN	COMMENT
100 to 300 (≈ 200) OUR ESTIMATE			
81± 13	¹ HUNT 19	DPWA	Multichannel
400±100	SOKHOYAN 15A	DPWA	Multichannel
90± 40	CUTKOSKY 80	IPWA	$\pi N \rightarrow \pi N$
110± 30	HOEHLER 79	IPWA	$\pi N \rightarrow \pi N$
••• We do not use the following data for averages, fits, limits, etc. •••			
390±140	ANISOVICH 12A	DPWA	Multichannel
56± 8	¹ SHRESTHA 12A	DPWA	Multichannel
134± 37	BATINIC 10	DPWA	$\pi N \rightarrow N\pi, N\eta$
175±133	VRANA 00	DPWA	Multichannel
¹ Statistical error only.			

N(1700) DECAY MODES

The following branching fractions are our estimates, not fits or averages.

Mode	Fraction (Γ_i/Γ)
Γ_1 $N\pi$	7-17 %
Γ_2 $N\eta$	1-2 %

Baryon Particle Listings

$N(1700)$

Γ_3	$N\omega$	10–34 %
Γ_4	ΛK	1–2 %
Γ_5	$N\pi\pi$	>89 %
Γ_6	$\Delta(1232)\pi$	55–85 %
Γ_7	$\Delta(1232)\pi, S\text{-wave}$	50–80 %
Γ_8	$\Delta(1232)\pi, D\text{-wave}$	4–14 %
Γ_9	$N\rho, S=3/2, S\text{-wave}$	32–44 %
Γ_{10}	$N\sigma$	2–14 %
Γ_{11}	$N(1440)\pi$	3–11 %
Γ_{12}	$N(1520)\pi$	<4 %
Γ_{13}	$p\gamma$	0.01–0.05 %
Γ_{14}	$p\gamma, \text{helicity}=1/2$	0.0–0.024 %
Γ_{15}	$p\gamma, \text{helicity}=3/2$	0.002–0.026 %
Γ_{16}	$n\gamma$	0.01–0.13 %
Γ_{17}	$n\gamma, \text{helicity}=1/2$	0.0–0.09 %
Γ_{18}	$n\gamma, \text{helicity}=3/2$	0.01–0.05 %

$N(1700)$ BRANCHING RATIOS

$\Gamma(N\pi)/\Gamma_{\text{total}}$	VALUE (%)	DOCUMENT ID	TECN	COMMENT	Γ_1/Γ
7 to 17 OUR ESTIMATE					
3.7 ± 0.1		¹ HUNT	19	DPWA Multichannel	
15 ± 6		SOKHOYAN	15A	DPWA Multichannel	
11 ± 5		CUTKOSKY	80	IPWA $\pi N \rightarrow \pi N$	
8 ± 3		HOEHLER	79	IPWA $\pi N \rightarrow \pi N$	
••• We do not use the following data for averages, fits, limits, etc. •••					
12 ± 5		ANISOVICH	12A	DPWA Multichannel	
2.8 ± 0.5		¹ SHRESTHA	12A	DPWA Multichannel	
9 ± 6		BATINIC	10	DPWA $\pi N \rightarrow N\pi, N\eta$	
4 ± 2		VRANA	00	DPWA Multichannel	
¹ Statistical error only.					

$\Gamma(N\eta)/\Gamma_{\text{total}}$	VALUE (%)	DOCUMENT ID	TECN	COMMENT	Γ_2/Γ
1–2 % OUR ESTIMATE					
1 ± 1		MUELLER	20	DPWA Multichannel	
1.1 ± 0.6		¹ HUNT	19	DPWA Multichannel	
••• We do not use the following data for averages, fits, limits, etc. •••					
14 ± 5		BATINIC	10	DPWA $\pi N \rightarrow N\pi, N\eta$	
10 ± 5		THOMA	08	DPWA Multichannel	
0 ± 1		VRANA	00	DPWA Multichannel	
¹ Statistical error only.					

$\Gamma(N\omega)/\Gamma_{\text{total}}$	VALUE (%)	DOCUMENT ID	TECN	COMMENT	Γ_3/Γ
22 ± 12		DENISENKO	16	DPWA Multichannel	

$\Gamma(\Lambda K)/\Gamma_{\text{total}}$	VALUE (%)	DOCUMENT ID	TECN	COMMENT	Γ_4/Γ
1–2 % OUR ESTIMATE					
1.3 ± 0.7		¹ HUNT	19	DPWA Multichannel	
¹ Statistical error only.					

$\Gamma(\Delta(1232)\pi, S\text{-wave})/\Gamma_{\text{total}}$	VALUE (%)	DOCUMENT ID	TECN	COMMENT	Γ_7/Γ
11 ± 8		¹ HUNT	19	DPWA Multichannel	
65 ± 15		SOKHOYAN	15A	DPWA Multichannel	
••• We do not use the following data for averages, fits, limits, etc. •••					
72 ± 23		ANISOVICH	12A	DPWA Multichannel	
31 ± 9		¹ SHRESTHA	12A	DPWA Multichannel	
11 ± 1		VRANA	00	DPWA Multichannel	
¹ Statistical error only.					

$\Gamma(\Delta(1232)\pi, D\text{-wave})/\Gamma_{\text{total}}$	VALUE (%)	DOCUMENT ID	TECN	COMMENT	Γ_8/Γ
13 ± 5		¹ HUNT	19	DPWA Multichannel	
9 ± 5		SOKHOYAN	15A	DPWA Multichannel	
••• We do not use the following data for averages, fits, limits, etc. •••					
<10		ANISOVICH	12A	DPWA Multichannel	
3 ± 2		¹ SHRESTHA	12A	DPWA Multichannel	
79 ± 56		VRANA	00	DPWA Multichannel	
¹ Statistical error only.					

$\Gamma(N\rho, S=3/2, S\text{-wave})/\Gamma_{\text{total}}$	VALUE (%)	DOCUMENT ID	TECN	COMMENT	Γ_9/Γ
7.5 ± 3.6		¹ HUNT	19	DPWA Multichannel	
••• We do not use the following data for averages, fits, limits, etc. •••					
38 ± 6		¹ SHRESTHA	12A	DPWA Multichannel	
7 ± 1		VRANA	00	DPWA Multichannel	
¹ Statistical error only.					

$\Gamma(N\sigma)/\Gamma_{\text{total}}$	VALUE (%)	DOCUMENT ID	TECN	COMMENT	Γ_{10}/Γ
62 ± 9		¹ HUNT	19	DPWA Multichannel	
8 ± 6		SOKHOYAN	15A	DPWA Multichannel	
••• We do not use the following data for averages, fits, limits, etc. •••					
24 ± 6		¹ SHRESTHA	12A	DPWA Multichannel	
18 ± 12		THOMA	08	DPWA Multichannel	
0 ± 1		VRANA	00	DPWA Multichannel	
¹ Statistical error only.					

$\Gamma(N(1440)\pi)/\Gamma_{\text{total}}$	VALUE (%)	DOCUMENT ID	TECN	COMMENT	Γ_{11}/Γ
7 ± 4		SOKHOYAN	15A	DPWA Multichannel	

$\Gamma(N(1520)\pi)/\Gamma_{\text{total}}$	VALUE (%)	DOCUMENT ID	TECN	COMMENT	Γ_{12}/Γ
<4		SOKHOYAN	15A	DPWA Multichannel	

$N(1700)$ PHOTON DECAY AMPLITUDES AT THE POLE

$N(1700) \rightarrow p\gamma, \text{helicity-1/2}$ amplitude $A_{1/2}$	MODULUS ($\text{GeV}^{-1/2}$)	PHASE ($^\circ$)	DOCUMENT ID	TECN	COMMENT
0.047 ± 0.016		75 ± 30	SOKHOYAN	15A	DPWA Multichannel

$N(1700) \rightarrow p\gamma, \text{helicity-3/2}$ amplitude $A_{3/2}$	MODULUS ($\text{GeV}^{-1/2}$)	PHASE ($^\circ$)	DOCUMENT ID	TECN	COMMENT
-0.041 ± 0.014		0 ± 20	SOKHOYAN	15A	DPWA Multichannel

$N(1700)$ BREIT-WIGNER PHOTON DECAY AMPLITUDES

$N(1700) \rightarrow p\gamma, \text{helicity-1/2}$ amplitude $A_{1/2}$	VALUE ($\text{GeV}^{-1/2}$)	DOCUMENT ID	TECN	COMMENT
0.032 ± 0.005		¹ HUNT	19	DPWA Multichannel
0.041 ± 0.017		ANISOVICH	12A	DPWA Multichannel
••• We do not use the following data for averages, fits, limits, etc. •••				
0.021 ± 0.005		¹ SHRESTHA	12A	DPWA Multichannel
¹ Statistical error only.				

$N(1700) \rightarrow p\gamma, \text{helicity-3/2}$ amplitude $A_{3/2}$	VALUE ($\text{GeV}^{-1/2}$)	DOCUMENT ID	TECN	COMMENT
0.034 ± 0.006		¹ HUNT	19	DPWA Multichannel
-0.037 ± 0.014		SOKHOYAN	15A	DPWA Multichannel
••• We do not use the following data for averages, fits, limits, etc. •••				
-0.034 ± 0.013		ANISOVICH	12A	DPWA Multichannel
0.050 ± 0.009		¹ SHRESTHA	12A	DPWA Multichannel
¹ Statistical error only.				

$N(1700) \rightarrow n\gamma, \text{helicity-1/2}$ amplitude $A_{1/2}$	VALUE ($\text{GeV}^{-1/2}$)	DOCUMENT ID	TECN	COMMENT
0.005 ± 0.011		¹ HUNT	19	DPWA Multichannel
0.025 ± 0.010		ANISOVICH	13B	DPWA Multichannel
••• We do not use the following data for averages, fits, limits, etc. •••				
-0.049 ± 0.008		¹ SHRESTHA	12A	DPWA Multichannel
¹ Statistical error only.				

$N(1700) \rightarrow n\gamma, \text{helicity-3/2}$ amplitude $A_{3/2}$	VALUE ($\text{GeV}^{-1/2}$)	DOCUMENT ID	TECN	COMMENT
-0.094 ± 0.017		¹ HUNT	19	DPWA Multichannel
-0.032 ± 0.018		ANISOVICH	13B	DPWA Multichannel
••• We do not use the following data for averages, fits, limits, etc. •••				
-0.092 ± 0.014		¹ SHRESTHA	12A	DPWA Multichannel
¹ Statistical error only.				

$N(1700)$ REFERENCES

For early references, see Physics Letters **111B** 1 (1982).

MUELLER	20	PL B803 135323	J. Mueller et al.	(CBELSA/TAPS Collab.)
HUNT	19	PR C99 055205	B. C. Hunt, D. M. Manley	
DENISENKO	16	PL B755 97	I. Denisenko et al.	
SOKHOYAN	15A	EPJ A51 95	V. Sokhoyan et al.	(CBELSA/TAPS Collab.)
PDG	14	CP C38 070001	K. Olive et al.	(PDG Collab.)
SVARC	14	PR C89 045205	A. Svarc et al.	(RBI Zagreb, UNI Tuzla)
ANISOVICH	13B	EPJ A49 67	A.V. Anisovich et al.	
ANISOVICH	12A	EPJ A48 15	A.V. Anisovich et al.	(BONN, PNPI)
SHRESTHA	12A	PR C86 055203	M. Shreshtha, D.M. Manley	(KSU)
BATINIC	10	PR C82 038203	M. Batinic et al.	(ZAGB)
THOMA	08	PL B659 87	U. Thoma et al.	(CB-ELSA Collab.)
VRANA	00	PRPL 328 181	T.P. Vrana, S.A. Dymant, T.-S.H. Lee	(PITT, ANL)
HOEHLER	93	πN Newsletter 9 1	G. Hohlner	(KARL)
CUTKOSKY	80	Toronto Conf. 19	R.E. Cutkosky et al.	(CMU, LBL) IJP
Albo		PR D20 2839	R.E. Cutkosky et al.	(CMU, LBL) IJP
HOEHLER	79	PDAT 12-1	G. Hohlner et al.	(KARLT) IJP
Albo		Toronto Conf. 3	R. Koch	(KARLT) IJP

N(1710) 1/2⁺

$I(J^P) = \frac{1}{2}(\frac{1}{2}^+)$ Status: * * * *

Older and obsolete values are listed and referenced in the 2014 edition, Chinese Physics C38 070001 (2014).

N(1710) POLE POSITION

REAL PART

VALUE (MeV)	DOCUMENT ID	TECN	COMMENT
1680 to 1720 (≈ 1700) OUR ESTIMATE			
1690 ± 15	ANISOVICH 17A	DPWA	Multichannel
1697 ± 23	¹ ANISOVICH 17A	L+P	$\gamma p, \pi^- p \rightarrow K\Lambda$
1770 ± 5 ± 2	² SVARC 14	L+P	$\pi N \rightarrow \pi N$
1690 ± 20	CUTKOSKY 80	IPWA	$\pi N \rightarrow \pi N$
• • • We do not use the following data for averages, fits, limits, etc. • • •			
1615	HUNT 19	DPWA	Multichannel
1651	ROENCHEN 15A	DPWA	Multichannel
1690 ± 15	SOKHOYAN 15A	DPWA	Multichannel
1690 ± 15	GUTZ 14	DPWA	Multichannel
1670	SHKLYAR 13	DPWA	Multichannel
1687 ± 17	ANISOVICH 12A	DPWA	Multichannel
1711 ± 15	³ BATINIC 10	DPWA	$\pi N \rightarrow N\pi, N\eta$
1679	VRANA 00	DPWA	Multichannel
1690	HOEHLER 93	SPED	$\pi N \rightarrow \pi N$
1698	CUTKOSKY 90	IPWA	$\pi N \rightarrow \pi N$

¹ Statistical error only.

² Fit to the amplitudes of HOEHLER 79.

³ BATINIC 10 finds evidence for a second P₁₁ state with all parameters except for the phase of the pole residue very similar to the parameters we give here.

-2xIMAGINARY PART

VALUE (MeV)	DOCUMENT ID	TECN	COMMENT
80 to 160 (≈ 120) OUR ESTIMATE			
155 ± 25	ANISOVICH 17A	DPWA	Multichannel
84 ± 34	¹ ANISOVICH 17A	L+P	$\gamma p, \pi^- p \rightarrow K\Lambda$
98 ± 8 ± 5	² SVARC 14	L+P	$\pi N \rightarrow \pi N$
80 ± 20	CUTKOSKY 80	IPWA	$\pi N \rightarrow \pi N$
• • • We do not use the following data for averages, fits, limits, etc. • • •			
169	HUNT 19	DPWA	Multichannel
121	ROENCHEN 15A	DPWA	Multichannel
170 ± 20	SOKHOYAN 15A	DPWA	Multichannel
170 ± 20	GUTZ 14	DPWA	Multichannel
159	SHKLYAR 13	DPWA	Multichannel
200 ± 25	ANISOVICH 12A	DPWA	Multichannel
174 ± 16	³ BATINIC 10	DPWA	$\pi N \rightarrow N\pi, N\eta$
132	VRANA 00	DPWA	Multichannel
200	HOEHLER 93	SPED	$\pi N \rightarrow \pi N$
88	CUTKOSKY 90	IPWA	$\pi N \rightarrow \pi N$

¹ Statistical error only.

² Fit to the amplitudes of HOEHLER 79.

³ BATINIC 10 finds evidence for a second P₁₁ state with all parameters except for the phase of the pole residue very similar to the parameters we give here.

N(1710) ELASTIC POLE RESIDUE

MODULUS |r|

VALUE (MeV)	DOCUMENT ID	TECN	COMMENT
4 to 10 (≈ 7) OUR ESTIMATE			
6 ± 3	SOKHOYAN 15A	DPWA	Multichannel
5 ± 1 ± 1	¹ SVARC 14	L+P	$\pi N \rightarrow \pi N$
8 ± 2	CUTKOSKY 80	IPWA	$\pi N \rightarrow \pi N$
• • • We do not use the following data for averages, fits, limits, etc. • • •			
3.2	ROENCHEN 15A	DPWA	Multichannel
6 ± 3	GUTZ 14	DPWA	Multichannel
11	SHKLYAR 13	DPWA	Multichannel
6 ± 4	ANISOVICH 12A	DPWA	Multichannel
24	² BATINIC 10	DPWA	$\pi N \rightarrow N\pi, N\eta$
15	HOEHLER 93	SPED	$\pi N \rightarrow \pi N$
9	CUTKOSKY 90	IPWA	$\pi N \rightarrow \pi N$

¹ Fit to the amplitudes of HOEHLER 79.

² BATINIC 10 finds evidence for a second P₁₁ state with all parameters except for the phase of the pole residue very similar to the parameters we give here.

PHASE θ

VALUE (°)	DOCUMENT ID	TECN	COMMENT
120 to 260 (≈ 190) OUR ESTIMATE			
130 ± 35	SOKHOYAN 15A	DPWA	Multichannel
-104 ± 7 ± 3	¹ SVARC 14	L+P	$\pi N \rightarrow \pi N$
175 ± 35	CUTKOSKY 80	IPWA	$\pi N \rightarrow \pi N$
• • • We do not use the following data for averages, fits, limits, etc. • • •			
55	ROENCHEN 15A	DPWA	Multichannel
120 ± 45	GUTZ 14	DPWA	Multichannel
9	SHKLYAR 13	DPWA	Multichannel
120 ± 70	ANISOVICH 12A	DPWA	Multichannel
20	² BATINIC 10	DPWA	$\pi N \rightarrow N\pi, N\eta$
-167	CUTKOSKY 90	IPWA	$\pi N \rightarrow \pi N$

¹ Fit to the amplitudes of HOEHLER 79.

² BATINIC 10 finds evidence for a second P₁₁ state with all parameters except for the phase of the pole residue very similar to the parameters we give here.

N(1710) INELASTIC POLE RESIDUE

The "normalized residue" is the residue divided by $\Gamma_{pole}/2$.

Normalized residue in Nπ → N(1710) → Nη

MODULUS	PHASE (°)	DOCUMENT ID	TECN	COMMENT
0.12 ± 0.04	0 ± 45	ANISOVICH 12A	DPWA	Multichannel
• • • We do not use the following data for averages, fits, limits, etc. • • •				
0.16	-180	ROENCHEN 15A	DPWA	Multichannel

Normalized residue in Nπ → N(1710) → ΛK

MODULUS	PHASE (°)	DOCUMENT ID	TECN	COMMENT
0.16 ± 0.05	-160 ± 25	ANISOVICH 17A	DPWA	Multichannel
0.12 ^{+0.24} _{-0.12}	-119 ± 83	¹ ANISOVICH 17A	L+P	$\gamma p, \pi^- p \rightarrow K\Lambda$
• • • We do not use the following data for averages, fits, limits, etc. • • •				
0.12	-32	ROENCHEN 15A	DPWA	Multichannel
0.17 ± 0.06	-110 ± 20	ANISOVICH 12A	DPWA	Multichannel

¹ Statistical error only.

Normalized residue in Nπ → N(1710) → ΣK

MODULUS	PHASE (°)	DOCUMENT ID	TECN	COMMENT
• • • We do not use the following data for averages, fits, limits, etc. • • •				
0.004	-43	ROENCHEN 15A	DPWA	Multichannel

Normalized residue in Nπ → N(1710) → N(1535)π

MODULUS	PHASE (°)	DOCUMENT ID	TECN	COMMENT
0.10 ± 0.04	140 ± 40	GUTZ 14	DPWA	Multichannel

N(1710) BREIT-WIGNER MASS

VALUE (MeV)	DOCUMENT ID	TECN	COMMENT
1680 to 1740 (≈ 1710) OUR ESTIMATE			
1648 ± 16	¹ HUNT 19	DPWA	Multichannel
1715 ± 20	SOKHOYAN 15A	DPWA	Multichannel
1737 ± 17	¹ SHKLYAR 13	DPWA	Multichannel
1700 ± 50	CUTKOSKY 80	IPWA	$\pi N \rightarrow \pi N$
1723 ± 9	HOEHLER 79	IPWA	$\pi N \rightarrow \pi N$
• • • We do not use the following data for averages, fits, limits, etc. • • •			
1715 ± 20	GUTZ 14	DPWA	Multichannel
1710 ± 20	ANISOVICH 12A	DPWA	Multichannel
1662 ± 7	¹ SHRESTHA 12A	DPWA	Multichannel
1729 ± 16	² BATINIC 10	DPWA	$\pi N \rightarrow N\pi, N\eta$
1752 ± 3	PENNER 02C	DPWA	Multichannel
1699 ± 65	VRANA 00	DPWA	Multichannel

¹ Statistical error only.

² BATINIC 10 finds evidence for a second P₁₁ state with all parameters except for the phase of the pole residue very similar to the parameters we give here.

N(1710) BREIT-WIGNER WIDTH

VALUE (MeV)	DOCUMENT ID	TECN	COMMENT
80 to 200 (≈ 140) OUR ESTIMATE			
195 ± 46	¹ HUNT 19	DPWA	Multichannel
175 ± 15	SOKHOYAN 15A	DPWA	Multichannel
368 ± 120	¹ SHKLYAR 13	DPWA	Multichannel
93 ± 30	CUTKOSKY 90	IPWA	$\pi N \rightarrow \pi N$
90 ± 30	CUTKOSKY 80	IPWA	$\pi N \rightarrow \pi N$
120 ± 15	HOEHLER 79	IPWA	$\pi N \rightarrow \pi N$
• • • We do not use the following data for averages, fits, limits, etc. • • •			
175 ± 15	GUTZ 14	DPWA	Multichannel
200 ± 18	ANISOVICH 12A	DPWA	Multichannel
116 ± 17	¹ SHRESTHA 12A	DPWA	Multichannel
180 ± 17	² BATINIC 10	DPWA	$\pi N \rightarrow N\pi, N\eta$
386 ± 59	PENNER 02C	DPWA	Multichannel
143 ± 100	VRANA 00	DPWA	Multichannel

¹ Statistical error only.

² BATINIC 10 finds evidence for a second P₁₁ state with all parameters except for the phase of the pole residue very similar to the parameters we give here.

N(1710) DECAY MODES

The following branching fractions are our estimates, not fits or averages.

Mode	Fraction (Γ _i /Γ)
Γ ₁ Nπ	5-20 %
Γ ₂ Nη	10-50 %
Γ ₃ Nω	1-5 %
Γ ₄ ΛK	5-25 %
Γ ₅ ΣK	seen

Baryon Particle Listings

$N(1710)$, $N(1720)$

Γ_6	$N\pi\pi$	14-48 %
Γ_7	$\Delta(1232)\pi$, P -wave	3-9 %
Γ_8	$N\rho$, $S=1/2$, P -wave	11-23 %
Γ_9	$N\sigma$	<16 %
Γ_{10}	$N(1535)\pi$	9-21 %
Γ_{11}	$\rho\gamma$, helicity=1/2	0.002-0.08 %
Γ_{12}	$n\gamma$, helicity=1/2	0.0-0.02%

$N(1710)$ BRANCHING RATIOS

$\Gamma(N\pi)/\Gamma_{total}$				Γ_1/Γ
VALUE (%)	DOCUMENT ID	TECN	COMMENT	
5 to 20 (≈ 10) OUR ESTIMATE				
12±6	¹ HUNT	19	DPWA	Multichannel
5±3	SOKHOYAN	15A	DPWA	Multichannel
2±2	¹ SHKLYAR	13	PWA	Multichannel
20±4	CUTKOSKY	80	IPWA	$\pi N \rightarrow \pi N$
12±4	HOEHLER	79	IPWA	$\pi N \rightarrow \pi N$
••• We do not use the following data for averages, fits, limits, etc. •••				
5±3	GUTZ	14	DPWA	Multichannel
5±4	ANISOVICH	12A	DPWA	Multichannel
15±4	¹ SHRESTHA	12A	DPWA	Multichannel
22±24	² BATINIC	10	DPWA	$\pi N \rightarrow N\pi$, $N\eta$
14±8	PENNER	02C	DPWA	Multichannel
27±13	VRANA	00	DPWA	Multichannel

¹ Statistical error only.
² BATINIC 10 finds evidence for a second P_{11} state with all parameters except for the phase of the pole residue very similar to the parameters we give here.

$\Gamma(N\eta)/\Gamma_{total}$				Γ_2/Γ
VALUE (%)	DOCUMENT ID	TECN	COMMENT	
10 to 50 (≈ 30) OUR ESTIMATE				
18±10	MUELLER	20	DPWA	Multichannel
17±8	¹ HUNT	19	DPWA	Multichannel
45±4	¹ SHKLYAR	13	DPWA	Multichannel
17±10	ANISOVICH	12A	DPWA	Multichannel
••• We do not use the following data for averages, fits, limits, etc. •••				
11±7	¹ SHRESTHA	12A	DPWA	Multichannel
6±8	² BATINIC	10	DPWA	$\pi N \rightarrow N\pi$, $N\eta$
36±11	PENNER	02C	DPWA	Multichannel
6±1	VRANA	00	DPWA	Multichannel

¹ Statistical error only.
² BATINIC 10 finds evidence for a second P_{11} state with all parameters except for the phase of the pole residue very similar to the parameters we give here.

$\Gamma(N\omega)/\Gamma_{total}$				Γ_3/Γ
VALUE (%)	DOCUMENT ID	TECN	COMMENT	
1 to 5 (≈ 3) OUR ESTIMATE				
2±2	DENISENKO	16	DPWA	Multichannel
3±2	¹ SHKLYAR	13	DPWA	Multichannel
••• We do not use the following data for averages, fits, limits, etc. •••				
13±2	PENNER	02C	DPWA	Multichannel

¹ Statistical error only.

$\Gamma(\Lambda K)/\Gamma_{total}$				Γ_4/Γ
VALUE (%)	DOCUMENT ID	TECN	COMMENT	
5 to 25 (≈ 15) OUR ESTIMATE				
1.8±1.5	¹ HUNT	19	DPWA	Multichannel
23±7	ANISOVICH	12A	DPWA	Multichannel
5±3	SHKLYAR	05	DPWA	Multichannel
••• We do not use the following data for averages, fits, limits, etc. •••				
8±4	¹ SHRESTHA	12A	DPWA	Multichannel
5±2	PENNER	02C	DPWA	Multichannel
10±10	VRANA	00	DPWA	Multichannel

¹ Statistical error only.

$\Gamma(\Sigma K)/\Gamma_{total}$				Γ_5/Γ
VALUE (%)	DOCUMENT ID	TECN	COMMENT	
••• We do not use the following data for averages, fits, limits, etc. •••				
7±7	PENNER	02C	DPWA	Multichannel

$\Gamma(\Delta(1232)\pi, P\text{-wave})/\Gamma_{total}$				Γ_7/Γ
VALUE (%)	DOCUMENT ID	TECN	COMMENT	
3-9 % OUR ESTIMATE				
28±9	¹ HUNT	19	DPWA	Multichannel
••• We do not use the following data for averages, fits, limits, etc. •••				
6±3	¹ SHRESTHA	12A	DPWA	Multichannel
39±8	VRANA	00	DPWA	Multichannel

¹ Statistical error only.

$\Gamma(N\rho, S=1/2, P\text{-wave})/\Gamma_{total}$				Γ_8/Γ
VALUE (%)	DOCUMENT ID	TECN	COMMENT	
11-23 % OUR ESTIMATE				
17±9	¹ HUNT	19	DPWA	Multichannel

••• We do not use the following data for averages, fits, limits, etc. •••

17±6	¹ SHRESTHA	12A	DPWA	Multichannel
17±1	VRANA	00	DPWA	Multichannel

¹ Statistical error only.

$\Gamma(N\sigma)/\Gamma_{total}$				Γ_9/Γ
VALUE (%)	DOCUMENT ID	TECN	COMMENT	
<16 % OUR ESTIMATE				
<16	¹ HUNT	19	DPWA	Multichannel

¹ Statistical error only.

$\Gamma(N(1535)\pi)/\Gamma_{total}$				Γ_{10}/Γ
VALUE (%)	DOCUMENT ID	TECN	COMMENT	
15±6	GUTZ	14	DPWA	Multichannel

$N(1710)$ PHOTON DECAY AMPLITUDES AT THE POLE

$N(1710) \rightarrow \rho\gamma$, helicity-1/2 amplitude $A_{1/2}$

MODULUS ($\text{GeV}^{-1/2}$)	PHASE ($^\circ$)	DOCUMENT ID	TECN	COMMENT
$0.028^{+0.009}_{-0.002}$	103^{+20}_{-6}	ROENCHEN	14	DPWA

••• We do not use the following data for averages, fits, limits, etc. •••

0.020	-83	ROENCHEN	15A	DPWA	Multichannel
-------	-----	----------	-----	------	--------------

$N(1710)$ BREIT-WIGNER PHOTON DECAY AMPLITUDES

$N(1710) \rightarrow \rho\gamma$, helicity-1/2 amplitude $A_{1/2}$

VALUE ($\text{GeV}^{-1/2}$)	DOCUMENT ID	TECN	COMMENT	
0.014 ± 0.008	¹ HUNT	19	DPWA	Multichannel
0.050 ± 0.010	SOKHOYAN	15A	DPWA	Multichannel
-0.050 ± 0.001	¹ SHKLYAR	13	DPWA	Multichannel
••• We do not use the following data for averages, fits, limits, etc. •••				
0.05 ± 0.01	GUTZ	14	DPWA	Multichannel
0.052 ± 0.015	ANISOVICH	12A	DPWA	Multichannel
-0.008 ± 0.003	¹ SHRESTHA	12A	DPWA	Multichannel
0.044	PENNER	02D	DPWA	Multichannel

¹ Statistical error only.

$N(1710) \rightarrow n\gamma$, helicity-1/2 amplitude $A_{1/2}$

VALUE ($\text{GeV}^{-1/2}$)	DOCUMENT ID	TECN	COMMENT	
0.0053 ± 0.0003	¹ HUNT	19	DPWA	Multichannel
-0.040 ± 0.020	ANISOVICH	13B	DPWA	Multichannel
••• We do not use the following data for averages, fits, limits, etc. •••				
0.017 ± 0.003	¹ SHRESTHA	12A	DPWA	Multichannel
-0.024	PENNER	02D	DPWA	Multichannel

¹ Statistical error only.

$N(1710)$ REFERENCES

For early references, see Physics Letters **111B** 1 (1982).

MUELLER	20	PL B803 135323	J. Mueller et al.	(CBELSA/TAPS Collab.)
HUNT	19	PR C9 055205	B.C. Hunt, D.M. Manley	
ANISOVICH	17A	PRL 119 062004	A.V. Anisovich et al.	
DENISENKO	16	EPL B755 97	I. Denisenko et al.	
ROENCHEN	15A	EPL A51 70	D. Roenchen et al.	
SOKHOYAN	15A	EPJ A51 95	V. Sokhoyan et al.	(CBELSA/TAPS Collab.)
GUTZ	14	EPJ A50 74	E. Gutz et al.	(CBELSA/TAPS Collab.)
PDG	14	CP C38 070001	K. Olive et al.	(PDG Collab.)
ROENCHEN	14	EPJ A50 101	D. Roenchen et al.	
Also		EPJ A51 63 (errata.)	D. Roenchen et al.	
SVARC	14	PR C89 045205	A. Svarc et al.	(RBI Zagreb, UNI Tuzla)
ANISOVICH	13B	EPJ A49 67	A.V. Anisovich et al.	
SHKLYAR	13	PR C87 015201	V. Shklyar, H. Lenske, U. Mosel	(GIES)
ANISOVICH	12A	EPJ A48 15	A.V. Anisovich et al.	(BONN, PNPI)
SHRESTHA	12A	PR C86 055203	M. Shrestha, D.M. Manley	(KSU)
BATINIC	10	PR C82 039203	M. Batinic et al.	(ZAGR)
SHKLYAR	05	PR C72 015210	V. Shklyar, H. Lenske, U. Mosel	(GIES)
PENNER	02C	PR C66 055211	G. Penner, U. Mosel	(GIES)
PENNER	02D	PR C66 055212	G. Penner, U. Mosel	(GIES)
VRANA	00	PRPL 328 181	T.P. Vrana, S.A. Dytman, T.-S.H. Lee	(PITT, ANL)
HOEHLER	93	πN Newsletter 9 1	G. Hoehler	(KARL)
CUTKOSKY	90	PR D42 235	R.E. Cutkosky, S. Wang	(CMU)
CUTKOSKY	80	Toronto Conf. 19	R.E. Cutkosky et al.	(CMU, LBL) IJP
Also		PR D20 2839	R.E. Cutkosky et al.	(CMU, LBL) IJP
HOEHLER	79	PDAT 12-1	G. Hoehler et al.	(KARL) IJP
Also		Toronto Conf. 3	R. Koch	(KARL) IJP

$$N(1720) 3/2^+$$

$$I(J^P) = \frac{1}{2}(3^+)_2 \text{ Status: } ***$$

Older and obsolete values are listed and referenced in the 2014 edition, Chinese Physics **C38** 070001 (2014).

$N(1720)$ POLE POSITION

REAL PART				
VALUE (MeV)	DOCUMENT ID	TECN	COMMENT	
1660 to 1690 (≈ 1675) OUR ESTIMATE				
1670±25	SOKHOYAN	15A	DPWA	Multichannel
1677±4±1	¹ SVARC	14	L+P	$\pi N \rightarrow \pi N$
1680±30	CUTKOSKY	80	IPWA	$\pi N \rightarrow \pi N$

• • • We do not use the following data for averages, fits, limits, etc. • • •

VALUE (MeV)	DOCUMENT ID	TECN	COMMENT
1654	HUNT 19	DPWA	Multichannel
1710	ROENCHEN 15A	DPWA	Multichannel
1670	SHKLYAR 13	DPWA	Multichannel
1660 ± 30	ANISOVICH 12A	DPWA	Multichannel
1691 ± 23	BATINIC 10	DPWA	$\pi N \rightarrow N\pi, N\eta$
1666	ARNDT 06	DPWA	$\pi N \rightarrow \pi N, \eta N$
1692	VRANA 00	DPWA	Multichannel
1686	HOEHLER 93	SPED	$\pi N \rightarrow \pi N$

¹ Fit to the amplitudes of HOEHLER 79.

-2xIMAGINARY PART

VALUE (MeV)	DOCUMENT ID	TECN	COMMENT
150 to 400 (≈ 250) OUR ESTIMATE			
430 ± 100	SOKHOYAN 15A	DPWA	Multichannel
184 ± 8 ± 1	¹ SVARC 14	L+P	$\pi N \rightarrow \pi N$
120 ± 40	CUTKOSKY 80	IPWA	$\pi N \rightarrow \pi N$
• • • We do not use the following data for averages, fits, limits, etc. • • •			
100	HUNT 19	DPWA	Multichannel
219	ROENCHEN 15A	DPWA	Multichannel
118	SHKLYAR 13	DPWA	Multichannel
450 ± 100	ANISOVICH 12A	DPWA	Multichannel
233 ± 23	BATINIC 10	DPWA	$\pi N \rightarrow N\pi, N\eta$
355	ARNDT 06	DPWA	$\pi N \rightarrow \pi N, \eta N$
94	VRANA 00	DPWA	Multichannel
187	HOEHLER 93	SPED	$\pi N \rightarrow \pi N$

¹ Fit to the amplitudes of HOEHLER 79.

$N(1720)$ ELASTIC POLE RESIDUE

MODULUS $|r|$

VALUE (MeV)	DOCUMENT ID	TECN	COMMENT
10 to 25 (≈ 15) OUR ESTIMATE			
26 ± 10	SOKHOYAN 15A	DPWA	Multichannel
13 ± 1	¹ SVARC 14	L+P	$\pi N \rightarrow \pi N$
8 ± 2	CUTKOSKY 80	IPWA	$\pi N \rightarrow \pi N$
• • • We do not use the following data for averages, fits, limits, etc. • • •			
4.2	ROENCHEN 15A	DPWA	Multichannel
12	SHKLYAR 13	DPWA	Multichannel
22 ± 8	ANISOVICH 12A	DPWA	Multichannel
20	BATINIC 10	DPWA	$\pi N \rightarrow N\pi, N\eta$
25	ARNDT 06	DPWA	$\pi N \rightarrow \pi N, \eta N$
15	HOEHLER 93	SPED	$\pi N \rightarrow \pi N$

¹ Fit to the amplitudes of HOEHLER 79.

PHASE θ

VALUE (°)	DOCUMENT ID	TECN	COMMENT
-160 to -100 (≈ -130) OUR ESTIMATE			
-100 ± 25	SOKHOYAN 15A	DPWA	Multichannel
-115 ± 3 ± 2	¹ SVARC 14	L+P	$\pi N \rightarrow \pi N$
-160 ± 30	CUTKOSKY 80	IPWA	$\pi N \rightarrow \pi N$
• • • We do not use the following data for averages, fits, limits, etc. • • •			
-47	ROENCHEN 15A	DPWA	Multichannel
-45	SHKLYAR 13	DPWA	Multichannel
-115 ± 30	ANISOVICH 12A	DPWA	Multichannel
-109	BATINIC 10	DPWA	$\pi N \rightarrow N\pi, N\eta$
-94	ARNDT 06	DPWA	$\pi N \rightarrow \pi N, \eta N$

¹ Fit to the amplitudes of HOEHLER 79.

$N(1720)$ INELASTIC POLE RESIDUE

The "normalized residue" is the residue divided by $\Gamma_{pole}/2$.

Normalized residue in $N\pi \rightarrow N(1720) \rightarrow N\eta$

MODULUS	PHASE (°)	DOCUMENT ID	TECN	COMMENT
0.03 ± 0.02		ANISOVICH 12A	DPWA	Multichannel
• • • We do not use the following data for averages, fits, limits, etc. • • •				
0.007	106	ROENCHEN 15A	DPWA	Multichannel

Normalized residue in $N\pi \rightarrow N(1720) \rightarrow \Lambda K$

MODULUS	PHASE (°)	DOCUMENT ID	TECN	COMMENT
0.06 ± 0.04	-150 ± 45	ANISOVICH 12A	DPWA	Multichannel
• • • We do not use the following data for averages, fits, limits, etc. • • •				
0.011	-70	ROENCHEN 15A	DPWA	Multichannel

Normalized residue in $N\pi \rightarrow N(1720) \rightarrow \Sigma K$

MODULUS	PHASE (°)	DOCUMENT ID	TECN	COMMENT
0.002	79	ROENCHEN 15A	DPWA	Multichannel

Normalized residue in $N\pi \rightarrow N(1720) \rightarrow \Delta\pi, P$ -wave

MODULUS	PHASE (°)	DOCUMENT ID	TECN	COMMENT
0.28 ± 0.09	95 ± 30	SOKHOYAN 15A	DPWA	Multichannel
• • • We do not use the following data for averages, fits, limits, etc. • • •				
0.29 ± 0.08	80 ± 40	ANISOVICH 12A	DPWA	Multichannel

Normalized residue in $N\pi \rightarrow N(1720) \rightarrow \Delta\pi, F$ -wave

MODULUS	PHASE (°)	DOCUMENT ID	TECN	COMMENT
0.07 ± 0.05		SOKHOYAN 15A	DPWA	Multichannel
• • • We do not use the following data for averages, fits, limits, etc. • • •				
0.03 ± 0.03		ANISOVICH 12A	DPWA	Multichannel

Normalized residue in $N\pi \rightarrow N(1720) \rightarrow N\sigma$

MODULUS	PHASE (°)	DOCUMENT ID	TECN	COMMENT
0.08 ± 0.04	-110 ± 35	SOKHOYAN 15A	DPWA	Multichannel

Normalized residue in $N\pi \rightarrow N(1720) \rightarrow N(1520)\pi, S$ -wave

MODULUS	PHASE (°)	DOCUMENT ID	TECN	COMMENT
0.05 ± 0.04	undefined	SOKHOYAN 15A	DPWA	Multichannel

$N(1720)$ BREIT-WIGNER MASS

VALUE (MeV)	DOCUMENT ID	TECN	COMMENT
1680 to 1750 (≈ 1720) OUR ESTIMATE			
1745 ± 6	GOLOVATCH 19	DPWA	$\gamma p \rightarrow \pi^+ \pi^- p$
1711 ± 4	¹ HUNT 19	DPWA	Multichannel
1690 ± 30	SOKHOYAN 15A	DPWA	Multichannel
1700 ± 10	¹ SHKLYAR 13	DPWA	Multichannel
1763.8 ± 4.6	ARNDT 06	DPWA	$\pi N \rightarrow \pi N, \eta N$
1700 ± 50	CUTKOSKY 80	IPWA	$\pi N \rightarrow \pi N$
1710 ± 20	HOEHLER 79	IPWA	$\pi N \rightarrow \pi N$
• • • We do not use the following data for averages, fits, limits, etc. • • •			
1748 ± 5	² MOKEEV 20	DPWA	$\gamma p \rightarrow \pi^+ \pi^- p$
1725 ± 10	³ MOKEEV 20	DPWA	$\gamma p \rightarrow \pi^+ \pi^- p$
1690 + ⁷⁰ - 35	ANISOVICH 12A	DPWA	Multichannel
1720 ± 5	¹ SHRESTHA 12A	DPWA	Multichannel
1720 ± 18	BATINIC 10	DPWA	$\pi N \rightarrow N\pi, N\eta$
1705 ± 10	PENNER 02C	DPWA	Multichannel
1716 ± 112	VRANA 00	DPWA	Multichannel

¹ Statistical error only.

² State a) of two states seen by the CLAS collaboration.

³ State b) of two states seen by the CLAS collaboration.

$N(1720)$ BREIT-WIGNER WIDTH

VALUE (MeV)	DOCUMENT ID	TECN	COMMENT
150 to 400 (≈ 250) OUR ESTIMATE			
116 ± 27	GOLOVATCH 19	DPWA	$\gamma p \rightarrow \pi^+ \pi^- p$
229 ± 22	¹ HUNT 19	DPWA	Multichannel
420 ± 80	SOKHOYAN 15A	DPWA	Multichannel
152 ± 2	¹ SHKLYAR 13	DPWA	Multichannel
210 ± 22	ARNDT 06	DPWA	$\pi N \rightarrow \pi N, \eta N$
125 ± 70	CUTKOSKY 80	IPWA	$\pi N \rightarrow \pi N$
190 ± 30	HOEHLER 79	IPWA	$\pi N \rightarrow \pi N$
• • • We do not use the following data for averages, fits, limits, etc. • • •			
114 ± 6	² MOKEEV 20	DPWA	$\gamma p \rightarrow \pi^+ \pi^- p$
120 ± 6	³ MOKEEV 20	DPWA	$\gamma p \rightarrow \pi^+ \pi^- p$
420 ± 100	ANISOVICH 12A	DPWA	Multichannel
200 ± 20	¹ SHRESTHA 12A	DPWA	Multichannel
244 ± 28	BATINIC 10	DPWA	$\pi N \rightarrow N\pi, N\eta$
237 ± 73	PENNER 02C	DPWA	Multichannel
121 ± 39	VRANA 00	DPWA	Multichannel

¹ Statistical error only.

² State a) of two states seen by the CLAS collaboration.

³ State b) of two states seen by the CLAS collaboration.

$N(1720)$ DECAY MODES

The following branching fractions are our estimates, not fits or averages.

Mode	Fraction (Γ_i/Γ)
Γ_1 $N\pi$	8-14 %
Γ_2 $N\eta$	1-5 %
Γ_3 $N\omega$	12-40 %
Γ_4 ΛK	4-19 %
Γ_5 $N\pi\pi$	>50 %
Γ_6 $\Delta(1232)\pi$	47-89 %
Γ_7 $\Delta(1232)\pi, P$ -wave	47-77 %
Γ_8 $\Delta(1232)\pi, F$ -wave	<12 %
Γ_9 $N\rho$	
Γ_{10} $N\rho, S=1/2, P$ -wave	1-2 %
Γ_{11} $N\sigma$	2-14 %
Γ_{12} $N(1440)\pi$	<2 %
Γ_{13} $N(1520)\pi, S$ -wave	1-5 %
Γ_{14} $p\gamma$	0.05-0.25 %
Γ_{15} $p\gamma, \text{helicity}=1/2$	0.05-0.15 %
Γ_{16} $p\gamma, \text{helicity}=3/2$	0.002-0.16 %

Baryon Particle Listings

 $N(1720)$

Γ_{17}	$n\gamma$	0.0-0.016 %
Γ_{18}	$n\gamma$, helicity=1/2	0.0-0.01 %
Γ_{19}	$n\gamma$, helicity=3/2	0.0-0.015 %

 $N(1720)$ BRANCHING RATIOS

$\Gamma(N\pi)/\Gamma_{\text{total}}$					Γ_1/Γ
VALUE (%)	DOCUMENT ID	TECN	COMMENT		
8 to 14 (≈ 11) OUR ESTIMATE					
18 \pm 2	¹ HUNT	19	DPWA	Multichannel	
11 \pm 4	SOKHOYAN	15A	DPWA	Multichannel	
17 \pm 2	¹ SHKLYAR	13	DPWA	Multichannel	
9.4 \pm 0.5	ARNDT	06	DPWA	$\pi N \rightarrow \pi N, \eta N$	
10 \pm 4	CUTKOSKY	80	IPWA	$\pi N \rightarrow \pi N$	
14 \pm 3	HOEHLER	79	IPWA	$\pi N \rightarrow \pi N$	
••• We do not use the following data for averages, fits, limits, etc. •••					
10 \pm 5	ANISOVICH	12A	DPWA	Multichannel	
13.6 \pm 0.6	¹ SHRESTHA	12A	DPWA	Multichannel	
18 \pm 3	BATINIC	10	DPWA	$\pi N \rightarrow N\pi, N\eta$	
17 \pm 2	PENNER	02C	DPWA	Multichannel	
5 \pm 5	VRANA	00	DPWA	Multichannel	

¹ Statistical error only.

$\Gamma(N\eta)/\Gamma_{\text{total}}$					Γ_2/Γ
VALUE (%)	DOCUMENT ID	TECN	COMMENT		
1 to 5 (≈ 3) OUR ESTIMATE					
3 \pm 2	MUELLER	20	DPWA	Multichannel	
3.8 \pm 0.5	¹ HUNT	19	DPWA	Multichannel	
< 1	SHKLYAR	13	DPWA	Multichannel	
3 \pm 2	ANISOVICH	12A	DPWA	Multichannel	
••• We do not use the following data for averages, fits, limits, etc. •••					
< 1	¹ SHRESTHA	12A	DPWA	Multichannel	
0 \pm 1	BATINIC	10	DPWA	$\pi N \rightarrow N\pi, N\eta$	
10 \pm 7	THOMA	08	DPWA	Multichannel	
0.2 \pm 0.2	PENNER	02C	DPWA	Multichannel	
4 \pm 1	VRANA	00	DPWA	Multichannel	

¹ Statistical error only.

$\Gamma(N\omega)/\Gamma_{\text{total}}$					Γ_3/Γ
VALUE (%)	DOCUMENT ID	TECN	COMMENT		
26 \pm 14	DENISENKO	16	DPWA	Multichannel	

$\Gamma(\Lambda K)/\Gamma_{\text{total}}$					Γ_4/Γ
VALUE (%)	DOCUMENT ID	TECN	COMMENT		
4-19 % OUR ESTIMATE					
16 \pm 3	¹ HUNT	19	DPWA	Multichannel	
4.3 \pm 0.4	SHKLYAR	05	DPWA	Multichannel	
••• We do not use the following data for averages, fits, limits, etc. •••					
2.8 \pm 0.4	¹ SHRESTHA	12A	DPWA	Multichannel	
12 \pm 9	THOMA	08	DPWA	Multichannel	
9 \pm 3	PENNER	02C	DPWA	Multichannel	

¹ Statistical error only.

$\Gamma(N\pi\pi)/\Gamma_{\text{total}}$					Γ_5/Γ
VALUE (%)	DOCUMENT ID	TECN	COMMENT		
>50 % OUR ESTIMATE					
84 \pm 16	GOLOVATCH	19	DPWA	$\gamma p \rightarrow \pi^+ \pi^- p$	

$\Gamma(\Delta(1232)\pi)/\Gamma_{\text{total}}$					Γ_6/Γ
VALUE (%)	DOCUMENT ID	TECN	COMMENT		
••• We do not use the following data for averages, fits, limits, etc. •••					
45 \pm 8	¹ MOKEEV	20	DPWA	$\gamma p \rightarrow \pi^+ \pi^- p$	
54 \pm 8	² MOKEEV	20	DPWA	$\gamma p \rightarrow \pi^+ \pi^- p$	

¹ State a) of two states seen by the CLAS collaboration.² State b) of two states seen by the CLAS collaboration.

$\Gamma(\Delta(1232)\pi, P\text{-wave})/\Gamma_{\text{total}}$					Γ_7/Γ
VALUE (%)	DOCUMENT ID	TECN	COMMENT		
62 \pm 15	SOKHOYAN	15A	DPWA	Multichannel	
••• We do not use the following data for averages, fits, limits, etc. •••					
75 \pm 15	ANISOVICH	12A	DPWA	Multichannel	

$\Gamma(\Delta(1232)\pi, F\text{-wave})/\Gamma_{\text{total}}$					Γ_8/Γ
VALUE (%)	DOCUMENT ID	TECN	COMMENT		
6 \pm 6	SOKHOYAN	15A	DPWA	Multichannel	

$\Gamma(N\rho)/\Gamma_{\text{total}}$					Γ_9/Γ
VALUE (%)	DOCUMENT ID	TECN	COMMENT		
••• We do not use the following data for averages, fits, limits, etc. •••					
38 \pm 8	¹ MOKEEV	20	DPWA	$\gamma p \rightarrow \pi^+ \pi^- p$	
7 \pm 3	² MOKEEV	20	DPWA	$\gamma p \rightarrow \pi^+ \pi^- p$	

¹ State a) of two states seen by the CLAS collaboration.² State b) of two states seen by the CLAS collaboration.

$\Gamma(N\rho, S=1/2, P\text{-wave})/\Gamma_{\text{total}}$					Γ_{10}/Γ
VALUE (%)	DOCUMENT ID	TECN	COMMENT		
1.4 \pm 0.5	¹ SHRESTHA	12A	DPWA	Multichannel	
••• We do not use the following data for averages, fits, limits, etc. •••					
91 \pm 1	VRANA	00	DPWA	Multichannel	

¹ Statistical error only.

$\Gamma(N\sigma)/\Gamma_{\text{total}}$					Γ_{11}/Γ
VALUE (%)	DOCUMENT ID	TECN	COMMENT		
8 \pm 6	SOKHOYAN	15A	DPWA	Multichannel	

$\Gamma(N(1440)\pi)/\Gamma_{\text{total}}$					Γ_{12}/Γ
VALUE (%)	DOCUMENT ID	TECN	COMMENT		
< 2	SOKHOYAN	15A	DPWA	Multichannel	

$\Gamma(N(1520)\pi, S\text{-wave})/\Gamma_{\text{total}}$					Γ_{13}/Γ
VALUE (%)	DOCUMENT ID	TECN	COMMENT		
3 \pm 2	SOKHOYAN	15A	DPWA	Multichannel	

 $N(1720)$ PHOTON DECAY AMPLITUDES AT THE POLE **$N(1720) \rightarrow p\gamma$, helicity-1/2 amplitude $A_{1/2}$**

MODULUS ($\text{GeV}^{-1/2}$)	PHASE ($^\circ$)	DOCUMENT ID	TECN	COMMENT
0.115 \pm 0.045	0 \pm 35	SOKHOYAN	15A	DPWA
0.051 \pm 0.005	57 \pm 9	ROENCHEN	14	DPWA
	-0.004			
••• We do not use the following data for averages, fits, limits, etc. •••				
0.039	5.3	ROENCHEN	15A	DPWA

 $N(1720) \rightarrow p\gamma$, helicity-3/2 amplitude $A_{3/2}$

MODULUS ($\text{GeV}^{-1/2}$)	PHASE ($^\circ$)	DOCUMENT ID	TECN	COMMENT
0.140 \pm 0.040	65 \pm 35	SOKHOYAN	15A	DPWA
0.014 \pm 0.009	102 \pm 29	ROENCHEN	14	DPWA
	-0.003			
••• We do not use the following data for averages, fits, limits, etc. •••				
0.032	66	ROENCHEN	15A	DPWA

 $N(1720)$ BREIT-WIGNER PHOTON DECAY AMPLITUDES **$N(1720) \rightarrow p\gamma$, helicity-1/2 amplitude $A_{1/2}$**

VALUE ($\text{GeV}^{-1/2}$)	DOCUMENT ID	TECN	COMMENT
0.080 to 0.120 (≈ 0.100) OUR ESTIMATE			
0.0809 \pm 0.0115	GOLOVATCH	19	DPWA
0.068 \pm 0.004	¹ HUNT	19	DPWA
0.115 \pm 0.045	SOKHOYAN	15A	DPWA
-0.065 \pm 0.002	¹ SHKLYAR	13	DPWA
0.095 \pm 0.002	WORKMAN	12A	DPWA
••• We do not use the following data for averages, fits, limits, etc. •••			
0.110 \pm 0.045	ANISOVICH	12A	DPWA
0.057 \pm 0.003	¹ SHRESTHA	12A	DPWA
0.073	DRECHSEL	07	DPWA
0.097 \pm 0.003	DUGGER	07	DPWA
-0.053	PENNER	02D	DPWA

¹ Statistical error only. **$N(1720) \rightarrow p\gamma$, helicity-3/2 amplitude $A_{3/2}$**

VALUE ($\text{GeV}^{-1/2}$)	DOCUMENT ID	TECN	COMMENT
-0.034 \pm 0.0076	GOLOVATCH	19	DPWA
0.028 \pm 0.003	¹ HUNT	19	DPWA
0.135 \pm 0.040	SOKHOYAN	15A	DPWA
0.035 \pm 0.002	¹ SHKLYAR	13	DPWA
-0.048 \pm 0.002	WORKMAN	12A	DPWA
••• We do not use the following data for averages, fits, limits, etc. •••			
0.150 \pm 0.030	ANISOVICH	12A	DPWA
-0.019 \pm 0.002	¹ SHRESTHA	12A	DPWA
-0.011	DRECHSEL	07	DPWA
-0.039 \pm 0.003	DUGGER	07	DPWA
0.027	PENNER	02D	DPWA

¹ Statistical error only. **$N(1720) \rightarrow n\gamma$, helicity-1/2 amplitude $A_{1/2}$**

VALUE ($\text{GeV}^{-1/2}$)	DOCUMENT ID	TECN	COMMENT
-0.064 \pm 0.006	¹ HUNT	19	DPWA
-0.080 \pm 0.050	ANISOVICH	13B	DPWA
••• We do not use the following data for averages, fits, limits, etc. •••			
-0.002 \pm 0.001	¹ SHRESTHA	12A	DPWA
-0.003	DRECHSEL	07	DPWA
-0.004	PENNER	02D	DPWA

¹ Statistical error only. **$N(1720) \rightarrow n\gamma$, helicity-3/2 amplitude $A_{3/2}$**

VALUE ($\text{GeV}^{-1/2}$)	DOCUMENT ID	TECN	COMMENT
-0.004 \pm 0.006	¹ HUNT	19	DPWA
-0.140 \pm 0.065	ANISOVICH	13B	DPWA

••• We do not use the following data for averages, fits, limits, etc. •••
 -0.001 ± 0.002 ¹ SHRESTHA 12A DPWA Multichannel
 -0.031 DRECHSEL 07 DPWA $\gamma N \rightarrow \pi N$
 0.003 PENNER 02D DPWA Multichannel
¹ Statistical error only.

N(1720) REFERENCES

For early references, see Physics Letters **111B 1** (1982).

MOKEEV 20	PL B805 135457	V. I. Mokeev <i>et al.</i>	(CLAS Collab.)
MUELLER 20	PL B803 135323	J. Mueller <i>et al.</i>	(CBELSA/TAPS Collab.)
GOLOVATCH 19	PR B788 371	E. Golovatch <i>et al.</i>	(CLAS Collab.)
HUNT 19	PR C9 05205	B. C. Hunt, D.M. Manley	
DENISENKO 16	PL B755 97	I. Denisenko <i>et al.</i>	
ROENCHEN 15A	EPJ A51 70	D. Roenchen <i>et al.</i>	
SOKHOYAN 15A	EPJ A51 95	V. Sokhoyan <i>et al.</i>	(CBELSA/TAPS Collab.)
PDG 14	CP C38 070001	K. Olive <i>et al.</i>	(PDG Collab.)
ROENCHEN 14	EPJ A50 101	D. Roenchen <i>et al.</i>	
Also	EPJ A51 63 (errata.)	D. Roenchen <i>et al.</i>	
SVARC 14	PR C89 045205	A. Svarc <i>et al.</i>	(RBI Zagreb, UNI Tuzla)
ANISOVICH 13B	EPJ A49 67	A.V. Anisovich <i>et al.</i>	(GIES)
SHKLYAR 13	PR C87 015201	V. Shklyar, H. Lenske, U. Mosel	(GIES)
ANISOVICH 12A	EPJ A48 15	A.V. Anisovich <i>et al.</i>	(BONN, PNPI)
SHRESTHA 12A	PR C86 055203	M. Shrestha, D.M. Manley	(KSU)
WORKMAN 12A	PR C86 015202	R. Workman <i>et al.</i>	(GWU)
BATINIC 10	PR C82 038203	M. Batinic <i>et al.</i>	(ZAGR)
THOMA 08	PL B659 87	U. Thoma <i>et al.</i>	(CB-ELSA Collab.)
DRECHSEL 07	EPJ A34 69	D. Drechsel, S.S. Kamalov, L. Tiator	(MAIN Z, JINR)
DUGGER 07	PR C76 025211	M. Dugger <i>et al.</i>	(JLab CLAS Collab.)
ARNDT 06	PR C74 045205	R.A. Arndt <i>et al.</i>	(GWU)
SHKLYAR 05	PR C72 015210	V. Shklyar, H. Lenske, U. Mosel	(GIES)
PENNER 02C	PR C66 055211	G. Penner, U. Mosel	(GIES)
PENNER 02D	PR C66 055212	G. Penner, U. Mosel	(GIES)
VRANA 00	PRPL 328 181	T. P. Vrana, S.A. Dytman, T.-S.H. Lee	(PITT, ANL)
HOEHLER 93	πN Newsletter 9 1	G. Hohlner	(KARL)
CUTKOSKY 80	Toronto Conf. 19	R.E. Cutkosky <i>et al.</i>	(CMU, LBL) IJP
Also	PR D20 2839	R.E. Cutkosky <i>et al.</i>	(CMU, LBL) IJP
HOEHLER 79	PDAT 12-1	G. Hohlner <i>et al.</i>	(KARLT) IJP
Also	Toronto Conf. 3	R. Koch	(KARLT) IJP

N(1860) 5/2⁺ $I(J^P) = \frac{1}{2}(\frac{5}{2}^+)$ Status: * *
 OMITTED FROM SUMMARY TABLE

Before the 2012 Review, all the evidence for a $J^P = 5/2^+$ state with a mass above 1800 MeV was filed under a two-star N(2000). There is now some evidence from ANISOVICH 12A for two $5/2^+$ states in this region, so we have split the older data (according to mass) between two two-star $5/2^+$ states, an N(1860) and an N(2000).

N(1860) POLE POSITION

REAL PART

VALUE (MeV)	DOCUMENT ID	TECN	COMMENT
1834 ± 19 ± 6	¹ SVARC 14	L+P	$\pi N \rightarrow \pi N$
1830 ± 120 - 60	ANISOVICH 12A	DPWA	Multichannel
••• We do not use the following data for averages, fits, limits, etc. •••			
1871	HUNT 19	DPWA	Multichannel
1807	ARNDT 06	DPWA	$\pi N \rightarrow \pi N, \eta N$

¹ Fit to the amplitudes of HOEHLER 79.

-2xIMAGINARY PART

VALUE (MeV)	DOCUMENT ID	TECN	COMMENT
122 ± 34 ± 7	² SVARC 14	L+P	$\pi N \rightarrow \pi N$
250 ± 150 - 50	ANISOVICH 12A	DPWA	Multichannel
••• We do not use the following data for averages, fits, limits, etc. •••			
337	HUNT 19	DPWA	Multichannel
109	ARNDT 06	DPWA	$\pi N \rightarrow \pi N, \eta N$

² Fit to the amplitudes of HOEHLER 79.

N(1860) ELASTIC POLE RESIDUE

MODULUS |r|

VALUE (MeV)	DOCUMENT ID	TECN	COMMENT
4 ± 1 ± 1	³ SVARC 14	L+P	$\pi N \rightarrow \pi N$
50 ± 20	ANISOVICH 12A	DPWA	Multichannel
••• We do not use the following data for averages, fits, limits, etc. •••			
60	ARNDT 06	DPWA	$\pi N \rightarrow \pi N, \eta N$

³ Fit to the amplitudes of HOEHLER 79.

PHASE θ

VALUE (°)	DOCUMENT ID	TECN	COMMENT
-39 ± 18 ± 9	⁴ SVARC 14	L+P	$\pi N \rightarrow \pi N$
-80 ± 40	ANISOVICH 12A	DPWA	Multichannel
••• We do not use the following data for averages, fits, limits, etc. •••			
-67	ARNDT 06	DPWA	$\pi N \rightarrow \pi N, \eta N$

⁴ Fit to the amplitudes of HOEHLER 79.

N(1860) BREIT-WIGNER MASS

VALUE (MeV)	DOCUMENT ID	TECN	COMMENT
1928 ± 21	⁵ HUNT 19	DPWA	Multichannel
1860 ± 120 - 60	ANISOVICH 12A	DPWA	Multichannel
1882 ± 10	HOEHLER 79	IPWA	$\pi N \rightarrow \pi N$
••• We do not use the following data for averages, fits, limits, etc. •••			
1900 ± 7	⁵ SHRESTHA 12A	DPWA	Multichannel
1817.7	ARNDT 06	DPWA	$\pi N \rightarrow \pi N, \eta N$

⁵ Statistical error only.

N(1860) BREIT-WIGNER WIDTH

VALUE (MeV)	DOCUMENT ID	TECN	COMMENT
376 ± 58	⁶ HUNT 19	DPWA	Multichannel
270 ± 140 - 50	ANISOVICH 12A	DPWA	Multichannel
95 ± 20	HOEHLER 79	IPWA	$\pi N \rightarrow \pi N$
••• We do not use the following data for averages, fits, limits, etc. •••			
219 ± 23	⁶ SHRESTHA 12A	DPWA	Multichannel
117.6	ARNDT 06	DPWA	$\pi N \rightarrow \pi N, \eta N$

⁶ Statistical error only.

N(1860) DECAY MODES

Mode	Fraction (Γ_i/Γ)
Γ_1 $N\pi$	4-20 %
Γ_2 $N\eta$	0-6 %
Γ_3 ΛK	<0.01 %
Γ_4 $N\pi\pi$	>61 %
Γ_5 $\Delta\pi$	20-54 %
Γ_6 $\Delta\pi, P$ -wave	4-16 %
Γ_7 $\Delta\pi, F$ -wave	16-38 %
Γ_8 $N\rho$	<8.6 %
Γ_9 $N\rho, S=3/2, P$ -wave	<8.5 %
Γ_{10} $N\rho, S=3/2, F$ -wave	<0.1 %
Γ_{11} $N\sigma$	41-61 %
Γ_{12} $p\gamma$	seen
Γ_{13} $p\gamma, \text{helicity}=1/2$	seen
Γ_{14} $p\gamma, \text{helicity}=3/2$	seen
Γ_{15} $n\gamma$	0.0017-0.062 %
Γ_{16} $n\gamma, \text{helicity}=1/2$	0.0003-0.019 %
Γ_{17} $n\gamma, \text{helicity}=3/2$	0.0014-0.043 %

N(1860) BRANCHING RATIOS

$\Gamma(N\pi)/\Gamma_{\text{total}}$	DOCUMENT ID	TECN	COMMENT	Γ_1/Γ
4-20 % OUR ESTIMATE				
8.0 ± 0.1	⁷ HUNT 19	DPWA	Multichannel	
20 ± 6	ANISOVICH 12A	DPWA	Multichannel	
4 ± 2	HOEHLER 79	IPWA	$\pi N \rightarrow \pi N$	
••• We do not use the following data for averages, fits, limits, etc. •••				
17 ± 1	⁷ SHRESTHA 12A	DPWA	Multichannel	
12.7	ARNDT 06	DPWA	$\pi N \rightarrow \pi N, \eta N$	

⁷ Statistical error only.

$\Gamma(N\eta)/\Gamma_{\text{total}}$	DOCUMENT ID	TECN	COMMENT	Γ_2/Γ
0-6 % OUR ESTIMATE				
0.11 ± 0.09	⁸ HUNT 19	DPWA	Multichannel	
••• We do not use the following data for averages, fits, limits, etc. •••				
4 ± 2	⁸ SHRESTHA 12A	DPWA	Multichannel	

⁸ Statistical error only.

$\Gamma(\Lambda K)/\Gamma_{\text{total}}$	DOCUMENT ID	TECN	COMMENT	Γ_3/Γ
<0.01 % OUR ESTIMATE				
<0.01	⁹ HUNT 19	DPWA	Multichannel	

⁹ Statistical error only.

$\Gamma(\Delta\pi, P\text{-wave})/\Gamma_{\text{total}}$	DOCUMENT ID	TECN	COMMENT	Γ_6/Γ
4-16 % OUR ESTIMATE				
10 ± 6	¹⁰ HUNT 19	DPWA	Multichannel	

¹⁰ Statistical error only.

$\Gamma(\Delta\pi, F\text{-wave})/\Gamma_{\text{total}}$	DOCUMENT ID	TECN	COMMENT	Γ_7/Γ
16-38 % OUR ESTIMATE				
27 ± 11	¹¹ HUNT 19	DPWA	Multichannel	

¹¹ Statistical error only.

Baryon Particle Listings

$N(1860)$, $N(1875)$

$\Gamma(N\rho, S=3/2, P\text{-wave})/\Gamma_{\text{total}}$ Γ_9/Γ

VALUE (%)	DOCUMENT ID	TECN	COMMENT
<8.5 % OUR ESTIMATE			
<8.5	12 HUNT	19	DPWA Multichannel
12			Statistical error only.

$\Gamma(N\rho, S=3/2, F\text{-wave})/\Gamma_{\text{total}}$ Γ_{10}/Γ

VALUE (%)	DOCUMENT ID	TECN	COMMENT
<0.1 % OUR ESTIMATE			
<0.1	13 HUNT	19	DPWA Multichannel
13			Statistical error only.

$\Gamma(N\sigma)/\Gamma_{\text{total}}$ Γ_{11}/Γ

VALUE (%)	DOCUMENT ID	TECN	COMMENT
41-61 % OUR ESTIMATE			
51 ± 10	14 HUNT	19	DPWA Multichannel
• • • We do not use the following data for averages, fits, limits, etc. • • •			
41 ± 6	14 SHRESTHA	12A	DPWA Multichannel
14			Statistical error only.

$N(1860)$ BREIT-WIGNER PHOTON DECAY AMPLITUDES

$N(1860) \rightarrow \rho\gamma$, helicity-1/2 amplitude $A_{1/2}$

VALUE (GeV ^{-1/2})	DOCUMENT ID	TECN	COMMENT
-0.022 ± 0.020	15 HUNT	19	DPWA Multichannel
• • • We do not use the following data for averages, fits, limits, etc. • • •			
-0.017 ± 0.003	15 SHRESTHA	12A	DPWA Multichannel
15			Statistical error only.

$N(1860) \rightarrow \rho\gamma$, helicity-3/2 amplitude $A_{3/2}$

VALUE	DOCUMENT ID	TECN	COMMENT
-0.032 ± 0.034	16 HUNT	19	DPWA Multichannel
• • • We do not use the following data for averages, fits, limits, etc. • • •			
0.029 ± 0.004	16 SHRESTHA	12A	DPWA Multichannel
16			Statistical error only.

$N(1860) \rightarrow n\gamma$, helicity-1/2 amplitude $A_{1/2}$

VALUE (GeV ^{-1/2})	DOCUMENT ID	TECN	COMMENT
0.021 ± 0.029	17 HUNT	19	DPWA Multichannel
0.021 ± 0.013	ANISOVICH	13B	DPWA Multichannel
• • • We do not use the following data for averages, fits, limits, etc. • • •			
0.010 ± 0.005	17 SHRESTHA	12A	DPWA Multichannel
17			Statistical error only.

$N(1860) \rightarrow n\gamma$, helicity-3/2 amplitude $A_{3/2}$

VALUE (GeV ^{-1/2})	DOCUMENT ID	TECN	COMMENT
0.070 ± 0.035	18 HUNT	19	DPWA Multichannel
0.034 ± 0.017	ANISOVICH	13B	DPWA Multichannel
• • • We do not use the following data for averages, fits, limits, etc. • • •			
-0.009 ± 0.005	18 SHRESTHA	12A	DPWA Multichannel
18			Statistical error only.

$N(1860)$ REFERENCES

HUNT	19	PR C99 055205	B.C. Hunt, D.M. Manley	
SVARC	14	PR C89 045205	A. Svarc et al.	(RBI Zagreb, UNI Tuzla)
ANISOVICH	13B	EPJ A49 67	A.V. Anisovich et al.	
ANISOVICH	12A	EPJ A48 15	A.V. Anisovich et al.	(BONN, PNPI)
SHRESTHA	12A	PR C86 055203	M. Shrestha, D.M. Manley	(KSU)
ARNDT	06	PR C74 045205	R.A. Arndt et al.	(GWU)
HOEHLER	79	PDAT 12-1	G. Hoehler et al.	(KARLT)

$N(1875) 3/2^-$

$I(J^P) = \frac{1}{2}(3/2^-)$ Status: * * *

Before the 2012 Review, all the evidence for a $J^P = 3/2^-$ state with a mass above 1800 MeV was filed under a two-star $N(2080)$. There is now evidence from ANISOVICH 12A for two $3/2^-$ states in this region, so we have split the older data (according to mass) between a three-star $N(1875)$ and a two-star $N(2120)$.

$N(1875)$ POLE POSITION

REAL PART

VALUE (MeV)	DOCUMENT ID	TECN	COMMENT
1850 to 1950 (≈ 1900) OUR ESTIMATE			
1870 ± 20	SOKHOYAN	15A	DPWA Multichannel
1880 ± 100	CUTKOSKY	80	IPWA $\pi N \rightarrow \pi N$ (lower m)
• • • We do not use the following data for averages, fits, limits, etc. • • •			
1993	HUNT	19	DPWA Multichannel
1810	SHKLYAR	13	DPWA Multichannel
1860 ± 25	ANISOVICH	12A	DPWA Multichannel
1957 ± 49	BATINIC	10	DPWA $\pi N \rightarrow N\pi, N\eta$
1824	VRANA	00	DPWA Multichannel

-2xIMAGINARY PART

VALUE (MeV)	DOCUMENT ID	TECN	COMMENT
100 to 220 (≈ 160) OUR ESTIMATE			
200 ± 15	SOKHOYAN	15A	DPWA Multichannel
160 ± 80	CUTKOSKY	80	IPWA $\pi N \rightarrow \pi N$ (lower m)
• • • We do not use the following data for averages, fits, limits, etc. • • •			
319	HUNT	19	DPWA Multichannel
98	SHKLYAR	13	DPWA Multichannel
200 ± 20	ANISOVICH	12A	DPWA Multichannel
467 ± 106	BATINIC	10	DPWA $\pi N \rightarrow N\pi, N\eta$
614	VRANA	00	DPWA Multichannel

$N(1875)$ ELASTIC POLE RESIDUE

MODULUS $|r|$

VALUE (MeV)	DOCUMENT ID	TECN	COMMENT
3 to 12 (≈ 10) OUR ESTIMATE			
3 ± 1.5	SOKHOYAN	15A	DPWA Multichannel
10 ± 5	CUTKOSKY	80	IPWA $\pi N \rightarrow \pi N$ (lower m)
• • • We do not use the following data for averages, fits, limits, etc. • • •			
3	SHKLYAR	13	DPWA Multichannel
2.5 ± 1.0	ANISOVICH	12A	DPWA Multichannel
53	BATINIC	10	DPWA $\pi N \rightarrow N\pi, N\eta$

PHASE θ

VALUE (°)	DOCUMENT ID	TECN	COMMENT
50 to 200 (≈ 100) OUR ESTIMATE			
160 ± 50	SOKHOYAN	15A	DPWA Multichannel
100 ± 80	CUTKOSKY	80	IPWA $\pi N \rightarrow \pi N$ (lower m)
• • • We do not use the following data for averages, fits, limits, etc. • • •			
-76	SHKLYAR	13	DPWA Multichannel
-65	BATINIC	10	DPWA $\pi N \rightarrow N\pi, N\eta$

$N(1875)$ INELASTIC POLE RESIDUE

The "normalized residue" is the residue divided by $\Gamma_{\text{pole}}/2$.

Normalized residue in $N\pi \rightarrow N(1875) \rightarrow \Lambda K$

MODULUS	PHASE (°)	DOCUMENT ID	TECN	COMMENT
0.015 ± 0.005		ANISOVICH	12A	DPWA Multichannel

Normalized residue in $N\pi \rightarrow N(1875) \rightarrow \Sigma K$

MODULUS	PHASE (°)	DOCUMENT ID	TECN	COMMENT
0.04 ± 0.02		ANISOVICH	12A	DPWA Multichannel

Normalized residue in $N\pi \rightarrow N(1875) \rightarrow N\sigma$

MODULUS	PHASE (°)	DOCUMENT ID	TECN	COMMENT
0.09 ± 0.03	-175 ± 45	SOKHOYAN	15A	DPWA Multichannel
• • • We do not use the following data for averages, fits, limits, etc. • • •				
0.08 ± 0.03	-170 ± 65	ANISOVICH	12A	DPWA Multichannel

Normalized residue in $N\pi \rightarrow N(1875) \rightarrow \Delta(1232)\pi, S\text{-wave}$

MODULUS	PHASE (°)	DOCUMENT ID	TECN	COMMENT
0.05 ± 0.03	undefined	SOKHOYAN	15A	DPWA Multichannel

Normalized residue in $N\pi \rightarrow N(1875) \rightarrow \Delta(1232)\pi, D\text{-wave}$

MODULUS	PHASE (°)	DOCUMENT ID	TECN	COMMENT
0.04 ± 0.02	undefined	SOKHOYAN	15A	DPWA Multichannel

Normalized residue in $N\pi \rightarrow N(1875) \rightarrow N(1440)\pi$

MODULUS	PHASE (°)	DOCUMENT ID	TECN	COMMENT
0.03 ± 0.02	undefined	SOKHOYAN	15A	DPWA Multichannel

$N(1875)$ BREIT-WIGNER MASS

VALUE (MeV)	DOCUMENT ID	TECN	COMMENT
1850 to 1920 (≈ 1875) OUR ESTIMATE			
2005 ± 12	¹ HUNT	19	DPWA Multichannel
1875 ± 20	SOKHOYAN	15A	DPWA Multichannel
1934 ± 10	¹ SHKLYAR	13	DPWA Multichannel
1880 ± 100	CUTKOSKY	80	IPWA $\pi N \rightarrow \pi N$
• • • We do not use the following data for averages, fits, limits, etc. • • •			
1880 ± 20	ANISOVICH	12A	DPWA Multichannel
1951 ± 27	¹ SHRESTHA	12A	DPWA Multichannel
2048 ± 65	BATINIC	10	DPWA $\pi N \rightarrow N\pi, N\eta$
1946 ± 1	PENNER	02C	DPWA Multichannel
1895	MART	00	DPWA $\gamma p \rightarrow \Lambda K^+$
2003 ± 18	VRANA	00	DPWA Multichannel
¹ Statistical error only.			

$N(1875)$ BREIT-WIGNER WIDTH

VALUE (MeV)	DOCUMENT ID	TECN	COMMENT
120 to 250 (≈ 200) OUR ESTIMATE			
321 ± 21	¹ HUNT	19	DPWA Multichannel
200 ± 25	SOKHOYAN	15A	DPWA Multichannel
857 ± 100	¹ SHKLYAR	13	DPWA Multichannel
180 ± 60	CUTKOSKY	80	IPWA $\pi N \rightarrow \pi N$ (lower m)

••• We do not use the following data for averages, fits, limits, etc. •••
 200 ± 25 ANISOVICH 12A DPWA Multichannel
 500 ± 45 ¹ SHRESTHA 12A DPWA Multichannel
 529 ± 128 BATINIC 10 DPWA $\pi N \rightarrow N\pi, N\eta$
 859 ± 7 PENNER 02c DPWA Multichannel
 372 MART 00 DPWA $\gamma p \rightarrow \Lambda K^+$
 1070 ± 858 VRANA 00 DPWA Multichannel
¹ Statistical error only.

N(1875) DECAY MODES

Mode	Fraction (Γ_i/Γ)
Γ_1 $N\pi$	3–11 %
Γ_2 $N\eta$	3–16 %
Γ_3 $N\omega$	15–25 %
Γ_4 ΛK	1–2 %
Γ_5 ΣK	0.3–1.1 %
Γ_6 $N\pi\pi$	>56 %
Γ_7 $\Delta(1232)\pi$	4–44 %
Γ_8 $\Delta(1232)\pi, S\text{-wave}$	2–21 %
Γ_9 $\Delta(1232)\pi, D\text{-wave}$	2–23 %
Γ_{10} $N\rho, S=3/2, S\text{-wave}$	36–56 %
Γ_{11} $N\sigma$	16–60 %
Γ_{12} $N(1440)\pi$	2–8 %
Γ_{13} $N(1520)\pi$	<2 %
Γ_{14} $\Lambda K^*(892)$	<0.2 %
Γ_{15} $p\gamma$	0.001–0.025 %
Γ_{16} $p\gamma, \text{helicity}=1/2$	0.001–0.021 %
Γ_{17} $p\gamma, \text{helicity}=3/2$	<0.003 %
Γ_{18} $n\gamma$	<0.040 %
Γ_{19} $n\gamma, \text{helicity}=1/2$	<0.007 %
Γ_{20} $n\gamma, \text{helicity}=3/2$	<0.033 %

N(1875) BRANCHING RATIOS

$\Gamma(N\pi)/\Gamma_{\text{total}}$	DOCUMENT ID	TECN	COMMENT	Γ_1/Γ
3 to 11 (≈ 7) OUR ESTIMATE				
7.5 ± 0.1	¹ HUNT	19	DPWA Multichannel	
4 ± 2	SOKHOYAN	15A	DPWA Multichannel	
11 ± 1	¹ SHKLYAR	13	DPWA Multichannel	
10 ± 4	CUTKOSKY	80	IPWA $\pi N \rightarrow \pi N$ (lower m)	
••• We do not use the following data for averages, fits, limits, etc. •••				
3 ± 2	ANISOVICH	12A	DPWA Multichannel	
7 ± 2	¹ SHRESTHA	12A	DPWA Multichannel	
17 ± 7	BATINIC	10	DPWA $\pi N \rightarrow N\pi, N\eta$	
12 ± 2	PENNER	02c	DPWA Multichannel	
13 ± 3	VRANA	00	DPWA Multichannel	

¹ Statistical error only.

$\Gamma(N\eta)/\Gamma_{\text{total}}$	DOCUMENT ID	TECN	COMMENT	Γ_2/Γ
3–16 % OUR ESTIMATE				
10 ± 6	MUELLER	20	DPWA Multichannel	
3.3 ± 0.8	¹ HUNT	19	DPWA Multichannel	
< 1	SHKLYAR	13	DPWA Multichannel	
••• We do not use the following data for averages, fits, limits, etc. •••				
8 ± 3	BATINIC	10	DPWA $\pi N \rightarrow N\pi, N\eta$	
7 ± 2	PENNER	02c	DPWA Multichannel	
0 ± 2	VRANA	00	DPWA Multichannel	

¹ Statistical error only.

$\Gamma(N\omega)/\Gamma_{\text{total}}$	DOCUMENT ID	TECN	COMMENT	Γ_3/Γ
1–2 % OUR ESTIMATE				
13 ± 7	DENISENKO	16	DPWA Multichannel	
20 ± 5	¹ SHKLYAR	13	DPWA Multichannel	
••• We do not use the following data for averages, fits, limits, etc. •••				
21 ± 7	PENNER	02c	DPWA Multichannel	

¹ Statistical error only.

$\Gamma(\Lambda K)/\Gamma_{\text{total}}$	DOCUMENT ID	TECN	COMMENT	Γ_4/Γ
1–2 % OUR ESTIMATE				
1.1 ± 0.4	¹ HUNT	19	DPWA Multichannel	
••• We do not use the following data for averages, fits, limits, etc. •••				
0.2 ± 0.2	PENNER	02c	DPWA Multichannel	

¹ Statistical error only.

$\Gamma(\Sigma K)/\Gamma_{\text{total}}$	DOCUMENT ID	TECN	COMMENT	Γ_5/Γ
0.3–1.1 % OUR ESTIMATE				
0.7 ± 0.4	PENNER	02c	DPWA Multichannel	

$\Gamma(\Delta(1232)\pi, S\text{-wave})/\Gamma_{\text{total}}$	DOCUMENT ID	TECN	COMMENT	Γ_8/Γ
2–21 % OUR ESTIMATE				
< 2	¹ HUNT	19	DPWA Multichannel	
14 ± 7	SOKHOYAN	15A	DPWA Multichannel	

••• We do not use the following data for averages, fits, limits, etc. •••
 87 ± 3 ¹ SHRESTHA 12A DPWA Multichannel
 40 ± 10 VRANA 00 DPWA Multichannel
¹ Statistical error only.

$\Gamma(\Delta(1232)\pi, D\text{-wave})/\Gamma_{\text{total}}$	DOCUMENT ID	TECN	COMMENT	Γ_9/Γ
2–23 % OUR ESTIMATE				
17 ± 6	¹ HUNT	19	DPWA Multichannel	
7 ± 5	SOKHOYAN	15A	DPWA Multichannel	

••• We do not use the following data for averages, fits, limits, etc. •••
 < 6 ¹ SHRESTHA 12A DPWA Multichannel
 17 ± 10 VRANA 00 DPWA Multichannel
¹ Statistical error only.

$\Gamma(N\rho, S=3/2, S\text{-wave})/\Gamma_{\text{total}}$	DOCUMENT ID	TECN	COMMENT	Γ_{10}/Γ
36–56 % OUR ESTIMATE				
46 ± 10	¹ HUNT	19	DPWA Multichannel	

••• We do not use the following data for averages, fits, limits, etc. •••
 < 5 ¹ SHRESTHA 12A DPWA Multichannel
 6 ± 6 VRANA 00 DPWA Multichannel
¹ Statistical error only.

$\Gamma(N\sigma)/\Gamma_{\text{total}}$	DOCUMENT ID	TECN	COMMENT	Γ_{11}/Γ
16–60 % OUR ESTIMATE				
24.3 ± 8.6	¹ HUNT	19	DPWA Multichannel	
45 ± 15	SOKHOYAN	15A	DPWA Multichannel	

••• We do not use the following data for averages, fits, limits, etc. •••
 < 4 ¹ SHRESTHA 12A DPWA Multichannel
 24 ± 24 VRANA 00 DPWA Multichannel
¹ Statistical error only.

$\Gamma(N(1440)\pi)/\Gamma_{\text{total}}$	DOCUMENT ID	TECN	COMMENT	Γ_{12}/Γ
16–60 % OUR ESTIMATE				
5 ± 3	SOKHOYAN	15A	DPWA Multichannel	

$\Gamma(N(1520)\pi)/\Gamma_{\text{total}}$	DOCUMENT ID	TECN	COMMENT	Γ_{13}/Γ
16–60 % OUR ESTIMATE				
< 2	SOKHOYAN	15A	DPWA Multichannel	

$\Gamma(\Lambda K^*(892))/\Gamma_{\text{total}}$	DOCUMENT ID	TECN	COMMENT	Γ_{14}/Γ
< 0.2 % OUR ESTIMATE				
< 0.2	ANISOVICH	17B	DPWA Multichannel	

N(1875) PHOTON DECAY AMPLITUDES AT THE POLE

N(1875) → pγ, helicity-1/2 amplitude A_{1/2}

MODULUS (GeV ^{-1/2})	PHASE (°)	DOCUMENT ID	TECN	COMMENT
0.017 ± 0.009	–110 ± 40	SOKHOYAN	15A	DPWA Multichannel

N(1875) → pγ, helicity-3/2 amplitude A_{3/2}

MODULUS (GeV ^{-1/2})	PHASE (°)	DOCUMENT ID	TECN	COMMENT
0.008 ± 0.004	180 ± 40	SOKHOYAN	15A	DPWA Multichannel

N(1875) BREIT-WIGNER PHOTON DECAY AMPLITUDES

N(1875) → pγ, helicity-1/2 amplitude A_{1/2}

VALUE (GeV ^{-1/2})	DOCUMENT ID	TECN	COMMENT
0.010 to 0.025 (≈ 0.015) OUR ESTIMATE			
–0.013 ± 0.008	¹ HUNT	19	DPWA Multichannel
0.011 ± 0.001	¹ SHKLYAR	13	DPWA Multichannel
0.018 ± 0.010	ANISOVICH	12A	DPWA Multichannel
••• We do not use the following data for averages, fits, limits, etc. •••			
0.007 ± 0.008	¹ SHRESTHA	12A	DPWA Multichannel
0.012	PENNER	02D	DPWA Multichannel

¹ Statistical error only.

Baryon Particle Listings

$N(1875)$, $N(1880)$

$N(1875) \rightarrow p\gamma$, helicity-3/2 amplitude $A_{3/2}$

VALUE (GeV ^{-1/2})	DOCUMENT ID	TECN	COMMENT
-0.010 to 0.025 (≈ -0.005) OUR ESTIMATE			
-0.093 ± 0.009	¹ HUNT	19	DPWA Multichannel
-0.007 ± 0.004	SOKHOYAN	15A	DPWA Multichannel
0.026 ± 0.001	¹ SHKLYAR	13	DPWA Multichannel
••• We do not use the following data for averages, fits, limits, etc. •••			
-0.009 ± 0.005	ANISOVICH	12A	DPWA Multichannel
0.043 ± 0.022	¹ SHRESTHA	12A	DPWA Multichannel
-0.010	PENNER	02D	DPWA Multichannel

¹ Statistical error only.

$N(1875) \rightarrow n\gamma$, helicity-1/2 amplitude $A_{1/2}$

VALUE (GeV ^{-1/2})	DOCUMENT ID	TECN	COMMENT
0.050 ± 0.009	¹ HUNT	19	DPWA Multichannel
0.010 ± 0.006	ANISOVICH	13B	DPWA Multichannel
••• We do not use the following data for averages, fits, limits, etc. •••			
0.055 ± 0.021	¹ SHRESTHA	12A	DPWA Multichannel
0.023	PENNER	02D	DPWA Multichannel

¹ Statistical error only.

$N(1875) \rightarrow n\gamma$, helicity-3/2 amplitude $A_{3/2}$

VALUE (GeV ^{-1/2})	DOCUMENT ID	TECN	COMMENT
0.141 ± 0.022	¹ HUNT	19	DPWA Multichannel
-0.020 ± 0.015	ANISOVICH	13B	DPWA Multichannel
••• We do not use the following data for averages, fits, limits, etc. •••			
-0.085 ± 0.031	¹ SHRESTHA	12A	DPWA Multichannel
-0.009	PENNER	02D	DPWA Multichannel

¹ Statistical error only.

$N(1875)$ REFERENCES

For early references, see Physics Letters **111B** 1 (1982).

MUELLER	20	PL B803 135323	J. Mueller et al.	(CBELSA/TAPS Collab.)
HUNT	19	PR C99 055205	B. C. Hunt, D.M. Manley	
ANISOVICH	17B	PL B771 142	A.V. Anisovich et al.	
DENISENKO	16	PL B755 97	I. Denisenko et al.	
SOKHOYAN	15A	EPJ A51 95	V. Sokhoyan et al.	(CBELSA/TAPS Collab.)
ANISOVICH	13B	EPJ A49 67	A.V. Anisovich et al.	
SHKLYAR	13	PR C87 015201	V. Shklyar, H. Lenske, U. Mosel	(GIES)
ANISOVICH	12A	EPJ A48 15	A.V. Anisovich et al.	(BONN, PNPI)
SHRESTHA	12A	PR C86 055203	M. Shrestha, D.M. Manley	(KSU)
BATINIC	10	PR C82 038203	M. Batinic et al.	(ZAGR)
PENNER	02C	PR C66 055211	G. Penner, U. Mosel	(GIES)
PENNER	02D	PR C66 055212	G. Penner, U. Mosel	(GIES)
MART	00	PR C61 012201	T. Mart, C. Beanhold	
VRANA	00	PRPL 328 181	T.P. Vrana, S.A. Dytman, T.-S.H. Lee	(PITT, ANL)
CUTKOSKY	80	Toronto Conf. 19	R.E. Cutkosky et al.	(CMU, LBL) JJP
		Also PR D20 2839	R.E. Cutkosky et al.	(CMU, LBL) JJP

$N(1880) 1/2^+$

 $I(J^P) = \frac{1}{2}(\frac{1}{2}^+)$ Status: ***

$N(1880)$ POLE POSITION

REAL PART

VALUE (MeV)	DOCUMENT ID	TECN	COMMENT
1820 to 1900 (≈ 1860) OUR ESTIMATE			
1860 ± 40	ANISOVICH	17A	DPWA Multichannel
••• We do not use the following data for averages, fits, limits, etc. •••			
1880	HUNT	19	DPWA Multichannel
1875 ± 11	¹ ANISOVICH	17A	L+P $\gamma p, \pi^- p \rightarrow K\Lambda$
1870 ± 40	SOKHOYAN	15A	DPWA Multichannel
1870 ± 40	GUTZ	14	DPWA Multichannel
1860 ± 35	ANISOVICH	12A	DPWA Multichannel

¹ Statistical error only.

-2×IMAGINARY PART

VALUE (MeV)	DOCUMENT ID	TECN	COMMENT
180 to 280 (≈ 230) OUR ESTIMATE			
230 ± 50	ANISOVICH	17A	DPWA Multichannel
••• We do not use the following data for averages, fits, limits, etc. •••			
429	HUNT	19	DPWA Multichannel
33 ± 9	² ANISOVICH	17A	L+P $\gamma p, \pi^- p \rightarrow K\Lambda$
220 ± 50	SOKHOYAN	15A	DPWA Multichannel
220 ± 50	GUTZ	14	DPWA Multichannel
250 ± 70	ANISOVICH	12A	DPWA Multichannel

² Statistical error only.

$N(1880)$ ELASTIC POLE RESIDUE

MODULUS |r|

VALUE (MeV)	DOCUMENT ID	TECN	COMMENT
6 ± 4	SOKHOYAN	15A	DPWA Multichannel
••• We do not use the following data for averages, fits, limits, etc. •••			
6 ± 4	GUTZ	14	DPWA Multichannel
6 ± 4	ANISOVICH	12A	DPWA Multichannel

PHASE θ

VALUE (°)	DOCUMENT ID	TECN	COMMENT
70 ± 60	SOKHOYAN	15A	DPWA Multichannel
••• We do not use the following data for averages, fits, limits, etc. •••			
70 ± 60	GUTZ	14	DPWA Multichannel
80 ± 65	ANISOVICH	12A	DPWA Multichannel

$N(1880)$ INELASTIC POLE RESIDUE

The "normalized residue" is the residue divided by $\Gamma_{pole}/2$.

Normalized residue in $N\pi \rightarrow N(1880) \rightarrow N\eta$

MODULUS	PHASE (°)	DOCUMENT ID	TECN	COMMENT
0.11 ± 0.07	-75 ± 55	ANISOVICH	12A	DPWA Multichannel

Normalized residue in $N\pi \rightarrow N(1880) \rightarrow \Lambda K$

MODULUS	PHASE (°)	DOCUMENT ID	TECN	COMMENT
0.05 ± 0.02	27 ± 30	ANISOVICH	17A	DPWA $\gamma p, \pi^- p \rightarrow K\Lambda$
••• We do not use the following data for averages, fits, limits, etc. •••				
0.3 ± 0.1	82 ± 9	³ ANISOVICH	17A	L+P $\gamma p, \pi^- p \rightarrow K\Lambda$
0.03 ± 0.02	40 ± 40	ANISOVICH	12A	DPWA Multichannel

³ Statistical error only.

Normalized residue in $N\pi \rightarrow N(1880) \rightarrow \Sigma K$

MODULUS	PHASE (°)	DOCUMENT ID	TECN	COMMENT
••• We do not use the following data for averages, fits, limits, etc. •••				
0.11 ± 0.06	95 ± 40	ANISOVICH	12A	DPWA Multichannel

Normalized residue in $N\pi \rightarrow N(1880) \rightarrow \Delta\pi, P$ -wave

MODULUS	PHASE (°)	DOCUMENT ID	TECN	COMMENT
0.14 ± 0.08	-150 ± 55	SOKHOYAN	15A	DPWA Multichannel
••• We do not use the following data for averages, fits, limits, etc. •••				
0.20 ± 0.08	-150 ± 50	ANISOVICH	12A	DPWA Multichannel

Normalized residue in $N\pi \rightarrow N(1880) \rightarrow N(1535)\pi$

MODULUS	PHASE (°)	DOCUMENT ID	TECN	COMMENT
0.09 ± 0.05	130 ± 60	GUTZ	14	DPWA Multichannel

Normalized residue in $N\pi \rightarrow N(1880) \rightarrow N\alpha_0(980)$

MODULUS	PHASE (°)	DOCUMENT ID	TECN	COMMENT
0.04 ± 0.03	40 ± 65	GUTZ	14	DPWA Multichannel

Normalized residue in $N\pi \rightarrow N(1880) \rightarrow N\sigma$

MODULUS	PHASE (°)	DOCUMENT ID	TECN	COMMENT
0.10 ± 0.05	-140 ± 55	SOKHOYAN	15A	DPWA Multichannel

$N(1880)$ BREIT-WIGNER MASS

VALUE (MeV)	DOCUMENT ID	TECN	COMMENT
1830 to 1930 (≈ 1880) OUR ESTIMATE			
1967 ± 20	⁴ HUNT	19	DPWA Multichannel
1875 ± 40	SOKHOYAN	15A	DPWA Multichannel
••• We do not use the following data for averages, fits, limits, etc. •••			
1875 ± 40	GUTZ	14	DPWA Multichannel
1870 ± 35	ANISOVICH	12A	DPWA Multichannel
1900 ± 36	⁴ SHRESTHA	12A	DPWA Multichannel

⁴ Statistical error only.

$N(1880)$ BREIT-WIGNER WIDTH

VALUE (MeV)	DOCUMENT ID	TECN	COMMENT
200 to 400 (≈ 300) OUR ESTIMATE			
500 ± 77	⁵ HUNT	19	DPWA Multichannel
230 ± 50	SOKHOYAN	15A	DPWA Multichannel
••• We do not use the following data for averages, fits, limits, etc. •••			
230 ± 50	GUTZ	14	DPWA Multichannel
235 ± 65	ANISOVICH	12A	DPWA Multichannel
485 ± 142	⁵ SHRESTHA	12A	DPWA Multichannel

⁵ Statistical error only.

$N(1880)$ DECAY MODES

Mode	Fraction (Γ_i/Γ)
Γ_1 $N\pi$	3-31 %
Γ_2 $N\eta$	1-55 %
Γ_3 $N\omega$	12-28 %
Γ_4 ΛK	1-3 %
Γ_5 ΣK	10-24 %
Γ_6 $N\pi\pi$	>32 %
Γ_7 $\Delta(1232)\pi$	5-42 %
Γ_8 $N\rho, S=1/2, P$ -wave	19-45 %

See key on page 1127

Baryon Particle Listings
N(1880), N(1895)

Γ_9	$N\sigma$	8-40 %
Γ_{10}	$N(1535)\pi$	4-12 %
Γ_{11}	$N_{a_0}(980)$	1-5 %
Γ_{12}	$\Lambda K^*(892)$	0.5-1.1 %
Γ_{13}	$p\gamma$, helicity=1/2	seen
Γ_{14}	$n\gamma$, helicity=1/2	0.002-0.63 %

N(1880) BRANCHING RATIOS

$\Gamma(N\pi)/\Gamma_{total}$	DOCUMENT ID	TECN	COMMENT	Γ_1/Γ
VALUE (%)				
3-31 % OUR ESTIMATE				
25 ± 6	6 HUNT	19	DPWA Multichannel	
6 ± 3	SOKHOYAN	15A	DPWA Multichannel	
• • • We do not use the following data for averages, fits, limits, etc. • • •				
6 ± 3	GUTZ	14	DPWA Multichannel	
5 ± 3	ANISOVICH	12A	DPWA Multichannel	
15 ± 5	6 SHRESTHA	12A	DPWA Multichannel	
6 Statistical error only.				

$\Gamma(N\eta)/\Gamma_{total}$	DOCUMENT ID	TECN	COMMENT	Γ_2/Γ
VALUE (%)				
1-55 % OUR ESTIMATE				
18 ± 8	MUELLER	20	DPWA Multichannel	
2 ± 1	7 HUNT	19	DPWA Multichannel	
25 ± 30	ANISOVICH	12A	DPWA Multichannel	
16 ± 7	7 SHRESTHA	12A	DPWA Multichannel	
• • • We do not use the following data for averages, fits, limits, etc. • • •				
7 Statistical error only.				

$\Gamma(N\omega)/\Gamma_{total}$	DOCUMENT ID	TECN	COMMENT	Γ_3/Γ
VALUE (%)				
12-28 % OUR ESTIMATE				
20 ± 8	DENISENKO	16	DPWA Multichannel	

$\Gamma(\Lambda K)/\Gamma_{total}$	DOCUMENT ID	TECN	COMMENT	Γ_4/Γ
VALUE (%)				
1-3 % OUR ESTIMATE				
2 ± 1	8 HUNT	19	DPWA Multichannel	
2 ± 1	ANISOVICH	12A	DPWA Multichannel	
• • • We do not use the following data for averages, fits, limits, etc. • • •				
32 ± 10	8 SHRESTHA	12A	DPWA Multichannel	
8 Statistical error only.				

$\Gamma(\Sigma K)/\Gamma_{total}$	DOCUMENT ID	TECN	COMMENT	Γ_5/Γ
VALUE (%)				
10-24 % OUR ESTIMATE				
17 ± 7	ANISOVICH	12A	DPWA Multichannel	

$\Gamma(\Delta(1232)\pi)/\Gamma_{total}$	DOCUMENT ID	TECN	COMMENT	Γ_7/Γ
VALUE (%)				
5-42 % OUR ESTIMATE				
11 ± 6	9 HUNT	19	DPWA Multichannel	
30 ± 12	SOKHOYAN	15A	DPWA Multichannel	
• • • We do not use the following data for averages, fits, limits, etc. • • •				
29 ± 12	ANISOVICH	12A	DPWA Multichannel	
< 2	9 SHRESTHA	12A	DPWA Multichannel	
9 Statistical error only.				

$\Gamma(N\rho, S=1/2, P\text{-wave})/\Gamma_{total}$	DOCUMENT ID	TECN	COMMENT	Γ_8/Γ
VALUE (%)				
19-45 % OUR ESTIMATE				
32 ± 13	10 HUNT	19	DPWA Multichannel	
10 Statistical error only.				

$\Gamma(N\sigma)/\Gamma_{total}$	DOCUMENT ID	TECN	COMMENT	Γ_9/Γ
VALUE (%)				
8-40 % OUR ESTIMATE				
< 9	11 HUNT	19	DPWA Multichannel	
25 ± 15	SOKHOYAN	15A	DPWA Multichannel	
• • • We do not use the following data for averages, fits, limits, etc. • • •				
8 ± 5	11 SHRESTHA	12A	DPWA Multichannel	
11 Statistical error only.				

$\Gamma(N(1535)\pi)/\Gamma_{total}$	DOCUMENT ID	TECN	COMMENT	Γ_{10}/Γ
VALUE (%)				
4-12 % OUR ESTIMATE				
8 ± 4	GUTZ	14	DPWA Multichannel	

$\Gamma(N_{a_0}(980))/\Gamma_{total}$	DOCUMENT ID	TECN	COMMENT	Γ_{11}/Γ
VALUE (%)				
1-5 % OUR ESTIMATE				
3 ± 2	GUTZ	14	DPWA Multichannel	

$\Gamma(\Lambda K^*(892))/\Gamma_{total}$	DOCUMENT ID	TECN	COMMENT	Γ_{12}/Γ
VALUE (%)				
0.5-1.1 % OUR ESTIMATE				
0.8 ± 0.3	ANISOVICH	17B	DPWA Multichannel	

N(1880) BREIT-WIGNER PHOTON DECAY AMPLITUDES

$N(1880) \rightarrow p\gamma$, helicity-1/2 amplitude $A_{1/2}$	DOCUMENT ID	TECN	COMMENT
VALUE (GeV ^{-1/2})			
0.119 ± 0.015	12 HUNT	19	DPWA Multichannel
• • • We do not use the following data for averages, fits, limits, etc. • • •			
0.021 ± 0.006	12 SHRESTHA	12A	DPWA Multichannel
12 Statistical error only.			

$N(1880) \rightarrow n\gamma$, helicity-1/2 amplitude $A_{1/2}$	DOCUMENT ID	TECN	COMMENT
VALUE (GeV ^{-1/2})			
0.016 ± 0.010	13 HUNT	19	DPWA Multichannel
-0.060 ± 0.050	ANISOVICH	13B	DPWA Multichannel
• • • We do not use the following data for averages, fits, limits, etc. • • •			
0.014 ± 0.007	13 SHRESTHA	12A	DPWA Multichannel
13 Statistical error only.			

N(1880) REFERENCES

MUELLER	20	PL B803 135323	J. Mueller <i>et al.</i>	(CBELSA/TAPS Collab.)
HUNT	19	PR C99 052005	B.C. Hunt, D.M. Manley	
ANISOVICH	17A	PRL 119 062004	A.V. Anisovich <i>et al.</i>	
ANISOVICH	17B	PL B771 142	A.V. Anisovich <i>et al.</i>	
DENISENKO	16	PL B755 97	L. Denisenko <i>et al.</i>	
SOKHOYAN	15A	EPJ A51 95	V. Sokhoyan <i>et al.</i>	(CBELSA/TAPS Collab.)
GUTZ	14	EPJ A50 74	E. Gutz <i>et al.</i>	(CBELSA/TAPS Collab.)
ANISOVICH	13B	EPJ A49 67	A.V. Anisovich <i>et al.</i>	
ANISOVICH	12A	EPJ A48 15	A.V. Anisovich <i>et al.</i>	(BONN, PNPI)
SHRESTHA	12A	PR C86 055203	M. Shrestha, D.M. Manley	(KSU)

N(1895) 1/2⁻

$I(J^P) = \frac{1}{2}(\frac{1}{2}^-)$ Status: * * * *

Before our 2012 Review, this state appeared in our Listings as the N(2090). Any structure in the S₁₁ wave above 1800 MeV is listed here. A few early results that are now obsolete have been omitted.

N(1895) POLE POSITION

REAL PART	DOCUMENT ID	TECN	COMMENT
VALUE (MeV)			
1890 to 1930 (≈ 1910) OUR ESTIMATE			
1907 ± 10	AFZAL	20	DPWA Multichannel
1895 ± 15	ANISOVICH	17A	DPWA Multichannel
1906 ± 17	1 ANISOVICH	17A	L+P $\gamma p, \pi^- p \rightarrow K\Lambda$
1917 ± 19 ± 1	2 SVARC	14	L+P $\pi N \rightarrow \pi N$
• • • We do not use the following data for averages, fits, limits, etc. • • •			
1956	HUNT	19	DPWA Multichannel
1907 ± 10	ANISOVICH	17C	DPWA Multichannel
1907 ± 10	SOKHOYAN	15A	DPWA Multichannel
1900 ± 15	ANISOVICH	12A	DPWA Multichannel
1797 ± 26	BATINIC	10	DPWA $\pi N \rightarrow N\pi, N\eta$
1795	VRANA	00	DPWA Multichannel
2150 ± 70	CUTKOSKY	80	IPWA $\pi N \rightarrow \pi N$
1 Statistical error only.			
2 Fit to the amplitudes of HOEHLER 79.			

-2xIMAGINARY PART	DOCUMENT ID	TECN	COMMENT
VALUE (MeV)			
80 to 140 (≈ 110) OUR ESTIMATE			
100 ± 40	AFZAL	20	DPWA Multichannel
132 ± 30	ANISOVICH	17A	DPWA Multichannel
100 ± 10	1 ANISOVICH	17A	L+P $\gamma p, \pi^- p \rightarrow K\Lambda$
101 ± 36 ± 1	1,2 SVARC	14	L+P $\pi N \rightarrow \pi N$
• • • We do not use the following data for averages, fits, limits, etc. • • •			
449	HUNT	19	DPWA Multichannel
100 ± 40	ANISOVICH	17C	DPWA Multichannel
100 ± 40	SOKHOYAN	15A	DPWA Multichannel
90 ± 30	ANISOVICH	12A	DPWA Multichannel
420 ± 45	BATINIC	10	DPWA $\pi N \rightarrow N\pi, N\eta$
220	VRANA	00	DPWA Multichannel
350 ± 100	CUTKOSKY	80	IPWA $\pi N \rightarrow \pi N$
1 Statistical error only.			
2 Fit to the amplitudes of HOEHLER 79.			

Baryon Particle Listings

 $N(1895)$ $N(1895)$ ELASTIC POLE RESIDUEMODULUS $|r|$

VALUE (MeV)	DOCUMENT ID	TECN	COMMENT
1 to 5 (≈ 3) OUR ESTIMATE			
3 ± 2	SOKHOYAN	15A	DPWA Multichannel
3.1 ± 1.4	¹ SVARC	14	L+P $\pi N \rightarrow \pi N$
••• We do not use the following data for averages, fits, limits, etc. •••			
1 ± 1	ANISOVICH	12A	DPWA Multichannel
60	BATINIC	10	DPWA $\pi N \rightarrow N\pi, N\eta$
40 ± 20	CUTKOSKY	80	IPWA $\pi N \rightarrow \pi N$

¹ Fit to the amplitudes of HOEHLER 79.PHASE θ

VALUE (°)	DOCUMENT ID	TECN	COMMENT
125 ± 45	SOKHOYAN	15A	DPWA Multichannel
$-107 \pm 23 \pm 2$	¹ SVARC	14	L+P $\pi N \rightarrow \pi N$
0 ± 90	CUTKOSKY	80	IPWA $\pi N \rightarrow \pi N$
••• We do not use the following data for averages, fits, limits, etc. •••			
-164	BATINIC	10	DPWA $\pi N \rightarrow N\pi, N\eta$

¹ Fit to the amplitudes of HOEHLER 79. $N(1895)$ INELASTIC POLE RESIDUEThe "normalized residue" is the residue divided by $\Gamma_{pole}/2$.Normalized residue in $N\pi \rightarrow N(1895) \rightarrow \Lambda K$

MODULUS	PHASE (°)	DOCUMENT ID	TECN	COMMENT
0.09 ± 0.03	8 ± 30	ANISOVICH	17A	DPWA Multichannel
0.06 ± 0.02	87 ± 27	¹ ANISOVICH	17A	L+P $\gamma p, \pi^- p \rightarrow K\Lambda$
••• We do not use the following data for averages, fits, limits, etc. •••				
0.05 ± 0.02	-90 ± 30	ANISOVICH	12A	DPWA Multichannel

¹ Statistical error only.Normalized residue in $N\pi \rightarrow N(1895) \rightarrow \Sigma K$

MODULUS	PHASE (°)	DOCUMENT ID	TECN	COMMENT
0.06 ± 0.02	40 ± 30	ANISOVICH	12A	DPWA Multichannel

Normalized residue in $N\pi \rightarrow N(1895) \rightarrow \Delta(1232)\pi$

MODULUS	PHASE (°)	DOCUMENT ID	TECN	COMMENT
0.05 ± 0.025	-100 ± 45	SOKHOYAN	15A	DPWA Multichannel

Normalized residue in $N\pi \rightarrow N(1895) \rightarrow N(1440)\pi$

MODULUS	PHASE (°)	DOCUMENT ID	TECN	COMMENT
0.05 ± 0.025	-100 ± 45	SOKHOYAN	15A	DPWA Multichannel

 $N(1895)$ BREIT-WIGNER MASS

VALUE (MeV)	DOCUMENT ID	TECN	COMMENT
1870 to 1920 (≈ 1895) OUR ESTIMATE			
2000 ± 29	¹ HUNT	19	DPWA Multichannel
1890^{+9}_{-23}	KASHEVAROV	17	DPWA $\gamma p \rightarrow \eta p, \eta' p$
1905 ± 12	SOKHOYAN	15A	DPWA Multichannel
1880 ± 20	HOEHLER	79	IPWA $\pi N \rightarrow \pi N$
••• We do not use the following data for averages, fits, limits, etc. •••			
1895 ± 15	ANISOVICH	12A	DPWA Multichannel
1910 ± 15	¹ SHRESTHA	12A	DPWA Multichannel
1812 ± 25	BATINIC	10	DPWA $\pi N \rightarrow N\pi, N\eta$
1822 ± 43	VRANA	00	DPWA Multichannel
2180 ± 80	CUTKOSKY	80	IPWA $\pi N \rightarrow \pi N$

¹ Statistical error only. $N(1895)$ BREIT-WIGNER WIDTH

VALUE (MeV)	DOCUMENT ID	TECN	COMMENT
80 to 200 (≈ 120) OUR ESTIMATE			
466 ± 72	¹ HUNT	19	DPWA Multichannel
150 ± 57	KASHEVAROV	17	DPWA $\gamma p \rightarrow \eta p, \eta' p$
100^{+30}_{-10}	SOKHOYAN	15A	DPWA Multichannel
95 ± 30	HOEHLER	79	IPWA $\pi N \rightarrow \pi N$
••• We do not use the following data for averages, fits, limits, etc. •••			
90^{+30}_{-15}	ANISOVICH	12A	DPWA Multichannel
502 ± 47	¹ SHRESTHA	12A	DPWA Multichannel
405 ± 40	BATINIC	10	DPWA $\pi N \rightarrow N\pi, N\eta$
248 ± 185	VRANA	00	DPWA Multichannel
350 ± 100	CUTKOSKY	80	IPWA $\pi N \rightarrow \pi N$

¹ Statistical error only. $N(1895)$ DECAY MODES

Mode	Fraction (Γ_i/Γ)
Γ_1 $N\pi$	2–18 %
Γ_2 $N\eta$	15–45 %
Γ_3 $N\eta'$	10–40 %
Γ_4 $N\omega$	16–40 %
Γ_5 ΛK	3–23 %
Γ_6 ΣK	6–20 %
Γ_7 $N\pi\pi$	17–74 %
Γ_8 $\Delta(1232)\pi, D$ -wave	3–11 %
Γ_9 $N\rho$	14–50 %
Γ_{10} $N\rho, S=1/2, S$ -wave	<18 %
Γ_{11} $N\rho, S=3/2, D$ -wave	14–32 %
Γ_{12} $N\sigma$	<13 %
Γ_{13} $N(1440)\pi$	2–12 %
Γ_{14} $\Lambda K^*(892)$	4–9 %
Γ_{15} $p\gamma, \text{helicity}=1/2$	0.01–0.06 %
Γ_{16} $n\gamma, \text{helicity}=1/2$	0.003–0.05 %

 $N(1895)$ BRANCHING RATIOS

$\Gamma(N\pi)/\Gamma_{total}$	VALUE (%)	DOCUMENT ID	TECN	COMMENT	Γ_1/Γ
2–18 % OUR ESTIMATE					
8 ± 4	¹ HUNT	19	DPWA Multichannel		
2.5 ± 1.5	SOKHOYAN	15A	DPWA Multichannel		
9 ± 5	HOEHLER	79	IPWA $\pi N \rightarrow \pi N$		
••• We do not use the following data for averages, fits, limits, etc. •••					
2 ± 1	ANISOVICH	12A	DPWA Multichannel		
17 ± 2	¹ SHRESTHA	12A	DPWA Multichannel		
32 ± 6	BATINIC	10	DPWA $\pi N \rightarrow N\pi, N\eta$		
17 ± 3	VRANA	00	DPWA Multichannel		
18 ± 8	CUTKOSKY	80	IPWA $\pi N \rightarrow \pi N$		

¹ Statistical error only.

$\Gamma(N\eta)/\Gamma_{total}$	VALUE (%)	DOCUMENT ID	TECN	COMMENT	Γ_2/Γ
15–45 % OUR ESTIMATE					
10 ± 5	MUELLER	20	DPWA Multichannel		
37 ± 9	¹ HUNT	19	DPWA Multichannel		
10 ± 5	ANISOVICH	17C	DPWA Multichannel		
20 ± 6	² KASHEVAROV	17	DPWA $\gamma p \rightarrow \eta p, \eta' p$		
••• We do not use the following data for averages, fits, limits, etc. •••					
21 ± 6	ANISOVICH	12A	DPWA Multichannel		
40 ± 4	¹ SHRESTHA	12A	DPWA Multichannel		
22 ± 10	BATINIC	10	DPWA $\pi N \rightarrow N\pi, N\eta$		
41 ± 4	VRANA	00	DPWA Multichannel		

¹ Statistical error only.² Assuming $A_{1/2} = -0.030 \text{ GeV}^{-1/2}$.

$\Gamma(N\eta')/\Gamma_{total}$	VALUE (%)	DOCUMENT ID	TECN	COMMENT	Γ_3/Γ
10–40 % OUR ESTIMATE					
13 ± 5	ANISOVICH	17C	DPWA Multichannel		
38 ± 20	¹ KASHEVAROV	17	DPWA $\gamma p \rightarrow \eta p, \eta' p$		

¹ Assuming $A_{1/2} = -0.030 \text{ GeV}^{-1/2}$.

$\Gamma(N\omega)/\Gamma_{total}$	VALUE (%)	DOCUMENT ID	TECN	COMMENT	Γ_4/Γ
16–40 % OUR ESTIMATE					
28 ± 12	DENISENKO	16	DPWA Multichannel		

$\Gamma(\Lambda K)/\Gamma_{total}$	VALUE (%)	DOCUMENT ID	TECN	COMMENT	Γ_5/Γ
3–23 % OUR ESTIMATE					
7 ± 4	¹ HUNT	19	DPWA Multichannel		
18 ± 5	ANISOVICH	12A	DPWA Multichannel		
••• We do not use the following data for averages, fits, limits, etc. •••					
1.8 ± 0.8	¹ SHRESTHA	12A	DPWA Multichannel		

¹ Statistical error only.

$\Gamma(\Sigma K)/\Gamma_{total}$	VALUE (%)	DOCUMENT ID	TECN	COMMENT	Γ_6/Γ
6–20 % OUR ESTIMATE					
13 ± 7	ANISOVICH	12A	DPWA Multichannel		

$\Gamma(\Delta(1232)\pi, D\text{-wave})/\Gamma_{total}$	VALUE (%)	DOCUMENT ID	TECN	COMMENT	Γ_8/Γ
3–11 % OUR ESTIMATE					
<10	¹ HUNT	19	DPWA Multichannel		
7 ± 4	SOKHOYAN	15A	DPWA Multichannel		

See key on page 1127

Baryon Particle Listings

$N(1895)$, $N(1900)$

••• We do not use the following data for averages, fits, limits, etc. •••

7 ± 3	¹ SHRESTHA	12A	DPWA	Multichannel
1 ± 1	VRANA	00	DPWA	Multichannel

¹ Statistical error only.

$\Gamma(N\rho, S=1/2, S\text{-wave})/\Gamma_{\text{total}}$ Γ_{10}/Γ

VALUE (%)	DOCUMENT ID	TECN	COMMENT
<18 % OUR ESTIMATE			
<18	¹ HUNT	19	DPWA Multichannel
••• We do not use the following data for averages, fits, limits, etc. •••			
< 2	¹ SHRESTHA	12A	DPWA Multichannel
36 ± 1	VRANA	00	DPWA Multichannel

¹ Statistical error only.

$\Gamma(N\rho, S=3/2, D\text{-wave})/\Gamma_{\text{total}}$ Γ_{11}/Γ

VALUE (%)	DOCUMENT ID	TECN	COMMENT
14-32 % OUR ESTIMATE			
23 ± 9	¹ HUNT	19	DPWA Multichannel
••• We do not use the following data for averages, fits, limits, etc. •••			
9 ± 3	¹ SHRESTHA	12A	DPWA Multichannel
1 ± 1	VRANA	00	DPWA Multichannel

¹ Statistical error only.

$\Gamma(N\sigma)/\Gamma_{\text{total}}$ Γ_{12}/Γ

VALUE (%)	DOCUMENT ID	TECN	COMMENT
<13 % OUR ESTIMATE			
<13	¹ HUNT	19	DPWA Multichannel
••• We do not use the following data for averages, fits, limits, etc. •••			
< 2	¹ SHRESTHA	12A	DPWA Multichannel
2 ± 1	VRANA	00	DPWA Multichannel

¹ Statistical error only.

$\Gamma(N(1440)\pi)/\Gamma_{\text{total}}$ Γ_{13}/Γ

VALUE (%)	DOCUMENT ID	TECN	COMMENT
2-12 % OUR ESTIMATE			
7 ± 5	¹ HUNT	19	DPWA Multichannel
2.5 ± 1.5	SOKHOYAN	15A	DPWA Multichannel
••• We do not use the following data for averages, fits, limits, etc. •••			
24 ± 4	¹ SHRESTHA	12A	DPWA Multichannel
2 ± 1	VRANA	00	DPWA Multichannel

¹ Statistical error only.

$\Gamma(\Lambda K^*(892))/\Gamma_{\text{total}}$ Γ_{14}/Γ

VALUE (%)	DOCUMENT ID	TECN	COMMENT
4-9 % OUR ESTIMATE			
6.3 ± 2.5	ANISOVICH	17B	DPWA Multichannel

$N(1895)$ PHOTON DECAY AMPLITUDES AT THE POLE

$N(1895) \rightarrow \rho\gamma$, helicity-1/2 amplitude $A_{1/2}$

MODULUS ($\text{GeV}^{-1/2}$)	PHASE ($^\circ$)	DOCUMENT ID	TECN	COMMENT
-0.015 ± 0.006	-35 ± 35	ANISOVICH	17C	DPWA Multichannel
••• We do not use the following data for averages, fits, limits, etc. •••				
0.015 ± 0.006	145 ± 35	SOKHOYAN	15A	DPWA Multichannel

$N(1895)$ BREIT-WIGNER PHOTON DECAY AMPLITUDES

$N(1895) \rightarrow \rho\gamma$, helicity-1/2 amplitude $A_{1/2}$

VALUE ($\text{GeV}^{-1/2}$)	DOCUMENT ID	TECN	COMMENT
0.017 ± 0.005	¹ HUNT	19	DPWA Multichannel
-0.016 ± 0.006	SOKHOYAN	15A	DPWA Multichannel
••• We do not use the following data for averages, fits, limits, etc. •••			
0.012 ± 0.006	¹ SHRESTHA	12A	DPWA Multichannel

¹ Statistical error only.

$N(1895) \rightarrow n\gamma$, helicity-1/2 amplitude $A_{1/2}$

VALUE ($\text{GeV}^{-1/2}$)	DOCUMENT ID	TECN	COMMENT
0.002 ± 0.013	¹ HUNT	19	DPWA Multichannel
0.013 ± 0.006	ANISOVICH	13B	DPWA Multichannel
••• We do not use the following data for averages, fits, limits, etc. •••			
0.003 ± 0.007	¹ SHRESTHA	12A	DPWA Multichannel

¹ Statistical error only.

$N(1895)$ REFERENCES

AFZAL	20	PRL 125 152002	F. Afzal et al.	(CBELSA/TAPS Collab.)
MUELLER	20	PL B803 135323	J. Mueller et al.	(CBELSA/TAPS Collab.)
HUNT	19	PR C99 055205	B.C. Hunt, D.M. Manley	
ANISOVICH	17A	PRL 119 062004	A.V. Anisovich et al.	
ANISOVICH	17B	PL B771 142	A.V. Anisovich et al.	
ANISOVICH	17C	PL B772 247	A.V. Anisovich et al.	
KASHEVAROV	17	PRL 118 212001	V.L. Kashevarov et al.	(A2/MAMI Collab.)
DENISENKO	16	PL B755 97	I. Denisenko et al.	
SOKHOYAN	15A	EPJ A51 95	V. Sokhoyan et al.	(CBELSA/TAPS Collab.)

SVARC	14	PR C89 045205	A. Svarc et al.	(RBI Zagreb, UNI Tuzla)
ANISOVICH	13B	EPJ A49 67	A.V. Anisovich et al.	
ANISOVICH	12A	EPJ A48 15	A.V. Anisovich et al.	(BONN, PNPI)
SHRESTHA	12A	PR C86 055203	M. Shrestha, D.M. Manley	(KSU)
BATINIC	10	PR C82 038203	M. Batinic et al.	(ZAGR)
VRANA	00	PRPL 328 181	T.P. Vrana, S.A. Dytman, T.-S.H. Lee	(PITT, ANL)
CUTKOSKY	80	Toronto Conf. 19	R.E. Cutkosky et al.	(CMU, LBL) IJP
Also		PR D20 2839	R.E. Cutkosky et al.	(CMU, LBL)
HOEHLER	79	PDAT 12-1	G. Hoehler et al.	(KARLT) IJP
Also		Toronto Conf. 3	R. Koch	(KARLT) IJP

$$N(1900) 3/2^+$$

$$I(J^P) = \frac{1}{2}(\frac{3}{2}^+) \text{ Status: } ***$$

$N(1900)$ POLE POSITION

REAL PART

VALUE (MeV)	DOCUMENT ID	TECN	COMMENT
1900 to 1940 (≈ 1920) OUR ESTIMATE			
1945 ± 35	ANISOVICH	17A	DPWA Multichannel
$1928 \pm 18 \pm 2$	¹ SVARC	14	L+P $\pi N \rightarrow \pi N$
••• We do not use the following data for averages, fits, limits, etc. •••			
1856	HUNT	19	DPWA Multichannel
1912 ± 30	² ANISOVICH	17A	L+P $\gamma\rho, \pi^-p \rightarrow K\Lambda$
1910 ± 30	SOKHOYAN	15A	DPWA Multichannel
1910 ± 30	GUTZ	14	DPWA Multichannel
1910	SHKLYAR	13	DPWA Multichannel
1900 ± 30	ANISOVICH	12A	DPWA Multichannel

¹ Fit to the amplitudes of HOEHLER 79.
² Statistical error only.

-2xIMAGINARY PART

VALUE (MeV)	DOCUMENT ID	TECN	COMMENT
100 to 200 (≈ 150) OUR ESTIMATE			
135 ± 70	ANISOVICH	17A	DPWA Multichannel
$152 \pm 40 \pm 9$	¹ SVARC	14	L+P $\pi N \rightarrow \pi N$
••• We do not use the following data for averages, fits, limits, etc. •••			
241	HUNT	19	DPWA Multichannel
166 ± 30	² ANISOVICH	17A	L+P $\gamma\rho, \pi^-p \rightarrow K\Lambda$
280 ± 50	SOKHOYAN	15A	DPWA Multichannel
280 ± 50	GUTZ	14	DPWA Multichannel
173	SHKLYAR	13	DPWA Multichannel
200 ± 100	ANISOVICH	12A	DPWA Multichannel

¹ Fit to the amplitudes of HOEHLER 79.
² Statistical error only.

$N(1900)$ ELASTIC POLE RESIDUE

MODULUS $|r|$

VALUE (MeV)	DOCUMENT ID	TECN	COMMENT
2 to 6 (≈ 4) OUR ESTIMATE			
4 ± 2	SOKHOYAN	15A	DPWA Multichannel
$4 \pm 1 \pm 1$	¹ SVARC	14	L+P $\pi N \rightarrow \pi N$
••• We do not use the following data for averages, fits, limits, etc. •••			
4 ± 2	GUTZ	14	DPWA Multichannel
10	SHKLYAR	13	DPWA Multichannel
3 ± 2	ANISOVICH	12A	DPWA Multichannel

¹ Fit to the amplitudes of HOEHLER 79.

PHASE θ

VALUE ($^\circ$)	DOCUMENT ID	TECN	COMMENT
-50 to 10 (≈ -20) OUR ESTIMATE			
-10 ± 40	SOKHOYAN	15A	DPWA Multichannel
$-29 \pm 15 \pm 2$	¹ SVARC	14	L+P $\pi N \rightarrow \pi N$
••• We do not use the following data for averages, fits, limits, etc. •••			
-10 ± 40	GUTZ	14	DPWA Multichannel
-64	SHKLYAR	13	DPWA Multichannel
10 ± 35	ANISOVICH	12A	DPWA Multichannel

¹ Fit to the amplitudes of HOEHLER 79.

$N(1900)$ INELASTIC POLE RESIDUE

The "normalized residue" is the residue divided by $\Gamma_{\text{pole}}/2$.

Normalized residue in $N\pi \rightarrow N(1900) \rightarrow N\eta$

MODULUS	PHASE ($^\circ$)	DOCUMENT ID	TECN	COMMENT
0.05 ± 0.02	70 ± 60	ANISOVICH	12A	DPWA Multichannel

Normalized residue in $N\pi \rightarrow N(1900) \rightarrow \Lambda K$

MODULUS	PHASE ($^\circ$)	DOCUMENT ID	TECN	COMMENT
0.03 ± 0.02	90 ± 40	ANISOVICH	17A	DPWA Multichannel
••• We do not use the following data for averages, fits, limits, etc. •••				
0.07 ± 0.03	135 ± 25	ANISOVICH	12A	DPWA Multichannel

Baryon Particle Listings

 $N(1900)$ Normalized residue in $N\pi \rightarrow N(1900) \rightarrow \Sigma K$

MODULUS	PHASE (°)	DOCUMENT ID	TECN	COMMENT
0.04±0.02	110 ± 30	ANISOVICH	12A	DPWA Multichannel

Normalized residue in $N\pi \rightarrow N(1900) \rightarrow N(1535)\pi$

MODULUS	PHASE (°)	DOCUMENT ID	TECN	COMMENT
0.04±0.01	170 ± 30	GUTZ	14	DPWA Multichannel

Normalized residue in $N\pi \rightarrow N(1900) \rightarrow \Delta(1232)\pi, P\text{-wave}$

MODULUS	PHASE (°)	DOCUMENT ID	TECN	COMMENT
0.07±0.04	-65 ± 30	SOKHOYAN	15A	DPWA Multichannel

Normalized residue in $N\pi \rightarrow N(1900) \rightarrow \Delta(1232)\pi, F\text{-wave}$

MODULUS	PHASE (°)	DOCUMENT ID	TECN	COMMENT
0.10±0.05	80 ± 30	SOKHOYAN	15A	DPWA Multichannel

Normalized residue in $N\pi \rightarrow N(1900) \rightarrow N(1520)\pi$

MODULUS	PHASE (°)	DOCUMENT ID	TECN	COMMENT
0.07±0.04	-105 ± 35	SOKHOYAN	15A	DPWA Multichannel

Normalized residue in $N\pi \rightarrow N(1900) \rightarrow N\sigma$

MODULUS	PHASE (°)	DOCUMENT ID	TECN	COMMENT
0.03±0.02	-110 ± 35	SOKHOYAN	15A	DPWA Multichannel

 $N(1900)$ BREIT-WIGNER MASS

VALUE (MeV)	DOCUMENT ID	TECN	COMMENT
-------------	-------------	------	---------

1890 to 1950 (≈ 1920) OUR ESTIMATE

1911 ± 6	¹ HUNT	19	DPWA Multichannel
1910 ± 30	SOKHOYAN	15A	DPWA Multichannel
1998 ± 3	¹ SHKLYAR	13	DPWA Multichannel

• • • We do not use the following data for averages, fits, limits, etc. • • •

1910 ± 30	GUTZ	14	DPWA Multichannel
1905 ± 30	ANISOVICH	12A	DPWA Multichannel
1900 ± 8	¹ SHRESTHA	12A	DPWA Multichannel
1951 ± 53	PENNER	02C	DPWA Multichannel

¹ Statistical error only.

 $N(1900)$ BREIT-WIGNER WIDTH

VALUE (MeV)	DOCUMENT ID	TECN	COMMENT
-------------	-------------	------	---------

100 to 320 (≈ 200) OUR ESTIMATE

292 ± 16	¹ HUNT	19	DPWA Multichannel
270 ± 50	SOKHOYAN	15A	DPWA Multichannel
359 ± 10	¹ SHKLYAR	13	DPWA Multichannel

• • • We do not use the following data for averages, fits, limits, etc. • • •

270 ± 50	GUTZ	14	DPWA Multichannel
250 ⁺¹²⁰ ₋₅₀	ANISOVICH	12A	DPWA Multichannel
101 ± 15	¹ SHRESTHA	12A	DPWA Multichannel
622 ± 42	PENNER	02C	DPWA Multichannel

¹ Statistical error only.

 $N(1900)$ DECAY MODES

Mode	Fraction (Γ_i/Γ)
Γ_1 $N\pi$	1-20 %
Γ_2 $N\eta$	2-14 %
Γ_3 $N\eta'$	4-8 %
Γ_4 $N\omega$	7-13 %
Γ_5 ΛK	2-20 %
Γ_6 ΣK	3-7 %
Γ_7 $N\pi\pi$	>56 %
Γ_8 $\Delta(1232)\pi$	30-70 %
Γ_9 $\Delta(1232)\pi, P\text{-wave}$	9-25 %
Γ_{10} $\Delta(1232)\pi, F\text{-wave}$	21-45 %
Γ_{11} $N\rho, S=1/2$	25-40 %
Γ_{12} $N\sigma$	1-7 %
Γ_{13} $N(1520)\pi$	7-23 %
Γ_{14} $N(1535)\pi$	4-10 %
Γ_{15} $\Lambda K^*(892)$	< 0.2 %
Γ_{16} $p\gamma$	0.001-0.025 %
Γ_{17} $p\gamma, \text{helicity}=1/2$	0.001-0.021 %
Γ_{18} $p\gamma, \text{helicity}=3/2$	< 0.003 %
Γ_{19} $n\gamma$	< 0.040 %
Γ_{20} $n\gamma, \text{helicity}=1/2$	< 0.007 %
Γ_{21} $n\gamma, \text{helicity}=3/2$	< 0.033 %

 $N(1900)$ BRANCHING RATIOS $\Gamma(N\pi)/\Gamma_{\text{total}}$ Γ_1/Γ

VALUE (%)	DOCUMENT ID	TECN	COMMENT
1-20 % OUR ESTIMATE			
1.9±0.1	¹ HUNT	19	DPWA Multichannel
3 ± 2	SOKHOYAN	15A	DPWA Multichannel
25 ± 1	¹ SHKLYAR	13	DPWA Multichannel
• • • We do not use the following data for averages, fits, limits, etc. • • •			
3 ± 2	GUTZ	14	DPWA Multichannel
3 ± 2	ANISOVICH	12A	DPWA Multichannel
7 ± 4	¹ SHRESTHA	12A	DPWA Multichannel
16 ± 2	PENNER	02C	DPWA Multichannel

¹ Statistical error only.

 $\Gamma(N\eta)/\Gamma_{\text{total}}$ Γ_2/Γ

VALUE (%)	DOCUMENT ID	TECN	COMMENT
2 ± 2	MUELLER	20	DPWA Multichannel
1.3±0.5	¹ HUNT	19	DPWA Multichannel
2 ± 2	¹ SHKLYAR	13	DPWA Multichannel
10 ± 4	ANISOVICH	12A	DPWA Multichannel
• • • We do not use the following data for averages, fits, limits, etc. • • •			
< 1	¹ SHRESTHA	12A	DPWA Multichannel
14 ± 5	PENNER	02C	DPWA Multichannel

¹ Statistical error only.

 $\Gamma(N\eta')/\Gamma_{\text{total}}$ Γ_3/Γ

VALUE (%)	DOCUMENT ID	TECN	COMMENT
4-8 % OUR ESTIMATE			
6±2	ANISOVICH	17C	DPWA Multichannel

 $\Gamma(N\omega)/\Gamma_{\text{total}}$ Γ_4/Γ

VALUE (%)	DOCUMENT ID	TECN	COMMENT
15 ± 8	DENISENKO	16	DPWA Multichannel
10 ± 3	¹ SHKLYAR	13	DPWA Multichannel
• • • We do not use the following data for averages, fits, limits, etc. • • •			
39 ± 9	PENNER	02C	DPWA Multichannel

¹ Statistical error only.

 $\Gamma(\Lambda K)/\Gamma_{\text{total}}$ Γ_5/Γ

VALUE (%)	DOCUMENT ID	TECN	COMMENT
13.7±0.3	¹ HUNT	19	DPWA Multichannel
16 ± 5	ANISOVICH	12A	DPWA Multichannel
2.4±0.3	¹ SHKLYAR	05	DPWA Multichannel
• • • We do not use the following data for averages, fits, limits, etc. • • •			
14 ± 5	¹ SHRESTHA	12A	DPWA Multichannel
5 to 15	NIKONOV	08	DPWA Multichannel
0.1±0.1	PENNER	02C	DPWA Multichannel

¹ Statistical error only.

 $\Gamma(\Sigma K)/\Gamma_{\text{total}}$ Γ_6/Γ

VALUE (%)	DOCUMENT ID	TECN	COMMENT
5 ± 2	ANISOVICH	12A	DPWA Multichannel
• • • We do not use the following data for averages, fits, limits, etc. • • •			
1 ± 1	PENNER	02C	DPWA Multichannel

 $\Gamma(\Delta(1232)\pi, P\text{-wave})/\Gamma_{\text{total}}$ Γ_9/Γ

VALUE (%)	DOCUMENT ID	TECN	COMMENT
17 ± 8	SOKHOYAN	15A	DPWA Multichannel

 $\Gamma(\Delta(1232)\pi, F\text{-wave})/\Gamma_{\text{total}}$ Γ_{10}/Γ

VALUE (%)	DOCUMENT ID	TECN	COMMENT
33 ± 12	SOKHOYAN	15A	DPWA Multichannel

 $\Gamma(N\rho, S=1/2)/\Gamma_{\text{total}}$ Γ_{11}/Γ

VALUE (%)	DOCUMENT ID	TECN	COMMENT
25-40 % OUR ESTIMATE			
32 ± 7	¹ HUNT	19	DPWA Multichannel

¹ Statistical error only.

 $\Gamma(N\sigma)/\Gamma_{\text{total}}$ Γ_{12}/Γ

VALUE (%)	DOCUMENT ID	TECN	COMMENT
4 ± 3	SOKHOYAN	15A	DPWA Multichannel

 $\Gamma(N(1520)\pi)/\Gamma_{\text{total}}$ Γ_{13}/Γ

VALUE (%)	DOCUMENT ID	TECN	COMMENT
15 ± 8	SOKHOYAN	15A	DPWA Multichannel

 $\Gamma(N(1535)\pi)/\Gamma_{\text{total}}$ Γ_{14}/Γ

VALUE (%)	DOCUMENT ID	TECN	COMMENT
7 ± 3	GUTZ	14	DPWA Multichannel

See key on page 1127

Baryon Particle Listings

$N(1900)$, $N(1990)$

$\Gamma(\Lambda K^*(892))/\Gamma_{total}$	DOCUMENT ID	TECN	COMMENT
VALUE (%)			
< 0.2 % OUR ESTIMATE			
<0.2	ANISOVICH	17B	DPWA Multichannel

$N(1900)$ PHOTON DECAY AMPLITUDES AT THE POLE

$N(1900) \rightarrow p\gamma$, helicity-1/2 amplitude $A_{1/2}$

MODULUS ($\text{GeV}^{-1/2}$)	PHASE ($^\circ$)	DOCUMENT ID	TECN	COMMENT
0.026 ± 0.014	60 ± 35	SOKHOYAN	15A	DPWA Multichannel

$N(1900) \rightarrow p\gamma$, helicity-3/2 amplitude $A_{3/2}$

MODULUS ($\text{GeV}^{-1/2}$)	PHASE ($^\circ$)	DOCUMENT ID	TECN	COMMENT
-0.070 ± 0.030	70 ± 50	SOKHOYAN	15A	DPWA Multichannel

$N(1900)$ BREIT-WIGNER PHOTON DECAY AMPLITUDES

$N(1900) \rightarrow p\gamma$, helicity-1/2 amplitude $A_{1/2}$

VALUE ($\text{GeV}^{-1/2}$)	DOCUMENT ID	TECN	COMMENT
0.040 ± 0.004	¹ HUNT	19	DPWA Multichannel
0.024 ± 0.014	SOKHOYAN	15A	DPWA Multichannel
-0.008 ± 0.001	¹ SHKLYAR	13	DPWA Multichannel
••• We do not use the following data for averages, fits, limits, etc. •••			
0.024 ± 0.014	GUTZ	14	DPWA Multichannel
0.026 ± 0.015	ANISOVICH	12A	DPWA Multichannel
0.041 ± 0.008	¹ SHRESTHA	12A	DPWA Multichannel
-0.017	PENNER	02D	DPWA Multichannel
¹ Statistical error only.			

$N(1900) \rightarrow p\gamma$, helicity-3/2 amplitude $A_{3/2}$

VALUE ($\text{GeV}^{-1/2}$)	DOCUMENT ID	TECN	COMMENT
-0.094 ± 0.007	¹ HUNT	19	DPWA Multichannel
-0.067 ± 0.030	SOKHOYAN	15A	DPWA Multichannel
< 0.001	SHKLYAR	13	DPWA Multichannel
••• We do not use the following data for averages, fits, limits, etc. •••			
-0.067 ± 0.030	GUTZ	14	DPWA Multichannel
-0.065 ± 0.030	ANISOVICH	12A	DPWA Multichannel
-0.004 ± 0.006	¹ SHRESTHA	12A	DPWA Multichannel
0.031	PENNER	02D	DPWA Multichannel
¹ Statistical error only.			

$N(1900) \rightarrow n\gamma$, helicity-1/2 amplitude $A_{1/2}$

VALUE ($\text{GeV}^{-1/2}$)	DOCUMENT ID	TECN	COMMENT
0.007 ± 0.014	¹ HUNT	19	DPWA Multichannel
0.000 ± 0.030	ANISOVICH	13B	DPWA Multichannel
••• We do not use the following data for averages, fits, limits, etc. •••			
-0.010 ± 0.004	¹ SHRESTHA	12A	DPWA Multichannel
-0.016	PENNER	02D	DPWA Multichannel
¹ Statistical error only.			

$N(1900) \rightarrow n\gamma$, helicity-3/2 amplitude $A_{3/2}$

VALUE ($\text{GeV}^{-1/2}$)	DOCUMENT ID	TECN	COMMENT
0.007 ± 0.011	¹ HUNT	19	DPWA Multichannel
-0.060 ± 0.045	ANISOVICH	13B	DPWA Multichannel
••• We do not use the following data for averages, fits, limits, etc. •••			
-0.011 ± 0.007	¹ SHRESTHA	12A	DPWA Multichannel
-0.002	PENNER	02D	DPWA Multichannel
¹ Statistical error only.			

$N(1900)$ REFERENCES

MUELLER	20	PL B803 135323	J. Mueller et al.	(CBELSA/TAPS Collab.)
HUNT	19	PR C99 055205	B.C. Hunt, D.M. Manley	
ANISOVICH	17A	PRL 119 062004	A.V. Anisovich et al.	
ANISOVICH	17B	PL B771 142	A.V. Anisovich et al.	
ANISOVICH	17C	PL B772 247	A.V. Anisovich et al.	
DENISENKO	16	PL B755 97	I. Denisenko et al.	
SOKHOYAN	15A	EPJ A51 95	V. Sokhoyan et al.	(CBELSA/TAPS Collab.)
GUTZ	14	EPJ A50 74	E. Gutz et al.	(CBELSA/TAPS Collab.)
SVARC	14	PR C89 045205	A. Svarc et al.	(RBI Zagreb, UNI Tuzla)
ANISOVICH	13B	EPJ A49 67	A.V. Anisovich et al.	
SHKLYAR	13	PR C87 015201	V. Shklyar, H. Lenske, U. Mosel	(GIES)
ANISOVICH	12A	EPJ A48 15	A.V. Anisovich et al.	(BONN, PNPI)
SHRESTHA	12A	PR C86 055203	M. Shrestha, D.M. Manley	(KSU)
NIKONOV	08	PL B662 245	V.A. Nikonov et al.	(Bonn, Gatchina)
SHKLYAR	05	PR C72 015210	V. Shklyar, H. Lenske, U. Mosel	(GIES)
PENNER	02C	PR C66 055211	G. Penner, U. Mosel	(GIES)
PENNER	02D	PR C66 055212	G. Penner, U. Mosel	(GIES)
HOEHLER	79	PDAT 12-1	G. Hohler et al.	(KARLT)

$N(1990) 7/2^+$

 $I(J^P) = \frac{1}{2}(7/2^+)$ Status: **
 OMITTED FROM SUMMARY TABLE
 Older and obsolete values are listed and referenced in the 2014 edition, Chinese Physics C38 070001 (2014).

$N(1990)$ POLE POSITION

REAL PART

VALUE (MeV)	DOCUMENT ID	TECN	COMMENT
2030 ± 65	ANISOVICH	12A	DPWA Multichannel
1900 ± 30	CUTKOSKY	80	IPWA $\pi N \rightarrow \pi N$
••• We do not use the following data for averages, fits, limits, etc. •••			
1913	HUNT	19	DPWA Multichannel
1738	ROENCHEN	15A	DPWA Multichannel
2301	VRANA	00	DPWA Multichannel

-2xIMAGINARY PART

VALUE (MeV)	DOCUMENT ID	TECN	COMMENT
240 ± 60	ANISOVICH	12A	DPWA Multichannel
260 ± 60	CUTKOSKY	80	IPWA $\pi N \rightarrow \pi N$
••• We do not use the following data for averages, fits, limits, etc. •••			
163	HUNT	19	DPWA Multichannel
188	ROENCHEN	15A	DPWA Multichannel
202	VRANA	00	DPWA Multichannel

$N(1990)$ ELASTIC POLE RESIDUE

MODULUS $|r|$

VALUE (MeV)	DOCUMENT ID	TECN	COMMENT
2 ± 1	ANISOVICH	12A	DPWA Multichannel
9 ± 3	CUTKOSKY	80	IPWA $\pi N \rightarrow \pi N$
••• We do not use the following data for averages, fits, limits, etc. •••			
4.3	ROENCHEN	15A	DPWA Multichannel

PHASE θ

VALUE ($^\circ$)	DOCUMENT ID	TECN	COMMENT
125 ± 65	ANISOVICH	12A	DPWA Multichannel
-60 ± 30	CUTKOSKY	80	IPWA $\pi N \rightarrow \pi N$
••• We do not use the following data for averages, fits, limits, etc. •••			
-70	ROENCHEN	15A	DPWA Multichannel

$\Delta(1990)$ INELASTIC POLE RESIDUE

The "normalized residue" is the residue divided by $\Gamma_{pole}/2$.

Normalized residue in $N\pi \rightarrow N(1990) \rightarrow N\eta$

MODULUS	PHASE ($^\circ$)	DOCUMENT ID	TECN	COMMENT
••• We do not use the following data for averages, fits, limits, etc. •••				
0.013	-82	ROENCHEN	15A	DPWA Multichannel

Normalized residue in $N\pi \rightarrow N(1990) \rightarrow \Lambda K$

MODULUS	PHASE ($^\circ$)	DOCUMENT ID	TECN	COMMENT
••• We do not use the following data for averages, fits, limits, etc. •••				
0.022	-111	ROENCHEN	15A	DPWA Multichannel

Normalized residue in $N\pi \rightarrow N(1990) \rightarrow \Sigma K$

MODULUS	PHASE ($^\circ$)	DOCUMENT ID	TECN	COMMENT
••• We do not use the following data for averages, fits, limits, etc. •••				
0.005	24	ROENCHEN	15A	DPWA Multichannel

$N(1990)$ BREIT-WIGNER MASS

1950 to 2100 (≈ 2020) OUR ESTIMATE

VALUE (MeV)	DOCUMENT ID	TECN	COMMENT
2028 ± 19	¹ HUNT	19	DPWA Multichannel
2060 ± 65	ANISOVICH	12A	DPWA Multichannel
1970 ± 50	CUTKOSKY	80	IPWA $\pi N \rightarrow \pi N$
2005 ± 150	HOEHLER	79	IPWA $\pi N \rightarrow \pi N$
••• We do not use the following data for averages, fits, limits, etc. •••			
1990 ± 45	¹ SHRESTHA	12A	DPWA Multichannel
2311 ± 16	VRANA	00	DPWA Multichannel
¹ Statistical error only.			

$N(1990)$ BREIT-WIGNER WIDTH

200 to 400 (≈ 300) OUR ESTIMATE

VALUE (MeV)	DOCUMENT ID	TECN	COMMENT
490 ± 110	¹ HUNT	19	DPWA Multichannel
240 ± 50	ANISOVICH	12A	DPWA Multichannel
350 ± 120	CUTKOSKY	80	IPWA $\pi N \rightarrow \pi N$
350 ± 100	HOEHLER	79	IPWA $\pi N \rightarrow \pi N$
••• We do not use the following data for averages, fits, limits, etc. •••			
203 ± 161	¹ SHRESTHA	12A	DPWA Multichannel
205 ± 72	VRANA	00	DPWA Multichannel
¹ Statistical error only.			

Baryon Particle Listings

 $N(1990)$, $N(2000)$ $N(1990)$ DECAY MODES

Mode	Fraction (Γ_i/Γ)
Γ_1 $N\pi$	2–6 %
Γ_2 $N\eta$	<3 %
Γ_3 ΛK	5.9–6.1 %
Γ_4 $p\gamma$	0.01–0.12%
Γ_5 $p\gamma$, helicity=1/2	0.003–0.042%
Γ_6 $p\gamma$, helicity=3/2	0.009–0.075 %
Γ_7 $n\gamma$	0.01–0.16 %
Γ_8 $n\gamma$, helicity=1/2	0.003–0.066 %
Γ_9 $n\gamma$, helicity=3/2	0.003–0.098 %

 $N(1990)$ BRANCHING RATIOS

$\Gamma(N\pi)/\Gamma_{\text{total}}$	DOCUMENT ID	TECN	COMMENT	Γ_1/Γ
VALUE (%)				
2–6 % OUR ESTIMATE				
1.9 ± 0.4	¹ HUNT	19	DPWA Multichannel	
2 ± 1	ANISOVICH	12A	DPWA Multichannel	
6 ± 2	CUTKOSKY	80	IPWA $\pi N \rightarrow \pi N$	
4 ± 2	HOEHLER	79	IPWA $\pi N \rightarrow \pi N$	
••• We do not use the following data for averages, fits, limits, etc. •••				
2 ± 1	¹ SHRESTHA	12A	DPWA Multichannel	
22 ± 11	VRANA	00	DPWA Multichannel	

¹ Statistical error only.

$\Gamma(N\eta)/\Gamma_{\text{total}}$	DOCUMENT ID	TECN	COMMENT	Γ_2/Γ
VALUE (%)				
<3 % OUR ESTIMATE				
1 ± 1	MUELLER	20	DPWA Multichannel	
1.7 ± 0.9	¹ HUNT	19	DPWA Multichannel	

¹ Statistical error only.

$\Gamma(\Lambda K)/\Gamma_{\text{total}}$	DOCUMENT ID	TECN	COMMENT	Γ_3/Γ
VALUE (%)				
5.9–6.1 % OUR ESTIMATE				
6.0 ± 0.1	¹ HUNT	19	DPWA Multichannel	

¹ Statistical error only. $N(1990)$ PHOTON DECAY AMPLITUDES AT THE POLE

$N(1990) \rightarrow p\gamma$, helicity-1/2 amplitude $A_{1/2}$				
MODULUS ($\text{GeV}^{-1/2}$)	PHASE ($^\circ$)	DOCUMENT ID	TECN	COMMENT
0.010 +0.011 –0.006	–103 +108 –155	ROENCHEN	14	DPWA
••• We do not use the following data for averages, fits, limits, etc. •••				
0.029	67	ROENCHEN	15A	DPWA Multichannel

$N(1990) \rightarrow p\gamma$, helicity-3/2 amplitude $A_{3/2}$				
MODULUS ($\text{GeV}^{-1/2}$)	PHASE ($^\circ$)	DOCUMENT ID	TECN	COMMENT
0.053 +0.023 –0.028	36 +17 –4	ROENCHEN	14	DPWA
••• We do not use the following data for averages, fits, limits, etc. •••				
0.033	39	ROENCHEN	15A	DPWA Multichannel

 $N(1990)$ BREIT-WIGNER PHOTON DECAY AMPLITUDES

$N(1990) \rightarrow p\gamma$, helicity-1/2 amplitude $A_{1/2}$				
VALUE ($\text{GeV}^{-1/2}$)	DOCUMENT ID	TECN	COMMENT	
0.006 ± 0.003	¹ HUNT	19	DPWA Multichannel	
0.040 ± 0.012	ANISOVICH	12A	DPWA Multichannel	

¹ Statistical error only.

$N(1990) \rightarrow p\gamma$, helicity-3/2 amplitude $A_{3/2}$				
VALUE ($\text{GeV}^{-1/2}$)	DOCUMENT ID	TECN	COMMENT	
–0.055 ± 0.008	¹ HUNT	19	DPWA Multichannel	
0.057 ± 0.012	ANISOVICH	12A	DPWA Multichannel	

¹ Statistical error only.

$N(1990) \rightarrow n\gamma$, helicity-1/2 amplitude $A_{1/2}$				
VALUE ($\text{GeV}^{-1/2}$)	DOCUMENT ID	TECN	COMMENT	
–0.027 ± 0.024	¹ HUNT	19	DPWA Multichannel	
–0.045 ± 0.020	ANISOVICH	13B	DPWA Multichannel	

¹ Statistical error only.

$N(1990) \rightarrow n\gamma$, helicity-3/2 amplitude $A_{3/2}$				
VALUE ($\text{GeV}^{-1/2}$)	DOCUMENT ID	TECN	COMMENT	
0.051 ± 0.020	¹ HUNT	19	DPWA Multichannel	
–0.052 ± 0.027	ANISOVICH	13B	DPWA Multichannel	

¹ Statistical error only. $N(1990)$ REFERENCESFor early references, see Physics Letters **111B** 1 (1982).

MUELLER	20	PL B803 135323	J. Mueller <i>et al.</i>	(CBELSA/TAPS Collab.)
HUNT	19	PR C99 055205	B. C. Hunt, D. M. Manley	
ROENCHEN	15A	EPJ A51 70	D. Roenchen <i>et al.</i>	
PDG	14	CP C38 070001	K. Olive <i>et al.</i>	(PDG Collab.)
ROENCHEN	14	EPJ A50 101	D. Roenchen <i>et al.</i>	
Also		EPJ A51 63 (errata.)	D. Roenchen <i>et al.</i>	
ANISOVICH	13B	EPJ A49 67	A. V. Anisovich <i>et al.</i>	
ANISOVICH	12A	EPJ A48 15	A. V. Anisovich <i>et al.</i>	(BONN, PNPI)
SHRESTHA	12A	PR C86 055203	M. Shrestha, D. M. Manley	(KSU)
VRANA	00	PRPL 328 181	T. P. Vrana, S. A. Dytman, T.-S. H. Lee	(PITT, ANL)
CUTKOSKY	80	Toronto Conf. 19	R. E. Cutkosky <i>et al.</i>	(CMU, LBL) IJP
Also		PR D20 2839	R. E. Cutkosky <i>et al.</i>	(CMU, LBL) IJP
HOEHLER	79	PDAT 12-1	G. Hoehler <i>et al.</i>	(KARLT) IJP
Also		Toronto Conf. 3	R. Koch	(KARLT) IJP

 $N(2000) 5/2^+$ $I(J^P) = \frac{1}{2}(\frac{5}{2}^+)$ Status: **

OMITTED FROM SUMMARY TABLE

Before the 2012 *Review*, all the evidence for a $J^P = 5/2^+$ state with a mass above 1800 MeV was filed under a two-star $N(2000)$. There is now some evidence from ANISOVICH 12A for two $5/2^+$ states in this region, so we have split the older data (according to mass) between two two-star $5/2^+$ states, an $N(1860)$ and an $N(2000)$.

 $N(2000)$ POLE POSITION

REAL PART	DOCUMENT ID	TECN	COMMENT
VALUE (MeV)			
2030 ± 40	SOKHOYAN	15A	DPWA Multichannel
••• We do not use the following data for averages, fits, limits, etc. •••			
1900	SHKLYAR	13	DPWA Multichannel
2030 ± 110	ANISOVICH	12A	DPWA Multichannel

–2×IMAGINARY PART

REAL PART	DOCUMENT ID	TECN	COMMENT
VALUE (MeV)			
380 ± 60	SOKHOYAN	15A	DPWA Multichannel
••• We do not use the following data for averages, fits, limits, etc. •••			
123	SHKLYAR	13	DPWA Multichannel
480 ± 100	ANISOVICH	12A	DPWA Multichannel

 $N(2000)$ ELASTIC POLE RESIDUE

MODULUS $ r $	DOCUMENT ID	TECN	COMMENT
VALUE (MeV)			
18 ± 8	SOKHOYAN	15A	DPWA Multichannel
••• We do not use the following data for averages, fits, limits, etc. •••			
11	SHKLYAR	13	DPWA Multichannel
35 +8 –15	ANISOVICH	12A	DPWA Multichannel

PHASE θ

PHASE θ	DOCUMENT ID	TECN	COMMENT
VALUE ($^\circ$)			
–15.0 ± 4.0	SOKHOYAN	15A	DPWA Multichannel
••• We do not use the following data for averages, fits, limits, etc. •••			
–6	SHKLYAR	13	DPWA Multichannel
–100 ± 40	ANISOVICH	12A	DPWA Multichannel

 $N(2000)$ INELASTIC POLE RESIDUEThe “normalized residue” is the residue divided by $\Gamma_{\text{pole}}/2$.

Normalized residue in $N\pi \rightarrow N(2000) \rightarrow \Delta(1232)\pi$, P-wave				
MODULUS	PHASE ($^\circ$)	DOCUMENT ID	TECN	COMMENT
0.16 ± 0.06	100 ± 50	SOKHOYAN	15A	DPWA Multichannel

Normalized residue in $N\pi \rightarrow N(2000) \rightarrow \Delta(1232)\pi$, F-wave				
MODULUS	PHASE ($^\circ$)	DOCUMENT ID	TECN	COMMENT
0.20 ± 0.10	–20 ± 45	SOKHOYAN	15A	DPWA Multichannel

Normalized residue in $N\pi \rightarrow N(2000) \rightarrow N\sigma$				
MODULUS	PHASE ($^\circ$)	DOCUMENT ID	TECN	COMMENT
0.12 ± 0.06	80 ± 40	SOKHOYAN	15A	DPWA Multichannel

Normalized residue in $N\pi \rightarrow N(2000) \rightarrow N(1520)\pi$, D-wave				
MODULUS	PHASE ($^\circ$)	DOCUMENT ID	TECN	COMMENT
0.17 ± 0.09	–60 ± 35	SOKHOYAN	15A	DPWA Multichannel

 $N(2000)$ BREIT-WIGNER MASS

VALUE (MeV)	DOCUMENT ID	TECN	COMMENT
2060 ± 30	SOKHOYAN	15A	DPWA Multichannel
1946 ± 4	¹ SHKLYAR	13	DPWA Multichannel

See key on page 1127

Baryon Particle Listings
 $N(2000)$, $N(2040)$

••• We do not use the following data for averages, fits, limits, etc. •••
 2090 ± 120 ANISOVICH 12A DPWA Multichannel
¹ Statistical error only.

$N(2000)$ BREIT-WIGNER WIDTH

VALUE (MeV)	DOCUMENT ID	TECN	COMMENT
390 ± 55	SOKHOYAN 15A	DPWA	Multichannel
198 ± 2	² SHKLYAR 13	DPWA	Multichannel
••• We do not use the following data for averages, fits, limits, etc. •••			
460 ± 100	ANISOVICH 12A	DPWA	Multichannel

² Statistical error only.

$N(2000)$ DECAY MODES

Mode	Fraction (Γ_i/Γ)
Γ_1 $N\pi$	6–10 %
Γ_2 $N\eta$	<4 %
Γ_3 $N\omega$	<2 %
Γ_4 $N\pi\pi$	35–90 %
Γ_5 $\Delta(1232)\pi$	30–80 %
Γ_6 $\Delta(1232)\pi$, P -wave	12–32 %
Γ_7 $\Delta(1232)\pi$, F -wave	19–49 %
Γ_8 $N\sigma$	5–15 %
Γ_9 $N(1520)\pi$, D -wave	11–31 %
Γ_{10} $N(1680)\pi$, P -wave	17–25 %
Γ_{11} $\Lambda K^*(892)$	1–3 %
Γ_{12} $p\gamma$	0.01–0.08 %
Γ_{13} $p\gamma$, helicity=1/2	0.003–0.031 %
Γ_{14} $p\gamma$, helicity=3/2	0.008–0.048 %
Γ_{15} $n\gamma$	0.002–0.07 %
Γ_{16} $n\gamma$, helicity=1/2	<0.017 %
Γ_{17} $n\gamma$, helicity=3/2	0.001–0.056 %

$N(2000)$ BRANCHING RATIOS

$\Gamma(N\pi)/\Gamma_{total}$	DOCUMENT ID	TECN	COMMENT	Γ_1/Γ
VALUE (%)				
6 to 10 (≈ 8) OUR ESTIMATE				
8 ± 4	SOKHOYAN 15A	DPWA	Multichannel	
10 ± 1	³ SHKLYAR 13	DPWA	Multichannel	
••• We do not use the following data for averages, fits, limits, etc. •••				
9 ± 4	ANISOVICH 12A	DPWA	Multichannel	

³ Statistical error only.

$\Gamma(N\eta)/\Gamma_{total}$	DOCUMENT ID	TECN	COMMENT	Γ_2/Γ
VALUE (%)				
2 ± 2	MUELLER 20	DPWA	Multichannel	
2 ± 2	⁴ SHKLYAR 13	DPWA	Multichannel	

⁴ Statistical error only.

$\Gamma(N\omega)/\Gamma_{total}$	DOCUMENT ID	TECN	COMMENT	Γ_3/Γ
VALUE (%)				
18 ± 8	DENISENKO 16	DPWA	Multichannel	
1 ± 1	⁵ SHKLYAR 13	DPWA	Multichannel	

⁵ Statistical error only.

$\Gamma(\Delta(1232)\pi, P\text{-wave})/\Gamma_{total}$	DOCUMENT ID	TECN	COMMENT	Γ_6/Γ
VALUE (%)				
22 ± 10	SOKHOYAN 15A	DPWA	Multichannel	

$\Gamma(\Delta(1232)\pi, F\text{-wave})/\Gamma_{total}$	DOCUMENT ID	TECN	COMMENT	Γ_7/Γ
VALUE (%)				
34 ± 15	SOKHOYAN 15A	DPWA	Multichannel	

$\Gamma(N\sigma)/\Gamma_{total}$	DOCUMENT ID	TECN	COMMENT	Γ_8/Γ
VALUE (%)				
10 ± 5	SOKHOYAN 15A	DPWA	Multichannel	

$\Gamma(N(1520)\pi, D\text{-wave})/\Gamma_{total}$	DOCUMENT ID	TECN	COMMENT	Γ_9/Γ
VALUE (%)				
21 ± 10	SOKHOYAN 15A	DPWA	Multichannel	

$\Gamma(N(1680)\pi, P\text{-wave})/\Gamma_{total}$	DOCUMENT ID	TECN	COMMENT	Γ_{10}/Γ
VALUE (%)				
16 ± 9	SOKHOYAN 15A	DPWA	Multichannel	

$\Gamma(\Lambda K^*(892))/\Gamma_{total}$	DOCUMENT ID	TECN	COMMENT	Γ_{11}/Γ
VALUE (%)				
1–3 % OUR EVALUATION				
2.2 ± 1.0	ANISOVICH 17B	DPWA	Multichannel	

$N(2000)$ PHOTON DECAY AMPLITUDES AT THE POLE

$N(2000) \rightarrow p\gamma$, helicity-1/2 amplitude $A_{1/2}$				
MODULUS ($\text{GeV}^{-1/2}$)	PHASE ($^\circ$)	DOCUMENT ID	TECN	COMMENT
0.033 ± 0.010	15 ± 25	SOKHOYAN 15A	DPWA	Multichannel

$N(2000) \rightarrow p\gamma$, helicity-3/2 amplitude $A_{3/2}$				
MODULUS ($\text{GeV}^{-1/2}$)	PHASE ($^\circ$)	DOCUMENT ID	TECN	COMMENT
0.045 ± 0.008	−140 ± 25	SOKHOYAN 15A	DPWA	Multichannel

$N(2000)$ BREIT-WIGNER PHOTON DECAY AMPLITUDES

$N(2000) \rightarrow p\gamma$, helicity-1/2 amplitude $A_{1/2}$				
VALUE ($\text{GeV}^{-1/2}$)	DOCUMENT ID	TECN	COMMENT	
0.031 ± 0.010	SOKHOYAN 15A	DPWA	Multichannel	
0.011 ± 0.001	⁶ SHKLYAR 13	DPWA	Multichannel	

⁶ Statistical error only.

$N(2000) \rightarrow p\gamma$, helicity-3/2 amplitude $A_{3/2}$				
VALUE ($\text{GeV}^{-1/2}$)	DOCUMENT ID	TECN	COMMENT	
−0.043 ± 0.008	SOKHOYAN 15A	DPWA	Multichannel	
0.025 ± 0.001	⁷ SHKLYAR 13	DPWA	Multichannel	

⁷ Statistical error only.

$N(2000) \rightarrow n\gamma$, helicity-1/2 amplitude $A_{1/2}$				
VALUE ($\text{GeV}^{-1/2}$)	DOCUMENT ID	TECN	COMMENT	
−0.018 ± 0.012	ANISOVICH 13B	DPWA	Multichannel	

$N(2000) \rightarrow n\gamma$, helicity-3/2 amplitude $A_{3/2}$				
VALUE ($\text{GeV}^{-1/2}$)	DOCUMENT ID	TECN	COMMENT	
−0.035 ± 0.020	ANISOVICH 13B	DPWA	Multichannel	

$N(2000)$ REFERENCES

MUELLER 20	PL B803 135323	J. Mueller et al.	(CBELSA/TAPS Collab.)
ANISOVICH 17B	PL B771 142	A.V. Anisovich et al.	
DENISENKO 16	PL B755 97	I. Denisenko et al.	
SOKHOYAN 15A	EPJ A51 95	V. Sokhoyan et al.	(CBELSA/TAPS Collab.)
ANISOVICH 13B	EPJ A49 67	A.V. Anisovich et al.	
SHKLYAR 13	PR C87 015201	V. Shklyar, H. Lenske, U. Mosel	(GIES)
ANISOVICH 12A	EPJ A48 15	A.V. Anisovich et al.	(BONN, PNPI)

$N(2040) 3/2^+$ $J^P = \frac{3}{2}^+$ Status: *

OMITTED FROM SUMMARY TABLE

$N(2040)$ MASS

VALUE (MeV)	DOCUMENT ID	TECN	COMMENT
2040 \pm $\frac{3}{4}$ ± 25	ABLIKIM 09B	BES2	$J/\psi \rightarrow p\bar{p}\pi^0$
2068 ± 3 \pm $\frac{15}{40}$	ABLIKIM 06K	BES2	$J/\psi \rightarrow p\bar{p}\pi^-, n\bar{p}\pi^+$
••• We do not use the following data for averages, fits, limits, etc. •••			
2244 ± 30	^{1,2} HUNT 19	DPWA	Multichannel

¹ Statistical error only.
² We list here candidates for high-mass $3/2^+$ states.

$N(2040)$ WIDTH

VALUE (MeV)	DOCUMENT ID	TECN	COMMENT
230 ± 8 ± 52	ABLIKIM 09B	BES2	$J/\psi \rightarrow p\bar{p}\pi^0$
165 ± 14 ± 40	ABLIKIM 06K	BES2	$J/\psi \rightarrow p\bar{p}\pi^-, n\bar{p}\pi^+$
••• We do not use the following data for averages, fits, limits, etc. •••			
530 ± 89	^{3,4} HUNT 19	DPWA	Multichannel

³ Statistical error only.
⁴ We list here candidates for high-mass $3/2^+$ states.

$N(2040)$ REFERENCES

HUNT 19	PR C99 055205	B.C. Hunt, D.M. Manley	
ABLIKIM 09B	PR D80 052004	M. Ablikim et al.	(BES II Collab.)
ABLIKIM 06K	PRL 97 062001	M. Ablikim et al.	(BES II Collab.)

Baryon Particle Listings

 $N(2060)$ $N(2060) 5/2^-$

$$I(J^P) = \frac{1}{2}(\frac{5}{2}^-) \text{ Status: } ***$$

Before our 2012 Review, this state appeared in our Listings as the $N(2200)$.

 $N(2060)$ POLE POSITION

REAL PART

VALUE (MeV)	DOCUMENT ID	TECN	COMMENT
2020 to 2130 (≈ 2070) OUR ESTIMATE			
2030 \pm 15	SOKHOYAN 15A	DPWA	Multichannel
2119 \pm 11 \pm 1	¹ SVARC 14	L+P	$\pi N \rightarrow \pi N$
2100 \pm 60	CUTKOSKY 80	IPWA	$\pi N \rightarrow \pi N$
••• We do not use the following data for averages, fits, limits, etc. •••			
2010	HUNT 19	DPWA	Multichannel
2040 \pm 15	ANISOVICH 12A	DPWA	Multichannel
2144 \pm 31	BATINIC 10	DPWA	$\pi N \rightarrow N\pi, N\eta$

¹ Fit to the amplitudes of HOEHLER 79.

-2xIMAGINARY PART

VALUE (MeV)	DOCUMENT ID	TECN	COMMENT
350 to 430 (≈ 400) OUR ESTIMATE			
400 \pm 35	SOKHOYAN 15A	DPWA	Multichannel
370 \pm 20 \pm 5	¹ SVARC 14	L+P	$\pi N \rightarrow \pi N$
360 \pm 80	CUTKOSKY 80	IPWA	$\pi N \rightarrow \pi N$
••• We do not use the following data for averages, fits, limits, etc. •••			
395	HUNT 19	DPWA	Multichannel
390 \pm 25	ANISOVICH 12A	DPWA	Multichannel
438 \pm 13	BATINIC 10	DPWA	$\pi N \rightarrow N\pi, N\eta$

¹ Fit to the amplitudes of HOEHLER 79.

 $N(2060)$ ELASTIC POLE RESIDUEMODULUS $|r|$

VALUE (MeV)	DOCUMENT ID	TECN	COMMENT
15 to 30 (≈ 20) OUR ESTIMATE			
25 \pm 8	SOKHOYAN 15A	DPWA	Multichannel
19 \pm 1 \pm 1	¹ SVARC 14	L+P	$\pi N \rightarrow \pi N$
20 \pm 10	CUTKOSKY 80	IPWA	$\pi N \rightarrow \pi N$
••• We do not use the following data for averages, fits, limits, etc. •••			
19 \pm 5	ANISOVICH 12A	DPWA	Multichannel
26	BATINIC 10	DPWA	$\pi N \rightarrow N\pi, N\eta$

¹ Fit to the amplitudes of HOEHLER 79.

PHASE θ

VALUE ($^\circ$)	DOCUMENT ID	TECN	COMMENT
-130 to -90 (≈ -110) OUR ESTIMATE			
-130 \pm 20	SOKHOYAN 15A	DPWA	Multichannel
-94 \pm 5 \pm 1	¹ SVARC 14	L+P	$\pi N \rightarrow \pi N$
-90 \pm 50	CUTKOSKY 80	IPWA	$\pi N \rightarrow \pi N$
••• We do not use the following data for averages, fits, limits, etc. •••			
-125 \pm 20	ANISOVICH 12A	DPWA	Multichannel
-71	BATINIC 10	DPWA	$\pi N \rightarrow N\pi, N\eta$

¹ Fit to the amplitudes of HOEHLER 79.

 $N(2060)$ INELASTIC POLE RESIDUE

The "normalized residue" is the residue divided by $\Gamma_{pole}/2$.

Normalized residue in $N\pi \rightarrow N(2060) \rightarrow N\eta$

MODULUS	PHASE ($^\circ$)	DOCUMENT ID	TECN	COMMENT
0.05 \pm 0.03	40 \pm 25	ANISOVICH 12A	DPWA	Multichannel

Normalized residue in $N\pi \rightarrow N(2060) \rightarrow \Lambda K$

MODULUS	DOCUMENT ID	TECN	COMMENT
0.01 \pm 0.005	ANISOVICH 12A	DPWA	Multichannel

Normalized residue in $N\pi \rightarrow N(2060) \rightarrow \Sigma K$

MODULUS	PHASE ($^\circ$)	DOCUMENT ID	TECN	COMMENT
0.04 \pm 0.02	-70 \pm 30	ANISOVICH 12A	DPWA	Multichannel

Normalized residue in $N\pi \rightarrow N(2060) \rightarrow \Delta(1232)\pi, D\text{-wave}$

MODULUS	PHASE ($^\circ$)	DOCUMENT ID	TECN	COMMENT
0.06 \pm 0.03	-90 \pm 40	SOKHOYAN 15A	DPWA	Multichannel

Normalized residue in $N\pi \rightarrow N(2060) \rightarrow N\sigma$

MODULUS	PHASE ($^\circ$)	DOCUMENT ID	TECN	COMMENT
0.12 \pm 0.06	80 \pm 40	SOKHOYAN 15A	DPWA	Multichannel

Normalized residue in $N\pi \rightarrow N(2060) \rightarrow N(1440)\pi$

MODULUS	PHASE ($^\circ$)	DOCUMENT ID	TECN	COMMENT
0.17 \pm 0.09	-60 \pm 35	SOKHOYAN 15A	DPWA	Multichannel

Normalized residue in $N\pi \rightarrow N(2060) \rightarrow N(1520)\pi, P\text{-wave}$

MODULUS	PHASE ($^\circ$)	DOCUMENT ID	TECN	COMMENT
0.14 \pm 0.06	-45 \pm 15	SOKHOYAN 15A	DPWA	Multichannel

 $N(2060)$ BREIT-WIGNER MASS

VALUE (MeV)	DOCUMENT ID	TECN	COMMENT
2030 to 2200 (≈ 2100) OUR ESTIMATE			
2111 \pm 17	¹ HUNT 19	DPWA	Multichannel
2045 \pm 15	SOKHOYAN 15A	DPWA	Multichannel
2180 \pm 80	CUTKOSKY 80	IPWA	$\pi N \rightarrow \pi N$
2228 \pm 30	HOEHLER 79	IPWA	$\pi N \rightarrow \pi N$
••• We do not use the following data for averages, fits, limits, etc. •••			
2060 \pm 15	ANISOVICH 12A	DPWA	Multichannel
2116 \pm 21	¹ SHRESTHA 12A	DPWA	Multichannel
2217 \pm 27	BATINIC 10	DPWA	$\pi N \rightarrow N\pi, N\eta$

¹ Statistical error only.

 $N(2060)$ BREIT-WIGNER WIDTH

VALUE (MeV)	DOCUMENT ID	TECN	COMMENT
300 to 450 (≈ 400) OUR ESTIMATE			
499 \pm 70	¹ HUNT 19	DPWA	Multichannel
420 \pm 30	SOKHOYAN 15A	DPWA	Multichannel
400 \pm 100	CUTKOSKY 80	IPWA	$\pi N \rightarrow \pi N$
310 \pm 50	HOEHLER 79	IPWA	$\pi N \rightarrow \pi N$
••• We do not use the following data for averages, fits, limits, etc. •••			
375 \pm 25	ANISOVICH 12A	DPWA	Multichannel
307 \pm 112	¹ SHRESTHA 12A	DPWA	Multichannel
481 \pm 17	BATINIC 10	DPWA	$\pi N \rightarrow N\pi, N\eta$

¹ Statistical error only.

 $N(2060)$ DECAY MODES

Mode	Fraction (Γ_i/Γ)
Γ_1 $N\pi$	7-12 %
Γ_2 $N\eta$	2-38 %
Γ_3 $N\omega$	1-7 %
Γ_4 ΛK	10-20 %
Γ_5 ΣK	1-5 %
Γ_6 $N\pi\pi$	12-52 %
Γ_7 $\Delta(1232)\pi, D\text{-wave}$	4-10 %
Γ_8 $N\rho$	5-33 %
Γ_9 $N\rho, S=1/2, P\text{-wave}$	<10 %
Γ_{10} $N\rho, S=3/2, D\text{-wave}$	5-23 %
Γ_{11} $N\sigma$	3-9 %
Γ_{12} $N(1440)\pi$	4-14 %
Γ_{13} $N(1520)\pi, P\text{-wave}$	9-21 %
Γ_{14} $N(1680)\pi, S\text{-wave}$	8-22 %
Γ_{15} $\Lambda K^*(892)$	0.3-1.3 %
Γ_{16} $p\gamma$	0.03-0.19 %
Γ_{17} $p\gamma, \text{helicity}=1/2$	0.02-0.08 %
Γ_{18} $p\gamma, \text{helicity}=3/2$	0.01-0.10 %
Γ_{19} $n\gamma$	0.003-0.07 %
Γ_{20} $n\gamma, \text{helicity}=1/2$	0.001-0.02 %
Γ_{21} $n\gamma, \text{helicity}=3/2$	0.002-0.05 %

 $N(2060)$ BRANCHING RATIOS

$\Gamma(N\pi)/\Gamma_{total}$	DOCUMENT ID	TECN	COMMENT	Γ_1/Γ
7 to 12 (≈ 10) OUR ESTIMATE				
5.3 \pm 1.4	¹ HUNT 19	DPWA	Multichannel	
11 \pm 2	SOKHOYAN 15A	DPWA	Multichannel	
10 \pm 3	CUTKOSKY 80	IPWA	$\pi N \rightarrow \pi N$	
7 \pm 2	HOEHLER 79	IPWA	$\pi N \rightarrow \pi N$	
••• We do not use the following data for averages, fits, limits, etc. •••				
8 \pm 2	ANISOVICH 12A	DPWA	Multichannel	
9 \pm 2	¹ SHRESTHA 12A	DPWA	Multichannel	
13 \pm 4	BATINIC 10	DPWA	$\pi N \rightarrow N\pi, N\eta$	

¹ Statistical error only.

$\Gamma(N\eta)/\Gamma_{total}$	DOCUMENT ID	TECN	COMMENT	Γ_2/Γ
2-38 % OUR ESTIMATE				
6 \pm 2	MUELLER 20	DPWA	Multichannel	
30 \pm 8	¹ HUNT 19	DPWA	Multichannel	
4 \pm 2	ANISOVICH 12A	DPWA	Multichannel	
••• We do not use the following data for averages, fits, limits, etc. •••				
< 1	¹ SHRESTHA 12A	DPWA	Multichannel	
0.2 \pm 1.0	BATINIC 10	DPWA	$\pi N \rightarrow N\pi, N\eta$	

¹ Statistical error only.

$\Gamma(N\omega)/\Gamma_{total}$	DOCUMENT ID	TECN	COMMENT	Γ_3/Γ
VALUE (%)				
4±3	DENISENKO 16	DPWA	Multichannel	
$\Gamma(\Lambda K)/\Gamma_{total}$	DOCUMENT ID	TECN	COMMENT	Γ_4/Γ
VALUE (%)				
10-20 % OUR ESTIMATE				
15±5	¹ HUNT 19	DPWA	Multichannel	
¹ Statistical error only.				
$\Gamma(\Sigma K)/\Gamma_{total}$	DOCUMENT ID	TECN	COMMENT	Γ_5/Γ
VALUE (%)				
3±2	ANISOVICH 12A	DPWA	Multichannel	
$\Gamma(\Delta(1232)\pi, D\text{-wave})/\Gamma_{total}$	DOCUMENT ID	TECN	COMMENT	Γ_7/Γ
VALUE (%)				
4-10 % OUR ESTIMATE				
15±6	¹ HUNT 19	DPWA	Multichannel	
7±3	SOKHOYAN 15A	DPWA	Multichannel	
••• We do not use the following data for averages, fits, limits, etc. •••				
40±13	¹ SHRESTHA 12A	DPWA	Multichannel	
¹ Statistical error only.				
$\Gamma(N\rho, S=1/2, P\text{-wave})/\Gamma_{total}$	DOCUMENT ID	TECN	COMMENT	Γ_9/Γ
VALUE (%)				
<10 % OUR ESTIMATE				
<10	¹ HUNT 19	DPWA	Multichannel	
••• We do not use the following data for averages, fits, limits, etc. •••				
21±15	¹ SHRESTHA 12A	DPWA	Multichannel	
¹ Statistical error only.				
$\Gamma(N\rho, S=3/2, D\text{-wave})/\Gamma_{total}$	DOCUMENT ID	TECN	COMMENT	Γ_{10}/Γ
VALUE (%)				
5-23 % OUR ESTIMATE				
14±9	¹ HUNT 19	DPWA	Multichannel	
¹ Statistical error only.				
$\Gamma(N\sigma)/\Gamma_{total}$	DOCUMENT ID	TECN	COMMENT	Γ_{11}/Γ
VALUE (%)				
6±3	SOKHOYAN 15A	DPWA	Multichannel	
$\Gamma(N(1440)\pi)/\Gamma_{total}$	DOCUMENT ID	TECN	COMMENT	Γ_{12}/Γ
VALUE (%)				
9±5	SOKHOYAN 15A	DPWA	Multichannel	
$\Gamma(N(1520)\pi, P\text{-wave})/\Gamma_{total}$	DOCUMENT ID	TECN	COMMENT	Γ_{13}/Γ
VALUE (%)				
15±6	SOKHOYAN 15A	DPWA	Multichannel	
$\Gamma(N(1680)\pi, S\text{-wave})/\Gamma_{total}$	DOCUMENT ID	TECN	COMMENT	Γ_{14}/Γ
VALUE (%)				
15±7	SOKHOYAN 15A	DPWA	Multichannel	
$\Gamma(\Lambda K^*(892))/\Gamma_{total}$	DOCUMENT ID	TECN	COMMENT	Γ_{15}/Γ
VALUE (%)				
0.3-1.3 % OUR ESTIMATE				
0.8±0.5	ANISOVICH 17B	DPWA	Multichannel	

N(2060) PHOTON DECAY AMPLITUDES AT THE POLE

N(2060) → pγ, helicity-1/2 amplitude A_{1/2}

MODULUS (GeV ^{-1/2})	PHASE (°)	DOCUMENT ID	TECN	COMMENT
0.064±0.010	12±8	SOKHOYAN 15A	DPWA	Multichannel

N(2060) → pγ, helicity-3/2 amplitude A_{3/2}

MODULUS (GeV ^{-1/2})	PHASE (°)	DOCUMENT ID	TECN	COMMENT
0.060±0.020	13±10	SOKHOYAN 15A	DPWA	Multichannel

N(2060) BREIT-WIGNER PHOTON DECAY AMPLITUDES

N(2060) → pγ, helicity-1/2 amplitude A_{1/2}

VALUE (GeV ^{-1/2})	DOCUMENT ID	TECN	COMMENT
-0.019±0.005	¹ HUNT 19	DPWA	Multichannel
0.062±0.010	SOKHOYAN 15A	DPWA	Multichannel
••• We do not use the following data for averages, fits, limits, etc. •••			
0.018±0.004	¹ SHRESTHA 12A	DPWA	Multichannel
¹ Statistical error only.			

N(2060) → pγ, helicity-3/2 amplitude A_{3/2}

VALUE (GeV ^{-1/2})	DOCUMENT ID	TECN	COMMENT
0.039±0.005	¹ HUNT 19	DPWA	Multichannel
0.062±0.020	SOKHOYAN 15A	DPWA	Multichannel
••• We do not use the following data for averages, fits, limits, etc. •••			
0.010±0.004	¹ SHRESTHA 12A	DPWA	Multichannel
¹ Statistical error only.			

N(2060) → nγ, helicity-1/2 amplitude A_{1/2}

VALUE (GeV ^{-1/2})	DOCUMENT ID	TECN	COMMENT
0.069±0.017	¹ HUNT 19	DPWA	Multichannel
0.025±0.011	ANISOVICH 13B	DPWA	Multichannel
••• We do not use the following data for averages, fits, limits, etc. •••			
-0.012±0.017	¹ SHRESTHA 12A	DPWA	Multichannel
¹ Statistical error only.			

N(2060) → nγ, helicity-3/2 amplitude A_{3/2}

VALUE (GeV ^{-1/2})	DOCUMENT ID	TECN	COMMENT
-0.023±0.020	¹ HUNT 19	DPWA	Multichannel
-0.037±0.017	ANISOVICH 13B	DPWA	Multichannel
••• We do not use the following data for averages, fits, limits, etc. •••			
-0.023±0.023	¹ SHRESTHA 12A	DPWA	Multichannel
¹ Statistical error only.			

N(2060) REFERENCES

MUELLER 20	PL B803 135323	J. Mueller et al.	(CBELSA/TAPS Collab.)
HUNT 19	PR C99 055205	B.C. Hunt, D.M. Manley	
ANISOVICH 17B	PL B771 142	A.V. Anisovich et al.	
DENISENKO 16	PL B755 97	I. Denisenko et al.	
SOKHOYAN 15A	EPJ A51 95	V. Sokhoyan et al.	(CBELSA/TAPS Collab.)
SVARC 14	PR C89 045205	A. Svarc et al.	(RBI Zagreb, UNI Tuzla)
ANISOVICH 13B	EPJ A49 67	A.V. Anisovich et al.	
ANISOVICH 12A	EPJ A48 15	A.V. Anisovich et al.	(BONN, PNPI)
SHRESTHA 12A	PR C86 055203	M. Shrestha, D.M. Manley	(KSU)
BATINIC 10	PR C82 038203	M. Batinic et al.	(ZAGR)
CUTKOSKY 80	Toronto Conf. 19	R.E. Cutkosky et al.	(CMU, LBL) IJF
	Also PR D20 2839	R.E. Cutkosky et al.	(CMU, LBL)
HOEHLER 79	PDAT 12-1	G. Hoehler et al.	(KARLT) IJF
	Also Toronto Conf. 3	R. Koch	(KARLT) IJF

N(2100) 1/2⁺

$I(J^P) = \frac{1}{2}(\frac{1}{2}^+)$ Status: ***

N(2100) POLE POSITION

REAL PART

VALUE (MeV)	DOCUMENT ID	TECN	COMMENT
2050 to 2150 (≈ 2100) OUR ESTIMATE			
2120±25	SOKHOYAN 15A	DPWA	Multichannel
2052±6±3	¹ SVARC 14	L+P	πN → πN
2120±40	CUTKOSKY 80	IPWA	πN → πN
••• We do not use the following data for averages, fits, limits, etc. •••			
2217	HUNT 19	DPWA	Multichannel
2120±47	BATINIC 10	DPWA	πN → Nπ, Nη
1810	VRANA 00	DPWA	Multichannel
¹ Fit to the amplitudes of HOEHLER 79.			

-2xIMAGINARY PART

VALUE (MeV)	DOCUMENT ID	TECN	COMMENT
240 to 340 (≈ 300) OUR ESTIMATE			
290±30	SOKHOYAN 15A	DPWA	Multichannel
337±10±4	¹ SVARC 14	L+P	πN → πN
240±80	CUTKOSKY 80	IPWA	πN → πN
••• We do not use the following data for averages, fits, limits, etc. •••			
545	HUNT 19	DPWA	Multichannel
346±80	BATINIC 10	DPWA	πN → Nπ, Nη
622	VRANA 00	DPWA	Multichannel
¹ Fit to the amplitudes of HOEHLER 79.			

N(2100) ELASTIC POLE RESIDUE

MODULUS |r|

VALUE (MeV)	DOCUMENT ID	TECN	COMMENT
15 to 30 (≈ 20) OUR ESTIMATE			
23±5	SOKHOYAN 15A	DPWA	Multichannel
30±1±1	¹ SVARC 14	L+P	πN → πN
14±7	CUTKOSKY 80	IPWA	πN → πN
••• We do not use the following data for averages, fits, limits, etc. •••			
33	BATINIC 10	DPWA	πN → Nπ, Nη
¹ Fit to the amplitudes of HOEHLER 79.			

PHASE θ

VALUE (°)	DOCUMENT ID	TECN	COMMENT
-100 to -60 (≈ -80) OUR ESTIMATE			
-70±25	SOKHOYAN 15A	DPWA	Multichannel
-92±3±2	¹ SVARC 14	L+P	πN → πN
35±25	CUTKOSKY 80	IPWA	πN → πN
••• We do not use the following data for averages, fits, limits, etc. •••			
-59	BATINIC 10	DPWA	πN → Nπ, Nη
¹ Fit to the amplitudes of HOEHLER 79.			

Baryon Particle Listings

 $N(2100)$ $N(2100)$ INELASTIC POLE RESIDUENormalized residue in $N\pi \rightarrow N(2100) \rightarrow \Delta(1232)\pi$

MODULUS	PHASE (°)	DOCUMENT ID	TECN	COMMENT
0.11±0.05	20 ± 60	SOKHOYAN 15A	DPWA	Multichannel

Normalized residue in $N\pi \rightarrow N(2100) \rightarrow N\sigma$

MODULUS	PHASE (°)	DOCUMENT ID	TECN	COMMENT
0.18±0.06	125 ± 25	SOKHOYAN 15A	DPWA	Multichannel

Normalized residue in $N\pi \rightarrow N(2100) \rightarrow N(1535)\pi$

MODULUS	PHASE (°)	DOCUMENT ID	TECN	COMMENT
0.22±0.06	-40 ± 25	SOKHOYAN 15A	DPWA	Multichannel

 $N(2100)$ BREIT-WIGNER MASS

VALUE (MeV)	DOCUMENT ID	TECN	COMMENT
2050 to 2150 (≈ 2100) OUR ESTIMATE			
2221 ± 92	¹ HUNT 19	DPWA	Multichannel
2115 ± 20	SOKHOYAN 15A	DPWA	Multichannel
2125 ± 75	CUTKOSKY 80	IPWA	$\pi N \rightarrow \pi N$
2050 ± 20	HOEHLER 79	IPWA	$\pi N \rightarrow \pi N$
••• We do not use the following data for averages, fits, limits, etc. •••			
2157 ± 42	BATINIC 10	DPWA	$\pi N \rightarrow N\pi, N\eta$
2068 ± 3 ⁺¹⁵ ₋₄₀	ABLIKIM 06K	BES2	$J/\psi \rightarrow (p\pi^-)\bar{p}$
2084 ± 93	VRANA 00	DPWA	Multichannel
¹ Statistical error only.			

 $N(2100)$ BREIT-WIGNER WIDTH

VALUE (MeV)	DOCUMENT ID	TECN	COMMENT
200 to 320 (≈ 260) OUR ESTIMATE			
545 ± 170	¹ HUNT 19	DPWA	Multichannel
290 ± 20	SOKHOYAN 15A	DPWA	Multichannel
260 ± 100	CUTKOSKY 80	IPWA	$\pi N \rightarrow \pi N$
200 ± 30	HOEHLER 79	IPWA	$\pi N \rightarrow \pi N$
••• We do not use the following data for averages, fits, limits, etc. •••			
355 ± 88	BATINIC 10	DPWA	$\pi N \rightarrow N\pi, N\eta$
165 ± 14 ± 40	ABLIKIM 06K	BES2	$J/\psi \rightarrow (p\pi^-)\bar{p}$
1077 ± 643	VRANA 00	DPWA	Multichannel
¹ Statistical error only.			

 $N(2100)$ DECAY MODES

Mode	Fraction (Γ_i/Γ)
Γ_1 $N\pi$	8–32 %
Γ_2 $N\eta$	5–45 %
Γ_3 $N\eta'$	5–11 %
Γ_4 $N\omega$	10–25 %
Γ_5 ΛK	<1.0 %
Γ_6 $N\pi\pi$	>55 %
Γ_7 $\Delta(1232)\pi, P$ -wave	6–14 %
Γ_8 $N\rho, S=1/2, P$ -wave	35–70 %
Γ_9 $N\sigma$	14–35 %
Γ_{10} $N(1535)\pi$	26–34 %
Γ_{11} $\Lambda K^*(892)$	3–11 %
Γ_{12} $p\gamma, \text{helicity}=1/2$	0.001–0.13 %
Γ_{13} $n\gamma, \text{helicity}=1/2$	0.004–0.09 %

 $N(2100)$ BRANCHING RATIOS

$\Gamma(N\pi)/\Gamma_{\text{total}}$	Γ_1/Γ
8–32 % OUR ESTIMATE	
21 ± 11	¹ HUNT 19 DPWA Multichannel
16 ± 5	SOKHOYAN 15A DPWA Multichannel
12 ± 3	CUTKOSKY 80 IPWA $\pi N \rightarrow \pi N$
10 ± 4	HOEHLER 79 IPWA $\pi N \rightarrow \pi N$
••• We do not use the following data for averages, fits, limits, etc. •••	
16 ± 5	BATINIC 10 DPWA $\pi N \rightarrow N\pi, N\eta$
2 ± 5	VRANA 00 DPWA Multichannel
¹ Statistical error only.	
$\Gamma(N\eta)/\Gamma_{\text{total}}$ Γ_2/Γ	
5–45 % OUR ESTIMATE	
30 ± 15	MUELLER 20 DPWA Multichannel
< 4.7	¹ HUNT 19 DPWA Multichannel
••• We do not use the following data for averages, fits, limits, etc. •••	
83 ± 5	BATINIC 10 DPWA $\pi N \rightarrow N\pi, N\eta$
61 ± 61	VRANA 00 DPWA Multichannel
¹ Statistical error only.	

 $\Gamma(N\eta')/\Gamma_{\text{total}}$

VALUE (%)	DOCUMENT ID	TECN	COMMENT	Γ_3/Γ
5–11 % OUR ESTIMATE				
8 ± 3	ANISOVICH 17C	DPWA	Multichannel	

 $\Gamma(N\omega)/\Gamma_{\text{total}}$

VALUE (%)	DOCUMENT ID	TECN	COMMENT	Γ_4/Γ
10–25 % OUR ESTIMATE				
15 ± 10	DENISENKO 16	DPWA	Multichannel	

 $\Gamma(\Lambda K)/\Gamma_{\text{total}}$

VALUE (%)	DOCUMENT ID	TECN	COMMENT	Γ_5/Γ
<1.0 % OUR ESTIMATE				
< 1.0	¹ HUNT 19	DPWA	Multichannel	
••• We do not use the following data for averages, fits, limits, etc. •••				
21 ± 20	VRANA 00	DPWA	Multichannel	
¹ Statistical error only.				

 $\Gamma(\Delta(1232)\pi, P\text{-wave})/\Gamma_{\text{total}}$

VALUE (%)	DOCUMENT ID	TECN	COMMENT	Γ_7/Γ
6–14 % OUR ESTIMATE				
< 7.5	¹ HUNT 19	DPWA	Multichannel	
10 ± 4	SOKHOYAN 15A	DPWA	Multichannel	
••• We do not use the following data for averages, fits, limits, etc. •••				
2 ± 1	VRANA 00	DPWA	Multichannel	
¹ Statistical error only.				

 $\Gamma(N\rho, S=1/2, P\text{-wave})/\Gamma_{\text{total}}$

VALUE (%)	DOCUMENT ID	TECN	COMMENT	Γ_8/Γ
35–70 % OUR ESTIMATE				
52 ± 19	¹ HUNT 19	DPWA	Multichannel	
••• We do not use the following data for averages, fits, limits, etc. •••				
4 ± 1	VRANA 00	DPWA	Multichannel	
¹ Statistical error only.				

 $\Gamma(\Lambda K^*(892))/\Gamma_{\text{total}}$

VALUE (%)	DOCUMENT ID	TECN	COMMENT	Γ_{11}/Γ
3–11 % OUR ESTIMATE				
7 ± 4	ANISOVICH 17B	DPWA	Multichannel	

 $\Gamma(N\sigma)/\Gamma_{\text{total}}$

VALUE (%)	DOCUMENT ID	TECN	COMMENT	Γ_9/Γ
14–35 % OUR ESTIMATE				
< 35	¹ HUNT 19	DPWA	Multichannel	
20 ± 6	SOKHOYAN 15A	DPWA	Multichannel	
••• We do not use the following data for averages, fits, limits, etc. •••				
10 ± 1	VRANA 00	DPWA	Multichannel	
¹ Statistical error only.				

 $\Gamma(N(1535)\pi)/\Gamma_{\text{total}}$

VALUE (%)	DOCUMENT ID	TECN	COMMENT	Γ_{10}/Γ
26–34 % OUR ESTIMATE				
30 ± 4	SOKHOYAN 15A	DPWA	Multichannel	

 $N(2100)$ PHOTON DECAY AMPLITUDES AT THE POLE $N(2100) \rightarrow p\gamma, \text{helicity-1/2 amplitude } A_{1/2}$

MODULUS (GeV ^{-1/2})	PHASE (°)	DOCUMENT ID	TECN	COMMENT
0.011 ± 0.004	65 ± 30	SOKHOYAN 15A	DPWA	Multichannel

 $N(2100)$ BREIT-WIGNER PHOTON DECAY AMPLITUDES $N(2100) \rightarrow p\gamma, \text{helicity-1/2 amplitude } A_{1/2}$

VALUE (GeV ^{-1/2})	DOCUMENT ID	TECN	COMMENT
0.032 ± 0.014	¹ HUNT 19	DPWA	Multichannel
0.010 ± 0.004	SOKHOYAN 15A	DPWA	Multichannel
¹ Statistical error only.			

 $N(2100) \rightarrow n\gamma, \text{helicity-1/2 amplitude } A_{1/2}$

VALUE (GeV ^{-1/2})	DOCUMENT ID	TECN	COMMENT
0.026 ± 0.013	¹ HUNT 19	DPWA	Multichannel
¹ Statistical error only.			

 $N(2100)$ REFERENCES

MUELLER 20	PL B803 135323	J. Mueller et al.	(CBELSA/TAPS Collab.)
HUNT 19	PR C99 055205	B. C. Hunt, D.M. Manley	
ANISOVICH 17B	PL B771 142	A.V. Anisovich et al.	
ANISOVICH 17C	PL B772 247	A.V. Anisovich et al.	
DENISENKO 16	PL B755 97	I. Denisenko et al.	
SOKHOYAN 15A	EPJ A51 95	V. Sokhoyan et al.	(CBELSA/TAPS Collab.)
SVARC 14	PR C89 045205	A. Svarc et al.	(RBI Zagreb, UNI Tuzla)
BATINIC 10	PR C82 038203	M. Batinic et al.	(ZAGR)
ABLIKIM 06K	PR L97 082001	M. Ablikim et al.	(BES-II Collab.)
VRANA 00	PR L97 082001	T.P. Vrana, S.A. Dytman, T.-S.H. Lee	(PITT, ANL)
CUTKOSKY 80	Toronto Conf. 19	R.E. Cutkosky et al.	(CMU, LBL) IJP
	PR D20 2839	R.E. Cutkosky et al.	(CMU, LBL)
		G. Hohler et al.	(KARLT) IJP
HOEHLER 79	PDAT 12-1	R. Koch	(KARLT) IJP
	Toronto Conf. 3		

See key on page 1127

Baryon Particle Listings
N(2120)

N(2120) 3/2⁻

$I(J^P) = \frac{1}{2}(\frac{3}{2}^-)$ Status: ***

Before the 2012 Review, all the evidence for a $J^P = 3/2^-$ state with a mass above 1800 MeV was filed under a two-star N(2080).

There is now evidence from ANISOVICH 12A for two 3/2⁻ states in this region, so we have split the older data (according to mass) between a three-star N(1875) and a two-star N(2120).

N(2120) POLE POSITION

REAL PART

VALUE (MeV)	DOCUMENT ID	TECN	COMMENT
2050 to 2150 (≈ 2100) OUR ESTIMATE			
2115 ± 40	SOKHOYAN 15A	DPWA	Multichannel
2094 ± 7 ± 11	SVARC 14	L+P	$\pi N \rightarrow \pi N$
2050 ± 70	CUTKOSKY 80	IPWA	$\pi N \rightarrow \pi N$ (higher <i>m</i>)
• • • We do not use the following data for averages, fits, limits, etc. • • •			
2357	HUNT 19	DPWA	Multichannel
2115 ± 40	GUTZ 14	DPWA	Multichannel
2110 ± 50	ANISOVICH 12A	DPWA	Multichannel

-2×IMAGINARY PART

VALUE (MeV)	DOCUMENT ID	TECN	COMMENT
200 to 360 (≈ 280) OUR ESTIMATE			
345 ± 35	SOKHOYAN 15A	DPWA	Multichannel
296 ± 15 ± 4	SVARC 14	L+P	$\pi N \rightarrow \pi N$
200 ± 80	CUTKOSKY 80	IPWA	$\pi N \rightarrow \pi N$ (higher <i>m</i>)
• • • We do not use the following data for averages, fits, limits, etc. • • •			
503	HUNT 19	DPWA	Multichannel
345 ± 35	GUTZ 14	DPWA	Multichannel
340 ± 45	ANISOVICH 12A	DPWA	Multichannel

N(2120) ELASTIC POLE RESIDUE

MODULUS |r|

VALUE (MeV)	DOCUMENT ID	TECN	COMMENT
10 to 30 (≈ 20) OUR ESTIMATE			
11 ± 6	SOKHOYAN 15A	DPWA	Multichannel
13 ± 1 ± 1	SVARC 14	L+P	$\pi N \rightarrow \pi N$
30 ± 20	CUTKOSKY 80	IPWA	$\pi N \rightarrow \pi N$ (higher <i>m</i>)
• • • We do not use the following data for averages, fits, limits, etc. • • •			
11 ± 6	GUTZ 14	DPWA	Multichannel
13 ± 3	ANISOVICH 12A	DPWA	Multichannel

PHASE θ

VALUE (°)	DOCUMENT ID	TECN	COMMENT
-40 to 20 (≈ -10) OUR ESTIMATE			
-30 ± 20	SOKHOYAN 15A	DPWA	Multichannel
-2 ± 4 ± 9	SVARC 14	L+P	$\pi N \rightarrow \pi N$
0 ± 100	CUTKOSKY 80	IPWA	$\pi N \rightarrow \pi N$ (higher <i>m</i>)
• • • We do not use the following data for averages, fits, limits, etc. • • •			
-30 ± 20	GUTZ 14	DPWA	Multichannel
-20 ± 10	ANISOVICH 12A	DPWA	Multichannel

N(2120) INELASTIC POLE RESIDUE

The "normalized residue" is the residue divided by $\Gamma_{pole}/2$.

Normalized residue in $N\pi \rightarrow N(2120) \rightarrow \Lambda K$

MODULUS	PHASE (°)	DOCUMENT ID	TECN	COMMENT
0.03 ± 0.01	100 ± 30	ANISOVICH 12A	DPWA	Multichannel

Normalized residue in $N\pi \rightarrow N(2120) \rightarrow \Sigma K$

MODULUS	PHASE (°)	DOCUMENT ID	TECN	COMMENT
0.02 ± 0.015	-50 ± 40	ANISOVICH 12A	DPWA	Multichannel

Normalized residue in $N\pi \rightarrow N(2120) \rightarrow N(1535)\pi$

MODULUS	PHASE (°)	DOCUMENT ID	TECN	COMMENT
0.15 ± 0.08	-90 ± 40	GUTZ 14	DPWA	Multichannel

Normalized residue in $N\pi \rightarrow N(2120) \rightarrow \Delta(1232)\pi, S\text{-wave}$

MODULUS	PHASE (°)	DOCUMENT ID	TECN	COMMENT
0.25 ± 0.10	undefined	SOKHOYAN 15A	DPWA	Multichannel

Normalized residue in $N\pi \rightarrow N(2120) \rightarrow \Delta(1232)\pi, D\text{-wave}$

MODULUS	PHASE (°)	DOCUMENT ID	TECN	COMMENT
0.15 ± 0.06	-35 ± 30	SOKHOYAN 15A	DPWA	Multichannel

Normalized residue in $N\pi \rightarrow N(2120) \rightarrow N\sigma$

MODULUS	PHASE (°)	DOCUMENT ID	TECN	COMMENT
0.09 ± 0.05	-80 ± 50	SOKHOYAN 15A	DPWA	Multichannel

N(2120) BREIT-WIGNER MASS

VALUE (MeV)	DOCUMENT ID	TECN	COMMENT
2060 to 2160 (≈ 2120) OUR ESTIMATE			
2353 ± 29	¹ HUNT 19	DPWA	Multichannel
2120 ± 45	SOKHOYAN 15A	DPWA	Multichannel
2060 ± 80	CUTKOSKY 80	IPWA	$\pi N \rightarrow \pi N$
2081 ± 20	HOEHLER 79	IPWA	$\pi N \rightarrow \pi N$
• • • We do not use the following data for averages, fits, limits, etc. • • •			
2120 ± 35	GUTZ 14	DPWA	Multichannel
2150 ± 60	ANISOVICH 12A	DPWA	Multichannel
¹ Statistical error only.			

N(2120) BREIT-WIGNER WIDTH

VALUE (MeV)	DOCUMENT ID	TECN	COMMENT
260 to 360 (≈ 300) OUR ESTIMATE			
503 ± 62	¹ HUNT 19	DPWA	Multichannel
340 ± 35	SOKHOYAN 15A	DPWA	Multichannel
300 ± 100	CUTKOSKY 80	IPWA	$\pi N \rightarrow \pi N$ (higher <i>m</i>)
265 ± 40	HOEHLER 79	IPWA	$\pi N \rightarrow \pi N$
• • • We do not use the following data for averages, fits, limits, etc. • • •			
340 ± 35	GUTZ 14	DPWA	Multichannel
330 ± 45	ANISOVICH 12A	DPWA	Multichannel
¹ Statistical error only.			

N(2120) DECAY MODES

Mode	Fraction (Γ_i/Γ)
Γ_1 $N\pi$	5-15 %
Γ_2 $N\eta$	1-5 %
Γ_3 $N\eta'$	2-6 %
Γ_4 $N\omega$	4-20 %
Γ_5 ΛK	6-11 %
Γ_6 $N\pi\pi$	>27 %
Γ_7 $\Delta(1232)\pi$	>23 %
Γ_8 $\Delta(1232)\pi, S\text{-wave}$	15-70 %
Γ_9 $\Delta(1232)\pi, D\text{-wave}$	8-45 %
Γ_{10} $N\rho, S=3/2, S\text{-wave}$	< 3 %
Γ_{11} $N\sigma$	4-15 %
Γ_{12} $N(1535)\pi$	7-23 %
Γ_{13} $\Lambda K^*(892)$	< 0.2 %
Γ_{14} $p\gamma$	0.16-2.1 %
Γ_{15} $p\gamma, \text{helicity}=1/2$	0.07-0.80 %
Γ_{16} $p\gamma, \text{helicity}=3/2$	0.09-1.3 %
Γ_{17} $n\gamma$	0.04-0.72 %
Γ_{18} $n\gamma, \text{helicity}=1/2$	0.04-0.60 %
Γ_{19} $n\gamma, \text{helicity}=3/2$	0.001-0.12 %

N(2120) BRANCHING RATIOS

$\Gamma(N\pi)/\Gamma_{total}$	VALUE (%)	DOCUMENT ID	TECN	COMMENT	Γ_1/Γ
5-15 % OUR ESTIMATE					
19 ± 2	¹ HUNT 19	DPWA	Multichannel		
5 ± 3	SOKHOYAN 15A	DPWA	Multichannel		
14 ± 7	CUTKOSKY 80	IPWA	$\pi N \rightarrow \pi N$ (higher <i>m</i>)		
6 ± 2	HOEHLER 79	IPWA	$\pi N \rightarrow \pi N$		
• • • We do not use the following data for averages, fits, limits, etc. • • •					
5 ± 3	GUTZ 14	DPWA	Multichannel		
6 ± 2	ANISOVICH 12A	DPWA	Multichannel		
¹ Statistical error only.					

$\Gamma(N\eta)/\Gamma_{total}$	VALUE (%)	DOCUMENT ID	TECN	COMMENT	Γ_2/Γ
1-5 % OUR ESTIMATE					
<1	MUELLER 20	DPWA	Multichannel		
3.1 ± 2.4	¹ HUNT 19	DPWA	Multichannel		
¹ Statistical error only.					

$\Gamma(N\eta')/\Gamma_{total}$	VALUE (%)	DOCUMENT ID	TECN	COMMENT	Γ_3/Γ
2-6 % OUR ESTIMATE					
4 ± 2	ANISOVICH 17c	DPWA	Multichannel		

$\Gamma(N\omega)/\Gamma_{total}$	VALUE (%)	DOCUMENT ID	TECN	COMMENT	Γ_4/Γ
4-20 % OUR ESTIMATE					
12 ± 8	DENISENKO 16	DPWA	Multichannel		

Baryon Particle Listings

 $N(2120)$, $N(2190)$

$\Gamma(\Lambda K)/\Gamma_{\text{total}}$				Γ_5/Γ
VALUE (%)	DOCUMENT ID	TECN	COMMENT	
6-11 % OUR ESTIMATE				
8.5 ± 2.5	1 HUNT	19	DPWA Multichannel	
¹ Statistical error only.				
$\Gamma(\Delta(1232)\pi, S\text{-wave})/\Gamma_{\text{total}}$				Γ_8/Γ
VALUE (%)	DOCUMENT ID	TECN	COMMENT	
15-70 % OUR ESTIMATE				
25 ± 11	1 HUNT	19	DPWA Multichannel	
50 ± 20	SOKHOYAN	15A	DPWA Multichannel	
¹ Statistical error only.				
$\Gamma(\Delta(1232)\pi, D\text{-wave})/\Gamma_{\text{total}}$				Γ_9/Γ
VALUE (%)	DOCUMENT ID	TECN	COMMENT	
8-45 % OUR ESTIMATE				
34 ± 11	1 HUNT	19	DPWA Multichannel	
20 ± 12	SOKHOYAN	15A	DPWA Multichannel	
¹ Statistical error only.				
$\Gamma(N\rho, S=3/2, S\text{-wave})/\Gamma_{\text{total}}$				Γ_{10}/Γ
VALUE (%)	DOCUMENT ID	TECN	COMMENT	
< 3 % OUR ESTIMATE				
< 3	1 HUNT	19	DPWA Multichannel	
¹ Statistical error only.				
$\Gamma(N\sigma)/\Gamma_{\text{total}}$				Γ_{11}/Γ
VALUE (%)	DOCUMENT ID	TECN	COMMENT	
4-15 % OUR ESTIMATE				
9 ± 5	1 HUNT	19	DPWA Multichannel	
11 ± 4	SOKHOYAN	15A	DPWA Multichannel	
¹ Statistical error only.				
$\Gamma(N(1535)\pi)/\Gamma_{\text{total}}$				Γ_{12}/Γ
VALUE (%)	DOCUMENT ID	TECN	COMMENT	
7-23 % OUR ESTIMATE				
15 ± 8	GUTZ	14	DPWA Multichannel	
$\Gamma(\Lambda K^*(892))/\Gamma_{\text{total}}$				Γ_{13}/Γ
VALUE (%)	DOCUMENT ID	TECN	COMMENT	
< 0.2 % OUR ESTIMATE				
< 0.2	ANISOVICH	17B	DPWA Multichannel	

 $N(2120)$ PHOTON DECAY AMPLITUDES AT THE POLE $N(2120) \rightarrow p\gamma$, helicity-1/2 amplitude $A_{1/2}$

MODULUS ($\text{GeV}^{-1/2}$)	PHASE ($^\circ$)	DOCUMENT ID	TECN	COMMENT
0.130 ± 0.045	-40 ± 25	SOKHOYAN	15A	DPWA Multichannel

 $N(2120) \rightarrow p\gamma$, helicity-3/2 amplitude $A_{3/2}$

MODULUS ($\text{GeV}^{-1/2}$)	PHASE ($^\circ$)	DOCUMENT ID	TECN	COMMENT
0.160 ± 0.060	-30 ± 15	SOKHOYAN	15A	DPWA Multichannel

 $N(2120)$ BREIT-WIGNER PHOTON DECAY AMPLITUDES $N(2120) \rightarrow p\gamma$, helicity-1/2 amplitude $A_{1/2}$

VALUE ($\text{GeV}^{-1/2}$)	DOCUMENT ID	TECN	COMMENT
0.047 ± 0.009	1 HUNT	19	DPWA Multichannel
0.130 ± 0.050	SOKHOYAN	15A	DPWA Multichannel
••• We do not use the following data for averages, fits, limits, etc. •••			
0.130 ± 0.050	GUTZ	14	DPWA Multichannel
¹ Statistical error only.			

 $N(2120) \rightarrow p\gamma$, helicity-3/2 amplitude $A_{3/2}$

VALUE ($\text{GeV}^{-1/2}$)	DOCUMENT ID	TECN	COMMENT
0.001 ± 0.007	1 HUNT	19	DPWA Multichannel
0.160 ± 0.065	SOKHOYAN	15A	DPWA Multichannel
••• We do not use the following data for averages, fits, limits, etc. •••			
0.160 ± 0.065	GUTZ	14	DPWA Multichannel
¹ Statistical error only.			

 $N(2120) \rightarrow n\gamma$, helicity-1/2 amplitude $A_{1/2}$

VALUE ($\text{GeV}^{-1/2}$)	DOCUMENT ID	TECN	COMMENT
-0.020 ± 0.013	1 HUNT	19	DPWA Multichannel
0.110 ± 0.045	ANISOVICH	13B	DPWA Multichannel
¹ Statistical error only.			

 $N(2120) \rightarrow n\gamma$, helicity-3/2 amplitude $A_{3/2}$

VALUE ($\text{GeV}^{-1/2}$)	DOCUMENT ID	TECN	COMMENT
-0.00 ± 0.02	1 HUNT	19	DPWA Multichannel
0.040 ± 0.030	ANISOVICH	13B	DPWA Multichannel
¹ Statistical error only.			

 $N(2120)$ REFERENCES

MUELLER	20	PL B803 135323	J. Mueller <i>et al.</i>	(CBELSA/TAPS Collab.)
HUNT	19	PR C39 055205	B.C. Hunt, D.M. Manley	
ANISOVICH	17B	PL B771 142	A.V. Anisovich <i>et al.</i>	
ANISOVICH	17C	PL B772 247	A.V. Anisovich <i>et al.</i>	
DENISENKO	16	PL B755 97	I. Denisenko <i>et al.</i>	
SOKHOYAN	15A	EPJ A51 95	V. Sokhoyan <i>et al.</i>	(CBELSA/TAPS Collab.)
GUTZ	14	EPJ A50 74	E. Gutz <i>et al.</i>	(CBELSA/TAPS Collab.)
SVARC	14	PR C89 045205	A. Svarc <i>et al.</i>	(RBI Zagreb, UNI Tuzla)
ANISOVICH	13B	EPJ A49 67	A.V. Anisovich <i>et al.</i>	
ANISOVICH	12A	EPJ A48 15	A.V. Anisovich <i>et al.</i>	(BONN, PNPI)
CUTKOSKY	80	Toronto Conf. 19	R.E. Cutkosky <i>et al.</i>	(CMU, LBL)
HOEHLER	79	PDAT 12-1	G. Hohler <i>et al.</i>	(KARLT)

 $N(2190) 7/2^-$

$$I(J^P) = \frac{1}{2} \left(\frac{7}{2}^-\right) \text{ Status: } ***$$

Older and obsolete values are listed and referenced in the 2014 edition, Chinese Physics **C38** 070001 (2014).

 $N(2190)$ POLE POSITION

REAL PART

VALUE (MeV)	DOCUMENT ID	TECN	COMMENT
2050 to 2150 (≈ 2100) OUR ESTIMATE			
2140 ± 20	AFZAL	20	DPWA Multichannel
2150 ± 25	SOKHOYAN	15A	DPWA Multichannel
2079 ± 4 ± 9	1 SVARC	14	L+P $\pi N \rightarrow \pi N$
2100 ± 50	CUTKOSKY	80	IPWA $\pi N \rightarrow \pi N$
••• We do not use the following data for averages, fits, limits, etc. •••			
2162	HUNT	19	DPWA Multichannel
2074	ROENCHEN	15A	DPWA Multichannel
2150 ± 25	ANISOVICH	12A	DPWA Multichannel
2063 ± 32	BATINIC	10	DPWA $\pi N \rightarrow N\pi, N\eta$
2070	ARNDT	06	DPWA $\pi N \rightarrow \pi N, \eta N$
2107	VRANA	00	DPWA Multichannel
2042	HOEHLER	93	SPED $\pi N \rightarrow \pi N$
¹ Fit to the amplitudes of HOEHLER 79.			

-2xIMAGINARY PART

VALUE (MeV)	DOCUMENT ID	TECN	COMMENT
300 to 500 (≈ 400) OUR ESTIMATE			
420 +120 - 40	AFZAL	20	DPWA Multichannel
325 ± 25	SOKHOYAN	15A	DPWA Multichannel
509 ± 7 ± 16	1 SVARC	14	L+P $\pi N \rightarrow \pi N$
400 ± 160	CUTKOSKY	80	IPWA $\pi N \rightarrow \pi N$
••• We do not use the following data for averages, fits, limits, etc. •••			
407	HUNT	19	DPWA Multichannel
327	ROENCHEN	15A	DPWA Multichannel
330 ± 30	ANISOVICH	12A	DPWA Multichannel
330 ± 101	BATINIC	10	DPWA $\pi N \rightarrow N\pi, N\eta$
520	ARNDT	06	DPWA $\pi N \rightarrow \pi N, \eta N$
380	VRANA	00	DPWA Multichannel
482	HOEHLER	93	SPED $\pi N \rightarrow \pi N$
¹ Fit to the amplitudes of HOEHLER 79.			

 $N(2190)$ ELASTIC POLE RESIDUEMODULUS $|r|$

VALUE (MeV)	DOCUMENT ID	TECN	COMMENT
25 to 70 (≈ 50) OUR ESTIMATE			
30 ± 4	SOKHOYAN	15A	DPWA Multichannel
54 ± 1 ± 3	1 SVARC	14	L+P $\pi N \rightarrow \pi N$
25 ± 10	CUTKOSKY	80	IPWA $\pi N \rightarrow \pi N$
••• We do not use the following data for averages, fits, limits, etc. •••			
35	ROENCHEN	15A	DPWA Multichannel
30 ± 5	ANISOVICH	12A	DPWA Multichannel
34	BATINIC	10	DPWA $\pi N \rightarrow N\pi, N\eta$
72	ARNDT	06	DPWA $\pi N \rightarrow \pi N, \eta N$
45	HOEHLER	93	SPED $\pi N \rightarrow \pi N$
¹ Fit to the amplitudes of HOEHLER 79.			

PHASE θ

VALUE ($^\circ$)	DOCUMENT ID	TECN	COMMENT
-30 to 30 (≈ 0) OUR ESTIMATE			
28 ± 10	SOKHOYAN	15A	DPWA Multichannel
-18 ± 1 ± 3	1 SVARC	14	L+P $\pi N \rightarrow \pi N$
-30 ± 50	CUTKOSKY	80	IPWA $\pi N \rightarrow \pi N$
••• We do not use the following data for averages, fits, limits, etc. •••			
-40	ROENCHEN	15A	DPWA Multichannel
30 ± 10	ANISOVICH	12A	DPWA Multichannel
-19	BATINIC	10	DPWA $\pi N \rightarrow N\pi, N\eta$
-32	ARNDT	06	DPWA $\pi N \rightarrow \pi N, \eta N$
¹ Fit to the amplitudes of HOEHLER 79.			

N(2190) INELASTIC POLE RESIDUE

The "normalized residue" is the residue divided by $\Gamma_{pole}/2$.

Normalized residue in $N\pi \rightarrow N(2190) \rightarrow \Lambda K$

MODULUS	PHASE (°)	DOCUMENT ID	TECN	COMMENT
0.03 ± 0.01	20 ± 15	ANISOVICH 12A	DPWA	Multichannel
•••				We do not use the following data for averages, fits, limits, etc. •••
0.005	-51	ROENCHEN 15A	DPWA	Multichannel

Normalized residue in $N\pi \rightarrow N(2190) \rightarrow \Sigma K$

MODULUS	PHASE (°)	DOCUMENT ID	TECN	COMMENT
•••				We do not use the following data for averages, fits, limits, etc. •••
0.013	-69	ROENCHEN 15A	DPWA	Multichannel

Normalized residue in $N\pi \rightarrow N(2190) \rightarrow N\eta$

MODULUS	PHASE (°)	DOCUMENT ID	TECN	COMMENT
•••				We do not use the following data for averages, fits, limits, etc. •••
0.016	129	ROENCHEN 15A	DPWA	Multichannel

Normalized residue in $N\pi \rightarrow N(2190) \rightarrow \Delta(1232)\pi, D\text{-wave}$

MODULUS	PHASE (°)	DOCUMENT ID	TECN	COMMENT
0.27 ± 0.04	-165 ± 20	SOKHOYAN 15A	DPWA	Multichannel

Normalized residue in $N\pi \rightarrow N(2190) \rightarrow N\sigma$

MODULUS	PHASE (°)	DOCUMENT ID	TECN	COMMENT
0.13 ± 0.05	50 ± 15	SOKHOYAN 15A	DPWA	Multichannel

N(2190) BREIT-WIGNER MASS

VALUE (MeV)	DOCUMENT ID	TECN	COMMENT
2140 to 2220 (≈ 2180) OUR ESTIMATE			
2222 ± 15	¹ HUNT 19	DPWA	Multichannel
2205 ± 18	SOKHOYAN 15A	DPWA	Multichannel
2152.4 ± 1.4	¹ ARNDT 06	DPWA	$\pi N \rightarrow \pi N, \eta N$
2200 ± 70	CUTKOSKY 80	IPWA	$\pi N \rightarrow \pi N$
2140 ± 12	HOEHLER 79	IPWA	$\pi N \rightarrow \pi N$
•••			We do not use the following data for averages, fits, limits, etc. •••
2180 ± 20	ANISOVICH 12A	DPWA	Multichannel
2150 ± 26	¹ SHRESTHA 12A	DPWA	Multichannel
2125 ± 61	BATINIC 10	DPWA	$\pi N \rightarrow N\pi, N\eta$
2168 ± 18	VRANA 00	DPWA	Multichannel

¹ Statistical error only.

N(2190) BREIT-WIGNER WIDTH

VALUE (MeV)	DOCUMENT ID	TECN	COMMENT
300 to 500 (≈ 400) OUR ESTIMATE			
442 ± 40	¹ HUNT 19	DPWA	Multichannel
355 ± 30	SOKHOYAN 15A	DPWA	Multichannel
484 ± 13	¹ ARNDT 06	DPWA	$\pi N \rightarrow \pi N, \eta N$
500 ± 150	CUTKOSKY 80	IPWA	$\pi N \rightarrow \pi N$
390 ± 30	HOEHLER 79	IPWA	$\pi N \rightarrow \pi N$
•••			We do not use the following data for averages, fits, limits, etc. •••
335 ± 40	ANISOVICH 12A	DPWA	Multichannel
500 ± 74	¹ SHRESTHA 12A	DPWA	Multichannel
381 ± 160	BATINIC 10	DPWA	$\pi N \rightarrow N\pi, N\eta$
453 ± 101	VRANA 00	DPWA	Multichannel

¹ Statistical error only.

N(2190) DECAY MODES

The following branching fractions are our estimates, not fits or averages.

Mode	Fraction (Γ_i/Γ)
Γ_1 $N\pi$	10–20 %
Γ_2 $N\eta$	1–5 %
Γ_3 $N\omega$	8–20 %
Γ_4 ΛK	0.2–0.8 %
Γ_5 $N\pi\pi$	22–51 %
Γ_6 $\Delta(1232)\pi, D\text{-wave}$	19–31 %
Γ_7 $N\rho, S=3/2, D\text{-wave}$	<11 %
Γ_8 $N\sigma$	3–9 %
Γ_9 $\Lambda K^*(892)$	0.2–0.8 %
Γ_{10} $p\gamma$	<0.08 %
Γ_{11} $p\gamma, \text{helicity}=1/2$	<0.06 %
Γ_{12} $p\gamma, \text{helicity}=3/2$	<0.02 %
Γ_{13} $n\gamma$	<0.04 %
Γ_{14} $n\gamma, \text{helicity}=1/2$	<0.01 %
Γ_{15} $n\gamma, \text{helicity}=3/2$	<0.03 %

N(2190) BRANCHING RATIOS

$\Gamma(N\pi)/\Gamma_{total}$	DOCUMENT ID	TECN	COMMENT	Γ_1/Γ
VALUE (%)				
10–20 % OUR ESTIMATE				
22.9 ± 0.6	¹ HUNT 19	DPWA	Multichannel	
16 ± 2	SOKHOYAN 15A	DPWA	Multichannel	
23.8 ± 0.1	¹ ARNDT 06	DPWA	$\pi N \rightarrow \pi N, \eta N$	
12 ± 6	CUTKOSKY 80	IPWA	$\pi N \rightarrow \pi N$	
14 ± 2	HOEHLER 79	IPWA	$\pi N \rightarrow \pi N$	
•••			We do not use the following data for averages, fits, limits, etc. •••	
16 ± 2	ANISOVICH 12A	DPWA	Multichannel	
20 ± 1	¹ SHRESTHA 12A	DPWA	Multichannel	
18 ± 12	BATINIC 10	DPWA	$\pi N \rightarrow N\pi, N\eta$	
20 ± 4	VRANA 00	DPWA	Multichannel	

¹ Statistical error only.

$\Gamma(N\eta)/\Gamma_{total}$	DOCUMENT ID	TECN	COMMENT	Γ_2/Γ
VALUE (%)				
1–5 % OUR ESTIMATE				
4 ± 2	MUELLER 20	DPWA	Multichannel	
2.7 ± 2.2	¹ HUNT 19	DPWA	Multichannel	
•••			We do not use the following data for averages, fits, limits, etc. •••	
2 ± 1	¹ SHRESTHA 12A	DPWA	Multichannel	
0.1 ± 0.3	BATINIC 10	DPWA	$\pi N \rightarrow N\pi, N\eta$	
0 ± 1	VRANA 00	DPWA	Multichannel	

¹ Statistical error only.

$\Gamma(N\omega)/\Gamma_{total}$	DOCUMENT ID	TECN	COMMENT	Γ_3/Γ
VALUE (%)				
8–20 % OUR ESTIMATE				
14 ± 6	DENISENKO 16	DPWA	Multichannel	
•••			We do not use the following data for averages, fits, limits, etc. •••	
seen	WILLIAMS 09	IPWA	$\gamma\rho \rightarrow \rho\omega$	

$\Gamma(\Lambda K)/\Gamma_{total}$	DOCUMENT ID	TECN	COMMENT	Γ_4/Γ
VALUE (%)				
0.2–0.8 % OUR ESTIMATE				
0.6 ± 0.1	¹ HUNT 19	DPWA	Multichannel	
0.5 ± 0.3	ANISOVICH 12A	DPWA	Multichannel	
•••			We do not use the following data for averages, fits, limits, etc. •••	
<1	¹ SHRESTHA 12A	DPWA	Multichannel	

¹ Statistical error only.

$\Gamma(\Delta(1232)\pi, D\text{-wave})/\Gamma_{total}$	DOCUMENT ID	TECN	COMMENT	Γ_6/Γ
VALUE (%)				
19–31 % OUR ESTIMATE				
25 ± 6	SOKHOYAN 15A	DPWA	Multichannel	

$\Gamma(N\rho, S=3/2, D\text{-wave})/\Gamma_{total}$	DOCUMENT ID	TECN	COMMENT	Γ_7/Γ
VALUE (%)				
<11 % OUR ESTIMATE				
<11	¹ HUNT 19	DPWA	Multichannel	
•••			We do not use the following data for averages, fits, limits, etc. •••	
29 ± 28	VRANA 00	DPWA	Multichannel	

¹ Statistical error only.

$\Gamma(N\sigma)/\Gamma_{total}$	DOCUMENT ID	TECN	COMMENT	Γ_8/Γ
VALUE (%)				
3–9 % OUR ESTIMATE				
6 ± 3	SOKHOYAN 15A	DPWA	Multichannel	

$\Gamma(\Lambda K^*(892))/\Gamma_{total}$	DOCUMENT ID	TECN	COMMENT	Γ_9/Γ
VALUE (%)				
0.2–0.8 % OUR ESTIMATE				
0.5 ± 0.3	ANISOVICH 17B	DPWA	Multichannel	

N(2190) PHOTON DECAY AMPLITUDES AT THE POLE

N(2190) → pγ, helicity-1/2 amplitude A_{1/2}

MODULUS (GeV ^{-1/2})	PHASE (°)	DOCUMENT ID	TECN	COMMENT
0.068 ± 0.005	-170 ± 12	SOKHOYAN 15A	DPWA	Multichannel
-0.083 + 0.007	-11 + 6	ROENCHEN 14	DPWA	
	-0.003 - 2			
•••				We do not use the following data for averages, fits, limits, etc. •••
-0.041	-21	ROENCHEN 15A	DPWA	Multichannel

N(2190) → pγ, helicity-3/2 amplitude A_{3/2}

MODULUS (GeV ^{-1/2})	PHASE (°)	DOCUMENT ID	TECN	COMMENT
0.025 ± 0.010	22 ± 10	SOKHOYAN 15A	DPWA	Multichannel
0.095 + 0.013	-3 + 3	ROENCHEN 14	DPWA	
	-0.010 - 5			
•••				We do not use the following data for averages, fits, limits, etc. •••
0.085	-22	ROENCHEN 15A	DPWA	Multichannel

Baryon Particle Listings

$N(2190)$, $N(2220)$

$N(2190)$ BREIT-WIGNER PHOTON DECAY AMPLITUDES

$N(2190) \rightarrow \rho\gamma$, helicity-1/2 amplitude $A_{1/2}$

VALUE (GeV ^{-1/2})	DOCUMENT ID	TECN	COMMENT
0.001 ± 0.002	¹ HUNT	19	DPWA Multichannel
-0.071 ± 0.006	SOKHOYAN	15A	DPWA Multichannel
••• We do not use the following data for averages, fits, limits, etc. •••			
-0.065 ± 0.008	ANISOVICH	12A	DPWA Multichannel

¹ Statistical error only.

$N(2190) \rightarrow \rho\gamma$, helicity-3/2 amplitude $A_{3/2}$

VALUE (GeV ^{-1/2})	DOCUMENT ID	TECN	COMMENT
0.015 ± 0.003	¹ HUNT	19	DPWA Multichannel
0.027 ± 0.010	SOKHOYAN	15A	DPWA Multichannel
••• We do not use the following data for averages, fits, limits, etc. •••			
0.035 ± 0.017	ANISOVICH	12A	DPWA Multichannel

¹ Statistical error only.

$N(2190) \rightarrow \rho\gamma$, ratio of helicity amplitudes $A_{3/2}/A_{1/2}$

VALUE	DOCUMENT ID	TECN	COMMENT
-0.17 ± 0.15	WILLIAMS	09	IPWA $\gamma\rho \rightarrow \rho\omega$

$N(2190) \rightarrow n\gamma$, helicity-1/2 amplitude $A_{1/2}$

VALUE (GeV ^{-1/2})	DOCUMENT ID	TECN	COMMENT
-0.01 ± 0.02	¹ HUNT	19	DPWA Multichannel
-0.015 ± 0.013	ANISOVICH	13B	DPWA Multichannel

¹ Statistical error only.

$N(2190) \rightarrow n\gamma$, helicity-3/2 amplitude $A_{3/2}$

VALUE (GeV ^{-1/2})	DOCUMENT ID	TECN	COMMENT
-0.023 ± 0.022	¹ HUNT	19	DPWA Multichannel
-0.034 ± 0.022	ANISOVICH	13B	DPWA Multichannel

¹ Statistical error only.

$N(2190)$ REFERENCES

For early references, see Physics Letters **111B** 1 (1982).

AFZAL	20	PRL 125 152002	F. Afzal et al.	(CBELSA/TAPS Collab.)
MUELLER	20	PL B803 135323	J. Mueller et al.	(CBELSA/TAPS Collab.)
HUNT	19	PR C99 055205	B. C. Hunt, D.M. Manley	
ANISOVICH	17B	PL B771 142	A.V. Anisovich et al.	
DENISENKO	16	PL B755 97	I. Denisenko et al.	
ROENCHEN	15A	EPJ A51 70	D. Roenchen et al.	
SOKHOYAN	15A	EPJ A51 95	V. Sokhoyan et al.	(CBELSA/TAPS Collab.)
PDC	14	CP C38 070001	K. Olive et al.	(PDG Collab.)
ROENCHEN	14	EPJ A50 101	D. Roenchen et al.	
Also		EPJ A51 63 (errat.)	D. Roenchen et al.	
SVARC	14	PR C89 045205	A. Svarc et al.	(RBI Zagreb, UNI Tuzla)
ANISOVICH	13B	EPJ A49 67	A.V. Anisovich et al.	
ANISOVICH	12A	EPJ A48 15	A.V. Anisovich et al.	(BONN, PNPI)
SHRESTHA	12A	PR C86 055203	M. Shrestha, D.M. Manley	(KSU)
BATINIC	10	PR C82 038203	M. Batinic et al.	(ZAGR)
WILLIAMS	09	PR C80 065209	M. Williams et al.	(JLab CLAS Collab.)
ARNDT	06	PR C74 045205	R.A. Arndt et al.	(GWU)
VRANA	00	PRPL 328 181	T.P. Vrana, S.A. Dytman, T.-S.H. Lee	(PITT, ANL)
HOEHLER	93	πN Newsletter 9 1	G. Hoehler	(KARL)
CUTKOSKY	80	Toronto Conf. 19	R.E. Cutkosky et al.	(CMU, LBL) IUP
Also		PR D20 2839	R.E. Cutkosky et al.	(CMU, LBL) IUP
HOEHLER	79	PDAT 12-1	G. Hoehler et al.	(KARLT) IUP
Also		Toronto Conf. 3	R. Koch	(KARLT) IUP

$N(2220) 9/2^+$

$$I(J^P) = \frac{1}{2}(\frac{9}{2}^+) \text{ Status: } ****$$

Older and obsolete values are listed and referenced in the 2014 edition, Chinese Physics **C38** 070001 (2014).

$N(2220)$ POLE POSITION

REAL PART

VALUE (MeV)	DOCUMENT ID	TECN	COMMENT
2130 to 2200 (≈ 2170) OUR ESTIMATE			
2127 ± 3 ± 24	¹ SVARC	14	L+P $\pi N \rightarrow \pi N$
2150 ± 35	ANISOVICH	12A	DPWA Multichannel
2160 ± 80	CUTKOSKY	80	IPWA $\pi N \rightarrow \pi N$
••• We do not use the following data for averages, fits, limits, etc. •••			
2171	ROENCHEN	15A	DPWA Multichannel
2199	ARNDT	06	DPWA $\pi N \rightarrow \pi N, \eta N$
2135	HOEHLER	93	ARGD $\pi N \rightarrow \pi N$

¹ Fit to the amplitudes of HOEHLER 79.

-2xIMAGINARY PART

VALUE (MeV)	DOCUMENT ID	TECN	COMMENT
360 to 480 (≈ 400) OUR ESTIMATE			
380 ± 7 ± 22	¹ SVARC	14	L+P $\pi N \rightarrow \pi N$
440 ± 40	ANISOVICH	12A	DPWA Multichannel
480 ± 100	CUTKOSKY	80	IPWA $\pi N \rightarrow \pi N$

••• We do not use the following data for averages, fits, limits, etc. •••

593	ROENCHEN	15A	DPWA Multichannel
372	ARNDT	06	DPWA $\pi N \rightarrow \pi N, \eta N$
400	HOEHLER	93	ARGD $\pi N \rightarrow \pi N$

¹ Fit to the amplitudes of HOEHLER 79.

$N(2220)$ ELASTIC POLE RESIDUE

MODULUS $|r|$

VALUE (MeV)	DOCUMENT ID	TECN	COMMENT
35 to 60 (≈ 45) OUR ESTIMATE			
38 ± 1 ± 5	¹ SVARC	14	L+P $\pi N \rightarrow \pi N$
60 ± 12	ANISOVICH	12A	DPWA Multichannel
45 ± 20	CUTKOSKY	80	IPWA $\pi N \rightarrow \pi N$
••• We do not use the following data for averages, fits, limits, etc. •••			
62	ROENCHEN	15A	DPWA Multichannel
33	ARNDT	06	DPWA $\pi N \rightarrow \pi N, \eta N$
40	HOEHLER	93	ARGD $\pi N \rightarrow \pi N$

¹ Fit to the amplitudes of HOEHLER 79.

PHASE θ

VALUE (°)	DOCUMENT ID	TECN	COMMENT
-60 to -30 (≈ -50) OUR ESTIMATE			
-52 ± 1 ± 14	¹ SVARC	14	L+P $\pi N \rightarrow \pi N$
-58 ± 12	ANISOVICH	12A	DPWA Multichannel
-45 ± 25	CUTKOSKY	80	IPWA $\pi N \rightarrow \pi N$
••• We do not use the following data for averages, fits, limits, etc. •••			
-59	ROENCHEN	15A	DPWA Multichannel
-33	ARNDT	06	DPWA $\pi N \rightarrow \pi N, \eta N$
-50	HOEHLER	93	ARGD $\pi N \rightarrow \pi N$

¹ Fit to the amplitudes of HOEHLER 79.

$N(2220)$ INELASTIC POLE RESIDUE

The "normalized residue" is the residue divided by $\Gamma_{pole}/2$.

Normalized residue in $N\pi \rightarrow N(2220) \rightarrow N\eta$

MODULUS	PHASE (°)	DOCUMENT ID	TECN	COMMENT
••• We do not use the following data for averages, fits, limits, etc. •••				
0.004	-101	ROENCHEN	15A	DPWA Multichannel

Normalized residue in $N\pi \rightarrow N(2220) \rightarrow \Lambda K$

MODULUS	PHASE (°)	DOCUMENT ID	TECN	COMMENT
••• We do not use the following data for averages, fits, limits, etc. •••				
0.007	62	ROENCHEN	15A	DPWA Multichannel

Normalized residue in $N\pi \rightarrow N(2220) \rightarrow \Sigma K$

MODULUS	PHASE (°)	DOCUMENT ID	TECN	COMMENT
••• We do not use the following data for averages, fits, limits, etc. •••				
0.009	-128	ROENCHEN	15A	DPWA Multichannel

$N(2220)$ BREIT-WIGNER MASS

VALUE (MeV)	DOCUMENT ID	TECN	COMMENT
2200 to 2300 (≈ 2250) OUR ESTIMATE			
2316.3 ± 2.9	¹ ARNDT	06	DPWA $\pi N \rightarrow \pi N, \eta N$
2230 ± 80	CUTKOSKY	80	IPWA $\pi N \rightarrow \pi N$
2205 ± 10	HOEHLER	79	IPWA $\pi N \rightarrow \pi N$

¹ Statistical error only.

$N(2220)$ BREIT-WIGNER WIDTH

VALUE (MeV)	DOCUMENT ID	TECN	COMMENT
350 to 500 (≈ 400) OUR ESTIMATE			
633 ± 17	¹ ARNDT	06	DPWA $\pi N \rightarrow \pi N, \eta N$
500 ± 150	CUTKOSKY	80	IPWA $\pi N \rightarrow \pi N$
365 ± 30	HOEHLER	79	IPWA $\pi N \rightarrow \pi N$

¹ Statistical error only.

$N(2220)$ DECAY MODES

The following branching fractions are our estimates, not fits or averages.

Mode	Fraction (Γ_i/Γ)
$\Gamma_1 N\pi$	15-30 %

$N(2220)$ BRANCHING RATIOS

$\Gamma(N\pi)/\Gamma_{total}$	Γ_1/Γ
15 to 30 (≈ 25) OUR ESTIMATE	
24 ± 5	ANISOVICH 12A DPWA Multichannel
24.6 ± 0.1	¹ ARNDT 06 DPWA $\pi N \rightarrow \pi N, \eta N$
15 ± 3	CUTKOSKY 80 IPWA $\pi N \rightarrow \pi N$
18.0 ± 1.5	HOEHLER 79 IPWA $\pi N \rightarrow \pi N$

¹ Statistical error only.

$N(2220)$ PHOTON DECAY AMPLITUDES AT THE POLE

$N(2220) \rightarrow p\gamma$, helicity-1/2 amplitude $A_{1/2}$

MODULUS ($\text{GeV}^{-1/2}$)	PHASE ($^\circ$)	DOCUMENT ID	TECN	COMMENT
$-0.233^{+0.084}_{-0.044}$	-47^{+10}_{-6}	ROENCHEN	14	DPWA
0.135	114	ROENCHEN	15A	DPWA Multichannel

••• We do not use the following data for averages, fits, limits, etc. •••

$N(2220) \rightarrow p\gamma$, helicity-3/2 amplitude $A_{3/2}$

MODULUS ($\text{GeV}^{-1/2}$)	PHASE ($^\circ$)	DOCUMENT ID	TECN	COMMENT
$0.162^{+0.041}_{-0.038}$	-27^{+26}_{-13}	ROENCHEN	14	DPWA
0.082	-41	ROENCHEN	15A	DPWA Multichannel

••• We do not use the following data for averages, fits, limits, etc. •••

$N(2220)$ REFERENCES

For early references, see Physics Letters **111B** 1 (1982).

ROENCHEN 15A EPJ A51 70	D. Roenchen et al.	
PDG 14 CP C38 070001	K. Olive et al.	(PDG Collab.)
ROENCHEN 14 EPJ A50 101	D. Roenchen et al.	
Also EPJ A51 63 (errat.)	D. Roenchen et al.	
SVARC 14 PR C39 045205	A. Svarc et al.	(RBI Zagreb, UNI Tuzla)
ANISOVICH 12A EPJ A48 15	A. V. Anisovich et al.	(BONN, PNPI)
ARNDT 06 PR C74 045205	R.A. Arndt et al.	(GWU)
HOEHLER 93 πN Newsletter 9 1	G. Hoehler	(KARL)
CUTKOSKY 80 Toronto Conf. 19	R.E. Cutkosky et al.	(CMU, LBL) IJP
Also PR D20 2839	R.E. Cutkosky et al.	(CMU, LBL) IJP
HOEHLER 79 PDAT 12-1	G. Hoehler et al.	(KARLT) IJP
Also Toronto Conf. 3	R. Koch	(KARLT) IJP

$N(2250) 9/2^-$

$I(J^P) = \frac{1}{2}(\frac{9}{2}^-)$ Status: * * * *

Older and obsolete values are listed and referenced in the 2014 edition, Chinese Physics **C38** 070001 (2014).

$N(2250)$ POLE POSITION

REAL PART

VALUE (MeV)	DOCUMENT ID	TECN	COMMENT
2150 to 2250 (≈ 2200) OUR ESTIMATE			
2195 \pm 45	AFZAL 20	DPWA	Multichannel
2157 \pm 3 \pm 14	¹ SVARC 14	L+P	$\pi N \rightarrow \pi N$
2195 \pm 45	ANISOVICH 12A	DPWA	Multichannel
2150 \pm 50	CUTKOSKY 80	IPWA	$\pi N \rightarrow \pi N$
••• We do not use the following data for averages, fits, limits, etc. •••			
2127	HUNT 19	DPWA	Multichannel
2062	ROENCHEN 15A	DPWA	Multichannel
2217	ARNDT 06	DPWA	$\pi N \rightarrow \pi N, \eta N$
2187	HOEHLER 93	SPED	$\pi N \rightarrow \pi N$

¹ Fit to the amplitudes of HOEHLER 79.

-2xIMAGINARY PART

VALUE (MeV)	DOCUMENT ID	TECN	COMMENT
350 to 500 (≈ 420) OUR ESTIMATE			
470 \pm 50	AFZAL 20	DPWA	Multichannel
412 \pm 7 \pm 44	¹ SVARC 14	L+P	$\pi N \rightarrow \pi N$
470 \pm 50	ANISOVICH 12A	DPWA	Multichannel
360 \pm 100	CUTKOSKY 80	IPWA	$\pi N \rightarrow \pi N$
••• We do not use the following data for averages, fits, limits, etc. •••			
262	HUNT 19	DPWA	Multichannel
403	ROENCHEN 15A	DPWA	Multichannel
431	ARNDT 06	DPWA	$\pi N \rightarrow \pi N, \eta N$
388	HOEHLER 93	SPED	$\pi N \rightarrow \pi N$

¹ Fit to the amplitudes of HOEHLER 79.

$N(2250)$ ELASTIC POLE RESIDUE

MODULUS $|r|$

VALUE (MeV)	DOCUMENT ID	TECN	COMMENT
20 to 30 (≈ 25) OUR ESTIMATE			
24 \pm 1 \pm 5	¹ SVARC 14	L+P	$\pi N \rightarrow \pi N$
26 \pm 5	ANISOVICH 12A	DPWA	Multichannel
20 \pm 6	CUTKOSKY 80	IPWA	$\pi N \rightarrow \pi N$
••• We do not use the following data for averages, fits, limits, etc. •••			
8.2	ROENCHEN 15A	DPWA	Multichannel
21	ARNDT 06	DPWA	$\pi N \rightarrow \pi N, \eta N$
21	HOEHLER 93	SPED	$\pi N \rightarrow \pi N$

¹ Fit to the amplitudes of HOEHLER 79.

PHASE θ

VALUE ($^\circ$)	DOCUMENT ID	TECN	COMMENT
-60 to -20 (≈ -40) OUR ESTIMATE			
-62 \pm 1 \pm 11	¹ SVARC 14	L+P	$\pi N \rightarrow \pi N$
-38 \pm 25	ANISOVICH 12A	DPWA	Multichannel
-50 \pm 20	CUTKOSKY 80	IPWA	$\pi N \rightarrow \pi N$
••• We do not use the following data for averages, fits, limits, etc. •••			
-64	ROENCHEN 15A	DPWA	Multichannel
-20	ARNDT 06	DPWA	$\pi N \rightarrow \pi N, \eta N$

¹ Fit to the amplitudes of HOEHLER 79.

$N(2250)$ INELASTIC POLE RESIDUE

The "normalized residue" is the residue divided by $\Gamma_{pole}/2$.

Normalized residue in $N\pi \rightarrow N(2250) \rightarrow N\eta$

MODULUS	PHASE ($^\circ$)	DOCUMENT ID	TECN	COMMENT
••• We do not use the following data for averages, fits, limits, etc. •••				
0.017	-89	ROENCHEN	15A	DPWA Multichannel

Normalized residue in $N\pi \rightarrow N(2250) \rightarrow \Lambda K$

MODULUS	PHASE ($^\circ$)	DOCUMENT ID	TECN	COMMENT
••• We do not use the following data for averages, fits, limits, etc. •••				
0.006	-101	ROENCHEN	15A	DPWA Multichannel

Normalized residue in $N\pi \rightarrow N(2250) \rightarrow \Sigma K$

MODULUS	PHASE ($^\circ$)	DOCUMENT ID	TECN	COMMENT
••• We do not use the following data for averages, fits, limits, etc. •••				
0.002	70	ROENCHEN	15A	DPWA Multichannel

$N(2250)$ BREIT-WIGNER MASS

VALUE (MeV)	DOCUMENT ID	TECN	COMMENT
2250 to 2320 (≈ 2280) OUR ESTIMATE			
2200 \pm 10	¹ HUNT 19	DPWA	Multichannel
2280 \pm 40	ANISOVICH 12A	DPWA	Multichannel
2302 \pm 6	¹ ARNDT 06	DPWA	$\pi N \rightarrow \pi N, \eta N$
2250 \pm 80	CUTKOSKY 80	IPWA	$\pi N \rightarrow \pi N$
2268 \pm 15	HOEHLER 79	IPWA	$\pi N \rightarrow \pi N$

¹ Statistical error only.

$N(2250)$ BREIT-WIGNER WIDTH

VALUE (MeV)	DOCUMENT ID	TECN	COMMENT
300 to 600 (≈ 500) OUR ESTIMATE			
343 \pm 51	¹ HUNT 19	DPWA	Multichannel
520 \pm 50	ANISOVICH 12A	DPWA	Multichannel
628 \pm 28	¹ ARNDT 06	DPWA	$\pi N \rightarrow \pi N, \eta N$
480 \pm 120	CUTKOSKY 80	IPWA	$\pi N \rightarrow \pi N$
300 \pm 40	HOEHLER 79	IPWA	$\pi N \rightarrow \pi N$

¹ Statistical error only.

$N(2250)$ DECAY MODES

The following branching fractions are our estimates, not fits or averages.

Mode	Fraction (Γ_i/Γ)
Γ_1 $N\pi$	5-15 %
Γ_2 $N\eta$	<5 %
Γ_3 ΛK	1-3 %

$N(2250)$ BRANCHING RATIOS

$\Gamma(N\pi)/\Gamma_{total}$	DOCUMENT ID	TECN	COMMENT	Γ_1/Γ
5-15 % OUR ESTIMATE				
8.5 \pm 0.4	¹ HUNT 19	DPWA	Multichannel	
12 \pm 4	ANISOVICH 12A	DPWA	Multichannel	
8.9 \pm 0.1	¹ ARNDT 06	DPWA	$\pi N \rightarrow \pi N, \eta N$	
10 \pm 2	CUTKOSKY 80	IPWA	$\pi N \rightarrow \pi N$	
10 \pm 2	HOEHLER 79	IPWA	$\pi N \rightarrow \pi N$	

¹ Statistical error only.

$\Gamma(N\eta)/\Gamma_{total}$	DOCUMENT ID	TECN	COMMENT	Γ_2/Γ
<5 % OUR ESTIMATE				
<5	¹ HUNT 19	DPWA	Multichannel	

¹ Statistical error only.

Baryon Particle Listings

 $N(2250)$, $N(2300)$, $N(2570)$, $N(2600)$, $N(2700)$

$\Gamma(AK)/\Gamma_{\text{total}}$	DOCUMENT ID	TECN	COMMENT	Γ_3/Γ
1-3 % OUR ESTIMATE				
2.0 ± 0.6	1 HUNT	19	DPWA Multichannel	

¹ Statistical error only. **$N(2250)$ PHOTON DECAY AMPLITUDES AT THE POLE** **$N(2250) \rightarrow p\gamma$, helicity-1/2 amplitude $A_{1/2}$**

MODULUS ($\text{GeV}^{-1/2}$)	PHASE ($^\circ$)	DOCUMENT ID	TECN	COMMENT
$-0.090^{+0.025}_{-0.022}$	-49^{+17}_{-11}	ROENCHEN	14	DPWA
• • • We do not use the following data for averages, fits, limits, etc. • • •				
0.026	-26	ROENCHEN	15A	DPWA Multichannel

 $N(2250) \rightarrow p\gamma$, helicity-3/2 amplitude $A_{3/2}$

MODULUS ($\text{GeV}^{-1/2}$)	PHASE ($^\circ$)	DOCUMENT ID	TECN	COMMENT
$0.049^{+0.031}_{-0.019}$	171^{+36}_{-43}	ROENCHEN	14	DPWA
• • • We do not use the following data for averages, fits, limits, etc. • • •				
0.119	-42	ROENCHEN	15A	DPWA Multichannel

 $N(2250)$ BREIT-WIGNER PHOTON DECAY AMPLITUDES **$N(2250) \rightarrow p\gamma$, helicity-1/2 amplitude $A_{1/2}$**

VALUE ($\text{GeV}^{-1/2}$)	DOCUMENT ID	TECN	COMMENT
0.0006 ± 0.0037	1 HUNT	19	DPWA Multichannel

¹ Statistical error only. **$N(2250) \rightarrow p\gamma$, helicity-3/2 amplitude $A_{3/2}$**

VALUE ($\text{GeV}^{-1/2}$)	DOCUMENT ID	TECN	COMMENT
0.013 ± 0.004	1 HUNT	19	DPWA Multichannel

¹ Statistical error only. **$N(2250)$ REFERENCES**

AFZAL	20	PRL 125 152002	F. Afzal et al.	(CBELSA/TAPS Collab.)
HUNT	19	PR C99 055205	B.C. Hunt, D.M. Manley	
ROENCHEN	15A	EPJ A51 70	D. Roenchen et al.	
PDG	14	CP C38 070001	K. Olive et al.	(PDG Collab.)
ROENCHEN	14	EPJ A50 101	D. Roenchen et al.	
Also		EPJ A51 63 (err.)	D. Roenchen et al.	
SVARC	14	PR C89 045205	A. Svarc et al.	(RBI Zagreb, UNI Tuzla)
ANISOVICH	12A	EPJ A48 15	A.V. Anisovich et al.	(BONN, PNPI)
ARNDT	06	PR C74 045205	R.A. Arndt et al.	(GWU)
HOEHLER	93	πN Newsletter 9 1	G. Hoehler	(KARL)
CUTKOSKY	80	Toronto Conf. 19	R.E. Cutkosky et al.	(CMU, LBL) IJP
Also		PR D20 2839	R.E. Cutkosky et al.	(CMU, LBL) IJP
HOEHLER	79	PDAT 12-1	G. Hoehler et al.	(KARL) IJP
Also		Toronto Conf. 3	R. Koch	(KARL) IJP

$N(2300) 1/2^+$ $I(J^P) = \frac{1}{2}(\frac{1}{2}^+)$ Status: **

OMITTED FROM SUMMARY TABLE

 $N(2300)$ MASS

VALUE (MeV)	DOCUMENT ID	TECN	COMMENT
$2300^{+40+109}_{-30-0}$	ABLIKIM	13A	BES3 $\psi(2S) \rightarrow p\bar{p}\pi^0$

 $N(2300)$ WIDTH

VALUE (MeV)	DOCUMENT ID	TECN	COMMENT
$340 \pm 30^{+110}_{-58}$	ABLIKIM	13A	BES3 $\psi(2S) \rightarrow p\bar{p}\pi^0$

 $N(2300)$ REFERENCES

ABLIKIM	13A	PRL 110 022001	M. Ablikim et al.	(BESIII Collab.)
---------	-----	----------------	-------------------	------------------

$N(2570) 5/2^-$ $I(J^P) = \frac{1}{2}(\frac{5}{2}^-)$ Status: **

OMITTED FROM SUMMARY TABLE

 $N(2570)$ MASS

VALUE (MeV)	DOCUMENT ID	TECN	COMMENT
2570^{+19+34}_{-10-10}	ABLIKIM	13A	BES3 $\psi(2S) \rightarrow p\bar{p}\pi^0$

 $N(2570)$ WIDTH

VALUE (MeV)	DOCUMENT ID	TECN	COMMENT
250^{+14+69}_{-24-21}	ABLIKIM	13A	BES3 $\psi(2S) \rightarrow p\bar{p}\pi^0$

 $N(2570)$ REFERENCES

ABLIKIM	13A	PRL 110 022001	M. Ablikim et al.	(BESIII Collab.)
---------	-----	----------------	-------------------	------------------

$N(2600) 11/2^-$ $I(J^P) = \frac{1}{2}(\frac{11}{2}^-)$ Status: ***

 $N(2600)$ BREIT-WIGNER MASS

VALUE (MeV)	DOCUMENT ID	TECN	COMMENT
2550 to 2750 (≈ 2600) OUR ESTIMATE			
2623 ± 197	ARNDT	06	DPWA $\pi N \rightarrow \pi N, \eta N$
2577 ± 50	HOEHLER	79	IPWA $\pi N \rightarrow \pi N$

 $N(2600)$ BREIT-WIGNER WIDTH

VALUE (MeV)	DOCUMENT ID	TECN	COMMENT
500 to 800 (≈ 650) OUR ESTIMATE			
1311 ± 996	ARNDT	06	DPWA $\pi N \rightarrow \pi N, \eta N$
400 ± 100	HOEHLER	79	IPWA $\pi N \rightarrow \pi N$

 $N(2600)$ DECAY MODES

Mode	Fraction (Γ_i/Γ)
Γ_1 $N\pi$	3-8 %

 $N(2600)$ BRANCHING RATIOS

$\Gamma(N\pi)/\Gamma_{\text{total}}$	DOCUMENT ID	TECN	COMMENT	Γ_1/Γ
3 to 8 (≈ 5) OUR ESTIMATE				
5.0 ± 1.8	ARNDT	06	DPWA $\pi N \rightarrow \pi N, \eta N$	
5 ± 1	HOEHLER	79	IPWA $\pi N \rightarrow \pi N$	

 $N(2600)$ REFERENCES

ARNDT	06	PR C74 045205	R.A. Arndt et al.	(GWU)
HOEHLER	79	PDAT 12-1	G. Hoehler et al.	(KARL) IJP
Also		Toronto Conf. 3	R. Koch	(KARL) IJP

$N(2700) 13/2^+$ $I(J^P) = \frac{1}{2}(\frac{13}{2}^+)$ Status: **

OMITTED FROM SUMMARY TABLE

 $N(2700)$ BREIT-WIGNER MASS

VALUE (MeV)	DOCUMENT ID	TECN	COMMENT
2612 ± 45	HOEHLER	79	IPWA $\pi N \rightarrow \pi N$

 $N(2700)$ BREIT-WIGNER WIDTH

VALUE (MeV)	DOCUMENT ID	TECN	COMMENT
350 ± 50	HOEHLER	79	IPWA $\pi N \rightarrow \pi N$

 $N(2700)$ DECAY MODES

Mode	Fraction (Γ_i/Γ)
Γ_1 $N\pi$	3-5 %

 $N(2700)$ BRANCHING RATIOS

$\Gamma(N\pi)/\Gamma_{\text{total}}$	DOCUMENT ID	TECN	COMMENT	Γ_1/Γ
4 ± 1	HOEHLER	79	IPWA $\pi N \rightarrow \pi N$	

 $N(2700)$ REFERENCES

HOEHLER	79	PDAT 12-1	G. Hoehler et al.	(KARL) IJP
Also		Toronto Conf. 3	R. Koch	(KARL) IJP

See key on page 1127

Baryon Particle Listings
 $N(\sim 3000)$

**$N(\sim 3000)$ Region
 Partial-Wave Analyses**

OMITTED FROM SUMMARY TABLE

We list here miscellaneous high-mass candidates for isospin-1/2 resonances found in partial-wave analyses.

Our 1982 edition had an $N(3245)$, an $N(3690)$, and an $N(3755)$, each a narrow peak seen in a production experiment. Since nothing has been heard from them since the 1960's, we declare them to be dead. There was also an $N(3030)$, deduced from total cross-section and 180° elastic cross-section measurements; it is the KOCH 80 $L_{1,15}$ state below.

$N(\sim 3000)$ BREIT-WIGNER MASS

VALUE (MeV)	DOCUMENT ID	TECN	COMMENT
≈ 3000 OUR ESTIMATE			
2600	KOCH 80	IPWA	$\pi N \rightarrow \pi N D_{13}$
3100	KOCH 80	IPWA	$\pi N \rightarrow \pi N L_{1,15}$ wave
3500	KOCH 80	IPWA	$\pi N \rightarrow \pi N M_{1,17}$ wave
3500 to 4000	KOCH 80	IPWA	$\pi N \rightarrow \pi N N_{1,19}$ wave
3500 \pm 200	HENDRY 78	MPWA	$\pi N \rightarrow \pi N L_{1,15}$ wave
3800 \pm 200	HENDRY 78	MPWA	$\pi N \rightarrow \pi N M_{1,17}$ wave
4100 \pm 200	HENDRY 78	MPWA	$\pi N \rightarrow \pi N N_{1,19}$ wave

$N(\sim 3000)$ BREIT-WIGNER WIDTH

VALUE (MeV)	DOCUMENT ID	TECN	COMMENT
1300 \pm 200	HENDRY 78	MPWA	$\pi N \rightarrow \pi N L_{1,15}$ wave
1600 \pm 200	HENDRY 78	MPWA	$\pi N \rightarrow \pi N M_{1,17}$ wave
1900 \pm 300	HENDRY 78	MPWA	$\pi N \rightarrow \pi N N_{1,19}$ wave

$N(\sim 3000)$ DECAY MODES

Mode	Fraction (Γ_i/Γ)
$\Gamma_1 N \pi$	2-8 %

$N(\sim 3000)$ BRANCHING RATIOS

$\Gamma(N\pi)/\Gamma_{total}$	DOCUMENT ID	TECN	COMMENT	Γ_1/Γ
2-8 % OUR ESTIMATE				
6 \pm 2	HENDRY 78	MPWA	$\pi N \rightarrow \pi N L_{1,15}$ wave	
4.0 \pm 1.5	HENDRY 78	MPWA	$\pi N \rightarrow \pi N M_{1,17}$ wave	
3.0 \pm 1.5	HENDRY 78	MPWA	$\pi N \rightarrow \pi N N_{1,19}$ wave	

$N(\sim 3000)$ REFERENCES

KOCH 80	Toronto Conf. 3	R. Koch	(KARLT) IJP
HENDRY 78	PRL 41 222	A.W. Hendry	(IND, LBL) IJP
Also	ANP 136 1	A.W. Hendry	(IND) IJP

Baryon Particle Listings

 $\Delta(1232)$ Δ BARYONS
($S = 0, I = 3/2$)

$$\Delta^{++} = uuu, \Delta^+ = uud, \Delta^0 = udd, \Delta^- = ddd$$

 $\Delta(1232) 3/2^+$

$$I(J^P) = \frac{3}{2}(\frac{3}{2}^+) \text{ Status: } ****$$

Older and obsolete values are listed and referenced in the 2014 edition, Chinese Physics C38 070001 (2014).

 $\Delta(1232)$ POLE POSITIONS

REAL PART, MIXED CHARGES

VALUE (MeV)	DOCUMENT ID	TECN	COMMENT
1209 to 1211 (≈ 1210) OUR ESTIMATE			
1211 $\pm 1 \pm 1$	¹ SVARC 14	L+P	$\pi N \rightarrow \pi N$
1210.5 ± 1.0	ANISOVICH 12A	DPWA	Multichannel
1210 ± 1	CUTKOSKY 80	IPWA	$\pi N \rightarrow \pi N$
••• We do not use the following data for averages, fits, limits, etc. •••			
1212.4	HUNT 19	DPWA	Multichannel
1218	ROENCHEN 15A	DPWA	Multichannel
1211 ± 1	ANISOVICH 10	DPWA	Multichannel
1211	ARNDT 06	DPWA	$\pi N \rightarrow \pi N, \eta N$
1210	ARNDT 04	DPWA	$\pi N \rightarrow \pi N, \eta N$
1209	² HOEHLER 93	ARGD	$\pi N \rightarrow \pi N$

¹ Fit to the amplitudes of HOEHLER 79.

² See HOEHLER 93 for a detailed discussion of the evidence for and the pole parameters of N and Δ resonances as determined from Argand diagrams of πN elastic partial-wave amplitudes and from plots of the speeds with which the amplitudes traverse the diagrams.

 $-2\times$ IMAGINARY PART, MIXED CHARGES

VALUE (MeV)	DOCUMENT ID	TECN	COMMENT
98 to 102 (≈ 100) OUR ESTIMATE			
98 $\pm 2 \pm 1$	¹ SVARC 14	L+P	$\pi N \rightarrow \pi N$
99 ± 2	ANISOVICH 12A	DPWA	Multichannel
100 ± 2	CUTKOSKY 80	IPWA	$\pi N \rightarrow \pi N$
••• We do not use the following data for averages, fits, limits, etc. •••			
96.8	HUNT 19	DPWA	Multichannel
92	ROENCHEN 15A	DPWA	Multichannel
100 ± 2	ANISOVICH 10	DPWA	Multichannel
99	ARNDT 06	DPWA	$\pi N \rightarrow \pi N, \eta N$
100	ARNDT 04	DPWA	$\pi N \rightarrow \pi N, \eta N$
100	² HOEHLER 93	ARGD	$\pi N \rightarrow \pi N$

¹ Fit to the amplitudes of HOEHLER 79.

² See HOEHLER 93 for a detailed discussion of the evidence for and the pole parameters of N and Δ resonances as determined from Argand diagrams of πN elastic partial-wave amplitudes and from plots of the speeds with which the amplitudes traverse the diagrams.

REAL PART, $\Delta(1232)^{++}$

VALUE (MeV)	DOCUMENT ID	COMMENT
••• We do not use the following data for averages, fits, limits, etc. •••		
1212.50 ± 0.24	BERNICHIA 96	Fit to PEDRONI 78

 $-2\times$ IMAGINARY PART, $\Delta(1232)^{++}$

VALUE (MeV)	DOCUMENT ID	COMMENT
••• We do not use the following data for averages, fits, limits, etc. •••		
97.37 ± 0.42	BERNICHIA 96	Fit to PEDRONI 78

REAL PART, $\Delta(1232)^+$

VALUE (MeV)	DOCUMENT ID	TECN	COMMENT
••• We do not use the following data for averages, fits, limits, etc. •••			
1211 ± 1 to 1212 ± 1	HANSTEIN 96	DPWA	$\gamma N \rightarrow \pi N$
1206.9 ± 0.9 to 1210.5 ± 1.8	MIROSHNIC... 79		Fit photoproduction

 $-2\times$ IMAGINARY PART, $\Delta(1232)^+$

VALUE (MeV)	DOCUMENT ID	TECN	COMMENT
••• We do not use the following data for averages, fits, limits, etc. •••			
102 ± 2 to 99 ± 2	¹ HANSTEIN 96	DPWA	$\gamma N \rightarrow \pi N$
111.2 ± 2.0 to 116.6 ± 2.2	MIROSHNIC... 79		Fit photoproduction

¹ The second (lower) value of HANSTEIN 96 here goes with the second (higher) value of the real part in the preceding data block.

REAL PART, $\Delta(1232)^0$

VALUE (MeV)	DOCUMENT ID	COMMENT
••• We do not use the following data for averages, fits, limits, etc. •••		
1213.20 ± 0.66	BERNICHIA 96	Fit to PEDRONI 78

 $-2\times$ IMAGINARY PART, $\Delta(1232)^0$

VALUE (MeV)	DOCUMENT ID	COMMENT
••• We do not use the following data for averages, fits, limits, etc. •••		
104.10 ± 1.01	BERNICHIA 96	Fit to PEDRONI 78

 $\Delta(1232)$ ELASTIC POLE RESIDUES

ABSOLUTE VALUE, MIXED CHARGES

VALUE (MeV)	DOCUMENT ID	TECN	COMMENT
49 to 52 (≈ 50) OUR ESTIMATE			
50 $\pm 1 \pm 1$	¹ SVARC 14	L+P	$\pi N \rightarrow \pi N$
51.6 ± 0.6	ANISOVICH 12A	DPWA	Multichannel
53 ± 2	CUTKOSKY 80	IPWA	$\pi N \rightarrow \pi N$
••• We do not use the following data for averages, fits, limits, etc. •••			
46	ROENCHEN 15A	DPWA	Multichannel
52	ARNDT 06	DPWA	$\pi N \rightarrow \pi N, \eta N$
53	ARNDT 04	DPWA	$\pi N \rightarrow \pi N, \eta N$
50	HOEHLER 93	ARGD	$\pi N \rightarrow \pi N$

PHASE, MIXED CHARGES

VALUE ($^\circ$)	DOCUMENT ID	TECN	COMMENT
-48 to -45 (≈ -46) OUR ESTIMATE			
-46 $\pm 1 \pm 1$	¹ SVARC 14	L+P	$\pi N \rightarrow \pi N$
-46 ± 1	ANISOVICH 12A	DPWA	Multichannel
-47 ± 1	CUTKOSKY 80	IPWA	$\pi N \rightarrow \pi N$
••• We do not use the following data for averages, fits, limits, etc. •••			
-36	ROENCHEN 15A	DPWA	Multichannel
-47	ARNDT 06	DPWA	$\pi N \rightarrow \pi N, \eta N$
-47	ARNDT 04	DPWA	$\pi N \rightarrow \pi N, \eta N$
-48	HOEHLER 93	ARGD	$\pi N \rightarrow \pi N$

¹ Fit to the amplitudes of HOEHLER 79.

 $\Delta(1232)$ BREIT-WIGNER MASSES

MIXED CHARGES

VALUE (MeV)	DOCUMENT ID	TECN	COMMENT
1230 to 1234 (≈ 1232) OUR ESTIMATE			
1230.8 ± 0.4	¹ HUNT 19	DPWA	Multichannel
1228 ± 2	ANISOVICH 12A	DPWA	Multichannel
1233.4 ± 0.4	¹ ARNDT 06	DPWA	$\pi N \rightarrow \pi N, \eta N$
1232 ± 3	CUTKOSKY 80	IPWA	$\pi N \rightarrow \pi N$
1233 ± 2	HOEHLER 79	IPWA	$\pi N \rightarrow \pi N$
••• We do not use the following data for averages, fits, limits, etc. •••			
1231.1 ± 0.2	¹ SHRESTHA 12A	DPWA	Multichannel
1230 ± 2	ANISOVICH 10	DPWA	Multichannel
1232.9 ± 1.2	ARNDT 04	DPWA	$\pi N \rightarrow \pi N, \eta N$
1228 ± 1	PENNER 02c	DPWA	Multichannel

¹ Statistical error only.

 $\Delta(1232)^{++}$ MASS

VALUE (MeV)	DOCUMENT ID	TECN	COMMENT
••• We do not use the following data for averages, fits, limits, etc. •••			
1230.55 ± 0.20	GRIDNEV 06	DPWA	$\pi N \rightarrow \pi N$
1231.88 ± 0.29	BERNICHIA 96		Fit to PEDRONI 78
1230.5 ± 0.2	ABAEV 95	IPWA	$\pi N \rightarrow \pi N$
1230.9 ± 0.3	KOCH 80b	IPWA	$\pi N \rightarrow \pi N$
1231.1 ± 0.2	PEDRONI 78		$\pi N \rightarrow \pi N$ 70-370 MeV

 $\Delta(1232)^+$ MASS

VALUE (MeV)	DOCUMENT ID	COMMENT
••• We do not use the following data for averages, fits, limits, etc. •••		
1234.9 ± 1.4	MIROSHNIC... 79	Fit photoproduction

 $\Delta(1232)^0$ MASS

VALUE (MeV)	DOCUMENT ID	TECN	COMMENT
••• We do not use the following data for averages, fits, limits, etc. •••			
1231.3 ± 0.6	BREITSCHOP...06	CNTR	Using new CHEX data
1233.40 ± 0.22	GRIDNEV 06	DPWA	$\pi N \rightarrow \pi N$
1234.35 ± 0.75	BERNICHIA 96		Fit to PEDRONI 78
1233.1 ± 0.3	ABAEV 95	IPWA	$\pi N \rightarrow \pi N$
1233.6 ± 0.5	KOCH 80b	IPWA	$\pi N \rightarrow \pi N$
1233.8 ± 0.2	PEDRONI 78		$\pi N \rightarrow \pi N$ 70-370 MeV

 $m_{\Delta^0} - m_{\Delta^{++}}$

VALUE (MeV)	DOCUMENT ID	TECN	COMMENT
••• We do not use the following data for averages, fits, limits, etc. •••			
2.86 ± 0.30	GRIDNEV 06	DPWA	$\pi N \rightarrow \pi N$
2.25 ± 0.68	BERNICHIA 96		Fit to PEDRONI 78
2.6 ± 0.4	ABAEV 95	IPWA	$\pi N \rightarrow \pi N$
2.7 ± 0.3	¹ PEDRONI 78		See the masses

¹ Using $\pi^\pm d$ as well, PEDRONI 78 determine $(M^- - M^{++}) + (M^0 - M^+)/3 = 4.6 \pm 0.2$ MeV.

$\Delta(1232)$ BREIT-WIGNER WIDTHS

MIXED CHARGES

VALUE (MeV)	DOCUMENT ID	TECN	COMMENT
114 to 120 (≈ 117) OUR ESTIMATE			
110.9 \pm 0.8	¹ HUNT 19	DPWA	Multichannel
110 \pm 3	ANISOVICH 12A	DPWA	Multichannel
118.7 \pm 0.6	¹ ARNDT 06	DPWA	$\pi N \rightarrow \pi N, \eta N$
120 \pm 5	CUTKOSKY 80	IPWA	$\pi N \rightarrow \pi N$
116 \pm 5	HOEHLER 79	IPWA	$\pi N \rightarrow \pi N$
••• We do not use the following data for averages, fits, limits, etc. •••			
113.0 \pm 0.5	¹ SHRESTHA 12A	DPWA	Multichannel
112 \pm 4	ANISOVICH 10	DPWA	Multichannel
118.0 \pm 2.2	ARNDT 04	DPWA	$\pi N \rightarrow \pi N, \eta N$
106 \pm 1	PENNER 02c	DPWA	Multichannel

¹ Statistical error only.

$\Delta(1232)^{++}$ WIDTH

VALUE (MeV)	DOCUMENT ID	TECN	COMMENT
••• We do not use the following data for averages, fits, limits, etc. •••			
112.2 \pm 0.7	GRIDNEV 06	DPWA	$\pi N \rightarrow \pi N$
109.07 \pm 0.48	BERNICHIA 96		Fit to PEDRONI 78
111.0 \pm 1.0	KOCH 80b	IPWA	$\pi N \rightarrow \pi N$
111.3 \pm 0.5	PEDRONI 78		$\pi N \rightarrow \pi N$ 70–370 MeV

$\Delta(1232)^+$ WIDTH

VALUE (MeV)	DOCUMENT ID	COMMENT
••• We do not use the following data for averages, fits, limits, etc. •••		
131.1 \pm 2.4	MIROSHNIC... 79	Fit photoproduction

$\Delta(1232)^0$ WIDTH

VALUE (MeV)	DOCUMENT ID	TECN	COMMENT
••• We do not use the following data for averages, fits, limits, etc. •••			
112.5 \pm 1.9	BREITSCHOP..06	CNTR	Using new CHEX data
116.9 \pm 0.7	GRIDNEV 06	DPWA	$\pi N \rightarrow \pi N$
117.58 \pm 1.16	BERNICHIA 96		Fit to PEDRONI 78
113.0 \pm 1.5	KOCH 80b	IPWA	$\pi N \rightarrow \pi N$
117.9 \pm 0.9	PEDRONI 78		$\pi N \rightarrow \pi N$ 70–370 MeV

Δ^0 - Δ^{++} WIDTH DIFFERENCE

VALUE (MeV)	DOCUMENT ID	TECN	COMMENT
••• We do not use the following data for averages, fits, limits, etc. •••			
4.66 \pm 1.0	GRIDNEV 06	DPWA	$\pi N \rightarrow \pi N$
8.45 \pm 1.11	BERNICHIA 96		Fit to PEDRONI 78
5.1 \pm 1.0	ABAEV 95	IPWA	$\pi N \rightarrow \pi N$
6.6 \pm 1.0	PEDRONI 78		See the widths

$\Delta(1232)$ DECAY MODES

The following branching fractions are our estimates, not fits or averages.

Mode	Fraction (Γ_j/Γ)
Γ_1 $N\pi$	99.4 %
Γ_2 $N\gamma$	0.55–0.65 %
Γ_3 $N\gamma$, helicity=1/2	0.11–0.13 %
Γ_4 $N\gamma$, helicity=3/2	0.44–0.52 %
Γ_5 pe^+e^-	(4.2 ± 0.7) $\times 10^{-5}$

$\Delta(1232)$ BRANCHING RATIOS

$\Gamma(N\pi)/\Gamma_{total}$	DOCUMENT ID	TECN	COMMENT	Γ_1/Γ
0.994 OUR ESTIMATE				
0.9939 \pm 0.0001	¹ HUNT 19	DPWA	Multichannel	
1.00	ARNDT 06	DPWA	$\pi N \rightarrow \pi N, \eta N$	
1.0	CUTKOSKY 80	IPWA	$\pi N \rightarrow \pi N$	
1.0	HOEHLER 79	IPWA	$\pi N \rightarrow \pi N$	
••• We do not use the following data for averages, fits, limits, etc. •••				
0.994	SHRESTHA 12A	DPWA	Multichannel	
1.0	ANISOVICH 10	DPWA	Multichannel	
1.000	ARNDT 04	DPWA	$\pi N \rightarrow \pi N, \eta N$	
1.00	PENNER 02c	DPWA	Multichannel	

¹ Statistical error only.

$\Gamma(pe^+e^-)/\Gamma_{total}$	DOCUMENT ID	COMMENT	Γ_5/Γ
4.19\pm0.34\pm0.62	¹ ADAMCZEW... 17		
••• We do not use the following data for averages, fits, limits, etc. •••			
¹ The systematic uncertainty includes the model dependence.			

$\Delta(1232)$ PHOTON DECAY AMPLITUDES AT THE POLE

$\Delta(1232) \rightarrow N\gamma$, helicity-1/2 amplitude $A_{1/2}$

MODULUS ($\text{GeV}^{-1/2}$)	PHASE ($^\circ$)	DOCUMENT ID	TECN	COMMENT
-0.114 $^{+0.010}_{-0.003}$	-9 $^{+4}_{-2}$	ROENCHEN 14	DPWA	
••• We do not use the following data for averages, fits, limits, etc. •••				
-0.117	-6.6	ROENCHEN 15A	DPWA	Multichannel

$\Delta(1232) \rightarrow N\gamma$, helicity-3/2 amplitude $A_{3/2}$

MODULUS ($\text{GeV}^{-1/2}$)	PHASE ($^\circ$)	DOCUMENT ID	TECN	COMMENT
-0.229 $^{+0.003}_{-0.004}$	3 $^{+0.3}_{-0.4}$	ROENCHEN 14	DPWA	
••• We do not use the following data for averages, fits, limits, etc. •••				
-0.226	2.8	ROENCHEN 15A	DPWA	Multichannel

$\Delta(1232)$ BREIT-WIGNER PHOTON DECAY AMPLITUDES

Papers on γN amplitudes predating 1981 may be found in our 2006 edition, Journal of Physics **G33** 1 (2006).

$\Delta(1232) \rightarrow N\gamma$, helicity-1/2 amplitude $A_{1/2}$

VALUE ($\text{GeV}^{-1/2}$)	DOCUMENT ID	TECN	COMMENT
-0.142 to -0.129 (≈ -0.135) OUR ESTIMATE			
-0.146 \pm 0.002	¹ HUNT 19	DPWA	Multichannel
-0.131 \pm 0.004	ANISOVICH 12A	DPWA	Multichannel
-0.139 \pm 0.002	¹ WORKMAN 12A	DPWA	$\gamma N \rightarrow N\pi$
-0.139 \pm 0.004	¹ DUGGER 07	DPWA	$\gamma N \rightarrow \pi N$
-0.137 \pm 0.005	AHRENS 04A	DPWA	$\tilde{\gamma}\tilde{p} \rightarrow N\pi$
-0.1357 \pm 0.0013 \pm 0.0037	BLANPIED 01	LEGS	$\gamma p \rightarrow p\gamma, p\pi^0, n\pi^+$
-0.131 \pm 0.001	¹ BECK 00	IPWA	$\tilde{\gamma}p \rightarrow p\pi^0, n\pi^+$
-0.140 \pm 0.005	KAMALOV 99	DPWA	$\gamma N \rightarrow \pi N$
-0.1294 \pm 0.0013	HANSTEIN 98	IPWA	$\gamma N \rightarrow \pi N$
-0.1278 \pm 0.0012	DAVIDSON 97	DPWA	$\gamma N \rightarrow \pi N$
••• We do not use the following data for averages, fits, limits, etc. •••			
-0.137 \pm 0.001	¹ SHRESTHA 12A	DPWA	Multichannel
-0.136 \pm 0.005	ANISOVICH 10	DPWA	Multichannel
-0.140	DRECHSEL 07	DPWA	$\gamma N \rightarrow \pi N$
-0.129 \pm 0.001	ARNDT 02	DPWA	$\gamma p \rightarrow N\pi$
-0.128	PENNER 02D	DPWA	Multichannel
-0.1312	HANSTEIN 98	DPWA	$\gamma N \rightarrow \pi N$

¹ Statistical error only.

$\Delta(1232) \rightarrow N\gamma$, helicity-3/2 amplitude $A_{3/2}$

VALUE ($\text{GeV}^{-1/2}$)	DOCUMENT ID	TECN	COMMENT
-0.262 to -0.248 (≈ -0.255) OUR ESTIMATE			
-0.250 \pm 0.002	¹ HUNT 19	DPWA	Multichannel
-0.254 \pm 0.005	ANISOVICH 12A	DPWA	Multichannel
-0.262 \pm 0.003	WORKMAN 12A	DPWA	$\gamma N \rightarrow N\pi$
-0.258 \pm 0.005	DUGGER 07	DPWA	$\gamma N \rightarrow \pi N$
-0.256 \pm 0.003	AHRENS 04A	DPWA	$\tilde{\gamma}\tilde{p} \rightarrow N\pi$
-0.2669 \pm 0.0016 \pm 0.0078	BLANPIED 01	LEGS	$\gamma p \rightarrow p\gamma, p\pi^0, n\pi^+$
-0.251 \pm 0.001	BECK 00	IPWA	$\tilde{\gamma}p \rightarrow p\pi^0, n\pi^+$
-0.258 \pm 0.006	KAMALOV 99	DPWA	$\gamma N \rightarrow \pi N$
-0.2466 \pm 0.0013	HANSTEIN 98	IPWA	$\gamma N \rightarrow \pi N$
-0.2524 \pm 0.0013	DAVIDSON 97	DPWA	$\gamma N \rightarrow \pi N$
••• We do not use the following data for averages, fits, limits, etc. •••			
-0.251 \pm 0.001	¹ SHRESTHA 12A	DPWA	Multichannel
-0.267 \pm 0.008	ANISOVICH 10	DPWA	Multichannel
-0.265	DRECHSEL 07	DPWA	$\gamma N \rightarrow \pi N$
-0.243 \pm 0.001	ARNDT 02	DPWA	$\gamma p \rightarrow N\pi$
-0.247	PENNER 02D	DPWA	Multichannel
-0.2522	HANSTEIN 98	DPWA	$\gamma N \rightarrow \pi N$

¹ Statistical error only.

$\Delta(1232) \rightarrow N\gamma$, E_2/M_1 ratio

VALUE	DOCUMENT ID	TECN	COMMENT
-0.030 to -0.020 (≈ -0.025) OUR ESTIMATE			
-0.0274 \pm 0.0003 \pm 0.0030	AHRENS 04A	DPWA	$\tilde{\gamma}\tilde{p} \rightarrow N\pi$
-0.020 \pm 0.002	ARNDT 02	DPWA	$\gamma p \rightarrow N\pi$
-0.0307 \pm 0.0026 \pm 0.0024	BLANPIED 01	LEGS	$\gamma p \rightarrow p\gamma, p\pi^0, n\pi^+$
-0.016 \pm 0.004 \pm 0.002	GALLER 01	DPWA	$\gamma p \rightarrow \gamma p$
-0.025 \pm 0.001 \pm 0.002	BECK 00	IPWA	$\tilde{\gamma}p \rightarrow p\pi^0, n\pi^+$
-0.0233 \pm 0.0017	HANSTEIN 98	IPWA	$\gamma N \rightarrow \pi N$
-0.015 \pm 0.005	¹ ARNDT 97	IPWA	$\gamma N \rightarrow \pi N$
-0.0319 \pm 0.0024	DAVIDSON 97	DPWA	$\gamma N \rightarrow \pi N$
••• We do not use the following data for averages, fits, limits, etc. •••			
-0.022	DRECHSEL 07	DPWA	$\gamma N \rightarrow \pi N$
-0.026	PENNER 02D	DPWA	Multichannel
-0.0254 \pm 0.0010	HANSTEIN 98	DPWA	$\gamma N \rightarrow \pi N$
-0.025 \pm 0.002 \pm 0.002	BECK 97	IPWA	$\gamma N \rightarrow \pi N$
-0.030 \pm 0.003 \pm 0.002	BLANPIED 97	DPWA	$\gamma N \rightarrow \pi N, \gamma N$

¹ This ARNDT 97 value is very sensitive to the database being fitted. The result is from a fit to the full pion photoproduction database, apart from the BLANPIED 97 cross-section measurements.

Baryon Particle Listings

 $\Delta(1232), \Delta(1600)$ $\Delta(1232) \rightarrow N\gamma$, absolute value of E_2/M_1 ratio at pole

VALUE	DOCUMENT ID	TECN	COMMENT
0.065 ± 0.007	ARNDT 97	DPWA	$\gamma N \rightarrow \pi N$
0.058	HANSTEIN 96	DPWA	$\gamma N \rightarrow \pi N$

 $\Delta(1232) \rightarrow N\gamma$, phase of E_2/M_1 ratio at pole

VALUE	DOCUMENT ID	TECN	COMMENT
-122 ± 5	ARNDT 97	DPWA	$\gamma N \rightarrow \pi N$
-127.2	HANSTEIN 96	DPWA	$\gamma N \rightarrow \pi N$

 $\Delta(1232)$ MAGNETIC MOMENTS $\Delta(1232)^{++}$ MAGNETIC MOMENT

The values are extracted from UCLA and SIN data on $\pi^+ p$ bremsstrahlung using a variety of different theoretical approximations and methods. Our estimate is *only* a rough guess of the range we expect the moment to lie within.

VALUE (μ_N)	DOCUMENT ID	TECN	COMMENT
6.14 ± 0.51	LOPEZCAST... 01	DPWA	$\pi^+ p \rightarrow \pi^+ p \gamma$
4.52 ± 0.50 ± 0.45	BOSSHARD 91		$\pi^+ p \rightarrow \pi^+ p \gamma$ (SIN data)
3.7 to 4.2	LIN 91B		$\pi^+ p \rightarrow \pi^+ p \gamma$ (from UCLA data)
4.6 to 4.9	LIN 91B		$\pi^+ p \rightarrow \pi^+ p \gamma$ (from SIN data)
5.6 to 7.5	WITTMAN 88		$\pi^+ p \rightarrow \pi^+ p \gamma$ (from UCLA data)
6.9 to 9.8	HELLER 87		$\pi^+ p \rightarrow \pi^+ p \gamma$ (from UCLA data)
4.7 to 6.7	NEFKENS 78		$\pi^+ p \rightarrow \pi^+ p \gamma$ (UCLA data)

 $\Delta(1232)^+$ MAGNETIC MOMENT

VALUE (μ_N)	DOCUMENT ID	COMMENT
2.7 ± 1.0 1.3 ± 1.5 ± 3	¹ KOTULLA 02	$\gamma p \rightarrow p \pi^0 \gamma'$

¹ The second error is systematic, the third is an estimate of theoretical uncertainties.

 $\Delta(1232)$ REFERENCES

For early references, see Physics Letters **111B** 1 (1982).

HUNT 19	PR C99 055205	B. C. Hunt, D.M. Manley	
ADAMCZEW... 17	PR C95 065205	J. Adamczewski-Musch et al.	(HADES Collab.)
ROENCHEN 15A	EPJ A51 70	D. Roenchen et al.	
PDG 14	CP C38 070001	K. Olive et al.	(PDG Collab.)
ROENCHEN 14	EPJ A50 101	D. Roenchen et al.	
Also	EPJ A51 63 (errata.)	D. Roenchen et al.	
SVARC 14	PR C89 045205	A. Svarc et al.	(RBI Zagreb, UNI Tuzla)
ANISOVICH 12A	EPJ A48 15	A.V. Anisovich et al.	(BONN, PNPI)
SHRESTHA 12A	PR C86 055203	M. Shrestha, D.M. Manley	(KSU)
WORKMAN 12A	PR C86 015202	R. Workman et al.	(GWU)
ANISOVICH 10	EPJ A44 203	A.V. Anisovich et al.	(BONN, PNPI)
DRECHSEL 07	EPJ A34 69	D. Drechsel, S.S. Kamalov, L. Tiator	(MAINZ, JINR)
DUGGER 07	PR C76 025211	M. Dugger et al.	(JLab CLAS Collab.)
ARNDT 06	PR C74 045205	R.A. Arndt et al.	(GWU)
BREITSCHOP... 06	PL B639 424	J. Breitschopf et al.	(TUBIN, HEBR, CSUS)
GRIDNEV 06	PAN 69 1542	A.B. Gridnev et al.	(PNPI, BONN, GWU)
PDG 06	JP G33 1	W.-M. Yao et al.	(PDG Collab.)
AHRENS 04A	EPJ A21 323	J. Ahrens et al.	(A2 Collab.)
ARNDT 04	PR C69 035213	R.A. Arndt et al.	(GWU, TRIU)
KOTULLA 02	PRL 89 272001	R.A. Arndt et al.	(GWU)
PENNER 02C	PR C64 055211	G. Penner, U. Mosel	(MAMI TAPS Collab.)
PENNER 02D	PR C64 055212	G. Penner, U. Mosel	(GIES)
BLANPIED 01	PR C64 025203	G. Blanpied et al.	(BNL LEGS Collab.)
GALLER 01	PL B503 245	G. Galler et al.	(Mainz LARA Collab.)
LOPEZCAST... 01	PL B517 339	G. Lopez Castro, A. Mariano	
Also	NP A697 440	G. Lopez Castro, A. Mariano	
BECK 00	PR C61 035204	R. Beck et al.	(Mainz Microtron DAPHNE Col.)
KAMALOV 99	PRL 83 4494	S.S. Kamalov, S.N. Yang	(Taiwan U.)
HANSTEIN 98	NP A632 561	O. Hanstein, D. Drechsel, L. Tiator	
ARNDT 97	PR C56 577	R.A. Arndt, I.I. Strakovsky, R.L. Workman	(VPI)
BECK 97	PRL 79 606	R. Beck et al.	(MAINZ, SACL, PAVI, GLAS)
Also	PRL 79 4510	R.L. Beck, H.P. Krahn	(MAINZ)
Also	PRL 79 4512	R.L. Beck, H.P. Krahn	(MAINZ)
Also	PRL 79 4515 (erratum)	R.L. Beck et al.	(MAINZ, SACL, PAVI, GLAS)
BLANPIED 97	PRL 79 4337	G.S. Blanpied et al.	(LEGS Collab.)
DAVIDSON 97	PRL 79 4509	R.M. Davidson, N.C.A. Mukhopadhyay	(RPI)
BERNICHIA 96	NP A597 623	A. Bernichia, G. Lopez Castro, J. Pestieau	(LOUV+)
HANSTEIN 96	PL B385 45	O. Hanstein, D. Drechsel, L. Tiator	(MAINZ)
ABAEV 95	ZPHY A352 85	V.V. Abaev, S.P. Kruglov	(PNPI)
HOEHLER 93	πN Newsletter 9 1	G. Hoehler	(KARL)
BOSSHARD 91	PR D44 1362	A. Boshard et al.	(ZURI, LBL, VILL+)
Also	PRL 64 2619	A. Boshard et al.	(CATH, LAUS, LBL+)
LIN 91B	PR C44 1819	D.H. Lin, M.K. Liou, Z.M. Ding	(CUINY, CSOK)
Also	PR C43 1930	D. Lin, M.K. Liou	(CUINY)
WITTMAN 88	PR C37 2075	R. Wittman	(TRIU)
HELLER 87	PR C35 718	L. Heller et al.	(LANL, MIT, ILL)
CUTKOSKY 80	Toronto Conf. 19	R.E. Cutkosky et al.	(CMU, LBL) IJP
Also	PR D20 2839	R.E. Cutkosky et al.	(CMU, LBL)
KOCH 80B	NP A336 331	R. Koch, E. Pietarinen	(KARLT) IJP
HOEHLER 79	PDAT 12-1	G. Hoehler et al.	(KARLT) IJP
Also	Toronto Conf. 3	R. Koch	(KARLT) IJP
MIROSHNIC... 79	SJNP 29 94	I.I. Miroshnichenko et al.	(KFTI) IJP
Also	Translated from YAF 29 188		
NEFKENS 78	PR D18 3911	B.M.K. Nefkens et al.	(UCLA, CATH) IJP
PEDRONI 78	NP A300 321	E. Pedroni et al.	(SIN, ISNG, KARLE+) IJP

 $\Delta(1600) 3/2^+$

$$I(J^P) = \frac{3}{2}(\frac{3}{2}^+) \text{ Status: } ***$$

Older and obsolete values are listed and referenced in the 2014 edition, Chinese Physics **C38** 070001 (2014).

 $\Delta(1600)$ POLE POSITION

REAL PART

VALUE (MeV)	DOCUMENT ID	TECN	COMMENT
1460 to 1560 (≈ 1510) OUR ESTIMATE			
1515 ± 20	SOKHOYAN 15A	DPWA	Multichannel
1469 ± 10 ± 5	¹ SVARC 14	L+P	$\pi N \rightarrow \pi N$
1550 ± 40	CUTKOSKY 80	IPWA	$\pi N \rightarrow \pi N$
• • • We do not use the following data for averages, fits, limits, etc. • • •			
1619	HUNT 19	DPWA	Multichannel
1552	ROENCHEN 15A	DPWA	Multichannel
1498 ± 25	ANISOVICH 12A	DPWA	Multichannel
1457	ARNDT 06	DPWA	$\pi N \rightarrow \pi N, \eta N$
1599	VRANA 00	DPWA	Multichannel
1550	HOEHLER 93	SPED	$\pi N \rightarrow \pi N$

¹ Fit to the amplitudes of HOEHLER 79.

-2xIMAGINARY PART

VALUE (MeV)	DOCUMENT ID	TECN	COMMENT
200 to 340 (≈ 270) OUR ESTIMATE			
250 ± 30	SOKHOYAN 15A	DPWA	Multichannel
314 ± 18 ± 8	¹ SVARC 14	L+P	$\pi N \rightarrow \pi N$
200 ± 60	CUTKOSKY 80	IPWA	$\pi N \rightarrow \pi N$
• • • We do not use the following data for averages, fits, limits, etc. • • •			
295	HUNT 19	DPWA	Multichannel
350	ROENCHEN 15A	DPWA	Multichannel
230 ± 50	ANISOVICH 12A	DPWA	Multichannel
400	ARNDT 06	DPWA	$\pi N \rightarrow \pi N, \eta N$
312	VRANA 00	DPWA	Multichannel

¹ Fit to the amplitudes of HOEHLER 79.

 $\Delta(1600)$ ELASTIC POLE RESIDUEMODULUS $|r|$

VALUE (MeV)	DOCUMENT ID	TECN	COMMENT
10 to 40 (≈ 25) OUR ESTIMATE			
13 ± 3	SOKHOYAN 15A	DPWA	Multichannel
38 ± 2 ± 2	¹ SVARC 14	L+P	$\pi N \rightarrow \pi N$
17 ± 4	CUTKOSKY 80	IPWA	$\pi N \rightarrow \pi N$
• • • We do not use the following data for averages, fits, limits, etc. • • •			
23	ROENCHEN 15A	DPWA	Multichannel
11 ± 6	ANISOVICH 12A	DPWA	Multichannel
44	ARNDT 06	DPWA	$\pi N \rightarrow \pi N, \eta N$

¹ Fit to the amplitudes of HOEHLER 79.

PHASE θ

VALUE (°)	DOCUMENT ID	TECN	COMMENT
150 to 210 (≈ 180) OUR ESTIMATE			
-155 ± 20	SOKHOYAN 15A	DPWA	Multichannel
-173 ± 5 ± 5	¹ SVARC 14	L+P	$\pi N \rightarrow \pi N$
-150 ± 30	CUTKOSKY 80	IPWA	$\pi N \rightarrow \pi N$
• • • We do not use the following data for averages, fits, limits, etc. • • •			
-155	ROENCHEN 15A	DPWA	Multichannel
-160 ± 33	ANISOVICH 12A	DPWA	Multichannel
+147	ARNDT 06	DPWA	$\pi N \rightarrow \pi N, \eta N$

¹ Fit to the amplitudes of HOEHLER 79.

 $\Delta(1600)$ INELASTIC POLE RESIDUE

The "normalized residue" is the residue divided by $\Gamma_{pole}/2$.

Normalized residue in $N\pi \rightarrow \Delta(1600) \rightarrow \Delta\pi, P$ -wave

MODULUS	PHASE (°)	DOCUMENT ID	TECN	COMMENT
0.15 ± 0.04	30 ± 35	SOKHOYAN 15A	DPWA	Multichannel
• • • We do not use the following data for averages, fits, limits, etc. • • •				
0.31	31	ROENCHEN 15A	DPWA	Multichannel
0.14 ± 0.10	154 ± 40	ANISOVICH 12A	DPWA	Multichannel

Normalized residue in $N\pi \rightarrow \Delta(1600) \rightarrow \Delta\pi, F$ -wave

MODULUS	PHASE (°)	DOCUMENT ID	TECN	COMMENT
0.010 ± 0.005		SOKHOYAN 15A	DPWA	Multichannel
• • • We do not use the following data for averages, fits, limits, etc. • • •				
0.013	29	ROENCHEN 15A	DPWA	Multichannel
0.010 ± 0.005		ANISOVICH 12A	DPWA	Multichannel

See key on page 1127

Baryon Particle Listings

$\Delta(1600)$, $\Delta(1620)$

Normalized residue in $N\pi \rightarrow \Delta(1600) \rightarrow \Sigma K$

MODULUS	PHASE (°)	DOCUMENT ID	TECN	COMMENT
0.13	-5.6	ROENCHEN	15A	DPWA Multichannel

$\Delta(1600)$ BREIT-WIGNER MASS

VALUE (MeV)	DOCUMENT ID	TECN	COMMENT
1500 to 1640 (≈ 1570) OUR ESTIMATE			
1664 ± 16	¹ HUNT	19	DPWA Multichannel
1520 ± 20	SOKHOYAN	15A	DPWA Multichannel
1600 ± 50	CUTKOSKY	80	IPWA $\pi N \rightarrow \pi N$
1522 ± 13	HOEHLER	79	IPWA $\pi N \rightarrow \pi N$
••• We do not use the following data for averages, fits, limits, etc. •••			
1510 ± 20	ANISOVICH	12A	DPWA Multichannel
1626 ± 8	¹ SHRESTHA	12A	DPWA Multichannel
1667 ± 1	PENNER	02C	DPWA Multichannel
1687 ± 44	VRANA	00	DPWA Multichannel

¹ Statistical error only.

$\Delta(1600)$ BREIT-WIGNER WIDTH

VALUE (MeV)	DOCUMENT ID	TECN	COMMENT
200 to 300 (≈ 250) OUR ESTIMATE			
322 ± 46	¹ HUNT	19	DPWA Multichannel
235 ± 30	SOKHOYAN	15A	DPWA Multichannel
300 ± 100	CUTKOSKY	80	IPWA $\pi N \rightarrow \pi N$
220 ± 40	HOEHLER	79	IPWA $\pi N \rightarrow \pi N$
••• We do not use the following data for averages, fits, limits, etc. •••			
220 ± 45	ANISOVICH	12A	DPWA Multichannel
225 ± 18	¹ SHRESTHA	12A	DPWA Multichannel
397 ± 10	PENNER	02C	DPWA Multichannel
493 ± 75	VRANA	00	DPWA Multichannel

¹ Statistical error only.

$\Delta(1600)$ DECAY MODES

The following branching fractions are our estimates, not fits or averages.

Mode	Fraction (Γ_i/Γ)
Γ_1 $N\pi$	8-24%
Γ_2 $N\pi\pi$	58-84%
Γ_3 $\Delta(1232)\pi$	58-82%
Γ_4 $\Delta(1232)\pi$, P-wave	72-82%
Γ_5 $\Delta(1232)\pi$, F-wave	<2%
Γ_6 $N(1440)\pi$	17-27%
Γ_7 $N\gamma$	0.001-0.035%
Γ_8 $N\gamma$, helicity=1/2	0.0-0.02%
Γ_9 $N\gamma$, helicity=3/2	0.001-0.015%

$\Delta(1600)$ BRANCHING RATIOS

$\Gamma(N\pi)/\Gamma_{total}$	DOCUMENT ID	TECN	COMMENT	Γ_1/Γ
8-24% OUR ESTIMATE				
10.7 ± 1.9	¹ HUNT	19	DPWA Multichannel	
14 ± 4	SOKHOYAN	15A	DPWA Multichannel	
18 ± 4	CUTKOSKY	80	IPWA $\pi N \rightarrow \pi N$	
21 ± 6	HOEHLER	79	IPWA $\pi N \rightarrow \pi N$	
••• We do not use the following data for averages, fits, limits, etc. •••				
12 ± 5	ANISOVICH	12A	DPWA Multichannel	
8 ± 2	¹ SHRESTHA	12A	DPWA Multichannel	
13 ± 1	PENNER	02C	DPWA Multichannel	
28 ± 5	VRANA	00	DPWA Multichannel	

¹ Statistical error only.

$\Gamma(\Delta(1232)\pi, P\text{-wave})/\Gamma_{total}$	DOCUMENT ID	TECN	COMMENT	Γ_4/Γ
72-82% OUR ESTIMATE				
64 ± 6	¹ HUNT	19	DPWA Multichannel	
77 ± 5	SOKHOYAN	15A	DPWA Multichannel	
••• We do not use the following data for averages, fits, limits, etc. •••				
78 ± 6	ANISOVICH	12A	DPWA Multichannel	
70 ± 3	¹ SHRESTHA	12A	DPWA Multichannel	
59 ± 10	VRANA	00	DPWA Multichannel	

¹ Statistical error only.

$\Gamma(\Delta(1232)\pi, F\text{-wave})/\Gamma_{total}$	DOCUMENT ID	TECN	COMMENT	Γ_5/Γ
<2% OUR ESTIMATE				
<2	SOKHOYAN	15A	DPWA Multichannel	

$\Gamma(N(1440)\pi)/\Gamma_{total}$	DOCUMENT ID	TECN	COMMENT	Γ_6/Γ
17-27% OUR ESTIMATE				
22 ± 5	¹ HUNT	19	DPWA Multichannel	
••• We do not use the following data for averages, fits, limits, etc. •••				
22 ± 3	¹ SHRESTHA	12A	DPWA Multichannel	
13 ± 4	VRANA	00	DPWA Multichannel	

¹ Statistical error only.

$\Delta(1600)$ PHOTON DECAY AMPLITUDES AT THE POLE

$\Delta(1600) \rightarrow N\gamma$, helicity-1/2 amplitude $A_{1/2}$	DOCUMENT ID	TECN	COMMENT
0.053 ± 0.010	130 ± 15	SOKHOYAN	15A DPWA Multichannel
0.193 ^{+0.023} _{-0.024}	151 ⁺⁹ ₋₁₅	ROENCHEN	14 DPWA
••• We do not use the following data for averages, fits, limits, etc. •••			
-0.230	-42	ROENCHEN	15A DPWA Multichannel

$\Delta(1600) \rightarrow N\gamma$, helicity-3/2 amplitude $A_{3/2}$	DOCUMENT ID	TECN	COMMENT
0.055 ± 0.010	152 ± 15	SOKHOYAN	15A DPWA Multichannel
-0.254 ^{+0.085} _{-0.086}	110 ⁺¹⁰ ₋₆	ROENCHEN	14 DPWA
••• We do not use the following data for averages, fits, limits, etc. •••			
0.332	-71	ROENCHEN	15A DPWA Multichannel

$\Delta(1600)$ BREIT-WIGNER PHOTON DECAY AMPLITUDES

$\Delta(1600) \rightarrow N\gamma$, helicity-1/2 amplitude $A_{1/2}$	DOCUMENT ID	TECN	COMMENT
VALUE (GeV^{-1/2})			
-0.060 to -0.030 (≈ -0.045) OUR ESTIMATE			
0.0082 ± 0.0014	¹ HUNT	19	DPWA Multichannel
-0.051 ± 0.010	SOKHOYAN	15A	DPWA Multichannel
-0.018 ± 0.015	¹ ARNDT	96	IPWA $\gamma N \rightarrow \pi N$
••• We do not use the following data for averages, fits, limits, etc. •••			
-0.050 ± 0.009	ANISOVICH	12A	DPWA Multichannel
0.006 ± 0.005	¹ SHRESTHA	12A	DPWA Multichannel
0.0	PENNER	02D	DPWA Multichannel

¹ Statistical error only.

$\Delta(1600) \rightarrow N\gamma$, helicity-3/2 amplitude $A_{3/2}$	DOCUMENT ID	TECN	COMMENT
VALUE (GeV^{-1/2})			
-0.050 to -0.020 (≈ -0.035) OUR ESTIMATE			
0.048 ± 0.014	¹ HUNT	19	DPWA Multichannel
-0.055 ± 0.010	SOKHOYAN	15A	DPWA Multichannel
-0.025 ± 0.015	¹ ARNDT	96	IPWA $\gamma N \rightarrow \pi N$
••• We do not use the following data for averages, fits, limits, etc. •••			
-0.040 ± 0.012	ANISOVICH	12A	DPWA Multichannel
0.052 ± 0.008	¹ SHRESTHA	12A	DPWA Multichannel
-0.024	PENNER	02D	DPWA Multichannel

¹ Statistical error only.

$\Delta(1600)$ REFERENCES

For early references, see Physics Letters **111B** 1 (1982).

HUNT	19	PR C99 055205	B. C. Hunt, D. M. Manley
ROENCHEN	15A	EPJ A51 70	D. Roenchen et al.
SOKHOYAN	15A	EPJ A51 95	V. Sokhoyan et al.
PDG	14	CP C38 070001	K. Olive et al.
ROENCHEN	14	EPJ A50 101	D. Roenchen et al.
		EPJ A51 63 (errata.)	D. Roenchen et al.
SVARC	14	PR C89 045205	A. Svarc et al.
ANISOVICH	12A	EPJ A48 15	A.V. Anisovich et al.
SHRESTHA	12A	PR C86 055203	M. Shrestha, D.M. Manley
ARNDT	06	PR C74 045205	R.A. Arndt et al.
PENNER	02C	PR C66 055211	G. Penner, U. Mosel
PENNER	02D	PR C66 055212	G. Penner, U. Mosel
VRANA	00	PRPL 329 181	T.P. Vrana, S.A. Dytman, T.-S.H. Lee
ARNDT	96	PR C53 430	R.A. Arndt, I.I. Strakovsky, R.L. Workman
HOEHLER	93	πN Newsletter 9 1	G. Hohlner
CUTKOSKY	80	Toronto Conf. 19	R.E. Cutkosky et al.
		PR D20 2839	R.E. Cutkosky et al.
HOEHLER	79	PDAT 12-1	G. Hohlner et al.
		Toronto Conf. 3	R. Koch
			(CBELSA/TAPS Collab.)
			(PDG Collab.)
			(RBI Zagreb, UNI Tuzla)
			(BONN, PNPI)
			(KSU)
			(GWU)
			(GIES)
			(PITT, ANL)
			(VPI)
			(KARL)
			(CMU, LBL) IJP
			(CMU, LBL) IJP
			(KARLT) IJP
			(KARLT) IJP

$$\Delta(1620) 1/2^-$$

$$J(P) = \frac{3}{2}(\frac{1}{2}^-) \text{ Status: } ***$$

Older and obsolete values are listed and referenced in the 2014 edition, Chinese Physics **C38** 070001 (2014).

$\Delta(1620)$ POLE POSITION

REAL PART	DOCUMENT ID	TECN	COMMENT
VALUE (MeV)			
1590 to 1610 (≈ 1600) OUR ESTIMATE			
1597 ± 5	SOKHOYAN	15A	DPWA Multichannel
1603 ± 7 ± 2	¹ SVARC	14	L+P $\pi N \rightarrow \pi N$
1600 ± 15	CUTKOSKY	80	IPWA $\pi N \rightarrow \pi N$

Baryon Particle Listings

 $\Delta(1620)$

• • • We do not use the following data for averages, fits, limits, etc. • • •

1577	HUNT	19	DPWA	Multichannel
1600	ROENCHEN	15A	DPWA	Multichannel
1597 ± 4	ANISOVICH	12A	DPWA	Multichannel
1595	ARNDT	06	DPWA	$\pi N \rightarrow \pi N, \eta N$
1607	VRANA	00	DPWA	Multichannel
1608	HOEHLER	93	SPED	$\pi N \rightarrow \pi N$

¹ Fit to the amplitudes of HOEHLER 79.

-2xIMAGINARY PART

VALUE (MeV)	DOCUMENT ID	TECN	COMMENT
-------------	-------------	------	---------

100 to 140 (≈ 120) OUR ESTIMATE

134 ± 8	SOKHOYAN	15A	DPWA	Multichannel
114 ± 12 ± 4	¹ SVARC	14	L+P	$\pi N \rightarrow \pi N$
120 ± 20	CUTKOSKY	80	IPWA	$\pi N \rightarrow \pi N$

• • • We do not use the following data for averages, fits, limits, etc. • • •

101	HUNT	19	DPWA	Multichannel
65	ROENCHEN	15A	DPWA	Multichannel
130 ± 9	ANISOVICH	12A	DPWA	Multichannel
135	ARNDT	06	DPWA	$\pi N \rightarrow \pi N, \eta N$
148	VRANA	00	DPWA	Multichannel
116	HOEHLER	93	SPED	$\pi N \rightarrow \pi N$

¹ Fit to the amplitudes of HOEHLER 79.

 $\Delta(1620)$ ELASTIC POLE RESIDUEMODULUS $|r|$

VALUE (MeV)	DOCUMENT ID	TECN	COMMENT
-------------	-------------	------	---------

15 to 20 (≈ 17) OUR ESTIMATE

20 ± 3	SOKHOYAN	15A	DPWA	Multichannel
17 ± 2 ± 1	¹ SVARC	14	L+P	$\pi N \rightarrow \pi N$
15 ± 2	CUTKOSKY	80	IPWA	$\pi N \rightarrow \pi N$

• • • We do not use the following data for averages, fits, limits, etc. • • •

16	ROENCHEN	15A	DPWA	Multichannel
18 ± 2	ANISOVICH	12A	DPWA	Multichannel
15	ARNDT	06	DPWA	$\pi N \rightarrow \pi N, \eta N$
19	HOEHLER	93	SPED	$\pi N \rightarrow \pi N$

¹ Fit to the amplitudes of HOEHLER 79.

PHASE θ

VALUE (°)	DOCUMENT ID	TECN	COMMENT
-----------	-------------	------	---------

-120 to -80 (≈ -100) OUR ESTIMATE

-90 ± 15	SOKHOYAN	15A	DPWA	Multichannel
-106 ± 10 ± 4	¹ SVARC	14	L+P	$\pi N \rightarrow \pi N$
-110 ± 20	CUTKOSKY	80	IPWA	$\pi N \rightarrow \pi N$

• • • We do not use the following data for averages, fits, limits, etc. • • •

-104	ROENCHEN	15A	DPWA	Multichannel
-100 ± 5	ANISOVICH	12A	DPWA	Multichannel
-92	ARNDT	06	DPWA	$\pi N \rightarrow \pi N, \eta N$
-95	HOEHLER	93	SPED	$\pi N \rightarrow \pi N$

¹ Fit to the amplitudes of HOEHLER 79.

 $\Delta(1620)$ INELASTIC POLE RESIDUE

The "normalized residue" is the residue divided by $\Gamma_{pole}/2$.

Normalized residue in $N\pi \rightarrow \Delta(1620) \rightarrow \Delta\pi, D\text{-wave}$

MODULUS	PHASE (°)	DOCUMENT ID	TECN	COMMENT
---------	-----------	-------------	------	---------

0.42 ± 0.06	-90 ± 20	SOKHOYAN	15A	DPWA	Multichannel
-------------	----------	----------	-----	------	--------------

• • • We do not use the following data for averages, fits, limits, etc. • • •

0.57	105	ROENCHEN	15A	DPWA	Multichannel
0.38 ± 0.09	-85 ± 30	ANISOVICH	12A	DPWA	Multichannel

Normalized residue in $N\pi \rightarrow \Delta(1620) \rightarrow \Sigma K$

MODULUS	PHASE (°)	DOCUMENT ID	TECN	COMMENT
---------	-----------	-------------	------	---------

0.22	-105	ROENCHEN	15A	DPWA	Multichannel
------	------	----------	-----	------	--------------

• • • We do not use the following data for averages, fits, limits, etc. • • •

Normalized residue in $N\pi \rightarrow \Delta(1620) \rightarrow N(1440)\pi$

MODULUS	PHASE (°)	DOCUMENT ID	TECN	COMMENT
---------	-----------	-------------	------	---------

0.10 ± 0.06	-65 ± 30	SOKHOYAN	15A	DPWA	Multichannel
-------------	----------	----------	-----	------	--------------

 $\Delta(1620)$ BREIT-WIGNER MASS

VALUE (MeV)	DOCUMENT ID	TECN	COMMENT
-------------	-------------	------	---------

1590 to 1630 (≈ 1610) OUR ESTIMATE

1635 ± 8	GOLOVATCH	19	DPWA	$\gamma p \rightarrow \pi^+ \pi^- p$
1589 ± 3	¹ HUNT	19	DPWA	Multichannel
1595 ± 8	SOKHOYAN	15A	DPWA	Multichannel
1615.2 ± 0.4	¹ ARNDT	06	DPWA	$\pi N \rightarrow \pi N, \eta N$
1620 ± 20	CUTKOSKY	80	IPWA	$\pi N \rightarrow \pi N$
1610 ± 7	HOEHLER	79	IPWA	$\pi N \rightarrow \pi N$

• • • We do not use the following data for averages, fits, limits, etc. • • •

1600 ± 8	ANISOVICH	12A	DPWA	Multichannel
1600 ± 1	¹ SHRESTHA	12A	DPWA	Multichannel
1612 ± 2	PENNER	02c	DPWA	Multichannel
1617 ± 15	VRANA	00	DPWA	Multichannel

¹ Statistical error only.

 $\Delta(1620)$ BREIT-WIGNER WIDTH

VALUE (MeV)	DOCUMENT ID	TECN	COMMENT
-------------	-------------	------	---------

110 to 150 (≈ 130) OUR ESTIMATE

144 ± 16	GOLOVATCH	19	DPWA	$\gamma p \rightarrow \pi^+ \pi^- p$
107 ± 7	¹ HUNT	19	DPWA	Multichannel
135 ± 9	SOKHOYAN	15A	DPWA	Multichannel
146.9 ± 1.9	¹ ARNDT	06	DPWA	$\pi N \rightarrow \pi N, \eta N$
140 ± 20	CUTKOSKY	80	IPWA	$\pi N \rightarrow \pi N$
139 ± 18	HOEHLER	79	IPWA	$\pi N \rightarrow \pi N$

• • • We do not use the following data for averages, fits, limits, etc. • • •

130 ± 11	ANISOVICH	12A	DPWA	Multichannel
112 ± 2	¹ SHRESTHA	12A	DPWA	Multichannel
202 ± 7	PENNER	02c	DPWA	Multichannel
143 ± 42	VRANA	00	DPWA	Multichannel

¹ Statistical error only.

 $\Delta(1620)$ DECAY MODES

The following branching fractions are our estimates, not fits or averages.

Mode	Fraction (Γ_i/Γ)
Γ_1 $N\pi$	25–35 %
Γ_2 $N\pi\pi$	>67 %
Γ_3 $\Delta(1232)\pi, D\text{-wave}$	44–72 %
Γ_4 $N\rho$	23–32%
Γ_5 $N\rho, S=1/2, S\text{-wave}$	23–32%
Γ_6 $N\rho, S=3/2, D\text{-wave}$	<0.04%
Γ_7 $N(1440)\pi$	<9 %
Γ_8 $N\gamma, \text{helicity}=1/2$	0.03–0.10 %

 $\Delta(1620)$ BRANCHING RATIOS

$\Gamma(N\pi)/\Gamma_{\text{total}}$	Γ_1/Γ
--------------------------------------	-------------------

VALUE (%)	DOCUMENT ID	TECN	COMMENT
-----------	-------------	------	---------

25 to 35 (≈ 30) OUR ESTIMATE

24 ± 2	¹ HUNT	19	DPWA	Multichannel
28 ± 3	SOKHOYAN	15A	DPWA	Multichannel
31.5 ± 0.1	¹ ARNDT	06	DPWA	$\pi N \rightarrow \pi N, \eta N$
25 ± 3	CUTKOSKY	80	IPWA	$\pi N \rightarrow \pi N$
35 ± 6	HOEHLER	79	IPWA	$\pi N \rightarrow \pi N$

• • • We do not use the following data for averages, fits, limits, etc. • • •

28 ± 3	ANISOVICH	12A	DPWA	Multichannel
33 ± 2	¹ SHRESTHA	12A	DPWA	Multichannel
34 ± 1	PENNER	02c	DPWA	Multichannel
45 ± 5	VRANA	00	DPWA	Multichannel

¹ Statistical error only.

$\Gamma(N\pi\pi)/\Gamma_{\text{total}}$	Γ_2/Γ
---	-------------------

VALUE (%)	DOCUMENT ID	TECN	COMMENT
-----------	-------------	------	---------

0.90 ± 0.10	GOLOVATCH	19	DPWA	$\gamma p \rightarrow \pi^+ \pi^- p$
-------------	-----------	----	------	--------------------------------------

$\Gamma(\Delta(1232)\pi, D\text{-wave})/\Gamma_{\text{total}}$	Γ_3/Γ
--	-------------------

VALUE (%)	DOCUMENT ID	TECN	COMMENT
-----------	-------------	------	---------

48 ± 4	¹ HUNT	19	DPWA	Multichannel
62 ± 10	SOKHOYAN	15A	DPWA	Multichannel

• • • We do not use the following data for averages, fits, limits, etc. • • •

60 ± 17	ANISOVICH	12A	DPWA	Multichannel
32 ± 2	¹ SHRESTHA	12A	DPWA	Multichannel
39 ± 2	VRANA	00	DPWA	Multichannel

¹ Statistical error only.

$\Gamma(N\rho, S=1/2, S\text{-wave})/\Gamma_{\text{total}}$	Γ_5/Γ
---	-------------------

VALUE (%)	DOCUMENT ID	TECN	COMMENT
-----------	-------------	------	---------

27 ± 4	¹ HUNT	19	DPWA	Multichannel
--------	-------------------	----	------	--------------

• • • We do not use the following data for averages, fits, limits, etc. • • •

26 ± 2	¹ SHRESTHA	12A	DPWA	Multichannel
14 ± 3	VRANA	00	DPWA	Multichannel

¹ Statistical error only.

See key on page 1127

Baryon Particle Listings

$\Delta(1620)$, $\Delta(1700)$

$\Gamma(N\rho, S=3/2, D\text{-wave})/\Gamma_{\text{total}}$ Γ_6/Γ

VALUE (%)	DOCUMENT ID	TECN	COMMENT
<0.04	¹ HUNT	19	DPWA Multichannel
••• We do not use the following data for averages, fits, limits, etc. •••			
2 ±1	VRANA	00	DPWA Multichannel

¹ Statistical error only.

$\Gamma(N(1440)\pi)/\Gamma_{\text{total}}$ Γ_7/Γ

VALUE (%)	DOCUMENT ID	TECN	COMMENT
<0.02	¹ HUNT	19	DPWA Multichannel
6 ±3	SOKHOYAN	15A	DPWA Multichannel
••• We do not use the following data for averages, fits, limits, etc. •••			
9 ±1	¹ SHRESTHA	12A	DPWA Multichannel
0 ±1	VRANA	00	DPWA Multichannel

¹ Statistical error only.

$\Delta(1620)$ PHOTON DECAY AMPLITUDES AT THE POLE

$\Delta(1620) \rightarrow N\gamma$, helicity-1/2 amplitude $A_{1/2}$

MODULUS ($\text{GeV}^{-1/2}$)	PHASE ($^\circ$)	DOCUMENT ID	TECN	COMMENT
0.054 ± 0.007	-6 ± 7	SOKHOYAN	15A	DPWA Multichannel
-0.028 ± 0.006	-166 ± 1	ROENCHEN	14	DPWA
-0.002 ± 0.002	-166 ± 4	ROENCHEN	14	DPWA
••• We do not use the following data for averages, fits, limits, etc. •••				
0.014	26	ROENCHEN	15A	DPWA Multichannel

$\Delta(1620)$ BREIT-WIGNER PHOTON DECAY AMPLITUDES

$\Delta(1620) \rightarrow N\gamma$, helicity-1/2 amplitude $A_{1/2}$

VALUE ($\text{GeV}^{-1/2}$)	DOCUMENT ID	TECN	COMMENT
0.030 to 0.060 (≈ 0.050) OUR ESTIMATE			
0.029 ± 0.0062	GOLOVATCH	19	DPWA $\gamma\rho \rightarrow \pi^+\pi^-\rho$
0.0124 ± 0.0007	¹ HUNT	19	DPWA Multichannel
0.055 ± 0.007	SOKHOYAN	15A	DPWA Multichannel
0.029 ± 0.003	¹ WORKMAN	12A	DPWA $\gamma N \rightarrow N\pi$
0.050 ± 0.002	¹ DUGGER	07	DPWA $\gamma N \rightarrow \pi N$
••• We do not use the following data for averages, fits, limits, etc. •••			
0.052 ± 0.005	ANISOVICH	12A	DPWA Multichannel
-0.003 ± 0.003	¹ SHRESTHA	12A	DPWA Multichannel
0.066	DRECHSEL	07	DPWA $\gamma N \rightarrow \pi N$
-0.050	PENNER	02D	DPWA Multichannel

¹ Statistical error only.

$\Delta(1620)$ REFERENCES

For early references, see Physics Letters **111B** 1 (1982).

GOLOVATCH	19	PL B788 371	E. Golovatch <i>et al.</i>	(CLAS Collab.)
HUNT	19	PR C99 055205	B. C. Hunt, D. M. Manley	
ROENCHEN	15A	EPJ A51 70	D. Roenchen <i>et al.</i>	
SOKHOYAN	15A	EPJ A51 95	V. Sokhoyan <i>et al.</i>	(CBELSA/TAPS Collab.)
PDG	14	CP C38 070001	K. Olive <i>et al.</i>	(PDG Collab.)
ROENCHEN	14	EPJ A50 101	D. Roenchen <i>et al.</i>	
Also		EPJ A51 63 (errat.)	D. Roenchen <i>et al.</i>	
SVARC	14	PR C89 045205	A. Svarc <i>et al.</i>	(RBI Zagreb, UNI Tuzla)
ANISOVICH	12A	EPJ A48 15	A. V. Anisovich <i>et al.</i>	(BONN, PNPI)
SHRESTHA	12A	PR C86 055203	M. Shrestha, D. M. Manley	(KSU)
WORKMAN	12A	PR C86 015202	R. Workman <i>et al.</i>	(GWU)
DRECHSEL	07	EPJ A34 69	D. Drechsel, S. S. Kamalov, L. Tiator	(MAINZ, JINR)
DUGGER	07	PR C76 025211	M. Dugger <i>et al.</i>	(JLab CLAS Collab.)
ARNDT	06	PR C74 045205	R. A. Arndt <i>et al.</i>	(GWU)
PENNER	02C	PR C66 055211	G. Penner, U. Mosel	(GIES)
PENNER	02D	PR C66 055212	G. Penner, U. Mosel	(GIES)
VRANA	00	PRPL 328 181	T. P. Vrana, S. A. Dytman, T.-S.H. Lee	(PITT, ANL)
HOEHLER	93	πN Newsletter 9 1	G. Hohlner	(KARL)
CUTKOSKY	80	Toronto Conf. 19	R. E. Cutkosky <i>et al.</i>	(CMU, LBL) IJP
Also		PR D20 2839	R. E. Cutkosky <i>et al.</i>	(CMU, LBL) IJP
HOEHLER	79	PDAT 12-1	G. Hohlner <i>et al.</i>	(KARLT) IJP
Also		Toronto Conf. 3	R. Koch	(KARLT) IJP

$\Delta(1700) 3/2^-$ $I(J^P) = \frac{3}{2}(\frac{3}{2}^-)$ Status: ***

Older and obsolete values are listed and referenced in the 2014 edition, Chinese Physics **C38** 070001 (2014).

$\Delta(1700)$ POLE POSITION

REAL PART

VALUE (MeV)	DOCUMENT ID	TECN	COMMENT
1640 to 1690 (≈ 1665) OUR ESTIMATE			
1685 ± 10	SOKHOYAN	15A	DPWA Multichannel
1643 ± 6 ± 3	¹ SVARC	14	L+P $\pi N \rightarrow \pi N$
1675 ± 25	CUTKOSKY	80	IPWA $\pi N \rightarrow \pi N$
••• We do not use the following data for averages, fits, limits, etc. •••			
1693	HUNT	19	DPWA Multichannel
1677	ROENCHEN	15A	DPWA Multichannel

1685 ± 10	GUTZ	14	DPWA Multichannel
1680 ± 10	ANISOVICH	12A	DPWA Multichannel
1632	ARNDT	06	DPWA $\pi N \rightarrow \pi N, \eta N$
1726	VRANA	00	DPWA Multichannel
1651	HOEHLER	93	SPED $\pi N \rightarrow \pi N$

¹ Fit to the amplitudes of HOEHLER 79.

-2xIMAGINARY PART

VALUE (MeV)	DOCUMENT ID	TECN	COMMENT
200 to 300 (≈ 250) OUR ESTIMATE			
300 ± 15	SOKHOYAN	15A	DPWA Multichannel
217 ± 10 ± 8	¹ SVARC	14	L+P $\pi N \rightarrow \pi N$
220 ± 40	CUTKOSKY	80	IPWA $\pi N \rightarrow \pi N$
••• We do not use the following data for averages, fits, limits, etc. •••			
213	HUNT	19	DPWA Multichannel
305	ROENCHEN	15A	DPWA Multichannel
300 ± 15	GUTZ	14	DPWA Multichannel
305 ± 15	ANISOVICH	12A	DPWA Multichannel
253	ARNDT	06	DPWA $\pi N \rightarrow \pi N, \eta N$
118	VRANA	00	DPWA Multichannel
159	HOEHLER	93	SPED $\pi N \rightarrow \pi N$

¹ Fit to the amplitudes of HOEHLER 79.

$\Delta(1700)$ ELASTIC POLE RESIDUE

MODULUS $|r|$

VALUE (MeV)	DOCUMENT ID	TECN	COMMENT
10 to 40 (≈ 25) OUR ESTIMATE			
40 ± 6	SOKHOYAN	15A	DPWA Multichannel
13 ± 1 ± 1	¹ SVARC	14	L+P $\pi N \rightarrow \pi N$
13 ± 3	CUTKOSKY	80	IPWA $\pi N \rightarrow \pi N$
••• We do not use the following data for averages, fits, limits, etc. •••			
24	ROENCHEN	15A	DPWA Multichannel
40 ± 6	GUTZ	14	DPWA Multichannel
42 ± 7	ANISOVICH	12A	DPWA Multichannel
18	ARNDT	06	DPWA $\pi N \rightarrow \pi N, \eta N$
10	HOEHLER	93	SPED $\pi N \rightarrow \pi N$

¹ Fit to the amplitudes of HOEHLER 79.

PHASE θ

VALUE ($^\circ$)	DOCUMENT ID	TECN	COMMENT
-40 to 0 (≈ -20) OUR ESTIMATE			
-1 ± 10	SOKHOYAN	15A	DPWA Multichannel
-30 ± 4 ± 3	¹ SVARC	14	L+P $\pi N \rightarrow \pi N$
-40	ARNDT	06	DPWA $\pi N \rightarrow \pi N, \eta N$
-20 ± 25	CUTKOSKY	80	IPWA $\pi N \rightarrow \pi N$
••• We do not use the following data for averages, fits, limits, etc. •••			
-7.3	ROENCHEN	15A	DPWA Multichannel
-1 ± 10	GUTZ	14	DPWA Multichannel
-3 ± 15	ANISOVICH	12A	DPWA Multichannel

¹ Fit to the amplitudes of HOEHLER 79.

$\Delta(1700)$ INELASTIC POLE RESIDUE

The "normalized residue" is the residue divided by $\Gamma_{\text{pole}}/2$.

Normalized residue in $N\pi \rightarrow \Delta(1700) \rightarrow \Delta\eta$

MODULUS	PHASE ($^\circ$)	DOCUMENT ID	TECN	COMMENT
0.12 ± 0.02	-60 ± 12	GUTZ	14	DPWA Multichannel
••• We do not use the following data for averages, fits, limits, etc. •••				
0.12 ± 0.03	-60 ± 15	ANISOVICH	12A	DPWA Multichannel

Normalized residue in $N\pi \rightarrow \Delta(1700) \rightarrow \Sigma K$

MODULUS	PHASE ($^\circ$)	DOCUMENT ID	TECN	COMMENT
••• We do not use the following data for averages, fits, limits, etc. •••				
0.011	-147	ROENCHEN	15A	DPWA Multichannel

Normalized residue in $N\pi \rightarrow \Delta(1700) \rightarrow N(1535)\pi$

MODULUS	PHASE ($^\circ$)	DOCUMENT ID	TECN	COMMENT
0.035 ± 0.015	-75 ± 30	GUTZ	14	DPWA Multichannel

Normalized residue in $N\pi \rightarrow \Delta(1700) \rightarrow \Delta(1232)\pi, S\text{-wave}$

MODULUS	PHASE ($^\circ$)	DOCUMENT ID	TECN	COMMENT
0.25 ± 0.12	135 ± 45	SOKHOYAN	15A	DPWA Multichannel
••• We do not use the following data for averages, fits, limits, etc. •••				
0.39	151	ROENCHEN	15A	DPWA Multichannel

Normalized residue in $N\pi \rightarrow \Delta(1700) \rightarrow \Delta(1232)\pi, D\text{-wave}$

MODULUS	PHASE ($^\circ$)	DOCUMENT ID	TECN	COMMENT
0.12 ± 0.06	-160 ± 30	SOKHOYAN	15A	DPWA Multichannel
••• We do not use the following data for averages, fits, limits, etc. •••				
0.054	166	ROENCHEN	15A	DPWA Multichannel

Baryon Particle Listings

 $\Delta(1700)$ Normalized residue in $N\pi \rightarrow \Delta(1700) \rightarrow N(1520)\pi, P\text{-wave}$

MODULUS	PHASE ($^\circ$)	DOCUMENT ID	TECN	COMMENT
0.10 ± 0.03	-10 ± 20	SOKHOYAN 15A	DPWA	Multichannel

 $\Delta(1700)$ BREIT-WIGNER MASS

VALUE (MeV)	DOCUMENT ID	TECN	COMMENT
1690 to 1730 (≈ 1710) OUR ESTIMATE			
1704 ± 8	GOLOVATCH 19	DPWA	$\gamma p \rightarrow \pi^+ \pi^- p$
1720 ± 5	¹ HUNT 19	DPWA	Multichannel
1715 ± 20	SOKHOYAN 15A	DPWA	Multichannel
1695.0 ± 1.3	¹ ARNDT 06	DPWA	$\pi N \rightarrow \pi N, \eta N$
1710 ± 30	CUTKOSKY 80	IPWA	$\pi N \rightarrow \pi N$
1680 ± 70	HOEHLER 79	IPWA	$\pi N \rightarrow \pi N$
••• We do not use the following data for averages, fits, limits, etc. •••			
1715 ± 20	GUTZ 14	DPWA	Multichannel
1715 ± 30 -15	ANISOVICH 12A	DPWA	Multichannel
1691 ± 4	¹ SHRESTHA 12A	DPWA	Multichannel
1678 ± 1	PENNER 02C	DPWA	Multichannel
1732 ± 23	VRANA 00	DPWA	Multichannel
¹ Statistical error only.			

 $\Delta(1700)$ BREIT-WIGNER WIDTH

VALUE (MeV)	DOCUMENT ID	TECN	COMMENT
220 to 380 (≈ 300) OUR ESTIMATE			
295 ± 35	GOLOVATCH 19	DPWA	$\gamma p \rightarrow \pi^+ \pi^- p$
226 ± 14	¹ HUNT 19	DPWA	Multichannel
300 ± 25	SOKHOYAN 15A	DPWA	Multichannel
375.5 ± 7.0	¹ ARNDT 06	DPWA	$\pi N \rightarrow \pi N, \eta N$
280 ± 80	CUTKOSKY 80	IPWA	$\pi N \rightarrow \pi N$
230 ± 80	HOEHLER 79	IPWA	$\pi N \rightarrow \pi N$
••• We do not use the following data for averages, fits, limits, etc. •••			
300 ± 25	GUTZ 14	DPWA	Multichannel
310 ± 40 -15	ANISOVICH 12A	DPWA	Multichannel
248 ± 9	¹ SHRESTHA 12A	DPWA	Multichannel
606 ± 15	PENNER 02C	DPWA	Multichannel
119 ± 70	VRANA 00	DPWA	Multichannel
¹ Statistical error only.			

 $\Delta(1700)$ DECAY MODES

The following branching fractions are our estimates, not fits or averages.

Mode	Fraction (Γ_i/Γ)
Γ_1 $N\pi$	10–20 %
Γ_2 $N\pi\pi$	>31 %
Γ_3 $\Delta(1232)\pi$	9–70 %
Γ_4 $\Delta(1232)\pi, S\text{-wave}$	5–54 %
Γ_5 $\Delta(1232)\pi, D\text{-wave}$	4–16 %
Γ_6 $N\rho, S=3/2, S\text{-wave}$	22–32%
Γ_7 $N(1520)\pi, P\text{-wave}$	1–5 %
Γ_8 $N(1535)\pi$	0.5–1.5 %
Γ_9 $\Delta(1232)\eta$	3–7 %
Γ_{10} $N\gamma$	0.22–0.60 %
Γ_{11} $N\gamma, \text{helicity}=1/2$	0.12–0.30 %
Γ_{12} $N\gamma, \text{helicity}=3/2$	0.10–0.30 %

 $\Delta(1700)$ BRANCHING RATIOS

$\Gamma(N\pi)/\Gamma_{\text{total}}$	DOCUMENT ID	TECN	COMMENT	Γ_1/Γ
10 to 20 OUR ESTIMATE				
15 ± 2	¹ HUNT 19	DPWA	Multichannel	
22 ± 4	SOKHOYAN 15A	DPWA	Multichannel	
15.6 ± 0.1	¹ ARNDT 06	DPWA	$\pi N \rightarrow \pi N, \eta N$	
12 ± 3	CUTKOSKY 80	IPWA	$\pi N \rightarrow \pi N$	
20 ± 3	HOEHLER 79	IPWA	$\pi N \rightarrow \pi N$	
••• We do not use the following data for averages, fits, limits, etc. •••				
22 ± 4	GUTZ 14	DPWA	Multichannel	
22 ± 4	ANISOVICH 12A	DPWA	Multichannel	
14 ± 1	¹ SHRESTHA 12A	DPWA	Multichannel	
14 ± 1	PENNER 02C	DPWA	Multichannel	
5 ± 1	VRANA 00	DPWA	Multichannel	
¹ Statistical error only.				

$\Gamma(N\pi\pi)/\Gamma_{\text{total}}$	DOCUMENT ID	TECN	COMMENT	Γ_2/Γ
0.89 ± 0.11	GOLOVATCH 19	DPWA	$\gamma p \rightarrow \pi^+ \pi^- p$	

 $\Gamma(\Delta(1232)\pi, S\text{-wave})/\Gamma_{\text{total}}$

VALUE (%)	DOCUMENT ID	TECN	COMMENT	Γ_4/Γ
49 ± 5	¹ HUNT 19	DPWA	Multichannel	
20 ± 15	SOKHOYAN 15A	DPWA	Multichannel	
••• We do not use the following data for averages, fits, limits, etc. •••				
20 ± 25 -13	ANISOVICH 12A	DPWA	Multichannel	
54 ± 3	¹ SHRESTHA 12A	DPWA	Multichannel	
90 ± 2	VRANA 00	DPWA	Multichannel	
¹ Statistical error only.				

 $\Gamma(\Delta(1232)\pi, D\text{-wave})/\Gamma_{\text{total}}$

VALUE (%)	DOCUMENT ID	TECN	COMMENT	Γ_5/Γ
7.6 ± 0.3	¹ HUNT 19	DPWA	Multichannel	
10 ± 6	SOKHOYAN 15A	DPWA	Multichannel	
••• We do not use the following data for averages, fits, limits, etc. •••				
12 ± 14 -7	ANISOVICH 12A	DPWA	Multichannel	
1 ± 1	¹ SHRESTHA 12A	DPWA	Multichannel	
4 ± 1	VRANA 00	DPWA	Multichannel	
¹ Statistical error only.				

 $\Gamma(N\rho, S=3/2, S\text{-wave})/\Gamma_{\text{total}}$

VALUE (%)	DOCUMENT ID	TECN	COMMENT	Γ_6/Γ
27 ± 5	¹ HUNT 19	DPWA	Multichannel	
••• We do not use the following data for averages, fits, limits, etc. •••				
30 ± 3	¹ SHRESTHA 12A	DPWA	Multichannel	
1 ± 1	VRANA 00	DPWA	Multichannel	
¹ Statistical error only.				

 $\Gamma(N(1520)\pi, P\text{-wave})/\Gamma_{\text{total}}$

VALUE (%)	DOCUMENT ID	TECN	COMMENT	Γ_7/Γ
3 ± 2	SOKHOYAN 15A	DPWA	Multichannel	

 $\Gamma(N(1535)\pi)/\Gamma_{\text{total}}$

VALUE (%)	DOCUMENT ID	TECN	COMMENT	Γ_8/Γ
1.0 ± 0.5	GUTZ 14	DPWA	Multichannel	
4 ± 2	HORN 08A	DPWA	Multichannel	

 $\Gamma(\Delta(1232)\eta)/\Gamma_{\text{total}}$

VALUE (%)	DOCUMENT ID	TECN	COMMENT	Γ_9/Γ
5 ± 2	GUTZ 14	DPWA	Multichannel	
••• We do not use the following data for averages, fits, limits, etc. •••				
5 ± 2	ANISOVICH 12A	DPWA	Multichannel	

 $\Gamma(N(1535)\pi)/\Gamma(\Delta(1232)\eta)$

VALUE	DOCUMENT ID	TECN	COMMENT	Γ_8/Γ_9
0.67	KASHEVAROV 09	CBAL	$\gamma p \rightarrow p\pi^0\eta$	

 $\Delta(1700)$ PHOTON DECAY AMPLITUDES AT THE POLE $\Delta(1700) \rightarrow N\gamma, \text{helicity-1/2 amplitude } A_{1/2}$

MODULUS ($\text{GeV}^{-1/2}$)	PHASE ($^\circ$)	DOCUMENT ID	TECN	COMMENT
0.175 ± 0.020	50 ± 10	SOKHOYAN 15A	DPWA	Multichannel
0.109 ± 0.010	-21 ± 12 -6	ROENCHEN 14	DPWA	
••• We do not use the following data for averages, fits, limits, etc. •••				
0.123	1.1	ROENCHEN 15A	DPWA	Multichannel

 $\Delta(1700) \rightarrow N\gamma, \text{helicity-3/2 amplitude } A_{3/2}$

MODULUS ($\text{GeV}^{-1/2}$)	PHASE ($^\circ$)	DOCUMENT ID	TECN	COMMENT
0.180 ± 0.020	45 ± 10	SOKHOYAN 15A	DPWA	Multichannel
0.111 ± 0.027 -0.006	12 ± 9 -11	ROENCHEN 14	DPWA	
••• We do not use the following data for averages, fits, limits, etc. •••				
0.124	22	ROENCHEN 15A	DPWA	Multichannel

 $\Delta(1700)$ BREIT-WIGNER PHOTON DECAY AMPLITUDES $\Delta(1700) \rightarrow N\gamma, \text{helicity-1/2 amplitude } A_{1/2}$

VALUE ($\text{GeV}^{-1/2}$)	DOCUMENT ID	TECN	COMMENT
0.100 to 0.160 (≈ 0.130) OUR ESTIMATE			
0.0872 ± 0.0189	GOLOVATCH 19	DPWA	$\gamma p \rightarrow \pi^+ \pi^- p$
0.156 ± 0.017	¹ HUNT 19	DPWA	Multichannel
0.165 ± 0.020	SOKHOYAN 15A	DPWA	Multichannel
0.132 ± 0.005	¹ DUGGER 13	DPWA	$\gamma N \rightarrow \pi N$
0.105 ± 0.005	¹ WORKMAN 12A	DPWA	$\gamma N \rightarrow \pi N$
••• We do not use the following data for averages, fits, limits, etc. •••			
0.165 ± 0.020	GUTZ 14	DPWA	Multichannel
0.160 ± 0.020	ANISOVICH 12A	DPWA	Multichannel
0.058 ± 0.010	¹ SHRESTHA 12A	DPWA	Multichannel
0.226	DRECHSEL 07	DPWA	$\gamma N \rightarrow \pi N$
0.125 ± 0.003	DUGGER 07	DPWA	$\gamma N \rightarrow \pi N$
0.096	PENNER 02D	DPWA	Multichannel
¹ Statistical error only.			

See key on page 1127

Baryon Particle Listings
Δ(1700), Δ(1750), Δ(1900)

Δ(1700) → Nγ, helicity-3/2 a amplitude A3/2

Table with columns: VALUE (GeV^-1/2), DOCUMENT ID, TECN, COMMENT. Includes entries for GOLOVATCH, HUNT, SOKHOYAN, DUGGER, WORKMAN, GUTZ, ANISOVICH, SHRESTHA, DRECHSEL, DUGGER, PENNER.

Δ(1700) REFERENCES

For early references, see Physics Letters 111B 1 (1982).

Reference table listing authors (e.g., Golovatch, Hunt, Roenchen, Sokhoyan, Gutz, PDG, Roenchen, Svarc, Dugger, Anisovich, Shrestha, Workman, Kashevarov, Horn, Drechsel, Dugger, Penner, Vrana, Hoehler, Cutkosky, Hoehler) and their associated publications and collaborations.

Δ(1750) 1/2+ I(J^P) = 3/2(1/2+) Status: *
OMITTED FROM SUMMARY TABLE

Δ(1750) POLE POSITION

Table for Δ(1750) pole position with columns: REAL PART, VALUE (MeV), DOCUMENT ID, TECN, COMMENT. Includes entries for ARNDT and VRANA.

Δ(1750) ELASTIC POLE RESIDUE

Table for Δ(1750) elastic pole residue with columns: MODULUS |r|, VALUE (MeV), DOCUMENT ID, TECN, COMMENT. Includes entry for ARNDT.

Δ(1750) BREIT-WIGNER MASS

Table for Δ(1750) Breit-Wigner mass with columns: VALUE (MeV), DOCUMENT ID, TECN, COMMENT. Includes entries for PENNER and VRANA.

Δ(1750) BREIT-WIGNER WIDTH

Table for Δ(1750) Breit-Wigner width with columns: VALUE (MeV), DOCUMENT ID, TECN, COMMENT. Includes entries for PENNER and VRANA.

Δ(1750) DECAY MODES

Table for Δ(1750) decay modes with columns: Mode, Fraction (Γi/Γ). Includes entries for Nπ, N(1440)π, ΣK.

Δ(1750) BRANCHING RATIOS

Table for Δ(1750) branching ratios with columns: Γ(Nπ)/Γtotal, Γ(N(1440)π)/Γtotal, Γ(ΣK)/Γtotal. Includes entries for PENNER and VRANA.

Δ(1750) BREIT-WIGNER PHOTON DECAY AMPLITUDES

Papers on γN amplitudes predating 1981 may be found in our 2006 edition, Journal of Physics G33 1 (2006).

Δ(1750) → Nγ, helicity-1/2 amplitude A1/2

Table for Δ(1750) helicity-1/2 amplitude with columns: VALUE (GeV^-1/2), DOCUMENT ID, TECN, COMMENT. Includes entry for PENNER.

Δ(1750) REFERENCES

Reference table listing authors (e.g., PDG, ARNDT, PENNER, Vrana) and their associated publications and collaborations.

Δ(1900) 1/2- I(J^P) = 3/2(1/2-) Status: ***

Older and obsolete values are listed and referenced in the 2014 edition, Chinese Physics C38 070001 (2014).

Δ(1900) POLE POSITION

Table for Δ(1900) pole position with columns: REAL PART, VALUE (MeV), DOCUMENT ID, TECN, COMMENT. Includes entries for SOKHOYAN, SVARC, CUTKOSKY, HUNT, GUTZ, ANISOVICH, VRANA, HOEHLER.

Δ(1900) ELASTIC POLE RESIDUE

Table for Δ(1900) elastic pole residue with columns: MODULUS |r|, VALUE (MeV), DOCUMENT ID, TECN, COMMENT. Includes entries for SOKHOYAN, SVARC, CUTKOSKY, HUNT, GUTZ, ANISOVICH, VRANA.

Δ(1900) ELASTIC POLE RESIDUE

Table for Δ(1900) elastic pole residue with columns: MODULUS |r|, VALUE (MeV), DOCUMENT ID, TECN, COMMENT. Includes entries for SOKHOYAN, SVARC, CUTKOSKY.

Baryon Particle Listings

 $\Delta(1900)$

••• We do not use the following data for averages, fits, limits, etc. •••

11 ± 2	GUTZ	14	DPWA	Multichannel
10 ± 3	ANISOVICH	12A	DPWA	Multichannel

¹ Fit to the amplitudes of HOEHLER 79.

PHASE θ

VALUE ($^\circ$)	DOCUMENT ID	TECN	COMMENT
-115 ± 20	SOKHOYAN	15A	DPWA Multichannel
$20 \pm 27 \pm 19$	¹ SVARC	14	L+P $\pi N \rightarrow \pi N$
$+20 \pm 40$	CUTKOSKY	80	IPWA $\pi N \rightarrow \pi N$

••• We do not use the following data for averages, fits, limits, etc. •••

-115 ± 20	GUTZ	14	DPWA	Multichannel
-125 ± 20	ANISOVICH	12A	DPWA	Multichannel

¹ Fit to the amplitudes of HOEHLER 79.

 $\Delta(1900)$ INELASTIC POLE RESIDUE

The "normalized residue" is the residue divided by $\Gamma_{pole}/2$.

Normalized residue in $N\pi \rightarrow \Delta(1900) \rightarrow \Sigma K$

MODULUS	PHASE ($^\circ$)	DOCUMENT ID	TECN	COMMENT
0.07 ± 0.02	-50 ± 30	ANISOVICH	12A	DPWA Multichannel

Normalized residue in $N\pi \rightarrow \Delta(1900) \rightarrow \Delta\pi, D\text{-wave}$

MODULUS	PHASE ($^\circ$)	DOCUMENT ID	TECN	COMMENT
0.18 ± 0.10	105 ± 25	SOKHOYAN	15A	DPWA Multichannel

••• We do not use the following data for averages, fits, limits, etc. •••

$0.12^{+0.08}_{-0.05}$	110 ± 20	ANISOVICH	12A	DPWA Multichannel
------------------------	--------------	-----------	-----	-------------------

Normalized residue in $N\pi \rightarrow \Delta(1900) \rightarrow \Delta(1232)\eta$

MODULUS	PHASE ($^\circ$)	DOCUMENT ID	TECN	COMMENT
0.013 ± 0.006	undefined	GUTZ	14	DPWA Multichannel

Normalized residue in $N\pi \rightarrow \Delta(1900) \rightarrow N(1440)\pi$

MODULUS	PHASE ($^\circ$)	DOCUMENT ID	TECN	COMMENT
0.11 ± 0.06	115 ± 30	SOKHOYAN	15A	DPWA Multichannel

Normalized residue in $N\pi \rightarrow \Delta(1900) \rightarrow N(1520)\pi$

MODULUS	PHASE ($^\circ$)	DOCUMENT ID	TECN	COMMENT
0.06 ± 0.03	undefined	SOKHOYAN	15A	DPWA Multichannel

 $\Delta(1900)$ BREIT-WIGNER MASS

VALUE (MeV)	DOCUMENT ID	TECN	COMMENT
-------------	-------------	------	---------

1840 to 1920 (≈ 1860) OUR ESTIMATE

1989 ± 22	¹ HUNT	19	DPWA Multichannel
1840 ± 20	SOKHOYAN	15A	DPWA Multichannel
1890 ± 50	CUTKOSKY	80	IPWA $\pi N \rightarrow \pi N$
1908 ± 30	HOEHLER	79	IPWA $\pi N \rightarrow \pi N$

••• We do not use the following data for averages, fits, limits, etc. •••

1840 ± 20	GUTZ	14	DPWA Multichannel
1840 ± 30	ANISOVICH	12A	DPWA Multichannel
1868 ± 12	¹ SHRESTHA	12A	DPWA Multichannel
1802 ± 87	VRANA	00	DPWA Multichannel

¹ Statistical error only.

 $\Delta(1900)$ BREIT-WIGNER WIDTH

VALUE (MeV)	DOCUMENT ID	TECN	COMMENT
-------------	-------------	------	---------

180 to 320 (≈ 250) OUR ESTIMATE

457 ± 60	¹ HUNT	19	DPWA Multichannel
295 ± 30	SOKHOYAN	15A	DPWA Multichannel
170 ± 50	CUTKOSKY	80	IPWA $\pi N \rightarrow \pi N$
140 ± 40	HOEHLER	79	IPWA $\pi N \rightarrow \pi N$

••• We do not use the following data for averages, fits, limits, etc. •••

295 ± 30	GUTZ	14	DPWA Multichannel
300 ± 45	ANISOVICH	12A	DPWA Multichannel
234 ± 27	¹ SHRESTHA	12A	DPWA Multichannel
48 ± 45	VRANA	00	DPWA Multichannel

¹ Statistical error only.

 $\Delta(1900)$ DECAY MODES

The following branching fractions are our estimates, not fits or averages.

Mode	Fraction (Γ_i/Γ)
Γ_1 $N\pi$	4–12%
Γ_2 ΣK	seen
Γ_3 $N\pi\pi$	> 52%

Γ_4	$\Delta(1232)\pi, D\text{-wave}$	30–70%
Γ_5	$N\rho$	22–60%
Γ_6	$N\rho, S=1/2, S\text{-wave}$	11–35%
Γ_7	$N\rho, S=3/2, D\text{-wave}$	11–25%
Γ_8	$N(1440)\pi$	3–32%
Γ_9	$N(1520)\pi$	2–10%
Γ_{10}	$\Delta(1232)\eta$	< 2%
Γ_{11}	$N\gamma, \text{helicity}=1/2$	0.06–0.43%

 $\Delta(1900)$ BRANCHING RATIOS **$\Gamma(N\pi)/\Gamma_{\text{total}}$**

VALUE (%)	DOCUMENT ID	TECN	COMMENT
-----------	-------------	------	---------

4–12% OUR ESTIMATE

3.7 ± 0.8	¹ HUNT	19	DPWA Multichannel
7 ± 2	SOKHOYAN	15A	DPWA Multichannel
10 ± 3	CUTKOSKY	80	IPWA $\pi N \rightarrow \pi N$
8 ± 4	HOEHLER	79	IPWA $\pi N \rightarrow \pi N$

••• We do not use the following data for averages, fits, limits, etc. •••

7 ± 2	GUTZ	14	DPWA Multichannel
7 ± 3	ANISOVICH	12A	DPWA Multichannel
8 ± 1	¹ SHRESTHA	12A	DPWA Multichannel
33 ± 10	VRANA	00	DPWA Multichannel

¹ Statistical error only.

 $\Gamma(\Delta(1232)\pi, D\text{-wave})/\Gamma_{\text{total}}$

VALUE (%)	DOCUMENT ID	TECN	COMMENT
-----------	-------------	------	---------

30–70% OUR ESTIMATE

42 ± 8	¹ HUNT	19	DPWA Multichannel
50 ± 20	SOKHOYAN	15A	DPWA Multichannel

••• We do not use the following data for averages, fits, limits, etc. •••

15^{+50}_{-10}	ANISOVICH	12A	DPWA Multichannel
56 ± 6	¹ SHRESTHA	12A	DPWA Multichannel
28 ± 1	VRANA	00	DPWA Multichannel

¹ Statistical error only.

 $\Gamma(N\rho, S=1/2, S\text{-wave})/\Gamma_{\text{total}}$

VALUE (%)	DOCUMENT ID	TECN	COMMENT
-----------	-------------	------	---------

11–35% OUR ESTIMATE

23 ± 12	¹ HUNT	19	DPWA Multichannel
12 ± 4	¹ SHRESTHA	12A	DPWA Multichannel
30 ± 2	VRANA	00	DPWA Multichannel

¹ Statistical error only.

 $\Gamma(N\rho, S=3/2, D\text{-wave})/\Gamma_{\text{total}}$

VALUE (%)	DOCUMENT ID	TECN	COMMENT
-----------	-------------	------	---------

11–25% OUR ESTIMATE

18 ± 7	¹ HUNT	19	DPWA Multichannel
23 ± 5	¹ SHRESTHA	12A	DPWA Multichannel
5 ± 1	VRANA	00	DPWA Multichannel

¹ Statistical error only.

 $\Gamma(N(1440)\pi)/\Gamma_{\text{total}}$

VALUE (%)	DOCUMENT ID	TECN	COMMENT
-----------	-------------	------	---------

3–32% OUR ESTIMATE

12 ± 9	¹ HUNT	19	DPWA Multichannel
20 ± 12	SOKHOYAN	15A	DPWA Multichannel
< 1	¹ SHRESTHA	12A	DPWA Multichannel
4 ± 1	VRANA	00	DPWA Multichannel

¹ Statistical error only.

 $\Gamma(N(1520)\pi)/\Gamma_{\text{total}}$

VALUE (%)	DOCUMENT ID	TECN	COMMENT
-----------	-------------	------	---------

2–10% OUR ESTIMATE

6 ± 4	SOKHOYAN	15A	DPWA Multichannel
-----------	----------	-----	-------------------

 $\Gamma(\Delta(1232)\eta)/\Gamma_{\text{total}}$

VALUE (%)	DOCUMENT ID	TECN	COMMENT
-----------	-------------	------	---------

< 2% OUR ESTIMATE

1 ± 1	GUTZ	14	DPWA Multichannel
-----------	------	----	-------------------

 $\Delta(1900)$ PHOTON DECAY AMPLITUDES AT THE POLE **$\Delta(1900) \rightarrow N\gamma, \text{helicity}=1/2$ amplitude $A_{1/2}$**

MODULUS (GeV $^{-1/2}$)	PHASE ($^\circ$)	DOCUMENT ID	TECN	COMMENT
--------------------------	--------------------	-------------	------	---------

0.064 ± 0.015	60 ± 20	SOKHOYAN	15A	DPWA Multichannel
-------------------	-------------	----------	-----	-------------------

See key on page 1127

Baryon Particle Listings

$\Delta(1900)$, $\Delta(1905)$

$\Delta(1900)$ BREIT-WIGNER PHOTON DECAY AMPLITUDES

$\Delta(1900) \rightarrow N\gamma$, helicity-1/2 amplitude $A_{1/2}$

VALUE (GeV ^{-1/2})	DOCUMENT ID	TECN	COMMENT
0.212 ± 0.029	¹ HUNT 19	DPWA	Multichannel
0.065 ± 0.015	SOKHOYAN 15A	DPWA	Multichannel
0.057 ± 0.014	GUTZ 14	DPWA	Multichannel
-0.082 ± 0.009	¹ SHRESTHA 12A	DPWA	Multichannel

• • • We do not use the following data for averages, fits, limits, etc. • • •

¹ Statistical error only.

$\Delta(1900)$ REFERENCES

For early references, see Physics Letters **111B** 1 (1982).

HUNT 19	PR C99 055205	B. C. Hunt, D.M. Manley	
SOKHOYAN 15A	EPJ A51 95	V. Sokhoyan et al.	(CBELSA/TAPS Collab.)
GUTZ 14	EPJ A50 74	E. Gutz et al.	(CBELSA/TAPS Collab.)
PDG 14	CP C38 070001	K. Olive et al.	(PDG Collab.)
SVARC 14	PR C89 045205	A. Svarc et al.	(RBI Zagreb, UNI Tuzla)
ANISOVICH 12A	EPJ A48 15	A.V. Anisovich et al.	(BONN, PNPI)
SHRESTHA 12A	PR C86 055203	M. Shrestha, D.M. Manley	(KSU)
VRANA 00	PRPL 328 181	T.P. Vrana, S.A. Dytman, T.-S.H. Lee	(PITT, ANL)
HOEHLER 93	π N Newsletter 9 1	G. Hoehler	(KARL)
CUTKOSKY 80	Toronto Conf. 19	R.E. Cutkosky et al.	(CMU, LBL) IJP
Also	PR D20 2839	R.E. Cutkosky et al.	(CMU, LBL) IJP
HOEHLER 79	PDAT 12-1	G. Hoehler et al.	(KARLT) IJP
Also	Toronto Conf. 3	R. Koch	(KARLT) IJP

$\Delta(1905) 5/2^+$

 $I(J^P) = \frac{3}{2}(\frac{5}{2}^+)$ Status: * * * *

Older and obsolete values are listed and referenced in the 2014 edition, Chinese Physics **C38** 070001 (2014).

$\Delta(1905)$ POLE POSITION

REAL PART

VALUE (MeV)	DOCUMENT ID	TECN	COMMENT
1770 to 1830 (≈ 1800) OUR ESTIMATE			
1800 ± 6	SOKHOYAN 15A	DPWA	Multichannel
1752 ± 3 ± 2	¹ SVARC 14	L+P	$\pi N \rightarrow \pi N$
1830 ± 40	CUTKOSKY 80	IPWA	$\pi N \rightarrow \pi N$
• • • We do not use the following data for averages, fits, limits, etc. • • •			
1819	HUNT 19	DPWA	Multichannel
1795	ROENCHEN 15A	DPWA	Multichannel
1800 ± 6	GUTZ 14	DPWA	Multichannel
1805 ± 10	ANISOVICH 12A	DPWA	Multichannel
1819	ARNDT 06	DPWA	$\pi N \rightarrow \pi N, \eta N$
1793	VRANA 00	DPWA	Multichannel
1829	HOEHLER 93	SPED	$\pi N \rightarrow \pi N$

¹ Fit to the amplitudes of HOEHLER 79.

-2xIMAGINARY PART

VALUE (MeV)	DOCUMENT ID	TECN	COMMENT
260 to 340 (≈ 300) OUR ESTIMATE			
290 ± 15	SOKHOYAN 15A	DPWA	Multichannel
346 ± 6 ± 2	¹ SVARC 14	L+P	$\pi N \rightarrow \pi N$
280 ± 60	CUTKOSKY 80	IPWA	$\pi N \rightarrow \pi N$
• • • We do not use the following data for averages, fits, limits, etc. • • •			
253	HUNT 19	DPWA	Multichannel
247	ROENCHEN 15A	DPWA	Multichannel
290 ± 15	GUTZ 14	DPWA	Multichannel
300 ± 15	ANISOVICH 12A	DPWA	Multichannel
247	ARNDT 06	DPWA	$\pi N \rightarrow \pi N, \eta N$
302	VRANA 00	DPWA	Multichannel
303	HOEHLER 93	SPED	$\pi N \rightarrow \pi N$

¹ Fit to the amplitudes of HOEHLER 79.

$\Delta(1905)$ ELASTIC POLE RESIDUE

MODULUS $|r|$

VALUE (MeV)	DOCUMENT ID	TECN	COMMENT
15 to 25 (≈ 20) OUR ESTIMATE			
19 ± 2	SOKHOYAN 15A	DPWA	Multichannel
24 ± 1 ± 1	¹ SVARC 14	L+P	$\pi N \rightarrow \pi N$
25 ± 8	CUTKOSKY 80	IPWA	$\pi N \rightarrow \pi N$
• • • We do not use the following data for averages, fits, limits, etc. • • •			
5.3	ROENCHEN 15A	DPWA	Multichannel
19 ± 2	GUTZ 14	DPWA	Multichannel
20 ± 2	ANISOVICH 12A	DPWA	Multichannel
15	ARNDT 06	DPWA	$\pi N \rightarrow \pi N, \eta N$
25	HOEHLER 93	SPED	$\pi N \rightarrow \pi N$

¹ Fit to the amplitudes of HOEHLER 79.

PHASE θ

VALUE (°)	DOCUMENT ID	TECN	COMMENT
-120 to -30 (≈ -50) OUR ESTIMATE			
-45 ± 4	SOKHOYAN 15A	DPWA	Multichannel
-114 ± 1 ± 2	¹ SVARC 14	L+P	$\pi N \rightarrow \pi N$
-50 ± 20	CUTKOSKY 80	IPWA	$\pi N \rightarrow \pi N$

• • • We do not use the following data for averages, fits, limits, etc. • • •

-89	ROENCHEN 15A	DPWA	Multichannel
-45 ± 4	GUTZ 14	DPWA	Multichannel
-44 ± 5	ANISOVICH 12A	DPWA	Multichannel
-30	ARNDT 06	DPWA	$\pi N \rightarrow \pi N, \eta N$

¹ Fit to the amplitudes of HOEHLER 79.

$\Delta(1905)$ INELASTIC POLE RESIDUE

The "normalized residue" is the residue divided by $\Gamma_{pole}/2$.

Normalized residue in $N\pi \rightarrow \Delta(1905) \rightarrow \Delta\pi, P$ -wave

MODULUS	PHASE (°)	DOCUMENT ID	TECN	COMMENT
0.19 ± 0.07	10 ± 30	SOKHOYAN 15A	DPWA	Multichannel
0.0870	72	ROENCHEN 15A	DPWA	Multichannel
0.25 ± 0.06	0 ± 15	ANISOVICH 12A	DPWA	Multichannel

• • • We do not use the following data for averages, fits, limits, etc. • • •

Normalized residue in $N\pi \rightarrow \Delta(1905) \rightarrow \Delta\pi, F$ -wave

MODULUS	PHASE (°)	DOCUMENT ID	TECN	COMMENT
0.009	64	ROENCHEN 15A	DPWA	Multichannel

• • • We do not use the following data for averages, fits, limits, etc. • • •

Normalized residue in $N\pi \rightarrow \Delta(1905) \rightarrow \Sigma K$

MODULUS	PHASE (°)	DOCUMENT ID	TECN	COMMENT
0.001	-155	ROENCHEN 15A	DPWA	Multichannel

• • • We do not use the following data for averages, fits, limits, etc. • • •

Normalized residue in $N\pi \rightarrow \Delta(1905) \rightarrow N(1535)\pi$

MODULUS	PHASE (°)	DOCUMENT ID	TECN	COMMENT
0.025 ± 0.010	130 ± 35	GUTZ 14	DPWA	Multichannel

Normalized residue in $N\pi \rightarrow \Delta(1905) \rightarrow \Delta(1232)\eta$

MODULUS	PHASE (°)	DOCUMENT ID	TECN	COMMENT
0.07 ± 0.02	40 ± 20	GUTZ 14	DPWA	Multichannel

$\Delta(1905)$ BREIT-WIGNER MASS

VALUE (MeV)	DOCUMENT ID	TECN	COMMENT
1855 to 1910 (≈ 1880) OUR ESTIMATE			
1883 ± 19	GOLOVATCH 19	DPWA	$\gamma p \rightarrow \pi^+ \pi^- p$
1866 ± 9	¹ HUNT 19	DPWA	Multichannel
1856 ± 6	SOKHOYAN 15A	DPWA	Multichannel
1857.8 ± 1.6	¹ ARNDT 06	DPWA	$\pi N \rightarrow \pi N, \eta N$
1910 ± 30	CUTKOSKY 80	IPWA	$\pi N \rightarrow \pi N$
1905 ± 20	HOEHLER 79	IPWA	$\pi N \rightarrow \pi N$
• • • We do not use the following data for averages, fits, limits, etc. • • •			
1856 ± 6	GUTZ 14	DPWA	Multichannel
1861 ± 6	ANISOVICH 12A	DPWA	Multichannel
1818 ± 8	¹ SHRESTHA 12A	DPWA	Multichannel
1873 ± 77	VRANA 00	DPWA	Multichannel

¹ Statistical error only.

$\Delta(1905)$ BREIT-WIGNER WIDTH

VALUE (MeV)	DOCUMENT ID	TECN	COMMENT
270 to 400 (≈ 330) OUR ESTIMATE			
327 ± 69	GOLOVATCH 19	DPWA	$\gamma p \rightarrow \pi^+ \pi^- p$
289 ± 20	¹ HUNT 19	DPWA	Multichannel
325 ± 15	SOKHOYAN 15A	DPWA	Multichannel
320.6 ± 8.6	¹ ARNDT 06	DPWA	$\pi N \rightarrow \pi N, \eta N$
400 ± 100	CUTKOSKY 80	IPWA	$\pi N \rightarrow \pi N$
260 ± 20	HOEHLER 79	IPWA	$\pi N \rightarrow \pi N$
• • • We do not use the following data for averages, fits, limits, etc. • • •			
325 ± 15	GUTZ 14	DPWA	Multichannel
335 ± 18	ANISOVICH 12A	DPWA	Multichannel
278 ± 18	¹ SHRESTHA 12A	DPWA	Multichannel
461 ± 111	VRANA 00	DPWA	Multichannel

¹ Statistical error only.

$\Delta(1905)$ DECAY MODES

The following branching fractions are our estimates, not fits or averages.

Mode	Fraction (Γ_i/Γ)
Γ_1 $N\pi$	9-15%
Γ_2 $N\pi\pi$	>65%
Γ_3 $\Delta(1232)\pi$	>48%
Γ_4 $\Delta(1232)\pi, P$ -wave	8-43%
Γ_5 $\Delta(1232)\pi, F$ -wave	40-58%
Γ_6 $N\rho, S=3/2, P$ -wave	17-35%
Γ_7 $N(1535)\pi$	< 1%
Γ_8 $N(1680)\pi, P$ -wave	5-15%

Baryon Particle Listings

 $\Delta(1905)$, $\Delta(1910)$

Γ_9	$\Delta(1232)\eta$	2-6%
Γ_{10}	$N\gamma$	0.012-0.036 %
Γ_{11}	$N\gamma$, helicity=1/2	0.002-0.006 %
Γ_{12}	$N\gamma$, helicity=3/2	0.01-0.03 %

 $\Delta(1905)$ BRANCHING RATIOS

$\Gamma(N\pi)/\Gamma_{\text{total}}$	DOCUMENT ID	TECN	COMMENT	Γ_1/Γ
9-15% OUR ESTIMATE				
17 ± 1	¹ HUNT	19	DPWA Multichannel	
13 ± 2	SOKHOYAN	15A	DPWA Multichannel	
12.2 ± 0.1	¹ ARNDT	06	DPWA $\pi N \rightarrow \pi N, \eta N$	
8 ± 3	CUTKOSKY	80	IPWA $\pi N \rightarrow \pi N$	
15 ± 2	HOEHLER	79	IPWA $\pi N \rightarrow \pi N$	
• • • We do not use the following data for averages, fits, limits, etc. • • •				
13 ± 2	GUTZ	14	DPWA Multichannel	
13 ± 2	ANISOVICH	12A	DPWA Multichannel	
6 ± 1	¹ SHRESTHA	12A	DPWA Multichannel	
9 ± 1	VRANA	00	DPWA Multichannel	
¹ Statistical error only.				

$\Gamma(N\pi\pi)/\Gamma_{\text{total}}$	DOCUMENT ID	TECN	COMMENT	Γ_2/Γ
>65% OUR ESTIMATE				
0.85 ± 0.15	GOLOVATCH	19	DPWA $\gamma p \rightarrow \pi^+ \pi^- p$	

$\Gamma(\Delta(1232)\pi, P\text{-wave})/\Gamma_{\text{total}}$	DOCUMENT ID	TECN	COMMENT	Γ_4/Γ
8-43% OUR ESTIMATE				
8.4 ± 0.5	¹ HUNT	19	DPWA Multichannel	
33 ± 10	SOKHOYAN	15A	DPWA Multichannel	
• • • We do not use the following data for averages, fits, limits, etc. • • •				
45 ± 14	ANISOVICH	12A	DPWA Multichannel	
28 ± 7	¹ SHRESTHA	12A	DPWA Multichannel	
23 ± 1	VRANA	00	DPWA Multichannel	
¹ Statistical error only.				

$\Gamma(\Delta(1232)\pi, F\text{-wave})/\Gamma_{\text{total}}$	DOCUMENT ID	TECN	COMMENT	Γ_5/Γ
40-58% OUR ESTIMATE				
49 ± 9	¹ HUNT	19	DPWA Multichannel	
• • • We do not use the following data for averages, fits, limits, etc. • • •				
64 ± 8	¹ SHRESTHA	12A	DPWA Multichannel	
44 ± 1	VRANA	00	DPWA Multichannel	
¹ Statistical error only.				

$\Gamma(N\rho, S=3/2, P\text{-wave})/\Gamma_{\text{total}}$	DOCUMENT ID	TECN	COMMENT	Γ_6/Γ
17-35% OUR ESTIMATE				
26 ± 9	¹ HUNT	19	DPWA Multichannel	
• • • We do not use the following data for averages, fits, limits, etc. • • •				
< 6	¹ SHRESTHA	12A	DPWA Multichannel	
24 ± 1	VRANA	00	DPWA Multichannel	
¹ Statistical error only.				

$\Gamma(N(1535)\pi)/\Gamma_{\text{total}}$	DOCUMENT ID	TECN	COMMENT	Γ_7/Γ
< 1% OUR ESTIMATE				
< 1	GUTZ	14	DPWA Multichannel	

$\Gamma(N(1680)\pi, P\text{-wave})/\Gamma_{\text{total}}$	DOCUMENT ID	TECN	COMMENT	Γ_8/Γ
5-15% OUR ESTIMATE				
10 ± 5	SOKHOYAN	15A	DPWA Multichannel	

$\Gamma(\Delta(1232)\eta)/\Gamma_{\text{total}}$	DOCUMENT ID	TECN	COMMENT	Γ_9/Γ
2-6% OUR ESTIMATE				
4 ± 2	GUTZ	14	DPWA Multichannel	

 $\Delta(1905)$ PHOTON DECAY AMPLITUDES AT THE POLE $\Delta(1905) \rightarrow N\gamma$, helicity-1/2 amplitude $A_{1/2}$

MODULUS ($\text{GeV}^{-1/2}$)	PHASE ($^\circ$)	DOCUMENT ID	TECN	COMMENT
0.025 ± 0.005	-28 ± 12	SOKHOYAN	15A	DPWA Multichannel
0.013 + 0.013 - 0.005	64 + 72 - 36	ROENCHEN	14	DPWA
• • • We do not use the following data for averages, fits, limits, etc. • • •				
0.053	89	ROENCHEN	15A	DPWA Multichannel

 $\Delta(1905) \rightarrow N\gamma$, helicity-3/2 amplitude $A_{3/2}$

MODULUS ($\text{GeV}^{-1/2}$)	PHASE ($^\circ$)	DOCUMENT ID	TECN	COMMENT
-0.050 ± 0.004	5 ± 10	SOKHOYAN	15A	DPWA Multichannel
0.072 ± 0.016	113 ± 13 7	ROENCHEN	14	DPWA
• • • We do not use the following data for averages, fits, limits, etc. • • •				
-0.030	80	ROENCHEN	15A	DPWA Multichannel

 $\Delta(1905)$ BREIT-WIGNER PHOTON DECAY AMPLITUDES $\Delta(1905) \rightarrow N\gamma$, helicity-1/2 amplitude $A_{1/2}$

VALUE ($\text{GeV}^{-1/2}$)	DOCUMENT ID	TECN	COMMENT
0.017 to 0.027 (≈ 0.022) OUR ESTIMATE			
0.019 ± 0.0076	GOLOVATCH	19	DPWA $\gamma p \rightarrow \pi^+ \pi^- p$
0.077 ± 0.010	¹ HUNT	19	DPWA Multichannel
0.025 ± 0.005	SOKHOYAN	15A	DPWA Multichannel
0.020 ± 0.002	¹ DUGGER	13	DPWA $\gamma N \rightarrow \pi N$
0.019 ± 0.002	¹ WORKMAN	12A	DPWA $\gamma N \rightarrow \pi N$
• • • We do not use the following data for averages, fits, limits, etc. • • •			
0.025 ± 0.005	GUTZ	14	DPWA Multichannel
0.025 ± 0.004	ANISOVICH	12A	DPWA Multichannel
0.066 ± 0.018	¹ SHRESTHA	12A	DPWA Multichannel
0.018	DRECHSEL	07	DPWA $\gamma N \rightarrow \pi N$
¹ Statistical error only.			

 $\Delta(1905) \rightarrow N\gamma$, helicity-3/2 amplitude $A_{3/2}$

VALUE ($\text{GeV}^{-1/2}$)	DOCUMENT ID	TECN	COMMENT
-0.055 to -0.035 (≈ -0.045) OUR ESTIMATE			
-0.0432 ± 0.0173	GOLOVATCH	19	DPWA $\gamma p \rightarrow \pi^+ \pi^- p$
-0.053 ± 0.029	¹ HUNT	19	DPWA Multichannel
-0.050 ± 0.005	SOKHOYAN	15A	DPWA Multichannel
-0.049 ± 0.005	¹ DUGGER	13	DPWA $\gamma N \rightarrow \pi N$
-0.038 ± 0.004	WORKMAN	12A	DPWA $\gamma N \rightarrow \pi N$
• • • We do not use the following data for averages, fits, limits, etc. • • •			
-0.050 ± 0.005	GUTZ	14	DPWA Multichannel
-0.049 ± 0.004	ANISOVICH	12A	DPWA Multichannel
-0.223 ± 0.029	¹ SHRESTHA	12A	DPWA Multichannel
-0.028	DRECHSEL	07	DPWA $\gamma N \rightarrow \pi N$
¹ Statistical error only.			

 $\Delta(1905)$ REFERENCESFor early references, see Physics Letters **111B** 1 (1982).

GOLOVATCH	19	PL B788 371	E. Golovatch et al.	(CLAS Collab.)
HUNT	19	PR C99 055205	B.C. Hunt, D.M. Manley	
ROENCHEN	15A	EPJ A51 70	D. Roenchen et al.	
SOKHOYAN	15A	EPJ A51 95	V. Sokhoyan et al.	(CBELSA/TAPS Collab.)
GUTZ	14	EPJ A50 74	E. Gutz et al.	(CBELSA/TAPS Collab.)
PDG	14	CP C38 070001	K. Olive et al.	(PDG Collab.)
ROENCHEN	14	EPJ A50 101	D. Roenchen et al.	
Also		EPJ A51 63 (errata.)	D. Roenchen et al.	
SVARC	14	PR C89 045205	A. Svarc et al.	(RBI Zagreb, UNI Tuzla)
DUGGER	13	PR C88 065203	M. Dugger et al.	(JLab CLAS Collab.)
ANISOVICH	12A	EPJ A48 15	A.V. Anisovich et al.	(BONN, PFI)
SHRESTHA	12A	PR C86 055203	M. Shrestha, D.M. Manley	(KSU)
WORKMAN	12A	PR C86 015202	R. Workman et al.	(GWU)
DRECHSEL	07	EPJ A34 69	D. Drechsel, S.S. Kamalov, L. Tiator	(MAINZ, JINR)
ARNDT	06	PR C74 045205	R.A. Arndt et al.	(GWU)
VRANA	00	PRPL 328 181	T.P. Vrana, S.A. Dytman, T.-S.H. Lee	(PITT, ANL)
HOEHLER	93	πN Newsletter 9 1	G. Hohlner	(KARL)
CUTKOSKY	80	Toronto Conf. 19	R.E. Cutkosky et al.	(CMU, LBL) IJP
Also		PR D20 2839	R.E. Cutkosky et al.	(CMU, LBL) IJP
HOEHLER	79	PDAT 12-1	G. Hohlner et al.	(KARLT) IJP
Also		Toronto Conf. 3	R. Koch	(KARLT) IJP

 $\Delta(1910) 1/2^+$

$$I(J^P) = \frac{3}{2}(1^+) \text{ Status: } ***$$

Older and obsolete values are listed and referenced in the 2014 edition, Chinese Physics **C38** 070001 (2014). $\Delta(1910)$ POLE POSITION

REAL PART

VALUE (MeV)	DOCUMENT ID	TECN	COMMENT
1830 to 1890 (≈ 1860) OUR ESTIMATE			
1840 ± 40	SOKHOYAN	15A	DPWA Multichannel
1896 ± 11	¹ SVARC	14	L+P $\pi N \rightarrow \pi N$
1880 ± 30	CUTKOSKY	80	IPWA $\pi N \rightarrow \pi N$
• • • We do not use the following data for averages, fits, limits, etc. • • •			
1801	HUNT	19	DPWA Multichannel
1799	ROENCHEN	15A	DPWA Multichannel
1840 ± 40	GUTZ	14	DPWA Multichannel
1850 ± 40	ANISOVICH	12A	DPWA Multichannel
1771	ARNDT	06	DPWA $\pi N \rightarrow \pi N, \eta N$
1880	VRANA	00	DPWA Multichannel
1874	HOEHLER	93	SPED $\pi N \rightarrow \pi N$
¹ Fit to the amplitudes of HOEHLER 79.			

Baryon Particle Listings
 $\Delta(1910)$

−2×IMAGINARY PART

VALUE (MeV)	DOCUMENT ID	TECN	COMMENT
200 to 400 (≈ 300) OUR ESTIMATE			
370±60	SOKHOYAN 15A	DPWA	Multichannel
302±22	¹ SVARC 14	L+P	$\pi N \rightarrow \pi N$
200±40	CUTKOSKY 80	IPWA	$\pi N \rightarrow \pi N$
••• We do not use the following data for averages, fits, limits, etc. •••			
224	HUNT 19	DPWA	Multichannel
648	ROENCHEN 15A	DPWA	Multichannel
370±60	GUTZ 14	DPWA	Multichannel
350±45	ANISOVICH 12A	DPWA	Multichannel
479	ARNDT 06	DPWA	$\pi N \rightarrow \pi N, \eta N$
496	VRANA 00	DPWA	Multichannel
283	HOEHLER 93	SPED	$\pi N \rightarrow \pi N$
¹ Fit to the amplitudes of HOEHLER 79.			

$\Delta(1910)$ ELASTIC POLE RESIDUE

MODULUS $|r|$

VALUE (MeV)	DOCUMENT ID	TECN	COMMENT
20 to 30 (≈ 25) OUR ESTIMATE			
25±6	SOKHOYAN 15A	DPWA	Multichannel
29±2	¹ SVARC 14	L+P	$\pi N \rightarrow \pi N$
20±4	CUTKOSKY 80	IPWA	$\pi N \rightarrow \pi N$
••• We do not use the following data for averages, fits, limits, etc. •••			
90	ROENCHEN 15A	DPWA	Multichannel
25±6	GUTZ 14	DPWA	Multichannel
24±6	ANISOVICH 12A	DPWA	Multichannel
45	ARNDT 06	DPWA	$\pi N \rightarrow \pi N, \eta N$
38	HOEHLER 93	SPED	$\pi N \rightarrow \pi N$
¹ Fit to the amplitudes of HOEHLER 79.			

PHASE θ

VALUE (°)	DOCUMENT ID	TECN	COMMENT
−180 to −80 (≈ −130) OUR ESTIMATE			
−155±30	SOKHOYAN 15A	DPWA	Multichannel
−83±4±1	¹ SVARC 14	L+P	$\pi N \rightarrow \pi N$
−90±30	CUTKOSKY 80	IPWA	$\pi N \rightarrow \pi N$
••• We do not use the following data for averages, fits, limits, etc. •••			
−83	ROENCHEN 15A	DPWA	Multichannel
−155±30	GUTZ 14	DPWA	Multichannel
−145±30	ANISOVICH 12A	DPWA	Multichannel
+172	ARNDT 06	DPWA	$\pi N \rightarrow \pi N, \eta N$
¹ Fit to the amplitudes of HOEHLER 79.			

$\Delta(1910)$ INELASTIC POLE RESIDUE

The “normalized residue” is the residue divided by $\Gamma_{pole}/2$.

Normalized residue in $N\pi \rightarrow \Delta(1910) \rightarrow \Sigma K$

MODULUS	PHASE (°)	DOCUMENT ID	TECN	COMMENT
0.07 ± 0.02	−110 ± 30	ANISOVICH 12A	DPWA	Multichannel
••• We do not use the following data for averages, fits, limits, etc. •••				
0.019	−123	ROENCHEN 15A	DPWA	Multichannel

Normalized residue in $N\pi \rightarrow \Delta(1910) \rightarrow \Delta\pi, P$ -wave

MODULUS	PHASE (°)	DOCUMENT ID	TECN	COMMENT
0.24 ± 0.10	85 ± 35	SOKHOYAN 15A	DPWA	Multichannel
••• We do not use the following data for averages, fits, limits, etc. •••				
0.58	131	ROENCHEN 15A	DPWA	Multichannel
0.16 ± 0.09	95 ± 40	ANISOVICH 12A	DPWA	Multichannel

Normalized residue in $N\pi \rightarrow \Delta(1910) \rightarrow \Delta(1232)\eta$

MODULUS	PHASE (°)	DOCUMENT ID	TECN	COMMENT
0.11 ± 0.04	−150 ± 50	GUTZ 14	DPWA	Multichannel

Normalized residue in $N\pi \rightarrow \Delta(1910) \rightarrow N(1440)\pi$

MODULUS	PHASE (°)	DOCUMENT ID	TECN	COMMENT
0.06 ± 0.03	170 ± 45	SOKHOYAN 15A	DPWA	Multichannel

$\Delta(1910)$ BREIT-WIGNER MASS

VALUE (MeV)	DOCUMENT ID	TECN	COMMENT
1850 to 1950 (≈ 1900) OUR ESTIMATE			
1846 ± 18	¹ HUNT 19	DPWA	Multichannel
1845 ± 40	SOKHOYAN 15A	DPWA	Multichannel
2067.9 ± 1.7	¹ ARNDT 06	DPWA	$\pi N \rightarrow \pi N, \eta N$
1910 ± 40	CUTKOSKY 80	IPWA	$\pi N \rightarrow \pi N$
1888 ± 20	HOEHLER 79	IPWA	$\pi N \rightarrow \pi N$
••• We do not use the following data for averages, fits, limits, etc. •••			
1845 ± 40	GUTZ 14	DPWA	Multichannel
1860 ± 40	ANISOVICH 12A	DPWA	Multichannel

1934 ± 5	¹ SHRESTHA 12A	DPWA	Multichannel
1995 ± 12	VRANA 00	DPWA	Multichannel

¹ Statistical error only.

$\Delta(1910)$ BREIT-WIGNER WIDTH

VALUE (MeV)	DOCUMENT ID	TECN	COMMENT
200 to 400 (≈ 300) OUR ESTIMATE			
260 ± 57	¹ HUNT 19	DPWA	Multichannel
360 ± 60	SOKHOYAN 15A	DPWA	Multichannel
543 ± 10	¹ ARNDT 06	DPWA	$\pi N \rightarrow \pi N, \eta N$
225 ± 50	CUTKOSKY 80	IPWA	$\pi N \rightarrow \pi N$
280 ± 50	HOEHLER 79	IPWA	$\pi N \rightarrow \pi N$
••• We do not use the following data for averages, fits, limits, etc. •••			
360 ± 60	GUTZ 14	DPWA	Multichannel
350 ± 55	ANISOVICH 12A	DPWA	Multichannel
211 ± 11	¹ SHRESTHA 12A	DPWA	Multichannel
713 ± 465	VRANA 00	DPWA	Multichannel
¹ Statistical error only.			

$\Delta(1910)$ DECAY MODES

The following branching fractions are our estimates, not fits or averages.

Mode	Fraction (Γ_i/Γ)
Γ_1 $N\pi$	10–30%
Γ_2 ΣK	4–14%
Γ_3 $\Delta(1232)\pi$	34–66%
Γ_4 $N(1440)\pi$	3–45%
Γ_5 $\Delta(1232)\eta$	5–13%
Γ_6 $N\gamma$, helicity=1/2	0.0–0.02%

$\Delta(1910)$ BRANCHING RATIOS

$\Gamma(N\pi)/\Gamma_{total}$	DOCUMENT ID	TECN	COMMENT	Γ_1/Γ
10–30% OUR ESTIMATE				
13 ± 3	¹ HUNT 19	DPWA	Multichannel	
12 ± 3	SOKHOYAN 15A	DPWA	Multichannel	
23.9 ± 0.1	¹ ARNDT 06	DPWA	$\pi N \rightarrow \pi N, \eta N$	
19 ± 3	CUTKOSKY 80	IPWA	$\pi N \rightarrow \pi N$	
24 ± 6	HOEHLER 79	IPWA	$\pi N \rightarrow \pi N$	
••• We do not use the following data for averages, fits, limits, etc. •••				
12 ± 3	GUTZ 14	DPWA	Multichannel	
12 ± 3	ANISOVICH 12A	DPWA	Multichannel	
17 ± 1	¹ SHRESTHA 12A	DPWA	Multichannel	
29 ± 21	VRANA 00	DPWA	Multichannel	
¹ Statistical error only.				

$\Gamma(\Sigma K)/\Gamma_{total}$	DOCUMENT ID	TECN	COMMENT	Γ_2/Γ
4–14% OUR ESTIMATE				
9 ± 5	ANISOVICH 12A	DPWA	Multichannel	

$\Gamma(\Delta(1232)\pi)/\Gamma_{total}$	DOCUMENT ID	TECN	COMMENT	Γ_3/Γ
34–66% OUR ESTIMATE				
50 ± 16	SOKHOYAN 15A	DPWA	Multichannel	
••• We do not use the following data for averages, fits, limits, etc. •••				
60 ± 28	ANISOVICH 12A	DPWA	Multichannel	

$\Gamma(N(1440)\pi)/\Gamma_{total}$	DOCUMENT ID	TECN	COMMENT	Γ_4/Γ
3–45% OUR ESTIMATE				
33 ± 12	¹ HUNT 19	DPWA	Multichannel	
6 ± 3	SOKHOYAN 15A	DPWA	Multichannel	
••• We do not use the following data for averages, fits, limits, etc. •••				
47 ± 6	¹ SHRESTHA 12A	DPWA	Multichannel	
56 ± 7	VRANA 00	DPWA	Multichannel	
¹ Statistical error only.				

$\Gamma(\Delta(1232)\eta)/\Gamma_{total}$	DOCUMENT ID	TECN	COMMENT	Γ_5/Γ
5–13% OUR ESTIMATE				
9 ± 4	GUTZ 14	DPWA	Multichannel	

$\Delta(1910)$ PHOTON DECAY AMPLITUDES AT THE POLE

$\Delta(1910) \rightarrow N\gamma$, helicity-1/2 amplitude $A_{1/2}$

MODULUS ($\text{GeV}^{-1/2}$)	PHASE (°)	DOCUMENT ID	TECN	COMMENT
0.027 ± 0.009	−30 ± 60	SOKHOYAN 15A	DPWA	Multichannel
−0.246 + 0.024 − 0.047	159 + 9 − 4	ROENCHEN 14	DPWA	

Baryon Particle Listings

 $\Delta(1910)$, $\Delta(1920)$

••• We do not use the following data for averages, fits, limits, etc. •••

0.321 39 ROENCHEN 15A DPWA Multichannel

 $\Delta(1910)$ BREIT-WIGNER PHOTON DECAY AMPLITUDES $\Delta(1910) \rightarrow N\gamma$, helicity-1/2 amplitude $A_{1/2}$

VALUE (GeV ^{-1/2})	DOCUMENT ID	TECN	COMMENT
0.010 to 0.030 (≈ 0.020) OUR ESTIMATE			
0.203 ± 0.056	¹ HUNT 19	DPWA	Multichannel
0.026 ± 0.008	SOKHOYAN 15A	DPWA	Multichannel
-0.002 ± 0.008	¹ ARNDT 96	IPWA	$\gamma N \rightarrow \pi N$
••• We do not use the following data for averages, fits, limits, etc. •••			
0.026 ± 0.008	GUTZ 14	DPWA	Multichannel
0.022 ± 0.009	ANISOVICH 12A	DPWA	Multichannel
0.030 ± 0.002	¹ SHRESTHA 12A	DPWA	Multichannel

¹ Statistical error only.

 $\Delta(1910)$ REFERENCES

For early references, see Physics Letters **111B** 1 (1982).

HUNT 19	PR C99 055205	B. C. Hunt, D.M. Manley
ROENCHEN 15A	EPJ A51 70	D. Roenchen <i>et al.</i>
SOKHOYAN 15A	EPJ A51 95	V. Sokhoyan <i>et al.</i>
GUTZ 14	EPJ A50 74	E. Gutz <i>et al.</i>
PDG 14	CP C38 070001	K. Olive <i>et al.</i>
ROENCHEN 14	EPJ A50 101	D. Roenchen <i>et al.</i>
Also	EPJ A51 63 (errata.)	D. Roenchen <i>et al.</i>
SVARC 14	PR C89 045205	A. Svarc <i>et al.</i>
ANISOVICH 12A	EPJ A48 15	A.V. Anisovich <i>et al.</i>
SHRESTHA 12A	PR C86 055203	M. Shrestha, D.M. Manley
ARNDT 06	PR C74 045205	R.A. Arndt <i>et al.</i>
VRANA 00	PRPL 328 181	T.P. Vrana, S.A. Dytman, T.-S.H. Lee
ARNDT 96	PR C53 430	R.A. Arndt, I.I. Strakovsky, R.L. Workman
HOEHLER 93	πN Newsletter 9 1	G. Hoehler
CUTKOSKY 80	Toronto Conf. 19	R.E. Cutkosky <i>et al.</i>
Also	PR D20 2839	R.E. Cutkosky <i>et al.</i>
HOEHLER 79	PDAT 12-1	G. Hoehler <i>et al.</i>
Also	Toronto Conf. 3	R. Koch

 $\Delta(1920)$ 3/2⁺

$$I(J^P) = \frac{3}{2}(\frac{3}{2}^+) \text{ Status: } ** *$$

Older and obsolete values are listed and referenced in the 2014 edition, Chinese Physics **C38** 070001 (2014).

 $\Delta(1920)$ POLE POSITION

REAL PART

VALUE (MeV)	DOCUMENT ID	TECN	COMMENT
1850 to 1950 (≈ 1900) OUR ESTIMATE			
1875 ± 30	SOKHOYAN 15A	DPWA	Multichannel
1906 ± 10 ± 2	¹ SVARC 14	L+P	$\pi N \rightarrow \pi N$
1900 ± 80	CUTKOSKY 80	IPWA	$\pi N \rightarrow \pi N$
••• We do not use the following data for averages, fits, limits, etc. •••			
1910	HUNT 19	DPWA	Multichannel
1715	ROENCHEN 15A	DPWA	Multichannel
1875 ± 30	GUTZ 14	DPWA	Multichannel
1890 ± 30	ANISOVICH 12A	DPWA	Multichannel
1880	VRANA 00	DPWA	Multichannel
1900	HOEHLER 93	SPED	$\pi N \rightarrow \pi N$

¹ Fit to the amplitudes of HOEHLER 79.

-2xIMAGINARY PART

VALUE (MeV)	DOCUMENT ID	TECN	COMMENT
200 to 400 (≈ 300) OUR ESTIMATE			
300 ± 40	SOKHOYAN 15A	DPWA	Multichannel
310 ± 20 ± 11	¹ SVARC 14	L+P	$\pi N \rightarrow \pi N$
300 ± 100	CUTKOSKY 80	IPWA	$\pi N \rightarrow \pi N$
••• We do not use the following data for averages, fits, limits, etc. •••			
472	HUNT 19	DPWA	Multichannel
882	ROENCHEN 15A	DPWA	Multichannel
300 ± 40	GUTZ 14	DPWA	Multichannel
300 ± 60	ANISOVICH 12A	DPWA	Multichannel
120	VRANA 00	DPWA	Multichannel

¹ Fit to the amplitudes of HOEHLER 79.

 $\Delta(1920)$ ELASTIC POLE RESIDUEMODULUS $|r|$

VALUE (MeV)	DOCUMENT ID	TECN	COMMENT
8 to 24 (≈ 16) OUR ESTIMATE			
16 ± 6	SOKHOYAN 15A	DPWA	Multichannel
26 ± 3 ± 2	¹ SVARC 14	L+P	$\pi N \rightarrow \pi N$
24 ± 4	CUTKOSKY 80	IPWA	$\pi N \rightarrow \pi N$
••• We do not use the following data for averages, fits, limits, etc. •••			
38	ROENCHEN 15A	DPWA	Multichannel
16 ± 6	GUTZ 14	DPWA	Multichannel
17 ± 8	ANISOVICH 12A	DPWA	Multichannel

¹ Fit to the amplitudes of HOEHLER 79.

PHASE θ

VALUE (°)	DOCUMENT ID	TECN	COMMENT
-150 to -50 (≈ -100) OUR ESTIMATE			
-50 ± 25	SOKHOYAN 15A	DPWA	Multichannel
-130 ± 5 ± 3	¹ SVARC 14	L+P	$\pi N \rightarrow \pi N$
-150 ± 30	CUTKOSKY 80	IPWA	$\pi N \rightarrow \pi N$
••• We do not use the following data for averages, fits, limits, etc. •••			
146	ROENCHEN 15A	DPWA	Multichannel
-50 ± 25	GUTZ 14	DPWA	Multichannel
-40 ± 20	ANISOVICH 12A	DPWA	Multichannel

¹ Fit to the amplitudes of HOEHLER 79.

 $\Delta(1920)$ INELASTIC POLE RESIDUE

The "normalized residue" is the residue divided by $\Gamma_{pole}/2$.

Normalized residue in $N\pi \rightarrow \Delta(1920) \rightarrow \Delta\eta$

MODULUS	PHASE (°)	DOCUMENT ID	TECN	COMMENT
0.15 ± 0.04	70 ± 20	GUTZ 14	DPWA	Multichannel
••• We do not use the following data for averages, fits, limits, etc. •••				
0.17 ± 0.08	70 ± 20	ANISOVICH 12A	DPWA	Multichannel

Normalized residue in $N\pi \rightarrow \Delta(1920) \rightarrow \Sigma K$

MODULUS	PHASE (°)	DOCUMENT ID	TECN	COMMENT
0.09 ± 0.03	80 ± 40	ANISOVICH 12A	DPWA	Multichannel
••• We do not use the following data for averages, fits, limits, etc. •••				
0.17	-35	ROENCHEN 15A	DPWA	Multichannel

Normalized residue in $N\pi \rightarrow \Delta(1920) \rightarrow \Delta\pi, P\text{-wave}$

MODULUS	PHASE (°)	DOCUMENT ID	TECN	COMMENT
0.20 ± 0.08	-105 ± 25	SOKHOYAN 15A	DPWA	Multichannel
••• We do not use the following data for averages, fits, limits, etc. •••				
0.069	131	ROENCHEN 15A	DPWA	Multichannel
0.20 ± 0.12	-120 ± 30	ANISOVICH 12A	DPWA	Multichannel

Normalized residue in $N\pi \rightarrow \Delta(1920) \rightarrow \Delta\pi, F\text{-wave}$

MODULUS	PHASE (°)	DOCUMENT ID	TECN	COMMENT
0.37 ± 0.10	-90 ± 20	SOKHOYAN 15A	DPWA	Multichannel
••• We do not use the following data for averages, fits, limits, etc. •••				
0.013	-115	ROENCHEN 15A	DPWA	Multichannel
0.28 ± 0.07	-95 ± 35	ANISOVICH 12A	DPWA	Multichannel

Normalized residue in $N\pi \rightarrow \Delta(1920) \rightarrow N(1535)\pi$

MODULUS	PHASE (°)	DOCUMENT ID	TECN	COMMENT
0.03 ± 0.02	35 ± 45	GUTZ 14	DPWA	Multichannel

Normalized residue in $N\pi \rightarrow \Delta(1920) \rightarrow N_{80}(980)$

MODULUS	PHASE (°)	DOCUMENT ID	TECN	COMMENT
0.03 ± 0.02	-85 ± 45	GUTZ 14	DPWA	Multichannel

Normalized residue in $N\pi \rightarrow \Delta(1920) \rightarrow N(1440)\pi$

MODULUS	PHASE (°)	DOCUMENT ID	TECN	COMMENT
0.04 ± 0.03	undefined	SOKHOYAN 15A	DPWA	Multichannel

Normalized residue in $N\pi \rightarrow \Delta(1920) \rightarrow N(1520)\pi, S\text{-wave}$

MODULUS	PHASE (°)	DOCUMENT ID	TECN	COMMENT
0.05 ± 0.05	undefined	SOKHOYAN 15A	DPWA	Multichannel

 $\Delta(1920)$ BREIT-WIGNER MASS

VALUE (MeV)	DOCUMENT ID	TECN	COMMENT
1870 to 1970 (≈ 1920) OUR ESTIMATE			
1976 ± 49	HUNT 19	DPWA	Multichannel
1880 ± 30	SOKHOYAN 15A	DPWA	Multichannel
2146 ± 32	¹ SHRESTHA 12A	DPWA	Multichannel
1920 ± 80	CUTKOSKY 80	IPWA	$\pi N \rightarrow \pi N$
1868 ± 10	HOEHLER 79	IPWA	$\pi N \rightarrow \pi N$
••• We do not use the following data for averages, fits, limits, etc. •••			
1880 ± 30	GUTZ 14	DPWA	Multichannel
1900 ± 30	ANISOVICH 12A	DPWA	Multichannel
2057 ± 1	PENNER 02c	DPWA	Multichannel
1889 ± 100	VRANA 00	DPWA	Multichannel

¹ Statistical error only.

 $\Delta(1920)$ BREIT-WIGNER WIDTH

VALUE (MeV)	DOCUMENT ID	TECN	COMMENT
240 to 360 (≈ 300) OUR ESTIMATE			
509 ± 170	HUNT 19	DPWA	Multichannel
300 ± 40	SOKHOYAN 15A	DPWA	Multichannel
400 ± 80	¹ SHRESTHA 12A	DPWA	Multichannel
300 ± 100	CUTKOSKY 80	IPWA	$\pi N \rightarrow \pi N$
220 ± 80	HOEHLER 79	IPWA	$\pi N \rightarrow \pi N$

See key on page 1127

Baryon Particle Listings
 $\Delta(1920)$

••• We do not use the following data for averages, fits, limits, etc. •••
 300 ± 40 GUTZ 14 DPWA Multichannel
 310 ± 60 ANISOVICH 12A DPWA Multichannel
 525 ± 32 PENNER 02C DPWA Multichannel
 123 ± 53 VRANA 00 DPWA Multichannel

¹ Statistical error only.

$\Delta(1920)$ DECAY MODES

The following branching fractions are our estimates, not fits or averages.

Mode	Fraction (Γ_i/Γ)
Γ_1 $N\pi$	5–20 %
Γ_2 ΣK	2–6 %
Γ_3 $N\pi\pi$	>46 %
Γ_4 $\Delta(1232)\pi$	>46 %
Γ_5 $\Delta(1232)\pi$, P -wave	2–28 %
Γ_6 $\Delta(1232)\pi$, F -wave	44–72 %
Γ_7 $N(1440)\pi$, P -wave	4–86 %
Γ_8 $N(1520)\pi$, S -wave	<5 %
Γ_9 $N(1535)\pi$	<2 %
Γ_{10} $N a_0(980)$	seen
Γ_{11} $\Delta(1232)\eta$	5–17 %
Γ_{12} $N\gamma$	0.01–0.84 %
Γ_{13} $N\gamma$, helicity=1/2	0.0–0.42 %
Γ_{14} $N\gamma$, helicity=3/2	0.01–0.42 %

$\Delta(1920)$ BRANCHING RATIOS

$\Gamma(N\pi)/\Gamma_{total}$	DOCUMENT ID	TECN	COMMENT	Γ_1/Γ
5–20 % OUR ESTIMATE				
10.5 ± 3.0	¹ HUNT	19	DPWA Multichannel	
8 ± 4	SOKHOYAN	15A	DPWA Multichannel	
20 ± 5	CUTKOSKY	80	IPWA $\pi N \rightarrow \pi N$	
14 ± 4	HOEHLER	79	IPWA $\pi N \rightarrow \pi N$	
••• We do not use the following data for averages, fits, limits, etc. •••				
8 ± 4	GUTZ	14	DPWA Multichannel	
8 ± 4	ANISOVICH	12A	DPWA Multichannel	
16 ± 4	¹ SHRESTHA	12A	DPWA Multichannel	
15 ± 1	PENNER	02C	DPWA Multichannel	
5 ± 4	VRANA	00	DPWA Multichannel	

¹ Statistical error only.

$\Gamma(\Sigma K)/\Gamma_{total}$	DOCUMENT ID	TECN	COMMENT	Γ_2/Γ
2–6 % OUR ESTIMATE				
4 ± 2	ANISOVICH	12A	DPWA Multichannel	
••• We do not use the following data for averages, fits, limits, etc. •••				
2.1 ± 0.3	PENNER	02C	DPWA Multichannel	

$\Gamma(\Delta(1232)\pi, P\text{-wave})/\Gamma_{total}$	DOCUMENT ID	TECN	COMMENT	Γ_5/Γ
2–28 % OUR ESTIMATE				
< 1.6	¹ HUNT	19	DPWA Multichannel	
18 ± 10	SOKHOYAN	15A	DPWA Multichannel	
••• We do not use the following data for averages, fits, limits, etc. •••				
22 ± 12	ANISOVICH	12A	DPWA Multichannel	
7 ± 5	¹ SHRESTHA	12A	DPWA Multichannel	
41 ± 3	VRANA	00	DPWA Multichannel	

¹ Statistical error only.

$\Gamma(\Delta(1232)\pi, F\text{-wave})/\Gamma_{total}$	DOCUMENT ID	TECN	COMMENT	Γ_6/Γ
44–72 % OUR ESTIMATE				
58 ± 14	SOKHOYAN	15A	DPWA Multichannel	
••• We do not use the following data for averages, fits, limits, etc. •••				
45 ± 20	ANISOVICH	12A	DPWA Multichannel	

$\Gamma(N(1440)\pi, P\text{-wave})/\Gamma_{total}$	DOCUMENT ID	TECN	COMMENT	Γ_7/Γ
4–86 % OUR ESTIMATE				
77 ± 9	¹ HUNT	19	DPWA Multichannel	
< 4	SOKHOYAN	15A	DPWA Multichannel	
••• We do not use the following data for averages, fits, limits, etc. •••				
< 20	¹ SHRESTHA	12A	DPWA Multichannel	
53 ± 8	VRANA	00	DPWA Multichannel	

¹ Statistical error only.

$\Gamma(N(1520)\pi, S\text{-wave})/\Gamma_{total}$	DOCUMENT ID	TECN	COMMENT	Γ_8/Γ
< 5 % OUR ESTIMATE				
< 5	SOKHOYAN	15A	DPWA Multichannel	

$\Gamma(N(1535)\pi)/\Gamma_{total}$	DOCUMENT ID	TECN	COMMENT	Γ_9/Γ
< 2 % OUR ESTIMATE				
< 2	GUTZ	14	DPWA Multichannel	

$\Gamma(N a_0(980))/\Gamma_{total}$	DOCUMENT ID	TECN	COMMENT	Γ_{10}/Γ
seen OUR ESTIMATE				
••• We do not use the following data for averages, fits, limits, etc. •••				
4 ± 2	HORN	08A	DPWA Multichannel	

$\Gamma(\Delta(1232)\eta)/\Gamma_{total}$	DOCUMENT ID	TECN	COMMENT	Γ_{11}/Γ
5–17 % OUR ESTIMATE				
11 ± 6	GUTZ	14	DPWA Multichannel	
••• We do not use the following data for averages, fits, limits, etc. •••				
15 ± 8	ANISOVICH	12A	DPWA Multichannel	

$\Delta(1920)$ PHOTON DECAY AMPLITUDES AT THE POLE

$\Delta(1920) \rightarrow N\gamma$, helicity-1/2 amplitude $A_{1/2}$	MODULUS ($\text{GeV}^{-1/2}$)	PHASE ($^\circ$)	DOCUMENT ID	TECN	COMMENT
	0.110 ± 0.030	–50 ± 20	SOKHOYAN	15A	DPWA Multichannel
	0.190 ± 0.050	–160 ± 24	ROENCHEN	14	DPWA
	–0.022	–11			
••• We do not use the following data for averages, fits, limits, etc. •••					
	–0.192	46	ROENCHEN	15A	DPWA Multichannel

$\Delta(1920) \rightarrow N\gamma$, helicity-3/2 amplitude $A_{3/2}$	MODULUS ($\text{GeV}^{-1/2}$)	PHASE ($^\circ$)	DOCUMENT ID	TECN	COMMENT
	–0.100 ± 0.040	0 ± 20	SOKHOYAN	15A	DPWA Multichannel
	–0.398 ± 0.070	–110 ± 4	ROENCHEN	14	DPWA
	–0.067	–5			
••• We do not use the following data for averages, fits, limits, etc. •••					
	0.522	67	ROENCHEN	15A	DPWA Multichannel

$\Delta(1920)$ BREIT-WIGNER PHOTON DECAY AMPLITUDES

$\Delta(1920) \rightarrow N\gamma$, helicity-1/2 amplitude $A_{1/2}$	VALUE ($\text{GeV}^{-1/2}$)	DOCUMENT ID	TECN	COMMENT
	–0.028 ± 0.010	¹ HUNT	19	DPWA Multichannel
	0.110 ± 0.030	SOKHOYAN	15A	DPWA Multichannel
••• We do not use the following data for averages, fits, limits, etc. •••				
	0.110 ± 0.030	GUTZ	14	DPWA Multichannel
	0.130 ± 0.030	ANISOVICH	12A	DPWA Multichannel
	–0.060			
	0.051 ± 0.010	¹ SHRESTHA	12A	DPWA Multichannel
	–0.007	PENNER	02D	DPWA Multichannel

¹ Statistical error only.

$\Delta(1920) \rightarrow N\gamma$, helicity-3/2 amplitude $A_{3/2}$	VALUE ($\text{GeV}^{-1/2}$)	DOCUMENT ID	TECN	COMMENT
	–0.043 ± 0.014	¹ HUNT	19	DPWA Multichannel
	–0.105 ± 0.035	SOKHOYAN	15A	DPWA Multichannel
••• We do not use the following data for averages, fits, limits, etc. •••				
	–0.105 ± 0.035	GUTZ	14	DPWA Multichannel
	–0.115 ± 0.025	ANISOVICH	12A	DPWA Multichannel
	–0.050			
	0.017 ± 0.015	¹ SHRESTHA	12A	DPWA Multichannel
	–0.001	PENNER	02D	DPWA Multichannel

¹ Statistical error only.

$\Delta(1920)$ REFERENCES

For early references, see Physics Letters **111B** 1 (1982).

HUNT	19	PR C99 055205	B.C. Hunt, D.M. Manley
ROENCHEN	15A	EPJ A51 70	D. Roenchen <i>et al.</i>
SOKHOYAN	15A	EPJ A51 95	V. Sokhoyan <i>et al.</i>
GUTZ	14	EPJ A50 74	E. Gutz <i>et al.</i>
PDG	14	CP C38 070001	K. Olive <i>et al.</i>
ROENCHEN	14	EPJ A50 101	D. Roenchen <i>et al.</i>
		Also EPJ A51 63 (errat.)	D. Roenchen <i>et al.</i>
SVARC	14	PR C89 045205	A. Svarc <i>et al.</i>
ANISOVICH	12A	EPJ A48 15	A.V. Anisovich <i>et al.</i>
SHRESTHA	12A	PR C86 055203	M. Shrestha, D.M. Manley
HORN	08A	EPJ A38 173	I. Horn <i>et al.</i>
		Also PRL 101 202002	I. Horn <i>et al.</i>
PENNER	02C	PR C66 055211	G. Penner, U. Mosel
PENNER	02D	PR C66 055212	G. Penner, U. Mosel
VRANA	00	PRPL 328 181	T.P. Vrana, S.A. Dytman, T.-S.H. Lee
HOEHLER	79	πN Newsletter 9 1	G. Hoehler
CUTKOSKY	80	Toronto Conf. 19	R.E. Cutkosky <i>et al.</i>
		Also PR D20 2839	R.E. Cutkosky <i>et al.</i>
HOEHLER	79	PDAT 12-1	G. Hoehler <i>et al.</i>
		Also Toronto Conf. 3	R. Koch
			(CBELSA/TAPS Collab.)
			(CBELSA/TAPS Collab.)
			(PDG Collab.)
			(RBI Zagreb, UNI Tuzla)
			(BONN, PNPI)
			(KSU)
			(CB-ELSA Collab.)
			(CB-ELSA Collab.)
			(GIES)
			(GIES)
			(PITT, ANL)
			(KARL)
			(CMU, LBL) IJP
			(CMU, LBL) IJP
			(KARL) IJP
			(KARL) IJP

Baryon Particle Listings

 $\Delta(1930)$ $\Delta(1930) 5/2^-$

$$I(J^P) = \frac{3}{2}(\frac{5}{2}^-) \text{ Status: } ***$$

Older and obsolete values are listed and referenced in the 2014 edition, Chinese Physics C38 070001 (2014).

 $\Delta(1930)$ POLE POSITION

REAL PART

VALUE (MeV)	DOCUMENT ID	TECN	COMMENT
1840 to 1920 (≈ 1880) OUR ESTIMATE			
$1848 \pm 9 \pm 19$	¹ SVARC 14	L+P	$\pi N \rightarrow \pi N$
1890 ± 50	CUTKOSKY 80	IPWA	$\pi N \rightarrow \pi N$
••• We do not use the following data for averages, fits, limits, etc. •••			
1863	HUNT 19	DPWA	Multichannel
1836	ROENCHEN 15A	DPWA	Multichannel
2001	ARNDT 06	DPWA	$\pi N \rightarrow \pi N, \eta N$
1883	VRANA 00	DPWA	Multichannel
1850	HOEHLER 93	SPED	$\pi N \rightarrow \pi N$

¹ Fit to the amplitudes of HOEHLER 79.

-2xIMAGINARY PART

VALUE (MeV)	DOCUMENT ID	TECN	COMMENT
230 to 330 (≈ 280) OUR ESTIMATE			
$321 \pm 17 \pm 7$	¹ SVARC 14	L+P	$\pi N \rightarrow \pi N$
260 ± 60	CUTKOSKY 80	IPWA	$\pi N \rightarrow \pi N$
••• We do not use the following data for averages, fits, limits, etc. •••			
260	HUNT 19	DPWA	Multichannel
724	ROENCHEN 15A	DPWA	Multichannel
387	ARNDT 06	DPWA	$\pi N \rightarrow \pi N, \eta N$
250	VRANA 00	DPWA	Multichannel
180	HOEHLER 93	SPED	$\pi N \rightarrow \pi N$

¹ Fit to the amplitudes of HOEHLER 79.

 $\Delta(1930)$ ELASTIC POLE RESIDUEMODULUS $|r|$

VALUE (MeV)	DOCUMENT ID	TECN	COMMENT
8 to 20 (≈ 14) OUR ESTIMATE			
$9 \pm 1 \pm 1$	¹ SVARC 14	L+P	$\pi N \rightarrow \pi N$
18 ± 6	CUTKOSKY 80	IPWA	$\pi N \rightarrow \pi N$
••• We do not use the following data for averages, fits, limits, etc. •••			
34	ROENCHEN 15A	DPWA	Multichannel
7	ARNDT 06	DPWA	$\pi N \rightarrow \pi N, \eta N$
20	HOEHLER 93	SPED	$\pi N \rightarrow \pi N$

¹ Fit to the amplitudes of HOEHLER 79.

PHASE θ

VALUE ($^\circ$)	DOCUMENT ID	TECN	COMMENT
-40 to -10 (≈ -30) OUR ESTIMATE			
$-37 \pm 3 \pm 7$	¹ SVARC 14	L+P	$\pi N \rightarrow \pi N$
-20 ± 40	CUTKOSKY 80	IPWA	$\pi N \rightarrow \pi N$
••• We do not use the following data for averages, fits, limits, etc. •••			
-155	ROENCHEN 15A	DPWA	Multichannel
-12	ARNDT 06	DPWA	$\pi N \rightarrow \pi N, \eta N$

¹ Fit to the amplitudes of HOEHLER 79.

 $\Delta(1930)$ INELASTIC POLE RESIDUE

The "normalized residue" is the residue divided by $\Gamma_{pole}/2$.

Normalized residue in $N\pi \rightarrow \Delta(1930) \rightarrow \Sigma K$

MODULUS	PHASE ($^\circ$)	DOCUMENT ID	TECN	COMMENT
••• We do not use the following data for averages, fits, limits, etc. •••				
0.043	-0.5	ROENCHEN 15A	DPWA	Multichannel

Normalized residue in $N\pi \rightarrow \Delta(1930) \rightarrow \Delta\pi, D\text{-wave}$

MODULUS	PHASE ($^\circ$)	DOCUMENT ID	TECN	COMMENT
••• We do not use the following data for averages, fits, limits, etc. •••				
0.15	30	ROENCHEN 15A	DPWA	Multichannel

Normalized residue in $N\pi \rightarrow \Delta(1930) \rightarrow \Delta\pi, G\text{-wave}$

MODULUS	PHASE ($^\circ$)	DOCUMENT ID	TECN	COMMENT
••• We do not use the following data for averages, fits, limits, etc. •••				
0.009	121	ROENCHEN 15A	DPWA	Multichannel

 $\Delta(1930)$ BREIT-WIGNER MASS

VALUE (MeV)	DOCUMENT ID	TECN	COMMENT
1900 to 2000 (≈ 1950) OUR ESTIMATE			
1988 ± 32	¹ HUNT 19	DPWA	Multichannel
2233 ± 53	¹ ARNDT 06	DPWA	$\pi N \rightarrow \pi N, \eta N$
1940 ± 30	CUTKOSKY 80	IPWA	$\pi N \rightarrow \pi N$
1901 ± 15	HOEHLER 79	IPWA	$\pi N \rightarrow \pi N$
••• We do not use the following data for averages, fits, limits, etc. •••			
1930 ± 12	¹ SHRESTHA 12A	DPWA	Multichannel
1932 ± 100	VRANA 00	DPWA	Multichannel

¹ Statistical error only.

 $\Delta(1930)$ BREIT-WIGNER WIDTH

VALUE (MeV)	DOCUMENT ID	TECN	COMMENT
200 to 400 (≈ 300) OUR ESTIMATE			
500 ± 160	¹ HUNT 19	DPWA	Multichannel
773 ± 187	ARNDT 06	DPWA	$\pi N \rightarrow \pi N, \eta N$
320 ± 60	CUTKOSKY 80	IPWA	$\pi N \rightarrow \pi N$
195 ± 60	HOEHLER 79	IPWA	$\pi N \rightarrow \pi N$
••• We do not use the following data for averages, fits, limits, etc. •••			
235 ± 39	¹ SHRESTHA 12A	DPWA	Multichannel
316 ± 237	VRANA 00	DPWA	Multichannel

¹ Statistical error only.

 $\Delta(1930)$ DECAY MODES

The following branching fractions are our estimates, not fits or averages.

Mode	Fraction (Γ_i/Γ)
$\Gamma_1 N\pi$	5-15 %
$\Gamma_2 N\gamma$	0.0-0.01 %
$\Gamma_3 N\gamma, \text{ helicity}=1/2$	0.0-0.005 %
$\Gamma_4 N\gamma, \text{ helicity}=3/2$	0.0-0.004 %

 $\Delta(1930)$ BRANCHING RATIOS

$\Gamma(N\pi)/\Gamma_{total}$	DOCUMENT ID	TECN	COMMENT	Γ/Γ
5 to 15 (≈ 10) OUR ESTIMATE				
9.5 ± 0.1	¹ HUNT 19	DPWA	Multichannel	
8.1 ± 1.2	¹ ARNDT 06	DPWA	$\pi N \rightarrow \pi N, \eta N$	
14 ± 4	CUTKOSKY 80	IPWA	$\pi N \rightarrow \pi N$	
4 ± 3	HOEHLER 79	IPWA	$\pi N \rightarrow \pi N$	
••• We do not use the following data for averages, fits, limits, etc. •••				
7.9 ± 0.4	¹ SHRESTHA 12A	DPWA	Multichannel	
9 ± 8	VRANA 00	DPWA	Multichannel	

¹ Statistical error only.

 $\Delta(1930)$ PHOTON DECAY AMPLITUDES AT THE POLE $\Delta(1930) \rightarrow N\gamma, \text{ helicity}=1/2$ amplitude $A_{1/2}$

MODULUS ($\text{GeV}^{-1/2}$)	PHASE ($^\circ$)	DOCUMENT ID	TECN	COMMENT
$0.130^{+0.073}_{-0.096}$	-50^{+77}_{-26}	ROENCHEN 14	DPWA	
••• We do not use the following data for averages, fits, limits, etc. •••				
-0.270	33	ROENCHEN 15A	DPWA	Multichannel

 $\Delta(1930) \rightarrow N\gamma, \text{ helicity}=3/2$ amplitude $A_{3/2}$

MODULUS ($\text{GeV}^{-1/2}$)	PHASE ($^\circ$)	DOCUMENT ID	TECN	COMMENT
$-0.056^{+0.003}_{-0.151}$	168^{+72}_{-76}	ROENCHEN 14	DPWA	
••• We do not use the following data for averages, fits, limits, etc. •••				
0.153	81	ROENCHEN 15A	DPWA	Multichannel

 $\Delta(1930)$ BREIT-WIGNER PHOTON DECAY AMPLITUDES $\Delta(1930) \rightarrow N\gamma, \text{ helicity}=1/2$ amplitude $A_{1/2}$

VALUE ($\text{GeV}^{-1/2}$)	DOCUMENT ID	TECN	COMMENT
-0.043 ± 0.008	¹ HUNT 19	DPWA	Multichannel
-0.007 ± 0.010	¹ ARNDT 96	IPWA	$\gamma N \rightarrow \pi N$
••• We do not use the following data for averages, fits, limits, etc. •••			
0.011 ± 0.003	¹ SHRESTHA 12A	DPWA	Multichannel

¹ Statistical error only.

 $\Delta(1930) \rightarrow N\gamma, \text{ helicity}=3/2$ amplitude $A_{3/2}$

VALUE ($\text{GeV}^{-1/2}$)	DOCUMENT ID	TECN	COMMENT
-0.020 ± 0.017	¹ HUNT 19	DPWA	Multichannel
0.005 ± 0.010	¹ ARNDT 96	IPWA	$\gamma N \rightarrow \pi N$
••• We do not use the following data for averages, fits, limits, etc. •••			
0.002 ± 0.002	¹ SHRESTHA 12A	DPWA	Multichannel

¹ Statistical error only.

 $\Delta(1930)$ REFERENCES

For early references, see Physics Letters **111B** 1 (1982).

HUNT 19	PR C99 055205	B.C. Hunt, D.M. Manley
ROENCHEN 15A	EPJ A51 70	D. Roenchen et al.
PDG 14	CP C38 070001	K. Olive et al.
ROENCHEN 14	EPJ A50 101	D. Roenchen et al.
Also	EPJ A51 63 (errata.)	D. Roenchen et al.
SVARC 14	PR C89 045205	A. Svarc et al.
SHRESTHA 12A	PR C86 055203	M. Shrestha, D.M. Manley
		(PDG Collab.)
		(RBI Zagreb, UNI Tuzla)
		(KSU)

See key on page 1127

Baryon Particle Listings
 $\Delta(1930)$, $\Delta(1940)$

ARNDT	06	PR C74 045205	R.A. Arndt et al.	(GWU)
VRANA	00	PRPL 328 181	T.P. Vrana, S.A. Dytman, T.-S.H. Lee	(PITT, ANL)
ARNDT	96	PR C53 430	R.A. Arndt, I.I. Strakovsky, R.L. Workman	(VPI)
HOEHLER	93	πN Newsletter 9 1	G. Höhler	(KARL)
CUTKOSKY	80	Toronto Conf. 19	R.E. Cutkosky et al.	(CMU, LBL) IJP
Also		PR D20 2839	R.E. Cutkosky et al.	(CMU, LBL) IJP
HOEHLER	79	PDAT 12-1	G. Höhler et al.	(KARL) IJP
Also		Toronto Conf. 3	R. Koch	(KARL) IJP

$\Delta(1940) 3/2^-$ $I(J^P) = \frac{3}{2}(\frac{3}{2}^-)$ Status: **

OMITTED FROM SUMMARY TABLE

$\Delta(1940)$ POLE POSITION

REAL PART

VALUE (MeV)	DOCUMENT ID	TECN	COMMENT
1850 to 2050 (\approx 1950) OUR ESTIMATE			
2040 \pm 50	SOKHOYAN 15A	DPWA	Multichannel
1878 \pm 11 \pm 5.5	¹ SVARC 14	L+P	$\pi N \rightarrow \pi N$
1900 \pm 100	CUTKOSKY 80	IPWA	$\pi N \rightarrow \pi N$
• • • We do not use the following data for averages, fits, limits, etc. • • •			
2139	HUNT 19	DPWA	Multichannel
2040 \pm 50	GUTZ 14	DPWA	Multichannel
1990 \pm 100	ANISOVICH 12A	DPWA	Multichannel

¹ Fit to the amplitudes of HOEHLER 79.

-2xIMAGINARY PART

VALUE (MeV)	DOCUMENT ID	TECN	COMMENT
200 to 500 (\approx 350) OUR ESTIMATE			
450 \pm 90	SOKHOYAN 15A	DPWA	Multichannel
212 \pm 21 \pm 6	¹ SVARC 14	L+P	$\pi N \rightarrow \pi N$
200 \pm 60	CUTKOSKY 80	IPWA	$\pi N \rightarrow \pi N$
• • • We do not use the following data for averages, fits, limits, etc. • • •			
400	HUNT 19	DPWA	Multichannel
450 \pm 90	GUTZ 14	DPWA	Multichannel
450 \pm 90	ANISOVICH 12A	DPWA	Multichannel

¹ Fit to the amplitudes of HOEHLER 79.

$\Delta(1940)$ ELASTIC POLE RESIDUE

MODULUS $|r|$

VALUE (MeV)	DOCUMENT ID	TECN	COMMENT
4 to 10 (\approx 7) OUR ESTIMATE			
6 \pm 3	SOKHOYAN 15A	DPWA	Multichannel
9 \pm 1 \pm 1	¹ SVARC 14	L+P	$\pi N \rightarrow \pi N$
8 \pm 3	CUTKOSKY 80	IPWA	$\pi N \rightarrow \pi N$
• • • We do not use the following data for averages, fits, limits, etc. • • •			
4 \pm 3	GUTZ 14	DPWA	Multichannel
4 \pm 4	ANISOVICH 12A	DPWA	Multichannel

¹ Fit to the amplitudes of HOEHLER 79.

PHASE θ

VALUE ($^\circ$)	DOCUMENT ID	TECN	COMMENT
150 to 250 (\approx 200) OUR ESTIMATE			
- 90 \pm 35	SOKHOYAN 15A	DPWA	Multichannel
140 \pm 7 \pm 7	¹ SVARC 14	L+P	$\pi N \rightarrow \pi N$
135 \pm 45	CUTKOSKY 80	IPWA	$\pi N \rightarrow \pi N$
• • • We do not use the following data for averages, fits, limits, etc. • • •			
- 50 \pm 35	GUTZ 14	DPWA	Multichannel

¹ Fit to the amplitudes of HOEHLER 79.

$\Delta(1940)$ INELASTIC POLE RESIDUE

The "normalized residue" is the residue divided by $\Gamma_{pole}/2$.

Normalized residue in $N\pi \rightarrow \Delta(1940) \rightarrow \Delta(1232)\pi$

MODULUS	PHASE ($^\circ$)	DOCUMENT ID	TECN	COMMENT
< 0.01	undefined	GUTZ 14	DPWA	Multichannel

Normalized residue in $N\pi \rightarrow \Delta(1940) \rightarrow N(1535)\pi$

MODULUS	PHASE ($^\circ$)	DOCUMENT ID	TECN	COMMENT
< 0.03	undefined	GUTZ 14	DPWA	Multichannel

Normalized residue in $N\pi \rightarrow \Delta(1940) \rightarrow \Delta(1232)\pi, S\text{-wave}$

MODULUS	PHASE ($^\circ$)	DOCUMENT ID	TECN	COMMENT
0.12 \pm 0.06	120 \pm 45	SOKHOYAN 15A	DPWA	Multichannel

Normalized residue in $N\pi \rightarrow \Delta(1940) \rightarrow \Delta(1232)\pi, D\text{-wave}$

MODULUS	PHASE ($^\circ$)	DOCUMENT ID	TECN	COMMENT
0.06 \pm 0.04	- 80 \pm 35	SOKHOYAN 15A	DPWA	Multichannel

$\Delta(1940)$ BREIT-WIGNER MASS

VALUE (MeV)	DOCUMENT ID	TECN	COMMENT
1940 to 2060 (\approx 2000) OUR ESTIMATE			
2137 \pm 13	¹ HUNT 19	DPWA	Multichannel
2050 \pm 40	SOKHOYAN 15A	DPWA	Multichannel
1940 \pm 100	CUTKOSKY 80	IPWA	$\pi N \rightarrow \pi N$
• • • We do not use the following data for averages, fits, limits, etc. • • •			
2050 \pm 40	GUTZ 14	DPWA	Multichannel
1995 \pm 105	ANISOVICH 12A	DPWA	Multichannel

¹ Statistical error only.

$\Delta(1940)$ BREIT-WIGNER WIDTH

VALUE (MeV)	DOCUMENT ID	TECN	COMMENT
300 to 500 (\approx 400) OUR ESTIMATE			
400 \pm 43	¹ HUNT 19	DPWA	Multichannel
450 \pm 70	SOKHOYAN 15A	DPWA	Multichannel
200 \pm 100	CUTKOSKY 80	IPWA	$\pi N \rightarrow \pi N$
• • • We do not use the following data for averages, fits, limits, etc. • • •			
450 \pm 70	GUTZ 14	DPWA	Multichannel
450 \pm 100	ANISOVICH 12A	DPWA	Multichannel

¹ Statistical error only.

$\Delta(1940)$ DECAY MODES

Mode	Fraction (Γ_i/Γ)
$\Gamma_1 N\pi$	1-20 %
$\Gamma_2 N\pi\pi$	>81 %
$\Gamma_3 \Delta(1232)\pi$	6-85 %
$\Gamma_4 \Delta(1232)\pi, S\text{-wave}$	1-65 %
$\Gamma_5 \Delta(1232)\pi, D\text{-wave}$	5-20 %
$\Gamma_6 N\rho, S=3/2, S\text{-wave}$	75-85 %
$\Gamma_7 N(1535)\pi$	2-14 %
$\Gamma_8 N a_0(980)$	seen
$\Gamma_9 \Delta(1232)\eta$	4-16 %
$\Gamma_{10} N\gamma$	0.06-2.53 %
$\Gamma_{11} N\gamma, \text{helicity}=1/2$	0.06-1.51 %
$\Gamma_{12} N\gamma, \text{helicity}=3/2$	0-1.02 %

$\Delta(1940)$ BRANCHING RATIOS

$\Gamma(N\pi)/\Gamma_{total}$	VALUE (%)	DOCUMENT ID	TECN	COMMENT	Γ_1/Γ
1-20 % OUR ESTIMATE					
16 \pm 4	¹ HUNT 19	DPWA	Multichannel		
2 \pm 1	SOKHOYAN 15A	DPWA	Multichannel		
5 \pm 2	CUTKOSKY 80	IPWA	$\pi N \rightarrow \pi N$		
• • • We do not use the following data for averages, fits, limits, etc. • • •					
2 \pm 1	GUTZ 14	DPWA	Multichannel		

¹ Statistical error only.

$\Gamma(\Delta(1232)\pi, S\text{-wave})/\Gamma_{total}$	VALUE (%)	DOCUMENT ID	TECN	COMMENT	Γ_4/Γ
1-65 % OUR ESTIMATE					
< 0.9	¹ HUNT 19	DPWA	Multichannel		
46 \pm 20	SOKHOYAN 15A	DPWA	Multichannel		
• • • We do not use the following data for averages, fits, limits, etc. • • •					
2 \pm 1	GUTZ 14	DPWA	Multichannel		

¹ Statistical error only.

$\Gamma(\Delta(1232)\pi, D\text{-wave})/\Gamma_{total}$	VALUE (%)	DOCUMENT ID	TECN	COMMENT	Γ_5/Γ
5-20 % OUR ESTIMATE					
< 6.3	¹ HUNT 19	DPWA	Multichannel		
12 \pm 7	SOKHOYAN 15A	DPWA	Multichannel		
• • • We do not use the following data for averages, fits, limits, etc. • • •					
1	GUTZ 14	DPWA	Multichannel		

¹ Statistical error only.

$\Gamma(N\rho, S=3/2, S\text{-wave})/\Gamma_{total}$	VALUE (%)	DOCUMENT ID	TECN	COMMENT	Γ_6/Γ
75-85 % OUR ESTIMATE					
80 \pm 5	¹ HUNT 19	DPWA	Multichannel		
• • • We do not use the following data for averages, fits, limits, etc. • • •					
1	GUTZ 14	DPWA	Multichannel		

¹ Statistical error only.

$\Gamma(N(1535)\pi)/\Gamma_{total}$	VALUE (%)	DOCUMENT ID	TECN	COMMENT	Γ_7/Γ
2-14 % OUR ESTIMATE					
8 \pm 6	GUTZ 14	DPWA	Multichannel		
• • • We do not use the following data for averages, fits, limits, etc. • • •					
2 \pm 1	HORN 08A	DPWA	Multichannel		

Baryon Particle Listings

$\Delta(1940), \Delta(1950)$

$\Gamma(N_{90}(980))/\Gamma_{total}$ Γ_8/Γ

VALUE (%)	DOCUMENT ID	TECN	COMMENT
seen OUR ESTIMATE			
••• We do not use the following data for averages, fits, limits, etc. •••			
2±1	HORN	08A	DPWA Multichannel

$\Gamma(\Delta(1232)\eta)/\Gamma_{total}$ Γ_9/Γ

VALUE (%)	DOCUMENT ID	TECN	COMMENT
4-16 % OUR ESTIMATE			
10±6	GUTZ	14	DPWA Multichannel
••• We do not use the following data for averages, fits, limits, etc. •••			
4±2	HORN	08A	DPWA Multichannel

$\Delta(1940)$ PHOTON DECAY AMPLITUDES AT THE POLE

$\Delta(1940) \rightarrow N\gamma$, helicity-1/2 amplitude $A_{1/2}$

MODULUS ($\text{GeV}^{-1/2}$)	PHASE ($^\circ$)	DOCUMENT ID	TECN	COMMENT
$0.170^{+0.120}_{-0.100}$	-10 ± 30	SOKHOYAN	15A	DPWA Multichannel

$\Delta(1940) \rightarrow N\gamma$, helicity-3/2 amplitude $A_{3/2}$

MODULUS ($\text{GeV}^{-1/2}$)	PHASE ($^\circ$)	DOCUMENT ID	TECN	COMMENT
0.150 ± 0.080	-10 ± 30	SOKHOYAN	15A	DPWA Multichannel

$\Delta(1940)$ BREIT-WIGNER PHOTON DECAY AMPLITUDES

$\Delta(1940) \rightarrow N\gamma$, helicity-1/2 amplitude $A_{1/2}$

VALUE ($\text{GeV}^{-1/2}$)	DOCUMENT ID	TECN	COMMENT
0.1614 ± 0.0031	¹ HUNT	19	DPWA Multichannel
$0.170^{+0.110}_{-0.080}$	SOKHOYAN	15A	DPWA Multichannel
••• We do not use the following data for averages, fits, limits, etc. •••			
$0.170^{+0.110}_{-0.080}$	GUTZ	14	DPWA Multichannel

¹ Statistical error only.

$\Delta(1940) \rightarrow N\gamma$, helicity-3/2 amplitude $A_{3/2}$

VALUE ($\text{GeV}^{-1/2}$)	DOCUMENT ID	TECN	COMMENT
-0.209 ± 0.023	¹ HUNT	19	DPWA Multichannel
0.150 ± 0.080	SOKHOYAN	15A	DPWA Multichannel
••• We do not use the following data for averages, fits, limits, etc. •••			
0.150 ± 0.080	GUTZ	14	DPWA Multichannel

¹ Statistical error only.

$\Delta(1940)$ REFERENCES

HUNT	19	PR C99 05205	B. C. Hunt, D.M. Manley
SOKHOYAN	15A	EPJ A51 95	V. Sokhoyan et al. (CBELSA/TAPS Collab.)
GUTZ	14	EPJ A50 74	E. Gutz et al. (CBELSA/TAPS Collab.)
SVARC	14	PR C09 045205	A. Svarc et al. (RBI Zagreb, UNI Tuzla)
ANISOVICH	12A	EPJ A48 15	A.V. Anisovich et al. (BONN, PNPI)
HORN	08A	EPJ A38 173	I. Horn et al. (CB-ELSA Collab.)
Also		PRL 101 202002	I. Horn et al. (CB-ELSA Collab.)
CUTKOSKY	80	Toronto Conf. 19	R.E. Cutkosky et al. (CMU, LBL) IJP
Also		PR D20 2839	R.E. Cutkosky et al. (CMU, LBL)
HOEHLER	79	PDAT 12-1	G. Hoehler et al. (KARLT)

$\Delta(1950) 7/2^+$

 $I(J^P) = \frac{3}{2}(\frac{7}{2}^+)$ Status: * * * *

Older and obsolete values are listed and referenced in the 2014 edition, Chinese Physics C38 070001 (2014).

$\Delta(1950)$ POLE POSITION

REAL PART

VALUE (MeV)	DOCUMENT ID	TECN	COMMENT
1870 to 1890 (≈ 1880) OUR ESTIMATE			
1888 ± 4	SOKHOYAN	15A	DPWA Multichannel
1877 ± 2±1	¹ SVARC	14	L+P $\pi N \rightarrow \pi N$
1890±15	CUTKOSKY	80	IPWA $\pi N \rightarrow \pi N$
••• We do not use the following data for averages, fits, limits, etc. •••			
1871	HUNT	19	DPWA Multichannel
1874	ROENCHEN	15A	DPWA Multichannel
1888 ± 4	GUTZ	14	DPWA Multichannel
1890 ± 4	ANISOVICH	12A	DPWA Multichannel
1876	ARNDT	06	DPWA $\pi N \rightarrow \pi N, \eta N$
1910	VRANA	00	DPWA Multichannel
1878	HOEHLER	93	ARGD $\pi N \rightarrow \pi N$
¹ Fit to the amplitudes of HOEHLER 79.			
-2xIMAGINARY PART			
VALUE (MeV)	DOCUMENT ID	TECN	COMMENT
220 to 260 (≈ 240) OUR ESTIMATE			
245 ± 8	SOKHOYAN	15A	DPWA Multichannel
223 ± 4±1	¹ SVARC	14	L+P $\pi N \rightarrow \pi N$
260±40	CUTKOSKY	80	IPWA $\pi N \rightarrow \pi N$

••• We do not use the following data for averages, fits, limits, etc. •••			
206	HUNT	19	DPWA Multichannel
239	ROENCHEN	15A	DPWA Multichannel
245 ± 8	GUTZ	14	DPWA Multichannel
243 ± 8	ANISOVICH	12A	DPWA Multichannel
227	ARNDT	06	DPWA $\pi N \rightarrow \pi N, \eta N$
230	VRANA	00	DPWA Multichannel
230	HOEHLER	93	ARGD $\pi N \rightarrow \pi N$

¹ Fit to the amplitudes of HOEHLER 79.

$\Delta(1950)$ ELASTIC POLE RESIDUE

MODULUS $|r|$

VALUE (MeV)	DOCUMENT ID	TECN	COMMENT
44 to 60 (≈ 52) OUR ESTIMATE			
58 ± 2	SOKHOYAN	15A	DPWA Multichannel
44 ± 1	¹ SVARC	14	L+P $\pi N \rightarrow \pi N$
50 ± 7	CUTKOSKY	80	IPWA $\pi N \rightarrow \pi N$
••• We do not use the following data for averages, fits, limits, etc. •••			
56	ROENCHEN	15A	DPWA Multichannel
58 ± 2	GUTZ	14	DPWA Multichannel
58 ± 2	ANISOVICH	12A	DPWA Multichannel
53	ARNDT	06	DPWA $\pi N \rightarrow \pi N, \eta N$
47	HOEHLER	93	ARGD $\pi N \rightarrow \pi N$

¹ Fit to the amplitudes of HOEHLER 79.

PHASE θ

VALUE ($^\circ$)	DOCUMENT ID	TECN	COMMENT
-40 to -24 (≈ -32) OUR ESTIMATE			
-24 ± 3	SOKHOYAN	15A	DPWA Multichannel
-39 ± 1±1	¹ SVARC	14	L+P $\pi N \rightarrow \pi N$
-33 ± 8	CUTKOSKY	80	IPWA $\pi N \rightarrow \pi N$
••• We do not use the following data for averages, fits, limits, etc. •••			
-33	ROENCHEN	15A	DPWA Multichannel
-24 ± 3	GUTZ	14	DPWA Multichannel
-24 ± 3	ANISOVICH	12A	DPWA Multichannel
-31	ARNDT	06	DPWA $\pi N \rightarrow \pi N, \eta N$
-32	HOEHLER	93	ARGD $\pi N \rightarrow \pi N$

¹ Fit to the amplitudes of HOEHLER 79.

$\Delta(1950)$ INELASTIC POLE RESIDUE

The "normalized residue" is the residue divided by $\Gamma_{pole}/2$.

Normalized residue in $N\pi \rightarrow \Delta(1950) \rightarrow \Sigma K$

MODULUS	PHASE ($^\circ$)	DOCUMENT ID	TECN	COMMENT
0.05 ± 0.01	-65 ± 25	ANISOVICH	12A	DPWA Multichannel
••• We do not use the following data for averages, fits, limits, etc. •••				
0.031	-87	ROENCHEN	15A	DPWA Multichannel

Normalized residue in $N\pi \rightarrow \Delta(1950) \rightarrow \Delta\pi, F$ -wave

MODULUS	PHASE ($^\circ$)	DOCUMENT ID	TECN	COMMENT
0.12 ± 0.04	undefined	SOKHOYAN	15A	DPWA Multichannel
••• We do not use the following data for averages, fits, limits, etc. •••				
0.54	131	ROENCHEN	15A	DPWA Multichannel
0.12 ± 0.04	12 ± 10	ANISOVICH	12A	DPWA Multichannel

Normalized residue in $N\pi \rightarrow \Delta(1950) \rightarrow \Delta\pi, H$ -wave

MODULUS	PHASE ($^\circ$)	DOCUMENT ID	TECN	COMMENT
••• We do not use the following data for averages, fits, limits, etc. •••				
0.033	-97	ROENCHEN	15A	DPWA Multichannel

Normalized residue in $N\pi \rightarrow \Delta(1950) \rightarrow \Delta(1232)\eta$

MODULUS	PHASE ($^\circ$)	DOCUMENT ID	TECN	COMMENT
0.035 ± 0.005	90 ± 25	GUTZ	14	DPWA Multichannel

$\Delta(1950)$ BREIT-WIGNER MASS

VALUE (MeV)	DOCUMENT ID	TECN	COMMENT
1915 to 1950 (≈ 1930) OUR ESTIMATE			
1943 ± 18	GOLOVATCH	19	DPWA $\gamma p \rightarrow \pi^+ \pi^- p$
1913 ± 4	¹ HUNT	19	DPWA Multichannel
1917 ± 4	ANISOVICH	17	DPWA Multichannel
1921.3 ± 0.2	¹ ARNDT	06	DPWA $\pi N \rightarrow \pi N, \eta N$
1950 ± 15	CUTKOSKY	80	IPWA $\pi N \rightarrow \pi N$
1913 ± 8	HOEHLER	79	IPWA $\pi N \rightarrow \pi N$
••• We do not use the following data for averages, fits, limits, etc. •••			
1917 ± 4	SOKHOYAN	15A	DPWA Multichannel
1917 ± 4	GUTZ	14	DPWA Multichannel
1915 ± 6	ANISOVICH	12A	DPWA Multichannel
1918 ± 1	¹ SHRESTHA	12A	DPWA Multichannel
1936 ± 5	VRANA	00	DPWA Multichannel

¹ Statistical error only. $\Delta(1950)$ BREIT-WIGNER WIDTH

VALUE (MeV)	DOCUMENT ID	TECN	COMMENT
235 to 335 (≈ 285) OUR ESTIMATE			
230 ± 88	GOLOVATCH 19	DPWA	$\gamma p \rightarrow \pi^+ \pi^- p$
241 ± 10	¹ HUNT 19	DPWA	Multichannel
251 ± 8	ANISOVICH 17	DPWA	Multichannel
271.1 ± 1.1	¹ ARNDT 06	DPWA	$\pi N \rightarrow \pi N, \eta N$
340 ± 5.0	CUTKOSKY 80	IPWA	$\pi N \rightarrow \pi N$
224 ± 10	HOEHLER 79	IPWA	$\pi N \rightarrow \pi N$
• • • We do not use the following data for averages, fits, limits, etc. • • •			
251 ± 8	SOKHOYAN 15A	DPWA	Multichannel
251 ± 8	GUTZ 14	DPWA	Multichannel
246 ± 10	ANISOVICH 12A	DPWA	Multichannel
259 ± 4	¹ SHRESTHA 12A	DPWA	Multichannel
245 ± 12	VRANA 00	DPWA	Multichannel

¹ Statistical error only. $\Delta(1950)$ DECAY MODES

The following branching fractions are our estimates, not fits or averages.

Mode	Fraction (Γ_i/Γ)
Γ_1 $N\pi$	35–45 %
Γ_2 ΣK	0.3–0.5 %
Γ_3 $N\pi\pi$	37–77 %
Γ_4 $\Delta(1232)\pi, F\text{-wave}$	1–9 %
Γ_5 $N(1680)\pi, P\text{-wave}$	3–9 %
Γ_6 $\Delta(1232)\eta$	< 0.6 %
Γ_7 $N\gamma$	0.06–0.14 %
Γ_8 $N\gamma, \text{helicity}=1/2$	0.03–0.05 %
Γ_9 $N\gamma, \text{helicity}=3/2$	0.04–0.09 %

 $\Delta(1950)$ BRANCHING RATIOS

$\Gamma(N\pi)/\Gamma_{\text{total}}$	DOCUMENT ID	TECN	COMMENT	Γ_1/Γ
35–45 % OUR ESTIMATE				
38 ± 2	¹ HUNT 19	DPWA	Multichannel	
46 ± 2	ANISOVICH 17	DPWA	Multichannel	
47.1 ± 0.1	¹ ARNDT 06	DPWA	$\pi N \rightarrow \pi N, \eta N$	
39 ± 4	CUTKOSKY 80	IPWA	$\pi N \rightarrow \pi N$	
38 ± 2	HOEHLER 79	IPWA	$\pi N \rightarrow \pi N$	
• • • We do not use the following data for averages, fits, limits, etc. • • •				
0.046 ± 0.002	SOKHOYAN 15A	DPWA	Multichannel	
46 ± 2	GUTZ 14	DPWA	Multichannel	
45 ± 2	ANISOVICH 12A	DPWA	Multichannel	
45.6 ± 0.4	¹ SHRESTHA 12A	DPWA	Multichannel	
44 ± 1	VRANA 00	DPWA	Multichannel	

¹ Statistical error only.

$\Gamma(N\pi\pi)/\Gamma_{\text{total}}$	DOCUMENT ID	TECN	COMMENT	Γ_3/Γ
57 ± 20	GOLOVATCH 19	DPWA	$\gamma p \rightarrow \pi^+ \pi^- p$	

$\Gamma(\Sigma K)/\Gamma_{\text{total}}$	DOCUMENT ID	TECN	COMMENT	Γ_2/Γ
0.6 ± 0.2	ANISOVICH 17	DPWA	Multichannel	
• • • We do not use the following data for averages, fits, limits, etc. • • •				
0.4 ± 0.1	ANISOVICH 12A	DPWA	Multichannel	

$\Gamma(\Delta(1232)\pi, F\text{-wave})/\Gamma_{\text{total}}$	DOCUMENT ID	TECN	COMMENT	Γ_4/Γ
5 ± 3	ANISOVICH 17	DPWA	Multichannel	
8 ± 1	¹ SHRESTHA 12A	DPWA	Multichannel	
• • • We do not use the following data for averages, fits, limits, etc. • • •				
5 ± 4	SOKHOYAN 15A	DPWA	Multichannel	
2.8 ± 1.4	ANISOVICH 12A	DPWA	Multichannel	
36 ± 1	VRANA 00	DPWA	Multichannel	

¹ Statistical error only.

$\Gamma(N(1680)\pi, P\text{-wave})/\Gamma_{\text{total}}$	DOCUMENT ID	TECN	COMMENT	Γ_5/Γ
6 ± 3	SOKHOYAN 15A	DPWA	Multichannel	

$\Gamma(\Delta(1232)\eta)/\Gamma_{\text{total}}$	DOCUMENT ID	TECN	COMMENT	Γ_6/Γ
0.3 ± 0.3	ANISOVICH 17	DPWA	Multichannel	
• • • We do not use the following data for averages, fits, limits, etc. • • •				
<1	GUTZ 14	DPWA	Multichannel	

 $\Delta(1950)$ PHOTON DECAY AMPLITUDES AT THE POLE $\Delta(1950) \rightarrow N\gamma, \text{helicity-1/2 amplitude } A_{1/2}$

MODULUS ($\text{GeV}^{-1/2}$)	PHASE ($^\circ$)	DOCUMENT ID	TECN	COMMENT
-0.067 ± 0.004	-10 ± 5	SOKHOYAN 15A	DPWA	Multichannel
-0.071 ± 0.004	-14^{+2}_{-4}	ROENCHEN 14	DPWA	
• • • We do not use the following data for averages, fits, limits, etc. • • •				
-0.068	-19	ROENCHEN 15A	DPWA	Multichannel

 $\Delta(1950) \rightarrow N\gamma, \text{helicity-3/2 amplitude } A_{3/2}$

MODULUS ($\text{GeV}^{-1/2}$)	PHASE ($^\circ$)	DOCUMENT ID	TECN	COMMENT
-0.095 ± 0.004	-10 ± 5	SOKHOYAN 15A	DPWA	Multichannel
$-0.089^{+0.008}_{-0.007}$	-10^{+3}_{-1}	ROENCHEN 14	DPWA	
• • • We do not use the following data for averages, fits, limits, etc. • • •				
-0.084	-19	ROENCHEN 15A	DPWA	Multichannel

 $\Delta(1950)$ BREIT-WIGNER PHOTON DECAY AMPLITUDES $\Delta(1950) \rightarrow N\gamma, \text{helicity-1/2 amplitude } A_{1/2}$

VALUE ($\text{GeV}^{-1/2}$)	DOCUMENT ID	TECN	COMMENT
-0.075 to -0.065 (≈ -0.070) OUR ESTIMATE			
-0.0698 ± 0.0141	GOLOVATCH 19	DPWA	$\gamma p \rightarrow \pi^+ \pi^- p$
-0.047 ± 0.002	¹ HUNT 19	DPWA	Multichannel
-0.067 ± 0.005	ANISOVICH 17	DPWA	Multichannel
-0.083 ± 0.004	WORKMAN 12A	DPWA	$\gamma N \rightarrow N\pi$
• • • We do not use the following data for averages, fits, limits, etc. • • •			
-0.067 ± 0.005	SOKHOYAN 15A	DPWA	Multichannel
-0.067 ± 0.005	GUTZ 14	DPWA	Multichannel
-0.071 ± 0.004	ANISOVICH 12A	DPWA	Multichannel
-0.065 ± 0.001	¹ SHRESTHA 12A	DPWA	Multichannel
-0.094	DRECHSEL 07	DPWA	$\gamma N \rightarrow \pi N$

¹ Statistical error only. $\Delta(1950) \rightarrow N\gamma, \text{helicity-3/2 amplitude } A_{3/2}$

VALUE ($\text{GeV}^{-1/2}$)	DOCUMENT ID	TECN	COMMENT
-0.100 to -0.080 (≈ -0.090) OUR ESTIMATE			
-0.1181 ± 0.0193	GOLOVATCH 19	DPWA	$\gamma p \rightarrow \pi^+ \pi^- p$
-0.074 ± 0.002	¹ HUNT 19	DPWA	Multichannel
-0.094 ± 0.004	ANISOVICH 17	DPWA	Multichannel
-0.096 ± 0.004	WORKMAN 12A	DPWA	$\gamma N \rightarrow N\pi$
• • • We do not use the following data for averages, fits, limits, etc. • • •			
-0.094 ± 0.004	SOKHOYAN 15A	DPWA	Multichannel
-0.094 ± 0.004	GUTZ 14	DPWA	Multichannel
-0.094 ± 0.005	ANISOVICH 12A	DPWA	Multichannel
-0.083 ± 0.001	¹ SHRESTHA 12A	DPWA	Multichannel
-0.121	DRECHSEL 07	DPWA	$\gamma N \rightarrow \pi N$

¹ Statistical error only. $\Delta(1950)$ REFERENCES

GOLOVATCH 19	PL B788 371	E. Golovatch et al.	(CLAS Collab.)
HUNT 19	PR C99 055205	B.C. Hunt, D.M. Manley	
ANISOVICH 17	PL B766 357	A.V. Anisovich et al.	
ROENCHEN 15A	EPJ A51 70	D. Roenchen et al.	
SOKHOYAN 15A	EPJ A51 95	V. Sokhoyan et al.	(CBELSA/TAPS Collab.)
GUTZ 14	EPJ A50 74	E. Gutz et al.	(CBELSA/TAPS Collab.)
PDG 14	CP C38 070001	K. Olive et al.	(PDG Collab.)
ROENCHEN 14	EPJ A50 101	D. Roenchen et al.	
Also	EPJ A51 63 (errata.)	D. Roenchen et al.	
SVARC 14	PR C89 045205	A. Svarc et al.	(RBI Zagreb, UNI Tuzla)
ANISOVICH 12A	EPJ A48 15	A.V. Anisovich et al.	(BONN, PNPI)
SHRESTHA 12A	PR C86 055203	M. Shrestha, D.M. Manley	(KSU)
WORKMAN 12A	PR C86 015202	R. Workman et al.	(GWU)
DRECHSEL 07	EPJ A34 69	D. Drechsel, S.S. Kamalov, L. Tiator	(MAINZ, JINR)
ARNDT 06	PR C74 045205	R.A. Arndt et al.	(GWU)
VRANA 00	PRPL 328 181	T.P. Vrana, S.A. Dytman, T.-S.H. Lee	(PITT, ANL)
HOEHLER 93	πN Newsletter 9 1	G. Hohlner	(KARL)
CUTKOSKY 80	Toronto Conf. 19	R.E. Cutkosky et al.	(CMU, LBL) IJP
Also	PR D20 2839	R.E. Cutkosky et al.	(CMU, LBL) IJP
HOEHLER 79	PDAT 12-1	G. Hohlner et al.	(KARLT) IJP
Also	Toronto Conf. 3	R. Koch	(KARLT) IJP

$$\Delta(2000) 5/2^+$$

$$I(J^P) = \frac{3}{2}(\frac{5}{2}^+) \text{ Status: } **$$

OMITTED FROM SUMMARY TABLE

 $\Delta(2000)$ POLE POSITION

REAL PART	DOCUMENT ID	TECN	COMMENT
1998 \pm 4 \pm 4	¹ SVARC 14	L+P	$\pi N \rightarrow \pi N$
1976	SHRESTHA 12A	DPWA	Multichannel
2150 \pm 100	CUTKOSKY 80	IPWA	$\pi N \rightarrow \pi N$
• • • We do not use the following data for averages, fits, limits, etc. • • •			
1697	VRANA 00	DPWA	Multichannel

¹ Fit to the amplitudes of HOEHLER 79.

Baryon Particle Listings

 $\Delta(2000)$, $\Delta(2150)$ **-2xIMAGINARY PART**

VALUE (MeV)	DOCUMENT ID	TECN	COMMENT
404 ± 10 ± 4	¹ SVARC 14	L+P	$\pi N \rightarrow \pi N$
350 ± 100	CUTKOSKY 80	IPWA	$\pi N \rightarrow \pi N$
● ● ● We do not use the following data for averages, fits, limits, etc. ● ● ●			
488	SHRESTHA 12A	DPWA	Multichannel
112	VRANA 00	DPWA	Multichannel
¹ Fit to the amplitudes of HOEHLER 79.			

 $\Delta(2000)$ ELASTIC POLE RESIDUE**MODULUS $|r|$**

VALUE (MeV)	DOCUMENT ID	TECN	COMMENT
34 ± 1 ± 1	¹ SVARC 14	L+P	$\pi N \rightarrow \pi N$
16 ± 5	CUTKOSKY 80	IPWA	$\pi N \rightarrow \pi N$
¹ Fit to the amplitudes of HOEHLER 79.			

PHASE θ

VALUE (°)	DOCUMENT ID	TECN	COMMENT
110 ± 1 ± 3	¹ SVARC 14	L+P	$\pi N \rightarrow \pi N$
150 ± 90	CUTKOSKY 80	IPWA	$\pi N \rightarrow \pi N$
¹ Fit to the amplitudes of HOEHLER 79.			

 $\Delta(2000)$ BREIT-WIGNER MASS

VALUE (MeV)	DOCUMENT ID	TECN	COMMENT
2015 ± 24	¹ SHRESTHA 12A	DPWA	Multichannel
2200 ± 125	CUTKOSKY 80	IPWA	$\pi N \rightarrow \pi N$
● ● ● We do not use the following data for averages, fits, limits, etc. ● ● ●			
1724 ± 61	VRANA 00	DPWA	Multichannel
1752 ± 32	MANLEY 92	IPWA	$\pi N \rightarrow \pi N$ & $N\pi\pi$
¹ Statistical error only.			

 $\Delta(2000)$ BREIT-WIGNER WIDTH

VALUE (MeV)	DOCUMENT ID	TECN	COMMENT
500 ± 52	¹ SHRESTHA 12A	DPWA	Multichannel
400 ± 125	CUTKOSKY 80	IPWA	$\pi N \rightarrow \pi N$
● ● ● We do not use the following data for averages, fits, limits, etc. ● ● ●			
138 ± 68	VRANA 00	DPWA	Multichannel
251 ± 93	MANLEY 92	IPWA	$\pi N \rightarrow \pi N$ & $N\pi\pi$
¹ Statistical error only.			

 $\Delta(2000)$ DECAY MODES

Mode	Fraction (Γ_i/Γ)
Γ_1 $N\pi$	3–11 %
Γ_2 $N\pi\pi$	>87 %
Γ_3 $\Delta(1232)\pi$	<9 %
Γ_4 $\Delta(1232)\pi$, P -wave	<6 %
Γ_5 $\Delta(1232)\pi$, F -wave	<3 %
Γ_6 $N\rho$, $S=3/2$, P -wave	seen
Γ_7 $N\gamma$	
Γ_8 $N\gamma$, helicity=1/2	seen
Γ_9 $N\gamma$, helicity=3/2	seen

 $\Delta(2000)$ BRANCHING RATIOS

$\Gamma(N\pi)/\Gamma_{\text{total}}$	DOCUMENT ID	TECN	COMMENT	Γ_1/Γ
7 ± 1	¹ SHRESTHA 12A	DPWA	Multichannel	
7 ± 4	CUTKOSKY 80	IPWA	$\pi N \rightarrow \pi N$	
● ● ● We do not use the following data for averages, fits, limits, etc. ● ● ●				
0 ± 1	VRANA 00	DPWA	Multichannel	
2 ± 1	MANLEY 92	IPWA	$\pi N \rightarrow \pi N$ & $N\pi\pi$	
¹ Statistical error only.				

$\Gamma(\Delta(1232)\pi, P\text{-wave})/\Gamma_{\text{total}}$	DOCUMENT ID	TECN	COMMENT	Γ_4/Γ
3 ± 3	¹ SHRESTHA 12A	DPWA	Multichannel	
● ● ● We do not use the following data for averages, fits, limits, etc. ● ● ●				
0 ± 1	VRANA 00	DPWA	Multichannel	
¹ Statistical error only.				

$\Gamma(\Delta(1232)\pi, F\text{-wave})/\Gamma_{\text{total}}$	DOCUMENT ID	TECN	COMMENT	Γ_5/Γ
< 3	SHRESTHA 12A	DPWA	Multichannel	
● ● ● We do not use the following data for averages, fits, limits, etc. ● ● ●				
40 ± 1	VRANA 00	DPWA	Multichannel	

 $\Gamma(N\rho, S=3/2, P\text{-wave})/\Gamma_{\text{total}}$

VALUE (%)	DOCUMENT ID	TECN	COMMENT	Γ_6/Γ
90 ± 3	¹ SHRESTHA 12A	DPWA	Multichannel	
● ● ● We do not use the following data for averages, fits, limits, etc. ● ● ●				
60 ± 60	VRANA 00	DPWA	Multichannel	
¹ Statistical error only.				

 $\Delta(2000)$ BREIT-WIGNER PHOTON DECAY AMPLITUDES **$\Delta(2000) \rightarrow p\gamma$, helicity-1/2 amplitude $A_{1/2}$**

VALUE ($\text{GeV}^{-1/2}$)	DOCUMENT ID	TECN	COMMENT
● ● ● We do not use the following data for averages, fits, limits, etc. ● ● ●			
-0.061 ± 0.018	¹ SHRESTHA 12A	DPWA	Multichannel
¹ Statistical error only.			

 $\Delta(2000) \rightarrow p\gamma$, helicity-3/2 amplitude $A_{3/2}$

VALUE ($\text{GeV}^{-1/2}$)	DOCUMENT ID	TECN	COMMENT
● ● ● We do not use the following data for averages, fits, limits, etc. ● ● ●			
0.158 ± 0.032	¹ SHRESTHA 12A	DPWA	Multichannel
¹ Statistical error only.			

 $\Delta(2000)$ REFERENCES

SVARC 14	PR C89 045205	A. Svarc <i>et al.</i>	(RBI Zagreb, UNI Tuzla)
SHRESTHA 12A	PR C86 055203	M. Shrestha, D.M. Manley	(KSU)
VRANA 00	PRPL 328 181	T.P. Vrana, S.A. Dytman, T.-S.H. Lee	(PITT, ANL)
MANLEY 92	PR D45 4002	D.M. Manley, E.M. Saleski	(KSU) IUP
	PR D30 904	D.M. Manley <i>et al.</i>	(VPI)
CUTKOSKY 80	Toronto Conf. 19	R.E. Cutkosky <i>et al.</i>	(CMU, LBL)
	PR D20 2839	R.E. Cutkosky <i>et al.</i>	(CMU, LBL)
HOEHLER 79	PDAT 12-1	G. Hoehler <i>et al.</i>	(KARLT)

 $\Delta(2150) 1/2^-$

$$I(J^P) = \frac{3}{2}(\frac{1}{2}^-) \text{ Status: *}$$

OMITTED FROM SUMMARY TABLE

 $\Delta(2150)$ POLE POSITION

REAL PART	DOCUMENT ID	TECN	COMMENT
2140 ± 80	CUTKOSKY 80	IPWA	$\pi N \rightarrow \pi N$
-2xIMAGINARY PART			
200 ± 80	CUTKOSKY 80	IPWA	$\pi N \rightarrow \pi N$

 $\Delta(2150)$ ELASTIC POLE RESIDUE

MODULUS $ r $	DOCUMENT ID	TECN	COMMENT
7 ± 2	CUTKOSKY 80	IPWA	$\pi N \rightarrow \pi N$
PHASE θ			
VALUE (°)	DOCUMENT ID	TECN	COMMENT
-60 ± 90	CUTKOSKY 80	IPWA	$\pi N \rightarrow \pi N$

 $\Delta(2150)$ BREIT-WIGNER MASS

VALUE (MeV)	DOCUMENT ID	TECN	COMMENT
2150 ± 100	CUTKOSKY 80	IPWA	$\pi N \rightarrow \pi N$

 $\Delta(2150)$ BREIT-WIGNER WIDTH

VALUE (MeV)	DOCUMENT ID	TECN	COMMENT
200 ± 100	CUTKOSKY 80	IPWA	$\pi N \rightarrow \pi N$

 $\Delta(2150)$ DECAY MODES

Mode	Fraction (Γ_i/Γ)
Γ_1 $N\pi$	6–10 %

 $\Delta(2150)$ BRANCHING RATIOS

$\Gamma(N\pi)/\Gamma_{\text{total}}$	DOCUMENT ID	TECN	COMMENT	Γ_1/Γ
8 ± 2	CUTKOSKY 80	IPWA	$\pi N \rightarrow \pi N$	

 $\Delta(2150)$ REFERENCES

CUTKOSKY 80	Toronto Conf. 19	R.E. Cutkosky <i>et al.</i>	(CMU, LBL) IUP
	PR D20 2839	R.E. Cutkosky <i>et al.</i>	(CMU, LBL)

See key on page 1127

Baryon Particle Listings
Δ(2200), Δ(2300)

Δ(2200) 7/2- I(J^P) = 3/2(7/2-) Status: ***

Δ(2200) POLE POSITION

Table with 4 columns: VALUE (MeV), DOCUMENT ID, TECN, COMMENT. Includes REAL PART and IMAGINARY PART data.

Δ(2200) ELASTIC POLE RESIDUE

Table with 4 columns: VALUE (MeV), DOCUMENT ID, TECN, COMMENT. Includes MODULUS |r| and PHASE θ data.

Δ(2200) INELASTIC POLE RESIDUE

The "normalized residue" is the residue divided by Γ_pole/2.

Table with 4 columns: MODULUS, PHASE (°), DOCUMENT ID, TECN, COMMENT. Includes Normalized residue in Nπ → Δ(2200) → ΣK, Δπ, D-wave, and G-wave.

Δ(2200) BREIT-WIGNER MASS

Table with 4 columns: VALUE (MeV), DOCUMENT ID, TECN, COMMENT. Includes 2150 to 2250 OUR ESTIMATE.

Δ(2200) BREIT-WIGNER WIDTH

Table with 4 columns: VALUE (MeV), DOCUMENT ID, TECN, COMMENT. Includes 200 to 500 OUR ESTIMATE.

Δ(2200) DECAY MODES

Table with 3 columns: Mode, Fraction (Γj/Γ), seen. Lists decay modes like Nπ, ΣK, Δπ, etc.

Δ(2200) BRANCHING RATIOS

Table with 4 columns: Γj/Γ, VALUE (%), DOCUMENT ID, TECN, COMMENT. Lists ratios for Nπ, ΣK, Δπ (D-wave), Δπ (G-wave), and Δη (D-wave).

Δ(2200) PHOTON DECAY AMPLITUDES AT THE POLE

Table with 4 columns: Δ(2200) → Nγ, helicity-1/2 amplitude A1/2, MODULUS (GeV^-1/2), PHASE (°), DOCUMENT ID, TECN, COMMENT.

Δ(2200) REFERENCES

Table with 4 columns: AUTHOR, YEAR, DOCUMENT ID, TECN, COMMENT. Lists references for Δ(2200).

Δ(2300) 9/2+ I(J^P) = 3/2(9/2+) Status: **

OMITTED FROM SUMMARY TABLE

Δ(2300) POLE POSITION

Table with 4 columns: REAL PART, VALUE (MeV), DOCUMENT ID, TECN, COMMENT. Includes 2370 ± 80 and IMAGINARY PART.

Δ(2300) ELASTIC POLE RESIDUE

Table with 4 columns: MODULUS |r|, VALUE (MeV), DOCUMENT ID, TECN, COMMENT. Includes PHASE θ.

Δ(2300) BREIT-WIGNER MASS

Table with 4 columns: VALUE (MeV), DOCUMENT ID, TECN, COMMENT. Includes 2400 ± 125 and 2217 ± 80.

Δ(2300) BREIT-WIGNER WIDTH

Table with 4 columns: VALUE (MeV), DOCUMENT ID, TECN, COMMENT. Includes 425 ± 150 and 300 ± 100.

Baryon Particle Listings

$\Delta(2300)$, $\Delta(2350)$, $\Delta(2390)$, $\Delta(2400)$

$\Delta(2300)$ DECAY MODES

Mode	Fraction (Γ_i/Γ)
Γ_1 $N\pi$	1-8 %

$\Delta(2300)$ BRANCHING RATIOS

$\Gamma(N\pi)/\Gamma_{\text{total}}$	DOCUMENT ID	TECN	COMMENT	Γ_1/Γ
6±2	CUTKOSKY 80	IPWA	$\pi N \rightarrow \pi N$	
3±2	HOEHLER 79	IPWA	$\pi N \rightarrow \pi N$	

$\Delta(2300)$ REFERENCES

CUTKOSKY 80	Toronto Conf. 19	R.E. Cutkosky et al.	(CMU, LBL) IJP
Also	PR D20 2839	R.E. Cutkosky et al.	(CMU, LBL)
HOEHLER 79	PDAT 12-1	G. Höhler et al.	(KARLT) IJP
Also	Toronto Conf. 3	R. Koch	(KARLT) IJP

$\Delta(2350)$ $5/2^-$

$$I(J^P) = \frac{3}{2}(\frac{5}{2}^-) \text{ Status: } *$$

OMITTED FROM SUMMARY TABLE

$\Delta(2350)$ POLE POSITION

REAL PART

VALUE (MeV)	DOCUMENT ID	TECN	COMMENT
2400±125	CUTKOSKY 80	IPWA	$\pi N \rightarrow \pi N$
●●● We do not use the following data for averages, fits, limits, etc. ●●●			
2427	VRANA 00	DPWA	Multichannel

-2xIMAGINARY PART

VALUE (MeV)	DOCUMENT ID	TECN	COMMENT
400±150	CUTKOSKY 80	IPWA	$\pi N \rightarrow \pi N$
●●● We do not use the following data for averages, fits, limits, etc. ●●●			
458	VRANA 00	DPWA	Multichannel

$\Delta(2350)$ ELASTIC POLE RESIDUE

MODULUS |r|

VALUE (MeV)	DOCUMENT ID	TECN	COMMENT
15±8	CUTKOSKY 80	IPWA	$\pi N \rightarrow \pi N$

PHASE θ

VALUE (°)	DOCUMENT ID	TECN	COMMENT
-70±70	CUTKOSKY 80	IPWA	$\pi N \rightarrow \pi N$

$\Delta(2350)$ BREIT-WIGNER MASS

VALUE (MeV)	DOCUMENT ID	TECN	COMMENT
2400±125	CUTKOSKY 80	IPWA	$\pi N \rightarrow \pi N$
2305±26	HOEHLER 79	IPWA	$\pi N \rightarrow \pi N$
●●● We do not use the following data for averages, fits, limits, etc. ●●●			
2459±100	VRANA 00	DPWA	Multichannel

$\Delta(2350)$ BREIT-WIGNER WIDTH

VALUE (MeV)	DOCUMENT ID	TECN	COMMENT
400±150	CUTKOSKY 80	IPWA	$\pi N \rightarrow \pi N$
300±70	HOEHLER 79	IPWA	$\pi N \rightarrow \pi N$
●●● We do not use the following data for averages, fits, limits, etc. ●●●			
480±360	VRANA 00	DPWA	Multichannel

$\Delta(2350)$ DECAY MODES

Mode	Fraction (Γ_i/Γ)
Γ_1 $N\pi$	4-30 %

$\Delta(2350)$ BRANCHING RATIOS

$\Gamma(N\pi)/\Gamma_{\text{total}}$	DOCUMENT ID	TECN	COMMENT	Γ_1/Γ
20±10	CUTKOSKY 80	IPWA	$\pi N \rightarrow \pi N$	
4±2	HOEHLER 79	IPWA	$\pi N \rightarrow \pi N$	
●●● We do not use the following data for averages, fits, limits, etc. ●●●				
7±14	VRANA 00	DPWA	Multichannel	

$\Delta(2350)$ REFERENCES

VRANA 00	PRPL 328 181	T.P. Vrana, S.A. Dytman, T.-S.H. Lee	(PITT, ANL)
CUTKOSKY 80	Toronto Conf. 19	R.E. Cutkosky et al.	(CMU, LBL) IJP
Also	PR D20 2839	R.E. Cutkosky et al.	(CMU, LBL)
HOEHLER 79	PDAT 12-1	G. Höhler et al.	(KARLT) IJP
Also	Toronto Conf. 3	R. Koch	(KARLT) IJP

$\Delta(2390)$ $7/2^+$

$$I(J^P) = \frac{3}{2}(\frac{7}{2}^+) \text{ Status: } *$$

OMITTED FROM SUMMARY TABLE

$\Delta(2390)$ POLE POSITION

REAL PART

VALUE (MeV)	DOCUMENT ID	TECN	COMMENT
2223±15±19	¹ SVARC 14	L+P	$\pi N \rightarrow \pi N$
2350±100	CUTKOSKY 80	IPWA	$\pi N \rightarrow \pi N$

-2xIMAGINARY PART

VALUE (MeV)	DOCUMENT ID	TECN	COMMENT
431±26±7	¹ SVARC 14	L+P	$\pi N \rightarrow \pi N$
260±100	CUTKOSKY 80	IPWA	$\pi N \rightarrow \pi N$

$\Delta(2390)$ ELASTIC POLE RESIDUE

MODULUS |r|

VALUE (MeV)	DOCUMENT ID	TECN	COMMENT
26±2±1	¹ SVARC 14	L+P	$\pi N \rightarrow \pi N$
12±6	CUTKOSKY 80	IPWA	$\pi N \rightarrow \pi N$

PHASE θ

VALUE (°)	DOCUMENT ID	TECN	COMMENT
-160±5±11	¹ SVARC 14	L+P	$\pi N \rightarrow \pi N$
-90±60	CUTKOSKY 80	IPWA	$\pi N \rightarrow \pi N$

$\Delta(2390)$ BREIT-WIGNER MASS

VALUE (MeV)	DOCUMENT ID	TECN	COMMENT
2350±100	CUTKOSKY 80	IPWA	$\pi N \rightarrow \pi N$
2425±60	HOEHLER 79	IPWA	$\pi N \rightarrow \pi N$

$\Delta(2390)$ BREIT-WIGNER WIDTH

VALUE (MeV)	DOCUMENT ID	TECN	COMMENT
300±100	CUTKOSKY 80	IPWA	$\pi N \rightarrow \pi N$
300±80	HOEHLER 79	IPWA	$\pi N \rightarrow \pi N$

$\Delta(2390)$ DECAY MODES

Mode	Fraction (Γ_i/Γ)
Γ_1 $N\pi$	3-12 %

$\Delta(2390)$ BRANCHING RATIOS

$\Gamma(N\pi)/\Gamma_{\text{total}}$	DOCUMENT ID	TECN	COMMENT	Γ_1/Γ
8±4	CUTKOSKY 80	IPWA	$\pi N \rightarrow \pi N$	
7±4	HOEHLER 79	IPWA	$\pi N \rightarrow \pi N$	

$\Delta(2390)$ FOOTNOTES

¹ Fit to the amplitudes of HOEHLER 79.

$\Delta(2390)$ REFERENCES

SVARC 14	PR C89 045205	A. Svarc et al.	(RBI Zagreb, UNI Tuzla)
CUTKOSKY 80	Toronto Conf. 19	R.E. Cutkosky et al.	(CMU, LBL) IJP
Also	PR D20 2839	R.E. Cutkosky et al.	(CMU, LBL)
HOEHLER 79	PDAT 12-1	G. Höhler et al.	(KARLT) IJP
Also	Toronto Conf. 3	R. Koch	(KARLT) IJP

$\Delta(2400)$ $9/2^-$

$$I(J^P) = \frac{3}{2}(\frac{9}{2}^-) \text{ Status: } **$$

OMITTED FROM SUMMARY TABLE

$\Delta(2400)$ POLE POSITION

REAL PART

VALUE (MeV)	DOCUMENT ID	TECN	COMMENT
2260±60	CUTKOSKY 80	IPWA	$\pi N \rightarrow \pi N$
●●● We do not use the following data for averages, fits, limits, etc. ●●●			
1931	ROENCHEN 15A	DPWA	Multichannel
1983	ARNDT 06	DPWA	$\pi N \rightarrow \pi N, \eta N$

-2xIMAGINARY PART

VALUE (MeV)	DOCUMENT ID	TECN	COMMENT
320±160	CUTKOSKY 80	IPWA	$\pi N \rightarrow \pi N$
●●● We do not use the following data for averages, fits, limits, etc. ●●●			
442	ROENCHEN 15A	DPWA	Multichannel
878	ARNDT 06	DPWA	$\pi N \rightarrow \pi N, \eta N$

$\Delta(2400)$ ELASTIC POLE RESIDUEMODULUS $|r|$

VALUE (MeV)	DOCUMENT ID	TECN	COMMENT
8 ± 4	CUTKOSKY 80	IPWA	$\pi N \rightarrow \pi N$
••• We do not use the following data for averages, fits, limits, etc. •••			
13	ROENCHEN 15A	DPWA	Multichannel
24	ARNDT 06	DPWA	$\pi N \rightarrow \pi N, \eta N$

PHASE θ

VALUE (°)	DOCUMENT ID	TECN	COMMENT
-25 ± 15	CUTKOSKY 80	IPWA	$\pi N \rightarrow \pi N$
••• We do not use the following data for averages, fits, limits, etc. •••			
-96	ROENCHEN 15A	DPWA	Multichannel
-139	ARNDT 06	DPWA	$\pi N \rightarrow \pi N, \eta N$

 $\Delta(2400)$ INELASTIC POLE RESIDUE

The "normalized residue" is the residue divided by $\Gamma_{pole}/2$.

Normalized residue in $N\pi \rightarrow \Delta(2400) \rightarrow \Sigma K$

MODULUS	PHASE (°)	DOCUMENT ID	TECN	COMMENT
0.009	25	ROENCHEN 15A	DPWA	Multichannel
••• We do not use the following data for averages, fits, limits, etc. •••				

Normalized residue in $N\pi \rightarrow \Delta(2400) \rightarrow \Delta\pi, G\text{-wave}$

MODULUS	PHASE (°)	DOCUMENT ID	TECN	COMMENT
0.18	-110	ROENCHEN 15A	DPWA	Multichannel
••• We do not use the following data for averages, fits, limits, etc. •••				

Normalized residue in $N\pi \rightarrow \Delta(2400) \rightarrow \Delta\pi, f\text{-wave}$

MODULUS	PHASE (°)	DOCUMENT ID	TECN	COMMENT
0.012	-1.0	ROENCHEN 15A	DPWA	Multichannel
••• We do not use the following data for averages, fits, limits, etc. •••				

 $\Delta(2400)$ BREIT-WIGNER MASS

VALUE (MeV)	DOCUMENT ID	TECN	COMMENT
2643 ± 141	¹ ARNDT 06	DPWA	$\pi N \rightarrow \pi N, \eta N$
2300 ± 100	CUTKOSKY 80	IPWA	$\pi N \rightarrow \pi N$
2468 ± 50	HOEHLER 79	IPWA	$\pi N \rightarrow \pi N$

¹ Statistical error only.

 $\Delta(2400)$ BREIT-WIGNER WIDTH

VALUE (MeV)	DOCUMENT ID	TECN	COMMENT
895 ± 432	² ARNDT 06	DPWA	$\pi N \rightarrow \pi N, \eta N$
330 ± 100	CUTKOSKY 80	IPWA	$\pi N \rightarrow \pi N$
480 ± 100	HOEHLER 79	IPWA	$\pi N \rightarrow \pi N$

² Statistical error only.

 $\Delta(2400)$ DECAY MODES

Mode	Fraction (Γ_i/Γ)
Γ_1 $N\pi$	3-9 %

 $\Delta(2400)$ BRANCHING RATIOS

$\Gamma(N\pi)/\Gamma_{total}$	DOCUMENT ID	TECN	COMMENT	Γ_1/Γ
6.4 ± 2.2	³ ARNDT 06	DPWA	$\pi N \rightarrow \pi N, \eta N$	
5 ± 2	CUTKOSKY 80	IPWA	$\pi N \rightarrow \pi N$	
6 ± 3	HOEHLER 79	IPWA	$\pi N \rightarrow \pi N$	

³ Statistical error only.

 $\Delta(2400)$ PHOTON DECAY AMPLITUDES AT THE POLE $\Delta(2400) \rightarrow N\gamma$, helicity-1/2 amplitude $A_{1/2}$

MODULUS ($\text{GeV}^{-1/2}$)	PHASE (°)	DOCUMENT ID	TECN	COMMENT
-0.128 ± 0.046 -0.012	118 ± 24 -3	ROENCHEN 14	DPWA	
••• We do not use the following data for averages, fits, limits, etc. •••				
-0.034	63	ROENCHEN 15A	DPWA	Multichannel

 $\Delta(2400) \rightarrow N\gamma$, helicity-3/2 amplitude $A_{3/2}$

MODULUS ($\text{GeV}^{-1/2}$)	PHASE (°)	DOCUMENT ID	TECN	COMMENT
-0.115 ± 0.042 -0.024	140 ± 17 -28	ROENCHEN 14	DPWA	
••• We do not use the following data for averages, fits, limits, etc. •••				
0.054	-75	ROENCHEN 15A	DPWA	Multichannel

 $\Delta(2400)$ REFERENCES

ROENCHEN 15A	EPJ A51 79	D. Roenchen et al.	
ROENCHEN 14	EPJ A50 101	D. Roenchen et al.	
Also	EPJ A51 63 (errat.)	D. Roenchen et al.	
ARNDT 06	PR C74 045205	R.A. Arndt et al.	(GWU)
CUTKOSKY 80	Toronto Conf. 19	R.E. Cutkosky et al.	(CMU, LBL) IJP
Also	PR D20 2839	R.E. Cutkosky et al.	(CMU, LBL)
HOEHLER 79	PDAT 12-1	G. Hohlner et al.	(KARLT) IJP
Also	Toronto Conf. 3	R. Koch	(KARLT) IJP

$\Delta(2420) 11/2^+$

$I(J^P) = \frac{3}{2}(11/2^+)$ Status: ***

Older and obsolete values are listed and referenced in the 2014 edition, Chinese Physics C38 070001 (2014).

 $\Delta(2420)$ POLE POSITION

REAL PART

VALUE (MeV)	DOCUMENT ID	TECN	COMMENT
2300 to 2500 (≈ 2400) OUR ESTIMATE			
$2454 \pm 4 \pm 11$	¹ SVARC 14	L+P	$\pi N \rightarrow \pi N$
2360 ± 100	CUTKOSKY 80	IPWA	$\pi N \rightarrow \pi N$
••• We do not use the following data for averages, fits, limits, etc. •••			
2529	ARNDT 06	DPWA	$\pi N \rightarrow \pi N, \eta N$
2300	HOEHLER 93	ARGD	$\pi N \rightarrow \pi N$

¹ Fit to the amplitudes of HOEHLER 79.

-2xIMAGINARY PART

VALUE (MeV)	DOCUMENT ID	TECN	COMMENT
350 to 550 (≈ 450) OUR ESTIMATE			
$462 \pm 8 \pm 50$	¹ SVARC 14	L+P	$\pi N \rightarrow \pi N$
420 ± 100	CUTKOSKY 80	IPWA	$\pi N \rightarrow \pi N$
••• We do not use the following data for averages, fits, limits, etc. •••			
621	ARNDT 06	DPWA	$\pi N \rightarrow \pi N, \eta N$
620	HOEHLER 93	ARGD	$\pi N \rightarrow \pi N$

¹ Fit to the amplitudes of HOEHLER 79.

 $\Delta(2420)$ ELASTIC POLE RESIDUEMODULUS $|r|$

VALUE (MeV)	DOCUMENT ID	TECN	COMMENT
20 to 40 (≈ 30) OUR ESTIMATE			
$30 \pm 1 \pm 7$	¹ SVARC 14	L+P	$\pi N \rightarrow \pi N$
18 ± 6	CUTKOSKY 80	IPWA	$\pi N \rightarrow \pi N$
••• We do not use the following data for averages, fits, limits, etc. •••			
33	ARNDT 06	DPWA	$\pi N \rightarrow \pi N, \eta N$
39	HOEHLER 93	ARGD	$\pi N \rightarrow \pi N$

¹ Fit to the amplitudes of HOEHLER 79.

PHASE θ

VALUE (°)	DOCUMENT ID	TECN	COMMENT
-60 to 20 (≈ -20) OUR ESTIMATE			
$11 \pm 1 \pm 8$	¹ SVARC 14	L+P	$\pi N \rightarrow \pi N$
-30 ± 40	CUTKOSKY 80	IPWA	$\pi N \rightarrow \pi N$
••• We do not use the following data for averages, fits, limits, etc. •••			
-45	ARNDT 06	DPWA	$\pi N \rightarrow \pi N, \eta N$
-60	HOEHLER 93	ARGD	$\pi N \rightarrow \pi N$

¹ Fit to the amplitudes of HOEHLER 79.

 $\Delta(2420)$ BREIT-WIGNER MASS

VALUE (MeV)	DOCUMENT ID	TECN	COMMENT
2300 to 2600 (≈ 2450) OUR ESTIMATE			
2633 ± 29	¹ ARNDT 06	DPWA	$\pi N \rightarrow \pi N, \eta N$
2400 ± 125	CUTKOSKY 80	IPWA	$\pi N \rightarrow \pi N$
2416 ± 17	HOEHLER 79	IPWA	$\pi N \rightarrow \pi N$

¹ Statistical error only.

 $\Delta(2420)$ BREIT-WIGNER WIDTH

VALUE (MeV)	DOCUMENT ID	TECN	COMMENT
300 to 700 (≈ 500) OUR ESTIMATE			
692 ± 47	¹ ARNDT 06	DPWA	$\pi N \rightarrow \pi N, \eta N$
450 ± 150	CUTKOSKY 80	IPWA	$\pi N \rightarrow \pi N$
340 ± 28	HOEHLER 79	IPWA	$\pi N \rightarrow \pi N$

¹ Statistical error only.

 $\Delta(2420)$ DECAY MODES

The following branching fractions are our estimates, not fits or averages.

Mode	Fraction (Γ_i/Γ)
Γ_1 $N\pi$	5-10 %

Baryon Particle Listings

 $\Delta(2420)$, $\Delta(2750)$, $\Delta(2950)$, $\Delta(\sim 3000)$ $\Delta(2420)$ BRANCHING RATIOS

$\Gamma(N\pi)/\Gamma_{\text{total}}$				Γ_1/Γ
VALUE (%)	DOCUMENT ID	TECN	COMMENT	
5 to 10 (≈ 8) OUR ESTIMATE				
8.5 ± 0.8	¹ ARNDT	06	DPWA $\pi N \rightarrow \pi N, \eta N$	
8 ± 3	CUTKOSKY	80	IPWA $\pi N \rightarrow \pi N$	
8.0 ± 1.5	HOEHLER	79	IPWA $\pi N \rightarrow \pi N$	

¹ Statistical error only. $\Delta(2420)$ REFERENCES

PDG	14	CP C38 070001	K. Olive et al.	(PDG Collab.)
SVARC	14	PR C89 045205	A. Svarc et al.	(RBI Zagreb, UNI Tuzla)
ARNDT	06	PR C74 045205	R.A. Arndt et al.	(GWU)
HOEHLER	93	πN Newsletter 9 1	G. Hohler	(KARL)
CUTKOSKY	80	Toronto Conf. 19	R.E. Cutkosky et al.	(CMU, LBL) IJP
Also		PR D20 2839	R.E. Cutkosky et al.	(CMU, LBL)
HOEHLER	79	PDAT 12-1	G. Hohler et al.	(KARLT) IJP
Also		Toronto Conf. 3	R. Koch	(KARLT) IJP

$$\Delta(2750) 13/2^- \quad I(J^P) = \frac{3}{2}(13/2^-) \text{ Status: } **$$

OMITTED FROM SUMMARY TABLE

 $\Delta(2750)$ BREIT-WIGNER MASS

VALUE (MeV)	DOCUMENT ID	TECN	COMMENT
2794 ± 80	HOEHLER	79	IPWA $\pi N \rightarrow \pi N$

 $\Delta(2750)$ BREIT-WIGNER WIDTH

VALUE (MeV)	DOCUMENT ID	TECN	COMMENT
350 ± 100	HOEHLER	79	IPWA $\pi N \rightarrow \pi N$

 $\Delta(2750)$ DECAY MODES

Mode	Fraction (Γ_i/Γ)
$\Gamma_1 N\pi$	2-6%

 $\Delta(2750)$ BRANCHING RATIOS

$\Gamma(N\pi)/\Gamma_{\text{total}}$				Γ_1/Γ
VALUE (%)	DOCUMENT ID	TECN	COMMENT	
4.0 ± 1.5	HOEHLER	79	IPWA $\pi N \rightarrow \pi N$	

 $\Delta(2750)$ REFERENCES

HOEHLER	79	PDAT 12-1	G. Hohler et al.	(KARLT) IJP
Also		Toronto Conf. 3	R. Koch	(KARLT) IJP

$$\Delta(2950) 15/2^+ \quad I(J^P) = \frac{3}{2}(15/2^+) \text{ Status: } **$$

OMITTED FROM SUMMARY TABLE

 $\Delta(2950)$ BREIT-WIGNER MASS

VALUE (MeV)	DOCUMENT ID	TECN	COMMENT
2990 ± 100	HOEHLER	79	IPWA $\pi N \rightarrow \pi N$

 $\Delta(2950)$ BREIT-WIGNER WIDTH

VALUE (MeV)	DOCUMENT ID	TECN	COMMENT
330 ± 100	HOEHLER	79	IPWA $\pi N \rightarrow \pi N$

 $\Delta(2950)$ DECAY MODES

Mode	Fraction (Γ_i/Γ)
$\Gamma_1 N\pi$	2-6%

 $\Delta(2950)$ BRANCHING RATIOS

$\Gamma(N\pi)/\Gamma_{\text{total}}$				Γ_1/Γ
VALUE (%)	DOCUMENT ID	TECN	COMMENT	
4 ± 2	HOEHLER	79	IPWA $\pi N \rightarrow \pi N$	

 $\Delta(2950)$ REFERENCES

HOEHLER	79	PDAT 12-1	G. Hohler et al.	(KARLT) IJP
Also		Toronto Conf. 3	R. Koch	(KARLT) IJP

 $\Delta(\sim 3000)$ Region
Partial-Wave Analyses

OMITTED FROM SUMMARY TABLE

We list here miscellaneous high-mass candidates for isospin-3/2 resonances found in partial-wave analyses.

Our 1982 edition also had a $\Delta(2850)$ and a $\Delta(3230)$. The evidence for them was deduced from total cross-section and 180° elastic cross-section measurements. The $\Delta(2850)$ has been resolved into the $\Delta(2750) 13_{13}$ and $\Delta(2950) K_{3,15}$. The $\Delta(3230)$ is perhaps related to the $K_{3,13}$ of HENDRY 78 and to the $L_{3,17}$ of KOCH 80.

 $\Delta(\sim 3000)$ BREIT-WIGNER MASS

VALUE (MeV)	DOCUMENT ID	TECN	COMMENT
3300	¹ KOCH	80	IPWA $\pi N \rightarrow \pi N L_{3,17}$ wave
3500	¹ KOCH	80	IPWA $\pi N \rightarrow \pi N M_{3,19}$ wave
2850 ± 150	HENDRY	78	MPWA $\pi N \rightarrow \pi N I_{3,11}$ wave
3200 ± 200	HENDRY	78	MPWA $\pi N \rightarrow \pi N K_{3,13}$ wave
3300 ± 200	HENDRY	78	MPWA $\pi N \rightarrow \pi N L_{3,17}$ wave
3700 ± 200	HENDRY	78	MPWA $\pi N \rightarrow \pi N M_{3,19}$ wave
4100 ± 300	HENDRY	78	MPWA $\pi N \rightarrow \pi N N_{3,21}$ wave

 $\Delta(\sim 3000)$ BREIT-WIGNER WIDTH

VALUE (MeV)	DOCUMENT ID	TECN	COMMENT
700 ± 200	HENDRY	78	MPWA $\pi N \rightarrow \pi N I_{3,11}$ wave
1000 ± 300	HENDRY	78	MPWA $\pi N \rightarrow \pi N K_{3,13}$ wave
1100 ± 300	HENDRY	78	MPWA $\pi N \rightarrow \pi N L_{3,17}$ wave
1300 ± 400	HENDRY	78	MPWA $\pi N \rightarrow \pi N M_{3,19}$ wave
1600 ± 500	HENDRY	78	MPWA $\pi N \rightarrow \pi N N_{3,21}$ wave

 $\Delta(\sim 3000)$ DECAY MODES

Mode	Fraction (Γ_i/Γ)
$\Gamma_1 N\pi$	1-8%

 $\Delta(\sim 3000)$ BRANCHING RATIOS

$\Gamma(N\pi)/\Gamma_{\text{total}}$				Γ_1/Γ
VALUE (%)	DOCUMENT ID	TECN	COMMENT	
1-8% OUR ESTIMATE				
6 ± 2	HENDRY	78	MPWA $\pi N \rightarrow \pi N I_{3,11}$ wave	
5 ± 2	HENDRY	78	MPWA $\pi N \rightarrow \pi N K_{3,13}$ wave	
3 ± 1	HENDRY	78	MPWA $\pi N \rightarrow \pi N L_{3,17}$ wave	
3 ± 1	HENDRY	78	MPWA $\pi N \rightarrow \pi N M_{3,19}$ wave	
2 ± 1	HENDRY	78	MPWA $\pi N \rightarrow \pi N N_{3,21}$ wave	

 $\Delta(\sim 3000)$ FOOTNOTES¹ In addition, KOCH 80 reports some evidence for an $S_{31} \Delta(2700)$ and a $P_{33} \Delta(2800)$. $\Delta(\sim 3000)$ REFERENCES

KOCH	80	Toronto Conf. 3	R. Koch	(KARLT) IJP
HENDRY	78	PRL 41 222	A.W. Hendry	(IND, LBL) IJP
Also		ANP 136 1	A.W. Hendry	(IND)

Λ BARYONS

$(S = -1, I = 0)$

$\Lambda^0 = uds$

Λ $I(J^P) = 0(\frac{1}{2}^+)$ Status: ****

We have omitted some results that have been superseded by later experiments. See our earlier editions.

Λ MASS

The fit uses Λ , Σ^+ , Σ^0 , Σ^- mass and mass-difference measurements.

VALUE (MeV)	EVTS	DOCUMENT ID	TECN	COMMENT
1115.683 ± 0.006 OUR FIT				
1115.683 ± 0.006 OUR AVERAGE				
1115.678 ± 0.006 ± 0.006	20k	HARTOUNI 94	SPEC	pp 27.5 GeV/c
1115.690 ± 0.008 ± 0.006	18k	¹ HARTOUNI 94	SPEC	pp 27.5 GeV/c
••• We do not use the following data for averages, fits, limits, etc. •••				
1115.59 ± 0.08	935	HYMAN 72	HEBC	
1115.39 ± 0.12	195	MAYEUR 67	EMUL	
1115.6 ± 0.4		LONDON 66	HBC	
1115.65 ± 0.07	488	² SCHMIDT 65	HBC	
1115.44 ± 0.12		³ BHOWMIK 63	RVUE	

¹We assume *CPT* invariance: this is the $\bar{\Lambda}$ mass as measured by HARTOUNI 94. See below for the fractional mass difference, testing *CPT*.

²The SCHMIDT 65 masses have been reevaluated using our April 1973 proton and K^\pm and π^\pm masses. P. Schmidt, private communication (1974).

³The mass has been raised 35 keV to take into account a 46 keV increase in the proton mass and an 11 keV decrease in the π^\pm mass (note added Reviews of Modern Physics **39** 1 (1967)).

$(m_\Lambda - m_{\bar{\Lambda}}) / m_\Lambda$

A test of *CPT* invariance.

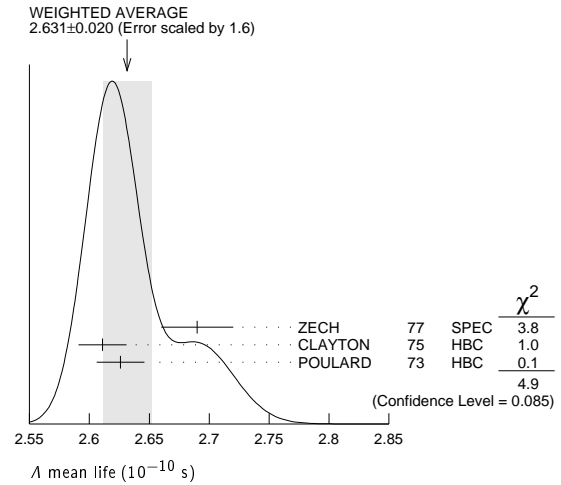
VALUE (units 10^{-5})	EVTS	DOCUMENT ID	TECN	COMMENT
- 0.1 ± 1.1 OUR AVERAGE				Error includes scale factor of 1.6.
+ 1.3 ± 1.2	31k	¹ RYBICKI 96	NA32	π^- Cu, 230 GeV
- 1.08 ± 0.90		HARTOUNI 94	SPEC	pp 27.5 GeV/c
4.5 ± 5.4		CHIEN 66	HBC	6.9 GeV/c $\bar{p}p$
••• We do not use the following data for averages, fits, limits, etc. •••				
-26 ± 13		BADIER 67	HBC	2.4 GeV/c $\bar{p}p$

¹RYBICKI 96 is an analysis of old ACCMOR (NA32) data.

Λ MEAN LIFE

Measurements with an error $\geq 0.1 \times 10^{-10}$ s have been omitted altogether, and only the latest high-statistics measurements are used for the average.

VALUE (10^{-10} s)	EVTS	DOCUMENT ID	TECN	COMMENT
2.632 ± 0.020 OUR AVERAGE				Error includes scale factor of 1.6. See the ideogram below.
2.69 ± 0.03	53k	ZECH 77	SPEC	Neutral hyperon beam
2.611 ± 0.020	34k	CLAYTON 75	HBC	0.96-1.4 GeV/c $K^- p$
2.626 ± 0.020	36k	POULARD 73	HBC	0.4-2.3 GeV/c $K^- p$
••• We do not use the following data for averages, fits, limits, etc. •••				
2.69 ± 0.05	6582	ALTHOFF 73B	OSPK	$\pi^+ n \rightarrow \Lambda K^+$
2.54 ± 0.04	4572	BALTAY 71B	HBC	$K^- p$ at rest
2.535 ± 0.035	8342	GRIMM 68	HBC	
2.47 ± 0.08	2600	HEPP 68	HBC	
2.35 ± 0.09	916	BURAN 66	HLBC	
2.452 ^{+0.056} _{-0.054}	2213	ENGELMANN 66	HBC	
2.59 ± 0.09	794	HUBBARD 64	HBC	
2.59 ± 0.07	1378	SCHWARTZ 64	HBC	
2.36 ± 0.06	2239	BLOCK 63	HEBC	



$(\tau_\Lambda - \tau_{\bar{\Lambda}}) / \tau_\Lambda$

A test of *CPT* invariance.

VALUE	DOCUMENT ID	TECN	COMMENT
-0.001 ± 0.009 OUR AVERAGE			
-0.0018 ± 0.0066 ± 0.0056	BARNES 96	CNTR	LEAR $\bar{p}p \rightarrow \bar{\Lambda}\Lambda$
0.044 ± 0.085	BADIER 67	HBC	2.4 GeV/c $\bar{p}p$

Λ MAGNETIC MOMENT

See the "Quark Model" review. Measurements with an error $\geq 0.15 \mu_N$ have been omitted.

VALUE (μ_N)	EVTS	DOCUMENT ID	TECN	COMMENT
-0.613 ± 0.004 OUR AVERAGE				
-0.606 ± 0.015	200k	COX 81	SPEC	
-0.6138 ± 0.0047	3M	SCHACHIN... 78	SPEC	
-0.59 ± 0.07	350k	HELLER 77	SPEC	
-0.57 ± 0.05	1.2M	BUNCE 76	SPEC	
-0.66 ± 0.07	1300	DAHL-JENSEN 71	EMUL	200 kG field

Λ ELECTRIC DIPOLE MOMENT

A nonzero value is forbidden by both *T* invariance and *P* invariance.

VALUE (10^{-16} ecm)	CL%	DOCUMENT ID	TECN
< 1.5	95	¹ PONDROM 81	SPEC
••• We do not use the following data for averages, fits, limits, etc. •••			
<100	95	² BARONI 71	EMUL
<500	95	GIBSON 66	EMUL

¹PONDROM 81 measures $(-3.0 \pm 7.4) \times 10^{-17}$ e-cm.

²BARONI 71 measures $(-5.9 \pm 2.9) \times 10^{-15}$ e-cm.

Λ DECAY MODES

Mode	Fraction (Γ_i/Γ)	Confidence level
Γ_1 $p\pi^-$	(63.9 ± 0.5) %	
Γ_2 $n\pi^0$	(35.8 ± 0.5) %	
Γ_3 $n\gamma$	(1.75 ± 0.15) × 10 ⁻³	
Γ_4 $p\pi^-\gamma$	[a] (8.4 ± 1.4) × 10 ⁻⁴	
Γ_5 $p e^- \bar{\nu}_e$	(8.32 ± 0.14) × 10 ⁻⁴	
Γ_6 $p \mu^- \bar{\nu}_\mu$	(1.57 ± 0.35) × 10 ⁻⁴	

Lepton (L) and/or Baryon (B) number violating decay modes

Γ_i	Mode	L, B	Upper Limit	90%
Γ_7	$\pi^+ e^-$	L, B	< 6	× 10 ⁻⁷ 90%
Γ_8	$\pi^+ \mu^-$	L, B	< 6	× 10 ⁻⁷ 90%
Γ_9	$\pi^- e^+$	L, B	< 4	× 10 ⁻⁷ 90%
Γ_{10}	$\pi^- \mu^+$	L, B	< 6	× 10 ⁻⁷ 90%
Γ_{11}	$K^+ e^-$	L, B	< 2	× 10 ⁻⁶ 90%
Γ_{12}	$K^+ \mu^-$	L, B	< 3	× 10 ⁻⁶ 90%
Γ_{13}	$K^- e^+$	L, B	< 2	× 10 ⁻⁶ 90%
Γ_{14}	$K^- \mu^+$	L, B	< 3	× 10 ⁻⁶ 90%
Γ_{15}	$K_S^0 \nu$	L, B	< 2	× 10 ⁻⁵ 90%
Γ_{16}	$\bar{p}\pi^+$	B	< 9	× 10 ⁻⁷ 90%

[a] See the Listings below for the pion momentum range used in this measurement.

Baryon Particle Listings

Λ

CONSTRAINED FIT INFORMATION

An overall fit to 5 branching ratios uses 20 measurements and one constraint to determine 5 parameters. The overall fit has a $\chi^2 = 10.5$ for 16 degrees of freedom.

The following *off-diagonal* array elements are the correlation coefficients $\langle \delta x_i \delta x_j \rangle / (\delta x_i \delta x_j)$, in percent, from the fit to the branching fractions, $x_i \equiv \Gamma_i / \Gamma_{\text{total}}$. The fit constrains the x_i whose labels appear in this array to sum to one.

x_2	-100			
x_3	-2	-1		
x_5	46	-46	-1	
x_6	0	0	0	0
	x_1	x_2	x_3	x_5

Λ BRANCHING RATIOS

$\Gamma(\rho\pi^-)/\Gamma(N\pi)$ $\Gamma_1/(\Gamma_1+\Gamma_2)$

VALUE	EVTS	DOCUMENT ID	TECN	COMMENT
0.641 ± 0.005 OUR FIT				
0.640 ± 0.005 OUR AVERAGE				
0.646 ± 0.008	4572	BALTAY	71B HBC	$K^- p$ at rest
0.635 ± 0.007	6736	DOYLE	69 HBC	$\pi^- p \rightarrow \Lambda K^0$
0.643 ± 0.016	903	HUMPHREY	62 HBC	
0.624 ± 0.030		CRAWFORD	59B HBC	$\pi^- p \rightarrow \Lambda K^0$

$\Gamma(n\pi^0)/\Gamma(N\pi)$ $\Gamma_2/(\Gamma_1+\Gamma_2)$

VALUE	EVTS	DOCUMENT ID	TECN	COMMENT
0.359 ± 0.005 OUR FIT				
0.310 ± 0.028 OUR AVERAGE				
0.35 ± 0.05		BROWN	63 HLBC	
0.291 ± 0.034	75	CHRETIEN	63 HLBC	

$\Gamma(n\gamma)/\Gamma_{\text{total}}$ Γ_3/Γ

VALUE (units 10^{-3})	EVTS	DOCUMENT ID	TECN	COMMENT
1.75 ± 0.15 OUR FIT				
1.75 ± 0.15	1816	LARSON	93 SPEC	$K^- p$ at rest
••• We do not use the following data for averages, fits, limits, etc. •••				
$1.78 \pm 0.24^{+0.14}_{-0.16}$	287	NOBLE	92 SPEC	See LARSON 93

$\Gamma(n\gamma)/\Gamma(n\pi^0)$ Γ_3/Γ_2

VALUE (units 10^{-3})	EVTS	DOCUMENT ID	TECN	COMMENT
••• We do not use the following data for averages, fits, limits, etc. •••				
$2.86 \pm 0.74 \pm 0.57$	24	BIAGI	86 SPEC	SPS hyperon beam

$\Gamma(\rho\pi^-\gamma)/\Gamma(\rho\pi^-)$ Γ_4/Γ_1

VALUE (units 10^{-3})	EVTS	DOCUMENT ID	TECN	COMMENT
1.32 ± 0.22	72	BAGGETT	72C HBC	$\pi^- < 95 \text{ MeV}/c$

$\Gamma(\rho e^- \bar{\nu}_e)/\Gamma(\rho\pi^-)$ Γ_5/Γ_1

VALUE (units 10^{-3})	EVTS	DOCUMENT ID	TECN	COMMENT
1.301 ± 0.019 OUR FIT				
1.301 ± 0.019 OUR AVERAGE				
1.335 ± 0.056	7111	BOURQUIN	83 SPEC	SPS hyperon beam
1.313 ± 0.024	10k	WISE	80 SPEC	
1.23 ± 0.11	544	LINDQUIST	77 SPEC	$\pi^- p \rightarrow K^0 \Lambda$
1.27 ± 0.07	1089	KATZ	73 HBC	
1.31 ± 0.06	1078	ALTHOFF	71 OSPK	
1.17 ± 0.13	86	¹ CANTER	71 HBC	$K^- p$ at rest
1.20 ± 0.12	143	² MALONEY	69 HBC	
1.17 ± 0.18	120	² BAGLIN	64 FBC	K^- freon 1.45 GeV/c
1.23 ± 0.20	150	² ELY	63 FBC	
••• We do not use the following data for averages, fits, limits, etc. •••				
1.32 ± 0.15	218	¹ LINDQUIST	71 OSPK	See LINDQUIST 77

¹ Changed by us from $\Gamma(\rho e^- \bar{\nu}_e)/\Gamma(N\pi)$ assuming the authors used $\Gamma(\Lambda \rightarrow p\pi^-)/\Gamma(\text{total}) = 2/3$.

² Changed by us from $\Gamma(\rho e^- \bar{\nu}_e)/\Gamma(N\pi)$ because $\Gamma(\rho e^- \nu)/\Gamma(\rho\pi^-)$ is the directly measured quantity.

$\Gamma(\rho\mu^- \bar{\nu}_\mu)/\Gamma_{\text{total}}$ Γ_6/Γ

VALUE (units 10^{-4})	EVTS	DOCUMENT ID	TECN	COMMENT
1.48 ± 0.21 ± 0.08	64	¹ ABLIKIM	21AG BES3	$J/\psi \rightarrow \Lambda \bar{\Lambda}$

¹ ABLIKIM 21AG use $\bar{\Lambda} \rightarrow \bar{p}\pi^+$ decay mode as the double tag identifier and thus as indirect normalization.

$\Gamma(\rho\mu^- \bar{\nu}_\mu)/\Gamma(N\pi)$ $\Gamma_6/(\Gamma_1+\Gamma_2)$

VALUE (units 10^{-4})	EVTS	DOCUMENT ID	TECN	COMMENT
1.57 ± 0.35 OUR FIT				
1.57 ± 0.35 OUR AVERAGE				
1.4 ± 0.5	14	BAGGETT	72B HBC	$K^- p$ at rest
2.4 ± 0.8	9	CANTER	71B HBC	$K^- p$ at rest
1.3 ± 0.7	3	LIND	64 RVUE	
1.5 ± 1.2	2	RONNE	64 FBC	

Lepton (L) and/or Baryon (B) number violating decay modes

$\Gamma(\pi^+ e^-)/\Gamma_{\text{total}}$ Γ_7/Γ

VALUE	CL%	DOCUMENT ID	TECN	COMMENT
<6 × 10⁻⁷	90	¹ MCCracken	15 CLAS	$\gamma p \rightarrow K^+ \Lambda$

¹ Uses $B(\Lambda \rightarrow p\pi^-) = (63.9 \pm 0.5)\%$ for normalization mode.

$\Gamma(\pi^+ \mu^-)/\Gamma_{\text{total}}$ Γ_8/Γ

VALUE	CL%	DOCUMENT ID	TECN	COMMENT
<6 × 10⁻⁷	90	¹ MCCracken	15 CLAS	$\gamma p \rightarrow K^+ \Lambda$

¹ Uses $B(\Lambda \rightarrow p\pi^-) = (63.9 \pm 0.5)\%$ for normalization mode.

$\Gamma(\pi^- e^+)/\Gamma_{\text{total}}$ Γ_9/Γ

VALUE	CL%	DOCUMENT ID	TECN	COMMENT
<4 × 10⁻⁷	90	¹ MCCracken	15 CLAS	$\gamma p \rightarrow K^+ \Lambda$

¹ Uses $B(\Lambda \rightarrow p\pi^-) = (63.9 \pm 0.5)\%$ for normalization mode.

$\Gamma(\pi^- \mu^+)/\Gamma_{\text{total}}$ Γ_{10}/Γ

VALUE	CL%	DOCUMENT ID	TECN	COMMENT
<6 × 10⁻⁷	90	¹ MCCracken	15 CLAS	$\gamma p \rightarrow K^+ \Lambda$

¹ Uses $B(\Lambda \rightarrow p\pi^-) = (63.9 \pm 0.5)\%$ for normalization mode.

$\Gamma(K^+ e^-)/\Gamma_{\text{total}}$ Γ_{11}/Γ

VALUE	CL%	DOCUMENT ID	TECN	COMMENT
<2 × 10⁻⁶	90	¹ MCCracken	15 CLAS	$\gamma p \rightarrow K^+ \Lambda$

¹ Uses $B(\Lambda \rightarrow p\pi^-) = (63.9 \pm 0.5)\%$ for normalization mode.

$\Gamma(K^+ \mu^-)/\Gamma_{\text{total}}$ Γ_{12}/Γ

VALUE	CL%	DOCUMENT ID	TECN	COMMENT
<3 × 10⁻⁶	90	¹ MCCracken	15 CLAS	$\gamma p \rightarrow K^+ \Lambda$

¹ Uses $B(\Lambda \rightarrow p\pi^-) = (63.9 \pm 0.5)\%$ for normalization mode.

$\Gamma(K^- e^+)/\Gamma_{\text{total}}$ Γ_{13}/Γ

VALUE	CL%	DOCUMENT ID	TECN	COMMENT
<2 × 10⁻⁶	90	¹ MCCracken	15 CLAS	$\gamma p \rightarrow K^+ \Lambda$

¹ Uses $B(\Lambda \rightarrow p\pi^-) = (63.9 \pm 0.5)\%$ for normalization mode.

$\Gamma(K^- \mu^+)/\Gamma_{\text{total}}$ Γ_{14}/Γ

VALUE	CL%	DOCUMENT ID	TECN	COMMENT
<3 × 10⁻⁶	90	¹ MCCracken	15 CLAS	$\gamma p \rightarrow K^+ \Lambda$

¹ Uses $B(\Lambda \rightarrow p\pi^-) = (63.9 \pm 0.5)\%$ for normalization mode.

$\Gamma(K_S^0 \nu)/\Gamma_{\text{total}}$ Γ_{15}/Γ

VALUE	CL%	DOCUMENT ID	TECN	COMMENT
<2 × 10⁻⁵	90	¹ MCCracken	15 CLAS	$\gamma p \rightarrow K^+ \Lambda$

¹ Uses $B(\Lambda \rightarrow p\pi^-) = (63.9 \pm 0.5)\%$ for normalization mode.

$\Gamma(\bar{p}\pi^+)/\Gamma_{\text{total}}$ Γ_{16}/Γ

VALUE	CL%	DOCUMENT ID	TECN	COMMENT
<9 × 10⁻⁷	90	¹ MCCracken	15 CLAS	$\gamma p \rightarrow K^+ \Lambda$

¹ Uses $B(\Lambda \rightarrow p\pi^-) = (63.9 \pm 0.5)\%$ for normalization mode.

Λ CP-violating decay-rate asymmetries

This is the difference between Λ and $\bar{\Lambda}$ decay rates to state f and \bar{f} divided by the sum of the rates:

$$A_{CP}(f) = [(B(\Lambda \rightarrow f)) - (B(\bar{\Lambda} \rightarrow \bar{f}))] / \text{Sum.}$$

$A_{CP}(\rho\mu^- \bar{\nu}_\mu)$ in $\Lambda \rightarrow \rho\mu^- \bar{\nu}_\mu, \bar{\Lambda} \rightarrow \bar{p}\mu^+ \nu_\mu$

VALUE	DOCUMENT ID	TECN	COMMENT
0.02 ± 0.14 ± 0.02	ABLIKIM	21AG BES3	$J/\psi \rightarrow \Lambda \bar{\Lambda}$

Λ DECAY PARAMETERS

See the "Note on Baryon Decay Parameters" in the neutron Listings. Some early results have been omitted.

α_- FOR $\Lambda \rightarrow p\pi^-$

VALUE	EVTS	DOCUMENT ID	TECN	COMMENT
0.732 ± 0.014 OUR AVERAGE				Error includes scale factor of 2.3.
0.750 ± 0.009 ± 0.004	420k	ABLIKIM	19BJ BES3	J/ψ to $\Lambda \bar{\Lambda}$
0.721 ± 0.006 ± 0.005		¹ IRELAND	19 CLAS	K production

••• We do not use the following data for averages, fits, limits, etc. •••

0.74 ^{+0.04} _{-0.03}		AAIJ	200 LHCB	$\Lambda_b \rightarrow J/\psi \Lambda$
0.584 ± 0.046	8500	ASTBURY	75 SPEC	
0.649 ± 0.023	10325	CLELAND	72 OSPK	
0.67 ± 0.06	3520	DAUBER	69 HBC	From Ξ decay
0.645 ± 0.017	10130	OVERSETH	67 OSPK	Λ from $\pi^- p$
0.62 ± 0.07	1156	CRONIN	63 CNTR	Λ from $\pi^- p$

¹ This is a new analysis based on existing kaon photoproduction data of the CLAS collaboration and using spin algebra constraints.

α₊ FOR $\bar{\Lambda} \rightarrow \bar{p}\pi^+$

VALUE	EVTS	DOCUMENT ID	TECN	COMMENT
-0.758 ± 0.010 ± 0.007	420k	ABLIKIM	19Bj BES3	J/ψ to ΛΛ
••• We do not use the following data for averages, fits, limits, etc. •••				
-0.755 ± 0.083 ± 0.063	≈ 8.7k	ABLIKIM	10 BES	J/ψ → ΛΛ
-0.63 ± 0.13	770	TIXIER	88 DM2	J/ψ → ΛΛ

α₀ FOR $\bar{\Lambda} \rightarrow \pi\pi^0$

VALUE	EVTS	DOCUMENT ID	TECN	COMMENT
-0.692 ± 0.016 ± 0.006	47k	ABLIKIM	19Bj BES3	J/ψ to ΛΛ

φ ANGLE FOR $\Lambda \rightarrow p\pi^-$

(tanφ = β / γ)

VALUE (°)	EVTS	DOCUMENT ID	TECN	COMMENT
-6.5 ± 3.5 OUR AVERAGE				
-7.0 ± 4.5	10325	CLELAND	72 OSPK	Λ from π ⁻ p
-8.0 ± 6.0	10130	OVERSETH	67 OSPK	Λ from π ⁻ p
13.0 ± 17.0	1156	CRONIN	63 OSPK	Λ from π ⁻ p

α₀ / α₋ = α(Λ → nπ⁰) / α(Λ → pπ⁻)

VALUE	EVTS	DOCUMENT ID	TECN	COMMENT
1.01 ± 0.07 OUR AVERAGE				
1.000 ± 0.068	4760	¹ OLSEN	70 OSPK	π ⁺ n → ΛK ⁺
1.10 ± 0.27		CORK	60 CNTR	

¹OLSEN 70 compares proton and neutron distributions from Λ decay.

α₀ / α₊ in $\bar{\Lambda} \rightarrow \pi\pi^0, \bar{\Lambda} \rightarrow \bar{p}\pi^+$

VALUE	EVTS	DOCUMENT ID	TECN	COMMENT
0.913 ± 0.028 ± 0.012	47k	ABLIKIM	19Bj BES3	J/ψ to ΛΛ

(α + ᾱ) / (α - ᾱ) in $\Lambda \rightarrow p\pi^-, \bar{\Lambda} \rightarrow \bar{p}\pi^+$

Zero if CP is conserved; α₋ and α₊ are the asymmetry parameters for Λ → pπ⁻ and $\bar{\Lambda} \rightarrow \bar{p}\pi^+$ decay. See also the Ξ⁻ for a similar test involving the decay chain Ξ⁻ → Λπ⁻, Λ → pπ⁻ and the corresponding antiparticle chain.

VALUE	EVTS	DOCUMENT ID	TECN	COMMENT
-0.002 ± 0.012 OUR AVERAGE				
-0.006 ± 0.012 ± 0.007	420k	ABLIKIM	19Bj BES3	J/ψ to ΛΛ
-0.081 ± 0.055 ± 0.059	≈ 8.7k	ABLIKIM	10 BES	J/ψ → ΛΛ
+0.013 ± 0.022	96k	BARNES	96 CNTR	LEAR $\bar{p}p \rightarrow \bar{\Lambda}\Lambda$
+0.01 ± 0.10	770	TIXIER	88 DM2	J/ψ → ΛΛ
-0.02 ± 0.14	10k	¹ CHAUVAT	85 CNTR	pp, $\bar{p}p$ ISR
••• We do not use the following data for averages, fits, limits, etc. •••				
-0.07 ± 0.09	4063	BARNES	87 CNTR	See BARNES 96

¹CHAUVAT 85 actually gives α₊($\bar{\Lambda}$) / α₋(Λ) = -1.04 ± 0.29. Assumes polarization is same in $\bar{p}p \rightarrow \bar{\Lambda}\Lambda$ and $pp \rightarrow \Lambda\Lambda$. Tests of this assumption, based on C-invariance and fragmentation, are satisfied by the data.

R = |G_E/G_M| in $\Lambda \rightarrow p\pi^-, \bar{\Lambda} \rightarrow \bar{p}\pi^+$

VALUE	DOCUMENT ID	TECN	COMMENT
0.96 ± 0.14 ± 0.02	¹ ABLIKIM	19Bf BES3	e ⁺ e ⁻ → $\bar{\Lambda}\Lambda$ at \sqrt{s} = 2.396 GeV

¹Determined using the latest BES-III value on the asymmetry parameter α = 0.750 ± 0.010.

Δφ = φ_E - φ_M in $\Lambda \rightarrow p\pi^-, \bar{\Lambda} \rightarrow \bar{p}\pi^+$

VALUE (degrees)	DOCUMENT ID	TECN	COMMENT
37 ± 12 ± 6	¹ ABLIKIM	19Bf BES3	e ⁺ e ⁻ → $\bar{\Lambda}\Lambda$ at \sqrt{s} = 2.396 GeV

¹Relative phase between GE and GM, determined using the latest BES-III value on the asymmetry parameter α = 0.750 ± 0.010.

g_A / g_V FOR $\Lambda \rightarrow p e^- \bar{\nu}_e$

Measurements with fewer than 500 events have been omitted. Where necessary, signs have been changed to agree with our conventions, which are given in the "Note on Baryon Decay Parameters" in the neutron Listings. The measurements all assume that the form factor g₂ = 0. See also the footnote on DWORKIN 90.

VALUE	EVTS	DOCUMENT ID	TECN	COMMENT
-0.718 ± 0.015 OUR AVERAGE				
-0.719 ± 0.016 ± 0.012	37k	¹ DWORKIN	90 SPEC	eν angular corr.
-0.70 ± 0.03	7111	BOURQUIN	83 SPEC	Ξ → Λπ ⁻
-0.734 ± 0.031	10k	² WISE	81 SPEC	eν angular correl.
••• We do not use the following data for averages, fits, limits, etc. •••				
-0.63 ± 0.06	817	ALTHOFF	73 OSPK	Polarized Λ

¹The tabulated result assumes the weak-magnetism coupling w ≡ g_w(0)/g_v(0) to be 0.97, as given by the CVC hypothesis and as assumed by the other listed measurements. However, DWORKIN 90 measures w to be 0.15 ± 0.30, and then g_A/g_V = -0.731 ± 0.016.
²This experiment measures only the absolute value of g_A/g_V.

Λ REFERENCES

We have omitted some papers that have been superseded by later experiments. See our earlier editions.

ABLIKIM	21AG	PRL 127 121802	M. Ablikim et al.	(BESIII Collab.)
AAJ	20O	JHEP 2006 110	R. Aaij et al.	(LHCb Collab.)
ABLIKIM	19BF	PRL 123 122003	M. Ablikim et al.	(BESIII Collab.)
ABLIKIM	19BJ	NATP 15 631	M. Ablikim et al.	(BESIII Collab.)
IRELAND	19	PRL 123 182301	D.G. Ireland et al.	(GLAS, GWU, JULI+)

MCCRACKEN	15	PR D92 072002	M.E. McCracken et al.	(JLab CLAS Collab.)
ABLIKIM	10	PR D81 012003	M. Ablikim et al.	(BES Collab.)
BARNES	96	PR C54 1877	P.D. Barnes et al.	(CERN PS-185 Collab.)
RYBICKI	96	APP B27 2155	K. Rybicki	
HARTOUNI	94	PRL 72 1322	E.P. Hartouni et al.	(BNL E766 Collab.)
Also		PRL 72 2821 (erratum)	E.P. Hartouni et al.	(BNL E766 Collab.)
LARSON	93	PR D47 799	K.D. Larson et al.	(BNL-811 Collab.)
NOBLE	92	PRL 69 414	A.J. Noble et al.	(BIRM, BOST, BRCO+)
DWORKIN	90	PR D41 780	J. Dworkin et al.	(MICH, WISC, RUTG+)
TIXIER	88	PL B212 523	M.H. Tixier et al.	(DM2 Collab.)
BARNES	87	PL B199 147	P.D. Barnes et al.	(CMU, SA CL, LANL+)
BIAGI	86	ZPHY C30 201	S.F. Biagi et al.	(BRIS, CERN, GEVA+)
CHAUVAT	85	PL 163B 273	P. Chauvat et al.	(CERN, CLER, UCLA+)
BOURQUIN	83	ZPHY C21 1	M.H. Bourquin et al.	(BRIS, GEVA, HEID+)
COX	81	PRL 46 877	P.T. Cox et al.	(MICH, WISC, RUTG, MINN+)
PONDROM	81	PR D23 814	L. Pondrom et al.	(WISC, MICH, RUTG+)
WISE	81	PL 98B 123	J.E. Wise et al.	(MASA, BNL)
WISE	80	PL 91B 165	J.E. Wise et al.	(MASA, BNL)
SCHACHIN...	78	PRL 41 1348	L. Schachinger et al.	(MICH, RUTG, WISC)
HELLER	77	PL 68B 480	K. Heller et al.	(MICH, WISC, HEIDH)
LINDQUIST	77	PR D16 2104	J. Lindquist et al.	(EFI, OSU, ANL)
Also		JP G2 L211	J. Lindquist et al.	(EFI, WUSL, OSU+)
ZECH	77	NP B124-413	G. Zech et al.	(SIEG, CERN, DORT, HEIDH)
BUNCE	76	PRL 36 1113	G.R.M. Bunce et al.	(WISC, MICH, RUTG)
ASTBURY	75	NP B99 30	P. Astbury et al.	(LOIC, CERN, ETH+)
CLAYTON	75	NP B95 130	E.F. Clayton et al.	(LOIC, RHEL)
ALTHOFF	73	PL 43B 237	K.H. Althoff et al.	(CERN, HEID)
ALTHOFF	73B	NP B66 29	K.H. Althoff et al.	(CERN, HEID)
KATZ	73	Thesis MDDP-TR-74-044	C.N. Katz	(UMD)
POULARD	73	PL 46B 135	G. Poulard, A. Givernaud, A.C. Borg	(SACL)
BAGGETT	72B	ZPHY 252 362	M.J. Baggett et al.	(HEID)
BAGGETT	72C	PL 42B 379	M.J. Baggett et al.	(HEID)
CLELAND	72	NP B40 221	W.E. Cleland et al.	(CERN, GEVA, LUND)
HYMAN	72	PR D5 1063	L.G. Hyman et al.	(ANL, CMU)
ALTHOFF	71	PL 37B 531	K.H. Althoff et al.	(CERN, HEID)
BALTAY	71B	PR D4 670	C. Baltay et al.	(COLU, BING)
BARONI	71	LCN 2 1256	G. Baroni, S. Petrella, G. Romano	(ROMA)
CANTER	71	PRL 26 868	J. Canter et al.	(STON, COLU)
CANTER	71B	PRL 27 59	J. Canter et al.	(STON, COLU)
DAHL-JENSEN	71	NC 3A 1	E. Dahl-Jensen et al.	(CERN, ANKA, LAUS+)
LINDQUIST	71	PRL 27 612	J. Lindquist et al.	(EFI, WUSL, OSU+)
OLSEN	70	PRL 24 843	S.L. Olsen et al.	(WISC, MICH)
DAUBER	69	PR 179 1262	F.M. Dauber et al.	(LRL)
DOYLE	69	Thesis UCLR 18139	J.C. Doyle	(LRL)
MALONEY	69	PRL 23 425	J.E. Maloney, B. Sechi-Zorn	(UMD)
GRIMM	68	NC 54A 187	H.J. Grimm	(HEID)
HEPP	68	ZPHY 214 71	V. Hepp, H. Schleich	(HEID)
MAYEUR	67	PL 25B 152	J. Badier et al.	(EPOL)
OVERSETH	67	U.Libr.Brux.Bul. 32	C. Mayeur, E. Tompa, J.H. Wickens	(BELG, LUC)
OVERSETH	67	PRL 19 391	O.E. Overseth, R.F. Roth	(MICH, PRIN)
PDG	67	RMP 39 1	A.H. Rosenfeld et al.	(LRL, CERN, YALE)
BURAN	66	PL 20 318	T. Buran et al.	(OSLO)
CHIEN	66	PR 152 1171	C.Y. Chien et al.	(YALE, BNL)
ENGELMANN	66	NC 45A 1038	R. Engelman et al.	(HEID, REHO)
GIBSON	66	NC 45A 882	W.M. Gibson, K. Green	(BRIS)
LONDON	66	PR 143 1034	G.W. London et al.	(BNL, SYRA)
SCHMIDT	65	PR 140 B1328	P. Schmidt	(COLU)
BAGLIN	64	NC 35 977	C. Baglin et al.	(EPOL, CERN, LOUC, RHEL+)
HUBBARD	64	PR 135 B183	J.R. Hubbard et al.	(LRL)
LIND	64	PR 135 B1483	V.G. Lind et al.	(WISC)
RONNE	64	PL 11 357	B.E. Ronne et al.	(CERN, EPOL, LOUC+)
SCHWARTZ	64	Thesis UCLR 11360	J.A. Schwartz	(LRL)
BHOWMIK	63	NC 28 1494	B. Bhowmik, D.P. Goyal	(DELH)
BLOCK	63	PR 130 766	M.M. Block et al.	(NWES, BGNA, SYRA+)
BROWN	63	PR 130 769	J.L. Brown et al.	(LRL, MICH)
CHRETIEN	63	PR 131 2208	M. Chretien et al.	(BRAN, BROW, HARV+)
CRONIN	63	PR 129 1795	J.W. Cronin, O.E. Overseth	(PRIN)
ELY	63	PR 131 868	R.P. Ely et al.	(LRL)
HUMPHREY	62	PR 127 1305	W.E. Humphrey, R.R. Ross	(LRL)
CORK	60	PR 120 1000	B. Cork et al.	(LRL, PRIN, BNL)
CRAWFORD	59B	PRL 2 266	F.S. Crawford et al.	(LRL)

See the related review(s):

Λ and Σ Resonances

Λ(1380) 1/2⁻

$J^P = \frac{1}{2}^-$ Status: * *

OMITTED FROM SUMMARY TABLE

See the related review on "Pole Structure of the Λ(1405) Region."

Λ(1380) POLE POSITION

REAL PART

VALUE (MeV)	DOCUMENT ID	TECN
••• We do not use the following data for averages, fits, limits, etc. •••		
1325 ± 15	¹ MAI	15 DPWA
1330 ⁺¹ - 4	² MAI	15 DPWA
1388 ± 9	GUO	13 DPWA
1381 ⁺¹⁸ - 6	IKEDA	12 DPWA

¹Solution number 4.
²Solution number 2.

-2xIMAGINARY PART

VALUE (MeV)	DOCUMENT ID	TECN
••• We do not use the following data for averages, fits, limits, etc. •••		
180 ⁺²⁴ - 36	¹ MAI	15 DPWA
112 ⁺³⁴ - 22	² MAI	15 DPWA
228 ⁺⁴⁸ - 50	GUO	13 DPWA
162 ⁺³⁸ - 16	IKEDA	12 DPWA

¹Solution number 4.
²Solution number 2.

Baryon Particle Listings

 $\Lambda(1380), \Lambda(1405)$ $\Lambda(1380)$ REFERENCES

MAI	15	EPJ A51 30	M. Mai, U.-G. Meißner	(BONN, JULI)
GUO	13	PR C07 035202	Z.-H. Guo, J. Oller	
IKEDA	12	NP A881 98	Y. Ikeda, T. Hyodo, W. Weise	(TUM, RIKEN, TINT)

 $\Lambda(1405) 1/2^-$

$$I(J^P) = 0(\frac{1}{2}^-) \text{ Status: } ****$$

In the 1998 Note on the $\Lambda(1405)$ in PDG 98, R.H. Dalitz discussed the S-shaped cusp behavior of the intensity at the $N\bar{K}$ threshold observed in THOMAS 73 and HEMINGWAY 85. He commented that this behavior "is characteristic of S-wave coupling; the other below threshold hyperon, the $\Sigma(1385)$, has no such threshold distortion because its $N\bar{K}$ coupling is P-wave. For $\Lambda(1405)$ this asymmetry is the sole direct evidence that $J^P = 1/2^-$."

A recent measurement by the CLAS collaboration, MORIYA 14, definitively established the long-assumed $J^P = 1/2^-$ spin-parity assignment of the $\Lambda(1405)$. The experiment produced the $\Lambda(1405)$ spin-polarized in the photoproduction process $\gamma p \rightarrow K^+ \Lambda(1405)$ and measured the decay of the $\Lambda(1405)$ (polarized) $\rightarrow \Sigma^+$ (polarized) π^- . The observed isotropic decay of $\Lambda(1405)$ is consistent with spin $J = 1/2$. The polarization transfer to the Σ^+ (polarized) direction revealed negative parity, and thus established $J^P = 1/2^-$.

See the related review(s):
Pole Structure of the $\Lambda(1405)$ Region

 $\Lambda(1405)$ POLE POSITION

REAL PART

VALUE (MeV)	DOCUMENT ID	TECN
$1429 \pm \frac{8}{7}$	¹ MAI 15	DPWA
1434 ± 2	² MAI 15	DPWA
$1421 \pm \frac{3}{2}$	GUO 13	DPWA
$1424 \pm \frac{7}{23}$	IKEDA 12	DPWA

¹ Solution number 4.
² Solution number 2.

-2xIMAGINARY PART

VALUE (MeV)	DOCUMENT ID	TECN
$24 \pm \frac{4}{6}$	¹ MAI 15	DPWA
$20 \pm \frac{4}{2}$	² MAI 15	DPWA
$38 \pm \frac{16}{10}$	GUO 13	DPWA
$52 \pm \frac{6}{28}$	IKEDA 12	DPWA

¹ Solution number 4.
² Solution number 2.

 $\Lambda(1405)$ MASS

PRODUCTION EXPERIMENTS

VALUE (MeV)	EVTS	DOCUMENT ID	TECN	COMMENT
$1405.1 \pm \frac{1.3}{1.0}$	OUR AVERAGE			
$1405 \pm \frac{11}{9}$		HASSANVAND 13	SPEC	$pp \rightarrow p\Lambda(1405)K^+$
$1405 \pm \frac{1.4}{1.0}$		ESMAILI 10	RVUE	$^4\text{He } K^- \rightarrow \Sigma^\pm \pi^\mp X$ at rest
1406.5 ± 4.0		¹ DALITZ 91		M-matrix fit
••• We do not use the following data for averages, fits, limits, etc. •••				
1391 ± 1	700	¹ HEMINGWAY 85	HBC	$K^- p$ 4.2 GeV/c
~ 1405	400	² THOMAS 73	HBC	$\pi^- p$ 1.69 GeV/c
1405	120	BARBARO... 68B	DBC	$K^- d$ 2.1-2.7 GeV/c
1400 ± 5	67	BIRMINGHAM 66	HBC	$K^- p$ 3.5 GeV/c
1382 ± 8		ENGLER 65	HDBC	$\pi^- p, \pi^+ d$ 1.68 GeV/c
1400 ± 24		MUSGRAVE 65	HBC	$\bar{p}p$ 3-4 GeV/c
1410		ALEXANDER 62	HBC	$\pi^- p$ 2.1 GeV/c
1405		ALSTON 62	HBC	$K^- p$ 1.2-0.5 GeV/c
1405		ALSTON 61B	HBC	$K^- p$ 1.15 GeV/c

¹ DALITZ 91 fits the HEMINGWAY 85 data.
² THOMAS 73 data is fit by CHAO 73 (see next section).

EXTRAPOLATIONS BELOW $N\bar{K}$ THRESHOLD

VALUE (MeV)	DOCUMENT ID	TECN	COMMENT
1407.56 or 1407.50	¹ KIMURA 00		potential model
1411	² MARTIN 81		K-matrix fit

1406	³ CHAO 73	DPWA	0-range fit (sol. B)
1421	MARTIN 70	RVUE	Constant K-matrix
1416 ± 4	MARTIN 69	HBC	Constant K-matrix
1403 ± 3	KIM 67	HBC	K-matrix fit
1407.5 ± 1.2	⁴ KITTEL 66	HBC	0-effective-range fit
1410.7 ± 1.0	KIM 65	HBC	0-effective-range fit
1409.6 ± 1.7	⁴ SAKITT 65	HBC	0-effective-range fit

¹ The KIMURA 00 values are from fits A and B from a coupled-channel potential model using low-energy $\bar{K}N$ and $\Sigma\pi$ data, kaonic-hydrogen x-ray measurements, and our $\Lambda(1405)$ mass and width. The results bear mainly on the nature of the $\Lambda(1405)$: three-quark state or $\bar{K}N$ bound state.

² The MARTIN 81 fit includes the $K^\pm p$ forward scattering amplitudes and the dispersion relations they must satisfy.

³ See also the accompanying paper of THOMAS 73.

⁴ Data of SAKITT 65 are used in the fit by KITTEL 66.

 $\Lambda(1405)$ WIDTH

PRODUCTION EXPERIMENTS

VALUE (MeV)	EVTS	DOCUMENT ID	TECN	COMMENT
50.5 ± 2.0	OUR AVERAGE			
62 ± 10		HASSANVAND 13	SPEC	$pp \rightarrow p\Lambda(1405)K^+$
50 ± 2		¹ DALITZ 91		M-matrix fit
••• We do not use the following data for averages, fits, limits, etc. •••				
$24 \pm \frac{4}{3}$		ESMAILI 10	RVUE	$^4\text{He } K^- \rightarrow \Sigma^\pm \pi^\mp X$ at rest
32 ± 1	700	¹ HEMINGWAY 85	HBC	$K^- p$ 4.2 GeV/c
45 to 55	400	² THOMAS 73	HBC	$\pi^- p$ 1.69 GeV/c
35	120	BARBARO... 68B	DBC	$K^- d$ 2.1-2.7 GeV/c
50 ± 10	67	BIRMINGHAM 66	HBC	$K^- p$ 3.5 GeV/c
89 ± 20		ENGLER 65	HDBC	
60 ± 20		MUSGRAVE 65	HBC	
35 ± 5		ALEXANDER 62	HBC	
50		ALSTON 62	HBC	
20		ALSTON 61B	HBC	

¹ DALITZ 91 fits the HEMINGWAY 85 data.

² THOMAS 73 data is fit by CHAO 73 (see next section).

EXTRAPOLATIONS BELOW $N\bar{K}$ THRESHOLD

VALUE (MeV)	DOCUMENT ID	TECN	COMMENT
••• We do not use the following data for averages, fits, limits, etc. •••			
50.24 or 50.26	¹ KIMURA 00		potential model
30	² MARTIN 81		K-matrix fit
55	^{3,4} CHAO 73	DPWA	0-range fit (sol. B)
20	MARTIN 70	RVUE	Constant K-matrix
29 ± 6	MARTIN 69	HBC	Constant K-matrix
50 ± 5	KIM 67	HBC	K-matrix fit
34.1 ± 4.1	⁵ KITTEL 66	HBC	
37.0 ± 3.2	KIM 65	HBC	
28.2 ± 4.1	⁵ SAKITT 65	HBC	

¹ The KIMURA 00 values are from fits A and B from a coupled-channel potential model using low-energy $\bar{K}N$ and $\Sigma\pi$ data, kaonic-hydrogen x-ray measurements, and our $\Lambda(1405)$ mass and width. The results bear mainly on the nature of the $\Lambda(1405)$: three-quark state or $\bar{K}N$ bound state.

² The MARTIN 81 fit includes the $K^\pm p$ forward scattering amplitudes and the dispersion relations they must satisfy.

³ An asymmetric shape, with $\Gamma/2 = 41$ MeV below resonance, 14 MeV above.

⁴ See also the accompanying paper of THOMAS 73.

⁵ Data of SAKITT 65 are used in the fit by KITTEL 66.

 $\Lambda(1405)$ DECAY MODES

Mode	Fraction (Γ_i/Γ)
$\Gamma_1 \Sigma\pi$	100 %
$\Gamma_2 \Lambda\gamma$	
$\Gamma_3 \Sigma^0\gamma$	
$\Gamma_4 N\bar{K}$	

 $\Lambda(1405)$ PARTIAL WIDTHS

$\Gamma(\Lambda\gamma)$	DOCUMENT ID	COMMENT	Γ_2
VALUE (keV)			
••• We do not use the following data for averages, fits, limits, etc. •••			
27 ± 8	BURKHARDT 91	Isobar model fit	
$\Gamma(\Sigma^0\gamma)$	DOCUMENT ID	COMMENT	Γ_3
VALUE (keV)			
••• We do not use the following data for averages, fits, limits, etc. •••			
10 ± 4 or 23 ± 7	BURKHARDT 91	Isobar model fit	

 $\Lambda(1405)$ BRANCHING RATIOS

$\Gamma(N\bar{K})/\Gamma(\Sigma\pi)$	CL%	DOCUMENT ID	TECN	COMMENT	Γ_4/Γ_1
VALUE					
••• We do not use the following data for averages, fits, limits, etc. •••					
<3	95	HEMINGWAY 85	HBC	$K^- p$ 4.2 GeV/c	

Baryon Particle Listings

$\Lambda(1405)$, $\Lambda(1520)$

$\Lambda(1405)$ REFERENCES

MAI	15	EPJ A51 30	M. Mai, U.-G. Meißner (BONN, JULI)
MORIYA	14	PRL 112 082004	K. Moriya et al. (CLAS Collab.) JP
GUO	13	PR C87 035202	Z.-H. Guo, J. Oller
HASSANVAND	13	PR C87 055202	M. Hassanvand et al.
Also		PR C88 019905 (errata)	M. Hassanvand et al.
IKEDA	12	NP A881 98	Y. Ikeda, T. Hyodo, W. Weise (TUM, RIKEN, TINT)
ESMALI	10	PL B686 23	J. Esmaili, Y. Akaishi, T. Yamazaki (RIKEN, ISUT+)
KIMURA	00	PR C62 015206	M. Kimura et al.
PDG	98	EPJ C3 1	C. Caso et al. (PDG Collab.)
BURKHARDT	91	PR C44 607	H. Burkhardt, J. Lowe (NOTT, UNM, BIRM)
DALITZ	91	JP G17 289	R.H. Dalitz, A. Deloff (OXFTP, WINR)
HENNINGWAY	85	NP B253 742	R.J. Hemingway (CERN)
MARTIN	81	NP B179 33	A.D. Martin (DURH)
CHAO	73	NP B56 46	Y.A. Chao et al. (RHEL, CMU, LOUC)
THOMAS	73	NP B56 15	D.W. Thomas et al. (CMU) J
MARTIN	70	NP B16 479	A.D. Martin, G.G. Ross (DURH)
MARTIN	69	PR 183 1352	B.R. Martin, M. Sakitt (LOUC, BNL)
Also		PR 183 1345	B.R. Martin, M. Sakitt (LOUC, BNL)
BARBARO...	68B	PRL 21 573	A. Barbaro-Galiteri et al. (LRL, SLAC)
KIM	67	PRL 19 1074	J.K. Kim (YALE)
BIRMINGHAM	66	PR 152 1148	M. Haque et al. (BIRM, GLS, LOIC, OXF+)
KITTEL	66	PL 21 349	W. Kittel, G. Otter, I. Wacek (VIEN)
ENGLER	65	PRL 15 224	A. Engler et al. (CMU, BNL, IJ)
KIM	65	PRL 14 29	J.K. Kim (COLU)
MUSGRAVE	65	NC 35 735	B. Musgrave et al. (BIRM, CERN, EPOL+)
SAKITT	65	PR 139 8719	M. Sakitt et al. (UMD, LRL)
ALEXANDER	62	PRL 8 447	G. Alexander et al. (LRL) I
ALSTON	62	CERN Conf. 311	M.H. Alston et al. (LRL) I
ALSTON	61B	PRL 6 698	M.H. Alston et al. (LRL) I

OTHER RELATED PAPERS

IWASAKI	97	PRL 78 3067	M. Iwasaki et al. (KEK 228 Collab.)
FINK	90	PR C41 2720	P.J.Jr. Fink et al. (IBMY, ORST, ANSM)
LEINWEBER	90	ANP 198 203	D.B. Leinweber (MCMS)
MUELLER-GR...	90	NP A513 557	A. Mueller-Groeling, K. Holinde, J. Speth (JULI)
BARRETT	89	NC 102A 179	R.C. Barrett (SURR)
BATTY	89	NC 102A 255	C.J. Batty, A. Gal (RAL, HEBR)
CAPSTICK	89	Excited Baryons 88, p.32	S. Capstick (GUEL)
LOWE	89	NC 102A 167	J. Lowe (BIRM)
WHITEHOUSE	89	PRL 63 1352	D.A. Whitehouse et al. (BIRM, BOST, BRCCO+)
SIEGEL	88	PR C38 2221	P.B. Siegel, W. Weise (REGE)
WORKMAN	88	PR D37 3117	R.L. Workman, H.W. Fearing (TRIUM)
SCHNICK	87	PRL 58 1719	J. Schnick, R.H. Landau (ORST)
CAPSTICK	86	PR D34 2809	S. Capstick, N. Isgur (TNTO)
JENNINGS	86	PL B176 229	B.K. Jennings (TRIUM)
MALTMAN	86	PR D34 1372	K. Maltman, N. Isgur (LANL, TNTO)
ZHONG	86	PL B171 471	Y.S. Zhong et al. (ADLD, TRIUM, SURR)
BURKHARDT	85	NP A440 653	H. Burkhardt, J. Lowe, A.S. Rosenthal (NOTT+)
DAREWYCH	85	PR D32 1765	J.W. Darewych, R. Koniuk, N. Isgur (YORKC, TNTO)
VEIT	85	PR D31 1033	E.A. Veit et al. (TRIUM, ADLD, SURR)
KIANG	84	PR C30 1638	D. Kiang et al. (DALH, MCMS)
MILLER	84	Conference paper	D.J. Miller (LOUC)
Conf. Intersections between Particle and Nuclear Physics, p. 783			
VANDIJK	84	PR D30 937	W. van Dijk (MCMS)
VEIT	84	PL 137B 415	E.A. Veit et al. (TRIUM, SURR, CERN)
DALITZ	82	Heid. Conf.	R.H. Dalitz et al. (OXFTP)
Heidelberg Conf., p. 201			
DALITZ	81	Kaon Conf.	R.H. Dalitz, J.G. McGinley (OXFTP)
Low and Intermediate Energy Kaon-Nucleon Physics, p.381			
MARTIN	81B	Kaon Conf.	A.D. Martin (DURH)
Low and Intermediate Energy Kaon-Nucleon Physics, p. 97			
OADES	77	NC 42A 482	G.C. Oades, G. Rasche (AARH, ZURI)
SHAW	73	Purdue Conf. 417	G.L. Shaw (UCI)
BARBARO...	72	LBL-555	A. Barbaro-Galiteri (LBL)
DOBSON	72	PR D6 3256	P.N. Dobson, R. McEthaney (HAWA)
RAJASEKARA...	72	PR D5 610	G. Rajasekaran (TATA)
Earlier papers also cited in RAJASEKARAN 72.			
CLINE	71	PRL 26 1194	D. Cline, R. Laumann, J. Mapp (WIS C)
MARTIN	71	PL 35B 62	A.D. Martin, A.D. Martin, G.G. Ross (DURH, LOUC+)
DALITZ	67	PR 153 1617	R.H. Dalitz, T.C. Wong, G. Rajasekaran (OXFTP+)
DONALD	66	PL 22 711	R.A. Donald et al. (LIVP)
KADYK	66	PRL 17 599	J.A. Kadyk et al. (LRL)
ABRAMS	65	PR 139 B454	G.S. Abrams, B. Sechi-Zorn (UMD)

$\Lambda(1520) \ 3/2^-$

 $\Gamma(J^P) = 0(\frac{3}{2}^-)$ Status: ***

Discovered by FERRO-LUZZI 62; the elaboration in WATSON 63 is the classic paper on the Breit-Wigner analysis of a multichannel resonance.

The measurements of the mass, width, and elasticity published before 1975 are now obsolete and have been omitted. They were last listed in our 1982 edition Physics Letters **111B** 1 (1982).

Production and formation experiments agree quite well, so they are listed together here.

$\Lambda(1520)$ POLE POSITION

REAL PART				
VALUE (MeV)	DOCUMENT ID	TECN	COMMENT	
1517 to 1518 (≈ 1517.5) OUR ESTIMATE				
1517.5 \pm 0.4 OUR AVERAGE				
1517.5 \pm 0.4	SARANTSEV	19	DPWA	$\bar{K}N$ multichannel
1517 +4 -4	¹ KAMANO	15	DPWA	$\bar{K}N$ multichannel
••• We do not use the following data for averages, fits, limits, etc. •••				
1518	ZHANG	13A	DPWA	$\bar{K}N$ multichannel
1518.8	QIANG	10	SPEC	$ep \rightarrow e'K^+X$ (fit to X)
¹ From the preferred solution A in KAMANO 15.				

-2xIMAGINARY PART

VALUE (MeV)	DOCUMENT ID	TECN	COMMENT	
14 to 18 (≈ 16) OUR ESTIMATE				
15.3 \pm 0.9 OUR AVERAGE				
15.3 \pm 0.9	SARANTSEV	19	DPWA	$\bar{K}N$ multichannel
15 +10 -8	¹ KAMANO	15	DPWA	$\bar{K}N$ multichannel
••• We do not use the following data for averages, fits, limits, etc. •••				
16	ZHANG	13A	DPWA	$\bar{K}N$ multichannel
17.2	QIANG	10	SPEC	$ep \rightarrow e'K^+X$ (fit to X)
¹ From the preferred solution A in KAMANO 15.				

$\Lambda(1520)$ POLE RESIDUES

The normalized residue is the residue divided by $\Gamma_{pole}/2$.

Normalized residue in $N\bar{K} \rightarrow \Lambda(1520) \rightarrow N\bar{K}$				
MODULUS	PHASE ($^\circ$)	DOCUMENT ID	TECN	COMMENT
0.45 \pm 0.01	-10 \pm 3	SARANTSEV	19	DPWA $\bar{K}N$ multichannel
••• We do not use the following data for averages, fits, limits, etc. •••				
0.431	-11	¹ KAMANO	15	DPWA $\bar{K}N$ multichannel
¹ From the preferred solution A in KAMANO 15.				

Normalized residue in $N\bar{K} \rightarrow \Lambda(1520) \rightarrow \Sigma\pi$				
MODULUS	PHASE ($^\circ$)	DOCUMENT ID	TECN	COMMENT
0.44 \pm 0.01	-15 \pm 3	SARANTSEV	19	DPWA $\bar{K}N$ multichannel
••• We do not use the following data for averages, fits, limits, etc. •••				
0.435	-10	¹ KAMANO	15	DPWA $\bar{K}N$ multichannel
¹ From the preferred solution A in KAMANO 15.				

Normalized residue in $N\bar{K} \rightarrow \Lambda(1520) \rightarrow \Lambda\eta$				
MODULUS	PHASE ($^\circ$)	DOCUMENT ID	TECN	COMMENT
0.013 \pm 0.003	116 \pm 3	SARANTSEV	19	DPWA $\bar{K}N$ multichannel

Normalized residue in $N\bar{K} \rightarrow \Lambda(1520) \rightarrow \Sigma(1385)\pi, S\text{-wave}$				
MODULUS	PHASE ($^\circ$)	DOCUMENT ID	TECN	COMMENT
••• We do not use the following data for averages, fits, limits, etc. •••				
0.431	-123	¹ KAMANO	15	DPWA $\bar{K}N$ multichannel
¹ From the preferred solution A in KAMANO 15.				

Normalized residue in $N\bar{K} \rightarrow \Lambda(1520) \rightarrow \Sigma(1385)\pi, D\text{-wave}$				
MODULUS	PHASE ($^\circ$)	DOCUMENT ID	TECN	COMMENT
••• We do not use the following data for averages, fits, limits, etc. •••				
0.0141	122	¹ KAMANO	15	DPWA $\bar{K}N$ multichannel
¹ From the preferred solution A in KAMANO 15.				

$\Lambda(1520)$ MASS

VALUE (MeV)	EVTs	DOCUMENT ID	TECN	COMMENT
1518 to 1520 (≈ 1519) OUR ESTIMATE				
1519.42 \pm 0.19 OUR AVERAGE				
1518.5 \pm 0.5		SARANTSEV	19	DPWA $\bar{K}N$ multichannel
1519.6 \pm 0.5		ZHANG	13A	DPWA $\bar{K}N$ multichannel
1520.4 \pm 0.6 \pm 1.5		QIANG	10	SPEC $ep \rightarrow e'K^+X$ (fit to X)
1517.3 \pm 1.5	300	BARBER	80D	SPEC $\gamma p \rightarrow \Lambda(1520)K^+$
1517.8 \pm 1.2	5k	BARLAG	79	HBC K^-p 4.2 GeV/c
1520.0 \pm 0.5		ALSTON...	78	DPWA $\bar{K}N \rightarrow \bar{K}N$
1519.7 \pm 0.3	4k	CAMERON	77	HBC K^-p 0.96-1.36 GeV/c
1519 \pm 1		GOPAL	77	DPWA $\bar{K}N$ multichannel
1519.4 \pm 0.3	2000	CORDEN	75	DBC K^-d 1.4-1.8 GeV/c

$\Lambda(1520)$ WIDTH

VALUE (MeV)	EVTs	DOCUMENT ID	TECN	COMMENT
15 to 17 (≈ 16) OUR ESTIMATE				
15.73 \pm 0.26 OUR AVERAGE				
15.7 \pm 1.0		SARANTSEV	19	DPWA $\bar{K}N$ multichannel
17 \pm 1		ZHANG	13A	DPWA $\bar{K}N$ multichannel
18.6 \pm 1.9 \pm 1.0		QIANG	10	SPEC $ep \rightarrow e'K^+X$ (fit to X)
16.3 \pm 3.3	300	BARBER	80D	SPEC $\gamma p \rightarrow \Lambda(1520)K^+$
16 \pm 1		GOPAL	80	DPWA $\bar{K}N \rightarrow \bar{K}N$
14 \pm 3	677	¹ BARLAG	79	HBC K^-p 4.2 GeV/c
15.4 \pm 0.5		ALSTON...	78	DPWA $\bar{K}N \rightarrow \bar{K}N$
16.3 \pm 0.5	4k	CAMERON	77	HBC K^-p 0.96-1.36 GeV/c
15.0 \pm 0.5		GOPAL	77	DPWA $\bar{K}N$ multichannel
15.5 \pm 1.6	2000	CORDEN	75	DBC K^-d 1.4-1.8 GeV/c
¹ From the best-resolution sample of $\Lambda\pi\pi$ events only.				

Baryon Particle Listings

 $\Lambda(1520)$ $\Lambda(1520)$ DECAY MODES

Mode	Fraction (Γ_i/Γ)
Γ_1 $N\bar{K}$	(45 ± 1) %
Γ_2 $\Sigma\pi$	(42 ± 1) %
Γ_3 $\Lambda\pi\pi$	(10 ± 1) %
Γ_4 $\Sigma(1385)\pi$, S-wave	
Γ_5 $\Sigma(1385)\pi$, D-wave	
Γ_6 $\Sigma(1385)\pi$	
Γ_7 $\Sigma(1385)\pi(\rightarrow\Lambda\pi\pi)$	
Γ_8 $\Lambda(\pi\pi)$ S-wave	
Γ_9 $\Sigma\pi\pi$	(0.9 ± 0.1) %
Γ_{10} $\Lambda\gamma$	(0.85 ± 0.15) %
Γ_{11} $\Sigma^0\gamma$	

 $\Lambda(1520)$ BRANCHING RATIOS

See "Sign conventions for resonance couplings" in the Note on Λ and Σ Resonances.

$\Gamma(N\bar{K})/\Gamma_{\text{total}}$	VALUE	DOCUMENT ID	TECN	COMMENT	Γ_1/Γ
0.45 to 0.47 OUR ESTIMATE					
0.45 ± 0.01		SARANTSEV	19	DPWA $\bar{K}N$ multichannel	
0.47 ± 0.04		ZHANG	13A	DPWA $\bar{K}N$ multichannel	
0.47 ± 0.02		GOPAL	80	DPWA $\bar{K}N \rightarrow \bar{K}N$	
0.45 ± 0.03		ALSTON...	78	DPWA $\bar{K}N \rightarrow \bar{K}N$	
0.448 ± 0.014		CORDEN	75	DBC K^-d 1.4-1.8 GeV/c	
••• We do not use the following data for averages, fits, limits, etc. •••					
0.43		¹ KAMANO	15	DPWA $\bar{K}N$ multichannel	
0.47 ± 0.01		GOPAL	77	DPWA See GOPAL 80	
0.42		MAST	76	HBC $K^-p \rightarrow \bar{K}^0n$	
¹ From the preferred solution A in KAMANO 15.					

$\Gamma(\Sigma\pi)/\Gamma_{\text{total}}$	VALUE	DOCUMENT ID	TECN	COMMENT	Γ_2/Γ
0.42 to 0.46 OUR ESTIMATE					
0.43 ± 0.01		SARANTSEV	19	DPWA $\bar{K}N$ multichannel	
0.47 ± 0.05		ZHANG	13A	DPWA $\bar{K}N$ multichannel	
0.426 ± 0.014		CORDEN	75	DBC K^-d 1.4-1.8 GeV/c	
0.418 ± 0.017		BARBARO...	69B	HBC K^-p 0.28-0.45 GeV/c	
••• We do not use the following data for averages, fits, limits, etc. •••					
0.446		¹ KAMANO	15	DPWA $\bar{K}N$ multichannel	
0.46		KIM	71	DPWA K-matrix analysis	
¹ From the preferred solution A in KAMANO 15.					

$\Gamma(\Sigma\pi)/\Gamma(N\bar{K})$	VALUE	DOCUMENT ID	TECN	COMMENT	Γ_2/Γ_1
0.9 to 1.0 OUR ESTIMATE					
0.98 ± 0.03		¹ GOPAL	77	DPWA $\bar{K}N$ multichannel	
0.82 ± 0.08		BURKHARDT	69	HBC K^-p 0.8-1.2 GeV/c	
1.06 ± 0.14		SCHEUER	68	DBC K^-N 3 GeV/c	
0.96 ± 0.20		DAHL	67	HBC π^-p 1.6-4 GeV/c	
0.73 ± 0.11		DAUBER	67	HBC K^-p 2 GeV/c	
••• We do not use the following data for averages, fits, limits, etc. •••					
1.06 ± 0.12		BERTHON	74	HBC Quasi-2-body σ	
1.72 ± 0.78		MUSGRAVE	65	HBC	
¹ The $\bar{K}N \rightarrow \Sigma\pi$ amplitude at resonance is +0.46 ± 0.01.					

$\Gamma(\Lambda\pi\pi)/\Gamma_{\text{total}}$	VALUE	DOCUMENT ID	TECN	COMMENT	Γ_3/Γ
0.09 to 0.11 OUR ESTIMATE					
0.091 ± 0.006		CORDEN	75	DBC K^-d 1.4-1.8 GeV/c	
0.11 ± 0.01		¹ MAST	73B	IPWA $K^-p \rightarrow \Lambda\pi\pi$	
¹ Assumes $\Gamma(N\bar{K})/\Gamma_{\text{total}} = 0.46 \pm 0.02$.					

$\Gamma(\Lambda\pi\pi)/\Gamma(N\bar{K})$	VALUE	DOCUMENT ID	TECN	COMMENT	Γ_3/Γ_1
0.18 to 0.22 OUR ESTIMATE					
0.22 ± 0.03		BURKHARDT	69	HBC K^-p 0.8-1.2 GeV/c	
0.19 ± 0.04		SCHEUER	68	DBC K^-N 3 GeV/c	
0.17 ± 0.05		DAHL	67	HBC π^-p 1.6-4 GeV/c	
0.21 ± 0.18		DAUBER	67	HBC K^-p 2 GeV/c	
••• We do not use the following data for averages, fits, limits, etc. •••					
0.27 ± 0.13		BERTHON	74	HBC Quasi-2-body σ	
0.2		KIM	71	DPWA K-matrix analysis	

$\Gamma(\Sigma\pi)/\Gamma(\Lambda\pi\pi)$	VALUE	DOCUMENT ID	TECN	COMMENT	Γ_2/Γ_3
3.4 to 4.4 OUR ESTIMATE					
3.9 ± 1.0		UHLIG	67	HBC K^-p 0.9-1.0 GeV/c	
3.3 ± 1.1		BIRMINGHAM	66	HBC K^-p 3.5 GeV/c	
4.5 ± 1.0		ARMENTEROS65c	HBC		

 $\Gamma(\Sigma(1385)\pi, S\text{-wave})/\Gamma_{\text{total}}$ Γ_4/Γ

VALUE	DOCUMENT ID	TECN	COMMENT
••• We do not use the following data for averages, fits, limits, etc. •••			
0.121	¹ KAMANO 15	15	DPWA $\bar{K}N$ multichannel
¹ From the preferred solution A in KAMANO 15.			

 $\Gamma(\Sigma(1385)\pi, D\text{-wave})/\Gamma_{\text{total}}$ Γ_5/Γ

VALUE	DOCUMENT ID	TECN	COMMENT
••• We do not use the following data for averages, fits, limits, etc. •••			
0.003	¹ KAMANO 15	15	DPWA Multichannel
¹ From the preferred solution A in KAMANO 15.			

 $\Gamma(\Sigma(1385)\pi)/\Gamma_{\text{total}}$ Γ_6/Γ

VALUE	DOCUMENT ID	TECN	COMMENT
0.041 ± 0.005	CHAN	72	HBC $K^-p \rightarrow \Lambda\pi\pi$

 $\Gamma(\Sigma(1385)\pi(\rightarrow\Lambda\pi\pi))/\Gamma(\Lambda\pi\pi)$ Γ_7/Γ_3

The $\Lambda\pi\pi$ mode is largely due to $\Sigma(1385)\pi$. Only the values of $(\Sigma(1385)\pi)/(\Lambda\pi\pi)$ given by MAST 73B and CORDEN 75 are based on real 3-body partial-wave analyses. The discrepancy between the two results is essentially due to the different hypotheses made concerning the shape of the $(\pi\pi)$ S-wave state.

VALUE	CL%	DOCUMENT ID	TECN	COMMENT
0.58 ± 0.22		CORDEN	75	DBC K^-d 1.4-1.8 GeV/c
0.82 ± 0.10		¹ MAST	73B	IPWA $K^-p \rightarrow \Lambda\pi\pi$
••• We do not use the following data for averages, fits, limits, etc. •••				
<0.44	90	WIELAND	11	SPHR $\gamma p \rightarrow K^+\Lambda(1520)$
0.39 ± 0.10		² BURKHARDT	71	HBC $K^-p \rightarrow (\Lambda\pi\pi)\pi$
¹ Both $\Sigma(1385)\pi DS_{03}$ and $\Sigma(\pi\pi) DP_{03}$ contribute.				
² The central bin (1514-1524 MeV) gives 0.74 ± 0.10 ; other bins are lower by 2-to-5 standard deviations.				

 $\Gamma(\Lambda(\pi\pi)S\text{-wave})/\Gamma(\Lambda\pi\pi)$ Γ_8/Γ_3

VALUE	DOCUMENT ID	TECN	COMMENT
0.20 ± 0.08	CORDEN	75	DBC K^-d 1.4-1.8 GeV/c

 $\Gamma(\Sigma\pi\pi)/\Gamma_{\text{total}}$ Γ_9/Γ

VALUE	DOCUMENT ID	TECN	COMMENT
0.007 to 0.011 OUR ESTIMATE			
0.007 ± 0.002	¹ CORDEN	75	DBC K^-d 1.4-1.8 GeV/c
0.0085 ± 0.0006	² MAST	73	MPWA $K^-p \rightarrow \Sigma\pi\pi$
0.010 ± 0.0015	BARBARO...	69B	HBC K^-p 0.28-0.45 GeV/c
¹ Much of the $\Sigma\pi\pi$ decay proceeds via $\Sigma(1385)\pi$.			
² Assumes $\Gamma(N\bar{K})/\Gamma_{\text{total}} = 0.46$.			

 $\Gamma(\Lambda\gamma)/\Gamma_{\text{total}}$ Γ_{10}/Γ

VALUE (units 10^{-3})	EVTS	DOCUMENT ID	TECN	COMMENT
7 to 11 OUR ESTIMATE				
10.7 ± 2.9 ^{+1.5} _{-0.4}	32	TAYLOR	05	CLAS $\gamma p \rightarrow K^+\Lambda\gamma$
10.2 ± 2.1 ± 1.5	290	ANTIP OV	04A	SPNX $pN(C) \rightarrow \Lambda(1520)K^+N(C)$
8.0 ± 1.4	238	MAST	68B	HBC Using $\Gamma(N\bar{K})/\Gamma_{\text{total}} = 0.45$

 $\Gamma(\Sigma^0\gamma)/\Gamma_{\text{total}}$ Γ_{11}/Γ

VALUE	DOCUMENT ID	TECN	COMMENT
0.02 ± 0.0035	¹ MAST	68B	HBC Not measured; see note
¹ Calculated from $\Gamma(\Lambda\gamma)/\Gamma_{\text{total}}$, assuming SU(3). Needed to constrain the sum of all the branching ratios to be unity.			

 $\Lambda(1520)$ REFERENCES

SARANTSEV 19	EPJ A55 180	A.V. Sarantsev <i>et al.</i>	(BONN, PNPI)
KAMANO 15	PR C92 025205	H. Kamano <i>et al.</i>	(ANL, OSAK)
ZHANG 13A	PR C88 035205	H. Zhang <i>et al.</i>	(KSU)
WIELAND 11	EPJ A47 47	F. Wieland <i>et al.</i>	(ELSA SAPHIR Collab.)
QIANG 10	PL B694 123	Y. Qiang <i>et al.</i>	(DUKE, JEFF, PNPI, GWU+)
TAYLOR 05	PR C71 054609	S. Taylor <i>et al.</i>	(JLab CLAS Collab.)
Also	PR C72 039902 (errat.)	S. Taylor <i>et al.</i>	(JLab CLAS Collab.)
ANTIP OV 04A	PL B604 22	Yu.M. Antipov <i>et al.</i>	(IHEP SPHINX Collab.)
PDG 82	PL 111B 1	M. Roos <i>et al.</i>	(HELS, CIT, CERN)
BARBER 80D	ZPHY C7 17	D.P. Barber <i>et al.</i>	(DARE, LANC, SHEF)
GOPAL 80	Toronto Conf. 159	G.P. Gopal	(RHEL) IJP
BARLAG 79	NP B149 220	S.J.M. Barlag <i>et al.</i>	(AMST, CERN, NIJ+)
ALSTON... 78	PR D18 182	M. Alston-Garnjost <i>et al.</i>	(LBL, MTHO+ IJP)
Also	PRL 38 1007	M. Alston-Garnjost <i>et al.</i>	(LBL, MTHO+ IJP)
CAMERON 77	NP B131 399	W. Cameron <i>et al.</i>	(RHEL, LOIC IJP)
GOPAL 77	NP B119 362	G.P. Gopal <i>et al.</i>	(LOIC, RHEL) IJP
MAST 76	PR D14 13	T.S. Mast <i>et al.</i>	(LBL)
CORDEN 75	NP B84 306	M.J. Corden <i>et al.</i>	(BIRM)
BERTHON 74	NC 21A 146	A. Berthon <i>et al.</i>	(CDEF, RHEL, SACL+)
MAST 73	PR D7 3212	T.S. Mast <i>et al.</i>	(LBL) IJP
MAST 73B	PR D7 5	T.S. Mast <i>et al.</i>	(LBL) IJP
CHAN 72	PRL 28 256	S.B. Chan <i>et al.</i>	(MASA, YALE)
BURKHARDT 71	NP B27 64	E. Burkhart <i>et al.</i>	(HEID, CERN, SACL)
KIM 71	PRL 27 356	J.K. Kim	(HARV) IJP
Also	Duke Conf. 161	J.K. Kim	(HARV) IJP
Hyperon Resonances, 1970			
BARBARO... 69B	Lund Conf. 352	A. Barbaro-Galtheri <i>et al.</i>	(LRL)
Also	Duke Conf. 95	R.D. Tripp	(LRL)
Hyperon Resonances 1970			
BURKHARDT 69	NP B14 106	E. Burkhart <i>et al.</i>	(HEID, EFI, CERN+)
MAST 68B	PRL 21 1715	T.S. Mast <i>et al.</i>	(LRL)
SCHEUER 68	NP B8 503	J.C. Scheuer <i>et al.</i>	(SABRE Collab.)
DAHL 67	PR 163 1377	O.I. Dahl <i>et al.</i>	(LRL)
DAUBER 67	PL 24B 925	P.M. Dauber <i>et al.</i>	(UCLA)

See key on page 1127

Baryon Particle Listings

$\Lambda(1520), \Lambda(1600)$

UHLIG 67 PR 155 1448 R.P. Uhlig et al. (UMD, NRL)
BIRMINGHAM 66 PR 152 1148 M. Haque et al. (BIRM, GLAS, LOIC, OXF+)
ARMENTEROS 65C PL 19 338 R. Armenteros et al. (CERN, HEID, SACL)
MUSGRAVE 65 NC 35 735 B. Musgrave et al. (BIRM, CERN, EPOL+)
WATSON 63 PR 131 2248 M.B. Watson, M. Ferro-Luzzi, R.D. Tripp (LRL) IJP
FERRO-LUZZI 62 PRL 8 28 M. Ferro-Luzzi, R.D. Tripp, M.B. Watson (LRL) IJP

$\Lambda(1600) 1/2^+$

 $I(J^P) = 0(\frac{1}{2}^+)$ Status: * * * *

$\Lambda(1600)$ POLE POSITION

REAL PART

VALUE (MeV)	DOCUMENT ID	TECN	COMMENT
1540 to 1560 (≈ 1550) OUR ESTIMATE			
1546 \pm 6 OUR AVERAGE	Error includes scale factor of 2.1.		
1562 \pm 8	SARANTSEV 19	DPWA	$\bar{K}N$ multichannel
1544 \pm 3	¹ KAMANO 15	DPWA	Multichannel

• • • We do not use the following data for averages, fits, limits, etc. • • •

1572	ZHANG 13A	DPWA	Multichannel
¹ From the preferred solution A in KAMANO 15.			

-2xIMAGINARY PART

VALUE (MeV)	DOCUMENT ID	TECN	COMMENT
120 to 240 (≈ 180) OUR ESTIMATE			
159 \pm 12 OUR AVERAGE	Error includes scale factor of 6.2.		
232 \pm 15	SARANTSEV 19	DPWA	$\bar{K}N$ multichannel
112 \pm 12	¹ KAMANO 15	DPWA	Multichannel

• • • We do not use the following data for averages, fits, limits, etc. • • •

138	ZHANG 13A	DPWA	Multichannel
¹ From the preferred solution A in KAMANO 15.			

$\Lambda(1600)$ POLE RESIDUES

The normalized residue is the residue divided by $\Gamma_{pole}/2$.

Normalized residue in $N\bar{K} \rightarrow \Lambda(1600) \rightarrow N\bar{K}$

MODULUS	PHASE ($^\circ$)	DOCUMENT ID	TECN	COMMENT
0.36 \pm 0.07	-63 \pm 10	SARANTSEV 19	DPWA	$\bar{K}N$ multichannel
• • • We do not use the following data for averages, fits, limits, etc. • • •				
0.105	-80	¹ KAMANO 15	DPWA	Multichannel
¹ From the preferred solution A in KAMANO 15.				

Normalized residue in $N\bar{K} \rightarrow \Lambda(1600) \rightarrow \Sigma\pi$

MODULUS	PHASE ($^\circ$)	DOCUMENT ID	TECN	COMMENT
0.39 \pm 0.08	148 \pm 10	SARANTSEV 19	DPWA	$\bar{K}N$ multichannel
• • • We do not use the following data for averages, fits, limits, etc. • • •				
0.232	108	¹ KAMANO 15	DPWA	Multichannel
¹ From the preferred solution A in KAMANO 15.				

Normalized residue in $N\bar{K} \rightarrow \Lambda(1600) \rightarrow \Lambda\eta$

MODULUS	PHASE ($^\circ$)	DOCUMENT ID	TECN	COMMENT
0.22 \pm 0.13	180 \pm 20	SARANTSEV 19	DPWA	$\bar{K}N$ multichannel

Normalized residue in $N\bar{K} \rightarrow \Lambda(1600) \rightarrow \Lambda\sigma$

MODULUS	PHASE ($^\circ$)	DOCUMENT ID	TECN	COMMENT
0.30 \pm 0.06	-70 \pm 10	SARANTSEV 19	DPWA	$\bar{K}N$ multichannel

Normalized residue in $N\bar{K} \rightarrow \Lambda(1600) \rightarrow \Sigma(1385)\pi$

MODULUS	PHASE ($^\circ$)	DOCUMENT ID	TECN	COMMENT
0.37 \pm 0.07	103 \pm 12	SARANTSEV 19	DPWA	$\bar{K}N$ multichannel
• • • We do not use the following data for averages, fits, limits, etc. • • •				
0.183	77	¹ KAMANO 15	DPWA	Multichannel
¹ From the preferred solution A in KAMANO 15.				

Normalized residue in $N\bar{K} \rightarrow \Lambda(1600) \rightarrow N\bar{K}^*(892), S=1/2, P\text{-wave}$

MODULUS	PHASE ($^\circ$)	DOCUMENT ID	TECN	COMMENT
0.02 \pm 0.01	126 \pm 45	SARANTSEV 19	DPWA	$\bar{K}N$ multichannel

Normalized residue in $N\bar{K} \rightarrow \Lambda(1600) \rightarrow N\bar{K}^*(892), S=3/2, P\text{-wave}$

MODULUS	PHASE ($^\circ$)	DOCUMENT ID	TECN	COMMENT
0.02 \pm 0.01	-135 \pm 45	SARANTSEV 19	DPWA	$\bar{K}N$ multichannel

$\Lambda(1600)$ MASS

VALUE (MeV)	DOCUMENT ID	TECN	COMMENT
1570 to 1630 (≈ 1600) OUR ESTIMATE			
1605 \pm 8	SARANTSEV 19	DPWA	$\bar{K}N$ multichannel
1592 \pm 10	ZHANG 13A	DPWA	Multichannel
1568 \pm 20	GOPAL 80	DPWA	$\bar{K}N \rightarrow \bar{K}N$
1703 \pm 100	ALSTON... 78	DPWA	$\bar{K}N \rightarrow \bar{K}N$
1573 \pm 25	GOPAL 77	DPWA	$\bar{K}N$ multichannel
1596 \pm 6	KANE 74	DPWA	$K^-p \rightarrow \Sigma\pi$
1620 \pm 10	LANGBEIN 72	IPWA	$\bar{K}N$ multichannel

• • • We do not use the following data for averages, fits, limits, etc. • • •

1572 or 1617	¹ MARTIN 77	DPWA	$\bar{K}N$ multichannel
1646 \pm 7	² CARROLL 76	DPWA	Isospin-0 total σ
	KIM 71	DPWA	K-matrix analysis

¹The two MARTIN 77 values are from a T-matrix pole and from a Breit-Wigner fit.
²A total cross-section bump with $(J+1/2) \Gamma_{el} / \Gamma_{total} = 0.04$.

$\Lambda(1600)$ WIDTH

VALUE (MeV)	DOCUMENT ID	TECN	COMMENT
150 to 250 (≈ 200) OUR ESTIMATE			
245 \pm 15	SARANTSEV 19	DPWA	$\bar{K}N$ multichannel
150 \pm 28	ZHANG 13A	DPWA	Multichannel
116 \pm 20	GOPAL 80	DPWA	$\bar{K}N \rightarrow \bar{K}N$
593 \pm 200	ALSTON... 78	DPWA	$\bar{K}N \rightarrow \bar{K}N$
147 \pm 50	GOPAL 77	DPWA	$\bar{K}N$ multichannel
175 \pm 20	KANE 74	DPWA	$K^-p \rightarrow \Sigma\pi$
60 \pm 10	LANGBEIN 72	IPWA	$\bar{K}N$ multichannel
• • • We do not use the following data for averages, fits, limits, etc. • • •			
247 or 271	¹ MARTIN 77	DPWA	$\bar{K}N$ multichannel
20	² CARROLL 76	DPWA	Isospin-0 total σ
50	KIM 71	DPWA	K-matrix analysis

¹The two MARTIN 77 values are from a T-matrix pole and from a Breit-Wigner fit.
²A total cross-section bump with $(J+1/2) \Gamma_{el} / \Gamma_{total} = 0.04$.

$\Lambda(1600)$ DECAY MODES

Mode	Fraction (Γ_i/Γ)
Γ_1 $N\bar{K}$	15-30 %
Γ_2 $\Sigma\pi$	10-60 %
Γ_3 $\Lambda\sigma$	(19 \pm 4) %
Γ_4 $\Sigma(1385)\pi$	(9 \pm 4) %

$\Lambda(1600)$ BRANCHING RATIOS

See "Sign conventions for resonance couplings" in the Note on Λ and Σ Resonances.

$\Gamma(N\bar{K})/\Gamma_{total}$	DOCUMENT ID	TECN	COMMENT	Γ_1/Γ
0.14 to 0.28 OUR ESTIMATE				
0.29 \pm 0.06	SARANTSEV 19	DPWA	$\bar{K}N$ multichannel	
0.14 \pm 0.04	ZHANG 13A	DPWA	Multichannel	
0.23 \pm 0.04	GOPAL 80	DPWA	$\bar{K}N \rightarrow \bar{K}N$	
0.14 \pm 0.05	ALSTON... 78	DPWA	$\bar{K}N \rightarrow \bar{K}N$	
0.25 \pm 0.15	LANGBEIN 72	IPWA	$\bar{K}N$ multichannel	
• • • We do not use the following data for averages, fits, limits, etc. • • •				
0.064	¹ KAMANO 15	DPWA	Multichannel	
0.24 \pm 0.04	GOPAL 77	DPWA	See GOPAL 80	
0.30 or 0.29	² MARTIN 77	DPWA	$\bar{K}N$ multichannel	

¹From the preferred solution A in KAMANO 15.
²The two MARTIN 77 values are from a T-matrix pole and from a Breit-Wigner fit.

$\Gamma(\Sigma\pi)/\Gamma_{total}$	DOCUMENT ID	TECN	COMMENT	Γ_2/Γ
0.37 \pm 0.07				
0.37 \pm 0.07	SARANTSEV 19	DPWA	$\bar{K}N$ multichannel	
• • • We do not use the following data for averages, fits, limits, etc. • • •				
0.851	¹ KAMANO 15	DPWA	Multichannel	
¹ From the preferred solution A in KAMANO 15.				

$\Gamma(\Lambda\sigma)/\Gamma_{total}$	DOCUMENT ID	TECN	COMMENT	Γ_3/Γ
0.19 \pm 0.04				
0.19 \pm 0.04	SARANTSEV 19	DPWA	$\bar{K}N$ multichannel	

$\Gamma(\Sigma(1385)\pi)/\Gamma_{total}$	DOCUMENT ID	TECN	COMMENT	Γ_4/Γ
0.09 \pm 0.04				
0.09 \pm 0.04	SARANTSEV 19	DPWA	$\bar{K}N$ multichannel	
• • • We do not use the following data for averages, fits, limits, etc. • • •				
0.085	¹ KAMANO 15	DPWA	Multichannel	
¹ From the preferred solution A in KAMANO 15.				

$(\Gamma_1\Gamma_2)^{1/2}/\Gamma_{total}$ in $N\bar{K} \rightarrow \Lambda(1600) \rightarrow \Sigma\pi$	DOCUMENT ID	TECN	COMMENT	$(\Gamma_1\Gamma_2)^{1/2}/\Gamma$
-0.23 \pm 0.03	ZHANG 13A	DPWA	Multichannel	
-0.16 \pm 0.04	GOPAL 77	DPWA	$\bar{K}N$ multichannel	
-0.33 \pm 0.11	KANE 74	DPWA	$K^-p \rightarrow \Sigma\pi$	
0.28 \pm 0.09	LANGBEIN 72	IPWA	$\bar{K}N$ multichannel	
• • • We do not use the following data for averages, fits, limits, etc. • • •				
-0.39 or -0.39	¹ MARTIN 77	DPWA	$\bar{K}N$ multichannel	
not seen	HEPP 76B	DPWA	$K^-N \rightarrow \Sigma\pi$	
¹ The two MARTIN 77 values are from a T-matrix pole and from a Breit-Wigner fit.				

Baryon Particle Listings

 $\Lambda(1600), \Lambda(1670)$ $\Lambda(1600)$ REFERENCES

SARANTSEV	19	EPJ A55 180	A.V. Sarantsev et al.	(BONN, PNPI)
KAMANO	15	PR C92 025205	H. Kamano et al.	(ANL, OSAK)
ZHANG	13A	PR C88 035205	H. Zhang et al.	(KSU)
GOPAL	80	Toronto Conf. 159	G.P. Gopal	(RHEL) IJP
ALSTON...	78	PR D18 182	M. Alston-Garnjost et al.	(LBL, MTHO+) IJP
Also		PRL 38 1007	M. Alston-Garnjost et al.	(LBL, MTHO+) IJP
GOPAL	77	NP B119 362	G.P. Gopal et al.	(LOIC, RHEL) IJP
MARTIN	77	NP B127 349	B.R. Martin, M.K. Pldcock, R.G. Moorhouse	(LOUC+) IJP
Also		NP B126 266	B.R. Martin, M.K. Pldcock	(LOUC) IJP
Also		NP B126 285	B.R. Martin, M.K. Pldcock	(LOUC) IJP
CARROLL	76	PRL 37 806	A.S. Carroll et al.	(BNL) I
HEPP	76B	PL 65B 487	V. Hepp et al.	(CERN, HEIDH, MPIM) IJP
KANE	74	LBL-2452	D.F. Kane	(LBL) IJP
LANGBEIN	72	NP B47 477	W. Langbein, F. Wagner	(MPIM) IJP
KIM	71	PRL 27 356	J.K. Kim	(HARV) IJP

 $\Lambda(1670) 1/2^-$

$$I(J^P) = 0(\frac{1}{2}^-) \text{ Status: } ***$$

The measurements of the mass, width, and elasticity published before 1974 are now obsolete and have been omitted. They were last listed in our 1982 edition Physics Letters **111B** 1 (1982).

 $\Lambda(1670)$ POLE POSITIONS

REAL PART

VALUE (MeV)	DOCUMENT ID	TECN	COMMENT
1670 to 1678 (≈ 1674) OUR ESTIMATE			
1676 ± 2	SARANTSEV 19	DPWA	$\bar{K}N$ multichannel
1669 $+3$ -8	¹ KAMANO 15	DPWA	$\bar{K}N$ multichannel
1677.5 ± 0.8	GARCIA-REC...03	DPWA	$\bar{K}N$ multichannel
•••	We do not use the following data for averages, fits, limits, etc. •••		
1667	ZHANG 13A	DPWA	$\bar{K}N$ multichannel
¹	From the preferred solution A in KAMANO 15.		

 $-2 \times$ IMAGINARY PART

VALUE (MeV)	DOCUMENT ID	TECN	COMMENT
28 to 36 (≈ 32) OUR ESTIMATE			
33 ± 4	SARANTSEV 19	DPWA	$\bar{K}N$ multichannel
19 $+18$ -2	¹ KAMANO 15	DPWA	$\bar{K}N$ multichannel
29.2 ± 1.4	GARCIA-REC...03	DPWA	$\bar{K}N$ multichannel
•••	We do not use the following data for averages, fits, limits, etc. •••		
26	ZHANG 13A	DPWA	$\bar{K}N$ multichannel
¹	From the preferred solution A in KAMANO 15.		

 $\Lambda(1670)$ POLE RESIDUES

The normalized residue is the residue divided by $\Gamma_{pole}/2$.

Normalized residue in $\bar{K}N \rightarrow \Lambda(1670) \rightarrow \bar{K}N$

MODULUS	PHASE ($^\circ$)	DOCUMENT ID	TECN	COMMENT
0.30 ± 0.06	-145 ± 11	SARANTSEV 19	DPWA	$\bar{K}N$ multichannel
•••	We do not use the following data for averages, fits, limits, etc. •••			
0.351	164	¹ KAMANO 15	DPWA	$\bar{K}N$ multichannel
¹	From the preferred solution A in KAMANO 15.			

Normalized residue in $N\bar{K} \rightarrow \Lambda(1670) \rightarrow \Sigma\pi$

MODULUS	PHASE ($^\circ$)	DOCUMENT ID	TECN	COMMENT
0.19 ± 0.06	145 ± 14	SARANTSEV 19	DPWA	$\bar{K}N$ multichannel
•••	We do not use the following data for averages, fits, limits, etc. •••			
0.327	125	¹ KAMANO 15	DPWA	$\bar{K}N$ multichannel
¹	From the preferred solution A in KAMANO 15.			

Normalized residue in $N\bar{K} \rightarrow \Lambda(1670) \rightarrow \Lambda\eta$

MODULUS	PHASE ($^\circ$)	DOCUMENT ID	TECN	COMMENT
0.26 ± 0.09	104 ± 14	SARANTSEV 19	DPWA	$\bar{K}N$ multichannel
•••	We do not use the following data for averages, fits, limits, etc. •••			
0.474	59	¹ KAMANO 15	DPWA	Multichannel
¹	From the preferred solution A in KAMANO 15.			

Normalized residue in $N\bar{K} \rightarrow \Lambda(1670) \rightarrow \Xi K$

MODULUS	PHASE ($^\circ$)	DOCUMENT ID	TECN	COMMENT
0.02 ± 0.02	100 ± 25	SARANTSEV 19	DPWA	$\bar{K}N$ multichannel

Normalized residue in $N\bar{K} \rightarrow \Lambda(1670) \rightarrow \Lambda\omega, S=1/2, S\text{-wave}$

MODULUS	PHASE ($^\circ$)	DOCUMENT ID	TECN	COMMENT
0.09 ± 0.04	-60 ± 35	SARANTSEV 19	DPWA	$\bar{K}N$ multichannel

Normalized residue in $N\bar{K} \rightarrow \Lambda(1670) \rightarrow \Lambda\omega, S=3/2, D\text{-wave}$

MODULUS	PHASE ($^\circ$)	DOCUMENT ID	TECN	COMMENT
0.05 ± 0.04		SARANTSEV 19	DPWA	$\bar{K}N$ multichannel

Normalized residue in $N\bar{K} \rightarrow \Lambda(1670) \rightarrow N\bar{K}^*(892), S=1/2, S\text{-wave}$

MODULUS	PHASE ($^\circ$)	DOCUMENT ID	TECN	COMMENT
0.31 ± 0.14	100 ± 45	SARANTSEV 19	DPWA	$\bar{K}N$ multichannel

Normalized residue in $N\bar{K} \rightarrow \Lambda(1670) \rightarrow N\bar{K}^*(892), S=3/2, D\text{-wave}$

MODULUS	PHASE ($^\circ$)	DOCUMENT ID	TECN	COMMENT
0.06 ± 0.03	-85 ± 40	SARANTSEV 19	DPWA	$\bar{K}N$ multichannel

Normalized residue in $N\bar{K} \rightarrow \Lambda(1670) \rightarrow \Lambda\sigma$

MODULUS	PHASE ($^\circ$)	DOCUMENT ID	TECN	COMMENT
0.25 ± 0.08	160 ± 15	SARANTSEV 19	DPWA	$\bar{K}N$ multichannel

Normalized residue in $N\bar{K} \rightarrow \Lambda(1670) \rightarrow \Sigma(1385)\pi$

MODULUS	PHASE ($^\circ$)	DOCUMENT ID	TECN	COMMENT
0.13 ± 0.06	110 ± 12	SARANTSEV 19	DPWA	$\bar{K}N$ multichannel
•••	We do not use the following data for averages, fits, limits, etc. •••			
0.0988	-104	¹ KAMANO 15	DPWA	Multichannel
¹	From the preferred solution A in KAMANO 15.			

 $\Lambda(1670)$ MASS

VALUE (MeV)	DOCUMENT ID	TECN	COMMENT
1670 to 1678 (≈ 1674) OUR ESTIMATE			
1674.3 $\pm 0.8 \pm 4.9$	LEE 21A	BELL	$\Lambda_C^+ \rightarrow \Lambda(1670) \pi^+$
1677 ± 2	SARANTSEV 19	DPWA	$\bar{K}N$ multichannel
1672 ± 3	ZHANG 13A	DPWA	Multichannel
1670.8 ± 1.7	KOISO 85	DPWA	$K^- p \rightarrow \Sigma\pi$
1667 ± 5	GOPAL 80	DPWA	$\bar{K}N \rightarrow \bar{K}N$
1671 ± 3	ALSTON... 78	DPWA	$\bar{K}N \rightarrow \bar{K}N$
1675 ± 2	HEPP 76B	DPWA	$K^- N \rightarrow \Sigma\pi$
1679 ± 1	KANE 74	DPWA	$K^- p \rightarrow \Sigma\pi$
1665 ± 5	PREVOST 74	DPWA	$K^- N \rightarrow \Sigma(1385)\pi$
•••	We do not use the following data for averages, fits, limits, etc. •••		
1673 ± 2	MANLEY 02	DPWA	$\bar{K}N$ multichannel
1668.9 ± 2.0	ABAEV 96	DPWA	$K^- p \rightarrow \Lambda\eta$
1670 ± 5	GOPAL 77	DPWA	$\bar{K}N$ multichannel
1664	¹ MARTIN 77	DPWA	$\bar{K}N$ multichannel
¹	MARTIN 77 obtains identical resonance parameters from a T-matrix pole and from a Breit-Wigner fit.		

 $\Lambda(1670)$ WIDTH

VALUE (MeV)	DOCUMENT ID	TECN	COMMENT
25 to 35 (≈ 30) OUR ESTIMATE			
36.1 $\pm 2.4 \pm 4.8$	LEE 21A	BELL	$\Lambda_C^+ \rightarrow \Lambda(1670) \pi^+$
33 ± 4	SARANTSEV 19	DPWA	$\bar{K}N$ multichannel
29 ± 5	ZHANG 13A	DPWA	$\bar{K}N$ multichannel
34.1 ± 3.7	KOISO 85	DPWA	$K^- p \rightarrow \Sigma\pi$
29 ± 5	GOPAL 80	DPWA	$\bar{K}N \rightarrow \bar{K}N$
29 ± 5	ALSTON... 78	DPWA	$\bar{K}N \rightarrow \bar{K}N$
46 ± 5	HEPP 76B	DPWA	$K^- N \rightarrow \Sigma\pi$
40 ± 3	KANE 74	DPWA	$K^- p \rightarrow \Sigma\pi$
19 ± 5	PREVOST 74	DPWA	$K^- N \rightarrow \Sigma(1385)\pi$
•••	We do not use the following data for averages, fits, limits, etc. •••		
23 ± 6	MANLEY 02	DPWA	$\bar{K}N$ multichannel
21.1 ± 3.6	ABAEV 96	DPWA	$K^- p \rightarrow \Lambda\eta$
45 ± 10	GOPAL 77	DPWA	$\bar{K}N$ multichannel
12	¹ MARTIN 77	DPWA	$\bar{K}N$ multichannel
¹	MARTIN 77 obtains identical resonance parameters from a T-matrix pole and from a Breit-Wigner fit.		

 $\Lambda(1670)$ DECAY MODES

Mode	Fraction (Γ_i/Γ)
Γ_1 $N\bar{K}$	20-30 %
Γ_2 $\Sigma\pi$	25-55 %
Γ_3 $\Lambda\eta$	10-25 %
Γ_4 $\Sigma(1385)\pi, D\text{-wave}$	(6.0 ± 2.0) %
Γ_5 $N\bar{K}^*(892), S=1/2, S\text{-wave}$	
Γ_6 $N\bar{K}^*(892), S=3/2, D\text{-wave}$	(5 ± 4) %
Γ_7 $\Lambda\sigma$	(20 ± 8) %

 $\Lambda(1670)$ BRANCHING RATIOS

See "Sign conventions for resonance couplings" in the Note on Λ and Σ Resonances.

$\Gamma(N\bar{K})/\Gamma_{total}$	DOCUMENT ID	TECN	COMMENT	Γ_1/Γ
0.20 to 0.30 OUR ESTIMATE				
0.33 ± 0.07	SARANTSEV 19	DPWA	$\bar{K}N$ multichannel	
0.26 ± 0.25	ZHANG 13A	DPWA	$\bar{K}N$ multichannel	
0.18 ± 0.03	GOPAL 80	DPWA	$\bar{K}N \rightarrow \bar{K}N$	
0.17 ± 0.03	ALSTON... 78	DPWA	$\bar{K}N \rightarrow \bar{K}N$	

• • • We do not use the following data for averages, fits, limits, etc. • • •

0.318	¹ KAMANO	15	DPWA	$\bar{K}N$ multichannel
0.37 ± 0.07	MANLEY	02	DPWA	$\bar{K}N$ multichannel
0.20 ± 0.03	GOPAL	77	DPWA	See GOPAL 80
0.15	² MARTIN	77	DPWA	$\bar{K}N$ multichannel

¹ From the preferred solution A in KAMANO 15.
² MARTIN 77 obtains identical resonance parameters from a T-matrix pole and from a Breit-Wigner fit.

$\Gamma(\Sigma\pi)/\Gamma_{\text{total}}$					Γ_2/Γ
<u>VALUE</u>	<u>DOCUMENT ID</u>	<u>TECN</u>	<u>COMMENT</u>		
0.12 ± 0.03	SARANTSEV	19	DPWA	$\bar{K}N$ multichannel	

• • • We do not use the following data for averages, fits, limits, etc. • • •

0.289	¹ KAMANO	15	DPWA	Multichannel
-------	---------------------	----	------	--------------

¹ From the preferred solution A in KAMANO 15.

$\Gamma(\Lambda\eta)/\Gamma_{\text{total}}$					Γ_3/Γ
<u>VALUE</u>	<u>DOCUMENT ID</u>	<u>TECN</u>	<u>COMMENT</u>		
0.20 ± 0.08	SARANTSEV	19	DPWA	$\bar{K}N$ multichannel	

• • • We do not use the following data for averages, fits, limits, etc. • • •

0.373	KAMANO	15	DPWA	Multichannel
0.30 ± 0.08	ABAEV	96	DPWA	$K^-p \rightarrow \Lambda\eta$

$\Gamma(\Sigma(1385)\pi, D\text{-wave})/\Gamma_{\text{total}}$					Γ_4/Γ
<u>VALUE</u>	<u>DOCUMENT ID</u>	<u>TECN</u>	<u>COMMENT</u>		
0.06 ± 0.02	SARANTSEV	19	DPWA	$\bar{K}N$ multichannel	

• • • We do not use the following data for averages, fits, limits, etc. • • •

0.019	KAMANO	15	DPWA	Multi-channel
-------	--------	----	------	---------------

$\Gamma(\Lambda\sigma)/\Gamma_{\text{total}}$					Γ_7/Γ
<u>VALUE</u>	<u>DOCUMENT ID</u>	<u>TECN</u>	<u>COMMENT</u>		
0.20 ± 0.08	SARANTSEV	19	DPWA	$\bar{K}N$ multichannel	

$\Gamma(N\bar{K}^*(892), S=1/2, S\text{-wave})/\Gamma_{\text{total}}$					Γ_5/Γ
<u>VALUE</u>	<u>DOCUMENT ID</u>	<u>TECN</u>	<u>COMMENT</u>		
• • • We do not use the following data for averages, fits, limits, etc. • • •					
not seen	¹ KAMANO	15	DPWA	Multichannel	

¹ Not seen in the preferred solution A in KAMANO 15.

$\Gamma(N\bar{K}^*(892), S=3/2, D\text{-wave})/\Gamma_{\text{total}}$					Γ_6/Γ
<u>VALUE</u>	<u>DOCUMENT ID</u>	<u>TECN</u>	<u>COMMENT</u>		
0.05 ± 0.04	ZHANG	13A	DPWA	Multichannel	

• • • We do not use the following data for averages, fits, limits, etc. • • •

not seen	¹ KAMANO	15	DPWA	Multichannel
----------	---------------------	----	------	--------------

¹ Not seen in the preferred solution A in KAMANO 15.

$(\Gamma_1\Gamma_f)^{1/2}/\Gamma_{\text{total}}$ in $N\bar{K} \rightarrow \Lambda(1670) \rightarrow \Sigma\pi$					$(\Gamma_1\Gamma_2)^{1/2}/\Gamma$
<u>VALUE</u>	<u>DOCUMENT ID</u>	<u>TECN</u>	<u>COMMENT</u>		

-0.29 ± 0.06	ZHANG	13A	DPWA	Multichannel
-0.26 ± 0.02	KOISO	85	DPWA	$K^-p \rightarrow \Sigma\pi$
-0.31 ± 0.03	GOPAL	77	DPWA	$\bar{K}N$ multichannel
-0.29 ± 0.03	HEPP	76B	DPWA	$K^-N \rightarrow \Sigma\pi$
-0.23 ± 0.03	LONDON	75	HLBC	$K^-p \rightarrow \Sigma^0\pi^0$
-0.27 ± 0.02	KANE	74	DPWA	$K^-p \rightarrow \Sigma\pi$

• • • We do not use the following data for averages, fits, limits, etc. • • •

-0.38 ± 0.03	MANLEY	02	DPWA	$\bar{K}N$ multichannel
-0.13	¹ MARTIN	77	DPWA	$\bar{K}N$ multichannel

¹ MARTIN 77 obtains identical resonance parameters from a T-matrix pole and from a Breit-Wigner fit.

$(\Gamma_1\Gamma_f)^{1/2}/\Gamma_{\text{total}}$ in $N\bar{K} \rightarrow \Lambda(1670) \rightarrow \Lambda\eta$					$(\Gamma_1\Gamma_3)^{1/2}/\Gamma$
<u>VALUE</u>	<u>DOCUMENT ID</u>	<u>TECN</u>	<u>COMMENT</u>		

-0.30 ± 0.10	ZHANG	13A	DPWA	Multichannel
+0.20 ± 0.05	BAXTER	73	DPWA	$K^-p \rightarrow$ neutrals

• • • We do not use the following data for averages, fits, limits, etc. • • •

+0.24 ± 0.04	MANLEY	02	DPWA	$\bar{K}N$ multichannel
0.24	KIM	71	DPWA	K-matrix analysis
0.26	ARMENTEROS69C		HBC	
0.20 or 0.23	BERLEY	65	HBC	

$(\Gamma_1\Gamma_f)^{1/2}/\Gamma_{\text{total}}$ in $N\bar{K} \rightarrow \Lambda(1670) \rightarrow \Sigma(1385)\pi, D\text{-wave}$					$(\Gamma_1\Gamma_4)^{1/2}/\Gamma$
<u>VALUE</u>	<u>DOCUMENT ID</u>	<u>TECN</u>	<u>COMMENT</u>		

-0.17 ± 0.06	MANLEY	02	DPWA	$\bar{K}N$ multichannel
-0.18 ± 0.05	PREVOST	74	DPWA	$K^-N \rightarrow \Sigma(1385)\pi$

 $\Lambda(1670)$ REFERENCES

LEE	21A	PR D103 052005	J.Y. Lee <i>et al.</i>	(BELLE Collab.)
SARANTSEV	19	EPJ A55 180	A.V. Sarantsev <i>et al.</i>	(BONN, PNPI)
KAMANO	15	PR C92 025205	H. Kamano <i>et al.</i>	(ANL, OSAK)
ZHANG	13A	PR C88 035205	H. Zhang <i>et al.</i>	(KSU)
GARCIA-RECIO...	03	PR D67 076009	C. Garcia-Recio <i>et al.</i>	(GRAN, VALE)
MANLEY	02	PRL 88 012002	D.M. Manley <i>et al.</i>	(BNL Crystal Ball Collab.)
ABAEV	96	PR C53 385	V.V. Abaev, B.M.K. Nefkens	(UCLA)
KOISO	85	NP A433 619	H. Koiso <i>et al.</i>	(TOKY, MASA)
PDG	82	PL 111B 1	M. Roos <i>et al.</i>	(HELSE, CIT, CERN)

GOPAL	80	Toronto Conf. 159	G.P. Gopal	(RHEL) IJP
ALSTON...	78	PR D18 182	M. Alston-Garnjost <i>et al.</i>	(LBL, MTHO+) IJP
Also		PRL 38 1007	M. Alston-Garnjost <i>et al.</i>	(LBL, MTHO+) IJP
GOPAL	77	NP B119 362	G.P. Gopal <i>et al.</i>	(LOIC, RHEL) IJP
MARTIN	77	NP B127 349	B.R. Martin, M.K. Pidcock, R.G. Moorhouse	(LOUC+) IJP
Also		NP B126 266	B.R. Martin, M.K. Pidcock	(LOUC) IJP
Also		NP B126 285	B.R. Martin, M.K. Pidcock	(LOUC) IJP
HEPP	76B	PL 65B 487	V. Hepp <i>et al.</i>	(CERN, HEIDH, MPIM) IJP
LONDON	75	NP B55 289	G.W. London <i>et al.</i>	(BNL, CERN, EPOL+) IJP
KANE	74	LBL-2452	D.F. Kane	(LBL) IJP
PREVOST	74	NP B69 246	J. Prevost <i>et al.</i>	(SACL, CERN, HEID)
BAXTER	73	NP B67 125	D.F. Baxter <i>et al.</i>	(OXF) IJP
KIM	71	PRL 27 356	J.K. Kim	(HARV) IJP
Also		Duke Conf. 161	J.K. Kim	(HARV) IJP
Hyperon Resonances, 1970				
ARMENTEROS 69C		Lund Paper 229	R. Armenteros <i>et al.</i>	(CERN, HEID, SACL) IJP
Values are quoted in LEVI-SETTI 69.				
BERLEY	65	PRL 15 641	D. Berley <i>et al.</i>	(BNL) IJP

 $\Lambda(1690) 3/2^-$

$$I(J^P) = 0(\frac{3}{2}^-) \text{ Status: } ***$$

The measurements of the mass, width, and elasticity published before 1974 are now obsolete and have been omitted. They were last listed in our 1982 edition Physics Letters **111B** 1 (1982).

 $\Lambda(1690)$ POLE POSITION**REAL PART**

<u>VALUE (MeV)</u>	<u>DOCUMENT ID</u>	<u>TECN</u>	<u>COMMENT</u>
1680 to 1700 (≈ 1690) OUR ESTIMATE			
1683 ± 3	SARANTSEV	19	DPWA $\bar{K}N$ multichannel
1697 ± ⁶ / ₆	¹ KAMANO	15	DPWA $\bar{K}N$ multichannel

• • • We do not use the following data for averages, fits, limits, etc. • • •

1689	ZHANG	13A	DPWA $\bar{K}N$ multichannel
------	-------	-----	------------------------------

¹ From the preferred solution A in KAMANO 15.

-2xIMAGINARY PART

<u>VALUE (MeV)</u>	<u>DOCUMENT ID</u>	<u>TECN</u>	<u>COMMENT</u>
60 to 80 (≈ 70) OUR ESTIMATE			
72 ± 5	SARANTSEV	19	DPWA $\bar{K}N$ multichannel
65 ± 14	¹ KAMANO	15	DPWA $\bar{K}N$ multichannel

• • • We do not use the following data for averages, fits, limits, etc. • • •

53	ZHANG	13A	DPWA $\bar{K}N$ multichannel
----	-------	-----	------------------------------

¹ From the preferred solution A in KAMANO 15.

 $\Lambda(1690)$ POLE RESIDUES

The normalized residue is the residue divided by $\Gamma_{\text{pole}}/2$.

Normalized residue in $N\bar{K} \rightarrow \Lambda(1690) \rightarrow N\bar{K}$

<u>MODULUS</u>	<u>PHASE ($^\circ$)</u>	<u>DOCUMENT ID</u>	<u>TECN</u>	<u>COMMENT</u>
0.24 ± 0.05	-28 ± 5	SARANTSEV	19	DPWA $\bar{K}N$ multichannel

• • • We do not use the following data for averages, fits, limits, etc. • • •

0.251	3	¹ KAMANO	15	DPWA Multichannel
-------	---	---------------------	----	-------------------

¹ From the preferred solution A in KAMANO 15.

Normalized residue in $N\bar{K} \rightarrow \Lambda(1690) \rightarrow \Sigma\pi$

<u>MODULUS</u>	<u>PHASE ($^\circ$)</u>	<u>DOCUMENT ID</u>	<u>TECN</u>	<u>COMMENT</u>
0.35 ± 0.07	175 ± 6	SARANTSEV	19	DPWA $\bar{K}N$ multichannel

• • • We do not use the following data for averages, fits, limits, etc. • • •

0.315	-173	¹ KAMANO	15	DPWA $\bar{K}N$ multichannel
-------	------	---------------------	----	------------------------------

¹ From the preferred solution A in KAMANO 15.

Normalized residue in $N\bar{K} \rightarrow \Lambda(1690) \rightarrow \Lambda\eta$

<u>MODULUS</u>	<u>PHASE ($^\circ$)</u>	<u>DOCUMENT ID</u>	<u>TECN</u>	<u>COMMENT</u>
0.05 ± 0.02	88 ± 8	SARANTSEV	19	DPWA $\bar{K}N$ multichannel

• • • We do not use the following data for averages, fits, limits, etc. • • •

0.00567	81	¹ KAMANO	15	DPWA Multichannel
---------	----	---------------------	----	-------------------

¹ From the preferred solution A in KAMANO 15.

Normalized residue in $N\bar{K} \rightarrow \Lambda(1690) \rightarrow \Lambda\sigma$

<u>MODULUS</u>	<u>PHASE ($^\circ$)</u>	<u>DOCUMENT ID</u>	<u>TECN</u>	<u>COMMENT</u>
0.08 ± 0.02	-10 ± 6	SARANTSEV	19	DPWA $\bar{K}N$ multichannel

Normalized residue in $N\bar{K} \rightarrow \Lambda(1690) \rightarrow \Sigma(1385)\pi, S\text{-wave}$

<u>MODULUS</u>	<u>PHASE ($^\circ$)</u>	<u>DOCUMENT ID</u>	<u>TECN</u>	<u>COMMENT</u>
0.11 ± 0.06	170 ± 70	SARANTSEV	19	DPWA $\bar{K}N$ multichannel

• • • We do not use the following data for averages, fits, limits, etc. • • •

0.134	168	¹ KAMANO	15	DPWA $\bar{K}N$ multichannel
-------	-----	---------------------	----	------------------------------

¹ From the preferred solution A in KAMANO 15.

Normalized residue in $N\bar{K} \rightarrow \Lambda(1690) \rightarrow \Sigma(1385)\pi, D\text{-wave}$

<u>MODULUS</u>	<u>PHASE ($^\circ$)</u>	<u>DOCUMENT ID</u>	<u>TECN</u>	<u>COMMENT</u>
0.06 ± 0.04	164 ± 15	SARANTSEV	19	DPWA $\bar{K}N$ multichannel

• • • We do not use the following data for averages, fits, limits, etc. • • •

0.319	-22	¹ KAMANO	15	DPWA $\bar{K}N$ multichannel
-------	-----	---------------------	----	------------------------------

¹ From the preferred solution A in KAMANO 15.

Baryon Particle Listings

 $\Lambda(1690)$ Normalized residue in $N\bar{K} \rightarrow \Lambda(1690) \rightarrow N\bar{K}^*(892)$, S-wave

VALUE	DOCUMENT ID	TECN	COMMENT
0.05 ± 0.04	SARANTSEV	19	DPWA $\bar{K}N$ multichannel

Normalized residue in $N\bar{K} \rightarrow \Lambda(1690) \rightarrow N\bar{K}^*(892)$, D-wave

VALUE	DOCUMENT ID	TECN	COMMENT
0.18 ± 0.05 @-110+45	SARANTSEV	19	DPWA $\bar{K}N$ multichannel

 $\Lambda(1690)$ MASS

VALUE (MeV)	DOCUMENT ID	TECN	COMMENT
1685 to 1695 (≈ 1690) OUR ESTIMATE			
1689 ± 3	SARANTSEV	19	DPWA $\bar{K}N$ multichannel
1691 ± 3	ZHANG	13A	DPWA $\bar{K}N$ multichannel
1695.7 ± 2.6	KOISO	85	DPWA $K^-p \rightarrow \Sigma\pi$
1690 ± 5	GOPAL	80	DPWA $\bar{K}N \rightarrow \bar{K}N$
1692 ± 5	ALSTON...	78	DPWA $\bar{K}N \rightarrow \bar{K}N$
1690 ± 3	HEPP	76B	DPWA $K^-N \rightarrow \Sigma\pi$
1689 ± 1	KANE	74	DPWA $K^-p \rightarrow \Sigma\pi$
••• We do not use the following data for averages, fits, limits, etc. •••			
1690 ± 5	GOPAL	77	DPWA $\bar{K}N$ multichannel
1687 or 1689	¹ MARTIN	77	DPWA $\bar{K}N$ multichannel
1692 ± 4	CARROLL	76	DPWA Isospin-0 total σ

¹The two MARTIN 77 values are from a T-matrix pole and from a Breit-Wigner fit. Another D_{03} Λ at 1966 MeV is also suggested by MARTIN 77, but is very uncertain.

 $\Lambda(1690)$ WIDTH

VALUE (MeV)	DOCUMENT ID	TECN	COMMENT
60 to 80 (≈ 70) OUR ESTIMATE			
75 ± 5	SARANTSEV	19	DPWA $\bar{K}N$ multichannel
54 ± 5	ZHANG	13A	DPWA $\bar{K}N$ multichannel
67.2 ± 5.6	KOISO	85	DPWA $K^-p \rightarrow \Sigma\pi$
61 ± 5	GOPAL	80	DPWA $\bar{K}N \rightarrow \bar{K}N$
64 ± 10	ALSTON...	78	DPWA $\bar{K}N \rightarrow \bar{K}N$
82 ± 8	HEPP	76B	DPWA $K^-N \rightarrow \Sigma\pi$
60 ± 4	KANE	74	DPWA $K^-p \rightarrow \Sigma\pi$
••• We do not use the following data for averages, fits, limits, etc. •••			
60 ± 5	GOPAL	77	DPWA $\bar{K}N$ multichannel
62 or 62	¹ MARTIN	77	DPWA $\bar{K}N$ multichannel
38	CARROLL	76	DPWA Isospin-0 total σ

¹The two MARTIN 77 values are from a T-matrix pole and from a Breit-Wigner fit. Another D_{03} Λ at 1966 MeV is also suggested by MARTIN 77, but is very uncertain.

 $\Lambda(1690)$ DECAY MODES

Mode	Fraction (Γ_i/Γ)
Γ_1 $N\bar{K}$	20–30 %
Γ_2 $\Sigma\pi$	20–40 %
Γ_3 $\Lambda\sigma$	(5.0 ± 2.0) %
Γ_4 $\Lambda\pi\pi$	~ 25 %
Γ_5 $\Sigma\pi\pi$	~ 20 %
Γ_6 $\Lambda\eta$	
Γ_7 $\Sigma(1385)\pi$, S-wave	(9 ± 5) %
Γ_8 $\Sigma(1385)\pi$, D-wave	(3.0 ± 2.0) %
Γ_9 $N\bar{K}^*(892)$, S=1/2, D-wave	
Γ_{10} $N\bar{K}^*(892)$, S=3/2, S-wave	
Γ_{11} $N\bar{K}^*(892)$, S=3/2, D-wave	

 $\Lambda(1690)$ BRANCHING RATIOS

$\Gamma(N\bar{K})/\Gamma_{total}$	DOCUMENT ID	TECN	COMMENT	Γ_1/Γ
0.20 to 0.28 OUR ESTIMATE				
0.23 ± 0.05	SARANTSEV	19	DPWA $\bar{K}N$ multichannel	
0.25 ± 0.04	ZHANG	13A	DPWA $\bar{K}N$ multichannel	
0.23 ± 0.03	GOPAL	80	DPWA $\bar{K}N \rightarrow \bar{K}N$	
0.22 ± 0.03	ALSTON...	78	DPWA $\bar{K}N \rightarrow \bar{K}N$	
••• We do not use the following data for averages, fits, limits, etc. •••				
0.239	¹ KAMANO	15	DPWA $\bar{K}N$ multichannel	
0.24 ± 0.03	GOPAL	77	DPWA See GOPAL 80	
0.28 or 0.26	² MARTIN	77	DPWA $\bar{K}N$ multichannel	

¹From the preferred solution A in KAMANO 15.

²The two MARTIN 77 values are from a T-matrix pole and from a Breit-Wigner fit. Another D_{03} Λ at 1966 MeV is also suggested by MARTIN 77, but is very uncertain.

 $\Gamma(\Sigma\pi)/\Gamma_{total}$

VALUE	DOCUMENT ID	TECN	COMMENT	Γ_2/Γ
0.50 ± 0.10	SARANTSEV	19	DPWA $\bar{K}N$ multichannel	
••• We do not use the following data for averages, fits, limits, etc. •••				
0.387	¹ KAMANO	15	DPWA $\bar{K}N$ multichannel	

¹From the preferred solution A in KAMANO 15.

 $\Gamma(\Lambda\eta)/\Gamma_{total}$

VALUE	DOCUMENT ID	TECN	COMMENT	Γ_6/Γ
~ 0.01	SARANTSEV	19	DPWA $\bar{K}N$ multichannel	
••• We do not use the following data for averages, fits, limits, etc. •••				
not seen	¹ KAMANO	15	DPWA Multichannel	

¹From the preferred solution A in KAMANO 15.

 $\Gamma(\Lambda\sigma)/\Gamma_{total}$

VALUE	DOCUMENT ID	TECN	COMMENT	Γ_3/Γ
0.05 ± 0.02	SARANTSEV	19	DPWA $\bar{K}N$ multichannel	

 $\Gamma(\Sigma(1385)\pi, S\text{-wave})/\Gamma_{total}$

VALUE	DOCUMENT ID	TECN	COMMENT	Γ_7/Γ
0.09 ± 0.05	SARANTSEV	19	DPWA $\bar{K}N$ multichannel	
••• We do not use the following data for averages, fits, limits, etc. •••				
0.062	¹ KAMANO	15	DPWA $\bar{K}N$ multichannel	

¹From the preferred solution A in KAMANO 15.

 $\Gamma(\Sigma(1385)\pi, D\text{-wave})/\Gamma_{total}$

VALUE	DOCUMENT ID	TECN	COMMENT	Γ_8/Γ
0.03 ± 0.02	SARANTSEV	19	DPWA $\bar{K}N$ multichannel	
••• We do not use the following data for averages, fits, limits, etc. •••				
0.308	¹ KAMANO	15	DPWA $\bar{K}N$ multichannel	

¹From the preferred solution A in KAMANO 15.

 $\Gamma(N\bar{K}^*(892), S=1/2, D\text{-wave})/\Gamma_{total}$

VALUE	DOCUMENT ID	TECN	COMMENT	Γ_9/Γ
••• We do not use the following data for averages, fits, limits, etc. •••				
not seen	SARANTSEV	19	DPWA $\bar{K}N$ multichannel	
not seen	¹ KAMANO	15	DPWA $\bar{K}N$ multichannel	

¹From the preferred solution A in KAMANO 15.

 $\Gamma(N\bar{K}^*(892), S=3/2, S\text{-wave})/\Gamma_{total}$

VALUE	DOCUMENT ID	TECN	COMMENT	Γ_{10}/Γ
••• We do not use the following data for averages, fits, limits, etc. •••				
0.003	KAMANO	15	DPWA Multichannel	

 $\Gamma(N\bar{K}^*(892), S=3/2, D\text{-wave})/\Gamma_{total}$

VALUE	DOCUMENT ID	TECN	COMMENT	Γ_{11}/Γ
••• We do not use the following data for averages, fits, limits, etc. •••				
not seen	¹ KAMANO	15	DPWA Multichannel	

¹From the preferred solution A in KAMANO 15.

 $(\Gamma_1\Gamma_7)^{1/2}/\Gamma_{total}$ in $N\bar{K} \rightarrow \Lambda(1690) \rightarrow \Sigma\pi$

VALUE	DOCUMENT ID	TECN	COMMENT	$(\Gamma_1\Gamma_2)^{1/2}/\Gamma$
-0.27 ± 0.03	ZHANG	13A	DPWA Multichannel	
-0.34 ± 0.02	KOISO	85	DPWA $K^-p \rightarrow \Sigma\pi$	
-0.25 ± 0.03	GOPAL	77	DPWA $\bar{K}N$ multichannel	
-0.29 ± 0.03	HEPP	76B	DPWA $K^-N \rightarrow \Sigma\pi$	
-0.28 ± 0.03	LONDON	75	HLBC $K^-p \rightarrow \Sigma^0\pi^0$	
-0.28 ± 0.02	KANE	74	DPWA $K^-p \rightarrow \Sigma\pi$	
••• We do not use the following data for averages, fits, limits, etc. •••				
-0.30 or -0.28	¹ MARTIN	77	DPWA $\bar{K}N$ multichannel	

¹The two MARTIN 77 values are from a T-matrix pole and from a Breit-Wigner fit. Another D_{03} Λ at 1966 MeV is also suggested by MARTIN 77, but is very uncertain.

 $(\Gamma_1\Gamma_7)^{1/2}/\Gamma_{total}$ in $N\bar{K} \rightarrow \Lambda(1690) \rightarrow \Lambda\pi\pi$

VALUE	DOCUMENT ID	TECN	COMMENT	$(\Gamma_1\Gamma_4)^{1/2}/\Gamma$
••• We do not use the following data for averages, fits, limits, etc. •••				
0.25 ± 0.02	¹ BARTLEY	68	HDBC $K^-p \rightarrow \Lambda\pi\pi$	

¹BARTLEY 68 uses only cross-section data. The enhancement is not seen by PREVOST 71.

 $(\Gamma_1\Gamma_7)^{1/2}/\Gamma_{total}$ in $N\bar{K} \rightarrow \Lambda(1690) \rightarrow \Sigma\pi\pi$

VALUE	DOCUMENT ID	TECN	COMMENT	$(\Gamma_1\Gamma_5)^{1/2}/\Gamma$
0.21	ARMENTEROS68C	HDBC	$K^-N \rightarrow \Sigma\pi\pi$	

 $(\Gamma_1\Gamma_7)^{1/2}/\Gamma_{total}$ in $N\bar{K} \rightarrow \Lambda(1690) \rightarrow \Lambda\eta$

VALUE	DOCUMENT ID	TECN	COMMENT	$(\Gamma_1\Gamma_6)^{1/2}/\Gamma$
0.00 ± 0.03	BAXTER	73	DPWA $K^-p \rightarrow$ neutrals	

 $(\Gamma_1\Gamma_7)^{1/2}/\Gamma_{total}$ in $N\bar{K} \rightarrow \Lambda(1690) \rightarrow \Sigma(1385)\pi, S\text{-wave}$

VALUE	DOCUMENT ID	TECN	COMMENT	$(\Gamma_1\Gamma_7)^{1/2}/\Gamma$
-0.28 ± 0.06	ZHANG	13A	DPWA Multichannel	
+0.27 ± 0.04	PREVOST	74	DPWA $K^-N \rightarrow \Sigma(1385)\pi$	

 $\Lambda(1690)$ REFERENCES

SARANTSEV	19	EPJ A55 180	A.V. Sarantsev et al.	(BONN, PNPI)
KAMANO	15	PR C92 025205	H. Kamano et al.	(ANL, OSAK)
ZHANG	13A	PR C88 035205	H. Zhang et al.	(KSU)
KOISO	85	NP A433 619	H. Koiso et al.	(TOKY, MASA)
PDG	82	PL 111B 1	M. Roos et al.	(HELS, CIT, CERN)
GOPAL	80	Toronto Conf. 159	G.P. Gopal	(RHEL)JUP

See key on page 1127

Baryon Particle Listings

$\Lambda(1690)$, $\Lambda(1710)$, $\Lambda(1800)$

ALSTON-...	78	PR D18 182	M. Alston-Garnjost <i>et al.</i>	(LBL, MTHO+) IJP
Also		PRL 38 1007	M. Alston-Garnjost <i>et al.</i>	(LBL, MTHO+) IJP
GOPAL	77	NP B119 362	G.P. Gopal <i>et al.</i>	(LOIC, RHEL) IJP
MARTIN	77	NP B127 349	B.R. Martin, M.K. Pidcock, R.G. Moorhouse	(LOUC+) IJP
Also		NP B126 266	B.R. Martin, M.K. Pidcock	(LOUC) IJP
Also		NP B126 285	B.R. Martin, M.K. Pidcock	(LOUC) IJP
CARROLL	76	PRL 37 806	A.S. Carroll <i>et al.</i>	(BNL) I
HEPP	76B	PL 65B 487	V. Hepp <i>et al.</i>	(CERN, HEID, MPIM) IJP
LONDON	75	NP B85 289	G.W. London <i>et al.</i>	(BNL, CERN, EPOL+) IJP
KANE	74	LBL-2452	D.F. Kane	(LBL) IJP
PREVOST	74	NP B69 246	J. Prevost <i>et al.</i>	(SACL, CERN, HEID) IJP
BAXTER	73	NP B67 125	D.F. Baxter <i>et al.</i>	(OXF) IJP
PREVOST	71	Amsterdam Conf.	J. Prevost	(CERN, HEID, SACL) IJP
ARMENTEROS	68C	NP B8 216	R. Armenteros <i>et al.</i>	(CERN, HEID, SACL) I
BARTLEY	68	PRL 21 1111	J.H. Bartley <i>et al.</i>	(TUFTS, FSU, BRAN) I

$\Lambda(1710) \ 1/2^+$

 $I(J^P) = 0(\frac{1}{2}^+) \text{ Status: } *$

OMITTED FROM SUMMARY TABLE

$\Lambda(1710)$ MASS

VALUE (MeV)	DOCUMENT ID	TECN	COMMENT
1713 ± 13	ZHANG	13A	DPWA Multichannel

$\Lambda(1710)$ WIDTH

VALUE (MeV)	DOCUMENT ID	TECN	COMMENT
180 ± 42	ZHANG	13A	DPWA Multichannel

$\Lambda(1710)$ DECAY MODES

Mode	Fraction (Γ_i/Γ)
$\Gamma_1 \ N\bar{K}$	(43 ± 4) %
$\Gamma_2 \ \Sigma \pi$	(21 ± 5) %
$\Gamma_3 \ \Sigma^*(1385) \pi, \ P\text{-wave}$	(20 ± 8) %
$\Gamma_4 \ N\bar{K}^*(892)$	
$\Gamma_5 \ N\bar{K}^*(892), \ S=1/2$	(5 ± 4) %
$\Gamma_6 \ N\bar{K}^*(892), \ S=3/2, \ P\text{-wave}$	(10 ± 8) %

$\Lambda(1710)$ BRANCHING RATIOS

$\Gamma(N\bar{K})/\Gamma_{\text{total}}$	Γ_1/Γ		
VALUE	DOCUMENT ID	TECN	COMMENT
0.43 ± 0.04	ZHANG	13A	DPWA Multichannel
$\Gamma(\Sigma \pi)/\Gamma_{\text{total}}$	Γ_2/Γ		
VALUE	DOCUMENT ID	TECN	COMMENT
0.21 ± 0.05	ZHANG	13A	DPWA Multichannel
$\Gamma(\Sigma^*(1385) \pi, \ P\text{-wave})/\Gamma_{\text{total}}$	Γ_3/Γ		
VALUE	DOCUMENT ID	TECN	COMMENT
0.20 ± 0.08	ZHANG	13A	DPWA Multichannel
$\Gamma(N\bar{K}^*(892), \ S=1/2)/\Gamma_{\text{total}}$	Γ_5/Γ		
VALUE	DOCUMENT ID	TECN	COMMENT
0.05 ± 0.04	ZHANG	13A	DPWA Multichannel
$\Gamma(N\bar{K}^*(892), \ S=3/2, \ P\text{-wave})/\Gamma_{\text{total}}$	Γ_6/Γ		
VALUE	DOCUMENT ID	TECN	COMMENT
0.10 ± 0.08	ZHANG	13A	DPWA Multichannel

$\Lambda(1710)$ REFERENCES

ZHANG	13A	PR C08 035205	H. Zhang <i>et al.</i>	(KSU)
-------	-----	---------------	------------------------	-------

$\Lambda(1800) \ 1/2^-$

 $I(J^P) = 0(\frac{1}{2}^-) \text{ Status: } ***$

$\Lambda(1800)$ POLE POSITION

REAL PART

VALUE (MeV)	DOCUMENT ID	TECN	COMMENT
1809 ± 9	SARANTSEV	19	DPWA $\bar{K}N$ multichannel
••• We do not use the following data for averages, fits, limits, etc. •••			
1729	ZHANG	13A	DPWA Multichannel

-2xIMAGINARY PART

VALUE (MeV)	DOCUMENT ID	TECN	COMMENT
205 ± 16	SARANTSEV	19	DPWA $\bar{K}N$ multichannel
••• We do not use the following data for averages, fits, limits, etc. •••			
198	ZHANG	13A	DPWA Multichannel

$\Lambda(1800)$ POLE RESIDUES

The normalized residue is the residue divided by $\Gamma_{\text{pole}}/2$.

Normalized residue in $N\bar{K} \rightarrow \Lambda(1800) \rightarrow N\bar{K}$

MODULUS	PHASE (°)	DOCUMENT ID	TECN	COMMENT
0.34 ± 0.07	103 ± 8	SARANTSEV	19	DPWA $\bar{K}N$ multichannel

Normalized residue in $N\bar{K} \rightarrow \Lambda(1800) \rightarrow \Sigma \pi$

MODULUS	PHASE (°)	DOCUMENT ID	TECN	COMMENT
0.30 ± 0.06	-123 ± 8	SARANTSEV	19	DPWA $\bar{K}N$ multichannel

Normalized residue in $N\bar{K} \rightarrow \Lambda(1800) \rightarrow \Lambda \eta$

MODULUS	PHASE (°)	DOCUMENT ID	TECN	COMMENT
0.06 ± 0.03	75 ± 10	SARANTSEV	19	DPWA $\bar{K}N$ multichannel

Normalized residue in $N\bar{K} \rightarrow \Lambda(1800) \rightarrow \Lambda \sigma$

MODULUS	PHASE (°)	DOCUMENT ID	TECN	COMMENT
0.24 ± 0.05	25 ± 10	SARANTSEV	19	DPWA $\bar{K}N$ multichannel

Normalized residue in $N\bar{K} \rightarrow \Lambda(1800) \rightarrow \Lambda \omega, \ S=1/2, \ S\text{-wave}$

MODULUS	PHASE (°)	DOCUMENT ID	TECN	COMMENT
0.12 ± 0.04	-114 ± 30	SARANTSEV	19	DPWA $\bar{K}N$ multichannel

Normalized residue in $N\bar{K} \rightarrow \Lambda(1800) \rightarrow \Lambda \omega, \ S=3/2, \ D\text{-wave}$

MODULUS	PHASE (°)	DOCUMENT ID	TECN	COMMENT
0.08 ± 0.03	-90 ± 17	SARANTSEV	19	DPWA $\bar{K}N$ multichannel

Normalized residue in $N\bar{K} \rightarrow \Lambda(1800) \rightarrow \Sigma(1385) \pi$

MODULUS	PHASE (°)	DOCUMENT ID	TECN	COMMENT
0.16 ± 0.06	-140 ± 35	SARANTSEV	19	DPWA $\bar{K}N$ multichannel

Normalized residue in $N\bar{K} \rightarrow \Lambda(1800) \rightarrow N\bar{K}^*(892), \ S=1/2, \ S\text{-wave}$

MODULUS	PHASE (°)	DOCUMENT ID	TECN	COMMENT
0.18 ± 0.06	65 ± 40	SARANTSEV	19	DPWA $\bar{K}N$ multichannel

Normalized residue in $N\bar{K} \rightarrow \Lambda(1800) \rightarrow N\bar{K}^*(892), \ S=3/2, \ D\text{-wave}$

MODULUS	PHASE (°)	DOCUMENT ID	TECN	COMMENT
0.09 ± 0.07		SARANTSEV	19	DPWA $\bar{K}N$ multichannel

$\Lambda(1800)$ MASS

VALUE (MeV)	DOCUMENT ID	TECN	COMMENT
1750 to 1850 (≈ 1800) OUR ESTIMATE			
1811 ± 10	SARANTSEV	19	DPWA $\bar{K}N$ multichannel
1783 ± 19	ZHANG	13A	DPWA $\bar{K}N$ multichannel
1841 ± 10	GOPAL	80	DPWA $\bar{K}N \rightarrow \bar{K}N$
1725 ± 20	ALSTON-...	78	DPWA $\bar{K}N \rightarrow \bar{K}N$
1830 ± 20	LANGBEIN	72	IPWA $\bar{K}N$ multichannel
••• We do not use the following data for averages, fits, limits, etc. •••			
1845 ± 10	MANLEY	02	DPWA $\bar{K}N$ multichannel
1825 ± 20	GOPAL	77	DPWA $\bar{K}N$ multichannel
1767 or 1842	¹ MARTIN	77	DPWA $\bar{K}N$ multichannel
1780	KIM	71	DPWA K-matrix analysis
1872 ± 10	BRICMAN	70B	DPWA $\bar{K}N \rightarrow \bar{K}N$

$\Lambda(1800)$ WIDTH

VALUE (MeV)	DOCUMENT ID	TECN	COMMENT
150 to 250 (≈ 200) OUR ESTIMATE			
209 ± 18	SARANTSEV	19	DPWA $\bar{K}N$ multichannel
256 ± 35	ZHANG	13A	DPWA $\bar{K}N$ multichannel
228 ± 20	GOPAL	80	DPWA $\bar{K}N \rightarrow \bar{K}N$
185 ± 20	ALSTON-...	78	DPWA $\bar{K}N \rightarrow \bar{K}N$
70 ± 15	LANGBEIN	72	IPWA $\bar{K}N$ multichannel
••• We do not use the following data for averages, fits, limits, etc. •••			
518 ± 84	MANLEY	02	DPWA $\bar{K}N$ multichannel
230 ± 20	GOPAL	77	DPWA $\bar{K}N$ multichannel
435 or 473	¹ MARTIN	77	DPWA $\bar{K}N$ multichannel
40	KIM	71	DPWA K-matrix analysis
100 ± 20	BRICMAN	70B	DPWA $\bar{K}N \rightarrow \bar{K}N$

$\Lambda(1800)$ DECAY MODES

Mode	Fraction (Γ_i/Γ)
$\Gamma_1 \ N\bar{K}$	25-40 %
$\Gamma_2 \ \Sigma \pi$	seen
$\Gamma_3 \ \Lambda \sigma$	(15 ± 4) %
$\Gamma_4 \ \Sigma(1385) \pi$	seen
$\Gamma_5 \ \Lambda \eta$	0.01 to 0.10
$\Gamma_6 \ N\bar{K}^*(892)$	seen
$\Gamma_7 \ N\bar{K}^*(892), \ S=1/2, \ S\text{-wave}$	
$\Gamma_8 \ N\bar{K}^*(892), \ S=3/2, \ D\text{-wave}$	

Baryon Particle Listings

 $\Lambda(1800), \Lambda(1810)$ $\Lambda(1800)$ BRANCHING RATIOS

See "Sign conventions for resonance couplings" in the Note on Λ and Σ Resonances.

 $\Gamma(N\bar{K})/\Gamma_{\text{total}}$

VALUE	DOCUMENT ID	TECN	COMMENT	Γ_1/Γ
0.25 to 0.40 OUR ESTIMATE				
0.35 ± 0.07	SARANTSEV 19	DPWA	$\bar{K}N$ multichannel	
0.13 ± 0.06	ZHANG 13A	DPWA	$\bar{K}N$ multichannel	
0.36 ± 0.04	GOPAL 80	DPWA	$\bar{K}N \rightarrow \bar{K}N$	
0.28 ± 0.05	ALSTON-... 78	DPWA	$\bar{K}N \rightarrow \bar{K}N$	
0.35 ± 0.15	LANGBEIN 72	IPWA	$\bar{K}N$ multichannel	
••• We do not use the following data for averages, fits, limits, etc. •••				
0.24 ± 0.10	MANLEY 02	DPWA	$\bar{K}N$ multichannel	
0.37 ± 0.05	GOPAL 77	DPWA	See GOPAL 80	
1.21 or 0.70	¹ MARTIN 77	DPWA	$\bar{K}N$ multichannel	
0.80	KIM 71	DPWA	K-matrix analysis	
0.18 ± 0.02	BRICMAN 70B	DPWA	$\bar{K}N \rightarrow \bar{K}N$	

 $\Gamma(\Sigma\pi)/\Gamma_{\text{total}}$

VALUE	DOCUMENT ID	TECN	COMMENT	Γ_2/Γ
0.27 ± 0.06	SARANTSEV 19	DPWA	$\bar{K}N$ multichannel	

 $\Gamma(\Lambda\sigma)/\Gamma_{\text{total}}$

VALUE	DOCUMENT ID	TECN	COMMENT	Γ_3/Γ
0.15 ± 0.04	SARANTSEV 19	DPWA	$\bar{K}N$ multichannel	

 $\Gamma(\Sigma(1385)\pi)/\Gamma_{\text{total}}$

VALUE	DOCUMENT ID	TECN	COMMENT	Γ_4/Γ
0.09 ± 0.04	SARANTSEV 19	DPWA	$\bar{K}N$ multichannel	

 $\Gamma(\Lambda\eta)/\Gamma_{\text{total}}$

VALUE	DOCUMENT ID	TECN	COMMENT	Γ_5/Γ
0.01 to 0.10 OUR ESTIMATE				
0.010 ± 0.005	SARANTSEV 19	DPWA	$\bar{K}N$ multichannel	
0.06 ± 0.05	ZHANG 13A	DPWA	Multichannel	

 $(\Gamma_1\Gamma_2)^{1/2}/\Gamma_{\text{total}}$ in $N\bar{K} \rightarrow \Lambda(1800) \rightarrow \Sigma\pi$

VALUE	DOCUMENT ID	TECN	COMMENT	$(\Gamma_1\Gamma_2)^{1/2}/\Gamma$
-0.07 ± 0.02	ZHANG 13A	DPWA	Multichannel	
-0.08 ± 0.05	GOPAL 77	DPWA	$\bar{K}N$ multichannel	
••• We do not use the following data for averages, fits, limits, etc. •••				
-0.74 or -0.43	¹ MARTIN 77	DPWA	$\bar{K}N$ multichannel	
0.24	KIM 71	DPWA	K-matrix analysis	

 $(\Gamma_1\Gamma_2)^{1/2}/\Gamma_{\text{total}}$ in $N\bar{K} \rightarrow \Lambda(1800) \rightarrow \Sigma(1385)\pi$

VALUE	DOCUMENT ID	TECN	COMMENT	$(\Gamma_1\Gamma_2)^{1/2}/\Gamma$
-0.09 ± 0.05	ZHANG 13A	DPWA	Multichannel	
+0.056 ± 0.028	² CAMERON 78	DPWA	$K^-p \rightarrow \Sigma(1385)\pi$	

 $(\Gamma_1\Gamma_2)^{1/2}/\Gamma_{\text{total}}$ in $N\bar{K} \rightarrow \Lambda(1800) \rightarrow N\bar{K}^*(892), S=1/2, S\text{-wave}$

VALUE	DOCUMENT ID	TECN	COMMENT	$(\Gamma_1\Gamma_2)^{1/2}/\Gamma$
-0.13 ± 0.02	ZHANG 13A	DPWA	Multichannel	
-0.17 ± 0.03	² CAMERON 78B	DPWA	$K^-p \rightarrow N\bar{K}^*$	

 $(\Gamma_1\Gamma_2)^{1/2}/\Gamma_{\text{total}}$ in $N\bar{K} \rightarrow \Lambda(1800) \rightarrow N\bar{K}^*(892), S=3/2, D\text{-wave}$

VALUE	DOCUMENT ID	TECN	COMMENT	$(\Gamma_1\Gamma_2)^{1/2}/\Gamma$
-0.13 ± 0.04	CAMERON 78B	DPWA	$K^-p \rightarrow N\bar{K}^*$	

 $\Lambda(1800)$ FOOTNOTES

- ¹ The two MARTIN 77 values are from a T-matrix pole and from a Breit-Wigner fit.
² The published sign has been changed to be in accord with the baryon-first convention.

 $\Lambda(1800)$ REFERENCES

SARANTSEV 19	EPJ A55 180	A.V. Sarantsev et al.	(BONN, PNPI)
ZHANG 13A	PR C88 035205	H. Zhang et al.	(KSU)
MANLEY 02	PRL 88 012002	D.M. Manley et al.	(BNL Crystal Ball Collab.)
GOPAL 80	Toronto Conf. 159	G.P. Gopal	(RHEL) IJP
ALSTON-... 78	PR D18 182	M. Alston-Garnjost et al.	(LBL, MTHO+) IJP
Also	PRL 38 1007	M. Alston-Garnjost et al.	(LBL, MTHO+) IJP
CAMERON 78	NP B143 189	W. Cameron et al.	(RHEL, LOIC) IJP
CAMERON 78B	NP B146 327	W. Cameron et al.	(RHEL, LOIC) IJP
GOPAL 77	NP B119 362	G.P. Gopal et al.	(LOIC, RHEL) IJP
MARTIN 77	NP B127 349	B.R. Martin, M.K. Pidcock, R.G. Moorhouse	(LOUC+) IJP
Also	NP B126 266	B.R. Martin, M.K. Pidcock	(LOUC) IJP
Also	NP B126 285	B.R. Martin, M.K. Pidcock	(LOUC) IJP
LANGBEIN 72	NP B47 477	W. Langbein, F. Wagner	(MPIM) IJP
KIM 71	PRL 27 356	J.K. Kim	(HARV) IJP
Also	Duke Conf. 161	J.K. Kim	(HARV) IJP
Hyperon Resonances, 1970			
BRICMAN 70B	PL 33B 511	C. Bricman, M. Ferro-Luzzi, J.P. Lagnaux	(CERN) IJP

 $\Lambda(1810)$ POLE POSITION

REAL PART

VALUE (MeV)	DOCUMENT ID	TECN	COMMENT
1773 ± 7	SARANTSEV 19	DPWA	$\bar{K}N$ multichannel
••• We do not use the following data for averages, fits, limits, etc. •••			
2097 ⁺⁴⁰ ₋₁	¹ KAMANO 15	DPWA	Multichannel
1780	ZHANG 13A	DPWA	Multichannel
¹ From the preferred solution A in KAMANO 15. Solution B reports $M = 1841^{+3}_{-4}$ MeV.			

-2xIMAGINARY PART

VALUE (MeV)	DOCUMENT ID	TECN	COMMENT
38 ± 14	SARANTSEV 19	DPWA	$\bar{K}N$ multichannel
••• We do not use the following data for averages, fits, limits, etc. •••			
166 ⁺⁶⁴ ₋₁₂	¹ KAMANO 15	DPWA	Multichannel
64	ZHANG 13A	DPWA	Multichannel
¹ From the preferred solution A in KAMANO 15. Solution B Reports $\Gamma = 62^{+6}_{-4}$ MeV.			

 $\Lambda(1810)$ POLE RESIDUES

The normalized residue is the residue divided by $\Gamma_{\text{pole}}/2$.

Normalized residue in $N\bar{K} \rightarrow \Lambda(1810) \rightarrow N\bar{K}$

MODULUS	PHASE (°)	DOCUMENT ID	TECN	COMMENT
0.018 ± 0.008	65 ± 26	SARANTSEV 19	DPWA	$\bar{K}N$ multichannel
••• We do not use the following data for averages, fits, limits, etc. •••				
0.205	-63	¹ KAMANO 15	DPWA	Multichannel
¹ From the preferred solution A in KAMANO 15.				

Normalized residue in $N\bar{K} \rightarrow \Lambda(1810) \rightarrow \Sigma\pi$

MODULUS	PHASE (°)	DOCUMENT ID	TECN	COMMENT
0.045 ± 0.020	-143 ± 24	SARANTSEV 19	DPWA	$\bar{K}N$ multichannel
••• We do not use the following data for averages, fits, limits, etc. •••				
0.0325	29	¹ KAMANO 15	DPWA	Multichannel
¹ From the preferred solution A in KAMANO 15.				

Normalized residue in $N\bar{K} \rightarrow \Lambda(1810) \rightarrow \Lambda\eta$

MODULUS	PHASE (°)	DOCUMENT ID	TECN	COMMENT
••• We do not use the following data for averages, fits, limits, etc. •••				
0.155	165	¹ KAMANO 15	DPWA	Multichannel
¹ From the preferred solution A in KAMANO 15.				

Normalized residue in $N\bar{K} \rightarrow \Lambda(1810) \rightarrow \Lambda\sigma$

MODULUS	PHASE (°)	DOCUMENT ID	TECN	COMMENT
0.055 ± 0.020	30 ± 16	SARANTSEV 19	DPWA	$\bar{K}N$ multichannel

Normalized residue in $N\bar{K} \rightarrow \Lambda(1810) \rightarrow \Xi K$

MODULUS	PHASE (°)	DOCUMENT ID	TECN	COMMENT
••• We do not use the following data for averages, fits, limits, etc. •••				
0.0937	-64	¹ KAMANO 15	DPWA	Multichannel
¹ From the preferred solution A in KAMANO 15.				

Normalized residue in $N\bar{K} \rightarrow \Lambda(1810) \rightarrow \Sigma(1385)\pi$

MODULUS	PHASE (°)	DOCUMENT ID	TECN	COMMENT
0.08 ± 0.03	-50 ± 30	SARANTSEV 19	DPWA	$\bar{K}N$ multichannel
••• We do not use the following data for averages, fits, limits, etc. •••				
0.244	-10	¹ KAMANO 15	DPWA	Multichannel
¹ From the preferred solution A in KAMANO 15.				

Normalized residue in $N\bar{K} \rightarrow \Lambda(1810) \rightarrow N\bar{K}^*(892), S=1/2, P\text{-wave}$

MODULUS	PHASE (°)	DOCUMENT ID	TECN	COMMENT
0.03 ± 0.03		SARANTSEV 19	DPWA	$\bar{K}N$ multichannel
••• We do not use the following data for averages, fits, limits, etc. •••				
0.159	-97	¹ KAMANO 15	DPWA	Multichannel
¹ From the preferred solution A in KAMANO 15.				

Normalized residue in $N\bar{K} \rightarrow \Lambda(1810) \rightarrow N\bar{K}^*(892), S=3/2, P\text{-wave}$

MODULUS	PHASE (°)	DOCUMENT ID	TECN	COMMENT
0.05 ± 0.04		SARANTSEV 19	DPWA	$\bar{K}N$ multichannel
••• We do not use the following data for averages, fits, limits, etc. •••				
0.0497	2	¹ KAMANO 15	DPWA	Multichannel
¹ From the preferred solution A in KAMANO 15.				

 $\Lambda(1810)$ MASS

VALUE (MeV)	DOCUMENT ID	TECN	COMMENT
1740 to 1840 (≈ 1790) OUR ESTIMATE			
1773 ± 7	SARANTSEV 19	DPWA	$\bar{K}N$ multichannel
1821 ± 10	ZHANG 13A	DPWA	Multichannel
1841 ± 20	GOPAL 80	DPWA	$\bar{K}N \rightarrow \bar{K}N$
1735 ± 5	CARROLL 76	DPWA	Isospin-0 total σ
1746 ± 10	PREVOST 74	DPWA	$K^-N \rightarrow \Sigma(1385)\pi$
1780 ± 20	LANGBEIN 72	IPWA	$\bar{K}N$ multichannel

$$\Lambda(1810) 1/2^+$$

$$I(J^P) = 0(\frac{1}{2}^+) \text{ Status: } ***$$

See key on page 1127

Baryon Particle Listings

$\Lambda(1810), \Lambda(1820)$

• • • We do not use the following data for averages, fits, limits, etc. • • •

1853 ± 20	GOPAL	77	DPWA	$\bar{K}N$ multichannel
1861 or 1953	¹ MARTIN	77	DPWA	$\bar{K}N$ multichannel
1755	KIM	71	DPWA	K-matrix analysis
1800	ARMENTEROS70	HBC	$\bar{K}N \rightarrow \bar{K}N$	
1750	ARMENTEROS70	HBC	$\bar{K}N \rightarrow \Sigma\pi$	
1690 ± 10	BARBARO...	70	HBC	$\bar{K}N \rightarrow \Sigma\pi$
1740	BAILEY	69	DPWA	$\bar{K}N \rightarrow \bar{K}N$
1745	ARMENTEROS68B	HBC	$\bar{K}N \rightarrow \bar{K}N$	

¹ The two MARTIN 77 values are from a T-matrix pole and from a Breit-Wigner fit.

$\Lambda(1810)$ WIDTH

VALUE (MeV)	DOCUMENT ID	TECN	COMMENT
50 to 170 (≈ 110) OUR ESTIMATE			
39 ± 15	SARANTSEV	19	DPWA $\bar{K}N$ multichannel
174 ± 5.0	ZHANG	13A	DPWA Multichannel
164 ± 20	GOPAL	80	DPWA $\bar{K}N \rightarrow \bar{K}N$
90 ± 20	CAMERON	78B	DPWA $K^-p \rightarrow N\bar{K}^*$
46 ± 20	PREVOST	74	DPWA $K^-N \rightarrow \Sigma(1385)\pi$
120 ± 10	LANGBEIN	72	IPWA $\bar{K}N$ multichannel
• • • We do not use the following data for averages, fits, limits, etc. • • •			
166 ± 20	GOPAL	77	DPWA $\bar{K}N$ multichannel
535 or 585	¹ MARTIN	77	DPWA $\bar{K}N$ multichannel
28	CARROLL	76	DPWA Isospin-0 total σ
35	KIM	71	DPWA K-matrix analysis
30	ARMENTEROS70	HBC	$\bar{K}N \rightarrow \bar{K}N$
70	ARMENTEROS70	HBC	$\bar{K}N \rightarrow \Sigma\pi$
22	BARBARO...	70	HBC $\bar{K}N \rightarrow \Sigma\pi$
300	BAILEY	69	DPWA $\bar{K}N \rightarrow \bar{K}N$
147	ARMENTEROS68B	HBC	

¹ The two MARTIN 77 values are from a T-matrix pole and from a Breit-Wigner fit.

$\Lambda(1810)$ DECAY MODES

Mode	Fraction (Γ_i/Γ)
Γ_1 $N\bar{K}$	0.05 to 0.35
Γ_2 $\Sigma\pi$	(16 ± 5) %
Γ_3 $\Lambda\eta$	
Γ_4 ΞK	
Γ_5 $\Sigma(1385)\pi$	(40 ± 15) %
Γ_6 $N\bar{K}^*(892)$	30–60 %
Γ_7 $N\bar{K}^*(892), S=1/2, P$ -wave	
Γ_8 $N\bar{K}^*(892), S=3/2, P$ -wave	

$\Lambda(1810)$ BRANCHING RATIOS

$\Gamma(N\bar{K})/\Gamma_{total}$	DOCUMENT ID	TECN	COMMENT	Γ_1/Γ
0.05 to 0.35 OUR ESTIMATE				
0.025 ± 0.013	SARANTSEV	19	DPWA $\bar{K}N$ multichannel	
0.19 ± 0.08	ZHANG	13A	DPWA $\bar{K}N$ multichannel	
0.24 ± 0.04	GOPAL	80	DPWA $\bar{K}N \rightarrow \bar{K}N$	
0.36 ± 0.05	LANGBEIN	72	IPWA $\bar{K}N$ multichannel	
• • • We do not use the following data for averages, fits, limits, etc. • • •				
0.225	¹ KAMANO	15	DPWA $\bar{K}N$ multichannel	
0.21 ± 0.04	GOPAL	77	DPWA See GOPAL 80	
0.52 or 0.49	² MARTIN	77	DPWA $\bar{K}N$ multichannel	
0.30	KIM	71	DPWA K-matrix analysis	
0.15	ARMENTEROS70	DPWA	$\bar{K}N \rightarrow \bar{K}N$	
0.55	BAILEY	69	DPWA $\bar{K}N \rightarrow \bar{K}N$	
0.4	ARMENTEROS68B	DPWA	$\bar{K}N \rightarrow \bar{K}N$	

¹ From the preferred solution A in KAMANO 15.

² The two MARTIN 77 values are from a T-matrix pole and from a Breit-Wigner fit.

$\Gamma(\Sigma\pi)/\Gamma_{total}$	DOCUMENT ID	TECN	COMMENT	Γ_2/Γ
0.16 ± 0.05				
	SARANTSEV	19	DPWA $\bar{K}N$ multichannel	

• • • We do not use the following data for averages, fits, limits, etc. • • •

0.009	¹ KAMANO	15	DPWA Multichannel
-------	---------------------	----	-------------------

¹ From the preferred solution A in KAMANO 15.

$\Gamma(\Lambda\eta)/\Gamma_{total}$	DOCUMENT ID	TECN	COMMENT	Γ_3/Γ
0.11				
	¹ KAMANO	15	DPWA Multichannel	

• • • We do not use the following data for averages, fits, limits, etc. • • •

¹ From the preferred solution A in KAMANO 15.

$\Gamma(\Xi K)/\Gamma_{total}$	DOCUMENT ID	TECN	COMMENT	Γ_4/Γ
0.051				
	¹ KAMANO	15	DPWA Multichannel	

¹ From the preferred solution A in KAMANO 15.

$\Gamma(\Sigma(1385)\pi)/\Gamma_{total}$ Γ_5/Γ

VALUE	DOCUMENT ID	TECN	COMMENT
0.40 ± 0.15			
	SARANTSEV	19	DPWA $\bar{K}N$ multichannel

• • • We do not use the following data for averages, fits, limits, etc. • • •

0.600	¹ KAMANO	15	DPWA Multichannel
-------	---------------------	----	-------------------

¹ From the preferred solution A in KAMANO 15.

$\Gamma(N\bar{K}^*(892), S=1/2, P$ -wave) $/\Gamma_{total}$ Γ_7/Γ

VALUE	DOCUMENT ID	TECN	COMMENT
• • • We do not use the following data for averages, fits, limits, etc. • • •			
0.003	¹ KAMANO	15	DPWA Multichannel

¹ From the preferred solution A in KAMANO 15.

$(\Gamma_i\Gamma_f)^{1/2}/\Gamma_{total}$ in $N\bar{K} \rightarrow \Lambda(1810) \rightarrow \Sigma\pi$ $(\Gamma_1\Gamma_2)^{1/2}/\Gamma$

VALUE	DOCUMENT ID	TECN	COMMENT
-0.08 ± 0.05	ZHANG	13A	DPWA Multichannel
-0.24 ± 0.04	GOPAL	77	DPWA $\bar{K}N$ multichannel

• • • We do not use the following data for averages, fits, limits, etc. • • •

+0.25 or +0.23	¹ MARTIN	77	DPWA $\bar{K}N$ multichannel
----------------	---------------------	----	------------------------------

< 0.01	LANGBEIN	72	IPWA $\bar{K}N$ multichannel
--------	----------	----	------------------------------

0.17	KIM	71	DPWA K-matrix analysis
------	-----	----	------------------------

+0.20	² ARMENTEROS70	DPWA	$\bar{K}N \rightarrow \Sigma\pi$
-------	---------------------------	------	----------------------------------

-0.13 ± 0.03	BARBARO...	70	DPWA $\bar{K}N \rightarrow \Sigma\pi$
--------------	------------	----	---------------------------------------

¹ The two MARTIN 77 values are from a T-matrix pole and from a Breit-Wigner fit.

² The published sign has been changed to be in accord with the baryon-first convention.

$(\Gamma_i\Gamma_f)^{1/2}/\Gamma_{total}$ in $N\bar{K} \rightarrow \Lambda(1810) \rightarrow \Sigma(1385)\pi$ $(\Gamma_1\Gamma_5)^{1/2}/\Gamma$

VALUE	DOCUMENT ID	TECN	COMMENT
+0.18 ± 0.10	PREVOST	74	DPWA $K^-N \rightarrow \Sigma(1385)\pi$

$(\Gamma_i\Gamma_f)^{1/2}/\Gamma_{total}$ in $N\bar{K} \rightarrow \Lambda(1810) \rightarrow N\bar{K}^*(892), S=1/2, P$ -wave $(\Gamma_1\Gamma_7)^{1/2}/\Gamma$

VALUE	DOCUMENT ID	TECN	COMMENT
-0.14 ± 0.03	¹ CAMERON	78B	DPWA $K^-p \rightarrow N\bar{K}^*$

¹ The published sign has been changed to be in accord with the baryon-first convention.

$(\Gamma_i\Gamma_f)^{1/2}/\Gamma_{total}$ in $N\bar{K} \rightarrow \Lambda(1810) \rightarrow N\bar{K}^*(892), S=3/2, P$ -wave $(\Gamma_1\Gamma_8)^{1/2}/\Gamma$

VALUE	DOCUMENT ID	TECN	COMMENT
+0.38 ± 0.06	ZHANG	13A	DPWA Multichannel
+0.35 ± 0.06	CAMERON	78B	DPWA $K^-p \rightarrow N\bar{K}^*$

$\Lambda(1810)$ REFERENCES

SARANTSEV	19	EPJ A55 180	A.V. Sarantsev et al.	(BONN, PNPI)
KAMANO	15	PR C92 025205	H. Kamano et al.	(ANL, OSAK)
ZHANG	13A	PR C88 035205	H. Zhang et al.	(KSU)
GOPAL	80	Toronto Conf. 159	G.P. Gopal	(RHEL) IJP
CAMERON	78B	NP B146 327	W. Cameron et al.	(RHEL, LOIC) IJP
GOPAL	77	NP B119 362	G.P. Gopal et al.	(LOIC, RHEL) IJP
MARTIN	77	NP B127 349	B.R. Martin, M.K. Pidcock, R.G. Moorhouse	(LOUC+) IJP
Also		NP B126 266	B.R. Martin, M.K. Pidcock	(LOUC) IJP
Also		NP B126 285	B.R. Martin, M.K. Pidcock	(LOUC) IJP
CARROLL	76	PRL 37 806	A.S. Carroll et al.	(BNL) I
PREVOST	74	NP B69 246	J. Prevost et al.	(SACL, CERN, HEID)
LANGBEIN	72	NP B47 477	W. Langbein, F. Wagner	(MPIM) IJP
KIM	71	PRL 27 356	J.K. Kim	(HARV) IJP
Also		Duke Conf. 161	J.K. Kim	(HARV) IJP
Hyperon Resonances, 1970				
ARMENTEROS 70		Duke Conf. 123	R. Armenteros et al.	(CERN, HEID, SACL) IJP
Hyperon Resonances, 1970				
BARBARO...	70	Duke Conf. 173	A. Barbaro-Galtri	(LRL) IJP
Hyperon Resonances, 1970				
BAILEY	69	Thesis UCRL 50617	J.M. Bailey	(LLL) IJP
ARMENTEROS 68B		NP B8 195	R. Armenteros et al.	(CERN, HEID, SACL) IJP

$\Lambda(1820) 5/2^+$

$$I(J^P) = 0(\frac{5}{2}^+) \text{ Status: } ***$$

This resonance is the cornerstone for all partial-wave analyses in this region. Most of the results published before 1973 are now obsolete and have been omitted. They may be found in our 1982 edition Physics Letters **111B** 1 (1982).

$\Lambda(1820)$ POLE POSITION

REAL PART

VALUE (MeV)	DOCUMENT ID	TECN	COMMENT
1812 to 1825 (≈ 1818) OUR ESTIMATE			
1813 ± 3	SARANTSEV	19	DPWA $\bar{K}N$ multichannel
1824 ± $\frac{2}{1}$	¹ KAMANO	15	DPWA $\bar{K}N$ multichannel

• • • We do not use the following data for averages, fits, limits, etc. • • •

1814	ZHANG	13A	DPWA $\bar{K}N$ multichannel
------	-------	-----	------------------------------

¹ From the preferred solution A in KAMANO 15.

-2xIMAGINARY PART

VALUE (MeV)	DOCUMENT ID	TECN	COMMENT
75 to 80 (≈ 77) OUR ESTIMATE			
78 ± 7	SARANTSEV	19	DPWA $\bar{K}N$ multichannel
77 ± 2	¹ KAMANO	15	DPWA $\bar{K}N$ multichannel

Baryon Particle Listings

 $\Lambda(1820)$

••• We do not use the following data for averages, fits, limits, etc. •••

85 ZHANG 13A DPWA $\bar{K}N$ multichannel

¹ From the preferred solution A in KAMANO 15.

 $\Lambda(1820)$ POLE RESIDUES

The normalized residue is the residue divided by $\Gamma_{pole}/2$.

Normalized residue in $N\bar{K} \rightarrow \Lambda(1820) \rightarrow N\bar{K}$

MODULUS	PHASE (°)	DOCUMENT ID	TECN	COMMENT
0.60 ± 0.12	-22 ± 5	SARANTSEV 19	DPWA	$\bar{K}N$ multichannel

••• We do not use the following data for averages, fits, limits, etc. •••

0.558 -13 ¹ KAMANO 15 DPWA $\bar{K}N$ multichannel

¹ From the preferred solution A in KAMANO 15.

Normalized residue in $N\bar{K} \rightarrow \Lambda(1820) \rightarrow \Sigma\pi$

MODULUS	PHASE (°)	DOCUMENT ID	TECN	COMMENT
0.34 ± 0.07	174 ± 5	SARANTSEV 19	DPWA	$\bar{K}N$ multichannel

••• We do not use the following data for averages, fits, limits, etc. •••

0.357 168 ¹ KAMANO 15 DPWA $\bar{K}N$ multichannel

¹ From the preferred solution A in KAMANO 15.

Normalized residue in $N\bar{K} \rightarrow \Lambda(1820) \rightarrow \Lambda\eta$

MODULUS	PHASE (°)	DOCUMENT ID	TECN	COMMENT
0.0184	-3	¹ KAMANO 15	DPWA	$\bar{K}N$ multichannel

••• We do not use the following data for averages, fits, limits, etc. •••

¹ From the preferred solution A in KAMANO 15.

Normalized residue in $N\bar{K} \rightarrow \Lambda(1820) \rightarrow \Xi K$

MODULUS	PHASE (°)	DOCUMENT ID	TECN	COMMENT
~ 0		SARANTSEV 19	DPWA	$\bar{K}N$ multichannel

••• We do not use the following data for averages, fits, limits, etc. •••

0.00111 70 ¹ KAMANO 15 DPWA $\bar{K}N$ multichannel

¹ From the preferred solution A in KAMANO 15.

Normalized residue in $N\bar{K} \rightarrow \Lambda(1820) \rightarrow \Sigma(1385)\pi, P\text{-wave}$

MODULUS	PHASE (°)	DOCUMENT ID	TECN	COMMENT
0.07 ± 0.02	-60 ± 50	SARANTSEV 19	DPWA	$\bar{K}N$ multichannel

••• We do not use the following data for averages, fits, limits, etc. •••

0.340 161 ¹ KAMANO 15 DPWA $\bar{K}N$ multichannel

¹ From the preferred solution A in KAMANO 15.

Normalized residue in $N\bar{K} \rightarrow \Lambda(1820) \rightarrow \Sigma(1385)\pi, F\text{-wave}$

MODULUS	PHASE (°)	DOCUMENT ID	TECN	COMMENT
0.11 ± 0.04	5 ± 45	SARANTSEV 19	DPWA	$\bar{K}N$ multichannel

••• We do not use the following data for averages, fits, limits, etc. •••

0.201 151 ¹ KAMANO 15 DPWA $\bar{K}N$ multichannel

¹ From the preferred solution A in KAMANO 15.

Normalized residue in $N\bar{K} \rightarrow \Lambda(1820) \rightarrow N\bar{K}^*(892), S=1/2, F\text{-wave}$

MODULUS	PHASE (°)	DOCUMENT ID	TECN	COMMENT
0.02 ± 0.02		SARANTSEV 19	DPWA	$\bar{K}N$ multichannel

••• We do not use the following data for averages, fits, limits, etc. •••

0.00750 41 ¹ KAMANO 15 DPWA $\bar{K}N$ multichannel

¹ From the preferred solution A in KAMANO 15.

Normalized residue in $N\bar{K} \rightarrow \Lambda(1820) \rightarrow N\bar{K}^*(892), S=3/2, P\text{-wave}$

MODULUS	PHASE (°)	DOCUMENT ID	TECN	COMMENT
0.35 ± 0.15	-30 ± 45	SARANTSEV 19	DPWA	$\bar{K}N$ multichannel

••• We do not use the following data for averages, fits, limits, etc. •••

0.171 -139 ¹ KAMANO 15 DPWA $\bar{K}N$ multichannel

¹ From the preferred solution A in KAMANO 15.

Normalized residue in $N\bar{K} \rightarrow \Lambda(1820) \rightarrow N\bar{K}^*(892), S=3/2, F\text{-wave}$

MODULUS	PHASE (°)	DOCUMENT ID	TECN	COMMENT
0.02 ± 0.02		SARANTSEV 19	DPWA	$\bar{K}N$ multichannel

••• We do not use the following data for averages, fits, limits, etc. •••

0.000517 161 ¹ KAMANO 15 DPWA $\bar{K}N$ multichannel

¹ From the preferred solution A in KAMANO 15.

 $\Lambda(1820)$ MASS

VALUE (MeV)	DOCUMENT ID	TECN	COMMENT
1815 to 1825 (≈ 1820) OUR ESTIMATE			
1822 ± 4	SARANTSEV 19	DPWA	$\bar{K}N$ multichannel
1823.5 ± 0.8	ZHANG 13A	DPWA	$\bar{K}N$ multichannel
1823 ± 3	GOPAL 80	DPWA	$\bar{K}N \rightarrow \bar{K}N$
1819 ± 2	ALSTON... 78	DPWA	$\bar{K}N \rightarrow \bar{K}N$
1821 ± 2	KANE 74	DPWA	$K^- p \rightarrow \Sigma\pi$

••• We do not use the following data for averages, fits, limits, etc. •••

1830 DECLAIS 77 DPWA $\bar{K}N \rightarrow \bar{K}N$

1822 ± 2 GOPAL 77 DPWA $\bar{K}N$ multichannel

1817 or 1819 ¹ MARTIN 77 DPWA $\bar{K}N$ multichannel

¹ The two MARTIN 77 values are from a T-matrix pole and from a Breit-Wigner fit.

 $\Lambda(1820)$ WIDTH

VALUE (MeV)	DOCUMENT ID	TECN	COMMENT
70 to 90 (≈ 80) OUR ESTIMATE			

80 ± 8 SARANTSEV 19 DPWA $\bar{K}N$ multichannel

89 ± 2 ZHANG 13A DPWA $\bar{K}N$ multichannel

77 ± 5 GOPAL 80 DPWA $\bar{K}N \rightarrow \bar{K}N$

72 ± 5 ALSTON... 78 DPWA $\bar{K}N \rightarrow \bar{K}N$

87 ± 3 KANE 74 DPWA $K^- p \rightarrow \Sigma\pi$

••• We do not use the following data for averages, fits, limits, etc. •••

82 DECLAIS 77 DPWA $\bar{K}N \rightarrow \bar{K}N$

81 ± 5 GOPAL 77 DPWA $\bar{K}N$ multichannel

76 or 76 ¹ MARTIN 77 DPWA $\bar{K}N$ multichannel

¹ The two MARTIN 77 values are from a T-matrix pole and from a Breit-Wigner fit.

 $\Lambda(1820)$ DECAY MODES

Mode	Fraction (Γ_i/Γ)
Γ_1 $N\bar{K}$	55–65 %
Γ_2 $\Sigma\pi$	8–14 %
Γ_3 $\Sigma(1385)\pi$	5–10 %
Γ_4 $\Sigma(1385)\pi, P\text{-wave}$	
Γ_5 $\Sigma(1385)\pi, F\text{-wave}$	(2.0 ± 1.0) %
Γ_6 $\Lambda\eta$	
Γ_7 ΞK	
Γ_8 $\Sigma\pi\pi$	
Γ_9 $N\bar{K}^*(892), S=1/2, F\text{-wave}$	
Γ_{10} $N\bar{K}^*(892), S=3/2, P\text{-wave}$	(3.0 ± 1.0) %
Γ_{11} $N\bar{K}^*(892), S=3/2, F\text{-wave}$	

 $\Lambda(1820)$ BRANCHING RATIOS

Errors quoted do not include uncertainties in the parametrizations used in the partial-wave analyses and are thus too small. See also "Sign conventions for resonance couplings" in the Note on Λ and Σ Resonances.

 $\Gamma(N\bar{K})/\Gamma_{total}$

VALUE	DOCUMENT ID	TECN	COMMENT
0.55 to 0.65 OUR ESTIMATE			

0.58 ± 0.12 SARANTSEV 19 DPWA $\bar{K}N$ multichannel

0.54 ± 0.01 ZHANG 13A DPWA $\bar{K}N$ multichannel

0.58 ± 0.02 GOPAL 80 DPWA $\bar{K}N \rightarrow \bar{K}N$

0.60 ± 0.03 ALSTON... 78 DPWA $\bar{K}N \rightarrow \bar{K}N$

••• We do not use the following data for averages, fits, limits, etc. •••

0.547 ¹ KAMANO 15 DPWA $\bar{K}N$ multichannel

0.51 DECLAIS 77 DPWA $\bar{K}N \rightarrow \bar{K}N$

0.57 ± 0.02 GOPAL 77 DPWA See GOPAL 80

0.59 or 0.58 ² MARTIN 77 DPWA $\bar{K}N$ multichannel

¹ From the preferred solution A in KAMANO 15.

² The two MARTIN 77 values are from a T-matrix pole and from a Breit-Wigner fit.

 $\Gamma(\Sigma\pi)/\Gamma_{total}$

VALUE	DOCUMENT ID	TECN	COMMENT
0.19 ± 0.04	SARANTSEV 19	DPWA	$\bar{K}N$ multichannel

••• We do not use the following data for averages, fits, limits, etc. •••

0.218 ¹ KAMANO 15 DPWA $\bar{K}N$ multichannel

¹ From the preferred solution A in KAMANO 15.

 $\Gamma(\Sigma(1385)\pi, P\text{-wave})/\Gamma_{total}$

VALUE	DOCUMENT ID	TECN	COMMENT
~ 0.01	SARANTSEV 19	DPWA	$\bar{K}N$ multichannel

••• We do not use the following data for averages, fits, limits, etc. •••

0.173 ¹ KAMANO 15 DPWA $\bar{K}N$ multichannel

¹ From the preferred solution A in KAMANO 15.

 $\Gamma(\Sigma(1385)\pi, F\text{-wave})/\Gamma_{total}$

VALUE	DOCUMENT ID	TECN	COMMENT
0.02 ± 0.01	SARANTSEV 19	DPWA	$\bar{K}N$ multichannel

••• We do not use the following data for averages, fits, limits, etc. •••

0.055 ¹ KAMANO 15 DPWA $\bar{K}N$ multichannel

¹ From the preferred solution A in KAMANO 15.

 $\Gamma(\Lambda\eta)/\Gamma_{total}$

VALUE	DOCUMENT ID	TECN	COMMENT
0.001	¹ KAMANO 15	DPWA	Multichannel

¹ From the preferred solution A in KAMANO 15.

See key on page 1127

Baryon Particle Listings

$\Lambda(1820), \Lambda(1830)$

$\Gamma(\Xi K)/\Gamma_{\text{total}}$ Γ_7/Γ

VALUE	DOCUMENT ID	TECN	COMMENT
not seen	¹ KAMANO 15	DPWA	Multichannel
¹ From the preferred solution A in KAMANO 15.			

$\Gamma(\Sigma \pi \pi)/\Gamma_{\text{total}}$ Γ_8/Γ

VALUE	DOCUMENT ID	TECN	COMMENT
no clear signal	¹ ARMENTEROS68C	HDBC	$K^- N \rightarrow \Sigma \pi \pi$
¹ There is a suggestion of a bump, enough to be consistent with what is expected from $\Sigma(1385) \rightarrow \Sigma \pi$ decay.			

$\Gamma(N\bar{K}^*(892), S=1/2, F\text{-wave})/\Gamma_{\text{total}}$ Γ_9/Γ

VALUE	DOCUMENT ID	TECN	COMMENT
not seen	¹ KAMANO 15	DPWA	Multichannel
¹ From the preferred solution A in KAMANO 15.			

$\Gamma(N\bar{K}^*(892), S=3/2, P\text{-wave})/\Gamma_{\text{total}}$ Γ_{10}/Γ

VALUE	DOCUMENT ID	TECN	COMMENT
0.03 ± 0.01	ZHANG 13A	DPWA	Multichannel
0.006	¹ KAMANO 15	DPWA	Multichannel
¹ From the preferred solution A in KAMANO 15.			

$\Gamma(N\bar{K}^*(892), S=3/2, F\text{-wave})/\Gamma_{\text{total}}$ Γ_{11}/Γ

VALUE	DOCUMENT ID	TECN	COMMENT
not seen	¹ KAMANO 15	DPWA	Multichannel
¹ From the preferred solution A in KAMANO 15.			

$(\Gamma_1 \Gamma_2)^{1/2}/\Gamma_{\text{total}}$ in $N\bar{K} \rightarrow \Lambda(1820) \rightarrow \Sigma \pi$ $(\Gamma_1 \Gamma_2)^{1/2}/\Gamma$

VALUE	DOCUMENT ID	TECN	COMMENT
-0.28 ± 0.01	ZHANG 13A	DPWA	Multichannel
-0.28 ± 0.03	GOPAL 77	DPWA	$\bar{K} N$ multichannel
-0.28 ± 0.01	KANE 74	DPWA	$K^- p \rightarrow \Sigma \pi$
-0.25 or -0.25	¹ MARTIN 77	DPWA	$\bar{K} N$ multichannel
¹ The two MARTIN 77 values are from a T-matrix pole and from a Breit-Wigner fit.			

$(\Gamma_1 \Gamma_2)^{1/2}/\Gamma_{\text{total}}$ in $N\bar{K} \rightarrow \Lambda(1820) \rightarrow \Sigma(1385) \pi, P\text{-wave}$ $(\Gamma_1 \Gamma_4)^{1/2}/\Gamma$

VALUE	DOCUMENT ID	TECN	COMMENT
-0.20 ± 0.02	ZHANG 13A	DPWA	Multichannel
-0.167 ± 0.054	¹ CAMERON 78	DPWA	$K^- p \rightarrow \Sigma(1385) \pi$
+0.27 ± 0.03	PREVOST 74	DPWA	$K^- N \rightarrow \Sigma(1385) \pi$
¹ The published sign has been changed to be in accord with the baryon-first convention.			

$(\Gamma_1 \Gamma_2)^{1/2}/\Gamma_{\text{total}}$ in $N\bar{K} \rightarrow \Lambda(1820) \rightarrow \Sigma(1385) \pi, F\text{-wave}$ $(\Gamma_1 \Gamma_5)^{1/2}/\Gamma$

VALUE	DOCUMENT ID	TECN	COMMENT
+0.065 ± 0.029	¹ CAMERON 78	DPWA	$K^- p \rightarrow \Sigma(1385) \pi$
¹ The published sign has been changed to be in accord with the baryon-first convention.			

$(\Gamma_1 \Gamma_2)^{1/2}/\Gamma_{\text{total}}$ in $N\bar{K} \rightarrow \Lambda(1820) \rightarrow \Lambda \eta$ $(\Gamma_1 \Gamma_6)^{1/2}/\Gamma$

VALUE	DOCUMENT ID	TECN	COMMENT
-0.096 ± 0.040 -0.020	RADER 73	MPWA	

$\Lambda(1820)$ REFERENCES

SARANTSEV 19	EPJ A55 180	A.V. Sarantsev et al.	(BONN, PNPI)
KAMANO 15	PR C92 025205	H. Kamano et al.	(ANL, OSAK)
ZHANG 13A	PR C88 035205	H. Zhang et al.	(KSU)
PDG 82	PL 11B 1	M. Roos et al.	(HEL5, CIT, CERN)
GOPAL 80	Toronto Conf. 159	G.P. Gopal	(RHEL) IJP
ALSTON... 78	PR D18 182	M. Alston-Garnjost et al.	(LBL, MTHO+) IJP
		PRL 38 1007	(LBL, MTHO+) IJP
CAMERON 78	NP B143 189	M. Alston-Garnjost et al.	(RHEL, LOIC) IJP
DECLAIS 77	CERN 77-16	Y. Declais et al.	(CAEN, CERN) IJP
GOPAL 77	NP B119 362	G.P. Gopal et al.	(LOIC, RHEL) IJP
MARTIN 77	NP B127 349	B.R. Martin, M.K. Pldcock, R.G. Moorhouse	(LOUC+) IJP
		NP B126 266	(LOUC) IJP
		NP B126 285	(LOUC) IJP
KANE 74	LBL-2452	D.F. Kane	(LBL) IJP
PREVOST 74	NP B69 246	J. Prevost et al.	(SACL, CERN, HEID)
RADER 73	NC 16A 178	R.K. Rader et al.	(SACL, HEID, CERN+)
ARMENTEROS 68C	NP B8 216	R. Armenteros et al.	(CERN, HEID, SACL)

$\Lambda(1830) 5/2^-$

 $I(J^P) = 0(\frac{5}{2}^-)$ Status: ***

For results published before 1973 (they are now obsolete), see our 1982 edition Physics Letters **111B** 1 (1982).

The best evidence for this resonance is in the $\Sigma \pi$ channel.

$\Lambda(1830)$ POLE POSITION

REAL PART

VALUE (MeV)	DOCUMENT ID	TECN	COMMENT
1800 to 1860 (≈ 1830) OUR ESTIMATE			
1819.5 ± 3.0	SARANTSEV 19	DPWA	$\bar{K} N$ multichannel
1899 +35 -37	¹ KAMANO 15	DPWA	Multichannel
1766 +37 -34	² KAMANO 15	DPWA	Multichannel
1809	ZHANG 13A	DPWA	Multichannel
¹ The preferred solution A in KAMANO 15 reports two poles. This entry is from the preferred solution A.			
² From the preferred solution A in KAMANO 15. Not seen in solution B.			

-2xIMAGINARY PART

VALUE (MeV)	DOCUMENT ID	TECN	COMMENT
50 to 80 (≈ 65) OUR ESTIMATE			
62 ± 5	SARANTSEV 19	DPWA	$\bar{K} N$ multichannel
80 +100 -34	¹ KAMANO 15	DPWA	Multichannel
212 +94 -62	² KAMANO 15	DPWA	Multichannel
109	ZHANG 13A	DPWA	Multichannel
¹ The preferred solution A in KAMANO 15 reports two poles. This entry is from the preferred solution A.			
² From the preferred solution A in KAMANO 15. Not seen in solution B.			

$\Lambda(1830)$ POLE RESIDUES

The normalized residue is the residue divided by $\Gamma_{\text{pole}}/2$.

Normalized residue in $N\bar{K} \rightarrow \Lambda(1830) \rightarrow N\bar{K}$

MODULUS	PHASE (°)	DOCUMENT ID	TECN	COMMENT
0.055 ± 0.010 20 ± 14		SARANTSEV 19	DPWA	$\bar{K} N$ multichannel
0.00502	-80	¹ KAMANO 15	DPWA	Multichannel
¹ From the preferred solution A in KAMANO 15.				

Normalized residue in $N\bar{K} \rightarrow \Lambda(1830) \rightarrow \Sigma \pi$

MODULUS	PHASE (°)	DOCUMENT ID	TECN	COMMENT
0.15 ± 0.03 180 ± 10		SARANTSEV 19	DPWA	$\bar{K} N$ multichannel
0.00581	179	¹ KAMANO 15	DPWA	Multichannel
¹ From the preferred solution A in KAMANO 15.				

Normalized residue in $N\bar{K} \rightarrow \Lambda(1830) \rightarrow \Lambda \eta$

MODULUS	PHASE (°)	DOCUMENT ID	TECN	COMMENT
0.00941	-65	¹ KAMANO 15	DPWA	Multichannel
¹ From the preferred solution A in KAMANO 15.				

Normalized residue in $N\bar{K} \rightarrow \Lambda(1830) \rightarrow \Xi K$

MODULUS	PHASE (°)	DOCUMENT ID	TECN	COMMENT
0.010 ± 0.005 65 ± 20		SARANTSEV 19	DPWA	$\bar{K} N$ multichannel
0.0477	94	¹ KAMANO 15	DPWA	Multichannel
¹ From the preferred solution A in KAMANO 15.				

Normalized residue in $N\bar{K} \rightarrow \Lambda(1830) \rightarrow \Sigma(1385) \pi, D\text{-wave}$

MODULUS	PHASE (°)	DOCUMENT ID	TECN	COMMENT
0.10 ± 0.04 10 ± 25		SARANTSEV 19	DPWA	$\bar{K} N$ multichannel
0.0237	113	¹ KAMANO 15	DPWA	Multichannel
¹ From the preferred solution A in KAMANO 15.				

Normalized residue in $N\bar{K} \rightarrow \Lambda(1830) \rightarrow \Sigma(1385) \pi, G\text{-wave}$

MODULUS	PHASE (°)	DOCUMENT ID	TECN	COMMENT
0.03 ± 0.02		SARANTSEV 19	DPWA	$\bar{K} N$ multichannel
0.000726	127	¹ KAMANO 15	DPWA	Multichannel
¹ From the preferred solution A in KAMANO 15.				

Normalized residue in $N\bar{K} \rightarrow \Lambda(1830) \rightarrow N\bar{K}^*(892), S=1/2, D\text{-wave}$

MODULUS	PHASE (°)	DOCUMENT ID	TECN	COMMENT
0.0278	-177	¹ KAMANO 15	DPWA	Multichannel
¹ From the preferred solution A in KAMANO 15.				

Baryon Particle Listings

 $\Lambda(1830)$ Normalized residue in $N\bar{K} \rightarrow \Lambda(1830) \rightarrow N\bar{K}^*(892)$, $S=3/2$, D -wave

MODULUS	PHASE ($^\circ$)	DOCUMENT ID	TECN	COMMENT
0.0255	3	¹ KAMANO 15	DPWA	Multichannel
¹ From the preferred solution A in KAMANO 15.				

Normalized residue in $N\bar{K} \rightarrow \Lambda(1830) \rightarrow N\bar{K}^*(892)$, $S=3/2$, G -wave

MODULUS	PHASE ($^\circ$)	DOCUMENT ID	TECN	COMMENT
0.00773	-17	¹ KAMANO 15	DPWA	Multichannel
¹ From the preferred solution A in KAMANO 15.				

Normalized residue in $N\bar{K} \rightarrow \Lambda(1830) \rightarrow \Lambda\omega$, $S=1/2$, D -wave

MODULUS	PHASE ($^\circ$)	DOCUMENT ID	TECN	COMMENT
0.04±0.03		SARANTSEV 19	DPWA	$\bar{K}N$ multichannel

Normalized residue in $N\bar{K} \rightarrow \Lambda(1830) \rightarrow \Lambda\omega$, $S=3/2$, D -wave

MODULUS	PHASE ($^\circ$)	DOCUMENT ID	TECN	COMMENT
0.05±0.03	-110 ± 35	SARANTSEV 19	DPWA	$\bar{K}N$ multichannel

 $\Lambda(1830)$ MASS

VALUE (MeV)	DOCUMENT ID	TECN	COMMENT
1820 to 1830 (\approx 1825) OUR ESTIMATE			
1821 ± 3	SARANTSEV 19	DPWA	$\bar{K}N$ multichannel
1820 ± 4	ZHANG 13A	DPWA	Multichannel
1831 ± 10	GOPAL 80	DPWA	$\bar{K}N \rightarrow \bar{K}N$
1825 ± 10	GOPAL 77	DPWA	$\bar{K}N$ multichannel
1825 ± 1	KANE 74	DPWA	$K^-p \rightarrow \Sigma\pi$
••• We do not use the following data for averages, fits, limits, etc. •••			
1817 or 1818	¹ MARTIN 77	DPWA	$\bar{K}N$ multichannel
¹ The two MARTIN 77 values are from a T-matrix pole and from a Breit-Wigner fit.			

 $\Lambda(1830)$ WIDTH

VALUE (MeV)	DOCUMENT ID	TECN	COMMENT
60 to 120 (\approx 90) OUR ESTIMATE			
64 ± 7	SARANTSEV 19	DPWA	$\bar{K}N$ multichannel
114 ± 10	ZHANG 13A	DPWA	Multichannel
100 ± 10	GOPAL 80	DPWA	$\bar{K}N \rightarrow \bar{K}N$
94 ± 10	GOPAL 77	DPWA	$\bar{K}N$ multichannel
119 ± 3	KANE 74	DPWA	$K^-p \rightarrow \Sigma\pi$
••• We do not use the following data for averages, fits, limits, etc. •••			
56 or 56	¹ MARTIN 77	DPWA	$\bar{K}N$ multichannel
¹ The two MARTIN 77 values are from a T-matrix pole and from a Breit-Wigner fit.			

 $\Lambda(1830)$ DECAY MODES

Mode	Fraction (Γ_i/Γ)	Scale factor
Γ_1 $N\bar{K}$	0.04 to 0.08	
Γ_2 $\Sigma\pi$	35–75 %	
Γ_3 ΞK		
Γ_4 $\Sigma(1385)\pi$	>15 %	
Γ_5 $\Sigma(1385)\pi$, D -wave	(40 ± 15) %	3.2
Γ_6 $\Sigma(1385)\pi$, G -wave		
Γ_7 $\Lambda\eta$		
Γ_8 $N\bar{K}^*(892)$, $S=1/2$, D -wave		
Γ_9 $N\bar{K}^*(892)$, $S=3/2$, D -wave		
Γ_{10} $N\bar{K}^*(892)$, $S=3/2$, G -wave		

 $\Lambda(1830)$ BRANCHING RATIOS

See "Sign conventions for resonance couplings" in the Note on Λ and Σ Resonances.

$\Gamma(N\bar{K})/\Gamma_{\text{total}}$	DOCUMENT ID	TECN	COMMENT	Γ_1/Γ
0.04 to 0.08 OUR ESTIMATE				
0.055 ± 0.010	SARANTSEV 19	DPWA	$\bar{K}N$ multichannel	
0.041 ± 0.005	ZHANG 13A	DPWA	Multichannel	
0.08 ± 0.03	GOPAL 80	DPWA	$\bar{K}N \rightarrow \bar{K}N$	
0.02 ± 0.02	ALSTON-...	78	DPWA $\bar{K}N \rightarrow \bar{K}N$	
••• We do not use the following data for averages, fits, limits, etc. •••				
0.006	¹ KAMANO 15	DPWA	Multichannel	
0.04 ± 0.03	GOPAL 77	DPWA	See GOPAL 80	
0.04 ± 0.04	² MARTIN 77	DPWA	$\bar{K}N$ multichannel	
¹ From the preferred solution A in KAMANO 15.				
² The two MARTIN 77 values are from a T-matrix pole and from a Breit-Wigner fit.				

 $\Gamma(\Sigma\pi)/\Gamma_{\text{total}}$

VALUE	DOCUMENT ID	TECN	COMMENT	Γ_2/Γ
0.42 ± 0.08	SARANTSEV 19	DPWA	$\bar{K}N$ multichannel	
••• We do not use the following data for averages, fits, limits, etc. •••				
0.017	¹ KAMANO 15	DPWA	Multichannel	
¹ From the preferred solution A in KAMANO 15.				

 $\Gamma(\Xi K)/\Gamma_{\text{total}}$

VALUE	DOCUMENT ID	TECN	COMMENT	Γ_3/Γ
••• We do not use the following data for averages, fits, limits, etc. •••				
0.562	¹ KAMANO 15	DPWA	Multichannel	
¹ From the preferred solution A in KAMANO 15.				

 $\Gamma(\Sigma(1385)\pi, D\text{-wave})/\Gamma_{\text{total}}$

VALUE	DOCUMENT ID	TECN	COMMENT	Γ_5/Γ
0.40 ± 0.15 OUR AVERAGE Error includes scale factor of 3.2.				
0.20 ± 0.08	SARANTSEV 19	DPWA	$\bar{K}N$ multichannel	
0.52 ± 0.06	ZHANG 13A	DPWA	Multichannel	
••• We do not use the following data for averages, fits, limits, etc. •••				
0.134	¹ KAMANO 15	DPWA	Multichannel	
¹ From the preferred solution A in KAMANO 15.				

 $\Gamma(\Sigma(1385)\pi, G\text{-wave})/\Gamma_{\text{total}}$

VALUE	DOCUMENT ID	TECN	COMMENT	Γ_6/Γ
0.020 ± 0.015	SARANTSEV 19	DPWA	$\bar{K}N$ multichannel	

 $\Gamma(\Lambda\eta)/\Gamma_{\text{total}}$

VALUE	DOCUMENT ID	TECN	COMMENT	Γ_7/Γ
••• We do not use the following data for averages, fits, limits, etc. •••				
0.024	¹ KAMANO 15	DPWA	Multichannel	
¹ From the preferred solution A in KAMANO 15.				

 $\Gamma(N\bar{K}^*(892), S=1/2, D\text{-wave})/\Gamma_{\text{total}}$

VALUE	DOCUMENT ID	TECN	COMMENT	Γ_8/Γ
••• We do not use the following data for averages, fits, limits, etc. •••				
0.134	¹ KAMANO 15	DPWA	Multichannel	
¹ From the preferred solution A in KAMANO 15.				

 $\Gamma(N\bar{K}^*(892), S=3/2, D\text{-wave})/\Gamma_{\text{total}}$

VALUE	DOCUMENT ID	TECN	COMMENT	Γ_9/Γ
••• We do not use the following data for averages, fits, limits, etc. •••				
0.115	¹ KAMANO 15	DPWA	Multichannel	
¹ From the preferred solution A in KAMANO 15.				

 $\Gamma(N\bar{K}^*(892), S=3/2, G\text{-wave})/\Gamma_{\text{total}}$

VALUE	DOCUMENT ID	TECN	COMMENT	Γ_{10}/Γ
••• We do not use the following data for averages, fits, limits, etc. •••				
0.009	¹ KAMANO 15	DPWA	Multichannel	
¹ From the preferred solution A in KAMANO 15.				

 $(\Gamma_1\Gamma_2)^{1/2}/\Gamma_{\text{total}}$ in $N\bar{K} \rightarrow \Lambda(1830) \rightarrow \Sigma\pi$

VALUE	DOCUMENT ID	TECN	COMMENT	$(\Gamma_1\Gamma_2)^{1/2}/\Gamma$
-0.13 ± 0.01	ZHANG 13A	DPWA	Multichannel	
-0.17 ± 0.03	GOPAL 77	DPWA	$\bar{K}N$ multichannel	
-0.15 ± 0.01	KANE 74	DPWA	$K^-p \rightarrow \Sigma\pi$	
••• We do not use the following data for averages, fits, limits, etc. •••				
-0.17 or -0.17	¹ MARTIN 77	DPWA	$\bar{K}N$ multichannel	
¹ The two MARTIN 77 values are from a T-matrix pole and from a Breit-Wigner fit.				

 $(\Gamma_1\Gamma_4)^{1/2}/\Gamma_{\text{total}}$ in $N\bar{K} \rightarrow \Lambda(1830) \rightarrow \Sigma(1385)\pi$

VALUE	DOCUMENT ID	TECN	COMMENT	$(\Gamma_1\Gamma_4)^{1/2}/\Gamma$
0.20 to 0.50 OUR ESTIMATE				
+0.141 ± 0.014	¹ CAMERON 78	DPWA	$K^-p \rightarrow \Sigma(1385)\pi$	
+0.13 ± 0.03	PREVOST 74	DPWA	$K^-N \rightarrow \Sigma(1385)\pi$	
¹ The CAMERON 78 upper limit on G -wave decay is 0.03. The published sign has been changed to be in accord with the baryon-first convention.				

 $(\Gamma_1\Gamma_7)^{1/2}/\Gamma_{\text{total}}$ in $N\bar{K} \rightarrow \Lambda(1830) \rightarrow \Lambda\eta$

VALUE	DOCUMENT ID	TECN	COMMENT	$(\Gamma_1\Gamma_7)^{1/2}/\Gamma$
-0.044 ± 0.020	RADER 73	MPWA		

 $\Lambda(1830)$ REFERENCES

SARANTSEV 19	EPJ A55 180	A.V. Sarantsev <i>et al.</i>	(BONN, PNPI)
KAMANO 15	PR C92 025205	H. Kamano <i>et al.</i>	(ANL, OSAK)
ZHANG 13A	PR C88 035205	H. Zhang <i>et al.</i>	(KSU)
PDG 82	PL 111B 1	M. Roos <i>et al.</i>	(HELS, CIT, CERN)
GOPAL 80	Toronto Conf. 159	G.P. Gopal	(RHEL) IJP
ALSTON-... 78	PR D18 182	M. Alston-Garnjost <i>et al.</i>	(LBL, MTHO+) IJP
Also	PRL 38 1007	M. Alston-Garnjost <i>et al.</i>	(LBL, MTHO+) IJP
CAMERON 78	NP B143 189	W. Cameron <i>et al.</i>	(RHEL, LOIC) IJP
GOPAL 77	NP B119 362	G.P. Gopal <i>et al.</i>	(LOIC, RHEL) IJP
MARTIN 77	NP B127 349	B.R. Martin, M.K. Pidcock, R.G. Moorhouse	(LOUC+) IJP
Also	NP B126 266	B.R. Martin, M.K. Pidcock	(LOUC)
Also	NP B126 285	B.R. Martin, M.K. Pidcock	(LOUC) IJP
KANE 74	LBL-2452	D.F. Kane	(LBL) IJP
PREVOST 74	NP B69 246	J. Prevost <i>et al.</i>	(SACL, CERN, HEID)
RADER 73	NC 16A 178	R.K. Rader <i>et al.</i>	(SACL, HEID, CERN+)

See key on page 1127

Baryon Particle Listings
 $\Lambda(1890)$ $\Lambda(1890) 3/2^+$ $J(P) = 0(\frac{3}{2}^+)$ Status: ****For results published before 1974 (they are now obsolete), see our 1982 edition Physics Letters **111B** 1 (1982). $\Lambda(1890)$ POLE POSITION

REAL PART

VALUE (MeV)	DOCUMENT ID	TECN	COMMENT
1872 ± 5	SARANTSEV 19	DPWA	$\bar{K}N$ multichannel
••• We do not use the following data for averages, fits, limits, etc. •••			
1859 ⁺⁵ ₋₇	¹ KAMANO 15	DPWA	Multichannel
1876	ZHANG 13A	DPWA	Multichannel
	¹ From the preferred solution A in KAMANO 15, incompatible with solution B.		

-2xIMAGINARY PART

VALUE (MeV)	DOCUMENT ID	TECN	COMMENT
101 ± 10	SARANTSEV 19	DPWA	$\bar{K}N$ multichannel
••• We do not use the following data for averages, fits, limits, etc. •••			
113 ⁺²⁰ ₋₄	¹ KAMANO 15	DPWA	$\bar{K}N$ multichannel
145	ZHANG 13A	DPWA	$\bar{K}N$ multichannel
	¹ From the preferred solution A in KAMANO 15, incompatible with solution B.		

 $\Lambda(1890)$ POLE RESIDUEThe "normalized residue" is the residue divided by $\Gamma_{pole}/2$.Normalized residue in $KN \rightarrow \Lambda(1890) \rightarrow KN$

MODULUS	PHASE (°)	DOCUMENT ID	TECN	COMMENT
0.30 ± 0.06	0 ± 10	SARANTSEV 19	DPWA	$\bar{K}N$ multichannel
••• We do not use the following data for averages, fits, limits, etc. •••				
0.241	-23	¹ KAMANO 15	DPWA	$\bar{K}N$ multichannel
	¹ From the preferred solution A in KAMANO 15.			

Normalized residue in $N\bar{K} \rightarrow \Lambda(1890) \rightarrow \Sigma\pi$

MODULUS	PHASE (°)	DOCUMENT ID	TECN	COMMENT
0.14 ± 0.05	148 ± 12	SARANTSEV 19	DPWA	$\bar{K}N$ multichannel
••• We do not use the following data for averages, fits, limits, etc. •••				
0.101	104	¹ KAMANO 15	DPWA	$\bar{K}N$ multichannel
	¹ From the preferred solution A in KAMANO 15.			

Normalized residue in $N\bar{K} \rightarrow \Lambda(1890) \rightarrow \Lambda\eta$

MODULUS	PHASE (°)	DOCUMENT ID	TECN	COMMENT
••• We do not use the following data for averages, fits, limits, etc. •••				
0.0485	-54	¹ KAMANO 15	DPWA	Multichannel
	¹ From the preferred solution A in KAMANO 15.			

Normalized residue in $N\bar{K} \rightarrow \Lambda(1890) \rightarrow \Xi K$

MODULUS	PHASE (°)	DOCUMENT ID	TECN	COMMENT
0.065 ± 0.020	160 ± 30	SARANTSEV 19	DPWA	$\bar{K}N$ multichannel
••• We do not use the following data for averages, fits, limits, etc. •••				
0.0562	-85	¹ KAMANO 15	DPWA	$\bar{K}N$ multichannel
	¹ From the preferred solution A in KAMANO 15.			

Normalized residue in $N\bar{K} \rightarrow \Lambda(1890) \rightarrow \Sigma(1385)\pi, P\text{-wave}$

MODULUS	PHASE (°)	DOCUMENT ID	TECN	COMMENT
0.11 ± 0.05	-160 ± 45	SARANTSEV 19	DPWA	$\bar{K}N$ multichannel
••• We do not use the following data for averages, fits, limits, etc. •••				
0.295	-40	¹ KAMANO 15	DPWA	$\bar{K}N$ multichannel
	¹ From the preferred solution A in KAMANO 15.			

Normalized residue in $N\bar{K} \rightarrow \Lambda(1890) \rightarrow \Sigma(1385)\pi, F\text{-wave}$

MODULUS	PHASE (°)	DOCUMENT ID	TECN	COMMENT
0.10 ± 0.04	10 ± 50	SARANTSEV 19	DPWA	$\bar{K}N$ multichannel
••• We do not use the following data for averages, fits, limits, etc. •••				
0.064	127	¹ KAMANO 15	DPWA	$\bar{K}N$ multichannel
	¹ From the preferred solution A in KAMANO 15.			

Normalized residue in $N\bar{K} \rightarrow \Lambda(1890) \rightarrow N\bar{K}^*(892), S=1/2, P\text{-wave}$

MODULUS	PHASE (°)	DOCUMENT ID	TECN	COMMENT
0.03 ± 0.03		SARANTSEV 19	DPWA	$\bar{K}N$ multichannel
••• We do not use the following data for averages, fits, limits, etc. •••				
0.188	-160	¹ KAMANO 15	DPWA	$\bar{K}N$ multichannel
	¹ From the preferred solution A in KAMANO 15.			

Normalized residue in $N\bar{K} \rightarrow \Lambda(1890) \rightarrow N\bar{K}^*(892), S=3/2, P\text{-wave}$

MODULUS	PHASE (°)	DOCUMENT ID	TECN	COMMENT
0.05 ± 0.03	180 ± 40	SARANTSEV 19	DPWA	$\bar{K}N$ multichannel

••• We do not use the following data for averages, fits, limits, etc. •••
 0.209 15 ¹KAMANO 15 DPWA $\bar{K}N$ multichannel
¹From the preferred solution A in KAMANO 15.

Normalized residue in $N\bar{K} \rightarrow \Lambda(1890) \rightarrow N\bar{K}^*(892), S=3/2, F\text{-wave}$

MODULUS	PHASE (°)	DOCUMENT ID	TECN	COMMENT
••• We do not use the following data for averages, fits, limits, etc. •••				
0.0141	129	¹ KAMANO 15	DPWA	Multichannel
	¹ From the preferred solution A in KAMANO 15.			

Normalized residue in $N\bar{K} \rightarrow \Lambda(1890) \rightarrow \Lambda\omega, S=1/2, P\text{-wave}$

MODULUS	PHASE (°)	DOCUMENT ID	TECN	COMMENT
0.24 ± 0.06	15 ± 20	SARANTSEV 19	DPWA	$\bar{K}N$ multichannel

Normalized residue in $N\bar{K} \rightarrow \Lambda(1890) \rightarrow \Lambda\omega, S=3/2, P\text{-wave}$

MODULUS	PHASE (°)	DOCUMENT ID	TECN	COMMENT
0.15 ± 0.08	-165 ± 20	SARANTSEV 19	DPWA	$\bar{K}N$ multichannel

 $\Lambda(1890)$ MASS

VALUE (MeV)	DOCUMENT ID	TECN	COMMENT
1870 to 1910 (≈ 1890) OUR ESTIMATE			
1873 ± 5	SARANTSEV 19	DPWA	$\bar{K}N$ multichannel
1900 ± 5	ZHANG 13A	DPWA	$\bar{K}N$ multichannel
1897 ± 5	GOPAL 80	DPWA	$\bar{K}N \rightarrow \bar{K}N$
1908 ± 10	ALSTON-...	78	DPWA $\bar{K}N \rightarrow \bar{K}N$
1894 ± 10	HEMINGWAY 75	DPWA	$K^-p \rightarrow \bar{K}N$
••• We do not use the following data for averages, fits, limits, etc. •••			
1900 ± 5	GOPAL 77	DPWA	$\bar{K}N$ multichannel
1856 or 1868	¹ MARTIN 77	DPWA	$\bar{K}N$ multichannel
1900	² NAKKASYAN 75	DPWA	$K^-p \rightarrow \Lambda\omega$
	¹ The two MARTIN 77 values are from a T-matrix pole and from a Breit-Wigner fit. ² Found in one of two best solutions.		

 $\Lambda(1890)$ WIDTH

VALUE (MeV)	DOCUMENT ID	TECN	COMMENT
80 to 160 (≈ 120) OUR ESTIMATE			
103 ± 10	SARANTSEV 19	DPWA	$\bar{K}N$ multichannel
161 ± 15	ZHANG 13A	DPWA	$\bar{K}N$ multichannel
74 ± 10	GOPAL 80	DPWA	$\bar{K}N \rightarrow \bar{K}N$
119 ± 20	ALSTON-...	78	DPWA $\bar{K}N \rightarrow \bar{K}N$
107 ± 10	HEMINGWAY 75	DPWA	$K^-p \rightarrow \bar{K}N$
••• We do not use the following data for averages, fits, limits, etc. •••			
72 ± 10	GOPAL 77	DPWA	$\bar{K}N$ multichannel
191 or 193	¹ MARTIN 77	DPWA	$\bar{K}N$ multichannel
100	² NAKKASYAN 75	DPWA	$K^-p \rightarrow \Lambda\omega$
	¹ The two MARTIN 77 values are from a T-matrix pole and from a Breit-Wigner fit. ² Found in one of two best solutions.		

 $\Lambda(1890)$ DECAY MODES

Mode	Fraction (Γ_i/Γ)
Γ_1 $N\bar{K}$	0.24 to 0.36
Γ_2 $\Sigma\pi$	3-10 %
Γ_3 $\Lambda\eta$	
Γ_4 ΞK	
Γ_5 $\Sigma(1385)\pi$	seen
Γ_6 $\Sigma(1385)\pi, P\text{-wave}$	(6.0 ± 3.0) %
Γ_7 $\Sigma(1385)\pi, F\text{-wave}$	(4.0 ± 2.0) %
Γ_8 $N\bar{K}^*(892)$	seen
Γ_9 $N\bar{K}^*(892), S=1/2$	
Γ_{10} $N\bar{K}^*(892), S=1/2, P\text{-wave}$	
Γ_{11} $N\bar{K}^*(892), S=3/2, P\text{-wave}$	
Γ_{12} $N\bar{K}^*(892), S=3/2, F\text{-wave}$	
Γ_{13} $\Lambda\omega$	

 $\Lambda(1890)$ BRANCHING RATIOSSee "Sign conventions for resonance couplings" in the Note on Λ and Σ Resonances.

$\Gamma(N\bar{K})/\Gamma_{total}$	DOCUMENT ID	TECN	COMMENT	Γ_1/Γ
0.24 to 0.36 OUR ESTIMATE				
0.30 ± 0.06	SARANTSEV 19	DPWA	$\bar{K}N$ multichannel	
0.37 ± 0.03	ZHANG 13A	DPWA	$\bar{K}N$ multichannel	
0.20 ± 0.02	GOPAL 80	DPWA	$\bar{K}N \rightarrow \bar{K}N$	
0.34 ± 0.05	ALSTON-...	78	DPWA $\bar{K}N \rightarrow \bar{K}N$	
0.24 ± 0.04	HEMINGWAY 75	DPWA	$K^-p \rightarrow \bar{K}N$	

Baryon Particle Listings

 $\Lambda(1890)$, $\Lambda(2000)$

• • • We do not use the following data for averages, fits, limits, etc. • • •

VALUE	DOCUMENT ID	TECN	COMMENT
0.305	¹ KAMANO 15	DPWA	$\bar{K}N$ multichannel
0.18 ± 0.02	GOPAL 77	DPWA	See GOPAL 80
0.36 or 0.34	² MARTIN 77	DPWA	$\bar{K}N$ multichannel

¹ From the preferred solution A in KAMANO 15.

² The two MARTIN 77 values are from a T-matrix pole and from a Breit-Wigner fit.

$\Gamma(\Sigma\pi)/\Gamma_{\text{total}}$ Γ_2/Γ

VALUE	DOCUMENT ID	TECN	COMMENT
6 ± 2	SARANTSEV 19	DPWA	$\bar{K}N$ multichannel
<0.03	LANGBEIN 72	IPWA	$\bar{K}N$ multichannel

• • • We do not use the following data for averages, fits, limits, etc. • • •

VALUE	DOCUMENT ID	TECN	COMMENT
0.04	¹ KAMANO 15	DPWA	$\bar{K}N$ multichannel

¹ From the preferred solution A in KAMANO 15.

$\Gamma(\Lambda\eta)/\Gamma_{\text{total}}$ Γ_3/Γ

• • • We do not use the following data for averages, fits, limits, etc. • • •

VALUE	DOCUMENT ID	TECN	COMMENT
0.012	¹ KAMANO 15	DPWA	$\bar{K}N$ multichannel

¹ From the preferred solution A in KAMANO 15.

$\Gamma(\Xi K)/\Gamma_{\text{total}}$ Γ_4/Γ

VALUE	DOCUMENT ID	TECN	COMMENT
~0.01	SARANTSEV 19	DPWA	$\bar{K}N$ multichannel

• • • We do not use the following data for averages, fits, limits, etc. • • •

VALUE	DOCUMENT ID	TECN	COMMENT
0.009	¹ KAMANO 15	DPWA	$\bar{K}N$ multichannel

¹ From the preferred solution A in KAMANO 15.

$\Gamma(\Sigma(1385)\pi, P\text{-wave})/\Gamma_{\text{total}}$ Γ_6/Γ

VALUE	DOCUMENT ID	TECN	COMMENT
0.06 ± 0.03	SARANTSEV 19	DPWA	$\bar{K}N$ multichannel

• • • We do not use the following data for averages, fits, limits, etc. • • •

VALUE	DOCUMENT ID	TECN	COMMENT
0.453	¹ KAMANO 15	DPWA	$\bar{K}N$ multichannel

¹ From the preferred solution A in KAMANO 15.

$\Gamma(\Sigma(1385)\pi, F\text{-wave})/\Gamma_{\text{total}}$ Γ_7/Γ

VALUE	DOCUMENT ID	TECN	COMMENT
0.04 ± 0.02	SARANTSEV 19	DPWA	$\bar{K}N$ multichannel

• • • We do not use the following data for averages, fits, limits, etc. • • •

VALUE	DOCUMENT ID	TECN	COMMENT
0.019	¹ KAMANO 15	DPWA	$\bar{K}N$ multichannel

¹ From the preferred solution A in KAMANO 15.

$\Gamma(N\bar{K}^*(892), S=1/2, P\text{-wave})/\Gamma_{\text{total}}$ Γ_{10}/Γ

VALUE	DOCUMENT ID	TECN	COMMENT
<0.01	SARANTSEV 19	DPWA	$\bar{K}N$ multichannel

• • • We do not use the following data for averages, fits, limits, etc. • • •

VALUE	DOCUMENT ID	TECN	COMMENT
0.073	¹ KAMANO 15	DPWA	$\bar{K}N$ multichannel

¹ From the preferred solution A in KAMANO 15.

$\Gamma(N\bar{K}^*(892), S=3/2, P\text{-wave})/\Gamma_{\text{total}}$ Γ_{11}/Γ

VALUE	DOCUMENT ID	TECN	COMMENT
~0.01	SARANTSEV 19	DPWA	$\bar{K}N$ multichannel

• • • We do not use the following data for averages, fits, limits, etc. • • •

VALUE	DOCUMENT ID	TECN	COMMENT
0.088	¹ KAMANO 15	DPWA	$\bar{K}N$ multichannel

¹ From the preferred solution A in KAMANO 15.

$\Gamma(N\bar{K}^*(892), S=3/2, F\text{-wave})/\Gamma_{\text{total}}$ Γ_{12}/Γ

VALUE	DOCUMENT ID	TECN	COMMENT
0.001	¹ KAMANO 15	DPWA	$\bar{K}N$ multichannel

¹ From the preferred solution A in KAMANO 15.

$(\Gamma_i\Gamma_f)^{1/2}/\Gamma_{\text{total}}$ in $N\bar{K} \rightarrow \Lambda(1890) \rightarrow \Sigma\pi$ $(\Gamma_1\Gamma_2)^{1/2}/\Gamma$

VALUE	DOCUMENT ID	TECN	COMMENT
-0.09 ± 0.02	ZHANG 13A	DPWA	$\bar{K}N$ multichannel
-0.09 ± 0.03	GOPAL 77	DPWA	$\bar{K}N$ multichannel

• • • We do not use the following data for averages, fits, limits, etc. • • •

VALUE	DOCUMENT ID	TECN	COMMENT
+0.15 or +0.14	¹ MARTIN 77	DPWA	$\bar{K}N$ multichannel

¹ The two MARTIN 77 values are from a T-matrix pole and from a Breit-Wigner fit.

$(\Gamma_i\Gamma_f)^{1/2}/\Gamma_{\text{total}}$ in $N\bar{K} \rightarrow \Lambda(1890) \rightarrow \Sigma(1385)\pi, P\text{-wave}$ $(\Gamma_1\Gamma_6)^{1/2}/\Gamma$

VALUE	DOCUMENT ID	TECN	COMMENT
<0.03	CAMERON 78	DPWA	$K^-p \rightarrow \Sigma(1385)\pi$

$(\Gamma_i\Gamma_f)^{1/2}/\Gamma_{\text{total}}$ in $N\bar{K} \rightarrow \Lambda(1890) \rightarrow \Sigma(1385)\pi, F\text{-wave}$ $(\Gamma_1\Gamma_7)^{1/2}/\Gamma$

VALUE	DOCUMENT ID	TECN	COMMENT
-0.31 ± 0.04	ZHANG 13A	DPWA	$\bar{K}N$ multichannel
-0.126 ± 0.055	¹ CAMERON 78	DPWA	$K^-p \rightarrow \Sigma(1385)\pi$

¹ The published sign has been changed to be in accord with the baryon-first convention.

$(\Gamma_i\Gamma_f)^{1/2}/\Gamma_{\text{total}}$ in $N\bar{K} \rightarrow \Lambda(1890) \rightarrow N\bar{K}^*(892), S=1/2$ $(\Gamma_1\Gamma_9)^{1/2}/\Gamma$

VALUE	DOCUMENT ID	TECN	COMMENT
-0.17 ± 0.05	ZHANG 13A	DPWA	$\bar{K}N$ multichannel
-0.07 ± 0.03	^{1,2} CAMERON 78B	DPWA	$K^-p \rightarrow N\bar{K}^*$

¹ Upper limits on the P_3 and F_3 waves are each 0.03.

² The published sign has been changed to be in accord with the baryon-first convention.

$(\Gamma_i\Gamma_f)^{1/2}/\Gamma_{\text{total}}$ in $N\bar{K} \rightarrow \Lambda(1890) \rightarrow N\bar{K}^*(892), S=3/2, F\text{-wave}$ $(\Gamma_1\Gamma_{12})^{1/2}/\Gamma$

VALUE	DOCUMENT ID	TECN	COMMENT
-0.11 ± 0.03	ZHANG 13A	DPWA	$\bar{K}N$ multichannel

$(\Gamma_i\Gamma_f)^{1/2}/\Gamma_{\text{total}}$ in $N\bar{K} \rightarrow \Lambda(1890) \rightarrow \Lambda\omega$ $(\Gamma_1\Gamma_{13})^{1/2}/\Gamma$

VALUE	DOCUMENT ID	TECN	COMMENT
seen	BACCARI 77	IPWA	$K^-p \rightarrow \Lambda\omega$
0.032	¹ NAKKASYAN 75	DPWA	$K^-p \rightarrow \Lambda\omega$

¹ Found in one of two best solutions.

$\Lambda(1890)$ REFERENCES

SARANTSEV 19	EPJ A55 180	A.V. Sarantsev <i>et al.</i>	(BONN, PNPI)
KAMANO 15	PR C92 025205	H. Kamano <i>et al.</i>	(ANL, OSAK)
ZHANG 13A	PR C88 035205	H. Zhang <i>et al.</i>	(KSU)
PDG 82	PL 111B 1	M. Roos <i>et al.</i>	(HELS, CIT, CERN)
GOPAL 80	Toronto Conf. 159	G.P. Gopal	(RHEL) IJP
ALSTON-... 78	PR D18 182	M. Alston-Garnjost <i>et al.</i>	(LBL, MTHO+) IJP
Also	PRL 38 1007	M. Alston-Garnjost <i>et al.</i>	(LBL, MTHO+) IJP
CAMERON 78	NP B143 189	W. Cameron <i>et al.</i>	(RHEL, LOIC) IJP
CAMERON 78B	NP B146 327	W. Cameron <i>et al.</i>	(RHEL, LOIC) IJP
BACCARI 77	NC 41A 96	B. Baccari <i>et al.</i>	(SACL, CDEF) IJP
GOPAL 77	NP B119 362	G.P. Gopal <i>et al.</i>	(LOIC, RHEL) IJP
MARTIN 77	NP B127 349	B.R. Martin, M.K. Pidcock, R.G. Moorhouse	(LOUC+) IJP
Also	NP B126 266	B.R. Martin, M.K. Pidcock	(LOUC) IJP
Also	NP B126 285	B.R. Martin, M.K. Pidcock	(LOUC) IJP
HEMINGWAY 75	NP B91 12	R.J. Hemingway <i>et al.</i>	(CERN, HEIDH, MPIM) IJP
NAKKASYAN 75	NP B93 85	A. Nakkasyan	(CERN) IJP
LANGBEIN 72	NP B47 477	W. Langbein, F. Wagner	(MPIM) IJP

$\Lambda(2000) 1/2^-$

$I(J^P) = 0(\frac{1}{2}^-)$ Status: *

OMITTED FROM SUMMARY TABLE

BARBARO-GALTIERI 70 (in $\Sigma\pi$) and BRANDSTETTER 72 (in $\Lambda\omega$) proposed a state at about this mass. Those analyses are considered to be obsolete, see NAKKASYAN 75 and PDG 18.

$\Lambda(2000)$ MASS

VALUE (MeV)	DOCUMENT ID	TECN	COMMENT
≈ 2000 OUR ESTIMATE			
2020 ± 16	ZHANG 13A	DPWA	Multichannel
2030 ± 30	CAMERON 78B	DPWA	$K^-p \rightarrow N\bar{K}^*$

$\Lambda(2000)$ WIDTH

VALUE (MeV)	DOCUMENT ID	TECN	COMMENT
255 ± 63	ZHANG 13A	DPWA	Multichannel
125 ± 25	CAMERON 78B	DPWA	$K^-p \rightarrow N\bar{K}^*$

$\Lambda(2000)$ DECAY MODES

Mode	Fraction (Γ_i/Γ)
Γ_1 $N\bar{K}$	(27 ± 6) %
Γ_2 $\Sigma\pi$	
Γ_3 $\Lambda\eta$	(16 ± 7) %
Γ_4 $N\bar{K}^*(892), S=1/2, S\text{-wave}$	
Γ_5 $N\bar{K}^*(892), S=3/2, D\text{-wave}$	

$\Lambda(2000)$ BRANCHING RATIOS

See "Sign conventions for resonance couplings" in the Note on Λ and Σ Resonances.

$\Gamma(N\bar{K})/\Gamma_{\text{total}}$	DOCUMENT ID	TECN	COMMENT
0.27 ± 0.06	ZHANG 13A	DPWA	Multichannel

$(\Gamma_i\Gamma_f)^{1/2}/\Gamma_{\text{total}}$ in $N\bar{K} \rightarrow \Lambda(2000) \rightarrow \Sigma\pi$ $(\Gamma_1\Gamma_2)^{1/2}/\Gamma$

VALUE	DOCUMENT ID	TECN	COMMENT
-0.07 ± 0.03	ZHANG 13A	DPWA	Multichannel

$\Gamma(\Lambda\eta)/\Gamma_{\text{total}}$ Γ_3/Γ

VALUE	DOCUMENT ID	TECN	COMMENT
0.16 ± 0.07	ZHANG 13A	DPWA	Multichannel

See key on page 1127

Baryon Particle Listings
 $\Lambda(2000)$, $\Lambda(2050)$, $\Lambda(2070)$

$(\Gamma_1 \Gamma_f)^{1/2} / \Gamma_{\text{total}}$ in $N\bar{K} \rightarrow \Lambda(2000) \rightarrow N\bar{K}^*(892)$, $S=1/2$, S -wave $(\Gamma_1 \Gamma_4)^{1/2} / \Gamma$

VALUE	DOCUMENT ID	TECN	COMMENT
-0.12 ± 0.03	1 CAMERON	78B	DPWA $K^- p \rightarrow N\bar{K}^*$

¹ The published sign has been changed to be in accord with the baryon-first convention.

$(\Gamma_1 \Gamma_f)^{1/2} / \Gamma_{\text{total}}$ in $N\bar{K} \rightarrow \Lambda(2000) \rightarrow N\bar{K}^*(892)$, $S=3/2$, D -wave $(\Gamma_1 \Gamma_5)^{1/2} / \Gamma$

VALUE	DOCUMENT ID	TECN	COMMENT
$+0.34 \pm 0.05$	ZHANG	13A	DPWA Multichannel
$+0.09 \pm 0.03$	CAMERON	78B	DPWA $K^- p \rightarrow N\bar{K}^*$

$\Lambda(2000)$ REFERENCES

PDG	18	PR D98 030001	M. Tanabashi et al.	(PDG Collab.)
ZHANG	13A	PR C88 035205	H. Zhang et al.	(KSU)
CAMERON	78B	NP B146 327	W. Cameron et al.	(RHEL, LOIC) IJP
NAKKASYAN	75	NP B93 85	A. Nakkasyan	(CERN) IJP
BRANDSTETTER...	72	NP B39 13	A.A. Brandstetter et al.	(RHEL, CDEF+) IJP
BARBARO...	70	Duke Conf. 173	A. Barbaro-Galieri	(LRL) IJP
Hyperon Resonances, 1970				

$\Lambda(2050) 3/2^-$ $I(J^P) = 0(\frac{3}{2}^-)$ Status: *

OMITTED FROM SUMMARY TABLE

$\Lambda(2050)$ MASS

VALUE (MeV)	DOCUMENT ID	TECN	COMMENT
2056 ± 22	ZHANG	13A	DPWA Multichannel

$\Lambda(2050)$ WIDTH

VALUE (MeV)	DOCUMENT ID	TECN	COMMENT
493 ± 61	ZHANG	13A	DPWA Multichannel

$\Lambda(2050)$ DECAY MODES

Mode	Fraction (Γ_i / Γ)
$\Gamma_1 N\bar{K}$	$(19 \pm 4) \%$
$\Gamma_2 \Sigma \pi$	$(6.0 \pm 3.0) \%$
$\Gamma_3 \Sigma^*(1385) \pi$, S -wave	$(8 \pm 6) \%$
$\Gamma_4 \Sigma^*(1385) \pi$, D -wave	$(4.0 \pm 3.0) \%$
$\Gamma_5 N\bar{K}^*(892)$, $S=1/2$	$(23 \pm 7) \%$

$\Lambda(2050)$ BRANCHING RATIOS

$\Gamma(N\bar{K}) / \Gamma_{\text{total}}$ Γ_1 / Γ

VALUE	DOCUMENT ID	TECN	COMMENT
0.19 ± 0.04	ZHANG	13A	DPWA Multichannel

$\Gamma(\Sigma \pi) / \Gamma_{\text{total}}$ Γ_2 / Γ

VALUE	DOCUMENT ID	TECN	COMMENT
0.06 ± 0.03	ZHANG	13A	DPWA Multichannel

$\Gamma(\Sigma^*(1385) \pi, S\text{-wave}) / \Gamma_{\text{total}}$ Γ_3 / Γ

VALUE	DOCUMENT ID	TECN	COMMENT
0.08 ± 0.06	ZHANG	13A	DPWA Multichannel

$\Gamma(\Sigma^*(1385) \pi, D\text{-wave}) / \Gamma_{\text{total}}$ Γ_4 / Γ

VALUE	DOCUMENT ID	TECN	COMMENT
0.04 ± 0.03	ZHANG	13A	DPWA Multichannel

$\Gamma(N\bar{K}^*(892), S=1/2) / \Gamma_{\text{total}}$ Γ_5 / Γ

VALUE	DOCUMENT ID	TECN	COMMENT
0.23 ± 0.07	ZHANG	13A	DPWA Multichannel

$\Lambda(2050)$ REFERENCES

ZHANG	13A	PR C88 035205	H. Zhang et al.	(KSU)
-------	-----	---------------	-----------------	-------

$\Lambda(2070) 3/2^+$ $J^P = \frac{3}{2}^+$ Status: *

OMITTED FROM SUMMARY TABLE

$\Lambda(2070)$ POLE POSITION

REAL PART

VALUE (MeV)	DOCUMENT ID	TECN	COMMENT
2044 ± 20	SARANTSEV	19	DPWA $\bar{K} N$ multichannel

$-2 \times \text{IMAGINARY PART}$

VALUE (MeV)	DOCUMENT ID	TECN	COMMENT
360 ± 45	SARANTSEV	19	DPWA $\bar{K} N$ multichannel

$\Lambda(2070)$ POLE RESIDUES

Normalized residue in $N\bar{K} \rightarrow \Lambda(2070) \rightarrow N\bar{K}$

MODULUS	PHASE ($^\circ$)	DOCUMENT ID	TECN	COMMENT
0.15 ± 0.05	-37 ± 10	SARANTSEV	19	DPWA $\bar{K} N$ multichannel

Normalized residue in $N\bar{K} \rightarrow \Lambda(2070) \rightarrow \Sigma \pi$

MODULUS	PHASE ($^\circ$)	DOCUMENT ID	TECN	COMMENT
0.10 ± 0.03	-47 ± 8	SARANTSEV	19	DPWA $\bar{K} N$ multichannel

Normalized residue in $N\bar{K} \rightarrow \Lambda(2070) \rightarrow \Xi K$

MODULUS	PHASE ($^\circ$)	DOCUMENT ID	TECN	COMMENT
0.11 ± 0.03	0 ± 25	SARANTSEV	19	DPWA $\bar{K} N$ multichannel

Normalized residue in $N\bar{K} \rightarrow \Lambda(2070) \rightarrow \Lambda \omega, S=1/2, P$ -wave

MODULUS	PHASE ($^\circ$)	DOCUMENT ID	TECN	COMMENT
0.10 ± 0.04	150 ± 17	SARANTSEV	19	DPWA $\bar{K} N$ multichannel

Normalized residue in $N\bar{K} \rightarrow \Lambda(2070) \rightarrow \Lambda \omega, S=3/2, P$ -wave

MODULUS	PHASE ($^\circ$)	DOCUMENT ID	TECN	COMMENT
0.08 ± 0.04	20 ± 30	SARANTSEV	19	DPWA $\bar{K} N$ multichannel

Normalized residue in $N\bar{K} \rightarrow \Lambda(2070) \rightarrow \Lambda \omega, S=3/2, F$ -wave

MODULUS	PHASE ($^\circ$)	DOCUMENT ID	TECN	COMMENT
0.04 ± 0.02	-175 ± 35	SARANTSEV	19	DPWA $\bar{K} N$ multichannel

Normalized residue in $N\bar{K} \rightarrow \Lambda(2070) \rightarrow \Sigma(1385) \pi, P$ -wave

MODULUS	PHASE ($^\circ$)	DOCUMENT ID	TECN	COMMENT
0.12 ± 0.07	-160 ± 55	SARANTSEV	19	DPWA $\bar{K} N$ multichannel

Normalized residue in $N\bar{K} \rightarrow \Lambda(2070) \rightarrow \Sigma(1385) \pi, F$ -wave

MODULUS	PHASE ($^\circ$)	DOCUMENT ID	TECN	COMMENT
0.07 ± 0.04	-145 ± 50	SARANTSEV	19	DPWA $\bar{K} N$ multichannel

Normalized residue in $N\bar{K} \rightarrow \Lambda(2070) \rightarrow N\bar{K}^*(892), S=1/2, P$ -wave

MODULUS	PHASE ($^\circ$)	DOCUMENT ID	TECN	COMMENT
0.36 ± 0.07	-45 ± 30	SARANTSEV	19	DPWA $\bar{K} N$ multichannel

Normalized residue in $N\bar{K} \rightarrow \Lambda(2070) \rightarrow N\bar{K}^*(892), S=3/2, P$ -wave

MODULUS	PHASE ($^\circ$)	DOCUMENT ID	TECN	COMMENT
0.16 ± 0.05	150 ± 35	SARANTSEV	19	DPWA $\bar{K} N$ multichannel

Normalized residue in $N\bar{K} \rightarrow \Lambda(2070) \rightarrow N\bar{K}^*(892), S=3/2, F$ -wave

MODULUS	PHASE ($^\circ$)	DOCUMENT ID	TECN	COMMENT
0.14 ± 0.08	-50 ± 30	SARANTSEV	19	DPWA $\bar{K} N$ multichannel

$\Lambda(2070)$ MASS

VALUE (MeV)	DOCUMENT ID	TECN	COMMENT
2070 ± 24	SARANTSEV	19	DPWA $\bar{K} N$ multichannel

$\Lambda(2070)$ WIDTH

VALUE (MeV)	DOCUMENT ID	TECN	COMMENT
370 ± 50	SARANTSEV	19	DPWA $\bar{K} N$ multichannel

$\Lambda(2070)$ DECAY MODES

Mode	Fraction (Γ_i / Γ)
$\Gamma_1 N\bar{K}$	$(12 \pm 5) \%$
$\Gamma_2 \Sigma \pi$	$(7.0 \pm 3.0) \%$
$\Gamma_3 \Xi K$	$(7.0 \pm 3.0) \%$
$\Gamma_4 \Lambda \omega, S=1/2, P$ -wave	$(7 \pm 4) \%$
$\Gamma_5 \Lambda \omega, S=3/2, P$ -wave	$(3.0 \pm 2.0) \%$
$\Gamma_6 \Lambda \omega, S=3/2, F$ -wave	$(1.0 \pm 1.0) \%$
$\Gamma_7 \Sigma(1385) \pi, P$ -wave	$(10 \pm 5) \%$
$\Gamma_8 \Sigma(1385) \pi, F$ -wave	$(2.0 \pm 2.0) \%$
$\Gamma_9 N\bar{K}^*(892), S=1/2, P$ -wave	$(42 \pm 8) \%$
$\Gamma_{10} N\bar{K}^*(892), S=3/2, P$ -wave	$(14 \pm 6) \%$
$\Gamma_{11} N\bar{K}^*(892), S=3/2, F$ -wave	$(10 \pm 6) \%$

$\Lambda(2070)$ BRANCHING RATIOS

$\Gamma(N\bar{K}) / \Gamma_{\text{total}}$ Γ_1 / Γ

VALUE	DOCUMENT ID	TECN	COMMENT
0.12 ± 0.05	SARANTSEV	19	DPWA $\bar{K} N$ multichannel

Baryon Particle Listings

 $\Lambda(2070)$, $\Lambda(2080)$

$\Gamma(\Sigma\pi)/\Gamma_{\text{total}}$	DOCUMENT ID	TECN	COMMENT	Γ_2/Γ
VALUE 0.07 ± 0.03	SARANTSEV	19	DPWA $\bar{K}N$ multichannel	
$\Gamma(\Xi K)/\Gamma_{\text{total}}$	DOCUMENT ID	TECN	COMMENT	Γ_3/Γ
VALUE 0.07 ± 0.03	SARANTSEV	19	DPWA $\bar{K}N$ multichannel	
$\Gamma(\Lambda\omega, S=1/2, P\text{-wave})/\Gamma_{\text{total}}$	DOCUMENT ID	TECN	COMMENT	Γ_4/Γ
VALUE 0.07 ± 0.04	SARANTSEV	19	DPWA $\bar{K}N$ multichannel	
$\Gamma(\Lambda\omega, S=3/2, P\text{-wave})/\Gamma_{\text{total}}$	DOCUMENT ID	TECN	COMMENT	Γ_5/Γ
VALUE 0.03 ± 0.02	SARANTSEV	19	DPWA $\bar{K}N$ multichannel	
$\Gamma(\Lambda\omega, S=3/2, F\text{-wave})/\Gamma_{\text{total}}$	DOCUMENT ID	TECN	COMMENT	Γ_6/Γ
VALUE 0.01 ± 0.01	SARANTSEV	19	DPWA $\bar{K}N$ multichannel	
$\Gamma(\Sigma(1385)\pi, P\text{-wave})/\Gamma_{\text{total}}$	DOCUMENT ID	TECN	COMMENT	Γ_7/Γ
VALUE 0.10 ± 0.05	SARANTSEV	19	DPWA $\bar{K}N$ multichannel	
$\Gamma(\Sigma(1385)\pi, F\text{-wave})/\Gamma_{\text{total}}$	DOCUMENT ID	TECN	COMMENT	Γ_8/Γ
VALUE 0.02 ± 0.02	SARANTSEV	19	DPWA $\bar{K}N$ multichannel	
$\Gamma(N\bar{K}^*(892), S=1/2, P\text{-wave})/\Gamma_{\text{total}}$	DOCUMENT ID	TECN	COMMENT	Γ_9/Γ
VALUE 0.42 ± 0.08	SARANTSEV	19	DPWA $\bar{K}N$ multichannel	
$\Gamma(N\bar{K}^*(892), S=3/2, P\text{-wave})/\Gamma_{\text{total}}$	DOCUMENT ID	TECN	COMMENT	Γ_{10}/Γ
VALUE 0.14 ± 0.06	SARANTSEV	19	DPWA $\bar{K}N$ multichannel	
$\Gamma(N\bar{K}^*(892), S=3/2, F\text{-wave})/\Gamma_{\text{total}}$	DOCUMENT ID	TECN	COMMENT	Γ_{11}/Γ
VALUE 0.10 ± 0.06	SARANTSEV	19	DPWA $\bar{K}N$ multichannel	

 $\Lambda(2070)$ REFERENCES

SARANTSEV 19 EPJ A55 180 A.V. Sarantsev et al. (BONN, PNPI)

$$\Lambda(2080) \ 5/2^- \quad J^P = \frac{5}{2}^- \quad \text{Status: } *$$

OMITTED FROM SUMMARY TABLE

 $\Lambda(2080)$ POLE POSITION

REAL PART	DOCUMENT ID	TECN	COMMENT
VALUE (MeV) 2070 ± 15	SARANTSEV	19	DPWA $\bar{K}N$ multichannel
$-2 \times$ IMAGINARY PART	DOCUMENT ID	TECN	COMMENT
VALUE (MeV) 172 ± 28	SARANTSEV	19	DPWA $\bar{K}N$ multichannel

 $\Lambda(2080)$ POLE RESIDUES

Normalized residue in $N\bar{K} \rightarrow \Lambda(2080) \rightarrow N\bar{K}$	DOCUMENT ID	TECN	COMMENT
MODULUS PHASE ($^\circ$) $0.12 \pm 0.03 \quad -35 \pm 22$	SARANTSEV	19	DPWA $\bar{K}N$ multichannel
Normalized residue in $N\bar{K} \rightarrow \Lambda(2080) \rightarrow \Sigma\pi$	DOCUMENT ID	TECN	COMMENT
MODULUS PHASE ($^\circ$) $0.07 \pm 0.03 \quad 11 \pm 16$	SARANTSEV	19	DPWA $\bar{K}N$ multichannel
Normalized residue in $N\bar{K} \rightarrow \Lambda(2080) \rightarrow \Xi K$	DOCUMENT ID	TECN	COMMENT
MODULUS PHASE ($^\circ$) $0.06 \pm 0.02 \quad 115 \pm 20$	SARANTSEV	19	DPWA $\bar{K}N$ multichannel
Normalized residue in $N\bar{K} \rightarrow \Lambda(2080) \rightarrow \Lambda\omega, S=1/2, D\text{-wave}$	DOCUMENT ID	TECN	COMMENT
MODULUS PHASE ($^\circ$) $0.06 \pm 0.03 \quad 115 \pm 25$	SARANTSEV	19	DPWA $\bar{K}N$ multichannel
Normalized residue in $N\bar{K} \rightarrow \Lambda(2080) \rightarrow \Lambda\omega, S=3/2, D\text{-wave}$	DOCUMENT ID	TECN	COMMENT
MODULUS PHASE ($^\circ$) $0.09 \pm 0.03 \quad -10 \pm 35$	SARANTSEV	19	DPWA $\bar{K}N$ multichannel
Normalized residue in $N\bar{K} \rightarrow \Lambda(2080) \rightarrow \Sigma(1385)\pi, D\text{-wave}$	DOCUMENT ID	TECN	COMMENT
MODULUS PHASE ($^\circ$) $0.14 \pm 0.04 \quad 155 \pm 45$	SARANTSEV	19	DPWA $\bar{K}N$ multichannel

Normalized residue in $N\bar{K} \rightarrow \Lambda(2080) \rightarrow \Sigma(1385)\pi, G\text{-wave}$	DOCUMENT ID	TECN	COMMENT
MODULUS PHASE ($^\circ$) $0.05 \pm 0.03 \quad 30 \pm 45$	SARANTSEV	19	$\bar{K}N$ multichannel
Normalized residue in $N\bar{K} \rightarrow \Lambda(2080) \rightarrow N\bar{K}^*(892), S=1/2, D\text{-wave}$	DOCUMENT ID	TECN	COMMENT
MODULUS PHASE ($^\circ$) $0.16 \pm 0.08 \quad -120 \pm 50$	SARANTSEV	19	DPWA $\bar{K}N$ multichannel
Normalized residue in $N\bar{K} \rightarrow \Lambda(2080) \rightarrow N\bar{K}^*(892), S=3/2, D\text{-wave}$	DOCUMENT ID	TECN	COMMENT
MODULUS PHASE ($^\circ$) $0.20 \pm 0.14 \quad 60 \pm 50$	SARANTSEV	19	DPWA $\bar{K}N$ multichannel

 $\Lambda(2080)$ MASS

VALUE (MeV)	DOCUMENT ID	TECN	COMMENT
2082 ± 13	SARANTSEV	19	DPWA $\bar{K}N$ multichannel

 $\Lambda(2080)$ WIDTH

VALUE (MeV)	DOCUMENT ID	TECN	COMMENT
181 ± 29	SARANTSEV	19	DPWA $\bar{K}N$ multichannel

 $\Lambda(2080)$ DECAY MODES

Mode	Fraction (Γ_i/Γ)
$\Gamma_1 \ N\bar{K}$	(11.0 \pm 3.0) %
$\Gamma_2 \ \Sigma\pi$	(5.0 \pm 2.0) %
$\Gamma_3 \ \Xi K$	(4.0 \pm 1.0) %
$\Gamma_4 \ \Lambda\omega, S=1/2, D\text{-wave}$	(4.0 \pm 2.0) %
$\Gamma_5 \ \Lambda\omega, S=3/2, D\text{-wave}$	(8.0 \pm 3.0) %
$\Gamma_6 \ \Sigma(1385)\pi, D\text{-wave}$	(15 \pm 5) %
$\Gamma_7 \ \Sigma(1385)\pi, G\text{-wave}$	(3.0 \pm 2.0) %
$\Gamma_8 \ N\bar{K}^*(892), S=1/2, D\text{-wave}$	(17 \pm 9) %
$\Gamma_9 \ N\bar{K}^*(892), S=3/2, D\text{-wave}$	(25 \pm 16) %

 $\Lambda(2080)$ BRANCHING RATIOS

$\Gamma(N\bar{K})/\Gamma_{\text{total}}$	DOCUMENT ID	TECN	COMMENT	Γ_1/Γ
VALUE 0.11 ± 0.03	SARANTSEV	19	DPWA $\bar{K}N$ multichannel	
$\Gamma(\Sigma\pi)/\Gamma_{\text{total}}$	DOCUMENT ID	TECN	COMMENT	Γ_2/Γ
VALUE 0.05 ± 0.02	SARANTSEV	19	DPWA $\bar{K}N$ multichannel	
$\Gamma(\Xi K)/\Gamma_{\text{total}}$	DOCUMENT ID	TECN	COMMENT	Γ_3/Γ
VALUE 0.04 ± 0.01	SARANTSEV	19	DPWA $\bar{K}N$ multichannel	
$\Gamma(\Lambda\omega, S=1/2, D\text{-wave})/\Gamma_{\text{total}}$	DOCUMENT ID	TECN	COMMENT	Γ_4/Γ
VALUE 0.04 ± 0.02	SARANTSEV	19	DPWA $\bar{K}N$ multichannel	
$\Gamma(\Lambda\omega, S=3/2, D\text{-wave})/\Gamma_{\text{total}}$	DOCUMENT ID	TECN	COMMENT	Γ_5/Γ
VALUE 0.08 ± 0.03	SARANTSEV	19	DPWA $\bar{K}N$ multichannel	
$\Gamma(\Sigma(1385)\pi, D\text{-wave})/\Gamma_{\text{total}}$	DOCUMENT ID	TECN	COMMENT	Γ_6/Γ
VALUE 0.15 ± 0.05	SARANTSEV	19	DPWA $\bar{K}N$ multichannel	
$\Gamma(\Sigma(1385)\pi, G\text{-wave})/\Gamma_{\text{total}}$	DOCUMENT ID	TECN	COMMENT	Γ_7/Γ
VALUE 0.03 ± 0.02	SARANTSEV	19	DPWA $\bar{K}N$ multichannel	
$\Gamma(N\bar{K}^*(892), S=1/2, D\text{-wave})/\Gamma_{\text{total}}$	DOCUMENT ID	TECN	COMMENT	Γ_8/Γ
VALUE 0.17 ± 0.09	SARANTSEV	19	DPWA $\bar{K}N$ multichannel	
$\Gamma(N\bar{K}^*(892), S=3/2, D\text{-wave})/\Gamma_{\text{total}}$	DOCUMENT ID	TECN	COMMENT	Γ_9/Γ
VALUE 0.25 ± 0.16	SARANTSEV	19	DPWA $\bar{K}N$ multichannel	

 $\Lambda(2080)$ REFERENCES

SARANTSEV 19 EPJ A55 180 A.V. Sarantsev et al. (BONN, PNPI)

$\Lambda(2085) 7/2^+$ $I(J^P) = 0(\frac{7}{2}^+)$ Status: **OMITTED FROM SUMMARY TABLE
was $\Lambda(2020)$

In LITCHFIELD 71, need for the state rests solely on a possibly inconsistent polarization measurement at 1.784 GeV/c. HEMINGWAY 75 does not require this state. GOPAL 77 does not need it in either $N\bar{K}$ or $\Sigma\pi$. With new K^-n angular distributions included, DECLAIS 77 sees it. However, this and other new data are included in GOPAL 80 and the state is not required. BACCARI 77 weakly supports it.

 $\Lambda(2085)$ POLE POSITION**REAL PART**

VALUE	DOCUMENT ID	TECN	COMMENT
••• We do not use the following data for averages, fits, limits, etc. •••			
1757	¹ KAMANO	15	DPWA Multichannel
¹ From the preferred solution A in KAMANO 15. Solution B reports $M = 2041^{+80}_{-82}$ MeV.			

-2xIMAGINARY PART

VALUE	DOCUMENT ID	TECN	COMMENT
••• We do not use the following data for averages, fits, limits, etc. •••			
146	¹ KAMANO	15	DPWA Multichannel
¹ From the preferred solution A in KAMANO 15. Solution B reports $M = 238^{+114}_{-34}$ MeV.			

 $\Lambda(2085)$ POLE RESIDUESThe normalized residue is the residue divided by $\Gamma_{pole}/2$.**Normalized residue in $N\bar{K} \rightarrow \Lambda(2085) \rightarrow N\bar{K}$**

MODULUS	PHASE (°)	DOCUMENT ID	TECN	COMMENT
••• We do not use the following data for averages, fits, limits, etc. •••				
0.000145	-77	¹ KAMANO	15	DPWA Multichannel
¹ From the preferred solution A in KAMANO 15.				

Normalized residue in $N\bar{K} \rightarrow \Lambda(2085) \rightarrow \Sigma\pi$

MODULUS	PHASE (°)	DOCUMENT ID	TECN	COMMENT
••• We do not use the following data for averages, fits, limits, etc. •••				
0.0112	120	¹ KAMANO	15	DPWA Multichannel
¹ From the preferred solution A in KAMANO 15.				

Normalized residue in $N\bar{K} \rightarrow \Lambda(2085) \rightarrow \Lambda\eta$

MODULUS	PHASE (°)	DOCUMENT ID	TECN	COMMENT
••• We do not use the following data for averages, fits, limits, etc. •••				
0.000786	-100	¹ KAMANO	15	DPWA Multichannel
¹ From the preferred solution A in KAMANO 15.				

Normalized residue in $N\bar{K} \rightarrow \Lambda(2085) \rightarrow \Sigma(1385)\pi, F\text{-wave}$

MODULUS	PHASE (°)	DOCUMENT ID	TECN	COMMENT
••• We do not use the following data for averages, fits, limits, etc. •••				
0.00451	-82	¹ KAMANO	15	DPWA Multichannel
¹ From the preferred solution A in KAMANO 15.				

Normalized residue in $N\bar{K} \rightarrow \Lambda(2085) \rightarrow \Sigma(1385)\pi, H\text{-wave}$

MODULUS	PHASE (°)	DOCUMENT ID	TECN	COMMENT
••• We do not use the following data for averages, fits, limits, etc. •••				
0.0000298	-128	¹ KAMANO	15	DPWA Multichannel
¹ From the preferred solution A in KAMANO 15.				

 $\Lambda(2085)$ MASS

VALUE (MeV)	DOCUMENT ID	TECN	COMMENT
≈ 2020 OUR ESTIMATE			
2043 ± 22	ZHANG 13A	DPWA	Multichannel
2140	BACCARI 77	DPWA	$K^-p \rightarrow \Lambda\omega$
2117	DECLAIS 77	DPWA	$\bar{K}N \rightarrow \bar{K}N$
2100 ± 30	LITCHFIELD 71	DPWA	$K^-p \rightarrow \bar{K}N$
2020 ± 20	BARBARO... 70	DPWA	$K^-p \rightarrow \Sigma\pi$

 $\Lambda(2085)$ WIDTH

VALUE (MeV)	DOCUMENT ID	TECN	COMMENT
200 ± 75	ZHANG 13A	DPWA	Multichannel
128	BACCARI 77	DPWA	$K^-p \rightarrow \Lambda\omega$
167	DECLAIS 77	DPWA	$\bar{K}N \rightarrow \bar{K}N$
120 ± 30	LITCHFIELD 71	DPWA	$K^-p \rightarrow \bar{K}N$
160 ± 30	BARBARO... 70	DPWA	$K^-p \rightarrow \Sigma\pi$

 $\Lambda(2085)$ DECAY MODES

Mode	Fraction (Γ_i/Γ)
Γ_1 $N\bar{K}$	
Γ_2 $\Sigma\pi$	
Γ_3 $\Lambda\eta$	
Γ_4 $\Sigma(1385)\pi, F\text{-wave}$	
Γ_5 $\Sigma(1385)\pi, H\text{-wave}$	
Γ_6 $N\bar{K}^*(892), S=1/2$	(30 ± 9) %
Γ_7 $N\bar{K}^*(892), S=1/2, F\text{-wave}$	
Γ_8 $N\bar{K}^*(892), S=3/2, F\text{-wave}$	
Γ_9 $N\bar{K}^*(892), S=3/2, H\text{-wave}$	
Γ_{10} $\Lambda\omega$	

 $\Lambda(2085)$ BRANCHING RATIOSSee "Sign conventions for resonance couplings" in the Note on Λ and Σ Resonances. **$\Gamma(N\bar{K})/\Gamma_{total}$**

VALUE	DOCUMENT ID	TECN	COMMENT	Γ_1/Γ
0.028 ± 0.005	ZHANG 13A	DPWA	Multichannel	
0.05	DECLAIS 77	DPWA	$\bar{K}N \rightarrow \bar{K}N$	
0.05 ± 0.02	LITCHFIELD 71	DPWA	$K^-p \rightarrow \bar{K}N$	
••• We do not use the following data for averages, fits, limits, etc. •••				
not seen	¹ KAMANO 15	DPWA	Multichannel	
¹ From the preferred solution A in KAMANO 15.				

 $\Gamma(\Sigma\pi)/\Gamma_{total}$

VALUE	DOCUMENT ID	TECN	COMMENT	Γ_2/Γ
••• We do not use the following data for averages, fits, limits, etc. •••				
0.891	¹ KAMANO 15	DPWA	Multichannel	
¹ From the preferred solution A in KAMANO 15.				

 $\Gamma(\Lambda\eta)/\Gamma_{total}$

VALUE	DOCUMENT ID	TECN	COMMENT	Γ_3/Γ
••• We do not use the following data for averages, fits, limits, etc. •••				
0.002	¹ KAMANO 15	DPWA	Multichannel	
¹ From the preferred solution A in KAMANO 15.				

 $\Gamma(\Sigma(1385)\pi, F\text{-wave})/\Gamma_{total}$

VALUE	DOCUMENT ID	TECN	COMMENT	Γ_4/Γ
••• We do not use the following data for averages, fits, limits, etc. •••				
0.105	¹ KAMANO 15	DPWA	Multichannel	
¹ From the preferred solution A in KAMANO 15.				

 $\Gamma(\Sigma(1385)\pi, H\text{-wave})/\Gamma_{total}$

VALUE	DOCUMENT ID	TECN	COMMENT	Γ_5/Γ
••• We do not use the following data for averages, fits, limits, etc. •••				
not seen	¹ KAMANO 15	DPWA	Multichannel	
¹ From the preferred solution A in KAMANO 15.				

 $\Gamma(N\bar{K}^*(892), S=1/2, F\text{-wave})/\Gamma_{total}$

VALUE	DOCUMENT ID	TECN	COMMENT	Γ_7/Γ
••• We do not use the following data for averages, fits, limits, etc. •••				
not seen	¹ KAMANO 15	DPWA	Multichannel	
¹ From the preferred solution A in KAMANO 15.				

 $\Gamma(N\bar{K}^*(892), S=3/2, F\text{-wave})/\Gamma_{total}$

VALUE	DOCUMENT ID	TECN	COMMENT	Γ_8/Γ
••• We do not use the following data for averages, fits, limits, etc. •••				
0.001	¹ KAMANO 15	DPWA	Multichannel	
¹ From the preferred solution A in KAMANO 15.				

 $\Gamma(N\bar{K}^*(892), S=3/2, H\text{-wave})/\Gamma_{total}$

VALUE	DOCUMENT ID	TECN	COMMENT	Γ_9/Γ
••• We do not use the following data for averages, fits, limits, etc. •••				
not seen	¹ KAMANO 15	DPWA	Multichannel	
¹ From the preferred solution A in KAMANO 15.				

 $\Gamma(N\bar{K}^*(892), S=1/2)/\Gamma_{total}$

VALUE	DOCUMENT ID	TECN	COMMENT	Γ_6/Γ
0.30 ± 0.09	ZHANG 13A	DPWA	Multichannel	

 $(\Gamma_1\Gamma_7)^{1/2}/\Gamma_{total}$ in $N\bar{K} \rightarrow \Lambda(2085) \rightarrow \Sigma\pi$

VALUE	DOCUMENT ID	TECN	COMMENT	$(\Gamma_1\Gamma_2)^{1/2}/\Gamma$
+0.02 ± 0.01	ZHANG 13A	DPWA	Multichannel	
-0.15 ± 0.02	BARBARO... 70	DPWA	$K^-p \rightarrow \Sigma\pi$	

Baryon Particle Listings

 $\Lambda(2085), \Lambda(2100)$

$(\Gamma_1 \Gamma_2)^{1/2} / \Gamma_{\text{total}}$ in $N\bar{K} \rightarrow \Lambda(2085) \rightarrow \Lambda\omega$	DOCUMENT ID	TECN	COMMENT
VALUE <0.05	BACCARI	77	DPWA $K^- p \rightarrow \Lambda\omega$

 $\Lambda(2085)$ REFERENCES

KAMANO	15	PR C92 025205	H. Kamano <i>et al.</i>	(ANL, OSAK)
ZHANG	13A	PR C88 035205	H. Zhang <i>et al.</i>	(KSU)
GOPAL	80	Toronto Conf. 159	G.P. Gopal	(RHEL)
BACCARI	77	NC 41A 96	B. Baccari <i>et al.</i>	(SACL, CDEF) IJP
DECLAIS	77	CERN 77-16	Y. Declais <i>et al.</i>	(CAEN, CERN) IJP
GOPAL	77	NP B119 362	G.P. Gopal <i>et al.</i>	(LOIC, RHEL)
HEMINGWAY	75	NP B91 12	R.J. Hemingway <i>et al.</i>	(CERN, HEIDH, MPIM) IJP
LITCHFIELD	71	NP B30 125	P.J. Litchfield <i>et al.</i>	(RHEL, CDEF, SACL) IJP
BARBARO...	70	Duke Conf. 173	A. Barbaro-Galieri	(LRL) IJP

Hyperon Resonances, 1970

 $\Lambda(2100) 7/2^-$

$$I(J^P) = 0(\frac{7}{2}^-) \text{ Status: } ****$$

Most of the results published before 1973 are now obsolete and have been omitted. They may be found in our 1982 edition Physics Letters **111B** 1 (1982).

This entry only includes results from partial-wave analyses. Parameters of peaks seen in cross sections and in invariant-mass distributions around 2100 MeV used to be listed in a separate entry immediately following. It may be found in our 1986 edition Physics Letters **170B** 1 (1986).

 $\Lambda(2100)$ POLE POSITION

REAL PART

VALUE (MeV)	DOCUMENT ID	TECN	COMMENT
2040 ± 14	SARANTSEV	19	DPWA $\bar{K}N$ multichannel
••• We do not use the following data for averages, fits, limits, etc. •••			
2023	ZHANG	13A	DPWA Multichannel

-2xIMAGINARY PART

VALUE (MeV)	DOCUMENT ID	TECN	COMMENT
215 ± 29	SARANTSEV	19	DPWA $\bar{K}N$ multichannel
••• We do not use the following data for averages, fits, limits, etc. •••			
239	ZHANG	13A	DPWA Multichannel

 $\Lambda(2100)$ POLE RESIDUE

The "normalized residue" is the residue divided by $\Gamma_{\text{pole}}/2$.

Normalized residue in $N\bar{K} \rightarrow \Lambda(2100) \rightarrow N\bar{K}$

MODULUS	PHASE (°)	DOCUMENT ID	TECN	COMMENT
0.28 ± 0.06	-40 ± 10	SARANTSEV	19	DPWA $\bar{K}N$ multichannel

Normalized residue in $N\bar{K} \rightarrow \Lambda(2100) \rightarrow \Sigma\pi$

MODULUS	PHASE (°)	DOCUMENT ID	TECN	COMMENT
0.09 ± 0.02	-35 ± 15	SARANTSEV	19	DPWA $\bar{K}N$ multichannel

Normalized residue in $N\bar{K} \rightarrow \Lambda(2100) \rightarrow \Sigma(1385)\pi, D\text{-wave}$

MODULUS	PHASE (°)	DOCUMENT ID	TECN	COMMENT
0.04 ± 0.03		SARANTSEV	19	DPWA $\bar{K}N$ multichannel

Normalized residue in $N\bar{K} \rightarrow \Lambda(2100) \rightarrow \Sigma(1385)\pi, G\text{-wave}$

MODULUS	PHASE (°)	DOCUMENT ID	TECN	COMMENT
0.06 ± 0.03	-45 ± 15	SARANTSEV	19	DPWA $\bar{K}N$ multichannel

Normalized residue in $N\bar{K} \rightarrow \Lambda(2100) \rightarrow N\bar{K}^*(892), S=3/2, D\text{-wave}$

MODULUS	PHASE (°)	DOCUMENT ID	TECN	COMMENT
0.11 ± 0.06	-30 ± 30	SARANTSEV	19	DPWA $\bar{K}N$ multichannel

 $\Lambda(2100)$ MASS

VALUE (MeV)	DOCUMENT ID	TECN	COMMENT
2090 to 2110 (≈ 2100) OUR ESTIMATE			
2090 ± 15	SARANTSEV	19	DPWA $\bar{K}N$ multichannel
2086 ± 6	ZHANG	13A	DPWA Multichannel
2104 ± 10	GOPAL	80	DPWA $\bar{K}N \rightarrow \bar{K}N$
2106 ± 30	DEBELLEFON	78	DPWA $\bar{K}N \rightarrow \bar{K}N$
2110 ± 10	GOPAL	77	DPWA $\bar{K}N$ multichannel
2105 ± 10	HEMINGWAY	75	DPWA $K^- p \rightarrow \bar{K}N$
2115 ± 10	KANE	74	DPWA $K^- p \rightarrow \Sigma\pi$
••• We do not use the following data for averages, fits, limits, etc. •••			
2094	BACCARI	77	DPWA $K^- p \rightarrow \Lambda\omega$
2094	DECLAIS	77	DPWA $\bar{K}N \rightarrow \bar{K}N$
2110 or 2089	¹ NAKKASYAN	75	DPWA $K^- p \rightarrow \Lambda\omega$

 $\Lambda(2100)$ WIDTH

VALUE (MeV)	DOCUMENT ID	TECN	COMMENT
100 to 250 (≈ 200) OUR ESTIMATE			
290 ± 30	SARANTSEV	19	DPWA $\bar{K}N$ multichannel
305 ± 16	ZHANG	13A	DPWA Multichannel
157 ± 40	DEBELLEFON	78	DPWA $\bar{K}N \rightarrow \bar{K}N$
250 ± 30	GOPAL	77	DPWA $\bar{K}N$ multichannel
241 ± 30	HEMINGWAY	75	DPWA $K^- p \rightarrow \bar{K}N$
152 ± 15	KANE	74	DPWA $K^- p \rightarrow \Sigma\pi$
••• We do not use the following data for averages, fits, limits, etc. •••			
98	BACCARI	77	DPWA $K^- p \rightarrow \Lambda\omega$
250	DECLAIS	77	DPWA $\bar{K}N \rightarrow \bar{K}N$
244 or 302	¹ NAKKASYAN	75	DPWA $K^- p \rightarrow \Lambda\omega$

 $\Lambda(2100)$ DECAY MODES

Mode	Fraction (Γ_i/Γ)
Γ_1 $N\bar{K}$	25–35 %
Γ_2 $\Sigma\pi$	~ 5 %
Γ_3 $\Lambda\eta$	<3 %
Γ_4 ΞK	<3 %
Γ_5 $\Lambda\omega$	<8 %
Γ_6 $\Sigma(1385)\pi, D\text{-wave}$	
Γ_7 $\Sigma(1385)\pi, G\text{-wave}$	(1.0 ± 1.0) %
Γ_8 $N\bar{K}^*(892)$	10–20 %
Γ_9 $N\bar{K}^*(892), S=3/2, D\text{-wave}$	(4.0 ± 2.0) %
Γ_{10} $N\bar{K}^*(892), S=1/2, G\text{-wave}$	
Γ_{11} $N\bar{K}^*(892), S=3/2, G\text{-wave}$	

 $\Lambda(2100)$ BRANCHING RATIOS

See "Sign conventions for resonance couplings" in the Note on Λ and Σ Resonances.

$\Gamma(N\bar{K})/\Gamma_{\text{total}}$	DOCUMENT ID	TECN	COMMENT	Γ_1/Γ
0.25 to 0.35 (≈ 0.30) OUR ESTIMATE				
0.24 ± 0.05	SARANTSEV	19	DPWA $\bar{K}N$ multichannel	
0.23 ± 0.01	ZHANG	13A	DPWA Multichannel	
0.34 ± 0.03	GOPAL	80	DPWA $\bar{K}N \rightarrow \bar{K}N$	
0.24 ± 0.06	DEBELLEFON	78	DPWA $\bar{K}N \rightarrow \bar{K}N$	
0.31 ± 0.03	HEMINGWAY	75	DPWA $K^- p \rightarrow \bar{K}N$	
••• We do not use the following data for averages, fits, limits, etc. •••				
0.29	DECLAIS	77	DPWA $\bar{K}N \rightarrow \bar{K}N$	
0.30 ± 0.03	GOPAL	77	DPWA See GOPAL 80	

$\Gamma(\Sigma\pi)/\Gamma_{\text{total}}$	DOCUMENT ID	TECN	COMMENT	Γ_2/Γ
VALUE 0.030 ± 0.015	SARANTSEV	19	DPWA $\bar{K}N$ multichannel	

$\Gamma(\Sigma(1385)\pi, D\text{-wave})/\Gamma_{\text{total}}$	DOCUMENT ID	TECN	COMMENT	Γ_6/Γ
VALUE <0.01	SARANTSEV	19	DPWA $\bar{K}N$ multichannel	

$\Gamma(\Sigma(1385)\pi, G\text{-wave})/\Gamma_{\text{total}}$	DOCUMENT ID	TECN	COMMENT	Γ_7/Γ
VALUE 0.01 ± 0.01	SARANTSEV	19	DPWA $\bar{K}N$ multichannel	

$\Gamma(N\bar{K}^*(892), S=3/2, D\text{-wave})/\Gamma_{\text{total}}$	DOCUMENT ID	TECN	COMMENT	Γ_9/Γ
VALUE 0.04 ± 0.02	SARANTSEV	19	DPWA $\bar{K}N$ multichannel	

$(\Gamma_1 \Gamma_2)^{1/2} / \Gamma_{\text{total}}$ in $N\bar{K} \rightarrow \Lambda(2100) \rightarrow \Sigma\pi$	DOCUMENT ID	TECN	COMMENT	$(\Gamma_1 \Gamma_2)^{1/2} / \Gamma$
VALUE +0.03 ± 0.01	ZHANG	13A	DPWA Multichannel	
+0.12 ± 0.04	GOPAL	77	DPWA $\bar{K}N$ multichannel	
+0.11 ± 0.01	KANE	74	DPWA $K^- p \rightarrow \Sigma\pi$	

$(\Gamma_1 \Gamma_3)^{1/2} / \Gamma_{\text{total}}$ in $N\bar{K} \rightarrow \Lambda(2100) \rightarrow \Lambda\eta$	DOCUMENT ID	TECN	COMMENT	$(\Gamma_1 \Gamma_3)^{1/2} / \Gamma$
VALUE -0.050 ± 0.020	RADER	73	MPWA $K^- p \rightarrow \Lambda\eta$	

$(\Gamma_1 \Gamma_4)^{1/2} / \Gamma_{\text{total}}$ in $N\bar{K} \rightarrow \Lambda(2100) \rightarrow \Xi K$	DOCUMENT ID	TECN	COMMENT	$(\Gamma_1 \Gamma_4)^{1/2} / \Gamma$
VALUE 0.035 ± 0.018	LITCHFIELD	71	DPWA $K^- p \rightarrow \Xi K$	
••• We do not use the following data for averages, fits, limits, etc. •••				
0.003	MULLER	69B	DPWA $K^- p \rightarrow \Xi K$	
0.05	TRIPP	67	RVUE $K^- p \rightarrow \Xi K$	

See key on page 1127

Baryon Particle Listings

$\Lambda(2100), \Lambda(2110)$

$(\Gamma_1 \Gamma_2)^{1/2} / \Gamma_{\text{total}}$ in $N\bar{K} \rightarrow \Lambda(2100) \rightarrow \Lambda\omega$ $(\Gamma_1 \Gamma_5)^{1/2} / \Gamma$

VALUE	DOCUMENT ID	TECN	COMMENT
-0.070	² BACCARI 77	DPWA	GD_{37} wave
+0.011	² BACCARI 77	DPWA	GG_{17} wave
+0.008	² BACCARI 77	DPWA	GG_{37} wave
0.122 or 0.154	¹ NAKKASYAN 75	DPWA	$K^- p \rightarrow \Lambda\omega$

$(\Gamma_1 \Gamma_2)^{1/2} / \Gamma_{\text{total}}$ in $N\bar{K} \rightarrow \Lambda(2100) \rightarrow N\bar{K}^*(892), S=3/2, D\text{-wave}$ $(\Gamma_1 \Gamma_9)^{1/2} / \Gamma$

VALUE	DOCUMENT ID	TECN	COMMENT
+0.16 ± 0.02	ZHANG 13A	DPWA	Multichannel
+0.21 ± 0.04	CAMERON 78B	DPWA	$K^- p \rightarrow N\bar{K}^*$

$(\Gamma_1 \Gamma_2)^{1/2} / \Gamma_{\text{total}}$ in $N\bar{K} \rightarrow \Lambda(2100) \rightarrow N\bar{K}^*(892), S=1/2, G\text{-wave}$ $(\Gamma_1 \Gamma_{10})^{1/2} / \Gamma$

VALUE	DOCUMENT ID	TECN	COMMENT
-0.03 ± 0.02	ZHANG 13A	DPWA	Multichannel
-0.04 ± 0.03	³ CAMERON 78B	DPWA	$K^- p \rightarrow N\bar{K}^*$

$(\Gamma_1 \Gamma_2)^{1/2} / \Gamma_{\text{total}}$ in $N\bar{K} \rightarrow \Lambda(2100) \rightarrow N\bar{K}^*(892), S=3/2, G\text{-wave}$ $(\Gamma_1 \Gamma_{11})^{1/2} / \Gamma$

VALUE	DOCUMENT ID	TECN	COMMENT
+0.08 ± 0.02	ZHANG 13A	DPWA	Multichannel

$\Lambda(2100)$ FOOTNOTES

- ¹ The NAKKASYAN 75 values are from the two best solutions found. Each has the $\Lambda(2100)$ and one additional resonance (P_3 or F_5).
- ² Note that the three for BACCARI 77 entries are for three different waves.
- ³ The published sign has been changed to be in accord with the baryon-first convention. The upper limit on the G_3 wave is 0.03.

$\Lambda(2100)$ REFERENCES

SARANTSEV 19	EPJ A55 180	A.V. Sarantsev et al.	(BONN, PNPI)
ZHANG 13A	PR C88 035205	H. Zhang et al.	(KSU)
FDG 86	PL 170B 1	M. Aguilar-Benitez et al.	(CERN, CIT+)
FDG 82	PL 111B 1	M. Roos et al.	(HEL5, CIT, CERN)
GOPAL 80	Toronto Conf. 159	G.P. Gopal	(RHEL) IJP
CAMERON 78B	NP B146 327	W. Cameron et al.	(RHEL, LOIC) IJP
DEBELLEFON 78	NC 42A 403	A. de Bellefon et al.	(CDEF, SAACL) IJP
BACCARI 77	NC 41A 96	B. Baccari et al.	(SACL, CDEF) IJP
DECLAIS 77	CERN 77-16	Y. Declais et al.	(CAEN, CERN) IJP
GOPAL 77	NP B119 362	G.P. Gopal et al.	(LOIC, RHEL) IJP
HEMINGWAY 75	NP B91 12	R.J. Hemingway et al.	(CERN, HEIDH, MPIM) IJP
NAKKASYAN 75	NP B93 85	A. Nakkasyan	(CERN) IJP
KANE 74	LBL-2452	D.F. Kane	(LBL) IJP
RADER 73	NC 16A 178	R.K. Rader et al.	(SACL, HEID, CERN+) IJP
LITCHFIELD 71	NP B30 125	P.J. Litchfield et al.	(RHEL, CDEF, SAACL) IJP
MULLER 69B	Thesis UCRL 19372	R.A. Muller	(LRL)
TRIPP 67	NP B3 10	R.D. Tripp et al.	(LRL, SLAC, CERN+) IJP

$\Lambda(2110) \ 5/2^+$

 $I(J^P) = 0(\frac{5}{2}^+)$ Status: ***

For results published before 1974 (they are now obsolete), see our 1982 edition Physics Letters **111B** 1 (1982). All the references have been retained.

This resonance is in the Baryon Summary Table, but the evidence for it could be better.

$\Lambda(2110)$ POLE POSITION

REAL PART

VALUE (MeV)	DOCUMENT ID	TECN	COMMENT
2048 ± 10	SARANTSEV 19	DPWA	$\bar{K}N$ multichannel
••• We do not use the following data for averages, fits, limits, etc. •••			
1970	ZHANG 13A	DPWA	$\bar{K}N$ multichannel

-2xIMAGINARY PART

VALUE (MeV)	DOCUMENT ID	TECN	COMMENT
255 ± 20	SARANTSEV 19	DPWA	$\bar{K}N$ multichannel
••• We do not use the following data for averages, fits, limits, etc. •••			
350	ZHANG 13A	DPWA	$\bar{K}N$ multichannel

$\Lambda(2110)$ POLE RESIDUE

The "normalized residue" is the residue divided by $\Gamma_{\text{pole}}/2$.

Normalized residue in $N\bar{K} \rightarrow \Lambda(2110) \rightarrow N\bar{K}$

MODULUS	PHASE (°)	DOCUMENT ID	TECN	COMMENT
0.020 ± 0.005	5 ± 15	SARANTSEV 19	DPWA	$\bar{K}N$ multichannel

Normalized residue in $N\bar{K} \rightarrow \Lambda(2110) \rightarrow \Sigma\pi$

MODULUS	PHASE (°)	DOCUMENT ID	TECN	COMMENT
0.13 ± 0.03	0 ± 15	SARANTSEV 19	DPWA	$\bar{K}N$ multichannel

Normalized residue in $N\bar{K} \rightarrow \Lambda(2110) \rightarrow \Xi K$

MODULUS	PHASE (°)	DOCUMENT ID	TECN	COMMENT
0.005 ± 0.005		SARANTSEV 19	DPWA	$\bar{K}N$ multichannel

Normalized residue in $N\bar{K} \rightarrow \Lambda(2110) \rightarrow \Lambda\omega, S=1/2, P\text{-wave}$

MODULUS	PHASE (°)	DOCUMENT ID	TECN	COMMENT
0.01 ± 0.01		SARANTSEV 19	DPWA	$\bar{K}N$ multichannel

Normalized residue in $N\bar{K} \rightarrow \Lambda(2110) \rightarrow \Lambda\omega, S=3/2, P\text{-wave}$

MODULUS	PHASE (°)	DOCUMENT ID	TECN	COMMENT
0.03 ± 0.01	-7 ± 16	SARANTSEV 19	DPWA	$\bar{K}N$ multichannel

Normalized residue in $N\bar{K} \rightarrow \Lambda(2110) \rightarrow \Lambda\omega, S=3/2, F\text{-wave}$

MODULUS	PHASE (°)	DOCUMENT ID	TECN	COMMENT
0.01 ± 0.01		SARANTSEV 19	DPWA	$\bar{K}N$ multichannel

$\Lambda(2110)$ MASS

VALUE (MeV)	DOCUMENT ID	TECN	COMMENT
2050 to 2130 (≈ 2090) OUR ESTIMATE			
2086 ± 12	SARANTSEV 19	DPWA	$\bar{K}N$ multichannel
2036 ± 13	ZHANG 13A	DPWA	$\bar{K}N$ multichannel
2092 ± 25	GOPAL 80	DPWA	$\bar{K}N \rightarrow \bar{K}N$
2125 ± 25	CAMERON 78B	DPWA	$K^- p \rightarrow N\bar{K}^*$
2106 ± 50	DEBELLEFON 78	DPWA	$\bar{K}N \rightarrow \bar{K}N$
2140 ± 20	DEBELLEFON 77	DPWA	$K^- p \rightarrow \Sigma\pi$
2100 ± 50	GOPAL 77	DPWA	$\bar{K}N$ multichannel
2112 ± 7	KANE 74	DPWA	$K^- p \rightarrow \Sigma\pi$
••• We do not use the following data for averages, fits, limits, etc. •••			
2137	BACCARI 77	DPWA	$K^- p \rightarrow \Lambda\omega$
2103	¹ NAKKASYAN 75	DPWA	$K^- p \rightarrow \Lambda\omega$

$\Lambda(2110)$ WIDTH

VALUE (MeV)	DOCUMENT ID	TECN	COMMENT
200 to 300 (≈ 250) OUR ESTIMATE			
274 ± 25	SARANTSEV 19	DPWA	$\bar{K}N$ multichannel
400 ± 38	ZHANG 13A	DPWA	$\bar{K}N$ multichannel
245 ± 25	GOPAL 80	DPWA	$\bar{K}N \rightarrow \bar{K}N$
160 ± 30	CAMERON 78B	DPWA	$K^- p \rightarrow N\bar{K}^*$
251 ± 50	DEBELLEFON 78	DPWA	$\bar{K}N \rightarrow \bar{K}N$
140 ± 20	DEBELLEFON 77	DPWA	$K^- p \rightarrow \Sigma\pi$
200 ± 50	GOPAL 77	DPWA	$\bar{K}N$ multichannel
190 ± 30	KANE 74	DPWA	$K^- p \rightarrow \Sigma\pi$
••• We do not use the following data for averages, fits, limits, etc. •••			
132	BACCARI 77	DPWA	$K^- p \rightarrow \Lambda\omega$
391	¹ NAKKASYAN 75	DPWA	$K^- p \rightarrow \Lambda\omega$

$\Lambda(2110)$ DECAY MODES

Mode	Fraction (Γ_i/Γ)
$\Gamma_1 \ N\bar{K}$	5-25 %
$\Gamma_2 \ \Sigma\pi$	10-40 %
$\Gamma_3 \ \Lambda\omega$	seen
$\Gamma_4 \ \Lambda\omega, S=1/2, P\text{-wave}$	
$\Gamma_5 \ \Lambda\omega, S=3/2, P\text{-wave}$	(5.0 ± 2.0) %
$\Gamma_6 \ \Lambda\omega, S=3/2, F\text{-wave}$	
$\Gamma_7 \ \Xi K$	
$\Gamma_8 \ \Sigma(1385)\pi$	seen
$\Gamma_9 \ \Sigma(1385)\pi, P\text{-wave}$	
$\Gamma_{10} \ N\bar{K}^*(892)$	10-60 %
$\Gamma_{11} \ N\bar{K}^*(892), S=1/2$	
$\Gamma_{12} \ N\bar{K}^*(892), S=3/2, P\text{-wave}$	

$\Lambda(2110)$ BRANCHING RATIOS

See "Sign conventions for resonance couplings" in the Note on Λ and Σ Resonances.

$\Gamma(N\bar{K})/\Gamma_{\text{total}}$

VALUE	DOCUMENT ID	TECN	COMMENT
0.05 to 0.25 OUR ESTIMATE			
0.020 ± 0.005	SARANTSEV 19	DPWA	$\bar{K}N$ multichannel
0.083 ± 0.005	ZHANG 13A	DPWA	$\bar{K}N$ multichannel
0.07 ± 0.03	GOPAL 80	DPWA	$\bar{K}N \rightarrow \bar{K}N$
0.27 ± 0.06	² DEBELLEFON 78	DPWA	$\bar{K}N \rightarrow \bar{K}N$
••• We do not use the following data for averages, fits, limits, etc. •••			
0.07 ± 0.03	GOPAL 77	DPWA	See GOPAL 80

$\Gamma(\Sigma\pi)/\Gamma_{\text{total}}$

VALUE	DOCUMENT ID	TECN	COMMENT
0.88 ± 0.20	SARANTSEV 19	DPWA	$\bar{K}N$ multichannel

Baryon Particle Listings

 $\Lambda(2110)$, $\Lambda(2325)$, $\Lambda(2350)$

$\Gamma(\Lambda\omega, S=1/2, P\text{-wave})/\Gamma_{\text{total}}$	DOCUMENT ID	TECN	COMMENT	Γ_4/Γ
VALUE				
<0.01	SARANTSEV	19	DPWA $\bar{K}N$ multichannel	

$\Gamma(\Lambda\omega, S=3/2, P\text{-wave})/\Gamma_{\text{total}}$	DOCUMENT ID	TECN	COMMENT	Γ_5/Γ
VALUE				
0.05 ± 0.02	SARANTSEV	19	DPWA $\bar{K}N$ multichannel	

$\Gamma(\Lambda\omega, S=3/2, F\text{-wave})/\Gamma_{\text{total}}$	DOCUMENT ID	TECN	COMMENT	Γ_6/Γ
VALUE				
<0.01	SARANTSEV	19	DPWA $\bar{K}N$ multichannel	

$\Gamma(\Xi K)/\Gamma_{\text{total}}$	DOCUMENT ID	TECN	COMMENT	Γ_7/Γ
VALUE				
~ 0	SARANTSEV	19	DPWA $\bar{K}N$ multichannel	

$(\Gamma_1\Gamma_2)^{1/2}/\Gamma_{\text{total}}$ in $N\bar{K} \rightarrow \Lambda(2110) \rightarrow \Sigma\pi$	DOCUMENT ID	TECN	COMMENT	$(\Gamma_1\Gamma_2)^{1/2}/\Gamma$
VALUE				
$+0.04 \pm 0.01$	ZHANG	13A	DPWA Multichannel	
$+0.14 \pm 0.01$	DEBELLEFON	77	DPWA $K^-p \rightarrow \Sigma\pi$	
$+0.20 \pm 0.03$	KANE	74	DPWA $K^-p \rightarrow \Sigma\pi$	
$\bullet\bullet\bullet$ We do not use the following data for averages, fits, limits, etc. $\bullet\bullet\bullet$				
$+0.10 \pm 0.03$	GOPAL	77	DPWA $\bar{K}N$ multichannel	

$(\Gamma_1\Gamma_2)^{1/2}/\Gamma_{\text{total}}$ in $N\bar{K} \rightarrow \Lambda(2110) \rightarrow \Lambda\omega$	DOCUMENT ID	TECN	COMMENT	$(\Gamma_1\Gamma_3)^{1/2}/\Gamma$
VALUE				
<0.05	BACCARI	77	DPWA $K^-p \rightarrow \Lambda\omega$	
0.112	1 NAKKASYAN	75	DPWA $K^-p \rightarrow \Lambda\omega$	

$(\Gamma_1\Gamma_2)^{1/2}/\Gamma_{\text{total}}$ in $N\bar{K} \rightarrow \Lambda(2110) \rightarrow \Sigma(1385)\pi, P\text{-wave}$	DOCUMENT ID	TECN	COMMENT	$(\Gamma_1\Gamma_9)^{1/2}/\Gamma$
VALUE				
$+0.04 \pm 0.01$	ZHANG	13A	DPWA Multichannel	
$+0.071 \pm 0.025$	3 CAMERON	78	DPWA $K^-p \rightarrow \Sigma(1385)\pi$	

$(\Gamma_1\Gamma_2)^{1/2}/\Gamma_{\text{total}}$ in $N\bar{K} \rightarrow \Lambda(2110) \rightarrow N\bar{K}^*(892), S=1/2$	DOCUMENT ID	TECN	COMMENT	$(\Gamma_1\Gamma_{11})^{1/2}/\Gamma$
VALUE				
-0.09 ± 0.01	ZHANG	13A	DPWA Multichannel	
-0.17 ± 0.04	4 CAMERON	78B	DPWA $K^-p \rightarrow N\bar{K}^*$	

$(\Gamma_1\Gamma_2)^{1/2}/\Gamma_{\text{total}}$ in $N\bar{K} \rightarrow \Lambda(2110) \rightarrow N\bar{K}^*(892), S=3/2, P\text{-wave}$	DOCUMENT ID	TECN	COMMENT	$(\Gamma_1\Gamma_{12})^{1/2}/\Gamma$
VALUE				
0.24 ± 0.01	ZHANG	13A	DPWA Multichannel	

 $\Lambda(2110)$ FOOTNOTES

- Found in one of two best solutions.
- The published error of 0.6 was a misprint.
- The CAMERON 78 upper limit on F -wave decay is 0.03. The sign here has been changed to be in accord with the baryon-first convention.
- The published sign has been changed to be in accord with the baryon-first convention. The CAMERON 78B upper limits on the P_3 and F_3 waves are each 0.03.

 $\Lambda(2110)$ REFERENCES

SARANTSEV	19	EPJ A55 180	A.V. Sarantsev <i>et al.</i>	(BONN, PNPI)
ZHANG	13A	PR C88 035205	H. Zhang <i>et al.</i>	(KSU)
PDG	82	PL 111B 1	M. Roos <i>et al.</i>	(HEL5, CIT, CERN)
GOPAL	80	Toronto Conf. 159	G.P. Gopal	(RHEL) IJF
CAMERON	78	NP B145 189	W. Cameron <i>et al.</i>	(RHEL, LOIC) IJF
CAMERON	78B	NP B146 327	W. Cameron <i>et al.</i>	(RHEL, LOIC) IJF
DEBELLEFON	78	NC 42A 403	A. de Bellefon <i>et al.</i>	(CDEF, SACL) IJF
BACCARI	77	NC 41A 96	B. Baccari <i>et al.</i>	(SACL, CDEF) IJF
DEBELLEFON	77	NC 37A 175	A. de Bellefon <i>et al.</i>	(CDEF, SACL) IJF
GOPAL	77	NP B119 362	G.P. Gopal <i>et al.</i>	(LOIC, RHEL) IJF
NAKKASYAN	75	NP B93 85	A. Nakkasyan	(CERN) IJF
KANE	74	LBL-2452	D.F. Kane	(LBL) IJF

$\Lambda(2325) 3/2^-$ $I(J^P) = 0(\frac{3}{2}^-)$ Status: *

OMITTED FROM SUMMARY TABLE

BACCARI 77 finds this state with either $J^P = 3/2^-$ or $3/2^+$ in a energy-dependent partial-wave analyses of $K^-p \rightarrow \Lambda\omega$ from 2070 to 2436 MeV. A subsequent semi-energy-independent analysis from threshold to 2436 MeV selects $3/2^-$. DEBELLEFON 78 (same group) also sees this state in an energy-dependent partial-wave analysis of $K^-p \rightarrow \bar{K}N$ data, and finds $J^P = 3/2^-$ or $3/2^+$. They again prefer $J^P = 3/2^-$, but only on the basis of model-dependent considerations.

 $\Lambda(2325)$ MASS

VALUE (MeV)	DOCUMENT ID	TECN	COMMENT
≈ 2325 OUR ESTIMATE			
2342 ± 30	DEBELLEFON	78	DPWA $\bar{K}N \rightarrow \bar{K}N$
2327 ± 20	BACCARI	77	DPWA $K^-p \rightarrow \Lambda\omega$

 $\Lambda(2325)$ WIDTH

VALUE (MeV)	DOCUMENT ID	TECN	COMMENT
177 ± 40	DEBELLEFON	78	DPWA $\bar{K}N \rightarrow \bar{K}N$
160 ± 40	BACCARI	77	IPWA $K^-p \rightarrow \Lambda\omega$

 $\Lambda(2325)$ DECAY MODES

Mode	Fraction (Γ_i/Γ)
Γ_1 $N\bar{K}$	$\sim 12\%$
Γ_2 $\Lambda\omega$	$\sim 10\%$

 $\Lambda(2325)$ BRANCHING RATIOS

$\Gamma(N\bar{K})/\Gamma_{\text{total}}$	DOCUMENT ID	TECN	COMMENT	Γ_1/Γ
VALUE				
0.19 ± 0.06	DEBELLEFON	78	DPWA $\bar{K}N \rightarrow \bar{K}N$	

$(\Gamma_1\Gamma_2)^{1/2}/\Gamma_{\text{total}}$ in $N\bar{K} \rightarrow \Lambda(2325) \rightarrow \Lambda\omega$	DOCUMENT ID	TECN	COMMENT	$(\Gamma_1\Gamma_2)^{1/2}/\Gamma$
VALUE				
0.06 ± 0.02	1 BACCARI	77	IPWA DS_{33} wave	
0.05 ± 0.02	1 BACCARI	77	DPWA DD_{13} wave	
0.08 ± 0.03	1 BACCARI	77	DPWA DD_{33} wave	

 $\Lambda(2325)$ FOOTNOTES

- 1 Note that the three BACCARI 77 entries are for three different waves.

 $\Lambda(2325)$ REFERENCES

DEBELLEFON	78	NC 42A 403	A. de Bellefon <i>et al.</i>	(CDEF, SACL) IJF
BACCARI	77	NC 41A 96	B. Baccari <i>et al.</i>	(SACL, CDEF) IJF

$\Lambda(2350) 9/2^+$

$I(J^P) = 0(\frac{9}{2}^+)$ Status: ** *

DAUM 68 favors $J^P = 7/2^-$ or $9/2^+$. BRICMAN 70 favors $9/2^+$. LASINSKI 71 suggests three states in this region using a Pomeron + resonances model. There are now also three formation experiments from the College de France-Saclay group, DEBELLEFON 77, BACCARI 77, and DEBELLEFON 78, which find $9/2^+$ in energy-dependent partial-wave analyses of $\bar{K}N \rightarrow \Sigma\pi, \Lambda\omega$, and $N\bar{K}$.

 $\Lambda(2350)$ MASS

VALUE (MeV)	DOCUMENT ID	TECN	COMMENT
2340 to 2370 (≈ 2350) OUR ESTIMATE			
2370 ± 50	DEBELLEFON	78	DPWA $\bar{K}N \rightarrow \bar{K}N$
2365 ± 20	DEBELLEFON	77	DPWA $K^-p \rightarrow \Sigma\pi$
2358 ± 6	BRICMAN	70	CNTR Total, charge exchange
$\bullet\bullet\bullet$ We do not use the following data for averages, fits, limits, etc. $\bullet\bullet\bullet$			
2372	BACCARI	77	DPWA $K^-p \rightarrow \Lambda\omega$
2344 ± 15	COOL	70	CNTR K^-p, K^-d total
2360 ± 20	LU	70	CNTR $\gamma p \rightarrow K^+Y^*$
2340 ± 7	BUGG	68	CNTR K^-p, K^-d total

 $\Lambda(2350)$ WIDTH

VALUE (MeV)	DOCUMENT ID	TECN	COMMENT
100 to 250 (≈ 150) OUR ESTIMATE			
204 ± 50	DEBELLEFON	78	DPWA $\bar{K}N \rightarrow \bar{K}N$
110 ± 20	DEBELLEFON	77	DPWA $K^-p \rightarrow \Sigma\pi$
324 ± 30	BRICMAN	70	CNTR Total, charge exchange
$\bullet\bullet\bullet$ We do not use the following data for averages, fits, limits, etc. $\bullet\bullet\bullet$			
257	BACCARI	77	DPWA $K^-p \rightarrow \Lambda\omega$
190	COOL	70	CNTR K^-p, K^-d total
55	LU	70	CNTR $\gamma p \rightarrow K^+Y^*$
140 ± 20	BUGG	68	CNTR K^-p, K^-d total

 $\Lambda(2350)$ DECAY MODES

Mode	Fraction (Γ_i/Γ)
Γ_1 $N\bar{K}$	$\sim 12\%$
Γ_2 $\Sigma\pi$	$\sim 10\%$
Γ_3 $\Lambda\omega$	

 $\Lambda(2350)$ BRANCHING RATIOS

See "Sign conventions for resonance couplings" in the Note on Λ and Σ Resonances.

$\Gamma(N\bar{K})/\Gamma_{\text{total}}$	DOCUMENT ID	TECN	COMMENT	Γ_1/Γ
VALUE				
~ 0.12 OUR ESTIMATE				
0.12 ± 0.04	DEBELLEFON	78	DPWA $\bar{K}N \rightarrow \bar{K}N$	

See key on page 1127

Baryon Particle Listings
 $\Lambda(2350)$, $\Lambda(2585)$ Bumps

$(\Gamma_1 \Gamma_2)^{1/2} / \Gamma_{\text{total}}$ in $N\bar{K} \rightarrow \Lambda(2350) \rightarrow \Sigma \pi$		$(\Gamma_1 \Gamma_2)^{1/2} / \Gamma$	
VALUE	DOCUMENT ID	TECN	COMMENT
-0.11 ± 0.02	DEBELLEFON 77	DPWA	$K^- p \rightarrow \Sigma \pi$

$(\Gamma_1 \Gamma_2)^{1/2} / \Gamma_{\text{total}}$ in $N\bar{K} \rightarrow \Lambda(2350) \rightarrow \Lambda \omega$		$(\Gamma_1 \Gamma_2)^{1/2} / \Gamma$	
VALUE	DOCUMENT ID	TECN	COMMENT
<0.05	BACCARI 77	DPWA	$K^- p \rightarrow \Lambda \omega$

$\Lambda(2350)$ REFERENCES

DEBELLEFON 78	NC 42A 403	A. de Bellefon <i>et al.</i>	(CDEF, SAACL) IJP
BACCARI 77	NC 41A 96	B. Baccari <i>et al.</i>	(SACL, CDEF) IJP
DEBELLEFON 77	NC 37A 175	A. de Bellefon <i>et al.</i>	(CDEF, SAACL) IJP
LASINSKI 71	NP B29 125	T.A. Lasinski	(EFI) IJP
BRICMAN 70	PL 31B 152	C. Bricman <i>et al.</i>	(CERN, CAEN, SAACL)
COOL 70	PR D1 1887	R.L. Cool <i>et al.</i>	(BNL) I
Also	PR L 16 1228	R.L. Cool <i>et al.</i>	(BNL) I
LU 70	PR D2 1846	D.C. Lu <i>et al.</i>	(YALE)
BUGG 68	PR 168 1466	D.V. Bugg <i>et al.</i>	(RHEL, BIRM, CAVE) I
DAUM 68	NP B7 19	C. Daum <i>et al.</i>	(CERN) JP

$\Lambda(2585)$ Bumps

$I(J^P) = 0(?^?)$ Status: *

OMITTED FROM SUMMARY TABLE

$\Lambda(2585)$ MASS (BUMPS)

VALUE (MeV)	DOCUMENT ID	TECN	COMMENT
≈ 2585 OUR ESTIMATE			
2585 ± 45	ABRAMS	70	CNTR $K^- p, K^- d$ total
2530 ± 25	LU	70	CNTR $\gamma p \rightarrow K^+ Y^*$

$\Lambda(2585)$ WIDTH (BUMPS)

VALUE (MeV)	DOCUMENT ID	TECN	COMMENT
300	ABRAMS	70	CNTR $K^- p, K^- d$ total
150	LU	70	CNTR $\gamma p \rightarrow K^+ Y^*$

$\Lambda(2585)$ DECAY MODES (BUMPS)

Mode	Γ_1
$N\bar{K}$	

$\Lambda(2585)$ BRANCHING RATIOS (BUMPS)

$(J+\frac{1}{2}) \times \Gamma(N\bar{K}) / \Gamma_{\text{total}}$	Γ_1 / Γ
<i>J</i> is not known, so only $(J+\frac{1}{2}) \times \Gamma(N\bar{K}) / \Gamma_{\text{total}}$ can be given.	

VALUE	DOCUMENT ID	TECN	COMMENT
1	ABRAMS	70	CNTR $K^- p, K^- d$ total
0.12 ± 0.12	¹ BRICMAN	70	CNTR Total, charge exchange

$\Lambda(2585)$ FOOTNOTES (BUMPS)

¹ The resonance is at the end of the region analyzed — no clear signal.

$\Lambda(2585)$ REFERENCES (BUMPS)

ABRAMS 70	PR D1 1917	R.J. Abrams <i>et al.</i>	(BNL) I
Also	PR L 16 1228	R.L. Cool <i>et al.</i>	(BNL) I
BRICMAN 70	PL 31B 152	C. Bricman <i>et al.</i>	(CERN, CAEN, SAACL)
LU 70	PR D2 1846	D.C. Lu <i>et al.</i>	(YALE)

Baryon Particle Listings

Σ^+

Σ BARYONS

($S = -1, I = 1$)

$\Sigma^+ = uus, \Sigma^0 = uds, \Sigma^- = dds$

Σ^+

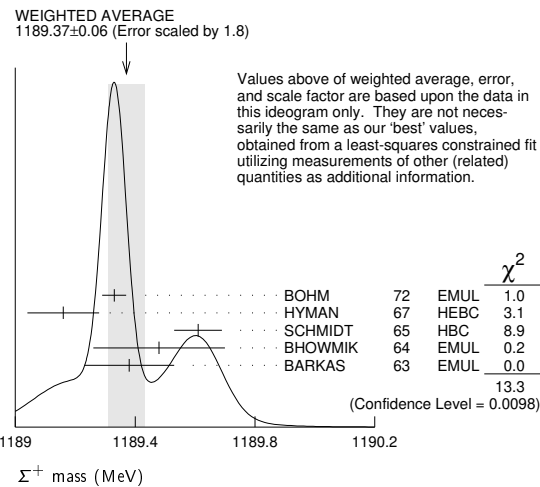
 $I(J^P) = 1(\frac{1}{2}^+)$ Status: ***

We have omitted some results that have been superseded by later experiments. See our earlier editions.

Σ^+ MASS

The fit uses $\Sigma^+, \Sigma^0, \Sigma^-$, and Λ mass and mass-difference measurements.

VALUE (MeV)	EVTS	DOCUMENT ID	TECN	COMMENT
1189.37 ± 0.07 OUR FIT				Error includes scale factor of 2.2.
1189.37 ± 0.06 OUR AVERAGE				Error includes scale factor of 1.8. See the ideogram below.
1189.33 ± 0.04	607	¹ BOHM	72	EMUL
1189.16 ± 0.12		HYMAN	67	HEBC
1189.61 ± 0.08	4205	SCHMIDT	65	HBC See note with Λ mass
1189.48 ± 0.22	58	² BHOWMIK	64	EMUL
1189.38 ± 0.15	144	² BARKAS	63	EMUL



¹ BOHM 72 is updated with our 1973 $K^-, \pi^-,$ and π^0 masses (Reviews of Modern Physics **45** S1 (1973)).
² These masses have been raised 30 keV to take into account a 46 keV increase in the proton mass and a 21 keV decrease in the π^0 mass (note added 1967 edition, Reviews of Modern Physics **39** 1 (1967)).

Σ^+ MEAN LIFE

Measurements with fewer than 1000 events have been omitted.

VALUE (10^{-10} s)	EVTS	DOCUMENT ID	TECN	COMMENT
0.8018 ± 0.0026 OUR AVERAGE				
0.8038 ± 0.0040 ± 0.0014		BARBOSA	00	E761 hyperons, 375 GeV
0.8043 ± 0.0080 ± 0.0014		¹ BARBOSA	00	E761 hyperons, 375 GeV
0.798 ± 0.005	30k	MARRAFFINO	80	HBC $K^- p$ 0.42-0.5 GeV/c
0.807 ± 0.013	5719	CONFORTO	76	HBC $K^- p$ 1-1.4 GeV/c
0.795 ± 0.010	20k	EISELE	70	HBC $K^- p$ at rest
0.803 ± 0.008	10664	BARLOUTAUD	69	HBC $K^- p$ 0.4-1.2 GeV/c
0.83 ± 0.032	1300	² CHANG	66	HBC

¹ This is a measurement of the Σ^- lifetime. Here we assume CPT invariance; see below for the fractional $\Sigma^+ - \Sigma^-$ lifetime difference obtained by BARBOSA 00.
² We have increased the CHANG 66 error of 0.018; see our 1970 edition, Reviews of Modern Physics **42** 87 (1970).

$$(\tau_{\Sigma^+} - \tau_{\Sigma^-}) / \tau_{\Sigma^+}$$

A test of CPT invariance.

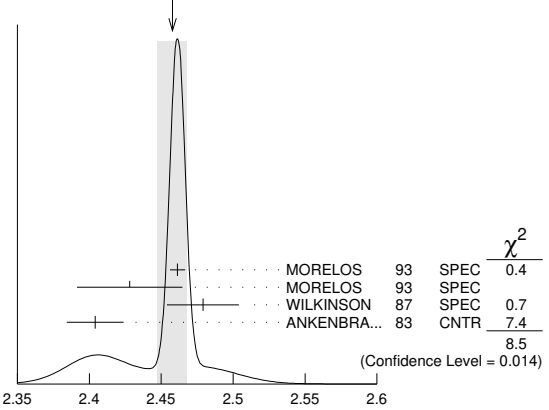
VALUE	DOCUMENT ID	TECN	COMMENT
(-6 ± 12) × 10⁻⁴	BARBOSA	00	E761 hyperons, 375 GeV

Σ^+ MAGNETIC MOMENT

See the "Quark Model" review. Measurements with an error $\geq 0.1 \mu_N$ have been omitted.

VALUE (μ_N)	EVTS	DOCUMENT ID	TECN	COMMENT
2.458 ± 0.010 OUR AVERAGE				Error includes scale factor of 2.1. See the ideogram below.
2.4613 ± 0.0034 ± 0.0040	250k	MORELOS	93	SPEC p Cu 800 GeV
2.428 ± 0.036 ± 0.007	12k	¹ MORELOS	93	SPEC p Cu 800 GeV
2.479 ± 0.012 ± 0.022	137k	WILKINSON	87	SPEC p Be 400 GeV
2.4040 ± 0.0198	44k	² ANKENBRA...	83	CNTR p Cu 400 GeV

WEIGHTED AVERAGE
2.458 ± 0.010 (Error scaled by 2.1)



¹ We assume CPT invariance: this is (minus) the Σ^- magnetic moment as measured by MORELOS 93. See below for the moment difference testing CPT .
² ANKENBRANDT 83 gives the value $2.38 \pm 0.02 \mu_N$. MORELOS 93 uses the same hyperon magnet and channel and claims to determine the field integral better, leading to the revised value given here.

$$(\mu_{\Sigma^+} + \mu_{\Sigma^-}) / \mu_{\Sigma^+}$$

A test of CPT invariance.

VALUE	DOCUMENT ID	TECN	COMMENT
0.014 ± 0.015	¹ MORELOS	93	SPEC p Cu 800 GeV

¹ This is our calculation from the MORELOS 93 measurements of the Σ^+ and Σ^- magnetic moments given above. The statistical error on μ_{Σ^-} dominates the error here.

Σ^+ DECAY MODES

Mode	Fraction (Γ_i/Γ)	Confidence level
Γ_1 $p\pi^0$	(51.57 ± 0.30) %	
Γ_2 $n\pi^+$	(48.31 ± 0.30) %	
Γ_3 $p\gamma$	(1.23 ± 0.05) × 10 ⁻³	
Γ_4 $n\pi^+\gamma$	[a] (4.5 ± 0.5) × 10 ⁻⁴	
Γ_5 $\Lambda e^+\nu_e$	(2.0 ± 0.5) × 10 ⁻⁵	

$\Delta S = \Delta Q$ (SQ) violating modes or
 $\Delta S = 1$ weak neutral current ($S1$) modes

Mode	Fraction	Confidence level
Γ_6 $n e^+ \nu_e$	$SQ < 5$	× 10 ⁻⁶ 90%
Γ_7 $n \mu^+ \nu_\mu$	$SQ < 3.0$	× 10 ⁻⁵ 90%
Γ_8 $p e^+ e^-$	$S1 < 7$	× 10 ⁻⁶
Γ_9 $p \mu^+ \mu^-$	$S1 (2.4 \pm 1.7) \times 10^{-8}$	

[a] See the Listings below for the pion momentum range used in this measurement.

CONSTRAINED FIT INFORMATION

An overall fit to 2 branching ratios uses 14 measurements and one constraint to determine 3 parameters. The overall fit has a $\chi^2 = 7.7$ for 12 degrees of freedom.

The following *off-diagonal* array elements are the correlation coefficients $\langle \delta x_i \delta x_j \rangle / (\delta x_i \delta x_j)$, in percent, from the fit to the branching fractions, $x_i \equiv \Gamma_i / \Gamma_{\text{total}}$. The fit constrains the x_i whose labels appear in this array to sum to one.

x_2	-100	
x_3	12	-14
x_1	x_2	

Σ^+ BRANCHING RATIOS

$\Gamma(n\pi^+)/\Gamma(N\pi)$ $\Gamma_2/(\Gamma_1+\Gamma_2)$

VALUE	EVTS	DOCUMENT ID	TECN	COMMENT
0.4836 ± 0.0030 OUR FIT				
0.4836 ± 0.0030 OUR AVERAGE				
0.4828 ± 0.0036	10k	¹ MARRAFFINO 80	HBC	$K^- p$ 0.42–0.5 GeV/c
0.488 ± 0.008	1861	NOWAK 78	HBC	
0.484 ± 0.015	537	TOVEE 71	EMUL	
0.488 ± 0.010	1331	BARLOUTAUD 69	HBC	$K^- p$ 0.4–1.2 GeV/c
0.46 ± 0.02	534	CHANG 66	HBC	
0.490 ± 0.024	308	HUMPHREY 62	HBC	

¹ MARRAFFINO 80 actually gives $\Gamma(p\pi^0)/\Gamma(\text{total}) = 0.5172 \pm 0.0036$.

$\Gamma(p\gamma)/\Gamma(p\pi^0)$ Γ_3/Γ_1

VALUE (units 10^{-3})	EVTS	DOCUMENT ID	TECN	COMMENT
2.38 ± 0.10 OUR FIT				
2.38 ± 0.10 OUR AVERAGE				
2.32 ± 0.11 ± 0.10	32k	TIMM 95	E761	Σ^+ 375 GeV
2.81 ± 0.39 $^{+0.21}_{-0.43}$	408	HESSEY 89	CNTR	$K^- p \rightarrow \Sigma^+ \pi^-$ at rest
2.52 ± 0.28	190	¹ KOBAYASHI 87	CNTR	$\pi^+ p \rightarrow \Sigma^+ K^+$
2.46 $^{+0.30}_{-0.35}$	155	BIAGI 85	CNTR	CERN hyperon beam
2.11 ± 0.38	46	MANZ 80	HBC	$K^- p \rightarrow \Sigma^+ \pi^-$
2.1 ± 0.3	45	ANG 69B	HBC	$K^- p$ at rest
2.76 ± 0.51	31	GERSHWIN 69B	HBC	$K^- p \rightarrow \Sigma^+ \pi^-$
3.7 ± 0.8	24	BAZIN 65	HBC	$K^- p$ at rest

¹ KOBAYASHI 87 actually gives $\Gamma(p\gamma)/\Gamma(\text{total}) = (1.30 \pm 0.15) \times 10^{-3}$.

$\Gamma(n\pi^+\gamma)/\Gamma(n\pi^+)$ Γ_4/Γ_2

The π^+ momentum cuts differ, so we do not average the results but simply use the latest value in the Summary Table.

VALUE (units 10^{-3})	EVTS	DOCUMENT ID	TECN	COMMENT
0.93 ± 0.10	180	EBENHOH 73	HBC	$\pi^+ < 150$ MeV/c
0.27 ± 0.05	29	ANG 69B	HBC	$\pi^+ < 110$ MeV/c
~ 1.8		BAZIN 65B	HBC	$\pi^+ < 116$ MeV/c

$\Gamma(\Lambda e^+ \nu_e)/\Gamma_{\text{total}}$ Γ_5/Γ

VALUE (units 10^{-5})	EVTS	DOCUMENT ID	TECN	COMMENT
2.0 ± 0.5 OUR AVERAGE				
1.6 ± 0.7	5	BALTAY 69	HBC	$K^- p$ at rest
2.9 ± 1.0	10	EISELE 69	HBC	$K^- p$ at rest
2.0 ± 0.8	6	BARASH 67	HBC	$K^- p$ at rest

$\Gamma(ne^+ \nu_e)/\Gamma(n\pi^+)$ Γ_6/Γ_2

Test of $\Delta S = \Delta Q$ rule. Experiments with an effective denominator less than 100,000 have been omitted.

EFFECTIVE DENOM.	EVTS	DOCUMENT ID	TECN	COMMENT
< 1.1 × 10⁻⁵ OUR LIMIT				Our 90% CL limit = (2.3 events)/(effective denominator sum). [Number of events increased to 2.3 for a 90% confidence level.]
111000	0	¹ EBENHOH 74	HBC	$K^- p$ at rest
105000	0	¹ SECHI-ZORN 73	HBC	$K^- p$ at rest

¹ Effective denominator calculated by us.

$\Gamma(n\mu^+ \nu_\mu)/\Gamma(n\pi^+)$ Γ_7/Γ_2

Test of $\Delta S = \Delta Q$ rule.

EFFECTIVE DENOM.	EVTS	DOCUMENT ID	TECN	COMMENT
< 6.2 × 10⁻⁵ OUR LIMIT				Our 90% CL limit = (6.7 events)/(effective denominator sum). [Number of events increased to 6.7 for a 90% confidence level.]
33800	0	BAGGETT 69B	HBC	
62000	2	EISELE 69B	HBC	
10150	0	² COURANT 64	HBC	
1710	0	² NAUENBERG 64	HBC	
120	1	GALTIERI 62	EMUL	

¹ Effective denominator calculated by us.

² Effective denominator taken from EISELE 67.

$\Gamma(pe^+ e^-)/\Gamma_{\text{total}}$ Γ_8/Γ

VALUE (units 10^{-6})	DOCUMENT ID	TECN	COMMENT
< 7	¹ ANG 69B	HBC	$K^- p$ at rest

¹ ANG 69B found three $pe^+ e^-$ events in agreement with $\gamma \rightarrow e^+ e^-$ conversion from $\Sigma^+ \rightarrow p\gamma$. The limit given here is for neutral currents.

$\Gamma(p\mu^+ \mu^-)/\Gamma_{\text{total}}$ Γ_9/Γ

A test for a $\Delta S = 1$ weak neutral current, but also allowed by higher-order electroweak interactions.

VALUE (units 10^{-8})	EVTS	DOCUMENT ID	TECN	COMMENT
2.4 $^{+1.7}_{-1.3}$ OUR AVERAGE				
2.2 $^{+0.9}_{-0.8}$ ± 1.5	10.2	¹ AAIJ 18E	LHCB	pp at 7, 8 TeV
8.6 $^{+6.6}_{-5.4}$ ± 5.5	3	² PARK 05	HYCP	p Cu, 800 GeV

¹ AAIJ 18E sees no structure in the dimuon mass distribution, contrary to PARK 05.

² The masses of the three dimuons of PARK 05 are within 1 MeV of one another, perhaps indicating the existence of a new state P^0 with mass 214.3 ± 0.5 MeV. In that case, the decay is $\Sigma^+ \rightarrow pP^0, P^0 \rightarrow \mu^+ \mu^-$, with a branching fraction of $(3.1 $^{+2.4}_{-1.9}$ ± 1.5) \times 10^{-8}$.

$\Gamma(\Sigma^+ \rightarrow ne^+ \nu_e)/\Gamma(\Sigma^- \rightarrow ne^- \bar{\nu}_e)$ Γ_6/Γ_3^-

VALUE	CL%	EVTS	DOCUMENT ID	TECN	COMMENT
< 0.009 OUR LIMIT					Our 90% CL limit, using $\Gamma(ne^+ \nu_e)/\Gamma(n\pi^+)$ above.
• • •					We do not use the following data for averages, fits, limits, etc. • • •
< 0.019	90	0	EBENHOH 74	HBC	$K^- p$ at rest
< 0.018	90	0	SECHI-ZORN 73	HBC	$K^- p$ at rest
< 0.12	95	0	COLE 71	HBC	$K^- p$ at rest
< 0.03	90	0	EISELE 69B	HBC	See EBENHOH 74

$\Gamma(\Sigma^+ \rightarrow n\mu^+ \nu_\mu)/\Gamma(\Sigma^- \rightarrow n\mu^- \bar{\nu}_\mu)$ Γ_7/Γ_4^-

VALUE	EVTS	DOCUMENT ID	TECN	COMMENT
< 0.12 OUR LIMIT				Our 90% CL limit, using $\Gamma(n\mu^+ \nu_\mu)/\Gamma(n\pi^+)$ above.
• • •				We do not use the following data for averages, fits, limits, etc. • • •
0.06 $^{+0.045}_{-0.03}$	2	EISELE 69B	HBC	$K^- p$ at rest

$\Gamma(\Sigma^+ \rightarrow n\ell^+ \nu)/\Gamma(\Sigma^- \rightarrow n\ell^- \bar{\nu}_\ell)$ $(\Gamma_6 + \Gamma_7)/(\Gamma_3^- + \Gamma_4^-)$

Test of $\Delta S = \Delta Q$ rule.

VALUE	EVTS	DOCUMENT ID	TECN	COMMENT
< 0.043 OUR LIMIT				Our 90% CL limit, using $[\Gamma(\Sigma^+ \rightarrow n\mu^+ \nu_\mu) + \Gamma(\Sigma^+ \rightarrow ne^+ \nu_e)]/\Gamma(\Sigma^+ \rightarrow n\pi^+)$.
• • •				We do not use the following data for averages, fits, limits, etc. • • •
< 0.08	1	NORTON 69	HBC	
< 0.034	0	BAGGETT 67	HBC	

Σ^+ DECAY PARAMETERS

See the "Note on Baryon Decay Parameters" in the neutron Listings. A few early results have been omitted.

α_0 FOR $\Sigma^+ \rightarrow p\pi^0$

VALUE	EVTS	DOCUMENT ID	TECN	COMMENT
-0.982 ± 0.014 OUR FIT				
-0.982 $^{+0.016}_{-0.013}$ OUR AVERAGE				
-0.998 ± 0.037 ± 0.009	93k	¹ ABLIKIM 20x	BES3	$J/\psi/\psi(2S) \rightarrow \Sigma^+ \Sigma^-$
-0.945 $^{+0.055}_{-0.042}$	1259	² LIPMAN 73	OSPK	$\pi^+ p \rightarrow \Sigma^+$
-0.940 ± 0.045	16k	BELLAMY 72	ASPK	$\pi^+ p \rightarrow \Sigma^+ K^+$
-0.98 $^{+0.05}_{-0.02}$	1335	³ HARRIS 70	OSPK	$\pi^+ p \rightarrow \Sigma^+ K^+$
-0.999 ± 0.022	32k	BANGERTER 69	HBC	$K^- p$ 0.4 GeV/c

¹ ABLIKIM 20x uses production through $e^+ e^- \rightarrow J/\psi \rightarrow \Sigma^+ \Sigma^-$ and $e^+ e^- \rightarrow \psi(2S) \rightarrow \Sigma^+ \Sigma^-$, with 87,815 and 5,327 events, respectively. Note that the reported values of decay parameters α_0 of Σ^+ and $\bar{\alpha}_0$ of Σ^- are correlated.

² Decay protons scattered off aluminum.

³ Decay protons scattered off carbon.

$\bar{\alpha}_0$ FOR $\Sigma^- \rightarrow \bar{p}\pi^0$

VALUE	EVTS	DOCUMENT ID	TECN	COMMENT
0.990 ± 0.037 ± 0.011	93k	¹ ABLIKIM 20x	BES3	$J/\psi/\psi(2S) \rightarrow \Sigma^+ \Sigma^-$

¹ ABLIKIM 20x uses production through $e^+ e^- \rightarrow J/\psi \rightarrow \Sigma^+ \Sigma^-$ and $e^+ e^- \rightarrow \psi(2S) \rightarrow \Sigma^+ \Sigma^-$, with 87,815 and 5,327 events, respectively. Note that the reported values of decay parameters α_0 of Σ^+ and $\bar{\alpha}_0$ of Σ^- are correlated.

$(\alpha_0 + \bar{\alpha}_0) / (\alpha_0 - \bar{\alpha}_0)$

VALUE	EVTS	DOCUMENT ID	TECN	COMMENT
0.004 ± 0.037 ± 0.010	93k	¹ ABLIKIM 20x	BES3	$J/\psi/\psi(2S) \rightarrow \Sigma^+ \Sigma^-$

¹ ABLIKIM 20x uses production through $e^+ e^- \rightarrow J/\psi \rightarrow \Sigma^+ \Sigma^-$ and $e^+ e^- \rightarrow \psi(2S) \rightarrow \Sigma^+ \Sigma^-$, with 87,815 and 5,327 events, respectively. Note that the reported values of decay parameters α_0 of Σ^+ and $\bar{\alpha}_0$ of Σ^- are correlated.

ϕ_0 ANGLE FOR $\Sigma^+ \rightarrow p\pi^0$ $(\tan \phi_0 = \beta/\gamma)$

VALUE (°)	EVTS	DOCUMENT ID	TECN	COMMENT
36 ± 34 OUR AVERAGE				
38.1 $^{+35.7}_{-37.1}$	1259	¹ LIPMAN 73	OSPK	$\pi^+ p \rightarrow \Sigma^+ K^+$
22 ± 90		² HARRIS 70	OSPK	$\pi^+ p \rightarrow \Sigma^+ K^+$

¹ Decay proton scattered off aluminum.

² Decay protons scattered off carbon.

α_+ / α_0

Older results have been omitted.

VALUE	EVTS	DOCUMENT ID	TECN	COMMENT
-0.069 ± 0.013 OUR FIT				
-0.073 ± 0.021	23k	MARRAFFINO 80	HBC	$K^- p$ 0.42–0.5 GeV/c

Baryon Particle Listings

Σ^+, Σ^0

α_+ FOR $\Sigma^+ \rightarrow n\pi^+$

VALUE	EVTS	DOCUMENT ID	TECN	COMMENT
0.068 ± 0.013 OUR FIT				
0.066 ± 0.016 OUR AVERAGE				
0.037 ± 0.049	4101	BERLEY	70B HBC	
0.069 ± 0.017	35k	BANGERTER	69 HBC	$K^- p$ 0.4 GeV/c

ϕ_+ ANGLE FOR $\Sigma^+ \rightarrow n\pi^+$ ($\tan \phi_+ = \beta/\gamma$)

VALUE (°)	EVTS	DOCUMENT ID	TECN	COMMENT
167 ± 20 OUR AVERAGE				Error includes scale factor of 1.1.
184 ± 24	1054	¹ BERLEY	70B HBC	
143 ± 29	560	BANGERTER	69B HBC	$K^- p$ 0.4 GeV/c

¹ Changed from 176 to 184° to agree with our sign convention.

α_γ FOR $\Sigma^+ \rightarrow p\gamma$

VALUE	EVTS	DOCUMENT ID	TECN	COMMENT
-0.76 ± 0.08 OUR AVERAGE				
-0.720 ± 0.086 ± 0.045	35k	¹ FOUCHER	92 SPEC	$\Sigma^+ 375$ GeV
-0.86 ± 0.13 ± 0.04	190	KOBAYASHI	87 CNTR	$\pi^+ p \rightarrow \Sigma^+ K^+$
-0.53 ^{+0.38} / _{-0.36}	46	MANZ	80 HBC	$K^- p \rightarrow \Sigma^+ \pi^-$
-1.03 ^{+0.52} / _{-0.42}	61	GERSHWIN	69B HBC	$K^- p \rightarrow \Sigma^+ \pi^-$

¹ See TIMM 95 for a detailed description of the analysis.

Σ^+ REFERENCES

We have omitted some papers that have been superseded by later experiments. See our earlier editions.

ABLIKIM	20X	PRL 125 052004	M. Ablikim <i>et al.</i>	(BESIII Collab.)
AAJ	18E	PRL 120 221803	R. Aaij <i>et al.</i>	(LHCb Collab.)
PARK	05	PRL 94 021801	H.K. Park <i>et al.</i>	(FNAL HyperCP Collab.)
BARBOSA	00	PR D61 031101	R.F. Barbosa <i>et al.</i>	(FNAL E761 Collab.)
TIMM	95	PR D51 4638	S. Timm <i>et al.</i>	(FNAL E761 Collab.)
MORELOS	93	PRL 71 3417	A. Morelos <i>et al.</i>	(FNAL E761 Collab.)
FOUCHER	92	PRL 68 3004	M. Foucher <i>et al.</i>	(FNAL E761 Collab.)
HESSEY	89	ZPHY C42 175	N.P. Hessey <i>et al.</i>	(BNL-811 Collab.)
KOBAYASHI	87	PRL 59 868	M. Kobayashi <i>et al.</i>	(KYOT)
WILKINSON	87	PRL 58 855	C.A. Wilkinson <i>et al.</i>	(WISC, MICH, RUTG+)
BIAGI	85	ZPHY C28 495	S.F. Biagi <i>et al.</i>	(CERN WA62 Collab.)
ANKENBRANDT	83	PRL 51 863	C.M. Ankenbrandt <i>et al.</i>	(FNAL, IOWA, ISU+)
MANZ	80	PL 96B 217	A. Manz <i>et al.</i>	(MPIM, VAND)
MARRAFFINO	80	PR D21 2501	J. Marraffino <i>et al.</i>	(VAND, MPIM)
NOWAK	78	NP B139 61	R.J. Nowak <i>et al.</i>	(LOUC, BELG, DURH+)
CONFORTO	76	NP B105 189	B. Conforto <i>et al.</i>	(RHEL, LOIC)
EBENHOH	74	ZPHY 266 367	H. Ebenhoh <i>et al.</i>	(HEIDT)
EBENHOH	73	ZPHY 264 413	W. Ebenhoh <i>et al.</i>	(HEIDT)
LIPMAN	73	PL 45B 89	N.H. Lipman <i>et al.</i>	(RHEL, SUSS, LOWC)
PDG	73	RMP 45 51	T.A. Lasinski <i>et al.</i>	(LBL, BRAN, CERN+)
SECHI-ZORN	73	PR D8 12	B. Sechi-Zorn, G.A. Snow	(UMD)
BELLAMY	72	PL 39B 299	E.H. Bellamy <i>et al.</i>	(LOWC, RHEL, SUSS)
BOHM	72	NP B48 1	G. Bohm <i>et al.</i>	(BERL, KIDR, BRUX, IASD+)
Also		IJHE-73.2 Nov	G. Bohm	(BERL, KIDR, BRUX, IASD, DUUC+)
COLE	71	PR D4 631	J. Cole <i>et al.</i>	(STON, COLU)
TOVEE	71	NP B33 493	D.N. Tovee <i>et al.</i>	(LOUC, KIDR, BERL+)
BERLEY	70B	PR D1 2015	D. Berley <i>et al.</i>	(BNL, MASA, YALE)
EISELE	70	ZPHY 238 372	F. Eisele <i>et al.</i>	(HEID)
HARRIS	70	PRL 24 165	F. Harris <i>et al.</i>	(MICH, WISC)
PDG	70	RMP 42 87	A. Barbaro-Galiteri <i>et al.</i>	(LRL, BRAN+)
ANG	69B	ZPHY 228 151	G. Ang <i>et al.</i>	(HEID)
BAGGETT	69B	Thesis MDDP-TR-973	N.V. Baggett <i>et al.</i>	(UMD)
BALTAY	69	PRL 22 615	C. Baltay <i>et al.</i>	(COLU, STON)
BANGERTER	69	Thesis UCRL 19244	R.O. Bangener	(LRL)
BANGERTER	69B	PR 187 1821	R.O. Bangener <i>et al.</i>	(LRL)
BARLOUTAUD	69	NP B14 153	R. Barloutaud <i>et al.</i>	(SACL, CERN, HEID)
EISELE	69	ZPHY 221 1	F. Eisele <i>et al.</i>	(HEID)
Also		PRL 13 291	W. Willis <i>et al.</i>	(BNL, CERN, HEID, UMD)
EISELE	69B	ZPHY 221 401	F. Eisele <i>et al.</i>	(HEID)
GERSHWIN	69B	PR 188 2077	L.K. Gershwin <i>et al.</i>	(LRL)
Also		Thesis UCRL 19246	L.K. Gershwin	(LRL)
NORTON	69	Thesis Nevis 175	H. Norton	(COLU)
BAGGETT	67	PRL 19 1459	N. Baggett <i>et al.</i>	(UMD)
Also		Vienna Abs. 374	N.V. Baggett, B. Kehoe	(UMD)
Also		Private Comm.	N.V. Baggett	(UMD)
BARASH	67	PRL 19 181	N. Barash <i>et al.</i>	(UMD)
EISELE	67	ZPHY 205 409	F. Eisele <i>et al.</i>	(HEID)
HYMAN	67	PL 25B 376	L.G. Hyman <i>et al.</i>	(ANL, CMU, NWES)
PDG	67	RMP 39 1	A.H. Rosenfeld <i>et al.</i>	(LRL, CERN, YALE)
CHANG	66	PR 151 1081	C.Y. Chang	(COLU)
Also		Thesis Nevis 145	C.Y. Chang	(COLU)
BAZIN	65	PRL 14 154	M. Bazin <i>et al.</i>	(PRIN, RUTG, COLU)
BAZIN	65B	PR 140 B1358	M. Bazin <i>et al.</i>	(PRIN, RUTG, COLU)
SCHMIDT	65	PR 140 B1328	P. Schmidt	(COLU)
BHOWMIK	64	NP 53 22	B. Bhowmik <i>et al.</i>	(DELH)
COURANT	64	PR 136 B1791	H. Courant <i>et al.</i>	(CERN, HEID, UMD+)
NAUENBERG	64	PRL 12 679	U. Nauenberg <i>et al.</i>	(COLU, RUTG, PRIN)
BARKAS	63	PRL 11 26	W.H. Barkas, J.N. Dyer, H.H. Heckman	(LRL)
Also		Thesis UCRL 9450	J.N. Dyer	(LRL)
GALTIERI	62	PRL 9 26	A. Barbaro-Galiteri <i>et al.</i>	(LRL)
HUMPHREY	62	PR 127 1305	W.E. Humphrey, R.R. Ross	(LRL)



$$J(P) = 1(\frac{1}{2}^+) \text{ Status: } ***$$

COURANT 63 and ALFF 65, using $\Sigma^0 \rightarrow \Lambda e^+ e^-$ decays (Dalitz decays), determined the Σ^0 parity to be positive, given that $J = 1/2$ and that certain very reasonable assumptions about form factors are true. The results of experiments involving the Primakoff effect, from which the Σ^0 mean life and $\Sigma^0 \rightarrow \Lambda$ transition magnetic moment come (see below), strongly support $J = 1/2$.

Σ^0 MASS

The fit uses $\Sigma^+, \Sigma^0, \Sigma^-,$ and Λ mass and mass-difference measurements.

VALUE (MeV)	EVTS	DOCUMENT ID	TECN	COMMENT
1192.642 ± 0.024 OUR FIT				
••• We do not use the following data for averages, fits, limits, etc. •••				
1192.65 ± 0.020 ± 0.014	3327	¹ WANG	97 SPEC	$\Sigma^0 \rightarrow \Lambda \gamma \rightarrow (p\pi^-)(e^+e^-)$

¹ This WANG 97 result is redundant with the Σ^0 - Λ mass-difference measurement below.

$m_{\Sigma^-} - m_{\Sigma^0}$

VALUE (MeV)	EVTS	DOCUMENT ID	TECN	COMMENT
4.807 ± 0.035 OUR FIT				Error includes scale factor of 1.1.
4.86 ± 0.08 OUR AVERAGE				Error includes scale factor of 1.2.
4.87 ± 0.12	37	DOSCH	65 HBC	
5.01 ± 0.12	12	SCHMIDT	65 HBC	See note with Λ mass
4.75 ± 0.1	18	BURNSTEIN	64 HBC	

$m_{\Sigma^0} - m_\Lambda$

VALUE (MeV)	EVTS	DOCUMENT ID	TECN	COMMENT
76.959 ± 0.023 OUR FIT				
76.966 ± 0.020 ± 0.013	3327	WANG	97 SPEC	$\Sigma^0 \rightarrow \Lambda \gamma \rightarrow (p\pi^-)(e^+e^-)$
••• We do not use the following data for averages, fits, limits, etc. •••				
76.23 ± 0.55	109	COLAS	75 HLBC	$\Sigma^0 \rightarrow \Lambda \gamma$
76.63 ± 0.28	208	SCHMIDT	65 HBC	See note with Λ mass

Σ^0 MEAN LIFE

These lifetimes are deduced from measurements of the cross sections for the Primakoff process $\Lambda \rightarrow \Sigma^0$ in nuclear Coulomb fields. An alternative expression of the same information is the Σ^0 - Λ transition magnetic moment given in the following section. The relation is $(\mu_{\Sigma\Lambda}/\mu_N)^2 \tau = 1.92951 \times 10^{-19}$ s (see DEVLIN 86).

VALUE (10^{-20} s)	DOCUMENT ID	TECN	COMMENT
7.4 ± 0.7 OUR EVALUATION			Using $\mu_{\Sigma\Lambda}$ (see the above note).
6.5 ^{+1.7} / _{-1.1}	² DEVLIN	86 SPEC	Primakoff effect
7.6 ± 0.5 ± 0.7	³ PETERSEN	86 SPEC	Primakoff effect
••• We do not use the following data for averages, fits, limits, etc. •••			
5.8 ± 1.3	² DYDAK	77 SPEC	See DEVLIN 86

² DEVLIN 86 is a recalculation of the results of DYDAK 77 removing a numerical approximation made in that work.
³ An additional uncertainty of the Primakoff formalism is estimated to be < 5%.

$|\mu(\Sigma^0 \rightarrow \Lambda)|$ TRANSITION MAGNETIC MOMENT

See the note in the Σ^0 mean-life section above. Also, See the "Quark Model" review.

VALUE (μ_N)	DOCUMENT ID	TECN	COMMENT
1.61 ± 0.08 OUR AVERAGE			
1.72 ^{+0.17} / _{-0.19}	⁴ DEVLIN	86 SPEC	Primakoff effect
1.59 ± 0.05 ± 0.07	⁵ PETERSEN	86 SPEC	Primakoff effect
••• We do not use the following data for averages, fits, limits, etc. •••			
1.82 ^{+0.25} / _{-0.18}	⁴ DYDAK	77 SPEC	See DEVLIN 86

⁴ DEVLIN 86 is a recalculation of the results of DYDAK 77 removing a numerical approximation made in that work.
⁵ An additional uncertainty of the Primakoff formalism is estimated to be < 2.5%.

Σ^0 DECAY MODES

Mode	Fraction (Γ_i/Γ)	Confidence level
$\Gamma_1 \Lambda \gamma$	100 %	
$\Gamma_2 \Lambda \gamma \gamma$	< 3 %	90%
$\Gamma_3 \Lambda e^+ e^-$	[a] 5 × 10 ⁻³	

[a] A theoretical value using QED.

Σ^0 BRANCHING RATIOS

VALUE	CL%	DOCUMENT ID	TECN	Γ_2/Γ
< 0.03	90	COLAS	75 HLBC	

See key on page 1127

Baryon Particle Listings

Σ^0, Σ^-

$\Gamma(\Lambda e^+ e^-)/\Gamma_{total}$ Γ_3/Γ
 See COURANT 63 and ALFF 65 for measurements of the invariant-mass spectrum of the Dalitz pairs.

VALUE	DOCUMENT ID	COMMENT
0.00545	FEINBERG 58	Theoretical QED calculation

Σ^0 REFERENCES

WANG 97	PR D56 2544	M.H.L.S. Wang <i>et al.</i>	(BNL-E766 Collab.)
DEVLIN 86	PR D34 1626	T. Devlin, P.C. Petersen, A. Beretvas	(RUTG)
PETERSEN 86	PRL 57 949	P.C. Petersen <i>et al.</i>	(RUTG, WISC, MICH+)
DYDAK 77	NP B118 1	F. Dydak <i>et al.</i>	(CERN, DORT, HEIDH)
COLAS 75	NP B91 253	J. Colas <i>et al.</i>	(ORSAY)
ALFF 65	PL 137 B1105	C. Alff <i>et al.</i>	(COLU, RUTG, BNL)P
DOSCH 65	PL 14 239	H.C. Dosch <i>et al.</i>	(HEID)
SCHMIDT 65	PR 140 B1328	P. Schmidt	(COLU)
BURNSTEIN 64	PRL 13 66	R.A. Burnstein <i>et al.</i>	(UMD)
COURANT 63	PRL 10 409	H. Courant <i>et al.</i>	(CERN, UMD)P
FEINBERG 58	PR 109 1019	G. Feinberg	(BNL)



$I(J^P) = 1(\frac{1}{2}^+)$ Status: * * * *

We have omitted some results that have been superseded by later experiments. See our earlier editions.

Σ^- MASS

The fit uses Σ^+ , Σ^0 , Σ^- , and Λ mass and mass-difference measurements.

VALUE (MeV)	EVTS	DOCUMENT ID	TECN	COMMENT
1197.449 ± 0.030 OUR FIT				Error includes scale factor of 1.2.
1197.45 ± 0.04 OUR AVERAGE				Error includes scale factor of 1.2.
1197.417 ± 0.040		GUREV 93	SPEC	Σ^- C atom, crystal diff.
1197.532 ± 0.057		GALL 88	CNTR	Σ^- Pb, Σ^- W atoms
1197.43 ± 0.08	3000	SCHMIDT 65	HBC	See note with Λ mass
• • • We do not use the following data for averages, fits, limits, etc. • • •				
1197.24 ± 0.15		¹ DUGAN 75	CNTR	Exotic atoms
¹ GALL 88 concludes that the DUGAN 75 mass needs to be reevaluated.				

$m_{\Sigma^-} - m_{\Sigma^+}$

VALUE (MeV)	EVTS	DOCUMENT ID	TECN
8.08 ± 0.08 OUR FIT			
8.09 ± 0.16 OUR AVERAGE			
7.91 ± 0.23	86	BOHM 72	EMUL
8.25 ± 0.25	2500	DOSCH 65	HBC
8.25 ± 0.40	87	BARKAS 63	EMUL

$m_{\Sigma^-} - m_{\Lambda}$

VALUE (MeV)	EVTS	DOCUMENT ID	TECN	COMMENT
81.766 ± 0.030 OUR FIT				Error includes scale factor of 1.2.
81.69 ± 0.07 OUR AVERAGE				
81.64 ± 0.09	2279	HEPP 68	HBC	
81.80 ± 0.13	85	SCHMIDT 65	HBC	See note with Λ mass
81.70 ± 0.19		BURNSTEIN 64	HBC	

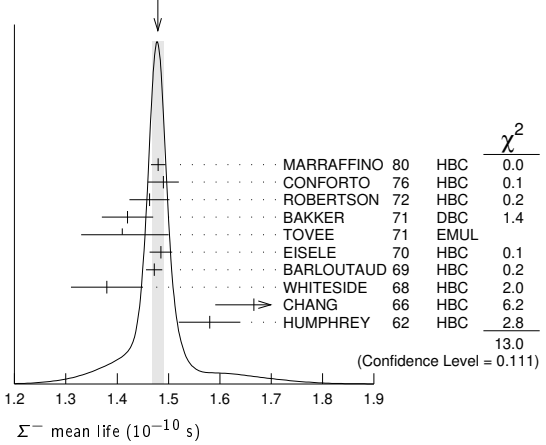
Σ^- MEAN LIFE

Measurements with an error $\geq 0.2 \times 10^{-10}$ s have been omitted.

VALUE (10^{-10} s)	EVTS	DOCUMENT ID	TECN	COMMENT
1.479 ± 0.011 OUR AVERAGE				Error includes scale factor of 1.3. See the ideogram below.
1.480 ± 0.014	16k	MARRAFFINO 80	HBC	$K^- p$ 0.42–0.5 GeV/c
1.49 ± 0.03	8437	CONFORTO 76	HBC	$K^- p$ 1–1.4 GeV/c
1.463 ± 0.039	2400	ROBERTSON 72	HBC	$K^- p$ 0.25 GeV/c
1.42 ± 0.05	1383	BAKKER 71	DBC	$K^- N \rightarrow \Sigma^- \pi \pi$
1.41 +0.09 -0.08		TOVEE 71	EMUL	
1.485 ± 0.022	100k	EISELE 70	HBC	$K^- p$ at rest
1.472 ± 0.016	10k	BARLOUTAUD 69	HBC	$K^- p$ 0.4–1.2 GeV/c
1.38 ± 0.07	506	WHITESIDE 68	HBC	$K^- p$ at rest
1.666 ± 0.075	3267	¹ CHANG 66	HBC	$K^- p$ at rest
1.58 ± 0.06	1208	HUMPHREY 62	HBC	$K^- p$ at rest

¹ We have increased the CHANG 66 error of 0.026; see our 1970 edition, Reviews of Modern Physics 42 87 (1970).

WEIGHTED AVERAGE
 1.479 ± 0.011 (Error scaled by 1.3)

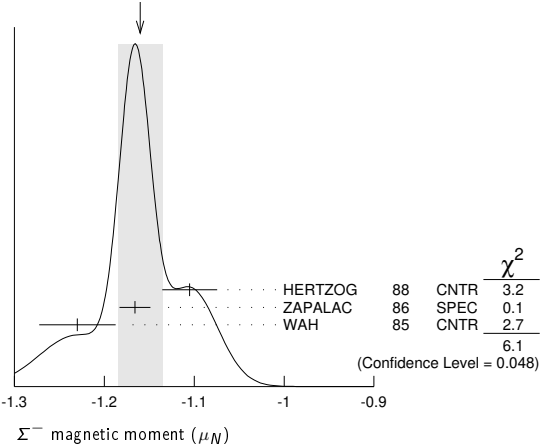


Σ^- MAGNETIC MOMENT

See the "Quark Model" review. Measurements with an error $\geq 0.3 \mu_N$ have been omitted.

VALUE (μ_N)	EVTS	DOCUMENT ID	TECN	COMMENT
-1.160 ± 0.025 OUR AVERAGE				Error includes scale factor of 1.7. See the ideogram below.
-1.105 ± 0.029 ± 0.010		HERTZOG 88	CNTR	Σ^- Pb, Σ^- W atoms
-1.166 ± 0.014 ± 0.010	671k	ZAPALAC 86	SPEC	$ne^- \nu, n\pi^-$ decays
-1.23 ± 0.03 ± 0.03		WAH 85	CNTR	$pCu \rightarrow \Sigma^- X$
• • • We do not use the following data for averages, fits, limits, etc. • • •				
-0.89 ± 0.14	516k	DECK 83	SPEC	$pBe \rightarrow \Sigma^- X$

WEIGHTED AVERAGE
 -1.160 ± 0.025 (Error scaled by 1.7)



Σ^- CHARGE RADIUS

VALUE (fm)	DOCUMENT ID	TECN	COMMENT
0.780 ± 0.080 ± 0.060	¹ ESCHRICH 01	SELX	$\Sigma^- e \rightarrow \Sigma^- e$
¹ ESCHRICH 01 actually gives $\langle r^2 \rangle = (0.61 \pm 0.12 \pm 0.09) \text{ fm}^2$.			

Σ^- DECAY MODES

Mode	Fraction (Γ_i/Γ)	Confidence level
Γ_1 $n\pi^-$	(99.848 ± 0.005) %	
Γ_2 $n\pi^- \gamma$	[a] (4.6 ± 0.6) × 10 ⁻⁴	
Γ_3 $n e^- \bar{\nu}_e$	(1.017 ± 0.034) × 10 ⁻³	
Γ_4 $n \mu^- \bar{\nu}_\mu$	(4.5 ± 0.4) × 10 ⁻⁴	
Γ_5 $\Lambda e^- \bar{\nu}_e$	(5.73 ± 0.27) × 10 ⁻⁵	
Γ_6 $\Sigma^+ X$	< 1.2	90%

Lepton number (L) violating modes

Γ_7 $p e^- e^-$	L	< 6.7	× 10 ⁻⁵	90%
------------------------	---	-------	--------------------	-----

[a] See the Listings below for the pion momentum range used in this measurement.

Baryon Particle Listings

Σ^-

CONSTRAINED FIT INFORMATION

An overall fit to 3 branching ratios uses 16 measurements and one constraint to determine 4 parameters. The overall fit has a $\chi^2 = 8.7$ for 13 degrees of freedom.

The following *off-diagonal* array elements are the correlation coefficients $\langle \delta x_i \delta x_j \rangle / (\delta x_i \delta x_j)$, in percent, from the fit to the branching fractions, $x_i \equiv \Gamma_i / \Gamma_{\text{total}}$. The fit constrains the x_i whose labels appear in this array to sum to one.

x_3	-64		
x_4	-77	0	
x_5	-5	0	0
	x_1	x_3	x_4

Σ^- BRANCHING RATIOS

$\Gamma(n\pi^- \gamma) / \Gamma(n\pi^-)$ Γ_2 / Γ_1
 The π^+ momentum cuts differ, so we do not average the results but simply use the latest value for the Summary Table.

VALUE (units 10^{-3})	EVTS	DOCUMENT ID	TECN	COMMENT
0.46 ± 0.06	292	EBENHOH 73	HBC	$\pi^+ < 150$ MeV/c
• • • We do not use the following data for averages, fits, limits, etc. • • •				
0.10 ± 0.02	23	ANG 69B	HBC	$\pi^- < 110$ MeV/c
~ 1.1		BAZIN 65B	HBC	$\pi^- < 166$ MeV/c

$\Gamma(n e^- \bar{\nu}_e) / \Gamma(n\pi^-)$ Γ_3 / Γ_1
 Measurements with an error $\geq 0.2 \times 10^{-3}$ have been omitted.

VALUE (units 10^{-3})	EVTS	DOCUMENT ID	TECN	COMMENT
1.019 ± 0.035				OUR FIT
$1.019^{+0.031}_{-0.040}$				OUR AVERAGE
0.96 ± 0.05	2847	BOURQUIN 83c	SPEC	SPS hyperon beam
$1.09^{+0.06}_{-0.08}$	601	¹ EBENHOH 74	HBC	$K^- p$ at rest
$1.05^{+0.07}_{-0.13}$	455	¹ SECHI-ZORN 73	HBC	$K^- p$ at rest
0.97 ± 0.15	57	COLE 71	HBC	$K^- p$ at rest
1.11 ± 0.09	180	BIERMAN 68	HBC	

¹ An additional negative systematic error is included for internal radiative corrections and latest form factors; see BOURQUIN 83c.

$\Gamma(n\mu^- \bar{\nu}_\mu) / \Gamma(n\pi^-)$ Γ_4 / Γ_1

VALUE (units 10^{-3})	EVTS	DOCUMENT ID	TECN	COMMENT
0.45 ± 0.04				OUR FIT
0.45 ± 0.04				OUR AVERAGE
0.38 ± 0.11	13	COLE 71	HBC	$K^- p$ at rest
0.43 ± 0.06	72	ANG 69	HBC	$K^- p$ at rest
0.43 ± 0.09	56	BAGGETT 69	HBC	$K^- p$ at rest
0.56 ± 0.20	11	BAZIN 65B	HBC	$K^- p$ at rest
0.66 ± 0.15	22	COURANT 64	HBC	

$\Gamma(\Lambda e^- \bar{\nu}_e) / \Gamma(n\pi^-)$ Γ_5 / Γ_1

VALUE (units 10^{-4})	EVTS	DOCUMENT ID	TECN	COMMENT
0.574 ± 0.027				OUR FIT
0.574 ± 0.027				OUR AVERAGE
0.561 ± 0.031	1620	¹ BOURQUIN 82	SPEC	SPS hyperon beam
0.63 ± 0.11	114	THOMPSON 80	ASPK	Hyperon beam
0.52 ± 0.09	31	BALTAY 69	HBC	$K^- p$ at rest
0.69 ± 0.12	31	EISELE 69	HBC	$K^- p$ at rest
0.64 ± 0.12	35	BARASH 67	HBC	$K^- p$ at rest
0.75 ± 0.28	11	COURANT 64	HBC	$K^- p$ at rest

¹ The value is from BOURQUIN 83B, and includes radiation corrections and new acceptance.

$\Gamma(\Sigma^+ X) / \Gamma_{\text{total}}$ Γ_6 / Γ

Here mode X can be any particle combination.

VALUE	CL%	DOCUMENT ID	TECN	COMMENT
$< 1.2 \times 10^{-4}$	90	ABLIKIM 21F	BES	1,311 M J/ψ decays

Lepton number (L) violating modes

$\Gamma(p e^- e^-) / \Gamma_{\text{total}}$ Γ_7 / Γ

This decay violates lepton number conservation with $\Delta Q = \Delta L = 2$.

VALUE	CL%	DOCUMENT ID	TECN	COMMENT
$< 6.7 \times 10^{-5}$	90	ABLIKIM 21F	BES	1,311 M J/ψ decays

Σ^- DECAY PARAMETERS

See the "Note on Baryon Decay Parameters" in the neutron Listings. Older, outdated results have been omitted.

α_- FOR $\Sigma^- \rightarrow n\pi^-$

VALUE	EVTS	DOCUMENT ID	TECN	COMMENT
-0.068 ± 0.008				OUR AVERAGE
-0.062 ± 0.024	28k	HANSL 78	HBC	$K^- p \rightarrow \Sigma^- \pi^+$
-0.067 ± 0.011	60k	BOGERT 70	HBC	$K^- p$ 0.4 GeV/c
-0.071 ± 0.012	51k	BANGERTER 69	HBC	$K^- p$ 0.4 GeV/c

ϕ ANGLE FOR $\Sigma^- \rightarrow n\pi^-$ $(\tan\phi = \beta / \gamma)$

VALUE (°)	EVTS	DOCUMENT ID	TECN	COMMENT
10 ± 15				OUR AVERAGE
$+5 \pm 23$	1092	¹ BERLEY 70B	HBC	n rescattering
14 ± 19	1385	BANGERTER 69B	HBC	$K^- p$ 0.4 GeV/c
¹ BERLEY 70B changed from -5 to $+5^\circ$ to agree with our sign convention.				

g_A/g_V FOR $\Sigma^- \rightarrow n e^- \bar{\nu}_e$

Measurements with fewer than 500 events have been omitted. Where necessary, signs have been changed to agree with our conventions, which are given in the "Note on Baryon Decay Parameters" in the neutron Listings. What is actually listed is $|g_1/f_1 - 0.237g_2/f_1|$. This reduces to $g_A/g_V \equiv g_1(0)/f_1(0)$ on making the usual assumption that $g_2 = 0$. See also the note on HSUEH 88.

VALUE	EVTS	DOCUMENT ID	TECN	COMMENT
0.340 ± 0.017				OUR AVERAGE
$+0.327 \pm 0.007 \pm 0.019$	50k	¹ HSUEH 88	SPEC	Σ^- 250 GeV
$+0.34 \pm 0.05$	4456	² BOURQUIN 83c	SPEC	SPS hyperon beam
0.385 ± 0.037	3507	³ TANENBAUM 74	ASPK	
• • • We do not use the following data for averages, fits, limits, etc. • • •				
0.29 ± 0.07	25k	HSUEH 85	SPEC	See HSUEH 88
$0.17^{+0.07}_{-0.09}$	519	DECAMP 77	ELEC	Hyperon beam

¹ The sign is, with our conventions, unambiguously positive. The value assumes, as usual, that $g_2 = 0$. If g_2 is included in the fit, than (with our sign convention) $g_2 = -0.56 \pm 0.37$, with a corresponding reduction of g_A/g_V to $+0.20 \pm 0.08$.

² BOURQUIN 83c favors the positive sign by at least 2.6 standard deviations.

³ TANENBAUM 74 gives 0.435 ± 0.035 , assuming no q^2 dependence in g_A and g_V . The listed result allows q^2 dependence, and is taken from HSUEH 88.

$f_2(0)/f_1(0)$ FOR $\Sigma^- \rightarrow n e^- \bar{\nu}_e$

The signs have been changed to be in accord with our conventions, given in the "Note on Baryon Decay Parameters" in the neutron Listings.

VALUE	EVTS	DOCUMENT ID	TECN	COMMENT
0.97 ± 0.14				OUR AVERAGE
$+0.96 \pm 0.07 \pm 0.13$	50k	HSUEH 88	SPEC	Σ^- 250 GeV
$+1.02 \pm 0.34$	4456	BOURQUIN 83c	SPEC	SPS hyperon beam

TRIPLE CORRELATION COEFFICIENT D for $\Sigma^- \rightarrow n e^- \bar{\nu}_e$

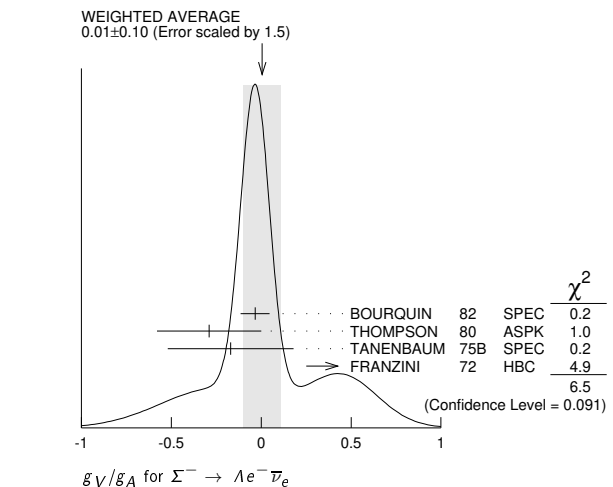
The coefficient D of the term $D \mathbf{P} \cdot (\hat{\mathbf{p}}_e \times \hat{\mathbf{p}}_\nu)$ in the $\Sigma^- \rightarrow n e^- \bar{\nu}_e$ decay angular distribution. A nonzero value would indicate a violation of time-reversal invariance.

VALUE	EVTS	DOCUMENT ID	TECN	COMMENT
0.11 ± 0.10	50k	HSUEH 88	SPEC	Σ^- 250 GeV

g_V/g_A FOR $\Sigma^- \rightarrow \Lambda e^- \bar{\nu}_e$

For the sign convention, see the "Note on Baryon Decay Parameters" in the neutron Listings. The value is predicted to be zero by conserved vector current theory. The values averaged assume CVC-SU(3) weak magnetism term.

VALUE	EVTS	DOCUMENT ID	TECN	COMMENT
0.01 ± 0.10				OUR AVERAGE
-0.034 ± 0.080	1620	¹ BOURQUIN 82	SPEC	SPS hyperon beam
-0.29 ± 0.29	114	THOMPSON 80	ASPK	BNL hyperon beam
-0.17 ± 0.35	55	TANENBAUM 75B	SPEC	BNL hyperon beam
$+0.45 \pm 0.20$	186	^{1,2} FRANZINI 72	HBC	



¹ The sign has been changed to agree with our convention.

Baryon Particle Listings
Sigma minus, Sigma (1385)

The FRANZINI 72 value includes the events of earlier papers.

gwm/ga FOR Sigma minus to Lambda e anti-nu_e

The values quoted assume the CVC prediction g_V = 0.

Table with columns: VALUE, EVTS, DOCUMENT ID, TECN, COMMENT. Contains data for various experiments like THOMPSON 80, TANENBAUM 75B, FRANZINI 72.

Sigma minus REFERENCES

We have omitted some papers that have been superseded by later experiments. See our earlier editions.

Large table of references for Sigma minus, listing authors, document IDs, and technical details.

Sigma (1385) plus -IMAGINARY PART

Table with columns: VALUE, DOCUMENT ID, COMMENT. Value: 17.5 +/- 1.5, Document: LICHTENBERG74.

Sigma (1385) minus REAL PART

Table with columns: VALUE, DOCUMENT ID, COMMENT. Value: 1383 +/- 1, Document: LICHTENBERG74.

Sigma (1385) minus -IMAGINARY PART

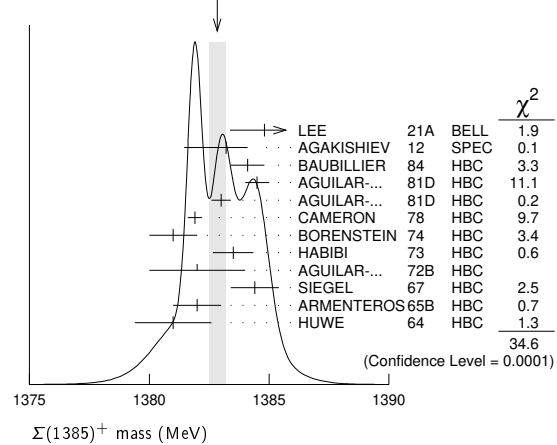
Table with columns: VALUE, DOCUMENT ID, COMMENT. Value: 22.5 +/- 1.5, Document: LICHTENBERG74.

Sigma (1385) MASSES

Sigma (1385) plus MASS

Table of Sigma (1385) plus masses from various experiments. Includes a weighted average plot and a list of excluded data points.

WEIGHTED AVERAGE 1382.83 +/- 0.34 (Error scaled by 1.9)



Sigma (1385) 3/2 plus

I(J^P) = 1(3/2+) Status: ***

Discovered by ALSTON 60. Early measurements of the mass and width for combined charge states have been omitted. They may be found in our 1984 edition Reviews of Modern Physics 56 S1 (1984).

We average only the most significant determinations. We do not average results from inclusive experiments with large backgrounds or results which are not accompanied by some discussion of experimental resolution. Nevertheless systematic differences between experiments remain. (See the ideograms in the Listings below.) These differences could arise from interference effects that change with production mechanism and/or beam momentum. They can also be accounted for in part by differences in the parametrizations employed. (See BORENSTEIN 74 for a discussion on this point.) Thus BORENSTEIN 74 uses a Breit-Wigner with energy-independent width, since a P-wave was found to give unsatisfactory fits. CAMERON 78 uses the same form. On the other hand HOLMGREN 77 obtains a good fit to their Lambda pi spectrum with a P-wave Breit-Wigner, but includes the partial width for the Sigma pi decay mode in the parametrization. AGUILAR-BENITEZ 81D gives masses and widths for five different Breit-Wigner shapes. The results vary considerably. Only the best-fit S-wave results are given here.

Sigma (1385) POLE POSITIONS

Sigma (1385) plus REAL PART

Table with columns: VALUE, DOCUMENT ID, COMMENT. Value: 1379 +/- 1, Document: LICHTENBERG74.

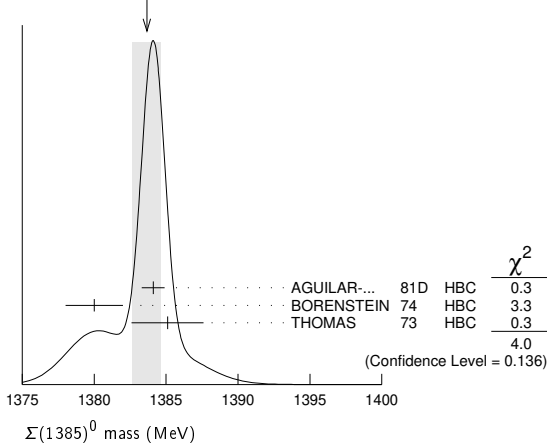
Sigma (1385) 0 MASS

Table of Sigma (1385) 0 masses from various experiments. Includes a weighted average and a list of excluded data points.

Baryon Particle Listings

$\Sigma(1385)$

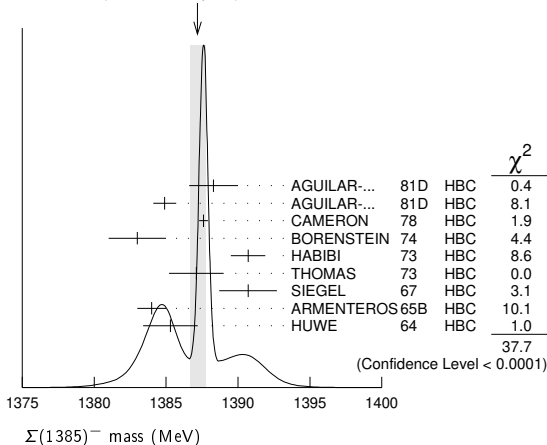
WEIGHTED AVERAGE
1383.7±1.0 (Error scaled by 1.4)



$\Sigma(1385)^-$ MASS

VALUE (MeV)	CL%	DOCUMENT ID	TECN	COMMENT
1387.2±0.5 OUR AVERAGE		Error includes scale factor of 2.2. See the ideogram below.		
1388.3±1.7	620	AGUILAR-...	81D	HBC $K^-p \rightarrow \Lambda\pi\pi$ 4.2 GeV/c
1384.9±0.8	3346	AGUILAR-...	81D	HBC $K^-p \rightarrow \Lambda^3\pi$ 4.2 GeV/c
1387.6±0.3	9720	CAMERON	78	HBC K^-p 0.96-1.36 GeV/c
1383 ± 2	2303	BORENSTEIN	74	HBC K^-p 2.18 GeV/c
1390.7±1.2	1900	HABIBI	73	HBC $K^-p \rightarrow \Lambda\pi\pi$
1387.1±1.9	630	4 THOMAS	73	HBC $\pi^-p \rightarrow \Lambda\pi^-K^+$
1390.7±2.0	370	SIEGEL	67	HBC K^-p 2.1 GeV/c
1384 ± 1	1380	ARMENTEROS65B	HBC	K^-p 0.9-1.2 GeV/c
1385.3±1.9	1086	4 HUWE	64	HBC K^-p 1.15-1.30 GeV/c
••• We do not use the following data for averages, fits, limits, etc. •••				
1383 ± 1	4.5k	1 BAUBILLIER	79B	HBC K^-p 8.25 GeV/c
1380 ± 6	150	1 SUGAHARA	79B	HBC π^-p 6 GeV/c
1387 ± 3	12k	1,2 BARREIRO	77B	HBC K^-p 4.2 GeV/c
1391 ± 3	193	HOLMGREN	77	HBC See AGUILAR-BENITEZ 81D
1383 ± 2		1 BARDADIN-...	75	HBC K^-p 14.3 GeV/c
1389 ± 1	3060	3 BERTHON	74	HBC K^-p 1263-1843 MeV/c
1389 ± 9	15	LONDON	66	HBC K^-p 2.24 GeV/c
1391.5±2.6	120	4 SMITH	65	HBC K^-p 1.8 GeV/c
1399.8±2.2	58	4 SMITH	65	HBC K^-p 1.95 GeV/c
1392.0±6.2	200	COOPER	64	HBC K^-p 1.45 GeV/c
1382 ± 3	93	DAHL	61	DBC K^-d 0.45 GeV/c
1376.0±4.4	224	4 ELY	61	HLBC K^-p 1.11 GeV/c

WEIGHTED AVERAGE
1387.2±0.5 (Error scaled by 2.2)



$m_{\Sigma(1385)^-} - m_{\Sigma(1385)^+}$

VALUE (MeV)	CL%	DOCUMENT ID	TECN	COMMENT
- 2 to +6	95	7 BORENSTEIN	74	HBC K^-p 2.18 GeV/c
7.2±1.4		7 HABIBI	73	HBC $K^-p \rightarrow \Lambda\pi\pi$
6.3±2.0		7 SIEGEL	67	HBC K^-p 2.1 GeV/c
11 ± 9		7 LONDON	66	HBC K^-p 2.24 GeV/c
9 ± 6		LONDON	66	HBC $\Lambda^3\pi$ events
2.0±1.5		7 ARMENTEROS65B	HBC	K^-p 0.9-1.2 GeV/c

7.2±2.1	7 SMITH	65	HBC	K^-p 1.8 GeV/c
17.2±2.0	7 SMITH	65	HBC	K^-p 1.95 GeV/c
17 ± 7	7 COOPER	64	HBC	K^-p 1.45 GeV/c
4.3±2.2	7 HUWE	64	HBC	K^-p 1.22 GeV/c
0.0±4.2	7 ELY	61	HLBC	K^-p 1.11 GeV/c

$m_{\Sigma(1385)^0} - m_{\Sigma(1385)^+}$

VALUE (MeV)	CL%	DOCUMENT ID	TECN	COMMENT
••• We do not use the following data for averages, fits, limits, etc. •••				
-4 to +4	95	7 BORENSTEIN	74	HBC K^-p 2.18 GeV/c

$m_{\Sigma(1385)^-} - m_{\Sigma(1385)^0}$

VALUE (MeV)	DOCUMENT ID	TECN	COMMENT
••• We do not use the following data for averages, fits, limits, etc. •••			
2.0±2.4	7 THOMAS	73	HBC $\pi^-p \rightarrow \Lambda\pi^-K^+$

$\Sigma(1385)$ WIDTHS

$\Sigma(1385)^+$ WIDTH

VALUE (MeV)	CL%	DOCUMENT ID	TECN	COMMENT
36.2± 0.7 OUR AVERAGE				
38.1± 1.5±2.1		LEE	21A	BELL $\Lambda^+ \rightarrow \eta\Sigma(1385)^+$
40.2± 2.1 ± 1.2 ± 2.8		AGAKISHIEV	12	SPEC $\rho p \rightarrow \Sigma(1385)^+ K^+ n$, 3.5 GeV
37.2± 2.0	1897	BAUBILLIER	84	HBC K^-p 8.25 GeV/c
35.1± 1.7	5256	AGUILAR-...	81D	HBC $K^-p \rightarrow \Lambda\pi\pi$ 4.2 GeV/c
37.5± 2.0	9361	AGUILAR-...	81D	HBC $K^-p \rightarrow \Lambda^3\pi$ 4.2 GeV/c
35.5± 1.9	6900	CAMERON	78	HBC K^-p 0.96-1.36 GeV/c
34.0± 1.6	6846	8 BORENSTEIN	74	HBC K^-p 2.18 GeV/c
38.3± 3.2	2300	9 HABIBI	73	HBC $K^-p \rightarrow \Lambda\pi\pi$
32.5± 6.0	400	AGUILAR-...	72B	HBC $K^-p \rightarrow \Lambda\pi's$
36 ± 4	1260	9 SIEGEL	67	HBC K^-p 2.1 GeV/c
32.0± 4.7	750	9 ARMENTEROS65B	HBC	K^-p 0.95-1.20 GeV/c
46.5± 6.4	859	9 HUWE	64	HBC K^-p 1.15-1.30 GeV/c
••• We do not use the following data for averages, fits, limits, etc. •••				
40 ± 3	600	BAKER	80	HYBR π^+p 7 GeV/c
37 ± 2	750	BAKER	80	HYBR K^-p 7 GeV/c
37 ± 2	7k	1 BAUBILLIER	79B	HBC K^-p 8.25 GeV/c
30 ± 4	2k	CAUTIS	79B	HYBR π^+p/K^-p 11.5 GeV
30 ± 6	100	1 SUGAHARA	79B	HBC π^-p 6 GeV/c
43 ± 5	22k	1,2 BARREIRO	77B	HBC K^-p 4.2 GeV/c
34 ± 2	2594	HOLMGREN	77	HBC See AGUILAR-BENITEZ 81D
40.0± 3.2		1 BARDADIN-...	75	HBC K^-p 14.3 GeV/c
48 ± 3	3740	3 BERTHON	74	HBC K^-p 1263-1843 MeV/c
33 ± 20	46	9 AGUILAR-...	70B	HBC $K^-p \rightarrow \Sigma\pi's$ 4 GeV/c
25 ± 32	62	9 BIRMINGHAM	66	HBC K^-p 3.5 GeV/c
30.3± 7.5	250	9 SMITH	65	HBC K^-p 1.8 GeV/c
33.1± 8.3	250	9 SMITH	65	HBC K^-p 1.95 GeV/c
51 ± 16	170	9 COOPER	64	HBC K^-p 1.45 GeV/c
48 ± 16	154	9 ELY	61	HLBC K^-p 1.11 GeV/c

$\Sigma(1385)^0$ WIDTH

VALUE (MeV)	CL%	DOCUMENT ID	TECN	COMMENT
36 ± 5 OUR AVERAGE				
34.8± 5.6	5722	AGUILAR-...	81D	HBC $K^-p \rightarrow \Lambda^3\pi$ 4.2 GeV/c
39.3±10.2	240	9 THOMAS	73	HBC $\pi^-p \rightarrow \Lambda\pi^0 K^0$
••• We do not use the following data for averages, fits, limits, etc. •••				
53 ± 8	3100	10 BORENSTEIN	74	HBC $K^-p \rightarrow \Lambda^3\pi$ 2.18 GeV/c
30 ± 9	106	CURTIS	63	OSPK π^-p 1.5 GeV/c

$\Sigma(1385)^-$ WIDTH

VALUE (MeV)	CL%	DOCUMENT ID	TECN	COMMENT
39.4± 2.1 OUR AVERAGE				
38.4±10.7	620	AGUILAR-...	81D	HBC $K^-p \rightarrow \Lambda\pi\pi$ 4.2 GeV/c
34.6± 4.2	3346	AGUILAR-...	81D	HBC $K^-p \rightarrow \Lambda^3\pi$ 4.2 GeV/c
39.2± 1.7	9720	CAMERON	78	HBC K^-p 0.96-1.36 GeV/c
35 ± 3	2303	8 BORENSTEIN	74	HBC K^-p 2.18 GeV/c
51.9± 4.8	1900	9 HABIBI	73	HBC $K^-p \rightarrow \Lambda\pi\pi$
48.2± 7.7	630	9 THOMAS	73	HBC $\pi^-p \rightarrow \Lambda\pi^-K^0$
31.0± 6.5	370	9 SIEGEL	67	HBC K^-p 2.1 GeV/c
38.0± 4.1	1382	9 ARMENTEROS65B	HBC	K^-p 0.95-1.20 GeV/c
62 ± 7	1086	HUWE	64	HBC K^-p 1.15-1.30 GeV/c
••• We do not use the following data for averages, fits, limits, etc. •••				
44 ± 4	4.5k	1 BAUBILLIER	79B	HBC K^-p 8.25 GeV/c
58 ± 4	150	1 SUGAHARA	79B	HBC π^-p 6 GeV/c
45 ± 5	12k	1,2 BARREIRO	77B	HBC K^-p 4.2 GeV/c
35 ± 10	193	HOLMGREN	77	HBC See AGUILAR-BENITEZ 81D
47 ± 6		1 BARDADIN-...	75	HBC K^-p 14.3 GeV/c
40 ± 3	3060	3 BERTHON	74	HBC K^-p 1263-1843 MeV/c

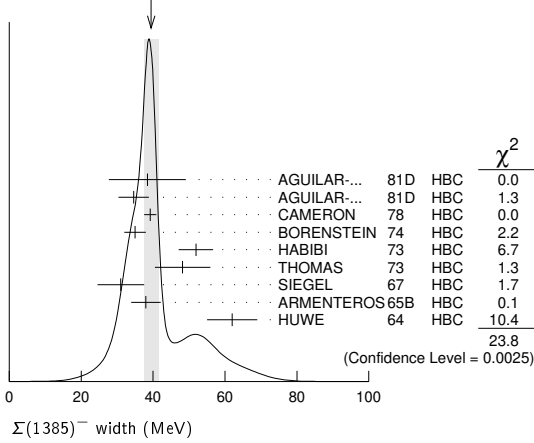
See key on page 1127

Baryon Particle Listings

$\Sigma(1385), \Sigma(1580)$

29.2±10.6	120	⁹ SMITH	65	HBC	K^-p 1.80 GeV/c
17.1± 8.9	58	⁹ SMITH	65	HBC	K^-p 1.95 GeV/c
88 ±24	200	⁹ COOPER	64	HBC	K^-p 1.45 GeV/c
40		DAHL	61	DBC	K^-d 0.45 GeV/c
66 ±18	224	⁹ ELY	61	HLBC	K^-p 1.11 GeV/c

WEIGHTED AVERAGE
39.4±2.1 (Error scaled by 1.7)



$\Sigma(1385)$ DECAY MODES

Mode	Fraction (Γ_i/Γ)	Confidence level
Γ_1 $\Lambda\pi$	(87.0 ± 1.5) %	
Γ_2 $\Sigma\pi$	(11.7 ± 1.5) %	
Γ_3 $\Lambda\gamma$	(1.25 ^{+0.13} _{-0.12}) %	
Γ_4 $\Sigma^+\gamma$	(7.0 ± 1.7) × 10 ⁻³	
Γ_5 $\Sigma^-\gamma$	< 2.4 × 10 ⁻⁴	90%
Γ_6 $N\bar{K}$		

$\Sigma(1385)$ BRANCHING RATIOS

$\Gamma(\Sigma\pi)/\Gamma(\Lambda\pi)$	DOCUMENT ID	TECN	CHG	COMMENT	Γ_2/Γ_1
0.135 ± 0.011 OUR AVERAGE					
0.20 ± 0.06	DIONISI 78B	HBC	±	$K^-p \rightarrow Y^* K\bar{K}$	
0.16 ± 0.03	BERTHON 74	HBC	±	K^-p 1.26–1.84 GeV/c	
0.11 ± 0.02	BERTHON 74	HBC	−	K^-p 1.26–1.84 GeV/c	
0.21 ± 0.05	BORENSTEIN 74	HBC	+	$K^-p \rightarrow \Lambda\pi^+\pi^-$, $\Sigma^0\pi^+\pi^-$	
0.18 ± 0.04	MAST 73	MPWA	±	$K^-p \rightarrow \Lambda\pi^+\pi^-$, $\Sigma^0\pi^+\pi^-$	
0.10 ± 0.05	THOMAS 73	HBC	−	$\pi^-p \rightarrow \Lambda K\pi, \Sigma K\pi$	
0.16 ± 0.07	AGUILAR... 72B	HBC	+	K^-p 3.9, 4.6 GeV/c	
0.13 ± 0.04	COLLEY 71B	DBC	−0	K^-N 1.5 GeV/c	
0.13 ± 0.04	PAN 69	HBC	+	$\pi^+p \rightarrow \Lambda K\pi, \Sigma K\pi$	
0.08 ± 0.06	LONDON 66	HBC	+	K^-p 2.24 GeV/c	
0.163±0.041	ARMENTEROS65B	HBC	±	K^-p 0.95–1.20 GeV/c	
0.09 ± 0.04	HUWE 64	HBC	±	K^-p 1.2–1.7 GeV	
••• We do not use the following data for averages, fits, limits, etc. •••					
<0.04	ALSTON 62	HBC	±	K^-p 1.15 GeV/c	
0.04 ± 0.04	BASTIEN 61	HBC	±		

$\Gamma(\Lambda\gamma)/\Gamma(\Lambda\pi)$ Γ_3/Γ_1

This ratio is of course for $\Sigma(1385)^0 \rightarrow \Lambda\gamma$ and $\Lambda\pi^0$.

VALUE (units 10 ⁻²)	EVTS	DOCUMENT ID	TECN	COMMENT
1.43^{+0.15}_{-0.13} OUR AVERAGE				
1.42±0.12 ^{+0.11} _{-0.07}	624 ± 25	KELLER 11	CLAS	$\gamma p \rightarrow K^+\Lambda\gamma, E_\gamma$ 1.6–3.8 GeV
1.53±0.39 ^{+0.15} _{-0.24}	61	TAYLOR 05	CLAS	$\gamma p \rightarrow K^+\Lambda\gamma$

$\Gamma(\Sigma^+\gamma)/\Gamma(\Sigma\pi)$ Γ_4/Γ_2

This ratio is for $\Sigma(1385)^+ \rightarrow \Sigma^+\gamma$ over $\Sigma(1385)^+ \rightarrow \Sigma\pi$.

VALUE (%)	DOCUMENT ID	TECN	COMMENT
5.98±1.11^{+0.27}_{-0.61}	11 KELLER 12	CLAS	$\gamma p \rightarrow K^0\Sigma(1385)^+$

$\Gamma(\Sigma^-\gamma)/\Gamma_{total}$ Γ_5/Γ

VALUE	CL%	DOCUMENT ID	TECN	CHG	COMMENT
<2.4 × 10⁻⁴	90	12 MOLCHANOV 04	SELX	−	$\Sigma^-Pb \rightarrow \Sigma(1385)^-$ Pb, 600 GeV
••• We do not use the following data for averages, fits, limits, etc. •••					
<6.1 × 10 ⁻⁴	90	13 ARIK 77	SPEC	−	$\Sigma^-Pb \rightarrow \Sigma(1385)^-$ Pb, 23 GeV

$(\Gamma_i/\Gamma)_{1/2}/\Gamma_{total}$ in $N\bar{K} \rightarrow \Sigma(1385) \rightarrow \Lambda\pi$	DOCUMENT ID	CHG	COMMENT	$(\Gamma_6/\Gamma_1)_{1/2}/\Gamma$
0.586±0.319	14 DEVENISH 74B	0	Fixed- t dispersion rel.	

$\Sigma(1385)$ FOOTNOTES

- From fit to inclusive $\Lambda\pi$ spectrum.
- Includes data of HOLMGREN 77.
- The errors are statistical only. The resolution is not unfolded.
- The error is enlarged to Γ/\sqrt{N} . See the note on the $K^*(892)$ mass in the 1984 edition.
- From a fit to $\Lambda\pi^0$ with the width fixed at 34 MeV.
- From fit to inclusive $\Lambda\pi^0$ spectrum with the width fixed at 40 MeV.
- Redundant with data in the mass Listings.
- Results from $\Lambda\pi^+\pi^-$ and $\Lambda\pi^+\pi^-\pi^0$ combined by us.
- The error is enlarged to $4\Gamma/\sqrt{N}$. See the note on the $K^*(892)$ mass in the 1984 edition.
- Consistent with +, 0, and − widths equal.
- KELLER 12 gives $\Gamma(\Sigma^+\gamma)/\Gamma(\Sigma^+\pi^0) = (11.95 \pm 2.21_{-1.21})\%$, using 1/2 our total $\Sigma(1385) \rightarrow \Sigma\pi$ fraction for $\Sigma^+\pi^0$. We divide the KELLER 12 value by two.
- We calculate this from the MOLCHANOV 04 upper limit of 9.5 keV on the $\Sigma^-\gamma$ width.
- We calculate this from the ARIK 77 upper limit of 24 keV on the $\Sigma^-\gamma$ width.
- An extrapolation of the parametrized amplitude below threshold.

$\Sigma(1385)$ REFERENCES

LEE 21A	PR D103 052005	J.Y. Lee et al.	(BELLE Collab.)
AGAKISHIEV 12	PR C85 035203	G. Agakishiev et al.	(HADES Collab.)
KELLER 12	PR D85 052004	D. Keller et al.	(JLab CLAS Collab.)
KELLER 11	PR D83 072004	D. Keller et al.	(JLab CLAS Collab.)
TAYLOR 05	PR C71 054609	S. Taylor et al.	(JLab CLAS Collab.)
Also	PR C72 039902 (err.)	S. Taylor et al.	(JLab CLAS Collab.)
MOLCHANOV 04	PL B590 1611	V.V. Molchanov et al.	(FNAL SELEX Collab.)
BAUBILLIER 84	ZPHY C23 213	M. Baubillier et al.	(BIRM, CERN, GLAS+)
PDG 84	RMP 56 51	C.G. Wohl et al.	(LBL, CIT, CERN)
AGUILAR... 81D	AFIS A77 144	M. Aguilar-Benitez, J. Salicio	(MADR)
BAKER 80	NP B166 207	P.A. Baker et al.	(LOIC)
BAUBILLIER 79B	NP B148 18	M. Baubillier et al.	(BIRM, CERN, GLAS+)
CAUTIS 79	NP B156 507	C.V. Cautis et al.	(SLAC)
SUGAHARA 79B	NP B156 237	R. Sugahara et al.	(KEK, OSKC, KINK)
CAMERON 78	NP B143 189	W. Cameron et al.	(RHEL, LOIC)
DIONISI 78B	PL 78B 154	C. Dionisi, R. Armenteros, J. Diaz	(CERN, AMST+)
ARIK 77	PRL 38 1000	E. Arik et al.	(PITT, BNL, MASA)
BARREIRO 77B	NP B126 319	F. Barreiro et al.	(CERN, AMST, NIM)
HOLMGREN 77	NP B119 261	S.O. Holmgren et al.	(CERN, AMST, NIM)
BARADIN... 75	NP B98 418	M. Baradin-Owinowska et al.	(SACL, EPOL+)
BERTHON 74	NC 21A 146	A. Berthon et al.	(CDEF, RHEL, SACL+)
BORENSTEIN 74	PR D9 3006	S.R. Borenstein et al.	(BNL, MICH)
DEVENISH 74B	NP B81 330	R.C.E. Devenish, C.D. Froggatt, B.R. Martin	(DESY+)
LICHTENBERG 74	PR D10 3865	D.B. Lichtenberg	(IND)
Also	Private Comm.	D.B. Lichtenberg	(IND)
HABIBI 73	Thesis Nevis 199	M. Habibi	(COLU)
Also	Purdue Conf. 387	C. Ballay et al.	(COLU, BING)
MAST 73	PR DT 3212	T.S. Mast et al.	(LBL) JIP
Also	PR D7 5	T.S. Mast et al.	(LBL) JIP
THOMAS 73	NP B56 15	D.W. Thomas et al.	(CMU) JIP
AGUILAR... 72B	PR D6 29	M. Aguilar-Benitez et al.	(BNL)
COLLEY 71B	NP B31 61	D.C. Colley et al.	(BIRM, EDIN, GLAS+)
AGUILAR... 70B	PRL 25 58	M. Aguilar-Benitez et al.	(BNL, SYRA)
PAN 69	PRL 23 808	Y.L. Pan, F.L. Forman	(PENN) I
SIEGEL 67	Thesis UCRL 18041	D.M. Siegel	(IND)
BIRMINGHAM 66	PR 152 1148	M. Haque et al.	(BIRM, GLAS, LOIC, OXF+)
LONDON 66	PR 143 1034	G.W. London et al.	(BNL, SYRA) J
ARMENTEROS 65B	PL 19 75	R. Armenteros et al.	(CERN, HEID, SACL)
SMITH 65	Thesis UCLA	L.T. Smith	(UCLA)
COOPER 64	PL 8 365	N.W.A. Cooper et al.	(CERN, AMST)
HUWE 64	Thesis UCRL 11291	D.O. Huwe	(LRL) JIP
Also	PR 181 1824	D.O. Huwe	(LRL)
CURTIS 63	PR 132 1771	L.J. Curtis et al.	(MICH) J
ALSTON 62	CERN Conf. 311	M.H. Alston et al.	(LRL)
BASTIEN 61	PRL 6 702	P.L. Bastien, M. Ferro-Luzzi, A.H. Rosenfeld	(LRL)
DAHL 61	PRL 6 142	O.I. Dahl et al.	(LRL)
ELY 61	PRL 7 461	R.P. Ely et al.	(LRL) J
ALSTON 60	PRL 5 520	M.H. Alston et al.	(LRL) I

$\Sigma(1580) 3/2^-$

$$J(P) = 1(\frac{3}{2}^-) \text{ Status: } *$$

OMITTED FROM SUMMARY TABLE

Seen in the isospin-1 $\bar{K}N$ cross section at BNL (LI 73, CARROLL 76) and in a partial-wave analysis of $K^-p \rightarrow \Lambda\pi^0$ for c.m. energies 1560–1600 MeV by LITCHFIELD 74. LITCHFIELD 74 finds $J^P = 3/2^-$. Not seen by ENGLER 78, CAMERON 78C, OLMSTED 04, nor by PRAKHOV 04.

Neither ZHANG 13A nor SARANTSEV 19 see any evidence for this state.

$\Sigma(1580)$ POLE POSITION

REAL PART

VALUE (MeV)	DOCUMENT ID	TECN	COMMENT
••• We do not use the following data for averages, fits, limits, etc. •••			
1607 ⁺¹³ ₋₁₁	1 KAMANO 15	DPWA	Multichannel

¹ From the preferred solution A in KAMANO 15. Solution B reports $M = 1492 \pm 4$ MeV.

-2xIMAGINARY PART

VALUE (MeV)	DOCUMENT ID	TECN	COMMENT
••• We do not use the following data for averages, fits, limits, etc. •••			
253 ⁺³⁰ ₋₁₈	2 KAMANO 15	DPWA	Multichannel

² From the preferred solution A in KAMANO 15. Solution B reports $M = 138 \pm 8$ MeV.

Baryon Particle Listings

 $\Sigma(1580), \Sigma(1620)$ $\Sigma(1580)$ POLE RESIDUES

The "normalized residue" is the residue divided by $\Gamma_{pole}/2$.

Normalized residue in $N\bar{K} \rightarrow \Sigma(1580) \rightarrow N\bar{K}$

MODULUS	PHASE ($^\circ$)	DOCUMENT ID	TECN	COMMENT
0.00778	51	³ KAMANO	15	DPWA Multichannel
³ From the preferred solution A in KAMANO 15.				

Normalized residue in $N\bar{K} \rightarrow \Sigma(1580) \rightarrow \Sigma\pi$

MODULUS	PHASE ($^\circ$)	DOCUMENT ID	TECN	COMMENT
0.0625	-6	⁴ KAMANO	15	DPWA Multichannel
⁴ From the preferred solution A in KAMANO 15.				

Normalized residue in $N\bar{K} \rightarrow \Sigma(1580) \rightarrow \Lambda\pi$

MODULUS	PHASE ($^\circ$)	DOCUMENT ID	TECN	COMMENT
0.059	156	⁵ KAMANO	15	DPWA Multichannel
⁵ From the preferred solution A in KAMANO 15.				

Normalized residue in $N\bar{K} \rightarrow \Sigma(1580) \rightarrow \Sigma(1385)\pi, S\text{-wave}$

MODULUS	PHASE ($^\circ$)	DOCUMENT ID	TECN	COMMENT
0.0368	-18	⁶ KAMANO	15	DPWA Multichannel
⁶ From the preferred solution A in KAMANO 15.				

Normalized residue in $N\bar{K} \rightarrow \Sigma(1580) \rightarrow \Sigma(1385)\pi, D\text{-wave}$

MODULUS	PHASE ($^\circ$)	DOCUMENT ID	TECN	COMMENT
0.0103	123	⁷ KAMANO	15	DPWA Multichannel
⁷ From the preferred solution A in KAMANO 15.				

 $\Sigma(1580)$ MASS

VALUE (MeV)	DOCUMENT ID	TECN	COMMENT
≈ 1580 OUR ESTIMATE			
1583 \pm 4	⁸ CARROLL	76	DPWA Isospin-1 total σ
1582 \pm 4	⁹ LITCHFIELD	74	DPWA $K^- p \rightarrow \Lambda\pi^0$
⁸ CARROLL 76 sees a total-cross-section bump with $(J+1/2) \Gamma_{el} / \Gamma_{total} = 0.06$.			
⁹ The main effect observed by LITCHFIELD 74 is in the $\Lambda\pi$ final state; the $\bar{K}N$ and $\Sigma\pi$ couplings are estimated from a multichannel fit including total-cross-section data of LI 73.			

 $\Sigma(1580)$ WIDTH

VALUE (MeV)	DOCUMENT ID	TECN	COMMENT
15	¹⁰ CARROLL	76	DPWA Isospin-1 total σ
11 \pm 4	¹¹ LITCHFIELD	74	DPWA $K^- p \rightarrow \Lambda\pi^0$
¹⁰ CARROLL 76 sees a total-cross-section bump with $(J+1/2) \Gamma_{el} / \Gamma_{total} = 0.06$.			
¹¹ The main effect observed by LITCHFIELD 74 is in the $\Lambda\pi$ final state; the $\bar{K}N$ and $\Sigma\pi$ couplings are estimated from a multichannel fit including total-cross-section data of LI 73.			

 $\Sigma(1580)$ DECAY MODES

Mode
Γ_1 $N\bar{K}$
Γ_2 $\Lambda\pi$
Γ_3 $\Sigma\pi$
Γ_4 $\Sigma(1385)\pi, S\text{-wave}$
Γ_5 $\Sigma(1385)\pi, D\text{-wave}$
Γ_6 $N\bar{K}^*(892), S=1/2, D\text{-wave}$
Γ_7 $N\bar{K}^*(892), S=3/2, S\text{-wave}$
Γ_8 $N\bar{K}^*(892), S=3/2, D\text{-wave}$

 $\Sigma(1580)$ BRANCHING RATIOS

See "Sign conventions for resonance couplings" in the Note on Λ and Σ Resonances.

$\Gamma(N\bar{K})/\Gamma_{total}$	DOCUMENT ID	TECN	COMMENT	Γ_1/Γ
$+0.03 \pm 0.01$	¹² LITCHFIELD	74	DPWA $\bar{K}N$ multichannel	
• • • We do not use the following data for averages, fits, limits, etc. • • •				
0.003	¹³ KAMANO	15	DPWA Multichannel	
¹² The main effect observed by LITCHFIELD 74 is in the $\Lambda\pi$ final state; the $\bar{K}N$ and $\Sigma\pi$ couplings are estimated from a multichannel fit including total-cross-section data of LI 73.				
¹³ From the preferred solution A in KAMANO 15.				

 $\Gamma(\Lambda\pi)/\Gamma_{total}$

VALUE	DOCUMENT ID	TECN	COMMENT	Γ_2/Γ
0.490	¹⁴ KAMANO	15	DPWA Multichannel	
¹⁴ From the preferred solution A in KAMANO 15.				

 $\Gamma(\Sigma\pi)/\Gamma_{total}$

VALUE	DOCUMENT ID	TECN	COMMENT	Γ_3/Γ
0.387	¹⁵ KAMANO	15	DPWA Multichannel	
¹⁵ From the preferred solution A in KAMANO 15.				

 $\Gamma(\Sigma(1385)\pi, S\text{-wave})/\Gamma_{total}$

VALUE	DOCUMENT ID	TECN	COMMENT	Γ_4/Γ
0.12	¹⁶ KAMANO	15	DPWA Multichannel	
¹⁶ From the preferred solution A in KAMANO 15.				

 $\Gamma(\Sigma(1385)\pi, D\text{-wave})/\Gamma_{total}$

VALUE	DOCUMENT ID	TECN	COMMENT	Γ_5/Γ
0.001	¹⁷ KAMANO	15	DPWA Multichannel	
¹⁷ From the preferred solution A in KAMANO 15.				

 $\Gamma(N\bar{K}^*(892), S=1/2, D\text{-wave})/\Gamma_{total}$

VALUE	DOCUMENT ID	TECN	COMMENT	Γ_6/Γ
not seen	¹⁸ KAMANO	15	DPWA Multichannel	
¹⁸ From the preferred solution A in KAMANO 15.				

 $\Gamma(N\bar{K}^*(892), S=3/2, S\text{-wave})/\Gamma_{total}$

VALUE	DOCUMENT ID	TECN	COMMENT	Γ_7/Γ
not seen	¹⁹ KAMANO	15	DPWA Multichannel	
¹⁹ From the preferred solution A in KAMANO 15.				

 $\Gamma(N\bar{K}^*(892), S=3/2, D\text{-wave})/\Gamma_{total}$

VALUE	DOCUMENT ID	TECN	COMMENT	Γ_8/Γ
not seen	²⁰ KAMANO	15	DPWA Multichannel	
²⁰ From the preferred solution A in KAMANO 15.				

 $(\Gamma_1\Gamma_2)^{1/2}/\Gamma_{total}$ in $N\bar{K} \rightarrow \Sigma(1580) \rightarrow \Lambda\pi$

VALUE	DOCUMENT ID	TECN	COMMENT	$(\Gamma_1\Gamma_2)^{1/2}/\Gamma$
not seen	CAMERON	78C	HBC $K_L^0 p \rightarrow \Lambda\pi^+$	
not seen	ENGLER	78	HBC $K_L^0 p \rightarrow \Lambda\pi^+$	
$+0.10 \pm 0.02$	²¹ LITCHFIELD	74	DPWA $K^- p \rightarrow \Lambda\pi^0$	

²¹ The main effect observed by LITCHFIELD 74 is in the $\Lambda\pi$ final state; the $\bar{K}N$ and $\Sigma\pi$ couplings are estimated from a multichannel fit including total-cross-section data of LI 73.

 $(\Gamma_1\Gamma_3)^{1/2}/\Gamma_{total}$ in $N\bar{K} \rightarrow \Sigma(1580) \rightarrow \Sigma\pi$

VALUE	DOCUMENT ID	TECN	COMMENT	$(\Gamma_1\Gamma_3)^{1/2}/\Gamma$
not seen	CAMERON	78C	HBC $K_L^0 p \rightarrow \Sigma^0\pi^+$	
not seen	ENGLER	78	HBC $K_L^0 p \rightarrow \Sigma^0\pi^+$	
$+0.03 \pm 0.04$	²² LITCHFIELD	74	DPWA $\bar{K}N$ multichannel	

²² The main effect observed by LITCHFIELD 74 is in the $\Lambda\pi$ final state; the $\bar{K}N$ and $\Sigma\pi$ couplings are estimated from a multichannel fit including total-cross-section data of LI 73.

 $\Sigma(1580)$ REFERENCES

SARANTSEV	19	EPJ A55 180	A.V. Sarantsev et al.	(BONN, PNPI)
KAMANO	15	PR C92 025205	H. Kamano et al.	(ANL, OSAK)
ZHANG	13A	PR C88 035205	H. Zhang et al.	(KSU)
OLMSTED	04	PL B588 29	J. Olmsted et al.	(BNL Crystal Ball Collab.)
PRAKHOV	04	PR C69 042202	S. Prakhov et al.	(BNL Crystal Ball Collab.)
CAMERON	78C	NP B132 189	W. Cameron et al.	(BGNA, EDIN, GLAS-1)
ENGLER	78	PR D18 3061	A. Engler et al.	(CMU, ANL)
CARROLL	76	PRL 37 806	A.S. Carroll et al.	(BNL)1
LITCHFIELD	74	PL 51B 509	P.J. Litchfield	(CERN)1P
LI	73	Purdue Conf. 283	K.K. Li	(BNL)1

 $\Sigma(1620) 1/2^-$

$$I(J^P) = 1(\frac{1}{2}^-) \text{ Status: *}$$

OMITTED FROM SUMMARY TABLE

The S_{11} state at 1697 MeV reported by VANHORN 75 is tentatively listed under the $\Sigma(1750)$. CARROLL 76 sees two bumps in the isospin-1 total cross section near this mass. GAO 12 sees no evidence for this resonance.

Production experiments are listed separately in the next entry.

Baryon Particle Listings
 $\Sigma(1620), \Sigma(1660)$

$\Sigma(1620)$ POLE POSITION

REAL PART			
VALUE (MeV)	DOCUMENT ID	TECN	COMMENT
1680 ± 8	SARANTSEV 19	DPWA	$\bar{K}N$ multichannel
• • • We do not use the following data for averages, fits, limits, etc. • • •			
1501	ZHANG 13A	DPWA	$\bar{K}N$ multichannel
-2xIMAGINARY PART			
VALUE (MeV)	DOCUMENT ID	TECN	COMMENT
39 ± 11	SARANTSEV 19	DPWA	$\bar{K}N$ multichannel
• • • We do not use the following data for averages, fits, limits, etc. • • •			
171	ZHANG 13A	DPWA	$\bar{K}N$ multichannel

$\Sigma(1620)$ POLE RESIDUE

The "normalized residue" is the residue divided by $\Gamma_{pole}/2$.

Normalized residue in $N\bar{K} \rightarrow \Sigma(1620) \rightarrow \Sigma\pi$			
MODULUS	PHASE (°)	DOCUMENT ID	TECN COMMENT
0.14 ± 0.03	-90 ± 25	SARANTSEV 19	DPWA $\bar{K}N$ multichannel
Normalized residue in $N\bar{K} \rightarrow \Sigma(1620) \rightarrow \Lambda\pi$			
MODULUS	PHASE (°)	DOCUMENT ID	TECN COMMENT
0.10 ± 0.03	75 ± 20	SARANTSEV 19	DPWA $\bar{K}N$ multichannel
Normalized residue in $N\bar{K} \rightarrow \Sigma(1620) \rightarrow \Xi K$			
MODULUS	PHASE (°)	DOCUMENT ID	TECN COMMENT
0.02 ± 0.01	120 ± 20	SARANTSEV 19	DPWA $\bar{K}N$ multichannel
Normalized residue in $N\bar{K} \rightarrow \Sigma(1620) \rightarrow \Lambda(1520)\pi$			
MODULUS	PHASE (°)	DOCUMENT ID	TECN COMMENT
0.12 ± 0.05	140 ± 40	SARANTSEV 19	DPWA $\bar{K}N$ multichannel
Normalized residue in $N\bar{K} \rightarrow \Sigma(1620) \rightarrow \Sigma(1385)\pi$			
MODULUS	PHASE (°)	DOCUMENT ID	TECN COMMENT
0.015 ± 0.010	155 ± 40	SARANTSEV 19	DPWA $\bar{K}N$ multichannel
Normalized residue in $N\bar{K} \rightarrow \Sigma(1620) \rightarrow N\bar{K}^*(892), S\text{-wave}$			
MODULUS	PHASE (°)	DOCUMENT ID	TECN COMMENT
0.05 ± 0.04		SARANTSEV 19	DPWA $\bar{K}N$ multichannel
Normalized residue in $N\bar{K} \rightarrow \Sigma(1620) \rightarrow N\bar{K}^*(892), D\text{-wave}$			
MODULUS	PHASE (°)	DOCUMENT ID	TECN COMMENT
0.01 ± 0.01		SARANTSEV 19	DPWA $\bar{K}N$ multichannel
Normalized residue in $N\bar{K} \rightarrow \Sigma(1620) \rightarrow N\bar{K}$			
VALUE	DOCUMENT ID	TECN	COMMENT
0.11 + 0.03 - 0.43 + 20	SARANTSEV 19	DPWA	$\bar{K}N$ multichannel

$\Sigma(1620)$ MASS

VALUE (MeV)	DOCUMENT ID	TECN	COMMENT
1600 to 1650 (≈ 1620) OUR ESTIMATE			
1681 ± 6	SARANTSEV 19	DPWA	$\bar{K}N$ multichannel
1600 ± 15	ZHANG 13A	DPWA	$\bar{K}N$ multichannel
1600 ± 6	¹ MORRIS 78	DPWA	$K^- n \rightarrow \Lambda\pi^-$
1608 ± 5	² CARROLL 76	DPWA	Isospin-1 total σ
1630 ± 10	LANGBEIN 72	IPWA	$\bar{K}N$ multichannel
1620	KIM 71	DPWA	K-matrix analysis
• • • We do not use the following data for averages, fits, limits, etc. • • •			
1633 ± 10	³ CARROLL 76	DPWA	Isospin-1 total σ

$\Sigma(1620)$ WIDTH

VALUE (MeV)	DOCUMENT ID	TECN	COMMENT
40 to 100 (≈ 70) OUR ESTIMATE			
40 ± 12	SARANTSEV 19	DPWA	$\bar{K}N$ multichannel
400 ± 152	ZHANG 13A	DPWA	$\bar{K}N$ multichannel
87 ± 19	¹ MORRIS 78	DPWA	$K^- n \rightarrow \Lambda\pi^-$
15	² CARROLL 76	DPWA	Isospin-1 total σ
65 ± 20	LANGBEIN 72	IPWA	$\bar{K}N$ multichannel
40	KIM 71	DPWA	K-matrix analysis
• • • We do not use the following data for averages, fits, limits, etc. • • •			
10	³ CARROLL 76	DPWA	Isospin-1 total σ

$\Sigma(1620)$ DECAY MODES

Mode	Fraction (Γ_i/Γ)
Γ_1 $N\bar{K}$	0.10 to 0.60
Γ_2 $\Lambda\pi$	(9.0 ± 3.0) %
Γ_3 $\Sigma\pi$	(17 ± 5) %
Γ_4 ΞK	
Γ_5 $\Lambda(1520)\pi$	(10 ± 5) %
Γ_6 $\Sigma(1385)\pi$	

$\Sigma(1620)$ BRANCHING RATIOS

$\Gamma(N\bar{K})/\Gamma_{total}$	Γ_1/Γ
VALUE	DOCUMENT ID TECN COMMENT
0.10 to 0.60 OUR ESTIMATE	
0.11 ± 0.03	SARANTSEV 19 DPWA $\bar{K}N$ multichannel
0.59 ± 0.10	ZHANG 13A DPWA $\bar{K}N$ multichannel
0.22 ± 0.02	LANGBEIN 72 IPWA $\bar{K}N$ multichannel
0.05	KIM 71 DPWA K-matrix analysis
$\Gamma(\Sigma\pi)/\Gamma_{total}$	Γ_3/Γ
VALUE	DOCUMENT ID TECN COMMENT
0.17 ± 0.05	SARANTSEV 19 DPWA $\bar{K}N$ multichannel
$\Gamma(\Lambda\pi)/\Gamma_{total}$	Γ_2/Γ
VALUE	DOCUMENT ID TECN COMMENT
0.09 ± 0.03	SARANTSEV 19 DPWA $\bar{K}N$ multichannel
$\Gamma(\Xi K)/\Gamma_{total}$	Γ_4/Γ
VALUE	DOCUMENT ID TECN COMMENT
~ 0	SARANTSEV 19 DPWA $\bar{K}N$ multichannel
$\Gamma(\Lambda(1520)\pi)/\Gamma_{total}$	Γ_5/Γ
VALUE	DOCUMENT ID TECN COMMENT
0.10 ± 0.05	SARANTSEV 19 DPWA $\bar{K}N$ multichannel
$\Gamma(\Sigma(1385)\pi)/\Gamma_{total}$	Γ_6/Γ
VALUE	DOCUMENT ID TECN COMMENT
< 0.01	SARANTSEV 19 DPWA $\bar{K}N$ multichannel
$(\Gamma_1\Gamma_2)^{1/2}/\Gamma_{total}$ in $N\bar{K} \rightarrow \Sigma(1620) \rightarrow \Lambda\pi$	$(\Gamma_1\Gamma_2)^{1/2}/\Gamma$
VALUE	DOCUMENT ID TECN COMMENT
0.12 ± 0.02	¹ MORRIS 78 DPWA $K^- n \rightarrow \Lambda\pi^-$
not seen	BAILLON 75 IPWA $\bar{K}N \rightarrow \Lambda\pi$
0.15	KIM 71 DPWA K-matrix analysis
$(\Gamma_1\Gamma_3)^{1/2}/\Gamma_{total}$ in $N\bar{K} \rightarrow \Sigma(1620) \rightarrow \Sigma\pi$	$(\Gamma_1\Gamma_3)^{1/2}/\Gamma$
VALUE	DOCUMENT ID TECN COMMENT
+ 0.32 ± 0.03	ZHANG 13A DPWA Multichannel
not seen	HEPP 76B DPWA $K^- N \rightarrow \Sigma\pi$
+ 0.40 ± 0.06	LANGBEIN 72 IPWA $\bar{K}N$ multichannel
+ 0.08	KIM 71 DPWA K-matrix analysis

$\Sigma(1620)$ FOOTNOTES

- ¹ MORRIS 78 obtains an equally good fit without including this resonance.
- ² Total cross-section bump with $(J+1/2) \Gamma_{el} / \Gamma_{total}$ is 0.06 seen by CARROLL 76.
- ³ Total cross-section bump with $(J+1/2) \Gamma_{el} / \Gamma_{total}$ is 0.04 seen by CARROLL 76.

$\Sigma(1620)$ REFERENCES

SARANTSEV 19 EPJ A55 180 A.V. Sarantsev et al. (BONN, PNPI)
 ZHANG 13A PR C88 035205 H. Zhang et al. (KSU)
 GAO 12 PR C86 025201 P. Gao, J. Shi, B.S. Zou (BHEP, BEJT+)
 Also NP A867 41 P. Gao, B.S. Zou, A. Sibirtsev (BHEP, BEJT+)
 MORRIS 78 PR D17 55 W.A. Morris et al. (FSU)JUP
 CARROLL 76 PRL 37 806 A.S. Carroll et al. (BNL)I
 HEPP 76B PL 65B 487 V. Hepp et al. (CERN, HEIDH, MPIM)JUP
 BAILLON 75 NP B94 39 P.H. Baillon, P.J. Lichfield (CERN, RHEL)JUP
 VANHORN 75 NP B87 145 A.J. van Horn (LBL)JUP
 Also NP B87 157 A.J. van Horn (LBL)JUP
 LANGBEIN 72 NP B47 477 W. Langbein, F. Wagner (MPIM)JUP
 KIM 71 PRL 27 356 J.K. Kim (HARV)JUP
 Also Duke Conf. 161 J.K. Kim (HARV)JUP
 Hyperon Resonances, 1970

$\Sigma(1660) 1/2^+$

$I(J^P) = 1(\frac{1}{2}^+)$ Status: * * *

For results published before 1974 (they are now obsolete), see our 1982 edition Physics Letters **111B** 1 (1982).

$\Sigma(1660)$ POLE POSITION

REAL PART			
VALUE (MeV)	DOCUMENT ID	TECN	COMMENT
1585 ± 20	SARANTSEV 19	DPWA	$\bar{K}N$ multichannel
• • • We do not use the following data for averages, fits, limits, etc. • • •			
1547 ± ¹¹¹ / ₅₉	¹ KAMANO 15	DPWA	$\bar{K}N$ multichannel
¹ From the preferred solution A in KAMANO 15. Solution B reports M = 1457 ± ⁵ / ₋₁ MeV.			
-2xIMAGINARY PART			
VALUE (MeV)	DOCUMENT ID	TECN	COMMENT
290 ± ¹⁴⁰/₄₀	SARANTSEV 19	DPWA	$\bar{K}N$ multichannel
• • • We do not use the following data for averages, fits, limits, etc. • • •			
183 ± ⁸⁶ / ₇₈	¹ KAMANO 15	DPWA	$\bar{K}N$ multichannel
¹ From the preferred solution A in KAMANO 15. Solution B reports $\Gamma = 78 ± 8/8 MeV.$			

Baryon Particle Listings

 $\Sigma(1660)$ $\Sigma(1660)$ POLE RESIDUES

The normalized residue is the residue divided by $\Gamma_{pole}/2$.

Normalized residue in $N\bar{K} \rightarrow \Sigma(1660) \rightarrow N\bar{K}$

MODULUS	PHASE ($^\circ$)	DOCUMENT ID	TECN	COMMENT
0.07 ± 0.03	-165 ± 35	SARANTSEV 19	DPWA	$\bar{K}N$ multichannel
0.0247	168	¹ KAMANO 15	DPWA	$\bar{K}N$ multichannel

¹ From the preferred solution A in KAMANO 15.

Normalized residue in $N\bar{K} \rightarrow \Sigma(1660) \rightarrow \Sigma\pi$

MODULUS	PHASE ($^\circ$)	DOCUMENT ID	TECN	COMMENT
0.17 ± 0.04	150 ± 20	SARANTSEV 19	DPWA	$\bar{K}N$ multichannel
0.16	78	¹ KAMANO 15	DPWA	$\bar{K}N$ multichannel

¹ From the preferred solution A in KAMANO 15.

Normalized residue in $N\bar{K} \rightarrow \Sigma(1660) \rightarrow \Lambda\pi$

MODULUS	PHASE ($^\circ$)	DOCUMENT ID	TECN	COMMENT
0.16 ± 0.05	0 ± 25	SARANTSEV 19	DPWA	$\bar{K}N$ multichannel
0.0614	-84	¹ KAMANO 15	DPWA	$\bar{K}N$ multichannel

¹ From the preferred solution A in KAMANO 15.

Normalized residue in $N\bar{K} \rightarrow \Sigma(1660) \rightarrow \Sigma\sigma$

MODULUS	PHASE ($^\circ$)	DOCUMENT ID	TECN	COMMENT
0.14 ± 0.06	-150 ± 30	SARANTSEV 19	DPWA	$\bar{K}N$ multichannel

Normalized residue in $N\bar{K} \rightarrow \Sigma(1660) \rightarrow \Sigma(1385)\pi$

MODULUS	PHASE ($^\circ$)	DOCUMENT ID	TECN	COMMENT
0.0513	-44	¹ KAMANO 15	DPWA	Multichannel

¹ From the preferred solution A in KAMANO 15.

Normalized residue in $N\bar{K} \rightarrow \Sigma(1660) \rightarrow \Lambda(1405)\pi$

MODULUS	PHASE ($^\circ$)	DOCUMENT ID	TECN	COMMENT
0.06 ± 0.03	-90 ± 25	SARANTSEV 19	DPWA	$\bar{K}N$ multichannel

Normalized residue in $N\bar{K} \rightarrow \Sigma(1660) \rightarrow \Lambda(1520)\pi$

MODULUS	PHASE ($^\circ$)	DOCUMENT ID	TECN	COMMENT
0.04 ± 0.02	5 ± 20	SARANTSEV 19	DPWA	$\bar{K}N$ multichannel

 $\Sigma(1660)$ MASS

VALUE (MeV)	DOCUMENT ID	TECN	COMMENT
1640 to 1680 (≈ 1660) OUR ESTIMATE			
1665 ± 20	SARANTSEV 19	DPWA	$\bar{K}N$ multichannel
1633 ± 3	GAO 12	DPWA	$\bar{K}N \rightarrow \Lambda\pi$
1665.1 ± 11.2	¹ KOISO 85	DPWA	$K^-p \rightarrow \Sigma\pi$
1670 ± 10	GOPAL 80	DPWA	$\bar{K}N \rightarrow \bar{K}N$
1679 ± 10	ALSTON-... 78	DPWA	$\bar{K}N \rightarrow \bar{K}N$
1668 ± 25	VANHORN 75	DPWA	$K^-p \rightarrow \Lambda\pi^0$
1670 ± 20	KANE 74	DPWA	$K^-p \rightarrow \Sigma\pi$
••• We do not use the following data for averages, fits, limits, etc. •••			
1676 ± 15	GOPAL 77	DPWA	$\bar{K}N$ multichannel
1565 or 1597	² MARTIN 77	DPWA	$\bar{K}N$ multichannel
1660 ± 30	³ BAILLON 75	IPWA	$\bar{K}N \rightarrow \Lambda\pi$
1671 ± 2	⁴ PONTE 75	DPWA	$K^-p \rightarrow \Lambda\pi^0$

¹ The evidence of KOISO 85 is weak.

² The two MARTIN 77 values are from a T-matrix pole and from a Breit-Wigner fit.

³ From solution 1 of BAILLON 75; not present in solution 2.

⁴ From solution 2 of PONTE 75; not present in solution 1.

 $\Sigma(1660)$ WIDTH

VALUE (MeV)	DOCUMENT ID	TECN	COMMENT
100 to 300 (≈ 200) OUR ESTIMATE			
300 +140 -40	SARANTSEV 19	DPWA	$\bar{K}N$ multichannel
121 + 4 -7	GAO 12	DPWA	$\bar{K}N \rightarrow \Lambda\pi$
81.5 ± 22.2	¹ KOISO 85	DPWA	$K^-p \rightarrow \Sigma\pi$
152 ± 20	GOPAL 80	DPWA	$\bar{K}N \rightarrow \bar{K}N$
38 ± 10	ALSTON-... 78	DPWA	$\bar{K}N \rightarrow \bar{K}N$
230 +165 -60	VANHORN 75	DPWA	$K^-p \rightarrow \Lambda\pi^0$
250 ± 110	KANE 74	DPWA	$K^-p \rightarrow \Sigma\pi$
••• We do not use the following data for averages, fits, limits, etc. •••			
120 ± 20	GOPAL 77	DPWA	$\bar{K}N$ multichannel
202 or 217	² MARTIN 77	DPWA	$\bar{K}N$ multichannel
80 ± 40	³ BAILLON 75	IPWA	$\bar{K}N \rightarrow \Lambda\pi$
81 ± 10	⁴ PONTE 75	DPWA	$K^-p \rightarrow \Lambda\pi^0$

¹ The evidence of KOISO 85 is weak.

² The two MARTIN 77 values are from a T-matrix pole and from a Breit-Wigner fit.

³ From solution 1 of BAILLON 75; not present in solution 2.

⁴ From solution 2 of PONTE 75; not present in solution 1.

 $\Sigma(1660)$ DECAY MODES

Mode	Fraction (Γ_i/Γ)
Γ_1 $N\bar{K}$	0.05 to 0.15 (≈ 010)
Γ_2 $\Lambda\pi$	(35 ± 12) %
Γ_3 $\Sigma\pi$	(37 ± 10) %
Γ_4 $\Sigma\sigma$	(20 ± 8) %
Γ_5 $\Sigma(1385)\pi$	
Γ_6 $\Lambda(1405)\pi$	(4.0 ± 2.0) %
Γ_7 $\Lambda(1520)\pi$	

 $\Sigma(1660)$ BRANCHING RATIOS

See "Sign conventions for resonance couplings" in the Note on Λ and Σ Resonances.

$\Gamma(N\bar{K})/\Gamma_{total}$	DOCUMENT ID	TECN	COMMENT	Γ_1/Γ
0.05 to 0.15 (≈ 010) OUR ESTIMATE				
0.07 ± 0.03	SARANTSEV 19	DPWA	$\bar{K}N$ multichannel	
0.12 ± 0.03	GOPAL 80	DPWA	$\bar{K}N \rightarrow \bar{K}N$	
0.10 ± 0.05	ALSTON-... 78	DPWA	$\bar{K}N \rightarrow \bar{K}N$	

••• We do not use the following data for averages, fits, limits, etc. •••				
0.005	¹ KAMANO 15	DPWA	$\bar{K}N$ multichannel	
<0.04	GOPAL 77	DPWA	See GOPAL 80	
0.27 or 0.29	² MARTIN 77	DPWA	$\bar{K}N$ multichannel	

¹ From the preferred solution A in KAMANO 15.

² The two MARTIN 77 values are from a T-matrix pole and from a Breit-Wigner fit.

$\Gamma(\Lambda\pi)/\Gamma_{total}$	DOCUMENT ID	TECN	COMMENT	Γ_2/Γ
0.35 ± 0.12	SARANTSEV 19	DPWA	$\bar{K}N$ multichannel	
0.128	¹ KAMANO 15	DPWA	$\bar{K}N$ multichannel	

¹ From the preferred solution A in KAMANO 15.

$\Gamma(\Sigma\pi)/\Gamma_{total}$	DOCUMENT ID	TECN	COMMENT	Γ_3/Γ
0.37 ± 0.10	SARANTSEV 19	DPWA	$\bar{K}N$ multichannel	
0.865	¹ KAMANO 15	DPWA	$\bar{K}N$ multichannel	

¹ From the preferred solution A in KAMANO 15.

$\Gamma(\Sigma\sigma)/\Gamma_{total}$	DOCUMENT ID	TECN	COMMENT	Γ_4/Γ
0.20 ± 0.08	SARANTSEV 19	DPWA	$\bar{K}N$ multichannel	

$\Gamma(\Sigma(1385)\pi)/\Gamma_{total}$	DOCUMENT ID	TECN	COMMENT	Γ_5/Γ
0.04 ± 0.02	SARANTSEV 19	DPWA	$\bar{K}N$ multichannel	
0.001	¹ KAMANO 15	DPWA	Multichannel	

¹ From the preferred solution A in KAMANO 15.

$\Gamma(\Lambda(1405)\pi)/\Gamma_{total}$	DOCUMENT ID	TECN	COMMENT	Γ_6/Γ
0.04 ± 0.02	SARANTSEV 19	DPWA	$\bar{K}N$ multichannel	

$\Gamma(\Lambda(1520)\pi)/\Gamma_{total}$	DOCUMENT ID	TECN	COMMENT	Γ_7/Γ
<0.01	SARANTSEV 19	DPWA	$\bar{K}N$ multichannel	

$(\Gamma_1\Gamma_2)^{1/2}/\Gamma_{total}$ in $N\bar{K} \rightarrow \Sigma(1660) \rightarrow \Lambda\pi$	DOCUMENT ID	TECN	COMMENT	$(\Gamma_1\Gamma_2)^{1/2}/\Gamma$
-0.064 + 0.005 -0.003	GAO 12	DPWA	$\bar{K}N \rightarrow \Lambda\pi$	
< 0.04	GOPAL 77	DPWA	$\bar{K}N$ multichannel	
0.12 + 0.12 -0.04	VANHORN 75	DPWA	$K^-p \rightarrow \Lambda\pi^0$	

••• We do not use the following data for averages, fits, limits, etc. •••				
-0.10 or -0.11	¹ MARTIN 77	DPWA	$\bar{K}N$ multichannel	
-0.04 ± 0.02	² BAILLON 75	IPWA	$\bar{K}N \rightarrow \Lambda\pi$	
+0.16 ± 0.01	³ PONTE 75	DPWA	$K^-p \rightarrow \Lambda\pi^0$	

¹ The two MARTIN 77 values are from a T-matrix pole and from a Breit-Wigner fit.

² From solution 1 of BAILLON 75; not present in solution 2.

³ From solution 2 of PONTE 75; not present in solution 1.

$(\Gamma_1\Gamma_2)^{1/2}/\Gamma_{total}$ in $N\bar{K} \rightarrow \Sigma(1660) \rightarrow \Sigma\pi$	DOCUMENT ID	TECN	COMMENT	$(\Gamma_1\Gamma_2)^{1/2}/\Gamma$
-0.13 ± 0.04	¹ KOISO 85	DPWA	$K^-p \rightarrow \Sigma\pi$	
-0.16 ± 0.03	GOPAL 77	DPWA	$\bar{K}N$ multichannel	
-0.11 ± 0.01	KANE 74	DPWA	$K^-p \rightarrow \Sigma\pi$	

••• We do not use the following data for averages, fits, limits, etc. •••				
-0.34 or -0.37	² MARTIN 77	DPWA	$\bar{K}N$ multichannel	
not seen	HEPP 768	DPWA	$K^-N \rightarrow \Sigma\pi$	

¹ The evidence of KOISO 85 is weak.

² The two MARTIN 77 values are from a T-matrix pole and from a Breit-Wigner fit.

³ From solution 2 of PONTE 75; not present in solution 1.

$\Sigma(1660)$ REFERENCES

SARANTSEV	19	EPJ A55 180	A.V. Sarantsev et al.	(BONN, PNPI)
KAMANO	15	PR C92 025205	H. Kamano et al.	(ANL, OSAK)
GAO	12	PR C86 025201	P. Gao, J. Shi, B.S. Zou	(BHEP, BEIJT)
Also		NP A867 41	P. Gao, B.S. Zou, A. Sibirtsev	(BHEP, BEIJT+)
KOISO	85	NP A433 619	H. Koiso et al.	(TOKY, MASA)
PDG	82	PL 111B 1	M. Roos et al.	(HEL5, CIT, CERN)
GOPAL	80	Toronto Conf. 159	G.P. Gopal	(RHEL) IJP
ALSTON-...	78	PR D18 182	M. Alston-Garnjost et al.	(LBL, MTHO+) IJP
Also		PRL 38 1007	M. Alston-Garnjost et al.	(LBL, MTHO+) IJP
GOPAL	77	NP B119 362	G.P. Gopal et al.	(LOIC, RHEL) IJP
MARTIN	77	NP B127 349	B.R. Martin, M.K. Pldcock, R.G. Moorhouse	(LOUC+) IJP
Also		NP B126 266	B.R. Martin, M.K. Pldcock	(LOUC) IJP
Also		NP B126 285	B.R. Martin, M.K. Pldcock	(LOUC) IJP
HEPP	76B	PL 65B 487	V. Hepp et al.	(CERN, HEIDH, MPIM) IJP
BAILLON	75	NP B94 39	P.H. Baillon, P.J. Litchfield	(CERN, RHEL) IJP
PONTE	75	PR D12 2597	R.A. Ponte et al.	(MASA, TENN, UCR) IJP
VANHORN	75	NP B87 145	A.J. van Horn	(LBL) IJP
Also		NP B87 157	A.J. van Horn	(LBL) IJP
KANE	74	LBL-2452	D.F. Kane	(LBL) IJP

$\Sigma(1670) 3/2^-$ $I(J^P) = 1(\frac{3}{2}^-)$ Status: * * * *

For most results published before 1974 (they are now obsolete), see our 1982 edition Physics Letters **111B** 1 (1982).

Results from production experiments are listed separately in the next entry.

$\Sigma(1670)$ POLE POSITION

REAL PART

VALUE (MeV)	DOCUMENT ID	TECN	COMMENT
1655 to 1675 (≈ 1662) OUR ESTIMATE			
1661 ± 3	SARANTSEV 19	DPWA	$\bar{K}N$ multichannel
1669 $^{+7}_{-7}$	¹ KAMANO 15	DPWA	$\bar{K}N$ multichannel
• • • We do not use the following data for averages, fits, limits, etc. • • •			
1674	ZHANG 13A	DPWA	$\bar{K}N$ multichannel

¹ From the preferred solution A in KAMANO 15.

-2xIMAGINARY PART

VALUE (MeV)	DOCUMENT ID	TECN	COMMENT
45 to 65 (≈ 55) OUR ESTIMATE			
52 ± 6	SARANTSEV 19	DPWA	$\bar{K}N$ multichannel
64 $^{+10}_{-14}$	¹ KAMANO 15	DPWA	$\bar{K}N$ multichannel
• • • We do not use the following data for averages, fits, limits, etc. • • •			
54	ZHANG 13A	DPWA	$\bar{K}N$ multichannel

¹ From the preferred solution A in KAMANO 15.

$\Sigma(1670)$ POLE RESIDUES

The normalized residue is the residue divided by $\Gamma_{pole}/2$.

Normalized residue in $N\bar{K} \rightarrow \Sigma(1670) \rightarrow N\bar{K}$

MODULUS	PHASE ($^\circ$)	DOCUMENT ID	TECN	COMMENT
0.10 ± 0.02	-31 ± 12	SARANTSEV 19	DPWA	$\bar{K}N$ multichannel
• • • We do not use the following data for averages, fits, limits, etc. • • •				
0.129	-20	¹ KAMANO 15	DPWA	$\bar{K}N$ multichannel

¹ From the preferred solution A in KAMANO 15.

Normalized residue in $N\bar{K} \rightarrow \Sigma(1670) \rightarrow \Sigma\pi$

MODULUS	PHASE ($^\circ$)	DOCUMENT ID	TECN	COMMENT
0.25 ± 0.05	-25 ± 10	SARANTSEV 19	DPWA	$\bar{K}N$ multichannel
• • • We do not use the following data for averages, fits, limits, etc. • • •				
0.249	-21	¹ KAMANO 15	DPWA	$\bar{K}N$ multichannel

¹ From the preferred solution A in KAMANO 15.

Normalized residue in $N\bar{K} \rightarrow \Sigma(1670) \rightarrow \Lambda\pi$

MODULUS	PHASE ($^\circ$)	DOCUMENT ID	TECN	COMMENT
0.09 ± 0.03	-52 ± 12	SARANTSEV 19	DPWA	$\bar{K}N$ multichannel
• • • We do not use the following data for averages, fits, limits, etc. • • •				
0.0818	-7	¹ KAMANO 15	DPWA	$\bar{K}N$ multichannel

¹ From the preferred solution A in KAMANO 15.

Normalized residue in $N\bar{K} \rightarrow \Sigma(1670) \rightarrow \Xi K$

MODULUS	PHASE ($^\circ$)	DOCUMENT ID	TECN	COMMENT
0.02 ± 0.01	160 ± 20	SARANTSEV 19	DPWA	$\bar{K}N$ multichannel

Normalized residue in $N\bar{K} \rightarrow \Sigma(1670) \rightarrow \Sigma\sigma$

MODULUS	PHASE ($^\circ$)	DOCUMENT ID	TECN	COMMENT
0.08 ± 0.03	-25 ± 15	SARANTSEV 19	DPWA	$\bar{K}N$ multichannel

Normalized residue in $N\bar{K} \rightarrow \Sigma(1670) \rightarrow \Sigma(1385)\pi, S$ -wave

MODULUS	PHASE ($^\circ$)	DOCUMENT ID	TECN	COMMENT
0.228	167	¹ KAMANO 15	DPWA	$\bar{K}N$ multichannel

¹ From the preferred solution A in KAMANO 15.

Normalized residue in $N\bar{K} \rightarrow \Sigma(1670) \rightarrow \Sigma(1385)\pi, D$ -wave

MODULUS	PHASE ($^\circ$)	DOCUMENT ID	TECN	COMMENT
• • • We do not use the following data for averages, fits, limits, etc. • • •				
0.0915	141	KAMANO 15	DPWA	$\bar{K}N$ multichannel

Normalized residue in $N\bar{K} \rightarrow \Sigma(1670) \rightarrow \Lambda(1405)\pi$

MODULUS	PHASE ($^\circ$)	DOCUMENT ID	TECN	COMMENT
0.03 ± 0.02	160 ± 15	SARANTSEV 19	DPWA	$\bar{K}N$ multichannel

Normalized residue in $N\bar{K} \rightarrow \Sigma(1670) \rightarrow \Lambda(1520)\pi, P$ -wave

MODULUS	PHASE ($^\circ$)	DOCUMENT ID	TECN	COMMENT
0.04 ± 0.02	120 ± 20	SARANTSEV 19	DPWA	$\bar{K}N$ multichannel

Normalized residue in $N\bar{K} \rightarrow \Sigma(1670) \rightarrow \Lambda(1520)\pi, F$ -wave

MODULUS	PHASE ($^\circ$)	DOCUMENT ID	TECN	COMMENT
0.01 ± 0.01		SARANTSEV 19	DPWA	$\bar{K}N$ multichannel

Normalized residue in $N\bar{K} \rightarrow \Sigma(1670) \rightarrow \Delta\bar{K}, S$ -wave

MODULUS	PHASE ($^\circ$)	DOCUMENT ID	TECN	COMMENT
0.01 ± 0.01		SARANTSEV 19	DPWA	$\bar{K}N$ multichannel

Normalized residue in $N\bar{K} \rightarrow \Sigma(1670) \rightarrow N\bar{K}^*(892), S=3/2, S$ -wave

VALUE	DOCUMENT ID	TECN	COMMENT
0.05 ± 0.03 0.50 ± 0.60	SARANTSEV 19	DPWA	$\bar{K}N$ multichannel

Normalized residue in $N\bar{K} \rightarrow \Sigma(1670) \rightarrow N\bar{K}^*(892), S=3/2, D$ -wave

MODULUS	PHASE ($^\circ$)	DOCUMENT ID	TECN	COMMENT
0.01 ± 0.01		SARANTSEV 19	DPWA	$\bar{K}N$ multichannel

Normalized residue in $N\bar{K} \rightarrow \Sigma(1670) \rightarrow N\bar{K}^*(892), S=1/2, D$ -wave

MODULUS	PHASE ($^\circ$)	DOCUMENT ID	TECN	COMMENT
0.03 ± 0.02		SARANTSEV 19	DPWA	$\bar{K}N$ multichannel

$\Sigma(1670)$ MASS

VALUE (MeV)	DOCUMENT ID	TECN	COMMENT
1665 to 1685 (≈ 1675) OUR ESTIMATE			
1665 ± 3	SARANTSEV 19	DPWA	$\bar{K}N$ multichannel
1678 ± 2	ZHANG 13A	DPWA	$\bar{K}N$ multichannel
1673 ± 1	GAO 12	DPWA	$\bar{K}N \rightarrow \Lambda\pi$
1665.1 ± 4.1	KOISO 85	DPWA	$K^-p \rightarrow \Sigma\pi$
1682 ± 5	GOPAL 80	DPWA	$\bar{K}N \rightarrow \bar{K}N$
1679 ± 10	ALSTON-... 78	DPWA	$\bar{K}N \rightarrow \bar{K}N$
1670 ± 5	GOPAL 77	DPWA	$\bar{K}N$ multichannel
1670 ± 6	HEPP 76B	DPWA	$K^-N \rightarrow \Sigma\pi$
1685 ± 20	BAILLON 75	IPWA	$\bar{K}N \rightarrow \Lambda\pi$
1659 $^{+12}_{-5}$	VANHORN 75	DPWA	$K^-p \rightarrow \Lambda\pi^0$
1670 ± 2	KANE 74	DPWA	$K^-p \rightarrow \Sigma\pi$
• • • We do not use the following data for averages, fits, limits, etc. • • •			
1667 or 1668	¹ MARTIN 77	DPWA	$\bar{K}N$ multichannel
1650	DEBELLEFON 76	IPWA	$K^-p \rightarrow \Lambda\pi^0$
1671 ± 3	PONTE 75	DPWA	$K^-p \rightarrow \Lambda\pi^0$ (sol. 1)
1655 ± 2	PONTE 75	DPWA	$K^-p \rightarrow \Lambda\pi^0$ (sol. 2)

¹ The two MARTIN 77 values are from a T-matrix pole and from a Breit-Wigner fit.

$\Sigma(1670)$ WIDTH

VALUE (MeV)	DOCUMENT ID	TECN	COMMENT
40 to 100 (≈ 70) OUR ESTIMATE			
54 ± 6	SARANTSEV 19	DPWA	$\bar{K}N$ multichannel
55 ± 4	ZHANG 13A	DPWA	$\bar{K}N$ multichannel
52 $^{+5}_{-2}$	GAO 12	DPWA	$\bar{K}N \rightarrow \Lambda\pi$
65.0 ± 7.3	KOISO 85	DPWA	$K^-p \rightarrow \Sigma\pi$
79 ± 10	GOPAL 80	DPWA	$\bar{K}N \rightarrow \bar{K}N$
56 ± 20	ALSTON-... 78	DPWA	$\bar{K}N \rightarrow \bar{K}N$
50 ± 5	GOPAL 77	DPWA	$\bar{K}N$ multichannel
56 ± 3	HEPP 76B	DPWA	$K^-N \rightarrow \Sigma\pi$
85 ± 25	BAILLON 75	IPWA	$\bar{K}N \rightarrow \Lambda\pi$
32 ± 11	VANHORN 75	DPWA	$K^-p \rightarrow \Lambda\pi^0$
79 ± 6	KANE 74	DPWA	$K^-p \rightarrow \Sigma\pi$
• • • We do not use the following data for averages, fits, limits, etc. • • •			
46 or 46	¹ MARTIN 77	DPWA	$\bar{K}N$ multichannel
80	DEBELLEFON 76	IPWA	$K^-p \rightarrow \Lambda\pi^0$
44 ± 11	PONTE 75	DPWA	$K^-p \rightarrow \Lambda\pi^0$ (sol. 1)
76 ± 5	PONTE 75	DPWA	$K^-p \rightarrow \Lambda\pi^0$ (sol. 2)

¹ The two MARTIN 77 values are from a T-matrix pole and from a Breit-Wigner fit.

$\Sigma(1670)$ DECAY MODES

Mode	Fraction (Γ_i/Γ)
$\Gamma_1 N\bar{K}$	0.06 to 0.12
$\Gamma_2 \Lambda\pi$	5-15 %

Baryon Particle Listings

 $\Sigma(1670)$

Γ_3	$\Sigma\pi$	30–60 %
Γ_4	$\Lambda\pi\pi$	
Γ_5	$\Sigma\pi\pi$	
Γ_6	$\Sigma\sigma$	(7.0 ± 3.0) %
Γ_7	$\Sigma(1385)\pi$	
Γ_8	$\Sigma(1385)\pi, S\text{-wave}$	
Γ_9	$\Sigma(1385)\pi, D\text{-wave}$	
Γ_{10}	$N\bar{K}^*(892), S=1/2, D\text{-wave}$	
Γ_{11}	$N\bar{K}^*(892), S=3/2, S\text{-wave}$	
Γ_{12}	$N\bar{K}^*(892), S=3/2, D\text{-wave}$	
Γ_{13}	$\Lambda(1405)\pi$	
Γ_{14}	$\Lambda(1520)\pi$	

 $\Sigma(1670)$ BRANCHING RATIOS

See “Sign conventions for resonance couplings” in the Note on Λ and Σ Resonances.

$\Gamma(N\bar{K})/\Gamma_{\text{total}}$	DOCUMENT ID	TECN	COMMENT	Γ_1/Γ
--	-------------	------	---------	-------------------

0.06 to 0.12 OUR ESTIMATE

0.10 ± 0.02	SARANTSEV	19	DPWA	$\bar{K}N$ multichannel
0.062 ± 0.007	ZHANG	13A	DPWA	$\bar{K}N$ multichannel
0.10 ± 0.03	GOPAL	80	DPWA	$\bar{K}N \rightarrow \bar{K}N$
0.11 ± 0.03	ALSTON-...	78	DPWA	$\bar{K}N \rightarrow \bar{K}N$

• • • We do not use the following data for averages, fits, limits, etc. • • •

0.121	¹ KAMANO	15	DPWA	$\bar{K}N$ multichannel
0.08 ± 0.03	GOPAL	77	DPWA	See GOPAL 80
0.07 or 0.07	² MARTIN	77	DPWA	$\bar{K}N$ multichannel

¹ From the preferred solution A in KAMANO 15.

² The two MARTIN 77 values are from a T-matrix pole and from a Breit-Wigner fit.

$\Gamma(\Lambda\pi)/\Gamma_{\text{total}}$	DOCUMENT ID	TECN	COMMENT	Γ_2/Γ
--	-------------	------	---------	-------------------

0.09 ± 0.02	SARANTSEV	19	DPWA	$\bar{K}N$ multichannel
-------------	-----------	----	------	-------------------------

• • • We do not use the following data for averages, fits, limits, etc. • • •

0.058	¹ KAMANO	15	DPWA	$\bar{K}N$ multichannel
-------	---------------------	----	------	-------------------------

¹ From the preferred solution A in KAMANO 15.

$\Gamma(\Sigma\pi)/\Gamma_{\text{total}}$	DOCUMENT ID	TECN	COMMENT	Γ_3/Γ
---	-------------	------	---------	-------------------

0.70 ± 0.15	SARANTSEV	19	DPWA	$\bar{K}N$ multichannel
-------------	-----------	----	------	-------------------------

• • • We do not use the following data for averages, fits, limits, etc. • • •

0.465	¹ KAMANO	15	DPWA	$\bar{K}N$ multichannel
-------	---------------------	----	------	-------------------------

¹ From the preferred solution A in KAMANO 15.

$\Gamma(\Lambda\pi\pi)/\Gamma_{\text{total}}$	DOCUMENT ID	TECN	COMMENT	Γ_4/Γ
---	-------------	------	---------	-------------------

• • • We do not use the following data for averages, fits, limits, etc. • • •

<0.11	ARMENTEROS68E	HBC	K^-p ($\Gamma_1=0.09$)
-------	---------------	-----	----------------------------

$\Gamma(\Sigma\pi\pi)/\Gamma_{\text{total}}$	DOCUMENT ID	TECN	COMMENT	Γ_5/Γ
--	-------------	------	---------	-------------------

• • • We do not use the following data for averages, fits, limits, etc. • • •

<0.14	¹ ARMENTEROS68E	HBC	K^-p, K^-d ($\Gamma_1=0.09$)
-------	----------------------------	-----	----------------------------------

¹ Ratio only for $\Sigma 2\pi$ system in $l=1$, which cannot be $\Sigma(1385)$.

$\Gamma(\Sigma\sigma)/\Gamma_{\text{total}}$	DOCUMENT ID	TECN	COMMENT	Γ_6/Γ
--	-------------	------	---------	-------------------

0.07 ± 0.03	SARANTSEV	19	DPWA	$\bar{K}N$ multichannel
-------------	-----------	----	------	-------------------------

$\Gamma(\Sigma(1385)\pi, S\text{-wave})/\Gamma_{\text{total}}$	DOCUMENT ID	TECN	COMMENT	Γ_8/Γ
--	-------------	------	---------	-------------------

• • • We do not use the following data for averages, fits, limits, etc. • • •

0.309	¹ KAMANO	15	DPWA	Multichannel
-------	---------------------	----	------	--------------

¹ From the preferred solution A in KAMANO 15.

$\Gamma(\Sigma(1385)\pi, D\text{-wave})/\Gamma_{\text{total}}$	DOCUMENT ID	TECN	COMMENT	Γ_9/Γ
--	-------------	------	---------	-------------------

• • • We do not use the following data for averages, fits, limits, etc. • • •

0.044	¹ KAMANO	15	DPWA	Multichannel
-------	---------------------	----	------	--------------

¹ From the preferred solution A in KAMANO 15.

$\Gamma(N\bar{K}^*(892), S=1/2, D\text{-wave})/\Gamma_{\text{total}}$	DOCUMENT ID	TECN	COMMENT	Γ_{10}/Γ
---	-------------	------	---------	----------------------

• • • We do not use the following data for averages, fits, limits, etc. • • •

0.001	¹ KAMANO	15	DPWA	Multichannel
-------	---------------------	----	------	--------------

¹ From the preferred solution A in KAMANO 15.

$\Gamma(N\bar{K}^*(892), S=3/2, S\text{-wave})/\Gamma_{\text{total}}$	DOCUMENT ID	TECN	COMMENT	Γ_{11}/Γ
---	-------------	------	---------	----------------------

• • • We do not use the following data for averages, fits, limits, etc. • • •

0.002	¹ KAMANO	15	DPWA	Multichannel
-------	---------------------	----	------	--------------

¹ From the preferred solution A in KAMANO 15.

$\Gamma(N\bar{K}^*(892), S=3/2, D\text{-wave})/\Gamma_{\text{total}}$	DOCUMENT ID	TECN	COMMENT	Γ_{12}/Γ
---	-------------	------	---------	----------------------

• • • We do not use the following data for averages, fits, limits, etc. • • •

0.001	¹ KAMANO	15	DPWA	Multichannel
-------	---------------------	----	------	--------------

¹ From the preferred solution A in KAMANO 15.

$\Gamma(\Lambda(1405)\pi)/\Gamma_{\text{total}}$	DOCUMENT ID	TECN	COMMENT	Γ_{13}/Γ
--	-------------	------	---------	----------------------

0.01 ± 0.01	SARANTSEV	19	DPWA	$\bar{K}N$ multichannel
-------------	-----------	----	------	-------------------------

• • • We do not use the following data for averages, fits, limits, etc. • • •

<0.06	ARMENTEROS68E	HBC	K^-p, K^-d ($\Gamma_1=0.09$)
-------	---------------	-----	----------------------------------

$\Gamma(\Lambda(1405)\pi)/\Gamma(\Sigma(1385)\pi)$	DOCUMENT ID	TECN	COMMENT	Γ_{13}/Γ_7
--	-------------	------	---------	------------------------

0.23 ± 0.08	BRUCKER	70	DBC	$K^-N \rightarrow \Sigma\pi\pi$
-------------	---------	----	-----	---------------------------------

$(\Gamma_i\Gamma_f)^{1/2}/\Gamma_{\text{total}}$ in $N\bar{K} \rightarrow \Sigma(1670) \rightarrow \Lambda\pi$	DOCUMENT ID	TECN	COMMENT	$(\Gamma_1\Gamma_2)^{1/2}/\Gamma$
--	-------------	------	---------	-----------------------------------

+0.08 ± 0.01	ZHANG	13A	DPWA	Multichannel
--------------	-------	-----	------	--------------

+0.081 ± 0.002 −0.004	GAO	12	DPWA	$\bar{K}N \rightarrow \Lambda\pi$
--------------------------	-----	----	------	-----------------------------------

+0.17 ± 0.03	¹ MORRIS	78	DPWA	$K^-n \rightarrow \Lambda\pi^-$
--------------	---------------------	----	------	---------------------------------

+0.13 ± 0.02	¹ MORRIS	78	DPWA	$K^-n \rightarrow \Lambda\pi^-$
--------------	---------------------	----	------	---------------------------------

+0.10 ± 0.02	GOPAL	77	DPWA	$\bar{K}N$ multichannel
--------------	-------	----	------	-------------------------

+0.06 ± 0.02	BAILLON	75	IPWA	$\bar{K}N \rightarrow \Lambda\pi$
--------------	---------	----	------	-----------------------------------

+0.09 ± 0.02	VANHORN	75	DPWA	$K^-p \rightarrow \Lambda\pi^0$
--------------	---------	----	------	---------------------------------

+0.018 ± 0.060	DEVENISH	74B		Fixed- t dispersion rel.
----------------	----------	-----	--	----------------------------

• • • We do not use the following data for averages, fits, limits, etc. • • •

+0.08 or +0.08	² MARTIN	77	DPWA	$\bar{K}N$ multichannel
----------------	---------------------	----	------	-------------------------

+0.05	DEBELLEFON	76	IPWA	$K^-p \rightarrow \Lambda\pi^0$
-------	------------	----	------	---------------------------------

+0.08 ± 0.01	PONTE	75	DPWA	$K^-p \rightarrow \Lambda\pi^0$ (sol. 1)
--------------	-------	----	------	--

+0.17 ± 0.01	PONTE	75	DPWA	$K^-p \rightarrow \Lambda\pi^0$ (sol. 2)
--------------	-------	----	------	--

¹ Results are with and without an S_{11} $\Sigma(1620)$ in the fit.

² The two MARTIN 77 values are from a T-matrix pole and from a Breit-Wigner fit.

$(\Gamma_i\Gamma_f)^{1/2}/\Gamma_{\text{total}}$ in $N\bar{K} \rightarrow \Sigma(1670) \rightarrow \Sigma\pi$	DOCUMENT ID	TECN	COMMENT	$(\Gamma_1\Gamma_3)^{1/2}/\Gamma$
---	-------------	------	---------	-----------------------------------

+0.20 ± 0.01	ZHANG	13A	DPWA	Multichannel
--------------	-------	-----	------	--------------

+0.20 ± 0.02	KOISO	85	DPWA	$K^-p \rightarrow \Sigma\pi$
--------------	-------	----	------	------------------------------

+0.21 ± 0.02	GOPAL	77	DPWA	$\bar{K}N$ multichannel
--------------	-------	----	------	-------------------------

+0.20 ± 0.01	HEPP	76B	DPWA	$K^-N \rightarrow \Sigma\pi$
--------------	------	-----	------	------------------------------

+0.21 ± 0.03	KANE	74	DPWA	$K^-p \rightarrow \Sigma\pi$
--------------	------	----	------	------------------------------

• • • We do not use the following data for averages, fits, limits, etc. • • •

+0.18 or +0.17	¹ MARTIN	77	DPWA	$\bar{K}N$ multichannel
----------------	---------------------	----	------	-------------------------

¹ The two MARTIN 77 values are from a T-matrix pole and from a Breit-Wigner fit.

$(\Gamma_i\Gamma_f)^{1/2}/\Gamma_{\text{total}}$ in $N\bar{K} \rightarrow \Sigma(1670) \rightarrow \Sigma(1385)\pi, S\text{-wave}$	DOCUMENT ID	TECN	COMMENT	$(\Gamma_1\Gamma_8)^{1/2}/\Gamma$
--	-------------	------	---------	-----------------------------------

+0.11 ± 0.03	PREVOST	74	DPWA	$K^-N \rightarrow \Sigma(1385)\pi$
--------------	---------	----	------	------------------------------------

• • • We do not use the following data for averages, fits, limits, etc. • • •

0.17 ± 0.02	¹ SIMS	68	DBC	$K^-N \rightarrow \Lambda\pi\pi$
-------------	-------------------	----	-----	----------------------------------

¹ SIMS 68 uses only cross-section data. Result used as upper limit only.

$\Gamma_i\Gamma_f/\Gamma_{\text{total}}^2$ in $N\bar{K} \rightarrow \Sigma(1670) \rightarrow \Lambda(1405)\pi$	DOCUMENT ID	TECN	COMMENT	$\Gamma_1\Gamma_{13}/\Gamma^2$
--	-------------	------	---------	--------------------------------

0.007 ± 0.002	¹ BRUCKER	70	DBC	$K^-N \rightarrow \Sigma\pi\pi$
---------------	----------------------	----	-----	---------------------------------

• • • We do not use the following data for averages, fits, limits, etc. • • •

<0.03	BERLEY	69	HBC	K^-p 0.6–0.82 GeV/ c
-------	--------	----	-----	--------------------------

¹ Assuming the $\Lambda(1405)\pi$ cross-section bump is due only to $3/2^-$ resonance.

$(\Gamma_i\Gamma_f)^{1/2}/\Gamma_{\text{total}}$ in $N\bar{K} \rightarrow \Sigma(1670) \rightarrow \Lambda(1520)\pi$	DOCUMENT ID	TECN	COMMENT	$(\Gamma_1\Gamma_{14})^{1/2}/\Gamma$
--	-------------	------	---------	--------------------------------------

0.081 ± 0.016	¹ CAMERON	77	DPWA	$P\text{-wave decay}$
---------------	----------------------	----	------	-----------------------

¹ The CAMERON 77 upper limit on $F\text{-wave decay}$ is 0.03.

 $\Sigma(1670)$ REFERENCES

SARANTSEV	19	EPJ A55 180	A.V. Sarantsev et al.	(BONN, PNPI)
KAMANO	15	PR C92 025205	H. Kamano et al.	(ANL, OSAK)
ZHANG	13A	PR C08 035205	H. Zhang et al.	(KSU)
GAO	12	PR C86 025201	P. Gao, J. Shi, B.S. Zou	(BHEP, BEIJT)
Also		NP A567 41	P. Gao, B.S. Zou, A. Sibirinev	(BHEP, BEIJT+)
KOISO	85	NP A433 619	H. Koiso et al.	(TOKY, MASA)
PDG	82	PL 111B 1	M. Roos et al.	(HEL5, CIT, CERN)
GOPAL	80	Toronto Conf. 159	G.P. Gopal	(RHEL) IJP
ALSTON-...	78	PR D18 182	M. Alston-Garnjost et al.	(LBL, MTHO+) IJP
Also		PRL 38 1007	M. Alston-Garnjost et al.	(LBL, MTHO+) IJP
MORRIS	78	PR D17 55	W.A. Morris et al.	(FSU) IJP
CAMERON	77	NP B131 399	W. Cameron et al.	(RHEL, LOIC) IJP
GOPAL	77	NP B119 362	G.P. Gopal et al.	(LOIC, RHEL) IJP

See key on page 1127

Baryon Particle Listings

$\Sigma(1670), \Sigma(1750)$

MARTIN	77	NP B127 349	B.R. Martin, M.K. Pidcock, R.G. Moorhouse (LOUC+) IJP
Also		NP B126 266	(LOUC)
Also		NP B126 285	(LOUC) IJP
DEBELLEFON	76	NP B109 129	A. de Bellefon, A. Berthon (CDEF) IJP
HEPP	76B	PL 65B 487	V. Hepp et al. (CERN, HEIDH, MPIM) IJP
BAILLON	75	NP B94 39	P.H. Baillon, P.J. Litchfield (CERN, RHEL) IJP
PONTE	75	PR D12 2597	R.A. Ponte et al. (MASA, TENN, UCR) IJP
VANHORN	75	NP B87 145	A.J. van Horn (LBL) IJP
Also		NP B87 157	A.J. van Horn (LBL) IJP
DEVENISH	74B	NP B91 330	R.C.E. Devenish, C.D. Froggatt, B.R. Martin (DESY+) IJP
KANE	74	LBL-2452	D.F. Kane (LBL) IJP
PREVOST	74	NP B69 246	J. Prevost et al. (SACL, CERN, HEID) IJP
BRUCKER	70	Duke Conf. 155	E.B. Brucker et al. (FSU) I
Hyperon Resonances, 1970			
BERLEY	69	PL 30B 430	D. Berley et al. (BNL)
ARMENTEROS	68E	PL 28B 521	R. Armenteros et al. (CERN, HEID, SACL) I
SIMS	68	PRL 21 1413	W.H. Sims et al. (FSU, TUFTS, BRAN)

$\Sigma(1750) 1/2^-$

$$I(J^P) = 1(\frac{1}{2}^-) \text{ Status: } ***$$

For most results published before 1974 (they are now obsolete), see our 1982 edition Physics Letters **111B** 1 (1982).

There is evidence for this state in many partial-wave analyses, but with wide variations in the mass, width, and couplings. The latest analyses indicated significant couplings to $N\bar{K}$ and $\Lambda\pi$, as well as to $\Sigma\eta$ whose threshold is at 1746 MeV (JONES 74).

$\Sigma(1750)$ POLE POSITION

REAL PART	DOCUMENT ID	TECN	COMMENT
VALUE (MeV)			
1689 ± 11	SARANTSEV 19	DPWA	$\bar{K}N$ multichannel
••• We do not use the following data for averages, fits, limits, etc. •••			
$1704 \pm \frac{3}{6}$	¹ KAMANO 15	DPWA	$\bar{K}N$ multichannel
1708	ZHANG 13A	DPWA	$\bar{K}N$ multichannel
¹ From the preferred solution A in KAMANO 15. Solution B reports two poles at M = $1551 \pm \frac{2}{9}$ MeV and $1940 \pm \frac{2}{2}$ MeV.			

-2xIMAGINARY PART	DOCUMENT ID	TECN	COMMENT
VALUE (MeV)			
206 ± 18	SARANTSEV 19	DPWA	$\bar{K}N$ multichannel
••• We do not use the following data for averages, fits, limits, etc. •••			
$86 \pm \frac{14}{4}$	¹ KAMANO 15	DPWA	$\bar{K}N$ multichannel
158	ZHANG 13A	DPWA	$\bar{K}N$ multichannel
¹ From the preferred solution A in KAMANO 15. Solution B Reports two poles with $\Gamma = 376 \pm \frac{12}{2}$ and $172 \pm \frac{4}{4}$ MeV.			

$\Sigma(1750)$ POLE RESIDUES

The normalized residue is the residue divided by $\Gamma_{pole}/2$.

Normalized residue in $N\bar{K} \rightarrow \Sigma(1750) \rightarrow N\bar{K}$	DOCUMENT ID	TECN	COMMENT
MODULUS PHASE (°)			
0.46 ± 0.09 -144 ± 15	SARANTSEV 19	DPWA	$\bar{K}N$ multichannel
••• We do not use the following data for averages, fits, limits, etc. •••			
0.0982 178	¹ KAMANO 15	DPWA	$\bar{K}N$ multichannel
¹ From the preferred solution A in KAMANO 15.			

Normalized residue in $N\bar{K} \rightarrow \Sigma(1750) \rightarrow \Sigma\pi$	DOCUMENT ID	TECN	COMMENT
MODULUS PHASE (°)			
0.27 ± 0.05 100 ± 18	SARANTSEV 19	DPWA	$\bar{K}N$ multichannel
••• We do not use the following data for averages, fits, limits, etc. •••			
0.192 137	¹ KAMANO 15	DPWA	Multichannel
¹ From the preferred solution A in KAMANO 15.			

Normalized residue in $N\bar{K} \rightarrow \Sigma(1750) \rightarrow \Sigma\eta$	DOCUMENT ID	TECN	COMMENT
MODULUS PHASE (°)			
0.05 ± 0.03	SARANTSEV 19	DPWA	$\bar{K}N$ multichannel

Normalized residue in $N\bar{K} \rightarrow \Sigma(1750) \rightarrow \Lambda\pi$	DOCUMENT ID	TECN	COMMENT
MODULUS PHASE (°)			
0.26 ± 0.06 115 ± 15	SARANTSEV 19	DPWA	$\bar{K}N$ multichannel
••• We do not use the following data for averages, fits, limits, etc. •••			
0.207 169	¹ KAMANO 15	DPWA	$\bar{K}N$ multichannel
¹ From the preferred solution A in KAMANO 15.			

Normalized residue in $N\bar{K} \rightarrow \Sigma(1750) \rightarrow \Xi K$	DOCUMENT ID	TECN	COMMENT
MODULUS PHASE (°)			
0.02 ± 0.02	SARANTSEV 19	DPWA	$\bar{K}N$ multichannel

Normalized residue in $N\bar{K} \rightarrow \Sigma(1750) \rightarrow \Sigma(1385)\pi, D\text{-wave}$	DOCUMENT ID	TECN	COMMENT
MODULUS PHASE (°)			
0.04 ± 0.03	SARANTSEV 19	DPWA	$\bar{K}N$ multichannel
••• We do not use the following data for averages, fits, limits, etc. •••			
0.0536 73	¹ KAMANO 15	DPWA	$\bar{K}N$ multichannel
¹ From the preferred solution A in KAMANO 15.			

Normalized residue in $N\bar{K} \rightarrow \Sigma(1750) \rightarrow \Lambda(1520)\pi$				
MODULUS	PHASE (°)	DOCUMENT ID	TECN	COMMENT
0.15 ± 0.07	-25 ± 40	SARANTSEV 19	DPWA	$\bar{K}N$ multichannel

Normalized residue in $N\bar{K} \rightarrow \Sigma(1750) \rightarrow N\bar{K}^*(892), S=1/2, S\text{-wave}$				
MODULUS	PHASE (°)	DOCUMENT ID	TECN	COMMENT
0.05 ± 0.03	-100 ± 35	SARANTSEV 19	DPWA	$\bar{K}N$ multichannel

$\Sigma(1750)$ MASS

VALUE (MeV)	DOCUMENT ID	TECN	COMMENT
1700 to 1800 (≈ 1750) OUR ESTIMATE			
1692 ± 11	SARANTSEV 19	DPWA	$\bar{K}N$ multichannel
1739 ± 8	ZHANG 13A	DPWA	$\bar{K}N$ multichannel
1756 ± 10	GOPAL 80	DPWA	$\bar{K}N \rightarrow \bar{K}N$
1770 ± 10	ALSTON-...	78	DPWA $\bar{K}N \rightarrow \bar{K}N$
••• We do not use the following data for averages, fits, limits, etc. •••			
1770 ± 15	GOPAL 77	DPWA	$\bar{K}N$ multichannel
1800 or 1813	¹ MARTIN 77	DPWA	$\bar{K}N$ multichannel
1715 ± 10	² CARROLL 76	DPWA	Isospin-1 total σ
1730	DEBELLEFON 76	IPWA	$K^-p \rightarrow \Lambda\pi^0$
1780 ± 30	BAILLON 75	IPWA	$\bar{K}N \rightarrow \Lambda\pi$ (sol. 1)
1700 ± 30	BAILLON 75	IPWA	$\bar{K}N \rightarrow \Lambda\pi$ (sol. 2)
$1697 \pm \frac{20}{10}$	VANHORN 75	DPWA	$K^-p \rightarrow \Lambda\pi^0$
1785 ± 12	CHU 74	DBC	Fits $\sigma(K^-n \rightarrow \Sigma^-\eta)$
1760 ± 5	³ JONES 74	HBC	Fits $\sigma(K^-p \rightarrow \Sigma^0\eta)$
1739 ± 10	PREVOST 74	DPWA	$K^-N \rightarrow \Sigma(1385)\pi$

¹ The two MARTIN 77 values are from a T-matrix pole and from a Breit-Wigner fit.
² A total cross-section bump with $(J+1/2) \Gamma_{el} / \Gamma_{total} = 0.30$.
³ An S-wave Breit-Wigner fit to the threshold cross section with no background and errors statistical only.

$\Sigma(1750)$ WIDTH

VALUE (MeV)	DOCUMENT ID	TECN	COMMENT
100 to 200 (≈ 150) OUR ESTIMATE			
208 ± 18	SARANTSEV 19	DPWA	$\bar{K}N$ multichannel
182 ± 60	ZHANG 13A	DPWA	$\bar{K}N$ multichannel
64 ± 10	GOPAL 80	DPWA	$\bar{K}N \rightarrow \bar{K}N$
161 ± 20	ALSTON-...	78	DPWA $\bar{K}N \rightarrow \bar{K}N$
••• We do not use the following data for averages, fits, limits, etc. •••			
60 ± 10	GOPAL 77	DPWA	$\bar{K}N$ multichannel
117 or 119	¹ MARTIN 77	DPWA	$\bar{K}N$ multichannel
10	² CARROLL 76	DPWA	Isospin-1 total σ
110	DEBELLEFON 76	IPWA	$K^-p \rightarrow \Lambda\pi^0$
140 ± 30	BAILLON 75	IPWA	$\bar{K}N \rightarrow \Lambda\pi$ (sol. 1)
160 ± 50	BAILLON 75	IPWA	$\bar{K}N \rightarrow \Lambda\pi$ (sol. 2)
$66 \pm \frac{14}{12}$	VANHORN 75	DPWA	$K^-p \rightarrow \Lambda\pi^0$
89 ± 33	CHU 74	DBC	Fits $\sigma(K^-n \rightarrow \Sigma^-\eta)$
92 ± 7	³ JONES 74	HBC	Fits $\sigma(K^-p \rightarrow \Sigma^0\eta)$
108 ± 20	PREVOST 74	DPWA	$K^-N \rightarrow \Sigma(1385)\pi$

¹ The two MARTIN 77 values are from a T-matrix pole and from a Breit-Wigner fit.
² A total cross-section bump with $(J+1/2) \Gamma_{el} / \Gamma_{total} = 0.30$.
³ An S-wave Breit-Wigner fit to the threshold cross section with no background and errors statistical only.

$\Sigma(1750)$ DECAY MODES

Mode	Fraction (Γ_i/Γ)
$\Gamma_1 N\bar{K}$	0.06 to 0.12
$\Gamma_2 \Lambda\pi$	(14 ± 5) %
$\Gamma_3 \Sigma\pi$	(16 ± 4) %
$\Gamma_4 \Sigma\eta$	15-55 %
$\Gamma_5 \Sigma(1385)\pi, D\text{-wave}$	< 1 %
$\Gamma_6 \Lambda(1520)\pi$	(2.0 ± 1.0) %
$\Gamma_7 N\bar{K}^*(892), S=1/2$	(8 ± 4) %
$\Gamma_8 N\bar{K}^*(892), S=3/2, D\text{-wave}$	

$\Sigma(1750)$ BRANCHING RATIOS

See "Sign conventions for resonance couplings" in the Note on Λ and Σ Resonances.

$\Gamma(N\bar{K})/\Gamma_{total}$	DOCUMENT ID	TECN	COMMENT	Γ_1/Γ
0.06 to 0.12 OUR ESTIMATE				
0.46 ± 0.09	SARANTSEV 19	DPWA	$\bar{K}N$ multichannel	
0.09 ± 0.07	ZHANG 13A	DPWA	Multichannel	
0.14 ± 0.03	GOPAL 80	DPWA	$\bar{K}N \rightarrow \bar{K}N$	
0.33 ± 0.05	ALSTON-...	78	DPWA $\bar{K}N \rightarrow \bar{K}N$	

Baryon Particle Listings

 $\Sigma(1750), \Sigma(1775)$

••• We do not use the following data for averages, fits, limits, etc. •••

VALUE	DOCUMENT ID	TECN	COMMENT
0.154	¹ KAMANO 15	DPWA	Multichannel
0.15 ± 0.03	GOPAL 77	DPWA	See GOPAL 80
0.06 or 0.05	² MARTIN 77	DPWA	$\bar{K}N$ multichannel

¹ From the preferred solution A in KAMANO 15.

² The two MARTIN 77 values are from a T-matrix pole and from a Breit-Wigner fit.

$\Gamma(\Lambda\pi)/\Gamma_{\text{total}}$	DOCUMENT ID	TECN	COMMENT	Γ_2/Γ
0.14 ± 0.05	SARANTSEV 19	DPWA	$\bar{K}N$ multichannel	

••• We do not use the following data for averages, fits, limits, etc. •••

0.435	¹ KAMANO 15	DPWA	$\bar{K}N$ multichannel
-------	------------------------	------	-------------------------

¹ From the preferred solution A in KAMANO 15.

$\Gamma(\Sigma\pi)/\Gamma_{\text{total}}$	DOCUMENT ID	TECN	COMMENT	Γ_3/Γ
0.16 ± 0.04	SARANTSEV 19	DPWA	$\bar{K}N$ multichannel	

••• We do not use the following data for averages, fits, limits, etc. •••

0.373	¹ KAMANO 15	DPWA	$\bar{K}N$ multichannel
-------	------------------------	------	-------------------------

¹ From the preferred solution A in KAMANO 15.

$\Gamma(\Lambda(1520)\pi)/\Gamma_{\text{total}}$	DOCUMENT ID	TECN	COMMENT	Γ_6/Γ
0.02 ± 0.01	SARANTSEV 19	DPWA	$\bar{K}N$ multichannel	

$\Gamma(\Sigma(1385)\pi, D\text{-wave})/\Gamma_{\text{total}}$	DOCUMENT ID	TECN	COMMENT	Γ_5/Γ
<0.01	SARANTSEV 19	DPWA	$\bar{K}N$ multichannel	

••• We do not use the following data for averages, fits, limits, etc. •••

0.024	¹ KAMANO 15	DPWA	$\bar{K}N$ multichannel
-------	------------------------	------	-------------------------

¹ From the preferred solution A in KAMANO 15.

$\Gamma(N\bar{K}^*(892), S=1/2)/\Gamma_{\text{total}}$	DOCUMENT ID	TECN	COMMENT	Γ_7/Γ
~ 0	SARANTSEV 19	DPWA	$\bar{K}N$ multichannel	

••• We do not use the following data for averages, fits, limits, etc. •••

0.004	¹ KAMANO 15	DPWA	$\bar{K}N$ multichannel
-------	------------------------	------	-------------------------

¹ From the preferred solution A in KAMANO 15.

$\Gamma(N\bar{K}^*(892), S=3/2, D\text{-wave})/\Gamma_{\text{total}}$	DOCUMENT ID	TECN	COMMENT	Γ_8/Γ
0.01	¹ KAMANO 15	DPWA	Multichannel	

¹ From the preferred solution A in KAMANO 15.

$(\Gamma_1\Gamma_f)^{1/2}/\Gamma_{\text{total}}$ in $N\bar{K} \rightarrow \Sigma(1750) \rightarrow \Lambda\pi$	DOCUMENT ID	TECN	COMMENT	$(\Gamma_1\Gamma_3)^{1/2}/\Gamma$
+0.10 ± 0.04	ZHANG 13A	DPWA	Multichannel	
0.04 ± 0.03	GOPAL 77	DPWA	$\bar{K}N$ multichannel	

••• We do not use the following data for averages, fits, limits, etc. •••

-0.10 or -0.09	¹ MARTIN 77	DPWA	$\bar{K}N$ multichannel
-0.12	DEBELLEFON 76	IPWA	$K^-p \rightarrow \Lambda\pi^0$
-0.12 ± 0.02	BAILLON 75	IPWA	$\bar{K}N \rightarrow \Lambda\pi$ (sol. 1)
-0.13 ± 0.03	BAILLON 75	IPWA	$\bar{K}N \rightarrow \Lambda\pi$ (sol. 2)
-0.13 ± 0.04	VANHORN 75	DPWA	$K^-p \rightarrow \Lambda\pi^0$
-0.120 ± 0.077	DEVENISH 74B		Fixed- t dispersion rel.

¹ The two MARTIN 77 values are from a T-matrix pole and from a Breit-Wigner fit.

$(\Gamma_1\Gamma_f)^{1/2}/\Gamma_{\text{total}}$ in $N\bar{K} \rightarrow \Sigma(1750) \rightarrow \Sigma\pi$	DOCUMENT ID	TECN	COMMENT	$(\Gamma_1\Gamma_3)^{1/2}/\Gamma$
+0.17 ± 0.07	ZHANG 13A	DPWA	Multichannel	
-0.09 ± 0.05	GOPAL 77	DPWA	$\bar{K}N$ multichannel	

••• We do not use the following data for averages, fits, limits, etc. •••

+0.06 or +0.06	¹ MARTIN 77	DPWA	$\bar{K}N$ multichannel
0.13 ± 0.02	LANGBEIN 72	IPWA	$\bar{K}N$ multichannel

¹ The two MARTIN 77 values are from a T-matrix pole and from a Breit-Wigner fit.

$(\Gamma_1\Gamma_f)^{1/2}/\Gamma_{\text{total}}$ in $N\bar{K} \rightarrow \Sigma(1750) \rightarrow \Sigma\eta$	DOCUMENT ID	TECN	COMMENT	$(\Gamma_1\Gamma_4)^{1/2}/\Gamma$
0.23 ± 0.01	¹ JONES 74	HBC	Fits $\sigma(K^-p \rightarrow \Sigma^0\eta)$	

••• We do not use the following data for averages, fits, limits, etc. •••

seen	CLINE 69	DBC	Threshold bump
------	----------	-----	----------------

¹ An S-wave Breit-Wigner fit to the threshold cross section with no background and errors statistical only.

$(\Gamma_1\Gamma_f)^{1/2}/\Gamma_{\text{total}}$ in $N\bar{K} \rightarrow \Sigma(1750) \rightarrow \Sigma(1385)\pi, D\text{-wave}$	DOCUMENT ID	TECN	COMMENT	$(\Gamma_1\Gamma_5)^{1/2}/\Gamma$
+0.17 ± 0.07	ZHANG 13A	DPWA	Multichannel	
+0.18 ± 0.15	PREVOST 74	DPWA	$K^-N \rightarrow \Sigma(1385)\pi$	

$(\Gamma_1\Gamma_f)^{1/2}/\Gamma_{\text{total}}$ in $N\bar{K} \rightarrow \Sigma(1750) \rightarrow \Lambda(1520)\pi$	DOCUMENT ID	TECN	COMMENT	$(\Gamma_1\Gamma_6)^{1/2}/\Gamma$
0.032 ± 0.021	CAMERON 77	DPWA	P-wave decay	

••• We do not use the following data for averages, fits, limits, etc. •••

 $\Sigma(1750)$ REFERENCES

SARANTSEV 19	EPJ A55 180	A.V. Sarantsev et al.	(BONN, PNPI)
KAMANO 15	PR C92 025205	H. Kamano et al.	(ANL, OSAK)
ZHANG 13A	PR C88 035205	H. Zhang et al.	(KSU)
PDG 82	PL 111B 1	M. Roos et al.	(HELS, CIT, CERN)
GOPAL 80	Toronto Conf. 159	G.P. Gopal	(RHEL) IJP
ALSTON... 78	PR D18 182	M. Alston-Garnjost et al.	(LBL, MTHO+) IJP
Also	PRL 38 1007	M. Alston-Garnjost et al.	(LBL, MTHO+) IJP
CAMERON 77	NP B131 399	W. Cameron et al.	(RHEL, LOIC) IJP
GOPAL 77	NP B119 362	G.P. Gopal et al.	(LOIC, RHEL) IJP
MARTIN 77	NP B127 349	B.R. Martin, M.K. Pidcock, R.G. Moorhouse	(LOUC+) IJP
Also	NP B126 266	B.R. Martin, M.K. Pidcock	(LOUC)
Also	NP B126 285	B.R. Martin, M.K. Pidcock	(LOUC) IJP
CARROLL 76	PRL 37 806	A.S. Carroll et al.	(BNL) I
DEBELLEFON 76	NP B109 129	A. de Bellefon, A. Berthon	(CDEF) IJP
BAILLON 75	NP B94 39	P.H. Baillon, P.J. Lichfield	(CERN, RHEL) IJP
VANHORN 75	NP B87 145	A.J. van Horn	(LBL) IJP
Also	NP B87 157	A.J. van Horn	(LBL) IJP
CHU 74	NC 20A 35	R.Y.L. Chu et al.	(PLAT, TUFTS, BRAN) IJP
DEVENISH 74B	NP B81 330	R.C.E. Devenish, C.D. Froggatt, B.R. Martin	(DESY+) IJP
JONES 74	NP B73 141	M.D. Jones	(CHIC) IJP
PREVOST 74	NP B69 246	J. Prevost et al.	(SACL, CERN, HEID) IJP
LANGBEIN 72	NP B47 477	W. Langbein, F. Wagner	(MFIM) IJP
CLINE 69	LCN 2 407	D. Cline, R. Laumann, J. Mapp	(WISC)

 $\Sigma(1775) 5/2^-$

$$I(J^P) = I(5/2^-) \text{ Status: } ***$$

Discovered by GALTIERI 63, this resonance plays the same role as cornerstone for isospin-1 analyses in this region as the $\Lambda(1820)F_{05}$ does in the isospin-0 channel.

For most results published before 1974 (they are now obsolete), see our 1982 edition Physics Letters **111B** 1 (1982).

 $\Sigma(1775)$ POLE POSITION

REAL PART

VALUE (MeV)	DOCUMENT ID	TECN	COMMENT
1760 to 1780 (≈ 1770) OUR ESTIMATE			

1767 ± 4	SARANTSEV 19	DPWA	$\bar{K}N$ multichannel
1767 ± $\frac{2}{2}$	¹ KAMANO 15	DPWA	$\bar{K}N$ multichannel

••• We do not use the following data for averages, fits, limits, etc. •••

1759	ZHANG 13A	DPWA	$\bar{K}N$ multichannel
------	-----------	------	-------------------------

¹ From the preferred solution A in KAMANO 15.

-2xIMAGINARY PART

VALUE (MeV)	DOCUMENT ID	TECN	COMMENT
45 to 65 (≈ 55) OUR ESTIMATE			

122 ± 8	SARANTSEV 19	DPWA	$\bar{K}N$ multichannel
128 ± $\frac{4}{2}$	¹ KAMANO 15	DPWA	$\bar{K}N$ multichannel

••• We do not use the following data for averages, fits, limits, etc. •••

118	ZHANG 13A	DPWA	$\bar{K}N$ multichannel
-----	-----------	------	-------------------------

¹ From the preferred solution A in KAMANO 15.

 $\Sigma(1775)$ POLE RESIDUES

The normalized residue is the residue divided by $\Gamma_{\text{pole}}/2$.

Normalized residue in $N\bar{K} \rightarrow \Sigma(1775) \rightarrow N\bar{K}$

MODULUS	PHASE (°)	DOCUMENT ID	TECN	COMMENT
0.44 ± 0.09	-17 ± 10	SARANTSEV 19	DPWA	$\bar{K}N$ multichannel

••• We do not use the following data for averages, fits, limits, etc. •••

0.371	-32	¹ KAMANO 15	DPWA	$\bar{K}N$ multichannel
-------	-----	------------------------	------	-------------------------

¹ From the preferred solution A in KAMANO 15.

Normalized residue in $N\bar{K} \rightarrow \Sigma(1775) \rightarrow \Sigma\pi$

MODULUS	PHASE (°)	DOCUMENT ID	TECN	COMMENT
0.13 ± 0.03	10 ± 12	SARANTSEV 19	DPWA	$\bar{K}N$ multichannel

••• We do not use the following data for averages, fits, limits, etc. •••

0.115	-24	¹ KAMANO 15	DPWA	$\bar{K}N$ multichannel
-------	-----	------------------------	------	-------------------------

¹ From the preferred solution A in KAMANO 15.

Normalized residue in $N\bar{K} \rightarrow \Sigma(1775) \rightarrow \Lambda\pi$

MODULUS	PHASE (°)	DOCUMENT ID	TECN	COMMENT
0.47 ± 0.10	130 ± 15	SARANTSEV 19	DPWA	$\bar{K}N$ multichannel

••• We do not use the following data for averages, fits, limits, etc. •••

0.325	157	¹ KAMANO 15	DPWA	$\bar{K}N$ multichannel
-------	-----	------------------------	------	-------------------------

¹ From the preferred solution A in KAMANO 15.

$\Sigma(1775)$

Normalized residue in $N\bar{K} \rightarrow \Sigma(1775) \rightarrow \Sigma(1385)\pi$, D-wave

MODULUS	PHASE (°)	DOCUMENT ID	TECN	COMMENT
0.391	137	¹ KAMANO 15	DPWA	$\bar{K}N$ multichannel

¹ From the preferred solution A in KAMANO 15.

Normalized residue in $N\bar{K} \rightarrow \Sigma(1775) \rightarrow \Sigma(1385)\pi$, G-wave

MODULUS	PHASE (°)	DOCUMENT ID	TECN	COMMENT
0.0129	-58	¹ KAMANO 15	DPWA	$\bar{K}N$ multichannel

¹ From the preferred solution A in KAMANO 15.

Normalized residue in $N\bar{K} \rightarrow \Sigma(1775) \rightarrow N\bar{K}^*(892)$, S=1/2, D-wave

MODULUS	PHASE (°)	DOCUMENT ID	TECN	COMMENT
0.04±0.02	-100±60	SARANTSEV 19	DPWA	$\bar{K}N$ multichannel

Normalized residue in $N\bar{K} \rightarrow \Sigma(1775) \rightarrow N\bar{K}^*(892)$, S=3/2, D-wave

MODULUS	PHASE (°)	DOCUMENT ID	TECN	COMMENT
0.09±0.06	10±50	SARANTSEV 19	DPWA	$\bar{K}N$ multichannel

Normalized residue in $N\bar{K} \rightarrow \Sigma(1775) \rightarrow N\bar{K}^*(892)$, S=3/2, G-wave

MODULUS	PHASE (°)	DOCUMENT ID	TECN	COMMENT
0.04±0.02	-100±60	SARANTSEV 19	DPWA	$\bar{K}N$ multichannel

Normalized residue in $N\bar{K} \rightarrow \Sigma(1775) \rightarrow \Xi K$

MODULUS	PHASE (°)	DOCUMENT ID	TECN	COMMENT
0.02±0.01	-90±35	SARANTSEV 19	DPWA	$\bar{K}N$ multichannel

Normalized residue in $N\bar{K} \rightarrow \Sigma(1775) \rightarrow \Lambda(1520)\pi$, P-wave

MODULUS	PHASE (°)	DOCUMENT ID	TECN	COMMENT
0.09±0.03	10±30	SARANTSEV 19	DPWA	$\bar{K}N$ multichannel

Normalized residue in $N\bar{K} \rightarrow \Sigma(1775) \rightarrow \Lambda(1520)\pi$, F-wave

VALUE	DOCUMENT ID	TECN	COMMENT
0.01±0.01	SARANTSEV 19	DPWA	$\bar{K}N$ multichannel

Normalized residue in $N\bar{K} \rightarrow \Sigma(1775) \rightarrow \Delta\bar{K}$, D-wave

VALUE	DOCUMENT ID	TECN	COMMENT
0.02±0.02	SARANTSEV 19	DPWA	$\bar{K}N$ multichannel

$\Sigma(1775)$ MASS

VALUE (MeV)	DOCUMENT ID	TECN	COMMENT
1770 to 1780 (≈ 1775) OUR ESTIMATE			
1776±4	SARANTSEV 19	DPWA	$\bar{K}N$ multichannel
1778±1	ZHANG 13A	DPWA	$\bar{K}N$ multichannel
1778±5	GOPAL 80	DPWA	$\bar{K}N \rightarrow \bar{K}N$
1777±5	ALSTON... 78	DPWA	$\bar{K}N \rightarrow \bar{K}N$
1775±10	BAILLON 75	IPWA	$\bar{K}N \rightarrow \Lambda\pi$
1774±10	VANHORN 75	DPWA	$K^-p \rightarrow \Lambda\pi^0$
1772±6	KANE 74	DPWA	$K^-p \rightarrow \Sigma\pi$
••• We do not use the following data for averages, fits, limits, etc. •••			
1774±5	GOPAL 77	DPWA	$\bar{K}N$ multichannel
1772 or 1777	¹ MARTIN 77	DPWA	$\bar{K}N$ multichannel
1765	DEBELLEFON 76	IPWA	$K^-p \rightarrow \Lambda\pi^0$

¹ The two MARTIN 77 values are from a T-matrix pole and from a Breit-Wigner fit.

$\Sigma(1775)$ WIDTH

VALUE (MeV)	DOCUMENT ID	TECN	COMMENT
105 to 135 (≈ 120) OUR ESTIMATE			
124±8	SARANTSEV 19	DPWA	$\bar{K}N$ multichannel
131±3	ZHANG 13A	DPWA	$\bar{K}N$ multichannel
137±10	GOPAL 80	DPWA	$\bar{K}N \rightarrow \bar{K}N$
116±10	ALSTON... 78	DPWA	$\bar{K}N \rightarrow \bar{K}N$
125±15	BAILLON 75	IPWA	$\bar{K}N \rightarrow \Lambda\pi$
146±18	VANHORN 75	DPWA	$K^-p \rightarrow \Lambda\pi^0$
154±10	KANE 74	DPWA	$K^-p \rightarrow \Sigma\pi$
••• We do not use the following data for averages, fits, limits, etc. •••			
130±10	GOPAL 77	DPWA	$\bar{K}N$ multichannel
102 or 103	¹ MARTIN 77	DPWA	$\bar{K}N$ multichannel
120	DEBELLEFON 76	IPWA	$K^-p \rightarrow \Lambda\pi^0$

¹ The two MARTIN 77 values are from a T-matrix pole and from a Breit-Wigner fit.

$\Sigma(1775)$ DECAY MODES

Mode	Fraction (Γ_i/Γ)
Γ_1 $N\bar{K}$	37–43%
Γ_2 $\Lambda\pi$	14–20%
Γ_3 $\Sigma\pi$	2–5%
Γ_4 $\Sigma(1385)\pi$	8–12%
Γ_5 $\Sigma(1385)\pi$, D-wave	
Γ_6 $\Sigma(1385)\pi$, G-wave	

Γ_7	$\Lambda(1520)\pi$, P-wave	17–23%
Γ_8	$\Sigma\pi\pi$	
Γ_9	$\Delta(1232)\bar{K}$, D-wave	
Γ_{10}	$N\bar{K}^*(892)$, S=1/2	
Γ_{11}	$N\bar{K}^*(892)$, S=1/2, D-wave	
Γ_{12}	$N\bar{K}^*(892)$, S=3/2, D-wave	
Γ_{13}	$N\bar{K}^*(892)$, S=3/2, G-wave	

$\Sigma(1775)$ BRANCHING RATIOS

See “Sign conventions for resonance couplings” in the Note on Λ and Σ Resonances. Also, the errors quoted do not include uncertainties due to the parametrization used in the partial-wave analyses and are thus too small.

$\Gamma(N\bar{K})/\Gamma_{total}$	VALUE	DOCUMENT ID	TECN	COMMENT	Γ_1/Γ
	0.37 to 0.43 OUR ESTIMATE				
	0.43±0.09	SARANTSEV 19	DPWA	$\bar{K}N$ multichannel	
	0.40±0.01	ZHANG 13A	DPWA	$\bar{K}N$ multichannel	
	0.40±0.02	GOPAL 80	DPWA	$\bar{K}N \rightarrow \bar{K}N$	
	0.37±0.03	ALSTON... 78	DPWA	$\bar{K}N \rightarrow \bar{K}N$	
	••• We do not use the following data for averages, fits, limits, etc. •••				
	0.402	¹ KAMANO 15	DPWA	Multichannel	
	0.41±0.03	GOPAL 77	DPWA	See GOPAL 80	
	0.37 or 0.36	² MARTIN 77	DPWA	$\bar{K}N$ multichannel	

¹ From the preferred solution A in KAMANO 15.
² The two MARTIN 77 values are from a T-matrix pole and from a Breit-Wigner fit.

$\Gamma(\Lambda\pi)/\Gamma_{total}$	VALUE	DOCUMENT ID	TECN	COMMENT	Γ_2/Γ
	0.49±0.10	SARANTSEV 19	DPWA	$\bar{K}N$ multichannel	
	••• We do not use the following data for averages, fits, limits, etc. •••				
	0.244	¹ KAMANO 15	DPWA	$\bar{K}N$ multichannel	

¹ From the preferred solution A in KAMANO 15.

$\Gamma(\Lambda\pi)/\Gamma(N\bar{K})$	VALUE	DOCUMENT ID	TECN	COMMENT	Γ_2/Γ_1
	0.33±0.05	UHLIG 67	HBC	K^-p 0.9 GeV/c	

$\Gamma(\Sigma\pi)/\Gamma_{total}$	VALUE	DOCUMENT ID	TECN	COMMENT	Γ_3/Γ
	0.035±0.010	SARANTSEV 19	DPWA	$\bar{K}N$ multichannel	
	••• We do not use the following data for averages, fits, limits, etc. •••				
	0.042	¹ KAMANO 15	DPWA	$\bar{K}N$ multichannel	

¹ From the preferred solution A in KAMANO 15.

$\Gamma(\Sigma(1385)\pi)/\Gamma(N\bar{K})$	VALUE	DOCUMENT ID	TECN	COMMENT	Γ_4/Γ_1
	0.25±0.09	UHLIG 67	HBC	K^-p 0.9 GeV/c	

$\Gamma(\Sigma(1385)\pi, D-wave)/\Gamma_{total}$	VALUE	DOCUMENT ID	TECN	COMMENT	Γ_5/Γ
	••• We do not use the following data for averages, fits, limits, etc. •••				
	0.309	¹ KAMANO 15	DPWA	Multichannel	

¹ From the preferred solution A in KAMANO 15.

$\Gamma(\Sigma(1385)\pi, G-wave)/\Gamma_{total}$	VALUE	DOCUMENT ID	TECN	COMMENT	Γ_6/Γ
	••• We do not use the following data for averages, fits, limits, etc. •••				
	not seen	¹ KAMANO 15	DPWA	Multichannel	

¹ From the preferred solution A in KAMANO 15.

$\Gamma(\Lambda(1520)\pi, P-wave)/\Gamma_{total}$	VALUE	DOCUMENT ID	TECN	COMMENT	Γ_7/Γ
	0.02±0.01	SARANTSEV 19	DPWA	$\bar{K}N$ multichannel	

$\Gamma(\Lambda(1520)\pi, P-wave)/\Gamma(N\bar{K})$	VALUE	DOCUMENT ID	TECN	COMMENT	Γ_7/Γ_1
	0.28±0.05	UHLIG 67	HBC	K^-p 0.9 GeV/c	

$\Gamma(\Sigma\pi\pi)/\Gamma_{total}$	VALUE	DOCUMENT ID	TECN	COMMENT	Γ_8/Γ
	••• We do not use the following data for averages, fits, limits, etc. •••				
	0.12	¹ ARMENTEROS68c	HDBC	$K^-N \rightarrow \Sigma\pi\pi$	

¹ For about 3/4 of this, the $\Sigma\pi$ system has $l=0$ and is almost entirely $\Lambda(1520)$. For the rest, the $\Sigma\pi$ has $l=1$, which is about what is expected from the known $\Sigma(1775) \rightarrow \Sigma(1385)\pi$ rate, as seen in $\Lambda\pi\pi$.

$\Gamma(N\bar{K}^*(892), S=1/2, D-wave)/\Gamma_{total}$	VALUE	DOCUMENT ID	TECN	COMMENT	Γ_{11}/Γ
	••• We do not use the following data for averages, fits, limits, etc. •••				
	not seen	¹ KAMANO 15	DPWA	Multichannel	

¹ From the preferred solution A in KAMANO 15.

Baryon Particle Listings

 $\Sigma(1775)$, $\Sigma(1780)$, $\Sigma(1880)$ $\Gamma(N\bar{K}^*(892), S=3/2, D\text{-wave})/\Gamma_{\text{total}}$ Γ_{12}/Γ

VALUE	DOCUMENT ID	TECN	COMMENT
0.003	1 KAMANO 15	DPWA	Multichannel

• • • We do not use the following data for averages, fits, limits, etc. • • •

¹ From the preferred solution A in KAMANO 15.

 $\Gamma(N\bar{K}^*(892), S=3/2, G\text{-wave})/\Gamma_{\text{total}}$ Γ_{13}/Γ

VALUE	DOCUMENT ID	TECN	COMMENT
not seen	1 KAMANO 15	DPWA	Multichannel

• • • We do not use the following data for averages, fits, limits, etc. • • •

¹ From the preferred solution A in KAMANO 15.

 $(\Gamma_1\Gamma_2)^{1/2}/\Gamma_{\text{total}}$ in $N\bar{K} \rightarrow \Sigma(1775) \rightarrow \Lambda\pi$ $(\Gamma_1\Gamma_2)^{1/2}/\Gamma$

VALUE	DOCUMENT ID	TECN	COMMENT
-0.31 ± 0.01	ZHANG 13A	DPWA	Multichannel
-0.28 ± 0.03	GOPAL 77	DPWA	$\bar{K}N$ multichannel
-0.25 ± 0.02	BAILLON 75	IPWA	$\bar{K}N \rightarrow \Lambda\pi$
-0.28 +0.04 -0.05	VANHORN 75	DPWA	$K^-p \rightarrow \Lambda\pi^0$
-0.259 ± 0.048	DEVENISH 74B	Fixed- t dispersion rel.	

• • • We do not use the following data for averages, fits, limits, etc. • • •

-0.29 or -0.28	1 MARTIN 77	DPWA	$\bar{K}N$ multichannel
-0.30	DEBELLEFON 76	IPWA	$K^-p \rightarrow \Lambda\pi^0$

¹ The two MARTIN 77 values are from a T-matrix pole and from a Breit-Wigner fit.

 $(\Gamma_1\Gamma_2)^{1/2}/\Gamma_{\text{total}}$ in $N\bar{K} \rightarrow \Sigma(1775) \rightarrow \Sigma\pi$ $(\Gamma_1\Gamma_2)^{1/2}/\Gamma$

VALUE	DOCUMENT ID	TECN	COMMENT
+0.08 ± 0.01	ZHANG 13A	DPWA	Multichannel
+0.13 ± 0.02	GOPAL 77	DPWA	$\bar{K}N$ multichannel
0.09 ± 0.01	KANE 74	DPWA	$K^-p \rightarrow \Sigma\pi$

• • • We do not use the following data for averages, fits, limits, etc. • • •

+0.08 or +0.08	1 MARTIN 77	DPWA	$\bar{K}N$ multichannel
----------------	-------------	------	-------------------------

¹ The two MARTIN 77 values are from a T-matrix pole and from a Breit-Wigner fit.

 $(\Gamma_1\Gamma_2)^{1/2}/\Gamma_{\text{total}}$ in $N\bar{K} \rightarrow \Sigma(1775) \rightarrow \Sigma(1385)\pi, D\text{-wave}$ $(\Gamma_1\Gamma_2)^{1/2}/\Gamma$

VALUE	DOCUMENT ID	TECN	COMMENT
-0.12 ± 0.01	ZHANG 13A	DPWA	Multichannel
-0.184 ± 0.011	1 CAMERON 78	DPWA	$K^-p \rightarrow \Sigma(1385)\pi$
+0.20 ± 0.02	PREVOST 74	DPWA	$K^-N \rightarrow \Sigma(1385)\pi$

• • • We do not use the following data for averages, fits, limits, etc. • • •

0.32 ± 0.06	SIMS 68	DBC	$K^-N \rightarrow \Lambda\pi\pi$
0.24 ± 0.03	ARMENTEROS67c	HBC	$K^-p \rightarrow \Lambda\pi\pi$

¹ The CAMERON 78 upper limit on G-wave decay is 0.03.

 $(\Gamma_1\Gamma_2)^{1/2}/\Gamma_{\text{total}}$ in $N\bar{K} \rightarrow \Sigma(1775) \rightarrow \Lambda(1520)\pi, P\text{-wave}$ $(\Gamma_1\Gamma_2)^{1/2}/\Gamma$

VALUE	DOCUMENT ID	TECN	COMMENT
-0.06 ± 0.01	ZHANG 13A	DPWA	Multichannel
-0.305 ± 0.010	1 CAMERON 77	DPWA	$K^-p \rightarrow \Lambda(1520)\pi^0$
0.31 ± 0.02	BARLETTA 72	DPWA	$K^-p \rightarrow \Lambda(1520)\pi^0$
0.27 ± 0.03	ARMENTEROS65c	HBC	$K^-p \rightarrow \Lambda(1520)\pi^0$

¹ This rate combines P-wave- and F-wave decays. The CAMERON 77 results for the separate P-wave- and F-wave decays are -0.303 ± 0.010 and -0.037 ± 0.014 . The published signs have been changed here to be in accord with the baryon-first convention.

 $(\Gamma_1\Gamma_2)^{1/2}/\Gamma_{\text{total}}$ in $N\bar{K} \rightarrow \Sigma(1775) \rightarrow \Delta(1232)\bar{K}, D\text{-wave}$ $(\Gamma_1\Gamma_2)^{1/2}/\Gamma$

VALUE	DOCUMENT ID	TECN	COMMENT
+0.06 ± 0.03	ZHANG 13A	DPWA	Multichannel

 $(\Gamma_1\Gamma_2)^{1/2}/\Gamma_{\text{total}}$ in $N\bar{K} \rightarrow \Sigma(1775) \rightarrow N\bar{K}^*(892), S=1/2$ $(\Gamma_1\Gamma_2)^{1/2}/\Gamma$

VALUE	DOCUMENT ID	TECN	COMMENT
+0.04 ± 0.01	ZHANG 13A	DPWA	Multichannel

 $(\Gamma_1\Gamma_2)^{1/2}/\Gamma_{\text{total}}$ in $N\bar{K} \rightarrow \Sigma(1775) \rightarrow N\bar{K}^*(892), S=3/2, D\text{-wave}$ $(\Gamma_1\Gamma_2)^{1/2}/\Gamma$

VALUE	DOCUMENT ID	TECN	COMMENT
+0.04 ± 0.01	ZHANG 13A	DPWA	Multichannel

 $\Sigma(1775)$ REFERENCES

SARANTSEV 19	EPJ A55 180	A.V. Sarantsev et al.	(BONN, PNPI)
KAMANO 15	PR C72 025205	H. Kamano et al.	(ANL, OSAK)
ZHANG 13A	PR C88 035205	H. Zhang et al.	(KSU)
PDG 82	PL 111B 1	M. Roos et al.	(HELSE, CIT, CERN)
GOPAL 77	Toronto Conf. 159	G.P. Gopal	(RHEL) IJP
ALSTON... 78	PR D18 182	M. Alston-Garnjost et al.	(LBL, MTHO+) IJP
Also	PRL 38 1007	M. Alston-Garnjost et al.	(LBL, MTHO+) IJP
CAMERON 78	NP B143 189	W. Cameron et al.	(RHEL, LOIC) IJP
CAMERON 77	NP B131 399	W. Cameron et al.	(RHEL, LOIC) IJP
GOPAL 77	NP B119 362	G.P. Gopal et al.	(LOIC, RHEL) IJP
MARTIN 77	NP B127 349	B.R. Martin, M.K. Pidcock, R.G. Moorhouse	(LOUC+) IJP
Also	NP B126 266	B.R. Martin, M.K. Pidcock	(LOUC) IJP
Also	NP B126 285	B.R. Martin, M.K. Pidcock	(LOUC) IJP
DEBELLEFON 76	NP B109 129	A. de Bellefon, A. Berthon	(CDEF) IJP
BAILLON 75	NP B94 39	P.H. Baillon, P.J. Lichfield	(CERN, RHEL) IJP

VANHORN 75	NP B87 145	A.J. van Horn	(LBL) IJP
Also	NP B87 157	A.J. van Horn	(LBL) IJP
DEVENISH 74B	NP B81 330	R.C.E. Devenish, C.D. Froggatt, B.R. Martin	(DESY+) IJP
KANE 74	LBL-2452	D.F. Kane	(LBL) IJP
PREVOST 74	NP B69 246	J. Prevost et al.	(SACL, CERN, HEID) IJP
BARLETTA 72	NP B40 45	W.A. Barletta	(EFI) IJP
Also	PRL 17 841	S. Fenster et al.	(CHIC, ANL, CERN) IJP
ARMENTEROS 68c	NP B8 216	R. Armenteros et al.	(CERN, HEID, SACL) IJP
SIMS 68	PRL 21 1413	W.H. Sims et al.	(FSU, TUFTS, BRAN) IJP
ARMENTEROS 67c	ZPHY 202 486	R. Armenteros et al.	(CERN, HEID, SACL) IJP
UHLIG 67	PR 155 1448	R.P. Uhlig et al.	(UMD, NRL) IJP
ARMENTEROS 65c	PL 19 338	R. Armenteros et al.	(CERN, HEID, SACL) IJP
GALTIERI 63	PL 6 296	A. Galtieri, A. Hussain, R. Tripp	(LRL) IJP

 $\Sigma(1780) 3/2^+$

$$I(J^P) = 1(\frac{3}{2}^+) \text{ Status: } *$$

OMITTED FROM SUMMARY TABLE
was $\Sigma(1730)$

 $\Sigma(1780)$ MASS

VALUE (MeV)	DOCUMENT ID	TECN	COMMENT
1730 to 1830 (≈ 1780) OUR ESTIMATE			
1727 ± 27	ZHANG 13A	DPWA	Multichannel
1798 or 1802	1 MARTIN 77	DPWA	$\bar{K}N$ multichannel
1720 ± 30	2 BAILLON 75	IPWA	$\bar{K}N \rightarrow \Lambda\pi$
1840 ± 10	LANGBEIN 72	IPWA	$\bar{K}N$ multichannel

¹ The two MARTIN 77 values are from a T-matrix pole and from a Breit-Wigner fit.
² From solution 1 of BAILLON 75; not present in solution 2.

 $\Sigma(1780)$ WIDTH

VALUE (MeV)	DOCUMENT ID	TECN	COMMENT
100 to 300 (≈ 200) OUR ESTIMATE			
276 ± 87	ZHANG 13A	DPWA	Multichannel
93 or 93	1 MARTIN 77	DPWA	$\bar{K}N$ multichannel
120 ± 30	2 BAILLON 75	IPWA	$\bar{K}N \rightarrow \Lambda\pi$
120 ± 10	LANGBEIN 72	IPWA	$\bar{K}N$ multichannel

¹ The two MARTIN 77 values are from a T-matrix pole and from a Breit-Wigner fit.
² From solution 1 of BAILLON 75; not present in solution 2.

 $\Sigma(1780)$ DECAY MODES

Mode	Fraction (Γ_i/Γ)
Γ_1 $N\bar{K}$	(2.0 ± 1.0) %
Γ_2 $\Lambda\pi$	(70 ± 17) %
Γ_3 $\Sigma\pi$	(12 ± 6) %

 $\Sigma(1780)$ BRANCHING RATIOS

$\Gamma(N\bar{K})/\Gamma_{\text{total}}$	DOCUMENT ID	TECN	COMMENT	Γ_1/Γ
0.02 ± 0.01	ZHANG 13A	DPWA	Multichannel	

$\Gamma(\Lambda\pi)/\Gamma_{\text{total}}$	DOCUMENT ID	TECN	COMMENT	Γ_2/Γ
0.70 ± 0.17	ZHANG 13A	DPWA	Multichannel	

$\Gamma(\Sigma\pi)/\Gamma_{\text{total}}$	DOCUMENT ID	TECN	COMMENT	Γ_3/Γ
0.12 ± 0.06	ZHANG 13A	DPWA	Multichannel	

 $\Sigma(1780)$ REFERENCES

ZHANG 13A	PR C88 035205	H. Zhang et al.	(KSU)
MARTIN 77	NP B127 349	B.R. Martin, M.K. Pidcock, R.G. Moorhouse	(LOUC+) IJP
BAILLON 75	NP B94 39	P.H. Baillon, P.J. Lichfield	(CERN, RHEL) IJP
LANGBEIN 72	NP B47 477	W. Langbein, F. Wagner	(MIMP) IJP

 $\Sigma(1880) 1/2^+$

$$I(J^P) = 1(\frac{1}{2}^+) \text{ Status: } **$$

OMITTED FROM SUMMARY TABLE

A P_{11} resonance is suggested by several partial-wave analyses, but with wide variations in the mass and other parameters. We list here all claims which lie well above the $P_{11} \Sigma(1770)$.

 $\Sigma(1880)$ POLE POSITION

VALUE (MeV)	DOCUMENT ID	TECN	COMMENT
1776	ZHANG 13A	DPWA	Multichannel

• • • We do not use the following data for averages, fits, limits, etc. • • •

Baryon Particle Listings
 $\Sigma(1880), \Sigma(1900)$

-2xIMAGINARY PART

VALUE (MeV)	DOCUMENT ID	TECN	COMMENT
• • • We do not use the following data for averages, fits, limits, etc. • • •			
270	ZHANG	13A	DPWA Multichannel

$\Sigma(1880)$ MASS

VALUE (MeV)	DOCUMENT ID	TECN	COMMENT
1820 to 1940 (≈ 1880) OUR ESTIMATE			
1821 \pm 17	ZHANG	13A	DPWA Multichannel
1826 \pm 20	GOPAL	80	DPWA $\bar{K}N \rightarrow \bar{K}N$
1870 \pm 10	CAMERON	78B	DPWA $K^-p \rightarrow N\bar{K}^*$
1847 or 1863	1 MARTIN	77	DPWA $\bar{K}N$ multichannel
1960 \pm 30	2 BAILLON	75	IPWA $\bar{K}N \rightarrow \Lambda\pi$
1985 \pm 50	VANHORN	75	DPWA $K^-p \rightarrow \Lambda\pi^0$
1898	3 LEA	73	DPWA Multichannel K-matrix
~ 1850	ARMENTEROS70	IPWA	$\bar{K}N \rightarrow \bar{K}N$
1950 \pm 50	BARBARO...	70	DPWA $K^-N \rightarrow \Lambda\pi$
1920 \pm 30	LITCHFIELD	70	DPWA $K^-N \rightarrow \Lambda\pi$
1850	BAILEY	69	DPWA $\bar{K}N \rightarrow \bar{K}N$
1882 \pm 40	SMART	68	DPWA $K^-N \rightarrow \Lambda\pi$

$\Sigma(1880)$ WIDTH

VALUE (MeV)	DOCUMENT ID	TECN	COMMENT
100 to 300 (≈ 200) OUR ESTIMATE			
300 \pm 59	ZHANG	13A	DPWA Multichannel
86 \pm 15	GOPAL	80	DPWA $\bar{K}N \rightarrow \bar{K}N$
80 \pm 10	CAMERON	78B	DPWA $K^-p \rightarrow N\bar{K}^*$
216 or 220	1 MARTIN	77	DPWA $\bar{K}N$ multichannel
260 \pm 40	2 BAILLON	75	IPWA $\bar{K}N \rightarrow \Lambda\pi$
220 \pm 140	VANHORN	75	DPWA $K^-p \rightarrow \Lambda\pi^0$
222	3 LEA	73	DPWA Multichannel K-matrix
~ 30	ARMENTEROS70	IPWA	$\bar{K}N \rightarrow \bar{K}N$
200 \pm 50	BARBARO...	70	DPWA $K^-N \rightarrow \Lambda\pi$
170 \pm 40	LITCHFIELD	70	DPWA $K^-N \rightarrow \Lambda\pi$
200	BAILEY	69	DPWA $\bar{K}N \rightarrow \bar{K}N$
222 \pm 150	SMART	68	DPWA $K^-N \rightarrow \Lambda\pi$

$\Sigma(1880)$ DECAY MODES

Mode	Fraction (Γ_i/Γ)
Γ_1 $N\bar{K}$	0.10 to 0.30 (≈ 0.20)
Γ_2 $\Lambda\pi$	
Γ_3 $\Sigma\pi$	
Γ_4 $\Lambda(1520)\pi, D$ -wave	(2.0 \pm 1.0) %
Γ_5 $N\bar{K}^*(892), S=1/2, P$ -wave	
Γ_6 $N\bar{K}^*(892), S=3/2, P$ -wave	
Γ_7 $\Delta(1232)\bar{K}, P$ -wave	(39 \pm 8) %

$\Sigma(1880)$ BRANCHING RATIOS

See "Sign conventions for resonance couplings" in the Note on Λ and Σ Resonances.

$\Gamma(N\bar{K})/\Gamma_{total}$	DOCUMENT ID	TECN	COMMENT	Γ_1/Γ
0.10 to 0.30 (≈ 0.20) OUR ESTIMATE				
0.10 \pm 0.03	ZHANG	13A	DPWA Multichannel	
0.06 \pm 0.02	GOPAL	80	DPWA $\bar{K}N \rightarrow \bar{K}N$	
0.27 or 0.27	1 MARTIN	77	DPWA $\bar{K}N$ multichannel	
0.31	3 LEA	73	DPWA Multichannel K-matrix	
0.20	ARMENTEROS70	IPWA	$\bar{K}N \rightarrow \bar{K}N$	
0.22	BAILEY	69	DPWA $\bar{K}N \rightarrow \bar{K}N$	

$(\Gamma_1\Gamma_7)^{1/2}/\Gamma_{total}$ in $N\bar{K} \rightarrow \Sigma(1880) \rightarrow \Lambda\pi$	DOCUMENT ID	TECN	COMMENT	$(\Gamma_1\Gamma_2)^{1/2}/\Gamma$
VALUE				
-0.24 or -0.24	1 MARTIN	77	DPWA $\bar{K}N$ multichannel	
-0.12 \pm 0.02	2 BAILLON	75	IPWA $\bar{K}N \rightarrow \Lambda\pi$	
+0.05 \pm 0.07	VANHORN	75	DPWA $K^-p \rightarrow \Lambda\pi^0$	
-0.169 \pm 0.119	DEVENISH	74B	Fixed- t dispersion rel.	
-0.30	3 LEA	73	DPWA Multichannel K-matrix	
-0.09 \pm 0.04	BARBARO...	70	DPWA $K^-N \rightarrow \Lambda\pi$	
-0.14 \pm 0.03	LITCHFIELD	70	DPWA $K^-N \rightarrow \Lambda\pi$	
-0.11 \pm 0.03	SMART	68	DPWA $K^-N \rightarrow \Lambda\pi$	

$(\Gamma_1\Gamma_7)^{1/2}/\Gamma_{total}$ in $N\bar{K} \rightarrow \Sigma(1880) \rightarrow \Sigma\pi$	DOCUMENT ID	TECN	COMMENT	$(\Gamma_1\Gamma_3)^{1/2}/\Gamma$
VALUE				
+0.30 or +0.29	1 MARTIN	77	DPWA $\bar{K}N$ multichannel	
not seen	3 LEA	73	DPWA Multichannel K-matrix	

$\Gamma(\Lambda(1520)\pi, D$ -wave)/ Γ_{total}	DOCUMENT ID	TECN	COMMENT	Γ_4/Γ
VALUE				
0.02 \pm 0.01	ZHANG	13A	DPWA Multichannel	

$(\Gamma_1\Gamma_7)^{1/2}/\Gamma_{total}$ in $N\bar{K} \rightarrow \Sigma(1880) \rightarrow N\bar{K}^*(892), S=1/2, P$ -wave ($\Gamma_1\Gamma_5$) ^{1/2} / Γ	DOCUMENT ID	TECN	COMMENT
VALUE			
-0.05 \pm 0.03	4 CAMERON	78B	DPWA $K^-p \rightarrow N\bar{K}^*$

$(\Gamma_1\Gamma_7)^{1/2}/\Gamma_{total}$ in $N\bar{K} \rightarrow \Sigma(1880) \rightarrow N\bar{K}^*(892), S=3/2, P$ -wave ($\Gamma_1\Gamma_6$) ^{1/2} / Γ	DOCUMENT ID	TECN	COMMENT
VALUE			
+0.11 \pm 0.03	CAMERON	78B	DPWA $K^-p \rightarrow N\bar{K}^*$

$\Gamma(\Delta(1232)\bar{K}, P$ -wave)/ Γ_{total}	DOCUMENT ID	TECN	COMMENT	Γ_7/Γ
VALUE				
0.39 \pm 0.08	ZHANG	13A	DPWA Multichannel	

$\Sigma(1880)$ FOOTNOTES

- The two MARTIN 77 values are from a T-matrix pole and from a Breit-Wigner fit.
- From solution 1 of BAILLON 75; not present in solution 2.
- Only unconstrained states from table 1 of LEA 73 are listed.
- The published sign has been changed to be in accord with the baryon-first convention.

$\Sigma(1880)$ REFERENCES

ZHANG	13A	PR C88 035205	H. Zhang et al.	(KSU)
GOPAL	80	Toronto Conf. 159	G.P. Gopal	(RHEL) IJP
CAMERON	78B	NP B146 327	W. Cameron et al.	(RHEL, LOIC) IJP
MARTIN	77	NP B127 349	B.R. Martin, M.K. Pidcock, R.G. Moorhouse	(LOUC+) IJP
		Also NP B126 266	B.R. Martin, M.K. Pidcock	(LOUC) IJP
		Also NP B126 285	B.R. Martin, M.K. Pidcock	(LOUC) IJP
BAILLON	75	NP B94 39	P.H. Baillon, P.J. Litchfield	(CERN, RHEL) IJP
VANHORN	75	NP B87 145	A.J. van Horn	(LBL) IJP
		Also NP B87 157	A.J. van Horn	(LBL) IJP
DEVENISH	74B	NP B81 330	R.C.E. Devenish, C.D. Froggatt, B.R. Martin	(DESY+) IJP
LEA	73	NP B56 77	A.T. Lea et al.	(RHEL, LOUC, GLAS, AARH) IJP
ARMENTEROS	70	Duke Conf. 123	R. Armenteros et al.	(CERN, HEID, SACL) IJP
		Hyperon Resonances, 1970		
BARBARO...	70	Duke Conf. 173	A. Barbaro-Galieri	(LRL) IJP
		Hyperon Resonances, 1970		
LITCHFIELD	70	NP B22 269	P.J. Litchfield	(RHEL) IJP
BAILEY	69	Thesis UCRL 50617	J.M. Bailey	(LLL) IJP
SMART	68	PR 169 1330	W.M. Smart	(LRL) IJP

$\Sigma(1900) 1/2^-$

$I(J^P) = 1(\frac{1}{2}^-)$ Status: **

OMITTED FROM SUMMARY TABLE

$\Sigma(1900)$ POLE POSITION

REAL PART	DOCUMENT ID	TECN	COMMENT
VALUE			
1936 \pm 10	SARANTSEV	19	DPWA $\bar{K}N$ multichannel

-2xIMAGINARY PART

VALUE	DOCUMENT ID	TECN	COMMENT
150 \pm 25	SARANTSEV	19	DPWA $\bar{K}N$ multichannel

$\Sigma(1900)$ POLE RESIDUES

The normalized residue is the residue divided by $\Gamma_{pole}/2$.

Normalized residue in $N\bar{K} \rightarrow \Sigma(1900) \rightarrow N\bar{K}$	DOCUMENT ID	TECN	COMMENT
MODULUS PHASE ($^\circ$)			
0.45 \pm 0.09 90 \pm 25	SARANTSEV	19	DPWA $\bar{K}N$ multichannel

Normalized residue in $N\bar{K} \rightarrow \Sigma(1900) \rightarrow \Sigma\pi$	DOCUMENT ID	TECN	COMMENT
MODULUS PHASE ($^\circ$)			
0.38 \pm 0.08 95 \pm 20	SARANTSEV	19	DPWA $\bar{K}N$ multichannel

Normalized residue in $N\bar{K} \rightarrow \Sigma(1900) \rightarrow \Sigma\eta$	DOCUMENT ID	TECN	COMMENT
MODULUS PHASE ($^\circ$)			
0.03 \pm 0.01 20 \pm 20	SARANTSEV	19	DPWA $\bar{K}N$ multichannel

Normalized residue in $N\bar{K} \rightarrow \Sigma(1900) \rightarrow \Lambda\pi$	DOCUMENT ID	TECN	COMMENT
MODULUS PHASE ($^\circ$)			
0.14 \pm 0.05 -160 \pm 50	SARANTSEV	19	DPWA $\bar{K}N$ multichannel

Normalized residue in $N\bar{K} \rightarrow \Sigma(1900) \rightarrow \Xi K$	DOCUMENT ID	TECN	COMMENT
MODULUS PHASE ($^\circ$)			
0.08 \pm 0.05 75 \pm 25	SARANTSEV	19	DPWA $\bar{K}N$ multichannel

Normalized residue in $N\bar{K} \rightarrow \Sigma(1900) \rightarrow \Sigma(1385)\pi$	DOCUMENT ID	TECN	COMMENT
MODULUS PHASE ($^\circ$)			
0.16 \pm 0.05 40 \pm 30	SARANTSEV	19	DPWA $\bar{K}N$ multichannel

Normalized residue in $N\bar{K} \rightarrow \Sigma(1900) \rightarrow \Lambda(1520)\pi$	DOCUMENT ID	TECN	COMMENT
MODULUS PHASE ($^\circ$)			
0.04 \pm 0.02 -25 \pm 40	SARANTSEV	19	DPWA $\bar{K}N$ multichannel

Baryon Particle Listings

 $\Sigma(1900)$, $\Sigma(1910)$ Normalized residue in $N\bar{K} \rightarrow \Sigma(1900) \rightarrow \Delta\bar{K}$

MODULUS	PHASE (°)	DOCUMENT ID	TECN	COMMENT
0.11 ± 0.04	60 ± 30	SARANTSEV 19	DPWA	$\bar{K}N$ multichannel

Normalized residue in $N\bar{K} \rightarrow \Sigma(1900) \rightarrow N\bar{K}^*(892)$, $S=1/2$, S -wave

MODULUS	PHASE (°)	DOCUMENT ID	TECN	COMMENT
0.17 ± 0.06	50 ± 50	SARANTSEV 19	DPWA	$\bar{K}N$ multichannel

Normalized residue in $N\bar{K} \rightarrow \Sigma(1900) \rightarrow N\bar{K}^*(892)$, $S=3/2$, D -wave

MODULUS	PHASE (°)	DOCUMENT ID	TECN	COMMENT
0.05 ± 0.04		SARANTSEV 19	DPWA	$\bar{K}N$ multichannel

 $\Sigma(1900)$ MASS

VALUE (MeV)	DOCUMENT ID	TECN	COMMENT
1900 to 1950 (≈ 1925) OUR ESTIMATE			
1938 ± 12	SARANTSEV 19	DPWA	$\bar{K}N$ multichannel
1900 ± 21	ZHANG 13A	DPWA	$\bar{K}N$ multichannel
1944 ± 15	GOPAL 80	DPWA	$\bar{K}N \rightarrow \bar{K}N$
1755 or 1834	¹ MARTIN 77	DPWA	$\bar{K}N$ multichannel
2004 ± 40	VANHORN 75	DPWA	$K^-p \rightarrow \Lambda\pi^0$
● ● ● We do not use the following data for averages, fits, limits, etc. ● ● ●			
1955 ± 15	GOPAL 77	DPWA	$\bar{K}N$ multichannel
¹ The two MARTIN 77 values are from a T-matrix pole and from a Breit-Wigner fit.			

 $\Sigma(1900)$ WIDTH

VALUE (MeV)	DOCUMENT ID	TECN	COMMENT
140 to 190 (≈ 165) OUR ESTIMATE			
155 ± 30	SARANTSEV 19	DPWA	$\bar{K}N$ multichannel
191 ± 47	ZHANG 13A	DPWA	$\bar{K}N$ multichannel
215 ± 25	GOPAL 80	DPWA	$\bar{K}N \rightarrow \bar{K}N$
413 or 450	¹ MARTIN 77	DPWA	$\bar{K}N$ multichannel
116 ± 40	VANHORN 75	DPWA	$K^-p \rightarrow \Lambda\pi^0$
● ● ● We do not use the following data for averages, fits, limits, etc. ● ● ●			
170 ± 40	GOPAL 77	DPWA	$\bar{K}N$ multichannel
¹ The two MARTIN 77 values are from a T-matrix pole and from a Breit-Wigner fit.			

 $\Sigma(1900)$ DECAY MODES

Mode	Fraction (Γ_i/Γ)
Γ_1 $N\bar{K}$	0.40 to 0.70 (≈ 0.55)
Γ_2 $\Sigma\pi$	0.10 to 0.40 (≈ 0.25)
Γ_3 $\Sigma\eta$	(1.0 \pm 1.0) %
Γ_4 $\Lambda\pi$	(6.0 \pm 2.0) %
Γ_5 ΞK	(3.0 \pm 2.0) %
Γ_6 $\Sigma(1385)\pi$	(7.0 \pm 3.0) %
Γ_7 $\Lambda(1520)\pi$	
Γ_8 $\Delta\bar{K}$	(2.5 \pm 1.0) %
Γ_9 $N\bar{K}^*(892)$, $S=1/2$, S -wave	(7.0 \pm 3.0) %
Γ_{10} $N\bar{K}^*(892)$, $S=3/2$, D -wave	

 $\Sigma(1900)$ BRANCHING RATIOS

$\Gamma(N\bar{K})/\Gamma_{\text{total}}$	DOCUMENT ID	TECN	COMMENT	Γ_1/Γ
0.40 to 0.70 (≈ 0.55) OUR ESTIMATE				
0.45 ± 0.09	SARANTSEV 19	DPWA	$\bar{K}N$ multichannel	
0.67 ± 0.17	ZHANG 13A	DPWA	$\bar{K}N$ multichannel	
$\Gamma(\Sigma\pi)/\Gamma_{\text{total}}$	DOCUMENT ID	TECN	COMMENT	Γ_2/Γ
0.10 to 0.40 (≈ 0.25) OUR ESTIMATE				
0.33 ± 0.07	SARANTSEV 19	DPWA	$\bar{K}N$ multichannel	
0.10 ± 0.05	ZHANG 13A	DPWA	$\bar{K}N$ multichannel	
$\Gamma(\Sigma\eta)/\Gamma_{\text{total}}$	DOCUMENT ID	TECN	COMMENT	Γ_3/Γ
0.01 \pm 0.01	SARANTSEV 19	DPWA	$\bar{K}N$ multichannel	
$\Gamma(\Lambda\pi)/\Gamma_{\text{total}}$	DOCUMENT ID	TECN	COMMENT	Γ_4/Γ
0.06 \pm 0.02	SARANTSEV 19	DPWA	$\bar{K}N$ multichannel	
$\Gamma(\Xi K)/\Gamma_{\text{total}}$	DOCUMENT ID	TECN	COMMENT	Γ_5/Γ
0.03 \pm 0.02	SARANTSEV 19	DPWA	$\bar{K}N$ multichannel	
$\Gamma(\Sigma(1385)\pi)/\Gamma_{\text{total}}$	DOCUMENT ID	TECN	COMMENT	Γ_6/Γ
0.07 \pm 0.03	SARANTSEV 19	DPWA	$\bar{K}N$ multichannel	

 $\Gamma(\Lambda(1520)\pi)/\Gamma_{\text{total}}$

VALUE	DOCUMENT ID	TECN	COMMENT	Γ_7/Γ
< 0.01	SARANTSEV 19	DPWA	$\bar{K}N$ multichannel	

 $\Gamma(\Delta\bar{K})/\Gamma_{\text{total}}$

VALUE	DOCUMENT ID	TECN	COMMENT	Γ_8/Γ
0.025 \pm 0.010	SARANTSEV 19	DPWA	$\bar{K}N$ multichannel	

 $\Gamma(N\bar{K}^*(892), S=1/2, S\text{-wave})/\Gamma_{\text{total}}$

VALUE	DOCUMENT ID	TECN	COMMENT	Γ_9/Γ
0.07 \pm 0.03	SARANTSEV 19	DPWA	$\bar{K}N$ multichannel	

 $\Gamma(N\bar{K}^*(892), S=3/2, D\text{-wave})/\Gamma_{\text{total}}$

VALUE	DOCUMENT ID	TECN	COMMENT	Γ_{10}/Γ
< 0.01	SARANTSEV 19	DPWA	$\bar{K}N$ multichannel	

 $\Sigma(1900)$ REFERENCES

SARANTSEV 19	EPJ A55 180	A.V. Sarantsev et al.	(BONN, PNPI)
ZHANG 13A	PR C88 035205	H. Zhang et al.	(KSU)
GOPAL 80	Toronto Conf. 159	G.P. Gopal et al.	(RHEL)
GOPAL 77	NP B119 362	G.P. Gopal et al.	(LOIC, RHEL)
MARTIN 77	NP B127 349	B.R. Martin, M.K. Pidcock, R.G. Moorhouse	(LOUC+)
VANHORN 75	NP B87 145	A.J. van Horn	(LBL)

 $\Sigma(1910) 3/2^-$

$$I(J^P) = 1(\frac{3}{2}^-) \text{ Status: } ***$$

was $\Sigma(1940)$

For results published before 1974 (they are now obsolete), see our 1982 edition Physics Letters **111B** 1 (1982).

Not all analyses require this state. It is not required by the GOYAL 77 analysis of $K^-n \rightarrow (\Sigma\pi)^-$ nor by the GOPAL 80 analysis of $K^-n \rightarrow K^-n$. See also HEMINGWAY 75.

 $\Sigma(1910)$ POLE RESIDUES

The normalized residue is the residue divided by $\Gamma_{\text{pole}}/2$.

Normalized residue in $N\bar{K} \rightarrow \Sigma(1910) \rightarrow N\bar{K}$

MODULUS	PHASE (°)	DOCUMENT ID	TECN	COMMENT
0.03 \pm 0.02	-95 ± 60	SARANTSEV 19	DPWA	$\bar{K}N$ multichannel

Normalized residue in $N\bar{K} \rightarrow \Sigma(1910) \rightarrow \Sigma\pi$

MODULUS	PHASE (°)	DOCUMENT ID	TECN	COMMENT
0.16 \pm 0.04	-160 ± 15	SARANTSEV 19	DPWA	$\bar{K}N$ multichannel

Normalized residue in $N\bar{K} \rightarrow \Sigma(1910) \rightarrow \Lambda\pi$

MODULUS	PHASE (°)	DOCUMENT ID	TECN	COMMENT
0.04 \pm 0.03	25 ± 25	SARANTSEV 19	DPWA	$\bar{K}N$ multichannel

Normalized residue in $N\bar{K} \rightarrow \Sigma(1910) \rightarrow \Xi\pi$

MODULUS	PHASE (°)	DOCUMENT ID	TECN	COMMENT
0.01 \pm 0.01		SARANTSEV 19	DPWA	$\bar{K}N$ multichannel

Normalized residue in $N\bar{K} \rightarrow \Sigma(1910) \rightarrow \Lambda(1520)\pi$, P -wave

MODULUS	PHASE (°)	DOCUMENT ID	TECN	COMMENT
0.01 \pm 0.01		SARANTSEV 19	DPWA	$\bar{K}N$ multichannel

Normalized residue in $N\bar{K} \rightarrow \Sigma(1910) \rightarrow \Lambda(1520)\pi$, F -wave

MODULUS	PHASE (°)	DOCUMENT ID	TECN	COMMENT
~ 0		SARANTSEV 19	DPWA	$\bar{K}N$ multichannel

Normalized residue in $N\bar{K} \rightarrow \Sigma(1910) \rightarrow \Delta\bar{K}$, S -wave

MODULUS	PHASE (°)	DOCUMENT ID	TECN	COMMENT
0.03 \pm 0.01	120 ± 20	SARANTSEV 19	DPWA	$\bar{K}N$ multichannel

Normalized residue in $N\bar{K} \rightarrow \Sigma(1910) \rightarrow N\bar{K}^*(892)$, $S=3/2$, S -wave

MODULUS	PHASE (°)	DOCUMENT ID	TECN	COMMENT
0.03 \pm 0.02	20 ± 35	SARANTSEV 19	DPWA	$\bar{K}N$ multichannel

Normalized residue in $N\bar{K} \rightarrow \Sigma(1910) \rightarrow N\bar{K}^*(892)$, $S=1/2$, D -wave

MODULUS	PHASE (°)	DOCUMENT ID	TECN	COMMENT
0.02 \pm 0.01		SARANTSEV 19	DPWA	$\bar{K}N$ multichannel

Normalized residue in $N\bar{K} \rightarrow \Sigma(1910) \rightarrow N\bar{K}^*(892)$, $S=3/2$, D -wave

MODULUS	PHASE (°)	DOCUMENT ID	TECN	COMMENT
0.01 \pm 0.01		SARANTSEV 19	DPWA	$\bar{K}N$ multichannel

 $\Sigma(1910)$ MASS

VALUE (MeV)	DOCUMENT ID	TECN	COMMENT
1870 to 1950 (≈ 1910) OUR ESTIMATE			
1878 ± 12	SARANTSEV 19	DPWA	$\bar{K}N$ multichannel
1920 ± 50	GOPAL 77	DPWA	$\bar{K}N$ multichannel
1950 ± 30	BAILLON 75	IPWA	$\bar{K}N \rightarrow \Lambda\pi$

See key on page 1127

Baryon Particle Listings
Σ(1910)

1949 ⁺⁴⁰ ₋₆₀	VANHORN	75	DPWA	$K^- p \rightarrow \Lambda \pi^0$
1935 ± 80	KANE	74	DPWA	$K^- p \rightarrow \Sigma \pi$
1940 ± 20	LITCHFIELD	74B	DPWA	$K^- p \rightarrow \Lambda(1520) \pi^0$
1950 ± 20	LITCHFIELD	74C	DPWA	$K^- p \rightarrow \Delta(1232) \bar{K}$
• • • We do not use the following data for averages, fits, limits, etc. • • •				
1886 or 1893	¹ MARTIN	77	DPWA	$\bar{K} N$ multichannel
1940	DEBELLEFON	76	IPWA	$K^- p \rightarrow \Lambda \pi^0, F_{17}$ wave

Σ(1910) WIDTH

VALUE (MeV)	DOCUMENT ID	TECN	COMMENT
150 to 300 (≈ 220) OUR ESTIMATE			
224 ± 25	SARANTSEV	19	DPWA $\bar{K} N$ multichannel
170 ± 25	CAMERON	78B	DPWA $K^- p \rightarrow N \bar{K}^*$
300 ± 80	GOPAL	77	DPWA $\bar{K} N$ multichannel
150 ± 75	BAILLON	75	IPWA $\bar{K} N \rightarrow \Lambda \pi$
160 ⁺⁷⁰ ₋₄₀	VANHORN	75	DPWA $K^- p \rightarrow \Lambda \pi^0$
330 ± 80	KANE	74	DPWA $K^- p \rightarrow \Sigma \pi$
60 ± 20	LITCHFIELD	74B	DPWA $K^- p \rightarrow \Lambda(1520) \pi^0$
70 ⁺³⁰ ₋₂₀	LITCHFIELD	74C	DPWA $K^- p \rightarrow \Delta(1232) \bar{K}$
• • • We do not use the following data for averages, fits, limits, etc. • • •			
157 or 159	¹ MARTIN	77	DPWA $\bar{K} N$ multichannel

Σ(1910) DECAY MODES

Mode	Fraction (Γ _i /Γ)
Γ ₁ $N \bar{K}$	0.01 to 0.05 (≈ 0.02)
Γ ₂ $\Lambda \pi$	(6 ± 4) %
Γ ₃ $\Sigma \pi$	(86 ± 21) %
Γ ₄ ΞK	
Γ ₅ $\Sigma(1385) \pi$	seen
Γ ₆ $\Sigma(1385) \pi, S$ -wave	
Γ ₇ $\Lambda(1520) \pi$	seen
Γ ₈ $\Lambda(1520) \pi, P$ -wave	
Γ ₉ $\Lambda(1520) \pi, F$ -wave	
Γ ₁₀ $\Delta(1232) \bar{K}$	(3.0 ± 1.0) %
Γ ₁₁ $\Delta(1232) \bar{K}, S$ -wave	
Γ ₁₂ $\Delta(1232) \bar{K}, D$ -wave	
Γ ₁₃ $N \bar{K}^*(892)$	seen
Γ ₁₄ $N \bar{K}^*(892), S=3/2, S$ -wave	
Γ ₁₅ $N \bar{K}^*(892), S=1/2, D$ -wave	(1.0 ± 1.0) %
Γ ₁₆ $N \bar{K}^*(892), S=3/2, D$ -wave	

Σ(1910) BRANCHING RATIOS

See "Sign conventions for resonance couplings" in the Note on Λ and Σ Resonances.

Γ(N \bar{K})/Γ _{total}	DOCUMENT ID	TECN	COMMENT	Γ ₁ /Γ
0.01 to 0.05 (≈ 0.02) OUR ESTIMATE				
0.03 ± 0.02	SARANTSEV	19	DPWA $\bar{K} N$ multichannel	
<0.04	GOPAL	77	DPWA $\bar{K} N$ multichannel	
0.14 or 0.13	¹ MARTIN	77	DPWA $\bar{K} N$ multichannel	

Γ(Λπ)/Γ _{total}	DOCUMENT ID	TECN	COMMENT	Γ ₂ /Γ
0.06 ± 0.04	SARANTSEV	19	DPWA $\bar{K} N$ multichannel	

Γ(Σπ)/Γ _{total}	DOCUMENT ID	TECN	COMMENT	Γ ₃ /Γ
0.86 ± 0.21	SARANTSEV	19	DPWA $\bar{K} N$ multichannel	

Γ(ΞK)/Γ _{total}	DOCUMENT ID	TECN	COMMENT	Γ ₄ /Γ
~ 0	SARANTSEV	19	DPWA $\bar{K} N$ multichannel	

Γ(Λ(1520)π, P-wave)/Γ _{total}	DOCUMENT ID	TECN	COMMENT	Γ ₈ /Γ
~ 0	SARANTSEV	19	DPWA $\bar{K} N$ multichannel	

Γ(Λ(1520)π, F-wave)/Γ _{total}	DOCUMENT ID	TECN	COMMENT	Γ ₉ /Γ
~ 0	SARANTSEV	19	DPWA $\bar{K} N$ multichannel	

Γ(Δ(1232)K̄)/Γ _{total}	DOCUMENT ID	TECN	COMMENT	Γ ₁₀ /Γ
0.03 ± 0.01	SARANTSEV	19	DPWA $\bar{K} N$ multichannel	

Γ(N $\bar{K}^*(892)$)/Γ _{total}	DOCUMENT ID	TECN	COMMENT	Γ ₁₃ /Γ
0.03 ± 0.02	SARANTSEV	19	DPWA $\bar{K} N$ multichannel	

Γ(N $\bar{K}^*(892), S=1/2, D$ -wave)/Γ _{total}	DOCUMENT ID	TECN	COMMENT	Γ ₁₅ /Γ
0.01 ± 0.01	SARANTSEV	19	DPWA $\bar{K} N$ multichannel	

Γ(N $\bar{K}^*(892), S=3/2, D$ -wave)/Γ _{total}	DOCUMENT ID	TECN	COMMENT	Γ ₁₆ /Γ
~ 0	SARANTSEV	19	DPWA $\bar{K} N$ multichannel	

(Γ _i Γ _f) ^{1/2} /Γ _{total} in $N \bar{K} \rightarrow \Sigma(1910) \rightarrow \Lambda \pi$	DOCUMENT ID	TECN	COMMENT	(Γ ₁ Γ ₂) ^{1/2} /Γ
-0.06 ± 0.03	GOPAL	77	DPWA $\bar{K} N$ multichannel	
-0.04 ± 0.02	BAILLON	75	IPWA $\bar{K} N \rightarrow \Lambda \pi$	
-0.05 ^{+0.03} _{-0.02}	VANHORN	75	DPWA $K^- p \rightarrow \Lambda \pi^0$	
-0.153 ± 0.070	DEVENISH	74B	Fixed- <i>t</i> dispersion rel.	
• • • We do not use the following data for averages, fits, limits, etc. • • •				
-0.15 or -0.14	¹ MARTIN	77	DPWA $\bar{K} N$ multichannel	

(Γ _i Γ _f) ^{1/2} /Γ _{total} in $N \bar{K} \rightarrow \Sigma(1910) \rightarrow \Sigma \pi$	DOCUMENT ID	TECN	COMMENT	(Γ ₁ Γ ₃) ^{1/2} /Γ
-0.08 ± 0.04	GOPAL	77	DPWA $\bar{K} N$ multichannel	
-0.14 ± 0.04	KANE	74	DPWA $K^- p \rightarrow \Sigma \pi$	
• • • We do not use the following data for averages, fits, limits, etc. • • •				
+0.16 or +0.16	¹ MARTIN	77	DPWA $\bar{K} N$ multichannel	

(Γ _i Γ _f) ^{1/2} /Γ _{total} in $N \bar{K} \rightarrow \Sigma(1910) \rightarrow \Sigma(1385) \pi$	DOCUMENT ID	TECN	COMMENT	(Γ ₁ Γ ₅) ^{1/2} /Γ
+0.066 ± 0.025	² CAMERON	78	DPWA $K^- p \rightarrow \Sigma(1385) \pi$	

(Γ _i Γ _f) ^{1/2} /Γ _{total} in $N \bar{K} \rightarrow \Sigma(1910) \rightarrow \Lambda(1520) \pi, P$ -wave	DOCUMENT ID	TECN	COMMENT	(Γ ₁ Γ ₈) ^{1/2} /Γ
< 0.03	CAMERON	77	DPWA $K^- p \rightarrow \Lambda(1520) \pi^0$	
-0.11 ± 0.04	LITCHFIELD	74B	DPWA $K^- p \rightarrow \Lambda(1520) \pi^0$	

(Γ _i Γ _f) ^{1/2} /Γ _{total} in $N \bar{K} \rightarrow \Sigma(1910) \rightarrow \Lambda(1520) \pi, F$ -wave	DOCUMENT ID	TECN	COMMENT	(Γ ₁ Γ ₉) ^{1/2} /Γ
0.062 ± 0.021	CAMERON	77	DPWA $K^- p \rightarrow \Lambda(1520) \pi^0$	
-0.08 ± 0.04	LITCHFIELD	74B	DPWA $K^- p \rightarrow \Lambda(1520) \pi^0$	

(Γ _i Γ _f) ^{1/2} /Γ _{total} in $N \bar{K} \rightarrow \Sigma(1910) \rightarrow \Delta(1232) \bar{K}, S$ -wave	DOCUMENT ID	TECN	COMMENT	(Γ ₁ Γ ₁₁) ^{1/2} /Γ
-0.16 ± 0.05	LITCHFIELD	74C	DPWA $K^- p \rightarrow \Delta(1232) \bar{K}$	

(Γ _i Γ _f) ^{1/2} /Γ _{total} in $N \bar{K} \rightarrow \Sigma(1910) \rightarrow \Delta(1232) \bar{K}, D$ -wave	DOCUMENT ID	TECN	COMMENT	(Γ ₁ Γ ₁₂) ^{1/2} /Γ
-0.14 ± 0.05	LITCHFIELD	74C	DPWA $K^- p \rightarrow \Delta(1232) \bar{K}$	

(Γ _i Γ _f) ^{1/2} /Γ _{total} in $N \bar{K} \rightarrow \Sigma(1910) \rightarrow N \bar{K}^*(892)$	DOCUMENT ID	TECN	COMMENT	(Γ ₁ Γ ₁₃) ^{1/2} /Γ
-0.09 ± 0.02	³ CAMERON	78B	DPWA $K^- p \rightarrow N \bar{K}^*$	

Σ(1910) FOOTNOTES

- The two MARTIN 77 values are from a T-matrix pole and from a Breit-Wigner fit.
- The published sign has been changed to be in accord with the baryon-first convention.
- Upper limits on the D₁ and D₃ waves are each 0.03.

Σ(1910) REFERENCES

SARANTSEV 19	EPJ A55 180	A.V. Sarantsev et al.	(BONN, PNPI)
PDG 82	PL 111B 1	M. Roos et al.	(HELS, CIT, CERN)
GOPAL 80	Toronto Conf. 159	G.P. Gopal	(RHEL)
CAMERON 78	NP B143 189	W. Cameron et al.	(RHEL, LOIC) IJP
CAMERON 78B	NP B146 327	W. Cameron et al.	(RHEL, LOIC) IJP
CAMERON 77	NP B131 399	W. Cameron et al.	(RHEL, LOIC) IJP
GOPAL 77	NP B119 362	G.P. Gopal et al.	(LOIC, RHEL) IJP
GOYAL 77	PR D16 2746	D.P. Goyal, A.V. Sodhi	(DELH)
MARTIN 77	NP B127 349	B.R. Martin, M.K. Pidcock, R.G. Moorhouse	(LOUC+) IJP
Also	NP B126 266	B.R. Martin, M.K. Pidcock	(LOUC)
Also	NP B126 285	B.R. Martin, M.K. Pidcock	(LOUC) IJP
DEBELLEFON 76	NP B109 129	A. de Bellefon, A. Berthon	(CDF) IJP
BAILLON 75	NP B94 39	P.H. Bailion, P.J. Litchfield	(CERN, RHEL) IJP
HEMINGWAY 75	NP B91 12	R.J. Hemingway et al.	(CERN, HEIDH, MPIM) IJP
VANHORN 75	NP B87 145	A.J. van Horn	(LBL) IJP
Also	NP B87 157	A.J. van Horn	(LBL) IJP
DEVENISH 74B	NP B81 330	R.C.E. Devenish, C.D. Froggatt, B.R. Martin	(DESY+) IJP
KANE 74	LBL-2452	D.F. Kane	(LBL) IJP
LITCHFIELD 74B	NP B74 19	P.J. Litchfield et al.	(CERN, HEIDH) IJP
LITCHFIELD 74C	NP B74 39	P.J. Litchfield et al.	(CERN, HEIDH) IJP

Baryon Particle Listings

 $\Sigma(1915)$ $\Sigma(1915) 5/2^+$

$$I(J^P) = 1(\frac{5}{2}^+) \text{ Status: } ****$$

Discovered by COOL 66. For results published before 1974 (they are now obsolete), see our 1982 edition Physics Letters **111B** 1 (1982).

This entry only includes results from partial-wave analyses. Parameters of peaks seen in cross sections and invariant-mass distributions in this region used to be listed in a separate entry immediately following. They may be found in our 1986 edition Physics Letters **170B** 1 (1986).

 $\Sigma(1915)$ POLE POSITION

REAL PART

VALUE (MeV)	DOCUMENT ID	TECN	COMMENT
1885 to 1915 (\approx 1900) OUR ESTIMATE			
1908 ± 7	SARANTSEV 19	DPWA	$\bar{K}N$ multichannel
$1890 \pm \frac{3}{2}$	¹ KAMANO 15	DPWA	$\bar{K}N$ multichannel
••• We do not use the following data for averages, fits, limits, etc. •••			
1897	ZHANG 13A	DPWA	$\bar{K}N$ multichannel
¹ From the preferred solution A in KAMANO 15.			

-2xIMAGINARY PART

VALUE (MeV)	DOCUMENT ID	TECN	COMMENT
90 to 110 (\approx 100) OUR ESTIMATE			
98 ± 12	SARANTSEV 19	DPWA	$\bar{K}N$ multichannel
$97 \pm \frac{4}{6}$	¹ KAMANO 15	DPWA	$\bar{K}N$ multichannel
••• We do not use the following data for averages, fits, limits, etc. •••			
133	ZHANG 13A	DPWA	$\bar{K}N$ multichannel
¹ From the preferred solution A in KAMANO 15.			

 $\Sigma(1915)$ POLE RESIDUES

The normalized residue is the residue divided by $\Gamma_{pole}/2$.

Normalized residue in $N\bar{K} \rightarrow \Sigma(1915) \rightarrow N\bar{K}$

MODULUS	PHASE ($^\circ$)	DOCUMENT ID	TECN	COMMENT
0.08 ± 0.02	-33 ± 15	SARANTSEV 19	DPWA	$\bar{K}N$ multichannel
••• We do not use the following data for averages, fits, limits, etc. •••				
0.0391	-15	¹ KAMANO 15	DPWA	$\bar{K}N$ multichannel
¹ From the preferred solution A in KAMANO 15.				

Normalized residue in $N\bar{K} \rightarrow \Sigma(1915) \rightarrow \Sigma\pi$

MODULUS	PHASE ($^\circ$)	DOCUMENT ID	TECN	COMMENT
0.09 ± 0.02	180 ± 12	SARANTSEV 19	DPWA	$\bar{K}N$ multichannel
••• We do not use the following data for averages, fits, limits, etc. •••				
0.157	157	¹ KAMANO 15	DPWA	$\bar{K}N$ multichannel
¹ From the preferred solution A in KAMANO 15.				

Normalized residue in $N\bar{K} \rightarrow \Sigma(1915) \rightarrow \Lambda\pi$

MODULUS	PHASE ($^\circ$)	DOCUMENT ID	TECN	COMMENT
0.07 ± 0.02	-170 ± 20	SARANTSEV 19	DPWA	$\bar{K}N$ multichannel
••• We do not use the following data for averages, fits, limits, etc. •••				
0.0757	166	¹ KAMANO 15	DPWA	$\bar{K}N$ multichannel
¹ From the preferred solution A in KAMANO 15.				

Normalized residue in $N\bar{K} \rightarrow \Sigma(1915) \rightarrow \Xi K$

MODULUS	PHASE ($^\circ$)	DOCUMENT ID	TECN	COMMENT
0.02 ± 0.01	-65 ± 35	SARANTSEV 19	DPWA	$\bar{K}N$ multichannel
••• We do not use the following data for averages, fits, limits, etc. •••				
0.002	-88	¹ KAMANO 15	DPWA	$\bar{K}N$ multichannel
¹ From the preferred solution A in KAMANO 15.				

Normalized residue in $N\bar{K} \rightarrow \Lambda(1915) \rightarrow \Sigma(1385)\pi, P\text{-wave}$

MODULUS	PHASE ($^\circ$)	DOCUMENT ID	TECN	COMMENT
0.02 ± 0.02		SARANTSEV 19	DPWA	$\bar{K}N$ multichannel
••• We do not use the following data for averages, fits, limits, etc. •••				
0.0724	161	¹ KAMANO 15	DPWA	$\bar{K}N$ multichannel
¹ From the preferred solution A in KAMANO 15.				

Normalized residue in $N\bar{K} \rightarrow \Lambda(1915) \rightarrow \Sigma(1385)\pi, F\text{-wave}$

MODULUS	PHASE ($^\circ$)	DOCUMENT ID	TECN	COMMENT
0.05 ± 0.03	-30 ± 50	SARANTSEV 19	DPWA	$\bar{K}N$ multichannel
••• We do not use the following data for averages, fits, limits, etc. •••				
0.0162	-163	¹ KAMANO 15	DPWA	$\bar{K}N$ multichannel
¹ From the preferred solution A in KAMANO 15.				

Normalized residue in $N\bar{K} \rightarrow \Sigma(1915) \rightarrow \Lambda(1520)\pi, D\text{-wave}$

MODULUS	PHASE ($^\circ$)	DOCUMENT ID	TECN	COMMENT
0.08 ± 0.02	-105 ± 50	SARANTSEV 19	DPWA	$\bar{K}N$ multichannel

Normalized residue in $N\bar{K} \rightarrow \Sigma(1915) \rightarrow \Delta\bar{K}, P\text{-wave}$

MODULUS	PHASE ($^\circ$)	DOCUMENT ID	TECN	COMMENT
0.12 ± 0.03	-10 ± 20	SARANTSEV 19	DPWA	$\bar{K}N$ multichannel

Normalized residue in $N\bar{K} \rightarrow \Sigma(1915) \rightarrow \Delta\bar{K}, F\text{-wave}$

MODULUS	PHASE ($^\circ$)	DOCUMENT ID	TECN	COMMENT
0.07 ± 0.02	-35 ± 25	SARANTSEV 19	DPWA	$\bar{K}N$ multichannel

Normalized residue in $N\bar{K} \rightarrow \Sigma(1915) \rightarrow \Lambda(1520)\pi, G\text{-wave}$

MODULUS	PHASE ($^\circ$)	DOCUMENT ID	TECN	COMMENT
0.01 ± 0.01		SARANTSEV 19	DPWA	$\bar{K}N$ multichannel

Normalized residue in $N\bar{K} \rightarrow \Sigma(1915) \rightarrow N\bar{K}^*(892), S=1/2, F\text{-wave}$

MODULUS	PHASE ($^\circ$)	DOCUMENT ID	TECN	COMMENT
0.07 ± 0.04	-60 ± 45	SARANTSEV 19	DPWA	$\bar{K}N$ multichannel
••• We do not use the following data for averages, fits, limits, etc. •••				
0.00476	4	¹ KAMANO 15	DPWA	$\bar{K}N$ multichannel
¹ From the preferred solution A in KAMANO 15.				

Normalized residue in $N\bar{K} \rightarrow \Sigma(1915) \rightarrow N\bar{K}^*(892), S=3/2, P\text{-wave}$

MODULUS	PHASE ($^\circ$)	DOCUMENT ID	TECN	COMMENT
••• We do not use the following data for averages, fits, limits, etc. •••				
0.0494	51	¹ KAMANO 15	DPWA	$\bar{K}N$ multichannel
¹ From the preferred solution A in KAMANO 15.				

Normalized residue in $N\bar{K} \rightarrow \Sigma(1915) \rightarrow N\bar{K}^*(892), S=3/2, F\text{-wave}$

MODULUS	PHASE ($^\circ$)	DOCUMENT ID	TECN	COMMENT
0.07 ± 0.03	-40 ± 45	SARANTSEV 19	DPWA	$\bar{K}N$ multichannel
••• We do not use the following data for averages, fits, limits, etc. •••				
0.000314	16	¹ KAMANO 15	DPWA	$\bar{K}N$ multichannel
¹ From the preferred solution A in KAMANO 15.				

 $\Sigma(1915)$ MASS

VALUE (MeV)	DOCUMENT ID	TECN	COMMENT
1900 to 1935 (\approx 1915) OUR ESTIMATE			
1918 ± 6	SARANTSEV 19	DPWA	$\bar{K}N$ multichannel
1920 ± 7	ZHANG 13A	DPWA	$\bar{K}N$ multichannel
1937 ± 20	ALSTON-...	78	DPWA $\bar{K}N \rightarrow \bar{K}N$
1894 ± 5	¹ CORDEN 77c		$K^- n \rightarrow \Sigma\pi$
1909 ± 5	¹ CORDEN 77c		$K^- n \rightarrow \Sigma\pi$
1920 ± 10	GOPAL 77	DPWA	$\bar{K}N$ multichannel
1920 ± 30	BAILLON 75	IPWA	$\bar{K}N \rightarrow \Lambda\pi$
1914 ± 10	HEMINGWAY 75	DPWA	$K^- p \rightarrow \bar{K}N$
$1920 \pm \frac{15}{20}$	VANHORN 75	DPWA	$K^- p \rightarrow \Lambda\pi^0$
1920 ± 5	KANE 74	DPWA	$K^- p \rightarrow \Sigma\pi$
••• We do not use the following data for averages, fits, limits, etc. •••			
not seen	DECLAIS 77	DPWA	$\bar{K}N \rightarrow \bar{K}N$
1925 or 1933	² MARTIN 77	DPWA	$\bar{K}N$ multichannel
1900 ± 4	³ CORDEN 76	DPWA	$K^- n \rightarrow \Lambda\pi^-$
1915	DEBELLEFON 76	IPWA	$K^- p \rightarrow \Lambda\pi^0$
¹ The two entries for CORDEN 77c are from two different acceptable solutions.			
² The two MARTIN 77 values are from a T-matrix pole and from a Breit-Wigner fit.			
³ Preferred solution 3; see CORDEN 76 for other possibilities.			

 $\Sigma(1915)$ WIDTH

VALUE (MeV)	DOCUMENT ID	TECN	COMMENT
80 to 160 (\approx 120) OUR ESTIMATE			
102 ± 12	SARANTSEV 19	DPWA	$\bar{K}N$ multichannel
149 ± 17	ZHANG 13A	DPWA	Multichannel
161 ± 20	ALSTON-...	78	DPWA $\bar{K}N \rightarrow \bar{K}N$
107 ± 14	¹ CORDEN 77c		$K^- n \rightarrow \Sigma\pi$
85 ± 13	¹ CORDEN 77c		$K^- n \rightarrow \Sigma\pi$
130 ± 10	GOPAL 77	DPWA	$\bar{K}N$ multichannel
70 ± 20	BAILLON 75	IPWA	$\bar{K}N \rightarrow \Lambda\pi$
85 ± 15	HEMINGWAY 75	DPWA	$K^- p \rightarrow \bar{K}N$
102 ± 18	VANHORN 75	DPWA	$K^- p \rightarrow \Lambda\pi^0$
162 ± 25	KANE 74	DPWA	$K^- p \rightarrow \Sigma\pi$
••• We do not use the following data for averages, fits, limits, etc. •••			
171 or 173	² MARTIN 77	DPWA	$\bar{K}N$ multichannel
75 ± 14	³ CORDEN 76	DPWA	$K^- n \rightarrow \Lambda\pi^-$
60	DEBELLEFON 76	IPWA	$K^- p \rightarrow \Lambda\pi^0$
¹ The two entries for CORDEN 77c are from two different acceptable solutions.			
² The two MARTIN 77 values are from a T-matrix pole and from a Breit-Wigner fit.			
³ Preferred solution 3; see CORDEN 76 for other possibilities.			

 $\Sigma(1915)$ DECAY MODES

Mode	Fraction (Γ_i/Γ)
Γ_1 $N\bar{K}$	0.05 to 0.15
Γ_2 $\Lambda\pi$	(6.0 \pm 2.0) %

Baryon Particle Listings
Σ(1915)

Table with 4 columns: Index, Resonance Name, Width, and Branching Ratio. Rows include Σπ, Σ(1385)π, Σ(1385)π, P-wave, Σ(1385)π, F-wave, Λ(1520)π, D-wave, Λ(1520)π, G-wave, N*(892), S=1/2, F-wave, N*(892), S=3/2, P-wave, N*(892), S=3/2, F-wave, ΔK, P-wave, and ΔK, F-wave.

Σ(1915) BRANCHING RATIOS

See "Sign conventions for resonance couplings" in the Note on Λ and Σ Resonances.

Table for Γ(NK*)/Γtotal with columns: VALUE, DOCUMENT ID, TECN, COMMENT. Includes 'OUR ESTIMATE' and data from SARANTSEV, ZHANG, GOPAL, ALSTON..., HEMINGWAY, KAMANO, and MARTIN.

1 The mass and width are fixed to the GOPAL 77 values due to the low elasticity.
2 From the preferred solution A in KAMANO 15.
3 The two MARTIN 77 values are from a T-matrix pole and from a Breit-Wigner fit.

Table for Γ(Λπ)/Γtotal with columns: VALUE, DOCUMENT ID, TECN, COMMENT. Includes data from SARANTSEV and KAMANO.

1 From the preferred solution A in KAMANO 15.

Table for Γ(Σπ)/Γtotal with columns: VALUE, DOCUMENT ID, TECN, COMMENT. Includes data from SARANTSEV and KAMANO.

1 From the preferred solution A in KAMANO 15.

Table for Γ(ΞK)/Γtotal with columns: VALUE, DOCUMENT ID, TECN, COMMENT. Includes data from SARANTSEV and KAMANO.

1 From the preferred solution A in KAMANO 15.

Table for Γ(Σ(1385)π, P-wave)/Γtotal with columns: VALUE, DOCUMENT ID, TECN, COMMENT. Includes data from SARANTSEV and KAMANO.

1 From the preferred solution A in KAMANO 15.

Table for Γ(Σ(1385)π, F-wave)/Γtotal with columns: VALUE, DOCUMENT ID, TECN, COMMENT. Includes data from SARANTSEV and KAMANO.

1 From the preferred solution A in KAMANO 15.

Table for Γ(Λ(1520)π, D-wave)/Γtotal with columns: VALUE, DOCUMENT ID, TECN, COMMENT. Includes data from SARANTSEV.

Table for Γ(Λ(1520)π, G-wave)/Γtotal with columns: VALUE, DOCUMENT ID, TECN, COMMENT. Includes data from SARANTSEV.

Table for Γ(N*(892), S=1/2, F-wave)/Γtotal with columns: VALUE, DOCUMENT ID, TECN, COMMENT. Includes data from SARANTSEV and KAMANO.

1 From the preferred solution A in KAMANO 15.

Table for Γ(N*(892), S=3/2, P-wave)/Γtotal with columns: VALUE, DOCUMENT ID, TECN, COMMENT. Includes data from KAMANO.

Table for Γ(N*(892), S=3/2, F-wave)/Γtotal with columns: VALUE, DOCUMENT ID, TECN, COMMENT. Includes data from SARANTSEV and KAMANO.

Table for Γ(ΔK, P-wave)/Γtotal with columns: VALUE, DOCUMENT ID, TECN, COMMENT. Includes data from SARANTSEV.

Table for Γ(ΔK, F-wave)/Γtotal with columns: VALUE, DOCUMENT ID, TECN, COMMENT. Includes data from SARANTSEV.

Table for (Γ1Γ2)1/2/Γtotal in N*K -> Σ(1915) -> Λπ with columns: VALUE, DOCUMENT ID, TECN, COMMENT. Includes data from GOPAL, CORDEN, BAILLON, VANHORN, DEVENISH, and MARTIN.

Table for (Γ1Γ2)1/2/Γtotal in N*K -> Σ(1915) -> Σπ with columns: VALUE, DOCUMENT ID, TECN, COMMENT. Includes data from ZHANG, CORDEN, GOPAL, KANE, and MARTIN.

Table for (Γ1Γ2)1/2/Γtotal in N*K -> Σ(1915) -> Σ(1385)π, P-wave with columns: VALUE, DOCUMENT ID, TECN, COMMENT. Includes data from CAMERON.

Table for (Γ1Γ2)1/2/Γtotal in N*K -> Σ(1915) -> Σ(1385)π, F-wave with columns: VALUE, DOCUMENT ID, TECN, COMMENT. Includes data from ZHANG and CAMERON.

Σ(1915) REFERENCES

List of references for Σ(1915) including authors like Sarantsev, Zhang, PDC, PDG, GOPAL, ALSTON..., CAMERON, CORDEN, DECLAIS, MARTIN, BAILLON, HEMINGWAY, VANHORN, DEVENISH, KANE, and COOL, along with their respective publications and institutions.

Baryon Particle Listings

 $\Sigma(1940), \Sigma(2010)$

$$\Sigma(1940) \ 3/2^+$$

$$I(J^P) = 1(\frac{3}{2}^+) \text{ Status: } *$$

OMITTED FROM SUMMARY TABLE

 $\Sigma(1940)$ MASS

VALUE (MeV)	DOCUMENT ID	TECN	COMMENT
1920 to 1960 (\approx 1940) OUR ESTIMATE			
1941 \pm 18	ZHANG	13A	DPWA $\bar{K}N$ multichannel
1925 \pm 20	VANHORN	75	DPWA $K^-p \rightarrow \Lambda\pi^0$

 $\Sigma(1940)$ WIDTH

VALUE (MeV)	DOCUMENT ID	TECN	COMMENT
100 to 400 (\approx 250) OUR ESTIMATE			
400 \pm 49	ZHANG	13A	DPWA $\bar{K}N$ multichannel
65 $^{+50}_{-20}$	VANHORN	75	DPWA $K^-p \rightarrow \Lambda\pi^0$

 $\Sigma(1940)$ DECAY MODES

Mode	Fraction (Γ_i/Γ)
Γ_1 $N\bar{K}$	(13.0 \pm 2.0) %
Γ_2 $\Sigma\pi$	(4.0 \pm 2.0) %
Γ_3 $\Sigma(1385)\pi$, P-wave	(22 \pm 7) %
Γ_4 $\Lambda(1520)\pi$, S-wave	(5.0 \pm 2.0) %

 $\Sigma(1940)$ BRANCHING RATIOS

$\Gamma(N\bar{K})/\Gamma_{\text{total}}$	Γ_1/Γ		
VALUE	DOCUMENT ID	TECN	COMMENT
0.13 \pm 0.02	ZHANG	13A	DPWA $\bar{K}N$ multichannel

$\Gamma(\Sigma\pi)/\Gamma_{\text{total}}$	Γ_2/Γ		
VALUE	DOCUMENT ID	TECN	COMMENT
0.04 \pm 0.02	ZHANG	13A	DPWA $\bar{K}N$ multichannel

$\Gamma(\Sigma(1385)\pi, \text{P-wave})/\Gamma_{\text{total}}$	Γ_3/Γ		
VALUE	DOCUMENT ID	TECN	COMMENT
0.22 \pm 0.07	ZHANG	13A	DPWA $\bar{K}N$ multichannel

$\Gamma(\Lambda(1520)\pi, \text{S-wave})/\Gamma_{\text{total}}$	Γ_4/Γ		
VALUE	DOCUMENT ID	TECN	COMMENT
0.05 \pm 0.02	ZHANG	13A	DPWA $\bar{K}N$ multichannel

 $\Sigma(1940)$ REFERENCES

ZHANG	13A	PR C88 035205	H. Zhang et al.	(KSU)
VANHORN	75	NP B87 145	A.J. van Horn	(LBL)

$$\Sigma(2010) \ 3/2^-$$

$$I(J^P) = 1(\frac{3}{2}^-) \text{ Status: } *$$

OMITTED FROM SUMMARY TABLE

 $\Sigma(2010)$ POLE POSITION

REAL PART	DOCUMENT ID	TECN	COMMENT
VALUE (MeV)			
1995 \pm 12	SARANTSEV	19	DPWA $\bar{K}N$ multichannel

-2xIMAGINARY PART	DOCUMENT ID	TECN	COMMENT
VALUE (MeV)			
175 \pm 24	SARANTSEV	19	DPWA $\bar{K}N$ multichannel

 $\Sigma(2010)$ POLE RESIDUESThe normalized residue is the residue divided by $\Gamma_{\text{pole}}/2$.

Normalized residue in $N\bar{K} \rightarrow \Sigma(2010) \rightarrow N\bar{K}$	DOCUMENT ID	TECN	COMMENT
MODULUS	PHASE ($^\circ$)		
0.07 \pm 0.03	-115 \pm 25	SARANTSEV	19 DPWA $\bar{K}N$ multichannel

Normalized residue in $N\bar{K} \rightarrow \Sigma(2010) \rightarrow \Sigma\pi$	DOCUMENT ID	TECN	COMMENT
MODULUS	PHASE ($^\circ$)		
0.04 \pm 0.02	130 \pm 22	SARANTSEV	19 DPWA $\bar{K}N$ multichannel

Normalized residue in $N\bar{K} \rightarrow \Sigma(2010) \rightarrow \Lambda\pi$	DOCUMENT ID	TECN	COMMENT
MODULUS	PHASE ($^\circ$)		
0.06 \pm 0.03	170 \pm 25	SARANTSEV	19 DPWA $\bar{K}N$ multichannel

Normalized residue in $N\bar{K} \rightarrow \Sigma(2010) \rightarrow \Xi K$

MODULUS	PHASE ($^\circ$)	DOCUMENT ID	TECN	COMMENT
0.04 \pm 0.02	-120 \pm 45	SARANTSEV	19	DPWA $\bar{K}N$ multichannel

Normalized residue in $N\bar{K} \rightarrow \Sigma(2010) \rightarrow \Lambda(1520)\pi$, P-wave

MODULUS	PHASE ($^\circ$)	DOCUMENT ID	TECN	COMMENT
0.03 \pm 0.02	80 \pm 35	SARANTSEV	19	DPWA $\bar{K}N$ multichannel

Normalized residue in $N\bar{K} \rightarrow \Sigma(2010) \rightarrow \Lambda(1520)\pi$, F-wave

MODULUS	PHASE ($^\circ$)	DOCUMENT ID	TECN	COMMENT
0.08 \pm 0.05	150 \pm 65	SARANTSEV	19	DPWA $\bar{K}N$ multichannel

Normalized residue in $N\bar{K} \rightarrow \Sigma(2010) \rightarrow \Sigma(1385)\pi$, P-wave

VALUE	DOCUMENT ID	TECN	COMMENT
0.04 $^{+0.02}_{-0.025} \pm$ 0.05	SARANTSEV	19	DPWA $\bar{K}N$ multichannel

Normalized residue in $N\bar{K} \rightarrow \Sigma(2010) \rightarrow \Sigma(1385)\pi$, F-wave

VALUE	DOCUMENT ID	TECN	COMMENT
0.02 \pm 0.02	SARANTSEV	19	DPWA $\bar{K}N$ multichannel

Normalized residue in $N\bar{K} \rightarrow \Sigma(2010) \rightarrow \Delta\bar{K}$, S-wave

MODULUS	PHASE ($^\circ$)	DOCUMENT ID	TECN	COMMENT
0.08 \pm 0.04	0 \pm 30	SARANTSEV	19	DPWA $\bar{K}N$ multichannel

Normalized residue in $N\bar{K} \rightarrow \Sigma(2010) \rightarrow \Delta\bar{K}$, D-wave

MODULUS	PHASE ($^\circ$)	DOCUMENT ID	TECN	COMMENT
0.02 \pm 0.02		SARANTSEV	19	DPWA $\bar{K}N$ multichannel

Normalized residue in $N\bar{K} \rightarrow \Sigma(2010) \rightarrow N\bar{K}^*(892)$, S-wave

VALUE	DOCUMENT ID	TECN	COMMENT
0.12 $^{+0.03}_{-0.030} \pm$ 0.06	SARANTSEV	19	DPWA $\bar{K}N$ multichannel

Normalized residue in $N\bar{K} \rightarrow \Sigma(2010) \rightarrow N\bar{K}^*(892)$, S=1/2, D-wave

MODULUS	PHASE ($^\circ$)	DOCUMENT ID	TECN	COMMENT
0.08 \pm 0.04	55 \pm 60	SARANTSEV	19	DPWA $\bar{K}N$ multichannel

Normalized residue in $N\bar{K} \rightarrow \Sigma(2010) \rightarrow N\bar{K}^*(892)$, S=3/2, D-wave

MODULUS	PHASE ($^\circ$)	DOCUMENT ID	TECN	COMMENT
0.08 \pm 0.04	15 \pm 60	SARANTSEV	19	DPWA $\bar{K}N$ multichannel

 $\Sigma(2010)$ MASS

VALUE (MeV)	DOCUMENT ID	TECN	COMMENT
2005 \pm 14	SARANTSEV	19	DPWA $\bar{K}N$ multichannel

 $\Sigma(2010)$ WIDTH

VALUE (MeV)	DOCUMENT ID	TECN	COMMENT
178 \pm 23	SARANTSEV	19	DPWA $\bar{K}N$ multichannel

 $\Sigma(2010)$ DECAY MODES

Mode	Fraction (Γ_i/Γ)
Γ_1 $N\bar{K}$	(7.0 \pm 3.0) %
Γ_2 $\Lambda\pi$	(5.0 \pm 2.0) %
Γ_3 $\Sigma\pi$	(3.0 \pm 2.0) %
Γ_4 ΞK	(3.0 \pm 2.0) %
Γ_5 $\Sigma(1385)\pi$, P-wave	(3.0 \pm 2.0) %
Γ_6 $\Sigma(1385)\pi$, F-wave	(2.0 \pm 2.0) %
Γ_7 $\Lambda(1520)\pi$, P-wave	(2.0 \pm 2.0) %
Γ_8 $\Lambda(1520)\pi$, F-wave	(12 \pm 6) %
Γ_9 $\Delta\bar{K}$, S-wave	(11 \pm 5) %
Γ_{10} $\Delta\bar{K}$, D-wave	(1.0 \pm 1.0) %
Γ_{11} $N\bar{K}^*(892)$, S=1/2, S-wave	(27 \pm 7) %
Γ_{12} $N\bar{K}^*(892)$, S=1/2, D-wave	(13 \pm 6) %
Γ_{13} $N\bar{K}^*(892)$, S=3/2, D-wave	(13 \pm 6) %

 $\Sigma(2010)$ BRANCHING RATIOSSee "Sign conventions for resonance couplings" in the Note on Λ and Σ Resonances.

$\Gamma(N\bar{K})/\Gamma_{\text{total}}$	Γ_1/Γ		
VALUE	DOCUMENT ID	TECN	COMMENT
0.07 \pm 0.03	SARANTSEV	19	DPWA $\bar{K}N$ multichannel

$\Gamma(\Lambda\pi)/\Gamma_{\text{total}}$	Γ_2/Γ		
VALUE	DOCUMENT ID	TECN	COMMENT
0.05 \pm 0.02	SARANTSEV	19	DPWA $\bar{K}N$ multichannel

$\Gamma(\Sigma\pi)/\Gamma_{\text{total}}$	Γ_3/Γ		
VALUE	DOCUMENT ID	TECN	COMMENT
0.03 \pm 0.02	SARANTSEV	19	DPWA $\bar{K}N$ multichannel

$\Gamma(\Xi K)/\Gamma_{\text{total}}$				Γ_4/Γ
VALUE	DOCUMENT ID	TECN	COMMENT	
0.03 ± 0.02	SARANTSEV	19	DPWA $\bar{K}N$ multichannel	
$\Gamma(\Sigma(1385)\pi, P\text{-wave})/\Gamma_{\text{total}}$				Γ_5/Γ
VALUE	DOCUMENT ID	TECN	COMMENT	
0.03 ± 0.02	SARANTSEV	19	DPWA $\bar{K}N$ multichannel	
$\Gamma(\Sigma(1385)\pi, F\text{-wave})/\Gamma_{\text{total}}$				Γ_6/Γ
VALUE	DOCUMENT ID	TECN	COMMENT	
0.02 ± 0.02	SARANTSEV	19	DPWA $\bar{K}N$ multichannel	
$\Gamma(\Lambda(1520)\pi, P\text{-wave})/\Gamma_{\text{total}}$				Γ_7/Γ
VALUE	DOCUMENT ID	TECN	COMMENT	
0.02 ± 0.02	SARANTSEV	19	DPWA $\bar{K}N$ multichannel	
$\Gamma(\Lambda(1520)\pi, F\text{-wave})/\Gamma_{\text{total}}$				Γ_8/Γ
VALUE	DOCUMENT ID	TECN	COMMENT	
0.12 ± 0.06	SARANTSEV	19	DPWA $\bar{K}N$ multichannel	
$\Gamma(\Delta\bar{K}, S\text{-wave})/\Gamma_{\text{total}}$				Γ_9/Γ
VALUE	DOCUMENT ID	TECN	COMMENT	
0.11 ± 0.05	SARANTSEV	19	DPWA $\bar{K}N$ multichannel	
$\Gamma(\Delta\bar{K}, D\text{-wave})/\Gamma_{\text{total}}$				Γ_{10}/Γ
VALUE	DOCUMENT ID	TECN	COMMENT	
0.01 ± 0.01	SARANTSEV	19	DPWA $\bar{K}N$ multichannel	
$\Gamma(N\bar{K}^*(892), S=1/2, S\text{-wave})/\Gamma_{\text{total}}$				Γ_{11}/Γ
VALUE	DOCUMENT ID	TECN	COMMENT	
0.27 ± 0.07	SARANTSEV	19	DPWA $\bar{K}N$ multichannel	
$\Gamma(N\bar{K}^*(892), S=1/2, D\text{-wave})/\Gamma_{\text{total}}$				Γ_{12}/Γ
VALUE	DOCUMENT ID	TECN	COMMENT	
0.13 ± 0.06	SARANTSEV	19	DPWA $\bar{K}N$ multichannel	
$\Gamma(N\bar{K}^*(892), S=3/2, D\text{-wave})/\Gamma_{\text{total}}$				Γ_{13}/Γ
VALUE	DOCUMENT ID	TECN	COMMENT	
0.13 ± 0.06	SARANTSEV	19	DPWA $\bar{K}N$ multichannel	

 $\Sigma(2010)$ REFERENCES

SARANTSEV 19 EPJ A55 100 A.V. Sarantsev et al. (BONN, PNPI)

$\Sigma(2030) 7/2^+$	$I(J^P) = 1(\frac{7}{2}^+)$ Status: ***
----------------------	---

Discovered by COOL 66 and by WOHL 66. For most results published before 1974 (they are now obsolete), see our 1982 edition Physics Letters **111B** 1 (1982).

This entry only includes results from partial-wave analyses. Parameters of peaks seen in cross sections and invariant-mass distributions around 2030 MeV may be found in our 1984 edition, Reviews of Modern Physics **56** S1 (1984).

 $\Sigma(2030)$ POLE POSITION

REAL PART			
VALUE (MeV)	DOCUMENT ID	TECN	COMMENT
2010 to 2030 (≈ 2020) OUR ESTIMATE			
2014 ± 6	SARANTSEV	19	DPWA $\bar{K}N$ multichannel
2025^{+10}_{-5}	¹ KAMANO	15	DPWA $\bar{K}N$ multichannel
••• We do not use the following data for averages, fits, limits, etc. •••			
1993	ZHANG	13A	DPWA $\bar{K}N$ multichannel
¹ From the preferred solution A in KAMANO 15.			
$-2 \times$ IMAGINARY PART			
VALUE (MeV)	DOCUMENT ID	TECN	COMMENT
130 to 190 (≈ 160) OUR ESTIMATE			
172 ± 12	SARANTSEV	19	DPWA $\bar{K}N$ multichannel
130^{+6}_{-24}	¹ KAMANO	15	DPWA $\bar{K}N$ multichannel
••• We do not use the following data for averages, fits, limits, etc. •••			
176	ZHANG	13A	DPWA $\bar{K}N$ multichannel
¹ From the preferred solution A in KAMANO 15.			

 $\Sigma(2030)$ POLE RESIDUES

The normalized residue is the residue divided by $\Gamma_{\text{pole}}/2$.

Normalized residue in $N\bar{K} \rightarrow \Sigma(2030) \rightarrow N\bar{K}$				
MODULUS	PHASE ($^\circ$)	DOCUMENT ID	TECN	COMMENT
0.20 ± 0.04	-38 ± 8	SARANTSEV	19	DPWA $\bar{K}N$ multichannel
••• We do not use the following data for averages, fits, limits, etc. •••				
0.220	-38	¹ KAMANO	15	DPWA $\bar{K}N$ multichannel
¹ From the preferred solution A in KAMANO 15.				

Normalized residue in $N\bar{K} \rightarrow \Sigma(2030) \rightarrow \Sigma\pi$				
MODULUS	PHASE ($^\circ$)	DOCUMENT ID	TECN	COMMENT
0.07 ± 0.02	165 ± 12	SARANTSEV	19	DPWA $\bar{K}N$ multichannel
••• We do not use the following data for averages, fits, limits, etc. •••				
0.0807	135	¹ KAMANO	15	DPWA $\bar{K}N$ multichannel
¹ From the preferred solution A in KAMANO 15.				

Normalized residue in $N\bar{K} \rightarrow \Sigma(2030) \rightarrow \Lambda\pi$				
MODULUS	PHASE ($^\circ$)	DOCUMENT ID	TECN	COMMENT
0.18 ± 0.04	-22 ± 12	SARANTSEV	19	DPWA $\bar{K}N$ multichannel
••• We do not use the following data for averages, fits, limits, etc. •••				
0.138	-24	¹ KAMANO	15	DPWA $\bar{K}N$ multichannel
¹ From the preferred solution A in KAMANO 15.				

Normalized residue in $N\bar{K} \rightarrow \Sigma(2030) \rightarrow \Xi K$				
MODULUS	PHASE ($^\circ$)	DOCUMENT ID	TECN	COMMENT
0.01 ± 0.01		SARANTSEV	19	DPWA $\bar{K}N$ multichannel
••• We do not use the following data for averages, fits, limits, etc. •••				
0.0348	129	¹ KAMANO	15	DPWA $\bar{K}N$ multichannel
¹ From the preferred solution A in KAMANO 15.				

Normalized residue in $N\bar{K} \rightarrow \Sigma(2030) \rightarrow \Sigma(1385)\pi, F\text{-wave}$				
MODULUS	PHASE ($^\circ$)	DOCUMENT ID	TECN	COMMENT
0.04 ± 0.03		SARANTSEV	19	DPWA $\bar{K}N$ multichannel
••• We do not use the following data for averages, fits, limits, etc. •••				
0.089	-23	¹ KAMANO	15	DPWA $\bar{K}N$ multichannel
¹ From the preferred solution A in KAMANO 15.				

Normalized residue in $N\bar{K} \rightarrow \Sigma(2030) \rightarrow \Sigma(1385)\pi, H\text{-wave}$				
MODULUS	PHASE ($^\circ$)	DOCUMENT ID	TECN	COMMENT
0.0245	132	¹ KAMANO	15	DPWA Multichannel
¹ From the preferred solution A in KAMANO 15.				

Normalized residue in $N\bar{K} \rightarrow \Sigma(2030) \rightarrow \Lambda(1520)\pi, D\text{-wave}$				
MODULUS	PHASE ($^\circ$)	DOCUMENT ID	TECN	COMMENT
0.03 ± 0.02	-100 ± 40	SARANTSEV	19	DPWA $\bar{K}N$ multichannel

Normalized residue in $N\bar{K} \rightarrow \Sigma(2030) \rightarrow \Lambda(1520)\pi, G\text{-wave}$				
MODULUS	PHASE ($^\circ$)	DOCUMENT ID	TECN	COMMENT
0.02 ± 0.02		SARANTSEV	19	DPWA $\bar{K}N$ multichannel

Normalized residue in $N\bar{K} \rightarrow \Sigma(2030) \rightarrow \Delta\bar{K}, F\text{-wave}$				
MODULUS	PHASE ($^\circ$)	DOCUMENT ID	TECN	COMMENT
0.16 ± 0.06	-130 ± 20	SARANTSEV	19	DPWA $\bar{K}N$ multichannel

Normalized residue in $N\bar{K} \rightarrow \Sigma(2030) \rightarrow \Delta\bar{K}, H\text{-wave}$				
MODULUS	PHASE ($^\circ$)	DOCUMENT ID	TECN	COMMENT
0.04 ± 0.02	-130 ± 35	SARANTSEV	19	DPWA $\bar{K}N$ multichannel

Normalized residue in $N\bar{K} \rightarrow \Sigma(2030) \rightarrow N\bar{K}^*(892), S=1/2, F\text{-wave}$				
MODULUS	PHASE ($^\circ$)	DOCUMENT ID	TECN	COMMENT
0.02 ± 0.02		SARANTSEV	19	DPWA $\bar{K}N$ multichannel
••• We do not use the following data for averages, fits, limits, etc. •••				
0.193	38	¹ KAMANO	15	DPWA $\bar{K}N$ multichannel
¹ From the preferred solution A in KAMANO 15.				

Normalized residue in $N\bar{K} \rightarrow \Sigma(2030) \rightarrow N\bar{K}^*(892), S=3/2, F\text{-wave}$				
MODULUS	PHASE ($^\circ$)	DOCUMENT ID	TECN	COMMENT
0.16 ± 0.09	-160 ± 40	SARANTSEV	19	DPWA $\bar{K}N$ multichannel
••• We do not use the following data for averages, fits, limits, etc. •••				
0.320	37	¹ KAMANO	15	DPWA $\bar{K}N$ multichannel
¹ From the preferred solution A in KAMANO 15.				

Normalized residue in $N\bar{K} \rightarrow \Sigma(2030) \rightarrow N\bar{K}^*(892), S=3/2, H\text{-wave}$				
MODULUS	PHASE ($^\circ$)	DOCUMENT ID	TECN	COMMENT
0.00358	22	¹ KAMANO	15	DPWA Multichannel
¹ From the preferred solution A in KAMANO 15.				

 $\Sigma(2030)$ MASS

VALUE (MeV)	DOCUMENT ID	TECN	COMMENT
2025 to 2040 (≈ 2030) OUR ESTIMATE			
2032 ± 6	SARANTSEV	19	DPWA $\bar{K}N$ multichannel
2030 ± 5	ZHANG	13A	DPWA $\bar{K}N$ multichannel
2036 ± 5	GOPAL	80	DPWA $\bar{K}N \rightarrow \bar{K}N$
2038 ± 10	CORDEN	77B	$K^-N \rightarrow N\bar{K}^*$
2030 ± 3	¹ CORDEN	76	DPWA $K^-n \rightarrow \Lambda\pi^-$
2035 ± 15	BAILLON	75	IPWA $\bar{K}N \rightarrow \Lambda\pi$
2038 ± 10	HEMINGWAY	75	DPWA $K^-p \rightarrow \bar{K}N$
2042 ± 11	VANHORN	75	DPWA $K^-p \rightarrow \Lambda\pi^0$
2020 ± 6	KANE	74	DPWA $K^-p \rightarrow \Sigma\pi$
2035 ± 10	LITCHFIELD	74B	DPWA $K^-p \rightarrow \Lambda(1520)\pi^0$
2020 ± 30	LITCHFIELD	74C	DPWA $K^-p \rightarrow \Delta(1232)\bar{K}$
2025 ± 10	LITCHFIELD	74D	DPWA $K^-p \rightarrow \Lambda(1820)\pi^0$

Baryon Particle Listings

 $\Sigma(2030)$

• • • We do not use the following data for averages, fits, limits, etc. • • •

2040 ± 5	GOPAL	77	DPWA	$\bar{K}N$ multichannel
2027 to 2057	GOYAL	77	DPWA	$K^-N \rightarrow \Sigma\pi$
2030	DEBELLEFON	76	IPWA	$K^-p \rightarrow \Lambda\pi^0$

¹ Preferred solution 3; see CORDEN 76 for other possibilities.

 $\Sigma(2030)$ WIDTH

VALUE (MeV)	DOCUMENT ID	TECN	COMMENT
150 to 200 (≈ 180) OUR ESTIMATE			
177 ± 12	SARANTSEV	19	DPWA $\bar{K}N$ multichannel
207 ± 17	ZHANG	13A	DPWA $\bar{K}N$ multichannel
172 ± 10	GOPAL	80	DPWA $\bar{K}N \rightarrow \bar{K}N$
137 ± 4.0	CORDEN	77B	$K^-N \rightarrow N\bar{K}^*$
201 ± 9	¹ CORDEN	76	DPWA $K^-n \rightarrow \Lambda\pi^-$
180 ± 20	BAILLON	75	IPWA $\bar{K}N \rightarrow \Lambda\pi$
172 ± 15	HEMINGWAY	75	DPWA $K^-p \rightarrow \bar{K}N$
178 ± 13	VANHORN	75	DPWA $K^-p \rightarrow \Lambda\pi^0$
111 ± 5	KANE	74	DPWA $K^-p \rightarrow \Sigma\pi$
160 ± 20	LITCHFIELD	74B	DPWA $K^-p \rightarrow \Lambda(1520)\pi^0$
200 ± 30	LITCHFIELD	74C	DPWA $K^-p \rightarrow \Delta(1232)\bar{K}$
• • • We do not use the following data for averages, fits, limits, etc. • • •			
260	DECLAIS	77	DPWA $\bar{K}N \rightarrow \bar{K}N$
190 ± 10	GOPAL	77	DPWA $\bar{K}N$ multichannel
126 to 195	GOYAL	77	DPWA $K^-N \rightarrow \Sigma\pi$
160	DEBELLEFON	76	IPWA $K^-p \rightarrow \Lambda\pi^0$
70 to 125	LITCHFIELD	74D	DPWA $K^-p \rightarrow \Lambda(1820)\pi^0$

¹ Preferred solution 3; see CORDEN 76 for other possibilities.

 $\Sigma(2030)$ DECAY MODES

Mode	Fraction (Γ_i/Γ)
Γ_1 $N\bar{K}$	17–23 %
Γ_2 $\Lambda\pi$	17–23 %
Γ_3 $\Sigma\pi$	5–10 %
Γ_4 ΞK	<2 %
Γ_5 $\Sigma(1385)\pi$	5–15 %
Γ_6 $\Sigma(1385)\pi, F\text{-wave}$	(1.0 ± 1.0) %
Γ_7 $\Sigma(1385)\pi, H\text{-wave}$	
Γ_8 $\Lambda(1520)\pi$	10–20 %
Γ_9 $\Lambda(1520)\pi, D\text{-wave}$	
Γ_{10} $\Lambda(1520)\pi, G\text{-wave}$	
Γ_{11} $\Delta(1232)\bar{K}$	10–20 %
Γ_{12} $\Delta(1232)\bar{K}, F\text{-wave}$	(15 ± 5) %
Γ_{13} $\Delta(1232)\bar{K}, H\text{-wave}$	(1.0 ± 1.0) %
Γ_{14} $N\bar{K}^*(892)$	
Γ_{15} $N\bar{K}^*(892), S=1/2, F\text{-wave}$	
Γ_{16} $N\bar{K}^*(892), S=3/2, F\text{-wave}$	(14 ± 8) %
Γ_{17} $N\bar{K}^*(892), S=3/2, H\text{-wave}$	
Γ_{18} $\Lambda(1820)\pi, P\text{-wave}$	

 $\Sigma(2030)$ BRANCHING RATIOS

See “Sign conventions for resonance couplings” in the Note on Λ and Σ Resonances.

$\Gamma(N\bar{K})/\Gamma_{\text{total}}$	DOCUMENT ID	TECN	COMMENT	Γ_1/Γ
0.17 to 0.23 OUR ESTIMATE				
0.20 ± 0.04	SARANTSEV	19	DPWA $\bar{K}N$ multichannel	
0.13 ± 0.01	ZHANG	13A	DPWA $\bar{K}N$ multichannel	
0.19 ± 0.03	GOPAL	80	DPWA $\bar{K}N \rightarrow \bar{K}N$	
0.18 ± 0.03	HEMINGWAY	75	DPWA $K^-p \rightarrow \bar{K}N$	
• • • We do not use the following data for averages, fits, limits, etc. • • •				
0.269	¹ KAMANO	15	DPWA Multichannel	
0.15	DECLAIS	77	DPWA $\bar{K}N \rightarrow \bar{K}N$	
0.24 ± 0.02	GOPAL	77	DPWA See GOPAL 80	

¹ From the preferred solution A in KAMANO 15.

$\Gamma(\Lambda\pi)/\Gamma_{\text{total}}$	DOCUMENT ID	TECN	COMMENT	Γ_2/Γ
0.17 ± 0.04				
• • • We do not use the following data for averages, fits, limits, etc. • • •				
0.080	¹ KAMANO	15	DPWA $\bar{K}N$ multichannel	

¹ From the preferred solution A in KAMANO 15.

$\Gamma(\Sigma\pi)/\Gamma_{\text{total}}$	DOCUMENT ID	TECN	COMMENT	Γ_3/Γ
0.025 ± 0.008				
• • • We do not use the following data for averages, fits, limits, etc. • • •				
0.037	¹ KAMANO	15	DPWA $\bar{K}N$ multichannel	

¹ From the preferred solution A in KAMANO 15.

$\Gamma(\Xi K)/\Gamma_{\text{total}}$	DOCUMENT ID	TECN	COMMENT	Γ_4/Γ
<0.01				
• • • We do not use the following data for averages, fits, limits, etc. • • •				
0.006	¹ KAMANO	15	DPWA $\bar{K}N$ multichannel	

¹ From the preferred solution A in KAMANO 15.

$\Gamma(\Lambda(1520)\pi, D\text{-wave})/\Gamma_{\text{total}}$	DOCUMENT ID	TECN	COMMENT	Γ_9/Γ
~ 0.01				
• • • We do not use the following data for averages, fits, limits, etc. • • •				
0.030	¹ KAMANO	15	DPWA $\bar{K}N$ multichannel	

$\Gamma(\Lambda(1520)\pi, G\text{-wave})/\Gamma_{\text{total}}$	DOCUMENT ID	TECN	COMMENT	Γ_{10}/Γ
<0.01				
• • • We do not use the following data for averages, fits, limits, etc. • • •				
0.030	¹ KAMANO	15	DPWA $\bar{K}N$ multichannel	

$\Gamma(\Sigma(1385)\pi, F\text{-wave})/\Gamma_{\text{total}}$	DOCUMENT ID	TECN	COMMENT	Γ_6/Γ
0.01 ± 0.01				
• • • We do not use the following data for averages, fits, limits, etc. • • •				
0.030	¹ KAMANO	15	DPWA $\bar{K}N$ multichannel	

¹ From the preferred solution A in KAMANO 15.

$\Gamma(\Sigma(1385)\pi, H\text{-wave})/\Gamma_{\text{total}}$	DOCUMENT ID	TECN	COMMENT	Γ_7/Γ
0.003				
• • • We do not use the following data for averages, fits, limits, etc. • • •				
0.003	¹ KAMANO	15	DPWA Multichannel	

¹ From the preferred solution A in KAMANO 15.

$\Gamma(\Delta(1232)\bar{K}, F\text{-wave})/\Gamma_{\text{total}}$	DOCUMENT ID	TECN	COMMENT	Γ_{12}/Γ
0.15 ± 0.05				
• • • We do not use the following data for averages, fits, limits, etc. • • •				
0.154	¹ KAMANO	15	DPWA $\bar{K}N$ multichannel	

$\Gamma(\Delta(1232)\bar{K}, H\text{-wave})/\Gamma_{\text{total}}$	DOCUMENT ID	TECN	COMMENT	Γ_{13}/Γ
0.01 ± 0.01				
• • • We do not use the following data for averages, fits, limits, etc. • • •				
0.422	¹ KAMANO	15	DPWA $\bar{K}N$ multichannel	

$\Gamma(N\bar{K}^*(892), S=1/2, F\text{-wave})/\Gamma_{\text{total}}$	DOCUMENT ID	TECN	COMMENT	Γ_{15}/Γ
<0.01				
• • • We do not use the following data for averages, fits, limits, etc. • • •				
0.154	¹ KAMANO	15	DPWA $\bar{K}N$ multichannel	

¹ From the preferred solution A in KAMANO 15.

$\Gamma(N\bar{K}^*(892), S=3/2, F\text{-wave})/\Gamma_{\text{total}}$	DOCUMENT ID	TECN	COMMENT	Γ_{16}/Γ
0.14 ± 0.08				
• • • We do not use the following data for averages, fits, limits, etc. • • •				
0.422	¹ KAMANO	15	DPWA $\bar{K}N$ multichannel	

¹ From the preferred solution A in KAMANO 15.

$\Gamma(N\bar{K}^*(892), S=3/2, H\text{-wave})/\Gamma_{\text{total}}$	DOCUMENT ID	TECN	COMMENT	Γ_{17}/Γ
not seen				
• • • We do not use the following data for averages, fits, limits, etc. • • •				
not seen	¹ KAMANO	15	DPWA $\bar{K}N$ multichannel	

¹ From the preferred solution A in KAMANO 15.

$(\Gamma_1\Gamma_7)^{1/2}/\Gamma_{\text{total}}$ in $N\bar{K} \rightarrow \Sigma(2030) \rightarrow \Lambda\pi$	DOCUMENT ID	TECN	COMMENT	$(\Gamma_1\Gamma_2)^{1/2}/\Gamma$
+0.15 ± 0.01	ZHANG	13A	DPWA Multichannel	
+0.18 ± 0.02	GOPAL	77	DPWA $\bar{K}N$ multichannel	
+0.20 ± 0.01	¹ CORDEN	76	DPWA $K^-n \rightarrow \Lambda\pi^-$	
+0.18 ± 0.02	BAILLON	75	IPWA $\bar{K}N \rightarrow \Lambda\pi$	
+0.20 ± 0.01	VANHORN	75	DPWA $K^-p \rightarrow \Lambda\pi^0$	
+0.195 ± 0.053	DEVENISH	74B	Fixed- t dispersion rel.	
• • • We do not use the following data for averages, fits, limits, etc. • • •				
0.20	DEBELLEFON	76	IPWA $K^-p \rightarrow \Lambda\pi^0$	

¹ Preferred solution 3; see CORDEN 76 for other possibilities.

$(\Gamma_1\Gamma_7)^{1/2}/\Gamma_{\text{total}}$ in $N\bar{K} \rightarrow \Sigma(2030) \rightarrow \Sigma\pi$	DOCUMENT ID	TECN	COMMENT	$(\Gamma_1\Gamma_3)^{1/2}/\Gamma$
-0.08 ± 0.01	ZHANG	13A	DPWA Multichannel	
-0.09 ± 0.01	¹ CORDEN	77c	$K^-n \rightarrow \Sigma\pi$	
-0.06 ± 0.01	¹ CORDEN	77c	$K^-n \rightarrow \Sigma\pi$	
-0.15 ± 0.03	GOPAL	77	DPWA $\bar{K}N$ multichannel	
-0.10 ± 0.01	KANE	74	DPWA $K^-p \rightarrow \Sigma\pi$	
• • • We do not use the following data for averages, fits, limits, etc. • • •				
-0.085 ± 0.02	² GOYAL	77	DPWA $K^-N \rightarrow \Sigma\pi$	

¹ The two entries for CORDEN 77c are from two different acceptable solutions.

² This coupling is extracted from unnormalized data.

See key on page 1127

Baryon Particle Listings

$\Sigma(2030), \Sigma(2070), \Sigma(2080)$

$(\Gamma_1 \Gamma_f) \frac{1}{2} / \Gamma_{\text{total}}$ in $N\bar{K} \rightarrow \Sigma(2030) \rightarrow \Xi K$ $(\Gamma_1 \Gamma_4) \frac{1}{2} / \Gamma$

VALUE	DOCUMENT ID	TECN	COMMENT
0.023	MULLER 69B	DPWA	$K^- p \rightarrow \Xi K$
<0.05	BURGUN 68	DPWA	$K^- p \rightarrow \Xi K$
<0.05	TRIPP 67	RVUE	$K^- p \rightarrow \Xi K$

$(\Gamma_1 \Gamma_f) \frac{1}{2} / \Gamma_{\text{total}}$ in $N\bar{K} \rightarrow \Sigma(2030) \rightarrow \Sigma(1385)\pi, F\text{-wave}$ $(\Gamma_1 \Gamma_6) \frac{1}{2} / \Gamma$

VALUE	DOCUMENT ID	TECN	COMMENT
+0.16 ± 0.01	ZHANG 13A	DPWA	Multichannel
+0.153 ± 0.026	¹ CAMERON 78	DPWA	$K^- p \rightarrow \Sigma(1385)\pi$

¹ The published sign has been changed to be in accord with the baryon-first convention.

$(\Gamma_1 \Gamma_f) \frac{1}{2} / \Gamma_{\text{total}}$ in $N\bar{K} \rightarrow \Sigma(2030) \rightarrow \Lambda(1520)\pi, D\text{-wave}$ $(\Gamma_1 \Gamma_9) \frac{1}{2} / \Gamma$

VALUE	DOCUMENT ID	TECN	COMMENT
+0.114 ± 0.010	¹ CAMERON 77	DPWA	$K^- p \rightarrow \Lambda(1520)\pi^0$
0.14 ± 0.03	LITCHFIELD 74B	DPWA	$K^- p \rightarrow \Lambda(1520)\pi^0$

• • • We do not use the following data for averages, fits, limits, etc. • • •

VALUE	DOCUMENT ID	TECN	COMMENT
0.10 ± 0.03	² CORDEN 75B	DBC	$K^- n \rightarrow N\bar{K}\pi^-$

¹ The published sign has been changed to be in accord with the baryon-first convention.
² An upper limit.

$(\Gamma_1 \Gamma_f) \frac{1}{2} / \Gamma_{\text{total}}$ in $N\bar{K} \rightarrow \Sigma(2030) \rightarrow \Lambda(1520)\pi, G\text{-wave}$ $(\Gamma_1 \Gamma_{10}) \frac{1}{2} / \Gamma$

VALUE	DOCUMENT ID	TECN	COMMENT
+0.146 ± 0.010	¹ CAMERON 77	DPWA	$K^- p \rightarrow \Lambda(1520)\pi^0$
0.02 ± 0.02	LITCHFIELD 74B	DPWA	$K^- p \rightarrow \Lambda(1520)\pi^0$

¹ The published sign has been changed to be in accord with the baryon-first convention.

$(\Gamma_1 \Gamma_f) \frac{1}{2} / \Gamma_{\text{total}}$ in $N\bar{K} \rightarrow \Sigma(2030) \rightarrow \Delta(1232)\bar{K}, F\text{-wave}$ $(\Gamma_1 \Gamma_{12}) \frac{1}{2} / \Gamma$

VALUE	DOCUMENT ID	TECN	COMMENT
+0.12 ± 0.02	ZHANG 13A	DPWA	Multichannel
0.16 ± 0.03	LITCHFIELD 74C	DPWA	$K^- p \rightarrow \Delta(1232)\bar{K}$

• • • We do not use the following data for averages, fits, limits, etc. • • •

VALUE	DOCUMENT ID	TECN	COMMENT
0.17 ± 0.03	¹ CORDEN 75B	DBC	$K^- n \rightarrow N\bar{K}\pi^-$

¹ An upper limit.

$(\Gamma_1 \Gamma_f) \frac{1}{2} / \Gamma_{\text{total}}$ in $N\bar{K} \rightarrow \Sigma(2030) \rightarrow \Delta(1232)\bar{K}, H\text{-wave}$ $(\Gamma_1 \Gamma_{13}) \frac{1}{2} / \Gamma$

VALUE	DOCUMENT ID	TECN	COMMENT
0.00 ± 0.02	LITCHFIELD 74C	DPWA	$K^- p \rightarrow \Delta(1232)\bar{K}$

$(\Gamma_1 \Gamma_f) \frac{1}{2} / \Gamma_{\text{total}}$ in $N\bar{K} \rightarrow \Sigma(2030) \rightarrow N\bar{K}^*(892), S=1/2, F\text{-wave}$ $(\Gamma_1 \Gamma_{15}) \frac{1}{2} / \Gamma$

VALUE	DOCUMENT ID	TECN	COMMENT
+0.06 ± 0.02	ZHANG 13A	DPWA	Multichannel
+0.06 ± 0.03	¹ CAMERON 78B	DPWA	$K^- p \rightarrow N\bar{K}^*$
-0.02 ± 0.01	CORDEN 77B		$K^- d \rightarrow NN\bar{K}^*$

¹ The published sign has been changed to be in accord with the baryon-first convention.

$(\Gamma_1 \Gamma_f) \frac{1}{2} / \Gamma_{\text{total}}$ in $N\bar{K} \rightarrow \Sigma(2030) \rightarrow N\bar{K}^*(892), S=3/2, F\text{-wave}$ $(\Gamma_1 \Gamma_{16}) \frac{1}{2} / \Gamma$

VALUE	DOCUMENT ID	TECN	COMMENT
+0.05 ± 0.01	ZHANG 13A	DPWA	Multichannel
+0.04 ± 0.03	¹ CAMERON 78B	DPWA	$K^- p \rightarrow N\bar{K}^*$
-0.12 ± 0.02	CORDEN 77B		$K^- d \rightarrow NN\bar{K}^*$

¹ The upper limit on the G_3 wave is 0.03.

$(\Gamma_1 \Gamma_f) \frac{1}{2} / \Gamma_{\text{total}}$ in $N\bar{K} \rightarrow \Sigma(2030) \rightarrow \Lambda(1820)\pi, P\text{-wave}$ $(\Gamma_1 \Gamma_{18}) \frac{1}{2} / \Gamma$

VALUE	DOCUMENT ID	TECN	COMMENT
0.14 ± 0.02	CORDEN 75B	DBC	$K^- n \rightarrow N\bar{K}\pi^-$
0.18 ± 0.04	LITCHFIELD 74D	DPWA	$K^- p \rightarrow \Lambda(1820)\pi^0$

$\Sigma(2030)$ REFERENCES

SARANTSEV 19	EPJ A55 180	A.V. Sarantsev et al.	(BONN, PNPI)
KAMANO 15	PR C92 025205	H. Kamano et al.	(ANL, OSAK)
ZHANG 13A	PR C88 035205	H. Zhang et al.	(KSU)
PDG 84	RMP 56 51	C.G. Wohl et al.	(LBL, CIT, CERN)
PDG 82	PL 11B 1	M. Roos et al.	(HELS, CIT, CERN)
GOPAL 80	Toronto Conf. 159	G.P. Gopal	(RHEL) IJP
CAMERON 78	NP B143 189	W. Cameron et al.	(RHEL, LOIC) IJP
CAMERON 78B	NP B146 327	W. Cameron et al.	(RHEL, LOIC) IJP
CAMERON 77	NP B131 399	W. Cameron et al.	(RHEL, LOIC) IJP
CORDEN 77B	NP B121 365	M.J. Corden et al.	(BIRM) IJP
CORDEN 77C	NP B125 61	M.J. Corden et al.	(BIRM) IJP
DECLAIS 77	CERN 77-16	Y. Declais et al.	(CAEN, CERN) IJP
GOPAL 77	NP B119 362	G.P. Gopal et al.	(LOIC, RHEL) IJP
GOYAL 77	PR D16 2746	D.P. Goyal, A.V. Sodhi	(DELH) IJP
CORDEN 76	NP B104 382	M.J. Corden et al.	(BIRM) IJP
DEBELLEFON 76	NP B109 129	A. de Bellefon, A. Berthon	(CDEF) IJP
BAILLON 75	NP B94 39	P.H. Baillon, P.J. Litchfield	(CERN, RHEL) IJP
CORDEN 75B	NP B92 365	M.J. Corden et al.	(BIRM) IJP
HEMINGWAY 75	NP B91 12	R.J. Hemingway et al.	(CERN, HEIDH, MPIM) IJP
VANHORN 75	NP B87 145	A.J. van Horn	(LBL) IJP
Also	NP B87 157	A.J. van Horn	(LBL) IJP

DEVENISH 74B	NP B81 330	R.C.E. Devenish, C.D. Froggatt, B.R. Martin	(DESY+) (LBL) IJP
KANE 74	LBL-2452	D.F. Kane	(CERN, HEIDH) IJP
LITCHFIELD 74B	NP B74 19	P.J. Litchfield et al.	(CERN, HEIDH) IJP
LITCHFIELD 74C	NP B74 39	P.J. Litchfield et al.	(CERN, HEIDH) IJP
LITCHFIELD 74D	NP B74 12	P.J. Litchfield et al.	(CERN, HEIDH) IJP
MULLER 69B	Thesis UCRL 19372	R.A. Muller	(LRL)
BURGUN 68	NP B8 447	G. Burgun et al.	(SACL, CDEF, RHEL)
TRIPP 67	NP B3 10	R.D. Tripp et al.	(LRL, SLAC, CERN+)
COOL 66	PRL 16 1228	R.L. Cool et al.	(BNL)
WOHL 66	PRL 17 107	C.G. Wohl, F.T. Solmitz, M.L. Stevenson	(LRL) IJP

$\Sigma(2070) 5/2^+$

$I(J^P) = 1(\frac{5}{2}^+)$ Status: *

OMITTED FROM SUMMARY TABLE

This state suggested by BERTHON 70B finds support in GOPAL 80 with new $K^- p$ polarization and $K^- n$ angular distributions. The very broad state seen in KANE 72 is not required in the later (KANE 74) analysis of $\bar{K}N \rightarrow \Sigma\pi$.

$\Sigma(2070)$ MASS

VALUE (MeV)	DOCUMENT ID	TECN	COMMENT
2020 to 2100 (≈ 2060) OUR ESTIMATE			
2051 ± 25	GOPAL 80	DPWA	$\bar{K}N \rightarrow \bar{K}N$
2070 ± 10	BERTHON 70B	DPWA	$K^- p \rightarrow \Sigma\pi$

• • • We do not use the following data for averages, fits, limits, etc. • • •

VALUE (MeV)	DOCUMENT ID	TECN	COMMENT
2057	KANE 72	DPWA	$K^- p \rightarrow \Sigma\pi$

$\Sigma(2070)$ WIDTH

VALUE (MeV)	DOCUMENT ID	TECN	COMMENT
100 to 300 (≈ 200) OUR ESTIMATE			
300 ± 30	GOPAL 80	DPWA	$\bar{K}N \rightarrow \bar{K}N$
140 ± 20	BERTHON 70B	DPWA	$K^- p \rightarrow \Sigma\pi$

• • • We do not use the following data for averages, fits, limits, etc. • • •

VALUE (MeV)	DOCUMENT ID	TECN	COMMENT
906	KANE 72	DPWA	$K^- p \rightarrow \Sigma\pi$

$\Sigma(2070)$ DECAY MODES

Mode	Γ_1 / Γ
Γ_1 $N\bar{K}$	
Γ_2 $\Sigma\pi$	

$\Sigma(2070)$ BRANCHING RATIOS

See "Sign conventions for resonance couplings" in the Note on Λ and Σ Resonances.

$\Gamma(N\bar{K}) / \Gamma_{\text{total}}$ Γ_1 / Γ

VALUE	DOCUMENT ID	TECN	COMMENT
0.08 ± 0.03	GOPAL 80	DPWA	$\bar{K}N \rightarrow \bar{K}N$

$(\Gamma_1 \Gamma_f) \frac{1}{2} / \Gamma_{\text{total}}$ in $N\bar{K} \rightarrow \Sigma(2070) \rightarrow \Sigma\pi$ $(\Gamma_1 \Gamma_2) \frac{1}{2} / \Gamma$

VALUE	DOCUMENT ID	TECN	COMMENT
0.12 ± 0.02	BERTHON 70B	DPWA	$K^- p \rightarrow \Sigma\pi$

• • • We do not use the following data for averages, fits, limits, etc. • • •

VALUE	DOCUMENT ID	TECN	COMMENT
0.104	KANE 72	DPWA	$K^- p \rightarrow \Sigma\pi$

$\Sigma(2070)$ REFERENCES

GOPAL 80	Toronto Conf. 159	G.P. Gopal	(RHEL) IJP
KANE 74	LBL-2452	D.F. Kane	(LBL)
KANE 72	PR D5 1583	D.F.J. Kane	(LBL)
BERTHON 70B	NP B24 417	A. Berthon et al.	(CDEF, RHEL, SACL) IJP

$\Sigma(2080) 3/2^+$

$I(J^P) = 1(\frac{3}{2}^+)$ Status: *

OMITTED FROM SUMMARY TABLE

Suggested by some but not all partial-wave analyses across this region.

$\Sigma(2080)$ MASS

VALUE (MeV)	DOCUMENT ID	TECN	COMMENT
2060 to 2120 (≈ 2090) OUR ESTIMATE			
2091 ± 7	¹ CORDEN 76	DPWA	$K^- n \rightarrow \Lambda\pi^-$
2070 to 2120	DEBELLEFON 76	IPWA	$K^- p \rightarrow \Lambda\pi^0$
2120 ± 40	BAILLON 75	IPWA	$\bar{K}N \rightarrow \Lambda\pi$ (sol. 1)
2140 ± 40	BAILLON 75	IPWA	$\bar{K}N \rightarrow \Lambda\pi$ (sol. 2)
2082 ± 4	COX 70	DPWA	See CORDEN 76
2070 ± 30	LITCHFIELD 70	DPWA	$K^- N \rightarrow \Lambda\pi$

Baryon Particle Listings

 $\Sigma(2080)$, $\Sigma(2100)$ $\Sigma(2080)$ WIDTH

VALUE (MeV)	DOCUMENT ID	TECN	COMMENT
100 to 240 (≈ 170) OUR ESTIMATE			
186 \pm 48	¹ CORDEN 76	DPWA	$K^- n \rightarrow \Lambda \pi^-$
100	DEBELLEFON 76	IPWA	$K^- p \rightarrow \Lambda \pi^0$
240 \pm 50	BAILLON 75	IPWA	$\bar{K} N \rightarrow \Lambda \pi$ (sol. 1)
200 \pm 50	BAILLON 75	IPWA	$\bar{K} N \rightarrow \Lambda \pi$ (sol. 2)
87 \pm 20	COX 70	DPWA	See CORDEN 76
250 \pm 40	LITCHFIELD 70	DPWA	$K^- N \rightarrow \Lambda \pi$

 $\Sigma(2080)$ DECAY MODES

Mode	
Γ_1	$N\bar{K}$
Γ_2	$\Lambda\pi$

 $\Sigma(2080)$ BRANCHING RATIOS

See "Sign conventions for resonance couplings" in the Note on Λ and Σ Resonances.

$(\Gamma_1\Gamma_2)^{1/2}/\Gamma_{\text{total}}$ in $N\bar{K} \rightarrow \Sigma(2080) \rightarrow \Lambda\pi$	DOCUMENT ID	TECN	COMMENT	$(\Gamma_1\Gamma_2)^{1/2}/\Gamma$
-0.10 \pm 0.03	¹ CORDEN 76	DPWA	$K^- n \rightarrow \Lambda \pi^-$	
-0.10	DEBELLEFON 76	IPWA	$K^- p \rightarrow \Lambda \pi^0$	
-0.13 \pm 0.04	BAILLON 75	IPWA	$\bar{K} N \rightarrow \Lambda \pi$ (sol. 1 and 2)	
-0.16 \pm 0.03	COX 70	DPWA	See CORDEN 76	
-0.09 \pm 0.03	LITCHFIELD 70	DPWA	$K^- N \rightarrow \Lambda \pi$	

 $\Sigma(2080)$ FOOTNOTES

¹ Preferred solution 3; see CORDEN 76 for other possibilities, including a D_{15} at this mass.

 $\Sigma(2080)$ REFERENCES

CORDEN 76	NP B104 382	M.J. Corden et al.	(BIRM) IJP
DEBELLEFON 76	NP B109 129	A. de Bellefon, A. Berthon	(CDEF) IJP
Also	NP B90 1	A. de Bellefon et al.	(CDEF, SAACL) IJP
BAILLON 75	NP B94 39	P.H. Baillon, P.J. Litchfield	(CERN, RHEL) IJP
COX 70	NP B19 61	G.F. Cox et al.	(BIRM, EDIN, GLAS, LOIC) IJP
LITCHFIELD 70	NP B22 269	P.J. Litchfield	(RHHEL) IJP

$$\Sigma(2100) 7/2^- \quad I(J^P) = 1(\frac{7}{2}^-) \text{ Status: } *$$

OMITTED FROM SUMMARY TABLE

 $\Sigma(2100)$ POLE POSITION

REAL PART	DOCUMENT ID	TECN	COMMENT
VALUE (MeV)			
2093\pm16	SARANTSEV 19	DPWA	$\bar{K} N$ multichannel
-2 \times IMAGINARY PART	DOCUMENT ID	TECN	COMMENT
VALUE (MeV)			
210\pm35	SARANTSEV 19	DPWA	$\bar{K} N$ multichannel

 $\Sigma(2100)$ POLE RESIDUES

Normalized residue in $N\bar{K} \rightarrow \Sigma(2100) \rightarrow N\bar{K}$	DOCUMENT ID	TECN	COMMENT
MODULUS PHASE ($^\circ$)			
0.09\pm0.02 -110 \pm 15	SARANTSEV 19	DPWA	$\bar{K} N$ multichannel
Normalized residue in $N\bar{K} \rightarrow \Sigma(2100) \rightarrow \Sigma\pi$	DOCUMENT ID	TECN	COMMENT
MODULUS PHASE ($^\circ$)			
0.04\pm0.02 -50 \pm 20	SARANTSEV 19	DPWA	$\bar{K} N$ multichannel
Normalized residue in $N\bar{K} \rightarrow \Sigma(2100) \rightarrow \Lambda\pi$	DOCUMENT ID	TECN	COMMENT
MODULUS PHASE ($^\circ$)			
0.03\pm0.02 -100 \pm 25	SARANTSEV 19	DPWA	$\bar{K} N$ multichannel
Normalized residue in $N\bar{K} \rightarrow \Sigma(2100) \rightarrow \Xi K$	DOCUMENT ID	TECN	COMMENT
MODULUS PHASE ($^\circ$)			
0.010\pm0.005 -120 \pm 35	SARANTSEV 19	DPWA	$\bar{K} N$ multichannel
Normalized residue in $N\bar{K} \rightarrow \Sigma(2100) \rightarrow \Lambda(1520)\pi, F\text{-wave}$	DOCUMENT ID	TECN	COMMENT
MODULUS PHASE ($^\circ$)			
0.02\pm0.01 -100 \pm 30	SARANTSEV 19	DPWA	$\bar{K} N$ multichannel
Normalized residue in $N\bar{K} \rightarrow \Sigma(2100) \rightarrow \Lambda(1520)\pi, H\text{-wave}$	DOCUMENT ID	TECN	COMMENT
MODULUS PHASE ($^\circ$)			
0.01\pm0.01	SARANTSEV 19	DPWA	$\bar{K} N$ multichannel

Normalized residue in $N\bar{K} \rightarrow \Sigma(2100) \rightarrow \Sigma(1385)\pi, D\text{-wave}$

MODULUS	PHASE ($^\circ$)	DOCUMENT ID	TECN	COMMENT
0.10\pm0.03	-60\pm30	SARANTSEV 19	DPWA	$\bar{K} N$ multichannel

Normalized residue in $N\bar{K} \rightarrow \Sigma(2100) \rightarrow \Sigma(1385)\pi, G\text{-wave}$

MODULUS	PHASE ($^\circ$)	DOCUMENT ID	TECN	COMMENT
0.03\pm0.01	-50\pm30	SARANTSEV 19	DPWA	$\bar{K} N$ multichannel

Normalized residue in $N\bar{K} \rightarrow \Sigma(2100) \rightarrow \Delta\bar{K}, G\text{-wave}$

MODULUS	PHASE ($^\circ$)	DOCUMENT ID	TECN	COMMENT
0.04\pm0.02	75\pm35	SARANTSEV 19	DPWA	$\bar{K} N$ multichannel

Normalized residue in $N\bar{K} \rightarrow \Sigma(2100) \rightarrow N\bar{K}^*(892), S=3/2, D\text{-wave}$

MODULUS	PHASE ($^\circ$)	DOCUMENT ID	TECN	COMMENT
0.08\pm0.04	20\pm50	SARANTSEV 19	DPWA	$\bar{K} N$ multichannel

 $\Sigma(2100)$ MASS

VALUE (MeV)	DOCUMENT ID	TECN	COMMENT
≈ 2100 OUR ESTIMATE			
2146 \pm 17	SARANTSEV 19	DPWA	$\bar{K} N$ multichannel
2060 \pm 20	BARBARO... 70	DPWA	$K^- p \rightarrow \Lambda \pi^0$
2120 \pm 30	BARBARO... 70	DPWA	$K^- p \rightarrow \Sigma \pi$

 $\Sigma(2100)$ WIDTH

VALUE (MeV)	DOCUMENT ID	TECN	COMMENT
260 \pm 40	SARANTSEV 19	DPWA	$\bar{K} N$ multichannel
70 \pm 30	BARBARO... 70	DPWA	$K^- p \rightarrow \Lambda \pi^0$
135 \pm 30	BARBARO... 70	DPWA	$K^- p \rightarrow \Sigma \pi$

 $\Sigma(2100)$ DECAY MODES

Mode	Fraction (Γ_i/Γ)
Γ_1	$N\bar{K}$ (8.0 \pm 2.0) %
Γ_2	$\Lambda\pi$ (1.5 \pm 1.0) %
Γ_3	$\Sigma\pi$ (2.0 \pm 1.0) %
Γ_4	ΞK
Γ_5	$\Sigma(1385)\pi, D\text{-wave}$ (12 \pm 6) %
Γ_6	$\Sigma(1385)\pi, G\text{-wave}$
Γ_7	$\Lambda(1520)\pi, F\text{-wave}$ (1.0 \pm 1.0) %
Γ_8	$\Lambda(1520)\pi, H\text{-wave}$
Γ_9	$N\bar{K}^*(892), S=3/2, D\text{-wave}$ (6.0 \pm 3.0) %
Γ_{10}	$\Delta\bar{K}, G\text{-wave}$ (1.0 \pm 1.0) %

 $\Sigma(2100)$ BRANCHING RATIOS

See "Sign conventions for resonance couplings" in the Note on Λ and Σ Resonances.

$(\Gamma_1\Gamma_2)^{1/2}/\Gamma_{\text{total}}$ in $N\bar{K} \rightarrow \Sigma(2100) \rightarrow \Lambda\pi$	DOCUMENT ID	TECN	COMMENT	$(\Gamma_1\Gamma_2)^{1/2}/\Gamma$
VALUE				
-0.07 \pm 0.02	BARBARO... 70	DPWA	$K^- p \rightarrow \Lambda \pi^0$	
$(\Gamma_1\Gamma_3)^{1/2}/\Gamma_{\text{total}}$ in $N\bar{K} \rightarrow \Sigma(2100) \rightarrow \Sigma\pi$	DOCUMENT ID	TECN	COMMENT	$(\Gamma_1\Gamma_3)^{1/2}/\Gamma$
VALUE				
+0.13 \pm 0.02	BARBARO... 70	DPWA	$K^- p \rightarrow \Sigma \pi$	
$\Gamma(N\bar{K})/\Gamma_{\text{total}}$	DOCUMENT ID	TECN	COMMENT	Γ_1/Γ
VALUE				
0.08\pm0.02	SARANTSEV 19	DPWA	$\bar{K} N$ multichannel	
$\Gamma(\Lambda\pi)/\Gamma_{\text{total}}$	DOCUMENT ID	TECN	COMMENT	Γ_2/Γ
VALUE				
0.015\pm0.01	SARANTSEV 19	DPWA	$\bar{K} N$ multichannel	
$\Gamma(\Sigma\pi)/\Gamma_{\text{total}}$	DOCUMENT ID	TECN	COMMENT	Γ_3/Γ
VALUE				
0.02\pm0.01	SARANTSEV 19	DPWA	$\bar{K} N$ multichannel	
$\Gamma(\Xi K)/\Gamma_{\text{total}}$	DOCUMENT ID	TECN	COMMENT	Γ_4/Γ
VALUE				
<0.01	SARANTSEV 19	DPWA	$\bar{K} N$ multichannel	
$\Gamma(\Sigma(1385)\pi, D\text{-wave})/\Gamma_{\text{total}}$	DOCUMENT ID	TECN	COMMENT	Γ_5/Γ
VALUE				
0.12\pm0.06	SARANTSEV 19	DPWA	$\bar{K} N$ multichannel	
$\Gamma(\Sigma(1385)\pi, G\text{-wave})/\Gamma_{\text{total}}$	DOCUMENT ID	TECN	COMMENT	Γ_6/Γ
VALUE				
~ 0.01	SARANTSEV 19	DPWA	$\bar{K} N$ multichannel	

See key on page 1127

Baryon Particle Listings
 $\Sigma(2100)$, $\Sigma(2110)$, $\Sigma(2230)$

$\Gamma(\Lambda(1520)\pi, F\text{-wave})/\Gamma_{\text{total}}$				Γ_7/Γ
VALUE	DOCUMENT ID	TECN	COMMENT	
0.01 ± 0.01	SARANTSEV	19	DPWA $\bar{K}N$ multichannel	

$\Gamma(\Lambda(1520)\pi, H\text{-wave})/\Gamma_{\text{total}}$				Γ_8/Γ
VALUE	DOCUMENT ID	TECN	COMMENT	
~ 0	SARANTSEV	19	DPWA $\bar{K}N$ multichannel	

$\Gamma(N\bar{K}^*(892), S=3/2, D\text{-wave})/\Gamma_{\text{total}}$				Γ_9/Γ
VALUE	DOCUMENT ID	TECN	COMMENT	
0.06 ± 0.03	SARANTSEV	19	DPWA $\bar{K}N$ multichannel	

$\Gamma(\Delta\bar{K}, G\text{-wave})/\Gamma_{\text{total}}$				Γ_{10}/Γ
VALUE	DOCUMENT ID	TECN	COMMENT	
0.01 ± 0.01	SARANTSEV	19	DPWA $\bar{K}N$ multichannel	

 $\Sigma(2100)$ REFERENCES

SARANTSEV 19	EPJ A55 180	A.V. Sarantsev et al.	(BONN, PNPI)
BARBARO...	70 Duke Conf. 173	A. Barbaro-Galieri	(LRL)JJP
Hyperon Resonances, 1970			

 $\Sigma(2110) 1/2^-$

$I(J^P) = 1(\frac{1}{2}^-)$ Status: *

OMITTED FROM SUMMARY TABLE
was $\Sigma(2160)$ $\Sigma(2110)$ POLE POSITION

REAL PART			
VALUE (MeV)	DOCUMENT ID	TECN	COMMENT
2158 ± 25	SARANTSEV	19	DPWA $\bar{K}N$ multichannel

$-2 \times$ IMAGINARY PART			
VALUE (MeV)	DOCUMENT ID	TECN	COMMENT
$300 \pm \frac{300}{60}$	SARANTSEV	19	DPWA $\bar{K}N$ multichannel

 $\Sigma(2110)$ POLE RESIDUES

Normalized residue in $N\bar{K} \rightarrow \Sigma(2110) \rightarrow N\bar{K}$			
MODULUS	PHASE ($^\circ$)	DOCUMENT ID	TECN COMMENT
0.29 ± 0.08	-20 ± 35	SARANTSEV 19	DPWA $\bar{K}N$ multichannel

Normalized residue in $N\bar{K} \rightarrow \Sigma(2110) \rightarrow \Sigma\pi$			
MODULUS	PHASE ($^\circ$)	DOCUMENT ID	TECN COMMENT
0.14 ± 0.04	-5 ± 35	SARANTSEV 19	DPWA $\bar{K}N$ multichannel

Normalized residue in $N\bar{K} \rightarrow \Sigma(2110) \rightarrow \Lambda\pi$			
MODULUS	PHASE ($^\circ$)	DOCUMENT ID	TECN COMMENT
0.39 ± 0.08	85 ± 25	SARANTSEV 19	DPWA $\bar{K}N$ multichannel

Normalized residue in $N\bar{K} \rightarrow \Sigma(2110) \rightarrow \Xi K$			
MODULUS	PHASE ($^\circ$)	DOCUMENT ID	TECN COMMENT
0.05 ± 0.02	-85 ± 35	SARANTSEV 19	DPWA $\bar{K}N$ multichannel

Normalized residue in $N\bar{K} \rightarrow \Sigma(2110) \rightarrow \Lambda(1520)\pi$			
MODULUS	PHASE ($^\circ$)	DOCUMENT ID	TECN COMMENT
0.025 ± 0.015		SARANTSEV 19	DPWA $\bar{K}N$ multichannel

Normalized residue in $N\bar{K} \rightarrow \Sigma(2110) \rightarrow \Sigma(1385)\pi$			
MODULUS	PHASE ($^\circ$)	DOCUMENT ID	TECN COMMENT
0.03 ± 0.02		SARANTSEV 19	DPWA $\bar{K}N$ multichannel

Normalized residue in $N\bar{K} \rightarrow \Sigma(2110) \rightarrow \Delta\bar{K}$			
MODULUS	PHASE ($^\circ$)	DOCUMENT ID	TECN COMMENT
0.035 ± 0.02	-30 ± 40	SARANTSEV 19	DPWA $\bar{K}N$ multichannel

Normalized residue in $N\bar{K} \rightarrow \Sigma(2110) \rightarrow N\bar{K}^*(892), S\text{-wave}$			
MODULUS	PHASE ($^\circ$)	DOCUMENT ID	TECN COMMENT
0.09 ± 0.03	-40 ± 50	SARANTSEV 19	DPWA $\bar{K}N$ multichannel

Normalized residue in $N\bar{K} \rightarrow \Sigma(2110) \rightarrow N\bar{K}^*(892), D\text{-wave}$			
MODULUS	PHASE ($^\circ$)	DOCUMENT ID	TECN COMMENT
0.04 ± 0.03		SARANTSEV 19	DPWA $\bar{K}N$ multichannel

 $\Sigma(2110)$ MASS

VALUE (MeV)	DOCUMENT ID	TECN	COMMENT
2105 ± 50 OUR AVERAGE	Error includes scale factor of 3.4.		
2165 ± 23	SARANTSEV 19	DPWA	$\bar{K}N$ multichannel
2060 ± 20	ZHANG 13A	DPWA	$\bar{K}N$ multichannel

 $\Sigma(2110)$ WIDTH

VALUE (MeV)	DOCUMENT ID	TECN	COMMENT
$313 \pm \frac{120}{50}$ OUR AVERAGE			
$320 \pm \frac{300}{60}$	SARANTSEV 19	DPWA	$\bar{K}N$ multichannel
300 ± 134	ZHANG 13A	DPWA	$\bar{K}N$ multichannel

 $\Sigma(2110)$ DECAY MODES

Mode	Fraction (Γ_i/Γ)
$\Gamma_1 N\bar{K}$	$(29 \pm 7) \%$
$\Gamma_2 \Sigma\pi$	$(7.0 \pm 2.0) \%$
$\Gamma_3 \Lambda\pi$	$(54 \pm 12) \%$
$\Gamma_4 N\bar{K}^*(892), S\text{-wave}$	$(3.0 \pm 1.0) \%$
$\Gamma_5 N\bar{K}^*(892), D\text{-wave}$	

 $\Sigma(2110)$ BRANCHING RATIOS

$\Gamma(N\bar{K})/\Gamma_{\text{total}}$				Γ_1/Γ
VALUE	DOCUMENT ID	TECN	COMMENT	
0.29 ± 0.07	SARANTSEV 19	DPWA	$\bar{K}N$ multichannel	

$\Gamma(\Sigma\pi)/\Gamma_{\text{total}}$				Γ_2/Γ
VALUE	DOCUMENT ID	TECN	COMMENT	
0.07 ± 0.02	SARANTSEV 19	DPWA	$\bar{K}N$ multichannel	

$\Gamma(\Lambda\pi)/\Gamma_{\text{total}}$				Γ_3/Γ
VALUE	DOCUMENT ID	TECN	COMMENT	
0.54 ± 0.12	SARANTSEV 19	DPWA	$\bar{K}N$ multichannel	

$\Gamma(N\bar{K}^*(892), S\text{-wave})/\Gamma_{\text{total}}$				Γ_4/Γ
VALUE	DOCUMENT ID	TECN	COMMENT	
0.03 ± 0.01	SARANTSEV 19	DPWA	$\bar{K}N$ multichannel	

$\Gamma(N\bar{K}^*(892), D\text{-wave})/\Gamma_{\text{total}}$				Γ_5/Γ
VALUE	DOCUMENT ID	TECN	COMMENT	
$\bullet \bullet \bullet$ We do not use the following data for averages, fits, limits, etc. $\bullet \bullet \bullet$				
~ 0.01	SARANTSEV 19	DPWA	$\bar{K}N$ multichannel	

 $\Sigma(2110)$ REFERENCES

SARANTSEV 19	EPJ A55 180	A.V. Sarantsev et al.	(BONN, PNPI)
ZHANG 13A	PR C88 035205	H. Zhang et al.	(KSU)

 $\Sigma(2230) 3/2^+$

$I(J^P) = 1(\frac{3}{2}^+)$ Status: *

OMITTED FROM SUMMARY TABLE

 $\Sigma(2230)$ POLE POSITION

REAL PART			
VALUE (MeV)	DOCUMENT ID	TECN	COMMENT
2234 ± 25	SARANTSEV 19	DPWA	$\bar{K}N$ multichannel

$-2 \times$ IMAGINARY PART			
VALUE (MeV)	DOCUMENT ID	TECN	COMMENT
340 ± 45	SARANTSEV 19	DPWA	$\bar{K}N$ multichannel

 $\Sigma(2230)$ POLE RESIDUES

Normalized residue in $N\bar{K} \rightarrow \Sigma(2230) \rightarrow N\bar{K}$			
MODULUS	PHASE ($^\circ$)	DOCUMENT ID	TECN COMMENT
0.07 ± 0.02	25 ± 15	SARANTSEV 19	DPWA $\bar{K}N$ multichannel

Normalized residue in $N\bar{K} \rightarrow \Sigma(2230) \rightarrow \Sigma\pi$			
MODULUS	PHASE ($^\circ$)	DOCUMENT ID	TECN COMMENT
0.03 ± 0.02	180 ± 25	SARANTSEV 19	DPWA $\bar{K}N$ multichannel

Normalized residue in $N\bar{K} \rightarrow \Sigma(2030) \rightarrow \Lambda\pi$			
MODULUS	PHASE ($^\circ$)	DOCUMENT ID	TECN COMMENT
0.11 ± 0.05	-16 ± 10	SARANTSEV 19	DPWA $\bar{K}N$ multichannel

Normalized residue in $N\bar{K} \rightarrow \Sigma(2230) \rightarrow \Xi K$			
MODULUS	PHASE ($^\circ$)	DOCUMENT ID	TECN COMMENT
0.04 ± 0.02	155 ± 20	SARANTSEV 19	DPWA $\bar{K}N$ multichannel

Normalized residue in $N\bar{K} \rightarrow \Sigma(2230) \rightarrow \Lambda(1520)\pi, S\text{-wave}$			
MODULUS	PHASE ($^\circ$)	DOCUMENT ID	TECN COMMENT
0.12 ± 0.05	-80 ± 25	SARANTSEV 19	DPWA $\bar{K}N$ multichannel

Baryon Particle Listings

 $\Sigma(2230)$, $\Sigma(2250)$ Normalized residue in $N\bar{K} \rightarrow \Sigma(2230) \rightarrow \Lambda(1520)\pi$, D -wave

MODULUS	PHASE (°)	DOCUMENT ID	TECN	COMMENT
0.03 ± 0.02	160 ± 30	SARANTSEV 19	DPWA	$\bar{K}N$ multichannel

Normalized residue in $N\bar{K} \rightarrow \Sigma(2230) \rightarrow \Sigma(1385)\pi$, P -wave

MODULUS	PHASE (°)	DOCUMENT ID	TECN	COMMENT
0.05 ± 0.02	60 ± 25	SARANTSEV 19	DPWA	$\bar{K}N$ multichannel

Normalized residue in $N\bar{K} \rightarrow \Sigma(2230) \rightarrow \Sigma(1385)\pi$, F -wave

MODULUS	PHASE (°)	DOCUMENT ID	TECN	COMMENT
0.05 ± 0.03	-70 ± 20	SARANTSEV 19	DPWA	$\bar{K}N$ multichannel

Normalized residue in $N\bar{K} \rightarrow \Sigma(2230) \rightarrow \Delta\bar{K}$, P -wave

MODULUS	PHASE (°)	DOCUMENT ID	TECN	COMMENT
0.11 ± 0.04	60 ± 15	SARANTSEV 19	DPWA	$\bar{K}N$ multichannel

Normalized residue in $N\bar{K} \rightarrow \Sigma(2230) \rightarrow \Delta\bar{K}$, F -wave

MODULUS	PHASE (°)	DOCUMENT ID	TECN	COMMENT
0.07 ± 0.03	90 ± 25	SARANTSEV 19	DPWA	$\bar{K}N$ multichannel

Normalized residue in $N\bar{K} \rightarrow \Sigma(2230) \rightarrow N\bar{K}^*(892)$, $S=1/2$, P -wave

MODULUS	PHASE (°)	DOCUMENT ID	TECN	COMMENT
0.08 ± 0.04	40 ± 45	SARANTSEV 19	DPWA	$\bar{K}N$ multichannel

Normalized residue in $N\bar{K} \rightarrow \Sigma(2230) \rightarrow N\bar{K}^*(892)$, $S=3/2$, P -wave

MODULUS	PHASE (°)	DOCUMENT ID	TECN	COMMENT
0.14 ± 0.03	-40 ± 45	SARANTSEV 19	DPWA	$\bar{K}N$ multichannel

Normalized residue in $N\bar{K} \rightarrow \Sigma(2230) \rightarrow N\bar{K}^*(892)$, $S=3/2$, F -wave

MODULUS	PHASE (°)	DOCUMENT ID	TECN	COMMENT
0.05 ± 0.03	35 ± 30	SARANTSEV 19	DPWA	$\bar{K}N$ multichannel

 $\Sigma(2230)$ MASS

VALUE (MeV)	DOCUMENT ID	TECN	COMMENT
2240 ± 27	SARANTSEV 19	DPWA	$\bar{K}N$ multichannel

 $\Sigma(2230)$ WIDTH

VALUE (MeV)	DOCUMENT ID	TECN	COMMENT
345 ± 50	SARANTSEV 19	DPWA	$\bar{K}N$ multichannel

 $\Sigma(2230)$ DECAY MODES

Mode	Fraction (Γ_i/Γ)
Γ_1 $N\bar{K}$	(6.0 ± 2.0) %
Γ_2 $\Sigma\pi$	(2.0 ± 1.0) %
Γ_3 $\Lambda\pi$	(12 ± 6) %
Γ_4 ΞK	(2.0 ± 1.0) %
Γ_5 $\Lambda(1520)\pi$, S -wave	(14 ± 5) %
Γ_6 $\Lambda(1520)\pi$, D -wave	
Γ_7 $\Sigma(1385)\pi$, P -wave	(4 ± 4) %
Γ_8 $\Sigma(1385)\pi$, F -wave	(3.0 ± 2.0) %
Γ_9 $\Delta\bar{K}$, P -wave	(14 ± 5) %
Γ_{10} $\Delta\bar{K}$, F -wave	(8.0 ± 2.0) %
Γ_{11} $N\bar{K}^*(892)$, $S=1/2$, F -wave	(8.0 ± 3.0) %
Γ_{12} $N\bar{K}^*(892)$, $S=3/2$, F -wave	(26 ± 5) %

 $\Sigma(2230)$ BRANCHING RATIOS

$\Gamma(N\bar{K})/\Gamma_{\text{total}}$	DOCUMENT ID	TECN	COMMENT	Γ_1/Γ
0.06 ± 0.02	SARANTSEV 19	DPWA	$\bar{K}N$ multichannel	

$\Gamma(\Sigma\pi)/\Gamma_{\text{total}}$	DOCUMENT ID	TECN	COMMENT	Γ_2/Γ
0.02 ± 0.01	SARANTSEV 19	DPWA	$\bar{K}N$ multichannel	

$\Gamma(\Lambda\pi)/\Gamma_{\text{total}}$	DOCUMENT ID	TECN	COMMENT	Γ_3/Γ
0.12 ± 0.06	SARANTSEV 19	DPWA	$\bar{K}N$ multichannel	

$\Gamma(\Xi K)/\Gamma_{\text{total}}$	DOCUMENT ID	TECN	COMMENT	Γ_4/Γ
0.02 ± 0.01	SARANTSEV 19	DPWA	$\bar{K}N$ multichannel	

$\Gamma(\Lambda(1520)\pi, S\text{-wave})/\Gamma_{\text{total}}$	DOCUMENT ID	TECN	COMMENT	Γ_5/Γ
0.14 ± 0.05	SARANTSEV 19	DPWA	$\bar{K}N$ multichannel	

 $\Gamma(\Lambda(1520)\pi, D\text{-wave})/\Gamma_{\text{total}}$

VALUE	DOCUMENT ID	TECN	COMMENT	Γ_6/Γ
0.04 ± 0.04	SARANTSEV 19	DPWA	$\bar{K}N$ multichannel	

 $\Gamma(\Sigma(1385)\pi, P\text{-wave})/\Gamma_{\text{total}}$

VALUE	DOCUMENT ID	TECN	COMMENT	Γ_7/Γ
0.04 ± 0.04	SARANTSEV 19	DPWA	$\bar{K}N$ multichannel	

 $\Gamma(\Sigma(1385)\pi, F\text{-wave})/\Gamma_{\text{total}}$

VALUE	DOCUMENT ID	TECN	COMMENT	Γ_8/Γ
0.03 ± 0.02	SARANTSEV 19	DPWA	$\bar{K}N$ multichannel	

 $\Gamma(\Delta\bar{K}, P\text{-wave})/\Gamma_{\text{total}}$

VALUE	DOCUMENT ID	TECN	COMMENT	Γ_9/Γ
0.14 ± 0.05	SARANTSEV 19	DPWA	$\bar{K}N$ multichannel	

 $\Gamma(\Delta\bar{K}, F\text{-wave})/\Gamma_{\text{total}}$

VALUE	DOCUMENT ID	TECN	COMMENT	Γ_{10}/Γ
0.08 ± 0.02	SARANTSEV 19	DPWA	$\bar{K}N$ multichannel	

 $\Gamma(N\bar{K}^*(892), S=1/2, F\text{-wave})/\Gamma_{\text{total}}$

VALUE	DOCUMENT ID	TECN	COMMENT	Γ_{11}/Γ
0.08 ± 0.03	SARANTSEV 19	DPWA	$\bar{K}N$ multichannel	

 $\Gamma(N\bar{K}^*(892), S=3/2, F\text{-wave})/\Gamma_{\text{total}}$

VALUE	DOCUMENT ID	TECN	COMMENT	Γ_{12}/Γ
0.26 ± 0.05	SARANTSEV 19	DPWA	$\bar{K}N$ multichannel	

 $\Sigma(2230)$ REFERENCES

SARANTSEV 19	EPJ A55 180	A.V. Sarantsev et al.	(BONN, PNPI)
--------------	-------------	-----------------------	--------------

 $\Sigma(2250)$

$$I(J^P) = 1(?^?) \quad \text{Status: } **$$

OMITTED FROM SUMMARY TABLE

Results from partial-wave analyses are too weak to warrant separating them from the production and cross-section experiments. LASINSKI 71 in $\bar{K}N$ using a Pomeron + resonances model, and DEBELLEFON 76, DEBELLEFON 77, and DEBELLEFON 78 in energy-dependent partial-wave analyses of $\bar{K}N \rightarrow \Lambda\pi$, $\Sigma\pi$, and $N\bar{K}$, respectively, suggest two resonances around this mass.

 $\Sigma(2250)$ MASS

VALUE (MeV)	DOCUMENT ID	TECN	COMMENT
2210 to 2280 (≈ 2250) OUR ESTIMATE			
2270 ± 50	DEBELLEFON 78	DPWA	D_5 wave
2210 ± 30	DEBELLEFON 78	DPWA	G_9 wave
2275 ± 20	DEBELLEFON 77	DPWA	D_5 wave
2215 ± 20	DEBELLEFON 77	DPWA	G_9 wave
2300 ± 30	¹ DEBELLEFON 75b	HBC	$K^-p \rightarrow \Xi^{*0}K^0$
2251 ± 30	VANHORN 75	DPWA	$K^-p \rightarrow \Lambda\pi^0, F_5$ wave
2280 ± 14	AGUILAR...	70b	HBC K^-p 3.9, 4.6 GeV/c
2237 ± 11	BRICMAN 70	CNTR	Total, charge exchange
2255 ± 10	COOL 70	CNTR	K^-p, K^-d total
2250 ± 7	BUGG 68	CNTR	K^-p, K^-d total
• • • We do not use the following data for averages, fits, limits, etc. • • •			
2260	DEBELLEFON 76	IPWA	D_5 wave
2215	DEBELLEFON 76	IPWA	G_9 wave
2250 ± 20	LU 70	CNTR	$\gamma p \rightarrow K^+Y^*$
2245	BLANPIED 65	CNTR	$\gamma p \rightarrow K^+Y^*$
2299 ± 6	BOCK 65	HBC	$\bar{p}p$ 5.7 GeV/c

 $\Sigma(2250)$ WIDTH

VALUE (MeV)	DOCUMENT ID	TECN	COMMENT
60 to 150 (≈ 100) OUR ESTIMATE			
120 ± 40	DEBELLEFON 78	DPWA	D_5 wave
80 ± 20	DEBELLEFON 78	DPWA	G_9 wave
70 ± 20	DEBELLEFON 77	DPWA	D_5 wave
60 ± 20	DEBELLEFON 77	DPWA	G_9 wave
130 ± 20	¹ DEBELLEFON 75b	HBC	$K^-p \rightarrow \Xi^{*0}K^0$
192 ± 30	VANHORN 75	DPWA	$K^-p \rightarrow \Lambda\pi^0, F_5$ wave
100 ± 20	AGUILAR...	70b	HBC K^-p 3.9, 4.6 GeV/c
164 ± 50	BRICMAN 70	CNTR	Total, charge exchange
230 ± 20	BUGG 68	CNTR	K^-p, K^-d total

See key on page 1127

Baryon Particle Listings

$\Sigma(2250)$, $\Sigma(2455)$ Bumps, $\Sigma(2620)$ Bumps

••• We do not use the following data for averages, fits, limits, etc. •••

100	DEBELLEFON 76	IPWA	D_5 wave
140	DEBELLEFON 76	IPWA	G_9 wave
170	COOL 70	CNTR	$K^- p, K^- d$ total
125	LU 70	CNTR	$\gamma p \rightarrow K^+ Y^*$
150	BLANPIED 65	CNTR	$\gamma p \rightarrow K^+ Y^*$
21^{+17}_{-21}	BOCK 65	HBC	$\bar{p} p$ 5.7 GeV/c

$\Sigma(2250)$ DECAY MODES

Mode	Fraction (Γ_i/Γ)
Γ_1 $N\bar{K}$	<10 %
Γ_2 $\Lambda\pi$	seen
Γ_3 $\Sigma\pi$	seen
Γ_4 $\Xi(1530)K$	

$\Sigma(2250)$ BRANCHING RATIOS

See "Sign conventions for resonance couplings" in the Note on Λ and Σ Resonances.

$\Gamma(N\bar{K})/\Gamma_{total}$ Γ_1/Γ

VALUE	DOCUMENT ID	TECN	COMMENT
<0.1 OUR ESTIMATE			
0.08 ± 0.02	DEBELLEFON 78	DPWA	D_5 wave
0.02 ± 0.01	DEBELLEFON 78	DPWA	G_9 wave

$(J+\frac{1}{2}) \times \Gamma(N\bar{K})/\Gamma_{total}$ Γ_1/Γ

VALUE	DOCUMENT ID	TECN	COMMENT
••• We do not use the following data for averages, fits, limits, etc. •••			
0.16 ± 0.12	BRICMAN 70	CNTR	Total, charge exchange
0.42	COOL 70	CNTR	$K^- p, K^- d$ total
0.47	BUGG 68	CNTR	

$(\Gamma_1\Gamma_2)^{1/2}/\Gamma_{total}$ in $N\bar{K} \rightarrow \Sigma(2250) \rightarrow \Lambda\pi$ $(\Gamma_1\Gamma_2)^{1/2}/\Gamma$

VALUE	DOCUMENT ID	TECN	COMMENT
-0.16 ± 0.03	VANHORN 75	DPWA	$K^- p \rightarrow \Lambda\pi^0, F_5$ wave

••• We do not use the following data for averages, fits, limits, etc. •••

+0.11	DEBELLEFON 76	IPWA	D_5 wave
-0.10	DEBELLEFON 76	IPWA	G_9 wave
-0.18	BARBARO... 70	DPWA	$K^- p \rightarrow \Lambda\pi^0, G_9$ wave

$(\Gamma_1\Gamma_2)^{1/2}/\Gamma_{total}$ in $N\bar{K} \rightarrow \Sigma(2250) \rightarrow \Sigma\pi$ $(\Gamma_1\Gamma_2)^{1/2}/\Gamma$

VALUE	DOCUMENT ID	TECN	COMMENT
$+0.06 \pm 0.02$	DEBELLEFON 77	DPWA	D_5 wave
-0.03 ± 0.02	DEBELLEFON 77	DPWA	G_9 wave
+0.07	BARBARO... 70	DPWA	$K^- p \rightarrow \Sigma\pi, G_9$ wave

$\Gamma(N\bar{K})/\Gamma(\Sigma\pi)$ Γ_1/Γ_3

VALUE	DOCUMENT ID	TECN	COMMENT
••• We do not use the following data for averages, fits, limits, etc. •••			
<0.18	BARNES 69	HBC	1 standard dev. limit

$\Gamma(\Lambda\pi)/\Gamma(\Sigma\pi)$ Γ_2/Γ_3

VALUE	DOCUMENT ID	TECN	COMMENT
••• We do not use the following data for averages, fits, limits, etc. •••			
<0.18	BARNES 69	HBC	1 standard dev. limit

$(\Gamma_1\Gamma_2)^{1/2}/\Gamma_{total}$ in $N\bar{K} \rightarrow \Sigma(2250) \rightarrow \Xi(1530)K$ $(\Gamma_1\Gamma_2)^{1/2}/\Gamma$

VALUE	DOCUMENT ID	TECN	COMMENT
0.18 ± 0.04	¹ DEBELLEFON 75B	HBC	$K^- p \rightarrow \Xi^* K^0$

$\Sigma(2250)$ FOOTNOTES

¹ Seen in the (initial and final state) D_5 wave. Isospin not determined.

$\Sigma(2250)$ REFERENCES

DEBELLEFON 78	NC 42A 403	A. de Bellefon et al.	(CDEF, SAACL) IJP
DEBELLEFON 77	NC 37A 175	A. de Bellefon et al.	(CDEF, SAACL) IJP
DEBELLEFON 76	NP B109 129	A. de Bellefon, A. Berthon	(CDEF) IJP
Also	NP B90 1	A. de Bellefon et al.	(CDEF, SAACL) IJP
DEBELLEFON 75B	NC 28A 289	A. de Bellefon et al.	(CDEF, SAACL) IJP
VANHORN 75	NP B87 145	A.J. van Horn	(LBL) IJP
Also	NP B87 157	A.J. van Horn	(LBL) IJP
LASINSKI 71	NP B29 125	T.A. Lasinski	(EFI) IJP
AGUILAR... 70B	PRL 25 58	M. Aguilar-Benitez et al.	(BNL, SYRA)
BARBARO... 70	Duke Conf. 173	A. Barbaro-Galiteri	(LRL) IJP
Hyperon Resonances, 1970			
BRICMAN 70	PL 31B 152	C. Bricman et al.	(CERN, CAEN, SAACL)
COOL 70	PR D1 1887	R.L. Cool et al.	(BNL) I
Also	PRL 16 1228	R.L. Cool et al.	(BNL) I
LU 70	PR D2 1846	D.C. Lu et al.	(YALE)
BARNES 69	PRL 22 479	V.E. Barnes et al.	(BNL, SYRA)
BUGG 68	PR 168 1466	D.V. Bugg et al.	(RHEL, BIRM, CAVE) I
BLANPIED 65	PRL 14 741	W.A. Blanpied et al.	(YALE, CEA)
BOCK 65	PL 17 166	R.K. Bock et al.	(CERN, SAACL)

$\Sigma(2455)$ Bumps

$I(J^P) = 1(?)^?$ Status: *

OMITTED FROM SUMMARY TABLE

There is also some slight evidence for Y^* states in this mass region from the reaction $\gamma p \rightarrow K^+ X$ — see GREENBERG 68.

$\Sigma(2455)$ MASS

VALUE (MeV)	DOCUMENT ID	TECN	COMMENT
≈ 2455 OUR ESTIMATE			
2455 ± 10	ABRAMS 70	CNTR	$K^- p, K^- d$ total
2455 ± 7	BUGG 68	CNTR	$K^- p, K^- d$ total

$\Sigma(2455)$ WIDTH

VALUE (MeV)	DOCUMENT ID	TECN	COMMENT
140	ABRAMS 70	CNTR	$K^- p, K^- d$ total
100 ± 20	BUGG 68	CNTR	

$\Sigma(2455)$ DECAY MODES

Mode	Fraction (Γ_i/Γ)
Γ_1 $N\bar{K}$	

$\Sigma(2455)$ BRANCHING RATIOS

$(J+\frac{1}{2}) \times \Gamma(N\bar{K})/\Gamma_{total}$ Γ_1/Γ

VALUE	DOCUMENT ID	TECN	COMMENT
0.39	ABRAMS 70	CNTR	$K^- p, K^- d$ total
0.05 ± 0.05	¹ BRICMAN 70	CNTR	Total, charge exchange
0.3	BUGG 68	CNTR	

$\Sigma(2455)$ FOOTNOTES

¹ Fit of total cross section given by BRICMAN 70 is poor in this region.

$\Sigma(2455)$ REFERENCES

ABRAMS 70	PR D1 1917	R.J. Abrams et al.	(BNL) I
Also	PRL 19 678	R.J. Abrams et al.	(BNL)
BRICMAN 70	PL 31B 152	C. Bricman et al.	(CERN, CAEN, SAACL)
BUGG 68	PR 168 1466	D.V. Bugg et al.	(RHEL, BIRM, CAVE) I
GREENBERG 68	PRL 20 221	J.S. Greenberg et al.	(YALE)

$\Sigma(2620)$ Bumps

$I(J^P) = 1(?)^?$ Status: *

OMITTED FROM SUMMARY TABLE

$\Sigma(2620)$ MASS

VALUE (MeV)	DOCUMENT ID	TECN	COMMENT
≈ 2620 OUR ESTIMATE			
2542 ± 22	DIBIANCA 75	DBC	$K^- N \rightarrow \Xi K\pi$
2620 ± 15	ABRAMS 70	CNTR	$K^- p, K^- d$ total

$\Sigma(2620)$ WIDTH

VALUE (MeV)	DOCUMENT ID	TECN	COMMENT
221 ± 81	DIBIANCA 75	DBC	$K^- N \rightarrow \Xi K\pi$
175	ABRAMS 70	CNTR	$K^- p, K^- d$ total

$\Sigma(2620)$ DECAY MODES

Mode	Fraction (Γ_i/Γ)
Γ_1 $N\bar{K}$	

$\Sigma(2620)$ BRANCHING RATIOS

$(J+\frac{1}{2}) \times \Gamma(N\bar{K})/\Gamma_{total}$ Γ_1/Γ

VALUE	DOCUMENT ID	TECN	COMMENT
0.32	ABRAMS 70	CNTR	$K^- p, K^- d$ total
0.36 ± 0.12	BRICMAN 70	CNTR	Total, charge exchange

$\Sigma(2620)$ REFERENCES

DIBIANCA 75	NP B98 137	F.A. Dibianca, R.J. Endorf	(CMU)
ABRAMS 70	PR D1 1917	R.J. Abrams et al.	(BNL) I
Also	PRL 19 678	R.J. Abrams et al.	(BNL)
BRICMAN 70	PL 31B 152	C. Bricman et al.	(CERN, CAEN, SAACL)

Baryon Particle Listings

 $\Sigma(3000)$ Bumps, $\Sigma(3170)$ Bumps **$\Sigma(3000)$ Bumps** $I(J^P) = 1(?^?)$ Status: *

OMITTED FROM SUMMARY TABLE

Seen as an enhancement in $\Lambda\pi$ and $\bar{K}N$ invariant mass spectra and in the missing mass of neutrals recoiling against a K^0 . $\Sigma(3000)$ MASS

VALUE (MeV)	DOCUMENT ID	TECN	CHG	COMMENT
≈ 3000 OUR ESTIMATE				
3000	EHRlich	66	HBC	0 $\pi^- p$ 7.91 GeV/c

 $\Sigma(3000)$ DECAY MODES

Mode	Fraction (Γ_i/Γ)
Γ_1 $N\bar{K}$	seen
Γ_2 $\Lambda\pi$	seen

 $\Sigma(3000)$ REFERENCES

EHRlich	66	PR 152 1194	R. Ehrlich, W. Selove, H. Yuta	(PENN)1
---------	----	-------------	--------------------------------	---------

 $\Sigma(3170)$ Bumps $I(J^P) = 1(?^?)$ Status: *

OMITTED FROM SUMMARY TABLE

Seen by AMIRZADEH 79 as a narrow 6.5-standard-deviation enhancement in the reaction $K^- p \rightarrow Y^{*+} \pi^-$ using data from independent high statistics bubble chamber experiments at 8.25 and 6.5 GeV/c. The dominant decay modes are multibody, multistrange final states and the production is via isospin-3/2 baryon exchange. Isospin 1 is favored.Not seen in a $K^- p$ experiment in LASS at 11 GeV/c (ASTON 85B). $\Sigma(3170)$ MASS
(PRODUCTION EXPERIMENTS)

VALUE (MeV)	EVTS	DOCUMENT ID	TECN	COMMENT
≈ 3170 OUR ESTIMATE				
3170 ± 5	35	AMIRZADEH	79	HBC $K^- p \rightarrow Y^{*+} \pi^-$

 $\Sigma(3170)$ WIDTH
(PRODUCTION EXPERIMENTS)

VALUE (MeV)	EVTS	DOCUMENT ID	TECN	COMMENT
<20	35	¹ AMIRZADEH	79	HBC $K^- p \rightarrow Y^{*+} \pi^-$

 $\Sigma(3170)$ DECAY MODES
(PRODUCTION EXPERIMENTS)

Mode	Fraction (Γ_i/Γ)
Γ_1 $\Lambda K \bar{K} \pi$'s	seen
Γ_2 $\Sigma K \bar{K} \pi$'s	seen
Γ_3 $\Xi K \pi$'s	seen

 $\Sigma(3170)$ BRANCHING RATIOS
(PRODUCTION EXPERIMENTS)

$\Gamma(\Lambda K \bar{K} \pi \text{'s})/\Gamma_{\text{total}}$	Γ_1/Γ		
VALUE	DOCUMENT ID	TECN	COMMENT
seen	AMIRZADEH	79	HBC $K^- p \rightarrow Y^{*+} \pi^-$
$\Gamma(\Sigma K \bar{K} \pi \text{'s})/\Gamma_{\text{total}}$	Γ_2/Γ		
VALUE	DOCUMENT ID	TECN	COMMENT
seen	AMIRZADEH	79	HBC $K^- p \rightarrow Y^{*+} \pi^-$
$\Gamma(\Xi K \pi \text{'s})/\Gamma_{\text{total}}$	Γ_3/Γ		
VALUE	DOCUMENT ID	TECN	COMMENT
seen	AMIRZADEH	79	HBC $K^- p \rightarrow Y^{*+} \pi^-$

 $\Sigma(3170)$ FOOTNOTES
(PRODUCTION EXPERIMENTS)¹ Observed width consistent with experimental resolution. $\Sigma(3170)$ REFERENCES
(PRODUCTION EXPERIMENTS)

ASTON	85B	PR D32 2270	D. Aston <i>et al.</i>	(SLAC, CARL, CNRC, CINC)
AMIRZADEH	79	PL 89B 125	J. Amirzadeh <i>et al.</i>	(BIRM, CERN, GLAS+) ¹
Also		Toronto Conf. 263	J.B. Kinson <i>et al.</i>	(BIRM, CERN, GLAS+) ¹

Ξ BARYONS

$(S = -2, I = 1/2)$

$\Xi^0 = uss, \Xi^- = dss$

Ξ^0

$I(J^P) = \frac{1}{2}(\frac{1}{2}^+)$ Status: ****

The parity has not actually been measured, but + is of course expected.

Ξ^0 MASS

The fit uses the $\Xi^0, \Xi^-,$ and Ξ^+ masses and the $\Xi^- - \Xi^0$ mass difference. It assumes that the Ξ^- and Ξ^+ masses are the same.

VALUE (MeV)	EVTS	DOCUMENT ID	TECN	COMMENT
1314.86 ± 0.20 OUR FIT				
1314.82 ± 0.06 ± 0.20	3120	FANTI	00 NA48	p Be, 450 GeV
• • • We do not use the following data for averages, fits, limits, etc. • • •				
1315.2 ± 0.92	49	WILQUET	72 HLBC	
1313.4 ± 1.8	1	PALMER	68 HBC	

$m_{\Xi^-} - m_{\Xi^0}$

The fit uses the $\Xi^0, \Xi^-,$ and Ξ^+ masses and the $\Xi^- - \Xi^0$ mass difference. It assumes that the Ξ^- and Ξ^+ masses are the same.

VALUE (MeV)	EVTS	DOCUMENT ID	TECN	COMMENT
6.85 ± 0.21 OUR FIT				
6.3 ± 0.7 OUR AVERAGE				
6.9 ± 2.2	29	LONDON	66 HBC	
6.1 ± 0.9	88	PJERROU	65B HBC	
6.8 ± 1.6	23	JAUNEAU	63 FBC	
• • • We do not use the following data for averages, fits, limits, etc. • • •				
6.1 ± 1.6	45	CARMONY	64B HBC	See PJERROU 65B

Ξ^0 MEAN LIFE

VALUE (10^{-10} s)	EVTS	DOCUMENT ID	TECN	COMMENT
2.90 ± 0.09 OUR AVERAGE				
2.83 ± 0.16	6300	1 ZECH	77 SPEC	Neutral hyperon beam
2.86 ^{+0.21} _{-0.19}	652	BALTAY	74 HBC	1.75 GeV/c $K^- p$
2.90 ^{+0.32} _{-0.27}	157	2 MAYEUR	72 HLBC	2.1 GeV/c K^-
3.07 ^{+0.22} _{-0.20}	340	DAUBER	69 HBC	
3.0 ± 0.5	80	PJERROU	65B HBC	
2.5 ^{+0.4} _{-0.3}	101	HUBBARD	64 HBC	
3.9 ^{+1.4} _{-0.8}	24	JAUNEAU	63 FBC	
• • • We do not use the following data for averages, fits, limits, etc. • • •				
3.5 ^{+1.0} _{-0.8}	45	CARMONY	64B HBC	See PJERROU 65B

¹The ZECH 77 result is $\tau_{\Xi^0} = [2.77 - (\tau_A - 2.69)] \times 10^{-10}$ s, in which we use $\tau_A = 2.63 \times 10^{-10}$ s.
²The MAYEUR 72 value is modified by the erratum.

Ξ^0 MAGNETIC MOMENT

See the "Quark Model" review.

VALUE (μ_N)	EVTS	DOCUMENT ID	TECN	COMMENT
-1.250 ± 0.014 OUR AVERAGE				
-1.253 ± 0.014	270k	COX	81 SPEC	
-1.20 ± 0.06	42k	BUNCE	79 SPEC	

Ξ^0 DECAY MODES

Mode	Fraction (Γ_i/Γ)	Confidence level
$\Gamma_1 \Lambda\pi^0$	(99.524 ± 0.012) %	
$\Gamma_2 \Lambda\gamma$	(1.17 ± 0.07) × 10 ⁻³	
$\Gamma_3 \Lambda e^+ e^-$	(7.6 ± 0.6) × 10 ⁻⁶	
$\Gamma_4 \Sigma^0 \gamma$	(3.33 ± 0.10) × 10 ⁻³	
$\Gamma_5 \Sigma^+ e^- \bar{\nu}_e$	(2.52 ± 0.08) × 10 ⁻⁴	
$\Gamma_6 \Sigma^+ \mu^- \bar{\nu}_\mu$	(2.33 ± 0.35) × 10 ⁻⁶	

$\Delta S = \Delta Q$ (SQ) violating modes or $\Delta S = 2$ forbidden (S2) modes

$\Gamma_7 \Sigma^- e^+ \nu_e$	SQ < 9	× 10 ⁻⁴	90%
$\Gamma_8 \Sigma^- \mu^+ \nu_\mu$	SQ < 9	× 10 ⁻⁴	90%
$\Gamma_9 p \pi^-$	S2 < 8	× 10 ⁻⁶	90%
$\Gamma_{10} p e^- \bar{\nu}_e$	S2 < 1.3	× 10 ⁻³	
$\Gamma_{11} p \mu^- \bar{\nu}_\mu$	S2 < 1.3	× 10 ⁻³	

CONSTRAINED FIT INFORMATION

An overall fit to 5 branching ratios uses 11 measurements and one constraint to determine 5 parameters. The overall fit has a $\chi^2 = 7.5$ for 7 degrees of freedom.

The following *off-diagonal* array elements are the correlation coefficients $\langle \delta x_i \delta x_j \rangle / (\delta x_i \delta x_j)$, in percent, from the fit to the branching fractions, $x_i \equiv \Gamma_i/\Gamma_{\text{total}}$. The fit constrains the x_i whose labels appear in this array to sum to one.

x_2	-57			
x_4	-82	0		
x_5	-7	0	0	
x_6	0	0	0	1
	x_1	x_2	x_4	x_5

Ξ^0 BRANCHING RATIOS

$\Gamma(\Lambda\gamma)/\Gamma(\Lambda\pi^0)$ Γ_2/Γ_1

VALUE (units 10 ⁻³)	EVTS	DOCUMENT ID	TECN	COMMENT
1.17 ± 0.07 OUR FIT				
1.17 ± 0.07 OUR AVERAGE				
1.17 ± 0.05 ± 0.06	672	³ LAI	04A NA48	p Be, 450 GeV
1.91 ± 0.34 ± 0.19	31	⁴ FANTI	00 NA48	p Be, 450 GeV
1.06 ± 0.12 ± 0.11	116	JAMES	90 SPEC	FNAL hyperons
³ LAI 04A used our 2002 value of 99.5% for the $\Xi^0 \rightarrow \Lambda\pi^0$ branching fraction to get $\Gamma(\Xi^0 \rightarrow \Lambda\gamma)/\Gamma_{\text{total}} = (1.16 \pm 0.05 \pm 0.06) \times 10^{-3}$. We adjust slightly to go back to what was directly measured.				
⁴ FANTI 00 used our 1998 value of 99.5% for the $\Xi^0 \rightarrow \Lambda\pi^0$ branching fraction to get $\Gamma(\Xi^0 \rightarrow \Lambda\gamma)/\Gamma_{\text{total}} = (1.90 \pm 0.34 \pm 0.19) \times 10^{-3}$. We adjust slightly to go back to what was directly measured.				

$\Gamma(\Lambda e^+ e^-)/\Gamma_{\text{total}}$ Γ_3/Γ

VALUE (units 10 ⁻⁶)	EVTS	DOCUMENT ID	TECN	COMMENT
7.6 ± 0.4 ± 0.5	397 ± 21	⁵ BATLEY	07c NA48	p Be, 400 GeV
⁵ This BATLEY 07c result is consistent with internal bremsstrahlung.				

$\Gamma(\Sigma^0 \gamma)/\Gamma(\Lambda\pi^0)$ Γ_4/Γ_1

VALUE (units 10 ⁻³)	EVTS	DOCUMENT ID	TECN	COMMENT
3.35 ± 0.10 OUR FIT				
3.35 ± 0.10 OUR AVERAGE				
3.34 ± 0.05 ± 0.09	4045	ALAVI-HARATI	01c KTEV	p nucleus, 800 GeV
3.16 ± 0.76 ± 0.32	17	⁶ FANTI	00 NA48	p Be, 450 GeV
3.56 ± 0.42 ± 0.10	85	TEIGE	89 SPEC	FNAL hyperons
⁶ FANTI 00 used our 1998 value of 99.5% for the $\Xi^0 \rightarrow \Lambda\pi^0$ branching fraction to get $\Gamma(\Xi^0 \rightarrow \Sigma^0 \gamma)/\Gamma_{\text{total}} = (3.14 \pm 0.76 \pm 0.32) \times 10^{-3}$. We adjust slightly to go back to what was directly measured.				

$\Gamma(\Sigma^+ e^- \bar{\nu}_e)/\Gamma_{\text{total}}$ Γ_5/Γ

VALUE (units 10 ⁻⁴)	EVTS	DOCUMENT ID	TECN	COMMENT
2.52 ± 0.08 OUR FIT				
2.53 ± 0.08 OUR AVERAGE				
2.51 ± 0.03 ± 0.09	6101	BATLEY	07 NA48	p Be, 400 GeV
2.55 ± 0.14 ± 0.10	419	⁷ BATLEY	07 NA48	p Be, 400 GeV
2.71 ± 0.22 ± 0.31	176	AFFOLDER	99 KTEV	p nucleus, 800 GeV
⁷ This BATLEY 07 result is for $\Xi^0 \rightarrow \Sigma^- e^+ \nu_e$ events.				

$\Gamma(\Sigma^+ \mu^- \bar{\nu}_\mu)/\Gamma_{\text{total}}$ Γ_6/Γ

VALUE (units 10 ⁻⁶)	EVTS	DOCUMENT ID	TECN	COMMENT
2.3 ± 0.4 OUR FIT				
2.17 ± 0.32 ± 0.17	66	⁸ BATLEY	13 NA48	p Be, 400 GeV
⁸ BATLEY 13 used $\Xi^0 \rightarrow \Sigma^+ e^- \bar{\nu}_e$ decay as a normalization mode and its branching fraction value of $(2.51 \pm 0.03 \pm 0.09) \times 10^{-4}$ from BATLEY 07.				

$\Gamma(\Sigma^+ \mu^- \bar{\nu}_\mu)/\Gamma(\Sigma^+ e^- \bar{\nu}_e)$ Γ_6/Γ_5

VALUE	EVTS	DOCUMENT ID	TECN	COMMENT
0.0092 ± 0.0015 OUR FIT				
0.018^{+0.007}_{-0.005} ± 0.002	9	ABOUZAID	05 KTEV	p nucleus 800 GeV

Baryon Particle Listings

=0

 $\Gamma(\Sigma^- e^+ \nu_e)/\Gamma(\Lambda\pi^0)$ Γ_7/Γ_1 Test of $\Delta S = \Delta Q$ rule.

VALUE (units 10^{-3})	CL%	EVTS	DOCUMENT ID	TECN	COMMENT
<0.9	90	0	YEH	74	HBC Effective denom.=2500
••• We do not use the following data for averages, fits, limits, etc. •••					
<1.5			DAUBER	69	HBC
<6			HUBBARD	66	HBC

 $\Gamma(\Sigma^- \mu^+ \nu_\mu)/\Gamma(\Lambda\pi^0)$ Γ_8/Γ_1 Test of $\Delta S = \Delta Q$ rule.

VALUE (units 10^{-3})	CL%	EVTS	DOCUMENT ID	TECN	COMMENT
<0.9	90	0	YEH	74	HBC Effective denom.=2500
••• We do not use the following data for averages, fits, limits, etc. •••					
<1.5			DAUBER	69	HBC
<6			HUBBARD	66	HBC

 $\Gamma(p\pi^-)/\Gamma(\Lambda\pi^0)$ Γ_9/Γ_1 $\Delta S=2$. Forbidden in first-order weak interaction.

VALUE (units 10^{-6})	CL%	EVTS	DOCUMENT ID	TECN	COMMENT
< 8.2	90		WHITE	05	HYCP p Cu, 800 GeV
••• We do not use the following data for averages, fits, limits, etc. •••					
< 36	90		GEWENIGER	75	SPEC
<1800	90	0	YEH	74	HBC Effective denom.=1300
< 900			DAUBER	69	HBC
<5000			HUBBARD	66	HBC

 $\Gamma(p e^- \bar{\nu}_e)/\Gamma(\Lambda\pi^0)$ Γ_{10}/Γ_1 $\Delta S=2$. Forbidden in first-order weak interaction.

VALUE (units 10^{-3})	CL%	EVTS	DOCUMENT ID	TECN	COMMENT
<1.3			DAUBER	69	HBC
••• We do not use the following data for averages, fits, limits, etc. •••					
<3.4	90	0	YEH	74	HBC Effective denom.=670
<6			HUBBARD	66	HBC

 $\Gamma(p\mu^- \bar{\nu}_\mu)/\Gamma(\Lambda\pi^0)$ Γ_{11}/Γ_1 $\Delta S=2$. Forbidden in first-order weak interaction.

VALUE (units 10^{-3})	CL%	EVTS	DOCUMENT ID	TECN	COMMENT
<1.3			DAUBER	69	HBC
••• We do not use the following data for averages, fits, limits, etc. •••					
<3.5	90	0	YEH	74	HBC Effective denom.=664
<6			HUBBARD	66	HBC

 Ξ^0 DECAY PARAMETERS

See the "Note on Baryon Decay Parameters" in the neutron Listings.

 $\alpha(\Xi^0) \alpha_-(\Lambda)$ This is a product of the $\Xi^0 \rightarrow \Lambda\pi^0$ and $\Lambda \rightarrow p\pi^-$ asymmetries.

VALUE	EVTS	DOCUMENT ID	TECN	COMMENT
-0.261 ± 0.006 OUR AVERAGE				
-0.276 ± 0.001 ± 0.035	4M	BATLEY	10B	NA48 p Be, 400 GeV
-0.260 ± 0.004 ± 0.005	300k	HANDLER	82	SPEC FNAL hyperons
••• We do not use the following data for averages, fits, limits, etc. •••				
-0.317 ± 0.027	6075	BUNCE	78	SPEC FNAL hyperons
-0.35 ± 0.06	505	BALTAY	74	HBC $K^- p$ 1.75 GeV/c
-0.28 ± 0.06	739	DAUBER	69	HBC $K^- p$ 1.7-2.6 GeV/c

 α FOR $\Xi^0 \rightarrow \Lambda\pi^0$ The above average, $\alpha(\Xi^0)\alpha_-(\Lambda) = -0.261 \pm 0.006$, divided by our current average $\alpha_-(\Lambda) = 0.732 \pm 0.014$, gives the following value for $\alpha(\Xi^0)$:

VALUE	DOCUMENT ID
-0.356 ± 0.011 OUR EVALUATION	

 ϕ ANGLE FOR $\Xi^0 \rightarrow \Lambda\pi^0$ ($\tan\phi = \beta/\gamma$)

VALUE (°)	EVTS	DOCUMENT ID	TECN	COMMENT
21 ± 12 OUR AVERAGE				
16 ± 17	652	BALTAY	74	HBC 1.75 GeV/c $K^- p$
38 ± 19	739	DAUBER	69	HBC
- 8 ± 30	146	BERGE	66	HBC

⁹DAUBER 69 uses $\alpha_\Lambda = 0.647 \pm 0.020$.¹⁰The errors have been multiplied by 1.2 due to approximations used for the Ξ polarization; see DAUBER 69 for a discussion.

RADIATIVE HYPERON DECAYS

Revised July 2011 by J.D. Jackson (LBNL).

The weak radiative decays of spin-1/2 hyperons, $B_i \rightarrow B_f \gamma$, yield information about matrix elements (form factors) similar to that gained from weak hadronic decays. For a polarized spin-1/2 hyperon decaying radiatively via a $\Delta Q = 0$, $\Delta S = 1$

transition, the angular distribution of the direction \hat{p} of the final spin-1/2 baryon in the hyperon rest frame is

$$\frac{dN}{d\Omega} = \frac{N}{4\pi} (1 + \alpha_\gamma \mathbf{P}_i \cdot \hat{p}). \quad (1)$$

Here \mathbf{P}_i is the polarization of the decaying hyperon, and α_γ is the asymmetry parameter. In terms of the form factors $F_1(q^2)$, $F_2(q^2)$, and $G(q^2)$ of the effective hadronic weak electromagnetic vertex,

$$F_1(q^2)\gamma_\lambda + iF_2(q^2)\sigma_{\lambda\mu}q^\mu + G(q^2)\gamma_\lambda\gamma_5,$$

 α_γ is

$$\alpha_\gamma = \frac{2 \operatorname{Re}[G(0)F_M^*(0)]}{|G(0)|^2 + |F_M(0)|^2}, \quad (2)$$

where $F_M = (m_i - m_f)[F_2 - F_1/(m_i + m_f)]$. If the decaying hyperon is unpolarized, the decay baryon has a longitudinal polarization given by $P_f = -\alpha_\gamma$ [1].

The angular distribution for the weak hadronic decay, $B_i \rightarrow B_f \pi$, has the same form as Eq. (1), but of course with a different asymmetry parameter, α_π . Now, however, if the decaying hyperon is unpolarized, the decay baryon has a longitudinal polarization given by $P_f = +\alpha_\pi$ [2,3]. The difference of sign is because the spins of the pion and photon are different.

$\Xi^0 \rightarrow \Lambda \gamma$ decay—The radiative decay $\Xi^0 \rightarrow \Lambda \gamma$ of an unpolarized Ξ^0 uses the hadronic decay $\Lambda \rightarrow p\pi^-$ as the analyzer. As noted above, the longitudinal polarization of the Λ will be $P_\Lambda = -\alpha_{\Xi\Lambda\gamma}$. Let α_- be the $\Lambda \rightarrow p\pi^-$ asymmetry parameter and $\theta_{\Lambda p}$ be the angle, as seen in the Λ rest frame, between the Λ line of flight and the proton momentum. Then the hadronic version of Eq. (1) applied to the $\Lambda \rightarrow p\pi^-$ decay gives

$$\frac{dN}{d \cos \theta_{\Lambda p}} = \frac{N}{2} (1 - \alpha_{\Xi\Lambda\gamma} \alpha_- \cos \theta_{\Lambda p}) \quad (3)$$

for the angular distribution of the proton in the Λ frame. Our current value, from the CERN NA48/1 experiment [4], is $\alpha_{\Xi\Lambda\gamma} = -0.704 \pm 0.019 \pm 0.064$.

$\Xi^0 \rightarrow \Sigma^0 \gamma$ decay—The asymmetry parameter here, $\alpha_{\Xi\Sigma\gamma}$, is measured by following the decay chain $\Xi^0 \rightarrow \Sigma^0 \gamma$, $\Sigma^0 \rightarrow \Lambda \gamma$, $\Lambda \rightarrow p\pi^-$. Again, for an unpolarized Ξ^0 , the longitudinal polarization of the Σ^0 will be $P_\Sigma = -\alpha_{\Xi\Sigma\gamma}$. In the $\Sigma^0 \rightarrow \Lambda \gamma$ decay, a parity-conserving magnetic-dipole transition, the polarization of the Σ^0 is transferred to the Λ , as may be seen as follows. Let $\theta_{\Sigma\Lambda}$ be the angle seen in the Σ^0 rest frame between the Σ^0 line of flight and the Λ momentum. For Σ^0 helicity +1/2, the probability amplitudes for positive and negative spin states of the Σ^0 along the Λ momentum are $\cos(\theta_{\Sigma\Lambda}/2)$ and $\sin(\theta_{\Sigma\Lambda}/2)$. Then the amplitude for a negative helicity photon and a negative helicity Λ is $\cos(\theta_{\Sigma\Lambda}/2)$, while the amplitude for positive helicities for the photon and Λ is $\sin(\theta_{\Sigma\Lambda}/2)$. For Σ^0 helicity -1/2, the amplitudes are interchanged. If the Σ^0 has longitudinal polarization P_Σ , the probabilities for Λ helicities $\pm 1/2$ are therefore

$$p(\pm 1/2) = \frac{1}{2}(1 \mp P_\Sigma) \cos^2(\theta_{\Sigma\Lambda}/2) + \frac{1}{2}(1 \pm P_\Sigma) \sin^2(\theta_{\Sigma\Lambda}/2), \quad (4)$$

and the longitudinal polarization of the Λ is

$$P_\Lambda = -P_\Sigma \cos \theta_{\Sigma\Lambda} = +\alpha_{\Xi\Sigma\gamma} \cos \theta_{\Sigma\Lambda} . \quad (5)$$

Using Eq. (1) for the $\Lambda \rightarrow p\pi^-$ decay again, we get for the joint angular distribution of the $\Sigma^0 \rightarrow \Lambda\gamma, \Lambda \rightarrow p\pi^-$ chain,

$$\frac{d^2N}{d\cos\theta_{\Sigma\Lambda} d\cos\theta_{\Lambda p}} = \frac{N}{4} (1 + \alpha_{\Xi\Sigma\gamma} \cos \theta_{\Sigma\Lambda} \alpha_- \cos \theta_{\Lambda p}) . \quad (6)$$

Our current average for $\alpha_{\Xi\Sigma\gamma}$ is -0.69 ± 0.06 [4,5].

References

1. R.E. Behrends, Phys. Rev. **111**, 1691 (1958); see Eq. (7) or (8).
2. In ancient times, the signs of the asymmetry term in the angular distributions of radiative and hadronic decays of polarized hyperons were sometimes opposite. For roughly 50 years, however, the overwhelming convention has been to make them the same. The aim, not always achieved, is to remove ambiguities.
3. For the definition of α_{π^-} , see the note on ‘‘Baryon Decay Parameters’’ in the Neutron Listings.
4. J.R. Batley *et al.*, Phys. Lett. **B693**, 241 (2010).
5. A. Alavi-Harati *et al.*, Phys. Rev. Lett. **86**, 3239 (2001).

α FOR $\Xi^0 \rightarrow \Lambda\gamma$

See the note above on ‘‘Radiative Hyperon Decays.’’

VALUE	EVTS	DOCUMENT ID	TECN	COMMENT
$-0.704 \pm 0.019 \pm 0.064$	52k	¹¹ BATLEY 10B	NA48	p Be, 400 GeV
•••				We do not use the following data for averages, fits, limits, etc. •••
$-0.78 \pm 0.18 \pm 0.06$	672	LAI 04A	NA48	See BATLEY 10B
-0.43 ± 0.44	87	¹² JAMES 90	SPEC	FNAL hyperons

- ¹¹ BATLEY 10B also measured the $\Xi^0 \rightarrow \bar{\Lambda}\gamma$ asymmetry to be -0.798 ± 0.064 (no systematic error given) with 4769 events.
- ¹² The sign has been changed; see the erratum, JAMES 02.

α FOR $\Xi^0 \rightarrow \Lambda e^+ e^-$

VALUE	EVTS	DOCUMENT ID	TECN	COMMENT
-0.8 ± 0.2	397 ± 21	¹³ BATLEY 07C	NA48	p Be, 400 GeV

¹³ This BATLEY 07C result is consistent with the asymmetry α for $\Xi^0 \rightarrow \Lambda\gamma$, as expected if the mechanism is internal bremsstrahlung.

α FOR $\Xi^0 \rightarrow \Sigma^0\gamma$

See the note above on ‘‘Radiative Hyperon Decays.’’

VALUE	EVTS	DOCUMENT ID	TECN	COMMENT
-0.69 ± 0.06	OUR AVERAGE			
$-0.729 \pm 0.030 \pm 0.076$	15k	¹⁴ BATLEY 10B	NA48	p Be, 400 GeV
$-0.63 \pm 0.08 \pm 0.05$	4045	ALAVI-HARATI01C	KTEV	p nucleus, 800 GeV
•••				We do not use the following data for averages, fits, limits, etc. •••
$+0.20 \pm 0.32 \pm 0.05$	85	¹⁵ TEIGE 89	SPEC	FNAL hyperons

- ¹⁴ BATLEY 10B also measured the $\Xi^0 \rightarrow \Sigma^0\gamma$ asymmetry to be -0.786 ± 0.104 (no systematic error given) with 1404 events.
- ¹⁵ This result has been withdrawn, due to an error. See the erratum, TEIGE 02.

$g_1(0)/f_1(0)$ FOR $\Xi^0 \rightarrow \Sigma^+ e^- \bar{\nu}_e$

VALUE	EVTS	DOCUMENT ID	TECN	COMMENT
1.22 ± 0.05	OUR AVERAGE			
1.21 ± 0.05		BATLEY 13	NA48	p Be, 400 GeV
$1.32^{+0.21}_{-0.17} \pm 0.05$	487	¹⁶ ALAVI-HARATI01i	KTEV	p nucleus, 800 GeV
•••				We do not use the following data for averages, fits, limits, etc. •••
$1.20 \pm 0.04 \pm 0.03$	6520	¹⁷ BATLEY 07	NA48	See BATLEY 13

- ¹⁶ ALAVI-HARATI 01i assumes here that the second-class current is zero and that the weak-magnetism term takes its exact SU(3) value.
- ¹⁷ This BATLEY 07 result uses our 2006 value of V_{US} from semileptonic kaon decays as input.

$g_2(0)/f_1(0)$ FOR $\Xi^0 \rightarrow \Sigma^+ e^- \bar{\nu}_e$

VALUE	EVTS	DOCUMENT ID	TECN	COMMENT
$-1.7^{+2.1}_{-2.0} \pm 0.5$	487	¹⁸ ALAVI-HARATI01i	KTEV	p nucleus, 800 GeV

- ¹⁸ ALAVI-HARATI 01i thus assumes that $g_2 = 0$ in calculating g_1/f_1 , above.

$f_2(0)/f_1(0)$ FOR $\Xi^0 \rightarrow \Sigma^+ e^- \bar{\nu}_e$

VALUE	EVTS	DOCUMENT ID	TECN	COMMENT
2.0 ± 0.9	OUR AVERAGE			
2.0 ± 1.3		BATLEY 13	NA48	p Be, 400 GeV
$2.0 \pm 1.2 \pm 0.5$	487	ALAVI-HARATI01i	KTEV	p nucleus, 800 GeV

Ξ^0 REFERENCES

BATLEY 13	PL B720 105	J.R. Batley <i>et al.</i>	(CERN NA48/1 Collab.)
BATLEY 10B	PL B693 241	J.R. Batley <i>et al.</i>	(CERN NA48/1 Collab.)
BATLEY 07	PL B645 36	J.R. Batley <i>et al.</i>	(CERN NA48/1 Collab.)
BATLEY 07C	PL B650 1	J.R. Batley <i>et al.</i>	(CERN NA48 Collab.)
ABOUZAID 05	PRL 95 081801	E. Abouzaid <i>et al.</i>	(FNAL KTeV Collab.)
WHITE 05	PRL 94 101804	C.G. White <i>et al.</i>	(FNAL HyperCP Collab.)
LAI 04A	PL B584 251	A. Lai <i>et al.</i>	(CERN NA48 Collab.)
JAMES 02	PRL 89 169901 (err.)	C. James <i>et al.</i>	(MINN, MICH, WISC, RUTG)
TEIGE 02	PRL 89 169902 (err.)	S. Teige <i>et al.</i>	(RUTG, MICH, MINN)
ALAVI-HARATI 01C	PRL 86 3239	A. Alavi-Harati <i>et al.</i>	(FNAL KTeV Collab.)
ALAVI-HARATI 01i	PRL 87 132001	A. Alavi-Harati <i>et al.</i>	(FNAL KTeV Collab.)
FANTI 00	EPJ C12 69	V. Fanti <i>et al.</i>	(CERN NA48 Collab.)
AFFOLDER 99	PRL 82 3751	A. Affolder <i>et al.</i>	(FNAL KTeV Collab.)
JAMES 90	PRL 64 843	C. James <i>et al.</i>	(MINN, MICH, WISC, RUTG)
TEIGE 89	PRL 63 2717	S. Teige <i>et al.</i>	(RUTG, MICH, MINN)
HANDLER 82	PR D25 639	R. Handler <i>et al.</i>	(WISC, MICH, MINN+)
COX 81	PRL 46 877	P.T. Cox <i>et al.</i>	(MICH, WISC, RUTG, MINN+)
BUNCE 79	PL 86B 336	G.R.M. Bunce <i>et al.</i>	(CERN NA48 Collab.)
BUNCE 78	PR D18 333	G.R.M. Bunce <i>et al.</i>	(WISC, MICH, RUTG)
ZECH 77	NP B124 413	G. Zech <i>et al.</i>	(SIEG, CERN, DORT, HEIDH)
GEWENIGER 75	PL 57B 193	C. Geweniger <i>et al.</i>	(CERN, HEIDH)
BALTAY 74	PR D9 49	C. Baltay <i>et al.</i>	(COLU, BING, J)
YEH 74	PR D10 3545	N. Yeh <i>et al.</i>	(BING, COLU)
MAYEUR 72	NP B47 333	C. Mayeur <i>et al.</i>	(BRUX, CERN, TUFTS, LOUC)
Also	NP B53 268 (erratum)	C. Mayeur	
WILQUET 72	PL 42B 372	G. Wilquet <i>et al.</i>	(BRUX, CERN, TUFTS+)
DAUBER 69	PR 179 1262	P.M. Dauber <i>et al.</i>	(LRL)
PALMER 68	PL 26B 323	R.B. Palmer <i>et al.</i>	(BNL, SYRA)
BERGE 66	PR 147 945	J.P. Berge <i>et al.</i>	(LRL)
HUBBARD 66	Thesis UCRL 11510	J.R. Hubbard	(LRL)
LONDON 66	PR 143 1034	G.W. London <i>et al.</i>	(BNL, SYRA)
PJERROU 65B	PRL 14 275	G.M. Pjerrou <i>et al.</i>	(UCLA)
Also	Thesis	G.M. Pjerrou	(UCLA)
CARMONY 64B	PRL 12 482	D.D. Carmony <i>et al.</i>	(UCLA)
HUBBARD 64	PR 135 B183	J.R. Hubbard <i>et al.</i>	(LRL)
JAUNEAU 63	PL 4 49	L. Jauneau <i>et al.</i>	(EPOL, CERN, LOUC+)
Also	Siena Conf. 1 1	L. Jauneau <i>et al.</i>	(EPOL, CERN, LOUC+)



$I(J^P) = \frac{1}{2}(\frac{1}{2}^+)$ Status: * * *

The parity has not actually been measured, but + is of course expected.

We have omitted some results that have been superseded by later experiments. See our earlier editions.

Ξ^- MASS

The fit uses the Ξ^-, Ξ^+ , and Ξ^0 masses and the $\Xi^- - \Xi^+$ mass difference. It assumes that the Ξ^- and Ξ^+ masses are the same.

VALUE (MeV)	EVTS	DOCUMENT ID	TECN	COMMENT
1321.71 ± 0.07	OUR FIT			
$1321.70 \pm 0.08 \pm 0.05$	2478 ± 68	ABDALLAH 06E	DLPH	from Z decays
•••				We do not use the following data for averages, fits, limits, etc. •••
1321.46 ± 0.34	632	DIBIANCA 75	DBC	4.9 GeV/c $K^- d$
1321.12 ± 0.41	268	WILQUET 72	HLBC	
1321.87 ± 0.51	195	¹ GOLDWASSER 70	HBC	5.5 GeV/c $K^- p$
1321.67 ± 0.52	6	CHIEN 66	HBC	6.9 GeV/c $\bar{p} p$
1321.4 ± 1.1	299	LONDON 66	HBC	
1321.3 ± 0.4	149	PJERROU 65B	HBC	
1321.1 ± 0.3	241	² BADIER 64	HBC	
1321.4 ± 0.4	517	² JAUNEAU 63D	FBC	
1321.1 ± 0.65	62	² SCHNEIDER 63	HBC	

- ¹ GOLDWASSER 70 uses $m_\Lambda = 1115.58$ MeV.
- ² These masses have been increased 0.09 MeV because the Λ mass increased.

Ξ^+ MASS

The fit uses the Ξ^-, Ξ^+ , and Ξ^0 masses and the $\Xi^- - \Xi^+$ mass difference. It assumes that the Ξ^- and Ξ^+ masses are the same.

VALUE (MeV)	EVTS	DOCUMENT ID	TECN	COMMENT
1321.71 ± 0.07	OUR FIT			
$1321.73 \pm 0.08 \pm 0.05$	2256 ± 63	ABDALLAH 06E	DLPH	from Z decays
•••				We do not use the following data for averages, fits, limits, etc. •••
1321.6 ± 0.8	35	VOTRUBA 72	HBC	10 GeV/c $K^+ p$
1321.2 ± 0.4	34	STONE 70	HBC	
1320.69 ± 0.93	5	CHIEN 66	HBC	6.9 GeV/c $\bar{p} p$

$(m_{\Xi^-} - m_{\Xi^+}) / m_{\Xi^-}$

A test of CPT invariance.

VALUE	DOCUMENT ID	TECN	COMMENT
$(-2.5 \pm 8.7) \times 10^{-5}$	ABDALLAH 06E	DLPH	from Z decays

Ξ^- MEAN LIFE

Measurements with an error $> 0.2 \times 10^{-10}$ s or with systematic errors not included have been omitted.

VALUE (10^{-10} s)	EVTS	DOCUMENT ID	TECN	COMMENT
1.639 ± 0.015	OUR AVERAGE			
$1.65 \pm 0.07 \pm 0.12$	2478 ± 68	ABDALLAH 06E	DLPH	from Z decays
1.652 ± 0.051	32k	BOURQUIN 84	SPEC	Hyperon beam

Baryon Particle Listings



1.665±0.065	41k	BOURQUIN	79	SPEC	Hyperon beam
1.609±0.028	4286	HEMINGWAY	78	HBC	4.2 GeV/c $K^- p$
1.67 ±0.08		DIBIANCA	75	DBC	4.9 GeV/c $K^- d$
1.63 ±0.03	4303	BALTAY	74	HBC	1.75 GeV/c $K^- p$
1.73 $\begin{smallmatrix} +0.08 \\ -0.07 \end{smallmatrix}$	680	MAYEUR	72	HLBC	2.1 GeV/c K^-
1.61 ±0.04	2610	DAUBER	69	HBC	
1.80 ±0.16	299	LONDON	66	HBC	
1.70 ±0.12	246	PJERROU	65B	HBC	
1.69 ±0.07	794	HUBBARD	64	HBC	
1.86 $\begin{smallmatrix} +0.15 \\ -0.14 \end{smallmatrix}$	517	JAUNEAU	63D	FBC	

Ξ⁺ MEAN LIFE

VALUE (10 ⁻¹⁰ s)	EVTS	DOCUMENT ID	TECN	COMMENT
1.70±0.08±0.12	2256 ± 63	ABDALLAH	06E	DLPH from Z decays
••• We do not use the following data for averages, fits, limits, etc. •••				
1.55 $\begin{smallmatrix} +0.35 \\ -0.20 \end{smallmatrix}$	35	³ VOTRUBA	72	HBC 10 GeV/c $K^+ p$
1.6 ±0.3	34	STONE	70	HBC
1.9 $\begin{smallmatrix} +0.7 \\ -0.5 \end{smallmatrix}$	12	³ SHEN	67	HBC
1.51±0.55	5	³ CHIEN	66	HBC 6.9 GeV/c $\bar{p} p$

$$(\tau_{\Xi^-} - \tau_{\Xi^+}) / \tau_{\Xi^-}$$

A test of CPT invariance.

VALUE	DOCUMENT ID	TECN	COMMENT
-0.01±0.07	ABDALLAH	06E	DLPH from Z decays

Ξ⁻ MAGNETIC MOMENT

See the "Quark Model" review.

VALUE (μ _N)	EVTS	DOCUMENT ID	TECN	COMMENT
-0.6507±0.0025 OUR AVERAGE				
-0.6505±0.0025	4.36M	DURYEA	92	SPEC 800 GeV p Be
-0.661 ±0.036 ±0.036	44k	TROST	89	SPEC Ξ ⁻ ~ 250 GeV
-0.69 ±0.04	218k	RAMEIKA	84	SPEC 400 GeV p Be
••• We do not use the following data for averages, fits, limits, etc. •••				
-0.674 ±0.021 ±0.020	122k	HO	90	SPEC See DURYEA 92
-2.1 ±0.8	2436	COOL	74	OSP K 1.8 GeV/c $K^- p$
-0.1 ±2.1	2724	BINGHAM	70B	OSP K 1.8 GeV/c $K^- p$

Ξ⁺ MAGNETIC MOMENT

See the "Quark Model" review.

VALUE (μ _N)	EVTS	DOCUMENT ID	TECN	COMMENT
+0.657±0.028±0.020	70k	HO	90	SPEC 800 GeV p Be

$$(\mu_{\Xi^-} + \mu_{\Xi^+}) / |\mu_{\Xi^-}|$$

A test of CPT invariance. We calculate this from the Ξ⁻ and Ξ⁺ magnetic moments above.

VALUE	DOCUMENT ID
+0.01±0.05 OUR EVALUATION	

Ξ⁻ DECAY MODES

Mode	Fraction (Γ _i /Γ)	Confidence level
Γ ₁ Λπ ⁻	(99.887±0.035) %	
Γ ₂ Σ ⁻ γ	(1.27 ±0.23) × 10 ⁻⁴	
Γ ₃ Λe ⁻ ν _e	(5.63 ±0.31) × 10 ⁻⁴	
Γ ₄ Λμ ⁻ ν _μ	(3.5 $\begin{smallmatrix} +3.5 \\ -2.2 \end{smallmatrix}$) × 10 ⁻⁴	
Γ ₅ Σ ⁰ e ⁻ ν _e	(8.7 ±1.7) × 10 ⁻⁵	
Γ ₆ Σ ⁰ μ ⁻ ν _μ	< 8	90%
Γ ₇ Σ ⁰ e ⁻ ν _e	< 2.59	90%
ΔS = 2 forbidden (S2) modes		
Γ ₈ nπ ⁻	S2 < 1.9	× 10 ⁻⁵ 90%
Γ ₉ ne ⁻ ν _e	S2 < 3.2	× 10 ⁻³ 90%
Γ ₁₀ nμ ⁻ ν _μ	S2 < 1.5	% 90%
Γ ₁₁ pπ ⁻ π ⁻	S2 < 4	× 10 ⁻⁴ 90%
Γ ₁₂ pπ ⁻ e ⁻ ν _e	S2 < 4	× 10 ⁻⁴ 90%
Γ ₁₃ pπ ⁻ μ ⁻ ν _μ	S2 < 4	× 10 ⁻⁴ 90%
Γ ₁₄ pμ ⁻ μ ⁻	L < 4	× 10 ⁻⁸ 90%

CONSTRAINED FIT INFORMATION

An overall fit to 4 branching ratios uses 5 measurements and one constraint to determine 5 parameters. The overall fit has a $\chi^2 = 1.0$ for 1 degrees of freedom.

The following *off-diagonal* array elements are the correlation coefficients $\langle \delta x_i \delta x_j \rangle / (\delta x_i \delta x_j)$, in percent, from the fit to the branching fractions, $x_i \equiv \Gamma_i / \Gamma_{\text{total}}$. The fit constrains the x_i whose labels appear in this array to sum to one.

x ₂	-6			
x ₃	-8	0		
x ₄	-99	0	-1	
x ₅	-5	0	0	0
	x ₁	x ₂	x ₃	x ₄

Ξ⁻ BRANCHING RATIOS

A number of early results have been omitted.

$$\Gamma(\Sigma^- \gamma) / \Gamma(\Lambda \pi^-) \quad \Gamma_2 / \Gamma_1$$

VALUE (units 10 ⁻⁴)	EVTS	DOCUMENT ID	TECN	COMMENT
1.27±0.24 OUR FIT				
1.27±0.23 OUR AVERAGE				
1.22±0.23±0.06	211	⁴ DUBBS	94	E761 Ξ ⁻ 375 GeV
2.27±1.02	9	BIAGI	87B	SPEC SPS hyperon beam
⁴ DUBBS 94 also finds weak evidence that the asymmetry parameter α _γ is positive (α _γ = 1.0 ± 1.3).				

$$\Gamma(\Lambda e^- \bar{\nu}_e) / \Gamma(\Lambda \pi^-) \quad \Gamma_3 / \Gamma_1$$

VALUE (units 10 ⁻³)	EVTS	DOCUMENT ID	TECN	COMMENT
0.564±0.031 OUR FIT				
0.564±0.031	2857	BOURQUIN	83	SPEC SPS hyperon beam
••• We do not use the following data for averages, fits, limits, etc. •••				
0.30 ±0.13	11	THOMPSON	80	ASPK Hyperon beam

$$\Gamma(\Lambda \mu^- \bar{\nu}_\mu) / \Gamma(\Lambda \pi^-) \quad \Gamma_4 / \Gamma_1$$

VALUE (units 10 ⁻³)	CL%	EVTS	DOCUMENT ID	TECN	COMMENT	
0.35 $\begin{smallmatrix} +0.35 \\ -0.22 \end{smallmatrix}$ OUR FIT						
0.35±0.35		1	YEH	74	HBC Effective denom.=2859	
••• We do not use the following data for averages, fits, limits, etc. •••						
< 2.3		90	0	THOMPSON	80	ASPK Effective denom.=1017
< 1.3				DAUBER	69	HBC
< 12				BERGE	66	HBC

$$\Gamma(\Sigma^0 e^- \bar{\nu}_e) / \Gamma(\Lambda \pi^-) \quad \Gamma_5 / \Gamma_1$$

VALUE (units 10 ⁻³)	EVTS	DOCUMENT ID	TECN	COMMENT
0.087±0.017 OUR FIT				
0.087±0.017	154	BOURQUIN	83	SPEC SPS hyperon beam

$$[\Gamma(\Lambda e^- \bar{\nu}_e) + \Gamma(\Sigma^0 e^- \bar{\nu}_e)] / \Gamma(\Lambda \pi^-) \quad (\Gamma_3 + \Gamma_5) / \Gamma_1$$

VALUE (units 10 ⁻³)	EVTS	DOCUMENT ID	TECN	COMMENT
••• We do not use the following data for averages, fits, limits, etc. •••				
0.651 ±0.031	3011	⁵ BOURQUIN	83	SPEC SPS hyperon beam
0.68 ±0.22	17	⁶ DUCLOS	71	OSP K

⁵ See the separate BOURQUIN 83 values for $\Gamma(\Lambda e^- \bar{\nu}_e) / \Gamma(\Lambda \pi^-)$ and $\Gamma(\Sigma^0 e^- \bar{\nu}_e) / \Gamma(\Lambda \pi^-)$ above.

⁶ DUCLOS 71 cannot distinguish Σ⁰'s from Λ's. The Cabibbo theory predicts the Σ⁰ rate is about a factor 6 smaller than the Λ rate.

$$\Gamma(\Sigma^0 \mu^- \bar{\nu}_\mu) / \Gamma(\Lambda \pi^-) \quad \Gamma_6 / \Gamma_1$$

VALUE (units 10 ⁻³)	CL%	EVTS	DOCUMENT ID	TECN	COMMENT	
<0.76		90	0	YEH	74	HBC Effective denom.=3026
••• We do not use the following data for averages, fits, limits, etc. •••						
<5				BERGE	66	HBC

$$\Gamma(\Xi^0 e^- \bar{\nu}_e) / \Gamma_{\text{total}} \quad \Gamma_7 / \Gamma$$

VALUE	CL%	DOCUMENT ID	TECN	COMMENT
<2.59 × 10⁻⁴		90	ABLKIM	21AH BES3 J/ψ → ΞΞ̄

$$\Gamma(\Xi^0 e^- \bar{\nu}_e) / \Gamma(\Lambda \pi^-) \quad \Gamma_7 / \Gamma_1$$

VALUE	CL%	DOCUMENT ID	TECN	COMMENT	
••• We do not use the following data for averages, fits, limits, etc. •••					
<2.3 × 10 ⁻³		90	YEH	74	HBC Effective denom.=1000

$$\Gamma(n \pi^-) / \Gamma(\Lambda \pi^-) \quad \Gamma_8 / \Gamma_1$$

VALUE (units 10 ⁻³)	CL%	EVTS	DOCUMENT ID	TECN	COMMENT	
ΔS=2. Forbidden in first-order weak interaction.						
<0.019		90	BIAGI	82B	SPEC SPS hyperon beam	
••• We do not use the following data for averages, fits, limits, etc. •••						
<3.0		90	0	YEH	74	HBC Effective denom.=760
<1.1				DAUBER	69	HBC
<5.0				FERRO-LUZZI	63	HBC

See key on page 1127

Baryon Particle Listings



$\Gamma(n e^- \bar{\nu}_e) / \Gamma(\Lambda \pi^-)$ **Γ_9 / Γ_1**
 $\Delta S=2$. Forbidden in first-order weak interaction.

VALUE (units 10^{-3})	CL%	EVTS	DOCUMENT ID	TECN	COMMENT
< 3.2	90	0	YEH 74	HBC	Effective denom.=715
<10	90		BINGHAM 65	RVUE	

••• We do not use the following data for averages, fits, limits, etc. •••

$\Gamma(n \mu^- \bar{\nu}_\mu) / \Gamma(\Lambda \pi^-)$ **Γ_{10} / Γ_1**
 $\Delta S=2$. Forbidden in first-order weak interaction.

VALUE (units 10^{-3})	CL%	EVTS	DOCUMENT ID	TECN	COMMENT
<15.3	90	0	YEH 74	HBC	Effective denom.=150

$\Gamma(p \pi^- \pi^-) / \Gamma(\Lambda \pi^-)$ **Γ_{11} / Γ_1**
 $\Delta S=2$. Forbidden in first-order weak interaction.

VALUE (units 10^{-4})	CL%	EVTS	DOCUMENT ID	TECN	COMMENT
<3.7	90	0	YEH 74	HBC	Effective denom.=6200

$\Gamma(p \pi^- e^- \bar{\nu}_e) / \Gamma(\Lambda \pi^-)$ **Γ_{12} / Γ_1**
 $\Delta S=2$. Forbidden in first-order weak interaction.

VALUE (units 10^{-4})	CL%	EVTS	DOCUMENT ID	TECN	COMMENT
<3.7	90	0	YEH 74	HBC	Effective denom.=6200

$\Gamma(p \pi^- \mu^- \bar{\nu}_\mu) / \Gamma(\Lambda \pi^-)$ **Γ_{13} / Γ_1**
 $\Delta S=2$. Forbidden in first-order weak interaction.

VALUE (units 10^{-4})	CL%	EVTS	DOCUMENT ID	TECN	COMMENT
<3.7	90	0	YEH 74	HBC	Effective denom.=6200

$\Gamma(p \mu^- \mu^-) / \Gamma(\Lambda \pi^-)$ **Γ_{14} / Γ_1**
 $\Delta L=2$ decay, forbidden by total lepton number conservation.

VALUE (units 10^{-8})	CL%	DOCUMENT ID	TECN	COMMENT
<4.0	90	RAJARAM 05	HYCP	p Cu, 800 GeV
<3.7 × 10 ⁴	90	LITTENBERG 92b	HBC	Uses YEH 74 data

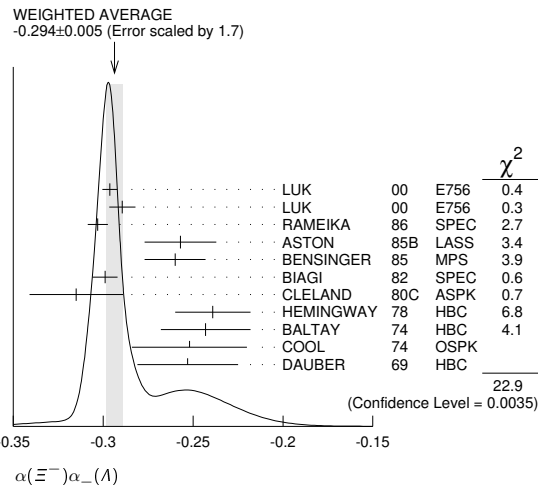
⁷This LITTENBERG 92b limit and the identical YEH 74 limits for the preceding three modes all result from nonobservance of any 3-prong decays of the Ξ^- . One could as well apply the limit to the sum of the four modes.

Ξ^- DECAY PARAMETERS

See the "Note on Baryon Decay Parameters" in the neutron Listings.

$\alpha(\Xi^-)\alpha_-(\Lambda)$

VALUE	EVTS	DOCUMENT ID	TECN	COMMENT
-0.294 ± 0.005 OUR AVERAGE				Error includes scale factor of 1.7. See the ideogram below.
-0.2963 ± 0.0042	189k	LUK	00	E756 p Be, 800 GeV
-0.2894 ± 0.0073	63k	⁸ LUK	00	E756 p Be, 800 GeV
-0.303 ± 0.004 ± 0.004	192k	RAMEIKA	86	SPEC 400 GeV pBe
-0.257 ± 0.020	11k	ASTON	85b	LASS 11 GeV/c K ⁻ p
-0.260 ± 0.017	21k	BENSINGER	85	MPS 5 GeV/c K ⁻ p
-0.299 ± 0.007	150k	BIAGI	82	SPEC SPS hyperon beam
-0.315 ± 0.026	9046	CLELAND	80c	ASPK BNL hyperon beam
-0.239 ± 0.021	6599	HEMINGWAY	78	HBC 4.2 GeV/c K ⁻ p
-0.243 ± 0.025	4303	BALTAY	74	HBC 1.75 GeV/c K ⁻ p
-0.252 ± 0.032	2436	COOL	74	OSPK 1.8 GeV/c K ⁻ p
-0.253 ± 0.028	2781	DAUBER	69	HBC



⁸This LUK 00 value is for $\alpha(\Xi^+)\alpha_+(\bar{\Lambda})$. We assume CP conservation here by including it in the average for $\alpha(\Xi^-)\alpha_-(\Lambda)$. But see the second data block below for the CP test.

α FOR $\Xi^- \rightarrow \Lambda \pi^-$
 The above average, $\alpha(\Xi^-)\alpha_-(\Lambda) = -0.294 \pm 0.005$, divided by our current average $\alpha_-(\Lambda) = 0.732 \pm 0.014$, gives the following value for $\alpha(\Xi^-)$:

-0.401 ± 0.010 OUR EVALUATION

$\frac{[\alpha(\Xi^-)\alpha_-(\Lambda) - \alpha(\Xi^+)\alpha_+(\bar{\Lambda})]}{[\alpha(\Xi^-)\alpha_-(\Lambda) + \alpha(\Xi^+)\alpha_+(\bar{\Lambda})]}$
 This is zero if CP is conserved. The α 's are the decay-asymmetry parameters for $\Xi^- \rightarrow \Lambda \pi^-$ and $\Lambda \rightarrow p \pi^-$ and for $\Xi^+ \rightarrow \bar{\Lambda} \pi^+$ and $\bar{\Lambda} \rightarrow \bar{p} \pi^+$.

VALUE (units 10^{-4})	EVTS	DOCUMENT ID	TECN	COMMENT
0.0 ± 5.1 ± 4.4	158M	HOLMSTROM 04	HYCP	p Cu, 800 GeV
+120 ± 140	252k	LUK	00	E756 p Be, 800 GeV

••• We do not use the following data for averages, fits, limits, etc. •••

ϕ ANGLE FOR $\Xi^- \rightarrow \Lambda \pi^-$ **(tan $\phi = \beta/\gamma$)**

VALUE (°)	EVTS	DOCUMENT ID	TECN	COMMENT
-2.1 ± 0.8 OUR AVERAGE				
-2.39 ± 0.64 ± 0.64	144M	⁹ HUANG 04	HYCP	p Cu, 800 GeV
-1.61 ± 2.66 ± 0.37	1.35M	¹⁰ CHAKRAVORTY 03	E756	p Be, 800 GeV
5 ± 10	11k	ASTON 85b	LASS	K ⁻ p
14.7 ± 16.0	21k	¹¹ BENSINGER 85	MPS	5 GeV/c K ⁻ p
11 ± 9	4303	BALTAY 74	HBC	1.75 GeV/c K ⁻ p
5 ± 16	2436	COOL 74	OSPK	1.8 GeV/c K ⁻ p
-14 ± 11	2781	DAUBER 69	HBC	Uses $\alpha_\Lambda = 0.647 \pm 0.020$
0 ± 12	1004	¹² BERGE 66	HBC	
-26 ± 30	2724	BINGHAM 70b	OSPK	
0 ± 20.4	364	¹² LONDON 66	HBC	Using $\alpha_\Lambda = 0.62$
54 ± 30	356	¹² CARMONY 64b	HBC	

••• We do not use the following data for averages, fits, limits, etc. •••

⁹From this result and α_Ξ , HUANG 04 gets $\beta_\Xi = -0.037 \pm 0.011 \pm 0.010$ and $\gamma_\Xi = 0.888 \pm 0.0004 \pm 0.006$. And the strong p-s phase difference for $\Lambda \pi^-$ scattering is $(4.6 \pm 1.4 \pm 1.2)^\circ$.
¹⁰From this result and α_Ξ , CHAKRAVORTY 03 obtains $\beta_\Xi = -0.025 \pm 0.042 \pm 0.006$ and $\gamma_\Xi = 0.889 \pm 0.001 \pm 0.007$. And the strong p-s phase difference for $\Lambda \pi^-$ scattering is $(3.17 \pm 5.28 \pm 0.73)^\circ$.
¹¹BENSINGER 85 used $\alpha_\Lambda = 0.642 \pm 0.013$.
¹²The errors have been multiplied by 1.2 due to approximations used for the Ξ polarization; see DAUBER 69 for a discussion.

g_A / g_V FOR $\Xi^- \rightarrow \Lambda e^- \bar{\nu}_e$

VALUE	EVTS	DOCUMENT ID	TECN	COMMENT
-0.25 ± 0.05	1992	¹³ BOURQUIN 83	SPEC	SPS hyperon beam

¹³BOURQUIN 83 assumes that $g_2 = 0$. Also, the sign has been changed to agree with our conventions, given in the "Note on Baryon Decay Parameters" in the neutron Listings.

Ξ^- REFERENCES

We have omitted some papers that have been superseded by later experiments. See our earlier editions.

ABLIKIM 21AH	PR D104 072007	M. Ablikim et al.	(BESIII Collab.)
ABDALLAH 06E	PL B639 179	J. Abdallah et al.	(DELPHI Collab.)
RAJARAM 05	PRL 94 181801	D. Rajaram et al.	(FNAL HyperCP Collab.)
HOLMSTROM 04	PRL 93 262001	T. Holmstrom et al.	(FNAL HyperCP Collab.)
HUANG 04	PRL 93 011802	M. Huang et al.	(FNAL HyperCP Collab.)
CHAKRAVORTY 03	PRL 91 031601	A. Chakravorty et al.	(FNAL E756 Collab.)
LUK 00	PRL 85 4860	K.B. Luk et al.	(FNAL E756 Collab.)
DUBBS 94	PRL 72 808	T. Dubbs et al.	(FNAL E761 Collab.)
DURYES 92	PRL 68 768	J. Duries et al.	(MINN, FNAL, MICH, RUTG)
LITTENBERG 92b	PR D46 892	L.S. Littenberg, R.E. Shrock	(BNL, STON)
HO 90	PRL 65 1713	P.M. Ho et al.	(MICH, FNAL, MINN, RUTG)
Also	PR D44 3402	P.M. Ho et al.	(MICH, FNAL, MINN, RUTG)
TROST 89	PR D40 1703	L.H. Trost et al.	(FNAL-715 Collab.)
BIAGI 87b	ZPHY C35 143	S.F. Biagi et al.	(BRIS, CERN, GEVA+)
RAMEIKA 86	PR D33 3172	R. Rameika et al.	(RUTG, MICH, WISC+)
ASTON 85b	PR D32 2270	D. Aston et al.	(SLAC, CARL, CNRC, CINC)
BENSINGER 85	NP B252 561	J.R. Bensingier et al.	(CHIC, ELMT, FNAL+)
BOURQUIN 84	NP B241 1	M.H. Bourquin et al.	(BRIS, GEVA, HEIDP+)
RAMEIKA 84	PRL 52 581	R. Rameika et al.	(RUTG, MICH, WISC+)
BOURQUIN 83	ZPHY C21 1	M.H. Bourquin et al.	(BRIS, GEVA, HEIDP+)
BIAGI 82b	PL 112B 265	S.F. Biagi et al.	(BRIS, CAVE, GEVA+)
BIAGI 82b	PL 112B 277	S.F. Biagi et al.	(LOMQ, GEVA, RL+)
CLELAND 80c	PR D21 12	W.E. Cleland et al.	(PITT, BNL)
THOMPSON 80	PR D21 25	J.A. Thompson et al.	(PITT, BNL)
BOURQUIN 78	PL 87B 297	M.H. Bourquin et al.	(BRIS, GEVA, HEIDP+)
HEMINGWAY 78	NP B142 205	R.J. Hemingway et al.	(CERN, ZEEM, NIJH+)
DIBIANCA 75	NP B98 137	F.A. Dibiaccia, R.J. Endorf	(CMU)
BALTAY 74	PR D9 49	C. Baltay et al.	(COLU, BING, J)
COOL 74	PR D10 792	R.L. Cool et al.	(BNL)
Also	PRL 29 1630	R.L. Cool et al.	(BNL)
YEH 74	PR D10 3545	N. Yeh et al.	(BING, COLU)
MAYEUR 72	NP B47 333	C. Mayeur et al.	(BRUX, CERN, TUFTS, LOUC)
VOTRUBA 72	NP B45 77	M.F. Votruba, A. Saffier, T.M. Ratcliffe	(BIRM+)
WILQUET 72	PL 42B 372	G. Wilquet et al.	(BRUX, CERN, TUFTS+)
DUCLÓS 71	NP B32 493	J. Duclós et al.	(CERN)
BINGHAM 70b	PR D1 3010	G.M. Bingham et al.	(UCSD, WASH)
GOLDWASSER 70	PR D1 1960	E.L. Goldwasser, P.F. Schultz	(ILL)
STONE 70	PL 32B 515	S.L. Stone et al.	(ROCH)
DAUBER 69	PR 179 1262	P.M. Dauber et al.	(LRL, J)
SHEN 67	PL 25B 443	B.C. Shen, A. Firestone, G. Goldhaber	(UCB+)
BERGE 66	PR 147 945	J.P. Berge et al.	(LRL)
CHIEN 66	PR 152 1171	C.Y. Chien et al.	(YALE, BNL)
LONDON 66	PR 143 1034	G.V. London et al.	(BNL, SYRA)
BINGHAM 65	PRSL 285 202	H.H. Bingham et al.	(CERN)
PIERROU 65b	PRL 14 275	G.M. Pierrou et al.	(UCLA)
Also	Thesis	G.M. Pierrou	(UCLA)

Baryon Particle Listings

$\Xi^-, \Xi's, \Xi(1530)$

BADIER 64	Dubna Conf. 1 593	J. Badier <i>et al.</i>	(EPOL, SACL, ZEEM)
CARMONY 64B	PRL 12 482	D.D. Carmony <i>et al.</i>	(UCLA)J
HUBBARD 64	PR 135 B183	J.R. Hubbard <i>et al.</i>	(LRL)
FERRO-LUZZI 63	PR 130 1568	M. Ferro-Luzzi <i>et al.</i>	(LRL)
JAUNEAU 63D	Siena Conf. 4	L. Jauneau <i>et al.</i>	(EPOL, CERN, LOUC+)
Also	PL 5 261	L. Jauneau <i>et al.</i>	(EPOL, CERN, LOUC+)
SCHNEIDER 63	PL 4 360	J. Schneider	(CERN)

Ξ RESONANCES

Revised 2004 by C.G. Wohl, (LBNL).

The accompanying table gives our evaluation of the present status of the Ξ resonances. Not much is known about Ξ resonances. This is because (1) they can only be produced as a part of a final state, and so the analysis is more complicated than if direct formation were possible, (2) the production cross sections are small (typically a few μb), and (3) the final states are topologically complicated and difficult to study with electronic techniques. Thus early information about Ξ resonances came entirely from bubble chamber experiments, where the numbers of events are small, and only in the 1980's did electronic experiments make any significant contributions. However, nothing of significance on Ξ resonances has been added since our 1988 edition.

For a detailed earlier review, see Meadows [1].

Table 1. The status of the Ξ resonances. Only those with an overall status of *** or **** are included in the Baryon Summary Table.

Particle	J^P	Overall status	Status as seen in —				
			$\Xi\pi$	ΛK	ΣK	$\Xi(1530)\pi$	Other channels
$\Xi(1318)$	$1/2^+$	****					Decays weakly
$\Xi(1530)$	$3/2^+$	****	****				
$\Xi(1620)$		*	*				
$\Xi(1690)$		***		***	**		
$\Xi(1820)$	$3/2^-$	***	**	***	**	**	
$\Xi(1950)$		***	**	**		*	
$\Xi(2030)$		***		**	***		
$\Xi(2120)$		*		*			
$\Xi(2250)$		**					3-body decays
$\Xi(2370)$		**					3-body decays
$\Xi(2500)$		*		*	*		3-body decays

**** Existence is certain, and properties are at least fairly well explored.
 *** Existence ranges from very likely to certain, but further confirmation is desirable and/or quantum numbers, branching fractions, etc. are not well determined.
 ** Evidence of existence is only fair.
 * Evidence of existence is poor.

Reference

- B.T. Meadows, in *Proceedings of the IVth International Conference on Baryon Resonances* (Toronto, 1980), ed. N. Isgur, p. 283.

$\Xi(1530) 3/2^+$

$$I(J^P) = \frac{1}{2}(\frac{3}{2}^+) \text{ Status: } ****$$

This is the only Ξ resonance whose properties are all reasonably well known. Assuming that the Λ_c^+ has $J^P = 1/2^+$, AUBERT 08AK, in a study of $\Lambda_c^+ \rightarrow \Xi^- \pi^+ K^+$, finds conclusively that the spin of the $\Xi(1530)^0$ is 3/2. In conjunction with SCHLEIN 63B and BUTTON-SHAFER 66, this proves also that the parity is +.

We use only those determinations of the mass and width that are accompanied by some discussion of systematics and resolution.

$\Xi(1530)$ POLE POSITIONS

$\Xi(1530)^0$ REAL PART

VALUE	DOCUMENT ID	COMMENT
1531.6 ± 0.4	LICHTENBERG74	Using HABIBI 73

$\Xi(1530)^0$ IMAGINARY PART

VALUE	DOCUMENT ID	COMMENT
4.45 ± 0.35	LICHTENBERG74	Using HABIBI 73

$\Xi(1530)^-$ REAL PART

VALUE	DOCUMENT ID	COMMENT
1534.4 ± 1.1	LICHTENBERG74	Using HABIBI 73

$\Xi(1530)^-$ IMAGINARY PART

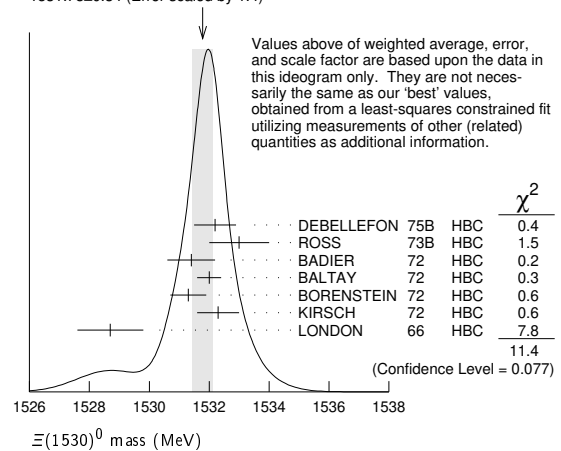
VALUE	DOCUMENT ID	COMMENT
$3.9^{+1.75}_{-3.9}$	LICHTENBERG74	Using HABIBI 73

$\Xi(1530)$ MASSES

$\Xi(1530)^0$ MASS

VALUE (MeV)	EVTS	DOCUMENT ID	TECN	COMMENT
1531.80 ± 0.32 OUR FIT				Error includes scale factor of 1.3.
1531.78 ± 0.34 OUR AVERAGE				Error includes scale factor of 1.4. See the ideogram below.
1532.2 ± 0.7		DEBELLEFON 75B	HBC	$K^- p \rightarrow \Xi^- \bar{K} \pi$
1533 ± 1		ROSS 73B	HBC	$K^- p \rightarrow \Xi \bar{K} \pi(\pi)$
1531.4 ± 0.8	59	BADIER 72	HBC	$K^- p$ 3.95 GeV/c
1532.0 ± 0.4	1262	BALTAY 72	HBC	$K^- p$ 1.75 GeV/c
1531.3 ± 0.6	324	BORENSTEIN 72	HBC	$K^- p$ 2.2 GeV/c
1532.3 ± 0.7	286	KIRSCH 72	HBC	$K^- p$ 2.87 GeV/c
1528.7 ± 1.1	76	LONDON 66	HBC	$K^- p$ 2.24 GeV/c
••• We do not use the following data for averages, fits, limits, etc. •••				
1532.1 ± 0.4	1244	ASTON 85B	LASS	$K^- p$ 11 GeV/c
1532.1 ± 0.6	2700	¹ BAUBILLIER 81B	HBC	$K^- p$ 8.25 GeV/c
1530 ± 1	450	BIAGI 81	SPEC	SPS hyperon beam
1527 ± 6	80	SIXEL 79	HBC	$K^- p$ 10 GeV/c
1535 ± 4	100	SIXEL 79	HBC	$K^- p$ 16 GeV/c
1533.6 ± 1.4	97	BERTHON 74	HBC	Quasi-2-body σ

WEIGHTED AVERAGE
 1531.78 ± 0.34 (Error scaled by 1.4)



$\Xi(1530)^-$ MASS

VALUE (MeV)	EVTS	DOCUMENT ID	TECN	COMMENT
1535.0 ± 0.6 OUR FIT				
1535.2 ± 0.8 OUR AVERAGE				
1534.5 ± 1.2		DEBELLEFON 75B	HBC	$K^- p \rightarrow \Xi^- \bar{K} \pi$
1535.3 ± 2.0		ROSS 73B	HBC	$K^- p \rightarrow \Xi \bar{K} \pi(\pi)$
1536.2 ± 1.6	185	KIRSCH 72	HBC	$K^- p$ 2.87 GeV/c
1535.7 ± 3.2	38	LONDON 66	HBC	$K^- p$ 2.24 GeV/c
••• We do not use the following data for averages, fits, limits, etc. •••				
1540 ± 3	48	BERTHON 74	HBC	Quasi-2-body σ
1534.7 ± 1.1	334	BALTAY 72	HBC	$K^- p$ 1.75 GeV/c

$m_{\Xi(1530)^-} - m_{\Xi(1530)}$

VALUE (MeV)	DOCUMENT ID	TECN	COMMENT
3.2 ± 0.6 OUR FIT			
2.9 ± 0.9 OUR AVERAGE			
2.7 ± 1.0	BALTAY 72	HBC	$K^- p$ 1.75 GeV/c
2.0 ± 3.2	MERRILL 66	HBC	$K^- p$ 1.7-2.7 GeV/c
5.7 ± 3.0	PJERROU 65B	HBC	$K^- p$ 1.8-1.95 GeV/c
••• We do not use the following data for averages, fits, limits, etc. •••			
3.9 ± 1.8	² KIRSCH 72	HBC	$K^- p$ 2.87 GeV/c
7 ± 4	² LONDON 66	HBC	$K^- p$ 2.24 GeV/c

$\Xi(1530)$ WIDTHS

See key on page 1127

Baryon Particle Listings

$\Xi(1530), \Xi(1620), \Xi(1690)$

 $\Xi(1530)^0$ WIDTH

VALUE (MeV)	EVTS	DOCUMENT ID	TECN	COMMENT
9.1±0.5 OUR AVERAGE				
9.5±1.2		DEBELLEFON 75B	HBC	$K^- p \rightarrow \Xi^- \bar{K} \pi$
9.1±2.4		ROSS 73B	HBC	$K^- p \rightarrow \Xi^- \bar{K} \pi(\pi)$
11 ± 2		BADIER 72	HBC	$K^- p$ 3.95 GeV/c
9.0±0.7		BALTAY 72	HBC	$K^- p$ 1.75 GeV/c
8.4±1.4		BORENSTEIN 72	HBC	$\Xi^- \pi^+$
11.0±1.8		KIRSCH 72	HBC	$\Xi^- \pi^+$
7 ± 7		BERGE 66	HBC	$K^- p$ 1.5–1.7 GeV/c
8.5±3.5		LONDON 66	HBC	$K^- p$ 2.24 GeV/c
7 ± 2		SCHLEIN 63B	HBC	$K^- p$ 1.8, 1.95 GeV/c
• • • We do not use the following data for averages, fits, limits, etc. • • •				
12.8±1.0	2700	¹ BAUBILLIER 81B	HBC	$K^- p$ 8.25 GeV/c
19 ± 6	80	³ SIXEL 79	HBC	$K^- p$ 10 GeV/c
14 ± 5	100	³ SIXEL 79	HBC	$K^- p$ 16 GeV/c

 $\Xi(1530)^-$ WIDTH

VALUE (MeV)	EVTS	DOCUMENT ID	TECN	COMMENT
9.9^{+1.7}_{-1.9} OUR AVERAGE				
9.6±2.8		DEBELLEFON 75B	HBC	$K^- p \rightarrow \Xi^- \bar{K} \pi$
8.3±3.6		ROSS 73B	HBC	$K^- p \rightarrow \Xi^- \bar{K} \pi(\pi)$
7.8 ^{+3.5} _{-7.8}		BALTAY 72	HBC	$K^- p$ 1.75 GeV/c
16.2±4.6		KIRSCH 72	HBC	$\Xi^- \pi^0, \Xi^0 \pi^-$

 $\Xi(1530)$ DECAY MODES

Mode	Fraction (Γ_i/Γ)	Confidence level
$\Gamma_1 \Xi \pi$	100 %	90%
$\Gamma_2 \Xi \gamma$	<3.7 %	

 $\Xi(1530)$ BRANCHING RATIOS

VALUE	CL%	DOCUMENT ID	TECN	COMMENT	Γ_2/Γ
<0.037	90	ABLIKIM 20	BES3	$J/\psi \rightarrow \Xi(1530)^- \Xi^+$	
• • • We do not use the following data for averages, fits, limits, etc. • • •					
<0.04	90	KALBFLEISCH 75	HBC	$K^- p$ 2.18 GeV/c	

 $\Xi(1530)$ FOOTNOTES

- ¹ BAUBILLIER 81B is a fit to the inclusive spectrum. The resolution (5 MeV) is not unfolded.
² Redundant with data in the mass Listings.
³ SIXEL 79 doesn't unfold the experimental resolution of 15 MeV.

 $\Xi(1530)$ REFERENCES

ABLIKIM 20	PR D101 012004	M. Ablikim <i>et al.</i>	(BESIII Collab.)
AUBERT 08AK	PR D78 034008	B. Aubert <i>et al.</i>	(BABAR Collab.)
ASTON 85B	PR D32 2270	D. Aston <i>et al.</i>	(SLAC, CARL, CNRC, CINC)
BAUBILLIER 81B	NP B192 1	M. Baubillier <i>et al.</i>	(BIRM, CERN, GLAS+)
BIAGI 81	ZPHY C9 305	S.F. Biagi <i>et al.</i>	(BRIS, CAVE, GEVA+)
SIXEL 79	NP B159 125	P. Sixel <i>et al.</i>	(AACH3, BERL, CERN, LOIC+)
DEBELLEFON 75B	NC 28A 289	A. de Bellefon <i>et al.</i>	(CDEF, SACL)
KALBFLEISCH 75	PR D11 987	G.R. Kalbfleisch, R.C. Strand, J.W. Chapman	(BNL+)
BERTHON 74	NC 21A 146	A. Berthon <i>et al.</i>	(CDEF, RHEL, SACL+)
LICHTENBERG 74	PR D10 3865	D.B. Lichtenberg	(IND)
Also	Private Comm.	D.B. Lichtenberg	(IND)
HABIBI 73	Thesis Nevis 199	M. Habibi	(COLU)
ROSS 73B	Purdue Conf. 355	R.T. Ross, J.L. Lloyd, D. Radojicic	(OXF)
BADIER 72	NP B37 429	J. Badier <i>et al.</i>	(EPOL)
BALTAY 72	PL 42B 129	C. Baltay <i>et al.</i>	(COLU, BING)
BORENSTEIN 72	PR D5 1559	S.R. Borenstein <i>et al.</i>	(BNL, MICH)I
KIRSCH 72	NP B40 349	L.E. Kirsch <i>et al.</i>	(BRAN, UMD, SYRA+)
BERGE 66	PR 147 945	J.P. Berge <i>et al.</i>	(LRL)I
BUTTON... 66	PR 142 983	J. Button-Shafer <i>et al.</i>	(LRL)JP
LONDON 66	PR 143 1034	G.W. London <i>et al.</i>	(BNL, SYRA)IJ
MERRILL 66	Thesis UCRL 16455	D.W. Merrill	(LRL)JP
PJERROU 65B	PRL 14 275	G.M. Pjerrou <i>et al.</i>	(UCLA)
SCHLEIN 63B	PRL 11 167	P.E. Schlein <i>et al.</i>	(UCLA)JP

OTHER RELATED PAPERS

MAZZUCATO 81	NP B178 1	M. Mazzucato <i>et al.</i>	(AMST, CERN, NIJM+)
BRIEFEL 77	PR D16 2706	E. Briefel <i>et al.</i>	(BRAN, UMD, SYRA+)
BRIEFEL 75	PR D12 1859	E. Briefel <i>et al.</i>	(BRAN, UMD, SYRA+)
HUNGERBU... 74	PR D10 2051	V. Hungerbuhler <i>et al.</i>	(YALE, FNAL, BNL+)
BUTTON... 66	PR 142 883	J. Button-Shafer <i>et al.</i>	(LRL)JP

 $\Xi(1620)$

$I(J^P) = \frac{1}{2}(?)$ Status: *
 J, P need confirmation.

OMITTED FROM SUMMARY TABLE

What little evidence there is consists of weak signals in the $\Xi \pi$ channel. A number of other experiments (e.g., BORENSTEIN 72 and HASSALL 81) have looked for but not seen any effect.

 $\Xi(1620)$ MASS

VALUE (MeV)	EVTS	DOCUMENT ID	TECN	COMMENT
≈ 1620 OUR ESTIMATE				
1624±3	31	BRIEFEL 77	HBC	$K^- p$ 2.87 GeV/c
1633±12	34	DEBELLEFON 75B	HBC	$K^- p \rightarrow \Xi^- \bar{K} \pi$
1606±6	29	ROSS 72	HBC	$K^- p$ 3.1–3.7 GeV/c

 $\Xi(1620)$ WIDTH

VALUE (MeV)	EVTS	DOCUMENT ID	TECN	COMMENT
22.5	31	¹ BRIEFEL 77	HBC	$K^- p$ 2.87 GeV/c
40 ± 15	34	DEBELLEFON 75B	HBC	$K^- p \rightarrow \Xi^- \bar{K} \pi$
21 ± 7	29	ROSS 72	HBC	$K^- p \rightarrow \Xi^- \pi^+ K^*0(892)$

 $\Xi(1620)$ DECAY MODES

Mode
$\Gamma_1 \Xi \pi$

 $\Xi(1620)$ FOOTNOTES

- ¹ The fit is insensitive to values between 15 and 30 MeV.

 $\Xi(1620)$ REFERENCES

HASSALL 81	NP B189 397	J.K. Hassall <i>et al.</i>	(CAVE, MSU)
BRIEFEL 77	PR D16 2706	E. Briefel <i>et al.</i>	(BRAN, UMD, SYRA+)
Also	Duke Conf. 317	E. Briefel <i>et al.</i>	(BRAN, UMD, SYRA+)
Hyperon Resonances, 1970			
Also	PR D12 1859	E. Briefel <i>et al.</i>	(BRAN, UMD, SYRA+)
DEBELLEFON 75B	NC 28A 289	A. de Bellefon <i>et al.</i>	(CDEF, SACL)
BORENSTEIN 72	PR D5 1559	S.R. Borenstein <i>et al.</i>	(BNL, MICH)I
ROSS 72	PL 38B 177	R.T. Ross <i>et al.</i>	(OXF)I

OTHER RELATED PAPERS

HUNGERBU... 74	PR D10 2051	V. Hungerbuhler <i>et al.</i>	(YALE, FNAL, BNL+)
SCHMIDT 73	Purdue Conf. 363	P.E. Schmidt	(BRAN)
KALBFLEISCH 70	Duke Conf. 331	G.R. Kalbfleisch	(BNL)I
Hyperon Resonances 1970			
APSELL 69	PRL 23 884	S.P. Apell <i>et al.</i>	(BRAN, UMD, SYRA+)
BARTSCH 69	PL 28B 439	J. Bartsch <i>et al.</i>	(AACH, BERL, CERN+)

 $\Xi(1690)$

$I(J^P) = \frac{1}{2}(?)$ Status: ***

AUBERT 08AK, in a study of $\Lambda_c^+ \rightarrow \Xi^- \pi^+ K^+$, finds some evidence that the $\Xi(1690)$ has $J^P = 1/2^-$.

DIONISI 78 sees a threshold enhancement in both the neutral and negatively charged $\Sigma \bar{K}$ mass spectra in $K^- p \rightarrow (\Sigma \bar{K}) K \pi$ at 4.2 GeV/c. The data from the $\Sigma \bar{K}$ channels alone cannot distinguish between a resonance and a large scattering length. Weaker evidence at the same mass is seen in the corresponding $\Lambda \bar{K}$ channels, and a coupled-channel analysis yields results consistent with a new Ξ .

BIAGI 81 sees an enhancement at 1700 MeV in the diffractively produced ΛK^- system. A peak is also observed in the ΛK^0 mass spectrum at 1660 MeV that is consistent with a 1720 MeV resonance decaying to $\Sigma^0 \bar{K}^0$, with the γ from the Σ^0 decay not detected.

BIAGI 87 provides further confirmation of this state in diffractive dissociation of Ξ^- into ΛK^- . The significance claimed is 6.7 standard deviations.

ADAMOVICH 98 sees a peak of 1400 ± 300 events in the $\Xi^- \pi^+$ spectrum produced by 345 GeV/c Σ^- -nucleus interactions.

 $\Xi(1690)$ MASSES

VALUE (MeV)	DOCUMENT ID
1690±10 OUR ESTIMATE This is only an educated guess; the error given is larger than the error on the average of the published values.	

 $\Xi(1690)^0$ MASS

VALUE (MeV)	EVTS	DOCUMENT ID	TECN	COMMENT
1686±4	1400	ADAMOVICH 98	WA89	Σ^- nucleus, 345 GeV/c
1699±5	175	¹ DIONISI 78	HBC	$K^- p$ 4.2 GeV/c
1684±5	183	² DIONISI 78	HBC	$K^- p$ 4.2 GeV/c

 $\Xi(1690)^-$ MASS

VALUE (MeV)	EVTS	DOCUMENT ID	TECN	COMMENT
1691.1 ± 1.9 ± 2.0	104	BIAGI 87	SPEC	Ξ^- Be 116 GeV
1700 ± 10	150	³ BIAGI 81	SPEC	Ξ^- H 100, 135 GeV
1694 ± 6	45	⁴ DIONISI 78	HBC	$K^- p$ 4.2 GeV/c

Baryon Particle Listings

 $\Xi(1690), \Xi(1820)$ $\Xi(1690)$ WIDTHS

MIXED CHARGES

VALUE (MeV)

DOCUMENT ID

20±15 OUR ESTIMATE

 $\Xi(1690)^0$ WIDTH

VALUE (MeV)	EVTS	DOCUMENT ID	TECN	COMMENT
10±6	1400	ADAMOVICH 98	WA89	Σ^- nucleus, 345 GeV/c
44±23	175	¹ DIONISI 78	HBC	$K^- p$ 4.2 GeV/c
20±4	183	² DIONISI 78	HBC	$K^- p$ 4.2 GeV/c

 $\Xi(1690)^-$ WIDTH

VALUE (MeV)	CL%	EVTS	DOCUMENT ID	TECN	COMMENT
<8	90	104	BIAGI 87	SPEC	Ξ^- Be 116 GeV
47±14		150	³ BIAGI 81	SPEC	Ξ^- H 100, 135 GeV
26±6		45	⁴ DIONISI 78	HBC	$K^- p$ 4.2 GeV/c

 $\Xi(1690)$ DECAY MODES

Mode	Fraction (Γ_i/Γ)
$\Gamma_1 \Lambda \bar{K}$	seen
$\Gamma_2 \Sigma \bar{K}$	seen
$\Gamma_3 \Xi \pi$	seen
$\Gamma_4 \Xi^- \pi^+ \pi^0$	
$\Gamma_5 \Xi^- \pi^+ \pi^-$	possibly seen
$\Gamma_6 \Xi(1530)\pi$	

 $\Xi(1690)$ BRANCHING RATIOS

$\Gamma(\Lambda \bar{K})/\Gamma_{\text{total}}$	Γ_1/Γ				
VALUE	EVTS	DOCUMENT ID	TECN	CHG	COMMENT
seen	104	BIAGI 87	SPEC	-	Ξ^- Be 116 GeV

$\Gamma(\Sigma \bar{K})/\Gamma(\Lambda \bar{K})$	Γ_2/Γ_1				
VALUE	EVTS	DOCUMENT ID	TECN	CHG	COMMENT
0.75±0.39	75	ABE 02c	BELL	-	$e^+e^- \approx \tau(4S)$
2.7±0.9		DIONISI 78	HBC	0	$K^- p$ 4.2 GeV/c
3.1±1.4		DIONISI 78	HBC	-	$K^- p$ 4.2 GeV/c

$\Gamma(\Xi \pi)/\Gamma(\Sigma \bar{K})$	Γ_3/Γ_2			
VALUE	DOCUMENT ID	TECN	CHG	COMMENT
<0.09	DIONISI 78	HBC	0	$K^- p$ 4.2 GeV/c

$\Gamma(\Xi \pi)/\Gamma_{\text{total}}$	Γ_3/Γ		
VALUE	DOCUMENT ID	TECN	COMMENT
seen	ADAMOVICH 98	WA89	Σ^- nucleus, 345 GeV/c

$\Gamma(\Xi^- \pi^+ \pi^0)/\Gamma(\Sigma \bar{K})$	Γ_4/Γ_2			
VALUE	DOCUMENT ID	TECN	CHG	COMMENT
<0.04	DIONISI 78	HBC	0	$K^- p$ 4.2 GeV/c

$\Gamma(\Xi^- \pi^+ \pi^-)/\Gamma_{\text{total}}$	Γ_5/Γ				
VALUE	EVTS	DOCUMENT ID	TECN	CHG	COMMENT
possibly seen	4	BIAGI 87	SPEC	-	Ξ^- Be 116 GeV

$\Gamma(\Xi^- \pi^+ \pi^-)/\Gamma(\Sigma \bar{K})$	Γ_5/Γ_2			
VALUE	DOCUMENT ID	TECN	CHG	COMMENT
<0.03	DIONISI 78	HBC	-	$K^- p$ 4.2 GeV/c

$\Gamma(\Xi(1530)\pi)/\Gamma(\Sigma \bar{K})$	Γ_6/Γ_2			
VALUE	DOCUMENT ID	TECN	CHG	COMMENT
<0.06	DIONISI 78	HBC	-	$K^- p$ 4.2 GeV/c

 $\Xi(1690)$ FOOTNOTES

- From a fit to the $\Sigma^+ K^-$ spectrum.
- From a coupled-channel analysis of the $\Sigma^+ K^-$ and $\Lambda \bar{K}^0$ spectra.
- A fit to the inclusive spectrum from $\Xi^- N \rightarrow \Lambda K^- X$.
- From a coupled-channel analysis of the $\Sigma^0 K^-$ and ΛK^- spectra.

 $\Xi(1690)$ REFERENCES

AUBERT	08AK PR D78 034008	B. Aubert <i>et al.</i>	(BABAR Collab.)
ABE	02C PL B524 33	K. Abe <i>et al.</i>	(KEK BELLE Collab.)
ADAMOVICH	98 EPJ C5 621	M.I. Adamovich <i>et al.</i>	(CERN WA89 Collab.)
BIAGI	87 ZPHY C34 15	S.F. Biagi <i>et al.</i>	(BRIS, CERN, GEVA+)
BIAGI	81 ZPHY C9 305	S.F. Biagi <i>et al.</i>	(BRIS, CAVE, GEVA+)
DIONISI	78 PL 80B 145	C. Dionisi <i>et al.</i>	(CERN, AMST, NIJM+)

 $\Xi(1820) 3/2^-$

$$I(J^P) = \frac{1}{2}(\frac{3}{2}^-) \text{ Status: } ***$$

The clearest evidence is an 8-standard-deviation peak in ΛK^- seen by GAY 76C. TEODORO 78 favors $J = 3/2$, but cannot make a parity discrimination. BIAGI 87C is consistent with $J = 3/2$ and favors negative parity for this J value.

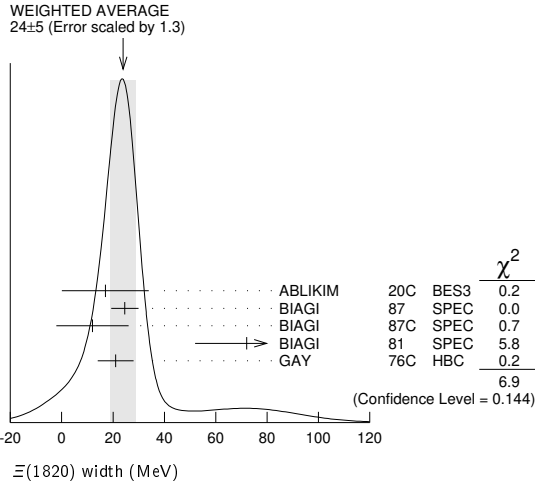
 $\Xi(1820)$ MASS

We only average the measurements that appear to us to be most significant and best determined.

VALUE (MeV)	EVTS	DOCUMENT ID	TECN	CHG	COMMENT
1823 ± 5 OUR ESTIMATE					
1823.5 ± 1.4 OUR AVERAGE					
1825.5 ± 4.7±4.7	288	ABLIKIM 20c	BES3	-	$e^+e^- \rightarrow \Xi(1820)^- \Xi^+$
1819.4 ± 3.1±2.0	280	¹ BIAGI 87	SPEC	0	$\Xi^- \text{Be} \rightarrow (\Lambda K^-) X$
1826 ± 3 ±1	54	BIAGI 87c	SPEC	0	$\Xi^- \text{Be} \rightarrow (\Lambda \bar{K}^0) X$
1822 ± 6		JENKINS 83	MPS	-	$K^- p \rightarrow K^+ (\text{MM})$
1830 ± 6	300	BIAGI 81	SPEC	-	SPS hyperon beam
1823 ± 2	130	GAY 76c	HBC	-	$K^- p$ 4.2 GeV/c
••• We do not use the following data for averages, fits, limits, etc. •••					
1817 ± 3		ADAMOVICH 99b	WA89		Σ^- nucleus, 345 GeV
1797 ±19	74	BRIEFEL 77	HBC	0	$K^- p$ 2.87 GeV/c
1829 ± 9	68	BRIEFEL 77	HBC	-0	$\Xi(1530)\pi$
1860 ±14	39	BRIEFEL 77	HBC	-	$\Sigma^- \bar{K}^0$
1870 ± 9	44	BRIEFEL 77	HBC	0	$\Lambda \bar{K}^0$
1813 ± 4	57	BRIEFEL 77	HBC	-	ΛK^-
1807 ±27		DIBIANCA 75	DBC	-0	$\Xi\pi, \Xi^*\pi$
1762 ± 8	28	² BADIER 72	HBC	-0	$\Xi\pi, \Xi\pi\pi, YK$
1838 ± 5	38	² BADIER 72	HBC	-0	$\Xi\pi, \Xi\pi\pi, YK$
1830 ±10	25	³ CRENNELL 70b	DBC	-0	3.6, 3.9 GeV/c
1826 ±12		⁴ CRENNELL 70b	DBC	-0	3.6, 3.9 GeV/c
1830 ±10	40	ALITTI 69	HBC	-	$\Lambda, \Sigma \bar{K}$
1814 ± 4	30	BADIER 65	HBC	0	$\Lambda \bar{K}^0$
1817 ± 7	29	SMITH 65c	HBC	-0	$\Lambda \bar{K}^0, \Lambda K^-$
1770		HALSTEINSLID63	FBC	-0	K^- freon 3.5 GeV/c

 $\Xi(1820)$ WIDTH

VALUE (MeV)	EVTS	DOCUMENT ID	TECN	CHG	COMMENT
24 +15 -10 OUR ESTIMATE					
24 ± 5 OUR AVERAGE					Error includes scale factor of 1.3. See the ideogram below.
17.0±15.0±7.9	288	ABLIKIM 20c	BES3	-	$e^+e^- \rightarrow \Xi(1820)^- \Xi^+$
24.6±5.3	280	¹ BIAGI 87	SPEC	0	$\Xi^- \text{Be} \rightarrow (\Lambda K^-) X$
12 ±14 ±1.7	54	BIAGI 87c	SPEC	0	$\Xi^- \text{Be} \rightarrow (\Lambda \bar{K}^0) X$
72 ±20	300	BIAGI 81	SPEC	-	SPS hyperon beam
21 ± 7	130	GAY 76c	HBC	-	$K^- p$ 4.2 GeV/c
••• We do not use the following data for averages, fits, limits, etc. •••					
23 ±13		ADAMOVICH 99b	WA89		Σ^- nucleus, 345 GeV
99 ±5.7	74	BRIEFEL 77	HBC	0	$K^- p$ 2.87 GeV/c
52 ±34	68	BRIEFEL 77	HBC	-0	$\Xi(1530)\pi$
72 ±17	39	BRIEFEL 77	HBC	-	$\Sigma^- \bar{K}^0$
44 ±11	44	BRIEFEL 77	HBC	0	$\Lambda \bar{K}^0$
26 ±11	57	BRIEFEL 77	HBC	-	ΛK^-
85 ±5.8		DIBIANCA 75	DBC	-0	$\Xi\pi, \Xi^*\pi$
51 ±13		² BADIER 72	HBC	-0	Lower mass
58 ±13		² BADIER 72	HBC	-0	Higher mass
103 +38 -24		³ CRENNELL 70b	DBC	-0	3.6, 3.9 GeV/c
48 +36 -19		⁴ CRENNELL 70b	DBC	-0	3.6, 3.9 GeV/c
55 +40 -20		ALITTI 69	HBC	-	$\Lambda, \Sigma \bar{K}$
12 ± 4		BADIER 65	HBC	0	$\Lambda \bar{K}^0$
30 ± 7		SMITH 65b	HBC	-0	$\Lambda \bar{K}$
<80		HALSTEINSLID63	FBC	-0	K^- freon 3.5 GeV/c



$\Xi(1820)$ DECAY MODES

Mode	Fraction (Γ_i/Γ)
$\Gamma_1 \Lambda\bar{K}$	large
$\Gamma_2 \Sigma\bar{K}$	small
$\Gamma_3 \Xi\pi$	small
$\Gamma_4 \Xi(1530)\pi$	small
$\Gamma_5 \Xi\pi\pi$ (not $\Xi(1530)\pi$)	

$\Xi(1820)$ BRANCHING RATIOS

The dominant modes seem to be $\Lambda\bar{K}$ and (perhaps) $\Xi(1530)\pi$, but the branching fractions are very poorly determined.

$\Gamma(\Lambda\bar{K})/\Gamma_{total}$	DOCUMENT ID	TECN	CHG	COMMENT	Γ_1/Γ
0.25 ± 0.05 OUR AVERAGE					
0.24 ± 0.05	ANISOVICH 12A	DPWA	—	Multichannel	
0.30 ± 0.15	ALITTI 69	HBC	—	$K^- p$ 3.9–5 GeV/c	

$\Gamma(\Xi\pi)/\Gamma_{total}$	DOCUMENT ID	TECN	CHG	COMMENT	Γ_3/Γ
0.10 ± 0.10					
	ALITTI 69	HBC	—	$K^- p$ 3.9–5 GeV/c	

$\Gamma(\Xi\pi)/\Gamma(\Lambda\bar{K})$	CL%	DOCUMENT ID	TECN	CHG	COMMENT	Γ_3/Γ_1
<0.36	95	GAY 76C	HBC	—	$K^- p$ 4.2 GeV/c	
0.20 ± 0.20		BADIER 65	HBC	0	$K^- p$ 3 GeV/c	

$\Gamma(\Xi\pi)/\Gamma(\Xi(1530)\pi)$	DOCUMENT ID	TECN	CHG	COMMENT	Γ_3/Γ_4
1.5^{+0.6}_{-0.4}	APSELL 70	HBC	0	$K^- p$ 2.87 GeV/c	

$\Gamma(\Sigma\bar{K})/\Gamma_{total}$	DOCUMENT ID	TECN	CHG	COMMENT	Γ_2/Γ
0.30 ± 0.15	ALITTI 69	HBC	—	$K^- p$ 3.9–5 GeV/c	
<0.02	TRIPP 67	RVUE	—	Use SMITH 65c	

$\Gamma(\Sigma\bar{K})/\Gamma(\Lambda\bar{K})$	DOCUMENT ID	TECN	CHG	COMMENT	Γ_2/Γ_1
0.24 ± 0.10	GAY 76C	HBC	—	$K^- p$ 4.2 GeV/c	

$\Gamma(\Xi(1530)\pi)/\Gamma_{total}$	DOCUMENT ID	TECN	CHG	COMMENT	Γ_4/Γ
0.30 ± 0.15	ALITTI 69	HBC	—	$K^- p$ 3.9–5 GeV/c	
seen	ASTON 85B	LASS	—	$K^- p$ 11 GeV/c	
not seen	⁵ HASSALL 81	HBC	—	$K^- p$ 6.5 GeV/c	
<0.25	⁶ DAUBER 69	HBC	—	$K^- p$ 2.7 GeV/c	

$\Gamma(\Xi(1530)\pi)/\Gamma(\Lambda\bar{K})$	DOCUMENT ID	TECN	CHG	COMMENT	Γ_4/Γ_1
0.38 ± 0.27 OUR AVERAGE				Error includes scale factor of 2.3.	
1.0 ± 0.3	GAY 76C	HBC	—	$K^- p$ 4.2 GeV/c	
0.26 ± 0.13	SMITH 65C	HBC	—0	$K^- p$ 2.45–2.7 GeV/c	

$\Gamma(\Xi\pi\pi$ (not $\Xi(1530)\pi$))/ $\Gamma(\Lambda\bar{K})$	DOCUMENT ID	TECN	CHG	COMMENT	Γ_5/Γ_1
0.30 ± 0.20	BIAGI 87	SPEC	—	Ξ^- Be 116 GeV	
<0.14	⁷ BADIER 65	HBC	0	1 st. dev. limit	
>0.1	SMITH 65C	HBC	—0	$K^- p$ 2.45–2.7 GeV/c	

$\Gamma(\Xi\pi\pi$ (not $\Xi(1530)\pi$))/ $\Gamma(\Xi(1530)\pi)$	DOCUMENT ID	TECN	CHG	COMMENT	Γ_5/Γ_4
consistent with zero	GAY 76C	HBC	—	$K^- p$ 4.2 GeV/c	
0.3 ± 0.5	⁸ APSELL 70	HBC	0	$K^- p$ 2.87 GeV/c	

$\Xi(1820)$ FOOTNOTES

- ¹BIAGI 87 also sees weak signals in the in the $\Xi^- \pi^+ \pi^-$ channel at 1782.6 ± 1.4 MeV ($\Gamma = 6.0 \pm 1.5$ MeV) and 1831.9 ± 2.8 MeV ($\Gamma = 9.6 \pm 9.9$ MeV).
- ²BADIER 72 adds all channels and divides the peak into lower and higher mass regions. The data can also be fitted with a single Breit-Wigner of mass 1800 MeV and width 150 MeV.
- ³From a fit to inclusive $\Xi\pi$, $\Xi\pi\pi$, and ΛK^- spectra.
- ⁴From a fit to inclusive $\Xi\pi$ and $\Xi\pi\pi$ spectra only.
- ⁵Including $\Xi\pi\pi$.
- ⁶DAUBER 69 uses in part the same data as SMITH 65c.
- ⁷For the decay mode $\Xi^- \pi^+ \pi^0$ only. This limit includes $\Xi(1530)\pi$.
- ⁸Or less. Upper limit for the 3-body decay.

$\Xi(1820)$ REFERENCES

ABLIKIM 20C	PRL 124 032002	M. Ablikim <i>et al.</i>	(BESIII Collab.)
ANISOVICH 12A	EPJ A48 15	A.V. Anisovich <i>et al.</i>	(BONN, PNPI)
ADAMOVIICH 99B	EPJ C11 271	M.I. Adamovich <i>et al.</i>	(CERN WA89 Collab.)
BIAGI 87	ZPHY C34 15	S.F. Biagi <i>et al.</i>	(BRIS, CERN, GEVA+)
BIAGI 87C	ZPHY C34 175	S.F. Biagi <i>et al.</i>	(BRIS, CERN, GEVA+)
ASTON 85B	PR D32 2270	D. Aston <i>et al.</i>	(SLAC, CARL, CNRC, CINIC)
JENKINS 83	PRL 51 951	C.M. Jenkins <i>et al.</i>	(FSU, BRAN, LBL+)
BIAGI 81	ZPHY C9 305	S.F. Biagi <i>et al.</i>	(BRIS, CAVE, GEVA+)
HASSALL 81	NP B189 397	J.K. Hassall <i>et al.</i>	(CAVE, MSU)
TEODORO 78	PL 77B 451	D. Teodoro <i>et al.</i>	(AMST, CERN, NIJM+)
BRIEFEL 77	PR D16 2706	E. Briefel <i>et al.</i>	(BRAN, UMD, SYRA+)
Also	PRL 23 884	S.P. Apseil <i>et al.</i>	(BRAN, UMD, SYRA+)
GAY 76C	PL 62B 477	J.B. Gay <i>et al.</i>	(AMST, CERN, NIJM) IU
DIBIANCA 75	NP B98 137	F.A. Dibiaccia, R.J. Endorf	(CMU)
BADIER 72	NP B37 429	J. Badier <i>et al.</i>	(EPOL)
APSELL 70	PRL 24 777	S.P. Apseil <i>et al.</i>	(BRAN, UMD, SYRA+)
CRENNELL 70B	PR D1 847	D.J. Crennell <i>et al.</i>	(BNL)
ALITTI 69	PRL 22 79	J. Alitti <i>et al.</i>	(BNL, SYRA) I
DAUBER 69	PR 179 1262	P.M. Dauber <i>et al.</i>	(LRL)
TRIPP 67	NP B3 10	R.D. Tripp <i>et al.</i>	(LRL, SLAC, CERN+)
BADIER 65	PL 16 171	J. Badier <i>et al.</i>	(EPOL, SAFL, AMST) I
SMITH 65B	Athens Conf. 251	G.A. Smith, J.S. Lindsey	(LRL)
SMITH 65C	PRL 14 25	G.A. Smith <i>et al.</i>	(LRL) IUP
HALSTEINSLID 63	Siena Conf. 1 73	A. Halsteinslid <i>et al.</i>	(BERG, CERN, EPOL+)

OTHER RELATED PAPERS

TEODORO 78	PL 77B 451	D. Teodoro <i>et al.</i>	(AMST, CERN, NIJM+)
BRIEFEL 75	PR D12 1859	E. Briefel <i>et al.</i>	(BRAN, UMD, SYRA+)
SCHMIDT 73	Purdue Conf. 363	P.E. Schmidt	(BRAN)
MERRILL 68	PR 167 1202	D.W. Merrill, J. Button-Shafer	(LRL)
SMITH 64	PRL 13 61	G.A. Smith <i>et al.</i>	(LRL) IUP

$\Xi(1950)$

$I(J^P) = \frac{1}{2}(??)$ Status: ***

We list here everything reported between 1875 and 2000 MeV. The accumulated evidence for a Ξ near 1950 MeV seems strong enough to include a $\Xi(1950)$ in the main Baryon Table, but not much can be said about its properties. In fact, there may be more than one Ξ near this mass.

$\Xi(1950)$ MASS

VALUE (MeV)	EVTS	DOCUMENT ID	TECN	COMMENT
1950 ± 15 OUR ESTIMATE				
1955 ± 6		ADAMOVIICH 99B	WA89	Σ^- nucleus, 345 GeV
1944 ± 9	129	BIAGI 87	SPEC	Ξ^- Be $\rightarrow (\Xi^- \pi^+) \pi^- X$
1963 ± 5 ± 2	63	BIAGI 87C	SPEC	Ξ^- Be $\rightarrow (\Lambda\bar{K}^0) X$
1937 ± 7	150	BIAGI 81	SPEC	SPS hyperon beam
1961 ± 18	139	BRIEFEL 77	HBC	$2.87 K^- p \rightarrow \Xi^- \pi^+ X$
1936 ± 22	44	BRIEFEL 77	HBC	$2.87 K^- p \rightarrow \Xi^0 \pi^- X$
1964 ± 10	56	BRIEFEL 77	HBC	$\Xi(1530)\pi$
1900 ± 12		DIBIANCA 75	DBC	$\Xi\pi$
1952 ± 11	25	ROSS 73C		$(\Xi\pi)^-$
1956 ± 6	29	BADIER 72	HBC	$\Xi\pi, \Xi\pi\pi, \Upsilon K$
1955 ± 14	21	GOLDWASSER 70	HBC	$\Xi\pi$
1894 ± 18	66	DAUBER 69	HBC	$\Xi\pi$
1930 ± 20	27	ALITTI 68	HBC	$\Xi^- \pi^+$
1933 ± 16	35	BADIER 65	HBC	$\Xi^- \pi^+$

Baryon Particle Listings

$\Xi(1950), \Xi(2030)$

$\Xi(1950)$ WIDTH

VALUE (MeV)	EVTS	DOCUMENT ID	TECN	COMMENT
60 ± 20 OUR ESTIMATE				
68 ± 22		ADAMOVIICH 99B	WA89	Σ^- nucleus, 345 GeV
100 ± 31	129	BIAGI 87	SPEC	$\Xi^- \text{Be} \rightarrow (\Xi^- \pi^+) \pi^- X$
25 ± 15 ± 1.2	63	BIAGI 87c	SPEC	$\Xi^- \text{Be} \rightarrow (\Lambda \bar{K}^0) X$
60 ± 8	150	BIAGI 81	SPEC	SPS hyperon beam
159 ± 57	139	BRIEFEL 77	HBC	2.87 $K^- p \rightarrow \Xi^- \pi^+ X$
87 ± 26	44	BRIEFEL 77	HBC	2.87 $K^- p \rightarrow \Xi^0 \pi^- X$
60 ± 39	56	BRIEFEL 77	HBC	$\Xi(1530) \pi$
63 ± 78		DIBIANCA 75	DBC	$\Xi \pi$
38 ± 10		ROSS 73c		$(\Xi \pi)^-$
35 ± 11	29	BADIER 72	HBC	$\Xi \pi, \Xi \pi \pi, \Upsilon K$
56 ± 26	21	GOLDWASSER 70	HBC	$\Xi \pi$
98 ± 23	66	DAUBER 69	HBC	$\Xi \pi$
80 ± 40	27	ALITTI 68	HBC	$\Xi^- \pi^+$
140 ± 35	35	BADIER 65	HBC	$\Xi^- \pi^+$

$\Xi(1950)$ DECAY MODES

Mode	Fraction (Γ_i/Γ)
$\Gamma_1 \Lambda \bar{K}$	seen
$\Gamma_2 \Sigma \bar{K}$	possibly seen
$\Gamma_3 \Xi \pi$	seen
$\Gamma_4 \Xi(1530) \pi$	
$\Gamma_5 \Xi \pi \pi$ (not $\Xi(1530) \pi$)	

$\Xi(1950)$ BRANCHING RATIOS

$\Gamma(\Sigma \bar{K})/\Gamma(\Lambda \bar{K})$			Γ_2/Γ_1		
VALUE	CL%	EVTS	DOCUMENT ID	TECN	COMMENT
<2.3	90	0	BIAGI 87c	SPEC	$\Xi^- \text{Be}$ 116 GeV
$\Gamma(\Sigma \bar{K})/\Gamma_{\text{total}}$			Γ_2/Γ		
VALUE	EVTS	DOCUMENT ID	TECN	COMMENT	
possibly seen	17	HASSALL 81	HBC	$K^- p$ 6.5 GeV/c	
$\Gamma(\Xi \pi)/\Gamma(\Xi(1530) \pi)$			Γ_3/Γ_4		
VALUE	DOCUMENT ID	TECN	COMMENT		
2.8 + 0.7 - 0.6	APSELL 70	HBC			
$\Gamma(\Xi \pi \pi \text{ (not } \Xi(1530) \pi))/\Gamma(\Xi(1530) \pi)$			Γ_5/Γ_4		
VALUE	DOCUMENT ID	TECN	COMMENT		
0.0 ± 0.3	APSELL 70	HBC			

$\Xi(1950)$ REFERENCES

ADAMOVIICH 99B	EPJ C11 271	M.I. Adamovich et al.	(CERN WA89 Collab.)
BIAGI 87	ZPHY C34 15	S.F. Biagi et al.	(BRIS, CERN, GEVA+)
BIAGI 87c	ZPHY C34 175	S.F. Biagi et al.	(BRIS, CERN, GEVA+)
BIAGI 81	ZPHY C9 305	S.F. Biagi et al.	(BRIS, CAVE, GEVA+)
HASSALL 81	NP B189 397	J.K. Hassall et al.	(CAVE, MSU)
BRIEFEL 77	PR D16 2706	E. Briefel et al.	(BRAN, UMD, SYRA+)
Also	Duke Conf. 317	E. Briefel et al.	(BRAN, UMD, SYRA+)
Hyperon Resonances, 1970			
DIBIANCA 75	NP B98 137	F.A. Dibianna, R.J. Endorf	(CMU)
ROSS 73c	Purdue Conf. 345	R.T. Ross, J.L. Lloyd, D. Radojicic	(OXF)
BADIER 72	NP B37 429	J. Badier et al.	(EPOL)
APSELL 70	PRL 24 777	S.P. Appell et al.	(BRAN, UMD, SYRA+)
GOLDWASSER 70	PR D1 1960	E.L. Goldwasser, P.F. Schultz	(ILL)
DAUBER 69	PR 179 1262	P.M. Dauber et al.	(LRL)
ALITTI 68	PRL 21 1119	J. Alitti et al.	(BNL, SYRA)
BADIER 65	PL 16 171	J. Badier et al.	(EPOL, SAACL, AMST)

$\Xi(2030)$

$$J(P) = \frac{1}{2} (\geq \frac{5}{2}) \text{ status: } ***$$

The evidence for this state has been much improved by HEMINGWAY 77, who see an eight standard deviation enhancement in $\Sigma \bar{K}$ and a weaker coupling to $\Lambda \bar{K}$. ALITTI 68 and HEMINGWAY 77 observe no signals in the $\Xi \pi \pi$ (or $\Xi(1530) \pi$) channel, in contrast to DIBIANCA 75. The decay $(\Lambda/\Sigma) \bar{K} \pi$ reported by BARTSCH 69 is also not confirmed by HEMINGWAY 77.

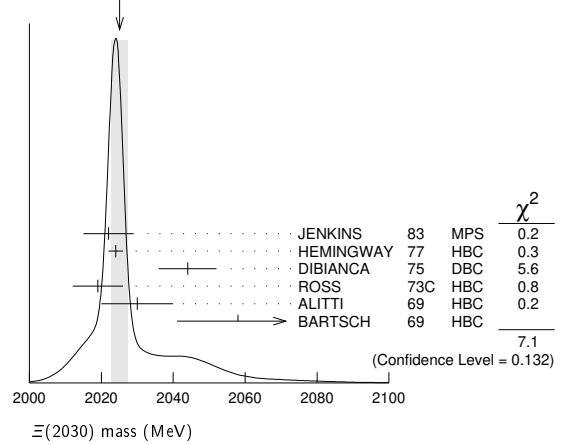
A moments analysis of the HEMINGWAY 77 data indicates at a level of three standard deviations that $J \geq 5/2$.

$\Xi(2030)$ MASS

VALUE (MeV)	EVTS	DOCUMENT ID	TECN	CHG	COMMENT
2025 ± 5 OUR ESTIMATE					
2025.1 ± 2.4 OUR AVERAGE Error includes scale factor of 1.3. See the ideogram below.					
2022 ± 7		JENKINS 83	MPS	-	$K^- p \rightarrow K^+ \text{MM}$
2024 ± 2	200	HEMINGWAY 77	HBC	-	$K^- p$ 4.2 GeV/c
2044 ± 8		DIBIANCA 75	DBC	-0	$\Xi \pi \pi, \Xi^* \pi$

2019 ± 7	15	ROSS 73c	HBC	-0	$\Sigma \bar{K}$
2030 ± 10	42	ALITTI 69	HBC	-	$K^- p$ 3.9-5 GeV/c
2058 ± 17	40	BARTSCH 69	HBC	-0	$K^- p$ 10 GeV/c

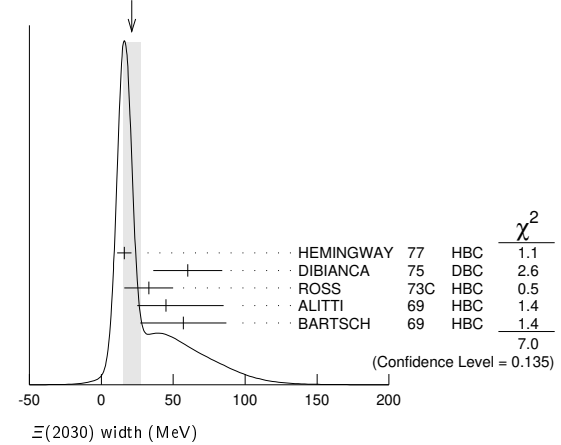
WEIGHTED AVERAGE
2025.1 ± 2.4 (Error scaled by 1.3)



$\Xi(2030)$ WIDTH

VALUE (MeV)	EVTS	DOCUMENT ID	TECN	CHG	COMMENT
20 ± 15 OUR ESTIMATE					
21 ± 6 OUR AVERAGE Error includes scale factor of 1.3. See the ideogram below.					
16 ± 5	200	HEMINGWAY 77	HBC	-	$K^- p$ 4.2 GeV/c
60 ± 24		DIBIANCA 75	DBC	-0	$\Xi \pi \pi, \Xi^* \pi$
33 ± 17	15	ROSS 73c	HBC	-0	$\Sigma \bar{K}$
45 + 40 - 20		ALITTI 69	HBC	-	$K^- p$ 3.9-5 GeV/c
57 ± 30		BARTSCH 69	HBC	-0	$K^- p$ 10 GeV/c

WEIGHTED AVERAGE
21 ± 6 (Error scaled by 1.3)



$\Xi(2030)$ DECAY MODES

Mode	Fraction (Γ_i/Γ)
$\Gamma_1 \Lambda \bar{K}$	~ 20 %
$\Gamma_2 \Sigma \bar{K}$	~ 80 %
$\Gamma_3 \Xi \pi$	small
$\Gamma_4 \Xi(1530) \pi$	small
$\Gamma_5 \Xi \pi \pi$ (not $\Xi(1530) \pi$)	small
$\Gamma_6 \Lambda \bar{K} \pi$	small
$\Gamma_7 \Sigma \bar{K} \pi$	small

$\Xi(2030)$ BRANCHING RATIOS

$\Gamma(\Xi \pi)/[\Gamma(\Lambda \bar{K}) + \Gamma(\Sigma \bar{K}) + \Gamma(\Xi \pi) + \Gamma(\Xi(1530) \pi)]$		$\Gamma_3/(\Gamma_1 + \Gamma_2 + \Gamma_3 + \Gamma_4)$		
VALUE	DOCUMENT ID	TECN	CHG	COMMENT
<0.30	ALITTI 69	HBC	-	1 standard dev. limit

••• We do not use the following data for averages, fits, limits, etc. •••

See key on page 1127

Baryon Particle Listings

$\Xi(2030)$, $\Xi(2120)$, $\Xi(2250)$, $\Xi(2370)$

$\Gamma(\Xi\pi)/\Gamma(\Sigma\bar{K})$		Γ_3/Γ_2	
VALUE	CL%	DOCUMENT ID	TECN
<0.19	95	HEMINGWAY 77	HBC

$\Gamma(\Lambda\bar{K})/[\Gamma(\Lambda\bar{K}) + \Gamma(\Sigma\bar{K}) + \Gamma(\Xi\pi) + \Gamma(\Xi(1530)\pi)]$		$\Gamma_1/(\Gamma_1 + \Gamma_2 + \Gamma_3 + \Gamma_4)$	
VALUE	CL%	DOCUMENT ID	TECN
0.25 ± 0.15		ALITTI 69	HBC

$\Gamma(\Lambda\bar{K})/\Gamma(\Sigma\bar{K})$		Γ_1/Γ_2	
VALUE	CL%	DOCUMENT ID	TECN
0.22 ± 0.09		HEMINGWAY 77	HBC

$\Gamma(\Sigma\bar{K})/[\Gamma(\Lambda\bar{K}) + \Gamma(\Sigma\bar{K}) + \Gamma(\Xi\pi) + \Gamma(\Xi(1530)\pi)]$		$\Gamma_2/(\Gamma_1 + \Gamma_2 + \Gamma_3 + \Gamma_4)$	
VALUE	CL%	DOCUMENT ID	TECN
0.75 ± 0.20		ALITTI 69	HBC

$\Gamma(\Xi(1530)\pi)/[\Gamma(\Lambda\bar{K}) + \Gamma(\Sigma\bar{K}) + \Gamma(\Xi\pi) + \Gamma(\Xi(1530)\pi)]$		$\Gamma_4/(\Gamma_1 + \Gamma_2 + \Gamma_3 + \Gamma_4)$	
VALUE	CL%	DOCUMENT ID	TECN
<0.15		ALITTI 69	HBC

• • • We do not use the following data for averages, fits, limits, etc. • • •

$[\Gamma(\Xi(1530)\pi) + \Gamma(\Xi\pi(\text{not } \Xi(1530)\pi))]/\Gamma(\Sigma\bar{K})$		$(\Gamma_4 + \Gamma_5)/\Gamma_2$	
VALUE	CL%	DOCUMENT ID	TECN
<0.11	95	1 HEMINGWAY 77	HBC

$\Gamma(\Lambda\bar{K}\pi)/\Gamma_{\text{total}}$		Γ_6/Γ	
VALUE	CL%	DOCUMENT ID	TECN
<0.32	95	HEMINGWAY 77	HBC

• • • We do not use the following data for averages, fits, limits, etc. • • •

$\Gamma(\Lambda\bar{K}\pi)/\Gamma(\Sigma\bar{K})$		Γ_6/Γ_2	
VALUE	CL%	DOCUMENT ID	TECN
<0.32	95	HEMINGWAY 77	HBC

$\Gamma(\Sigma\bar{K}\pi)/\Gamma_{\text{total}}$		Γ_7/Γ	
VALUE	CL%	DOCUMENT ID	TECN
<0.04	95	2 HEMINGWAY 77	HBC

• • • We do not use the following data for averages, fits, limits, etc. • • •

$\Gamma(\Sigma\bar{K}\pi)/\Gamma(\Sigma\bar{K})$		Γ_7/Γ_2	
VALUE	CL%	DOCUMENT ID	TECN
<0.04	95	2 HEMINGWAY 77	HBC

 $\Xi(2030)$ FOOTNOTES

- ¹ For the decay mode $\Xi^- \pi^+ \pi^-$ only.
² For the decay mode $\Sigma^\pm K^- \pi^\mp$ only.

 $\Xi(2030)$ REFERENCES

JENKINS 83	PRL 51 951	C.M. Jenkins <i>et al.</i>	(FSU, BRAN, LBL+)
HEMINGWAY 77	PL 68B 197	R.J. Hemingway <i>et al.</i>	(AMST, CERN, NIJM+)
	Also PL 62B 477	J.B. Gay <i>et al.</i>	(AMST, CERN, NIJM)
DIBIANCA 75	NP B30 137	F.A. Dibanca, R.J. Endorf	(CMU)
ROSS 73C	Purdue Conf. 345	R.T. Ross, J.L. Lloyd, D. Radojicic	(OXF)
ALITTI 69	PRL 22 79	J. Alitti <i>et al.</i>	(BNL, SYRA)
BARTSCH 69	PL 28B 439	J. Bartsch <i>et al.</i>	(AACH, BERL, CERN+)
ALITTI 68	PRL 21 1119	J. Alitti <i>et al.</i>	(BNL, SYRA)

 $\Xi(2120)$

$$I(J^P) = \frac{1}{2}(?)^? \text{ Status: } * * \\ J, P \text{ need confirmation.}$$

OMITTED FROM SUMMARY TABLE

 $\Xi(2120)$ MASS

VALUE (MeV)	EVTS	DOCUMENT ID	TECN	COMMENT
≈ 2120 OUR ESTIMATE				
2137 ± 4	18	1 CHLIAPNIK... 79	HBC	$K^+ p$ 32 GeV/c
2123 ± 7		2 GAY 76c	HBC	$K^- p$ 4.2 GeV/c

 $\Xi(2120)$ WIDTH

VALUE (MeV)	EVTS	DOCUMENT ID	TECN	COMMENT
<20	18	1 CHLIAPNIK... 79	HBC	$K^+ p$ 32 GeV/c
25 ± 12		2 GAY 76c	HBC	$K^- p$ 4.2 GeV/c

 $\Xi(2120)$ DECAY MODES

Mode	Fraction (Γ_j/Γ)
Γ_1 $\Lambda\bar{K}$	seen

 $\Xi(2120)$ BRANCHING RATIOS

$\Gamma(\Lambda\bar{K})/\Gamma_{\text{total}}$		Γ_1/Γ	
VALUE	CL%	DOCUMENT ID	TECN
seen		1 CHLIAPNIK... 79	HBC
seen		2 GAY 76c	HBC

 $\Xi(2120)$ FOOTNOTES

- ¹ CHLIAPNIKOV 79 does not uniquely identify the K^+ in the $(\Lambda\bar{K}^+) X$ final state. It also reports bumps with fewer events at 2240, 2540, and 2830 MeV.
² GAY 76c sees a 4-standard deviation signal. However, HEMINGWAY 77, with more events from the same experiment points out that the signal is greatly reduced if a cut is made on the 4-momentum u . This suggests an anomalous production mechanism if the $\Xi(2120)$ is real.

 $\Xi(2120)$ REFERENCES

CHLIAPNIK... 79	NP B158 253	P.V. Chliapnikov <i>et al.</i>	(CERN, BELG, MONS)
HEMINGWAY 77	PL 68B 197	R.J. Hemingway <i>et al.</i>	(AMST, CERN, NIJM+)
GAY 76c	PL 62B 477	J.B. Gay <i>et al.</i>	(AMST, CERN, NIJM)

 $\Xi(2250)$

$$I(J^P) = \frac{1}{2}(?)^? \text{ Status: } * * \\ J, P \text{ need confirmation.}$$

OMITTED FROM SUMMARY TABLE

The evidence for this state is mixed. BARTSCH 69 sees a bump of not much statistical significance in $\Lambda\bar{K}\pi$, $\Sigma\bar{K}\pi$, and $\Xi\pi\pi$ mass spectra. GOLDWASSER 70 sees a narrower bump in $\Xi\pi\pi$ at a higher mass. Not seen by HASSALL 81 with 45 events/ μb at 6.5 GeV/c. Seen by JENKINS 83. Perhaps seen by BIAGI 87.

 $\Xi(2250)$ MASS

VALUE (MeV)	EVTS	DOCUMENT ID	TECN	CHG	COMMENT
≈ 2250 OUR ESTIMATE					
2189 ± 7	66	BIAGI 87	SPEC	—	$\Xi^- \text{Be} \rightarrow (\Xi^- \pi^+ \pi^-) X$
2214 ± 5		JENKINS 83	MPS	—	$K^- p \rightarrow K^+ \text{MM}$
2295 ± 15	18	GOLDWASSER 70	HBC	—	$K^- p$ 5.5 GeV/c
2244 ± 52	35	BARTSCH 69	HBC	—	$K^- p$ 10 GeV/c

 $\Xi(2250)$ WIDTH

VALUE (MeV)	EVTS	DOCUMENT ID	TECN	CHG	COMMENT
46 ± 27	66	BIAGI 87	SPEC	—	$\Xi^- \text{Be} \rightarrow (\Xi^- \pi^+ \pi^-) X$
< 30		GOLDWASSER 70	HBC	—	$K^- p$ 5.5 GeV/c
130 ± 80		BARTSCH 69	HBC	—	

 $\Xi(2250)$ DECAY MODES

Mode	Fraction (Γ_j/Γ)
Γ_1 $\Xi\pi\pi$	
Γ_2 $\Lambda\bar{K}\pi$	
Γ_3 $\Sigma\bar{K}\pi$	

 $\Xi(2250)$ REFERENCES

BIAGI 87	ZPHY C34 15	S.F. Biagi <i>et al.</i>	(BRIS, CERN, GEVA+)
JENKINS 83	PRL 51 951	C.M. Jenkins <i>et al.</i>	(FSU, BRAN, LBL+)
HASSALL 81	NP B189 397	J.K. Hassall <i>et al.</i>	(CAVE, MSU)
GOLDWASSER 70	PR D1 1960	E.L. Goldwasser, P.F. Schultz	(ILL)
BARTSCH 69	PL 28B 439	J. Bartsch <i>et al.</i>	(AACH, BERL, CERN+)

 $\Xi(2370)$

$$I(J^P) = \frac{1}{2}(?)^? \text{ Status: } * * \\ J, P \text{ need confirmation.}$$

OMITTED FROM SUMMARY TABLE

 $\Xi(2370)$ MASS

VALUE (MeV)	EVTS	DOCUMENT ID	TECN	CHG	COMMENT
≈ 2370 OUR ESTIMATE					
2356 ± 10		JENKINS 83	MPS	—	$K^- p \rightarrow K^+ \text{MM}$
2370	50	HASSALL 81	HBC	—	$K^- p$ 6.5 GeV/c
2373 ± 8	94	AMIRZADEH 80	HBC	—	$K^- p$ 8.25 GeV/c
2392 ± 27		DIBIANCA 75	DBC	—	$\Xi\pi\pi$

 $\Xi(2370)$ WIDTH

VALUE (MeV)	EVTS	DOCUMENT ID	TECN	CHG	COMMENT
80	50	HASSALL 81	HBC	—	$K^- p$ 6.5 GeV/c
80 ± 25	94	AMIRZADEH 80	HBC	—	$K^- p$ 8.25 GeV/c
75 ± 69		DIBIANCA 75	DBC	—	$\Xi\pi\pi$

Baryon Particle Listings

 $\Xi(2370)$, $\Xi(2500)$ $\Xi(2370)$ DECAY MODES

Mode	Fraction (Γ_i/Γ)
Γ_1 $\Lambda\bar{K}\pi$ Includes $\Gamma_4 + \Gamma_6$.	seen
Γ_2 $\Sigma\bar{K}\pi$ Includes $\Gamma_5 + \Gamma_6$.	seen
Γ_3 Ω^-K	
Γ_4 $\Lambda\bar{K}^*(892)$	
Γ_5 $\Sigma\bar{K}^*(892)$	
Γ_6 $\Sigma(1385)\bar{K}$	

 $\Xi(2370)$ BRANCHING RATIOS

$\Gamma(\Lambda\bar{K}\pi)/\Gamma_{\text{total}}$					Γ_1/Γ
VALUE	DOCUMENT ID	TECN	CHG	COMMENT	
seen	AMIRZADEH 80	HBC	-0	K^-p 8.25 GeV/c	
$\Gamma(\Sigma\bar{K}\pi)/\Gamma_{\text{total}}$					Γ_2/Γ
VALUE	DOCUMENT ID	TECN	CHG	COMMENT	
seen	AMIRZADEH 80	HBC	-0	K^-p 8.25 GeV/c	
$[\Gamma(\Lambda\bar{K}\pi) + \Gamma(\Sigma\bar{K}\pi)]/\Gamma_{\text{total}}$					$(\Gamma_1+\Gamma_2)/\Gamma$
VALUE	EVTS	DOCUMENT ID	TECN	CHG	COMMENT
seen	50	HASSALL 81	HBC	-0	K^-p 6.5 GeV/c
$\Gamma(\Omega^-K)/\Gamma_{\text{total}}$					Γ_3/Γ
VALUE	DOCUMENT ID	TECN	CHG	COMMENT	
0.09±0.04	¹ KINSON 80	HBC	-	K^-p 8.25 GeV/c	
$[\Gamma(\Lambda\bar{K}^*(892)) + \Gamma(\Sigma\bar{K}^*(892))]/\Gamma_{\text{total}}$					$(\Gamma_4+\Gamma_5)/\Gamma$
VALUE	DOCUMENT ID	TECN	CHG	COMMENT	
0.22±0.13	¹ KINSON 80	HBC	-	K^-p 8.25 GeV/c	
$\Gamma(\Sigma(1385)\bar{K})/\Gamma_{\text{total}}$					Γ_6/Γ
VALUE	DOCUMENT ID	TECN	CHG	COMMENT	
0.12±0.08	¹ KINSON 80	HBC	-	K^-p 8.25 GeV/c	

 $\Xi(2370)$ FOOTNOTES

vglue.lin

¹ KINSON 80 is a reanalysis of AMIRZADEH 80 with 50% more events. $\Xi(2370)$ REFERENCES

JENKINS 83	PRL 51 951	C.M. Jenkins et al.	(FSU, BRAN, LBL+)
HASSALL 81	NP B189 397	J.K. Hassall et al.	(CAVE, MSU)
AMIRZADEH 80	PL 90B 324	J. Amirzadeh et al.	(BIRM, CERN, GLAS+) ¹
KINSON 80	Toronto Conf. 263	J.B. Kinson et al.	(BIRM, CERN, GLAS+) ¹
DIBIANCA 75	NP B98 137	F.A. Dibianca, R.J. Endorf	(CMU)

 $\Xi(2500)$
 $I(J^P) = \frac{1}{2}(?)^?$ Status: *
 J, P need confirmation.

OMITTED FROM SUMMARY TABLE

The ALITTI 69 peak might be instead the $\Xi(2370)$ or might be neither the $\Xi(2370)$ nor the $\Xi(2500)$. $\Xi(2500)$ MASS

VALUE (MeV)	EVTS	DOCUMENT ID	TECN	CHG	COMMENT
≈ 2500 OUR ESTIMATE					
2505±10		JENKINS 83	MPS	-	$K^-p \rightarrow K^+$ MM
2430±20	30	ALITTI 69	HBC	-	K^-p 4.6-5 GeV/c
2500±10	45	BARTSCH 69	HBC	-0	K^-p 10 GeV/c

 $\Xi(2500)$ WIDTH

VALUE (MeV)	DOCUMENT ID	TECN	CHG
150 ⁺⁶⁰ ₋₄₀	ALITTI 69	HBC	-
59±27	BARTSCH 69	HBC	-0

 $\Xi(2500)$ DECAY MODES

Mode	Fraction (Γ_i/Γ)
Γ_1 $\Xi\pi$	
Γ_2 $\Lambda\bar{K}$	
Γ_3 $\Sigma\bar{K}$	
Γ_4 $\Xi\pi\pi$	seen
Γ_5 $\Xi(1530)\pi$	
Γ_6 $\Lambda\bar{K}\pi + \Sigma\bar{K}\pi$	seen

 $\Xi(2500)$ BRANCHING RATIOS

$\Gamma(\Xi\pi)/[\Gamma(\Xi\pi) + \Gamma(\Lambda\bar{K}) + \Gamma(\Sigma\bar{K}) + \Gamma(\Xi(1530)\pi)]$					$\Gamma_1/(\Gamma_1+\Gamma_2+\Gamma_3+\Gamma_5)$
VALUE	DOCUMENT ID	TECN	CHG	COMMENT	
<0.5	ALITTI 69	HBC	-	1 standard dev. limit	
$\Gamma(\Lambda\bar{K})/[\Gamma(\Xi\pi) + \Gamma(\Lambda\bar{K}) + \Gamma(\Sigma\bar{K}) + \Gamma(\Xi(1530)\pi)]$					$\Gamma_2/(\Gamma_1+\Gamma_2+\Gamma_3+\Gamma_5)$
VALUE	DOCUMENT ID	TECN	CHG	COMMENT	
0.5±0.2	ALITTI 69	HBC	-		
$\Gamma(\Sigma\bar{K})/[\Gamma(\Xi\pi) + \Gamma(\Lambda\bar{K}) + \Gamma(\Sigma\bar{K}) + \Gamma(\Xi(1530)\pi)]$					$\Gamma_3/(\Gamma_1+\Gamma_2+\Gamma_3+\Gamma_5)$
VALUE	DOCUMENT ID	TECN	CHG	COMMENT	
0.5±0.2	ALITTI 69	HBC	-		
$\Gamma(\Xi(1530)\pi)/[\Gamma(\Xi\pi) + \Gamma(\Lambda\bar{K}) + \Gamma(\Sigma\bar{K}) + \Gamma(\Xi(1530)\pi)]$					$\Gamma_5/(\Gamma_1+\Gamma_2+\Gamma_3+\Gamma_5)$
VALUE	DOCUMENT ID	TECN	CHG	COMMENT	
<0.2	ALITTI 69	HBC	-	1 standard dev. limit	
$\Gamma(\Xi\pi\pi)/\Gamma_{\text{total}}$					Γ_4/Γ
VALUE	DOCUMENT ID	TECN	CHG	COMMENT	
seen	BARTSCH 69	HBC	-0		
$[\Gamma(\Lambda\bar{K}\pi) + \Gamma(\Sigma\bar{K}\pi)]/\Gamma_{\text{total}}$					Γ_6/Γ
VALUE	DOCUMENT ID	TECN	CHG	COMMENT	
seen	BARTSCH 69	HBC	-0		

 $\Xi(2500)$ REFERENCES

JENKINS 83	PRL 51 951	C.M. Jenkins et al.	(FSU, BRAN, LBL+)
ALITTI 69	PRL 22 79	J. Alitti et al.	(BNL, SYRA) ¹
BARTSCH 69	PL 28B 439	J. Bartsch et al.	(AACH, BERL, CERN+)

Ω BARYONS

($S = -3, I = 0$)

$\Omega^- = sss$



$I(J^P) = 0(\frac{3}{2}^+)$ Status: * * * *

The unambiguous discovery in both production and decay was by BARNES 64. The quantum numbers follow from the assignment of the particle to the baryon decuplet. DEUTSCHMANN 78 and BAUBILLIER 78 rule out $J = 1/2$ and find consistency with $J = 3/2$. AUBERT, BE 06 finds from the decay angular distributions of $\Xi_c^0 \rightarrow \Omega^- K^+$ and $\Omega_c^0 \rightarrow \Omega^- K^+$ that $J = 3/2$; this depends on the spins of the Ξ_c^0 and Ω_c^0 being $J = 1/2$, their supposed values. ABLIKIM 21E determines the Ω^- spin to be $J = 3/2$ from the decay angular distributions of the complete decay chain $\psi(3686) \rightarrow \Omega^- \bar{\Omega}^+$, with subsequent decays $\Omega^- \rightarrow K^- \Lambda$ and $\bar{\Omega}^+ \rightarrow K^+ \bar{\Lambda}$. We have omitted some results that have been superseded by later experiments. See our earlier editions.

Ω^- MASS

The fit assumes the Ω^- and $\bar{\Omega}^+$ masses are the same, and averages them together.

VALUE (MeV)	EVTS	DOCUMENT ID	TECN	COMMENT
1672.45 ± 0.29 OUR FIT				
1672.43 ± 0.32 OUR AVERAGE				
1673 ± 1	100	HARTOUNI 85	SPEC	80–280 GeV $K_L^0 C$
1673.0 ± 0.8	41	BAUBILLIER 78	HBC	8.25 GeV/c $K^- p$
1671.7 ± 0.6	27	HEMINGWAY 78	HBC	4.2 GeV/c $K^- p$
1673.4 ± 1.7	4	¹ DIBIANCA 75	DBC	4.9 GeV/c $K^- d$
1673.3 ± 1.0	3	PALMER 68	HBC	$K^- p$ 4.6, 5 GeV/c
1671.8 ± 0.8	3	SCHULTZ 68	HBC	$K^- p$ 5.5 GeV/c
1674.2 ± 1.6	5	SCOTTER 68	HBC	$K^- p$ 6 GeV/c
1672.1 ± 1.0	1	² FRY 55	EMUL	
• • • We do not use the following data for averages, fits, limits, etc. • • •				
1671.43 ± 0.78	13	³ DEUTSCH... 73	HBC	$K^- p$ 10 GeV/c
1671.9 ± 1.2	6	³ SPETH 69	HBC	See DEUTSCHMANN 73
1673.0 ± 0.8	1	ABRAMS 64	HBC	$\rightarrow \Xi^- \pi^0$
1670.6 ± 1.0	1	² FRY 55B	EMUL	
1675	1	⁴ EISENBERG 54	EMUL	

¹DIBIANCA 75 gives a mass for each event. We quote the average.
²The FRY 55 and FRY 55B events were identified as Ω^- by ALVAREZ 73. The masses assume decay to ΛK^- at rest. For FRY 55B, decay from an atomic orbit could Doppler shift the K^- energy and the resulting Ω^- mass by several MeV. This shift is negligible for FRY 55 because the Ω decay is approximately perpendicular to its orbital velocity, as is known because the Λ strikes the nucleus (L. Alvarez, private communication 1973). We have calculated the error assuming that the orbital n is 4 or larger.
³Excluded from the average; the Ω^- lifetimes measured by the experiments differ significantly from other measurements.
⁴The EISENBERG 54 mass was calculated for decay in flight. ALVAREZ 73 has shown that the Ω interacted with an Ag nucleus to give $K^- \Xi Ag$.

$\bar{\Omega}^+$ MASS

The fit assumes the Ω^- and $\bar{\Omega}^+$ masses are the same, and averages them together.

VALUE (MeV)	EVTS	DOCUMENT ID	TECN	COMMENT
1672.45 ± 0.29 OUR FIT				
1672.5 ± 0.7 OUR AVERAGE				
1672 ± 1	72	HARTOUNI 85	SPEC	80–280 GeV $K_L^0 C$
1673.1 ± 1.0	1	FIRESTONE 71B	HBC	12 GeV/c $K^+ d$

$(m_{\Omega^-} - m_{\bar{\Omega}^+}) / m_{\Omega^-}$

A test of CPT invariance.

VALUE	DOCUMENT ID	TECN	COMMENT
$(-1.44 \pm 7.98) \times 10^{-5}$	CHAN 98	E756	p Be, 800 GeV

Ω^- MEAN LIFE

Measurements with an error $> 0.1 \times 10^{-10}$ s have been omitted. The fit assumes the Ω^- and $\bar{\Omega}^+$ mean lives are the same, and averages them together.

VALUE (10^{-10} s)	EVTS	DOCUMENT ID	TECN	COMMENT
0.821 ± 0.011 OUR FIT				
0.821 ± 0.011 OUR AVERAGE				
0.817 ± 0.013 ± 0.018	6934	CHAN	98 E756	p Be, 800 GeV
0.811 ± 0.037	1096	LUK	88 SPEC	p Be 400 GeV
0.823 ± 0.013	12k	BOURQUIN 84	SPEC	SPS hyperon beam

• • • We do not use the following data for averages, fits, limits, etc. • • •
 0.822 ± 0.028 2437 BOURQUIN 79B SPEC See BOURQUIN 84

$\bar{\Omega}^+$ MEAN LIFE

The fit assumes the Ω^- and $\bar{\Omega}^+$ mean lives are the same, and averages them together.

VALUE (10^{-10} s)	EVTS	DOCUMENT ID	TECN	COMMENT
0.821 ± 0.011 OUR FIT				
0.823 ± 0.031 ± 0.022	1801	CHAN	98 E756	p Be, 800 GeV

$(\tau_{\Omega^-} - \tau_{\bar{\Omega}^+}) / \tau_{\Omega^-}$

A test of CPT invariance. Our calculation, from the averages in the preceding two data blocks.

VALUE	DOCUMENT ID
0.00 ± 0.05 OUR ESTIMATE	

Ω^- MAGNETIC MOMENT

VALUE (μ_N)	EVTS	DOCUMENT ID	TECN	COMMENT
-2.02 ± 0.05 OUR AVERAGE				
-2.024 ± 0.056	235k	WALLACE 95	SPEC	Ω^- 300–550 GeV
-1.94 ± 0.17 ± 0.14	25k	DIEHL 91	SPEC	Spin-transfer production

Ω^- DECAY MODES

Mode	Fraction (Γ_i/Γ)	Confidence level
$\Gamma_1 \Lambda K^-$	(67.8 ± 0.7) %	
$\Gamma_2 \Xi^0 \pi^-$	(23.6 ± 0.7) %	
$\Gamma_3 \Xi^- \pi^0$	(8.6 ± 0.4) %	
$\Gamma_4 \Xi^- \pi^+ \pi^-$	$(3.7^{+0.7}_{-0.6}) \times 10^{-4}$	
$\Gamma_5 \Xi(1530)^0 \pi^-$	$< 7 \times 10^{-5}$	90%
$\Gamma_6 \Xi^0 e^- \bar{\nu}_e$	$(5.6 \pm 2.8) \times 10^{-3}$	
$\Gamma_7 \Xi^- \gamma$	$< 4.6 \times 10^{-4}$	90%

$\Delta S = 2$ forbidden (S_2) modes

$\Gamma_8 \Lambda \pi^-$	S_2	$< 2.9 \times 10^{-6}$	90%
--------------------------	-------	------------------------	-----

Ω^- BRANCHING RATIOS

The BOURQUIN 84 values (which include results of BOURQUIN 79B, a separate experiment) are much more accurate than any other results, and so the other results have been omitted.

$\Gamma(\Lambda K^-)/\Gamma_{total}$	EVTS	DOCUMENT ID	TECN	COMMENT	Γ_1/Γ
0.678 ± 0.007	14k	BOURQUIN 84	SPEC	SPS hyperon beam	
0.686 ± 0.013	1920	BOURQUIN 79B	SPEC	See BOURQUIN 84	

• • • We do not use the following data for averages, fits, limits, etc. • • •

$\Gamma(\Xi^0 \pi^-)/\Gamma_{total}$	EVTS	DOCUMENT ID	TECN	COMMENT	Γ_2/Γ
0.236 ± 0.007	1947	BOURQUIN 84	SPEC	SPS hyperon beam	
0.234 ± 0.013	317	BOURQUIN 79B	SPEC	See BOURQUIN 84	

• • • We do not use the following data for averages, fits, limits, etc. • • •

$\Gamma(\Xi^- \pi^0)/\Gamma_{total}$	EVTS	DOCUMENT ID	TECN	COMMENT	Γ_3/Γ
0.086 ± 0.004	759	BOURQUIN 84	SPEC	SPS hyperon beam	
0.080 ± 0.008	145	BOURQUIN 79B	SPEC	See BOURQUIN 84	

• • • We do not use the following data for averages, fits, limits, etc. • • •

$\Gamma(\Xi^- \pi^+ \pi^-)/\Gamma_{total}$	EVTS	DOCUMENT ID	TECN	COMMENT	Γ_4/Γ
$3.74^{+0.67}_{-0.56}$	100	⁵ KAMAEV 10	HYCP	p Cu, 800 GeV	
4.3 $^{+3.4}_{-1.3}$	4	BOURQUIN 84	SPEC	SPS hyperon beam	

• • • We do not use the following data for averages, fits, limits, etc. • • •

⁵This KAMAEV 10 value uses 76 $\Omega^- \rightarrow \Xi^- \pi^+ \pi^-$ and 24 $\bar{\Omega}^+ \rightarrow \Xi^+ \pi^- \pi^+$ decays. The Ω^- and $\bar{\Omega}^+$ branching fractions measurements are statistically equal. The errors given combine statistical and systematic contributions. The CP branching-fraction asymmetry, $(\Omega^- - \bar{\Omega}^+)/\text{sum}$, is $+0.12 \pm 0.20$.

$\Gamma(\Xi(1530)^0 \pi^-)/\Gamma_{total}$	CL%	EVTS	DOCUMENT ID	TECN	COMMENT	Γ_5/Γ
< 0.7	90		KAMAEV 10	HYCP	p Cu, 800 GeV	

Baryon Particle Listings

 $\Omega^-, \Omega(2012)^-$

••• We do not use the following data for averages, fits, limits, etc. •••

$6.4^{+5.1}_{-2.0}$ 4 ⁶ BOURQUIN 84 SPEC SPS hyperon beam

⁶The same 4 events as in the previous mode, with the isospin factor to take into account $\Xi(1530)^0 \rightarrow \Xi^0 \pi^0$ decays included. BOURQUIN 84 adopted a theoretical assumption that $\Xi(1530)^0 \pi^-$ would dominate $\Xi^- \pi^+ \pi^-$ decay.

$\Gamma(\Xi^0 e^- \nu_e)/\Gamma_{\text{total}}$ Γ_6/Γ

VALUE (units 10^{-3})	EVTS	DOCUMENT ID	TECN	COMMENT
5.6 ± 2.8	14	BOURQUIN 84	SPEC	SPS hyperon beam

••• We do not use the following data for averages, fits, limits, etc. •••

~ 10 3 BOURQUIN 79B SPEC See BOURQUIN 84

$\Gamma(\Xi^- \gamma)/\Gamma_{\text{total}}$ Γ_7/Γ

VALUE (units 10^{-4})	CL%	EVTS	DOCUMENT ID	TECN	COMMENT
< 4.6	90	0	ALBUQUERQ..94	E761	Ω^- 375 GeV

••• We do not use the following data for averages, fits, limits, etc. •••

< 22 90 9 BOURQUIN 84 SPEC SPS hyperon beam

< 31 90 0 BOURQUIN 79B SPEC See BOURQUIN 84

$\Gamma(\Lambda \pi^-)/\Gamma_{\text{total}}$ Γ_8/Γ

$\Delta S=2$. Forbidden in first-order weak interaction.

VALUE (units 10^{-6})	CL%	DOCUMENT ID	TECN	COMMENT
< 2.9	90	WHITE 05	HYCP	p Cu, 800 GeV

••• We do not use the following data for averages, fits, limits, etc. •••

< 190 90 BOURQUIN 84 SPEC SPS hyperon beam

< 1300 90 BOURQUIN 79B SPEC See BOURQUIN 84

 Ω^- DECAY PARAMETERS

$\alpha(\Omega^-) \alpha_-(\Lambda)$ FOR $\Omega^- \rightarrow \Lambda K^-$

Some early results have been omitted.

VALUE	EVTS	DOCUMENT ID	TECN	COMMENT
0.0115 ± 0.0015	OUR AVERAGE			
$0.0133 \pm 0.0033 \pm 0.0052$	960k	⁷ CHEN 05	HYCP	p Cu, 800 GeV
$0.0114 \pm 0.0012 \pm 0.0010$	4.5M	⁷ LU 05A	HYCP	p Cu, 800 GeV

••• We do not use the following data for averages, fits, limits, etc. •••

-0.018 ± 0.030 6953 CHAN 98 E756 p Be, 800 GeV

-0.022 ± 0.051 1743 LUK 88 SPEC p Be 400 GeV

-0.016 ± 0.018 12k BOURQUIN 84 SPEC SPS hyperon beam

⁷The results of CHEN 05 and LU 05A are from different experimental runs.

α FOR $\Omega^- \rightarrow \Lambda K^-$

The above average, $\alpha(\Omega^-) \alpha_-(\Lambda) = 0.0115 \pm 0.0015$, divided by our current average

$\alpha_-(\Lambda) = 0.732 \pm 0.014$ gives $\alpha(\Omega^-)$:

VALUE	DOCUMENT ID
0.0157 ± 0.0021	OUR EVALUATION

$\bar{\alpha}$ FOR $\bar{\Omega}^+ \rightarrow \bar{\Lambda} K^+$

VALUE	EVTS	DOCUMENT ID	TECN	COMMENT
$-0.0181 \pm 0.0028 \pm 0.0026$	1.89M	LU 06	HYCP	p Cu, 800 GeV

••• We do not use the following data for averages, fits, limits, etc. •••

$+0.017 \pm 0.077$ 1823 CHAN 98 E756 p Be, 800 GeV

$(\alpha + \bar{\alpha})/(\alpha - \bar{\alpha})$ in $\Omega^- \rightarrow \Lambda K^-, \bar{\Omega}^+ \rightarrow \bar{\Lambda} K^+$

Zero if CP is conserved.

VALUE	DOCUMENT ID	TECN	COMMENT
$-0.016 \pm 0.092 \pm 0.089$	⁸ LU 06	HYCP	p Cu, 800 GeV

⁸This value uses the results of CHEN 05, LU 05A, and LU 06.

α FOR $\Omega^- \rightarrow \Xi^0 \pi^-$

VALUE	EVTS	DOCUMENT ID	TECN	COMMENT
$+0.09 \pm 0.14$	1630	BOURQUIN 84	SPEC	SPS hyperon beam

α FOR $\Omega^- \rightarrow \Xi^- \pi^0$

VALUE	EVTS	DOCUMENT ID	TECN	COMMENT
$+0.05 \pm 0.21$	614	BOURQUIN 84	SPEC	SPS hyperon beam

 Ω^- REFERENCES

We have omitted some papers that have been superseded by later experiments. See our earlier editions.

ABLIKIM 21E	PRL 126 092002	M. Ablikim et al.	(BESIII Collab.)
KAMAEV 10	PL B693 236	O. Kamaev et al.	(FNAL HyperCP Collab.)
AUBERT, BE 06	PRL 97 112001	B. Aubert et al.	(BABAR Collab.)
LU 06	PRL 96 242001	L.C. Lu et al.	(FNAL HyperCP Collab.)
CHEN 05	PR D71 051102	Y.C. Chen et al.	(FNAL HyperCP Collab.)
LU 05A	PL B617 11	L.C. Lu et al.	(FNAL HyperCP Collab.)
WHITE 05	PRL 94 101904	C.G. White et al.	(FNAL HyperCP Collab.)
CHAN 98	PR D58 072002	A.W. Chan et al.	(FNAL E756 Collab.)
WALLACE 95	PRL 74 3732	N.B. Wallace et al.	(MINN, ARIZ, MICH+)
ALBUQUERQ... 94	PR D50 18	I.F. Albuquerque et al.	(FNAL E761 Collab.)
DIHEL 91	PRL 67 804	H.T. Diehl et al.	(RUTG, FNAL, MICH+)
LUK 88	PR D38 19	K.B. Luk et al.	(RUTG, WIS C, MICH, MINN)
HARTOUNI 85	PRL 54 628	E.P. Hartouni et al.	(COLU, ILL, FNAL)
BOURQUIN 84	NP B241 1	M.H. Bouquin et al.	(BRIS, GEVA, HEIDP+)
Also	PL B78 297	M.H. Bouquin et al.	(BRIS, GEVA, HEIDP+)
BOURQUIN 79B	PL B88 192	M.H. Bouquin et al.	(BRIS, GEVA, HEIDP+)
BAUBILLIER 78	PL 78B 342	M. Baubillier et al.	(BIRM, CERN, GLAS+)

DEUTSCH... 78	PL 73B 96	M. Deuschmann et al.	(AACH3, BERL, CERN+)
HEMINGWAY 78	NP B142 205	R.J. Hemingway et al.	(CERN, ZEEM, NUM+)
DIBIAN CA 75	NP B98 137	F.A. Dibianca, R.J. Endorf	(CMU)
ALVAREZ 73	PR D8 702	L.W. Alvarez	(LBL)
DEUTSCH... 73	NP B61 102	M. Deuschmann et al.	(ABCLV Collab.)
FIRESTONE 71B	PRL 26 410	L. Firestone et al.	(LRL)
SPETH 69	PL 29B 252	R. Speth et al.	(AACH, BERL, CERN, LOIC+)
PALMER 68	PL 26B 323	R.B. Palmer et al.	(BNL, SYRA)
SCHULTZ 68	PR 168 1509	P.F. Schultz et al.	(ILL, ANL, NVES+)
SCOTTER 68	PL 26B 474	D. Scotter et al.	(BIRM, GLAS, LOIC+)
ABRAMS 64	PRL 13 670	G.S. Abrams et al.	(UMD, NRL)
BARNES 64	PRL 12 204	V.E. Barnes et al.	(BNL)
FRY 55	PR 97 1189	W.F. Fry, J. Schneps, M.S. Swami	(WISC)
FRY 55B	NC 2 346	W.F. Fry, J. Schneps, M.S. Swami	(WISC)
EISENBERG 54	PR 96 541	Y. Eisenberg	(CORN)

 $\Omega(2012)^-$

$I(J^P) = 0(?)^-$ Status: ***

Seen in $\Xi^0 K^-$ and $\Xi^- K_S^0$ decays with a combined significance of 8.3 standard deviations.

 $\Omega(2012)^-$ MASS

VALUE (MeV)	EVTS	DOCUMENT ID	TECN	COMMENT
$2012.4 \pm 0.7 \pm 0.6$	520	YELTON 18A	BELL	In $\Upsilon(1S), \Upsilon(2S), \Upsilon(3S)$

 $\Omega(2012)^-$ WIDTH

VALUE (MeV)	EVTS	DOCUMENT ID	TECN	COMMENT
$6.4^{+2.5}_{-2.0} \pm 1.6$	520	YELTON 18A	BELL	In $\Upsilon(1S), \Upsilon(2S), \Upsilon(3S)$

 $\Omega(2012)^-$ DECAY MODES

Branching fractions are given relative to the one DEFINED AS 1.

Mode	Fraction (Γ_i/Γ)	Confidence level
$\Gamma_1 \Xi^- K$		
$\Gamma_2 (\Xi^- \pi) K$		
$\Gamma_3 \Xi^0 K^-$	DEFINED AS 1	
$\Gamma_4 \Xi^- \bar{K}^0$	0.83 ± 0.21	
$\Gamma_5 \Xi^0 \pi^0 K^-$	< 0.30	90%
$\Gamma_6 \Xi^0 \pi^- \bar{K}^0$	< 0.21	90%
$\Gamma_7 \Xi^- \pi^0 \bar{K}^0$	< 0.7	90%
$\Gamma_8 \Xi^- \pi^+ K^-$	< 0.08	90%

 $\Omega(2012)^-$ BRANCHING RATIOS

$\Gamma((\Xi \pi) K)/\Gamma(\Xi K)$	Γ_2/Γ_1
< 0.119	90
	JIA 19 BELL In $\Upsilon(1S, 2S, 3S)$

$\Gamma(\Xi^0 K^-)/\Gamma(\Xi^- \bar{K}^0)$	Γ_3/Γ_4
1.2 ± 0.3	
	YELTON 18A BELL In $\Upsilon(1S, 2S, 3S)$

$\Gamma(\Xi^0 \pi^0 K^-)/\Gamma(\Xi^0 K^-)$	Γ_5/Γ_3
< 0.304	90
	JIA 19 BELL In $\Upsilon(1S, 2S, 3S)$

$\Gamma(\Xi^0 \pi^- \bar{K}^0)/\Gamma(\Xi^0 K^-)$	Γ_6/Γ_3
< 0.213	90
	JIA 19 BELL In $\Upsilon(1S, 2S, 3S)$

$\Gamma(\Xi^0 \pi^- \bar{K}^0)/\Gamma(\Xi^- \bar{K}^0)$	Γ_6/Γ_4
< 0.256	90
	JIA 19 BELL In $\Upsilon(1S, 2S, 3S)$

$\Gamma(\Xi^- \pi^0 \bar{K}^0)/\Gamma(\Xi^- \bar{K}^0)$	Γ_7/Γ_4
< 0.811	90
	JIA 19 BELL In $\Upsilon(1S, 2S, 3S)$

$\Gamma(\Xi^- \pi^+ K^-)/\Gamma(\Xi^0 K^-)$	Γ_8/Γ_3
< 0.078	90
	JIA 19 BELL In $\Upsilon(1S, 2S, 3S)$

$\Gamma(\Xi^- \pi^+ K^-)/\Gamma(\Xi^- \bar{K}^0)$	Γ_8/Γ_4
< 0.093	90
	JIA 19 BELL In $\Upsilon(1S, 2S, 3S)$

 $\Omega(2012)^-$ REFERENCES

JIA 19	PR D100 032006	S. Jia et al.	(BELLE Collab.)
YELTON 18A	PRL 121 052003	J. Yelton et al.	(BELLE Collab.)

See key on page 1127

Baryon Particle Listings
 $\Omega(2250)^-, \Omega(2380)^-, \Omega(2470)^-$

$\Omega(2250)^-$ $I(J^P) = 0(?^?)$ Status: ***

$\Omega(2250)^-$ MASS

VALUE (MeV)	EVTS	DOCUMENT ID	TECN	COMMENT
2252 ± 9 OUR AVERAGE				
2253 ± 13	44	ASTON	87B LASS	$K^- p$ 11 GeV/c
2251 ± 9 ± 8	78	BIAGI	86B SPEC	SPS Ξ^- beam

$\Omega(2250)^-$ WIDTH

VALUE (MeV)	EVTS	DOCUMENT ID	TECN	COMMENT
55 ± 18 OUR AVERAGE				
81 ± 38	44	ASTON	87B LASS	$K^- p$ 11 GeV/c
48 ± 20	78	BIAGI	86B SPEC	SPS Ξ^- beam

$\Omega(2250)^-$ DECAY MODES

Mode	Fraction (Γ_i/Γ)
$\Gamma_1 \Xi^- \pi^+ K^-$	seen
$\Gamma_2 \Xi(1530)^0 K^-$	seen

$\Omega(2250)^-$ BRANCHING RATIOS

$\Gamma(\Xi(1530)^0 K^-)/\Gamma(\Xi^- \pi^+ K^-)$ Γ_2/Γ_1

VALUE	EVTS	DOCUMENT ID	TECN	COMMENT
~ 1.0	44	ASTON	87B LASS	$K^- p$ 11 GeV/c
0.70 ± 0.20	49	BIAGI	86B SPEC	Ξ^- Be 116 GeV/c

$\Omega(2250)^-$ REFERENCES

ASTON	87B	PL B194 579	D. Aston <i>et al.</i>	(SLAC, NAGO, CINC, INUS)
BIAGI	86B	ZPHY C31 33	S.F. Biagi <i>et al.</i>	(LOQM, GEVA, RAL+)

$\Omega(2380)^-$ Status: **

OMITTED FROM SUMMARY TABLE

$\Omega(2380)^-$ MASS

VALUE (MeV)	EVTS	DOCUMENT ID	TECN	COMMENT
≈ 2380 OUR ESTIMATE				
2384 ± 9 ± 8	45	BIAGI	86B SPEC	SPS Ξ^- beam

$\Omega(2380)^-$ WIDTH

VALUE (MeV)	EVTS	DOCUMENT ID	TECN	COMMENT
26 ± 23	45	BIAGI	86B SPEC	SPS Ξ^- beam

$\Omega(2380)^-$ DECAY MODES

Mode	Fraction (Γ_i/Γ)
$\Gamma_1 \Xi^- \pi^+ K^-$	seen
$\Gamma_2 \Xi(1530)^0 K^-$	
$\Gamma_3 \Xi^- \bar{K}^*(892)^0$	

$\Omega(2380)^-$ BRANCHING RATIOS

$\Gamma(\Xi(1530)^0 K^-)/\Gamma(\Xi^- \pi^+ K^-)$ Γ_2/Γ_1

VALUE	CL%	EVTS	DOCUMENT ID	TECN	COMMENT
< 0.44	90	9	BIAGI	86B SPEC	Ξ^- Be 116 GeV/c

$\Gamma(\Xi^- \bar{K}^*(892)^0)/\Gamma(\Xi^- \pi^+ K^-)$ Γ_3/Γ_1

VALUE	EVTS	DOCUMENT ID	TECN	COMMENT
0.5 ± 0.3	21	BIAGI	86B SPEC	Ξ^- Be 116 GeV/c

$\Omega(2380)^-$ REFERENCES

BIAGI	86B	ZPHY C31 33	S.F. Biagi <i>et al.</i>	(LOQM, GEVA, RAL+)
-------	-----	-------------	--------------------------	--------------------

$\Omega(2470)^-$ Status: **

OMITTED FROM SUMMARY TABLE

A peak in the $\Omega^- \pi^+ \pi^-$ mass spectrum with a signal significance claimed to be at least 5.5 standard deviations. There is no reason to seriously doubt the existence of this state, but unless the evidence is overwhelming we usually wait for confirmation from a second experiment before elevating peaks to the Summary Table.

$\Omega(2470)^-$ MASS

VALUE (MeV)	EVTS	DOCUMENT ID	TECN	COMMENT
2474 ± 12	59	ASTON	88G LASS	$K^- p$ 11 GeV/c

$\Omega(2470)^-$ WIDTH

VALUE (MeV)	EVTS	DOCUMENT ID	TECN	COMMENT
72 ± 33	59	ASTON	88G LASS	$K^- p$ 11 GeV/c

$\Omega(2470)^-$ DECAY MODES

Mode	Fraction (Γ_i/Γ)
$\Gamma_1 \Omega^- \pi^+ \pi^-$	

$\Omega(2470)^-$ REFERENCES

ASTON	88G	PL B215 799	D. Aston <i>et al.</i>	(SLAC, NAGO, CINC, INUS)
-------	-----	-------------	------------------------	--------------------------

Baryon Particle Listings

Charmed Baryons, Λ_c^+

CHARMED BARYONS ($C = +1$)

$$\Lambda_c^+ = udc, \quad \Sigma_c^{++} = uuc, \quad \Sigma_c^+ = udc, \quad \Sigma_c^0 = ddc, \\ \Xi_c^+ = usc, \quad \Xi_c^0 = dsc, \quad \Omega_c^0 = ssc$$

Λ_c^+

$$I(J^P) = 0(\frac{1}{2}^+) \text{ Status: } ****$$

The parity of the Λ_c^+ is defined to be positive (as are the parities of the proton, neutron, and Λ). The quark content is udc . Results of an analysis of $pK^-\pi^+$ decays (JEZABEK 92) are consistent with $J = 1/2$. ABLIKIM 21N determines the Λ_c^+ spin to be $J = 1/2$, from an angular analysis of various 2-body Λ_c^+ decays in $e^+e^- \rightarrow \Lambda_c^+ \bar{\Lambda}_c^-$.

We have omitted some results that have been superseded by later experiments. The omitted results may be found in earlier editions.

Λ_c^+ MASS

Our value in 2004, 2284.9 ± 0.6 MeV, was the average of the measurements now filed below as "not used." The BABAR measurement is so much better that we use it alone. Note that it is about 2.6 (old) standard deviations above the 2004 value.

The fit also includes $\Sigma_c^-\Lambda_c^+$ and $\Lambda_c^{*+}-\Lambda_c^+$ mass-difference measurements, but this doesn't affect the Λ_c^+ mass. The new (in 2006) Λ_c^+ mass simply pushes all those other masses higher.

VALUE (MeV)	EVTS	DOCUMENT ID	TECN	COMMENT
2286.46 ± 0.14 OUR FIT				
2286.46 ± 0.14	4891	¹ AUBERT,B	05s BABR	$\Lambda_c^0 K^+$ and $\Sigma^0 K_S^0 K^+$
• • • We do not use the following data for averages, fits, limits, etc. • • •				
2284.7 ± 0.6 ± 0.7	1134	VERY	91 CLEO	Six modes
2281.7 ± 2.7 ± 2.6	29	ALVAREZ	90b NA14	$pK^-\pi^+$
2285.8 ± 0.6 ± 1.2	101	BARLAG	89 NA32	$pK^-\pi^+$
2284.7 ± 2.3 ± 0.5	5	AGUILAR...	88b LEBE	$pK^-\pi^+$
2283.1 ± 1.7 ± 2.0	628	ALBRECHT	88c ARG	$pK^-\pi^+$, $p\bar{K}^0$, $\Lambda 3\pi$
2286.2 ± 1.7 ± 0.7	97	ANJOS	88b E691	$pK^-\pi^+$
2281 ± 3	2	JONES	87 HBC	$pK^-\pi^+$
2283 ± 3	3	BOSETTI	82 HBC	$pK^-\pi^+$
2290 ± 3	1	CALICCHIO	80 HYBR	$pK^-\pi^+$

¹AUBERT,B 05s uses low-Q $\Lambda_c^0 K^+$ and $\Sigma^0 K_S^0 K^+$ decays to minimize systematic errors. The error above includes systematic as well as statistical errors. Many cross checks and adjustments to properties of the BABAR detector, as well as the large number of clean events, make this by far the best measurement of the Λ_c^+ mass.

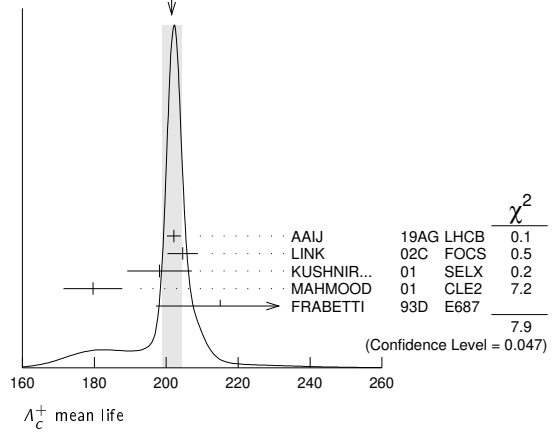
Λ_c^+ MEAN LIFE

Measurements with an error $\geq 100 \times 10^{-15}$ s or with fewer than 20 events have been omitted from the Listings.

VALUE (10^{-15} s)	EVTS	DOCUMENT ID	TECN	COMMENT
201.5 ± 2.7 OUR AVERAGE				Error includes scale factor of 1.6. See the ideogram below.
202.1 ± 1.7 ± 0.9	304k	¹ AAIJ	19AG LHCB	$\Lambda_c^+ \rightarrow pK^-\pi^+$
204.6 ± 3.4 ± 2.5	8034	LINK	02c FOCS	$\Lambda_c^+ \rightarrow pK^-\pi^+$
198.1 ± 7.0 ± 5.6	1630	KUSHNIR...	01 SELX	$\Lambda_c^+ \rightarrow pK^-\pi^+$
179.6 ± 6.9 ± 4.4	4749	MAHMOOD	01 CLE2	$e^+e^- \approx \tau(4S)$
215 ± 16 ± 8	1340	FRABETTI	93D E687	$\gamma\text{Be}, \Lambda_c^+ \rightarrow pK^-\pi^+$
• • • We do not use the following data for averages, fits, limits, etc. • • •				
180 ± 30 ± 30	29	ALVAREZ	90 NA14	$\gamma, \Lambda_c^+ \rightarrow pK^-\pi^+$
200 ± 30 ± 30	90	FRABETTI	90 E687	$\gamma\text{Be}, \Lambda_c^+ \rightarrow pK^-\pi^+$
196 $\begin{smallmatrix} +23 \\ -20 \end{smallmatrix}$	101	BARLAG	89 NA32	$pK^-\pi^+$ + c.c.
220 ± 30 ± 20	97	ANJOS	88b E691	$pK^-\pi^+$ + c.c.

¹AAIJ 19AG reports $[A_c^+ \text{ MEAN LIFE}] / [D^\pm \text{ MEAN LIFE}] = 0.1956 \pm 0.0010 \pm 0.0013$ which we multiply by our best value $D^\pm \text{ MEAN LIFE} = (1.033 \pm 0.005) \times 10^{-12}$ s. Our first error is their experiment's error and our second error is the systematic error from using our best value.

WEIGHTED AVERAGE
201.5±2.7 (Error scaled by 1.6)



Λ_c^+ DECAY MODES

Branching fractions marked with a footnote, e.g. [a], have been corrected for decay modes not observed in the experiments. For example, the sub-mode fraction $\Lambda_c^+ \rightarrow p\bar{K}^*(892)^0$ seen in $\Lambda_c^+ \rightarrow pK^-\pi^+$ has been multiplied up to include $\bar{K}^*(892)^0 \rightarrow \bar{K}^0\pi^0$ decays.

Mode	Fraction (Γ_i/Γ)	Scale factor/ Confidence level
Hadronic modes with a p or n: S = -1 final states		
Γ_1 pK_S^0	(1.59 ± 0.08) %	S=1.1
Γ_2 $pK^-\pi^+$	(6.28 ± 0.32) %	S=1.4
Γ_3 $p\bar{K}^*(892)^0$	[a] (1.96 ± 0.27) %	
Γ_4 $\Delta(1232)^{++}K^-$	(1.08 ± 0.25) %	
Γ_5 $\Lambda(1520)\pi^+$	[a] (2.2 ± 0.5) %	
Γ_6 $pK^-\pi^+$ nonresonant	(3.5 ± 0.4) %	
Γ_7 $pK_S^0\pi^0$	(1.97 ± 0.13) %	S=1.1
Γ_8 $n\bar{K}^0\pi^+$	(1.82 ± 0.25) %	
Γ_9 $p\bar{K}^0\eta$	(8.3 ± 1.8) × 10 ⁻³	
Γ_{10} $pK_S^0\pi^+\pi^-$	(1.60 ± 0.12) %	S=1.1
Γ_{11} $pK^-\pi^+\pi^0$	(4.46 ± 0.30) %	S=1.5
Γ_{12} $pK^*(892)^-\pi^+$	[a] (1.4 ± 0.5) %	
Γ_{13} $p(K^-\pi^+)_{\text{nonresonant}}\pi^0$	(4.6 ± 0.8) %	
Γ_{14} $\Delta(1232)\bar{K}^*(892)$	seen	
Γ_{15} $pK^-\pi^+\pi^-$	(1.4 ± 0.9) × 10 ⁻³	
Γ_{16} $pK^-\pi^+2\pi^0$	(1.0 ± 0.5) %	
Hadronic modes with a p: S = 0 final states		
Γ_{17} $p\pi^0$	< 8 × 10 ⁻⁵	CL=90%
Γ_{18} $p\eta$	(1.42 ± 0.12) × 10 ⁻³	
Γ_{19} $p\omega(782)^0$	(8.3 ± 1.1) × 10 ⁻⁴	
Γ_{20} $p\pi^+\pi^-$	(4.61 ± 0.28) × 10 ⁻³	
Γ_{21} $p f_0(980)$	[a] (3.5 ± 2.3) × 10 ⁻³	
Γ_{22} $p2\pi^+2\pi^-$	(2.3 ± 1.4) × 10 ⁻³	
Γ_{23} pK^+K^-	(1.06 ± 0.06) × 10 ⁻³	
Γ_{24} $p\phi$	[a] (1.06 ± 0.14) × 10 ⁻³	
Γ_{25} $pK^+K^-\text{non-}\phi$	(5.3 ± 1.2) × 10 ⁻⁴	
Γ_{26} $p\phi\pi^0$	(10 ± 4) × 10 ⁻⁵	
Γ_{27} $pK^+K^-\pi^0$ nonresonant	< 6.3 × 10 ⁻⁵	CL=90%
Hadronic modes with a hyperon: S = -1 final states		
Γ_{28} $\Lambda\pi^+$	(1.30 ± 0.07) %	S=1.1
Γ_{29} $\Lambda(1670)\pi^+, \Lambda(1670) \rightarrow \eta\Lambda$	(3.5 ± 0.5) × 10 ⁻³	
Γ_{30} $\Lambda\pi^+\pi^0$	(7.1 ± 0.4) %	S=1.1
Γ_{31} $\Lambda\rho^+$	< 6 %	CL=95%
Γ_{32} $\Lambda\pi^-2\pi^+$	(3.64 ± 0.29) %	S=1.4
Γ_{33} $\Sigma(1385)^+\pi^+\pi^-, \Sigma^{*+} \rightarrow \Lambda\pi^+$	(1.0 ± 0.5) %	
Γ_{34} $\Sigma(1385)^-2\pi^+, \Sigma^{*-} \rightarrow \Lambda\pi^-$	(7.6 ± 1.4) × 10 ⁻³	
Γ_{35} $\Lambda\pi^+\rho^0$	(1.5 ± 0.6) %	
Γ_{36} $\Sigma(1385)^+\rho^0, \Sigma^{*+} \rightarrow \Lambda\pi^+$	(5 ± 4) × 10 ⁻³	
Γ_{37} $\Lambda\pi^-2\pi^+$ nonresonant	< 1.1 %	CL=90%
Γ_{38} $\Lambda\pi^-\pi^02\pi^+$ total	(2.3 ± 0.8) %	
Γ_{39} $\Lambda\pi^+\eta$	[a] (1.84 ± 0.26) %	
Γ_{40} $\Sigma(1385)^+\eta$	[a] (9.1 ± 2.0) × 10 ⁻³	
Γ_{41} $\Lambda\pi^+\omega$	[a] (1.5 ± 0.5) %	

Γ_{42}	$\Lambda\pi^-\pi^0 2\pi^+$, no η or ω	< 8	$\times 10^{-3}$	CL=90%
Γ_{43}	$\Lambda K^+ \overline{K}^0$	(5.7 ± 1.1)	$\times 10^{-3}$	S=1.9
Γ_{44}	$\Xi(1690)^0 K^+, \Xi^{*0} \rightarrow \Lambda \overline{K}^0$	(1.6 ± 0.5)	$\times 10^{-3}$	
Γ_{45}	$\Sigma^0 \pi^+$	(1.29 ± 0.07)	%	S=1.1
Γ_{46}	$\Sigma^0 \pi^+ \eta$	(7.5 ± 0.8)	$\times 10^{-3}$	
Γ_{47}	$\Sigma^+ \pi^0$	(1.25 ± 0.10)	%	
Γ_{48}	$\Sigma^+ \eta$	(4.4 ± 2.0)	$\times 10^{-3}$	
Γ_{49}	$\Sigma^+ \eta'$	(1.5 ± 0.6)	%	
Γ_{50}	$\Sigma^+ \pi^+ \pi^-$	(4.50 ± 0.25)	%	S=1.3
Γ_{51}	$\Sigma^+ \rho^0$	< 1.7	%	CL=95%
Γ_{52}	$\Sigma^- 2\pi^+$	(1.87 ± 0.18)	%	
Γ_{53}	$\Sigma^0 \pi^+ \pi^0$	(3.5 ± 0.4)	%	
Γ_{54}	$\Sigma^+ \pi^0 \pi^0$	(1.55 ± 0.15)	%	
Γ_{55}	$\Sigma^0 \pi^- 2\pi^+$	(1.11 ± 0.30)	%	
Γ_{56}	$\Sigma^+ \pi^+ \pi^- \pi^0$	—		
Γ_{57}	$\Sigma^+ \omega$	[a] (1.70 ± 0.21)	%	
Γ_{58}	$\Sigma^- \pi^0 2\pi^+$	(2.1 ± 0.4)	%	
Γ_{59}	$\Sigma^+ K^+ K^-$	(3.5 ± 0.4)	$\times 10^{-3}$	S=1.1
Γ_{60}	$\Sigma^+ \phi$	[a] (3.9 ± 0.6)	$\times 10^{-3}$	S=1.1
Γ_{61}	$\Xi(1690)^0 K^+, \Xi^{*0} \rightarrow \Sigma^+ K^-$	(1.02 ± 0.25)	$\times 10^{-3}$	
Γ_{62}	$\Sigma^+ K^+ K^-$ nonresonant	< 8	$\times 10^{-4}$	CL=90%
Γ_{63}	$\Xi^0 K^+$	(5.5 ± 0.7)	$\times 10^{-3}$	
Γ_{64}	$\Xi^- K^+ \pi^+$	(6.2 ± 0.6)	$\times 10^{-3}$	S=1.1
Γ_{65}	$\Xi(1530)^0 K^+$	(4.3 ± 0.9)	$\times 10^{-3}$	S=1.1

Hadronic modes with a hyperon: S = 0 final states

Γ_{66}	ΛK^+	(6.1 ± 1.2)	$\times 10^{-4}$	
Γ_{67}	$\Lambda K^+ \pi^+ \pi^-$	< 5	$\times 10^{-4}$	CL=90%
Γ_{68}	$\Sigma^0 K^+$	(5.2 ± 0.8)	$\times 10^{-4}$	
Γ_{69}	$\Sigma^0 K^+ \pi^+ \pi^-$	< 2.6	$\times 10^{-4}$	CL=90%
Γ_{70}	$\Sigma^+ K^+ \pi^-$	(2.1 ± 0.6)	$\times 10^{-3}$	
Γ_{71}	$\Sigma^+ K^*(892)^0$	[a] (3.5 ± 1.0)	$\times 10^{-3}$	
Γ_{72}	$\Sigma^- K^+ \pi^+$	< 1.2	$\times 10^{-3}$	CL=90%

Doubly Cabibbo-suppressed modes

Γ_{73}	$\rho K^+ \pi^-$	(1.11 ± 0.18)	$\times 10^{-4}$	
---------------	------------------	-------------------	------------------	--

Semileptonic modes

Γ_{74}	$\Lambda e^+ \nu_e$	(3.6 ± 0.4)	%	
Γ_{75}	$\Lambda \mu^+ \nu_\mu$	(3.5 ± 0.5)	%	

Inclusive modes

Γ_{76}	e^+ anything	(3.95 ± 0.35)	%	
Γ_{77}	p anything	(50 ± 16)	%	
Γ_{78}	n anything	(50 ± 16)	%	
Γ_{79}	Λ anything	$(38.2^{+2.9}_{-2.4})$	%	
Γ_{80}	K_S^0 anything	(9.9 ± 0.7)	%	
Γ_{81}	3prongs	(24 ± 8)	%	

 $\Delta C = 1$ weak neutral current (C1) modes, or Lepton Family number (LF), or Lepton number (L), or Baryon number (B) violating modes

Γ_{82}	$p e^+ e^-$	C1	< 5.5	$\times 10^{-6}$	CL=90%
Γ_{83}	$p \mu^+ \mu^-$ non-resonant	C1	< 7.7	$\times 10^{-8}$	CL=90%
Γ_{84}	$p e^+ \mu^-$	LF	< 9.9	$\times 10^{-6}$	CL=90%
Γ_{85}	$p e^- \mu^+$	LF	< 1.9	$\times 10^{-5}$	CL=90%
Γ_{86}	$\overline{p} 2e^+$	L,B	< 2.7	$\times 10^{-6}$	CL=90%
Γ_{87}	$\overline{p} 2\mu^+$	L,B	< 9.4	$\times 10^{-6}$	CL=90%
Γ_{88}	$\overline{p} e^+ \mu^+$	L,B	< 1.6	$\times 10^{-5}$	CL=90%
Γ_{89}	$\Sigma^- \mu^+ \mu^+$	L	< 7.0	$\times 10^{-4}$	CL=90%

[a] This branching fraction includes all the decay modes of the final-state resonance.

CONSTRAINED FIT INFORMATION

An overall fit to 41 branching ratios uses 62 measurements and one constraint to determine 21 parameters. The overall fit has a $\chi^2 = 47.4$ for 42 degrees of freedom.

The following *off-diagonal* array elements are the correlation coefficients $\langle \delta x_i \delta x_j \rangle / (\delta x_i \delta x_j)$, in percent, from the fit to the branching fractions, $x_i \equiv \Gamma_i / \Gamma_{\text{total}}$. The fit constrains the x_i whose labels appear in this array to sum to one.

x_2	54									
x_7	46	55								
x_{10}	44	64	39							
x_{11}	51	61	40	60						
x_{28}	54	66	44	42	43					
x_{30}	45	61	41	38	36	65				
x_{32}	51	37	28	41	60	45	36			
x_{43}	16	22	14	14	14	26	19	12		
x_{45}	51	55	38	37	40	74	58	44	20	
x_{47}	38	39	30	25	29	34	33	23	10	29
x_{50}	51	88	50	60	61	59	55	39	20	50
x_{52}	5	9	5	6	6	6	6	3	2	5
x_{55}	13	14	9	12	15	13	11	20	4	12
x_{57}	19	30	18	23	26	19	18	18	6	16
x_{59}	23	41	23	28	28	27	25	18	9	23
x_{60}	19	32	19	22	23	22	20	14	7	18
x_{63}	8	15	8	10	9	10	9	6	3	8
x_{64}	29	39	25	25	25	51	35	24	14	38
x_{65}	6	11	6	7	7	7	7	4	2	6
	x_1	x_2	x_7	x_{10}	x_{11}	x_{28}	x_{30}	x_{32}	x_{43}	x_{45}
	x_{50}									
	x_{52}									
	x_{55}									
	x_{57}									
	x_{59}									
	x_{60}									
	x_{63}									
	x_{64}									
	x_{65}									
	x_{47}	x_{50}	x_{52}	x_{55}	x_{57}	x_{59}	x_{60}	x_{63}	x_{64}	

 Λ_c^+ BRANCHING RATIOS

A few really obsolete results have been omitted.

Hadronic modes with a p : S = -1 final states

$\Gamma(pK_S^0)/\Gamma_{\text{total}}$						Γ_1/Γ
VALUE (%)	EVTs	DOCUMENT ID	TECN	COMMENT		
1.59±0.08 OUR FIT				Error includes scale factor of 1.1.		
1.52±0.08±0.03	1243	ABLIKIM	16 BES3	$e^+ e^- \rightarrow \Lambda_c \bar{\Lambda}_c$, 4.599 GeV		
$\Gamma(pK_S^0)/\Gamma(K^- \pi^+)$						Γ_1/Γ_2
Measurements given as a \overline{K}^0 ratio have been divided by 2 to convert to a K_S^0 ratio.						
VALUE	EVTs	DOCUMENT ID	TECN	COMMENT		
0.254±0.012 OUR FIT				Error includes scale factor of 1.4.		
0.234±0.020 OUR AVERAGE						
0.23 ± 0.01 ± 0.02		ALAM	98 CLE2	$e^+ e^- \approx \mathcal{T}(4S)$		
0.22 ± 0.04 ± 0.03	133	AVERY	91 CLE0	$e^+ e^-$ 10.5 GeV		
0.28 ± 0.09 ± 0.07	45	ANJOS	90 E691	$\gamma\text{Be } 70\text{-}260$ GeV		
0.31 ± 0.08 ± 0.02	73	ALBRECHT	88c ARG	$e^+ e^-$ 10 GeV		

$\Gamma(pK^- \pi^+)/\Gamma_{\text{total}}$						Γ_2/Γ
VALUE (%)	EVTs	DOCUMENT ID	TECN	COMMENT		
6.28±0.32 OUR FIT				Error includes scale factor of 1.4.		
6.3 ± 0.5 OUR AVERAGE				Error includes scale factor of 2.0.		
5.84 ± 0.27 ± 0.23	6.3k	ABLIKIM	16 BES3	$e^+ e^- \rightarrow \Lambda_c \bar{\Lambda}_c$, 4.599 GeV		
6.84 ± 0.24 $\pm_{0.27}^{0.21}$	1.4k	1 ZUPANC	14 BELL	$e^+ e^- \rightarrow D^{(*)-} \overline{p} \pi^+$ recoil		

• • • We do not use the following data for averages, fits, limits, etc. • • •

5.0 ± 1.3 2 PDG See footnote

¹ This ZUPANC 14 value is the FIRST-EVER model-independent measurement of a Λ_c^+ branching fraction.

² See the note by P. Burchat, “ Λ_c^+ Branching Fractions,” in any edition of the Review from 2002 through 2014 for how this value was obtained. It is now obsolete.

$\Gamma(p\overline{K}^*(892)^0)/\Gamma(K^- \pi^+)$						Γ_3/Γ_2
VALUE	EVTs	DOCUMENT ID	TECN	COMMENT		
0.31±0.04 OUR AVERAGE						
0.29 ± 0.04 ± 0.03		1 AITALA	00 E791	$\pi^- N$, 500 GeV		
0.35 $\pm_{-0.07}^{+0.06}$ ± 0.03	39	BOZEK	93 NA32	$\pi^- \text{Cu}$ 230 GeV		
0.42 ± 0.24	12	BASILE	81b CNTR	$pp \rightarrow \Lambda_c^+ e^- X$		
0.35 ± 0.11		BARLAG	90d NA32	See BOZEK 93		

Unseen decay modes of the $\overline{K}^*(892)^0$ are included.

• • • We do not use the following data for averages, fits, limits, etc. • • •

¹ AITALA 00 makes a coherent 5-dimensional amplitude analysis of $946 \pm 38 \Lambda_c^+ \rightarrow p K^- \pi^+$ decays.

Baryon Particle Listings

Λ_C^+					Λ_C^+					
$\Gamma(\Delta(1232)^{++}K^-)/\Gamma(pK^-\pi^+)$					Γ_4/Γ_2					
VALUE	EVTS	DOCUMENT ID	TECN	COMMENT	VALUE	EVTS	DOCUMENT ID	TECN	COMMENT	
0.17±0.04 OUR AVERAGE		Error includes scale factor of 1.1.			0.73±0.12±0.05	67	BOZEK	93	NA32 π^- Cu 230 GeV	
0.18±0.03±0.03		¹ AITALA	00	E791 π^- N, 500 GeV	$\Gamma(\Delta(1232)\bar{K}^*(892))/\Gamma_{total}$					
0.12± $_{-0.05}^{+0.04}$	14	BOZEK	93	NA32 π^- Cu 230 GeV	VALUE	EVTS	DOCUMENT ID	TECN	COMMENT	
0.40±0.17	17	BASILE	81B	CNTR $p\bar{p} \rightarrow \Lambda_C^+ e^- X$	seen	35	AMENDOLIA	87	SPEC γ Ge-Si	
¹ AITALA 00 makes a coherent 5-dimensional amplitude analysis of $946 \pm 38 \Lambda_C^+ \rightarrow pK^-\pi^+$ decays.					$\Gamma(pK^-2\pi^+\pi^-)/\Gamma(pK^-\pi^+)$					
$\Gamma(\Lambda(1520)\pi^+)/\Gamma(pK^-\pi^+)$					Γ_{15}/Γ_2					
Unseen decay modes of the $\Lambda(1520)$ are included.					VALUE	EVTS	DOCUMENT ID	TECN	COMMENT	
VALUE	EVTS	DOCUMENT ID	TECN	COMMENT	0.022±0.015		BARLAG	90D	NA32 π^- 230 GeV	
0.35±0.08 OUR AVERAGE					$\Gamma(pK^-\pi^+2\pi^0)/\Gamma(pK^-\pi^+)$					
0.34±0.08±0.05		¹ AITALA	00	E791 π^- N, 500 GeV	VALUE	EVTS	DOCUMENT ID	TECN	COMMENT	
0.40± $_{-0.13}^{+0.18}$	12	BOZEK	93	NA32 π^- Cu 230 GeV	0.16±0.07±0.03	15	BOZEK	93	NA32 π^- Cu 230 GeV	
¹ AITALA 00 makes a coherent 5-dimensional amplitude analysis of $946 \pm 38 \Lambda_C^+ \rightarrow pK^-\pi^+$ decays.					Hadronic modes with a p : $S = 0$ final states					
$\Gamma(pK^-\pi^+ \text{ nonresonant})/\Gamma(pK^-\pi^+)$					$\Gamma(p\pi^0)/\Gamma_{total}$					
VALUE	EVTS	DOCUMENT ID	TECN	COMMENT	VALUE	CL%	DOCUMENT ID	TECN	COMMENT	
0.55±0.06 OUR AVERAGE					$\bullet\bullet\bullet$ We do not use the following data for averages, fits, limits, etc. $\bullet\bullet\bullet$					
0.55±0.06±0.04		¹ AITALA	00	E791 π^- N, 500 GeV	<2.7 × 10 ⁻⁴	90	ABLIKIM	17Q	BES3 e^+e^- at 4.6 GeV	
0.56± $_{-0.09}^{+0.07}$	71	BOZEK	93	NA32 π^- Cu 230 GeV	$\Gamma(p\pi^0)/\Gamma(pK^-\pi^+)$					
¹ AITALA 00 makes a coherent 5-dimensional amplitude analysis of $946 \pm 38 \Lambda_C^+ \rightarrow pK^-\pi^+$ decays.					VALUE	CL%	EVTS	DOCUMENT ID	TECN	COMMENT
$\Gamma(pK_S^0\pi^0)/\Gamma_{total}$					Γ_{17}/Γ_2					
VALUE (%)	EVTS	DOCUMENT ID	TECN	COMMENT	<1.273 × 10 ⁻³	90	7.7k	¹ LI	21	BELL e^+e^- at Υ (nS)
1.97±0.13 OUR FIT		Error includes scale factor of 1.1.			¹ Uses $B(\pi^0 \rightarrow \gamma\gamma) = 0.9882 \pm 0.0003$.					
1.87±0.13±0.05	558	ABLIKIM	16	BES3 $e^+e^- \rightarrow \Lambda_C\bar{\Lambda}_C$, 4.599 GeV	$\Gamma(p\eta)/\Gamma_{total}$					
$\Gamma(pK_S^0\pi^0)/\Gamma(pK^-\pi^+)$					Unseen decay modes of the η are included.					
VALUE	EVTS	DOCUMENT ID	TECN	COMMENT	VALUE (units 10 ⁻³)	EVTS	DOCUMENT ID	TECN	COMMENT	
0.314±0.018 OUR FIT					$\bullet\bullet\bullet$ We do not use the following data for averages, fits, limits, etc. $\bullet\bullet\bullet$					
0.33 ± 0.03 ± 0.04	774	ALAM	98	CLE2 $e^+e^- \approx \Upsilon(4S)$	1.24±0.28±0.10	52	ABLIKIM	17Q	BES3 $\eta \rightarrow 2\gamma, \pi^+\pi^0\pi^-$	
$\Gamma(nK_S^0\pi^+)/\Gamma_{total}$					$\Gamma(p\eta)/\Gamma(pK^-\pi^+)$					
VALUE (%)	EVTS	DOCUMENT ID	TECN	COMMENT	VALUE (units 10 ⁻²)	EVTS	DOCUMENT ID	TECN	COMMENT	
1.82±0.23±0.11	83	ABLIKIM	17H	BES3 e^+e^- at 4.6 GeV	2.258±0.077±0.122	7.7k	¹ LI	21	BELL e^+e^- at Υ (nS)	
$\Gamma(p\bar{K}^0\eta)/\Gamma(pK^-\pi^+)$					¹ Uses $B(\eta \rightarrow \gamma\gamma) = 0.3941 \pm 0.0020$.					
VALUE	EVTS	DOCUMENT ID	TECN	COMMENT	$\Gamma(p\omega(782)^0)/\Gamma_{total}$					
0.25±0.04±0.04	57	AMMAR	95	CLE2 $e^+e^- \approx \Upsilon(4S)$	VALUE (units 10 ⁻⁴)	EVTS	DOCUMENT ID	TECN	COMMENT	
$\Gamma(p\bar{K}^0\eta)/\Gamma_{total}$					$\bullet\bullet\bullet$ We do not use the following data for averages, fits, limits, etc. $\bullet\bullet\bullet$					
VALUE (%)	EVTS	DOCUMENT ID	TECN	COMMENT	9.4±3.2±2.2	13	AAIJ	18N	LHCB Seen in $\Lambda_C^+ \rightarrow p\mu^+\mu^-$	
0.828±0.168±0.056	42	¹ ABLIKIM	21H	BES3 e^+e^- at 4.6 GeV	$\Gamma(p\omega(782)^0)/\Gamma(pK^-\pi^+)$					
¹ ABLIKIM 21H measures $B(\Lambda_C^+ \rightarrow pK_S^0\eta) = (0.414 \pm 0.084 \pm 0.028)\%$.					VALUE (units 10 ⁻²)	EVTS	DOCUMENT ID	TECN	COMMENT	
$\Gamma(pK_S^0\pi^+\pi^-)/\Gamma_{total}$					1.32±0.12±0.10	1.8k	¹ LI	21E	BELL e^+e^- at Υ (nS)	
VALUE (%)	EVTS	DOCUMENT ID	TECN	COMMENT	¹ LI 21E reconstructs the $\omega(782)$ via $\omega \rightarrow \pi^+\pi^-\pi^0$ and $\pi^0 \rightarrow \gamma\gamma$.					
1.60±0.12 OUR FIT		Error includes scale factor of 1.1.			$\Gamma(p\pi^+\pi^-)/\Gamma(pK^-\pi^+)$					
1.53±0.11±0.09	485	ABLIKIM	16	BES3 $e^+e^- \rightarrow \Lambda_C\bar{\Lambda}_C$, 4.599 GeV	VALUE (units 10 ⁻²)	EVTS	DOCUMENT ID	TECN	COMMENT	
$\Gamma(pK_S^0\pi^+\pi^-)/\Gamma(pK^-\pi^+)$					7.35±0.24 OUR AVERAGE		Error includes scale factor of 1.3.			
VALUE	EVTS	DOCUMENT ID	TECN	COMMENT	7.44±0.08±0.18	20k	AAIJ	18V	LHCB $\Lambda_b^0 \rightarrow \Lambda_C^+\mu^-X$	
0.257±0.031 OUR AVERAGE					6.70±0.48±0.25	495	ABLIKIM	16U	BES3 e^+e^- at 4.599 GeV	
0.26 ± 0.02 ± 0.03	985	ALAM	98	CLE2 $e^+e^- \approx \Upsilon(4S)$	6.9 ± 3.6	5	BARLAG	90D	NA32 π^- 230 GeV	
0.22 ± 0.06 ± 0.02	83	AVERY	91	CLEO $e^+e^- = 10.5$ GeV	$\Gamma(p\bar{K}^0(980))/\Gamma(pK^-\pi^+)$					
0.49 ± 0.18 ± 0.04	12	BARLAG	90D	NA32 π^- 230 GeV	Unseen decay modes of the $\bar{K}^0(980)$ are included.					
$\Gamma(pK^-\pi^+\pi^0)/\Gamma_{total}$					VALUE	EVTS	DOCUMENT ID	TECN	COMMENT	
VALUE (%)	EVTS	DOCUMENT ID	TECN	COMMENT	0.055±0.036		BARLAG	90D	NA32 π^- 230 GeV	
4.46±0.30 OUR FIT		Error includes scale factor of 1.5.			$\Gamma(p2\pi^+2\pi^-)/\Gamma(pK^-\pi^+)$					
4.53±0.23±0.30	1849	ABLIKIM	16	BES3 $e^+e^- \rightarrow \Lambda_C\bar{\Lambda}_C$, 4.599 GeV	VALUE	EVTS	DOCUMENT ID	TECN	COMMENT	
$\Gamma(pK^-\pi^+\pi^0)/\Gamma(pK^-\pi^+)$					0.036±0.023		BARLAG	90D	NA32 π^- 230 GeV	
VALUE (%)	EVTS	DOCUMENT ID	TECN	COMMENT	$\Gamma(pK^+K^-)/\Gamma(pK^-\pi^+)$					
0.71 ± 0.04 OUR FIT		Error includes scale factor of 2.4.			VALUE (units 10 ⁻²)	EVTS	DOCUMENT ID	TECN	COMMENT	
0.685±0.019 OUR AVERAGE					1.70±0.04 OUR AVERAGE					
0.685 ± 0.007 ± 0.018	242k	PAL	17	BELL $e^+e^- \approx \Upsilon(4S), \Upsilon(5S)$	1.70 ± 0.03 ± 0.03	3.4k	AAIJ	18V	LHCB $\Lambda_b^0 \rightarrow \Lambda_C^+\mu^-X$	
0.67 ± 0.04 ± 0.11	2.6k	ALAM	98	CLE2 $e^+e^- \approx \Upsilon(4S)$	1.4 ± 0.2 ± 0.2	676	ABE	02C	BELL $e^+e^- \approx \Upsilon(4S)$	
$\Gamma(pK^*(892)^-\pi^+)/\Gamma(pK_S^0\pi^+\pi^-)$					3.9 ± 0.9 ± 0.7	214	ALEXANDER	96C	CLE2 $e^+e^- \approx \Upsilon(4S)$	
VALUE	EVTS	DOCUMENT ID	TECN	COMMENT	$\bullet\bullet\bullet$ We do not use the following data for averages, fits, limits, etc. $\bullet\bullet\bullet$					
0.88±0.28	17	ALEEV	94	BIS2 n N 20–70 GeV	9.6 ± 2.9 ± 1.0	30	FRABETTI	93H	E687 γ Be, \bar{E}_γ 220 GeV	
Unseen decay modes of the $K^*(892)^-$ are included.					4.8 ± 2.7		BARLAG	90D	NA32 π^- 230 GeV	
VALUE	EVTS	DOCUMENT ID	TECN	COMMENT	$\Gamma(p\phi)/\Gamma(pK^-\pi^+)$					
0.88±0.28					Unseen decay modes of the ϕ are included.					
VALUE (units 10 ⁻²)	EVTS	DOCUMENT ID	TECN	COMMENT	VALUE (units 10 ⁻²)	EVTS	DOCUMENT ID	TECN	COMMENT	
1.70±0.21 OUR AVERAGE					1.70±0.21 OUR AVERAGE					
1.81±0.33±0.13	44	ABLIKIM	16U	BES3 e^+e^- at 4.599 GeV	1.81 ± 0.33 ± 0.13	44	ABLIKIM	16U	BES3 e^+e^- at 4.599 GeV	
1.5 ± 0.2 ± 0.2	345	ABE	02C	BELL $e^+e^- \approx \Upsilon(4S)$	1.5 ± 0.2 ± 0.2	345	ABE	02C	BELL $e^+e^- \approx \Upsilon(4S)$	
2.4 ± 0.6 ± 0.3	54	ALEXANDER	96C	CLE2 $e^+e^- \approx \Upsilon(4S)$	2.4 ± 0.6 ± 0.3	54	ALEXANDER	96C	CLE2 $e^+e^- \approx \Upsilon(4S)$	
$\bullet\bullet\bullet$ We do not use the following data for averages, fits, limits, etc. $\bullet\bullet\bullet$					$\bullet\bullet\bullet$ We do not use the following data for averages, fits, limits, etc. $\bullet\bullet\bullet$					
4.0 ± 2.7		BARLAG	90D	NA32 π^- 230 GeV	4.0 ± 2.7		BARLAG	90D	NA32 π^- 230 GeV	

$\Gamma(\rho K^+ K^- \text{ non-}\phi)/\Gamma(\rho K^- \pi^+)$ Γ_{25}/Γ_2

VALUE (units 10^{-3})	EVTS	DOCUMENT ID	TECN	COMMENT
8.4 ± 1.8 OUR AVERAGE				
9.36 ± 2.22 ± 0.71	38	ABLIKIM	16u BES3	$e^+ e^-$ at 4.599 GeV
7 ± 2 ± 2	344	ABE	02c BELL	$e^+ e^- \approx \Upsilon(4S)$

 $\Gamma(\rho\phi\pi^0)/\Gamma(\rho K^- \pi^+)$ Γ_{26}/Γ_2

VALUE (units 10^{-3})	DOCUMENT ID	TECN	COMMENT
1.538 ± 0.641^{+0.077}_{-0.100}	PAL	17 BELL	$e^+ e^- \approx \Upsilon(4S), \Upsilon(5S)$

 $\Gamma(\rho K^+ K^- \pi^0 \text{ nonresonant})/\Gamma_{\text{total}}$ Γ_{27}/Γ

VALUE	CL%	DOCUMENT ID	TECN	COMMENT
< 6.3 × 10⁻⁵	90	PAL	17 BELL	$e^+ e^- \approx \Upsilon(4S), \Upsilon(5S)$

————— Hadronic modes with a hyperon: $S = -1$ final states —————

 $\Gamma(\Lambda\pi^+)/\Gamma_{\text{total}}$ Γ_{28}/Γ

VALUE (%)	EVTS	DOCUMENT ID	TECN	COMMENT
1.30 ± 0.07 OUR FIT				Error includes scale factor of 1.1.
1.24 ± 0.07 ± 0.03	706	ABLIKIM	16 BES3	$e^+ e^- \rightarrow \Lambda_c \bar{\Lambda}_c, 4.599$ GeV

 $\Gamma(\Lambda\pi^+)/\Gamma(\rho K^- \pi^+)$ Γ_{28}/Γ_2

VALUE	EVTS	DOCUMENT ID	TECN	COMMENT
0.207 ± 0.009 OUR FIT				Error includes scale factor of 1.2.
0.204 ± 0.019 OUR AVERAGE				
0.217 ± 0.013 ± 0.020	750	LINK	05F FOCS	γ nucleus, $\bar{E}_\gamma \approx 180$ GeV
0.18 ± 0.03 ± 0.04		ALBRECHT	92 ARG	$e^+ e^- \approx 10.4$ GeV
0.18 ± 0.03 ± 0.03	87	AVERY	91 CLEO	$e^+ e^- 10.5$ GeV

 $\Gamma(\Lambda(1670)\pi^+, \Lambda(1670) \rightarrow \eta\Lambda)/\Gamma(\rho K^- \pi^+)$ Γ_{29}/Γ_2

VALUE (units 10^{-2})	EVTS	DOCUMENT ID	TECN	COMMENT
5.54 ± 0.29 ± 0.73	9.7k	LEE	21A BELL	$e^+ e^- \approx \Upsilon(nS)$

 $\Gamma(\Lambda\pi^+\pi^0)/\Gamma_{\text{total}}$ Γ_{30}/Γ

VALUE (%)	EVTS	DOCUMENT ID	TECN	COMMENT
7.1 ± 0.4 OUR FIT				Error includes scale factor of 1.1.
7.01 ± 0.37 ± 0.19	1497	ABLIKIM	16 BES3	$e^+ e^- \rightarrow \Lambda_c \bar{\Lambda}_c, 4.599$ GeV

 $\Gamma(\Lambda\pi^+\pi^0)/\Gamma(\rho K^- \pi^+)$ Γ_{30}/Γ_2

VALUE	EVTS	DOCUMENT ID	TECN	COMMENT
1.12 ± 0.05 OUR FIT				Error includes scale factor of 1.1.
0.73 ± 0.09 ± 0.16	464	AVERY	94 CLE2	$e^+ e^- \approx \Upsilon(3S), \Upsilon(4S)$

 $\Gamma(\Lambda\rho^+)/\Gamma(\rho K^- \pi^+)$ Γ_{31}/Γ_2

VALUE	CL%	DOCUMENT ID	TECN	COMMENT
< 0.95	95	AVERY	94 CLE2	$e^+ e^- \approx \Upsilon(3S), \Upsilon(4S)$

 $\Gamma(\Lambda\pi^- 2\pi^+)/\Gamma_{\text{total}}$ Γ_{32}/Γ

VALUE (%)	EVTS	DOCUMENT ID	TECN	COMMENT
3.64 ± 0.29 OUR FIT				Error includes scale factor of 1.4.
3.81 ± 0.24 ± 0.18	609	ABLIKIM	16 BES3	$e^+ e^- \rightarrow \Lambda_c \bar{\Lambda}_c, 4.599$ GeV

 $\Gamma(\Lambda\pi^- 2\pi^+)/\Gamma(\rho K^- \pi^+)$ Γ_{32}/Γ_2

VALUE	EVTS	DOCUMENT ID	TECN	COMMENT
0.58 ± 0.04 OUR FIT				Error includes scale factor of 1.9.
0.522 ± 0.032 OUR AVERAGE				
0.508 ± 0.024 ± 0.024	1356	LINK	05F FOCS	γ nucleus, $\bar{E}_\gamma \approx 180$ GeV
0.65 ± 0.11 ± 0.12	289	AVERY	91 CLEO	$e^+ e^- 10.5$ GeV
0.82 ± 0.29 ± 0.27	44	ANJOS	90 E691	γ Be 70–260 GeV
0.94 ± 0.41 ± 0.13	10	BARLAG	90D NA32	$\pi^- 230$ GeV
0.61 ± 0.16 ± 0.04	105	ALBRECHT	88c ARG	$e^+ e^- 10$ GeV

 $\Gamma(\Sigma(1385)^+\pi^+\pi^-, \Sigma^{*+} \rightarrow \Lambda\pi^+)/\Gamma(\Lambda\pi^- 2\pi^+)$ Γ_{33}/Γ_{32}

VALUE	DOCUMENT ID	TECN	COMMENT
0.28 ± 0.10 ± 0.08	LINK	05F FOCS	γ nucleus, $\bar{E}_\gamma \approx 180$ GeV

 $\Gamma(\Sigma(1385)^- 2\pi^+, \Sigma^{*-} \rightarrow \Lambda\pi^-)/\Gamma(\Lambda\pi^- 2\pi^+)$ Γ_{34}/Γ_{32}

VALUE	DOCUMENT ID	TECN	COMMENT
0.21 ± 0.03 ± 0.02	LINK	05F FOCS	γ nucleus, $\bar{E}_\gamma \approx 180$ GeV

 $\Gamma(\Lambda\pi^+\rho^0)/\Gamma(\Lambda\pi^- 2\pi^+)$ Γ_{35}/Γ_{32}

VALUE	DOCUMENT ID	TECN	COMMENT
0.40 ± 0.12 ± 0.12	LINK	05F FOCS	γ nucleus, $\bar{E}_\gamma \approx 180$ GeV

 $\Gamma(\Sigma(1385)^+\rho^0, \Sigma^{*+} \rightarrow \Lambda\pi^+)/\Gamma(\Lambda\pi^- 2\pi^+)$ Γ_{36}/Γ_{32}

VALUE	DOCUMENT ID	TECN	COMMENT
0.14 ± 0.09 ± 0.07	LINK	05F FOCS	γ nucleus, $\bar{E}_\gamma \approx 180$ GeV

 $\Gamma(\Lambda\pi^- 2\pi^+ \text{ nonresonant})/\Gamma(\Lambda\pi^- 2\pi^+)$ Γ_{37}/Γ_{32}

VALUE	CL%	DOCUMENT ID	TECN	COMMENT
< 0.3	90	LINK	05F FOCS	γ nucleus, $\bar{E}_\gamma \approx 180$ GeV

 $\Gamma(\Lambda\pi^- \pi^0 2\pi^+ \text{ total})/\Gamma(\rho K^- \pi^+)$ Γ_{38}/Γ_2

VALUE	EVTS	DOCUMENT ID	TECN	COMMENT
0.36 ± 0.09 ± 0.09	50	¹ CRONIN-HEN..03	CLE3	$e^+ e^- \approx \Upsilon(4S)$
				¹ CRONIN-HENNESSY 03 finds this channel to be dominantly $\Lambda\eta\pi^+$ and $\Lambda\omega\pi^+$; see below.

 $\Gamma(\Lambda\pi^+\eta)/\Gamma_{\text{total}}$ Γ_{39}/Γ

VALUE (units 10^{-2})	EVTS	DOCUMENT ID	TECN	COMMENT
1.84 ± 0.21 ± 0.15	154	ABLIKIM	19Y BES3	$e^+ e^-$ at 4.6 GeV

 $\Gamma(\Lambda\pi^+\eta)/\Gamma(\rho K^- \pi^+)$ Γ_{39}/Γ_2

VALUE	EVTS	DOCUMENT ID	TECN	COMMENT
0.295 ± 0.014 OUR AVERAGE				Unseen decay modes of the η are included.
0.293 ± 0.003 ± 0.014	51k	LEE	21A BELL	$e^+ e^- \approx \Upsilon(nS)$
0.41 ± 0.17 ± 0.10	11	CRONIN-HEN..03	CLE3	$e^+ e^- \approx \Upsilon(4S)$
0.35 ± 0.05 ± 0.06	116	AMMAR	95 CLE2	$e^+ e^- \approx \Upsilon(4S)$

 $\Gamma(\Sigma(1385)^+\eta)/\Gamma_{\text{total}}$ Γ_{40}/Γ

VALUE (units 10^{-2})	EVTS	DOCUMENT ID	TECN	COMMENT
0.91 ± 0.18 ± 0.09	54	ABLIKIM	19Y BES3	$e^+ e^-$ at 4.6 GeV

 $\Gamma(\Sigma(1385)^+\eta)/\Gamma(\rho K^- \pi^+)$ Γ_{40}/Γ_2

VALUE	EVTS	DOCUMENT ID	TECN	COMMENT
0.190 ± 0.016 OUR AVERAGE				Unseen decay modes of the $\Sigma(1385)^+$ and η are included.
0.192 ± 0.006 ± 0.016	29k	LEE	21A BELL	$e^+ e^- \approx \Upsilon(nS)$
0.17 ± 0.04 ± 0.03	54	AMMAR	95 CLE2	$e^+ e^- \approx \Upsilon(4S)$

 $\Gamma(\Lambda\pi^+\omega)/\Gamma(\rho K^- \pi^+)$ Γ_{41}/Γ_2

VALUE	EVTS	DOCUMENT ID	TECN	COMMENT
0.24 ± 0.06 ± 0.06	32	CRONIN-HEN..03	CLE3	$e^+ e^- \approx \Upsilon(4S)$

 $\Gamma(\Lambda\pi^- \pi^0 2\pi^+, \text{ no } \eta \text{ or } \omega)/\Gamma(\rho K^- \pi^+)$ Γ_{42}/Γ_2

VALUE	CL%	DOCUMENT ID	TECN	COMMENT
< 0.13	90	CRONIN-HEN..03	CLE3	$e^+ e^- \approx \Upsilon(4S)$

 $\Gamma(\Lambda K^+ \bar{K}^0)/\Gamma(\rho K^- \pi^+)$ Γ_{43}/Γ_2

VALUE	EVTS	DOCUMENT ID	TECN	COMMENT
0.090 ± 0.017 OUR FIT				Error includes scale factor of 1.9.
0.131 ± 0.020 OUR AVERAGE				
0.142 ± 0.018 ± 0.022	251	LINK	05F FOCS	γ nucleus, $\bar{E}_\gamma \approx 180$ GeV
0.12 ± 0.02 ± 0.02	59	AMMAR	95 CLE2	$e^+ e^- \approx \Upsilon(4S)$

 $\Gamma(\Xi(1690)^0 K^+, \Xi^{*0} \rightarrow \Lambda \bar{K}^0)/\Gamma(\Lambda K^+ \bar{K}^0)$ Γ_{44}/Γ_{43}

VALUE	EVTS	DOCUMENT ID	TECN	COMMENT
0.28 ± 0.07 OUR AVERAGE				
0.32 ± 0.10 ± 0.04	84 ± 24	LINK	05F FOCS	γ nucleus, $\bar{E}_\gamma \approx 180$ GeV
0.26 ± 0.08 ± 0.03	93	ABE	02c BELL	$e^+ e^- \approx \Upsilon(4S)$

 $\Gamma(\Lambda K^+ \bar{K}^0)/\Gamma(\Lambda\pi^+)$ Γ_{43}/Γ_{28}

VALUE	EVTS	DOCUMENT ID	TECN	COMMENT
0.44 ± 0.08 OUR FIT				Error includes scale factor of 2.0.
0.395 ± 0.026 ± 0.036	460 ± 30	AUBERT	07u BABR	$e^+ e^- \approx \Upsilon(4S)$

 $\Gamma(\Sigma^0 \pi^+)/\Gamma_{\text{total}}$ Γ_{45}/Γ

VALUE (%)	EVTS	DOCUMENT ID	TECN	COMMENT
1.29 ± 0.07 OUR FIT				Error includes scale factor of 1.1.
1.27 ± 0.08 ± 0.03	522	ABLIKIM	16 BES3	$e^+ e^- \rightarrow \Lambda_c \bar{\Lambda}_c, 4.599$ GeV

 $\Gamma(\Sigma^0 \pi^+)/\Gamma(\rho K^- \pi^+)$ Γ_{45}/Γ_2

VALUE	EVTS	DOCUMENT ID	TECN	COMMENT
0.206 ± 0.010 OUR FIT				Error includes scale factor of 1.2.
0.20 ± 0.04 OUR AVERAGE				
0.21 ± 0.02 ± 0.04	196	AVERY	94 CLE2	$e^+ e^- \approx \Upsilon(3S), \Upsilon(4S)$
0.17 ± 0.06 ± 0.04		ALBRECHT	92 ARG	$e^+ e^- \approx 10.4$ GeV

 $\Gamma(\Sigma^0 \pi^+)/\Gamma(\Lambda\pi^+)$ Γ_{45}/Γ_{28}

VALUE	EVTS	DOCUMENT ID	TECN	COMMENT
0.99 ± 0.04 OUR FIT				
0.98 ± 0.05 OUR AVERAGE				
0.977 ± 0.015 ± 0.051	33k	AUBERT	07u BABR	$e^+ e^- \approx \Upsilon(4S)$
1.09 ± 0.11 ± 0.19	750	LINK	05F FOCS	γ nucleus, $\bar{E}_\gamma \approx 180$ GeV

 $\Gamma(\Sigma^0 \pi^+\eta)/\Gamma(\rho K^- \pi^+)$ Γ_{46}/Γ_2

VALUE	EVTS	DOCUMENT ID	TECN	COMMENT
0.120 ± 0.006 ± 0.010	17k	LEE	21A BELL	$e^+ e^- \approx \Upsilon(nS)$

 $\Gamma(\Sigma^+ \pi^0)/\Gamma_{\text{total}}$ Γ_{47}/Γ

VALUE (%)	EVTS	DOCUMENT ID	TECN	COMMENT
1.25 ± 0.10 OUR FIT				
1.18 ± 0.10 ± 0.03	309	ABLIKIM	16 BES3	$e^+ e^- \rightarrow \Lambda_c \bar{\Lambda}_c, 4.599$ GeV

Baryon Particle Listings

Λ_c^+

$\Gamma(\Sigma^+\pi^0)/\Gamma(\rho K^-\pi^+)$					Γ_{47}/Γ_2
VALUE	EVTS	DOCUMENT ID	TECN	COMMENT	
0.199±0.015 OUR FIT					
0.20 ±0.03 ±0.03	93	KUBOTA	93	CLE2	$e^+e^- \approx \Upsilon(4S)$

$\Gamma(\Sigma^+\eta)/\Gamma(\rho K^-\pi^+)$					Γ_{48}/Γ_2
Unseen decay modes of the η are included.					
VALUE	EVTS	DOCUMENT ID	TECN	COMMENT	
0.11±0.03±0.02	26	AMMAR	95	CLE2	$e^+e^- \approx \Upsilon(4S)$

$\Gamma(\Sigma^+\eta)/\Gamma(\Sigma^+\pi^0)$					Γ_{48}/Γ_{47}
VALUE	EVTS	DOCUMENT ID	TECN	COMMENT	
0.35±0.16±0.02	15	¹ ABLIKIM	19x	BES3	e^+e^- at 4.6 GeV
¹ ABLIKIM 19x report evidence for the observation of the decay $\Lambda_c^+ \rightarrow \Sigma^+\eta$ at 2.5 σ significance.					

$\Gamma(\Sigma^+\eta')/\Gamma(\Sigma^+\omega)$					Γ_{49}/Γ_{57}
VALUE	EVTS	DOCUMENT ID	TECN	COMMENT	
0.86±0.34±0.04	13	¹ ABLIKIM	19x	BES3	e^+e^- at 4.6 GeV
¹ ABLIKIM 19x report evidence for the observation of the decay $\Lambda_c^+ \rightarrow \Sigma^+\eta'$ at 3.2 σ significance.					

$\Gamma(\Sigma^+\pi^+\pi^-)/\Gamma_{total}$					Γ_{50}/Γ
VALUE (%)	EVTS	DOCUMENT ID	TECN	COMMENT	
4.50±0.25 OUR FIT					Error includes scale factor of 1.3.
4.25±0.24±0.20	1156	ABLIKIM	16	BES3	$e^+e^- \rightarrow \Lambda_c^+\bar{\Lambda}_c, 4.599$ GeV

$\Gamma(\Sigma^+\pi^+\pi^-)/\Gamma(\rho K^-\pi^+)$					Γ_{50}/Γ_2
VALUE	EVTS	DOCUMENT ID	TECN	COMMENT	
0.716±0.019 OUR FIT					
0.720±0.024 OUR AVERAGE					
0.719±0.003±0.024	2.7M	BERGER	18	BELL	$e^+e^- \approx \Upsilon(4S)$
0.74±0.07±0.09	487	KUBOTA	93	CLE2	$e^+e^- \approx \Upsilon(4S)$
••• We do not use the following data for averages, fits, limits, etc. •••					
0.72 ±0.14	47 ± 9	VAZQUEZ-JA...08	SELX	Σ^- nucleus, 600 GeV	
0.54 ^{+0.18} / _{-0.15}	11	BARLAG	92	NA32	π^- Cu 230 GeV

$\Gamma(\Sigma^+\rho^0)/\Gamma(\rho K^-\pi^+)$					Γ_{51}/Γ_2
VALUE	CL%	DOCUMENT ID	TECN	COMMENT	
<0.27	95	KUBOTA	93	CLE2	$e^+e^- \approx \Upsilon(4S)$

$\Gamma(\Sigma^-2\pi^+)/\Gamma_{total}$					Γ_{52}/Γ
VALUE (%)	EVTS	DOCUMENT ID	TECN	COMMENT	
1.87±0.18 OUR FIT					
1.81±0.17±0.09	161	ABLIKIM	17y	BES3	e^+e^- at 4.6 GeV

$\Gamma(\Sigma^-2\pi^+)/\Gamma(\rho K^-\pi^+)$					Γ_{52}/Γ_2
VALUE	EVTS	DOCUMENT ID	TECN	COMMENT	
0.297±0.030 OUR FIT					Error includes scale factor of 1.1.
0.314±0.067	30 ± 6	VAZQUEZ-JA...08	SELX	Σ^- nucleus, 600 GeV	

$\Gamma(\Sigma^-2\pi^+)/\Gamma(\Sigma^+\pi^+\pi^-)$					Γ_{52}/Γ_{50}
VALUE	EVTS	DOCUMENT ID	TECN	COMMENT	
0.42±0.04 OUR FIT					Error includes scale factor of 1.1.
0.53±0.15±0.07	56	FRABETTI	94E	E687	γ Be, \bar{E}_γ 220 GeV

$\Gamma(\Sigma^0\pi^+\pi^0)/\Gamma(\rho K^-\pi^+)$					Γ_{53}/Γ_2
VALUE	EVTS	DOCUMENT ID	TECN	COMMENT	
0.56 ±0.05 OUR AVERAGE					Error includes scale factor of 1.5.
0.575±0.005±0.036	2.7M	BERGER	18	BELL	$e^+e^- \approx \Upsilon(4S)$
0.36 ±0.09 ±0.10	117	AVERY	94	CLE2	$e^+e^- \approx \Upsilon(3S), \Upsilon(4S)$

$\Gamma(\Sigma^+\pi^0\pi^0)/\Gamma(\rho K^-\pi^+)$					Γ_{54}/Γ_2
VALUE	EVTS	DOCUMENT ID	TECN	COMMENT	
0.247±0.006±0.019	925k	BERGER	18	BELL	$e^+e^- \approx \Upsilon(4S)$

$\Gamma(\Sigma^0\pi^-2\pi^+)/\Gamma(\rho K^-\pi^+)$					Γ_{55}/Γ_2
VALUE	EVTS	DOCUMENT ID	TECN	COMMENT	
0.18±0.05 OUR FIT					
0.21±0.05±0.05	90	AVERY	94	CLE2	$e^+e^- \approx \Upsilon(3S), \Upsilon(4S)$

$\Gamma(\Sigma^0\pi^-2\pi^+)/\Gamma(\Lambda\pi^-2\pi^+)$					Γ_{55}/Γ_{32}
VALUE	EVTS	DOCUMENT ID	TECN	COMMENT	
0.31±0.08 OUR FIT					
0.26±0.06±0.09	480	LINK	05F	FOCS	γ nucleus, $\bar{E}_\gamma \approx 180$ GeV

$\Gamma(\Sigma^+\omega)/\Gamma_{total}$					Γ_{57}/Γ
VALUE (%)	EVTS	DOCUMENT ID	TECN	COMMENT	
1.70±0.21 OUR FIT					
1.56±0.20±0.07	157	ABLIKIM	16	BES3	$e^+e^- \rightarrow \Lambda_c^+\bar{\Lambda}_c, 4.599$ GeV

$\Gamma(\Sigma^+\omega)/\Gamma(\rho K^-\pi^+)$					Γ_{57}/Γ_2
Unseen decay modes of the ω are included.					
VALUE	EVTS	DOCUMENT ID	TECN	COMMENT	
0.271±0.031 OUR FIT					
0.54 ±0.13 ±0.06	107	KUBOTA	93	CLE2	$e^+e^- \approx \Upsilon(4S)$

$\Gamma(\Sigma^-\pi^02\pi^+)/\Gamma_{total}$					Γ_{58}/Γ
VALUE (%)	EVTS	DOCUMENT ID	TECN	COMMENT	
2.11±0.33±0.14	88	ABLIKIM	17y	BES3	e^+e^- at 4.6 GeV

$\Gamma(\Sigma^+K^+K^-)/\Gamma(\rho K^-\pi^+)$					Γ_{59}/Γ_2
VALUE	EVTS	DOCUMENT ID	TECN	COMMENT	
0.056±0.006 OUR FIT					
0.070±0.011±0.011	59	AVERY	93	CLE2	$e^+e^- \approx 10.5$ GeV

$\Gamma(\Sigma^+K^+K^-)/\Gamma(\Sigma^+\pi^+\pi^-)$					Γ_{59}/Γ_{50}
VALUE	EVTS	DOCUMENT ID	TECN	COMMENT	
0.078±0.008 OUR FIT					
0.074±0.009 OUR AVERAGE					
0.076±0.007±0.009	246	ABE	02c	BELL	$e^+e^- \approx \Upsilon(4S)$
0.071±0.011±0.011	103	LINK	02G	FOCS	γ nucleus, ≈ 180 GeV

$\Gamma(\Sigma^+\phi)/\Gamma(\rho K^-\pi^+)$					Γ_{60}/Γ_2
Unseen decay modes of the ϕ are included.					
VALUE	EVTS	DOCUMENT ID	TECN	COMMENT	
0.062±0.009 OUR FIT					
0.069±0.023±0.016	26	AVERY	93	CLE2	$e^+e^- \approx 10.5$ GeV

$\Gamma(\Sigma^+\phi)/\Gamma(\Sigma^+\pi^+\pi^-)$					Γ_{60}/Γ_{50}
Unseen decay modes of the ϕ are included.					
VALUE	EVTS	DOCUMENT ID	TECN	COMMENT	
0.087±0.012 OUR FIT					
0.086±0.012 OUR AVERAGE					
0.085±0.012±0.012	129	ABE	02c	BELL	$e^+e^- \approx \Upsilon(4S)$
0.087±0.016±0.006	57	LINK	02G	FOCS	γ nucleus, ≈ 180 GeV

$\Gamma(\Xi(1690)^0 K^+, \Xi^{*0} \rightarrow \Sigma^+ K^-)/\Gamma(\Sigma^+\pi^+\pi^-)$					Γ_{61}/Γ_{50}
VALUE	EVTS	DOCUMENT ID	TECN	COMMENT	
0.023±0.005 OUR AVERAGE					
0.023±0.005±0.005	75	ABE	02c	BELL	$e^+e^- \approx \Upsilon(4S)$
0.022±0.006±0.006	34	LINK	02G	FOCS	γ nucleus, ≈ 180 GeV

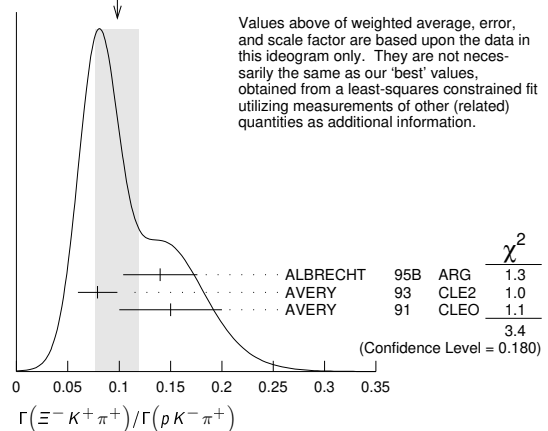
$\Gamma(\Sigma^+K^+K^- \text{ nonresonant})/\Gamma(\Sigma^+\pi^+\pi^-)$					Γ_{62}/Γ_{50}
VALUE	CL%	DOCUMENT ID	TECN	COMMENT	
<0.018	90	ABE	02c	BELL	$e^+e^- \approx \Upsilon(4S)$
••• We do not use the following data for averages, fits, limits, etc. •••					
<0.028	90	LINK	02G	FOCS	γ nucleus, ≈ 180 GeV

$\Gamma(\Xi^0 K^+)/\Gamma_{total}$					Γ_{63}/Γ
VALUE (units 10^{-3})	EVTS	DOCUMENT ID	TECN	COMMENT	
5.5 ±0.7 OUR FIT					
5.90±0.86±0.39	68	ABLIKIM	18y	BES3	e^+e^- at 4.6 GeV

$\Gamma(\Xi^0 K^+)/\Gamma(\rho K^-\pi^+)$					Γ_{63}/Γ_2
VALUE	EVTS	DOCUMENT ID	TECN	COMMENT	
0.088±0.012 OUR FIT					
0.078±0.013±0.013	56	AVERY	93	CLE2	$e^+e^- \approx 10.5$ GeV

$\Gamma(\Xi^- K^+\pi^+)/\Gamma(\rho K^-\pi^+)$					Γ_{64}/Γ_2
VALUE	EVTS	DOCUMENT ID	TECN	COMMENT	
0.099±0.009 OUR FIT					
0.098±0.021 OUR AVERAGE					Error includes scale factor of 1.3. See the ideogram below.
0.14 ±0.03 ±0.02	34	ALBRECHT	95B	ARG	$e^+e^- \approx 10.4$ GeV
0.079±0.013±0.014	60	AVERY	93	CLE2	$e^+e^- \approx 10.5$ GeV
0.15 ±0.04 ±0.03	30	AVERY	91	CLEO	$e^+e^- 10.5$ GeV

WEIGHTED AVERAGE
0.098±0.021 (Error scaled by 1.3)



$\Gamma(\Xi^- K^+ \pi^+)/\Gamma(\Lambda \pi^+)$ Γ_{64}/Γ_{28}

VALUE	EVTS	DOCUMENT ID	TECN	COMMENT
0.48 ± 0.04 OUR FIT				
0.480 ± 0.016 ± 0.039	2665 ± 84	AUBERT	07u BABR	$e^+ e^- \approx \Upsilon(4S)$

$\Gamma(\Xi(1530)^0 K^+)/\Gamma_{total}$ Γ_{65}/Γ

VALUE (units 10^{-3})	EVTS	DOCUMENT ID	TECN	COMMENT
4.3 ± 0.9 OUR FIT				Error includes scale factor of 1.1.
5.02 ± 0.99 ± 0.31	60	ABLIKIM	18y BES3	$e^+ e^-$ at 4.6 GeV

$\Gamma(\Xi(1530)^0 K^+)/\Gamma(\rho K^- \pi^+)$ Γ_{65}/Γ_2

VALUE	EVTS	DOCUMENT ID	TECN	COMMENT
0.068 ± 0.014 OUR FIT				Error includes scale factor of 1.1.
0.053 ± 0.016 ± 0.010	24	AVERY	93 CLE2	$e^+ e^- \approx 10.5$ GeV
0.05 ± 0.02 ± 0.01	11	ALBRECHT	95b ARG	$e^+ e^- \approx 10.4$ GeV

Hadronic modes with a hyperon: S = 0 final states

$\Gamma(\Lambda K^+)/\Gamma(\Lambda \pi^+)$ Γ_{66}/Γ_{28}

VALUE	EVTS	DOCUMENT ID	TECN	COMMENT
0.047 ± 0.009 OUR AVERAGE				Error includes scale factor of 1.8.
0.044 ± 0.004 ± 0.003	1162 ± 101	AUBERT	07u BABR	$e^+ e^- \approx \Upsilon(4S)$
0.074 ± 0.010 ± 0.012	265	ABE	02c BELL	$e^+ e^- \approx \Upsilon(4S)$

$\Gamma(\Lambda K^+ \pi^+ \pi^-)/\Gamma(\Lambda \pi^+)$ Γ_{67}/Γ_{28}

VALUE	CL%	DOCUMENT ID	TECN	COMMENT
< 4.1 × 10⁻²	90	AUBERT	07u BABR	$e^+ e^- \approx \Upsilon(4S)$

$\Gamma(\Sigma^0 K^+)/\Gamma(\Sigma^0 \pi^+)$ Γ_{68}/Γ_{45}

VALUE	EVTS	DOCUMENT ID	TECN	COMMENT
0.040 ± 0.006 OUR AVERAGE				
0.038 ± 0.005 ± 0.003	366 ± 52	AUBERT	07u BABR	$e^+ e^- \approx \Upsilon(4S)$
0.056 ± 0.014 ± 0.008	75	ABE	02c BELL	$e^+ e^- \approx \Upsilon(4S)$

$\Gamma(\Sigma^0 K^+ \pi^+ \pi^-)/\Gamma(\Sigma^0 \pi^+)$ Γ_{69}/Γ_{45}

VALUE	CL%	DOCUMENT ID	TECN	COMMENT
< 2.0 × 10⁻²	90	AUBERT	07u BABR	$e^+ e^- \approx \Upsilon(4S)$

$\Gamma(\Sigma^+ K^+ \pi^-)/\Gamma(\Sigma^+ \pi^+ \pi^-)$ Γ_{70}/Γ_{50}

VALUE	EVTS	DOCUMENT ID	TECN	COMMENT
0.047 ± 0.011 ± 0.008	105	ABE	02c BELL	$e^+ e^- \approx \Upsilon(4S)$

$\Gamma(\Sigma^+ K^*(892)^0)/\Gamma(\Sigma^+ \pi^+ \pi^-)$ Γ_{71}/Γ_{50}

Unseen decay modes of the $K^*(892)^0$ are included.

VALUE	EVTS	DOCUMENT ID	TECN	COMMENT
0.078 ± 0.018 ± 0.013	49	LINK	02g FOCS	γ nucleus, ≈ 180 GeV

$\Gamma(\Sigma^- K^+ \pi^+)/\Gamma(\Sigma^+ K^*(892)^0)$ Γ_{72}/Γ_{71}

VALUE	CL%	DOCUMENT ID	TECN	COMMENT
< 0.35	90	LINK	02g FOCS	γ nucleus, ≈ 180 GeV

Doubly Cabibbo-suppressed modes

$\Gamma(\rho K^+ \pi^-)/\Gamma(\rho K^- \pi^+)$ Γ_{73}/Γ_2

VALUE (units 10^{-3})	EVTS	DOCUMENT ID	TECN	COMMENT
1.77 ± 0.27 OUR AVERAGE				Error includes scale factor of 1.9.
1.65 ± 0.15 ± 0.05	392	AAIJ	18v LHCb	$\Lambda_b^0 \rightarrow \Lambda_c^+ \mu^- X$
2.35 ± 0.27 ± 0.21	3379	YANG	16 BELL	At or near T 's

Semileptonic modes

$\Gamma(\Lambda e^+ \nu_e)/\Gamma_{total}$ Γ_{74}/Γ

VALUE (%)	EVTS	DOCUMENT ID	TECN	COMMENT
3.63 ± 0.38 ± 0.20	104	ABLIKIM	15y BES3	567 pb ⁻¹ , 4.599 GeV

$\Gamma(\Lambda e^+ \nu_e)/\Gamma(e^+ \text{ anything})$ Γ_{74}/Γ_{76}

VALUE (%)	EVTS	DOCUMENT ID	TECN	COMMENT
91.9 ± 12.5 ± 5.4	214	ABLIKIM	18Af BES3	$e^+ e^-$ 4.6 GeV

$\Gamma(\Lambda e^+ \nu_e)/\Gamma(\rho K^- \pi^+)$ Γ_{74}/Γ_2

VALUE	EVTS	DOCUMENT ID	TECN	COMMENT
0.43 ± 0.08		1,2 BERGFELD	94 CLE2	$e^+ e^- \approx \Upsilon(4S)$
0.38 ± 0.14		2,3 ALBRECHT	91g ARG	$e^+ e^- \approx 10.4$ GeV
1 BERGFELD 94 measures $\sigma(e^+ e^- \rightarrow \Lambda_c^+ X) \cdot B(\Lambda_c^+ \rightarrow \Lambda e^+ \nu_e) = (4.87 \pm 0.28 \pm 0.69)$ pb. 2 To extract $\Gamma(\Lambda_c^+ \rightarrow \Lambda e^+ \nu_e)/\Gamma(\Lambda_c^+ \rightarrow \rho K^- \pi^+)$, we use $\sigma(e^+ e^- \rightarrow \Lambda_c^+ X) \cdot B(\Lambda_c^+ \rightarrow \rho K^- \pi^+) = (11.2 \pm 1.3)$ pb, which is the weighted average of measurements from ARGUS (ALBRECHT 96e) and CLEO (AVERY 91). 3 ALBRECHT 91g measures $\sigma(e^+ e^- \rightarrow \Lambda_c^+ X) \cdot B(\Lambda_c^+ \rightarrow \Lambda e^+ \nu_e) = (4.20 \pm 1.28 \pm 0.71)$ pb.				

$\Gamma(\Lambda \mu^+ \nu_\mu)/\Gamma_{total}$ Γ_{75}/Γ

VALUE (%)	EVTS	DOCUMENT ID	TECN	COMMENT
3.49 ± 0.46 ± 0.27	79	ABLIKIM	17D BES3	$e^+ e^-$ at 4.6 GeV

$\Gamma(\Lambda \mu^+ \nu_\mu)/\Gamma(\rho K^- \pi^+)$ Γ_{75}/Γ_2

VALUE	DOCUMENT ID	TECN	COMMENT
0.40 ± 0.09	1,2 BERGFELD	94 CLE2	$e^+ e^- \approx \Upsilon(4S)$
0.35 ± 0.20	2,3 ALBRECHT	91g ARG	$e^+ e^- \approx 10.4$ GeV
• • • We do not use the following data for averages, fits, limits, etc. • • • 1 BERGFELD 94 measures $\sigma(e^+ e^- \rightarrow \Lambda_c^+ X) \cdot B(\Lambda_c^+ \rightarrow \Lambda \mu^+ \nu_\mu) = (4.43 \pm 0.51 \pm 0.64)$ pb. 2 To extract $\Gamma(\Lambda_c^+ \rightarrow \Lambda \mu^+ \nu_\mu)/\Gamma(\Lambda_c^+ \rightarrow \rho K^- \pi^+)$, we use $\sigma(e^+ e^- \rightarrow \Lambda_c^+ X) \cdot B(\Lambda_c^+ \rightarrow \rho K^- \pi^+) = (11.2 \pm 1.3)$ pb, which is the weighted average of measurements from ARGUS (ALBRECHT 96e) and CLEO (AVERY 91). 3 ALBRECHT 91g measures $\sigma(e^+ e^- \rightarrow \Lambda_c^+ X) \cdot B(\Lambda_c^+ \rightarrow \Lambda \mu^+ \nu_\mu) = (3.91 \pm 2.02 \pm 0.90)$ pb.			

$\Gamma(\Lambda \mu^+ \nu_\mu)/\Gamma(\Lambda e^+ \nu_e)$ Γ_{75}/Γ_{74}

VALUE	DOCUMENT ID	TECN	COMMENT
0.96 ± 0.16 ± 0.04	1 ABLIKIM	17D BES3	$e^+ e^-$ at 4.6 GeV
• • • We do not use the following data for averages, fits, limits, etc. • • • 1 This is the ratio of the ABLIKIM 17D $\Lambda \mu^+ \nu_e$ branching fraction and the ABLIKIM 15y $\Lambda e^+ \nu_e$ branching fraction (see above), and so is not an independent measurement.			

Inclusive modes

$\Gamma(e^+ \text{ anything})/\Gamma_{total}$ Γ_{76}/Γ

VALUE (%)	EVTS	DOCUMENT ID	TECN	COMMENT
3.95 ± 0.34 ± 0.09	214	ABLIKIM	18Af BES3	$e^+ e^-$ 4.6 GeV

$\Gamma(\rho \text{ anything})/\Gamma_{total}$ Γ_{77}/Γ

VALUE	DOCUMENT ID	TECN	COMMENT
0.50 ± 0.08 ± 0.14	1 CRAWFORD	92 CLEO	$e^+ e^-$ 10.5 GeV
1 This CRAWFORD 92 value includes protons from Λ decay. The value is model dependent, but account is taken of this in the systematic error.			

$\Gamma(n \text{ anything})/\Gamma_{total}$ Γ_{78}/Γ

VALUE	DOCUMENT ID	TECN	COMMENT
0.50 ± 0.08 ± 0.14	1 CRAWFORD	92 CLEO	$e^+ e^-$ 10.5 GeV
1 This CRAWFORD 92 value includes neutrons from Λ decay. The value is model dependent, but account is taken of this in the systematic error.			

$\Gamma(\Lambda \text{ anything})/\Gamma_{total}$ Γ_{79}/Γ

VALUE (%)	EVTS	DOCUMENT ID	TECN	COMMENT
38.2^{+2.8}_{-2.2} ± 0.9	700	ABLIKIM	18e BES3	$e^+ e^-$ at 4.6 GeV

$\Gamma(K_S^0 \text{ anything})/\Gamma_{total}$ Γ_{80}/Γ

VALUE (%)	EVTS	DOCUMENT ID	TECN	COMMENT
9.9 ± 0.6 ± 0.4	478	ABLIKIM	20Aj BES3	$e^+ e^-$ at 4.6 GeV

$\Gamma(3\text{prongs})/\Gamma_{total}$ Γ_{81}/Γ

VALUE	DOCUMENT ID	TECN	COMMENT
0.24 ± 0.07 ± 0.04	KAYIS-TOPAK.03	CHRS	ν_μ emulsion, $\bar{E}=27$ GeV

Rare or forbidden modes

$\Gamma(\rho e^+ e^-)/\Gamma_{total}$ Γ_{82}/Γ

A test for the $\Delta C=1$ weak neutral current. Allowed by higher-order electroweak interactions.

VALUE	CL%	EVTS	DOCUMENT ID	TECN	COMMENT
< 5.5 × 10⁻⁶	90	4.0 ± 7.1	LEES	11g BABR	$e^+ e^- \approx \Upsilon(4S)$

$\Gamma(\rho \mu^+ \mu^- \text{ non-resonant})/\Gamma_{total}$ Γ_{83}/Γ

A test for the $\Delta C=1$ weak neutral current. Allowed by higher-order electroweak interactions.

VALUE	CL%	DOCUMENT ID	TECN	COMMENT
< 7.7 × 10⁻⁸	90	AAIJ	18N LHCb	Ratio to $p\phi, \phi \rightarrow \mu^+ \mu^-$
• • • We do not use the following data for averages, fits, limits, etc. • • • < 4.4 × 10 ⁻⁵ 90 LEES 11g BABR $e^+ e^- \approx \Upsilon(4S)$ < 3.4 × 10 ⁻⁴ 90 KODAMA 95 E653 π^- emulsion 600 GeV				

$\Gamma(\rho e^+ \mu^-)/\Gamma_{total}$ Γ_{84}/Γ

A test of lepton family-number conservation.

VALUE	CL%	EVTS	DOCUMENT ID	TECN	COMMENT
< 9.9 × 10⁻⁶	90	-0.7 ± 3.0	LEES	11g BABR	$e^+ e^- \approx \Upsilon(4S)$

$\Gamma(\rho e^- \mu^+)/\Gamma_{total}$ Γ_{85}/Γ

A test of lepton family-number conservation.

VALUE	CL%	EVTS	DOCUMENT ID	TECN	COMMENT
< 19 × 10⁻⁶	90	6.2 ± 4.9	LEES	11g BABR	$e^+ e^- \approx \Upsilon(4S)$

Baryon Particle Listings

$$\Lambda_c^+$$

$\Gamma(\bar{p}2e^+)/\Gamma_{total}$ Γ_{86}/Γ
 A test of lepton- and baryon-number conservation.

VALUE	CL%	EVTS	DOCUMENT ID	TECN	COMMENT
$<2.7 \times 10^{-6}$	90	-1.5 ± 4.5	LEES	11G BABR	$e^+e^- \approx \mathcal{T}(4S)$

$\Gamma(\bar{p}2\mu^+)/\Gamma_{total}$ Γ_{87}/Γ
 A test of lepton- and baryon-number conservation and of lepton family-number conservation.

VALUE	CL%	EVTS	DOCUMENT ID	TECN	COMMENT
$<9.4 \times 10^{-6}$	90	0.0 ± 2.2	LEES	11G BABR	$e^+e^- \approx \mathcal{T}(4S)$

$\Gamma(\bar{p}e^+\mu^+)/\Gamma_{total}$ Γ_{88}/Γ
 A test of lepton- and baryon-number conservation and of lepton family-number conservation.

VALUE	CL%	EVTS	DOCUMENT ID	TECN	COMMENT
$<16 \times 10^{-6}$	90	10.1 ± 6.8	LEES	11G BABR	$e^+e^- \approx \mathcal{T}(4S)$

$\Gamma(\Sigma^-\mu^+\mu^+)/\Gamma_{total}$ Γ_{89}/Γ
 A test of lepton-number conservation.

VALUE	CL%	EVTS	DOCUMENT ID	TECN	COMMENT
$<7.0 \times 10^{-4}$	90	0	KODAMA	95 E653	π^- emulsion 600 GeV

Λ_c^+ DECAY PARAMETERS

See the note on "Baryon Decay Parameters" in the neutron Listings.

α FOR $\Lambda_c^+ \rightarrow \Lambda\pi^+$

VALUE	CL%	EVTS	DOCUMENT ID	TECN	COMMENT
-0.84 ± 0.09	OUR AVERAGE				
$-0.80 \pm 0.11 \pm 0.02$			ABLIKIM	19AX BES3	e^+e^- at 4.6 GeV
$-0.78 \pm 0.16 \pm 0.19$			LINK	06A FOCUS	$\gamma A, \bar{E}_\gamma \approx 180$ GeV
$-0.94 \pm 0.21 \pm 0.12$	414		¹ BISHAI	95 CLE2	$e^+e^- \approx \mathcal{T}(4S)$
-0.96 ± 0.42			ALBRECHT	92 ARG	$e^+e^- \approx 10.4$ GeV
-1.1 ± 0.4	86		AVERY	90B CLEO	$e^+e^- \approx 10.6$ GeV

¹BISHAI 95 actually gives $\alpha = -0.94 + 0.21 + 0.12 - 0.06 - 0.06$, chopping the errors at the physical limit -1.0 . However, for $\alpha \approx -1.0$, some experiments should get unphysical values ($\alpha < -1.0$), and for averaging with other measurements such values (or errors that extend below -1.0) should not be chopped.

α FOR $\Lambda_c^+ \rightarrow \Sigma^+\pi^0$

VALUE	CL%	EVTS	DOCUMENT ID	TECN	COMMENT
-0.55 ± 0.11	OUR AVERAGE				
$-0.57 \pm 0.10 \pm 0.07$			ABLIKIM	19AX BES3	e^+e^- at 4.6 GeV
$-0.45 \pm 0.31 \pm 0.06$	89		BISHAI	95 CLE2	$e^+e^- \approx \mathcal{T}(4S)$

α FOR $\Lambda_c^+ \rightarrow \Sigma^0\pi^+$

VALUE	CL%	EVTS	DOCUMENT ID	TECN	COMMENT
$-0.73 \pm 0.17 \pm 0.07$			ABLIKIM	19AX BES3	e^+e^- at 4.6 GeV

α FOR $\Lambda_c^+ \rightarrow \Lambda e^+\nu_e$

The experiments don't cover the complete (or same incomplete) $M(\Lambda e^+)$ range, but we average them together anyway.

VALUE	CL%	EVTS	DOCUMENT ID	TECN	COMMENT
-0.86 ± 0.04	OUR AVERAGE				
$-0.86 \pm 0.03 \pm 0.02$	3201		¹ HINSON	05 CLEO	$e^+e^- \approx \mathcal{T}(4S)$
$-0.91 \pm 0.42 \pm 0.25$			² ALBRECHT	94B ARG	$e^+e^- \approx 10$ GeV
$-0.82 \pm 0.09 + 0.06 - 0.06 - 0.03$	700		³ CRAWFORD	95 CLE2	See HINSON 05
$-0.89 \pm 0.17 + 0.09 - 0.11 - 0.05$	350		⁴ BERGFELD	94 CLE2	See CRAWFORD 95

¹HINSON 05 measures the form-factor ratio $R \equiv f_2/f_1$ for $\Lambda_c^+ \rightarrow \Lambda e^+\nu_e$ events to be $-0.31 \pm 0.05 \pm 0.04$ and the pole mass to be $2.21 \pm 0.08 \pm 0.14$ GeV/ c^2 , and from these calculates α , averaged over q^2 , where $\langle q^2 \rangle = 0.67$ (GeV/ c^2).

²ALBRECHT 94B uses Λe^+ and $\Lambda\mu^+$ events in the mass range $1.85 < M(\Lambda e^+) < 2.20$ GeV.

³CRAWFORD 95 measures the form-factor ratio $R \equiv f_2/f_1$ for $\Lambda_c^+ \rightarrow \Lambda e^+\nu_e$ events to be $-0.25 \pm 0.14 \pm 0.08$ and from this calculates α , averaged over q^2 , to be the above.

⁴BERGFELD 94 uses Λe^+ events.

α FOR $\Lambda_c^+ \rightarrow \rho K_S^0$

VALUE	CL%	EVTS	DOCUMENT ID	TECN	COMMENT
$0.18 \pm 0.43 \pm 0.14$			ABLIKIM	19AX BES3	e^+e^- at 4.6 GeV

$\Lambda_c^+, \bar{\Lambda}_c^-$ CP-VIOLATING DECAY ASYMMETRIES

$(\alpha + \bar{\alpha})/(\alpha - \bar{\alpha})$ in $\Lambda_c^+ \rightarrow \Lambda\pi^+, \bar{\Lambda}_c^- \rightarrow \bar{\Lambda}\pi^-$

This is zero if CP is conserved.

VALUE	CL%	EVTS	DOCUMENT ID	TECN	COMMENT
$-0.07 \pm 0.19 \pm 0.24$			LINK	06A FOCUS	$\gamma A, \bar{E}_\gamma \approx 180$ GeV

$(\alpha + \bar{\alpha})/(\alpha - \bar{\alpha})$ in $\Lambda_c^+ \rightarrow \Lambda e^+\nu_e, \bar{\Lambda}_c^- \rightarrow \bar{\Lambda}e^-\bar{\nu}_e$

This is zero if CP is conserved.

VALUE	CL%	EVTS	DOCUMENT ID	TECN	COMMENT
$0.00 \pm 0.03 \pm 0.02$			HINSON	05 CLEO	$e^+e^- \approx \mathcal{T}(4S)$

$A_{CP}(\Lambda X)$ in $\Lambda_c \rightarrow \Lambda X, \bar{\Lambda}_c \rightarrow \bar{\Lambda} X$

VALUE (%)	CL%	EVTS	DOCUMENT ID	TECN	COMMENT
$2.1 \pm 7.0 - 6.6 \pm 1.6$		700	ABLIKIM	18E BES3	e^+e^- at 4.6 GeV

$\Delta A_{CP} = A_{CP}(\Lambda_c^+ \rightarrow \rho K^+ K^-) - A_{CP}(\Lambda_c^+ \rightarrow \rho\pi^+\pi^-)$

VALUE (%)	CL%	EVTS	DOCUMENT ID	TECN	COMMENT
$0.30 \pm 0.91 \pm 0.61$			¹ AAIJ	18R LHCB	$p\bar{p}$ 7, 8 TeV

¹AAIJ 18R applies phase-space-dependent weights to the $\Lambda_c^+ \rightarrow \rho\pi^+\pi^-$ sample to align its kinematics with the $\Lambda_c^+ \rightarrow \rho K^+ K^-$ sample.

Λ_c^+ REFERENCES

We have omitted some papers that have been superseded by later experiments. The omitted papers may be found in our 1992 edition (Physical Review D45, 1 June, Part II) or in earlier editions.

ABLIKIM	21H	PL B817 136327	M. Ablikim et al.	(BESIII Collab.)
ABLIKIM	21N	PR D103 1091101	M. Ablikim et al.	(BESIII Collab.)
LEE	21A	PR D103 052005	J.Y. Lee et al.	(BELLE Collab.)
LI	21	PR D103 072004	S.X. Li et al.	(BELLE Collab.)
LI	21E	PR D104 072008	S.X. Li et al.	(BELLE Collab.)
ABLIKIM	20AJ	EPJ C80 935	M. Ablikim et al.	(BESIII Collab.)
AAIJ	19AG	PR D100 032001	R. Aaij et al.	(LHCb Collab.)
ABLIKIM	19AX	PR D100 072004	M. Ablikim et al.	(BESIII Collab.)
ABLIKIM	19X	CP 443 083002	M. Ablikim et al.	(BESIII Collab.)
ABLIKIM	19Y	PR D99 032010	M. Ablikim et al.	(BESIII Collab.)
AAIJ	18N	PR D97 091101	R. Aaij et al.	(LHCb Collab.)
AAIJ	18R	JHEP 1803 182	R. Aaij et al.	(LHCb Collab.)
AAIJ	18V	JHEP 1803 043	R. Aaij et al.	(LHCb Collab.)
ABLIKIM	18AF	PRL 121 251801	M. Ablikim et al.	(BESIII Collab.)
ABLIKIM	18E	PRL 121 062003	M. Ablikim et al.	(BESIII Collab.)
ABLIKIM	18Y	PL B783 200	M. Ablikim et al.	(BESIII Collab.)
BERGER	18	PR D98 112006	M. Berger et al.	(BELLE Collab.)
ABLIKIM	17D	PL B767 42	M. Ablikim et al.	(BESIII Collab.)
ABLIKIM	17H	PRL 118 112001	M. Ablikim et al.	(BESIII Collab.)
ABLIKIM	17Q	PR D95 111102	M. Ablikim et al.	(BESIII Collab.)
ABLIKIM	17Y	PL B772 388	M. Ablikim et al.	(BESIII Collab.)
PAL	17	PR D96 051102	B. Pal et al.	(BELLE Collab.)
ABLIKIM	16	PRL 116 052001	M. Ablikim et al.	(BESIII Collab.)
ABLIKIM	16U	PRL 117 232002	M. Ablikim et al.	(BESIII Collab.)
YANG	16	PRL 117 011801	S.B. Yang et al.	(BELLE Collab.)
ABLIKIM	15Y	PRL 115 221805	M. Ablikim et al.	(BESIII Collab.)
ZUPANC	14	PRL 113 042002	A. Zupanc et al.	(BELLE Collab.)
LEES	11G	PR D84 072006	J.P. Lees et al.	(BABAR Collab.)
VAZQUEZ-JA...	08	PL B666 299	E. Vazquez-Jauregui et al.	(SELEX Collab.)
AUBERT	07U	PR D75 052002	B. Aubert et al.	(BABAR Collab.)
LINK	06A	PL B634 165	J.M. Link et al.	(FNAL FOCUS Collab.)
AUBERT.B	05S	PR D72 052006	B. Aubert et al.	(BABAR Collab.)
HINSON	05	PRL 94 191801	J.W. Hinson et al.	(CLEO Collab.)
LINK	05F	PL B624 221	J.M. Link et al.	(FNAL FOCUS Collab.)
CRONIN-HEN...	03	PR D67 012001	D. Cronin-Hennessy et al.	(CLEO Collab.)
KAYIS-TOPAK...	03	PL B555 156	A. Kayis-Topaksu et al.	(CERN CHORUS Collab.)
ABE	02C	PL B524 33	K. Abe et al.	(KEK BELLE Collab.)
LINK	02C	PRL 88 161801	J.M. Link et al.	(FNAL FOCUS Collab.)
LINK	02G	PL B540 25	J.M. Link et al.	(FNAL FOCUS Collab.)
PDG	02	PR D66 010001	K. Hagiwara et al.	(PDG Collab.)
KUSHNIR...	01	PRL 86 5243	A. Kushnirenko et al.	(FNAL SELEX Collab.)
MAHMOOD	01	PRL 86 2232	A.H. Mahmood et al.	(CLEO Collab.)
AITALA	00	PL B471 449	E.M. Aitala et al.	(FNAL E791 Collab.)
ALAM	98	PR D57 4467	M.S. Alam et al.	(CLEO Collab.)
ALBRECHT	96E	PR D57 273 223	H. Albrecht et al.	(ARGUS Collab.)
ALEXANDER	96C	PR D53 10113	J.P. Alexander et al.	(CLEO Collab.)
ALBRECHT	95B	PL B342 397	H. Albrecht et al.	(ARGUS Collab.)
AMMAR	95	PRL 74 3534	R. Ammar et al.	(CLEO Collab.)
BISHAI	95	PL B350 256	M. Bishai et al.	(CLEO Collab.)
CRAWFORD	95	PRL 75 624	G. Crawford et al.	(CLEO Collab.)
KODAMA	95	PL B345 85	K. Kodama et al.	(FNAL E653 Collab.)
ALBRECHT	94B	PL B326 320	H. Albrecht et al.	(ARGUS Collab.)
ALEEV	94	PAN 57 1370	A.N. Aleev et al.	(Serpukhov B1S-2 Collab.)
AVERY	94	Translated from YF 57 1443.	P. Avery et al.	(CLEO Collab.)
BERGFELD	94	PL B325 237	T. Bergfeld et al.	(CLEO Collab.)
FRABETTI	94E	PL B328 193	P.L. Frabetti et al.	(FNAL E687 Collab.)
AVERY	93	PRL 71 2391	P. Avery et al.	(CLEO Collab.)
BOZEK	93	PL B312 247	A. Bozek et al.	(CERN NA32 Collab.)
FRABETTI	93D	PRL 70 1755	P.L. Frabetti et al.	(FNAL E687 Collab.)
FRABETTI	93H	PL B314 477	P.L. Frabetti et al.	(FNAL E687 Collab.)
KUBOTA	93	PRL 71 3255	Y. Kubota et al.	(CLEO Collab.)
ALBRECHT	92	PL B274 239	H. Albrecht et al.	(ARGUS Collab.)
BARLAG	92	PL B283 465	S. Barlag et al.	(ACCMOR Collab.)
CRAWFORD	92	PR D45 752	G. Crawford et al.	(CLEO Collab.)
JEZABEK	92	PL B286 175	M. Jezabek, K. Rybicki, R. Rylko	(CRAC Collab.)
ALBRECHT	91G	PL B269 234	H. Albrecht et al.	(ARGUS Collab.)
AVERY	91	PR D43 3599	P. Avery et al.	(CLEO Collab.)
ALVAREZ	90	ZPHY C47 539	M.P. Alvarez et al.	(CERN NA14/2 Collab.)
ALVAREZ	90B	PL B246 256	M.P. Alvarez et al.	(CERN NA14/2 Collab.)
ANJOS	90	PR D41 801	J.C. Anjos et al.	(FNAL E691 Collab.)
AVERY	90B	PRL 65 2842	P. Avery et al.	(CLEO Collab.)
BARLAG	90D	ZPHY C48 29	S. Barlag et al.	(ACCMOR Collab.)
FRABETTI	90	PL B251 639	P.L. Frabetti et al.	(FNAL E687 Collab.)
BARLAG	89	PL B218 374	S. Barlag et al.	(ACCMOR Collab.)
AGUILAR...	88B	ZPHY C40 321	M. Aguilar-Benitez et al.	(LEBC-EHS Collab.)
Also		PL B359 254	M. Aguilar-Benitez et al.	(LEBC-EHS Collab.)
Also		PL B199 462	M. Aguilar-Benitez et al.	(LEBC-EHS Collab.)
Also		SJNP 48 833	M. Begalli et al.	(LEBC-EHS Collab.)
ALBRECHT	88C	PL B207 109	H. Albrecht et al.	(ARGUS Collab.)
ANJOS	88B	PRL 60 1379	J.C. Anjos et al.	(FNAL E691 Collab.)
AMENODOLA	87	ZPHY C36 513	S.R. Amendolia et al.	(CERN NA1 Collab.)
JONES	87	ZPHY C36 593	G.T. Jones et al.	(CERN WA21 Collab.)
BOSETTI	82	PL 109B 234	P.C. Bosetti et al.	(AACH3, BONN, CERN+)
BASILIE	81B	NC 62A 14	M. Basile et al.	(CERN, BONA, PIGA, FRAS)
CALICCHIO	80	PL 93B 521	M. Calicchio et al.	(BARI, BIRM, BRUX+)

OTHER RELATED PAPERS

MIGLIOZZI	99	PL B462 217	P. Migliozi et al.
DUNIETZ	98	PR D58 094010	I. Dunietz

See key on page 1127

Baryon Particle Listings

$\Lambda_c(2595)^+$, $\Lambda_c(2625)^+$

$\Lambda_c(2595)^+$ $J(P) = 0(\frac{1}{2}^-)$ Status: ***

The $\Lambda_c^+ \pi^+ \pi^-$ mode is largely, and perhaps entirely, $\Sigma_c \pi$, which is just at threshold; since the Σ_c has $J^P = 1/2^+$, the J^P here is almost certainly $1/2^-$. This result is in accord with the theoretical expectation that this is the charm counterpart of the strange $\Lambda(1405)$.

$\Lambda_c(2595)^+$ MASS

The mass is obtained from the $\Lambda_c(2595)^+ - \Lambda_c^+$ mass-difference measurements below.

VALUE (MeV)	DOCUMENT ID
2592.25 ± 0.28 OUR FIT	

$\Lambda_c(2595)^+ - \Lambda_c^+$ MASS DIFFERENCE

VALUE (MeV)	EVTS	DOCUMENT ID	TECN	COMMENT
305.79 ± 0.24 OUR FIT				
305.6 ± 0.3	3.5k	AALTONEN 11H	CDF	$p\bar{p}$ at 1.96 TeV
309.7 ± 0.9 ± 0.4	19	ALBRECHT 97	ARG	$e^+e^- \approx 10$ GeV
309.2 ± 0.7 ± 0.3	14 ± 4.5	FRABETTI 96	E687	γ Be, $\bar{E}_\gamma \approx 220$ GeV
307.5 ± 0.4 ± 1.0	112 ± 17	EDWARDS 95	CLE2	$e^+e^- \approx 10.5$ GeV

• • • We do not use the following data for averages, fits, limits, etc. • • •

¹ BLECHMAN 03 finds that a more sophisticated treatment than a simple Breit-Wigner for the proximity of the threshold of the dominant decay, $\Sigma_c(2455)\pi$, lowers the $\Lambda_c(2595)^+ - \Lambda_c^+$ mass difference by 2 or 3 MeV. The analysis of AALTONEN 11H bears this out.

$\Lambda_c(2595)^+$ WIDTH

VALUE (MeV)	EVTS	DOCUMENT ID	TECN	COMMENT
2.59 ± 0.30 ± 0.47	3.5k	² AALTONEN 11H	CDF	$p\bar{p}$ at 1.96 TeV
2.9 $^{+2.9}_{-2.1}$ $^{+1.8}_{-1.4}$	19	ALBRECHT 97	ARG	$e^+e^- \approx 10$ GeV
3.9 $^{+1.4}_{-1.2}$ $^{+2.0}_{-1.0}$	112 ± 17	EDWARDS 95	CLE2	$e^+e^- \approx 10.5$ GeV

• • • We do not use the following data for averages, fits, limits, etc. • • •

² AALTONEN 11H treats the three charged modes $\Lambda_c(2595)^+ \rightarrow \Sigma_c(2455)^+ \pi^-$, $\Sigma_c(2455)^+ \pi^0$, $\Sigma_c(2455)^0 \pi^+$ separately in terms of a common coupling constant h_2 and obtains $h_2^2 = 0.36 \pm 0.08$. From this the width is determined.

$\Lambda_c(2595)^+$ DECAY MODES

$\Lambda_c^+ \pi \pi$ and its submode $\Sigma_c(2455)\pi$ — the latter just barely — are the only strong decays allowed to an excited Λ_c^+ having this mass; and the submode seems to dominate.

Mode	Fraction (Γ_i/Γ)
Γ_1 $\Lambda_c^+ \pi^+ \pi^-$	[a] —
Γ_2 $\Sigma_c(2455)^{++} \pi^-$	24 ± 7 %
Γ_3 $\Sigma_c(2455)^0 \pi^+$	24 ± 7 %
Γ_4 $\Lambda_c^+ \pi^+ \pi^-$ 3-body	18 ± 10 %
Γ_5 $\Lambda_c^+ \pi^0$	[b] not seen
Γ_6 $\Lambda_c^+ \gamma$	not seen

[a] See AALTONEN 11H, Fig. 8, for the calculated ratio of $\Lambda_c^+ \pi^0 \pi^0$ and $\Lambda_c^+ \pi^+ \pi^-$ partial widths as a function of the $\Lambda_c(2595)^+ - \Lambda_c^+$ mass difference. At our value of the mass difference, the ratio is about 4.

[b] A test that the isospin is indeed 0, so that the particle is indeed a Λ_c^+ .

$\Lambda_c(2595)^+$ BRANCHING RATIOS

$\Gamma(\Sigma_c(2455)^{++} \pi^-) / \Gamma(\Lambda_c^+ \pi^+ \pi^-)$ Γ_2/Γ_1

VALUE	DOCUMENT ID	TECN	COMMENT
0.36 ± 0.10 OUR AVERAGE			
0.37 ± 0.12 ± 0.13	ALBRECHT 97	ARG	$e^+e^- \approx 10$ GeV
0.36 ± 0.09 ± 0.09	EDWARDS 95	CLE2	$e^+e^- \approx 10.5$ GeV

$\Gamma(\Sigma_c(2455)^0 \pi^+) / \Gamma(\Lambda_c^+ \pi^+ \pi^-)$ Γ_3/Γ_1

VALUE	DOCUMENT ID	TECN	COMMENT
0.37 ± 0.10 OUR AVERAGE			
0.29 ± 0.10 ± 0.11	ALBRECHT 97	ARG	$e^+e^- \approx 10$ GeV
0.42 ± 0.09 ± 0.09	EDWARDS 95	CLE2	$e^+e^- \approx 10.5$ GeV

$[\Gamma(\Sigma_c(2455)^{++} \pi^-) + \Gamma(\Sigma_c(2455)^0 \pi^+)] / \Gamma(\Lambda_c^+ \pi^+ \pi^-)$ $(\Gamma_2 + \Gamma_3)/\Gamma_1$

VALUE	CL%	DOCUMENT ID	TECN	COMMENT
0.66 $^{+0.13}_{-0.16}$ ± 0.07		ALBRECHT 97	ARG	$e^+e^- \approx 10$ GeV
>0.51	90	³ FRABETTI 96	E687	γ Be, $\bar{E}_\gamma \approx 220$ GeV

³ The results of FRABETTI 96 are consistent with this ratio being 100%.

$\Gamma(\Lambda_c^+ \pi^0) / \Gamma(\Lambda_c^+ \pi^+ \pi^-)$ Γ_5/Γ_1

$\Lambda_c^+ \pi^0$ decay is forbidden by isospin conservation if this state is in fact a Λ_c .

VALUE	CL%	DOCUMENT ID	TECN	COMMENT
<3.53	90	EDWARDS 95	CLE2	$e^+e^- \approx 10.5$ GeV

$\Gamma(\Lambda_c^+ \gamma) / \Gamma(\Lambda_c^+ \pi^+ \pi^-)$ Γ_6/Γ_1

VALUE	CL%	DOCUMENT ID	TECN	COMMENT
<0.98	90	EDWARDS 95	CLE2	$e^+e^- \approx 10.5$ GeV

$\Lambda_c(2595)^+$ REFERENCES

AALTONEN 11H	PR D84 012003	T. Aaltonen et al.	(CDF Collab.)
BLECHMAN 03	PR D67 074033	A.E. Blechman et al.	(JHU, FLOR)
ALBRECHT 97	PL B402 207	H. Albrecht et al.	(ARGUS Collab.)
FRABETTI 96	PL B365 461	P.L. Frabetti et al.	(FNAL E687 Collab.)
EDWARDS 95	PRL 74 3331	K.W. Edwards et al.	(CLEO Collab.)

$\Lambda_c(2625)^+$ $J(P) = 0(\frac{3}{2}^-)$ Status: ***

The spin-parity has not been measured but is expected to be $3/2^-$; this is presumably the charm counterpart of the strange $\Lambda(1520)$.

$\Lambda_c(2625)^+$ MASS

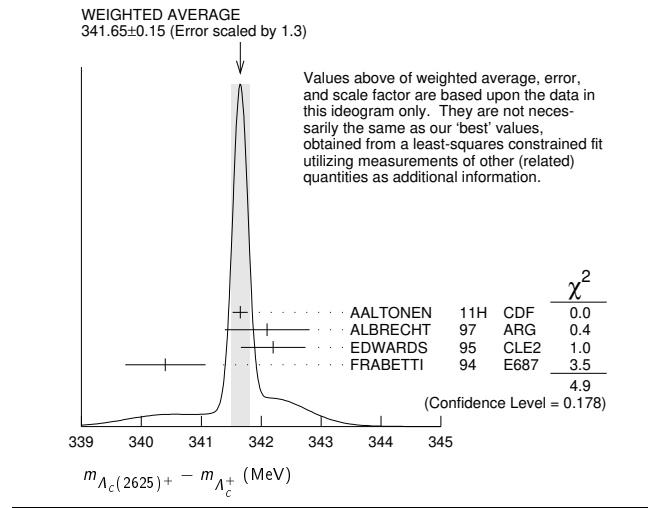
The mass is obtained from the $\Lambda_c(2625)^+ - \Lambda_c^+$ mass-difference measurements below.

VALUE (MeV)	EVTS	DOCUMENT ID	TECN	COMMENT
2628.11 ± 0.19 OUR FIT				Error includes scale factor of 1.1.
2626.6 ± 0.5 ± 1.5	42 ± 9	ALBRECHT 93F	ARG	See ALBRECHT 97

• • • We do not use the following data for averages, fits, limits, etc. • • •

$\Lambda_c(2625)^+ - \Lambda_c^+$ MASS DIFFERENCE

VALUE (MeV)	EVTS	DOCUMENT ID	TECN	COMMENT
341.65 ± 0.13 OUR FIT				Error includes scale factor of 1.1.
341.65 ± 0.15 OUR AVERAGE				Error includes scale factor of 1.3. See the ideogram below.
341.65 ± 0.04 ± 0.12	6.2k	AALTONEN 11H	CDF	$p\bar{p}$ at 1.96 TeV
342.1 ± 0.5 ± 0.5	51	ALBRECHT 97	ARG	$e^+e^- \approx 10$ GeV
342.2 ± 0.2 ± 0.5	245 ± 19	EDWARDS 95	CLE2	$e^+e^- \approx 10.5$ GeV
340.4 ± 0.6 ± 0.3	40 ± 9	FRABETTI 94	E687	γ Be, $\bar{E}_\gamma \approx 220$ GeV



$\Lambda_c(2625)^+$ WIDTH

VALUE (MeV)	CL%	EVTS	DOCUMENT ID	TECN	COMMENT
<0.97	90	6.2k	AALTONEN 11H	CDF	$p\bar{p}$ at 1.96 TeV
• • • We do not use the following data for averages, fits, limits, etc. • • •					
<1.9	90	245 ± 19	EDWARDS 95	CLE2	$e^+e^- \approx 10.5$ GeV
<3.2	90		ALBRECHT 93F	ARG	$e^+e^- \approx \gamma(4S)$

Baryon Particle Listings

 $\Lambda_c(2625)^+$, $\Lambda_c(2765)^+$, $\Lambda_c(2860)^+$, $\Lambda_c(2880)^+$ $\Lambda_c(2625)^+$ DECAY MODES

$\Lambda_c^+ \pi \pi$ and its submode $\Sigma(2455)\pi$ are the only strong decays allowed to an excited Λ_c^+ having this mass.

Mode	Fraction (Γ_i/Γ)	Confidence level
Γ_1 $\Lambda_c^+ \pi^+ \pi^-$	$\approx 67\%$	
Γ_2 $\Sigma_c(2455)^{++} \pi^-$	<5	90%
Γ_3 $\Sigma_c(2455)^0 \pi^+$	<5	90%
Γ_4 $\Lambda_c^+ \pi^+ \pi^-$ 3-body	large	
Γ_5 $\Lambda_c^+ \pi^0$	[a] not seen	
Γ_6 $\Lambda_c^+ \gamma$	not seen	

[a] A test that the isospin is indeed 0, so that the particle is indeed a Λ_c^+ .

 $\Lambda_c(2625)^+$ BRANCHING RATIOS

$\Gamma(\Sigma_c(2455)^{++} \pi^-)/\Gamma(\Lambda_c^+ \pi^+ \pi^-)$ Γ_2/Γ_1				
VALUE	CL%	DOCUMENT ID	TECN	COMMENT
<0.08	90	EDWARDS	95	CLE2 $e^+ e^- \approx 10.5$ GeV

$\Gamma(\Sigma_c(2455)^0 \pi^+)/\Gamma(\Lambda_c^+ \pi^+ \pi^-)$ Γ_3/Γ_1				
VALUE	CL%	DOCUMENT ID	TECN	COMMENT
<0.07	90	EDWARDS	95	CLE2 $e^+ e^- \approx 10.5$ GeV

$[\Gamma(\Sigma_c(2455)^{++} \pi^-) + \Gamma(\Sigma_c(2455)^0 \pi^+)]/\Gamma(\Lambda_c^+ \pi^+ \pi^-)$ $(\Gamma_2 + \Gamma_3)/\Gamma_1$					
VALUE	CL%	EVTS	DOCUMENT ID	TECN	COMMENT
<0.36	90		FRABETTI	94	E687 γ Be, $\bar{E}_\gamma = 220$ GeV
0.46 ± 0.14		21	ALBRECHT	93F	ARG $e^+ e^- \approx \Upsilon(4S)$

$\Gamma(\Lambda_c^+ \pi^+ \pi^- \text{ 3-body})/\Gamma(\Lambda_c^+ \pi^+ \pi^-)$ Γ_4/Γ_1				
VALUE	EVTS	DOCUMENT ID	TECN	COMMENT
0.54 ± 0.14	16	ALBRECHT	93F	ARG $e^+ e^- \approx \Upsilon(4S)$

$\Gamma(\Lambda_c^+ \pi^0)/\Gamma(\Lambda_c^+ \pi^+ \pi^-)$ Γ_5/Γ_1				
VALUE	CL%	DOCUMENT ID	TECN	COMMENT
<0.91	90	EDWARDS	95	CLE2 $e^+ e^- \approx 10.5$ GeV

$\Gamma(\Lambda_c^+ \gamma)/\Gamma(\Lambda_c^+ \pi^+ \pi^-)$ Γ_6/Γ_1				
VALUE	CL%	DOCUMENT ID	TECN	COMMENT
<0.52	90	EDWARDS	95	CLE2 $e^+ e^- \approx 10.5$ GeV

 $\Lambda_c(2625)^+$ REFERENCES

AALTONEN	11H	PR D84 012003	T. Aaltonen et al.	(CDF Collab.)
ALBRECHT	97	PL B402 207	H. Albrecht et al.	(ARGUS Collab.)
EDWARDS	95	PRL 74 3331	K.W. Edwards et al.	(CLEO Collab.)
FRABETTI	94	PRL 72 961	P.L. Frabetti et al.	(FNAL E687 Collab.)
ALBRECHT	93F	PL B317 227	H. Albrecht et al.	(ARGUS Collab.)

$\Lambda_c(2765)^+$ or $\Sigma_c(2765)$ $I(J^P) = ?(??)$ Status: *

OMITTED FROM SUMMARY TABLE

A broad, statistically significant peak (997^{+141}_{-129} events) seen in $\Lambda_c^+ \pi^+ \pi^-$. However, nothing at all is known about its quantum numbers, including whether it is a Λ_c^+ or a Σ_c , or whether the width might be due to overlapping states.

 $\Lambda_c(2765)^+$ MASS

The mass is obtained from the $\Lambda_c(2765)^+ - \Lambda_c^+$ mass-difference measurement below.

VALUE (MeV)	DOCUMENT ID
2766.6 ± 2.4 OUR FIT	

 $\Lambda_c(2765)^+ - \Lambda_c^+$ MASS DIFFERENCE

VALUE (MeV)	EVTS	DOCUMENT ID	TECN	COMMENT
480.1 ± 2.4 OUR FIT				
480.1 ± 2.4	997^{+141}_{-129}	ARTUSO	01	CLE2 $e^+ e^- \approx \Upsilon(4S)$

 $\Lambda_c(2765)^+$ WIDTH

VALUE (MeV)	DOCUMENT ID	TECN	COMMENT
50	ARTUSO	01	CLE2 $e^+ e^- \approx \Upsilon(4S)$

 $\Lambda_c(2765)^+$ DECAY MODES

Mode	Fraction (Γ_i/Γ)
Γ_1 $\Lambda_c^+ \pi^+ \pi^-$	seen

 $\Lambda_c(2765)^+$ REFERENCES

ARTUSO	01	PRL 86 4479	M. Artuso et al.	(CLEO Collab.)
--------	----	-------------	------------------	----------------

$\Lambda_c(2860)^+$

$I(J^P) = 0(\frac{3}{2}^+)$ Status: ***

 $\Lambda_c(2860)^+$ MASS

VALUE (MeV)	DOCUMENT ID	TECN	COMMENT
$2856.1^{+2.0}_{-1.7} \pm 0.5^{+1.1}_{-5.6}$	¹ AAIJ	17s	LHCB in $\Lambda_b^0 \rightarrow D^0 p \pi^-$

¹The third AAJ 17s uncertainty comes from modeling the resonant shape of the nearby $\Lambda_c(2880)^+$ and the background (non-resonant) amplitudes.

 $\Lambda_c(2860)^+$ WIDTH

VALUE (MeV)	DOCUMENT ID	TECN	COMMENT
$67.6^{+10.1}_{-8.1} \pm 1.4^{+5.9}_{-20.0}$	¹ AAIJ	17s	LHCB in $\Lambda_b^0 \rightarrow D^0 p \pi^-$

¹The third AAJ 17s uncertainty comes from modeling the resonant shape of the nearby $\Lambda_c(2880)^+$ and the background (non-resonant) amplitudes.

 $\Lambda_c(2860)^+$ DECAY MODES

Mode	Fraction (Γ_i/Γ)
Γ_1 $D^0 p$	seen

 $\Lambda_c(2860)^+$ BRANCHING RATIOS

$\Gamma(D^0 p)/\Gamma_{\text{total}}$ Γ_1/Γ			
VALUE	DOCUMENT ID	TECN	COMMENT
seen	AAIJ	17s	LHCB in $\Lambda_b^0 \rightarrow D^0 p \pi^-$

 $\Lambda_c(2860)^+$ REFERENCES

AAIJ	17s	JHEP 1705 030	R. Aaij et al.	(LHCb Collab.)JP
------	-----	---------------	----------------	------------------

$\Lambda_c(2880)^+$

$I(J^P) = 0(\frac{5}{2}^+)$ Status: ***

A narrow peak seen in $\Lambda_c^+ \pi^+ \pi^-$ and in $p D^0$. It is not seen in $p D^+$, and therefore it is a Λ_c^+ and not a Σ_c .

 $\Lambda_c(2880)^+$ MASS

VALUE (MeV)	EVTS	DOCUMENT ID	TECN	COMMENT
2881.63 \pm 0.24 OUR FIT				
2881.62 \pm 0.24 OUR AVERAGE				

$2881.75 \pm 0.29 \pm 0.07^{+0.14}_{-0.20}$	¹ AAIJ	17s	LHCB	in $\Lambda_b^0 \rightarrow D^0 p \pi^-$
$2881.9 \pm 0.1 \pm 0.5$	2.8k	AUBERT	07	BABR in $p D^0$
$2881.2 \pm 0.2 \pm 0.4$	690	MIZUK	07	BELL in $\Sigma_c(2455)^{0,++} \pi^\pm$

¹The third AAJ 17s uncertainty comes from modeling the resonant shape of the $\Lambda_c(2880)^+$ and the background (non-resonant) amplitudes.

 $\Lambda_c(2880)^+ - \Lambda_c^+$ MASS DIFFERENCE

VALUE (MeV)	EVTS	DOCUMENT ID	TECN	COMMENT
595.17 \pm 0.28 OUR FIT				
596 \pm 1 \pm 2	350	ARTUSO	01	CLE2 in $\Lambda_c^+ \pi^+ \pi^-$

 $\Lambda_c(2880)^+$ WIDTH

VALUE (MeV)	CL%	EVTS	DOCUMENT ID	TECN	COMMENT
5.6 $^{+0.8}_{-0.6}$ OUR AVERAGE					

$5.43^{+0.77+0.81}_{-0.71-0.29}$	² AAIJ	17s	LHCB	in $\Lambda_b^0 \rightarrow D^0 p \pi^-$
$5.8 \pm 1.5 \pm 1.1$	2.8k	AUBERT	07	BABR in $p D^0$
$5.8 \pm 0.7 \pm 1.1$	690	MIZUK	07	BELL in $\Sigma_c(2455)^{0,++} \pi^\pm$

See key on page 1127

Baryon Particle Listings

$\Lambda_c(2880)^+$, $\Lambda_c(2940)^+$, $\Sigma_c(2455)$

••• We do not use the following data for averages, fits, limits, etc. •••

<8 90 ARTUSO 01 CLEO in $\Lambda_c^+ \pi^+ \pi^-$
 2 AAIJ 17s reports $5.43^{+0.77}_{-0.71} \pm 0.29^{+0.75}_{-0.00}$ MeV value where the third uncertainty comes from modeling the resonant shape of the $\Lambda_c(2880)^+$ and the background (non-resonant) amplitudes. We have combined in quadrature the systematic uncertainties.

$\Lambda_c(2880)^+$ DECAY MODES

Mode	Fraction (Γ_i/Γ)
Γ_1 $\Lambda_c^+ \pi^+ \pi^-$	seen
Γ_2 $\Sigma_c(2455)^{0,++} \pi^\pm$	seen
Γ_3 $\Sigma_c(2520)^{0,++} \pi^\pm$	seen
Γ_4 ρD^0	seen

$\Lambda_c(2880)^+$ BRANCHING RATIOS

$\Gamma(\Sigma_c(2455)^{0,++} \pi^\pm) / \Gamma(\Lambda_c^+ \pi^+ \pi^-)$					Γ_2/Γ_1
VALUE	EVTS	DOCUMENT ID	TECN	COMMENT	
0.392 ± 0.031 OUR AVERAGE		Error includes scale factor of 1.3.			
0.404 ± 0.021 ± 0.014		MIZUK 07 BELL		in $\Sigma_c(2455)^{0,++} \pi^\pm$	
0.31 ± 0.06 ± 0.03	96	ARTUSO 01 CLE2		$e^+ e^- \approx \mathcal{T}(4S)$	

$\Gamma(\Sigma_c(2520)^{0,++} \pi^\pm) / \Gamma(\Lambda_c^+ \pi^+ \pi^-)$					Γ_3/Γ_1
VALUE	CL%	DOCUMENT ID	TECN	COMMENT	
0.091 ± 0.025 ± 0.010		MIZUK 07 BELL		in $\Sigma_c(2455)^{0,++} \pi^\pm$	

••• We do not use the following data for averages, fits, limits, etc. •••

<0.11 90 ARTUSO 01 CLE2 $e^+ e^- \approx \mathcal{T}(4S)$

$\Gamma(\Sigma_c(2520)^{0,++} \pi^\pm) / \Gamma(\Sigma_c(2455)^{0,++} \pi^\pm)$					Γ_3/Γ_2
VALUE	DOCUMENT ID	TECN	COMMENT		
0.225 ± 0.062 ± 0.025	3 MIZUK 07 BELL		in $\Sigma_c(2455)^{0,++} \pi^\pm$		

••• We do not use the following data for averages, fits, limits, etc. •••

³This MIZUK 07 ratio is redundant with MIZUK 07 ratios given above.

$\Lambda_c(2880)^+$ REFERENCES

AAIJ 17s	JHEP 1705 030	R. Aaij et al.	(LHCb Collab.) JP
AUBERT 07	PRL 98 012001	B. Aubert et al.	(BABAR Collab.)
MIZUK 07	PRL 98 262001	R. Mizuk et al.	(BELLE Collab.)
ARTUSO 01	PRL 86 4479	M. Artuso et al.	(CLEO Collab.)

$\Lambda_c(2940)^+$

$I(J^P) = 0(\frac{3}{2}^-)$ Status: ***

A narrow peak seen in ρD^0 and in $\Lambda_c^+ \pi^+ \pi^-$. It is not seen in ρD^+ , and therefore it is a Λ_c^+ and not a Σ_c . $J^P = 3/2^-$ is favored, but not certain.

$\Lambda_c(2940)^+$ MASS

VALUE (MeV)	EVTS	DOCUMENT ID	TECN	COMMENT
2939.6^{+1.3}_{-1.5} OUR AVERAGE				
2944.8 ^{+3.5} _{-2.5} ± 0.4 ^{+0.1} _{-4.6}	1	AAIJ 17s	LHCB	in $\Lambda_b^0 \rightarrow D^0 \rho \pi^-$
2939.8 ± 1.3 ± 1.0	2.2k	AUBERT 07	BABR	in ρD^0
2938.0 ± 1.3 ^{+2.0} _{-4.0}	220	MIZUK 07	BELL	in $\Sigma_c(2455)^{0,++} \pi^\pm$

¹The third AAIJ 17s uncertainty comes from modeling the resonant shape of the nearby $\Lambda_c(2880)^+$ and the background (non-resonant) amplitudes.

$\Lambda_c(2940)^+$ WIDTH

VALUE (MeV)	EVTS	DOCUMENT ID	TECN	COMMENT
20⁺⁶₋₅ OUR AVERAGE				
27.7 ^{+8.2} _{-6.0} ± 0.9 ^{+5.2} _{-10.4}	2	AAIJ 17s	LHCB	in $\Lambda_b^0 \rightarrow D^0 \rho \pi^-$
17.5 ± 5.2 ± 5.9	2.2k	AUBERT 07	BABR	in ρD^0
13 ⁺⁸ ₋₅ ⁺²⁷ ₋₇	220	MIZUK 07	BELL	in $\Sigma_c(2455)^{0,++} \pi^\pm$

²The third AAIJ 17s uncertainty comes from modeling the resonant shape of the nearby $\Lambda_c(2880)^+$ and the background (non-resonant) amplitudes.

$\Lambda_c(2940)^+$ DECAY MODES

Mode	Fraction (Γ_i/Γ)
Γ_1 ρD^0	seen
Γ_2 $\Sigma_c(2455)^{0,++} \pi^\pm$	seen

$\Lambda_c(2940)^+$ REFERENCES

AAIJ 17s	JHEP 1705 030	R. Aaij et al.	(LHCb Collab.) JP
AUBERT 07	PRL 98 012001	B. Aubert et al.	(BABAR Collab.)
MIZUK 07	PRL 98 262001	R. Mizuk et al.	(BELLE Collab.)

$\Sigma_c(2455)$

$I(J^P) = 1(\frac{1}{2}^+)$ Status: ***

The angular distribution of $B^- \rightarrow \Sigma_c(2455)^0 \bar{p}$ favors $J = 1/2$ (as the quark model predicts). $J = 3/2$ is excluded by more than four standard deviations; see AUBERT 08BN.

$\Sigma_c(2455)$ MASSES

The masses are obtained from the mass-difference measurements that follow.

$\Sigma_c(2455)^{++}$ MASS

VALUE (MeV)	DOCUMENT ID
2453.97 ± 0.14 OUR FIT	

$\Sigma_c(2455)^+$ MASS

VALUE (MeV)	DOCUMENT ID
2452.65^{+0.22}_{-0.16} OUR FIT	

$\Sigma_c(2455)^0$ MASS

VALUE (MeV)	DOCUMENT ID
2453.75 ± 0.14 OUR FIT	

$\Sigma_c(2455) - \Lambda_c^+$ MASS DIFFERENCES

$m_{\Sigma_c(2455)^{++}} - m_{\Lambda_c^+}$

VALUE (MeV)	EVTS	DOCUMENT ID	TECN	COMMENT
167.510 ± 0.017 OUR FIT				
167.510 ± 0.022 OUR AVERAGE				
167.51 ± 0.01 ± 0.02	36k	LEE 14	BELL	$e^+ e^-$ at $\mathcal{T}(4S)$
167.44 ± 0.04 ± 0.12	13.8k	AALTONEN 11H	CDF	$p\bar{p}$ at 1.96 TeV
167.4 ± 0.1 ± 0.2	2k	ARTUSO 02	CLE2	$e^+ e^- \approx \mathcal{T}(4S)$
167.35 ± 0.19 ± 0.12	461	LINK 00c	FOCS	$\gamma A, \bar{E}_\gamma, 180$ GeV
167.76 ± 0.29 ± 0.15	122	AITALA 96B	E791	$\pi^- N, 500$ GeV
167.6 ± 0.6 ± 0.6	56	FRABETTI 96	E687	$\gamma Be, \bar{E}_\gamma \approx 220$ GeV
168.2 ± 0.3 ± 0.2	126	CRAWFORD 93	CLE2	$e^+ e^- \approx \mathcal{T}(4S)$
167.8 ± 0.4 ± 0.3	54	BOWCOCK 89	CLEO	$e^+ e^- \approx 10$ GeV
168.2 ± 0.5 ± 1.6	92	ALBRECHT 88D	ARG	$e^+ e^- 10$ GeV
167.4 ± 0.5 ± 2.0	46	DIESBURG 87	SPEC	$nA \sim 600$ GeV
••• We do not use the following data for averages, fits, limits, etc. •••				
167 ± 1	2	JONES 87	HBC	νp in BEBC
166 ± 1	1	BOSETTI 82	HBC	See JONES 87
168 ± 3	6	BALTAY 79	HLBC	$\nu Ne-H$ in 15-ft
166 ± 15	1	CAZZOLI 75	HBC	νp in BNL 7-ft

$m_{\Sigma_c(2455)^+} - m_{\Lambda_c^+}$

VALUE (MeV)	EVTS	DOCUMENT ID	TECN	COMMENT
166.19^{+0.16}_{-0.08} OUR FIT				
166.19^{+0.15}_{-0.08} OUR AVERAGE				
166.17 ± 0.05 ^{+0.16} _{-0.07}		YELTON 21	BELL	$e^+ e^-$ at $\mathcal{T}(nS)$
166.4 ± 0.2 ± 0.3	661	AMMAR 01	CLE2	$e^+ e^- \approx \mathcal{T}(4S)$
••• We do not use the following data for averages, fits, limits, etc. •••				
168.5 ± 0.4 ± 0.2	111	CRAWFORD 93	CLE2	See AMMAR 01
168 ± 3	1	CALICCHIO 80	HBC	νp in BEBC-TST

$m_{\Sigma_c(2455)^0} - m_{\Lambda_c^+}$

VALUE (MeV)	EVTS	DOCUMENT ID	TECN	COMMENT
167.290 ± 0.017 OUR FIT				
167.290 ± 0.022 OUR AVERAGE				
167.29 ± 0.01 ± 0.02	32k	LEE 14	BELL	$e^+ e^-$ at $\mathcal{T}(4S)$
167.28 ± 0.03 ± 0.12	15.9k	AALTONEN 11H	CDF	$p\bar{p}$ at 1.96 TeV
167.2 ± 0.1 ± 0.2	2k	ARTUSO 02	CLE2	$e^+ e^- \approx \mathcal{T}(4S)$
167.38 ± 0.21 ± 0.13	362	LINK 00c	FOCS	$\gamma A, \bar{E}_\gamma, 180$ GeV
167.38 ± 0.29 ± 0.15	143	AITALA 96B	E791	$\pi^- N, 500$ GeV
167.8 ± 0.6 ± 0.2		ALEEV 96	SPEC	n nucleus, 50 GeV/c
166.6 ± 0.5 ± 0.6	69	FRABETTI 96	E687	$\gamma Be, \bar{E}_\gamma \approx 220$ GeV
167.1 ± 0.3 ± 0.2	124	CRAWFORD 93	CLE2	$e^+ e^- \approx \mathcal{T}(4S)$
168.4 ± 1.0 ± 0.3	14	ANJOS 89D	E691	$\gamma Be 90-260$ GeV
••• We do not use the following data for averages, fits, limits, etc. •••				
167.9 ± 0.5 ± 0.3	48	1 BOWCOCK 89	CLEO	$e^+ e^- 10$ GeV
167.0 ± 0.5 ± 1.6	70	1 ALBRECHT 88D	ARG	$e^+ e^- 10$ GeV
178.2 ± 0.4 ± 2.0	85	2 DIESBURG 87	SPEC	$nA \sim 600$ GeV
163 ± 2	1	AMMAR 86	EMUL	νA

Baryon Particle Listings

$\Sigma_c(2455), \Sigma_c(2520)$

¹ This result enters the fit through $m_{\Sigma_c^{++}} - m_{\Sigma_c^0}$ given below.
² See the note on DIESBURG 87 in the $m_{\Sigma_c^{++}} - m_{\Sigma_c^0}$ section below.

$\Sigma_c(2455)$ MASS DIFFERENCES

$m_{\Sigma_c(2455)^{++}} - m_{\Sigma_c(2455)^0}$

VALUE (MeV)	DOCUMENT ID	TECN	COMMENT
0.220 ± 0.013 OUR FIT			
0.221 ± 0.014 OUR AVERAGE			
0.22 ± 0.01 ± 0.01	LEE	14	BELL e^+e^- at $\Upsilon(4S)$
0.2 ± 0.1 ± 0.1	ARTUSO	02	CLE2 $e^+e^- \approx \Upsilon(4S)$
-0.03 ± 0.28 ± 0.11	LINK	00c	FOCS $\gamma A, \bar{E}_\gamma \approx 180$ GeV
0.38 ± 0.40 ± 0.15	AITALA	96B	E791 $\pi^- N, 500$ GeV
1.1 ± 0.4 ± 0.1	CRAWFORD	93	CLE2 $e^+e^- \approx \Upsilon(4S)$
-0.1 ± 0.6 ± 0.1	BOWCOCK	89	CLEO $e^+e^- \approx 10$ GeV
1.2 ± 0.7 ± 0.3	ALBRECHT	88D	ARG $e^+e^- \approx 10$ GeV
••• We do not use the following data for averages, fits, limits, etc. •••			
-10.8 ± 2.9	³ DIESBURG	87	SPEC $nA \sim 600$ GeV

³DIESBURG 87 is completely incompatible with the other experiments, which is surprising since it agrees with them about $m_{\Sigma_c(2455)^{++}} - m_{\Lambda_c^+}$. We go with the majority here.

$m_{\Sigma_c(2455)^+} - m_{\Sigma_c(2455)^0}$

VALUE (MeV)	DOCUMENT ID	TECN	COMMENT
-1.10 ± 0.16 OUR FIT			
-1.10 ± 0.08 OUR FIT			
••• We do not use the following data for averages, fits, limits, etc. •••			
1.4 ± 0.5 ± 0.3	CRAWFORD	93	CLE2 See AMMAR 01

$\Sigma_c(2455)$ WIDTHS

$\Sigma_c(2455)^{++}$ WIDTH

VALUE (MeV)	EVTS	DOCUMENT ID	TECN	COMMENT
1.89 ± 0.09 OUR AVERAGE				Error includes scale factor of 1.1.
1.84 ± 0.04 ± 0.07	36k	LEE	14	BELL e^+e^- at $\Upsilon(4S)$
2.34 ± 0.13 ± 0.45	13.8k	AALTONEN	11H	CDF $p\bar{p}$ at 1.96 TeV
2.3 ± 0.2 ± 0.3	2k	ARTUSO	02	CLE2 $e^+e^- \approx \Upsilon(4S)$
2.05 ± 0.41 ± 0.38	1110	LINK	02	FOCS $\gamma A, \bar{E}_\gamma \approx 180$ GeV

$\Sigma_c(2455)^+$ WIDTH

VALUE (MeV)	CL%	EVTS	DOCUMENT ID	TECN	COMMENT
2.3 ± 0.3 ± 0.3			YELTON	21	BELL e^+e^- at $\Upsilon(nS)$
••• We do not use the following data for averages, fits, limits, etc. •••					
<4.6	90	661	AMMAR	01	CLE2 $e^+e^- \approx \Upsilon(4S)$

$\Sigma_c(2455)^0$ WIDTH

VALUE (MeV)	EVTS	DOCUMENT ID	TECN	COMMENT
1.83 ± 0.11 OUR AVERAGE				Error includes scale factor of 1.2.
1.76 ± 0.04 ± 0.09	32k	LEE	14	BELL e^+e^- at $\Upsilon(4S)$
1.65 ± 0.11 ± 0.49	15.9k	AALTONEN	11H	CDF $p\bar{p}$ at 1.96 TeV
2.6 ± 0.5 ± 0.3		AUBERT	08BN	BABR $B^- \rightarrow \bar{p}\Lambda_c^+\pi^-$
2.5 ± 0.2 ± 0.3	2k	ARTUSO	02	CLE2 $e^+e^- \approx \Upsilon(4S)$
1.55 ± 0.41 ± 0.37	913	LINK	02	FOCS $\gamma A, \bar{E}_\gamma \approx 180$ GeV

$\Sigma_c(2455)$ DECAY MODES

$\Lambda_c^+\pi$ is the only strong decay allowed to a Σ_c having this mass.

Mode	Fraction (Γ_i/Γ)
$\Gamma_1 \Lambda_c^+\pi$	$\approx 100\%$

$\Sigma_c(2455)$ REFERENCES

YELTON	21	PR D104 052003	J. Yelton et al.	(BELLE Collab.)
LEE	14	PR D89 091102	S.-H. Lee et al.	(BELLE Collab.)
AALTONEN	11H	PR D84 012003	T. Aaltonen et al.	(CDF Collab.)
AUBERT	08BN	PR D78 112003	B. Aubert et al.	(BABAR Collab.)
ARTUSO	02	PR D65 071101	M. Artuso et al.	(CLEO Collab.)
LINK	02	PL B525 205	J.M. Link et al.	(FNAL FOCUS Collab.)
AMMAR	01	PRL 86 1167	R. Ammar et al.	(CLEO Collab.)
LINK	00c	PL B488 218	J.M. Link et al.	(FNAL FOCUS Collab.)
AITALA	96B	PL B379 292	E.M. Aitala et al.	(FNAL E791 Collab.)
ALEEV	96	JINRRC 3-77 31	A.N. Aleev et al.	(Serpuukhov EXCHARM Collab.)
FRABETTI	96	PL B365 461	P.L. Frabetti et al.	(FNAL E687 Collab.)
CRAWFORD	93	PRL 71 3259	G. Crawford et al.	(CLEO Collab.)
ANJOS	89D	PL 62 1721	J.C. Anjos et al.	(FNAL E691 Collab.)
BOWCOCK	89	PRL 62 1240	T.J.V. Bowcock et al.	(CLEO Collab.)
ALBRECHT	88D	PL B211 489	H. Albrecht et al.	(ARGUS Collab.)
DIESBURG	87	PRL 59 2711	M. Diesburg et al.	(FNAL E400 Collab.)
JONES	87	ZPHY C36 593	G.T. Jones et al.	(CERN WA21 Collab.)
AMMAR	86	JETPL 43 515	R. Ammar et al.	(ITFP)
BOSETTI	82	PL 103B 234	P.C. Bosetti et al.	(AACH3, BONN, CERN+)
CALICCHIO	80	PL 93B 521	M. Calicchio et al.	(BARI, BIRM, BRUX+)
BALTAY	79	PRL 42 1721	C. Baltay et al.	(COLU, BNL)
CAZZOLI	75	PRL 34 1125	E.G. Cazzoli et al.	(BNL)

$\Sigma_c(2520)$

$$I(J^P) = 1(\frac{3}{2}^+) \text{ Status: } ***$$

Seen in the $\Lambda_c^+\pi^\pm$ mass spectrum. The natural assignment is that this is the $J^P = 3/2^+$ excitation of the $\Sigma_c(2455)$, the charm counterpart of the $\Sigma(1385)$, but neither J nor P has been measured.

$\Sigma_c(2520)$ MASSES

The masses are obtained from the mass-difference measurements that follow.

$\Sigma_c(2520)^{++}$ MASS

VALUE (MeV)	EVTS	DOCUMENT ID	TECN	COMMENT
2518.41 ± 0.22 OUR FIT				Error includes scale factor of 1.1.
••• We do not use the following data for averages, fits, limits, etc. •••				
2530 ± 5 ± 5	6	¹ AMMOSOV	93	HLBC $\nu p \rightarrow \mu^- \Sigma_c(2530)^{++}$
		¹ AMMOSOV	93	sees a cluster of 6 events and estimates the background to be 1 event.

$\Sigma_c(2520)^+$ MASS

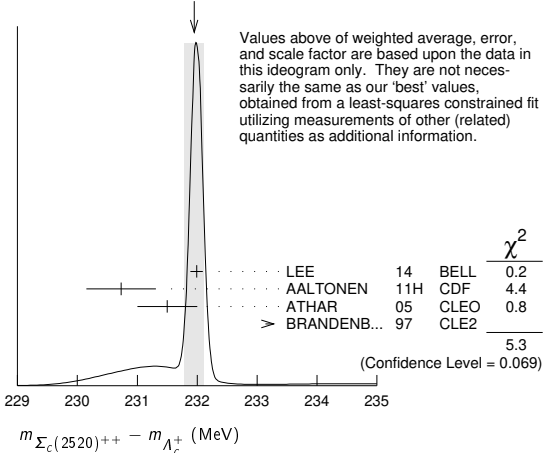
VALUE (MeV)	DOCUMENT ID
2517.4 ± 0.7 OUR FIT	
$\Sigma_c(2520)^0$ MASS	
VALUE (MeV)	DOCUMENT ID
2518.48 ± 0.20 OUR FIT	
	Error includes scale factor of 1.1.

$\Sigma_c(2520)$ MASS DIFFERENCES

$m_{\Sigma_c(2520)^{++}} - m_{\Lambda_c^+}$

VALUE (MeV)	EVTS	DOCUMENT ID	TECN	COMMENT
231.95 ± 0.18 OUR FIT				Error includes scale factor of 1.3.
231.95 ± 0.16 OUR AVERAGE				Error includes scale factor of 1.6. See the ideogram below.
231.99 ± 0.10 ± 0.02	44k	LEE	14	BELL e^+e^- at $\Upsilon(4S)$
230.73 ± 0.56 ± 0.16	8.8k	AALTONEN	11H	CDF $p\bar{p}$ at 1.96 TeV
231.5 ± 0.4 ± 0.3	1.3k	ATHAR	05	CLEO e^+e^- , 9.4-11.5 GeV
234.5 ± 1.1 ± 0.8	677	BRANDENB...	97	CLE2 $e^+e^- \approx \Upsilon(4S)$

WEIGHTED AVERAGE
231.95 ± 0.16 (Error scaled by 1.6)



$m_{\Sigma_c(2520)^+} - m_{\Lambda_c^+}$

VALUE (MeV)	EVTS	DOCUMENT ID	TECN	COMMENT
230.9 ± 0.7 OUR FIT				
230.9 ± 0.7 OUR AVERAGE				
230.9 ± 0.5 ± 0.5		YELTON	21	BELL e^+e^- at $\Upsilon(nS)$
231.0 ± 1.1 ± 2.0	327	AMMAR	01	CLE2 $e^+e^- \approx \Upsilon(4S)$

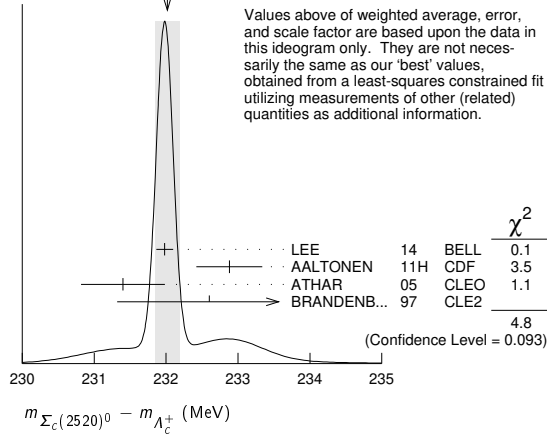
$m_{\Sigma_c(2520)^0} - m_{\Lambda_c^+}$

VALUE (MeV)	EVTS	DOCUMENT ID	TECN	COMMENT
232.02 ± 0.16 OUR FIT				Error includes scale factor of 1.3.
232.02 ± 0.17 OUR AVERAGE				Error includes scale factor of 1.5. See the ideogram below.
231.98 ± 0.11 ± 0.04	41k	LEE	14	BELL e^+e^- at $\Upsilon(4S)$
232.88 ± 0.43 ± 0.16	9.0k	AALTONEN	11H	CDF $p\bar{p}$ at 1.96 TeV
231.4 ± 0.5 ± 0.3	1.3k	ATHAR	05	CLEO e^+e^- , 9.4-11.5 GeV
232.6 ± 1.0 ± 0.8	504	BRANDENB...	97	CLE2 $e^+e^- \approx \Upsilon(4S)$

See key on page 1127

Baryon Particle Listings
 $\Sigma_c(2520), \Sigma_c(2800)$

WEIGHTED AVERAGE
 232.02±0.17 (Error scaled by 1.5)



Values above of weighted average, error, and scale factor are based upon the data in this ideogram only. They are not necessarily the same as our 'best' values, obtained from a least-squares constrained fit utilizing measurements of other (related) quantities as additional information.

$m_{\Sigma_c(2520)^{++}} - m_{\Sigma_c(2520)^0}$

VALUE (MeV)	EVTs	DOCUMENT ID	TECN	COMMENT
0.01 ± 0.15 ± 0.03	44/41k	LEE	14	BELL e^+e^- at $\Upsilon(4S)$
••• We do not use the following data for averages, fits, limits, etc. •••				
0.1 ± 0.8 ± 0.3		² ATHAR	05	CLEO e^+e^- , 9.4–11.5 GeV
1.9 ± 1.4 ± 1.0		³ BRANDENB...	97	CLE2 $e^+e^- \approx \Upsilon(4S)$

²This ATHAR 05 result is redundant with measurements in earlier entries.
³This BRANDENBURG 97 result is redundant with measurements in earlier entries.

$\Sigma_c(2520)$ WIDTHS

$\Sigma_c(2520)^{++}$ WIDTH

VALUE (MeV)	EVTs	DOCUMENT ID	TECN	COMMENT
14.78^{+0.30}_{-0.40} OUR AVERAGE				
14.77 ± 0.25 ^{+0.18} _{-0.30}	44k	LEE	14	BELL e^+e^- at $\Upsilon(4S)$
15.03 ± 2.12 ± 1.36	8.8k	AALTONEN	11H	CDF $p\bar{p}$ at 1.96 TeV
14.4 ^{+1.6} _{-1.5} ± 1.4	1.3k	ATHAR	05	CLEO e^+e^- , 9.4–11.5 GeV
17.9 ^{+3.8} _{-3.2} ± 4.0	677	BRANDENB...	97	CLE2 $e^+e^- \approx \Upsilon(4S)$

$\Sigma_c(2520)^+$ WIDTH

VALUE (MeV)	CL%	EVTs	DOCUMENT ID	TECN	COMMENT
17.2^{+2.3+3.1}_{-2.1-0.7}			YELTON	21	BELL e^+e^- at $\Upsilon(nS)$
••• We do not use the following data for averages, fits, limits, etc. •••					
<17	90	327	AMMAR	01	CLE2 $e^+e^- \approx \Upsilon(4S)$

$\Sigma_c(2520)^0$ WIDTH

VALUE (MeV)	EVTs	DOCUMENT ID	TECN	COMMENT
15.3^{+0.4}_{-0.5} OUR AVERAGE				
15.41 ± 0.41 ^{+0.20} _{-0.32}	41k	LEE	14	BELL e^+e^- at $\Upsilon(4S)$
12.51 ± 1.82 ± 1.37	9.0k	AALTONEN	11H	CDF $p\bar{p}$ at 1.96 TeV
16.6 ^{+1.9} _{-1.7} ± 1.4	1.3k	ATHAR	05	CLEO e^+e^- , 9.4–11.5 GeV
13.0 ^{+3.7} _{-3.0} ± 4.0	504	BRANDENB...	97	CLE2 $e^+e^- \approx \Upsilon(4S)$

$\Sigma_c(2520)$ DECAY MODES

$\Lambda_c^+ \pi$ is the only strong decay allowed to a Σ_c having this mass.

Mode	Fraction (Γ_i/Γ)
$\Gamma_1 \Lambda_c^+ \pi$	≈ 100 %

$\Sigma_c(2520)$ REFERENCES

YELTON	21	PR D104 052003	J. Yelton et al.	(BELLE Collab.)
LEE	14	PR D89 091102	S.-H. Lee et al.	(BELLE Collab.)
AALTONEN	11H	PR D84 012003	T. Aaltonen et al.	(CDF Collab.)
ATHAR	05	PR D71 051101	S.B. Athar et al.	(CLEO Collab.)
AMMAR	01	PRL 86 1167	R. Ammar et al.	(CLEO Collab.)
BRANDENB...	97	PRL 78 2304	G. Brandenburg et al.	(CLEO Collab.)
AMMOSOV	93	JETPL 58 247	V.V. Ammosov et al.	(SERP)

Translated from ZETFP 58 241.

$\Sigma_c(2800)$

$I(J^P) = 1(?)^?$ Status: ***

Seen in the $\Lambda_c^+ \pi^+$, $\Lambda_c^+ \pi^0$, and $\Lambda_c^+ \pi^-$ mass spectra.

$\Sigma_c(2800)$ MASSES

The charged ++ and + masses are obtained from the mass-difference measurements that follow. The neutral mass is dominated by the mass-difference measurement, but is pulled up somewhat by the less well-determined but considerably higher direct-mass measurement. It is possible, in fact, that AUBERT 08BN is seeing a different Σ_c .

$\Sigma_c(2800)^{++}$ MASS

VALUE (MeV)	DOCUMENT ID
2801⁺⁴₋₆ OUR FIT	

$\Sigma_c(2800)^+$ MASS

VALUE (MeV)	DOCUMENT ID
2792⁺¹⁴₋₅ OUR FIT	

$\Sigma_c(2800)^0$ MASS

VALUE (MeV)	DOCUMENT ID	TECN	COMMENT
2806⁺⁵₋₇ OUR FIT			Error includes scale factor of 1.3.
2846 ± 8 ± 10	AUBERT	08BN BABR	$B^- \rightarrow \bar{p} \Lambda_c^+ \pi^-$

$\Sigma_c(2800)$ MASS DIFFERENCES

$m_{\Sigma_c(2800)^{++}} - m_{\Lambda_c^+}$

VALUE (MeV)	EVTs	DOCUMENT ID	TECN	COMMENT
514⁺⁴₋₆ OUR FIT				
514.5^{+3.4+2.8}_{-3.1-4.9}	2810 ⁺¹⁰⁹⁰ ₋₇₇₅	MIZUK	05	BELL $e^+e^- \approx \Upsilon(4S)$

$m_{\Sigma_c(2800)^+} - m_{\Lambda_c^+}$

VALUE (MeV)	EVTs	DOCUMENT ID	TECN	COMMENT
505⁺¹⁴₋₅ OUR FIT				
505.4^{+5.8+12.4}_{-4.6-2.0}	1540 ⁺¹⁷⁵⁰ ₋₁₀₅₀	MIZUK	05	BELL $e^+e^- \approx \Upsilon(4S)$

$m_{\Sigma_c(2800)^0} - m_{\Lambda_c^+}$

VALUE (MeV)	EVTs	DOCUMENT ID	TECN	COMMENT
519⁺⁵₋₇ OUR FIT				Error includes scale factor of 1.3.
515.4^{+3.2+2.1}_{-3.1-6.0}	2240 ⁺¹³⁰⁰ ₋₇₄₀	MIZUK	05	BELL $e^+e^- \approx \Upsilon(4S)$

$\Sigma_c(2800)$ WIDTHS

$\Sigma_c(2800)^{++}$ WIDTH

VALUE (MeV)	EVTs	DOCUMENT ID	TECN	COMMENT
75⁺¹⁸⁺¹²₋₁₃₋₁₁	2810 ⁺¹⁰⁹⁰ ₋₇₇₅	MIZUK	05	BELL $e^+e^- \approx \Upsilon(4S)$

$\Sigma_c(2800)^+$ WIDTH

VALUE (MeV)	EVTs	DOCUMENT ID	TECN	COMMENT
62⁺³⁷⁺⁵²₋₂₃₋₃₈	1540 ⁺¹⁷⁵⁰ ₋₁₀₅₀	MIZUK	05	BELL $e^+e^- \approx \Upsilon(4S)$

$\Sigma_c(2800)^0$ WIDTH

VALUE (MeV)	EVTs	DOCUMENT ID	TECN	COMMENT
72⁺²²₋₁₅ OUR AVERAGE				
86 ⁺³³ ₋₂₂ ± 12		AUBERT	08BN BABR	$B^- \rightarrow \bar{p} \Lambda_c^+ \pi^-$
61 ⁺¹⁸⁺²² ₋₁₃₋₁₃	2240 ⁺¹³⁰⁰ ₋₇₄₀	MIZUK	05	BELL $e^+e^- \approx \Upsilon(4S)$

$\Sigma_c(2800)$ DECAY MODES

Mode	Fraction (Γ_i/Γ)
$\Gamma_1 \Lambda_c^+ \pi$	seen

$\Sigma_c(2800)$ REFERENCES

AUBERT	08BN	PR D78 112003	B. Aubert et al.	(BABAR Collab.)
MIZUK	05	PRL 94 122002	R. Mizuk et al.	(BELLE Collab.)

Baryon Particle Listings



$$I(J^P) = \frac{1}{2}(\frac{1}{2}^+) \text{ Status: } ***$$

Neither of J or P has actually been measured.

Ξ_c^+ MASS

The fit uses the Ξ_c^+ and Ξ_c^0 mass and mass-difference measurements.

VALUE (MeV)	EVTS	DOCUMENT ID	TECN	COMMENT
2467.71 ± 0.23 OUR FIT		Error includes scale factor of 1.3.		
2467.95 ± 0.19 OUR AVERAGE				
2467.97 ± 0.14 ± 0.17	3.8k	¹ AAIJ	14z	LHCB pp at 7, 8 TeV
2468.00 ± 0.18 ± 0.51	5.1k	AALTONEN	14b	CDF $p\bar{p}$ at 1.96 TeV
2468.1 ± 0.4 ± 0.2	4.9k	² LESIAK	05	BELL e^+e^- , $\Upsilon(4S)$
2468.8 ± 1.9 ± 2.5	90	FRABETTI	98	E687 γ Be, $\bar{E}_\gamma = 220$ GeV
2467.0 ± 1.6 ± 2.0	147	EDWARDS	96	CLE2 $e^+e^- \approx \Upsilon(4S)$
2465.1 ± 3.6 ± 1.9	30	ALBRECHT	90F	ARG e^+e^- at $\Upsilon(4S)$
2467 ± 3 ± 4	23	ALAM	89	CLEO e^+e^- 10.6 GeV
2466.5 ± 2.7 ± 1.2	5	BARLAG	89c	ACCM π^- Cu 230 GeV
• • • We do not use the following data for averages, fits, limits, etc. • • •				
2464.4 ± 2.0 ± 1.4	30	FRABETTI	93b	E687 See FRABETTI 98
2459 ± 5 ± 30	56	³ COTEUS	87	SPEC $nA \approx 600$ GeV
2460 ± 25	82	BIAGI	83	SPEC Σ^- Be 135 GeV

¹ AAIJ 14z systematic error includes in quadrature the 0.14 MeV uncertainty from the $m(\Lambda_c^+)$ mass value.

² The systematic error was (wrongly) given the other way round in LESIAK 05; see the erratum.

³ Although COTEUS 87 claims to agree well with BIAGI 83 on the mass and width, there appears to be a discrepancy between the two experiments. BIAGI 83 sees a single peak (statistical significance about 6 standard deviations) in the $\Lambda K^- \pi^+ \pi^+$ mass spectrum. COTEUS 87 sees two peaks in the same spectrum, one at the Ξ_c^+ mass, the other 75 MeV lower. The latter is attributed to $\Xi_c^+ \rightarrow \Sigma^0 K^- \pi^+ \pi^+ \rightarrow (\Lambda \gamma) K^- \pi^+ \pi^+$, with the γ unseen. The combined significance of the double peak is stated to be 5.5 standard deviations. But the absence of any trace of a lower peak in BIAGI 83 seems to us to throw into question the interpretation of the lower peak of COTEUS 87.

Ξ_c^+ MEAN LIFE

VALUE (10^{-15} s)	EVTS	DOCUMENT ID	TECN	COMMENT
453 ± 5 OUR AVERAGE				
454 ± 5 ± 2	56k	¹ AAIJ	19AG	LHCB $\Xi_c^+ \rightarrow pK^- \pi^+$
503 ± 47 ± 18	250	MAHMOOD	02	CLE2 $e^+e^- \approx \Upsilon(4S)$
439 ± 22 ± 9	532	LINK	01d	FOCS γ nucleus, $\bar{E}_\gamma \approx 180$ GeV
340 ± 70 ± 20	56	FRABETTI	98	E687 γ Be, $\bar{E}_\gamma = 220$ GeV
400 ± 180 ± 100	102	COTEUS	87	SPEC $nA \approx 600$ GeV
480 ± 210 ± 200	53	BIAGI	85c	SPEC Σ^- Be 135 GeV
• • • We do not use the following data for averages, fits, limits, etc. • • •				
410 ± 110 ± 80 ± 20	30	FRABETTI	93b	E687 See FRABETTI 98
200 ± 110 ± 60	6	BARLAG	89c	ACCM π^- (K^-) Cu 230 GeV

¹ AAIJ 19AG reports $[\Xi_c^+ \text{ MEAN LIFE}] / [D^\pm \text{ MEAN LIFE}] = 0.4392 \pm 0.0034 \pm 0.0028$ which we multiply by our best value $D^\pm \text{ MEAN LIFE} = (1.033 \pm 0.005) \times 10^{-12}$ s. Our first error is their experiment's error and our second error is the systematic error from using our best value.

Ξ_c^+ DECAY MODES

Branching fractions marked with a footnote, e.g. [a], have been corrected for decay modes not observed in the experiments. For example, the sub-mode fraction $\Xi_c^+ \rightarrow \Sigma^+ \bar{K}^*(892)^0$ seen in $\Xi_c^+ \rightarrow \Sigma^+ K^- \pi^+$ has been multiplied up to include $\bar{K}^*(892)^0 \rightarrow \bar{K}^0 \pi^0$ decays.

Mode	Fraction (Γ_i/Γ)	Scale factor/ Confidence level
------	--------------------------------	-----------------------------------

Cabibbo-favored ($S = -2$) decays

Γ_1	$p2K_S^0$	$(2.5 \pm 1.3) \times 10^{-3}$	
Γ_2	$\Lambda \bar{K}^0 \pi^+$	—	
Γ_3	$\Sigma(1385)^+ \bar{K}^0$	[a] $(2.9 \pm 2.0) \%$	
Γ_4	$\Lambda K^- 2\pi^+$	$(9 \pm 4) \times 10^{-3}$	
Γ_5	$\Lambda \bar{K}^*(892)^0 \pi^+$	[a] $< 5 \times 10^{-3}$	CL=90%
Γ_6	$\Sigma(1385)^+ K^- \pi^+$	[a] $< 6 \times 10^{-3}$	CL=90%
Γ_7	$\Sigma^+ K^- \pi^+$	$(2.7 \pm 1.2) \%$	
Γ_8	$\Sigma^+ \bar{K}^*(892)^0$	[a] $(2.3 \pm 1.1) \%$	
Γ_9	$\Sigma^0 K^- 2\pi^+$	$(8 \pm 5) \times 10^{-3}$	

Γ_{10}	$\Xi^0 \pi^+$	$(1.6 \pm 0.8) \%$	
Γ_{11}	$\Xi^- 2\pi^+$	$(2.9 \pm 1.3) \%$	
Γ_{12}	$\Xi(1530)^0 \pi^+$	[a] $< 2.9 \times 10^{-3}$	CL=90%
Γ_{13}	$\Xi(1620)^0 \pi^+$	seen	
Γ_{14}	$\Xi(1690)^0 \pi^+$	seen	
Γ_{15}	$\Xi^0 \pi^+ \pi^0$	$(6.7 \pm 3.5) \%$	
Γ_{16}	$\Xi^0 \pi^- 2\pi^+$	$(5.0 \pm 2.6) \%$	
Γ_{17}	$\Xi^0 e^+ \nu_e$	$(7 \pm 4) \%$	
Γ_{18}	$\Omega^- K^+ \pi^+$	$(2.0 \pm 1.5) \times 10^{-3}$	

Cabibbo-suppressed decays

Γ_{19}	$pK^- \pi^+$	$(6.2 \pm 3.0) \times 10^{-3}$	S=1.5
Γ_{20}	$p\bar{K}^*(892)^0$	[a] $(3.3 \pm 1.7) \times 10^{-3}$	
Γ_{21}	$\Sigma^+ \pi^+ \pi^-$	$(1.4 \pm 0.8) \%$	
Γ_{22}	$\Sigma^- 2\pi^+$	$(5.1 \pm 3.4) \times 10^{-3}$	
Γ_{23}	$\Sigma^+ K^+ K^-$	$(4.3 \pm 2.5) \times 10^{-3}$	
Γ_{24}	$\Sigma^+ \phi$	[a] $< 3.2 \times 10^{-3}$	CL=90%
Γ_{25}	$\Xi(1690)^0 K^+, \Xi^0 \rightarrow \Sigma^+ K^-$	$< 1.3 \times 10^{-3}$	CL=90%
Γ_{26}	$p\phi(1020)$	$(1.2 \pm 0.6) \times 10^{-4}$	

[a] This branching fraction includes all the decay modes of the final-state resonance.

Ξ_c^+ BRANCHING RATIOS

Cabibbo-favored ($S = -2$) decays

$\Gamma(p2K_S^0)/\Gamma(\Xi^- 2\pi^+)$	Γ_1/Γ_{11}			
VALUE	EVTS	DOCUMENT ID	TECN	COMMENT
0.087 ± 0.016 ± 0.014	168 ± 27	LESIAK	05	BELL e^+e^- , $\Upsilon(4S)$

$\Gamma(\Sigma(1385)^+ \bar{K}^0)/\Gamma(\Xi^- 2\pi^+)$	Γ_3/Γ_{11}			
Unseen decay modes of the $\Sigma(1385)^+$ are included.				
VALUE	EVTS	DOCUMENT ID	TECN	COMMENT
1.00 ± 0.49 ± 0.24	20	LINK	03e	FOCS $< 1.72, 90\%$ CL

$\Gamma(\Lambda K^- 2\pi^+)/\Gamma(\Xi^- 2\pi^+)$	Γ_4/Γ_{11}			
VALUE				
EVTS				
DOCUMENT ID				
TECN				
COMMENT				
0.323 ± 0.033 OUR AVERAGE				
0.32 ± 0.03 ± 0.02	1177 ± 55	LESIAK	05	BELL e^+e^- , $\Upsilon(4S)$
0.28 ± 0.06 ± 0.06	58	LINK	03e	FOCS γ nucleus, $\bar{E}_\gamma \approx 180$ GeV
0.58 ± 0.16 ± 0.07	61	BERGFELD	96	CLE2 $e^+e^- \approx \Upsilon(4S)$

$\Gamma(\Lambda \bar{K}^*(892)^0 \pi^+)/\Gamma(\Lambda K^- 2\pi^+)$	Γ_5/Γ_4			
Unseen decay modes of the $\bar{K}^*(892)^0$ are included.				
VALUE	CL%	DOCUMENT ID	TECN	COMMENT
< 0.5	90	BERGFELD	96	CLE2 $e^+e^- \approx \Upsilon(4S)$

$\Gamma(\Sigma(1385)^+ K^- \pi^+)/\Gamma(\Lambda K^- 2\pi^+)$	Γ_6/Γ_4			
Unseen decay modes of the $\Sigma(1385)^+$ are included.				
VALUE	CL%	DOCUMENT ID	TECN	COMMENT
< 0.7	90	BERGFELD	96	CLE2 $e^+e^- \approx \Upsilon(4S)$

$\Gamma(\Sigma^+ K^- \pi^+)/\Gamma(\Xi^- 2\pi^+)$	Γ_7/Γ_{11}			
VALUE				
EVTS				
DOCUMENT ID				
TECN				
COMMENT				
0.94 ± 0.10 OUR AVERAGE				
0.91 ± 0.11 ± 0.04	251	LINK	03e	FOCS γ nucleus, $\bar{E}_\gamma \approx 180$ GeV
0.92 ± 0.20 ± 0.07		¹ JUN	00	SELX Σ^- nucleus, 600 GeV
1.18 ± 0.26 ± 0.17	119	BERGFELD	96	CLE2 $e^+e^- \approx \Upsilon(4S)$

¹ This JUN 00 result is redundant with other results given below.

$\Gamma(\Sigma^+ \bar{K}^*(892)^0)/\Gamma(\Xi^- 2\pi^+)$	Γ_8/Γ_{11}			
Unseen decay modes of the $\bar{K}^*(892)^0$ are included.				
VALUE	EVTS	DOCUMENT ID	TECN	COMMENT
0.81 ± 0.15 OUR AVERAGE				
0.78 ± 0.16 ± 0.06	119	LINK	03e	FOCS γ nucleus, $\bar{E}_\gamma \approx 180$ GeV
0.92 ± 0.27 ± 0.14	61	BERGFELD	96	CLE2 $e^+e^- \approx \Upsilon(4S)$

$\Gamma(\Sigma^0 K^- 2\pi^+)/\Gamma(\Lambda K^- 2\pi^+)$	Γ_9/Γ_4			
VALUE	EVTS	DOCUMENT ID	TECN	COMMENT
0.84 ± 0.36	47	¹ COTEUS	87	SPEC $nA \approx 600$ GeV

¹ See, however, the note on the COTEUS 87 Ξ_c^+ mass measurement.

$\Gamma(\Xi^0 \pi^+)/\Gamma(\Xi^- 2\pi^+)$	Γ_{10}/Γ_{11}			
VALUE	EVTS	DOCUMENT ID	TECN	COMMENT
0.55 ± 0.13 ± 0.09	39	EDWARDS	96	CLE2 $e^+e^- \approx \Upsilon(4S)$

$\Gamma(\Xi^- 2\pi^+)/\Gamma_{\text{total}}$	Γ_{11}/Γ			
VALUE (units 10^{-2})	EVTS	DOCUMENT ID	TECN	COMMENT
2.86 ± 1.21 ± 0.38	24	¹ LI	19c	BELL $e^+e^- \approx \Upsilon(4S)$

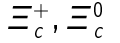


Table with 6 columns: status, value, document ID, TECN, COMMENT. Rows include BERGFELD 96 CLE2, AVERY 95 CLE2, FRABETTI 93B E687, ALBRECHT 90F ARG, ALAM 89 CLEO.

1 Li 19c report a significance of 6.8 sigma for the observation of this decay mode, observed in Xi_c^+ from B^0 -> Xi_c^+ Xi_c^+.

Gamma(Xi(1530)^0 pi^+)/Gamma(Xi^- 2pi^+) Gamma_12/Gamma_11

Table with 6 columns: VALUE, CL%, DOCUMENT ID, TECN, COMMENT. Row: <0.1, 90, LINK, 03E, FOCUS, gamma nucleus, E_gamma approx 180 GeV.

••• We do not use the following data for averages, fits, limits, etc. ••• <0.2, 90, BERGFELD 96 CLE2 e+e- approx T(4S)

Gamma(Xi(1620)^0 pi^+)/Gamma_total Gamma_13/Gamma

Table with 6 columns: VALUE, DOCUMENT ID, TECN, COMMENT. Row: SUMIHAMA 19 BELL e+e- mostly at T(4S)

Gamma(Xi(1690)^0 pi^+)/Gamma_total Gamma_14/Gamma

Table with 6 columns: VALUE, DOCUMENT ID, TECN, COMMENT. Row: SUMIHAMA 19 BELL e+e- mostly at T(4S)

Gamma(Xi^0 pi^+ pi^0)/Gamma(Xi^- 2pi^+) Gamma_15/Gamma_11

Table with 6 columns: VALUE, EVTS, DOCUMENT ID, TECN, COMMENT. Row: 2.34 +/- 0.57 +/- 0.37, 81, EDWARDS 96 CLE2 e+e- approx T(4S)

Gamma(Xi(1530)^0 pi^+)/Gamma(Xi^0 pi^+ pi^0) Gamma_12/Gamma_15

Table with 6 columns: VALUE, CL%, DOCUMENT ID, TECN, COMMENT. Row: <0.3, 90, EDWARDS 96 CLE2 e+e- approx T(4S)

Gamma(Xi^0 pi^- 2pi^+)/Gamma(Xi^- 2pi^+) Gamma_16/Gamma_11

Table with 6 columns: VALUE, EVTS, DOCUMENT ID, TECN, COMMENT. Row: 1.74 +/- 0.42 +/- 0.27, 57, EDWARDS 96 CLE2 e+e- approx T(4S)

Gamma(Xi^0 e+ nu_e)/Gamma(Xi^- 2pi^+) Gamma_17/Gamma_11

Table with 6 columns: VALUE, EVTS, DOCUMENT ID, TECN, COMMENT. Row: 2.3 +/- 0.6 +/- 0.3 / 0.6, 41, ALEXANDER 95B CLE2 e+e- approx T(4S)

Gamma(Omega^- K^+ pi^+)/Gamma(Xi^- 2pi^+) Gamma_18/Gamma_11

Table with 6 columns: VALUE, EVTS, DOCUMENT ID, TECN, COMMENT. Row: 0.07 +/- 0.03 +/- 0.03, 14, LINK 03E FOCUS <0.12, 90% CL

Gamma(p K^- pi^+)/Gamma_total Gamma_19/Gamma

Table with 6 columns: VALUE (units 10^-3), EVTS, DOCUMENT ID, TECN, COMMENT. Row: 6.2 +/- 3.0 OUR AVERAGE, Error includes scale factor of 1.5.

1 AAIJ 20AH extracts B(Xi_c^+ -> p K^- pi^+) assuming production fraction ratios f_Xi_c^0/f_Lambda_c^+ = (9.7 +/- 0.9 +/- 3.1) x 10^-2 (from AAIJ 19AB plus heavy quark symmetry arguments) as well as f_Xi_c^0/f_Xi_c^+ = 1.00 +/- 0.01, and uses the input B(Lambda_c^+ -> p K^- pi^+) = (6.23 +/- 0.33) x 10^-2. Its correlation with B(Xi_c^0 -> Lambda_c^+ pi^-), as measured in AAIJ 20AH, is 0.414.

2 Li 19c report a significance of 4.4 sigma for the observation of this decay mode, observed in Xi_c^+ from B^0 -> Xi_c^+ Xi_c^+.

Cabibbo-suppressed decays

Gamma(p K^- pi^+)/Gamma(Xi^- 2pi^+) Gamma_19/Gamma_11

Table with 6 columns: VALUE, EVTS, DOCUMENT ID, TECN, COMMENT. Row: 0.21 +/- 0.04 OUR AVERAGE, 0.194 +/- 0.054, 47 +/- 11, VAZQUEZ-JA...08 SELX Sigma^- nucleus, 600 GeV.

Gamma(p K*(892)^0)/Gamma(p K^- pi^+) Gamma_20/Gamma_19

Table with 6 columns: VALUE, EVTS, DOCUMENT ID, TECN, COMMENT. Row: 0.54 +/- 0.09 +/- 0.05, LINK 01B FOCUS gamma nucleus

Gamma(Sigma^+ pi^+ pi^-)/Gamma(Xi^- 2pi^+) Gamma_21/Gamma_11

Table with 6 columns: VALUE, EVTS, DOCUMENT ID, TECN, COMMENT. Row: 0.48 +/- 0.20, 21 +/- 8, VAZQUEZ-JA...08 SELX Sigma^- nucleus, 600 GeV

Gamma(Sigma^- 2pi^+)/Gamma(Xi^- 2pi^+) Gamma_22/Gamma_11

Table with 6 columns: VALUE, EVTS, DOCUMENT ID, TECN, COMMENT. Row: 0.18 +/- 0.09, 10 +/- 4, VAZQUEZ-JA...08 SELX Sigma^- nucleus, 600 GeV

Gamma(Sigma^+ K^+ K^-)/Gamma(Sigma^+ K^- pi^+) Gamma_23/Gamma_7

Table with 6 columns: VALUE, EVTS, DOCUMENT ID, TECN, COMMENT. Row: 0.16 +/- 0.06 +/- 0.01, 17, LINK 03E FOCUS gamma nucleus, E_gamma approx 180 GeV

Gamma(Sigma^+ phi)/Gamma(Sigma^+ K^- pi^+) Gamma_24/Gamma_7

Table with 6 columns: VALUE, CL%, DOCUMENT ID, TECN, COMMENT. Row: <0.12, 90, LINK 03E FOCUS gamma nucleus, E_gamma approx 180 GeV

Gamma(p phi(1020))/Gamma(p K^- pi^+) Gamma_26/Gamma_19

Table with 6 columns: VALUE (units 10^-3), EVTS, DOCUMENT ID, TECN, COMMENT. Row: 19.8 +/- 0.7 +/- 0.9 +/- 0.2, 3.4k, 1 AAIJ 19I LHCb pp at 8 TeV

1 The last uncertainty is due to the uncertainty in the phi -> K^+ K^- branching fraction.

Gamma(Xi(1690)^0 K^+ X B(Xi(1690)^0 -> Sigma^+ K^-))/Gamma(Sigma^+ K^- pi^+) Gamma_25/Gamma_7

Table with 6 columns: VALUE, CL%, DOCUMENT ID, TECN, COMMENT. Row: <0.05, 90, LINK 03E FOCUS gamma nucleus, E_gamma approx 180 GeV

Xi_c^+ REFERENCES

AAIJ 20AH PR D102 071101 R. Aaij et al. (LHCb Collab.)
AAIJ 19AB PR D99 052006 R. Aaij et al. (LHCb Collab.)
AAIJ 19AG PR D100 032001 R. Aaij et al. (LHCb Collab.)
AAIJ 19I JHEP 1904 084 R. Aaij et al. (LHCb Collab.)
LI 19C PR D100 031101 Y.B. Li et al. (BELLE Collab.)
SUMIHAMA 19 PRL 122 072501 M. Sumihama et al. (BELLE Collab.)
AAIJ 14Z PRL 113 032001 R. Aaij et al. (LHCb Collab.)
AALTONEN 14B CDF E687 (CDF Collab.)
VAZQUEZ-JA...08 PL B666 299 E. Vazquez-Jauregui et al. (SELX Collab.)
LESIAK 05 PL B605 237 T. Lesiak et al. (BELLE Collab.)
Also PL B617 198 (errata.) T. Lesiak et al. (BELLE Collab.)
LINK 03E PL B571 139 J.M. Link et al. (FNAL FOCUS Collab.)
MAHMOOD 02 PR D65 031102 A.H. Mahmood et al. (CLEO Collab.)
LINK 01B PL B512 277 J.M. Link et al. (FNAL FOCUS Collab.)
LINK 01D PL B523 53 J.M. Link et al. (FNAL FOCUS Collab.)
JUN 00 PRL 84 1857 S.Y. Jun et al. (FNAL SELEX Collab.)
FRABETTI 98 PL B427 211 P.L. Frabetti et al. (FNAL E687 Collab.)
BERGFELD 96 PL B365 431 T. Bergfeld et al. (CLEO Collab.)
EDWARDS 96 PL B373 261 K.W. Edwards et al. (CLEO Collab.)
ALEXANDER 95B PRL 74 3113 J. Alexander et al. (CLEO Collab.)
Also PRL 75 4155 (erratum.) J. Alexander et al. (CLEO Collab.)
AVERY 95 PRL 75 4364 P. Avery et al. (CLEO Collab.)
FRABETTI 93B PRL 70 1381 P.L. Frabetti et al. (FNAL E687 Collab.)
ALBRECHT 90F PL B247 121 H. Albrecht et al. (ARGUS Collab.)
ALAM 89 PL B226 401 M.S. Alam et al. (CLEO Collab.)
BARLAG 89C PL B233 522 S. Barlag et al. (ACCMOR Collab.)
COTEUS 87 PRL 59 1530 P. Coteus et al. (FNAL E400 Collab.)
BIAGI 85C PL 150B 230 S.F. Biagi et al. (CERN WA62 Collab.)
BIAGI 83 PL 122B 455 S.F. Biagi et al. (CERN WA62 Collab.)



I(J^P) = 1/2(1/2^+) Status: ***

Neither J or P has actually been measured.

Xi_c^0 MASS

The fit uses the Xi_c^0 and Xi_c^+ mass and mass-difference measurements.

Table with 6 columns: VALUE (MeV), EVTS, DOCUMENT ID, TECN, COMMENT. Row: 2470.44 +/- 0.28 OUR FIT Error includes scale factor of 1.2.

2470.99 +/- 0.30 - 0.50 OUR AVERAGE

Table with 6 columns: VALUE, EVTS, DOCUMENT ID, TECN, COMMENT. Rows include AALTONEN 14B CDF, LESIAK 05 BELL, FRABETTI 98B E687, HENDERSON 92B CLEO, ALBRECHT 90F ARG, BARLAG 90 ACCM, ALAM 89 CLEO.

••• We do not use the following data for averages, fits, limits, etc. ••• 2462.1 +/- 3.1 +/- 1.4, 42, 2 FRABETTI 93C E687 See FRABETTI 98B, 2471 +/- 3 +/- 4, 14, AVERY 89 CLEO See ALAM 89

1 The systematic error was (wrongly) given the other way round in LESIAK 05.

2 The FRABETTI 93C mass is well below the other measurements.

Xi_c^0 - Xi_c^+ MASS DIFFERENCE

Table with 6 columns: VALUE (MeV), EVTS, DOCUMENT ID, TECN, COMMENT. Row: 2.72 +/- 0.23 OUR FIT Error includes scale factor of 1.1.

Table with 6 columns: VALUE, EVTS, DOCUMENT ID, TECN, COMMENT. Rows include 2.91 +/- 0.26 OUR AVERAGE, 2.85 +/- 0.30 +/- 0.04, 5.1/3.4k, AALTONEN 14B CDF, LESIAK 05 BELL, ALBRECHT 90F ARG, BARLAG 90 ACCM, ALAM 89 CLEO.

Baryon Particle Listings

$$\Xi_c^0$$

Ξ_c^0 MEAN LIFE				
VALUE (10^{-15} s)	EVTS	DOCUMENT ID	TECN	COMMENT
151.9 ± 2.4 OUR AVERAGE				
153.4 ± 2.4 ± 0.7	22k	¹ AAIJ	19AG LHCb	$\Xi_c^0 \rightarrow p K^- K^- \pi^+$
118 $^{+14}_{-12}$ ± 5	110	LINK	02H FOCS	γ nucleus, ≈ 180 GeV
101 $^{+25}_{-17}$ ± 5	42	FRABETTI	93c E687	γ Be, $\overline{E}_\gamma = 220$ GeV
82 $^{+59}_{-30}$	4	BARLAG	90 ACCM	$\pi^- (K^-)$ Cu 230 GeV

¹AAIJ 19AG reports [Ξ_c^0 MEAN LIFE] / [D^\pm MEAN LIFE] = $0.1485 \pm 0.0017 \pm 0.0016$ which we multiply by our best value D^\pm MEAN LIFE = $(1.033 \pm 0.005) \times 10^{-12}$ s. Our first error is their experiment's error and our second error is the systematic error from using our best value.

 Ξ_c^0 DECAY MODES

Mode	Fraction (Γ_i/Γ)	Scale factor
Cabibbo-favored decays		
Γ_1 $p K^- K^- \pi^+$	$(4.8 \pm 1.2) \times 10^{-3}$	1.1
Γ_2 $p K^- \overline{K}^*(892)^0, \overline{K}^{*0} \rightarrow K^- \pi^+$	$(2.0 \pm 0.6) \times 10^{-3}$	
Γ_3 $p K^- K^- \pi^+$ (no \overline{K}^{*0})	$(3.0 \pm 0.9) \times 10^{-3}$	
Γ_4 ΛK_S^0	$(3.2 \pm 0.7) \times 10^{-3}$	
Γ_5 $\Lambda K^- \pi^+$	$(1.45 \pm 0.33) \%$	1.1
Γ_6 $\Lambda \overline{K}^*(892)^0$	$(2.6 \pm 0.7) \times 10^{-3}$	
Γ_7 $\Lambda \overline{K}^0 \pi^+ \pi^-$	seen	
Γ_8 $\Lambda K^- \pi^+ \pi^+ \pi^-$	seen	
Γ_9 $\Sigma^0 K_S^0$	$(5.4 \pm 1.6) \times 10^{-4}$	
Γ_{10} $\Sigma^+ K^-$	$(1.8 \pm 0.4) \times 10^{-3}$	
Γ_{11} $\Sigma^0 \overline{K}^*(892)^0$	$(9.8 \pm 2.3) \times 10^{-3}$	
Γ_{12} $\Sigma^+ K^*(892)^-$	$(4.9 \pm 1.4) \times 10^{-3}$	
Γ_{13} $\Xi^- \pi^+$	$(1.43 \pm 0.32) \%$	1.1
Γ_{14} $\Xi^- \pi^+ \pi^+ \pi^-$	$(4.8 \pm 2.3) \%$	
Γ_{15} $\Xi^0 K^+ K^-$		
Γ_{16} $\Xi^0 \phi, \phi \rightarrow K^+ K^-$	$(5.1 \pm 1.3) \times 10^{-4}$	
Γ_{17} $\Xi^0 K^+ K^-$ nonresonant	$(5.6 \pm 1.4) \times 10^{-4}$	
Γ_{18} $\Omega^- K^+$	$(4.2 \pm 1.0) \times 10^{-3}$	
Γ_{19} $\Xi^- e^+ \nu_e$	$(1.04 \pm 0.24) \%$	
Γ_{20} $\Xi^- \mu^+ \nu_\mu$	$(1.01 \pm 0.25) \%$	
Cabibbo-suppressed decays		
Γ_{21} $\Lambda_c^+ \pi^-$	$(5.5 \pm 1.8) \times 10^{-3}$	
Γ_{22} $\Xi^- K^+$	$(3.9 \pm 1.2) \times 10^{-4}$	
Γ_{23} $\Lambda K^+ K^-$ (no ϕ)	$(4.1 \pm 1.4) \times 10^{-4}$	
Γ_{24} $\Lambda \phi$	$(4.9 \pm 1.5) \times 10^{-4}$	

CONSTRAINED FIT INFORMATION

An overall fit to 5 branching ratios uses 6 measurements and one constraint to determine 4 parameters. The overall fit has a $\chi^2 = 1.4$ for 3 degrees of freedom.

The following *off-diagonal* array elements are the correlation coefficients $\langle \delta x_i \delta x_j \rangle / (\delta x_i \delta x_j)$, in percent, from the fit to the branching fractions, $x_i \equiv \Gamma_i / \Gamma_{\text{total}}$. The fit constrains the x_i whose labels appear in this array to sum to one.

x_5	68
x_{13}	89 76
	x_1 x_5

 Ξ_c^0 BRANCHING RATIOS

Cabibbo-favored (S = -2) decays

$\Gamma(p K^- K^- \pi^+) / \Gamma_{\text{total}}$					Γ_1 / Γ
VALUE (%)	EVTS	DOCUMENT ID	TECN	COMMENT	
0.48 ± 0.12 OUR FIT	Error includes scale factor of 1.1.				
0.58 ± 0.05	17 ± 5	LI	19A	BELL	$e^+ e^-$ at $\Upsilon(4S)$
$\Gamma(p K^- K^- \pi^+) / \Gamma(\Xi^- \pi^+)$					Γ_1 / Γ_{13}
VALUE (%)	EVTS	DOCUMENT ID	TECN	COMMENT	
0.34 ± 0.04 OUR AVERAGE					
0.33 ± 0.03 ± 0.03	1908 ± 62	LESIAK	05	BELL	$e^+ e^-$, $\Upsilon(4S)$
0.35 ± 0.06 ± 0.03	148 ± 18	DANKO	04	CLEO	$e^+ e^-$
$\Gamma(p K^- \overline{K}^*(892)^0, \overline{K}^{*0} \rightarrow K^- \pi^+) / \Gamma(\Xi^- \pi^+)$					Γ_2 / Γ_{13}
VALUE (%)	EVTS	DOCUMENT ID	TECN	COMMENT	
0.14 ± 0.03 ± 0.01		DANKO	04	CLEO	$e^+ e^-$

$\Gamma(p K^- K^- \pi^+ (\text{no } \overline{K}^{*0})) / \Gamma(\Xi^- \pi^+)$					Γ_3 / Γ_{13}
VALUE (%)	EVTS	DOCUMENT ID	TECN	COMMENT	
0.21 ± 0.04 ± 0.02		DANKO	04	CLEO	$e^+ e^-$

$\Gamma(\Lambda K_S^0) / \Gamma(\Xi^- \pi^+)$					Γ_4 / Γ_{13}
VALUE (%)	EVTS	DOCUMENT ID	TECN	COMMENT	
0.225 ± 0.013 OUR AVERAGE					
0.229 ± 0.008 ± 0.012	5.6k	LI	21F	BELL	$e^+ e^-$ at $\Upsilon(nS)$
0.21 ± 0.02 ± 0.02	465 ± 37	LESIAK	05	BELL	$e^+ e^-$, $\Upsilon(4S)$

$\Gamma(\Lambda K^- \pi^+) / \Gamma_{\text{total}}$					Γ_5 / Γ
VALUE (%)	EVTS	DOCUMENT ID	TECN	COMMENT	
1.45 ± 0.33 OUR FIT	Error includes scale factor of 1.1.				
1.17 ± 0.37 ± 0.09	24 ± 6	LI	19A	BELL	$e^+ e^-$ at $\Upsilon(4S)$

$\Gamma(\Lambda K^- \pi^+) / \Gamma(\Xi^- \pi^+)$					Γ_5 / Γ_{13}
VALUE (%)	EVTS	DOCUMENT ID	TECN	COMMENT	
1.02 ± 0.15 OUR FIT	Error includes scale factor of 1.2.				
1.07 ± 0.12 ± 0.07	2979 ± 211	LESIAK	05	BELL	$e^+ e^-$, $\Upsilon(4S)$

$\Gamma(\Lambda \overline{K}^*(892)^0) / \Gamma(\Xi^- \pi^+)$					Γ_6 / Γ_{13}
VALUE (%)	EVTS	DOCUMENT ID	TECN	COMMENT	
0.18 ± 0.02 ± 0.01	4k	JIA	21	BELL	$e^+ e^-$ at $\Upsilon(nS)$

$\Gamma(\Lambda \overline{K}^0 \pi^+ \pi^-) / \Gamma_{\text{total}}$					Γ_7 / Γ
VALUE (%)	EVTS	DOCUMENT ID	TECN	COMMENT	
seen		FRABETTI	98B	E687	γ Be, $\overline{E}_\gamma = 220$ GeV

$\Gamma(\Lambda K^- \pi^+ \pi^+ \pi^-) / \Gamma_{\text{total}}$					Γ_8 / Γ
VALUE (%)	EVTS	DOCUMENT ID	TECN	COMMENT	
seen		FRABETTI	98B	E687	γ Be, $\overline{E}_\gamma = 220$ GeV

$\Gamma(\Sigma^0 K_S^0) / \Gamma(\Xi^- \pi^+)$					Γ_9 / Γ_{13}
VALUE (units 10^{-2})	EVTS	DOCUMENT ID	TECN	COMMENT	
3.8 ± 0.6 ± 0.4	279	LI	21F	BELL	$e^+ e^-$ at $\Upsilon(nS)$

$\Gamma(\Sigma^+ K^-) / \Gamma(\Xi^- \pi^+)$					$\Gamma_{10} / \Gamma_{13}$
VALUE (units 10^{-2})	EVTS	DOCUMENT ID	TECN	COMMENT	
12.3 ± 0.7 ± 1.0	889	LI	21F	BELL	$e^+ e^-$ at $\Upsilon(nS)$

$\Gamma(\Sigma^0 \overline{K}^*(892)^0) / \Gamma(\Xi^- \pi^+)$					$\Gamma_{11} / \Gamma_{13}$
VALUE (%)	EVTS	DOCUMENT ID	TECN	COMMENT	
0.69 ± 0.03 ± 0.03	6.3k	JIA	21	BELL	$e^+ e^-$ at $\Upsilon(nS)$

$\Gamma(\Sigma^+ K^*(892)^-) / \Gamma(\Xi^- \pi^+)$					$\Gamma_{12} / \Gamma_{13}$
VALUE (%)	EVTS	DOCUMENT ID	TECN	COMMENT	
0.34 ± 0.06 ± 0.02	373	JIA	21	BELL	$e^+ e^-$ at $\Upsilon(nS)$

$\Gamma(\Xi^- \pi^+) / \Gamma_{\text{total}}$					Γ_{13} / Γ
VALUE (%)	EVTS	DOCUMENT ID	TECN	COMMENT	
1.43 ± 0.32 OUR FIT	Error includes scale factor of 1.1.				
1.80 ± 0.50 ± 0.14	45 ± 7	LI	19A	BELL	$e^+ e^-$ at $\Upsilon(4S)$

$\Gamma(\Xi^- \pi^+) / \Gamma(\Xi^- \pi^+ \pi^+ \pi^-)$					$\Gamma_{13} / \Gamma_{14}$
VALUE (%)	EVTS	DOCUMENT ID	TECN	COMMENT	
0.30 ± 0.12 ± 0.05		ALBRECHT	90F	ARG	$e^+ e^-$ at $\Upsilon(4S)$

$\Gamma(\Omega^- K^+) / \Gamma(\Xi^- \pi^+)$					$\Gamma_{18} / \Gamma_{13}$
VALUE (%)	EVTS	DOCUMENT ID	TECN	COMMENT	
0.294 ± 0.018 ± 0.016	650	AUBERT,B	05M	BABR	$e^+ e^- \approx \Upsilon(4S)$

$\Gamma(\Xi^0 \phi, \phi \rightarrow K^+ K^-) / \Gamma(\Xi^- \pi^+)$					$\Gamma_{16} / \Gamma_{13}$
VALUE (%)	EVTS	DOCUMENT ID	TECN	COMMENT	
0.036 ± 0.004 ± 0.002	311	¹ MCNEIL	21	BELL	$e^+ e^-$ at $\Upsilon(nS)$

¹MCNEIL 21 assumes an azimuthally symmetric amplitude model to recover resonant and nonresonant contributions to $\Xi_c^0 \rightarrow \Xi^0 K^+ K^-$.

$\Gamma(\Xi^0 K^+ K^- \text{ nonresonant}) / \Gamma(\Xi^- \pi^+)$					$\Gamma_{17} / \Gamma_{13}$
VALUE (%)	EVTS	DOCUMENT ID	TECN	COMMENT	
0.039 ± 0.004 ± 0.002	311	¹ MCNEIL	21	BELL	$e^+ e^-$ at $\Upsilon(nS)$

¹MCNEIL 21 assumes an azimuthally symmetric amplitude model to recover resonant and nonresonant contributions to $\Xi_c^0 \rightarrow \Xi^0 K^+ K^-$.

$\Gamma(\Xi^- e^+ \nu_e) / \Gamma(\Xi^- \pi^+)$					$\Gamma_{19} / \Gamma_{13}$
VALUE (%)	EVTS	DOCUMENT ID	TECN	COMMENT	
0.730 ± 0.021 ± 0.039		¹ LI	21c	BELL	$e^+ e^-$ at 10.52, 10.58 GeV
• • • We do not use the following data for averages, fits, limits, etc. • • •					
1.38 ± 0.14 ± 0.22		ACHARYA	21A	ALCE	pp at 13 TeV
3.1 ± 1.0 $^{+0.3}_{-0.5}$	54	ALEXANDER	95B	CLE2	$e^+ e^- \approx \Upsilon(4S)$
0.96 ± 0.43 ± 0.18	18	² ALBRECHT	93B	ARG	$e^+ e^- \approx 10.4$ GeV

¹LI 21c measures ratio $B(\Xi_c^0 \rightarrow \Xi^- e^+ \nu_e) / B(\Xi_c^0 \rightarrow \Xi^- \mu^+ \nu_\mu) = 1.03 \pm 0.05 \pm 0.07$.

²This ALBRECHT 93B value is the average of the $(\Xi^- e^+ \text{ anything}) / \Xi^- \pi^+$ and $(\Xi^- \mu^+ \text{ anything}) / \Xi^- \pi^+$ ratios. Here we average it with the $\Xi^- e^+ \nu_e / \Xi^- \pi^+$ ratio.

See key on page 1127

Baryon Particle Listings

$$\Xi_c^0, \Xi_c^{'+}, \Xi_c^{\prime 0}$$

$\Gamma(\Xi_c^{\prime -} \mu^+ \nu_\mu) / \Gamma(\Xi_c^{\prime -} \pi^+) \quad \Gamma_{20} / \Gamma_{13}$

VALUE	DOCUMENT ID	TECN	COMMENT
0.708 ± 0.033 ± 0.056	¹ LI	21c	BELL e ⁺ e ⁻ at 10.52, 10.58 GeV
¹ LI 21c measures ratio $B(\Xi_c^0 \rightarrow \Xi_c^{\prime -} e^+ \nu_e) / B(\Xi_c^0 \rightarrow \Xi_c^{\prime -} \mu^+ \nu_\mu) = 1.03 \pm 0.05 \pm 0.07$.			

$\Gamma(\Xi_c^{\prime -} e^+ \nu_e) / \Gamma(\Xi_c^{\prime -} \mu^+ \nu_\mu) \quad \Gamma_{19} / \Gamma_{20}$

VALUE	DOCUMENT ID	TECN	COMMENT
• • • We do not use the following data for averages, fits, limits, etc. • • •			
1.03 ± 0.05 ± 0.07	¹ LI	21c	BELL e ⁺ e ⁻ at 10.52, 10.58 GeV
¹ LI 21c value is not independent from other quoted measurements.			

Cabibbo-suppressed decays

$\Gamma(\Lambda_c^+ \pi^-) / \Gamma_{total} \quad \Gamma_{21} / \Gamma$

VALUE (units 10 ⁻³)	EVTS	DOCUMENT ID	TECN	COMMENT
5.5 ± 0.2 ± 1.8	6.3k	¹ AAJ	20AH LHCB	pp at 13 TeV
¹ AAJ 20AH extracts $B(\Xi_c^0 \rightarrow \Lambda_c^+ \pi^-)$ using two different normalization modes: $\Lambda_c^+ \rightarrow p K^- \pi^+$ and $\Xi_c^+ \rightarrow p K^- \pi^+$. The mean value of both results, taking their correlations into account, is presented as the final result. The measurement assumes production fraction ratios $f_{\Xi_c^0} / f_{\Lambda_c^+} = (9.7 \pm 0.9 \pm 3.1) \times 10^{-2}$ (from AAJ 19AB plus heavy quark symmetry arguments) as well as $f_{\Xi_c^+} / f_{\Xi_c^0} = 1.00 \pm 0.01$. It further uses the inputs $B(\Lambda_c^+ \rightarrow p K^- \pi^+) = (6.23 \pm 0.33) \times 10^{-2}$ and $B(\Xi_c^+ \rightarrow p K^- \pi^+) = (4.5 \pm 2.1 \pm 0.7) \times 10^{-3}$ (from LI 19C). Its correlation with $B(\Xi_c^+ \rightarrow p K^- \pi^+)$, as measured in AAJ 20AH, is 0.414.				

$\Gamma(\Xi_c^{\prime -} K^+) / \Gamma(\Xi_c^{\prime -} \pi^+) \quad \Gamma_{22} / \Gamma_{13}$

VALUE (units 10 ⁻²)	EVTS	DOCUMENT ID	TECN	COMMENT
2.75 ± 0.51 ± 0.25	314 ± 58	CHISTOV	13	BELL e ⁺ e ⁻ ≈ $\mathcal{T}(4S)$

$\Gamma(\Lambda K^+ K^- (no \phi)) / \Gamma(\Xi_c^{\prime -} \pi^+) \quad \Gamma_{23} / \Gamma_{13}$

VALUE (units 10 ⁻²)	EVTS	DOCUMENT ID	TECN	COMMENT
2.86 ± 0.61 ± 0.37	510 ± 110	CHISTOV	13	BELL e ⁺ e ⁻ ≈ $\mathcal{T}(4S)$

$\Gamma(\Lambda \phi) / \Gamma(\Xi_c^{\prime -} \pi^+) \quad \Gamma_{24} / \Gamma_{13}$

VALUE (units 10 ⁻²)	EVTS	DOCUMENT ID	TECN	COMMENT
3.43 ± 0.58 ± 0.32	316 ± 54	CHISTOV	13	BELL e ⁺ e ⁻ ≈ $\mathcal{T}(4S)$

Ξ_c^0 DECAY PARAMETERS

See the note on "Baryon Decay Parameters" in the neutron Listings.

α FOR $\Xi_c^0 \rightarrow \Xi_c^{\prime -} \pi^+$

VALUE	EVTS	DOCUMENT ID	TECN	COMMENT
-0.64 ± 0.05 ± 0.01		LI	21c	BELL e ⁺ e ⁻ at 10.52, 10.58 GeV
• • • We do not use the following data for averages, fits, limits, etc. • • •				
-0.56 ± 0.39 ^{+0.10} _{-0.09}	138	CHAN	01	CLE2 e ⁺ e ⁻ ≈ $\mathcal{T}(4S)$

α FOR $\Xi_c^0 \rightarrow \Xi_c^{\prime +} \pi^-$

VALUE	DOCUMENT ID	TECN	COMMENT
0.61 ± 0.05 ± 0.01	LI	21c	BELL e ⁺ e ⁻ at 10.52, 10.58 GeV

α FOR $\Xi_c^0 \rightarrow \Lambda \bar{K}^*(892)^0$

VALUE	EVTS	DOCUMENT ID	TECN	COMMENT
0.15 ± 0.22 ± 0.04	4k	¹ JIA	21	BELL e ⁺ e ⁻ at $\mathcal{T}(nS)$
¹ JIA 21 measures $\alpha(\Xi_c^0 \rightarrow \Lambda \bar{K}^*(892)^0) \alpha(\Lambda \rightarrow p \pi^-) = 0.115 \pm 0.164 \pm 0.031$, and uses $\alpha(\Lambda \rightarrow p \pi^-) = 0.747 \pm 0.010$.				

α FOR $\Xi_c^0 \rightarrow \Sigma^+ K^*(892)^-$

VALUE	EVTS	DOCUMENT ID	TECN	COMMENT
-0.52 ± 0.30 ± 0.02	373	¹ JIA	21	BELL e ⁺ e ⁻ at $\mathcal{T}(nS)$
¹ JIA 21 measures $\alpha(\Xi_c^0 \rightarrow \Sigma^+ \bar{K}^*(892)^-) \alpha(\Sigma^+ \rightarrow p \pi^0) = 0.514 \pm 0.295 \pm 0.012$, and uses $\alpha(\Sigma^+ \rightarrow p \pi^0) = -0.980 \pm 0.017$.				

Ξ_c^0 REFERENCES

ACHARYA	21A	PRL 127 272001	S. Acharya et al.	(ALICE Collab.)
JIA	21	JHEP 2106 160	S. Jia et al.	(BELLE Collab.)
LI	21C	PRL 127 121803	Y.B. Li et al.	(BELLE Collab.)
LI	21F	PR D105 L011102	Y. Li et al.	(BELLE Collab.)
MCNEIL	21	PR D103 112002	J.T. McNeil et al.	(BELLE Collab.)
AAJ	20AH	PR D102 071101	R. Aaij et al.	(LHCb Collab.)
AAJ	19AB	PR D99 052006	R. Aaij et al.	(LHCb Collab.)
AAJ	19AG	PR D100 032001	R. Aaij et al.	(LHCb Collab.)
LI	19A	PRL 122 082001	Y.B. Li et al.	(BELLE Collab.)
LI	19C	PR D100 031101	Y.B. Li et al.	(BELLE Collab.)
AALTONEN	14B	PR D89 072014	T. Aaltonen et al.	(CDF Collab.)
CHISTOV	13	PR D88 071103	R. Chistov et al.	(BELLE Collab.)
AUBERT,B	05M	PRL 95 142003	B. Aubert et al.	(BABAR Collab.)
LESIAK	05	PL B605 237	T. Lesiak et al.	(BELLE Collab.)
Also		PL B617 198 (errata.)	T. Lesiak et al.	(BELLE Collab.)

DANKO	04	PR D69 052004	I. Danko et al.	(CLEO Collab.)
LINK	02H	PL B541 211	J.M. Link et al.	(FNAL FOCUS Collab.)
CHAN	01	PR D63 111102	S. Chan et al.	(CLEO Collab.)
FRABETTI	98B	PL B426 403	P.L. Frabetti et al.	(FNAL E687 Collab.)
ALEXANDER	95B	PRL 74 3113	J. Alexander et al.	(CLEO Collab.)
Also		PRL 75 4155 (erratum)	J. Alexander et al.	(CLEO Collab.)
ALBRECHT	93B	PL B303 368	H. Albrecht et al.	(ARGUS Collab.)
FRABETTI	93C	PRL 70 2058	P.L. Frabetti et al.	(FNAL E687 Collab.)
HENDERSON	92B	PL B283 161	S. Henderson et al.	(CLEO Collab.)
ALBRECHT	90F	PL B247 121	H. Albrecht et al.	(ARGUS Collab.)
BARLAG	89	PL B236 495	S. Barlag et al.	(ACCMOR Collab.)
ALAM	89	PL B226 401	M.S. Alam et al.	(CLEO Collab.)
AVERY	89	PRL 62 863	P. Avery et al.	(CLEO Collab.)

$$\Xi_c^{\prime +}$$

$$I(J^P) = \frac{1}{2}(\frac{1}{2}^+) \text{ Status: } ***$$

The $\Xi_c^{\prime +}$ and $\Xi_c^{\prime 0}$ presumably complete the SU(3) sextet whose other members are the $\Sigma_c^{\prime +}$, $\Sigma_c^{\prime 0}$, and $\Omega_c^{\prime 0}$; see Fig. 5 in the "Quark Model" review. The quantum numbers given above come from this presumption but have not been measured.

$\Xi_c^{\prime +}$ MASS

The mass is obtained from the mass-difference measurement that follows.

VALUE (MeV)	DOCUMENT ID
2578.2 ± 0.5 OUR FIT	Error includes scale factor of 1.1.

$\Xi_c^{\prime +} - \Xi_c^{\prime 0}$ MASS DIFFERENCE

VALUE (MeV)	EVTS	DOCUMENT ID	TECN	COMMENT
110.5 ± 0.4 OUR FIT				
110.5 ± 0.1 ± 0.4	7k	YELTON	16	BELL e ⁺ e ⁻ , \mathcal{T} regions
• • • We do not use the following data for averages, fits, limits, etc. • • •				
107.8 ± 1.7 ± 2.5	25	JESSOP	99	CLE2 e ⁺ e ⁻ ≈ $\mathcal{T}(4S)$

$\Xi_c^{\prime +} - \Xi_c^0$ MASS DIFFERENCE

VALUE (MeV)	DOCUMENT ID	TECN	COMMENT
-0.5 ± 0.6 OUR FIT			
• • • We do not use the following data for averages, fits, limits, etc. • • •			
-0.8 ± 0.1 ± 0.5	YELTON	16	BELL 7055 and 11,560 evts

$\Xi_c^{\prime +}$ DECAY MODES

The $\Xi_c^{\prime +} - \Xi_c^{\prime 0}$ mass difference is too small for any strong decay to occur.

Mode	Fraction (Γ_i / Γ)
$\Gamma_1 \Xi_c^{\prime +} \gamma$	seen

$\Xi_c^{\prime +}$ REFERENCES

YELTON	16	PR D94 052011	J. Yelton et al.	(BELLE Collab.)
JESSOP	99	PRL 82 492	C.P. Jessop et al.	(CLEO Collab.)

$$\Xi_c^0$$

$$I(J^P) = \frac{1}{2}(\frac{1}{2}^+) \text{ Status: } ***$$

The Ξ_c^0 and $\Xi_c^{\prime +}$ presumably complete the SU(3) sextet whose other members are the $\Sigma_c^{\prime +}$, $\Sigma_c^{\prime 0}$, and $\Omega_c^{\prime 0}$; see Fig. 5 in the "Quark Model" review. The quantum numbers given above come from this presumption but have not been measured.

Ξ_c^0 MASS

The mass is obtained from the mass-difference measurement that follows.

VALUE (MeV)	DOCUMENT ID
2578.7 ± 0.5 OUR FIT	

$\Xi_c^0 - \Xi_c^{\prime 0}$ MASS DIFFERENCE

VALUE (MeV)	EVTS	DOCUMENT ID	TECN	COMMENT
108.3 ± 0.4 OUR FIT				
108.3 ± 0.1 ± 0.4	11.5k	YELTON	16	BELL e ⁺ e ⁻ , \mathcal{T} regions
• • • We do not use the following data for averages, fits, limits, etc. • • •				
107.0 ± 1.4 ± 2.5	28	JESSOP	99	CLE2 e ⁺ e ⁻ ≈ $\mathcal{T}(4S)$

Baryon Particle Listings

 $\Xi_c^{\prime 0}$, $\Xi_c(2645)$, $\Xi_c(2790)$ $\Xi_c^{\prime 0}$ DECAY MODESThe $\Xi_c^{\prime 0} - \Xi_c^0$ mass difference is too small for any strong decay to occur.

Mode	Fraction (Γ_i/Γ)
$\Gamma_1 \Xi_c^0 \gamma$	seen

 $\Xi_c^{\prime 0}$ REFERENCES

YELTON	16	PR D94 052011	J. Yelton <i>et al.</i>	(BELLE Collab.)
JESSOP	99	PRL 82 492	C.P. Jessop <i>et al.</i>	(CLEO Collab.)

 $\Xi_c(2645)$ $I(J^P) = \frac{1}{2}(\frac{3}{2}^+)$ Status: ***The natural assignment is that this is the $J^P = 3/2^+$ excitation of the Ξ_c in the same SU(4) multiplet as the $\Delta(1232)$, but the quantum numbers have not been measured. $\Xi_c(2645)$ MASSES $\Xi_c(2645)^+$ MASS

VALUE (MeV)	EVTs	DOCUMENT ID	TECN	COMMENT
2645.10 ± 0.30 OUR FIT				Error includes scale factor of 1.2.
2645.6 ± 0.2 ± 0.6 0.8	578 ± 32	LESIAK	08	BELL $e^+e^- \approx \mathcal{T}(4S)$

 $\Xi_c(2645)^0$ MASS

VALUE (MeV)	EVTs	DOCUMENT ID	TECN	COMMENT
2646.16 ± 0.25 OUR FIT				Error includes scale factor of 1.3.
2645.7 ± 0.2 ± 0.6 0.7	611 ± 32	LESIAK	08	BELL $e^+e^- \approx \mathcal{T}(4S)$

 $\Xi_c(2645) - \Xi_c$ MASS DIFFERENCES $m_{\Xi_c(2645)^+} - m_{\Xi_c^0}$

VALUE (MeV)	EVTs	DOCUMENT ID	TECN	COMMENT
174.67 ± 0.09 OUR FIT				
174.66 ± 0.06 ± 0.07	1260	YELTON	16	BELL e^+e^- in \mathcal{T} regions ••• We do not use the following data for averages, fits, limits, etc. •••
177.1 ± 0.5 ± 1.1	47	FRABETTI	98B	E687 γ Be, $\bar{E}\gamma = 220$ GeV
174.3 ± 0.5 ± 1.0	34	GIBBONS	96	CLE2 $e^+e^- \approx \mathcal{T}(4S)$

 $m_{\Xi_c(2645)^0} - m_{\Xi_c^+}$

VALUE (MeV)	EVTs	DOCUMENT ID	TECN	COMMENT
178.45 ± 0.10 OUR FIT				
178.46 ± 0.07 ± 0.07	975	YELTON	16	BELL e^+e^- in \mathcal{T} regions ••• We do not use the following data for averages, fits, limits, etc. •••
178.2 ± 0.5 ± 1.0	55	AVERY	95	CLE2 $e^+e^- \approx \mathcal{T}(4S)$

 $\Xi_c(2645)^+ - \Xi_c(2645)^0$ MASS DIFFERENCE

VALUE (MeV)	DOCUMENT ID	TECN	COMMENT
-1.06 ± 0.27 OUR FIT			Error includes scale factor of 1.1.
-0.85 ± 0.09 ± 0.49	YELTON 16	BELL	1260 and 975 evts
-0.1 ± 0.3 ± 0.6	LESIAK 08	BELL	≈ 600 evts each

 $\Xi_c(2645)$ WIDTHS $\Xi_c(2645)^+$ WIDTH

VALUE (MeV)	CL%	EVTs	DOCUMENT ID	TECN	COMMENT
2.14 ± 0.19 OUR AVERAGE					Error includes scale factor of 1.1.
2.06 ± 0.13 ± 0.13	1260	YELTON	16	BELL	e^+e^- in \mathcal{T} regions
2.6 ± 0.2 ± 0.4	3.7k	KATO	14	BELL	$e^+e^- \mathcal{T}(1S) - \mathcal{T}(5S)$
<3.1	90	GIBBONS	96	CLE2	$e^+e^- \approx \mathcal{T}(4S)$

 $\Xi_c(2645)^0$ WIDTH

VALUE (MeV)	CL%	EVTs	DOCUMENT ID	TECN	COMMENT
2.35 ± 0.18 ± 0.13					
<5.5	90	55	AVERY	95	CLE2 $e^+e^- \approx \mathcal{T}(4S)$

 $\Xi_c(2645)$ DECAY MODES $\Xi_c \pi$ is the only strong decay allowed to a Ξ_c resonance having this mass.

Mode	Fraction (Γ_i/Γ)
$\Gamma_1 \Xi_c^0 \pi^+$	seen
$\Gamma_2 \Xi_c^+ \pi^-$	seen

 $\Xi_c(2645)$ REFERENCES

YELTON	16	PR D94 052011	J. Yelton <i>et al.</i>	(BELLE Collab.)
KATO	14	PR D89 052003	Y. Kato <i>et al.</i>	(BELLE Collab.)
LESIAK	08	PL B665 9	T. Lesiak <i>et al.</i>	(BELLE Collab.)
FRABETTI	98B	PL B426 403	P.L. Frabetti <i>et al.</i>	(FNAL E687 Collab.)
GIBBONS	96	PRL 77 810	L.K. Gibbons <i>et al.</i>	(CLEO Collab.)
AVERY	95	PRL 75 4364	P. Avery <i>et al.</i>	(CLEO Collab.)

 $\Xi_c(2790)$ $I(J^P) = \frac{1}{2}(\frac{1}{2}^-)$ Status: ***Seen in $\Xi_c' \pi$ decays. The simplest assignment, based on the mass, width, and decay mode, is that this belongs in the same SU(4) multiplet as the $\Lambda(1405)$ and the $\Lambda_c(2595)^+$, but the spin and parity have not been measured. $\Xi_c(2790)$ MASSES

The masses are obtained from the mass-difference measurements that follow.

 $\Xi_c(2790)^+$ MASS

VALUE (MeV)	DOCUMENT ID
2791.9 ± 0.5 OUR FIT	

 $\Xi_c(2790)^0$ MASS

VALUE (MeV)	DOCUMENT ID
2793.9 ± 0.5 OUR FIT	

 $\Xi_c(2790) - \Xi_c'$ MASS DIFFERENCES $m_{\Xi_c(2790)^+} - m_{\Xi_c^0}$

VALUE (MeV)	EVTs	DOCUMENT ID	TECN	COMMENT
213.20 ± 0.22 OUR FIT				
213.2 ± 0.2 ± 0.1		YELTON 16	BELL	2231 and 11,560 evts
••• We do not use the following data for averages, fits, limits, etc. •••				
211.2 ± 1.3 ± 1.0	18	CSORNA	01	CLEO $e^+e^- \approx \mathcal{T}(4S)$

 $m_{\Xi_c(2790)^0} - m_{\Xi_c^+}$

VALUE (MeV)	EVTs	DOCUMENT ID	TECN	COMMENT
215.70 ± 0.22 OUR FIT				
215.7 ± 0.2 ± 0.1		YELTON 16	BELL	1241 and 7055 evts
••• We do not use the following data for averages, fits, limits, etc. •••				
216.2 ± 1.3 ± 1.0	14	CSORNA	01	CLEO $e^+e^- \approx \mathcal{T}(4S)$

 $\Xi_c(2790)^+ - \Xi_c(2790)^0$ MASS DIFFERENCE

VALUE (MeV)	DOCUMENT ID	TECN	COMMENT
-2.0 ± 0.7 OUR FIT			
••• We do not use the following data for averages, fits, limits, etc. •••			
-3.3 ± 0.4 ± 0.5	YELTON 16	BELL	2231 and 1241 evts

 $\Xi_c(2790)$ WIDTHS $\Xi_c(2790)^+$ WIDTH

VALUE (MeV)	CL%	EVTs	DOCUMENT ID	TECN	COMMENT
8.9 ± 0.6 ± 0.8		2231	YELTON 16	BELL	e^+e^- , \mathcal{T} regions
••• We do not use the following data for averages, fits, limits, etc. •••					
<15	90		CSORNA 01	CLEO	$e^+e^- \approx \mathcal{T}(4S)$

 $\Xi_c(2790)^0$ WIDTH

VALUE (MeV)	CL%	EVTs	DOCUMENT ID	TECN	COMMENT
10.0 ± 0.7 ± 0.8		1241	YELTON 16	BELL	e^+e^- , \mathcal{T} regions
••• We do not use the following data for averages, fits, limits, etc. •••					
<12	90		CSORNA 01	CLEO	$e^+e^- \approx \mathcal{T}(4S)$

 $\Xi_c(2790)$ DECAY MODES

Mode	Fraction (Γ_i/Γ)
$\Gamma_1 \Xi_c' \pi$	seen
$\Gamma_2 \Xi_c^0 \gamma$	
$\Gamma_3 \Xi_c^+ \gamma$	

 $\Xi_c(2790)$ BRANCHING RATIOS

$\Gamma(\Xi_c' \pi)/\Gamma_{\text{total}}$	Γ_1/Γ		
seen			
seen			
••• We do not use the following data for averages, fits, limits, etc. •••			
seen	YELTON 16	BELL	e^+e^- , \mathcal{T} regions
seen	CSORNA 01	CLEO	$e^+e^- \approx \mathcal{T}(4S)$

See key on page 1127

Baryon Particle Listings

$\Xi_c(2790)$, $\Xi_c(2815)$, $\Xi_c(2923)$

$\Gamma(\Xi_c^0 \gamma)/\Gamma(\Xi_c^+ \pi)$		Γ_2/Γ_1	
VALUE	EVTS	DOCUMENT ID	TECN
0.13 ± 0.03 ± 0.02	401	¹ YELTON	20 BELL
1 Assumes $B(\Xi_c^+ \rightarrow \Xi_c^+ \gamma) = 100\%$, noting no strong decay of the Ξ_c^+ is permitted in the available phase space. YELTON 20 measures $B(\Xi_c(2790)^0 \rightarrow \Xi_c^0 \gamma)/B(\Xi_c(2790)^0 \rightarrow \Xi_c^+ \pi^- \rightarrow \Xi_c^+ \gamma \pi^-)$.			

$\Gamma(\Xi_c^+ \gamma)/\Gamma(\Xi_c^+ \pi)$		Γ_3/Γ_1	
VALUE	CL%	DOCUMENT ID	TECN
<0.06	90	¹ YELTON	20 BELL
1 Assumes $B(\Xi_c^0 \rightarrow \Xi_c^0 \gamma) = 100\%$, noting no strong decay of the Ξ_c^+ is permitted in the available phase space. YELTON 20 measures $B(\Xi_c(2790)^+ \rightarrow \Xi_c^+ \gamma)/B(\Xi_c(2790)^+ \rightarrow \Xi_c^0 \pi^+ \rightarrow \Xi_c^0 \gamma \pi^+)$.			

$\Xi_c(2790)$ REFERENCES

YELTON	20	PR D102 071103	J. Yelton et al.	(BELLE Collab.)
YELTON	16	PR D94 052011	J. Yelton et al.	(BELLE Collab.)
CSORNA	01	PRL 86 4243	S.E. Csorna et al.	(CLEO Collab.)

$\Xi_c(2815)$

$$I(J^P) = \frac{1}{2}(\frac{3}{2}^-) \text{ Status: } ***$$

Seen in both $\Xi_c^+ \pi$ and $\Xi_c \pi \pi$ decays. The simplest assignment is that this belongs to the same SU(4) multiplet as the $\Lambda(1520)$ and the $\Lambda_c(2625)$, but the spin and parity have not been measured.

$\Xi_c(2815)$ MASSES

The masses are obtained from the mass-difference measurements that follow.

$\Xi_c(2815)^+$ MASS

VALUE (MeV)	EVTS	DOCUMENT ID	TECN	COMMENT
2816.51 ± 0.25 OUR FIT				Error includes scale factor of 1.2.
• • • We do not use the following data for averages, fits, limits, etc. • • •				
2817.0 ± 1.2 ^{+0.7} / _{-0.8}	73 ± 10	LESIAK	08 BELL	$e^+ e^- \approx \Upsilon(4S)$

$\Xi_c(2815)^0$ MASS

VALUE (MeV)	EVTS	DOCUMENT ID	TECN	COMMENT
2819.79 ± 0.30 OUR FIT				Error includes scale factor of 1.1.
• • • We do not use the following data for averages, fits, limits, etc. • • •				
2820.4 ± 1.4 ^{+0.9} / _{-1.0}	48 ± 8	LESIAK	08 BELL	$e^+ e^- \approx \Upsilon(4S)$

$\Xi_c(2815) - \Xi_c$ MASS DIFFERENCES

$m_{\Xi_c(2815)^+} - m_{\Xi_c^+}$

VALUE (MeV)	EVTS	DOCUMENT ID	TECN	COMMENT
348.80 ± 0.10 OUR FIT				
348.80 ± 0.08 ± 0.06	941	YELTON	16 BELL	$e^+ e^-$, Υ regions
• • • We do not use the following data for averages, fits, limits, etc. • • •				
348.6 ± 0.6 ± 1.0	20	ALEXANDER	99b CLE2	$e^+ e^- \approx \Upsilon(4S)$

$m_{\Xi_c(2815)^0} - m_{\Xi_c^0}$

VALUE (MeV)	EVTS	DOCUMENT ID	TECN	COMMENT
349.35 ± 0.11 OUR FIT				
349.35 ± 0.08 ± 0.07	1258	YELTON	16 BELL	$e^+ e^-$, Υ regions
• • • We do not use the following data for averages, fits, limits, etc. • • •				
347.2 ± 0.7 ± 2.0	9	ALEXANDER	99b CLE2	$e^+ e^- \approx \Upsilon(4S)$

$\Xi_c(2815)^+ - \Xi_c(2815)^0$ MASS DIFFERENCE

$m_{\Xi_c(2815)^+} - m_{\Xi_c(2815)^0}$

VALUE (MeV)	DOCUMENT ID	TECN	COMMENT
-3.27 ± 0.27 OUR FIT			
• • • We do not use the following data for averages, fits, limits, etc. • • •			
-3.47 ± 0.12 ± 0.48	YELTON	16 BELL	941 and 1258 evts
-3.4 ± 1.9 ± 0.9	LESIAK	08 BELL	73 & 48 events

$\Xi_c(2815)$ WIDTHS

$\Xi_c(2815)^+$ WIDTH

VALUE (MeV)	CL%	EVTS	DOCUMENT ID	TECN	COMMENT
2.43 ± 0.20 ± 0.17		941	YELTON	16 BELL	$e^+ e^-$, Υ regions
• • • We do not use the following data for averages, fits, limits, etc. • • •					
<3.5		90	ALEXANDER	99b CLE2	$e^+ e^- \approx \Upsilon(4S)$

$\Xi_c(2815)^0$ WIDTH

VALUE (MeV)	CL%	EVTS	DOCUMENT ID	TECN	COMMENT
2.54 ± 0.18 ± 0.17		1258	YELTON	16 BELL	$e^+ e^-$, Υ regions
• • • We do not use the following data for averages, fits, limits, etc. • • •					
<6.5		90	ALEXANDER	99b CLE2	$e^+ e^- \approx \Upsilon(4S)$

$\Xi_c(2815)$ DECAY MODES

The $\Xi_c \pi \pi$ modes are consistent with being entirely via $\Xi_c(2645) \pi$.

Mode	Fraction (Γ_i/Γ)
$\Gamma_1 \Xi_c^+ \pi$	seen
$\Gamma_2 \Xi_c(2645) \pi$	seen
$\Gamma_3 \Xi_c^0 \gamma$	seen
$\Gamma_4 \Xi_c^+ \gamma$	

$\Gamma(\Xi_c^+ \pi)/\Gamma_{total}$

VALUE	DOCUMENT ID	TECN	COMMENT
seen	YELTON	16 BELL	$e^+ e^-$, Υ regions
seen	ALEXANDER	99b CLE2	$e^+ e^- \approx \Upsilon(4S)$

$\Gamma(\Xi_c(2645) \pi)/\Gamma_{total}$

VALUE	DOCUMENT ID	TECN	COMMENT
seen	YELTON	16 BELL	$e^+ e^-$, Υ regions
seen	LESIAK	08 BELL	$e^+ e^- \approx \Upsilon(4S)$

$\Gamma(\Xi_c^0 \gamma)/\Gamma(\Xi_c(2645) \pi)$

VALUE	EVTS	DOCUMENT ID	TECN	CHG	COMMENT
0.41 ± 0.05 ± 0.03	222	¹ YELTON	20 BELL	0	$e^+ e^-$ at $\Upsilon(4S)$
1 Assumes $B(\Xi_c(2645)^+ \rightarrow \Xi_c^0 \pi^+) = 100\%$, which is the only strong decay of the $\Xi_c(2645)$ permitted in the available phase space. YELTON 20 measures $B(\Xi_c(2815)^0 \rightarrow \Xi_c^0 \gamma)/B(\Xi_c(2815)^0 \rightarrow \Xi_c(2645)^+ \pi^- \rightarrow \Xi_c^0 \pi^+ \pi^-)$.					

$\Gamma(\Xi_c^+ \gamma)/\Gamma(\Xi_c(2645) \pi)$

VALUE	CL%	DOCUMENT ID	TECN	CHG	COMMENT
<0.09		¹ YELTON	20 BELL	+	$e^+ e^-$ at $\Upsilon(4S)$
1 Assumes $B(\Xi_c(2645)^0 \rightarrow \Xi_c^+ \pi^-) = 100\%$, which is the only strong decay of the $\Xi_c(2645)$ permitted in the available phase space. YELTON 20 measures $B(\Xi_c(2815)^+ \rightarrow \Xi_c^+ \gamma)/B(\Xi_c(2815)^+ \rightarrow \Xi_c(2645)^0 \pi^+ \rightarrow \Xi_c^+ \pi^- \pi^+)$.					

$\Xi_c(2815)$ REFERENCES

YELTON	20	PR D102 071103	J. Yelton et al.	(BELLE Collab.)
YELTON	16	PR D94 052011	J. Yelton et al.	(BELLE Collab.)
LESIAK	08	PL B665 9	T. Lesiak et al.	(BELLE Collab.)
ALEXANDER	99b	PRL 83 3390	J.P. Alexander et al.	(CLEO Collab.)

$\Xi_c(2923)$

$$I(J^P) = ?(??) \text{ Status: } **$$

OMITTED FROM SUMMARY TABLE

$\Xi_c(2923)$ MASSES

$\Xi_c(2923)^0$ MASS

VALUE (MeV)	EVTS	DOCUMENT ID	TECN	COMMENT
2923.04 ± 0.25 ± 0.24	5.4k	¹ AAIJ	20x LHCB	pp at 13 TeV
1 AAIJ 20x reports $2923.04 \pm 0.25 \pm 0.20 \pm 0.14$ MeV where the last uncertainty is due to the Λ_c^+ mass.				

$\Xi_c(2923)$ WIDTHS

$\Xi_c(2923)^0$ WIDTH

VALUE (MeV)	EVTS	DOCUMENT ID	TECN	COMMENT
7.1 ± 0.8 ± 1.8	5.4k	AAIJ	20x LHCB	pp at 13 TeV

$\Xi_c(2923)$ DECAY MODES

Mode	Fraction (Γ_i/Γ)
$\Gamma_1 \Lambda_c^+ K^-$	seen

$\Xi_c(2923)$ BRANCHING RATIOS

$\Gamma(\Lambda_c^+ K^-)/\Gamma_{total}$

VALUE	EVTS	DOCUMENT ID	TECN	COMMENT
seen	5.4k	AAIJ	20x LHCB	pp at 13 TeV

$\Xi_c(2923)$ REFERENCES

AAIJ	20x	PRL 124 222001	R. Aaij et al.	(LHCb Collab.)
------	-----	----------------	----------------	----------------

Baryon Particle Listings

$\Xi_c(2930), \Xi_c(2970)$

$\Xi_c(2930)$

$$I(J^P) = ?(??) \text{ Status: } **$$

OMITTED FROM SUMMARY TABLE

$\Xi_c(2930)$ MASSES

$\Xi_c(2930)^+$ MASS

VALUE (MeV)	EVTS	DOCUMENT ID	TECN	COMMENT
2942.3 ± 4.4 ± 1.5	21	LI	18D	BELL e^+e^- at $\Upsilon(4S)$

$\Xi_c(2930)^0$ MASS

VALUE (MeV)	EVTS	DOCUMENT ID	TECN	COMMENT
2938.55 ± 0.21 ± 0.22	10.4k	¹ AAIJ	20X	LHCB pp at 13 TeV

••• We do not use the following data for averages, fits, limits, etc. •••

2928.9 ± 3.0 +0.9 -12.0	61	LI	18A	BELL e^+e^- at $\Upsilon(4S)$
2931 ± 3 ± 5	34	AUBERT	08H	BABR $\Upsilon(4S) \rightarrow B\bar{B}$

¹AAIJ 20X reports 2938.55 ± 0.21 ± 0.17 ± 0.14 MeV where the last uncertainty is due to the Λ_c^+ mass. Observes that the broader resonance at 2930 MeV seen in $B^- \rightarrow K^-\Lambda_c^+\bar{\Lambda}_c^-$ by LI 18A and AUBERT 08H resolves into two narrower peaks at approximately 2939 MeV and 2923 MeV.

$\Xi_c(2930)^+ - \Xi_c(2930)^0$ MASS DIFFERENCE

VALUE (MeV)	EVTS	DOCUMENT ID	TECN	COMMENT
13.4 ± 5.3 +1.7 -12.1	21	¹ LI	18D	BELL e^+e^- at $\Upsilon(4S)$

¹This LI 18D value is not independent of the mass measurements.

$\Xi_c(2930)$ WIDTHS

$\Xi_c(2930)^+$ WIDTH

VALUE (MeV)	EVTS	DOCUMENT ID	TECN	COMMENT
14.8 ± 8.8 ± 2.5	21	LI	18D	BELL e^+e^- at $\Upsilon(4S)$

$\Xi_c(2930)^0$ WIDTH

VALUE (MeV)	EVTS	DOCUMENT ID	TECN	COMMENT
10.2 ± 0.8 ± 1.1	10.4k	¹ AAIJ	20X	LHCB pp at 13 TeV

••• We do not use the following data for averages, fits, limits, etc. •••

19.5 ± 8.4 +5.9 -7.9	61	LI	18A	BELL e^+e^- at $\Upsilon(4S)$
36 ± 7 ± 11	34	AUBERT	08H	BABR $\Upsilon(4S) \rightarrow B\bar{B}$

¹AAIJ 20X observes that the broader resonance at 2930 MeV seen in $B^- \rightarrow K^-\Lambda_c^+\bar{\Lambda}_c^-$ by LI 18A and AUBERT 08H resolves into two narrower peaks at approximately 2939 MeV and 2923 MeV.

$\Xi_c(2930)$ DECAY MODES

Mode	Fraction (Γ_i/Γ)
$\Gamma_1 \Lambda_c^+ K^-$	seen
$\Gamma_2 \Lambda_c^+ K_S^0$	seen

$\Xi_c(2930)$ BRANCHING RATIOS

$\Gamma(\Lambda_c^+ K^-)/\Gamma_{\text{total}}$	Γ_1/Γ			
VALUE	EVTS	DOCUMENT ID	TECN	COMMENT
seen	10.4k	AAIJ	20X	LHCB pp at 13 TeV
seen	61	LI	18A	BELL Significance 5.1 std
seen	34	AUBERT	08H	BABR e^+e^- at $\Upsilon(4S)$

$\Gamma(\Lambda_c^+ K_S^0)/\Gamma_{\text{total}}$	Γ_2/Γ			
VALUE	EVTS	DOCUMENT ID	TECN	COMMENT
seen	21	LI	18D	BELL Significance 4.1 std

$\Xi_c(2930)$ REFERENCES

AAIJ	20X	PRL 124 222001	R. Aaij et al.	(LHCB Collab.)
LI	18A	EPJ C78 252	Y.B. Li et al.	(BELLE Collab.)
LI	18D	EPJ C78 928	Y.B. Li et al.	(BELLE Collab.)
AUBERT	08H	PR D77 031101	B. Aubert et al.	(BABAR Collab.)

$\Xi_c(2970)$

$$I(J^P) = \frac{1}{2}(\frac{1}{2}^+) \text{ Status: } ***$$

was $\Xi_c(2980)$

$J^P = 1/2^+$ is favored by MOON 21.

$\Xi_c(2970)$ MASSES

$\Xi_c(2970)^+$ MASS

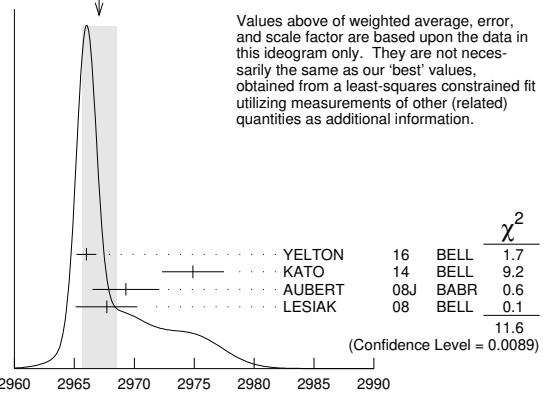
VALUE (MeV)	EVTS	DOCUMENT ID	TECN	COMMENT
2964.3 ± 1.5 OUR FIT				Error includes scale factor of 3.9.
2967.1 ± 1.4 OUR AVERAGE				Error includes scale factor of 2.0. See the ideogram below.

2966.0 ± 0.8 ± 0.2	0.9k	YELTON	16	BELL $e^+e^- \rightarrow \Upsilon(4S), \Upsilon(5S)$ and continuum
2974.9 ± 1.5 ± 2.1	244 ± 39	KATO	14	BELL $e^+e^- \Upsilon(1S)$ to $\Upsilon(5S)$
2969.3 ± 2.2 ± 1.7	756 ± 206	AUBERT	08J	BABR $e^+e^- \approx 10.58$ GeV
2967.7 ± 2.3 +1.1 -1.2	78 ± 13	LESIAK	08	BELL $e^+e^- \approx \Upsilon(4S)$

••• We do not use the following data for averages, fits, limits, etc. •••

2978.5 ± 2.1 ± 2.0	405 ± 51	CHISTOV	06	BELL See KATO 14
--------------------	----------	---------	----	------------------

WEIGHTED AVERAGE
2967.1 ± 1.4 (Error scaled by 2.0)



$\Xi_c(2970)^+$ MASS (MeV)

$\Xi_c(2970)^0$ MASS

The evidence is statistically weaker for this charge state.

VALUE (MeV)	EVTS	DOCUMENT ID	TECN	COMMENT
2967.1 ± 1.7 OUR FIT				Error includes scale factor of 6.7.
2965.9 ± 2.2 OUR AVERAGE				Error includes scale factor of 7.4.

2964.88 ± 0.26 ± 0.20	11.7k	¹ AAIJ	20X	LHCB pp at 13 TeV
2970.8 ± 0.7 ± 0.2	1.4k	YELTON	16	BELL $e^+e^- \rightarrow \Upsilon(4S), \Upsilon(5S), \text{continuum}$
2972.9 ± 4.4 ± 1.6	67 ± 44	AUBERT	08J	BABR $e^+e^- \approx 10.58$ GeV
2965.7 ± 2.4 +1.1 -1.2	57 ± 13	LESIAK	08	BELL $e^+e^- \approx \Upsilon(4S)$
2977.1 ± 8.8 ± 3.5	42 ± 24	CHISTOV	06	BELL $e^+e^- \approx \Upsilon(4S)$

¹AAIJ 20X reports 2964.88 ± 0.26 ± 0.14 ± 0.14 MeV where the last uncertainty is due to the Λ_c^+ mass. Further studies are required to establish whether the narrow resonance at 2965 MeV is a different baryon from the narrow resonance at 2970 MeV seen by YELTON 16.

$\Xi_c(2970) - \Xi_c$ MASS DIFFERENCES

$m_{\Xi_c(2970)^+} - m_{\Xi_c^+}$

VALUE (MeV)	EVTS	DOCUMENT ID	TECN	COMMENT
496.6 ± 1.5 OUR FIT				Error includes scale factor of 3.7.
498.1 ± 0.8 ± 0.2	916	YELTON	16	BELL e^+e^- , Υ regions

$m_{\Xi_c(2970)^0} - m_{\Xi_c^0}$

VALUE (MeV)	EVTS	DOCUMENT ID	TECN	COMMENT
496.7 ± 1.8 OUR FIT				Error includes scale factor of 5.3.
499.9 ± 0.7 ± 0.2	1.4k	YELTON	16	BELL e^+e^- , Υ regions

$\Xi_c(2970)^+ - \Xi_c(2970)^0$ MASS DIFFERENCE

VALUE (MeV)	DOCUMENT ID	TECN	COMMENT
-2.8 ± 1.9 OUR FIT			Error includes scale factor of 4.8.
-4.8 ± 0.1 ± 0.5	YELTON 16	BELL	916 and 1443 evts

$\Xi_c(2970)$ WIDTHS

$\Xi_c(2970)^+$ WIDTH

VALUE (MeV)	EVTS	DOCUMENT ID	TECN	COMMENT
20.9 +2.4 -3.5 OUR AVERAGE				Error includes scale factor of 1.2.

28.1 ± 2.4 +1.0 -5.0	916	YELTON	16	BELL e^+e^- , Υ regions
14.8 ± 2.5 ± 4.1	244 ± 39	KATO	14	BELL $e^+e^- \Upsilon(1S)$ to $\Upsilon(5S)$
27 ± 8 ± 2	756 ± 206	AUBERT	08J	BABR $e^+e^- \approx 10.58$ GeV
18 ± 6 ± 3	78 ± 13	LESIAK	08	BELL $e^+e^- \approx \Upsilon(4S)$

••• We do not use the following data for averages, fits, limits, etc. •••

43.5 ± 7.5 ± 7.0	405 ± 51	CHISTOV	06	BELL See KATO 14
------------------	----------	---------	----	------------------

$\Xi_c(2970)^0$ WIDTH

VALUE (MeV)	EVTS	DOCUMENT ID	TECN	COMMENT
14.1 ± 0.9 ± 1.3	11.7k	¹ AAIJ	20X	LHCB pp at 13 TeV
30.3 ± 2.3 +1.0 -1.8	1443	YELTON	16	BELL e^+e^- , Υ regions

See key on page 1127

Baryon Particle Listings

$\Xi_c(2970), \Xi_c(3055), \Xi_c(3080)$

••• We do not use the following data for averages, fits, limits, etc. •••

31 ± 7 ± 8	67 ± 44	AUBERT	08J	BABR	$e^+e^- \approx 10.58$ GeV
15 ± 6 ± 3	57 ± 13	LESIAK	08	BELL	$e^+e^- \approx \Upsilon(4S)$

¹ Further studies are required to establish whether the narrow resonance at 2965 MeV is a different baryon from the narrow resonance at 2970 MeV seen by YELTON 16.

$\Xi_c(2970)$ DECAY MODES

Mode	Fraction (Γ_i/Γ)
$\Gamma_1 \Lambda_c^+ \bar{K} \pi$	seen
$\Gamma_2 \Sigma_c(2455) \bar{K}$	seen
$\Gamma_3 \Lambda_c^+ \bar{K}$	not seen
$\Gamma_4 \Lambda_c^+ K^-$	seen
$\Gamma_5 \Xi_c 2\pi$	seen
$\Gamma_6 \Xi_c' \pi$	seen
$\Gamma_7 \Xi_c(2645) \pi$	seen

$\Xi_c(2970)$ BRANCHING RATIOS

$\Gamma(\Lambda_c^+ \bar{K} \pi)/\Gamma_{\text{total}}$	Γ_1/Γ		
VALUE	DOCUMENT ID	TECN	COMMENT
seen	AUBERT	08J	BABR $e^+e^- \approx \Upsilon(4S)$
seen	CHISTOV	06	BELL $e^+e^- \approx \Upsilon(4S)$

$\Gamma(\Lambda_c^+ K^-)/\Gamma_{\text{total}}$	Γ_4/Γ		
VALUE	DOCUMENT ID	TECN	COMMENT
seen	1 AAIJ	20x	LHCB pp at 13 TeV

¹ Further studies are required to establish whether the narrow resonance at 2965 MeV is a different baryon from the narrow resonance at 2970 MeV seen by YELTON 16.

$\Gamma(\Sigma_c(2455) \bar{K})/\Gamma(\Lambda_c^+ \bar{K} \pi)$	Γ_2/Γ_1		
VALUE	DOCUMENT ID	TECN	COMMENT
$0.55 \pm 0.07 \pm 0.13$	AUBERT	08J	BABR $e^+e^- \approx \Upsilon(4S)$

$\Gamma(\Xi_c' \pi)/\Gamma_{\text{total}}$	Γ_6/Γ		
VALUE	DOCUMENT ID	TECN	COMMENT
seen	YELTON	16	BELL e^+e^- , Υ regions

$\Gamma(\Xi_c(2645) \pi)/\Gamma_{\text{total}}$	Γ_7/Γ		
VALUE	DOCUMENT ID	TECN	COMMENT
seen	LESIAK	08	BELL $e^+e^- \approx \Upsilon(4S)$

$\Gamma(\Xi_c' \pi)/\Gamma(\Xi_c(2645) \pi)$	Γ_6/Γ_7		
VALUE	DOCUMENT ID	TECN	COMMENT
$1.67 \pm 0.29 \pm 0.15 \pm 0.09 \pm 0.25$	1 MOON	21	BELL e^+e^- at $\Upsilon(nS)$

¹ Measurement of the ratio of $\Xi_c(2970)^+ \rightarrow \Xi_c(2645)^0 \pi^+$ versus $\Xi_c(2970)^+ \rightarrow \Xi_c^0 \pi^+$. The last uncertainty is from possible isospin-symmetry-breaking effects. MOON 21 determines from an angular analysis of the $\Xi_c^+ \pi^+ \pi^-$ final state that the spin of the $\Xi_c(2970)^+$ is strongly compatible with $J = 1/2$, assuming domination by the lowest partial wave in $\Xi_c(2970)^+ \rightarrow \Xi_c(2645)^0 \pi^+$. When further combined with the size of this ratio, MOON 21 determines from heavy quark symmetry that the spin-parity of the $\Xi_c(2970)^+$ is favored to be $J^P = 1/2^+$, with light degrees of freedom in the 0^+ state.

$\Xi_c(2970)$ REFERENCES

MOON	21	PR D103 L111101	T.J. Moon <i>et al.</i>	(BELLE Collab.) JP
AAIJ	20X	PRL 124 222001	R. Aaij <i>et al.</i>	(LHCb Collab.)
YELTON	16	PR D94 052011	J. Yelton <i>et al.</i>	(BELLE Collab.)
KATO	14	PR D89 052003	Y. Kato <i>et al.</i>	(BELLE Collab.)
AUBERT	08J	PR D77 012002	B. Aubert <i>et al.</i>	(BABAR Collab.)
LESIAK	08	PL B665 9	T. Lesiak <i>et al.</i>	(BELLE Collab.)
CHISTOV	06	PRL 97 162001	R. Chistov <i>et al.</i>	(BELLE Collab.)

$\Xi_c(3055)$

$I(J^P) = ?(??)$ Status: ***

$\Xi_c(3055)$ MASSES

$\Xi_c(3055)^+$ MASS	VALUE (MeV)	EVTs	DOCUMENT ID	TECN	COMMENT
3055.9 ± 0.4	894		KATO	16	BELL $e^+e^- \Upsilon$ region
••• We do not use the following data for averages, fits, limits, etc. •••					
$3058.1 \pm 1.0 \pm 2.1$	199 ± 46		KATO	14	BELL See KATO 16
$3054.2 \pm 1.2 \pm 0.5$	218 ± 95		AUBERT	08J	BABR $e^+e^- \approx 10.58$ GeV

$\Xi_c(3055)$ WIDTHS

$\Xi_c(3055)^+$ WIDTH	VALUE (MeV)	EVTs	DOCUMENT ID	TECN	COMMENT
$7.8 \pm 1.2 \pm 1.5$			KATO	16	BELL $e^+e^- \Upsilon$ region

••• We do not use the following data for averages, fits, limits, etc. •••

$9.7 \pm 3.4 \pm 3.3$	199 ± 46	KATO	14	BELL	$e^+e^- \Upsilon(1S)$ to $\Upsilon(5S)$
$17 \pm 6 \pm 11$	218 ± 95	AUBERT	08J	BABR	$e^+e^- \approx 10.58$ GeV

$\Xi_c(3055)$ DECAY MODES

Mode	Fraction (Γ_i/Γ)
$\Gamma_1 \Sigma^{++} K^-$	seen
$\Gamma_2 \Lambda D^+$	seen

$\Xi_c(3055)$ BRANCHING RATIOS

$\Gamma(\Lambda D^+)/\Gamma(\Sigma^{++} K^-)$	Γ_2/Γ_1		
VALUE	DOCUMENT ID	TECN	COMMENT
$5.09 \pm 1.01 \pm 0.76$	KATO	16	BELL 721 and 103 evts

$\Xi_c(3055)$ REFERENCES

KATO	16	PR D94 032002	Y. Kato <i>et al.</i>	(BELLE Collab.)
KATO	14	PR D89 052003	Y. Kato <i>et al.</i>	(BELLE Collab.)
AUBERT	08J	PR D77 012002	B. Aubert <i>et al.</i>	(BABAR Collab.)

$\Xi_c(3080)$

$I(J^P) = \frac{1}{2}(??)$ Status: ***

$\Xi_c(3080)$ MASSES

$\Xi_c(3080)^+$ MASS	VALUE (MeV)	EVTs	DOCUMENT ID	TECN	COMMENT
3077.2 ± 0.4 OUR AVERAGE					
3077.9 ± 0.9	596		KATO	16	BELL $e^+e^- \Upsilon$ region
$3077.0 \pm 0.4 \pm 0.2$	403 ± 60		AUBERT	08J	BABR $e^+e^- \approx 10.58$ GeV
••• We do not use the following data for averages, fits, limits, etc. •••					
$3076.9 \pm 0.3 \pm 0.2$	210 ± 30		KATO	14	BELL See KATO 16
$3076.7 \pm 0.9 \pm 0.5$	326 ± 40		CHISTOV	06	BELL See KATO 14

$\Xi_c(3080)^0$ MASS	VALUE (MeV)	EVTs	DOCUMENT ID	TECN	COMMENT
3079.9 ± 1.4 OUR AVERAGE					Error includes scale factor of 1.3.
$3079.3 \pm 1.1 \pm 0.2$	90 ± 27		AUBERT	08J	BABR $e^+e^- \approx 10.58$ GeV
$3082.8 \pm 1.8 \pm 1.5$	67 ± 20		CHISTOV	06	BELL $e^+e^- \approx \Upsilon(4S)$

$\Xi_c(3080)$ WIDTHS

$\Xi_c(3080)^+$ WIDTH	VALUE (MeV)	EVTs	DOCUMENT ID	TECN	COMMENT
3.6 ± 1.1 OUR AVERAGE					Error includes scale factor of 1.5.
$3.0 \pm 0.7 \pm 0.4$	596		KATO	16	BELL $e^+e^- \Upsilon$ region
$5.5 \pm 1.3 \pm 0.6$	403 ± 60		AUBERT	08J	BABR $e^+e^- \approx 10.58$ GeV
••• We do not use the following data for averages, fits, limits, etc. •••					
$2.4 \pm 0.9 \pm 1.6$	210 ± 30		KATO	14	BELL See KATO 16
$6.2 \pm 1.2 \pm 0.8$	326 ± 40		CHISTOV	06	BELL See KATO 14

$\Xi_c(3080)^0$ WIDTH	VALUE (MeV)	EVTs	DOCUMENT ID	TECN	COMMENT
5.6 ± 2.2 OUR AVERAGE					
$5.9 \pm 2.3 \pm 1.5$	90 ± 27		AUBERT	08J	BABR $e^+e^- \approx 10.58$ GeV
$5.2 \pm 3.1 \pm 1.8$	67 ± 20		CHISTOV	06	BELL $e^+e^- \approx \Upsilon(4S)$

$\Xi_c(3080)$ DECAY MODES

Mode	Fraction (Γ_i/Γ)
$\Gamma_1 \Lambda_c^+ \bar{K} \pi$	seen
$\Gamma_2 \Sigma_c(2455) \bar{K}$	seen
$\Gamma_3 \Sigma_c(2455)^{++} K^-$	seen
$\Gamma_4 \Sigma_c(2520)^{++} K^-$	seen
$\Gamma_5 \Sigma_c(2455) \bar{K} + \Sigma_c(2520) \bar{K}$	seen
$\Gamma_6 \Lambda_c^+ \bar{K}$	not seen
$\Gamma_7 \Lambda_c^+ \bar{K} \pi^+ \pi^-$	not seen
$\Gamma_8 \Lambda D^+$	seen

$\Xi_c(3080)$ BRANCHING RATIOS

$\Gamma(\Sigma_c(2455) \bar{K})/\Gamma(\Lambda_c^+ \bar{K} \pi)$	Γ_2/Γ_1		
VALUE	DOCUMENT ID	TECN	COMMENT
0.45 ± 0.06 OUR AVERAGE			
$0.45 \pm 0.05 \pm 0.05$	AUBERT	08J	BABR in $\Lambda_c^+ K^- \pi^+$
$0.44 \pm 0.12 \pm 0.07$	AUBERT	08J	BABR in $\Lambda_c^+ K_S^0 \pi^-$

Baryon Particle Listings

$\Xi_c(3080), \Xi_c(3123), \Omega_c^0$

$\Gamma(\Sigma_c(2520)^{++} K^-)/\Gamma(\Sigma_c(2455)^{++} K^-)$				Γ_4/Γ_3
VALUE	DOCUMENT ID	TECN	COMMENT	
1.07 ± 0.27 ± 0.04	KATO	16	BELL	234 and 176 evts

$[\Gamma(\Sigma_c(2455) \bar{K}) + \Gamma(\Sigma_c(2520) \bar{K})]/\Gamma(\Lambda_c^+ \bar{K} \pi)$				Γ_5/Γ_1
VALUE	DOCUMENT ID	TECN	COMMENT	
0.89 ± 0.12 OUR AVERAGE				
0.95 ± 0.14 ± 0.06	AUBERT	08J	BABR	in $\Lambda_c^+ K^- \pi^+$
0.78 ± 0.21 ± 0.05	AUBERT	08J	BABR	in $\Lambda_c^+ K_S^0 \pi^-$

$\Gamma(\Lambda^+)/\Gamma(\Sigma_c(2455)^{++} K^-)$				Γ_8/Γ_3
VALUE	DOCUMENT ID	TECN	COMMENT	
1.29 ± 0.30 ± 0.15	KATO	16	BELL	186 and 176 evts

$\Xi_c(3080)$ REFERENCES

KATO	16	PR D94 032002	Y. Kato <i>et al.</i>	(BELLE Collab.)
KATO	14	PR D89 052003	Y. Kato <i>et al.</i>	(BELLE Collab.)
AUBERT	08J	PR D77 012002	B. Aubert <i>et al.</i>	(BABAR Collab.)
CHISTOV	06	PRL 97 162001	R. Chistov <i>et al.</i>	(BELLE Collab.)

$\Xi_c(3123)$

$$I(J^P) = ?(??) \text{ Status: } *$$

OMITTED FROM SUMMARY TABLE

A peak in the $\Sigma_c(2520)^{++} K^- \rightarrow \Lambda_c^+ K^- \pi^+$ mass spectrum with a significance of 3.6 standard deviations. KATO 14 finds no evidence for this state.

$\Xi_c(3123)$ MASSES

$\Xi_c(3123)^+$ MASS

VALUE (MeV)	EVTs	DOCUMENT ID	TECN	COMMENT
3122.9 ± 1.3 ± 0.3	101 ± 35	AUBERT	08J	BABR $e^+ e^- \approx 10.58$ GeV

$\Xi_c(3123)$ WIDTHS

$\Xi_c(3123)^+$ WIDTH

VALUE (MeV)	EVTs	DOCUMENT ID	TECN	COMMENT
4.4 ± 3.4 ± 1.7	101 ± 35	AUBERT	08J	BABR $e^+ e^- \approx 10.58$ GeV

$\Xi_c(3123)$ REFERENCES

KATO	14	PR D89 052003	Y. Kato <i>et al.</i>	(BELLE Collab.)
AUBERT	08J	PR D77 012002	B. Aubert <i>et al.</i>	(BABAR Collab.)

Ω_c^0

$$I(J^P) = 0(\frac{1}{2}^+) \text{ Status: } ***$$

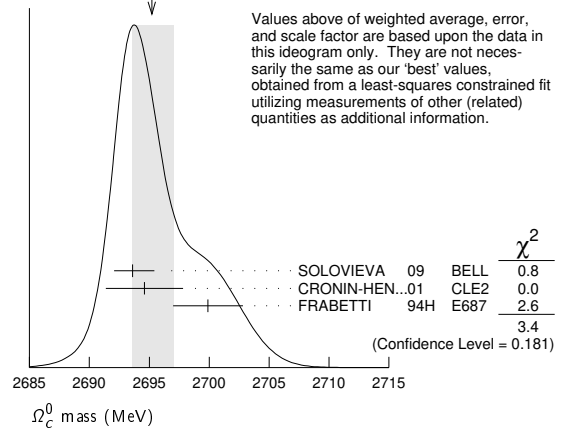
The quantum numbers have not been measured, but are simply assigned in accord with the quark model, in which the Ω_c^0 is the ssc ground state. No absolute branching fractions have been measured.

Ω_c^0 MASS

VALUE (MeV)	EVTs	DOCUMENT ID	TECN	COMMENT
2695.2 ± 1.7 OUR FIT				Error includes scale factor of 1.3.
2695.2 ± 1.8 OUR AVERAGE				Error includes scale factor of 1.3. See the ideogram below.
2693.6 ± 0.3 ± 1.8	725	SOLOVIEVA	09	BELL $\Omega^- \pi^+$ in $e^+ e^- \rightarrow \Upsilon(4S)$
2694.6 ± 2.6 ± 1.9	40	¹ CRONIN-HEN..01	CLE2	$e^+ e^- \approx 10.6$ GeV
2699.9 ± 1.5 ± 2.5	42	² FRABETTI	94H	E687 γ Be, $\bar{E}_\gamma = 221$ GeV
• • • We do not use the following data for averages, fits, limits, etc. • • •				
2705.9 ± 3.3 ± 2.0	10	³ FRABETTI	93	E687 γ Be, $\bar{E}_\gamma = 221$ GeV
2719.0 ± 7.0 ± 2.5	11	⁴ ALBRECHT	92H	ARG $e^+ e^- \approx 10.6$ GeV
2740 ± 20	3	BIAGI	85B	SPEC Σ^- Be 135 GeV/c

¹ CRONIN-HENNESSY 01 sees 40.4 ± 9.0 events in a sum over five channels.
² FRABETTI 94H claims a signal of $42.5 \pm 8.8 \Sigma^+ K^- K^- \pi^+$ events. The background is about 24 events.
³ FRABETTI 93 claims a signal of $10.3 \pm 3.9 \Omega^- \pi^+$ events above a background of 5.8 events.
⁴ ALBRECHT 92H claims a signal of $11.5 \pm 4.3 \Xi^- K^- \pi^+ \pi^+$ events. The background is about 5 events.

WEIGHTED AVERAGE
2695.2 ± 1.8 - 1.6 (Error scaled by 1.3)



Ω_c^0 MEAN LIFE

VALUE (10^{-15} s)	EVTs	DOCUMENT ID	TECN	COMMENT
268 ± 24 ± 10	978	¹ AAIJ	18J	LHCB $p K^- K^- \pi^+$
• • • We do not use the following data for averages, fits, limits, etc. • • •				
72 ± 11 ± 11	64	LINK	03C	FOCS $\Omega^- \pi^+, \Xi^- K^- \pi^+ \pi^+$
55 ⁺¹³ ₋₁₁ ± 18 ⁺¹⁸ ₋₂₃	86	ADAMOVICH	95B	VVA89 $\Omega^- \pi^- \pi^+ \pi^+, \Xi^- K^- \pi^+ \pi^+$
86 ⁺²⁷ ₋₂₀ ± 28	25	FRABETTI	95D	E687 $\Sigma^+ K^- K^- \pi^+$

¹ AAIJ 18J, with nearly five times more events than the previous three experiments combined, gets a lifetime that is nearly four times larger than the average of those experiments, $(69 \pm 12) \times 10^{-15}$ s. We go with the larger data sample.

Ω_c^0 DECAY MODES

No absolute branching fractions have been measured. The following are branching ratios relative to $\Omega^- \pi^+$.

Mode	Fraction (Γ_i/Γ)	Confidence level
Cabibbo-favored ($S = -3$) decays — relative to $\Omega^- \pi^+$		
Γ_1 $\Omega^- \pi^+$	DEFINED AS 1	
Γ_2 $\Omega^- \pi^+ \pi^0$	1.80 ± 0.33	
Γ_3 $\Omega^- \rho^+$	> 1.3	90%
Γ_4 $\Omega^- \pi^- 2\pi^+$	0.31 ± 0.05	
Γ_5 $\Omega^- e^+ \nu_e$	2.4 ± 1.2	
Γ_6 $\Xi^0 \bar{K}^0$	1.64 ± 0.29	
Γ_7 $\Xi^0 K^- \pi^+$	1.20 ± 0.18	
Γ_8 $\Xi^0 \bar{K}^{*0}, \bar{K}^{*0} \rightarrow K^- \pi^+$	0.68 ± 0.16	
Γ_9 $\Omega(2012)^- \pi^+, \Omega(2012)^- \rightarrow \Xi^0 K^-$	0.12 ± 0.05	
Γ_{10} $\Xi^- \bar{K}^0 \pi^+$	2.12 ± 0.28	
Γ_{11} $\Omega(2012)^- \pi^+, \Omega(2012)^- \rightarrow \Xi^- \bar{K}^0$	0.12 ± 0.06	
Γ_{12} $\Xi^- K^- 2\pi^+$	0.63 ± 0.09	
Γ_{13} $\Xi(1530)^0 K^- \pi^+, \Xi^{*0} \rightarrow \Xi^- \bar{K}^0 \pi^+$	0.21 ± 0.06	
Γ_{14} $\Xi^- \bar{K}^{*0} \pi^+$	0.34 ± 0.11	
Γ_{15} $p K^- K^- \pi^+$	seen	
Γ_{16} $\Sigma^+ K^- K^- \pi^+$	< 0.32	90%
Γ_{17} $\Lambda \bar{K}^0 \bar{K}^0$	1.72 ± 0.35	

Ω_c^0 BRANCHING RATIOS

A few early but now obsolete measurements have been omitted. See K.A. Olive, *et al.* (Particle Data Group), Chinese Physics **C38** 070001 (2014).

$\Gamma(\Omega^- \pi^+ \pi^0)/\Gamma(\Omega^- \pi^+)$				Γ_2/Γ_1
VALUE	EVTs	DOCUMENT ID	TECN	COMMENT
1.80 ± 0.33 OUR AVERAGE				Error includes scale factor of 1.9.
2.00 ± 0.17 ± 0.11	403	YELTON	18	BELL $e^+ e^- \rightarrow \Upsilon(4S), +$ higher
1.27 ± 0.31 ± 0.11	64	AUBERT	07AH	BABR $e^+ e^- \approx \Upsilon(4S)$

See key on page 1127

Baryon Particle Listings

$\Omega_c^0, \Omega_c(2770)^0, \Omega_c(3000)^0$

$\Gamma(\Omega^- \rho^+)/\Gamma(\Omega^- \pi^+ \pi^0)$ Γ_3/Γ_2

VALUE	CL%	DOCUMENT ID	TECN	COMMENT
>0.71	90	¹ YELTON 18	BELL	$e^+ e^- \rightarrow \Upsilon(4S)$, +higher

¹ This submode fraction is evaluated from a background-subtracted signal in a mass plot. Result ignores interference effects and systematic uncertainties, which YELTON 18 claim are both small.

$\Gamma(\Omega^- \pi^- 2\pi^+)/\Gamma(\Omega^- \pi^+)$ Γ_4/Γ_1

VALUE	EVTS	DOCUMENT ID	TECN	COMMENT
0.31 ± 0.05 OUR AVERAGE				
0.32 ± 0.05 ± 0.02	108	YELTON 18	BELL	$e^+ e^- \rightarrow \Upsilon(4S)$, +higher
0.28 ± 0.09 ± 0.01	25	AUBERT 07AH	BABR	$e^+ e^- \approx \Upsilon(4S)$

$\Gamma(\Omega^- \pi^+)/\Gamma(\Omega^- e^+ \nu_e)$ Γ_1/Γ_5

VALUE	EVTS	DOCUMENT ID	TECN	COMMENT
0.41 ± 0.19 ± 0.04	11	AMMAR 02	CLE2	$e^+ e^- \approx \Upsilon(4S)$

$\Gamma(\Xi^0 \bar{K}^0)/\Gamma(\Omega^- \pi^+)$ Γ_6/Γ_1

VALUE	EVTS	DOCUMENT ID	TECN	COMMENT
1.64 ± 0.26 ± 0.12	98	YELTON 18	BELL	$e^+ e^- \rightarrow \Upsilon(4S)$, +higher

$\Gamma(\Xi^0 K^- \pi^+)/\Gamma(\Omega^- \pi^+)$ Γ_7/Γ_1

VALUE	EVTS	DOCUMENT ID	TECN	COMMENT
1.20 ± 0.16 ± 0.08	168	YELTON 18	BELL	$e^+ e^- \rightarrow \Upsilon(4S)$, +higher

$\Gamma(\Xi^0 \bar{K}^{*0}, \bar{K}^{*0} \rightarrow K^- \pi^+)/\Gamma(\Xi^0 K^- \pi^+)$ Γ_8/Γ_7

VALUE	EVTS	DOCUMENT ID	TECN	COMMENT
0.57 ± 0.10	95	¹ YELTON 18	BELL	$e^+ e^- \rightarrow \Upsilon(4S)$, +higher

¹ This submode fraction is evaluated from a background-subtracted signal in a mass plot. Result ignores interference effects and systematic uncertainties, which YELTON 18 claim are both small.

$\Gamma(\Omega(2012)^- \pi^+, \Omega(2012)^- \rightarrow \Xi^0 K^-)/\Gamma(\Xi^0 K^- \pi^+)$ Γ_9/Γ_7

VALUE (units 10 ⁻²)	EVTS	DOCUMENT ID	TECN	COMMENT
9.6 ± 3.2 ± 1.8	28	¹ LI 21D	BELL	$e^+ e^-$ at $\Upsilon(ns)$

¹ LI 21D reports the significance of the $\Omega(2012)$ signal is 4.2 σ including systematic uncertainties. Also measures $B(\Omega_c^0 \rightarrow \Omega(2012)^- \pi^+, \Omega(2012)^- \rightarrow (\bar{K}\Xi^-))/B(\Omega_c^0 \rightarrow \Xi^0 K^- \pi^+) = 0.220 \pm 0.059 \pm 0.035$.

$\Gamma(\Xi^- \bar{K}^0 \pi^+)/\Gamma(\Omega^- \pi^+)$ Γ_{10}/Γ_1

VALUE	EVTS	DOCUMENT ID	TECN	COMMENT
2.12 ± 0.24 ± 0.14	349	YELTON 18	BELL	$e^+ e^- \rightarrow \Upsilon(4S)$, +higher

$\Gamma(\Omega(2012)^- \pi^+, \Omega(2012)^- \rightarrow \Xi^- \bar{K}^0)/\Gamma(\Xi^- \bar{K}^0 \pi^+)$ Γ_{11}/Γ_{10}

VALUE (units 10 ⁻²)	EVTS	DOCUMENT ID	TECN	COMMENT
5.5 ± 2.8 ± 0.7	18	¹ LI 21D	BELL	$e^+ e^-$ at $\Upsilon(ns)$

¹ LI 21D reports the significance of the $\Omega(2012)$ signal is 4.2 σ including systematic uncertainties. Also measures $B(\Omega_c^0 \rightarrow \Omega(2012)^- \pi^+, \Omega(2012)^- \rightarrow (\bar{K}\Xi^-))/B(\Omega_c^0 \rightarrow \Xi^0 K^- \pi^+) = 0.220 \pm 0.059 \pm 0.035$.

$\Gamma(\Xi^- K^- 2\pi^+)/\Gamma(\Omega^- \pi^+)$ Γ_{12}/Γ_1

VALUE	EVTS	DOCUMENT ID	TECN	COMMENT
0.63 ± 0.09 OUR AVERAGE				Error includes scale factor of 1.4.
0.68 ± 0.07 ± 0.03	278	YELTON 18	BELL	$e^+ e^- \rightarrow \Upsilon(4S)$, +higher
0.46 ± 0.13 ± 0.03	45	AUBERT 07AH	BABR	$e^+ e^- \approx \Upsilon(4S)$

$\Gamma(\Xi(1530)^0 K^- \pi^+, \Xi^{*0} \rightarrow \Xi^- \pi^+)/\Gamma(\Xi^- K^- 2\pi^+)$ Γ_{13}/Γ_{12}

VALUE	EVTS	DOCUMENT ID	TECN	COMMENT
0.33 ± 0.09	74	¹ YELTON 18	BELL	$e^+ e^- \rightarrow \Upsilon(4S)$, +higher

¹ This submode fraction is evaluated from a background-subtracted signal in a mass plot. Result ignores interference effects and systematic uncertainties, which YELTON 18 claim are both small.

$\Gamma(\Xi^- \bar{K}^{*0} \pi^+)/\Gamma(\Xi^- K^- 2\pi^+)$ Γ_{14}/Γ_{12}

VALUE	EVTS	DOCUMENT ID	TECN	COMMENT
0.55 ± 0.16	136	¹ YELTON 18	BELL	$e^+ e^- \rightarrow \Upsilon(4S)$, +higher

¹ This submode fraction is evaluated from a background-subtracted signal in a mass plot. Result ignores interference effects and systematic uncertainties, which YELTON 18 claim are both small.

$\Gamma(p K^- K^- \pi^+)/\Gamma_{total}$ Γ_{15}/Γ

VALUE	DOCUMENT ID	TECN	COMMENT
seen	AAIJ 160	LHCB	pp at 7, 8 TeV

$\Gamma(\Sigma^+ K^- K^- \pi^+)/\Gamma(\Omega^- \pi^+)$ Γ_{16}/Γ_1

VALUE	CL%	EVTS	DOCUMENT ID	TECN	COMMENT
<0.32	90	17	YELTON 18	BELL	$e^+ e^- \rightarrow \Upsilon(4S)$, +higher

$\Gamma(\Lambda \bar{K}^0 \bar{K}^0)/\Gamma(\Omega^- \pi^+)$ Γ_{17}/Γ_1

VALUE	EVTS	DOCUMENT ID	TECN	COMMENT
1.72 ± 0.32 ± 0.14	95	YELTON 18	BELL	$e^+ e^- \rightarrow \Upsilon(4S)$, +higher

Ω_c^0 REFERENCES

LI 21D	PR D104 052005	Y.B. Li <i>et al.</i>	(BELLE Collab.)
AAIJ 18J	PRL 121 092003	R. Aaij <i>et al.</i>	(LHCb Collab.)
YELTON 18	PR D97 032001	J. Yelton <i>et al.</i>	(BELLE Collab.)
AAIJ 16O	PR D93 092007	R. Aaij <i>et al.</i>	(LHCb Collab.)
PDG 14	CP C38 070001	K. Olive <i>et al.</i>	(PDG Collab.)
SOLOVIEVA 09	PL B672 1	E. Solovieva <i>et al.</i>	(BELLE Collab.)
AUBERT 07AH	PRL 99 062001	B. Aubert <i>et al.</i>	(BABAR Collab.)
LINK 03C	PL B561 41	J.M. Link <i>et al.</i>	(FNAL FOCUS Collab.)
AMMAR 02	PRL 89 171803	R. Ammar <i>et al.</i>	(CLEO Collab.)
CRONIN-HEN... 01	PRL 86 3730	D. Cronin-Hennessy <i>et al.</i>	(CLEO Collab.)
ADAMOVICH 95B	PL B358 151	M.I. Adamovich <i>et al.</i>	(CERN WA89 Collab.)
FRABETTI 95D	PL B357 678	P.L. Frabetti <i>et al.</i>	(FNAL E687 Collab.)
FRABETTI 94H	PL B338 106	P.L. Frabetti <i>et al.</i>	(FNAL E687 Collab.)
FRABETTI 93	PL B300 190	P.L. Frabetti <i>et al.</i>	(FNAL E687 Collab.)
ALBRECHT 92H	PL B288 367	H. Albrecht <i>et al.</i>	(ARGUS Collab.)
BIAGI 85B	ZPHY C28 175	S.F. Biagi <i>et al.</i>	(CERN WA62 Collab.)

$\Omega_c(2770)^0$

$I(J^P) = 0(\frac{3}{2}^+)$ Status: ***

The natural assignment is that this goes with the $\Sigma_c(2520)$ and $\Xi_c(2645)$ to complete the lowest mass $J^P = \frac{3}{2}^+$ SU(3) sextet, part of the SU(4) 20-plet that includes the $\Delta(1232)$. But J and P have not been measured.

$\Omega_c(2770)^0$ MASS

The mass is obtained from the mass-difference measurement that follows.

VALUE (MeV)	DOCUMENT ID
2765.9 ± 2.0 OUR FIT	Error includes scale factor of 1.2.

$\Omega_c(2770)^0 - \Omega_c^0$ MASS DIFFERENCE

VALUE (MeV)	EVTS	DOCUMENT ID	TECN	COMMENT
70.7^{+0.8}_{-0.9} OUR FIT				
70.7^{+0.8}_{-1.0} OUR AVERAGE				
70.7 ± 0.9 ^{+0.1} _{-0.1}	54 ± 9	SOLOVIEVA 09	BELL	$\Omega_c^0 \gamma$ in $e^+ e^- \rightarrow \Upsilon(4S)$
70.8 ± 1.0 ± 1.1	105 ± 22	AUBERT, BE 06i	BABR	$e^+ e^- \approx \Upsilon(4S)$

$\Omega_c(2770)^0$ DECAY MODES

The $\Omega_c(2770)^0 - \Omega_c^0$ mass difference is too small for any strong decay to occur.

Mode	Fraction (Γ_i/Γ)
$\Gamma_1 \Omega_c^0 \gamma$	presumably 100%

$\Omega_c(2770)^0$ REFERENCES

SOLOVIEVA 09	PL B672 1	E. Solovieva <i>et al.</i>	(BELLE Collab.)
AUBERT, BE 06i	PRL 97 232001	B. Aubert <i>et al.</i>	(BABAR Collab.)

$\Omega_c(3000)^0$

$I(J^P) = ?(?^?)$ Status: ***

$\Omega_c(3000)^0$ MASS

VALUE (MeV)	EVTS	DOCUMENT ID	TECN	COMMENT
3000.41 ± 0.22 OUR AVERAGE				
3000.7 ± 1.0 ± 0.2	38	YELTON 18B	BELL	$e^+ e^-$ at $\Upsilon(4S)$
3000.4 ± 0.2 ± 0.1	1.3k	AAIJ	17AH LHCB	pp at 7, 8, 13 TeV
• • • We do not use the following data for averages, fits, limits, etc. • • •				
2999.2 ± 0.9 ± 0.9 ^{+0.19} _{-0.22}	24	¹ AAIJ	21AC LHCB	pp at 7, 8, 13 TeV

¹ Measured via $\Omega_b^- \rightarrow \Omega_c^{*0} \pi^- \rightarrow \Xi_c^+ K^- \pi^-$. The third uncertainty is due to the uncertainty in the Ξ_c^+ mass.

$\Omega_c(3000)^0$ WIDTH

VALUE (MeV)	EVTS	DOCUMENT ID	TECN	COMMENT
4.5 ± 0.6 ± 0.3	1.3k	AAIJ	17AH LHCB	pp at 7, 8, 13 TeV
• • • We do not use the following data for averages, fits, limits, etc. • • •				
4.8 ± 2.1 ± 2.5	24	AAIJ	21AC LHCB	pp at 7, 8, 13 TeV

$\Omega_c(3000)^0$ DECAY MODES

Mode	Fraction (Γ_i/Γ)
$\Gamma_1 \Xi_c^+ K^-$	seen

Baryon Particle Listings

$\Omega_c(3000)^0, \Omega_c(3050)^0, \Omega_c(3065)^0, \Omega_c(3090)^0$

$\Omega_c(3000)^0$ BRANCHING RATIOS

$\Gamma(\Xi_c^+ K^-)/\Gamma_{\text{total}}$					Γ_1/Γ
VALUE	EVTS	DOCUMENT ID	TECN	COMMENT	
seen	24	¹ AAIJ	21AC LHCb	pp at 7, 8, 13 TeV	
seen	38	² YELTON	18B BELLE	e^+e^- at $\Upsilon(4S)$	
seen	1.3k	³ AAIJ	17AH LHCb	pp at 7, 8, 13 TeV	

¹ AAIJ 21AC report a significance of 6.2 σ .
² YELTON 18B report a significance of 3.9 σ .
³ AAIJ 17AH report a significance of 20.4 σ .

$\Omega_c(3000)^0$ REFERENCES

AAIJ	21AC PR D104 L091102	R. Aaij <i>et al.</i>	(LHCb Collab.)
YELTON	18B PR D97 051102	J. Yelton <i>et al.</i>	(BELLE Collab.)
AAIJ	17AH PRL 118 182001	R. Aaij <i>et al.</i>	(LHCb Collab.)

$\Omega_c(3050)^0$

 $I(J^P) = ?(??)$ Status: ***
 AAIJ 21AC rejects $J = 1/2$ hypothesis at 2.2 σ .

$\Omega_c(3050)^0$ MASS

VALUE (MeV)	CL%	DOCUMENT ID	TECN	COMMENT
3050.19 ± 0.13 OUR AVERAGE				
$3050.1 \pm 0.3 \pm 0.2^{+0.19}_{-0.22}$	33	¹ AAIJ	21AC LHCb	pp at 7, 8, 13 TeV
$3050.2 \pm 0.4 \pm 0.2$	28	YELTON	18B BELLE	e^+e^- at $\Upsilon(4S)$
$3050.2 \pm 0.1 \pm 0.1$	970	AAIJ	17AH LHCb	pp at 7, 8, 13 TeV

¹ Measured via $\Omega_b^- \rightarrow \Omega_c^{*0} \pi^- \rightarrow \Xi_c^+ K^- \pi^-$. The third uncertainty is due to the uncertainty in the Ξ_c^+ mass.

$\Omega_c(3050)^0$ WIDTH

VALUE (MeV)	CL%	DOCUMENT ID	TECN	COMMENT
<1.2	95	AAIJ	17AH LHCb	pp at 7, 8, 13 TeV
• • • We do not use the following data for averages, fits, limits, etc. • • •				
<1.6	95	AAIJ	21AC LHCb	pp at 7, 8, 13 TeV

$\Omega_c(3050)^0$ DECAY MODES

Mode	Fraction (Γ_i/Γ)
$\Gamma_1 \Xi_c^+ K^-$	seen

$\Omega_c(3050)^0$ BRANCHING RATIOS

$\Gamma(\Xi_c^+ K^-)/\Gamma_{\text{total}}$					Γ_1/Γ
VALUE	EVTS	DOCUMENT ID	TECN	COMMENT	
seen	33	¹ AAIJ	21AC LHCb	pp at 7, 8, 13 TeV	
seen	28	² YELTON	18B BELLE	e^+e^- at $\Upsilon(4S)$	
seen	970	³ AAIJ	17AH LHCb	pp at 7, 8, 13 TeV	

¹ AAIJ 21AC report a significance of 9.9 σ .
² YELTON 18B report a significance of 4.6 σ .
³ AAIJ 17AH report a significance of 20.4 σ .

$\Omega_c(3050)^0$ REFERENCES

AAIJ	21AC PR D104 L091102	R. Aaij <i>et al.</i>	(LHCb Collab.)
YELTON	18B PR D97 051102	J. Yelton <i>et al.</i>	(BELLE Collab.)
AAIJ	17AH PRL 118 182001	R. Aaij <i>et al.</i>	(LHCb Collab.)

$\Omega_c(3065)^0$

 $I(J^P) = ?(??)$ Status: ***
 AAIJ 21AC rejects $J = 1/2$ hypothesis at 3.6 σ .

$\Omega_c(3065)^0$ MASS

VALUE (MeV)	CL%	DOCUMENT ID	TECN	COMMENT
3065.54 ± 0.26 OUR AVERAGE				
$3065.9 \pm 0.4 \pm 0.4^{+0.19}_{-0.22}$	51	¹ AAIJ	21AC LHCb	pp at 7, 8, 13 TeV
$3064.9 \pm 0.6 \pm 0.2$	82	YELTON	18B BELLE	e^+e^- at $\Upsilon(4S)$
$3065.6 \pm 0.1 \pm 0.3$	1.74k	AAIJ	17AH LHCb	pp at 7, 8, 13 TeV

¹ Measured via $\Omega_b^- \rightarrow \Omega_c^{*0} \pi^- \rightarrow \Xi_c^+ K^- \pi^-$. The third uncertainty is due to the uncertainty in the Ξ_c^+ mass.

$\Omega_c(3065)^0$ WIDTH

VALUE (MeV)	CL%	DOCUMENT ID	TECN	COMMENT
3.3 ± 0.6 OUR AVERAGE				Error includes scale factor of 1.5.
$1.7 \pm 1.0 \pm 0.5$	51	AAIJ	21AC LHCb	pp at 7, 8, 13 TeV
$3.5 \pm 0.4 \pm 0.2$	1.74k	AAIJ	17AH LHCb	pp at 7, 8, 13 TeV

$\Omega_c(3065)^0$ DECAY MODES

Mode	Fraction (Γ_i/Γ)
$\Gamma_1 \Xi_c^+ K^-$	seen

$\Omega_c(3065)^0$ BRANCHING RATIOS

$\Gamma(\Xi_c^+ K^-)/\Gamma_{\text{total}}$					Γ_1/Γ
VALUE	EVTS	DOCUMENT ID	TECN	COMMENT	
seen	51	¹ AAIJ	21AC LHCb	pp at 7, 8, 13 TeV	
seen	82	YELTON	18B BELLE	e^+e^- at $\Upsilon(4S)$	
seen	1.74k	² AAIJ	17AH LHCb	pp at 7, 8, 13 TeV	

¹ AAIJ 21AC report a significance of 11.9 σ .
² AAIJ 17AH report a significance of 23.9 σ .

$\Omega_c(3065)^0$ REFERENCES

AAIJ	21AC PR D104 L091102	R. Aaij <i>et al.</i>	(LHCb Collab.)
YELTON	18B PR D97 051102	J. Yelton <i>et al.</i>	(BELLE Collab.)
AAIJ	17AH PRL 118 182001	R. Aaij <i>et al.</i>	(LHCb Collab.)

$\Omega_c(3090)^0$

 $I(J^P) = ?(??)$ Status: ***

$\Omega_c(3090)^0$ MASS

VALUE (MeV)	CL%	DOCUMENT ID	TECN	COMMENT
3090.1 ± 0.5 OUR AVERAGE				
$3091.0 \pm 1.1 \pm 1.0^{+0.19}_{-0.22}$	41	¹ AAIJ	21AC LHCb	pp at 7, 8, 13 TeV
$3089.3 \pm 1.2 \pm 0.2$	87	YELTON	18B BELLE	e^+e^- at $\Upsilon(4S)$
$3090.2 \pm 0.3 \pm 0.5$	2.0k	AAIJ	17AH LHCb	pp at 7, 8, 13 TeV

¹ Measured via $\Omega_b^- \rightarrow \Omega_c^{*0} \pi^- \rightarrow \Xi_c^+ K^- \pi^-$. The third uncertainty is due to the uncertainty in the Ξ_c^+ mass.

$\Omega_c(3090)^0$ WIDTH

VALUE (MeV)	CL%	DOCUMENT ID	TECN	COMMENT
$8.7 \pm 1.0 \pm 0.8$	2.0k	AAIJ	17AH LHCb	pp at 7, 8, 13 TeV
• • • We do not use the following data for averages, fits, limits, etc. • • •				
$7.4 \pm 3.1 \pm 2.8$	41	AAIJ	21AC LHCb	pp at 7, 8, 13 TeV

$\Omega_c(3090)^0$ DECAY MODES

Mode	Fraction (Γ_i/Γ)
$\Gamma_1 \Xi_c^+ K^-$	seen

$\Omega_c(3090)^0$ BRANCHING RATIOS

$\Gamma(\Xi_c^+ K^-)/\Gamma_{\text{total}}$					Γ_1/Γ
VALUE	EVTS	DOCUMENT ID	TECN	COMMENT	
seen	41	¹ AAIJ	21AC LHCb	pp at 7, 8, 13 TeV	
seen	87	YELTON	18B BELLE	e^+e^- at $\Upsilon(4S)$	
seen	2.0k	² AAIJ	17AH LHCb	pp at 7, 8, 13 TeV	

¹ AAIJ 21AC report a significance of 7.8 σ .
² AAIJ 17AH report a significance of 21.1 σ .

$\Omega_c(3090)^0$ REFERENCES

AAIJ	21AC PR D104 L091102	R. Aaij <i>et al.</i>	(LHCb Collab.)
YELTON	18B PR D97 051102	J. Yelton <i>et al.</i>	(BELLE Collab.)
AAIJ	17AH PRL 118 182001	R. Aaij <i>et al.</i>	(LHCb Collab.)

See key on page 1127

Baryon Particle Listings

$\Omega_c(3120)^0$

$\Omega_c(3120)^0$

$I(J^P) = ?(??)$ Status: ***

$\Omega_c(3120)^0$ MASS

VALUE (MeV)	EVTS	DOCUMENT ID	TECN	COMMENT
$3119.1 \pm 0.3 \pm 0.9 \pm 0.3$	480	¹ AAIJ	17AH LHCb	pp at 7, 8, 13 TeV

¹ The third error is the uncertainty on the Ξ_c^+ mass. (AAIJ 17AH gave $+0.3$ MeV here, but as of 2018 it is ± 0.3 .)

$\Omega_c(3120)^0$ WIDTH

VALUE (MeV)	CL%	DOCUMENT ID	TECN	COMMENT
<2.6	95	AAIJ	17AH LHCb	pp at 7, 8, 13 TeV

$\Omega_c(3120)^0$ DECAY MODES

Mode	Fraction (Γ_i/Γ)
$\Gamma_1 \Xi_c^+ K^-$	seen

$\Omega_c(3120)^0$ BRANCHING RATIOS

$\Gamma(\Xi_c^+ K^-)/\Gamma_{\text{total}}$	DOCUMENT ID	TECN	COMMENT	Γ_1/Γ
seen	¹ AAIJ	17AH LHCb	pp at 7, 8, 13 TeV	

¹ AAIJ 17AH report a significance of 10.4 σ .

$\Omega_c(3120)^0$ REFERENCES

AAIJ	17AH PRL 118 182001	R. Aaij <i>et al.</i>	(LHCb Collab.)
------	---------------------	-----------------------	----------------

Baryon Particle Listings

 Ξ_{cc}^+ Ξ_{cc}^{++}

DOUBLY CHARMED BARYONS

(C = +2)

$$\Xi_{cc}^{++} = ucc, \Xi_{cc}^+ = dcc, \Omega_{cc}^+ = scc$$

 Ξ_{cc}^+

$$I(J^P) = ?(?)^? \text{ Status: } *$$

OMITTED FROM SUMMARY TABLE

Nominally the isospin partner of the Ξ_{cc}^{++} (ccu). While the SELEX experiment (MATTSON 02, OCHERASHVILI 05) claimed an observation of this state, subsequent searches by BABAR (AUBERT, B 06D), Belle (CHISTOV 06, KATO 14), and LHCb (AAIJ 13CD, AAIJ 20AX) did not find any significant signal or evidence for the Ξ_{cc}^+ . However, AAIJ 21AE reports that its search for $\Xi_{cc}^+ \rightarrow \Xi_c^+ \pi^+ \pi^-$, when combined with a prior search for $\Xi_{cc}^+ \rightarrow \Lambda_c^+ K^- \pi^+$ decays in AAIJ 20AX, yields a signal at 2.9 σ global significance (4.0 σ local).

 Ξ_{cc}^+ MASS

VALUE (MeV)	EVTS	DOCUMENT ID	TECN	COMMENT
3518.9 ± 0.9 OUR AVERAGE				
3518 ± 3	6	¹ OCHERASHVILI.05	SELX	Σ^- nucleus \approx 600 GeV
3519 ± 1	16	² MATTSON 02	SELX	Σ^- nucleus \approx 600 GeV
• • • We do not use the following data for averages, fits, limits, etc. • • •				
3623.0 ± 1.4	368 ± 193	³ AAIJ 21AE	LHCb	pp at 7, 8, 13 TeV

- ¹ OCHERASHVILI 05 claims “an excess of 5.62 events over ... 1.38 ± 0.13 events” for a significance of 4.8 σ in $pD^+ K^-$ events.
- ² MATTSON 02 claims “an excess of 15.9 events over an expected background of 6.1 ± 0.5 events, a statistical significance of 6.3 σ ” in the $\Lambda_c^+ K^- \pi^+$ invariant-mass spectrum. The probability that the peak is a fluctuation increases from 1.0 × 10⁻⁶ to 1.1 × 10⁻⁴ when the number of bins searched is considered.
- ³ Uncertainties are statistical only. Because of undetermined systematic uncertainties in the extraction of this result it cannot be considered a mass measurement. AAIJ 21AE performs a combined fit to its $\Xi_{cc}^+ \rightarrow \Xi_c^+ \pi^+ \pi^-$ data and the $\Xi_{cc}^+ \rightarrow \Lambda_c^+ K^- \pi^+$ data from AAIJ 20AX, finding a global significance of 2.9 σ (4.0 σ local).

 Ξ_{cc}^+ MEAN LIFE

VALUE (10 ⁻¹⁵ s)	CL%	DOCUMENT ID	TECN	COMMENT
<33	90	MATTSON 02	SELX	Σ^- nucleus, \approx 600 GeV
• • • We do not use the following data for averages, fits, limits, etc. • • •				

 Ξ_{cc}^+ DECAY MODES

Mode	Fraction (Γ_i/Γ)
Γ_1 $\Lambda_c^+ K^- \pi^+$	not seen
Γ_2 $\Xi_c^+ \pi^+ \pi^-$	not seen
Γ_3 $pD^+ K^-$	

$\Gamma(pD^+ K^-)/\Gamma(\Lambda_c^+ K^- \pi^+)$	Γ_3/Γ_1
0.36 ± 0.21	
6	0CHERASHVILI.05
	SELX $\Sigma^- \approx$ 600 GeV
• • • We do not use the following data for averages, fits, limits, etc. • • •	

$\Gamma(\Lambda_c^+ K^- \pi^+)/\Gamma_{\text{total}}$	Γ_1/Γ
not seen	
¹ AAIJ 20AX	LHCb pp at 7, 8, 13 TeV
¹ No significant signal is observed in the mass range 3.4–3.8 GeV	

$\Gamma(\Xi_c^+ \pi^+ \pi^-)/\Gamma_{\text{total}}$	Γ_2/Γ
not seen	
95	145 ± 139
¹ AAIJ 21AE	LHCb pp at 7, 8, 13 TeV

¹ No significant signal is seen in the mass range 3.4–3.8 GeV. AAIJ 21AE performs a combined fit to its $\Xi_{cc}^+ \rightarrow \Xi_c^+ \pi^+ \pi^-$ data and the $\Xi_{cc}^+ \rightarrow \Lambda_c^+ K^- \pi^+$ data from AAIJ 20AX, finding a global significance of 2.9 σ (4.0 σ local).

 Ξ_{cc}^+ REFERENCES

AAIJ 21AE	JHEP 2112 107	R. Aaij et al.	(LHCb Collab.)
AAIJ 20AX	SCPMA 63 221062	R. Aaij et al.	(LHCb Collab.)
KATO 14	PR D89 052003	Y. Kato et al.	(BELLE Collab.)
AAIJ 13CD	JHEP 1312 090	R. Aaij et al.	(LHCb Collab.)
AUBERT, B 06D	PR D74 011103	B. Aubert et al.	(BABAR Collab.)
CHISTOV 06	PRL 97 162001	R. Chistov et al.	(BELLE Collab.)
UCHERASHVILI.05	PL B628 18	A. Ocherashvili et al.	(FNAL SELEX Collab.)
MATTSON 02	PRL 89 112001	M. Mattson et al.	(FNAL SELEX Collab.)

 Ξ_{cc}^{++}

$$I(J^P) = ?(?)^? \text{ Status: } ***$$

 Ξ_{cc}^{++} MASS

VALUE (MeV)	EVTS	DOCUMENT ID	TECN	COMMENT
3621.55 ± 0.23 ± 0.30	2k	¹ AAIJ 20J	LHCb	pp at 13 TeV
• • • We do not use the following data for averages, fits, limits, etc. • • •				
3620.6 ± 1.5 ± 0.4 ± 0.3	91	² AAIJ 18BA	LHCb	pp at 13 TeV
3621.40 ± 0.72 ± 0.27 ± 0.14	313	³ AAIJ 17bc	LHCb	pp at 13 TeV

¹ AAIJ 20J combines mass measurements 3621.53 ± 0.24 ± 0.29 MeV from $\Xi_{cc}^{++} \rightarrow \Lambda_c^+ K^- \pi^+ \pi^+$ and 3621.95 ± 0.60 ± 0.49 MeV from $\Xi_{cc}^{++} \rightarrow \Xi_c^+ \pi^+$. Supersedes AAIJ 18BA and AAIJ 17bc.

² The third error in AAIJ 18BA value is from the uncertainty of the Ξ_c^+ mass.

³ The third error in AAIJ 17bc value is from the uncertainty of the Λ_c^+ mass. The width of the signal is 6.6 ± 0.8 MeV, consistent with the experimental resolution.

 Ξ_{cc}^{++} MEAN LIFE

VALUE (10 ⁻¹⁵ s)	EVTS	DOCUMENT ID	TECN	COMMENT
256⁺²⁴₋₂₂ ± 14	304	AAIJ 18G	LHCb	pp at 13 TeV

 Ξ_{cc}^{++} DECAY MODES

Mode	Fraction (Γ_i/Γ)
Γ_1 $\Lambda_c^+ K^- \pi^+ \pi^+$	seen
Γ_2 $\Xi_c^+ \pi^+, \Xi_c^+ \rightarrow pK^- \pi^+$	seen
Γ_3 $D^+ pK^- \pi^+$	

$\Gamma(\Lambda_c^+ K^- \pi^+ \pi^+)/\Gamma_{\text{total}}$	Γ_1/Γ
seen	
AAIJ 17bc	LHCb 12 std significance

$\Gamma(\Xi_c^+ \pi^+, \Xi_c^+ \rightarrow pK^- \pi^+)/\Gamma_{\text{total}}$	Γ_2/Γ
seen	
91	AAIJ 18BA LHCb 5.9 std significance

$\Gamma(\Xi_c^+ \pi^+, \Xi_c^+ \rightarrow pK^- \pi^+)/\Gamma(\Lambda_c^+ K^- \pi^+ \pi^+)$	Γ_2/Γ_1
2.2 ± 0.6 ± 0.1	
⁴ AAIJ 18BA	LHCb Ratio 91 over 289 events

⁴ AAIJ 18BA reports $[\Gamma(\Xi_{cc}^{++} \rightarrow \Xi_c^+ \pi^+, \Xi_c^+ \rightarrow pK^- \pi^+)/\Gamma(\Xi_{cc}^{++} \rightarrow \Lambda_c^+ K^- \pi^+ \pi^+)] / [\Gamma(\Lambda_c^+ \rightarrow pK^- \pi^+)] = (3.5 ± 0.9 ± 0.3) × 10^{-2}$ which we multiply by our best value $B(\Lambda_c^+ \rightarrow pK^- \pi^+) = (6.28 ± 0.32) × 10^{-2}$. Our first error is their experiment's error and our second error is the systematic error from using our best value.

$\Gamma(D^+ pK^- \pi^+)/\Gamma(\Lambda_c^+ K^- \pi^+ \pi^+)$	Γ_3/Γ_1
<1.7 × 10 ⁻²	
90	AAIJ 19AO LHCb pp at 13 TeV

 Ξ_{cc}^{++} REFERENCES

AAIJ 20J	JHEP 2002 049	R. Aaij et al.	(LHCb Collab.)
AAIJ 19AO	JHEP 1910 124	R. Aaij et al.	(LHCb Collab.)
AAIJ 18BA	PRL 121 162002	R. Aaij et al.	(LHCb Collab.)
AAIJ 18G	PRL 121 052002	R. Aaij et al.	(LHCb Collab.)
AAIJ 17BC	PRL 119 112001	R. Aaij et al.	(LHCb Collab.)

See key on page 1127

Baryon Particle Listings

Λ_b^0

BOTTOM BARYONS
($B = -1$)

$\Lambda_b^0 = udb, \Xi_b^0 = usb, \Xi_b^- = dsb, \Omega_b^- = sss$

Λ_b^0

$I(J^P) = 0(\frac{1}{2}^+)$ Status: ***

In the quark model, a Λ_b^0 is an isospin-0 udb state. The lowest Λ_b^0 ought to have $J^P = 1/2^+$. None of $I, J,$ or P have actually been measured.

Λ_b^0 MASS

$m_{\Lambda_b^0}$	VALUE (MeV)	EVTs	DOCUMENT ID	TECN	COMMENT
5619.60 ± 0.17 OUR AVERAGE					
5619.62 ± 0.16 ± 0.13			1 AAIJ	17AM LHCb	pp at 7, 8 TeV
5619.30 ± 0.34			2 AAIJ	14AA LHCb	pp at 7 TeV
5620.15 ± 0.31 ± 0.47			3 AALTONEN	14B CDF	$p\bar{p}$ at 1.96 TeV
5619.7 ± 0.7 ± 1.1			4 AAD	13U ATLS	pp at 7 TeV
5621 ± 4 ± 3			5 ABE	97B CDF	$p\bar{p}$ at 1.8 TeV
5668 ± 16 ± 8		4	6 ABREU	96N DLPH	$e^+e^- \rightarrow Z$
5614 ± 21 ± 4		4	7 BUSKULIC	96L ALEP	$e^+e^- \rightarrow Z$
• • • We do not use the following data for averages, fits, limits, etc. • • •					
5619.65 ± 0.17 ± 0.17			6 AAIJ	16Y LHCb	Repl. by AAIJ 17AM
5619.44 ± 0.13 ± 0.38			3 AAIJ	13AV LHCb	Repl. by AAIJ 17AM
5619.19 ± 0.70 ± 0.30			3 AAIJ	12E LHCb	Repl. by AAIJ 13AV
5619.7 ± 1.2 ± 1.2			7 ACOSTA	06 CDF	Repl. by AALTONEN 14B
not seen			8 ABE	93B CDF	Repl. by ABE 97B
5640 ± 50 ± 30		16	9 ALBAJAR	91E UA1	$p\bar{p}$ 630 GeV
5640 $\begin{smallmatrix} +100 \\ -210 \end{smallmatrix}$		52	BARI	91 SFM	$\Lambda_b^0 \rightarrow \rho D^0 \pi^-$
5650 $\begin{smallmatrix} +150 \\ -200 \end{smallmatrix}$		90	BARI	91 SFM	$\Lambda_b^0 \rightarrow \Lambda_c^+ \pi^+ \pi^- \pi^-$

- Uses $\Lambda_b^0 \rightarrow \chi_{c1} p K^-, \Lambda_b^0 \rightarrow \chi_{c2} p K^-, \Lambda_b^0 \rightarrow J/\psi \Lambda, \Lambda_b^0 \rightarrow p \psi(2S) K^-, \Lambda_b^0 \rightarrow p J/\psi \pi^+ \pi^- K^-,$ and $\Lambda_b^0 \rightarrow p J/\psi K^-$ decays.
- Uses exclusively reconstructed final states $\Lambda_b^0 \rightarrow \Lambda_c^+ D_s^-, \Lambda_c^+ D^-$ and $\bar{B}^0 \rightarrow D^+ D_s^-$ decays. The uncertainty includes both statistical and systematic contributions.
- Uses $\Lambda_b^0 \rightarrow J/\psi \Lambda$ fully reconstructed decays.
- ABE 97B observed 38 events with a background of 18 ± 1.6 events in the mass range 5.60–5.65 GeV/ c^2 , a significance of > 3.4 standard deviations.
- Uses 4 fully reconstructed Λ_b^0 events.
- Uses $\Lambda_b^0 \rightarrow p \psi(2S) K^-, \Lambda_b^0 \rightarrow p J/\psi \pi^+ \pi^- K^-,$ and $\Lambda_b^0 \rightarrow p J/\psi K^-$ decays.
- Uses exclusively reconstructed final states containing a $J/\psi \rightarrow \mu^+ \mu^-$ decays.
- ABE 93B states that, based on the signal claimed by ALBAJAR 91E, CDF should have found $30 \pm 23 \Lambda_b^0 \rightarrow J/\psi(1S) \Lambda$ events. Instead, CDF found not more than 2 events.
- ALBAJAR 91E claims 16 ± 5 events above a background of 9 ± 1 events, a significance of about 5 standard deviations.

$m_{\Lambda_b^0} - m_{B^0}$

VALUE (MeV)	DOCUMENT ID	TECN	COMMENT
339.2 ± 1.4 ± 0.1	1 ACOSTA	06 CDF	$p\bar{p}$ at 1.96 TeV
1 Uses exclusively reconstructed final states containing $J/\psi \rightarrow \mu^+ \mu^-$ decays.			

$m_{\Lambda_b^0} - m_{B^+}$

VALUE (MeV)	DOCUMENT ID	TECN	COMMENT
339.72 ± 0.28 OUR AVERAGE			
339.72 ± 0.24 ± 0.18	1 AAIJ	14AA LHCb	pp at 7 TeV
339.71 ± 0.71 ± 0.09	2 AAIJ	12E LHCb	pp at 7 TeV
1 Uses exclusively reconstructed final states $\Lambda_b^0 \rightarrow \Lambda_c^+ D_s^-, \Lambda_c^+ D^-$ and $\bar{B}^0 \rightarrow D^+ D_s^-$ decays.			
2 Uses exclusively reconstructed final states containing $J/\psi \rightarrow \mu^+ \mu^-$ decays.			

Λ_b^0 MEAN LIFE

See b -baryon Admixture section for data on b -baryon mean life average over species of b -baryon particles.

“OUR EVALUATION” is an average using rescaled values of the data listed below. The average and rescaling were performed by the Heavy Flavor Averaging Group (HFLAV) and are described at <https://hflav.web.cern.ch/>. The averaging/rescaling procedure takes into account correlations between the measurements and asymmetric lifetime errors.

VALUE (10^{-12} s)	EVTs	DOCUMENT ID	TECN	COMMENT
1.471 ± 0.009 OUR EVALUATION				
1.477 ± 0.027 ± 0.009	1	SIRUNYAN	18BY CMS	pp at 8 TeV
1.415 ± 0.027 ± 0.006	2	AAIJ	14E LHCb	pp at 7 TeV
1.479 ± 0.009 ± 0.010	3	AAIJ	14U LHCb	pp at 7, 8 TeV
1.565 ± 0.035 ± 0.020	2	AALTONEN	14B CDF	$p\bar{p}$ at 1.96 TeV

1.449 ± 0.036 ± 0.017	2	AAD	13U ATLS	pp at 7 TeV
1.503 ± 0.052 ± 0.031	2	CHATRCHYAN	13AC CMS	pp at 7 TeV
1.303 ± 0.075 ± 0.035	2	ABAZOV	12U D0	$p\bar{p}$ at 1.96 TeV
1.401 ± 0.046 ± 0.035	4	AALTONEN	10B CDF	$p\bar{p}$ at 1.96 TeV
1.27 $\begin{smallmatrix} +0.35 \\ -0.29 \end{smallmatrix}$ ± 0.09		ABREU	95S DLPH	Excess $p\mu^-$, decay lengths
• • • We do not use the following data for averages, fits, limits, etc. • • •				
1.482 ± 0.018 ± 0.012	5	AAIJ	13BB LHCb	Repl. by AAIJ 14U
1.537 ± 0.045 ± 0.014	2	AALTONEN	11 CDF	Repl. by AALTONEN 14B
1.218 $\begin{smallmatrix} +0.130 \\ -0.115 \end{smallmatrix}$ ± 0.042	2	ABAZOV	07S D0	Repl. by ABAZOV 12U
1.290 $\begin{smallmatrix} +0.119 \\ -0.110 \end{smallmatrix}$ ± 0.087 ± 0.091	6	ABAZOV	07U D0	$p\bar{p}$ at 1.96 TeV
1.593 $\begin{smallmatrix} +0.083 \\ -0.078 \end{smallmatrix}$ ± 0.033	2	ABULENCIA	07A CDF	Repl. by AALTONEN 11
1.22 $\begin{smallmatrix} +0.22 \\ -0.18 \end{smallmatrix}$ ± 0.04	2	ABAZOV	05C D0	Repl. by ABAZOV 07S
1.11 $\begin{smallmatrix} +0.19 \\ -0.18 \end{smallmatrix}$ ± 0.05	7	ABREU	99W DLPH	$e^+e^- \rightarrow Z$
1.29 $\begin{smallmatrix} +0.24 \\ -0.22 \end{smallmatrix}$ ± 0.06	7	ACKERSTAFF	98G OPAL	$e^+e^- \rightarrow Z$
1.21 ± 0.11	7	BARATE	98D ALEP	$e^+e^- \rightarrow Z$
1.32 ± 0.15 ± 0.07	8	ABE	96M CDF	$p\bar{p}$ at 1.8 TeV
1.19 $\begin{smallmatrix} +0.21 \\ -0.18 \end{smallmatrix}$ ± 0.07		ABREU	96D DLPH	Repl. by ABREU 99W
1.14 $\begin{smallmatrix} +0.22 \\ -0.19 \end{smallmatrix}$ ± 0.07	69	AKERS	95K OPAL	Repl. by ACKERSTAFF 98G
1.02 $\begin{smallmatrix} +0.23 \\ -0.18 \end{smallmatrix}$ ± 0.06	44	BUSKULIC	95L ALEP	Repl. by BARATE 98D

- Measured using $\Lambda_b^0 \rightarrow J/\psi \Lambda$ decays.
- Measured mean life using fully reconstructed $\Lambda_b^0 \rightarrow J/\psi \Lambda$ decays.
- Used $\Lambda_b^0 \rightarrow J/\psi p K^-$ decays.
- Measured mean life using fully reconstructed $\Lambda_b^0 \rightarrow \Lambda_c^+ \pi^-$ decays.
- Measured the lifetime ratio of decays $\Lambda_b^0 \rightarrow J/\psi p K^-$ to $B^0 \rightarrow J/\psi \pi^+ K^-$ to be $0.976 \pm 0.012 \pm 0.006$ with $\tau_{B^0} = 1.519 \pm 0.007$ ps.
- Measured using semileptonic decays $\Lambda_b^0 \rightarrow \Lambda_c^+ \mu \nu X$ and $\Lambda_c^+ \rightarrow K_S^0 p$.
- Measured using $\Lambda_c \ell^-$ and $\Lambda \ell^+ \ell^-$.
- Excess $\Lambda_c \ell^-$, decay lengths.

$\tau_{\Lambda_b^0} / \tau_{B^0}$

VALUE	DOCUMENT ID	TECN	COMMENT
0.940 ± 0.035 ± 0.006	1 AAIJ	14E LHCb	pp at 7 TeV
1 Measured using $\Lambda_b^0 \rightarrow J/\psi \Lambda$ decays.			

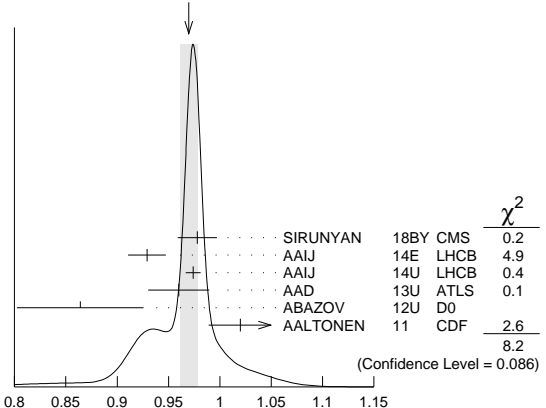
$\tau_{\Lambda_b^0} / \tau_{B^0}$ MEAN LIFE RATIO

$\tau_{\Lambda_b^0} / \tau_{B^0}$ (direct measurements)

“OUR EVALUATION” has been obtained by the Heavy Flavor Averaging Group (HFLAV) by including both B^0 and B^+ decays.

VALUE	DOCUMENT ID	TECN	COMMENT
0.964 ± 0.007 OUR EVALUATION			
0.970 ± 0.009 OUR AVERAGE			Error includes scale factor of 1.4. See the ideogram below.
0.978 ± 0.018 ± 0.006	1	SIRUNYAN	18BY CMS pp at 8 TeV
0.929 ± 0.018 ± 0.004	1	AAIJ	14E LHCb pp at 7 TeV
0.974 ± 0.006 ± 0.004	2	AAIJ	14U LHCb pp at 7, 8 TeV
0.960 ± 0.025 ± 0.016	3	AAD	13U ATLS pp at 7 TeV
0.864 ± 0.052 ± 0.033	4,5	ABAZOV	12U D0 $p\bar{p}$ at 1.96 TeV
1.020 ± 0.030 ± 0.008	4	AALTONEN	11 CDF $p\bar{p}$ at 1.96 TeV
• • • We do not use the following data for averages, fits, limits, etc. • • •			
0.976 ± 0.012 ± 0.006	6	AAIJ	13BB LHCb Repl. by AAIJ 14U
0.811 $\begin{smallmatrix} +0.096 \\ -0.087 \end{smallmatrix}$ ± 0.034	4,5	ABAZOV	07S D0 Repl. by ABAZOV 12U
1.041 ± 0.057	7	ABULENCIA	07A CDF Repl. by AALTONEN 11
0.87 $\begin{smallmatrix} +0.17 \\ -0.14 \end{smallmatrix}$ ± 0.03	7	ABAZOV	05C D0 Repl. by ABAZOV 07S

WEIGHTED AVERAGE
0.970 ± 0.009 (Error scaled by 1.4)



$\tau_{\Lambda_b^0} / \tau_{B^0}$ (direct measurements)

Baryon Particle Listings

Λ_b^0

- ¹ Measured using $\Lambda_b^0 \rightarrow J/\psi \Lambda$ and $B^0 \rightarrow J/\psi K^*(892)^0$ decays.
- ² Used $\Lambda_b^0 \rightarrow J/\psi p K^-$ and $B^0 \rightarrow J/\psi K^*(892)^0$ decays.
- ³ Measured with $\Lambda_b^0 \rightarrow J/\psi(\mu^+ \mu^-) \Lambda^0(p\pi^-)$ decays.
- ⁴ Uses fully reconstructed $\Lambda_b \rightarrow J/\psi \Lambda$ decays.
- ⁵ Uses $B^0 \rightarrow J/\psi K_S^0$ decays for denominator.
- ⁶ Measures $1/\tau_{\Lambda_b^0} - 1/\tau_{B^0}$ and uses $\tau_{B^0} = 1.519 \pm 0.007$ ps to extract lifetime ratio.
- ⁷ Measured mean life ratio using fully reconstructed decays.

Λ_b^0 DECAY MODES

The branching fractions $B(b\text{-baryon} \rightarrow \Lambda \ell^- \bar{\nu}_\ell \text{anything})$ and $B(\Lambda_b^0 \rightarrow \Lambda_c^+ \ell^- \bar{\nu}_\ell \text{anything})$ are not pure measurements because the underlying measured products of these with $B(b \rightarrow b\text{-baryon})$ were used to determine $B(b \rightarrow b\text{-baryon})$, as described in the note "Production and Decay of b -Flavored Hadrons."

For inclusive branching fractions, e.g., $\Lambda_b \rightarrow \bar{\Lambda}_c \text{anything}$, the values usually are multiplicities, not branching fractions. They can be greater than one.

Mode	Fraction (Γ_i/Γ)	Scale factor/ Confidence level
Γ_1 $J/\psi(1S) \Lambda \times B(b \rightarrow \Lambda_b^0)$	$(5.8 \pm 0.8) \times 10^{-5}$	
Γ_2 $J/\psi(1S) \Lambda$		
Γ_3 $J/\psi(1S) \Lambda \phi$		
Γ_4 $\psi(2S) \Lambda$		
Γ_5 $p D^0 \pi^-$	$(6.3 \pm 0.6) \times 10^{-4}$	
Γ_6 $\Lambda_c(2860)^+ \pi^-$, $\Lambda_c^+ \rightarrow D^0 p$		
Γ_7 $\Lambda_c(2880)^+ \pi^-$, $\Lambda_c^+ \rightarrow D^0 p$		
Γ_8 $\Lambda_c(2940)^+ \pi^-$, $\Lambda_c^+ \rightarrow D^0 p$		
Γ_9 $p D^0 K^-$	$(4.6 \pm 0.8) \times 10^{-5}$	
Γ_{10} $p D K^-$, $D \rightarrow K^- \pi^+$		
Γ_{11} $p D K^-$, $D \rightarrow K^+ \pi^-$		
Γ_{12} $p J/\psi \pi^-$	$(2.6 \pm 0.4) \times 10^{-5}$	
Γ_{13} $p \pi^- J/\psi$, $J/\psi \rightarrow \mu^+ \mu^-$	$(1.6 \pm 0.8) \times 10^{-6}$	
Γ_{14} $p J/\psi K^-$	$(3.2 \pm 0.5) \times 10^{-4}$	
Γ_{15} $p \eta_c(1S) K^-$	$(1.06 \pm 0.26) \times 10^{-4}$	
Γ_{16} $P_c(4312)^+ K^-$, $P_c(4312)^+ \rightarrow p \eta_c(1S)$	$< 2.5 \times 10^{-5}$	CL=95%
Γ_{17} $P_c(4380)^+ K^-$, $P_c \rightarrow p J/\psi$	$(2.7 \pm 1.4) \times 10^{-5}$	[a]
Γ_{18} $P_c(4450)^+ K^-$, $P_c \rightarrow p J/\psi$	$(1.3 \pm 0.4) \times 10^{-5}$	[a]
Γ_{19} $\chi_{c1}(1P) p K^-$	$(7.6 \pm 1.5) \times 10^{-5}$	
Γ_{20} $\chi_{c1}(1P) p \pi^-$	$(5.0 \pm 1.1) \times 10^{-6}$	
Γ_{21} $\chi_{c2}(1P) p K^-$	$(7.9 \pm 1.6) \times 10^{-5}$	
Γ_{22} $\chi_{c2}(1P) p \pi^-$	$(4.8 \pm 1.9) \times 10^{-6}$	
Γ_{23} $p J/\psi(1S) \pi^+ \pi^- K^-$	$(6.6 \pm 1.1) \times 10^{-5}$	
Γ_{24} $p \psi(2S) K^-$	$(6.6 \pm 1.2) \times 10^{-5}$	
Γ_{25} $\chi_{c1}(3872) p K^-$	$(3.2 \pm 1.4) \times 10^{-5}$	
Γ_{26} $\chi_{c1}(3872) \Lambda(1520)$	$(1.9 \pm 0.9) \times 10^{-5}$	
Γ_{27} $\psi(2S) p \pi^-$	$(7.5 \pm 1.6) \times 10^{-6}$	
Γ_{28} $p \bar{K}^0 \pi^-$	$(1.3 \pm 0.4) \times 10^{-5}$	
Γ_{29} $p K^0 K^-$	$< 3.5 \times 10^{-6}$	CL=90%
Γ_{30} $\Lambda_c^+ \pi^-$	$(4.9 \pm 0.4) \times 10^{-3}$	S=1.2
Γ_{31} $\Lambda_c^+ K^-$	$(3.56 \pm 0.28) \times 10^{-4}$	S=1.2
Γ_{32} $\Lambda_c^+ a_1(1260)^-$	seen	
Γ_{33} $\Lambda_c^+ D^-$	$(4.6 \pm 0.6) \times 10^{-4}$	
Γ_{34} $\Lambda_c^+ D_s^-$	$(1.10 \pm 0.10) \%$	
Γ_{35} $\Lambda_c^+ \pi^+ \pi^- \pi^-$	$(7.6 \pm 1.1) \times 10^{-3}$	S=1.1
Γ_{36} $\Lambda_c(2595)^+ \pi^-$, $\Lambda_c(2595)^+ \rightarrow \Lambda_c^+ \pi^+ \pi^-$	$(3.4 \pm 1.4) \times 10^{-4}$	
Γ_{37} $\Lambda_c(2625)^+ \pi^-$, $\Lambda_c(2625)^+ \rightarrow \Lambda_c^+ \pi^+ \pi^-$	$(3.3 \pm 1.3) \times 10^{-4}$	
Γ_{38} $\Sigma_c(2455)^0 \pi^+ \pi^-$, $\Sigma_c^0 \rightarrow \Lambda_c^+ \pi^-$	$(5.7 \pm 2.2) \times 10^{-4}$	
Γ_{39} $\Sigma_c(2455)^{++} \pi^- \pi^-$, $\Sigma_c^{++} \rightarrow \Lambda_c^+ \pi^+$	$(3.2 \pm 1.5) \times 10^{-4}$	
Γ_{40} $\Lambda_c^+ K^+ K^- \pi^-$	$(1.02 \pm 0.11) \times 10^{-3}$	
Γ_{41} $\Lambda_c^+ p \bar{p} \pi^-$	$(2.63 \pm 0.27) \times 10^{-4}$	
Γ_{42} $\Sigma_c(2455)^0 p \bar{p}$, $\Sigma_c^0 \rightarrow \Lambda_c^+ \pi^-$	$(2.3 \pm 0.5) \times 10^{-5}$	

Γ_{43} $\Sigma_c(2520)^0 p \bar{p}$, $\Sigma_c(2520)^0 \rightarrow \Lambda_c^+ \pi^-$	$(3.1 \pm 0.7) \times 10^{-5}$	
Γ_{44} $\Lambda K^0 2\pi^+ 2\pi^-$		
Γ_{45} $\Lambda_c^+ \ell^- \bar{\nu}_\ell \text{anything}$	[b] $(10.9 \pm 2.2) \%$	
Γ_{46} $\Lambda_c^+ \ell^- \bar{\nu}_\ell$	$(6.2 \pm 1.4) \%$	
Γ_{47} $\Lambda_c^+ \pi^+ \pi^- \ell^- \bar{\nu}_\ell$	$(5.6 \pm 3.1) \%$	
Γ_{48} $\Lambda_c(2595)^+ \ell^- \bar{\nu}_\ell$	$(7.9 \pm 4.0) \times 10^{-3}$	
Γ_{49} $\Lambda_c(2625)^+ \ell^- \bar{\nu}_\ell$	$(1.3 \pm 0.6) \%$	
Γ_{50} $\Sigma_c(2455)^0 \pi^+ \ell^- \bar{\nu}_\ell$		
Γ_{51} $\Sigma_c(2455)^{++} \pi^- \ell^- \bar{\nu}_\ell$		
Γ_{52} $p h^-$	[c] $< 2.3 \times 10^{-5}$	CL=90%
Γ_{53} $p \pi^-$	$(4.5 \pm 0.8) \times 10^{-6}$	
Γ_{54} $p K^-$	$(5.4 \pm 1.0) \times 10^{-6}$	
Γ_{55} $p D_s^-$	$< 4.8 \times 10^{-4}$	CL=90%
Γ_{56} $p \mu^- \bar{\nu}_\mu$	$(4.1 \pm 1.0) \times 10^{-4}$	
Γ_{57} $\Lambda \mu^+ \mu^-$	$(1.08 \pm 0.28) \times 10^{-6}$	
Γ_{58} $p \pi^- \mu^+ \mu^-$	$(6.9 \pm 2.5) \times 10^{-8}$	
Γ_{59} $p K^- e^+ e^-$	$(3.1 \pm 0.6) \times 10^{-7}$	
Γ_{60} $p K^- \mu^+ \mu^-$	$(2.6 \pm 0.5) \times 10^{-7}$	
Γ_{61} $\Lambda \gamma$	$(7.1 \pm 1.7) \times 10^{-6}$	
Γ_{62} $\Lambda \eta$	$(9 \pm 7) \times 10^{-6}$	
Γ_{63} $\Lambda \eta'(958)$	$< 3.1 \times 10^{-6}$	CL=90%
Γ_{64} $\Lambda \pi^+ \pi^-$	$(4.6 \pm 1.9) \times 10^{-6}$	
Γ_{65} $\Lambda K^+ \pi^-$	$(5.6 \pm 1.2) \times 10^{-6}$	
Γ_{66} $\Lambda K^+ K^-$	$(1.60 \pm 0.22) \times 10^{-5}$	
Γ_{67} $\Lambda \phi$	$(9.8 \pm 2.6) \times 10^{-6}$	
Γ_{68} $p \pi^- \pi^+ \pi^-$	$(2.10 \pm 0.22) \times 10^{-5}$	
Γ_{69} $p K^- K^+ \pi^-$	$(4.0 \pm 0.6) \times 10^{-6}$	
Γ_{70} $p K^- \pi^+ \pi^-$	$(5.0 \pm 0.5) \times 10^{-5}$	
Γ_{71} $p K^- K^+ K^-$	$(1.26 \pm 0.13) \times 10^{-5}$	

[a] P_c^+ is a pentaquark-charmonium state.

[b] Not a pure measurement. See note at head of Λ_b^0 Decay Modes.

[c] Here h^- means π^- or K^- .

CONSTRAINED FIT INFORMATION

An overall fit to 10 branching ratios uses 12 measurements and one constraint to determine 7 parameters. The overall fit has a $\chi^2 = 10.8$ for 6 degrees of freedom.

The following *off-diagonal* array elements are the correlation coefficients $\langle \delta x_i \delta x_j \rangle / (\delta x_i \delta x_j)$, in percent, from the fit to the branching fractions, $x_i \equiv \Gamma_i/\Gamma_{\text{total}}$. The fit constrains the x_i whose labels appear in this array to sum to one.

x_{31}	92				
x_{35}	46	43			
x_{46}	13	12	6		
x_{53}	0	0	0	0	
x_{54}	0	0	0	0	82
	x_{30}	x_{31}	x_{35}	x_{46}	x_{53}

Λ_b^0 BRANCHING RATIOS

$\Gamma(J/\psi(1S) \Lambda \times B(b \rightarrow \Lambda_b^0)) / \Gamma_{\text{total}}$	Γ_1/Γ
VALUE (units 10^{-5})	
5.8 ± 0.8 OUR AVERAGE	
6.01 ± 0.60 ± 0.58 ± 0.28	1 ABAZOV 11o D0 $p\bar{p}$ at 1.96 TeV
4.7 ± 2.3 ± 0.2	2 ABE 97b CDF $p\bar{p}$ at 1.8 TeV
••• We do not use the following data for averages, fits, limits, etc. •••	
180 ± 60 ± 90	16 ALBAJAR 91e UA1 $p\bar{p}$ at 630 GeV
¹ ABAZOV 11o uses $B(B^0 \rightarrow J/\psi K_S^0) \times B(b \rightarrow B^0) = (1.74 \pm 0.08) \times 10^{-4}$ to obtain the result. The $(\pm 0.08) \times 10^{-4}$ uncertainty of this product is listed as the last uncertainty of the measurement, $(\pm 0.28) \times 10^{-5}$.	
² ABE 97b reports $[B(\Lambda_b^0 \rightarrow J/\psi \Lambda) \times B(b \rightarrow \Lambda_b^0)] / [B(B^0 \rightarrow J/\psi K_S^0) \times B(b \rightarrow B^0)] = 0.27 \pm 0.12 \pm 0.05$. We multiply by our best value $B(B^0 \rightarrow J/\psi K_S^0) \times B(b \rightarrow B^0) = (1.74 \pm 0.08) \times 10^{-4}$. Our first error is their experiment error and our second error is the systematic error from using our best value.	

$\Gamma(\psi(2S)\Lambda)/\Gamma(J/\psi(1S)\Lambda)$ Γ_4/Γ_2

VALUE	DOCUMENT ID	TECN	COMMENT
0.508±0.023 OUR AVERAGE			
0.513±0.023±0.019	¹ AAIJ	19F LHCb	pp at 7, 8 TeV
0.50 ± 0.03 ± 0.02	² AAD	15CH ATLS	pp at 8 TeV

¹ AAIJ 19F uses $B(J/\psi \rightarrow \mu^+ \mu^-) = (5.961 \pm 0.033) \times 10^{-2}$ and $B(\psi(2S) \rightarrow e^+ e^-) = (7.93 \pm 0.17) \times 10^{-3}$ from PDG 18 with assumption of lepton universality. AAIJ 19F reports this result as $0.513 \pm 0.023 \pm 0.016 \pm 0.011$, where the last uncertainty is the contribution due to the external input of branching fractions used in the analysis.

² AAD 15CH uses $B(J/\psi \rightarrow \mu^+ \mu^-) = (5.961 \pm 0.033) \times 10^{-2}$ and $B(\psi(2S) \rightarrow \mu^+ \mu^-) = (7.89 \pm 0.17) \times 10^{-3}$ from PDG 14 with assumption of lepton universality.

$\Gamma(J/\psi(1S)\Lambda\phi)/\Gamma(\psi(2S)\Lambda)$ Γ_3/Γ_4

VALUE (units 10 ⁻²)	DOCUMENT ID	TECN	COMMENT
8.26±0.90±0.69	SIRUNYAN	20H CMS	pp at 13 TeV

$\Gamma(pD^0\pi^-)/\Gamma_{total}$ Γ_5/Γ

VALUE	EVTS	DOCUMENT ID	TECN	COMMENT
• • • We do not use the following data for averages, fits, limits, etc. • • •				
seen	52	BARJ	91 SFM	$D^0 \rightarrow K^- \pi^+$
seen		BASILE	81 SFM	$D^0 \rightarrow K^- \pi^+$

$\Gamma(\Lambda_c(2860)^+ \pi^-, \Lambda_c^+ \rightarrow D^0 p)/\Gamma(\Lambda_c(2880)^+ \pi^-, \Lambda_c^+ \rightarrow D^0 p)$ Γ_6/Γ_7

VALUE	DOCUMENT ID	TECN	COMMENT
4.54^{+0.51+0.21}_{-0.39-0.59}	AAIJ	17s LHCb	pp at 7, 8 TeV

$\Gamma(\Lambda_c(2940)^+ \pi^-, \Lambda_c^+ \rightarrow D^0 p)/\Gamma(\Lambda_c(2880)^+ \pi^-, \Lambda_c^+ \rightarrow D^0 p)$ Γ_8/Γ_7

VALUE	DOCUMENT ID	TECN	COMMENT
0.83^{+0.31+0.18}_{-0.10-0.43}	AAIJ	17s LHCb	pp at 7, 8 TeV

$\Gamma(pD^0K^-)/\Gamma(pD^0\pi^-)$ Γ_9/Γ_5

VALUE (units 10 ⁻²)	DOCUMENT ID	TECN	COMMENT
7.3±0.8^{+0.5}_{-0.6}	AAIJ	14H LHCb	pp at 7 TeV

$\Gamma(pDK^-, D \rightarrow K^- \pi^+)/\Gamma(pDK^-, D \rightarrow K^+ \pi^-)$ Γ_{10}/Γ_{11}

VALUE	DOCUMENT ID	TECN	COMMENT
7.1±0.8^{+0.4}_{-0.3}	¹ AAIJ	21AD LHCb	pp at 7, 8, 13 TeV

¹ Measured in the full phase space.

$\Gamma(pJ/\psi\pi^-)/\Gamma(pJ/\psi K^-)$ Γ_{12}/Γ_{14}

VALUE (units 10 ⁻²)	DOCUMENT ID	TECN	COMMENT
8.24±0.25±0.42	AAIJ	14K LHCb	pp at 7, 8 TeV

$\Gamma(pJ/\psi K^-)/\Gamma_{total}$ Γ_{14}/Γ

VALUE (units 10 ⁻⁴)	DOCUMENT ID	TECN	COMMENT
3.17±0.04^{+0.57}_{-0.45}	¹ AAIJ	16A LHCb	pp at 7, 8 TeV

¹ AAIJ 16A reported the measurement of $(3.17 \pm 0.04 \pm 0.07 \pm 0.34^{+0.45}_{-0.28}) \times 10^{-4}$ where the first uncertainty is statistical, the second is systematic, the third is due to the branching fraction of $B^0 \rightarrow J/\psi K^*(892)^0$, and the fourth is due to the knowledge of $f_{\Lambda_b^0}/f_{\psi}$. We combined in quadrature second to fourth uncertainties to a total systematic uncertainty.

$\Gamma(p\eta_c(1S)K^-)/\Gamma(pJ/\psi K^-)$ Γ_{15}/Γ_{14}

VALUE	DOCUMENT ID	TECN	COMMENT
0.333±0.050±0.037	¹ AAIJ	20AK LHCb	pp at 13 TeV

¹ AAIJ 20AK reported the measurement of $0.333 \pm 0.050 \pm 0.019 \pm 0.032$, where the last uncertainty is due to uncertainties of the used branching fractions of $J/\psi \rightarrow p\bar{p}$ and $\eta_c \rightarrow p\bar{p}$ decays. We combined in quadrature the systematic uncertainties.

$\Gamma(P_c(4312)^+ K^-, P_c(4312)^+ \rightarrow p\eta_c(1S))/\Gamma(p\eta_c(1S)K^-)$ Γ_{16}/Γ_{15}

VALUE	CL%	DOCUMENT ID	TECN	COMMENT
<0.24	95	AAIJ	20AK LHCb	pp at 13 TeV

$\Gamma(P_c(4380)^+ K^-, P_c \rightarrow pJ/\psi)/\Gamma_{total}$ Γ_{17}/Γ

VALUE (units 10 ⁻⁵)	DOCUMENT ID	TECN	COMMENT
2.66±0.22±1.41_{-1.38}	¹ AAIJ	16A LHCb	pp at 7, 8 TeV

¹ AAIJ 16 total systematic includes the uncertainties on $f(P_c^+)$ and $B(\Lambda_b \rightarrow pJ/\psi K^-)$.

$\Gamma(P_c(4450)^+ K^-, P_c \rightarrow pJ/\psi)/\Gamma_{total}$ Γ_{18}/Γ

VALUE (units 10 ⁻⁵)	DOCUMENT ID	TECN	COMMENT
1.30±0.16^{+0.42}_{-0.39}	¹ AAIJ	16A LHCb	pp at 7, 8 TeV

¹ AAIJ 16 total systematic includes the uncertainties on $f(P_c^+)$ and $B(\Lambda_b \rightarrow pJ/\psi K^-)$.

$\Gamma(\chi_{c1}(1P)pK^-)/\Gamma(pJ/\psi K^-)$ Γ_{19}/Γ_{14}

VALUE	DOCUMENT ID	TECN	COMMENT
0.239±0.019±0.007	¹ AAIJ	17AMLHCb	pp at 7, 8 TeV

¹ AAIJ 17AM reports $0.242 \pm 0.014 \pm 0.016$ from a measurement of $[\Gamma(\Lambda_b^0 \rightarrow \chi_{c1}(1P)pK^-)/\Gamma(\Lambda_b^0 \rightarrow pJ/\psi K^-)] \times [B(\chi_{c1}(1P) \rightarrow \gamma J/\psi(1S))]$ assuming $B(\chi_{c1}(1P) \rightarrow \gamma J/\psi(1S)) = (33.9 \pm 1.2) \times 10^{-2}$, which we rescale to our best value $B(\chi_{c1}(1P) \rightarrow \gamma J/\psi(1S)) = (34.3 \pm 1.0) \times 10^{-2}$. Our first error is their experiment's error and our second error is the systematic error from using our best value.

$\Gamma(\chi_{c1}(1P)p\pi^-)/\Gamma(\chi_{c1}(1P)pK^-)$ Γ_{20}/Γ_{19}

VALUE (units 10 ⁻²)	DOCUMENT ID	TECN	COMMENT
6.59±1.01±0.22	AAIJ	21R LHCb	pp at 13 TeV

$\Gamma(\chi_{c2}(1P)pK^-)/\Gamma(pJ/\psi K^-)$ Γ_{21}/Γ_{14}

VALUE	DOCUMENT ID	TECN	COMMENT
0.250±0.025±0.007	¹ AAIJ	17AMLHCb	pp at 7, 8 TeV

¹ AAIJ 17AM reports $0.248 \pm 0.02 \pm 0.017$ from a measurement of $[\Gamma(\Lambda_b^0 \rightarrow \chi_{c2}(1P)pK^-)/\Gamma(\Lambda_b^0 \rightarrow pJ/\psi K^-)] \times [B(\chi_{c2}(1P) \rightarrow \gamma J/\psi(1S))]$ assuming $B(\chi_{c2}(1P) \rightarrow \gamma J/\psi(1S)) = (19.2 \pm 0.7) \times 10^{-2}$, which we rescale to our best value $B(\chi_{c2}(1P) \rightarrow \gamma J/\psi(1S)) = (19.0 \pm 0.5) \times 10^{-2}$. Our first error is their experiment's error and our second error is the systematic error from using our best value.

$\Gamma(\chi_{c2}(1P)pK^-)/\Gamma(\chi_{c1}(1P)pK^-)$ Γ_{21}/Γ_{19}

VALUE	DOCUMENT ID	TECN	COMMENT
1.06±0.05±0.04±0.04	¹ AAIJ	21R LHCb	pp at 13 TeV

¹ The first uncertainty is statistical, the second is systematic and the third is related to the uncertainties in the branching fractions of the $\chi_{cJ} \rightarrow J/\psi\gamma$ decays.

$\Gamma(\chi_{c2}(1P)p\pi^-)/\Gamma(\chi_{c1}(1P)p\pi^-)$ Γ_{22}/Γ_{20}

VALUE	DOCUMENT ID	TECN	COMMENT
0.95±0.30±0.04±0.04	¹ AAIJ	21R LHCb	pp at 13 TeV

¹ Evidence for the $\Lambda_b^0 \rightarrow \chi_{c2} p \pi^-$ decay is obtained with a significance of 3.5 standard deviations. The first uncertainty is statistical, the second is systematic and the third is related to the uncertainties in the branching fractions of the $\chi_{cJ} \rightarrow J/\psi\gamma$ decays.

$\Gamma(pJ/\psi(1S)\pi^+\pi^-K^-)/\Gamma(pJ/\psi K^-)$ Γ_{23}/Γ_{14}

VALUE	DOCUMENT ID	TECN	COMMENT
0.2086±0.0096±0.0134	¹ AAIJ	16Y LHCb	pp at 7, 8 TeV

¹ Excludes $\psi(2S) \rightarrow J/\psi\pi^+\pi^-$.

$\Gamma(p\psi(2S)K^-)/\Gamma(pJ/\psi K^-)$ Γ_{24}/Γ_{14}

VALUE	DOCUMENT ID	TECN	COMMENT
0.2070±0.0076±0.0059	¹ AAIJ	16Y LHCb	pp at 7, 8 TeV

¹ AAIJ 16Y reports a measurement of $0.2070 \pm 0.0076 \pm 0.0046 \pm 0.0037$ where the third uncertainty is due to the knowledge of J/ψ and $\psi(2S)$ branching fractions. We have combined both systematic uncertainties in quadrature.

$\Gamma(\chi_{c1}(3872)\Lambda(1520))/\Gamma(\chi_{c1}(3872)pK^-)$ Γ_{26}/Γ_{25}

VALUE	DOCUMENT ID	TECN	COMMENT
0.58±0.15	AAIJ	19AN LHCb	pp at 7, 8, 13 TeV

$\Gamma(\chi_{c1}(3872)pK^-)/\Gamma(p\psi(2S)K^-)$ Γ_{25}/Γ_{24}

VALUE	DOCUMENT ID	TECN	COMMENT
0.49±0.10±0.16	¹ AAIJ	19AN LHCb	pp at 7, 8, 13 TeV

¹ AAIJ 19AN reports $[\Gamma(\Lambda_b^0 \rightarrow \chi_{c1}(3872)pK^-)/\Gamma(\Lambda_b^0 \rightarrow p\psi(2S)K^-)] \times [B(\chi_{c1}(3872) \rightarrow \pi^+\pi^-J/\psi(1S))] / [B(\psi(2S) \rightarrow J/\psi(1S)\pi^+\pi^-)] = (5.4 \pm 1.1 \pm 0.2) \times 10^{-2}$ which we multiply or divide by our best values $B(\chi_{c1}(3872) \rightarrow \pi^+\pi^-J/\psi(1S)) = (3.8 \pm 1.2) \times 10^{-2}$, $B(\psi(2S) \rightarrow J/\psi(1S)\pi^+\pi^-) = (34.68 \pm 0.30) \times 10^{-2}$. Our first error is their experiment's error and our second error is the systematic error from using our best values.

$\Gamma(\psi(2S)p\pi^-)/\Gamma(p\psi(2S)K^-)$ Γ_{27}/Γ_{24}

VALUE (%)	DOCUMENT ID	TECN	COMMENT
11.4±1.3±0.2	AAIJ	18AF LHCb	pp at 7, 8, 13 TeV

$\Gamma(p\bar{K}^0\pi^-)/\Gamma_{total}$ Γ_{28}/Γ

VALUE (units 10 ⁻⁵)	DOCUMENT ID	TECN	COMMENT
1.26±0.19±0.36	¹ AAIJ	14Q LHCb	pp at 7 TeV

¹ Used the normalizing mode branching fraction value of $B(B^0 \rightarrow K^0\pi^+\pi^-) = (4.96 \pm 0.20) \times 10^{-5}$.

$\Gamma(pK^0K^-)/\Gamma_{total}$ Γ_{29}/Γ

VALUE	CL%	DOCUMENT ID	TECN	COMMENT
<3.5 × 10⁻⁶	90	AAIJ	14Q LHCb	pp at 7 TeV

$\Gamma(\Lambda_c^+ \pi^-)/\Gamma_{total}$ Γ_{30}/Γ

VALUE (units 10 ⁻³)	EVTS	DOCUMENT ID	TECN	COMMENT
4.9 ± 0.4 OUR FIT				Error includes scale factor of 1.2.
4.8 ± 0.5 OUR AVERAGE				Error includes scale factor of 1.5.
4.60 ^{+0.31} _{-0.30} ± 0.14		¹ AAIJ	14I LHCb	pp at 7 TeV
5.97 ± 0.28 ± 0.81		² AAIJ	14Q LHCb	pp at 7 TeV
8.8 ± 2.8 ± 1.5		³ ABULENCIA	07B CDF	p \bar{p} at 1.96 TeV

Baryon Particle Listings

 Λ_b^0

• • • We do not use the following data for averages, fits, limits, etc. • • •

seen	3	ABREU	96N	DLPH	$\Lambda_c^+ \rightarrow pK^- \pi^+$
seen	4	BUSKULIC	96L	ALEP	$\Lambda_c^+ \rightarrow pK^- \pi^+$, $\rho^0 \bar{K}^0, \Lambda \pi^+ \pi^+ \pi^-$

¹ AAIJ 14I reports $(4.30 \pm 0.03 \pm_{-0.11}^{+0.12} \pm 0.26 \pm 0.21) \times 10^{-3}$ from a measurement of $[\Gamma(\Lambda_b^0 \rightarrow \Lambda_c^+ \pi^-) / \Gamma_{\text{total}}] \times [B(B^0 \rightarrow D^- \pi^+)]$ assuming $B(B^0 \rightarrow D^- \pi^+) = (2.68 \pm 0.13) \times 10^{-3}$, which we rescale to our best value $B(B^0 \rightarrow D^- \pi^+) = (2.51 \pm 0.08) \times 10^{-3}$. Our first error is their experiment's error and our second error is the systematic error from using our best value. Uses information on f_{baryon}/f_d from measurement in semileptonic decays by the same authors.

² Obtained using the branching fraction of $\Lambda_c^+ \rightarrow pK^- \pi^+$ decay.

³ The result is obtained from $(f_{\text{baryon}}/f_d) (B(\Lambda_b^0 \rightarrow \Lambda_c^+ \pi^-) / B(\bar{B}^0 \rightarrow D^+ \pi^-)) = 0.82 \pm 0.08 \pm 0.11 \pm 0.22$, assuming $f_{\text{baryon}}/f_d = 0.25 \pm 0.04$ and $B(\bar{B}^0 \rightarrow D^+ \pi^-) = (2.68 \pm 0.13) \times 10^{-3}$.

$\Gamma(\rho D^0 \pi^-) / \Gamma(\Lambda_c^+ \pi^-)$ Γ_5 / Γ_{30}

VALUE	DOCUMENT ID	TECN	COMMENT
$0.128 \pm 0.007 \pm_{-0.007}^{+0.006}$	¹ AAIJ	14H	LHCB pp at 7 TeV

¹ AAIJ 14H reports $[\Gamma(\Lambda_b^0 \rightarrow \rho D^0 \pi^-) / \Gamma(\Lambda_b^0 \rightarrow \Lambda_c^+ \pi^-)] \times [B(D^0 \rightarrow K^- \pi^+)] / [B(\Lambda_c^+ \rightarrow pK^- \pi^+)] = (8.06 \pm 0.23 \pm 0.35) \times 10^{-2}$ which we multiply or divide by our best values $B(D^0 \rightarrow K^- \pi^+) = (3.947 \pm 0.030) \times 10^{-2}$, $B(\Lambda_c^+ \rightarrow pK^- \pi^+) = (6.28 \pm 0.32) \times 10^{-2}$. Our first error is their experiment's error and our second error is the systematic error from using our best values.

$\Gamma(\Lambda_c^+ K^-) / \Gamma_{\text{total}}$ Γ_{31} / Γ

VALUE (units 10^{-4})	DOCUMENT ID	TECN	COMMENT
3.56 ± 0.28 OUR FIT			Error includes scale factor of 1.2.
$3.55 \pm 0.44 \pm 0.50$	¹ AAIJ	14Q	LHCB pp at 7 TeV

¹ Obtained using the branching fraction of $\Lambda_c^+ \rightarrow pK^- \pi^+$ decay.

$\Gamma(\Lambda_c^+ K^-) / \Gamma(\Lambda_c^+ \pi^-)$ $\Gamma_{31} / \Gamma_{30}$

VALUE (units 10^{-2})	DOCUMENT ID	TECN	COMMENT
7.31 ± 0.22 OUR FIT			
$7.31 \pm 0.16 \pm 0.16$	AAIJ	14H	LHCB pp at 7 TeV

$\Gamma(\Lambda_c^+ a_1(1260)^-) / \Gamma_{\text{total}}$ Γ_{32} / Γ

VALUE	EVTS	DOCUMENT ID	TECN	COMMENT
seen	1	ABREU	96N	DLPH $\Lambda_c^+ \rightarrow pK^- \pi^+$, $a_1^- \rightarrow \rho^0 \pi^- \rightarrow \pi^+ \pi^- \pi^-$

$\Gamma(\Lambda_c^+ D_s^-) / \Gamma_{\text{total}}$ Γ_{34} / Γ

VALUE (units 10^{-2})	DOCUMENT ID	TECN	COMMENT
1.1 ± 0.1	¹ AAIJ	14AA	LHCB pp at 7 TeV

¹ Uses $B(\bar{B}^0 \rightarrow D^+ D_s^-) = (7.2 \pm 0.8) \times 10^{-3}$ and their measured $B(\Lambda_b^0 \rightarrow \Lambda_c^+ \pi^-) / B(\bar{B}^0 \rightarrow D^+ \pi^-)$ values.

$\Gamma(\Lambda_c^+ D^-) / \Gamma(\Lambda_c^+ D_s^-)$ $\Gamma_{33} / \Gamma_{34}$

VALUE	DOCUMENT ID	TECN	COMMENT
$0.042 \pm 0.003 \pm 0.003$	AAIJ	14AA	LHCB pp at 7 TeV

$\Gamma(\Lambda_c^+ \pi^+ \pi^- \pi^-) / \Gamma_{\text{total}}$ Γ_{35} / Γ

VALUE (units 10^{-3})	EVTS	DOCUMENT ID	TECN	COMMENT
7.6 ± 1.1 OUR FIT				Error includes scale factor of 1.1.
$14.8 \pm_{-3.1}^{+3.8} \pm 1.1$	¹ AALTONEN	12A	CDF	$p\bar{p}$ at 1.96 TeV

• • • We do not use the following data for averages, fits, limits, etc. • • •

seen	90	BARI	91	SFM	$\Lambda_c^+ \rightarrow pK^- \pi^+$
------	----	------	----	-----	--------------------------------------

¹ AALTONEN 12A reports $[\Gamma(\Lambda_b^0 \rightarrow \Lambda_c^+ \pi^+ \pi^- \pi^-) / \Gamma_{\text{total}}] / [B(\Lambda_b^0 \rightarrow \Lambda_c^+ \pi^-)] = 3.04 \pm 0.33 \pm_{-0.55}^{+0.70}$ which we multiply by our best value $B(\Lambda_b^0 \rightarrow \Lambda_c^+ \pi^-) = (4.9 \pm 0.4) \times 10^{-3}$. Our first error is their experiment's error and our second error is the systematic error from using our best value.

$\Gamma(\Lambda_c^+ \pi^+ \pi^- \pi^-) / \Gamma(\Lambda_c^+ \pi^-)$ $\Gamma_{35} / \Gamma_{30}$

VALUE	DOCUMENT ID	TECN	COMMENT
1.57 ± 0.21 OUR FIT			
$1.43 \pm 0.16 \pm 0.13$	AAIJ	11E	LHCB pp at 7 TeV

$\Gamma(\Lambda_c(2595)^+ \pi^-, \Lambda_c(2595)^+ \rightarrow \Lambda_c^+ \pi^+ \pi^-) / \Gamma(\Lambda_c^+ \pi^+ \pi^- \pi^-)$ $\Gamma_{36} / \Gamma_{35}$

VALUE (units 10^{-2})	DOCUMENT ID	TECN	COMMENT
$4.4 \pm 1.7 \pm_{-0.4}^{+0.6}$	AAIJ	11E	LHCB pp at 7 TeV

$\Gamma(\Lambda_c(2625)^+ \pi^-, \Lambda_c(2625)^+ \rightarrow \Lambda_c^+ \pi^+ \pi^-) / \Gamma(\Lambda_c^+ \pi^+ \pi^- \pi^-)$ $\Gamma_{37} / \Gamma_{35}$

VALUE (units 10^{-2})	DOCUMENT ID	TECN	COMMENT
$4.3 \pm 1.5 \pm 0.4$	AAIJ	11E	LHCB pp at 7 TeV

$\Gamma(\Sigma_c(2455)^0 \pi^+ \pi^-, \Sigma_c^0 \rightarrow \Lambda_c^+ \pi^-) / \Gamma(\Lambda_c^+ \pi^+ \pi^- \pi^-)$ $\Gamma_{38} / \Gamma_{35}$

VALUE (units 10^{-2})	DOCUMENT ID	TECN	COMMENT
$7.4 \pm 2.4 \pm 1.2$	AAIJ	11E	LHCB pp at 7 TeV

$\Gamma(\Sigma_c(2455)^{++} \pi^- \pi^-, \Sigma_c^{++} \rightarrow \Lambda_c^+ \pi^+) / \Gamma(\Lambda_c^+ \pi^+ \pi^- \pi^-)$ $\Gamma_{39} / \Gamma_{35}$

VALUE (units 10^{-2})	DOCUMENT ID	TECN	COMMENT
$4.2 \pm 1.8 \pm 0.7$	AAIJ	11E	LHCB pp at 7 TeV

$\Gamma(\Lambda_c^+ K^+ K^- \pi^-) / \Gamma(\Lambda_c^+ D_s^-)$ $\Gamma_{40} / \Gamma_{34}$

VALUE (units 10^{-2})	DOCUMENT ID	TECN	COMMENT
$9.26 \pm 0.29 \pm 0.53$	¹ AAIJ	21B	LHCB pp at 7 and 8 TeV

¹ AAIJ 21B systematic uncertainty includes the contribution from the $D_s^- \rightarrow K^+ K^- \pi^-$ branching fraction.

$\Gamma(\Lambda_c^+ \rho \bar{p} \pi^-) / \Gamma(\Lambda_c^+ \pi^-)$ $\Gamma_{41} / \Gamma_{30}$

VALUE (units 10^{-2})	DOCUMENT ID	TECN	COMMENT
$5.40 \pm 0.23 \pm 0.32$	AAIJ	18AW	LHCB pp at 7 and 8 TeV

$\Gamma(\Sigma_c(2455)^0 \rho \bar{p}, \Sigma_c^0 \rightarrow \Lambda_c^+ \pi^-) / \Gamma(\Lambda_c^+ \rho \bar{p} \pi^-)$ $\Gamma_{42} / \Gamma_{41}$

VALUE (units 10^{-2})	DOCUMENT ID	TECN	COMMENT
$8.9 \pm 1.5 \pm 0.6$	AAIJ	18AW	LHCB pp at 7 and 8 TeV

$\Gamma(\Sigma_c(2520)^0 \rho \bar{p}, \Sigma_c(2520)^0 \rightarrow \Lambda_c^+ \pi^-) / \Gamma(\Lambda_c^+ \rho \bar{p} \pi^-)$ $\Gamma_{43} / \Gamma_{41}$

VALUE	DOCUMENT ID	TECN	COMMENT
$0.119 \pm 0.020 \pm 0.014$	AAIJ	18AW	LHCB pp at 7 and 8 TeV

$\Gamma(\Lambda K^0 2\pi^+ 2\pi^-) / \Gamma_{\text{total}}$ Γ_{44} / Γ

VALUE	EVTS	DOCUMENT ID	TECN	COMMENT
• • • We do not use the following data for averages, fits, limits, etc. • • •				
seen	4	¹ ARENTON	86	FMP5 $\Lambda K_S^0 2\pi^+ 2\pi^-$

¹ See the footnote to the ARENTON 86 mass value.

$\Gamma(\Lambda_c^+ \ell^- \bar{\nu}_\ell \text{ anything}) / \Gamma_{\text{total}}$ Γ_{45} / Γ

The values and averages in this section serve only to show what values result if one assumes our $B(b \rightarrow b\text{-baryon})$. They cannot be thought of as measurements since the underlying product branching fractions were also used to determine $B(b \rightarrow b\text{-baryon})$ as described in the note on "Production and Decay of B-Flavored Hadrons."

$\Gamma(\Lambda_c^+ \ell^- \bar{\nu}_\ell \text{ anything}) / \Gamma_{\text{total}}$ Γ_{45} / Γ

VALUE	EVTS	DOCUMENT ID	TECN	COMMENT
0.109 ± 0.022 OUR AVERAGE				
$0.102 \pm 0.019 \pm 0.013$		¹ BARATE	98D	ALEP $e^+ e^- \rightarrow Z$
$0.14 \pm_{-0.04}^{+0.05} \pm 0.02$	29	² ABREU	95S	DLPH $e^+ e^- \rightarrow Z$

• • • We do not use the following data for averages, fits, limits, etc. • • •

$0.090 \pm 0.022 \pm 0.012$	55	³ BUSKULIC	95L	ALEP Repl. by BARATE 98D
$0.18 \pm 0.07 \pm 0.02$	21	⁴ BUSKULIC	92E	ALEP $\Lambda_c^+ \rightarrow pK^- \pi^+$

¹ BARATE 98D reports $[\Gamma(\Lambda_b^0 \rightarrow \Lambda_c^+ \ell^- \bar{\nu}_\ell \text{ anything}) / \Gamma_{\text{total}}] \times [B(\bar{b} \rightarrow b\text{-baryon})] = 0.0086 \pm 0.0007 \pm 0.0014$ which we divide by our best value $B(\bar{b} \rightarrow b\text{-baryon}) = (8.4 \pm 1.1) \times 10^{-2}$. Our first error is their experiment's error and our second error is the systematic error from using our best value. Measured using $\Lambda_c \ell^-$ and $\Lambda \ell^+ \ell^-$.

² ABREU 95S reports $[\Gamma(\Lambda_b^0 \rightarrow \Lambda_c^+ \ell^- \bar{\nu}_\ell \text{ anything}) / \Gamma_{\text{total}}] \times [B(\bar{b} \rightarrow b\text{-baryon})] = 0.0118 \pm 0.0026 \pm_{-0.0021}^{+0.0031}$ which we divide by our best value $B(\bar{b} \rightarrow b\text{-baryon}) = (8.4 \pm 1.1) \times 10^{-2}$. Our first error is their experiment's error and our second error is the systematic error from using our best value.

³ BUSKULIC 95L reports $[\Gamma(\Lambda_b^0 \rightarrow \Lambda_c^+ \ell^- \bar{\nu}_\ell \text{ anything}) / \Gamma_{\text{total}}] \times [B(\bar{b} \rightarrow b\text{-baryon})] = 0.00755 \pm 0.0014 \pm 0.0012$ which we divide by our best value $B(\bar{b} \rightarrow b\text{-baryon}) = (8.4 \pm 1.1) \times 10^{-2}$. Our first error is their experiment's error and our second error is the systematic error from using our best value.

⁴ BUSKULIC 92E reports $[\Gamma(\Lambda_b^0 \rightarrow \Lambda_c^+ \ell^- \bar{\nu}_\ell \text{ anything}) / \Gamma_{\text{total}}] \times [B(\bar{b} \rightarrow b\text{-baryon})] = 0.015 \pm 0.0035 \pm 0.0045$ which we divide by our best value $B(\bar{b} \rightarrow b\text{-baryon}) = (8.4 \pm 1.1) \times 10^{-2}$. Our first error is their experiment's error and our second error is the systematic error from using our best value. Superseded by BUSKULIC 95L.

$\Gamma(\Lambda_c^+ \ell^- \bar{\nu}_\ell) / \Gamma_{\text{total}}$ Γ_{46} / Γ

VALUE	DOCUMENT ID	TECN	COMMENT
$0.062 \pm_{-0.013}^{+0.014}$ OUR FIT			

$0.050 \pm_{-0.008}^{+0.011} \pm_{-0.012}^{+0.016}$	¹ ABDALLAH	04A	DLPH $e^+ e^- \rightarrow Z^0$
---	-----------------------	-----	--------------------------------

¹ Derived from a combined likelihood and event rate fit to the distribution of the $l\text{sgur}$ -wise variable and using HQET. The slope of the form factor is measured to be $\rho^2 = 2.03 \pm 0.46 \pm_{-1.00}^{+0.72}$.

$\Gamma(\Lambda_c^+ \ell^- \bar{\nu}_\ell) / \Gamma(\Lambda_c^+ \pi^-)$ $\Gamma_{46} / \Gamma_{30}$

VALUE	DOCUMENT ID	TECN	COMMENT
$12.8 \pm_{-2.7}^{+3.0}$ OUR FIT			

$16.6 \pm 3.0 \pm_{-3.6}^{+2.8}$	AALTONEN	09E	CDF $p\bar{p}$ at 1.96 TeV
----------------------------------	----------	-----	----------------------------

$\Gamma(\Lambda_c^+ \pi^+ \pi^- \ell^- \bar{\nu}_\ell) / \Gamma_{\text{total}}$ Γ_{47} / Γ

VALUE	DOCUMENT ID	TECN	COMMENT
0.056 ± 0.031 -0.030	¹ ABDALLAH	04A	DLPH $e^+ e^- \rightarrow Z^0$

¹ Derived from the fraction of $\Gamma(\Lambda_b^0 \rightarrow \Lambda_c^+ \ell^- \bar{\nu}_\ell) / (\Gamma(\Lambda_b^0 \rightarrow \Lambda_c^+ \ell^- \bar{\nu}_\ell) + \Gamma(\Lambda_b^0 \rightarrow \Lambda_c^+ \pi^+ \pi^- \ell^- \bar{\nu}_\ell)) = 0.47 \pm 0.10 + 0.07$
 $-0.08 - 0.06$.

$\Gamma(\Lambda_c^+ \ell^- \bar{\nu}_\ell) / [\Gamma(\Lambda_c^+ \ell^- \bar{\nu}_\ell) + \Gamma(\Lambda_c^+ \pi^+ \pi^- \ell^- \bar{\nu}_\ell)]$ $\Gamma_{46} / (\Gamma_{46} + \Gamma_{47})$

VALUE	DOCUMENT ID	TECN	COMMENT
$0.47 \pm 0.10 + 0.07$ $-0.08 - 0.06$	ABDALLAH	04A	DLPH $e^+ e^- \rightarrow Z^0$

$\Gamma(\Lambda_c(2595)^+ \ell^- \bar{\nu}_\ell) / \Gamma(\Lambda_c^+ \ell^- \bar{\nu}_\ell)$ $\Gamma_{48} / \Gamma_{46}$

VALUE	DOCUMENT ID	TECN	COMMENT
$0.126 \pm 0.033 \pm 0.047$ -0.038	¹ AALTONEN	09E	CDF $p\bar{p}$ at 1.96 TeV

¹ AALTONEN 09E assumes isospin conservation for $\Lambda_c(2595) \rightarrow \Lambda_c \pi^+ \pi^+$ and $\Lambda_c(2595) \rightarrow \Lambda_c \pi^0 \pi^0$. Significant isospin violation from thresholds in $\Lambda_c(2595) \rightarrow \Sigma_c(2455) \pi \rightarrow \Lambda_c \pi \pi$ may alter the recovered ratio.

$\Gamma(\Lambda_c(2625)^+ \ell^- \bar{\nu}_\ell) / \Gamma(\Lambda_c^+ \ell^- \bar{\nu}_\ell)$ $\Gamma_{49} / \Gamma_{46}$

VALUE	DOCUMENT ID	TECN	COMMENT
$0.210 \pm 0.042 \pm 0.071$ -0.050	AALTONEN	09E	CDF $p\bar{p}$ at 1.96 TeV

$[\frac{1}{2} \Gamma(\Sigma_c(2455)^0 \pi^+ \ell^- \bar{\nu}_\ell) + \frac{1}{2} \Gamma(\Sigma_c(2455)^{++} \pi^- \ell^- \bar{\nu}_\ell)] / \Gamma(\Lambda_c^+ \ell^- \bar{\nu}_\ell)$
 $(\frac{1}{2} \Gamma_{50} + \frac{1}{2} \Gamma_{51}) / \Gamma_{46}$

VALUE	DOCUMENT ID	TECN	COMMENT
$0.054 \pm 0.022 \pm 0.021$ -0.018	AALTONEN	09E	CDF $p\bar{p}$ at 1.96 TeV

$\Gamma(p h^-) / \Gamma_{\text{total}}$ Γ_{52} / Γ

VALUE	CL%	DOCUMENT ID	TECN	COMMENT
$< 2.3 \times 10^{-5}$	90	¹ ACOSTA	05o	CDF $p\bar{p}$ at 1.96 TeV

¹ Assumes $f_A / f_d = 0.25$, and equal momentum distribution for Λ_b and B mesons.

$\Gamma(p \pi^-) / \Gamma_{\text{total}}$ Γ_{53} / Γ

VALUE (units 10^{-6})	CL%	DOCUMENT ID	TECN	COMMENT
4.5 ± 0.8 OUR FIT		¹ AALTONEN	09c	CDF $p\bar{p}$ at 1.96 TeV
$4.0 \pm 0.9 \pm 0.5$				

••• We do not use the following data for averages, fits, limits, etc. **••••**

VALUE	DOCUMENT ID	TECN	COMMENT
< 50	90	² BUSKULIC	96v ALEP $e^+ e^- \rightarrow Z$

¹ AALTONEN 09c reports $[\Gamma(\Lambda_b^0 \rightarrow p \pi^-) / \Gamma_{\text{total}}] / [B(B^0 \rightarrow K^+ \pi^-)] \times [B(\bar{B} \rightarrow b\text{-baryon})] / [B(\bar{B} \rightarrow B^0)] = 0.042 \pm 0.007 \pm 0.006$ which we multiply or divide by our best values $B(B^0 \rightarrow K^+ \pi^-) = (1.96 \pm 0.05) \times 10^{-5}$, $B(\bar{B} \rightarrow b\text{-baryon}) = (8.4 \pm 1.1) \times 10^{-2}$, $B(\bar{B} \rightarrow B^0) = (40.8 \pm 0.7) \times 10^{-2}$. Our first error is their experiment's error and our second error is the systematic error from using our best values.

² BUSKULIC 96v assumes PDG 96 production fractions for B^0, B^+, B_s, b baryons.

$\Gamma(p K^-) / \Gamma_{\text{total}}$ Γ_{54} / Γ

VALUE (units 10^{-6})	CL%	DOCUMENT ID	TECN	COMMENT
5.4 ± 1.0 OUR FIT		¹ AALTONEN	09c	CDF $p\bar{p}$ at 1.96 TeV
$6.3 \pm 1.1 \pm 0.8$				

••• We do not use the following data for averages, fits, limits, etc. **••••**

VALUE	DOCUMENT ID	TECN	COMMENT
< 360	90	² ADAM	96D DLPH $e^+ e^- \rightarrow Z$
< 50	90	³ BUSKULIC	96v ALEP $e^+ e^- \rightarrow Z$

¹ AALTONEN 09c reports $[\Gamma(\Lambda_b^0 \rightarrow p K^-) / \Gamma_{\text{total}}] / [B(B^0 \rightarrow K^+ \pi^-)] \times [B(\bar{B} \rightarrow b\text{-baryon})] / [B(\bar{B} \rightarrow B^0)] = 0.066 \pm 0.009 \pm 0.008$ which we multiply or divide by our best values $B(B^0 \rightarrow K^+ \pi^-) = (1.96 \pm 0.05) \times 10^{-5}$, $B(\bar{B} \rightarrow b\text{-baryon}) = (8.4 \pm 1.1) \times 10^{-2}$, $B(\bar{B} \rightarrow B^0) = (40.8 \pm 0.7) \times 10^{-2}$. Our first error is their experiment's error and our second error is the systematic error from using our best values.

² ADAM 96D assumes $f_{B^0} = f_{B^-} = 0.39$ and $f_{B_s} = 0.12$.

³ BUSKULIC 96v assumes PDG 96 production fractions for B^0, B^+, B_s, b baryons.

$\Gamma(p \pi^-) / \Gamma(p K^-)$ $\Gamma_{53} / \Gamma_{54}$

VALUE	DOCUMENT ID	TECN	COMMENT
0.84 ± 0.09 OUR FIT			
$0.86 \pm 0.08 \pm 0.05$	AAIJ	12AR	LHCB pp at 7 TeV

$\Gamma(p D_s^-) / \Gamma_{\text{total}}$ Γ_{55} / Γ

VALUE	CL%	DOCUMENT ID	TECN	COMMENT
$< 4.8 \times 10^{-4}$	90	AAIJ	14Q	LHCB pp at 7 TeV

$\Gamma(p \mu^- \bar{\nu}_\mu) / \Gamma_{\text{total}}$ Γ_{56} / Γ

VALUE (units 10^{-4})	DOCUMENT ID	TECN	COMMENT
4.1 ± 1.0	¹ AAIJ	15Bg	LHCB pp at 8 TeV

¹ The ratio of $B(\Lambda_b^0 \rightarrow p \mu^- \bar{\nu}_\mu)$ to $B(\Lambda_b^0 \rightarrow \Lambda_c^+ \mu^- \bar{\nu}_\mu)$ is measured within a restricted q^2 region. Combined with theoretical calculations of the form factors and the previously measured value of $|V_{cb}|$, the first $|V_{ub}| = (3.27 \pm 0.15 \pm 0.16 \pm 0.06) \times 10^{-3}$ measurement from the Λ_b decay is obtained, consistent with the exclusively measured world averages.

$\Gamma(p \mu^- \bar{\nu}_\mu) / \Gamma(\Lambda_c^+ \ell^- \bar{\nu}_\ell)$ $\Gamma_{56} / \Gamma_{46}$

VALUE (units 10^{-2})	DOCUMENT ID	TECN	COMMENT
$1.0 \pm 0.04 \pm 0.08$	¹ AAIJ	15Bg	LHCB pp at 8 TeV

••• We do not use the following data for averages, fits, limits, etc. **••••**

¹ This measurement is a ratio of $\Gamma(\Lambda_b^0 \rightarrow p \mu^- \bar{\nu}_\mu)[q^2 > 15 \text{ GeV}/c^2]$ to $\Gamma(\Lambda_b^0 \rightarrow \Lambda_c^+ \mu^- \bar{\nu}_\mu)[q^2 > 7 \text{ GeV}/c^2]$ within a restricted q^2 region. Combined with theoretical calculations of the form factors and the previously measured value of $|V_{cb}|$, the first $|V_{ub}| = (3.27 \pm 0.15 \pm 0.16 \pm 0.06) \times 10^{-3}$ measurement from the Λ_b decay is obtained, consistent with the exclusively measured world averages.

$\Gamma(\Lambda \mu^+ \mu^-) / \Gamma_{\text{total}}$ Γ_{57} / Γ

VALUE (units 10^{-7})	DOCUMENT ID	TECN	COMMENT
10.8 ± 2.8 OUR AVERAGE			
$9.6 \pm 1.6 \pm 2.5$	¹ AAIJ	13AJ	LHCB pp at 7 TeV
$17.3 \pm 4.2 \pm 5.5$	AALTONEN	11AI	CDF $p\bar{p}$ at 1.96 TeV

¹ Uses $B(\Lambda_b^0 \rightarrow J/\psi \Lambda) = (6.2 \pm 1.4) \times 10^{-4}$. This measurement comes from the sum of the differential rates in q^2 regions excluding those corresponding to J/ψ and $\psi(2S)$ $[[8.68, 10.09] \text{ and } [12.86, 14.18] \text{ GeV}^2/c^4]$.

$\Gamma(p \pi^- \mu^+ \mu^-) / \Gamma_{\text{total}}$ Γ_{58} / Γ

VALUE (units 10^{-8})	DOCUMENT ID	TECN	COMMENT
$6.9 \pm 1.9 \pm 1.7$ -1.5	¹ AAIJ	17P	LHCB pp at 7, 8 TeV

¹ Excludes J/ψ and $\psi(2S)$ decays to $\mu^+ \mu^-$.

$\Gamma(p \pi^- \mu^+ \mu^-) / \Gamma(p \pi^- J/\psi, J/\psi \rightarrow \mu^+ \mu^-)$ $\Gamma_{58} / \Gamma_{13}$

VALUE (units 10^{-7})	DOCUMENT ID	TECN	COMMENT
$4.4 \pm 1.2 \pm 0.7$	¹ AAIJ	17P	LHCB pp at 7, 8 TeV

¹ The $p \pi^- \mu^+ \mu^-$ mode excludes J/ψ and $\psi(2S)$ decays to $\mu^+ \mu^-$.

$\Gamma(p K^- e^+ e^-) / \Gamma_{\text{total}}$ Γ_{59} / Γ

VALUE (units 10^{-6})	DOCUMENT ID	TECN	COMMENT
$0.310 \pm 0.040 \pm 0.054$ -0.047	^{1,2} AAIJ	20M	LHCB pp at 7, 8, 13 TeV

¹ Measured over $0.1 < q^2 < 6.0 \text{ GeV}/c^2$, and $m_{pK} < 2.6 \text{ GeV}/c^2$.

² The first uncertainty is the statistical uncertainty and the second is the combination of all systematic uncertainties including those related to the normalization of $\Lambda_b^0 \rightarrow J/\psi p K^-$.

$\Gamma(p K^- \mu^+ \mu^-) / \Gamma_{\text{total}}$ Γ_{60} / Γ

VALUE (units 10^{-6})	DOCUMENT ID	TECN	COMMENT
$0.265 \pm 0.014 \pm 0.049$ -0.039	^{1,2} AAIJ	20M	LHCB pp at 7, 8, 13 TeV

¹ Measured over $0.1 < q^2 < 6.0 \text{ GeV}/c^2$, and $m_{pK} < 2.6 \text{ GeV}/c^2$.

² The first uncertainty is the statistical uncertainty and the second is the combination of all systematic uncertainties including those related to the normalization of $\Lambda_b^0 \rightarrow J/\psi p K^-$.

$\Gamma(p K^- \mu^+ \mu^-) / \Gamma(p K^- e^+ e^-)$ $\Gamma_{60} / \Gamma_{59}$

VALUE	DOCUMENT ID	TECN	COMMENT
$0.86 \pm 0.14 \pm 0.05$ -0.11	¹ AAIJ	20M	LHCB pp at 7, 8, 13 TeV

¹ Measured over $0.1 < q^2 < 6.0 \text{ GeV}/c^2$, and $m_{pK} < 2.6 \text{ GeV}/c^2$.

$\Gamma(p K^- e^+ e^-) / \Gamma(p J/\psi K^-)$ $\Gamma_{59} / \Gamma_{14}$

VALUE (units 10^{-4})	DOCUMENT ID	TECN	COMMENT
$9.8 \pm 1.4 \pm 0.8$ -1.3	¹ AAIJ	20M	LHCB pp at 7, 8, 13 TeV

¹ Measured over $0.1 < q^2 < 6.0 \text{ GeV}/c^2$, and $m_{pK} < 2.6 \text{ GeV}/c^2$.

$\Gamma(p K^- \mu^+ \mu^-) / \Gamma(p J/\psi K^-)$ $\Gamma_{60} / \Gamma_{14}$

VALUE (units 10^{-4})	DOCUMENT ID	TECN	COMMENT
$8.4 \pm 0.4 \pm 0.4$	¹ AAIJ	20M	LHCB pp at 7, 8, 13 TeV

¹ Measured over $0.1 < q^2 < 6.0 \text{ GeV}/c^2$, and $m_{pK} < 2.6 \text{ GeV}/c^2$.

$\Gamma(\Lambda \gamma) / \Gamma_{\text{total}}$ Γ_{61} / Γ

VALUE (units 10^{-6})	CL%	DOCUMENT ID	TECN	COMMENT
$7.1 \pm 1.5 \pm 0.9$		¹ AAIJ	19z	LHCB pp at 13 TeV

••• We do not use the following data for averages, fits, limits, etc. **••••**

VALUE	CL%	DOCUMENT ID	TECN	COMMENT
< 1300	90	ACOSTA	02G	CDF $p\bar{p}$ at 1.8 TeV

¹ AAIJ 19z normalized to $B^0 \rightarrow K^{*0} \gamma$ and used an integrated luminosity of 1.7 fb^{-1} .

$\Gamma(\Lambda \eta) / \Gamma_{\text{total}}$ Γ_{62} / Γ

VALUE (units 10^{-6})	DOCUMENT ID	TECN	COMMENT
$9 \pm 7 \pm 1$	¹ AAIJ	15AH	LHCB pp at 7, 8 TeV

¹ AAIJ 15AH reports $[\Gamma(\Lambda_b^0 \rightarrow \Lambda \eta) / \Gamma_{\text{total}}] / [B(B^0 \rightarrow \eta' K^0)] = 0.142 \pm 0.11$ which we multiply by our best value $B(B^0 \rightarrow \eta' K^0) = (6.6 \pm 0.4) \times 10^{-5}$. Our first error is their experiment's error and our second error is the systematic error from using our best value. The single uncertainty quoted with the original measurement combines in quadrature statistical and systematic uncertainties.

Baryon Particle Listings

 Λ_b^0 $\Gamma(\Lambda\eta'(958))/\Gamma_{\text{total}}$ Γ_{63}/Γ

VALUE	CL%	DOCUMENT ID	TECN	COMMENT
$<3.1 \times 10^{-6}$	90	¹ AAIJ	15AH LHCb	pp at 7, 8 TeV
¹ AAIJ 15AH reports $[\Gamma(\Lambda_b^0 \rightarrow \Lambda\eta'(958))/\Gamma_{\text{total}}] / [B(B^0 \rightarrow \eta' K^0)] < 0.047$ which we multiply by our best value $B(B^0 \rightarrow \eta' K^0) = 6.6 \times 10^{-5}$.				

 $\Gamma(\Lambda\pi^+\pi^-)/\Gamma(\Lambda_c^+\pi^-)$ Γ_{64}/Γ_{30}

VALUE (units 10^{-4})	DOCUMENT ID	TECN	COMMENT
$9.5 \pm 3.8 \pm 0.5$	¹ AAIJ	16W LHCb	pp at 7, 8 TeV
¹ AAIJ 16W reports $[\Gamma(\Lambda_b^0 \rightarrow \Lambda\pi^+\pi^-)/\Gamma(\Lambda_b^0 \rightarrow \Lambda_c^+\pi^-)] / [B(\Lambda_c^+ \rightarrow \Lambda\pi^+)] = (7.3 \pm 1.9 \pm 2.2) \times 10^{-2}$ which we multiply by our best value $B(\Lambda_c^+ \rightarrow \Lambda\pi^+) = (1.30 \pm 0.07) \times 10^{-2}$. Our first error is their experiment's error and our second error is the systematic error from using our best value.			

 $\Gamma(\Lambda K^+\pi^-)/\Gamma(\Lambda_c^+\pi^-)$ Γ_{65}/Γ_{30}

VALUE (units 10^{-4})	DOCUMENT ID	TECN	COMMENT
$11.6 \pm 2.3 \pm 0.6$	¹ AAIJ	16W LHCb	pp at 7, 8 TeV
¹ AAIJ 16W reports $[\Gamma(\Lambda_b^0 \rightarrow \Lambda K^+\pi^-)/\Gamma(\Lambda_b^0 \rightarrow \Lambda_c^+\pi^-)] / [B(\Lambda_c^+ \rightarrow \Lambda\pi^+)] = (8.9 \pm 1.2 \pm 1.3) \times 10^{-2}$ which we multiply by our best value $B(\Lambda_c^+ \rightarrow \Lambda\pi^+) = (1.30 \pm 0.07) \times 10^{-2}$. Our first error is their experiment's error and our second error is the systematic error from using our best value.			

 $\Gamma(\Lambda K^+K^-)/\Gamma(\Lambda_c^+\pi^-)$ Γ_{66}/Γ_{30}

VALUE (units 10^{-3})	DOCUMENT ID	TECN	COMMENT
$3.29 \pm 0.35 \pm 0.17$	¹ AAIJ	16W LHCb	pp at 7, 8 TeV
¹ AAIJ 16W reports $[\Gamma(\Lambda_b^0 \rightarrow \Lambda K^+K^-)/\Gamma(\Lambda_b^0 \rightarrow \Lambda_c^+\pi^-)] / [B(\Lambda_c^+ \rightarrow \Lambda\pi^+)] = (25.3 \pm 1.9 \pm 1.9) \times 10^{-2}$ which we multiply by our best value $B(\Lambda_c^+ \rightarrow \Lambda\pi^+) = (1.30 \pm 0.07) \times 10^{-2}$. Our first error is their experiment's error and our second error is the systematic error from using our best value.			

 $\Gamma(\Lambda\phi)/\Gamma_{\text{total}}$ Γ_{67}/Γ

VALUE (units 10^{-6})	DOCUMENT ID	TECN	COMMENT
$9.8 \pm 2.1 \pm 1.6$ -1.5	¹ AAIJ	16J LHCb	pp at 7, 8 TeV
¹ AAIJ 16J reports $[\Gamma(\Lambda_b^0 \rightarrow \Lambda\phi)/\Gamma_{\text{total}}] / [B(B^0 \rightarrow K^0\phi)] \times [B(\bar{B} \rightarrow b\text{-baryon})] / [B(\bar{B} \rightarrow B^0)] = 0.275 \pm 0.055 \pm 0.020$ which we multiply or divide by our best values $B(B^0 \rightarrow K^0\phi) = (7.3 \pm 0.7) \times 10^{-6}$, $B(\bar{B} \rightarrow b\text{-baryon}) = (8.4 \pm 1.1) \times 10^{-2}$, $B(\bar{B} \rightarrow B^0) = (40.8 \pm 0.7) \times 10^{-2}$. Our first error is their experiment's error and our second error is the systematic error from using our best values.			

 $\Gamma(p\pi^-\pi^+\pi^-)/\Gamma(\Lambda_c^+\pi^-)$ Γ_{68}/Γ_{30}

VALUE (units 10^{-3})	DOCUMENT ID	TECN	COMMENT
$4.30 \pm 0.24 \pm 0.22$ -0.23	¹ AAIJ	18Q LHCb	pp at 7, 8 TeV
¹ AAIJ 18Q reports $[\Gamma(\Lambda_b^0 \rightarrow p\pi^-\pi^+\pi^-)/\Gamma(\Lambda_b^0 \rightarrow \Lambda_c^+\pi^-)] / [B(\Lambda_c^+ \rightarrow pK^-\pi^+)] = (6.85 \pm 0.19 \pm 0.08 \pm 0.32) \times 10^{-2}$ which we multiply by our best value $B(\Lambda_c^+ \rightarrow pK^-\pi^+) = (6.28 \pm 0.32) \times 10^{-2}$. Our first error is their experiment's error and our second error is the systematic error from using our best value.			

 $\Gamma(pK^-K^+\pi^-)/\Gamma(\Lambda_c^+\pi^-)$ Γ_{69}/Γ_{30}

VALUE (units 10^{-3})	DOCUMENT ID	TECN	COMMENT
$0.83 \pm 0.10 \pm 0.04$	¹ AAIJ	18Q LHCb	pp at 7, 8 TeV
¹ AAIJ 18Q reports $[\Gamma(\Lambda_b^0 \rightarrow pK^-K^+\pi^-)/\Gamma(\Lambda_b^0 \rightarrow \Lambda_c^+\pi^-)] / [B(\Lambda_c^+ \rightarrow pK^-\pi^+)] = (1.32 \pm 0.09 \pm 0.09 \pm 0.10) \times 10^{-2}$ which we multiply by our best value $B(\Lambda_c^+ \rightarrow pK^-\pi^+) = (6.28 \pm 0.32) \times 10^{-2}$. Our first error is their experiment's error and our second error is the systematic error from using our best value.			

 $\Gamma(pK^-\pi^+\pi^-)/\Gamma(\Lambda_c^+\pi^-)$ Γ_{70}/Γ_{30}

VALUE (units 10^{-3})	DOCUMENT ID	TECN	COMMENT
$10.3 \pm 0.5 \pm 0.5$	¹ AAIJ	18Q LHCb	pp at 7, 8 TeV
¹ AAIJ 18Q reports $[\Gamma(\Lambda_b^0 \rightarrow pK^-\pi^+\pi^-)/\Gamma(\Lambda_b^0 \rightarrow \Lambda_c^+\pi^-)] / [B(\Lambda_c^+ \rightarrow pK^-\pi^+)] = (16.4 \pm 0.3 \pm 0.2 \pm 0.7) \times 10^{-2}$ which we multiply by our best value $B(\Lambda_c^+ \rightarrow pK^-\pi^+) = (6.28 \pm 0.32) \times 10^{-2}$. Our first error is their experiment's error and our second error is the systematic error from using our best value.			

 $\Gamma(pK^-K^+K^-)/\Gamma(\Lambda_c^+\pi^-)$ Γ_{71}/Γ_{30}

VALUE (units 10^{-3})	DOCUMENT ID	TECN	COMMENT
$2.58 \pm 0.15 \pm 0.13$ -0.14	¹ AAIJ	18Q LHCb	pp at 7, 8 TeV
¹ AAIJ 18Q reports $[\Gamma(\Lambda_b^0 \rightarrow pK^-K^+K^-)/\Gamma(\Lambda_b^0 \rightarrow \Lambda_c^+\pi^-)] / [B(\Lambda_c^+ \rightarrow pK^-\pi^+)] = (4.11 \pm 0.12 \pm 0.06 \pm 0.19) \times 10^{-2}$ which we multiply by our best value $B(\Lambda_c^+ \rightarrow pK^-\pi^+) = (6.28 \pm 0.32) \times 10^{-2}$. Our first error is their experiment's error and our second error is the systematic error from using our best value.			

PARTIAL BRANCHING FRACTIONS IN $\Lambda_b \rightarrow \Lambda\mu^+\mu^-$ $B(\Lambda_b \rightarrow \Lambda\mu^+\mu^-) (q^2 < 2.0 \text{ GeV}^2/c^4)$

VALUE (units 10^{-7})	DOCUMENT ID	TECN	COMMENT
0.71 ± 0.27 OUR AVERAGE			
0.72 ± 0.24 -0.22 ± 0.14	¹ AAIJ	15AE LHCb	pp at 7, 8 TeV
$0.15 \pm 2.01 \pm 0.05$	AALTONEN	11AI CDF	$p\bar{p}$ at 1.96 TeV
• • • We do not use the following data for averages, fits, limits, etc. • • •			
$0.56 \pm 0.76 \pm 0.80$	² AAIJ	13AJ LHCb	Repl. by AAIJ 15AE
¹ AAIJ 15AE measurement covers $0.1 < q^2 < 2.0 \text{ GeV}^2/c^4$.			
² Uses $B(\Lambda_b^0 \rightarrow J/\psi\Lambda) = (6.2 \pm 1.4) \times 10^{-4}$.			

 $B(\Lambda_b \rightarrow \Lambda\mu^+\mu^-) (2.0 < q^2 < 4.3 \text{ GeV}^2/c^4)$

VALUE (units 10^{-7})	DOCUMENT ID	TECN	COMMENT
0.28 ± 0.28 -0.21 OUR AVERAGE			
0.253 ± 0.276 -0.207 ± 0.046	¹ AAIJ	15AE LHCb	pp at 7, 8 TeV
$1.8 \pm 1.7 \pm 0.6$	AALTONEN	11AI CDF	$p\bar{p}$ at 1.96 TeV
• • • We do not use the following data for averages, fits, limits, etc. • • •			
$0.71 \pm 0.60 \pm 0.23$	² AAIJ	13AJ LHCb	Repl. by AAIJ 15AE
¹ AAIJ 15AE measurement covers $2.0 < q^2 < 4.0 \text{ GeV}^2/c^4$.			
² Uses $B(\Lambda_b^0 \rightarrow J/\psi\Lambda) = (6.2 \pm 1.4) \times 10^{-4}$.			

 $B(\Lambda_b \rightarrow \Lambda\mu^+\mu^-) (q^2 < 4.3 \text{ GeV}^2/c^4)$

VALUE (units 10^{-7})	DOCUMENT ID	TECN	COMMENT
$2.7 \pm 2.5 \pm 0.9$	AALTONEN	11AI CDF	$p\bar{p}$ at 1.96 TeV

 $B(\Lambda_b \rightarrow \Lambda\mu^+\mu^-) (4.0 < q^2 < 6.0 \text{ GeV}^2/c^4)$

VALUE (units 10^{-7})	DOCUMENT ID	TECN	COMMENT
0.04 ± 0.18 -0.00 ± 0.02	AAIJ	15AE LHCb	pp at 7, 8 TeV

 $B(\Lambda_b \rightarrow \Lambda\mu^+\mu^-) (1.0 < q^2 < 6.0 \text{ GeV}^2/c^4)$

VALUE (units 10^{-7})	DOCUMENT ID	TECN	COMMENT
0.47 ± 0.31 -0.27 OUR AVERAGE			
0.45 ± 0.30 -0.25 ± 0.10	¹ AAIJ	15AE LHCb	pp at 7 and 8 TeV
$1.3 \pm 2.1 \pm 0.4$	AALTONEN	11AI CDF	$p\bar{p}$ at 1.96 TeV
¹ AAIJ 15AE measurement covers $1.1 < q^2 < 6.0 \text{ GeV}^2/c^4$.			

 $B(\Lambda_b \rightarrow \Lambda\mu^+\mu^-) (6.0 < q^2 < 8.0 \text{ GeV}^2/c^4)$

VALUE (units 10^{-7})	DOCUMENT ID	TECN	COMMENT
0.50 ± 0.24 -0.22 ± 0.10	AAIJ	15AE LHCb	pp at 7, 8 TeV

 $B(\Lambda_b \rightarrow \Lambda\mu^+\mu^-) (4.3 < q^2 < 8.68 \text{ GeV}^2/c^4)$

VALUE (units 10^{-7})	DOCUMENT ID	TECN	COMMENT
0.5 ± 0.7 OUR AVERAGE			
$0.66 \pm 0.74 \pm 0.18$	¹ AAIJ	13AJ LHCb	pp at 7 TeV
$-0.2 \pm 1.6 \pm 0.1$	AALTONEN	11AI CDF	$p\bar{p}$ at 1.96 TeV
¹ Uses $B(\Lambda_b^0 \rightarrow J/\psi\Lambda) = (6.2 \pm 1.4) \times 10^{-4}$.			

 $B(\Lambda_b \rightarrow \Lambda\mu^+\mu^-) (10.09 < q^2 < 12.86 \text{ GeV}^2/c^4)$

VALUE (units 10^{-7})	DOCUMENT ID	TECN	COMMENT
2.2 ± 0.6 OUR AVERAGE			
2.08 ± 0.42 -0.39 ± 0.42	¹ AAIJ	15AE LHCb	pp at 7, 8 TeV
$3.0 \pm 1.5 \pm 1.0$	AALTONEN	11AI CDF	$p\bar{p}$ at 1.96 TeV
• • • We do not use the following data for averages, fits, limits, etc. • • •			
$1.55 \pm 0.58 \pm 0.55$	² AAIJ	13AJ LHCb	Repl. by AAIJ 15AE
¹ AAIJ 15AE measurement covers $11.0 < q^2 < 12.5 \text{ GeV}^2/c^4$.			
² Uses $B(\Lambda_b^0 \rightarrow J/\psi\Lambda) = (6.2 \pm 1.4) \times 10^{-4}$.			

 $B(\Lambda_b \rightarrow \Lambda\mu^+\mu^-) (14.18 < q^2 < 16.0 \text{ GeV}^2/c^4)$

VALUE (units 10^{-7})	DOCUMENT ID	TECN	COMMENT
1.7 ± 0.5 OUR AVERAGE			Error includes scale factor of 1.1.
2.04 ± 0.35 -0.33 ± 0.42	¹ AAIJ	15AE LHCb	pp at 7, 8 TeV
$1.0 \pm 0.7 \pm 0.3$	AALTONEN	11AI CDF	$p\bar{p}$ at 1.96 TeV
• • • We do not use the following data for averages, fits, limits, etc. • • •			
$1.44 \pm 0.44 \pm 0.42$	² AAIJ	13AJ LHCb	Repl. by AAIJ 15AE
¹ AAIJ 15AE measurement covers $15.0 < q^2 < 16.0 \text{ GeV}^2/c^4$.			
² Uses $B(\Lambda_b^0 \rightarrow J/\psi\Lambda) = (6.2 \pm 1.4) \times 10^{-4}$.			

 $B(\Lambda_b \rightarrow \Lambda\mu^+\mu^-) (16.0 < q^2 \text{ GeV}^2/c^4)$

VALUE (units 10^{-7})	DOCUMENT ID	TECN	COMMENT
$7.0 \pm 1.9 \pm 2.2$	AALTONEN	11AI CDF	$p\bar{p}$ at 1.96 TeV
• • • We do not use the following data for averages, fits, limits, etc. • • •			
$4.73 \pm 0.77 \pm 1.25$	^{1,2} AAIJ	13AJ LHCb	Repl. by AAIJ 15AE
¹ Uses $B(\Lambda_b^0 \rightarrow J/\psi\Lambda) = (6.2 \pm 1.4) \times 10^{-4}$.			
² Requires $16.00 < q^2 < 20.30 \text{ GeV}^2/c^4$.			

See key on page 1127

Baryon Particle Listings

 Λ_b^0 $B(\Lambda_b \rightarrow \Lambda \mu^+ \mu^-)$ ($18.0 < q^2 < 20.0 \text{ GeV}^2/c^4$)

VALUE (units 10^{-7})	DOCUMENT ID	TECN	COMMENT
$2.44 \pm 0.28 \pm 0.50$	AAIJ	15AE LHCb	pp at 7, 8 TeV

 $B(\Lambda_b \rightarrow \Lambda \mu^+ \mu^-)$ ($15.0 < q^2 < 20.0 \text{ GeV}^2/c^4$)

VALUE (units 10^{-7})	DOCUMENT ID	TECN	COMMENT
$6.00 \pm 0.45 \pm 1.25$	AAIJ	15AE LHCb	pp at 7, 8 TeV

CP VIOLATION

 A_{CP} is defined as

$$A_{CP} = \frac{B(\Lambda_b^0 \rightarrow f) - B(\bar{\Lambda}_b^0 \rightarrow \bar{f})}{B(\Lambda_b^0 \rightarrow f) + B(\bar{\Lambda}_b^0 \rightarrow \bar{f})},$$

the CP-violation asymmetry of exclusive Λ_b^0 and $\bar{\Lambda}_b^0$ decay. $A_{CP}(\Lambda_b \rightarrow p \pi^-)$

VALUE	DOCUMENT ID	TECN	COMMENT
-0.025 ± 0.029 OUR AVERAGE	Error includes scale factor of 1.2.		
$-0.035 \pm 0.017 \pm 0.020$	AAIJ	18AX LHCb	pp at 7 and 8 TeV
$0.06 \pm 0.07 \pm 0.03$	AALTONEN	14P CDF	$p\bar{p}$ at 1.96 TeV
• • • We do not use the following data for averages, fits, limits, etc. • • •			
$0.03 \pm 0.17 \pm 0.05$	AALTONEN	11N CDF	Repl. by AALTONEN 14P

 $A_{CP}(\Lambda_b \rightarrow p K^-)$

VALUE	DOCUMENT ID	TECN	COMMENT
-0.025 ± 0.022 OUR AVERAGE			
$-0.020 \pm 0.013 \pm 0.019$	AAIJ	18AX LHCb	pp at 7 and 8 TeV
$-0.10 \pm 0.08 \pm 0.04$	AALTONEN	14P CDF	$p\bar{p}$ at 1.96 TeV
• • • We do not use the following data for averages, fits, limits, etc. • • •			
$0.37 \pm 0.17 \pm 0.03$	AALTONEN	11N CDF	Repl. by AALTONEN 14P

 $A_{CP}(\Lambda_b \rightarrow D p K^-)$

VALUE	DOCUMENT ID	TECN	COMMENT
$0.12 \pm 0.09 \pm 0.02$ 0.03	1 AAIJ	21AD LHCb	pp at 7, 8, 13 TeV

A_{CP} is measured from $(B(\Lambda_b^0 \rightarrow [K^+ \pi^-]_D p K^-) - B(\bar{\Lambda}_b^0 \rightarrow [K^- \pi^+]_D \bar{p} K^+)) / (B(\Lambda_b^0 \rightarrow [K^+ \pi^-]_D p K^-) + B(\bar{\Lambda}_b^0 \rightarrow [K^- \pi^+]_D \bar{p} K^+))$ in the full phase space.

 $\Delta A_{CP}(\rho K^- / \pi^-)$

VALUE	DOCUMENT ID	TECN	COMMENT
$\Delta A_{CP} \equiv A_{CP}(\rho K^-) - A_{CP}(\pi^-)$			
$0.014 \pm 0.022 \pm 0.010$	AAIJ	18AX LHCb	pp at 7 and 8 TeV

 $A_{CP}(\Lambda_b \rightarrow p \bar{K}^0 \pi^-)$

VALUE	DOCUMENT ID	TECN	COMMENT
$0.22 \pm 0.13 \pm 0.03$	AAIJ	14Q LHCb	pp at 7 TeV

 $\Delta A_{CP}(J/\psi p \pi^- / K^-)$

VALUE (units 10^{-2})	DOCUMENT ID	TECN	COMMENT
$\Delta A_{CP} \equiv A_{CP}(J/\psi p \pi^-) - A_{CP}(J/\psi p K^-)$			
$5.7 \pm 2.4 \pm 1.2$	AAIJ	14K LHCb	pp at 7, 8 TeV

 $A_{CP}(\Lambda_b \rightarrow \Lambda K^+ \pi^-)$

VALUE	DOCUMENT ID	TECN	COMMENT
$-0.53 \pm 0.23 \pm 0.11$	1 AAIJ	16W LHCb	pp at 7, 8 TeV
¹ Measured relative to $\Lambda_b^0 \rightarrow \Lambda_c^+ \pi^-$ decay.			

 $A_{CP}(\Lambda_b \rightarrow \Lambda K^+ K^-)$

VALUE	DOCUMENT ID	TECN	COMMENT
$-0.28 \pm 0.10 \pm 0.07$	1 AAIJ	16W LHCb	pp at 7, 8 TeV
¹ Measured relative to $\Lambda_b^0 \rightarrow \Lambda_c^+ \pi^-$ decay.			

 $\Delta A_{CP}(\Lambda_b^0 \rightarrow p K^- \mu^+ \mu^-)$

VALUE (units 10^{-2})	DOCUMENT ID	TECN	COMMENT
$\Delta A_{CP} \equiv A_{CP}(p K^- \mu^+ \mu^-) - A_{CP}(p K^- J/\psi)$			
$-3.5 \pm 5.0 \pm 0.2$	AAIJ	17T LHCb	pp at 7, 8 TeV

 $\Delta A_{CP}(\Lambda_b^0 \rightarrow p \pi^- \pi^+ \pi^-)$

VALUE (units 10^{-2})	DOCUMENT ID	TECN	COMMENT
$\Delta A_{CP} \equiv A_{CP}(\Lambda_b^0 \rightarrow p \pi^- \pi^+ \pi^-) - A_{CP}(\Lambda_b^0 \rightarrow (\Lambda_c^+ \rightarrow p \pi^- \pi^+) \pi^-)$			
$1.1 \pm 2.5 \pm 0.6$	1 AAIJ	19AH LHCb	pp at 7 and 8 TeV
¹ Full phase space.			

 $\Delta A_{CP}(\Lambda_b^0 \rightarrow (p \pi^- \pi^+ \pi^-)_{LBM})$

VALUE (units 10^{-2})	DOCUMENT ID	TECN	COMMENT
$\Delta A_{CP} \equiv A_{CP}(\Lambda_b^0 \rightarrow (p \pi^- \pi^+ \pi^-)_{LBM}) - A_{CP}(\Lambda_b^0 \rightarrow (\Lambda_c^+ \rightarrow p \pi^- \pi^+) \pi^-)$. Two-body low invariant-mass region (LBM): $m(p \pi^-) < 2000 \text{ MeV}$ and $m(\pi^+ \pi^-) < 1640 \text{ MeV}$.			
$3.7 \pm 4.1 \pm 0.5$	1 AAIJ	19AH LHCb	pp at 7 and 8 TeV
¹ Measurement done with $m(p \pi^-) < 2000 \text{ MeV}/c^2$ and $m(\pi^+ \pi^-) < 1640 \text{ MeV}/c^2$.			

 $\Delta A_{CP}(\Lambda_b^0 \rightarrow p a_1(1260)^-)$

$\Delta A_{CP} \equiv A_{CP}(\Lambda_b^0 \rightarrow p a_1(1260)^-) - A_{CP}(\Lambda_b^0 \rightarrow (\Lambda_c^+ \rightarrow p \pi^- \pi^+) \pi^-)$. $419 < m(\pi^+ \pi^- \pi^+) < 1500 \text{ MeV}$.

VALUE (units 10^{-2})	DOCUMENT ID	TECN	COMMENT
$-1.5 \pm 4.2 \pm 0.6$	AAIJ	19AH LHCb	pp at 7 and 8 TeV

 $\Delta A_{CP}(\Lambda_b^0 \rightarrow N(1520)^0 \rho(770)^0)$

$\Delta A_{CP} \equiv A_{CP}(\Lambda_b^0 \rightarrow N(1520)^0 \rho(770)^0) - A_{CP}(\Lambda_b^0 \rightarrow (\Lambda_c^+ \rightarrow p \pi^- \pi^+) \pi^-)$. $1078 < m(p \pi^-) < 1800 \text{ MeV}$ and $m(\pi^+ \pi^-) < 1100 \text{ MeV}$.

VALUE (units 10^{-2})	DOCUMENT ID	TECN	COMMENT
$2.0 \pm 4.9 \pm 0.4$	AAIJ	19AH LHCb	pp at 7 and 8 TeV

 $\Delta A_{CP}(\Lambda_b^0 \rightarrow \Delta(1232)^{++} \pi^- \pi^-)$

$\Delta A_{CP} \equiv A_{CP}(\Lambda_b^0 \rightarrow \Delta(1232)^{++} \pi^- \pi^-) - A_{CP}(\Lambda_b^0 \rightarrow (\Lambda_c^+ \rightarrow p \pi^- \pi^+) \pi^-)$. $1078 < m(p \pi^+) < 1432 \text{ MeV}$.

VALUE (units 10^{-2})	DOCUMENT ID	TECN	COMMENT
$0.1 \pm 3.2 \pm 0.6$	AAIJ	19AH LHCb	pp at 7 and 8 TeV

 $\Delta A_{CP}(\Lambda_b^0 \rightarrow p K^- \pi^+ \pi^-)$

$\Delta A_{CP} \equiv A_{CP}(\Lambda_b^0 \rightarrow p K^- \pi^+ \pi^-) - A_{CP}(\Lambda_b^0 \rightarrow (\Lambda_c^+ \rightarrow p K^- \pi^+) \pi^-)$

VALUE (units 10^{-2})	DOCUMENT ID	TECN	COMMENT
$3.2 \pm 1.1 \pm 0.6$	1 AAIJ	19AH LHCb	pp at 7 and 8 TeV
¹ Full phase space.			

 $\Delta A_{CP}(\Lambda_b^0 \rightarrow (p K^- \pi^+ \pi^-)_{LBM})$

$\Delta A_{CP} \equiv A_{CP}(\Lambda_b^0 \rightarrow (p K^- \pi^+ \pi^-)_{LBM}) - A_{CP}(\Lambda_b^0 \rightarrow (\Lambda_c^+ \rightarrow p K^- \pi^+) \pi^-)$. Two-body low invariant-mass region (LBM): $m(p K^-) < 2000 \text{ MeV}$ and $m(\pi^+ \pi^-) < 1640 \text{ MeV}$.

VALUE (units 10^{-2})	DOCUMENT ID	TECN	COMMENT
$3.5 \pm 1.5 \pm 0.5$	1 AAIJ	19AH LHCb	pp at 7 and 8 TeV
¹ Measurement done with $m(p K^-) < 2000 \text{ MeV}/c^2$ and $m(\pi^+ \pi^-) < 1640 \text{ MeV}/c^2$.			

 $\Delta A_{CP}(\Lambda_b^0 \rightarrow N(1520)^0 K^*(892)^0)$

$\Delta A_{CP} \equiv A_{CP}(\Lambda_b^0 \rightarrow N(1520)^0 K^*(892)^0) - A_{CP}(\Lambda_b^0 \rightarrow (\Lambda_c^+ \rightarrow p K^- \pi^+) \pi^-)$. $1078 < m(p \pi^-) < 1800 \text{ MeV}$ and $750 < m(\pi^+ K^-) < 1100 \text{ MeV}$.

VALUE (units 10^{-2})	DOCUMENT ID	TECN	COMMENT
$5.5 \pm 2.5 \pm 0.5$	AAIJ	19AH LHCb	pp at 7 and 8 TeV

 $\Delta A_{CP}(\Lambda_b^0 \rightarrow \Lambda(1520) \rho(770)^0)$

$\Delta A_{CP} \equiv A_{CP}(\Lambda_b^0 \rightarrow \Lambda(1520) \rho(770)^0) - A_{CP}(\Lambda_b^0 \rightarrow (\Lambda_c^+ \rightarrow p K^- \pi^+) \pi^-)$. $1460 < m(p K^-) < 1580 \text{ MeV}$ and $m(\pi^+ \pi^-) < 1100 \text{ MeV}$.

VALUE (units 10^{-2})	DOCUMENT ID	TECN	COMMENT
$0.6 \pm 6.0 \pm 0.5$	AAIJ	19AH LHCb	pp at 7 and 8 TeV

 $\Delta A_{CP}(\Lambda_b^0 \rightarrow \Delta(1232)^{++} K^- \pi^-)$

$\Delta A_{CP} \equiv A_{CP}(\Lambda_b^0 \rightarrow \Delta(1232)^{++} K^- \pi^-) - A_{CP}(\Lambda_b^0 \rightarrow (\Lambda_c^+ \rightarrow p K^- \pi^+) \pi^-)$. $1078 < m(p \pi^+) < 1432 \text{ MeV}$.

VALUE (units 10^{-2})	DOCUMENT ID	TECN	COMMENT
$4.4 \pm 2.6 \pm 0.6$	AAIJ	19AH LHCb	pp at 7 and 8 TeV

 $\Delta A_{CP}(\Lambda_b^0 \rightarrow p K_1(1410)^-)$

$\Delta A_{CP} \equiv A_{CP}(\Lambda_b^0 \rightarrow p K_1(1410)^-) - A_{CP}(\Lambda_b^0 \rightarrow (\Lambda_c^+ \rightarrow p K^- \pi^+) \pi^-)$. $1200 < m(K^- \pi^+) < 1600 \text{ MeV}$.

VALUE (units 10^{-2})	DOCUMENT ID	TECN	COMMENT
$4.7 \pm 3.5 \pm 0.8$	AAIJ	19AH LHCb	pp at 7 and 8 TeV

 $\Delta A_{CP}(\Lambda_b^0 \rightarrow p K^- K^+ \pi^-)$

$\Delta A_{CP} \equiv A_{CP}(\Lambda_b^0 \rightarrow p K^- K^+ \pi^-) - A_{CP}(\Lambda_b^0 \rightarrow (\Lambda_c^+ \rightarrow p \pi^- \pi^+) \pi^-)$

VALUE (units 10^{-2})	DOCUMENT ID	TECN	COMMENT
$-6.9 \pm 4.9 \pm 0.8$	1 AAIJ	19AH LHCb	pp at 7 and 8 TeV
¹ Full phase space.			

 $\Delta A_{CP}(\Lambda_b^0 \rightarrow p K^- K^+ K^-)$

$\Delta A_{CP} \equiv A_{CP}(\Lambda_b^0 \rightarrow p K^- K^+ K^-) - A_{CP}(\Lambda_b^0 \rightarrow (\Lambda_c^+ \rightarrow p K^- \pi^+) \pi^-)$

VALUE (units 10^{-2})	DOCUMENT ID	TECN	COMMENT
$0.2 \pm 1.8 \pm 0.6$	1 AAIJ	19AH LHCb	pp at 7 and 8 TeV
¹ Full phase space.			

 $\Delta A_{CP}(\Lambda_b^0 \rightarrow \Lambda(1520) \phi(1020))$

$\Delta A_{CP} \equiv A_{CP}(\Lambda_b^0 \rightarrow \Lambda(1520) \phi(1020)) - A_{CP}(\Lambda_b^0 \rightarrow (\Lambda_c^+ \rightarrow p K^- \pi^+) \pi^-)$. $1460 < m(p K^-) < 1600 \text{ MeV}$ and $1005 < m(K^+ K^-) < 1040 \text{ MeV}$.

VALUE (units 10^{-2})	DOCUMENT ID	TECN	COMMENT
$4.3 \pm 5.6 \pm 0.4$	AAIJ	19AH LHCb	pp at 7 and 8 TeV

 $\Delta A_{CP}(\Lambda_b^0 \rightarrow (p K^-)_{\text{highmass}} \phi(1020))$

$\Delta A_{CP} \equiv A_{CP}(\Lambda_b^0 \rightarrow (p K^-)_{\text{highmass}} \phi(1020)) - A_{CP}(\Lambda_b^0 \rightarrow (\Lambda_c^+ \rightarrow p K^- \pi^+) \pi^-)$. $m(p K^-) > 1600 \text{ MeV}$ and $1005 < m(K^+ K^-) < 1040 \text{ MeV}$.

VALUE (units 10^{-2})	DOCUMENT ID	TECN	COMMENT
$-0.7 \pm 3.3 \pm 0.7$	1 AAIJ	19AH LHCb	pp at 7 and 8 TeV
¹ Measurement done with $m(p K^-) > 1600 \text{ MeV}/c^2$.			

Baryon Particle Listings

 Λ_b^0 $\Delta A_{CP}(\Lambda_b^0 \rightarrow (\rho K^- K^+ K^-)_{LBM})$

$\Delta A_{CP} \equiv A_{CP}(\Lambda_b^0 \rightarrow (\rho K^- K^+ K^-)_{LBM}) - A_{CP}(\Lambda_b^0 \rightarrow (\Lambda_c^+ \rightarrow \rho K^- \pi^+) \pi^-)$. Two-body low invariant-mass region (LBM): $m(\rho K^-) < 2000$ MeV and $m(K^+ K^-) < 1675$ MeV.

VALUE (units 10^{-2})	DOCUMENT ID	TECN	COMMENT
$2.7 \pm 2.3 \pm 0.6$	1 AAIJ	19AH LHCb	pp at 7 and 8 TeV

¹ Measurement done with $m(\rho K^-) < 2000$ MeV/ c^2 and $m(K^+ K^-) < 1675$ MeV/ c^2 .

CP AND T VIOLATION PARAMETERS

Measured values of the triple-product asymmetry parameters, odd under time-reversal, are defined as $A_{c(s)}(\Lambda/\phi) = (N_{c(s)}^+ - N_{c(s)}^-) / (\text{sum})$ where $N_{c(s)}^+$, $N_{c(s)}^-$ are the number of Λ or ϕ candidates for which the $\cos(\Phi)$ and $\sin(\Phi)$ observables are positive and negative, respectively. Angles $\cos(\Phi)$ and $\sin(\Phi)$ are defined as in LEITNER 07.

 $A_c(\Lambda)$

VALUE	DOCUMENT ID	TECN	COMMENT
$-0.22 \pm 0.12 \pm 0.06$	AAIJ	16J LHCb	pp at 7, 8 TeV

 $A_s(\Lambda)$

VALUE	DOCUMENT ID	TECN	COMMENT
$0.13 \pm 0.12 \pm 0.05$	AAIJ	16J LHCb	pp at 7, 8 TeV

 $A_c(\phi)$

VALUE	DOCUMENT ID	TECN	COMMENT
$-0.01 \pm 0.12 \pm 0.03$	AAIJ	16J LHCb	pp at 7, 8 TeV

 $A_s(\phi)$

VALUE	DOCUMENT ID	TECN	COMMENT
$-0.07 \pm 0.12 \pm 0.01$	AAIJ	16J LHCb	pp at 7, 8 TeV

 $a_{CP}(\Lambda_b^0 \rightarrow \rho \pi^- \pi^+ \pi^-)$

Observable calculated as half of the difference between triple products for Λ_b^0 and $\bar{\Lambda}_b^0$, which is sensitive to CP violation.

VALUE (%)	DOCUMENT ID	TECN	COMMENT
$-0.7 \pm 0.7 \pm 0.2$	1 AAIJ	20AB LHCb	pp at 7, 8, 13 TeV

• • • We do not use the following data for averages, fits, limits, etc. • • •

$1.15 \pm 1.45 \pm 0.32$	2 AAIJ	17H LHCb	Repl. by AAIJ 20AB
--------------------------	--------	----------	--------------------

¹ Used both triple product asymmetries and the unbinned energy test method.
² Measured over full phase space of the decay.

 $a_{CP}(\Lambda_b^0 \rightarrow \rho K^- \pi^+ \pi^-)$

Observable calculated as half of the difference between triple products for Λ_b^0 and $\bar{\Lambda}_b^0$, which is sensitive to CP violation.

VALUE (%)	DOCUMENT ID	TECN	COMMENT
$-0.81 \pm 0.84 \pm 0.31$	1 AAIJ	18AG LHCb	pp at 7, 8 TeV

¹ Measured over full phase space of the decay.

 $a_{CP}(\Lambda_b^0 \rightarrow \rho K^- K^+ \pi^-)$

Observable calculated as half of the difference between triple products for Λ_b^0 and $\bar{\Lambda}_b^0$, which is sensitive to CP violation.

VALUE (%)	DOCUMENT ID	TECN	COMMENT
$-0.93 \pm 4.54 \pm 0.42$	1 AAIJ	17H LHCb	pp at 7, 8 TeV

¹ Measured over full phase space of the decay.

 $a_{CP}(\Lambda_b^0 \rightarrow \rho K^- K^+ K^-)$

Observable calculated as half of the difference between triple products for Λ_b^0 and $\bar{\Lambda}_b^0$, which is sensitive to CP violation.

VALUE (%)	DOCUMENT ID	TECN	COMMENT
$1.12 \pm 1.51 \pm 0.32$	1 AAIJ	18AG LHCb	pp at 7, 8 TeV

¹ Measured over full phase space of the decay.

 $a_{CP}(\Lambda_b^0 \rightarrow \rho K^- \mu^+ \mu^-)$

VALUE (%)	DOCUMENT ID	TECN	COMMENT
$1.2 \pm 5.0 \pm 0.7$	AAIJ	17T LHCb	pp at 7, 8 TeV

P VIOLATION PARAMETERS

Observables calculated as average of the triple products for Λ_b^0 and $\bar{\Lambda}_b^0$, which is sensitive to parity violation.

 $a_P(\Lambda_b^0 \rightarrow \rho \pi^- \pi^+ \pi^-)$

VALUE (%)	DOCUMENT ID	TECN	COMMENT
$-4.0 \pm 0.7 \pm 0.2$	1 AAIJ	20AB LHCb	pp at 7, 8, 13 TeV

• • • We do not use the following data for averages, fits, limits, etc. • • •

$-3.71 \pm 1.45 \pm 0.32$	2 AAIJ	17H LHCb	Repl. by AAIJ 20AB
---------------------------	--------	----------	--------------------

¹ Used both triple product asymmetries and the unbinned energy test method.
² Measured over full phase space of the decay.

 $a_P(\Lambda_b^0 \rightarrow \rho K^- \pi^+ \pi^-)$

VALUE (%)	DOCUMENT ID	TECN	COMMENT
$-0.60 \pm 0.84 \pm 0.31$	1 AAIJ	18AG LHCb	pp at 7, 8 TeV

¹ Measured over full phase space of the decay.

 $a_P(\Lambda_b^0 \rightarrow \rho K^- K^+ \pi^-)$

VALUE (%)	DOCUMENT ID	TECN	COMMENT
$3.62 \pm 4.54 \pm 0.42$	1 AAIJ	17H LHCb	pp at 7, 8 TeV

¹ Measured over full phase space of the decay.

 $a_P(\Lambda_b^0 \rightarrow \rho K^- K^+ K^-)$

VALUE (%)	DOCUMENT ID	TECN	COMMENT
$-1.56 \pm 1.51 \pm 0.32$	1 AAIJ	18AG LHCb	pp at 7, 8 TeV

¹ Measured over full phase space of the decay.

 $a_P(\Lambda_b^0 \rightarrow \rho K^- \mu^+ \mu^-)$

VALUE (%)	DOCUMENT ID	TECN	COMMENT
$-4.8 \pm 5.0 \pm 0.7$	AAIJ	17T LHCb	pp at 7, 8 TeV

 Λ_b^0 DECAY PARAMETERS

See the note on "Baryon Decay Parameters" in the neutron Listings.

 α decay parameter for $\Lambda_b \rightarrow J/\psi \Lambda$

VALUE	DOCUMENT ID	TECN	COMMENT
-0.017 ± 0.026 OUR AVERAGE			

$-0.022^{+0.027}_{-0.026}$ 1 AAIJ 20o LHCb pp at 7, 8, 13 TeV

$-0.14 \pm 0.14 \pm 0.10$ 2 SIRUNYAN 18R CMS pp at 7, 8 TeV

$0.30 \pm 0.16 \pm 0.06$ 3 AAD 14L ATLAS pp at 7 TeV

• • • We do not use the following data for averages, fits, limits, etc. • • •

$0.05 \pm 0.17 \pm 0.07$ 4 AAIJ 13AG LHCb Repl. by AAIJ 20o

¹ Extracted using a Bayesian analysis. The most probable value is given as -0.022 , with a 68% credibility interval $[-0.048, 0.005]$. Transverse polarizations of Λ_b^0 of -0.004 (68% credibility interval $[-0.064, 0.051]$), 0.001 (68% credibility interval $[-0.035, 0.045]$), and 0.032 (68% credibility interval $[-0.011, 0.065]$) are also reported at 7 TeV, 8 TeV and 13 TeV, respectively. Note that both statistical and systematic uncertainties are included.

² An angular analysis of $\Lambda_b \rightarrow J/\psi \Lambda$ decay is performed. Note that the sign of α in CMS definition is the opposite to that used by AAIJ 13AG and AAD 14L. Λ_b transverse production polarization of $0.00 \pm 0.06 \pm 0.06$ is also reported, as well as squares of the helicity amplitudes.

³ An angular analysis of $\Lambda_b \rightarrow J/\psi \Lambda$ decay is performed and magnitudes of all helicity amplitudes are also reported.

⁴ An angular analysis of $\Lambda_b \rightarrow J/\psi \Lambda$ decay is performed and a Λ_b transverse production polarization of $0.06 \pm 0.07 \pm 0.02$ is also reported.

 $f_L(\mu\mu)$ longitudinal polarization fraction in $\Lambda_b \rightarrow \Lambda \mu^+ \mu^-$

VALUE	DOCUMENT ID	TECN	COMMENT
$0.61^{+0.11}_{-0.14} \pm 0.03$	1 AAIJ	15AE LHCb	pp at 7, 8 TeV

¹ AAIJ 15AE measurement covers $15.0 < q^2 < 20.0$ GeV²/ c^4 .

FORWARD-BACKWARD ASYMMETRIES

The forward-backward asymmetry is defined as $A_{FB}(\Lambda_b^0) = [N(F) - N(B)] / [N(F) + N(B)]$, where the forward (F) direction corresponds to a particle (Λ_b^0 or $\bar{\Lambda}_b^0$) sharing valence quark flavors with a beam particle with the same sign of rapidity.

 $A_{FB}(\Lambda_b^0 \rightarrow J/\psi \Lambda)$

VALUE	DOCUMENT ID	TECN	COMMENT
$0.04 \pm 0.07 \pm 0.02$	1 ABZOV	15i D0	pp at 1.96 TeV

¹ The measured asymmetry integrated over rapidity y in the range of $0.1 < |y| < 2.0$.

 $A_{FB}^{\ell}(\mu\mu)$ in $\Lambda_b \rightarrow \Lambda \mu^+ \mu^-$

VALUE	DOCUMENT ID	TECN	COMMENT
$-0.39 \pm 0.04 \pm 0.01$	1 AAIJ	18AP LHCb	pp at 7, 8, 13 TeV

• • • We do not use the following data for averages, fits, limits, etc. • • •

$-0.05 \pm 0.09 \pm 0.03$ 2 AAIJ 15AE LHCb Repl. by AAIJ 18AP.

¹ The measurement covers $15.0 < q^2 < 20.0$ GeV²/ c^4 .

² AAIJ 15AE measurement covers $15.0 < q^2 < 20.0$ GeV²/ c^4 .

 $\Delta(A_{FB}^{\ell}(\mu\mu))$ in $\Lambda_b \rightarrow \Lambda \mu^+ \mu^-$

Difference of asymmetries $A_{FB}^{\ell}(\mu\mu)$ in $\Lambda_b \rightarrow \Lambda \mu^+ \mu^-$ between Λ_b and $\bar{\Lambda}_b$ decays

VALUE	DOCUMENT ID	TECN	COMMENT
$-0.05 \pm 0.09 \pm 0.03$	AAIJ	18Ao LHCb	pp at 7, 8 TeV

 $A_{FB}^{h}(\rho\pi)$ in $\Lambda_b \rightarrow \Lambda(\rho\pi) \mu^+ \mu^-$

VALUE	DOCUMENT ID	TECN	COMMENT
$-0.30 \pm 0.05 \pm 0.02$	1 AAIJ	18AP LHCb	pp at 7, 8, 13 TeV

• • • We do not use the following data for averages, fits, limits, etc. • • •

$-0.29 \pm 0.07 \pm 0.03$ 2 AAIJ 15AE LHCb Repl. by AAIJ 18AP.

¹ The measurement covers $15.0 < q^2 < 20.0$ GeV²/ c^4 .

² AAIJ 15AE measurement covers $15.0 < q^2 < 20.0$ GeV²/ c^4 .

 $A_{FB}^{h}(\mu\mu)$ in $\Lambda_b \rightarrow \Lambda \mu^+ \mu^-$

VALUE	DOCUMENT ID	TECN	COMMENT
$0.25 \pm 0.04 \pm 0.01$	1 AAIJ	18AP LHCb	pp at 7, 8, 13 TeV

¹ The measurement covers $15.0 < q^2 < 20.0$ GeV²/ c^4 .

See key on page 1127

Baryon Particle Listings

$\Lambda_b^0, \Lambda_b(5912)^0, \Lambda_b(5920)^0$

$\Lambda_b^0 - \bar{\Lambda}_b^0$ Production Asymmetry

$$A_P(\Lambda_b^0) = [\sigma(\Lambda_b^0) - \sigma(\bar{\Lambda}_b^0)] / [\sigma(\Lambda_b^0) + \sigma(\bar{\Lambda}_b^0)]$$

$A_P(\Lambda_b^0)$

VALUE (units 10^{-2})	DOCUMENT ID	TECN	COMMENT
1.4 ± 0.4 OUR AVERAGE	Error includes scale factor of 1.8.		
1.92 ± 0.35	¹ AAIJ	21AJ LHCb	pp at 7 TeV
1.09 ± 0.29	¹ AAIJ	21AJ LHCb	pp at 8 TeV
-0.11 ± 2.53 ± 1.08	² AAIJ	17BF LHCb	pp at 7 TeV
3.44 ± 1.61 ± 0.76	² AAIJ	17BF LHCb	pp at 8 TeV

¹ Integrated over the kinematic range $2 < p_T < 27$ GeV/c and $2.15 < y < 4.10$.
² Indirect determination in kinematic range $2 < p_T < 30$ GeV/c and $2.1 < \eta < 4.5$ from production asymmetries of B^+, B^0 and B_s^0 .

Λ_b^0 REFERENCES

AAIJ	21AD	PR D104 112008	R. Aaij et al.	(LHCb Collab.)
AAIJ	21AJ	JHEP 2110 060	R. Aaij et al.	(LHCb Collab.)
AAIJ	21B	PL B815 136172	R. Aaij et al.	(LHCb Collab.)
AAIJ	21R	JHEP 2105 095	R. Aaij et al.	(LHCb Collab.)
AAIJ	20AB	PR D102 051101	R. Aaij et al.	(LHCb Collab.)
AAIJ	20AK	PR D102 112012	R. Aaij et al.	(LHCb Collab.)
AAIJ	20M	JHEP 2005 040	R. Aaij et al.	(LHCb Collab.)
AAIJ	20O	JHEP 2006 110	R. Aaij et al.	(LHCb Collab.)
SIRUNYAN	20H	PL B802 135203	A.M. Sirunyan et al.	(CMS Collab.)
AAIJ	19AH	EPJ C79 745	R. Aaij et al.	(LHCb Collab.)
AAIJ	19AN	JHEP 1909 028	R. Aaij et al.	(LHCb Collab.)
AAIJ	19F	JHEP 1903 126	R. Aaij et al.	(LHCb Collab.)
AAIJ	19Z	PRL 123 031801	R. Aaij et al.	(LHCb Collab.)
AAIJ	18AF	JHEP 1808 131	R. Aaij et al.	(LHCb Collab.)
AAIJ	18AG	JHEP 1808 039	R. Aaij et al.	(LHCb Collab.)
AAIJ	18AO	JHEP 1809 145 (errat.)	R. Aaij et al.	(LHCb Collab.)
AAIJ	18AP	JHEP 1809 146	R. Aaij et al.	(LHCb Collab.)
AAIJ	18AW	PL B784 101	R. Aaij et al.	(LHCb Collab.)
AAIJ	18AX	PL B787 124	R. Aaij et al.	(LHCb Collab.)
AAIJ	18Q	JHEP 1802 098	R. Aaij et al.	(LHCb Collab.)
PDG	18	PR D98 030001	M. Tanabashi et al.	(PDG Collab.)
SIRUNYAN	18BY	EPJ C78 457	A.M. Sirunyan et al.	(CMS Collab.)
SIRUNYAN	18R	PR D97 072010	A.M. Sirunyan et al.	(CMS Collab.)
AAIJ	17AM	PRL 119 062001	R. Aaij et al.	(LHCb Collab.)
AAIJ	17BF	PL B774 139	R. Aaij et al.	(LHCb Collab.)
AAIJ	17H	NATP 13 391	R. Aaij et al.	(LHCb Collab.)
AAIJ	17P	JHEP 1704 029	R. Aaij et al.	(LHCb Collab.)
AAIJ	17S	JHEP 1705 030	R. Aaij et al.	(LHCb Collab.)
AAIJ	17T	JHEP 1706 109	R. Aaij et al.	(LHCb Collab.)
AAIJ	16	JHEP 1601 012	R. Aaij et al.	(LHCb Collab.)
AAIJ	16A	CP C40 011001	R. Aaij et al.	(LHCb Collab.)
AAIJ	16J	PL B759 282	R. Aaij et al.	(LHCb Collab.)
AAIJ	16W	JHEP 1605 081	R. Aaij et al.	(LHCb Collab.)
AAIJ	16Y	JHEP 1605 132	R. Aaij et al.	(LHCb Collab.)
AAD	15CH	PL B751 63	G. Aad et al.	(ATLAS Collab.)
AAIJ	15AE	JHEP 1506 115	R. Aaij et al.	(LHCb Collab.)
Also	JHEP 1809 145 (errat.)	R. Aaij et al.	(LHCb Collab.)	
AAIJ	15AH	JHEP 1509 006	R. Aaij et al.	(LHCb Collab.)
AAIJ	15B	NATP 11 743	R. Aaij et al.	(LHCb Collab.)
ABAZOV	15I	PR D91 072008	V.M. Abazov et al.	(D0 Collab.)
AAD	14L	PR D89 092009	G. Aad et al.	(ATLAS Collab.)
AAIJ	14AA	PRL 112 202001	R. Aaij et al.	(LHCb Collab.)
AAIJ	14E	JHEP 1404 114	R. Aaij et al.	(LHCb Collab.)
AAIJ	14H	PR D89 032001	R. Aaij et al.	(LHCb Collab.)
AAIJ	14I	JHEP 1408 143	R. Aaij et al.	(LHCb Collab.)
AAIJ	14K	JHEP 1407 103	R. Aaij et al.	(LHCb Collab.)
AAIJ	14Q	JHEP 1404 087	R. Aaij et al.	(LHCb Collab.)
AAIJ	14U	PL B734 122	R. Aaij et al.	(LHCb Collab.)
AALTONEN	14B	PR D89 072014	T. Aaltonen et al.	(CDF Collab.)
AALTONEN	14P	PRL 113 242001	T. Aaltonen et al.	(CDF Collab.)
PDG	14	CP C38 070001	K. Olive et al.	(PDG Collab.)
AAD	13U	PR D87 032002	G. Aad et al.	(ATLAS Collab.)
AAIJ	13AG	PL B724 27	R. Aaij et al.	(LHCb Collab.)
AAIJ	13AJ	PL B725 25	R. Aaij et al.	(LHCb Collab.)
AAIJ	13AV	PRL 110 182001	R. Aaij et al.	(LHCb Collab.)
AAIJ	13BB	PRL 111 102003	R. Aaij et al.	(LHCb Collab.)
CHATRCHYAN	13AC	JHEP 1307 163	S. Chatrchyan et al.	(CMS Collab.)
AAIJ	12AR	JHEP 1210 037	R. Aaij et al.	(LHCb Collab.)
AAIJ	12E	PL B708 241	R. Aaij et al.	(LHCb Collab.)
AALTONEN	12A	PR D85 032003	T. Aaltonen et al.	(CDF Collab.)
ABAZOV	12U	PR D85 112003	V.M. Abazov et al.	(D0 Collab.)
AAIJ	11E	PR D84 092001	R. Aaij et al.	(LHCb Collab.)
Also	PR D85 039904 (errat.)	R. Aaij et al.	(LHCb Collab.)	
AALTONEN	11	PRL 106 121804	T. Aaltonen et al.	(CDF Collab.)
AALTONEN	11AI	PRL 107 201802	T. Aaltonen et al.	(CDF Collab.)
AALTONEN	11N	PRL 106 181802	T. Aaltonen et al.	(CDF Collab.)
ABAZOV	11O	PR D84 031102	V.M. Abazov et al.	(D0 Collab.)
AALTONEN	10B	PRL 104 102002	T. Aaltonen et al.	(CDF Collab.)
AALTONEN	09C	PRL 103 031801	T. Aaltonen et al.	(CDF Collab.)
AALTONEN	09E	PR D79 032001	T. Aaltonen et al.	(CDF Collab.)
ABAZOV	07S	PRL 99 142001	V.M. Abazov et al.	(D0 Collab.)
ABAZOV	07U	PR 99 182001	V.M. Abazov et al.	(D0 Collab.)
ABULENCIA	07A	PR 98 122001	A. Abulencia et al.	(FNAL CDF Collab.)
ABULENCIA	07B	PRL 98 122002	A. Abulencia et al.	(FNAL CDF Collab.)
LEITNER	07	NPBPS 174 169	O. Leitner, Z.J. Ajaltouni	(CDF Collab.)
ACOSTA	06	PRL 96 202001	D. Acosta et al.	(CDF Collab.)
ABAZOV	05C	PRL 94 102001	V.M. Abazov et al.	(D0 Collab.)
ACOSTA	05O	PR D72 051104	D. Acosta et al.	(CDF Collab.)
ABDALLAH	04A	PL B585 63	J. Abdallah et al.	(DELPHI Collab.)
ACOSTA	02G	PR D66 112002	D. Acosta et al.	(CDF Collab.)
ABREU	99W	EPJ C10 185	P. Abreu et al.	(DELPHI Collab.)
ACKERS STAFF	98G	PL B426 161	K. Ackersstaff et al.	(OPAL Collab.)
BARATE	98D	EPJ C2 197	R. Barate et al.	(ALEPH Collab.)
ABE	97B	PR D55 1142	F. Abe et al.	(CDF Collab.)
ABE	96M	PRL 77 1439	F. Abe et al.	(CDF Collab.)
ABREU	96D	ZPHY C71 199	P. Abreu et al.	(DELPHI Collab.)
ABREU	96N	PL B374 351	P. Abreu et al.	(DELPHI Collab.)
ADAM	96D	ZPHY C72 207	W. Adam et al.	(DELPHI Collab.)
BUSKULIC	96L	PL B380 442	D. Buskulic et al.	(ALEPH Collab.)
BUSKULIC	96V	PL B384 471	D. Buskulic et al.	(ALEPH Collab.)
PDG	96	PR D54 1	R. M. Barnett et al.	(PDG Collab.)
ABREU	95S	ZPHY C68 375	P. Abreu et al.	(DELPHI Collab.)
AKERS	95K	PL B353 402	R. Akers et al.	(OPAL Collab.)
BUSKULIC	95L	PL B357 685	D. Buskulic et al.	(ALEPH Collab.)
ABE	93B	PR D47 2639	F. Abe et al.	(CDF Collab.)

BUSKULIC	92E	PL B294 145	D. Buskulic et al.	(ALEPH Collab.)
ALBAJAR	91E	PL B273 540	C. Albajar et al.	(UA1 Collab.)
BARI	91	NC 104A 1787	G. Bari et al.	(CERN R422 Collab.)
ARENTON	86	NP B274 707	M.W. Arenton et al.	(ARIZ, NDAM, VAND)
BASILE	81	LNC 31 97	M. Basile et al.	(CERN R415 Collab.)

$\Lambda_b(5912)^0$

$J^P = \frac{1}{2}^-$ Status: ***

Quantum numbers are based on quark model expectations.

$\Lambda_b(5912)^0$ MASS

VALUE (MeV)	DOCUMENT ID	TECN	COMMENT
5912.19 ± 0.17 OUR AVERAGE			
5912.19 ± 0.03 ± 0.17	¹ AAIJ	20Q LHCb	pp at 7, 8, 13 TeV
5912.32 ± 0.12 ± 0.17	² SIRUNYAN	20K CMS	pp at 13 TeV
5912.20 ± 0.13 ± 0.17	^{3,4} AAIJ	12AL LHCb	Repl. by AAIJ 20q

- • • We do not use the following data for averages, fits, limits, etc. • • •
- ¹ AAIJ 20q measures $m(\Lambda_b(5912)^0) - m(\Lambda_b^0) = 292.589 \pm 0.029 \pm 0.010$ MeV. We have adjusted the measurement to our best value of $m(\Lambda_b^0) = 5619.60 \pm 0.17$ MeV. Our first error is their experiment's error and our second error is the systematic error from using our best values.
- ² SIRUNYAN 20k measures $m(\Lambda_b(5912)^0) - m(\Lambda_b^0) = 292.72 \pm 0.12 \pm 0.01$ MeV. We have adjusted the measurement to our best value of $m(\Lambda_b^0) = 5619.60 \pm 0.17$ MeV. Our first error is their experiment's error and our second error is the systematic error from using our best values.
- ³ Observed in $\Lambda_b(5912)^0 \rightarrow \Lambda_b^0 \pi^+ \pi^-$ decays with 17.6 ± 4.8 candidates with a significance of 5.2 sigma.
- ⁴ AAIJ 12AL measures $m(\Lambda_b(5912)^0) - m(\Lambda_b^0) = 292.60 \pm 0.12 \pm 0.04$ MeV. We have adjusted the measurement to our best value of $m(\Lambda_b^0) = 5619.60 \pm 0.17$ MeV. Our first error is their experiment's error and our second error is the systematic error from using our best values.

$\Lambda_b(5912)^0$ WIDTH

VALUE (MeV)	CL%	DOCUMENT ID	TECN	COMMENT
< 0.25	90	AAIJ	20Q LHCb	pp at 7, 8, 13 TeV
< 0.66	90	AAIJ	12AL LHCb	Repl. by AAIJ 20q

$\Lambda_b(5912)^0$ DECAY MODES

Mode	Fraction (Γ_i/Γ)
$\Gamma_1 \Lambda_b^0 \pi^+ \pi^-$	seen

$\Lambda_b(5912)^0$ BRANCHING RATIOS

$\Gamma(\Lambda_b^0 \pi^+ \pi^-)/\Gamma_{total}$	DOCUMENT ID	TECN	COMMENT	Γ_1/Γ
seen	AAIJ	20Q LHCb	pp at 7, 8, 13 TeV	
seen	SIRUNYAN	20K CMS	pp at 13 TeV	
seen	AAIJ	12AL LHCb	pp at 7 TeV	

$\Lambda_b(5912)^0$ REFERENCES

AAIJ	20Q	JHEP 2006 136	R. Aaij et al.	(LHCb Collab.)
SIRUNYAN	20K	PL B803 135345	A.M. Sirunyan et al.	(CMS Collab.)
AAIJ	12AL	PRL 109 172003	R. Aaij et al.	(LHCb Collab.)

$\Lambda_b(5920)^0$

$J^P = \frac{3}{2}^-$ Status: ***

Quantum numbers are based on quark model expectations.

$\Lambda_b(5920)^0$ MASS

VALUE (MeV)	DOCUMENT ID	TECN	COMMENT
5920.09 ± 0.17 OUR AVERAGE			
5920.09 ± 0.02 ± 0.17	¹ AAIJ	20Q LHCb	pp at 7, 8, 13 TeV
5920.16 ± 0.07 ± 0.17	² SIRUNYAN	20K CMS	pp at 13 TeV
5919.4 ± 0.5 ± 0.2	^{3,4} AALTONEN	13V CDF	p \bar{p} at 1.96 TeV
5920.00 ± 0.09 ± 0.17	^{5,6} AAIJ	12AL LHCb	Repl. by AAIJ 20q

- • • We do not use the following data for averages, fits, limits, etc. • • •
- ¹ AAIJ 20q measures $m(\Lambda_b(5920)^0) - m(\Lambda_b^0) = 300.492 \pm 0.019 \pm 0.010$ MeV. We have adjusted the measurement to our best value of $m(\Lambda_b^0) = 5619.60 \pm 0.17$ MeV. Our first error is their experiment's error and our second error is the systematic error from using our best values.
- ² SIRUNYAN 20k measures $m(\Lambda_b(5920)^0) - m(\Lambda_b^0) = 300.56 \pm 0.07 \pm 0.01$ MeV. We have adjusted the measurement to our best value of $m(\Lambda_b^0) = 5619.60 \pm 0.17$ MeV. Our first error is their experiment's error and our second error is the systematic error from using our best values.

Baryon Particle Listings

 $\Lambda_b(5920)^0, \Lambda_b(6070)^0, \Lambda_b(6146)^0, \Lambda_b(6152)^0$

³ Measured in $\Lambda_b(5920)^0 \rightarrow \Lambda_b^0 \pi^+ \pi^-$ decays with $17.3^{+5.3}_{-4.6}$ events, with a significance of 3.5 sigma.

⁴ AALTONEN 13v measures $m(\Lambda_b(5920)^0) - m(\Lambda_b^0) - 2m(\pi) = 20.68 \pm 0.35 \pm 0.30$ MeV.

We have adjusted the measurement to our best values of $m(\Lambda_b^0) = 5619.60 \pm 0.17$ MeV and $m(\pi) = 139.57039 \pm 0.00018$ MeV. Our first error is their experiment's error and our second error is the systematic error from using our best values.

⁵ Observed in $\Lambda_b(5920)^0 \rightarrow \Lambda_b^0 \pi^+ \pi^-$ decays with 52.5 ± 8.1 candidates with a significance of 10.2 sigma.

⁶ AAIJ 12AL measures $m(\Lambda_b(5920)^0) - m(\Lambda_b^0) = 300.40 \pm 0.08 \pm 0.04$ MeV. We have adjusted the measurement to our best value of $m(\Lambda_b^0) = 5619.60 \pm 0.17$ MeV. Our first error is their experiment's error and our second error is the systematic error from using our best values.

 $\Lambda_b(5920)^0$ WIDTH

VALUE (MeV)	CL%	DOCUMENT ID	TECN	COMMENT
<0.19	90	AAIJ	20Q LHCb	pp at 7, 8, 13 TeV
• • •				We do not use the following data for averages, fits, limits, etc. • • •
<0.63	90	AAIJ	12AL LHCb	Repl. by AAIJ 20Q

 $\Lambda_b(5920)^0$ DECAY MODES

Mode	Fraction (Γ_i/Γ)
$\Gamma_1 \Lambda_b^0 \pi^+ \pi^-$	seen

 $\Lambda_b(5920)^0$ BRANCHING RATIOS

$\Gamma(\Lambda_b^0 \pi^+ \pi^-)/\Gamma_{\text{total}}$	Γ_1/Γ		
VALUE	DOCUMENT ID	TECN	COMMENT
seen	AAIJ	20Q LHCb	pp at 7, 8, 13 TeV
seen	SIRUNYAN	20K LHCb	pp at 13 TeV
seen	AALTONEN	13V CDF	$p\bar{p}$ at 1.96 TeV
seen	AAIJ	12AL LHCb	pp at 7 TeV

 $\Lambda_b(5920)^0$ REFERENCES

AAIJ	20Q	JHEP 2006 136	R. Aaij <i>et al.</i>	(LHCb Collab.)
SIRUNYAN	20K	PL B803 135345	A.M. Sirunyan <i>et al.</i>	(CMS Collab.)
AALTONEN	13V	PR D88 071101	T. Aaltonen <i>et al.</i>	(CDF Collab.)
AAIJ	12AL	PRL 109 172003	R. Aaij <i>et al.</i>	(LHCb Collab.)

$$\Lambda_b(6070)^0 \quad J^P = \frac{1}{2}^+ \quad \text{Status: } ***$$

Quantum numbers are based on quark model expectations.

 $\Lambda_b(6070)^0$ MASS

VALUE (MeV)	DOCUMENT ID	TECN	COMMENT
6072.3 ± 2.9 ± 0.2	¹ AAIJ	20Q LHCb	pp at 7, 8, 13 TeV

¹ AAIJ 20Q measures $m(\Lambda_b(6070)^0) - m(\Lambda_b^0) = 452.7 \pm 2.9 \pm 0.5$ MeV. We have adjusted the measurement to our best value of $m(\Lambda_b^0) = 5619.60 \pm 0.17$ MeV. Our first error is their experiment's error and our second error is the systematic error from using our best values.

 $\Lambda_b(6070)^0$ WIDTH

VALUE (MeV)	DOCUMENT ID	TECN	COMMENT
72 ± 11 ± 2	AAIJ	20Q LHCb	pp at 7, 8, 13 TeV

 $\Lambda_b(6070)^0$ DECAY MODES

Mode	Fraction (Γ_i/Γ)
$\Gamma_1 \Lambda_b^0 \pi^+ \pi^-$	seen

 $\Lambda_b(6070)^0$ BRANCHING RATIOS

$\Gamma(\Lambda_b^0 \pi^+ \pi^-)/\Gamma_{\text{total}}$	Γ_1/Γ		
VALUE	DOCUMENT ID	TECN	COMMENT
seen	AAIJ	20Q LHCb	pp at 7, 8, 13 TeV

 $\Lambda_b(6070)^0$ REFERENCES

AAIJ	20Q	JHEP 2006 136	R. Aaij <i>et al.</i>	(LHCb Collab.)
------	-----	---------------	-----------------------	----------------

$$\Lambda_b(6146)^0 \quad J^P = \frac{3}{2}^+ \quad \text{Status: } ***$$

Quantum numbers are based on quark model expectations.

 $\Lambda_b(6146)^0$ MASS $\Lambda_b(6146)^0$ MASS

VALUE (MeV)	DOCUMENT ID	TECN	COMMENT
6146.2 ± 0.4 OUR AVERAGE			
6146.5 ± 2.1 ± 0.2	¹ SIRUNYAN	20K CMS	pp at 13 TeV
6146.17 ± 0.33 ± 0.27	² AAIJ	19AJ LHCb	pp at 7, 8, 13 TeV

¹ SIRUNYAN 20K measures $m(\Lambda_b(6146)^0) - m(\Lambda_b^0) = 526.9 \pm 1.9 \pm 0.8$ MeV. We have adjusted the measurement to our best value of $m(\Lambda_b^0) = 5619.60 \pm 0.17$ MeV. Our first error is their experiment's error and our second error is the systematic error from using our best values.

² Observed in $\Lambda_b^0 \pi^+ \pi^-$ mode.

 $m\Lambda_b(6146)^0 - m\Lambda_b^0$

VALUE (MeV)	DOCUMENT ID	TECN	COMMENT
526.55 ± 0.33 ± 0.10	¹ AAIJ	19AJ LHCb	pp at 7, 8, 13 TeV

¹ Observed in $\Lambda_b^0 \pi^+ \pi^-$ mode.

 $\Lambda_b(6146)^0$ WIDTH

VALUE (MeV)	DOCUMENT ID	TECN	COMMENT
2.9 ± 1.3 ± 0.3	¹ AAIJ	19AJ LHCb	pp at 7, 8, 13 TeV

¹ Observed in $\Lambda_b^0 \pi^+ \pi^-$ mode.

 $\Lambda_b(6146)^0$ DECAY MODES

Mode	Fraction (Γ_i/Γ)
$\Gamma_1 \Lambda_b^0 \pi^+ \pi^-$	seen

 $\Lambda_b(6146)^0$ BRANCHING RATIOS

$\Gamma(\Lambda_b^0 \pi^+ \pi^-)/\Gamma_{\text{total}}$	Γ_1/Γ		
VALUE	DOCUMENT ID	TECN	COMMENT
seen	SIRUNYAN	20K LHCb	pp at 13 TeV
seen	AAIJ	19AJ LHCb	pp at 7, 8, 13 TeV

 $\Lambda_b(6146)^0$ REFERENCES

SIRUNYAN	20K	PL B803 135345	A.M. Sirunyan <i>et al.</i>	(CMS Collab.)
AAIJ	19AJ	PRL 123 152001	R. Aaij <i>et al.</i>	(LHCb Collab.)

$$\Lambda_b(6152)^0 \quad J^P = \frac{5}{2}^+ \quad \text{Status: } ***$$

Quantum numbers are based on quark model expectations.

 $\Lambda_b(6152)^0$ MASS $\Lambda_b(6152)^0$ MASS

VALUE (MeV)	DOCUMENT ID	TECN	COMMENT
6152.5 ± 0.4 OUR AVERAGE			
6152.7 ± 1.2 ± 0.2	¹ SIRUNYAN	20K CMS	pp at 13 TeV
6152.51 ± 0.26 ± 0.27	² AAIJ	19AJ LHCb	pp at 7, 8, 13 TeV

¹ SIRUNYAN 20K measures $m(\Lambda_b(6152)^0) - m(\Lambda_b^0) = 533.1 \pm 1.1 \pm 0.4$ MeV. We have adjusted the measurement to our best value of $m(\Lambda_b^0) = 5619.60 \pm 0.17$ MeV. Our first error is their experiment's error and our second error is the systematic error from using our best values.

² Observed in $\Lambda_b^0 \pi^+ \pi^-$ mode.

 $m\Lambda_b(6152)^0 - m\Lambda_b^0$

VALUE (MeV)	DOCUMENT ID	TECN	COMMENT
532.89 ± 0.26 ± 0.10	¹ AAIJ	19AJ LHCb	pp at 7, 8, 13 TeV

¹ Observed in $\Lambda_b^0 \pi^+ \pi^-$ mode.

 $m\Lambda_b(6152)^0 - m\Lambda_b(6146)^0$

VALUE (MeV)	DOCUMENT ID	TECN	COMMENT
6.34 ± 0.32 ± 0.02	AAIJ	19AJ LHCb	pp at 7, 8, 13 TeV

 $\Lambda_b(6152)^0$ WIDTH

VALUE (MeV)	DOCUMENT ID	TECN	COMMENT
2.1 ± 0.8 ± 0.3	¹ AAIJ	19AJ LHCb	pp at 7, 8, 13 TeV

¹ Observed in $\Lambda_b^0 \pi^+ \pi^-$ mode.

 $\Lambda_b(6152)^0$ DECAY MODES

Mode	Fraction (Γ_i/Γ)
$\Gamma_1 \Lambda_b^0 \pi^+ \pi^-$	seen

$\Lambda_b(6152)^0$ BRANCHING RATIOS

$\Gamma(\Lambda_b^0 \pi^+ \pi^-)/\Gamma_{\text{total}}$	DOCUMENT ID	TECN	COMMENT	Γ_1/Γ	
seen	SIRUNYAN	20K	LHCB	pp at 13 TeV	
seen	AAIJ	19AJ	LHCB	pp at 7, 8, 13 TeV	

 $\Lambda_b(6152)^0$ REFERENCES

SIRUNYAN	20K	PL B803 135345	A. M. Sirunyan et al.	(CMS Collab.)
AAIJ	19AJ	PRL 123 152001	R. Aaij et al.	(LHCb Collab.)

 Σ_b

$I(J^P) = 1(\frac{1}{2}^+)$ Status: ***
I, J, P need confirmation.

In the quark model Σ_b^+ , Σ_b^0 , Σ_b^- are an isotriplet (uub , udb , ddb) state. The lowest Σ_b ought to have $J^P = 1/2^+$. None of I, J, or P have actually been measured.

 Σ_b MASS Σ_b^+ MASS

VALUE (MeV)	DOCUMENT ID	TECN	COMMENT
5810.56 ± 0.25 OUR AVERAGE			
5810.55 ± 0.11 ± 0.23	¹ AAIJ	19A	LHCB pp at 7, 8 TeV
5811.3 $^{+0.9}_{-0.8}$ ± 1.7	² AALTONEN	12F	CDF $p\bar{p}$ at 1.96 TeV
• • • We do not use the following data for averages, fits, limits, etc. • • •			
5807.8 $^{+2.0}_{-2.2}$ ± 1.7	³ AALTONEN	07K	CDF Repl. by AALTONEN 12F

- Measured using fully reconstructed $\Lambda_b^0 \rightarrow \Lambda_c^+ \pi^-$ and $\Lambda_c^+ \rightarrow p K^- \pi^+$ decays.
- Measured using fully reconstructed $\Lambda_b^0 \rightarrow \Lambda_c^+ \pi^-$ and $\Lambda_c^+ \rightarrow K^- \pi^+$ decays.
- Observed four $\Lambda_b^0 \pi^\pm$ resonances in the fully reconstructed decay mode $\Lambda_b^0 \rightarrow \Lambda_c^+ \pi^-$, where $\Lambda_c^+ \rightarrow p K^- \pi^+$.

 Σ_b^- MASS

VALUE (MeV)	DOCUMENT ID	TECN	COMMENT
5815.64 ± 0.27 OUR AVERAGE			
5815.64 ± 0.14 ± 0.24	¹ AAIJ	19A	LHCB pp at 7, 8 TeV
5815.5 $^{+0.6}_{-0.5}$ ± 1.7	² AALTONEN	12F	CDF $p\bar{p}$ at 1.96 TeV
• • • We do not use the following data for averages, fits, limits, etc. • • •			
5815.2 ± 1.0 ± 1.7	³ AALTONEN	07K	CDF Repl. by AALTONEN 12F

- Measured using fully reconstructed $\Lambda_b^0 \rightarrow \Lambda_c^+ \pi^-$ and $\Lambda_c^+ \rightarrow p K^- \pi^+$ decays.
- Measured using fully reconstructed $\Lambda_b^0 \rightarrow \Lambda_c^+ \pi^-$ and $\Lambda_c^+ \rightarrow K^- \pi^+$ decays.
- Observed four $\Lambda_b^0 \pi^\pm$ resonances in the fully reconstructed decay mode $\Lambda_b^0 \rightarrow \Lambda_c^+ \pi^-$, where $\Lambda_c^+ \rightarrow p K^- \pi^+$.

 $m_{\Sigma_b^+} - m_{\Sigma_b^-}$

VALUE (MeV)	DOCUMENT ID	TECN	COMMENT
-5.06 ± 0.18 OUR AVERAGE			
-5.09 ± 0.18 ± 0.01	¹ AAIJ	19A	LHCB pp at 7, 8 TeV
-4.2 $^{+1.1}_{-1.0}$ ± 0.1	² AALTONEN	12F	CDF $p\bar{p}$ at 1.96 TeV
¹ Measured using fully reconstructed $\Lambda_b^0 \rightarrow \Lambda_c^+ \pi^-$ and $\Lambda_c^+ \rightarrow p K^- \pi^+$ decays.			
² Measured using fully reconstructed $\Lambda_b^0 \rightarrow \Lambda_c^+ \pi^-$ and $\Lambda_c^+ \rightarrow K^- \pi^+$ decays.			

 Σ_b WIDTH Σ_b^+ WIDTH

VALUE (MeV)	DOCUMENT ID	TECN	COMMENT
5.0 ± 0.5 OUR AVERAGE			
4.83 ± 0.31 ± 0.37	¹ AAIJ	19A	LHCB pp at 7, 8 TeV
9.7 $^{+3.8}_{-2.8}$ $^{+1.2}_{-1.1}$	² AALTONEN	12F	CDF $p\bar{p}$ at 1.96 TeV
¹ Measured using fully reconstructed $\Lambda_b^0 \rightarrow \Lambda_c^+ \pi^-$ and $\Lambda_c^+ \rightarrow p K^- \pi^+$ decays.			
² Measured using fully reconstructed $\Lambda_b^0 \rightarrow \Lambda_c^+ \pi^-$ and $\Lambda_c^+ \rightarrow K^- \pi^+$ decays.			

 Σ_b^- WIDTH

VALUE (MeV)	DOCUMENT ID	TECN	COMMENT
5.3 ± 0.5 OUR AVERAGE			
5.33 ± 0.42 ± 0.37	¹ AAIJ	19A	LHCB pp at 7, 8 TeV
4.9 $^{+3.1}_{-2.1}$ ± 1.1	² AALTONEN	12F	CDF $p\bar{p}$ at 1.96 TeV
¹ Measured using fully reconstructed $\Lambda_b^0 \rightarrow \Lambda_c^+ \pi^-$ and $\Lambda_c^+ \rightarrow p K^- \pi^+$ decays.			
² Measured using fully reconstructed $\Lambda_b^0 \rightarrow \Lambda_c^+ \pi^-$ and $\Lambda_c^+ \rightarrow K^- \pi^+$ decays.			

 Σ_b DECAY MODES

Mode	Fraction (Γ_i/Γ)
$\Gamma_1 \Lambda_b^0 \pi$	dominant

 Σ_b BRANCHING RATIOS

$\Gamma(\Lambda_b^0 \pi)/\Gamma_{\text{total}}$	DOCUMENT ID	TECN	COMMENT	Γ_1/Γ
dominant	AALTONEN	07K	CDF	$p\bar{p}$ at 1.96 TeV

 Σ_b REFERENCES

AAIJ	19A	PRL 122 012001	R. Aaij et al.	(LHCb Collab.)
AALTONEN	12F	PR D85 092011	T. Aaltonen et al.	(CDF Collab.)
AALTONEN	07K	PRL 99 202001	T. Aaltonen et al.	(CDF Collab.)

 Σ_b^*

$I(J^P) = 1(\frac{3}{2}^+)$ Status: ***
I, J, P need confirmation.

I, J, P need confirmation. Quantum numbers shown are quark-model predictions.

 Σ_b^+ MASS

VALUE (MeV)	DOCUMENT ID	TECN	COMMENT
5830.32 ± 0.27 OUR AVERAGE			
5830.28 ± 0.14 ± 0.24	¹ AAIJ	19A	LHCB pp at 7, 8 TeV
5832.1 ± 0.7 $^{+1.7}_{-1.8}$	² AALTONEN	12F	CDF $p\bar{p}$ at 1.96 TeV
¹ Measured using fully reconstructed $\Lambda_b^0 \rightarrow \Lambda_c^+ \pi^-$ and $\Lambda_c^+ \rightarrow p K^- \pi^+$ decays.			
² Measured using fully reconstructed $\Lambda_b^0 \rightarrow \Lambda_c^+ \pi^-$ and $\Lambda_c^+ \rightarrow K^- \pi^+$ decays.			

 Σ_b^- MASS

VALUE (MeV)	DOCUMENT ID	TECN	COMMENT
5834.74 ± 0.30 OUR AVERAGE			
5834.73 ± 0.17 ± 0.25	¹ AAIJ	19A	LHCB pp at 7, 8 TeV
5835.1 ± 0.6 $^{+1.7}_{-1.8}$	² AALTONEN	12F	CDF $p\bar{p}$ at 1.96 TeV
¹ Measured using fully reconstructed $\Lambda_b^0 \rightarrow \Lambda_c^+ \pi^-$ and $\Lambda_c^+ \rightarrow p K^- \pi^+$ decays.			
² Measured using fully reconstructed $\Lambda_b^0 \rightarrow \Lambda_c^+ \pi^-$ and $\Lambda_c^+ \rightarrow K^- \pi^+$ decays.			

 $m_{\Sigma_b^{*+}} - m_{\Sigma_b^{*-}}$

VALUE (MeV)	DOCUMENT ID	TECN	COMMENT
-4.37 ± 0.33 OUR AVERAGE			Error includes scale factor of 1.6.
-4.45 ± 0.22 ± 0.01	¹ AAIJ	19A	LHCB pp at 7, 8 TeV
-3.0 $^{+1.0}_{-0.9}$ ± 0.1	² AALTONEN	12F	CDF $p\bar{p}$ at 1.96 TeV
¹ Measured using fully reconstructed $\Lambda_b^0 \rightarrow \Lambda_c^+ \pi^-$ and $\Lambda_c^+ \rightarrow p K^- \pi^+$ decays.			
² Measured using fully reconstructed $\Lambda_b^0 \rightarrow \Lambda_c^+ \pi^-$ and $\Lambda_c^+ \rightarrow K^- \pi^+$ decays.			

 $m_{\Sigma_b^{*+}} - m_{\Sigma_b^+}$

VALUE	DOCUMENT ID	TECN	COMMENT
19.73 ± 0.18 ± 0.01			
19.73 ± 0.18 ± 0.01	¹ AAIJ	19A	LHCB pp at 7, 8 TeV
¹ Measured using fully reconstructed $\Lambda_b^0 \rightarrow \Lambda_c^+ \pi^-$ and $\Lambda_c^+ \rightarrow p K^- \pi^+$ decays.			

 $m_{\Sigma_b^{*-}} - m_{\Sigma_b^-}$

VALUE	DOCUMENT ID	TECN	COMMENT
19.09 ± 0.22 ± 0.02			
19.09 ± 0.22 ± 0.02	¹ AAIJ	19A	LHCB pp at 7, 8 TeV
¹ Measured using fully reconstructed $\Lambda_b^0 \rightarrow \Lambda_c^+ \pi^-$ and $\Lambda_c^+ \rightarrow p K^- \pi^+$ decays.			

 Σ_b^* WIDTH Σ_b^{*+} WIDTH

VALUE (MeV)	DOCUMENT ID	TECN	COMMENT
9.4 ± 0.5 OUR AVERAGE			
9.34 ± 0.47 ± 0.26	¹ AAIJ	19A	LHCB pp at 7, 8 TeV
11.5 $^{+2.7}_{-2.2}$ $^{+1.0}_{-1.5}$	² AALTONEN	12F	CDF $p\bar{p}$ at 1.96 TeV
¹ Measured using fully reconstructed $\Lambda_b^0 \rightarrow \Lambda_c^+ \pi^-$ and $\Lambda_c^+ \rightarrow p K^- \pi^+$ decays.			
² Measured using fully reconstructed $\Lambda_b^0 \rightarrow \Lambda_c^+ \pi^-$ and $\Lambda_c^+ \rightarrow K^- \pi^+$ decays.			

 Σ_b^{*-} WIDTH

VALUE (MeV)	DOCUMENT ID	TECN	COMMENT
10.4 ± 0.8 OUR AVERAGE			Error includes scale factor of 1.3.
10.68 ± 0.60 ± 0.33	¹ AAIJ	19A	LHCB pp at 7, 8 TeV

Baryon Particle Listings

Σ_b^* , $\Sigma_b(6097)^+$, $\Sigma_b(6097)^-$, Ξ_b^-

7.5 $^{+2.2}_{-1.8}$ $^{+0.9}_{-1.4}$	2 AALTONEN	12F	CDF	$p\bar{p}$ at 1.96 TeV
1 Measured using fully reconstructed $\Lambda_b^0 \rightarrow \Lambda_c^+ \pi^-$ and $\Lambda_c^+ \rightarrow p K^- \pi^+$ decays.				
2 Measured using fully reconstructed $\Lambda_b^0 \rightarrow \Lambda_c^+ \pi^-$ and $\Lambda_c^+ \rightarrow K^- \pi^+$ decays.				

$m_{\Sigma_b^*} - m_{\Sigma_b}$

VALUE (MeV)	DOCUMENT ID	TECN	COMMENT
21.2 $^{+2.0}_{-1.9}$ $^{+0.4}_{-0.3}$	1 AALTONEN	07K	CDF $p\bar{p}$ at 1.96 TeV
1 Observed four $\Lambda_b^0 \pi^\pm$ resonances in the fully reconstructed decay mode $\Lambda_b^0 \rightarrow \Lambda_c^+ \pi^-$, where $\Lambda_c^+ \rightarrow p K^- \pi^+$. Assumes $m_{\Sigma_b^{*+}} - m_{\Sigma_b^+} = m_{\Sigma_b^{*-}} - m_{\Sigma_b^-}$.			

Σ_b^* DECAY MODES

Mode	Fraction (Γ_i/Γ)
Γ_1 $\Lambda_b^0 \pi$	dominant

Σ_b^* BRANCHING RATIOS

$\Gamma(\Lambda_b^0 \pi)/\Gamma_{\text{total}}$	DOCUMENT ID	TECN	COMMENT	Γ_1/Γ
dominant	AALTONEN	07K	CDF $p\bar{p}$ at 1.96 TeV	

Σ_b^* REFERENCES

AAIJ	19A	PRL 122 012001	R. Aaij et al.	(LHCb Collab.)
AALTONEN	12F	PR D85 092011	T. Aaltonen et al.	(CDF Collab.)
AALTONEN	07K	PRL 99 202001	T. Aaltonen et al.	(CDF Collab.)

$\Sigma_b(6097)^+$	$J^P = ??$	Status: ***
--------------------	------------	-------------

$\Sigma_b(6097)^+$ MASS

VALUE (MeV)	DOCUMENT ID	TECN	COMMENT
6095.8 $\pm 1.7 \pm 0.4$	1 AAIJ	19A	LHCB pp at 7, 8 TeV
1 Measured using fully reconstructed $\Lambda_b^0 \rightarrow \Lambda_c^+ \pi^-$ and $\Lambda_c^+ \rightarrow p K^- \pi^+$ decays.			

$m_{\Sigma_b(6097)^+} - m_{\Sigma_b(6097)^-}$

VALUE	DOCUMENT ID	TECN	COMMENT
-2.2 $^{+2.4}_{-0.3}$ MeV	1 AAIJ	19A	LHCB pp at 7, 8 TeV
1 Measured using fully reconstructed $\Lambda_b^0 \rightarrow \Lambda_c^+ \pi^-$ and $\Lambda_c^+ \rightarrow p K^- \pi^+$ decays.			

$\Sigma_b(6097)^+$ WIDTH

VALUE (MeV)	DOCUMENT ID	TECN	COMMENT
31.0 $\pm 5.5 \pm 0.7$	1 AAIJ	19A	LHCB pp at 7, 8 TeV
1 Measured using fully reconstructed $\Lambda_b^0 \rightarrow \Lambda_c^+ \pi^-$ and $\Lambda_c^+ \rightarrow p K^- \pi^+$ decays.			

$\Sigma_b(6097)^+$ DECAY MODES

Mode	Fraction (Γ_i/Γ)
Γ_1 $\Lambda_b \pi^+ \times B(b \rightarrow \Sigma_b(6097)^+)$	seen

$\Sigma_b(6097)^+$ BRANCHING RATIOS

$\Gamma(\Lambda_b \pi^+ \times B(b \rightarrow \Sigma_b(6097)^+))/\Gamma_{\text{total}}$	DOCUMENT ID	TECN	COMMENT	Γ_1/Γ
seen	AAIJ	19A	LHCB pp at 7, 8 TeV	

$\Sigma_b(6097)^+$ REFERENCES

AAIJ	19A	PRL 122 012001	R. Aaij et al.	(LHCb Collab.)
------	-----	----------------	----------------	----------------

$\Sigma_b(6097)^-$	$J^P = ??$	Status: ***
--------------------	------------	-------------

$\Sigma_b(6097)^-$ MASS

VALUE (MeV)	DOCUMENT ID	TECN	COMMENT
6098.0 $\pm 1.7 \pm 0.5$	1 AAIJ	19A	LHCB pp at 7, 8 TeV
1 Measured using fully reconstructed $\Lambda_b^0 \rightarrow \Lambda_c^+ \pi^-$ and $\Lambda_c^+ \rightarrow p K^- \pi^+$ decays.			

$\Sigma_b(6097)^-$ WIDTH

VALUE (MeV)	DOCUMENT ID	TECN	COMMENT
28.9 $\pm 4.2 \pm 0.9$	1 AAIJ	19A	LHCB pp at 7, 8 TeV
1 Measured using fully reconstructed $\Lambda_b^0 \rightarrow \Lambda_c^+ \pi^-$ and $\Lambda_c^+ \rightarrow p K^- \pi^+$ decays.			

$\Sigma_b(6097)^-$ DECAY MODES

Mode	Fraction (Γ_i/Γ)
Γ_1 $\Lambda_b \pi^- \times B(b \rightarrow \Sigma_b(6097)^-)$	seen

$\Sigma_b(6097)^-$ BRANCHING RATIOS

$\Gamma(\Lambda_b \pi^- \times B(b \rightarrow \Sigma_b(6097)^-))/\Gamma_{\text{total}}$	DOCUMENT ID	TECN	COMMENT	Γ_1/Γ
seen	AAIJ	19A	LHCB pp at 7, 8 TeV	

$\Sigma_b(6097)^-$ REFERENCES

AAIJ	19A	PRL 122 012001	R. Aaij et al.	(LHCb Collab.)
------	-----	----------------	----------------	----------------



$I(J^P) = \frac{1}{2}(\frac{1}{2}^+)$ Status: ***
I, J, P need confirmation.

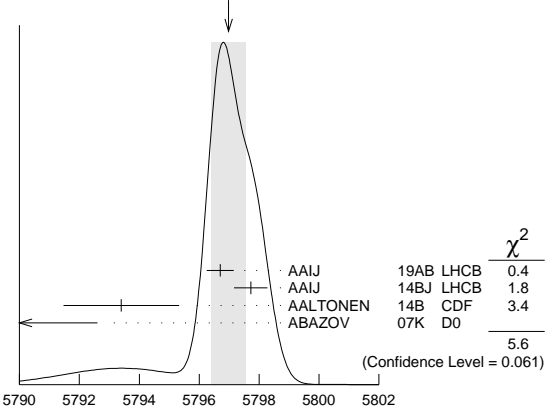
In the quark model, Ξ_b^0 and Ξ_b^- are an iso doublet (*usb*, *dsb*) state; the lowest Ξ_b^0 and Ξ_b^- ought to have $J^P = 1/2^+$. None of I, J, or P have actually been measured.

Ξ_b^- MASS

Ξ_b^- MASS

VALUE (MeV)	DOCUMENT ID	TECN	COMMENT
5797.0 ± 0.6 OUR AVERAGE	Error includes scale factor of 1.7. See the ideogram below.		
5796.70 $\pm 0.39 \pm 0.23$	AAIJ	19AB	LHCB pp at 7, 8 and 13 TeV
5797.72 $\pm 0.46 \pm 0.31$	1 AAIJ	14BJ	LHCB pp at 7, 8 TeV
5793.4 $\pm 1.8 \pm 0.7$	2 AALTONEN	14B	CDF $p\bar{p}$ at 1.96 TeV
5774 $\pm 11 \pm 15$	3 ABAZOV	07K	D0 $p\bar{p}$ at 1.96 TeV
• • • We do not use the following data for averages, fits, limits, etc. • • •			
5795.8 $\pm 0.9 \pm 0.4$	4 AAIJ	13AV	LHCB Repl. by AAIJ 19AB
5796.7 $\pm 5.1 \pm 1.4$	5 AALTONEN	11X	CDF Repl. by AALTONEN 14B
5790.9 $\pm 2.6 \pm 0.8$	6 AALTONEN	09AP	CDF Repl. by AALTONEN 14B
5792.9 $\pm 2.5 \pm 1.7$	7 AALTONEN	07A	CDF Repl. by AALTONEN 09AP

WEIGHTED AVERAGE
5797.0 \pm 0.6 (Error scaled by 1.7)



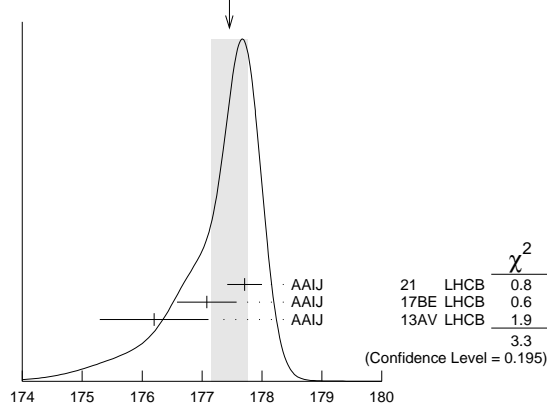
Ξ_b^- MASS (MeV)

- 1 Reconstructed in $\Xi_b^- \rightarrow \Xi_c^0 \pi^-$, $\Xi_c^0 \rightarrow p K^- K^- \pi^+$ decays. Reference Λ_b^0 mass 5619.30 \pm 0.34 MeV from AAIJ 14AA.
- 2 Uses $\Xi_b^- \rightarrow J/\psi \Xi^-$ and $\Xi_c^0 \pi^-$ decays.
- 3 Observed in $\Xi_b^- \rightarrow J/\psi \Xi^-$ decays with 15.2 \pm 4.4 $^{+1.9}_{-0.4}$ candidates, a significance of 5.5 sigma.
- 4 Measured in $\Xi_b^- \rightarrow J/\psi \Xi^-$ decays.
- 5 Measured in $\Xi_b^- \rightarrow \Xi_c^0 \pi^-$ with 25.8 $^{+5.5}_{-5.2}$ candidates.
- 6 Measured in $\Xi_b^- \rightarrow J/\psi \Xi^-$ decays with 66 $^{+14}_{-9}$ candidates.
- 7 Observed in $\Xi_b^- \rightarrow J/\psi \Xi^-$ decays with 17.5 \pm 4.3 candidates, a significance of 7.7 sigma.

$m_{\Xi_b^-} - m_{\Lambda_b^0}$

VALUE (MeV)	DOCUMENT ID	TECN	COMMENT
177.46 ± 0.31 OUR AVERAGE	Error	includes scale factor of 1.3.	See the ideogram below.
177.71 ± 0.24 ± 0.16	¹ AAIJ	21 LHCb	pp at 7, 8, 13 TeV
177.08 ± 0.47 ± 0.16	² AAIJ	17BE LHCb	pp at 7, 8 TeV
176.2 ± 0.9 ± 0.1	³ AAIJ	13AV LHCb	pp at 7 TeV
• • • We do not use the following data for averages, fits, limits, etc. • • •			
177.73 ± 0.33 ± 0.14	⁴ AAIJ	17BE LHCb	pp at 7, 8 TeV
178.36 ± 0.46 ± 0.16	^{1,5} AAIJ	14BJ LHCb	Repl. by AAIJ 2021

WEIGHTED AVERAGE
177.46 ± 0.31 (Error scaled by 1.3)



$m_{\Xi_b^-} - m_{\Lambda_b^0}$ (MeV)

- 1 Reconstructed in $\Xi_b^- \rightarrow \Xi_c^0 \pi^-, \Xi_c^0 \rightarrow p K^- K^- \pi^+$ decays. Reference decays $\Lambda_b^0 \rightarrow \Lambda^+ \pi^-$ were used.
- 2 Reconstructed in $\Xi_b^- \rightarrow J/\psi \Lambda K^-$ decays. Reference decays $\Lambda_b^0 \rightarrow J/\psi \Lambda$ were used.
- 3 Reconstructed in $\Xi_b^- \rightarrow J/\psi \Xi^-$ decays.
- 4 Combination of the original statistically independent measurements of AAIJ 17BE and AAIJ 14BJ taking into account correlation between systematic uncertainties.
- 5 Combined with AAIJ 17BE.

$m_{\Xi_b^-} - m_{\Xi_b^0}$

VALUE (MeV)	DOCUMENT ID	TECN	COMMENT
5.9 ± 0.6 OUR AVERAGE			
5.92 ± 0.60 ± 0.23	¹ AAIJ	14BJ LHCb	pp at 7, 8 TeV
3.1 ± 5.6 ± 1.3	² AALTONEN	11x CDF	pP at 1.96 TeV

- 1 Reconstructed in $\Xi_b^- \rightarrow \Xi_c^0 \pi^-, \Xi_c^0 \rightarrow p K^- K^- \pi^+$ decays. Uses $m(\Xi_b^0) - m(\Lambda_b^0) = 172.44 \pm 0.39 \pm 0.17$ MeV from AAIJ 14Z.
- 2 Derived from measurements in $\Xi_b^0 \rightarrow \Xi_c^+ \pi^-$ and $\Xi_b^- \rightarrow J/\psi \Xi^-$ from AALTONEN 09AP taking correlated systematic uncertainties into account.

Ξ_b^- MEAN LIFE

“OUR EVALUATION” is an average using rescaled values of the data listed below. The average and rescaling were performed by the Heavy Flavor Averaging Group (HFLAV) and are described at <https://hflav.web.cern.ch/>. The averaging/rescaling procedure takes into account correlations between the measurements and asymmetric lifetime errors.

Ξ_b^- MEAN LIFE

VALUE (10^{-12} s)	DOCUMENT ID	TECN	COMMENT
1.572 ± 0.040 OUR EVALUATION			
1.57 ± 0.04 OUR AVERAGE	Error	includes scale factor of 1.1.	
1.599 ± 0.041 ± 0.022	¹ AAIJ	14BJ LHCb	pp at 7, 8 TeV
1.55 $^{+0.10}_{-0.09}$ ± 0.03	² AAIJ	14T LHCb	pp at 7, 8 TeV
1.36 ± 0.15 ± 0.02	AALTONEN	14B CDF	pP at 1.96 TeV
• • • We do not use the following data for averages, fits, limits, etc. • • •			
1.56 $^{+0.27}_{-0.25}$ ± 0.02	³ AALTONEN	09AP CDF	Repl. by AALTONEN 14B

- 1 Reconstructed in $\Xi_b^- \rightarrow \Xi_c^0 \pi^-, \Xi_c^0 \rightarrow p K^- K^- \pi^+$ decays. Reference Λ_b^0 lifetime $1.479 \pm 0.009 \pm 0.010$ ps from AAIJ 14U.
- 2 Measured in $\Xi_b^- \rightarrow J/\psi \Xi^-$ decays.
- 3 Measured in $\Xi_b^- \rightarrow J/\psi \Xi^-$ decays with 66^{+14}_{-9} candidates.

MEAN LIFE RATIOS

$\tau_{\Xi_b^-} / \tau_{\Lambda_b^0}$ mean life ratio

VALUE	DOCUMENT ID	TECN	COMMENT
1.089 ± 0.026 ± 0.011	¹ AAIJ	14BJ LHCb	pp at 7, 8 TeV

1 Reconstructed in $\Xi_b^- \rightarrow \Xi_c^0 \pi^-, \Xi_c^0 \rightarrow p K^- K^- \pi^+$ decays. Reference $\Lambda_b^0 \rightarrow \Lambda^+ \pi^-$.

$\tau_{\Xi_b^-} / \tau_{\Xi_b^0}$ mean life ratio

VALUE	DOCUMENT ID	TECN	COMMENT
1.083 ± 0.032 ± 0.016	¹ AAIJ	14BJ LHCb	pp at 7, 8 TeV

1 Reconstructed in $\Xi_b^- \rightarrow \Xi_c^0 \pi^-, \Xi_c^0 \rightarrow p K^- K^- \pi^+$ decays. Uses Ξ_b^0 measurements from AAIJ 14Z.

Ξ_b^- DECAY MODES

Mode	Fraction (Γ_i/Γ)
Γ_1 $J/\psi \Xi^- \times B(b \rightarrow \Xi_b^-)$	$(1.02^{+0.26}_{-0.21}) \times 10^{-5}$
Γ_2 $J/\psi \Lambda K^- \times B(b \rightarrow \Xi_b^-)$	$(2.5 \pm 0.4) \times 10^{-6}$
Γ_3 $p K^- K^- \times B(b \rightarrow \Xi_b^-)$	$(3.7 \pm 0.8) \times 10^{-8}$
Γ_4 $p K^- K^-$	seen
Γ_5 $p \pi^- \pi^-$	seen
Γ_6 $p K^- \pi^-$	seen
Γ_7 $\Lambda_b^0 \pi^- \times B(b \rightarrow \Xi_b^-) / B(b \rightarrow \Lambda_b^0)$	$(5.7 \pm 2.0) \times 10^{-4}$
Γ_8 $\Xi_c^0 \pi^-$	seen
Γ_9 $\Sigma(1385) K^-$	$(2.6 \pm 2.3) \times 10^{-7}$
Γ_{10} $\Lambda(1405) K^-$	$(1.9 \pm 1.2) \times 10^{-7}$
Γ_{11} $\Lambda(1520) K^-$	$(7.6 \pm 3.2) \times 10^{-7}$
Γ_{12} $\Lambda(1670) K^-$	$(4.5 \pm 2.3) \times 10^{-7}$
Γ_{13} $\Sigma(1775) K^-$	$(2.2 \pm 1.5) \times 10^{-7}$
Γ_{14} $\Sigma(1915) K^-$	$(2.6 \pm 2.5) \times 10^{-7}$

Ξ_b^- BRANCHING RATIOS

$\Gamma(J/\psi \Xi^- \times B(b \rightarrow \Xi_b^-)) / \Gamma_{total}$ Γ_1/Γ

VALUE (units 10^{-4})	DOCUMENT ID	TECN	COMMENT
0.102 $^{+0.026}_{-0.021}$ OUR AVERAGE			
0.098 $^{+0.023}_{-0.016}$ ± 0.014	¹ AALTONEN	09AP CDF	pP at 1.96 TeV
0.16 ± 0.07 ± 0.02	² ABAZOV	07k D0	pP at 1.96 TeV

- 1 AALTONEN 09AP reports $[\Gamma(\Xi_b^- \rightarrow J/\psi \Xi^- \times B(b \rightarrow \Xi_b^-)) / \Gamma_{total}] / [B(\Lambda_b^0 \rightarrow J/\psi(1S) \Lambda \times B(b \rightarrow \Lambda_b^0))] = 0.167^{+0.037}_{-0.025} \pm 0.012$ which we multiply by our best value $B(\Lambda_b^0 \rightarrow J/\psi(1S) \Lambda \times B(b \rightarrow \Lambda_b^0)) = (5.8 \pm 0.8) \times 10^{-5}$. Our first error is their experiment's error and our second error is the systematic error from using our best value.
- 2 ABAZOV 07k reports $[\Gamma(\Xi_b^- \rightarrow J/\psi \Xi^- \times B(b \rightarrow \Xi_b^-)) / \Gamma_{total}] / [B(\Lambda_b^0 \rightarrow J/\psi(1S) \Lambda \times B(b \rightarrow \Lambda_b^0))] = 0.28 \pm 0.09^{+0.09}_{-0.08}$ which we multiply by our best value $B(\Lambda_b^0 \rightarrow J/\psi(1S) \Lambda \times B(b \rightarrow \Lambda_b^0)) = (5.8 \pm 0.8) \times 10^{-5}$. Our first error is their experiment's error and our second error is the systematic error from using our best value.

$\Gamma(J/\psi \Lambda K^- \times B(b \rightarrow \Xi_b^-)) / \Gamma_{total}$ Γ_2/Γ

VALUE (units 10^{-6})	DOCUMENT ID	TECN	COMMENT
2.45 ± 0.19 ± 0.35	^{1,2} AAIJ	17BE LHCb	pp at 7 and 8 TeV

- 1 AAIJ 17BE reports $[\Gamma(\Xi_b^- \rightarrow J/\psi \Lambda K^- \times B(b \rightarrow \Xi_b^-)) / \Gamma_{total}] / [B(\Lambda_b^0 \rightarrow J/\psi(1S) \Lambda \times B(b \rightarrow \Lambda_b^0))] = (4.19 \pm 0.29 \pm 0.15) \times 10^{-2}$ which we multiply by our best value $B(\Lambda_b^0 \rightarrow J/\psi(1S) \Lambda \times B(b \rightarrow \Lambda_b^0)) = (5.8 \pm 0.8) \times 10^{-5}$. Our first error is their experiment's error and our second error is the systematic error from using our best value.
- 2 Integrated over the b -baryon transverse momentum $p_T < 25$ GeV and rapidity $2.0 < y < 4.5$.

$\Gamma(p K^- K^- \times B(b \rightarrow \Xi_b^-)) / \Gamma_{total}$ Γ_3/Γ

VALUE (units 10^{-8})	DOCUMENT ID	TECN	COMMENT
3.7 ± 0.8 ± 0.2	¹ AAIJ	17F LHCb	pp at 7, 8 TeV

- 1 AAIJ 17F reports $[\Gamma(\Xi_b^- \rightarrow p K^- K^- \times B(\bar{b} \rightarrow \Xi_b^-)) / \Gamma_{total}] / [B(B^+ \rightarrow K^+ K^- K^+) / [B(\bar{b} \rightarrow B^+)]] = (2.65 \pm 0.35 \pm 0.47) \times 10^{-3}$ which we multiply by our best values $B(B^+ \rightarrow K^+ K^- K^+) = (3.40 \pm 0.14) \times 10^{-5}$, $B(\bar{b} \rightarrow B^+) = (40.8 \pm 0.7) \times 10^{-2}$. Our first error is their experiment's error and our second error is the systematic error from using our best values.

$\Gamma(p K^- K^-) / \Gamma_{total}$ Γ_4/Γ

VALUE (units 10^{-6})	DOCUMENT ID	TECN	COMMENT
2.3 ± 0.9	¹ AAIJ	21AH LHCb	pp at 7, 8, 13 TeV

- 1 Obtained using the ratio of fragmentation and branching fractions relative to the $B^- \rightarrow K^+ K^- K^-$ decay.

$\Gamma(p \pi^- \pi^-) / \Gamma(p K^- K^-)$ Γ_5/Γ_4

VALUE	CL%	DOCUMENT ID	TECN	COMMENT
< 0.56	90	¹ AAIJ	17F LHCb	pp at 7, 8 TeV

- 1 Measures the ratio as $0.28 \pm 0.16 \pm 0.13$.

$\Gamma(p K^- \pi^-) / \Gamma(p K^- K^-)$ Γ_6/Γ_4

VALUE	DOCUMENT ID	TECN	COMMENT
0.98 ± 0.27 ± 0.09	AAIJ	17F LHCb	pp at 7, 8 TeV

Baryon Particle Listings

$$\Xi_b^-, \Xi_b^0$$

$\Gamma(\Lambda_b^0 \pi^- \times B(b \rightarrow \Xi_b^-)/B(b \rightarrow \Lambda_b^0))/\Gamma_{\text{total}}$	Γ_7/Γ		
VALUE (units 10^{-4})	DOCUMENT ID	TECN	COMMENT

$5.7 \pm 1.8^{+0.8}_{-0.9}$ ¹AAIJ 15BA LHCB *pp* at 7, 8 TeV

¹ A signal is reported with a significance of 3.2 standard deviations in the decay chain of $\Xi_b^- \rightarrow \Lambda_b^0 \pi^-$, $\Lambda_b^0 \rightarrow \Lambda_c^+ \pi^-$, and $\Lambda_c^+ \rightarrow p K^- \pi^+$.

$\Gamma(\Xi_b^0 \pi^-)/\Gamma_{\text{total}}$	Γ_8/Γ		
VALUE	DOCUMENT ID	TECN	COMMENT

seen AAIJ 16a LHCB *pp* at 7, 8 TeV

$\Gamma(\Sigma(1385) K^-)/\Gamma_{\text{total}}$	Γ_9/Γ		
VALUE (units 10^{-6})	DOCUMENT ID	TECN	COMMENT

$0.26 \pm 0.11 \pm 0.20$ ¹AAIJ 21AH LHCB *pp* at 7, 8 and 13 TeV

¹ Obtained from an amplitude analysis of quasi-two-body contributions to the $\Xi_b^- \rightarrow R K^-$ decay, with $R \rightarrow p K^-$.

$\Gamma(\Lambda(1405) K^-)/\Gamma_{\text{total}}$	Γ_{10}/Γ		
VALUE (units 10^{-6})	DOCUMENT ID	TECN	COMMENT

$0.19 \pm 0.06 \pm 0.10$ ¹AAIJ 21AH LHCB *pp* at 7, 8 and 13 TeV

¹ Obtained from an amplitude analysis of quasi-two-body contributions to the $\Xi_b^- \rightarrow R K^-$ decay, with $R \rightarrow p K^-$.

$\Gamma(\Lambda(1520) K^-)/\Gamma_{\text{total}}$	Γ_{11}/Γ		
VALUE (units 10^{-6})	DOCUMENT ID	TECN	COMMENT

$0.76 \pm 0.09 \pm 0.31$ ¹AAIJ 21AH LHCB *pp* at 7, 8 and 13 TeV

¹ Obtained from an amplitude analysis of quasi-two-body contributions to the $\Xi_b^- \rightarrow R K^-$ decay, with $R \rightarrow p K^-$.

$\Gamma(\Lambda(1670) K^-)/\Gamma_{\text{total}}$	Γ_{12}/Γ		
VALUE (units 10^{-6})	DOCUMENT ID	TECN	COMMENT

$0.45 \pm 0.07 \pm 0.22$ ¹AAIJ 21AH LHCB *pp* at 7, 8 and 13 TeV

¹ Obtained from an amplitude analysis of quasi-two-body contributions to the $\Xi_b^- \rightarrow R K^-$ decay, with $R \rightarrow p K^-$.

$\Gamma(\Sigma(1775) K^-)/\Gamma_{\text{total}}$	Γ_{13}/Γ		
VALUE (units 10^{-6})	DOCUMENT ID	TECN	COMMENT

$0.22 \pm 0.08 \pm 0.13$ ¹AAIJ 21AH LHCB *pp* at 7, 8 and 13 TeV

¹ Obtained from an amplitude analysis of quasi-two-body contributions to the $\Xi_b^- \rightarrow R K^-$ decay, with $R \rightarrow p K^-$.

$\Gamma(\Sigma(1915) K^-)/\Gamma_{\text{total}}$	Γ_{14}/Γ		
VALUE (units 10^{-6})	DOCUMENT ID	TECN	COMMENT

$0.26 \pm 0.09 \pm 0.23$ ¹AAIJ 21AH LHCB *pp* at 7, 8 and 13 TeV

¹ Obtained from an amplitude analysis of quasi-two-body contributions to the $\Xi_b^- \rightarrow R K^-$ decay, with $R \rightarrow p K^-$.

P VIOLATION ASYMMETRY

 $A_P(\Xi_b), \Xi_b^- - \Xi_b^+$ production asymmetry

$$A_P(\Xi_b) = [\sigma(\Xi_b^-) - \sigma(\Xi_b^+)] / [\sigma(\Xi_b^-) + \sigma(\Xi_b^+)]$$

VALUE (units 10^{-2})	DOCUMENT ID	TECN	COMMENT
--------------------------	-------------	------	---------

-2 ± 4 OUR AVERAGE
 $1.1 \pm 5.6 \pm 1.9$ ^{1,2}AAIJ 19AB LHCB *pp* at 7 and 8 TeV
 $-3.9 \pm 4.9 \pm 2.5$ ^{1,2}AAIJ 19AB LHCB *pp* at 13 TeV

¹ Baryon kinematic range $p_T < 20$ GeV/c and $2 < \eta < 6$.

² Measured using previous measurements of $A_P(\Lambda_b)$ in AAJ 17BF.

CP VIOLATION in Ξ_b decays

$$A_{CP}(\Xi_b) = [B(\Xi_b^- \rightarrow f) - B(\Xi_b^+ \rightarrow \bar{f})] / \text{Sum}$$

$A_{CP}(\Xi_b^- \rightarrow \Sigma(1385) K^-)$	DOCUMENT ID	TECN	COMMENT
VALUE			

$(-27 \pm 34 \pm 73) \times 10^{-2}$ AAIJ 21AH LHCB *pp* at 7, 8, 13 TeV

$A_{CP}(\Xi_b^- \rightarrow \Lambda(1405) K^-)$	DOCUMENT ID	TECN	COMMENT
VALUE			

$(-1 \pm 24 \pm 32) \times 10^{-2}$ AAIJ 21AH LHCB *pp* at 7, 8, 13 TeV

$A_{CP}(\Xi_b^- \rightarrow \Lambda(1520) K^-)$	DOCUMENT ID	TECN	COMMENT
VALUE			

$(-5 \pm 9 \pm 8) \times 10^{-2}$ AAIJ 21AH LHCB *pp* at 7, 8, 13 TeV

$A_{CP}(\Xi_b^- \rightarrow \Lambda(1670) K^-)$	DOCUMENT ID	TECN	COMMENT
VALUE			

$(3 \pm 14 \pm 10) \times 10^{-2}$ AAIJ 21AH LHCB *pp* at 7, 8, 13 TeV

$A_{CP}(\Xi_b^- \rightarrow \Sigma(1775) K^-)$	DOCUMENT ID	TECN	COMMENT
VALUE			

$(-47 \pm 26 \pm 14) \times 10^{-2}$ AAIJ 21AH LHCB *pp* at 7, 8, 13 TeV

$A_{CP}(\Xi_b^- \rightarrow \Sigma(1915) K^-)$	DOCUMENT ID	TECN	COMMENT
VALUE			

$(11 \pm 26 \pm 22) \times 10^{-2}$ AAIJ 21AH LHCB *pp* at 7, 8, 13 TeV

 Ξ_b^- REFERENCES

AAIJ	21	PR D103 012004	R. Aaij et al.	(LHCb Collab.)
AAIJ	21AH	PR D104 052010	R. Aaij et al.	(LHCb Collab.)
AAIJ	19AB	PR D99 052006	R. Aaij et al.	(LHCb Collab.)
AAIJ	17BE	PL B772 265	R. Aaij et al.	(LHCb Collab.)
AAIJ	17BF	PL B774 139	R. Aaij et al.	(LHCb Collab.)
AAIJ	17F	PRL 118 071801	R. Aaij et al.	(LHCb Collab.)
AAIJ	16O	PR D93 092007	R. Aaij et al.	(LHCb Collab.)
AAIJ	15BA	PRL 115 241801	R. Aaij et al.	(LHCb Collab.)
AAIJ	14AA	PRL 112 202001	R. Aaij et al.	(LHCb Collab.)
AAIJ	14BJ	PRL 113 242002	R. Aaij et al.	(LHCb Collab.)
AAIJ	14T	PL B736 154	R. Aaij et al.	(LHCb Collab.)
AAIJ	14U	PL B734 122	R. Aaij et al.	(LHCb Collab.)
AAIJ	14Z	PRL 113 032001	R. Aaij et al.	(LHCb Collab.)
AALTONEN	14B	PR D89 072014	T. Aaltonen et al.	(CDF Collab.)
AAIJ	13AV	PRL 110 182001	R. Aaij et al.	(LHCb Collab.)
AALTONEN	11X	PRL 107 102001	T. Aaltonen et al.	(CDF Collab.)
AALTONEN	09AP	PR D80 072003	T. Aaltonen et al.	(CDF Collab.)
AALTONEN	07A	PRL 99 052002	T. Aaltonen et al.	(CDF Collab.)
ABAZOV	07K	PRL 99 052001	V.M. Abazov et al.	(D0 Collab.)

$$\Xi_b^0$$

$I(J^P) = \frac{1}{2}(\frac{1}{2}^+)$ Status: ***
 I, J, P need confirmation.

In the quark model, Ξ_b^0 and Ξ_b^- are an isodoublet (usb, dsb) state; the lowest Ξ_b^0 and Ξ_b^- ought to have $J^P = 1/2^+$. None of $I, J, or P$ have actually been measured.

 Ξ_b^0 MASS

Ξ_b^0 MASS	DOCUMENT ID	TECN	COMMENT
VALUE (MeV)			

5791.9 ± 0.5 OUR AVERAGE

$5794.3 \pm 2.4 \pm 0.7$ AAIJ 14H LHCB *pp* at 7 TeV
 $5791.80 \pm 0.39 \pm 0.31$ ¹AAIJ 14Z LHCB *pp* at 7, 8 TeV
 $5788.7 \pm 4.3 \pm 1.4$ ²AALTONEN 14B CDF $p\bar{p}$ at 1.96 TeV

• • • We do not use the following data for averages, fits, limits, etc. • • •
 $5787.8 \pm 5.0 \pm 1.3$ ³AALTONEN 11X CDF Repl. by AALTONEN 14B

¹ Uses $\Xi_b^0 \rightarrow \Xi_c^+ \pi^-$ and $\Xi_c^+ \rightarrow p K^- \pi^+$ decays. The measurement comes from the mass difference of Ξ_b^0 and Λ_b^0 .

² Uses $\Xi_b^0 \rightarrow \Xi_c^+ \pi^-$ decays.

³ Measured in $\Xi_b^0 \rightarrow \Xi_c^+ \pi^-$ with $25.3_{-5.4}^{+5.6}$ candidates.

 $m_{\Xi_b^0} - m_{\Lambda_b^0}$

VALUE (MeV)	DOCUMENT ID	TECN	COMMENT
-------------	-------------	------	---------

172.5 ± 0.4 OUR AVERAGE

$174.8 \pm 2.4 \pm 0.5$ AAIJ 14H LHCB *pp* at 7 TeV
 $172.44 \pm 0.39 \pm 0.17$ ¹AAIJ 14Z LHCB *pp* at 7, 8 TeV

¹ Uses $\Xi_b^0 \rightarrow \Xi_c^+ \pi^-$ and $\Xi_c^+ \rightarrow p K^- \pi^+$ decays.

 Ξ_b^0 MEAN LIFE

"OUR EVALUATION" is an average using rescaled values of the data listed below. The average and rescaling were performed by the Heavy Flavor Averaging Group (HFLAV) and are described at <https://hflav.web.cern.ch/>. The averaging/rescaling procedure takes into account correlations between the measurements and asymmetric lifetime errors.

 Ξ_b^0 MEAN LIFE

VALUE (10^{-12} s)	DOCUMENT ID	TECN	COMMENT
-----------------------	-------------	------	---------

1.480 ± 0.030 OUR EVALUATION

$1.477 \pm 0.026 \pm 0.019$ ¹AAIJ 14Z LHCB *pp* at 7, 8 TeV

¹ Uses $\Xi_b^0 \rightarrow \Xi_c^+ \pi^-$ and $\Xi_c^+ \rightarrow p K^- \pi^+$ decays. The measurement comes from the value of relative lifetime of Ξ_b^0 to Λ_b^0 .

 $\tau_{\text{mix}} (1/2\pi)$ times the oscillation period

VALUE (s)	DOCUMENT ID	TECN	COMMENT
-----------	-------------	------	---------

$> 13 \times 10^{-12}$ ¹AAIJ 17BH LHCB *pp* at 7, 8 TeV

¹ Uses Ξ_b^{*+} and $\Xi_b^{\prime-}$ decays to $\Xi_b^0 \pi^-$, where $\Xi_b^0 \rightarrow \Xi_c^+ \pi^-$, $\Xi_c^+ \rightarrow p K^- \pi^+$.

 Ξ_b^0 DECAY MODES

Mode	Fraction (Γ_i/Γ)	Confidence level
Γ_1 $p D^0 K^- \times B(b \rightarrow \Xi_b^0)$	$(1.7 \pm 0.5) \times 10^{-6}$	
Γ_2 $p \bar{K}^0 \pi^- \times B(b \rightarrow \Xi_b^0)/B(\bar{b} \rightarrow B^0)$	$< 1.6 \times 10^{-6}$	90%

See key on page 1127

Baryon Particle Listings

$\Xi_b^0, \Xi_b'(5935)^-$

Γ_3	$\rho K^0 K^- \times B(b \rightarrow \Xi_b^0)/B(\bar{b} \rightarrow B^0)$	< 1.1	$\times 10^{-6}$	90%
Γ_4	$\Lambda \pi^+ \pi^- \times B(b \rightarrow \Xi_b^0)/B(b \rightarrow \Lambda_b^0)$	< 1.7	$\times 10^{-6}$	90%
Γ_5	$\Lambda K^- \pi^+ \times B(b \rightarrow \Xi_b^0)/B(b \rightarrow \Lambda_b^0)$	< 8	$\times 10^{-7}$	90%
Γ_6	$\Lambda K^+ K^- \times B(b \rightarrow \Xi_b^0)/B(b \rightarrow \Lambda_b^0)$	< 3	$\times 10^{-7}$	90%
Γ_7	$J/\psi \Lambda$	seen		
Γ_8	$J/\psi \Xi^0$	seen		
Γ_9	$\Lambda_c^+ K^- \times B(b \rightarrow \Xi_b^0)$	(6 ± 4)	$\times 10^{-7}$	
Γ_{10}	$\rho K^- \pi^+ \pi^- \times B(b \rightarrow \Xi_b^0)/B(b \rightarrow \Lambda_b^0)$	(1.9 ± 0.4)	$\times 10^{-6}$	
Γ_{11}	$\rho K^- K^+ \pi^- \times B(b \rightarrow \Xi_b^0)/B(b \rightarrow \Lambda_b^0)$	(1.71 ± 0.31)	$\times 10^{-6}$	
Γ_{12}	$\rho K^- K^+ K^- \times B(b \rightarrow \Xi_b^0)/B(b \rightarrow \Lambda_b^0)$	(1.7 ± 1.0)	$\times 10^{-7}$	

Ξ_b^0 BRANCHING RATIOS

$\Gamma(\rho D^0 K^- \times B(b \rightarrow \Xi_b^0))/\Gamma_{total}$	Γ_1/Γ		
VALUE (units 10^{-6})	DOCUMENT ID	TECN	COMMENT
1.7 ± 0.4 ± 0.4	¹ AAIJ	14H	LHCB <i>pp</i> at 7 TeV
¹ AAIJ 14H reports $[\Gamma(\Xi_b \rightarrow \rho D^0 K^- \times B(\bar{b} \rightarrow \Xi_b))/\Gamma_{total}] / [B(\bar{b} \rightarrow b\text{-baryon})] / [B(\Lambda_b^0 \rightarrow \rho D^0 K^-)] = 0.44 \pm 0.09 \pm 0.06$ which we multiply by our best values $B(\bar{b} \rightarrow b\text{-baryon}) = (8.4 \pm 1.1) \times 10^{-2}$, $B(\Lambda_b^0 \rightarrow \rho D^0 K^-) = (4.6 \pm 0.8) \times 10^{-5}$. Our first error is their experiment's error and our second error is the systematic error from using our best values.			

$\Gamma(\rho \bar{K}^0 \pi^- \times B(b \rightarrow \Xi_b^0)/B(\bar{b} \rightarrow B^0))/\Gamma_{total}$	Γ_2/Γ			
VALUE	CL%	DOCUMENT ID	TECN	COMMENT
< 1.6 × 10⁻⁶	90	AAIJ	14Q	LHCB <i>pp</i> at 7 TeV

$\Gamma(\rho K^0 K^- \times B(b \rightarrow \Xi_b^0)/B(\bar{b} \rightarrow B^0))/\Gamma_{total}$	Γ_3/Γ			
VALUE	CL%	DOCUMENT ID	TECN	COMMENT
< 1.1 × 10⁻⁶	90	AAIJ	14Q	LHCB <i>pp</i> at 7 TeV

$\Gamma(\Lambda \pi^+ \pi^- \times B(b \rightarrow \Xi_b^0)/B(b \rightarrow \Lambda_b^0))/\Gamma_{total}$	Γ_4/Γ			
VALUE	CL%	DOCUMENT ID	TECN	COMMENT
< 1.7 × 10⁻⁶	90	AAIJ	16W	LHCB <i>pp</i> at 7, 8 TeV

$\Gamma(\Lambda K^- \pi^+ \times B(b \rightarrow \Xi_b^0)/B(b \rightarrow \Lambda_b^0))/\Gamma_{total}$	Γ_5/Γ			
VALUE	CL%	DOCUMENT ID	TECN	COMMENT
< 0.8 × 10⁻⁶	90	AAIJ	16W	LHCB <i>pp</i> at 7, 8 TeV

$\Gamma(\Lambda K^+ K^- \times B(b \rightarrow \Xi_b^0)/B(b \rightarrow \Lambda_b^0))/\Gamma_{total}$	Γ_6/Γ			
VALUE	CL%	DOCUMENT ID	TECN	COMMENT
< 0.3 × 10⁻⁶	90	AAIJ	16W	LHCB <i>pp</i> at 7, 8 TeV

$\Gamma(J/\psi \Lambda)/\Gamma(J/\psi \Xi^0)$	Γ_7/Γ_8		
VALUE (units 10^{-3})	DOCUMENT ID	TECN	COMMENT
8.2 ± 2.1 ± 0.9	¹ AAIJ	20U	LHCB <i>pp</i> at 7, 8 and 13 TeV
¹ The Cabibbo suppressed $\Xi_b \rightarrow J/\psi \Lambda$ decay is observed for the first time.			

$\Gamma(\Lambda_c^+ K^- \times B(b \rightarrow \Xi_b^0))/\Gamma(\rho D^0 K^- \times B(b \rightarrow \Xi_b^0))$	Γ_9/Γ_1		
VALUE	DOCUMENT ID	TECN	COMMENT
0.36 ± 0.19 ± 0.02	¹ AAIJ	14H	LHCB <i>pp</i> at 7 TeV
¹ AAIJ 14H reports $[\Gamma(\Xi_b \rightarrow \Lambda_c^+ K^- \times B(\bar{b} \rightarrow \Xi_b))/\Gamma(\Xi_b \rightarrow \rho D^0 K^- \times B(\bar{b} \rightarrow \Xi_b))] \times [B(\Lambda_c^+ \rightarrow \rho K^- \pi^+)] / [B(D^0 \rightarrow K^- \pi^+)] = 0.57 \pm 0.22 \pm 0.21$ which we multiply or divide by our best values $B(\Lambda_c^+ \rightarrow \rho K^- \pi^+) = (6.28 \pm 0.32) \times 10^{-2}$, $B(D^0 \rightarrow K^- \pi^+) = (3.947 \pm 0.030) \times 10^{-2}$. Our first error is their experiment's error and our second error is the systematic error from using our best values.			

$\Gamma(\rho K^- \pi^+ \pi^- \times B(b \rightarrow \Xi_b^0)/B(b \rightarrow \Lambda_b^0))/\Gamma_{total}$	Γ_{10}/Γ		
VALUE (units 10^{-6})	DOCUMENT ID	TECN	COMMENT
1.90 ± 0.35 ± 0.17	¹ AAIJ	18Q	LHCB <i>pp</i> at 7, 8 TeV
¹ AAIJ 18Q reports $[\Gamma(\Xi_b \rightarrow \rho K^- \pi^+ \pi^- \times B(b \rightarrow \Xi_b^0)/B(b \rightarrow \Lambda_b^0))/\Gamma_{total}] / [B(\Lambda_c^+ \rightarrow \rho K^- \pi^+)] / [B(\Lambda_b^0 \rightarrow \Lambda_c^+ \pi^-)] = (6.2 \pm 0.8 \pm 0.2 \pm 0.8) \times 10^{-3}$ which we multiply by our best values $B(\Lambda_c^+ \rightarrow \rho K^- \pi^+) = (6.28 \pm 0.32) \times 10^{-2}$, $B(\Lambda_b^0 \rightarrow \Lambda_c^+ \pi^-) = (4.9 \pm 0.4) \times 10^{-3}$. Our first error is their experiment's error and our second error is the systematic error from using our best values.			

$\Gamma(\rho K^- K^- \pi^+ \times B(b \rightarrow \Xi_b^0)/B(b \rightarrow \Lambda_b^0))/\Gamma_{total}$	Γ_{11}/Γ		
VALUE (units 10^{-6})	DOCUMENT ID	TECN	COMMENT
1.71 ± 0.27 ± 0.15	¹ AAIJ	18Q	LHCB <i>pp</i> at 7, 8 TeV
¹ AAIJ 18Q reports $[\Gamma(\Xi_b \rightarrow \rho K^- K^- \pi^+ \times B(b \rightarrow \Xi_b^0)/B(b \rightarrow \Lambda_b^0))/\Gamma_{total}] / [B(\Lambda_c^+ \rightarrow \rho K^- \pi^+)] / [B(\Lambda_b^0 \rightarrow \Lambda_c^+ \pi^-)] = (5.6 \pm 0.6 \pm 0.4 \pm 0.5) \times 10^{-3}$ which we multiply by our best values $B(\Lambda_c^+ \rightarrow \rho K^- \pi^+) = (6.28 \pm 0.32) \times 10^{-2}$, $B(\Lambda_b^0 \rightarrow \Lambda_c^+ \pi^-) = (4.9 \pm 0.4) \times 10^{-3}$. Our first error is their experiment's error and our second error is the systematic error from using our best values.			

$\Gamma(\rho K^- K^+ K^- \times B(b \rightarrow \Xi_b^0)/B(b \rightarrow \Lambda_b^0))/\Gamma_{total}$	Γ_{12}/Γ		
VALUE (units 10^{-6})	DOCUMENT ID	TECN	COMMENT
0.17 ± 0.09 ± 0.02	^{1,2} AAIJ	18Q	LHCB <i>pp</i> at 7, 8 TeV
¹ AAIJ 18Q reports $[\Gamma(\Xi_b \rightarrow \rho K^- K^+ K^- \times B(b \rightarrow \Xi_b^0)/B(b \rightarrow \Lambda_b^0))/\Gamma_{total}] / [B(\Lambda_c^+ \rightarrow \rho K^- \pi^+)] / [B(\Lambda_b^0 \rightarrow \Lambda_c^+ \pi^-)] = (0.57 \pm 0.28 \pm 0.08 \pm 0.10) \times 10^{-3}$ which we multiply by our best values $B(\Lambda_c^+ \rightarrow \rho K^- \pi^+) = (6.28 \pm 0.32) \times 10^{-2}$, $B(\Lambda_b^0 \rightarrow \Lambda_c^+ \pi^-) = (4.9 \pm 0.4) \times 10^{-3}$. Our first error is their experiment's error and our second error is the systematic error from using our best values.			
² AAIJ 18Q sees excess with a significance of 2.3σ . Using $B(\Lambda_b^0 \rightarrow \Lambda_c^+ \pi^-) = (0.430 \pm 0.036) \times 10^{-2}$ and $B(\Lambda_c^+ \rightarrow \rho K^- \pi^+) = (6.46 \pm 0.24) \times 10^{-2}$ the authors set two sided limit [0.11-0.25] at 90% C.L.			

P AND CP VIOLATION ASYMMETRIES

$a_P(\Xi_b^0 \rightarrow \rho K^- K^- \pi^+)$			
Observable calculated as average of the triple products for Ξ_b^0 and Ξ_b^0 , which is sensitive to parity violation.			
VALUE (%)	DOCUMENT ID	TECN	COMMENT
-3.04 ± 5.19 ± 0.36	¹ AAIJ	18AG	LHCB <i>pp</i> at 7, 8 TeV
¹ Measured over full phase space of the decay.			

$a_{CP}(\Xi_b^0 \rightarrow \rho K^- K^- \pi^+)$			
Observable calculated as half of the difference between triple products for Ξ_b^0 and Ξ_b^0 , which is sensitive to CP violation.			
VALUE (%)	DOCUMENT ID	TECN	COMMENT
-3.58 ± 5.19 ± 0.36	¹ AAIJ	18AG	LHCB <i>pp</i> at 7, 8 TeV
¹ Measured over full phase space of the decay.			

$\Delta A_{CP}(\Xi_b^0 \rightarrow \rho K^- \pi^+ \pi^-)$			
$\Delta A_{CP} \equiv A_{CP}(\Xi_b^0 \rightarrow \rho K^- \pi^+ \pi^-) - A_{CP}(\Xi_b^0 \rightarrow (\Xi_c^+ \rightarrow \rho K^- \pi^+) \pi^-)$			
VALUE (units 10^{-2})	DOCUMENT ID	TECN	COMMENT
-17 ± 11 ± 1	¹ AAIJ	19AH	LHCB <i>pp</i> at 7 and 8 TeV
¹ Full phase space.			

$\Delta A_{CP}(\Xi_b^0 \rightarrow \rho K^- \pi^+ K^-)$			
$\Delta A_{CP} \equiv A_{CP}(\Xi_b^0 \rightarrow \rho K^- \pi^+ K^-) - A_{CP}(\Xi_b^0 \rightarrow (\Xi_c^+ \rightarrow \rho K^- \pi^+) K^-)$			
VALUE (units 10^{-2})	DOCUMENT ID	TECN	COMMENT
-6.8 ± 8.0 ± 0.8	¹ AAIJ	19AH	LHCB <i>pp</i> at 7 and 8 TeV
¹ Full phase space.			

Ξ_b^0 REFERENCES

AAIJ	20U	PRL 124 111802	R. Aaij et al.	(LHCb Collab.)
AAIJ	19AH	EPJ C79 745	R. Aaij et al.	(LHCb Collab.)
AAIJ	18AG	JHEP 1808 039	R. Aaij et al.	(LHCb Collab.)
AAIJ	18Q	JHEP 1802 098	R. Aaij et al.	(LHCb Collab.)
AAIJ	17BH	PRL 119 181807	R. Aaij et al.	(LHCb Collab.)
AAIJ	16W	JHEP 1605 081	R. Aaij et al.	(LHCb Collab.)
AAIJ	14H	PR D89 032001	R. Aaij et al.	(LHCb Collab.)
AAIJ	14Q	JHEP 1404 087	R. Aaij et al.	(LHCb Collab.)
AAIJ	14Z	PRL 113 032001	R. Aaij et al.	(LHCb Collab.)
AALTONEN	14B	PR D89 072014	T. Aaltonen et al.	(CDF Collab.)
AALTONEN	11X	PRL 107 102001	T. Aaltonen et al.	(CDF Collab.)

$\Xi_b'(5935)^-$

$J^P = \frac{1}{2}^+$ Status: ***

$\Xi_b'(5935)^-$ MASS

VALUE (MeV)	DOCUMENT ID	TECN	COMMENT
5935.02 ± 0.02 ± 0.05	¹ AAIJ	15H	LHCB <i>pp</i> at 7, 8 TeV
¹ Not independent of the mass difference measurement below. Observed in $\Xi_b^0 \pi^-$ channel with $\Xi_b^0 \rightarrow \Xi_c^+ \pi^-$ and $\Xi_c^+ \rightarrow \rho K^- \pi^+$.			

$m_{\Xi_b'(5935)^-} - m_{\Xi_b^0} - m_{\pi^-}$

VALUE (MeV)	DOCUMENT ID	TECN	COMMENT
3.653 ± 0.018 ± 0.006	² AAIJ	15H	LHCB <i>pp</i> at 7, 8 TeV
² Observed in $\Xi_b^0 \pi^-$ channel with $\Xi_b^0 \rightarrow \Xi_c^+ \pi^-$ and $\Xi_c^+ \rightarrow \rho K^- \pi^+$.			

Baryon Particle Listings

 $\Xi'_b(5935)^-, \Xi_b(5945)^0, \Xi_b(5955)^-, \Xi_b(6100)^-, \Xi_b(6227)^-$ $\Xi'_b(5935)^-$ WIDTH

VALUE (MeV)	CL%	DOCUMENT ID	TECN	COMMENT
<0.08	95	³ AAIJ	15H LHCb	pp at 7, 8 TeV

³ Observed in $\Xi_b^0 \pi^-$ channel with $\Xi_b^0 \rightarrow \Xi_c^+ \pi^-$ and $\Xi_c^+ \rightarrow p K^- \pi^+$.

 $\Xi'_b(5935)^-$ DECAY MODES

Mode	Fraction (Γ_i/Γ)
$\Gamma_1 \quad \Xi_b^0 \pi^- \times B(\bar{b} \rightarrow \Xi'_b(5935)^-)/B(\bar{b} \rightarrow \Xi_b^0)$	(11.8±1.8) %

 $\Xi'_b(5935)^-$ BRANCHING RATIOS

$\Gamma(\Xi_b^0 \pi^- \times B(\bar{b} \rightarrow \Xi'_b(5935)^-)/B(\bar{b} \rightarrow \Xi_b^0))/\Gamma_{\text{total}}$	Γ_1/Γ		
0.118±0.017±0.007			
VALUE	DOCUMENT ID	TECN	COMMENT
	⁴ AAIJ	15H LHCb	pp at 7, 8 TeV

⁴ Observed in $\Xi_b^0 \pi^-$ channel with $\Xi_b^0 \rightarrow \Xi_c^+ \pi^-$ and $\Xi_c^+ \rightarrow p K^- \pi^+$.

 $\Xi'_b(5935)^-$ REFERENCES

AAIJ 15H PRL 114 062004 R. Aaij et al. (LHCb Collab.)

$\Xi_b(5945)^0$	$J^P = \frac{3}{2}^+$	Status: ***
-----------------------------------	-----------------------	-------------

Quantum numbers are based on quark model expectations.

 $\Xi_b(5945)^0$ MASS

VALUE (MeV)	DOCUMENT ID	TECN	COMMENT
5952.3±0.6 OUR AVERAGE			
5952.3±0.1±0.6	¹ AAIJ	16AE LHCb	pp at 7, 8 TeV
5951.4±0.8±0.6	² CHATRCHYAN12s	CMS	pp at 7 TeV, 5.3 fb ⁻¹

¹ AAIJ 16AE measures $m(\Xi_b(5945)^0) - m(\Xi_b^-) - m(\pi^+) = 15.727 \pm 0.068 \pm 0.023$ MeV. We have adjusted the measurement to our best values of $m(\Xi_b^-) = 5797.0 \pm 0.6$ MeV, $m(\pi^+) = 139.57039 \pm 0.00018$ MeV. Our first error is their experiment's error and our second error is the systematic error from using our best values.

² CHATRCHYAN 12s measures $m(\Xi_b(5945)^0) - m(\Xi_b^-) - m(\pi^+) = 14.84 \pm 0.74 \pm 0.28$ MeV. We have adjusted the measurement to our best values of $m(\Xi_b^-) = 5797.0 \pm 0.6$ MeV, $m(\pi^+) = 139.57039 \pm 0.00018$ MeV. Our first error is their experiment's error and our second error is the systematic error from using our best values.

 $\Xi_b(5945)^0$ WIDTH

VALUE (MeV)	DOCUMENT ID	TECN	COMMENT
0.90±0.16±0.08	³ AAIJ	16AE LHCb	pp at 7, 8 TeV

••• We do not use the following data for averages, fits, limits, etc. •••

2.1 ±1.7 ⁴ CHATRCHYAN12s CMS pp at 7 TeV, 5.3 fb⁻¹

³ Measured using $\Xi_b(5945)^0 \rightarrow \Xi_b^- \pi^+, \Xi_b^- \rightarrow \Xi_c^0 \pi^-, \Xi_c^0 \rightarrow p K^- K^- \pi^+$ decays.

⁴ Systematic uncertainty not evaluated.

 $\Xi_b(5945)^0$ DECAY MODES

Mode	Fraction (Γ_i/Γ)
$\Gamma_1 \quad \Xi_b^- \pi^+$	seen

 $\Xi_b(5945)^0$ BRANCHING RATIOS

$\Gamma(\Xi_b^- \pi^+)/\Gamma_{\text{total}}$	Γ_1/Γ		
seen			
seen			
VALUE	DOCUMENT ID	TECN	COMMENT
	AAIJ	16AE ATLS	pp at 7, 8 TeV
	CHATRCHYAN12s	CMS	pp at 7 TeV, 5.3 fb ⁻¹

 $\Xi_b(5945)^0$ REFERENCESAAIJ 16AE JHEP 1605 161 R. Aaij et al. (LHCb Collab.)
CHATRCHYAN 12s PRL 108 252002 S. Chatrchyan et al. (CMS Collab.)

$\Xi_b(5955)^-$	$J^P = \frac{3}{2}^+$	Status: ***
-----------------------------------	-----------------------	-------------

 $\Xi_b(5955)^-$ MASS

VALUE (MeV)	DOCUMENT ID	TECN	COMMENT
5955.33±0.12±0.05	¹ AAIJ	15H LHCb	pp at 7, 8 TeV

¹ Not independent of the mass difference measurement below. Observed in $\Xi_b^0 \pi^-$ channel with $\Xi_b^0 \rightarrow \Xi_c^+ \pi^-$ and $\Xi_c^+ \rightarrow p K^- \pi^+$.

 $m_{\Xi_b(5955)^-} - m_{\Xi_b^0} - m_{\pi^-}$

VALUE (MeV)	DOCUMENT ID	TECN	COMMENT
23.96±0.12±0.06	¹ AAIJ	15H LHCb	pp at 7, 8 TeV

¹ Observed in $\Xi_b^0 \pi^-$ channel with $\Xi_b^0 \rightarrow \Xi_c^+ \pi^-$ and $\Xi_c^+ \rightarrow p K^- \pi^+$.

 $\Xi_b(5955)^-$ WIDTH

VALUE (MeV)	DOCUMENT ID	TECN	COMMENT
1.65±0.31±0.10	¹ AAIJ	15H LHCb	pp at 7, 8 TeV

¹ Observed in $\Xi_b^0 \pi^-$ channel with $\Xi_b^0 \rightarrow \Xi_c^+ \pi^-$ and $\Xi_c^+ \rightarrow p K^- \pi^+$.

 $\Xi_b(5955)^-$ DECAY MODES

Mode	Fraction (Γ_i/Γ)
$\Gamma_1 \quad \Xi_b^0 \pi^- \times B(\bar{b} \rightarrow \Xi_b^*(5955)^-)/B(\bar{b} \rightarrow \Xi_b^0)$	(20.7±3.5) %

 $\Xi_b(5955)^-$ BRANCHING RATIOS

$\Gamma(\Xi_b^0 \pi^- \times B(\bar{b} \rightarrow \Xi_b^*(5955)^-)/B(\bar{b} \rightarrow \Xi_b^0))/\Gamma_{\text{total}}$	Γ_1/Γ		
0.207±0.032±0.015			
VALUE	DOCUMENT ID	TECN	COMMENT
	¹ AAIJ	15H LHCb	pp at 7, 8 TeV

¹ Observed in $\Xi_b^0 \pi^-$ channel with $\Xi_b^0 \rightarrow \Xi_c^+ \pi^-$ and $\Xi_c^+ \rightarrow p K^- \pi^+$.

 $\Xi_b(5955)^-$ REFERENCES

AAIJ 15H PRL 114 062004 R. Aaij et al. (LHCb Collab.)

$\Xi_b(6100)^-$	$J^P = \frac{3}{2}^-$	Status: ***
-----------------------------------	-----------------------	-------------

J, P need confirmation.

 $\Xi_b(6100)^-$ MASS

VALUE (MeV)	DOCUMENT ID	TECN	COMMENT
6100.3±0.2±0.6	¹ SIRUNYAN	21F CMS	pp at 13 TeV

¹ Observed in $\Xi_b(6100)^- \rightarrow \Xi_b^- \pi^+ \pi^-$ decays.

 $m_{\Xi_b(6100)^-} - m_{\Xi_b^-} - 2 m_{\pi^+}$

VALUE (MeV)	DOCUMENT ID	TECN	COMMENT
24.14±0.22±0.09	¹ SIRUNYAN	21F CMS	pp at 13 TeV

¹ Observed in $\Xi_b(6100)^- \rightarrow \Xi_b^- \pi^+ \pi^-$ decays.

 $\Xi_b(6100)^-$ WIDTH

VALUE (MeV)	CL%	DOCUMENT ID	TECN	COMMENT
<1.9	95	¹ SIRUNYAN	21F CMS	pp at 13 TeV

¹ Observed in $\Xi_b(6100)^- \rightarrow \Xi_b^- \pi^+ \pi^-$ decays.

 $\Xi_b(6100)^-$ DECAY MODES

Mode	Fraction (Γ_i/Γ)
$\Gamma_1 \quad \Xi_b^- \pi^+ \pi^-$	seen

 $\Xi_b(6100)^-$ BRANCHING RATIOS

$\Gamma(\Xi_b^- \pi^+ \pi^-)/\Gamma_{\text{total}}$	Γ_1/Γ			
seen				
VALUE	EVTS	DOCUMENT ID	TECN	COMMENT
	60	SIRUNYAN	21F CMS	pp at 13 TeV

 $\Xi_b(6100)^-$ REFERENCES

SIRUNYAN 21F PRL 126 252003 A.M. Sirunyan et al. (CMS Collab.)

$\Xi_b(6227)^-$	$J^P = ?^?$	Status: ***
-----------------------------------	-------------	-------------

 $\Xi_b(6227)^-$ MASS

VALUE (MeV)	DOCUMENT ID	TECN	COMMENT
6227.9±0.9±0.2	¹ AAIJ	21 LHCb	pp at 7, 8, 13 TeV

See key on page 1127

Baryon Particle Listings

$\Xi_b(6227)^-, \Xi_b(6227)^0, \Omega_b^-$

••• We do not use the following data for averages, fits, limits, etc. •••
 6226.9 ± 2.0 ± 0.4 ^{2,3} AAIJ 18H LHCb Repl. by AAIJ 2021
¹ AAIJ 21 measures $m(\Xi_b(6227)^-) - m(\Lambda_b^0) = 608.3 \pm 0.8 \pm 0.4$ MeV. We have adjusted the measurement to our best value of $m(\Lambda_b^0) = 5619.60 \pm 0.17$ MeV. Our first error is their experiment's error and our second error is the systematic error from using our best values.
² Uses $\Lambda_b^0 K^-$ and $\Xi_b^0 \pi^-$ modes.
³ Measures mass difference $m(\Xi_b(6227)^-) - m(\Lambda_b^0) = 607.3 \pm 2.0 \pm 0.3$ MeV and uses $m(\Lambda_b^0) = 5619.58 \pm 0.17$ MeV.

$\Xi_b(6227)^-$ WIDTH

VALUE (MeV)	DOCUMENT ID	TECN	COMMENT
19.9 ± 2.1 ± 1.5	¹ AAIJ	21	LHCb pp at 7, 8, 13 TeV
••• We do not use the following data for averages, fits, limits, etc. •••			
18.1 ± 5.4 ± 1.8	² AAIJ	18H	LHCb Repl. by AAIJ 2021
¹ Uses $\Lambda_b^0 K^-$ decays.			
² Uses $\Lambda_b^0 K^-$ and $\Xi_b^0 \pi^-$ modes.			

$\Xi_b(6227)^-$ DECAY MODES

Mode	Fraction (Γ_i/Γ)	Scale factor
Γ_1 $\Lambda_b^0 K^- \times B(b \rightarrow \Xi_b(6227)^-)/B(b \rightarrow \Lambda_b^0)$	$(3.20 \pm 0.35) \times 10^{-3}$	
Γ_2 $\Xi_b^0 \pi^- \times B(b \rightarrow \Xi_b(6227)^-)/B(b \rightarrow \Xi_b^0)$	$(2.8 \pm 1.1) \%$	1.8

$\Xi_b(6227)^-$ BRANCHING RATIOS

$\Gamma(\Lambda_b^0 K^- \times B(b \rightarrow \Xi_b(6227)^-)/B(b \rightarrow \Lambda_b^0))/\Gamma_{total}$	Γ_1/Γ
3.20 ± 0.35 OUR AVERAGE	
3.0 ± 0.3 ± 0.4	AAIJ 18H LHCb pp at 7, 8 TeV
3.4 ± 0.3 ± 0.4	AAIJ 18H LHCb pp at 13 TeV

$\Gamma(\Xi_b^0 \pi^- \times B(b \rightarrow \Xi_b(6227)^-)/B(b \rightarrow \Xi_b^0))/\Gamma_{total}$	Γ_2/Γ
28 ± 11 OUR AVERAGE Error includes scale factor of 1.8.	
47 ± 10 ± 7	AAIJ 18H LHCb pp at 7, 8 TeV
22 ± 6 ± 3	AAIJ 18H LHCb pp at 13 TeV

$\Xi_b(6227)^-$ REFERENCES

AAIJ 21 PR D103 012004 R. Aaij et al. (LHCb Collab.)	AAIJ 18H PRL 121 072002 R. Aaij et al. (LHCb Collab.)
--	---

$\Xi_b(6227)^0$ $J^P = ?^?$ Status: ***

$\Xi_b(6227)^0$ MASS

VALUE (MeV)	DOCUMENT ID	TECN	COMMENT
6226.8^{+1.4}_{-1.5} ± 0.6	^{1,2} AAIJ	21	LHCb pp at 7, 8, 13 TeV
¹ AAIJ 21 measures $m(\Xi_b(6227)^0) - m(\Xi_b^-) = 429.8+1.4-1.5 ± 0.3$ MeV. We have adjusted the measurement to our best value of $m(\Xi_b^-) = 5797.0 \pm 0.6$ MeV. Our first error is their experiment's error and our second error is the systematic error from using our best values.			
² Uses $\Xi_b^- \pi^+$ decays.			

$\Xi_b(6227)^0$ WIDTH

VALUE (MeV)	DOCUMENT ID	TECN	COMMENT
18.6^{+5.0}_{-4.1} ± 1.4	¹ AAIJ	21	LHCb pp at 7, 8, 13 TeV
¹ Uses $\Xi_b^- \pi^+$ decays.			

$\Xi_b(6227)^0$ DECAY MODES

Mode	Fraction (Γ_i/Γ)
Γ_1 $\Xi_b^- \pi^+ \times B(b \rightarrow \Xi_b(6227)^0)/B(b \rightarrow \Xi_b^-)$	$(4.5 \pm 0.9) \%$

$\Xi_b(6227)^0$ BRANCHING RATIOS

$\Gamma(\Xi_b^- \pi^+ \times B(b \rightarrow \Xi_b(6227)^0)/B(b \rightarrow \Xi_b^-))/\Gamma_{total}$	Γ_1/Γ
4.5 ± 0.8 ± 0.4	
VALUE (%)	DOCUMENT ID TECN COMMENT
4.5 ± 0.8 ± 0.4	AAIJ 21 LHCb pp at 7, 8, 13 TeV

$\Xi_b(6227)^0$ REFERENCES

AAIJ 21 PR D103 012004 R. Aaij et al. (LHCb Collab.)
--

Ξ_b^0

$J^P = \frac{1}{2}^+$

OMITTED FROM SUMMARY TABLE

Ξ_b^0 DECAY MODES

Mode	Fraction (Γ_i/Γ)	Confidence level
Γ_1 $D^0 p K^- \times B(b \rightarrow \Xi_b^0)/B(b \rightarrow \Lambda_b)$	$< 1.4 \times 10^{-5}$	95%

Ξ_b^0 BRANCHING RATIOS

$\Gamma(D^0 p K^- \times B(b \rightarrow \Xi_b^0)/B(b \rightarrow \Lambda_b))/\Gamma_{total}$	Γ_1/Γ
< 1.4 × 10⁻⁵	
VALUE (%)	DOCUMENT ID TECN COMMENT
< 1.4 × 10 ⁻⁵	95 ^{1,2} AAIJ 20AMLHCb pp at 13 TeV
¹ AAIJ 20AM reports upper limits for $[\Gamma(\Xi_b^0 \rightarrow D^0 p K^- \times B(b \rightarrow \Xi_b^0)/B(b \rightarrow \Lambda_b))/\Gamma_{total}] / [B(\Lambda_b^0 \rightarrow p D^0 K^-)] < 3.0 \times 10^{-1} - 1.7 \times 10^{-2}$ for the considered Ξ_b^0 mass and lifetime hypotheses ranging from 6.7 to 7.2 GeV and from 100 to 500 fs. We use the 3.0×10^{-1} limit for the quoted result.	
² AAIJ 20AM reports $[\Gamma(\Xi_b^0 \rightarrow D^0 p K^- \times B(b \rightarrow \Xi_b^0)/B(b \rightarrow \Lambda_b))/\Gamma_{total}] / [B(\Lambda_b^0 \rightarrow p D^0 K^-)] < 3.0 \times 10^{-1}$ which we multiply by our best value $B(\Lambda_b^0 \rightarrow p D^0 K^-) = 4.6 \times 10^{-5}$.	

Ξ_b^0 REFERENCES

AAIJ 20AM JHEP 2011 095 R. Aaij et al. (LHCb Collab.)

Ω_b^-

$I(J^P) = 0(\frac{1}{2}^+)$ Status: ***
 I, J, P need confirmation.

In the quark model Ω_b^- is ssb ground state. None of its quantum numbers has been measured.

Ω_b^- MASS

VALUE (MeV)	DOCUMENT ID	TECN	COMMENT
6045.2 ± 1.2 OUR AVERAGE			
6044.30 ± 1.20 ± 1.12	¹ AAIJ	21AC	LHCb pp at 7, 8, 13 TeV
6045.1 ± 3.2 ± 0.8	² AAIJ	16o	LHCb pp at 7, 8 TeV
6047.5 ± 3.8 ± 0.6	³ AALTONEN	14B	CDF $p\bar{p}$ at 1.96 TeV
6046.0 ± 2.2 ± 0.5	⁴ AAIJ	13AV	LHCb pp at 7 TeV
••• We do not use the following data for averages, fits, limits, etc. •••			
6054.4 ± 6.8 ± 0.9	⁵ AALTONEN	09AP	CDF Repl. by AALTONEN 14B
6165 ± 10 ± 13	⁶ ABAZOV	08AL	D0 $p\bar{p}$ at 1.96 TeV

¹ Uses $\Omega_b^- \rightarrow \Xi_c^+ K^- \pi^-$ and $\Xi_c^+ \rightarrow p K^- \pi^+$ decays. Reports the value of $6044.3 \pm 1.2 \pm 1.1^{+0.19}_{-0.22}$ MeV where the last uncertainty is due to the mass of Ξ_c^+ . We have combined the two systematic uncertainties in quadrature.
² Reconstructed in $\Omega_b^- \rightarrow \Omega_c^0 \pi^-$, $\Omega_c^0 \rightarrow p K^- K^- \pi^+$ decays. Reference Ξ_b^- mass 5797.72 ± 0.6 MeV from AAIJ 14B.
³ Uses $\Omega_b^- \rightarrow J/\psi \Omega^-$ and $\Omega_c^0 \pi^-$ decays, with the first evidence for $\Omega_b^- \rightarrow \Omega_c^0 \pi^-$ at 3.3 σ significance.
⁴ Measured in $\Omega_b^- \rightarrow J/\psi \Omega^-$ with 19 ± 5 events.
⁵ Observed in $\Omega_b^- \rightarrow J/\psi \Omega^-$ decays with 16⁺⁶₋₄ candidates, a significance of 5.5 sigma from a combined mass-lifetime fit.
⁶ Observed in $\Omega_b^- \rightarrow J/\psi \Omega^-$ decays with 17.8 ± 4.9 ± 0.8 candidates, a significance of 5.4 sigma.

$m_{\Omega_b^-} - m_{\Lambda_b^0}$	DOCUMENT ID	TECN	COMMENT
426.4 ± 2.2 ± 0.4	AAIJ	13AV	LHCb pp at 7 TeV

$m_{\Omega_b^-} - m_{\Xi_b^-}$	DOCUMENT ID	TECN	COMMENT
247.3 ± 3.2 ± 0.5	¹ AAIJ	16o	LHCb pp at 7, 8 TeV

Baryon Particle Listings

 $\Omega_b^-, \Omega_b(6316)^-$

¹ Uses $\Omega_b^- \rightarrow \Omega_c^0 \pi^-, \Omega_c^0 \rightarrow p K^- K^- \pi^+$ and $\Xi_b^- \rightarrow \Xi_c^0 \pi^-, \Xi_c^0 \rightarrow p K^- K^- \pi^+$ decays.

 Ω_b MEAN LIFE

"OUR EVALUATION" has been provided by the Heavy Flavor Averaging Group (HFLAV, <https://hflav.web.cern.ch/>).

VALUE (10^{-12} s)	DOCUMENT ID	TECN	COMMENT
-----------------------	-------------	------	---------

1.64^{+0.19}_{-0.17} OUR EVALUATION

1.65^{+0.19}_{-0.16} OUR AVERAGE

1.78 ± 0.26 ± 0.05 ± 0.06 ¹ AAIJ 160 LHCb pp at 7, 8 TeV

1.54^{+0.26}_{-0.21} ± 0.05 ² AAIJ 14T LHCb pp at 7, 8 TeV

1.66^{+0.53}_{-0.40} ± 0.02 ² AALTONEN 14B CDF $p\bar{p}$ at 1.96 TeV

• • • We do not use the following data for averages, fits, limits, etc. • • •

1.13^{+0.53}_{-0.40} ± 0.02 ³ AALTONEN 09AP CDF Repl. by AALTONEN 14B

¹ Measured in $\Omega_b^- \rightarrow \Omega_c^0 \pi^-, \Omega_c^0 \rightarrow p K^- K^- \pi^+$ decays relative to $\Xi_b^- \rightarrow \Xi_c^0 \pi^-, \Xi_c^0 \rightarrow p K^- K^- \pi^+$ decays with reference Ξ_b^- mean life 1.599 ± 0.06 ps from AAIJ 14B.

² Measured in $\Omega_b^- \rightarrow J/\psi \Omega^-$ decays.

³ Observed in $\Omega_b^- \rightarrow J/\psi \Omega^-$ decays with 16⁺⁶₋₄ candidates, a significance of 5.5 sigma from a combined mass-lifetime fit.

 $\tau(\Omega_b^-)/\tau(\Xi_b^-)$ mean life ratio

VALUE	DOCUMENT ID	TECN	COMMENT
-------	-------------	------	---------

1.11 ± 0.16 ± 0.03 ¹ AAIJ 160 LHCb pp at 7, 8 TeV

¹ Uses $\Omega_b^- \rightarrow \Omega_c^0 \pi^-, \Omega_c^0 \rightarrow p K^- K^- \pi^+$ and $\Xi_b^- \rightarrow \Xi_c^0 \pi^-, \Xi_c^0 \rightarrow p K^- K^- \pi^+$ decays.

 Ω_b^- DECAY MODES

Mode	Fraction (Γ_i/Γ)	Confidence level
Γ_1 $J/\psi \Omega^- \times B(b \rightarrow \Omega_b)$	(2.9 ^{+1.1} _{-0.8}) × 10 ⁻⁶	
Γ_2 $p K^- K^- \times B(\bar{b} \rightarrow \Omega_b)$	< 2.3 × 10 ⁻⁹	90%
Γ_3 $p \pi^- \pi^- \times B(\bar{b} \rightarrow \Omega_b)$	< 1.5 × 10 ⁻⁸	90%
Γ_4 $p K^- \pi^- \times B(\bar{b} \rightarrow \Omega_b)$	< 7 × 10 ⁻⁹	90%
Γ_5 $\Omega_c^0 \pi^-$	seen	
Γ_6 $\Omega_c^0 \pi^-, \Omega_c^0 \rightarrow p K^- K^- \pi^+$	seen	
Γ_7 $\Xi_c^+ K^- \pi^-$	seen	

 Ω_b^- BRANCHING RATIOS

$\Gamma(J/\psi \Omega^- \times B(b \rightarrow \Omega_b))/\Gamma_{\text{total}}$ Γ_1/Γ

VALUE (units 10 ⁻⁴)	DOCUMENT ID	TECN	COMMENT
---------------------------------	-------------	------	---------

0.029^{+0.011}_{-0.008} OUR AVERAGE

0.026^{+0.010}_{-0.007} ± 0.004 ¹ AALTONEN 09AP CDF $p\bar{p}$ at 1.96 TeV

0.08 ± 0.04 ± 0.02 ² ABAZOV 08AL D0 $p\bar{p}$ at 1.96 TeV

¹ AALTONEN 09AP reports [$\Gamma(\Omega_b^- \rightarrow J/\psi \Omega^- \times B(b \rightarrow \Omega_b))/\Gamma_{\text{total}}$] / [$B(\Lambda_b^0 \rightarrow J/\psi(1S) \Lambda \times B(b \rightarrow \Lambda_b^0))$] = 0.045^{+0.017}_{-0.012} ± 0.004 which we multiply by our best value $B(\Lambda_b^0 \rightarrow J/\psi(1S) \Lambda \times B(b \rightarrow \Lambda_b^0)) = (5.8 \pm 0.8) \times 10^{-5}$. Our first error is their experiment's error and our second error is the systematic error from using our best value.

² ABAZOV 08AL reports [$\Gamma(\Omega_b^- \rightarrow J/\psi \Omega^- \times B(b \rightarrow \Omega_b))/\Gamma_{\text{total}}$] / [$B(\Xi_b^- \rightarrow J/\psi \Xi^- \times B(b \rightarrow \Xi_b^-))$] = 0.80 ± 0.32^{+0.14}_{-0.22} which we multiply by our best value $B(\Xi_b^- \rightarrow J/\psi \Xi^- \times B(b \rightarrow \Xi_b^-)) = (1.02^{+0.26}_{-0.21}) \times 10^{-5}$. Our first error is their experiment's error and our second error is the systematic error from using our best value.

$\Gamma(p K^- K^- \times B(\bar{b} \rightarrow \Omega_b))/\Gamma_{\text{total}}$ Γ_2/Γ

VALUE (units 10 ⁻⁵)	CL%	DOCUMENT ID	TECN	COMMENT
---------------------------------	-----	-------------	------	---------

<2.3 × 10⁻⁴ 90 ¹ AAIJ 21AH LHCb pp at 7, 8, 13 TeV

• • • We do not use the following data for averages, fits, limits, etc. • • •

<2.5 × 10⁻⁴ 90 ² AAIJ 17F LHCb pp at 7, 8 TeV

¹ AAIJ 21AH reports [$\Gamma(\Omega_b^- \rightarrow p K^- K^- \times B(\bar{b} \rightarrow \Omega_b))/\Gamma_{\text{total}}$] / [$B(\Xi_b^- \rightarrow p K^- K^- \times B(b \rightarrow \Xi_b^-))$] < 62 × 10⁻³ which we multiply by our best value $B(\Xi_b^- \rightarrow p K^- K^- \times B(b \rightarrow \Xi_b^-)) = 3.7 \times 10^{-8}$.

² AAIJ 17F reports [$\Gamma(\Omega_b^- \rightarrow p K^- K^- \times B(\bar{b} \rightarrow \Omega_b))/\Gamma_{\text{total}}$] / [$B(B^+ \rightarrow K^+ K^- K^+) / [B(\bar{b} \rightarrow B^+)] < 18 \times 10^{-5}$ which we multiply by our best values $B(B^+ \rightarrow K^+ K^- K^+) = 3.40 \times 10^{-5}$, $B(\bar{b} \rightarrow B^+) = 40.8 \times 10^{-2}$.

$\Gamma(p \pi^- \pi^- \times B(\bar{b} \rightarrow \Omega_b))/\Gamma_{\text{total}}$ Γ_3/Γ

VALUE (units 10 ⁻⁵)	CL%	DOCUMENT ID	TECN	COMMENT
---------------------------------	-----	-------------	------	---------

<1.5 × 10⁻³ 90 ¹ AAIJ 17F LHCb pp at 7, 8 TeV

¹ AAIJ 17F reports [$\Gamma(\Omega_b^- \rightarrow p \pi^- \pi^- \times B(\bar{b} \rightarrow \Omega_b))/\Gamma_{\text{total}}$] / [$B(B^+ \rightarrow K^+ K^- K^+) / [B(\bar{b} \rightarrow B^+)] < 109 \times 10^{-5}$ which we multiply by our best values $B(B^+ \rightarrow K^+ K^- K^+) = 3.40 \times 10^{-5}$, $B(\bar{b} \rightarrow B^+) = 40.8 \times 10^{-2}$.

$\Gamma(p K^- \pi^- \times B(\bar{b} \rightarrow \Omega_b))/\Gamma_{\text{total}}$ Γ_4/Γ

VALUE (units 10 ⁻⁵)	CL%	DOCUMENT ID	TECN	COMMENT
---------------------------------	-----	-------------	------	---------

<7 × 10⁻⁴ 90 ¹ AAIJ 17F LHCb pp at 7, 8 TeV

¹ AAIJ 17F reports [$\Gamma(\Omega_b^- \rightarrow p K^- \pi^- \times B(\bar{b} \rightarrow \Omega_b))/\Gamma_{\text{total}}$] / [$B(B^+ \rightarrow K^+ K^- K^+) / [B(\bar{b} \rightarrow B^+)] < 51 \times 10^{-5}$ which we multiply by our best values $B(B^+ \rightarrow K^+ K^- K^+) = 3.40 \times 10^{-5}$, $B(\bar{b} \rightarrow B^+) = 40.8 \times 10^{-2}$.

$\Gamma(\Omega_c^0 \pi^-)/\Gamma_{\text{total}}$ Γ_5/Γ

VALUE	DOCUMENT ID	TECN	COMMENT
-------	-------------	------	---------

seen AAIJ 160 LHCb pp at 7, 8 TeV

$\Gamma(\Xi_c^+ K^- \pi^-)/\Gamma(\Omega_c^0 \pi^-), \Omega_c^0 \rightarrow p K^- K^- \pi^+$ Γ_7/Γ_6

VALUE (units 10 ²)	DOCUMENT ID	TECN	COMMENT
--------------------------------	-------------	------	---------

2.2 ± 0.2 ± 1.0 ¹ AAIJ 21AC LHCb pp at 7, 8, 13 TeV

¹ AAIJ 21AC reports [$\Gamma(\Omega_b^- \rightarrow \Xi_c^+ K^- \pi^-)/\Gamma(\Omega_b^- \rightarrow \Omega_c^0 \pi^-), \Omega_c^0 \rightarrow p K^- K^- \pi^+$] × [$B(\Xi_c^+ \rightarrow p K^- \pi^+)] = 1.35 \pm 0.11 \pm 0.05$ which we divide by our best value $B(\Xi_c^+ \rightarrow p K^- \pi^+) = (6.2 \pm 3.0) \times 10^{-3}$. Our first error is their experiment's error and our second error is the systematic error from using our best value.

 Ω_b^- REFERENCES

AAIJ	21AC	PR D104 L091102	R. Aaij et al.	(LHCb Collab.)
AAIJ	21AH	PR D104 052010	R. Aaij et al.	(LHCb Collab.)
AAIJ	17F	PRL 118 071801	R. Aaij et al.	(LHCb Collab.)
AAIJ	16O	PR D93 092007	R. Aaij et al.	(LHCb Collab.)
AAIJ	14B	PL B728 234	R. Aaij et al.	(LHCb Collab.)
AAIJ	14T	PL B736 154	R. Aaij et al.	(LHCb Collab.)
AALTONEN	14B	PR D89 072014	T. Aaltonen et al.	(CDF Collab.)
AAIJ	13AV	PRL 110 182001	R. Aaij et al.	(LHCb Collab.)
AALTONEN	09AP	PR D80 072003	T. Aaltonen et al.	(CDF Collab.)
ABAZOV	08AL	PRL 101 232002	V.M. Abazov et al.	(D0 Collab.)

 $\Omega_b(6316)^-$

$I(J^P) = ?(??)$ Status: *
I, J, P need confirmation.

OMITTED FROM SUMMARY TABLE

 $\Omega_b(6316)^-$ MASS

VALUE (MeV)	DOCUMENT ID	TECN	COMMENT
-------------	-------------	------	---------

6315.6 ± 0.3 ± 0.5 ¹ AAIJ 20T LHCb pp at 7, 8, 13 TeV

¹ AAIJ 20T measures $m(\Omega_b(6316)^-) - m(\Xi_b^0) = 523.74 \pm 0.31 \pm 0.07$ MeV. We have adjusted the measurement to our best values of $m(\Xi_b^0) = 5791.9 \pm 0.5$ MeV. Our first error is their experiment's error and our second error is the systematic error from using our best values.

 $\Omega_b(6316)^-$ WIDTH

VALUE (MeV)	CL%	DOCUMENT ID	TECN	COMMENT
-------------	-----	-------------	------	---------

<4.2 95 AAIJ 20T LHCb pp at 7, 8, 13 TeV

 $\Omega_b(6316)^-$ DECAY MODES

Mode	Fraction (Γ_i/Γ)
Γ_1 $\Xi_b^0 K^-$	seen

 $\Omega_b(6316)^-$ BRANCHING RATIOS

$\Gamma(\Xi_b^0 K^-)/\Gamma_{\text{total}}$ Γ_1/Γ

VALUE	DOCUMENT ID	TECN	COMMENT
-------	-------------	------	---------

seen ¹ AAIJ 20T LHCb pp at 7, 8, 13 TeV

¹ AAIJ 20T establishes the decay at 2.1 σ significance level.

 $\Omega_b(6316)^-$ REFERENCES

AAIJ	20T	PRL 124 082002	R. Aaij et al.	(LHCb Collab.)
------	-----	----------------	----------------	----------------

See key on page 1127

Baryon Particle Listings

$\Omega_b(6330)^-, \Omega_b(6340)^-, \Omega_b(6350)^-, b$ -baryon ADMIXTURE ($\Lambda_b, \Xi_b, \Omega_b$)

$\Omega_b(6330)^-$ $I(J^P) = ?(?^?)$ Status: *
I, J, P need confirmation.
 OMITTED FROM SUMMARY TABLE

$\Omega_b(6330)^-$ MASS

VALUE (MeV)	DOCUMENT ID	TECN	COMMENT
$6330.3 \pm 0.3 \pm 0.5$	¹ AAIJ	20T LHCb	<i>pp</i> at 7, 8, 13 TeV

¹ AAIJ 20T measures $m(\Omega_b(6330)^-) - m(\Xi_b^0) = 538.40 \pm 0.28 \pm 0.07$ MeV. We have adjusted the measurement to our best values of $m(\Xi_b^0) = 5791.9 \pm 0.5$ MeV. Our first error is their experiment's error and our second error is the systematic error from using our best values.

$\Omega_b(6330)^-$ WIDTH

VALUE (MeV)	CL%	DOCUMENT ID	TECN	COMMENT
<4.7	95	AAIJ	20T LHCb	<i>pp</i> at 7, 8, 13 TeV

$\Omega_b(6330)^-$ DECAY MODES

Mode	Fraction (Γ_i/Γ)
$\Gamma_1 \Xi_b^0 K^-$	seen

$\Omega_b(6330)^-$ BRANCHING RATIOS

$\Gamma(\Xi_b^0 K^-)/\Gamma_{total}$	Γ_1/Γ
seen	seen

¹ AAIJ 20T establishes the decay at 2.6 σ significance level.

$\Omega_b(6330)^-$ REFERENCES

AAIJ	20T	PRL 124 082002	R. Aaij et al.	(LHCb Collab.)
------	-----	----------------	----------------	----------------

$\Omega_b(6340)^-$ $I(J^P) = ?(?^?)$ Status: *
I, J, P need confirmation.
 OMITTED FROM SUMMARY TABLE

$\Omega_b(6340)^-$ MASS

VALUE (MeV)	DOCUMENT ID	TECN	COMMENT
$6339.7 \pm 0.3 \pm 0.5$	¹ AAIJ	20T LHCb	<i>pp</i> at 7, 8, 13 TeV

¹ AAIJ 20T measures $m(\Omega_b(6340)^-) - m(\Xi_b^0) = 547.81 \pm 0.26 \pm 0.05$ MeV. We have adjusted the measurement to our best values of $m(\Xi_b^0) = 5791.9 \pm 0.5$ MeV. Our first error is their experiment's error and our second error is the systematic error from using our best values.

$\Omega_b(6340)^-$ WIDTH

VALUE (MeV)	CL%	DOCUMENT ID	TECN	COMMENT
<1.8	95	AAIJ	20T LHCb	<i>pp</i> at 7, 8, 13 TeV

$\Omega_b(6340)^-$ DECAY MODES

Mode	Fraction (Γ_i/Γ)
$\Gamma_1 \Xi_b^0 K^-$	seen

$\Omega_b(6340)^-$ BRANCHING RATIOS

$\Gamma(\Xi_b^0 K^-)/\Gamma_{total}$	Γ_1/Γ
seen	seen

$\Omega_b(6340)^-$ REFERENCES

AAIJ	20T	PRL 124 082002	R. Aaij et al.	(LHCb Collab.)
------	-----	----------------	----------------	----------------

$\Omega_b(6350)^-$ $I(J^P) = ?(?^?)$ Status: *
I, J, P need confirmation.
 OMITTED FROM SUMMARY TABLE

$\Omega_b(6350)^-$ MASS

VALUE (MeV)	DOCUMENT ID	TECN	COMMENT
$6349.8 \pm 0.4 \pm 0.5$	¹ AAIJ	20T LHCb	<i>pp</i> at 7, 8, 13 TeV

¹ AAIJ 20T measures $m(\Omega_b(6350)^-) - m(\Xi_b^0) = 557.98 \pm 0.35 \pm 0.05$ MeV. We have adjusted the measurement to our best values of $m(\Xi_b^0) = 5791.9 \pm 0.5$ MeV. Our first error is their experiment's error and our second error is the systematic error from using our best values.

$\Omega_b(6350)^-$ WIDTH

VALUE (MeV)	CL%	DOCUMENT ID	TECN	COMMENT
<3.2	95	AAIJ	20T LHCb	<i>pp</i> at 7, 8, 13 TeV

$\Omega_b(6350)^-$ DECAY MODES

Mode	Fraction (Γ_i/Γ)
$\Gamma_1 \Xi_b^0 K^-$	seen

$\Omega_b(6350)^-$ BRANCHING RATIOS

$\Gamma(\Xi_b^0 K^-)/\Gamma_{total}$	Γ_1/Γ
seen	seen

$\Omega_b(6350)^-$ REFERENCES

AAIJ	20T	PRL 124 082002	R. Aaij et al.	(LHCb Collab.)
------	-----	----------------	----------------	----------------

b -baryon ADMIXTURE ($\Lambda_b, \Xi_b, \Omega_b$)

b -baryon ADMIXTURE MEAN LIFE

Each measurement of the b -baryon mean life is an average over an admixture of various b baryons which decay weakly. Different techniques emphasize different admixtures of produced particles, which could result in a different b -baryon mean life. More b -baryon flavor specific channels are not included in the measurement.

VALUE (10^{-12} s)	EVTS	DOCUMENT ID	TECN	COMMENT
• • • We do not use the following data for averages, fits, limits, etc. • • •				
$1.218^{+0.130}_{-0.115} \pm 0.042$		¹ ABAZOV	07s D0	Repl. by ABAZOV 12u
$1.22^{+0.22}_{-0.18} \pm 0.04$		¹ ABAZOV	05c D0	Repl. by ABAZOV 07s
$1.16 \pm 0.20 \pm 0.08$		² ABREU	99w DLPH	$e^+e^- \rightarrow Z$
$1.19 \pm 0.14 \pm 0.07$		³ ABREU	99w DLPH	$e^+e^- \rightarrow Z$
$1.14 \pm 0.08 \pm 0.04$		⁴ ABREU	99w DLPH	$e^+e^- \rightarrow Z$
$1.11^{+0.19}_{-0.18} \pm 0.05$		⁵ ABREU	99w DLPH	$e^+e^- \rightarrow Z$
$1.29^{+0.24}_{-0.22} \pm 0.06$		⁵ ACKERSTAFF	98g OPAL	$e^+e^- \rightarrow Z$
$1.20 \pm 0.08 \pm 0.06$		⁶ BARATE	98d ALEP	$e^+e^- \rightarrow Z$
1.21 ± 0.11		⁵ BARATE	98d ALEP	$e^+e^- \rightarrow Z$
$1.32 \pm 0.15 \pm 0.07$		⁷ ABE	96m CDF	$p\bar{p}$ at 1.8 TeV
$1.46^{+0.22}_{-0.21} \pm 0.07$		ABREU	96d DLPH	Repl. by ABREU 99w
$1.10^{+0.19}_{-0.17} \pm 0.09$		⁵ ABREU	96d DLPH	$e^+e^- \rightarrow Z$
$1.16 \pm 0.11 \pm 0.06$		⁵ AKERS	96 OPAL	$e^+e^- \rightarrow Z$
$1.27^{+0.35}_{-0.29} \pm 0.09$		ABREU	95s DLPH	Repl. by ABREU 99w
$1.05^{+0.12}_{-0.11} \pm 0.09$	290	BUSKULIC	95L ALEP	Repl. by BARATE 98d
$1.04^{+0.48}_{-0.38} \pm 0.10$	11	⁸ ABREU	93F DLPH	Excess $\Lambda\mu^-$, decay lengths
$1.05^{+0.23}_{-0.20} \pm 0.08$	157	⁹ AKERS	93 OPAL	Excess $\Lambda\ell^-$, decay lengths
$1.12^{+0.32}_{-0.29} \pm 0.16$	101	¹⁰ BUSKULIC	92i ALEP	Excess $\Lambda\ell^-$, impact parameters

¹ Measured mean life using fully reconstructed $\Lambda_b^0 \rightarrow J/\psi\Lambda$ decays.
² Measured using $\Lambda\ell^-$ decay length.
³ Measured using $p\ell^-$ decay length.
⁴ This ABREU 99w result is the combined result of the $\Lambda\ell^-$, $p\ell^-$, and excess $\Lambda\mu^-$ impact parameter measurements.
⁵ Measured using $\Lambda_c\ell^-$ and $\Lambda\ell^+\ell^-$.
⁶ Measured using the excess of $\Lambda\ell^-$, lepton impact parameter.

Baryon Particle Listings

 b -baryon ADMIXTURE ($\Lambda_b, \Xi_b, \Omega_b$)⁷ Measured using $\Lambda_c \ell^-$.⁸ ABREU 93F superseded by ABREU 96D.⁹ AKERS 93 superseded by AKERS 96.¹⁰ BUSKULIC 92i superseded by BUSKULIC 95L. **b -baryon ADMIXTURE DECAY MODES**
($\Lambda_b, \Xi_b, \Omega_b$)

These branching fractions are actually an average over weakly decaying b -baryons weighted by their production rates at the LHC, LEP, and Tevatron, branching ratios, and detection efficiencies. They scale with the b -baryon production fraction $B(b \rightarrow b\text{-baryon})$.

The branching fractions $B(b\text{-baryon} \rightarrow \Lambda \ell^- \bar{\nu}_\ell \text{ anything})$ and $B(\Lambda_b^0 \rightarrow \Lambda_c^+ \ell^- \bar{\nu}_\ell \text{ anything})$ are not pure measurements because the underlying measured products of these with $B(b \rightarrow b\text{-baryon})$ were used to determine $B(b \rightarrow b\text{-baryon})$, as described in the note "Production and Decay of b -Flavored Hadrons."

For inclusive branching fractions, e.g., $B \rightarrow D^\pm \text{ anything}$, the values usually are multiplicities, not branching fractions. They can be greater than one.

Mode	Fraction (Γ_i/Γ)	Scale factor
Γ_1 $p\mu^- \bar{\nu}$ anything	$(5.8 \pm \frac{2.3}{2.0})\%$	
Γ_2 $p\ell \bar{\nu}_\ell$ anything	$(5.6 \pm 1.2)\%$	
Γ_3 p anything	$(70 \pm 22)\%$	
Γ_4 $\Lambda \ell^- \bar{\nu}_\ell$ anything	$(3.8 \pm 0.6)\%$	
Γ_5 $\Lambda \ell^+ \nu_\ell$ anything	$(3.2 \pm 0.8)\%$	
Γ_6 Λ anything	$(39 \pm 7)\%$	
Γ_7 $\Xi^- \ell^- \bar{\nu}_\ell$ anything	$(4.6 \pm 1.4) \times 10^{-3}$	1.2

 b -baryon ADMIXTURE ($\Lambda_b, \Xi_b, \Omega_b$) BRANCHING RATIOS

$\Gamma(p\mu^- \bar{\nu} \text{ anything})/\Gamma_{\text{total}}$	Γ_1/Γ
VALUE (%)	EVTS
$5.8 \pm \frac{2.3}{1.9} \pm 0.8$	125

¹ ABREU 95s reports $[\Gamma(b\text{-baryon} \rightarrow p\mu^- \bar{\nu} \text{ anything})/\Gamma_{\text{total}}] \times [B(\bar{b} \rightarrow b\text{-baryon})] = 0.0049 \pm 0.0011 \pm \frac{0.0015}{0.0011}$ which we divide by our best value $B(\bar{b} \rightarrow b\text{-baryon}) = (8.4 \pm 1.1) \times 10^{-2}$. Our first error is their experiment's error and our second error is the systematic error from using our best value.

$\Gamma(p\ell \bar{\nu}_\ell \text{ anything})/\Gamma_{\text{total}}$	Γ_2/Γ
VALUE (%)	EVTS
$5.6 \pm 0.9 \pm 0.7$	262

¹ BARATE 98v reports $[\Gamma(b\text{-baryon} \rightarrow p\ell \bar{\nu}_\ell \text{ anything})/\Gamma_{\text{total}}] \times [B(\bar{b} \rightarrow b\text{-baryon})] = (4.72 \pm 0.66 \pm 0.44) \times 10^{-3}$ which we divide by our best value $B(\bar{b} \rightarrow b\text{-baryon}) = (8.4 \pm 1.1) \times 10^{-2}$. Our first error is their experiment's error and our second error is the systematic error from using our best value.

$\Gamma(p\ell \bar{\nu}_\ell \text{ anything})/\Gamma(p \text{ anything})$	Γ_2/Γ_3
VALUE (%)	EVTS
$8.0 \pm 1.2 \pm 1.4$	290

$\Gamma(\Lambda \ell^- \bar{\nu}_\ell \text{ anything})/\Gamma_{\text{total}}$	Γ_4/Γ
VALUE (%)	EVTS
$3.8 \pm 0.6 \text{ OUR AVERAGE}$	262

The values and averages in this section serve only to show what values result if one assumes our $B(b \rightarrow b\text{-baryon})$. They cannot be thought of as measurements since the underlying product branching fractions were also used to determine $B(b \rightarrow b\text{-baryon})$ as described in the note on "Production and Decay of b -Flavored Hadrons."

VALUE (%)	EVTS	DOCUMENT ID	TECN	COMMENT
$3.9 \pm 0.5 \pm 0.5$		¹ BARATE	98D ALEP	$e^+ e^- \rightarrow Z$
$3.5 \pm 0.4 \pm 0.5$		² AKERS	96 OPAL	Excess of $\Lambda \ell^-$ over $\Lambda \ell^+$
$3.6 \pm 0.9 \pm 0.5$	262	³ ABREU	95s DLPH	Excess of $\Lambda \ell^-$ over $\Lambda \ell^+$
$7.3 \pm 1.4 \pm 1.0$	290	⁴ BUSKULIC	95L ALEP	Excess of $\Lambda \ell^-$ over $\Lambda \ell^+$
••• We do not use the following data for averages, fits, limits, etc. •••				
seen	157	⁵ AKERS	93 OPAL	Excess of $\Lambda \ell^-$ over $\Lambda \ell^+$
$8.3 \pm 2.5 \pm 1.1$	101	⁶ BUSKULIC	92i ALEP	Excess of $\Lambda \ell^-$ over $\Lambda \ell^+$

¹ BARATE 98D reports $[\Gamma(b\text{-baryon} \rightarrow \Lambda \ell^- \bar{\nu}_\ell \text{ anything})/\Gamma_{\text{total}}] \times [B(\bar{b} \rightarrow b\text{-baryon})] = 0.00326 \pm 0.00016 \pm 0.00039$ which we divide by our best value $B(\bar{b} \rightarrow b\text{-baryon}) = (8.4 \pm 1.1) \times 10^{-2}$. Our first error is their experiment's error and our second error is the systematic error from using our best value. Measured using the excess of $\Lambda \ell^-$, lepton impact parameter.

² AKERS 96 reports $[\Gamma(b\text{-baryon} \rightarrow \Lambda \ell^- \bar{\nu}_\ell \text{ anything})/\Gamma_{\text{total}}] \times [B(\bar{b} \rightarrow b\text{-baryon})] = 0.00291 \pm 0.00023 \pm 0.00025$ which we divide by our best value $B(\bar{b} \rightarrow b\text{-baryon}) = (8.4 \pm 1.1) \times 10^{-2}$. Our first error is their experiment's error and our second error is the systematic error from using our best value.

³ ABREU 95s reports $[\Gamma(b\text{-baryon} \rightarrow \Lambda \ell^- \bar{\nu}_\ell \text{ anything})/\Gamma_{\text{total}}] \times [B(\bar{b} \rightarrow b\text{-baryon})] = 0.0030 \pm 0.0006 \pm 0.0004$ which we divide by our best value $B(\bar{b} \rightarrow b\text{-baryon}) = (8.4 \pm 1.1) \times 10^{-2}$. Our first error is their experiment's error and our second error is the systematic error from using our best value.

⁴ BUSKULIC 95L reports $[\Gamma(b\text{-baryon} \rightarrow \Lambda \ell^- \bar{\nu}_\ell \text{ anything})/\Gamma_{\text{total}}] \times [B(\bar{b} \rightarrow b\text{-baryon})] = 0.0061 \pm 0.0006 \pm 0.0010$ which we divide by our best value $B(\bar{b} \rightarrow b\text{-baryon}) = (8.4 \pm 1.1) \times 10^{-2}$. Our first error is their experiment's error and our second error is the systematic error from using our best value.

⁵ AKERS 93 superseded by AKERS 96.

⁶ BUSKULIC 92i reports $[\Gamma(b\text{-baryon} \rightarrow \Lambda \ell^- \bar{\nu}_\ell \text{ anything})/\Gamma_{\text{total}}] \times [B(\bar{b} \rightarrow b\text{-baryon})] = 0.0070 \pm 0.0010 \pm 0.0018$ which we divide by our best value $B(\bar{b} \rightarrow b\text{-baryon}) = (8.4 \pm 1.1) \times 10^{-2}$. Our first error is their experiment's error and our second error is the systematic error from using our best value. Superseded by BUSKULIC 95L.

 $\Gamma(\Lambda \ell^+ \nu_\ell \text{ anything})/\Gamma(\Lambda \text{ anything})$

VALUE (units 10^{-2})	DOCUMENT ID	TECN	COMMENT
$8.0 \pm 1.2 \pm 0.8$	ABBIENDI	99L OPAL	$e^+ e^- \rightarrow Z$
••• We do not use the following data for averages, fits, limits, etc. •••			
$7.0 \pm 1.2 \pm 0.7$	ACKERSTAFF	97N OPAL	Repl. by ABBIENDI 99L

 $\Gamma(\Lambda \text{ anything})/\Gamma_{\text{total}}$

VALUE (%)	DOCUMENT ID	TECN	COMMENT
$39 \pm 7 \text{ OUR AVERAGE}$			
$42 \pm 6 \pm 5$	¹ ABBIENDI	99L OPAL	$e^+ e^- \rightarrow Z$
$27 \pm \frac{15}{9} \pm 3$	² ABREU	95c DLPH	$e^+ e^- \rightarrow Z$

••• We do not use the following data for averages, fits, limits, etc. •••

³ ACKERSTAFF 97N OPAL Repl. by ABBIENDI 99L

⁴ ABBIENDI 99L reports $[\Gamma(b\text{-baryon} \rightarrow \Lambda \text{ anything})/\Gamma_{\text{total}}] \times [B(\bar{b} \rightarrow b\text{-baryon})] = 0.035 \pm 0.0032 \pm 0.0035$ which we divide by our best value $B(\bar{b} \rightarrow b\text{-baryon}) = (8.4 \pm 1.1) \times 10^{-2}$. Our first error is their experiment's error and our second error is the systematic error from using our best value.

² ABREU 95c reports $0.28 \pm \frac{0.17}{0.12}$ from a measurement of $[\Gamma(b\text{-baryon} \rightarrow \Lambda \text{ anything})/\Gamma_{\text{total}}] \times [B(\bar{b} \rightarrow b\text{-baryon})]$ assuming $B(\bar{b} \rightarrow b\text{-baryon}) = 0.08 \pm 0.02$, which we rescale to our best value $B(\bar{b} \rightarrow b\text{-baryon}) = (8.4 \pm 1.1) \times 10^{-2}$. Our first error is their experiment's error and our second error is the systematic error from using our best value.

³ ACKERSTAFF 97N reports $[\Gamma(b\text{-baryon} \rightarrow \Lambda \text{ anything})/\Gamma_{\text{total}}] \times [B(\bar{b} \rightarrow b\text{-baryon})] = 0.0393 \pm 0.0046 \pm 0.0037$ which we divide by our best value $B(\bar{b} \rightarrow b\text{-baryon}) = (8.4 \pm 1.1) \times 10^{-2}$. Our first error is their experiment's error and our second error is the systematic error from using our best value.

 $\Gamma(\Xi^- \ell^- \bar{\nu}_\ell \text{ anything})/\Gamma_{\text{total}}$

VALUE (units 10^{-3})	DOCUMENT ID	TECN	COMMENT
$4.6 \pm 1.4 \text{ OUR AVERAGE}$			Error includes scale factor of 1.2.
$3.6 \pm 1.2 \pm 0.5$	¹ ABDALLAH	05c DLPH	$e^+ e^- \rightarrow Z^0$
$6.4 \pm 1.6 \pm 0.8$	² BUSKULIC	96T ALEP	Excess $\Xi^- \ell^-$ over $\Xi^- \ell^+$
••• We do not use the following data for averages, fits, limits, etc. •••			
$7.0 \pm 2.8 \pm 0.9$	³ ABREU	95v DLPH	Repl. by ABDALLAH 05c

¹ ABDALLAH 05c reports $[\Gamma(b\text{-baryon} \rightarrow \Xi^- \ell^- \bar{\nu}_\ell \text{ anything})/\Gamma_{\text{total}}] \times [B(\bar{b} \rightarrow b\text{-baryon})] = (3.0 \pm 1.0 \pm 0.3) \times 10^{-4}$ which we divide by our best value $B(\bar{b} \rightarrow b\text{-baryon}) = (8.4 \pm 1.1) \times 10^{-2}$. Our first error is their experiment's error and our second error is the systematic error from using our best value.

² BUSKULIC 96T reports $[\Gamma(b\text{-baryon} \rightarrow \Xi^- \ell^- \bar{\nu}_\ell \text{ anything})/\Gamma_{\text{total}}] \times [B(\bar{b} \rightarrow b\text{-baryon})] = (5.4 \pm 1.1 \pm 0.8) \times 10^{-4}$ which we divide by our best value $B(\bar{b} \rightarrow b\text{-baryon}) = (8.4 \pm 1.1) \times 10^{-2}$. Our first error is their experiment's error and our second error is the systematic error from using our best value.

³ ABREU 95v reports $[\Gamma(b\text{-baryon} \rightarrow \Xi^- \ell^- \bar{\nu}_\ell \text{ anything})/\Gamma_{\text{total}}] \times [B(\bar{b} \rightarrow b\text{-baryon})] = (5.9 \pm 2.1 \pm 1.0) \times 10^{-4}$ which we divide by our best value $B(\bar{b} \rightarrow b\text{-baryon}) = (8.4 \pm 1.1) \times 10^{-2}$. Our first error is their experiment's error and our second error is the systematic error from using our best value.

 b -baryon ADMIXTURE ($\Lambda_b, \Xi_b, \Omega_b$) REFERENCES

ABAZOV	12U	PR D95 112003	V.M. Abazov et al.	(D0 Collab.)
ABAZOV	07S	PRL 99 142001	V.M. Abazov et al.	(D0 Collab.)
ABAZOV	05C	PRL 94 102001	V.M. Abazov et al.	(D0 Collab.)
ABDALLAH	05C	EPJ C44 299	J. Abdallah et al.	(DELPHI Collab.)
ABBIENDI	99L	EPJ C9 1	G. Abbiendi et al.	(OPAL Collab.)
ABREU	99W	EPJ C10 185	P. Abreu et al.	(DELPHI Collab.)
ACKERSTAFF	98G	PL B426 161	K. Ackerstaff et al.	(OPAL Collab.)
BARATE	98D	EPJ C2 197	R. Barate et al.	(ALEPH Collab.)
BARATE	98V	EPJ C5 205	R. Barate et al.	(ALEPH Collab.)
ACKERSTAFF	97N	ZPHY C74 423	K. Ackerstaff et al.	(OPAL Collab.)
ABE	96M	PRL 77 1439	F. Abe et al.	(CDF Collab.)
ABREU	96D	ZPHY C71 199	P. Abreu et al.	(DELPHI Collab.)
AKERS	96	ZPHY C69 195	R. Akers et al.	(OPAL Collab.)
BUSKULIC	96T	PL B384 449	D. Buskulic et al.	(ALEPH Collab.)
ABREU	95C	PL B347 447	P. Abreu et al.	(DELPHI Collab.)
ABREU	95S	ZPHY C68 375	P. Abreu et al.	(DELPHI Collab.)
ABREU	95V	ZPHY C68 541	P. Abreu et al.	(DELPHI Collab.)
BUSKULIC	95L	PL B357 685	D. Buskulic et al.	(ALEPH Collab.)
ABREU	93F	PL B311 379	P. Abreu et al.	(DELPHI Collab.)
AKERS	93	PL B316 435	R. Akers et al.	(OPAL Collab.)
BUSKULIC	92I	PL B297 449	D. Buskulic et al.	(ALEPH Collab.)

See key on page 1127

Baryon Particle Listings

Pentaquarks, $P_c(4312)^+$, $P_c(4380)^+$, $P_c(4440)^+$, $P_c(4457)^+$

EXOTIC BARYONS

See the related review(s):

Pentaquarks

$P_c(4312)^+$ Status: *

$P_c(4312)^+$ MASS

VALUE (MeV)	DOCUMENT ID	TECN	COMMENT
$4311.9 \pm 0.7^{+6.8}_{-0.6}$	AAIJ	19W LHCb	pp at 7, 8, 13 TeV

$P_c(4312)^+$ WIDTH

VALUE (MeV)	DOCUMENT ID	TECN	COMMENT
$9.8 \pm 2.7^{+3.7}_{-4.5}$	AAIJ	19W LHCb	pp at 7, 8, 13 TeV

$P_c(4312)^+$ DECAY MODES

Mode	Fraction (Γ_i/Γ)
Γ_1 $J/\psi p$	seen

$P_c(4312)^+$ BRANCHING RATIOS

$\Gamma(J/\psi p)/\Gamma_{total}$	DOCUMENT ID	TECN	COMMENT	Γ_1/Γ
seen	AAIJ	19W LHCb	pp at 7, 8, 13 TeV	

$P_c(4312)^+$ REFERENCES

AAIJ	19W	PRL 122 222001	R. Aaij et al.	(LHCb Collab.)
------	-----	----------------	----------------	----------------

$P_c(4380)^+$ Status: *

A resonance seen in $\Lambda_b^0 \rightarrow P_c^+ K^-$, then $P_c \rightarrow J/\psi p$, with a significance of 9 standard deviations. The $J/\psi p$ quark content is $uudc\bar{c}$, a pentaquark. See also the $P_c(4450)^+$. In the best amplitude fit, the two states have opposite parity, one having $J = 3/2$, the other $J = 5/2$.

Extraction of the pentaquark signals requires some understanding of the dominant $K^- p$ background. AAIJ 15P used a model-dependent approach. AAIJ 16AG reanalyzed the data making minimal assumptions about the $K^- p$ background, and thus confirmed the strong significance of the pentaquark signals.

$P_c(4380)^+$ MASS

VALUE (MeV)	DOCUMENT ID	TECN	COMMENT
$4380 \pm 8 \pm 29$	AAIJ	15P LHCb	pp at 7, 8 TeV

$P_c(4380)^+$ WIDTH

VALUE (MeV)	DOCUMENT ID	TECN	COMMENT
$205 \pm 18 \pm 86$	AAIJ	15P LHCb	pp at 7, 8 TeV

$P_c(4380)^+$ DECAY MODES

Mode	Fraction (Γ_i/Γ)
Γ_1 $J/\psi p$	seen

$P_c(4380)^+$ BRANCHING RATIOS

$\Gamma(J/\psi p)/\Gamma_{total}$	DOCUMENT ID	TECN	COMMENT	Γ_1/Γ
seen	AAIJ	15P LHCb	pp at 7, 8 TeV	

$P_c(4380)^+$ REFERENCES

AAIJ	16AG	PRL 117 082002	R. Aaij et al.	(LHCb Collab.)
AAIJ	15P	PRL 115 072001	R. Aaij et al.	(LHCb Collab.)

$P_c(4440)^+$ Status: *

$P_c(4440)^+$ MASS

VALUE (MeV)	DOCUMENT ID	TECN	COMMENT
$4440.3 \pm 1.3^{+4.1}_{-4.7}$	AAIJ	19W LHCb	pp at 7, 8, 13 TeV

$P_c(4440)^+$ WIDTH

VALUE (MeV)	DOCUMENT ID	TECN	COMMENT
$20.6 \pm 4.9^{+8.7}_{-10.1}$	AAIJ	19W LHCb	pp at 7, 8, 13 TeV

$P_c(4440)^+$ DECAY MODES

Mode	Fraction (Γ_i/Γ)
Γ_1 $J/\psi p$	seen

$P_c(4440)^+$ BRANCHING RATIOS

$\Gamma(J/\psi p)/\Gamma_{total}$	DOCUMENT ID	TECN	COMMENT	Γ_1/Γ
seen	¹ POPOV	21 D0	$p\bar{p}$ at 1.96 TeV	
seen	AAIJ	19W LHCb	pp at 7, 8, 13 TeV	

¹ Search for J/ψ inclusive production in association with a charged particle, assumed to be a proton. POPOV 21 observes a resonant signal consistent with a superposition of the $P_c(4440)^+$ and $P_c(4457)^+$, using masses and widths measured by AAIJ 19W, at significance of 3σ .

$P_c(4440)^+$ REFERENCES

POPOV	21	PAN 83 1383	A.V. Popov et al.	(D0 Collab.)
AAIJ	19W	PRL 122 222001	R. Aaij et al.	(LHCb Collab.)

$P_c(4457)^+$ Status: *

was $P_c(4450)$

A resonance seen in $\Lambda_b^0 \rightarrow P_c^+ K^-$, then $P_c \rightarrow J/\psi p$, with a significance of 12 standard deviations. The $J/\psi p$ quark content is $uudc\bar{c}$, a pentaquark. See also the $P_c(4380)^+$. In the best amplitude fit, the two states have opposite parity, one having $J = 3/2$, the other $J = 5/2$.

Extraction of the pentaquark signals requires some understanding of the dominant $K^- p$ background. AAIJ 15P used a model-dependent approach. AAIJ 16AG reanalyzed the data making minimal assumptions about the $K^- p$ background, and thus confirmed the strong significance of the pentaquark signals.

$P_c(4457)^+$ MASS

VALUE (MeV)	DOCUMENT ID	TECN	COMMENT
$4457.3 \pm 0.6^{+4.1}_{-1.7}$	AAIJ	19W LHCb	pp at 7, 8, 13 TeV

••• We do not use the following data for averages, fits, limits, etc. •••
 $4449.8 \pm 1.7 \pm 2.5$ ¹ AAIJ 15P LHCb Repl. by AAIJ 19W
¹ Considering $P_c(4440)$ and $P_c(4457)$ as a single resonance.

$P_c(4457)^+$ WIDTH

VALUE (MeV)	DOCUMENT ID	TECN	COMMENT
$6.4 \pm 2.0^{+5.7}_{-1.9}$	AAIJ	19W LHCb	pp at 7, 8, 13 TeV

••• We do not use the following data for averages, fits, limits, etc. •••
 $39 \pm 5 \pm 19$ ¹ AAIJ 15P LHCb Repl. by AAIJ 19W
¹ Considering $P_c(4440)$ and $P_c(4457)$ as a single resonance.

$P_c(4457)^+$ DECAY MODES

Mode	Fraction (Γ_i/Γ)
Γ_1 $J/\psi p$	seen

$P_c(4457)^+$ BRANCHING RATIOS

$\Gamma(J/\psi p)/\Gamma_{total}$	DOCUMENT ID	TECN	COMMENT	Γ_1/Γ
seen	¹ POPOV	21 D0	$p\bar{p}$ at 1.96 TeV	

Baryon Particle Listings

 $P_c(4457)^+$

seen AAIJ 19W LHCb pp at 7, 8, 13 TeV
 seen AAIJ 15P LHCb pp at 7, 8 TeV

¹ Search for J/ψ inclusive production in association with a charged particle, assumed to be a proton. POPOV 21 observes a resonant signal consistent with a superposition of the $P_c(4440)^+$ and $P_c(4457)^+$, using masses and widths measured by AAIJ 19W, at significance of 3σ .

 $P_c(4457)^+$ REFERENCES

POPOV	21	PAN 83 1383	A.V. Popov <i>et al.</i>	(D0 Collab.)
AAIJ	19W	PRL 122 222001	R. Aaij <i>et al.</i>	(LHCb Collab.)
AAIJ	16AG	PRL 117 082002	R. Aaij <i>et al.</i>	(LHCb Collab.)
AAIJ	15P	PRL 115 072001	R. Aaij <i>et al.</i>	(LHCb Collab.)

Magnetic Monopole Searches	2185
Supersymmetric Particle Searches	2187
Technicolor	2238
Quark and Lepton Compositeness	2239
Extra Dimensions	2243
WIMP and Dark Matter Searches	2249
Other Particle Searches	2263

SEARCHES IN OTHER SECTIONS

Neutral Higgs Bosons, Searches for	1187
Charged Higgs Bosons (H^\pm and $H^{\pm\pm}$), Searches for	1196
New Heavy Bosons	1200
Axions (A^0) and Other Very Light Bosons	1217
Heavy Charged Lepton Searches	1272
Double- β Decay	1284
Heavy Neutral Leptons, Searches for	1307
b' (Fourth Generation) Quark	1337
t' (Fourth Generation) Quark	1339
Free Quark Searches	1341

Related Reviews in Volume 1

85. Extra dimensions (rev.)	983
86. W' -boson searches (rev.)	991
87. Z' -boson searches (rev.)	995
88. Supersymmetry: theory (rev.)	1000
89. Supersymmetry: experiment (rev.)	1019
90. Axions and other similar particles (rev.)	1038
91. Quark and lepton compositeness, searches for (rev.)	1055
92. Dynamical electroweak symmetry	1061
breaking: implications of the H^0 (rev.)	
93. Grand unified theories	1076
94. Leptoquarks (rev.)	1090
95. Magnetic monopoles (rev.)	1093



SEARCHES
not in other sections

Magnetic Monopole Searches

See the related review(s):
Magnetic Monopoles

Monopole Production Cross Section — Accelerator Searches

X-SECT (cm ²)	MASS (GeV)	CHG (g)	ENERGY (GeV)	BEAM	DOCUMENT ID	TECN
<3 E-38	750-1910	1-5	13000	pp	1 ACHARYA 21	INDU
<1.3E-40	200-4000	1	13000	pp	2 AAD 20G	ATLS
<5.6E-40	500-4000	2	13000	pp	2 AAD 20G	ATLS
	200-5000	2	13000	pp	3 ACHARYA 19B	INDU
	200-5000	1	13000	pp	4 ACHARYA 18A	INDU
<2.5E-37	200-6000	1	13000	pp	5 ACHARYA 17	INDU
<2E-37	200-6000	2	13000	pp	5 ACHARYA 17	INDU
<4E-37	200-5000	3	13000	pp	5 ACHARYA 17	INDU
<1.5E-36	400-4000	4	13000	pp	5 ACHARYA 17	INDU
<7E-36	1000-3000	5	13000	pp	5 ACHARYA 17	INDU
<5E-40	200-2500	0.5-2.0	8000	pp	6 AAD 16AB	ATLS
<2E-37	100-3500	1	8000	pp	7 ACHARYA 16	INDU
<2E-37	100-3500	2	8000	pp	7 ACHARYA 16	INDU
<6E-37	500-3000	3	8000	pp	7 ACHARYA 16	INDU
<7E-36	1000-2000	4	8000	pp	7 ACHARYA 16	INDU
<1.6E-38	200-1200	1	7000	pp	8 AAD 12CS	ATLS
<5E-38	45-102	1	206	e ⁺ e ⁻	9 ABBIENDI 08	OPAL
<0.2E-36	200-700	1	1960	p \bar{p}	10 ABULENCIA 06K	CNTR
<2E-36		1	300	e ⁺ p	11,12 AKTAS 05A	INDU
<0.2 E-36		2	300	e ⁺ p	11,12 AKTAS 05A	INDU
<0.09E-36		3	300	e ⁺ p	11,12 AKTAS 05A	INDU
<0.05E-36		≥ 6	300	e ⁺ p	11,12 AKTAS 05A	INDU
<2.E-36		1	300	e ⁺ p	11,13 AKTAS 05A	INDU
<0.2E-36		2	300	e ⁺ p	11,13 AKTAS 05A	INDU
<0.07E-36		3	300	e ⁺ p	11,13 AKTAS 05A	INDU
<0.06E-36		≥ 6	300	e ⁺ p	11,13 AKTAS 05A	INDU
<0.6E-36	>265	1	1800	p \bar{p}	14 KALBFLEISCH 04	INDU
<0.2E-36	>355	2	1800	p \bar{p}	14 KALBFLEISCH 04	INDU
<0.07E-36	>410	3	1800	p \bar{p}	14 KALBFLEISCH 04	INDU
<0.2E-36	>375	6	1800	p \bar{p}	14 KALBFLEISCH 04	INDU
<0.7E-36	>295	1	1800	p \bar{p}	15,16 KALBFLEISCH 00	INDU
<7.8E-36	>260	2	1800	p \bar{p}	15,16 KALBFLEISCH 00	INDU
<2.3E-36	>325	3	1800	p \bar{p}	15,17 KALBFLEISCH 00	INDU
<0.11E-36	>420	6	1800	p \bar{p}	15,17 KALBFLEISCH 00	INDU
<0.65E-33	<3.3	≥ 2	11A	197Au	18,19 HE 97	
<1.90E-33	<8.1	≥ 2	160A	208Pb	18,19 HE 97	
<3.E-37	<45.0	1.0	88-94	e ⁺ e ⁻	PINFOLD 93	PLAS
<3.E-37	<41.6	2.0	88-94	e ⁺ e ⁻	PINFOLD 93	PLAS
<7.E-35	<44.9	0.2-1.0	89-93	e ⁺ e ⁻	KINOSHITA 92	PLAS
<2.E-34	<850	≥ 0.5	1800	p \bar{p}	BERTANI 90	PLAS
<1.2E-33	<800	≥ 1	1800	p \bar{p}	PRICE 90	PLAS
<1.E-37	<29	1	50-61	e ⁺ e ⁻	KINOSHITA 89	PLAS
<1.E-37	<18	2	50-61	e ⁺ e ⁻	KINOSHITA 89	PLAS
<1.E-38	<17	<1	35	e ⁺ e ⁻	BRAUNSC... 88B	CNTR
<8.E-37	<24	1	50-52	e ⁺ e ⁻	KINOSHITA 88	PLAS
<1.3E-35	<22	2	50-52	e ⁺ e ⁻	KINOSHITA 88	PLAS
<9.E-37	<4	<0.15	10.6	e ⁺ e ⁻	GENSOLE 87	CLEO
<3.E-37	<800	≥ 1	1800	p \bar{p}	PRICE 87	PLAS
<3.E-38	<3	<3	29	e ⁺ e ⁻	FRYBERGER 84	PLAS
<1.E-31	<1.3	1.3	540	p \bar{p}	AUBERT 83B	PLAS
<4.E-38	<10	<6	34	e ⁺ e ⁻	MUSSET 83	PLAS
<8.E-36	<20		52	pp	20 DELL 82	CNTR
<9.E-37	<30	<3	29	e ⁺ e ⁻	KINOSHITA 82	PLAS
<1.E-37	<20	<24	63	pp	CARRIGAN 78	CNTR
<1.E-37	<30	<3	56	pp	HOFFMANN 78	PLAS
			62	pp	20 DELL 76	SPRK
<4.E-33			300	p	20 STEVENS 76B	SPRK
<1.E-40	<5	<2	70	p	21 ZRELOV 76	CNTR
<2.E-30			300	n	20 BURKE 75	OSPK
<1.E-38			8	ν	22 CARRIGAN 75	HLCB
<5.E-43	<12	<10	400	p	EBERHARD 75B	INDU
<2.E-36	<30	<3	60	pp	GIACOMELLI 75	PLAS
<5.E-42	<13	<24	400	p	CARRIGAN 74	CNTR
<6.E-42	<12	<24	300	p	CARRIGAN 73	CNTR
<2.E-36		1	0.001	γ	21 BARTLETT 72	CNTR
<1.E-41	<5		70	p	GUREVICH 72	EMUL
<1.E-40	<3	<2	28	p	A MALDI 63	EMUL
<2.E-40	<3	<2	30	p	PURCELL 63	CNTR
<1.E-35	<3	<4	28	p	FIDECARO 61	CNTR
<2.E-35	<1	1	6	p	BRADNER 59	EMUL

- ACHARYA 21 search for dyons at LHC. Using a production model limits (we report the lowest) are set for dyons with magnetic charge up to 5 gD, electric charges up to 200 e and spins 0, 1/2, 1. The corresponding mass limits for magnetic monopoles are in the range 870-2040 GeV for magnetic charges in the same range.
- AAD 20G give limits for Drell-Yan production with spin-0 and spin-1/2 monopoles. The above limit is for spin = 0 at mass = 3 TeV.
- ACHARYA 19B limits both β-dependent and β-independent on monopoles with spins 0, 1/2, and 1 and with magnetic charges ranging from one to five times the Dirac charge in mass ranges between 200 GeV and 5000 GeV.
- ACHARYA 18A provide limits on monopoles with spins 0, 1/2, and 1 and with magnetic charges ranging from two to five times the Dirac charge.
- The search was sensitive to monopoles which had stopped in aluminium trapping volumes. Monopoles with spins 0 and 1/2 were considered; mass-dependent spin 1/2 monopole limits are quoted here.
- AAD 16AB model-independent 95% CL limits estimated using a fiducial region of approximately constant acceptance. Limits are mass-dependent.
- ACHARYA 16 limits at 95% CL estimated using a Drell-Yan-like production mechanism for scalar monopoles.
- AAD 12CS searched for monopoles as highly ionising objects. The cross section limits are based on an assumed Drell-Yan-like production process for spin 1/2 monopoles. The limits are mass- and scenario-dependent.
- ABBIENDI 08 assume production of spin 1/2 monopoles with effective charge gβ (n=1), via e⁺e⁻ → γ* → M \bar{M} , so that the cross section is proportional to (1 + cos²θ). There is no z information for such highly saturated tracks, so a parabolic track in the jet chamber is projected onto the xy plane. Charge per hit in the chamber produces a clean separation of signal and background.
- ABULENCIA 06K searches for high-ionizing signals in CDF central outer tracker and time-of-flight detector. For Drell-Yan M \bar{M} production, the cross section limit implies M > 360 GeV at 95% CL.
- AKTAS 05A model-dependent limits as a function of monopole mass shown for arbitrary mass of 60 GeV. Based on search for stopped monopoles in the H1 Al beam pipe.
- AKTAS 05A limits with assumed elastic spin 0 monopole pair production.
- AKTAS 05A limits with assumed inelastic spin 1/2 monopole pair production.
- KALBFLEISCH 04 reports searches for stopped magnetic monopoles in Be, Al, and Pb samples obtained from discarded material from the upgrading of DØ and CDF. A large-aperture warm-bore cryogenic detector was used. The approach was an extension of the methods of KALBFLEISCH 00. Cross section results moderately model dependent; interpretation as a mass lower limit depends on possibly invalid perturbation expansion.
- KALBFLEISCH 00 used an induction method to search for stopped monopoles in pieces of the DØ (FNAL) beryllium beam pipe and in extensions to the drift chamber aluminum support cylinder. Results are model dependent.
- KALBFLEISCH 00 result is for aluminum.
- KALBFLEISCH 00 result is for beryllium.
- HE 97 used a lead target and barium phosphate glass detectors. Cross-section limits are well below those predicted via the Drell-Yan mechanism.
- This work has also been reinterpreted in the framework of monopole production via the thermal Schwinger process (GOULD 17); this gives rise to lower mass limits.
- Multiphoton events.
- Cherenkov radiation polarization.
- Re-examines CERN neutrino experiments.

Monopole Production — Other Accelerator Searches

MASS (GeV)	CHG (g)	SPIN	ENERGY (GeV)	BEAM	DOCUMENT ID	TECN
> 610	≥ 1	0	1800	p \bar{p}	1 ABBOTT 98K	D0
> 870	≥ 1	1/2	1800	p \bar{p}	1 ABBOTT 98K	D0
>1580	≥ 1	1	1800	p \bar{p}	1 ABBOTT 98K	D0
> 510			88-94	e ⁺ e ⁻	2 ACCIARRI 95C	L3

- ABBOTT 98K search for heavy pointlike Dirac monopoles via central production of a pair of photons with high transverse energies.
- ACCIARRI 95C finds a limit B(Z → γγ) < 0.8 × 10⁻⁵ (which is possible via a monopole loop) at 95% CL and sets the mass limit via a cross section model.

Monopole Flux — Cosmic Ray Searches

"Caty" in the charge column indicates a search for monopole-catalyzed nucleon decay.

FLUX (cm ⁻² sr ⁻¹ s ⁻¹)	MASS (GeV)	CHG (g)	COMMENTS (β = v/c)	DOCUMENT ID	TECN
<2E-19		1	0.86 < β < 0.995	1 ABBASI 22	ICCB
<2E-14	>5E8		6E-4 < β < 5E-3	2 ACERO 21	NOVA
<1E-17		Caty	1E-5 < β < 1E-3	3 GAPONENKO 21	BAIK
<1.5E-18			β > 0.6	4 ALBERT 17	ANTR
<2.5E-21		1	1E8 < γ < 1E13	5 AAB 16	AUGE
<1.55E-18			β > 0.51	6 AARTSEN 16B	ICCB
<1E-17		Caty	1E-3 < β < 1E-2	7 AARTSEN 14	ICCB
<3E-18		1	β > 0.8	8 ABBASI 13	ICCB
<1.3E-17		1	β > 0.625	9 ADRIAN-MAR.	12A ANTR
<6E-28	<1E17	Caty	1E-5 < β < 0.04	10 UENO 12	SKAM
<1E-19		1	γ > 1E10	11 DETRIXHE 11	ANIT
<3.8E-17		1	β > 0.76	8 ABBASI 10A	ICCB
<1.3E-15	1E4 < M < 5E13	1	β > 0.05	12 BALESTRA 08	PLAS
<0.65E-15	>5E13	1	β > 0.05	12 BALESTRA 08	PLAS
<1E-18		1	γ > 1 E8	11 HOGAN 08	RICE
<1.4E-16		1	1.1E-4 < β < 1	13 AMBROSIO 02B	MCRO
<3E-16		Caty	1.1E-4 < β < 5E-3	14 AMBROSIO 02C	MCRO
<1.5E-15		1	5E-3 < β < 0.99	15 AMBROSIO 02D	MCRO
<1E-15		1	1.1 × 10 ⁻⁴ -0.1	16 AMBROSIO 97	MCRO
<5.6E-15		1	(0.18-3.0)E-3	17 AHLN 94	MCRO
<2.7E-15		Caty	β ~ 1 × 10 ⁻³	18 BECKER-SZ..	94 IMB
<8.7E-15		1	>2.E-3	THRON 92	SODU
<4.4E-12		1	all β	GARDNER 91	INDU

Searches Particle Listings

Magnetic Monopole Searches

<7.2E-13	1	all β	HUBER	91	INDU
<3.7E-15	>E12	1 $\beta=1.E-4$	19 ORITO	91	PLAS
<3.2E-16	>E10	1 $\beta > 0.05$	19 ORITO	91	PLAS
<3.2E-16	>E10-E12	2,3	19 ORITO	91	PLAS
<3.8E-13	1	all β	BERMON	90	INDU
<5.E-16	Caty	1 all β	18 BEZRUKOV	90	CHER
<1.8E-14	1	1 $\beta > 1.1E-4$	20 BUCKLAND	90	HEPT
<1.E-18	1	3.E-4 < β < 1.5E-3	21 GHOSH	90	MICA
<7.2E-13	1	all β	HUBER	90	INDU
<5.E-12	>E7	1 3.E-4 < β < 5.E-3	BARISH	87	CNTR
<1.E-13	Caty	1 1.E-5 < β < 1	18 BARTELT	87	SOUND
<1.E-10	1	all β	EBISU	87	INDU
<2.E-13	1	1.E-4 < β < 6.E-4	MASEK	87	HEPT
<2.E-14	1	4.E-5 < β < 2.E-4	NAKAMURA	87	PLAS
<2.E-14	1	1.E-3 < β < 1	NAKAMURA	87	PLAS
<5.E-14	1	9.E-4 < β < 1.E-2	SHEPKO	87	CNTR
<2.E-13	1	4.E-4 < β < 1	TSUKAMOTO	87	CNTR
<5.E-14	1	all β	22 CAPLIN	86	INDU
<5.E-12	1	all β	CROMAR	86	INDU
<1.E-13	1	7.E-4 < β	HARA	86	CNTR
<7.E-11	1	all β	INCANDELA	86	INDU
<1.E-18	1	4.E-4 < β < 1.E-3	21 PRICE	86	MICA
<5.E-12	1	all β	BERMON	85	INDU
<6.E-12	1	all β	CAPLIN	85	INDU
<6.E-10	1	all β	EBISU	85	INDU
<3.E-15	Caty	5.E-5 < $\beta \leq 1.E-3$	18 KAJITA	85	KAMI
<2.E-21	Caty	1 $\beta < 1.E-3$	18,23 KAJITA	85	KAMI
<3.E-15	Caty	1.E-3 < β < 1.E-1	18 PARK	85B	CNTR
<5.E-12	1	1.E-4 < β < 1	BATTISTONI	84	NUSX
<7.E-12	1	all β	INCANDELA	84	INDU
<7.E-13	1	3.E-4 < β	20 KAJINO	84	CNTR
<2.E-12	1	3.E-4 < β < 1.E-1	KAJINO	84B	CNTR
<6.E-13	1	5.E-4 < β < 1	KAWAGOE	84	CNTR
<2.E-14	1	1.E-3 < β	18 KRISHNA...	84	CNTR
<4.E-13	1	6.E-4 < β < 2.E-3	LISS	84	CNTR
<1.E-16	1	3.E-4 < β < 1.E-3	21 PRICE	84	MICA
<1.E-13	1	1.E-4 < β	PRICE	84B	PLAS
<4.E-13	1	6.E-4 < β < 2.E-3	TARLE	84	CNTR
<4.E-13	1	1.E-2 < β < 1.E-3	24 ANDERSON	83	EMUL
<1.E-12	1	7.E-3 < β < 1	BARTELT	83B	CNTR
<3.E-13	1	1.E-3 < β < 4.E-1	BONARELLI	83	PLAS
<3.E-12	Caty	5.E-4 < β < 5.E-2	18 BOSETTI	83	CNTR
<4.E-11	1	all β	CABRERA	83	INDU
<5.E-15	1	1.E-2 < β < 1	DOKE	83	PLAS
<8.E-15	Caty	1.E-4 < β < 1.E-1	18 ERREDE	83	IMB
<5.E-12	1	1.E-4 < β < 3.E-2	GROOM	83	CNTR
<2.E-12	1	6.E-4 < β < 1	MASHIMO	83	CNTR
<1.E-13	1	1 $\beta=3.E-3$	ALEXEYEV	82	CNTR
<2.E-12	1	7.E-3 < β < 6.E-1	BONARELLI	82	CNTR
6.E-10	1	all β	25 CABRERA	82	INDU
<2.E-11	1	1.E-2 < β < 1.E-1	MASHIMO	82	CNTR
<2.E-15	concentrator	concentrator	BARTLETT	81	PLAS
<1.E-13	>1	1.E-3 < β	KINOSHITA	81B	PLAS
<5.E-11	<E17	3.E-4 < β < 1.E-3	ULLMAN	81	CNTR
<2.E-11	concentrator	concentrator	BARTLETT	78	PLAS
1.E-1	>200	2	26 PRICE	75	PLAS
<2.E-13	>2	>2	FLEISCHER	71	PLAS
<1.E-19	>2	obsidian, mica	FLEISCHER	69C	PLAS
<5.E-15	<15	<3 concentrator	CARITHERS	66	ELEC
<2.E-11	<1-3	concentrator	MALKUS	51	EMUL

- ¹ABBASI 22 search was based on Cherenkov light detection in an array of optical modules in the Antarctic ice cap. Limits are speed-dependent.
- ²ACERO 21 employ NOVA experiment to set reported 90% CL upper limit on the cosmic monopoles flux for velocity $6 \times 10^{-4} < \beta < 5 \times 10^{-3}$ and mass $> 5 \times 10^8$ GeV.
- ³GAPONENKO 21 use data of NT200 two-year operation at Baikal to give speed-dependent limits for different assumed catalysis cross sections. Reported limit is for $\sigma = 10$ mb.
- ⁴ALBERT 17 limits were estimated using a Cherenkov light in an array of optical modules under the Mediterranean Sea. The limits are for MM masses between 10^{10} and 10^{14} GeV. The limits are speed-dependent.
- ⁵AAB 16 search was made with a set of telescopes sampling the longitudinal profile of fluorescence light emitted by extensive air showers. Limits are speed dependent.
- ⁶AARTSEN 16b was based on a Cherenkov signature in an array of optical modules which were sunk in the Antarctic ice cap. Limits are speed-dependent.
- ⁷Beyond the monopole speed, the limits of AARTSEN 14 depend on the catalysis cross section (σ) which corresponds to the monopole radiating \bar{l} times the light per track length compared to the Cherenkov light from a single electrically charged, relativistic particle. The values quoted here correspond to $\sigma = 1$ barn or $\bar{l} = 30$.
- ⁸ABBASI 13 and ABBASI 10a were based on a Cherenkov signature in an array of optical modules which were sunk in the Antarctic ice cap. Limits are speed-dependent.
- ⁹ADRIAN-MARTINEZ 12a measurements were based on a Cherenkov signature in an underwater telescope in the Western Mediterranean Sea. Limits are speed-dependent.
- ¹⁰The limits from UENO 12 depend on the monopole speed and are also sensitive to assumed values of monopole mass and the catalysis cross section.
- ¹¹HOGAN 08 and DETRIXHE 11 limits on relativistic monopoles are based on nonobservation of radio Cherenkov signals at the South Pole. Limits are speed-dependent.
- ¹²BALESTRA 08 exposed of nuclear track detector modules totaling 400 m² for 4 years at the Chacaltaya Laboratory (5230 m) in search for intermediate-mass monopoles with $\beta > 0.05$. The analysis is mainly based on three CR39 modules. For $M > 5 \times 10^{13}$ GeV there

- can be upward-going monopoles as well, hence the flux limit is half that obtained for less massive monopoles. Previous experiments (e.g. MACRO and OHYA (ORITO 91)) had set limits only for $M > 1 \times 10^9$ GeV.
- ¹³AMBROSIO 02b direct search final result for $m \geq 10^{17}$ GeV, based upon 4.2 to 9.5 years of running, depending upon the subsystem. Limit with CR39 track-etch detector extends the limit from $\beta=4 \times 10^{-5}$ (3.1×10^{-16} cm⁻²sr⁻¹s⁻¹) to $\beta=1 \times 10^{-4}$ (2.1×10^{-16} cm⁻²sr⁻¹s⁻¹). Limit curve in paper is piecewise continuous due to different detection techniques for different β ranges.
- ¹⁴AMBROSIO 02c limit for catalysis of nucleon decay with catalysis cross section of ≈ 1 mb. The flux limit increases by ~ 3 at the higher β limit, and increases to 1×10^{-14} cm⁻²sr⁻¹s⁻¹ if the catalysis cross section is 0.01 mb. Based upon 71193 hr of data with the streamer detector, with an acceptance of 4250 m²sr.
- ¹⁵AMBROSIO 02d result for "more than two years of data." Ionization search using several subsystems. Limit curve as a function of β not given. Included in AMBROSIO 02b.
- ¹⁶AMBROSIO 97 global MACRO 90%CL is 0.78×10^{-15} at $\beta=1.1 \times 10^{-4}$, goes through a minimum at 0.61×10^{-15} near $\beta=(1.1-2.7) \times 10^{-3}$, then rises to 0.84×10^{-15} at $\beta=0.1$. The global limit in this region is below the Parker bound at 10^{-15} . Less stringent limits are established for $4 \times 10^{-5} < \beta < 1 \times 10^{-4}$. Limits set by various triggers and different subdetectors are given in the paper. All limits assume a catalysis cross section smaller than a few mb.
- ¹⁷AHLEN 94 limit for dyons extends down to $\beta=0.9E-4$ and a limit of $1.3E-14$ extends to $\beta=0.8E-4$. Also see comment by PRICE 94 and reply of BARISH 94. One loophole in the AHLEN 94 result is that in the case of monopoles catalyzing nucleon decay, relativistic particles could veto the events. See AMBROSIO 97 for additional results.
- ¹⁸Catalysis of nucleon decay; sensitive to assumed catalysis cross section.
- ¹⁹ORITO 91 limits are functions of velocity. Lowest limits are given here.
- ²⁰Used DKMPR mechanism and Penning effect.
- ²¹Assumes monopole attaches fermion nucleus.
- ²²Limit from combining data of CAPLIN 86, BERMON 85, INCANDELA 84, and CABRERA 83. For a discussion of controversy about CAPLIN 86 observed event, see GUY 87. Also see SCHOUTEN 87.
- ²³Based on lack of high-energy solar neutrinos from catalysis in the sun.
- ²⁴Anomalous long-range α (⁴He) tracks.
- ²⁵CABRERA 82 candidate event has single Dirac charge within $\pm 5\%$.
- ²⁶ALVEREZ 75, FLEISCHER 75, and FRIEDLANDER 75 explain as fragmenting nucleus. EBERHARD 75 and ROSS 76 discuss conflict with other experiments. HAGSTROM 77 reinterprets as antinucleus. PRICE 78 reassesses.

Monopole Flux — Astrophysics

FLUX (cm ⁻² sr ⁻¹ s ⁻¹)	MASS (GeV)	CHG ($\beta = v/c$)	COMMENTS	DOCUMENT ID	TECN
<1.3E-20			faint white dwarf	1 FREESE	99 ASTR
<1.E-16	E17	1	galactic field	2 ADAMS	93 COSM
<1.E-23			Jovian planets	1 ARAFUNE	85 ASTR
<1.E-16	E15		solar trapping	BRACCI	85B ASTR
<1.E-18		1		1 HARVEY	84 COSM
<3.E-23			neutron stars	KOLB	84 ASTR
<7.E-22			pulsars	1 FREESE	83B ASTR
<1.E-18	<E18	1	intergalactic field	1 REPHAELI	83 COSM
<1.E-23			neutron stars	1 DIMOPOUL...	82 COSM
<5.E-22			neutron stars	1 KOLB	82 COSM
<5.E-15	>E21		galactic halo	SALPETER	82 COSM
<1.E-12	E19	1	$\beta=3.E-3$	3 TURNER	82 COSM
<1.E-16		1	galactic field	PARKER	70 COSM

- ¹Catalysis of nucleon decay.
- ²ADAMS 93 limit based on "survival and growth of a small galactic seed field" is 10^{-16} ($m/10^{17}$ GeV) cm⁻²sr⁻¹s⁻¹. Above 10^{17} GeV, limit 10^{-16} (10^{17} GeV/m) cm⁻²sr⁻¹s⁻¹ (from requirement that monopole density does not overclose the universe) is more stringent.
- ³Re-evaluates PARKER 70 limit for GUT monopoles.

Monopole Density — Matter Searches

DENSITY	CHG (g)	MATERIAL	DOCUMENT ID	TECN
<9.8E-5/gram	≥ 1	Polar rock	BENDTZ	13 INDU
<6.9E-6/gram	>1/3	Meteorites and other	JEON	95 INDU
<2.E-7/gram	>0.6	Fe ore	1 EBISU	87 INDU
<4.6E-6/gram	>0.5	deep schist	KOVALIK	86 INDU
<1.6E-6/gram	>0.5	manganese nodules	2 KOVALIK	86 INDU
<1.3E-6/gram	>0.5	seawater	KOVALIK	86 INDU
>1.E+14/gram	>1/3	iron aerosols	Mikhailov	83 SPEC
<6.E-4/gram	<140	air, seawater	CARRIGAN	76 CNTR
<5.E-1/gram	>0.04	11 materials	CABRERA	75 INDU
<2.E-4/gram	>0.05	moon rock	ROSS	73 INDU
<6.E-7/gram	<120	seawater	KOLM	71 CNTR
<1.E-2/gram	<120	manganese nodules	FLEISCHER	69 PLAS
<1.E-4/gram	>0	manganese	FLEISCHER	69B PLAS
<2.E-3/gram	<1-3	magnetite, meteor	GOTO	63 EMUL
<2.E-2/gram		meteorite	PETUKHOV	63 CNTR

- ¹Mass 1×10^{14} – 1×10^{17} GeV.
- ²KOVALIK 86 examined 498 kg of schist from two sites which exhibited clear mineralogical evidence of having been buried at least 20 km deep and held below the Curie temperature.

See key on page 1127

Searches Particle Listings

Magnetic Monopole Searches, Supersymmetric Particle Searches

Monopole Density — Astrophysics

Table with columns: DENSITY, CHG (g), MATERIAL, DOCUMENT ID, TECN. Rows include <1.E-9/gram, <6.E-33/nuc1, <2.E-28/nuc1, <2.E-4/prot, <2.E-13/m3.

1 Catalysis of nucleon decay.

REFERENCES FOR Magnetic Monopole Searches

ABBASI 22 PRL 128 051101 R. Abbasi et al. (IceCube Collab.)
ACERO 21 PR D103 012007 M.A. Acero et al. (NOVA Collab.)
ACHARYA 21 PRL 126 071801 B. Acharya et al. (MOEDAL Collab.)

ARAFUNE 83 PL 133B 380 J. Arafune, M. Fukugita (ICRR, KYOTO)
AUBERT 83B PL 120B 465 B. Aubert et al. (CERN, LAPP)
BARTELT 83B PRL 50 655 J.E. Bartelt et al. (MINN, ANL)
BARWICK 83 PR D28 2338 S.W. Barwick, K. Kinoshita, P.B. Price (UCB)
BONARELLI 83 PL 126B 137 R. Bonarelli, P. Capiluppi, I. d'Antone (BGNA)

OTHER RELATED PAPERS

GROOM 86 PRPL 140 323 D.E. Groom (UTAH) Review

Supersymmetric Particle Searches

The exclusion of particle masses within a mass range (m1, m2) will be denoted with the notation "none m1-m2" in the VALUE column of the following Listings. The latest unpublished results are described in the "Supersymmetry: Experiment" review.

See the related review(s): Supersymmetry, Part I (Theory) Supersymmetry, Part II (Experiment)

CONTENTS:

- chi_1^0 (Lightest Neutralino) mass limit
- Accelerator limits for stable chi_1^0
- Bounds on chi_1^0 from dark matter searches
- chi_1^0-p elastic cross section
Spin-dependent interactions
Spin-independent interactions
- Other bounds on chi_1^0 from astrophysics and cosmology
- Unstable chi_1^0 (Lightest Neutralino) mass limit
chi_2^0, chi_3^0, chi_4^0 (Neutralinos) mass limits
chi_1^pm, chi_2^pm (Charginos) mass limits

Downloaded from https://academic.oup.com/ptep/article/2022/8/083C01/6651666 by CERN Library user on 11 October 2022

Searches Particle Listings

Supersymmetric Particle Searches

Long-lived $\tilde{\chi}^\pm$ (Chargino) mass limit
 $\tilde{\nu}$ (Sneutrino) mass limit
 Charged sleptons
 – R-parity conserving \tilde{e} (Selectron) mass limit
 – R-parity violating \tilde{e} (Selectron) mass limit
 – R-parity conserving $\tilde{\mu}$ (Smuon) mass limit
 – R-parity violating $\tilde{\mu}$ (Smuon) mass limit
 – R-parity conserving $\tilde{\tau}$ (Stau) mass limit
 – R-parity violating $\tilde{\tau}$ (Stau) mass limit
 – Long-lived $\tilde{\ell}$ (Slepton) mass limit
 \tilde{q} (Squark) mass limit
 – R-parity conserving \tilde{q} (Squark) mass limit
 – R-parity violating \tilde{q} (Squark) mass limit
 Long-lived \tilde{q} (Squark) mass limit
 \tilde{b} (Sbottom) mass limit
 – R-parity conserving \tilde{b} (Sbottom) mass limit
 – R-parity violating \tilde{b} (Sbottom) mass limit
 \tilde{t} (Stop) mass limit
 – R-parity conserving \tilde{t} (Stop) mass limit
 – R-parity violating \tilde{t} (Stop) mass limit
 Heavy \tilde{g} (Glauino) mass limit
 – R-parity conserving heavy \tilde{g} (Glauino) mass limit
 – R-parity violating heavy \tilde{g} (Glauino) mass limit
 Long-lived \tilde{g} (Glauino) mass limit
 Light \tilde{G} (Gravitino) mass limits from collider experiments
 Supersymmetry miscellaneous results

The results shown below, unless stated otherwise, are based on the Minimal Supersymmetric Standard Model (MSSM), as described in the Note on Supersymmetry. Unless otherwise indicated, this includes the assumption of common gaugino and scalar masses at the scale of Grand Unification (GUT), and use of the resulting relations in the spectrum and decay branching ratios. Unless otherwise indicated, it is also assumed that R -parity (R) is conserved and that:

- 1) The $\tilde{\chi}_1^0$ is the lightest supersymmetric particle (LSP),
- 2) $m_{\tilde{f}_L} = m_{\tilde{f}_R}$, where $\tilde{f}_{L,R}$ refer to the scalar partners of left- and right-handed fermions.

Limits involving different assumptions are identified in the Comments or in the Footnotes, in particular also the many simplified models, see definitions below. We summarize here the notations used in this Chapter to characterize some of the most common deviations from the MSSM (for further details, see the Note on Supersymmetry).

Theories with R -parity violation (RPV) are characterized by a superpotential of the form: $\lambda_{ijk} L_i L_j e_k^c + \lambda'_{ijk} L_i Q_j d_k^c + \lambda''_{ijk} u_i^c d_j^c d_k^c$, where i, j, k are generation indices. The presence of any of these couplings is often identified in the following by the symbols $LL\tilde{E}$, $LQ\tilde{D}$, and $U\tilde{D}\tilde{D}$. Mass limits in the presence of RPV will often refer to “direct” and “indirect” decays. Direct refers to RPV decays of the particle in consideration. Indirect refers to cases where RPV appears in the decays of the LSP. The LSP need not be the $\tilde{\chi}_1^0$.

In several models, most notably in theories with so-called Gauge Mediated Supersymmetry Breaking (GMSB), the gravitino (\tilde{G}) is the LSP. It is usually much lighter than any other massive particle in the spectrum, and $m_{\tilde{G}}$ is then neglected in all decay processes involving gravitinos. In these scenarios, particles other than the neutralino are sometimes considered as the next-to-lightest supersymmetric particle (NLSP), and are assumed to decay to their even- R partner plus \tilde{G} . If the lifetime is short enough for the decay to take place within the detector, \tilde{G} is assumed to be undetected and to give rise to missing energy (\cancel{E}) or missing transverse energy (\cancel{E}_T) signatures.

When needed, specific assumptions on the eigenstate content of $\tilde{\chi}^0$ and $\tilde{\chi}^\pm$ states are indicated, using the notation $\tilde{\gamma}$ (photino), \tilde{H} (higgsino), \tilde{W} (wino), and \tilde{Z} (zino) to signal that the limit of pure states was used. The term gaugino is also used, to generically indicate wino-like charginos and zino-like neutralinos.

In the listings we have made use of the following abbreviations for simplified models employed by the experimental collaborations in supersymmetry searches published in the past year.

WARNING: Experimental lower mass limits determined within simplified models are to be treated with extreme care as they might not be directly applicable to realistic models. This is outlined in detail in the publications and we recommend consulting them before using bounds. For example, branching ratios, typically fixed to specific values in simplified models, can vary substantially in more elaborate models.

Simplified Models Table

- Tglu1A:** gluino pair production with $\tilde{g} \rightarrow q\tilde{q}\tilde{\chi}_1^0$.
Tglu1B: gluino pair production with $\tilde{g} \rightarrow q\tilde{q}'\tilde{\chi}_1^\pm$, $\tilde{\chi}_1^\pm \rightarrow W^\pm\tilde{\chi}_1^0$.
Tglu1C: gluino pair production with a 2/3 probability of having a $\tilde{g} \rightarrow q\tilde{q}'\tilde{\chi}_1^\pm$, $\tilde{\chi}_1^\pm \rightarrow W^\pm\tilde{\chi}_1^0$ decay and a 1/3 probability of having a $\tilde{g} \rightarrow q\tilde{q}\tilde{\chi}_2^0$, $\tilde{\chi}_2^0 \rightarrow Z^\pm\tilde{\chi}_1^0$ decay.
Tglu1D: gluino pair production with one gluino decaying to $q\tilde{q}'\tilde{\chi}_1^\pm$ with $\tilde{\chi}_1^\pm \rightarrow W^\pm + \tilde{G}$, and the other gluino decaying to $q\tilde{q}\tilde{\chi}_1^0$ with $\tilde{\chi}_1^0 \rightarrow \gamma + \tilde{G}$.
Tglu1E: gluino pair production with $\tilde{g} \rightarrow q\tilde{q}'\tilde{\chi}_1^\pm$, $\tilde{\chi}_1^\pm \rightarrow W^\pm\tilde{\chi}_2^0$ and $\tilde{\chi}_2^0 \rightarrow Z^\pm\tilde{\chi}_1^0$ where $m_{\tilde{\chi}_1^\pm} = (m_{\tilde{g}} + m_{\tilde{\chi}_1^0})/2$, $m_{\tilde{\chi}_2^0} = (m_{\tilde{\chi}_1^\pm} + m_{\tilde{\chi}_1^0})/2$.
Tglu1F: gluino pair production with $\tilde{g} \rightarrow q\tilde{q}'\tilde{\chi}_1^\pm$ or $\tilde{g} \rightarrow q\tilde{q}\tilde{\chi}_2^0$ with equal branching ratios, where $\tilde{\chi}_1^\pm$ decays through an intermediate scalar tau lepton or sneutrino to $\tau\nu\tilde{\chi}_1^0$ and where $\tilde{\chi}_2^0$ decays through an intermediate scalar tau lepton or sneutrino to $\tau^+\tau^-\tilde{\chi}_1^0$ or $\nu\bar{\nu}\tilde{\chi}_1^0$; the mass hierarchy is such that $m_{\tilde{\chi}_1^\pm} \sim m_{\tilde{\chi}_2^0} = (m_{\tilde{g}} + m_{\tilde{\chi}_1^0})/2$ and $m_{\tilde{\tau},\tilde{\nu}} = (m_{\tilde{\chi}_1^\pm} + m_{\tilde{\chi}_1^0})/2$.
Tglu1G: gluino pair production with $\tilde{g} \rightarrow q\tilde{q}\tilde{\chi}_2^0$, and $\tilde{\chi}_2^0$ decaying through an intermediate slepton or sneutrino to $l^+l^-\tilde{\chi}_1^0$ or $\nu\bar{\nu}\tilde{\chi}_1^0$ where $m_{\tilde{\chi}_2^0} = (m_{\tilde{g}} + m_{\tilde{\chi}_1^0})/2$ and $m_{\tilde{e},\tilde{\nu}} = (m_{\tilde{\chi}_2^0} + m_{\tilde{\chi}_1^0})/2$.
Tglu1H: gluino pair production with $\tilde{g} \rightarrow q\tilde{q}\tilde{\chi}_2^0$, and $\tilde{\chi}_2^0 \rightarrow \tilde{\chi}_1^0 Z^{0(*)}$.
Tglu1I: gluino pair production with $\tilde{g} \rightarrow q\tilde{q}\tilde{\chi}_2^0$, and $\tilde{\chi}_2^0 \rightarrow \tilde{\chi}_1^0 H$.
Tglu1J: gluino pair production with $\tilde{g} \rightarrow q\tilde{q}\tilde{\chi}_2^0$, and $\text{BR}(\tilde{\chi}_2^0 \rightarrow \tilde{\chi}_1^0 Z^{0(*)}) = \text{BR}(\tilde{\chi}_2^0 \rightarrow \tilde{\chi}_1^0 H) = 0.5$.
Tglu1LL gluino pair production where $\tilde{g} \rightarrow q\tilde{q}\tilde{\chi}_1^0$ happens with 1/3 probability and $\tilde{g} \rightarrow q\tilde{q}'\tilde{\chi}_1^\pm$ happens with 2/3 probability. The $\tilde{\chi}_1^\pm$ is assumed to be few hundreds of MeV heavier than the $\tilde{\chi}_1^0$, and decays to $\tilde{\chi}_1^0$ via a pion.
Tglu2A: gluino pair production with $\tilde{g} \rightarrow b\tilde{b}\tilde{\chi}_1^0$.
Tglu3A: gluino pair production with $\tilde{g} \rightarrow t\tilde{t}\tilde{\chi}_1^0$.
Tglu3B: gluino pair production with $\tilde{g} \rightarrow t\tilde{t}$ where \tilde{t} decays exclusively to $t\tilde{\chi}_1^0$.
Tglu3C: gluino pair production with $\tilde{g} \rightarrow t\tilde{t}$ where \tilde{t} decays exclusively to $c\tilde{\chi}_1^0$.
Tglu3D: gluino pair production with $\tilde{g} \rightarrow t\tilde{b}\tilde{\chi}_1^\pm$ with $\tilde{\chi}_1^\pm \rightarrow W^\pm\tilde{\chi}_1^0$.
Tglu3E: gluino pair production where the gluino decays 25% of the time through $\tilde{g} \rightarrow b\tilde{b}\tilde{\chi}_1^0$ and 50% of the time through $\tilde{g} \rightarrow t\tilde{b}\tilde{\chi}_1^\pm$ with $\tilde{\chi}_1^\pm \rightarrow W^\pm\tilde{\chi}_1^0$.
Tglu3F: gluino pair production with wino-like couplings to electroweakinos, that is: $\tilde{g} \rightarrow t\tilde{t}\tilde{\chi}_{1,2}^0$ with BR 17%, $\tilde{g} \rightarrow b\tilde{b}\tilde{\chi}_{1,2}^0$ with BR 17%, $\tilde{g} \rightarrow t\tilde{t}\tilde{\chi}_1^\pm$ with BR 66%.
Tglu3G: gluino pair production with higgsino-like couplings to electroweakinos, that is: $\tilde{g} \rightarrow t\tilde{t}\tilde{\chi}_{1,2}^0$ with BR 50%, $\tilde{g} \rightarrow t\tilde{t}\tilde{\chi}_1^\pm$ with BR 50%.
Tglu4A: gluino pair production with one gluino decaying to $q\tilde{q}'\tilde{\chi}_1^\pm$ with $\tilde{\chi}_1^\pm \rightarrow W^\pm + \tilde{G}$, and the other gluino decaying to $q\tilde{q}\tilde{\chi}_1^0$ with $\tilde{\chi}_1^0 \rightarrow \gamma + \tilde{G}$.

- Tglu4B:** gluino pair production with gluinos decaying to $q\bar{q}\tilde{\chi}_1^0$ and $\tilde{\chi}_1^0 \rightarrow \gamma + \tilde{G}$.
- Tglu4C:** gluino pair production with gluinos decaying to $\tilde{g} \rightarrow q\bar{q}\tilde{\chi}_1^0$ and $\tilde{\chi}_1^0 \rightarrow Z + \tilde{G}$.
- Tglu4D:** gluino pair production with $\tilde{g} \rightarrow q\bar{q}\tilde{\chi}_1^0$ where the $\tilde{\chi}_1^0$ decays with equal probability to $\tilde{\chi}_1^0 \rightarrow \gamma + \tilde{G}$ or to $\tilde{\chi}_1^0 \rightarrow H + \tilde{G}$.
- Tglu4E:** gluino pair production with $\tilde{g} \rightarrow b\bar{b}\tilde{\chi}_1^0$ where the $\tilde{\chi}_1^0$ decays with equal probability to $\tilde{\chi}_1^0 \rightarrow \gamma + \tilde{G}$ or to $\tilde{\chi}_1^0 \rightarrow Z + \tilde{G}$.
- Tglu4F:** gluino pair production with $\tilde{g} \rightarrow t\bar{t}\tilde{\chi}_1^0$ where the $\tilde{\chi}_1^0$ decays with equal probability to $\tilde{\chi}_1^0 \rightarrow \gamma + \tilde{G}$ or to $\tilde{\chi}_1^0 \rightarrow Z + \tilde{G}$.
- Tglu1RPV:** gluino pair production with $\tilde{g} \rightarrow uds$ via RPV coupling λ''_{112} .
- Tglu2RPV:** gluino pair production with $\tilde{g} \rightarrow (tbd, tbs)$ via RPV coupling λ''_{313} or λ''_{323} .
-
- Tsqk1:** squark pair production with $\tilde{q} \rightarrow q\tilde{\chi}_1^0$.
- Tsqk1LL:** squark pair production where $\tilde{q} \rightarrow q\tilde{\chi}_1^0$ and $\tilde{q} \rightarrow q'\tilde{\chi}_1^\pm$ each happen with 50% probability. The $\tilde{\chi}_1^\pm$ is assumed to be few hundreds of MeV heavier than the $\tilde{\chi}_1^0$, and decays to $\tilde{\chi}_1^0$ via a pion.
- Tsqk2:** squark pair production with $\tilde{q} \rightarrow q\tilde{\chi}_2^0$ and $\tilde{\chi}_2^0 \rightarrow Z + \tilde{\chi}_1^0$.
- Tsqk2A:** squark pair production with $\tilde{q} \rightarrow q\tilde{\chi}_2^0$, where one of the $\tilde{\chi}_2^0 \rightarrow Z^*(\tilde{\chi}_1^0 \rightarrow f\bar{f}\tilde{\chi}_1^0)$ and the other $\tilde{\chi}_2^0 \rightarrow \tilde{\ell}\ell^+ \rightarrow \ell^+\ell^-\tilde{\chi}_1^0$.
- Tsqk3:** squark pair production with $\tilde{q} \rightarrow q'\tilde{\chi}_1^\pm$, $\tilde{\chi}_1^\pm \rightarrow W^\pm\tilde{\chi}_1^0$ (like Tglu1B but for squarks)
- Tsqk4:** squark pair production with squarks decaying to $q\tilde{\chi}_1^0$ and $\tilde{\chi}_1^0 \rightarrow \gamma + \tilde{G}$.
- Tsqk4A:** squark pair production with one squark decaying to $q\tilde{\chi}_1^\pm$ with $\tilde{\chi}_1^\pm \rightarrow W^\pm + \tilde{G}$, and the other squark decaying to $q\tilde{\chi}_1^0$ with $\tilde{\chi}_1^0 \rightarrow \gamma + \tilde{G}$.
- Tsqk4B:** squark pair production with squarks decaying to $q\tilde{\chi}_1^0$ and $\tilde{\chi}_1^0 \rightarrow \gamma + \tilde{G}$.
-
- Tstop1:** stop pair production with $\tilde{t} \rightarrow t\tilde{\chi}_1^0$.
- Tstop1LL:** stop pair production where $\tilde{t} \rightarrow t\tilde{\chi}_1^0$ and $\tilde{t} \rightarrow b\tilde{\chi}_1^\pm$ each happen with 50% probability. The $\tilde{\chi}_1^\pm$ is assumed to be few hundreds of MeV heavier than the $\tilde{\chi}_1^0$, and decays to $\tilde{\chi}_1^0$ via a pion.
- Tstop2:** stop pair production with $\tilde{t} \rightarrow b\tilde{\chi}_1^\pm$ with $\tilde{\chi}_1^\pm \rightarrow W^\pm\tilde{\chi}_1^0$.
- Tstop3:** stop pair production with the subsequent four-body decay $\tilde{t} \rightarrow bff'\tilde{\chi}_1^0$ where f represents a lepton or a quark.
- Tstop4:** stop pair production with $\tilde{t} \rightarrow c\tilde{\chi}_1^0$.
- Tstop5:** stop pair production with $\tilde{t} \rightarrow b\tilde{\tau}$ with $\tilde{\tau} \rightarrow \tau\tilde{G}$.
- Tstop6:** stop pair production with $\tilde{t} \rightarrow t + \tilde{\chi}_2^0$, where $\tilde{\chi}_2^0 \rightarrow Z + \tilde{\chi}_1^0$ or $H + \tilde{\chi}_1^0$ each with BR 50%.
- Tstop7:** stop pair production with $\tilde{t}_2 \rightarrow \tilde{t}_1 + H/Z$, where $\tilde{t}_1 \rightarrow t + \tilde{\chi}_1^0$.
- Tstop8:** stop pair production with equal probability of the stop decaying via $\tilde{t} \rightarrow t\tilde{\chi}_1^0$ or via $\tilde{t} \rightarrow b\tilde{\chi}_1^\pm$ with $\tilde{\chi}_1^\pm \rightarrow W^\pm\tilde{\chi}_1^0$.
- Tstop9:** stop pair production with equal probability of the stop decaying via $\tilde{t} \rightarrow c\tilde{\chi}_1^0$ or via the four-body decay $\tilde{t} \rightarrow bff'\tilde{\chi}_1^0$ where f represents a lepton or a quark.
- Tstop10:** stop pair production with $\tilde{t} \rightarrow b\tilde{\chi}_1^\pm$ and $\tilde{\chi}_1^\pm \rightarrow W^\pm\tilde{\chi}_1^0 \rightarrow (f\bar{f}') + \tilde{\chi}_1^0$ with a virtual W -boson.
- Tstop11:** stop pair production with $\tilde{t} \rightarrow b\tilde{\chi}_1^\pm$ with $\tilde{\chi}_1^\pm$ decaying through an intermediate slepton to $\nu\tilde{\chi}_1^0$.
- Tstop12:** stop pair production with $\tilde{t} \rightarrow t\tilde{\chi}_1^0$ and $\tilde{\chi}_1^0 \rightarrow \gamma + \tilde{G}$.
- Tstop13:** stop pair production with $\tilde{t} \rightarrow t\tilde{\chi}_1^0$ where the $\tilde{\chi}_1^0$ can decay with equal probability to $\tilde{\chi}_1^0 \rightarrow \gamma + \tilde{G}$ or to $\tilde{\chi}_1^0 \rightarrow Z + \tilde{G}$.
- Tstop14:** stop pair production with wino-like couplings to electroweakinos, that is: $\tilde{t} \rightarrow t\tilde{\chi}_{1,2}^0$ with BR 33%, $\tilde{g} \rightarrow b\tilde{\chi}_1^\pm$ with BR 67%.
- Tstop15:** stop pair production with higgsino-like couplings to electroweakinos, that is: $\tilde{t} \rightarrow t\tilde{\chi}_{1,2}^0$ with BR 50%, $\tilde{g} \rightarrow b\tilde{\chi}_1^\pm$ with BR 50%.
- Tstop1RPV:** stop pair production with $\tilde{t} \rightarrow b\bar{s}$ via RPV coupling λ''_{323} .
- Tstop2RPV:** stop pair production with $\tilde{t} \rightarrow b\bar{\ell}$, via RPV coupling λ''_{333} .
- Tstop3RPV:** stop pair production with $\tilde{t} \rightarrow qm$, via RPV coupling λ''_{23k} .
- Tstop4RPV:** stop pair production with $\tilde{t} \rightarrow b\tilde{\chi}_1^\pm$, $\tilde{\chi}_1^\pm \rightarrow bbs$ via RPV coupling λ''_{323} .
- Tstop5RPV:** stop pair production with $\tilde{t} \rightarrow t\tilde{\chi}_{1,2}^0$, $\tilde{\chi}_{1,2}^0 \rightarrow tbs$ via RPV coupling λ''_{323} .
-
- Tsbot1:** sbottom pair production with $\tilde{b} \rightarrow b\tilde{\chi}_1^0$.
- Tsbot2:** sbottom pair production with $\tilde{b} \rightarrow t\tilde{\chi}_1^-, \tilde{\chi}_1^- \rightarrow W^-\tilde{\chi}_1^0$.
- Tsbot3:** sbottom pair production with $\tilde{b} \rightarrow b\tilde{\chi}_2^0$, where one of the $\tilde{\chi}_2^0 \rightarrow Z^*(\tilde{\chi}_1^0 \rightarrow f\bar{f}\tilde{\chi}_1^0)$ and the other $\tilde{\chi}_2^0 \rightarrow \tilde{\ell}\ell^+ \rightarrow \ell^+\ell^-\tilde{\chi}_1^0$.
- Tsbot4:** sbottom pair production with $\tilde{b} \rightarrow b\tilde{\chi}_2^0$, with $\tilde{\chi}_2^0 \rightarrow H\tilde{\chi}_1^0$.
-
- Tchi1chi1A:** electroweak pair and associated production of nearly mass-degenerate charginos $\tilde{\chi}_1^\pm$ and neutralinos $\tilde{\chi}_1^0$, where $\tilde{\chi}_1^\pm$ decays to $\tilde{\chi}_1^0$ plus soft radiation, and where one of the $\tilde{\chi}_1^0$ decays to $\gamma + \tilde{G}$ while the other one decays to $Z/H + \tilde{G}$ (with equal probability).
- Tchi1chi1B:** electroweak pair production of charginos $\tilde{\chi}_1^\pm$, where $\tilde{\chi}_1^\pm$ decays through an intermediate slepton or sneutrino to $\nu\tilde{\chi}_1^0$ and where the slepton or sneutrino mass is 5%, 25%, 50%, 75% and 95% of the $\tilde{\chi}_1^\pm$ mass.
- Tchi1chi1C:** electroweak pair production of charginos $\tilde{\chi}_1^\pm$, where $\tilde{\chi}_1^\pm$ decays through an intermediate slepton or sneutrino to $\nu\tilde{\chi}_1^0$ and where $m_{\tilde{\ell},\tilde{\nu}} = (m_{\tilde{\chi}_1^\pm} + m_{\tilde{\chi}_1^0})/2$.
- Tchi1chi1D:** electroweak associated pair production of charginos $\tilde{\chi}_1^\pm$, where $\tilde{\chi}_1^\pm$ decays through an intermediate scalar tau lepton or sneutrino to $\tau\nu\tilde{\chi}_1^0$ and where $m_{\tilde{\tau},\tilde{\nu}} = (m_{\tilde{\chi}_1^\pm} + m_{\tilde{\chi}_1^0})/2$.
- Tchi1chi1F:** electroweak pair and associated production of nearly mass-degenerate charginos $\tilde{\chi}_1^\pm$ and neutralinos $\tilde{\chi}_1^0$ (i.e. $\tilde{\chi}_1^\pm\tilde{\chi}_1^\pm$ and $\tilde{\chi}_1^\pm\tilde{\chi}_1^0$ production) where the $\tilde{\chi}_1^\pm$ decays exclusively to $\tilde{\chi}_1^0$ plus soft radiation and the $\tilde{\chi}_1^0$ decays to $\gamma/Z + \tilde{G}$.
- Tchi1chi1G:** electroweak pair production of charginos $\tilde{\chi}_1^\pm$, which are nearly mass-degenerate with neutralinos $\tilde{\chi}_1^0$. The $\tilde{\chi}_1^\pm$ decays either to $W^\pm + \tilde{G}$, or to $\tilde{\chi}_1^0$ plus soft radiation. The $\tilde{\chi}_1^0$ decays exclusively to $\gamma + \tilde{G}$.
- Tchi1chi1H:** electroweak pair production of charginos $\tilde{\chi}_1^\pm$, with $\tilde{\chi}_1^\pm \rightarrow W^\pm + \tilde{\chi}_1^0$ and $W^\pm \rightarrow \ell^\pm + \nu$.
- Tchi1chi1I:** electroweak pair production of charginos $\tilde{\chi}_1^\pm$ with $\tilde{\chi}_1^\pm \rightarrow W^\pm\tilde{\chi}_1^0$ and $W^\pm \rightarrow q\bar{q}'$.
-
- Tchi1n1A:** electroweak associated production of mass-degenerate charginos $\tilde{\chi}_1^\pm$ and neutralinos $\tilde{\chi}_1^0$, where $\tilde{\chi}_1^\pm$ decays exclusively to $W^\pm + \tilde{G}$ and $\tilde{\chi}_1^0$ decays exclusively to $\gamma + \tilde{G}$.
- Tchi1n2A:** electroweak associated production of mass-degenerate charginos $\tilde{\chi}_1^\pm$ and neutralinos $\tilde{\chi}_2^0$, where $\tilde{\chi}_1^\pm$ decays through an intermediate slepton or sneutrino to $\nu\tilde{\chi}_1^0$ and where $\tilde{\chi}_2^0$ decays through an intermediate slepton or sneutrino to $l^+\tilde{\chi}_1^0$ or $\nu\nu\tilde{\chi}_1^0$.
- Tchi1n2B:** electroweak associated production of mass-degenerate charginos $\tilde{\chi}_1^\pm$ and neutralinos $\tilde{\chi}_2^0$, where $\tilde{\chi}_1^\pm$ decays through an intermediate slepton or sneutrino to $\nu\tilde{\chi}_1^0$ and where $\tilde{\chi}_2^0$ decays through an intermediate slepton or sneutrino to $l^+\tilde{\chi}_1^0$ or $\nu\nu\tilde{\chi}_1^0$ and where the slepton or sneutrino mass is 5%, 25%, 50%, 75% and 95% of the $\tilde{\chi}_1^\pm$ mass.
- Tchi1n2C:** electroweak associated production of mass-degenerate charginos $\tilde{\chi}_1^\pm$ and neutralinos $\tilde{\chi}_2^0$, where $\tilde{\chi}_1^\pm$ decays through an intermediate slepton or sneutrino to $\nu\tilde{\chi}_1^0$ and where $\tilde{\chi}_2^0$ decays through an intermediate slepton or sneutrino to $l^+\tilde{\chi}_1^0$ or $\nu\nu\tilde{\chi}_1^0$ and where $m_{\tilde{\ell},\tilde{\nu}} = (m_{\tilde{\chi}_1^\pm} + m_{\tilde{\chi}_1^0})/2$.
- Tchi1n2D:** electroweak associated production of mass-degenerate charginos $\tilde{\chi}_1^\pm$ and neutralinos $\tilde{\chi}_2^0$, where $\tilde{\chi}_1^\pm$ decays through an intermediate scalar tau lepton or sneutrino to $\tau\nu\tilde{\chi}_1^0$ and where $\tilde{\chi}_2^0$ decays through an intermediate scalar tau lepton or sneutrino to $\tau^+\tau^-\tilde{\chi}_1^0$ or $\nu\nu\tilde{\chi}_1^0$ and where $m_{\tilde{\tau},\tilde{\nu}} = (m_{\tilde{\chi}_1^\pm} + m_{\tilde{\chi}_1^0})/2$.
- Tchi1n2E:** electroweak associated production of mass-degenerate charginos $\tilde{\chi}_1^\pm$ and neutralinos $\tilde{\chi}_2^0$, where $\tilde{\chi}_1^\pm \rightarrow W^\pm + \tilde{\chi}_1^0$ and $\tilde{\chi}_2^0 \rightarrow H + \tilde{\chi}_1^0$.
- Tchi1n2F:** electroweak associated production of mass-degenerate wino-like charginos $\tilde{\chi}_1^\pm$ and neutralinos $\tilde{\chi}_2^0$, where $\tilde{\chi}_1^\pm$ decays through an intermediate W^{**} to $\nu\tilde{\chi}_1^0$ and where $\tilde{\chi}_2^0$ decays through an intermediate Z^* to $l^+\tilde{\chi}_1^0$ or $\nu\nu\tilde{\chi}_1^0$.
- Tchi1n2Fa:** electroweak associated production of mass-degenerate wino-like charginos $\tilde{\chi}_1^\pm$ and neutralinos $\tilde{\chi}_2^0$, where $\tilde{\chi}_1^\pm$ decays through an intermediate W^{**} to $q\bar{q}\tilde{\chi}_1^0$ and where $\tilde{\chi}_2^0$ decays through an intermediate Z^* to $l^+\tilde{\chi}_1^0$ or $\nu\nu\tilde{\chi}_1^0$.
- Tchi1n2Fb:** electroweak associated production of mass-degenerate wino-like charginos $\tilde{\chi}_1^\pm$ and neutralinos $\tilde{\chi}_2^0$, where $\tilde{\chi}_1^\pm$ decays through an intermediate $W^{(*)}$ to $q\bar{q}\tilde{\chi}_1^0$ and where $\tilde{\chi}_2^0$ decays through an intermediate $Z^{(*)}$ to $q\bar{q}\tilde{\chi}_1^0$.
- Tchi1n2G:** electroweak associated production of Higgsino-like charginos $\tilde{\chi}_1^\pm$ and neutralinos $\tilde{\chi}_2^0$, and electroweak associated production of $\tilde{\chi}_2^0$ and $\tilde{\chi}_1^0$, where $m_{\tilde{\chi}_1^\pm} = (m_{\tilde{\chi}_2^0} + m_{\tilde{\chi}_1^0})/2$ and where $\tilde{\chi}_1^\pm$

Searches Particle Listings

Supersymmetric Particle Searches

- decays through an intermediate $W^{\pm*}$ to $q\bar{q}\tilde{\chi}_1^0$ and where $\tilde{\chi}_2^0$ decays through an intermediate Z^* to $l^+l^-\tilde{\chi}_1^0$.
- Tchi1n2Ga:** electroweak associated production of Higgsino-like charginos $\tilde{\chi}_1^\pm$ and neutralinos $\tilde{\chi}_2^0$, and electroweak associated production of $\tilde{\chi}_2^0$ and $\tilde{\chi}_1^0$, where $m_{\tilde{\chi}_1^\pm} = (m_{\tilde{\chi}_2^0} + m_{\tilde{\chi}_1^0})/2$ and where $\tilde{\chi}_1^\pm$ decays through an intermediate $W^{\pm*}$ to $l\nu\tilde{\chi}_1^0$ and where $\tilde{\chi}_2^0$ decays through an intermediate Z^* to $l^+l^-\tilde{\chi}_1^0$.
- Tchi1n2H:** electroweak associated production of mass-degenerate charginos $\tilde{\chi}_1^\pm$ and neutralinos $\tilde{\chi}_2^0$, where $\tilde{\chi}_1^\pm$ decays through an intermediate slepton or sneutrino to $l\nu\tilde{\chi}_1^0$ and where $\tilde{\chi}_2^0$ decays through an intermediate scalar tau lepton or sneutrino to $\tau^+\tau^-\tilde{\chi}_1^0$ or $\nu\bar{\nu}\tilde{\chi}_1^0$.
- Tchi1n2I:** electroweak associated production of mass-degenerate charginos $\tilde{\chi}_1^\pm$ and neutralinos $\tilde{\chi}_2^0$, where $\tilde{\chi}_1^\pm$ decays to $W^\pm + \tilde{\chi}_1^0$ and where $\tilde{\chi}_2^0$ decays 50% of the time to $Z + \tilde{\chi}_1^0$ and 50% of the time to $H + \tilde{\chi}_1^0$.
- Tchi1n12_GGM:** in the framework of General Gauge Mediation (GGM): electroweak pair and associated production of nearly mass-degenerate charginos $\tilde{\chi}_1^\pm$ and neutralinos $\tilde{\chi}_1^0, \tilde{\chi}_2^0$ (i.e. $\tilde{\chi}_1^\pm\tilde{\chi}_1^\pm, \tilde{\chi}_1^\pm\tilde{\chi}_1^0$ and $\tilde{\chi}_1^\pm\tilde{\chi}_2^0$ production) where the $\tilde{\chi}_1^\pm$ decays exclusively to $W^\pm + \tilde{G}$, the $\tilde{\chi}_2^0$ decays to $Z/H + \tilde{G}$ and the $\tilde{\chi}_1^0$ decays to $\gamma/Z + \tilde{G}$. The branching ratios depend on the composition of the gauge eigenstates of the neutralinos in the GGM scenario.
- TwinoLSPBL:** Electroweak pair production of wino-like $\tilde{\chi}_1^\pm$ and $\tilde{\chi}_1^0$ (i.e. $\tilde{\chi}_1^\pm\tilde{\chi}_1^\pm$ and $\tilde{\chi}_1^0\tilde{\chi}_1^0$). The $\tilde{\chi}_1^\pm$ can decay via bi-linear RPV into Zl, Hl or $W\nu$; the $\tilde{\chi}_1^0$ can decay into $Z\nu, H\nu$ or Wl .
- Tn1n1A:** electroweak pair and associated production of nearly mass-degenerate Higgsino-like charginos $\tilde{\chi}_1^\pm$ and neutralinos $\tilde{\chi}_1^0$ and $\tilde{\chi}_2^0$, where $\tilde{\chi}_1^\pm$ and $\tilde{\chi}_2^0$ decay to $\tilde{\chi}_1^0$ plus soft radiation and where both of the $\tilde{\chi}_1^0$ decay to $H + \tilde{G}$.
- Tn1n1B:** electroweak pair and associated production of nearly mass-degenerate Higgsino-like charginos $\tilde{\chi}_1^\pm$ and neutralinos $\tilde{\chi}_1^0$ and $\tilde{\chi}_2^0$, where $\tilde{\chi}_1^\pm$ and $\tilde{\chi}_2^0$ decay to $\tilde{\chi}_1^0$ plus soft radiation and where the $\tilde{\chi}_1^0$ decays 50% of the time to $H + \tilde{G}$ and 50 % of the time to $Z + \tilde{G}$.
- Tn1n1C:** electroweak pair and associated production of nearly mass-degenerate Higgsino-like charginos $\tilde{\chi}_1^\pm$ and neutralinos $\tilde{\chi}_1^0$ and $\tilde{\chi}_2^0$, where $\tilde{\chi}_1^\pm$ and $\tilde{\chi}_2^0$ decay to $\tilde{\chi}_1^0$ plus soft radiation and where both of the $\tilde{\chi}_1^0$ decay to $Z + \tilde{G}$.
- Tn1n1D:** electroweak pair and associated production of nearly mass-degenerate Higgsino-like charginos $\tilde{\chi}_1^\pm$ and neutralinos $\tilde{\chi}_1^0, \tilde{\chi}_2^0$.
- Tn1n1E:** electroweak pair and associated production of nearly mass-degenerate wino-like charginos $\tilde{\chi}_1^\pm$ and neutralinos $\tilde{\chi}_1^0$.
- Tn2n3A:** electroweak associated production of mass-degenerate neutralinos $\tilde{\chi}_2^0$ and $\tilde{\chi}_3^0$, where $\tilde{\chi}_2^0$ and $\tilde{\chi}_3^0$ decay through intermediate sleptons to $l^+l^-\tilde{\chi}_1^0$ and where the slepton mass is 5%, 25%, 50%, 75% and 95% of the $\tilde{\chi}_2^0$ mass.
- Tn2n3B:** electroweak associated production of mass-degenerate neutralinos $\tilde{\chi}_2^0$ and $\tilde{\chi}_3^0$, where $\tilde{\chi}_2^0$ and $\tilde{\chi}_3^0$ decay through intermediate sleptons to $l^+l^-\tilde{\chi}_1^0$ and where $m_{\tilde{l}} = (m_{\tilde{\chi}_2^0} + m_{\tilde{\chi}_1^0})/2$.
- TWinoBinoA:** electroweak pair production of mass-degenerate wino-like doublet ($\tilde{\chi}_2^0, \tilde{\chi}_1^\pm$) (including all pair-production mechanisms) decaying into a bino singlet ($\tilde{\chi}_1^0$). Decays happen via Standard Model bosons, assumed to decay via hadrons.
- TWinoHinoA:** electroweak pair production of mass-degenerate wino-like doublet ($\tilde{\chi}_2^0, \tilde{\chi}_2^\pm$) (including all possible pair-production mechanisms) decaying into a quasi-mass-degenerate Higgsino triplet ($\tilde{\chi}_1^0, \tilde{\chi}_2^0, \tilde{\chi}_1^\pm$). Decays happen via Standard Model bosons, assumed to decay via hadrons.
- THinoBinoA:** electroweak pair production of quasi-mass-degenerate higgsino-like triplet ($\tilde{\chi}_2^0, \tilde{\chi}_2^\pm, \tilde{\chi}_1^\pm$) (including all possible pair-production mechanisms) decaying into a bino singlet ($\tilde{\chi}_1^0$). Decays happen via Standard Model bosons, assumed to decay via hadrons.
- HinoWinoA:** electroweak pair production of quasi-mass-degenerate higgsino-like triplet ($\tilde{\chi}_2^0, \tilde{\chi}_2^\pm, \tilde{\chi}_2^\pm$) (including all possible pair-production mechanisms) decaying into a mass-degenerate wino doublet ($\tilde{\chi}_1^0, \tilde{\chi}_1^\pm$). Decays happen via Standard Model bosons, assumed to decay via hadrons.

$\tilde{\chi}_1^0$ is often assumed to be the lightest supersymmetric particle (LSP). See also the $\tilde{\chi}_2^0, \tilde{\chi}_3^0, \tilde{\chi}_4^0$ section below.

We have divided the $\tilde{\chi}_1^0$ listings below into five sections:

- 1) Accelerator limits for stable $\tilde{\chi}_1^0$,
- 2) Bounds on $\tilde{\chi}_1^0$ from dark matter searches,
- 3) $\tilde{\chi}_1^0 - p$ elastic cross section (spin-dependent, spin-independent interactions),
- 4) Other bounds on $\tilde{\chi}_1^0$ from astrophysics and cosmology, and
- 5) Unstable $\tilde{\chi}_1^0$ (Lightest Neutralino) mass limit.

Accelerator limits for stable $\tilde{\chi}_1^0$

Unless otherwise stated, results in this section assume spectra, production rates, decay modes, and branching ratios as evaluated in the MSSM, with gaugino and sfermion mass unification at the GUT scale. These papers generally study production of $\tilde{\chi}_i^0\tilde{\chi}_j^0$ ($i \geq 1, j \geq 2$), $\tilde{\chi}_1^\pm\tilde{\chi}_1^\mp$, and (in the case of hadronic collisions) $\tilde{\chi}_1^\pm\tilde{\chi}_2^0$ pairs. The mass limits on $\tilde{\chi}_1^0$ are either direct, or follow indirectly from the constraints set by the non-observation of $\tilde{\chi}_1^\pm$ and $\tilde{\chi}_2^0$ states on the gaugino and higgsino MSSM parameters M_2 and μ . In some cases, information is used from the nonobservation of slepton decays.

Obsolete limits obtained from e^+e^- collisions up to $\sqrt{s}=184$ GeV have been removed from this compilation and can be found in the 2000 Edition (The European Physical Journal **C15** 1 (2000)) of this Review. $\Delta m = m_{\tilde{\chi}_2^0} - m_{\tilde{\chi}_1^0}$.

VALUE (GeV)	CL%	DOCUMENT ID	TECN	COMMENT
none 450–930	95	1 AAD	21AX ATLS	jets + large-R jets + E_T , Tn1n1C
none 200–320	95	2 AAD	21BF ATLS	$e^\pm + b$ -jets + many jets, Tn1n1D, RPV, λ_{323}^{ν} electroweakino decay, degenerate Higgsino triplet
none 200–370	95	2 AAD	21BF ATLS	$e^\pm + b$ -jets + many jets, Tn1n1E, RPV, λ_{323}^{ν} electroweakino decay, degenerate Wino doublet
>40	95	3 DREINER	09 THEO	
>42.4	95	4 ABBIENDI	04H OPAL	all $\tan\beta$, $\Delta m > 5$ GeV, $m_0 > 500$ GeV, $A_0 = 0$
>39.2	95	5 HEISTER	04 ALEP	all $\tan\beta$, all Δm , all m_0
>32.5	95	6 ABDALLAH	03M DLPH	all $\tan\beta$, $m_{\tilde{\nu}} > 500$ GeV
>46	95	7 ABDALLAH	03M DLPH	all $\tan\beta$, all Δm , all m_0
>32.5	95	8 ACCIARRI	00D L3	$\tan\beta > 0.7$, $\Delta m > 3$ GeV, all m_0
>24		9 AAD	14K ATLS	
>24		10 CALIBBI	13	thermal relic abundance, MSSM particle content

1 AAD 21AX searched in 139 fb^{-1} of pp collisions at $\sqrt{s} = 13$ TeV for pair production of electroweakinos decaying to the LSP via the emission of Standard Model bosons (Higgs, W, Z) decaying into hadrons. The final state in all cases characterised by the presence of E_T , jets, and large-R jets tagged according to the boson of interest. Different assumptions (Higgsino, Wino, Bino) are made for the pair produced electroweakinos and for the LSP multiplet. No significant excess above the Standard Model predictions is observed. Limits are set on the electroweakino masses as a function of the model parameters (in particular $m_{\tilde{\chi}_1^0}$). See Fig. 16.

2 AAD 21BF searched in 139 fb^{-1} of pp collisions at $\sqrt{s} = 13$ TeV for pair production of gluinos, stops, electroweakinos decaying RPV either directly or indirectly via the LSP. The final state in all cases is one or two leptons, many jets (up to fifteen) and b -jets. Different models with different branching fractions of the gluino or stop follow from the assumptions on the nature of the electroweakinos. No significant excess above the Standard Model predictions is observed. Limits are set on the $gluino, \tilde{t}_1$, electroweakino masses as a function of the $\tilde{\chi}_1^0$ mass in several scenarios of gluino, stop and electroweakino pair production.

3 DREINER 09 show that in the general MSSM with non-universal gaugino masses there exists no model-independent laboratory bound on the mass of the lightest neutralino. An essentially massless $\tilde{\chi}_1^0$ is allowed by the experimental and observational data, imposing some constraints on other MSSM parameters, including M_2, μ and the slepton and squark masses.

4 ABBIENDI 04H search for charginos and neutralinos in events with acoplanar leptons+jets and multi-jet final states in the 192–209 GeV data, combined with the results on leptonic final states from ABBIENDI 04. The results hold for a scan over the parameter space covering the region $0 < M_2 < 5000$ GeV, $-1000 < \mu < 1000$ GeV and $\tan\beta$ from 1 to 40. This limit supersedes ABBIENDI 00H.

5 HEISTER 04 data collected up to 209 GeV. Updates earlier analysis of selections from HEISTER 02e, includes a new analysis of charginos and neutralinos decaying into stau and uses results on charginos with initial state radiation from HEISTER 02j. The limit is based on the direct search for charginos and neutralinos, the constraints from the slepton search and the Higgs mass limits from HEISTER 02 using a top mass of 175 GeV, interpreted in a framework with universal gaugino and sfermion masses. Assuming the mixing in the stau sector to be negligible, the limit improves to 43.1 GeV. Under the assumption of MSUGRA with unification of the Higgs and sfermion masses, the limit improves to 50 GeV, and reaches 53 GeV for $A_0 = 0$. These limits include and update the results of BARATE 01.

6 ABDALLAH 03M uses data from $\sqrt{s} = 192\text{--}208$ GeV. A limit on the mass of $\tilde{\chi}_1^0$ is derived from direct searches for neutralinos combined with the chargino search. Neutralinos are searched in the production of $\tilde{\chi}_1^0\tilde{\chi}_2^0, \tilde{\chi}_1^0\tilde{\chi}_3^0$, as well as $\tilde{\chi}_2^0\tilde{\chi}_3^0$ and $\tilde{\chi}_2^0\tilde{\chi}_4^0$ giving rise to

$\tilde{\chi}_1^0$ (Lightest Neutralino) mass limit

cascade decays, and $\tilde{\chi}_1^0 \tilde{\chi}_2^0$ and $\tilde{\chi}_1^0 \tilde{\chi}_2^0$, followed by the decay $\tilde{\chi}_2^0 \rightarrow \tilde{\tau} \tau$. The results hold for the parameter space defined by values of $M_2 < 1$ TeV, $|\mu| \leq 2$ TeV with the $\tilde{\chi}_1^0$ as LSP. The limit is obtained for $\tan\beta = 1$ and large m_0 , where $\tilde{\chi}_2^0 \tilde{\chi}_4^0$ and chargino pair production are important. If the constraint from Higgs searches is also imposed, the limit improves to 49.0 GeV in the m_h^{\max} scenario with $m_t=174.3$ GeV. These limits update the results of ABREU 00.

⁷ ABDALLAH 03M uses data from $\sqrt{s} = 192\text{--}208$ GeV. An indirect limit on the mass of $\tilde{\chi}_1^0$ is derived by constraining the MSSM parameter space by the results from direct searches for neutralinos (including cascade decays and $\tilde{\tau}\tau$ final states), for charginos (for all Δm_{\pm}) and for sleptons, stop and sbottom. The results hold for the full parameter space defined by values of $M_2 < 1$ TeV, $|\mu| \leq 2$ TeV with the $\tilde{\chi}_1^0$ as LSP. Constraints from the Higgs search in the m_h^{\max} scenario assuming $m_t=174.3$ GeV are included. The limit is obtained for $\tan\beta \geq 5$ when stau mixing leads to mass degeneracy between $\tilde{\tau}_1$ and $\tilde{\chi}_1^0$ and the limit is based on $\tilde{\chi}_2^0$ production followed by its decay to $\tilde{\tau}_1 \tau$. In the pathological scenario where m_0 and $|\mu|$ are large, so that the $\tilde{\chi}_2^0$ production cross section is negligible, and where there is mixing in the stau sector but not in stop nor sbottom, the limit is based on charginos with soft decay products and an ISR photon. The limit then degrades to 39 GeV. See Figs. 40–42 for the dependence of the limit on $\tan\beta$ and $m_{\tilde{\tau}}$. These limits update the results of ABREU 00w.

⁸ ACCIARRI 00d data collected at $\sqrt{s}=189$ GeV. The results hold over the full parameter space defined by $0.7 \leq \tan\beta \leq 60$, $0 \leq M_2 \leq 2$ TeV, $m_0 \leq 500$ GeV, $|\mu| \leq 2$ TeV. The minimum mass limit is reached for $\tan\beta=1$ and large m_0 . The results of slepton searches from ACCIARRI 99w are used to help set constraints in the region of small m_0 . The limit improves to 48 GeV for $m_0 \geq 200$ GeV and $\tan\beta \geq 10$. See their Figs. 6–8 for the $\tan\beta$ and m_0 dependence of the limits. Updates ACCIARRI 98f.

⁹ AAD 14k sets limits on the χ -nucleon spin-dependent and spin-independent cross sections out to $m_\chi = 10$ TeV.

¹⁰ CALIBBI 13 use the fact that if the relic abundance of $\tilde{\chi}_1^0$ does not overclose the universe, scalar lepton and Higgsino masses must be relatively small. Using 8 TeV ATLAS constraints on the scalar tau mass and on invisible Higgs decays, they estimate a lower bound for the $\tilde{\chi}_1^0$ mass.

Bounds on $\tilde{\chi}_1^0$ from dark matter searches

These papers generally exclude regions in the $M_2 - \mu$ parameter plane assuming that $\tilde{\chi}_1^0$ is the dominant form of dark matter in the galactic halo. These limits are based on the lack of detection in laboratory experiments, telescopes, or by the absence of a signal in underground neutrino detectors. The latter signal is expected if $\tilde{\chi}_1^0$ accumulates in the Sun or the Earth and annihilates into high-energy ν 's.

VALUE DOCUMENT ID TECN

• • • We do not use the following data for averages, fits, limits, etc. • • •

1	ABDALLAH	21	HESS
2	ABAZAJIAN	20	FLAT
3	ABDALLAH	20	HESS
4	ABE	20G	SKAM
5	ALBERT	20	HAWC
6	ALBERT	20A	ANTR
7	ALBERT	20C	ANIC
8	ALVAREZ	20	FLAT
9	HOOF	20	FLAT
10	DI-MAURO	19	FLAT
11	JOHNSON	19	FLAT
12	LI	19D	FLAT
13	ABDALLAH	18	HESS
14	AHNEN	18	MGIC
15	ALBERT	18B	HAWC
16	ALBERT	18C	HAWC
17	AARTSEN	17	ICCB
18	AARTSEN	17A	ICCB
19	AARTSEN	17C	ICCB
20	ARCHAMBAU.	17	VRTS
21	ADRIAN-MAR.	16	ANTR
22	AHNEN	16	MGFL
23	AVRORIN	16	BAIK
24	CIRELLI	16	THEO
24	LEITE	16	THEO
25	ACKERMANN	15	FLAT
26	ACKERMANN	15A	FLAT
27	ACKERMANN	15B	FLAT
28	BUCKLEY	15	THEO
29	CHOI	15	SKAM
30	ALEKSIC	14	MGIC
31	AVRORIN	14	BAIK
32	AARTSEN	13C	ICCB
33	BERGSTROM	13	COSM
34	BOLIEV	13	BAKS
33	JIN	13	ASTR
33	KOPP	13	COSM
35	ACKERMANN	10	FLAT
36	ACHTERBERG	06	AMND
37	ACKERMANN	06	AMND
38	DEBOER	06	RVUE
39	DESAI	04	SKAM
39	AMBROSIO	99	MCRO

40	LOSECCO	95	RVUE
41	MORI	93	KAMI
42	BOTTINO	92	COSM
43	BOTTINO	91	RVUE
44	GELMINI	91	COSM
45	KAMIONKOW.	91	RVUE
46	MORI	91B	KAMI
47	OLIVE	88	COSM

none 4–15 GeV

¹ ABDALLAH 21 places constraints on the dark matter annihilation cross section for annihilations into gamma-rays from the dwarf irregular galaxy WLM for masses between 0.15 to 10 TeV.

² ABAZAJIAN 20 sets constraints on the dark matter annihilation from gamma-ray searches from Fermi LAT observations of the Galactic center.

³ ABDALLAH 20 places constraints on the dark matter annihilation cross section for annihilations into gamma-rays from Milky Way dwarf galaxy satellites for masses between 0.2 to 40 TeV.

⁴ ABE 20G is based on SuperKamiokande data taken from 1996 to 2016 searching for neutrinos produced from dark matter annihilations in the galactic center or halo. They place constraints on the dark matter-nucleon scattering cross section for dark matter masses between 1 GeV and 10 TeV.

⁵ ALBERT 20 sets limits on the annihilation cross section of dark matter with mass between 1 and 100 TeV from gamma-ray observations of the local dwarf spheroidal galaxies.

⁶ ALBERT 20A set limits on the dark matter annihilation cross section from neutrinos observations in the Galactic center using 11 years of ANTARES data.

⁷ ALBERT 20C set limits on the dark matter annihilation cross section from neutrinos observations in the Galactic center combining Antares and IceCube data.

⁸ ALVAREZ 20 set limits on the dark matter annihilation from gamma-ray searches from Fermi LAT observations in the directions of dwarf spheroidal galaxies.

⁹ HOOF 20 set limits on the dark matter annihilation from gamma-ray searches from Fermi LAT observations in the directions of dwarf spheroidal galaxies.

¹⁰ DI-MAURO 19 sets limits on the dark matter annihilation from gamma-ray searches in M31 and M33 galaxies using Fermi LAT data.

¹¹ JOHNSON 19 sets limits on p-wave dark matter annihilations in the galactic center using Fermi data.

¹² LI 19D sets limits on dark matter annihilation cross sections searching for line-like signals in the all-sky Fermi data.

¹³ ABDALLAH 18 places constraints on the dark matter annihilation cross section for annihilations into gamma-rays in the Galactic center for masses between 300 GeV to 70 TeV. This updates ABDALLAH 16.

¹⁴ AHNEN 18 uses observations of the dwarf satellite galaxy Ursa Major II to obtain upper limits on annihilation cross sections for dark matter in various channels for masses between 0.1–100 TeV.

¹⁵ ALBERT 18B sets limits on the annihilation cross section of dark matter with mass between 1 and 100 TeV from gamma-ray observations of the Andromeda galaxy.

¹⁶ ALBERT 18C sets limits on the spin-dependent coupling of dark matter to protons from dark matter annihilation in the Sun.

¹⁷ AARTSEN 17 is based on data collected during 327 days of detector livetime with IceCube. They looked for interactions of ν 's resulting from neutralino annihilations in the Earth over a background of atmospheric neutrinos and set 90% CL limits on the spin independent neutralino-proton cross section for neutralino masses in the range 10–10000 GeV.

¹⁸ AARTSEN 17A is based on data collected during 532 days of livetime with the IceCube 86-string detector including the DeepCore sub-array. They looked for interactions of ν 's from neutralino annihilations in the Sun over a background of atmospheric neutrinos and set 90% CL limits on the spin dependent neutralino-proton cross section for neutralino masses in the range 10–10000 GeV. This updates AARTSEN 16c.

¹⁹ AARTSEN 17C is based on 1005 days of running with the IceCube detector. They set a limit on the annihilation cross section for dark matter with masses between 10–1000 GeV annihilating in the Galactic center assuming an NFW profile. The limit is of $1.2 \times 10^{23} \text{ cm}^3 \text{ s}^{-1}$ in the $\tau^+ \tau^-$ channel. Supersedes AARTSEN 15E.

²⁰ ARCHAMBAULT 17 performs a joint statistical analysis of four dwarf galaxies with VERITAS looking for gamma-ray emission from neutralino annihilation. They set limits on the neutralino annihilation cross section.

²¹ ADRIAN-MARTINEZ 16 is based on data from the ANTARES neutrino telescope. They looked for interactions of ν 's from neutralino annihilations in the Sun over a background of atmospheric neutrinos and set 90% CL limits on the muon neutrino flux. They also obtain limits on the spin dependent and spin independent neutralino-proton cross section for neutralino masses in the range 50 to 5,000 GeV. This updates ADRIAN-MARTINEZ 13.

²² AHNEN 16 combines 158 hours of Segue 1 observations with MAGIC with 6 year observations of 15 dwarf satellite galaxies by Fermi-LAT to set limits on annihilation cross sections for dark matter masses between 10 GeV and 100 TeV.

²³ AVRORIN 16 is based on 2.76 years with Lake Baikal neutrino telescope. They derive 90% upper limits on the annihilation cross section from dark matter annihilations in the Galactic center.

²⁴ CIRELLI 16 and LEITE 16 derive bounds on the annihilation cross section from radio observations.

²⁵ ACKERMANN 15 is based on 5.8 years of data with Fermi-LAT and search for monochromatic gamma-rays in the energy range of 0.2–500 GeV from dark matter annihilations. This updates ACKERMANN 13A.

²⁶ ACKERMANN 15A is based on 50 months of data with Fermi-LAT and search for dark matter annihilation signals in the isotropic gamma-ray background as well as galactic subhalos in the energy range of a few GeV to a few tens of TeV.

²⁷ ACKERMANN 15B is based on 6 years of data with Fermi-LAT observations of Milky Way dwarf spheroidal galaxies. Set limits on the annihilation cross section from $m_\chi = 2$ GeV to 10 TeV. This updates ACKERMANN 14.

²⁸ BUCKLEY 15 is based on 5 years of Fermi-LAT data searching for dark matter annihilation signals from Large Magellanic Cloud.

²⁹ CHOI 15 is based on 3903 days of SuperKamiokande data searching for neutrinos produced from dark matter annihilations in the sun. They place constraints on the dark matter-nucleon scattering cross section for dark matter masses between 4–200 GeV.

³⁰ ALEKSIC 14 is based on almost 160 hours of observations of Segue 1 satellite dwarf galaxy using the MAGIC telescopes between 2011 and 2013. Sets limits on the annihilation cross section out to $m_\chi = 10$ TeV.

³¹ AVRORIN 14 is based on almost 2.76 years with Lake Baikal neutrino telescope. They derive 90% upper limits on the fluxes of muons and muon neutrinos from dark matter annihilations in the Sun.

Searches Particle Listings

Supersymmetric Particle Searches

- ³² AARTSEN 13c is based on data collected during 339.8 effective days with the IceCube 59-string detector. They looked for interactions of ν_μ 's from neutralino annihilations in nearby galaxies and galaxy clusters. They obtain limits on the neutralino annihilation cross section for neutralino masses in the range 30–100,000 GeV.
- ³³ BERGSTROM 13, JIN 13, and KOPP 13 derive limits on the mass and annihilation cross section using AMS-02 data. JIN 13 also sets a limit on the lifetime of the dark matter particle.
- ³⁴ BOLIEV 13 is based on data collected during 24.12 years of live time with the Bakson Underground Scintillator Telescope. They looked for interactions of ν_μ 's from neutralino annihilations in the Sun over a background of atmospheric neutrinos and set 90% CL limits on the muon flux. They also obtain limits on the spin dependent and spin independent neutralino-proton cross section for neutralino masses in the range 10–1000 GeV.
- ³⁵ ACKERMANN 10 place upper limits on the annihilation cross section with $b\bar{b}$ or $\mu^+\mu^-$ final states.
- ³⁶ ACHTERBERG 06 is based on data collected during 421.9 effective days with the AMANDA detector. They looked for interactions of ν_μ 's from the centre of the Earth over a background of atmospheric neutrinos and set 90% CL limits on the muon flux. Their limit is compared with the muon flux expected from neutralino annihilations into W^+W^- and $b\bar{b}$ at the centre of the Earth for MSSM parameters compatible with the relic dark matter density, see their Fig. 7.
- ³⁷ ACKERMANN 06 is based on data collected during 143.7 days with the AMANDA-II detector. They looked for interactions of ν_μ 's from the Sun over a background of atmospheric neutrinos and set 90% CL limits on the muon flux. Their limit is compared with the muon flux expected from neutralino annihilations into W^+W^- in the Sun for SUSY model parameters compatible with the relic dark matter density, see their Fig. 3.
- ³⁸ DEBOER 06 interpret an excess of diffuse Galactic gamma rays observed with the EGRET satellite as originating from π^0 decays from the annihilation of neutralinos into quark jets. They analyze the corresponding parameter space in a supergravity inspired MSSM model with radiative electroweak symmetry breaking, see their Fig. 3 for the preferred region in the $(m_0, m_{1/2})$ plane of a scenario with large $\tan\beta$.
- ³⁹ AMBROSIO 99 and DESAI 04 set new neutrino flux limits which can be used to limit the parameter space in supersymmetric models based on neutralino annihilation in the Sun and the Earth.
- ⁴⁰ LOSECCO 95 reanalyzed the IMB data and places lower limit on $m_{\tilde{\chi}_1^0}$ of 18 GeV if the LSP is a photino and 10 GeV if the LSP is a higgsino based on LSP annihilation in the sun producing high-energy neutrinos and the limits on neutrino fluxes from the IMB detector.
- ⁴¹ MORI 93 excludes some region in $M_2-\mu$ parameter space depending on $\tan\beta$ and lightest scalar Higgs mass for neutralino dark matter $m_{\tilde{\chi}_1^0} > m_W$, using limits on upgoing muons produced by energetic neutrinos from neutralino annihilation in the Sun and the Earth.
- ⁴² BOTTINO 92 excludes some region $M_2-\mu$ parameter space assuming that the lightest neutralino is the dark matter, using upgoing muons at Kamiokande, direct searches by Ge detectors, and by LEP experiments. The analysis includes top radiative corrections on Higgs parameters and employs two different hypotheses for nucleon-Higgs coupling. Effects of rescaling in the local neutralino density according to the neutralino relic abundance are taken into account.
- ⁴³ BOTTINO 91 excluded a region in $M_2-\mu$ plane using upgoing muon data from Kamioka experiment, assuming that the dark matter surrounding us is composed of neutralinos and that the Higgs boson is not too heavy.
- ⁴⁴ GELMINI 91 exclude a region in $M_2-\mu$ plane using dark matter searches.
- ⁴⁵ KAMIONKOWSKI 91 excludes a region in the $M_2-\mu$ plane using IMB limit on upgoing muons originated by energetic neutrinos from neutralino annihilation in the sun, assuming that the dark matter is composed of neutralinos and that $m_{H_1^0} \lesssim 50$ GeV. See Fig. 8 in the paper.
- ⁴⁶ MORI 91b exclude a part of the region in the $M_2-\mu$ plane with $m_{\tilde{\chi}_1^0} \lesssim 80$ GeV using a limit on upgoing muons originated by energetic neutrinos from neutralino annihilation in the earth, assuming that the dark matter surrounding us is composed of neutralinos and that $m_{H_1^0} \lesssim 80$ GeV.
- ⁴⁷ OLIVE 88 result assumes that photinos make up the dark matter in the galactic halo. Limit is based on annihilations in the sun and is due to an absence of high energy neutrinos detected in underground experiments. The limit is model dependent.

$\tilde{\chi}_1^0-p$ elastic cross section

Experimental results on the $\tilde{\chi}_1^0-p$ elastic cross section are evaluated at $m_{\tilde{\chi}_1^0}=100$ GeV. The experimental results on the cross section are often mass dependent. Therefore, the mass and cross section results are also given where the limit is strongest, when appropriate. Results are quoted separately for spin-dependent interactions (based on an effective 4-Fermi Lagrangian of the form $\tilde{\chi}_1^0 \gamma^\mu \tilde{\chi}_1^0 \chi \bar{\chi} \gamma_\mu \mu^5 q$) and spin-independent interactions ($\tilde{\chi}_1^0 \chi \bar{\chi} q$). For calculational details see GRIEST 88b, ELLIS 88b, BARBIERI 89c, DREES 93b, ARNOWITT 96, BERGSTROM 96, and BAER 97 in addition to the theory papers listed in the Tables. For a description of the theoretical assumptions and experimental techniques underlying most of the listed papers, see the review on "Dark matter" in this "Review of Particle Physics," and references therein. Most of the following papers use galactic halo and nuclear interaction assumptions from (LEWIN 96).

Spin-dependent interactions

VALUE (pb)	CL%	DOCUMENT ID	TECN	COMMENT
< 4 × 10 ⁻⁵	90	1 AMOLE	19 PICO	C ₃ F ₈
< 5 × 10 ⁻⁴	90	2 APRILE	19A XE1T	Xe
< 7 × 10 ⁻⁴	90	3 XIA	19A PNDX	Xe
< 8 × 10 ⁻⁴	90	4 AKERIB	17A LUX	Xe
< 0.28	90	5 BATTAT	17 DRFT	CS ₂ ; CF ₄
< 0.027	90	6 BEHNKE	17 PICA	C ₄ F ₁₀
< 5 × 10 ⁻⁴	90	7 AMOLE	16 PICO	CF ₃ I
< 6.8 × 10 ⁻³	90	8 APRILE	16b X100	Xe

• • • We do not use the following data for averages, fits, limits, etc. • • •

< 6.3 × 10 ⁻³	90	9 FELIZARDO	14 SMPL	C ₂ ClF ₅
< 0.01	90	10 AKIMOV	12 ZEP3	Xe
< 7 × 10 ⁻³		11 BEHNKE	12 COUP	CF ₃ I
< 8.5 × 10 ⁻³		12 FELIZARDO	12 SMPL	C ₂ ClF ₅
< 0.016	90	13 KIM	12 KIMS	Csl
5 × 10 ⁻¹⁰ to 10 ⁻⁵	95	14 BUCHMUEL...	11b THEO	
< 1	90	15 ANGLE	08A XE10	Xe
< 0.055		16 BEDNYAKOV	08 HDMS	Ge
< 0.33	90	17 BEHNKE	08 COUP	CF ₃ I
< 5		18 AKERIB	06 CDMS	Ge
< 2		19 SHIMIZU	06a CNTR	CaF ₂
< 0.4		20 ALNER	05 NAIA	Nal Spin Dep.
< 2		21 BARNABE-HE.	05 PICA	C
2 × 10 ⁻¹¹ to 1 × 10 ⁻⁴		22 ELLIS	04 THEO	$\mu > 0$
< 0.8		23 AHMED	03 NAIA	Nal Spin Dep.
< 40		24 TAKEDA	03 BOLO	NaF Spin Dep.
< 10		25 ANGLÖHER	02 CRES	Saphire
8 × 10 ⁻⁷ to 2 × 10 ⁻⁵		26 ELLIS	01c THEO	$\tan\beta \leq 10$
< 3.8		27 BERNABEI	00b DAMA	Xe
< 0.8		28 SPOONER	00 UKDM	Nal
< 4.8		29 BELL	99c DAMA	F
< 100		29 OOTANI	99 BOLO	LIF
< 0.6		29 BERNABEI	98c DAMA	Xe
< 5		28 BERNABEI	97 DAMA	F

- The strongest limit is $< 2.5 \times 10^{-5}$ pb at $m_\chi = 25$ GeV. This updates AMOLE 17.
- The strongest limit is $< 2 \times 10^{-4}$ pb at $m_\chi = 30$ GeV. For scatterings on neutrons, the strongest limit is $< 6.3 \times 10^{-6}$ pb at $m_\chi = 30$ GeV.
- The strongest limit is $< 4.4 \times 10^{-4}$ pb at $m_\chi = 40$ GeV. This updates FU 17.
- The strongest limit is 5×10^{-4} pb at $m_\chi = 35$ GeV. The limit for scattering on neutrons is 3×10^{-5} pb at 100 GeV and is 1.6×10^{-5} pb at 35 GeV. This updates AKERIB 16A.
- Directional recoil detector. This updates DAW 12.
- This result updates ARCHAMBAULT 12. The strongest limit is 0.013 pb at $m_\chi = 20$ GeV.
- The strongest limit is 5×10^{-4} pb at $m_\chi = 80$ GeV.
- The strongest limit is 5.2×10^{-3} pb at 50 GeV. The limit for scattering on neutrons is 2.8×10^{-4} pb at 100 GeV and the strongest limit is 2.0×10^{-4} pb at 50 GeV. This updates APRILE 13.
- The strongest limit is 0.0043 pb and occurs at $m_\chi = 35$ GeV. FELIZARDO 14 also presents limits for the scattering on neutrons. At $m_\chi = 100$ GeV, the upper limit is 0.13 pb and the strongest limit is 0.066 pb at $m_\chi = 35$ GeV.
- This result updates LEBEDENKO 09A. The strongest limit is 8×10^{-3} pb at $m_\chi = 50$ GeV. Limit applies to the neutralino neutron elastic cross section.
- The strongest limit is 6×10^{-3} pb at $m_\chi = 60$ GeV.
- The strongest limit is 5.7×10^{-3} pb at $m_\chi = 35$ GeV.
- This result updates LEE 07A. The strongest limit is at $m_\chi = 80$ GeV.
- Predictions for the spin-dependent elastic cross section based on a frequentist approach to electroweak observables in the framework of $N=1$ supergravity models with radiative breaking of the electroweak gauge symmetry.
- The strongest limit is 0.6 pb and occurs at $m_\chi = 30$ GeV. The limit for scattering on neutrons is 0.01 pb at $m_\chi = 100$ GeV, and the strongest limit is 0.0045 pb at $m_\chi = 30$ GeV.
- Limit applies to neutron elastic cross section.
- The strongest upper limit is 0.25 pb and occurs at $m_\chi \simeq 40$ GeV.
- The strongest upper limit is 4 pb and occurs at $m_\chi \simeq 60$ GeV. The limit on the neutron spin-dependent elastic cross section is 0.07 pb. This latter limit is improved in AHMED 09, where a limit of 0.02 pb is obtained at $m_\chi = 100$ GeV. The strongest limit in AHMED 09 is 0.018 pb and occurs at $m_\chi = 60$ GeV.
- The strongest upper limit is 1.2 pb and occurs at $m_\chi \simeq 40$ GeV. The limit on the neutron spin-dependent cross section is 35 pb.
- The strongest upper limit is 0.35 pb and occurs at $m_\chi \simeq 60$ GeV.
- The strongest upper limit is 1.2 pb and occurs $m_\chi \simeq 30$ GeV.
- ELLIS 04 calculates the χp elastic scattering cross section in the framework of $N=1$ supergravity models with radiative breaking of the electroweak gauge symmetry, but without universal scalar masses. In the case of universal squark and slepton masses, but non-universal Higgs masses, the limit becomes 2×10^{-4} , see ELLIS 03e.
- The strongest upper limit is 0.75 pb and occurs at $m_\chi \simeq 70$ GeV.
- The strongest upper limit is 30 pb and occurs at $m_\chi \simeq 20$ GeV.
- The strongest upper limit is 8 pb and occurs at $m_\chi \simeq 30$ GeV.
- ELLIS 01c calculates the $\chi-p$ elastic scattering cross section in the framework of $N=1$ supergravity models with radiative breaking of the electroweak gauge symmetry. In models with nonuniversal Higgs masses, the upper limit to the cross section is 6×10^{-4} .
- The strongest upper limit is 3 pb and occurs at $m_\chi \simeq 60$ GeV. The limits are for inelastic scattering $\chi^0 + {}^{129}\text{Xe} \rightarrow \chi^0 + {}^{129}\text{Xe}^* (39.58 \text{ keV})$.
- The strongest upper limit is 4.4 pb and occurs at $m_\chi \simeq 60$ GeV.
- The strongest upper limit is about 35 pb and occurs at $m_\chi \simeq 15$ GeV.

Spin-independent interactions

VALUE (pb)	CL%	DOCUMENT ID	TECN	COMMENT
• • • We do not use the following data for averages, fits, limits, etc. • • •				
$< 6.5 \times 10^{-11}$	90	1 MENG	21B PNDX	Xe
$< 5 \times 10^{-10}$	90	2 WANG	20G PNDX	Xe
$< 2.5 \times 10^{-8}$	90	3 ABE	19 XMAS	Xe
$< 3.9 \times 10^{-9}$	90	4 AJAJ	19 DEAP	Ar
$< 2 \times 10^{-8}$	90	5 AMOLE	19 PICO	C ₃ F ₈
$< 2.25 \times 10^{-6}$	90	6 ADHIKARI	18 C100	Nal
$< 1.14 \times 10^{-8}$	90	7 AGNES	18A DS50	Ar
$< 1.6 \times 10^{-8}$	90	8 AGNESE	18A CDMS	Ge
$< 9 \times 10^{-11}$	90	9 APRILE	18 XE1T	Xe
$< 1.8 \times 10^{-10}$	90	10 AKERIB	17 LUX	Xe
$< 1.5 \times 10^{-9}$	90	11 APRILE	16B X100	Xe
$< 1.5 \times 10^{-9}$	90	12 AKERIB	14 LUX	Xe
$10^{-11}-10^{-7}$	95	13 BUCHMUEL...	14A THEO	
$< 4.6 \times 10^{-6}$	90	14 FELIZARDO	14 SMPL	C ₂ ClF ₅
$10^{-11}-10^{-8}$	95	15 ROSZKOWSKI	14 THEO	
$< 2.2 \times 10^{-6}$	90	16 AGNESE	13 CDMS	Si
$< 5 \times 10^{-8}$	90	17 AKIMOV	12 ZEP3	Xe
$1.6 \times 10^{-6}; 3.7 \times 10^{-5}$		18 ANGLÖHER	12 CRES	CaWO ₄
3×10^{-12} to 3×10^{-9}	95	19 BECHTLE	12 THEO	
$< 1.6 \times 10^{-7}$		20 BEHNKE	12 COUP	CF ₃ I
$< 2.3 \times 10^{-7}$	90	21 KIM	12 KIMS	Csl
$< 3.3 \times 10^{-8}$	90	22 AHMED	11A	Ge
$< 4.4 \times 10^{-8}$	90	23 ARMENGAUD	11 EDE2	Ge
$< 1 \times 10^{-7}$	90	24 ANGLE	08 XE10	Xe
$< 1 \times 10^{-6}$	90	25 BENETTI	08 WARP	Ar
$< 7.5 \times 10^{-7}$	90	26 ALNER	07A ZEP2	Xe
$< 2 \times 10^{-7}$		27 AKERIB	06A CDMS	Ge
$< 9 \times 10^{-7}$		28 ALNER	05 NAIA	Nal Spin Indep.
$< 12 \times 10^{-7}$		29 ALNER	05A ZEPL	
$< 14 \times 10^{-7}$		30 SANGIARD	05 EDEL	Ge
$< 4 \times 10^{-7}$		31 AKERIB	04 CDMS	Ge
2×10^{-11} to 1.5×10^{-7}	95	32 BALTZ	04 THEO	
2×10^{-11} to 8×10^{-6}		33 ELLIS	04 THEO	$\mu > 0$
$< 5 \times 10^{-8}$		34 PIERCE	04A THEO	
$< 2 \times 10^{-5}$		35 AHMED	03 NAIA	Nal Spin Indep.
$< 3 \times 10^{-6}$		36 AKERIB	03 CDMS	Ge
2×10^{-13} to 2×10^{-7}		37 BAER	03A THEO	
$< 1.4 \times 10^{-5}$		38 KLAPDOR-K...	03 HDMS	Ge
$< 6 \times 10^{-6}$		39 ABRAMS	02 CDMS	Ge
1×10^{-12} to 7×10^{-6}		40 KIM	02B THEO	
$< 3 \times 10^{-5}$		41 MORALES	02B CSME	Ge
$< 1 \times 10^{-5}$		42 MORALES	02C IGEX	Ge
$< 1 \times 10^{-6}$		43 BALTZ	01 THEO	
$< 3 \times 10^{-5}$		44 BAUDIS	01 HDMS	Ge
$< 7 \times 10^{-6}$		45 BOTTINO	01 THEO	
$< 1 \times 10^{-8}$		46 CORSETTI	01 THEO	$\tan\beta \leq 25$
5×10^{-10} to 1.5×10^{-8}		47 ELLIS	01C THEO	$\tan\beta \leq 10$
$< 4 \times 10^{-6}$		48 GOMEZ	01 THEO	
2×10^{-10} to 1×10^{-7}		49 LAHANAS	01 THEO	
$< 3 \times 10^{-6}$		50 ABUSAIDI	00 CDMS	Ge, Si
$< 6 \times 10^{-7}$		51 ACCOMANDO	00 THEO	
2.5×10^{-9} to 3.5×10^{-8}		52 BERNABEI	00 DAMA	Nal
$< 1.5 \times 10^{-5}$		53 FENG	00 THEO	$\tan\beta=10$
$< 4 \times 10^{-5}$		54 MORALES	00 IGEX	Ge
$< 7 \times 10^{-6}$		55 SPOONER	00 UKDM	Nal
$< 7 \times 10^{-6}$		56 BAUDIS	99 HDMO	⁷⁶ Ge
$< 7 \times 10^{-6}$		57 BERNABEI	98C DAMA	Xe

- 1 Commissioning Run for PandaX-4T. The strongest limit is 3.8×10^{-11} pb at $m_\chi = 40$ GeV.
- 2 WANG 20G strongest limit is 2.2×10^{-10} pb at 30 GeV using 132 ton-day full exposure of PandaX-II. This updates CUI 17A, though the results here provide weaker constraints.
- 3 The strongest upper limit is 2.2×10^{-8} pb at 60 GeV.
- 4 This updates AMAUDRUZ 18.
- 5 This updates AMOLE 16.
- 6 The strongest limit is 2.05×10^{-6} at $m = 60$ GeV.
- 7 The strongest limit is 1.09×10^{-8} pb at $m_\chi = 126$ GeV. This updates AGNES 15.
- 8 The strongest limit is 1.0×10^{-8} pb at $m_\chi = 46$ GeV. This updates AGNESE 15B.
- 9 Based on 278.8 days of data collection. The strongest limit is 4.1×10^{-11} pb at $m_\chi = 30$ GeV. This updates APRILE 17C.
- 10 AKERIB 17. The strongest limit is 1.1×10^{-10} pb at 50 GeV. This updates AKERIB 16.
- 11 The strongest limit is 1.1×10^{-9} pb at 50 GeV. This updates APRILE 12.
- 12 The strongest upper limit is 7.6×10^{-10} at $m_\chi = 33$ GeV.
- 13 Predictions for the spin-independent elastic cross section based on a frequentist approach to electroweak observables in the framework of $N = 1$ supergravity models with radiative breaking of the electroweak gauge symmetry using the 20 fb⁻¹ 8 TeV and the 5 fb⁻¹ 7 TeV LHC data and the LUX data.
- 14 The strongest limit is 3.6×10^{-6} pb and occurs at $m_\chi = 35$ GeV. Felizardo 2014 updates Felizardo 2012.
- 15 Predictions for the spin-independent elastic cross section based on a Bayesian approach to electroweak observables in the framework of $N = 1$ supergravity models with radiative breaking of the electroweak gauge symmetry using the 20 fb⁻¹ LHC data and LUX.

- 16 AGNESE 13 presents 90% CL limits on the elastic cross section for masses in the range 7–100 GeV using the Si based detector. The strongest upper limit is 1.8×10^{-6} pb at $m_\chi = 50$ GeV. This limit is improved to 7×10^{-7} pb in AGNESE 13A.
- 17 This result updates LEBEDENKO 09. The strongest limit is 3.9×10^{-8} pb at $m_\chi = 52$ GeV.
- 18 ANGLÖHER 12 presents results of 730 kg days from the CRESST-II dark matter detector. They find two maxima in the likelihood function corresponding to best fit WIMP masses of 25.3 and 11.6 GeV with elastic cross sections of 1.6×10^{-6} and 3.7×10^{-5} pb respectively, see their Table 4. The statistical significance is more than 4σ . ANGLÖHER 12 updates ANGLÖHER 09.
- 19 Predictions for the spin-independent elastic cross section based on a frequentist approach to electroweak observables in the framework of $N = 1$ supergravity models with radiative breaking of the electroweak gauge symmetry using the 5 fb⁻¹ LHC data and XENON100.
- 20 The strongest limit is 1.4×10^{-7} at $m_\chi = 60$ GeV.
- 21 This result updates LEE 07A. The strongest limit is 2.1×10^{-7} at $m_\chi = 70$ GeV.
- 22 AHMED 11A gives combined results from CDMS and EDELWEISS. The strongest limit is at $m_\chi = 90$ GeV.
- 23 ARMENGAUD 11 updates result of ARMENGAUD 10. Strongest limit at $m_\chi = 85$ GeV.
- 24 The strongest upper limit is 5.1×10^{-8} pb and occurs at $m_\chi \approx 30$ GeV. The values quoted here are based on the analysis performed in ANGLE 08 with the update from SORESENSEN 09.
- 25 The strongest upper limit is 6.6×10^{-7} pb and occurs at $m_\chi \approx 65$ GeV.
- 26 AKERIB 06A updates the results of AKERIB 05. The strongest upper limit is 1.6×10^{-7} pb and occurs at $m_\chi \approx 60$ GeV.
- 27 The strongest upper limit is also close to 1.0×10^{-6} pb and occurs at $m_\chi \approx 70$ GeV. BENOIT 06 claim that the discrimination power of ZEPLIN-I measurement (ALNER 05A) is not reliable enough to obtain a limit better than 1×10^{-3} pb. However, SMITH 06 do not agree with the criticisms of BENOIT 06.
- 28 AKERIB 04 is incompatible with BERNABEI 00 most likely value, under the assumption of standard WIMP-halo interactions. The strongest upper limit is 4×10^{-7} pb and occurs at $m_\chi \approx 60$ GeV.
- 29 Predictions for the spin-independent elastic cross section in the framework of $N = 1$ supergravity models with radiative breaking of the electroweak gauge symmetry.
- 30 KIM 02 and ELLIS 04 calculate the χp elastic scattering cross section in the framework of $N=1$ supergravity models with radiative breaking of the electroweak gauge symmetry, but without universal scalar masses.
- 31 In the case of universal squark and slepton masses, but non-universal Higgs masses, the limit becomes 2×10^{-6} (2×10^{-11} when constraint from the BNL $g-2$ experiment are included), see ELLIS 03E. ELLIS 05 display the sensitivity of the elastic scattering cross section to the π -Nucleon Σ term.
- 32 PIERCE 04A calculates the χp elastic scattering cross section in the framework of models with very heavy scalar masses. See Fig. 2 of the paper.
- 33 The strongest upper limit is 1.8×10^{-5} pb and occurs at $m_\chi \approx 80$ GeV.
- 34 Under the assumption of standard WIMP-halo interactions, Akerib 03 is incompatible with BERNABEI 00 most likely value at the 99.98% CL. See Fig. 4.
- 35 BAER 03A calculates the χp elastic scattering cross section in several models including the framework of $N=1$ supergravity models with radiative breaking of the electroweak gauge symmetry.
- 36 The strongest upper limit is 7×10^{-6} pb and occurs at $m_\chi \approx 30$ GeV.
- 37 ABRAMS 02 is incompatible with the DAMA most likely value at the 99.9% CL. The strongest upper limit is 3×10^{-6} pb and occurs at $m_\chi \approx 30$ GeV.
- 38 The strongest upper limit is 2×10^{-5} pb and occurs at $m_\chi \approx 40$ GeV.
- 39 The strongest upper limit is 7×10^{-6} pb and occurs at $m_\chi \approx 46$ GeV.
- 40 The strongest upper limit is 1.8×10^{-5} pb and occurs at $m_\chi \approx 32$ GeV.
- 41 BOTTINO 01 calculates the $\chi-p$ elastic scattering cross section in the framework of the following supersymmetric models: $N=1$ supergravity with the radiative breaking of the electroweak gauge symmetry, $N=1$ supergravity with nonuniversal scalar masses and an effective MSSM model at the electroweak scale.
- 42 Calculates the $\chi-p$ elastic scattering cross section in the framework of $N=1$ supergravity models with radiative breaking of the electroweak gauge symmetry.
- 43 ELLIS 01C calculates the $\chi-p$ elastic scattering cross section in the framework of $N=1$ supergravity models with radiative breaking of the electroweak gauge symmetry. ELLIS 02B find a range $2 \times 10^{-8}-1.5 \times 10^{-7}$ at $\tan\beta=50$. In models with nonuniversal Higgs masses, the upper limit to the cross section is 4×10^{-7} .
- 44 ACCOMANDO 00 calculate the $\chi-p$ elastic scattering cross section in the framework of minimal $N=1$ supergravity models with radiative breaking of the electroweak gauge symmetry. The limit is relaxed by at least an order of magnitude when models with nonuniversal scalar masses are considered. A subset of the authors in ARNOWITT 02 updated the limit to $< 9 \times 10^{-8}$ ($\tan\beta < 55$).
- 45 BERNABEI 00 search for annual modulation of the WIMP signal. The data favor the hypothesis of annual modulation at 4σ and are consistent, for a particular model framework quoted there, with $m_{\chi 0} = 44 \pm 19$ GeV and a spin-independent X^0 -proton cross section of $(5.4 \pm 1.0) \times 10^{-6}$ pb. See also BERNABEI 01 and BERNABEI 00C.
- 46 FENG 00 calculate the $\chi-p$ elastic scattering cross section in the framework of $N=1$ supergravity models with radiative breaking of the electroweak gauge symmetry with a particular emphasis on focus point models. At $\tan\beta=50$, the range is $8 \times 10^{-8}-4 \times 10^{-7}$.

Other bounds on $\tilde{\chi}_1^0$ from astrophysics and cosmology

Most of these papers generally exclude regions in the $M_2 - \mu$ parameter plane by requiring that the $\tilde{\chi}_1^0$ contribution to the overall cosmological density is less than some maximal value to avoid overclosure of the Universe. Those not based on the cosmological density are indicated. Many of these papers also include LEP and/or other bounds.

VALUE	DOCUMENT ID	TECN	COMMENT
>46 GeV	1 ELLIS	00	RVUE

Searches Particle Listings

Supersymmetric Particle Searches

• • • We do not use the following data for averages, fits, limits, etc. • • •

	2	ATHRON	17B	COSM
	3	BECHTLE	16	COSM
	4	BAGNASCHI	15	COSM
	5	BUCHMUEL...	14	COSM
	6	BUCHMUEL...	14A	COSM
	7	ROSZKOWSKI	14	COSM
	8	CABRERA	13	COSM
	9	ELLIS	13B	COSM
	8	STREGE	13	COSM
	5	AKULA	12	COSM
	5	ARBEY	12A	COSM
	5	BAER	12	COSM
	10	BALAZS	12	COSM
	11	BECHTLE	12	COSM
	12	BESKIDT	12	COSM
> 18 GeV	13	BOTTINO	12	COSM
	5	BUCHMUEL...	12	COSM
	5	CAO	12A	COSM
	5	ELLIS	12B	COSM
	14	FENG	12B	COSM
	5	KADASTIK	12	COSM
	10	STREGE	12	COSM
	15	BUCHMUEL...	11	COSM
	16	ROSZKOWSKI	11	COSM
	17	ELLIS	10	COSM
	18	BUCHMUEL...	09	COSM
	19	DREINER	09	THEO
	20	BUCHMUEL...	08	COSM
	16	ELLIS	08	COSM
	21	CALIBBI	07	COSM
	22	ELLIS	07	COSM
	23	ALLANACH	06	COSM
	24	DE-AUSTRI	06	COSM
	16	BAER	05	COSM
	25	BALTZ	04	COSM
> 6 GeV	13,26	BELANGER	04	THEO
	27	ELLIS	04B	COSM
	28	PIERCE	04A	COSM
	29	BAER	03	COSM
> 6 GeV	13	BOTTINO	03	COSM
	29	CHATTOPAD...	03	COSM
	30	ELLIS	03	COSM
	16	ELLIS	03B	COSM
	29	ELLIS	03C	COSM
	29	LAHANAS	03	COSM
	31	LAHANAS	02	COSM
	32	BARGER	01C	COSM
	33	ELLIS	01B	COSM
	30	BOEHM	00B	COSM
	34	FENG	00	COSM
< 600 GeV	35	ELLIS	98B	COSM
	36	EDSJO	97	COSM Co-annihilation
	37	BAER	96	COSM
	16	BEREZINSKY	95	COSM
	38	FALK	95	COSM CP-violating phases
	39	DREES	93	COSM Minimal supergravity
	40	FALK	93	COSM Sfermion mixing
	39	KELLEY	93	COSM Minimal supergravity
	41	MIZUTA	93	COSM Co-annihilation
	42	LOPEZ	92	COSM Minimal supergravity, $m_0=A=0$
	43	MCDONALD	92	COSM
	44	GRIEST	91	COSM
	45	NOJIRI	91	COSM Minimal supergravity
	46	OLIVE	91	COSM
	47	ROSZKOWSKI	91	COSM
	48	GRIEST	90	COSM
	46	OLIVE	89	COSM
none 100 eV - 15 GeV		SREDNICKI	88	COSM $\tilde{\tau}; m_{\tilde{\tau}}=100$ GeV
none 100 eV-5 GeV		ELLIS	84	COSM $\tilde{\tau};$ for $m_{\tilde{\tau}}=100$ GeV
		GOLDBERG	83	COSM $\tilde{\tau}$
	49	KRAUSS	83	COSM $\tilde{\tau}$
		VYSOTSKI	83	COSM $\tilde{\tau}$

¹ ELLIS 00 updates ELLIS 98. Uses LEP e^+e^- data at $\sqrt{s}=202$ and 204 GeV to improve bound on neutralino mass to 51 GeV when scalar mass universality is assumed and 46 GeV when Higgs mass universality is relaxed. Limits on $\tan\beta$ improve to > 2.7 ($\mu > 0$), > 2.2 ($\mu < 0$) when scalar mass universality is assumed and > 1.9 (both signs of μ) when Higgs mass universality is relaxed.

² ATHRON 17b places constraints on the SUSY parameter space in the framework of $N=1$ supergravity models with radiative breaking of the electroweak gauge symmetry using all Run I and the 13 fb^{-1} 13 TeV Run II LHC searches and other experimental data.

³ BECHTLE 16 places constraints on the SUSY parameter space in the framework of $N=1$ supergravity models with radiative breaking of the electroweak gauge symmetry using all Run I LHC searches.

⁴ BAGNASCHI 15 places constraints on the SUSY parameter space in the framework of $N=1$ supergravity models with radiative breaking of the electroweak gauge symmetry using all Run I LHC searches.

⁵ Implications of the LHC result on the Higgs mass and on the SUSY parameter space in the framework of $N=1$ supergravity models with radiative breaking of the electroweak gauge symmetry.

⁶ BUCHMUELLER 14A places constraints on the SUSY parameter space in the framework of $N=1$ supergravity models with radiative breaking of the electroweak gauge symmetry using indirect experimental searches using the 20 fb^{-1} 8 TeV and the 5 fb^{-1} 7 TeV LHC and the LUX data.

⁷ ROSZKOWSKI 14 places constraints on the SUSY parameter space in the framework of $N=1$ supergravity models with radiative breaking of the electroweak gauge symmetry using Bayesian statistics and indirect experimental searches using the 20 fb^{-1} LHC and the LUX data.

⁸ CABRERA 13 and STREGE 13 place constraints on the SUSY parameter space in the framework of $N=1$ supergravity models with radiative breaking of the electroweak gauge symmetry with and without non-universal Higgs masses using the 5.8 fb^{-1} , $\sqrt{s}=7$ TeV ATLAS supersymmetry searches and XENON100 results.

⁹ ELLIS 13B place constraints on the SUSY parameter space in the framework of $N=1$ supergravity models with radiative breaking of the electroweak gauge symmetry with and without Higgs mass universality. Models with universality below the GUT scale are also considered.

¹⁰ BALAZS 12 and STREGE 12 place constraints on the SUSY parameter space in the framework of $N=1$ supergravity models with radiative breaking of the electroweak gauge symmetry using the 1 fb^{-1} LHC supersymmetry searches, the 5 fb^{-1} Higgs mass constraints, both with $\sqrt{s}=7$ TeV, and XENON100 results.

¹¹ BECHTLE 12 places constraints on the SUSY parameter space in the framework of $N=1$ supergravity models with radiative breaking of the electroweak gauge symmetry using indirect experimental searches, using the 5 fb^{-1} LHC and XENON100 data.

¹² BESKIDT 12 places constraints on the SUSY parameter space in the framework of $N=1$ supergravity models with radiative breaking of the electroweak gauge symmetry using indirect experimental searches, the 5 fb^{-1} LHC and the XENON100 data.

¹³ BELANGER 04 and BOTTINO 12 (see also BOTTINO 03, BOTTINO 03A and BOTTINO 04) do not assume gaugino or scalar mass unification.

¹⁴ FENG 12b places constraints on the SUSY parameter space in the framework of $N=1$ supergravity models with radiative breaking of the electroweak gauge symmetry and large sfermion masses using the 1 fb^{-1} LHC supersymmetry searches, the 5 fb^{-1} LHC Higgs mass constraints both with $\sqrt{s}=7$ TeV, and XENON100 results.

¹⁵ BUCHMUELLER 11 places constraints on the SUSY parameter space in the framework of $N=1$ supergravity models with radiative breaking of the electroweak gauge symmetry using indirect experimental searches and including supersymmetry breaking relations between A and B parameters.

¹⁶ Places constraints on the SUSY parameter space in the framework of $N=1$ supergravity models with radiative breaking of the electroweak gauge symmetry but non-Universal Higgs masses.

¹⁷ ELLIS 10 places constraints on the SUSY parameter space in the framework of $N=1$ supergravity models with radiative breaking of the electroweak gauge symmetry with universality above the GUT scale.

¹⁸ BUCHMUELLER 09 places constraints on the SUSY parameter space in the framework of $N=1$ supergravity models with radiative breaking of the electroweak gauge symmetry using indirect experimental searches.

¹⁹ DREINER 09 show that in the general MSSM with non-universal gaugino masses there exists no model-independent laboratory bound on the mass of the lightest neutralino. An essentially massless χ_1^0 is allowed by the experimental and observational data, imposing some constraints on other MSSM parameters, including M_2 , μ and the slepton and squark masses.

²⁰ BUCHMUELLER 08 places constraints on the SUSY parameter space in the framework of $N=1$ supergravity models with radiative breaking of the electroweak gauge symmetry using indirect experimental searches.

²¹ CALIBBI 07 places constraints on the SUSY parameter space in the framework of $N=1$ supergravity models with radiative breaking of the electroweak gauge symmetry with universality above the GUT scale including the effects of right-handed neutrinos.

²² ELLIS 07 places constraints on the SUSY parameter space in the framework of $N=1$ supergravity models with radiative breaking of the electroweak gauge symmetry with universality below the GUT scale.

²³ ALLANACH 06 places constraints on the SUSY parameter space in the framework of $N=1$ supergravity models with radiative breaking of the electroweak gauge symmetry.

²⁴ DE-AUSTRI 06 places constraints on the SUSY parameter space in the framework of $N=1$ supergravity models with radiative breaking of the electroweak gauge symmetry.

²⁵ BALTZ 04 places constraints on the SUSY parameter space in the framework of $N=1$ supergravity models with radiative breaking of the electroweak gauge symmetry.

²⁶ Limit assumes a pseudo scalar mass < 200 GeV. For larger pseudo scalar masses, $m_\chi > 18(29)$ GeV for $\tan\beta = 50(10)$. Bounds from WMAP, $(g-2)_\mu$, $b \rightarrow s\gamma$, LEP.

²⁷ ELLIS 04b places constraints on the SUSY parameter space in the framework of $N=1$ supergravity models with radiative breaking of the electroweak gauge symmetry including supersymmetry breaking relations between A and B parameters. See also ELLIS 03d.

²⁸ PIERCE 04a places constraints on the SUSY parameter space in the framework of models with very heavy scalar masses.

²⁹ BAER 03, CHATTOPADHYAY 03, ELLIS 03c and LAHANAS 03 place constraints on the SUSY parameter space in the framework of $N=1$ supergravity models with radiative breaking of the electroweak gauge symmetry based on WMAP results for the cold dark matter density.

³⁰ BOEHM 00b and ELLIS 03 place constraints on the SUSY parameter space in the framework of minimal $N=1$ supergravity models with radiative breaking of the electroweak gauge symmetry. Includes the effect of χ - t co-annihilations.

³¹ LAHANAS 02 places constraints on the SUSY parameter space in the framework of minimal $N=1$ supergravity models with radiative breaking of the electroweak gauge symmetry. Focuses on the role of pseudo-scalar Higgs exchange.

³² BARGER 01c use the cosmic relic density inferred from recent CMB measurements to constrain the parameter space in the framework of minimal $N=1$ supergravity models with radiative breaking of the electroweak gauge symmetry.

³³ ELLIS 01b places constraints on the SUSY parameter space in the framework of minimal $N=1$ supergravity models with radiative breaking of the electroweak gauge symmetry. Focuses on models with large $\tan\beta$.

³⁴ FENG 00 explores cosmologically allowed regions of MSSM parameter space with multi-TeV masses.

³⁵ ELLIS 98b assumes a universal scalar mass and radiative supersymmetry breaking with universal gaugino masses. The upper limit to the LSP mass is increased due to the inclusion of $\chi - \tilde{\tau}_R$ coannihilations.

- 36 EDSJO 97 included all coannihilation processes between neutralinos and charginos for any neutralino mass and composition.
- 37 Notes the location of the neutralino Z resonance and h resonance annihilation corridors in minimal supergravity models with radiative electroweak breaking.
- 38 Mass of the bino (=LSP) is limited to $m_{\tilde{B}} \lesssim 350$ GeV for $m_t = 174$ GeV.
- 39 DREES 93, KELLEY 93 compute the cosmic relic density of the LSP in the framework of minimal $N=1$ supergravity models with radiative breaking of the electroweak gauge symmetry.
- 40 FALK 93 relax the upper limit to the LSP mass by considering sfermion mixing in the MSSM.
- 41 MIZUTA 93 include coannihilations to compute the relic density of Higgsino dark matter.
- 42 LOPEZ 92 calculate the relic LSP density in a minimal SUSY GUT model.
- 43 MCDONALD 92 calculate the relic LSP density in the MSSM including exact tree-level annihilation cross sections for all two-body final states.
- 44 GRIEST 91 improve relic density calculations to account for coannihilations, pole effects, and threshold effects.
- 45 NOJIRI 91 uses minimal supergravity mass relations between squarks and sleptons to narrow cosmologically allowed parameter space.
- 46 Mass of the bino (=LSP) is limited to $m_{\tilde{B}} \lesssim 350$ GeV for $m_t \leq 200$ GeV. Mass of the higgsino (=LSP) is limited to $m_{\tilde{H}} \lesssim 1$ TeV for $m_t \leq 200$ GeV.
- 47 ROSZKOWSKI 91 calculates LSP relic density in mixed gaugino/higgsino region.
- 48 Mass of the bino (=LSP) is limited to $m_{\tilde{B}} \lesssim 550$ GeV. Mass of the higgsino (=LSP) is limited to $m_{\tilde{H}} \lesssim 3.2$ TeV.
- 49 KRAUSS 83 finds $m_{\tilde{\gamma}}$ not 30 eV to 2.5 GeV. KRAUSS 83 takes into account the gravitino decay. Find that limits depend strongly on reheated temperature. For example a new allowed region $m_{\tilde{\gamma}} = 4-20$ MeV exists if $m_{\text{gravitino}} < 40$ TeV. See figure 2.

Unstable $\tilde{\chi}_1^0$ (Lightest Neutralino) mass limit

Unless otherwise stated, results in this section assume spectra and production rates as evaluated in the MSSM. Unless otherwise stated, the goldstino or gravitino mass $m_{\tilde{G}}$ is assumed to be negligible relative to all other masses. In the following, \tilde{G} is assumed to be undetected and to give rise to a missing energy (\cancel{E}) signature.

Some earlier papers are now obsolete and have been omitted. They were last listed in our PDG 14 edition: K. Olive, et al. (Particle Data Group), Chinese Physics **C38** 070001 (2014) (<http://pdg.lbl.gov>).

VALUE (GeV)	CL%	DOCUMENT ID	TECN	COMMENT
> 540	95	1 AAD	21Y ATLS	$\geq 4\ell$, Tchi1n12-GGM, $\tilde{\chi}_1^0 \rightarrow Z\tilde{G}$
none 7-50	95	2 AAIJ	21V LHCB	$e^{\pm}\mu^{\mp}$, RPV $\tilde{\chi}_1^0 \rightarrow e^{\pm}\mu^{\mp}\nu$, 2 ps $< \tau < 50$ ps
>1100	95	3 SIRUNYAN	21AF CMS	long-lived $\tilde{\chi}_1^0$, RPV $\tilde{\chi}_1^0 \rightarrow tbs$, χ'_{323} coupling, 0.6 mm $< c\tau < 70$ mm
> 800	95	4 SIRUNYAN	21M CMS	$\ell^{\pm}\ell^{\mp} + \cancel{E}_T$, Tn1n1C
> 650	95	4 SIRUNYAN	21M CMS	$\ell^{\pm}\ell^{\mp} + \cancel{E}_T$, Tn1n1B
> 380	95	5 AAD	20AN ATLS	$2\gamma + \cancel{E}_T$, Tn1n1A, GMSB
> 525	95	6 SIRUNYAN	19CA CMS	$\tilde{\chi}_1^0 \rightarrow \gamma\tilde{G}$, GMSB, SPS8, $c\tau=1$ m
> 290	95	7 SIRUNYAN	19ci CMS	$\geq 1 H (\rightarrow \gamma\gamma) + \text{jets} + \cancel{E}_T$, Tn1n1A, GMSB
> 230	95	7 SIRUNYAN	19ci CMS	$\geq 1 H (\rightarrow \gamma\gamma) + \text{jets} + \cancel{E}_T$, Tn1n1B, GMSB
> 930	95	8 SIRUNYAN	19K CMS	$\gamma + \text{lepton} + \cancel{E}_T$, Tchi1n1A
none 130-230, 290-880	95	9 AABOUD	18ck ATLS	$2H (\rightarrow bb) + \cancel{E}_T$, Tn1n1A, GMSB
> 295	95	10 AABOUD	18Z ATLS	$\geq 4\ell$, GMSB, Tn1n1C
> 180	95	11 SIRUNYAN	18Ao CMS	$\ell^{\pm}\ell^{\pm}$ or $\geq 3\ell$, Tn1n1A
> 260	95	11 SIRUNYAN	18Ao CMS	$\ell^{\pm}\ell^{\pm}$ or $\geq 3\ell$, Tn1n1B
> 450	95	11 SIRUNYAN	18Ao CMS	$\ell^{\pm}\ell^{\pm}$ or $\geq 3\ell$, Tn1n1C
> 750	95	12 SIRUNYAN	18AP CMS	Combination of searches, GMSB, Tn1n1A
> 650	95	12 SIRUNYAN	18AP CMS	Combination of searches, GMSB, Tn1n1B
> 690	95	12 SIRUNYAN	18AP CMS	Combination of searches, GMSB, Tn1n1C
> 500	95	13 SIRUNYAN	18AR CMS	$\ell^{\pm}\ell^{\mp} + \text{jets} + \cancel{E}_T$, GMSB, Tn1n1B
> 650	95	13 SIRUNYAN	18AR CMS	$\ell^{\pm}\ell^{\mp} + \text{jets} + \cancel{E}_T$, GMSB, Tn1n1C
none 230-770	95	14 SIRUNYAN	18O CMS	$2H (\rightarrow bb) + \cancel{E}_T$, Tn1n1A, GMSB
> 205	95	15 SIRUNYAN	18X CMS	$\geq 1 H (\rightarrow \gamma\gamma) + \text{jets} + \cancel{E}_T$, Tn1n1A, GMSB
> 130	95	15 SIRUNYAN	18X CMS	$\geq 1 H (\rightarrow \gamma\gamma) + \text{jets} + \cancel{E}_T$, Tn1n1B, GMSB
> 380	95	16 KHACHATRY..14L	CMS	$\tilde{\chi}_1^0 \rightarrow Z\tilde{G}$ simplified models, GMSB, RPV
• • • We do not use the following data for averages, fits, limits, etc. • • •				
none 300-1000	95	17 AAD	20D	$\tilde{q} \rightarrow q\tilde{\chi}_1^0, \tilde{\chi}_1^0 \rightarrow \ell\ell\nu$, RPV, λ_{121} or $\lambda_{122} \neq 0$
		18 AABOUD	19G ATLS	$\tilde{\chi}_1^0 \rightarrow Z\tilde{G}$ from gluinos as in Tglu1A, GMSB, depending on $c\tau$
		19 AAIJ	17Z	displaced vertex with associated μ
		20 KHACHATRY..16Bx	CMS	$\geq 3\ell^{\pm}$, RPV, λ or λ' couplings, wino- or higgsino-like neutralinos
		21 AAD	14BH ATLS	$2\gamma + \cancel{E}_T$, GMSB, SPS8
		22 AAD	13AP ATLS	$2\gamma + \cancel{E}_T$, GMSB, SPS8
none 220-380	95	23 AAD	13Q ATLS	$\gamma + b + \cancel{E}_T$, higgsino-like neutralino, GMSB
		24 AAD	13R ATLS	$\tilde{\chi}_1^0 \rightarrow \mu j j$, RPV, $\lambda'_{211} \neq 0$

		25 AALTONEN	13i CDF	$\tilde{\chi}_1^0 \rightarrow \gamma\tilde{G}, \cancel{E}_T$, GMSB
> 220	95	26 CHATARCHYAN13AH	CMS	$\tilde{\chi}_1^0 \rightarrow \gamma\tilde{G}$, GMSB, SPS8, $c\tau < 500$ mm
		27 AAD	12CP ATLS	$2\gamma + \cancel{E}_T$, GMSB
		28 AAD	12CT ATLS	$\geq 4\ell^{\pm}$, RPV
		29 AAD	12R ATLS	$\tilde{\chi}_1^0 \rightarrow \mu j j$, RPV, $\lambda'_{211} \neq 0$
		30 ABAZOV	12AD D0	$\tilde{\chi}_1^0 \rightarrow \gamma Z\tilde{G}$, GMSB
		31 CHATARCHYAN12BK	CMS	$2\gamma + \cancel{E}_T$, GMSB
		32 CHATARCHYAN11B	CMS	$\tilde{W}^0 \rightarrow \gamma\tilde{G}, \tilde{W}^{\pm} \rightarrow \ell^{\pm}\tilde{G}$, GMSB
> 149	95	33 AALTONEN	10 CDF	$p\bar{p} \rightarrow \tilde{\chi}\tilde{\chi}, \tilde{\chi}=\tilde{\chi}_2^0, \tilde{\chi}_1^{\pm}, \tilde{\chi}_1^0 \rightarrow \gamma\tilde{G}$, GMSB
> 175	95	34 ABAZOV	10P D0	$\tilde{\chi}_1^0 \rightarrow \gamma\tilde{G}$, GMSB
> 125	95	35 ABAZOV	08F D0	$p\bar{p} \rightarrow \tilde{\chi}\tilde{\chi}, \tilde{\chi}=\tilde{\chi}_2^0, \tilde{\chi}_1^{\pm}, \tilde{\chi}_1^0 \rightarrow \gamma\tilde{G}$, GMSB
> 96.8	95	36 ABULENCIA	07H CDF	RPV, $LL\bar{E}$
		37 ABBIENDI	06B OPAL	$e^+e^- \rightarrow \tilde{B}\tilde{B}, (\tilde{B} \rightarrow \tilde{G}\gamma)$
		38 ABDALLAH	05B DLPH	$e^+e^- \rightarrow \tilde{G}\tilde{\chi}_1^0, (\tilde{\chi}_1^0 \rightarrow \tilde{G}\gamma)$
> 96	95	39 ABDALLAH	05B DLPH	$e^+e^- \rightarrow \tilde{B}\tilde{B}, (\tilde{B} \rightarrow \tilde{G}\gamma)$

- 1 AAD 21Y searched in 139 fb^{-1} of pp collisions at $\sqrt{s} = 13$ TeV for supersymmetry in events with four or more leptons (electrons, muons and tau-leptons). No significant excess above the Standard Model expectations is observed. Limits are set on Tchi1n12-GGM, and RPV models similar to Tchi1n2l, Tglu1A (with $q = u, d, s, c, b$, with equal branching fractions), and $\tilde{\ell}_L/\tilde{\nu} \rightarrow \ell/\nu\tilde{\chi}_1^0$ (mass-degenerate $\tilde{\ell}_L$ and $\tilde{\nu}$ of all 3 generations), all with $\tilde{\chi}_1^0 \rightarrow \ell^{\pm}\ell^{\mp}\nu$ via λ_{12k} or λ_{j33} (where $i, k \in 1, 2$), see their Figure 11.
- 2 AAIJ 21v searched in 5.38 fb^{-1} of pp collisions at $\sqrt{s} = 13$ TeV for long-lived particles (LLP) decaying to $e^{\pm}\mu^{\mp}\nu$. The LLP can be a $\tilde{\chi}_1^0$ in RPV SUSY, or a right-handed neutrino, and can be produced in pairs, in the decay of the Higgs boson, or from charged current processes. No significant excess above the Standard Model expectations is observed. Limits are set on the cross section times branching ratio for all three production mechanisms, see their Figures 6-8.
- 3 SIRUNYAN 21AF searched in 140 fb^{-1} of pp collisions at $\sqrt{s} = 13$ TeV for supersymmetry in events with two displaced vertices from long-lived particles decaying into multijet or dijet final states. No significant excess above the Standard Model expectations is observed. Limits are set on the gluino mass in the simplified model Tglu2RPV with χ'_{323} coupling, on the $\tilde{\chi}_1^0$ mass in an RPV model with $\tilde{\chi}_1^0$ pair production and the RPV decay $\tilde{\chi}_1^0 \rightarrow tbs$ with χ'_{323} coupling and on the \tilde{t} mass in an RPV model with top squark pair production and the RPV decay $\tilde{t} \rightarrow \tilde{d}_i\tilde{d}_j$ with χ'_{3ij} coupling, see their Figure 7.
- 4 SIRUNYAN 21M searched in 137 fb^{-1} of pp collisions at $\sqrt{s} = 13$ TeV for supersymmetry in events with two opposite-sign same-flavor leptons (electrons, muons) and \cancel{E}_T . No significant excess above the Standard Model expectations is observed. Limits are set on the gluino mass in the simplified model Tglu4C, see their Figure 10, on the $\tilde{\chi}_2^0$ and $\tilde{\chi}_1^{\pm}$ mass in Tchi1n2Fa, see their Figure 11, on the $\tilde{\chi}_1^0$ mass in Tn1n1C and Tn1n1B for $m_{-0}=m_{\tilde{\chi}_1^{\pm}}=m_{-0}$, see their Figure 12. Limits are also set on the light squark mass in the simplified model Tsqk2A, on the sbottom mass in Tsb0t3, see their Figure 13, and on the slepton mass in direct electroweak pair production of mass-degenerate left- and right-handed sleptons (selectrons and smuons), see their Figure 14.
- 5 AAD 20AN searched in 139 fb^{-1} of pp collisions at $\sqrt{s} = 13$ TeV for events with two photons and missing transverse momentum. Events are further categorised in terms of lepton or jet multiplicity. No significant excess over the expected background is observed. Limits at 95% C.L. are set on the Higgsino mass in the Tn1n1A simplified model, see their Figure 11.
- 6 SIRUNYAN 19CA searched in 77.4 fb^{-1} of pp collisions at $\sqrt{s} = 13$ TeV for events containing delayed photons in both single and diphoton plus \cancel{E}_T final states. No excess is observed above the background expected from Standard Model processes. The results are used to set 95% C.L. exclusion limits in the context of GMSB, using the SPS8 benchmark model. For neutralino proper decay lengths of 0.1, 1, 10, and 100 m, masses up to about 320, 525, 360, and 215 GeV are excluded, respectively. See their Fig. 5. The searches involve the simplified models Tglu1D, Tglu4A,B,C, Tsqk4,4A,4B.
- 7 SIRUNYAN 19ci searched in 77.5 fb^{-1} of pp collisions at $\sqrt{s} = 13$ TeV for events with one or more high-momentum Higgs bosons, decaying to pairs of photons, jets and \cancel{E}_T . No significant excess above the Standard Model expectations is observed. Limits are set on the sbottom mass in the Tsb0t4 simplified model, see Figure 3, and on the wino mass in the Tchi1n2E simplified model, see their Figure 4. Limits are also set on the higgsino mass in the Tn1n1A and Tn1n1B simplified models, see their Figure 5.
- 8 SIRUNYAN 19K searched in 35.9 fb^{-1} of pp collisions at $\sqrt{s} = 13$ TeV for events with a photon, an electron or muon, and large \cancel{E}_T . No significant excess above the Standard Model expectations is observed. In the framework of GMSB, limits are set on the chargino and neutralino mass in the Tchi1n1A simplified model, see their Figure 6. Limits are also set on the gluino mass in the Tglu4A simplified model, and on the squark mass in the Tsqk4A simplified model, see their Figure 7.
- 9 AABOUD 18ck searched for events with at least 3 b-jets and large missing transverse energy in two datasets of pp collisions at $\sqrt{s} = 13$ TeV of 36.1 fb^{-1} and 24.3 fb^{-1} depending on the trigger requirements. The analyses aimed to reconstruct two Higgs bosons decaying to pairs of b-quarks. No significant excess above the Standard Model expectations is observed. Limits are set on the Higgsino mass in the Tn1n1A simplified model, see their Figure 15(a). Constraints are also presented as a function of the BR of Higgsino decaying into a higgs boson and a gravitino, see their Figure 15(b).
- 10 AABOUD 18z searched in 36.1 fb^{-1} of pp collisions at $\sqrt{s} = 13$ TeV for events containing four or more charged leptons (electrons, muons and up to two hadronically decaying taus). No significant deviation from the expected SM background is observed. Limits are set on the Higgsino mass in simplified models of general gauge mediated supersymmetry Tn1n1A/Tn1n1B/Tn1n1C, see their Figure 9. Limits are also set on the wino, slepton, sneutrino and gluino mass in a simplified model of NLSP pair production with R-parity violating decays of the LSP via λ_{12k} or λ_{j33} to charged leptons, see their Figures 7, 8.
- 11 SIRUNYAN 18Ao searched in 35.9 fb^{-1} of pp collisions at $\sqrt{s} = 13$ TeV for direct electroweak production of charginos and higgsinos in events with either two or more leptons (electrons or muons) of the same electric charge, or with three or more leptons, which can include up to two hadronically decaying tau leptons. No significant excess above

Searches Particle Listings

Supersymmetric Particle Searches

- the Standard Model expectations is observed. Limits are set on the chargino/neutralino mass in the Tchi1n2A, Tchi1n2H, Tchi1n2D, Tchi1n2E and Tchi1n2F simplified models, see their Figures 14, 15, 16, 17 and 18. Limits are also set on the higgsino mass in the Tn1n1A, Tn1n1B and Tn1n1C simplified models, see their Figure 19.
- 12 SIRUNYAN 18AP searched in 35.9 fb^{-1} of pp collisions at $\sqrt{s} = 13 \text{ TeV}$ for direct electroweak production of charginos and neutralinos by combining a number of previous and new searches. No significant excess above the Standard Model expectations is observed. Limits are set on the chargino/neutralino mass in the Tchi1n2E, Tchi1n2F and Tchi1n2I simplified models, see their Figures 7, 8, 9 and 10. Limits are also set on the higgsino mass in the Tn1n1A, Tn1n1B and Tn1n1C simplified models, see their Figure 11, 12, 13 and 14.
- 13 SIRUNYAN 18AR searched in 35.9 fb^{-1} of pp collisions at $\sqrt{s} = 13 \text{ TeV}$ for events containing two opposite-charge, same-flavour leptons (electrons or muons), jets and \cancel{E}_T . No significant excess above the Standard Model expectations is observed. Limits are set on the gluino mass in the Tglu4C simplified model, see their Figure 7. Limits are also set on the chargino/neutralino mass in the Tchi1n2F simplified models, see their Figure 8, and on the higgsino mass in the Tn1n1B and Tn1n1C simplified models, see their Figure 9. Finally, limits are set on the sbottom mass in the Tsb0t3 simplified model, see their Figure 10.
- 14 SIRUNYAN 18o searched in 35.9 fb^{-1} of pp collisions at $\sqrt{s} = 13 \text{ TeV}$ for events with two Higgs bosons, decaying to pairs of b -quarks, and large \cancel{E}_T . No significant excess above the Standard Model expectations is observed. Limits are set on the Higgsino mass in the T1n1n1A simplified model, see their Figure 9.
- 15 SIRUNYAN 18x searched in 35.9 fb^{-1} of pp collisions at $\sqrt{s} = 13 \text{ TeV}$ for events with one or more high-momentum Higgs bosons, decaying to pairs of photons, jets and \cancel{E}_T . The razor variables (M_R and R^2) are used to categorise the events. No significant excess above the Standard Model expectations is observed. Limits are set on the sbottom mass in the Tsb0t4 simplified model and on the wino mass in the Tchi1n2E simplified model, see their Figure 5. Limits are also set on the higgsino mass in the Tn1n1A and Tn1n1B simplified models, see their Figure 6.
- 16 KHACHATRYAN 14L searched in 19.5 fb^{-1} of pp collisions at $\sqrt{s} = 8 \text{ TeV}$ for evidence of direct pair production of neutralinos with Higgs or Z -bosons in the decay chain, leading to HH , HZ and ZZ final states with missing transverse energy. The decays of 16–20. a Higgs boson to a b -quark pair, to a photon pair, and to final states with leptons are considered in conjunction with hadronic and leptonic decay modes of the Z and W bosons. No significant excesses over the expected SM backgrounds are observed. The results are interpreted in the context of GMSB simplified models where the decays $\tilde{\chi}_1^0 \rightarrow H\bar{G}$ or $\tilde{\chi}_1^0 \rightarrow Z\bar{G}$ take place either 100% or 50% of the time, see Figs. 16–20.
- 17 AAD 20b searched in 32.8 fb^{-1} of pp collisions at $\sqrt{s} = 13 \text{ TeV}$ for events containing an oppositely charge lepton pair ($e\bar{e}$, $\mu\bar{\mu}$ or $e\mu$) coming from long-lived neutralinos decaying through the R -parity-violating decay $\tilde{\chi}_1^0 \rightarrow \ell\ell\nu$ with $\lambda_{121} \neq 0$ or $\lambda_{122} \neq 0$. No excess over the expected background is observed. Limits are derived for decay lengths of the neutralino between 1 mm and 10 m in a scenario where a squark-antisquark pair is produced, with the squark decaying to a quark and a $\tilde{\chi}_1^0$, with either $\tilde{\chi}_1^0 \rightarrow e\bar{e}\nu/e\mu\nu$ ($\lambda_{121} \neq 0$) or $\tilde{\chi}_1^0 \rightarrow e\mu\nu/\mu\mu\nu$ ($\lambda_{122} \neq 0$), see their Figures 4 and 5.
- 18 AABOUD 19G searched in 32.9 fb^{-1} of pp collisions at $\sqrt{s} = 13 \text{ TeV}$ for evidence of neutralinos decaying into a Z -boson and a gravitino, in events characterized by the presence of dimuon vertices with displacements from the pp interaction point in the range of 1400 cm. Neutralinos are assumed to be produced in the decay chain of gluinos as in Tglu1A models. No significant excess is observed in the number of vertices relative to the predicted background. In GGM with a gluino mass of 1100 GeV, neutralino masses in the range 300–1000 GeV are excluded for certain values of $c\tau$, see their Figure 7.
- 19 AAIJ 17z searched in 1 fb^{-1} of pp collisions at $\sqrt{s} = 7 \text{ TeV}$ and in 2 fb^{-1} of pp collisions at $\sqrt{s} = 8 \text{ TeV}$ for events containing a displaced vertex with one associated high transverse momentum μ . No excess is observed above the background expected from Standard Model processes. The results are used to set 95% C.L. upper limits on the cross section times branching fractions of pair-produced neutralinos decaying non-promptly into a muon and two quarks. Long-lived particles in a mass range 23–198 GeV are considered, see their Fig. 5 and Fig. 6.
- 20 KHACHATRYAN 16BX searched in 19.5 fb^{-1} of pp collisions at $\sqrt{s} = 8 \text{ TeV}$ for events containing 3 or more leptons coming from the electroweak production of wino- or higgsino-like neutralinos, assuming non-zero R -parity-violating leptonic couplings λ_{122} , λ_{123} , and λ_{233} or semileptonic couplings λ'_{31} , λ'_{233} , λ'_{331} , and λ'_{333} . No excess over the expected background is observed and limits are derived on the neutralino mass, see Figs. 24 and 25.
- 21 AAD 14BH searched in 20.3 fb^{-1} of pp collisions at $\sqrt{s} = 8 \text{ TeV}$ for events containing non-pointing photons in a diphoton plus missing transverse energy final state. No excess is observed above the background expected from Standard Model processes. The results are used to set 95% C.L. exclusion limits in the context of gauge-mediated supersymmetric breaking models, with the lightest neutralino being the next-to-lightest supersymmetric particle and decaying with a lifetime in the range from 0.25 ns to about 100 ns into a photon and a gravitino. For limits on the NLSP lifetime versus Λ plane, for the SPS8 model, see their Fig. 7.
- 22 AAD 13AP searched in 4.8 fb^{-1} of pp collisions at $\sqrt{s} = 7 \text{ TeV}$ for events containing non-pointing photons in a diphoton plus missing transverse energy final state. No excess is observed above the background expected from Standard Model processes. The results are used to set 95% C.L. exclusion limits in the context of gauge-mediated supersymmetric breaking models, with the lightest neutralino being the next-to-lightest supersymmetric particle and decaying with a lifetime in excess of 0.25 ns into a photon and a gravitino. For limits in the NLSP lifetime versus Λ plane, for the SPS8 model, see their Fig. 8.
- 23 AAD 13Q searched in 4.7 fb^{-1} of pp collisions at $\sqrt{s} = 7 \text{ TeV}$ for events containing a high- p_T isolated photon, at least one jet identified as originating from a bottom quark, and high missing transverse momentum. Such signatures may originate from supersymmetric models with gauge-mediated supersymmetry breaking in events in which one of a pair of higgsino-like neutralinos decays into a photon and a gravitino while the other decays into a Higgs boson and a gravitino. No significant excess above the expected background was found and limits were set on the neutralino mass in a generalized GMSB model (GGM) with a higgsino-like neutralino NLSP, see their Fig. 4. Intermediate neutralino masses between 220 and 380 GeV are excluded at 95% C.L. regardless of the squark and gluino masses, purely on the basis of the expected weak production.
- 24 AAD 13R looked in 4.4 fb^{-1} of pp collisions at $\sqrt{s} = 7 \text{ TeV}$ for events containing new, heavy particles that decay at a significant distance from their production point into a final state containing a high-momentum muon and charged hadrons. No excess over the expected background is observed and limits are placed on the production cross-section of neutralinos via squarks for various $m_{\tilde{q}}$, $m_{\tilde{\chi}_1^0}$ in an R -parity violating scenario with $\lambda'_{211} \neq 0$, as a function of the neutralino lifetime, see their Fig. 6.
- 25 AALTONEN 13i searched in 6.3 fb^{-1} of $p\bar{p}$ collisions at $\sqrt{s} = 1.96 \text{ TeV}$ for events containing \cancel{E}_T and a delayed photon that arrives late in the detector relative to the time expected from prompt production. No evidence of delayed photon production is observed.
- 26 CHATRCHYAN 13AH searched in 4.9 fb^{-1} of pp collisions at $\sqrt{s} = 7 \text{ TeV}$ for events containing \cancel{E}_T and a delayed photon that arrives late in the detector relative to the time expected from prompt production. No significant excess above the expected background was found and limits were set on the pair production of $\tilde{\chi}_1^0$ depending on the neutralino proper decay length, see Fig. 8. Supersedes CHATRCHYAN 12BK.
- 27 AAD 12CP searched in 4.8 fb^{-1} of pp collisions at $\sqrt{s} = 7 \text{ TeV}$ for events with two photons and large \cancel{E}_T due to $\tilde{\chi}_1^0 \rightarrow \gamma\bar{G}$ decays in a GMSB framework. No significant excess above the expected background was found and limits were set on the neutralino mass in a generalized GMSB model (GGM) with a bino-like neutralino NLSP, see Figs. 6 and 7. The other sparticle masses were decoupled, $\tan\beta = 2$ and $c\tau_{NLSP} < 0.1 \text{ mm}$. Also, in the framework of the SPS8 model, limits are presented in Fig. 8.
- 28 AAD 12CT searched in 4.7 fb^{-1} of pp collisions at $\sqrt{s} = 7 \text{ TeV}$ for events containing four or more leptons (electrons or muons) and either moderate values of missing transverse momentum or large effective mass. No significant excess is found in the data. Limits are presented in a simplified model of R -parity violating supersymmetry in which charginos are pair-produced and then decay into a W -boson and a $\tilde{\chi}_1^0$, which in turn decays through an RPV coupling into two charged leptons ($e^\pm e^\mp$ or $\mu^\pm \mu^\mp$) and a neutrino. In this model, limits are set on the neutralino mass as a function of the chargino mass, see Fig. 3a. Limits are also set in an R -parity violating mSUGRA model, see Fig. 3b.
- 29 AAD 12R looked in 33 pb^{-1} of pp collisions at $\sqrt{s} = 7 \text{ TeV}$ for events containing new, heavy particles that decay at a significant distance from their production point into a final state containing a high-momentum muon and charged hadrons. No excess over the expected background is observed and limits are placed on the production cross-section of neutralinos via squarks for various ($m_{\tilde{q}}$, $m_{\tilde{\chi}_1^0}$) in an R -parity violating scenario with $\lambda'_{211} \neq 0$, as a function of the neutralino lifetime, see their Fig. 8. Superseded by AAD 13R.
- 30 ABZOV 12AD looked in 6.2 fb^{-1} of pp collisions at $\sqrt{s} = 1.96 \text{ TeV}$ for events with a photon, a Z -boson, and large \cancel{E}_T in the final state. This topology corresponds to a GMSB model where pairs of neutralino NLSPs are either pair produced promptly or from decays of other supersymmetric particles and then decay to either $Z\bar{G}$ or $\gamma\bar{G}$. No significant excess over the SM expectation is observed and a limit at 95% C.L. on the cross section is derived as a function of the effective SUSY breaking scale Λ , see Fig. 3. Assuming $N_{mes} = 2$, $M_{mes} = 3 \Lambda$, $\tan\beta = 3$, $\mu = 0.75 M_1$, and $C_{grav} = 1$, the model is excluded at 95% C.L. for values of $\Lambda < 87 \text{ TeV}$.
- 31 CHATRCHYAN 12BK searched in 2.23 fb^{-1} of pp collisions at $\sqrt{s} = 7 \text{ TeV}$ for events with two photons and large \cancel{E}_T due to $\tilde{\chi}_1^0 \rightarrow \gamma\bar{G}$ decays in a GMSB framework. No significant excess above the expected background was found and limits were set on the pair production of $\tilde{\chi}_1^0$ depending on the neutralino lifetime, see Fig. 6.
- 32 CHATRCHYAN 11B looked in 35 pb^{-1} of pp collisions at $\sqrt{s} = 7 \text{ TeV}$ for events with an isolated lepton (e or μ), a photon and \cancel{E}_T which may arise in a generalized gauge mediated model from the decay of Wino-like NLSPs. No evidence for an excess over the expected background is observed. Limits are derived in the plane of squark/gluino mass versus Wino mass (see Fig. 4). Mass degeneracy of the produced squarks and gluinos is assumed.
- 33 AALTONEN 10 searched in 2.6 fb^{-1} of $p\bar{p}$ collisions at $\sqrt{s} = 1.96 \text{ TeV}$ for diphoton events with large \cancel{E}_T . They may originate from the production of $\tilde{\chi}^\pm$ in pairs or associated to a $\tilde{\chi}_1^0$, decaying into $\tilde{\chi}_1^0$ which itself decays in GMSB to $\tilde{\chi}_1^0 \rightarrow \gamma\bar{G}$. There is no excess of events beyond expectation. An upper limit on the cross section is calculated in the GMSB model as a function of the $\tilde{\chi}_1^0$ mass and lifetime, see their Fig. 2. A limit is derived on the $\tilde{\chi}_1^0$ mass of 149 GeV for $\tau_{\tilde{\chi}_1^0} \ll 1 \text{ ns}$, which improves the results of previous searches.
- 34 ABZOV 10P looked in 6.3 fb^{-1} of $p\bar{p}$ collisions at $\sqrt{s} = 1.96 \text{ TeV}$ for events with at least two isolated γ s and large \cancel{E}_T . These could be the signature of $\tilde{\chi}_2^0$ and $\tilde{\chi}_1^\pm$ production, decaying to $\tilde{\chi}_1^0$ and finally $\tilde{\chi}_1^0 \rightarrow \gamma\bar{G}$ in a GMSB framework. No significant excess over the SM expectation is observed, and a limit at 95% C.L. on the cross section is derived for $N_{mes} = 1$, $\tan\beta = 15$ and $\mu > 0$, see their Fig. 2. This allows them to set a limit on the effective SUSY breaking scale $\Lambda > 124 \text{ TeV}$, from which the excluded $\tilde{\chi}_1^0$ mass range is obtained.
- 35 ABZOV 08F looked in 1.1 fb^{-1} of $p\bar{p}$ collisions at $\sqrt{s} = 1.96 \text{ TeV}$ for diphoton events with large \cancel{E}_T . They may originate from the production of $\tilde{\chi}^\pm$ in pairs or associated to a $\tilde{\chi}_1^0$, decaying to a $\tilde{\chi}_1^0$ which itself decays promptly in GMSB to $\tilde{\chi}_1^0 \rightarrow \gamma\bar{G}$. No significant excess was found compared to the background expectation. A limit is derived on the masses of SUSY particles in the GMSB framework for $M = 2\Lambda$, $N = 1$, $\tan\beta = 15$ and $\mu > 0$, see Figure 2. It also excludes $\Lambda < 91.5 \text{ TeV}$. Supersedes the results of ABZOV 05A. Superseded by ABZOV 10P.
- 36 ABULENCIA 07H searched in 346 pb^{-1} of $p\bar{p}$ collisions at $\sqrt{s} = 1.96 \text{ TeV}$ for events with at least three leptons (e or μ) from the decay of $\tilde{\chi}_1^0$ via $LL\bar{E}$ couplings. The results are consistent with the hypothesis of no signal. Upper limits on the cross-section are extracted and a limit is derived in the framework of mSUGRA on the masses of $\tilde{\chi}_1^0$ and $\tilde{\chi}_1^\pm$, see e.g. their Fig. 3 and Tab. II.
- 37 ABBIENDI 06b use 600 pb^{-1} of data from $\sqrt{s} = 189\text{--}209 \text{ GeV}$. They look for events with diphotons + \cancel{E} final states originating from prompt decays of pair-produced neutralinos in a GMSB scenario with $\tilde{\chi}_1^0$ NLSP. Limits on the cross-section are computed as a function of $m(\tilde{\chi}_1^0)$, see their Fig. 14. The limit on the $\tilde{\chi}_1^0$ mass is for a pure Bino state assuming a prompt decay, with lifetimes up to 10^{-9} s. Supersedes the results of ABBIENDI 04N.
- 38 ABDALLAH 05b use data from $\sqrt{s} = 180\text{--}209 \text{ GeV}$. They look for events with single photons + \cancel{E} final states. Limits are computed in the plane ($m(\tilde{G})$, $m(\tilde{\chi}_1^0)$), shown in their Fig. 9b for a pure Bino state in the GMSB framework and in Fig. 9c for a no-scale supergravity model. Supersedes the results of ABREU 00z.
- 39 ABDALLAH 05b use data from $\sqrt{s} = 130\text{--}209 \text{ GeV}$. They look for events with diphotons + \cancel{E} final states and single photons not pointing to the vertex, expected in GMSB when

See key on page 1127

Searches Particle Listings

Supersymmetric Particle Searches

the $\tilde{\chi}_1^0$ is the NLSP. Limits are computed in the plane $(m(\tilde{G}), m(\tilde{\chi}_1^0))$, see their Fig. 10. The lower limit is derived on the $\tilde{\chi}_1^0$ mass for a pure Bino state assuming a prompt decay and $m_{\tilde{e}_R} = m_{\tilde{e}_L} = 2 m_{\tilde{\chi}_1^0}$. It improves to 100 GeV for $m_{\tilde{e}_R} = m_{\tilde{e}_L} = 1.1 m_{\tilde{\chi}_1^0}$ and the limit in the plane $(m(\tilde{\chi}_1^0), m(\tilde{e}_R))$ is shown in Fig. 10b. For long-lived neutralinos, cross-section limits are displayed in their Fig 11. Supersedes the results of ABREU 00Z.

$\tilde{\chi}_2^0, \tilde{\chi}_3^0, \tilde{\chi}_4^0$ (Neutralinos) mass limits

Neutralinos are unknown mixtures of photinos, z-inos, and neutral higgsinos (the supersymmetric partners of photons and of Z and Higgs bosons). The limits here apply only to $\tilde{\chi}_2^0, \tilde{\chi}_3^0$, and $\tilde{\chi}_4^0$. $\tilde{\chi}_1^0$ is the lightest supersymmetric particle (LSP); see $\tilde{\chi}_1^0$ Mass Limits. It is not possible to quote rigorous mass limits because they are extremely model dependent; i.e. they depend on branching ratios of various $\tilde{\chi}^0$ decay modes, on the masses of decay products ($\tilde{e}, \tilde{\gamma}, \tilde{q}, \tilde{g}$), and on the \tilde{e} mass exchanged in $e^+e^- \rightarrow \tilde{\chi}_i^0 \tilde{\chi}_j^0$. Limits arise either from direct searches, or from the MSSM constraints set on the gaugino and higgsino mass parameters M_2 and μ through searches for lighter charginos and neutralinos. Often limits are given as contour plots in the $m_{\tilde{\chi}_0} - m_{\tilde{e}}$ plane vs other parameters. When specific assumptions are made, e.g. the neutralino is a pure photino ($\tilde{\gamma}$), pure z-ino (\tilde{Z}), or pure neutral higgsino (\tilde{H}^0), the neutralinos will be labelled as such.

Limits obtained from e^+e^- collisions at energies up to 136 GeV, as well as other limits from different techniques, are now superseded and have not been included in this compilation. They can be found in the 1998 Edition (The European Physical Journal **C3** 1 (1998)) of this Review. Some later papers are now obsolete and have been omitted. They were last listed in our PDG 14 edition: K. Olive, *et al.* (Particle Data Group), Chinese Physics **C38** 070001 (2014) (<http://pdg.lbl.gov>).

VALUE (GeV)	CL%	DOCUMENT ID	TECN	COMMENT
> 640	95	1 AAD	21BG ATLS	$3\ell + \cancel{E}_T$, Tchi1n2F, wino cross section, $m_{\tilde{\chi}_1^0} = 0$ GeV
> 300	95	1 AAD	21BG ATLS	$3\ell + \cancel{E}_T$, Tchi1n2F, wino cross section, $m_{\tilde{\chi}_2^0} - m_{\tilde{\chi}_1^0} = m_Z$
> 240	95	1 AAD	21BG ATLS	$3\ell + \cancel{E}_T$, Tchi1n2F, wino cross section, $m_{\tilde{\chi}_2^0} - m_{\tilde{\chi}_1^0} = 10$ GeV
> 195	95	1 AAD	21BG ATLS	$3\ell + \cancel{E}_T$, Tchi1n2Ga, higgsino cross section, $m_{\tilde{\chi}_2^0} - m_{\tilde{\chi}_1^0} = 10$ GeV
> 190	95	1 AAD	21BG ATLS	$3\ell + \cancel{E}_T$, Tchi1n2E, wino cross section, $m_{\tilde{\chi}_1^0} = 0$ GeV
>1600	95	2 AAD	21Y ATLS	$\geq 4\ell$, RPV Tchi1n2l with $\tilde{\chi}_1^0 \rightarrow \ell^\pm \ell^\mp \nu, \lambda_{12k} \neq 0, m_{\tilde{\chi}_1^0} = 1200$ GeV
>1100	95	2 AAD	21Y ATLS	$\geq 4\ell$, RPV Tchi1n2l with $\tilde{\chi}_1^0 \rightarrow \ell^\pm \ell^\mp \nu, \lambda_{i33} \neq 0, m_{\tilde{\chi}_1^0} = 1000$ GeV
> 750	95	3 SIRUNYAN	21M CMS	$\ell^\pm \ell^\mp + \cancel{E}_T$, Tchi1n2Fa, $m_{\tilde{\chi}_1^0} < 100$ GeV
none 400-820	95	4 TUMASYAN	21c CMS	$1 \ell^\pm + 2b$ -jets + \cancel{E}_T , Tchi1n2E, $\tilde{\chi}_1^0 = 200$ GeV
none 160-820	95	4 TUMASYAN	21c CMS	$1 \ell^\pm + 2b$ -jets + \cancel{E}_T , Tchi1n2E, $\tilde{\chi}_1^0 = 0$ GeV
> 380	95	5 AAD	20AN ATLS	$2\gamma + \cancel{E}_T$, Tn1n1A, GMSB
> 193	95	6 AAD	20I ATLS	2ℓ (soft), jets, \cancel{E}_T ; Tchi1n2Ga, higgsino, $m_{\tilde{\chi}_2^0} - m_{\tilde{\chi}_1^0} = 9.3$ GeV
> 240	95	7 AAD	20I ATLS	2ℓ (soft), jets, \cancel{E}_T ; Tchi1n2Fa, wino, $m_{\tilde{\chi}_2^0} - m_{\tilde{\chi}_1^0} = 7$ GeV
> 345	95	8 AAD	20K ATLS	$3\ell + \cancel{E}_T$, Tchi1n2F, $m_{\tilde{\chi}_1^0} = 0$ GeV
> 740	95	9 AAD	20R ATLS	$1\ell + 2b$ -jets + \cancel{E}_T , Tchi1n2E, $m_{\tilde{\chi}_1^0} = 0$ GeV
> 290	95	10 SIRUNYAN	20AU CMS	soft $\tau + \text{jet} + \cancel{E}_T$, Tchi1n2D, wino, $m_{\tilde{\chi}_1^+} - m_{\tilde{\chi}_1^0} = 50$ GeV
> 680	95	11 AABOUD	19AU ATL	0, 1, 2 or more ℓ , $H \rightarrow \gamma\gamma, bb, WW^*, ZZ^*, \tau\tau$ (various searches), Tchi1n2E, $m_{\tilde{\chi}_1^0} = 0$ GeV
> 112	95	12 SIRUNYAN	19BU CMS	$pp \rightarrow \tilde{\chi}_1^+ \tilde{\chi}_2^0 + 2$ jets, $\tilde{\chi}_2^0 \rightarrow \ell^+ \ell^- \tilde{\chi}_1^0$, heavy sleptons, $m_{\tilde{\chi}_2^0} - m_{\tilde{\chi}_1^0} = 1$ GeV, $m_{\tilde{\chi}_2^0} = \tilde{m}_{\tilde{\chi}_1^+}$
> 215	95	12 SIRUNYAN	19BU CMS	$pp \rightarrow \tilde{\chi}_1^+ \tilde{\chi}_2^0 + 2$ jets, $\tilde{\chi}_2^0 \rightarrow \ell^+ \ell^- \tilde{\chi}_1^0$, heavy sleptons, $m_{\tilde{\chi}_2^0} - m_{\tilde{\chi}_1^0} = 30$ GeV, $m_{\tilde{\chi}_2^0} = \tilde{m}_{\tilde{\chi}_1^+}$
> 760	95	13 AABOUD	18AY ATLS	$2\tau + \cancel{E}_T$, Tchi1n2D and $\tilde{\tau}_L$ -only, $m_{\tilde{\chi}_1^0} = 0$ GeV
>1125	95	14 AABOUD	18BT ATLS	$2,3\ell + \cancel{E}_T$, Tchi1n2C, $m_{\tilde{\chi}_1^0} = 0$ GeV
> 580	95	15 AABOUD	18BT ATLS	$2,3\ell + \cancel{E}_T$, Tchi1n2F, $m_{\tilde{\chi}_1^0} = 0$ GeV

none 130-230, 290-880	95	16 AABOUD	18CK ATLS	$2H \rightarrow bb + \cancel{E}_T$, Tn1n1A, GMSB
none 220-600	95	17 AABOUD	18CO ATLS	$2,3\ell + \cancel{E}_T$, recursive jigsaw, Tchi1n2F, $m_{\tilde{\chi}_1^0} = 0$ GeV
> 145	95	18 AABOUD	18R ATLS	2ℓ (soft) + \cancel{E}_T , Tchi1n2G, higgsino, $m_{\tilde{\chi}_2^0} - m_{\tilde{\chi}_1^0} = 5$ GeV
> 175	95	19 AABOUD	18R ATLS	2ℓ (soft) + \cancel{E}_T , Tchi1n2F, wino, $m_{\tilde{\chi}_2^0} - m_{\tilde{\chi}_1^0} = 10$ GeV
>1060	95	20 AABOUD	18U ATLS	$2\gamma + \cancel{E}_T$, GGM, Tchi1chi1A, any NLSP mass
> 167	95	21 SIRUNYAN	18AJ CMS	2ℓ (soft) + \cancel{E}_T , Tchi1n2G, higgsino, $m_{\tilde{\chi}_2^0} - m_{\tilde{\chi}_1^0} = 15$ GeV
> 710	95	22 SIRUNYAN	18DP CMS	$2\tau + \cancel{E}_T$, Tchi1n2D, $m_{\tilde{\chi}_1^0} = 0$ GeV
none 220-490	95	23 SIRUNYAN	17AW CMS	$1\ell + 2$ b-jets + \cancel{E}_T , Tchi1n2E, $m_{\tilde{\chi}_1^0} = 0$ GeV
> 600	95	24 AAD	16AA ATLS	$3,4\ell + \cancel{E}_T$, Tn2n3A, $m_{\tilde{\chi}_1^0} = 0$ GeV
> 670	95	24 AAD	16AA ATLS	$3,4\ell + \cancel{E}_T$, Tn2n3B, $m_{\tilde{\chi}_1^0} < 200$ GeV
> 250	95	25 AAD	15BA ATLS	$m_{\tilde{\chi}_1^\pm} = m_{\tilde{\chi}_2^0}, m_{\tilde{\chi}_1^0} = 0$ GeV
> 380	95	26 AAD	14H ATLS	$\tilde{\chi}_1^\pm \tilde{\chi}_2^0 \rightarrow \tau^\pm \nu \tilde{\chi}_1^0 \tau^\pm \tau^\mp \tilde{\chi}_1^0$, simplified model, $m_{\tilde{\chi}_1^\pm} = m_{\tilde{\chi}_2^0}, m_{\tilde{\chi}_1^0} = 0$ GeV
> 700	95	26 AAD	14H ATLS	$\tilde{\chi}_1^\pm \tilde{\chi}_2^0 \rightarrow \ell^\pm \nu \tilde{\chi}_1^0 \ell^\pm \ell^\mp \tilde{\chi}_1^0$, simplified model, $m_{\tilde{\chi}_1^\pm} = m_{\tilde{\chi}_2^0}, m_{\tilde{\chi}_1^0} = 0$ GeV
> 345	95	26 AAD	14H ATLS	$\tilde{\chi}_1^\pm \tilde{\chi}_2^0 \rightarrow W \tilde{\chi}_1^0 Z \tilde{\chi}_1^0$, simplified model, $m_{\tilde{\chi}_1^\pm} = m_{\tilde{\chi}_2^0}, m_{\tilde{\chi}_1^0} = 0$ GeV
> 148	95	26 AAD	14H ATLS	$\tilde{\chi}_1^\pm \tilde{\chi}_2^0 \rightarrow W \tilde{\chi}_1^0 H \tilde{\chi}_1^0$, simplified model, $m_{\tilde{\chi}_1^\pm} = m_{\tilde{\chi}_2^0}, m_{\tilde{\chi}_1^0} = 0$ GeV
> 620	95	27 AAD	14X ATLS	$\geq 4\ell^\pm, \tilde{\chi}_{2,3}^0 \rightarrow \ell^\pm \ell^\mp \tilde{\chi}_1^0, m_{\tilde{\chi}_1^0} = 0$ GeV
> 62.4	95	28 AAD	13 ATLS	$3\ell^\pm + \cancel{E}_T$, pMSSM, SMS
> 99.9	95	29 CHATARCHYAN	12BJ CMS	$\geq 2 \ell$, jets + \cancel{E}_T , $pp \rightarrow \tilde{\chi}_1^\pm \tilde{\chi}_2^0$
> 116.0	95	30 ABREU	00W DLPH	$\tilde{\chi}_2^0, 1 \leq \tan\beta \leq 40$, all Δm , all m_0
	95	30 ABREU	00W DLPH	$\tilde{\chi}_3^0, 1 \leq \tan\beta \leq 40$, all Δm , all m_0
	95	30 ABREU	00W DLPH	$\tilde{\chi}_4^0, 1 \leq \tan\beta \leq 40$, all Δm , all m_0
•••				We do not use the following data for averages, fits, limits, etc. •••
> 310	95	31 AAD	20AN ATLS	$2\gamma + \cancel{E}_T$, Tchi1n2E, $m_{\tilde{\chi}_1^0} = 0$ GeV
none 180-355	95	32 AAD	14G ATLS	$\tilde{\chi}_1^\pm \tilde{\chi}_2^0 \rightarrow W \tilde{\chi}_1^0 Z \tilde{\chi}_1^0$, simplified model, $m_{\tilde{\chi}_1^\pm} = m_{\tilde{\chi}_2^0}, m_{\tilde{\chi}_1^0} = 0$ GeV
		33 KHACHATRYAN	14I CMS	$\tilde{\chi}_2^0 \rightarrow (Z, H) \tilde{\chi}_1^0 \tilde{\ell} \tilde{\ell}$, simplified model
		34 AAD	12AS ATLS	$3\ell^\pm + \cancel{E}_T$, pMSSM
		35 AAD	12T ATLS	$\ell^\pm \ell^\pm + \cancel{E}_T, pp \rightarrow \tilde{\chi}_1^\pm \tilde{\chi}_2^0$

1 AAD 21BG searched in 139 fb⁻¹ of pp collisions at $\sqrt{s} = 13$ TeV for pair production $\tilde{\chi}_2^0 \tilde{\chi}_1^\pm$ in final states with three leptons, with and without assuming the presence of a $Z \rightarrow \ell\ell$ decay. No significant excess above the Standard Model predictions is observed. Limits are set on the $\tilde{\chi}_2^0$ and $\tilde{\chi}_1^\pm$ mass in Tchi1n2E, Tchi1n2F and Tchi1n2Ga. See their Fig. 16.

2 AAD 21Y searched in 139 fb⁻¹ of pp collisions at $\sqrt{s} = 13$ TeV for supersymmetry in events with four or more leptons (electrons, muons and tau-leptons). No significant excess above the Standard Model expectations is observed. Limits are set on Tchi1n2-GGM, and RPV models similar to Tchi1n2l, Tglu1A (with $q = u, d, s, c, b$, with equal branching fractions), and $\tilde{\ell}_L/\tilde{\nu} \rightarrow \ell/\nu \tilde{\chi}_1^0$ (mass-degenerate $\tilde{\ell}_L$ and $\tilde{\nu}$ of all 3 generations), all with $\tilde{\chi}_1^0 \rightarrow \ell^\pm \ell^\mp \nu$ via λ_{12k} or λ_{i33} (where $i, k \in 1, 2$), see their Figure 11.

3 SIRUNYAN 21M searched in 137 fb⁻¹ of pp collisions at $\sqrt{s} = 13$ TeV for supersymmetry in events with two opposite-sign same-flavor leptons (electrons, muons) and \cancel{E}_T . No significant excess above the Standard Model expectations is observed. Limits are set on the gluino mass in the simplified model Tglu4C, see their Figure 10, on the $\tilde{\chi}_2^0$ and $\tilde{\chi}_1^\pm$ mass in Tchi1n2Fa, see their Figure 11, on the $\tilde{\chi}_1^0$ mass in Tn1n1C and Tn1n1B for $m_{\tilde{\chi}_2^0} = m_{\tilde{\chi}_1^\pm} = m_{\tilde{\chi}_1^0}$, see their Figure 12. Limits are also set on the light squark mass for the simplified model Tsqk2A, on the sbottom mass in Tsb0t3, see their Figure 13, and on the slepton mass in direct electroweak pair production of mass-degenerate left- and right-handed sleptons (selectrons and smuons), see their Figure 14.

4 TUMASYAN 21C searched in 137 fb⁻¹ of pp collisions at $\sqrt{s} = 13$ TeV for supersymmetry in events with one lepton, a Higgs boson decaying to a pair of bottom quarks, and large \cancel{E}_T . No significant excess above the Standard Model expectations is observed. Lower limits are set on the masses of $\tilde{\chi}_2^0$ and $\tilde{\chi}_1^\pm$ in the simplified model Tchi1n2E, see their Figure 6.

5 AAD 20AN searched in 139 fb⁻¹ of pp collisions at $\sqrt{s} = 13$ TeV for events with two photons and missing transverse momentum. Events are further categorised in terms of lepton or jet multiplicity. No significant excess over the expected background is observed. Limits at 95% C.L. are set on the Higgsino mass in the Tn1n1A simplified model, see their Figure 11.

Searches Particle Listings

Supersymmetric Particle Searches

- 6 AAD 20i reported on ATLAS searches for electroweak production in models with compressed mass spectra as Tchi1n2Ga. A dataset of pp collisions at $\sqrt{s} = 13$ TeV corresponding to an integrated luminosity of 139 fb^{-1} was used. Events with \cancel{E}_T , two same-flavour, opposite-charge, low-transverse-momentum leptons, and jets from initial-state radiation or characteristic of vector-boson fusion production are selected. Constraints at 95% C.L. are placed in Higgsino models on the mass of the $\tilde{\chi}_2^0$ (the $\tilde{\chi}_1^{\pm}$ mass is halfway between the $\tilde{\chi}_2^0$ and $\tilde{\chi}_1^0$ masses) at 193 GeV for a mass splitting between $\tilde{\chi}_2^0$ and $\tilde{\chi}_1^0$ of 9.3 GeV and extend down to a mass splitting of 2.4 GeV at the LEP chargino mass limit. See their Fig. 14(a).
- 7 AAD 20i reported on ATLAS searches for electroweak production in models with compressed mass spectra as Tchi1n2Fa. A dataset of pp collisions at $\sqrt{s} = 13$ TeV corresponding to an integrated luminosity of 139 fb^{-1} was used. Events with \cancel{E}_T , two same-flavour, opposite-charge, low-transverse-momentum leptons, and jets from initial-state radiation or characteristic of vector-boson fusion production are selected. Constraints at 95% C.L. are placed in Wino-Bino models on the mass of the $\tilde{\chi}_2^0$ (degenerate with $\tilde{\chi}_1^{\pm}$) at 240 GeV for a mass splitting between $\tilde{\chi}_2^0$ and $\tilde{\chi}_1^0$ of 7 GeV and extend down to a mass splitting of 1.5 GeV at the LEP chargino mass limit of 92.4 GeV. See their Fig. 14(b,c).
- 8 AAD 20k reported on a search for electroweak production in models with mass splittings near the electroweak scale as Tchi1n2F and exploiting three-lepton final state events with an emulated recursive jigsaw reconstruction method. The analysis uses a dataset of pp collisions at $\sqrt{s} = 13$ TeV corresponding to an integrated luminosity of 139 fb^{-1} . Exclusion limits at 95% C.L. are derived on next-to-lightest neutralinos and charginos with masses up to 345 GeV for a massless lightest neutralino, see their Fig. 7.
- 9 AAD 20r searched for electroweak production in the model Tchi1n2E, selecting events with a pair of b -tagged jets consistent with those from a Higgs boson decay, either an electron or a muon from the W boson decay and \cancel{E}_T . The analysis uses a dataset of pp collisions at $\sqrt{s} = 13$ TeV corresponding to an integrated luminosity of 139 fb^{-1} . Exclusion limits at 95% C.L. are derived on next-to-lightest neutralinos and charginos with masses up to 740 GeV for a massless lightest neutralino, assuming pure wino cross-sections. See their Fig. 6.
- 10 SIRUNYAN 20AU searched in 77.2 fb^{-1} of pp collisions at $\sqrt{s} = 13$ TeV for events containing one soft, hadronically decaying tau lepton, one energetic jet from initial-state radiation, and large \cancel{E}_T . No excess over the expected background is observed. Limits are derived on the wino mass in the Tchi1n2D simplified model, see their Figure 2.
- 11 AABOUD 19AU searched in 36.1 fb^{-1} of pp collisions at $\sqrt{s} = 13$ TeV for direct electroweak production of charginos and next-to-lightest neutralinos decaying into lightest neutralinos and a W and a Higgs boson, respectively. Fully hadronic, semileptonic, diphoton, and multilepton (electrons, muons) final states with missing transverse momentum are considered in this search. Observations are consistent with the Standard Model expectations, and 95% confidence-level limits of up to 680 GeV on the chargino/next-to-lightest neutralino masses are set (Tchi1n2E model). See their Figure 14 for an overlay of exclusion contours from all searches.
- 12 SIRUNYAN 19BU searched for pair production of gauginos via vector boson fusion assuming the gaugino spectrum is compressed, in 35.9 fb^{-1} of pp collisions at $\sqrt{s} = 13$ TeV. The final states explored included zero leptons plus two jets, one lepton plus two jets, and one hadronic tau plus two jets. A similar bound is obtained in the light slepton limit.
- 13 AABOUD 18AY searched in 36.1 fb^{-1} of pp collisions at $\sqrt{s} = 13$ TeV for direct electroweak production of charginos and neutralinos as in Tchi1n2D models, in events characterised by the presence of at least two hadronically decaying tau leptons and large missing transverse energy. No significant deviation from the expected SM background is observed. Assuming decays via intermediate $\tilde{\tau}_L$ and $m_{\tilde{\chi}_1^{\pm}} = m_{\tilde{\chi}_2^0}$, the observed limits rule out $\tilde{\chi}_2^0$ masses up to 760 GeV for a massless $\tilde{\chi}_1^0$. See their Fig.7 (right). Interpretations are also provided in Fig 8 (bottom) for different assumptions on the ratio between $m_{\tilde{\tau}}$ and $m_{\tilde{\chi}_2^0} + m_{\tilde{\chi}_1^0}$.
- 14 AABOUD 18BT searched in 36.1 fb^{-1} of pp collisions at $\sqrt{s} = 13$ TeV for direct electroweak production of charginos, chargino and next-to-lightest neutralinos and sleptons in events with two or three leptons (electrons or muons), with or without jets, and large missing transverse energy. No significant excess above the Standard Model expectations is observed. Limits are set on the next-to-lightest neutralino mass up to 1100 GeV for massless $\tilde{\chi}_1^0$ in the Tchi1n2C simplified model exploiting the 3ℓ signature, see their Figure 8(c).
- 15 AABOUD 18BT searched in 36.1 fb^{-1} of pp collisions at $\sqrt{s} = 13$ TeV for direct electroweak production of charginos, chargino and next-to-lightest neutralinos and sleptons in events with two or three leptons (electrons or muons), with or without jets, and large missing transverse energy. No significant excess above the Standard Model expectations is observed. Limits are set on the next-to-lightest neutralino mass up to 580 GeV for massless $\tilde{\chi}_1^0$ in the Tchi1n2F simplified model exploiting the $2\ell+2$ jets and 3ℓ signatures, see their Figure 8(d).
- 16 AABOUD 18CK searched for events with at least 3 b -jets and large missing transverse energy in two datasets of pp collisions at $\sqrt{s} = 13$ TeV of 36.1 fb^{-1} and 24.3 fb^{-1} depending on the trigger requirements. The analyses aimed to reconstruct two Higgs bosons decaying to pairs of b -quarks. No significant excess above the Standard Model expectations is observed. Limits are set on the Higgsino mass in the T1n1A simplified model, see their Figure 15(a). Constraints are also presented as a function of the BR of Higgsino decaying into an higgs boson and a gravitino, see their Figure 15(b).
- 17 AABOUD 18CO searched in 36.1 fb^{-1} of pp collisions at $\sqrt{s} = 13$ TeV for direct electroweak production of mass-degenerate charginos and next-to-lightest neutralinos in events with two or three leptons (electrons or muons), with or without jets, and large missing transverse energy. The search channels are based on recursive jigsaw reconstruction. Limits are set on the next-to-lightest neutralinos mass up to 600 GeV for massless neutralinos in the Tchi1n2F simplified model exploiting the statistical combination of $2\ell+2$ jets and 3ℓ channels. Next-to-lightest neutralinos masses below 220 GeV are not excluded due to an excess of events above the SM prediction in the dedicated regions. See their Figure 13(d).
- 18 AABOUD 18R searched in 36.1 fb^{-1} of pp collisions at $\sqrt{s} = 13$ TeV for electroweak production in scenarios with compressed mass spectra in final states with two low-momentum leptons and missing transverse momentum. The data are found to be consistent with the SM prediction. Results are interpreted in Tchi1n2G higgsino models, and $\tilde{\chi}_2^0$ masses are excluded up to 145 GeV for $m_{\tilde{\chi}_2^0} - m_{\tilde{\chi}_1^0} = 5$ GeV. The exclusion limits extend down to mass splittings of 2.5 GeV, see their Fig. 10 (top). Results are also interpreted in terms of exclusion bounds on the production cross-sections for the NUHM2 scenario as a function of the universal gaugino mass $m_{1/2}$ and $m_{\tilde{\chi}_2^0} - m_{\tilde{\chi}_1^0}$, see their Fig. 12.
- 19 AABOUD 18R searched in 36.1 fb^{-1} of pp collisions at $\sqrt{s} = 13$ TeV for electroweak production in scenarios with compressed mass spectra in final states with two low-momentum leptons and missing transverse momentum. The data are found to be consistent with the SM prediction. Results are interpreted in Tchi1n2F wino models, and $\tilde{\chi}_2^0$ masses are excluded up to 175 GeV for $m_{\tilde{\chi}_2^0} - m_{\tilde{\chi}_1^0} = 10$ GeV. The exclusion limits extend down to mass splittings of 2 GeV, see their Fig. 10 (bottom). Results are also interpreted in terms of exclusion bounds on the production cross-sections for the NUHM2 scenario as a function of the universal gaugino mass $m_{1/2}$ and $m_{\tilde{\chi}_2^0} - m_{\tilde{\chi}_1^0}$, see their Fig. 12.
- 20 AABOUD 18U searched in 36.1 fb^{-1} of pp collisions at $\sqrt{s} = 13$ TeV in events with at least one isolated photon, possibly jets and significant transverse momentum targeting generalised models of gauge-mediated SUSY breaking. No significant excess of events is observed above the SM prediction. Results of the diphoton channel are interpreted in terms of lower limits on the masses of gauginos Tchi1ch1A models, which reach as high as 1.3 TeV. Gaugino masses below 1060 GeV are excluded for any NLSP mass, see their Fig. 10.
- 21 SIRUNYAN 18AU searched in 35.9 fb^{-1} of pp collisions at $\sqrt{s} = 13$ TeV for events containing two low-momentum, oppositely charged leptons (electrons or muons) and \cancel{E}_T . No excess over the expected background is observed. Limits are derived on the wino mass in the Tchi1n2F simplified model, see their Figure 5. Limits are also set on the stop mass in the Tstop10 simplified model, see their Figure 6. Finally, limits are set on the Higgsino mass in the Tchi1n2G simplified model, see Figure 8 and in the pMSSM, see Figure 7.
- 22 SIRUNYAN 18DP searched in 35.9 fb^{-1} of pp collisions at $\sqrt{s} = 13$ TeV for direct electroweak production of charginos and neutralinos or of chargino pairs in events with a tau lepton pair and significant missing transverse momentum. Both hadronic and leptonic decay modes are considered for the tau lepton. No significant excess above the Standard Model expectations is observed. Limits are set on the chargino mass in the Tchi1ch1D and Tchi1n2 simplified models, see their Figures 14 and 15. Also, excluded stau pair production cross sections are shown in Figures 11, 12, and 13.
- 23 SIRUNYAN 17AW searched in 35.9 fb^{-1} of pp collisions at $\sqrt{s} = 13$ TeV for events with a charged lepton (electron or muon), two jets identified as originating from a b -quark, and large \cancel{E}_T . No significant excess above the Standard Model expectations is observed. Limits are set on the mass of the chargino and the next-to-lightest neutralino in the Tchi1n2E simplified model, see their Figure 6.
- 24 AAD 16AA summarized and extended ATLAS searches for electroweak supersymmetry in final states containing several charged leptons, \cancel{E}_T , with or without hadronic jets, in 20 fb^{-1} of pp collisions at $\sqrt{s} = 8$ TeV. The paper reports the results of new interpretations and statistical combinations of previously published analyses, as well as new analyses. Exclusion limits at 95% C.L. are set on mass-degenerate $\tilde{\chi}_2^0$ and $\tilde{\chi}_3^0$ masses in the Tn2n3A and Tn2n3B simplified models. See their Fig. 15.
- 25 AAD 15BA searched in 20.3 fb^{-1} of pp collisions at $\sqrt{s} = 8$ TeV for electroweak production of charginos and neutralinos decaying to a final state containing a W boson and a 125 GeV Higgs boson, plus missing transverse momentum. No excess beyond the Standard Model expectation is observed. Exclusion limits are derived in simplified models of direct chargino and next-to-lightest neutralino production, with the decays $\tilde{\chi}_1^{\pm} \rightarrow W^{\pm} \tilde{\chi}_1^0$ and $\tilde{\chi}_2^0 \rightarrow H \tilde{\chi}_1^0$ having 100% branching fraction, see Fig. 8. A combination of the multiple final states for the Higgs decay yields the best limits (Fig. 8d).
- 26 AAD 14H searched in 20.3 fb^{-1} of pp collisions at $\sqrt{s} = 8$ TeV for electroweak production of charginos and neutralinos decaying to a final state with three leptons and missing transverse momentum. No excess beyond the Standard Model expectation is observed. Exclusion limits are derived in simplified models of direct chargino and next-to-lightest neutralino production, with decays to the lightest neutralino via either all three generations of leptons, staus only, gauge bosons, or Higgs bosons, see Fig. 7. An interpretation in the pMSSM is also given, see Fig. 8.
- 27 AAD 14X searched in 20.3 fb^{-1} of pp collisions at $\sqrt{s} = 8$ TeV for events with at least four leptons (electrons, muons, taus) in the final state. No significant excess above the Standard Model expectations is observed. Limits are set on the neutralino mass in an R-parity conserving simplified model where the decay $\tilde{\chi}_{2,3}^0 \rightarrow \ell^{\pm} \ell^{\mp} \tilde{\chi}_1^0$ takes place with a branching ratio of 100%, see Fig. 10.
- 28 AAD 13 searched in 4.7 fb^{-1} of pp collisions at $\sqrt{s} = 7$ TeV for charginos and neutralinos decaying to a final state with three leptons (e and μ) and missing transverse energy. No excess beyond the Standard Model expectation is observed. Exclusion limits are derived in the phenomenological MSSM, see Fig. 2 and 3, and in simplified models, see Fig. 4. For the simplified models with intermediate slepton decays, degenerate $\tilde{\chi}_1^{\pm}$ and $\tilde{\chi}_2^0$ masses up to 500 GeV are excluded at 95% C.L. for very large mass differences with the $\tilde{\chi}_1^0$. Supersedes AAD 12AS.
- 29 CHATRCHYAN 12BJ searched in 4.98 fb^{-1} of pp collisions at $\sqrt{s} = 7$ TeV for direct electroweak production of charginos and neutralinos in events with at least two leptons, jets and missing transverse momentum. No significant excesses over the expected SM backgrounds are observed and 95% C.L. limits on the production cross section of $\tilde{\chi}_1^{\pm} \tilde{\chi}_2^0$ pair production were set in a number of simplified models, see Figs. 7 to 12. Most limits are for exactly 3 jets.
- 30 ABREU 00w combines data collected at $\sqrt{s}=189$ GeV with results from lower energies. The mass limit is obtained by constraining the MSSM parameter space with gaugino and fermion mass universality at the GUT scale, using the results of negative direct searches for neutralinos (including cascade decays and $\tilde{\tau}$ final states) from ABREU 01, for charginos from ABREU 00j and ABREU 00t (for all Δm_{\pm}), and for charged sleptons from ABREU 01b. The results hold for the full parameter space defined by all values of M_2 and $|\mu| \leq 2$ TeV with the $\tilde{\chi}_1^0$ as LSP.
- 31 AAD 20AN searched in 139 fb^{-1} of pp collisions at $\sqrt{s} = 13$ TeV for events with two photons and missing transverse momentum. Events are further categorised in terms of lepton or jet multiplicity. No significant excess over the expected background is observed. Limits at 95% C.L. are derived in Tchi1n2E simplified models. Next-to-lightest neutralinos and charginos with masses up to 310 GeV for a massless lightest neutralino are excluded. See their Fig. 10.
- 32 AAD 14c searched in 20.3 fb^{-1} of pp collisions at $\sqrt{s} = 8$ TeV for electroweak production of chargino-neutralino pairs, decaying to a final state with two leptons (e and μ) and missing transverse momentum. No excess beyond the Standard Model expectation is

observed. Exclusion limits are derived in simplified models of chargino and next-to-lightest neutralino production, with decays to the lightest neutralino via gauge bosons, see Fig. 7. An interpretation in the pMSSM is also given, see Fig. 10.

³³ KHACHATRYAN 14i searched in 19.5 fb^{-1} of pp collisions at $\sqrt{s} = 8 \text{ TeV}$ for electroweak production of charginos and neutralinos decaying to a final state with three leptons (e or μ) and missing transverse momentum, or with a Z-boson, dijets and missing transverse momentum. No excess beyond the Standard Model expectation is observed. Exclusion limits are derived in simplified models, see Figs. 12–16.

³⁴ AAD 12As searched in 2.06 fb^{-1} of pp collisions at $\sqrt{s} = 7 \text{ TeV}$ for charginos and neutralinos decaying to a final state with three leptons (e and μ) and missing transverse energy. No excess beyond the Standard Model expectation is observed. Exclusion limits are derived in the phenomenological MSSM, see Fig. 2 (top), and in simplified models, see Fig. 2 (bottom).

³⁵ AAD 12T looked in 1 fb^{-1} of pp collisions at $\sqrt{s} = 7 \text{ TeV}$ for the production of supersymmetric particles decaying into final states with missing transverse momentum and exactly two isolated leptons (e or μ). Same-sign dilepton events were separately studied. Additionally, in opposite-sign events, a search was made for an excess of same-flavor over different-flavor lepton pairs. No excess over the expected background is observed and limits are placed on the effective production cross section of opposite-sign dilepton events with $E_T > 250 \text{ GeV}$ and on same-sign dilepton events with $E_T > 100 \text{ GeV}$. The latter limit is interpreted in a simplified electroweak gaugino production model.

$\tilde{\chi}_1^\pm, \tilde{\chi}_2^\pm$ (Charginos) mass limits

Charginos are unknown mixtures of w-inos and charged higgsinos (the supersymmetric partners of W and Higgs bosons). A lower mass limit for the lightest chargino ($\tilde{\chi}_1^\pm$) of approximately 45 GeV, independent of the field composition and of the decay mode, has been obtained by the LEP experiments from the analysis of the Z width and decays. These results, as well as other now superseded limits from e^+e^- collisions at energies below 136 GeV, and from hadronic collisions, can be found in the 1998 Edition (The European Physical Journal **C3** 1 (1998)) of this Review.

Unless otherwise stated, results in this section assume spectra, production rates, decay modes and branching ratios as evaluated in the MSSM, with gaugino and stfermion mass unification at the GUT scale. These papers generally study production of $\tilde{\chi}_1^0 \tilde{\chi}_2^0, \tilde{\chi}_1^+ \tilde{\chi}_1^-$ and (in the case of hadronic collisions) $\tilde{\chi}_1^+ \tilde{\chi}_2^0$ pairs, including the effects of cascade decays. The mass limits on $\tilde{\chi}_1^\pm$ are either direct, or follow indirectly from the constraints set by the non-observation of $\tilde{\chi}_2^0$ states on the gaugino and higgsino MSSM parameters M_2 and μ . For generic values of the MSSM parameters, limits from high-energy e^+e^- collisions coincide with the highest value of the mass allowed by phase-space, namely $m_{\tilde{\chi}_1^\pm} \lesssim \sqrt{s}/2$. The still unpublished combination of the results of the four LEP collaborations from the 2000 run of LEP2 at \sqrt{s} up to $\approx 209 \text{ GeV}$ yields a lower mass limit of 103.5 GeV valid for general MSSM models. The limits become however weaker in certain regions of the MSSM parameter space where the detection efficiencies or production cross sections are suppressed. For example, this may happen when: (i) the mass differences $\Delta m_{\pm} = m_{\tilde{\chi}_1^\pm} - m_{\tilde{\chi}_2^0}$ or $\Delta m_{\nu} = m_{\tilde{\chi}_1^\pm} - m_{\tilde{\nu}}$ are very small, and the detection efficiency is reduced; (ii) the electron sneutrino mass is small, and the $\tilde{\chi}_1^\pm$ production rate is suppressed due to a destructive interference between s and t channel exchange diagrams. The regions of MSSM parameter space where the following limits are valid are indicated in the comment lines or in the footnotes.

Some earlier papers are now obsolete and have been omitted. They were last listed in our PDG 14 edition: K. Olive, *et al.* (Particle Data Group), Chinese Physics **C38** 070001 (2014) (<http://pdg.lbl.gov>).

VALUE (GeV)	CL%	DOCUMENT ID	TECN	COMMENT
>1080	95	1 AAD	21Ax ATLS	jets + large-R jets + E_T , TWinoBinoA, nearly independent of $B(\tilde{\chi}_2^0 \rightarrow Z\tilde{\chi}_1^0), m_{\tilde{\chi}_1^0} = 0 \text{ GeV}$
>1060	95	1 AAD	21Ax ATLS	jets + large-R jets + E_T , TWinoHinoA, $\tan \beta = 10, \mu > 0, m_{\tilde{\chi}_1^0} = 0 \text{ GeV}$
> 900	95	1 AAD	21Ax ATLS	jets + large-R jets + E_T , THinoBinoA, nearly independent of $B(\tilde{\chi}_2^0 \rightarrow Z\tilde{\chi}_1^0), m_{\tilde{\chi}_1^0} = 0 \text{ GeV}$
> 900	95	1 AAD	21Ax ATLS	jets + large-R jets + E_T , THinoWinoA, $\tan \beta = 10, \mu > 0, m_{\tilde{\chi}_1^0} = 0 \text{ GeV}$
>1060	95	1 AAD	21Ax ATLS	jets + large-R jets + E_T , Tchi1n2E, full hadronic final state, $m_{\tilde{\chi}_1^0} = 0 \text{ GeV}$
> 960	95	1 AAD	21Ax ATLS	jets + large-R jets + E_T , Tchi1n2Fb, $m_{\tilde{\chi}_1^0} = 0 \text{ GeV}$
none 620–740	95	1 AAD	21Ax ATLS	jets + large-R jets + E_T , Tchi1chi1l, $m_{\tilde{\chi}_1^0} = 0 \text{ GeV}$
> 640	95	2 AAD	21Bg ATLS	$3\ell + E_T$, Tchi1n2F, wino cross section, $m_{\tilde{\chi}_1^0} = 0 \text{ GeV}$
> 300	95	2 AAD	21Bg ATLS	$3\ell + E_T$, Tchi1n2F, wino cross section, $m_{\tilde{\chi}_2^0} - m_{\tilde{\chi}_1^0} = m_Z$
> 240	95	2 AAD	21Bg ATLS	$3\ell + E_T$, Tchi1n2F, wino cross section, $m_{\tilde{\chi}_2^0} - m_{\tilde{\chi}_1^0} = 10 \text{ GeV}$
> 190	95	2 AAD	21Bg ATLS	$3\ell + E_T$, Tchi1n2E, wino cross section, $m_{\tilde{\chi}_1^0} = 0 \text{ GeV}$

>1100	95	3 AAD	21E ATLS	$3\ell, Z\ell$ resonances, TWinoL-SPBL, RPV, $B(\tilde{\chi}_1^\pm \rightarrow Z e) = B(\tilde{\chi}_1^0 \rightarrow Z \nu) = 1$
>1050	95	3 AAD	21E ATLS	$3\ell, Z\ell$ resonances, TWinoL-SPBL, RPV, $B(\tilde{\chi}_1^\pm \rightarrow Z \mu) = B(\tilde{\chi}_1^0 \rightarrow Z \nu) = 1$
> 625	95	3 AAD	21E ATLS	$3\ell, Z\ell$ resonances, TWinoL-SPBL, RPV, $B(\tilde{\chi}_1^\pm \rightarrow Z \tau) = B(\tilde{\chi}_1^0 \rightarrow Z \nu) = 1$
> 975	95	3 AAD	21E ATLS	$3\ell, Z\ell$ resonances, TWinoL-SPBL, RPV, $B(\tilde{\chi}_1^\pm \rightarrow Z \ell) = B(\tilde{\chi}_1^0 \rightarrow Z \nu) = 1$ and $\ell = e, \mu, \tau$
>1600	95	4 AAD	21Y ATLS	$\geq 4\ell$, RPV Tchi1n2l with $\tilde{\chi}_1^0 \rightarrow \ell^\pm \ell^\mp \nu, \lambda_{12k} \neq 0, m_{\tilde{\chi}_1^0} = 1200 \text{ GeV}$
>1100	95	4 AAD	21Y ATLS	$\geq 4\ell$, RPV Tchi1n2l with $\tilde{\chi}_1^0 \rightarrow \ell^\pm \ell^\mp \nu, \lambda_{133} \neq 0, m_{\tilde{\chi}_1^0} = 1000 \text{ GeV}$
> 750	95	5 SIRUNYAN	21M CMS	$\ell^\pm \ell^\mp + E_T$, Tchi1n2Fa, $m_{\tilde{\chi}_1^0} < 100 \text{ GeV}$
none 400–820	95	6 TUMASYAN	21c CMS	$1 \ell^\pm + 2b\text{-jets} + E_T$, Tchi1n2E, $\tilde{\chi}_1^0 = 200 \text{ GeV}$
none 160–820	95	6 TUMASYAN	21c CMS	$1 \ell^\pm + 2b\text{-jets} + E_T$, Tchi1n2E, $\tilde{\chi}_1^0 = 0 \text{ GeV}$
> 380	95	7 AAD	20An ATLS	$2\gamma + E_T$, Tn1n1A, GMSB
> 240	95	8 AAD	20l ATLS	2ℓ (soft), jets, E_T ; Tchi1n2Fa, wino, $m_{\tilde{\chi}_1^\pm} - m_{\tilde{\chi}_1^0} = 7 \text{ GeV}$
> 345	95	9 AAD	20k ATLS	$3\ell + E_T$, Tchi1n2F, $m_{\tilde{\chi}_1^0} = 0 \text{ GeV}$
> 420	95	10 AAD	20o ATLS	$2\ell + E_T$, Tchi1chi1H, $m_{\tilde{\chi}_1^0} = 0 \text{ GeV}$
>1000	95	11 AAD	20o ATLS	$2\ell + E_T$, Tchi1chi1C, $m_{\tilde{\chi}_1^0} = 0 \text{ GeV}$
> 740	95	12 AAD	20R ATLS	$1\ell + 2b\text{-jets} + E_T$, Tchi1n2E, $m_{\tilde{\chi}_1^0} = 0 \text{ GeV}$
> 290	95	13 SIRUNYAN	20Au CMS	soft $\tau + \text{jet} + E_T$, Tchi1n2D, wino, $m_{\tilde{\chi}_1^\pm} - m_{\tilde{\chi}_1^0} = 50 \text{ GeV}$
>1050	95	14 SIRUNYAN	20B CMS	$\geq 1\gamma + E_T$, Tchi1chi1F, $\tilde{\chi}_1^0 \rightarrow \gamma \tilde{G}$
> 825	95	14 SIRUNYAN	20B CMS	$\geq 1\gamma + E_T$, Tchi1chi1G, $\tilde{\chi}_1^\pm \rightarrow \tilde{\chi}_1^0 + \text{soft}$
> 840	95	14 SIRUNYAN	20B CMS	$\geq 1\gamma + E_T$, Tchi1n12-GGM, $120 \text{ GeV} < m_{\tilde{\chi}_1^0} < 720 \text{ GeV}$
> 680	95	15 AABOUD	19Au ATL	0, 1, 2 or more $\ell, H (\rightarrow \gamma\gamma, b\bar{b}, W W^*, Z Z^*, \tau\tau)$ (various searches), Tchi1n2E, $m_{\tilde{\chi}_1^0} = 0 \text{ GeV}$
> 112	95	16 SIRUNYAN	19Bu CMS	$pp \rightarrow \tilde{\chi}_1^+ \tilde{\chi}_2^0 + 2\text{jets}, \tilde{\chi}_1^+ \rightarrow \ell^+ \nu \tilde{\chi}_1^0$, heavy sleptons, $m_{\tilde{\chi}_1^\pm} - m_{\tilde{\chi}_1^0} = 1 \text{ GeV}, m_{\tilde{\chi}_1^+} = m_{\tilde{\chi}_2^0}$
> 215	95	16 SIRUNYAN	19Bu CMS	$pp \rightarrow \tilde{\chi}_1^+ \tilde{\chi}_2^0 + 2\text{jets}, \tilde{\chi}_1^+ \rightarrow \ell^+ \nu \tilde{\chi}_1^0$, heavy sleptons, $m_{\tilde{\chi}_1^\pm} - m_{\tilde{\chi}_1^0} = 30 \text{ GeV}, m_{\tilde{\chi}_1^+} = m_{\tilde{\chi}_2^0}$
> 235	95	17 SIRUNYAN	19Ci CMS	$\geq 1 H (\rightarrow \gamma\gamma) + \text{jets} + E_T$, Tchi1n2E, $m_{\tilde{\chi}_1^0} = 1 \text{ GeV}$
> 930	95	18 SIRUNYAN	19K CMS	$\gamma + \text{lepton} + E_T$, Tchi1n1A
> 630	95	19 AABOUD	18Ay ATLS	$2\tau + E_T$, Tchi1chi1D and $\tilde{\tau}_L$ -only, $m_{\tilde{\chi}_1^0} = 0 \text{ GeV}$
> 760	95	20 AABOUD	18Ay ATLS	$2\tau + E_T$, Tchi1n2D and $\tilde{\tau}_L$ -only, $m_{\tilde{\chi}_1^0} = 0 \text{ GeV}$
> 740	95	21 AABOUD	18Bt ATLS	$2\ell + E_T$, Tchi1chi1C, $m_{\tilde{\chi}_1^0} = 0 \text{ GeV}$
>1125	95	22 AABOUD	18Bt ATLS	$2,3\ell + E_T$, Tchi1n2C, $m_{\tilde{\chi}_1^0} = 0 \text{ GeV}$
> 580	95	23 AABOUD	18Bt ATLS	$2,3\ell + E_T$, Tchi1n2F, $m_{\tilde{\chi}_1^0} = 0 \text{ GeV}$
none 130–230, 290–880	95	24 AABOUD	18Ck ATLS	$2H (\rightarrow b\bar{b}) + E_T$, Tn1n1A, GMSB
none 220–600	95	25 AABOUD	18Co ATLS	$2,3\ell + E_T$, recursive jigsaw, Tchi1n2F, $m_{\tilde{\chi}_1^0} = 0 \text{ GeV}$
> 175	95	26 AABOUD	18R ATLS	2ℓ (soft) + E_T , Tchi1n2F, wino, $m_{\tilde{\chi}_1^\pm} - m_{\tilde{\chi}_1^0} = 10 \text{ GeV}$
> 145	95	27 AABOUD	18R ATLS	2ℓ (soft) + E_T , Tchi1n2G, higgsino, $m_{\tilde{\chi}_1^\pm} - m_{\tilde{\chi}_1^0} = 5 \text{ GeV}$
>1060	95	28 AABOUD	18U ATLS	$2\gamma + E_T$, GGM, Tchi1chi1A, any NLSF mass

Searches Particle Listings

Supersymmetric Particle Searches

>1400	95	29	AABOUD	18Z ATLS	$\geq 4\ell$, RPV, $\lambda_{12k} \neq 0$, $m_{\tilde{\chi}_1^0} > 500$ GeV	none	95	44	AAD	15CA ATLS	$\geq 1 \gamma + e, \mu + \cancel{E}_T$, GGM, wino-like NLSP
>1320	95	29	AABOUD	18Z ATLS	$\geq 4\ell$, RPV, $\lambda_{12k} \neq 0$, $m_{\tilde{\chi}_1^0} > 400$ GeV	> 700	95	45	AAD	14H ATLS	$\tilde{\chi}_1^{\pm} \tilde{\chi}_2^0 \rightarrow \ell^{\pm} \nu \tilde{\chi}_1^0 \ell^{\pm} \tilde{\chi}_1^0$, simplified model, $m_{\tilde{\chi}_1^{\pm}} = m_{\tilde{\chi}_2^0}$, $m_{\tilde{\chi}_1^0} = 0$ GeV
> 980	95	29	AABOUD	18Z ATLS	$\geq 4\ell$, RPV, $\lambda_{j33} \neq 0$, 400 GeV < $m_{\tilde{\chi}_1^0} < 700$ GeV	> 345	95	45	AAD	14H ATLS	$\tilde{\chi}_1^{\pm} \tilde{\chi}_2^0 \rightarrow W \tilde{\chi}_1^0 Z \tilde{\chi}_1^0$, simplified model, $m_{\tilde{\chi}_1^{\pm}} = m_{\tilde{\chi}_2^0}$, $m_{\tilde{\chi}_1^0} = 0$ GeV
> 980	95	30	SIRUNYAN	18AA CMS	$\geq 1\gamma + \cancel{E}_T$, GGM, wino-like $\tilde{\chi}_2^0 \tilde{\chi}_1^{\pm}$ pair production, nearly degenerate wino and bino masses	> 148	95	45	AAD	14H ATLS	$\tilde{\chi}_1^{\pm} \tilde{\chi}_2^0 \rightarrow W \tilde{\chi}_1^0 H \tilde{\chi}_1^0$, simplified model, $m_{\tilde{\chi}_1^{\pm}} = m_{\tilde{\chi}_2^0}$, $m_{\tilde{\chi}_1^0} = 0$ GeV
> 780	95	30	SIRUNYAN	18AA CMS	$\geq 1\gamma + \cancel{E}_T$, Tchi1n1A	> 380	95	45	AAD	14H ATLS	$\tilde{\chi}_1^{\pm} \tilde{\chi}_2^0 \rightarrow \tau^{\pm} \nu \tilde{\chi}_1^0 \tau^{\pm} \tilde{\chi}_1^0$, simplified model, $m_{\tilde{\chi}_1^{\pm}} = m_{\tilde{\chi}_2^0}$, $m_{\tilde{\chi}_1^0} = 0$ GeV
> 950	95	30	SIRUNYAN	18AA CMS	$\geq 1\gamma + \cancel{E}_T$, Tchi1chi1A	> 750	95	46	AAD	14X ATLS	RPV, $\geq 4\ell^{\pm}$, $\tilde{\chi}_1^{\pm} \rightarrow W^{(*)\pm} \tilde{\chi}_1^0$, $\tilde{\chi}_1^0 \rightarrow \ell^{\pm} \tilde{\chi}_1^{\mp} \nu$
> 230	95	31	SIRUNYAN	18AJ CMS	2ℓ (soft) + \cancel{E}_T , Tchi1n2F, wino, $m_{\tilde{\chi}_2^0} - m_{\tilde{\chi}_1^0} = 20$ GeV	> 210	95	47	KHACHATRY...14L	CMS	$\tilde{\chi}_2^0 \rightarrow H \tilde{\chi}_1^0$ and $\tilde{\chi}_1^{\pm} \rightarrow W^{\pm} \tilde{\chi}_1^0$ simplified models, $m_{\tilde{\chi}_2^0} = m_{\tilde{\chi}_1^{\pm}}$, $m_{\tilde{\chi}_1^0} = 0$ GeV
>1150	95	32	SIRUNYAN	18AO CMS	$\ell^{\pm} \ell^{\pm}$ or $\geq 3\ell$, Tchi1n2A, $m_{\tilde{\ell}} = m_{\tilde{\nu}} = m_{\tilde{\chi}_1^0} + 0.5 (m_{\tilde{\chi}_1^{\pm}} - m_{\tilde{\chi}_1^0})$, $m_{\tilde{\chi}_1^0} = 0$ GeV	> 540	95	48	AAD	13 ATLS	$3\ell^{\pm} + \cancel{E}_T$, pMSSM, SMS
>1120	95	32	SIRUNYAN	18AO CMS	$\ell^{\pm} \ell^{\pm}$ or $\geq 3\ell$, Tchi1n2A, $m_{\tilde{\ell}} = m_{\tilde{\nu}} = m_{\tilde{\chi}_1^0} + 0.05 (m_{\tilde{\chi}_1^{\pm}} - m_{\tilde{\chi}_1^0})$, $m_{\tilde{\chi}_1^0} = 0$ GeV	> 540	95	49	AAD	13B ATLS	$2\ell^{\pm} + \cancel{E}_T$, pMSSM, SMS
>1050	95	32	SIRUNYAN	18AO CMS	$\ell^{\pm} \ell^{\pm}$ or $\geq 3\ell$, Tchi1n2A, $m_{\tilde{\ell}} = m_{\tilde{\nu}} = m_{\tilde{\chi}_1^0} + 0.95 (m_{\tilde{\chi}_1^{\pm}} - m_{\tilde{\chi}_1^0})$, $m_{\tilde{\chi}_1^0} = 0$ GeV	> 540	95	50	AAD	12CT ATLS	$\geq 4\ell^{\pm}$, RPV, $m_{\tilde{\chi}_1^0} > 300$ GeV
>1080	95	32	SIRUNYAN	18AO CMS	$\ell^{\pm} \ell^{\pm}$ or $\geq 3\ell$, Tchi1n2H, $m_{\tilde{\ell}} = m_{\tilde{\chi}_1^0} + 0.5 (m_{\tilde{\chi}_1^{\pm}} - m_{\tilde{\chi}_1^0})$, $m_{\tilde{\chi}_1^0} = 0$ GeV	> 94	95	51	CHATRCHYAN12BJ	CMS	$\geq 2\ell$, jets + \cancel{E}_T , $\Delta p \rightarrow \tilde{\chi}_1^{\pm} \tilde{\chi}_2^0$
>1030	95	32	SIRUNYAN	18AO CMS	$\ell^{\pm} \ell^{\pm}$ or $\geq 3\ell$, Tchi1n2H, $m_{\tilde{\ell}} = m_{\tilde{\chi}_1^0} + 0.05 (m_{\tilde{\chi}_1^{\pm}} - m_{\tilde{\chi}_1^0})$, $m_{\tilde{\chi}_1^0} = 0$ GeV	> 310	95	52	ABDALLAH	03M DLPH	$\tilde{\chi}_1^{\pm}$, $\tan\beta \leq 40$, $\Delta p_{\pm} > 3$ GeV, all m_0
>1050	95	32	SIRUNYAN	18AO CMS	$\ell^{\pm} \ell^{\pm}$ or $\geq 3\ell$, Tchi1n2H, $m_{\tilde{\ell}} = m_{\tilde{\chi}_1^0} + 0.95 (m_{\tilde{\chi}_1^{\pm}} - m_{\tilde{\chi}_1^0})$, $m_{\tilde{\chi}_1^0} = 0$ GeV	> 570	95	53	AAD	20AN ATLS	$2\gamma + \cancel{E}_T$, Tchi1n2E, $m_{\tilde{\chi}_1^0} = 0$ GeV
> 625	95	32	SIRUNYAN	18AO CMS	$\ell^{\pm} \ell^{\pm}$ or $\geq 3\ell$, Tchi1n2D, $m_{\tilde{\ell}} = m_{\tilde{\chi}_1^0} + 0.5 (m_{\tilde{\chi}_1^{\pm}} - m_{\tilde{\chi}_1^0})$, $m_{\tilde{\chi}_1^0} = 0$ GeV	> 680	95	54	KHACHATRY...16AA	CMS	$\geq 1\gamma$ + jets + \cancel{E}_T , Tchi1chi1A
> 180	95	32	SIRUNYAN	18AO CMS	$\ell^{\pm} \ell^{\pm}$ or $\geq 3\ell$, Tchi1n2E, $m_{\tilde{\chi}_1^0} = 0$ GeV	> 710	95	54	KHACHATRY...16AA	CMS	$\geq 1\gamma$ + jets + \cancel{E}_T , GGM, $\tilde{\chi}_2^0 \tilde{\chi}_1^{\pm}$ pair production, wino-like NLSP
> 450	95	32	SIRUNYAN	18AO CMS	$\ell^{\pm} \ell^{\pm}$ or $\geq 3\ell$, Tchi1n2F, $m_{\tilde{\chi}_1^0} = 0$ GeV	>1000	95	55	KHACHATRY...16R	CMS	$\geq 1\gamma + 1 e$ or $\mu + \cancel{E}_T$, Tglu1F, $m_{\tilde{\chi}_1^{\pm}} = m_{\tilde{\chi}_2^0} > 200$ GeV
> 480	95	33	SIRUNYAN	18AP CMS	Combination of searches, Tchi1n2E, $m_{\tilde{\chi}_1^0} = 0$ GeV	> 307	95	56	KHACHATRY...16Y	CMS	1,2 soft ℓ^{\pm} + jets + \cancel{E}_T , Tchi1n2A, $m_{\tilde{\chi}_1^{\pm}} - m_{\tilde{\chi}_1^0} = 20$ GeV
> 650	95	33	SIRUNYAN	18AP CMS	Combination of searches, Tchi1n2F, $m_{\tilde{\chi}_1^0} = 0$ GeV	> 410	95	57	AAD	14AV ATLS	$\geq 2\tau + \cancel{E}_T$, direct $\tilde{\chi}_1^{\pm} \tilde{\chi}_2^0$, $\tilde{\chi}_1^{\pm} \tilde{\chi}_1^{\mp}$ production, $m_{\tilde{\chi}_2^0} = m_{\tilde{\chi}_1^{\pm}}$, $m_{\tilde{\chi}_1^0} = 0$ GeV
> 535	95	33	SIRUNYAN	18AP CMS	Combination of searches, Tchi1n2I, $m_{\tilde{\chi}_1^0} = 0$ GeV	> 345	95	58	AAD	14AV ATLS	$\geq 2\tau + \cancel{E}_T$, direct $\tilde{\chi}_1^{\pm} \tilde{\chi}_1^{\mp}$ production, $m_{\tilde{\chi}_1^0} = 0$ GeV
none 160-610	95	34	SIRUNYAN	18AR CMS	$\ell^{\pm} \ell^{\mp}$ + jets + \cancel{E}_T , Tchi1n2F, $m_{\tilde{\chi}_1^0} = 0$ GeV	none 100-105, 120-135, 145-160	95	59	AAD	14G ATLS	$\tilde{\chi}_1^{\pm} \tilde{\chi}_1^{\mp} \rightarrow W^{\pm} \tilde{\chi}_1^0 W^{\mp} \tilde{\chi}_1^0$, simplified model, $m_{\tilde{\chi}_1^0} = 0$ GeV
none 170-200	95	35	SIRUNYAN	18DN CMS	$\ell^{\pm} \ell^{\mp}$, Tchi1chi1E, $m_{\tilde{\chi}_1^0} = 1$ GeV	none 140-465	95	59	AAD	14G ATLS	$\tilde{\chi}_1^{\pm} \tilde{\chi}_1^{\mp} \rightarrow \ell^{\pm} \nu \tilde{\chi}_1^0 \ell^{\mp} \tilde{\chi}_1^0$, simplified model, $m_{\tilde{\chi}_1^0} = 0$ GeV
> 810	95	35	SIRUNYAN	18DN CMS	$\ell^{\pm} \ell^{\mp}$, Tchi1chi1C, $m_{\tilde{\chi}_1^0} = 0$ GeV	none 180-355	95	59	AAD	14G ATLS	$\tilde{\chi}_1^{\pm} \tilde{\chi}_2^0 \rightarrow W \tilde{\chi}_1^0 Z \tilde{\chi}_1^0$, simplified model, $m_{\tilde{\chi}_1^{\pm}} = m_{\tilde{\chi}_2^0}$, $m_{\tilde{\chi}_1^0} = 0$ GeV
> 630	95	36	SIRUNYAN	18DP CMS	$2\tau + \cancel{E}_T$, Tchi1chi1D, $m_{\tilde{\chi}_1^0} = 0$ GeV	> 168	95	60	AALTONEN	14 CDF	$3\ell^{\pm} + \cancel{E}_T$, $\tilde{\chi}_1^{\pm} \rightarrow \ell \nu \tilde{\chi}_1^0$, mSUGRA with $m_0 = 60$ GeV
> 710	95	36	SIRUNYAN	18DP CMS	$2\tau + \cancel{E}_T$, Tchi1n2D, $m_{\tilde{\chi}_1^0} = 0$ GeV	> 61	95	61	KHACHATRY...14I	CMS	$\tilde{\chi}_1^{\pm} \rightarrow W \tilde{\chi}_1^0$, $\tilde{\ell} \nu$, $\tilde{\ell} \nu$, simplified model
> 170	95	37	SIRUNYAN	18X CMS	$\geq 1 H (\rightarrow \gamma\gamma) + \text{jets} + \cancel{E}_T$, Tchi1n2E, $m_{\tilde{\chi}_1^0} < 25$ GeV	> 62	95	62	AALTONEN	13Q CDF	$\tilde{\chi}_1^{\pm} \rightarrow \tau X$, simplified gravity- and gauge-mediated models
> 420	95	38	KHACHATRY...17L	CMS	$2\tau + \cancel{E}_T$, Tchi1chi1C and $\tilde{\tau}$ -only, $m_{\tilde{\chi}_1^0} = 0$ GeV	63	95	63	AAD	12AS ATLS	$3\ell^{\pm} + \cancel{E}_T$, pMSSM
none 220-490	95	39	SIRUNYAN	17AW CMS	$1\ell + 2b$ -jets + \cancel{E}_T , Tchi1n2E, $m_{\tilde{\chi}_1^0} = 0$ GeV	64	95	64	AAD	12T ATLS	$\ell^{\pm} \ell^{\mp} + \cancel{E}_T$, $\ell^{\pm} \ell^{\pm} + \cancel{E}_T$, $pp \rightarrow \tilde{\chi}_1^{\pm} \tilde{\chi}_2^0$
> 500	95	40	AAD	16AA ATLS	$2\ell^{\pm} + \cancel{E}_T$, Tchi1chi1B, $m_{\tilde{\chi}_1^0} = 0$ GeV	> 163	95	65	CHATRCHYAN11B	CMS	$\tilde{W}^0 \rightarrow \gamma \tilde{G}, \tilde{W}^{\pm} \rightarrow \ell^{\pm} \tilde{G}$, GMSB
> 220	95	40	AAD	16AA ATLS	$2\ell^{\pm} + \cancel{E}_T$, Tchi1chi1C, low Δm for $\tilde{\chi}_1^{\pm}, \tilde{\chi}_1^0$	> 66	95	66	CHATRCHYAN11V	CMS	$\tan\beta=3$, $m_0=60$ GeV, $A_0=0$, $\mu > 0$
> 700	95	41	AAD	16AA ATLS	$3,4\ell + \cancel{E}_T$, Tchi1n2B, $m_{\tilde{\chi}_1^0} = 0$ GeV						
> 700	95	41	AAD	16AA ATLS	$3,4\ell + \cancel{E}_T$, Tchi1n2C, $m_{\tilde{\ell}} = m_{\tilde{\chi}_1^0} + 0.5$ (or 0.95) $(m_{\tilde{\chi}_1^{\pm}} - m_{\tilde{\chi}_1^0})$						
> 400	95	41	AAD	16AA ATLS	2 hadronic $\tau + \cancel{E}_T$ & $3\ell + \cancel{E}_T$ combination, Tchi1n2D, $m_{\tilde{\chi}_1^0} = 0$ GeV						
> 540	95	42	KHACHATRY...16R	CMS	$\geq 1\gamma + 1 e$ or $\mu + \cancel{E}_T$, Tchi1n1A						
> 250	95	43	AAD	15BA ATLS	$m_{\tilde{\chi}_1^{\pm}} = m_{\tilde{\chi}_2^0}$, $m_{\tilde{\chi}_1^0} = 0$ GeV						
> 590	95	44	AAD	15CA ATLS	$\geq 2\gamma + \cancel{E}_T$, GGM, bino-like NLSP, any NLSP mass						

1 AAD 21AX searched in 139 fb⁻¹ of pp collisions at $\sqrt{s} = 13$ TeV for pair production of electroweakinos decaying to the LSP via the emission of Standard Model bosons (Higgs, W, Z) decaying into hadrons. The final state in all cases characterised by the presence of \cancel{E}_T , jets, and large-R jets tagged according to the boson of interest. Different assumptions (Higgsino, Wino, Bino) are made for the pair produced electroweakinos and for the LSP multiplet. No significant excess above the Standard Model predictions is observed. Limits are set on the electroweakino masses as a function of the model parameters (in particular $m_{\tilde{\chi}_1^0}$). See Figs. 12, 14, 15.

2 AAD 21BG searched in 139 fb⁻¹ of pp collisions at $\sqrt{s} = 13$ TeV for pair production $\tilde{\chi}_2^0 \tilde{\chi}_1^{\pm}$ in final states with three leptons, with and without assuming the presence of a Z⁰ → $\ell\ell$ decay. No significant excess above the Standard Model predictions is observed. Limits are set on the $\tilde{\chi}_2^0$ and $\tilde{\chi}_1^{\pm}$ mass in Tchi1n2E, Tchi1n2F and Tchi1n2Ga. See their Fig. 16.

- ³ AAD 21E searched in 139 fb^{-1} of pp collisions at $\sqrt{s} = 13 \text{ TeV}$ for production of wino-like $\tilde{\chi}_1^\pm \tilde{\chi}_1^\pm$ and $\tilde{\chi}_1^\pm \tilde{\chi}_1^0$, followed by the RPV decay of $\tilde{\chi}_1^\pm$ into $Z\ell$, $H\ell$ or $W\nu$ and of $\tilde{\chi}_1^0$ into $Z\nu$, $H\nu$ or $W\ell$, in events with three leptons, looking for $Z\ell$ resonances. No significant excess above the Standard Model predictions is observed. Limits are set on the common $m_{\tilde{\chi}_1^\pm}/m_{\tilde{\chi}_1^0}$ mass in the TwnoLSPRPV simplified model, as a function of the common $\tilde{\chi}_1^\pm/\tilde{\chi}_1^0$ branching fraction to a Z boson. See Figure 9.
- ⁴ AAD 21Y searched in 139 fb^{-1} of pp collisions at $\sqrt{s} = 13 \text{ TeV}$ for supersymmetry in events with four or more leptons (electrons, muons and tau-leptons). No significant excess above the Standard Model expectations is observed. Limits are set on Tchi1n2-GGM, and RPV models similar to Tchi1n2I, Tglu1A (with $q = u, d, s, c, b$, with equal branching fractions), and $\tilde{\ell}_L/\tilde{\nu} \rightarrow \ell/\nu \tilde{\chi}_1^0$ (mass-degenerate $\tilde{\ell}_L$ and $\tilde{\nu}$ of all 3 generations), all with $\tilde{\chi}_1^0 \rightarrow \ell^\pm \tilde{\ell}^\mp \nu$ via λ_{12k} or λ_{133} (where $i, k = 1, 2$), see their Figure 11.
- ⁵ SIRUNYAN 21m searched in 137 fb^{-1} of pp collisions at $\sqrt{s} = 13 \text{ TeV}$ for supersymmetry in events with two opposite-sign same-flavor leptons (electrons, muons) and \cancel{E}_T . No significant excess above the Standard Model expectations is observed. Limits are set on the gluino mass in the simplified model Tglu4C, see their Figure 10, on the $\tilde{\chi}_2^0$ and $\tilde{\chi}_1^\pm$ mass in Tchi1n2Fa, see their Figure 11, on the $\tilde{\chi}_1^0$ mass in Tn1n1C and Tn1n1B for $m_{\tilde{\chi}_2^0} = m_{\tilde{\chi}_1^\pm} = m_{\tilde{\chi}_1^0}$, see their Figure 12. Limits are also set on the light squark mass for the simplified model Tsqk2A, on the sbottom mass in Tsb0t3, see their Figure 13, and on the slepton mass in direct electroweak pair production of mass-degenerate left- and right-handed sleptons (selectrons and smuons), see their Figure 14.
- ⁶ TUMASYAN 21c searched in 137 fb^{-1} of pp collisions at $\sqrt{s} = 13 \text{ TeV}$ for supersymmetry in events with one lepton, a Higgs boson decaying to a pair of bottom quarks, and large \cancel{E}_T . No significant excess above the Standard Model expectations is observed. Lower limits are set on the masses of $\tilde{\chi}_2^0$ and $\tilde{\chi}_1^\pm$ in the simplified model Tchi1n2E, see their Figure 6.
- ⁷ AAD 20AN searched in 139 fb^{-1} of pp collisions at $\sqrt{s} = 13 \text{ TeV}$ for events with two photons and missing transverse momentum. Events are further categorised in terms of lepton or jet multiplicity. No significant excess over the expected background is observed. Limits at 95% C.L. are set on the Higgsino mass in the T1n1n1A simplified model, see their Figure 11.
- ⁸ AAD 20I reported on ATLAS searches for electroweak production in models with compressed mass spectra as Tchi1n2Fa. A dataset of pp collisions at $\sqrt{s} = 13 \text{ TeV}$ corresponding to an integrated luminosity of 139 fb^{-1} was used. Events with \cancel{E}_T , two same-flavour, opposite-charge, low-transverse-momentum leptons, and jets from initial-state radiation or characteristic of vector-boson fusion production are selected. Constraints at 95% C.L. are placed on the mass of the $\tilde{\chi}_1^\pm$ (degenerate with $\tilde{\chi}_2^0$) at 240 GeV for a mass splitting between $\tilde{\chi}_1^\pm$ and $\tilde{\chi}_1^0$ of 7 GeV and extend down to a mass splitting of 1.5 GeV at the LEP chargino mass limit of 92.4 GeV. See their Fig. 14(b,c).
- ⁹ AAD 20K reported on a search for electroweak production in models with mass splittings near the electroweak scale as Tchi1n2F and exploiting three-lepton final state events with an emulated recursive jigsaw reconstruction method. The analysis uses a dataset of pp collisions at $\sqrt{s} = 13 \text{ TeV}$ corresponding to an integrated luminosity of 139 fb^{-1} . Exclusion limits at 95% C.L. are derived on next-to-lightest neutralinos and charginos with masses up to 345 GeV for a massless lightest neutralino, see their Fig. 7.
- ¹⁰ AAD 20O reported on a search for electroweak production in models with charginos and sleptons decaying into final states with exactly two oppositely charged leptons and missing transverse momentum. A dataset of pp collisions at $\sqrt{s} = 13 \text{ TeV}$ corresponding to an integrated luminosity of 139 fb^{-1} was used. Exclusion limits at 95% C.L. are derived on $m_{\tilde{\chi}_1^\pm}$ decaying according to the Tchi1chi1H simplified model. Chargino masses up to 420 GeV are excluded for a massless lightest neutralino, see their Fig. 7(a).
- ¹¹ AAD 20Q reported on a search for electroweak production in models with charginos and sleptons decaying into final states with exactly two oppositely charged leptons and missing transverse momentum. A dataset of pp collisions at $\sqrt{s} = 13 \text{ TeV}$ corresponding to an integrated luminosity of 139 fb^{-1} was used. Exclusion limits at 95% C.L. are derived on $m_{\tilde{\chi}_1^\pm}$ decaying according to the Tchi1chi1C simplified model. Chargino masses up to 1000 GeV are excluded for a massless lightest neutralino, see their Fig. 7(b).
- ¹² AAD 20R searched for electroweak production in the model Tchi1n2E, selecting events with a pair of b -tagged jets consistent with those from a Higgs boson decay, either an electron or a muon from the W boson decay and \cancel{E}_T . The analysis uses a dataset of pp collisions at $\sqrt{s} = 13 \text{ TeV}$ corresponding to an integrated luminosity of 139 fb^{-1} . Exclusion limits at 95% C.L. are derived on next-to-lightest neutralinos and charginos with masses up to 740 GeV for a massless lightest neutralino, assuming pure wino cross-sections. See their Fig. 6.
- ¹³ SIRUNYAN 20AU searched in 77.2 fb^{-1} of pp collisions at $\sqrt{s} = 13 \text{ TeV}$ for events containing one soft, hadronically decaying tau lepton, one energetic jet from initial-state radiation, and large \cancel{E}_T . No excess over the expected background is observed. Limits are derived on the wino mass in the Tchi1n2D simplified model, see their Figure 2.
- ¹⁴ SIRUNYAN 20B searched in 35.9 fb^{-1} of pp collisions at $\sqrt{s} = 13 \text{ TeV}$ for events with at least one photon and large \cancel{E}_T . No significant excess above the Standard Model expectations is observed. Limits are set on chargino masses in a general gauge-mediated SUSY breaking (GGM) scenario Tchi1n12-GGM, see Figure 4. Limits are also set on the NLSF mass in the Tchi1chi1F and Tchi1chi1G simplified models, see their Figure 5. Finally, limits are set on the gluino mass in the Tglu4A simplified model, see Figure 6.
- ¹⁵ AABOUD 19AU searched in 36.1 fb^{-1} of pp collisions at $\sqrt{s} = 13 \text{ TeV}$ for direct electroweak production of charginos and next-to-lightest neutralinos decaying into lightest neutralinos and a W , and a Higgs boson, respectively. Fully hadronic, semileptonic, diphoton, and multilepton (electrons, muons) final states with missing transverse momentum are considered in this search. Observations are consistent with the Standard Model expectations, and 95% confidence-level limits of up to 680 GeV on the chargino/next-to-lightest neutralino masses are set (Tchi1n2E model). See their Figure 14 for an overlay of exclusion contours from all searches.
- ¹⁶ SIRUNYAN 19BU searched for pair production of gauginos via vector boson fusion assuming the gaugino spectrum is compressed, in 35.9 fb^{-1} of pp collisions at $\sqrt{s} = 13 \text{ TeV}$. The final states explored included zero leptons plus two jets, one lepton plus two jets, and one hadronic tau plus two jets. A similar bound is obtained in the light slepton limit.
- ¹⁷ SIRUNYAN 19CI searched in 77.5 fb^{-1} of pp collisions at $\sqrt{s} = 13 \text{ TeV}$ for events with one or more high-momentum Higgs bosons, decaying to pairs of photons, jets and \cancel{E}_T . No significant excess above the Standard Model expectations is observed. Limits are set on the wino mass in the higgsino mass in the Tchi1n2E simplified model, see their Figure 5.
- ¹⁸ SIRUNYAN 19K searched in 35.9 fb^{-1} of pp collisions at $\sqrt{s} = 13 \text{ TeV}$ for events with a photon, an electron or muon, and large \cancel{E}_T . No significant excess above the Standard Model expectations is observed. In the framework of GMSB, limits are set on the chargino and neutralino mass in the Tchi1n1A simplified model, see their Figure 6. Limits are also set on the gluino mass in the Tglu4A simplified model, and on the squark mass in the Tsqk4A simplified model, see their Figure 7.
- ¹⁹ AABOUD 18AY searched in 36.1 fb^{-1} of pp collisions at $\sqrt{s} = 13 \text{ TeV}$ for direct electroweak production of charginos as in Tchi1chi1D models in events characterised by the presence of at least two hadronically decaying tau leptons and large missing transverse energy. No significant deviation from the expected SM background is observed. In the Tchi1chi1D model, assuming decays via intermediate $\tilde{\tau}_1$, the observed limits rule out $\tilde{\chi}_1^\pm$ masses up to 630 GeV for a massless $\tilde{\chi}_1^0$. See their Fig.7 (left). Interpretations are also provided in Fig 8 (top) for different assumptions on the ratio between $m_{\tilde{\tau}_1}$ and $m_{\tilde{\chi}_1^\pm} + m_{\tilde{\chi}_1^0}$.
- ²⁰ AABOUD 18AY searched in 36.1 fb^{-1} of pp collisions at $\sqrt{s} = 13 \text{ TeV}$ for direct electroweak production of charginos and neutralinos as in Tchi1n2D models, in events characterised by the presence of at least two hadronically decaying tau leptons and large missing transverse energy. No significant deviation from the expected SM background is observed. Assuming decays via intermediate $\tilde{\tau}_1$ and $m_{\tilde{\chi}_1^\pm} = m_{\tilde{\chi}_2^0}$, the observed limits rule out $\tilde{\chi}_1^\pm$ masses up to 760 GeV for a massless $\tilde{\chi}_1^0$. See their Fig.7 (right). Interpretations are also provided in Fig 8 (bottom) for different assumptions on the ratio between $m_{\tilde{\tau}_1}$ and $m_{\tilde{\chi}_1^\pm} + m_{\tilde{\chi}_1^0}$.
- ²¹ AABOUD 18BT searched in 36.1 fb^{-1} of pp collisions at $\sqrt{s} = 13 \text{ TeV}$ for direct electroweak production of charginos, chargino and next-to-lightest neutralinos and sleptons in events with two or three leptons (electrons or muons), with or without jets and large missing transverse energy. No significant excess above the Standard Model expectations is observed. Limits are set on the chargino mass up to 750 GeV for massless neutralinos in the Tchi1chi1C simplified model exploiting $2\ell + 0$ jets signatures, see their Figure 8(a).
- ²² AABOUD 18BT searched in 36.1 fb^{-1} of pp collisions at $\sqrt{s} = 13 \text{ TeV}$ for direct electroweak production of charginos, chargino and next-to-lightest neutralinos and sleptons in events with two or three leptons (electrons or muons), with or without jets, and large missing transverse energy. No significant excess above the Standard Model expectations is observed. Limits are set on the chargino mass up to 1100 GeV for massless neutralinos in the Tchi1n2C simplified model exploiting 3ℓ signature, see their Figure 8(c).
- ²³ AABOUD 18BT searched in 36.1 fb^{-1} of pp collisions at $\sqrt{s} = 13 \text{ TeV}$ for direct electroweak production of charginos, chargino and next-to-lightest neutralinos and sleptons in events with two or three leptons (electrons or muons), with or without jets, and large missing transverse energy. No significant excess above the Standard Model expectations is observed. Limits are set on the chargino mass up to 580 GeV for massless neutralinos in the Tchi1n2F simplified model exploiting $2\ell+2$ jets and 3ℓ signatures, see their Figure 8(d).
- ²⁴ AABOUD 18CK searched for events with at least 3 b -jets and large missing transverse energy in two datasets of pp collisions at $\sqrt{s} = 13 \text{ TeV}$ of 36.1 fb^{-1} and 24.3 fb^{-1} depending on the trigger requirements. The analyses aimed to reconstruct two Higgs bosons decaying to pairs of b -quarks. No significant excess above the Standard Model expectations is observed. Limits are set on the Higgsino mass in the T1n1n1A simplified model, see their Figure 15(a). Constraints are also presented as a function of the BR of Higgsino decaying into a Higgs boson and a gravitino, see their Figure 15(b).
- ²⁵ AABOUD 18CO searched in 36.1 fb^{-1} of pp collisions at $\sqrt{s} = 13 \text{ TeV}$ for direct electroweak production of mass-degenerate charginos and next-to-lightest neutralinos in events with two or three leptons (electrons or muons), with or without jets, and large missing transverse energy. The search channels are based on recursive jigsaw reconstruction. Limits are set on the chargino mass up to 600 GeV for massless neutralinos in the Tchi1n2F simplified model exploiting the statistical combination of $2\ell+2$ jets and 3ℓ channels. Chargino masses below 220 GeV are not excluded due to an excess of events above the SM prediction in the dedicated regions. See their Figure 13(d).
- ²⁶ AABOUD 18R searched in 36.1 fb^{-1} of pp collisions at $\sqrt{s} = 13 \text{ TeV}$ for electroweak production in scenarios with compressed mass spectra in final states with two low-momentum leptons and missing transverse momentum. The data are found to be consistent with the SM prediction. Results are interpreted in Tchi1n2G wino models and $\tilde{\chi}_1^\pm$ masses are excluded up to 175 GeV for $m_{\tilde{\chi}_1^\pm} - m_{\tilde{\chi}_1^0} = 10 \text{ GeV}$. The exclusion limits extend down to mass splittings of 2 GeV, see their Fig. 10 (bottom).
- ²⁷ AABOUD 18R searched in 36.1 fb^{-1} of pp collisions at $\sqrt{s} = 13 \text{ TeV}$ for electroweak production in scenarios with compressed mass spectra in final states with two low-momentum leptons and missing transverse momentum. The data are found to be consistent with the SM prediction. Results are interpreted in Tchi1n2G higgsino models and $\tilde{\chi}_1^\pm$ masses are excluded up to 145 GeV for $m_{\tilde{\chi}_1^\pm} - m_{\tilde{\chi}_1^0} = 5 \text{ GeV}$. The exclusion limits extend down to mass splittings of 2.5 GeV, see their Fig. 10 (top).
- ²⁸ AABOUD 18U searched in 36.1 fb^{-1} of pp collisions at $\sqrt{s} = 13 \text{ TeV}$ in events with at least one isolated photon, possibly jets and significant transverse momentum targeting generalised models of gauge-mediated SUSY breaking. No significant excess of events is observed above the SM prediction. Results of the diphoton channel are interpreted in terms of lower limits on the masses of gauginos Tchi1chi1A models, which reach as high as 1.3 TeV. Gaugino masses below 1060 GeV are excluded for any NLSF mass, see their Figure 10.
- ²⁹ AABOUD 18Z searched in 36.1 fb^{-1} of pp collisions at $\sqrt{s} = 13 \text{ TeV}$ for events containing four or more charged leptons (electrons, muons and up to two hadronically decaying taus). No significant deviation from the expected SM background is observed. Limits are set on the Higgsino mass in simplified models of general gauge mediated supersymmetry Tn1n1A/Tn1n1B/Tn1n1C, see their Figure 9. Limits are also set on the wino, slepton, sneutrino and gluino mass in a simplified model of NLSF pair production with R-parity violating decays of the LSP via λ_{12k} or λ_{133} to charged leptons, see their Figures 7, 8.
- ³⁰ SIRUNYAN 18AA searched in 35.9 fb^{-1} of pp collisions at $\sqrt{s} = 13 \text{ TeV}$ for events with at least one photon and large \cancel{E}_T . No significant excess above the Standard Model expectations is observed. Limits are set on wino masses in a general gauge-mediated SUSY breaking (GGM) scenario with bino-like $\tilde{\chi}_1^0$ and wino-like $\tilde{\chi}_1^\pm$ and $\tilde{\chi}_2^0$, see Figure

Searches Particle Listings

Supersymmetric Particle Searches

7. Limits are also set on the NLSP mass in the Tchi1n1A and Tchi1ch1A simplified models, see their Figure 8. Finally, limits are set on the gluino mass in the Tglu4A and Tglu4B simplified models, see their Figure 9, and on the squark mass in the Tskq4A and Tskq4B simplified models, see their Figure 10.
- 31 SIRUNYAN 18AJ searched in 35.9 fb^{-1} of pp collisions at $\sqrt{s} = 13 \text{ TeV}$ for events containing two low-momentum, oppositely charged leptons (electrons or muons) and \cancel{E}_T . No excess over the expected background is observed. Limits are derived on the wino mass in the Tchi1n2F simplified model, see their Figure 5. Limits are also set on the stop mass in the Tstop10 simplified model, see their Figure 6. Finally, limits are set on the Higgsino mass in the Tchi1n2G simplified model, see Figure 8 and in the pMSSM, see Figure 7.
- 32 SIRUNYAN 18AO searched in 35.9 fb^{-1} of pp collisions at $\sqrt{s} = 13 \text{ TeV}$ for direct electroweak production of charginos and neutralinos in events with either two or more leptons (electrons or muons) of the same electric charge, or with three or more leptons, which can include up to two hadronically decaying tau leptons. No significant excess above the Standard Model expectations is observed. Limits are set on the chargino/neutralino mass in the Tchi1n2A, Tchi1n2H, Tchi1n2D, Tchi1n2E and Tchi1n2F simplified models, see their Figures 14, 15, 16, 17 and 18. Limits are also set on the higgsino mass in the Tn1n1A, Tn1n1B and Tn1n1C simplified models, see their Figure 19.
- 33 SIRUNYAN 18AP searched in 35.9 fb^{-1} of pp collisions at $\sqrt{s} = 13 \text{ TeV}$ for direct electroweak production of charginos and neutralinos by combining a number of previous and new searches. No significant excess above the Standard Model expectations is observed. Limits are set on the chargino/neutralino mass in the Tchi1n2E, Tchi1n2F and Tchi1n2I simplified models, see their Figures 7, 8, 9 and 10. Limits are also set on the higgsino mass in the Tn1n1A, Tn1n1B and Tn1n1C simplified models, see their Figure 11, 12, 13 and 14.
- 34 SIRUNYAN 18AR searched in 35.9 fb^{-1} of pp collisions at $\sqrt{s} = 13 \text{ TeV}$ for events containing two opposite-charge, same-flavour leptons (electrons or muons), jets and \cancel{E}_T . No significant excess above the Standard Model expectations is observed. Limits are set on the gluino mass in the Tglu4C simplified model, see their Figure 7. Limits are also set on the chargino/neutralino mass in the Tchi1n2F simplified models, see their Figure 8, and on the higgsino mass in the Tn1n1B and Tn1n1C simplified models, see their Figure 9. Finally, limits are set on the sbottom mass in the Tsb0t3 simplified model, see their Figure 10.
- 35 SIRUNYAN 18DN searched in 35.9 fb^{-1} of pp collisions at $\sqrt{s} = 13 \text{ TeV}$ for direct electroweak production of charginos and for pair production of top squarks in events with two leptons (electrons or muons) of the opposite electric charge. No significant excess above the Standard Model expectations is observed. Limits are set on the chargino mass in the Tchi1ch1C and Tchi1ch1E simplified models, see their Figure 8. Limits are also set on the stop mass in the Tstop1 and Tstop2 simplified models, see their Figure 9.
- 36 SIRUNYAN 18DP searched in 35.9 fb^{-1} of pp collisions at $\sqrt{s} = 13 \text{ TeV}$ for direct electroweak production of charginos and neutralinos or of chargino pairs in events with a tau lepton pair and significant missing transverse momentum. Both hadronic and leptonic decay modes are considered for the tau lepton. No significant excess above the Standard Model expectations is observed. Limits are set on the chargino mass in the Tchi1ch1D and Tchi1n2 simplified models, see their Figures 14 and 15. Also, excluded stau pair production cross sections are shown in Figures 11, 12, and 13.
- 37 SIRUNYAN 18X searched in 35.9 fb^{-1} of pp collisions at $\sqrt{s} = 13 \text{ TeV}$ for events with one or more high-momentum Higgs bosons, decaying to pairs of photons, jets and \cancel{E}_T . The razor variables (M_R and R^2) are used to categorise the events. No significant excess above the Standard Model expectations is observed. Limits are set on the sbottom mass in the Tsb0t4 simplified model and on the wino mass in the Tchi1n2E simplified model, see their Figure 5. Limits are also set on the higgsino mass in the Tn1n1A and Tn1n1B simplified models, see their Figure 6.
- 38 KHACHATRYAN 17L searched in about 19 fb^{-1} of pp collisions at $\sqrt{s} = 8 \text{ TeV}$ for events with two τ (at least one decaying hadronically) and \cancel{E}_T . In the Tchi1ch1C model, assuming decays via intermediate $\tilde{\tau}$ or $\tilde{\nu}_\tau$ with equivalent mass, the observed limits rule out $\tilde{\chi}_1^\pm$ masses up to 420 GeV for a massless $\tilde{\chi}_1^0$. See their Fig. 5.
- 39 SIRUNYAN 17AV searched in 35.9 fb^{-1} of pp collisions at $\sqrt{s} = 13 \text{ TeV}$ for events with a charged lepton (electron or muon), two jets identified as originating from a b -quark, and large \cancel{E}_T . No significant excess above the Standard Model expectations is observed. Limits are set on the mass of the chargino and the next-to-lightest neutralino in the Tchi1n2E simplified model, see their Figure 6.
- 40 AAD 16AA summarized and extended ATLAS searches for electroweak supersymmetry in final states containing several charged leptons, \cancel{E}_T , with or without hadronic jets, in 20 fb^{-1} of pp collisions at $\sqrt{s} = 8 \text{ TeV}$. The paper reports the results of new interpretations and statistical combinations of previously published analyses, as well as new analyses. Exclusion limits at 95% C.L. are set on the $\tilde{\chi}_1^\pm$ mass in the Tchi1ch1B and Tchi1ch1C simplified models. See their Fig. 13.
- 41 AAD 16AA summarized and extended ATLAS searches for electroweak supersymmetry in final states containing several charged leptons, \cancel{E}_T , with or without hadronic jets, in 20 fb^{-1} of pp collisions at $\sqrt{s} = 8 \text{ TeV}$. The paper reports the results of new interpretations and statistical combinations of previously published analyses, as well as new analyses. Exclusion limits at 95% C.L. are set on mass-degenerate $\tilde{\chi}_1^\pm$ and $\tilde{\chi}_2^0$ masses in the Tchi1n2B, Tchi1n2C, and Tchi1n2D simplified models. See their Figs. 16, 17, and 18. Interpretations in phenomenological-MSSM, two-parameter Non Universal Higgs Masses (NUHM2), and gauge-mediated symmetry breaking (GMSB) models are also given in their Figs. 20, 21 and 22.
- 42 KHACHATRYAN 16R searched in 19.7 fb^{-1} of pp collisions at $\sqrt{s} = 8 \text{ TeV}$ for events with one or more photons, one electron or muon, and \cancel{E}_T . No significant excess above the Standard Model expectations is observed. Limits are set on wino masses in a general gauge-mediated SUSY breaking model (GGM), for a wino-like neutralino NLSP scenario, see Fig. 5. Limits are also set in the Tglu1D and Tchi1n1A simplified models, see Fig. 6. The Tchi1n1A limit is reduced to 340 GeV for a branching ratio reduced by the weak mixing angle.
- 43 AAD 15BA searched in 20.3 fb^{-1} of pp collisions at $\sqrt{s} = 8 \text{ TeV}$ for electroweak production of charginos and neutralinos decaying to a final state containing a W boson and a 125 GeV Higgs boson, plus missing transverse momentum. No excess beyond the Standard Model expectation is observed. Exclusion limits are derived in simplified models of direct chargino and next-to-lightest neutralino production, with the decays $\tilde{\chi}_1^\pm \rightarrow W^\pm \tilde{\chi}_1^0$ and $\tilde{\chi}_2^0 \rightarrow H^\pm \tilde{\chi}_1^0$ having 100% branching fraction, see Fig. 8. A combination of the multiple final states for the Higgs decay yields the best limits (Fig. 8d).
- 44 AAD 15CA searched in 20.3 fb^{-1} of pp collisions at $\sqrt{s} = 8 \text{ TeV}$ for events with one or more photons and \cancel{E}_T , with or without leptons (e, μ). No significant excess above the Standard Model expectations is observed. Limits are set on wino masses in the general gauge-mediated SUSY breaking model (GGM), for wino-like NLSP, see Fig. 9, 12
- 45 AAD 14H searched in 20.3 fb^{-1} of pp collisions at $\sqrt{s} = 8 \text{ TeV}$ for electroweak production of charginos and neutralinos decaying to a final state with three leptons and missing transverse momentum. No excess beyond the Standard Model expectation is observed. Exclusion limits are derived in simplified models of direct chargino and next-to-lightest neutralino production, with decays to the lightest neutralino via either all three generations of leptons, staus only, gauge bosons, or Higgs bosons, see Fig. 7. An interpretation in the pMSSM is also given, see Fig. 8.
- 46 AAD 14X searched in 20.3 fb^{-1} of pp collisions at $\sqrt{s} = 8 \text{ TeV}$ for events with at least four leptons (electrons, muons, taus) in the final state. No significant excess above the Standard Model expectations is observed. Limits are set on the wino-like chargino mass in an R-parity violating simplified model where the decay $\tilde{\chi}_1^\pm \rightarrow W^{(*)\pm} \tilde{\chi}_1^0$, with $\tilde{\chi}_1^0 \rightarrow \ell^\pm \ell^\mp \nu$, takes place with a branching ratio of 100%, see Fig. 8.
- 47 KHACHATRYAN 14L searched in 19.5 fb^{-1} of pp collisions at $\sqrt{s} = 8 \text{ TeV}$ for evidence of chargino-neutralino $\tilde{\chi}_1^\pm \tilde{\chi}_2^0$ pair production with Higgs or W -bosons in the decay chain, leading to HW final states with missing transverse energy. The decays of a Higgs boson to a photon pair are considered in conjunction with hadronic and leptonic decay modes of the W bosons. No significant excesses over the expected SM backgrounds are observed. The results are interpreted in the context of simplified models where the decays $\tilde{\chi}_2^0 \rightarrow H \tilde{\chi}_1^0$ and $\tilde{\chi}_1^\pm \rightarrow W^\pm \tilde{\chi}_1^0$ take place 100% of the time, see Figs. 22–23.
- 48 AAD 13C searched in 4.7 fb^{-1} of pp collisions at $\sqrt{s} = 7 \text{ TeV}$ for charginos and neutralinos decaying to a final state with three leptons (e and μ) and missing transverse energy. No excess beyond the Standard Model expectation is observed. Exclusion limits are derived in the phenomenological MSSM, see Fig. 2 and 3, and in simplified models, see Fig. 4. For the simplified models with intermediate slepton decays, degenerate $\tilde{\chi}_1^\pm$ and $\tilde{\chi}_2^0$ masses up to 500 GeV are excluded at 95% C.L. for very large mass differences with the $\tilde{\chi}_1^0$. Supersedes AAD 12AS.
- 49 AAD 13B searched in 4.7 fb^{-1} of pp collisions at $\sqrt{s} = 7 \text{ TeV}$ for gauginos decaying to a final state with two leptons (e and μ) and missing transverse energy. No excess beyond the Standard Model expectation is observed. Limits are derived in a simplified model of wino-like chargino pair production, where the chargino always decays to the lightest neutralino via an intermediate on-shell charged slepton, see Fig. 2(b). Chargino masses between 110 and 340 GeV are excluded at 95% C.L. for $m_{\tilde{\chi}_1^0} = 10 \text{ GeV}$. Exclusion limits are also derived in the phenomenological MSSM, see Fig. 3.
- 50 AAD 12CT searched in 4.7 fb^{-1} of pp collisions at $\sqrt{s} = 7 \text{ TeV}$ for events containing four or more leptons (electrons or muons) and either moderate values of missing transverse momentum or large effective mass. No significant excess is found in the data. Limits are presented in a simplified model of R-parity violating supersymmetry in which charginos are pair-produced and then decay into a W -boson and a $\tilde{\chi}_1^0$, which in turn decays through an RPV coupling into two charged leptons ($e^\pm e^\mp$ or $e^\pm \mu^\mp$) and a neutrino. In this model, chargino masses up to 540 GeV are excluded at 95% C.L. for $m_{\tilde{\chi}_1^0}$ above 300 GeV, see Fig. 3a. The limit deteriorates for lighter $\tilde{\chi}_1^0$. Limits are also set in an R-parity violating MSUGRA model, see Fig. 3b.
- 51 KHACHATRYAN 12BJ searched in 4.98 fb^{-1} of pp collisions at $\sqrt{s} = 7 \text{ TeV}$ for direct electroweak production of charginos and neutralinos in events with at least two leptons, jets and missing transverse momentum. No significant excesses over the expected SM backgrounds are observed and 95% C.L. limits on the production cross section of $\tilde{\chi}_1^\pm \tilde{\chi}_2^0$ pair production were set in a number of simplified models, see Figs. 7 to 12.
- 52 ABDALLAH 03M uses data from $\sqrt{s} = 192\text{--}208 \text{ GeV}$ in the framework of the MSSM with gaugino and sfermion mass universality at the GUT scale. An indirect limit on the mass of charginos is derived by constraining the MSSM parameter space by the results from direct searches for neutralinos (including cascade decays), for charginos and for sleptons. These limits are valid for values of $M_2 < 1 \text{ TeV}$, $|\mu| \leq 2 \text{ TeV}$ with the $\tilde{\chi}_1^0$ as LSP. Constraints from the Higgs search in the m_h^{max} scenario assuming $m_t = 174.3 \text{ GeV}$ are included. The quoted limit applies if there is no mixing in the third family or when $m_{\tilde{t}_1} - m_{\tilde{\chi}_1^0} > 6 \text{ GeV}$. If mixing is included the limit degrades to 90 GeV. See Fig. 43 for the mass limits as a function of $\tan\beta$. These limits update the results of ABREU 00W.
- 53 AAD 20AN searched in 139 fb^{-1} of pp collisions at $\sqrt{s} = 13 \text{ TeV}$ for events with two photons and missing transverse momentum. Events are further categorised in terms of lepton or jet multiplicity. No significant excess over the expected background is observed. Limits at 95% C.L. are derived in Tchi1n2E simplified models. Next-to-lightest neutralinos and charginos with masses up to 310 GeV for a massless lightest neutralino are excluded. See their Fig. 10.
- 54 KHACHATRYAN 16AA searched in 7.4 fb^{-1} of pp collisions at $\sqrt{s} = 8 \text{ TeV}$ for events with one or more photons, hadronic jets and \cancel{E}_T . No significant excess above the Standard Model expectations is observed. Limits are set on wino masses in the general gauge-mediated SUSY breaking model (GGM), for a wino-like neutralino NLSP scenario and with the wino mass fixed at 10 GeV above the bino mass, see Fig. 4. Limits are also set in the Tchi1ch1A and Tchi1n1A simplified models, see Fig. 3.
- 55 KHACHATRYAN 16R searched in 19.7 fb^{-1} of pp collisions at $\sqrt{s} = 8 \text{ TeV}$ for events with one or more photons, one electron or muon, and \cancel{E}_T . No significant excess above the Standard Model expectations is observed. Limits are also set in the Tglu1F simplified model, see Fig. 6.
- 56 KHACHATRYAN 16Y searched in 19.7 fb^{-1} of pp collisions at $\sqrt{s} = 8 \text{ TeV}$ for events with one or two soft isolated leptons, hadronic jets, and \cancel{E}_T . No significant excess above the Standard Model expectations is observed. Limits are set on the $\tilde{\chi}_1^\pm$ mass (which is degenerate with the $\tilde{\chi}_2^0$) in the Tchi1n2A simplified model, see Fig. 4.
- 57 AAD 14AV searched in 20.3 fb^{-1} of pp collisions at $\sqrt{s} = 8 \text{ TeV}$ for the direct production of charginos, neutralinos and staus in events containing at last two hadronically decaying τ -leptons, large missing transverse momentum and low jet activity. The quoted limit was derived for direct $\tilde{\chi}_1^\pm \tilde{\chi}_2^0$ and $\tilde{\chi}_1^\pm \tilde{\chi}_1^\mp$ production with $\tilde{\chi}_2^0 \rightarrow \tilde{\tau} \tau \rightarrow \tau \tau \tilde{\chi}_1^0$ and $\tilde{\chi}_1^\pm \rightarrow \tilde{\tau} \nu(\tilde{\nu} \tau) \rightarrow \tau \nu \tilde{\chi}_1^0$, $m_{\tilde{\chi}_2^0} = m_{\tilde{\chi}_1^\pm}$, $m_{\tilde{\tau}} = 0.5 (m_{\tilde{\chi}_1^\pm} + m_{\tilde{\chi}_1^0})$, $m_{\tilde{\chi}_1^0} = 0 \text{ GeV}$. No excess over the expected SM background is observed. Exclusion limits are set in simplified models of $\tilde{\chi}_1^\pm \tilde{\chi}_1^\mp$ and $\tilde{\chi}_1^\pm \tilde{\chi}_2^0$ pair production, see their Figure 7. Upper limits on the cross section and signal strength for direct di-stau production are derived, see Figures 8 and 9. Also, limits are derived in a pMSSM model where the only light slepton is the $\tilde{\tau}_R$, see Figure 10.

See key on page 1127

Searches Particle Listings
Supersymmetric Particle Searches

⁵⁸ AAD 14AV searched in 20.3 fb^{-1} of pp collisions at $\sqrt{s} = 8 \text{ TeV}$ for the direct production of charginos, neutralinos and staus in events containing at least two hadronically decaying τ -leptons, large missing transverse momentum and low jet activity. The quoted limit was derived for direct $\tilde{\chi}_1^\pm \tilde{\chi}_1^\mp$ production with $\tilde{\chi}_1^\pm \rightarrow \tau \nu (\bar{\nu} \tau) \rightarrow \tau \nu \tilde{\chi}_1^0$, $m_{\tilde{\tau}} = 0.5 (m_{\tilde{\chi}_1^\pm} + m_{\tilde{\chi}_1^0})$, $m_{\tilde{\chi}_1^0} = 0 \text{ GeV}$. No excess over the expected SM background is observed.

Exclusion limits are set in simplified models of $\tilde{\chi}_1^\pm \tilde{\chi}_1^\mp$ and $\tilde{\chi}_1^\pm \tilde{\chi}_2^0$ pair production, see their Figure 7. Upper limits on the cross section and signal strength for direct di-stau production are derived, see Figures 8 and 9. Also, limits are derived in a pMSSM model where the only light slepton is the $\tilde{\tau}_R$, see Figure 10.

⁵⁹ AAD 14G searched in 20.3 fb^{-1} of pp collisions at $\sqrt{s} = 8 \text{ TeV}$ for electroweak production of chargino pairs, or chargino-neutralino pairs, decaying to a final state with two leptons (e and μ) and missing transverse momentum. No excess beyond the Standard Model expectation is observed. Exclusion limits are derived in simplified models of chargino pair production, with chargino decays to the lightest neutralino via either sleptons or gauge bosons, see Fig 5.; or in simplified models of chargino and next-to-lightest neutralino production, with decays to the lightest neutralino via gauge bosons, see Fig. 7. An interpretation in the pMSSM is also given, see Fig. 10.

⁶⁰ AALTONEN 14 searched in 5.8 fb^{-1} of $p\bar{p}$ collisions at $\sqrt{s} = 1.96 \text{ TeV}$ for evidence of chargino and next-to-lightest neutralino associated production in final states consisting of three leptons (electrons, muons or taus) and large missing transverse momentum. The results are consistent with the Standard Model predictions within 1.85σ . Limits on the chargino mass are derived in an mSUGRA model with $m_0 = 60 \text{ GeV}$, $\tan\beta = 3$, $A_0 = 0$ and $\mu > 0$, see their Fig. 2.

⁶¹ KHACHATRYAN 14i searched in 19.5 fb^{-1} of pp collisions at $\sqrt{s} = 8 \text{ TeV}$ for electroweak production of chargino pairs decaying to a final state with opposite-sign lepton pairs (e or μ) and missing transverse momentum. No excess beyond the Standard Model expectation is observed. Exclusion limits are derived in simplified models, see Fig. 18.

⁶² AALTONEN 13Q searched in 6.0 fb^{-1} of $p\bar{p}$ collisions at $\sqrt{s} = 1.96 \text{ TeV}$ for evidence of chargino-neutralino associated production in like-sign dilepton final states. One lepton is identified as the hadronic decay of a tau lepton, while the other is an electron or muon. Good agreement with the Standard Model predictions is observed and limits are set on the chargino-neutralino cross section for simplified gravity- and gauge-mediated models, see their Figs. 2 and 3.

⁶³ AAD 12AS searched in 2.06 fb^{-1} of pp collisions at $\sqrt{s} = 7 \text{ TeV}$ for charginos and neutralinos decaying to a final state with three leptons (e and μ) and missing transverse energy. No excess beyond the Standard Model expectation is observed. Exclusion limits are derived in the phenomenological MSSM, see Fig. 2 (top), and in simplified models, see Fig. 2 (bottom).

⁶⁴ AAD 12T looked in 1 fb^{-1} of pp collisions at $\sqrt{s} = 7 \text{ TeV}$ for the production of supersymmetric particles decaying into final states with missing transverse momentum and exactly two isolated leptons (e or μ). Opposite-sign and same-sign dilepton events were separately studied. Additionally, in opposite-sign events, a search was made for an excess of same-flavor over different-flavor lepton pairs. No excess over the expected background is observed and limits are placed on the effective production cross section of opposite-sign dilepton events with $E_{Tl} > 250 \text{ GeV}$ and on same-sign dilepton events with $E_{Tl} > 100 \text{ GeV}$. The latter limit is interpreted in a simplified electroweak gaugino production model as a lower chargino mass limit.

⁶⁵ CHATRCHYAN 11B looked in 35 pb^{-1} of pp collisions at $\sqrt{s} = 7 \text{ TeV}$ for events with an isolated lepton (e or μ), a photon and E_{Tl} which may arise in a generalized gauge mediated model from the decay of Wino-like NLSPs. No evidence for an excess over the expected background is observed. Limits are derived in the plane of squark/gluino mass versus Wino mass (see Fig. 4). Mass degeneracy of the produced squarks and gluinos is assumed.

⁶⁶ CHATRCHYAN 11V looked in 35 pb^{-1} of pp collisions at $\sqrt{s} = 7 \text{ TeV}$ for events with > 3 isolated leptons (e , μ or τ), with or without jets and E_{Tl} . No evidence for an excess over the expected background is observed. Limits are derived in the CMSSM ($m_0, m_{1/2}$) plane for $\tan\beta = 3$ (see Fig. 5).

Long-lived $\tilde{\chi}^\pm$ (Chargino) mass limit

Limits on charginos which leave the detector before decaying.

VALUE (GeV)	CL%	DOCUMENT ID	TECN	COMMENT
> 884	95	1 SIRUNYAN 20N CMS		$\tilde{\chi}^\pm \rightarrow \tilde{\chi}_1^0 \pi^\pm$, wino LSP, AMSB, $\tan\beta = 5$, $\mu > 0$, $\tau = 3 \text{ ns}$
> 474	95	1 SIRUNYAN 20N CMS		$\tilde{\chi}^\pm \rightarrow \tilde{\chi}_1^0 \pi^\pm$, wino LSP, AMSB, $\tan\beta = 5$, $\mu > 0$, $\tau = 0.2 \text{ ns}$
> 750	95	1 SIRUNYAN 20N CMS		$\tilde{\chi}^\pm \rightarrow \tilde{\chi}_1^0 \pi^\pm$, higgsino LSP, AMSB, $\tan\beta = 5$, $\mu > 0$, $\tau = 3 \text{ ns}$
> 175	95	1 SIRUNYAN 20N CMS		$\tilde{\chi}^\pm \rightarrow \tilde{\chi}_1^0 \pi^\pm$, higgsino LSP, AMSB, $\tan\beta = 5$, $\mu > 0$, $\tau = 0.05 \text{ ns}$
> 1090	95	2 AABOUD 19AT ATLS		long-lived $\tilde{\chi}_1^\pm$ mAMSB
> 460	95	3 AABOUD 18AS ATLS		$\tilde{\chi}^\pm \rightarrow \tilde{\chi}_1^0 \pi^\pm$, lifetime 0.2 ns, $m_{\tilde{\chi}^\pm} - m_{\tilde{\chi}_1^0} = 160 \text{ MeV}$
> 715	95	4 SIRUNYAN 18BR CMS		$\tilde{\chi}^\pm \rightarrow \tilde{\chi}_1^0 \pi^\pm$, AMSB, $\tan\beta = 5$ and $\mu > 0$, $\tau = 3 \text{ ns}$
> 695	95	4 SIRUNYAN 18BR CMS		$\tilde{\chi}^\pm \rightarrow \tilde{\chi}_1^0 \pi^\pm$, AMSB, $\tan\beta = 5$ and $\mu > 0$, $\tau = 7 \text{ ns}$
> 505	95	4 SIRUNYAN 18BR CMS		$\tilde{\chi}^\pm \rightarrow \tilde{\chi}_1^0 \pi^\pm$, AMSB, $\tan\beta = 5$, $\mu > 0$, $0.5 \text{ ns} > \tau > 60 \text{ ns}$
> 620	95	5 AAD 15AE ATLS		stable $\tilde{\chi}^\pm$
> 534	95	6 AAD 15BMATLS		stable $\tilde{\chi}^\pm$
> 239	95	6 AAD 15BMATLS		$\tilde{\chi}^\pm \rightarrow \tilde{\chi}_1^0 \pi^\pm$, lifetime 1 ns, $m_{\tilde{\chi}^\pm} - m_{\tilde{\chi}_1^0} = 0.14 \text{ GeV}$
> 482	95	6 AAD 15BMATLS		$\tilde{\chi}^\pm \rightarrow \tilde{\chi}_1^0 \pi^\pm$, lifetime 15 ns, $m_{\tilde{\chi}^\pm} - m_{\tilde{\chi}_1^0} = 0.14 \text{ GeV}$
> 103	95	7 AAD 13H ATLS		long-lived $\tilde{\chi}^\pm \rightarrow \tilde{\chi}_1^0 \pi^\pm$, mAMSB, $\Delta m_{\tilde{\chi}_1^0} = 160 \text{ MeV}$
> 92	95	8 AAD 12BJ ATLS		long-lived $\tilde{\chi}^\pm \rightarrow \pi^\pm \tilde{\chi}_1^0$, mAMSB
> 171	95	9 ABYZOV 09M D0		\tilde{H}
> 102	95	10 ABBIENDI 03L OPAL		$m_{\tilde{D}} > 500 \text{ GeV}$
none 2-93.0	95	11 ABREU 00T DLPH		\tilde{H}^\pm or $m_{\tilde{D}} > m_{\tilde{\chi}^\pm}$

••• We do not use the following data for averages, fits, limits, etc. •••

> 260	95	12 KHACHATRYAN...15AB CMS		$\tilde{\chi}_1^\pm \rightarrow \tilde{\chi}_1^0 \pi^\pm$, $\tau_{\tilde{\chi}_1^\pm} = 0.2 \text{ ns}$, AMSB
> 800	95	13 KHACHATRYAN...15AO CMS		long-lived $\tilde{\chi}_1^\pm$, mAMSB, $\tau > 100 \text{ ns}$
> 100	95	13 KHACHATRYAN...15AO CMS		long-lived $\tilde{\chi}_1^\pm$, mAMSB, $\tau > 3 \text{ ns}$
	95	14 KHACHATRYAN...15W CMS		long-lived $\tilde{\chi}_1^\pm$, $\tilde{q} \rightarrow q \tilde{\chi}_1^0$, $\tilde{\chi}_1^0 \rightarrow \ell^+ \ell^- \nu$, RPV disappearing-track signature, AMSB
> 270	95	15 AAD 13BD ATLS		long-lived $\tilde{\chi}^\pm$, gaugino-like
> 278	95	16 ABYZOV 13B D0		long-lived $\tilde{\chi}^\pm$, higgsino-like
> 244	95	16 ABYZOV 13B D0		long-lived $\tilde{\chi}^\pm$, higgsino-like

¹ SIRUNYAN 20N searched in 101 fb^{-1} of pp collisions at $\sqrt{s} = 13 \text{ TeV}$ for direct electroweak production of long-lived charginos in events containing isolated tracks with missing hits in the outer layer of the silicon tracker and little or no associated calorimetric energy deposits (disappearing tracks). No significant excess above the Standard Model expectations is observed. In an AMSB context and assuming a wino LSP, limits are set on the cross section of direct chargino production through $pp \rightarrow \tilde{\chi}^\pm \tilde{\chi}^\mp$ and $pp \rightarrow \tilde{\chi}^\pm \tilde{\chi}_1^0$, assuming $B(\tilde{\chi}^\pm \rightarrow \tilde{\chi}_1^0 \pi^\pm) = 100\%$, as a function of the chargino mass and mean proper lifetime, see Figure 2. In the case of a Higgsino LSP, limits are set on the cross section of direct chargino production through $pp \rightarrow \tilde{\chi}^\pm \tilde{\chi}^\mp$ and $pp \rightarrow \tilde{\chi}^\pm \tilde{\chi}_{1,2}^0$, assuming $B(\tilde{\chi}^\pm \rightarrow \tilde{\chi}_1^0 \pi^\pm) = 95.5\%$, $B(\tilde{\chi}^\pm \rightarrow \tilde{\chi}_1^0 e^\pm) = 3\%$, $B(\tilde{\chi}^\pm \rightarrow \tilde{\chi}_1^0 \mu^\pm) = 1.5\%$, as a function of the chargino mass and mean proper lifetime, see Figure 3.

² AABOUD 19AT searched in 36.1 fb^{-1} of pp collisions at $\sqrt{s} = 13 \text{ TeV}$ for metastable R-hadrons. Multiple search strategies for a wide range of lifetimes, corresponding to path lengths of a few meters, are defined. No significant deviations from the expected Standard Model background are observed. Results are interpreted in terms of direct electroweak production of long-lived charginos in the context of AMSB scenarios. Chargino masses are excluded at 95% C.L. below 1090 GeV . See their Figure 10 (right).

³ AABOUD 18AS searched in 36.1 fb^{-1} of pp collisions at $\sqrt{s} = 13 \text{ TeV}$ for direct electroweak production of long-lived charginos in the context of AMSB or phenomenological MSSM scenarios with wino-like LSP. Events with a disappearing track due to a low-momentum pion accompanied by at least one jet with high transverse momentum from initial-state radiation are considered. No significant excess above the Standard Model expectations is observed. Exclusion limits are set at 95% confidence level on the mass of charginos for different chargino lifetimes. For a pure wino with a lifetime of about 0.2 ns , corresponding to a mass-splitting between the charged and neutral wino of around 160 MeV , chargino masses up to 460 GeV are excluded, see their Fig. 8.

⁴ SIRUNYAN 18BR searched in 38.4 fb^{-1} of pp collisions at $\sqrt{s} = 13 \text{ TeV}$ for direct electroweak production of long-lived charginos in events containing isolated tracks with missing hits in the outer layer of the silicon tracker and little or no associated calorimetric energy deposits (disappearing tracks). No significant excess above the Standard Model expectations is observed. In an AMSB context, limits are set on the cross section of direct chargino production through $pp \rightarrow \tilde{\chi}^\pm \tilde{\chi}^\mp$ and $pp \rightarrow \tilde{\chi}^\pm \tilde{\chi}_1^0$, assuming $\text{BR}(\tilde{\chi}^\pm \rightarrow \tilde{\chi}_1^0 \pi^\pm) = 100\%$, as a function of the chargino mass and mean proper lifetime, see Figures 3, 4 and 5.

⁵ AAD 15AE searched in 19.1 fb^{-1} of pp collisions at $\sqrt{s} = 8 \text{ TeV}$ for heavy long-lived charged particles, measured through their specific ionization energy loss in the ATLAS pixel detector or their time-of-flight in the ALTAS muon system. In the absence of an excess of events above the expected backgrounds, limits are set on stable charginos, see Fig. 10.

⁶ AAD 15BM searched in 18.4 fb^{-1} of pp collisions at $\sqrt{s} = 8 \text{ TeV}$ for stable and metastable non-relativistic charged particles through their anomalous specific ionization energy loss in the ATLAS pixel detector. In absence of an excess of events above the expected backgrounds, limits are set on stable charginos (see Table 5) and on metastable charginos decaying to $\tilde{\chi}_1^0 \pi^\pm$, see Fig. 11.

⁷ AAD 13H searched in 4.7 fb^{-1} of pp collisions at $\sqrt{s} = 7 \text{ TeV}$ for direct electroweak production of long-lived charginos in the context of AMSB scenarios. The search is based on the signature of a high-momentum isolated track with few associated hits in the outer part of the tracking system, arising from a chargino decay into a neutralino and a low-momentum pion. The p_T spectrum of the tracks was found to be consistent with the SM expectations. Constraints on the lifetime and the production cross section were obtained, see Fig. 6. In the minimal AMSB framework with $\tan\beta = 5$, and $\mu > 0$, a chargino having a mass below $103 (85) \text{ GeV}$ for a chargino-neutralino mass splitting $\Delta m_{\tilde{\chi}_1^0}$ of $160 (170) \text{ MeV}$ is excluded at the 95% C.L. See Fig. 7 for more precise bounds.

⁸ AAD 12BJ looked in 1.02 fb^{-1} of pp collisions at $\sqrt{s} = 7 \text{ TeV}$ for signatures of decaying charginos resulting in isolated tracks with few associated hits in the outer region of the tracking system. The p_T spectrum of the tracks was found to be consistent with the SM expectations. Constraints on the lifetime and the production cross section were obtained. In the minimal AMSB framework with $m_{3/2} < 32 \text{ TeV}$, $m_0 < 1.5 \text{ TeV}$, $\tan\beta = 5$, and $\mu > 0$, a chargino having a mass below 92 GeV and a lifetime between 0.5 ns and 2 ns is excluded at the 95% C.L. See their Fig. 8 for more precise bounds.

⁹ ABYZOV 09M searched in 1.1 fb^{-1} of $p\bar{p}$ collisions at $\sqrt{s} = 1.96 \text{ TeV}$ for events with direct production of a pair of charged massive stable particles identified by their TOF. The number of the observed events is consistent with the predicted background. The data are used to constrain the production cross section as a function of the $\tilde{\chi}_1^\pm$ mass, see their Fig. 2. The quoted limit improves to 206 GeV for gaugino-like charginos.

¹⁰ ABBIENDI 03L used $e^+ e^-$ data at $\sqrt{s} = 130\text{--}209 \text{ GeV}$ to select events with two high momentum tracks with anomalous dE/dx . The excluded cross section is compared to the theoretical expectation as a function of the heavy particle mass in their Fig. 3. The bounds are valid for colorless fermions with lifetime longer than 10^{-6} s . Supersedes the results from ACKERSTAFF 98P.

¹¹ ABREU 00T searches for the production of heavy stable charged particles, identified by their ionization or Cherenkov radiation, using data from $\sqrt{s} = 130$ to 189 GeV . These limits include and update the results of ABREU 98P.

¹² KHACHATRYAN 15AB searched in 19.5 fb^{-1} of pp collisions at $\sqrt{s} = 8 \text{ TeV}$ for events containing tracks with little or no associated calorimetric energy deposits and with missing hits in the outer layers of the tracking system (disappearing-track signature). Such disappearing tracks can result from the decay of charginos that are nearly mass degenerate with the lightest neutralino. The number of observed events is in agreement with the background expectation. Limits are set on the cross section of electroweak chargino production in terms of the chargino mass and mean proper lifetime, see Fig. 4. In the minimal AMSB model, a chargino mass below 260 GeV is excluded at 95% C.L., see their Fig. 5.

Searches Particle Listings

Supersymmetric Particle Searches

- 13** KHACHATRYAN 15o searched in 18.8 fb^{-1} of pp collisions at $\sqrt{s} = 8 \text{ TeV}$ for evidence of long-lived charginos in the context of AMSB and pMSSM scenarios. The results are based on a previously published search for heavy stable charged particles at 7 and 8 TeV. In the minimal AMSB framework with $\tan\beta = 5$ and $\mu \geq 0$, constraints on the chargino mass and lifetime were placed, see Fig. 5. Charginos with a mass below 800 (100) GeV are excluded at the 95% C.L. for lifetimes above 100 ns (3 ns). Constraints are also placed on the pMSSM parameter space, see Fig. 3.
- 14** KHACHATRYAN 15w searched in up to 20.5 fb^{-1} of pp collisions at $\sqrt{s} = 8 \text{ TeV}$ for evidence of long-lived neutralinos produced through \tilde{q} -pair production, with $\tilde{q} \rightarrow q\tilde{\chi}^0$ and $\tilde{\chi}^0 \rightarrow \ell^+\ell^-\nu$ (RPV: $\lambda_{121}, \lambda_{122} \neq 0$). 95% C.L. exclusion limits on cross section times branching ratio are set as a function of mean proper decay length of the neutralino, see Figs. 6 and 9.
- 15** AAD 13BD searched in 20.3 fb^{-1} of pp collisions at $\sqrt{s} = 8 \text{ TeV}$ for events containing tracks with no associated hits in the outer region of the tracking system resulting from the decay of charginos that are nearly mass degenerate with the lightest neutralino, as is often the case in AMSB scenarios. No significant excess above the background expectation is observed for candidate tracks with large transverse momentum. Constraints on chargino properties are obtained and in the minimal AMSB model, a chargino mass below 270 GeV is excluded at 95% C.L., see their Fig. 7.
- 16** ABAZOV 13b looked in 6.3 fb^{-1} of $p\bar{p}$ collisions at $\sqrt{s} = 1.96 \text{ TeV}$ for charged massive long-lived particles in events with muon-like particles that have both speed and ionization energy loss inconsistent with muons produced in beam collisions. In the absence of an excess, limits are set at 95% C.L. on gaugino- and higgsino-like charginos, see their Table 20 and Fig. 23.

$\tilde{\nu}$ (Sneutrino) mass limit

The limits may depend on the number, $N(\tilde{\nu})$, of sneutrinos assumed to be degenerate in mass. Only $\tilde{\nu}_L$ (not $\tilde{\nu}_R$) is assumed to exist. It is possible that $\tilde{\nu}$ could be the lightest supersymmetric particle (LSP).

We report here, but do not include in the Listings, the limits obtained from the fit of the final results obtained by the LEP Collaborations on the invisible width of the Z boson ($\Delta\Gamma_{\text{inv.}} < 2.0 \text{ MeV}$, LEP-SLC 06): $m_{\tilde{\nu}} > 43.7 \text{ GeV}$ ($N(\tilde{\nu})=1$) and $m_{\tilde{\nu}} > 44.7 \text{ GeV}$ ($N(\tilde{\nu})=3$).

Some earlier papers are now obsolete and have been omitted. They were last listed in our PDG 14 edition: K. Olive, et al. (Particle Data Group), Chinese Physics **C38** 070001 (2014) (<http://pdg.lbl.gov>).

VALUE (GeV)	CL%	DOCUMENT ID	TECN	COMMENT
>3400	95	1 AABOUD	18CM ATLS	RPV, $\tilde{\nu}_\tau \rightarrow e\mu$, $\lambda_{312} = \lambda_{321} = 0.07$, $\lambda'_{311} = 0.11$
>2900	95	2 AABOUD	18CM ATLS	RPV, $\tilde{\nu}_\tau \rightarrow e\tau$, $\lambda_{313} = \lambda_{331} = 0.07$, $\lambda'_{311} = 0.11$
>2600	95	3 AABOUD	18CM ATLS	RPV, $\tilde{\nu}_\tau \rightarrow \mu\tau$, $\lambda_{323} = \lambda_{332} = 0.07$, $\lambda'_{311} = 0.11$
>1060	95	4 AABOUD	18Z ATLS	RPV, $\geq 4\ell$, $\lambda_{12k} \neq 0$, $m_{\tilde{\chi}_1^0} = 600 \text{ GeV}$ (mass-degenerate left-handed sleptons and sneutrinos of all 3 generations)
> 780	95	4 AABOUD	18Z ATLS	RPV, $\geq 4\ell$, $\lambda_{133} \neq 0$, $m_{\tilde{\chi}_1^0} = 300 \text{ GeV}$ (mass-degenerate left-handed sleptons and sneutrinos of all 3 generations)
>1700	95	5 SIRUNYAN	18AT CMS	RPV, $\tilde{\nu}_\tau \rightarrow e\mu$, $\lambda_{132} = \lambda_{231} = \lambda'_{311} = 0.01$
>3800	95	5 SIRUNYAN	18AT CMS	RPV, $\tilde{\nu}_\tau \rightarrow e\mu$, $\lambda_{132} = \lambda_{231} = \lambda'_{311} = 0.1$
>2300	95	6 AABOUD	16P ATLS	RPV, $\tilde{\nu}_\tau \rightarrow e\mu$, $\lambda'_{311} = 0.11$
>2200	95	6 AABOUD	16P ATLS	RPV, $\tilde{\nu}_\tau \rightarrow e\tau$, $\lambda'_{311} = 0.11$
>1900	95	6 AABOUD	16P ATLS	RPV, $\tilde{\nu}_\tau \rightarrow \mu\tau$, $\lambda'_{311} = 0.11$
> 400	95	7 AAD	14X ATLS	RPV, $\geq 4\ell^\pm$, $\tilde{\nu} \rightarrow \nu\tilde{\chi}_1^0$, $\tilde{\chi}_1^0 \rightarrow \ell^\pm\ell^\mp\nu$
> 94	95	8 AAD	11Z ATLS	RPV, $\tilde{\nu}_\tau \rightarrow e\mu$
> 41	95	9 ABDALLAH	03M DLPH	$1 \leq \tan\beta \leq 40$, $m_{\tilde{e}_R} - m_{\tilde{\nu}_R} > 10 \text{ GeV}$
> 84	95	10 HEISTER	02N ALEP	$\tilde{\nu}_e$, any Δm
> 41	95	11 DECAMP	92 ALEP	$\Gamma(Z \rightarrow \text{invisible})$; $N(\tilde{\nu})=3$, model independent
• • •		We do not use the following data for averages, fits, limits, etc. • • •		
>1280	95	12 SIRUNYAN	19AO	RPV, $\mu^\pm\mu^\pm + \geq 2\text{jets}$, $\lambda'_{211} \neq 0$, $\tilde{\nu}_\mu \rightarrow \mu\tilde{\chi}_1^\pm$, $\tilde{\chi}_1^\pm \rightarrow \mu q\bar{q}q\bar{q}$
>2300	95	13 KHACHATRYAN...16BE	CMS	RPV, $\tilde{\nu}_\tau \rightarrow e\mu$, $\lambda_{132} = \lambda_{231} = \lambda'_{311} = 0.01$
>2000	95	13 KHACHATRYAN...16BE	CMS	RPV, $\tilde{\nu}_\tau \rightarrow e\mu$, $\lambda_{132} = \lambda_{231} = 0.07$, $\lambda'_{311} = 0.11$
>1700	95	14 AAD	15o ATLS	RPV ($e\mu$), $\tilde{\nu}_\tau$, $\lambda'_{311} = 0.11$, $\lambda_{i3k} = 0.07$
		14 AAD	15o ATLS	RPV ($\tau\mu$, $e\tau$), $\tilde{\nu}_\tau$, $\lambda'_{311} = 0.11$, $\lambda_{i3k} = 0.07$
		15 AAD	13Al ATLS	RPV, $\tilde{\nu}_\tau \rightarrow e\mu$, $e\tau$, $\mu\tau$
		16 AAD	11H ATLS	RPV, $\tilde{\nu}_\tau \rightarrow e\mu$

17 AALTONEN	10Z CDF	RPV, $\tilde{\nu}_\tau \rightarrow e\mu$, $e\tau$, $\mu\tau$	
18 ABAZOV	10M D0	RPV, $\tilde{\nu}_\tau \rightarrow e\mu$	
19 ABDALLAH	04H DLPH	AMSB, $\mu > 0$	
> 37.1	95	20 ADRIANI	93M L3 $\Gamma(Z \rightarrow \text{invisible})$; $N(\tilde{\nu})=1$
> 36	95	ABREU	91F DLPH $\Gamma(Z \rightarrow \text{invisible})$; $N(\tilde{\nu})=1$
> 31.2	95	21 ALEXANDER	91F OPAL $\Gamma(Z \rightarrow \text{invisible})$; $N(\tilde{\nu})=1$

- 1** AABOUD 18CM searched in 36.1 fb^{-1} of pp collisions at $\sqrt{s} = 13 \text{ TeV}$ for heavy particles decaying into an $e\mu$, $e\tau$, $\mu\tau$ final state. No significant deviation from the expected SM background is observed. Limits are set on the mass of a stau neutrino with R-parity-violating couplings. For $\tilde{\nu}_\tau \rightarrow e\mu$, masses below 3.4 TeV are excluded at 95% CL, see their Figure 4(b). Upper limits on the RPV couplings $|\lambda_{312}|$ versus $|\lambda'_{311}|$ are also performed, see their Figure 8(a-b).
- 2** AABOUD 18CM searched in 36.1 fb^{-1} of pp collisions at $\sqrt{s} = 13 \text{ TeV}$ for heavy particles decaying into an $e\mu$, $e\tau$, $\mu\tau$ final state. No significant deviation from the expected SM background is observed. Limits are set on the mass of a stau neutrino with R-parity-violating couplings. For $\tilde{\nu}_\tau \rightarrow e\tau$, masses below 2.9 TeV are excluded at 95% CL, see their Figure 5(b). Upper limits on the RPV couplings $|\lambda_{313}|$ versus $|\lambda'_{311}|$ are also performed, see their Figure 8(c).
- 3** AABOUD 18CM searched in 36.1 fb^{-1} of pp collisions at $\sqrt{s} = 13 \text{ TeV}$ for heavy particles decaying into an $e\mu$, $e\tau$, $\mu\tau$ final state. No significant deviation from the expected SM background is observed. Limits are set on the mass of a stau neutrino with R-parity-violating couplings. For $\tilde{\nu}_\tau \rightarrow \mu\tau$, masses below 2.6 TeV are excluded at 95% CL, see their Figure 6(b). Upper limits on the RPV couplings $|\lambda_{323}|$ versus $|\lambda'_{311}|$ are also performed, see their Figure 8(d).
- 4** AABOUD 18Z searched in 36.1 fb^{-1} of pp collisions at $\sqrt{s} = 13 \text{ TeV}$ for events containing four or more charged leptons (electrons, muons and up to two hadronically decaying taus). No significant deviation from the expected SM background is observed. Limits are set on the Higgsino mass in simplified models of general gauge mediated supersymmetry Tn1n1A/Tn1n1B/Tn1n1C, see their Figure 9. Limits are also set on the wino, slepton, sneutrino and gluino mass in a simplified model of NLSB pair production with R-parity violating decays of the LSP via λ_{12k} or λ_{133} to charged leptons, see their Figures 7, 8.
- 5** SIRUNYAN 18AT searched in 35.9 fb^{-1} of pp collisions at $\sqrt{s} = 13 \text{ TeV}$ for heavy resonances decaying into $e\mu$ final states. No significant excess above the Standard Model expectation is observed and 95% C.L. exclusions are placed on the cross section times branching ratio for the R-parity-violating production and decay of a supersymmetric tau sneutrino, see their Fig. 3.
- 6** AABOUD 16P searched in 3.2 fb^{-1} of pp collisions at $\sqrt{s} = 13 \text{ TeV}$ for events with different flavour dilepton pairs ($e\mu$, $e\tau$, $\mu\tau$) from the production of $\tilde{\nu}_\tau$ via an RPV λ'_{311} coupling and followed by a decay via $\lambda_{312} = \lambda_{321} = 0.07$ for $e + \mu$, via $\lambda_{313} = \lambda_{331} = 0.07$ for $e + \tau$ and via $\lambda_{323} = \lambda_{332} = 0.07$ for $\mu + \tau$. No evidence for a dilepton resonance over the SM expectation is observed, and limits are derived on $m_{\tilde{\nu}}$ at 95% CL, see their Figs. 2(b), 3(b), 4(b), and Table 3.
- 7** AAD 14X searched in 20.3 fb^{-1} of pp collisions at $\sqrt{s} = 8 \text{ TeV}$ for events with at least four leptons (electrons, muons, taus) in the final state. No significant excess above the Standard Model expectations is observed. Limits are set on the sneutrino mass in an R-parity violating simplified model where the decay $\tilde{\nu} \rightarrow \nu\tilde{\chi}_1^0$, with $\tilde{\chi}_1^0 \rightarrow \ell^\pm\ell^\mp\nu$, takes place with a branching ratio of 100%, see Fig. 9.
- 8** AAD 11Z looked in 1.07 fb^{-1} of pp collisions at $\sqrt{s} = 7 \text{ TeV}$ for events with one electron and one muon of opposite charge from the production of $\tilde{\nu}_\tau$ via an RPV λ'_{311} coupling and followed by a decay via λ_{312} into $e + \mu$. No evidence for an (e, μ) resonance over the SM expectation is observed, and a limit is derived in the plane of λ'_{311} versus $m_{\tilde{\nu}}$ for three values of λ_{312} , see their Fig. 2. Masses $m_{\tilde{\nu}} < 1.32$ (1.45) TeV are excluded for $\lambda'_{311} = 0.10$ and $\lambda_{312} = 0.05$ ($\lambda'_{311} = 0.11$ and $\lambda_{312} = 0.07$).
- 9** ABDALLAH 03M uses data from $\sqrt{s} = 192$ -208 GeV to obtain limits in the framework of the MSSM with gaugino and sfermion mass universality at the GUT scale. An indirect limit on the mass is derived by constraining the MSSM parameter space by the results from direct searches for neutralinos (including cascade decays) and for sleptons. These limits are valid for values of $M_2 < 1 \text{ TeV}$, $|\mu| \leq 1 \text{ TeV}$ with the $\tilde{\chi}_1^0$ as LSP. The quoted limit is obtained when there is no mixing in the third family. See Fig. 43 for the mass limits as a function of $\tan\beta$. These limits update the results of ABREU 00w.
- 10** HEISTER 02N derives a bound on $m_{\tilde{\nu}_e}$ by exploiting the mass relation between the $\tilde{\nu}_e$ and \tilde{e} , based on the assumption of universal GUT scale gaugino and scalar masses $m_{1/2}$ and m_0 and the search described in the \tilde{e} section. In the MSUGRA framework with radiative electroweak symmetry breaking, the limit improves to $m_{\tilde{\nu}_e} > 130 \text{ GeV}$, assuming a trilinear coupling $A_0=0$ at the GUT scale. See Figs. 5 and 7 for the dependence of the limits on $\tan\beta$.
- 11** DECAMP 92 limit is from $\Gamma(\text{invisible})/\Gamma(\ell\ell) = 5.91 \pm 0.15$ ($N_{\nu_i} = 2.97 \pm 0.07$).
- 12** SIRUNYAN 19AO searched in 35.9 fb^{-1} of pp collisions at $\sqrt{s} = 13 \text{ TeV}$ for events containing two same-sign muons and at last two jets, originating from resonant production of second-generation sleptons ($\tilde{\mu}_L, \tilde{\nu}_\mu$) via the R-parity violating coupling λ'_{211} to quarks. No significant excess above the Standard Model expectations is observed. Upper limits on cross sections are derived in the context of two simplified models, see their Figure 4. The cross section limits are translated into limits on λ'_{211} for a modified CMSSM, see their Figure 5.
- 13** KHACHATRYAN 16BE searched in 19.7 fb^{-1} of pp collisions at $\sqrt{s} = 8 \text{ TeV}$ for evidence of narrow resonances decaying into $e\mu$ final states. No significant excess above the Standard Model expectation is observed and 95% C.L. exclusions are placed on the cross section times branching ratio for the production of an R-parity-violating supersymmetric tau sneutrino, see their Fig. 3.
- 14** AAD 15o searched in 20.3 fb^{-1} of pp collisions at $\sqrt{s} = 8 \text{ TeV}$ for evidence of heavy particles decaying into $e\mu$, $e\tau$ or $\mu\tau$ final states. No significant excess above the Standard Model expectation is observed, and 95% C.L. exclusions are placed on the cross section times branching ratio for the production of an R-parity-violating supersymmetric tau sneutrino, applicable to any sneutrino flavour, see their Fig. 2.
- 15** AAD 13Al searched in 4.6 fb^{-1} of pp collisions at $\sqrt{s} = 7 \text{ TeV}$ for evidence of heavy particles decaying into $e\mu$, $e\tau$ or $\mu\tau$ final states. No significant excess above the Standard Model expectation is observed, and 95% C.L. exclusions are placed on the cross section times branching ratio for the production of an R-parity-violating supersymmetric tau sneutrino, see their Fig. 2. For couplings $\lambda'_{311} = 0.10$ and $\lambda_{i3k} = 0.05$, the lower limits on the $\tilde{\nu}_\tau$ mass are 1610, 1110, 1100 GeV in the $e\mu$, $e\tau$, and $\mu\tau$ channels, respectively.

See key on page 1127

Searches Particle Listings Supersymmetric Particle Searches

- 16 AAD 11H looked in 35 pb⁻¹ of pp collisions at $\sqrt{s} = 7$ TeV for events with one electron and one muon of opposite charge from the production of $\tilde{\nu}_\tau$ via an RPV λ'_{311} coupling and followed by a decay via λ_{312} into $e + \mu$. No evidence for an excess over the SM expectation is observed, and a limit is derived in the plane of λ'_{311} versus $m_{\tilde{\nu}}$ for several values of λ_{312} , see their Fig. 2. Superseded by AAD 11Z.
- 17 AALTONEN 10Z searched in 1 fb⁻¹ of $p\bar{p}$ collisions at $\sqrt{s} = 1.96$ TeV for events from the production $d\bar{d} \rightarrow \tilde{\nu}_\tau$ with the subsequent decays $\tilde{\nu}_\tau \rightarrow e\mu, \mu\tau, e\tau$ in the MSSM framework with RPV. Two isolated leptons of different flavor and opposite charges are required, with τ s identified by their hadronic decay. No statistically significant excesses are observed over the SM background. Upper limits on λ_{311}^2 times the branching ratio are listed in their Table III for various $\tilde{\nu}_\tau$ masses. Limits on the cross section times branching ratio for $\lambda'_{311} = 0.10$ and $\lambda_{i3k} = 0.05$, displayed in Fig. 2, are used to set limits on the $\tilde{\nu}_\tau$ mass of 558 GeV for the $e\mu$, 441 GeV for the $\mu\tau$ and 442 GeV for the $e\tau$ channels.
- 18 ABAZOV 10M looked in 5.3 fb⁻¹ of $p\bar{p}$ collisions at $\sqrt{s} = 1.96$ TeV for events with exactly one pair of high p_T isolated $e\mu$ and a veto against hard jets. No evidence for an excess over the SM expectation is observed, and a limit at 95% C.L. on the cross section times branching ratio is derived, see their Fig. 3. These limits are translated into limits on couplings as a function of $m_{\tilde{\nu}_\tau}$ as shown on their Fig. 4. As an example, for $m_{\tilde{\nu}_\tau} = 100$ GeV and $\lambda_{312} \leq 0.07$, couplings $\lambda'_{311} > 7.7 \times 10^{-4}$ are excluded.
- 19 ABDALLAH 04H use data from LEP 1 and $\sqrt{s} = 192\text{--}208$ GeV. They re-use results or re-analyze the data from ABDALLAH 03M to put limits on the parameter space of anomaly-mediated supersymmetry breaking (AMSB), which is scanned in the region $1 < m_{3/2} < 50$ TeV, $0 < m_0 < 1000$ GeV, $1.5 < \tan\beta < 35$, both signs of μ . The constraints are obtained from the searches for mass degenerate chargino and neutralino, for SM-like and invisible Higgs, for leptonically decaying charginos and from the limit on non-SM Z width of 3.2 MeV. The limit is for $m_t = 174.3$ GeV (see Table 2 for other m_t values). The limit improves to 114 GeV for $\mu < 0$.
- 20 ADRIANI 93M limit from $\Delta\Gamma(Z)(\text{invisible}) < 16.2$ MeV.
- 21 ALEXANDER 91F limit is for one species of $\tilde{\nu}$ and is derived from $\Gamma(\text{invisible, new})/\Gamma(\ell\ell) < 0.38$.

Charged sleptons

This section contains limits on charged scalar leptons ($\tilde{\ell}$, with $\ell=e,\mu,\tau$). Studies of width and decays of the Z boson (use is made here of $\Delta\Gamma_{\text{inv}} < 2.0$ MeV, LEP 00) conclusively rule out $m_{\tilde{\ell}_R} < 40$ GeV (41 GeV for $\tilde{\ell}_L$), independently of decay modes, for each individual slepton. The limits improve to 43 GeV (43.5 GeV for $\tilde{\ell}_L$) assuming all 3 flavors to be degenerate. Limits on higher mass sleptons depend on model assumptions and on the mass splitting $\Delta m = m_{\tilde{\ell}} - m_{\tilde{\chi}_1^0}$. The mass and composition of $\tilde{\chi}_1^0$ may affect the electron production rate in e^+e^- collisions through t-channel exchange diagrams. Production rates are also affected by the potentially large mixing angle of the lightest mass eigenstate $\tilde{\ell}_1 = \tilde{\ell}_R \sin\theta_{\tilde{\ell}} + \tilde{\ell}_L \cos\theta_{\tilde{\ell}}$. It is generally assumed that only $\tilde{\tau}$ may have significant mixing. The coupling to the Z vanishes for $\theta_{\tilde{\ell}}=0.82$. In the high-energy limit of e^+e^- collisions the interference between γ and Z exchange leads to a minimal cross section for $\theta_{\tilde{\ell}}=0.91$, a value which is sometimes used in the following entries relative to data taken at LEP2. When limits on $m_{\tilde{\ell}_R}$ are quoted, it is understood that limits on $m_{\tilde{\ell}_L}$ are usually at least as strong.

Possibly open decays involving gauginos other than $\tilde{\chi}_1^0$ will affect the detection efficiencies. Unless otherwise stated, the limits presented here result from the study of $\tilde{\ell}^+\tilde{\ell}^-$ production, with production rates and decay properties derived from the MSSM. Limits made obsolete by the recent analyses of e^+e^- collisions at high energies can be found in previous Editions of this Review.

For decays with final state gravitinos (\tilde{G}), $m_{\tilde{G}}$ is assumed to be negligible relative to all other masses.

R-parity conserving \tilde{e} (Selectron) mass limit

Some earlier papers are now obsolete and have been omitted. They were last listed in our PDG 14 edition: K. Olive, et al. (Particle Data Group), Chinese Physics **C38** 070001 (2014) (<http://pdg.lbl.gov>).

VALUE (GeV)	CL%	DOCUMENT ID	TECN	COMMENT
>700	95	1 SIRUNYAN 21M	CMS	$\ell^\pm \ell^\mp + \cancel{E}_T, m_{\tilde{\nu}_\tau} = m_{\tilde{\ell}_L}$ and $\tilde{\ell} = \tilde{e}, \tilde{\mu}, m_{\tilde{\chi}_1^0} = 0$ GeV
>700	95	2 AAD 20a	ATLS	$2\ell + \cancel{E}_T, m_{\tilde{\ell}_R} = m_{\tilde{\ell}_L}$ and $\tilde{\ell} = \tilde{e}, \tilde{\mu}, m_{\tilde{\chi}_1^0} = 0$ GeV
>250	95	3 SIRUNYAN 19Aw	CMS	$\ell^\pm \ell^\mp + \cancel{E}_T, \tilde{e}_R, m_{\tilde{\chi}_1^0} = 0$ GeV
>310	95	3 SIRUNYAN 19Aw	CMS	$\ell^\pm \ell^\mp + \cancel{E}_T, \tilde{e}_L, m_{\tilde{\chi}_1^0} = 0$ GeV
>350	95	3 SIRUNYAN 19Aw	CMS	$\ell^\pm \ell^\mp + \cancel{E}_T, m_{\tilde{e}_R} = m_{\tilde{e}_L}, m_{\tilde{\chi}_1^0} = 0$ GeV
>290	95	3 SIRUNYAN 19Aw	CMS	$\ell^\pm \ell^\mp + \cancel{E}_T, \tilde{e}_R, \tilde{e}_L$ and $\tilde{\ell} = \tilde{e}, \tilde{\mu}, m_{\tilde{\chi}_1^0} = 0$ GeV
>400	95	3 SIRUNYAN 19Aw	CMS	$\ell^\pm \ell^\mp + \cancel{E}_T, \tilde{\ell}_L$ and $\tilde{\ell} = \tilde{e}, \tilde{\mu}, m_{\tilde{\chi}_1^0} = 0$ GeV
>450	95	3 SIRUNYAN 19Aw	CMS	$\ell^\pm \ell^\mp + \cancel{E}_T, m_{\tilde{\ell}_R} = m_{\tilde{\ell}_L}$ and $\tilde{\ell} = \tilde{e}, \tilde{\mu}, m_{\tilde{\chi}_1^0} = 0$ GeV

>500	95	4 AABOUD 18B	ATLS	$2\ell + \cancel{E}_T, m_{\tilde{\ell}_R} = m_{\tilde{\ell}_L}$ and $\tilde{\ell} = \tilde{e}, \tilde{\mu}, \tilde{\tau}$, with $m_{\tilde{\chi}_1^0} = 0$ GeV
>190	95	5 AABOUD 18R	ATLS	2ℓ (soft) + $\cancel{E}_T, m_{\tilde{e}} = m_{\tilde{\mu}}, m_{\tilde{\tau}} = m_{\tilde{\chi}_1^0} = 5$ GeV
> 97.5		6 CHATRCHYAN 14R	CMS	$\geq 3\ell^\pm, \tilde{\ell} \rightarrow \ell^\pm \tau^\mp \tau^\mp \tilde{G}$ simplified model, GMSB, stau (N)NLSF scenario
> 94.4		7 AAD 13B	ATLS	$2\ell^\pm + \cancel{E}_T, \text{SMS, pMSSM}$
> 71.3		8 ABBIENDI 04	OPAL	$\tilde{e}_R, \Delta m > 11$ GeV, $ \mu > 100$ GeV, $\tan\beta=1.5$
none 30-94	95	9 ACHARD 04	L3	$\tilde{e}_R, \Delta m > 10$ GeV, $ \mu > 200$ GeV, $\tan\beta \geq 2$
> 94	95	9 ACHARD 04	L3	$\tilde{e}_R, \text{all } \Delta m$
> 95	95	10 ABDALLAH 03M	DLPH	$\Delta m > 15$ GeV, $\tilde{e}_R^+ \tilde{e}_R^-$
> 73	95	11 ABDALLAH 03M	DLPH	$\tilde{e}_R, 1 \leq \tan\beta \leq 40, \Delta m > 10$ GeV
> 95	95	12 HEISTER 02E	ALEP	$\Delta m > 15$ GeV, $\tilde{e}_R^+ \tilde{e}_R^-$
> 73	95	13 HEISTER 02N	ALEP	$\tilde{e}_R, \text{any } \Delta m$
>107	95	13 HEISTER 02N	ALEP	$\tilde{e}_L, \text{any } \Delta m$
●●● We do not use the following data for averages, fits, limits, etc. ●●●				
>101	95	14 AAD 20i	ATLS	2ℓ (soft), jets, $\cancel{E}_T, \tilde{e}_R$ only, $m_{\tilde{e}_R} - m_{\tilde{\chi}_1^0} = 7.5$ GeV
>169	95	15 AAD 20i	ATLS	2ℓ (soft), jets, $\cancel{E}_T, \tilde{e}_L$ only, $m_{\tilde{e}_L} - m_{\tilde{\chi}_1^0} = 7.1$ GeV
none 90-325	95	16 AAD 14G	ATLS	$\tilde{\ell}\tilde{\ell} \rightarrow \ell^+ \tilde{\chi}_1^0 \ell^- \tilde{\chi}_1^0$, simplified model, $m_{\tilde{\ell}} = m_{\tilde{\tau}}, m_{\tilde{\chi}_1^0} = 0$ GeV
		17 KHACHATRY...14i	CMS	$\tilde{\ell} \rightarrow \ell \tilde{\chi}_1^0$, simplified model

- 1 SIRUNYAN 21M searched in 137 fb⁻¹ of pp collisions at $\sqrt{s} = 13$ TeV for supersymmetry in events with two opposite-sign same-flavor leptons (electrons, muons) and \cancel{E}_T . No significant excess above the Standard Model expectations is observed. Limits are set on the gluino mass in the simplified model Tglu4C, see their Figure 10, on the $\tilde{\chi}_1^0$ and $\tilde{\chi}_1^\pm$ mass in Tchi1n2Fa, see their Figure 11, on the $\tilde{\chi}_1^0$ mass in Tn1n1C and Tn1n1B for $m_{\tilde{\chi}_2^0} = m_{\tilde{\chi}_1^\pm} = m_{\tilde{\chi}_1^0}$, see their Figure 12. Limits are also set on the light squark mass for the simplified model Tsqk2A, on the sbottom mass in Tsbot3, see their Figure 13, and on the slepton mass in direct electroweak pair production of mass-degenerate left- and right-handed sleptons (selectrons and smuons), see their Figure 14.
- 2 AAD 20o reported on a search for electroweak production in models with charginos and sleptons decaying into final states with exactly two oppositely charged leptons and missing transverse momentum. A dataset of pp collisions at $\sqrt{s} = 13$ TeV corresponding to an integrated luminosity of 139 fb⁻¹ was used. Light-flavour sleptons \tilde{e} and $\tilde{\mu}$ are constrained at 95% C.L. to have masses above 700 GeV for massless lightest neutralino, see their Fig. 7(c). Exclusion limits are also set for selectrons and smuons separately, considering either right- or left-handed components, by including only the di-electron and di-muon same-flavour signal regions defined in the search, see their Fig. 8.
- 3 SIRUNYAN 19Aw searched in 35.9 fb⁻¹ of pp collisions at $\sqrt{s} = 13$ TeV for direct electroweak pair production of selectrons or smuons in events with two leptons (electrons or muons) of the opposite electric charge and same flavour, no jets and large \cancel{E}_T . No significant excess above the Standard Model expectations is observed. Limits are set on the slepton mass assuming left-handed, right-handed or both left- and right-handed (mass degenerate) production, see their Figure 6. Similarly, limits are set on the smuon mass, see their Figure 7. Limits are also set on slepton masses under the assumption that the selectron and smuon are mass degenerate, see their Figure 5.
- 4 AABOUD 18B searched in 36.1 fb⁻¹ of pp collisions at $\sqrt{s} = 13$ TeV for direct electroweak production of charginos, chargino and next-to-lightest neutralinos and sleptons in events with two or three leptons (electrons or muons), with or without jets, and large missing transverse energy. No significant excess above the Standard Model expectations is observed. Limits are set on the slepton mass up to 500 GeV for massless $\tilde{\chi}_1^0$, assuming degeneracy of $\tilde{e}, \tilde{\mu}$, and $\tilde{\tau}$ and exploiting the 2ℓ signature, see their Figure 8(b).
- 5 AABOUD 18R searched in 36.1 fb⁻¹ of pp collisions at $\sqrt{s} = 13$ TeV for electroweak production in scenarios with compressed mass spectra in final states with two low-momentum leptons and missing transverse momentum. The data are found to be consistent with the SM prediction. Results are interpreted in slepton pair production models with a fourfold degeneracy assumed in selectron and smuon masses. The \tilde{e} masses are excluded up to 190 GeV for $m_{\tilde{e}} - m_{\tilde{\chi}_1^0} = 5$ GeV. The exclusion limits extend down to mass splittings of 1 GeV, see their Fig. 11.
- 6 CHATRCHYAN 14R searched in 19.5 fb⁻¹ of pp collisions at $\sqrt{s} = 8$ TeV for events with at least three leptons (electrons, muons, taus) in the final state. No significant excess above the Standard Model expectations is observed. Limits are set on the slepton mass in a stau (N)NLSF simplified model (GMSB) where the decay $\tilde{\ell} \rightarrow \ell^\pm \tau^\pm \tau^\mp \tilde{G}$ takes place with a branching ratio of 100%, see Fig. 8.
- 7 AAD 13B searched in 4.7 fb⁻¹ of pp collisions at $\sqrt{s} = 7$ TeV for sleptons decaying to a final state with two leptons (e and μ) and missing transverse energy. No excess beyond the Standard Model expectation is observed. Limits are derived in a simplified model of direct left-handed slepton pair production, where left-handed slepton masses between 85 and 195 GeV are excluded at 95% C.L. for $m_{\tilde{\chi}_1^0} = 20$ GeV. See also Fig. 2(a). Exclusion limits are also derived in the phenomenological MSSM, see Fig. 3.
- 8 ABBIENDI 04 search for $\tilde{e}_R \tilde{e}_R$ production in acoplanar di-electron final states in the 183-208 GeV data. See Fig. 13 for the dependence of the limits on $m_{\tilde{\chi}_1^0}$ and for the limit at $\tan\beta=35$. This limit supersedes ABBIENDI 00g.
- 9 ACHARD 04 search for $\tilde{e}_R \tilde{e}_L$ and $\tilde{e}_R \tilde{e}_R$ production in single- and acoplanar di-electron final states in the 192-209 GeV data. Absolute limits on $m_{\tilde{e}_R}$ are derived from a scan over the MSSM parameter space with universal GUT scale gaugino and scalar masses $m_{1/2}$ and m_0 , $1 \leq \tan\beta \leq 60$ and $-2 \leq \mu \leq 2$ TeV. See Fig. 4 for the dependence of the limits on $m_{\tilde{\chi}_1^0}$. This limit supersedes ACCIARRI 99w.
- 10 ABDALLAH 03M looked for acoplanar dielectron + \cancel{E} final states at $\sqrt{s} = 189\text{--}208$ GeV. The limit assumes $\mu = -200$ GeV and $\tan\beta=1.5$ in the calculation of the production cross

Searches Particle Listings

Supersymmetric Particle Searches

section and $B(\bar{e} \rightarrow e\tilde{\chi}_1^0)$. See Fig. 15 for limits in the $(m_{\tilde{e}_R}, m_{\tilde{\chi}_1^0})$ plane. These limits

include and update the results of ABREU 01

¹¹ ABDALLAH 03M uses data from $\sqrt{s} = 192\text{--}208$ GeV to obtain limits in the framework of the MSSM with gaugino and sfermion mass universality at the GUT scale. An indirect limit on the mass is derived by constraining the MSSM parameter space by the results from direct searches for neutralinos (including cascade decays) and for sleptons. These limits are valid for values of $M_2 < 1$ TeV, $|\mu| \leq 1$ TeV with the $\tilde{\chi}_1^0$ as LSP. The quoted limit is obtained when there is no mixing in the third family. See Fig. 43 for the mass limits as a function of $\tan\beta$. These limits update the results of ABREU 00w.

¹² HEISTER 02E looked for acoplanar dielectron + \cancel{E}_T final states from e^+e^- interactions between 183 and 209 GeV. The mass limit assumes $\mu < -200$ GeV and $\tan\beta=2$ for the production cross section and $B(\bar{e} \rightarrow e\tilde{\chi}_1^0)=1$. See their Fig. 4 for the dependence of the limit on Δm . These limits include and update the results of BARATE 01.

¹³ HEISTER 02N search for $\tilde{e}_R \tilde{e}_L$ and $\tilde{e}_R \tilde{e}_R$ production in single- and acoplanar dielectron final states in the 183–208 GeV data. Absolute limits on $m_{\tilde{e}_R}$ are derived from a scan over the MSSM parameter space with universal GUT scale gaugino and scalar masses $m_{1/2}$ and m_0 , $1 \leq \tan\beta \leq 50$ and $-10 \leq \mu \leq 10$ TeV. The region of small $|\mu|$, where cascade decays are important, is covered by a search for $\tilde{\chi}_1^0 \tilde{\chi}_3^0$ in final states with leptons and possibly photons. Limits on $m_{\tilde{e}_L}$ are derived by exploiting the mass relation between the \tilde{e}_L and \tilde{e}_R , based on universal m_0 and $m_{1/2}$. When the constraint from the mass limit of the lightest Higgs from HEISTER 02 is included, the bounds improve to $m_{\tilde{e}_R} > 77(75)$ GeV and $m_{\tilde{e}_L} > 115(115)$ GeV for a top mass of 175(180) GeV. In the MSUGRA framework with radiatively broken electroweak symmetry breaking, the limits improve further to $m_{\tilde{e}_R} > 95$ GeV and $m_{\tilde{e}_L} > 152$ GeV, assuming a trilinear coupling $A_0=0$ at the GUT scale. See Figs. 4, 5, 7 for the dependence of the limits on $\tan\beta$.

¹⁴ AAD 20i reported on ATLAS searches for slepton pair production in models with compressed mass spectra. A dataset of pp collisions at $\sqrt{s} = 13$ TeV corresponding to an integrated luminosity of 139 fb^{-1} was used. Events with \cancel{E}_T , two same-flavour, opposite-charge, low-transverse-momentum leptons, and jets from initial-state radiation or characteristic of vector-boson fusion production are selected. Light-flavour sleptons \tilde{e} and $\tilde{\mu}$ are constrained at 95% C.L. to have masses above 251 GeV for a mass splitting slepton– $\tilde{\chi}_1^0$ of 10 GeV, with constraints extending down to mass splittings of 550 MeV at the LEP slepton limits (73 GeV), see their Fig. 16(a). If only selectrons are considered, and $\tilde{e} = \tilde{e}_R$, masses below 101 GeV are excluded for mass splitting $\tilde{e}_R, \tilde{\chi}_1^0$ of 7.5 GeV. See their Fig. 16(b).

¹⁵ AAD 20j reported on ATLAS searches for slepton pair production in models with compressed mass spectra. A dataset of pp collisions at $\sqrt{s} = 13$ TeV corresponding to an integrated luminosity of 139 fb^{-1} was used. Events with \cancel{E}_T , two same-flavour, opposite-charge, low-transverse-momentum leptons, and jets from initial-state radiation or characteristic of vector-boson fusion production are selected. Light-flavour sleptons \tilde{e} and $\tilde{\mu}$ are constrained at 95% C.L. to have masses above 251 GeV for a mass splitting slepton– $\tilde{\chi}_1^0$ of 10 GeV, with constraints extending down to mass splittings of 550 MeV at the LEP slepton limits (73 GeV). See their Fig. 16(a). If only selectron are considered, and $\tilde{e} = \tilde{e}_L$, masses below 169 GeV are excluded for mass splitting $\tilde{e}_L, \tilde{\chi}_1^0$ of 7.1 GeV. See their Fig. 16(b).

¹⁶ AAD 14g searched in 20.3 fb^{-1} of pp collisions at $\sqrt{s} = 8$ TeV for electroweak production of slepton pairs, decaying to a final state with two leptons (e and μ) and missing transverse momentum. No excess beyond the Standard Model expectation is observed. Exclusion limits are derived in simplified models of slepton pair production, see Fig. 8. An interpretation in the pMSSM is also given, see Fig. 10.

¹⁷ KHACHATRYAN 14i searched in 19.5 fb^{-1} of pp collisions at $\sqrt{s} = 8$ TeV for electroweak production of slepton pairs decaying to a final state with opposite-sign lepton pairs (e or μ) and missing transverse momentum. No excess beyond the Standard Model expectation is observed. Exclusion limits are derived in simplified models, see Fig. 18.

R-parity violating \tilde{e} (Selectron) mass limit

Some earlier papers are now obsolete and have been omitted. They were last listed in our PDG 14 edition: K. Olive, et al. (Particle Data Group), Chinese Physics **C38** 070001 (2014) (<http://pdg.lbl.gov>).

VALUE (GeV)	CL%	DOCUMENT ID	TECN	COMMENT
>1200	95	¹ AAD	21Y ATLS	$\geq 4\ell, \lambda_{12k} \neq 0, m_{\tilde{\chi}_1^0} = 900$ GeV (mass-degenerate $\tilde{\ell}_L$ and $\tilde{\nu}$ of all 3 generations)
> 870	95	¹ AAD	21Y ATLS	$\geq 4\ell, \lambda_{i33} \neq 0, m_{\tilde{\chi}_1^0} = 450$ GeV (mass-degenerate $\tilde{\ell}_L$ and $\tilde{\nu}$ of all 3 generations)
>1065	95	² AABOUD	18Z ATLS	$\geq 4\ell, \lambda_{12k} \neq 0, m_{\tilde{\chi}_1^0} = 600$ GeV (mass-degenerate left-handed sleptons and sneutrinos of all 3 generations)
> 780	95	² AABOUD	18Z ATLS	$\geq 4\ell, \lambda_{i33} \neq 0, m_{\tilde{\chi}_1^0} = 300$ GeV (mass-degenerate left-handed sleptons and sneutrinos of all 3 generations)
> 410	95	³ AAD	14x ATLS	$\geq 4\ell^\pm, \tilde{\ell} \rightarrow l\tilde{\chi}_1^0, \tilde{\chi}_1^0 \rightarrow \ell^\pm \tilde{\ell}^* \nu$
•••				We do not use the following data for averages, fits, limits, etc. •••
> 89	95	⁴ ABBIENDI	04F OPAL	\tilde{e}_L
> 92	95	⁵ ABDALLAH	04M DLPH	\tilde{e}_R , indirect, $\Delta m > 5$ GeV

¹ AAD 21Y searched in 139 fb^{-1} of pp collisions at $\sqrt{s} = 13$ TeV for supersymmetry in events with four or more leptons (electrons, muons and tau-leptons). No significant excess above the Standard Model expectations is observed. Limits are set on Tch1n2-GGM, and RPV models similar to Tch1n2l, Tglu1A (with $q = u, d, s, c, b$, with equal branching fractions), and $\tilde{\ell}_L / \tilde{\nu} \rightarrow \ell / \nu \tilde{\chi}_1^0$ (mass-degenerate $\tilde{\ell}_L$ and $\tilde{\nu}$ of all 3 generations), all with $\tilde{\chi}_1^0 \rightarrow \ell^\pm \tilde{\ell}^* \nu$ via λ_{12k} or λ_{i33} (where $i, k = 1, 2$), see their Figure 11.

² AABOUD 18Z searched in 36.1 fb^{-1} of pp collisions at $\sqrt{s} = 13$ TeV for events containing four or more charged leptons (electrons, muons and up to two hadronically decaying

taus). No significant deviation from the expected SM background is observed. Limits are set on the Higgsino mass in simplified models of general gauge mediated supersymmetry Tn1n1A/Tn1n1B/Tn1n1C, see their Figure 9. Limits are also set on the wino, slepton, sneutrino and gluino mass in a simplified model of NLSP pair production with R-parity violating decays of the LSP via λ_{12k} or λ_{i33} to charged leptons, see their Figures 7, 8.

³ AAD 14x searched in 20.3 fb^{-1} of pp collisions at $\sqrt{s} = 8$ TeV for events with at least four leptons (electrons, muons, taus) in the final state. No significant excess above the Standard Model expectations is observed. Limits are set on the slepton mass in an R-parity violating simplified model where the decay $\tilde{\ell} \rightarrow \ell \tilde{\chi}_1^0$, with $\tilde{\chi}_1^0 \rightarrow \ell^\pm \tilde{\ell}^* \nu$, takes place with a branching ratio of 100%, see Fig. 9.

⁴ ABBIENDI 04F use data from $\sqrt{s} = 189\text{--}209$ GeV. They derive limits on sparticle masses under the assumption of RPV with $LL\tilde{E}$ or $LQ\tilde{D}$ couplings. The results are valid for $\tan\beta = 1.5$, $\mu = -200$ GeV, with, in addition, $\Delta m > 5$ GeV for indirect decays via $LQ\tilde{D}$. The limit quoted applies to direct decays via $LL\tilde{E}$ or $LQ\tilde{D}$ couplings. For indirect decays, the limits on the \tilde{e}_R mass are respectively 99 and 92 GeV for $LL\tilde{E}$ and $LQ\tilde{D}$ couplings and $m_{\tilde{\chi}_1^0} = 10$ GeV and degrade slightly for larger $\tilde{\chi}_1^0$ mass. Supersedes the results of ABBIENDI 00.

⁵ ABDALLAH 04M use data from $\sqrt{s} = 192\text{--}208$ GeV to derive limits on sparticle masses under the assumption of RPV with $LL\tilde{E}$ or $U\tilde{D}\tilde{D}$ couplings. The results are valid for $\mu = -200$ GeV, $\tan\beta = 1.5$, $\Delta m > 5$ GeV and assuming a BR of 1 for the given decay. The limit quoted is for indirect $U\tilde{D}\tilde{D}$ decays using the neutralino constraint of 39.5 GeV for $LL\tilde{E}$ and of 38.0 GeV for $U\tilde{D}\tilde{D}$ couplings, also derived in ABDALLAH 04M. For indirect decays via $LL\tilde{E}$ the limit improves to 95 GeV if the constraint from the neutralino is used and to 94 GeV if it is not used. For indirect decays via $U\tilde{D}\tilde{D}$ couplings it remains unchanged when the neutralino constraint is not used. Supersedes the result of ABREU 00u.

R-parity conserving $\tilde{\mu}$ (Smuon) mass limit

VALUE (GeV)	CL%	DOCUMENT ID	TECN	COMMENT
>700	95	¹ SIRUNYAN	21M CMS	$\ell^\pm \tilde{\ell}^* + \cancel{E}_T, m_{\tilde{e}} = m_{\tilde{\mu}_L}$ and $\tilde{\ell} = \tilde{e}, \tilde{\mu}, m_{\tilde{\chi}_1^0} = 0$ GeV
>150	95	² AAD	20i ATLS	2ℓ (soft), jets, $\cancel{E}_T, \tilde{\mu}_R$ only, $m_{\tilde{\mu}_R} - m_{\tilde{\chi}_1^0} = 8.2$ GeV
>216	95	³ AAD	20i ATLS	2ℓ (soft), jets, $\cancel{E}_T, \tilde{\mu}_L$ only, $m_{\tilde{\mu}_L} - m_{\tilde{\chi}_1^0} = 10$ GeV
>700	95	⁴ AAD	20o ATLS	$2\ell + \cancel{E}_T, m_{\tilde{e}_R} = m_{\tilde{\mu}_L}$ and $\tilde{\ell} = \tilde{e}, \tilde{\mu}, m_{\tilde{\chi}_1^0} = 0$ GeV
>210	95	⁵ SIRUNYAN	19AW CMS	$\ell^\pm \tilde{\ell}^* + \cancel{E}_T, \tilde{\mu}_R, m_{\tilde{\chi}_1^0} = 0$ GeV
>280	95	⁵ SIRUNYAN	19AW CMS	$\ell^\pm \tilde{\ell}^* + \cancel{E}_T, \tilde{\mu}_L, m_{\tilde{\chi}_1^0} = 0$ GeV
>290	95	⁵ SIRUNYAN	19AW CMS	$\ell^\pm \tilde{\ell}^* + \cancel{E}_T, \tilde{e}_R$ and $\tilde{\ell} = \tilde{e}, \tilde{\mu}, m_{\tilde{\chi}_1^0} = 0$ GeV
>400	95	⁵ SIRUNYAN	19AW CMS	$\ell^\pm \tilde{\ell}^* + \cancel{E}_T, \tilde{e}_L$ and $\tilde{\ell} = \tilde{e}, \tilde{\mu}, m_{\tilde{\chi}_1^0} = 0$ GeV
>450	95	⁵ SIRUNYAN	19AW CMS	$\ell^\pm \tilde{\ell}^* + \cancel{E}_T, m_{\tilde{e}_R} = m_{\tilde{\mu}_L}$ and $\tilde{\ell} = \tilde{e}, \tilde{\mu}, m_{\tilde{\chi}_1^0} = 0$ GeV
>310	95	⁵ SIRUNYAN	19AW CMS	$\ell^\pm \tilde{\ell}^* + \cancel{E}_T, m_{\tilde{\mu}_R} = m_{\tilde{\mu}_L}, m_{\tilde{\chi}_1^0} = 0$ GeV
>190	95	⁶ AABOUD	18R ATLS	2ℓ (soft) + $\cancel{E}_T, m_{\tilde{e}} = m_{\tilde{\mu}}, m_{\tilde{\mu}} - m_{\tilde{\chi}_1^0} = 5$ GeV
		⁷ CHATRCHYAN 14R	CMS	$\geq 3\ell^\pm, \tilde{\ell} \rightarrow \ell^\pm \tau^* \tau^* \tilde{G}$ simplified model, GMSB, stau (N)NLSP scenario
> 91.0		⁸ AAD	13B ATLS	$2\ell^\pm + \cancel{E}_T, \text{SMS, pMSSM}$
> 86.7		⁹ ABBIENDI	04 OPAL	$\Delta m > 3$ GeV, $\tilde{\mu}_R^+ \tilde{\mu}_R^-$, $ \mu > 100$ GeV, $\tan\beta = 1.5$
> 86.7		¹⁰ ACHARD	04 L3	$\Delta m > 10$ GeV, $\tilde{\mu}_R^+ \tilde{\mu}_R^-$, $ \mu > 200$ GeV, $\tan\beta \geq 2$
> 94	95	¹¹ ABDALLAH	03M DLPH	$\Delta m > 5$ GeV, $\tilde{\mu}_R^+ \tilde{\mu}_R^-$
> 88	95	¹² ABDALLAH	03M DLPH	$\tilde{\mu}_R 1 \leq \tan\beta \leq 40, \Delta m > 10$ GeV
> 88	95	¹³ HEISTER	02E ALEP	$\Delta m > 15$ GeV, $\tilde{\mu}_R^+ \tilde{\mu}_R^-$
•••				We do not use the following data for averages, fits, limits, etc. •••
>500	95	¹⁴ AABOUD	18BT ATLS	$2\ell + \cancel{E}_T, m_{\tilde{e}_R} = m_{\tilde{\mu}_L}$ and $\tilde{\ell} = \tilde{e}, \tilde{\mu}, \tilde{\tau}$, with $m_{\tilde{\chi}_1^0} = 0$ GeV
none 90–325	95	¹⁵ AAD	14G ATLS	$\tilde{\ell}\tilde{\ell} \rightarrow \ell^+ \tilde{\chi}_1^0 \ell^- \tilde{\chi}_1^0$, simplified model, $m_{\tilde{e}_L} = m_{\tilde{\mu}_R}, m_{\tilde{\chi}_1^0} = 0$ GeV
> 80	95	¹⁶ KHACHATRYAN 14i	CMS	$\tilde{\ell} \rightarrow \ell \tilde{\chi}_1^0$, simplified model
> 80	95	¹⁷ ABREU	00V DLPH	$\tilde{\mu}_R \tilde{\mu}_R (\tilde{\mu}_R \rightarrow \mu \tilde{G}), m_{\tilde{G}} > 8$ eV

¹ SIRUNYAN 21M searched in 137 fb^{-1} of pp collisions at $\sqrt{s} = 13$ TeV for supersymmetry in events with two opposite-sign same-flavor leptons (electrons, muons) and \cancel{E}_T . No significant excess above the Standard Model expectations is observed. Limits are set on the gluino mass in the simplified model Tglu4C, see their Figure 10, on the $\tilde{\chi}_2^0$ and $\tilde{\chi}_1^\pm$ mass in Tch1n2Fa, see their Figure 11, on the $\tilde{\chi}_1^0$ mass in Tn1n1C and Tn1n1B for $m_{\tilde{\chi}_2^0} = m_{\tilde{\chi}_1^\pm} = m_{\tilde{\chi}_1^0}$, see their Figure 12. Limits are also set on the light squark mass for the simplified model Tsqk2A, on the sbottom mass in Tsb0t3, see their Figure 13, and on the slepton mass in direct electroweak pair production of mass-degenerate left- and right-handed sleptons (selectrons and smuons), see their Figure 14.

- ² AAD 20i reported on ATLAS searches for slepton pair production in models with compressed mass spectra. A dataset of pp collisions at $\sqrt{s} = 13$ TeV corresponding to an integrated luminosity of 139 fb^{-1} was used. Events with \cancel{E}_T , two same-flavour, opposite-charge, low-transverse-momentum leptons, and jets from initial-state radiation or characteristic of vector-boson fusion production are selected. Light-flavour sleptons \tilde{e} and $\tilde{\mu}$ are constrained at 95% C.L. to have masses above 251 GeV for a mass splitting slepton- $\tilde{\chi}_1^0$ of 10 GeV, with constraints extending down to mass splittings of 550 MeV at the LEP slepton limits (73 GeV). See their Fig. 16(a). If only smuon are considered, and $\tilde{\mu} = \tilde{\mu}_R$, masses below 150 GeV are excluded for mass splitting $\tilde{\mu}_R, \tilde{\chi}_1^0$ of 8.2 GeV. See their Fig. 16(b).
- ³ AAD 20i reported on ATLAS searches for slepton pair production in models with compressed mass spectra. A dataset of pp collisions at $\sqrt{s} = 13$ TeV corresponding to an integrated luminosity of 139 fb^{-1} was used. Events with \cancel{E}_T , two same-flavour, opposite-charge, low-transverse-momentum leptons, and jets from initial-state radiation or characteristic of vector-boson fusion production are selected. Light-flavour sleptons \tilde{e} and $\tilde{\mu}$ are constrained at 95% C.L. to have masses above 251 GeV for a mass splitting slepton- $\tilde{\chi}_1^0$ of 10 GeV, with constraints extending down to mass splittings of 550 MeV at the LEP slepton limits (73 GeV). See their Fig. 16(a). If only smuon are considered, and $\tilde{\mu} = \tilde{\mu}_L$, masses below 216 GeV are excluded for mass splitting $\tilde{\mu}_L, \tilde{\chi}_1^0$ of 10 GeV. See their Fig. 16(b).
- ⁴ AAD 20o reported on a search for electroweak production in models with charginos and sleptons decaying into final states with exactly two oppositely charged leptons and missing transverse momentum. A dataset of pp collisions at $\sqrt{s} = 13$ TeV corresponding to an integrated luminosity of 139 fb^{-1} was used. Light-flavour sleptons \tilde{e} and $\tilde{\mu}$ are constrained at 95% C.L. to have masses above 700 GeV for massless lightest neutralino, see their Fig. 7(c). Exclusion limits are also set for selectrons and smuons separately, considering either right- or left-handed components, by including only the di-electron and di-muon same-flavour signal regions defined in the search, see their Fig. 8.
- ⁵ SIRUNYAN 19AW searched in 35.9 fb^{-1} of pp collisions at $\sqrt{s} = 13$ TeV for direct electroweak pair production of selectrons or smuons in events with two leptons (electrons or muons) of the opposite electric charge and same flavour, no jets and large \cancel{E}_T . No significant excess above the Standard Model expectations is observed. Limits are set on the selectron mass assuming left-handed, right-handed or both left- and right-handed (mass degenerate) production, see their Figure 6. Similarly, limits are set on the smuon mass, see their Figure 7. Limits are also set on slepton masses under the assumption that the selectron and smuon are mass degenerate, see their Figure 5.
- ⁶ AABOUD 18R searched in 36.1 fb^{-1} of pp collisions at $\sqrt{s} = 13$ TeV for electroweak production in scenarios with compressed mass spectra in final states with two low-momentum leptons and missing transverse momentum. The data are found to be consistent with the SM prediction. Results are interpreted in slepton pair production models with a fourfold degeneracy assumed in selectron and smuon masses. The $\tilde{\mu}$ masses are excluded up to 190 GeV for $m_{\tilde{\mu}} - m_{\tilde{\chi}_1^0} = 5$ GeV. The exclusion limits extend down to mass splittings of 1 GeV, see their Fig. 11.
- ⁷ CHATRCHYAN 14R searched in 19.5 fb^{-1} of pp collisions at $\sqrt{s} = 8$ TeV for events with at least three leptons (electrons, muons, taus) in the final state. No significant excess above the Standard Model expectations is observed. Limits are set on the slepton mass in a stau (N)NLSP simplified model (GMSB) where the decay $\tilde{e} \rightarrow e^{\pm} \tau^{\pm} \tilde{\nu} \tilde{G}$ takes place with a branching ratio of 100%, see Fig. 8.
- ⁸ AAD 13s searched in 4.7 fb^{-1} of pp collisions at $\sqrt{s} = 7$ TeV for sleptons decaying to a final state with two leptons (e and μ) and missing transverse energy. No excess beyond the Standard Model expectation is observed. Limits are derived in a simplified model of direct left-handed slepton pair production, where left-handed slepton masses between 85 and 195 GeV are excluded at 95% C.L. for $m_{\tilde{\chi}_1^0} = 20$ GeV. See also Fig. 2(a). Exclusion limits are also derived in the phenomenological MSSM, see Fig. 3.
- ⁹ ABBIENDI 04 search for $\tilde{\mu}_R \tilde{\mu}_R$ production in acoplanar di-muon final states in the 183–208 GeV data. See Fig. 14 for the dependence of the limits on $m_{\tilde{\chi}_1^0}$ and for the limit at $\tan\beta=35$. Under the assumption of 100% branching ratio for $\tilde{\mu}_R \rightarrow \mu \tilde{\chi}_1^0$, the limit improves to 94.0 GeV for $\Delta m > 4$ GeV. See Fig. 11 for the dependence of the limits on $m_{\tilde{\chi}_1^0}$ at several values of the branching ratio. This limit supersedes ABBIENDI 00g.
- ¹⁰ ACHARD 04 search for $\tilde{\mu}_R \tilde{\mu}_R$ production in acoplanar di-muon final states in the 192–209 GeV data. Limits on $m_{\tilde{\mu}_R}$ are derived from a scan over the MSSM parameter space with universal GUT scale gaugino and scalar masses $m_{1/2}$ and m_0 , $1 \leq \tan\beta \leq 60$ and $-2 \leq \mu \leq 2$ TeV. See Fig. 4 for the dependence of the limits on $m_{\tilde{\chi}_1^0}$. This limit supersedes ACCIARRI 99w.
- ¹¹ ABDALLAH 03M looked for acoplanar dimuon + \cancel{E} final states at $\sqrt{s} = 189$ –208 GeV. The limit assumes $B(\tilde{\mu} \rightarrow \mu \tilde{\chi}_1^0) = 100\%$. See Fig. 16 for limits on the $(m_{\tilde{\mu}_R}, m_{\tilde{\chi}_1^0})$ plane. These limits include and update the results of ABREU 01.
- ¹² ABDALLAH 03M uses data from $\sqrt{s} = 192$ –208 GeV to obtain limits in the framework of the MSSM with gaugino and sfermion mass universality at the GUT scale. An indirect limit on the mass is derived by constraining the MSSM parameter space by the results from direct searches for neutralinos (including cascade decays) and for sleptons. These limits are valid for values of $M_2 < 1$ TeV, $|\mu| \leq 1$ TeV with the $\tilde{\chi}_1^0$ as LSP. The quoted limit is obtained when there is no mixing in the third family. See Fig. 43 for the mass limits as a function of $\tan\beta$. These limits update the results of ABREU 00w.
- ¹³ HEISTER 02E looked for acoplanar dimuon + \cancel{E}_T final states from e^+e^- interactions between 183 and 209 GeV. The mass limit assumes $B(\tilde{\mu} \rightarrow \mu \tilde{\chi}_1^0) = 1$. See their Fig. 4 for the dependence of the limit on Δm . These limits include and update the results of BARATE 01.
- ¹⁴ AABOUD 18BT searched in 36.1 fb^{-1} of pp collisions at $\sqrt{s} = 13$ TeV for direct electroweak production of charginos, chargino and next-to-lightest neutralinos and sleptons in events with two or three leptons (electrons or muons), with or without jets, and large missing transverse energy. No significant excess above the Standard Model expectations is observed. Limits are set on the slepton mass up to 500 GeV for massless $\tilde{\chi}_1^0$, assuming degeneracy of $\tilde{e}, \tilde{\mu}$, and $\tilde{\tau}$ and exploiting the 2ℓ signature, see their Figure 8(b).
- ¹⁵ AAD 14G searched in 20.3 fb^{-1} of pp collisions at $\sqrt{s} = 8$ TeV for electroweak production of slepton pairs, decaying to a final state with two leptons (e and μ) and missing transverse momentum. No excess beyond the Standard Model expectation is observed. Exclusion limits are derived in simplified models of slepton pair production, see Fig. 8. An interpretation in the pMSSM is also given, see Fig. 10.

- ¹⁶ KHACHATRYAN 14i searched in 19.5 fb^{-1} of pp collisions at $\sqrt{s} = 8$ TeV for electroweak production of slepton pairs decaying to a final state with opposite-sign lepton pairs (e or μ) and missing transverse momentum. No excess beyond the Standard Model expectation is observed. Exclusion limits are derived in simplified models, see Fig. 18.
- ¹⁷ ABREU 00v use data from $\sqrt{s} = 130$ –189 GeV to search for tracks with large impact parameter or visible decay vertices. Limits are obtained as function of $m_{\tilde{e}}$, after combining these results with the search for slepton pair production in the SUGRA framework from ABREU 01 to cover prompt decays and on stable particle searches from ABREU 00q. For limits at different $m_{\tilde{e}}$, see their Fig. 12.

R-parity violating $\tilde{\mu}$ (Smuon) mass limit

VALUE (GeV)	CL%	DOCUMENT ID	TECN	COMMENT
>1200	95	¹ AAD	21Y ATLS	$\geq 4\ell, \lambda_{12k} \neq 0, m_{\tilde{\chi}_1^0} = 900$ GeV (mass-degenerate \tilde{L} and $\tilde{\nu}$ of all 3 generations)
> 870	95	¹ AAD	21Y ATLS	$\geq 4\ell, \lambda_{133} \neq 0, m_{\tilde{\chi}_1^0} = 450$ GeV (mass-degenerate \tilde{L} and $\tilde{\nu}$ of all 3 generations)
> 780	95	² AABOUD	18Z ATLS	$\geq 4\ell, \lambda_{133} \neq 0, m_{\tilde{\chi}_1^0} = 300$ GeV (mass-degenerate left-handed sleptons and sneutrinos of all 3 generations)
>1060	95	² AABOUD	18Z ATLS	$\geq 4\ell, \lambda_{12k} \neq 0, m_{\tilde{\chi}_1^0} = 600$ GeV (mass-degenerate left-handed sleptons and sneutrinos of all 3 generations)
> 410	95	³ AAD	14X ATLS	RPV, $\geq 4\ell^{\pm}, \tilde{e} \rightarrow \ell \tilde{\chi}_1^0, \tilde{\chi}_1^0 \rightarrow \ell^{\pm} \tilde{e} \tilde{\nu}$ • • • We do not use the following data for averages, fits, limits, etc. • • •
		⁴ SIRUNYAN	19Ao	$\mu^{\pm} \mu^{\pm} + \geq 2\text{jets}, \lambda'_{211} \neq 0,$ $\tilde{\mu}_L \rightarrow \mu \tilde{\chi}_1^0, \tilde{\chi}_1^0 \rightarrow \mu q \bar{q}$
> 87	95	⁵ ABDALLAH	04M DLPH	RPV, $\tilde{\mu}_R$, indirect, $\Delta m > 5$ GeV
> 81	95	⁶ HEISTER	03G ALEP	RPV, $\tilde{\mu}_L$

- ¹ AAD 21Y searched in 139 fb^{-1} of pp collisions at $\sqrt{s} = 13$ TeV for supersymmetry in events with four or more leptons (electrons, muons and tau-leptons). No significant excess above the Standard Model expectations is observed. Limits are set on Tch1n12-GGM, and RPV models similar to Tch1n2l, Tglu1A (with $q = u, d, s, c, b$, with equal branching fractions), and $\tilde{e}_L/\tilde{\nu} \rightarrow \ell/\nu \tilde{\chi}_1^0$ (mass-degenerate \tilde{e}_L and $\tilde{\nu}$ of all 3 generations), all with $\tilde{\chi}_1^0 \rightarrow \ell^{\pm} \tilde{e} \tilde{\nu}$ via λ_{12k} or λ_{133} (where $i, k \in 1, 2$), see their Figure 11.
- ² AABOUD 18Z searched in 36.1 fb^{-1} of pp collisions at $\sqrt{s} = 13$ TeV for events containing four or more charged leptons (electrons, muons and up to two hadronically decaying taus). No significant deviation from the expected SM background is observed. Limits are set on the Higgsino mass in simplified models of general gauge mediated supersymmetry Tn1n1A/Tn1n1B/Tn1n1C, see their Figure 9. Limits are also set on the wino, slepton, sneutrino and gluino mass in a simplified model of NLSP pair production with R-parity violating decays of the LSP via λ_{12k} or λ_{133} to charged leptons, see their Figures 7, 8.
- ³ AAD 14x searched in 20.3 fb^{-1} of pp collisions at $\sqrt{s} = 8$ TeV for events with at least four leptons (electrons, muons, taus) in the final state. No significant excess above the Standard Model expectations is observed. Limits are set on the slepton mass in an R-parity violating simplified model where the decay $\tilde{e} \rightarrow \ell \tilde{\chi}_1^0$, with $\tilde{\chi}_1^0 \rightarrow \ell^{\pm} \tilde{e} \tilde{\nu}$, takes place with a branching ratio of 100%, see Fig. 9.
- ⁴ SIRUNYAN 19Ao searched in 35.9 fb^{-1} of pp collisions at $\sqrt{s} = 13$ TeV for events containing two same-sign muons and at last two jets, originating from resonant production of second-generation sleptons ($\tilde{\mu}_L, \tilde{\nu}_\mu$) via the R-parity violating coupling λ'_{211} to quarks. No significant excess above the Standard Model expectations is observed. Upper limits on cross sections are derived in the context of two simplified models, see their Figure 4. The cross section limits are translated into limits on λ'_{211} for a modified CMSSM, see their Figure 5.
- ⁵ ABDALLAH 04M use data from $\sqrt{s} = 192$ –208 GeV to derive limits on sparticle masses under the assumption of RPV with $L\tilde{E}$ or $\tilde{U}\tilde{D}\tilde{D}$ couplings. The results are valid for $\mu = -200$ GeV, $\tan\beta = 1.5$, $\Delta m \geq 5$ GeV and assuming a BR of 1 for the given decay. The limit quoted is for indirect $\tilde{U}\tilde{D}\tilde{D}$ decays using the neutralino constraint of 39.5 GeV for $L\tilde{E}$ and of 38.0 GeV for $\tilde{U}\tilde{D}\tilde{D}$ couplings, also derived in ABDALLAH 04M. For indirect decays via $L\tilde{E}$ the limit improves to 90 GeV if the constraint from the neutralino is used and remains at 87 GeV if it is not used. For indirect decays via $\tilde{U}\tilde{D}\tilde{D}$ couplings it degrades to 85 GeV when the neutralino constraint is not used. Supersedes the result of ABREU 00u.
- ⁶ HEISTER 03G searches for the production of smuons in the case of RPV prompt decays with $L\tilde{E}, L\tilde{Q}\tilde{D}$ or $\tilde{U}\tilde{D}\tilde{D}$ couplings at $\sqrt{s} = 189$ –209 GeV. The search is performed for direct and indirect decays, assuming one coupling at a time to be non-zero. The limit holds for direct decays mediated by RPV $L\tilde{Q}\tilde{D}$ couplings and improves to 90 GeV for indirect decays (for $\Delta m > 10$ GeV). Limits are also given for $L\tilde{E}$ direct ($m_{\tilde{\mu}_R} > 87$ GeV) and indirect decays ($m_{\tilde{\mu}_R} > 96$ GeV for $m(\tilde{\chi}_1^0) > 23$ GeV from BARATE 98s) and for $\tilde{U}\tilde{D}\tilde{D}$ indirect decays ($m_{\tilde{\mu}_R} > 85$ GeV for $\Delta m > 10$ GeV). Supersedes the results from BARATE 01s.

R-parity conserving $\tilde{\tau}$ (Stau) mass limit

Some earlier papers are now obsolete and have been omitted. They were last listed in our PDG 14 edition: K. Olive, *et al.* (Particle Data Group), Chinese Physics **C38** 070001 (2014) (<http://pdg.lbl.gov>).

VALUE (GeV)	CL%	DOCUMENT ID	TECN	COMMENT
none 120–390	95	¹ AAD	20H	2 hadronic $\tau + \cancel{E}_T, \tilde{\tau}_{R/L} \rightarrow \tau \tilde{\chi}_1^0, m_{\tilde{\chi}_1^0} = 0$ GeV

Searches Particle Listings

Supersymmetric Particle Searches

none	90–150	95	2	SIRUNYAN	20P	CMS	$2\tau + \cancel{E}_T, \tau h \tau h$ and $\ell \tau h$, $m_{\tilde{\tau}_R} = m_{\tilde{\tau}_L}, m_{\tilde{\chi}_1^0} = 1 \text{ GeV}$
>	85.2		3	ABBIENDI	04	OPAL	$\Delta m > 6 \text{ GeV}, \theta_\tau = \pi/2, \mu > 100 \text{ GeV}, \tan\beta = 1.5$
>	78.3		4	ACHARD	04	L3	$\Delta m > 15 \text{ GeV}, \theta_\tau = \pi/2, \mu > 200 \text{ GeV}, \tan\beta \geq 2$
>	81.9	95	5	ABDALLAH	03M	DLPH	$\Delta m > 15 \text{ GeV}$, all θ_τ
>	79	95	6	HEISTER	02E	ALEP	$\Delta m > 15 \text{ GeV}, \theta_\tau = \pi/2$
>	76	95	6	HEISTER	02E	ALEP	$\Delta m > 15 \text{ GeV}, \theta_\tau = 0.91$
• • •	We do not use the following data for averages, fits, limits, etc. • • •						
>	>500	95	7	AABOUD	18BT	ATLS	$2\ell + \cancel{E}_T, m_{\tilde{\ell}_R} = m_{\tilde{\ell}_L}, \tilde{\ell} = \tilde{e}, \tilde{\mu}, \tilde{\tau}, m_{\tilde{\chi}_1^0} = 0 \text{ GeV}$
none	109	95	8	KHACHATRYAN	17L	CMS	$2\tau + \cancel{E}_T, \tilde{\tau}_L \rightarrow \tau \tilde{\chi}_1^0, m_{\tilde{\chi}_1^0} = 0 \text{ GeV}$
none		95	9	AAD	16AA	ATLS	2 hadronic $\tau + \cancel{E}_T, \tilde{\tau}_R/L \rightarrow \tau \tilde{\chi}_1^0, m_{\tilde{\chi}_1^0} = 0 \text{ GeV}$
			10	AAD	12AF	ATLS	$2\tau + \text{jets} + \cancel{E}_T, \text{GMSB}$
			11	AAD	12AG	ATLS	$\geq 1\tau_h + \text{jets} + \cancel{E}_T, \text{GMSB}$
			12	AAD	12CM	ATLS	$\geq 1\tau + \text{jets} + \cancel{E}_T, \text{GMSB}$
>	87.4	95	13	ABBIENDI	06B	OPAL	$\tilde{\tau}_R \rightarrow \tau \tilde{G}$, all $\tau(\tilde{\tau}_R)$
>	68	95	14	ABDALLAH	04H	DLPH	AMSB, $\mu > 0$
none	$m_{\tilde{\tau}} - 26.3$	95	5	ABDALLAH	03M	DLPH	$\Delta m > m_{\tilde{\tau}}$, all θ_τ

¹ AAD 20H presented ATLAS searches for direct production of $\tilde{\tau}$ in final states with two hadronically decaying leptons and \cancel{E}_T . The analysis uses a dataset of pp collisions at $\sqrt{s} = 13 \text{ TeV}$ corresponding to an integrated luminosity of 139 fb^{-1} . Exclusion limits at 95% C.L. are derived in scenarios of direct production of $\tilde{\tau}$ pairs with each $\tilde{\tau}$ decaying into a τ and the lightest neutralino $\tilde{\chi}_1^0$ in simplified models where the $\tilde{\tau}_R$ and $\tilde{\tau}_L$ mass eigenstates are degenerate. Stau masses from 120 GeV to 390 GeV are excluded for a massless lightest neutralino, see their Fig. 7(a). If $\tilde{\tau}_1$ -only pair production is considered, the exclusion region extends between 155 GeV to 310 GeV, see their Fig. 7(b).

² SIRUNYAN 20P searched in 77.2 fb^{-1} of pp collisions at $\sqrt{s} = 13 \text{ TeV}$ for direct pair production of tau sleptons in events with a tau lepton pair and significant missing transverse momentum. Final states with two double hadronic decay of the tau leptons are considered, as well as where one of the tau leptons decays into an electron or a muon. No significant excess above the Standard Model expectations is observed. Limits are set on the stau mass in a simplified models where two tau sleptons are pair produced and decay to a tau lepton and the lightest neutralino, assuming either only left-handed stau production, see Figure 8, or assuming degenerate left- and right-handed stau production, see Figure 9.

³ ABBIENDI 04 search for $\tilde{\tau}\tilde{\tau}$ production in acoplanar di-tau final states in the 183–208 GeV data. See Fig. 15 for the dependence of the limits on $m_{\tilde{\chi}_1^0}$ and for the limit at $\tan\beta = 35$. Under the assumption of 100% branching ratio for $\tilde{\tau}_R \rightarrow \tau \tilde{\chi}_1^0$, the limit improves to 89.8 GeV for $\Delta m > 8 \text{ GeV}$. See Fig. 12 for the dependence of the limits on $m_{\tilde{\chi}_1^0}$ at several values of the branching ratio and for their dependence on θ_τ . This limit supersedes ABBIENDI 00c.

⁴ ACHARD 04 search for $\tilde{\tau}\tilde{\tau}$ production in acoplanar di-tau final states in the 192–209 GeV data. Limits on $m_{\tilde{\tau}_R}$ are derived from a scan over the MSSM parameter space with universal GUT scale gaugino and scalar masses $m_{1/2}$ and m_0 , $1 \leq \tan\beta \leq 60$ and $-2 \leq \mu \leq 2 \text{ TeV}$. See Fig. 4 for the dependence of the limits on $m_{\tilde{\chi}_1^0}$.

⁵ ABDALLAH 03M looked for acoplanar $\tilde{\tau}\tilde{\tau}$ final states at $\sqrt{s} = 130\text{--}208 \text{ GeV}$. A dedicated search was made for low mass $\tilde{\tau}\tilde{\tau}$ decoupling from the Z^0 . The limit assumes $B(\tilde{\tau} \rightarrow \tau \tilde{\chi}_1^0) = 100\%$. See Fig. 20 for limits on the $(m_{\tilde{\tau}}, m_{\tilde{\chi}_1^0})$ plane and as function of the $\tilde{\chi}_1^0$ mass and of the branching ratio. The limit in the low-mass region improves to 29.6 and 31.1 GeV for $\tilde{\tau}_R$ and $\tilde{\tau}_L$, respectively, at $\Delta m > m_{\tilde{\tau}}$. The limit in the high-mass region improves to 84.7 GeV for $\tilde{\tau}_R$ and $\Delta m > 15 \text{ GeV}$. These limits include and update the results of ABREU 01.

⁶ HEISTER 02E looked for acoplanar ditau + \cancel{E}_T final states from e^+e^- interactions between 183 and 209 GeV. The mass limit assumes $B(\tilde{\tau} \rightarrow \tau \tilde{\chi}_1^0) = 1$. See their Fig. 4 for the dependence of the limit on Δm . These limits include and update the results of BARATE 01.

⁷ AABOUD 18BT searched in 36.1 fb^{-1} of pp collisions at $\sqrt{s} = 13 \text{ TeV}$ for direct electroweak production of charginos, chargino and next-to-lightest neutralinos and sleptons in events with two or three leptons (electrons or muons), with or without jets, and large missing transverse energy. No significant excess above the Standard Model expectations is observed. Limits are set on the slepton mass up to 500 GeV for massless $\tilde{\chi}_1^0$ assuming degeneracy of $\tilde{e}, \tilde{\mu}$, and $\tilde{\tau}$ and exploiting the 2ℓ signature, see their Figure 8(b).

⁸ KHACHATRYAN 17L searched in about 19 fb^{-1} of pp collisions at $\sqrt{s} = 8 \text{ TeV}$ for events with two τ (at least one decaying hadronically) and \cancel{E}_T . Results were interpreted to set constraints on the cross section for production of $\tilde{\tau}_L$ pairs for $m_{\tilde{\chi}_1^0} = 1 \text{ GeV}$. No mass constraints are set, see their Fig. 7.

⁹ AAD 16AA summarized and extended ATLAS searches for electroweak supersymmetry in final states containing several charged leptons, \cancel{E}_T , with or without hadronic jets, in 20 fb^{-1} of pp collisions at $\sqrt{s} = 8 \text{ TeV}$. The paper reports 95% C.L. exclusion limits on the cross-section for production of $\tilde{\tau}_R$ and $\tilde{\tau}_L$ pairs for various $m_{\tilde{\chi}_1^0}$, using the 2 hadronic $\tau + \cancel{E}_T$ analysis. The $m_{\tilde{\tau}_R/L} = 109 \text{ GeV}$ is excluded for $m_{\tilde{\chi}_1^0} = 0 \text{ GeV}$, with the constraints being stronger for $\tilde{\tau}_R$. See their Fig. 12.

¹⁰ AAD 12AF searched in 2 fb^{-1} of pp collisions at $\sqrt{s} = 7 \text{ TeV}$ for events with two tau leptons, jets and large \cancel{E}_T in a GMSB framework. No significant excess above the expected background was found and an upper limit on the visible cross section for new phenomena is set. A 95% C.L. lower limit of 32 TeV on the mGMSB breaking scale Λ is set for $M_{mess} = 250 \text{ TeV}, N_S = 3, \mu > 0$ and $C_{grav} = 1$, independent of $\tan\beta$.

¹¹ AAD 12AG searched in 2.05 fb^{-1} of pp collisions at $\sqrt{s} = 7 \text{ TeV}$ for events with at least one hadronically decaying tau lepton, jets, and large \cancel{E}_T in a GMSB framework.

No significant excess above the expected background was found and an upper limit on the visible cross section for new phenomena is set. A 95% C.L. lower limit of 30 TeV on the mGMSB breaking scale Λ is set for $M_{mess} = 250 \text{ TeV}, N_S = 3, \mu > 0$ and $C_{grav} = 1$, independent of $\tan\beta$. For large values of $\tan\beta$, the limit on Λ increases to 43 TeV.

¹² AAD 12CM searched in 4.7 fb^{-1} of pp collisions at $\sqrt{s} = 7 \text{ TeV}$ for events with at least one tau lepton, zero or one additional light lepton (e/μ) jets, and large \cancel{E}_T in a GMSB framework. No significant excess above the expected background was found and an upper limit on the visible cross section for new phenomena is set. A 95% C.L. lower limit of 54 TeV on the mGMSB breaking scale Λ is set for $M_{mess} = 250 \text{ TeV}, N_S = 3, \mu > 0$ and $C_{grav} = 1$, for $\tan\beta > 20$. Here the $\tilde{\tau}_1$ is the NLSP.

¹³ ABBIENDI 06B use 600 pb^{-1} of data from $\sqrt{s} = 189\text{--}209 \text{ GeV}$. They look for events from pair-produced staus in a GMSB scenario with $\tilde{\tau}$ NLSP including prompt $\tilde{\tau}$ decays to ditau + \cancel{E} final states, large impact parameters, kinked tracks and heavy stable charged particles. Limits on the cross-section are computed as a function of $m(\tilde{\tau})$ and the lifetime, see their Fig. 7. The limit is compared to the $\sigma \cdot BR^2$ from a scan over the GMSB parameter space.

¹⁴ ABDALLAH 04H use data from LEP 1 and $\sqrt{s} = 192\text{--}208 \text{ GeV}$. They re-use results or re-analyze the data from ABDALLAH 03M to put limits on the parameter space of anomaly-mediated supersymmetry breaking (AMSB), which is scanned in the region $1 < m_{3/2} < 50 \text{ TeV}, 0 < m_0 < 1000 \text{ GeV}, 1.5 < \tan\beta < 35$, both signs of μ . The constraints are obtained from the searches for mass degenerate chargino and neutralino, for SM-like and invisible Higgs, for leptonically decaying charginos and from the limit on non-SM Z width of 3.2 MeV. The limit is for $m_t = 174.3 \text{ GeV}$ (see Table 2 for other m_t values). The limit improves to 75 GeV for $\mu < 0$.

R-parity violating $\tilde{\tau}$ (Stau) mass limit

Some earlier papers are now obsolete and have been omitted. They were last listed in our PDG 14 edition: K. Olive, et al. (Particle Data Group), Chinese Physics **C38** 070001 (2014) (<http://pdg.lbl.gov>).

VALUE (GeV)	CL%	DOCUMENT ID	TECN	COMMENT
>1200	95	¹ AAD	21Y ATLS	$\geq 4\ell, \lambda_{12k} \neq 0, m_{\tilde{\chi}_1^0} = 900 \text{ GeV}$ (mass-degenerate $\tilde{\ell}_L$ and $\tilde{\nu}$ of all 3 generations)
> 870	95	¹ AAD	21Y ATLS	$\geq 4\ell, \lambda_{i33} \neq 0, m_{\tilde{\chi}_1^0} = 450 \text{ GeV}$ (mass-degenerate $\tilde{\ell}_L$ and $\tilde{\nu}$ of all 3 generations)
>1060	95	² AABOUD	18z ATLS	$\geq 4\ell, \lambda_{12k} \neq 0, m_{\tilde{\chi}_1^0} = 600 \text{ GeV}$ (mass-degenerate left-handed sleptons and sneutrinos of all 3 generations)
> 780	95	² AABOUD	18z ATLS	$\geq 4\ell, \lambda_{i33} \neq 0, m_{\tilde{\chi}_1^0} = 300 \text{ GeV}$ (mass-degenerate left-handed sleptons and sneutrinos of all 3 generations)
> 90	95	³ ABDALLAH	04M DLPH	$\tilde{\tau}_R$, indirect, $\Delta m > 5 \text{ GeV}$
• • •	We do not use the following data for averages, fits, limits, etc. • • •			
> 74	95	⁴ ABBIENDI	04F OPAL	$\tilde{\tau}_L$

¹ AAD 21Y searched in 139 fb^{-1} of pp collisions at $\sqrt{s} = 13 \text{ TeV}$ for supersymmetry in events with four or more leptons (electrons, muons and tau-leptons). No significant excess above the Standard Model expectations is observed. Limits are set on Tchi1n2-GGM, and RPV models similar to Tchi1n2L, Tglu1A (with $q = u, d, s, c, b$, with equal branching fractions), and $\tilde{\ell}_L/\tilde{\nu} \rightarrow \ell/\nu \tilde{\chi}_1^0$ (mass-degenerate $\tilde{\ell}_L$ and $\tilde{\nu}$ of all 3 generations), all with $\tilde{\chi}_1^0 \rightarrow \ell^\pm e^\mp \nu$ via λ_{12k} or λ_{i33} (where $i, k \in 1, 2$), see their Figure 11.

² AABOUD 18z searched in 36.1 fb^{-1} of pp collisions at $\sqrt{s} = 13 \text{ TeV}$ for events containing four or more charged leptons (electrons, muons and up to two hadronically decaying taus). No significant deviation from the expected SM background is observed. Limits are set on the Higgsino mass in simplified models of general gauge mediated supersymmetry Tn1n1A/Tn1n1B/Tn1n1C, see their Figure 9. Limits are also set on the wino, slepton, sneutrino and gluino mass in a simplified model of NLSP pair production with R-parity violating decays of the LSP via λ_{12k} or λ_{i33} to charged leptons, see their Figures 7, 8.

³ ABDALLAH 04M use data from $\sqrt{s} = 192\text{--}208 \text{ GeV}$ to derive limits on sparticle masses under the assumption of RPV with $LL\bar{E}$ couplings. The results are valid for $\mu = -200 \text{ GeV}, \tan\beta = 1.5, \Delta m > 5 \text{ GeV}$ and assuming a BR of 1 for the given decay. The limit quoted is for indirect decays using the neutralino constraint of 39.5 GeV, also derived in ABDALLAH 04M. For indirect decays via $LL\bar{E}$ the limit decreases to 86 GeV if the constraint from the neutralino is not used. Supersedes the result of ABREU 00u.

⁴ ABBIENDI 04F use data from $\sqrt{s} = 189\text{--}209 \text{ GeV}$. They derive limits on sparticle masses under the assumption of RPV with $LL\bar{E}$ or $LQ\bar{D}$ couplings. The results are valid for $\tan\beta = 1.5, \mu = -200 \text{ GeV}$, with, in addition, $\Delta m > 5 \text{ GeV}$ for indirect decays via $LQ\bar{D}$. The limit quoted applies to direct decays with $LL\bar{E}$ couplings and improves to 75 GeV for $LQ\bar{D}$ couplings. The limit on the $\tilde{\tau}_R$ mass for indirect decays is 92 GeV for $LL\bar{E}$ couplings at $m_{\tilde{\chi}_1^0} = 10 \text{ GeV}$ and no exclusion is obtained for $LQ\bar{D}$ couplings. Supersedes the results of ABBIENDI 00.

Long-lived $\tilde{\ell}$ (Slepton) mass limit

Limits on scalar leptons which leave detector before decaying. Limits from Z decays are independent of lepton flavor. Limits from continuum e^+e^- annihilation are also independent of flavor for smuons and staus. Selection limits from e^+e^- collisions in the continuum depend on MSSM parameters because of the additional neutralino exchange contribution.

VALUE (GeV)	CL%	DOCUMENT ID	TECN	COMMENT
>720	95	¹ AAD	21AL ATLS	2ℓ displaced, long-lived $\tilde{e}, \tilde{e} \rightarrow e\tilde{G}, m_{\tilde{e}_R} = m_{\tilde{e}_L}, \tau_{\tilde{e}} = 0.1 \text{ ns}$
>680	95	¹ AAD	21AL ATLS	2ℓ displaced, long-lived $\tilde{\mu}, \tilde{\mu} \rightarrow \mu\tilde{G}, m_{\tilde{\mu}_R} = m_{\tilde{\mu}_L}, \tau_{\tilde{\mu}} = 0.1 \text{ ns}$
>340	95	¹ AAD	21AL ATLS	2ℓ displaced, long-lived $\tilde{\tau}, \tilde{\tau} \rightarrow \tau\tilde{G}, \text{mixing } \sin\theta_{\tilde{\tau}} = 0.95, \tau_{\tilde{\tau}} = 0.1 \text{ ns}$

>820	95	1	AAD	21AL ATLS	2 ℓ displaced, long-lived $\tilde{\ell}, \tilde{\ell} \rightarrow \ell \tilde{G}, m_{\tilde{\ell}R} = m_{\tilde{\ell}L}, m_{\tilde{e}} = m_{\tilde{\mu}} = m_{\tilde{\tau}}, \tau_{\tilde{\ell}} = 0.1$ ns
>430	95	2	AABOUD	19AT ATLS	long-lived $\tilde{\tau}$, GMSB
>490	95	3	KHACHATRYAN	16BW CMS	long-lived $\tilde{\tau}$ from inclusive production, mGMSB SPS line 7 scenario
>240	95	3	KHACHATRYAN	16BW CMS	long-lived $\tilde{\tau}$ from direct pair production, mGMSB SPS line 7 scenario
>440	95	4	AAD	15AE ATLS	mGMSB, $M_{mess} = 250$ TeV, $N_5 = 3, \mu > 0, C_{grav} = 5000, \tan\beta = 10$
>385	95	4	AAD	15AE ATLS	mGMSB, $M_{mess} = 250$ TeV, $N_5 = 3, \mu > 0, C_{grav} = 5000, \tan\beta = 50$
>286	95	4	AAD	15AE ATLS	direct $\tilde{\tau}$ production
none 124–309	95	5	AAIJ	15BD LHCB	long-lived $\tilde{\tau}$, mGMSB, SP57
> 98	95	6	ABBIENDI	03L OPAL	$\tilde{\mu}_R, \tilde{\tau}_R$
none 2–87.5	95	7	ABREU	00Q DLPH	$\tilde{\mu}_R, \tilde{\tau}_R$
> 81.2	95	8	ACCIARRI	99H L3	$\tilde{\mu}_R, \tilde{\tau}_R$
> 81	95	9	BARATE	98K ALEP	$\tilde{\mu}_R, \tilde{\tau}_R$
• • •					We do not use the following data for averages, fits, limits, etc. • • •
>300	95	10	AAD	13AA ATLS	long-lived $\tilde{\tau}$, GMSB, $\tan\beta = 5-20$
>339	95	11	ABAZOV	13B D0	long-lived $\tilde{\tau}$, $100 < m_{\tilde{\tau}} < 300$ GeV
>500	95	12,13	CHATRCHYAN	13AB CMS	long-lived $\tilde{\tau}$, direct $\tilde{\tau}_1$ pair prod., minimal GMSB, SPS line 7
>314	95	12,14	CHATRCHYAN	13AB CMS	long-lived $\tilde{\tau}, \tilde{\tau}_1$ from direct pair prod. and from decay of heavier SUSY particles, minimal GMSB, SPS line 7
>136	95	15	CHATRCHYAN	12L CMS	long-lived $\tilde{\tau}, \tilde{\tau}_1$ from decay of heavier SUSY particles, minimal GMSB, SPS line 7
>136	95	16	AAD	11P ATLS	stable $\tilde{\tau}$, GMSB scenario, $\tan\beta=5$

1 AAD 21AL searched in 139 fb^{-1} of pp collisions at $\sqrt{s} = 13$ TeV for pair production of long-lived sleptons in events with highly displaced leptons. No significant excess above the Standard Model predictions is observed. Limits are set on $m_{\tilde{e}}, m_{\tilde{\mu}}, m_{\tilde{\tau}}$ as a function of the slepton lifetime, assuming the $\tilde{\ell} \rightarrow \ell \tilde{G}$ decay and mass-degenerate $\tilde{\ell}_L$ and $\tilde{\ell}_R$. See Figures 2.

2 AABOUD 19AT searched in 36.1 fb^{-1} of pp collisions at $\sqrt{s} = 13$ TeV for metastable and stable R -hadrons. Multiple search strategies for a wide range of lifetimes, corresponding to path lengths of a few meters, are defined. No significant deviations from the expected Standard Model background are observed. Results are interpreted in terms of exclusion limits on long-lived stau in the context of GMSB models. Lower limits on the mass for direct production of staus are set at 430 GeV, see their Fig. 10 (left).

3 KHACHATRYAN 16BW searched in 2.5 fb^{-1} of pp collisions at $\sqrt{s} = 13$ TeV for events with heavy stable charged particles, identified by their anomalously high energy deposits in the silicon tracker and/or long time-of-flight measurements by the muon system. No evidence for an excess over the expected background is observed. Limits are derived for pair production of tau sleptons as a function of mass, depending on their direct or inclusive production in a minimal GMSB scenario along the Snowmass Points and Slopes (SPS) line 7, see Fig. 4 and Table 7.

4 AAD 15AE searched in 19.1 fb^{-1} of pp collisions at $\sqrt{s} = 8$ TeV for heavy long-lived charged particles, measured through their specific ionization energy loss in the ATLAS pixel detector or their time-of-flight in the ALTA5 muon system. In the absence of an excess of events above the expected backgrounds, limits are set on stable $\tilde{\tau}$ sleptons in various scenarios, see Figs. 5–7.

5 AAIJ 15BD searched in 3.0 fb^{-1} of pp collisions at $\sqrt{s} = 7$ and 8 TeV for evidence of Drell-Yan pair production of long-lived $\tilde{\tau}$ particles. No evidence for such particles is observed and 95% C.L. upper limits on the cross section of $\tilde{\tau}$ pair production are derived, see Fig. 7. In the mGMSB, assuming the SP57 benchmark scenario $\tilde{\tau}$ masses between 124 and 309 GeV are excluded at 95% C.L.

6 ABBIENDI 03L used e^+e^- data at $\sqrt{s} = 130-209$ GeV to select events with two high momentum tracks with anomalous dE/dx . The excluded cross section is compared to the theoretical expectation as a function of the heavy particle mass in their Fig. 3. The limit improves to 98.5 GeV for $\tilde{\mu}_L$ and $\tilde{\tau}_L$. The bounds are valid for colorless spin 0 particles with lifetimes longer than 10^{-6} s. Supersedes the results from ACKERSTAFF 98P.

7 ABREU 00Q searches for the production of pairs of heavy, charged stable particles in e^+e^- annihilation at $\sqrt{s} = 130-189$ GeV. The upper bound improves to 88 GeV for $\tilde{\mu}_L, \tilde{\tau}_L$. These limits include and update the results of ABREU 98P.

8 ACCIARRI 99H searched for production of pairs of back-to-back heavy charged particles at $\sqrt{s} = 130-183$ GeV. The upper bound improves to 82.2 GeV for $\tilde{\mu}_L, \tilde{\tau}_L$.

9 The BARATE 98K mass limit improves to 82 GeV for $\tilde{\mu}_L, \tilde{\tau}_L$. Data collected at $\sqrt{s} = 161-184$ GeV.

10 AAD 13AA searched in 4.7 fb^{-1} of pp collisions at $\sqrt{s} = 7$ TeV for events containing long-lived massive particles in a GMSB framework. No significant excess above the expected background was found. A 95% C.L. lower limit of 300 GeV is placed on long-lived $\tilde{\tau}$'s in the GMSB model with $M_{mess} = 250$ TeV, $N_5 = 3, \mu > 0$, for $\tan\beta = 5-20$. The lower limit on the GMSB breaking scale Λ was found to be 99–110 TeV, for $\tan\beta$ values between 5 and 40, see Fig. 4 (top). Also, directly produced long-lived sleptons, or sleptons decaying to long-lived ones, are excluded at 95% C.L. up to a $\tilde{\tau}$ mass of 278 GeV for models with slepton splittings smaller than 50 GeV.

11 ABAZOV 13B looked in 6.3 fb^{-1} of $p\bar{p}$ collisions at $\sqrt{s} = 1.96$ TeV for charged massive long-lived particles in events with muon-like particles that have both speed and ionization energy loss inconsistent with muons produced in beam collisions. In the absence of an excess, limits are set at 95% C.L. on the production cross section of stau leptons in the mass range 100–300 GeV, see their Table 20 and Fig. 23.

12 CHATRCHYAN 13AB looked in 5.0 fb^{-1} of pp collisions at $\sqrt{s} = 7$ TeV and in 18.8 fb^{-1} of pp collisions at $\sqrt{s} = 8$ TeV for events with heavy stable particles, identified by their anomalous dE/dx in the tracker or additionally requiring that it be identified as muon in the muon chambers, from pair production of $\tilde{\tau}_1$'s. No evidence for an excess over the expected background is observed. Supersedes CHATRCHYAN 12L.

- 13 CHATRCHYAN 13AB limits are derived for pair production of $\tilde{\tau}_1$ as a function of mass in minimal GMSB scenarios along the Snowmass Points and Slopes (SPS) line 7 (see Fig. 8 and Table 7). The limit given here is valid for direct pair $\tilde{\tau}_1$ production.
- 14 CHATRCHYAN 13AB limits are derived for the production of $\tilde{\tau}_1$ as a function of mass in minimal GMSB scenarios along the Snowmass Points and Slopes (SPS) line 7 (see Fig. 8 and Table 7). The limit given here is valid for the production of $\tilde{\tau}_1$ from both direct pair production and from the decay of heavier supersymmetric particles.
- 15 CHATRCHYAN 12L looked in 5.0 fb^{-1} of pp collisions at $\sqrt{s} = 7$ TeV for events with heavy stable particles, identified by their anomalous dE/dx in the tracker or additionally requiring that it be identified as muon in the muon chambers, from pair production of $\tilde{\tau}_1$'s. No evidence for an excess over the expected background is observed. Limits are derived for the production of $\tilde{\tau}_1$ as a function of mass in minimal GMSB scenarios along the Snowmass Points and Slopes (SPS) line 7 (see Fig. 3). The limit given here is valid for the production of $\tilde{\tau}_1$ in the decay of heavier supersymmetric particles.
- 16 AAD 11P looked in 37 pb^{-1} of pp collisions at $\sqrt{s} = 7$ TeV for events with two heavy stable particles, reconstructed in the Inner tracker and the Muon System and identified by their time of flight in the Muon System. No evidence for an excess over the SM expectation is observed. Limits on the mass are derived, see Fig. 3, for $\tilde{\tau}$ in a GMSB scenario and for sleptons produced by electroweak processes only, in which case the limit degrades to 110 GeV.

\tilde{q} (Squark) mass limit

For $m_{\tilde{q}} > 60-70$ GeV, it is expected that squarks would undergo a cascade decay via a number of neutralinos and/or charginos rather than undergo a direct decay to photinos as assumed by some papers. Limits obtained when direct decay is assumed are usually higher than limits when cascade decays are included.

Limits from e^+e^- collisions depend on the mixing angle of the lightest mass eigenstate $\tilde{q}_1 = \tilde{q}_R \sin\theta_{\tilde{q}} + \tilde{q}_L \cos\theta_{\tilde{q}}$. It is usually assumed that only the sbottom and stop squarks have non-trivial mixing angles (see the stop and sbottom sections). Here, unless otherwise noted, squarks are always taken to be either left/right degenerate, or purely of left or right type. Data from Z decays have set squark mass limits above 40 GeV, in the case of $\tilde{q} \rightarrow q \tilde{\chi}_1^0$ decays if $\Delta m = m_{\tilde{q}} - m_{\tilde{\chi}_1^0} \gtrsim 5$ GeV. For smaller values of Δm , current constraints on the invisible width of the Z ($\Delta\Gamma_{\text{inv}} < 2.0$ MeV, LEP 00) exclude $m_{\tilde{u}_{L,R}} < 44$ GeV, $m_{\tilde{d}} < 33$ GeV, $m_{\tilde{d}_L} < 44$ GeV and, assuming all squarks degenerate, $m_{\tilde{q}} < 45$ GeV.

Some earlier papers are now obsolete and have been omitted. They were last listed in our PDG 14 edition: K. Olive, et al. (Particle Data Group), Chinese Physics **C38** 070001 (2014) (<http://pdg.lbl.gov>).

R-parity conserving \tilde{q} (Squark) mass limit

VALUE (GeV)	CL%	DOCUMENT ID	TECN	COMMENT
>1400	95	1	AAD	21AK ATLS $\ell^{\pm} + \text{jets} + \cancel{E}_T, \text{Ts}qk3, 4$ degenerate light $\tilde{q}_\ell, m_{\tilde{\chi}_1^{\pm}} = (m_{\tilde{q}} + m_{\tilde{\chi}_1^0})/2, m_{\tilde{\chi}_1^0} < 200$ GeV
>1040	95	1	AAD	21AK ATLS $\ell^{\pm} + \text{jets} + \cancel{E}_T, \text{Ts}qk3, 1$ light $\tilde{q}_\ell, m_{\tilde{\chi}_1^{\pm}} = (m_{\tilde{q}} + m_{\tilde{\chi}_1^0})/2, m_{\tilde{\chi}_1^0} < 200$ GeV
> 925	95	2	AAD	21F ATLS ≥ 1 jet + $\cancel{E}_T, \text{Ts}qk1, m_{\tilde{q}} - m_{\tilde{\chi}_1^0} = 5$ GeV
> 550	95	2	AAD	21F ATLS ≥ 1 jet + $\cancel{E}_T, \text{Tstop}3, m_{\tilde{t}} - m_{\tilde{\chi}_1^0} = 5$ GeV
> 550	95	2	AAD	21F ATLS ≥ 1 jet + $\cancel{E}_T, \text{Tstop}4, m_{\tilde{t}} - m_{\tilde{\chi}_1^0} = 5$ GeV
> 545	95	2	AAD	21F ATLS ≥ 1 jet + $\cancel{E}_T, \text{Tsb}01, m_{\tilde{b}} - m_{\tilde{\chi}_1^0} = 5$ GeV
>1850	95	3	AAD	21L ATLS jets + $\cancel{E}_T, \text{Ts}qk1, 8$ degenerate $\tilde{q}, m_{\tilde{\chi}_1^0} = 0$ GeV
>1220	95	3	AAD	21L ATLS jets + $\cancel{E}_T, \text{Ts}qk1, 1$ non-degenerate $\tilde{q}, m_{\tilde{\chi}_1^0} = 0$ GeV
>1310	95	3	AAD	21L ATLS jets + $\cancel{E}_T, \text{Ts}qk3, 4$ degenerate $\tilde{q}_i, m_{\tilde{\chi}_1^{\pm}} = (m_{\tilde{q}} + m_{\tilde{\chi}_1^0})/2, m_{\tilde{\chi}_1^0} = 0$ GeV
>3000	95	3	AAD	21L ATLS jets + \cancel{E}_T , combined $\tilde{g}\tilde{g}, \tilde{g}\tilde{q}, \tilde{q}\tilde{q}$ production, $\tilde{g} \rightarrow qq'\tilde{\chi}_1^0, \tilde{q} \rightarrow q\tilde{\chi}_1^0, m_{\tilde{q}} = m_{\tilde{g}}, m_{\tilde{\chi}_1^0} = 0$ GeV
>1800	95	4	SIRUNYAN	21M CMS $\ell^{\pm} \tilde{e}^{\mp} + \cancel{E}_T, \text{Ts}qk2A, m_{\tilde{\chi}_1^0} = 1500$ GeV, $m_{\tilde{\chi}_1^0} = 100$ GeV
>1590	95	5	SIRUNYAN	19AG CMS $2\gamma + \cancel{E}_T, \text{Ts}qk4B, 500$ GeV $< m_{\tilde{\chi}_1^0} < 1500$ GeV
>1130	95	6	SIRUNYAN	19CH CMS jets + $\cancel{E}_T, \text{Ts}qk1, 1$ light flavour, $m_{\tilde{\chi}_1^0} = 0$ GeV
>1630	95	6	SIRUNYAN	19CH CMS jets + $\cancel{E}_T, \text{Ts}qk1, 8$ degenerate light flavours, $m_{\tilde{\chi}_1^0} = 0$ GeV
>1430	95	7	SIRUNYAN	19K CMS $\gamma + \ell + \cancel{E}_T, \text{Ts}qk4A, m_{\tilde{\chi}_1^0} = 1200$ GeV

Searches Particle Listings

Supersymmetric Particle Searches

>1200	95	8	AABOUD	18BJ ATLS	$\ell^\pm \ell^\mp + \text{jets} + \cancel{E}_T, \text{Tsqr}2, m_{\tilde{\chi}_1^0} = 1 \text{ GeV}, \text{any } m_{\tilde{\chi}_2^0}$	> 780	95	32	CHATRCHYAN14I	CMS	multijets + $\cancel{E}_T, \tilde{q} \rightarrow q\tilde{\chi}_1^0$ simplified model, $m_{\tilde{\chi}_1^0} < 200 \text{ GeV}$
> 850	95	9	AABOUD	18BV ATLS	$c\text{-jets} + \cancel{E}_T, \text{Tsqr}1 \text{ (charm only)}, m_{\tilde{\chi}_1^0} = 0 \text{ GeV}$	>1360	95	33	AAD	13L ATLS	jets + $\cancel{E}_T, \text{CMSSM}, m_{\tilde{g}} = m_{\tilde{q}}$
> 710	95	10	AABOUD	18I ATLS	$\geq 1 \text{ jets} + \cancel{E}_T, \text{Tsqr}1, m_{\tilde{q}} \sim m_{\tilde{\chi}_1^0}$	>1200	95	34	AAD	13Q ATLS	$\gamma + b + \cancel{E}_T, \text{higgsino-like neutralino}, m_{\tilde{\chi}_1^0} > 220 \text{ GeV}, \text{GMSB}$
>1820	95	11	AABOUD	18U ATLS	$2\gamma + \cancel{E}_T, \text{GGM}, \text{Tsqr}4B, \text{any NLSP mass}$	>1250	95	35	CHATRCHYAN13	CMS	$\ell^\pm \ell^\mp + \text{jets} + \cancel{E}_T, \text{CMSSM}, m_{\tilde{q}} = m_{\tilde{g}}$
>1550	95	12	AABOUD	18V ATLS	$\text{jets} + \cancel{E}_T, \text{Tsqr}1, m_{\tilde{\chi}_1^0} = 0 \text{ GeV}$	>1430	95	36	CHATRCHYAN13G	CMS	$0,1,2, \geq 3 \text{ b-jets} + \cancel{E}_T, \text{CMSSM}, m_{\tilde{q}} = m_{\tilde{g}}$
>1150	95	13	AABOUD	18V ATLS	$\text{jets} + \cancel{E}_T, \text{Tsqr}3, m_{\tilde{\chi}_1^\pm} = 0.5(m_{\tilde{q}} + m_{\tilde{\chi}_1^0}), m_{\tilde{\chi}_1^0} = 0 \text{ GeV}$	> 750	95	37	CHATRCHYAN13H	CMS	$2\gamma + \geq 4 \text{ jets} + \text{low } \cancel{E}_T, \text{stealth SUSY model}$
>1650	95	14	SIRUNYAN	18AA CMS	$\geq 1\gamma + \cancel{E}_T, \text{Tsqr}4A$	> 820	95	39	AAD	12AX ATLS	$\ell + \text{jets} + \cancel{E}_T, \text{CMSSM}, m_{\tilde{q}} = m_{\tilde{g}}$
>1750	95	14	SIRUNYAN	18AA CMS	$\geq 1\gamma + \cancel{E}_T, \text{Tsqr}4B$	>1200	95	40	AAD	12CJ ATLS	$\ell^\pm + \text{jets} + \cancel{E}_T, \text{CMSSM}, m_{\tilde{q}} = m_{\tilde{g}}$
> 675	95	15	SIRUNYAN	18AY CMS	$\text{jets} + \cancel{E}_T, \text{Tsqr}1, 1 \text{ light flavor state}, m_{\tilde{\chi}_1^0} = 0 \text{ GeV}$	> 870	95	41	AAD	12CP ATLS	$2\gamma + \cancel{E}_T, \text{GMSB}, \text{bino NLSP}, m_{\tilde{\chi}_1^0} > 50 \text{ GeV}$
>1320	95	15	SIRUNYAN	18AY CMS	$\text{jets} + \cancel{E}_T, \text{Tsqr}1, 8 \text{ degenerate light flavor states}, m_{\tilde{\chi}_1^0} = 0 \text{ GeV}$	> 950	95	42	AAD	12W ATLS	$\text{jets} + \cancel{E}_T, \text{CMSSM}, m_{\tilde{q}} = m_{\tilde{g}}$
>1220	95	16	AABOUD	17AR ATLS	$1\ell + \text{jets} + \cancel{E}_T, \text{Tsqr}3, m_{\tilde{\chi}_1^0} = 0 \text{ GeV}$	> 760	95	43	CHATRCHYAN12	CMS	$e, \mu, \text{jets}, \text{razor}, \text{CMSSM}$
>1000	95	17	AABOUD	17N ATLS	$2 \text{ same-flavour, opposite-sign } \ell + \text{jets} + \cancel{E}_T, \text{Tsqr}2, m_{\tilde{\chi}_1^0} = 0 \text{ GeV}$	>1110	95	44	CHATRCHYAN12AE	CMS	$\text{jets} + \cancel{E}_T, \tilde{q} \rightarrow q\tilde{\chi}_1^0, m_{\tilde{\chi}_1^0} < 200 \text{ GeV}$
>1150	95	18	KHACHATRY...17P	CMS	$1 \text{ or more jets} + \cancel{E}_T, \text{Tsqr}1, 4(\text{flavor}) \times 2(\text{isospin}) = 8 \text{ mass degenerate states}, m_{\tilde{\chi}_1^0} = 0 \text{ GeV}$	>1180	95	45	CHATRCHYAN12AT	CMS	$\text{jets} + \cancel{E}_T, \text{CMSSM}, m_{\tilde{q}} = m_{\tilde{g}}$
> 575	95	18	KHACHATRY...17P	CMS	$1 \text{ or more jets} + \cancel{E}_T, \text{Tsqr}1, \text{one light flavor state}, m_{\tilde{\chi}_1^0} = 0 \text{ GeV}$	>1080	95	46	AABOUD	18V ATLS	$\text{jets} + \cancel{E}_T, \text{Tsqr}5, (m_{\tilde{\chi}_2^0} - m_{\tilde{\chi}_1^0}) / (m_{\tilde{q}} - m_{\tilde{\chi}_1^0}) < 0.95, m_{\tilde{\chi}_1^0} = 60 \text{ GeV}$
>1370	95	19	KHACHATRY...17V	CMS	$2\gamma + \cancel{E}_T, \text{GGM}, \text{Tsqr}4, \text{any NLSP mass}$	> 300	95	47	KHACHATRY...16BT	CMS	$19\text{-parameter pMSSM model, global Bayesian analysis, flat prior}$
>1600	95	20	SIRUNYAN	17AY CMS	$\gamma + \text{jets} + \cancel{E}_T, \text{Tsqr}4B, m_{\tilde{\chi}_1^0} = 0 \text{ GeV}$	>1650	95	48	AAD	15AI ATLS	$\ell^\pm + \text{jets} + \cancel{E}_T$
>1370	95	20	SIRUNYAN	17AY CMS	$\gamma + \text{jets} + \cancel{E}_T, \text{Tsqr}4A, m_{\tilde{\chi}_1^0} = 0 \text{ GeV}$	> 790	95	26	AAD	15BV ATLS	$\text{jets} + \cancel{E}_T, m_{\tilde{g}} = m_{\tilde{q}}, m_{\tilde{\chi}_1^0} = 1 \text{ GeV}$
>1050	95	21	SIRUNYAN	17AZ CMS	$\geq 1 \text{ jets} + \cancel{E}_T, \text{Tsqr}1, \text{single light flavor state}, m_{\tilde{\chi}_1^0} = 0 \text{ GeV}$	> 820	95	26	AAD	15BV ATLS	$\text{jets} + \cancel{E}_T, \tilde{q} \rightarrow qW\tilde{\chi}_1^0, m_{\tilde{\chi}_1^0} = 100 \text{ GeV}$
>1550	95	21	SIRUNYAN	17AZ CMS	$\geq 1 \text{ jets} + \cancel{E}_T, \text{Tsqr}1, 4(\text{flavor}) \times 2(\text{isospin}) = 8 \text{ degenerate mass states}, m_{\tilde{\chi}_1^0} = 0 \text{ GeV}$	> 850	95	26	AAD	15BV ATLS	$2 \text{ or } 3 \text{ leptons} + \text{jets}, \tilde{q} \text{ decays via staus}, m_{\tilde{\chi}_1^0} = 100 \text{ GeV}$
>1390	95	22	SIRUNYAN	17P CMS	$\text{jets} + \cancel{E}_T, \text{Tsqr}1, 4(\text{flavor}) \times 2(\text{isospin}) = 8 \text{ degenerate mass states}, m_{\tilde{\chi}_1^0} = 0 \text{ GeV}$	> 700	95	49	KHACHATRY...15AR	CMS	$\tilde{q} \rightarrow q\tilde{\chi}_1^0, \tilde{\chi}_1^0 \rightarrow \tilde{S}g, \tilde{S} \rightarrow S\tilde{G}, S \rightarrow gg, m_{\tilde{S}} = 100 \text{ GeV}, m_{\tilde{S}} = 90 \text{ GeV}$
> 950	95	22	SIRUNYAN	17P CMS	$\text{jets} + \cancel{E}_T, \text{Tsqr}1, \text{one light flavor state}, m_{\tilde{\chi}_1^0} = 0 \text{ GeV}$	> 550	95	49	KHACHATRY...15AR	CMS	$\ell^\pm, \tilde{q} \rightarrow q\tilde{\chi}_1^\pm, \tilde{\chi}_1^\pm \rightarrow \tilde{S}W^\pm, \tilde{S} \rightarrow S\tilde{G}, S \rightarrow gg, m_{\tilde{S}} = 100 \text{ GeV}, m_{\tilde{S}} = 90 \text{ GeV}$
> 608	95	23	AABOUD	16D ATLS	$\geq 1 \text{ jet} + \cancel{E}_T, \text{Tsqr}1, m_{\tilde{q}} - m_{\tilde{\chi}_1^0} \geq 5 \text{ GeV}$	>1500	95	50	KHACHATRY...15AZ	CMS	$\geq 2\gamma, \geq 1 \text{ jet}, (\text{Razor}), \text{bino-like NLSP}, m_{\tilde{\chi}_1^0} = 375 \text{ GeV}$
>1030	95	24	AABOUD	16N ATLS	$\geq 2 \text{ jets} + \cancel{E}_T, \text{Tsqr}1, m_{\tilde{\chi}_1^0} = 0 \text{ GeV}$	>1000	95	50	KHACHATRY...15AZ	CMS	$\geq 1\gamma, \geq 2 \text{ jet}, \text{wino-like NLSP}, m_{\tilde{\chi}_1^0} = 375 \text{ GeV}$
> 600	95	25	KHACHATRY...16BS	CMS	$\text{jets} + \cancel{E}_T, \text{Tsqr}1, \text{single light squark}, m_{\tilde{\chi}_1^0} = 0 \text{ GeV}$	> 670	95	51	AAD	14E ATLS	$\ell^\pm \ell^\pm (\ell^\mp) + \text{jets}, \tilde{q} \rightarrow q'\tilde{\chi}_1^\pm, \tilde{\chi}_1^\pm \rightarrow W^{(*)}\tilde{\chi}_2^0, \tilde{\chi}_2^0 \rightarrow Z^{(*)}\tilde{\chi}_1^0$ simplified model, $m_{\tilde{\chi}_1^0} < 300 \text{ GeV}$
>1260	95	25	KHACHATRY...16BS	CMS	$\text{jets} + \cancel{E}_T, \text{Tsqr}1, 8 \text{ degenerate light squarks}, m_{\tilde{\chi}_1^0} = 0 \text{ GeV}$	> 780	95	51	AAD	14E ATLS	$\ell^\pm \ell^\pm (\ell^\mp) + \text{jets}, \tilde{q} \rightarrow q'\tilde{\chi}_1^\pm / \tilde{\chi}_2^0, \tilde{\chi}_1^\pm \rightarrow \ell^\pm \nu \tilde{\chi}_1^0, \tilde{\chi}_2^0 \rightarrow \ell^\pm \ell^\mp (\nu\nu)\tilde{\chi}_1^0$ simplified model
> 850	95	26	AAD	15BV ATLS	$\text{jets} + \cancel{E}_T, \tilde{q} \rightarrow q\tilde{\chi}_1^0, m_{\tilde{\chi}_1^0} = 100 \text{ GeV}$	> 700	95	52	CHATRCHYAN13A0	CMS	$\ell^\pm \ell^\mp + \text{jets} + \cancel{E}_T, \text{CMSSM}, m_0 < 700 \text{ GeV}$
> 250	95	27	AAD	15CS ATLS	$\text{photon} + \cancel{E}_T, pp \rightarrow \tilde{q}\tilde{q}^* \gamma, \tilde{q} \rightarrow q\tilde{\chi}_1^0, m_{\tilde{q}} - m_{\tilde{\chi}_1^0} = m_c$	>1350	95	53	CHATRCHYAN13AV	CMS	$\text{jets} (+ \text{leptons}) + \cancel{E}_T, \text{CMSSM}, m_{\tilde{g}} = m_{\tilde{q}}$
> 490	95	28	AAD	15K ATLS	$\tilde{c} \rightarrow c\tilde{\chi}_1^0, m_{\tilde{\chi}_1^0} < 200 \text{ GeV}$	> 800	95	54	CHATRCHYAN13W	CMS	$\geq 1 \text{ photons} + \text{jets} + \cancel{E}_T, \text{GGM}, \text{wino-like NLSP}, m_{\tilde{\chi}_1^0} = 375 \text{ GeV}$
> 875	95	29	KHACHATRY...15AF	CMS	$\tilde{q} \rightarrow q\tilde{\chi}_1^0, \text{simplified model}, 8 \text{ degenerate light } \tilde{q}, m_{\tilde{\chi}_1^0} = 0$	>1000	95	54	CHATRCHYAN13W	CMS	$\geq 2 \text{ photons} + \text{jets} + \cancel{E}_T, \text{GGM}, \text{bino-like NLSP}, m_{\tilde{\chi}_1^0} = 375 \text{ GeV}$
> 520	95	29	KHACHATRY...15AF	CMS	$\tilde{q} \rightarrow q\tilde{\chi}_1^0, \text{simplified model}, \text{single light squark}, m_{\tilde{\chi}_1^0} = 0$	> 340	95	55	DREINER	12A THEO	$m_{\tilde{q}} \sim m_{\tilde{\chi}_1^0}$
>1450	95	29	KHACHATRY...15AF	CMS	$\text{CMSSM}, \tan\beta = 30, A_0 = -2\max(m_0, m_{1/2}), \mu > 0$	> 650	95	56	DREINER	12A THEO	$m_{\tilde{q}} = m_{\tilde{g}} \sim m_{\tilde{\chi}_1^0}$
> 850	95	30	AAD	14AE ATLS	$\text{jets} + \cancel{E}_T, \tilde{q} \rightarrow q\tilde{\chi}_1^0 \text{ simplified model}, \text{mass degenerate first and second generation squarks}, m_{\tilde{\chi}_1^0} = 0 \text{ GeV}$						
> 440	95	30	AAD	14AE ATLS	$\text{jets} + \cancel{E}_T, \tilde{q} \rightarrow q\tilde{\chi}_1^0 \text{ simplified model}, \text{single light-flavour squark}, m_{\tilde{\chi}_1^0} = 0 \text{ GeV}$						
>1700	95	30	AAD	14AE ATLS	$\text{jets} + \cancel{E}_T, \text{mSUGRA/CMSSM}, m_{\tilde{q}} = m_{\tilde{g}}$						
> 800	95	31	CHATRCHYAN14AH	CMS	$\text{jets} + \cancel{E}_T, \tilde{q} \rightarrow q\tilde{\chi}_1^0 \text{ simplified model}, m_{\tilde{\chi}_1^0} = 50 \text{ GeV}$						

1 AAD 21AK searched in 139 fb^{-1} of pp collisions at $\sqrt{s} = 13 \text{ TeV}$ for pair production of gluinos and squarks in events with a single isolated electron or muon, originating from the decay of a W boson, multiple jets and significant \cancel{E}_T . No significant excess above the Standard Model expectations is observed. Limits are set on the gluino mass in the Tglu1B simplified model and on the squark mass in the Tsqr3 simplified model, see their Figure 8.

2 AAD 21F searched in 139 fb^{-1} of pp collisions at $\sqrt{s} = 13 \text{ TeV}$ for pair production of squarks in events with a high- p_T jet and \cancel{E}_T . No significant excess above the Standard Model predictions is observed. Limits are set on the \tilde{t} mass in the Tstop3 and Tstop4, on the \tilde{b} mass in the Tstop1, and on the \tilde{q} mass in the Tsqr1 simplified model (four-flavour, two chirality states degeneracy).

- ³ AAD 21L searched in 139 fb^{-1} of pp collisions at $\sqrt{s} = 13 \text{ TeV}$ for pair production of gluinos and squarks in events with jets, large missing transverse momentum but no electrons or muons. No significant excess above the Standard Model expectations is observed. Limits are set on the gluino mass in the Tglu1A and Tglu1B simplified models, on the squark mass in the Tsqk1 and Tsqk3 simplified models and in a simplified model for gluino-squark production, see their Figures 13-17.
- ⁴ SIRUNYAN 21M searched in 137 fb^{-1} of pp collisions at $\sqrt{s} = 13 \text{ TeV}$ for supersymmetry in events with two opposite-sign same-flavor leptons (electrons, muons) and \cancel{E}_T . No significant excess above the Standard Model expectations is observed. Limits are set on the gluino mass in the simplified model Tglu4C, see their Figure 10, on the $\tilde{\chi}_2^0$ and $\tilde{\chi}_1^\pm$ mass in Tch1n2Fa, see their Figure 11, on the $\tilde{\chi}_1^0$ mass in Tn1n1C and Tn1n1B for $m_{\tilde{\chi}_2^0} = m_{\tilde{\chi}_1^\pm} = m_{\tilde{\chi}_1^0}$, see their Figure 12. Limits are also set on the light squark mass for the simplified model Tsqk2A, on the sbottom mass in Tsb0t3, see their Figure 13, and on the slepton mass in direct electroweak pair production of mass-degenerate left- and right-handed sleptons (selectrons and smuons), see their Figure 14.
- ⁵ SIRUNYAN 19AG searched in 35.9 fb^{-1} of pp collisions at $\sqrt{s} = 13 \text{ TeV}$ for events with two photons and large \cancel{E}_T . No significant excess above the Standard Model expectations is observed. Limits are set on the gluino mass in the Tglu4B simplified model and on the squark mass in the Tsqk4B simplified model, see their Figure 3.
- ⁶ SIRUNYAN 19CH searched in 137 fb^{-1} of pp collisions at $\sqrt{s} = 13 \text{ TeV}$ for events containing multiple jets and large \cancel{E}_T . No significant excess above the Standard Model expectations is observed. Limits are set on the gluino mass in the Tglu1A, Tglu1C, Tglu2A and Tglu3A simplified models, see their Figure 13. Limits are also set on squark, sbottom and stop masses in the Tsqk1, Tsb0t1, Tstop1 simplified models, see their Figure 14.
- ⁷ SIRUNYAN 19K searched in 35.9 fb^{-1} of pp collisions at $\sqrt{s} = 13 \text{ TeV}$ for events with a photon, an electron or muon, and large \cancel{E}_T . No significant excess above the Standard Model expectations is observed. In the framework of GMSB, limits are set on the chargino and neutralino mass in the Tch1n1A simplified model, see their Figure 6. Limits are also set on the gluino mass in the Tglu4A simplified model, and on the squark mass in the Tsqk4A simplified model, see their Figure 7.
- ⁸ AABOUD 18BJ searched in 36.1 fb^{-1} of pp collisions at $\sqrt{s} = 13 \text{ TeV}$ in events with two opposite-sign charged leptons (electrons and muons), jets and missing transverse momentum, with various requirements to be sensitive to signals with different kinematic endpoint values in the dilepton invariant mass distribution. The data are found to be consistent with the SM expectation. Results are interpreted in the Tsqk2 model in case of $m_{\tilde{\chi}_1^0} = 1 \text{ GeV}$: for any $m_{\tilde{\chi}_2^0}$, squark masses below 1200 GeV are excluded, see their Fig. 14(b).
- ⁹ AABOUD 18BV searched in 36.1 fb^{-1} of pp collisions at $\sqrt{s} = 13 \text{ TeV}$ for events with at least one jet identified as c -jet, large missing transverse energy and no leptons. Good agreement is observed between the number of events in data and Standard Model predictions. The results are translated into exclusion limits in Tsqk1 models considering only \tilde{c}_1 . In scenarios with massless neutralinos, scharm masses below 850 GeV are excluded. If the differences of the \tilde{c}_1 and $\tilde{\chi}_1^0$ masses is below 100 GeV , scharm masses below 500 GeV are excluded. See their Fig.6 and Fig.7.
- ¹⁰ AABOUD 18I searched in 36.1 fb^{-1} of pp collisions at $\sqrt{s} = 13 \text{ TeV}$ for events with at least one jet with a transverse momentum above 250 GeV and no leptons. Good agreement is observed between the number of events in data and Standard Model predictions. The results are translated into exclusion limits in Tsqk1 models. In the compressed scenario with similar squark and neutralino masses, squark masses below 710 GeV are excluded. See their Fig.10(b).
- ¹¹ AABOUD 18U searched in 36.1 fb^{-1} of pp collisions at $\sqrt{s} = 13 \text{ TeV}$ in events with at least one isolated photon, possibly jets and significant transverse momentum targeting generalised models of gauge-mediated SUSY breaking. No significant excess of events is observed above the SM prediction. Results are interpreted in terms of lower limits on the masses of squark in Tsqk4B models. Masses below 1820 GeV are excluded for any NLSP mass, see their Fig. 9.
- ¹² AABOUD 18V searched in 36.1 fb^{-1} of pp collisions at $\sqrt{s} = 13 \text{ TeV}$ in events with no charged leptons, jets and missing transverse momentum. The data are found to be consistent with the SM expectation. Results are interpreted in the Tsqk1 model: squark masses below 1550 GeV are excluded for massless LSP, see their Fig. 13(a).
- ¹³ AABOUD 18V searched in 36.1 fb^{-1} of pp collisions at $\sqrt{s} = 13 \text{ TeV}$ in events with no charged leptons, jets and missing transverse momentum. The data are found to be consistent with the SM expectation. Results are interpreted in the Tsqk3 model. Assuming that $m_{\tilde{\chi}_1^\pm} = 0.5 (m_{\tilde{q}} + m_{\tilde{\chi}_1^0})$, squark masses below 1150 GeV are excluded for massless LSP, see their Fig. 14(a). Exclusions are also shown assuming $m_{\tilde{\chi}_1^0} = 60 \text{ GeV}$, see their Fig. 14(b).
- ¹⁴ SIRUNYAN 18AA searched in 35.9 fb^{-1} of pp collisions at $\sqrt{s} = 13 \text{ TeV}$ for events with at least one photon and large \cancel{E}_T . No significant excess above the Standard Model expectations is observed. Limits are set on wino masses in a general gauge-mediated SUSY breaking (GGM) scenario with bino-like $\tilde{\chi}_1^0$ and wino-like $\tilde{\chi}_1^\pm$ and $\tilde{\chi}_2^0$, see Figure 7. Limits are also set on the NLSP mass in the Tch1n1A and Tch1ch1A simplified models, see their Figure 8. Finally, limits are set on the gluino mass in the Tglu4A and Tglu4B simplified models, see their Figure 9, and on the squark mass in the Tsqk4A and Tsqk4B simplified models, see their Figure 10.
- ¹⁵ SIRUNYAN 18AY searched in 35.9 fb^{-1} of pp collisions at $\sqrt{s} = 13 \text{ TeV}$ for events containing one or more jets and significant \cancel{E}_T . No significant excess above the Standard Model expectations is observed. Limits are set on the gluino mass in the Tglu1A, Tglu2A and Tglu3A simplified models, see their Figure 3. Limits are also set on squark, sbottom and stop masses in the Tsqk1, Tsb0t1, Tstop1 and Tstop4 simplified models, see their Figure 3. Finally, limits are set on long-lived gluino masses in a Tglu1A simplified model where the gluino is metastable or long-lived with proper decay lengths in the range $10^{-3} \text{ mm} < c\tau < 10^5 \text{ mm}$, see their Figure 4.
- ¹⁶ AABOUD 17AR searched in 36.1 fb^{-1} of pp collisions at $\sqrt{s} = 13 \text{ TeV}$ for events with one isolated lepton, at least two jets and large missing transverse momentum. No significant excess above the Standard Model expectations is observed. Limits up to 1.25 TeV are set on the 1st and 2nd generation squark masses in Tsqk3 simplified models, with $x = (m_{\tilde{\chi}_1^\pm} - m_{\tilde{\chi}_1^0}) / (m_{\tilde{q}} - m_{\tilde{\chi}_1^0}) = 1/2$. Similar limits are obtained for variable x and fixed neutralino mass, $m_{\tilde{\chi}_1^0} = 60 \text{ GeV}$. See their Figure 13.
- ¹⁷ AABOUD 17N searched in 14.7 fb^{-1} of pp collisions at $\sqrt{s} = 13 \text{ TeV}$ for events with 2 same-flavour, opposite-sign leptons (electrons or muons), jets and large missing transverse momentum. The results are interpreted as 95% C.L. limits in Tsqk2 models, assuming $m_{\tilde{\chi}_1^0} = 0 \text{ GeV}$ and $m_{\tilde{\chi}_2^0} = 600 \text{ GeV}$. See their Fig. 12 for exclusion limits as a function of $m_{\tilde{\chi}_2^0}$.
- ¹⁸ KHACHATRYAN 17P searched in 2.3 fb^{-1} of pp collisions at $\sqrt{s} = 13 \text{ TeV}$ for events with one or more jets and large \cancel{E}_T . No significant excess above the Standard Model expectations is observed. Limits are set on the gluino mass in the Tglu1A, Tglu2A, Tglu3A, Tglu3B, Tglu3C and Tglu3D simplified models, see their Figures 7 and 8. Limits are also set on the squark mass in the Tsqk1 simplified model, see their Fig. 7, and on the sbottom mass in the Tsb0t1 simplified model, see Fig. 8. Finally, limits are set on the stop mass in the Tstop1, Tstop3, Tstop4, Tstop6 and Tstop7 simplified models, see Fig. 8.
- ¹⁹ KHACHATRYAN 17V searched in 2.3 fb^{-1} of pp collisions at $\sqrt{s} = 13 \text{ TeV}$ for events with two photons and large \cancel{E}_T . No significant excess above the Standard Model expectations is observed. Limits are set on the gluino and squark mass in the context of general gauge mediation models Tglu4B and Tsqk4, see their Fig. 4.
- ²⁰ SIRUNYAN 17AY searched in 35.9 fb^{-1} of pp collisions at $\sqrt{s} = 13 \text{ TeV}$ for events with at least one photon, jets and large \cancel{E}_T . No significant excess above the Standard Model expectations is observed. Limits are set on the gluino mass in the Tglu4A and Tglu4B simplified models, and on the squark mass in the Tsqk4A and Tsqk4B simplified models, see their Figure 6.
- ²¹ SIRUNYAN 17AZ searched in 35.9 fb^{-1} of pp collisions at $\sqrt{s} = 13 \text{ TeV}$ for events with one or more jets and large \cancel{E}_T . No significant excess above the Standard Model expectations is observed. Limits are set on the gluino mass in the Tglu1A, Tglu2A, Tglu3A simplified models, see their Figures 6. Limits are also set on the squark mass in the Tsqk1 simplified model (for single light squark and for 8 degenerate light squarks), on the sbottom mass in the Tsb0t1 simplified model and on the stop mass in the Tstop1 simplified model, see their Fig. 7. Finally, limits are set on the stop mass in the Tstop2, Tstop4 and Tstop8 simplified models, see Fig. 8.
- ²² SIRUNYAN 17P searched in 35.9 fb^{-1} of pp collisions at $\sqrt{s} = 13 \text{ TeV}$ for events with multiple jets and large \cancel{E}_T . No significant excess above the Standard Model expectations is observed. Limits are set on the gluino mass in the Tglu1A, Tglu1C, Tglu2A, Tglu3A and Tglu3D simplified models, see their Fig. 12. Limits are also set on the squark mass in the Tsqk1 simplified model, on the stop mass in the Tstop1 simplified model, and on the sbottom mass in the Tsb0t1 simplified model, see Fig. 13.
- ²³ AABOUD 16D searched in 3.2 fb^{-1} of pp collisions at $\sqrt{s} = 13 \text{ TeV}$ for events with an energetic jet and large missing transverse momentum. The results are interpreted as 95% C.L. limits on masses of first and second generation squarks decaying into a quark and the lightest neutralino in scenarios with $m_{\tilde{q}} - m_{\tilde{\chi}_1^0} < 25 \text{ GeV}$. See their Fig. 6.
- ²⁴ AABOUD 16N searched in 3.2 fb^{-1} of pp collisions at $\sqrt{s} = 13 \text{ TeV}$ for events containing hadronic jets, large \cancel{E}_T , and no electrons or muons. No significant excess above the Standard Model expectations is observed. First- and second-generation squark masses below 1030 GeV are excluded at the 95% C.L. decaying to quarks and a massless lightest neutralino. See their Fig. 7a.
- ²⁵ KHACHATRYAN 16BS searched in 2.3 fb^{-1} of pp collisions at $\sqrt{s} = 13 \text{ TeV}$ for events with at least one energetic jet, no isolated leptons, and significant \cancel{E}_T , using the transverse mass variable M_{T2} to discriminate between signal and background processes. No significant excess above the Standard Model expectations is observed. Limits are set on the squark mass in the Tsqk1 simplified model, both in the assumption of a single light squark and of 8 degenerate squarks, see Fig. 11 and Table 3.
- ²⁶ AAD 15BV summarized and extended ATLAS searches for gluinos and first- and second-generation squarks in final states containing jets and missing transverse momentum, with or without leptons or b -jets in the $\sqrt{s} = 8 \text{ TeV}$ data set collected in 2012. The paper reports the results of new interpretations and statistical combinations of previously published analyses, as well as new analyses. Exclusion limits at 95% C.L. are set on the squark mass in several R-parity conserving models. See their Figs. 9, 11, 18, 22, 24, 27, 28.
- ²⁷ AAD 15CS searched in 20.3 fb^{-1} of pp collisions at $\sqrt{s} = 8 \text{ TeV}$ for evidence of pair production of squarks, decaying into a quark and a neutralino, where a photon was radiated either from an initial-state quark, from an intermediate squark, or from a final-state quark. No evidence was found for an excess above the expected level of Standard Model background and a 95% C.L. exclusion limit was set on the squark mass as a function of the squark-neutralino mass difference, see Fig. 19.
- ²⁸ AAD 15K searched in 20.3 fb^{-1} of pp collisions at $\sqrt{s} = 8 \text{ TeV}$ for events containing at least two jets, where the two leading jets are each identified as originating from c -quarks, and large missing transverse momentum. No excess of events above the expected level of Standard Model background was found. Exclusion limits at 95% C.L. are set on the mass of superpartners of charm quarks (\tilde{c}). Assuming that the decay $\tilde{c} \rightarrow c\tilde{\chi}_1^0$ takes place 100% of the time, a scalar charm mass below 490 GeV is excluded for $m_{\tilde{\chi}_1^0} < 200 \text{ GeV}$. For more details, see their Fig. 2.
- ²⁹ KHACHATRYAN 15AF searched in 19.5 fb^{-1} of pp collisions at $\sqrt{s} = 8 \text{ TeV}$ for events with at least two energetic jets and significant \cancel{E}_T , using the transverse mass variable M_{T2} to discriminate between signal and background processes. No significant excess above the Standard Model expectations is observed. Limits are set on the squark mass in simplified models where the decay $\tilde{q} \rightarrow q\tilde{\chi}_1^0$ takes place with a branching ratio of 100%, both for the case of a single light squark or 8 degenerate squarks, see Fig. 12. See also Table 5. Exclusions in the CMSSM, assuming $\tan\beta = 30$, $A_0 = -2 \max(m_0, m_{1/2})$ and $\mu > 0$, are also presented, see Fig. 15.
- ³⁰ AAD 14AE searched in 20.3 fb^{-1} of pp collisions at $\sqrt{s} = 8 \text{ TeV}$ for strongly produced supersymmetric particles in events containing jets and large missing transverse momentum, and no electrons or muons. No excess over the expected SM background is observed. Exclusion limits are derived in simplified models containing squarks that decay via $\tilde{q} \rightarrow q\tilde{\chi}_1^0$, where either a single light state or two degenerate generations of squarks are assumed, see Fig. 10.
- ³¹ CHATRCHYAN 14AH searched in 4.7 fb^{-1} of pp collisions at $\sqrt{s} = 7 \text{ TeV}$ for events with at least two energetic jets and significant \cancel{E}_T , using the razor variables (M_R and R^2) to discriminate between signal and background processes. No significant excess above the Standard Model expectations is observed. Limits are set on squark masses in simplified models where the decay $\tilde{q} \rightarrow q\tilde{\chi}_1^0$ takes place with a branching ratio of 100%, see Fig. 28. Exclusions in the CMSSM, assuming $\tan\beta = 10$, $A_0 = 0$ and $\mu > 0$, are also presented, see Fig. 26.
- ³² CHATRCHYAN 14I searched in 19.5 fb^{-1} of pp collisions at $\sqrt{s} = 8 \text{ TeV}$ for events containing multijets and large \cancel{E}_T . No excess over the expected SM background is observed. Exclusion limits are derived in simplified models containing squarks that decay via $\tilde{q} \rightarrow q\tilde{\chi}_1^0$, where either a single light state or two degenerate generations of squarks are assumed, see Fig. 7a.

Searches Particle Listings

Supersymmetric Particle Searches

- 33 AAD 13L searched in 4.7 fb^{-1} of pp collisions at $\sqrt{s} = 7 \text{ TeV}$ for the production of squarks and gluinos in events containing jets, missing transverse momentum and no high- p_T electrons or muons. No excess over the expected SM background is observed. In mSUGRA/CMSSM models with $\tan\beta = 10$, $A_0 = 0$ and $\mu > 0$, squarks and gluinos of equal mass are excluded for masses below 1360 GeV at 95% C.L. In a simplified model containing only squarks of the first two generations, a gluino octet and a massless neutralino, squark masses below 1320 GeV are excluded at 95% C.L. for gluino masses below 2 TeV. See Figures 10–15 for more precise bounds.
- 34 AAD 13Q searched in 4.7 fb^{-1} of pp collisions at $\sqrt{s} = 7 \text{ TeV}$ for events containing a high- p_T isolated photon, at least one jet identified as originating from a bottom quark, and high missing transverse momentum. Such signatures may originate from supersymmetric models with gauge-mediated supersymmetry breaking in events in which one of a pair of higgsino-like neutralinos decays into a photon and a gravitino while the other decays into a Higgs boson and a gravitino. No significant excess above the expected background was found and limits were set on the squark mass as a function of the neutralino mass in a generalized GMSB model (GGM) with a higgsino-like neutralino NLSP, see their Fig. 4. For neutralino masses greater than 220 GeV, squark masses below 1020 GeV are excluded at 95% C.L.
- 35 CHATRCHYAN 13 looked in 4.98 fb^{-1} of pp collisions at $\sqrt{s} = 7 \text{ TeV}$ for events with two opposite-sign leptons (e, μ, τ), jets and missing transverse energy. No excess beyond the Standard Model expectation is observed. Exclusion limits are derived in the mSUGRA/CMSSM model with $\tan\beta = 10$, $A_0 = 0$ and $\mu > 0$, see Fig. 6.
- 36 CHATRCHYAN 13G searched in 4.98 fb^{-1} of pp collisions at $\sqrt{s} = 7 \text{ TeV}$ for the production of squarks and gluinos in events containing 0,1,2, ≥ 3 b -jets, missing transverse momentum and no electrons or muons. No excess over the expected SM background is observed. In mSUGRA/CMSSM models with $\tan\beta = 10$, $A_0 = 0$, and $\mu > 0$, squarks and gluinos of equal mass are excluded for masses below 1250 GeV at 95% C.L. Exclusions are also derived in various simplified models, see Fig. 7.
- 37 CHATRCHYAN 13H searched in 4.96 fb^{-1} of pp collisions at $\sqrt{s} = 7 \text{ TeV}$ for events with two photons, ≥ 4 jets and low $E_{\cancel{T}}$ due to $\tilde{q} \rightarrow \gamma \tilde{\chi}_1^0$ decays in a stealth SUSY framework, where the $\tilde{\chi}_1^0$ decays through a singlino (\tilde{S}) intermediate state to $\gamma S \tilde{G}$, with the singlet state S decaying to two jets. No significant excess above the expected background was found and limits were set in a particular R-parity conserving stealth SUSY model. The model assumes $m_{\tilde{\chi}_1^0} = 0.5 m_{\tilde{q}}$, $m_S = 100 \text{ GeV}$ and $m_{\tilde{S}} = 90 \text{ GeV}$. Under these assumptions, squark masses less than 1430 GeV were excluded at the 95% C.L.
- 38 CHATRCHYAN 13T searched in 11.7 fb^{-1} of pp collisions at $\sqrt{s} = 8 \text{ TeV}$ for events with at least two energetic jets and significant $E_{\cancel{T}}$, using the α_T variable to discriminate between processes with genuine and misreconstructed $E_{\cancel{T}}$. No significant excess above the Standard Model expectations is observed. Limits are set on squark masses in simplified models where the decay $\tilde{q} \rightarrow q \tilde{\chi}_1^0$ takes place with a branching ratio of 100%, assuming an eightfold degeneracy of the masses of the first two generation squarks, see Fig. 8 and Table 9. Also limits in the case of a single light squark are given.
- 39 AAD 12AX searched in 1.04 fb^{-1} of pp collisions at $\sqrt{s} = 7 \text{ TeV}$ for supersymmetry in events containing jets, missing transverse momentum and one isolated electron or muon. No excess over the expected SM background is observed and model-independent limits are set on the cross section of new physics contributions to the signal regions. In mSUGRA/CMSSM models with $\tan\beta = 10$, $A_0 = 0$ and $\mu > 0$, squarks and gluinos of equal mass are excluded for masses below 820 GeV at 95% C.L. Limits are also set on simplified models for squark production and decay via an intermediate chargino and on supersymmetric models with bilinear R-parity violation. Supersedes AAD 11G.
- 40 AAD 12CJ searched in 4.7 fb^{-1} of pp collisions at $\sqrt{s} = 7 \text{ TeV}$ for events containing one or more isolated leptons (electrons or muons), jets and $E_{\cancel{T}}$. The observations are in good agreement with the SM expectations and exclusion limits have been set in number of SUSY models. In the mSUGRA/CMSSM model with $\tan\beta = 10$, $A_0 = 0$, and $\mu > 0$, 95% C.L. exclusion limits have been derived for $m_{\tilde{q}} < 1200 \text{ GeV}$, assuming equal squark and gluino masses. In minimal GMSB, values of the effective SUSY breaking scale $\Lambda < 50 \text{ TeV}$ are excluded at 95% C.L. for $\tan\beta < 45$. Also exclusion limits in a number of simplified models have been presented, see Figs. 10 and 12.
- 41 AAD 12CP searched in 4.8 fb^{-1} of pp collisions at $\sqrt{s} = 7 \text{ TeV}$ for events with two photons and large $E_{\cancel{T}}$ due to $\tilde{\chi}_1^0 \rightarrow \gamma \tilde{G}$ decays in a GMSB framework. No significant excess above the expected background was found and limits were set on the squark mass as a function of the neutralino mass in a generalized GMSB model (GGM) with a bino-like neutralino NLSP. The other sparticle masses were decoupled, $\tan\beta = 2$ and $c\tau_{NLSP} < 0.1 \text{ mm}$. Also, in the framework of the SP58 model, a 95% C.L. lower limit was set on the breaking scale Λ of 196 TeV.
- 42 AAD 12W searched in 1.04 fb^{-1} of pp collisions at $\sqrt{s} = 7 \text{ TeV}$ for the production of squarks and gluinos in events containing jets, missing transverse momentum and no electrons or muons. No excess over the expected SM background is observed. In mSUGRA/CMSSM models with $\tan\beta = 10$, $A_0 = 0$ and $\mu > 0$, squarks and gluinos of equal mass are excluded for masses below 950 GeV at 95% C.L. In a simplified model containing only squarks of the first two generations, a gluino octet and a massless neutralino, squark masses below 875 GeV are excluded at 95% C.L.
- 43 CHATRCHYAN 12 looked in 35 pb^{-1} of pp collisions at $\sqrt{s} = 7 \text{ TeV}$ for events with e and/or μ and/or jets, a large total transverse energy, and $E_{\cancel{T}}$. The event selection is based on the dimensionless razor variable R , related to the $E_{\cancel{T}}$ and M_{R2} , an indicator of the heavy particle mass scale. No evidence for an excess over the expected background is observed. Limits are derived in the CMSSM ($m_0, m_{1/2}$) plane for $\tan\beta = 3, 10$ and 50 (see Fig. 7 and 8). Limits are also obtained for Simplified Model Spectra.
- 44 CHATRCHYAN 12AE searched in 4.98 fb^{-1} of pp collisions at $\sqrt{s} = 7 \text{ TeV}$ for events with at least three jets and large missing transverse momentum. No significant excesses over the expected SM backgrounds are observed and 95% C.L. limits on the production cross section of squarks in a scenario where $\tilde{q} \rightarrow q \tilde{\chi}_1^0$ with a 100% branching ratio, see Fig. 3. For $m_{\tilde{\chi}_1^0} < 200 \text{ GeV}$, values of $m_{\tilde{q}}$ below 760 GeV are excluded at 95% C.L. Also limits in the CMSSM are presented, see Fig. 2.
- 45 CHATRCHYAN 12AT searched in 4.73 fb^{-1} of pp collisions at $\sqrt{s} = 7 \text{ TeV}$ for the production of squarks and gluinos in events containing jets, missing transverse momentum and no electrons or muons. No excess over the expected SM background is observed. In mSUGRA/CMSSM models with $\tan\beta = 10$, $A_0 = 0$ and $\mu > 0$, squarks with masses below 1110 GeV are excluded at 95% C.L. Squarks and gluinos of equal mass are excluded for masses below 1180 GeV at 95% C.L. Exclusions are also derived in various simplified models, see Fig. 6.
- 46 AABOUD 18v searched in 36.1 fb^{-1} of pp collisions at $\sqrt{s} = 13 \text{ TeV}$ in events with no charged leptons, jets and missing transverse momentum. The data are found to be consistent with the SM expectation. Results are interpreted in the Tsqk5 model. Squark masses below 1100 GeV are excluded if $(m_{\tilde{\chi}_2^0} - m_{\tilde{\chi}_1^0})/(m_{\tilde{q}} - m_{\tilde{\chi}_1^0}) < 0.95$ and $m_{\tilde{\chi}_1^0} = 60 \text{ GeV}$, see their Fig. 16(a).
- 47 KHACHATRYAN 16BT performed a global Bayesian analysis of a wide range of CMS results obtained with data samples corresponding to 5.0 fb^{-1} of pp collisions at $\sqrt{s} = 7 \text{ TeV}$ and in 19.5 fb^{-1} of pp collisions at $\sqrt{s} = 8 \text{ TeV}$. The set of searches considered, both individually and in combination, includes those with all-hadronic final states, same-sign and opposite-sign dileptons, and multi-lepton final states. An interpretation was given in a scan of the 19-parameter pMSSM. No scan points with a gluino mass less than 500 GeV survived and 98% of models with a squark mass less than 300 GeV were excluded.
- 48 AAD 15AI searched in 20 fb^{-1} of pp collisions at $\sqrt{s} = 8 \text{ TeV}$ for events containing at least one isolated lepton (electron or muon), jets, and large missing transverse momentum. No excess of events above the expected level of Standard Model background was found. Exclusion limits at 95% C.L. are set on the squark masses in the CMSSM/mSUGRA, see Fig. 15, in the NUHM2, see Fig. 16, and in various simplified models, see Figs. 19–21.
- 49 KHACHATRYAN 15AR searched in 19.7 fb^{-1} of pp collisions at $\sqrt{s} = 8 \text{ TeV}$ for events containing jets, either a charged lepton or a photon, and low missing transverse momentum. No significant excess above the Standard Model expectations is observed. Limits are set on the squark mass in a stealth SUSY model where the decays $\tilde{q} \rightarrow q \tilde{\chi}_1^{\pm}$, $\tilde{\chi}_1^{\pm} \rightarrow \tilde{S} W^{\pm}$, $\tilde{S} \rightarrow S \tilde{G}$ and $S \rightarrow g g$, with $m_{\tilde{S}} = 100 \text{ GeV}$ and $m_S = 90 \text{ GeV}$, take place with a branching ratio of 100%. See Fig. 6 for γ or Fig. 7 for e^{\pm} analyses.
- 50 KHACHATRYAN 15AZ searched in 19.7 fb^{-1} of pp collisions at $\sqrt{s} = 8 \text{ TeV}$ for events with either at least one photon, hadronic jets and $E_{\cancel{T}}$ (single photon channel) or with at least two photons and at least one jet and using the razor variables. No significant excess above the Standard Model expectations is observed. Limits are set on gluino masses in the general gauge-mediated SUSY breaking model (GGM), for both a bino-like and wino-like neutralino NLSP scenario, see Fig. 8 and 9.
- 51 AAD 14E searched in 20.3 fb^{-1} of pp collisions at $\sqrt{s} = 8 \text{ TeV}$ for strongly produced supersymmetric particles in events containing jets and two same-sign leptons or three leptons. The search also utilises jets originating from b -quarks, missing transverse momentum and other variables. No excess over the expected SM background is observed. Exclusion limits are derived in simplified models containing gluinos and squarks, see Figures 5 and 6. In the $\tilde{q} \rightarrow q' \tilde{\chi}_1^{\pm}$, $\tilde{\chi}_1^{\pm} \rightarrow W^{(*)\pm} \tilde{\chi}_2^0$, $\tilde{\chi}_2^0 \rightarrow Z^{(*)} \tilde{\chi}_1^0$ simplified model, the following assumptions have been made: $m_{\tilde{\chi}_1^{\pm}} = 0.5 m_{\tilde{\chi}_1^0} + m_{\tilde{g}}$, $m_{\tilde{\chi}_2^0} = 0.5 (m_{\tilde{\chi}_1^0} + m_{\tilde{q}})$. In the $\tilde{q} \rightarrow q' \tilde{\chi}_1^{\pm}$ or $\tilde{q} \rightarrow q' \tilde{\chi}_2^0$, $\tilde{\chi}_1^{\pm} \rightarrow e^{\pm} \nu \tilde{\chi}_1^0$ or $\tilde{\chi}_2^0 \rightarrow e^{\pm} \ell^{\mp} (\nu \nu) \tilde{\chi}_1^0$ simplified model, the following assumptions have been made: $m_{\tilde{\chi}_1^{\pm}} = m_{\tilde{\chi}_2^0} = 0.5 (m_{\tilde{\chi}_1^0} + m_{\tilde{q}})$, $m_{\tilde{\chi}_1^0} < 460 \text{ GeV}$. Limits are also derived in the mSUGRA/CMSSM, bRPV and GMSB models, see their Fig. 8.
- 52 CHATRCHYAN 13AO searched in 4.98 fb^{-1} of pp collisions at $\sqrt{s} = 7 \text{ TeV}$ for events with two opposite-sign isolated leptons accompanied by hadronic jets and $E_{\cancel{T}}$. No significant excesses over the expected SM backgrounds are observed and 95% C.L. exclusion limits are derived in the mSUGRA/CMSSM model with $\tan\beta = 10$, $A_0 = 0$ and $\mu > 0$, see Fig. 8.
- 53 CHATRCHYAN 13AV searched in 4.7 fb^{-1} of pp collisions at $\sqrt{s} = 7 \text{ TeV}$ for new heavy particle pairs decaying into jets (possibly b -tagged), leptons and $E_{\cancel{T}}$ using the Razor variables. No significant excesses over the expected SM backgrounds are observed and 95% C.L. exclusion limits are derived in the mSUGRA/CMSSM model with $\tan\beta = 10$, $A_0 = 0$ and $\mu > 0$, see Fig. 3. The results are also interpreted in various simplified models, see Fig. 4.
- 54 CHATRCHYAN 13W searched in 4.93 fb^{-1} of pp collisions at $\sqrt{s} = 7 \text{ TeV}$ for events with one or more photons, hadronic jets and $E_{\cancel{T}}$. No significant excess above the Standard Model expectations is observed. Limits are set on squark masses in the general gauge-mediated SUSY breaking model (GGM), for both a wino-like and bino-like neutralino NLSP scenario, see Fig. 5.
- 55 DREINER 12A reassesses constraints from CMS (at 7 TeV, $\sim 4.4 \text{ fb}^{-1}$) under the assumption that the first and second generation squarks and the lightest SUSY particle are quasi-degenerate in mass (compressed spectrum).
- 56 DREINER 12A reassesses constraints from CMS (at 7 TeV, $\sim 4.4 \text{ fb}^{-1}$) under the assumption that the first and second generation squarks, the gluino, and the lightest SUSY particle are quasi-degenerate in mass (compressed spectrum).

R-parity violating \tilde{q} (squark) mass limit

VALUE (GeV)	CL%	DOCUMENT ID	TECN	COMMENT	
none	100–720	95	1 SIRUNYAN	18EA CMS	2 large jets with four-parton substructure, $\tilde{q} \rightarrow 4q$
>1600	95	2 KHACHATRYAN..16BX	CMS	$\tilde{q} \rightarrow q \tilde{\chi}_1^0, \tilde{\chi}_1^0 \rightarrow \ell \ell \nu, \lambda_{121} \neq 0, m_{\tilde{g}} = 2400 \text{ GeV}$	
>1000	95	3 AAD	15CB ATLS	jets, $\tilde{q} \rightarrow q \tilde{\chi}_1^0, \tilde{\chi}_1^0 \rightarrow \ell q q, m_{\tilde{\chi}_1^0} = 108 \text{ GeV}$ and $2.5 < c\tau_{\tilde{\chi}_1^0} < 200 \text{ mm}$	
		4 AAD	12AX ATLS	ℓ +jets + $E_{\cancel{T}}$, CMSSM, $m_{\tilde{q}} = m_{\tilde{g}}$	
		5 CHATRCHYAN12AL	CMS	$\geq 3\ell^{\pm}$	

- 1 SIRUNYAN 18EA searched in 38.2 fb^{-1} of pp collisions at $\sqrt{s} = 13 \text{ TeV}$ for the pair production of resonances, each decaying to at least four quarks. Reconstructed particles are clustered into two large jets of similar mass, each consistent with four-parton substructure. No statistically significant excess over the Standard Model expectation is observed. Limits are set on the squark and gluino mass in RPV supersymmetry models where squarks (gluinos) decay, through intermediate higgsinos, to four (five) quarks, see their Figure 4.
- 2 KHACHATRYAN 16BX searched in 19.5 fb^{-1} of pp collisions at $\sqrt{s} = 8 \text{ TeV}$ for events containing 4 leptons coming from R-parity-violating decays of $\tilde{\chi}_1^0 \rightarrow \ell \ell \nu$ with $\lambda_{121} \neq 0$ or $\lambda_{122} \neq 0$. No excess over the expected background is observed. Limits are derived on the gluino, squark and stop masses, see Fig. 23.
- 3 AAD 15CB searched for events containing at least one long-lived particle that decays at a significant distance from its production point (displaced vertex, DV) into two leptons or into five or more charged particles in 20.3 fb^{-1} of pp collisions at $\sqrt{s} = 8 \text{ TeV}$. The dilepton signature is characterised by DV formed from at least two leptons candidates.

Four different final states were considered for the multitrack signature, in which the DV must be accompanied by a high-transverse momentum muon or electron candidate that originates from the DV, jets or missing transverse momentum. No events were observed in any of the signal regions. Results were interpreted in SUSY scenarios involving R -parity violation, split supersymmetry, and gauge mediation. See their Fig. 14–20.

⁴ AAD 12Ax searched in 1.04 fb^{-1} of pp collisions at $\sqrt{s} = 7 \text{ TeV}$ for supersymmetry in events containing jets, missing transverse momentum and one isolated electron or muon. No excess over the expected SM background is observed and model-independent limits are set on the cross section of new physics contributions to the signal regions. In mSUGRA/CMSSM models with $\tan\beta = 10$, $A_0 = 0$ and $\mu > 0$, squarks and gluinos of equal mass are excluded for masses below 820 GeV at 95% C.L. Limits are also set on simplified models for squark production and decay via an intermediate chargino and on supersymmetric models with bilinear R -parity violation. Supersedes AAD 11g.

⁵ CHATRCHYAN 12AL looked in 4.98 fb^{-1} of pp collisions at $\sqrt{s} = 7 \text{ TeV}$ for anomalous production of events with three or more isolated leptons. Limits on squark and gluino masses are set in RPV SUSY models with leptonic $LL\bar{E}$ couplings, $\lambda_{123} > 0.05$, and hadronic UDD couplings, $\lambda_{112} > 0.05$, see their Fig. 5. In the UDD case the leptons arise from supersymmetric cascade decays. A very specific supersymmetric spectrum is assumed. All decays are prompt.

Long-lived \tilde{q} (Squark) mass limit

The following are bounds on long-lived scalar squarks, assumed to hadronize into hadrons with lifetime long enough to escape the detector prior to a possible decay. Limits may depend on the mixing angle of mass eigenstates: $\tilde{q}_1 = \tilde{q}_L \cos\theta_q + \tilde{q}_R \sin\theta_q$.

The coupling to the Z^0 boson vanishes for up-type squarks when $\theta_u = 0.98$, and for down type squarks when $\theta_d = 1.17$.

VALUE (GeV)	CL%	DOCUMENT ID	TECN	COMMENT
>1250	95	¹ AABOUD	19AT ATLS	\tilde{b} R -hadrons
>1340	95	² AABOUD	19AT ATLS	\tilde{t} R -hadrons
>1600	95	³ SIRUNYAN	19BH CMS	long-lived \tilde{t} , RPV, $\tilde{t} \rightarrow \tilde{d}\tilde{d}$, $10 \text{ mm} < c\tau < 110 \text{ mm}$
>1350	95	³ SIRUNYAN	19BH CMS	long-lived \tilde{t} , RPV, $\tilde{t} \rightarrow b\ell$, $7 \text{ mm} < c\tau < 110 \text{ mm}$
> 805	95	⁴ AABOUD	16B ATLS	\tilde{b} R -hadrons
> 890	95	⁵ AABOUD	16B ATLS	\tilde{t} R -hadrons
>1040	95	⁶ KHACHATRYAN	16BW CMS	\tilde{t} R -hadrons, cloud interaction model
>1000	95	⁶ KHACHATRYAN	16BW CMS	\tilde{t} R -hadrons, charge-suppressed interaction model
> 845	95	⁷ AAD	15AE ATLS	\tilde{b} R -hadron, stable, Regge model
> 900	95	⁷ AAD	15AE ATLS	\tilde{t} R -hadron, stable, Regge model
>1500	95	⁷ AAD	15AE ATLS	\tilde{g} decaying to 300 GeV stable sleptons, LeptoSUSY model
> 751	95	⁸ AAD	15BM ATLS	\tilde{b} R -hadron, stable, Regge model
> 766	95	⁸ AAD	15BM ATLS	\tilde{t} R -hadron, stable, Regge model
> 525	95	⁹ KHACHATRYAN	15AK CMS	\tilde{t} R -hadrons, $1 \mu\text{s} < \tau < 1000 \text{ s}$
> 470	95	⁹ KHACHATRYAN	15AK CMS	\tilde{t} R -hadrons, $1 \mu\text{s} < \tau < 1000 \text{ s}$
> 683	95	¹⁰ AAD	13AA ATLS	\tilde{t} , R -hadrons, generic interaction model
> 612	95	¹¹ AAD	13AA ATLS	\tilde{b} , R -hadrons, generic interaction model
> 344	95	¹² AAD	13BC ATLS	R -hadrons, $\tilde{t} \rightarrow b\tilde{\chi}_1^0$, Regge model, lifetime between 10^{-5} and 10^3 s , $m_{\tilde{\chi}_1^0} = 100 \text{ GeV}$
> 379	95	¹³ AAD	13BC ATLS	R -hadrons, $\tilde{t} \rightarrow t\tilde{\chi}_1^0$, Regge model, lifetime between 10^{-5} and 10^3 s , $m_{\tilde{\chi}_1^0} = 100 \text{ GeV}$
> 935	95	¹⁴ CHATRCHYAN	13AB CMS	long-lived \tilde{t} forming R -hadrons, cloud interaction model

¹ AABOUD 19AT searched in 36.1 fb^{-1} of pp collisions at $\sqrt{s} = 13 \text{ TeV}$ for metastable and stable R -hadrons. Multiple search strategies for a wide range of lifetimes, corresponding to path lengths of a few meters, are defined. No significant deviations from the expected Standard Model background are observed. Sbottom R -hadrons are excluded at 95% C.L. for masses below 1250 GeV. Less stringent constraints are achieved with the muon-spectrometer agnostic analysis. See their Figure 9 (bottom-left).

² AABOUD 19AT searched in 36.1 fb^{-1} of pp collisions at $\sqrt{s} = 13 \text{ TeV}$ for metastable and stable R -hadrons. Multiple search strategies for a wide range of lifetimes, corresponding to path lengths of a few meters, are defined. No significant deviations from the expected Standard Model background are observed. Stop R -hadrons are excluded at 95% C.L. for masses below 1340 GeV. Similar constraints are achieved with the muon-spectrometer agnostic analysis. See their Figure 9 (bottom-right).

³ SIRUNYAN 19BH searched in 35.9 fb^{-1} of pp collisions at $\sqrt{s} = 13 \text{ TeV}$ for long-lived particles decaying into jets, with each long-lived particle having a decay vertex well displaced from the production vertex. The selected events are found to be consistent with standard model predictions. Limits are set on the gluino mass in a GMSB model where the gluino is decaying via $\tilde{g} \rightarrow \tilde{g}G$, see their Figure 4 and in an RPV model of supersymmetry where the gluino is decaying via $\tilde{g} \rightarrow T\tilde{D}\tilde{S}$, see their Figures 5. Limits are also set on the stop mass in two RPV models, see their Figure 6 (for $\tilde{t} \rightarrow b\ell$ decays) and Figure 7 (for $\tilde{t} \rightarrow \tilde{d}\tilde{d}$ decays).

⁴ AABOUD 16B searched in 3.2 fb^{-1} of pp collisions at $\sqrt{s} = 13 \text{ TeV}$ for long-lived R -hadrons using observables related to large ionization losses and slow propagation velocities, which are signatures of heavy charged particles traveling significantly slower than the speed of light. Exclusion limits at 95% C.L. are set on the long-lived sbottom masses exceeding 805 GeV. See their Fig. 5.

⁵ AABOUD 16B searched in 3.2 fb^{-1} of pp collisions at $\sqrt{s} = 13 \text{ TeV}$ for long-lived R -hadrons using observables related to large ionization losses and slow propagation velocities, which are signatures of heavy charged particles traveling significantly slower than the speed of light. Exclusion limits at 95% C.L. are set on the long-lived stop masses exceeding 890 GeV. See their Fig. 5.

⁶ KHACHATRYAN 16BW searched in 2.5 fb^{-1} of pp collisions at $\sqrt{s} = 13 \text{ TeV}$ for events with heavy stable charged particles, identified by their anomalously high energy deposits

in the silicon tracker and/or long time-of-flight measurements by the muon system. No evidence for an excess over the expected background is observed. Limits are derived for pair production of top squarks as a function of mass, depending on the interaction model, see Fig. 4 and Table 7.

⁷ AAD 15AE searched in 19.1 fb^{-1} of pp collisions at $\sqrt{s} = 8 \text{ TeV}$ for heavy long-lived charged particles, measured through their specific ionization energy loss in the ATLAS pixel detector or their time-of-flight in the ATLAS muon system. In the absence of an excess of events above the expected backgrounds, limits are set R -hadrons in various scenarios, see Fig. 11. Limits are also set in LeptoSUSY models where the gluino decays to stable 300 GeV leptons, see Fig. 9.

⁸ AAD 15BM searched in 18.4 fb^{-1} of pp collisions at $\sqrt{s} = 8 \text{ TeV}$ for stable and metastable non-relativistic charged particles through their anomalous specific ionization energy loss in the ATLAS pixel detector. In absence of an excess of events above the expected backgrounds, limits are set on stable bottom and top squark R -hadrons, see Table 5.

⁹ KHACHATRYAN 15AK looked in a data set corresponding to fb^{-1} of pp collisions at $\sqrt{s} = 8 \text{ TeV}$, and a search interval corresponding to 281 h of trigger lifetime, for long-lived particles that have stopped in the CMS detector. No evidence for an excess over the expected background in a cloud interaction model is observed. Assuming the decay $\tilde{t} \rightarrow t\tilde{\chi}_1^0$ and lifetimes between $1 \mu\text{s}$ and 1000 s , limits are derived on \tilde{t} production as a function of $m_{\tilde{\chi}_1^0}$, see Figs. 4 and 7. The exclusions require that $m_{\tilde{\chi}_1^0}$ is kinematically consistent with the minimum values of the jet energy thresholds used.

¹⁰ AAD 13AA searched in 4.7 fb^{-1} of pp collisions at $\sqrt{s} = 7 \text{ TeV}$ for events containing colored long-lived particles that hadronize forming R -hadrons. No significant excess above the expected background was found. Long-lived R -hadrons containing a \tilde{t} are excluded for masses up to 683 GeV at 95% C.L. in a general interaction model. Also, limits independent of the fraction of R -hadrons that arrive charged in the muon system were derived, see Fig. 6.

¹¹ AAD 13AA searched in 4.7 fb^{-1} of pp collisions at $\sqrt{s} = 7 \text{ TeV}$ for events containing colored long-lived particles that hadronize forming R -hadrons. No significant excess above the expected background was found. Long-lived R -hadrons containing a \tilde{b} are excluded for masses up to 612 GeV at 95% C.L. in a general interaction model. Also, limits independent of the fraction of R -hadrons that arrive charged in the muon system were derived, see Fig. 6.

¹² AAD 13BC searched in 5.0 fb^{-1} of pp collisions at $\sqrt{s} = 7 \text{ TeV}$ and in 22.9 fb^{-1} of pp collisions at $\sqrt{s} = 8 \text{ TeV}$ for bottom squark R -hadrons that have come to rest within the ATLAS calorimeter and decay at some later time to hadronic jets and a neutralino. In absence of an excess of events above the expected backgrounds, limits are set on sbottom masses for the decay $\tilde{b} \rightarrow b\tilde{\chi}_1^0$ for different lifetimes, and for a neutralino mass of 100 GeV, see their Table 6 and Fig. 10.

¹³ AAD 13BC searched in 5.0 fb^{-1} of pp collisions at $\sqrt{s} = 7 \text{ TeV}$ and in 22.9 fb^{-1} of pp collisions at $\sqrt{s} = 8 \text{ TeV}$ for bottom squark R -hadrons that have come to rest within the ATLAS calorimeter and decay at some later time to hadronic jets and a neutralino. In absence of an excess of events above the expected backgrounds, limits are set on stop masses for the decay $\tilde{t} \rightarrow t\tilde{\chi}_1^0$ for different lifetimes, and for a neutralino mass of 100 GeV, see their Table 6 and Fig. 10.

¹⁴ CHATRCHYAN 13AB looked in 5.0 fb^{-1} of pp collisions at $\sqrt{s} = 7 \text{ TeV}$ and in 18.8 fb^{-1} of pp collisions at $\sqrt{s} = 8 \text{ TeV}$ for events with heavy stable particles, identified by their anomalous dE/dx in the tracker and additionally requiring that it be identified as muon in the muon chambers, from pair production of \tilde{t}_1 's. No evidence for an excess over the expected background is observed. Limits are derived for pair production of stops as a function of mass in the cloud interaction model (see Fig. 8 and Table 6). In the charge-suppressed model, the limit decreases to 818 GeV.

\tilde{b} (Sbottom) mass limit

Limits in e^+e^- depend on the mixing angle of the mass eigenstate $\tilde{b}_1 = \tilde{b}_L \cos\theta_b + \tilde{b}_R \sin\theta_b$. Coupling to the Z vanishes for $\theta_b \sim 1.17$. As a consequence, no absolute constraint in the mass region $\lesssim 40 \text{ GeV}$ is available in the literature at this time from e^+e^- collisions. In the Listings below, we use $\Delta m = m_{\tilde{b}_1} - m_{\tilde{\chi}_1^0}$.

Some earlier papers are now obsolete and have been omitted. They were last listed in our PDG 14 edition: K. Olive, *et al.* (Particle Data Group), Chinese Physics **C38** 070001 (2014) (<http://pdg.lbl.gov>).

R-parity conserving \tilde{b} (Sbottom) mass limit

VALUE (GeV)	CL%	DOCUMENT ID	TECN	COMMENT
> 850	95	¹ AAD	21AM ATLS	$\tau^{\pm}s + b\text{-jets} + \cancel{E}_T$, Tsb04, $m_{\tilde{\chi}_2^0} - m_{\tilde{\chi}_1^0} = 130 \text{ GeV}$, $m_{\tilde{\chi}_2^0} < 180 \text{ GeV}$
>1270	95	² AAD	21s ATLS	$b\text{-jets} + \cancel{E}_T$, Tsb01, $m_{\tilde{\chi}_1^0} = 0 \text{ GeV}$
> 660	95	² AAD	21s ATLS	$b\text{-jets} + \cancel{E}_T$, Tsb01, $m_{\tilde{b}_1} - m_{\tilde{\chi}_1^0} = 10 \text{ GeV}$
>1600	95	³ SIRUNYAN	21M CMS	$\ell^{\pm}\ell^{\mp} + \cancel{E}_T$, Tsb03, $m_{\tilde{\chi}_2^0} = 1500 \text{ GeV}$, $m_{\tilde{\chi}_1^0} = 100 \text{ GeV}$
> 750	95	⁴ AAD	20v ATLS	same-sign $\ell^{\pm}\ell^{\pm} + \text{jets}$, Tsb02, $m_{\tilde{\chi}_1^0} = m_{\tilde{\chi}_2^0} + 100 \text{ GeV}$, $m_{\tilde{\chi}_1^0} \sim 50 \text{ GeV}$
> 850	95	⁵ SIRUNYAN	20T CMS	same-sign $\ell^{\pm}\ell^{\pm}$ or $\geq 3\ell^{\pm} + \text{jets}$, Tsb02, $m_{\tilde{\chi}_1^0} < 800 \text{ GeV}$, $m_{\tilde{\chi}_1^0} = 50 \text{ GeV}$
>1500	95	⁶ AAD	19H ATLS	$\geq 3 b\text{-jets} + \cancel{E}_T$, Tsb04, $\geq 1 h(\rightarrow b\tilde{b})$, $m_{\tilde{\chi}_1^0} = 60 \text{ GeV}$
>1300	95	⁷ AAD	19H ATLS	$\geq 3 b\text{-jets} + \cancel{E}_T$, Tsb04, $\geq 1 h(\rightarrow b\tilde{b})$, $m_{\tilde{\chi}_2^0} = m_{\tilde{\chi}_1^0} + 130 \text{ GeV}$

Searches Particle Listings

Supersymmetric Particle Searches

>1220	95	⁸ SIRUNYAN	19CH CMS	jets+ \cancel{E}_T , Tsb0t1, $m_{\tilde{\chi}_1^0} = 0$ GeV	38 KHACHATRY...15AD CMS	$\ell^\pm \ell^\mp + \text{jets} + \cancel{E}_T, \tilde{b} \rightarrow$ $b \ell^\pm \ell^\mp \tilde{\chi}_1^0$			
> 530	95	⁹ SIRUNYAN	19CI CMS	$\geq 1 H (\rightarrow \gamma\gamma) + \text{jets} + \cancel{E}_T$, Tsb0t4, $m_{\tilde{\chi}_2^0} = m_{\tilde{\chi}_1^0} + 130$ GeV, $m_{\tilde{\chi}_1^0} = 1$ GeV	none 340–600 95	³⁹ AAD	14AX ATLS	$\geq 3 b\text{-jets} + \cancel{E}_T, \tilde{b} \rightarrow b \tilde{\chi}_2^0$ simplified model with $\tilde{\chi}_2^0 \rightarrow h \tilde{\chi}_1^0$, $m_{\tilde{\chi}_1^0} = 60$ GeV, $m_{\tilde{\chi}_2^0} = 300$ GeV	
> 430	95	¹⁰ AABOUD	18I ATLS	$\geq 1 \text{jets} + \cancel{E}_T$, Tsb0t1, $m_{\tilde{b}} - m_{\tilde{\chi}_1^0} \sim m_b$	> 440	95	⁴⁰ AAD	14E ATLS	$\ell^\pm \ell^\pm (\ell^\mp) + \text{jets}, \tilde{b}_1 \rightarrow t \tilde{\chi}_1^\pm$ with $\tilde{\chi}_1^\pm \rightarrow W^{(*)\pm} \tilde{\chi}_1^0$ simplified model, $m_{\tilde{\chi}_1^\pm} = 2 m_{\tilde{\chi}_1^0}$
> 840	95	¹¹ SIRUNYAN	18AL CMS	$\geq 3 \ell^\pm + \text{jets} + \cancel{E}_T$, Tsb0t2, $m_{\tilde{\chi}_1^0} = 50$ GeV	> 500	95	⁴¹ CHATRCHYAN14H	CMS	same-sign $\ell^\pm \ell^\pm, \tilde{b} \rightarrow t \tilde{\chi}_1^\pm, \tilde{\chi}_1^\pm \rightarrow W^\pm \tilde{\chi}_1^0$ simplified model, $m_{\tilde{\chi}_1^\pm} = 2$ GeV, $m_{\tilde{\chi}_1^0} = 100$ GeV
> 975	95	¹² SIRUNYAN	18AR CMS	$\ell^\pm \ell^\mp + \text{jets} + \cancel{E}_T$, Tsb0t3, $m_{\tilde{\chi}_1^0} = (m_{\tilde{\chi}_2^0} + m_{\tilde{\chi}_1^0})/2, m_{\tilde{\chi}_1^0} = 100$ GeV	> 620	95	⁴² AAD	13AU ATLS	2 $b\text{-jets} + \cancel{E}_T, \tilde{b}_1 \rightarrow b \tilde{\chi}_1^0, m_{\tilde{\chi}_1^0} < 120$ GeV
>1060	95	¹³ SIRUNYAN	18AY CMS	jets+ \cancel{E}_T , Tsb0t1, $m_{\tilde{\chi}_1^0} = 0$ GeV	> 550	95	⁴³ CHATRCHYAN13AT	CMS	jets + $\cancel{E}_T, \tilde{b} \rightarrow b \tilde{\chi}_1^0$ simplified model, $m_{\tilde{\chi}_1^0} = 50$ GeV
>1230	95	¹⁴ SIRUNYAN	18B CMS	jets+ \cancel{E}_T , Tsb0t1, $m_{\tilde{\chi}_1^0} = 0$ GeV	> 600	95	⁴⁴ CHATRCHYAN13T	CMS	jets + $\cancel{E}_T, \tilde{b} \rightarrow b \tilde{\chi}_1^0$ simplified model, $m_{\tilde{\chi}_1^0} = 0$ GeV
> 420	95	¹⁵ SIRUNYAN	18X CMS	$\geq 1 H (\rightarrow \gamma\gamma) + \text{jets} + \cancel{E}_T$, Tsb0t4, $m_{\tilde{\chi}_2^0} = m_{\tilde{\chi}_1^0} + 130$ GeV, $m_{\tilde{\chi}_1^0} < 225$ GeV	> 450	95	⁴⁵ CHATRCHYAN13V	CMS	same-sign $\ell^\pm \ell^\pm + \geq 2 b\text{-jets}, \tilde{b} \rightarrow t \tilde{\chi}_1^\pm, \tilde{\chi}_1^\pm \rightarrow W^\pm \tilde{\chi}_1^0$ simplified model, $m_{\tilde{\chi}_1^0} = 50$ GeV
> 700	95	¹⁶ AABOUD	17AJ ATLS	same-sign $\ell^\pm \ell^\pm / 3 \ell + \text{jets} + \cancel{E}_T$, Tsb0t2, $m_{\tilde{\chi}_1^0} = 0$ GeV	> 390	95	⁴⁶ AAD	12AN ATLS	$\tilde{b}_1 \rightarrow b \tilde{\chi}_1^0$, simplified model, $m_{\tilde{\chi}_1^0} < 60$ GeV
> 950	95	¹⁷ AABOUD	17AX ATLS	2 $b\text{-jets} + \cancel{E}_T$, Tsb0t1, $m_{\tilde{\chi}_1^0} = 0$ GeV	> 410	95	⁴⁷ CHATRCHYAN12AI	CMS	$\ell^\pm \ell^\pm + b\text{-jets} + \cancel{E}_T$
> 880	95	¹⁸ AABOUD	17AX ATLS	2 $b\text{-jets} + \cancel{E}_T$, mixture Tsb0t1 and Tsb0t2 BR=50%, $m_{\tilde{\chi}_1^0} = 0$ GeV, $m_{\tilde{\chi}_1^\pm} - m_{\tilde{\chi}_1^0} = 1$ GeV	> 294	95	⁴⁸ CHATRCHYAN12BO	CMS	$\tilde{b}_1 \rightarrow b \tilde{\chi}_1^0$, simplified model, $m_{\tilde{\chi}_1^0} = 50$ GeV
> 315	95	¹⁹ KHACHATRY...17A	CMS	2 VBF jets + \cancel{E}_T , Tsb0t1, $m_{\tilde{b}} - m_{\tilde{\chi}_1^0} = 5$ GeV	> 230	95	⁴⁹ AAD	11K ATLS	stable b
> 450	95	²⁰ KHACHATRY...17AW	CMS	$\geq 3 \ell^\pm, 2 \text{jets}, \text{Tsb0t2}, m_{\tilde{\chi}_1^0} = 50$ GeV, $m_{\tilde{\chi}_1^\pm} = 200$ GeV	> 247	95	⁵⁰ AAD	11O ATLS	$\tilde{g} \rightarrow \tilde{b}_1 b, \tilde{b}_1 \rightarrow b \tilde{\chi}_1^0, m_{\tilde{\chi}_1^0} = 60$ GeV
> 800	95	²¹ KHACHATRY...17P	CMS	1 or more jets+ \cancel{E}_T , Tsb0t1, $m_{\tilde{\chi}_1^0} = 0$ GeV	> 520	95	⁵¹ CHATRCHYAN11D	CMS	$\tilde{b}, \tilde{t} \rightarrow b$
>1175	95	²² SIRUNYAN	17AZ CMS	$\geq 1 \text{jets} + \cancel{E}_T$, Tsb0t1, $m_{\tilde{\chi}_1^0} = 0$ GeV	> 230	95	⁵² AALTONEN	10R CDF	$\tilde{b}_1 \rightarrow b \tilde{\chi}_1^0, m_{\tilde{\chi}_1^0} < 70$ GeV
> 890	95	²³ SIRUNYAN	17K CMS	jets+ \cancel{E}_T , Tsb0t1, $m_{\tilde{\chi}_1^0} = 0$ GeV	> 247	95	⁵³ ABAZOV	10L D0	$\tilde{b}_1 \rightarrow b \tilde{\chi}_1^0, m_{\tilde{\chi}_1^0} = 0$ GeV
> 810	95	²⁴ SIRUNYAN	17S CMS	same-sign $\ell^\pm \ell^\pm + \text{jets} + \cancel{E}_T$, Tsb0t2, $m_{\tilde{\chi}_1^0} = 50$ GeV, $m_{\tilde{\chi}_1^\pm} = 100$ GeV					
> 323	95	²⁵ AABOUD	16D ATLS	$\geq 1 \text{jet} + \cancel{E}_T$, Tsb0t1, $m_{\tilde{b}} - m_{\tilde{\chi}_1^0} = 5$ GeV					
> 840	95	²⁶ AABOUD	16Q ATLS	2 $b\text{-jets} + \cancel{E}_T$, Tsb0t1, $m_{\tilde{\chi}_1^0} = 100$ GeV					
> 540	95	²⁷ AAD	16BB ATLS	2 same-sign $3\ell + \text{jets} + \cancel{E}_T$, Tsb0t2, $m_{\tilde{\chi}_1^0} < 55$ GeV					
> 680	95	²⁸ KHACHATRY...16BJ	CMS	same-sign $\ell^\pm \ell^\pm$, Tsb0t2, $m_{\tilde{\chi}_1^\pm} < 550$ GeV, $m_{\tilde{\chi}_1^0} = 50$ GeV					
> 500	95	²⁸ KHACHATRY...16BJ	CMS	same-sign $\ell^\pm \ell^\pm$, Tsb0t2, $m_{\tilde{b}} - m_{\tilde{\chi}_1^\pm} < 100$ GeV, $m_{\tilde{\chi}_1^0} = 50$ GeV					
> 880	95	²⁹ KHACHATRY...16BS	CMS	jets + \cancel{E}_T , Tsb0t1, $m_{\tilde{\chi}_1^0} = 0$ GeV					
> 550	95	³⁰ KHACHATRY...16BY	CMS	opposite-sign $\ell^\pm \ell^\pm$, Tsb0t3, $m_{\tilde{\chi}_1^0} = 100$ GeV					
> 600	95	³¹ AAD	15CJ ATLS	$\tilde{b} \rightarrow b \tilde{\chi}_1^0, m_{\tilde{\chi}_1^0} < 250$ GeV					
> 440	95	³¹ AAD	15CJ ATLS	$\tilde{b} \rightarrow t \tilde{\chi}_1^\pm, \tilde{\chi}_1^\pm \rightarrow W^{(*)\pm} \tilde{\chi}_1^0, m_{\tilde{\chi}_1^0} = 60$ GeV, $m_{\tilde{b}} - m_{\tilde{\chi}_1^\pm} < m_t$					
none 300–650	95	³¹ AAD	15CJ ATLS	$\tilde{b} \rightarrow \tilde{b} \tilde{\chi}_2^0, \tilde{\chi}_2^0 \rightarrow h \tilde{\chi}_1^0, m_{\tilde{\chi}_1^0} = 60$ GeV, $m_{\tilde{\chi}_2^0} > 250$ GeV					
> 640	95	³² KHACHATRY...15AF	CMS	$\tilde{b} \rightarrow b \tilde{\chi}_1^0, m_{\tilde{\chi}_1^0} = 0$					
> 650	95	³³ KHACHATRY...15AH	CMS	$\tilde{b} \rightarrow b \tilde{\chi}_1^0, m_{\tilde{\chi}_1^0} = 0$					
> 250	95	³³ KHACHATRY...15AH	CMS	$\tilde{b} \rightarrow b \tilde{\chi}_1^0, m_{\tilde{b}} - m_{\tilde{\chi}_1^0} < 10$ GeV					
> 570	95	³⁴ KHACHATRY...15I	CMS	$\tilde{b} \rightarrow t \tilde{\chi}_1^\pm, \tilde{\chi}_1^\pm \rightarrow W^\pm \tilde{\chi}_1^0, m_{\tilde{\chi}_1^0} = 50$ GeV, $150 < m_{\tilde{\chi}_1^\pm} < 300$ GeV					
> 255	95	³⁵ AAD	14T ATLS	$\tilde{b}_1 \rightarrow b \tilde{\chi}_1^0, m_{\tilde{b}_1} - m_{\tilde{\chi}_1^0} \approx m_b$					
> 400	95	³⁶ CHATRCHYAN14AH	CMS	jets + $\cancel{E}_T, \tilde{b} \rightarrow b \tilde{\chi}_1^0$ simplified model, $m_{\tilde{\chi}_1^0} = 50$ GeV					
		³⁷ CHATRCHYAN14R	CMS	$\geq 3 \ell^\pm, \tilde{b} \rightarrow t \tilde{\chi}_1^\pm, \tilde{\chi}_1^\pm \rightarrow W^\pm \tilde{\chi}_1^0$ simplified model, $m_{\tilde{\chi}_1^0} = 50$ GeV					

• • • We do not use the following data for averages, fits, limits, etc. • • •

¹ AAD 21AM searched in 139 fb⁻¹ of pp collisions at $\sqrt{s} = 13$ TeV for pair production of bottom squarks in events with hadronically decaying τ^\pm -leptons, b -tagged jets, and large \cancel{E}_T . No significant excess above the Standard Model expectations is observed. Limits are set on the bottom squark mass in the Tsb0t4 simplified model, assuming $m_{\tilde{\chi}_2^0} - m_{\tilde{\chi}_1^0} = 130$ GeV, see their Figure 8.

² AAD 21s searched in 139 fb⁻¹ of pp collisions at $\sqrt{s} = 13$ TeV for pair production of sbottoms, LQ or dark matter in events with b -jets and \cancel{E}_T , also using dedicated secondary-vertex-finding techniques. No significant excess above the Standard Model predictions is observed. Limits are set on $m_{\tilde{b}_1}$ in the Tsb0t1 simplified model, on the LQ masses depending on the BR in $b\nu$, on scalar and pseudoscalar dark matter mediator masses. See Figures 8, 9, 10.

³ SIRUNYAN 21M searched in 137 fb⁻¹ of pp collisions at $\sqrt{s} = 13$ TeV for supersymmetry in events with two opposite-sign same-flavor leptons (electrons, muons) and \cancel{E}_T . No significant excess above the Standard Model expectations is observed. Limits are set on the gluino mass in the simplified model Tglu4C, see their Figure 10, on the $\tilde{\chi}_1^0$ and $\tilde{\chi}_1^\pm$ mass in Tchi1n2Fa, see their Figure 11, on the $\tilde{\chi}_1^0$ mass in Tn1n1C and Tn1n1B for $m_{\tilde{\chi}_2^0} = m_{\tilde{\chi}_1^\pm} = m_{\tilde{\chi}_1^0}$, see their Figure 12. Limits are also set on the light squark mass for the simplified model Tsqk2A, on the sbottom mass in Tsb0t3, see their Figure 13, and on the slepton mass in direct electroweak pair production of mass-degenerate left- and right-handed sleptons (selectrons and smuons), see their Figure 14.

⁴ AAD 20V searched in 139 fb⁻¹ of pp collisions at $\sqrt{s} = 13$ TeV for events with two same-sign charged leptons (electrons or muons) and jets. No significant excess above the Standard Model expectations is observed. Exclusion limits at 95% C.L. are set on the bottom squark masses in the Tsb0t2 simplified model for $m_{\tilde{\chi}_1^\pm} = m_{\tilde{\chi}_1^0} + 100$ GeV, see their Fig. 8(a).

⁵ SIRUNYAN 20T searched in 137 fb⁻¹ of pp collisions at $\sqrt{s} = 13$ TeV for events with at least two jets, and two isolated same-sign or three or more charged leptons (electrons or muons). No significant excess above the Standard Model expectations is observed. Limits are set on the gluino mass in the Tglu3A, Tglu3B, Tglu3C and Tglu3D simplified models, see their Figure 7, and in the Tglu1C and Tglu1B simplified models, see their Figures 8 and 9. Limits are also set on the sbottom mass in the Tsb0t2 simplified model, see their Figure 10, and on the stop mass in the Tstop7 simplified model, see their Figure 11. Finally, limits are set on the gluino mass in RPV simplified models where the gluino decays either via $\tilde{g} \rightarrow q\bar{q}\bar{q}$ + $e/\mu/\tau$ or via $\tilde{g} \rightarrow tbs$, see Figure 12.

⁶ AAD 19H searched in 139 fb⁻¹ of pp collisions at $\sqrt{s} = 13$ TeV for events with no charged leptons, three or more b -jets, and large \cancel{E}_T . Higgs boson candidates are reconstructed as b -jet pairs. No significant excess above the Standard Model expectations is observed. Limits up to 1500 GeV are set on the sbottom mass in the Tsb0t4 simplified model, see Figure 8(a), for fixed $m_{\tilde{\chi}_1^0} = 60$ GeV and for $m_{\tilde{\chi}_2^0}$ up to 1200 GeV.

⁷ AAD 19H searched in 139 fb⁻¹ of pp collisions at $\sqrt{s} = 13$ TeV for events with no charged leptons, three or more b -jets, and large \cancel{E}_T . Higgs boson candidates are reconstructed as b -jet pairs. No significant excess above the Standard Model expectations is observed. Limits up to 1300 GeV are set on the sbottom mass in the Tsb0t4 simplified model, see Figure 8(b), for $m_{\tilde{\chi}_2^0} = m_{\tilde{\chi}_1^0} + 130$ GeV and $m_{\tilde{\chi}_2^0}$ from 200 to 750 GeV.

⁸ SIRUNYAN 19CH searched in 137 fb⁻¹ of pp collisions at $\sqrt{s} = 13$ TeV for events containing multiple jets and large \cancel{E}_T . No significant excess above the Standard Model expectations is observed. Limits are set on the gluino mass in the Tglu1A, Tglu1C, Tglu2A and Tglu3A simplified models, see their Figure 13. Limits are also set on squark,

- sbottom and stop masses in the Tsqk1, Tsb0t1, Tstop1 simplified models, see their Figure 14.
- ⁹ SIRUNYAN 19cl searched in 77.5 fb^{-1} of pp collisions at $\sqrt{s} = 13 \text{ TeV}$ for events with one or more high-momentum Higgs bosons, decaying to pairs of photons, jets and \cancel{E}_T . No significant excess above the Standard Model expectations is observed. Limits are set on the sbottom mass in the Tsb0t4 simplified model, see Figure 3, and on the wino mass in the Tch1n2E simplified model, see their Figure 4. Limits are also set on the higgsino mass in the Tn1n1A and Tn1n1B simplified models, see their Figure 5.
- ¹⁰ AABOUD 18j searched in 36.1 fb^{-1} of pp collisions at $\sqrt{s} = 13 \text{ TeV}$ for events with at least one jet with a transverse momentum above 250 GeV and no leptons. Good agreement is observed between the number of events in data and Standard Model predictions. The results are translated into exclusion limits in Tsb0t1 models. In the compressed scenario with sbottom and neutralino masses differing by m_b , sbottom masses below 430 GeV are excluded. For $m_{\tilde{\chi}_1^0} = 0$ they exclude sbottom masses up to 610 GeV. See their Fig.10(a).
- ¹¹ SIRUNYAN 18Al searched in 35.9 fb^{-1} of pp collisions at $\sqrt{s} = 13 \text{ TeV}$ for events with at least three charged leptons, in any combination of electrons and muons, jets and significant \cancel{E}_T . No significant excess above the Standard Model expectations is observed. Limits are set on the gluino mass in the Tglu3A and Tglu1C simplified models, see their Figure 5. Limits are also set on the sbottom mass in the Tsb0t2 simplified model, see their Figure 6, and on the stop mass in the Tstop7 simplified model, see their Figure 7.
- ¹² SIRUNYAN 18AR searched in 35.9 fb^{-1} of pp collisions at $\sqrt{s} = 13 \text{ TeV}$ for events containing two opposite-charge, same-flavour leptons (electrons or muons), jets and \cancel{E}_T . No significant excess above the Standard Model expectations is observed. Limits are set on the gluino mass in the Tglu4C simplified model, see their Figure 7. Limits are also set on the chargino/neutralino mass in the Tch1n2F simplified model, see their Figure 8, and on the neutralino mass in the Tn1n1B and Tn1n1C simplified models, see their Figure 9. Finally, limits are set on the sbottom mass in the Tsb0t3 simplified model, see their Figure 10.
- ¹³ SIRUNYAN 18AY searched in 35.9 fb^{-1} of pp collisions at $\sqrt{s} = 13 \text{ TeV}$ for events containing one or more jets and significant \cancel{E}_T . No significant excess above the Standard Model expectations is observed. Limits are set on the gluino mass in the Tglu1A, Tglu2A and Tglu3A simplified models, see their Figure 3. Limits are also set on squark, sbottom and stop masses in the Tsqk1, Tsb0t1, Tstop1 and Tstop4 simplified models, see their Figure 3. Finally, limits are set on long-lived gluino masses in a Tglu1A simplified model where the gluino is metastable or long-lived with proper decay lengths in the range $10^{-3} \text{ mm} < c\tau < 10^5 \text{ mm}$, see their Figure 4.
- ¹⁴ SIRUNYAN 18B searched in 35.9 fb^{-1} of pp collisions at $\sqrt{s} = 13 \text{ TeV}$ for the pair production of third-generation squarks in events with jets and large \cancel{E}_T . No significant excess above the Standard Model expectations is observed. Limits are set on the sbottom mass in the Tsb0t1 simplified model, see their Figure 5, and on the stop mass in the Tstop4 simplified model, see their Figure 6.
- ¹⁵ SIRUNYAN 18x searched in 35.9 fb^{-1} of pp collisions at $\sqrt{s} = 13 \text{ TeV}$ for events with one or more high-momentum Higgs bosons, decaying to pairs of photons, jets and \cancel{E}_T . The razor variables (M_R and R^2) are used to categorise the events. No significant excess above the Standard Model expectations is observed. Limits are set on the sbottom mass in the Tsb0t4 simplified model and on the wino mass in the Tch1n2E simplified model, see their Figure 5. Limits are also set on the higgsino mass in the Tn1n1A and Tn1n1B simplified models, see their Figure 6.
- ¹⁶ AABOUD 17AJ searched in 36.1 fb^{-1} of pp collisions at $\sqrt{s} = 13 \text{ TeV}$ for events with two same-sign or three leptons, jets and large missing transverse momentum. No significant excess above the Standard Model expectations is observed. Limits up to 700 GeV are set on the bottom squark mass in Tsb0t2 simplified models assuming $m_{\tilde{\chi}_1^0} = 0 \text{ GeV}$. See their Figure 4(d).
- ¹⁷ AABOUD 17AX searched in 36 fb^{-1} of pp collisions at $\sqrt{s} = 13 \text{ TeV}$ for events containing two jets identified as originating from b -quarks and large missing transverse momentum. No excess of events above the expected level of Standard Model background was found. Exclusion limits at 95% C.L. are set on the masses of bottom squarks. In the Tsb0t1 simplified model, a b_1 mass below 950 GeV is excluded for $m_{\tilde{\chi}_1^0} = 0$ (<420) GeV. See their Fig. 7(a).
- ¹⁸ AABOUD 17AX searched in 36 fb^{-1} of pp collisions at $\sqrt{s} = 13 \text{ TeV}$ for events containing two jets identified as originating from b -quarks and large missing transverse momentum, with or without leptons. No excess of events above the expected level of Standard Model background was found. Exclusion limits at 95% C.L. are set on the masses of bottom squarks. Assuming 50% BR for Tsb0t1 and Tsb0t2 simplified models, a b_1 mass below 880 (860) GeV is excluded for $m_{\tilde{\chi}_1^0} = 0$ (<250) GeV. See their Fig. 7(b).
- ¹⁹ KHACHATRYAN 17A searched in 18.5 fb^{-1} of pp collisions at $\sqrt{s} = 8 \text{ TeV}$ for events with two forward jets, produced through vector boson fusion, and missing transverse momentum. No significant excess above the Standard Model expectations is observed. A limit is set on sbottom masses in the Tsb0t1 simplified model, see Fig. 3.
- ²⁰ KHACHATRYAN 17AW searched in 2.3 fb^{-1} of pp collisions at $\sqrt{s} = 13 \text{ TeV}$ for events with at least three charged leptons, in any combination of electrons and muons, and significant \cancel{E}_T . No significant excess above the Standard Model expectations is observed. Limits are set on the gluino mass in the Tglu3A and Tglu1C simplified models, and on the sbottom mass in the Tsb0t2 simplified model, see their Figure 4.
- ²¹ KHACHATRYAN 17P searched in 2.3 fb^{-1} of pp collisions at $\sqrt{s} = 13 \text{ TeV}$ for events with one or more jets and large \cancel{E}_T . No significant excess above the Standard Model expectations is observed. Limits are set on the gluino mass in the Tglu1A, Tglu2A, Tglu3A, Tglu3B, Tglu3C and Tglu3D simplified models, see their Figures 7 and 8. Limits are also set on the squark mass in the Tsqk1 simplified model, see their Fig. 7, and on the sbottom mass in the Tsb0t1 simplified model, see Fig. 8. Finally, limits are set on the stop mass in the Tstop1, Tstop3, Tstop4, Tstop6 and Tstop7 simplified models, see Fig. 8.
- ²² SIRUNYAN 17AZ searched in 35.9 fb^{-1} of pp collisions at $\sqrt{s} = 13 \text{ TeV}$ for events with one or more jets and large \cancel{E}_T . No significant excess above the Standard Model expectations is observed. Limits are set on the gluino mass in the Tglu1A, Tglu2A, Tglu3A simplified models, see their Figures 6. Limits are also set on the squark mass in the Tsqk1 simplified model (for single light squark and for 8 degenerate light squarks), on the sbottom mass in the Tsb0t1 simplified model and on the stop mass in the Tstop1 simplified model, see their Fig. 7. Finally, limits are set on the stop mass in the Tstop2, Tstop4 and Tstop8 simplified models, see Fig. 8.
- ²³ SIRUNYAN 17k searched in 2.3 fb^{-1} of pp collisions at $\sqrt{s} = 13 \text{ TeV}$ for direct production of stop or sbottom pairs in events with multiple jets and significant \cancel{E}_T . A second search also requires an isolated lepton and is combined with the all-hadronic search. No significant excess above the Standard Model expectations is observed. Limits are set on
- the stop mass in the Tstop1, Tstop8 and Tstop4 simplified models, see their Figures 7, 8 and 9 (for the Tstop4 limits, only the results of the all-hadronic search are used). Limits are also set on the sbottom mass in the Tsb0t1 simplified model, see Fig. 10 (also here, only the results of the all-hadronic search are used).
- ²⁴ SIRUNYAN 17s searched in 35.9 fb^{-1} of pp collisions at $\sqrt{s} = 13 \text{ TeV}$ for events with two isolated same-sign leptons, jets, and large \cancel{E}_T . No significant excess above the Standard Model expectations is observed. Limits are set on the mass of the gluino mass in the Tglu3A, Tglu3B, Tglu3C, Tglu3D and Tglu1B simplified models, see their Figures 5 and 6, and on the sbottom mass in the Tsb0t2 simplified model, see their Figure 6.
- ²⁵ AABOUD 16D searched in 3.2 fb^{-1} of pp collisions at $\sqrt{s} = 13 \text{ TeV}$ for events with an energetic jet and large missing transverse momentum. The results are interpreted as 95% C.L. limits on mass of sbottom decaying into a b -quark and the lightest neutralino in scenarios with $m_{\tilde{b}_1} - m_{\tilde{\chi}_1^0}$ between 5 and 20 GeV. See their Fig. 6.
- ²⁶ AABOUD 16Q searched in 3.2 fb^{-1} of pp collisions at $\sqrt{s} = 13 \text{ TeV}$ for events containing two jets identified as originating from b -quarks and large missing transverse momentum. No excess of events above the expected level of Standard Model background was found. Exclusion limits at 95% C.L. are set on the masses of third-generation squarks. Assuming that the decay $\tilde{b}_1 \rightarrow b\tilde{\chi}_1^0$ (Tsb0t1) takes place 100% of the time, a b_1 mass below 840 (800) GeV is excluded for $m_{\tilde{\chi}_1^0} < 100$ (360) GeV. Differences in mass above 100 GeV between the \tilde{b}_1 and the $\tilde{\chi}_1^0$ are excluded up to a \tilde{b}_1 mass of 500 GeV. For more details, see their Fig. 4.
- ²⁷ AAD 16BB searched in 3.2 fb^{-1} of pp collisions at $\sqrt{s} = 13 \text{ TeV}$ for events with exactly two same-sign leptons or at least three leptons, multiple hadronic jets, b -jets, and \cancel{E}_T . No significant excess over the Standard Model expectation is found. Exclusion limits at 95% C.L. are set on the sbottom mass for the Tsb0t2 model, assuming $m_{\tilde{\chi}_1^\pm} = m_{\tilde{\chi}_1^0} + 100 \text{ GeV}$. See their Fig. 4c.
- ²⁸ KHACHATRYAN 16BJ searched in 2.3 fb^{-1} of pp collisions at $\sqrt{s} = 13 \text{ TeV}$ for events with two isolated same-sign dileptons and jets in the final state. No significant excess above the Standard Model expectations is observed. Limits are set on the sbottom mass in the Tsb0t2 simplified model, see Fig. 6.
- ²⁹ KHACHATRYAN 16BS searched in 2.3 fb^{-1} of pp collisions at $\sqrt{s} = 13 \text{ TeV}$ for events with at least one energetic jet, no isolated leptons, and significant \cancel{E}_T , using the transverse mass variable M_{T2} to discriminate between signal and background processes. No significant excess above the Standard Model expectations is observed. Limits are set on the sbottom mass in the Tsb0t1 simplified model, see Fig. 11 and Table 3.
- ³⁰ KHACHATRYAN 16BY searched in 2.3 fb^{-1} of pp collisions at $\sqrt{s} = 13 \text{ TeV}$ for events with two opposite-sign, same-flavour leptons, jets, and missing transverse momentum. No significant excess above the Standard Model expectations is observed. Limits are set on the gluino mass in the Tglu4C simplified model, see Fig. 4, and on sbottom masses in the Tsb0t3 simplified model, see Fig. 5.
- ³¹ AAD 15CJ searched in 20 fb^{-1} of pp collisions at $\sqrt{s} = 8 \text{ TeV}$ for evidence of third generation squarks by combining a large number of searches covering various final states. Limits on the sbottom mass are shown, either assuming the $\tilde{b} \rightarrow b\tilde{\chi}_1^0$ decay, see Fig. 11, or assuming the $\tilde{b} \rightarrow t\tilde{\chi}_1^\pm$ decay, with $\tilde{\chi}_1^\pm \rightarrow W^{(*)}\tilde{\chi}_1^0$, see Fig. 12a, or assuming the $\tilde{b} \rightarrow b\tilde{\chi}_2^0$ decay, with $\tilde{\chi}_2^0 \rightarrow h\tilde{\chi}_1^0$, see Fig. 12b. Interpretations in the pMSSM are also discussed, see Figures 13–15.
- ³² KHACHATRYAN 15AF searched in 19.5 fb^{-1} of pp collisions at $\sqrt{s} = 8 \text{ TeV}$ for events with at least two energetic jets and significant \cancel{E}_T , using the transverse mass variable M_{T2} to discriminate between signal and background processes. No significant excess above the Standard Model expectations is observed. Limits are set on the sbottom mass in simplified models where the decay $\tilde{b} \rightarrow b\tilde{\chi}_1^0$ takes place with a branching ratio of 100%, see Fig. 12. See also Table 5. Exclusions in the CMSSM, assuming $\tan\beta = 30$, $A_0 = -2 \max(m_0, m_{1/2})$ and $\mu > 0$, are also presented, see Fig. 15.
- ³³ KHACHATRYAN 15AH searched in 19.4 or 19.7 fb^{-1} of pp collisions at $\sqrt{s} = 8 \text{ TeV}$ for events containing either a fully reconstructed top quark, or events containing dijets requiring one or both jets to originate from b -quarks, or events containing a mono-jet. No significant excess above the Standard Model expectations is observed. Limits are set on the sbottom mass in simplified models where the decay $\tilde{b} \rightarrow b\tilde{\chi}_1^0$ takes place with a branching ratio of 100%, see Fig. 12. Limits are also set in a simplified model where the decay $\tilde{b} \rightarrow c\tilde{\chi}_1^0$ takes place with a branching ratio of 100%, see Fig. 12.
- ³⁴ KHACHATRYAN 15I searched in 19.5 fb^{-1} of pp collisions at $\sqrt{s} = 8 \text{ TeV}$ for events in which b -jets and four W -bosons are produced. Five individual search channels are combined (fully hadronic, single lepton, same-sign dilepton, opposite-sign dilepton, multi-lepton). No significant excess above the Standard Model expectations is observed. Limits are set on the sbottom mass in a simplified model where the decay $\tilde{b} \rightarrow t\tilde{\chi}_1^\pm$, with $\tilde{\chi}_1^\pm \rightarrow W^\pm\tilde{\chi}_1^0$, takes place with a branching ratio of 100%, see Fig. 7.
- ³⁵ AAD 14T searched in 20.3 fb^{-1} of pp collisions at $\sqrt{s} = 8 \text{ TeV}$ for monojet-like events. No excess of events above the expected level of Standard Model background was found. Exclusion limits at 95% C.L. are set on the masses of third-generation squarks in simplified models which assume that the decay $\tilde{b}_1 \rightarrow b\tilde{\chi}_1^0$ takes place 100% of the time, see Fig. 12.
- ³⁶ CHATRCHYAN 14AH searched in 4.7 fb^{-1} of pp collisions at $\sqrt{s} = 7 \text{ TeV}$ for events with at least two energetic jets and significant \cancel{E}_T , using the razor variables (M_R and R^2) to discriminate between signal and background processes. A second analysis requires at least one of the jets to be originating from a b -quark. No significant excess above the Standard Model expectations is observed. Limits are set on sbottom masses in simplified models where the decay $\tilde{b} \rightarrow b\tilde{\chi}_1^0$ takes place with a branching ratio of 100%, see Figs. 28 and 29. Exclusions in the CMSSM, assuming $\tan\beta = 10$, $A_0 = 0$ and $\mu > 0$, are also presented, see Fig. 26.
- ³⁷ CHATRCHYAN 14R searched in 19.5 fb^{-1} of pp collisions at $\sqrt{s} = 8 \text{ TeV}$ for events with at least three leptons (electrons, muons, taus) in the final state. No significant excess above the Standard Model expectations is observed. Limits are set on the gluino mass in a simplified model where the decay $\tilde{b} \rightarrow t\tilde{\chi}_1^\pm$, with $\tilde{\chi}_1^\pm \rightarrow W^\pm\tilde{\chi}_1^0$, takes place with a branching ratio of 100%, see Fig. 11.
- ³⁸ KHACHATRYAN 15AD searched in 19.4 fb^{-1} of pp collisions at $\sqrt{s} = 8 \text{ TeV}$ for events with two opposite-sign same flavor isolated leptons featuring either a kinematic edge, or a peak at the Z -boson mass, in the invariant mass spectrum. No evidence for a statistically significant excess over the expected SM backgrounds is observed and 95% C.L. exclusion limits are derived in a simplified model of sbottom pair production where the sbottom decays into a b -quark, two opposite-sign dileptons and a neutralino LSP,

Searches Particle Listings

Supersymmetric Particle Searches

- through an intermediate state containing either an off-shell Z-boson or a slepton, see Fig. 8.
- ³⁹ AAD 14Ax searched in 20.1 fb^{-1} of pp collisions at $\sqrt{s} = 8 \text{ TeV}$ for the strong production of supersymmetric particles in events containing either zero or at last one high- p_T lepton, large missing transverse momentum, high jet multiplicity and at least three jets identified as originating from b -quarks. No excess over the expected SM background is observed. Limits are derived in mSUGRA/CMSSM models with $\tan\beta = 30$, $A_0 = -2 m_0$ and $\mu > 0$, see their Fig. 14. Also, exclusion limits are set in simplified models containing scalar bottom quarks, where the decay $\bar{b} \rightarrow b\bar{\chi}_2^0$ and $\bar{\chi}_2^0 \rightarrow h\bar{\chi}_1^0$ takes place with a branching ratio of 100%, see their Figures 11.
- ⁴⁰ AAD 14E searched in 20.3 fb^{-1} of pp collisions at $\sqrt{s} = 8 \text{ TeV}$ for strongly produced supersymmetric particles in events containing jets and two same-sign leptons or three leptons. The search also utilises jets originating from b -quarks, missing transverse momentum and other variables. No excess over the expected SM background is observed. Exclusion limits are derived in simplified models containing bottom, see Fig. 7. Limits are also derived in the mSUGRA/CMSSM, bRPV and GMSB models, see their Fig. 8.
- ⁴¹ CHATRCHYAN 14H searched in 19.5 fb^{-1} of pp collisions at $\sqrt{s} = 8 \text{ TeV}$ for events with two isolated same-sign dileptons and jets in the final state. No significant excess above the Standard Model expectations is observed. Limits are set on the sbottom mass in a simplified models where the decay $\bar{b} \rightarrow t\bar{\chi}_1^\pm, \bar{\chi}_1^\pm \rightarrow W^\pm\bar{\chi}_1^0$ takes place with a branching ratio of 100%, with varying mass of the $\bar{\chi}_1^\pm$, for $m_{\bar{\chi}_1^0} = 50 \text{ GeV}$, see Fig. 6.
- ⁴² AAD 13AU searched in 20.1 fb^{-1} of pp collisions at $\sqrt{s} = 8 \text{ TeV}$ for events containing two jets identified as originating from b -quarks and large missing transverse momentum. No excess of events above the expected level of Standard Model background was found. Exclusion limits at 95% C.L. are set on the masses of third-generation squarks. Assuming that the decay $\bar{b}_1 \rightarrow b\bar{\chi}_1^0$ takes place 100% of the time, a b_1 mass below 620 GeV is excluded for $m_{\bar{\chi}_1^0} < 120 \text{ GeV}$. For more details, see their Fig. 5.
- ⁴³ CHATRCHYAN 13AT provides interpretations of various searches for supersymmetry by the CMS experiment based on $4.73\text{--}4.98 \text{ fb}^{-1}$ of pp collisions at $\sqrt{s} = 7 \text{ TeV}$ in the framework of simplified models. Limits are set on the sbottom mass in a simplified models where sbottom quarks are pair-produced and the decay $\bar{b} \rightarrow b\bar{\chi}_1^0$ takes place with a branching ratio of 100%, see Fig. 4.
- ⁴⁴ CHATRCHYAN 13T searched in 11.7 fb^{-1} of pp collisions at $\sqrt{s} = 8 \text{ TeV}$ for events with at least two energetic jets and significant E_T , using the α_T variable to discriminate between processes with genuine and misreconstructed E_T . No significant excess above the Standard Model expectations is observed. Limits are set on sbottom masses in simplified models where the decay $\bar{b} \rightarrow b\bar{\chi}_1^0$ takes place with a branching ratio of 100%, see Fig. 8 and Table 9.
- ⁴⁵ CHATRCHYAN 13v searched in 10.5 fb^{-1} of pp collisions at $\sqrt{s} = 8 \text{ TeV}$ for events with two isolated same-sign dileptons and at least two b -jets in the final state. No significant excess above the Standard Model expectations is observed. Limits are set on the bottom mass in a simplified models where the decay $\bar{b} \rightarrow t\bar{\chi}_1^\pm, \bar{\chi}_1^\pm \rightarrow W^\pm\bar{\chi}_1^0$ takes place with a branching ratio of 100%, with varying mass of the $\bar{\chi}_1^\pm$, for $m_{\bar{\chi}_1^0} = 50 \text{ GeV}$, see Fig. 4.
- ⁴⁶ AAD 12AN searched in 2.05 fb^{-1} of pp collisions at $\sqrt{s} = 7 \text{ TeV}$ for scalar bottom quarks in events with large missing transverse momentum and two b -jets in the final state. The data are found to be consistent with the Standard Model expectations. Limits are set in an R-parity conserving minimal supersymmetric scenario, assuming $B(\bar{b}_1 \rightarrow b\bar{\chi}_1^0) = 100\%$, see their Fig. 2.
- ⁴⁷ CHATRCHYAN 12AI looked in 4.98 fb^{-1} of pp collisions at $\sqrt{s} = 7 \text{ TeV}$ for events with two same-sign leptons (e, μ), but not necessarily same flavor, at least 2 b -jets and missing transverse energy. No excess beyond the Standard Model expectation is observed. Exclusion limits are derived in a simplified model for sbottom pair production, where the sbottom decays through $\bar{b}_1 \rightarrow t\bar{\chi}_1 W$, see Fig. 8.
- ⁴⁸ CHATRCHYAN 12BO searched in 4.7 fb^{-1} of pp collisions at $\sqrt{s} = 7 \text{ TeV}$ for scalar bottom quarks in events with large missing transverse momentum and two b -jets in the final state. The data are found to be consistent with the Standard Model expectations. Limits are set in an R-parity conserving minimal supersymmetric scenario, assuming $B(\bar{b}_1 \rightarrow b\bar{\chi}_1^0) = 100\%$, see their Fig. 2.
- ⁴⁹ AAD 11K looked in 34 pb^{-1} of pp collisions at $\sqrt{s} = 7 \text{ TeV}$ for events with heavy stable particles, identified by their anomalous dE/dx in the tracker or time of flight in the tile calorimeter, from pair production of \bar{b} . No evidence for an excess over the SM expectation is observed and limits on the mass are derived for pair production of sbottom, see Fig. 4.
- ⁵⁰ AAD 11o looked in 35 pb^{-1} of pp collisions at $\sqrt{s} = 7 \text{ TeV}$ for events with jets, of which at least one is a b -jet, and E_T . No excess above the Standard Model was found. Limits are derived in the $(m_{\bar{g}}, m_{\bar{b}_1})$ plane (see Fig. 2) under the assumption of 100% branching ratios and \bar{b}_1 being the lightest squark. The quoted limit is valid for $m_{\bar{b}_1} < 500 \text{ GeV}$. A similar approach for \bar{t}_1 as the lightest squark with $\bar{g} \rightarrow \bar{t}_1 t$ and $\bar{t}_1 \rightarrow b\bar{\chi}_1^\pm$ with 100% branching ratios leads to a gluino mass limit of 520 GeV for $130 < m_{\bar{t}_1} < 300 \text{ GeV}$. Limits are also derived in the CMSSM $(m_0, m_{1/2})$ plane for $\tan\beta = 40$, see Fig. 4, and in scenarios based on the gauge group $SO(10)$.
- ⁵¹ CHATRCHYAN 11D looked in 35 pb^{-1} of pp collisions at $\sqrt{s} = 7 \text{ TeV}$ for events with ≥ 2 jets, at least one of which is b -tagged, and E_T , where the b -jets are decay products of \bar{t} or \bar{b} . No evidence for an excess over the expected background is observed. Limits are derived in the CMSSM $(m_0, m_{1/2})$ plane for $\tan\beta = 50$ (see Fig. 2).
- ⁵² AALTONEN 10R searched in 2.65 fb^{-1} of $p\bar{p}$ collisions at $\sqrt{s} = 1.96 \text{ TeV}$ for events with E_T and exactly two jets, at least one of which is b -tagged. The results are in agreement with the SM prediction, and a limit on the cross section of 0.1 pb is obtained for the range of masses $80 < m_{\bar{b}_1} < 280 \text{ GeV}$ assuming that the sbottom decays exclusively to $b\bar{\chi}_1^0$. The excluded mass region in the framework of conserved R_p is shown in a plane of $(m_{\bar{b}_1}, m_{\bar{\chi}_1^0})$, see their Fig. 2.
- ⁵³ ABAZOV 10L looked in 5.2 fb^{-1} of $p\bar{p}$ collisions at $\sqrt{s} = 1.96 \text{ TeV}$ for events with at least 2 b -jets and E_T and the production of $\bar{b}_1\bar{b}_1$. No evidence for an excess over the SM expectation is observed, and a limit on the cross section is derived under the assumption of 100% branching ratio. The excluded mass region in the framework of

conserved R_p is shown in a plane of $(m_{\bar{b}_1}, m_{\bar{\chi}_1^0})$, see their Fig. 3b. The exclusion also extends to $m_{\bar{\chi}_1^0} = 110 \text{ GeV}$ for $160 < m_{\bar{b}_1} < 200 \text{ GeV}$.

R-parity violating \tilde{b} (Sbottom) mass limit

VALUE (GeV)	CL%	DOCUMENT ID	TECN	COMMENT
>307	95	¹ KHACHATRYAN...16BX CMS	RPV, $\bar{b} \rightarrow td$ or ts, λ_{332}'' or λ_{331}'' coupling	
		² AAD	14E ATLS	$\ell^\pm \ell^\pm (\ell\bar{\tau}) + \text{jets}, \bar{b}_1 \rightarrow t\bar{\chi}_1^\pm$ with $\bar{\chi}_1^\pm \rightarrow W^{(*)\pm}\bar{\chi}_1^0$ simplified model, $m_{\bar{\chi}_1^\pm} = 2 m_{\bar{\chi}_1^0}$

• • • We do not use the following data for averages, fits, limits, etc. • • •

- ¹ KHACHATRYAN 16BX searched in 19.5 fb^{-1} of pp collisions at $\sqrt{s} = 8 \text{ TeV}$ for events containing 2 leptons coming from R-parity-violating decays of supersymmetric particles. No excess over the expected background is observed. Limits are derived on the sbottom mass, assuming the RPV $\bar{b} \rightarrow td$ or $\bar{b} \rightarrow ts$ decay, see Fig. 15.
- ² AAD 14E searched in 20.3 fb^{-1} of pp collisions at $\sqrt{s} = 8 \text{ TeV}$ for strongly produced supersymmetric particles in events containing jets and two same-sign leptons or three leptons. The search also utilises jets originating from b -quarks, missing transverse momentum and other variables. No excess over the expected SM background is observed. Exclusion limits are derived in simplified models containing bottom, see Fig. 7. Limits are also derived in the mSUGRA/CMSSM, bRPV and GMSB models, see their Fig. 8.

\tilde{t} (Stop) mass limit

Limits depend on the decay mode. In e^+e^- collisions they also depend on the mixing angle of the mass eigenstate $\tilde{t}_1 = \tilde{t}_L \cos\theta_t + \tilde{t}_R \sin\theta_t$. The coupling to the Z vanishes when $\theta_t = 0.98$. In the Listings below, we use $\Delta m \equiv m_{\tilde{t}_1} - m_{\bar{\chi}_1^0}$ or $\Delta m \equiv m_{\tilde{t}_1} - m_{\tilde{c}}$, depending on relevant decay mode. See also bounds in “ \tilde{q} (Squark) MASS LIMIT.”

Some earlier papers are now obsolete and have been omitted. They were last listed in our PDG 14 edition: K. Olive, *et al.* (Particle Data Group), Chinese Physics **C38** 070001 (2014) (<http://pdg.lbl.gov>).

R-parity conserving \tilde{t} (Stop) mass limit

VALUE (GeV)	CL%	DOCUMENT ID	TECN	COMMENT
>1400	95	¹ AAD	21AW ATLS	$\tau^\pm + \text{jets} + b\text{-jets} + E_T, \text{Tstop5}, m_{\tilde{t}_1} = 1200 \text{ GeV}$
>1200	95	² AAD	21o ATLS	$\ell^\pm + \text{jet} + E_T, \text{Tstop1}, m_{\bar{\chi}_1^0} = 0 \text{ GeV}$
> 710	95	² AAD	21o ATLS	$\ell^\pm + \text{jet} + E_T, \text{Tstop1}, m_{\bar{\chi}_1^0} = 580 \text{ GeV}$
> 640	95	² AAD	21o ATLS	$\ell^\pm + \text{jet} + E_T, \text{Tstop3}, m_{\bar{\chi}_1^0} = 580 \text{ GeV}$
>1000	95	³ AAD	21P ATLS	$\ell^\pm \ell^\pm + \text{jets} + E_T, \text{Tstop1}, m_{\bar{\chi}_1^0} = 0 \text{ GeV}$
> 600	95	³ AAD	21P ATLS	$\ell^\pm \ell^\pm + \text{jets} + E_T, \text{Tstop2}, m_{\bar{\chi}_1^0} = 500 \text{ GeV}$
> 550	95	³ AAD	21P ATLS	$\ell^\pm \ell^\pm + \text{jets} + E_T, \text{Tstop3}, m_{\bar{\chi}_1^0} = 500 \text{ GeV}$
>1310	95	⁴ SIRUNYAN	21AD CMS	$\text{jets} + E_T, \text{Tstop1}, m_{\bar{\chi}_1^0} < 300 \text{ GeV}$
>1170	95	⁴ SIRUNYAN	21AD CMS	$\text{jets} + E_T, \text{Tstop2}, m_{\bar{\chi}_1^\pm} = (m_{\tilde{t}} + m_{\bar{\chi}_1^0})/2, m_{\bar{\chi}_1^0} < 100 \text{ GeV}$
>1150	95	⁴ SIRUNYAN	21AD CMS	$\text{jets} + E_T, \text{Tstop1} (50\%) \text{ or } \text{Tstop2} (50\%), m_{\bar{\chi}_1^\pm} = m_{\bar{\chi}_1^0} = 5 \text{ GeV}, m_{\bar{\chi}_1^0} = 100 \text{ GeV}$
> 640	95	⁴ SIRUNYAN	21AD CMS	$\text{jets} + E_T, \text{Tstop3}, m_{\tilde{t}} - m_{\bar{\chi}_1^0} = 50 \text{ GeV}$
> 620	95	⁴ SIRUNYAN	21AD CMS	$\text{jets} + E_T, \text{Tstop3}, 10 \text{ GeV} < m_{\tilde{t}} - m_{\bar{\chi}_1^0} < 60 \text{ GeV}$
> 740	95	⁴ SIRUNYAN	21AD CMS	$\text{jets} + E_T, \text{Tstop2}, m_{\tilde{t}} - m_{\bar{\chi}_1^0} = 80 \text{ GeV}$
> 720	95	⁴ SIRUNYAN	21AD CMS	$\text{jets} + E_T, \text{Tstop2}, 40 \text{ GeV} < m_{\tilde{t}} - m_{\bar{\chi}_1^0} < 80 \text{ GeV}$
> 595	95	⁴ SIRUNYAN	21AD CMS	$\text{jets} + E_T, \text{Tstop2}, m_{\tilde{t}} - m_{\bar{\chi}_1^0} = 10 \text{ GeV}$
> 630	95	⁴ SIRUNYAN	21AD CMS	$\text{jets} + E_T, \text{Tstop4}, m_{\tilde{t}} - m_{\bar{\chi}_1^0} = 20 \text{ GeV}$
none 200–920	95	⁵ SIRUNYAN	21B CMS	$\ell^\pm \ell^\pm + b\text{-jets} + E_T, \text{Tstop1}, m_{\bar{\chi}_1^0} = 0 \text{ GeV}$
none 250–810	95	⁵ SIRUNYAN	21B CMS	$\ell^\pm \ell^\pm + b\text{-jets} + E_T, \text{Tstop2}, m_{\bar{\chi}_1^\pm} = (m_{\tilde{t}} + m_{\bar{\chi}_1^0})/2, m_{\bar{\chi}_1^0} = 0 \text{ GeV}$

>1300	95	5	SIRUNYAN	21B	CMS	$\ell^\pm \ell^\mp + b\text{-jets} + \cancel{E}_T, T_{\text{stop1}}, m_{\tilde{\chi}_1^\pm} = (m_{\tilde{\tau}} + m_{\tilde{\chi}_1^0})/2, m_{\tilde{\ell}} = (m_{\tilde{\chi}_1^\pm} - m_{\tilde{\chi}_1^0})/2 + m_{\tilde{\chi}_1^0}, m_{\tilde{\chi}_1^0} = 0$	> 760	95	14	SIRUNYAN	20T	CMS	same-sign $\ell^\pm \ell^\pm$ or $\geq 3\ell^\pm + \text{jets}, T_{\text{stop7}}, m_{\tilde{\tau}_1} - m_{\tilde{\chi}_1^0} = 175 \text{ GeV}, m_{\tilde{\tau}_1} = 200 \text{ GeV}, B(\tilde{\tau}_2 \rightarrow \tilde{\tau}_1 Z) = B(\tilde{\tau}_2 \rightarrow \tilde{\tau}_1 H) = 50\%$
none 400-1180	95	5	SIRUNYAN	21B	CMS	$\ell^\pm \ell^\mp + b\text{-jets} + \cancel{E}_T, T_{\text{stop1}}, m_{\tilde{\chi}_1^\pm} = (m_{\tilde{\tau}} + m_{\tilde{\chi}_1^0})/2, m_{\tilde{\ell}} = 0.05 (m_{\tilde{\chi}_1^\pm} - m_{\tilde{\chi}_1^0}) + m_{\tilde{\chi}_1^0}, m_{\tilde{\chi}_1^0} = 0$	>1100	95	15	SIRUNYAN	20U	CMS	$\tau^\pm \tau^\mp + b\text{-jets} + \cancel{E}_T, T_{\text{stop1}}, m_{\tilde{\chi}_1^\pm} = 0.5 (m_{\tilde{\tau}} + m_{\tilde{\chi}_1^0}), m_{\tilde{\tau}} = 0.5 m_{\tilde{\chi}_1^\pm}, m_{\tilde{\chi}_1^0} = 0$
>1400	95	5	SIRUNYAN	21B	CMS	$\ell^\pm \ell^\mp + b\text{-jets} + \cancel{E}_T, T_{\text{stop1}}, m_{\tilde{\chi}_1^\pm} = (m_{\tilde{\tau}} + m_{\tilde{\chi}_1^0})/2, m_{\tilde{\ell}} = 0.95 (m_{\tilde{\chi}_1^\pm} - m_{\tilde{\chi}_1^0}) + m_{\tilde{\chi}_1^0}, m_{\tilde{\chi}_1^0} = 0$	>1110	95	16	SIRUNYAN	19AU	CMS	$\gamma + \text{jets} + b\text{-jets} + \cancel{E}_T, T_{\text{stop13}}, m_{\tilde{\chi}_1^0} = 1 \text{ GeV}$
>1325	95	6	TUMASYAN	21I	CMS	$\geq 2 \text{ jets} + \cancel{E}_T + 0, 1, 2 \ell, T_{\text{stop1}}, m_{\tilde{\chi}_1^0} = 0 \text{ GeV}$	>1190	95	16	SIRUNYAN	19AU	CMS	$\gamma + \text{jets} + b\text{-jets} + \cancel{E}_T, T_{\text{stop13}}, m_{\tilde{\chi}_1^0} = 800 \text{ GeV}$
>1150	95	6	TUMASYAN	21I	CMS	$\geq 2 \text{ jets} + \cancel{E}_T + 0, 1, 2 \ell, T_{\text{stop1}}, m_{\tilde{\chi}_1^0} = 700 \text{ GeV}$	>1140	95	17	SIRUNYAN	19CH	CMS	$\text{jets} + \cancel{E}_T, T_{\text{stop1}}, m_{\tilde{\chi}_1^0} = 0 \text{ GeV}$
>1260	95	6	TUMASYAN	21I	CMS	$\geq 2 \text{ jets} + \cancel{E}_T + 0, 1, 2 \ell, T_{\text{stop2}}, m_{\tilde{\chi}_1^0} = 0 \text{ GeV}$	> 208	95	18	SIRUNYAN	19S	CMS	$1 \text{ or } 2 \ell + \text{jets} + \cancel{E}_T, T_{\text{stop1}}, m_{\tilde{\chi}_1^0} < 200 \text{ GeV}$
>1000	95	6	TUMASYAN	21I	CMS	$\geq 2 \text{ jets} + \cancel{E}_T + 0, 1, 2 \ell, T_{\text{stop2}}, m_{\tilde{\chi}_1^0} < 575 \text{ GeV}$	> 235	95	19	SIRUNYAN	19U	CMS	$e^\pm \mu^\mp + \geq 1b\text{-jet}, T_{\text{stop1}}, m_{\tilde{\tau}_1} - m_{\tilde{\chi}_1^0} = 175 \text{ GeV}$
>1175	95	6	TUMASYAN	21I	CMS	$\geq 2 \text{ jets} + \cancel{E}_T + 0, 1, 2 \ell, T_{\text{stop1}} (50\%) \text{ or } T_{\text{stop2}} (50\%), m_{\tilde{\chi}_1^0} = 0 \text{ GeV}$	> 242	95	19	SIRUNYAN	19U	CMS	$e^\pm \mu^\mp + \geq 1b\text{-jet}, T_{\text{stop1}}, m_{\tilde{\tau}_1} - m_{\tilde{\chi}_1^0} = 182.5 \text{ GeV}$
>1000	95	6	TUMASYAN	21I	CMS	$\geq 2 \text{ jets} + \cancel{E}_T + 0, 1, 2 \ell, T_{\text{stop1}} (50\%) \text{ or } T_{\text{stop2}} (50\%), \tilde{\chi}_1^0 = 570 \text{ GeV}$	> 940	95	19	SIRUNYAN	19U	CMS	$e^\pm \mu^\mp + \geq 1b\text{-jet}, T_{\text{stop1}}, m_{\tilde{\tau}_1} - m_{\tilde{\chi}_1^0} = 167.5 \text{ GeV}$
none 145-295	95	6	TUMASYAN	21I	CMS	$\geq 2 \text{ jets} + \cancel{E}_T + 0, 1, 2 \ell, T_{\text{stop1}} (50\%) \text{ or } T_{\text{stop2}} (50\%), \tilde{\chi}_1^0 = 570 \text{ GeV}$	> 270	95	20	AABOUD	18AQ	ATLS	$1\ell + \text{jets} + \cancel{E}_T, T_{\text{stop1}}, m_{\tilde{\chi}_1^0} = 0 \text{ GeV}$
none, 170-230	95	7	AABOUD	20	ATLS	$e^\pm \mu^\mp + \geq 1b\text{-jet}, T_{\text{stop1}}, m_{\tilde{\chi}_1^0} = 0.5 \text{ GeV}$	> 840	95	21	AABOUD	18AQ	ATLS	$1\ell + \text{jets} + \cancel{E}_T, T_{\text{stop3}}, m_{\tilde{\tau}_1} - m_{\tilde{\chi}_1^0} = 20 \text{ GeV}$
none, 170-220	95	7	AABOUD	20	ATLS	$e^\pm \mu^\mp + \geq 1b\text{-jet}, T_{\text{stop1}}, m_{\tilde{\chi}_1^0} < 62 \text{ GeV}$	> 500	95	22	AABOUD	18AQ	ATLS	$1\ell + \text{jets} + \cancel{E}_T, T_{\text{stop2}}, m_{\tilde{\tau}_1} - m_{\tilde{\chi}_1^0} = 10 \text{ GeV}$
>1220	95	8	AAD	20AS	ATLS	$\ell^\pm \ell^\mp$ or $2 b\text{-jets} \text{ and } \cancel{E}_T, T_{\text{stop6}}, m_{\tilde{\chi}_2^0} = 900 \text{ GeV}$	> 850	95	23	AABOUD	18BV	ATLS	$c\text{-jets} + \cancel{E}_T, T_{\text{stop4}}, m_{\tilde{\tau}_1} - m_{\tilde{\chi}_1^0} < 100 \text{ GeV}$
> 860	95	9	AAD	20AS	ATLS	$\ell^\pm \ell^\mp$ or $2 b\text{-jets} \text{ and } \cancel{E}_T, \tilde{\tau}_2 \text{ with } \tilde{\tau}_2 \rightarrow \tilde{\tau}_1 Z, \tilde{\tau}_1 \rightarrow b f f' \tilde{\chi}_1^0, \Delta m(\tilde{\tau}_1, \tilde{\chi}_1^0) = 40 \text{ GeV}$	> 390	95	24	AABOUD	18BV	ATLS	$c\text{-jets} + \cancel{E}_T, T_{\text{stop4}}, m_{\tilde{\chi}_1^0} = 0 \text{ GeV}$
none 400-1250	95	10	AAD	20S	ATLS	$\text{jets} + \cancel{E}_T, T_{\text{stop1}}, m_{\tilde{\chi}_1^0} = 0 \text{ GeV}$	> 430	95	25	AABOUD	18I	ATLS	$\geq 1 \text{ jets} + \cancel{E}_T, T_{\text{stop3}}, m_{\tilde{\tau}_1} \sim m_{\tilde{\chi}_1^0}$
none 300-660	95	11	AAD	20S	ATLS	$\text{jets} + \cancel{E}_T, T_{\text{stop3}}, m_{\tilde{\chi}_1^0} = 0 \text{ GeV}$	> 450	95	26	AABOUD	18I	ATLS	$\geq 1 \text{ jets} + \cancel{E}_T, T_{\text{stop4}}, m_{\tilde{\tau}_1} - m_{\tilde{\chi}_1^0} = 5 \text{ GeV}$
> 765	95	12	AAD	20V	ATLS	same-sign $\ell^\pm \ell^\pm + \text{jets}, \tilde{\tau}_1 \rightarrow t \tilde{\chi}_2^0, \tilde{\chi}_2^0 \rightarrow \tilde{\chi}_1^\pm W, \tilde{\chi}_1^\pm \rightarrow \tilde{\chi}_1^0 W, m_{\tilde{\chi}_1^\pm} \sim m_{\tilde{\chi}_1^0}$	>1160	95	27	AABOUD	18Y	ATLS	$2\ell (\geq 1 \text{ hadronic } \tau) + b\text{-jets} + \cancel{E}_T, T_{\text{stop5}}, m_{\tilde{\tau}_1} \sim 800 \text{ GeV}$
>1200	95	13	SIRUNYAN	20AH	CMS	$\ell^\pm + \text{jet} + \cancel{E}_T, T_{\text{stop1}}, m_{\tilde{\chi}_1^0} = 0 \text{ GeV}$	> 450	95	28	SIRUNYAN	18AJ	CMS	$2\ell (\text{soft}) + \cancel{E}_T, T_{\text{stop10}}, m_{\tilde{\chi}_1^\pm} = (m_{\tilde{\tau}} + m_{\tilde{\chi}_1^0})/2, m_{\tilde{\tau}_1} - m_{\tilde{\chi}_1^0} = 40 \text{ GeV}$
>1175	95	13	SIRUNYAN	20AH	CMS	$\ell^\pm + \text{jet} + \cancel{E}_T, T_{\text{stop1}}, m_{\tilde{\chi}_1^0} < 425 \text{ GeV}$	> 720	95	29	SIRUNYAN	18AL	CMS	$\geq 3\ell^\pm + \text{jets} + \cancel{E}_T, T_{\text{stop7}}, m_{\tilde{\tau}_1} - m_{\tilde{\chi}_1^0} = 175 \text{ GeV}, m_{\tilde{\tau}_1} = 200 \text{ GeV}, BR(\tilde{\tau}_2 \rightarrow \tilde{\tau}_1 H) = 100\%$
none 230-1140	95	13	SIRUNYAN	20AH	CMS	$\ell^\pm + \text{jet} + \cancel{E}_T, T_{\text{stop2}}, m_{\tilde{\chi}_1^\pm} = (m_{\tilde{\tau}} + m_{\tilde{\chi}_1^0})/2, m_{\tilde{\chi}_1^0} = 0 \text{ GeV}$	> 780	95	29	SIRUNYAN	18AL	CMS	$\geq 3\ell^\pm + \text{jets} + \cancel{E}_T, T_{\text{stop7}}, m_{\tilde{\tau}_1} - m_{\tilde{\chi}_1^0} = 175 \text{ GeV}, m_{\tilde{\tau}_1} = 200 \text{ GeV}, BR(\tilde{\tau}_2 \rightarrow \tilde{\tau}_1 Z) = 100\%$
>1100	95	13	SIRUNYAN	20AH	CMS	$\ell^\pm + \text{jet} + \cancel{E}_T, T_{\text{stop2}}, m_{\tilde{\chi}_1^\pm} = (m_{\tilde{\tau}} + m_{\tilde{\chi}_1^0})/2, 50 < m_{\tilde{\chi}_1^0} < 425 \text{ GeV}$	> 710	95	29	SIRUNYAN	18AL	CMS	$\geq 3\ell^\pm + \text{jets} + \cancel{E}_T, T_{\text{stop7}}, m_{\tilde{\tau}_1} - m_{\tilde{\chi}_1^0} = 175 \text{ GeV}, m_{\tilde{\tau}_1} = 200 \text{ GeV}, BR(\tilde{\tau}_2 \rightarrow \tilde{\tau}_1 Z) = BR(\tilde{\tau}_2 \rightarrow \tilde{\tau}_1 H) = 50\%$
>1070	95	13	SIRUNYAN	20AH	CMS	$\ell^\pm + \text{jet} + \cancel{E}_T, T_{\text{stop8}}, m_{\tilde{\chi}_1^\pm} - m_{\tilde{\chi}_1^0} = 5 \text{ GeV}, m_{\tilde{\chi}_1^0} = 0 \text{ GeV}$	> 730	95	30	SIRUNYAN	18AN	CMS	$1 \text{ or } 2 \gamma + \ell + \text{jets}, \text{GGM}, T_{\text{stop12}}, m_{\tilde{\chi}_1^0} = 150 \text{ GeV}$
>1050	95	13	SIRUNYAN	20AH	CMS	$\ell^\pm + \text{jet} + \cancel{E}_T, T_{\text{stop8}}, m_{\tilde{\chi}_1^\pm} - m_{\tilde{\chi}_1^0} = 5 \text{ GeV}, m_{\tilde{\chi}_1^0} < 350 \text{ GeV}$	> 650	95	30	SIRUNYAN	18AN	CMS	$1 \text{ or } 2 \gamma + \ell + \text{jets}, \text{GGM}, T_{\text{stop12}}, m_{\tilde{\chi}_1^0} = 500 \text{ GeV}$
> 730	95	14	SIRUNYAN	20T	CMS	same-sign $\ell^\pm \ell^\pm$ or $\geq 3\ell^\pm + \text{jets}, T_{\text{stop7}}, m_{\tilde{\tau}_1} - m_{\tilde{\chi}_1^0} = 175 \text{ GeV}, m_{\tilde{\tau}_1} = 200 \text{ GeV}, B(\tilde{\tau}_2 \rightarrow \tilde{\tau}_1 H) = 100\%$	> 800	95	31	SIRUNYAN	18AY	CMS	$\text{jets} + \cancel{E}_T, T_{\text{stop1}}, m_{\tilde{\chi}_1^0} = 0 \text{ GeV}$
> 890	95	14	SIRUNYAN	20T	CMS	same-sign $\ell^\pm \ell^\pm$ or $\geq 3\ell^\pm + \text{jets}, T_{\text{stop7}}, m_{\tilde{\tau}_1} - m_{\tilde{\chi}_1^0} = 175 \text{ GeV}, m_{\tilde{\tau}_1} = 200 \text{ GeV}, B(\tilde{\tau}_2 \rightarrow \tilde{\tau}_1 Z) = 100\%$	> 750	95	31	SIRUNYAN	18AY	CMS	$\text{jets} + \cancel{E}_T, T_{\text{stop4}}, m_{\tilde{\chi}_1^0} = 420 \text{ GeV}$
							>1050	95	32	SIRUNYAN	18B	CMS	$\text{jets} + \cancel{E}_T, T_{\text{stop4}}, m_{\tilde{\tau}_1} - m_{\tilde{\chi}_1^0} = 10 \text{ GeV}$
								95	33	SIRUNYAN	18C	CMS	$\ell^\pm \ell^\mp + b\text{-jets} + \cancel{E}_T, T_{\text{stop1}}, m_{\tilde{\chi}_1^0} = 0$
								95	33	SIRUNYAN	18C	CMS	$\ell^\pm \ell^\mp + b\text{-jets} + \cancel{E}_T, T_{\text{stop2}}, m_{\tilde{\chi}_1^\pm} = (m_{\tilde{\tau}} + m_{\tilde{\chi}_1^0})/2, m_{\tilde{\chi}_1^0} = 0$
								95	33	SIRUNYAN	18C	CMS	Combination of all-hadronic, $1 \ell^\pm$ and $\ell^\pm \ell^\mp$ searches, $T_{\text{stop1}}, m_{\tilde{\chi}_1^0} = 0$

Searches Particle Listings
Supersymmetric Particle Searches

>1000	95	33	SIRUNYAN	18c	CMS	Combination of all-hadronic, 1 ℓ^\pm and $\ell^\pm \bar{\ell} \mp$ searches, Tstop2, $m_{\tilde{\chi}_1^\pm} = (m_{\tilde{t}} +$ $m_{\tilde{\chi}_1^0})/2$, $m_{\tilde{\chi}_1^0} = 0$	> 280	95	48	KHACHATRY...17P	CMS	1 or more jets+ E_T , Tstop3, 10 GeV < $m_{\tilde{t}} - m_{\tilde{\chi}_1^0} < 80$ GeV	
>1200	95	33	SIRUNYAN	18c	CMS	$\ell^\pm \bar{\ell} \mp + b$ -jets + E_T , Tstop11, $m_{\tilde{\chi}_1^\pm} = 0.5 (m_{\tilde{t}} + m_{\tilde{\chi}_1^0})$, $m_{\tilde{\ell}} = 0.5 m_{\tilde{\chi}_1^\pm}$, $m_{\tilde{\chi}_1^0} = 0$	> 320	95	48	KHACHATRY...17P	CMS	1 or more jets+ E_T , Tstop9, 10 GeV < $m_{\tilde{t}} - m_{\tilde{\chi}_1^0} < 80$ GeV	
>1300	95	33	SIRUNYAN	18c	CMS	$\ell^\pm \bar{\ell} \mp + b$ -jets + E_T , Tstop11, $m_{\tilde{\chi}_1^\pm} = 0.5 (m_{\tilde{t}} + m_{\tilde{\chi}_1^0})$, $m_{\tilde{\ell}} = 0.95 m_{\tilde{\chi}_1^\pm}$, $m_{\tilde{\chi}_1^0} = 0$	> 240	95	49	KHACHATRY...17s	CMS	jets+ E_T , Tstop4, $m_{\tilde{t}} - m_{\tilde{\chi}_1^0} =$ 10 GeV	
none 460-1060	95	33	SIRUNYAN	18c	CMS	$\ell^\pm \bar{\ell} \mp + b$ -jets + E_T , Tstop11, $m_{\tilde{\chi}_1^\pm} = 0.5 (m_{\tilde{t}} + m_{\tilde{\chi}_1^0})$, $m_{\tilde{\ell}} = 0.05 m_{\tilde{\chi}_1^\pm}$, $m_{\tilde{\chi}_1^0} = 0$	> 225	95	50	KHACHATRY...17s	CMS	jets+ E_T , Tstop3, $m_{\tilde{t}} - m_{\tilde{\chi}_1^0} =$ 10 GeV	
>1020	95	34	SIRUNYAN	18D	CMS	top quark (hadronically decay- ing) + jets + E_T , Tstop1, $m_{\tilde{\chi}_1^0} = 0$ GeV	> 325	95	51	KHACHATRY...17s	CMS	jets+ E_T , Tstop2, $m_{\tilde{\chi}_1^\pm} = 0.25$ $m_{\tilde{t}} + 0.75 m_{\tilde{\chi}_1^0}$, $m_{\tilde{\chi}_1^0} = 225$ GeV	
> 420	95	35	SIRUNYAN	18DI	CMS	$\ell^\pm + \text{jet} + E_T$, Tstop3, $m_{\tilde{t}} - m_{\tilde{\chi}_1^0} = 10$ GeV	> 400	95	52	KHACHATRY...17s	CMS	jets+ E_T , Tstop2, $m_{\tilde{\chi}_1^\pm} = 0.75$ $m_{\tilde{t}} + 0.25 m_{\tilde{\chi}_1^0}$, $m_{\tilde{\chi}_1^0} = 0$ GeV	
> 560	95	35	SIRUNYAN	18DI	CMS	$\ell^\pm + \text{jet} + E_T$, Tstop3, $m_{\tilde{t}} - m_{\tilde{\chi}_1^0} = 80$ GeV	> 500	95	53	KHACHATRY...17s	CMS	jets+ E_T , Tstop1, $m_{\tilde{\chi}_1^0} = 0$ GeV	
> 540	95	35	SIRUNYAN	18DI	CMS	ℓ^\pm , Tstop10, $m_{\tilde{\chi}_1^\pm} = (m_{\tilde{t}} +$ $m_{\tilde{\chi}_1^0})/2$, $m_{\tilde{t}} - m_{\tilde{\chi}_1^0} = 40$ GeV	>1120	95	54	SIRUNYAN	17As	CMS	1 ℓ +jets+ E_T , Tstop1, $m_{\tilde{\chi}_1^0} = 0$ GeV
> 590	95	35	SIRUNYAN	18DI	CMS	Combination of all-hadronic and 1 ℓ^\pm searches, Tstop3, $m_{\tilde{t}} - m_{\tilde{\chi}_1^0} = 30$ GeV	>1000	95	54	SIRUNYAN	17As	CMS	1 ℓ +jets+ E_T , Tstop2, $m_{\tilde{\chi}_1^\pm} =$ $(m_{\tilde{t}} + m_{\tilde{\chi}_1^0})/2$, $m_{\tilde{\chi}_1^0} = 0$ GeV
> 670	95	35	SIRUNYAN	18DI	CMS	Combination of all-hadronic and 1 ℓ^\pm searches, Tstop10, $m_{\tilde{\chi}_1^\pm} = (m_{\tilde{t}} + m_{\tilde{\chi}_1^0})/2$, $m_{\tilde{t}} - m_{\tilde{\chi}_1^0} = 60$ GeV	> 980	95	54	SIRUNYAN	17As	CMS	1 ℓ +jets+ E_T , Tstop8, $m_{\tilde{\chi}_1^\pm} - m_{\tilde{\chi}_1^0} = 5$ GeV, $m_{\tilde{\chi}_1^0} = 0$ GeV
> 450	95	36	SIRUNYAN	18DN	CMS	$\ell^\pm \bar{\ell} \mp$, Tstop1, $m_{\tilde{t}} - m_{\tilde{\chi}_1^0} =$ m_W	>1040	95	55	SIRUNYAN	17AT	CMS	jets+ E_T , Tstop1, $m_{\tilde{\chi}_1^0} = 0$ GeV
none 225-325	95	36	SIRUNYAN	18DN	CMS	$\ell^\pm \bar{\ell} \mp$, Tstop2, $m_{\tilde{\chi}_1^\pm} = (m_{\tilde{t}} +$ $m_{\tilde{\chi}_1^0})/2$, $m_{\tilde{t}} - m_{\tilde{\chi}_1^0} = 2$ m_W	> 750	95	55	SIRUNYAN	17AT	CMS	jets+ E_T , Tstop2, $m_{\tilde{\chi}_1^\pm} = (m_{\tilde{t}} +$ $m_{\tilde{\chi}_1^0})/2$, $m_{\tilde{\chi}_1^0} = 0$ GeV
none 210-690	95	36	SIRUNYAN	18DN	CMS	$\ell^\pm \bar{\ell} \mp$, Tstop1, $m_{\tilde{\chi}_1^0} = 0$ GeV	> 940	95	55	SIRUNYAN	17AT	CMS	jets+ E_T , Tstop8, $m_{\tilde{\chi}_1^\pm} - m_{\tilde{\chi}_1^0} =$ 5 GeV, $m_{\tilde{\chi}_1^0} = 100$ GeV
none 250-600	95	36	SIRUNYAN	18DN	CMS	$\ell^\pm \bar{\ell} \mp$, Tstop2, $m_{\tilde{\chi}_1^\pm} = (m_{\tilde{t}} +$ $m_{\tilde{\chi}_1^0})/2$, $m_{\tilde{\chi}_1^0} = 0$ GeV	> 540	95	55	SIRUNYAN	17AT	CMS	jets+ E_T , Tstop3, 10 GeV < $m_{\tilde{t}} - m_{\tilde{\chi}_1^0} < 80$ GeV
> 700	95	37	AABOUD	17AJ	ATLS	same-sign $\ell^\pm \ell^\pm / 3 \ell + \text{jets} +$ E_T , Tstop11, $m_{\tilde{\chi}_2^0} = m_{\tilde{\chi}_1^0}$	> 480	95	55	SIRUNYAN	17AT	CMS	jets+ E_T , Tstop4, 10 GeV < $m_{\tilde{t}} - m_{\tilde{\chi}_1^0} < 80$ GeV
> 880	95	38	AABOUD	17AX	ATLS	+ 100 GeV b -jets+ E_T , mixture Tstop1 and Tstop2 with BR=50%, $m_{\tilde{\chi}_1^0}$ $= 0$ GeV, $m_{\tilde{\chi}_1^\pm} - m_{\tilde{\chi}_1^0} = 1$ GeV	> 530	95	55	SIRUNYAN	17AT	CMS	jets+ E_T , Tstop10, $m_{\tilde{\chi}_1^\pm} =$ $(m_{\tilde{t}} + m_{\tilde{\chi}_1^0})/2$, 10 GeV < $m_{\tilde{t}} - m_{\tilde{\chi}_1^0} < 80$ GeV
none 250-1000	95	39	AABOUD	17AY	ATLS	jets+ E_T , Tstop1, $m_{\tilde{\chi}_1^0} = 0$ GeV	>1070	95	56	SIRUNYAN	17Az	CMS	≥ 1 jets+ E_T , Tstop1, $m_{\tilde{\chi}_1^0} =$ 0 GeV
none 450-850	95	40	AABOUD	17AY	ATLS	jets+ E_T , mixture of Tstop1 and Tstop2 with BR=50%, $m_{\tilde{\chi}_1^\pm} - m_{\tilde{\chi}_1^0} = 1$ GeV	> 900	95	56	SIRUNYAN	17Az	CMS	≥ 1 jets+ E_T , Tstop2, $m_{\tilde{\chi}_1^\pm} =$ $(m_{\tilde{t}} + m_{\tilde{\chi}_1^0})/2$, $m_{\tilde{\chi}_1^0} = 0$ GeV
> 720	95	41	AABOUD	17BE	ATLS	$\ell^\pm \bar{\ell} \mp + E_T$, Tstop1, $m_{\tilde{\chi}_1^0} = 0$ GeV	>1020	95	56	SIRUNYAN	17Az	CMS	≥ 1 jets+ E_T , Tstop8, $m_{\tilde{\chi}_1^\pm} - m_{\tilde{\chi}_1^0} = 5$ GeV, $m_{\tilde{\chi}_1^0} =$ 100 GeV
> 400	95	42	AABOUD	17BE	ATLS	$\ell^\pm \bar{\ell} \mp + E_T$, Tstop3, $m_{\tilde{t}} - m_{\tilde{\chi}_1^0} = 40$ GeV	> 540	95	56	SIRUNYAN	17Az	CMS	≥ 1 jets+ E_T , Tstop4, 10 GeV < $m_{\tilde{t}} - m_{\tilde{\chi}_1^0} < 80$ GeV
> 430	95	43	AABOUD	17BE	ATLS	$\ell^\pm \bar{\ell} \mp + E_T$, Tstop1 (offshell t), $m_{\tilde{t}} - m_{\tilde{\chi}_1^0} \sim m_W$	none 280-830	95	57	SIRUNYAN	17k	CMS	0, 1 ℓ^\pm +jets+ E_T (combina- tion), Tstop1, $m_{\tilde{\chi}_1^0} = 0$ GeV
> 700	95	44	AABOUD	17BE	ATLS	$\ell^\pm \bar{\ell} \mp + E_T$, Tstop2, $m_{\tilde{t}} - m_{\tilde{\chi}_1^\pm} = 10$ GeV, $m_{\tilde{\chi}_1^0}$ $= 0$ GeV	> 700	95	57	SIRUNYAN	17k	CMS	0, 1 ℓ^\pm +jets+ E_T (combina- tion), Tstop8, $m_{\tilde{\chi}_1^\pm} - m_{\tilde{\chi}_1^0} =$ 5 GeV, $m_{\tilde{\chi}_1^0} = 100$ GeV
> 750	95	45	KHACHATRY...17	CMS	jets+ E_T , Tstop1, $m_{\tilde{\chi}_1^0} = 100$ GeV	> 160	95	57	SIRUNYAN	17k	CMS	jets+ E_T , Tstop4, 10 < $m_{\tilde{t}} - m_{\tilde{\chi}_1^0} < 80$ GeV	
none 250-740	95	46	KHACHATRY...17AD	CMS	jets+ b -jets+ E_T , Tstop1, $m_{\tilde{\chi}_1^0}$ $= 0$ GeV	none 230-960	95	58	SIRUNYAN	17P	CMS	jets+ E_T , Tstop1, $m_{\tilde{\chi}_1^0} = 0$ GeV	
> 610	95	47	KHACHATRY...17AD	CMS	jets+ b -jets+ E_T , mixture Tstop1 and Tstop2 with BR=50%, $m_{\tilde{\chi}_1^0} = 60$ GeV	> 990	95	58	SIRUNYAN	17P	CMS	jets+ E_T , Tstop1, $m_{\tilde{\chi}_1^0} = 0$ GeV	
> 590	95	48	KHACHATRY...17P	CMS	1 or more jets+ E_T , Tstop8, $m_{\tilde{\chi}_1^\pm} - m_{\tilde{\chi}_1^0} = 5$ GeV, $m_{\tilde{\chi}_1^0}$ $= 100$ GeV	> 323	95	59	AABOUD	16D	ATLS	≥ 1 jet + E_T , Tstop4, $m_{\tilde{t}} - m_{\tilde{\chi}_1^0} = 5$ GeV	
none 280-640	95	48	KHACHATRY...17P	CMS	1 or more jets+ E_T , Tstop1, $m_{\tilde{\chi}_1^0} = 0$ GeV	none, 745-780	95	60	AABOUD	16J	ATLS	1 $\ell^\pm + \geq 4$ jets + E_T , Tstop1, $m_{\tilde{\chi}_1^0} = 0$ GeV	
> 350	95	48	KHACHATRY...17P	CMS	1 or more jets+ E_T , Tstop4, 10 GeV < $m_{\tilde{t}} - m_{\tilde{\chi}_1^0} < 80$ GeV	> 700	95	61	AAD	16AY	ATLS	2 ℓ (including hadronic τ) + E_T , Tstop5, 87 GeV < $m_{\tilde{\tau}} < m_{\tilde{t}}$	
						> 775	95	62	KHACHATRY...16AV	CMS	1 or 2 ℓ^\pm +jets+ b -jets+ E_T , Tstop1, $m_{\tilde{\chi}_1^0} < 250$ GeV		
						> 620	95	62	KHACHATRY...16AV	CMS	1 or 2 ℓ^\pm +jets+ b -jets E_T , Tstop2, $m_{\tilde{\chi}_1^0} = 0$ GeV, $m_{\tilde{\chi}_1^\pm} =$ $0.75 m_{\tilde{t}} + 0.25 m_{\tilde{\chi}_1^0}$		
						> 800	95	63	KHACHATRY...16BK	CMS	jets+ E_T , Tstop1, $m_{\tilde{\chi}_1^0} < 200$ GeV		
							95	63	KHACHATRY...16BK	CMS	jets+ E_T , Tstop2, $m_{\tilde{\chi}_1^0} = 0$ GeV		
							95	64	KHACHATRY...16Bs	CMS	jets+ E_T , Tstop1, $m_{\tilde{\chi}_1^0} = 0$ GeV		

> 316	95	65	KHACHATRY...16Y	CMS	1 or 2 soft $\ell^{\pm} + \text{jets} + \cancel{E}_T$, Tstop3, $m_{\tilde{t}} - m_{\tilde{\chi}_1^0} = 25$ GeV	> 360	95	83	CHATRCHYAN14u	CMS	$\tilde{t}_1 \rightarrow b\tilde{\chi}_1^{\pm}r, \tilde{\chi}_1^{\pm} \rightarrow f f' \tilde{\chi}_1^0$, $\tilde{\chi}_1^0 \rightarrow H\tilde{G}$ simplified model, $m_{\tilde{\chi}_1^{\pm}} - m_{\tilde{\chi}_1^0} = 5$ GeV, GMSB
> 250	95	66	AAD	15CJ ATLS	$B(\tilde{t} \rightarrow c\tilde{\chi}_1^0) + B(\tilde{t} \rightarrow b f f' \tilde{\chi}_1^0) = 1, m_{\tilde{t}} - m_{\tilde{\chi}_1^0} = 10$ GeV	> 215	95	CZAKON	14	$\tilde{t} \rightarrow t\tilde{\chi}_1^0, m_{\tilde{\chi}_1^0} < 10$ GeV	
> 270	95	66	AAD	15CJ ATLS	$\tilde{t} \rightarrow c\tilde{\chi}_1^0, m_{\tilde{t}} - m_{\tilde{\chi}_1^0} = 80$ GeV	84	KHACHATRY...14c	CMS	$\tilde{t}_2 \rightarrow H\tilde{t}_1$ or $\tilde{t}_2 \rightarrow Z\tilde{t}_1$ simplified model		
none, 200–700	95	66	AAD	15CJ ATLS	$\tilde{t} \rightarrow t\tilde{\chi}_1^0, m_{\tilde{\chi}_1^0} = 0$	1 AAD 21AW searched in 139 fb^{-1} of pp collisions at $\sqrt{s} = 13$ TeV for pair production of stops in events with one or two hadronically decaying τ leptons, jets, b -jets and \cancel{E}_T . No significant excess above the Standard Model predictions is observed. Limits are set on the \tilde{t}_1 mass as a function of the $\tilde{\tau}_1$ in the Tstop5 scenario. See their Fig. 8.					
> 500	95	66	AAD	15CJ ATLS	$B(\tilde{t} \rightarrow t\tilde{\chi}_1^0) + B(\tilde{t} \rightarrow b\tilde{\chi}_1^{\pm}) = 1, \tilde{\chi}_1^{\pm} \rightarrow W^{(*)}\tilde{\chi}_1^0, m_{\tilde{\chi}_1^{\pm}} = 2m_{\tilde{\chi}_1^0}, m_{\tilde{\chi}_1^0} < 160$ GeV	2 AAD 21o searched in 139 fb^{-1} of pp collisions at $\sqrt{s} = 13$ TeV for pair production of top squarks in events with one electron or muon, jets, and large missing transverse momentum. No significant excess above the Standard Model expectations is observed. Limits are set on the top squark mass in the Tstop1 and Tstop3 simplified models and dark matter models, see their Figures 13, 14 and 15.					
> 600	95	66	AAD	15CJ ATLS	$\tilde{t}_2 \rightarrow Z\tilde{t}_1, m_{\tilde{t}_2} - m_{\tilde{\chi}_1^0} = 180$ GeV, $m_{\tilde{\chi}_1^0} = 0$	3 AAD 21P searched in 139 fb^{-1} of pp collisions at $\sqrt{s} = 13$ TeV for pair production of top squarks in events with two opposite-sign leptons, jets, and large missing transverse momentum. No significant excess above the Standard Model expectations is observed. Limits are set on the top squark mass in the Tstop1, Tstop2, and Tstop3 simplified models, see their Figures 14.					
> 600	95	66	AAD	15CJ ATLS	$\tilde{t}_2 \rightarrow h\tilde{t}_1, m_{\tilde{t}_2} - m_{\tilde{\chi}_1^0} = 180$ GeV, $m_{\tilde{\chi}_1^0} = 0$	4 SIRUNYAN 21AD searched in 137 fb^{-1} of pp collisions at $\sqrt{s} = 13$ TeV for supersymmetry in events with multiple jets, no leptons, and large \cancel{E}_T . No significant excess above the Standard Model expectations is observed. Limits are set on the top squark mass in the simplified models Tstop1, Tstop2 with $m_{\tilde{\chi}_1^{\pm}} = (m_{\tilde{t}} + m_{\tilde{\chi}_1^0})/2$, and a 50:50 mixture of these with $m_{\tilde{\chi}_1^{\pm}} - m_{\tilde{\chi}_1^0} = 5$ GeV, see their Figure 8. Limits are also set on the top squark mass for $10 \text{ GeV} < m_{\tilde{t}} - m_{\tilde{\chi}_1^{\pm}} < 80$ GeV in the simplified models Tstop2, Tstop 3, and Tstop4, see their Figure 9. For indirect top squark production, limits are set on the gluino mass in the simplified models Tglu3A, Tglu3C with $m_{\tilde{t}} - m_{\tilde{\chi}_1^0} = 20$ GeV, and Tglu3D with $m_{\tilde{\chi}_1^{\pm}} - m_{\tilde{\chi}_1^0} = 5$ GeV, see their Figure 10.					
none, 172.5–191	95	67	AAD	15J ATLS	$\tilde{t} \rightarrow t\tilde{\chi}_1^0, m_{\tilde{\chi}_1^0} = 1$ GeV	5 SIRUNYAN 21B searched in 137 fb^{-1} of pp collisions at $\sqrt{s} = 13$ TeV for the pair production of top squarks in events with two oppositely charged leptons (electrons or muons), jets identified as originating from a b -quark and significant \cancel{E}_T . No significant excess above the Standard Model expectations is observed. Limits are set on the top stop mass in the Tstop1, Tstop2 and Tstop11 simplified models, see their Figures 6 and 7.					
> 450	95	68	KHACHATRY...15AF	CMS	$\tilde{t} \rightarrow t\tilde{\chi}_1^0, m_{\tilde{\chi}_1^0} = 0, m_{\tilde{t}} > m_{\tilde{\chi}_1^0} + m_{\tilde{\chi}_1^0}$	6 TUMASYAN 21i searched in 137 fb^{-1} of pp collisions at $\sqrt{s} = 13$ TeV for evidence of top squarks in events with at least two jets and large \cancel{E}_T , categorized into events with 0, 1, or 2 leptons. No significant excess above the Standard Model expectations is observed. Limits are set on the top squark mass in the simplified model Tstop1 in the top corridor $ m_{\tilde{t}} - m_{\tilde{\chi}_1^0} - 175 \text{ GeV} < 30$ GeV using dilepton events, see their Figure 7. Limits are also set for a combination of earlier searches with 0, 1, and 2 leptons in the models Tstop1, Tstop2 and a 50:50 mixture of these models, see their Figure 9. The results are interpreted in an alternative signal model of dark matter production via a spin-0 mediator in association with a top quark pair as well.					
> 560	95	69	KHACHATRY...15AH	CMS	$\tilde{t} \rightarrow t\tilde{\chi}_1^0, m_{\tilde{\chi}_1^0} = 0, m_{\tilde{t}} > m_{\tilde{\chi}_1^0} + m_{\tilde{\chi}_1^0}$	7 AABOU 20 searched in 36.1 fb^{-1} of pp collisions at $\sqrt{s} = 13$ TeV for events containing one electron-muon pair with opposite charge. The search targets a region of parameter space where the kinematics of top squark pair production and top quark pair production is very similar and makes use of the double-differential angular distributions of the leptons. No excess above the Standard Model expectations is observed. Limits are set on the stop mass in the Tstop1 model, see Figures 16 and 17.					
> 250	95	70	KHACHATRY...15AH	CMS	$\tilde{t} \rightarrow c\tilde{\chi}_1^0, m_{\tilde{t}} - m_{\tilde{\chi}_1^0} < 10$ GeV	8 AAD 20As searched in 139 fb^{-1} of pp collisions at $\sqrt{s} = 13$ TeV for evidence of top squarks in events containing either a pair of jets consistent with SM Higgs boson decay into b -quarks or a same-flavour opposite-sign dilepton pair with an invariant mass consistent with a Z boson. No significant excess over the expected background is observed. Limits at 95% C.L. are set in Tstop6 simplified model. Assuming $m_{\tilde{\chi}_1^0} = 0$ GeV, \tilde{t}_1 masses up to 1220 GeV are excluded for $m_{\tilde{\chi}_2^0}$ around 900 GeV. Limits reduce down to \tilde{t}_1 masses up to 900 GeV for $m_{\tilde{\chi}_2^0} = 130$ GeV. See their Fig. 10. Limits are presented also in case of $B(\tilde{\chi}_2^0 \rightarrow \tilde{\chi}_1^0 h) = 0$ and 1, see their Fig. 11.					
> 730	95	71	KHACHATRY...15X	CMS	$\tilde{t} \rightarrow t\tilde{\chi}_1^0, m_{\tilde{\chi}_1^0} = 100$ GeV, $m_{\tilde{t}} > m_{\tilde{\chi}_1^0} + m_{\tilde{\chi}_1^0}$	9 AAD 20As searched in 139 fb^{-1} of pp collisions at $\sqrt{s} = 13$ TeV for evidence of top squarks in events containing either a pair of jets consistent with SM Higgs boson decay into b -quarks or a same-flavour opposite-sign dilepton pair with an invariant mass consistent with a Z boson. No significant excess over the expected background is observed. Limits at 95% C.L. are set in simplified model featuring \tilde{t}_2 pair production, $\tilde{t}_2 \rightarrow \tilde{t}_1 Z$ and $\tilde{t}_1 \rightarrow b f f' \tilde{\chi}_1^0$. Assuming $m_{\tilde{\chi}_1^0} = 300$ GeV, and a mass difference between \tilde{t}_1 and $\tilde{\chi}_1^0$ of 40 GeV, \tilde{t}_2 masses up to 860 GeV are excluded. See their Fig. 12.					
none 400–645	95	71	KHACHATRY...15X	CMS	$\tilde{t} \rightarrow t\tilde{\chi}_1^0$ or $\tilde{t} \rightarrow b\tilde{\chi}_1^{\pm}, m_{\tilde{\chi}_1^0} = 100$ GeV, $m_{\tilde{\chi}_1^{\pm}} - m_{\tilde{\chi}_1^0} = 5$ GeV	10 AAD 20s searched in 139 fb^{-1} of pp collisions at $\sqrt{s} = 13$ TeV for events containing multiple jets and large \cancel{E}_T . No significant excess above the Standard Model expectations is observed. Exclusion limits at 95% C.L. are set on top squark masses in the Tstop1 model up to 1250 GeV for lightest neutralino masses below 200 GeV. Additional constraints are set in the case where $m_{\tilde{t}} - m_{\tilde{\chi}_1^0} \sim m_{\tilde{t}}$ for which top squark masses in the range 300–630 GeV are excluded. See their Fig. 13.					
none 270–645	95	72	AAD	14AJ ATLS	≥ 4 jets + $\cancel{E}_T, \tilde{t}_1 \rightarrow t\tilde{\chi}_1^0, m_{\tilde{\chi}_1^0} < 30$ GeV	11 AAD 20s searched in 139 fb^{-1} of pp collisions at $\sqrt{s} = 13$ TeV for events containing multiple jets and large \cancel{E}_T . No significant excess above the Standard Model expectations is observed. Exclusion limits at 95% C.L. are set on top squark masses in the Tstop3 model in the range 300–660 GeV. In case $m_{\tilde{t}} - m_{\tilde{\chi}_1^0} \sim 5$ GeV or above, $m_{\tilde{t}}$ below 500 GeV are excluded. See their Fig. 13(b).					
none 250–550	95	72	AAD	14AJ ATLS	≥ 4 jets + $\cancel{E}_T, B(\tilde{t}_1 \rightarrow b\tilde{\chi}_1^{\pm}) = 50\%, m_{\tilde{\chi}_1^{\pm}} = 2m_{\tilde{\chi}_1^0}, m_{\tilde{\chi}_1^0} < 60$ GeV	12 AAD 20v searched in 139 fb^{-1} of pp collisions at $\sqrt{s} = 13$ TeV for events with two same-sign charged leptons (electrons or muons) and jets. No significant excess above the Standard Model expectations is observed. Exclusion limits at 95% C.L. are set on the top squark mass up to 765 GeV assuming $\tilde{t}_1 \rightarrow t\tilde{\chi}_2^0$ with $\tilde{\chi}_2^0 \rightarrow \tilde{\chi}_1^{\pm} W$ and $\tilde{\chi}_1^{\pm} \rightarrow \tilde{\chi}_1^0 W$. Masses of the charginos and lightest neutralinos are set as $m_{\tilde{\chi}_1^0} = m_{\tilde{\tau}_1} - 275$ GeV, $m_{\tilde{\chi}_2^0} = m_{\tilde{\chi}_1^0} + 100$ GeV and $m_{\tilde{\chi}_1^{\pm}} \sim m_{\tilde{\chi}_1^0}$. See their Fig. 8(b).					
none 210–640	95	73	AAD	14BD ATLS	$\ell^{\pm} + \text{jets} + \cancel{E}_T, \tilde{t}_1 \rightarrow t\tilde{\chi}_1^0, m_{\tilde{\chi}_1^0} = 0$ GeV						
> 500	95	73	AAD	14BD ATLS	$\ell^{\pm} + \text{jets} + \cancel{E}_T, \tilde{t}_1 \rightarrow b\tilde{\chi}_1^{\pm}, m_{\tilde{\chi}_1^{\pm}} = 2m_{\tilde{\chi}_1^0}, 100 \text{ GeV} < m_{\tilde{\chi}_1^0} < 150$ GeV						
none 150–445	95	74	AAD	14F ATLS	$\ell^{\pm}\ell^{\mp}$ final state, $\tilde{t}_1 \rightarrow b\tilde{\chi}_1^{\pm}, m_{\tilde{t}_1} - m_{\tilde{\chi}_1^{\pm}} = 10$ GeV, $m_{\tilde{\chi}_1^0} = 1$ GeV						
none 215–530	95	74	AAD	14F ATLS	$\ell^{\pm}\ell^{\mp}$ final state, $\tilde{t}_1 \rightarrow t\tilde{\chi}_1^0, m_{\tilde{\chi}_1^0} = 1$ GeV						
> 270	95	75	AAD	14T ATLS	$\tilde{t}_1 \rightarrow c\tilde{\chi}_1^0, m_{\tilde{\chi}_1^0} = 200$ GeV						
> 240	95	75	AAD	14T ATLS	$\tilde{t}_1 \rightarrow c\tilde{\chi}_1^0, m_{\tilde{t}_1} - m_{\tilde{\chi}_1^0} < 85$ GeV						
> 255	95	75	AAD	14T ATLS	$\tilde{t}_1 \rightarrow b f f' \tilde{\chi}_1^0, m_{\tilde{t}_1} - m_{\tilde{\chi}_1^0} \approx m_b$						
> 400	95	76	CHATRCHYAN14AH	CMS	jets + $\cancel{E}_T, \tilde{t} \rightarrow t\tilde{\chi}_1^0$ simplified model, $m_{\tilde{\chi}_1^0} = 50$ GeV						
••• We do not use the following data for averages, fits, limits, etc. •••		77	CHATRCHYAN14R	CMS	$\geq 3\ell^{\pm}, \tilde{t} \rightarrow (b\tilde{\chi}_1^{\pm}/t\tilde{\chi}_1^0), \tilde{\chi}_1^{\pm} \rightarrow (qq'/\ell\nu)\tilde{\chi}_1^0, \tilde{\chi}_1^0 \rightarrow (H/Z)\tilde{G}, \text{GMSB, natural higgsino NLP scenario}$						
> 850	95	78	AABOU	17AF ATLS	$2\ell + \text{jets} + b\text{-jets} + \cancel{E}_T, \text{Tstop6}, m_{\tilde{\chi}_1^0} = 0$						
> 800	95	79	AABOU	17AF ATLS	$2\ell + \text{jets} + b\text{-jets} + \cancel{E}_T, \text{Tstop7 with } 100\% \text{ decays via } Z, m_{\tilde{\chi}_1^0} = 50$ GeV						
> 880	95	80	AABOU	17AF ATLS	$2\ell + \text{jets} + b\text{-jets} + \cancel{E}_T, \text{Tstop7 with } 100\% \text{ decays via higgs}, m_{\tilde{\chi}_1^0} = 50$ GeV						
> 230	95	81	AABOU ROLBIECKI	17AY ATLS 15 THEO	jets + \cancel{E}_T , pMSSM-inspired WW xsection, $\tilde{t}_1 \rightarrow bW\tilde{\chi}_1^0, m_{\tilde{t}_1} \approx m_b + m_W + m_{\tilde{\chi}_1^0}$						
> 600	95	82	AAD	14B ATLS	$Z + b\cancel{E}_T, \tilde{t}_2 \rightarrow Z\tilde{t}_1, \tilde{t}_1 \rightarrow t\tilde{\chi}_1^0, m_{\tilde{\chi}_1^0} < 200$ GeV						
> 540	95	82	AAD	14B ATLS	$Z + b\cancel{E}_T, \tilde{t}_1 \rightarrow t\tilde{\chi}_1^0, \tilde{\chi}_1^0 \rightarrow Z\tilde{G}, \text{natural GMSB, } 100 \text{ GeV} < m_{\tilde{\chi}_1^0} < m_{\tilde{t}_1} - 10$ GeV						

Searches Particle Listings

Supersymmetric Particle Searches

- 13 SIRUNYAN 20AH searched in 137 fb^{-1} of pp collisions at $\sqrt{s} = 13 \text{ TeV}$ for pair production of top squarks in events with a single isolated electron or muon, multiple jets and large \cancel{E}_T . No significant excess above the Standard Model expectations is observed. Limits are set on the stop mass in the Tstop1, Tstop2 and Tstop8 simplified models, see Figures 6, 7 and 8, respectively.
- 14 SIRUNYAN 20T searched in 137 fb^{-1} of pp collisions at $\sqrt{s} = 13 \text{ TeV}$ for events with at least two jets, and two isolated same-sign or three or more charged leptons (electrons or muons). No significant excess above the Standard Model expectations is observed. Limits are set on the gluino mass in the Tglu3A, Tglu3B, Tglu3C and Tglu3D simplified models, see their Figure 7, and in the Tglu1C and Tglu1B simplified models, see their Figures 8 and 9. Limits are also set on the sbottom mass in the Tsb02 simplified model, see their Figure 10, and on the stop mass in the Tstop7 simplified model, see their Figure 11. Finally, limits are set on the gluino mass in RPV simplified models where the gluino decays either via $\tilde{g} \rightarrow qq\bar{q}\bar{q} + e/\mu/\tau$ or via $\tilde{g} \rightarrow tbs$, see Figure 12.
- 15 SIRUNYAN 20U searched in 77.2 fb^{-1} of pp collisions at $\sqrt{s} = 13 \text{ TeV}$ for the pair production of top squarks in events with two hadronically decaying taus, jets identified as originating from a b -quark and large \cancel{E}_T . No significant excess above the Standard Model expectations is observed. Limits are set on the stop mass in the Tstop11 simplified model assuming the final state leptons are taus. Different values of the scalar tau mass are considered; the impact on the lower bound is negligible.
- 16 SIRUNYAN 19AU searched in 35.9 fb^{-1} of pp collisions at $\sqrt{s} = 13 \text{ TeV}$ for events with at least one photon, jets, some of which are identified as originating from b -quarks, and large \cancel{E}_T . No significant excess above the Standard Model expectations is observed. In the framework of GMSB, limits are set on the gluino mass in the Tglu4C, Tglu4D and Tglu4E simplified models, and on the top squark mass in the Tstop13 simplified model, see their Figure 5.
- 17 SIRUNYAN 19CH searched in 137 fb^{-1} of pp collisions at $\sqrt{s} = 13 \text{ TeV}$ for events containing multiple jets and large \cancel{E}_T . No significant excess above the Standard Model expectations is observed. Limits are set on the gluino mass in the Tglu1A, Tglu1C, Tglu2A and Tglu3A simplified models, see their Figure 13. Limits are also set on squark, sbottom and stop masses in the Tsqk1, Tsb01, Tstop1 simplified models, see their Figure 14.
- 18 SIRUNYAN 19S searched in 35.9 fb^{-1} of pp collisions at $\sqrt{s} = 13 \text{ TeV}$ for events with zero or one charged leptons, jets and \cancel{E}_T . The razor variables (M_R and R^2) are used to categorize the events. No significant excess above the Standard Model expectations is observed. Limits are set on the gluino mass in the Tglu3A and Tglu3C simplified models, see Figures 22 and 23, and on the stop mass in the Tstop1 simplified model, see their Figure 24.
- 19 SIRUNYAN 19U searched in 35.9 fb^{-1} of pp collisions at $\sqrt{s} = 13 \text{ TeV}$ for events containing one electron-muon pair with opposite charge. The search targets a region of parameter space where the kinematics of top squark pair production and top quark pair production is very similar, due to the mass difference between the top squark and the neutralino being close to the top quark mass. No excess above the Standard Model expectations is observed. Limits are set on the stop mass in the Tstop1 model, with $m_{\tilde{t}_1} - m_{\tilde{\chi}_1^0}$ close to m_t , see Figure 5.
- 20 AABOUD 18AQ searched in 36.1 fb^{-1} of pp collisions at $\sqrt{s} = 13 \text{ TeV}$ for top squark pair production in final states with one isolated electron or muon, several energetic jets, and missing transverse momentum. No significant excess over the Standard Model prediction is observed. In case of Tstop1 models, top squark masses up to 940 GeV are excluded assuming $m_{\tilde{t}_1} - m_{\tilde{\chi}_1^0} = 0 \text{ GeV}$, see their Fig. 20. If the top quark is not on-shell (3-body) decay, exclusions up to 500 GeV are obtained for $m_{\tilde{\chi}_1^0} = 300 \text{ GeV}$. Exclusions as a function of $m_{\tilde{t}_1} - m_{\tilde{\chi}_1^0}$ are given in their Fig. 21.
- 21 AABOUD 18AQ searched in 36.1 fb^{-1} of pp collisions at $\sqrt{s} = 13 \text{ TeV}$ for top squark pair production in final states with one isolated electron or muon, several energetic jets, and missing transverse momentum. No significant excess over the Standard Model prediction is observed. In case of Tstop3 models (4-body), top squark masses up to 370 GeV are excluded for $m_{\tilde{t}_1} - m_{\tilde{\chi}_1^0}$ as low as 20 GeV. Top squark masses below 195 GeV are excluded for all $m_{\tilde{\chi}_1^0}$, see their Fig. 20 and Fig. 21.
- 22 AABOUD 18AQ searched in 36.1 fb^{-1} of pp collisions at $\sqrt{s} = 13 \text{ TeV}$ for top squark pair production in final states with one isolated electron or muon, several energetic jets, and missing transverse momentum. No significant excess over the Standard Model prediction is observed. In case of Tstop2 models, top squark masses up to 840 GeV are excluded for $m_{\tilde{t}_1} - m_{\tilde{\chi}_1^0} = 10 \text{ GeV}$. See their Fig. 23. Exclusion limits for this decay mode are presented also in the context of Higgsino-LSP phenomenological MSSM models, where $m_{\tilde{\chi}_1^\pm} - m_{\tilde{\chi}_1^0} = 5 \text{ GeV}$, see their Fig. 26.
- 23 AABOUD 18BV searched in 36.1 fb^{-1} of pp collisions at $\sqrt{s} = 13 \text{ TeV}$ for events with at least one jet identified as c -jet, large missing transverse energy and no leptons. Good agreement is observed between the number of events in data and Standard Model predictions. The results are translated into exclusion limits in Tstop4 models. In scenarios with differences of the stop and neutralino masses below 100 GeV, stop masses below 500 GeV are excluded. See their Fig. 6 and Fig. 7.
- 24 AABOUD 18BV searched in 36.1 fb^{-1} of pp collisions at $\sqrt{s} = 13 \text{ TeV}$ for events with at least one jet identified as c -jet, large missing transverse energy and no leptons. Good agreement is observed between the number of events in data and Standard Model predictions. The results are translated into exclusion limits in Tstop1 models. In scenarios with massless neutralinos, top squark masses below 850 GeV are excluded. See their Fig. 6.
- 25 AABOUD 18I searched in 36.1 fb^{-1} of pp collisions at $\sqrt{s} = 13 \text{ TeV}$ for events with at least one jet with a transverse momentum above 250 GeV and no leptons. Good agreement is observed between the number of events in data and Standard Model predictions. The results are translated into exclusion limits in Tstop3 models. Stop masses below 390 GeV are excluded for $m_{\tilde{t}_1} - m_{\tilde{\chi}_1^0} = m_b$. See their Fig. 9(b).
- 26 AABOUD 18I searched in 36.1 fb^{-1} of pp collisions at $\sqrt{s} = 13 \text{ TeV}$ for events with at least one jet with a transverse momentum above 250 GeV and no leptons. Good agreement is observed between the number of events in data and Standard Model predictions. The results are translated into exclusion limits in Tstop4 models. In scenarios with differences of the stop and neutralino masses around 5 GeV, stop masses below 430 GeV are excluded. See their Fig. 9(a).
- 27 AABOUD 18Y searched in 36.1 fb^{-1} of pp collisions at $\sqrt{s} = 13 \text{ TeV}$ for direct pair production of top squarks in final states with two tau leptons, b -jets, and missing transverse momentum. At least one hadronic τ is required. No significant deviation from the SM predictions is observed in the data. The analysis results are interpreted in Tstop5 models with a nearly massless gravitino. Top squark masses up to 1.16 TeV and tau slepton masses up to 1 TeV are excluded, see their Fig. 7.
- 28 SIRUNYAN 18AJ searched in 35.9 fb^{-1} of pp collisions at $\sqrt{s} = 13 \text{ TeV}$ for events containing two low-momentum, oppositely charged leptons (electrons or muons) and \cancel{E}_T . No excess over the expected background is observed. Limits are derived on the wino mass in the Tch1n2F simplified model, see their Figure 5. Limits are also set on the stop mass in the Tstop10 simplified model, see their Figure 6. Finally, limits are set on the Higgsino mass in the Tch1n2G simplified model, see Figure 8 and in the pMSSM, see Figure 7.
- 29 SIRUNYAN 18AL searched in 35.9 fb^{-1} of pp collisions at $\sqrt{s} = 13 \text{ TeV}$ for events with at least three charged leptons, in any combination of electrons and muons, jets and significant \cancel{E}_T . No significant excess above the Standard Model expectations is observed. Limits are set on the gluino mass in the Tglu3A and Tglu1C simplified models, see their Figure 5. Limits are also set on the sbottom mass in the Tsb02 simplified model, see their Figure 6, and on the stop mass in the Tstop7 simplified model, see their Figure 7.
- 30 SIRUNYAN 18AN searched in 19.7 fb^{-1} of pp collisions at $\sqrt{s} = 8 \text{ TeV}$ for events containing one or two photons and a pair of top quarks from the decay of a pair of top squark in a natural gauge-mediated scenario. The final state consists of a lepton (electron or muon), jets and one or two photons. No significant excess above the Standard Model expectations is observed. Limits are set on the stop mass in the Tstop12 simplified model, see their Figure 6.
- 31 SIRUNYAN 18AY searched in 35.9 fb^{-1} of pp collisions at $\sqrt{s} = 13 \text{ TeV}$ for events containing one or more jets and significant \cancel{E}_T . No significant excess above the Standard Model expectations is observed. Limits are set on the gluino mass in the Tglu1A, Tglu2A and Tglu3A simplified models, see their Figure 3. Limits are also set on squark, sbottom and stop masses in the Tsqk1, Tsb01, Tstop1 and Tstop4 simplified models, see their Figure 3. Finally, limits are set on long-lived gluino masses in a Tglu1A simplified model where the gluino is metastable or long-lived with proper decay lengths in the range $10^{-3} \text{ mm} < c\tau < 10^5 \text{ mm}$, see their Figure 4.
- 32 SIRUNYAN 18B searched in 35.9 fb^{-1} of pp collisions at $\sqrt{s} = 13 \text{ TeV}$ for the pair production of third-generation squarks in events with jets and large \cancel{E}_T . No significant excess above the Standard Model expectations is observed. Limits are set on the sbottom mass in the Tsb01 simplified model, see their Figure 5, and on the stop mass in the Tstop4 simplified model, see their Figure 6.
- 33 SIRUNYAN 18C searched in 35.9 fb^{-1} of pp collisions at $\sqrt{s} = 13 \text{ TeV}$ for the pair production of top squarks in events with two oppositely charged leptons (electrons or muons), jets identified as originating from a b -quark and large \cancel{E}_T . No significant excess above the Standard Model expectations is observed. Limits are set on the stop mass in the Tstop1, Tstop2 and Tstop11 simplified models, see their Figures 11 and 12. The Tstop1 and Tstop2 results are combined with complementary searches in the all-hadronic and single lepton channels, see their Figures 13 and 14.
- 34 SIRUNYAN 18D searched in 35.9 fb^{-1} of pp collisions at $\sqrt{s} = 13 \text{ TeV}$ for events containing identified hadronically decaying top quarks, no leptons, and \cancel{E}_T . No significant excess above the Standard Model expectations is observed. Limits are set on the stop mass in the Tstop1 simplified model, see their Figure 8, and on the gluino mass in the Tglu3A, Tglu3B, Tglu3C and Tglu3E simplified models, see their Figure 9.
- 35 SIRUNYAN 18DI searched in 35.9 fb^{-1} of pp collisions at $\sqrt{s} = 13 \text{ TeV}$ for pair production of top squarks in events with a low transverse momentum lepton (electron or muon), a high-momentum jet and significant missing transverse momentum. No significant excess above the Standard Model expectations is observed. Limits are set on the stop mass in the Tstop3 and Tstop10 simplified models, see their Figures 7 and 8. A combination of this search with the all-hadronic search is presented in Figure 9.
- 36 SIRUNYAN 18DN searched in 35.9 fb^{-1} of pp collisions at $\sqrt{s} = 13 \text{ TeV}$ for direct electroweak production of charginos and for pair production of top squarks in events with two leptons (electrons or muons) of the opposite electric charge. No significant excess above the Standard Model expectations is observed. Limits are set on the chargino mass in the Tch1ch1C and Tch1ch1E simplified models, see their Figure 8. Limits are also set on the stop mass in the Tstop1 and Tstop2 simplified models, see their Figure 9.
- 37 AABOUD 17AJ searched in 36.1 fb^{-1} of pp collisions at $\sqrt{s} = 13 \text{ TeV}$ for events with two same-sign or three leptons, jets and large missing transverse momentum. No significant excess above the Standard Model expectations is observed. Limits up to 700 GeV are set on the top squark mass in Tstop11 simplified models, assuming $m_{\tilde{\chi}_1^0} = m_{\tilde{t}_1} - 275 \text{ GeV}$ and $m_{\tilde{\chi}_2^0} = m_{\tilde{\chi}_1^0} + 100 \text{ GeV}$. See their Figure 4(e).
- 38 AABOUD 17AX searched in 36 fb^{-1} of pp collisions at $\sqrt{s} = 13 \text{ TeV}$ for events containing two jets identified as originating from b -quarks and large missing transverse momentum, with or without leptons. No excess of events above the expected level of Standard Model background was found. Exclusion limits at 95% C.L. are set on the masses of top squarks. Assuming 50% BR for Tstop1 and Tstop2 simplified models, a \tilde{t}_1 mass below 880 (860) GeV is excluded for $m_{\tilde{\chi}_1^0} = 0$ (<250) GeV. See their Fig. 7(b).
- 39 AABOUD 17AY searched in 36.1 fb^{-1} of pp collisions at $\sqrt{s} = 13 \text{ TeV}$ for events with at least four jets and large missing transverse momentum. No significant excess above the Standard Model expectations is observed. Limits in the range 250–1000 GeV are set on the top squark mass in Tstop1 simplified models. For the first time, additional constraints are set for the region $m_{\tilde{t}_1} \sim m_t + m_{\tilde{\chi}_1^0}$, with exclusion of the \tilde{t}_1 mass range 235–590 GeV. See their Figure 8.
- 40 AABOUD 17AY searched in 36.1 fb^{-1} of pp collisions at $\sqrt{s} = 13 \text{ TeV}$ for events with at least four jets and large missing transverse momentum. No significant excess above the Standard Model expectations is observed. Limits in the range 450–850 GeV are set on the top squark mass in a mixture of Tstop1 and Tstop2 simplified models with BR=50% and assuming $m_{\tilde{\chi}_1^\pm} - m_{\tilde{\chi}_1^0} = 1 \text{ GeV}$ and $m_{\tilde{\chi}_1^0} < 240 \text{ GeV}$. Constraints are given for various values of the BR. See their Figure 9.
- 41 AABOUD 17BE searched in 36.1 fb^{-1} of pp collisions at $\sqrt{s} = 13 \text{ TeV}$ for events with two opposite-charge leptons (electrons and muons) and large missing transverse momentum. No significant excess above the Standard Model expectations is observed. Limits up to 720 GeV are set on the top squark mass in Tstop1 simplified models, assuming massless neutralinos. See their Figure 9 (2-body area).
- 42 AABOUD 17BE searched in 36.1 fb^{-1} of pp collisions at $\sqrt{s} = 13 \text{ TeV}$ for events with two opposite-charge leptons (electrons and muons) and large missing transverse momentum. No significant excess above the Standard Model expectations is observed. Limits up to 400 GeV are set on the top squark mass in Tstop3 simplified models, assuming $m_{\tilde{t}_1} - m_{\tilde{\chi}_1^0} = 40 \text{ GeV}$. See their Figure 9 (4-body area).
- 43 AABOUD 17BE searched in 36.1 fb^{-1} of pp collisions at $\sqrt{s} = 13 \text{ TeV}$ for events with two opposite-charge leptons (electrons and muons) and large missing transverse momentum. No significant excess above the Standard Model expectations is observed.

- Limits up to 430 GeV are set on the top squark mass in Tstop1 simplified models where top quarks are offshell, assuming $m_{\tilde{t}_1} - m_{\tilde{\chi}_1^0}$ close to the W mass. See their Figure 9 (3-body area).
- 44 AABOUD 17E searched in 36.1 fb^{-1} of pp collisions at $\sqrt{s} = 13 \text{ TeV}$ for events with two opposite-charge leptons (electrons and muons) and large missing transverse momentum. No significant excess above the Standard Model expectations is observed. Limits up to 700 GeV are set on the top squark mass in Tstop2 simplified models, assuming $m_{\tilde{t}_1} - m_{\tilde{\chi}_1^0} = 10 \text{ GeV}$ and massless neutralinos. See their Figure 10.
- 45 KHACHATRYAN 17 searched in 2.3 fb^{-1} of pp collisions at $\sqrt{s} = 13 \text{ TeV}$ for events containing four or more jets, no more than one lepton, and missing transverse momentum, using the razor variables (M_R and R^2) to discriminate between signal and background processes. No evidence for an excess over the expected background is observed. Limits are derived on the stop mass in the Tstop1 simplified model, see Fig. 17.
- 46 KHACHATRYAN 17AD searched in 2.3 fb^{-1} of pp collisions at $\sqrt{s} = 13 \text{ TeV}$ for events containing at least four jets (including b -jets), missing transverse momentum and tagged top quarks. No evidence for an excess over the expected background is observed. Top squark masses in the range 250–740 GeV and neutralino masses up to 240 GeV are excluded at 95% C.L. See Fig. 12.
- 47 KHACHATRYAN 17AD searched in 2.3 fb^{-1} of pp collisions at $\sqrt{s} = 13 \text{ TeV}$ for events containing at least four jets (including b -jets), missing transverse momentum and tagged top quarks. No evidence for an excess over the expected background is observed. Limits are derived on the \tilde{t} mass in simplified models that are a mixture of Tstop1 and Tstop2 with branching fractions 50% for each of the two decay modes: top squark masses of up to 610 GeV and neutralino masses up to 190 GeV are excluded at 95% C.L. The $\tilde{\chi}_1^{\pm}$ and the $\tilde{\chi}_1^0$ are assumed to be nearly degenerate in mass, with a 5 GeV difference between their masses. See Fig. 12.
- 48 KHACHATRYAN 17P searched in 2.3 fb^{-1} of pp collisions at $\sqrt{s} = 13 \text{ TeV}$ for events with one or more jets and large \cancel{E}_T . No significant excess above the Standard Model expectations is observed. Limits are set on the gluino mass in the Tglu1A, Tglu2A, Tglu3A, Tglu3B, Tglu3C and Tglu3D simplified models, see their Figures 7 and 8. Limits are also set on the squark mass in the Tsqk1 simplified model, see their Fig. 7, and on the sbottom mass in the Tsb0t1 simplified model, see Fig. 8. Finally, limits are set on the stop mass in the Tstop1, Tstop3, Tstop4, Tstop6 and Tstop7 simplified models, see Fig. 8.
- 49 KHACHATRYAN 17s searched in 18.5 fb^{-1} of pp collisions at $\sqrt{s} = 8 \text{ TeV}$ for events containing multiple jets and missing transverse momentum, using the α_T variable to discriminate between signal and background processes. No evidence for an excess over the expected background is observed. Limits are derived on the stop mass in the Tstop4 model: for $\Delta m = m_{\tilde{t}} - m_{\tilde{\chi}_1^0}$ equal to 10 and 80 GeV, masses of stop below 240 and 260 GeV are excluded, respectively. See their Fig. 3.
- 50 KHACHATRYAN 17s searched in 18.5 fb^{-1} of pp collisions at $\sqrt{s} = 8 \text{ TeV}$ for events containing multiple jets and missing transverse momentum, using the α_T variable to discriminate between signal and background processes. No evidence for an excess over the expected background is observed. Limits are derived on the stop mass in the Tstop3 model: for $\Delta m = m_{\tilde{t}} - m_{\tilde{\chi}_1^0}$ equal to 10 and 80 GeV, masses of stop below 225 and 130 GeV are excluded, respectively. See their Fig. 3.
- 51 KHACHATRYAN 17s searched in 18.5 fb^{-1} of pp collisions at $\sqrt{s} = 8 \text{ TeV}$ for events containing multiple jets and missing transverse momentum, using the α_T variable to discriminate between signal and background processes. No evidence for an excess over the expected background is observed. Limits are derived on the stop mass in the Tstop2 model: assuming $m_{\tilde{\chi}_1^{\pm}} = 0.25 m_{\tilde{t}} + 0.75 m_{\tilde{\chi}_1^0}$, masses of stop up to 325 GeV and masses of the neutralino up to 225 GeV are excluded. See their Fig. 3.
- 52 KHACHATRYAN 17s searched in 18.5 fb^{-1} of pp collisions at $\sqrt{s} = 8 \text{ TeV}$ for events containing multiple jets and missing transverse momentum, using the α_T variable to discriminate between signal and background processes. No evidence for an excess over the expected background is observed. Limits are derived on the stop mass in the Tstop2 model: assuming $m_{\tilde{\chi}_1^{\pm}} = 0.75 m_{\tilde{t}} + 0.25 m_{\tilde{\chi}_1^0}$, masses of stop up to 400 GeV are excluded for low neutralino masses. See their Fig. 3.
- 53 KHACHATRYAN 17s searched in 18.5 fb^{-1} of pp collisions at $\sqrt{s} = 8 \text{ TeV}$ for events containing multiple jets and missing transverse momentum, using the α_T variable to discriminate between signal and background processes. No evidence for an excess over the expected background is observed. Limits are derived on the stop mass in the Tstop1 model: assuming masses of stop up to 500 GeV and masses of the neutralino up to 105 GeV are excluded. See their Fig. 3.
- 54 SIRUNYAN 17As searched in 35.9 fb^{-1} of pp collisions at $\sqrt{s} = 13 \text{ TeV}$ for events with a single lepton (electron or muon), jets, and large \cancel{E}_T . No significant excess above the Standard Model expectations is observed. Limits are set on the stop mass in the Tstop1, Tstop2 and Tstop8 simplified models, see their Figures 5, 6 and 7.
- 55 SIRUNYAN 17AT searched in 35.9 fb^{-1} of pp collisions at $\sqrt{s} = 13 \text{ TeV}$ for direct production of top squarks in events with jets and large \cancel{E}_T . No significant excess above the Standard Model expectations is observed. Limits are set on the stop mass in the Tstop1, Tstop2, Tstop4, Tstop8 and Tstop10 simplified models, see their Figures 9 to 14.
- 56 SIRUNYAN 17AZ searched in 35.9 fb^{-1} of pp collisions at $\sqrt{s} = 13 \text{ TeV}$ for events with one or more jets and large \cancel{E}_T . No significant excess above the Standard Model expectations is observed. Limits are set on the gluino mass in the Tglu1A, Tglu2A, Tglu3A simplified models, see their Figures 6. Limits are also set on the squark mass in the Tsqk1 simplified model (for single light squark and for 8 degenerate light squarks), on the sbottom mass in the Tsb0t1 simplified model and on the stop mass in the Tstop1 simplified model, see their Fig. 7. Finally, limits are set on the stop mass in the Tstop2, Tstop4 and Tstop8 simplified models, see Fig. 8.
- 57 SIRUNYAN 17k searched in 2.3 fb^{-1} of pp collisions at $\sqrt{s} = 13 \text{ TeV}$ for direct production of stop or sbottom pairs in events with multiple jets and significant \cancel{E}_T . A second search also requires an isolated lepton and is combined with the all-hadronic search. No significant excess above the Standard Model expectations is observed. Limits are set on the stop mass in the Tstop1, Tstop8 and Tstop4 simplified models, see their Figures 7, 8 and 9 (for the Tstop4 limits, only the results of the all-hadronic search are used). Limits are also set on the sbottom mass in the Tsb0t1 simplified model, see Fig. 10 (also here, only the results of the all-hadronic search are used).
- 58 SIRUNYAN 17P searched in 35.9 fb^{-1} of pp collisions at $\sqrt{s} = 13 \text{ TeV}$ for events with multiple jets and large \cancel{E}_T . No significant excess above the Standard Model expectations is observed. Limits are set on the gluino mass in the Tglu1A, Tglu1C, Tglu2A, Tglu3A and Tglu3D simplified models, see their Fig. 12. Limits are also set on the squark mass in the Tsqk1 simplified model, on the stop mass in the Tstop1 simplified model, and on the sbottom mass in the Tsb0t1 simplified model, see Fig. 13.
- 59 AABOUD 16D searched in 3.2 fb^{-1} of pp collisions at $\sqrt{s} = 13 \text{ TeV}$ in events with an energetic jet and large missing transverse momentum. The results are interpreted as 95% C.L. limits on mass of stop decaying into a charm-quark and the lightest neutralino in scenarios with $m_{\tilde{t}_1} - m_{\tilde{\chi}_1^0}$ between 5 and 20 GeV. See their Fig. 5.
- 60 AABOUD 16J searched in 3.2 fb^{-1} of pp collisions at $\sqrt{s} = 13 \text{ TeV}$ in final states with one isolated electron or muon, jets, and missing transverse momentum. For the direct stop pair production model where the stop decays via top and lightest neutralino, the results exclude at 95% C.L. stop masses between 745 GeV and 780 GeV for a massless $\tilde{\chi}_1^0$. See their Fig. 8.
- 61 AAD 16AY searched in 20 fb^{-1} of pp collisions at $\sqrt{s} = 8 \text{ TeV}$ for events with either two hadronically decaying tau leptons, one hadronically decaying tau and one light lepton, or two light leptons. No significant excess over the Standard Model expectation is found. Exclusion limits at 95% C.L. on the mass of top squarks decaying via \tilde{t} to a nearly massless gravitino are placed depending on $m_{\tilde{t}}$ which is ranging from the 87 GeV LEP limit to $m_{\tilde{t}_1}$. See their Figs. 9 and 10.
- 62 KHACHATRYAN 16AV searched in 19.7 fb^{-1} of pp collisions at $\sqrt{s} = 8 \text{ TeV}$ for events with one or two isolated leptons, hadronic jets, b -jets and \cancel{E}_T . No significant excess above the Standard Model expectations is observed. Limits are set on the stop mass in the Tstop1 and Tstop2 simplified models, see Fig. 11.
- 63 KHACHATRYAN 16BK searched in 18.9 fb^{-1} of pp collisions at $\sqrt{s} = 8 \text{ TeV}$ for events with hadronic jets and \cancel{E}_T . No significant excess above the Standard Model expectations is observed. Limits are set on the stop mass in the Tstop1 and Tstop2 simplified models, see Fig. 16.
- 64 KHACHATRYAN 16BS searched in 2.3 fb^{-1} of pp collisions at $\sqrt{s} = 13 \text{ TeV}$ for events with at least one energetic jet, no isolated leptons, and significant \cancel{E}_T , using the transverse mass variable M_{T2} to discriminate between signal and background processes. No significant excess above the Standard Model expectations is observed. Limits are set on the stop mass in the Tstop1 simplified model, see Fig. 11 and Table 3.
- 65 KHACHATRYAN 16Y searched in 19.7 fb^{-1} of pp collisions at $\sqrt{s} = 8 \text{ TeV}$ for events with one or two soft isolated leptons, hadronic jets, and \cancel{E}_T . No significant excess above the Standard Model expectations is observed. Limits are set on the stop mass in the Tstop3 simplified model, see Fig. 3.
- 66 AAD 15CJ searched in 20 fb^{-1} of pp collisions at $\sqrt{s} = 8 \text{ TeV}$ for evidence of third generation squarks by combining a large number of searches covering various final states. Stop decays with and without charginos in the decay chain are considered and summaries of all ATLAS Run 1 searches for direct stop production can be found in Fig. 4 (no intermediate charginos) and Fig. 7 (intermediate charginos). Limits are set on stop masses in compressed mass regions, with $B(\tilde{t} \rightarrow c\tilde{\chi}_1^0) + B(\tilde{t} \rightarrow b\tilde{t}'\tilde{\chi}_1^0) = 1$, see Fig. 5. Limits are also set on stop masses assuming that both the decay $\tilde{t} \rightarrow t\tilde{\chi}_1^0$ and $\tilde{t} \rightarrow b\tilde{\chi}_1^{\pm}$ are possible, with both their branching ratios summing up to 1, assuming $\tilde{\chi}_1^{\pm} \rightarrow W^{(*)}\tilde{\chi}_1^0$ and $m_{\tilde{\chi}_1^{\pm}} = 2 m_{\tilde{\chi}_1^0}$, see Fig. 6. Limits on the mass of the next-to-lightest stop \tilde{t}_2 , decaying either to $Z\tilde{t}_1$, $h\tilde{t}_1$ or $t\tilde{\chi}_1^0$, are also presented, see Figs. 9 and 10. Interpretations in the pMSSM are also discussed, see Figs 13–15.
- 67 AAD 15J interpreted the measurement of spin correlations in $\tilde{t}\tilde{t}$ production using 20.3 fb^{-1} of pp collisions at $\sqrt{s} = 8 \text{ TeV}$ in exclusion limits on the pair production of light \tilde{t}_1 squarks with masses similar to the top quark mass. The \tilde{t}_1 is assumed to decay through $\tilde{t}_1 \rightarrow t\tilde{\chi}_1^0$ with predominantly right-handed top and a 100% branching ratio. The data are found to be consistent with the Standard Model expectations and masses between the top quark mass and 191 GeV are excluded, see their Fig. 2.
- 68 KHACHATRYAN 15AF searched in 19.5 fb^{-1} of pp collisions at $\sqrt{s} = 8 \text{ TeV}$ for events with at least two energetic jets and significant \cancel{E}_T , using the transverse mass variable M_{T2} to discriminate between signal and background processes. No significant excess above the Standard Model expectations is observed. Limits are set on the stop mass in simplified models where the decay $\tilde{t} \rightarrow t\tilde{\chi}_1^0$ takes place with a branching ratio of 100%, see Fig. 12. See also Table 5. Exclusions in the CMSSM, assuming $\tan\beta = 30$, $A_0 = -2 \max(m_0, m_{1/2})$ and $\mu > 0$, are also presented, see Fig. 15.
- 69 KHACHATRYAN 15AH searched in 19.4 or 19.7 fb^{-1} of pp collisions at $\sqrt{s} = 8 \text{ TeV}$ for events containing either a fully reconstructed top quark, or events containing dijets requiring one or both jets to originate from b -quarks, or events containing a mono-jet. No significant excess above the Standard Model expectations is observed. Limits are set on the stop mass in simplified models where the decay $\tilde{t} \rightarrow t\tilde{\chi}_1^0$ takes place with a branching ratio of 100%, see Fig. 9. Limits are also set in simplified models where the decays $\tilde{t} \rightarrow t\tilde{\chi}_1^0$ and $\tilde{t} \rightarrow b\tilde{\chi}_1^{\pm}$, with $m_{\tilde{\chi}_1^{\pm}} - m_{\tilde{\chi}_1^0} = 5 \text{ GeV}$, each take place with a branching ratio of 50%, see Fig. 10, or with other fractions, see Fig. 11. Finally, limits are set in a simplified model where the decay $\tilde{t} \rightarrow c\tilde{\chi}_1^0$ takes place with a branching ratio of 100%, see Figs. 9, 10 and 11.
- 70 KHACHATRYAN 15AH searched in 19.4 or 19.7 fb^{-1} of pp collisions at $\sqrt{s} = 8 \text{ TeV}$ for events containing either a fully reconstructed top quark, or events containing dijets requiring one or both jets to originate from b -quarks, or events containing a mono-jet. No significant excess above the Standard Model expectations is observed. Limits are set on the stop mass in simplified models where the decay $\tilde{t} \rightarrow t\tilde{\chi}_1^0$ takes place with a branching ratio of 100%, see Fig. 9. Limits are also set in simplified models where the decays $\tilde{t} \rightarrow t\tilde{\chi}_1^0$ and $\tilde{t} \rightarrow b\tilde{\chi}_1^{\pm}$, with $m_{\tilde{\chi}_1^{\pm}} - m_{\tilde{\chi}_1^0} = 5 \text{ GeV}$, each take place with a branching ratio of 50%, see Fig. 10, or with other fractions, see Fig. 11. Finally, limits are set in a simplified model where the decay $\tilde{t} \rightarrow c\tilde{\chi}_1^0$ takes place with a branching ratio of 100%, see Figs. 9, 10, and 11.
- 71 KHACHATRYAN 15x searched in 19.3 fb^{-1} of pp collisions at $\sqrt{s} = 8 \text{ TeV}$ for events with at least two energetic jets, at least one of which is required to originate from a b quark, possibly a lepton, and significant \cancel{E}_T , using the razor variables (M_R and R^2) to discriminate between signal and background processes. No significant excess above the Standard Model expectations is observed. Limits are set on the stop mass in simplified models where the decay $\tilde{t} \rightarrow t\tilde{\chi}_1^0$ and the decay $\tilde{t} \rightarrow b\tilde{\chi}_1^{\pm}$, with $m_{\tilde{\chi}_1^{\pm}} - m_{\tilde{\chi}_1^0} = 5 \text{ GeV}$, take place with branching ratios varying between 0 and 100%, see Figs. 15, 16 and 17.
- 72 AAD 14AJ searched in 20.1 fb^{-1} of pp collisions at $\sqrt{s} = 8 \text{ TeV}$ for events containing four or more jets and large missing transverse momentum. No excess of events above

Searches Particle Listings

Supersymmetric Particle Searches

- the expected level of Standard Model background was found. Exclusion limits at 95% C.L. are set on the masses of third-generation squarks in simplified models which either assume that the decay $\tilde{t}_1 \rightarrow t\tilde{\chi}_1^0$ takes place 100% of the time, see Fig. 8, or that this decay takes place 50% of the time, while the decay $\tilde{t}_1 \rightarrow b\tilde{\chi}_1^\pm$ takes place the other 50% of the time, see Fig. 9.
- ⁷³ AAD 14BD searched in 20 fb⁻¹ of pp collisions at $\sqrt{s} = 8$ TeV for events containing one isolated lepton, jets and large missing transverse momentum. No excess of events above the expected level of Standard Model background was found. Exclusion limits at 95% C.L. are set on the masses of third-generation squarks in simplified models which either assume that the decay $\tilde{t}_1 \rightarrow t\tilde{\chi}_1^0$ takes place 100% of the time, see Fig. 15, or the decay $\tilde{t}_1 \rightarrow b\tilde{\chi}_1^\pm$ takes place 100% of the time, see Fig. 16–22. For the mixed decay scenario, see Fig. 23.
- ⁷⁴ AAD 14F searched in 20.3 fb⁻¹ of pp collisions at $\sqrt{s} = 8$ TeV for events containing two leptons (e or μ), and possibly jets and missing transverse momentum. No excess of events above the expected level of Standard Model background was found. Exclusion limits at 95% C.L. are set on the masses of third-generation squarks in simplified models which either assume that the decay $\tilde{t}_1 \rightarrow b\tilde{\chi}_1^\pm$ takes place 100% of the time, see Figs. 14–17 and 20, or that the decay $\tilde{t}_1 \rightarrow t\tilde{\chi}_1^0$ takes place 100% of the time, see Figs. 18 and 19.
- ⁷⁵ AAD 14T searched in 20.3 fb⁻¹ of pp collisions at $\sqrt{s} = 8$ TeV for monojet-like and c -tagged events. No excess of events above the expected level of Standard Model background was found. Exclusion limits at 95% C.L. are set on the masses of third-generation squarks in simplified models which assume that the decay $\tilde{t}_1 \rightarrow c\tilde{\chi}_1^0$ takes place 100% of the time, see Fig. 9 and 10. The results of the monojet-like analysis are also interpreted in terms of stop pair production in the four-body decay $\tilde{t}_1 \rightarrow bff'\tilde{\chi}_1^0$, see Fig. 11.
- ⁷⁶ CHATRCHYAN 14AH searched in 4.7 fb⁻¹ of pp collisions at $\sqrt{s} = 7$ TeV for events with at least two energetic jets and significant \cancel{E}_T , using the razor variables (M_R and R^2) to discriminate between signal and background processes. A second analysis requires at least one of the jets to be originating from a b -quark. No significant excess above the Standard Model expectations is observed. Limits are set on sbottom masses in simplified models where the decay $\tilde{t} \rightarrow t\tilde{\chi}_1^0$ takes place with a branching ratio of 100%, see Figs. 28 and 29. Exclusions in the CMSSM, assuming $\tan\beta = 10$, $A_0 = 0$ and $\mu > 0$, are also presented, see Fig. 26.
- ⁷⁷ CHATRCHYAN 14R searched in 19.5 fb⁻¹ of pp collisions at $\sqrt{s} = 8$ TeV for events with at least three leptons (electrons, muons, taus) in the final state. No significant excess above the Standard Model expectations is observed. Limits are set on the stop mass in a natural higgsino NLSP simplified model (GMSB) where the decay $\tilde{t} \rightarrow b\tilde{\chi}_1^\pm$, with $\tilde{\chi}_1^\pm \rightarrow (qq'/\ell\nu)H$, $Z\tilde{G}$, takes place with a branching ratio of 100% (the particles between brackets have a soft p_T spectrum), see Figs. 4–6.
- ⁷⁸ AABOUD 17AF searched in 36 fb⁻¹ of pp collisions at $\sqrt{s} = 13$ TeV for evidence of top squarks in events containing 2 leptons, jets, b -jets and \cancel{E}_T . In Tstop6 model, assuming $m_{\tilde{\chi}_1^0} = 0$ GeV, \tilde{t}_1 masses up to 850 GeV are excluded for $m_{\tilde{\chi}_2^0} > 200$ GeV.
- ⁷⁹ AABOUD 17AF searched in 36 fb⁻¹ of pp collisions at $\sqrt{s} = 13$ TeV for evidence of \tilde{t}_2 in events containing 2 leptons, jets, b -jets and \cancel{E}_T . In Tstop7 model, assuming $m_{\tilde{\chi}_1^0} = 50$ GeV and 100% decays via Z boson, \tilde{t}_2 masses up to 800 GeV are excluded. Exclusion limits are also shown as a function of the \tilde{t}_2 branching ratios in their Figure 7.
- ⁸⁰ AABOUD 17AF searched in 36 fb⁻¹ of pp collisions at $\sqrt{s} = 13$ TeV for evidence of \tilde{t}_2 in events containing 2 leptons, jets, b -jets and \cancel{E}_T . In Tstop7 model, assuming $m_{\tilde{\chi}_1^0} = 50$ GeV and 100% decays via higgs boson, \tilde{t}_2 masses up to 880 GeV are excluded. Exclusion limits are also shown as a function of the \tilde{t}_2 branching ratios in their Figure 7.
- ⁸¹ AABOUD 17AY searched in 36.1 fb⁻¹ of pp collisions at $\sqrt{s} = 13$ TeV for events with at least four jets and large missing transverse momentum. No significant excess above the Standard Model expectations is observed. Limits are set on the top squark mass assuming three pMSSM-inspired models. The first one, referred to as Higgsino LSP model, assumes $m_{\tilde{\chi}_1^\pm} - m_{\tilde{\chi}_1^0} = 5$ GeV and $m_{\tilde{\chi}_2^0} - m_{\tilde{\chi}_1^0} = 10$ GeV, with a mixture of decay modes as in Tstop1, Tstop2 and Tstop6. See their Figure 10. The second and third models are referred to as Wino NLSP and well-tempered pMSSM models, respectively. See their Figure 11 and Figure 12, and text for details on assumptions.
- ⁸² AAD 14B searched in 20.3 fb⁻¹ of pp collisions at $\sqrt{s} = 8$ TeV for events containing a Z boson, with or without additional leptons, plus jets originating from b -quarks and significant missing transverse momentum. No excess over the expected SM background is observed. Limits are derived in simplified models featuring \tilde{t}_2 production, with $\tilde{t}_2 \rightarrow Z\tilde{t}_1$, $\tilde{t}_1 \rightarrow t\tilde{\chi}_1^0$ with a 100% branching ratio, see Fig. 4, and in the framework of natural GMSB, see Fig. 6.
- ⁸³ CHATRCHYAN 14U searched in 19.7 fb⁻¹ of pp collisions at $\sqrt{s} = 8$ TeV for evidence of direct pair production of top squarks, with Higgs bosons in the decay chain. The search is performed using a selection of events containing two Higgs bosons, each decaying to a photon pair, missing transverse energy and possibly b -quark jets. No significant excesses over the expected SM backgrounds are observed. The results are interpreted in the context of a “natural SUSY” simplified model where the decays $\tilde{t}_1 \rightarrow b\tilde{\chi}_1^\pm$, with $\tilde{\chi}_1^\pm \rightarrow ff'\tilde{\chi}_1^0$, and $\tilde{\chi}_1^0 \rightarrow H\tilde{G}$, all happen with 100% branching ratio, see Fig. 4.
- ⁸⁴ KHACHATRYAN 14C searched in 19.5 fb⁻¹ of pp collisions at $\sqrt{s} = 8$ TeV for evidence of direct pair production of top squarks, with Higgs or Z -bosons in the decay chain. The search is performed using a selection of events containing leptons and b -quark jets. No significant excesses over the expected SM backgrounds are observed. The results are interpreted in the context of a simplified model with pair production of a heavier top-squark mass eigenstate \tilde{t}_2 decaying to a lighter top-squark eigenstate \tilde{t}_1 via either $\tilde{t}_2 \rightarrow H\tilde{t}_1$ or $\tilde{t}_2 \rightarrow Z\tilde{t}_1$, followed in both cases by $\tilde{t}_1 \rightarrow t\tilde{\chi}_1^0$. The interpretation is performed in the region where the mass difference between the \tilde{t}_1 and $\tilde{\chi}_1^0$ is approximately equal to the top-quark mass, which is not probed by searches for direct \tilde{t}_1 pair production, see Figs. 5 and 6. The analysis excludes top squarks with masses $m_{\tilde{t}_2} < 575$ GeV and $m_{\tilde{t}_1} < 400$ GeV at 95% C.L.

R-parity violating \tilde{t} (Stop) mass limit

VALUE (GeV)	CL%	DOCUMENT ID	TECN	COMMENT
>1100	95	¹ AAD	21BF ATLS	$\ell^\pm + b$ -jets + many jets, Tstop14, $\lambda_{323}^{\prime\prime}$ electroweakino decay, 500 GeV $< m_{\tilde{\chi}_1^0} < 800$ GeV
>1150	95	¹ AAD	21BF ATLS	$\ell^\pm + b$ -jets + many jets, Tstop15, $\lambda_{323}^{\prime\prime}$ electroweakino decay, 600 GeV $< m_{\tilde{\chi}_1^0} < 900$ GeV
>1300	95	¹ AAD	21BF ATLS	$\ell^\pm + b$ -jets + many jets, Tstop1, $\lambda_{323}^{\prime\prime}$ electroweakino decay, 500 GeV $< m_{\tilde{\chi}_1^0} < 1000$ GeV
>1600	95	² SIRUNYAN	21AF CMS	long-lived \tilde{t} , $\tilde{t} \rightarrow \overline{d}d$, $\lambda_{313}^{\prime\prime}$ coupling, 0.4 mm $< c\tau < 80$ mm
>1600	95	³ SIRUNYAN	21U CMS	long-lived \tilde{t} , $\tilde{t} \rightarrow b\bar{t}$, 5 $< c\tau < 240$ mm
>1600	95	³ SIRUNYAN	21U CMS	long-lived \tilde{t} , $\tilde{t} \rightarrow d\bar{t}$, $\lambda_{331}^{\prime\prime}$ coupling, 3 $< c\tau < 360$ mm
>1600	95	³ SIRUNYAN	21U CMS	long-lived \tilde{t} , $\tilde{t} \rightarrow \overline{d}d$, $\eta_{111}^{\prime\prime}$ coupling, 2 $< c\tau < 1320$ mm
> 670	95	⁴ SIRUNYAN	21V CMS	$\ell^\pm + \geq 7$ jets, Tstop1 with $\tilde{\chi}_1^0 \rightarrow qq, \lambda_{abc}^{\prime\prime}$ coupling, $a,b,c \in 1,2$
> 870	95	⁴ SIRUNYAN	21V CMS	$\ell^\pm + \geq 7$ jets, stealth SYY model
>1700	95	⁵ AAD	20M ATLS	$\tilde{t} \rightarrow q\mu$, long-lived, Tstop3RPV, $\tau = 0.1$ ns
>1150	95	⁶ SIRUNYAN	19Bi ATLS	$\tilde{t} \rightarrow b\mu$, long-lived, Tstop2RPV, $c\tau = 0.1$ cm
>1100	95	⁷ SIRUNYAN	19Bj CMS	$\tilde{t} \rightarrow be$, Tstop2RPV, prompt
none 100–410	95	⁸ AABOUD	18BB ATLS	4 jets, Tstop1RPV with $\tilde{t} \rightarrow d, s, \lambda_{12}^{\prime\prime}$ coupling
none 100–470, 480–610	95	⁹ AABOUD	18BB ATLS	4 jets, Tstop1RPV, $\lambda_{323}^{\prime\prime}$ coupling
≥ 600 –1500	95	¹⁰ AABOUD	18P ATLS	$2\ell + b$ -jets, Tstop2RPV, depending on $\lambda_{333}^{\prime\prime}$ coupling ($i = 1, 2, 3$)
>1130	95	¹¹ SIRUNYAN	18AD CMS	$\tilde{t} \rightarrow b\ell$, long-lived, $c\tau = 70$ –100 mm
> 550	95	¹¹ SIRUNYAN	18AD CMS	$\tilde{t} \rightarrow b\ell$, long-lived, $c\tau = 1$ –1000 mm
>1400	95	¹² SIRUNYAN	18Dv CMS	long-lived \tilde{t} , $\tilde{t} \rightarrow \overline{d}d$, 0.6 mm $< c\tau < 80$ mm
none 80–520	95	¹³ SIRUNYAN	18Dy CMS	2, 4 jets, Tstop3RPV, $\lambda_{312}^{\prime\prime}$ coupling
none 80–270, 285–340, 400–525	95	¹³ SIRUNYAN	18Dy CMS	2, 4 jets, Tstop1RPV, $\lambda_{323}^{\prime\prime}$ coupling
>1200	95	¹⁴ AABOUD	17Ai ATLS	$\geq 1\ell + \geq 8$ jets, Tstop1 with $\tilde{\chi}_1^0 \rightarrow tbs$, $\lambda_{323}^{\prime\prime}$ coupling, $m_{\tilde{\chi}_1^0} = 500$ GeV
none, 100–315	95	¹⁵ AAD	16AMATLS	2 large-radius jets, Tstop1RPV
none, 200–350	95	¹⁶ KHACHATRY...15L	CMS	$\tilde{t} \rightarrow qq$, $\lambda_{312}^{\prime\prime} \neq 0$
none, 200–385	95	¹⁶ KHACHATRY...15L	CMS	$\tilde{t} \rightarrow qb$, $\lambda_{323}^{\prime\prime} \neq 0$
> 740	95	¹⁷ KHACHATRY...14T	CMS	$\tau + b$ -jets, $LQ\overline{D}$, $\lambda_{333}^{\prime\prime} \neq 0$, $\tilde{t} \rightarrow \tau b$ simplified model
> 580	95	¹⁷ KHACHATRY...14T	CMS	$\tau + b$ -jets, $LQ\overline{D}$, $\lambda_{3jk}^{\prime\prime} \neq 0$ ($j \neq 3$), $\tilde{t} \rightarrow \tilde{\chi}_1^\pm b$, $\tilde{\chi}_1^\pm \rightarrow qq\tau^\pm$ simplified model
••• We do not use the following data for averages, fits, limits, etc. •••				
> 770	95	¹⁸ AAD	21B ATLS	≥ 8 jets, ≥ 5 b -jets, Tstop4RPV
> 890	95	¹⁹ KHACHATRY...16AC	CMS	$e^+e^- + \geq 5$ jets; $\tilde{t} \rightarrow b\tilde{\chi}_1^\pm$; $\tilde{\chi}_1^\pm \rightarrow \ell^\pm jj$, $\lambda_{ijk}^{\prime\prime}$
>1000	95	¹⁹ KHACHATRY...16AC	CMS	$\mu^+\mu^- + \geq 5$ jets; $\tilde{t} \rightarrow b\tilde{\chi}_1^\pm$; $\tilde{\chi}_1^\pm \rightarrow \ell^\pm jj$, $\lambda_{ijk}^{\prime\prime}$
> 950	95	²⁰ KHACHATRY...16BX	CMS	$\tilde{t} \rightarrow t\tilde{\chi}_1^0, \tilde{\chi}_1^0 \rightarrow \ell\nu, \lambda_{121}$ or $\lambda_{122} \neq 0$
> 790	95	²¹ KHACHATRY...15E	CMS	$\tilde{t}_1 \rightarrow b\ell$, $c\tau = 2$ cm

¹ AAD 21BF searched in 139 fb⁻¹ of pp collisions at $\sqrt{s} = 13$ TeV for pair production of gluinos, stops, electroweakinos decaying RPV either directly or indirectly via the LSP. The final state in all cases is one or two leptons, many jets (up to fifteen) and b -jets. Different models with different branching fractions of the gluino or stop follow from the assumptions on the nature of the electroweakinos. No significant excess above the Standard Model predictions is observed. Limits are set on the $gluino$, \tilde{t}_1 , electroweakino masses as a function of the $\tilde{\chi}_1^0$ mass in several scenarios of gluino, stop and electroweakino pair production.

- 2 SIRUNYAN 21AF searched in 140 fb^{-1} of pp collisions at $\sqrt{s} = 13 \text{ TeV}$ for supersymmetry in events with two displaced vertices from long-lived particles decaying into multijet or dijet final states. No significant excess above the Standard Model expectations is observed. Limits are set on the gluino mass in the simplified model Tglu2RPV with λ''_{323} coupling, on the $\tilde{\chi}_1^0$ mass in an RPV model with $\tilde{\chi}_1^0$ pair production and the RPV decay $\tilde{\chi}_1^0 \rightarrow tbs$ with λ''_{323} coupling and on the \tilde{t} mass in an RPV model with top squark pair production and the RPV decay $\tilde{t} \rightarrow \bar{d}_i \bar{d}_j$ with λ''_{3ij} coupling, see their Figure 7.
- 3 SIRUNYAN 21u searched in 132 fb^{-1} of pp collisions at $\sqrt{s} = 13 \text{ TeV}$ for supersymmetry in events with displaced tracks and displaced vertices associated with a dijet system. No significant excess above the Standard Model expectations is observed. Limits are set on long-lived gluinos in an RPC GMSB SUSY model of gluino pair production, with $\tilde{g} \rightarrow gG$, see their Figure 9, in Tglu1A in a mini-split model, see their Figure 10, and in an RPV model of gluino pair production, with $\tilde{g} \rightarrow tbs$ with coupling λ''_{323} , see their Figure 11. Limits are also set on long-lived top squarks in Tstop2RPV, see their Figure 12, in an RPV model with $\tilde{t} \rightarrow d\bar{d}$ and λ''_{331} coupling, see their Figure 13, and in a dynamical RPV model with $\tilde{t} \rightarrow \bar{d}\bar{d}$ via a nonholomorphic RPV coupling λ''_{311} , see their Figure 14. The best mass limit is achieved in all cases at $c\tau = 30 \text{ mm}$.
- 4 SIRUNYAN 21v searched in 137 fb^{-1} of pp collisions at $\sqrt{s} = 13 \text{ TeV}$ for supersymmetry in events with one charged lepton (e^\pm or μ^\pm) and ≥ 7 jets. No significant excess above the Standard Model expectations is observed. Limits are set on an RPV SUSY model like Tstop1 with the additional decay $\tilde{\chi}_1^0 \rightarrow qq\bar{q}$ with coupling λ''_{abc} , with $a, b, c \in 1, 2$, and on a stealth SUSY model called SY, with one scalar particle \tilde{S} with even R-parity and its superpartner \tilde{S} , both singlets under all SM interactions, and with a portal mediated by loop interactions involving a new vectorlike messenger field (Y), where pair produced top squarks decay as $\tilde{t} \rightarrow t\tilde{S}$, and $\tilde{S} \rightarrow G\tilde{S}$, and $\tilde{S} \rightarrow g\tilde{g}$, see their Figure 6 and 7.
- 5 AAD 20M searched for long-lived particles decaying into hadrons and at least one muon in events containing a displaced muon track and a displaced vertex. The analysis uses a dataset of pp collisions at $\sqrt{s} = 13 \text{ TeV}$ corresponding to an integrated luminosity of 136 fb^{-1} . Using the Tstop3RPV simplified model, top squarks with masses up to 1.7 TeV are excluded for a lifetime of 0.1 ns , and masses below 1.3 TeV are excluded for lifetimes between 0.01 ns and 30 ns , see their Figure 7. The dependence on the RPV coupling λ''_{23k} multiplied by $\cos\theta_{\tilde{t}}$, with $\theta_{\tilde{t}}$ the mixing angle between the left- and right-handed \tilde{t} squarks, is also shown, see their Fig. 7.
- 6 SIRUNYAN 19Bi searched in 35.9 fb^{-1} of pp collisions at $\sqrt{s} = 13 \text{ TeV}$ in final states with two muons and two jets, or with one muon, two jets, and missing transverse momentum. Limits are set in a model of pair-produced, prompt or long-lived top squarks with R-parity violating decays to a b -quark and a lepton (Tstop2RPV), branching fraction of $\tilde{t} \rightarrow b\mu$ equal to $1/3$ and $c\tau$ between 0.1 cm and 10 cm in the case of long-lived top squarks. See their Fig. 10.
- 7 SIRUNYAN 19Bj searched in 35.9 fb^{-1} of pp collisions at $\sqrt{s} = 13 \text{ TeV}$ in final states with two electrons and two jets, or with one electron, two jets, and missing transverse momentum. Limits are set in a model of pair-produced, prompt top squarks with R-parity violating decays to a b -quark and a lepton (Tstop2RPV), assuming branching fraction of $\tilde{t} \rightarrow be$ equal to $1/3$ and $c\tau = 0 \text{ cm}$. See their Fig. 10.
- 8 AABOUD 18BB searched in 36.7 fb^{-1} of pp collisions at $\sqrt{s} = 13 \text{ TeV}$ for massive coloured resonances which are pair-produced and decay into two jets. No significant deviation from the background prediction is observed. Results are interpreted in a SUSY simplified model as Tstop1RPV with $\tilde{t} \rightarrow d\bar{s}$. Top squarks with masses in the range $100\text{--}410 \text{ GeV}$ are excluded, see their Figure 9(a). The λ''_{312} coupling is assumed to be sufficiently large for the decays to be prompt, but small enough to neglect the single-top-squark resonant production through RPV couplings.
- 9 AABOUD 18BB searched in 36.7 fb^{-1} of pp collisions at $\sqrt{s} = 13 \text{ TeV}$ for massive coloured resonances which are pair-produced and decay into two jets. No significant deviation from the background prediction is observed. Results are interpreted in Tstop1RPV. Top squarks with masses in the range $100\text{--}470 \text{ GeV}$ or $480\text{--}610 \text{ GeV}$ are excluded, see their Figure 9(b). The λ''_{323} coupling is assumed to be sufficiently large for the decays to be prompt, but small enough to neglect the single-top-squark resonant production through RPV couplings.
- 10 AABOUD 18P searched in 36.1 fb^{-1} of pp collisions at $\sqrt{s} = 13 \text{ TeV}$ for pair-produced top squarks that decay through RPV λ''_{i33} ($i = 1, 2, 3$) couplings to a final state with two leptons and two jets, at least one of which is identified as a b -jet. No significant excess is observed over the SM background. In the Tstop2RPV model, lower limits on the top squark masses between 600 and 1500 GeV are set depending on the branching fraction to be , $b\mu$, and $b\tau$ final states. See their Figs 6 and 7.
- 11 SIRUNYAN 18AD searched in 2.6 fb^{-1} of pp collisions at $\sqrt{s} = 13 \text{ TeV}$ for long-lived particles by exploiting the multiplicity of displaced jets to search for the presence of signal decays occurring at distances between 1 and 1000 mm . Limits are set in a model of pair-produced, long-lived top squarks with R-parity violating decays to a b -quark and a lepton, see their Figure 3.
- 12 SIRUNYAN 18Dv searched in 38.5 fb^{-1} of pp collisions at $\sqrt{s} = 13 \text{ TeV}$ for long-lived particles in events with multiple jets and two displaced vertices composed of many tracks. No events with two well-separated high-track-multiplicity vertices were observed. Limits are set on the stop and the gluino mass in RPV models of supersymmetry where the stop (gluino) is decaying solely into dijet (multijet) final states, see their Figures 6 and 7.
- 13 SIRUNYAN 18Dv searched in 35.9 fb^{-1} of pp collisions at $\sqrt{s} = 13 \text{ TeV}$ for the pair production of resonances, each decaying to two quarks. The search is conducted separately in a boosted (two-jet) and resolved (four-jet) jet topology. The mass spectra are found to be consistent with the Standard Model expectations. Limits are set on the stop mass in the Tstop3RPV and Tstop1RPV simplified models, see their Figure 11.
- 14 AABOUD 17AI searched in 36.1 fb^{-1} of pp collisions at $\sqrt{s} = 13 \text{ TeV}$ for events with one or more isolated lepton, at least eight jets, either zero or many b -jets, for evidence of R-parity violating decays of the top squark. No significant excess above the Standard Model expectations is observed. Limits up to 1.25 (1.10) TeV are set on the top squark mass in R-parity-violating supersymmetry models where \tilde{t}_1 decays for a bino LSP as: $\tilde{t} \rightarrow t\tilde{\chi}_1^0$ and for a higgsino LSP as $\tilde{t} \rightarrow t\tilde{\chi}_{1,2}^0/b\tilde{\chi}_1^+$. These is followed by the decays through the non-zero λ''_{323} coupling $\tilde{\chi}_{1,2}^0 \rightarrow tbs$, $\tilde{\chi}_1^+ \rightarrow bbs$. See their Figure 10 and text for details on model assumptions.
- 15 AAD 16AM searched in 17.4 fb^{-1} of pp collisions at $\sqrt{s} = 8 \text{ TeV}$ for events containing two large-radius hadronic jets. No deviation from the background prediction is observed. Top squarks with masses between 100 and 315 GeV are excluded at 95% C.L. in the

- hypothesis that they both decay via R-parity violating coupling λ''_{323} to b - and s -quarks. See their Fig. 10.
- 16 KHACHATRYAN 15L searched in 19.4 fb^{-1} of pp collisions at $\sqrt{s} = 8 \text{ TeV}$ for pair production of heavy resonances decaying to pairs of jets in four jet events. No significant excess above the Standard Model expectations is observed. Limits are set on the stop mass in R-parity-violating supersymmetry models where $\tilde{t} \rightarrow qq$ ($\lambda''_{312} \neq 0$), see Fig. 6 (top) and $\tilde{t} \rightarrow qb$ ($\lambda''_{323} \neq 0$), see Fig. 6 (bottom).
- 17 KHACHATRYAN 14T searched in 19.7 fb^{-1} of pp collisions at $\sqrt{s} = 8 \text{ TeV}$ for events with τ -leptons and b -quark jets, possibly with extra light-flavour jets. No excess above the Standard Model expectations is observed. Limits are set on stop masses in RPV SUSY models with $LQ\bar{D}$ couplings, in two simplified models. In the first model, the decay $\tilde{t} \rightarrow \tau b$ is considered, with $\lambda''_{333} \neq 0$, see Fig. 3. In the second model, the decay $\tilde{t} \rightarrow \tilde{\chi}^\pm b$, with the subsequent decay $\tilde{\chi}^\pm \rightarrow qq\tau^\pm$ is considered, with $\lambda''_{3jk} \neq 0$ and the mass splitting between the top squark and the charging chosen to be 100 GeV , see Fig. 4.
- 18 AAD 21B searched in 139 fb^{-1} of pp collisions at $\sqrt{s} = 13 \text{ TeV}$ for events with at least eight jets and at least 5 b -jets, for evidence of R-parity violating decays of the top squark. No significant excess above the Standard Model expectations is observed. Limits up to 950 GeV are set on the top squark mass in Tstop4RPV simplified model. See their Figure 7 for more detailed mass bounds.
- 19 KHACHATRYAN 16AC searched in 19.7 fb^{-1} of pp collisions at $\sqrt{s} = 8 \text{ TeV}$ for events with low missing transverse momentum, two oppositely charged electrons or muons, and at least five jets, at least one of which is a b -jet, for evidence of R-parity violating, charging-mediated decays of the top squark. No significant excess above the Standard Model expectations is observed. Limits are set on the stop mass in R-parity-violating supersymmetry models where $\tilde{t} \rightarrow b\tilde{\chi}_1^\pm$ with $\tilde{\chi}_1^\pm \rightarrow e^\pm jj$, $\lambda''_{ijk} \neq 0$ ($i, j, k \leq 2$), and with $m_{\tilde{t}} - m_{\tilde{\chi}_1^\pm} = 100 \text{ GeV}$, see Fig. 3.
- 20 KHACHATRYAN 16BX searched in 19.5 fb^{-1} of pp collisions at $\sqrt{s} = 8 \text{ TeV}$ for events containing 4 leptons coming from R-parity-violating decays of $\tilde{\chi}_1^0 \rightarrow \ell\ell\nu$ with $\lambda_{121} \neq 0$ or $\lambda_{122} \neq 0$. No excess over the expected background is observed. Limits are derived on the gluino, squark and stop masses, see Fig. 23.
- 21 KHACHATRYAN 15E searched for long-lived particles decaying to leptons in 19.7 fb^{-1} of pp collisions at $\sqrt{s} = 8 \text{ TeV}$. Events were selected with an electron and muon with opposite charges and each with transverse impact parameter values between 0.02 and 2 cm . Limits are set on SUSY benchmark models with pair production of top squarks decaying into an $e\mu$ final state via RPV interactions. See their Fig. 2

Heavy \tilde{g} (Gluino) mass limit

For $m_{\tilde{g}} > 60\text{--}70 \text{ GeV}$, it is expected that gluinos would undergo a cascade decay via a number of neutralinos and/or charginos rather than undergo a direct decay to photons as assumed by some papers. Limits obtained when direct decay is assumed are usually higher than limits when cascade decays are included.

Some earlier papers are now obsolete and have been omitted. They were last listed in our PDG 14 edition: K. Olive, *et al.* (Particle Data Group), Chinese Physics **C38** 070001 (2014) (<http://pdg.lbl.gov>).

R-parity conserving heavy \tilde{g} (Gluino) mass limit

VALUE (GeV)	CL%	DOCUMENT ID	TECN	COMMENT
>2200	95	1 AAD	21AK ATLS	$\ell^\pm + \text{jets} + \cancel{E}_T$, Tglu1B, $m_{\tilde{\chi}_1^\pm} = (m_{\tilde{g}} + m_{\tilde{\chi}_1^0})/2$, $m_{\tilde{\chi}_1^0} < 400 \text{ GeV}$
none	95	1 AAD	21AK ATLS	$\ell^\pm + \text{jets} + \cancel{E}_T$, Tglu1B, $m_{\tilde{\chi}_1^\pm} = (m_{\tilde{g}} + m_{\tilde{\chi}_1^0})/2$, $m_{\tilde{\chi}_1^0} < 1000 \text{ GeV}$
>2300	95	2 AAD	21L ATLS	$\text{jets} + \cancel{E}_T$, Tglu1A, $m_{\tilde{\chi}_1^0} < 200 \text{ GeV}$
>3000	95	2 AAD	21L ATLS	$\text{jets} + \cancel{E}_T$, combined $\tilde{g}\tilde{g}$, $\tilde{g}\tilde{q}$, $\tilde{q}\tilde{q}$ production, $\tilde{g} \rightarrow qd\tilde{\chi}_1^0$, $\tilde{q} \rightarrow q\tilde{\chi}_1^0$, $m_{\tilde{q}} = m_{\tilde{g}}$, $m_{\tilde{\chi}_1^0} = 0 \text{ GeV}$
>2200	95	2 AAD	21L ATLS	$\text{jets} + \cancel{E}_T$, Tglu1B, $m_{\tilde{\chi}_1^0} = 0 \text{ GeV}$
>1400	95	3 AAD	21X ATLS	jets in empty bunch crossings, Tglu1A, long-lived R-hadron, $m_{\tilde{\chi}_1^0} = 100 \text{ GeV}$, $10^{-5} < \tau_{\text{R-hadron}} < 10^3 \text{ s}$
> 870	95	3 AAD	21X ATLS	jets in empty bunch crossings, Tglu1A, long-lived R-hadron, $m_{\tilde{g}} - m_{\tilde{\chi}_1^0} = 100 \text{ GeV}$, $10^{-5} < \tau_{\text{R-hadron}} < 10^3 \text{ s}$
>2260	95	4 SIRUNYAN	21AD CMS	$\text{jets} + \cancel{E}_T$, Tglu3A, $m_{\tilde{\chi}_1^0} < 1050 \text{ GeV}$
>2150	95	4 SIRUNYAN	21AD CMS	$\text{jets} + \cancel{E}_T$, Tglu3C, $m_{\tilde{\chi}_1^0} = 600 \text{ GeV}$, $m_{\tilde{t}} - m_{\tilde{\chi}_1^0} = 20 \text{ GeV}$
>2250	95	4 SIRUNYAN	21AD CMS	$\text{jets} + \cancel{E}_T$, Tglu3D, $m_{\tilde{\chi}_1^0} = 700 \text{ GeV}$, $m_{\tilde{\chi}_1^\pm} - m_{\tilde{\chi}_1^0} = 5 \text{ GeV}$
>1870	95	5 SIRUNYAN	21M CMS	$\ell^\pm \ell^\mp + \cancel{E}_T$, Tglu4C, $m_{\tilde{\chi}_1^0} = 1100 \text{ GeV}$

Searches Particle Listings

Supersymmetric Particle Searches

>1980	95	6	AAD	20AL ATLS	8 or more jets + \cancel{E}_T , Tglu1E, $m_{\tilde{\chi}_1^0} = 100$ GeV		>1970	95	19	AABOUD	18AR ATLS	jets+ $\geq 3b$ -jets+ \cancel{E}_T , Tglu3A, $m_{\tilde{\chi}_1^0} < 300$ GeV
>1820	95	6	AAD	20AL ATLS	8 or more jets + \cancel{E}_T , Tglu3A, $m_{\tilde{\chi}_1^0} = 100$ GeV		>1920	95	20	AABOUD	18AR ATLS	jets+ $\geq 3b$ -jets+ \cancel{E}_T , Tglu2A, $m_{\tilde{\chi}_1^0} < 600$ GeV
>1600	95	7	AAD	20V ATLS	same-sign $\ell^\pm \ell^\pm$ + jets, Tglu1E, $m_{\tilde{\chi}_1^0} = 100$ GeV		>1650	95	21	AABOUD	18As ATLS	≥ 4 jets and disappearing tracks from $\tilde{\chi}^\pm \rightarrow \tilde{\chi}_1^0 \pi^\pm$, modified Tglu1A or Tglu1B, $\tilde{\chi}^\pm$ lifetime 0.2 ns, $m_{\tilde{\chi}^\pm} = 460$ GeV
>1975	95	8	SIRUNYAN	20B CMS	$\geq 1\gamma + \cancel{E}_T$, Tglu4A, BR($\tilde{g} \rightarrow$ $q\bar{q}\tilde{\chi}_1^\pm$)=0.5, $m_{\tilde{\chi}_1^0} \simeq m_{\tilde{g}}$		>1850	95	22	AABOUD	18BJ ATLS	$\ell^\pm \ell^\mp$ + jets + \cancel{E}_T , Tglu1G, $m_{\tilde{\chi}_1^0} = 100$ GeV
>1920	95	9	SIRUNYAN	20BJ CMS	jets+ \cancel{E}_T , Tglu1H, $m_{\tilde{g}} - m_{\tilde{\chi}_2^0} =$ 50 GeV, $m_{\tilde{\chi}_1^0} = 1$ GeV		>1650	95	23	AABOUD	18BJ ATLS	$\ell^\pm \ell^\mp$ + jets + \cancel{E}_T , Tglu1H, $m_{\tilde{\chi}_1^0} = 100$ GeV
>2150	95	10	SIRUNYAN	20E CMS	1 ℓ +jets, Tglu3A, $m_{\tilde{\chi}_1^0} < 700$ GeV		>2150	95	24	AABOUD	18U ATLS	2 γ + \cancel{E}_T , GGM, Tglu4B, any NLSP mass
>2050	95	10	SIRUNYAN	20E CMS	1 ℓ +jets, Tglu3A, $m_{\tilde{\chi}_1^0} < 1100$ GeV		>1600	95	25	AABOUD	18U ATLS	γ + jets + \cancel{E}_T , GGM higgsino- bino, mix of Tglu4B and Tglu4C, any NLSP mass
>1650	95	10	SIRUNYAN	20E CMS	1 ℓ + jets, Tglu3C, $m_{\tilde{\tau}} - m_{\tilde{\chi}_1^0} =$ 175 GeV, $m_{\tilde{\chi}_1^0} < 1150$ GeV		>2030	95	26	AABOUD	18V ATLS	jets+ \cancel{E}_T , Tglu1A, $m_{\tilde{\chi}_1^0} = 0$ GeV
>1700	95	11	SIRUNYAN	20T CMS	same-sign $\ell^\pm \ell^\pm$ or $\geq 3\ell^\pm$ + jets, Tglu3A, $m_{\tilde{\chi}_1^0} = 0$ GeV		>1980	95	27	AABOUD	18V ATLS	jets+ \cancel{E}_T , Tglu1B, $m_{\tilde{\chi}_1^\pm} = 0.5(m_{\tilde{g}} + m_{\tilde{\chi}_1^0})$, $m_{\tilde{\chi}_1^0}$ $= 0$ GeV
>1610	95	11	SIRUNYAN	20T CMS	same-sign $\ell^\pm \ell^\pm$ or $\geq 3\ell^\pm$ + jets, Tglu3B, $m_{\tilde{\tau}_1} - m_{\tilde{\chi}_1^0} = 175$ GeV, $m_{\tilde{\chi}_1^0} = 0$ GeV		>1750	95	28	AABOUD	18V ATLS	jets+ \cancel{E}_T , Tglu1C, $m_{\tilde{\chi}_1^0} = 1$ GeV, any $m_{\tilde{\chi}_2^0} > 100$ GeV
>1300	95	11	SIRUNYAN	20T CMS	same-sign $\ell^\pm \ell^\pm$ or $\geq 3\ell^\pm$ + jets, Tglu3C, $m_{\tilde{\tau}_1} - m_{\tilde{\chi}_1^0} = 20$ GeV, $m_{\tilde{\chi}_1^0} = 0$ GeV		>2000	95	29	SIRUNYAN	18AA CMS	$\geq 1\gamma + \cancel{E}_T$, Tglu4A
>1500	95	11	SIRUNYAN	20T CMS	same-sign $\ell^\pm \ell^\pm$ or $\geq 3\ell^\pm$ + jets, Tglu3D, $m_{\tilde{\chi}_1^\pm} = m_{\tilde{\chi}_1^0} +$ 5 GeV, $m_{\tilde{\chi}_1^0} = 0$ GeV		>2100	95	29	SIRUNYAN	18AA CMS	$\geq 1\gamma + \cancel{E}_T$, Tglu4B
>1350	95	11	SIRUNYAN	20T CMS	same-sign $\ell^\pm \ell^\pm$ or $\geq 3\ell^\pm$ + jets, Tglu1C, $m_{\tilde{\chi}_2^0} = m_{\tilde{\chi}_1^\pm} =$ $(m_{\tilde{g}} + m_{\tilde{\chi}_1^0})/2$, $m_{\tilde{\chi}_1^0} = 0$ GeV		>1800	95	30	SIRUNYAN	18AC CMS	1 ℓ +jets, Tglu3A, $m_{\tilde{\chi}_1^0} < 650$ GeV
>1250	95	11	SIRUNYAN	20T CMS	same-sign $\ell^\pm \ell^\pm$ or $\geq 3\ell^\pm$ + jets, Tglu1C, $m_{\tilde{\chi}_2^0} = m_{\tilde{\chi}_1^\pm} =$ $m_{\tilde{\chi}_1^0} + 20$ GeV, $m_{\tilde{\chi}_1^0} = 0$ GeV		>1700	95	30	SIRUNYAN	18AC CMS	1 ℓ +jets, Tglu3A, $m_{\tilde{\chi}_1^0} < 1040$ GeV
>1425	95	11	SIRUNYAN	20T CMS	same-sign $\ell^\pm \ell^\pm$ or $\geq 3\ell^\pm$ + jets, Tglu1B, $m_{\tilde{\chi}_1^\pm} = (m_{\tilde{g}} +$ $m_{\tilde{\chi}_1^0})/2$, $m_{\tilde{\chi}_1^0} = 0$ GeV		>1900	95	30	SIRUNYAN	18AC CMS	1 ℓ + jets, Tglu1B, $m_{\tilde{\chi}_1^\pm} = (m_{\tilde{g}} +$ $m_{\tilde{\chi}_1^0})/2$, $m_{\tilde{\chi}_1^0} < 300$ GeV
>1425	95	11	SIRUNYAN	20T CMS	same-sign $\ell^\pm \ell^\pm$ or $\geq 3\ell^\pm$ + jets, Tglu1B, $m_{\tilde{\chi}_1^\pm} = (m_{\tilde{g}} +$ $m_{\tilde{\chi}_1^0})/2$, $m_{\tilde{\chi}_1^0} = 0$ GeV		>1250	95	30	SIRUNYAN	18AC CMS	1 ℓ + jets, Tglu1B, $m_{\tilde{\chi}_1^\pm} = (m_{\tilde{g}} +$ $m_{\tilde{\chi}_1^0})/2$, $m_{\tilde{\chi}_1^0} < 950$ GeV
>1425	95	11	SIRUNYAN	20T CMS	same-sign $\ell^\pm \ell^\pm$ or $\geq 3\ell^\pm$ + jets, Tglu1B, $m_{\tilde{\chi}_1^\pm} = m_{\tilde{\chi}_1^0} +$ 20 GeV, $m_{\tilde{\chi}_1^0} = 0$ GeV		>1610	95	31	SIRUNYAN	18AL CMS	$\geq 3\ell^\pm$ + jets + \cancel{E}_T , Tglu3A, $m_{\tilde{\chi}_1^0} = 0$ GeV
>2000	95	12	AABOUD	19I ATL	≥ 2 jets + 1 or 2 τ + \cancel{E}_T , Tglu1F, $m_{\tilde{\chi}_1^0} = 100$ GeV		>1160	95	31	SIRUNYAN	18AL CMS	$\geq 3\ell^\pm$ + jets + \cancel{E}_T , Tglu1C, $m_{\tilde{\chi}_2^0} = m_{\tilde{\chi}_1^\pm} = (m_{\tilde{g}} +$ $m_{\tilde{\chi}_1^0})/2$, $m_{\tilde{\chi}_1^0} = 0$ GeV
>1860	95	13	SIRUNYAN	19AG CMS	2 γ + \cancel{E}_T , Tglu4B, 500 GeV $< m_{\tilde{\chi}_1^0} < 1500$ GeV		>1500	95	32	SIRUNYAN	18AR CMS	$\ell^\pm \ell^\mp$ + jets + \cancel{E}_T , GMSB, Tglu4C, $m_{\tilde{\chi}_1^0} = 100$ GeV
>1920	95	14	SIRUNYAN	19AU CMS	γ + jets + b -jets + \cancel{E}_T , Tglu4D, $m_{\tilde{\chi}_1^0} = 127$ GeV		>1770	95	32	SIRUNYAN	18AR CMS	$\ell^\pm \ell^\mp$ + jets + \cancel{E}_T , GMSB, Tglu4C, $m_{\tilde{\chi}_1^0} = 1400$ GeV
>1950	95	14	SIRUNYAN	19AU CMS	γ + jets + b -jets + \cancel{E}_T , Tglu4E, $m_{\tilde{\chi}_1^0} = 1$ GeV		>1625	95	33	SIRUNYAN	18AY CMS	jets+ \cancel{E}_T , Tglu1A, $m_{\tilde{\chi}_1^0} = 0$ GeV
>1800	95	14	SIRUNYAN	19AU CMS	γ + jets + b -jets + \cancel{E}_T , Tglu4F, $m_{\tilde{\chi}_1^0} = 1$ GeV		>1825	95	33	SIRUNYAN	18AY CMS	jets+ \cancel{E}_T , Tglu2A, $m_{\tilde{\chi}_1^0} = 0$ GeV
>2090	95	14	SIRUNYAN	19AU CMS	γ + jets + b -jets + \cancel{E}_T , Tglu4D, $m_{\tilde{\chi}_1^0} = 1200$ GeV		>1625	95	33	SIRUNYAN	18AY CMS	jets+ \cancel{E}_T , Tglu3A, $m_{\tilde{\chi}_1^0} = 0$ GeV
>2120	95	14	SIRUNYAN	19AU CMS	γ + jets + b -jets + \cancel{E}_T , Tglu4E, $m_{\tilde{\chi}_1^0} = 1200$ GeV		>2040	95	34	SIRUNYAN	18D CMS	top quark (hadronically decaying) + jets + \cancel{E}_T , Tglu3A, $m_{\tilde{\chi}_1^0} =$ 0 GeV
>1970	95	14	SIRUNYAN	19AU CMS	γ + jets + b -jets + \cancel{E}_T , Tglu4F, $m_{\tilde{\chi}_1^0} = 1200$ GeV		>1930	95	34	SIRUNYAN	18D CMS	top quark (hadronically decaying) + jets + \cancel{E}_T , Tglu3B, $m_{\tilde{\tau}_1} - m_{\tilde{\chi}_1^0} = 175$ GeV, $m_{\tilde{\chi}_1^0}$ $= 200$ GeV
>1700	95	15	SIRUNYAN	19CE CMS	2 jets, Stealth SUSY, Tglu1A and $\tilde{\chi}_1^0 \rightarrow \tilde{S} \gamma$ ($\tilde{S} \rightarrow S \tilde{G}$), $m_{\tilde{\chi}_1^0}$ $= 200$ GeV		>1690	95	34	SIRUNYAN	18D CMS	top quark (hadronically decaying) + jets + \cancel{E}_T , Tglu3C, $m_{\tilde{\tau}_1} - m_{\tilde{\chi}_1^0} = 20$ GeV, $m_{\tilde{\chi}_1^0} =$ 0 GeV
>2000	95	16	SIRUNYAN	19CH CMS	jets+ \cancel{E}_T , Tglu1A, $m_{\tilde{\chi}_1^0} = 0$ GeV		>1990	95	34	SIRUNYAN	18D CMS	top quark (hadronically decaying) + jets + \cancel{E}_T , Tglu3E, $m_{\tilde{\chi}_1^\pm}$ $= m_{\tilde{\chi}_1^0} + 5$ GeV, $m_{\tilde{\chi}_1^0} = 100$ GeV
>2030	95	16	SIRUNYAN	19CH CMS	jets+ \cancel{E}_T , Tglu1C, $m_{\tilde{\chi}_1^\pm} = m_{\tilde{\chi}_2^0} =$ $0.5(m_{\tilde{g}} + m_{\tilde{\chi}_1^0})$, $m_{\tilde{\chi}_1^0} = 0$ GeV		>2010	95	35	SIRUNYAN	18M CMS	$\geq 1 H (\rightarrow bb) + \cancel{E}_T$, Tglu1I
>2270	95	16	SIRUNYAN	19CH CMS	jets+ \cancel{E}_T , Tglu2A, $m_{\tilde{\chi}_1^0} = 0$ GeV		>1825	95	35	SIRUNYAN	18M CMS	$\geq 1 H (\rightarrow bb) + \cancel{E}_T$, Tglu1J
>2180	95	16	SIRUNYAN	19CH CMS	jets+ \cancel{E}_T , Tglu3A, $m_{\tilde{\chi}_1^0} = 0$ GeV		>1750	95	36	AABOUD	17AJ ATLS	same-sign $\ell^\pm \ell^\pm$ / 3 ℓ + jets + \cancel{E}_T , Tglu3A, $m_{\tilde{\chi}_1^0} = 100$ GeV
>1750	95	17	SIRUNYAN	19K CMS	$\gamma + \ell + \cancel{E}_T$, Tglu4A, $m_{\tilde{\chi}_1^0} = 1500$ GeV		>1570	95	37	AABOUD	17AJ ATLS	same-sign $\ell^\pm \ell^\pm$ / 3 ℓ + jets + \cancel{E}_T , Tglu1E, $m_{\tilde{\chi}_1^0} = 100$ GeV
>2000	95	18	SIRUNYAN	19S CMS	1 or 2 ℓ + jets + \cancel{E}_T , Tglu3A, $m_{\tilde{\chi}_1^0} < 700$ GeV		>1860	95	38	AABOUD	17AJ ATLS	same-sign $\ell^\pm \ell^\pm$ / 3 ℓ + jets + \cancel{E}_T , Tglu1G, $m_{\tilde{\chi}_1^0} = 200$ GeV
>1900	95	18	SIRUNYAN	19S CMS	1 or 2 ℓ + jets + \cancel{E}_T , Tglu3C, 150 GeV $< m_{\tilde{\chi}_1^0} < 950$ GeV		>2100	95	39	AABOUD	17AR ATLS	1 ℓ +jets+ \cancel{E}_T , Tglu1B, $m_{\tilde{\chi}_1^0} = 0$ GeV
							>1740	95	40	AABOUD	17AR ATLS	1 ℓ +jets+ \cancel{E}_T , Tglu1E, $m_{\tilde{\chi}_1^0} = 0$ GeV
							>1800	95	41	AABOUD	17AY ATLS	jets+ \cancel{E}_T , Tglu3A, $m_{\tilde{\tau}_1} - m_{\tilde{\chi}_1^0} =$ 5 GeV
							>1800	95	42	AABOUD	17AZ ATLS	≥ 7 jets+ \cancel{E}_T , large R-jets and/or b -jets, Tglu1E, $m_{\tilde{\chi}_1^0}$ $= 100$ GeV

See key on page 1127

Searches Particle Listings
Supersymmetric Particle Searches

>1540	95	43	AABOUD	17AZ ATLS	≥ 7 jets+ E_T , large R-jets and/or b-jets, Tglu3A, $m_{\chi_1^0} = 0$ GeV	>1200	95	58	SIRUNYAN	17s CMS	same-sign $\ell^\pm \ell^\pm +$ jets + E_T , Tglu3D, $m_{\chi_1^\pm} = m_{\chi_1^0} + 5$ GeV, $m_{\chi_1^0} = 100$ GeV
>1340	95	44	AABOUD	17N ATLS	2 same-flavor, opposite-sign $\ell +$ jets + E_T , Tglu1H, $m_{\chi_1^0} = 0$ GeV	>1370	95	58	SIRUNYAN	17s CMS	same-sign $\ell^\pm \ell^\pm +$ jets + E_T , Tglu3B, $m_{\tilde{t}_1} - m_{\chi_1^0} = 175$ GeV, $m_{\chi_1^0} = 50$ GeV
>1310	95	45	AABOUD	17N ATLS	2 same-flavor, opposite-sign $\ell +$ jets + E_T , Tglu1H, $m_{\chi_2^0} = (m_{\tilde{g}} + m_{\chi_1^0})/2$, $m_{\chi_1^0} < 400$ GeV	>1180	95	58	SIRUNYAN	17s CMS	same-sign $\ell^\pm \ell^\pm +$ jets + E_T , Tglu3C, $m_{\tilde{t}_1} - m_{\chi_1^0} = 20$ GeV, $m_{\chi_1^0} = 0$ GeV
>1700	95	46	AABOUD	17N ATLS	2 same-flavor, opposite-sign $\ell +$ jets + E_T , Tglu1G, $m_{\chi_1^0} \sim 1$ GeV	>1280	95	58	SIRUNYAN	17s CMS	same-sign $\ell^\pm \ell^\pm +$ jets + E_T , Tglu1B, $m_{\chi_1^\pm} = (m_{\tilde{g}} + m_{\chi_1^0})/2$, $m_{\chi_1^0} = 0$ GeV
>1400	95	47	KHACHATRY...17	CMS	jets+ E_T , Tglu1A, $m_{\chi_1^0} = 200$ GeV	>1300	95	58	SIRUNYAN	17s CMS	same-sign $\ell^\pm \ell^\pm +$ jets + E_T , Tglu1B, $m_{\tilde{t}_1} - m_{\chi_1^0} = 20$ GeV, $m_{\chi_1^0} = 100$ GeV
>1650	95	47	KHACHATRY...17	CMS	jets+ E_T , Tglu2A, $m_{\chi_1^0} = 200$ GeV	>1570	95	59	AABOUD	16Ac ATLS	≥ 2 jets + 1 or 2 $\tau + E_T$, Tglu1F, $m_{\chi_1^0} = 100$ GeV
>1600	95	47	KHACHATRY...17	CMS	jets+ E_T , Tglu3A, $m_{\chi_1^0} = 200$ GeV	>1460	95	60	AABOUD	16J ATLS	1 $\ell^\pm + \geq 4$ jets + E_T , Tglu3C, $m_{\tilde{t}_1} - m_{\chi_1^0} = 5$ GeV
>1550	95	48	KHACHATRY...17AD	CMS	jets+b-jets+ E_T , Tglu3A, $m_{\chi_1^0} = 0$ GeV	>1650	95	61	AABOUD	16M ATLS	2 $\gamma + E_T$, Tglu1D, any NLS mass
>1450	95	49	KHACHATRY...17AD	CMS	jets+b-jets+ E_T , Tglu3C, 200 < $m_{\chi_1^0} < 400$ GeV	>1510	95	62	AABOUD	16N ATLS	≥ 4 jets + E_T , Tglu1A, $m_{\chi_1^0} = 0$ GeV
>1570	95	50	KHACHATRY...17As	CMS	1 ℓ , Tglu3A, $m_{\chi_1^0} < 600$ GeV	>1500	95	63	AABOUD	16N ATLS	≥ 4 jets + E_T , Tglu1B, $m_{\chi_1^\pm} = (m_{\tilde{g}} + m_{\chi_1^0})/2$, $m_{\chi_1^0} = 200$ GeV
>1500	95	50	KHACHATRY...17As	CMS	1 ℓ , Tglu3A, $m_{\chi_1^0} < 775$ GeV	>1780	95	64	AAD	16AD ATLS	0 ℓ , ≥ 3 b-jets + E_T , Tglu2A, $m_{\chi_1^0} < 800$ GeV
>1400	95	50	KHACHATRY...17As	CMS	1 ℓ , Tglu1B, $m_{\chi_1^\pm} = (m_{\tilde{g}} + m_{\chi_1^0})/2$, $m_{\chi_1^0} < 725$ GeV	>1760	95	65	AAD	16AD ATLS	1 ℓ , ≥ 3 b-jets + E_T , Tglu3A, $m_{\chi_1^0} < 700$ GeV
none	95	50	KHACHATRY...17As	CMS	1 ℓ , Tglu1B, $m_{\chi_1^\pm} = (m_{\tilde{g}} + m_{\chi_1^0})/2$, $m_{\chi_1^0} < 850$ GeV	>1300	95	66	AAD	16BB ATLS	2 same-sign/3 $\ell +$ jets + E_T , Tglu1D, $m_{\chi_1^0} < 600$ GeV
1050-1350	95	50	KHACHATRY...17As	CMS	1 ℓ , Tglu1B, $m_{\chi_1^\pm} = (m_{\tilde{g}} + m_{\chi_1^0})/2$, $m_{\chi_1^0} < 850$ GeV	>1100	95	66	AAD	16BB ATLS	2 same-sign/3 $\ell +$ jets + E_T , Tglu1E, $m_{\chi_1^0} < 300$ GeV
>1175	95	51	KHACHATRY...17AW	CMS	$\geq 3\ell^\pm$, 2 jets, Tglu3A, $m_{\chi_1^0} = 0$ GeV	>1200	95	66	AAD	16BB ATLS	2 same-sign/3 $\ell +$ jets + E_T , Tglu3A, $m_{\chi_1^0} < 600$ GeV
> 825	95	51	KHACHATRY...17AW	CMS	$\geq 3\ell^\pm$, 2 jets, Tglu1C, $m_{\chi_1^\pm} = (m_{\tilde{g}} + m_{\chi_1^0})/2$, $m_{\chi_1^0} = 0$ GeV	>1600	95	67	AAD	16Bg ATLS	1 ℓ , ≥ 4 jets, E_T , Tglu1B, $m_{\chi_1^\pm} = (m_{\tilde{g}} + m_{\chi_1^0})/2$, $m_{\chi_1^0} = 100$ GeV
>1350	95	52	KHACHATRY...17P	CMS	1 or more jets+ E_T , Tglu1A, $m_{\chi_1^0} = 0$ GeV	>1400	95	68	AAD	16V ATLS	≥ 7 to ≥ 10 jets + E_T , Tglu1E, $m_{\chi_1^0} < 200$ GeV
>1545	95	52	KHACHATRY...17P	CMS	1 or more jets+ E_T , Tglu2A, $m_{\chi_1^0} = 0$ GeV	>1400	95	68	AAD	16V ATLS	≥ 7 to ≥ 10 jets + E_T , pMSSM $M_1 = 60$ GeV, $M_2 = 3$ TeV, $\tan\beta=10$, $\mu < 0$
>1120	95	52	KHACHATRY...17P	CMS	1 or more jets+ E_T , Tglu3A, $m_{\chi_1^0} = 0$ GeV	>1100	95	69	KHACHATRY...16AM	CMS	boosted $W+b$, Tglu3C, $m_{\tilde{t}_1} - m_{\chi_1^0} < 80$ GeV, $m_{\chi_1^0} < 400$ GeV
>1300	95	52	KHACHATRY...17P	CMS	1 or more jets+ E_T , Tglu3D, $m_{\chi_1^\pm} = m_{\chi_1^0} + 5$ GeV, $m_{\chi_1^0} = 100$ GeV	> 700	95	69	KHACHATRY...16AM	CMS	boosted $W+b$, Tglu3B, $m_{\tilde{t}_1} - m_{\chi_1^0} = 175$ GeV, $m_{\chi_1^0} = 0$ GeV
> 780	95	52	KHACHATRY...17P	CMS	1 or more jets+ E_T , Tglu3B, $m_{\tilde{t}_1} - m_{\chi_1^0} = 175$ GeV, $m_{\chi_1^0} = 50$ GeV	>1050	95	70	KHACHATRY...16Bj	CMS	same-sign $\ell^\pm \ell^\pm$, Tglu3A, $m_{\chi_1^0} < 800$ GeV
> 790	95	52	KHACHATRY...17P	CMS	1 or more jets+ E_T , Tglu3C, $m_{\tilde{t}_1} - m_{\chi_1^0} = 20$ GeV, $m_{\chi_1^0} = 0$ GeV	>1300	95	70	KHACHATRY...16Bj	CMS	same-sign $\ell^\pm \ell^\pm$, Tglu3A, $m_{\chi_1^0} = 0$
>1650	95	53	KHACHATRY...17V	CMS	2 $\gamma + E_T$, GGM, Tglu4B, any NLS mass	>1140	95	70	KHACHATRY...16Bj	CMS	same-sign $\ell^\pm \ell^\pm$, Tglu3B, $m_{\tilde{t}_1} - m_{\chi_1^0} = 20$ GeV, $m_{\chi_1^0} = 0$
>1900	95	54	SIRUNYAN	17AF CMS	1 ℓ +jets+b-jets+ E_T , Tglu3A, $m_{\chi_1^0} = 0$ GeV	> 850	95	70	KHACHATRY...16Bj	CMS	same-sign $\ell^\pm \ell^\pm$, Tglu3B, $m_{\tilde{t}_1} - m_{\chi_1^0} = 20$ GeV, $m_{\chi_1^0} < 700$ GeV
>1600	95	54	SIRUNYAN	17AF CMS	1 ℓ +jets+b-jets+ E_T , Tglu3B, $m_{\tilde{t}_1} - m_{\chi_1^0} = 175$ GeV, $m_{\chi_1^0} = 50$ GeV	> 950	95	70	KHACHATRY...16Bj	CMS	same-sign $\ell^\pm \ell^\pm$, Tglu3D, $m_{\chi_1^\pm} = m_{\chi_1^0} + 5$ GeV
>1800	95	55	SIRUNYAN	17AY CMS	$\gamma +$ jets+ E_T , Tglu4B, $m_{\chi_1^0} = 0$ GeV	>1100	95	70	KHACHATRY...16Bj	CMS	same-sign $\ell^\pm \ell^\pm$, Tglu1B, $m_{\chi_1^\pm} = 0.5(m_{\tilde{g}} + m_{\chi_1^0})$, $m_{\chi_1^0} < 400$ GeV
>1600	95	55	SIRUNYAN	17AY CMS	$\gamma +$ jets+ E_T , Tglu4A, $m_{\chi_1^0} = 0$ GeV	> 830	95	70	KHACHATRY...16Bj	CMS	same-sign $\ell^\pm \ell^\pm$, Tglu1B, $m_{\chi_1^\pm} = 0.5(m_{\tilde{g}} + m_{\chi_1^0})$, $m_{\chi_1^0} < 700$ GeV
>1860	95	56	SIRUNYAN	17AZ CMS	≥ 1 jets + E_T , Tglu1A, $m_{\chi_1^0} = 0$ GeV	>1300	95	70	KHACHATRY...16Bj	CMS	same-sign $\ell^\pm \ell^\pm$, Tglu3B, $m_{\tilde{t}_1} - m_{\chi_1^0} = m_t$, $m_{\chi_1^0} = 0$
>2025	95	56	SIRUNYAN	17AZ CMS	≥ 1 jets+ E_T , Tglu2A, $m_{\chi_1^0} = 0$ GeV	>1050	95	70	KHACHATRY...16Bj	CMS	same-sign $\ell^\pm \ell^\pm$, Tglu3B, $m_{\tilde{t}_1} - m_{\chi_1^0} = m_t$, $m_{\chi_1^0} < 800$ GeV
>1900	95	56	SIRUNYAN	17AZ CMS	≥ 1 jets+ E_T , Tglu3A, $m_{\chi_1^0} = 0$ GeV	>1725	95	71	KHACHATRY...16Bs	CMS	jets + E_T , Tglu1A, $m_{\chi_1^0} = 0$
>1825	95	57	SIRUNYAN	17P CMS	jets+ E_T , Tglu1A, $m_{\chi_1^0} = 0$ GeV	>1750	95	71	KHACHATRY...16Bs	CMS	jets + E_T , Tglu2A, $m_{\chi_1^0} = 0$
>1950	95	57	SIRUNYAN	17P CMS	jets+ E_T , Tglu2A, $m_{\chi_1^0} = 0$ GeV	>1550	95	71	KHACHATRY...16Bs	CMS	jets + E_T , Tglu3A, $m_{\chi_1^0} = 0$
>1960	95	57	SIRUNYAN	17P CMS	jets+ E_T , Tglu3A, $m_{\chi_1^0} = 0$ GeV	>1280	95	72	KHACHATRY...16By	CMS	opposite-sign $\ell^\pm \ell^\pm$, Tglu4C, $m_{\chi_1^0} = 1000$ GeV
>1800	95	57	SIRUNYAN	17P CMS	jets+ E_T , Tglu1C, $m_{\chi_1^\pm} = m_{\chi_2^0} = (m_{\tilde{g}} + m_{\chi_1^0})/2$, $m_{\chi_1^0} = 0$ GeV						
>1870	95	57	SIRUNYAN	17P CMS	jets+ E_T , Tglu3D, $m_{\chi_1^\pm} = m_{\chi_1^0} + 5$ GeV, $m_{\chi_1^0} = 1000$ GeV						
>1520	95	58	SIRUNYAN	17s CMS	same-sign $\ell^\pm \ell^\pm +$ jets + E_T , Tglu3A, $m_{\chi_1^0} = 0$ GeV						

Searches Particle Listings

Supersymmetric Particle Searches

>1030	95	72	KHACHATRY...16BY CMS	opposite-sign $\ell^\pm \ell^\pm$, Tglu4C, $m_{\tilde{\chi}_1^0} = 0$ GeV	> 500	95	95	KHACHATRY...16BT CMS	19-parameter pMSSM model, global Bayesian analysis, flat prior	
>1440	95	73	KHACHATRY...16V CMS	jets + \cancel{E}_T , Tglu1A, $m_{\tilde{\chi}_1^0} = 0$		95	96	AAD	15AB ATLS $\tilde{g} \rightarrow \tilde{S}g, c\tau = 1$ m, $\tilde{S} \rightarrow \tilde{S}\tilde{G}$ and $\tilde{S} \rightarrow gg, BR = 100\%$	
>1600	95	73	KHACHATRY...16V CMS	jets + \cancel{E}_T , Tglu2A, $m_{\tilde{\chi}_1^0} = 0$		95	97	AAD	15AI ATLS $\ell^\pm +$ jets + \cancel{E}_T	
>1550	95	73	KHACHATRY...16V CMS	jets + \cancel{E}_T , Tglu3A, $m_{\tilde{\chi}_1^0} = 0$	>1600	95	75	AAD	15BV ATLS pMSSM, $M_1 = 60$ GeV, $m_{\tilde{q}} < 1500$ GeV	
>1450	95	73	KHACHATRY...16V CMS	jets + \cancel{E}_T , Tglu1C, $m_{\tilde{\chi}_1^0} = 0$	>1280	95	75	AAD	15BV ATLS mSUGRA, $m_0 > 2$ TeV	
> 820	95	74	AAD	15BG ATLS GGM, $\tilde{g} \rightarrow q\tilde{q}Z\tilde{G}, \tan\beta = 30, \mu > 600$ GeV	>1100	95	75	AAD	15BV ATLS via $\tilde{\tau}$, natural GMSB, all $m_{\tilde{\tau}}$	
> 850	95	74	AAD	15BG ATLS GGM, $\tilde{g} \rightarrow q\tilde{q}Z\tilde{G}, \tan\beta = 1.5, \mu > 450$ GeV	>1330	95	75	AAD	15BV ATLS jets + $\cancel{E}_T, \tilde{g} \rightarrow q\tilde{q}\tilde{\chi}_1^0, m_{\tilde{\chi}_1^0} = 1$ GeV	
>1150	95	75	AAD	15BV ATLS general RPC \tilde{g} decays, $m_{\tilde{\chi}_1^0} < 100$ GeV	>1500	95	75	AAD	15BV ATLS jets + $\cancel{E}_T, \tilde{g} \rightarrow \tilde{q}q, \tilde{q} \rightarrow q\tilde{\chi}_1^0, m_{\tilde{\chi}_1^0} = 1$ GeV	
> 700	95	76	AAD	15BX ATLS $\tilde{g} \rightarrow X\tilde{\chi}_1^0$, independent of $m_{\tilde{\chi}_1^0}$	>1650	95	75	AAD	15BV ATLS jets + $\cancel{E}_T, m_{\tilde{g}} = m_{\tilde{q}}, m_{\tilde{\chi}_1^0} = 1$ GeV	
>1290	95	77	AAD	15CA ATLS $\geq 2 \gamma + \cancel{E}_T$, GGM, bino-like NLSP, any NLSP mass	> 850	95	75	AAD	15BV ATLS jets + $\cancel{E}_T, \tilde{g} \rightarrow g\tilde{\chi}_1^0, m_{\tilde{\chi}_1^0} < 550$ GeV	
>1260	95	77	AAD	15CA ATLS $\geq 1 \gamma + b$ -jets + \cancel{E}_T , GGM, higgsino-bino admix. NLSP and $\mu < 0, m(\text{NLSP}) > 450$ GeV	>1270	95	75	AAD	15BV ATLS jets + $\cancel{E}_T, \tilde{g} \rightarrow q\tilde{q}W\tilde{\chi}_1^0, m_{\tilde{\chi}_1^0} = 100$ GeV	
>1140	95	77	AAD	15CA ATLS $\geq 1 \gamma +$ jets + \cancel{E}_T , GGM, higgsino-bino admixture NLSP, all $\mu > 0$	>1150	95	75	AAD	15BV ATLS jets + $\ell^\pm \ell^\pm, \tilde{g}$ decays via sleptons, $m_{\tilde{\chi}_1^0} = 100$ GeV	
>1225	95	78	KHACHATRY...15AF CMS	$\tilde{g} \rightarrow q\tilde{q}\tilde{\chi}_1^0, m_{\tilde{\chi}_1^0} = 0$	>1320	95	75	AAD	15BV ATLS τ, \tilde{q} decays via staus, $m_{\tilde{\chi}_1^0} = 100$ GeV	
>1300	95	78	KHACHATRY...15AF CMS	$\tilde{g} \rightarrow b\tilde{b}\tilde{\chi}_1^0, m_{\tilde{\chi}_1^0} = 0$	>1220	95	75	AAD	15BV ATLS b -jets, $\tilde{g} \rightarrow t\tilde{\tau}\tilde{\chi}_1^0, m_{\tilde{\chi}_1^0} < 400$ GeV	
>1225	95	78	KHACHATRY...15AF CMS	$\tilde{g} \rightarrow t\tilde{\tau}\tilde{\chi}_1^0, m_{\tilde{\chi}_1^0} = 0$	>1220	95	75	AAD	15BV ATLS b -jets, $\tilde{g} \rightarrow \tilde{t}_1 t$ and $\tilde{t}_1 \rightarrow t\tilde{\chi}_1^0, m_{\tilde{\chi}_1^0} < 1000$ GeV	
>1550	95	78	KHACHATRY...15AF CMS	CMSSM, $\tan\beta=30, m_{\tilde{g}}=m_{\tilde{q}}, A_0=-2\max(m_0, m_1/2), \mu > 0$	>1310	95	75	AAD	15BV ATLS b -jets, $\tilde{g} \rightarrow \tilde{t}_1 t$ and $\tilde{t}_1 \rightarrow b\tilde{\chi}_1^0, m_{\tilde{\chi}_1^0} < 1000$ GeV, $m_{\tilde{\tau}_1} < 1000$ GeV, $m_{\tilde{\chi}_1^0} = 60$ GeV	
>1150	95	78	KHACHATRY...15AF CMS	CMSSM, $\tan\beta=30, A_0=-2\max(m_0, m_1/2), \mu > 0$	>1220	95	75	AAD	15BV ATLS b -jets, $\tilde{g} \rightarrow \tilde{t}_1 t$ and $\tilde{g} \rightarrow c\tilde{\chi}_1^0$	
>1280	95	79	KHACHATRY...15I CMS	$\tilde{g} \rightarrow t\tilde{\tau}\tilde{\chi}_1^0, m_{\tilde{\chi}_1^0} = 0$	>1180	95	75	AAD	15BV ATLS b -jets, $\tilde{g} \rightarrow \tilde{t}_1 t$ and $\tilde{g} \rightarrow b_1 b$ and $\tilde{b}_1 \rightarrow b\tilde{\chi}_1^0, m_{\tilde{\chi}_1^0} < 1000$ GeV	
>1310	95	80	KHACHATRY...15X CMS	$\tilde{g} \rightarrow b\tilde{b}\tilde{\chi}_1^0, m_{\tilde{\chi}_1^0} = 100$ GeV	>1260	95	75	AAD	15BV ATLS b -jets, $\tilde{g} \rightarrow \tilde{t}_1 t$ and $\tilde{g} \rightarrow c\tilde{\chi}_1^0$	
>1175	95	80	KHACHATRY...15X CMS	$\tilde{g} \rightarrow t\tilde{\tau}\tilde{\chi}_1^0, m_{\tilde{\chi}_1^0} = 100$ GeV	>1200	95	75	AAD	15BV ATLS b -jets, $\tilde{g} \rightarrow \tilde{b}_1 b$ and $\tilde{b}_1 \rightarrow b\tilde{\chi}_1^0, m_{\tilde{\chi}_1^0} < 1000$ GeV	
>1330	95	81	AAD	14AE ATLS jets + $\cancel{E}_T, \tilde{g} \rightarrow q\tilde{q}\tilde{\chi}_1^0$ simplified model, $m_{\tilde{\chi}_1^0} = 0$ GeV	>1200	95	75	AAD	15BV ATLS b -jets, $\tilde{g} \rightarrow \tilde{b}_1 b$ and $\tilde{b}_1 \rightarrow b\tilde{\chi}_1^0, m_{\tilde{\chi}_1^0} < 1000$ GeV	
>1700	95	81	AAD	14AE ATLS jets + \cancel{E}_T , mSUGRA/CMSSM, $m_{\tilde{q}} = m_{\tilde{g}}$	>1250	95	75	AAD	15BV ATLS b -jets, $\tilde{g} \rightarrow b\tilde{\chi}_1^0, m_{\tilde{\chi}_1^0} < 400$ GeV	
>1090	95	82	AAD	14AG ATLS $\tau +$ jets + \cancel{E}_T , natural Gauge Mediation	none,	95	75	AAD	15BV ATLS b -jets, \tilde{g} decay via offshell \tilde{t}_1 and $\tilde{b}_1, m_{\tilde{\chi}_1^0} < 500$ GeV	
>1600	95	82	AAD	14AG ATLS $\tau +$ jets + \cancel{E}_T , mGMSB, $M_{mess} = 250$ GeV, $N_5 = 3, \mu > 0, C_{grav} = 1$	750-1250	95	98	AAD	15CB ATLS jets, $\tilde{g} \rightarrow q\tilde{q}\tilde{\chi}_1^0, \tilde{\chi}_1^0 \rightarrow Z\tilde{G}, \text{GGM}, m_{\tilde{\chi}_1^0} = 400$ GeV and $3 < c\tau_{\tilde{\chi}_1^0} < 500$ mm	
> 640	95	83	AAD	14X ATLS $\geq 4\ell^\pm, \tilde{g} \rightarrow q\tilde{q}\tilde{\chi}_1^0, \tilde{\chi}_1^0 \rightarrow \ell^\pm \ell^\mp \tilde{G}, \tan\beta = 30, \text{GGM}$	>1100	95	98	AAD	15CB ATLS jets or $\cancel{E}_T, \tilde{g} \rightarrow q\tilde{q}\tilde{\chi}_1^0$, Split SUSY, $m_{\tilde{\chi}_1^0} = 100$ GeV and $15 < c\tau < 300$ mm	
>1000	95	84	CHATRCHYAN14AH CMS	jets + $\cancel{E}_T, \tilde{g} \rightarrow q\tilde{q}\tilde{\chi}_1^0$ simplified model, $m_{\tilde{\chi}_1^0} = 50$ GeV	>1400	95	98	AAD	15CB ATLS $\cancel{E}_T, \tilde{g} \rightarrow q\tilde{q}\tilde{\chi}_1^0$, Split SUSY, $m_{\tilde{\chi}_1^0} = 100$ GeV and $20 < c\tau < 250$ mm	
>1350	95	84	CHATRCHYAN14AH CMS	jets + \cancel{E}_T , CMSSM, $m_{\tilde{g}} = m_{\tilde{q}}$	>1500	95	98	AAD	99 KHACHATRY...15AD CMS $\ell^\pm \ell^\mp +$ jets + \cancel{E}_T , GMSB, $\tilde{g} \rightarrow q\tilde{q}Z\tilde{G}$	
>1000	95	85	CHATRCHYAN14AH CMS	jets + $\cancel{E}_T, \tilde{g} \rightarrow b\tilde{b}\tilde{\chi}_1^0$ simplified model, $m_{\tilde{\chi}_1^0} = 50$ GeV	>1300	100	98	AAD	100 KHACHATRY...15AZ CMS $\geq 2 \gamma, \geq 1$ jet, (Razor), bino-like NLSP, $m_{\tilde{\chi}_1^0} = 375$ GeV	
>1000	95	86	CHATRCHYAN14AH CMS	jets + $\cancel{E}_T, \tilde{g} \rightarrow t\tilde{\tau}\tilde{\chi}_1^0$ simplified model, $m_{\tilde{\chi}_1^0} = 50$ GeV	> 800	95	100	98	AAD	100 KHACHATRY...15AZ CMS $\geq 1 \gamma, \geq 2$ jet, wino-like NLSP, $m_{\tilde{\chi}_1^0} = 375$ GeV
>1160	95	87	CHATRCHYAN14I CMS	jets + $\cancel{E}_T, \tilde{g} \rightarrow q\tilde{q}\tilde{\chi}_1^0$ simplified model, $m_{\tilde{\chi}_1^0} < 100$ GeV	>1280	95	101	98	AAD	14AX ATLS $\geq 3 b$ -jets + \cancel{E}_T , CMSSM
>1130	95	87	CHATRCHYAN14I CMS	multijets + $\cancel{E}_T, \tilde{g} \rightarrow t\tilde{\tau}\tilde{\chi}_1^0$ simplified model, $m_{\tilde{\chi}_1^0} < 100$ GeV	>1250	95	101	98	AAD	14AX ATLS $\geq 3 b$ -jets + $\cancel{E}_T, \tilde{g} \rightarrow \tilde{b}_1 b\tilde{\chi}_1^0$ simplified model, $\tilde{b}_1 \rightarrow b\tilde{\chi}_1^0, m_{\tilde{\chi}_1^0} = 60$ GeV, $m_{\tilde{\tau}_1} < 900$ GeV
>1210	95	87	CHATRCHYAN14I CMS	multijets + $\cancel{E}_T, \tilde{g} \rightarrow q\tilde{q}W/Z\tilde{\chi}_1^0$ simplified model, $m_{\tilde{\chi}_1^0} < 100$ GeV	>1190	95	101	98	AAD	14AX ATLS $\geq 3 b$ -jets + $\cancel{E}_T, \tilde{g} \rightarrow \tilde{t}_1 t\tilde{\chi}_1^0$ simplified model, $\tilde{t}_1 \rightarrow t\tilde{\chi}_1^0, m_{\tilde{\chi}_1^0} = 60$ GeV, $m_{\tilde{\tau}_1} < 1000$ GeV
>1260	95	88	CHATRCHYAN14N CMS	$1\ell^\pm +$ jets + $\geq 2b$ -jets, $\tilde{g} \rightarrow t\tilde{\tau}\tilde{\chi}_1^0$ simplified model, $m_{\tilde{\chi}_1^0} = 0$ GeV, $m_{\tilde{\tau}_1} > m_{\tilde{g}}$	>1180	95	101	98	AAD	14AX ATLS $\geq 3 b$ -jets + $\cancel{E}_T, \tilde{g} \rightarrow \tilde{t}_1 t\tilde{\chi}_1^0$ simplified model, $\tilde{t}_1 \rightarrow b\tilde{\chi}_1^0, m_{\tilde{\chi}_1^0} = 2m_{\tilde{\chi}_1^0}, m_{\tilde{\chi}_1^0} = 60$ GeV, $m_{\tilde{\tau}_1} < 1000$ GeV
		89	CHATRCHYAN14R CMS	$\geq 3\ell^\pm, (\tilde{g}/\tilde{q}) \rightarrow q\ell^\pm \ell^\mp \tilde{G}$ simplified model, GMSB, slepton co-NLSP scegaro						
		90	CHATRCHYAN14R CMS	$\geq 3\ell^\pm, \tilde{g} \rightarrow t\tilde{\tau}\tilde{\chi}_1^0$ simplified model						
• • •	We do not use the following data for averages, fits, limits, etc. • • •									
>1500	95	91	AABOUD	18BJ ATLS $\ell^\pm \ell^\mp +$ jets + \cancel{E}_T , Tglu1H, $m_{\tilde{\chi}_1^0} = 1$ GeV, any $m_{\tilde{\chi}_2^0}$	>1250	95	101	98	AAD	14AX ATLS $\geq 3 b$ -jets + $\cancel{E}_T, \tilde{g} \rightarrow b\tilde{b}\tilde{\chi}_1^0$ simplified model, $m_{\tilde{\chi}_1^0} < 400$ GeV
>1770	95	92	AABOUD	18V ATLS jets + \cancel{E}_T , Tglu1C-like, 1/2 BR per decay mode, any $m_{\tilde{\chi}_2^0} - m_{\tilde{\chi}_1^0}, m_{\tilde{\chi}_1^0} = 60$ GeV	>1340	95	101	98	AAD	14AX ATLS $\geq 3 b$ -jets + $\cancel{E}_T, \tilde{g} \rightarrow t\tilde{\tau}\tilde{\chi}_1^0$ simplified model, $m_{\tilde{\chi}_1^0} < 400$ GeV
>1600	95	93	AABOUD	17AZ ATLS ≥ 7 jets + \cancel{E}_T , large R-jets and/or b -jets, pMSSM, $m_{\tilde{\chi}_1^\pm} = 200$ GeV						
>1600	95	94	KHACHATRY...16AY CMS	$1\ell^\pm +$ jets + b -jets + \cancel{E}_T , Tglu3A, $m_{\tilde{\chi}_1^0} = 0$ GeV						

See key on page 1127

Searches Particle Listings

Supersymmetric Particle Searches

>1300	95	101	AAD	14AX ATLS	≥ 3 b -jets + \cancel{E}_T , $\tilde{g} \rightarrow t\bar{b}\tilde{\chi}_1^\pm$ simplified model, $\tilde{\chi}_1^\pm \rightarrow t\bar{t}'\tilde{\chi}_1^0$, $m_{\tilde{\chi}_1^\pm} - m_{\tilde{\chi}_1^0} = 2$ GeV, $m_{\tilde{g}} < 300$ GeV
> 950	95	102	AAD	14E ATLS	$\ell^\pm \ell^\pm (\ell^\mp)$ + jets, $\tilde{g} \rightarrow t\bar{t}\tilde{\chi}_1^0$ simplified model
>1000	95	102	AAD	14E ATLS	$\ell^\pm \ell^\pm (\ell^\mp)$ + jets, $\tilde{g} \rightarrow t\bar{t}_1$ with $\tilde{t}_1 \rightarrow b\tilde{\chi}_1^\pm$ simplified model, $m_{\tilde{t}_1} < 200$ GeV, $m_{\tilde{\chi}_1^\pm} = 118$ GeV, $m_{\tilde{\chi}_1^0} = 60$ GeV
> 640	95	102	AAD	14E ATLS	$\ell^\pm \ell^\pm (\ell^\mp)$ + jets, $\tilde{g} \rightarrow t\bar{t}_1$ with $\tilde{t}_1 \rightarrow c\tilde{\chi}_1^0$ simplified model, $m_{\tilde{t}_1} = m_{\tilde{\chi}_1^0} + 20$ GeV
> 860	95	102	AAD	14E ATLS	$\ell^\pm \ell^\pm (\ell^\mp)$ + jets, $\tilde{g} \rightarrow qq'\tilde{\chi}_1^\pm$, $\tilde{\chi}_1^\pm \rightarrow W^{(*)}\tilde{\chi}_1^0$ simplified model, $m_{\tilde{\chi}_1^\pm} = 2 m_{\tilde{\chi}_1^0}$, $m_{\tilde{\chi}_1^0} < 400$ GeV
>1040	95	102	AAD	14E ATLS	$\ell^\pm \ell^\pm (\ell^\mp)$ + jets, $\tilde{g} \rightarrow qq'\tilde{\chi}_1^\pm$, $\tilde{\chi}_1^\pm \rightarrow W^{(*)}\tilde{\chi}_1^0$, $\tilde{\chi}_2^0 \rightarrow Z^{(*)}\tilde{\chi}_1^0$ simplified model, $m_{\tilde{\chi}_1^0} < 520$ GeV
>1200	95	102	AAD	14E ATLS	$\ell^\pm \ell^\pm (\ell^\mp)$ + jets, $\tilde{g} \rightarrow qq'\tilde{\chi}_1^\pm/\tilde{\chi}_2^0$, $\tilde{\chi}_1^\pm \rightarrow \ell^\pm \nu \tilde{\chi}_1^0$, $\tilde{\chi}_2^0 \rightarrow \ell^\pm \ell^\mp (\nu\nu)\tilde{\chi}_1^0$ simplified model
>1050	95	103	CHATRCHYAN14H	CMS	same-sign $\ell^\pm \ell^\pm$, $\tilde{g} \rightarrow t\bar{t}\tilde{\chi}_1^0$ simplified model, massless $\tilde{\chi}_1^0$
> 900	95	104	CHATRCHYAN14H	CMS	same-sign $\ell^\pm \ell^\pm$, $\tilde{g} \rightarrow qq'\tilde{\chi}_1^\pm$, $\tilde{\chi}_1^\pm \rightarrow W^\pm \tilde{\chi}_1^0$ simplified model, $m_{\tilde{\chi}_1^\pm} = 0.5 m_{\tilde{g}}$, massless $\tilde{\chi}_1^0$
>1050	95	105	CHATRCHYAN14H	CMS	same-sign $\ell^\pm \ell^\pm$, $\tilde{g} \rightarrow b\bar{t}\tilde{\chi}_1^\pm$, $\tilde{\chi}_1^\pm \rightarrow W^\pm \tilde{\chi}_1^0$ simplified model, $m_{\tilde{\chi}_1^\pm} = 300$ GeV, $m_{\tilde{\chi}_1^0} = 50$ GeV

¹ AAD 21AK searched in 139 fb^{-1} of pp collisions at $\sqrt{s} = 13$ TeV for pair production of gluinos and squarks in events with a single isolated electron or muon, originating from the decay of a W boson, multiple jets and significant \cancel{E}_T . No significant excess above the Standard Model expectations is observed. Limits are set on the gluino mass in the Tglu1B simplified model and on the squark mass in the Tsqk3 simplified model, see their Figure 8.

² AAD 21L searched in 139 fb^{-1} of pp collisions at $\sqrt{s} = 13$ TeV for pair production of gluinos and squarks in events with jets, large missing transverse momentum but no electrons or muons. No significant excess above the Standard Model expectations is observed. Limits are set on the gluino mass in the Tglu1A and Tglu1B simplified models, on the squark mass in the Tsqk1 and Tsqk3 simplified models and in a simplified model for gluino-squark production, see their Figures 13-17.

³ AAD 21X searched in 139 fb^{-1} of pp collisions at $\sqrt{s} = 13$ TeV for the decay of long-lived R-hadrons stopped by the calorimeter, producing high-momentum jets resulting in large out-of-time energy deposits in the calorimeters. These decays are detected using data collected during periods in the LHC bunch structure when collisions are absent. No significant excess above the predicted background is observed. Limits are set on the R-hadron mass in the Tglu1A simplified model as a function of the R-hadron lifetime, for different $m_{\tilde{\chi}_1^0}$. See Figures 9, 10.

⁴ SIRUNYAN 21AD searched in 137 fb^{-1} of pp collisions at $\sqrt{s} = 13$ TeV for supersymmetry in events with multiple jets, no leptons, and large \cancel{E}_T . No significant excess above the Standard Model expectations is observed. Limits are set on the top squark mass in the simplified models Tstop1, Tstop2 with $m_{\tilde{t}_\pm} = (m_{\tilde{t}} + m_{\tilde{\chi}_1^0})/2$, and a 50:50 mixture of these with $m_{\tilde{t}_\pm} - m_{\tilde{\chi}_1^0} = 5$ GeV, see their Figure 8. Limits are also set on the top squark mass for $10 \text{ GeV} < m_{\tilde{t}} - m_{\tilde{\chi}_1^0} < 80 \text{ GeV}$ in the simplified models Tstop2, Tstop3, and Tstop4, see their Figure 9. For indirect top squark production, limits are set on the gluino mass in the simplified models Tglu3A, Tglu3C with $m_{\tilde{t}} - m_{\tilde{\chi}_1^0} = 20$ GeV, and Tglu3D with $m_{\tilde{t}_\pm} - m_{\tilde{\chi}_1^0} = 5$ GeV, see their Figure 10.

⁵ SIRUNYAN 21M searched in 137 fb^{-1} of pp collisions at $\sqrt{s} = 13$ TeV for supersymmetry in events with two opposite-sign same-flavor leptons (electrons, muons) and \cancel{E}_T . No significant excess above the Standard Model expectations is observed. Limits are set on the gluino mass in the simplified model Tglu4C, see their Figure 10, on the $\tilde{\chi}_2^0$ and $\tilde{\chi}_1^\pm$ mass in Tchl1n2Fa, see their Figure 11, on the $\tilde{\chi}_1^0$ mass in Tchl1n1C and Tchl1n1B for $m_{\tilde{\chi}_2^0} = m_{\tilde{\chi}_1^\pm} = m_{\tilde{\chi}_1^0}$, see their Figure 12. Limits are also set on the light squark mass for the simplified model Tsqk2A, on the sbottom mass in Tsb0t3, see their Figure 13, and on the slepton mass in direct electroweak pair production of mass-degenerate left- and right-handed sleptons (selectrons and smuons), see their Figure 14.

⁶ AAD 20AL searched in 139 fb^{-1} of pp collisions at $\sqrt{s} = 13$ TeV for events with 8 or more jets and moderate missing transverse momentum. The selection makes requirements according to the number of b -tagged jets and the scalar sum of masses of large-radius jets. No significant excess above the Standard Model expectations is observed. Limits up to about 2 TeV are set on the gluino mass in Tglu1E simplified model. Limits up to about 1.8 TeV are set on the gluino mass in Tglu3A simplified model. See their Fig. 10(a).

⁷ AAD 20V searched in 139 fb^{-1} of pp collisions at $\sqrt{s} = 13$ TeV in final states with same-sign charged leptons (electrons or muons) and jets. No significant excess over the Standard Model expectation is observed. In the Tglu1E model, considering off-shell intermediate W and Z bosons in the decay chains, gluino masses are excluded at 95% C.L. up to 1600 GeV for neutralino masses of 100 GeV or above (up to 1000 GeV). See their Fig. 7(a).

⁸ SIRUNYAN 20B searched in 35.9 fb^{-1} of pp collisions at $\sqrt{s} = 13$ TeV for events with at least one photon and large \cancel{E}_T . No significant excess above the Standard Model expectations is observed. Limits are set on chargino masses in a general gauge-mediated SUSY breaking (GGM) scenario Tchl1n12-GGM, see Figure 4. Limits are also set on the NLSP mass in the Tchl1ch1F and Tchl1ch1G simplified models, see their Figure 5. Finally, limits are set on the gluino mass in the Tglu4A simplified model, see Figure 6.

⁹ SIRUNYAN 20BJ searched in 137 fb^{-1} of pp collisions at $\sqrt{s} = 13$ TeV for events containing two hadronically decaying, highly energetic Z bosons and large \cancel{E}_T . No significant excess above the Standard Model expectations is observed. Limits are set on the gluino mass in the Tglu1H simplified model, see their Figure 9.

¹⁰ SIRUNYAN 20E searched in 137 fb^{-1} of pp collisions at $\sqrt{s} = 13$ TeV for events with a single electron or muon and multiple jets, including at least one identified as originating from a b -quark, and large \cancel{E}_T . No significant excess above the Standard Model expectations is observed. Limits are set on the gluino mass in the Tglu3A simplified model, see their Fig. 10, and the Tglu3C simplified model, see their Fig. 11.

¹¹ SIRUNYAN 20T searched in 137 fb^{-1} of pp collisions at $\sqrt{s} = 13$ TeV for events with at least two jets, and two isolated same-sign or three or more charged leptons (electrons or muons). No significant excess above the Standard Model expectations is observed. Limits are set on the gluino mass in the Tglu3A, Tglu3B, Tglu3C and Tglu3D simplified models, see their Figure 7, and in the Tglu1C and Tglu1B simplified models, see their Figures 8 and 9. Limits are also set on the sbottom mass in the Tsb0t2 simplified model, see their Figure 10, and on the stop mass in the Tstop7 simplified model, see their Figure 11. Finally, limits are set on the gluino mass in RPV simplified models where the gluino decays either via $\tilde{g} \rightarrow qq\bar{q}\bar{q} + e/\mu/\tau$ or via $\tilde{g} \rightarrow tbs$, see Figure 12.

¹² AABOUD 19J searched in 36.1 fb^{-1} of pp collisions at $\sqrt{s} = 13$ TeV in final states with hadronic jets, 1 or two hadronically decaying τ and \cancel{E}_T . In Tglu1F, gluino masses are excluded at 95% C.L. up to 2000 GeV for neutralino masses of 100 GeV or below. Neutralino masses up to 1000 GeV are excluded for all gluino masses below 1400 GeV. See their Fig. 9. Limits are also presented in the context of Gauge-Mediated Symmetry Breaking models: in this case, values of A below 110 TeV are excluded at the 95% CL for all values of $\tan\beta$ in the range $2 < \tan\beta < 60$, see their Fig. 10.

¹³ SIRUNYAN 19AG searched in 35.9 fb^{-1} of pp collisions at $\sqrt{s} = 13$ TeV for events with two photons and large \cancel{E}_T . No significant excess above the Standard Model expectations is observed. Limits are set on the gluino mass in the Tglu4B simplified model and on the squark mass in the Tsqk4B simplified model, see their Figure 3.

¹⁴ SIRUNYAN 19AU searched in 35.9 fb^{-1} of pp collisions at $\sqrt{s} = 13$ TeV for events with at least one photon, jets, some of which are identified as originating from b -quarks, and large \cancel{E}_T . No significant excess above the Standard Model expectations is observed. In the framework of GMSB, limits are set on the gluino mass in the Tglu4C, Tglu4D and Tglu4E simplified models, and on the top squark mass in the Tstop13 simplified model, see their Figure 5.

¹⁵ SIRUNYAN 19CE searched in 35.9 fb^{-1} of pp collisions at $\sqrt{s} = 13$ TeV for new particles decaying to a photon and two gluons in events with at least three large-radius jets of which two have substructure and are composed of a photon and two gluons. No statistically significant excess is observed above the SM background expectation. Upper limits at 95% confidence level on the cross section for gluino pair production are set, using a simplified Tglu1A-like stealth SUSY model. Gluino masses up to 1500-1700 GeV are excluded, depending on the neutralino mass, with the highest exclusion set for $m_{\tilde{\chi}_1^0} = 200$ GeV. See their Fig. 4.

¹⁶ SIRUNYAN 19CH searched in 137 fb^{-1} of pp collisions at $\sqrt{s} = 13$ TeV for events containing multiple jets and large \cancel{E}_T . No significant excess above the Standard Model expectations is observed. Limits are set on the gluino mass in the Tglu1A, Tglu1C, Tglu2A and Tglu3A simplified models, see their Figure 13. Limits are also set on squark, sbottom and stop masses in the Tsqk1, Tsb0t1, Tstop1 simplified models, see their Figure 14.

¹⁷ SIRUNYAN 19K searched in 35.9 fb^{-1} of pp collisions at $\sqrt{s} = 13$ TeV for events with a photon, an electron or muon, and large \cancel{E}_T . No significant excess above the Standard Model expectations is observed. In the framework of GMSB, limits are set on the chargino and neutralino mass in the Tchl1n1A simplified model, see their Figure 6. Limits are also set on the gluino mass in the Tglu4A simplified model, and on the squark mass in the Tsqk4A simplified model, see their Figure 7.

¹⁸ SIRUNYAN 19S searched in 35.9 fb^{-1} of pp collisions at $\sqrt{s} = 13$ TeV for events with zero or one charged leptons, jets and \cancel{E}_T . The razor variables (M_R and R^2) are used to categorize the events. No significant excess above the Standard Model expectations is observed. Limits are set on the gluino mass in the Tglu3A and Tglu3C simplified models, see Figures 22 and 23, and on the stop mass in the Tstop1 simplified model, see their Figure 24.

¹⁹ AABOUD 18AR searched in 36.1 fb^{-1} of pp collisions at $\sqrt{s} = 13$ TeV for gluino pair production in events containing large missing transverse momentum and several energetic jets, at least three of which must be identified as originating from b -quarks. No excess is found above the predicted background. In Tglu3A models, gluino masses of less than 1.97 TeV are excluded for $m_{\tilde{\chi}_1^0}$ below 300 GeV, see their Fig. 10(a). Interpretations are also provided for scenarios where Tglu3A modes mix with Tglu2A and Tglu3D, see their Fig. 11.

²⁰ AABOUD 18AR searched in 36.1 fb^{-1} of pp collisions at $\sqrt{s} = 13$ TeV for gluino pair production in events containing large missing transverse momentum and several energetic jets, at least three of which must be identified as originating from b -quarks. No excess is found above the predicted background. In Tglu2A models, gluino masses of less than 1.92 TeV are excluded for $m_{\tilde{\chi}_1^0}$ below 600 GeV, see their Fig. 10(b). Interpretations are also provided for scenarios where Tglu2A modes mix with Tglu3A and Tglu3D, see their Fig. 11.

²¹ AABOUD 18AS searched in 36.1 fb^{-1} of pp collisions at $\sqrt{s} = 13$ TeV for gluino pair production in the context of AMSB or phenomenological MSSM scenarios with wino-like

Searches Particle Listings

Supersymmetric Particle Searches

- LSP and long-lived charginos. Events with a disappearing track due to a low-momentum pion accompanied by at least four jets are considered. No significant excess above the Standard Model expectations is observed. Exclusion limits are set at 95% confidence level on the mass of gluinos for different chargino lifetimes. Gluino masses up to 1.65 TeV are excluded assuming a chargino mass of 460 GeV and lifetime of 0.2 ns, corresponding to a mass-splitting between the charged and neutral wino of around 160 MeV. See their Fig. 9.
- 22 AABOUD 18BJ searched in 36.1 fb^{-1} of pp collisions at $\sqrt{s} = 13 \text{ TeV}$ in events with two opposite-sign charged leptons (electrons and muons), jets and missing transverse momentum, with various requirements to be sensitive to signals with different kinematic endpoint values in the dilepton invariant mass distribution. The data are found to be consistent with the SM expectation. Results are interpreted in the Tglu1G model: gluino masses below 1850 GeV are excluded for $m_{\tilde{\chi}_1^0} = 100 \text{ GeV}$, see their Fig. 12(a).
- 23 AABOUD 18BJ searched in 36.1 fb^{-1} of pp collisions at $\sqrt{s} = 13 \text{ TeV}$ in events with two opposite-sign charged leptons (electrons and muons), jets and missing transverse momentum, with various requirements to be sensitive to signals with different kinematic endpoint values in the dilepton invariant mass distribution. The data are found to be consistent with the SM expectation. Results are interpreted in the Tglu1H model: gluino masses below 1650 GeV are excluded for $m_{\tilde{\chi}_1^0} = 100 \text{ GeV}$, see their Fig. 13(a).
- 24 AABOUD 18U searched in 36.1 fb^{-1} of pp collisions at $\sqrt{s} = 13 \text{ TeV}$ in events with at least one isolated photon, possibly jets and significant transverse momentum targeting generalised models of gauge-mediated SUSY breaking. No significant excess of events is observed above the SM prediction. Results for the di-photon channel are interpreted in terms of lower limits on the masses of gluinos in Tglu4B models, which reach as high as 2.3 TeV. Gluinos with masses below 2.15 TeV are excluded for any NLSP mass, see their Fig. 8.
- 25 AABOUD 18U searched in 36.1 fb^{-1} of pp collisions at $\sqrt{s} = 13 \text{ TeV}$ in events with at least one isolated photon, possibly jets and significant transverse momentum targeting generalised models of gauge-mediated SUSY breaking. No significant excess of events is observed above the SM prediction. Results of the $\gamma + \text{jets} + \cancel{E}_T$ channel are interpreted in terms of lower limits on the masses of gluinos in GGM higgsino-bino models (mix of Tglu4B and Tglu4C), which reach as high as 2050 GeV. Gluino masses below 1600 GeV are excluded for any NLSP mass provided that $m_{\tilde{g}} - m_{\tilde{\chi}_1^0} > 50 \text{ GeV}$. See their Fig. 11.
- 26 AABOUD 18V searched in 36.1 fb^{-1} of pp collisions at $\sqrt{s} = 13 \text{ TeV}$ in events with no charged leptons, jets and missing transverse momentum. The data are found to be consistent with the SM expectation. Results are interpreted in the Tglu1A model: gluino masses below 2030 GeV are excluded for massless LSP, see their Fig. 13(b).
- 27 AABOUD 18V searched in 36.1 fb^{-1} of pp collisions at $\sqrt{s} = 13 \text{ TeV}$ in events with no charged leptons, jets and missing transverse momentum. The data are found to be consistent with the SM expectation. Results are interpreted in the Tglu1B model. Assuming that $m_{\tilde{\chi}_1^\pm} = 0.5 (m_{\tilde{g}} + m_{\tilde{\chi}_1^0})$, gluino masses below 1980 GeV are excluded for massless LSP, see their Fig. 14(c). Exclusions are also shown assuming $m_{\tilde{\chi}_1^0} = 60 \text{ GeV}$, see their Fig. 14(d).
- 28 AABOUD 18V searched in 36.1 fb^{-1} of pp collisions at $\sqrt{s} = 13 \text{ TeV}$ in events with no charged leptons, jets and missing transverse momentum. The data are found to be consistent with the SM expectation. Results are interpreted in the Tglu1E model: gluino masses below 1750 GeV are excluded for $m_{\tilde{\chi}_1^0} = 1 \text{ GeV}$ and any $m_{\tilde{\chi}_2^0}$ above 100 GeV, see their Fig. 15. Gluino mass exclusion up to 2 TeV is found for $m_{\tilde{\chi}_2^0} = 1 \text{ TeV}$.
- 29 SIRUNYAN 18AA searched in 35.9 fb^{-1} of pp collisions at $\sqrt{s} = 13 \text{ TeV}$ for events with at least one photon and large \cancel{E}_T . No significant excess above the Standard Model expectations is observed. Limits are set on wino masses in a general gauge-mediated SUSY breaking (GGM) scenario with bino-like $\tilde{\chi}_1^0$ and wino-like $\tilde{\chi}_1^\pm$ and $\tilde{\chi}_2^0$, see Figure 7. Limits are also set on the NLSP mass in the Tch1n1A and Tch1ch1A simplified models, see their Figure 8. Finally, limits are set on the gluino mass in the Tglu4A and Tglu4B simplified models, see their Figure 9, and on the squark mass in the Tskq4A and Tskq4B simplified models, see their Figure 10.
- 30 SIRUNYAN 18AC searched in 35.9 fb^{-1} of pp collisions at $\sqrt{s} = 13 \text{ TeV}$ for events with a single electron or muon and multiple jets. No significant excess above the Standard Model expectations is observed. Limits are set on the gluino mass in the Tglu3A and Tglu1B simplified models, see their Figure 5.
- 31 SIRUNYAN 18AL searched in 35.9 fb^{-1} of pp collisions at $\sqrt{s} = 13 \text{ TeV}$ for events with at least three charged leptons, in any combination of electrons and muons, jets and significant \cancel{E}_T . No significant excess above the Standard Model expectations is observed. Limits are set on the gluino mass in the Tglu3A and Tglu1C simplified models, see their Figure 5. Limits are also set on the sbottom mass in the Tstop2 simplified model, see their Figure 6, and on the stop mass in the Tstop7 simplified model, see their Figure 7.
- 32 SIRUNYAN 18AR searched in 35.9 fb^{-1} of pp collisions at $\sqrt{s} = 13 \text{ TeV}$ for events containing two opposite-charge, same-flavour leptons (electrons or muons), jets and \cancel{E}_T . No significant excess above the Standard Model expectations is observed. Limits are set on the gluino mass in the Tglu4C simplified model, see their Figure 7. Limits are also set on the chargino/neutralino mass in the Tch1n2F simplified models, see their Figure 8, and on the higgsino mass in the Tn1n1B and Tn1n1C simplified models, see their Figure 9. Finally, limits are set on the sbottom mass in the Tstop3 simplified model, see their Figure 10.
- 33 SIRUNYAN 18AV searched in 35.9 fb^{-1} of pp collisions at $\sqrt{s} = 13 \text{ TeV}$ for events containing one or more jets and significant \cancel{E}_T . No significant excess above the Standard Model expectations is observed. Limits are set on the gluino mass in the Tglu1A, Tglu2A and Tglu3A simplified models, see their Figure 3. Limits are also set on squark, sbottom and stop masses in the Tskq1, Tstop1, Tstop1 and Tstop4 simplified models, see their Figure 3. Finally, limits are set on long-lived gluino masses in a Tglu1A simplified model where the gluino is metastable or long-lived with proper decay lengths in the range $10^{-3} \text{ mm} < c\tau < 10^5 \text{ mm}$, see their Figure 4.
- 34 SIRUNYAN 18D searched in 35.9 fb^{-1} of pp collisions at $\sqrt{s} = 13 \text{ TeV}$ for events containing identified hadronically decaying top quarks, no leptons, and \cancel{E}_T . No significant excess above the Standard Model expectations is observed. Limits are set on the stop mass in the Tstop1 simplified model, see their Figure 8, and on the gluino mass in the Tglu3A, Tglu3B, Tglu3C and Tglu3E simplified models, see their Figure 9.
- 35 SIRUNYAN 18M searched in 35.9 fb^{-1} of pp collisions at $\sqrt{s} = 13 \text{ TeV}$ for events with one or more high-momentum Higgs bosons, decaying to pairs of b -quarks, and large \cancel{E}_T . No significant excess above the Standard Model expectations is observed. Limits are set on the gluino mass in the Tglu1I and Tglu1J simplified models, see their Figure 3.
- 36 AABOUD 17AJ searched in 36.1 fb^{-1} of pp collisions at $\sqrt{s} = 13 \text{ TeV}$ for events with two same-sign or three leptons, jets and large missing transverse momentum. No significant excess above the Standard Model expectations is observed. Limits up to 1.75 TeV are set on the gluino mass in Tglu3A simplified models in case of off-shell top squarks and for $m_{\tilde{\chi}_1^0} = 100 \text{ GeV}$. See their Figure 4(a).
- 37 AABOUD 17AJ searched in 36.1 fb^{-1} of pp collisions at $\sqrt{s} = 13 \text{ TeV}$ for events with two same-sign or three leptons, jets and large missing transverse momentum. No significant excess above the Standard Model expectations is observed. Limits up to 1.57 TeV are set on the gluino mass in Tglu1E simplified models (2-step models) for $m_{\tilde{\chi}_1^0} = 100 \text{ GeV}$. See their Figure 4(b).
- 38 AABOUD 17AJ searched in 36.1 fb^{-1} of pp collisions at $\sqrt{s} = 13 \text{ TeV}$ for events with two same-sign or three leptons, jets and large missing transverse momentum. No significant excess above the Standard Model expectations is observed. Limits up to 1.86 TeV are set on the gluino mass in Tglu1G simplified models for $m_{\tilde{\chi}_1^0} = 200 \text{ GeV}$. See their Figure 4(c).
- 39 AABOUD 17AR searched in 36.1 fb^{-1} of pp collisions at $\sqrt{s} = 13 \text{ TeV}$ for events with one isolated lepton, at least two jets and large missing transverse momentum. No significant excess above the Standard Model expectations is observed. Limits up to 2.1 TeV are set on the gluino mass in Tglu1B simplified models, with $x = (m_{\tilde{\chi}_1^\pm} - m_{\tilde{\chi}_1^0}) / (m_{\tilde{g}} - m_{\tilde{\chi}_1^0}) = 1/2$. Similar limits are obtained for variable x and fixed neutralino mass, $m_{\tilde{\chi}_1^0} = 60 \text{ GeV}$. See their Figure 13.
- 40 AABOUD 17AR searched in 36.1 fb^{-1} of pp collisions at $\sqrt{s} = 13 \text{ TeV}$ for events with one isolated lepton, at least two jets and large missing transverse momentum. No significant excess above the Standard Model expectations is observed. Limits up to 1.74 TeV are set on the gluino mass in Tglu1E simplified model. Limits up to 1.7 TeV are also set on pMSSM models leading to similar signal event topologies. See their Figure 13.
- 41 AABOUD 17AY searched in 36.1 fb^{-1} of pp collisions at $\sqrt{s} = 13 \text{ TeV}$ for events with at least four jets and large missing transverse momentum. No significant excess above the Standard Model expectations is observed. Limits up to 1.8 TeV are set on the gluino mass in Tglu3A simplified models assuming $m_{\tilde{t}_1} - m_{\tilde{\chi}_1^0} = 5 \text{ GeV}$. See their Figure 13.
- 42 AABOUD 17AZ searched in 36.1 fb^{-1} of pp collisions at $\sqrt{s} = 13 \text{ TeV}$ for events with at least seven jets and large missing transverse momentum. Selected events are further classified based on the presence of large R -jets or b -jets and no leptons. No significant excess above the Standard Model expectations is observed. Limits up to 1.8 TeV are set on the gluino mass in Tglu1E simplified models. See their Figure 6b.
- 43 AABOUD 17AZ searched in 36.1 fb^{-1} of pp collisions at $\sqrt{s} = 13 \text{ TeV}$ for events with at least seven jets and large missing transverse momentum. Selected events are further classified based on the presence of large R -jets or b -jets and no leptons. No significant excess above the Standard Model expectations is observed. Limits up to 1.54 TeV are set on the gluino mass in Tglu3A simplified models. See their Figure 7a.
- 44 AABOUD 17N searched in 14.7 fb^{-1} of pp collisions at $\sqrt{s} = 13 \text{ TeV}$ in final states with 2 same-flavor, opposite-sign leptons (electrons or muons), jets and large missing transverse momentum. In Tglu1J models, gluino masses are excluded at 95% C.L. up to 1300 GeV for $m_{\tilde{\chi}_1^0} = 0 \text{ GeV}$ and $m_{\tilde{\chi}_2^0} = 1100 \text{ GeV}$. See their Fig. 12 for exclusion limits as a function of $m_{\tilde{\chi}_2^0}$. Limits are also presented assuming $m_{\tilde{\chi}_2^0} = m_{\tilde{\chi}_1^0} + 100 \text{ GeV}$, see their Fig. 13.
- 45 AABOUD 17N searched in 14.7 fb^{-1} of pp collisions at $\sqrt{s} = 13 \text{ TeV}$ in final states with 2 same-flavor, opposite-sign leptons (electrons or muons), jets and large missing transverse momentum. In Tglu1H models, gluino masses are excluded at 95% C.L. up to 1310 GeV for $m_{\tilde{\chi}_1^0} < 400 \text{ GeV}$ and assuming $m_{\tilde{\chi}_2^0} = (m_{\tilde{g}} + m_{\tilde{\chi}_1^0})/2$. See their Fig. 15.
- 46 AABOUD 17N searched in 14.7 fb^{-1} of pp collisions at $\sqrt{s} = 13 \text{ TeV}$ in final states with 2 same-flavor, opposite-sign leptons (electrons or muons), jets and large missing transverse momentum. In Tglu1G models, gluino masses are excluded at 95% C.L. up to 1700 GeV for small $m_{\tilde{\chi}_1^0}$. The results probe kinematic endpoints as small as $m_{\tilde{\chi}_2^0} - m_{\tilde{\chi}_1^0} = (m_{\tilde{g}} - m_{\tilde{\chi}_1^0})/2 = 50 \text{ GeV}$. See their Fig. 14.
- 47 KHACHATRYAN 17 searched in 2.3 fb^{-1} of pp collisions at $\sqrt{s} = 13 \text{ TeV}$ for events containing four or more jets, no more than one lepton, and missing transverse momentum, using the razor variables (M_R and R^2) to discriminate between signal and background processes. No evidence for an excess over the expected background is observed. Limits are derived on the gluino mass in the Tglu1A, Tglu2A and Tglu3A simplified models, see Figs. 16 and 17. Also, assuming gluinos decay only via three-body processes involving third-generation quarks plus a neutralino/chargino, and assuming $m_{\tilde{\chi}_1^\pm} = m_{\tilde{\chi}_1^0} + 5 \text{ GeV}$, a branching ratio-independent limit on the gluino mass is given, see Fig. 16.
- 48 KHACHATRYAN 17AD searched in 2.3 fb^{-1} of pp collisions at $\sqrt{s} = 13 \text{ TeV}$ for events containing at least four jets (including b -jets), missing transverse momentum and tagged top quarks. No evidence for an excess over the expected background is observed. Gluino masses up to 1550 GeV and neutralino masses up to 900 GeV are excluded at 95% C.L. See Fig. 13.
- 49 KHACHATRYAN 17AD searched in 2.3 fb^{-1} of pp collisions at $\sqrt{s} = 13 \text{ TeV}$ for events containing at least four jets (including b -jets), missing transverse momentum and tagged top quarks. No evidence for an excess over the expected background is observed. Gluino masses up to 1450 GeV and neutralino masses up to 820 GeV are excluded at 95% C.L. See Fig. 13.
- 50 KHACHATRYAN 17AS searched in 2.3 fb^{-1} of pp collisions at $\sqrt{s} = 13 \text{ TeV}$ for events with a single electron or muon and multiple jets. No significant excess above the Standard Model expectations is observed. Limits are set on the gluino mass in the Tglu3A and Tglu1B simplified models, see their Fig. 7.
- 51 KHACHATRYAN 17AW searched in 2.3 fb^{-1} of pp collisions at $\sqrt{s} = 13 \text{ TeV}$ for events with at least three charged leptons, in any combination of electrons and muons, and significant \cancel{E}_T . No significant excess above the Standard Model expectations is observed. Limits are set on the gluino mass in the Tglu3A and Tglu1C simplified models, and on the sbottom mass in the Tstop2 simplified model, see their Figure 4.
- 52 KHACHATRYAN 17P searched in 2.3 fb^{-1} of pp collisions at $\sqrt{s} = 13 \text{ TeV}$ for events with one or more jets and large \cancel{E}_T . No significant excess above the Standard Model expectations is observed. Limits are set on the gluino mass in the Tglu1A, Tglu2A, Tglu3A, Tglu3B, Tglu3C and Tglu3D simplified models, see their Figures 7 and 8. Limits are also set on the squark mass in the Tskq1 simplified model, see their Fig. 7, and on the sbottom mass in the Tstop1 simplified model, see Fig. 8. Finally, limits are set on the stop mass in the Tstop1, Tstop3, Tstop4, Tstop6 and Tstop7 simplified models, see Fig. 8.

- ⁵³ KHACHATRYAN 17v searched in 2.3 fb^{-1} of pp collisions at $\sqrt{s} = 13 \text{ TeV}$ for events with two photons and large $E_{\cancel{T}}$. No significant excess above the Standard Model expectations is observed. Limits are set on the gluino and squark mass in the context of general gauge mediation models Tglu4B and Tsqk4, see their Fig. 4.
- ⁵⁴ SIRUNYAN 17AF searched in 35.9 fb^{-1} of pp collisions at $\sqrt{s} = 13 \text{ TeV}$ for events with a single lepton (electron or muon), jets, including at least one jet originating from a b -quark, and large $E_{\cancel{T}}$. No significant excess above the Standard Model expectations is observed. Limits are set on the gluino mass in the Tglu3A and Tglu3B simplified models, see their Figure 2.
- ⁵⁵ SIRUNYAN 17AY searched in 35.9 fb^{-1} of pp collisions at $\sqrt{s} = 13 \text{ TeV}$ for events with at least one photon, jets and large $E_{\cancel{T}}$. No significant excess above the Standard Model expectations is observed. Limits are set on the gluino mass in the Tglu4A and Tglu4B simplified models, and on the squark mass in the Tskq4A and Tskq4B simplified models, see their Figure 6.
- ⁵⁶ SIRUNYAN 17AZ searched in 35.9 fb^{-1} of pp collisions at $\sqrt{s} = 13 \text{ TeV}$ for events with one or more jets and large $E_{\cancel{T}}$. No significant excess above the Standard Model expectations is observed. Limits are set on the gluino mass in the Tglu1A, Tglu2A, Tglu3A simplified models, see their Figures 6. Limits are also set on the squark mass in the Tskq1 simplified model (for single light squark and for 8 degenerate light squarks), on the sbottom mass in the Tsb0t1 simplified model and on the stop mass in the Tstop1 simplified model, see their Fig. 7. Finally, limits are set on the stop mass in the Tstop2, Tstop4 and Tstop8 simplified models, see Fig. 8.
- ⁵⁷ SIRUNYAN 17P searched in 35.9 fb^{-1} of pp collisions at $\sqrt{s} = 13 \text{ TeV}$ for events with multiple jets and large $E_{\cancel{T}}$. No significant excess above the Standard Model expectations is observed. Limits are set on the gluino mass in the Tglu1A, Tglu1C, Tglu2A, Tglu3A and Tglu3D simplified models, see their Fig. 12. Limits are also set on the squark mass in the Tskq1 simplified model, on the stop mass in the Tstop1 simplified model, and on the sbottom mass in the Tsb0t1 simplified model, see Fig. 13.
- ⁵⁸ SIRUNYAN 17S searched in 35.9 fb^{-1} of pp collisions at $\sqrt{s} = 13 \text{ TeV}$ for events with two isolated same-sign leptons, jets, and large $E_{\cancel{T}}$. No significant excess above the Standard Model expectations is observed. Limits are set on the mass of the gluino mass in the Tglu3A, Tglu3B, Tglu3C, Tglu3D and Tglu1B simplified models, see their Figures 5 and 6, and on the sbottom mass in the Tsb0t2 simplified model, see their Figure 6.
- ⁵⁹ AABOUD 16AC searched in 3.2 fb^{-1} of pp collisions at $\sqrt{s} = 13 \text{ TeV}$ in final states with hadronic jets, 1 or two hadronically decaying τ and $E_{\cancel{T}}$. In Tglu1F, gluino masses are excluded at 95% C.L. up to 1570 GeV for neutralino masses of 100 GeV or below. Neutralino masses up to 700 GeV are excluded for all gluino masses between 800 GeV and 1500 GeV, while the strongest neutralino-mass exclusion of 750 GeV is achieved for gluino masses around 1400 GeV. See their Fig. 8. Limits are also presented in the context of Gauge-Mediated Symmetry Breaking models: in this case, values of A below 92 TeV are excluded at the 95% CL, corresponding to gluino masses below 2000 GeV. See their Fig. 9.
- ⁶⁰ AABOUD 16I searched in 3.2 fb^{-1} of pp collisions at $\sqrt{s} = 13 \text{ TeV}$ in final states with one isolated electron or muon, hadronic jets, and $E_{\cancel{T}}$. Gluino-mediated pair production of stops with a nearly mass-degenerate stop and neutralino are targeted and gluino masses are excluded at 95% C.L. up to 1460 GeV. A 100% of stops decaying via charm + neutralino is assumed. The results are also valid in case of 4-body decays $\tilde{t}_1 \rightarrow f\bar{f}'b\tilde{\chi}_1^0$. See their Fig. 8.
- ⁶¹ AABOUD 16M searched in 3.2 fb^{-1} of pp collisions at $\sqrt{s} = 13 \text{ TeV}$ for events with two photons, hadronic jets and $E_{\cancel{T}}$. No significant excess above the Standard Model expectations is observed. Exclusion limits at 95% C.L. are set on gluino masses in the general gauge-mediated SUSY breaking model (GGM), for bino-like NLSP. See their Fig. 3.
- ⁶² AABOUD 16N searched in 3.2 fb^{-1} of pp collisions at $\sqrt{s} = 13 \text{ TeV}$ for events containing hadronic jets, large $E_{\cancel{T}}$, and no electrons or muons. No significant excess above the Standard Model expectations is observed. Gluino masses below 1510 GeV are excluded at the 95% C.L. in a simplified model with only gluinos and the lightest neutralino. See their Fig. 7b.
- ⁶³ AABOUD 16N searched in 3.2 fb^{-1} of pp collisions at $\sqrt{s} = 13 \text{ TeV}$ for events containing hadronic jets, large $E_{\cancel{T}}$, and no electrons or muons. No significant excess above the Standard Model expectations is observed. Gluino masses below 1500 GeV are excluded at the 95% C.L. in a simplified model with gluinos decaying via an intermediate $\tilde{\chi}_1^\pm$ to two quarks, a W boson and a $\tilde{\chi}_1^0$, for $m_{\tilde{\chi}_1^0} = 200 \text{ GeV}$. See their Fig. 8.
- ⁶⁴ AAD 16AD searched in 3.2 fb^{-1} of pp collisions at $\sqrt{s} = 13 \text{ TeV}$ for events containing several energetic jets, of which at least three must be identified as b -jets, large $E_{\cancel{T}}$ and no electrons or muons. No significant excess above the Standard Model expectations is observed. For $\tilde{\chi}_1^0$ below 800 GeV, gluino masses below 1780 GeV are excluded at 95% C.L. for gluinos decaying via bottom squarks. See their Fig. 7a.
- ⁶⁵ AAD 16AD searched in 3.2 fb^{-1} of pp collisions at $\sqrt{s} = 13 \text{ TeV}$ for events containing several energetic jets, of which at least three must be identified as b -jets, large $E_{\cancel{T}}$ and one electron or muon. Large-radius jets with a high mass are also used to identify highly boosted top quarks. No significant excess above the Standard Model expectations is observed. For $\tilde{\chi}_1^0$ below 700 GeV, gluino masses below 1760 GeV are excluded at 95% C.L. for gluinos decaying via top squarks. See their Fig. 7b.
- ⁶⁶ AAD 16BB searched in 3.2 fb^{-1} of pp collisions at $\sqrt{s} = 13 \text{ TeV}$ for events with exactly two same-sign leptons or at least three leptons, multiple hadronic jets, b -jets, and $E_{\cancel{T}}$. No significant excess over the Standard Model expectation is found. Exclusion limits at 95% C.L. are set on the gluino mass in various simplified models (Tglu1D, Tglu1E, Tglu3A). See their Figs. 4.a, 4.b, and 4.d.
- ⁶⁷ AAD 16BC searched in 3.2 fb^{-1} of pp collisions at $\sqrt{s} = 13 \text{ TeV}$ in final states with one isolated electron or muon, hadronic jets, and $E_{\cancel{T}}$. The data agree with the SM background expectation in the six signal selections defined in the search, and the largest deviation is a 2.1 standard deviation excess. Gluinos are excluded at 95% C.L. up to 1600 GeV assuming they decay via the lightest chargino to the lightest neutralino as in the model Tglu1B for $m_{\tilde{\chi}_1^0} = 100 \text{ GeV}$, assuming $m_{\tilde{\chi}_1^\pm} = (m_{\tilde{g}} + m_{\tilde{\chi}_1^0})/2$. See their Fig. 6.
- ⁶⁸ AAD 16V searched in 3.2 fb^{-1} of pp collisions at $\sqrt{s} = 13 \text{ TeV}$ for events with $E_{\cancel{T}}$ various hadronic jet multiplicities from ≥ 7 to ≥ 10 and with various b -jet multiplicity requirements. No significant excess over the Standard Model expectation is found. Exclusion limits at 95% C.L. are set on the gluino mass in one simplified model (Tglu1E) and a pMSSM-inspired model. See their Fig. 5.
- ⁶⁹ KHACHATRYAN 16AM searched in 19.7 fb^{-1} of pp collisions at $\sqrt{s} = 8 \text{ TeV}$ for events with highly boosted W -bosons and b -jets, using the razor variables (M_R and R^2) to discriminate between signal and background processes. No significant excess above the Standard Model expectations is observed. Limits are set on the gluino mass in the Tglu3C and Tglu3B simplified models, see Fig. 12.
- ⁷⁰ KHACHATRYAN 16BJ searched in 2.3 fb^{-1} of pp collisions at $\sqrt{s} = 13 \text{ TeV}$ for events with two isolated same-sign dileptons and jets in the final state. No significant excess above the Standard Model expectations is observed. Limits are set on the gluino mass in the following simplified models: Tglu3A and Tglu3D, see Fig. 4, Tglu3B and Tglu3C, see Fig. 5, and Tglu1B, see Fig. 7.
- ⁷¹ KHACHATRYAN 16BS searched in 2.3 fb^{-1} of pp collisions at $\sqrt{s} = 13 \text{ TeV}$ for events with at least one energetic jet, no isolated leptons, and significant $E_{\cancel{T}}$, using the transverse mass variable M_{T2} to discriminate between signal and background processes. No significant excess above the Standard Model expectations is observed. Limits are set on the gluino mass in the Tglu1A, Tglu2A and Tglu3A simplified models, see Fig. 10 and Table 3.
- ⁷² KHACHATRYAN 16BY searched in 2.3 fb^{-1} of pp collisions at $\sqrt{s} = 13 \text{ TeV}$ for events with two opposite-sign, same-flavour leptons, jets, and missing transverse momentum. No significant excess above the Standard Model expectations is observed. Limits are set on the gluino mass in the Tglu4C simplified model, see Fig. 4, and on sbottom masses in the Tsb0t3 simplified model, see Fig. 5.
- ⁷³ KHACHATRYAN 16V searched in 2.3 fb^{-1} of pp collisions at $\sqrt{s} = 13 \text{ TeV}$ for events with at least four energetic jets and significant $E_{\cancel{T}}$, no identified isolated electron or muon or charged track. No significant excess above the Standard Model expectations is observed. Limits are set on the gluino mass in the Tglu1A, Tglu1C, Tglu2A, and Tglu3A simplified models, see Fig. 8.
- ⁷⁴ AAD 15BC searched in 20.3 fb^{-1} of pp collisions at $\sqrt{s} = 8 \text{ TeV}$ for events with jets, missing $E_{\cancel{T}}$, and two opposite-sign same flavour isolated leptons featuring either a kinematic edge, or a peak at the Z -boson mass, in the invariant mass spectrum. No evidence for a statistically significant excess over the expected SM backgrounds are observed and 95% C.L. exclusion limits are derived in a GGM simplified model of gluino pair production where the gluino decays into quarks, a Z -boson, and a massless gravitino LSP, see Fig. 12. Also, limits are set in simplified models with slepton / sneutrino intermediate states, see Fig. 13.
- ⁷⁵ AAD 15BV summarized and extended ATLAS searches for gluinos and first- and second-generation squarks in final states containing jets and missing transverse momentum, with or without leptons or b -jets in the $\sqrt{s} = 8 \text{ TeV}$ data set collected in 2012. The paper reports the results of new interpretations and statistical combinations of previously published analyses, as well as new analyses. Exclusion limits at 95% C.L. are set on the gluino mass in several R -parity conserving models, leading to a generalized constraint on gluino masses exceeding 1150 GeV for lightest supersymmetric particle masses below 100 GeV. See their Figs. 10, 19, 20, 21, 23, 25, 26, 29-37.
- ⁷⁶ AAD 15BX interpreted the results of a wide range of ATLAS direct searches for supersymmetry, during the first run of the LHC using the $\sqrt{s} = 7 \text{ TeV}$ and $\sqrt{s} = 8 \text{ TeV}$ data set collected in 2012, within the wider framework of the phenomenological MSSM (pMSSM). The integrated luminosity was up to 20.3 fb^{-1} . From an initial random sampling of 500 million pMSSM points, generated from the 19-parameter pMSSM, a total of 310,327 model points with $\tilde{\chi}_1^0$ LSP were selected each of which satisfies constraints from previous collider searches, precision measurements, cold dark matter energy density measurements and direct dark matter searches. The impact of the ATLAS Run 1 searches on this space was presented, considering the fraction of model points surviving, after projection into two-dimensional spaces of sparticle masses. Good complementarity is observed between different ATLAS analyses, with almost all showing regions of unique sensitivity. ATLAS searches have good sensitivity at LSP mass below 800 GeV.
- ⁷⁷ AAD 15CA searched in 20.3 fb^{-1} of pp collisions at $\sqrt{s} = 8 \text{ TeV}$ for events with one or more photons, hadronic jets or b -jets and $E_{\cancel{T}}$. No significant excess above the Standard Model expectations is observed. Limits are set on gluino masses in the general gauge-mediated SUSY breaking model (GGM), for bino-like or higgsino-bino admixtures NLSP, see Fig. 8, 10, 11.
- ⁷⁸ KHACHATRYAN 15AF searched in 19.5 fb^{-1} of pp collisions at $\sqrt{s} = 8 \text{ TeV}$ for events with at least two energetic jets and significant $E_{\cancel{T}}$, using the transverse mass variable M_{T2} to discriminate between signal and background processes. No significant excess above the Standard Model expectations is observed. Limits are set on the gluino mass in simplified models where the decay $\tilde{g} \rightarrow q\bar{q}\tilde{\chi}_1^0$ takes place with a branching ratio of 100%, see Fig. 13(a), or where the decay $\tilde{g} \rightarrow b\bar{b}\tilde{\chi}_1^0$ takes place with a branching ratio of 100%, see Fig. 13(b), or where the decay $\tilde{g} \rightarrow t\bar{t}\tilde{\chi}_1^0$ takes place with a branching ratio of 100%, see Fig. 13(c). See also Table 5. Exclusions in the CMSSM, assuming $\tan\beta = 30$, $A_0 = -2 \max(m_0, m_{1/2})$ and $\mu > 0$, are also presented, see Fig. 15.
- ⁷⁹ KHACHATRYAN 15I searched in 19.5 fb^{-1} of pp collisions at $\sqrt{s} = 8 \text{ TeV}$ for events in which b -jets and four W -bosons are produced. Five individual search channels are combined (fully hadronic, single lepton, same-sign dilepton, opposite-sign dilepton, multilepton). No significant excess above the Standard Model expectations is observed. Limits are set on the gluino mass in a simplified model where the decay $\tilde{g} \rightarrow t\bar{t}\tilde{\chi}_1^0$ takes place with a branching ratio of 100%, see Fig. 5. Also a simplified model with gluinos decaying into on-shell top squarks is considered, see Fig. 6.
- ⁸⁰ KHACHATRYAN 15X searched in 19.3 fb^{-1} of pp collisions at $\sqrt{s} = 8 \text{ TeV}$ for events with at least two energetic jets, at least one of which is required to originate from a b quark, and significant $E_{\cancel{T}}$, using the razor variables (M_R and R^2) to discriminate between signal and background processes. No significant excess above the Standard Model expectations is observed. Limits are set on the gluino mass in simplified models where the decay $\tilde{g} \rightarrow b\bar{b}\tilde{\chi}_1^0$ and the decay $\tilde{g} \rightarrow t\bar{t}\tilde{\chi}_1^0$ take place with branching ratios varying between 0, 50 and 100%, see Figs. 13 and 14.
- ⁸¹ AAD 14AE searched in 20.3 fb^{-1} of pp collisions at $\sqrt{s} = 8 \text{ TeV}$ for strongly produced supersymmetric particles in events containing jets and large missing transverse momentum, and no electrons or muons. No excess over the expected SM background is observed. Exclusion limits are derived in simplified models containing gluinos and squarks, see Figures 5, 6 and 7. Limits are also derived in the mSUGRA/CMSSM with parameters $\tan\beta = 30$, $A_0 = -2 m_0$ and $\mu > 0$, see their Fig. 8.
- ⁸² AAD 14AG searched in 20.3 fb^{-1} of pp collisions at $\sqrt{s} = 8 \text{ TeV}$ for events containing one hadronically decaying τ -lepton, zero or one additional light leptons (electrons or muons), jets and large missing transverse momentum. No excess of events above the expected level of Standard Model background was found. Exclusion limits at 95% C.L. are set in several SUSY scenarios. For an interpretation in the minimal GMSB model, see their Fig. 8. For an interpretation in the mSUGRA/CMSSM with parameters $\tan\beta = 30$, $A_0 = -2 m_0$ and $\mu > 0$, see their Fig. 9. For an interpretation in the framework of natural Gauge Mediation, see Fig. 10. For an interpretation in the bRPV scenario, see their Fig. 11.
- ⁸³ AAD 14X searched in 20.3 fb^{-1} of pp collisions at $\sqrt{s} = 8 \text{ TeV}$ for events with at least four leptons (electrons, muons, taus) in the final state. No significant excess above the

Searches Particle Listings

Supersymmetric Particle Searches

- Standard Model expectations is observed. Limits are set on the gluino mass in a general gauge-mediation model (GGM) where the decay $\tilde{g} \rightarrow q\bar{q}\tilde{\chi}_1^0$, with $\tilde{\chi}_1^0 \rightarrow \ell^\pm\ell^\mp\tilde{G}$, takes place with a branching ratio of 100%, for two choices of $\tan\beta = 1.5$ and 30, see Fig. 11. Also some constraints on the higgsino mass parameter μ are discussed.
- 84 CHATRCHYAN 14AH searched in 4.7 fb^{-1} of pp collisions at $\sqrt{s} = 7 \text{ TeV}$ for events with at least two energetic jets and significant \cancel{E}_T , using the razor variables (M_R and R^2) to discriminate between signal and background processes. No significant excess above the Standard Model expectations is observed. Limits are set on sbottom masses in simplified models where the decay $\tilde{g} \rightarrow q\bar{q}\tilde{\chi}_1^0$ takes place with a branching ratio of 100%, see Fig. 28. Exclusions in the CMSSM, assuming $\tan\beta = 10$, $A_0 = 0$ and $\mu > 0$, are also presented, see Fig. 26.
- 85 CHATRCHYAN 14AH searched in 4.7 fb^{-1} of pp collisions at $\sqrt{s} = 7 \text{ TeV}$ for events with at least two energetic jets and significant \cancel{E}_T , using the razor variables (M_R and R^2) to discriminate between signal and background processes. A second analysis requires at least one of the jets to be originating from a b -quark. No significant excess above the Standard Model expectations is observed. Limits are set on sbottom masses in simplified models where the decay $\tilde{g} \rightarrow b\bar{b}\tilde{\chi}_1^0$ takes place with a branching ratio of 100%, see Figs. 28 and 29. Exclusions in the CMSSM, assuming $\tan\beta = 10$, $A_0 = 0$ and $\mu > 0$, are also presented, see Fig. 26.
- 86 CHATRCHYAN 14AH searched in 4.7 fb^{-1} of pp collisions at $\sqrt{s} = 7 \text{ TeV}$ for events with at least two energetic jets and significant \cancel{E}_T , using the razor variables (M_R and R^2) to discriminate between signal and background processes. A second analysis requires at least one of the jets to be originating from a b -quark. No significant excess above the Standard Model expectations is observed. Limits are set on sbottom masses in simplified models where the decay $\tilde{g} \rightarrow t\bar{t}\tilde{\chi}_1^0$ takes place with a branching ratio of 100%, see Figs. 28 and 29. Exclusions in the CMSSM, assuming $\tan\beta = 10$, $A_0 = 0$ and $\mu > 0$, are also presented, see Fig. 26.
- 87 CHATRCHYAN 14I searched in 19.5 fb^{-1} of pp collisions at $\sqrt{s} = 8 \text{ TeV}$ for events containing multijets and large \cancel{E}_T . No excess over the expected SM background is observed. Exclusion limits are derived in simplified models containing gluinos that decay via $\tilde{g} \rightarrow q\bar{q}\tilde{\chi}_1^0$ with a 100% branching ratio, see Fig. 7b, or via $\tilde{g} \rightarrow t\bar{t}\tilde{\chi}_1^0$ with a 100% branching ratio, see Fig. 7c, or via $\tilde{g} \rightarrow q\bar{q}W/Z\tilde{\chi}_1^0$, see Fig. 7d.
- 88 CHATRCHYAN 14N searched in 19.3 fb^{-1} of pp collisions at $\sqrt{s} = 8 \text{ TeV}$ for events containing a single isolated electron or muon and multiple jets, at least two of which are identified as originating from a b -quark. No significant excesses over the expected SM backgrounds are observed. The results are interpreted in three simplified models of gluino pair production with subsequent decay into virtual or on-shell top squarks, where each of the top squarks decays in turn into a top quark and a $\tilde{\chi}_1^0$, see Fig. 4. The models differ in which masses are allowed to vary.
- 89 CHATRCHYAN 14R searched in 19.5 fb^{-1} of pp collisions at $\sqrt{s} = 8 \text{ TeV}$ for events with at least three leptons (electrons, muons, taus) in the final state. No significant excess above the Standard Model expectations is observed. Limits are set on the gluino mass in a slepton co-NLSP simplified model (GMSB) where the decay $\tilde{g} \rightarrow q\ell^\pm\ell^\mp\tilde{G}$ takes place with a branching ratio of 100%, see Fig. 8.
- 90 CHATRCHYAN 14R searched in 19.5 fb^{-1} of pp collisions at $\sqrt{s} = 8 \text{ TeV}$ for events with at least three leptons (electrons, muons, taus) in the final state. No significant excess above the Standard Model expectations is observed. Limits are set on the gluino mass in a simplified model where the decay $\tilde{g} \rightarrow t\bar{t}\tilde{\chi}_1^0$ takes place with a branching ratio of 100%, see Fig. 11.
- 91 AABOUD 18BJ searched in 36.1 fb^{-1} of pp collisions at $\sqrt{s} = 13 \text{ TeV}$ in events with two opposite-sign charged leptons (electrons and muons), jets and missing transverse momentum, with various requirements to be sensitive to signals with different kinematic endpoint values in the dilepton invariant mass distribution. The data are found to be consistent with the SM expectation. Results are interpreted in the Tglu1H model in case of $m_{\tilde{\chi}_1^0} = 1 \text{ GeV}$: for any $m_{\tilde{\chi}_2^0}$, gluino masses below 1500 GeV are excluded, see their Fig. 14(a).
- 92 AABOUD 18V searched in 36.1 fb^{-1} of pp collisions at $\sqrt{s} = 13 \text{ TeV}$ in events with no charged leptons, jets and missing transverse momentum. The data are found to be consistent with the SM expectation. Results are interpreted in a Tglu1C-like model, assuming 50% BR for each gluino decay mode. Gluino masses below 1770 GeV are excluded for any $m_{\tilde{\chi}_2^0} - m_{\tilde{\chi}_1^0}$ and $m_{\tilde{\chi}_1^0} = 60 \text{ GeV}$, see their Fig. 16(b).
- 93 AABOUD 17AZ searched in 36.1 fb^{-1} of pp collisions at $\sqrt{s} = 13 \text{ TeV}$ for events with at least seven jets and large missing transverse momentum. Selected events are further classified based on the presence of large R-jets or b -jets and no leptons. No significant excess above the Standard Model expectations is observed. Limits are set for pMSSM models with $M_1 = 60 \text{ GeV}$, $\tan(\beta) = 10$, $\mu < 0$ varying the soft-breaking parameters M_3 and μ . Gluino masses up to 1600 GeV are excluded for $m_{\tilde{\chi}_1^0} = 200 \text{ GeV}$. See their Figure 6a and text for details on the model.
- 94 KHACHATRYAN 16AY searched in 2.3 fb^{-1} of pp collisions at $\sqrt{s} = 13 \text{ TeV}$ for events with one isolated high transverse momentum lepton (e or μ), hadronic jets of which at least one is identified as coming from a b -quark, and large \cancel{E}_T . No significant excess above the Standard Model expectations is observed. Limits are set on the gluino mass in the Tglu3A simplified model, see Fig. 10, and in the Tglu3B model, see Fig. 11.
- 95 KHACHATRYAN 16BT performed a global Bayesian analysis of a wide range of CMS results obtained with data samples corresponding to 5.0 fb^{-1} of pp collisions at $\sqrt{s} = 7 \text{ TeV}$ and in 19.5 fb^{-1} of pp collisions at $\sqrt{s} = 8 \text{ TeV}$. The set of searches considered, both individually and in combination, includes those with all-hadronic final states, same-sign and opposite-sign dileptons, and multi-lepton final states. An interpretation was given in a scan of the 19-parameter pMSSM. No scan points with a gluino mass less than 500 GeV survived and 98% of models with a squark mass less than 300 GeV were excluded.
- 96 AAD 15AB searched for the decay of neutral, weakly interacting, long-lived particles in 20.3 fb^{-1} of pp collisions at $\sqrt{s} = 8 \text{ TeV}$. Signal events require at least two reconstructed vertices possibly originating from long-lived particles decaying to jets in the inner tracking detector and muon spectrometer. No significant excess of events over the expected background was found. Results were interpreted in Stealth SUSY benchmark models where a pair of gluinos decay to long-lived singlinos, \tilde{S} , which in turn each decay to a low-mass gravitino and a pair of jets. The 95% confidence-level limits are set on the cross section \times branching ratio for the decay $\tilde{g} \rightarrow \tilde{S}g$, as a function of the singlino proper lifetime (τ). See their Fig. 10(f)
- 97 AAD 15AI searched in 20 fb^{-1} of pp collisions at $\sqrt{s} = 8 \text{ TeV}$ for events containing at least one isolated lepton (electron or muon), jets, and large missing transverse momentum. No excess of events above the expected level of Standard Model background was found. Exclusion limits at 95% C.L. are set on the gluino mass in the CMSSM/mSUGRA, see Fig. 15, in the NUHM2, see Fig. 16, and in various simplified models, see Figs. 18–22.
- 98 AAD 15CB searched for events containing at least one long-lived particle that decays at a significant distance from its production point (displaced vertex, DV) into two leptons or into five or more charged particles in 20.3 fb^{-1} of pp collisions at $\sqrt{s} = 8 \text{ TeV}$. The dilepton signature is characterised by DV formed from at least two lepton candidates. Four different final states were considered for the multitrack signature, in which the DV must be accompanied by a high-transverse momentum muon or electron candidate that originates from the DV, jets or missing transverse momentum. No events were observed in any of the signal regions. Results were interpreted in SUSY scenarios involving R -parity violation, split supersymmetry, and gauge mediation. See their Fig. 12–20.
- 99 KHACHATRYAN 15AD searched in 19.4 fb^{-1} of pp collisions at $\sqrt{s} = 8 \text{ TeV}$ for events with two opposite-sign same flavor isolated leptons featuring either a kinematic edge, or a peak at the Z -boson mass, in the invariant mass spectrum. No evidence for a statistically significant excess over the expected SM backgrounds is observed and 95% C.L. exclusion limits are derived in a simplified model of gluino pair production where the gluino decays into quarks, a Z -boson, and a massless gravitino LSP, see Fig. 9.
- 100 KHACHATRYAN 15AZ searched in 19.7 fb^{-1} of pp collisions at $\sqrt{s} = 8 \text{ TeV}$ for events with either at least one photon, hadronic jets and \cancel{E}_T (single photon channel) or with at least two photons and at least one jet and using the razor variables. No significant excess above the Standard Model expectations is observed. Limits are set on gluino masses in the general gauge-mediated SUSY breaking model (GGM), for both a bino-like and wino-like neutralino NLSP scenario, see Fig. 8 and 9.
- 101 AAD 14AX searched in 20.1 fb^{-1} of pp collisions at $\sqrt{s} = 8 \text{ TeV}$ for the strong production of supersymmetric particles in events containing either zero or at least one high p_T lepton, large missing transverse momentum, high jet multiplicity and at least three jets identified as originating from b -quarks. No excess over the expected SM background is observed. Limits are derived in mSUGRA/CMSSM models with $\tan\beta = 30$, $A_0 = -2m_0$ and $\mu > 0$, see their Fig. 14. Also, exclusion limits in simplified models containing gluinos and scalar top and bottom quarks are set, see their Figures 12, 13.
- 102 AAD 14E searched in 20.3 fb^{-1} of pp collisions at $\sqrt{s} = 8 \text{ TeV}$ for strongly produced supersymmetric particles in events containing jets and two same-sign leptons or three leptons. The search also utilises jets originating from b -quarks, missing transverse momentum and other variables. No excess over the expected SM background is observed. Exclusion limits are derived in simplified models containing gluinos and squarks, see Figures 5 and 6. In the $\tilde{g} \rightarrow q\bar{q}\tilde{\chi}_1^\pm, \tilde{\chi}_1^\pm \rightarrow W^{(*)}\tilde{\chi}_2^0, \tilde{\chi}_2^0 \rightarrow Z^{(*)}\tilde{\chi}_1^0$ simplified model, the following assumptions have been made: $m_{\tilde{\chi}_1^\pm} = 0.5 m_{\tilde{\chi}_1^0} + m_{\tilde{g}}^0$, $m_{\tilde{\chi}_2^0} = 0.5 (m_{\tilde{\chi}_1^0} + m_{\tilde{\chi}_2^\pm})$, $m_{\tilde{\chi}_1^0} < 520 \text{ GeV}$. In the $\tilde{g} \rightarrow q\bar{q}\tilde{\chi}_1^\pm, \tilde{\chi}_1^\pm \rightarrow \ell^\pm\nu_{\tilde{\chi}_1^0}$ or $\tilde{g} \rightarrow q\bar{q}\tilde{\chi}_2^0, \tilde{\chi}_2^0 \rightarrow \ell^\pm\ell^\mp(\nu\nu)\tilde{\chi}_1^0$ simplified model, the following assumptions have been made: $m_{\tilde{\chi}_1^\pm} = m_{\tilde{\chi}_2^0} = 0.5 (m_{\tilde{\chi}_1^0} + m_{\tilde{g}}^0)$, $m_{\tilde{\chi}_1^0} < 660 \text{ GeV}$. Limits are also derived in the mSUGRA/CMSSM, bRPV and GMSB models, see their Fig. 8.
- 103 CHATRCHYAN 14H searched in 19.5 fb^{-1} of pp collisions at $\sqrt{s} = 8 \text{ TeV}$ for events with two isolated same-sign dileptons and jets in the final state. No significant excess above the Standard Model expectations is observed. Limits are set on the gluino mass in simplified models where the decay $\tilde{g} \rightarrow t\bar{t}\tilde{\chi}_1^0$ takes place with a branching ratio of 100%, or where the decay $\tilde{g} \rightarrow \tilde{t}t, \tilde{t} \rightarrow t\tilde{\chi}_1^0$ takes place with a branching ratio of 100%, with varying mass of the $\tilde{\chi}_1^0$, or where the decay $\tilde{g} \rightarrow b\bar{b}, \tilde{b} \rightarrow t\tilde{\chi}_1^\pm, \tilde{\chi}_1^\pm \rightarrow W^\pm\tilde{\chi}_1^0$ takes place with a branching ratio of 100%, with varying mass of the $\tilde{\chi}_1^\pm$, see Fig. 5.
- 104 CHATRCHYAN 14H searched in 19.5 fb^{-1} of pp collisions at $\sqrt{s} = 8 \text{ TeV}$ for events with two isolated same-sign dileptons and jets in the final state. No significant excess above the Standard Model expectations is observed. Limits are set on the gluino mass in simplified models where the decay $\tilde{g} \rightarrow q\bar{q}\tilde{\chi}_1^\pm, \tilde{\chi}_1^\pm \rightarrow W^\pm\tilde{\chi}_1^0$ takes place with a branching ratio of 100%, with varying mass of the $\tilde{\chi}_1^\pm$ and $\tilde{\chi}_1^0$, see Fig. 7.
- 105 CHATRCHYAN 14H searched in 19.5 fb^{-1} of pp collisions at $\sqrt{s} = 8 \text{ TeV}$ for events with two isolated same-sign dileptons and jets in the final state. No significant excess above the Standard Model expectations is observed. Limits are set on the gluino mass in simplified models where the decay $\tilde{g} \rightarrow b\bar{b}\tilde{\chi}_1^\pm, \tilde{\chi}_1^\pm \rightarrow W^\pm\tilde{\chi}_1^0$ takes place with a branching ratio of 100%, for two choices of $m_{\tilde{\chi}_1^\pm}$ and fixed $m_{\tilde{\chi}_1^0}$, see Fig. 6.

R-parity violating heavy \tilde{g} (Gluino) mass limit

VALUE (GeV)	CL%	DOCUMENT ID	TECN	COMMENT
>2200	95	1 AAD	21BF ATLS	$\ell^\pm + b$ -jets + many jets, Tglu3F, λ_{323} electroweakino decay, $500 \text{ GeV} < m_{\tilde{\chi}_1^0} < 1600 \text{ GeV}$
>2250	95	1 AAD	21BF ATLS	$\ell^\pm + b$ -jets + many jets, Tglu3G, λ_{323} electroweakino decay, $600 \text{ GeV} < m_{\tilde{\chi}_1^0} < 1600 \text{ GeV}$
>2200	95	1 AAD	21BF ATLS	$\ell^\pm + b$ -jets + many jets, Tglu3B, λ_{323} electroweakino decay, $600 \text{ GeV} < m_{\tilde{\chi}_1^0} < 1600 \text{ GeV}$
>1800	95	1 AAD	21BF ATLS	$\ell^\pm + b$ -jets + many jets, Tglu3B, λ_{323}, \tilde{t} decay, $m_{\tilde{t}} < 1200 \text{ GeV}$
>2200	95	1 AAD	21BF ATLS	$\ell^\pm + b$ -jets + many jets, Tglu1A, $\chi', \tilde{\chi}_1^0$ decay with equal probability into e, μ, ν_e, ν_μ , $400 \text{ GeV} < m_{\tilde{\chi}_1^0} < 1700 \text{ GeV}$

Mass	Year	Pub	Exp	Search	Notes
>2500	95	2 AAD	21Y ATLS	$\geq 4\ell, Tglu1A$ with $\tilde{\chi}_1^0 \rightarrow \ell^\pm \ell^\mp \nu, \lambda_{12k} \neq 0, m_{\tilde{\chi}_1^0} = 2200$ GeV	••• We do not use the following data for averages, fits, limits, etc. •••
>1900	95	2 AAD	21Y ATLS	$\geq 4\ell, Tglu1A$ with $\tilde{\chi}_1^0 \rightarrow \ell^\pm \ell^\mp \nu, \lambda_{j33} \neq 0, m_{\tilde{\chi}_1^0} = 1550$ GeV	
>1600	95	3 AAD	20AL ATLS	8 or more jets + $\cancel{E}_T, Tglu2RPV$	jets and large R-jets, $Tglu2RPV$ and $\tilde{\chi}_1^0 \rightarrow qq\bar{q}, \lambda''$ coupling, $m_{\tilde{\chi}_1^0} = 1000$ GeV
>1600	95	4 AAD	20V ATLS	same-sign $\ell^\pm \ell^\pm$ + jets, $\tilde{g} \rightarrow t\bar{b}d$ simplified model	
>2150	95	5 SIRUNYAN	20T CMS	same-sign $\ell^\pm \ell^\pm$ or $\geq 3\ell^\pm$ + jets, $\tilde{g} \rightarrow qq\bar{q}\bar{q} + e/\mu/\tau$ simplified model	$\tilde{g} \rightarrow qq\bar{q}\bar{q}, \tilde{\chi}_1^0 \rightarrow \ell\ell\nu, \lambda_{121}$ or $\lambda_{122} \neq 0, m_{\tilde{\chi}_1^0} > 400$ GeV
>1725	95	5 SIRUNYAN	20T CMS	same-sign $\ell^\pm \ell^\pm$ or $\geq 3\ell^\pm$ + jets, $\tilde{g} \rightarrow t\bar{b}s$ simplified model	
>1500	95	6 SIRUNYAN	19F CMS	$\tilde{g} \rightarrow jjj$	pMSSM, $M_1 = 60$ GeV, $m_{\tilde{q}} < 1500$ GeV
>2260	95	7 AABOUD	18Z ATLS	$\geq 4\ell, \lambda_{12k} \neq 0, m_{\tilde{\chi}_1^0} > 1000$ GeV	
>1650	95	7 AABOUD	18Z ATLS	$\geq 4\ell, \lambda_{j33} \neq 0, m_{\tilde{\chi}_1^0} > 500$ GeV	b-jets, $\tilde{g} \rightarrow \tilde{t}_1 t$ and $\tilde{t}_1 \rightarrow t\tilde{\chi}_1^0$, $m_{\tilde{T}_1} < 1000$ GeV
>1610	95	8 SIRUNYAN	18AK CMS	$\tilde{g} \rightarrow t\bar{b}s, \lambda''_{332}$ coupling	b-jets, $\tilde{g} \rightarrow \tilde{t}_1 t$ and $\tilde{t}_1 \rightarrow b\tilde{\chi}_1^\pm, m_{\tilde{T}_1} < 1000$ GeV, $m_{\tilde{\chi}_1^0} = 60$ GeV
>1690	95	9 SIRUNYAN	18D CMS	top quark (hadronically decaying) + jets + $\cancel{E}_T, Tglu3C, m_{\tilde{t}_1} - m_{\tilde{\chi}_1^0} = 20$ GeV, $m_{\tilde{\chi}_1^0} = 0$ GeV	jets, $\tilde{g} \rightarrow \tilde{t}_1 t$ and $\tilde{t}_1 \rightarrow sb, 400 < m_{\tilde{t}_1} < 1000$ GeV
none 100-1410	95	10 SIRUNYAN	18EA CMS	2 large jets with four-parton sub-structure, $\tilde{g} \rightarrow 5q$	$\ell, \tilde{g} \rightarrow (e/\mu)qq$, benchmark gluino, neutralino masses
>2100	95	11 AABOUD	17AI ATLS	$\geq 1\ell + \geq 8$ jets, $Tglu3A$ and $\tilde{\chi}_1^0 \rightarrow u\bar{d}s, \lambda''_{112}$ coupling, $m_{\tilde{\chi}_1^0} = 1000$ GeV	$\ell\ell/Z, \tilde{g} \rightarrow (e/e/\mu/\mu/e/\mu)qq, m_{\tilde{\chi}_1^0} = 400$ GeV and $0.7 < c\tau_{\tilde{\chi}_1^0} < 3 \times 10^5$ mm
>1650	95	12 AABOUD	17AI ATLS	$\geq 1\ell + \geq 8$ jets, $\tilde{g} \rightarrow t\bar{t}, \tilde{t} \rightarrow b\bar{s}, \lambda''_{323}$ coupling, $m_{\tilde{\tau}} = 1000$ GeV	≥ 10 jets, $\tilde{g} \rightarrow qq\bar{q}\tilde{\chi}_1^0, \tilde{\chi}_1^0 \rightarrow qq\bar{q}, m_{\tilde{\chi}_1^0} = 500$ GeV
>1800	95	13 AABOUD	17AI ATLS	$\geq 1\ell + \geq 8$ jets, $Tglu1A$ and $\tilde{\chi}_1^0 \rightarrow q\bar{q}\ell, \lambda'$ coupling, $m_{\tilde{\chi}_1^0} = 1000$ GeV	$\geq 6,7$ jets, $\tilde{g} \rightarrow qq\bar{q}$, (light-quark, λ'' couplings)
>1800	95	14 AABOUD	17AJ ATLS	same-sign $\ell^\pm \ell^\pm / 3\ell +$ jets + $\cancel{E}_T, Tglu3A, \lambda''_{112}$ coupling, $m_{\tilde{\chi}_1^0} = 50$ GeV	$\geq 6,7$ jets, $\tilde{g} \rightarrow qq\bar{q}$, (b-quark, λ'' couplings)
>1750	95	15 AABOUD	17AJ ATLS	same-sign $\ell^\pm \ell^\pm / 3\ell +$ jets + $\cancel{E}_T, Tglu1A$ and $\tilde{\chi}_1^0 \rightarrow qq\ell, \lambda'$ coupling	≥ 3 b-jets + $\cancel{E}_T, \tilde{g} \rightarrow \tilde{t}_1 t\tilde{\chi}_1^\pm$ simplified model, $\tilde{t}_1 \rightarrow b\tilde{\chi}_1^\pm, m_{\tilde{\tau}_\pm} = 2m_{\tilde{\chi}_1^0}, m_{\tilde{\chi}_1^0} = 60$ GeV, $m_{\tilde{\tau}_1} < 1000$ GeV
>1450	95	16 AABOUD	17AJ ATLS	same-sign $\ell^\pm \ell^\pm / 3\ell +$ jets + $\cancel{E}_T, \tilde{g} \rightarrow t\bar{t}_1$ and $\tilde{t}_1 \rightarrow s\bar{d}, \lambda''_{321}$ coupling	$\ell^\pm \ell^\pm (\ell^\mp) +$ jets, $\tilde{g} \rightarrow t\bar{t}_1$ with $\tilde{t}_1 \rightarrow b\bar{s}$ simplified model
>1450	95	17 AABOUD	17AJ ATLS	same-sign $\ell^\pm \ell^\pm / 3\ell +$ jets + $\cancel{E}_T, \tilde{g} \rightarrow t\bar{t}_1$ and $\tilde{t}_1 \rightarrow b\bar{d}, \lambda''_{313}$ coupling	same-sign $\ell^\pm \ell^\pm, \tilde{g} \rightarrow t\bar{b}s$ simplified model
> 400	95	18 AABOUD	17AJ ATLS	same-sign $\ell^\pm \ell^\pm / 3\ell +$ jets + $\cancel{E}_T, \bar{d}_R \rightarrow t\bar{b}(t\bar{s}), \lambda''_{313} (\lambda''_{321})$ coupling	
none 625-1375	95	19 AABOUD	17AZ ATLS	≥ 7 jets + \cancel{E}_T , large R-jets and/or b-jets, $\tilde{g} \rightarrow t\bar{t}_1$ and $\tilde{t}_1 \rightarrow b\bar{s}, \lambda''_{323}$ coupling	
none 600-650	95	20 KHACHATRY...17Y	CMS	$\tilde{g} \rightarrow qq\bar{q}\bar{q}, \lambda''_{212}$ coupling, $m_{\tilde{q}} = 100$ GeV	
none 600-1030	95	20 KHACHATRY...17Y	CMS	$\tilde{g} \rightarrow qq\bar{q}\bar{q}, \lambda''_{212}$ coupling, $m_{\tilde{q}} = 900$ GeV	
none 600-650	95	20 KHACHATRY...17Y	CMS	$\tilde{g} \rightarrow qq\bar{q}\bar{b}, \lambda''_{213}$ coupling, $m_{\tilde{q}} = 100$ GeV	
none 600-1080	95	20 KHACHATRY...17Y	CMS	$\tilde{g} \rightarrow qq\bar{q}\bar{b}, \lambda''_{213}$ coupling, $m_{\tilde{q}} = 900$ GeV	
none 600-680	95	20 KHACHATRY...17Y	CMS	$\tilde{g} \rightarrow qq\bar{q}\bar{b}, \lambda''_{212}$ coupling, $m_{\tilde{q}} = 100$ GeV	
none 600-1080	95	20 KHACHATRY...17Y	CMS	$\tilde{g} \rightarrow qq\bar{q}\bar{b}, \lambda''_{212}$ coupling, $m_{\tilde{q}} = 900$ GeV	
none 600-650	95	20 KHACHATRY...17Y	CMS	$\tilde{g} \rightarrow qq\bar{b}\bar{b}, \lambda''_{213}$ coupling, $m_{\tilde{q}} = 100$ GeV	
none 600-1100	95	20 KHACHATRY...17Y	CMS	$\tilde{g} \rightarrow qq\bar{b}\bar{b}, \lambda''_{213}$ coupling, $m_{\tilde{q}} = 900$ GeV	
>1050	95	21 KHACHATRY...16BX	CMS	same-sign $\ell^\pm \ell^\pm, Tglu3A, m_{\tilde{\chi}_1^0} < 800$ GeV	
>1140	95	21 KHACHATRY...16BX	CMS	same-sign $\ell^\pm \ell^\pm, Tglu3B, m_{\tilde{\tau}} - m_{\tilde{\chi}_1^0} = 20$ GeV, $m_{\tilde{\chi}_1^0} = 0$	
>1030	95	22 KHACHATRY...16BX	CMS	$\tilde{g} \rightarrow t\bar{b}s, \lambda''_{332}$ coupling	
>1150	95	23 AAD	15BV ATLS	general RPC \tilde{g} decays, $m_{\tilde{\chi}_1^0} < 100$ GeV	
>1350	95	24 AAD	14X ATLS	$\geq 4\ell^\pm, \tilde{g} \rightarrow qq\bar{q}\tilde{\chi}_1^0, \tilde{\chi}_1^0 \rightarrow \ell^\pm \ell^\mp \nu$	
> 650	95	25 CHATRCHYAN 14P	CMS	$\tilde{g} \rightarrow jjj$	
none 200-835	95	25 CHATRCHYAN 14P	CMS	$\tilde{g} \rightarrow bjj$	

Searches Particle Listings

Supersymmetric Particle Searches

- 8** SIRUNYAN 18AK searched in 35.9 fb^{-1} of pp collisions at $\sqrt{s} = 13 \text{ TeV}$ for events containing a single lepton, large jet and b -quark jet multiplicities, coming from R-parity-violating decays of gluinos. No excess over the expected background is observed. Limits are derived on the gluino mass, assuming the RPV $\tilde{g} \rightarrow tbs$ decay, see their Figure 9.
- 9** SIRUNYAN 18D searched in 35.9 fb^{-1} of pp collisions at $\sqrt{s} = 13 \text{ TeV}$ for events containing identified hadronically decaying top quarks, no leptons, and E_T . No significant excess above the Standard Model expectations is observed. Limits are set on the stop mass in the Tstop1 simplified model, see their Figure 8, and on the gluino mass in the Tglu3A, Tglu3B, Tglu3C and Tglu3E simplified models, see their Figure 9.
- 10** SIRUNYAN 18EA searched in 38.2 fb^{-1} of pp collisions at $\sqrt{s} = 13 \text{ TeV}$ for the pair production of resonances, each decaying to at least four quarks. Reconstructed particles are clustered into two large jets of similar mass, each consistent with four-parton substructure. No statistically significant excess over the Standard Model expectation is observed. Limits are set on the squark and gluino mass in RPV supersymmetry models where squarks (gluinos) decay, through intermediate higgsinos, to four (five) quarks, see their Figure 4.
- 11** AABOUD 17AI searched in 36.1 fb^{-1} of pp collisions at $\sqrt{s} = 13 \text{ TeV}$ for events with one or more isolated lepton, at least eight jets, either zero or many b -jets, for evidence of R-parity violating decays of the gluino. No significant excess above the Standard Model expectations is observed. Limits up to 2.1 TeV are set on the gluino mass in R-parity-violating supersymmetry models as Tglu3A with LSP decay through the non-zero λ''_{112} coupling as $\tilde{\chi}_1^0 \rightarrow uds$. See their Figure 9.
- 12** AABOUD 17AJ searched in 36.1 fb^{-1} of pp collisions at $\sqrt{s} = 13 \text{ TeV}$ for events with one or more isolated lepton, at least eight jets, either zero or many b -jets, for evidence of R-parity violating decays of the gluino. No significant excess above the Standard Model expectations is observed. Limits up to 1.65 TeV are set on the gluino mass in R-parity-violating supersymmetry models with $\tilde{g} \rightarrow t\bar{t}$, $\tilde{t} \rightarrow bs$ through the non-zero λ''_{323} coupling. See their Figure 9.
- 13** AABOUD 17AL searched in 36.1 fb^{-1} of pp collisions at $\sqrt{s} = 13 \text{ TeV}$ for events with one or more isolated lepton, at least eight jets, either zero or many b -jets, for evidence of R-parity violating decays of the gluino. No significant excess above the Standard Model expectations is observed. Limits up to 1.8 TeV are set on the gluino mass in R-parity-violating supersymmetry models as Tglu1A with the LSP decay through the non-zero λ' coupling as $\tilde{\chi}_1^0 \rightarrow qq\ell$. See their Figure 9.
- 14** AABOUD 17AJ searched in 36.1 fb^{-1} of pp collisions at $\sqrt{s} = 13 \text{ TeV}$ for events with two same-sign or three leptons, jets and large missing transverse momentum. No significant excess above the Standard Model expectations is observed. Limits up to 1.8 TeV are set on the gluino mass in R-parity-violating supersymmetry models as Tglu3A with LSP decaying through the non-zero λ''_{112} coupling as $\tilde{\chi}_1^0 \rightarrow uds$. See their Figure 5(d).
- 15** AABOUD 17AJ searched in 36.1 fb^{-1} of pp collisions at $\sqrt{s} = 13 \text{ TeV}$ for events with two same-sign or three leptons, jets and large missing transverse momentum. No significant excess above the Standard Model expectations is observed. Limits up to 1.75 TeV are set on the gluino mass in R-parity-violating supersymmetry models as Tglu1A with LSP decaying through the non-zero λ' coupling as $\tilde{\chi}_1^0 \rightarrow qq\ell$. See their Figure 5(c).
- 16** AABOUD 17AJ searched in 36.1 fb^{-1} of pp collisions at $\sqrt{s} = 13 \text{ TeV}$ for events with two same-sign or three leptons, jets and large missing transverse momentum. No significant excess above the Standard Model expectations is observed. Limits up to 1.45 TeV are set on the gluino mass in R-parity-violating supersymmetry models where $\tilde{g} \rightarrow t\bar{t}_1$ and $\tilde{t}_1 \rightarrow sd$ through the non-zero λ''_{321} coupling. See their Figure 5(b).
- 17** AABOUD 17AJ searched in 36.1 fb^{-1} of pp collisions at $\sqrt{s} = 13 \text{ TeV}$ for events with two same-sign or three leptons, jets and large missing transverse momentum. No significant excess above the Standard Model expectations is observed. Limits up to 1.45 TeV are set on the gluino mass in R-parity-violating supersymmetry models where $\tilde{g} \rightarrow t\bar{t}_1$ and $\tilde{t}_1 \rightarrow bd$ through the non-zero λ''_{313} coupling. See their Figure 5(a).
- 18** AABOUD 17AJ searched in 36.1 fb^{-1} of pp collisions at $\sqrt{s} = 13 \text{ TeV}$ for events with two same-sign or three leptons, jets and large missing transverse momentum. No significant excess above the Standard Model expectations is observed. Limits up to 400 GeV are set on the down type squark (\tilde{d}_R) mass in R-parity-violating supersymmetry models where $\tilde{d}_R \rightarrow t\bar{b}$ through the non-zero λ''_{313} coupling or $\tilde{d}_R \rightarrow ts$ through the non-zero λ''_{321} . See their Figure 5(e) and 5(f).
- 19** AABOUD 17AZ searched in 36.1 fb^{-1} of pp collisions at $\sqrt{s} = 13 \text{ TeV}$ for events with at least seven jets and large missing transverse momentum. Selected events are further classified based on the presence of large R-jets or b -jets and no leptons. No significant excess above the Standard Model expectations is observed. Limits are set for R-parity violating decays of the gluino assuming $\tilde{g} \rightarrow t\bar{t}_1$ and $\tilde{t}_1 \rightarrow bs$ through the non-zero λ''_{323} couplings. The range 625–1375 GeV is excluded for $m_{\tilde{t}_1} = 400 \text{ GeV}$. See their Figure 7b.
- 20** KHACHATRYAN 17Y searched in 19.7 fb^{-1} of pp collisions at $\sqrt{s} = 8 \text{ TeV}$ for events containing at least 8 or 10 jets, possibly b -tagged, coming from R-parity-violating decays of supersymmetric particles. No excess over the expected background is observed. Limits are derived on the gluino mass, assuming various RPV decay modes, see Fig. 7.
- 21** KHACHATRYAN 16BJ searched in 2.3 fb^{-1} of pp collisions at $\sqrt{s} = 13 \text{ TeV}$ for events with two isolated same-sign dileptons and jets in the final state. No significant excess above the Standard Model expectations is observed. Limits are set on the gluino mass in the following simplified models: Tglu3A and Tglu3D, see Fig. 4, Tglu3B and Tglu3C, see Fig. 5, and Tglu1B, see Fig. 7.
- 22** KHACHATRYAN 16BX searched in 19.5 fb^{-1} of pp collisions at $\sqrt{s} = 8 \text{ TeV}$ for events containing 0 or 1 leptons and b -tagged jets, coming from R-parity-violating decays of supersymmetric particles. No excess over the expected background is observed. Limits are derived on the gluino mass, assuming the RPV $\tilde{g} \rightarrow tbs$ decay, see Fig. 7 and 10.
- 23** AAD 15bv summarized and extended ATLAS searches for gluinos and first- and second-generation squarks in final states containing jets and missing transverse momentum, with or without leptons or b -jets in the $\sqrt{s} = 8 \text{ TeV}$ data set collected in 2012. The paper reports the results of new interpretations and statistical combinations of previously published analyses, as well as new analyses. Exclusion limits at 95% C.L. are set on the gluino mass in several R-parity conserving models, leading to a generalized constraint on gluino masses exceeding 1150 GeV for lightest supersymmetric particle masses below 100 GeV. See their Figs. 10, 19, 20, 21, 23, 25, 26, 29–37.
- 24** AAD 14x searched in 20.3 fb^{-1} of pp collisions at $\sqrt{s} = 8 \text{ TeV}$ for events with at least four leptons (electrons, muons, taus) in the final state. No significant excess above the Standard Model expectations is observed. Limits are set on the gluino mass in an R-parity violating simplified model where the decay $\tilde{g} \rightarrow q\bar{q}\tilde{\chi}_1^0$, with $\tilde{\chi}_1^0 \rightarrow \ell^\pm \ell^\mp \nu$, takes place with a branching ratio of 100%, see Fig. 8.
- 25** CHATRCHYAN 14P searched in 19.4 fb^{-1} of pp collisions at $\sqrt{s} = 8 \text{ TeV}$ for three-jet resonances produced in the decay of a gluino in R-parity violating supersymmetric models. No excess over the expected SM background is observed. Assuming a 100% branching ratio for the gluino decay into three light-flavour jets, limits are set on the cross section of gluino pair production, see Fig. 7, and gluino masses below 650 GeV are excluded at 95% C.L. Assuming a 100% branching ratio for the gluino decaying to one b -quark jet and two light-flavour jets, gluino masses between 200 GeV and 835 GeV are excluded at 95% C.L.
- 26** AABOUD 18CF searched in 36.1 fb^{-1} of pp collisions at $\sqrt{s} = 13 \text{ TeV}$ for events with several jets, possibly b -jets, and large-radius jets for evidence of R-parity violating decays of the gluino. No significant excess above the Standard Model expectations is observed. Limits between 1000 and 1875 GeV are set on the gluino mass in R-parity-violating supersymmetry models as Tglu2RPV with the LSP decay through the non-zero λ'' coupling as $\tilde{\chi}_1^0 \rightarrow qq\ell$. The most stringent limit is obtained for $m_{\tilde{\chi}_1^0} = 1000 \text{ GeV}$, the weakest for $m_{\tilde{\chi}_1^0} = 50 \text{ GeV}$. See their Figure 7(b). Figure 7(a) presents results for gluinos directly decaying into 3 quarks, Tglu1RPV.
- 27** KHACHATRYAN 16BX searched in 19.5 fb^{-1} of pp collisions at $\sqrt{s} = 8 \text{ TeV}$ for events containing 4 leptons coming from R-parity-violating decays of $\tilde{\chi}_1^0 \rightarrow \ell\ell\nu$ with $\lambda_{121} \neq 0$ or $\lambda_{122} \neq 0$. No excess over the expected background is observed. Limits are derived on the gluino, squark and stop masses, see Fig. 23.
- 28** AAD 15CB searched for events containing at least one long-lived particle that decays at a significant distance from its production point (displaced vertex, DV) into two leptons or into five or more charged particles in 20.3 fb^{-1} of pp collisions at $\sqrt{s} = 8 \text{ TeV}$. The dilepton signature is characterised by DV formed from at least two lepton candidates. Four different final states were considered for the multitrack signature, in which the DV must be accompanied by a high-transverse momentum muon or electron candidate that originates from the DV, jets or missing transverse momentum. No events were observed in any of the signal regions. Results were interpreted in SUSY scenarios involving R-parity violation, split supersymmetry, and gauge mediation. See their Fig. 12–20.
- 29** AAD 15X searched in 20.3 fb^{-1} of pp collisions at $\sqrt{s} = 8 \text{ TeV}$ for events containing large number of jets, no requirements on missing transverse momentum and no isolated electrons or muons. The sensitivity of the search is enhanced by considering the number of b -tagged jets and the scalar sum of masses of large-radius jets in an event. No evidence was found for excesses above the expected level of Standard Model background. Exclusion limits at 95% C.L. are set on the gluino mass assuming the gluino decays to various quark flavors, and for various neutralino masses. See their Fig. 11–16.
- 30** AAD 14Ax searched in 20.1 fb^{-1} of pp collisions at $\sqrt{s} = 8 \text{ TeV}$ for the strong production of supersymmetric particles in events containing either zero or at least one high p_T lepton, large missing transverse momentum, high jet multiplicity and at least three jets identified as originating from b -quarks. No excess over the expected SM background is observed. Limits are derived in mSUGRA/CMSSM models with $\tan\beta = 30$, $A_0 = -2m_0$ and $\mu > 0$, see their Fig. 14. Also, exclusion limits in simplified models containing gluinos and scalar top and bottom quarks are set, see their Figures 12, 13.
- 31** AAD 14E searched in 20.3 fb^{-1} of pp collisions at $\sqrt{s} = 8 \text{ TeV}$ for strongly produced supersymmetric particles in events containing jets and two same-sign leptons or three leptons. The search also utilises jets originating from b -quarks, missing transverse momentum and other variables. No excess over the expected SM background is observed. Exclusion limits are derived in simplified models containing gluinos and squarks, see Figures 5 and 6. In the $\tilde{g} \rightarrow q\bar{q}\tilde{\chi}_1^\pm$, $\tilde{\chi}_1^\pm \rightarrow W^{(*)\pm}\tilde{\chi}_2^0$, $\tilde{\chi}_2^0 \rightarrow Z^{(*)}\tilde{\chi}_1^0$ simplified model, the following assumptions have been made: $m_{\tilde{\chi}_1^\pm} = 0.5 m_{\tilde{\chi}_1^0} + m_{\tilde{g}}$, $m_{\tilde{\chi}_2^0} = 0.5 (m_{\tilde{\chi}_1^0} + m_{\tilde{g}})$, $m_{\tilde{\chi}_1^0} < 520 \text{ GeV}$. In the $\tilde{g} \rightarrow q\bar{q}\tilde{\chi}_1^\pm$, $\tilde{\chi}_1^\pm \rightarrow \ell^\pm \nu \tilde{\chi}_1^0$ or $\tilde{g} \rightarrow q\bar{q}\tilde{\chi}_2^0$, $\tilde{\chi}_2^0 \rightarrow \ell^\pm \ell^\mp (\nu\nu)\tilde{\chi}_1^0$ simplified model, the following assumptions have been made: $m_{\tilde{\chi}_1^\pm} = m_{\tilde{\chi}_2^0} = 0.5 (m_{\tilde{\chi}_1^0} + m_{\tilde{g}})$, $m_{\tilde{\chi}_1^0} < 660 \text{ GeV}$. Limits are also derived in the mSUGRA/CMSSM, bRPV and GMSB models, see their Fig. 8.
- 32** CHATRCHYAN 14H searched in 19.5 fb^{-1} of pp collisions at $\sqrt{s} = 8 \text{ TeV}$ for events with two isolated same-sign dileptons and jets in the final state. No significant excess above the Standard Model expectations is observed. Limits are set on the gluino mass in simplified models where the R-parity violating decay $\tilde{g} \rightarrow tbs$ takes place with a branching ratio of 100%, see Fig. 8.

Long-lived \tilde{g} (Gluino) mass limit

Limits on light gluinos ($m_{\tilde{g}} < 5 \text{ GeV}$) were last listed in our PDG 14 edition: K. Olive, et al. (Particle Data Group), Chinese Physics C38 070001 (2014) (<http://pdg.lbl.gov>).

VALUE (GeV)	CL%	DOCUMENT ID	TECN	COMMENT
>2500	95	1 SIRUNYAN	21AF CMS	long-lived \tilde{g} , Tglu2RPV, λ''_{223} coupling, $0.6 \text{ mm} < c\tau < 90 \text{ mm}$
>2450	95	2 SIRUNYAN	21U CMS	long-lived \tilde{g} , $pp \rightarrow \tilde{g}\tilde{g}$, $\tilde{g} \rightarrow g\tilde{G}$, GMSB, $6 < c\tau < 550 \text{ mm}$
>2500	95	2 SIRUNYAN	21U CMS	long-lived \tilde{g} , $pp \rightarrow \tilde{g}\tilde{g}$, $\tilde{g} \rightarrow q\bar{q}\tilde{\chi}_1^0$ mini-split, $m_{\tilde{\chi}_1^0} = 100 \text{ GeV}$, $7 < c\tau < 360 \text{ mm}$
>2500	95	2 SIRUNYAN	21U CMS	long-lived \tilde{g} , $pp \rightarrow \tilde{g}\tilde{g}$, $\tilde{g} \rightarrow tbs$, λ''_{323} coupling, $3 < c\tau < 1000 \text{ mm}$
>1980	95	3 AABOUD	19AT ATLS	R-hadrons, Tglu1A, metastable
>2060	95	4 AABOUD	19C ATLS	R-hadrons, Tglu1A, $\tau \geq 10 \text{ ns}$, $m_{\tilde{\chi}_1^0} = 100 \text{ GeV}$
>1890	95	4 AABOUD	19C ATLS	R-hadrons, Tglu1A, stable
>2400	95	5 SIRUNYAN	19BH CMS	long-lived \tilde{g} , RPV, $\tilde{g} \rightarrow \bar{T}\bar{b}$, $10 \text{ mm} < c\tau < 250 \text{ mm}$
>2300	95	5 SIRUNYAN	19BH CMS	long-lived \tilde{g} , GMSB, $\tilde{g} \rightarrow g\tilde{G}$, $20 \text{ mm} < c\tau < 110 \text{ mm}$

See key on page 1127

Searches Particle Listings

Supersymmetric Particle Searches

>2100	95	6	SIRUNYAN	19BT CMS	long-lived \tilde{g} , GMSB, $\tilde{g} \rightarrow g\tilde{G}$, $0.3 \text{ m} < c\tau < 30 \text{ m}$
>2500	95	6	SIRUNYAN	19BT CMS	long-lived \tilde{g} , GMSB, $\tilde{g} \rightarrow g\tilde{G}$, $c\tau = 1 \text{ m}$
>1900	95	6	SIRUNYAN	19BT CMS	long-lived \tilde{g} , GMSB, $\tilde{g} \rightarrow g\tilde{G}$, $c\tau = 100 \text{ m}$
>2370	95	7	AABOUD	18s ATLS	displaced vertex + \cancel{E}_T , long-lived Tglu1A, $m_{\tilde{\chi}_1^0} = 100 \text{ GeV}$, and $\tau = 0.17 \text{ ns}$
>1600	95	8	SIRUNYAN	18AY CMS	jets + \cancel{E}_T , Tglu1A, $c\tau < 0.1 \text{ mm}$, $m_{\tilde{\chi}_1^0} = 100 \text{ GeV}$
>1750	95	8	SIRUNYAN	18AY CMS	jets + \cancel{E}_T , Tglu1A, $c\tau = 1 \text{ mm}$, $m_{\tilde{\chi}_1^0} = 100 \text{ GeV}$
>1640	95	8	SIRUNYAN	18AY CMS	jets + \cancel{E}_T , Tglu1A, $c\tau = 10 \text{ mm}$, $m_{\tilde{\chi}_1^0} = 100 \text{ GeV}$
>1490	95	8	SIRUNYAN	18AY CMS	jets + \cancel{E}_T , Tglu1A, $c\tau = 100 \text{ mm}$, $m_{\tilde{\chi}_1^0} = 100 \text{ GeV}$
>1300	95	8	SIRUNYAN	18AY CMS	jets + \cancel{E}_T , Tglu1A, $c\tau = 1 \text{ m}$, $m_{\tilde{\chi}_1^0} = 100 \text{ GeV}$
> 960	95	8	SIRUNYAN	18AY CMS	jets + \cancel{E}_T , Tglu1A, $c\tau = 10 \text{ m}$, $m_{\tilde{\chi}_1^0} = 100 \text{ GeV}$
> 900	95	8	SIRUNYAN	18AY CMS	jets + \cancel{E}_T , Tglu1A, $c\tau = 100 \text{ m}$, $m_{\tilde{\chi}_1^0} = 100 \text{ GeV}$
>2200	95	9	SIRUNYAN	18DV CMS	long-lived \tilde{g} , RPV, $\tilde{g} \rightarrow \bar{t}\bar{d}\bar{s}$, $0.6 \text{ mm} < c\tau < 80 \text{ mm}$
>1000	95	10	KHACHATRY...17AR CMS	long-lived \tilde{g} , RPV, $\tilde{g} \rightarrow \bar{t}\bar{d}\bar{s}$, $c\tau = 0.3 \text{ mm}$	
>1300	95	10	KHACHATRY...17AR CMS	long-lived \tilde{g} , RPV, $\tilde{g} \rightarrow \bar{t}\bar{d}\bar{s}$, $c\tau = 1.0 \text{ mm}$	
>1400	95	10	KHACHATRY...17AR CMS	long-lived \tilde{g} , RPV, $\tilde{g} \rightarrow \bar{t}\bar{d}\bar{s}$, $2 \text{ mm} < c\tau < 30 \text{ mm}$	
>1580	95	11	AABOUD	16B ATLS	long-lived R-hadrons
> 740–1590	95	12	AABOUD	16C ATLS	R-hadrons, Tglu1A, $\tau \geq 0.4 \text{ ns}$, $m_{\tilde{\chi}_1^0} = 100 \text{ GeV}$
>1570	95	12	AABOUD	16C ATLS	R-hadrons, Tglu1A, stable
>1610	95	13	KHACHATRY...16BWCMS	long-lived \tilde{g} forming R-hadrons, $f = 0.1$, cloud interaction model	
>1580	95	13	KHACHATRY...16BWCMS	long-lived \tilde{g} forming R-hadrons, $f = 0.1$, charge-suppressed interaction model	
>1520	95	13	KHACHATRY...16BWCMS	long-lived \tilde{g} forming R-hadrons, $f = 0.5$, cloud interaction model	
>1540	95	13	KHACHATRY...16BWCMS	long-lived \tilde{g} forming R-hadrons, $f = 0.5$, charge-suppressed interaction model	
>1270	95	14	AAD	15AE ATLS	\tilde{g} R-hadron, generic R-hadron model
>1360	95	14	AAD	15AE ATLS	\tilde{g} decaying to 300 GeV stable sleptons, LeptoSUSY model
>1115	95	15	AAD	15BMATLS	\tilde{g} R-hadron, stable
>1185	95	15	AAD	15BMATLS	$\tilde{g} \rightarrow (g/q\bar{q})\tilde{\chi}_1^0$, lifetime 10 ns, $m_{\tilde{\chi}_1^0} = 100 \text{ GeV}$
>1099	95	15	AAD	15BMATLS	$\tilde{g} \rightarrow (g/q\bar{q})\tilde{\chi}_1^0$, lifetime 10 ns, $m_{\tilde{g}} - m_{\tilde{\chi}_1^0} = 100 \text{ GeV}$
>1182	95	15	AAD	15BMATLS	$\tilde{g} \rightarrow t\bar{t}\tilde{\chi}_1^0$, lifetime 10 ns, $m_{\tilde{\chi}_1^0} = 100 \text{ GeV}$
>1157	95	15	AAD	15BMATLS	$\tilde{g} \rightarrow t\bar{t}\tilde{\chi}_1^0$, lifetime 10 ns, $m_{\tilde{g}} - m_{\tilde{\chi}_1^0} = 480 \text{ GeV}$
> 869	95	15	AAD	15BMATLS	$\tilde{g} \rightarrow (g/q\bar{q})\tilde{\chi}_1^0$, lifetime 1 ns, $m_{\tilde{\chi}_1^0} = 100 \text{ GeV}$
> 821	95	15	AAD	15BMATLS	$\tilde{g} \rightarrow (g/q\bar{q})\tilde{\chi}_1^0$, lifetime 1 ns, $m_{\tilde{g}} - m_{\tilde{\chi}_1^0} = 100 \text{ GeV}$
> 836	95	15	AAD	15BMATLS	$\tilde{g} \rightarrow t\bar{t}\tilde{\chi}_1^0$, lifetime 1 ns, $m_{\tilde{\chi}_1^0} = 100 \text{ GeV}$
> 836	95	15	AAD	15BMATLS	$\tilde{g} \rightarrow t\bar{t}\tilde{\chi}_1^0$, lifetime 10 ns, $m_{\tilde{g}} - m_{\tilde{\chi}_1^0} = 480 \text{ GeV}$
>1000	95	16	KHACHATRY...15AK CMS	\tilde{g} R-hadrons, $10 \mu\text{s} < \tau < 1000 \text{ s}$	
> 880	95	16	KHACHATRY...15AK CMS	\tilde{g} R-hadrons, $1 \mu\text{s} < \tau < 1000 \text{ s}$, limits, etc.	
••• We do not use the following data for averages, fits, limits, etc. •••					
> 985	95	17	AAD	13AA ATLS	\tilde{g} , R-hadrons, generic interaction model
> 832	95	18	AAD	13BC ATLS	R-hadrons, $\tilde{g} \rightarrow g/q\bar{q}\tilde{\chi}_1^0$, generic R-hadron model, lifetime between 10^{-5} and 10^3 s , $m_{\tilde{\chi}_1^0} = 100 \text{ GeV}$
>1322	95	19	CHATRCHYAN13AB CMS	long-lived \tilde{g} forming R-hadrons, $f = 0.1$, cloud interaction model	
none 200–341	95	20	AAD	12P ATLS	long-lived $\tilde{g} \rightarrow g\tilde{\chi}_1^0$, $m_{\tilde{\chi}_1^0} = 100 \text{ GeV}$

> 640	95	21	CHATRCHYAN12AN CMS	long-lived $\tilde{g} \rightarrow g\tilde{\chi}_1^0$	
>1098	95	22	CHATRCHYAN12L CMS	long-lived \tilde{g} forming R-hadrons, $f = 0.1$	
> 586	95	23	AAD	11K ATLS	stable \tilde{g}
> 544	95	24	AAD	11P ATLS	stable \tilde{g} , GMSB scenario, $\tan\beta=5$
> 370	95	25	KHACHATRY...11C CMS	long lived \tilde{g}	
> 398	95	26	KHACHATRY...11C CMS	stable \tilde{g}	

- SIRUNYAN 21AF searched in 140 fb^{-1} of pp collisions at $\sqrt{s} = 13 \text{ TeV}$ for supersymmetry in events with two displaced vertices from long-lived particles decaying into multijet or dijet final states. No significant excess above the Standard Model expectations is observed. Limits are set on the gluino mass in the simplified model Tglu2RPV with λ_{323}'' coupling, on the $\tilde{\chi}_1^0$ mass in an RPV model with $\tilde{\chi}_1^0$ pair production and the RPV decay $\tilde{\chi}_1^0 \rightarrow tbs$ with λ_{323}'' coupling and on the \tilde{t} mass in an RPV model with top squark pair production and the RPV decay $\tilde{t} \rightarrow \bar{d}_i\bar{d}_j$ with λ_{3ij}'' coupling, see their Figure 7.
- SIRUNYAN 21U searched in 132 fb^{-1} of pp collisions at $\sqrt{s} = 13 \text{ TeV}$ for supersymmetry in events with displaced tracks and displaced vertices associated with a dijet system. No significant excess above the Standard Model expectations is observed. Limits are set on long-lived gluinos in an RPC GMSB SUSY model of gluino pair production, with $\tilde{g} \rightarrow g\tilde{G}$, see their Figure 9, in Tglu1A in a mini-split model, see their Figure 10, and in an RPV model of gluino pair production, with $\tilde{g} \rightarrow tbs$ with coupling λ_{323}'' , see their Figure 11. Limits are also set on long-lived top squarks in Tstop2RPV, see their Figure 12, in an RPV model with $\tilde{t} \rightarrow d\bar{d}$ and λ_{x31}' coupling, see their Figure 13, and in a dynamical RPV model with $\tilde{t} \rightarrow \bar{d}\bar{d}$ via a nonholomorphic RPV coupling η_{311}'' , see their Figure 14. The best mass limit is achieved in all cases at $c\tau = 30 \text{ mm}$.
- AABOUD 19AT searched in 36.1 fb^{-1} of pp collisions at $\sqrt{s} = 13 \text{ TeV}$ for metastable and stable R-hadrons. Multiple search strategies for a wide range of lifetimes, corresponding to path lengths of a few meters, are defined. No significant deviations from the expected Standard Model background are observed. Gluino R-hadrons with lifetimes of the order of 50 ns are excluded at 95% C.L. for masses below 1980 GeV using the muon-spectrometer agnostic analysis. Using the full-detector search, the observed lower limits on the mass are 2000 GeV. See their Figure 9 (top).
- AABOUD 19C searched in 36.1 fb^{-1} of pp collisions at $\sqrt{s} = 13 \text{ TeV}$ for metastable and stable R-hadrons arising as excesses in the mass distribution of reconstructed tracks with high transverse momentum and large dE/dx . Gluino R-hadrons with lifetimes above 10 ns are excluded at 95% C.L. with lower mass limit range between 1000 GeV and 2060 GeV, see their Figure 5(a). Masses smaller than 1290 GeV are excluded for a lifetime of 1 ns, see their Figure 6. In the case of stable R-hadrons, the lower mass limit is 1890 GeV, see their Figure 5(b).
- SIRUNYAN 19BH searched in 35.9 fb^{-1} of pp collisions at $\sqrt{s} = 13 \text{ TeV}$ for long-lived particles decaying into jets, with each long-lived particle having a decay vertex well displaced from the production vertex. The selected events are found to be consistent with standard model predictions. Limits are set on the gluino mass in a GMSB model where the gluino is decaying via $\tilde{g} \rightarrow g\tilde{G}$, see their Figure 4 and in an RPV model of supersymmetry where the gluino is decaying via $\tilde{g} \rightarrow \bar{t}\bar{d}\bar{s}$, see their Figures 5. Limits are also set on the stop mass in two RPV models, see their Figure 6 (for $\tilde{t} \rightarrow b\bar{l}$ decays) and Figure 7 (for $\tilde{t} \rightarrow \bar{d}\bar{d}$ decays).
- SIRUNYAN 19BT searched in 137 fb^{-1} of pp collisions at $\sqrt{s} = 13 \text{ TeV}$ for long-lived particles decaying to displaced, nonprompt jets and missing transverse momentum. Candidate signal events are identified using the timing capabilities of the CMS electromagnetic calorimeter. The results of the search are found to be consistent with the background predictions. Limits are set on the gluino mass in a GMSB model where long-lived gluinos are pair produced and decaying via $\tilde{g} \rightarrow g\tilde{G}$, see their Figures 4 and 5.
- AABOUD 18s searched in 32.8 fb^{-1} of pp collisions at $\sqrt{s} = 13 \text{ TeV}$ for long-lived gluinos in final states with large missing transverse momentum and at least one high-mass displaced vertex with five or more tracks. The observed yield is consistent with the expected background. Exclusion limits are derived for Tglu1A models predicting the existence of long-lived gluinos reaching roughly $m(\tilde{g}) = 2000 \text{ GeV}$ to 2370 GeV for $m(\tilde{\chi}_1^0) = 100 \text{ GeV}$ and gluino lifetimes between 0.02 and 10 ns, see their Fig. 8. Limits are presented also as a function of the lifetime (for a fixed gluino-neutralino mass difference of 100 GeV) and of the gluino and neutralino masses (for a fixed lifetime of 1 ns). See their Fig. 9 and 10 respectively.
- SIRUNYAN 18AY searched in 35.9 fb^{-1} of pp collisions at $\sqrt{s} = 13 \text{ TeV}$ for events containing one or more jets and significant \cancel{E}_T . No significant excess above the Standard Model expectations is observed. Limits are set on the gluino mass in the Tglu1A, Tglu2A and Tglu3A simplified models, see their Figure 3. Limits are also set on squark, sbottom and stop masses in the Tsqk1, Tsbol1, Tstop1 and Tstop4 simplified models, see their Figure 3. Finally, limits are set on long-lived gluino masses in a Tglu1A simplified model where the gluino is metastable or long-lived with proper decay lengths in the range $10^{-3} \text{ mm} < c\tau < 10^5 \text{ mm}$, see their Figure 4.
- SIRUNYAN 18DV searched in 38.5 fb^{-1} of pp collisions at $\sqrt{s} = 13 \text{ TeV}$ for long-lived particles in events with multiple jets and two displaced vertices composed of many tracks. No events with two well-separated high-track-multiplicity vertices were observed. Limits are set on the stop and the gluino mass in RPV models of supersymmetry where the stop (gluino) is decaying solely into dijet (multijet) final states, see their Figures 6 and 7.
- KHACHATRYAN 17AR searched in 17.6 fb^{-1} of pp collisions at $\sqrt{s} = 8 \text{ TeV}$ for R-parity-violating SUSY in which long-lived neutralinos or gluinos decay into multijet final states. No significant excess above the Standard Model expectations is observed. Limits are set on the gluino mass for a range of mean proper decay lengths ($c\tau$), see their Fig. 7. The upper limits on the production cross section times branching ratio squared (Fig. 7) are also applicable to long-lived neutralinos.
- AABOUD 16B searched in 3.2 fb^{-1} of pp collisions at $\sqrt{s} = 13 \text{ TeV}$ for long-lived R-hadrons using observables related to large ionization losses and slow propagation velocities, which are signatures of heavy charged particles traveling significantly slower than the speed of light. Exclusion limits at 95% C.L. are set on the long-lived gluino masses exceeding 1580 GeV. See their Fig. 5.
- AABOUD 16C searched in 3.2 fb^{-1} of pp collisions at $\sqrt{s} = 13 \text{ TeV}$ for long-lived and stable R-hadrons identified by anomalous specific ionization energy loss in the ATLAS Pixel detector. Gluino R-hadrons with lifetimes above 0.4 ns are excluded at 95% C.L. with lower mass limit range between 740 GeV and 1590 GeV. In the case of stable R-hadrons, the lower mass limit is 1570 GeV. See their Figs. 5 and 6.

Searches Particle Listings

Supersymmetric Particle Searches

- 13 KHACHATRYAN 16BW searched in 2.5 fb^{-1} of pp collisions at $\sqrt{s} = 13 \text{ TeV}$ for events with heavy stable charged particles, identified by their anomalously high energy deposits in the silicon tracker and/or long time-of-flight measurements by the muon system. No evidence for an excess over the expected background is observed. Limits are derived for pair production of gluinos as a function of mass, depending on the interaction model and on the fraction f , of produced gluinos hadronizing into a \tilde{g} -gluon state, see Fig. 4 and Table 7.
- 14 AAD 15AE searched in 19.1 fb^{-1} of pp collisions at $\sqrt{s} = 8 \text{ TeV}$ for heavy long-lived charged particles, measured through their specific ionization energy loss in the ATLAS pixel detector or their time-of-flight in the ALTA muon system. In the absence of an excess of events above the expected backgrounds, limits are set for R -hadrons in various scenarios, see Fig. 11. Limits are also set in LeptoSUSY models where the gluino decays to stable 300 GeV leptons, see Fig. 9.
- 15 AAD 15BM searched in 18.4 fb^{-1} of pp collisions at $\sqrt{s} = 8 \text{ TeV}$ for stable and metastable non-relativistic charged particles through their anomalously specific ionization energy loss in the ATLAS pixel detector. In the absence of an excess of events above the expected backgrounds, limits are set within a generic R -hadron model, on stable gluino R -hadrons (see Table 5) and on metastable gluino R -hadrons decaying to $(g/\bar{q}\bar{q})$ plus a light $\tilde{\chi}_1^0$ (see Fig. 7) and decaying to $t\bar{t}$ plus a light $\tilde{\chi}_1^0$ (see Fig. 9).
- 16 KHACHATRYAN 15AK looked in a data set corresponding to 18.6 fb^{-1} of pp collisions at $\sqrt{s} = 8 \text{ TeV}$, and a search interval corresponding to 281 h of trigger lifetime, for long-lived particles that have stopped in the CMS detector. No evidence for an excess over the expected background in a cloud interaction model is observed. Assuming the decay $\tilde{g} \rightarrow g\tilde{\chi}_1^0$ and lifetimes between 1 μs and 1000 s, limits are derived on \tilde{g} production as a function of $m_{\tilde{\chi}_1^0}$, see Figs. 4 and 6. The exclusions require that $m_{\tilde{\chi}_1^0}$ is kinematically consistent with the minimum values of the jet energy thresholds used.
- 17 AAD 13AA searched in 4.7 fb^{-1} of pp collisions at $\sqrt{s} = 7 \text{ TeV}$ for events containing colored long-lived particles that hadronize forming R -hadrons. No significant excess above the expected background was found. Long-lived R -hadrons containing a \tilde{g} are excluded for masses up to 985 GeV at 95% C.L. in a general interaction model. Also, limits independent of the fraction of R -hadrons that arrive charged in the muon system were derived, see Fig. 6.
- 18 AAD 13bc searched in 5.0 fb^{-1} of pp collisions at $\sqrt{s} = 7 \text{ TeV}$ and in 22.9 fb^{-1} of pp collisions at $\sqrt{s} = 8 \text{ TeV}$ for bottom squark R -hadrons that have come to rest within the ATLAS calorimeter and decay at some later time to hadronic jets and a neutralino. In the absence of an excess of events above the expected backgrounds, limits are set on gluino masses for different decays, lifetimes, and neutralino masses, see their Table 6 and Fig. 10.
- 19 CHATRCHYAN 13AB looked in 5.0 fb^{-1} of pp collisions at $\sqrt{s} = 7 \text{ TeV}$ and in 18.8 fb^{-1} of pp collisions at $\sqrt{s} = 8 \text{ TeV}$ for events with heavy stable particles, identified by their anomalously dE/dx in the tracker or additionally requiring that it be identified as muon in the muon chambers, from pair production of \tilde{g} 's. No evidence for an excess over the expected background is observed. Limits are derived for pair production of gluinos as a function of mass (see Fig. 8 and Table 5), depending on the fraction, f , of formation of $\tilde{g}-g$ (R -gluonball) states. The quoted limit is for $f = 0.1$, while for $f = 0.5$ it degrades to 1276 GeV. In the conservative scenario where every hadronic interaction causes it to become neutral, the limit decreases to 928 GeV for $f = 0.1$.
- 20 AAD 12P looked in 31 pb^{-1} of pp collisions at $\sqrt{s} = 7 \text{ TeV}$ for events with pair production of long-lived gluinos. The hadronization of the gluinos leads to R -hadrons which may stop inside the detector and later decay via $\tilde{g} \rightarrow g\tilde{\chi}_1^0$ during gaps between the proton bunches. No significant excess over the expected background is observed. From a counting experiment, a limit at 95% C.L. on the cross section as a function of $m_{\tilde{g}}$ is derived for $m_{\tilde{\chi}_1^0} = 100 \text{ GeV}$, see Fig. 4. The limit is valid for lifetimes between 10^{-5} and 10^3 seconds and assumes the *Generic* matter interaction model for the production cross section.
- 21 CHATRCHYAN 12AN looked in 4.0 fb^{-1} of pp collisions at $\sqrt{s} = 7 \text{ TeV}$ for events with pair production of long-lived gluinos. The hadronization of the gluinos leads to R -hadrons which may stop inside the detector and later decay via $\tilde{g} \rightarrow g\tilde{\chi}_1^0$ during gaps between the proton bunches. No significant excess over the expected background is observed. From a counting experiment, a limit at 95% C.L. on the cross section as a function of $m_{\tilde{g}}$ is derived, see Fig. 3. The mass limit is valid for lifetimes between 10^{-5} and 10^3 seconds, for what they call "the daughter gluon energy $E_{\tilde{g}} > 100 \text{ GeV}$ and assuming the *cloud* interaction model for R -hadrons. Supersedes KHACHATRYAN 11.
- 22 CHATRCHYAN 12L looked in 5.0 fb^{-1} of pp collisions at $\sqrt{s} = 7 \text{ TeV}$ for events with heavy stable particles, identified by their anomalously dE/dx in the tracker or additionally requiring that it be identified as muon in the muon chambers, from pair production of \tilde{g} 's. No evidence for an excess over the expected background is observed. Limits are derived for pair production of gluinos as a function of mass (see Fig. 3), depending on the fraction, f , of formation of $\tilde{g}-g$ (R -glueball) states. The quoted limit is for $f = 0.1$, while for $f = 0.5$ it degrades to 1046 GeV. In the conservative scenario where every hadronic interaction causes it to become neutral, the limit decreases to 928 GeV for $f = 0.1$. Supersedes KHACHATRYAN 11c.
- 23 AAD 11k looked in 34 pb^{-1} of pp collisions at $\sqrt{s} = 7 \text{ TeV}$ for events with heavy stable particles, identified by their anomalously dE/dx in the tracker or time of flight in the tile calorimeter, from pair production of \tilde{g} . No evidence for an excess over the SM expectation is observed. Limits are derived for pair production of gluinos as a function of mass (see Fig. 4), for a fraction, $f = 10\%$, of formation of $\tilde{g}-g$ (R -gluonball). If instead of a phase space driven approach for the hadronic scattering of the R -hadrons, a triple-Regge model or a bag-model is used, the limit degrades to 566 and 562 GeV, respectively.
- 24 AAD 11P looked in 37 pb^{-1} of pp collisions at $\sqrt{s} = 7 \text{ TeV}$ for events with heavy stable particles, reconstructed and identified by their time of flight in the Muon System. There is no requirement on their observation in the tracker to increase the sensitivity to cases where gluinos have a large fraction, f , of formation of neutral $\tilde{g}-g$ (R -gluonball). No evidence for an excess over the SM expectation is observed. Limits are derived as a function of mass (see Fig. 4), for $f = 0.1$. For fractions $f = 0.5$ and 1.0 the limit degrades to 537 and 530 GeV, respectively.
- 25 KHACHATRYAN 11 looked in 10 pb^{-1} of pp collisions at $\sqrt{s} = 7 \text{ TeV}$ for events with pair production of long-lived gluinos. The hadronization of the gluinos leads to R -hadrons which may stop inside the detector and later decay via $\tilde{g} \rightarrow g\tilde{\chi}_1^0$ during gaps between the proton bunches. No significant excess over the expected background is observed. From a counting experiment, a limit at 95% C.L. on the cross section times branching ratio is derived for $m_{\tilde{g}} - m_{\tilde{\chi}_1^0} > 100 \text{ GeV}$, see their Fig. 2. Assuming 100% branching

ratio, lifetimes between 75 ns and $3 \times 10^5 \text{ s}$ are excluded for $m_{\tilde{g}} = 300 \text{ GeV}$. The \tilde{g} mass exclusion is obtained with the same assumptions for lifetimes between 10 μs and 1000 s, but shows some dependence on the model for R -hadron interactions with matter, illustrated in Fig. 3. From a time-profile analysis, the mass exclusion is 382 GeV for a lifetime of 10 μs under the same assumptions as above.

- 26 KHACHATRYAN 11c looked in 3.1 pb^{-1} of pp collisions at $\sqrt{s} = 7 \text{ TeV}$ for events with heavy stable particles, identified by their anomalously dE/dx in the tracker or additionally requiring that it be identified as muon in the muon chambers, from pair production of \tilde{g} . No evidence for an excess over the expected background is observed. Limits are derived for pair production of gluinos as a function of mass (see Fig. 3), depending on the fraction, f , of formation of $\tilde{g}-g$ (R -gluonball). The quoted limit is for $f = 0.1$, while for $f = 0.5$ it degrades to 357 GeV. In the conservative scenario where every hadronic interaction causes it to become neutral, the limit decreases to 311 GeV for $f = 0.1$.

Light \tilde{G} (Gravitino) mass limits from collider experiments

The following are bounds on light ($\ll 1 \text{ eV}$) gravitino indirectly inferred from its coupling to matter suppressed by the gravitino decay constant.

Unless otherwise stated, all limits assume that other supersymmetric particles besides the gravitino are too heavy to be produced. The gravitino is assumed to be undetected and to give rise to a missing energy (\cancel{E}) signature.

Some earlier papers are now obsolete and have been omitted. They were last listed in our PDG 14 edition: K. Olive, *et al.* (Particle Data Group), Chinese Physics **C38** 070001 (2014) (<http://pdg.lbl.gov>).

VALUE (eV)	CL%	DOCUMENT ID	TECN	COMMENT
• • • We do not use the following data for averages, fits, limits, etc. • • •				
$> 3.5 \times 10^{-4}$	95	1 AAD	15BH ATLS	jet + \cancel{E}_T , $pp \rightarrow (\tilde{q}/\tilde{g})\tilde{G}$, $m_{\tilde{q}} = m_{\tilde{g}} = 500 \text{ GeV}$
$> 3 \times 10^{-4}$	95	1 AAD	15BH ATLS	jet + \cancel{E}_T , $pp \rightarrow (\tilde{q}/\tilde{g})\tilde{G}$, $m_{\tilde{q}} = m_{\tilde{g}} = 1000 \text{ GeV}$
$> 2 \times 10^{-4}$	95	1 AAD	15BH ATLS	jet + \cancel{E}_T , $pp \rightarrow (\tilde{q}/\tilde{g})\tilde{G}$, $m_{\tilde{q}} = m_{\tilde{g}} = 1500 \text{ GeV}$
$> 1.09 \times 10^{-5}$	95	2 ABDALLAH	05B DLPH	$e^+e^- \rightarrow \tilde{G}\tilde{G}\gamma$
$> 1.35 \times 10^{-5}$	95	3 ACHARD	04E L3	$e^+e^- \rightarrow \tilde{G}\tilde{G}\gamma$
$> 1.3 \times 10^{-5}$	95	4 HEISTER	03C ALEP	$e^+e^- \rightarrow \tilde{G}\tilde{G}\gamma$
$> 11.7 \times 10^{-6}$	95	5 ACOSTA	02H CDF	$p\bar{p} \rightarrow \tilde{G}\tilde{G}\gamma$
$> 8.7 \times 10^{-6}$	95	6 ABBIENDI,G	00D OPAL	$e^+e^- \rightarrow \tilde{G}\tilde{G}\gamma$

- 1 AAD 15BH searched in 20.3 fb^{-1} of pp collisions at $\sqrt{s} = 8 \text{ TeV}$ for associated production of a light gravitino and a squark or gluino. The squark (gluino) is assumed to decay exclusively to a quark (gluon) and a gravitino. No evidence was found for an excess above the expected level of Standard Model background and 95% C.L. lower limits were set on the gravitino mass as a function of the squark/gluino mass, both in the case of degenerate and non-degenerate squark/gluino masses, see Figs. 14 and 15.
- 2 ABDALLAH 05B use data from $\sqrt{s} = 180\text{--}208 \text{ GeV}$. They look for events with a single photon + \cancel{E} final states from which a cross section limit of $\sigma < 0.18 \text{ pb}$ at 208 GeV is obtained, allowing a limit on the mass to be set. Supersedes the results of ABREU 00Z.
- 3 ACHARD 04E use data from $\sqrt{s} = 189\text{--}209 \text{ GeV}$. They look for events with a single photon + \cancel{E} final states from which a limit on the Gravitino mass is set corresponding to $\sqrt{F} > 238 \text{ GeV}$. Supersedes the results of ACCIARRI 99R.
- 4 HEISTER 03C use the data from $\sqrt{s} = 189\text{--}209 \text{ GeV}$ to search for $\gamma\cancel{E}_T$ final states.
- 5 ACOSTA 02H looked in 87 pb^{-1} of $p\bar{p}$ collisions at $\sqrt{s} = 1.8 \text{ TeV}$ for events with a high- E_T photon and \cancel{E}_T . They compared the data with a GMSB model where the final state could arise from $q\bar{q} \rightarrow \tilde{G}\tilde{G}$. Since the cross section for this process scales as $1/|F|^4$, a limit at 95% CL is derived on $|F|^{1/2} > 221 \text{ GeV}$. A model independent limit for the above topology is also given in the paper.
- 6 ABBIENDI,G 00D searches for $\gamma\cancel{E}$ final states from $\sqrt{s} = 189 \text{ GeV}$.

Supersymmetry miscellaneous results

Results that do not appear under other headings or that make nonminimal assumptions.

Some earlier papers are now obsolete and have been omitted. They were last listed in our PDG 14 edition: K. Olive, *et al.* (Particle Data Group), Chinese Physics **C38** 070001 (2014) (<http://pdg.lbl.gov>).

VALUE	CL%	DOCUMENT ID	TECN	COMMENT
• • • We do not use the following data for averages, fits, limits, etc. • • •				
		1 AAD	20C ATLS	habemus MSSM, $m_A - \tan\beta$ plane
none 450–1400	95	2 AAD	20L ATLS	heavy neutral Higgs bosons, hMSSM, $m_A - \tan\beta$ plane
> 65	95	3 AABOUD	16AF ATLS	selected ATLAS searches on EWK sector
none 0–2	95	4 AAD	16AG ATLS	dark photon, γ_d , in SUSY- and Higgs-portal models
		5 AAD	13P ATLS	dark γ , hidden valley
		6 AALTONEN	12AB CDF	hidden-valley Higgs
none 100–185	95	7 AAD	11AA ATLS	scalar gluons
		8 CHATRCHYAN11E	CMS	$\mu\mu$ resonances
		9 ABAZOV	10N D0	γ_D , hidden valley

- 1 AAD 20C uses a statistical combination of six final states $b\bar{b}b\bar{b}$, $b\bar{b}W\bar{W}$, $b\bar{b}\tau\tau$, $W\bar{W}W\bar{W}$, $b\bar{b}\gamma\gamma$, and $W\bar{W}\gamma\gamma$ to search for non-resonant and resonant production of Higgs boson pairs. The search uses 36.1 fb^{-1} of pp collisions data at $\sqrt{s} = 13 \text{ TeV}$. Constraints in the habemus Minimal Supersymmetric Standard Model in the $(m_A, \tan\beta)$ parameter space are placed, see their Figure 7(b).

See key on page 1127

Searches Particle Listings Supersymmetric Particle Searches

- 2 AAD 20L used 27.8 fb⁻¹ of pp collision data at $\sqrt{s} = 13$ TeV to search for heavy neutral Higgs bosons produced in association with at least one b-quark and decaying into a pair of b-quarks. The data are compatible with SM expectations, yielding no significant excess of events in the mass range 450–1400 GeV, see their Fig. 11. Exclusion limits at 95% C.L. were derived in hMSSM scenarios as a function of m_A and $\tan\beta$, see their Fig. 9 and 10.
- 3 AABOU 16AF uses a selection of searches by ATLAS for the electroweak production of SUSY particles studying resulting constraints on dark matter candidates. They use 20 fb⁻¹ of pp collisions at $\sqrt{s} = 8$ TeV. A likelihood-driven scan of an effective model focusing on the gaugino-higgsino and Higgs sector of the pMSSM is performed. The ATLAS searches impact models where $m_0 < 65$ GeV, excluding 86% of them. See their Figs. 2, 4, and 6.
- 4 AAD 16AG searches for prompt lepton-jets using 20 fb⁻¹ of pp collisions at $\sqrt{s} = 8$ TeV collected with the ATLAS detector. Lepton-jets are expected from decays of low-mass dark photons in SUSY-portal and Higgs-portal models. No significant excess of events is observed and 95% CL upper limits are computed on the production cross section times branching ratio for two prompt lepton-jets in models predicting 2 or 4 γ_D via SUSY-portal topologies, for γ_D mass values between 0 and 2 GeV. See their Figs 9 and 10. The results are also interpreted in terms of a 90% CL exclusion region in kinetic mixing and dark-photon mass parameter space. See their Fig. 13.
- 5 AAD 13P searched in 5 fb⁻¹ of pp collisions at $\sqrt{s} = 7$ TeV for single lepton-jets with at least four muons; pairs of lepton-jets, each with two or more muons; and pairs of lepton-jets with two or more electrons. All of these could be signatures of Hidden Valley supersymmetric models. No statistically significant deviations from the Standard Model expectations are found. 95% C.L. limits are placed on the production cross section times branching ratio of dark photons for several parameter sets of a Hidden Valley model.
- 6 AALTONEN 12AB looked in 5.1 fb⁻¹ of pp collisions at $\sqrt{s} = 1.96$ TeV for anomalous production of multiple low-energy leptons in association with a W or Z boson. Such events may occur in hidden valley models in which a supersymmetric Higgs boson is produced in association with a W or Z boson, with $H \rightarrow \tilde{\chi}_1^0 \tilde{\chi}_1^0$ pair and with the $\tilde{\chi}_1^0$ further decaying into a dark photon (γ_D) and the unobservable lightest SUSY particle of the hidden sector. As the γ_D is expected to be light, it may decay into a lepton pair. No significant excess over the SM expectation is observed and a limit at 95% C.L. is set on the cross section for a benchmark model of supersymmetric hidden-valley Higgs production.
- 7 AAD 11AA looked in 34 pb⁻¹ of pp collisions at $\sqrt{s} = 7$ TeV for events with ≥ 4 jets originating from pair production of scalar gluons, each decaying to two gluons. No two-jet resonances are observed over the SM background. Limits are derived on the cross section times branching ratio (see Fig. 3). Assuming 100% branching ratio for the decay to two gluons, the quoted exclusion range is obtained, except for a 5 GeV mass window around 140 GeV.
- 8 CHATRCHYAN 11E looked in 35 pb⁻¹ of pp collisions at $\sqrt{s} = 7$ TeV for events with collimated μ pairs (leptonic jets) from the decay of hidden sector states. No evidence for new resonance production is found. Limits are derived and compared to various SUSY models (see Fig. 4) where the LSP, either the $\tilde{\chi}_1^0$ or a \tilde{q} , decays to dark sector particles.
- 9 ABAZOV 10N looked in 5.8 fb⁻¹ of pp collisions at $\sqrt{s} = 1.96$ TeV for events from hidden valley models in which a $\tilde{\chi}_1^0$ decays into a dark photon, γ_D , and the unobservable lightest SUSY particle of the hidden sector. As the γ_D is expected to be light, it may decay into a tightly collimated lepton pair, called lepton jet. They searched for events with E_T and two isolated lepton jets observable by an opposite charged lepton pair $e\bar{e}$, $e\mu$ or $\mu\bar{\mu}$. No significant excess over the SM expectation is observed, and a limit at 95% C.L. on the cross section times branching ratio is derived, see their Table I. They also examined the invariant mass of the lepton jets for a narrow resonance, see their Fig. 4, but found no evidence for a signal.

REFERENCES FOR Supersymmetric Particle Searches

AAD	21AK	EPL C81 600	G. Aad et al.	(ATLAS Collab.)
AAD	21AL	PRL 127 051802	G. Aad et al.	(ATLAS Collab.)
AAD	21AM	PR D104 032014	G. Aad et al.	(ATLAS Collab.)
AAD	21AW	PR D104 112005	G. Aad et al.	(ATLAS Collab.)
AAD	21AX	PR D104 112010	G. Aad et al.	(ATLAS Collab.)
AAD	21B	EPL C81 111	G. Aad et al.	(ATLAS Collab.)
Also	EPL C81 249 (errata.)	G. Aad et al.	(ATLAS Collab.)	
AAD	21BF	EPL C81 1023	G. Aad et al.	(ATLAS Collab.)
AAD	21BG	EPL C81 1118	G. Aad et al.	(ATLAS Collab.)
AAD	21E	PR D103 112003	G. Aad et al.	(ATLAS Collab.)
AAD	21F	PR D103 112006	G. Aad et al.	(ATLAS Collab.)
AAD	21L	JHEP 2102 143	G. Aad et al.	(ATLAS Collab.)
AAD	21O	JHEP 2104 174	G. Aad et al.	(ATLAS Collab.)
AAD	21P	JHEP 2104 165	G. Aad et al.	(ATLAS Collab.)
AAD	21S	JHEP 2105 093	G. Aad et al.	(ATLAS Collab.)
AAD	21X	JHEP 2107 173	G. Aad et al.	(ATLAS Collab.)
AAD	21Y	JHEP 2107 167	G. Aad et al.	(ATLAS Collab.)
AALJ	21V	EPL C81 261	R. Aaij et al.	(LHCb Collab.)
ABDALLAH	21	PR D103 102002	H. Abdallah et al.	(H.E.S.S. Collab.)
MENG	21B	PRL 127 261802	Y. Meng et al.	(PandaX-4T Collab.)
SIRUNYAN	21AD	PR D104 052001	A.M. Sirunyan et al.	(CMS Collab.)
SIRUNYAN	21AF	PR D104 052011	A.M. Sirunyan et al.	(CMS Collab.)
SIRUNYAN	21B	EPL C81 3	A.M. Sirunyan et al.	(CMS Collab.)
SIRUNYAN	21M	JHEP 2104 123	A.M. Sirunyan et al.	(CMS Collab.)
SIRUNYAN	21U	PR D104 012015	A.M. Sirunyan et al.	(CMS Collab.)
SIRUNYAN	21V	PR D104 032006	A.M. Sirunyan et al.	(CMS Collab.)
TUMASYAN	21C	JHEP 2110 045	A. Tumasyan et al.	(CMS Collab.)
TUMASYAN	21I	EPL C81 970	A. Tumasyan et al.	(CMS Collab.)
AABOU	20	EPL C80 754	M. Aaboud et al.	(ATLAS Collab.)
AAD	20AL	JHEP 2010 062	G. Aad et al.	(ATLAS Collab.)
AAD	20AN	JHEP 2010 005	G. Aad et al.	(ATLAS Collab.)
AAD	20AS	EPL C80 1080	G. Aad et al.	(ATLAS Collab.)
AAD	20C	PL B800 135103	G. Aad et al.	(ATLAS Collab.)
AAD	20D	PL B801 135114	G. Aad et al.	(ATLAS Collab.)
AAD	20H	PR D101 032009	G. Aad et al.	(CMS Collab.)
AAD	20I	PR D101 052005	G. Aad et al.	(ATLAS Collab.)
AAD	20K	PR D101 072001	G. Aad et al.	(ATLAS Collab.)
AAD	20L	PR D102 032004	G. Aad et al.	(ATLAS Collab.)
AAD	20M	PR D102 032006	G. Aad et al.	(ATLAS Collab.)
AAD	20O	EPL C80 123	G. Aad et al.	(ATLAS Collab.)
AAD	20R	EPL C80 691	G. Aad et al.	(ATLAS Collab.)
AAD	20S	EPL C80 737	G. Aad et al.	(ATLAS Collab.)
AAD	20V	JHEP 2006 046	G. Aad et al.	(ATLAS Collab.)
ABAZAJIAN	20	PR D102 043012	K.N. Abazajian et al.	(UCI, VPI, TOKY+)
ABDALLAH	20	PR D102 062001	H. Abdallah et al.	(H.E.S.S. Collab.)
ABE	20G	PR D102 072002	K. Abe et al.	(Super-Kamiokande Collab.)
ALBERT	20	PR D101 103001	A. Albert et al.	(HAWC Collab.)
ALBERT	20A	PL B805 135439	A. Albert et al.	(ANTARES Collab.)
ALBERT	20C	PR D102 082002	A. Albert et al.	(ANTARES and IceCube Collab.)

ALVAREZ	20	JCAP 2009 004	A. Alvarez et al.	(GOET+)
HOOF	20	JCAP 2002 012	S. Hoof, A. Geringer-Sameth, R. Trotta	(CMS Collab.)
SIRUNYAN	20AH	JHEP 2005 032	A.M. Sirunyan et al.	(CMS Collab.)
SIRUNYAN	20AU	PRL 124 041803	A.M. Sirunyan et al.	(CMS Collab.)
SIRUNYAN	20B	PL B801 135183	A.M. Sirunyan et al.	(CMS Collab.)
SIRUNYAN	20BJ	JHEP 2009 149	A.M. Sirunyan et al.	(CMS Collab.)
SIRUNYAN	20E	PR D101 052010	A.M. Sirunyan et al.	(CMS Collab.)
SIRUNYAN	20N	PL B806 135502	A.M. Sirunyan et al.	(CMS Collab.)
SIRUNYAN	20P	EPL C80 189	A.M. Sirunyan et al.	(CMS Collab.)
SIRUNYAN	20T	EPL C80 752	A.M. Sirunyan et al.	(CMS Collab.)
SIRUNYAN	20U	JHEP 2002 015	A.M. Sirunyan et al.	(CMS Collab.)
WANG	20G	CP C44 125001	Q. Wang et al.	(PandaX-II Collab.)
AABOU	19AT	PR D99 092007	M. Aaboud et al.	(ATLAS Collab.)
AABOU	19AU	PR D100 012006	M. Aaboud et al.	(ATLAS Collab.)
AABOU	19C	PL B788 96	M. Aaboud et al.	(ATLAS Collab.)
AABOU	19G	PR D99 012001	M. Aaboud et al.	(ATLAS Collab.)
AABOU	19H	PR D99 012009	M. Aaboud et al.	(ATLAS Collab.)
AAD	19I	JHEP 1912 060	G. Aad et al.	(ATLAS Collab.)
ABE	19	PL B789 45	K. Abe et al.	(XMASS Collab.)
AJAJ	19	PR D100 022004	R. Ajaj et al.	(DEAP-3600 Collab.)
AMOLE	19	PR D100 022001	C. Amole et al.	(PICO Collab.)
APRILE	19A	PRL 122 141301	E. Aprile et al.	(XENONIT Collab.)
DI-MAURO	19	PR D99 123027	M. Di Mauro et al.	
JOHNSON	19	PR D99 103007	C. Johnson et al.	
LI	19D	PR D99 123519	S. Li et al.	
SIRUNYAN	19AG	JHEP 1906 143	A.M. Sirunyan et al.	(CMS Collab.)
SIRUNYAN	19AO	EPL C79 305	A.M. Sirunyan et al.	(CMS Collab.)
SIRUNYAN	19AU	EPL C79 444	A.M. Sirunyan et al.	(CMS Collab.)
SIRUNYAN	19AW	PL B790 140	A.M. Sirunyan et al.	(CMS Collab.)
SIRUNYAN	19BH	PR D99 032011	A.M. Sirunyan et al.	(CMS Collab.)
SIRUNYAN	19BI	PR D99 032014	A.M. Sirunyan et al.	(CMS Collab.)
SIRUNYAN	19BJ	PR D99 052002	A.M. Sirunyan et al.	(CMS Collab.)
SIRUNYAN	19BT	PL B797 134876	A.M. Sirunyan et al.	(CMS Collab.)
SIRUNYAN	19BU	JHEP 1908 150	A.M. Sirunyan et al.	(CMS Collab.)
SIRUNYAN	19CA	PR D100 112003	A.M. Sirunyan et al.	(CMS Collab.)
SIRUNYAN	19CE	PRL 123 241801	A.M. Sirunyan et al.	(CMS Collab.)
SIRUNYAN	19CH	JHEP 1910 244	A.M. Sirunyan et al.	(CMS Collab.)
SIRUNYAN	19CI	JHEP 1911 109	A.M. Sirunyan et al.	(CMS Collab.)
SIRUNYAN	19F	PR D99 012010	A.M. Sirunyan et al.	(CMS Collab.)
SIRUNYAN	19K	JHEP 1901 154	A.M. Sirunyan et al.	(CMS Collab.)
SIRUNYAN	19S	JHEP 1903 031	A.M. Sirunyan et al.	(CMS Collab.)
SIRUNYAN	19U	JHEP 1903 101	A.M. Sirunyan et al.	(CMS Collab.)
XIA	19A	PL B792 199	J. Xia et al.	(PandaX-II Collab.)
AABOU	18AQ	JHEP 1806 108	M. Aaboud et al.	(ATLAS Collab.)
AABOU	18AR	JHEP 1806 107	M. Aaboud et al.	(ATLAS Collab.)
AABOU	18AS	JHEP 1806 022	M. Aaboud et al.	(ATLAS Collab.)
AABOU	18AY	EPL C78 154	M. Aaboud et al.	(ATLAS Collab.)
AABOU	18BB	EPL C78 250	M. Aaboud et al.	(ATLAS Collab.)
AABOU	18BJ	EPL C78 625	M. Aaboud et al.	(ATLAS Collab.)
AABOU	18BT	EPL C78 995	M. Aaboud et al.	(ATLAS Collab.)
AABOU	18BV	JHEP 1809 050	M. Aaboud et al.	(ATLAS Collab.)
AABOU	18CF	PL B785 136	M. Aaboud et al.	(ATLAS Collab.)
AABOU	18CK	PR D98 092002	M. Aaboud et al.	(ATLAS Collab.)
AABOU	18CM	PR D98 092008	M. Aaboud et al.	(ATLAS Collab.)
AABOU	18CO	PR D98 092012	M. Aaboud et al.	(ATLAS Collab.)
AABOU	18I	JHEP 1801 126	M. Aaboud et al.	(ATLAS Collab.)
AABOU	18P	PR D97 032003	M. Aaboud et al.	(ATLAS Collab.)
AABOU	18R	PR D97 052010	M. Aaboud et al.	(ATLAS Collab.)
AABOU	18S	PR D97 052012	M. Aaboud et al.	(ATLAS Collab.)
AABOU	18U	PR D97 092006	M. Aaboud et al.	(ATLAS Collab.)
AABOU	18V	PR D97 112001	M. Aaboud et al.	(ATLAS Collab.)
AABOU	18Y	PR D98 032008	M. Aaboud et al.	(ATLAS Collab.)
AABOU	18Z	PR D98 032009	M. Aaboud et al.	(ATLAS Collab.)
ABDALLAH	18	PRL 120 051101	H. Abdallah et al.	(H.E.S.S. Collab.)
ADHIKARI	18	NAT 564 83	G. Adhikari et al.	(COSINE-100 Collab.)
AGNES	18A	PR D98 102006	P. Agnes et al.	(DarkSide-50 Collab.)
AGNESE	18A	PRL 120 061802	R. Agnese et al.	(SuperCDMS Collab.)
AHNEN	18	JCAP 1803 009	M.L. Ahnen et al.	(MAGIC Collab.)
ALBERT	18B	JCAP 1806 043	A. Albert et al.	(HAWC Collab.)
ALBERT	18C	PR D98 123012	A. Albert et al.	(HAWC Collab.)
AMAUDRUZ	18	PRL 121 071801	P.A. Amaudruz et al.	(DEAP-3600 Collab.)
APRILE	18	PRL 121 111302	E. Aprile et al.	(XENONIT Collab.)
SIRUNYAN	18AA	PL B780 118	A.M. Sirunyan et al.	(CMS Collab.)
SIRUNYAN	18AC	PL B780 384	A.M. Sirunyan et al.	(CMS Collab.)
SIRUNYAN	18AD	PL B780 432	A.M. Sirunyan et al.	(CMS Collab.)
SIRUNYAN	18AJ	PL B780 440	A.M. Sirunyan et al.	(CMS Collab.)
SIRUNYAN	18AK	PL B783 114	A.M. Sirunyan et al.	(CMS Collab.)
SIRUNYAN	18AL	JHEP 1802 067	A.M. Sirunyan et al.	(CMS Collab.)
SIRUNYAN	18AN	JHEP 1803 167	A.M. Sirunyan et al.	(CMS Collab.)
SIRUNYAN	18AO	JHEP 1803 166	A.M. Sirunyan et al.	(CMS Collab.)
SIRUNYAN	18AP	JHEP 1803 160	A.M. Sirunyan et al.	(CMS Collab.)
SIRUNYAN	18AR	JHEP 1803 076	A.M. Sirunyan et al.	(CMS Collab.)
SIRUNYAN	18AT	JHEP 1804 073	A.M. Sirunyan et al.	(CMS Collab.)
SIRUNYAN	18AY	JHEP 1805 025	A.M. Sirunyan et al.	(CMS Collab.)
SIRUNYAN	18B	PL B778 263	A.M. Sirunyan et al.	(CMS Collab.)
SIRUNYAN	18BR	JHEP 1808 016	A.M. Sirunyan et al.	(CMS Collab.)
SIRUNYAN	18C	PR D97 032009	A.M. Sirunyan et al.	(CMS Collab.)
SIRUNYAN	18D	PR D97 012007	A.M. Sirunyan et al.	(CMS Collab.)
SIRUNYAN	18DI	JHEP 1809 065	A.M. Sirunyan et al.	(CMS Collab.)
SIRUNYAN	18DN	JHEP 1811 079	A.M. Sirunyan et al.	(CMS Collab.)
SIRUNYAN	18DP	JHEP 1811 151	A.M. Sirunyan et al.	(CMS Collab.)
SIRUNYAN	18DV	PR D98 092011	A.M. Sirunyan et al.	(CMS Collab.)
SIRUNYAN	18DY	PR D98 112014	A.M. Sirunyan et al.	(CMS Collab.)
SIRUNYAN	18EA	PRL 121 141802	A.M. Sirunyan et al.	(CMS Collab.)
SIRUNYAN	18EM	PRL 120 241801	A.M. Sirunyan et al.	(CMS Collab.)
SIRUNYAN	18X	PR D97 032007	A.M. Sirunyan et al.	(CMS Collab.)
SIRUNYAN	18Y	PL B779 166	A.M. Sirunyan et al.	(CMS Collab.)
AABOU	17AF	JHEP 1708 006	M. Aaboud et al.	(ATLAS Collab.)
AABOU	17AJ	JHEP 1709 088	M. Aaboud et al.	(ATLAS Collab.)
AABOU	17AJ	JHEP 1709 084	M. Aaboud et al.	(ATLAS Collab.)
Also	JHEP 1908 121 (errata.)	M. Aaboud et al.	(ATLAS Collab.)	
AABOU	17AR	PR D96 112010	M. Aaboud et al.	(ATLAS Collab.)
AABOU	17AX	JHEP 1711 195	M. Aaboud et al.	(ATLAS Collab.)
AABOU	17AY	JHEP 1712 085	M. Aaboud et al.	(ATLAS Collab.)
AABOU	17AZ	JHEP 1712 034	M. Aaboud et al.	(ATLAS Collab.)
AABOU	17BE	EPL C77 898	M. Aaboud et al.	(ATLAS Collab.)
AABOU	17N	EPL C77 144	M. Aaboud et al.	(ATLAS Collab.)
AAJ	17Z	EPL C77 224	R. Aaij et al.	(LHCb Collab.)
AARTSEN	17	EPL C77 92	M.G. Aartsen et al.	(IceCube Collab.)
AARTSEN	17A	EPL C77 146	M.G. Aartsen et al.	(IceCube Collab.)
Also	EPL C79 214 (errata.)	M.G. Aartsen et al.	(IceCube Collab.)	
AARTSEN	17C	EPL C77 627	M.G. Aartsen et al.	(IceCube Collab.)
AKERIB	17	PRL 118 021303	D.S. Akerib et al.	(LUX Collab.)
AKERIB	17A	PRL 118 251302	D.S. Akerib et al.	(LUX Collab.)
AMOLE	17	PRL 118 251301	C. Amole et al.	(PICO Collab.)
APRILE	17G	PRL 119 181301	E. Aprile et al.	(XENON Collab.)
ARCHAMBAULT	17	PR D95 082001	S. Archambault et al.	(VERITAS Collab.)
ATHRON	17B	EPL C77 824	P. Athron et al.	(GAMBIT Collab.)
BATTAT	17	ASP 91 65	J.B.R. Battat et al.	(DRIFT-II Collab.)
BEHNKE	17	ASP 90 95	E. Behnke et al.	(PICASSO Collab.)
CUI	17A	PRL 119 181302	X. Cui et al.	(PandaX-II Collab.)

Searches Particle Listings
Supersymmetric Particle Searches

FU	17	PRL 118 071301	C. Fu et al.	(PandaX-II Collab.)	AAD	14F	JHEP 1406 124	G. Aad et al.	(ATLAS Collab.)
Also		PRL 120 049902 (err.)	C. Fu et al.	(PandaX-II Collab.)	AAD	14G	JHEP 1405 071	G. Aad et al.	(ATLAS Collab.)
KHACHATRY...	17	PR D95 012003	V. Khachatryan et al.	(CMS Collab.)	AAD	14H	JHEP 1404 169	G. Aad et al.	(ATLAS Collab.)
KHACHATRY...	17A	PRL 118 021802	V. Khachatryan et al.	(CMS Collab.)	AAD	14K	PR D90 012004	G. Aad et al.	(ATLAS Collab.)
KHACHATRY...	17AD	PR D96 012004	V. Khachatryan et al.	(CMS Collab.)	AAD	14T	PR D90 052008	G. Aad et al.	(ATLAS Collab.)
KHACHATRY...	17AR	PR D95 012009	V. Khachatryan et al.	(CMS Collab.)	AAD	14X	PR D90 052001	G. Aad et al.	(ATLAS Collab.)
KHACHATRY...	17AS	PR D95 012011	V. Khachatryan et al.	(CMS Collab.)	AALTONEN	14	PR D90 012011	T. Aaltonen et al.	(CDF Collab.)
KHACHATRY...	17AW	EPJ C77 635	V. Khachatryan et al.	(CMS Collab.)	ACKERMANN	14	PR D89 042001	M. Ackermann et al.	(Fermi-LAT Collab.)
KHACHATRY...	17L	JHEP 1704 018	V. Khachatryan et al.	(CMS Collab.)	AKERIB	14	PRL 112 091303	D.S. Akerib et al.	(LUX Collab.)
KHACHATRY...	17P	EPJ C77 294	V. Khachatryan et al.	(CMS Collab.)	ALEKSIC	14	JCAP 1402 008	J. Aleksic et al.	(MAGIC Collab.)
KHACHATRY...	17S	PL B767 403	V. Khachatryan et al.	(CMS Collab.)	AVRORIN	14	ASP 62 12	A.D. Avrorin et al.	(BAIKAL Collab.)
KHACHATRY...	17V	PL B769 391	V. Khachatryan et al.	(CMS Collab.)	BUCHMUELL...	14	EPJ C74 2809	O. Buchmuller et al.	(CDF Collab.)
KHACHATRY...	17Y	PL B770 257	V. Khachatryan et al.	(CMS Collab.)	BUCHMUELL...	14A	EPJ C74 2922	O. Buchmuller et al.	(CDF Collab.)
SIRUNYAN	17AF	PRL 119 151802	A.M. Sirunyan et al.	(CMS Collab.)	CHATRCHYAN	14AH	PR D90 112001	S. Chatrchyan et al.	(CMS Collab.)
SIRUNYAN	17AS	JHEP 1710 019	A.M. Sirunyan et al.	(CMS Collab.)	CHATRCHYAN	14H	JHEP 1401 163	S. Chatrchyan et al.	(CMS Collab.)
SIRUNYAN	17AT	JHEP 1710 005	A.M. Sirunyan et al.	(CMS Collab.)	CHATRCHYAN	14I	JHEP 1406 055	S. Chatrchyan et al.	(CMS Collab.)
SIRUNYAN	17AW	JHEP 1711 029	A.M. Sirunyan et al.	(CMS Collab.)	CHATRCHYAN	14N	PL B733 328	S. Chatrchyan et al.	(CMS Collab.)
SIRUNYAN	17AY	JHEP 1712 142	A.M. Sirunyan et al.	(CMS Collab.)	CHATRCHYAN	14P	PL B730 193	S. Chatrchyan et al.	(CMS Collab.)
SIRUNYAN	17AZ	EPJ C77 710	A.M. Sirunyan et al.	(CMS Collab.)	CHATRCHYAN	14R	PR D90 032006	S. Chatrchyan et al.	(CMS Collab.)
SIRUNYAN	17K	EPJ C77 327	A.M. Sirunyan et al.	(CMS Collab.)	CHATRCHYAN	14U	PRL 112 161802	S. Chatrchyan et al.	(CMS Collab.)
SIRUNYAN	17P	PR D96 032003	A.M. Sirunyan et al.	(CMS Collab.)	CZAKON	14	PRL 113 201803	M. Czakon et al.	(AACH, CAMB, UCB, LBL+)
SIRUNYAN	17S	EPJ C77 578	A.M. Sirunyan et al.	(CMS Collab.)	FELIZARDO	14	PR D89 072013	M. Felizardo et al.	(SIMPLE Collab.)
AABOUD	16AC	EPJ C76 683	M. Aaboud et al.	(ATLAS Collab.)	KHACHATRY...	14C	PL B736 371	V. Khachatryan et al.	(CMS Collab.)
AABOUD	16AF	JHEP 1609 175	M. Aaboud et al.	(ATLAS Collab.)	KHACHATRY...	14I	EPJ C74 3036	V. Khachatryan et al.	(CMS Collab.)
AABOUD	16B	PL B760 647	M. Aaboud et al.	(ATLAS Collab.)	KHACHATRY...	14L	PR D90 092007	V. Khachatryan et al.	(CMS Collab.)
AABOUD	16C	PR D93 112015	M. Aaboud et al.	(ATLAS Collab.)	KHACHATRY...	14T	PL B739 229	V. Khachatryan et al.	(CMS Collab.)
AABOUD	16D	PR D94 032005	M. Aaboud et al.	(ATLAS Collab.)	PDG	14	CP C38 070001	K. Olive et al.	(PDG Collab.)
AABOUD	16J	PR D94 052009	M. Aaboud et al.	(ATLAS Collab.)	ROSKOWSKI	14	JHEP 1408 067	L. Roszkowski, E.M. Sessolo, A.J. Williams	(WINR Collab.)
AABOUD	16M	EPJ C76 517	M. Aaboud et al.	(ATLAS Collab.)	AAD	13	PL B718 841	G. Aad et al.	(ATLAS Collab.)
AABOUD	16N	EPJ C76 392	M. Aaboud et al.	(ATLAS Collab.)	AAD	13AA	PL B720 277	G. Aad et al.	(ATLAS Collab.)
AABOUD	16O	EPJ C76 541	M. Aaboud et al.	(ATLAS Collab.)	AAD	13AI	JHEP 1307 186	G. Aad et al.	(ATLAS Collab.)
AABOUD	16Q	EPJ C76 547	M. Aaboud et al.	(ATLAS Collab.)	AAD	13AP	PR D88 012001	G. Aad et al.	(ATLAS Collab.)
AAD	16AA	PR D93 052002	G. Aad et al.	(ATLAS Collab.)	AAD	13AU	JHEP 1310 189	G. Aad et al.	(ATLAS Collab.)
AAD	16AD	PR D94 032003	G. Aad et al.	(ATLAS Collab.)	AAD	13B	PL B718 879	G. Aad et al.	(ATLAS Collab.)
AAD	16AG	JHEP 1602 062	G. Aad et al.	(ATLAS Collab.)	AAD	13BC	PR D88 112003	G. Aad et al.	(ATLAS Collab.)
AAD	16AM	JHEP 1606 067	G. Aad et al.	(ATLAS Collab.)	AAD	13BD	PR D88 112006	G. Aad et al.	(ATLAS Collab.)
AAD	16AY	EPJ C76 81	G. Aad et al.	(ATLAS Collab.)	AAD	13H	JHEP 1301 131	G. Aad et al.	(ATLAS Collab.)
AAD	16BB	EPJ C76 259	G. Aad et al.	(ATLAS Collab.)	AAD	13L	PR D87 012008	G. Aad et al.	(ATLAS Collab.)
AAD	16B	EPJ C76 565	G. Aad et al.	(ATLAS Collab.)	AAD	13P	PL B719 299	G. Aad et al.	(ATLAS Collab.)
AAD	16V	PL B757 334	G. Aad et al.	(ATLAS Collab.)	AAD	13Q	PL B719 261	G. Aad et al.	(ATLAS Collab.)
AARTSEN	16C	JCAP 1604 022	M.G. Aartsen et al.	(IceCube Collab.)	AAD	13R	PL B719 280	G. Aad et al.	(ATLAS Collab.)
ABDALLAH	16	PRL 117 111301	H. Abdallah et al.	(HE-S Collab.)	AALTONEN	13I	JHEP 1307 182	T. Aaltonen et al.	(CDF Collab.)
ADRIAN-MAR...	16	PR B759 69	S. Adrian-Martinez et al.	(ANTARES Collab.)	AALTONEN	13J	PRL 110 201802	T. Aaltonen et al.	(CDF Collab.)
AHNEN	16	JCAP 1602 039	M.L. Ahnen et al.	(MAGIC and Fermi-LAT Collab.)	AARTSEN	13C	PR D88 122001	M.G. Aartsen et al.	(IceCube Collab.)
AKERIB	16	PRL 116 161301	D.S. Akerib et al.	(LUX Collab.)	ABAZOV	13B	PR D87 052011	V.M. Abazov et al.	(DO Collab.)
AKERIB	16A	PRL 116 161302	D.S. Akerib et al.	(LUX Collab.)	ACKERMANN	13A	PR D88 082002	M. Ackermann et al.	(Fermi-LAT Collab.)
AMOLE	16	PR D93 052014	C. Amole et al.	(PICCO Collab.)	ADRIAN-MAR...	13	JCAP 1311 032	S. Adrian-Martinez et al.	(ANTARES Collab.)
APRILE	16B	PR D94 122001	E. Aprile et al.	(XENON100 Collab.)	AGNESE	13	PR D88 031104	R. Agnese et al.	(CDMS Collab.)
AVRORIN	16	ASP 81 12	A.D. Avrorin et al.	(BAIKAL Collab.)	AGNESE	13A	PRL 111 251301	R. Agnese et al.	(CDMS Collab.)
BECHTLE	16	EPJ C76 96	P. Bechtel et al.	(LPNHE, MADE Collab.)	APRILE	13	PRL 111 021301	E. Aprile et al.	(XENON100 Collab.)
CIRELLI	16	JCAP 1607 041	M. Cirelli, M. Taoso	(LPNHE, MADE Collab.)	BERGSTROM	13	PRL 111 171101	L. Bergstrom et al.	(CDF Collab.)
KHACHATRY...	16AA	PL B759 479	V. Khachatryan et al.	(CMS Collab.)	BOLIV	13	JCAP 1309 019	M. Boliev et al.	(CDF Collab.)
KHACHATRY...	16AC	PL B760 378	V. Khachatryan et al.	(CMS Collab.)	CABRERA	13	JHEP 1307 186	M. Cabrera, J. Casas, R. de Austri	(CDF Collab.)
KHACHATRY...	16AM	PR D93 092009	V. Khachatryan et al.	(CMS Collab.)	CALIBBI	13	JHEP 1310 132	L. Calibbi et al.	(CDF Collab.)
KHACHATRY...	16AV	JHEP 1607 027	V. Khachatryan et al.	(CMS Collab.)	CHATRCHYAN	13	PL B718 815	S. Chatrchyan et al.	(CMS Collab.)
KHACHATRY...	16AY	JHEP 1608 122	V. Khachatryan et al.	(CMS Collab.)	CHATRCHYAN	13AB	JHEP 1307 122	S. Chatrchyan et al.	(CMS Collab.)
KHACHATRY...	16BE	EPJ C76 317	V. Khachatryan et al.	(CMS Collab.)	CHATRCHYAN	13AH	PL B722 273	S. Chatrchyan et al.	(CMS Collab.)
KHACHATRY...	16BJ	EPJ C76 439	V. Khachatryan et al.	(CMS Collab.)	CHATRCHYAN	13AO	PR D87 072001	S. Chatrchyan et al.	(CMS Collab.)
KHACHATRY...	16BK	EPJ C76 460	V. Khachatryan et al.	(CMS Collab.)	CHATRCHYAN	13AT	PR D88 052017	S. Chatrchyan et al.	(CMS Collab.)
KHACHATRY...	16BS	JHEP 1610 006	V. Khachatryan et al.	(CMS Collab.)	CHATRCHYAN	13AV	PRL 111 081802	S. Chatrchyan et al.	(CMS Collab.)
KHACHATRY...	16BT	JHEP 1610 129	V. Khachatryan et al.	(CMS Collab.)	CHATRCHYAN	13G	JHEP 1301 077	S. Chatrchyan et al.	(CMS Collab.)
KHACHATRY...	16BW	PR D94 112004	V. Khachatryan et al.	(CMS Collab.)	CHATRCHYAN	13H	PL B719 42	S. Chatrchyan et al.	(CMS Collab.)
KHACHATRY...	16BX	PR D94 112009	V. Khachatryan et al.	(CMS Collab.)	CHATRCHYAN	13T	EPJ C73 2568	S. Chatrchyan et al.	(CMS Collab.)
KHACHATRY...	16BY	JHEP 1612 013	V. Khachatryan et al.	(CMS Collab.)	CHATRCHYAN	13V	JHEP 1303 037	S. Chatrchyan et al.	(CMS Collab.)
KHACHATRY...	16R	PL B757 6	V. Khachatryan et al.	(CMS Collab.)	Also		JHEP 1307 041 (err.)	S. Chatrchyan et al.	(CMS Collab.)
KHACHATRY...	16V	PL B758 152	V. Khachatryan et al.	(CMS Collab.)	CHATRCHYAN	13W	JHEP 1303 111	S. Chatrchyan et al.	(CMS Collab.)
KHACHATRY...	16Y	PL B759 9	V. Khachatryan et al.	(CMS Collab.)	ELLIS	13B	EPJ C73 2403	J. Ellis et al.	(CDF Collab.)
LEITE	16	JCAP 1611 021	N. Leite et al.	(LPNHE, MADE Collab.)	JIN	13	JCAP 1311 026	H.-B. Jin, Y.-L. Wu, Y.-F. Zhou	(CDF Collab.)
AAD	15AB	PR D92 012010	G. Aad et al.	(ATLAS Collab.)	KOPP	13	PR D88 076013	J. Kopp	(CDF Collab.)
AAD	15AE	JHEP 1501 068	G. Aad et al.	(ATLAS Collab.)	STREGE	13	JCAP 1304 013	C. Stregge et al.	(CDF Collab.)
AAD	15AI	JHEP 1504 116	G. Aad et al.	(ATLAS Collab.)	AAD	12AF	PL B714 180	G. Aad et al.	(ATLAS Collab.)
AAD	15BA	EPJ C75 208	G. Aad et al.	(ATLAS Collab.)	AAD	12AG	PL B714 197	G. Aad et al.	(ATLAS Collab.)
AAD	15BG	EPJ C75 318	G. Aad et al.	(ATLAS Collab.)	AAD	12AN	PRL 108 181802	G. Aad et al.	(ATLAS Collab.)
Also		EPJ C75 463	G. Aad et al.	(ATLAS Collab.)	AAD	12AS	PRL 108 261804	G. Aad et al.	(ATLAS Collab.)
AAD	15BH	EPJ C75 299	G. Aad et al.	(ATLAS Collab.)	AAD	12AX	PR D85 012006	G. Aad et al.	(ATLAS Collab.)
Also		EPJ C75 408 (err.)	G. Aad et al.	(ATLAS Collab.)	Also		PR D87 099903 (err.)	G. Aad et al.	(ATLAS Collab.)
AAD	15BM	EPJ C75 407	G. Aad et al.	(ATLAS Collab.)	AAD	12BJ	EPJ C72 1993	G. Aad et al.	(ATLAS Collab.)
AAD	15BV	JHEP 1510 054	G. Aad et al.	(ATLAS Collab.)	AAD	12CJ	PR D86 092002	G. Aad et al.	(ATLAS Collab.)
AAD	15BX	JHEP 1510 134	G. Aad et al.	(ATLAS Collab.)	AAD	12CM	EPJ C72 2215	G. Aad et al.	(ATLAS Collab.)
AAD	15CA	PR D92 072001	G. Aad et al.	(ATLAS Collab.)	AAD	12CP	PL B718 411	G. Aad et al.	(ATLAS Collab.)
AAD	15CB	PR D92 072004	G. Aad et al.	(ATLAS Collab.)	AAD	12CT	JHEP 1212 124	G. Aad et al.	(ATLAS Collab.)
AAD	15CJ	EPJ C75 510	G. Aad et al.	(ATLAS Collab.)	AAD	12D	EPJ C72 1965	G. Aad et al.	(ATLAS Collab.)
AAD	15CS	PR D91 012008	G. Aad et al.	(ATLAS Collab.)	AAD	12R	PL B707 478	G. Aad et al.	(ATLAS Collab.)
Also		PR D92 059903 (err.)	G. Aad et al.	(ATLAS Collab.)	AAD	12T	PL B709 137	G. Aad et al.	(ATLAS Collab.)
AAD	15J	PRL 114 142001	G. Aad et al.	(ATLAS Collab.)	AAD	12W	PL B710 67	G. Aad et al.	(ATLAS Collab.)
AAD	15K	PRL 114 161901	G. Aad et al.	(ATLAS Collab.)	AALTONEN	12B	PR D85 092001	T. Aaltonen et al.	(CDF Collab.)
AAD	15O	PRL 115 031801	G. Aad et al.	(ATLAS Collab.)	ABAZOV	12AD	PR D86 071701	V.M. Abazov et al.	(DO Collab.)
AAD	15X	PR D91 112016	G. Aad et al.	(ATLAS Collab.)	AKIMOV	12	PL B709 14	D.Yu. Akimov et al.	(ZEPLIN-III Collab.)
AALJ	15BD	EPJ C75 595	R. Aaij et al.	(LHCb Collab.)	AKULA	12	PR D85 075001	S. Akula et al.	(NEAS, MICH Collab.)
AARTSEN	15E	EPJ C75 492	M.G. Aartsen et al.	(IceCube Collab.)	ANGLOHER	12	EPJ C72 1971	G. Angloher et al.	(CRESS-TII Collab.)
ACKERMANN	15	PR D91 122002	M. Ackermann et al.	(Fermi-LAT Collab.)	APRILE	12	PRL 109 181301	E. Aprile et al.	(XENON100 Collab.)
ACKERMANN	15A	JCAP 1509 008	M. Ackermann et al.	(Fermi-LAT Collab.)	ARBEY	12A	PL B708 162	A. Arbey et al.	(CDF Collab.)
ACKERMANN	15B	PRL 115 231301	M. Ackermann et al.	(Fermi-LAT Collab.)	ARCHAMBAU...	12	PL B711 153	S. Archambault et al.	(PICASSO Collab.)
AGNESE	15	PL B743 456	P. Agnese et al.	(DarkSide-50 Collab.)	BAER	12	JHEP 1205 091	H. Baer, V. Barger, A. Mustafayev	(OKLA, WIS+ Collab.)
AGNESE	15B	PR D92 072003	R. Agnese et al.	(SuperCDMS Collab.)	BALAZS	12	EPJ C73 2563	C. Balazs et al.	(CDF Collab.)
BAGNASCHI	15	EPJ C75 900	E.A. Bagnaschi et al.	(CDF Collab.)	BECHTLE	12	JHEP 1206 098	P. Bechtel et al.	(CDF Collab.)
BUCKLEY	15	PR D91 102001	M.R. Buckley et al.	(CDF Collab.)	BEHNKE	12	PR D86 052001	E. Behnke et al.	(COUPP Collab.)
CHOI	15	PRL 114 141301	K. Choi et al.	(Super-Kamiokande Collab.)	Also		PR D90 072002 (err.)	G. Aad et al.	(CDF Collab.)
KHACHATRY...	15AB	JHEP 1501 096	V. Khachatryan et al.	(CMS Collab.)	BESKIDT	12	EPJ C72 2166	C. Beskidt et al.	(KARLE, JINR, ITEP Collab.)
KHACHATRY...	15AD	JHEP 1504 124	V. Khachatryan et al.	(CMS Collab.)	BOTTINO	12	PR D85 095013	A. Bottino, N. Fornengo, S. Scopel	(TORI, SOGA Collab.)
KHACHATRY...	15AF	JHEP 1505 078	V. Khachatryan et al.	(CMS Collab.)	BUCHMUELL...	12	EPJ C72 2020	O. Buchmuller et al.	(CDF Collab.)
KHACHATRY...	15AH	JHEP 1506 116	V. Khachatryan et al.	(CMS Collab.)	CAO	12A	PL B710 665	J. Cao et al.	(CDF Collab.)
KHACHATRY...	15AK	EPJ C75 151	V. Khachatryan et al.	(CMS Collab.)	CHATRCHYAN	12	PR D85 012004	S. Chatrchyan et al.	(CMS Collab.)
KHACHATRY...	15AO	EPJ C75 325	V. Khachatryan et al.	(CMS Collab.)	CHATRCHYAN	12AE	PRL 109 171803	S. Chatrchyan et al.	(CMS Collab.)
KHACHATRY...	15AR	PL B743 503	V. Khachatryan et al.	(CMS Collab.)	CHATRCHYAN	12AI	JHEP 1208 110	S. Chatrchyan et al.	(CMS Collab.)
KHACHATRY...	15AZ	PR D92 072006	V. Khachatryan et al.	(CMS Collab.)	CHATRCHYAN	12AL	JHEP 1206 169	S. Chatrchyan et al.	(CMS Collab.)
KHACHATRY...	15E	PRL 114 061801	V. Khachatryan et al.	(CMS Collab.)	CHATRCHYAN	12AN	JHEP 1208 026	S. Chatrchyan et al.	(CMS Collab.)
KHACHATRY...	15I	PL B745 5	V. Khachatryan et al.	(CMS Collab.)	CHATRCHYAN	12AT	JHEP 1210 018	S. Chatrchyan et al.	(CMS Collab.)
KHACHATRY...	15L	PL B747 98	V. Khachatryan et al.	(CMS Collab.)	CHATRCHYAN	12BJ	JHEP 1211 147	S. Chatrchyan et al.	(CMS Collab.)
KHACHATRY...	15O	PL B748 255	V. Khachatryan et al.	(CMS Collab.)	CHATRCHYAN	12BK	JHEP 1211 172	S. Chatrchyan et al.	(CMS Collab.)
KHACHATRY...	15W	PR D91 052012	V. Khachatryan et al.	(CMS Collab.)	CHATRCHYAN	12BO	JHEP 1212 055	S. Chatrchyan et al.	(CMS Collab.)
KHACHATRY...	15X	PR D91 052018	V. Khachatryan et al.	(CMS Collab.)	CHATRCHYAN	12L	PL B713 408	S. Chatrchyan et al.	(CMS Collab.)
ROLBIECKI	15	PL B750 247	K. Rolbiecki, J. Tattersall	(MADE, HEID Collab.)	DAW	12	ASP 35 397	E. Daw et al.	(DRIFT-III Collab.)
AAD	14AE	JHEP 1409 176	G. Aad et al.	(ATLAS Collab.)	DRREINER	12A	EPL		

See key on page 1127

Searches Particle Listings
Supersymmetric Particle Searches

Table listing particle searches with columns for author names, publication codes, and collaboration names. Includes entries for AAD, ABREU, ACCIARRI, etc., with various codes like PRL, EPJ, and PL, and collaborations like ATLAS, CMS, DELPHI, etc.

Searches Particle Listings

Technicolor

Technicolor

See the related review(s):
 Dynamical Electroweak Symmetry Breaking: Implications of the H^0

The latest unpublished results are described in "Dynamical Electroweak Symmetry Breaking" review.

MASS LIMITS for Resonances in Models of Dynamical Electroweak Symmetry Breaking

VALUE (GeV)	CL%	DOCUMENT ID	TECN	COMMENT
• • • We do not use the following data for averages, fits, limits, etc. • • •				
>3900	95	1 AAD 20AM ATLS	top-color Z'	
		2 AAD 20W ATLS	$\rho_T \rightarrow W\pi_T \rightarrow \ell\nu q\bar{q}$	
		3 AAD 16W ATLS	color octet vector resonance	
>2400	95	4 KHACHATRYAN...16E CMS	top-color Z'	
		5 AAD 15AB ATLS	$h \rightarrow \pi_V \pi_V$	
>1800	95	6 AAD 15AO ATLS	top-color Z'	
		7 AAD 15BB ATLS	$\rho\rho \rightarrow \rho_T/a_{1T} \rightarrow Wh$ or Zh	
		8 AAD 15Q ATLS	$h \rightarrow \pi_V \pi_V$	
		9 AAIJ 15AN LHCB	$h \rightarrow \pi_V \pi_V$	
>1140	95	10 KHACHATRYAN...15C CMS	$\rho_T \rightarrow WZ$	
		11 KHACHATRYAN...15W CMS	$H \rightarrow \pi_V \pi_V$	
none 200–700, 750–890	95	12 AAD 14AT ATLS	$\rho\rho \rightarrow \omega_T \rightarrow Z\gamma$	
none 275–960	95	12 AAD 14AT ATLS	$\rho\rho \rightarrow a_T \rightarrow W\gamma$	
		13 AAD 14V ATLS	color singlet techni-vector	
		14 AAD 13AN ATLS	$\rho\rho \rightarrow a_T \rightarrow W\gamma$	
> 703		15 AAD 13AN ATLS	$\rho\rho \rightarrow \omega_T \rightarrow Z\gamma$	
> 494		16 AAD 13AQ ATLS	top-color Z'	
none 500–1740	95	17 CHATRCHYAN13AP CMS	top-color Z'	
>1300	95	16 CHATRCHYAN13BM CMS	top-color Z'	
>2100	95	18 BAAK 12 RVUE	QCD-like technicolor	
		19 CHATRCHYAN12AF CMS	$\rho_T \rightarrow WZ$	
none 167–687	95	16 AALTONEN 11AD CDF	top-color Z'	
> 805	95	16 AALTONEN 11AE CDF	top-color Z'	
> 805	95	20 CHIVUKULA 11 RVUE	top-Higgs	
		21 CHIVUKULA 11A RVUE	techni- π	
		22 AALTONEN 10I CDF	$\rho\bar{\rho} \rightarrow \rho_T/\omega_T \rightarrow W\pi_T$	
none 208–408	95	23 ABAZOV 10A D0	$\rho_T \rightarrow WZ$	
		24 ABAZOV 07I D0	$\rho\bar{\rho} \rightarrow \rho_T/\omega_T \rightarrow W\pi_T$	
> 280	95	25 ABULENCIA 05A CDF	$\rho_T \rightarrow e^+e^-, \mu^+\mu^-$	
		26 CHEKANOV 02B ZEUS	color octet techni- π	
> 207	95	27 ABAZOV 01B D0	$\rho_T \rightarrow e^+e^-$	
none 90–206.7	95	28 ABDALLAH 01 DLPH	$e^+e^- \rightarrow \rho_T$	
		29 AFFOLDER 00F CDF	color-singlet techni- ρ , $\rho_T \rightarrow W\pi_T, 2\pi_T$	
> 600	95	30 AFFOLDER 00K CDF	color-octet techni- ρ , $\rho_{T8} \rightarrow 2\pi_{LQ}$	
none 350–440	95	31 ABE 99F CDF	color-octet techni- ρ , $\rho_{T8} \rightarrow \bar{b}b$	
		32 ABE 99N CDF	techni- ω , $\omega_T \rightarrow \gamma\bar{b}b$	
none 260–480	95	33 ABE 97G CDF	color-octet techni- ρ , $\rho_{T8} \rightarrow 2j\text{ets}$	

1 AAD 20AM search for a top-color Z' decaying to $t\bar{t}$ in pp collisions at $\sqrt{s} = 13$ TeV. The quoted limit is for $\Gamma_{Z'}/M_{Z'}$ = 0.01. The limit becomes $M_{Z'} > 4700$ GeV for $\Gamma_{Z'}/M_{Z'} = 0.03$.

2 AAD 20W search for techni- ρ decaying to $\pi_T W$ in pp collisions at $\sqrt{s} = 13$ TeV. See their Fig. 5a for limits on σ_B .

3 AAD 16W search for color octet vector resonance decaying to $b\bar{b}$ in pp collisions at $\sqrt{s} = 8$ TeV. The vector like quark B is assumed to decay to bH . See their Fig.3 and Fig.4 for limits on σ_B .

4 KHACHATRYAN 16E search for top-color Z' decaying to $t\bar{t}$. The quoted limit is for $\Gamma_{Z'}/M_{Z'}$ = 0.012. Also exclude $M_{Z'} < 2.9$ TeV for wider topcolor Z' with $\Gamma_{Z'}/M_{Z'} = 0.1$.

5 AAD 15AB search for long-lived hidden valley π_V particles which are produced in pairs by the decay of a scalar boson. π_V is assumed to decay into dijets. See their Fig. 10 for the limit on σ_B .

6 AAD 15AO search for top-color Z' decaying to $t\bar{t}$. The quoted limit is for $\Gamma_{Z'}/M_{Z'} = 0.012$.

7 AAD 15BB search for minimal walking technicolor (MWT) isotriplet vector and axial-vector resonances decaying to Wh or Zh . See their Fig. 3 for the exclusion limit in the MWT parameter space.

8 AAD 15Q search for long-lived hidden valley π_V particles which are produced in pairs by the decay of scalar boson. π_V is assumed to decay into dijets. See their Fig. 5 and Fig. 6 for the limit on σ_B .

9 AAIJ 15AN search for long-lived hidden valley π_V particles which are produced in pairs by the decay of scalar boson with a mass of 120GeV. π_V is assumed to decay into dijets. See their Fig. 4 for the limit on σ_B .

10 KHACHATRYAN 15C search for a vector techni-resonance decaying to WZ . The limit assumes $M_{\pi_T} = (3/4) M_{\rho_T} = 25$ GeV. See their Fig.3 for the limit in $M_{\pi_T} - M_{\rho_T}$ plane of the low scale technicolor model.

11 KHACHATRYAN 15W search for long-lived hidden valley π_V particles which are produced in pairs in the decay of heavy higgs boson H . π_V is assumed to decay into $\ell^+\ell^-$. See their Fig. 7 and Fig. 8 for the limits on σ_B .

12 AAD 14AT search for techni- ω and techni- a resonances decaying to $V\gamma$ with $V = W(\rightarrow \ell\nu)$ or $Z(\rightarrow \ell^+\ell^-)$.

13 AAD 14V search for vector techni-resonances decaying into electron or muon pairs in pp collisions at $\sqrt{s} = 8$ TeV. See their table IX for exclusion limits with various assumptions.

14 AAD 13AN search for vector techni-resonance a_T decaying into $W\gamma$.

15 AAD 13AN search for vector techni-resonance ω_T decaying into $Z\gamma$.

16 Search for top-color Z' decaying to $t\bar{t}$. The quoted limit is for $\Gamma_{Z'}/M_{Z'} = 0.012$.

17 CHATRCHYAN 13AP search for top-color leptophobic Z' decaying to $t\bar{t}$. The quoted limit is for $\Gamma_{Z'}/M_{Z'} = 0.012$.

18 BAAK 12 give electroweak oblique parameter constraints on the QCD-like technicolor models. See their Fig. 28.

19 CHATRCHYAN 12AF search for a vector techni-resonance decaying to WZ . The limit assumes $M_{\pi_T} = (3/4) M_{\rho_T} = 25$ GeV. See their Fig. 3 for the limit in $M_{\pi_T} - M_{\rho_T}$ plane of the low scale technicolor model.

20 Using the LHC limit on the Higgs boson production cross section, CHIVUKULA 11 obtain a limit on the top-Higgs mass > 300 GeV at 95% CL assuming 150 GeV top-pion mass.

21 Using the LHC limit on the Higgs boson production cross section, CHIVUKULA 11A obtain a limit on the technipion mass ruling out the region $110 \text{ GeV} < m_P < 2m_t$. Existence of color techni-fermions, top-color mechanism, and $N_{TC} \geq 3$ are assumed.

22 AALTONEN 10I search for the vector techni-resonances (ρ_T, ω_T) decaying into $W\pi_T$ with $W \rightarrow \ell\nu$ and $\pi_T \rightarrow b\bar{b}, b\bar{c},$ or $b\bar{s}$. See their Fig.3 for the exclusion plot in $M_{\pi_T} - M_{\rho_T}$ plane.

23 ABAZOV 10A search for a vector techni-resonance decaying into WZ . The limit assumes $M_{\rho_T} < M_{\pi_T} + M_W$.

24 ABAZOV 07I search for the vector techni-resonances (ρ_T, ω_T) decaying into $W\pi_T$ with $W \rightarrow e\nu$ and $\pi_T \rightarrow b\bar{b}$ or $b\bar{c}$. See their Fig. 2 for the exclusion plot in $M_{\pi_T} - M_{\rho_T}$ plane.

25 ABULENCIA 05A search for resonances decaying to electron or muon pairs in $p\bar{p}$ collisions. at $\sqrt{s} = 1.96$ TeV. The limit assumes Technicolor-scale mass parameters $M_V = M_A = 500$ GeV.

26 CHEKANOV 02B search for color octet techni- π P decaying into dijets in ep collisions. See their Fig. 5 for the limit on $\sigma(ep \rightarrow ePX) \cdot B(P \rightarrow 2j)$.

27 ABAZOV 01B searches for vector techni-resonances (ρ_T, ω_T) decaying to e^+e^- . The limit assumes $M_{\rho_T} = M_{\omega_T} < M_{\pi_T} + M_W$.

28 The limit is independent of the π_T mass. See their Fig. 9 and Fig. 10 for the exclusion plot in the $M_{\rho_T} - M_{\pi_T}$ plane. ABDALLAH 01 limit on the techni-pion mass is $M_{\pi_T} > 79.8$ GeV for $N_D = 2$, assuming its point-like coupling to gauge bosons.

29 AFFOLDER 00F search for ρ_T decaying into $W\pi_T$ or $\pi_T\pi_T$ with $W \rightarrow \ell\nu$ and $\pi_T \rightarrow \bar{b}b, \bar{b}c$. See Fig. 1 in the above Note on "Dynamical Electroweak Symmetry Breaking" for the exclusion plot in the $M_{\rho_T} - M_{\pi_T}$ plane.

30 AFFOLDER 00K search for the ρ_{T8} decaying into $\pi_{LQ}\pi_{LQ}$ with $\pi_{LQ} \rightarrow b\nu$. For $\pi_{LQ} \rightarrow c\nu$, the limit is $M_{\rho_{T8}} > 510$ GeV. See their Fig. 2 and Fig. 3 for the exclusion plot in the $M_{\rho_{T8}} - M_{\pi_{LQ}}$ plane.

31 ABE 99F search for a new particle X decaying into $b\bar{b}$ in $p\bar{p}$ collisions at $E_{cm} = 1.8$ TeV. See Fig. 7 in the above Note on "Dynamical Electroweak Symmetry Breaking" for the upper limit on $\sigma(p\bar{p} \rightarrow X) \times B(X \rightarrow b\bar{b})$. ABE 99F also exclude top gluons of width $\Gamma = 0.3M$ in the mass interval $280 < M < 670$ GeV, of width $\Gamma = 0.5M$ in the mass interval $340 < M < 640$ GeV, and of width $\Gamma = 0.7M$ in the mass interval $375 < M < 560$ GeV.

32 ABE 99N search for the techni- ω decaying into $\gamma\pi_T$. The technipion is assumed to decay $\pi_T \rightarrow b\bar{b}$. See Fig. 2 in the above Note on "Dynamical Electroweak Symmetry Breaking" for the exclusion plot in the $M_{\omega_T} - M_{\pi_T}$ plane.

33 ABE 97G search for a new particle X decaying into dijets in $p\bar{p}$ collisions at $E_{cm} = 1.8$ TeV. See Fig. 5 in the above Note on "Dynamical Electroweak Symmetry Breaking" for the upper limit on $\sigma(p\bar{p} \rightarrow X) \times B(X \rightarrow 2j)$.

REFERENCES FOR Technicolor

AAD 20AM	JHEP 2010 061	G. Aad et al.	(ATLAS Collab.)
AAD 20W	JHEP 2006 151	G. Aad et al.	(ATLAS Collab.)
AAD 16W	PL B758 249	G. Aad et al.	(ATLAS Collab.)
KHACHATRYAN...16E	PR D93 012001	V. Khachatryan et al.	(CMS Collab.)
AAD 15AB	PR D92 012010	G. Aad et al.	(ATLAS Collab.)
AAD 15AO	JHEP 1508 148	G. Aad et al.	(ATLAS Collab.)
AAD 15BB	EPJ C75 263	G. Aad et al.	(ATLAS Collab.)
AAD 15Q	PL B743 15	G. Aad et al.	(ATLAS Collab.)
AAIJ 15AN	EPJ C75 152	R. Aaij et al.	(LHCb Collab.)
KHACHATRYAN...15C	PL B740 83	V. Khachatryan et al.	(CMS Collab.)
KHACHATRYAN...15W	PR D91 052012	V. Khachatryan et al.	(CMS Collab.)
AAD 14AT	PL B738 428	G. Aad et al.	(ATLAS Collab.)
AAD 14V	PR D90 052005	G. Aad et al.	(ATLAS Collab.)
AAD 13AN	PR D87 112003	G. Aad et al.	(ATLAS Collab.)
Also	PR D91 119901 (errat.)	G. Aad et al.	(ATLAS Collab.)
AAD 13AQ	PR D88 012004	G. Aad et al.	(ATLAS Collab.)
CHATRCHYAN 13AP	PR D87 072002	S. Chatrchyan et al.	(CMS Collab.)
CHATRCHYAN 13BM	PRL 111 211804	S. Chatrchyan et al.	(CMS Collab.)
Also	PRL 112 119903 (errat.)	S. Chatrchyan et al.	(CMS Collab.)
BAAK 12	EPJ C72 2003	M. Baak et al.	(Glitter Group)
CHATRCHYAN 12AF	PRL 109 141801	S. Chatrchyan et al.	(CMS Collab.)
AALTONEN 11AD	PR D84 072003	T. Aaltonen et al.	(CDF Collab.)
AALTONEN 11AE	PR D84 072004	T. Aaltonen et al.	(CDF Collab.)
CHIVUKULA 11	PR D84 095022	R.S. Chivukula et al.	(CDF Collab.)
CHIVUKULA 11A	PR D84 115025	R. S. Chivukula et al.	(CDF Collab.)
AALTONEN 10I	PRL 104 111802	T. Aaltonen et al.	(CDF Collab.)
ABAZOV 10A	PRL 104 061801	V.M. Abazov et al.	(DO Collab.)
ABAZOV 07I	PRL 98 221801	V.M. Abazov et al.	(DO Collab.)
ABULENCIA 05A	PRL 95 252001	A. Abulencia et al.	(CDF Collab.)
CHEKANOV 02B	PL B531 9	S. Chekanov et al.	(ZEUS Collab.)
ABAZOV 01B	PR 87 061802	V.M. Abazov et al.	(DO Collab.)
ABDALLAH 01	EPJ C22 17	J. Abdallah et al.	(DELPHI Collab.)
AFFOLDER 00F	PRL 84 1110	T. Affolder et al.	(CDF Collab.)
AFFOLDER 00K	PRL 85 2056	T. Affolder et al.	(CDF Collab.)
ABE 99F	PRL 82 2038	F. Abe et al.	(CDF Collab.)
ABE 99N	PR 83 3124	F. Abe et al.	(CDF Collab.)
ABE 97G	PR D55 5263	F. Abe et al.	(CDF Collab.)

Quark and Lepton Compositeness, Searches for

The latest unpublished results are described in the "Quark and Lepton Compositeness" review.
See the related review(s):
Searches for Quark and Lepton Compositeness

CONTENTS:

- Scale Limits for Contact Interactions: $\Lambda(eeee)$
- Scale Limits for Contact Interactions: $\Lambda(e\mu\mu\mu)$
- Scale Limits for Contact Interactions: $\Lambda(ee\tau\tau)$
- Scale Limits for Contact Interactions: $\Lambda(\ell\ell\ell\ell)$
- Scale Limits for Contact Interactions: $\Lambda(eeqq)$
- Scale Limits for Contact Interactions: $\Lambda(\mu\mu qq)$
- Scale Limits for Contact Interactions: $\Lambda(\ell\nu\ell\nu)$
- Scale Limits for Contact Interactions: $\Lambda(e\nu qq)$
- Scale Limits for Contact Interactions: $\Lambda(qqqq)$
- Scale Limits for Contact Interactions: $\Lambda(\nu\nu qq)$
- Mass Limits for Excited e (e^*)
 - Limits for Excited e (e^*) from Pair Production
 - Limits for Excited e (e^*) from Single Production
 - Limits for Excited e (e^*) from $e^+e^- \rightarrow \gamma\gamma$
 - Indirect Limits for Excited e (e^*)
- Mass Limits for Excited μ (μ^*)
 - Limits for Excited μ (μ^*) from Pair Production
 - Limits for Excited μ (μ^*) from Single Production
 - Indirect Limits for Excited μ (μ^*)
- Mass Limits for Excited τ (τ^*)
 - Limits for Excited τ (τ^*) from Pair Production
 - Limits for Excited τ (τ^*) from Single Production
- Mass Limits for Excited Neutrino (ν^*)
 - Limits for Excited ν (ν^*) from Pair Production
 - Limits for Excited ν (ν^*) from Single Production
- Mass Limits for Excited q (q^*)
 - Limits for Excited q (q^*) from Pair Production
 - Limits for Excited q (q^*) from Single Production
- Mass Limits for Color Sextet Quarks (q_6)
- Mass Limits for Color Octet Charged Leptons (ℓ_8)
- Mass Limits for Color Octet Neutrinos (ν_8)
- Mass Limits for W_8 (Color Octet W Boson)

SCALE LIMITS for Contact Interactions: $\Lambda(eeee)$

Limits are for $\Lambda_{LL}^{\pm\pm}$ only. For other cases, see each reference.

$\Lambda_{LL}^+(TeV)$	$\Lambda_{LL}^-(TeV)$	CL%	DOCUMENT ID	TECN	COMMENT
>8.3	>10.3	95	¹ BOURILKOV 01	RVUE	$E_{cm} = 192-208$ GeV
•••			We do not use the following data for averages, fits, limits, etc. •••		
>4.5	>7.0	95	² SCHAEEL 07A	ALEP	$E_{cm} = 189-209$ GeV
>5.3	>6.8	95	ABDALLAH 06c	DLPH	$E_{cm} = 130-207$ GeV
>4.7	>6.1	95	³ ABBIENDI 04G	OPAL	$E_{cm} = 130-207$ GeV
>4.3	>4.9	95	ACCIARRI 00P	L3	$E_{cm} = 130-189$ GeV

¹ A combined analysis of the data from ALEPH, DELPHI, L3, and OPAL.
² SCHAEEL 07A limits are from R_{σ} , Q_{FB}^{depl} , and hadronic cross section measurements.
³ ABBIENDI 04G limits are from $e^+e^- \rightarrow e^+e^-$ cross section at $\sqrt{s} = 130-207$ GeV.

SCALE LIMITS for Contact Interactions: $\Lambda(e\mu\mu\mu)$

Limits are for $\Lambda_{LL}^{\pm\pm}$ only. For other cases, see each reference.

$\Lambda_{LL}^+(TeV)$	$\Lambda_{LL}^-(TeV)$	CL%	DOCUMENT ID	TECN	COMMENT
>6.6	>9.5	95	¹ SCHAEEL 07A	ALEP	$E_{cm} = 189-209$ GeV
> 8.5	>3.8	95	ACCIARRI 00P	L3	$E_{cm} = 130-189$ GeV
•••			We do not use the following data for averages, fits, limits, etc. •••		
>7.3	>7.6	95	ABDALLAH 06c	DLPH	$E_{cm} = 130-207$ GeV
>8.1	>7.3	95	² ABBIENDI 04G	OPAL	$E_{cm} = 130-207$ GeV

¹ SCHAEEL 07A limits are from R_{σ} , Q_{FB}^{depl} , and hadronic cross section measurements.
² ABBIENDI 04G limits are from $e^+e^- \rightarrow \mu\mu$ cross section at $\sqrt{s} = 130-207$ GeV.

SCALE LIMITS for Contact Interactions: $\Lambda(ee\tau\tau)$

Limits are for $\Lambda_{LL}^{\pm\pm}$ only. For other cases, see each reference.

$\Lambda_{LL}^+(TeV)$	$\Lambda_{LL}^-(TeV)$	CL%	DOCUMENT ID	TECN	COMMENT
>7.9	>5.8	95	¹ SCHAEEL 07A	ALEP	$E_{cm} = 189-209$ GeV
>7.9	>4.6	95	ABDALLAH 06c	DLPH	$E_{cm} = 130-207$ GeV
>4.9	>7.2	95	² ABBIENDI 04G	OPAL	$E_{cm} = 130-207$ GeV
•••			We do not use the following data for averages, fits, limits, etc. •••		
>5.4	>4.7	95	ACCIARRI 00P	L3	$E_{cm} = 130-189$ GeV

¹ SCHAEEL 07A limits are from R_{σ} , Q_{FB}^{depl} , and hadronic cross section measurements.
² ABBIENDI 04G limits are from $e^+e^- \rightarrow \tau\tau$ cross section at $\sqrt{s} = 130-207$ GeV.

SCALE LIMITS for Contact Interactions: $\Lambda(\ell\ell\ell\ell)$

Lepton universality assumed. Limits are for $\Lambda_{LL}^{\pm\pm}$ only. For other cases, see each reference.

$\Lambda_{LL}^+(TeV)$	$\Lambda_{LL}^-(TeV)$	CL%	DOCUMENT ID	TECN	COMMENT
>7.9	> 10.3	95	¹ SCHAEEL 07A	ALEP	$E_{cm} = 189-209$ GeV
>9.1	>8.2	95	ABDALLAH 06c	DLPH	$E_{cm} = 130-207$ GeV
•••			We do not use the following data for averages, fits, limits, etc. •••		
>7.7	>9.5	95	² ABBIENDI 04G	OPAL	$E_{cm} = 130-207$ GeV
			³ BABICH 03	RVUE	
			ACCIARRI 00P	L3	$E_{cm} = 130-189$ GeV

¹ SCHAEEL 07A limits are from R_{σ} , Q_{FB}^{depl} , and hadronic cross section measurements.
² ABBIENDI 04G limits are from $e^+e^- \rightarrow \ell^+\ell^-$ cross section at $\sqrt{s} = 130-207$ GeV.
³ BABICH 03 obtain a bound $-0.175 \text{ TeV}^{-2} < 1/\Lambda_{LL}^2 < 0.095 \text{ TeV}^{-2}$ (95%CL) in a model independent analysis allowing all of $\Lambda_{LL}, \Lambda_{LR}, \Lambda_{RL}, \Lambda_{RR}$ to coexist.

SCALE LIMITS for Contact Interactions: $\Lambda(eeqq)$

Limits are for $\Lambda_{LL}^{\pm\pm}$ only. For other cases, see each reference.

$\Lambda_{LL}^+(TeV)$	$\Lambda_{LL}^-(TeV)$	CL%	DOCUMENT ID	TECN	COMMENT
>23.5	>26.1	95	¹ AAD 21Q	ATLS	($eeqq$)
>19.5	>24.0	95	² SIRUNYAN 21N	CMS	($eeqq$)
>23.5	>26.1	95	³ AAD 20AP	ATLS	($eeqq$)
> 4.5	>12.8	95	⁴ ABRAMOWICZ19	ZEUS	($eeqq$)
>16.8	>23.9	95	⁵ SIRUNYAN 19AC	CMS	($eeqq$)
>24	>37	95	⁶ AABOUD 17AT	ATLS	($eeqq$)
> 8.4	>10.2	95	⁷ ABDALLAH 09	DLPH	($eebb$)
> 9.4	>5.6	95	⁸ SCHAEEL 07A	ALEP	($eecc$)
> 9.4	>4.9	95	⁷ SCHAEEL 07A	ALEP	($eebb$)
>23.3	>12.5	95	⁹ CHEUNG 01B	RVUE	($eeuu$)
>11.1	>26.4	95	⁹ CHEUNG 01B	RVUE	($eedd$)
•••			We do not use the following data for averages, fits, limits, etc. •••		
> 7.1	>7.1	95	¹⁰ AAD 21AU	ATLS	($eebs$)
>15.5	>19.5	95	¹¹ AABOUD 16U	ATLS	($eeqq$)
>13.5	>18.3	95	¹² KHACHATRYAN15AE	CMS	($eeqq$)
>16.4	>20.7	95	¹³ AAD 14BE	ATLS	($eeqq$)
> 9.5	>12.1	95	¹⁴ AAD 13E	ATLS	($eeqq$)
>10.1	>9.4	95	¹⁵ AAD 12AB	ATLS	($eeqq$)
> 4.2	>4.0	95	¹⁶ AARON 11C	H1	($eeqq$)
> 3.8	>3.8	95	¹⁷ ABDALLAH 11	DLPH	($ee\tau c$)
>12.9	>7.2	95	¹⁸ SCHAEEL 07A	ALEP	($eeqq$)
> 3.7	>5.9	95	¹⁹ ABULENCIA 06L	CDF	($eeqq$)

¹ AAD 21Q limits are from pp collisions at $\sqrt{s} = 13$ TeV. A frequentist statistical framework is used to remove the prior dependence.
² SIRUNYAN 21N limits are from e^+e^- mass distribution in pp collisions at $\sqrt{s} = 13$ TeV.
³ AAD 20AP limits are from e^+e^- mass distribution in pp collisions at $\sqrt{s} = 13$ TeV.
⁴ ABRAMOWICZ 19 limits are from Q^2 spectrum measurements of $e^\pm p \rightarrow e^\pm X$.
⁵ SIRUNYAN 19AC limits are from e^+e^- mass distribution in pp collisions at $\sqrt{s} = 13$ TeV.
⁶ AABOUD 17AT limits are from pp collisions at $\sqrt{s} = 13$ TeV. The quoted limit uses a uniform positive prior in $1/\Lambda^2$.
⁷ ABDALLAH 09 and SCHAEEL 07A limits are from R_D, A_{FB}^b .
⁸ SCHAEEL 07A limits are from $R_{\sigma}, Q_{FB}^{depl}$, and hadronic cross section measurements.
⁹ CHEUNG 01B is an update of BARGER 98E.
¹⁰ AAD 21AU search for new phenomena in final states with e^+e^- and one or no b -tagged jets in pp collisions at $\sqrt{s} = 13$ TeV. The quoted limits assume $g_*^2 = 4$.
¹¹ AABOUD 16U limits are from pp collisions at $\sqrt{s} = 13$ TeV. The quoted limit uses a uniform positive prior in $1/\Lambda^2$.
¹² KHACHATRYAN 15AE limit is from e^+e^- mass distribution in pp collisions at $E_{cm} = 8$ TeV.
¹³ AAD 14BE limits are from pp collisions at $\sqrt{s} = 8$ TeV. The quoted limit uses a uniform positive prior in $1/\Lambda^2$.
¹⁴ AAD 13E limits are from e^+e^- mass distribution in pp collisions at $E_{cm} = 7$ TeV.
¹⁵ AAD 12AB limits are from e^+e^- mass distribution in pp collisions at $E_{cm} = 7$ TeV.
¹⁶ AARON 11C limits are from Q^2 spectrum measurements of $e^\pm p \rightarrow e^\pm X$.
¹⁷ ABDALLAH 11 limit is from $e^+e^- \rightarrow t\bar{c}$ cross section. $\Lambda_{LL} = \Lambda_{LR} = \Lambda_{RL} = \Lambda_{RR}$ is assumed.
¹⁸ SCHAEEL 07A limit assumes quark flavor universality of the contact interactions.
¹⁹ ABULENCIA 06L limits are from $p\bar{p}$ collisions at $\sqrt{s} = 1.96$ TeV.

SCALE LIMITS for Contact Interactions: $\Lambda(\mu\mu qq)$

$\Lambda_{LL}^+(TeV)$	$\Lambda_{LL}^-(TeV)$	CL%	DOCUMENT ID	TECN	COMMENT
>22.3	>32.7	95	¹ AAD 21Q	ATLS	($\mu\mu qq$)
>23.3	> 40.0	95	² SIRUNYAN 21N	CMS	($\mu\mu qq$)
>22.3	>32.7	95	³ AAD 20AP	ATLS	($\mu\mu qq$)
>20.4	>30.4	95	⁴ SIRUNYAN 19AC	CMS	($\mu\mu qq$)
>20	>30	95	⁵ AABOUD 17AT	ATLS	($\mu\mu qq$)

Searches Particle Listings

Quark and Lepton Compositeness

••• We do not use the following data for averages, fits, limits, etc. •••

> 8.5	>8.5	95	6 AAD	21AU ATLS	($\mu b s$)
>15.8	>21.8	95	7 AABOUD	16U ATLS	($\mu\mu q q$)
>12.0	>15.2	95	8 KHACHATRYAN...15AE	CMS	($\mu\mu q q$)
>12.5	>16.7	95	9 AAD	14BE ATLS	($\mu\mu q q$)
> 9.6	>12.9	95	10 AAD	13E ATLS	($\mu\mu q q$) (isosinglet)
> 9.5	>13.1	95	11 CHATRCHYAN13K	CMS	($\mu\mu q q$) (isosinglet)
> 8.0	>7.0	95	12 AAD	12AB ATLS	($\mu\mu q q$) (isosinglet)

- 1 AAD 21q limits are from pp collisions at $\sqrt{s} = 13$ TeV. A frequentist statistical framework is used to remove the prior dependence.
- 2 SIRUNYAN 21N limits are from $\mu^+\mu^-$ mass distribution in pp collisions at $\sqrt{s} = 13$ TeV.
- 3 AAD 20AP limits are from $\mu^+\mu^-$ mass distribution in pp collisions at $\sqrt{s} = 13$ TeV.
- 4 SIRUNYAN 19AC limits are from $\mu^+\mu^-$ mass distribution in pp collisions at $\sqrt{s} = 13$ TeV.
- 5 AABOUD 17AT limits are from pp collisions at $\sqrt{s} = 13$ TeV. The quoted limit uses a uniform positive prior in $1/\Lambda^2$.
- 6 AAD 21AU search for new phenomena in final states with $\mu^+\mu^-$ and one or no b -tagged jets in pp collisions at $\sqrt{s} = 13$ TeV. The quoted limits assume $g_*^2 = 4\pi$.
- 7 AABOUD 16U limits are from pp collisions at $\sqrt{s} = 13$ TeV. The quoted limit uses a uniform positive prior in $1/\Lambda^2$.
- 8 KHACHATRYAN 15AE limit is from $\mu^+\mu^-$ mass distribution in pp collisions at $E_{cm} = 8$ TeV.
- 9 AAD 14BE limits are from pp collisions at $\sqrt{s} = 8$ TeV. The quoted limit uses a uniform positive prior in $1/\Lambda^2$.
- 10 AAD 13E limits are from $\mu^+\mu^-$ mass distribution in pp collisions at $E_{cm} = 7$ TeV.
- 11 CHATRCHYAN 13K limits are from $\mu^+\mu^-$ mass distribution in pp collisions at $E_{cm} = 7$ TeV.
- 12 AAD 12AB limits are from $\mu^+\mu^-$ mass distribution in pp collisions at $E_{cm} = 7$ TeV.

SCALE LIMITS for Contact Interactions: $\Lambda(\ell\nu\ell\nu)$

VALUE (TeV)	CL%	DOCUMENT ID	TECN	COMMENT
>3.10	90	1 JODIDIO	86	SPEC $\Lambda_{LR}^\pm(\nu_\mu\nu_e\mu e)$

••• We do not use the following data for averages, fits, limits, etc. •••

>3.8		2 DIAZCRUZ	94	RVUE $\Lambda_{LL}^\pm(\tau\nu_\tau e\nu_e)$
>8.1		2 DIAZCRUZ	94	RVUE $\Lambda_{LL}^\pm(\tau\nu_\tau e\nu_e)$
>4.1		3 DIAZCRUZ	94	RVUE $\Lambda_{LL}^\pm(\tau\nu_\tau\mu\nu_\mu)$
>6.5		3 DIAZCRUZ	94	RVUE $\Lambda_{LL}^\pm(\tau\nu_\tau\mu\nu_\mu)$

- 1 JODIDIO 86 limit is from $\mu^+ \rightarrow \bar{\nu}_\mu e^+ \nu_e$. Chirality invariant interactions $L = (g^2/\Lambda^2)$ with $[\eta_{LL} (\bar{\nu}_\mu L \gamma^\alpha \mu_L) (\bar{e}_L \gamma_\alpha \nu_{eL}) + \eta_{LR} (\bar{\nu}_\mu L \gamma^\alpha \nu_{eL} (\bar{e}_R \gamma_\alpha \mu_R)]$ with $g^2/4\pi = 1$ and $(\eta_{LL}, \eta_{LR}) = (0, \pm 1)$ are taken. No limits are given for Λ_{LR}^\pm with $(\eta_{LL}, \eta_{LR}) = (\pm 1, 0)$. For more general constraints with right-handed neutrinos and chirality nonconserving contact interactions, see their text.
- 2 DIAZCRUZ 94 limits are from $\Gamma(\tau \rightarrow e\nu\nu)$ and assume flavor-dependent contact interactions with $\Lambda(\tau\nu_\tau e\nu_e) \ll \Lambda(\mu\nu_\mu e\nu_e)$.
- 3 DIAZCRUZ 94 limits are from $\Gamma(\tau \rightarrow \mu\nu\nu)$ and assume flavor-dependent contact interactions with $\Lambda(\tau\nu_\tau\mu\nu_\mu) \ll \Lambda(\mu\nu_\mu e\nu_e)$.

SCALE LIMITS for Contact Interactions: $\Lambda(e\nu qq)$

VALUE (TeV)	CL%	DOCUMENT ID	TECN
>2.81	95	1 AFFOLDER	01i CDF

- 1 AFFOLDER 00i bound is for a scalar interaction $\bar{q}_R q_L \bar{\nu}_L \nu_{eL}$.

SCALE LIMITS for Contact Interactions: $\Lambda(qqqq)$

$\Lambda_{LL}^+(TeV)$	$\Lambda_{LL}^-(TeV)$	CL%	DOCUMENT ID	TECN	COMMENT
>13.1 none	17.4–29.5	>21.8	95	1 AABOUD	17AK ATLS pp dijet angl.
>12.8	>17.5	95	2 AABOUD	18AV ATLS	$pp \rightarrow t\bar{t}t\bar{t}$
>11.5	>14.7	95	3 SIRUNYAN	18DD CMS	pp dijet angl.
>12.0	>17.5	95	4 SIRUNYAN	17F CMS	pp dijet angl.
			5 AAD	16S ATLS	pp dijet angl.
			6 AAD	15AR ATLS	$pp \rightarrow t\bar{t}t\bar{t}$
			7 AAD	15BY ATLS	$pp \rightarrow t\bar{t}t\bar{t}$
			8 AAD	15L ATLS	pp dijet angl.
> 8.1	>12.0	95	9 KHACHATRYAN...15J	CMS	pp dijet angl.
> 9.0	>11.7	95	10 FABBRICHESI	14 RVUE	$q\bar{q}t\bar{t}$
> 5					

- 1 AABOUD 17AK limit is from dijet angular distribution in pp collisions at $\sqrt{s} = 13$ TeV. u, d , and s quarks are assumed to be composite.
- 2 AABOUD 18AV obtain limit on t_R compositeness $2\pi/\Lambda_{RR}^2 < 1.6 \text{ TeV}^{-2}$ at 95% CL from $t\bar{t}t\bar{t}$ production in the pp collisions at $E_{cm} = 13$ TeV.
- 3 SIRUNYAN 18DD limit is from dijet angular distribution in pp collisions at $\sqrt{s} = 13$ TeV.
- 4 SIRUNYAN 17F limit is from dijet angular cross sections in pp collisions at $E_{cm} = 13$ TeV. All quarks are assumed to be composite.
- 5 AAD 16S limit is from dijet angular selections in pp collisions at $E_{cm} = 13$ TeV. u, d , and s quarks are assumed to be composite.
- 6 AAD 15AR obtain limit on the t_R compositeness $2\pi/\Lambda_{RR}^2 < 6.6 \text{ TeV}^{-2}$ at 95% CL from the $t\bar{t}t\bar{t}$ production in the pp collisions at $E_{cm} = 8$ TeV.
- 7 AAD 15BY obtain limit on the t_R compositeness $2\pi/\Lambda_{RR}^2 < 15.1 \text{ TeV}^{-2}$ at 95% CL from the $t\bar{t}t\bar{t}$ production in the pp collisions at $E_{cm} = 8$ TeV.

- 8 AAD 15L limit is from dijet angular distribution in pp collisions at $E_{cm} = 8$ TeV. u, d , and s quarks are assumed to be composite.
- 9 KHACHATRYAN 15J limit is from dijet angular distribution in pp collisions at $E_{cm} = 8$ TeV. u, d, s, c , and b quarks are assumed to be composite.
- 10 FABBRICHESI 14 obtain bounds on chromoelectric and chromomagnetic form factors of the top-quark using $pp \rightarrow t\bar{t}$ and $p\bar{p} \rightarrow t\bar{t}$ cross sections. The quoted limit on the $q\bar{q}t\bar{t}$ contact interaction is derived from their bound on the chromoelectric form factor.

SCALE LIMITS for Contact Interactions: $\Lambda(\nu\nu qq)$

Limits are for Λ_{LL}^\pm only. For other cases, see each reference.

$\Lambda_{LL}^+(TeV)$	$\Lambda_{LL}^-(TeV)$	CL%	DOCUMENT ID	TECN	COMMENT
>5.0	>5.4	95	1 MCFARLAND	98 CCFR	νN scattering

- 1 MCFARLAND 98 assumed a flavor universal interaction. Neutrinos were mostly of muon type.

MASS LIMITS for Excited e (e^*)

Most e^+e^- experiments assume one-photon or Z exchange. The limits from some e^+e^- experiments which depend on λ have assumed transition couplings which are chirality violating ($\eta_L = \eta_R$). However they can be interpreted as limits for chirality-conserving interactions after multiplying the coupling value λ by $\sqrt{2}$; see Note.

Excited leptons have the same quantum numbers as other ortholeptons. See also the searches for ortholeptons in the "Searches for Heavy Leptons" section.

Limits for Excited e (e^*) from Pair Production

These limits are obtained from $e^+e^- \rightarrow e^+e^*$ and thus rely only on the (electroweak) charge of e^* . Form factor effects are ignored unless noted. For the case of limits from Z decay, the e^* coupling is assumed to be of sequential type. Possible t channel contribution from transition magnetic coupling is neglected. All limits assume a dominant $e^* \rightarrow e\gamma$ decay except the limits from $\Gamma(Z)$.

For limits prior to 1987, see our 1992 edition (Physical Review **D45** 51 (1992)).

VALUE (GeV)	CL%	DOCUMENT ID	TECN	COMMENT
>103.2	95	1 ABBIENDI	02G OPAL	$e^+e^- \rightarrow e^*e^*$ Homodoublet type
>102.8	95	2 ACHARD	03B L3	$e^+e^- \rightarrow e^*e^*$ Homodoublet type

- 1 From e^+e^- collisions at $\sqrt{s} = 183\text{--}209$ GeV. $f = f'$ is assumed.
- 2 From e^+e^- collisions at $\sqrt{s} = 189\text{--}209$ GeV. $f = f'$ is assumed. ACHARD 03b also obtain limit for $f = -f'$: $m_{e^*} > 96.6$ GeV.

Limits for Excited e (e^*) from Single Production

These limits are from $e^+e^- \rightarrow e^*e, W \rightarrow e^*\nu$, or $p \rightarrow e^*X$ and depend on transition magnetic coupling between e and e^* . All limits assume $e^* \rightarrow e\gamma$ decay except as noted. Limits from LEP, UA2, and H1 are for chiral coupling, whereas all other limits are for nonchiral coupling, $\eta_L = \eta_R = 1$. In most papers, the limit is expressed in the form of an excluded region in the $\lambda\text{--}m_{e^*}$ plane. See the original papers.

For limits prior to 1987, see our 1992 edition (Physical Review **D45** 51 (1992)).

VALUE (GeV)	CL%	DOCUMENT ID	TECN	COMMENT
>5600	95	1 SIRUNYAN	20AJ CMS	$pp \rightarrow e^*e^*X$
>4800	95	2 AABOUD	19AZ ATLS	$pp \rightarrow e^*e^*X$
>3900	95	3 SIRUNYAN	19Z CMS	$pp \rightarrow e^*e^*X$
>2450	95	4 KHACHATRYAN...16AQ	CMS	$pp \rightarrow e^*e^*X$
>3000	95	5 AAD	15AP ATLS	$pp \rightarrow e^{(*)}e^*X$
>2200	95	6 AAD	13BB ATLS	$pp \rightarrow e^*e^*X$
>1900	95	7 CHATRCHYAN	13AE CMS	$pp \rightarrow e^*e^*X$
>1870	95	8 AAD	12AZ ATLS	$pp \rightarrow e^{(*)}e^*X$

- 1 SIRUNYAN 20AJ search for e^* production in $2e2j$ final states in pp collisions at $\sqrt{s} = 13$ TeV. The quoted limit assumes $\Lambda = m_{e^*}$, $f = f' = 1$. The contact interaction is included. See their Fig.11 for exclusion limits in $m_{e^*}\text{--}\Lambda$ plane.
- 2 AABOUD 19AZ search for single e^* production in pp collisions at $\sqrt{s} = 13$ TeV. The limit quoted above is from $e^* \rightarrow e\bar{q}\bar{q}$ and $e^* \rightarrow \nu W$ decays assuming $f = f' = 1$ and $m_{e^*} = \Lambda$. The contact interaction is included in e^* production and decay amplitudes. See their Fig.6 for exclusion limits in $m_{e^*}\text{--}\Lambda$ plane.
- 3 SIRUNYAN 19Z search for e^* production in $\ell\ell\gamma$ final states in pp collisions at $\sqrt{s} = 13$ TeV. The quoted limit assumes $\Lambda = m_{e^*}$, $f = f' = 1$. The contact interaction is included in the e^* production and decay amplitudes.
- 4 KHACHATRYAN 16AQ search for single e^* production in pp collisions at $\sqrt{s} = 8$ TeV. The limit above is from the $e^* \rightarrow e\gamma$ search channel assuming $f = f' = 1$, $m_{e^*} = \Lambda$. See their Table 7 for limits in other search channels or with different assumptions.
- 5 AAD 15AP search for e^* production in events with three or more charged leptons in pp collisions at $\sqrt{s} = 8$ TeV. The quoted limit assumes $\Lambda = m_{e^*}$, $f = f' = 1$. The contact interaction is included in the e^* production and decay amplitudes.
- 6 AAD 13BB search for single e^* production in pp collisions with $e^* \rightarrow e\gamma$ decay. $f = f' = 1$, and e^* production via contact interaction with $\Lambda = m_{e^*}$ are assumed.
- 7 CHATRCHYAN 13AE search for single e^* production in pp collisions with $e^* \rightarrow e\gamma$ decay. $f = f' = 1$, and e^* production via contact interaction with $\Lambda = m_{e^*}$ are assumed.
- 8 AAD 12AZ search for e^* production via four-fermion contact interaction in pp collisions with $e^* \rightarrow e\gamma$ decay. The quoted limit assumes $\Lambda = m_{e^*}$. See their Fig. 8 for the exclusion plot in the mass-coupling plane.

Limits for Excited e (e^*) from $e^+e^- \rightarrow \gamma\gamma$

These limits are derived from indirect effects due to e^* exchange in the t channel and depend on transition magnetic coupling between e and e^* . All limits are for $\lambda_\gamma = 1$. All limits except ABE 89j and ACHARD 02D are for nonchiral coupling with $\eta_L = \eta_R = 1$. We choose the chiral coupling limit as the best limit and list it in the Summary Table.

For limits prior to 1987, see our 1992 edition (Physical Review **D45** S1 (1992)).

VALUE (GeV)	CL%	DOCUMENT ID	TECN	COMMENT
>356	95	¹ ABDALLAH 04N	DLPH	$\sqrt{s} = 161\text{--}208$ GeV
• • •		We do not use the following data for averages, fits, limits, etc. • • •		
>310	95	ACHARD 02D	L3	$\sqrt{s} = 192\text{--}209$ GeV

¹ ABDALLAH 04N also obtain a limit on the excited electron mass with $e e^*$ chiral coupling, $m_{e^*} > 295$ GeV at 95% CL.

Indirect Limits for Excited e (e^*)

These limits make use of loop effects involving e^* and are therefore subject to theoretical uncertainty.

VALUE (GeV)	DOCUMENT ID	TECN	COMMENT
• • •	We do not use the following data for averages, fits, limits, etc. • • •		
	¹ DORENBOS... 89	CHRM	$\mathcal{T}_{\mu e} \rightarrow \mathcal{T}_{\mu e}, \nu_{\mu e} \rightarrow \nu_{\mu e}$
	² GRIFOLS 86	THEO	$\nu_{\mu e} \rightarrow \nu_{\mu e}$
	³ RENARD 82	THEO	$g\text{--}2$ of electron

¹ DORENBOSCH 89 obtain the limit $\lambda_\gamma^2 \Lambda_{\text{cut}}^2 / m_{e^*}^2 < 2.6$ (95% CL), where Λ_{cut} is the cutoff scale, based on the one-loop calculation by GRIFOLS 86. If one assumes that $\Lambda_{\text{cut}} = 1$ TeV and $\lambda_\gamma = 1$, one obtains $m_{e^*} > 620$ GeV. However, one generally expects $\lambda_\gamma \approx m_{e^*} / \Lambda_{\text{cut}}$ in composite models.

² GRIFOLS 86 uses $\nu_{\mu e} \rightarrow \nu_{\mu e}$ and $\mathcal{T}_{\mu e} \rightarrow \mathcal{T}_{\mu e}$ data from CHARM Collaboration to derive mass limits which depend on the scale of compositeness.

³ RENARD 82 derived from $g\text{--}2$ data limits on mass and couplings of e^* and μ^* . See figures 2 and 3 of the paper.

MASS LIMITS for Excited μ (μ^*)

Limits for Excited μ (μ^*) from Pair Production

These limits are obtained from $e^+e^- \rightarrow \mu^* \mu^*$ and thus rely only on the (electroweak) charge of μ^* . Form factor effects are ignored unless noted. For the case of limits from Z decay, the μ^* coupling is assumed to be of sequential type. All limits assume a dominant $\mu^* \rightarrow \mu\gamma$ decay except the limits from $\Gamma(Z)$.

For limits prior to 1987, see our 1992 edition (Physical Review **D45** S1 (1992)).

VALUE (GeV)	CL%	DOCUMENT ID	TECN	COMMENT
>103.2	95	¹ ABBIENDI 02G	OPAL	$e^+e^- \rightarrow \mu^* \mu^*$ Homodoublet type
• • •	We do not use the following data for averages, fits, limits, etc. • • •			
>102.8	95	² ACHARD 03B	L3	$e^+e^- \rightarrow \mu^* \mu^*$ Homodoublet type

¹ From e^+e^- collisions at $\sqrt{s} = 183\text{--}209$ GeV. $f = f'$ is assumed.

² From e^+e^- collisions at $\sqrt{s} = 189\text{--}209$ GeV. $f = f'$ is assumed. ACHARD 03B also obtain limit for $f = -f'$: $m_{\mu^*} > 96.6$ GeV.

Limits for Excited μ (μ^*) from Single Production

These limits are from $e^+e^- \rightarrow \mu^* \mu$ and depend on transition magnetic coupling between μ and μ^* . All limits assume $\mu^* \rightarrow \mu\gamma$ decay. Limits from LEP are for chiral coupling, whereas all other limits are for nonchiral coupling, $\eta_L = \eta_R = 1$. In most papers, the limit is expressed in the form of an excluded region in the $\lambda\text{--}m_{\mu^*}$ plane. See the original papers.

For limits prior to 1987, see our 1992 edition (Physical Review **D45** S1 (1992)).

VALUE (GeV)	CL%	DOCUMENT ID	TECN	COMMENT
>5700	95	¹ SIRUNYAN 20AJ	CMS	$pp \rightarrow \mu \mu^* X$
• • •	We do not use the following data for averages, fits, limits, etc. • • •			
>3800	95	² SIRUNYAN 19Z	CMS	$pp \rightarrow \mu \mu^* X$
>2800	95	³ AAD 16BMATLS	pp	$\rightarrow \mu \mu^* X$
>2470	95	⁴ KHACHATRYAN...16AQ	CMS	$pp \rightarrow \mu \mu^* X$
>3000	95	⁵ AAD 15AP	ATLS	$pp \rightarrow \mu^{(*)} \mu^* X$
>2200	95	⁶ AAD 13BB	ATLS	$pp \rightarrow \mu \mu^* X$
>1900	95	⁷ CHATRCHYAN13AE	CMS	$pp \rightarrow \mu \mu^* X$
>1750	95	⁸ AAD 12AZ	ATLS	$pp \rightarrow \mu^{(*)} \mu^* X$

¹ SIRUNYAN 20AJ search for μ^* production in $2\mu 2j$ final states in pp collisions at $\sqrt{s} = 13$ TeV. The quoted limit assumes $\Lambda = m_{\mu^*}$, $f = f' = 1$. The contact interaction is included. See their Fig.11 for exclusion limits in $m_{\mu^*}\text{--}\Lambda$ plane.

² SIRUNYAN 19Z search for μ^* production in $\ell\ell\gamma$ final states in pp collisions at $\sqrt{s} = 13$ TeV. The quoted limit assumes $\Lambda = m_{\mu^*}$, $f = f' = 1$. The contact interaction is included in the μ^* production and decay amplitudes.

³ AAD 16BM search for μ^* production in $\mu\mu jj$ events in pp collisions at $\sqrt{s} = 8$ TeV. Both the production and decay are assumed to occur via a contact interaction with $\Lambda = m_{\mu^*}$.

⁴ KHACHATRYAN 16AQ search for single μ^* production in pp collisions at $\sqrt{s} = 8$ TeV. The limit above is from the $\mu^* \rightarrow \mu\gamma$ search channel assuming $f = f' = 1$, $m_{\mu^*} = \Lambda$. See their Table 7 for limits in other search channels or with different assumptions.

⁵ AAD 15AP search for μ^* production in evens with three or more charged leptons in pp collisions at $\sqrt{s} = 8$ TeV. The quoted limit assumes $\Lambda = m_{\mu^*}$, $f = f' = 1$. The contact interaction is included in the μ^* production and decay amplitudes.

⁶ AAD 13BB search for single μ^* production in pp collisions with $\mu^* \rightarrow \mu\gamma$ decay. $f = f' = 1$, and μ^* production via contact interaction with $\Lambda = m_{\mu^*}$ are assumed.

⁷ CHATRCHYAN 13AE search for single μ^* production in pp collisions with $\mu^* \rightarrow \mu\gamma$ decay. $f = f' = 1$, and μ^* production via contact interaction with $\Lambda = m_{\mu^*}$ are assumed.

⁸ AAD 12AZ search for μ^* production via four-fermion contact interaction in pp collisions with $\mu^* \rightarrow \mu\gamma$ decay. The quoted limit assumes $\Lambda = m_{\mu^*}$. See their Fig. 8 for the exclusion plot in the mass-coupling plane.

Indirect Limits for Excited μ (μ^*)

These limits make use of loop effects involving μ^* and are therefore subject to theoretical uncertainty.

VALUE (GeV)	DOCUMENT ID	TECN	COMMENT
• • •	We do not use the following data for averages, fits, limits, etc. • • •		
	¹ RENARD 82	THEO	$g\text{--}2$ of muon

¹ RENARD 82 derived from $g\text{--}2$ data limits on mass and couplings of e^* and μ^* . See figures 2 and 3 of the paper.

MASS LIMITS for Excited τ (τ^*)

Limits for Excited τ (τ^*) from Pair Production

These limits are obtained from $e^+e^- \rightarrow \tau^* \tau^*$ and thus rely only on the (electroweak) charge of τ^* . Form factor effects are ignored unless noted. For the case of limits from Z decay, the τ^* coupling is assumed to be of sequential type. All limits assume a dominant $\tau^* \rightarrow \tau\gamma$ decay except the limits from $\Gamma(Z)$.

For limits prior to 1987, see our 1992 edition (Physical Review **D45** S1 (1992)).

VALUE (GeV)	CL%	DOCUMENT ID	TECN	COMMENT
>103.2	95	¹ ABBIENDI 02G	OPAL	$e^+e^- \rightarrow \tau^* \tau^*$ Homodoublet type
• • •	We do not use the following data for averages, fits, limits, etc. • • •			
>102.8	95	² ACHARD 03B	L3	$e^+e^- \rightarrow \tau^* \tau^*$ Homodoublet type

¹ From e^+e^- collisions at $\sqrt{s} = 183\text{--}209$ GeV. $f = f'$ is assumed.

² From e^+e^- collisions at $\sqrt{s} = 189\text{--}209$ GeV. $f = f'$ is assumed. ACHARD 03B also obtain limit for $f = -f'$: $m_{\tau^*} > 96.6$ GeV.

Limits for Excited τ (τ^*) from Single Production

These limits are from $e^+e^- \rightarrow \tau^* \tau$ and depend on transition magnetic coupling between τ and τ^* . All limits assume $\tau^* \rightarrow \tau\gamma$ decay. Limits from LEP are for chiral coupling, whereas all other limits are for nonchiral coupling, $\eta_L = \eta_R = 1$. In most papers, the limit is expressed in the form of an excluded region in the $\lambda\text{--}m_{\tau^*}$ plane. See the original papers.

VALUE (GeV)	CL%	DOCUMENT ID	TECN	COMMENT
>2500	95	¹ AAD 15AP	ATLS	$pp \rightarrow \tau^{(*)} \tau^* X$
• • •	We do not use the following data for averages, fits, limits, etc. • • •			
> 180	95	² ACHARD 03B	L3	$e^+e^- \rightarrow \tau \tau^*$
> 185	95	³ ABBIENDI 02G	OPAL	$e^+e^- \rightarrow \tau \tau^*$

¹ AAD 15AP search for τ^* production in events with three or more charged leptons in pp collisions at $\sqrt{s} = 8$ TeV. The quoted limit assumes $\Lambda = m_{\tau^*}$, $f = f' = 1$. The contact interaction is included in the τ^* production and decay amplitudes.

² ACHARD 03B result is from e^+e^- collisions at $\sqrt{s} = 189\text{--}209$ GeV. $f = f' = \Lambda / m_{\tau^*}$ is assumed. See their Fig. 4 for the exclusion plot in the mass-coupling plane.

³ ABBIENDI 02G result is from e^+e^- collisions at $\sqrt{s} = 183\text{--}209$ GeV. $f = f' = \Lambda / m_{\tau^*}$ is assumed for τ^* coupling. See their Fig. 4c for the exclusion limit in the mass-coupling plane.

MASS LIMITS for Excited Neutrino (ν^*)

Limits for Excited ν (ν^*) from Pair Production

These limits are obtained from $e^+e^- \rightarrow \nu^* \nu^*$ and thus rely only on the (electroweak) charge of ν^* . Form factor effects are ignored unless noted. The ν^* coupling is assumed to be of sequential type unless otherwise noted. All limits assume a dominant $\nu^* \rightarrow \nu\gamma$ decay except the limits from $\Gamma(Z)$.

VALUE (GeV)	CL%	DOCUMENT ID	TECN	COMMENT
>1600	95	¹ AAD 15AP	ATLS	$pp \rightarrow \nu^* \nu^* X$
• • •	We do not use the following data for averages, fits, limits, etc. • • •			
> 102.6	95	² ABBIENDI 04N	OPAL	
		³ ACHARD 03B	L3	$e^+e^- \rightarrow \nu^* \nu^*$ Homodoublet type

¹ AAD 15AP search for ν^* pair production in events with three or more charged leptons in pp collisions at $\sqrt{s} = 8$ TeV. The quoted limit assumes $\Lambda = m_{\nu^*}$, $f = f' = 1$. The contact interaction is included in the ν^* production and decay amplitudes.

² From e^+e^- collisions at $\sqrt{s} = 192\text{--}209$ GeV, ABBIENDI 04N obtain limit on $\sigma(e^+e^- \rightarrow \nu^* \nu^*) B^2(\nu^* \rightarrow \nu\gamma)$. See their Fig.2. The limit ranges from 20 to 45 fb for $m_{\nu^*} > 45$ GeV.

³ From e^+e^- collisions at $\sqrt{s} = 189\text{--}209$ GeV. $f = -f'$ is assumed. ACHARD 03B also obtain limit for $f = f'$: $m_{\nu_e^*} > 101.7$ GeV, $m_{\nu_\mu^*} > 101.8$ GeV, and $m_{\nu_\tau^*} > 92.9$ GeV. See their Fig. 4 for the exclusion plot in the mass-coupling plane.

Searches Particle Listings

Quark and Lepton Compositeness

Limits for Excited ν (ν^*) from Single Production

These limits are from $e^+e^- \rightarrow \nu\nu^*$, $Z \rightarrow \nu\nu^*$, or $ep \rightarrow \nu^*X$ and depend on transition magnetic coupling between ν/e and ν^* . Assumptions about ν^* decay mode are given in footnotes.

VALUE (GeV)	CL%	DOCUMENT ID	TECN	COMMENT
>213	95	1 AARON	08 H1	$ep \rightarrow \nu^*X$
>190	95	2 ACHARD	03B L3	$e^+e^- \rightarrow \nu\nu^*$
none 50-150	95	3 ADLOFF	02 H1	$ep \rightarrow \nu^*X$
>158	95	4 CHEKANOV	02D ZEUS	$ep \rightarrow \nu^*X$

- We do not use the following data for averages, fits, limits, etc. •••
- 1 AARON 08 search for single ν^* production in ep collisions with the decays $\nu^* \rightarrow \nu\gamma$, νZ , eW . The quoted limit assumes $f = -f' = \Lambda/m_{\nu^*}$. See their Fig. 3 and Fig. 4 for the exclusion plots in the mass-coupling plane.
- 2 ACHARD 03B result is from e^+e^- collisions at $\sqrt{s} = 189-209$ GeV. The quoted limit is for ν_e^* . $f = -f' = \Lambda/m_{\nu^*}$ is assumed. See their Fig. 4 for the exclusion plot in the mass-coupling plane.
- 3 ADLOFF 02 search for single ν^* production in ep collisions with the decays $\nu^* \rightarrow \nu\gamma$, νZ , eW . The quoted limit assumes $f = -f' = \Lambda/m_{\nu^*}$. See their Fig. 1 for the exclusion plots in the mass-coupling plane.
- 4 CHEKANOV 02D search for single ν^* production in ep collisions with the decays $\nu^* \rightarrow \nu\gamma$, νZ , eW . $f = -f' = \Lambda/m_{\nu^*}$ is assumed for the e^* coupling. CHEKANOV 02D also obtain limit for $f = f' = \Lambda/m_{\nu^*}$; $m_{\nu^*} > 135$ GeV. See their Fig. 5c and Fig. 5d for the exclusion plot in the mass-coupling plane.

MASS LIMITS for Excited q (q^*)

Limits for Excited q (q^*) from Pair Production

These limits are mostly obtained from $e^+e^- \rightarrow q^*\bar{q}^*$ and thus rely only on the (electroweak) charge of the q^* . Form factor effects are ignored unless noted. Assumptions about the q^* decay are given in the comments and footnotes.

VALUE (GeV)	CL%	DOCUMENT ID	TECN	COMMENT
>338	95	1 AALTONEN	10H CDF	$q^* \rightarrow tW^-$
none 700-1200	95	2 SIRUNYAN	18v CMS	$pp \rightarrow t^*_{3/2} \bar{t}^*_{3/2} \rightarrow t\bar{t}g\bar{g}$
> 45.6	95	4 ADRIANI	93M L3	$Z \rightarrow q^*q^*$
> 41.7	95	5 BARDADIN...	92 RVUE	u or d type, $Z \rightarrow q^*q^*$
> 44.7	95	5 BARDADIN...	92 RVUE	d -type, $\Gamma(Z)$
> 40.6	95	6 DECAAMP	92 ALEP	u -type, $\Gamma(Z)$
> 44.2	95	6 DECAAMP	92 ALEP	d -type, $\Gamma(Z)$
> 45	95	7 DECAAMP	92 ALEP	u or d type, $Z \rightarrow q^*q^*$
> 45	95	6 ABREU	91F DLPH	u -type, $\Gamma(Z)$
> 45	95	6 ABREU	91F DLPH	d -type, $\Gamma(Z)$

- We do not use the following data for averages, fits, limits, etc. •••
- 1 AALTONEN 10H obtain limits on the q^*q^* production cross section in $p\bar{p}$ collisions. See their Fig. 3.
- 2 SIRUNYAN 18v search for pair production of spin 3/2 excited top quarks. $B(t^*_{3/2} \rightarrow t\bar{g}) = 1$ is assumed.
- 3 BARATE 98u obtain limits on the form factor. See their Fig. 16 for limits in mass-form factor plane.
- 4 ADRIANI 93M limit is valid for $B(q^* \rightarrow qg) > 0.25$ (0.17) for up (down) type.
- 5 BARDADIN-OTWINOWSKA 92 limit based on $\Delta\Gamma(Z) < 36$ MeV.
- 6 These limits are independent of decay modes.
- 7 Limit is for $B(q^* \rightarrow qg) + B(q^* \rightarrow q\gamma) = 1$.

Limits for Excited q (q^*) from Single Production

These limits are from $e^+e^- \rightarrow q^*\bar{q}$, $p\bar{p} \rightarrow q^*X$, or $pp \rightarrow q^*X$ and depend on transition magnetic couplings between q and q^* . Assumptions about q^* decay mode are given in the footnotes and comments.

VALUE (GeV)	CL%	DOCUMENT ID	TECN	COMMENT
>6700 (CL = 95%) OUR LIMIT				
none 2000-6700	95	1 AAD	20T ATLS	$pp \rightarrow q^*X, q^* \rightarrow qg$
none 1250-3200	95	1 AAD	20T ATLS	$pp \rightarrow b^*X, b^* \rightarrow bg, b\gamma, bZ, tW$
none 1800-6300	95	2 SIRUNYAN	20AI CMS	$pp \rightarrow q^*X, q^* \rightarrow qg$
none 1500-2600	95	3 AABOUD	18AB ATLS	$pp \rightarrow b^*X, b^* \rightarrow bg$
none 1500-5300	95	4 AABOUD	18BA ATLS	$pp \rightarrow q^*X, q^* \rightarrow q\gamma$
none 1000-5500	95	5 SIRUNYAN	18AG CMS	$pp \rightarrow q^*X, q^* \rightarrow q\gamma$
none 1000-1800	95	6 SIRUNYAN	18AG CMS	$pp \rightarrow b^*X, b^* \rightarrow b\gamma$
none 600-6000	95	7 SIRUNYAN	18BO CMS	$pp \rightarrow q^*X, q^* \rightarrow qg$
none 1200-5000	95	8 SIRUNYAN	18P CMS	$pp \rightarrow q^*X, q^* \rightarrow qW$
none 1200-4700	95	8 SIRUNYAN	18P CMS	$pp \rightarrow q^*X, q^* \rightarrow qZ$
>6000	95	9 AABOUD	17AK ATLS	$pp \rightarrow q^*X, q^* \rightarrow qg$
>2600	95	10 SIRUNYAN	21AG CMS	$pp \rightarrow b^*X, b^* \rightarrow tW$
none 600-5400	95	11 KHACHATRY...	17W CMS	$pp \rightarrow q^*X, q^* \rightarrow qg$
none 1100-2100	95	12 AABOUD	16 ATLS	$pp \rightarrow b^*X, b^* \rightarrow bg$
>1500	95	13 AAD	16AH ATLS	$pp \rightarrow b^*X, b^* \rightarrow tW$
>4400	95	14 AAD	16AI ATLS	$pp \rightarrow q^*X, q^* \rightarrow q\gamma$
		15 AAD	16AV ATLS	$pp \rightarrow q^*X, q^* \rightarrow Wb$
>5200	95	16 AAD	16S ATLS	$pp \rightarrow q^*X, q^* \rightarrow qg$
>1390	95	17 KHACHATRY...	16I CMS	$pp \rightarrow b^*X, b^* \rightarrow tW$
>5000	95	18 KHACHATRY...	16K CMS	$pp \rightarrow q^*X, q^* \rightarrow qg$

- We do not use the following data for averages, fits, limits, etc. •••
- 10 SIRUNYAN 21AG search for resonances decaying into dijets in pp collisions at $\sqrt{s} = 13$ TeV. Assume $\Lambda = m_{q^*}$, $f_5 = f = f' = 1$.
- 11 KHACHATRY...17W search for resonances decaying into dijets in pp collisions at $\sqrt{s} = 13$ TeV. Assume $\Lambda = m_{q^*}$, $f_5 = f = f' = 1$.
- 12 AABOUD 16 ATLS assume $\Lambda = m_{b^*}$, $f_5 = f = f' = 1$. The contact interactions are not included in b^* production and decay amplitudes.
- 13 AAD 16AH ATLS assume $\Lambda = m_{q^*}$, $f_5 = f = f' = 1$. The contact interactions are not included in q^* production and decay amplitudes.
- 14 AAD 16AI ATLS assume $\Lambda = m_{q^*}$, $f_5 = f = f' = 1$. The contact interactions are not included in q^* production and decay amplitudes.
- 15 AAD 16AV ATLS assume $\Lambda = m_{q^*}$, $f_5 = f = f' = 1$. The contact interactions are not included in q^* production and decay amplitudes.
- 16 AAD 16S ATLS assume $\Lambda = m_{q^*}$, $f_5 = f = f' = 1$. The contact interactions are not included in q^* production and decay amplitudes.
- 17 KHACHATRY...16I search for resonances decaying into dijets in pp collisions at $\sqrt{s} = 8$ TeV using the data scouting technique which increases the sensitivity to the low mass resonances.
- 18 KHACHATRY...16K assume $\Lambda = m_{q^*}$, $f_5 = f = f' = 1$. The contact interactions are not included in q^* production and decay amplitudes.

none 500-1600	95	19 KHACHATRY...	16L CMS	$pp \rightarrow q^*X, q^* \rightarrow qg$
>4060	95	20 AAD	15V ATLS	$pp \rightarrow q^*X, q^* \rightarrow qg$
>3500	95	21 KHACHATRY...	15V CMS	$pp \rightarrow q^*X, q^* \rightarrow qg$
>3500	95	22 AAD	14A ATLS	$pp \rightarrow q^*X, q^* \rightarrow q\gamma$
>3200	95	23 KHACHATRY...	14 CMS	$pp \rightarrow q^*X, q^* \rightarrow qW$
>2900	95	24 KHACHATRY...	14 CMS	$pp \rightarrow q^*X, q^* \rightarrow qZ$
none 700-3500	95	25 KHACHATRY...	14J CMS	$pp \rightarrow q^*X, q^* \rightarrow q\gamma$
>2380	95	26 CHATRCHYAN	13AJ CMS	$pp \rightarrow q^*X, q^* \rightarrow qW$
>2150	95	27 CHATRCHYAN	13AJ CMS	$pp \rightarrow q^*X, q^* \rightarrow qZ$

- 1 AAD 20T search for resonances decaying into dijets in pp collisions at $\sqrt{s} = 13$ TeV. Assume $\Lambda = m_{q^*}$, $f_5 = f = f' = 1$.
- 2 SIRUNYAN 20AI search for resonances decaying into dijets in pp collisions at $\sqrt{s} = 13$ TeV. Assume $\Lambda = m_{q^*}$, $f_5 = f = f' = 1$.
- 3 AABOUD 18AB assume $\Lambda = m_{b^*}$, $f_5 = f = f' = 1$. The contact interactions are not included in b^* production and decay amplitudes.
- 4 AABOUD 18BA search for first-generation excited quarks (u^* and d^*) with degenerate mass, assuming $\Lambda = m_{q^*}$, $f_5 = f = f' = 1$. The contact interactions are not included in q^* production and decay amplitudes.
- 5 SIRUNYAN 18AG search for first-generation excited quarks (u^* and d^*) with degenerate mass, assuming $\Lambda = m_{q^*}$, $f_5 = f = f' = 1$.
- 6 SIRUNYAN 18AG search for excited b quark assuming $\Lambda = m_{q^*}$, $f_5 = f = f' = 1$.
- 7 SIRUNYAN 18BO assume $\Lambda = m_{q^*}$, $f_5 = f = f' = 1$. The contact interactions are not included in q^* production and decay amplitudes.
- 8 SIRUNYAN 18P use the hadronic decay of W or Z , assuming $\Lambda = m_{q^*}$, $f_5 = f = f' = 1$.
- 9 AABOUD 17AK assume $\Lambda = m_{q^*}$, $f_5 = f = f' = 1$. The contact interactions are not included in q^* production and decay amplitudes. Only the decay of $q^* \rightarrow gu$ and $q^* \rightarrow gd$ is simulated as the benchmark signals in the analysis.
- 10 SIRUNYAN 21AG search for b^* decaying to tW in pp collisions at $\sqrt{s} = 13$ TeV. The limit quoted above assumes $\kappa_L^b = g_L = 1, \kappa_R^b = g_R = 0$. The limit becomes $m_{b^*} > 2.8$ TeV (> 3.1 TeV) if we assume $\kappa_L^b = g_L = 0, \kappa_R^b = g_R = 1$ ($\kappa_L^b = g_L = \kappa_R^b = g_R = 1$). See their Fig. 5 for limits on $\sigma \cdot B$.
- 11 KHACHATRYAN 17W assume $\Lambda = m_{q^*}$, $f_5 = f = f' = 1$. The contact interactions are not included in q^* production and decay amplitudes.
- 12 AABOUD 16 assume $\Lambda = m_{b^*}$, $f_5 = f = f' = 1$. The contact interactions are not included in the b^* production and decay amplitudes.
- 13 AAD 16AH search for b^* decaying to tW in pp collisions at $\sqrt{s} = 8$ TeV. $f_g = f_L = f_R = 1$ are assumed. See their Fig. 12b for limits on $\sigma \cdot B$.
- 14 AAD 16AI assume $\Lambda = m_{q^*}$, $f_5 = f = f' = 1$.
- 15 AAD 16AV search for single production of vector-like quarks decaying to Wb in pp collisions. See their Fig. 8 for the limits on couplings and mixings.
- 16 AAD 16S assume $\Lambda = m_{q^*}$, $f_5 = f = f' = 1$. The contact interactions are not included in q^* production and decay amplitudes.
- 17 KHACHATRYAN 16I search for b^* decaying to tW in pp collisions at $\sqrt{s} = 8$ TeV. $\kappa_L^b = g_L = 1, \kappa_R^b = g_R = 0$ are assumed. See their Fig. 8 for limits on $\sigma \cdot B$.
- 18 KHACHATRYAN 16K assume $\Lambda = m_{q^*}$, $f_5 = f = f' = 1$. The contact interactions are not included in q^* production and decay amplitudes.
- 19 KHACHATRYAN 16L search for resonances decaying into dijets in pp collisions at $\sqrt{s} = 8$ TeV using the data scouting technique which increases the sensitivity to the low mass resonances.
- 20 AAD 15V assume $\Lambda = m_{q^*}$, $f_5 = f = f' = 1$. The contact interactions are not included in q^* production and decay amplitudes.
- 21 KHACHATRYAN 15V assume $\Lambda = m_{q^*}$, $f_5 = f = f' = 1$. The contact interactions are not included in q^* production and decay amplitudes.
- 22 AAD 14A assume $\Lambda = m_{q^*}$, $f_5 = f = f' = 1$.
- 23 KHACHATRYAN 14 use the hadronic decay of W , assuming $\Lambda = m_{q^*}$, $f_5 = f = f' = 1$.
- 24 KHACHATRYAN 14 use the hadronic decay of Z , assuming $\Lambda = m_{q^*}$, $f_5 = f = f' = 1$.
- 25 KHACHATRYAN 14J assume $f_5 = f = f' = \Lambda / m_{q^*}$.
- 26 CHATRCHYAN 13AJ use the hadronic decay of W .
- 27 CHATRCHYAN 13AJ use the hadronic decay of Z .

MASS LIMITS for Color Sextet Quarks (q_6)

VALUE (GeV)	CL%	DOCUMENT ID	TECN	COMMENT
>84	95	1 ABE	89D CDF	$p\bar{p} \rightarrow q_6\bar{q}_6$

- 1 ABE 89D look for pair production of unit-charged particles which leave the detector before decaying. In the above limit the color sextet quark is assumed to fragment into a unit-charged or neutral hadron with equal probability and to have long enough lifetime not to decay within the detector. A limit of 121 GeV is obtained for a color decuplet.

MASS LIMITS for Color Octet Charged Leptons (ℓ_8)

VALUE (GeV)	CL%	DOCUMENT ID	TECN	COMMENT
>86	95	1 ABE	89D CDF	Stable ℓ_8 : $p\bar{p} \rightarrow \ell_8\bar{\ell}_8$

- We do not use the following data for averages, fits, limits, etc. •••
- 2 ABE 93 H1 $e\bar{e} \rightarrow e\bar{e}X$

See key on page 1127

Searches Particle Listings

Quark and Lepton Compositeness, Extra Dimensions

- 1 ABE 89D look for pair production of unit-charged particles which leave the detector before decaying. In the above limit the color octet lepton is assumed to fragment into a unit-charged or neutral hadron with equal probability and to have long enough lifetime not to decay within the detector. The limit improves to 99 GeV if it always fragments into a unit-charged hadron.
2 ABT 93 search for e8 production via e-gluon fusion in ep collisions with e8 -> eg. See their Fig. 3 for exclusion plot in the me8-lambda plane for me8 = 35-220 GeV.

MASS LIMITS for Color Octet Neutrinos (nu8)

Table with columns: VALUE (GeV), CL%, DOCUMENT ID, TECN, COMMENT. Includes entries for BARGER 89, KIM 90, and BARTEL 87b with detailed comments on assumptions and cross-sections.

MASS LIMITS for W8 (Color Octet W Boson)

Table with columns: VALUE (GeV), DOCUMENT ID, TECN, COMMENT. Includes entry for ALBAJAR 89 with comment on sigma(W8 -> W+jet)/sigma(W) < 0.019.

REFERENCES FOR Searches for Quark and Lepton Compositeness

Extensive list of references for quark and lepton compositeness searches, including AAD, SIRUNYAN, ABOUD, etc., with document IDs and technical details.

Extensive list of references for extra dimensions searches, including ADLOFF, CHEKANOV, AFFOLDER, etc., with document IDs and technical details.

Extra Dimensions

For explanation of terms used and discussion of significant model dependence of following limits, see the "Extra Dimensions" review. Footnotes describe originally quoted limit. delta indicates the number of extra dimensions.

Limits not encoded here are summarized in the "Extra Dimensions" review, where the latest unpublished results are also described.

See the related review(s):

Extra Dimensions

CONTENTS:

- Limits on R from Deviations in Gravitational Force Law
Limits on R from On-Shell Production of Gravitons: delta = 2
Mass Limits on M_TT
Limits on 1/R = M_c
Limits on Kaluza-Klein Gravitons in Warped Extra Dimensions
Limits on Kaluza-Klein Gluons in Warped Extra Dimensions
Black Hole Production Limits
- Semiclassical Black Holes
- Quantum Black Holes

Limits on R from Deviations in Gravitational Force Law

This section includes limits on the size of extra dimensions from deviations in the Newtonian (1/r^2) gravitational force law at short distances. Deviations are parameterized by a gravitational potential of the form V = -(Gm m'/r) [1 + alpha exp(-r/R)]. For delta toroidal extra dimensions of equal size, alpha = 8delta/3. Quoted bounds are for delta = 2 unless otherwise noted.

Table with columns: VALUE (um), CL%, DOCUMENT ID, TECN, COMMENT. Lists various experiments like BLAKEMORE, HEACOCK, LEE, etc., and their constraints on R.

- 1 BLAKEMORE 21 obtain constraints on non-Newtonian forces with strengths |alpha| >= 10^8 and length scales R > 10 um. See their Fig. 4 for more details including comparison with previous searches.
2 HEACOCK 21 obtain constraints on non-Newtonian forces with strengths 10^18 <= |alpha| <= 10^25 and length scales R approx 0.02-10 nm. See their Figure 3 for more details. This improves the results of HADDOCK 18. These constraints do not place limits on the size of extra flat dimensions.

Searches Particle Listings

Extra Dimensions

- ³ LEE 20 search for new forces probing a range of $|\alpha| \simeq 0.1\text{--}10^5$ and length scales $R \simeq 7\text{--}90 \mu\text{m}$. For $\delta = 1$ the bound on R is $30 \mu\text{m}$. See their Fig. 5 for details on the bound.
- ⁴ TAN 20A search for new forces probing a range of $|\alpha| \simeq 4 \times 10^{-3}\text{--}1 \times 10^2$ and length scales $R \simeq 40\text{--}350 \mu\text{m}$. See their Fig. 6 for details on the bound.
- ⁵ BERGE 18 uses results from the MICROSCOPE experiment to obtain constraints on non-Newtonian forces with strengths $10^{-11} \lesssim |\alpha| \lesssim 10^{-7}$ and length scales $R \gtrsim 10^5 \text{ m}$. See their Figure 1 for more details. These constraints do not place limits on the size of extra flat dimensions.
- ⁶ FAYET 18A uses results from the MICROSCOPE experiment to obtain constraints on an EP-violating force possibly arising from a new U(1) gauge boson. For $R \gtrsim 10^7 \text{ m}$ the limits are $|\alpha| \lesssim$ a few 10^{-13} to a few 10^{-11} depending on the coupling, corresponding to $|c| \gtrsim 10^{-24}$ for the coupling of the new spin-1 or spin-0 mediator. These constraints do not place limits on the size of extra flat dimensions. This extends the results of FAYET 18.
- ⁷ KLIMCHITSKAYA 17A uses an experiment that measures the difference of Casimir forces to obtain bounds on non-Newtonian forces with strengths $|\alpha| \simeq 10^5\text{--}10^{17}$ and length scales $R = 0.03\text{--}10 \mu\text{m}$. See their Fig. 3. These constraints do not place limits on the size of extra flat dimensions.
- ⁸ XU 13 obtain constraints on non-Newtonian forces with strengths $|\alpha| \simeq 10^{34}\text{--}10^{36}$ and length scales $R \simeq 1\text{--}10 \text{ fm}$. See their Fig. 4 for more details. These constraints do not place limits on the size of extra flat dimensions.
- ⁹ BEZERRA 11 obtain constraints on non-Newtonian forces with strengths $10^{11} \lesssim |\alpha| \lesssim 10^{18}$ and length scales $R = 30\text{--}1260 \text{ nm}$. See their Fig. 2 for more details. These constraints do not place limits on the size of extra flat dimensions.
- ¹⁰ SUSHKOV 11 obtain improved limits on non-Newtonian forces with strengths $10^7 \lesssim |\alpha| \lesssim 10^{11}$ and length scales $0.4 \mu\text{m} < R < 4 \mu\text{m}$ (95% CL). See their Fig. 2. These bounds do not place limits on the size of extra flat dimensions. However, a model dependent bound of $M_* > 70 \text{ TeV}$ is obtained assuming gauge bosons that couple to baryon number also propagate in $(4 + \delta)$ dimensions.
- ¹¹ BEZERRA 10 obtain improved constraints on non-Newtonian forces with strengths $10^{19} \lesssim |\alpha| \lesssim 10^{29}$ and length scales $R = 1.6\text{--}14 \text{ nm}$ (95% CL). See their Fig. 1. This bound does not place limits on the size of extra flat dimensions.
- ¹² MASUDA 09 obtain improved constraints on non-Newtonian forces with strengths $10^9 \lesssim |\alpha| \lesssim 10^{11}$ and length scales $R = 1.0\text{--}2.9 \mu\text{m}$ (95% CL). See their Fig. 3. This bound does not place limits on the size of extra flat dimensions.
- ¹³ GERACI 08 obtain improved constraints on non-Newtonian forces with strengths $|\alpha| > 14,000$ and length scales $R = 5\text{--}15 \mu\text{m}$. See their Fig. 9. This bound does not place limits on the size of extra flat dimensions.
- ¹⁴ TRENKEL 08 uses two independent measurements of Newton's constant G to constrain new forces with strength $|\alpha| \simeq 10^{-4}$ and length scales $R = 0.02\text{--}1 \text{ m}$. See their Fig. 1. This bound does not place limits on the size of extra flat dimensions.
- ¹⁵ DECCA 07A search for new forces and obtain bounds in the region with strengths $|\alpha| \simeq 10^{13}\text{--}10^{18}$ and length scales $R = 20\text{--}86 \text{ nm}$. See their Fig. 6. This bound does not place limits on the size of extra flat dimensions.
- ¹⁶ KAPNER 07 search for new forces, probing a range of $|\alpha| \simeq 10^{-3}\text{--}10^5$ and length scales $R \simeq 10\text{--}1000 \mu\text{m}$. For $\delta = 1$ the bound on R is $44 \mu\text{m}$. For $\delta = 2$, the bound is expressed in terms of M_* , here translated to a bound on the radius. See their Fig. 6 for details on the bound.
- ¹⁷ TU 07 search for new forces probing a range of $|\alpha| \simeq 10^{-1}\text{--}10^5$ and length scales $R \simeq 20\text{--}1000 \mu\text{m}$. For $\delta = 1$ the bound on R is $53 \mu\text{m}$. See their Fig. 3 for details on the bound.
- ¹⁸ SMULLIN 05 search for new forces, and obtain bounds in the region with strengths $\alpha \simeq 10^3\text{--}10^8$ and length scales $R = 6\text{--}20 \mu\text{m}$. See their Figs. 1 and 16 for details on the bound. This work does not place limits on the size of extra flat dimensions.
- ¹⁹ HOYLE 04 search for new forces, probing α down to 10^{-2} and distances down to $10 \mu\text{m}$. Quoted bound on R is for $\delta = 2$. For $\delta = 1$, bound goes to $160 \mu\text{m}$. See their Fig. 34 for details on the bound.
- ²⁰ CHIAVERINI 03 search for new forces, probing α above 10^4 and λ down to $3 \mu\text{m}$, finding no signal. See their Fig. 4 for details on the bound. This bound does not place limits on the size of extra flat dimensions.
- ²¹ LONG 03 search for new forces, probing α down to 3, and distances down to about $10 \mu\text{m}$. See their Fig. 4 for details on the bound.
- ²² HOYLE 01 search for new forces, probing α down to 10^{-2} and distances down to $20 \mu\text{m}$. See their Fig. 4 for details on the bound. The quoted bound is for $\alpha \geq 3$.
- ²³ HOSKINS 85 search for new forces, probing distances down to 4 mm . See their Fig. 13 for details on the bound. This bound does not place limits on the size of extra flat dimensions.

Limits on R from On-Shell Production of Gravitons: $\delta = 2$

This section includes limits on on-shell production of gravitons in collider and astrophysical processes. Bounds quoted are on R , the assumed common radius of the flat extra dimensions, for $\delta = 2$ extra dimensions. Studies often quote bounds in terms of derived parameter; experiments are actually sensitive to the masses of the KK gravitons: $m_{\vec{n}} = |\vec{n}|/R$. See the Review on "Extra Dimensions" for details. Bounds are given in μm for $\delta = 2$.

VALUE (μm)	CL%	DOCUMENT ID	TECN	COMMENT
< 3.8	95	1 AAD 21F ATLS	pp	$\rightarrow jG$
< 0.00016	95	2 HANNESTAD 03		Neutron star heating
••• We do not use the following data for averages, fits, limits, etc. •••				
< 56	95	3 SIRUNYAN 21A CMS	pp	$\rightarrow ZG$
< 4.1	95	4 TUMASYAN 21D CMS	pp	$\rightarrow jG$
		5 SIRUNYAN 17AQ CMS	pp	$\rightarrow \gamma G$
		6 AABOUD 16F ATLS	pp	$\rightarrow \gamma G$
		7 KHACHATRYAN 16N CMS	pp	$\rightarrow \gamma G$
		8 AAD 15CS ATLS	pp	$\rightarrow \gamma G$
< 127	95	9 AAD 13C ATLS	pp	$\rightarrow \gamma G$
< 34.4	95	10 AAD 13D ATLS	pp	$\rightarrow jj$
< 0.0087	95	11 AJELLO 12 FLAT		Neutron star γ sources
< 245	95	12 AALTONEN 08AC CDF	pp	$\rightarrow \gamma G, jG$
< 615	95	13 ABAZOV 08S D0	pp	$\rightarrow \gamma G$
< 0.916	95	14 DAS 08		Supernova cooling

< 350	95	15 ABULENCIA, A 06 CDF	pp	$\rightarrow jG$
< 270	95	16 ABDALLAH 05B DLPH	e^+e^-	$\rightarrow \gamma G$
< 210	95	17 ACHARD 04E L3	e^+e^-	$\rightarrow \gamma G$
< 480	95	18 ACOSTA 04C CDF	pp	$\rightarrow jG$
< 0.00038	95	19 CASSE 04		Neutron star γ sources
< 610	95	20 ABAZOV 03 D0	pp	$\rightarrow jG$
< 0.96	95	21 HANNESTAD 03		Supernova cooling
< 0.096	95	22 HANNESTAD 03		Diffuse γ background
< 0.051	95	23 HANNESTAD 03		Neutron star γ sources
< 300	95	24 HEISTER 03c ALEP	e^+e^-	$\rightarrow \gamma G$
		25 FAIRBAIRN 01		Cosmology
< 0.66	95	26 HANHART 01		Supernova cooling
		27 CASSISI 00		Red giants
< 1300	95	28 ACCIARRI 99S L3	e^+e^-	$\rightarrow ZG$

- ¹ AAD 21F search for $pp \rightarrow jG$, using 139 fb^{-1} of data at $\sqrt{s} = 13 \text{ TeV}$ to place lower limits on M_D for two to six extra dimensions (see their Table X), from which this bound on R is derived. This limit supersedes that in AABOUD 18I.
- ² HANNESTAD 03 obtain a limit on R from the heating of old neutron stars by the surrounding cloud of trapped KK gravitons. Limits for all $\delta \leq 7$ are given in their Tables V and VI. These limits supersede those in HANNESTAD 02.
- ³ SIRUNYAN 21A search for $pp \rightarrow ZG$, using 137 fb^{-1} of data at $\sqrt{s} = 13 \text{ TeV}$ to place lower limits on M_D for two to seven extra dimensions (see their Figure 12), from which this bound on R is derived. These limits supersede those obtained in SIRUNYAN 18BV.
- ⁴ TUMASYAN 21D search for $pp \rightarrow jG$, using 137 fb^{-1} of data at $\sqrt{s} = 13 \text{ TeV}$ to place lower limits on M_D for two to seven extra dimensions (see their Table 3), from which this bound on R is derived. This limit supersedes that in SIRUNYAN 18S.
- ⁵ SIRUNYAN 17AQ search for $pp \rightarrow \gamma G$, using 12.9 fb^{-1} of data at $\sqrt{s} = 13 \text{ TeV}$ to place limits on M_D for three to six extra dimensions (see their Table 3).
- ⁶ AABOUD 16F search for $pp \rightarrow \gamma G$, using 3.2 fb^{-1} of data at $\sqrt{s} = 13 \text{ TeV}$ to place limits on M_D for two to six extra dimensions (see their Figure 9), from which this bound on R is derived.
- ⁷ KHACHATRYAN 16N search for $pp \rightarrow \gamma G$, using 19.6 fb^{-1} of data at $\sqrt{s} = 8 \text{ TeV}$ to place limits on M_D for three to six extra dimensions (see their Table 5).
- ⁸ AAD 15CS search for $pp \rightarrow \gamma G$, using 20.3 fb^{-1} of data at $\sqrt{s} = 8 \text{ TeV}$ to place lower limits on M_D for two to six extra dimensions (see their Fig. 18).
- ⁹ AAD 13C search for $pp \rightarrow \gamma G$, using 4.6 fb^{-1} of data at $\sqrt{s} = 7 \text{ TeV}$ to place bounds on M_D for two to six extra dimensions, from which this bound on R is derived.
- ¹⁰ AAD 13D search for the dijet decay of quantum black holes in 4.8 fb^{-1} of data produced in pp collisions at $\sqrt{s} = 7 \text{ TeV}$ to place bounds on M_D for two to seven extra dimensions, from which these bounds on R are derived. Limits on M_D for all $\delta \leq 7$ are given in their Table 3.
- ¹¹ AJELLO 12 obtain a limit on R from the gamma-ray emission of point γ sources that arise from the photon decay of KK gravitons which are gravitationally bound around neutron stars. Limits for all $\delta \leq 7$ are given in their Table 7.
- ¹² AALTONEN 08AC search for $pp \rightarrow \gamma G$ and $pp \rightarrow jG$ at $\sqrt{s} = 1.96 \text{ TeV}$ with 2.0 fb^{-1} and 1.1 fb^{-1} respectively, in order to place bounds on the fundamental scale and size of the extra dimensions. See their Table III for limits on all $\delta \leq 6$.
- ¹³ ABAZOV 08S search for $pp \rightarrow \gamma G$, using 1 fb^{-1} of data at $\sqrt{s} = 1.96 \text{ TeV}$ to place bounds on M_D for two to eight extra dimensions, from which these bounds on R are derived. See their paper for intermediate values of δ .
- ¹⁴ DAS 08 obtain a limit on R from Kaluza-Klein graviton cooling of SN1987A due to plasmon-plasmon annihilation.
- ¹⁵ ABULENCIA, A 06 search for $pp \rightarrow jG$ using 368 pb^{-1} of data at $\sqrt{s} = 1.96 \text{ TeV}$. See their Table II for bounds for all $\delta \leq 6$.
- ¹⁶ ABDALLAH 05B search for $e^+e^- \rightarrow \gamma G$ at $\sqrt{s} = 180\text{--}209 \text{ GeV}$ to place bounds on the size of extra dimensions and the fundamental scale. Limits for all $\delta \leq 6$ are given in their Table 6. These limits supersede those in ABREU 00Z.
- ¹⁷ ACHARD 04E search for $e^+e^- \rightarrow \gamma G$ at $\sqrt{s} = 189\text{--}209 \text{ GeV}$ to place bounds on the size of extra dimensions and the fundamental scale. See their Table 8 for limits with $\delta \leq 8$. These limits supersede those in ACCIARRI 99R.
- ¹⁸ ACOSTA 04C search for $pp \rightarrow jG$ at $\sqrt{s} = 1.8 \text{ TeV}$ to place bounds on the size of extra dimensions and the fundamental scale. See their paper for bounds on $\delta = 4, 6$.
- ¹⁹ CASSE 04 obtain a limit on R from the gamma-ray emission of point γ sources that arises from the photon decay of gravitons around newly born neutron stars, applying the technique of HANNESTAD 03 to neutron stars in the galactic bulge. Limits for all $\delta \leq 7$ are given in their Table I.
- ²⁰ ABAZOV 03 search for $pp \rightarrow jG$ at $\sqrt{s} = 1.8 \text{ TeV}$ to place bounds on M_D for 2 to 7 extra dimensions, from which these bounds on R are derived. See their paper for bounds on intermediate values of δ . We quote results without the approximate NLO scaling introduced in the paper.
- ²¹ HANNESTAD 03 obtain a limit on R from graviton cooling of supernova SN1987A. Limits for all $\delta \leq 7$ are given in their Tables V and VI.
- ²² HANNESTAD 03 obtain a limit on R from gravitons emitted in supernovae and which subsequently decay, contaminating the diffuse cosmic γ background. Limits for all $\delta \leq 7$ are given in their Tables V and VI. These limits supersede those in HANNESTAD 02.
- ²³ HANNESTAD 03 obtain a limit on R from gravitons emitted in two recent supernovae and which subsequently decay, creating point γ sources. Limits for all $\delta \leq 7$ are given in their Tables V and VI. These limits are corrected in the published erratum.
- ²⁴ HEISTER 03c use the process $e^+e^- \rightarrow \gamma G$ at $\sqrt{s} = 189\text{--}209 \text{ GeV}$ to place bounds on the size of extra dimensions and the scale of gravity. See their Table 4 for limits with $\delta \leq 6$ for derived limits on M_D .
- ²⁵ FAIRBAIRN 01 obtains bounds on R from over production of KK gravitons in the early universe. Bounds are quoted in paper in terms of fundamental scale of gravity. Bounds depend strongly on temperature of QCD phase transition and range from $R < 0.13 \mu\text{m}$ to $0.001 \mu\text{m}$ for $\delta=2$; bounds for $\delta=3,4$ can be derived from Table 1 in the paper.
- ²⁶ HANHART 01 obtain bounds on R from limits on graviton cooling of supernova SN 1987A using numerical simulations of proto-neutron star neutrino emission.
- ²⁷ CASSISI 00 obtain rough bounds on M_D (and thus R) from red giant cooling for $\delta=2,3$. See their paper for details.
- ²⁸ ACCIARRI 99S search for $e^+e^- \rightarrow ZG$ at $\sqrt{s} = 189 \text{ GeV}$. Limits on the gravity scale are found in their Table 2, for $\delta \leq 4$.

Mass Limits on M_{TT}

This section includes limits on the cut-off mass scale, M_{TT} , of dimension-8 operators from KK graviton exchange in models of large extra dimensions. Ambiguities in the UV-divergent summation are absorbed into the parameter λ , which is taken to be $\lambda = \pm 1$ in the following analyses. Bounds for $\lambda = -1$ are shown in parenthesis after the bound for $\lambda = +1$, if appropriate. Different papers use slightly different definitions of the mass scale. The definition used here is related to another popular convention by $M_{TT}^4 = (2/\pi) \Lambda_4^4$, as discussed in the above Review on "Extra Dimensions."

VALUE (TeV)	CL%	DOCUMENT ID	TECN	COMMENT
> 9.02	95	1 SIRUNYAN	18DD CMS	$pp \rightarrow$ dijet, ang. distrib.
> 20.6	(> 15.7)	2 GIUDICE	03 RVUE	Dim-6 operators
> 6.7	95	3 SIRUNYAN	21N CMS	$pp \rightarrow e^+e^-, \mu^+\mu^-$
> 6.9	95	4 SIRUNYAN	19AC CMS	$pp \rightarrow e^+e^-, \mu^+\mu^-, \gamma\gamma$
> 7.0	(> 5.6)	5 SIRUNYAN	18DU CMS	$pp \rightarrow \gamma\gamma$
> 6.5	95	6 AABOUD	17AP ATLS	$pp \rightarrow \gamma\gamma$
> 3.8	95	7 AAD	14BE ATLS	$pp \rightarrow e^+e^-, \mu^+\mu^-$
> 3.2	95	8 AAD	13E ATLS	$pp \rightarrow e^+e^-, \mu^+\mu^-, \gamma\gamma$
> 0.90	(> 0.92)	9 BAAK	12 RVUE	Electroweak
> 1.48	95	10 AARON	11c H1	$e^\pm p \rightarrow e^\pm X$
> 1.45	95	11 ABAZOV	09AE D0	$p\bar{p} \rightarrow$ dijet, ang. distrib.
> 1.1	(> 1.0)	12 ABAZOV	09D D0	$p\bar{p} \rightarrow e^+e^-, \gamma\gamma$
> 0.898	(> 0.998)	13 SCHAEEL	07A ALEP	$e^+e^- \rightarrow e^+e^-$
> 0.853	(> 0.939)	14 ABDALLAH	06C DLPH	$e^+e^- \rightarrow \ell^+\ell^-$
> 0.96	(> 0.93)	15 GERDES	06	$p\bar{p} \rightarrow e^+e^-, \gamma\gamma$
> 0.78	(> 0.79)	16 ABAZOV	05V D0	$p\bar{p} \rightarrow \mu^+\mu^-$
> 0.805	(> 0.956)	17 CHEKANOV	04B ZEUS	$e^\pm p \rightarrow e^\pm X$
> 0.7	(> 0.7)	18 ABBIENDI	03D OPAL	$e^+e^- \rightarrow \gamma\gamma$
> 0.82	(> 0.78)	19 ACHARD	03D L3	$e^+e^- \rightarrow ZZ$
> 1.28	(> 1.25)	20 ADLOFF	03 H1	$e^\pm p \rightarrow e^\pm X$
> 0.80	(> 0.85)	21 GIUDICE	03 RVUE	
> 0.84	(> 0.99)	22 HEISTER	03C ALEP	$e^+e^- \rightarrow \gamma\gamma$
> 1.2	(> 1.1)	23 ACHARD	02D L3	$e^+e^- \rightarrow \gamma\gamma$
> 0.60	(> 0.63)	24 ABBOTT	01 D0	$p\bar{p} \rightarrow e^+e^-, \gamma\gamma$
> 0.63	(> 0.50)	25 ABBIENDI	00R OPAL	$e^+e^- \rightarrow \mu^+\mu^-$
> 0.68	(> 0.61)	25 ABBIENDI	00R OPAL	$e^+e^- \rightarrow \tau^+\tau^-$
> 0.680	(> 0.542)	26 ABREU	00A DLPH	$e^+e^- \rightarrow \gamma\gamma$
> 15-28	99.7	27 ABREU	00S DLPH	$e^+e^- \rightarrow \mu^+\mu^-, \tau^+\tau^-$
> 0.98	95	28 CHANG	00B RVUE	Electroweak
> 0.29-0.38	95	29 CHEUNG	00 RVUE	$e^+e^- \rightarrow \gamma\gamma$
> 0.50-1.1	95	30 GRAESSER	00 RVUE	$(g-2)_\mu$
> 2.0	(> 2.0)	31 HAN	00 RVUE	Electroweak
> 1.0	(> 1.1)	32 MATHEWS	00 RVUE	$p\bar{p} \rightarrow jj$
		33 MELE	00 RVUE	$e^+e^- \rightarrow VV$
		34 ABBIENDI	99P OPAL	
		35 ACCIARRI	99M L3	
		36 ACCIARRI	99S L3	
		37 BOURILKOV	99	$e^+e^- \rightarrow e^+e^-$

- 1 SIRUNYAN 18DD use dijet angular distributions in 35.9 fb^{-1} of data from pp collisions at $\sqrt{s} = 13 \text{ TeV}$ to place a lower bound on Λ_T , here converted to M_{TT} . This updates the results of SIRUNYAN 17f.
- 2 GIUDICE 03 place bounds on Λ_6 , the coefficient of the gravitationally-induced dimension-6 operator $(2\pi\lambda/\Lambda_6^2)(\sum \bar{F}_i \gamma_\mu^5 F_i)(\sum \bar{F}_j \mu \gamma^5 F_j)$, using data from a variety of experiments. Results are quoted for $\lambda = \pm 1$ and are independent of δ .
- 3 SIRUNYAN 21N use 137 (140) fb^{-1} of data from pp collisions at $\sqrt{s} = 13 \text{ TeV}$ in the dielectron (dimuon) channels to place a lower limit on Λ_T , here converted to M_{TT} . Bounds on individual channels can be found in their Table 7.
- 4 SIRUNYAN 19AC use $35.9 (36.3) \text{ fb}^{-1}$ of data from pp collisions at $\sqrt{s} = 13 \text{ TeV}$ in the dielectron (dimuon) channels to place a lower limit on Λ_T , here converted to M_{TT} . The dielectron and dimuon channels are combined with previous results in the diphoton channel to set the best limit. Bounds on individual channels and different priors can be found in their Table 2. This updates the results in KHACHATRYAN 15AE.
- 5 SIRUNYAN 18DU use 35.9 fb^{-1} of data from pp collisions at $\sqrt{s} = 13 \text{ TeV}$ to place lower limits on M_{TT} (equivalent to their M_S). This updates the results of CHATRCHYAN 12R.
- 6 AABOUD 17AP use 36.7 fb^{-1} of data from pp collisions at $\sqrt{s} = 13 \text{ TeV}$ to place lower limits on M_{TT} (equivalent to their M_S). This updates the results of AAD 13AS.
- 7 AAD 14BE use 20 fb^{-1} of data from pp collisions at $\sqrt{s} = 8 \text{ TeV}$ in the dielectron channel to place lower limits on M_{TT} (equivalent to their M_S).
- 8 AAD 13E use 4.9 and 5.0 fb^{-1} of data from pp collisions at $\sqrt{s} = 7 \text{ TeV}$ in the dielectron and dimuon channels, respectively, to place lower limits on M_{TT} (equivalent to their M_S). The dielectron and dimuon channels are combined with previous results in the diphoton channel to set the best limit. Bounds on individual channels and different priors can be found in their Table VIII.
- 9 BAAK 12 use electroweak precision observables to place bounds on the ratio Λ_T/M_D as a function of M_D . See their Fig. 22 for constraints with a Higgs mass of 120 GeV .
- 10 AARON 11c search for deviations in the differential cross section of $e^\pm p \rightarrow e^\pm X$ in 446 pb^{-1} of data taken at $\sqrt{s} = 301$ and 319 GeV to place a bound on M_{TT} .
- 11 ABAZOV 09AE use dijet angular distributions in 0.7 fb^{-1} of data from $p\bar{p}$ collisions at $\sqrt{s} = 1.96 \text{ TeV}$ to place lower bounds on Λ_T (equivalent to their M_S), here converted to M_{TT} .
- 12 ABAZOV 09D use 1.05 fb^{-1} of data from $p\bar{p}$ collisions at $\sqrt{s} = 1.96 \text{ TeV}$ to place lower bounds on Λ_T (equivalent to their M_S), here converted to M_{TT} .
- 13 SCHAEEL 07A use e^+e^- collisions at $\sqrt{s} = 189-209 \text{ GeV}$ to place lower limits on Λ_T , here converted to limits on M_{TT} .
- 14 ABDALLAH 06c use e^+e^- collisions at $\sqrt{s} \sim 130-207 \text{ GeV}$ to place lower limits on M_{TT} , which is equivalent to their definition of M_S . Bound shown includes all possible

- final state leptons, $\ell = e, \mu, \tau$. Bounds on individual leptonic final states can be found in their Table 31.
- 15 GERDES 06 use 100 to 110 pb^{-1} of data from $p\bar{p}$ collisions at $\sqrt{s} = 1.8 \text{ TeV}$, as recorded by the CDF Collaboration during Run I of the Tevatron. Bound shown includes a K -factor of 1.3 . Bounds on individual e^+e^- and $\gamma\gamma$ final states are found in their Table 1.
- 16 ABAZOV 05V use 246 pb^{-1} of data from $p\bar{p}$ collisions at $\sqrt{s} = 1.96 \text{ TeV}$ to search for deviations in the differential cross section to $\mu^+\mu^-$ from graviton exchange.
- 17 CHEKANOV 04B search for deviations in the differential cross section of $e^\pm p \rightarrow e^\pm X$ with 130 pb^{-1} of combined data and Q^2 values up to $40,000 \text{ GeV}^2$ to place a bound on M_{TT} .
- 18 ABBIENDI 03D use e^+e^- collisions at $\sqrt{s} = 181-209 \text{ GeV}$ to place bounds on the ultraviolet scale M_{TT} , which is equivalent to their definition of M_S .
- 19 ACHARD 03D look for deviations in the cross section for $e^+e^- \rightarrow ZZ$ from $\sqrt{s} = 200-209 \text{ GeV}$ to place a bound on M_{TT} .
- 20 ADLOFF 03 search for deviations in the differential cross section of $e^\pm p \rightarrow e^\pm X$ at $\sqrt{s} = 301$ and 319 GeV to place bounds on M_{TT} .
- 21 GIUDICE 03 review existing experimental bounds on M_{TT} and derive a combined limit.
- 22 HEISTER 03c use e^+e^- collisions at $\sqrt{s} = 189-209 \text{ GeV}$ to place bounds on the scale of dim-8 gravitational interactions. Their M_S^2 is equivalent to our M_{TT} with $\lambda = \pm 1$.
- 23 ACHARD 02 search for s-channel graviton exchange effects in $e^+e^- \rightarrow \gamma\gamma$ at $E_{\text{cm}} = 192-209 \text{ GeV}$.
- 24 ABBOTT 01 search for variations in differential cross sections to e^+e^- and $\gamma\gamma$ final states at the Tevatron.
- 25 ABBIENDI 00R uses e^+e^- collisions at $\sqrt{s} = 189 \text{ GeV}$.
- 26 ABREU 00A search for s-channel graviton exchange effects in $e^+e^- \rightarrow \gamma\gamma$ at $E_{\text{cm}} = 189-202 \text{ GeV}$.
- 27 ABREU 00S uses e^+e^- collisions at $\sqrt{s} = 183$ and 189 GeV . Bounds on μ and τ individual final states given in paper.
- 28 CHANG 00B derive 3σ limit on M_{TT} of $(28, 19, 15) \text{ TeV}$ for $\delta = (2, 4, 6)$ respectively assuming the presence of a torsional coupling in the gravitational action. Highly model dependent.
- 29 CHEUNG 00 obtains limits from anomalous diphoton production at OPAL due to graviton exchange. Original limit for $\delta = 4$. However, unknown UV theory renders δ -dependence unreliable. Original paper works in HLZ convention.
- 30 GRAESSER 00 obtains a bound from graviton contributions to $g-2$ of the muon through loops of 0.29 TeV for $\delta = 2$ and 0.38 TeV for $\delta = 4, 6$. Limits scale as $\lambda^{1/2}$. However calculational scheme not well-defined without specification of high-scale theory. See the "Extra Dimensions Review."
- 31 HAN 00 calculates corrections to gauge boson self-energies from KK graviton loops and constrain them using S and T . Bounds on M_{TT} range from 0.5 TeV ($\delta = 6$) to 1.1 TeV ($\delta = 2$); see text. Limits have strong dependence, $\lambda^{\delta+2}$, on unknown λ coefficient.
- 32 MATHEWS 00 search for evidence of graviton exchange in CDF and DØ dijet production data. See their Table 2 for slightly stronger δ -dependent bounds. Limits expressed in terms of $\bar{M}_S^4 = M_{TT}^4/8$.
- 33 MELE 00 obtains bound from KK graviton contributions to $e^+e^- \rightarrow VV$ ($V = \gamma, W, Z$) at LEP. Authors use Hewett conventions.
- 34 ABBIENDI 99P search for s-channel graviton exchange effects in $e^+e^- \rightarrow \gamma\gamma$ at $E_{\text{cm}} = 189 \text{ GeV}$. The limits $G_\pm > 660 \text{ GeV}$ and $G_\pm > 634 \text{ GeV}$ are obtained from combined $E_{\text{cm}} = 183$ and 189 GeV data, where G_\pm is a scale related to the fundamental gravity scale.
- 35 ACCIARRI 99M search for the reaction $e^+e^- \rightarrow \gamma G$ and s-channel graviton exchange effects in $e^+e^- \rightarrow \gamma\gamma, W^+W^-, ZZ, e^+e^-, \mu^+\mu^-, \tau^+\tau^-, q\bar{q}$ at $E_{\text{cm}} = 183 \text{ GeV}$. Limits on the gravity scale are listed in their Tables 1 and 2.
- 36 ACCIARRI 99S search for the reaction $e^+e^- \rightarrow ZG$ and s-channel graviton exchange effects in $e^+e^- \rightarrow \gamma\gamma, W^+W^-, ZZ, e^+e^-, \mu^+\mu^-, \tau^+\tau^-, q\bar{q}$ at $E_{\text{cm}} = 189 \text{ GeV}$. Limits on the gravity scale are listed in their Tables 1 and 2.
- 37 BOURILKOV 99 performs global analysis of LEP data on e^+e^- collisions at $\sqrt{s} = 183$ and 189 GeV . Bound is on Λ_T .

Limits on $1/R = M_c$

This section includes limits on $1/R = M_c$, the compactification scale in models with one TeV-sized extra dimension, due to exchange of Standard Model KK excitations. Bounds assume fermions are not in the bulk, unless stated otherwise. See the "Extra Dimensions" review for discussion of model dependence.

VALUE (TeV)	CL%	DOCUMENT ID	TECN	COMMENT
> 4.16	95	1 AAD	12CC ATLS	$pp \rightarrow \ell\bar{\ell}$
> 6.1		2 BARBIERI	04 RVUE	Electroweak
> 3.8	95	3 AVNISH	21 RVUE	$pp \rightarrow$ multijet
> 3.40	95	4 AABOUD	18AV ATLS	$pp \rightarrow t\bar{t}t\bar{t}$
		5 AABOUD	18CE ATLS	$pp \rightarrow t\bar{t}t\bar{t}$
		6 ACCOMANDO	15 RVUE	Electroweak
		7 KHACHATRYAN	15T CMS	$pp \rightarrow \ell X$
		8 CHATRCHYAN	13AQ CMS	$pp \rightarrow \ell X$
		9 CHATRCHYAN	13W CMS	$pp \rightarrow \gamma\gamma, \delta = 6, M_D = 5 \text{ TeV}$
		10 EDELHAUSER	13 RVUE	$pp \rightarrow \ell\bar{\ell} + X$
		11 AAD	12CP ATLS	$pp \rightarrow \gamma\gamma, \delta = 6, M_D = 5 \text{ TeV}$
		12 AAD	12X ATLS	$pp \rightarrow \gamma\gamma, \delta = 6, M_D = 5 \text{ TeV}$
		13 ABAZOV	12M D0	$p\bar{p} \rightarrow \mu\mu$
		14 BAAK	12 RVUE	Electroweak
		15 FLACKE	12 RVUE	Electroweak
		16 NISHIWAKI	12 RVUE	$H \rightarrow WW, \gamma\gamma$
		17 AAD	11F ATLS	$pp \rightarrow \gamma\gamma, \delta = 6, M_D = 5 \text{ TeV}$
		18 AAD	11X ATLS	$pp \rightarrow \gamma\gamma, \delta = 6, M_D = 5 \text{ TeV}$
		19 ABAZOV	10P D0	$p\bar{p} \rightarrow \gamma\gamma, \delta = 6, M_D = 5 \text{ TeV}$
		20 ABAZOV	09AE D0	$p\bar{p} \rightarrow$ dijet, angular dist.
		21 HAISCH	07 RVUE	$\bar{B} \rightarrow X_s \gamma$
		22 GOGOLADZE	06 RVUE	Electroweak
		23 CORNET	00 RVUE	Electroweak
		24 RIZZO	00 RVUE	Electroweak

• • • We do not use the following data for averages, fits, limits, etc. • • •

Searches Particle Listings

Extra Dimensions

- 1 AAD 12cc use 4.9 and 5.0 fb⁻¹ of data from pp collisions at $\sqrt{s} = 7$ TeV in the dielectron and dimuon channels, respectively, to place a lower bound on the mass of the lightest KK Z/γ boson (equivalent to $1/R = M_C$). The limit quoted here assumes a flat prior corresponding to when the pure Z/γ KK cross section term dominates. See their Section 15 for more details.
- 2 BARBIERI 04 use electroweak precision observables to place a lower bound on the compactification scale $1/R$. Both the gauge bosons and the Higgs boson are assumed to propagate in the bulk.
- 3 AVNISH 21 perform a study on the ATLAS collaboration search for multiple jets plus missing transverse energy from pp collisions at $\sqrt{s} = 13$ TeV and integrated luminosity of 139 fb⁻¹, to place constraints on the compactification scale and cutoff scale Λ in universal extra dimension models with Standard Model fields propagating in the bulk.
- 4 AABOUD 18av use 36.1 fb⁻¹ of data from pp collisions at $\sqrt{s} = 13$ TeV in final states with multiple b-jets, to place a lower bound on the compactification scale in a model with two universal extra dimensions. Assuming the radii of the two extra dimensions are equal, a lower limit of 1.8 TeV for the Kaluza-Klein mass is obtained.
- 5 AABOUD 18cc use 36.1 fb⁻¹ of data from pp collisions at $\sqrt{s} = 13$ TeV in final states with same-charge leptons and b-jets, to place a lower bound on the compactification scale in a model with two universal extra dimensions. Assuming the radii of the two extra dimensions are equal, a lower limit of 1.45 TeV for the Kaluza-Klein mass is obtained.
- 6 ACCOMANDO 15 use electroweak precision observables to place a lower bound on the compactification scale $1/R$. See their Fig. 2 for the bound as a function of $\sin\beta$, which parametrizes the VEV contribution from brane and bulk Higgs fields. The quoted value is for the minimum bound which occurs at $\sin\beta = 0.45$.
- 7 KHACHATRYAN 15t use 19.7 fb⁻¹ of data from pp collisions at $\sqrt{s} = 8$ TeV to place a lower bound on the compactification scale $1/R$.
- 8 CHATRCHYAN 13aq use 5.0 fb⁻¹ of data from pp collisions at $\sqrt{s} = 7$ TeV and a further 3.7 fb⁻¹ of data at $\sqrt{s} = 8$ TeV to place a lower bound on the compactification scale $1/R$, in models with universal extra dimensions and Standard Model fields propagating in the bulk. See their Fig. 5 for the bound as a function of the universal bulk fermion mass parameter μ .
- 9 CHATRCHYAN 13w use diphoton events with large missing transverse momentum in 4.93 fb⁻¹ of data produced from pp collisions at $\sqrt{s} = 7$ TeV to place a lower bound on the compactification scale in a universal extra dimension model with gravitational decays. The bound assumes that the cutoff scale Λ , for the radiative corrections to the Kaluza-Klein masses, satisfies $\Lambda/M_C = 20$. The model parameters are chosen such that the decay $\gamma^* \rightarrow G\gamma$ occurs with an appreciable branching fraction.
- 10 EDELHAUSER 13 use 19.6 and 20.6 fb⁻¹ of data from pp collisions at $\sqrt{s} = 8$ TeV analyzed by the CMS Collaboration in the dielectron and dimuon channels, respectively, to place a lower bound on the mass of the second lightest Kaluza-Klein Z/γ boson (converted to a limit on $1/R = M_C$). The bound assumes Standard Model fields propagating in the bulk and that the cutoff scale Λ , for the radiative corrections to the Kaluza-Klein masses, satisfies $\Lambda/M_C = 20$.
- 11 AAD 12cp use diphoton events with large missing transverse momentum in 4.8 fb⁻¹ of data produced from pp collisions at $\sqrt{s} = 7$ TeV to place a lower bound on the compactification scale in a universal extra dimension model with gravitational decays. The bound assumes that the cutoff scale Λ , for the radiative corrections to the Kaluza-Klein masses, satisfies $\Lambda/M_C = 20$. The model parameters are chosen such that the decay $\gamma^* \rightarrow G\gamma$ occurs with an appreciable branching fraction.
- 12 AAD 12x use diphoton events with large missing transverse momentum in 1.07 fb⁻¹ of data produced from pp collisions at $\sqrt{s} = 7$ TeV to place a lower bound on the compactification scale in a universal extra dimension model with gravitational decays. The bound assumes that the cutoff scale Λ , for the radiative corrections to the Kaluza-Klein masses, satisfies $\Lambda/M_C = 20$. The model parameters are chosen such that the decay $\gamma^* \rightarrow G\gamma$ occurs with an appreciable branching fraction.
- 13 ABAZOV 12m use same-sign dimuon events in 7.3 fb⁻¹ of data from $p\bar{p}$ collisions at $\sqrt{s} = 1.96$ TeV to place a lower bound on the compactification scale $1/R$, in models with universal extra dimensions where all Standard Model fields propagate in the bulk.
- 14 BAAK 12 use electroweak precision observables to place a lower bound on the compactification scale $1/R$, in models with universal extra dimensions and Standard Model fields propagating in the bulk. Bound assumes a 125 GeV Higgs mass. See their Fig. 25 for the bound as a function of the Higgs mass.
- 15 FLACKE 12 use electroweak precision observables to place a lower bound on the compactification scale $1/R$, in models with universal extra dimensions and Standard Model fields propagating in the bulk. See their Fig. 1 for the bound as a function of the universal bulk fermion mass parameter μ .
- 16 NISHIWAKI 12 use up to 2 fb⁻¹ of data from the ATLAS and CMS experiments that constrains the production cross section of a Higgs-like particle to place a lower bound on the compactification scale $1/R$ in universal extra dimension models. The quoted bound assumes Standard Model fields propagating in the bulk and a 125 GeV Higgs mass. See their Fig. 1 for the bound as a function of the Higgs mass.
- 17 AAD 11f use diphoton events with large missing transverse energy in 3.1 pb⁻¹ of data produced from pp collisions at $\sqrt{s} = 7$ TeV to place a lower bound on the compactification scale in a universal extra dimension model with gravitational decays. The bound assumes that the cutoff scale Λ , for the radiative corrections to the Kaluza-Klein masses, satisfies $\Lambda/M_C = 20$. The model parameters are chosen such that the decay $\gamma^* \rightarrow G\gamma$ occurs with an appreciable branching fraction.
- 18 AAD 11x use diphoton events with large missing transverse energy in 36 pb⁻¹ of data produced from pp collisions at $\sqrt{s} = 7$ TeV to place a lower bound on the compactification scale in a universal extra dimension model with gravitational decays. The bound assumes that the cutoff scale Λ , for the radiative corrections to the Kaluza-Klein masses, satisfies $\Lambda/M_C = 20$. The model parameters are chosen such that the decay $\gamma^* \rightarrow G\gamma$ occurs with an appreciable branching fraction.
- 19 ABAZOV 10p use diphoton events with large missing transverse energy in 6.3 fb⁻¹ of data produced from $p\bar{p}$ collisions at $\sqrt{s} = 1.96$ TeV to place a lower bound on the compactification scale in a universal extra dimension model with gravitational decays. The bound assumes that the cutoff scale Λ , for the radiative corrections to the Kaluza-Klein masses, satisfies $\Lambda/M_C = 20$. The model parameters are chosen such that the decay $\gamma^* \rightarrow G\gamma$ occurs with an appreciable branching fraction.
- 20 ABAZOV 09ae use dijet angular distributions in 0.7 fb⁻¹ of data from $p\bar{p}$ collisions at $\sqrt{s} = 1.96$ TeV to place a lower bound on the compactification scale.
- 21 HAISCH 07 use inclusive B -meson decays to place a Higgs mass independent bound on the compactification scale $1/R$ in the minimal universal extra dimension model.
- 22 GOGOLADZE 06 use electroweak precision observables to place a lower bound on the compactification scale in models with universal extra dimensions. Bound assumes a 115 GeV Higgs mass. See their Fig. 3 for the bound as a function of the Higgs mass.

- 23 CORNET 00 translates a bound on the coefficient of the 4-fermion operator $(\bar{\ell}\gamma_\mu\tau^\alpha\ell)(\bar{\ell}\gamma^\mu\tau^\alpha\ell)$ derived by Hagiwara and Matsumoto into a limit on the mass scale of KK W bosons.
- 24 RIZZO 00 obtains limits from global electroweak fits in models with a Higgs in the bulk (3.8 TeV) or on the standard brane (3.3 TeV).

Limits on Kaluza-Klein Gravitons in Warped Extra Dimensions

This section places limits on the mass of the first Kaluza-Klein (KK) excitation of the graviton in the warped extra dimension model of Randall and Sundrum. Bounds in parenthesis assume Standard Model fields propagate in the bulk. Experimental bounds depend strongly on the warp parameter, k . See the "Extra Dimensions" review for a full discussion.

Here we list limits for the value of the warp parameter $k/\overline{M}_P = 0.1$.

VALUE (TeV)	CL%	DOCUMENT ID	TECN	COMMENT
>4.78	95	1 SIRUNYAN	21N CMS	$pp \rightarrow G \rightarrow e^+e^-, \mu^+\mu^-$
••• We do not use the following data for averages, fits, limits, etc. •••				
>4.5	95	2 AAD	21AF ATLS	$pp \rightarrow G \rightarrow ZZ$
		3 AAD	21AY ATLS	$pp \rightarrow G \rightarrow \gamma\gamma$
		4 AAD	20AT ATLS	$pp \rightarrow G \rightarrow WW, ZZ$
		5 AAD	20C ATLS	$pp \rightarrow G \rightarrow HH$
		6 AAD	20T ATLS	$pp \rightarrow G \rightarrow b\bar{b}$
>2.6	95	7 SIRUNYAN	20A1 CMS	$pp \rightarrow G \rightarrow jj$
		8 SIRUNYAN	20F CMS	$pp \rightarrow G \rightarrow HH$
		9 SIRUNYAN	20Q CMS	$pp \rightarrow G \rightarrow WW, ZZ$
		10 AABOUD	19A ATLS	$pp \rightarrow G \rightarrow HH$
		11 AABOUD	19o ATLS	$pp \rightarrow G \rightarrow HH$
		12 AAD	19d ATLS	$pp \rightarrow G \rightarrow WW, ZZ$
		13 SIRUNYAN	19 CMS	$pp \rightarrow G \rightarrow HH$
		14 SIRUNYAN	19Be CMS	$pp \rightarrow G \rightarrow HH$
		15 SIRUNYAN	19cf CMS	$pp \rightarrow G \rightarrow HH$
		16 AABOUD	18B1 ATLS	$pp \rightarrow G \rightarrow t\bar{t}$
		17 AABOUD	18CJ ATLS	$pp \rightarrow G \rightarrow VV, VH, \ell\bar{\ell}$
		18 AABOUD	18CQ ATLS	$pp \rightarrow G \rightarrow HH$
		19 AABOUD	18CW ATLS	$pp \rightarrow G \rightarrow HH$
		20 SIRUNYAN	18AF CMS	$pp \rightarrow G \rightarrow HH$
		21 SIRUNYAN	18As CMS	$pp \rightarrow G \rightarrow ZZ$
		22 SIRUNYAN	18Ax CMS	$pp \rightarrow G \rightarrow WW$
		23 SIRUNYAN	18Bk CMS	$pp \rightarrow G \rightarrow ZZ$
		24 SIRUNYAN	18CW CMS	$pp \rightarrow G \rightarrow HH$
		25 SIRUNYAN	18DJ CMS	$pp \rightarrow G \rightarrow ZZ$
>4.1	95	26 SIRUNYAN	18DU CMS	$pp \rightarrow G \rightarrow \gamma\gamma$
		27 SIRUNYAN	18F CMS	$pp \rightarrow G \rightarrow HH$
		28 SIRUNYAN	18I CMS	$pp \rightarrow G \rightarrow b\bar{b}$
		29 AAD	16R ATLS	$pp \rightarrow G \rightarrow WW, ZZ$
		30 AAD	15AZ ATLS	$pp \rightarrow G \rightarrow WW$
		31 AAD	15CT ATLS	$pp \rightarrow G \rightarrow WW, ZZ$
>2.68	95	32 AAD	14V ATLS	$pp \rightarrow G \rightarrow e^+e^-, \mu^+\mu^-$
>1.23 (>0.84)	95	33 AAD	13A ATLS	$pp \rightarrow G \rightarrow WW$
>0.94 (>0.71)	95	34 AAD	13Ao ATLS	$pp \rightarrow G \rightarrow WW$
>2.23	95	35 AAD	13AS ATLS	$pp \rightarrow \gamma\gamma, e^+e^-, \mu^+\mu^-$
>0.845	95	36 AAD	12AD ATLS	$pp \rightarrow G \rightarrow ZZ$
		37 AALTONEN	12V CDF	$p\bar{p} \rightarrow G \rightarrow ZZ$
		38 BAAK	12 RVUE	Electroweak
		39 AALTONEN	11G CDF	$p\bar{p} \rightarrow G \rightarrow ZZ$
>1.058	95	40 AALTONEN	11R CDF	$p\bar{p} \rightarrow G \rightarrow e^+e^-, \gamma\gamma$
>0.754	95	41 ABAZOV	11H D0	$p\bar{p} \rightarrow G \rightarrow WW$
>0.607		42 AALTONEN	10N CDF	$p\bar{p} \rightarrow G \rightarrow WW$
>1.05		43 ABAZOV	10F D0	$p\bar{p} \rightarrow G \rightarrow e^+e^-, \gamma\gamma$
		44 AALTONEN	08S CDF	$p\bar{p} \rightarrow G \rightarrow ZZ$
>0.90		45 ABAZOV	08J D0	$p\bar{p} \rightarrow G \rightarrow e^+e^-, \gamma\gamma$
		46 AALTONEN	07G CDF	$p\bar{p} \rightarrow G \rightarrow \gamma\gamma$
>0.889		47 AALTONEN	07H CDF	$p\bar{p} \rightarrow G \rightarrow e\bar{e}$
>0.785		48 ABAZOV	05N D0	$p\bar{p} \rightarrow G \rightarrow \ell\ell, \gamma\gamma$
>0.71		49 ABULENCIA	05A CDF	$p\bar{p} \rightarrow G \rightarrow \ell\bar{\ell}$

- 1 SIRUNYAN 21n use 137 (140) fb⁻¹ of data from pp collisions at $\sqrt{s} = 13$ TeV to search for dilepton resonances in the dielectron (dimuon) channel. See Table 6 for other limits with warp parameter values $k/\overline{M}_P = 0.01$ and 0.05. This updates the results of SIRUNYAN 18bB.
- 2 AAD 21AF use 139 fb⁻¹ of data from pp collisions at $\sqrt{s} = 13$ TeV to search for ZZ resonances in the $\ell\ell\ell\ell$ and $\ell\ell\nu\bar{\nu}$ final states ($\ell = e, \mu$). See their Figure 8 for the limit on the cross section times branching fraction as a function of the KK graviton mass, including theoretical values for $k/\overline{M}_P = 1$. This updates the results of AAD 15AU and AABOUD 18BF.
- 3 AAD 21AY use 139 fb⁻¹ of data from pp collisions at $\sqrt{s} = 13$ TeV in the diphoton channel to place a lower limit on the mass of the lightest KK graviton. This updates the results of AABOUD 17AP.
- 4 AAD 20AT use 139 fb⁻¹ of data from pp collisions at $\sqrt{s} = 13$ TeV to search for diboson resonances in semileptonic final states ($\ell\nu q q, \ell\ell q q, \nu\nu q q$). See their Figure 15 for the limit on the cross section times branching fraction as a function of the KK graviton mass. Lower limits on the graviton mass are also given for $k/\overline{M}_P = 1$. This updates the results of AABOUD 18AK and AABOUD 18AL.
- 5 AAD 20c use 36.1 fb⁻¹ of data from pp collisions at $\sqrt{s} = 13$ TeV to search for Higgs boson pair production in the $b\bar{b}b\bar{b}, b\bar{b}W^+W^-,$ and $b\bar{b}\tau^+\tau^-$ final states. See their Figure 5(b)(c) for limits on the cross section as a function of the KK graviton mass. In the case of $k/\overline{M}_P = 1$ and 2, gravitons are excluded in the mass range 260–3000 GeV and 260–1760 GeV, respectively.

- 6 AAD 20t use 139 fb^{-1} of data from pp collisions at $\sqrt{s} = 13 \text{ TeV}$ to search for narrow resonances decaying to bottom quark pairs. See their Figure 7 for the limit on the product of the cross section, branching fraction, acceptance and b -tagging efficiency as a function of the KK graviton mass. In the case of $k/\overline{M}_P = 0.2$, KK gravitons in the mass range 1.25–2.8 TeV are excluded.
- 7 SIRUNYAN 20Ai use 137 fb^{-1} of data from pp collisions at $\sqrt{s} = 13 \text{ TeV}$ to search for dijet resonances. See their Figure 6 for the limit on the product of the cross section, branching fraction and acceptance as a function of the KK graviton mass. This updates the results of SIRUNYAN 18Bq.
- 8 SIRUNYAN 20F use 35.9 fb^{-1} of data from pp collisions at $\sqrt{s} = 13 \text{ TeV}$ to search for Higgs boson pair production in the $b\bar{b}ZZ$ final state. See their Figure 4 for limits on the cross section times branching fraction as a function of the KK graviton mass, and Figure 5 for limits as a function of k/\overline{M}_P .
- 9 SIRUNYAN 20q use 77.3 fb^{-1} of data from pp collisions at $\sqrt{s} = 13 \text{ TeV}$ to search for diboson resonances with dijet final states. See their Figure 12 for the limit on the cross section times branching fraction as a function of the KK graviton mass, including the theoretical prediction for $k/\overline{M}_P = 0.5$. This updates the results of SIRUNYAN 18P.
- 10 AABOUD 19A use 36.1 fb^{-1} of data from pp collisions at $\sqrt{s} = 13 \text{ TeV}$ to search for Higgs boson pair production in the $b\bar{b}b\bar{b}$ final state. See their Figure 9 for limits on the cross section times branching fraction as a function of the KK graviton mass. Assuming $k/\overline{M}_P = 1$, gravitons in the mass range 313–1362 GeV are excluded. This updates the results of AABOUD 16i.
- 11 AABOUD 19o use 36.1 fb^{-1} of data from pp collisions at $\sqrt{s} = 13 \text{ TeV}$ to search for Higgs boson pair production in the $b\bar{b}WW$ final state. See their Figure 12 for limits on the cross section times branching fraction as a function of the KK graviton mass for $k/\overline{M}_P = 1$ and $k/\overline{M}_P = 2$.
- 12 AAD 19b use 139 fb^{-1} of data from pp collisions at $\sqrt{s} = 13 \text{ TeV}$ to search for diboson resonances in the all-hadronic final state. See their Figure 9(b) for the limit on the cross section times branching fraction as a function of the KK graviton mass, including theoretical values for $k/\overline{M}_P = 1$. This updates the results of AABOUD 18f.
- 13 SIRUNYAN 19 use 35.9 fb^{-1} of data from pp collisions at $\sqrt{s} = 13 \text{ TeV}$ to search for Higgs boson pair production in the $b\bar{b}\tau\tau$ final state. See their Figure 9 for limits on the cross section times branching fraction as a function of the KK graviton mass. Assuming $k/\overline{M}_P = 1$, gravitons in the mass range 290–810 GeV are excluded. This updates the result of KHACHATRYAN 16Bq.
- 14 SIRUNYAN 19BE use 35.9 fb^{-1} of data from pp collisions at $\sqrt{s} = 13 \text{ TeV}$ to search for Higgs boson pair production by combining the results from four final states: $b\bar{b}\gamma\gamma$, $b\bar{b}\tau\tau$, $b\bar{b}b\bar{b}$, and $b\bar{b}VV$. See their Figure 7 for limits on the cross section times branching fraction as a function of the KK graviton mass.
- 15 SIRUNYAN 19CF use 35.9 fb^{-1} of data from pp collisions at $\sqrt{s} = 13 \text{ TeV}$ to search for Higgs boson pair production in the $b\bar{b}q\bar{q}\ell\nu$ final state. See their Figure 7 for limits on the cross section times branching fraction as a function of the KK graviton mass, including theoretical values for $k/\overline{M}_P = 0.1$ and 0.3.
- 16 AABOUD 18BI use 36.1 fb^{-1} of data from pp collisions at $\sqrt{s} = 13 \text{ TeV}$ to search for top-quark pairs decaying into the lepton-plus jets topology. See their Figure 16 for the limit on the KK graviton mass as a function of the cross section times branching fraction, including theoretical values for $k/\overline{M}_P = 1$.
- 17 AABOUD 18CJ combine the searches for heavy resonances decaying into bosonic and leptonic final states from 36.1 fb^{-1} of pp collision data at $\sqrt{s} = 13 \text{ TeV}$. The lower limit on the KK graviton mass, with $k/\overline{M}_P = 1$, is 2.3 TeV.
- 18 AABOUD 18CQ use 36.1 fb^{-1} of data from pp collisions at $\sqrt{s} = 13 \text{ TeV}$ to search for Higgs boson pair production in the $b\bar{b}\tau^+\tau^-$ final state. See their Figure 2 for limits on the cross section times branching fraction as a function of the KK graviton mass. Assuming $k/\overline{M}_P = 1$, gravitons in the mass range 325–885 GeV are excluded.
- 19 AABOUD 18CW use 36.1 fb^{-1} of data from pp collisions at $\sqrt{s} = 13 \text{ TeV}$ to search for Higgs boson pair production in the $\gamma\gamma b\bar{b}$ final state. See their Figure 7 for limits on the cross section times branching fraction as a function of the KK graviton mass.
- 20 SIRUNYAN 18AF use 35.9 fb^{-1} of data from pp collisions at $\sqrt{s} = 13 \text{ TeV}$ to search for Higgs boson pair production in the $b\bar{b}b\bar{b}$ final state. See their Figure 9 for limits on the cross section times branching fraction as a function of the KK graviton mass, including theoretical values for $k/\overline{M}_P = 0.5$. This updates the results of KHACHATRYAN 15r.
- 21 SIRUNYAN 18As use 35.9 fb^{-1} of data from pp collisions at $\sqrt{s} = 13 \text{ TeV}$ to search for ZZ resonances in the $\ell\nu\bar{\nu}$ final state ($\ell = e, \mu$). See their Figure 5 for the limit on the KK graviton mass as a function of the cross section times branching fraction, including theoretical values for $k/\overline{M}_P = 0.1, 0.5, \text{ and } 1.0$.
- 22 SIRUNYAN 18AX use 35.9 fb^{-1} of data from pp collisions at $\sqrt{s} = 13 \text{ TeV}$ to search for WW resonances in $\ell\nu q\bar{q}$ final states ($\ell = e, \mu$). See their Figure 6 for the limit on the KK graviton mass as a function of the cross section times branching fraction, including theoretical values for $k/\overline{M}_P = 0.5$. This updates the results of KHACHATRYAN 14A.
- 23 SIRUNYAN 18BK use 35.9 fb^{-1} of data from pp collisions at $\sqrt{s} = 13 \text{ TeV}$ to search for ZZ resonances in the $\nu\bar{\nu}q\bar{q}$ final state. See their Figure 4 for the limit on the KK graviton mass as a function of the cross section times branching fraction, including theoretical values for $k/\overline{M}_P = 0.5$.
- 24 SIRUNYAN 18CW use 35.9 fb^{-1} of data from pp collisions at $\sqrt{s} = 13 \text{ TeV}$ to search for Higgs boson pair production in the $b\bar{b}b\bar{b}$ final state. See their Figure 8 for limits on the cross section times branching fraction as a function of the KK graviton mass, including theoretical values for $k/\overline{M}_P = 0.5$.
- 25 SIRUNYAN 18DJ use 35.9 fb^{-1} of data from pp collisions at $\sqrt{s} = 13 \text{ TeV}$ to search for ZZ resonances in $2\ell 2q$ final states ($\ell = e, \mu$). See their Figure 6 for the limit on the KK graviton mass as a function of the cross section times branching fraction. Assuming $k/\overline{M}_P = 0.5$, a graviton mass is excluded below 925 GeV.
- 26 SIRUNYAN 18DU use 35.9 fb^{-1} of data from pp collisions at $\sqrt{s} = 13 \text{ TeV}$, in the diphoton channel to place a lower limit on the mass of the lightest KK graviton. See their paper for limits with other warp parameter values $k/\overline{M}_P = 0.01$ and 0.2. This updates the results of KHACHATRYAN 16i.
- 27 SIRUNYAN 18F use 35.9 fb^{-1} of data from pp collisions at $\sqrt{s} = 13 \text{ TeV}$ to search for Higgs boson pair production in the $b\bar{b}\ell\nu\ell\nu$ final state. See their Figure 7 for limits on the cross section times branching fraction as a function of the KK graviton mass, including theoretical values for $k/\overline{M}_P = 0.1$.
- 28 SIRUNYAN 18I use 19.7 fb^{-1} of data from pp collisions at $\sqrt{s} = 8 \text{ TeV}$ to search for narrow resonances decaying to bottom quark pairs. See their Figure 3 for the limit on the KK graviton mass as a function of the cross section times branching fraction in the mass range of 325–1200 GeV.
- 29 AAD 16R use 20.3 fb^{-1} of data from pp collisions at $\sqrt{s} = 8 \text{ TeV}$ to place a lower bound on the mass of the lightest KK graviton. See their Figure 4 for the limit on the KK graviton mass as a function of the cross section times branching fraction.
- 30 AAD 15AZ use 20.3 fb^{-1} of data from pp collisions at $\sqrt{s} = 8 \text{ TeV}$ to place a lower bound on the mass of the lightest KK graviton. See their Figure 2 for limits on the KK graviton mass as a function of the cross section times branching ratio.
- 31 AAD 15CT use 20.3 fb^{-1} of data from pp collisions at $\sqrt{s} = 8 \text{ TeV}$ to place a lower bound on the mass of the lightest KK graviton. See their Figures 6b and 6c for the limit on the KK graviton mass as a function of the cross section times branching fraction.
- 32 AAD 14V use $20.3 (20.5) \text{ fb}^{-1}$ of data from pp collisions at $\sqrt{s} = 8 \text{ TeV}$ in the dilepton (dimuon) channels to place a lower bound on the mass of the lightest KK graviton. This updates the results of AAD 12cc.
- 33 AAD 13A use 4.7 fb^{-1} of data from pp collisions at $\sqrt{s} = 7 \text{ TeV}$ in the $\ell\nu\ell\nu$ channel, to place a lower bound on the mass of the lightest KK graviton.
- 34 AAD 13AO use 4.7 fb^{-1} of data from pp collisions at $\sqrt{s} = 7 \text{ TeV}$ in the $\ell\nu jj$ channel, to place a lower bound on the mass of the lightest KK graviton.
- 35 AAD 13AS use 4.9 fb^{-1} of data from pp collisions at $\sqrt{s} = 7 \text{ TeV}$ in the diphoton channel to place lower limits on the mass of the lightest KK graviton. The diphoton channel is combined with previous results in the dilepton and dimuon channels to set the best limit. See their Table 2 for warp parameter values k/\overline{M}_P between 0.01 and 0.1. This updates the results of AAD 12y.
- 36 AAD 12AD use 1.02 fb^{-1} of data from pp collisions at $\sqrt{s} = 7 \text{ TeV}$ to search for KK gravitons in a warped extra dimension decaying to ZZ dibosons in the $lljj$ and $llll$ channels ($\ell = e, \mu$). The limit is quoted for the combined $lljj + llll$ channels. See their Figure 5 for limits on the cross section $\sigma(G \rightarrow ZZ)$ as a function of the graviton mass.
- 37 AALTONEN 12v use 6 fb^{-1} of data from $p\bar{p}$ collisions at $\sqrt{s} = 1.96 \text{ TeV}$ to search for KK gravitons in a warped extra dimension decaying to ZZ dibosons in the $lljj$ and $llll$ channels ($\ell = e, \mu$). It provides improved limits over the previous analysis in AALTONEN 11G. See their Figure 16 for limits from all channels combined on the cross section times branching ratio $\sigma(p\bar{p} \rightarrow G^* \rightarrow ZZ)$ as a function of the graviton mass.
- 38 BAAK 12 use electroweak precision observables to place a lower bound on the compactification scale $k e^{-\pi k R}$, assuming Standard Model fields propagate in the bulk and the Higgs is confined to the IR brane. See their Fig. 27 for more details.
- 39 AALTONEN 11G use $2.5\text{--}2.9 \text{ fb}^{-1}$ of data from $p\bar{p}$ collisions at $\sqrt{s} = 1.96 \text{ TeV}$ to search for KK gravitons in a warped extra dimension decaying to ZZ dibosons via the $e\bar{e}e, e\bar{e}\mu\mu, \mu\bar{\mu}\mu\mu, e\bar{e}j, \text{ and } \mu\bar{\mu}jj$ channels. See their Fig. 20 for limits on the cross section $\sigma(G \rightarrow ZZ)$ as a function of the graviton mass.
- 40 AALTONEN 11R uses 5.7 fb^{-1} of data from $p\bar{p}$ collisions at $\sqrt{s} = 1.96 \text{ TeV}$ in the dilepton channel to place a lower bound on the mass of the lightest graviton. It provides combined limits with the diphoton channel analysis of AALTONEN 11U. For warp parameter values k/\overline{M}_P between 0.01 to 0.1 the lower limit on the mass of the lightest graviton is between 612 and 1058 GeV. See their Table 1 for more details.
- 41 ABAZOV 11H use 5.4 fb^{-1} of data from $p\bar{p}$ collisions at $\sqrt{s} = 1.96 \text{ TeV}$ to place a lower bound on the mass of the lightest graviton. Their 95% C.L. exclusion limit does not include masses less than 300 GeV.
- 42 AALTONEN 10N use 2.9 fb^{-1} of data from $p\bar{p}$ collisions at $\sqrt{s} = 1.96 \text{ TeV}$ to place a lower bound on the mass of the lightest graviton.
- 43 ABAZOV 10F use 5.4 fb^{-1} of data from $p\bar{p}$ collisions at $\sqrt{s} = 1.96 \text{ TeV}$ to place a lower bound on the mass of the lightest graviton. For warp parameter values of k/\overline{M}_P between 0.01 and 0.1 the lower limit on the mass of the lightest graviton is between 560 and 1050 GeV. See their Fig. 3 for more details.
- 44 AALTONEN 08s use $p\bar{p}$ collisions at $\sqrt{s} = 1.96 \text{ TeV}$ to search for KK gravitons in warped extra dimensions. They search for graviton resonances decaying to four electrons via two Z bosons using 1.1 fb^{-1} of data. See their Fig. 8 for limits on $\sigma_B(G \rightarrow ZZ)$ versus the graviton mass.
- 45 ABAZOV 08I use $p\bar{p}$ collisions at $\sqrt{s} = 1.96 \text{ TeV}$ to search for KK gravitons in warped extra dimensions. They search for graviton resonances decaying to electrons and photons using 1 fb^{-1} of data. For warp parameter values of k/\overline{M}_P between 0.01 and 0.1 the lower limit on the mass of the lightest excitation is between 300 and 900 GeV. See their Fig. 4 for more details.
- 46 AALTONEN 07G use $p\bar{p}$ collisions at $\sqrt{s} = 1.96 \text{ TeV}$ to search for KK gravitons in warped extra dimensions. They search for graviton resonances decaying to photons using 1.2 fb^{-1} of data. For warp parameter values of $k/\overline{M}_P = 0.1, 0.05, \text{ and } 0.01$ the bounds on the graviton mass are 850, 694, and 230 GeV, respectively. See their Fig. 3 for more details. See also AALTONEN 07H.
- 47 AALTONEN 07H use $p\bar{p}$ collisions at $\sqrt{s} = 1.96 \text{ TeV}$ to search for KK gravitons in warped extra dimensions. They search for graviton resonances decaying to electrons using 1.3 fb^{-1} of data. For a warp parameter value of $k/\overline{M}_P = 0.1$ the bound on the graviton mass is 807 GeV. See their Fig. 4 for more details. A combined analysis with the diphoton data of AALTONEN 07G yields for $k/\overline{M}_P = 0.1$ a graviton mass lower bound of 889 GeV.
- 48 ABAZOV 05N use $p\bar{p}$ collisions at $\sqrt{s} = 1.96 \text{ TeV}$ to search for KK gravitons in warped extra dimensions. They search for graviton resonances decaying to muons, electrons or photons, using 260 pb^{-1} of data. For warp parameter values of $k/\overline{M}_P = 0.1, 0.05, \text{ and } 0.01$, the bounds on the graviton mass are 785, 650 and 250 GeV respectively. See their Fig. 3 for more details.
- 49 ABULENCIA 05A use $p\bar{p}$ collisions at $\sqrt{s} = 1.96 \text{ TeV}$ to search for KK gravitons in warped extra dimensions. They search for graviton resonances decaying to muons or electrons, using 200 pb^{-1} of data. For warp parameter values of $k/\overline{M}_P = 0.1, 0.05, \text{ and } 0.01$, the bounds on the graviton mass are 710, 510 and 170 GeV respectively.

Limits on Kaluza-Klein Gluons in Warped Extra Dimensions

This section places limits on the mass of the first Kaluza-Klein (KK) excitation of the gluon in warped extra dimension models with Standard Model fields propagating in the bulk. Bounds are given for a specific benchmark model with $\Gamma/m = 15.3\%$ where Γ is the width and m the mass of the KK gluon. See the "Extra Dimensions" review for more discussion.

VALUE (TeV)	CL%	DOCUMENT ID	TECN	COMMENT
>3.8	95	1 AABOUD 18BI ATLS		$g_{KK} \rightarrow t\bar{t} \rightarrow \ell j$
•••		We do not use the following data for averages, fits, limits, etc. •••		
		2 AABOUD 19AS ATLS		$g_{KK} \rightarrow t\bar{t} \rightarrow jj$
		3 SIRUNYAN 19AL CMS		$g_{KK} \rightarrow t\bar{t}$
>2.5	95	4 CHATRCHYAN13BM CMS		$g_{KK} \rightarrow t\bar{t}$
		5 CHEN 13A		$\bar{B} \rightarrow X_S \gamma$
>1.5	95	6 AAD 12BV ATLS		$g_{KK} \rightarrow t\bar{t} \rightarrow \ell j$

Searches Particle Listings

Extra Dimensions

- AABOUD 18B1 use 36.1 fb^{-1} of data from pp collisions at $\sqrt{s} = 13 \text{ TeV}$. This result updates AAD 13AQ.
- AABOUD 19AS use 36.1 fb^{-1} of data from pp collisions at $\sqrt{s} = 13 \text{ TeV}$. An upper bound of 3.4 TeV is placed on the KK gluon mass for $\Gamma/m = 30\%$.
- SIRUNYAN 19AL use 35.9 fb^{-1} of data from pp collisions at $\sqrt{s} = 13 \text{ TeV}$ to place limits on a KK gluon decaying to a top quark and a heavy vector-like fermion, T. KK gluon masses between 1.5 and 2.3 TeV and between 2.0 and 2.4 TeV are excluded for T masses of 1.2 and 1.5 TeV, respectively.
- CHATRCHYAN 13BM use 19.7 fb^{-1} of data from pp collisions at $\sqrt{s} = 8 \text{ TeV}$. Bound is for a width of approximately 15–20% of the KK gluon mass.
- CHEN 13A place limits on the KK mass scale for a specific warped model with custodial symmetry and bulk fermions. See their Figures 4 and 5.
- AAD 12BV use 2.05 fb^{-1} of data from pp collisions at $\sqrt{s} = 7 \text{ TeV}$.

Black Hole Production Limits

Semiclassical Black Holes

VALUE (GeV)	DOCUMENT ID	TECN	COMMENT
• • • We do not use the following data for averages, fits, limits, etc. • • •			
1	SIRUNYAN 18DA CMS	$pp \rightarrow \text{multijet}$	
2	AAD 16N ATLS	$pp \rightarrow \text{multijet}$	
3	AAD 16O ATLS	$pp \rightarrow \ell + (\ell\ell/\ell j/jj)$	
4	AAD 13AW ATLS	$pp \rightarrow \mu\mu$	
1	SIRUNYAN 18DA use 35.9 fb^{-1} of data from pp collisions at $\sqrt{s} = 13 \text{ TeV}$ to search for semiclassical black holes decaying to multijet final states. No excess of events above the expected level of standard model background was observed. Exclusion limits at 95% C.L. are set on the mass threshold for black hole production as a function of the higher-dimensional Planck scale for rotating and nonrotating black holes under several model assumptions (ADD, 2, 4, 6 extra dimensions model) in the 7.1–10.3 TeV range. These limits supersede those in SIRUNYAN 17CP.		
2	AAD 16N use 3.6 fb^{-1} of data from pp collisions at $\sqrt{s} = 13 \text{ TeV}$ to search for semiclassical black hole decays to multijet final states. No excess of events above the expected level of Standard Model background was observed. Exclusion contours at 95% C.L. are set on the mass threshold for black hole production versus higher-dimensional Planck scale for rotating black holes (ADD, 6 extra dimensions model).		
3	AAD 16O use 3.2 fb^{-1} of data from pp collisions at $\sqrt{s} = 13 \text{ TeV}$ to search for semiclassical black hole decays to high-mass final states with leptons and jets. No excess of events above the expected level of Standard Model background was observed. Exclusion contours at 95% C.L. are set on the mass threshold for black hole production versus higher-dimensional Planck scale for rotating black holes (ADD, 2 to 6 extra dimensions).		
4	AAD 13AW use 20.3 fb^{-1} of data from pp collisions at $\sqrt{s} = 8 \text{ TeV}$ to search for semiclassical black hole decays to like-sign dimuon final states using large track multiplicity. No excess of events above the expected level of Standard Model background was observed. Exclusion contours at 95% C.L. are set on the mass threshold for black hole production versus higher-dimensional Planck scale in various extra dimensions, rotating and non-rotating models.		

Quantum Black Holes

VALUE (GeV)	DOCUMENT ID	TECN	COMMENT
• • • We do not use the following data for averages, fits, limits, etc. • • •			
1	AAD 20T ATLS	$pp \rightarrow jj$	
2	AABOUD 18BA ATLS	$pp \rightarrow \gamma j$	
3	AABOUD 18CM ATLS	$pp \rightarrow e\mu, e\tau, \mu\tau$	
4	SIRUNYAN 18AT CMS	$pp \rightarrow e\mu$	
5	SIRUNYAN 18DD CMS	$pp \rightarrow \text{dijet, ang. distrib.}$	
6	SIRUNYAN 17CP CMS	$pp \rightarrow jj$	
7	KHACHATRYAN...16BE CMS	$pp \rightarrow e\mu$	
8	KHACHATRYAN...15V CMS	$pp \rightarrow jj$	
9	AAD 14AL ATLS	$pp \rightarrow \ell j$	
10	AAD 14V ATLS	$pp \rightarrow ee, \mu\mu$	
11	CHATRCHYAN 13A CMS	$pp \rightarrow jj$	
1	AAD 20T use 139 fb^{-1} of data from pp collisions at $\sqrt{s} = 13 \text{ TeV}$ to search for quantum black hole decays to final states with dijets. No excess of events above the expected level of Standard Model background was observed. Exclusion limits at 95% C.L. are set on mass thresholds for black hole production in an ADD (6 extra dimensions) model. Assuming the black hole mass threshold is equal to the higher-dimensional Planck scale, mass thresholds below 9.4 TeV are excluded. This limit supersedes AABOUD 17AK.		
2	AABOUD 18BA use 36.7 fb^{-1} of data from pp collisions at $\sqrt{s} = 13 \text{ TeV}$ to search for quantum black hole decays to final states with a photon and a jet. No excess of events above the expected level of Standard Model background was observed. Exclusion limits at 95% C.L. are set on mass thresholds for black hole production in ADD (6 extra dimensions) and RS1 models. Assuming the black hole mass threshold is equal to the Planck scale, mass thresholds below 7.1 TeV and 4.4 TeV are excluded for the ADD and RS1 models, respectively. These limits supersede those in AAD 16A1.		
3	AABOUD 18CM use 36.1 fb^{-1} of data from pp collisions at $\sqrt{s} = 13 \text{ TeV}$ to search for quantum black hole decays with different-flavor high-mass dilepton final states. No excess of events above the expected level of Standard Model background was observed. Exclusion limits at 95% C.L. are set on mass thresholds for black hole production in ADD (6 extra dimensions) and RS1 models. Assuming the black hole mass threshold is equal to the Planck scale, mass thresholds below 7.1 TeV and 4.4 TeV are excluded for the ADD and RS1 models, respectively. These limits supersede those in AAD 16A1.		
4	SIRUNYAN 18AT use 35.9 fb^{-1} of data from pp collisions at $\sqrt{s} = 13 \text{ TeV}$ to search for quantum black hole decays to $e\mu$ final states. In Figure 4, lower mass limits of 5.3, 5.5 and 5.6 TeV are placed in a model with 4, 5 and 6 extra dimensions, respectively, and a lower mass limit of 3.6 TeV is found for a single warped dimension.		
5	SIRUNYAN 18DD use 35.9 fb^{-1} of data from pp collisions at $\sqrt{s} = 13 \text{ TeV}$ to search for quantum black hole decays in dijet angular distributions. A lower mass limit of 5.9 (8.2) TeV is placed in the RS (ADD) model with one (six) extra dimension(s).		
6	SIRUNYAN 17CP use 2.3 fb^{-1} of data from pp collisions at $\sqrt{s} = 13 \text{ TeV}$ to search for quantum black holes decaying to dijet final states. No excess of events above the expected level of standard model background was observed. Limits on the quantum black hole mass threshold are set as a function of the higher-dimensional Planck scale, under		

the assumption that the mass threshold must exceed the above Planck scale. Depending on the model, mass thresholds in the range up to 5.1–9.0 TeV are excluded.

- KHACHATRYAN 16BE use 19.7 fb^{-1} of data from pp collisions at $\sqrt{s} = 8 \text{ TeV}$ to search for quantum black holes undergoing lepton flavor violating decay to the $e\mu$ final state. No excess of events above the expected level of standard model background was observed. Exclusion limits at 95% CL are set on mass thresholds for black hole production in the ADD (2–6 flat extra dimensions), RS1 (1 warped extra dimension), and a model with a Planck scale at the TeV scale from a renormalization of the gravitational constant (no extra dimensions). Limits on the black hole mass threshold are set assuming that it is equal to the higher-dimensional Planck scale. Mass thresholds for quantum black holes in the range up to 3.15–3.63 TeV are excluded in the ADD model. In the RS1 model, mass thresholds below 2.81 TeV are excluded in the PDG convention for the Schwarzschild radius. In the model with no extra dimensions, mass thresholds below 1.99 TeV are excluded.
- KHACHATRYAN 15V use 19.7 fb^{-1} of data from pp collisions at $\sqrt{s} = 8 \text{ TeV}$ to search for quantum black holes decaying to dijet final states. No excess of events above the expected level of standard model background was observed. Exclusion limits at 95% CL are set on mass thresholds for black hole production in the ADD (2–6 flat extra dimensions) and RS1 (1 warped extra dimension) model. Limits on the black hole mass threshold are set as a function of the higher-dimensional Planck scale, under the assumption that the mass threshold must exceed the above Planck scale. Depending on the model, mass thresholds in the range up to 5.0–6.3 TeV are excluded. This paper supersedes CHATRCHYAN 13AD.
- AAD 14AL use 20.3 fb^{-1} of data from pp collisions at $\sqrt{s} = 8 \text{ TeV}$ to search for quantum black hole decays to final states with high-invariant-mass lepton + jet. No excess of events above the expected level of Standard Model background was observed. Exclusion limits at 95% C.L. are set on mass thresholds for black hole production in an ADD (6 extra dimensions) model. Assuming the black hole mass threshold is equal to the higher-dimensional Planck scale, mass thresholds below 5.3 TeV are excluded.
- AAD 14V use $20.3 (20.5) \text{ fb}^{-1}$ of data in the dielectron (dimuon) channels from pp collisions at $\sqrt{s} = 8 \text{ TeV}$ to search for quantum black hole decays involving high-mass dilepton resonances. No excess of events above the expected level of Standard Model background was observed. Exclusion limits at 95% C.L. are set on mass thresholds for black hole production in ADD (6 extra dimensions) and RS1 models. Assuming the black hole mass threshold is equal to the higher-dimensional Planck scale, mass thresholds below 3.65 TeV and 2.24 TeV are excluded for the ADD and RS1 models, respectively.
- CHATRCHYAN 13A use 5 fb^{-1} of data from pp collisions at $\sqrt{s} = 7 \text{ TeV}$ to search for quantum black holes decaying to dijet final states. No excess of events above the expected level of standard model background was observed. Exclusion limits at 95% CL are set on mass thresholds for black hole production in the ADD (2–6 flat extra dimensions) and RS (1 warped extra dimension) model. Limits on the black hole mass threshold are set as a function of the higher-dimensional Planck scale, under assumption that the mass threshold must exceed the above Planck scale. Depending on the model, mass thresholds in the range up to 4.0–5.3 TeV are excluded.

REFERENCES FOR Extra Dimensions

AAD	21AF	EPJ C81 332	G. Aad et al.	(ATLAS Collab.)
AAD	21AY	PL B822 136651	G. Aad et al.	(ATLAS Collab.)
AAD	21F	PR D103 112006	G. Aad et al.	(ATLAS Collab.)
AVNISH	21	PR D103 115011	Avnish et al.	
BLAKEMORE	21	PR D104 L061101	C.P. Blakemore et al.	(STAN)
HEACOCK	21	SCI 373 1239	B. Heacock et al.	(MIST, RIKEN, NAGO+)
SIRUNYAN	21A	EPJ C81 13	A.M. Sirunyan et al.	(CMS Collab.)
Also		EPJ C81 333 (errat.)	A.M. Sirunyan et al.	(CMS Collab.)
SIRUNYAN	21N	JHEP 2107 208	A.M. Sirunyan et al.	(CMS Collab.)
TUMASYAN	21D	JHEP 2111 153	A. Tumasyan et al.	(CMS Collab.)
AAD	20AT	EPJ C80 1165	G. Aad et al.	(ATLAS Collab.)
AAD	20C	PL B800 135103	G. Aad et al.	(ATLAS Collab.)
AAD	20T	JHEP 2003 145	G. Aad et al.	(ATLAS Collab.)
LEE	20	PRL 124 101101	J.G. Lee et al.	(WASH)
SIRUNYAN	20AI	JHEP 2005 033	A.M. Sirunyan et al.	(CMS Collab.)
SIRUNYAN	20F	PR D102 032003	A.M. Sirunyan et al.	(CMS Collab.)
SIRUNYAN	20Q	EPJ C80 237	A.M. Sirunyan et al.	(CMS Collab.)
Also		PRL 124 051301	W.-H. Tan et al.	
AABOUD	19A	JHEP 1901 030	M. Aaboud et al.	(ATLAS Collab.)
AABOUD	19AS	PR D99 092004	M. Aaboud et al.	(ATLAS Collab.)
AABOUD	19D	JHEP 1904 092	M. Aaboud et al.	(ATLAS Collab.)
AAD	19D	JHEP 1909 091	G. Aad et al.	(ATLAS Collab.)
Also		JHEP 2006 042 (errat.)	G. Aad et al.	(ATLAS Collab.)
SIRUNYAN	19	PL B788 7	A.M. Sirunyan et al.	(CMS Collab.)
SIRUNYAN	19AC	JHEP 1904 114	A.M. Sirunyan et al.	(CMS Collab.)
SIRUNYAN	19AL	EPJ C79 208	A.M. Sirunyan et al.	(CMS Collab.)
SIRUNYAN	19BE	PRL 122 121803	A.M. Sirunyan et al.	(CMS Collab.)
SIRUNYAN	19CF	JHEP 1910 125	A.M. Sirunyan et al.	(CMS Collab.)
AABOUD	18AK	JHEP 1803 042	M. Aaboud et al.	(ATLAS Collab.)
AABOUD	18AL	JHEP 1803 009	M. Aaboud et al.	(ATLAS Collab.)
AABOUD	18AV	JHEP 1807 089	M. Aaboud et al.	(ATLAS Collab.)
AABOUD	18BA	EPJ C78 102	M. Aaboud et al.	(ATLAS Collab.)
AABOUD	18BF	EPJ C78 293	M. Aaboud et al.	(ATLAS Collab.)
AABOUD	18BI	EPJ C78 565	M. Aaboud et al.	(ATLAS Collab.)
AABOUD	18CE	JHEP 1812 039	M. Aaboud et al.	(ATLAS Collab.)
AABOUD	18CJ	PR D98 052008	M. Aaboud et al.	(ATLAS Collab.)
AABOUD	18CM	PR D98 092008	M. Aaboud et al.	(ATLAS Collab.)
AABOUD	18CQ	PRL 121 191801	M. Aaboud et al.	(ATLAS Collab.)
AABOUD	18CW	JHEP 1811 040	M. Aaboud et al.	(ATLAS Collab.)
AABOUD	18F	PL B777 21	M. Aaboud et al.	(ATLAS Collab.)
AABOUD	18I	JHEP 1801 126	M. Aaboud et al.	(ATLAS Collab.)
BERGE	18	PRL 120 141101	J. Berge et al.	(MICROSCOPE Collab.)
FAYET	18	PR D97 055039	P. Fayet	(EPOL)
FAYET	18A	PR D99 055043	P. Fayet	(ENSP, EPOL)
HADDOCK	18	PR D97 062002	C. Haddock et al.	(NAGO, KEK, OSAK+)
SIRUNYAN	18AF	PL B781 244	A.M. Sirunyan et al.	(CMS Collab.)
SIRUNYAN	18AS	JHEP 1803 003	A.M. Sirunyan et al.	(CMS Collab.)
SIRUNYAN	18AT	JHEP 1804 073	A.M. Sirunyan et al.	(CMS Collab.)
SIRUNYAN	18AX	JHEP 1805 088	A.M. Sirunyan et al.	(CMS Collab.)
SIRUNYAN	18BB	JHEP 1806 120	A.M. Sirunyan et al.	(CMS Collab.)
SIRUNYAN	18BK	JHEP 1807 075	A.M. Sirunyan et al.	(CMS Collab.)
SIRUNYAN	18BO	JHEP 1808 130	A.M. Sirunyan et al.	(CMS Collab.)
SIRUNYAN	18BV	EPJ C78 291	A.M. Sirunyan et al.	(CMS Collab.)
SIRUNYAN	18CW	JHEP 1808 152	A.M. Sirunyan et al.	(CMS Collab.)
SIRUNYAN	18DA	JHEP 1811 042	A.M. Sirunyan et al.	(CMS Collab.)
SIRUNYAN	18DD	EPJ C78 789	A.M. Sirunyan et al.	(CMS Collab.)
SIRUNYAN	18DJ	JHEP 1809 101	A.M. Sirunyan et al.	(CMS Collab.)
SIRUNYAN	18DU	PR D98 092001	A.M. Sirunyan et al.	(CMS Collab.)
SIRUNYAN	18F	JHEP 1801 054	A.M. Sirunyan et al.	(CMS Collab.)
SIRUNYAN	18I	PRL 120 201801	A.M. Sirunyan et al.	(CMS Collab.)
SIRUNYAN	18P	PR D97 072006	A.M. Sirunyan et al.	(CMS Collab.)
SIRUNYAN	18S	PR D97 092005	A.M. Sirunyan et al.	(CMS Collab.)
AABOUD	17AK	PR D96 052004	M. Aaboud et al.	(ATLAS Collab.)
AABOUD	17AP	PL B775 105	M. Aaboud et al.	(ATLAS Collab.)

See key on page 1127

Searches Particle Listings

Extra Dimensions, WIMP and Dark Matter Searches

KLIMCHITSK... 17A	PR D95 123013	G.L. Klimchitskaya, V.M. Mostepanenko	(CMS Collab.)
SIRUNYAN 17AQ	JHEP 1710 073	A.M. Sirunyan et al.	(CMS Collab.)
SIRUNYAN 17CP	PL B774 279	A.M. Sirunyan et al.	(CMS Collab.)
SIRUNYAN 17F	JHEP 1707 013	A.M. Sirunyan et al.	(CMS Collab.)
ABOUD 16F	JHEP 1606 059	M. Aaboud et al.	(ATLAS Collab.)
ABOUD 16I	PR D94 052002	M. Aaboud et al.	(ATLAS Collab.)
ABOUD 16P	EPJ C76 541	M. Aaboud et al.	(ATLAS Collab.)
AAD 16AI	JHEP 1603 041	G. Aad et al.	(ATLAS Collab.)
AAD 16N	JHEP 1603 026	G. Aad et al.	(ATLAS Collab.)
AAD 16O	PL B760 520	G. Aad et al.	(ATLAS Collab.)
AAD 16R	PL B755 285	G. Aad et al.	(ATLAS Collab.)
KHACHATRY... 16BE	EPJ C76 317	V. Khachatryan et al.	(CMS Collab.)
KHACHATRY... 16BQ	PR D94 052012	V. Khachatryan et al.	(CMS Collab.)
KHACHATRY... 16M	PRL 117 051802	V. Khachatryan et al.	(CMS Collab.)
KHACHATRY... 16N	PL B755 102	V. Khachatryan et al.	(CMS Collab.)
AAD 15AU	EPJ C75 69	G. Aad et al.	(ATLAS Collab.)
AAD 15AZ	EPJ C75 209	G. Aad et al.	(ATLAS Collab.)
Also	EPJ C75 370 (errat.)	G. Aad et al.	(ATLAS Collab.)
AAD 15CS	PR D91 032008	G. Aad et al.	(ATLAS Collab.)
Also	PR D92 059903 (errat.)	G. Aad et al.	(ATLAS Collab.)
AAD 15CT	JHEP 1512 055	G. Aad et al.	(ATLAS Collab.)
ACCOMANDO 15	MPL A30 1540010	E. Accomando	(SHMP)
KHACHATRY... 15AE	JHEP 1504 025	V. Khachatryan et al.	(CMS Collab.)
KHACHATRY... 15R	PL B749 560	V. Khachatryan et al.	(CMS Collab.)
KHACHATRY... 15T	PR D91 092005	V. Khachatryan et al.	(CMS Collab.)
KHACHATRY... 15V	PR D91 052009	V. Khachatryan et al.	(CMS Collab.)
AAD 14AL	PRL 112 091804	G. Aad et al.	(ATLAS Collab.)
AAD 14BE	EPJ C74 3134	G. Aad et al.	(ATLAS Collab.)
AAD 14V	PR D90 052005	G. Aad et al.	(ATLAS Collab.)
KHACHATRY... 14A	JHEP 1408 174	V. Khachatryan et al.	(CMS Collab.)
AAD 13A	PL B710 860	G. Aad et al.	(ATLAS Collab.)
AAD 13AQ	PR D87 112006	G. Aad et al.	(ATLAS Collab.)
AAD 13AQ	PR D88 012004	G. Aad et al.	(ATLAS Collab.)
AAD 13AS	NJP 15 043007	G. Aad et al.	(ATLAS Collab.)
AAD 13AW	PR D88 072001	G. Aad et al.	(ATLAS Collab.)
AAD 13C	PRL 110 011802	G. Aad et al.	(ATLAS Collab.)
AAD 13D	JHEP 1301 029	G. Aad et al.	(ATLAS Collab.)
AAD 13E	PR D87 015010	G. Aad et al.	(ATLAS Collab.)
CHATRCHYAN 13A	JHEP 1301 013	S. Chatrchyan et al.	(CMS Collab.)
CHATRCHYAN 13AD	JHEP 1307 178	S. Chatrchyan et al.	(CMS Collab.)
CHATRCHYAN 13AQ	PR D87 072005	S. Chatrchyan et al.	(CMS Collab.)
CHATRCHYAN 13BM	PRL 111 211804	S. Chatrchyan et al.	(CMS Collab.)
Also	PRL 112 119903 (errat.)	S. Chatrchyan et al.	(CMS Collab.)
CHATRCHYAN 13W	JHEP 1303 111	S. Chatrchyan et al.	(CMS Collab.)
CHEN 13A	CP C37 063102	J.-B. Chen et al.	(DALI)
EDELHAUSER 13	JHEP 1308 091	L. Edelhauser, T. Flacke, M. Kramer	(AACH, KAIST)
XU 13	JP G40 035107	J. Xu et al.	
AAD 12AD	PL B712 331	G. Aad et al.	(ATLAS Collab.)
AAD 12BV	JHEP 1209 041	G. Aad et al.	(ATLAS Collab.)
AAD 12CC	JHEP 1211 138	G. Aad et al.	(ATLAS Collab.)
AAD 12CP	PL B718 411	G. Aad et al.	(ATLAS Collab.)
AAD 12X	PL B710 519	G. Aad et al.	(ATLAS Collab.)
AAD 12Y	PL B710 538	G. Aad et al.	(ATLAS Collab.)
AALTONEN 12V	PR D85 012008	T. Aaltonen et al.	(CDF Collab.)
ABAZOV 12M	PRL 108 131802	V.M. Abazov et al.	(DO Collab.)
AJELLO 12	JCAP 1202 012	M. Ajello et al.	(Fermi-LAT Collab.)
BAAK 12	EPJ C72 2003	M. Baak et al.	(Glitter Group)
CHATRCHYAN 12R	PRL 108 111801	S. Chatrchyan et al.	(CMS Collab.)
FLACKE 12	PR D85 126007	T. Flacke, C. Pasold	(WURZ)
NISHIWAKI 12	PL B707 506	K. Nishiwaki et al.	(KOBE, OSAK)
AAD 11F	PRL 106 121803	G. Aad et al.	(ATLAS Collab.)
AAD 11X	EPJ C71 1744	G. Aad et al.	(ATLAS Collab.)
AALTONEN 11G	PR D83 122008	T. Aaltonen et al.	(CDF Collab.)
AALTONEN 11H	PRL 107 051801	T. Aaltonen et al.	(CDF Collab.)
AALTONEN 11I	PR D83 011102	T. Aaltonen et al.	(CDF Collab.)
AARON 11C	PL B705 52	F. D. Aaron et al.	(HI Collab.)
ABAZOV 11H	PRL 107 011801	V.M. Abazov et al.	(DO Collab.)
BEZERRA 11	PR D83 075004	V.B. Bezerra et al.	(DO Collab.)
SUSHKOV 11	PRL 107 171101	A.O. Sushkov et al.	(CDF Collab.)
AALTONEN 10N	PRL 104 241801	T. Aaltonen et al.	(CDF Collab.)
ABAZOV 10F	PRL 104 241802	V.M. Abazov et al.	(DO Collab.)
ABAZOV 10P	PRL 105 221802	V.M. Abazov et al.	(DO Collab.)
BEZERRA 10	PR D81 055003	V.B. Bezerra et al.	(DO Collab.)
ABAZOV 09AE	PRL 103 191803	V.M. Abazov et al.	(DO Collab.)
ABAZOV 09D	PRL 102 051801	V.M. Abazov et al.	(DO Collab.)
MASUDA 09	PRL 102 171101	M. Masuda, M. Sasaki	(ICRR)
AALTONEN 08AC	PRL 101 181602	T. Aaltonen et al.	(CDF Collab.)
AALTONEN 08S	PR D78 012008	T. Aaltonen et al.	(CDF Collab.)
ABAZOV 08J	PRL 100 091802	V.M. Abazov et al.	(DO Collab.)
ABAZOV 08S	PRL 101 011601	V.M. Abazov et al.	(DO Collab.)
DAS 08	PR D78 063011	P.K. Das, V.H.S. Kumar, P.K. Suresh	
GERACI 08	PR D78 022002	A.A. Geraci et al.	(STAN)
TRENKEL 08	PR D77 122001	C. Trenkel	(CDF Collab.)
AALTONEN 07G	PRL 99 171801	T. Aaltonen et al.	(CDF Collab.)
AALTONEN 07H	PR 99 171802	T. Aaltonen et al.	(CDF Collab.)
DECCA 07A	EPJ C51 963	R.S. Decca et al.	
HAISCH 07	PR D76 034014	U. Haisch, A. Weiler	
KAPNER 07	PRL 98 021101	D.J. Kapner et al.	
SCHAEL 07A	EPJ C49 411	S. Schael et al.	(ALEPH Collab.)
TU 07	PRL 98 201101	L.-C. Tu et al.	
ABDALLAH 06C	EPJ C45 589	J. Abdallah et al.	(DELPHI Collab.)
ABULENCIA, A 06	PRL 97 171802	A. Abulencia et al.	(CDF Collab.)
GERDES 06	PR D73 112008	D. Gerdes et al.	
GOGOLADZE 06	PR D74 093012	I. Gogoladze, C. Macesanu	
ABAZOV 05N	PRL 95 091801	V.M. Abazov et al.	(DO Collab.)
ABAZOV 05V	PRL 95 161602	V.M. Abazov et al.	(DO Collab.)
ABDALLAH 05B	EPJ C38 395	J. Abdallah et al.	(DELPHI Collab.)
ABULENCIA, A 05A	PRL 95 252001	A. Abulencia et al.	(CDF Collab.)
SMULLIN 05	PR D72 122001	S.J. Smullin et al.	
ACHARD 04E	PL B587 16	P. Achard et al.	(L3 Collab.)
ACOSTA 04C	PRL 92 121802	D. Acosta et al.	(CDF Collab.)
BARBIERI 04	NP B703 127	R. Barbieri et al.	
CASSE 04	PRL 92 111102	M. Casse et al.	
CHEKANOV 04B	PL B591 23	S. Chekanov et al.	(ZEUS Collab.)
HOYLE 04	PR D70 042004	C.D. Hoyle et al.	(WASH)
ABAZOV 03	PRL 90 251802	V.M. Abazov et al.	(DO Collab.)
ABBIENDI 03D	EPJ C26 331	G. Abbiendi et al.	(OPAL Collab.)
ACHARD 03D	PL B572 133	P. Achard et al.	(L3 Collab.)
ADLOFF 03	PL B568 35	C. Adloff et al.	(HI Collab.)
CHIAVERINI 03	PRL 90 151101	J. Chilverini et al.	
GUIDICE 03	NP B643 377	G.F. Giudice, A. Strumia	
HANNENSTAD 03	PR D67 125008	S. Hannestad, G.G. Raffelt	
Also	PR D69 029901 (errat.)	S. Hannestad, G.G. Raffelt	
HEISTER 03C	EPJ C28 1	A. Heister et al.	(ALEPH Collab.)
LONG 03	NAT 421 922	J.C. Long et al.	
ACHARD 02	PL B524 65	P. Achard et al.	(L3 Collab.)
ACHARD 02D	PL B531 28	P. Achard et al.	(L3 Collab.)
HANNENSTAD 02	PRL 88 071301	S. Hannestad, G. Raffelt	
ABBOTT 01	PRL 86 1156	B. Abbott et al.	(DO Collab.)
FAIRBAIRN 01	PL B508 335	M. Fairbairn	
HANHART 01	PL B509 1	C. Hanhart et al.	
HOYLE 01	PRL 86 1418	C.D. Hoyle et al.	
ABBIENDI 00R	EPJ C13 553	G. Abbiendi et al.	(OPAL Collab.)
ABREU 00A	PL B491 67	P. Abreu et al.	(DELPHI Collab.)
ABREU 00S	PL B485 45	P. Abreu et al.	(DELPHI Collab.)
ABREU 00Z	EPJ C17 53	P. Abreu et al.	(DELPHI Collab.)
CASSISI 00	PL B481 323	S. Cassisi et al.	
CHANG 00B	PRL 85 3765	L.N. Chang et al.	
CHEUNG 00	PR D61 015005	K. Cheung	
CORNET 00	PR D61 037701	F. Cornet, M. Relano, J. Rico	
GRAESSER 00	PR D61 074019	M.L. Graesser	
HAN 00	PR D62 125018	T. Han, D. Marfatia, R.-J. Zhang	
MATHEWS 00	JHEP 0007 008	P. Mathews, S. Raychaudhuri, K. Sridhar	
MELE 00	PR D61 117901	S. Mele, E. Sanchez	
RIZZO 00	PR D61 016007	T.G. Rizzo, J.D. Wells	
ABBIENDI 99P	PL B465 303	G. Abbiendi et al.	(OPAL Collab.)
ACCIARRI 99M	PL B464 135	M. Acciari et al.	(L3 Collab.)
ACCIARRI 99S	PL B470 268	M. Acciari et al.	(L3 Collab.)
ACCIARRI 99S	PL B470 281	M. Acciari et al.	(L3 Collab.)
BOURLIKOV 99	JHEP 9908 006	D. Bourlikov	
HOSKINS 85	PR D32 3084	J.K. Hoskins et al.	

WIMP and Dark Matter Searches

We omit papers on CHAMP's, millicharged particles, and other exotic particles.

GALACTIC WIMP SEARCHES

These limits are for weakly-interacting stable particles that may constitute the invisible mass in the galaxy. Unless otherwise noted, a local mass density of $0.3 \text{ GeV}/\text{cm}^3$ is assumed; see each paper for velocity distribution assumptions. In the papers the limit is given as a function of the χ^0 mass. Here we list limits only for typical mass values of sub-GeV, GeV, 20 GeV, 100 GeV, and 1 TeV. Specific limits on supersymmetric dark matter particles may be found in the Supersymmetry section.

Spin-Independent Cross Section Limits for Dark Matter Particle (χ^0) on Nucleon

For m_{χ^0} in GeV range

We provide here limits for $m_{\chi^0} < 5 \text{ GeV}$

VALUE (pb)	CL%	DOCUMENT ID	TECN	COMMENT
• • • We do not use the following data for averages, fits, limits, etc. • • •				
$< 2 \times 10^{-7}$	95	1 AKERIB 21A	LUX	low mass WIMPs
$< 5 \times 10^6$	90	2 ALKHATIB 21	SCDM	light DM
$< 1 \times 10^8$	95	3 ANDRIAMIR... 21A		sub-GeV DM on nucleon
$< 1 \times 10^{-8}$	90	4 APRILE 21	XE1T	GeV scale DM
$< 8 \times 10^{-4}$	90	5 AGUILAR-AR... 20C	DMIC	WIMP SI scatter on Si
$< 8 \times 10^{-2}$	90	6 AKERIB 20A	LUX	GeV-scale WIMP search
$< 1 \times 10^{-2}$	90	7 ABDELHAME... 19A	CRES	CaWO ₄
$< 5.4 \times 10^{-6}$	90	8 AGNESE 19A	SCDM	GeV-scale WIMPs on Ge
< 1	90	9 AKERIB 19	LUX	light DM on Xe via Migdal/brem effect
$< 1 \times 10^{-6}$	90	10 AMOLE 19	PICO	C ₃ F ₈
$< 1.6 \times 10^{-3}$	90	11 APRILE 19C	XE1T	DM on Xe
$< 1 \times 10^{-7}$	90	12 APRILE 19D	XE1T	DM on Xe
< 0.1	90	13 ARMENGAUD 19	EDEL	GeV-scale WIMPs on Ge
$< 1.6 \times 10^3$	90	14 KOBAYASHI 19	XMAS	annual modulation Xe
$< 7 \times 10^2$	90	15 LIU 19b	CDEX	GeV; sub-GeV DM via Migdal
$< 7 \times 10^{-7}$	90	16 AGNES 18	DS50	GeV-scale WIMPs on Ar
$< 1.5 \times 10^{-5}$	95	17 AGNESE 18	SCDM	GeV-scale WIMPs on Ge
$< 2 \times 10^{-8}$	90	18 APRILE 18	XE1T	Xe, SI
$< 4.5 \times 10^{-3}$	90	19 ANAUD 18	NEWS	low mass WIMP, Ne
$< 8 \times 10^{-6}$	90	20 JIANG 18	CDEX	GeV-scale WIMPs on Ge
$< 3 \times 10^{-5}$	90	21 YANG 18	CDEX	WIMPs on Ge
$< 1 \times 10^{-6}$	90	22 AKERIB 17	LUX	Xe
$< 1 \times 10^2$	90	23 ANGLOHER 17A	CRES	GeV-scale WIMPs
$< 7 \times 10^{-5}$	90	24 ANGLOHER 16	CRES	CaWO ₄
$< 3 \times 10^{-5}$	90	25 APRILE 16	X100	Xe
$< 4.3 \times 10^{-4}$	90	26 ARMENGAUD 16	EDE3	GeV-scale WIMPs on Ge
$< 7 \times 10^{-5}$	90	27 HEHN 16	EDE3	SI WIMP on Ge
$< 6 \times 10^{-5}$	90	28 ZHAO 16	CDEX	GeV-scale WIMPs on Ge
$< 1 \times 10^{-4}$	90	29 AMOLE 15	PICO	C ₃ F ₈
$< 8 \times 10^{-5}$	90	30 XIAO 15	PNDX	WIMPs on Xe
$< 3 \times 10^{-5}$	90	31 AGNESE 14	SCDM	GeV-scale WIMPs
$< 1 \times 10^{-3}$	90	32 AKERIB 14	LUX	WIMP on Xe
$< 9 \times 10^{-4}$	90	33 LI 13b	TEXO	WIMPs on Ge
$< 3 \times 10^{-4}$	90	34 ARCHAMBAU... 12	PICO	C ₄ F ₁₀
$< 2 \times 10^{-4}$	90	35 AALSETH 11	CGNT	GeV WIMPs on Ge
$< 5 \times 10^{-4}$	90	36 AHMED 11B	CDM2	GeV-scale WIMPs on Ge
$< 8 \times 10^{-4}$	90	37 ANGLE 11	XE10	Xe
$< 5 \times 10^{-4}$	90	38 AKERIB 10	CDM2	WIMPs on Ge/Si

1 AKERIB 21A present new technique for low mass WIMP detection. Require $\sigma^{SI}(\rho_\chi) < 2 \times 10^{-7} \text{ pb}$ for $m(\text{WIMP}) 10 \text{ GeV}$.
 2 ALKHATIB 21 search for light DM using SuperCDMS; require $\sigma^{SI}(\rho_\chi) < 5 \times 10^6$ for $m(\text{DM}) = 0.1 \text{ GeV}$.
 3 ANDRIAMIRADO 21A search for upscattered (boosted) sub-GeV DM interacting with proton in PROSPECT detector. No signal observed. Limits placed in $\sigma(\chi N)$ vs. $m(\text{DM})$ plane for $m(\text{DM}) \sim 1 \text{ keV} - 0.5 \text{ GeV}$. The listed limit is for $m(\text{DM}) = 1 \text{ keV}$.

Searches Particle Listings

WIMP and Dark Matter Searches

4 APRILE 21 search for low recoil energy GeV-scale DM in XENON1T with 1.6 keV threshold. No signal in 0.6 t yr exposure. Limits placed in $\sigma^{SI}(\chi N)$ vs. $m(\text{DM})$ plane for $m(\text{DM})$ between 3–12 GeV. The listed limit is for $m(\text{DM}) = 5$ GeV.	$<2.2 \times 10^{-10}$	90	3 WANG	20g	PNDX	Xe TPC
5 AGUILAR-AREVALO 20c search for WIMP SI scatter on Si using DAMIC at SNOLab; some excess; limits placed in σ vs $m(\text{DM})$ for $m(\text{DM})$ in 1.2–10 GeV; quoted limit for $m(\text{WIMP}) = 2$ GeV.	$<7 \times 10^{-5}$	90	4 ANGLÖHER	19	CRES	CaWO ₄
6 AKERIB 20A search for GeV-scale WIMPs via WIMP-nucleon scatter with single photon emission; no signal; limits placed in $m(\text{WIMP})$ vs $\sigma^{SI}(\chi N)$ plane: for example $\sigma^{SI}(\chi N) < 8 \times 10^{-4}$ pb for $m(\text{WIMP}) = 2.5$ GeV.	$<3 \times 10^{-7}$	90	5 KIM	19A	KIMS	Nal
7 ABDELHAMEED 19A search for GeV scale dark matter SI scatter on CaWO ₄ ; no signal, limits placed in σ vs. mass plane for $m(\text{DM}) \sim 0.1$ –10 GeV. The listed limit is for $m(\text{DM}) = 1$ GeV.	$<3.5 \times 10^{-5}$	90	6 KOBAYASHI	19	XMAS	SI WIMP on Xe
8 AGNESE 19A search for 1.5–10 GeV WIMP scatter on Ge in CDMSlite dataset. Limits set in a likelihood analysis. No signal was observed. Limit reported for $m(\chi) = 5$ GeV.	$<2 \times 10^{-7}$	90	7 SEONG	19	BELL	$\tau \rightarrow \gamma A, A \rightarrow \chi \chi$
9 AKERIB 19 search for 0.4–5 GeV DM using bremsstrahlung photons and "Migdal" electrons; 1.4×10^4 kg d exposure of liquid Xe; constraint $\sigma^{SI}(\chi N) < 1$ pb for $m(\chi) = 5$ GeV in light scalar mediator model.	$<2 \times 10^{-7}$	90	8 YANG	19	CDEX	annual modulation Ge
10 AMOLE 19 search for SI WIMP scatter on C ₃ F ₈ in PICO-60 bubble chamber; no signal; set limit for spin independent coupling $\sigma^{SI}(\chi N) < 1 \times 10^{-6}$ pb for $m(\chi) = 5$ GeV.	$<2 \times 10^{-7}$	90	9 ABE	18c	XMAS	X ⁰ -Xe modulation
11 APRILE 19c search for light DM scatter on Xe via atomic excitation, ionization (Migdal effect) or bremsstrahlung; no signal, limits placed in σ vs. $m(\text{DM})$ plane for $m(\text{DM}) \sim 0.085$ –2 GeV. The listed limit is for $m(\text{DM}) = 1$ GeV.	$<1.44 \times 10^{-5}$	90	10 ADHIKARI	18	C100	Nal
12 APRILE 19d search for light DM scatter on Xe via ionization to probe SI, SD, and χ_e cross sections; with 22 t d exposure, limits placed in various σ vs. $m(\text{DM})$ planes. Quoted limit is for $m(\text{DM}) = 5$ GeV.	$<3 \times 10^{-7}$	90	11 AGNES	18	D550	X ⁰ -Ar
13 ARMENGAUD 19search for GeV scale WIMP scatter on Ge; limits placed in $\sigma^{SI}(\chi N)$ vs. $m(\chi)$ plane for $m(\chi) \sim 0.045$ –10 GeV; quoted limit is for $m(\chi) = 5$ GeV.	$<5 \times 10^{-6}$	95	12 AGNESE	18	SCDM	Ge
14 KOBAYASHI 19 search for sub-GeV WIMP annual modulation in Xe via brems; no signal; limits placed in $\sigma^{SI}(\chi N)$ vs. $m(\chi)$ plane for $m \sim 0.3$ –1 GeV; quoted limit is for $m(\chi) = 0.5$ GeV.	$<4 \times 10^{-8}$	90	13 AGNESE	18A	SCDM	Ge
15 LIU 19b search for sub-GeV DM using Migdal effect on Ge at CDEX-IB; no signal, require $\sigma^{SI}(\chi N) < 7 \times 10^2$ pb for $m(\chi) = 0.1$ GeV.	$<6 \times 10^{-11}$	90	14 APRILE	18	XE1T	Xe, SI
16 AGNES 18 search for 1.8–20 GeV WIMP SI scatter on Ar; quoted limit is for $m(\chi) = 5$ GeV.	$<4.5 \times 10^{-3}$	90	15 ARNAUD	18	NEWS	GeV WIMPs on Ne
17 AGNESE 18 search for GeV scale WIMPs using CDMSlite; limits placed in $\sigma^{SI}(\chi N)$ vs. $m(\chi)$ plane for $m \sim 1.5$ –20 GeV; quoted limit is for $m(\chi) = 5$ GeV.	$<2 \times 10^{-6}$	90	16 AARTSEN	17	ICCB	ν , earth
18 APRILE 18 search for WIMP scatter on 1 t yr Xe; no signal, limits set in $\sigma(\chi N)$ vs. $m(\chi)$ plane for $m(\chi) \sim 6$ –1000 GeV; quoted limit is for $m = 6$ GeV.	$<2 \times 10^{-10}$	90	17 AKERIB	17	LUX	Xe
19 ARNAUD 18 search for low mass WIMP scatter on Ne via SPC at NEWS-G; limits set in $\sigma^{SI}(\chi N)$ vs. $m(\chi)$ plane for $m \sim 0.5$ –20 GeV; quoted limit is for $m = 5$ GeV.	$<1 \times 10^{-3}$	90	18 BARBOSA-D...	17	ICCB	Nal
20 JIANG 18 search for GeV scale WIMP scatter on Ge; limits placed in $\sigma^{SI}(\chi N)$ vs. $m(\chi)$ plane for $m(\chi) \sim 3$ –10 GeV; quoted limit is for $m(\chi) = 5$ GeV.	$<1.7 \times 10^{-10}$	90	19 CUI	17A	PNDX	WIMPs on Xe
21 YANG 18 search for WIMP scatter on Ge; limits placed in $\sigma^{SI}(\chi N)$ vs. $m(\chi)$ plane for $m(\chi) \sim 2$ –10 GeV; quoted limit is for $m(\chi) = 5$ GeV.	$<7.3 \times 10^{-7}$	90			AGNES	16 D550 Ar
22 AKERIB 17 search for WIMP scatter on Xe; limits placed in $\sigma^{SI}(\chi N)$ vs. $m(\chi)$ plane for $m(\chi) \sim 5$ –1 $\times 10^3$ GeV; quoted limit is for $m(\chi) = 5$ GeV.	$<1 \times 10^{-5}$	90	20 AGNESE	16	CDMS	Ge
23 ANGLÖHER 17A search for GeV scale WIMP scatter on Al ₂ O ₃ crystal; limits placed in $\sigma^{SI}(\chi N)$ vs. $m(\chi)$ plane for $m(\chi) \sim 0.15$ –10 GeV; quoted limit is for $m(\chi) = 5$ GeV.	$<2 \times 10^{-4}$	90	21 AGUILAR-AR...	16	DMIC	Si CCDs
24 ANGLÖHER 16 search for GeV scale WIMP scatter on CaWO ₄ ; limits placed in $\sigma^{SI}(\chi N)$ vs. $m(\chi)$ plane for $m(\chi) \sim 0.5$ –30 GeV; quoted limit is for $m(\chi) = 5$ GeV.	$<4.5 \times 10^{-5}$	90	22 ANGLÖHER	16	CRES	CaWO ₄
25 ARMENGAUD 16 search for GeV scale WIMP scatter on Ge; limits placed in $\sigma^{SI}(\chi N)$ vs. $m(\chi)$ plane for $m(\chi) \sim 4$ –30 GeV; quoted limit is for $m(\chi) = 5$ GeV.	$<2 \times 10^{-6}$	90	23 APRILE	16	X100	Xe
26 HEHN 16 search for low mass WIMPs via SI scatter on Ge target using profile likelihood analysis; limits placed in $\sigma^{SI}(\chi N)$ vs. $m(\chi)$ plane for $m(\chi) \sim 4$ –30 GeV; quoted limit is for $m(\chi) = 5$ GeV.	$<9.4 \times 10^{-8}$	90	24 ARMENGAUD	16	EDE3	Ge
27 ZHAO 16 search for GeV-scale WIMP scatter on Ge; limits placed in $\sigma^{SI}(\chi N)$ vs. $m(\chi)$ plane for $m(\chi) \sim 4$ –30 GeV; quoted limit is for $m(\chi) = 5$ GeV.	$<1.0 \times 10^{-7}$	90	25 HEHN	16	EDE3	Ge
28 AGNESE 15 search for 1.5–10 GeV WIMP scatter on Ge in CDMS II; limits placed in $\sigma^{SI}(\chi N)$ vs. $m(\chi)$ plane for $m(\chi) \sim 3.5$ –30 GeV; quoted limit is for $m(\chi) = 5$ GeV.	$<5 \times 10^{-6}$	90	26 ZHAO	16	CDEX	Ge
29 AMOLE 15 search for WIMP scatter on C ₃ F ₈ in PICO-2L; limits placed in $\sigma^{SI}(\chi N)$ vs. $m(\chi)$ plane for $m(\chi) \sim 4$ –25 GeV; quoted limit is for $m(\chi) = 5$ GeV.	$<1 \times 10^{-5}$	90			AGNES	15 D550 Ar
30 XIAO 15 search for WIMP scatter on Xe with PandaX-I; limits placed in $\sigma^{SI}(\chi N)$ vs. $m(\chi)$ plane for $m(\chi) \sim 5$ –100 GeV; quoted limit is for $m(\chi) = 5$ GeV.	$<1.5 \times 10^{-6}$	90	27 AGNESE	15A	CDM2	Ge
31 AGNESE 14 search for GeV scale WIMPs SI scatter at SuperCDMS; no signal, limits placed in $\sigma^{SI}(\chi N)$ vs. $m(\chi)$ plane for $m(\chi) \sim 3.5$ –30 GeV; quoted limit is for $m(\chi) = 5$ GeV.	$<1.5 \times 10^{-7}$	90	28 AGNESE	15B	CDM2	Ge
32 AKERIB 14 search for WIMP scatter on Xe; limits placed in $\sigma^{SI}(\chi N)$ vs. $m(\chi)$ plane for $m(\chi) \sim 5$ –5000 GeV. Limit given for $m(\chi) = 5$ GeV.	$<2 \times 10^{-6}$	90	29 AMOLE	15	PICO	C ₃ F ₈
33 LI 13b search for WIMP scatter on Ge; limits placed in $\sigma^{SI}(\chi N)$ vs. $m(\chi)$ plane for $m(\chi) \sim 4$ –100 GeV; quoted limit is for $m(\chi) = 5$ GeV.	$<1.2 \times 10^{-5}$	90			CHOI	15 SKAM H, solar $\nu(b\bar{b})$
34 ARCHAMBAULT 12 search for low mass WIMP scatter on C ₄ F ₁₀ ; limits set in $\sigma^{SI}(\chi N)$ vs. $m(\chi)$ plane for $m \sim 4$ –12 GeV; quoted limit is for $m = 5$ GeV.	$<1.19 \times 10^{-6}$	90	30 XIAO	15	PNDX	Xe
35 AALSETH 11 search for GeV-scale SI WIMP scatter on Ge; limits placed on $\sigma^{SI}(\chi N)$ for $m(\chi) \sim 3.5$ –100 GeV; quoted limit is for $m(\chi) = 5$ GeV.	$<2 \times 10^{-8}$	90	31 AGNESE	14	SCDM	Ge
36 AHMED 11b search for GeV scale WIMP scatter on Ge in CDMS II; limits placed in $\sigma^{SD}(\chi n)$ vs. $m(\chi)$ plane for $m \sim 4$ –12 GeV.	$<3.7 \times 10^{-5}$	90	32 AGNESE	14A	SCDM	Ge
37 ANGLE 11 search for GeV scale WIMPs in Xenon-10; limits placed in $\sigma^{SI}(\chi N)$ vs. $m(\chi)$ plane for $m(\chi) \sim 4$ –20 GeV; quoted limit is for $m(\chi) = 5$ GeV.	$<1 \times 10^{-9}$	90	33 AKERIB	14	LUX	Xe
38 AKERIB 10 search for WIMP scatter on Ge/Si in CDMS II; limits place in $\sigma_{SI}(\chi N)$ vs. $m(\chi)$ plane for $m \sim 3$ –100 GeV. Limit given for $m(\text{DM}) = 5$ GeV.	$<2 \times 10^{-6}$	90	34 ANGLÖHER	14	CRES	CaWO ₄
					FELIZARDO	14 SMPL C ₂ ClF ₅
			35 LEE	14A	KIMS	Csl
			36 LIU	14A	CDEX	Ge
			37 YUE	14	CDEX	Ge
			38 AARTSEN	13	ICCB	H, solar $\nu(\tau^+ \tau^-)$
			39 ABE	13B	XMAS	Xe
			40 AGNESE	13	CDM2	Si
			41 AGNESE	13A	CDM2	Si
			42 AGNESE	13A	CDM2	Si
			43 BERNABEI	13A	DAMA	Nal modulation
			44 LI	13B	TEXO	Ge
			45 ZHAO	13	CDEX	Ge
			46 AKIMOV	12	ZEP3	Xe
			47 ANGLÖHER	12	CRES	CaWO ₄
			48 ANGLÖHER	12	CRES	CaWO ₄
			49 APRILE	12	X100	Xe
			50 ARMENGAUD	12	EDE2	Ge
			51 BARRETO	12	DMIC	CCD
			52 BEHNKE	12	COUP	CF ₃ I
			53 FELIZARDO	12	SMPL	C ₂ ClF ₅
			54 KIM	12	KIMS	Csl
			55 AALSETH	11	CGNT	Ge
			56 AALSETH	11A	CGNT	Ge
			57 AHMED	11	CDM2	Ge, inelastic
			58 AHMED	11A	RVUE	Ge
			59 ANGLE	11	XE10	Xe
			60 APRILE	11	X100	Xe
			61 APRILE	11A	X100	Xe, inelastic
			62 APRILE	11B	X100	Xe
			63 HORN	11	ZEP3	Xe
			64 AHMED	10	CDM2	Ge
			65 AKERIB	10	CDM2	Si, Ge, low threshold
			66 APRILE	10	X100	Xe
			67 ARMENGAUD	10	EDE2	Ge
			68 FELIZARDO	10	SMPL	C ₂ ClF ₃
			69 AHMED	09	CDM2	Ge
			70 LIN	09	TEXO	Ge
			71 AALSETH	08	CGNT	Ge

For $m_{\chi 0} = 20$ GeV

For limits from χ^0 annihilation in the Sun, the assumed annihilation final state is shown in parenthesis in the comment.

VALUE (pb)	CL%	DOCUMENT ID	TECN	COMMENT
$<5 \times 10^{-11}$	90	1 MENG	21b	PNDX Xe WIMP search
$<5 \times 10^{-5}$		2 FELIZARDO	20	SMPL C ₂ ClF ₅

• • • We do not use the following data for averages, fits, limits, etc. • • •

- MENG 21b search for SI WIMP interaction with 3.7 t Xe and 0.63 t yr exposure. No signal observed. Limits placed in $m(\text{DM})$ vs. σ^{SI} plane.
- FELIZARDO 20 presents 2014 SIMPLE bounds on WIMP DM using C₂ClF₅ target.
- WANG 20g search for SI WIMP scatter on Xe with 132 t d exposure of PANDAX-II.
- ANGLÖHER 19 search for low mass WIMP scatter on CaWO₄; no signal; limits placed on Wilson coefficients for $m(\chi) = 0.6$ –60 GeV.
- KIM 19A search for WIMP scatter in Nal KIMS experiment; no signal; require $\sigma^{SI}(\chi N) < 7 \times 10^{-5}$ pb for $m(\chi) = 20$ GeV.
- KOBAYASHI 19 search for WIMP scatter in XMAS single-phase liquid Xe detector; no signal; require $\sigma^{SI}(\chi N) < 3 \times 10^{-7}$ pb for $m(\chi) = 20$ GeV.

See key on page 1127

Searches Particle Listings

WIMP and Dark Matter Searches

- 7 SEONG 19 search for $T \rightarrow \gamma A$, $A \rightarrow \chi\chi$ via CP-odd Higgs; no signal; limits on BF set; model dependent conversion to WIMP-nucleon scattering cross section limits $\sigma^{SI} < 10^{-36} \text{ cm}^2$ for $m(\chi) = 0.01\text{--}1 \text{ GeV}$.
- 8 YANG 19 search for low mass wimps via annual modulation in Ge; no signal; require $\sigma^{SI}(\chi N) < 3.5 \times 10^{-9} \text{ pb}$ for $m(\chi) = 20 \text{ GeV}$.
- 9 ABE 18c search for WIMP annual modulation signal for $m(\text{WIMP})$: 6–20 GeV; limits set on SI WIMP-nucleon cross section: see Fig. 6.
- 10 ADHIKARI 18 search for WIMP scatter on NaI; no signal; require $\sigma^{SI} < 1.44 \times 10^{-5} \text{ pb}$ for $m(\text{WIMP}) = 20 \text{ GeV}$; inconsistent with DAMA/LIBRA result.
- 11 AGNES 18 search low mass $m(\text{WIMP})$: 1.8–20 GeV scatter on Ar; limits on SI WIMP-nucleon cross section set in Fig. 8.
- 12 AGNESE 18 give limits for $\sigma^{SI}(\chi N)$ for $m(\text{WIMP})$ between 1.5 and 20 GeV using CDMSlite mode data.
- 13 AGNESE 18a search for WIMP scatter on Ge at SuperCDMS; 1 event, consistent with expected background; set limit in $\sigma^{SI}(\chi N)$ vs. $m(\chi)$ plane for $m \sim 10\text{--}250 \text{ GeV}$.
- 14 APRILE 18 search for WIMP scatter on 1 t yr Xe; no signal, limits placed in $\sigma^{SI}(\chi N)$ vs. $m(\chi)$ plane for $m(\chi) \sim 6\text{--}1000 \text{ GeV}$.
- 15 ARNAUD 18 search for low mass WIMP scatter on Ne via SPC at NEWS-G; limits set in $\sigma^{SI}(\chi N)$ vs. $m(\chi)$ plane for $m \sim 0.5\text{--}20 \text{ GeV}$.
- 16 AARTSEN 17 obtain $\sigma(\text{SI}) < 6 \times 10^{-6} \text{ pb}$ for $m(\text{wimp}) = 20 \text{ GeV}$ from ν from earth.
- 17 AKERIB 17 search for WIMP scatter on Xe; limits placed in $\sigma^{SI}(\chi N)$ vs. $m(\chi)$ plane for $m(\chi) \sim 5\text{--}1 \times 10^5 \text{ GeV}$.
- 18 BARBOSA-DE-SOUZA 17 search for annual modulation of WIMP scatter on NaI using an exposure of 61 kg yr of DM-Ice17 for recoil energy in the 4–20 keV range (DAMA found modulation for recoil energy $< 5 \text{ keV}$). No modulation seen. Sensitivity insufficient to distinguish DAMA signal from null.
- 19 CUI 17a search for SI WIMP scatter; limits placed in $\sigma^{SI}(\chi N)$ vs. $m(\chi)$ plane for $m \sim 10\text{--}1 \times 10^4 \text{ GeV}$ using 54 ton-day exposure of Xe.
- 20 AGNESE 16 CDMSlite excludes low mass WIMPs 1.6–5.5 GeV and SI scattering cross section depending on $m(\text{WIMP})$; see Fig. 4.
- 21 AGUILAR-AREVALO 16 search low mass 1–10 GeV WIMP scatter on Si CCDs; set limits Fig. 11.
- 22 ANGLÖHER 16 search for GeV scale WIMP scatter on CaWO_4 ; limits placed in $\sigma^{SI}(\chi N)$ vs. $m(\chi)$ plane for $m(\chi) \sim 0.5\text{--}30 \text{ GeV}$.
- 23 APRILE 16 search for low mass WIMPs via ionization at XENON100; limits placed in $\sigma^{SI}(\chi N)$ vs. $m(\chi)$ plane for $m \sim 3.5\text{--}20 \text{ GeV}$.
- 24 ARMENGAUD 16 search for GeV scale WIMP scatter on Ge; limits placed in $\sigma^{SI}(\chi N)$ vs. $m(\chi)$ plane for $m(\chi) \sim 4\text{--}30 \text{ GeV}$.
- 25 HEHN 16 search for low mass WIMPs via SI scatter on Ge target using profile likelihood analysis; limits placed in $\sigma^{SI}(\chi N)$ vs. $m(\chi)$ plane for $m(\chi) \sim 4\text{--}30 \text{ GeV}$.
- 26 ZHAO 16 search for GeV-scale WIMP scatter on Ge; limits placed in $\sigma^{SI}(\chi N)$ vs. $m(\chi)$ plane for $m(\chi) \sim 4\text{--}30 \text{ GeV}$.
- 27 AGNESE 15a reanalyse AHMED 11b low threshold data. See their Fig. 12 (left) for improved limits extending down to 5 GeV.
- 28 AGNESE 15b reanalyse AHMED 10 data.
- 29 See their Fig. 7 for limits extending down to 4 GeV.
- 30 XIAO 15 search for WIMP scatter on Xe with PandaX-I; limits placed in $\sigma^{SI}(\chi N)$ vs. $m(\chi)$ plane for $m(\chi) \sim 5\text{--}100 \text{ GeV}$.
- 31 This limit value is provided by the authors. See their Fig. 4 for limits extending down to $m_{\chi^0} = 3.5 \text{ GeV}$.
- 32 This limit value is provided by the authors. AGNESE 14a result is from CDMSlite mode operation with enhanced sensitivity to low mass m_{χ^0} . See their Fig. 3 for limits extending down to $m_{\chi^0} = 3.5 \text{ GeV}$ (see also Fig. 4 in AGNESE 14).
- 33 See their Fig. 5 for limits extending down to $m_{\chi^0} = 5.5 \text{ GeV}$.
- 34 See their Fig. 5 for limits extending down to $m_{\chi^0} = 1 \text{ GeV}$.
- 35 See their Fig. 5 for limits extending down to $m_{\chi^0} = 5 \text{ GeV}$.
- 36 LIU 14a result is based on prototype CDEX-0 detector. See their Fig. 13 for limits extending down to $m_{\chi^0} = 2 \text{ GeV}$.
- 37 See their Fig. 4 for limits extending down to $m_{\chi^0} = 4.5 \text{ GeV}$.
- 38 AARTSEN 13 search for neutrinos from the Sun arising from the pair annihilation of X^0 trapped by the sun in data taken between June 2010 and May 2011.
- 39 See their Fig. 8 for limits extending down to $m_{\chi^0} = 7 \text{ GeV}$.
- 40 This limit value is provided by the authors. AGNESE 13 use data taken between Oct. 2006 and July 2007. See their Fig. 4 for limits extending down to $m_{\chi^0} = 7 \text{ GeV}$.
- 41 This limit value is provided by the authors. AGNESE 13a use data taken between July 2007 and Sep. 2008. Three candidate events are seen. Assuming these events are real, the best fit parameters are $m_{\chi^0} = 8.6 \text{ GeV}$ and $\sigma = 1.9 \times 10^{-5} \text{ pb}$.
- 42 This limit value is provided by the authors. Limit from combined data of AGNESE 13 and AGNESE 13a. See their Fig. 4 for limits extending down to $m_{\chi^0} = 5.5 \text{ GeV}$.
- 43 BERNABEI 13a search for annual modulation of counting rate in the 2–6 keV recoil energy interval, in a 14 yr live time exposure of 1.33 t yr. Find a modulation of $0.0112 \pm 0.0012 \text{ counts}/(\text{day kg keV})$ with 9.3 sigma C.L. Find period and phase in agreement with expectations from DM particles.
- 44 LI 13b search for WIMP scatter on Ge; limits placed in $\sigma^{SI}(\chi N)$ vs. $m(\chi)$ plane for $m(\chi) \sim 4\text{--}100 \text{ GeV}$.
- 45 See their Fig. 5 for limits for $m_{\chi^0} = 4\text{--}12 \text{ GeV}$.
- 46 ANGLÖHER 12 observe excess events above the expected background which are consistent with X^0 with mass $\sim 25 \text{ GeV}$ (or 12 GeV) and spin-independent X^0 -nucleon cross section of $2 \times 10^{-6} \text{ pb}$ (or $4 \times 10^{-5} \text{ pb}$).
- 47 Reanalysis of ANGLÖHER 09 data with all three nuclides. See also BROWN 12.
- 48 See also APRILE 14a.
- 49 See their Fig. 4 for limits extending down to $m_{\chi^0} = 7 \text{ GeV}$.
- 50 See their Fig. 13 for cross section limits for m_{χ^0} between 1.2 and 10 GeV.
- 51 See also DAHL 12 for a criticism.
- 52 See their Fig. 4 for limits extending to $m_{\chi^0} = 3.5 \text{ GeV}$.
- 53 AALSETH 11a find indications of annual modulation of the data, the energy spectrum being compatible with X^0 mass around 8 GeV. See also AALSETH 13.

- 54 AHMED 11 search for X^0 inelastic scattering. See their Fig. 8–10 for limits. The inelastic cross section reduces to the elastic cross section at the limit of zero mass splitting (Fig. 8, left).
- 55 AHMED 11a combine CDMS II and EDELWEISS data.
- 56 ANGLE 11 show limits down to $m_{\chi^0} = 4 \text{ GeV}$ on Fig. 3.
- 57 APRILE 11 reanalyze APRILE 10 data.
- 58 APRILE 11a search for X^0 inelastic scattering. See their Fig. 2 and 3 for limits. See also APRILE 14a.
- 59 HORN 11 perform detector calibration by neutrons. Earlier results are only marginally affected.
- 60 See their Fig. 10 and 12 for limits extending to X^0 mass of 1 GeV.
- 61 Superseded by AHMED 10.
- 62 See their Fig. 6(a) for cross section limits for m_{χ^0} extending down to 2 GeV.
- 63 See their Fig. 2 for cross section limits for m_{χ^0} between 4 and 10 GeV.

For $m_{\chi^0} = 100 \text{ GeV}$

For limits from X^0 annihilation in the Sun, the assumed annihilation final state is shown in parenthesis in the comment.

VALUE (pb)	CL%	DOCUMENT ID	TECN	COMMENT
$< 6 \times 10^{-11}$	90	1 MENG	21B	PNDX Xe WIMP search
		2 ADHIKARI	20	DEAP Ar
		3 FELIZARDO	20	SMP L W
$< 5 \times 10^{-5}$		4 WANG	20G	PNDX Xe TPC
$< 4.2 \times 10^{-10}$	90	5 ABE	19	XMAS Xe
$< 4 \times 10^{-8}$	90	6 AJAJ	19	DEAP Ar
$< 3.9 \times 10^{-9}$	90	7 ADHIKARI	18	C100 NaI
$< 2.3 \times 10^{-6}$	90	8 AGNES	18A	D550 Ar
$< 1.14 \times 10^{-8}$	90	9 AGNESE	18A	CDMS Ge
$< 2 \times 10^{-8}$	90	10 AMAUDRUZ	18	DEAP Ar
$< 1.2 \times 10^{-8}$	90	11 APRILE	18	XE1T Xe
$< 9.12 \times 10^{-11}$	90	12 REN	18	PNDX SiDM at PDX-II
$< 1.7 \times 10^{-10}$	90	13 AKERIB	17	LUX Xe
$< 1.2 \times 10^{-10}$	90	14 APRILE	17G	XE1T Xe
$< 1.2 \times 10^{-10}$	90	15 CUI	17A	PNDX Xe
$< 2.0 \times 10^{-8}$	90	16 AGNES	16	D550 Ar
$< 1 \times 10^{-9}$	90	17 AKERIB	16	LUX Xe
$< 1 \times 10^{-9}$	90	18 APRILE	16B	X100 Xe
$< 2 \times 10^{-8}$	90	19 TAN	16	PNDX Xe
$< 4 \times 10^{-10}$	90	20 TAN	16B	PNDX Xe
$< 6 \times 10^{-8}$	90	21 AGNES	15	D550 Ar
$< 4 \times 10^{-8}$	90	22 AGNESE	15B	CDM2 Ge
$< 7.13 \times 10^{-6}$	90	23 CHOI	15	SKAM H, solar ν ($b\bar{b}$)
$< 6.26 \times 10^{-7}$	90	24 CHOI	15	SKAM H, solar ν ($W^+ W^-$)
$< 2.76 \times 10^{-7}$	90	25 CHOI	15	SKAM H, solar ν ($\tau^+ \tau^-$)
$< 1.5 \times 10^{-8}$	90	26 XIAO	15	PNDX Xe
$< 1 \times 10^{-9}$	90	27 AKERIB	14	LUX Xe
$< 4.0 \times 10^{-6}$	90	28 AVRORIN	14	BAIK H, solar ν ($W^+ W^-$)
$< 1.0 \times 10^{-4}$	90	29 AVRORIN	14	BAIK H, solar ν ($b\bar{b}$)
$< 1.6 \times 10^{-6}$	90	30 AVRORIN	14	BAIK H, solar ν ($\tau^+ \tau^-$)
$< 5 \times 10^{-6}$	90	31 FELIZARDO	14	SMP L C ₂ ClF ₅
$< 6.01 \times 10^{-7}$	90	32 AARTSEN	13	ICCB H, solar ν ($W^+ W^-$)
$< 3.30 \times 10^{-5}$	90	33 AARTSEN	13	ICCB H, solar ν ($b\bar{b}$)
$< 1.9 \times 10^{-6}$	90	34 ADRIAN-MAR.13	13	ANTR H, solar ν ($W^+ W^-$)
$< 1.2 \times 10^{-4}$	90	35 ADRIAN-MAR.13	13	ANTR H, solar ν ($b\bar{b}$)
$< 7.6 \times 10^{-7}$	90	36 ADRIAN-MAR.13	13	ANTR H, solar ν ($\tau^+ \tau^-$)
$< 2 \times 10^{-6}$	90	37 AGNESE	13	CDM2 Si
$< 1.6 \times 10^{-6}$	90	38 BOLIEV	13	BAKS H, solar ν ($W^+ W^-$)
$< 1.9 \times 10^{-5}$	90	39 BOLIEV	13	BAKS H, solar ν ($b\bar{b}$)
$< 7.1 \times 10^{-7}$	90	40 BOLIEV	13	BAKS H, solar ν ($\tau^+ \tau^-$)
$< 3.2 \times 10^{-4}$	90	41 LI	13B	TEXO WIMPs on Ge
$< 1.67 \times 10^{-6}$	90	42 ABBASI	12	ICCB H, solar ν ($W^+ W^-$)
$< 1.07 \times 10^{-4}$	90	43 ABBASI	12	ICCB H, solar ν ($b\bar{b}$)
$< 4 \times 10^{-8}$	90	44 AKIMOV	12	ZEP3 Xe
$< 1.4 \times 10^{-6}$	90	45 ANGLÖHER	12	CRES CaWO_4
$< 3 \times 10^{-9}$	90	46 APRILE	12	X100 Xe
$< 3 \times 10^{-7}$	90	47 BEHNKE	12	COUP CF ₃ I
$< 7 \times 10^{-6}$	90	48 FELIZARDO	12	SMP L C ₂ ClF ₅
$< 2.5 \times 10^{-7}$	90	49 KIM	12	KIMS Csl
$< 2 \times 10^{-4}$	90	50 AALSETH	11	CGNT Ge
		51 AHMED	11	CDM2 Ge, inelastic
		52 AHMED	11A	RVUE Ge
		53 AJELLO	11	FLAT
$< 3 \times 10^{-8}$	90	54 APRILE	11	X100 Xe
		55 APRILE	11A	X100 Xe, inelastic
		56 APRILE	11B	X100 Xe
$< 1 \times 10^{-8}$	90	57 ARMENGAUD	11	EDE2 Ge
$< 5 \times 10^{-8}$	90	58 HORN	11	ZEP3 Xe
		59 AHMED	10	CDM2 Ge
		60 AKERIB	10	CDM2 Si, Ge, low threshold
		61 AKIMOV	10	ZEP3 Xe, inelastic
$< 5 \times 10^{-8}$	90	62 APRILE	10	X100 Xe
$< 1 \times 10^{-7}$	90	63 ARMENGAUD	10	EDE2 Ge
$< 3 \times 10^{-5}$	90	64 FELIZARDO	10	SMP L C ₂ ClF ₃
$< 5 \times 10^{-8}$	90	65 AHMED	09	CDM2 Ge
		66 ANGLE	09	XE10 Xe, inelastic
		67 LIN	09	TEXO Ge
$< 3 \times 10^{-4}$	90	68 GIULIANI	05	RVUE

Searches Particle Listings

WIMP and Dark Matter Searches

- 1 MENG 21b search for SI WIMP interaction with 3.7 t Xe and 0.63 t yr exposure. No signal observed. Limits placed in m(DM) vs. σ^{SI} plane.
- 2 ADHIKARI 20 search for SI WIMP scatter from Ar in AJAJ 19 data. No signal observed. Limits placed on σ^P vs. m(WIMP) for various assumed operators and models.
- 3 FELIZARDO 20 presents 2014 SIMPLE bounds on WIMP DM using C₂ClF₅ target .
- 4 WANG 20g search for SI WIMP scatter on Xe with 132 t d exposure of PANDAX-II .
- 5 ABE 19 search for SI DD in single phase Xe; no signal; require $\sigma^{SI}(\chi p) < 4 \times 10^{-8}$ pb for $m(\chi) \sim 100$ GeV.
- 6 AJAJ 19 search for SI WIMP-nucleon scatter with 758 tonne day exposure of single phase liquid Ar; no signal; require $\sigma^{SI}(\chi N) < 3.9 \times 10^{-9}$ pb for $m(\chi) = 100$ GeV.
- 7 ADHIKARI 18 search for WIMP scatter on Na; limit set $\sigma^{SI}(\chi p) < 2.3 \times 10^{-6}$ pb for $m(\chi) = 100$ GeV.
- 8 AGNES 18a search for WIMP scatter on 46.4 kg Ar; no signal; require $\sigma^{SI}(\chi N) < 1.14 \times 10^{-8}$ pb for $m(\chi) = 100$ GeV.
- 9 AGNESE 18a set limit $\sigma^{SI}(\chi N) < 2 \times 10^{-8}$ pb for m(WIMP) = 100 GeV.
- 10 AMAUDRUZ 18 search for WIMP scatter on Ar with DEAP-3600; limits set: $\sigma^{SI}(\chi p) < 1.2 \times 10^{-8}$ pb for m(WIMP) = 100 GeV.
- 11 APRILE 18 search for WIMP scatter on 1.3 t liquid Xe; no signal; require $\sigma^{SI}(\chi p) < 9.12 \times 10^{-11}$ pb for $m(\chi) = 100$ GeV.
- 12 REN 18 search for self-interacting DM at Panda-X-II with a total exposure of 54 ton day; limits set in m(DM) vs. m(mediator) plane.
- 13 AKERIB 17 exclude SI cross section $> 1.7 \times 10^{-10}$ pb for m(WIMP) = 100 GeV. Uses complete LUX data set.
- 14 APRILE 17g set limit $\sigma^{SI}(\chi p) < 1.2 \times 10^{-10}$ pb for m(WIMP) = 100 GeV using 1 ton fiducial mass Xe TPC. Exposure is 34.2 live days.
- 15 CUI 17a search for SI WIMP scatter; limits placed in $\sigma^{SI}(\chi N)$ vs. $m(\chi)$ plane for $m \sim 10^{-1} \times 10^4$ GeV using 54 ton-day exposure of Xe.
- 16 AKERIB 16 re-analysis of 2013 data exclude SI cross section $> 1 \times 10^{-9}$ pb for m(WIMP) = 100 GeV on Xe target.
- 17 APRILE 16b combined 447 live days using Xe target exclude $\sigma(SI) > 1.1 \times 10^{-9}$ pb for m(WIMP) = 50 GeV.
- 18 TAN 16 search for WIMP scatter off Xe target; see SI exclusion plot Fig. 6.
- 19 TAN 16b search for WIMP-p scatter off Xe target; see Fig. 5 for SI exclusion.
- 20 AGNESE 15b reanalyse AHMED 10 data.
- 21 XIAO 15 search for WIMP scatter on Xe with PandaX-I; limits placed in $\sigma^{SI}(\chi N)$ vs. $m(\chi)$ plane for $m(\chi) \sim 5-100$ GeV.
- 22 AVRORIN 14 search for neutrinos from the Sun arising from the pair annihilation of X^0 trapped by the Sun in data taken between 1998 and 2003. See their Table 1 for limits assuming annihilation into neutrino pairs.
- 23 AARTSEN 13 search for neutrinos from the Sun arising from the pair annihilation of X^0 trapped by the sun in data taken between June 2010 and May 2011.
- 24 ADRIAN-MARTINEZ 13 search for neutrinos from the Sun arising from the pair annihilation of X^0 trapped by the sun in data taken between Jan. 2007 and Dec. 2008.
- 25 AGNESE 13 use data taken between Oct. 2006 and July 2007.
- 26 BOLIEV 13 search for neutrinos from the Sun arising from the pair annihilation of X^0 trapped by the sun in data taken from 1978 to 2009. See also SUVOROVA 13 for an older analysis of the same data.
- 27 LI 13b search for WIMP scatter on Ge; limits placed in $\sigma^{SI}(\chi N)$ vs. $m(\chi)$ plane for $m(\chi) \sim 4-100$ GeV.
- 28 ABBASI 12 search for neutrinos from the Sun arising from the pair annihilation of X^0 trapped by the Sun. The amount of X^0 depends on the X^0 -proton cross section.
- 29 Reanalysis of ANGLOHER 09 data with all three nuclides. See also BROWN 12.
- 30 See also APRILE 14a.
- 31 See their Fig. 6 for a limit on inelastically scattering X^0 for $m_{X^0} = 70$ GeV.
- 32 AHMED 11 search for X^0 inelastic scattering. See their Fig. 8-10 for limits.
- 33 AHMED 11a combine CDMS and EDELWEISS data.
- 34 AJELLO 11 search for e^\pm flux from X^0 annihilations in the Sun. Models in which X^0 annihilates into an intermediate long-lived weakly interacting particles or X^0 scatters inelastically are constrained. See their Fig. 6-8 for limits.
- 35 APRILE 11 reanalyse APRILE 10 data.
- 36 APRILE 11a search for X^0 inelastic scattering. See their Fig. 2 and 3 for limits. See also APRILE 14a.
- 37 Supersedes ARMENGAUD 10. A limit on inelastic cross section is also given.
- 38 HORN 11 perform detector calibration by neutrons. Earlier results are only marginally affected.
- 39 AKIMOV 10 give cross section limits for inelastically scattering dark matter. See their Fig. 4.
- 40 Superseded by AHMED 10.
- 41 ANGLE 09 search for X^0 inelastic scattering. See their Fig. 4 for limits.
- 42 GIULIANI 05 analyzes the spin-independent X^0 -nucleon cross section limits with both isoscalar and isovector couplings. See their Fig. 3 and 4 for limits on the couplings.

For $m_{X^0} = 1$ TeV

For limits from X^0 annihilation in the Sun, the assumed annihilation final state is shown in parenthesis in the comment.

VALUE (pb)	CL%	DOCUMENT ID	TECN	COMMENT
$< 5 \times 10^{-10}$	90	1 MENG 21b	PNDX	Xe WIMP search
$< 4 \times 10^{-9}$	90	2 ADHIKARI 20	DEAP	Ar
$< 3 \times 10^{-6}$	90	3 WANG 20g	PNDX	Xe TPC
$< 3.8 \times 10^{-8}$	90	4 YAGUNA 19	Ar;	l-spin viol DM
$< 8.24 \times 10^{-10}$	90	5 AGNES 18a	DS50	Ar
$< 2 \times 10^{-9}$	90	6 APRILE 18	XE1T	Xe
< 0.3	90	7 AKERIB 17	LUX	Xe
$< 1.2 \times 10^{-9}$	90	8 CHEN 17E	PNDX	$\chi N \rightarrow \chi^* \rightarrow \chi \gamma$
$< 8.6 \times 10^{-8}$	90	9 CUI 17a	PNDX	SI WIMPs on Xe
$< 2 \times 10^{-7}$	90	AGNES 16	DS50	Ar
$< 2 \times 10^{-7}$	90	AGNES 15	DS50	Ar
$< 1 \times 10^{-8}$	90	10 AGNESE 15b	CDM2	Ge
$< 1 \times 10^{-8}$	90	AKERIB 14	LUX	Xe

$< 2.2 \times 10^{-6}$	90	11 AVRORIN 14	BAIK	H, solar ν ($W^+ W^-$)
$< 5.5 \times 10^{-5}$	90	11 AVRORIN 14	BAIK	H, solar ν ($b \bar{b}$)
$< 6.8 \times 10^{-7}$	90	11 AVRORIN 14	BAIK	H, solar ν ($\tau^+ \tau^-$)
$< 3.46 \times 10^{-7}$	90	12 AARTSEN 13	ICCB	H, solar ν ($W^+ W^-$)
$< 7.75 \times 10^{-6}$	90	12 AARTSEN 13	ICCB	H, solar ν ($b \bar{b}$)
$< 6.9 \times 10^{-7}$	90	13 ADRIAN-MAR.13	ANTR	H, solar ν ($W^+ W^-$)
$< 1.5 \times 10^{-5}$	90	13 ADRIAN-MAR.13	ANTR	H, solar ν ($b \bar{b}$)
$< 1.8 \times 10^{-7}$	90	13 ADRIAN-MAR.13	ANTR	H, solar ν ($\tau^+ \tau^-$)
$< 4.3 \times 10^{-6}$	90	14 BOLIEV 13	BAKS	H, solar ν ($W^+ W^-$)
$< 3.4 \times 10^{-5}$	90	14 BOLIEV 13	BAKS	H, solar ν ($b \bar{b}$)
$< 1.2 \times 10^{-6}$	90	14 BOLIEV 13	BAKS	H, solar ν ($\tau^+ \tau^-$)
$< 2.12 \times 10^{-7}$	90	15 ABBASI 12	ICCB	H, solar ν ($W^+ W^-$)
$< 6.56 \times 10^{-6}$	90	15 ABBASI 12	ICCB	H, solar ν ($b \bar{b}$)
$< 4 \times 10^{-7}$	90	AKIMOV 12	ZEP3	Xe
$< 1.1 \times 10^{-5}$	90	16 ANGLOHER 12	CRES	CaWO ₄
$< 2 \times 10^{-8}$	90	17 APRILE 12	X100	Xe
$< 2 \times 10^{-6}$	90	BEHNKE 12	COUP	CF ₃ I
$< 4 \times 10^{-6}$	90	FELIZARDO 12	SMPL	C ₂ ClF ₅
$< 1.5 \times 10^{-6}$	90	KIM 12	KIMS	Csl
$< 1.5 \times 10^{-7}$	90	18 AHMED 11A	RVUE	Ge, inelastic
$< 2 \times 10^{-7}$	90	20 APRILE 11	X100	Xe
$< 8 \times 10^{-8}$	90	17 APRILE 11b	X100	Xe
$< 2 \times 10^{-7}$	90	21 ARMENGAUD 11	EDE2	Ge
$< 2 \times 10^{-7}$	90	22 HORN 11	ZEP3	Xe
$< 2 \times 10^{-7}$	90	AHMED 10	CDM2	Ge
$< 4 \times 10^{-7}$	90	APRILE 10	X100	Xe
$< 6 \times 10^{-7}$	90	ARMENGAUD 10	EDE2	Ge
$< 3.5 \times 10^{-7}$	90	23 AHMED 09	CDM2	Ge

- 1 MENG 21b search for SI WIMP interaction with 3.7 t Xe and 0.63 t yr exposure. No signal observed. Limits placed in m(DM) vs. σ^{SI} plane.
- 2 ADHIKARI 20 search for SI WIMP scatter from Ar in AJAJ 19 data. No signal observed. Limits placed on σ^P vs. m(WIMP) for various assumed operators and models.
- 3 WANG 20g search for SI WIMP scatter on Xe with 132 t d exposure of PANDAX-II .
- 4 YAGUNA 19 recasts DEAP-3600 single-phase liquid argon results in limit for isospin violating DM; for $f_n/f_p = -0.69$, requires $\sigma^{SI}(\chi p) < 3 \times 10^{-6}$ pb for $m(\chi) = 1$ TeV.
- 5 AGNES 18a search for WIMP scatter on 46.4 kg Ar; no signal; require $\sigma^{SI}(\chi N) < 3.8 \times 10^{-8}$ pb for $m(\chi) = 1$ TeV.
- 6 APRILE 18 search for WIMP scatter on 1.3 t Xe; no signal seen; require $\sigma^{SI}(\chi p) < 8.24 \times 10^{-10}$ pb for $m(\chi) = 1$ TeV.
- 7 AKERIB 17 search for WIMP scatter on Xe using complete LUX data set; limits placed in $\sigma^{SI}(\chi N)$ vs. $m(\chi)$ plane for $m(\chi) \sim 5-1 \times 10^5$ GeV.
- 8 CHEN 17E search for inelastic WIMP scatter on Xe; require $\sigma^{SI}(\chi N) < 0.3$ pb for $m(\chi) = 1$ TeV and (mass difference) = 300 keV.
- 9 CUI 17a search for WIMP scatter using 54 ton-day exposure of Xe; limits placed in $\sigma^{SI}(\chi N)$ vs. $m(\chi)$ plane for $m \sim 10^{-1} \times 10^4$ GeV.
- 10 AGNESE 15b reanalyse AHMED 10 data.
- 11 AVRORIN 14 search for neutrinos from the Sun arising from the pair annihilation of X^0 trapped by the Sun in data taken between 1998 and 2003. See their Table 1 for limits assuming annihilation into neutrino pairs.
- 12 AARTSEN 13 search for neutrinos from the Sun arising from the pair annihilation of X^0 trapped by the sun in data taken between June 2010 and May 2011.
- 13 ADRIAN-MARTINEZ 13 search for neutrinos from the Sun arising from the pair annihilation of X^0 trapped by the sun in data taken between Jan. 2007 and Dec. 2008.
- 14 BOLIEV 13 search for neutrinos from the Sun arising from the pair annihilation of X^0 trapped by the sun in data taken from 1978 to 2009. See also SUVOROVA 13 for an older analysis of the same data.
- 15 ABBASI 12 search for neutrinos from the Sun arising from the pair annihilation of X^0 trapped by the Sun. The amount of X^0 depends on the X^0 -proton cross section.
- 16 Reanalysis of ANGLOHER 09 data with all three nuclides. See also BROWN 12.
- 17 See also APRILE 14a.
- 18 AHMED 11 search for X^0 inelastic scattering. See their Fig. 8-10 for limits.
- 19 AHMED 11a combine CDMS and EDELWEISS data.
- 20 APRILE 11 reanalyse APRILE 10 data.
- 21 Supersedes ARMENGAUD 10. A limit on inelastic cross section is also given.
- 22 HORN 11 perform detector calibration by neutrons. Earlier results are only marginally affected.
- 23 Superseded by AHMED 10.

Spin-Dependent Cross Section Limits for Dark Matter Particle (X^0) on Proton

For m_{X^0} in GeV range

We provide here limits for $m_{X^0} < 5$ GeV

VALUE (pb)	CL%	DOCUMENT ID	TECN	COMMENT
$< 8 \times 10^4$	90	1 ABDELHAME..20A	CRES	LiAlO ₂
$< 1 \times 10^6$	95	2 ABDELHAME..19	CRES	GeV-scale WIMPs on Li
$< 3 \times 10^{-4}$	90	3 AMOLE 19	PICO	C ₃ F ₈
$< 1.7 \times 10^4$	90	4 APRILE 19c	XE1T	light DM on Xe via Migdal/brem effect
$< 8 \times 10^6$	90	5 ARMENGAUD 19	EDEL	GeV-scale WIMPs on Ge
< 70	90	6 XIA 19A	PNDX	SD WIMP on Xe
< 100	90	7 AGNESE 18	SCDM	GeV-scale WIMPs on Ge
< 1	90	8 AKERIB 17A	LUX	Xe
< 0.6	90	9 FU 17	PNDX	SD WIMP on Xe
< 0.2	90	10 AMOLE 15	PICO	C ₃ F ₈
$< 1.6 \times 10^{-1}$	90	11 ARCHAMBAU.12	PICA	19F

- ¹ ABDELHAMEED 20A use LiAlO₂ target in CRESST to search for SD WIMP scatter on p; no signal; quoted limit is for m(DM) = 1 GeV.
- ² ABDELHAMEED 19 search for SD WIMP scatter on ⁷Li; limits placed on $\sigma^{SD}(\chi p)$ for m(χ) ~ 0.8–20 GeV; quoted limit is for m(χ) = 1 GeV.
- ³ AMOLE 19 search for SD WIMP scatter on C₃F₈ in PICO-60 bubble chamber; no signal; set limit for spin dependent coupling $\sigma^{SD}(\chi p) < 2 \times 10^{-4}$ pb for m(χ) = 5 GeV.
- ⁴ APRILE 19c search for light DM on Xe via Migdal/brem effect; no signal, require $\sigma^{SD}(\chi p) < 1.7 \times 10^4$ pb for m(χ) = 1 GeV.
- ⁵ ARMENGAUD 19 search for GeV scale WIMP scatter on Ge; limits placed in $\sigma^{SD}(\chi p)$ vs. m(χ) plane for m(χ) ~ 0.5–10 GeV; quoted limit is for m(χ) = 5 GeV.
- ⁶ XIA 19A search for WIMP scatter on Xe in PandaX-II; limits placed in $\sigma^{SD}(\chi p)$ vs. m(χ) plane for m(χ) ~ 5–1 × 10⁵ GeV; quoted limit is for m(χ) = 5 GeV.
- ⁷ AGNESE 18 search for GeV scale WIMPs with CDMSlite; limits placed in $\sigma^{SD}(\chi p)$ vs. m(χ) plane for m(χ) ~ 1.5–20 GeV; quoted limit is for m(χ) = 5 GeV.
- ⁸ AKERIB 17A search for SD WIMP scatter on Xe using 129.5 kg yr exposure; limits placed in $\sigma^{SD}(\chi p)$ vs. m(χ) plane for m(χ) ~ 6–1 × 10⁵ GeV.
- ⁹ FU 17 search for SD WIMP scatter on Xe; limits set in $\sigma^{SD}(\chi p)$ vs. m(χ) plane for m(χ) ~ 4–1 × 10³ GeV; quoted limit is for m(χ) = 5 GeV.
- ¹⁰ AMOLE 15 search for WIMP scatter on C₃F₈ in PICO-2L; limits placed in $\sigma^{SD}(\chi p)$ vs. m(χ) plane for m(χ) ~ 4–1 × 10⁴ GeV; quoted limit is for m(χ) = 5 GeV.
- ¹¹ ARCHAMBAULT 12 search for SD WIMP scatter in ¹⁹F with PICASSO; limits set in $\sigma^{SD}(\chi p)$ vs. m(χ) plane for m ~ 4–500 GeV; quoted limit is for m(χ) = 5 GeV.

For m_{χ0} = 20 GeV

For limits from X⁰ annihilation in the Sun, the assumed annihilation final state is shown in parenthesis in the comment.

VALUE (pb)	CL%	DOCUMENT ID	TECN	COMMENT
••• We do not use the following data for averages, fits, limits, etc. •••				
< 9 × 10 ⁻⁵	90	¹ AARTSEN 20c	ICCB	SD WIMP on p
< 2 × 10 ⁵	90	² ABDELHAMEED..20A	CRES	LiAlO ₂
< 5 × 10 ⁻³	90	³ FELIZARDO 20	SMP L	WIMPs via SIMPLE
< 3 × 10 ⁵	95	⁴ ABDELHAMEED..19	CRES	⁷ Li
< 2.5 × 10 ⁻⁵	90	⁵ AMOLE 19	PICO	C ₃ F ₈
< 2.5 × 10 ⁻⁴	90	⁶ APRILE 19A	XE1T	Xe, SD
< 1 × 10 ⁻³	90	⁷ XIA 19A	PNDX	SD WIMP on Xe
< 30	95	⁸ AGNESE 18	SCDM	Ge
< 1 × 10 ⁻³	90	⁹ AKERIB 17A	LUX	Xe
< 1.32 × 10 ⁻²	90	¹⁰ BEHNKE 17	PICA	C ₄ F ₁₀
< 2 × 10 ⁻³	90	¹¹ FU 17	PNDX	SD WIMP on Xe
< 5 × 10 ⁻⁴	90	¹² AMOLE 16A	PICO	C ₃ F ₈
< 2 × 10 ⁻⁶	90	¹³ KHACHATRY..16AJ	CMS	8 TeV pp → Z+ET; Z → ℓℓ
< 1.2 × 10 ⁻³	90	AMOLE 15	PICO	C ₃ F ₈
< 1.43 × 10 ⁻³	90	CHOI 15	SKAM	H, solar ν (b \bar{b})
< 1.42 × 10 ⁻⁴	90	CHOI 15	SKAM	H, solar ν (τ ⁺ τ ⁻)
< 5 × 10 ⁻³	90	FELIZARDO 14	SMP L	C ₂ ClF ₅
< 1.29 × 10 ⁻²	90	¹⁴ AARTSEN 13	ICCB	H, solar ν (τ ⁺ τ ⁻)
< 3.17 × 10 ⁻²	90	¹⁵ APRILE 13	X100	Xe
< 3 × 10 ⁻²	90	¹⁶ ARCHAMBAU..12	PICA	F (C ₄ F ₁₀)
< 6 × 10 ⁻²	90	BEHNKE 12	COUP	CF ₃ I
< 20	90	DAW 12	DRFT	F (CF ₄)
< 7 × 10 ⁻³	90	FELIZARDO 12	SMP L	C ₂ ClF ₅
< 0.15	90	KIM 12	KIMS	CsI
< 1 × 10 ⁵	90	¹⁷ AHLEN 11	DMP T	F (CF ₄)
< 0.1	90	¹⁷ BEHNKE 11	COUP	CF ₃ I
< 1.5 × 10 ⁻²	90	¹⁸ TANAKA 11	SKAM	H, solar ν (b \bar{b})
< 0.2	90	ARCHAMBAU..09	PICA	F
< 4	90	LEBEDENKO 09A	ZEP3	Xe
< 0.6	90	ANGLE 08A	XE10	Xe
< 100	90	ALNER 07	ZEP2	Xe
< 1	90	LEE 07A	KIMS	CsI
< 20	90	¹⁹ AKERIB 06	CDMS	⁷³ Ge, ²⁹ Si
< 2	90	SHIMIZU 06A	CNTR	F (CaF ₂)
< 0.5	90	ALNER 05	NAIA	NaI
< 1.5	90	BARNABE-HE..05	PICA	F (C ₄ F ₁₀)
< 1.5	90	GIRARD 05	SMP L	F (C ₂ ClF ₅)
< 35	90	MIUCHI 03	BOLO	LIF
< 30	90	TAKEDA 03	BOLO	NaF

- ¹ AARTSEN 20c place combined IceCube and Pico-60 velocity-independent limits on spin-dependent WIMP-p scatter $\sigma^{SD}(\chi p) < 9-5$ pb for m(WIMP) = 20 GeV assuming dominant annihilation to ττ.
- ² ABDELHAMEED 20A use LiAlO₂ target in CRESST to search for spin-dependent WIMP scatter on p; limits set for m(WIMP): 0.3–30 GeV in Fig. 8. Quoted limit is for m(WIMP) = 30 GeV.
- ³ FELIZARDO 20 presents 2014 SIMPLE bounds on WIMP DM using C₂ClF₅ target.
- ⁴ ABDELHAMEED 19 uses Li₂MoO₄ target to set limit for spin dependent coupling $\sigma^{SD}(\chi p) < 3 \times 10^5$ pb for m(χ) = 20 GeV.
- ⁵ AMOLE 19 search for SD WIMP scatter on C₃F₈ in PICO-60 bubble chamber; no signal; set limit for spin dependent coupling $\sigma^{SD}(\chi p) < 2.5 \times 10^{-5}$ pb for m(χ) = 20 GeV.
- ⁶ APRILE 19A search for SD WIMP scatter on 1 t yr Xe; no signal, limits placed in $\sigma^{SD}(\chi p)$ vs. m(χ) plane for m ~ 6–1000 GeV.
- ⁷ XIA 19A search for WIMP scatter on Xe in PandaX-II; limits placed in $\sigma^{SD}(\chi p)$ vs. m(χ) plane for m(χ) ~ 5–1 × 10⁵ GeV.
- ⁸ AGNESE 18 give limits for $\sigma^{SD}(\rho \chi)$ for m(WIMP) between 1.5 and 20 GeV using CDMSlite mode data.

- ⁹ AKERIB 17A search for SD WIMP scatter on Xe using 129.5 kg yr exposure; limits placed in $\sigma^{SD}(\chi p)$ vs. m(χ) plane for m(χ) ~ 6–1 × 10⁵ GeV.
- ¹⁰ BEHNKE 17 show final Picasso results based on 231.4 kg d exposure at SNOLab for WIMP scatter on C₄F₁₀ search via superheated droplet; require $\sigma(SD) < 1.32 \times 10^{-2}$ pb for m(WIMP) = 20 GeV.
- ¹¹ FU 17 search for SD WIMP scatter on Xe; limits set in $\sigma^{SD}(\chi p)$ vs. m(χ) plane for m(χ) ~ 4–1 × 10³ GeV.
- ¹² AMOLE 16A require SD WIMP-p scattering $< 5 \times 10^{-4}$ pb for m(WIMP) = 20 GeV; bubbles from C₃F₈ target.
- ¹³ KHACHATRYAN 16AJ require SD WIMP-p $< 2 \times 10^{-6}$ pb for m(WIMP) = 20 GeV from pp → Z + ET; Z → ℓℓ signal.
- ¹⁴ AARTSEN 13 search for neutrinos from the Sun arising from the pair annihilation of X⁰ trapped by the sun in data taken between June 2010 and May 2011.
- ¹⁵ The value has been provided by the authors. APRILE 13 note that the proton limits on Xe are highly sensitive to the theoretical model used. See also APRILE 14A.
- ¹⁶ ARCHAMBAULT 12 search for WIMP scatter on C₄F₁₀; limits set in $\sigma^{SD}(\chi p)$ vs. m(χ) plane for m ~ 4–500 GeV.
- ¹⁷ Use a direction-sensitive detector.
- ¹⁸ TANAKA 11 search for neutrinos from the Sun arising from the pair annihilation of X⁰ trapped by the Sun. The amount of X⁰ depends on the X⁰-proton cross section.
- ¹⁹ See also AKERIB 05.

For m_{χ0} = 100 GeV

For limits from X⁰ annihilation in the Sun, the assumed annihilation final state is shown in parenthesis in the comment.

VALUE (pb)	CL%	DOCUMENT ID	TECN	COMMENT
••• We do not use the following data for averages, fits, limits, etc. •••				
< 50	90	¹ IKEDA 21	NAGE	directional gas TPC
< 3.34 × 10 ⁻⁴	90	² AARTSEN 20c	ICCB	SD WIMP on p
< 6.5 × 10 ⁻³	90	³ FELIZARDO 20	SMP L	WIMPs via SIMPLE
< 4 × 10 ⁻⁵	90	⁴ AMOLE 19	PICO	C ₃ F ₈
< 4 × 10 ⁻⁴	90	⁵ APRILE 19A	XE1T	Xe, SD
< 8 × 10 ⁻⁴	90	⁶ XIA 19A	PNDX	SD WIMP on Xe
< 8 × 10 ⁻⁴	90	⁷ AKERIB 17A	LUX	Xe
< 5 × 10 ⁻⁵	90	⁸ AMOLE 17	PICO	C ₃ F ₈
< 3.3 × 10 ⁻²	90	⁹ APRILE 17A	X100	Xe inelastic
< 2.8 × 10 ⁻¹	90	¹⁰ BATTAT 17	DRFT	CS ₂
< 1.5 × 10 ⁻³	90	¹¹ FU 17	PNDX	Xe
< 0.553–0.019	95	¹² AABOUD 16b	ATLS	pp → j + ET
< 1 × 10 ⁻⁵	90	¹³ AABOUD 16f	ATLS	pp → γ + ET
< 1 × 10 ⁻⁴	90	¹⁴ AARTSEN 16c	ICCB	solar ν (W ⁺ W ⁻)
< 2 × 10 ⁻⁴	90	¹⁵ ADRIAN-MAR..16	ANTR	solar ν (WW, b \bar{b} , ττ)
< 3 × 10 ⁻³	90	¹⁶ AKERIB 16A	LUX	Xe
< 5 × 10 ⁻⁴	90	¹⁷ AMOLE 16	PICO	CF ₃ I
< 1.5 × 10 ⁻³	90	AMOLE 15	PICO	C ₃ F ₈
< 3.19 × 10 ⁻³	90	CHOI 15	SKAM	H, solar ν (b \bar{b})
< 2.80 × 10 ⁻⁴	90	CHOI 15	SKAM	H, solar ν (W ⁺ W ⁻)
< 1.24 × 10 ⁻⁴	90	CHOI 15	SKAM	H, solar ν (τ ⁺ τ ⁻)
< 8 × 10 ²	90	¹⁸ NAKAMURA 15	NAGE	CF ₄
< 1.7 × 10 ⁻³	90	¹⁹ AVRORIN 14	BAIK	H, solar ν (W ⁺ W ⁻)
< 4.5 × 10 ⁻²	90	¹⁹ AVRORIN 14	BAIK	H, solar ν (b \bar{b})
< 7.1 × 10 ⁻⁴	90	¹⁹ AVRORIN 14	BAIK	H, solar ν (τ ⁺ τ ⁻)
< 6 × 10 ⁻³	90	FELIZARDO 14	SMP L	C ₂ ClF ₅
< 2.68 × 10 ⁻⁴	90	²⁰ AARTSEN 13	ICCB	H, solar ν (W ⁺ W ⁻)
< 1.47 × 10 ⁻²	90	²⁰ AARTSEN 13	ICCB	H, solar ν (b \bar{b})
< 8.5 × 10 ⁻⁴	90	²¹ ADRIAN-MAR..13	ANTR	H, solar ν (W ⁺ W ⁻)
< 5.5 × 10 ⁻²	90	²¹ ADRIAN-MAR..13	ANTR	H, solar ν (b \bar{b})
< 3.4 × 10 ⁻⁴	90	²¹ ADRIAN-MAR..13	ANTR	H, solar ν (τ ⁺ τ ⁻)
< 1.00 × 10 ⁻²	90	²² APRILE 13	X100	Xe
< 7.1 × 10 ⁻⁴	90	²³ BOLIEV 13	BAKS	H, solar ν (W ⁺ W ⁻)
< 8.4 × 10 ⁻³	90	²³ BOLIEV 13	BAKS	H, solar ν (b \bar{b})
< 8.4 × 10 ⁻³	90	²³ BOLIEV 13	BAKS	H, solar ν (τ ⁺ τ ⁻)
< 3.1 × 10 ⁻⁴	90	²⁴ ABBASI 12	ICCB	H, solar ν (W ⁺ W ⁻)
< 7.07 × 10 ⁻⁴	90	²⁴ ABBASI 12	ICCB	H, solar ν (b \bar{b})
< 4.53 × 10 ⁻²	90	²⁴ ABBASI 12	ICCB	H, solar ν (τ ⁺ τ ⁻)
< 7 × 10 ⁻²	90	²⁵ ARCHAMBAU..12	PICA	F (C ₄ F ₁₀)
< 1 × 10 ⁻²	90	BEHNKE 12	COUP	CF ₃ I
< 1.8	90	DAW 12	DRFT	F (CF ₄)
< 9 × 10 ⁻³	90	FELIZARDO 12	SMP L	C ₂ ClF ₅
< 2 × 10 ⁻²	90	KIM 12	KIMS	CsI
< 2 × 10 ³	90	¹⁸ AHLEN 11	DMP T	F (CF ₄)
< 7 × 10 ⁻²	90	BEHNKE 11	COUP	CF ₃ I
< 2.7 × 10 ⁻⁴	90	²⁶ TANAKA 11	SKAM	H, solar ν (W ⁺ W ⁻)
< 4.5 × 10 ⁻³	90	²⁶ TANAKA 11	SKAM	H, solar ν (b \bar{b})
< 6 × 10 ³	90	²⁷ FELIZARDO 10	SMP L	C ₂ ClF ₃
< 0.4	90	¹⁸ MIUCHI 10	NAGE	CF ₄
< 0.8	90	ARCHAMBAU..09	PICA	F
< 1.0	90	LEBEDENKO 09A	ZEP3	Xe
< 15	90	ANGLE 08A	XE10	Xe
< 0.2	90	ALNER 07	ZEP2	Xe
< 1 × 10 ⁴	90	LEE 07A	KIMS	CsI
< 5	90	¹⁸ MIUCHI 07	NAGE	F (CF ₄)
< 2	90	²⁸ AKERIB 06	CDMS	⁷³ Ge, ²⁹ Si
< 0.3	90	SHIMIZU 06A	CNTR	F (CaF ₂)
< 2	90	ALNER 05	NAIA	NaI
< 2	90	BARNABE-HE..05	PICA	F (C ₄ F ₁₀)

Searches Particle Listings

WIMP and Dark Matter Searches

<100	90	BENOIT	05	EDEL	⁷³ Ge
< 1.5	90	GIRARD	05	SMPL	F (C ₂ ClF ₅)
< 0.7		²⁹ GIULIANI	05A	RVUE	
		³⁰ GIULIANI	04	RVUE	
		³¹ GIULIANI	04A	RVUE	
< 35	90	MIUCHI	03	BOLO	LiF
< 40	90	TAKEDA	03	BOLO	NaF

- 1 IKEDA 21 use direction sensitive TPC NEWAGE to search for SD WIMPs. No signal observed. Limits set in $\sigma^{SD}(\chi p)$ vs. m plane; $\sigma^{SD}(\chi p) < 50$ pb for $m(\text{DM}) = 100$ GeV.
- 2 AARTSEN 20c place combined IceCube and Pico-60 velocity-independent limits on spin-dependent WIMP- p scatter $\sigma^{SD}(\chi p) < 3.34 \times 10^{-4}$ pb for $m(\text{WIMP}) = 100$ GeV assuming dominant annihilation to $\tau\bar{\tau}$.
- 3 FELIZARDO 20 presents 2014 SIMPLE bounds on WIMP DM using C₂ClF₅ target.
- 4 AMOLE 19 search for SD WIMP scatter on C₃F₈ in PICO-60 bubble chamber; no signal; set limit for spin dependent coupling $\sigma^{SD}(\chi p) < 4 \times 10^{-5}$ pb for $m(\chi) = 100$ GeV.
- 5 APRILE 19A search for SD WIMP scatter on 1 t yr Xe; no signal, limits placed in $\sigma^{SD}(\chi p)$ vs. $m(\chi)$ plane for $m \sim 6$ –1000 GeV.
- 6 XIA 19A search for WIMP scatter on Xe in PandaX-II; limits placed in $\sigma^{SD}(\chi p)$ vs. $m(\chi)$ plane for $m(\chi) \sim 5$ – 1×10^5 GeV.
- 7 AKERIB 17A search for SD WIMP scatter on Xe using 129.5 kg yr exposure; limits placed in $\sigma^{SD}(\chi p)$ vs. $m(\chi)$ plane for $m(\chi) \sim 6$ – 1×10^5 GeV.
- 8 AMOLE 17 require $\sigma(\text{WIMP-}p)^{SD} < 5 \times 10^{-5}$ pb for $m(\text{WIMP}) = 100$ GeV using PICO-60 1167 kg-days exposure at SNOLab.
- 9 APRILE 17A require $\sigma(\text{WIMP-}p)(\text{inelastic})^{SD} < 3.3 \times 10^{-2}$ pb for $m(\text{WIMP}) = 100$ GeV, based on 7640 kg day exposure at LNGS.
- 10 BATTAT 17 use directional detection of CS₂ ions to require $\sigma(\text{SD}) < 2.8 \times 10^{-1}$ pb for 100 GeV WIMP with a 55 days exposure at the Boulby Underground Science Facility.
- 11 FU 17 from a 33000 kg d exposure at CJPL, PANDAX II derive for $m(\text{DM}) = 100$ GeV, $\sigma^{SD}(\text{WIMP-}p) < 2 \times 10^{-3}$ pb.
- 12 AABOUD 16D use ATLAS 13 TeV 3.2 fb⁻¹ of data to search for monojet plus missing E_T ; agree with SM rates; present limits on large extra dimensions, compressed SUSY spectra and wimp pair production.
- 13 AABOUD 16F search for monophoton plus missing E_T events at ATLAS with 13 Tev and 3.2 fb⁻¹; signal agrees with SM background; place limits on SD WIMP-proton scattering vs. mediator mass and large extra dimension models.
- 14 AARTSEN 16c search for high energy ν s from WIMP annihilation in solar core; limits set on SD WIMP- p scattering (Fig. 8).
- 15 ADRIAN-MARTINEZ 16 search for WIMP annihilation into ν s from solar core; exclude SD cross section < few 10^{-4} depending on $m(\text{WIMP})$.
- 16 AKERIB 16A using 2013 data exclude SD WIMP-proton scattering $> 3 \times 10^{-3}$ pb for $m(\text{WIMP}) = 100$ GeV.
- 17 AMOLE 16 use bubble technique on CF₃I target to exclude SD WIMP- p scattering $> 5 \times 10^{-4}$ pb for $m(\text{WIMP}) = 100$ GeV.
- 18 Use a direction-sensitive detector.
- 19 AVRORIN 14 search for neutrinos from the Sun arising from the pair annihilation of X^0 trapped by the Sun in data taken between 1998 and 2003. See their Table 1 for limits assuming annihilation into neutrino pairs.
- 20 AARTSEN 13 search for neutrinos from the Sun arising from the pair annihilation of X^0 trapped by the sun in data taken between June 2010 and May 2011.
- 21 ADRIAN-MARTINEZ 13 search for neutrinos from the Sun arising from the pair annihilation of X^0 trapped by the sun in data taken between Jan. 2007 and Dec. 2008.
- 22 The value has been provided by the authors. APRILE 13 note that the proton limits on Xe are highly sensitive to the theoretical model used. See also APRILE 14A.
- 23 BOLIEV 13 search for neutrinos from the Sun arising from the pair annihilation of X^0 trapped by the sun in data taken from 1978 to 2009. See also SUVOROVA 13 for an older analysis of the same data.
- 24 ABBASI 12 search for neutrinos from the Sun arising from the pair annihilation of X^0 trapped by the Sun. The amount of X^0 depends on the X^0 -proton cross section.
- 25 ARCHAMBAULT 12 search for WIMP scatter on C₄F₁₀; limits set in $\sigma^{SD}(\chi p)$ vs. $m(\chi)$ plane for $m \sim 4$ –500 GeV.
- 26 TANAKA 11 search for neutrinos from the Sun arising from the pair annihilation of X^0 trapped by the Sun. The amount of X^0 depends on the X^0 -proton cross section.
- 27 See their Fig. 3 for limits on spin-dependent proton couplings for X^0 mass of 50 GeV.
- 28 See also AKERIB 05.
- 29 GIULIANI 05A analyze available data and give combined limits.
- 30 GIULIANI 04 reanalyze COLLAR 00 data and give limits for spin-dependent X^0 -proton coupling.
- 31 GIULIANI 04A give limits for spin-dependent X^0 -proton couplings from existing data.

For $m_{X^0} = 1$ TeV

For limits from X^0 annihilation in the Sun, the assumed annihilation final state is shown in parenthesis in the comment.

VALUE (pb)	CL%	DOCUMENT ID	TECN	COMMENT
••• We do not use the following data for averages, fits, limits, etc. •••				
<200	90	1 IKEDA	21	NAGE directional gas TPC
< 4.81×10^{-3}	90	2 AARTSEN	20c	ICCB SD WIMP on p
< 3×10^{-4}	90	3 AMOLE	19	PICO C ₃ F ₈
< 4×10^{-3}	90	4 APRILE	19A	XE1T Xe, SD
< 5×10^{-3}	90	5 XIA	19A	PNDX SD WIMP on Xe
		6 ALBERT	18c	HAWK DM annihilation in Sun to long-lived mediator
< 2.05×10^{-5}	90	7 AARTSEN	17A	ICCB ν , sun
< 7×10^{-3}	90	8 AKERIB	17A	LUX Xe
< 2×10^{-2}	90	9 FU	17	PNDX SD WIMP on Xe
		10 ADRIAN-MAR.	16B	ANTR solar μ from WIMP annih.
< 1×10^{-2}	90	AMOLE	15	PICO C ₃ F ₈
< 1.5×10^3	90	NAKAMURA	15	NAGE CF ₄
< 2.7×10^{-3}	90	11 AVRORIN	14	BAIK H, solar ν ($W^+ W^-$)

< 6.9×10^{-2}	90	11 AVRORIN	14	BAIK H, solar ν ($b\bar{b}$)
< 8.4×10^{-4}	90	11 AVRORIN	14	BAIK H, solar ν ($\tau^+ \tau^-$)
< 4.48×10^{-4}	90	12 AARTSEN	13	ICCB H, solar ν ($W^+ W^-$)
< 1.00×10^{-2}	90	12 AARTSEN	13	ICCB H, solar ν ($b\bar{b}$)
< 8.9×10^{-4}	90	13 ADRIAN-MAR.	13	ANTR H, solar ν ($W^+ W^-$)
< 2.0×10^{-2}	90	13 ADRIAN-MAR.	13	ANTR H, solar ν ($b\bar{b}$)
< 2.3×10^{-4}	90	13 ADRIAN-MAR.	13	ANTR H, solar ν ($\tau^+ \tau^-$)
< 7.57×10^{-2}	90	14 APRILE	13	X100 Xe
< 5.4×10^{-3}	90	15 BOLIEV	13	BAKS H, solar ν ($W^+ W^-$)
< 4.2×10^{-2}	90	15 BOLIEV	13	BAKS H, solar ν ($b\bar{b}$)
< 1.5×10^{-3}	90	15 BOLIEV	13	BAKS H, solar ν ($\tau^+ \tau^-$)
< 2.50×10^{-4}	90	16 ABBASI	12	ICCB H, solar ν ($W^+ W^-$)
< 7.86×10^{-3}	90	16 ABBASI	12	ICCB H, solar ν ($b\bar{b}$)
< 8×10^{-2}	90	BEHNKE	12	COUP CF ₃ I
< 8	90	DAW	12	DRFT F (CF ₄)
< 6×10^{-2}	90	FELIZARDO	12	SMPL C ₂ ClF ₅
< 8×10^{-2}	90	KIM	12	KIMS Csl
< 8×10^3	90	17 AHLEN	11	DMTP F (CF ₄)
< 0.4	90	BEHNKE	11	COUP CF ₃ I
< 2×10^{-3}	90	18 TANAKA	11	SKAM H, solar ν ($b\bar{b}$)
< 2×10^{-2}	90	18 TANAKA	11	SKAM H, solar ν ($W^+ W^-$)
< 1×10^{-3}	90	19 ABBASI	10	ICCB KK dark matter
< 2×10^4	90	17 MIUCHI	10	NAGE CF ₄
< 8.7×10^{-4}	90	ABBASI	09B	ICCB H, solar ν ($W^+ W^-$)
< 2.2×10^{-2}	90	ABBASI	09B	ICCB H, solar ν ($b\bar{b}$)
< 3	90	ARCHAMBAU.	09	PICA F
< 6	90	LEBEDENKO	09A	ZEP3 Xe
< 9	90	ANGLE	08A	XE10 Xe
<100	90	ALNER	07	ZEP2 Xe
< 0.8	90	LEE	07A	KIMS Csl
< 4×10^4	90	17 MIUCHI	07	NAGE F (CF ₄)
< 30	90	20 AKERIB	06	CDMS ⁷³ Ge, ²⁹ Si
< 1.5	90	ALNER	05	NAIA NaI
< 15	90	BARNABE-HE.	05	PICA F (C ₄ F ₁₀)
<600	90	BENOIT	05	EDEL ⁷³ Ge
< 10	90	GIRARD	05	SMPL F (C ₂ ClF ₅)
<260	90	MIUCHI	03	BOLO LiF
<150	90	TAKEDA	03	BOLO NaF

- 1 IKEDA 21 use direction sensitive TPC NEWAGE to search for SD WIMPs. No signal observed. Limits set in $\sigma^{SD}(\chi p)$ vs. m plane; $\sigma^{SD}(\chi p) < 200$ pb for $m(\text{DM}) = 1000$ GeV.
- 2 AARTSEN 20c place combined IceCube and Pico-60 velocity-independent limits on spin-dependent WIMP- p scatter $\sigma^{SD}(\chi p) < 3 \times 10^{-3}$ pb for $m(\text{WIMP}) = 1$ TeV assuming dominant annihilation to $W W$.
- 3 AMOLE 19 search for SD WIMP scatter on C₃F₈ in PICO-60 bubble chamber; no signal; set limit for spin dependent coupling $\sigma^{SD}(\chi p) < 3 \times 10^{-4}$ pb for $m(\chi) = 1000$ GeV.
- 4 APRILE 19A search for SD WIMP scatter on 1 t yr Xe; no signal, limits placed in $\sigma^{SD}(\chi p)$ vs. $m(\chi)$ plane for $m \sim 6$ –1000 GeV.
- 5 XIA 19A search for WIMP scatter on Xe in PandaX-II; limits placed in $\sigma^{SD}(\chi p)$ vs. $m(\chi)$ plane for $m(\chi) \sim 5$ – 1×10^5 GeV.
- 6 ALBERT 18c search for DM annihilation in Sun to long-lived mediator (LLM) which decays outside Sun, for DM masses above 1 TeV; assuming LLM, limits set on $\sigma^{SD}(\chi p)$.
- 7 AARTSEN 17A search for neutrinos from solar WIMP annihilation into $\tau^+ \tau^-$ in 532 days of live time.
- 8 AKERIB 17A search for SD WIMP scatter on Xe using 129.5 kg yr exposure; limits placed in $\sigma^{SD}(\chi p)$ vs. $m(\chi)$ plane for $m(\chi) \sim 6$ – 1×10^5 GeV.
- 9 FU 17 search for SD WIMP scatter on Xe; limits set in $\sigma^{SD}(\chi p)$ vs. $m(\chi)$ plane for $m(\chi) \sim 4$ – 1×10^3 GeV.
- 10 ADRIAN-MARTINEZ 16B search for secluded DM via WIMP annihilation in solar core into light mediator which later decays to μ or ν s; limits presented in Figures 3 and 4.
- 11 AVRORIN 14 search for neutrinos from the Sun arising from the pair annihilation of X^0 trapped by the Sun in data taken between 1998 and 2003. See their Table 1 for limits assuming annihilation into neutrino pairs.
- 12 AARTSEN 13 search for neutrinos from the Sun arising from the pair annihilation of X^0 trapped by the sun in data taken between June 2010 and May 2011.
- 13 ADRIAN-MARTINEZ 13 search for neutrinos from the Sun arising from the pair annihilation of X^0 trapped by the sun in data taken between Jan. 2007 and Dec. 2008.
- 14 The value has been provided by the authors. APRILE 13 note that the proton limits on Xe are highly sensitive to the theoretical model used. See also APRILE 14A.
- 15 BOLIEV 13 search for neutrinos from the Sun arising from the pair annihilation of X^0 trapped by the sun in data taken from 1978 to 2009. See also SUVOROVA 13 for an older analysis of the same data.
- 16 ABBASI 12 search for neutrinos from the Sun arising from the pair annihilation of X^0 trapped by the Sun. The amount of X^0 depends on the X^0 -proton cross section.
- 17 Use a direction-sensitive detector.
- 18 TANAKA 11 search for neutrinos from the Sun arising from the pair annihilation of X^0 trapped by the Sun. The amount of X^0 depends on the X^0 -proton cross section.
- 19 ABBASI 10 search for ν_μ from annihilations of Kaluza-Klein photon dark matter in the Sun.
- 20 See also AKERIB 05.

———— Spin-Dependent Cross Section Limits ————
———— for Dark Matter Particle (χ^0) on Neutron ————

For m_{χ^0} in GeV rangeWe provide here limits for $m_{\chi^0} < 5$ GeV

VALUE (pb)	CL%	DOCUMENT ID	TECN	COMMENT
< 1 × 10 ⁸	90	1 ABDELHAMEE..20A	CRES	LiAlO ₂
< 1 × 10 ¹⁰	95	2 ABDELHAMEE..19	CRES	SD low mass DM on Li
< 2.3 × 10 ²	90	3 APRILE	19C	XE1T light DM on Xe via Migdal/brem effect
< 1 × 10 ⁻²	90	4 APRILE	19D	XE1T light DM on Xe via ionization
< 4 × 10 ⁴	90	5 ARMENGAUD	19	EDEL GeV-scale WIMPs on Ge
< 8 × 10 ⁻²	90	6 XIA	19A	PNDX SD WIMP on Xe
< 3	90	7 AGNESE	18	SCDM GeV-scale WIMPs on Ge
< 3	90	8 JIANG	18	CDEX GeV-scale WIMPs on Ge
< 10	90	9 YANG	18	CDEX WIMPs on Ge
< 1 × 10 ⁻¹	90	10 AKERIB	17A	LUX Xe
< 0.1	90	11 FU	17	PNDX SD WIMP on Xe
< 20	90	12 ZHAO	16	CDEX GeV-scale WIMPs on Ge
< 150	90	13 AHMED	11B	CDM2 GeV-scale WIMPs on Ge

- • • We do not use the following data for averages, fits, limits, etc. • • •
- ABDELHAMEED 20A use LiAlO₂ target in CRESST to search for SD WIMP scatter; no signal; quoted limit is for $m(\text{DM}) = 1$ GeV.
 - ABDELHAMEED 19 search for GeV-scale WIMP SD scatter on ⁷Li crystal; set limit $\sigma^{SD}(\chi n)$ for $m(\chi) \sim 0.8\text{--}20$ GeV; quoted limit for $m(\chi) = 1$ GeV.
 - APRILE 19C search for light DM on Xe via Migdal/bremstrahlung effect; no signal, require $\sigma^{SD}(\chi n) < 230$ pb for $m(\chi) = 1$ GeV.
 - APRILE 19D search for light DM scatter on Xe via ionization; no signal, limits placed in σ vs. $m(\text{DM}) \sim 3\text{--}6$ GeV; quoted limit is for $m(\text{DM}) = 5$ GeV.
 - ARMENGAUD 19 search for GeV scale WIMP scatter on Ge; limits placed in $\sigma^{SD}(\chi n)$ vs. $m(\chi)$ plane for $m(\chi) \sim 0.5\text{--}10$ GeV; quoted limit is for $m(\chi) = 5$ GeV.
 - XIA 19A search for WIMP scatter on Xe in PandaX-II; limits placed in $\sigma^{SD}(\chi n)$ vs. $m(\chi)$ plane for $m(\chi) \sim 5\text{--}1 \times 10^5$ GeV; quoted limit is for $m(\chi) = 5$ GeV.
 - AGNESE 18 search for GeV scale WIMPs scatter at CDMSlite; limits placed in $\sigma^{SD}(\chi n)$ vs. $m(\chi)$ plane for $m \sim 1.5\text{--}20$ GeV; quoted limit is for $m(\chi) = 5$ GeV.
 - JIANG 18 search for GeV scale WIMP scatter on Ge; limits placed in $\sigma^{SD}(\chi n)$ vs. $m(\chi)$ plane for $m(\chi) \sim 3\text{--}10$ GeV; quoted limit is for $m(\chi) = 5$ GeV.
 - YANG 18 search for WIMP scatter on Ge; limits placed in $\sigma^{SD}(\chi n)$ vs. $m(\chi)$ plane for $m(\chi) \sim 2\text{--}10$ GeV; quoted limit is for $m(\chi) = 5$ GeV.
 - AKERIB 17A search for SD WIMP scatter on Xe with 129.5 kg yr exposure; limits placed in $\sigma^{SD}(\chi n)$ vs. $m(\chi)$ plane for $m(\chi) \sim 5\text{--}1 \times 10^5$ GeV; quoted limit is for $m(\chi) = 5$ GeV.
 - FU 17 search for SD WIMP scatter on Xe; limits set in $\sigma^{SD}(\chi n)$ vs. $m(\chi)$ plane for $m(\chi) \sim 4\text{--}1 \times 10^3$ GeV; quoted limit is for $m(\chi) = 5$ GeV.
 - ZHAO 16 search for GeV-scale WIMP scatter on Ge; limits placed in $\sigma^{SD}(\chi n)$ vs. $m(\chi)$ plane for $m(\chi) \sim 4\text{--}30$ GeV; quoted limit is for $m(\chi) = 5$ GeV.
 - AHMED 11B search for GeV scale WIMP scatter on Ge in CDMS II; limits placed in $\sigma^{SD}(\chi n)$ vs. $m(\chi)$ plane for $m \sim 4\text{--}12$ GeV. Limit given for $m(\chi) = 5$ GeV.

For $m_{\chi^0} = 20$ GeV

VALUE (pb)	CL%	DOCUMENT ID	TECN	COMMENT
< 5 × 10 ⁷	90	1 ABDELHAMEE..20A	CRES	LiAlO ₂
< 1 × 10 ⁻¹	90	2 FELIZARDO	20	SMP L WIMPs via SIMPLE
< 8 × 10 ⁻⁶	90	3 APRILE	19A	XE1T Xe, SD
< 3 × 10 ⁻⁵	90	4 XIA	19A	PNDX SD WIMP on Xe
< 1.5	95	5 AGNESE	18	SCDM Ge
< 2.5 × 10 ⁻⁵	90	6 AKERIB	17A	LUX Xe
< 7 × 10 ⁻⁵	90	7 FU	17	PNDX SD WIMP on Xe
< 2	90	8 ZHAO	16	CDEX GeV-scale WIMPs on Ge
< 0.09	90	9 FELIZARDO	14	SMP L C ₂ ClF ₅
< 8	90	10 UCHIDA	14	XMAS ¹²⁹ Xe, inelastic
< 1.13 × 10 ⁻³	90	11 APRILE	13	X100 Xe
< 0.02	90	12 AKIMOV	12	ZEP3 Xe
< 0.06	90	13 AHMED	09	CDM2 Ge
< 0.04	90	14 LEBEDENKO	09A	ZEP3 Xe
< 50	90	15 LIN	09	TEXO Ge
< 6 × 10 ⁻³	90	16 ANGLE	08A	XE10 Xe
< 0.5	90	17 ALNER	07	ZEP2 Xe
< 25	90	18 LEE	07A	KIMS Csl
< 0.3	90	19 AKERIB	06	CDMS ⁷³ Ge, ²⁹ Si
< 30	90	20 SHIMIZU	06A	CNTR F (CaF ₂)
< 60	90	21 ALNER	05	NAIA NaI
< 20	90	22 BARNABE-HE..05	PICA	F (C ₄ F ₁₀)
< 10	90	23 BENOIT	05	EDEL ⁷³ Ge
< 4	90	24 KLAPDOR-K...05	HDM S	⁷³ Ge (enriched)
< 600	90	25 TAKEDA	03	BOLO NaF

- • • We do not use the following data for averages, fits, limits, etc. • • •
- ABDELHAMEED 20A use LiAlO₂ target in CRESST to search for SD WIMP scatter on n ; limits placed for $m(\text{WIMP})$: 0.3–30 GeV in Fig. 8. Quoted limit is for $M(\text{WIMP}) = 30$ GeV.
 - FELIZARDO 20 presents 2014 SIMPLE bounds on WIMP DM using C₂ClF₅ target.
 - APRILE 19A search for SD WIMP scatter on 1 t yr Xe; no signal; limits placed in $\sigma^{SD}(\chi n)$ vs. $m(\chi)$ plane for $m \sim 6\text{--}1000$ GeV.
 - XIA 19A search for WIMP scatter on Xe in PandaX-II; limits placed in $\sigma^{SD}(\chi n)$ vs. $m(\chi)$ plane for $m(\chi) \sim 5\text{--}1 \times 10^5$ GeV.

- AGNESE 18 give limits for $\sigma^{SD}(n\chi)$ for $m(\text{WIMP})$ between 1.5 and 20 GeV using CDMSlite mode data.
- AKERIB 17A search for SD WIMP scatter on Xe with 129.5 kg yr exposure; limits placed in $\sigma^{SD}(\chi n)$ vs. $m(\chi)$ plane for $m(\chi) \sim 5\text{--}1 \times 10^5$ GeV.
- FU 17 search for SD WIMP scatter on Xe; limits set in $\sigma^{SD}(\chi n)$ vs. $m(\chi)$ plane for $m(\chi) \sim 4\text{--}1 \times 10^3$ GeV.
- ZHAO 16 search for GeV-scale WIMP scatter on Ge; limits placed in $\sigma^{SD}(\chi n)$ vs. $m(\chi)$ plane for $m(\chi) \sim 4\text{--}30$ GeV.
- Derived limit from search for inelastic scattering $\chi^0 + ^{129}\text{Xe} \rightarrow \chi^0 + ^{129}\text{Xe}^*$ (39.58 keV).
- The value has been provided by the authors. See also APRILE 14A.
- See their Fig. 6(b) for cross section limits for m_{χ^0} extending down to 2 GeV.
- See also AKERIB 05.

For $m_{\chi^0} = 100$ GeV

VALUE (pb)	CL%	DOCUMENT ID	TECN	COMMENT
< 1.5 × 10 ⁻¹	90	1 FELIZARDO	20	SMP L WIMPs via SIMPLE
< 1.5 × 10 ⁻⁵	90	2 APRILE	19A	XE1T Xe, SD
< 4 × 10 ⁻³	90	3 SUZUKI	19	XMAS ¹²⁹ Xe, inelastic
< 2 × 10 ⁻⁵	90	4 XIA	19A	PNDX SD WIMP on Xe
< 2.5 × 10 ⁻⁵	90	5 AKERIB	17A	LUX Xe
< 7 × 10 ⁻⁵	90	6 FU	17	PNDX SD WIMP on Xe
< 0.1	90	7 FELIZARDO	14	SMP L C ₂ ClF ₅
< 0.05	90	8 UCHIDA	14	XMAS ¹²⁹ Xe, inelastic
< 4.68 × 10 ⁻⁴	90	9 APRILE	13	X100 Xe
< 0.01	90	10 AKIMOV	12	ZEP3 Xe
< 0.02	90	11 FELIZARDO	10	SMP L C ₂ ClF ₃
< 0.01	90	12 AHMED	09	CDM2 Ge
< 100	90	13 LEBEDENKO	09A	ZEP3 Xe
< 0.01	90	14 LIN	09	TEXO Ge
< 0.05	90	15 ANGLE	08A	XE10 Xe
< 0.08	90	16 ALNER	07	ZEP2 Xe
< 6	90	17 LEE	07A	KIMS Csl
< 0.07	90	18 AKERIB	06	CDMS ⁷³ Ge, ²⁹ Si
< 30	90	19 SHIMIZU	06A	CNTR F (CaF ₂)
< 10	90	20 ALNER	05	NAIA NaI
< 30	90	21 BARNABE-HE..05	PICA	F (C ₄ F ₁₀)
< 0.7	90	22 BENOIT	05	EDEL ⁷³ Ge
< 0.2	90	23 GIULIANI	05A	RVUE
< 1.5	90	24 KLAPDOR-K...05	HDM S	⁷³ Ge (enriched)
< 800	90	25 GIULIANI	04	RVUE
		26 GIULIANI	04A	RVUE
		27 MIUCHI	03	BOLO LiF
		28 TAKEDA	03	BOLO NaF

- • • We do not use the following data for averages, fits, limits, etc. • • •
- FELIZARDO 20 presents 2014 SIMPLE bounds on WIMP DM using C₂ClF₅ target.
 - APRILE 19A search for SD WIMP scatter on 1 t yr Xe; no signal, limits placed in $\sigma^{SD}(\chi n)$ vs. $m(\chi)$ plane for $m \sim 6\text{--}1000$ GeV.
 - SUZUKI 19 search in single phase liquid xenon detector for inelastic scattering $\chi^0 + ^{129}\text{Xe} \rightarrow \chi^0 + ^{129}\text{Xe}^*$ (39.58 keV); no signal; require $\sigma(\chi n)^{SD} < 4 \times 10^{-3}$ pb for $m(\chi) = 100$ GeV.
 - XIA 19A search for WIMP scatter on Xe in PandaX-II; limits placed in $\sigma^{SD}(\chi n)$ vs. $m(\chi)$ plane for $m(\chi) \sim 5\text{--}1 \times 10^5$ GeV.
 - AKERIB 17A search for SD WIMP scatter on Xe with 129.5 kg yr exposure; limits placed in $\sigma^{SD}(\chi n)$ vs. $m(\chi)$ plane for $m(\chi) \sim 5\text{--}1 \times 10^5$ GeV.
 - FU 17 search for SD WIMP scatter on Xe; limits set in $\sigma^{SD}(\chi n)$ vs. $m(\chi)$ plane for $m(\chi) \sim 4\text{--}1 \times 10^3$ GeV.
 - UCHIDA 14 derived limit from search for inelastic scattering $\chi^0 + ^{129}\text{Xe} \rightarrow \chi^0 + ^{129}\text{Xe}^*$ (39.58 keV).
 - The value has been provided by the authors. See also APRILE 14A.
 - See their Fig. 3 for limits on spin-dependent neutron couplings for X^0 mass of 50 GeV.
 - BEDNYAKOV 08 reanalyze KLAPDOR-KLEINGROTHAUS 05 and BAUDIS 01 data.
 - See also AKERIB 05.
 - GIULIANI 05A analyze available data and give combined limits.
 - GIULIANI 04 reanalyze COLLAR 00 data and give limits for spin-dependent X^0 -neutron coupling.
 - GIULIANI 04A give limits for spin-dependent X^0 -neutron couplings from existing data.
 - MIUCHI 03 give model-independent limit for spin-dependent X^0 -proton and neutron cross sections. See their Fig. 5.

For $m_{\chi^0} = 1$ TeV

VALUE (pb)	CL%	DOCUMENT ID	TECN	COMMENT
< 7 × 10 ⁻¹	90	1 FELIZARDO	20	SMP L WIMPs via SIMPLE
< 1.2 × 10 ⁻⁴	90	2 APRILE	19A	XE1T Xe, SD
< 2 × 10 ⁻⁴	90	3 XIA	19A	PNDX Xe
< 2.5 × 10 ⁻⁴	90	4 AKERIB	17A	LUX Xe
< 4 × 10 ⁻⁴	90	5 FU	17	PNDX SD WIMP on Xe
< 0.07	90	6 FELIZARDO	14	SMP L C ₂ ClF ₅
< 2	90	7 UCHIDA	14	XMAS ¹²⁹ Xe, inelastic
< 3.6 × 10 ⁻³	90	8 APRILE	13	X100 Xe
< 0.08	90	9 AKIMOV	12	ZEP3 Xe
< 0.2	90	10 AHMED	09	CDM2 Ge
< 0.1	90	11 LEBEDENKO	09A	ZEP3 Xe

Searches Particle Listings

WIMP and Dark Matter Searches

VALUE	90	ANGLE	08A	XE10	Xe
< 0.1	90	ANGLE	08A	XE10	Xe
< 0.25	90	⁸ BEDNYAKOV	08	RVUE	Ge
< 0.6	90	ALNER	07	ZEP2	Xe
< 30	90	LEE	07A	KIMS	Csl
< 0.5	90	⁹ AKERIB	06	CDMS	⁷³ Ge, ²⁹ Si
< 40	90	ALNER	05	NAIA	Nal
<200	90	BARNABE-HE.05	PICA	F (C ₄ F ₁₀)	
< 4	90	BENOIT	05	EDEL	⁷³ Ge
< 10	90	KLAPDOR-K...	05	HDMS	⁷³ Ge (enriched)
< 4 × 10 ³	90	TA KEDA	03	BOLO	NaF

- ¹FELIZARDO 20 presents 2014 SIMPLE bounds on WIMP DM using C₂F₅ target .
- ²APRILE 19A search for SD WIMP scatter on 1 t yr Xe; no signal, limits placed in $\sigma^{SD}(\chi n)$ vs. $m(\chi)$ plane for $m \sim 6$ -1000 GeV.
- ³XIA 19A search for WIMP scatter on Xe in PandaX-II; limits placed in $\sigma^{SD}(\chi n)$ vs. $m(\chi)$ plane for $m(\chi) \sim 5$ -1 × 10⁵ GeV.
- ⁴AKERIB 17A search for SD WIMP scatter on Xe with 129.5 kg yr exposure; limits placed in $\sigma^{SD}(\chi n)$ vs. $m(\chi)$ plane for $m(\chi) \sim 5$ -1 × 10⁵ GeV.
- ⁵FU 17 search for SD WIMP scatter on Xe; limits set in $\sigma^{SD}(\chi n)$ vs. $m(\chi)$ plane for $m(\chi) \sim 4$ -1 × 10³ GeV.
- ⁶Derived limit from search for inelastic scattering $X^0 + ^{129}\text{Xe}^* \rightarrow X^0 + ^{129}\text{Xe}^*$ (39.58 keV).
- ⁷The value has been provided by the authors. See also APRILE 14A.
- ⁸BEDNYAKOV 08 reanalyze KLAPDOR-KLEINGROTHAUS 05 and BAUDIS 01 data.
- ⁹See also AKERIB 05.

Cross-Section Limits for Dark Matter Particles (X⁰) on electronFor m_{X^0} in GeV range

We provide here limits for $m_{X^0} < 5$ GeV

VALUE (pb)	CL%	DOCUMENT ID	TECN	COMMENT
< 10	90	¹ CHENG	21	PNDX MeV-scale DM on e
< 8.7 × 10 ²	90	² AKERIB	20	LUX mirror DM with Xe
< 100	90	³ AMARAL	20	SCDM light DM scatter on e in Si
< 0.6	90	⁴ APRILE	20	XE1T excess keV electron recoil in Xe
< 2 × 10 ⁶	90	⁵ ARNAUD	20	EDEL MeV DM scatter on e in Ge
< 1 × 10 ⁻⁴	90	⁶ BARAK	20	SENS MeV scale DM scatter from e in Si
< 9 × 10 ⁻³	90	⁷ ABRAMOFF	19	SENS WIMP-e scatter on Si
< 1 × 10 ⁴	90	⁸ AGUILAR-AR...	19A	DMIC MeV scale DM scatter on e in Si
< 5 × 10 ³	90	⁹ APRILE	19D	XE1T light DM on Xe via ionization
	90	¹⁰ AGNES	18B	DS50 Ar
	90	¹¹ AGNESE	18B	SCDM e χ scatter
	90	¹² CRISLER	18	SENS Si CCD
	90	¹³ APRILE	17	X100 Xe, annual modulation

- ¹CHENG 21 search for MeV-scale DM scatter from e in PANDAX-II. No signal detected. Limits set in $\sigma(\chi e)$ vs. $m(\text{DM})$ plane for two choices of form factors; $\sigma(\chi e) < 10$ pb for $m(\chi) = 10$ MeV and $F_{DM} = 1$.
- ²AKERIB 20 search for mirror DM with LUX 95 d × 118 kg data for mirror e scatter from Xe; no signal, limits placed in kinetic mixing parameter vs. mirror e temperature $T \sim 0.1$ -0.9 keV plane.
- ³AMARAL 20 search SuperCDMS data for low mass DM scatter from e in Si; no signal; quoted limit $\sigma_e < 8.7 \times 10^2$ pb for $m(\text{DM}) = 10$ MeV with form factor $F_{DM} = 1$.
- ⁴APRILE 20 report excess at electron recoil around 2-3 keV in Xe; data compared to unforeseen tritium background, and various signal models (bosonic DM, solar axion, and neutrino magnetic moment).
- ⁵ARNAUD 20 search for MeV DM scatter from e in Ge; no signal; quoted limit is for $m(\text{DM}) = 10$ MeV with form factor $F_{DM} = 1$.
- ⁶BARAK 20 report search for MeV scale DM scatter from e in Si; limits placed in σ_e vs. $m(\text{DM})$ plane; quoted limit is for $m(\text{DM}) = 10$ MeV and form factor $F_{DM} = 1$.
- ⁷ABRAMOFF 19 search for MeV-scale WIMP scatter from Si skipper-CCD; limits placed on $\sigma(\chi e)$ for $m(\chi) \sim 0.5$ -100 MeV depending on DM form factors. Limit given for $m(\text{DM}) = 1$ MeV.
- ⁸AGUILAR-AREVALO 19A search for MeV scale DM scatter from e in Si CCDs at SNO-LAB; no signal, limits placed in $\sigma(e)$ vs. $m(\text{DM})$ plane for $m(\text{DM}) \sim 0.6$ -100 MeV.
- ⁹APRILE 19D search for light DM scatter on Xe via ionization; no signal, limits placed in σ on nucleus vs. $m(\text{DM})$ plane for $m(\text{DM}) \sim 0.02$ -10 GeV; quoted limit is for $m(\text{DM}) = 0.2$ GeV.
- ¹⁰AGNES 18B search for MeV scale WIMP scatter from e in Ar; no signal, limits set in σ_e vs. $m(\chi)$ plane for $m \sim 20$ -1000 MeV and two choices of form factor $F(\text{DM})$; quoted limit for $m(\chi) = 100$ MeV and $F = 1$.
- ¹¹AGNESE 18B search for e χ scatter in SuperCDMS; limits placed in $\sigma(e\chi)$ vs. $m(\chi)$ plane for $m \sim 0.3$ -1 × 10⁴ MeV for two assumed form factors and also in $m(\text{dark photon})$ vs. kinetic mixing plane. Limit given for $m(\chi) = 1$ GeV and $F=1$.
- ¹²CRISLER 18 search for $\chi e \rightarrow \chi e$ scatter in Si CCD; place limits on MeV DM in σ_e vs. $m(\chi)$ plane for $m \sim 0.5$ -1000 MeV for different form factors; quoted limit is for $F(\text{DM}) = 1$ and $m(\chi) = 10$ MeV.
- ¹³APRILE 17 search for WIMP-e annual modulation signal for recoil energy in the 2.0-5.8 keV interval using 4 years data with Xe. No significant effect seen.

Cross-Section Limits for Dark Matter Particles (X⁰) on NucleiFor m_{X^0} in GeV range

We provide here limits for $m_{X^0} < 5$ GeV

For $m_{X^0} = 20$ GeV

VALUE (nb)	CL%	DOCUMENT ID	TECN	COMMENT
< 0.03	90	¹ UCHIDA	14	XMAS ¹²⁹ Xe, inelastic
< 0.08	90	² ANGLOHER	02	CRES AI
< 0.04	95	³ BENOIT	00	EDEL Ge
< 0.8	96	⁴ KLIMENKO	98	CNTR ⁷³ Ge, inel.
< 6	96	ALESSAND...	96	CNTR O
< 0.02	90	⁵ BELLI	96	CNTR ¹²⁹ Xe, inel.
< 4 × 10 ⁻³	90	⁶ BELLI	96c	CNTR ¹²⁹ Xe
< 0.3	90	⁷ BERNABE	96	CNTR Na
< 0.2	95	⁸ SARSA	96	CNTR Na
< 0.015	90	⁹ SMITH	96	CNTR Na
< 0.05	95	¹⁰ GARCIA	95	CNTR Natural Ge
< 0.1	95	QUENBY	95	CNTR Na
< 90	90	¹¹ SNOWDEN...	95	MICA ¹⁶ O
< 4 × 10 ³	90	¹² SNOWDEN...	95	MICA ³⁹ K
< 0.7	90	BACCI	92	CNTR Na
< 0.12	90	¹² REUSSER	91	CNTR Natural Ge
< 0.06	95	CALDWELL	88	CNTR Natural Ge

- • • We do not use the following data for averages, fits, limits, etc. • • •
- ¹UCHIDA 14 limit is for inelastic scattering $X^0 + ^{129}\text{Xe}^* \rightarrow X^0 + ^{129}\text{Xe}^*$ (39.58 keV).
- ²ANGLOHER 02 limit is for spin-dependent WIMP-Aluminum cross section.
- ³BENOIT 00 find four event categories in Ge detectors and suggest that low-energy surface nuclear recoils can explain anomalous events reported by UKDMC and Slacly Nal experiments.
- ⁴KLIMENKO 98 limit is for inelastic scattering $X^0 \text{ } ^{73}\text{Ge} \rightarrow X^0 \text{ } ^{73}\text{Ge}^*$ (13.26 keV).
- ⁵BELLI 96 limit for inelastic scattering $X^0 \text{ } ^{129}\text{Xe} \rightarrow X^0 \text{ } ^{129}\text{Xe}^*$ (39.58 keV).
- ⁶BELLI 96c use background subtraction and obtain $\sigma < 150$ pb (< 1.5 fb) (90% CL) for spin-dependent (independent) X^0 -proton cross section. The confidence level is from R. Bernabei, private communication, May 20, 1999.
- ⁷BERNABE 96 use pulse shape discrimination to enhance the possible signal. The limit here is from R. Bernabei, private communication, September 19, 1997.
- ⁸SARSA 96 search for annual modulation of WIMP signal. See SARSA 97 for details of the analysis. The limit here is from M.L. Sarsa, private communication, May 26, 1997.
- ⁹SMITH 96 use pulse shape discrimination to enhance the possible signal. A dark matter density of 0.4 GeV cm^{-3} is assumed.
- ¹⁰GARCIA 95 limit is from the event rate. A weaker limit is obtained from searches for diurnal and annual modulation.
- ¹¹SNOWDEN-FFT 95 look for recoil tracks in an ancient mica crystal. Similar limits are also given for ²⁷Al and ²⁸Si. See COLLAR 96 and SNOWDEN-FFT 96 for discussion on potential backgrounds.
- ¹²REUSSER 91 limit here is changed from published (0.04) after reanalysis by authors. J.L. Vuilleumier, private communication, March 29, 1996.

For $m_{X^0} = 100$ GeV

VALUE (nb)	CL%	DOCUMENT ID	TECN	COMMENT
< 3.3 × 10 ⁻⁶	90	¹ APRILE	21A	XE1T ¹²⁹ Xe, inelastic
< 3 × 10 ⁻³	90	² UCHIDA	14	XMAS ¹²⁹ Xe, inelastic
< 0.3	90	³ ANGLOHER	02	CRES AI
		⁴ BELLI	02	RVUE
		⁵ BERNABE	02c	DAMA
		⁶ GREEN	02	RVUE
		⁷ ULLIO	01	RVUE
		⁸ BENOIT	00	EDEL Ge
< 4 × 10 ⁻³	90	⁹ BERNABE	00D	¹²⁹ Xe, inelastic
		¹⁰ AMBROSIO	99	MCRO
		¹¹ BRHLIK	99	RVUE
< 8 × 10 ⁻³	95	¹² KLIMENKO	98	CNTR ⁷³ Ge, inelastic
< 0.08	95	¹³ KLIMENKO	98	CNTR ⁷³ Ge, inelastic
< 4	96	ALESSAND...	96	CNTR O
< 25	96	ALESSAND...	96	CNTR Te
< 6 × 10 ⁻³	90	¹⁴ BELLI	96	CNTR ¹²⁹ Xe, inelastic
		¹⁵ BELLI	96c	CNTR ¹²⁹ Xe
< 1 × 10 ⁻³	90	¹⁶ BERNABE	96	CNTR Na
< 0.3	90	¹⁶ BERNABE	96	CNTR I
< 0.7	95	¹⁷ SARSA	96	CNTR Na
< 0.03	90	¹⁸ SMITH	96	CNTR Na
< 0.8	90	¹⁸ SMITH	96	CNTR I
< 0.35	95	¹⁹ GARCIA	95	CNTR Natural Ge
< 0.6	95	QUENBY	95	CNTR Na
< 3	95	QUENBY	95	CNTR I
< 1.5 × 10 ²	90	²⁰ SNOWDEN...	95	MICA ¹⁶ O
< 4 × 10 ²	90	²⁰ SNOWDEN...	95	MICA ³⁹ K
< 0.08	90	²¹ BECK	94	CNTR ⁷⁶ Ge
< 2.5	90	BACCI	92	CNTR Na
< 3	90	BACCI	92	CNTR I
< 0.9	90	²² REUSSER	91	CNTR Natural Ge
< 0.7	95	CALDWELL	88	CNTR Natural Ge

See key on page 1127

Searches Particle Listings

WIMP and Dark Matter Searches

- 1 APRILE 21A search for inelastic DM scatter off ^{129}Xe nuclei with 0.83 yr exposure. No signal observed. Limits placed in $\sigma(\chi\text{Xe})$ vs. $m(\text{DM})$ plane for WIMP mass between 20 GeV and 10 TeV.
- 2 UCHIDA 14 limit is for inelastic scattering $\chi^0 + ^{129}\text{Xe}^* \rightarrow \chi^0 + ^{129}\text{Xe}^*(39.58 \text{ keV})$.
- 3 ANGIOHER 02 limit is for spin-dependent WIMP-Aluminum cross section.
- 4 BELLI 02 discuss dependence of the extracted WIMP cross section on the assumptions of the galactic halo structure.
- 5 BERNABEI 02c analyze the DAMA data in the scenario in which χ^0 scatters into a slightly heavier state as discussed by SMITH 01.
- 6 GREEN 02 discusses dependence of extracted WIMP cross section limits on the assumptions of the galactic halo structure.
- 7 ULLIO 01 disfavor the possibility that the BERNABEI 99 signal is due to spin-dependent WIMP coupling.
- 8 BENOIT 00 find four event categories in Ge detectors and suggest that low-energy surface nuclear recoils can explain anomalous events reported by UKDMC and Saclay Nal experiments.
- 9 BERNABEI 00d limit is for inelastic scattering $\chi^0 ^{129}\text{Xe} \rightarrow \chi^0 ^{129}\text{Xe}$ (39.58 keV).
- 10 AMBROSIO 99 search for ongoing muon events induced by neutrinos originating from WIMP annihilations in the Sun and Earth.
- 11 BRHLIK 99 discuss the effect of astrophysical uncertainties on the WIMP interpretation of the BERNABEI 99 signal.
- 12 KLIMENKO 98 limit is for inelastic scattering $\chi^0 ^{73}\text{Ge} \rightarrow \chi^0 ^{73}\text{Ge}^*$ (13.26 keV).
- 13 KLIMENKO 98 limit is for inelastic scattering $\chi^0 ^{73}\text{Ge} \rightarrow \chi^0 ^{73}\text{Ge}^*$ (66.73 keV).
- 14 BELLI 96 limit for inelastic scattering $\chi^0 ^{129}\text{Xe} \rightarrow \chi^0 ^{129}\text{Xe}^*(39.58 \text{ keV})$.
- 15 BELLI 96c use background subtraction and obtain $\sigma < 0.35 \text{ pb}$ ($< 0.15 \text{ fb}$) (90% CL) for spin-dependent (independent) χ^0 -proton cross section. The confidence level is from R. Bernabei, private communication, May 20, 1999.
- 16 BERNABEI 96 use pulse shape discrimination to enhance the possible signal. The limit here is from R. Bernabei, private communication, September 19, 1997.
- 17 SARSA 96 search for annual modulation of WIMP signal. See SARSA 97 for details of the analysis. The limit here is from M.L. Sarsa, private communication, May 26, 1997.
- 18 SMITH 96 use pulse shape discrimination to enhance the possible signal. A dark matter density of 0.4 GeV cm^{-3} is assumed.
- 19 GARCIA 95 limit is from the event rate. A weaker limit is obtained from searches for diurnal and annual modulation.
- 20 SNOWDEN-IFFT 95 look for recoil tracks in an ancient mica crystal. Similar limits are also given for ^{27}Al and ^{28}Si . See COLLAR 96 and SNOWDEN-IFFT 96 for discussion on potential backgrounds.
- 21 BECK 94 uses enriched ^{76}Ge (86% purity).
- 22 REUSSER 91 limit here is changed from published (0.3) after reanalysis by authors. J.L. Vuilleumier, private communication, March 29, 1996.

For $m_{\chi^0} = 1 \text{ TeV}$

VALUE (nb)	CL%	DOCUMENT ID	TECN	COMMENT
• • • We do not use the following data for averages, fits, limits, etc. • • •				
< 0.03	90	1 UCHIDA 14	XMAS	^{129}Xe , inelastic
< 3	90	2 ANGIOHER 02	CRES	Al
		3 BENOIT 00	EDEL	Ge
		4 BERNABEI 99d	CNTR	SIMP
		5 DERBIN 99	CNTR	SIMP
< 0.06	95	6 KLIMENKO 98	CNTR	^{73}Ge , inel.
< 0.4	95	7 KLIMENKO 98	CNTR	^{73}Ge , inel.
< 40		ALESSAND... 96	CNTR	O
< 700		ALESSAND... 96	CNTR	Te
< 0.05	90	8 BELLI 96	CNTR	^{129}Xe , inel.
< 1.5	90	9 BELLI 96	CNTR	^{129}Xe , inel.
		10 BELLI 96c	CNTR	^{129}Xe
< 0.01	90	11 BERNABEI 96	CNTR	Na
< 9	90	11 BERNABEI 96	CNTR	l
< 7	95	12 SARSA 96	CNTR	Na
< 0.3	90	13 SMITH 96	CNTR	Na
< 6	90	13 SMITH 96	CNTR	l
< 6	95	14 GARCIA 95	CNTR	Natural Ge
< 8	95	QUENBY 95	CNTR	Na
< 50	95	QUENBY 95	CNTR	l
< 700	90	15 SNOWDEN... 95	MICA	^{16}O
< 1 $\times 10^3$	90	15 SNOWDEN... 95	MICA	^{39}K
< 0.8	90	16 BECK 94	CNTR	^{76}Ge
< 30	90	BACCI 92	CNTR	Na
< 30	90	BACCI 92	CNTR	l
< 15	90	17 REUSSER 91	CNTR	Natural Ge
< 6	95	CALDWELL 88	CNTR	Natural Ge

- 1 UCHIDA 14 limit is for inelastic scattering $\chi^0 + ^{129}\text{Xe}^* \rightarrow \chi^0 + ^{129}\text{Xe}^*$ (39.58 keV).
- 2 ANGIOHER 02 limit is for spin-dependent WIMP-Aluminum cross section.
- 3 BENOIT 00 find four event categories in Ge detectors and suggest that low-energy surface nuclear recoils can explain anomalous events reported by UKDMC and Saclay Nal experiments.
- 4 BERNABEI 99d search for SIMPs (Strongly Interacting Massive Particles) in the mass range 10^3 – 10^{16} GeV. See their Fig. 3 for cross-section limits.
- 5 DERBIN 99 search for SIMPs (Strongly Interacting Massive Particles) in the mass range 10^2 – 10^{14} GeV. See their Fig. 3 for cross-section limits.
- 6 KLIMENKO 98 limit is for inelastic scattering $\chi^0 ^{73}\text{Ge} \rightarrow \chi^0 ^{73}\text{Ge}^*$ (13.26 keV).
- 7 KLIMENKO 98 limit is for inelastic scattering $\chi^0 ^{73}\text{Ge} \rightarrow \chi^0 ^{73}\text{Ge}^*$ (66.73 keV).
- 8 BELLI 96 limit for inelastic scattering $\chi^0 ^{129}\text{Xe} \rightarrow \chi^0 ^{129}\text{Xe}^*(39.58 \text{ keV})$.
- 9 BELLI 96 limit for inelastic scattering $\chi^0 ^{129}\text{Xe} \rightarrow \chi^0 ^{129}\text{Xe}^*(236.14 \text{ keV})$.
- 10 BELLI 96c use background subtraction and obtain $\sigma < 0.7 \text{ pb}$ ($< 0.7 \text{ fb}$) (90% CL) for spin-dependent (independent) χ^0 -proton cross section. The confidence level is from R. Bernabei, private communication, May 20, 1999.

- 11 BERNABEI 96 use pulse shape discrimination to enhance the possible signal. The limit here is from R. Bernabei, private communication, September 19, 1997.
- 12 SARSA 96 search for annual modulation of WIMP signal. See SARSA 97 for details of the analysis. The limit here is from M.L. Sarsa, private communication, May 26, 1997.
- 13 SMITH 96 use pulse shape discrimination to enhance the possible signal. A dark matter density of 0.4 GeV cm^{-3} is assumed.
- 14 GARCIA 95 limit is from the event rate. A weaker limit is obtained from searches for diurnal and annual modulation.
- 15 SNOWDEN-IFFT 95 look for recoil tracks in an ancient mica crystal. Similar limits are also given for ^{27}Al and ^{28}Si . See COLLAR 96 and SNOWDEN-IFFT 96 for discussion on potential backgrounds.
- 16 BECK 94 uses enriched ^{76}Ge (86% purity).
- 17 REUSSER 91 limit here is changed from published (5) after reanalysis by authors. J.L. Vuilleumier, private communication, March 29, 1996.

Miscellaneous Results from Underground Dark Matter Searches

VALUE	CL%	DOCUMENT ID	TECN	COMMENT
• • • We do not use the following data for averages, fits, limits, etc. • • •				
		1 ADHIKARI 22	DEAP	Planck scale DM multiple scatter on Ar
		2 AKERIB 21b	LUX	limits on WIMP EFT couplings
		3 AMARE 21	ANAL	annual modulation on Nal
		4 AGOSTINI 20	HPGE	keV-MeV scale super-WIMP absorption in Ge
		5 ANDRIANAV... 20	FUNK	hidden photon DM search
		6 CLARK 20	20	superheavy MIMP DM
		7 ABRAMOFF 19	SENS	MeV DM e-Si; dark photon Si absorption
		8 ADHIKARI 19	C100	annual modulation Nal
		9 AMARE 19	ANAL	annual modulation Nal
< 6.4×10^{-10}	90	10 APRILE 19	XE1T	π (Xe)
		11 BRINGMANN 19		cosmic ray DM
		12 BRUNE 19		Majoron DM
		13 CHOI 19	THEO	290 TeV IceCube ν
		14 HA 19	C100	inelastic boosted dark γ
		15 KLOPF 19		$n \rightarrow \chi e^+ e^-$
		16 AARTSEN 18d	ICCB	relic WIMP $\chi \rightarrow \nu X$
		17 ABE 18f	XMAS	$A' e \rightarrow A' e$
		18 AGNES 18b	D550	Ar
		19 AGNESE 18b	SCDM	MeV DM e-Si; dark photon Si absorption
		20 AKERIB 18a	LUX	Xe
		21 ARMENGAUD 18	EDE3	Ge
		22 KACHULIS 18	SKAM	boosted DM on e
< 1×10^{-12}	90	23 AGUILAR-AR... 17	DMIC	γ' on Si
		24 APRILE 17	X100	Xe
		25 APRILE 17b	X100	Xe
		26 APRILE 17h	X100	keV bosonic DM search
		27 APRILE 17k	X100	$\chi N \rightarrow \chi^* \rightarrow \chi \gamma$
< 4×10^{-3}	90	28 ANGIOHER 16a	CRES	CaWO_4
		29 APRILE 15	X100	Event rate modulation
		30 APRILE 15a	X100	Electron scattering

- 1 ADHIKARI 22 search for multiple scatter of Planck scale DM on Ar using DEAP detector. No signal observed. Limits placed in mass vs. cross section plane for $m(\text{DM})$: 10^7 – 10^{19} GeV.
- 2 AKERIB 21b place limits on 15 WIMP non-relativistic EFT couplings for $m(\text{DM})$: 10–4000 GeV using 3.14 kg d exposure.
- 3 AMARE 21 search for WIMP annual modulation signal on Nal target in the Canfranc Underground Laboratory (LSC). With an effective exposure of 313.95 kg y, and a sensitivity of 2.5σ no signal is observed. Incompatible with DAMA/LIBRA at 3.3σ level.
- 4 AGOSTINI 20 search for keV–MeV scale super-WIMP absorption in Ge in GERDA; no signal; limits placed on keV–MeV scale bosonic super-WIMPs in coupling vs. mass plane.
- 5 ANDRIANAVALOMAHEFA 20 search for hidden photon DM in eV range; place limits in $m(\text{DM})$ vs $\ln(\chi)$ plane: exclude coupling $\chi \lesssim 1 \times 10^{-12}$ for $m(\text{DM}) \sim 2.5$ –7 eV.
- 6 CLARK 20 use Majorana and Xe-1-ton data to constrain superheavy multiply interacting dark matter (MIMP) in range $m \sim 10^8$ – 10^{17} GeV depending on interaction cross section.
- 7 ABRAMOFF 19 search for MeV scale DM via DM–e scattering and dark photon DM via absorption in Si; limits set in coupling vs. $m(\chi)$ plane and on dark photon in $m(A)$ vs. kinetic mixing parameter plane.
- 8 ADHIKARI 19 search for annual modulation signal from WIMP scatter on Nal with 1.7 yr exposure; result consistent with both DAMA/LIBRA and null hypothesis.
- 9 AMARE 19 is ANAIS-112 search for WIMP scatter annual modulation on Nal; 157.55 kg yr exposure; result compatible with null hypothesis; confirm goal of reaching sensitivity at 3σ to DAMA/LIBRA result in 5 years.
- 10 APRILE 19 search for WIMP-pion scattering in Xe; no signal: require $\sigma(\chi\pi) < 6.4 \times 10^{-10} \text{ pb}$ for $m(\chi) = 30 \text{ GeV}$.
- 11 BRINGMANN 19 derive theoretically limits on GeV and sub-GeV mass dark matter, in its high energy component generated by interaction with cosmic rays; place limits on σ_{SI} and $\sigma_{SD} < 10^9 \text{ pb}$.
- 12 BRUNE 19 examine possibility of Majoron dark matter; limits placed on Majoron mass vs. coupling from SN1987a and ν -less double beta decay.
- 13 CHOI 19 from multimessenger observation finds limit on $\sigma(\nu\chi)/m(\text{DM}) < 5.1 \times 10^{-23} \text{ cm}^2/\text{GeV}$ based on 290 TeV IceCube neutrino event.
- 14 HA 19 search for inelastic boosted MeV scale dark photon using COSINE-100 data; limits placed in m vs. epsilon plane for various mediators.
- 15 KLOPF 19 search for DM via $n \rightarrow \chi e^+ e^-$; no signal: limits placed in branching fraction vs. $m(e^+ e^-)$ plane.
- 16 AARTSEN 18d search for long-lived DM particles decaying $\chi \rightarrow \nu X$; no excess seen; for DM masses above 10 TeV, excluding lifetimes shorter than 10^{28} s .

Searches Particle Listings

WIMP and Dark Matter Searches

- 17 ABE 18f search for keV mass ALPs and hidden photons (HP) scatter on electrons; limits set on mass vs. coupling.
- 18 AGNES 18b search for MeV-scale DM scatter on electrons in Ar; no signal; require $\sigma(\chi e) < 9 \times 10^{-3}$ pb for DM form factor $F(\text{DM}) = 1$ and < 300 pb for $F(\text{DM})$ proportional to $1/q^2$ for $m(\chi) = 100$ MeV.
- 19 AGNESE 18b search for MeV scale DM via DM- e scattering and dark photon DM via absorption in Si; limits set on MeV DM in coupling vs. $m(\chi)$ plane and on dark photon in $m(A')$ vs. kinetic mixing plane.
- 20 AKERIB 18a search for annual and diurnal modulation of DM scattering rate on electrons for recoil energy between 2 and 6 keVee; no signal found.
- 21 ARMENGAUD 18 search for ALP from the Sun and galactic bosonic DM, interacting in Ge; no signal; limits set for 0.8–500 keV DM particles.
- 22 KACHULIS 18 search for an excess of elastically scattered electrons above the atmospheric neutrino background in Super-K; limits placed for simple annihilation or decay in the Sun or galactic center producing "boosted" dark matter.
- 23 AGUILAR-AREVALO 17 search for hidden photon DM scatter on Si target CCD; limit kinetic mixing $\kappa < 1 \times 10^{-12}$ for $m = 10$ eV.
- 24 APRILE 17 search for WIMP- e annual modulation signal for recoil energy in the 2.0–5.8 keV interval using 4 years data with Xe. No significant effect seen.
- 25 APRILE 17d set limits on 14 WIMP-nucleon different interaction operators. No deviations found using 225 live days in the 6.6–240 keV recoil energy range.
- 26 APRILE 17h search for keV bosonic DM via $e\chi \rightarrow e$, looking for electronic recoils with 224.6 live days of data and 34 kg of LXe. Limits set on $\chi e e$ coupling for $m(\chi) = 8$ –125 keV.
- 27 APRILE 17k search for magnetic inelastic DM via $\chi N \rightarrow \chi^* \rightarrow \chi\gamma$. Limits set in DM magnetic moment vs. mass splitting plane for two DM masses corresponding to the DAMA/LIBRA best fit values.
- 28 ANGLOHER 16a require q^2 dependent scattering $< 8 \times 10^{-3}$ pb for asymmetric DM $m(\text{WIMP}) = 3$ GeV on CaWO_4 target. It uses a local dark matter density of 0.38 GeV/cm^3 .
- 29 APRILE 15 search for periodic variation of electronic recoil event rate in the data between Feb. 2011 and Mar. 2012. No significant modulation is found for periods up to 500 days.
- 30 APRILE 15a search for χ^0 scattering off electrons. See their Fig. 4 for limits on cross section through axial-vector coupling for m_{χ^0} between 0.6 GeV and 1 TeV. For $m_{\chi^0} = 2$ GeV, $\sigma < 60$ pb (90%CL) is obtained.

 χ^0 Annihilation Cross SectionLimits are on σv for χ^0 pair annihilation at threshold.

VALUE (cm^2s^{-1})	CL%	DOCUMENT ID	TECN	COMMENT
• • • We do not use the following data for averages, fits, limits, etc. • • •				
$< 5 \times 10^{-24}$	95	1 ABDALLAH 21	HESS	WIMP annihilation in dwarf irregular galaxy
		2 CIRELLI 21		light DM annihilation producing X-rays
		3 JOHN 21		cosmic positron spectra limits on leptophilic DM
$< 2.5 \times 10^{-27}$	95	4 ABAZAJIAN 20	FLAT	γ from galactic center
		5 ABDALLAH 20	HESS	WIMP annihilation in dwarf satellite galaxies
$< 1.2 \times 10^{-24}$	90	6 ABE 20g	SKAM	WIMP annihilation to neutrinos
$< 2.2 \times 10^{-24}$	95	7 ALBERT 20	HAWC	WIMP annihilation to γ
$< 5 \times 10^{-24}$	90	8 ALBERT 20a	ANTR	WIMP annihilation to $\nu\bar{\nu}$ in galactic center
$< 1 \times 10^{-23}$	90	9 ALBERT 20c	ANTR	Antares/IceCube search for WIMP annihilation to $\nu\bar{\nu}$
$< 8 \times 10^{-26}$		10 ALVAREZ 20	FLAT	dwarf spheroidal; J-distribution
$< 2 \times 10^{-26}$	90	11 HOOF 20	FLAT	WIMP annihilation to γ
		12 MAZZIOTTA 20	FLAT	DM annihilation in Sun to γ
		13 ABEYSEKARA 19	HAWC	DM annihilation to $\gamma\bar{\gamma}$ within galactic substructure
$< 0.8 \times 10^{-22}$	95	14 ALBERT 19b	HAWC	annihilation/decay to γ in M31
$< 4 \times 10^{-26}$	95	15 CHEUNG 19	EDGS	$\chi\chi \rightarrow e^+e^-$ and $b\bar{b}$
$< 7 \times 10^{-27}$	95	16 DI-MAURO 19	FLAT	Fermi-LAT M31 and M33
		17 JOHNSON 19	FLAT	P-wave DM; Fermi-LAT
$< 2 \times 10^{-26}$	95	18 LI 19d	FLAT	$\chi\chi \rightarrow \gamma$
$< 1 \times 10^{-32}$		19 NG 19		sterile ν decay/annihilation
		20 QUEIROZ 19		semi-annihilating DM
$< 4 \times 10^{-28}$	95	21 ABDALLAH 18	HESS	$\chi^0\chi^0 \rightarrow \gamma X$; galactic halo
$< 1 \times 10^{-23}$	95	22 AHNEN 18	MGIC	$\chi^0\chi^0 \rightarrow \gamma X$; Ursa Major II
$< 1 \times 10^{-22}$	95	23 ALBERT 18b	HAWC	$\chi^0\chi^0 \rightarrow \gamma X$; Andromeda
$< 1 \times 10^{-26}$	95	24 CHANG 18a		$\chi\chi \rightarrow b\bar{b} \rightarrow \gamma$
		25 LISANTI 18	THEO	Fermi, γ ; galaxy groups
		26 MAZZIOTTA 18	FLAT	Fermi-LAT CRE data
$< 1.2 \times 10^{-23}$	95	27 AARTSEN 17c	ICCB	$\chi\chi \rightarrow$ neutrinos
$< 1 \times 10^{-23}$	95	28 ALBERT 17a	ANTR	ν , DM annihilation
$< 1.32 \times 10^{-25}$	95	29 ARCHAMBAU.17	VRTS	γ dwarf galaxies
$< 7 \times 10^{-21}$	90	30 AVRORIN 17	BAIK	cosmic ν
$< 1 \times 10^{-28}$		31 BOUDAUD 17		MeV DM to e^+e^-
		32 AARTSEN 16d	ICCB	ν , galactic center
$< 6 \times 10^{-26}$	95	33 ABDALLAH 16	HESS	Central Galactic Halo
$< 1 \times 10^{-27}$	95	34 ABDALLAH 16a	HESS	WIMP+WIMP $\rightarrow \gamma\gamma$; galactic center
$< 3 \times 10^{-26}$	95	35 AHNEN 16	MGFL	Satellite galaxy, $m(\text{WIMP})=100$ GeV
$< 1.9 \times 10^{-21}$	90	36 AVRORIN 16	BAIK	$\nu\bar{\nu}$ from galactic center
$< 3 \times 10^{-26}$	95	37 CAPUTO 16	FLAT	small Magellanic cloud
$< 1 \times 10^{-25}$	95	38 FORNASA 16	FLAT	Fermi-LAT γ -ray anisotropy
$< 5 \times 10^{-27}$		39 LEITE 16		WIMP, radio

$< 2 \times 10^{-26}$	95	40 LI 16	FLAT	dwarf galaxies
$< 1 \times 10^{-25}$	95	41 LI 16a	FLAT	Fermi-LAT; M31
$< 1 \times 10^{-26}$		42 LIANG 16	FLAT	Fermi-LAT, gamma line
$< 1 \times 10^{-25}$	95	43 LU 16	FLAT	Fermi-LAT and AMS-02
$< 1 \times 10^{-23}$	95	44 SHIRASAKI 16	FLAT	extra galactic
		45 AARTSEN 15c	ICCB	ν , Galactic halo
		46 AARTSEN 15e	ICCB	ν , Galactic center
		47 ABRAMOWSKI15	HESS	Galactic center
		48 ACKERMANN 15	FLAT	monochromatic γ
		49 ACKERMANN 15a	FLAT	isotropic γ background
		50 ACKERMANN 15b	FLAT	Satellite galaxy
		51 ADRIAN-MAR.15	ANTR	ν , Galactic center
$< 2.90 \times 10^{-26}$	95	52,53 ACKERMANN 14	FLAT	Satellite galaxy, $m = 10$ GeV
$< 1.84 \times 10^{-25}$	95	52,54 ACKERMANN 14	FLAT	Satellite galaxy, $m = 100$ GeV
$< 1.75 \times 10^{-24}$	95	52,54 ACKERMANN 14	FLAT	Satellite galaxy, $m = 1$ TeV
$< 4.52 \times 10^{-24}$	95	55 ALEKSIC 14	MGIC	Segue 1, $m = 1.35$ TeV
		56 AARTSEN 13c	ICCB	Galaxies
		57 ABRAMOWSKI13	HESS	Central Galactic Halo
		58 ACKERMANN 13a	FLAT	Galaxy
		59 ABRAMOWSKI12	HESS	Fornax Cluster
		60 ACKERMANN 12	FLAT	Galaxy
		61 ACKERMANN 12	FLAT	Galaxy
		62 ALIU 12	VRTS	Segue 1
$< 1 \times 10^{-22}$	90	63 ABBASI 11c	ICCB	Galactic halo, $m=1$ TeV
$< 3 \times 10^{-25}$	95	64 ABRAMOWSKI11	HESS	Near Galactic center, $m=1$ TeV
$< 1 \times 10^{-26}$	95	65 ACKERMANN 11	FLAT	Satellite galaxy, $m=10$ GeV
$< 1 \times 10^{-25}$	95	65 ACKERMANN 11	FLAT	Satellite galaxy, $m=100$ GeV
$< 1 \times 10^{-24}$	95	65 ACKERMANN 11	FLAT	Satellite galaxy, $m=1$ TeV

- 1 ABDALLAH 21 search for WIMP-WIMP annihilation into 2 monoenergetic γ rays in WLM dwarf irregular galaxy using HESS data. No signal. Limits placed in $\langle\sigma v\rangle$ vs. $m(\text{WIMP})$ plane for a mass of 370 GeV.
- 2 CIRELLI 21 derive limits on light DM annihilation to $ee, \mu\mu, \pi\pi$ that then produce X-rays using data published by INTEGRAL telescope. Limits placed in $\langle\sigma v\rangle$ vs. $m(\text{DM})$ plane for $m(\text{DM}) = 1$ –5000 MeV.
- 3 JOHN 21 derive limits on leptophilic DM annihilating to positrons by comparing expected spectra to AMS-02 data. The range $m(\text{DM}): 60$ –300 GeV appears excluded for this type of model, see Fig. 3.
- 4 ABAZAJIAN 20 derive new limits on WIMP annihilation in galactic center (GC): $\sigma \cdot v < 2.5 \times 10^{-27} \text{ cm}^3/\text{s}$ for $m(\text{WIMP}) = 50$ GeV; seems to rule out WIMP explanation for GC γ excess, favouring an astrophysics origin.
- 5 ABDALLAH 20 search for WIMP annihilation in newly discovered by DES dwarf satellite galaxies using HESS; limits placed in $\langle\sigma v\rangle$ vs. $m(\text{DM})$ plane depending on annihilation channel and which dwarf satellite.
- 6 ABE 20c search Super-Kamiokande data for WIMP annihilation to neutrinos in galactic center/halo; no signal; limits placed in $\langle\sigma v\rangle$ vs. $m(\text{DM})$ plane depending on annihilation channel and $m(\text{WIMP})$. Reported limit for annihilation to $\nu\bar{\nu}$ at 1 GeV.
- 7 ALBERT 20 search for TeV-scale WIMP annihilation to $\gamma\gamma$ in dwarf spheroidal galaxies; no signal; limits placed in σv vs $m(\text{WIMP})$ plane: e.g. $\sigma v < 2.2 \times 10^{-24} \text{ cm}^3/\text{s}$ for $m(\text{WIMP}) = 1$ TeV.
- 8 ALBERT 20a search for WIMP annihilation to $\nu\bar{\nu}$ in galactic center using Antares; limits placed in $\sigma \cdot v$ vs $m(\text{WIMP})$ plane e.g. $\sigma \cdot v < 5 \times 10^{-24} \text{ cm}^3/\text{s}$ for $m(\text{WIMP}) = 1$ TeV assuming annihilation dominantly to $\tau\bar{\tau}$.
- 9 ALBERT 20c report combined Antares + IceCube search for WIMP annihilation to $\tau\bar{\tau}$; for NFW halo profile report $\sigma v < 1 \times 10^{-23} \text{ cm}^3/\text{s}$ for $m(\text{WIMP}) = 100$ GeV.
- 10 ALVAREZ 20 use profiling over J-factor distributions and background to derive new limits on $\sigma \cdot v$; e.g. $\sigma \cdot v < 8 \times 10^{-26} \text{ cm}^3/\text{s}$ for $m(\text{WIMP}) = 100$ GeV.
- 11 HOOF 20 examine γ rays from 27 dwarf spheroidals using Fermi-LAT data; place limits in $\sigma \cdot v$ vs $m(\text{WIMP})$ plane using profile likelihood and marginalized posterior techniques for DM annihilation to $\tau\bar{\tau}$ and $b\bar{b}$; quoted limit uses first technique and $b\bar{b}$ channel for $m(\text{WIMP}) = 100$ GeV; results rule out WIMP explanation of galactic center excess.
- 12 MAZZIOTTA 20 use Fermi-LAT pointed-at-Sun data to search for DM annihilation in the Sun to long-lived mediators decaying into gamma rays, i.e. $\chi\chi \rightarrow \phi\phi \rightarrow 4\gamma$. Limits placed on the SI and SD DM-nucleon cross sections in the σ -DM mass plane for DM masses in the range 3 GeV – 1.8 TeV. Limits are evaluated in both cases of equilibrium and non-equilibrium.
- 13 ABEYSEKARA 19 search for $\gamma\bar{\gamma}$ from DM annihilation in galactic substructures with HAWC; no signal, limits placed in $J(\sigma v)$ vs. declination plane for $m(\text{DM}) \sim 1$ –108 TeV.
- 14 ALBERT 19b search for DM signal from M31 galaxy in μ, τ, t, b, W channels using HAWC for $m(\text{DM}) \sim 1$ –100 TeV; no signal, limits placed in $\langle\sigma v\rangle$ vs. $m(\text{DM})$ plane.
- 15 CHEUNG 19 derive model-dependent bounds on $\langle\sigma v\rangle$ from EDGES data: $< 4 \times 10^{-26} \text{ cm}^3/\text{s}$ for e^+e^- and $b\bar{b}$ for $m(\chi) = 100$ GeV (including boost factor).
- 16 DI-MAURO 19 place limits on WIMP annihilation via Fermi-LAT observation of M31 and M33 galaxies: $\langle\sigma v\rangle < 7 \times 10^{-27} \text{ cm}^3/\text{s}$ for $m(\chi) = 20$ GeV from M31.
- 17 JOHNSON 19 search for γ -rays, 10–600 GeV energy, from P-wave annihilating DM around SgrA* BH using Fermi-LAT; limits set for various models.
- 18 LI 19d search for $\chi\chi \rightarrow \gamma$ in Fermi-LAT data; no signal, require $\langle\sigma v\rangle < 2 \times 10^{-26} \text{ cm}^3/\text{s}$ for $m(\chi) = 100$ GeV.
- 19 NG 19 search for X-ray line from sterile ν decay/annihilation using NuStar M-31; no signal: limits placed in $m(\nu)$ vs mixing angle and $\langle\sigma v\rangle$ vs $m(\nu)$.
- 20 QUEIROZ 19 examine $\chi\chi \rightarrow \chi SM$ semi-annihilation of DM reaction; limits placed for various assumed SM particles in $\langle\sigma v\rangle$ vs. $m(\chi)$ plane.
- 21 ABDALLAH 18 search for WIMP WIMP $\rightarrow \gamma X$ in central galactic halo, 10 years of data; limits placed in $\langle\sigma v\rangle$ vs. $m(\text{WIMP})$ plane for $m(\text{WIMP}): 0.3$ –70 TeV.
- 22 AHNEN 18 search for WIMP WIMP $\rightarrow \gamma X$ from Ursa Major II; limits set in $\langle\sigma v\rangle$ vs. $m(\text{WIMP})$ plane for $b\bar{b}, W^+W^-, \tau^+\tau^-,$ and $\mu^+\mu^-$ annihilation modes.
- 23 ALBERT 18b search for TeV-scale WIMPs with WIMP WIMP $\rightarrow \gamma X$ in Andromeda galaxy using HAWC Observatory; limits set in $\langle\sigma v\rangle$ vs $m(\text{WIMP})$ plane.

- 24 CHANG 18A examine $\chi\chi \rightarrow b\bar{b} \rightarrow \gamma$ using Fermi Pass 8 data; no signal; require $\langle\sigma v\rangle < 10^{-26} \text{ cm}^3/\text{s}$ for $m(\chi) = 50 \text{ GeV}$.
- 25 LISANTI 18 examine Fermi Pass 8 γ -ray data from galaxy groups; report $m(\text{WIMP}) > 30 \text{ GeV}$ for annihilation in $b\bar{b}$ channel.
- 26 MAZZIOTTA 18 examine Fermi-LAT electron and positron spectra searching for features originating from DM particles annihilation into e^+e^- pairs, from 45 GeV to 2 TeV; no signal found, limits are obtained.
- 27 AARTSEN 17c use 1005 days of IceCube data to search for $\chi\chi \rightarrow$ neutrinos via various annihilation channels. Limits set.
- 28 ALBERT 17A search for DM annihilation to νs using ANTARES data from 2007–2015. No signal. Limits set in $\langle\sigma v\rangle$ vs. $m(\text{DM})$ plane for $m(\text{DM}) \sim 10\text{--}10^5 \text{ GeV}$. The listed limit is for $m(\text{DM}) = 100 \text{ TeV}$.
- 29 ARCHAMBAULT 17 set limits for WIMP mass between 100 GeV and 1 TeV on $\langle\sigma v\rangle$ for $W^+W^-, ZZ, b\bar{b}, s\bar{s}, u\bar{u}, d\bar{d}, t\bar{t}, e^+e^-, gg, c\bar{c}, hh, \gamma\gamma, \mu^+\mu^-, \tau^+\tau^-$ annihilation channels.
- 30 AVORIN 17 find upper limits for the annihilation cross section in various channels for DM particle mass between 30 GeV and 10 TeV. Strongest upper limits coming from the two neutrino channel require $\langle\sigma v\rangle < 6 \times 10^{-20} \text{ cm}^3/\text{s}$ in dwarf galaxies and $\langle\sigma v\rangle < 7 \times 10^{-21} \text{ cm}^3/\text{s}$ in LMC for 5 TeV WIMP mass.
- 31 BOUDAUD 17 use data from the spacecraft Voyager 1, beyond the heliopause, and from AMS02 on $\chi\chi \rightarrow e^+e^-$ to require $\langle\sigma v\rangle < 1. \times 10^{-28} \text{ cm}^3/\text{s}$ for $m(\chi) = 10 \text{ MeV}$.
- 32 AARTSEN 16d search for GeV νs from WIMP annihilation in galaxy; limits set on $\langle\sigma v\rangle$ in Fig. 6, 7.
- 33 ABDALLAH 16 require $\langle\sigma v\rangle < 6 \times 10^{-26} \text{ cm}^3/\text{s}$ for $m(\text{WIMP}) = 1.5 \text{ TeV}$ from 254 hours observation (WW channel) and $< 2 \times 10^{-26} \text{ cm}^3/\text{s}$ for $m(\text{WIMP}) = 1.0 \text{ TeV}$ in $\tau^+\tau^-$ channel.
- 34 ABDALLAH 16a search for line spectra from WIMP + WIMP $\rightarrow \gamma\gamma$ in 18 hr HESS data; rule out previous 130 GeV WIMP hint from Fermi-LAT data.
- 35 AHNEN 16 require $\langle\sigma v\rangle < 3 \times 10^{-26} \text{ cm}^3/\text{s}$ for $m(\text{WIMP}) = 100 \text{ GeV}$ (WW channel).
- 36 AVORIN 16 require $\langle\sigma v\rangle < 1.91 \times 10^{-21} \text{ cm}^3/\text{s}$ from WIMP annihilation to νs via WW channel for $m(\text{WIMP}) = 1 \text{ TeV}$.
- 37 CAPUTO 16 place limits on WIMPs from annihilation to gamma rays in Small Magellanic Cloud using Fermi-LAT data: $\langle\sigma v\rangle < 3 \times 10^{-26} \text{ cm}^3/\text{s}$ for $m(\text{WIMP}) = 10 \text{ GeV}$.
- 38 FORNASE 16 use anisotropies in the γ -ray diffuse emission detected by Fermi-LAT to bound $\langle\sigma v\rangle < 10^{-25} \text{ cm}^3/\text{s}$ for $m(\text{WIMP}) = 100 \text{ GeV}$ in $b\bar{b}$ channel: see Fig. 28. The limit is driven by dark-matter subhalos in the Milky Way and it refers to their Most Constraining Scenario.
- 39 LEITE 16 constrain WIMP annihilation via search for radio emissions from Smith cloud; $\langle\sigma v\rangle < 5 \times 10^{-27} \text{ cm}^3/\text{s}$ in ee channel for $m(\text{WIMP}) = 5 \text{ GeV}$.
- 40 LI 16 re-analyze Fermi-LAT data on 8 dwarf spheroidal; set limit $\langle\sigma v\rangle < 2 \times 10^{-26} \text{ cm}^3/\text{s}$ for $m(\text{WIMP}) = 100 \text{ GeV}$ in $b\bar{b}$ mode with substructures included.
- 41 LI 16a constrain $\langle\sigma v\rangle < 10^{-25} \text{ cm}^3/\text{s}$ in $b\bar{b}$ channel for $m(\text{WIMP}) = 100 \text{ GeV}$ using Fermi-LAT data from M31; see Fig. 6.
- 42 LIANG 16 search dwarf spheroidal galaxies, Large Magellanic Cloud, and Small Magellanic Cloud for γ -line in Fermi-LAT data.
- 43 LU 16 re-analyze Fermi-LAT and AMS-02 data; require $\langle\sigma v\rangle < 10^{-25} \text{ cm}^3/\text{s}$ for $m(\text{WIMP}) = 1 \text{ TeV}$ in $b\bar{b}$ channel.
- 44 SHIRASAKI 16 re-analyze Fermi-LAT extra-galactic data; require $\langle\sigma v\rangle < 10^{-23} \text{ cm}^3/\text{s}$ for $m(\text{WIMP}) = 1 \text{ TeV}$ in $b\bar{b}$ channel; see Fig. 8.
- 45 AARTSEN 15c search for neutrinos from X^0 annihilation in the Galactic halo. See their Figs. 16 and 17, and Table 5 for limits on $\sigma \cdot v$ for X^0 mass between 100 GeV and 100 TeV.
- 46 AARTSEN 15e search for neutrinos from X^0 annihilation in the Galactic center. See their Figs. 7 and 9, and Table 3 for limits on $\sigma \cdot v$ for X^0 mass between 30 GeV and 10 TeV.
- 47 ABRAMOWSKI 15 search for γ from X^0 annihilation in the Galactic center. See their Fig. 4 for limits on $\sigma \cdot v$ for X^0 mass between 250 GeV and 10 TeV.
- 48 ACKERMANN 15 search for monochromatic γ from X^0 annihilation in the Galactic halo. See their Fig. 8 and Tables 2–4 for limits on $\sigma \cdot v$ for X^0 mass between 0.2 GeV and 500 GeV.
- 49 ACKERMANN 15a search for γ from X^0 annihilation (both Galactic and extragalactic) in the isotropic γ background. See their Fig. 7 for limits on $\sigma \cdot v$ for X^0 mass between 10 GeV and 30 TeV.
- 50 ACKERMANN 15b search for γ from X^0 annihilation in 15 dwarf spheroidal satellite galaxies of the Milky Way. See their Figs. 1 and 2 for limits on $\sigma \cdot v$ for X^0 mass between 2 GeV and 10 TeV.
- 51 ADRIAN-MARTINEZ 15 search for neutrinos from X^0 annihilation in the Galactic center. See their Figs. 10 and 11 and Tables 1 and 2 for limits on $\sigma \cdot v$ for X^0 mass between 25 GeV and 10 TeV.
- 52 ACKERMANN 14 search for γ from X^0 annihilation in 25 dwarf spheroidal satellite galaxies of the Milky Way. See their Tables II–VII for limits assuming annihilation into $e^+e^-, \mu^+\mu^-, \tau^+\tau^-, u\bar{u}, b\bar{b}$, and W^+W^- , for X^0 mass ranging from 2 GeV to 10 TeV.
- 53 Limit assuming X^0 pair annihilation into $b\bar{b}$.
- 54 Limit assuming X^0 pair annihilation into W^+W^- .
- 55 ALEKSIC 14 search for γ from X^0 annihilation in the dwarf spheroidal galaxy Segue 1. The listed limit assumes annihilation into W^+W^- . See their Figs. 6, 7, and 16 for limits on $\sigma \cdot v$ for annihilation channels $\mu^+\mu^-, \tau^+\tau^-, b\bar{b}, t\bar{t}, \gamma\gamma, \gamma Z, W^+W^-, ZZ$ for X^0 mass between 10^2 and 10^4 GeV .
- 56 AARTSEN 13c search for neutrinos from X^0 annihilation in nearby galaxies and galaxy clusters. See their Figs. 5–7 for limits on $\sigma \cdot v$ for $X^0 X^0 \rightarrow \nu\bar{\nu}, \mu^+\mu^-, \tau^+\tau^-$, and W^+W^- for X^0 mass between 300 GeV and 100 TeV.
- 57 ABRAMOWSKI 13 search for monochromatic γ from X^0 annihilation in the Milky Way halo in the central region. Limit on $\sigma \cdot v$ between 10^{-28} and $10^{-25} \text{ cm}^3 \text{ s}^{-1}$ (95% CL) is obtained for X^0 mass between 500 GeV and 20 TeV for $X^0 X^0 \rightarrow \gamma\gamma$. X^0 density distribution in the Galaxy by Einasto is assumed. See their Fig. 4.
- 58 ACKERMANN 13a search for monochromatic γ from X^0 annihilation in the Milky Way. Limit on $\sigma \cdot v$ for the process $X^0 X^0 \rightarrow \gamma\gamma$ in the range 10^{-29} – $10^{-27} \text{ cm}^3 \text{ s}^{-1}$ (95% CL) is obtained for X^0 mass between 5 and 300 GeV. The limit depends slightly on

the assumed density profile of X^0 in the Galaxy. See their Tables VII–X and Fig. 10. Supersedes ACKERMANN 12.

- 59 ABRAMOWSKI 12 search for γ 's from X^0 annihilation in the Fornax galaxy cluster. See their Fig. 7 for limits on $\sigma \cdot v$ for X^0 mass between 0.1 and 100 TeV for the annihilation channels $\tau^+\tau^-, b\bar{b}$, and W^+W^- .
- 60 ACKERMANN 12 search for monochromatic γ from X^0 annihilation in the Milky Way. Limit on $\sigma \cdot v$ in the range 10^{-28} – $10^{-26} \text{ cm}^3 \text{ s}^{-1}$ (95% CL) is obtained for X^0 mass between 7 and 200 GeV if X^0 annihilates into $\gamma\gamma$. The limit depends slightly on the assumed density profile of X^0 in the Galaxy. See their Table III and Fig. 15.
- 61 ACKERMANN 12 search for γ from X^0 annihilation in the Milky Way in the diffuse γ background. Limit on $\sigma \cdot v$ of 10^{-24} – $10^{-26} \text{ cm}^3 \text{ s}^{-1}$ or larger is obtained for X^0 mass between 5 GeV and 10 TeV for various annihilation channels including $W^+W^-, b\bar{b}, gg, e^+e^-, \mu^+\mu^-, \tau^+\tau^-$. The limit depends slightly on the assumed density profile of X^0 in the Galaxy. See their Figs. 17–20.
- 62 ALIU 12 search for γ 's from X^0 annihilation in the dwarf spheroidal galaxy Segue 1. Limit on $\sigma \cdot v$ in the range 10^{-24} – $10^{-20} \text{ cm}^3 \text{ s}^{-1}$ (95% CL) is obtained for X^0 mass between 10 GeV and 2 TeV for annihilation channels $e^+e^-, \mu^+\mu^-, \tau^+\tau^-, b\bar{b}$, and W^+W^- . See their Fig. 3.
- 63 ABBASI 11c search for $\nu\mu$ from X^0 annihilation in the outer halo of the Milky Way. The limit assumes annihilation into $\nu\nu$. See their Fig. 9 for limits with other annihilation channels.
- 64 ABRAMOWSKI 11 search for γ from X^0 annihilation near the Galactic center. The limit assumes Einasto DM density profile.
- 65 ACKERMANN 11 search for γ from X^0 annihilation in ten dwarf spheroidal satellite galaxies of the Milky Way. The limit for $m = 10 \text{ GeV}$ assumes annihilation into $b\bar{b}$, the others W^+W^- . See their Fig. 2 for limits with other final states. See also GERINGER-SAMETH 11 for a different analysis of the same data.

Dark Matter Particle (X^0) Production in Hadron Collisions

Searches for X^0 production in association with observable particles (γ , jets, ...) in high energy hadron collisions. If a specific form of effective interaction Lagrangian is assumed, the limits may be translated into limits on X^0 -nucleon scattering cross section.

VALUE	DOCUMENT ID	TECN	COMMENT
•••	We do not use the following data for averages, fits, limits, etc. •••		
1	AAD	21AZ ATLS	DM search in $H \cancel{E}_T \rightarrow \gamma\gamma \cancel{E}_T$
2	AAD	21BB ATLS	DM search in $H \cancel{E}_T \rightarrow b\bar{b} \cancel{E}_T$
3	AAD	21D ATLS	Dark Higgs
4	AAD	21F ATLS	jet + missing momentum
5	AAD	21K ATLS	photon + DM
6	AAD	21O ATLS	$\ell + \text{jets} + \cancel{E}_T$ to search for t-pairs + DM
7	AAD	21P ATLS	$\ell^+ \ell^- + \text{jets} + \cancel{E}_T$
8	AAD	21S ATLS	b-jets + \cancel{E}_T
9	SIRUNYAN	21A CMS	$pp \rightarrow Z\chi\chi; Z \rightarrow \ell\bar{\ell}$
10	TUMASYAN	21D CMS	DM search in jets + \cancel{E}_T
11	SIRUNYAN	20X CMS	$pp \rightarrow Z' \rightarrow A(Z')h \rightarrow h + \cancel{E}_T$
12	AABOUD	19AA ATLS	multi-channel BSM search
13	AABOUD	19AI ATLS	$H \rightarrow \chi\chi$
14	AABOUD	19AL ATLS	$H \rightarrow \chi\chi$
15	AABOUD	19Q ATLS	single $t + \cancel{E}_T$
16	AABOUD	19V ATLS	revised mediator based DM searches
17	BANERJEE	19 NA64	$eN \rightarrow eN + \cancel{E}$
18	SIRUNYAN	19AN CMS	$H\chi\chi \rightarrow b\bar{b} \cancel{E}_T$
19	SIRUNYAN	19BC CMS	LQ LQ $\rightarrow \mu j \cancel{E}_T$
20	SIRUNYAN	19Bo CMS	$VV \rightarrow Hqq; H \rightarrow \text{DM}$
21	SIRUNYAN	19C CMS	$pp \rightarrow t\bar{t}\chi\chi$
22	SIRUNYAN	19o CMS	$pp \rightarrow \gamma \cancel{E}_T$
23	SIRUNYAN	19X CMS	$pp \rightarrow t\bar{t} + \cancel{E}_T; pp \rightarrow t(\bar{t}) + \cancel{E}_T$
24	AABOUD	18 ATLS	$pp \rightarrow Z\chi\chi; Z \rightarrow \ell\bar{\ell}$
25	AABOUD	18A ATLS	$pp \rightarrow t\bar{t} \cancel{E}_T; pp \rightarrow b\bar{b} \cancel{E}_T$
26	AABOUD	18Ca ATLS	$pp \rightarrow V\chi\chi; V \rightarrow jj$
27	AABOUD	18i ATLS	$pp \rightarrow \text{jet}(s) + \cancel{E}_T$
28	AGUILAR-AR...	18B MBNE	$pN \rightarrow \chi\chi, \chi = e, \pi, \text{ or } N$
29	KHACHATRY...	18 CMS	$pp \rightarrow Z(\ell\ell) + \cancel{E}_T$
30	SIRUNYAN	18BF CMS	$pp \rightarrow t \cancel{E}_T$
31	SIRUNYAN	18Bo CMS	dijet resonance search
32	SIRUNYAN	18BV CMS	$pp \rightarrow Z \cancel{E}_T$
33	SIRUNYAN	18c CMS	$pp \rightarrow t\bar{t} \cancel{E}_T$
34	SIRUNYAN	18cu CMS	$pp \rightarrow Z \cancel{E}_T$
35	SIRUNYAN	18DH CMS	$pp \rightarrow \chi\chi h; h \rightarrow \gamma\gamma \text{ or } \tau\tau$
36	SIRUNYAN	18s CMS	$pp \rightarrow \text{jets} \cancel{E}_T$
37	AABOUD	17A ATLS	$pp (H \rightarrow b\bar{b} + \text{WIMP pair})$
38	AABOUD	17AM ATLS	$pp \rightarrow Z' \rightarrow Ah \rightarrow h(b\bar{b}) + \cancel{E}_T$
39	AABOUD	17AQ ATLS	$pp \rightarrow h(\gamma\gamma) + \cancel{E}_T$
40	AABOUD	17Bd ATLS	$pp \rightarrow \text{jet}(s) + \cancel{E}_T$
41	AABOUD	17R ATLS	$pp \rightarrow \gamma \cancel{E}_T$
42	AGUILAR-AR...	17A MBNE	$pN \rightarrow \chi\chi X; \chi N \rightarrow \chi N$
43	BANERJEE	17 NA64	$eN \rightarrow eN \gamma'$
44	KHACHATRY...	17A CMS	forward jets + \cancel{E}_T
45	KHACHATRY...	17F CMS	$H \rightarrow \text{invisibles}$
46	SIRUNYAN	17 CMS	$Z + \cancel{E}_T$
47	SIRUNYAN	17AP CMS	$pp \rightarrow Z' \rightarrow Ah \rightarrow h + \cancel{E}_T$
48	SIRUNYAN	17AQ CMS	$pp \rightarrow \gamma + \cancel{E}_T$
49	SIRUNYAN	17Bb CMS	$pp \rightarrow t\bar{t} + \cancel{E}_T; pp \rightarrow b\bar{b} + \cancel{E}_T$

Searches Particle Listings

WIMP and Dark Matter Searches

- | | | | | | | | | |
|----|-------------|------|------|--|----|-----------------|------|---|
| 50 | SIRUNYAN | 17G | CMS | $pp \rightarrow j + E_T$ | 28 | AGUILAR-AREVALO | 18B | search for WIMP production in MiniBooNE p beam dump; no signal; limits set for $m(\chi) \sim 5\text{--}50$ MeV in vector portal DM model. |
| 51 | SIRUNYAN | 17U | CMS | $pp \rightarrow Z\chi\chi; Z \rightarrow \ell\bar{\ell}$ | 29 | KHACHATRYAN | 18 | search for $pp \rightarrow Z(\ell\ell) + E_T$; no signal; limits set on effective dark matter interactions and other exotic physics models. |
| 52 | AABOUD | 16AD | ATLS | $(W \text{ or } Z \rightarrow \text{jets}) + E_T$ | 30 | SIRUNYAN | 18BF | search for $pp \rightarrow t E_T$ at 13 TeV and 36 fb^{-1} ; no signal; limits placed on DM models involving a flavor changing neutral current, scalar resonance decaying to top quark and DM. |
| 53 | AAD | 16AF | ATLS | $VV \rightarrow \text{forward jets} + E_T$ | 31 | SIRUNYAN | 18B0 | search for high mass dijet resonances at 13 TeV and 36 fb^{-1} ; no signal; limits placed on various models, including simplified DM models involving a spin = 1 Z' mediator. |
| 54 | AAD | 16AG | ATLS | $\ell + \text{jets}$ | 32 | SIRUNYAN | 18BV | search for $pp \rightarrow Z E_T$ at 13 TeV; no signal; limits placed for various exotic physics models including DM. |
| 55 | AAD | 16M | ATLS | $pp \rightarrow H + E_T, H \rightarrow b\bar{b}$ | 33 | SIRUNYAN | 18C | search for new physics in $pp \rightarrow$ final states with two oppositely charged leptons at 13 TeV with 35.9 fb^{-1} . Limits placed on $m(\text{mediator})$ and top squark for various simplified models. |
| 56 | KHACHATRYAN | 16BZ | CMS | $\text{jet}(s) + E_T$ | 34 | SIRUNYAN | 18CU | search for $pp \rightarrow Z E_T$ at 13 TeV and 2.3 fb^{-1} ; no signal; limits placed for various exotic models including DM. |
| 57 | KHACHATRYAN | 16CA | CMS | $\text{jets} + E_T$ | 35 | SIRUNYAN | 18DH | search for $pp \rightarrow \chi\chi h; h \rightarrow \gamma\gamma \text{ or } \tau\tau$ at 13 TeV, 35.9 fb^{-1} ; no signal; limits placed on massive boson mediator Z' in the context of $Z'+2\text{HDM}$ and baryonic Z' models. Limits also cast in terms of spin-independent WIMP-nucleon cross section for masses 1–200 GeV. |
| 58 | KHACHATRYAN | 16N | CMS | $pp \rightarrow \gamma + E_T$ | 36 | SIRUNYAN | 18S | search for $pp \rightarrow$ jets E_T at 13 TeV; no signal; limits placed on simplified dark matter models, on the branching ratio of the Higgs boson to invisible particles, and on several other exotic physics models including fermion portal DM. |
| 59 | AAD | 15AS | ATLS | $b(\bar{b}) + E_T, t(\bar{t}) + E_T$ | 37 | AABOUD | 17A | search for $H \rightarrow b\bar{b} + E_T$. See Fig. 4b for limits set on VB mediator vs WIMP mass. |
| 60 | AAD | 15BH | ATLS | $\text{jet} + E_T$ | 38 | AABOUD | 17AM | search for $pp \rightarrow Z' \rightarrow Ah \rightarrow h(b\bar{b}) + E_T$ at 13 TeV. Limits set in $m(Z')$ vs. $m(A)$ plane and on the visible cross section of $h(b\bar{b}) + E_T$ events in bins of E_T . |
| 61 | AAD | 15CF | ATLS | $H^0 + E_T$ | 39 | AABOUD | 17AQ | search for WIMP in $pp \rightarrow h(\gamma\gamma) + E_T$ in 36.1 fb^{-1} of data. Limits on the visible cross section are also provided. Model dependent limits on spin independent DM - Nucleon cross-section are also presented, which are more stringent than those from direct searches for DM mass smaller than 2.5 GeV. |
| 62 | AAD | 15CS | ATLS | $\gamma + E_T$ | 40 | AABOUD | 17BD | search for $pp \rightarrow \text{jet}(s) + E_T$ at 13 TeV with 3.2 fb^{-1} of data. Limits set for simplified models. Observables corrected for detector effects can be used to constrain other models. |
| 63 | KHACHATRYAN | 15AG | CMS | $t\bar{t} + E_T$ | 41 | AABOUD | 17R | for an axial vector mediator in the s-channel, excludes $m(\text{mediator}) < 750\text{--}1200$ GeV for $m(\text{DM}) < 230\text{--}480$ GeV, depending on the couplings. |
| 64 | KHACHATRYAN | 15AL | CMS | $\text{jet} + E_T$ | 42 | AGUILAR-AREVALO | 17A | search for DM produced in 8 GeV proton collisions with steel beam dump followed by DM-nucleon scattering in MiniBooNE detector. Limit placed on DM cross section parameter $Y < 2 \times 10^{-8}$ for $\alpha_D = 0.5$ and for $0.01 < m(\text{DM}) < 0.3$ GeV. |
| 65 | KHACHATRYAN | 15T | CMS | $\ell + E_T$ | 43 | BANERJEE | 17 | search for dark photon invisible decay via eN scattering; exclude $m(\gamma') < 100$ MeV as an explanation of $(g_\mu - 2)$ muon anomaly. |
| 66 | AAD | 14AI | ATLS | $W + E_T$ | 44 | KHACHATRYAN | 17A | search for WIMPs in forward jets + E_T channel with 18.5 fb^{-1} at 8 TeV; limits set in effective theory model, Fig. 3. |
| 67 | AAD | 14BK | ATLS | $W, Z + E_T$ | 45 | KHACHATRYAN | 17F | search for $H \rightarrow$ invisibles in pp collisions at 7, 8, and 13 TeV; place limits on Higgs portal DM. |
| 68 | AAD | 14K | ATLS | $Z + E_T$ | 46 | SIRUNYAN | 17 | search for $pp \rightarrow Z + E_T$ with 2.3 fb^{-1} at 13 TeV; no signal seen; limits placed on WIMPs and unparticles. |
| 69 | AAD | 14O | ATLS | $Z + E_T$ | 47 | SIRUNYAN | 17AP | search for $pp \rightarrow Z' \rightarrow Ah \rightarrow h + E_T$ with $h \rightarrow b\bar{b}$ or $\gamma\gamma$ and $A \rightarrow \chi\chi$ with 2.3 fb^{-1} at 13 TeV. Limits set in $m(Z')$ vs. $m(A)$ plane. |
| 70 | AAD | 13AD | ATLS | $\text{jet} + E_T$ | 48 | SIRUNYAN | 17AQ | search for $pp \rightarrow \gamma + E_T$ at 13 TeV with 12.9 fb^{-1} . Limits derived for simplified DM models, effective electroweak-DM interaction and Extra Dimensions models. |
| 71 | AAD | 13C | ATLS | $\gamma + E_T$ | 49 | SIRUNYAN | 17BB | search for WIMPs via $pp \rightarrow t\bar{t} + E_T, pp \rightarrow b\bar{b} + E_T$ at 13 TeV with 2.2 fb^{-1} . Limits derived for various simplified models. |
| 72 | AALTONEN | 12K | CDF | $t + E_T$ | 50 | SIRUNYAN | 17G | search for $pp \rightarrow j + E_T$ with 12.9 fb^{-1} at 13 TeV; limits placed on WIMP mass/mediators in DM simplified models. |
| 73 | AALTONEN | 12M | CDF | $\text{jet} + E_T$ | 51 | SIRUNYAN | 17U | search for WIMPs/unparticles via $pp \rightarrow Z\chi\chi, Z \rightarrow \ell\bar{\ell}$ at 13 TeV with 2.3 fb^{-1} . Limits derived for various simplified models. |
| 74 | CHATRCHYAN | 12AP | CMS | $\text{jet} + E_T$ | 52 | AABOUD | 16AD | place limits on $VV\chi\chi$ effective theory via search for hadronic W or Z plus WIMP pair production. See Fig. 5. |
| 75 | CHATRCHYAN | 12T | CMS | $\gamma + E_T$ | 53 | AAD | 16AF | search for $VV \rightarrow (H \rightarrow \text{WIMP pair}) + \text{forward jets}$ with 20.3 fb^{-1} at 8 TeV; set limits in Higgs portal model, Fig. 8. |
- 1 AAD 21AZ search for DM in $H E_T \rightarrow \gamma\gamma E_T$ events with 139 fb^{-1} at 13 TeV. No signal observed. Limits placed for several simplified models.
- 2 AAD 21BB search for DM in $H E_T \rightarrow b\bar{b} E_T$ events with 139 fb^{-1} at 13 TeV. No signal observed. Limits placed for several simplified models.
- 3 AAD 21b search for $VV + \chi\chi, V \rightarrow q\bar{q}$ with 139 fb^{-1} at 13 TeV LHC. No signal detected. Limits placed in dark Higgs boson mass vs. $m(Z')$ plane. Here VV stand for $W^\pm W^\mp, ZZ$.
- 4 AAD 21F search for monojet recoiling against invisibles with 139 fb^{-1} at 13 TeV LHC. No signal detected. Limits placed in various simplified dark matter models.
- 5 AAD 21K search for a photon recoiling against dark matter with 139 fb^{-1} at 13 TeV LHC. No signal detected. Limits placed on parameter space of various simplified models.
- 6 AAD 21o search for $\ell + \text{jets} + E_T$ to search for t -pairs + DM particles with 139 fb^{-1} at LHC 13 TeV LHC. No signal detected. Limits placed in the cross-section vs. mediator mass plane, assuming light DM states.
- 7 AAD 21P search for $\ell^+\ell^- + \text{jets} + E_T$ in context of various BSM models with 139 fb^{-1} at 13 TeV LHC. No signal observed. Limits placed in parameter space of dark matter models and SUSY.
- 8 AAD 21s search for b -jets + E_T signal from BSM/DM models with 139 fb^{-1} at 13 TeV LHC. No signal observed. Limits placed on parameter space of DM models.
- 9 SIRUNYAN 21A search for DM production in association with leptonically decaying Z boson in 137 fb^{-1} at 13 TeV; no signal; limits set in large variety of simplified DM models.
- 10 TUMASYAN 21D search for DM and other exotica at CMS in jets + E_T events with 137 fb^{-1} at 13 TeV. No signal observed. Limits placed for a variety of simplified models.
- 11 SIRUNYAN 20K search for DM in $pp \rightarrow Z' \rightarrow A(Z')h \rightarrow h + E_T$ in CMS at 13 TeV with 35.9 fb^{-1} ; no signal; limits placed in σ^{SI} vs. $m(\chi)$, and $\sigma, m(A)$ and $\tan\beta$ vs $m(Z')$ for considered DM models.
- 12 AABOUD 19AA searches for BSM physics in more than 700 event classes with more than 10^5 regions at 13 TeV with 3.2 fb^{-1} ; no significant signal.
- 13 AABOUD 19AI searches for vector boson fusion $pp \rightarrow Hqq, H \rightarrow$ invisible at 13 TeV with 36.1 fb^{-1} ; no signal; require $B(H \rightarrow \text{invisible}) < 0.37$ (0.28 expected).
- 14 AABOUD 19AL perform search in three different channels for $H \rightarrow \chi\chi$ at 7, 8 and 13 TeV; combined result $\text{BF}(H \rightarrow \text{invisible}) < 0.26$ (0.17 expected).
- 15 AABOUD 19Q search for single $t + E_T$ at 13 TeV with 36.1 fb^{-1} of data; no signal; limits set in σ or coupling vs. mass plane for simplified models.
- 16 AABOUD 19v review ATLAS results from 7, 8 and 13 TeV searches for mediator-based DM and DE scalar which couples to gravity; no signal; limits set for large variety of simplified models.
- 17 BANERJEE 19 search for dark photon via $eN \rightarrow eN + E$ in NA64; no signal, limits placed in kinetic mixing ϵ vs. $m(\text{DM})$ plane for $m(\text{DM}) \sim 0.001\text{--}1$ GeV.
- 18 SIRUNYAN 19AN search at 13 TeV with 35.9 fb^{-1} for $pp \rightarrow H\chi\chi \rightarrow b\bar{b} E_T$; no signal; limits set in the context of a 2HDM + pseudoscalar (a) model and a baryonic Z' model.
- 19 SIRUNYAN 19bc search for DM via LeptoQuark pair annihilation $LQ LQ \rightarrow \mu j\chi\chi \rightarrow \mu j E_T$ with 77.4 fb^{-1} , 13 TeV; no signal; limits placed in $m(\chi)$ vs. $m(LQ)$ plane. Model dependent limits on DM mass up to 600 GeV depending on $m(LQ)$ placed.
- 20 SIRUNYAN 19B0 search for vector boson fusion $VV \rightarrow qqH$ with $H \rightarrow \chi\chi$ at 13 TeV with 38.2 fb^{-1} ; no signal; limits placed for several models. Also search for $H \rightarrow$ invisible at 7, 8, and 13 TeV; no signal; limit placed on $\text{BF} < 0.19$.
- 21 SIRUNYAN 19C search for DM via $pp \rightarrow t\bar{t}\chi\chi$ at 13 TeV, 35.9 fb^{-1} ; no signal; limits placed on coupling vs. mediator mass for various simplified models.
- 22 SIRUNYAN 19o search for $pp \rightarrow \gamma$ at 13 TeV with 35.9 fb^{-1} ; no signal; limits placed on parameters of various models.
- 23 SIRUNYAN 19x search for $pp \rightarrow t\bar{t} E_T$ and $pp \rightarrow t E_T + \dots$ at 13 TeV with 35.9 fb^{-1} ; no signal; limits placed on χ production σ for various simplified models with $m(\chi) = 1$ GeV.
- 24 AABOUD 18 search for $pp \rightarrow Z + E_T$ with $Z \rightarrow \ell\ell$ at 13 TeV with 36.1 fb^{-1} of data. Limits set for simplified models.
- 25 AABOUD 18A search for $pp \rightarrow t\bar{t} E_T$ or $pp \rightarrow b\bar{b} E_T$ at 13 TeV, 36.1 fb^{-1} of data. Limits set for simplified models.
- 26 AABOUD 18CA search for $pp \rightarrow V\chi\chi$ with $V \rightarrow jj$ at 13 TeV, 36.1 fb^{-1} ; no signal; limits set in $m(\text{DM})$ vs $m(\text{mediator})$ simplified model plane.
- 27 AABOUD 18i search for $pp \rightarrow j + E_T$ at 13 TeV with 36.1 fb^{-1} of data. Limits set for simplified models with pair-produced weakly interacting dark-matter candidates.
- 959 Downloaded from https://academic.oup.com/ptep/article/2022/8/083C01/6651666 by CERN Library user on 11 October 2022

- 64 KHACHATRYAN 15AL search for events with a jet and missing E_T in pp collisions at $E_{cm} = 8$ TeV with $L = 19.7 \text{ fb}^{-1}$. See their Fig. 5 and Tables 4-6 for translated limits on X^0 -nucleon cross section for $m = 1-1000$ GeV.
- 65 KHACHATRYAN 15T search for events with a lepton and missing E_T in pp collisions at $E_{cm} = 8$ TeV with $L = 19.7 \text{ fb}^{-1}$. See their Fig. 17 for translated limits on X^0 -proton cross section for $m = 1-1000$ GeV.
- 66 AAD 14AI search for events with a W and missing E_T in pp collisions at $E_{cm} = 8$ TeV with $L = 20.3 \text{ fb}^{-1}$. See their Fig. 4 for translated limits on X^0 -nucleon cross section for $m = 1-1500$ GeV.
- 67 AAD 14EK search for hadronically decaying W , Z in association with E_T in 20.3 fb^{-1} at $8 \text{ TeV } pp$ collisions. Fig. 5 presents exclusion results for SI and SD scattering cross section. In addition, cross section limits on the anomalous production of W or Z bosons with large missing transverse momentum are also set in two fiducial regions.
- 68 AAD 14K search for events with a Z and missing E_T in pp collisions at $E_{cm} = 8$ TeV with $L = 20.3 \text{ fb}^{-1}$. See their Fig. 5 and 6 for translated limits on X^0 -nucleon cross section for $m = 1-10^3$ GeV.
- 69 AAD 14O search for ZH^0 production with H^0 decaying to invisible final states. See their Fig. 4 for translated limits on X^0 -nucleon cross section for $m = 1-60$ GeV in Higgs-portal X^0 scenario.
- 70 AAD 13AD search for events with a jet and missing E_T in pp collisions at $E_{cm} = 7$ TeV with $L = 4.7 \text{ fb}^{-1}$. See their Figs. 5 and 6 for translated limits on X^0 -nucleon cross section for $m = 1-1300$ GeV.
- 71 AAD 13C search for events with a photon and missing E_T in pp collisions at $E_{cm} = 7$ TeV with $L = 4.6 \text{ fb}^{-1}$. See their Fig. 3 for translated limits on X^0 -nucleon cross section for $m = 1-1000$ GeV.
- 72 AALTONEN 12K search for events with a top quark and missing E_T in $p\bar{p}$ collisions at $E_{cm} = 1.96$ TeV with $L = 7.7 \text{ fb}^{-1}$. Upper limits on $\sigma(tX^0)$ in the range $0.4-2$ pb (95% CL) is given for $m_{X^0} = 0-150$ GeV.
- 73 AALTONEN 12M search for events with a jet and missing E_T in $p\bar{p}$ collisions at $E_{cm} = 1.96$ TeV with $L = 6.7 \text{ fb}^{-1}$. Upper limits on the cross section in the range $2-10$ pb (90% CL) is given for $m_{X^0} = 1-300$ GeV. See their Fig. 2 for translated limits on X^0 -nucleon cross section.
- 74 CHATRCHYAN 12AP search for events with a jet and missing E_T in pp collisions at $E_{cm} = 7$ TeV with $L = 5.0 \text{ fb}^{-1}$. See their Fig. 4 for translated limits on X^0 -nucleon cross section for $m_{X^0} = 0.1-1000$ GeV.
- 75 CHATRCHYAN 12T search for events with a photon and missing E_T in pp collisions at $E_{cm} = 7$ TeV with $L = 5.0 \text{ fb}^{-1}$. Upper limits on the cross section in the range $13-15$ fb (90% CL) is given for $m_{X^0} = 1-1000$ GeV. See their Fig. 2 for translated limits on X^0 -nucleon cross section.

REFERENCES FOR WIMP and Dark Matter Searches

ADHIKARI	22	PRL 120 011801	P. Adhikari et al.	(DEAP Collab.)
AAD	21A2	JHEP 2110 0113	G. Aad et al.	(ATLAS Collab.)
AAD	21BB	JHEP 2111 209	G. Aad et al.	(ATLAS Collab.)
AAD	21D	PRL 126 121802	G. Aad et al.	(ATLAS Collab.)
AAD	21F	PR D103 112006	G. Aad et al.	(ATLAS Collab.)
AAD	21K	JHEP 2102 226	G. Aad et al.	(ATLAS Collab.)
AAD	21O	JHEP 2104 174	G. Aad et al.	(ATLAS Collab.)
AAD	21P	JHEP 2104 165	G. Aad et al.	(ATLAS Collab.)
AAD	21S	JHEP 2105 093	G. Aad et al.	(ATLAS Collab.)
ABDALLAH	21	PR D103 102002	H. Abdallah et al.	(H.E.S.S. Collab.)
AKERIB	21A	PR D104 012011	D.S. Akerib et al.	(LUX Collab.)
AKERIB	21B	PR D104 062005	D.S. Akerib et al.	(LUX Collab.)
ALKHATIB	21	PRL 127 061801	I. Alkhatib et al.	(SuperCDMS Collab.)
AMARE	21	PR D103 102005	J. Amare et al.	(ANAIS Collab.)
ANDRIAMIR...	21A	PR D104 012009	M. Andriamirado et al.	(PROSPECT Collab.)
APRILE	21	PRL 126 091301	E. Aprile et al.	(XENONIT Collab.)
APRILE	21A	PR D103 063028	E. Aprile et al.	(XENONIT Collab.)
CHENG	21	PRL 126 211803	C. Cheng et al.	(XENONIT Collab.)
CIRELLI	21	PR D103 063022	M. Cirelli et al.	(Pandax-II Collab.)
IKEDA	21	PTEP 2021 063F01	T. Ikeda et al.	(NEWAGE Collab.)
JOHN	21	JCAP 2112 007	I. John, T. Linden	(STOH Collab.)
MENG	21B	PRL 127 261802	Y. Meng et al.	(Pandax-4T Collab.)
SIRUNYAN	21A	EPJ C81 13	A.M. Sirunyan et al.	(CMS Collab.)
	Also	EPJ C81 333 (errata)	A.M. Sirunyan et al.	(CMS Collab.)
TUMASYAN	21D	JHEP 2111 153	A. Tumasyan et al.	(CMS Collab.)
AARTSEN	20C	EPJ C80 819	M.G. Aartsen et al.	(IceCube, PICO Collabs)
ABAZJIAN	20	PR D102 043012	K.N. Abazajian et al.	(UCI, VPI, TOKY+)
ABDALLAH	20	PR D102 062001	H. Abdallah et al.	(H.E.S.S. Collab.)
ABDELHAMEE...	20A	EPJ C80 834	A.H. Abdelhameed et al.	(CRESST Collab.)
ABE	20G	PR D102 072002	K. Abe et al.	(Super-Kamiokande Collab.)
ADHIKARI	20	PR D102 082001	P. Adhikari et al.	(DEAP-3600 Collab.)
AGOSTINI	20	PRL 125 011801	M. Agostini et al.	(GERDA Collab.)
AGUILAR-AR...	20C	PRL 125 241803	A. Aguilar-Arevalo et al.	(DAMIC Collab.)
AKERIB	20	PR D101 012003	D.S. Akerib et al.	(LUX Collab.)
AKERIB	20A	PR D101 042001	D.S. Akerib et al.	(LUX Collab.)
ALBERT	20	PR D101 103001	A. Albert et al.	(HAWC Collab.)
ALBERT	20A	PL B805 135439	A. Albert et al.	(ANTARES Collab.)
ALBERT	20C	PR D102 082002	A. Albert et al.	(ANTARES and IceCube Collab.)
ALVAREZ	20	JCAP 2009 004	A. Alvarez et al.	
AMARAL	20	PR D102 091101	D.W. Amaral et al.	(SuperCDMS Collab.)
ANDRIANAV...	20	PR D102 042001	A. Andrianavalomahafa et al.	(FUNK Collab.)
APRILE	20	PR D102 072004	E. Aprile et al.	(XENON Collab.)
ARNAUD	20	PRL 125 141301	Q. Arnaud et al.	(EDELWEISS Collab.)
BARAK	20	PRL 125 171802	L. Barak et al.	(SENSEI Collab.)
CLARK	20	PR D102 123026	M. Clark et al.	(PURD Collab.)
	Also	PR D104 129903 (errata)	M. Clark et al.	(Purd Collab.)
FELIZARDO	20	JCAP 2002 012	S. Hoof, A. Geringer-Sameth, R. Trotta	(SIMPLE Collab.)
HOOF	20	JCAP 2002 012	S. Hoof, A. Geringer-Sameth, R. Trotta	(GOET+ Collab.)
MAZZIOTTA	20	PR D102 022003	M.N. Mazziotta et al.	(CMS Collab.)
SIRUNYAN	20X	JHEP 2003 025	A.M. Sirunyan et al.	(CMS Collab.)
WANG	20G	CP C44 125001	Q. Wang et al.	(Pandax-II Collab.)
AABOUD	19A	EPJ C79 120	M. Aaboud et al.	(ATLAS Collab.)
AABOUD	19AL	PL B793 499	M. Aaboud et al.	(ATLAS Collab.)
AABOUD	19AL	PRL 122 231801	M. Aaboud et al.	(ATLAS Collab.)
AABOUD	19Q	JHEP 1905 041	M. Aaboud et al.	(ATLAS Collab.)
AABOUD	19V	JHEP 1905 142	M. Aaboud et al.	(ATLAS Collab.)
ABDELHAMEE...	19	EPJ C79 630	A.H. Abdelhameed et al.	(CRESST Collab.)
ABDELHAMEE...	19A	PR D100 102002	A.H. Abdelhameed et al.	(CRESST Collab.)
ABE	19	PL B789 45	K. Abe et al.	(XMASS Collab.)
ABEYSEKARA	19	JCAP 1907 022	A.U. Abeysekara et al.	(HAWC Collab.)
ABRAMOFF	19	PRL 122 141801	O. Abramoff et al.	(SENSEI Collab.)
ADHIKARI	19	PRL 123 031302	G. Adhikari et al.	(COSINE-100 Collab.)
AGNESE	19A	PR D99 062001	R. Agnese et al.	(CMS Collab.)

AGUILAR-AR...	19A	PRL 123 181802	A. Aguilar-Arevalo et al.	(DAMIC Collab.)
AJAJ	19	PR D100 022004	R. Ajaj et al.	(DEAP-3600 Collab.)
AKERIB	19	PRL 122 131301	D.S. Akerib et al.	(LUX Collab.)
ALBERT	19B	JCAP 1904 E01	A. Albert et al.	(HAWC Collab.)
AMARE	19	PRL 123 031301	J. Amare et al.	(ANAIS Collab.)
AMOLE	19	PR D100 022001	C. Amole et al.	(PICO Collab.)
ANGLOHER	19	EPJ C79 43	G. Angloher et al.	(CRESST-II Collab.)
APRILE	19	PRL 122 071301	E. Aprile et al.	(XENONIT Collab.)
APRILE	19A	PRL 122 141301	E. Aprile et al.	(XENONIT Collab.)
APRILE	19C	PRL 123 241803	E. Aprile et al.	(XENONIT Collab.)
APRILE	19D	PRL 123 251801	E. Aprile et al.	(XENONIT Collab.)
ARMENGAUD	19	PR D99 082003	E. Armengaud et al.	(EDELWEISS Collab.)
BANERJEE	19	PRL 123 121801	D. Banerjee et al.	(NA64 Collab.)
BRINGMANN	19	PRL 122 171801	T. Bringmann, M. Pospelov	(OSLO, VICT Collab.)
BRUNE	19	PR D99 096005	T. Brune, H. Pas	(DORT Collab.)
CHEUNG	19	PL B789 137	K. Cheung et al.	
CHOI	19	PR D99 083018	K.-Y. Choi, J. Kim, C. Rott	(SUNG Collab.)
DI-MAURO	19	PR D99 123027	M. Di Mauro et al.	
HA	19	PRL 122 131802	C. Ha et al.	(COSINE-100 Collab.)
JOHNSON	19	PR D99 103007	C. Johnson et al.	
KIM	19A	JHEP 1903 194	K.W. Kim et al.	(KIMS Collab.)
KLOPF	19	PRL 122 222503	M. Klopff et al.	(PERKEO II Collab.)
KOBAYASHI	19	PL B795 308	M. Kobayashi et al.	(XMASS Collab.)
LI	19D	PR D99 123519	S. Li et al.	
LIU	19B	PRL 123 161301	Z.Z. Liu et al.	(CDEX Collab.)
NG	19	PR D99 083005	K.C.Y. Ng et al.	
QUEIROZ	19	JCAP 1904 048	F.S. Queiroz, C. Siqueira	
SEONG	19	PRL 122 011801	I.S. Seong et al.	(BELLE Collab.)
SIRUNYAN	19AM	EPJ C79 280	A.M. Sirunyan et al.	(CMS Collab.)
SIRUNYAN	19B	PL B795 76	A.M. Sirunyan et al.	(CMS Collab.)
SIRUNYAN	19C	PL B795 520	A.M. Sirunyan et al.	(CMS Collab.)
SIRUNYAN	19C	PRL 122 011803	A.M. Sirunyan et al.	(CMS Collab.)
SIRUNYAN	19O	JHEP 1902 074	A.M. Sirunyan et al.	(CMS Collab.)
SIRUNYAN	19X	JHEP 1903 141	A.M. Sirunyan et al.	(CMS Collab.)
SUZUKI	19	ASP 110 1	T. Suzuki et al.	(XMASS Collab.)
XIA	19A	PL B792 193	J. Xia et al.	(Pandax-II Collab.)
YAGUNA	19	JCAP 1904 041	C. Yaguna	
YANG	19	PRL 123 221301	L.T. Yang et al.	(CDEX Collab.)
AABOUD	18	PL B776 318	M. Aaboud et al.	(ATLAS Collab.)
AABOUD	18A	EPJ C78 180	M. Aaboud et al.	(ATLAS Collab.)
AABOUD	18CA	JHEP 1810 180	M. Aaboud et al.	(ATLAS Collab.)
AABOUD	18C	JHEP 1801 126	M. Aaboud et al.	(ATLAS Collab.)
AARTSEN	18D	EPJ C78 831	M.G. Aartsen et al.	(IceCube Collab.)
ABDALLAH	18	PRL 120 201101	H. Abdallah et al.	(H.E.S.S. Collab.)
ABE	18C	PR D97 102006	K. Abe et al.	(XMASS Collab.)
ABE	18F	PL B787 153	K. Abe et al.	(XMASS Collab.)
ADHIKARI	18	NAT 564 83	G. Adhikari et al.	(COSINE-100 Collab.)
AGNES	18	PRL 121 081307	P. Agnes et al.	(DarkSide-50 Collab.)
AGNES	18A	PR D98 102006	P. Agnes et al.	(DarkSide-50 Collab.)
AGNES	18B	PRL 121 111303	P. Agnes et al.	(DarkSide-50 Collab.)
AGNESE	18	PR D97 022002	R. Agnese et al.	(SuperCDMS Collab.)
AGNESE	18A	PRL 120 061802	R. Agnese et al.	(SuperCDMS Collab.)
AGNESE	18B	PRL 120 061801	R. Agnese et al.	(SuperCDMS Collab.)
	Also	PRL 122 061901 (errata)	R. Agnese et al.	(SuperCDMS Collab.)
AGUILAR-AR...	18B	PR D98 112004	A.A. Aguilar-Arevalo	(MiniBooNE Collab.)
AHNEN	18	JCAP 1803 009	M.L. Ahnen et al.	(MAGIC Collab.)
AKERIB	18A	PR D98 062005	D.S. Akerib et al.	(LUX Collab.)
ALBERT	18B	JCAP 1806 043	A. Albert et al.	(HAWC Collab.)
ALBERT	18C	PR D98 123012	A. Albert et al.	(HAWC Collab.)
AMAUDRUZ	18	PRL 121 071801	P.A. Amaudruz et al.	(DEAP-3600 Collab.)
APRILE	18	PRL 121 111302	E. Aprile et al.	(XENONIT Collab.)
ARMENGAUD	18	PR D98 082004	E. Armengaud et al.	(EDELWEISS-III Collab.)
ARNAUD	18	ASP 97 54	Q. Arnaud et al.	(NEWS-5 Collab.)
CHANG	18A	PR D98 123004	L.J. Chang, M. Lisanti, S. Mishra-Sharma	(PRIN Collab.)
CRISLER	18	PRL 121 061803	M. Crisler et al.	(SENSEI Collab.)
JIANG	18	PRL 120 241301	H. Jiang et al.	(CDEX Collab.)
KACHULIS	18	PRL 120 221301	C. Kachulis et al.	(Super-Kamiokande Collab.)
KHACHATRY...	18	PR D97 099903	V. Khachatryan et al.	(CMS Collab.)
LISANTI	18	PRL 120 101101	M. Lisanti et al.	(PRIN, MIT, MICH Collab.)
MAZZIOTTA	18	PR D98 022006	M. Mazziotta et al.	(Fermi-LAT Collab.)
REN	18	PRL 121 021304	X. Ren et al.	(Pandax-II Collab.)
SIRUNYAN	18B	JHEP 1806 027	A.M. Sirunyan et al.	(CMS Collab.)
SIRUNYAN	18B	JHEP 1808 130	A.M. Sirunyan et al.	(CMS Collab.)
SIRUNYAN	18B	EPJ C78 291	A.M. Sirunyan et al.	(CMS Collab.)
SIRUNYAN	18C	PR D97 022009	A.M. Sirunyan et al.	(CMS Collab.)
SIRUNYAN	18C	JHEP 1801 056	A.M. Sirunyan et al.	(CMS Collab.)
SIRUNYAN	18D	JHEP 1809 046	A.M. Sirunyan et al.	(CMS Collab.)
SIRUNYAN	18S	PR D97 092005	A.M. Sirunyan et al.	(CMS Collab.)
YANG	18	CP C42 023002	L.T. Yang et al.	(CDEX Collab.)
AABOUD	17A	PL B765 11	M. Aaboud et al.	(ATLAS Collab.)
AABOUD	17AM	PRL 119 181804	M. Aaboud et al.	(ATLAS Collab.)
AABOUD	17AQ	PR D96 112004	M. Aaboud et al.	(ATLAS Collab.)
AABOUD	17B	EPJ C77 765	M. Aaboud et al.	(ATLAS Collab.)
AABOUD	17D	EPJ C77 393	M. Aaboud et al.	(ATLAS Collab.)
AARTSEN	17	EPJ C77 82	M.G. Aartsen et al.	(IceCube Collab.)
AARTSEN	17A	EPJ C77 146	M.G. Aartsen et al.	(IceCube Collab.)
	Also	EPJ C79 214 (errata)	M.G. Aartsen et al.	(IceCube Collab.)
AARTSEN	17C	EPJ C77 627	M.G. Aartsen et al.	(IceCube Collab.)
AGUILAR-AR...	17A	PRL 118 141803	A. Aguilar-Arevalo et al.	(DAMIC Collab.)
AGUILAR-AR...	17A	PRL 118 221803	A.A. Aguilar-Arevalo et al.	(MiniBooNE Collab.)
AKERIB	17	PRL 118 021303	D.S. Akerib et al.	(LUX Collab.)
AKERIB	17A	PRL 118 251302	D.S. Akerib et al.	(LUX Collab.)
ALBERT	17A	PL B769 249	A. Albert et al.	(ANTARES Collab.)
	Also	PL B796 253 (errata)	A. Albert et al.	(ANTARES Collab.)
AMOLE	17	PRL 118 251301	C. Amole et al.	(PICO Collab.)
ANGLOHER	17A	EPJ C77 631	G. Angloher et al.	(CRESST Collab.)
APRILE	17	PRL 119 101101	E. Aprile et al.	(XENON100 Collab.)
APRILE	17A	PR D96 022008	E. Aprile et al.	(XENON100 Collab.)
APRILE	17D	PR D96 042004	E. Aprile et al.	(XENON100 Collab.)
APRILE	17G	PRL 119 181301	E. Aprile et al.	(XENON Collab.)
APRILE	17H	PR D96 122002	E. Aprile et al.	(XENON100 Collab.)
APRILE	17K	JCAP 1710 039	E. Aprile et al.	(XENON100 Collab.)
ARCHAMBAU...	17	PR D95 082001	S. Archambault et al.	(VERITAS Collab.)
AVORIN	17	JETP 125 80	A.D. Avorin et al.	(BAIKAL Collab.)
BANERJEE	17	PRL 118 011802	D. Banerjee et al.	(NA64 Collab.)
BARBOSA-D...	17	PR D95 032006	E. Barbosa de Souza et al.	(DM17 Collab.)
BATTAT	17	ASP 91 65	J.B.R. Battat et al.	(DRIFT-III Collab.)
BEHNKE	17	ASP 90 85	E. Behnke et al.	(PICASSO Collab.)
BOUDAUD	17	PRL 119 021103	M. Boudaud, J. Lavallo, P. Salati	
CHEN	17E	PR D96 102007	X. Chen et al.	(Pandax-II Collab.)
CHUI	17A	PRL 119 181302	X. Cui et al.	(Pandax-II Collab.)
FU	17	PRL 118 071301	C. Fu et al.	(Pandax-II Collab.)
	Also	PRL 120 049902 (errata)	C. Fu et al.	(Pandax-II Collab.)
KHACHATRY...	17A	PRL 118 021802	V. Khachatryan et al.	(CMS Collab.)
KHACHATRY...	17F	JHEP 1702 135	V. Khachatryan et al.	(CMS Collab.)
SIRUNYAN	17	JHEP 1703 061	A.M. Sirunyan et al.	(CMS Collab.)
SIRUNYAN	17AP	JHEP 1710 180	A.M. Sirunyan et al.	(CMS Collab.)
SIRUNYAN	17AQ	JHEP 1710 073	A.M. Sirunyan et al.	(CMS Collab.)
SIRUNYAN	17B	EPJ C77 345	A.M. Sirunyan et al.	(CMS Collab.)
SIRUNYAN	17G	JHEP 1707 014	A.M. Sirunyan et al.	(CMS Collab.)
SIRUNYAN	17U	JHEP 1709 106	A.M. Sirunyan et al.	

Searches Particle Listings

WIMP and Dark Matter Searches

ABOUD	16D	PR D94 032005	M. Aaboud <i>et al.</i>	(ATLAS Collab.)	FELIZARDO	12	PRL 108 201302	M. Felizardo <i>et al.</i>	(SIMPLE Collab.)
ABOUD	16F	JHEP 1606 055	M. Aaboud <i>et al.</i>	(ATLAS Collab.)	KIM	12	PRL 108 181301	S.C. Kim <i>et al.</i>	(KIMS Collab.)
AAD	16AF	JHEP 1601 172	G. Aad <i>et al.</i>	(ATLAS Collab.)	AALSETH	11	PRL 106 131301	C.E. Aalseth <i>et al.</i>	(CoGENT Collab.)
AAD	16AG	JHEP 1602 062	G. Aad <i>et al.</i>	(ATLAS Collab.)	AALSETH	11A	PRL 107 141301	C.E. Aalseth <i>et al.</i>	(CoGENT Collab.)
AAD	16M	PR D93 072007	G. Aad <i>et al.</i>	(ATLAS Collab.)	ABBASI	11C	PR D84 022004	R. Abbasi <i>et al.</i>	(IceCube Collab.)
AARTSEN	16C	JCAP 1604 022	M.G. Aartsen <i>et al.</i>	(IceCube Collab.)	ABRAMOWSKI	11	PRL 106 161301	A. Abramowski <i>et al.</i>	(H.E.S.S. Collab.)
AARTSEN	16D	EPJ C76 531	M.G. Aartsen <i>et al.</i>	(IceCube Collab.)	ACKERMANN	11	PRL 107 241302	M. Ackermann <i>et al.</i>	(Fermi-LAT Collab.)
ABDALLAH	16	PRL 117 111301	H. Abdallah <i>et al.</i>	(H.E.S.S. Collab.)	AHLEN	11	PL B695 124	S. Ahlen <i>et al.</i>	(DMTPC Collab.)
ABDALLAH	16A	PRL 117 151302	H. Abdallah <i>et al.</i>	(H.E.S.S. Collab.)	AHMED	11	PR D83 112002	Z. Ahmed <i>et al.</i>	(CDMS Collab.)
ADRIAN-MAR...	16	PL B759 69	S. Adrian-Martinez <i>et al.</i>	(ANTARES Collab.)	AHMED	11A	PR D84 011102	Z. Ahmed <i>et al.</i>	(CDMS and EDELWEISS Collabs.)
ADRIAN-MAR...	16B	JCAP 1605 016	S. Adrian-Martinez <i>et al.</i>	(ANTARES Collab.)	AHMED	11B	PRL 106 131302	Z. Ahmed <i>et al.</i>	(CDMS Collab.)
AGNES	16	PR D93 081101	P. Agnes <i>et al.</i>	(DarkSide-50 Collab.)	AJELLO	11	PR D84 032007	M. Ajello <i>et al.</i>	(Fermi-LAT Collab.)
AGNESE	16	PRL 116 071301	R. Agnese <i>et al.</i>	(SuperCDMS Collab.)	ANGLE	11	PRL 107 051301	J. Angle <i>et al.</i>	(XENON10 Collab.)
AGUILAR-AR...	16	PR D94 082006	A. Aguilar-Arevalo <i>et al.</i>	(DAMIC Collab.)	Also		PRL 110 249901 (err.)	J. Angle <i>et al.</i>	(XENON10 Collab.)
AHNEN	16	JCAP 1602 039	M.L. Ahnen <i>et al.</i>	(MAGIC and Fermi-LAT Collab.)	APRILE	11	PR D84 052003	E. Aprile <i>et al.</i>	(XENON100 Collab.)
AKERIB	16	PRL 116 161301	D.S. Akerib <i>et al.</i>	(LUX Collab.)	APRILE	11A	PR D84 061101	E. Aprile <i>et al.</i>	(XENON100 Collab.)
AKERIB	16A	PRL 116 161302	D.S. Akerib <i>et al.</i>	(LUX Collab.)	APRILE	11B	PRL 107 131302	E. Aprile <i>et al.</i>	(XENON100 Collab.)
AMOLE	16	PR D93 052014	C. Amole <i>et al.</i>	(PICO Collab.)	ARMENGAUD	11	PL B702 329	E. Armengaud <i>et al.</i>	(EDELWEISS-II Collab.)
AMOLE	16A	PR D93 061101	C. Amole <i>et al.</i>	(PICO Collab.)	GERINGER-SA...	11	PRL 107 241303	A. Gerlinger-Sameth, S.M. Koushiappas	(COUPP Collab.)
ANGLOHER	16	EPJ C76 25	G. Angloher <i>et al.</i>	(CRESSST-II Collab.)	HORN	11	PL B705 471	M. Horn <i>et al.</i>	(ZEPLIN-III Collab.)
ANGLOHER	16A	PRL 117 021303	G. Angloher <i>et al.</i>	(CRESSST-II Collab.)	TANAKA	11	APJ 742 78	T. Tanaka <i>et al.</i>	(Super-Kamiokande Collab.)
APRILE	16	PR D94 092001	E. Aprile <i>et al.</i>	(XENON100 Collab.)	ABBASI	10	PR D81 057101	R. Abbasi <i>et al.</i>	(IceCube Collab.)
APRILE	16B	PR D94 122001	E. Aprile <i>et al.</i>	(XENON100 Collab.)	AHMED	10	SCI 327 1619	Z. Ahmed <i>et al.</i>	(CDMS II Collab.)
ARMENGAUD	16	JCAP 1605 019	E. Armengaud <i>et al.</i>	(EDELWEISS-III Collab.)	AKERIB	10	PR D82 122004	D.S. Akerib <i>et al.</i>	(CDMS II Collab.)
AVRORIN	16	ASP 81 12	A.D. Avrorin <i>et al.</i>	(BAIKAL Collab.)	AKIMOV	10	PL B692 180	D.Yu. Akimov <i>et al.</i>	(ZEPLIN-III Collab.)
CAPUTO	16	PR D93 062004	R. Caputo <i>et al.</i>	(Fermi-LAT Collab.)	APRILE	10	PRL 105 131302	E. Aprile <i>et al.</i>	(XENON100 Collab.)
FORNASA	16	PR D94 123005	M. Fornasa <i>et al.</i>	(Fermi-LAT Collab.)	ARMENGAUD	10	PL B687 294	E. Armengaud <i>et al.</i>	(EDELWEISS-II Collab.)
HEHN	16	EPJ C76 548	L. Hehn <i>et al.</i>	(EDELWEISS-III Collab.)	FELIZARDO	10	PRL 105 211301	M. Felizardo <i>et al.</i>	(The SIMPLE Collab.)
KHACHATRY...	16AJ	PR D93 052011	V. Khachatryan <i>et al.</i>	(CMS Collab.)	MENOI	10	PL B686 11	K. Benoit <i>et al.</i>	(NEWAGE Collab.)
KHACHATRY...	16BZ	JHEP 1612 083	V. Khachatryan <i>et al.</i>	(CMS Collab.)	ABBASI	09B	PRL 102 201302	R. Abbasi <i>et al.</i>	(IceCube Collab.)
Also		JHEP 1708 035 (err.)	V. Khachatryan <i>et al.</i>	(CMS Collab.)	AHMED	09	PRL 102 011301	Z. Ahmed <i>et al.</i>	(CDMS Collab.)
KHACHATRY...	16CA	JHEP 1612 088	V. Khachatryan <i>et al.</i>	(CMS Collab.)	ANGLE	09	PR D80 115005	J. Angle <i>et al.</i>	(XENON10 Collab.)
KHACHATRY...	16N	PL B755 102	V. Khachatryan <i>et al.</i>	(CMS Collab.)	ANGLOHER	09	ASP 31 270	G. Angloher <i>et al.</i>	(CRESSST Collab.)
LEITE	16	JCAP 1611 021	N. Leite <i>et al.</i>	(PICO Collab.)	ARCHAMBAU...	09	PL B682 185	S. Archambault <i>et al.</i>	(PICASSO Collab.)
LI	16	PR D93 043518	S. Li <i>et al.</i>	(PICO Collab.)	LEBEDENKO	09A	PRL 103 151302	V.N. Lebedenko <i>et al.</i>	(ZEPLIN-III Collab.)
LI	16A	JCAP 1612 028	Z. Li <i>et al.</i>	(PICO Collab.)	LIN	09	PR D79 061101	S.T. Lin <i>et al.</i>	(TEXONO Collab.)
LIANG	16	PR D94 103502	Y.-F. Liang <i>et al.</i>	(PICO Collab.)	Also		PRL 101 251301	C.E. Aalseth <i>et al.</i>	(CoGENT Collab.)
LU	16	PR D93 103517	B.-Q. Lu, H.-S. Zong	(PICO Collab.)	ANGLE	08A	PRL 101 091301	J. Angle <i>et al.</i>	(XENON10 Collab.)
SHIRASAKI	16	PR D94 063522	M. Shirasaki <i>et al.</i>	(PandaX Collab.)	BEDNYAKOV	08	PAN 71 111	V.A. Bednyakov, H.P. Klapdor-Klingrothaus, I.V. Krivosheina	(ZEPLIN-III Collab.)
TAN	16	PR D93 122009	T.H. Tan <i>et al.</i>	(PandaX Collab.)	ALNER	07	PL B653 161	G.J. Alner <i>et al.</i>	(ZEPLIN-III Collab.)
TAN	16B	PRL 117 121303	A. Tan <i>et al.</i>	(PandaX Collab.)	LEE	07A	PRL 99 091301	H.S. Lee <i>et al.</i>	(KIMS Collab.)
ZHAO	16	PR D93 092003	W. Zhao <i>et al.</i>	(CDX Collab.)	MIUCHI	07	PL B654 58	K. Miuchi <i>et al.</i>	(KIMS Collab.)
AAD	15AS	EPJ C75 92	G. Aad <i>et al.</i>	(ATLAS Collab.)	AKERIB	06	PR D73 011102	D.S. Akerib <i>et al.</i>	(CDMS Collab.)
AAD	15BH	EPJ C75 299	G. Aad <i>et al.</i>	(ATLAS Collab.)	SHIMIZU	06A	PL B633 195	Y. Shimizu <i>et al.</i>	(CDMS Collab.)
Also		EPJ C75 408 (err.)	G. Aad <i>et al.</i>	(ATLAS Collab.)	AKERIB	05	PR D72 052009	D.S. Akerib <i>et al.</i>	(CDMS Collab.)
AAD	15CF	PRL 115 131801	G. Aad <i>et al.</i>	(ATLAS Collab.)	ALNER	05	PL B616 17	G.J. Alner <i>et al.</i>	(UK Dark Matter Collab.)
AAD	15CS	PR D91 012008	G. Aad <i>et al.</i>	(ATLAS Collab.)	BARNABE-HE...	05	PL B624 186	M. Barnabe-Heider <i>et al.</i>	(PICASSO Collab.)
Also		PR D92 059903 (err.)	G. Aad <i>et al.</i>	(ATLAS Collab.)	BENOIT	05	PL B616 25	A. Benoit <i>et al.</i>	(EDELWEISS Collab.)
AARTSEN	15C	EPJ C75 20	M.G. Aartsen <i>et al.</i>	(IceCube Collab.)	GIRARD	05	PL B621 233	T.A. Girard <i>et al.</i>	(SIMPLE Collab.)
AARTSEN	15E	EPJ C75 492	M.G. Aartsen <i>et al.</i>	(IceCube Collab.)	GIULIANI	05	PL B621 233	F. Giuliani	(SIMPLE Collab.)
ABRAMOWSKI	15	PRL 114 081301	A. Abramowski <i>et al.</i>	(H.E.S.S. Collab.)	GIULIANI	05A	PR D71 123503	F. Giuliani, T.A. Girard	(SIMPLE Collab.)
ACKERMANN	15	PR D91 122002	M. Ackermann <i>et al.</i>	(Fermi-LAT Collab.)	KLAPDOR-K...	05	PL B609 226	H.V. Klapdor-Klingrothaus, I.V. Krivosheina, C. Tomei	(SIMPLE Collab.)
ACKERMANN	15A	JCAP 1509 008	M. Ackermann <i>et al.</i>	(Fermi-LAT Collab.)	GIULIANI	04	PL B588 151	F. Giuliani, T.A. Girard	(SIMPLE Collab.)
ACKERMANN	15B	PRL 115 231301	M. Ackermann <i>et al.</i>	(Fermi-LAT Collab.)	GIULIANI	04A	PRL 93 161301	F. Giuliani	(SIMPLE Collab.)
ADRIAN-MAR...	15	JCAP 1510 068	S. Adrian-Martinez <i>et al.</i>	(ANTARES Collab.)	MIUCHI	03	ASP 19 135	K. Miuchi <i>et al.</i>	(KIMS Collab.)
AGNES	15	PL B743 456	P. Agnes <i>et al.</i>	(DarkSide-50 Collab.)	TAKEDA	03	PL B572 145	A. Takeda <i>et al.</i>	(KIMS Collab.)
AGNESE	15A	PR D91 052021	R. Agnese <i>et al.</i>	(SuperCDMS Collab.)	ANGLOHER	02	ASP 18 43	G. Angloher <i>et al.</i>	(CRESSST Collab.)
AGNESE	15B	PR D92 072003	R. Agnese <i>et al.</i>	(SuperCDMS Collab.)	BELLI	02	PR D66 043503	P. Belli <i>et al.</i>	(DAMA Collab.)
AMOLE	15	PRL 114 231302	C. Amole <i>et al.</i>	(PICO Collab.)	BERNABE	02C	EPJ C23 611	R. Bernabei <i>et al.</i>	(DAMA Collab.)
APRILE	15	PRL 115 091302	E. Aprile <i>et al.</i>	(XENON Collab.)	GREEN	02	PR D66 083003	A.M. Green	(DAMA Collab.)
APRILE	15A	SCI 349 851	E. Aprile <i>et al.</i>	(XENON Collab.)	BAUDIS	01	PR D63 022001	L. Baudis <i>et al.</i>	(Heidelberg-Moscow Collab.)
CHOI	15	PRL 114 141301	K. Choi <i>et al.</i>	(Super-Kamiokande Collab.)	SMITH	01	PR D64 043502	D. Smith, N. Weiner	(Heidelberg-Moscow Collab.)
KHACHATRY...	15AG	JHEP 1506 121	V. Khachatryan <i>et al.</i>	(CMS Collab.)	ULLIO	01	JHEP 0107 044	P. Ullio, M. Kamionkowski, P. Vogel	(Heidelberg-Moscow Collab.)
KHACHATRY...	15AL	EPJ C76 235	V. Khachatryan <i>et al.</i>	(CMS Collab.)	BENOIT	00	PL B479 8	A. Benoit <i>et al.</i>	(EDELWEISS Collab.)
KHACHATRY...	15T	PR D91 092005	V. Khachatryan <i>et al.</i>	(CMS Collab.)	BERNABE	00D	NJP 2 15	R. Bernabei <i>et al.</i>	(DAMA Collab.)
NAKAMURA	15	PTEP 2015 4 043F01	K. Nakamura <i>et al.</i>	(NEWAGE Collab.)	COLLAR	00	PR 85 3083	J.I. Collar <i>et al.</i>	(SIMPLE Collab.)
XIAO	15	PR D92 052004	X. Xiao <i>et al.</i>	(PandaX Collab.)	AMBROSIO	99	PR D60 082002	M. Ambrosio <i>et al.</i>	(Macro Collab.)
AAD	14A1	JHEP 1409 037	G. Aad <i>et al.</i>	(ATLAS Collab.)	BERNABE	99	PL B450 448	R. Bernabei <i>et al.</i>	(DAMA Collab.)
AAD	14B	PRL 112 041802	G. Aad <i>et al.</i>	(ATLAS Collab.)	BERNABE	99D	PRL 83 4918	R. Bernabei <i>et al.</i>	(DAMA Collab.)
AAD	14C	PR D90 012004	G. Aad <i>et al.</i>	(ATLAS Collab.)	BRHLIK	99	PL B464 303	M. Brhlik, L. Roszkowski	(DAMA Collab.)
AAD	14O	PRL 112 201802	G. Aad <i>et al.</i>	(ATLAS Collab.)	DERBIN	99	PAN 62 1896	A.V. Derbin <i>et al.</i>	(DAMA Collab.)
ACKERMANN	14	PR D89 042001	M. Ackermann <i>et al.</i>	(Fermi-LAT Collab.)	KLIMENKO	98	JETPL 67 875	A.A. Klimenko <i>et al.</i>	(DAMA Collab.)
AGNESE	14	PRL 112 241302	R. Agnese <i>et al.</i>	(SuperCDMS Collab.)	Also		Translated from ZETFP 67 835.	M.L. Sarsa <i>et al.</i>	(ZARA Collab.)
AGNESE	14A	PRL 112 041302	R. Agnese <i>et al.</i>	(SuperCDMS Collab.)	SARSA	97	PR D56 1856	A. Alessandrello <i>et al.</i>	(MILA, MILA, SASSO Collabs.)
AKERIB	14	PRL 112 091303	D.S. Akerib <i>et al.</i>	(LUX Collab.)	Also		PR B387 222 (erratum)	P. Belli <i>et al.</i>	(DAMA Collab.)
ALEKSIC	14	JCAP 1402 008	J. Aleksic <i>et al.</i>	(MAGIC Collab.)	BELLI	96C	NC C19 537	P. Belli <i>et al.</i>	(DAMA Collab.)
ANGLOHER	14	EPJ C74 3184	G. Angloher <i>et al.</i>	(CRESSST-II Collab.)	BERNABE	96	PL B389 757	R. Bernabei <i>et al.</i>	(DAMA Collab.)
APRILE	14A	ASP 54 11	E. Aprile <i>et al.</i>	(XENON100 Collab.)	COLLAR	96	PRL 76 331	J.I. Collar	(SCUC Collab.)
AVRORIN	14	ASP 62 12	A.D. Avrorin <i>et al.</i>	(BAIKAL Collab.)	SARSA	96	PL B386 458	M.L. Sarsa <i>et al.</i>	(ZARA Collab.)
FELIZARDO	14	PR D89 072013	M. Felizardo <i>et al.</i>	(SIMPLE Collab.)	Also		PR D56 1856	M.L. Sarsa <i>et al.</i>	(ZARA Collab.)
LEE	14A	PR D90 052006	H.S. Lee <i>et al.</i>	(KIMS Collab.)	SMITH	96	PL B379 299	P.F. Smith <i>et al.</i>	(RAL, SHEF, LOIC+ Collabs.)
LIU	14A	PR D90 032003	S.K. Liu <i>et al.</i>	(CDX Collab.)	SNOWDEN...	96	PRL 76 332	D.P. Snowden-Ifft, E.S. Freeman, P.B. Price	(UBC Collab.)
UCHIDA	14	PTEP 2014 063C01	H. Uchida <i>et al.</i>	(XMASS Collab.)	GARCIA	95	PR D51 1458	E. Garcia <i>et al.</i>	(ZARA, SCUC, PNC Collabs.)
YUE	14	PR D90 091701	K. Yue <i>et al.</i>	(CDX Collab.)	QUENBY	95	PL B351 70	J.J. Quenby <i>et al.</i>	(LOIC, RAL, SHEF+ Collabs.)
AAD	13AD	JHEP 1304 075	G. Aad <i>et al.</i>	(ATLAS Collab.)	SNOWDEN...	95	PRL 74 4133	D.P. Snowden-Ifft, E.S. Freeman, P.B. Price	(UBC Collab.)
AAD	13C	PRL 110 018002	G. Aad <i>et al.</i>	(ATLAS Collab.)	Also		PRL 76 331	J.I. Collar	(SCUC Collab.)
AALSETH	13	PR D88 012002	C.E. Aalseth <i>et al.</i>	(CoGENT Collab.)	BECK	94	PL B336 141	M. Beck <i>et al.</i>	(MPIK, KIAE, SASSO Collabs.)
AARTSEN	13	PRL 110 131302	M.G. Aartsen <i>et al.</i>	(IceCube Collab.)	BACCI	92	PL B293 460	C. Bacci <i>et al.</i>	(Beijing-Roma-Saclay Collab.)
AARTSEN	13C	PR D88 122001	M.G. Aartsen <i>et al.</i>	(IceCube Collab.)	REUSSER	91	PL B255 143	D. Reusser <i>et al.</i>	(NEUC, CIT, PSI Collabs.)
ABE	13B	PL B719 78	K. Abe <i>et al.</i>	(XMASS Collab.)	CALDWELL	88	PRL 61 510	D.O. Caldwell <i>et al.</i>	(UCSB, UCB, LBL Collabs.)
ABRAMOWSKI	13	PRL 110 041301	A. Abramowski <i>et al.</i>	(H.E.S.S. Collab.)					
ACKERMANN	13A	PR D88 082002	M. Ackermann <i>et al.</i>	(Fermi-LAT Collab.)					
ADRIAN-MAR...	13	JCAP 1311 032	S. Adrian-Martinez <i>et al.</i>	(ANTARES Collab.)					
AGNESE	13	PR D88 031104	R. Agnese <i>et al.</i>	(CDMS Collab.)					
AGNESE	13A	PRL 111 251301	R. Agnese <i>et al.</i>	(CDMS Collab.)					
APRILE	13	PRL 111 021301	E. Aprile <i>et al.</i>	(XENON100 Collab.)					
BERNABE	13A	EPJ C73 2648	R. Bernabei <i>et al.</i>	(DAMA Collab.)					
BOLIV	13	JCAP 1309 019	M. Boliv <i>et al.</i>	(DAMA Collab.)					
LI	13B	PRL 110 261301	H.B. Li <i>et al.</i>	(TEXONO Collab.)					
SUVOROVA	13	PAN 76 1367	O.V. Suvorova <i>et al.</i>	(INRM Collab.)					
Also		Translated from YAF 76 1433.							
ZHAO	13	PR D88 052004	W. Zhao <i>et al.</i>	(CDX Collab.)					
AALTONEN	12K	PRL 108 201802	T. Aaltonen <i>et al.</i>	(CDF Collab.)					
AALTONEN	12M	PRL 108 211804	T. Aaltonen <i>et al.</i>	(CDF Collab.)					
ABBASI	12	PR D85 042002	R. Abbasi <i>et al.</i>	(IceCube Collab.)					
ABRAMOWSKI	12	APJ 750 123	A. Abramowski <i>et al.</i>	(H.E.S.S. Collab.)					
ACKERMANN	12	PR D86 022002	M. Ackermann <i>et al.</i>	(Fermi-LAT Collab.)					
AKIMOV	12	PL B709 14	D.Yu. Akimov <i>et al.</i>	(ZEPLIN-III Collab.)					
ALIU	12	PR D85 062001	E. Aliu <i></i>						

See key on page 1127

Searches Particle Listings

Other Particle Searches

Other Particle Searches

OMITTED FROM SUMMARY TABLE

OTHER PARTICLE SEARCHES

Revised February 2018 by K. Hikasa (Tohoku University).

We collect here those searches which do not appear in any other search categories. These are listed in the following order:

- Concentration of stable particles in matter
- General new physics searches
- Limits on jet-jet resonance in hadron collisions
- Limits on neutral particle production at accelerators
- Limits on charged particles in e^+e^- collisions
- Limits on charged particles in hadron reactions
- Limits on charged particles in cosmic rays
- Searches for quantum black hole production

Note that searches appear in separate sections elsewhere for Higgs bosons (and technipions), other heavy bosons (including W_R , W' , Z' , leptiquarks, axiguons), axions (including pseudo-Goldstone bosons, Majorons, familons), WIMPs, heavy leptons, heavy neutrinos, free quarks, monopoles, supersymmetric particles, and compositeness.

We no longer list for limits on tachyons and centauros. See our 1994 edition for these limits.

CONCENTRATION OF STABLE PARTICLES IN MATTER

Concentration of Heavy (Charge +1) Stable Particles in Matter

VALUE	CL%	DOCUMENT ID	TECN	COMMENT
••• We do not use the following data for averages, fits, limits, etc. •••				
$<4 \times 10^{-17}$	95	1 YAMAGATA	93 SPEC	Deep sea water, $M=5-1600m_p$
$<6 \times 10^{-15}$	95	2 VERKERK	92 SPEC	Water, $M=10^5$ to 3×10^7 GeV
$<7 \times 10^{-15}$	95	2 VERKERK	92 SPEC	Water, $M=10^4$, 6×10^7 GeV
$<9 \times 10^{-15}$	95	2 VERKERK	92 SPEC	Water, $M=10^8$ GeV
$<3 \times 10^{-23}$	90	3 HEMMICK	90 SPEC	Water, $M=1000m_p$
$<2 \times 10^{-21}$	90	3 HEMMICK	90 SPEC	Water, $M=5000m_p$
$<3 \times 10^{-20}$	90	3 HEMMICK	90 SPEC	Water, $M=10000m_p$
$<1. \times 10^{-29}$		SMITH	82B SPEC	Water, $M=30-400m_p$
$<2. \times 10^{-28}$		SMITH	82B SPEC	Water, $M=12-1000m_p$
$<1. \times 10^{-14}$		SMITH	82B SPEC	Water, $M>1000 m_p$
$<(0.2-1.) \times 10^{-21}$		SMITH	79 SPEC	Water, $M=6-350 m_p$

¹ YAMAGATA 93 used deep sea water at 4000 m since the concentration is enhanced in deep sea due to gravity.

² VERKERK 92 looked for heavy isotopes in sea water and put a bound on concentration of stable charged massive particle in sea water. The above bound can be translated into into a bound on charged dark matter particle (5×10^6 GeV), assuming the local density, $\rho=0.3$ GeV/cm³, and the mean velocity (v)=300 km/s.

³ See HEMMICK 90 Fig. 7 for other masses 100-10000 m_p .

Concentration of Heavy Stable Particles Bound to Nuclei

VALUE	CL%	DOCUMENT ID	TECN	COMMENT
••• We do not use the following data for averages, fits, limits, etc. •••				
$< 2 \times 10^{-17}/\text{nucleon}$	95	1 AFEK	21	millicharged particle search
$<1.2 \times 10^{-11}$	95	2 JAVORSEK	01 SPEC	Au, $M=3$ GeV
$<6.9 \times 10^{-10}$	95	2 JAVORSEK	01 SPEC	Au, $M=144$ GeV
$<1 \times 10^{-11}$	95	3 JAVORSEK	01B SPEC	Au, $M=188$ GeV
$<1 \times 10^{-8}$	95	3 JAVORSEK	01B SPEC	Au, $M=1669$ GeV
$<6 \times 10^{-9}$	95	3 JAVORSEK	01B SPEC	Fe, $M=188$ GeV
$<1 \times 10^{-8}$	95	3 JAVORSEK	01B SPEC	Fe, $M=647$ GeV
$<4 \times 10^{-20}$	90	4 HEMMICK	90 SPEC	C, $M=100m_p$
$<8 \times 10^{-20}$	90	4 HEMMICK	90 SPEC	C, $M=1000m_p$
$<2 \times 10^{-16}$	90	4 HEMMICK	90 SPEC	C, $M=10000m_p$
$<6 \times 10^{-13}$	90	4 HEMMICK	90 SPEC	Li, $M=1000m_p$
$<1 \times 10^{-11}$	90	4 HEMMICK	90 SPEC	Be, $M=1000m_p$
$<6 \times 10^{-14}$	90	4 HEMMICK	90 SPEC	B, $M=1000m_p$
$<4 \times 10^{-17}$	90	4 HEMMICK	90 SPEC	O, $M=1000m_p$
$<4 \times 10^{-15}$	90	4 HEMMICK	90 SPEC	F, $M=1000m_p$
$<1.5 \times 10^{-13}/\text{nucleon}$	68	5 NORMAN	89 SPEC	$^{206}\text{Pb}X^-$
$<1.2 \times 10^{-12}/\text{nucleon}$	68	5 NORMAN	87 SPEC	$^{56,58}\text{Fe}X^-$

- ¹ AFEK 21 search for millicharged particles bound to matter using an optomechanical device. No signal was observed. Limits placed in the abundance vs. charge plane (Fig. 3). This is translated to the mass versus charge plane by requiring bound states to be stable.
- ² JAVORSEK 01 search for (neutral) SIMPs (strongly interacting massive particles) bound to Au nuclei. Here M is the effective SIMP mass.
- ³ JAVORSEK 01B search for (neutral) SIMPs (strongly interacting massive particles) bound to Au and Fe nuclei from various origins with exposures on the earth's surface, in a satellite, heavy ion collisions, etc. Here M is the mass of the anomalous nucleus. See also JAVORSEK 02.
- ⁴ See HEMMICK 90 Fig. 7 for other masses 100-10000 m_p .
- ⁵ Bound valid up to $m_{X^-} \sim 100$ TeV.

GENERAL NEW PHYSICS SEARCHES

This subsection lists some of the search experiments which look for general signatures characteristic of new physics, independent of the framework of a specific model.

The observed events are compatible with Standard Model expectation, unless noted otherwise.

VALUE	DOCUMENT ID	TECN	COMMENT
••• We do not use the following data for averages, fits, limits, etc. •••			
1	ALKHATIB 21A	SCDM	CDMSlite search for fractionally charged relics
2	AGUILAR-AR...20B	CONN	ν elastic scatter on nuclei
3	FEDDERKE 20		CHAMPs from white dwarfs
4	SIRUNYAN 20A	CMS	SUSY/LQ search with mT2 or long-lived charged particles
5	ALCANTARA 19		Auger, superheavy DM
6	PORAYKO 18	PPTA	pulsar timing fuzzy DM search
7	AAD 15AT	ATLS	$t + \cancel{E}_T$
8	KHACHATRY...15F	CMS	$t + \cancel{E}_T$
9	AALTONEN 14J	CDF	$W + 2$ jets
10	AAD 13A	ATLS	$WW \rightarrow \ell\nu\ell\nu$
11	AAD 13C	ATLS	$\gamma + \cancel{E}_T$
12	AALTONEN 13I	CDF	Delayed $\gamma + \cancel{E}_T$
13	CHATRCHYAN13	CMS	$\ell^+\ell^- + \text{jets} + \cancel{E}_T$
14	AAD 12C	ATLS	$t\bar{t} + \cancel{E}_T$
15	AALTONEN 12M	CDF	jet + \cancel{E}_T
16	CHATRCHYAN12AP	CMS	jet + \cancel{E}_T
17	CHATRCHYAN12Q	CMS	$Z + \text{jets} + \cancel{E}_T$
18	CHATRCHYAN12T	CMS	$\gamma + \cancel{E}_T$
19	AAD 11S	ATLS	jet + \cancel{E}_T
20	AALTONEN 11AF	CDF	$\ell^\pm\ell^\pm$
21	CHATRCHYAN11C	CMS	$\ell^+\ell^- + \text{jets} + \cancel{E}_T$
22	CHATRCHYAN11U	CMS	jet + \cancel{E}_T
23	AALTONEN 10AF	CDF	$\gamma\gamma + \ell, \cancel{E}_T$
24	AALTONEN 09AF	CDF	$\ell\gamma b \cancel{E}_T$
25	AALTONEN 09G	CDF	$\ell\ell\ell \cancel{E}_T$

¹ ALKHATIB 21A search for lightly ionizing fractionally charged relics scattering from Ge. No signal observed. Limits plotted in fractional charge f vs. vertical intensity plane for $m \sim 5$ MeV to 100 TeV.

² AGUILAR-AREVALO 20B search for light BSM mediator effect on ν elastic scatter on nuclei; no signal; limits placed in $m(\text{mediator})$ vs. coupling plane for two models of MeV-scale mediators.

³ FEDDERKE 20 place limits on cosmic relic charged massive particles (CHAMPs) due to their capture and subsequent disruption of old white dwarf stars; limits placed in the $m(\text{CHAMP})$ vs. relic density parameter plane.

⁴ SIRUNYAN 20A search for SUSY and LQ production using mT2 or presence of long-lived charged particle; no signal, limits placed in various mass planes for different BSM scenarios and various assumed lifetimes.

⁵ ALCANTARA 19 place limits on $m(\text{WIMPzilla}=X)$ vs lifetime from upper bound on ultra high energy cosmic rays at Auger experiment: e.g. $\tau(X) < 4 \times 10^{22}$ yr for $m(X) = 10^{16}$ GeV.

⁶ PORAYKO 18 search for deviations in the residuals of pulsar timing data using PPTA. No signal observed. Limits set on fuzzy DM with $3 \times 10^{-24} < m(\text{DM}) < 2 \times 10^{-22}$ eV.

⁷ AAD 15AT search for events with a top quark and missing E_T in pp collisions at $E_{\text{cm}} = 8$ TeV with $L = 20.3 \text{ fb}^{-1}$.

⁸ KHACHATRYAN 15F search for events with a top quark and missing E_T in pp collisions at $E_{\text{cm}} = 8$ TeV with $L = 19.7 \text{ fb}^{-1}$.

⁹ AALTONEN 14J examine events with a W and two jets in $p\bar{p}$ collisions at $E_{\text{cm}} = 1.96$ TeV with $L = 8.9 \text{ fb}^{-1}$. Invariant mass distributions of the two jets are consistent with the Standard Model expectation.

¹⁰ AAD 13A search for resonant WW production in pp collisions at $E_{\text{cm}} = 7$ TeV with $L = 4.7 \text{ fb}^{-1}$.

¹¹ AAD 13C search for events with a photon and missing \cancel{E}_T in pp collisions at $E_{\text{cm}} = 7$ TeV with $L = 4.6 \text{ fb}^{-1}$.

¹² AALTONEN 13I search for events with a photon and missing E_T , where the photon is detected after the expected timing, in $p\bar{p}$ collisions at $E_{\text{cm}} = 1.96$ TeV with $L = 6.3 \text{ fb}^{-1}$. The data are consistent with the Standard Model expectation.

¹³ CHATRCHYAN 13 search for events with an opposite-sign lepton pair, jets, and missing E_T in pp collisions at $E_{\text{cm}} = 7$ TeV with $L = 4.98 \text{ fb}^{-1}$.

¹⁴ AAD 12C search for events with a $t\bar{t}$ pair and missing \cancel{E}_T in pp collisions at $E_{\text{cm}} = 7$ TeV with $L = 1.04 \text{ fb}^{-1}$.

¹⁵ AALTONEN 12M search for events with a jet and missing E_T in $p\bar{p}$ collisions at $E_{\text{cm}} = 1.96$ TeV with $L = 6.7 \text{ fb}^{-1}$.

Searches Particle Listings

Other Particle Searches

- 16 CHATRCHYAN 12AP search for events with a jet and missing E_T in pp collisions at $E_{cm} = 7$ TeV with $L = 5.0$ fb $^{-1}$.
- 17 CHATRCHYAN 12Q search for events with a Z , jets, and missing E_T in pp collisions at $E_{cm} = 7$ TeV with $L = 4.98$ fb $^{-1}$.
- 18 CHATRCHYAN 12T search for events with a photon and missing E_T in pp collisions at $E_{cm} = 7$ TeV with $L = 5.0$ fb $^{-1}$.
- 19 AAD 11s search for events with one jet and missing E_T in pp collisions at $E_{cm} = 7$ TeV with $L = 33$ pb $^{-1}$.
- 20 AALTONEN 11AF search for high- p_T like-sign dileptons in $p\bar{p}$ collisions at $E_{cm} = 1.96$ TeV with $L = 6.1$ fb $^{-1}$.
- 21 CHATRCHYAN 11C search for events with an opposite-sign lepton pair, jets, and missing E_T in pp collisions at $E_{cm} = 7$ TeV with $L = 34$ pb $^{-1}$.
- 22 CHATRCHYAN 11U search for events with one jet and missing E_T in pp collisions at $E_{cm} = 7$ TeV with $L = 36$ pb $^{-1}$.
- 23 AALTONEN 10AF search for $\gamma\gamma$ events with e, μ, τ , or missing E_T in $p\bar{p}$ collisions at $E_{cm} = 1.96$ TeV with $L = 1.1$ – 2.0 fb $^{-1}$.
- 24 AALTONEN 09AF search for $\ell\gamma$ events with missing E_T in $p\bar{p}$ collisions at $E_{cm} = 1.96$ TeV with $L = 1.9$ fb $^{-1}$. The observed events are compatible with Standard Model expectation including $t\bar{t}\gamma$ production.
- 25 AALTONEN 09G search for $\mu\mu\mu$ and $\mu\mu e$ events with missing E_T in $p\bar{p}$ collisions at $E_{cm} = 1.96$ TeV with $L = 976$ pb $^{-1}$.

LIMITS ON JET-JET RESONANCES

Heavy Particle Production Cross Section

Limits are for a particle decaying to two hadronic jets.

Units(pb)	CL%	Mass(GeV)	DOCUMENT ID	TECN	COMMENT
•••	•••	•••	•••	•••	•••
			1 AAD	20AD ATLS	pp at 13 TeV, dijet resonance
			2 AAD	20T ATLS	dijet resonance search
			3 AAD	20W ATLS	dijet resonance plus lepton
			4 SIRUNYAN	20AI CMS	dijet resonance search
			5 AABOUD	19AJ ATLS	$pp \rightarrow \gamma X, X \rightarrow jj$
			6 SIRUNYAN	19B CMS	$pp \rightarrow jA, A \rightarrow b\bar{b}$
			7 SIRUNYAN	19CD CMS	$pp \rightarrow Z'\gamma, Z' \rightarrow jj$
			8 AABOUD	18AD ATLS	$pp \rightarrow Y \rightarrow HX \rightarrow (bb) + (qq)$
			9 AABOUD	18CK ATLS	$pp \rightarrow bbb + E_T$
			10 AABOUD	18CL ATLS	$pp \rightarrow$ vector-like quarks
			11 AABOUD	18N ATLS	$pp \rightarrow jj$ resonance
			12 SIRUNYAN	18DJ CMS	$pp \rightarrow ZZ$ or $WZ \rightarrow \ell\bar{\ell}jj$
			13 SIRUNYAN	18DY CMS	$pp \rightarrow RR; R \rightarrow jj$
			14 KHACHATRYAN...17W	CMS	$pp \rightarrow jj$ resonance
			15 KHACHATRYAN...17Y	CMS	$pp \rightarrow (8-10) j + E_T$
			16 SIRUNYAN	17F CMS	$pp \rightarrow jj$ angular distribution
			17 AABOUD	16 ATLS	$pp \rightarrow b + \text{jet}$
			18 AAD	16N ATLS	$pp \rightarrow 3$ high E_T jets
			19 AAD	16S ATLS	$pp \rightarrow jj$ resonance
			20 KHACHATRYAN...16K	CMS	$pp \rightarrow jj$ resonance
			21 KHACHATRYAN...16L	CMS	$pp \rightarrow jj$ resonance
			22 AAD	13D ATLS	7 TeV $pp \rightarrow 2$ jets
			23 AALTONEN	13R CDF	1.96 TeV $p\bar{p} \rightarrow 4$ jets
			24 CHATRCHYAN13A	CMS	7 TeV $pp \rightarrow 2$ jets
			25 CHATRCHYAN13A	CMS	7 TeV $pp \rightarrow b\bar{b}X$
			26 AAD	12S ATLS	7 TeV $pp \rightarrow 2$ jets
			27 CHATRCHYAN12BL	CMS	7 TeV $pp \rightarrow t\bar{t}X$
			28 AAD	11AG ATLS	7 TeV $pp \rightarrow 2$ jets
			29 AALTONEN	11M CDF	1.96 TeV $p\bar{p} \rightarrow W + 2$ jets
			30 ABAZOV	11I D0	1.96 TeV $p\bar{p} \rightarrow W + 2$ jets
			31 AAD	10 ATLS	7 TeV $pp \rightarrow 2$ jets
			32 KHACHATRYAN...10	CMS	7 TeV $pp \rightarrow 2$ jets
			33 ABE	99F CDF	1.8 TeV $p\bar{p} \rightarrow b\bar{b} + \text{anything}$
			34 ABE	97G CDF	1.8 TeV $p\bar{p} \rightarrow 2$ jets
			35 ABE	93G CDF	1.8 TeV $p\bar{p} \rightarrow 2$ jets
			35 ABE	93G CDF	1.8 TeV $p\bar{p} \rightarrow 2$ jets
< 2603	95	200			
< 44	95	400			
< 7	95	600			

- 1 AAD 20AD search for weakly supervised dijet resonance in ATLAS with 139 fb $^{-1}$ at 13 TeV; no signal; various limits placed depending on kinematics and production cross section.
- 2 AAD 20T search for dijet resonance with or without b -jets at 13 TeV and 139 fb $^{-1}$; no signal; limits placed in $\sigma \cdot \text{BF}$ vs mass plane for various BSM models.
- 3 AAD 20W search for dijet resonance plus lepton with ATLAS at 13 TeV and 139 fb $^{-1}$; no signal; limits placed in $\sigma \cdot \text{BF}$ vs. mass plane for various BSM models.
- 4 SIRUNYAN 20AI search for dijet resonance in CMS at 13 TeV with 137 fb $^{-1}$; no signal; limits set in σ vs. mass plane for various BSM models.
- 5 AABOUD 19AJ search for low mass dijet resonance in $pp \rightarrow \gamma X, X \rightarrow jj$ at 13 TeV with 79.8 fb $^{-1}$ of data; no signal found; limits placed on Z' model in coupling vs. $m(Z')$ plane.
- 6 SIRUNYAN 19B search for low mass resonance $pp \rightarrow jA, A \rightarrow b\bar{b}$ at 13 TeV using 35.9 fb $^{-1}$; no signal; exclude resonances 50–350 GeV depending on production and decay.
- 7 SIRUNYAN 19CD search for $pp \rightarrow Z'\gamma, Z' \rightarrow jj$ with fat jet (jj); no signal, limits placed in $m(Z')$ vs. coupling plane for Z' masses from 10 to 125 GeV.
- 8 AABOUD 18AD search for new heavy particle $Y \rightarrow HX \rightarrow (bb) + (qq)$. No signal observed. Limits set on $m(Y)$ vs. $m(X)$ in the ranges of $m(Y)$ in 1–4 TeV and $m(X)$ in 50–1000 GeV.

- 9 AABOUD 18CK search for SUSY Higgsinos in gauge-mediation via $pp \rightarrow bbb + E_T$ at 13 TeV using two complementary analyses with 24.3/36.1 fb $^{-1}$; no signal is found and Higgsinos with masses between 130 and 230 GeV and between 290 and 880 GeV are excluded at the 95% confidence level.
- 10 AABOUD 18CL search for $pp \rightarrow$ vector-like quarks \rightarrow jets at 13 TeV with 36 fb $^{-1}$; no signal seen; limits set on various VLQ scenarios. For pure $B \rightarrow Hb$ or $T \rightarrow Ht$, set the mass limit $m > 1010$ GeV.
- 11 AABOUD 18N search for dijet resonance at ATLAS with 13 TeV and 29.3 fb $^{-1}$; limits set on $m(Z')$ in the mass range of 450–1800 GeV.
- 12 SIRUNYAN 18DJ search for $pp \rightarrow ZZ$ or $WZ \rightarrow \ell\bar{\ell}jj$ resonance at 13 TeV, 35.9 fb $^{-1}$; no signal; limits set in the 400–4500 GeV mass range, exclusion of W' up to 2270 GeV in the HVT model A, and up to 2330 GeV for HVT model B. WED bulk graviton exclusion up to 925 GeV.
- 13 SIRUNYAN 18DY search for $pp \rightarrow RR; R \rightarrow jj$ two dijet resonances at 13 TeV 35.9 fb $^{-1}$; no signal; limits placed on RPV top-squark pair production.
- 14 KHACHATRYAN 17W search for dijet resonance in 12.9 fb $^{-1}$ data at 13 TeV; see Fig. 2 for limits on axiguons, diquarks, dark matter mediators etc.
- 15 KHACHATRYAN 17Y search for $pp \rightarrow (8-10) j$ in 19.7 fb $^{-1}$ at 8 TeV. No signal seen. Limits set on colorons, axiguons, RPV, and SUSY.
- 16 SIRUNYAN 17F measure $pp \rightarrow jj$ angular distribution in 2.6 fb $^{-1}$ at 13 TeV; limits set on LEDs and quantum black holes.
- 17 AABOUD 16 search for resonant dijets including one or two b -jets with 3.2 fb $^{-1}$ at 13 TeV; exclude excited b^* quark from 1.1–2.1 TeV; exclude leptophilic Z' with SM couplings from 1.1–1.5 TeV.
- 18 AAD 16N search for ≥ 3 jets with 3.6 fb $^{-1}$ at 13 TeV; limits placed on micro black holes (Fig. 10) and string balls (Fig. 11).
- 19 AAD 16S search for high mass jet-jet resonance with 3.6 fb $^{-1}$ at 13 TeV; exclude portions of excited quarks, W', Z' and contact interaction parameter space.
- 20 KHACHATRYAN 16K search for dijet resonance in 2.4 fb $^{-1}$ data at 13 TeV; see Fig. 3 for limits on axiguons, diquarks etc.
- 21 KHACHATRYAN 16L use data scouting technique to search for jj resonance on 18.8 fb $^{-1}$ of data at 8 TeV. Limits on the coupling of a leptophobic Z' to quarks are set, improving on the results by other experiments in the mass range between 500–800 GeV.
- 22 AAD 13D search for dijet resonances in pp collisions at $E_{cm} = 7$ TeV with $L = 4.8$ fb $^{-1}$. The observed events are compatible with Standard Model expectation. See their Fig. 6 and Table 2 for limits on resonance cross section in the range $m = 1.0$ – 4.0 TeV.
- 23 AALTONEN 13R search for production of a pair of jet-jet resonances in $p\bar{p}$ collisions at $E_{cm} = 1.96$ TeV with $L = 6.6$ fb $^{-1}$. See their Fig. 5 and Tables I, II for cross section limits.
- 24 CHATRCHYAN 13A search for $qq, qg,$ and gg resonances in pp collisions at $E_{cm} = 7$ TeV with $L = 4.8$ fb $^{-1}$. See their Fig. 3 and Table 1 for limits on resonance cross section in the range $m = 1.0$ – 4.3 TeV.
- 25 CHATRCHYAN 13A search for $b\bar{b}$ resonances in pp collisions at $E_{cm} = 7$ TeV with $L = 4.8$ fb $^{-1}$. See their Fig. 8 and Table 4 for limits on resonance cross section in the range $m = 1.0$ – 4.0 TeV.
- 26 AAD 12S search for dijet resonances in pp collisions at $E_{cm} = 7$ TeV with $L = 1.0$ fb $^{-1}$. See their Fig. 3 and Table 2 for limits on resonance cross section in the range $m = 0.9$ – 4.0 TeV.
- 27 CHATRCHYAN 12BL search for $t\bar{t}$ resonances in pp collisions at $E_{cm} = 7$ TeV with $L = 4.4$ fb $^{-1}$. See their Fig. 4 for limits on resonance cross section in the range $m = 0.5$ – 3.0 TeV.
- 28 AAD 11AG search for dijet resonances in pp collisions at $E_{cm} = 7$ TeV with $L = 36$ pb $^{-1}$. Limits on number of events for $m = 0.6$ – 4 TeV are given in their Table 3.
- 29 AALTONEN 11M find a peak in two jet invariant mass distribution around 140 GeV in $W + 2$ jet events in $p\bar{p}$ collisions at $E_{cm} = 1.96$ TeV with $L = 4.3$ fb $^{-1}$.
- 30 ABAZOV 11I search for two-jet resonances in $W + 2$ jet events in $p\bar{p}$ collisions at $E_{cm} = 1.96$ TeV with $L = 4.3$ fb $^{-1}$ and give limits $\sigma < (2.6-1.3)$ pb (95% CL) for $m = 110$ – 170 GeV. The result is incompatible with AALTONEN 11M.
- 31 AAD 10 search for narrow dijet resonances in pp collisions at $E_{cm} = 7$ TeV with $L = 315$ nb $^{-1}$. Limits on the cross section in the range 10 – 10^3 pb is given for $m = 0.3$ – 1.7 TeV.
- 32 KHACHATRYAN 10 search for narrow dijet resonances in pp collisions at $E_{cm} = 7$ TeV with $L = 2.9$ pb $^{-1}$. Limits on the cross section in the range 1 – 300 pb is given for $m = 0.5$ – 2.6 TeV separately in the final states $qq, qg,$ and gg .
- 33 ABE 99F search for narrow $b\bar{b}$ resonances in $p\bar{p}$ collisions at $E_{cm} = 1.8$ TeV. Limits on $\sigma(p\bar{p} \rightarrow X + \text{anything}) \times \text{B}(X \rightarrow b\bar{b})$ in the range 3 – 10^3 pb (95% CL) are given for $m_X = 200$ – 750 GeV. See their Table I.
- 34 ABE 97G search for narrow dijet resonances in $p\bar{p}$ collisions with 106 pb $^{-1}$ of data at $E_{cm} = 1.8$ TeV. Limits on $\sigma(p\bar{p} \rightarrow X + \text{anything}) \times \text{B}(X \rightarrow jj)$ in the range 10^4 – 10^{-1} pb (95% CL) are given for dijet mass $m = 200$ – 1150 GeV with both jets having $|\eta| < 2.0$ and the dijet system having $|\cos\theta^*| < 0.67$. See their Table I for the list of limits. Supersedes ABE 93c.
- 35 ABE 93c give cross section times branching ratio into light (d, u, s, c, b) quarks for $\Gamma = 0.02$ M. Their Table II gives limits for $M = 200$ – 900 GeV and $\Gamma = (0.02-0.2)$ M.

LIMITS ON NEUTRAL PARTICLE PRODUCTION

Production Cross Section of Radiatively-Decaying Neutral Particle

VALUE (pb)	CL%	DOCUMENT ID	TECN	COMMENT
•••	•••	•••	•••	•••
		1 ALBERT	18c HAWC	γ from Sun
		2 KHACHATRYAN...17D	CMS	$Z\gamma$ resonance
< 0.0008	95	3 AAD	16AI ATLS	$pp \rightarrow \gamma + \text{jet}$
		4 KHACHATRYAN...16M	CMS	$pp \rightarrow \gamma\gamma$ resonance
< (0.043-0.17)	95	5 ABBIENDI	00D OPAL	$e^+e^- \rightarrow X^0\gamma^0,$ $X^0 \rightarrow \gamma^0\gamma^0$
< (0.05-0.8)	95	6 ABBIENDI	00D OPAL	$e^+e^- \rightarrow X^0X^0,$ $X^0 \rightarrow \gamma^0\gamma^0$
< (2.5-0.5)	95	7 ACKERSTAFF	97B OPAL	$e^+e^- \rightarrow X^0\gamma^0,$ $X^0 \rightarrow \gamma^0\gamma^0$
< (1.6-0.9)	95	8 ACKERSTAFF	97B OPAL	$e^+e^- \rightarrow X^0X^0,$ $X^0 \rightarrow \gamma^0\gamma^0$

- 1 ALBERT 18c search for WIMP annihilation in Sun to long-lived, radiatively decaying mediator; no signal; limits set on $\sigma^{SD}(\chi p)$ assuming long-lived mediator.
- 2 KHACHATRYAN 17D search for new scalar resonance decaying to $Z\gamma$ with $Z \rightarrow e^+e^-$, $\mu^+\mu^-$ in pp collisions at 8 and 13 TeV; no signal seen.
- 3 AAD 16A search for excited quarks (EQ) and quantum black holes (QBH) in 3.2 fb⁻¹ at 13 TeV of data; exclude EQ below 4.4 TeV and QBH below 3.8 (6.2) TeV for RS1 (ADD) models. The visible cross section limit was obtained for 5 TeV resonance with $\sigma_G/M_G = 2\%$.
- 4 KHACHATRYAN 16M search for $\gamma\gamma$ resonance using 19.7 fb⁻¹ at 8 TeV and 3.3 fb⁻¹ at 13 TeV; slight excess at 750 GeV noted; limit set on RS graviton.
- 5 ABBIENDI 00D associated production limit is for $m_{X0} = 90\text{--}188$ GeV, $m_{Y0}=0$ at $E_{cm}=189$ GeV. See also their Fig. 9.
- 6 ABBIENDI 00D pair production limit is for $m_{X0} = 45\text{--}94$ GeV, $m_{Y0}=0$ at $E_{cm}=189$ GeV. See also their Fig. 12.
- 7 ACKERSTAFF 97B associated production limit is for $m_{X0} = 80\text{--}160$ GeV, $m_{Y0}=0$ from 10.0 pb⁻¹ at $E_{cm} = 161$ GeV. See their Fig. 3(a).
- 8 ACKERSTAFF 97B pair production limit is for $m_{X0} = 40\text{--}80$ GeV, $m_{Y0}=0$ from 10.0 pb⁻¹ at $E_{cm} = 161$ GeV. See their Fig. 3(b).

Heavy Particle Production Cross Section

VALUE (cm ² /N)	CL%	DOCUMENT ID	TECN	COMMENT
• • • We do not use the following data for averages, fits, limits, etc. • • •				
		1 AAD	21F ATLS	monojet search
		2 AAIJ	20AL LHCB	pp at 13 TeV, dimuon resonance
		3 SIRUNYAN	20AY CMS	$\Upsilon(1S)\mu^+\mu^-$ decay states
		4 SIRUNYAN	20Z CMS	multilepton BSM search, 13 TeV
		5 AABOUD	19H ATLS	di-photon-jet resonance
		6 AABOUD	19V ATLS	ATLAS review, mediator-based DM
		7 SIRUNYAN	19Q CMS	$pp \rightarrow \gamma \cancel{E}_T$
		8 AABOUD	18CJ ATLS	$pp \rightarrow VV/\ell\ell/\ell\nu, V = W, Z, h$
		9 AABOUD	18CM ATLS	$pp \rightarrow e\mu/e\tau/\mu\tau$
		10 AAIJ	18AJ LHCB	$pp \rightarrow A' \rightarrow \mu^+\mu^-$; dark photon
		11 BANERJEE	18 NA64	$eZ \rightarrow eZX(A')$
		12 BANERJEE	18A NA64	$eZ \rightarrow eZA', A' \rightarrow \chi\chi$
		13 MARSICANO	18 E137	$e^+e^- \rightarrow A'(\gamma)$ visible decay
		14 SIRUNYAN	18BB CMS	$pp \rightarrow Z' \rightarrow \ell^+\ell^-$ at 13 TeV
		15 SIRUNYAN	18DA CMS	$pp \rightarrow$ Black Hole, string ball, sphaleron
		16 SIRUNYAN	18DD CMS	$pp \rightarrow jj$
		17 SIRUNYAN	18DR CMS	$pp \rightarrow b\mu\bar{\mu}$
		18 SIRUNYAN	18DU CMS	$pp \rightarrow \gamma\gamma$
		19 SIRUNYAN	18ED CMS	$pp \rightarrow V \rightarrow Wh; h \rightarrow b\bar{b}; W \rightarrow \ell\nu$
		20 AABOUD	17B ATLS	WH, ZH resonance
		21 AAIJ	17BR LHCB	$pp \rightarrow \pi\nu\pi\nu, \pi\nu \rightarrow jj$
		22 AAD	16O ATLS	$\ell + (\ell s \text{ or jets})$
		23 AAD	16R ATLS	WW, WZ, ZZ resonance
		24 KRASZNAHO..16		$p^7\text{Li} \rightarrow {}^8\text{Be} \rightarrow X(17)N, X(17) \rightarrow e^+e^-$
		25 LEES	15E BABR	e^+e^- collisions
		26 ADAMS	97B KTEV	$m = 1.2\text{--}5$ GeV
		27 GALLAS	95 TOF	$m = 0.5\text{--}20$ GeV
		28 AKESSON	91 CNTR	$m = 0\text{--}5$ GeV
		29 BADIER	86 BDMP	$\tau = (0.05\text{--}1.) \times 10^{-8}$ s
		30 GUSTAFSON	76 CNTR	$\tau > 10^{-7}$ s
$< 10^{-36}\text{--}10^{-33}$	90			
$< (4\text{--}0.3) \times 10^{-31}$	95			
$< 2 \times 10^{-36}$	90			
$< 2.5 \times 10^{-35}$				

- 1 AAD 21F search for hard monojet production at ATLAS with 139⁻¹ of 13 TeV data. No signal observed. Limits placed on invisible production cross-section recoiling against ISR and interpreted in variety of BSM models.
- 2 AAIJ 20AL search for dimuon resonance from promptly decaying X particle; no signal; limits placed on $m(X)$ up to 60 GeV depending on mixing in 2HDM.
- 3 SIRUNYAN 20AY measured $\Upsilon(1S)$ pair production cross section and searched for new states decaying into $\Upsilon(1S)\mu^+\mu^-$ at CMS with 13 TeV with 35.9 fb⁻¹. No signal is found and limits are set in σ -BF vs. mass plane for tetra- b -quarks with masses between 17.5 and 19 GeV and for generic search for narrow resonances with mass between 16.5 and 27 GeV.
- 4 SIRUNYAN 20Z search for BSM physics via multilepton production with CMS at 13 TeV with 137 fb⁻¹; no signal is found and limits are set on type-III seesaw and other BSM models.
- 5 AABOUD 19H searches for di-photon-jet resonance at 13 TeV and 36.7 fb⁻¹ of data; no signal found and limits placed on σ -BR vs. mass plane for various simplified models.
- 6 AABOUD 19V review ATLAS searches for mediator-based DM at 7, 8, and 13 TeV with up to 37 fb⁻¹ of data; no signal found and limits set for wide variety of simplified models of dark matter.
- 7 SIRUNYAN 19Q search for $pp \rightarrow \gamma \cancel{E}_T$ at 13 TeV with 36.1 fb⁻¹; no signal found and limits set for various simplified models.
- 8 AABOUD 18CJ make multichannel search for $pp \rightarrow VV/\ell\ell/\ell\nu, V = W, Z, h$ at 13 TeV, 36.1 fb⁻¹; no signal found; limits placed for several BSM models.
- 9 AABOUD 18CM search for lepton-flavor violating resonance in $pp \rightarrow e\mu/e\tau/\mu\tau$ at 13 TeV, 36.1 fb⁻¹; no signal is found and limits placed for various BSM models.
- 10 AAIJ 18AJ search for prompt and delayed dark photon decay $A' \rightarrow \mu^+\mu^-$ at LHCB detector using 1.6 fb⁻¹ of pp collisions at 13 TeV; limits on $m(A')$ vs. kinetic mixing are set.

- 11 BANERJEE 18 search for dark photon $A'/16.7$ MeV boson X at NA64 via $eZ \rightarrow eZX(A')$; no signal found and limits set on the X - e^- coupling ϵ_e in the range $1.3 \times 10^{-4} \leq \epsilon_e \leq 4.2 \times 10^{-4}$ excluding part of the allowed parameter space.
- 12 BANERJEE 18A search for invisibly decaying dark photons in $eZ \rightarrow eZA', A' \rightarrow$ invisible; no signal found and limits set on mixing for $m(A') < 1$ GeV.
- 13 MARSICANO 18 search for dark photon $e^+e^- \rightarrow A'(\gamma)$ visible decay in SLAC E137 e beam dump data. No signal observed and limits set in ϵ coupling vs $m(A')$ plane, see their figure 7.
- 14 SIRUNYAN 18BB search for high mass dilepton resonance; no signal found and exclude portions of p -space of Z', KK graviton models.
- 15 SIRUNYAN 18DA search for $pp \rightarrow$ Black Hole, string ball, sphaleron via high multiplicity events at 13 TeV, 35.9 fb⁻¹; no signal, require e.g. $m(\text{BH}) > 10.1$ TeV.
- 16 SIRUNYAN 18DD search for $pp \rightarrow jj$ deviations in dijet angular distribution. No signal observed. Set limits on large extra dimensions, black holes and DM mediators e.g. $m(\text{BH}) > 5.9\text{--}8.2$ TeV.
- 17 SIRUNYAN 18DR search for dimuon resonance in $pp \rightarrow b\mu\bar{\mu}$ at 8 and 13 TeV. Slight excess seen at $m(\mu\bar{\mu}) \sim 28$ GeV in some channels.
- 18 SIRUNYAN 18DU search for high mass diphoton resonance in $pp \rightarrow \gamma\gamma$ at 13 TeV using 35.9 fb⁻¹; no signal; limits placed on RS Graviton, LED, and clockwork.
- 19 SIRUNYAN 18ED search for $pp \rightarrow V \rightarrow Wh; h \rightarrow b\bar{b}; W \rightarrow \ell\nu$ at 13 TeV with 35.9 fb⁻¹; no signal; limits set on $m(W')$ > 2.9 TeV.
- 20 AABOUD 17B exclude $m(W', Z') < 1.49\text{--}2.31$ TeV depending on the couplings and W'/Z' degeneracy assumptions via WH, ZH search in pp collisions at 13 TeV with 3.2 fb⁻¹ of data.
- 21 AAIJ 17BR search for long-lived hidden valley pions from Higgs decay. Limits are set on the signal strength as a function of the mass and lifetime of the long-lived particle in their Fig. 4 and Tab. 4.
- 22 AAD 16O search for high $E_T \ell + (\ell s \text{ or jets})$ with 3.2 fb⁻¹ at 13 TeV; exclude micro black holes mass < 8 TeV (Fig. 3) for models with two extra dimensions.
- 23 AAD 16R search for WW, WZ, ZZ resonance in 20.3 fb⁻¹ at 8 TeV data; limits placed on massive RS graviton (Fig. 4).
- 24 KRASZNAHORKAY 16 report $p\text{Li} \rightarrow \text{Be} \rightarrow e\bar{\nu}N$ 5 σ resonance at 16.7 MeV— possible evidence for nuclear interference or new light boson. However, such nuclear interference was ruled out already by ZANG 17.
- 25 LEES 15E search for long-lived neutral particles produced in e^+e^- collisions in the Upsilon region, which decays into $e^+e^-, \mu^+\mu^-, e^+\mu^\mp, \pi^+\pi^-, K^+K^-, \text{ or } \pi^\pm K^\mp$. See their Fig. 2 for cross section limits.
- 26 ADAMS 97B search for a hadron-like neutral particle produced in pN interactions, which decays into a p^0 and a weakly interacting massive particle. Upper limits are given for the ratio to K_L production for the mass range 1.2–5 GeV and lifetime $10^{-9}\text{--}10^{-4}$ s. See also our Light Gluino Section.
- 27 GALLAS 95 limit is for a weakly interacting neutral particle produced in 800 GeV/c pN interactions decaying with a lifetime of $10^{-4}\text{--}10^{-8}$ s. See their Figs. 8 and 9. Similar limits are obtained for a stable particle with interaction cross section $10^{-29}\text{--}10^{-33}$ cm². See Fig. 10.
- 28 AKESSON 91 limit is from weakly interacting neutral long-lived particles produced in pN reaction at 450 GeV/c performed at CERN SPS. Bourquin-Gaillard formula is used as the production model. The above limit is for $\tau > 10^{-7}$ s. For $\tau > 10^{-9}$ s, $\sigma < 10^{-30}$ cm²/nucleon is obtained.
- 29 BADIER 86 looked for long-lived particles at 300 GeV π^- beam dump. The limit applies for nonstrongly interacting neutral or charged particles with mass > 2 GeV. The limit applies for particle modes, $\mu^+\pi^-, \mu^+\mu^-, \pi^+\pi^-, X, \pi^+\pi^-\pi^\pm$ etc. See their figure 5 for the contours of limits in the mass- τ plane for each mode.
- 30 GUSTAFSON 76 is a 300 GeV FNAL experiment looking for heavy ($m > 2$ GeV) long-lived neutral hadrons in the M4 neutral beam. The above typical value is for $m = 3$ GeV and assumes an interaction cross section of 1 mb. Values as a function of mass and interaction cross section are given in figure 2.

Production of New Penetrating Non- ν Like States in Beam Dump

VALUE	DOCUMENT ID	TECN	COMMENT
• • • We do not use the following data for averages, fits, limits, etc. • • •			
	1 ANDREEV	21 NA64	search for new boson X in $eZ \rightarrow eZX$
	2 LOSECCO	81 CALO	28 GeV protons
	1 ANDREEV	21	search for new invisibly decaying boson X in $eZ \rightarrow eZX$ at NA64. No signal observed. Limits set in coupling vs. $m(X)$ plane for $m(X) \sim 10^{-3}$ to 1 GeV.
	2		No excess neutral-current events leads to $\sigma(\text{production}) \times \sigma(\text{interaction}) \times \text{acceptance} < 2.26 \times 10^{-71}$ cm ² /nucleon ² (CL = 90%) for light neutrals. Acceptance depends on models (0.1 to 4. $\times 10^{-4}$).

LIMITS ON CHARGED PARTICLES IN e^+e^- Heavy Particle Production Cross Section in e^+e^-

Ratio to $\sigma(e^+e^- \rightarrow \mu^+\mu^-)$ unless noted. See also entries in Free Quark Search and Magnetic Monopole Searches.

VALUE	CL%	DOCUMENT ID	TECN	COMMENT
• • • We do not use the following data for averages, fits, limits, etc. • • •				
$< 1 \times 10^{-3}$	90	1 KILE	18 ALEP	$e^+e^- \rightarrow 4$ jets
		2 ABLIKIM	17AA BES3	$e^+e^- \rightarrow \ell\bar{\ell}\gamma$
		3 ACKERSTAFF	98P OPAL	$Q=1,2/3, m=45\text{--}89.5$ GeV
		4 ABREU	97D DLPH	$Q=1,2/3, m=45\text{--}84$ GeV
		5 BARATE	97K ALEP	$Q=1, m=45\text{--}85$ GeV
		6 AKERS	95R OPAL	$Q=1, m=5\text{--}45$ GeV
		7 AKERS	95R OPAL	$Q=2, m=5\text{--}45$ GeV
		8 BUSKULIC	93C ALEP	$Q=1, m=32\text{--}72$ GeV
		9 ADACHI	90C TOPZ	$Q=1, m=1\text{--}16, 18\text{--}27$ GeV
		10 ADACHI	90E TOPZ	$Q=1, m=5\text{--}25$ GeV
		11 KINOSHITA	82 PLAS	$Q=3\text{--}180, m < 14.5$ GeV
		12 BARTEL	80 JADE	$Q=(3,4,5)/3$ 2–12 GeV

Searches Particle Listings

Other Particle Searches

- ¹ KILE 18 investigate archived ALEPH $e^+e^- \rightarrow 4$ jets data and see 4–5 σ excess at 110 GeV.
- ² ABLIKIM 17AA search for dark photon $A \rightarrow \ell\bar{\ell}$ at 3.773 GeV with 2.93 fb⁻¹. Limits are set in ϵ vs $m(A)$ plane.
- ³ ACKERSTAFF 98P search for pair production of long-lived charged particles at E_{cm} between 130 and 183 GeV and give limits $\sigma < (0.05-0.2)$ pb (95%CL) for spin-0 and spin-1/2 particles with $m=45-89.5$ GeV, charge 1 and 2/3. The limit is translated to the cross section at $E_{cm}=183$ GeV with the s dependence described in the paper. See their Figs. 2–4.
- ⁴ ABREU 97D search for pair production of long-lived particles and give limits $\sigma < (0.4-2.3)$ pb (95%CL) for various center-of-mass energies $E_{cm}=130-136, 161,$ and 172 GeV, assuming an almost flat production distribution in $\cos\theta$.
- ⁵ BARATE 97K search for pair production of long-lived charged particles at $E_{cm} = 130, 136, 161,$ and 172 GeV and give limits $\sigma < (0.2-0.4)$ pb (95%CL) for spin-0 and spin-1/2 particles with $m=45-85$ GeV. The limit is translated to the cross section at $E_{cm}=172$ GeV with the E_{cm} dependence described in the paper. See their Figs. 2 and 3 for limits on $J = 1/2$ and $J = 0$ cases.
- ⁶ AKERS 95R is a CERN-LEP experiment with $W_{cm} \sim m_Z$. The limit is for the production of a stable particle in multihadron events normalized to $\sigma(e^+e^- \rightarrow \text{hadrons})$. Constant phase space distribution is assumed. See their Fig. 3 for bounds for $Q = \pm 2/3, \pm 4/3$.
- ⁷ BUSKULIC 93c is a CERN-LEP experiment with $W_{cm} = m_Z$. The limit is for a pair or single production of heavy particles with unusual ionization loss in TPC. See their Fig. 5 and Table 1.
- ⁸ ADACHI 90C is a KEK-TRISTAN experiment with $W_{cm} = 52-60$ GeV. The limit is for pair production of a scalar or spin-1/2 particle. See Figs. 3 and 4.
- ⁹ ADACHI 90E is KEK-TRISTAN experiment with $W_{cm} = 52-61.4$ GeV. The above limit is for inclusive production cross section normalized to $\sigma(e^+e^- \rightarrow \mu^+\mu^-) \cdot \beta(3-\beta^2)/2$, where $\beta = (1 - 4m^2/W_{cm}^2)^{1/2}$. See the paper for the assumption about the production mechanism.
- ¹⁰ KINOSHITA 82 is SLAC PEP experiment at $W_{cm} = 29$ GeV using lexan and ³⁹Cr plastic sheets sensitive to highly ionizing particles.
- ¹¹ BARTEL 80 is DESY-PETRA experiment with $W_{cm} = 27-35$ GeV. Above limit is for inclusive pair production and ranges between $1. \times 10^{-1}$ and $1. \times 10^{-2}$ depending on mass and production momentum distributions. (See their figures 9, 10, 11).

Branching Fraction of Z^0 to a Pair of Stable Charged Heavy Fermions

VALUE	CL%	DOCUMENT ID	TECN	COMMENT
$< 5 \times 10^{-6}$	95	¹ AKERS 95R	OPAL	$m = 40.4-45.6$ GeV
$< 1 \times 10^{-3}$	95	AKRAWY 90O	OPAL	$m = 29-40$ GeV

• • • We do not use the following data for averages, fits, limits, etc. • • •

¹ AKERS 95R give the 95% CL limit $\sigma(X\bar{X})/\sigma(\mu\mu) < 1.8 \times 10^{-4}$ for the pair production of singly- or doubly-charged stable particles. The limit applies for the mass range 40.4–45.6 GeV for X^\pm and < 45.6 GeV for $X^{\pm\pm}$. See the paper for bounds for $Q = \pm 2/3, \pm 4/3$.

LIMITS ON CHARGED PARTICLES IN HADRONIC REACTIONS

MASS LIMITS for Long-Lived Charged Heavy Fermions

Limits are for spin 1/2 particles with no color and SU(2)_L charge. The electric charge Q of the particle (in the unit of e) is therefore equal to its weak hypercharge. Pair production by Drell-Yan like γ and Z exchange is assumed to derive the limits.

VALUE (GeV)	CL%	DOCUMENT ID	TECN	COMMENT
> 660	95	¹ SIRUNYAN 20N	CMS	disappearing track LLP
> 200	95	² AAD 15BJ	ATLS	$ Q = 2$
> 480	95	³ CHATRCHYAN13AB	CMS	$ Q = 1/3$
> 574	95	³ CHATRCHYAN13AB	CMS	$ Q = 2/3$
> 685	95	³ CHATRCHYAN13AB	CMS	$ Q = 1$
> 140	95	³ CHATRCHYAN13AB	CMS	$ Q = 2$
> 310	95	⁴ CHATRCHYAN13AR	CMS	$ Q = 1/3$
	95	⁴ CHATRCHYAN13AR	CMS	$ Q = 2/3$

• • • We do not use the following data for averages, fits, limits, etc. • • •

- ¹ SIRUNYAN 20N search for LLPs using disappearing track signature at CMS at 13 TeV with 101 fb⁻¹; no signal; limits placed on long-lived winos and higgsinos from SUSY depending on mass and lifetime: e.g. at 95% CL, for a purely higgsino neutralino, $m(\text{chargino}) > 750$ (175) GeV for $\tau = 3$ (0.05) ns, and for a purely wino neutralino, $m(\text{chargino}) > 884$ (474) GeV for $\tau = 3$ (0.2) ns.
- ² AAD 15BJ use 20.3 fb⁻¹ of pp collisions at $E_{cm} = 8$ TeV. See paper for limits for $|Q| = 3, 4, 5, 6$.
- ³ CHATRCHYAN 13AB use 5.0 fb⁻¹ of pp collisions at $E_{cm} = 7$ TeV and 18.8 fb⁻¹ at $E_{cm} = 8$ TeV. See paper for limits for $|Q| = 3, 4, \dots, 8$.
- ⁴ CHATRCHYAN 13AR use 5.0 fb⁻¹ of pp collisions at $E_{cm} = 7$ TeV.

Heavy Particle Production Cross Section

VALUE (nb)	CL%	DOCUMENT ID	TECN	COMMENT
		¹ SIRUNYAN 21T	CMS	model independent search
		² SIRUNYAN 20C	CMS	4t search via multileptons
		³ AABOUD 19AA	ATLS	BSM search
		⁴ AABOUD 19Q	ATLS	single top + MET
		⁵ AABOUD 17D	ATLS	anomalous $WWjj, WZjj$
		⁶ AABOUD 17L	ATLS	$m > 870$ GeV, $Z(\rightarrow \nu\nu)tX$
		⁷ SIRUNYAN 17B	CMS	tH
		⁸ SIRUNYAN 17C	CMS	$Z + (t \text{ or } b)$
		⁹ SIRUNYAN 17J	CMS	$X_{5/3} \rightarrow tW$
		¹⁰ AAIJ 15BD	LHCb	$m=124-309$ GeV

• • • We do not use the following data for averages, fits, limits, etc. • • •

$< 1.2 \times 10^{-3}$	95	¹¹ AAD	13AH	ATLS	$ q =(2-6)e, m=50-600$ GeV
$< 1.0 \times 10^{-5}$	95	¹² AAD	11I	ATLS	$ q =10e, m=0.2-1$ TeV
$< 4.8 \times 10^{-5}$	95	^{13,14} AALTONEN	09Z	CDF	$m > 100$ GeV, noncolored
$< 0.31-0.04 \times 10^{-3}$	95	^{13,15} AALTONEN	09Z	CDF	$m > 100$ GeV, colored
< 0.19	95	¹⁶ ABAZOV	09M	D0	pair production
< 0.05	95	¹⁷ AKTAS	04c	H1	$m=3-10$ GeV
< 0.05	95	¹⁸ ABE	92J	CDF	$m=50-200$ GeV
$< 30-130$		¹⁹ CARROLL	78	SPEC	$m=2-2.5$ GeV
< 100		²⁰ LEIPUNER	73	CNTR	$m=3-11$ GeV

- ¹ SIRUNYAN 21T perform model unspecific search for deviations from SM with CMS at 13 TeV with 35.9 fb⁻¹ data in numerous signature channels. No deviations from SM found.
- ² SIRUNYAN 20c search for four top-quark production with decay to multileptons at CMS at 13 TeV with 137 fb⁻¹; no signal is found and limits are placed on the Higgs boson oblique parameter in the effective field theory framework (EFT) and the model parameters ($\tan\beta$).
- ³ AABOUD 19AA search for BSM physics at 13 TeV with 3.2 fb⁻¹ in $> 10^5$ regions of > 700 event classes; no significant signal found.
- ⁴ AABOUD 19Q search for single top+MET events at 13 TeV with 36.1 fb⁻¹ of data; no signal found and limits set in σ or coupling vs. mass plane for variety of simplified models including DM and vector-like top quark T .
- ⁵ AABOUD 17D search for $WWjj, WZjj$ in pp collisions at 8 TeV with 3.2 fb⁻¹; set limits on anomalous couplings.
- ⁶ AABOUD 17L search for the pair production of heavy vector-like T quarks in the $Z(\rightarrow \nu\nu)tX$ final state.
- ⁷ SIRUNYAN 17b search for vector-like quark $pp \rightarrow TX \rightarrow tHX$ in 2.3 fb⁻¹ at 13 TeV; no signal seen; limits placed.
- ⁸ SIRUNYAN 17c search for vector-like quark $pp \rightarrow TX \rightarrow Z + (t \text{ or } b)$ in 2.3 fb⁻¹ at 13 TeV; no signal seen; limits placed.
- ⁹ SIRUNYAN 17j search for $pp \rightarrow X_{5/3}X_{5/3} \rightarrow tWtW$ with 2.3 fb⁻¹ at 13 TeV. No signal seen: $m(X) > 1020$ (990) GeV for RH (LH) new charge 5/3 quark.
- ¹⁰ AAIJ 15BD search for production of long-lived particles in pp collisions at $E_{cm} = 7$ and 8 TeV. See their Table 6 for cross section limits.
- ¹¹ AAD 13AH search for production of long-lived particles with $|q|=(2-6)e$ in pp collisions at $E_{cm} = 7$ TeV with 4.4 fb⁻¹. See their Fig. 8 for cross section limits.
- ¹² AAD 11I search for production of highly ionizing massive particles in pp collisions at $E_{cm} = 7$ TeV with $L = 3.1$ pb⁻¹. See their Table 5 for similar limits for $|q| = 6e$ and $17e$, Table 6 for limits on pair production cross section.
- ¹³ AALTONEN 09Z search for long-lived charged particles in $p\bar{p}$ collisions at $E_{cm} = 1.96$ TeV with $L = 1.0$ fb⁻¹. The limits are on production cross section for a particle of mass above 100 GeV in the region $|\eta| \lesssim 0.7, p_T > 40$ GeV, and $0.4 < \beta < 1.0$.
- ¹⁴ Limit for weakly interacting charge-1 particle.
- ¹⁵ Limit for up-quark like particle.
- ¹⁶ ABAZOV 09M search for pair production of long-lived charged particles in $p\bar{p}$ collisions at $E_{cm} = 1.96$ TeV with $L = 1.1$ fb⁻¹. Limit on the cross section of (0.31–0.04) pb (95% CL) for the mass range of 60–300 GeV, assuming the kinematics of stau pair production.
- ¹⁷ AKTAS 04c look for charged particle photoproduction at HERA with mean c.m. energy of 200 GeV.
- ¹⁸ ABE 92J look for pair production of unit-charged particles which leave detector before decaying. Limit shown here is for $m=50$ GeV. See their Fig. 5 for different charges and stronger limits for higher mass.
- ¹⁹ CARROLL 78 look for neutral, $S = -2$ dihyperon resonance in $pp \rightarrow 2K^+X$. Cross section varies within above limits over mass range and $p_{lab} = 5.1-5.9$ GeV/c.
- ²⁰ LEIPUNER 73 is an NAL 300 GeV p experiment. Would have detected particles with lifetime greater than 200 ns.

Heavy Particle Production Differential Cross Section

VALUE (cm ² sr ⁻¹ GeV ⁻¹)	CL%	DOCUMENT ID	TECN	CHG	COMMENT
$< 2.6 \times 10^{-36}$	90	¹ BALDIN 76	CNTR	–	$Q = 1, m=2.1-9.4$ GeV
$< 2.2 \times 10^{-33}$	90	² ALBROW 75	SPEC	±	$Q = \pm 1, m=4-15$ GeV
$< 1.1 \times 10^{-33}$	90	² ALBROW 75	SPEC	±	$Q = \pm 2, m=6-27$ GeV
$< 8. \times 10^{-35}$	90	³ JOVANOVIĆ 75	CNTR	±	$m=15-26$ GeV
$< 1.5 \times 10^{-34}$	90	³ JOVANOVIĆ 75	CNTR	±	$Q = \pm 2, m=3-10$ GeV
$< 6. \times 10^{-35}$	90	³ JOVANOVIĆ 75	CNTR	±	$Q = \pm 2, m=10-26$ GeV
$< 1. \times 10^{-31}$	90	⁴ APPEL 74	CNTR	±	$m=3.2-7.2$ GeV
$< 5.8 \times 10^{-34}$	90	⁵ ALPER 73	SPEC	±	$m=1.5-24$ GeV
$< 1.2 \times 10^{-35}$	90	⁶ ANTIPOV 71B	CNTR	–	$Q = -, m=2.2-2.8$
$< 2.4 \times 10^{-35}$	90	⁷ ANTIPOV 71C	CNTR	–	$Q = -, m=1.2-1.7, 2.1-4$
$< 2.4 \times 10^{-35}$	90	⁸ BINON 69	CNTR	–	$Q = -, m=1-1.8$ GeV
$< 1.5 \times 10^{-36}$		⁸ DORFAN 65	CNTR		Be target $m=3-7$ GeV
$< 3.0 \times 10^{-36}$		⁸ DORFAN 65	CNTR		Fe target $m=3-7$ GeV

• • • We do not use the following data for averages, fits, limits, etc. • • •

- ¹ BALDIN 76 is a 70 GeV Serpukhov experiment. Value is per Al nucleus at $\theta = 0$. For other charges in range -0.5 to -3.0 , CL = 90% limit is $(2.6 \times 10^{-36})/|(charge)|$ for mass range (2.1–9.4 GeV) $\times |(charge)|$. Assumes stable particle interacting with matter as do antiprotons.
- ² ALBROW 75 is a CERN ISR experiment with $E_{cm} = 53$ GeV. $\theta = 40$ mr. See figure 5 for mass ranges up to 35 GeV.
- ³ JOVANOVIĆ 75 is a CERN ISR 26+26 and 15+15 GeV pp experiment. Figure 4 covers ranges $Q = 1/3$ to 2 and $m = 3$ to 26 GeV. Value is per GeV momentum.
- ⁴ APPEL 74 is NAL 300 GeV pW experiment. Studies forward production of heavy (up to 24 GeV) charged particles with momenta 24–200 GeV (–charge) and 40–150 GeV (+charge). Above typical value is for 75 GeV and is per GeV momentum per nucleon.
- ⁵ ALPER 73 is CERN ISR 26+26 GeV pp experiment. $p > 0.9$ GeV, $0.2 < \beta < 0.65$.
- ⁶ ANTIPOV 71B is from same 70 GeV p experiment as ANTIPOV 71C and BINON 69.
- ⁷ ANTIPOV 71C limit inferred from flux ratio. 70 GeV p experiment.
- ⁸ DORFAN 65 is a 30 GeV/c p experiment at BNL. Units are per GeV momentum per nucleus.

Long-Lived Heavy Particle Invariant Cross Section

VALUE (cm ² /GeV ² /N)	CL%	DOCUMENT ID	TECN	CHG	COMMENT
••• We do not use the following data for averages, fits, limits, etc. •••					
< 5-700 × 10 ⁻³⁵	90	1 BERNSTEIN 88	CNTR		
< 5-700 × 10 ⁻³⁷	90	1 BERNSTEIN 88	CNTR		
< 2.5 × 10 ⁻³⁶	90	2 THRON 85	CNTR	-	Q = 1, m = 4-12 GeV
< 1. × 10 ⁻³⁵	90	2 THRON 85	CNTR	+	Q = 1, m = 4-12 GeV
< 6. × 10 ⁻³³	90	3 ARMITAGE 79	SPEC		m = 1.87 GeV
< 1.5 × 10 ⁻³³	90	3 ARMITAGE 79	SPEC		m = 1.5-3.0 GeV
		4 BOZZOLI 79	CNTR	±	Q = (2/3, 1, 4/3, 2)
< 1.1 × 10 ⁻³⁷	90	5 CUTTS 78	CNTR		m = 4-10 GeV
< 3.0 × 10 ⁻³⁷	90	6 VIDAL 78	CNTR		m = 4.5-6 GeV

- BERNSTEIN 88 limits apply at $x = 0.2$ and $p_T = 0$. Mass and lifetime dependence of limits are shown in the regions: $m = 1.5-7.5$ GeV and $\tau = 10^{-8}-2 \times 10^{-6}$ s. First number is for hadrons; second is for weakly interacting particles.
- THRON 85 is FNAL 400 GeV proton experiment. Mass determined from measured velocity and momentum. Limits are for $\tau > 3 \times 10^{-9}$ s.
- ARMITAGE 79 is CERN-ISR experiment at $E_{cm} = 53$ GeV. Value is for $x = 0.1$ and $p_T = 0.15$. Observed particles at $m = 1.87$ GeV are found all consistent with being antideuterons.
- BOZZOLI 79 is CERN-SPS 200 GeV pN experiment. Looks for particle with τ larger than 10^{-8} s. See their figure 11-18 for production cross-section upper limits vs mass.
- CUTTS 78 is pBe experiment at FNAL sensitive to particles of $\tau > 5 \times 10^{-8}$ s. Value is for $-0.3 < x < 0$ and $p_T = 0.175$.
- VIDAL 78 is FNAL 400 GeV proton experiment. Value is for $x = 0$ and $p_T = 0$. Puts lifetime limit of $< 5 \times 10^{-8}$ s on particle in this mass range.

**Long-Lived Heavy Particle Production
($\sigma(\text{Heavy Particle}) / \sigma(\pi)$)**

VALUE	EVTS	DOCUMENT ID	TECN	CHG	COMMENT
••• We do not use the following data for averages, fits, limits, etc. •••					
< 10 ⁻⁸		1 NAKAMURA 89	SPEC	±	Q = (-5/3, ±2)
	0	2 BUSSIÈRE 80	CNTR	±	Q = (2/3, 1, 4/3, 2)

1 NAKAMURA 89 is KEK experiment with 12 GeV protons on Pt target. The limit applies for mass $\lesssim 1.6$ GeV and lifetime $\gtrsim 10^{-7}$ s.
2 BUSSIÈRE 80 is CERN-SPS experiment with 200-240 GeV protons on Be and Al target. See their figures 6 and 7 for cross-section ratio vs mass.

Production and Capture of Long-Lived Massive Particles

VALUE (10 ⁻³⁶ cm ²)	DOCUMENT ID	TECN	COMMENT
••• We do not use the following data for averages, fits, limits, etc. •••			
	1 AAD 21X	ATLS	search for captured LLPs
	2 ACHARYA 21	INDU	dyons production, capture
< 20 to 800	3 ALEKSEEV 76	ELEC	$\tau = 5$ ms to 1 day
< 200 to 2000	3 ALEKSEEV 76B	ELEC	$\tau = 100$ ms to 1 day
< 1.4 to 9	4 FRANKEL 75	CNTR	$\tau = 50$ ms to 10 hours
< 1.0 to 9	5 FRANKEL 74	CNTR	$\tau = 1$ to 1000 hours

- AAAD 21X search for LLPs which come to rest in ATLAS detector to deposit energy between collisions. No signal observed in 111 fb⁻¹ of data. Limits placed in lifetime vs. mass plane assuming model with gluino hadrons: e.g. $m > 1.4$ TeV for $\tau \sim 10^{-5}$ to 10^3 sec.
- ACHARYA 21 search for dyons (carrying electric and magnetic charge) and monopoles via production and capture in 6.46 fb⁻¹ of 13 TeV LHC data. No signal observed. Limits placed in mass vs. magnetic charge plane.
- ALEKSEEV 76 and ALEKSEEV 76B are 61-70 GeV p Serpukhov experiment. Cross section is per Pb nucleus.
- FRANKEL 75 is extension of FRANKEL 74.
- FRANKEL 74 looks for particles produced in thick Al targets by 300-400 GeV/c protons.

Long-Lived Particle (LLP) Search at Hadron Collisions

Limits are for cross section times branching ratio.

VALUE (fb)	CL%	DOCUMENT ID	TECN	COMMENT
••• We do not use the following data for averages, fits, limits, etc. •••				
		1 AAD 21AL	ATLS	charged LLPs search
		2 AAD 21BA	ATLS	LLP from higgs decay search
		3 AAIJ 21V	LHCB	LLP $\rightarrow e\mu\nu$ search
		4 SIRUNYAN 21AF	CMS	LLP search via displaced jets
		5 SIRUNYAN 21U	CMS	LLP search via displaced jets
< 0.07	95	6 TUMASYAN 21	CMS	LLP endcap muon detector searches
		7 AAD 20D	ATLS	$pp \rightarrow$ LLPs at 13 TeV
		8 AAD 20J	ATLS	scalar boson decay to LLPs
		9 AAD 20M	ATLS	LLP top squark decay to μ
		10 AAD 20P	ATLS	LLP dark photon search
		11 AAIJ 20AL	LHCB	pp dimuon resonance
		12 BALL 20		LLP milli-charged particles at LHC
		13 AABOUD 19AE	ATLS	pp at 13 TeV
		14 AABOUD 19AK	ATLS	$pp \rightarrow \Phi \rightarrow ZZ_d$
		15 AABOUD 19AM	ATLS	DY multi-charged LLP production
		16 AABOUD 19AO	ATLS	LLP via displaced jets
		17 AABOUD 19AT	ATLS	heavy, charged LLPs
		18 AABOUD 19G	ATLS	LLP decay to $\mu^+\mu^-$
		19 SIRUNYAN 19BH	CMS	LLP via displaced jets
		20 SIRUNYAN 19BT	CMS	LLP via displaced jets+MET
		21 SIRUNYAN 19CA	CMS	LLP $\rightarrow \gamma$ search
		22 SIRUNYAN 19Q	CMS	$pp \rightarrow j +$ displaced dark quark jet
		23 SIRUNYAN 18AW	CMS	Long-lived particle search
		24 AAIJ 16AR	LHCB	$H \rightarrow XX$ LLPs
		25 KHACHATRYAN 16BW	CMS	direct production: HSCPs
< 2000	90	26 BADIER 86	BDMP	$\tau = (0.05-1.) \times 10^{-8}$ s

- AAAD 21AL reports on ATLAS search for long-lived charged particles with 139 fb⁻¹ at 13 TeV. No signal observed. Limits placed in lifetime vs. mass plane: e.g. for $\tau(\text{LLP}) \sim 0.1$ ns, $m(\text{electron}) > 720$ GeV.
- AAAD 21BA search for long-lived particles from ZH production ($H \rightarrow b\bar{b}$) with 2 displaced vertices in 139 fb⁻¹ of data at 13 TeV. No signal detected. Limits placed in branching fraction vs. lifetime plane.
- AAIJ 21V search for $pp \rightarrow \text{LLP} + \text{LLP}$ with $\text{LLP} \rightarrow e\mu\nu$ in the lifetime range between 2 and 50 ps at LHCB with 5.4 fb⁻¹ at 13 TeV. No signal observed. Limits placed in LLP cross section vs. mass or lifetime plane for $m(\text{LLP}) \sim 7$ to 50 GeV.
- SIRUNYAN 21AF search for LLPs at CMS via jets with 2 displaced vertices in 140 fb⁻¹ of data at 13 TeV. No signal observed. Limits placed for RPV SUSY models in which a long-lived neutralino or gluino decays into a multijet final state with top, bottom, and strange quarks.
- SIRUNYAN 21U search for long-lived particles (LLPs) via displaced jets at CMS with LHCB and 132 fb⁻¹. No signal detected. Limits placed on simplified model production of LLP $X \rightarrow q\bar{q}$ with $\sigma < 0.07$ fb for $m(X) > 500$ GeV and $c\tau \sim 2$ to 250 mm.
- TUMASYAN 21 search for long-lived particles in CMS muon endcap detector in 137 fb⁻¹ of data at 13 TeV. No signal detected. Limits are placed depending on the branching fraction of Higgs boson to LLP decaying to $dd, bb,$ and $\tau^+\tau^-$, depending on proper decay length, and LLP masses.
- AAAD 20D search for opposite-sign dileptons originating from long-lived particles in pp collisions at 13 TeV with 32.8 fb⁻¹; limits placed in squark cross section vs. $c\tau$ plane for RPV SUSY.
- AAAD 20J search for scalar boson decay to two long-lived particles; no signal; limits placed in BF vs $c\tau$ plane for various mass hypotheses. This search is also combined with other ATLAS displaced-jet searches.
- AAAD 20M search for long-lived top-squarks decay to μ and hadrons; no signal; limits placed in cross section vs. mass and mass vs. lifetime planes.
- AAAD 20P search for long-lived dark photons produced from the decay of a scalar boson, with each dark photon decaying into displaced collimated leptons or light hadrons at 13 TeV with 36 fb⁻¹; no signal; limits placed in $\sigma \cdot \text{BF}$ vs. $c\tau$ and other planes.
- AAIJ 20AL search for long-lived $X \rightarrow \mu^+\mu^-$ decays in 5.1 fb⁻¹ of LHCB data at 13 TeV; no signal; limits placed on $m(X)$ up to 3 GeV depending on kinetic mixing.
- BALL 20 search for long-lived milli-charged particles produced at LHC; limits placed in charge vs. mass plane (Fig. 8).
- AABOUD 19AE search for long-lived particles via displaced jets using 10.8 fb⁻¹ or 33.0 fb⁻¹ data (depending on a trigger) at 13 TeV; no signal found and limits set in branching ratio vs. decay length plane.
- AABOUD 19AK searches for long-lived particle Z_d via $pp \rightarrow \Phi \rightarrow ZZ_d$ at 13 TeV with 36.1 fb⁻¹; no signal found and limits set in $\sigma \times \text{BR}$ vs. lifetime plane for simplified model.
- AABOUD 19AM search for Drell-Yan (DY) production of long-lived multi-charge particles at 13 TeV with 36.1 fb⁻¹ of data; no signal found and exclude 50 GeV $< m(\text{LLMCP}) < 980-1220$ GeV for electric charge $|q| = (2-7)e$.
- AABOUD 19AO search for neutral long-lived particles producing displaced jets at 13 TeV with 36.1 fb⁻¹ of data; no signal found and exclude regions of $\sigma \cdot \text{BR}$ vs. lifetime plane for various models.
- AABOUD 19AT search for heavy, charged long-lived particles at 13 TeV with 36.1 fb⁻¹; no signal found and upper limits set on masses of various hypothetical particles.
- AABOUD 19G search for long-lived particle with decay to $\mu^+\mu^-$ at 13 TeV with 32.9 fb⁻¹; no signal found and limits set in combinations of lifetime, mass and coupling planes for various simplified models.
- SIRUNYAN 19BH search for long-lived SUSY particles via displaced jets at 13 TeV with 35.9 fb⁻¹; no signal found and limits placed in mass vs lifetime plane for various hypothetical models.
- SIRUNYAN 19BT search for displaced jet(s)+ E_T at 13 TeV with 137 fb⁻¹; no signal found and limits placed in mass vs lifetime plane for gauge mediated SUSY breaking models.
- SIRUNYAN 19CA search for gluino/squark decay to long-lived neutralino, decay to γ in GMSB; no signal, limits placed in $m(X)$ vs. lifetime plane for SP58 GMSB benchmark point.
- SIRUNYAN 19Q search for $pp \rightarrow j +$ displaced jet via dark quark with 13 TeV at 16.1 fb⁻¹; no signal found and limits set in mass vs lifetime plane for dark quark/dark pion model.
- SIRUNYAN 18AW search for very long lived particles (LLPs) decaying hadronically or to $\mu\pi$ in CMS detector; none seen/limits set on lifetime vs. cross section.
- AAIJ 16AR search for long lived particles from $H \rightarrow XX$ with displaced X decay vertex using 0.62 fb⁻¹ at 7 TeV; limits set in Fig. 7.
- KHACHATRYAN 16BW search for heavy stable charged particles via ToF with 2.5 fb⁻¹ at 13 TeV; require stable $m(\text{gluino}) > 1610$ GeV.
- BADIER 86 looked for long-lived particles at 300 GeV π^- beam dump. The limit applies for particle modes, $\mu^+\pi^-, \mu^+\mu^-, \pi^+\pi^-, \pi^+\pi^+X, \pi^+\pi^-\pi^+$ etc. See their figure 5 for the contours of limits in the mass- τ plane for each mode.

Long-Lived Heavy Particle Cross Section

VALUE (pb/sr)	CL%	DOCUMENT ID	TECN	COMMENT
••• We do not use the following data for averages, fits, limits, etc. •••				
< 34	95	1 RAM 94	SPEC	1015 $< m_{X^{++}} < 1085$ MeV
< 75	95	1 RAM 94	SPEC	920 $< m_{X^{++}} < 1025$ MeV

1 RAM 94 search for a long-lived doubly-charged fermion X^{++} with mass between m_N and $m_N + m_\pi$ and baryon number +1 in the reaction $pp \rightarrow X^{++}n$. No candidate is found. The limit is for the cross section at 15° scattering angle at 460 MeV incident energy and applies for $\tau(X^{++}) \gg 0.1 \mu\text{s}$.

Searches Particle Listings

Other Particle Searches

LIMITS ON CHARGED PARTICLES IN COSMIC RAYS

Heavy Particle Flux in Cosmic Rays

VALUE ($\text{cm}^{-2}\text{s}^{-1}\text{s}^{-1}$)	CL%	EVTs	DOCUMENT ID	TECN	COMMENT
••• We do not use the following data for averages, fits, limits, etc. •••					
< 1	$\times 10^{-8}$	90	1 ALVIS	18 MAJD	Fractionally charged
			2 AGNESE	15 CDM2	$Q = 1/6$
~ 6	$\times 10^{-9}$	2	3 SAITO	90	$Q \approx 14, m \approx 370 m_p$
< 1.4	$\times 10^{-12}$	90	0	4 MINCER	85 CALO $m \geq 1$ TeV
			5 SAKUYAMA	83B PLAS	$m \sim 1$ TeV
< 1.7	$\times 10^{-11}$	99	0	6 BHAT	82 CC
< 1.	$\times 10^{-9}$	90	0	7 MARINI	82 CNTR $Q=1, m \sim 4.5 m_p$
2.	$\times 10^{-9}$		3	8 YOCK	81 SPRK $Q=1, m \sim 4.5 m_p$
			3	8 YOCK	81 SPRK Fractionally charged
3.0	$\times 10^{-9}$		3	9 YOCK	80 SPRK $m \sim 4.5 m_p$
$(4 \pm 1) \times 10^{-11}$			3	GOODMAN	79 ELEC $m \geq 5$ GeV
< 1.3	$\times 10^{-9}$	90	0	10 BHAT	78 CNTR $m > 1$ GeV
< 1.0	$\times 10^{-9}$		0	BRIATORE	76 ELEC
< 7.	$\times 10^{-10}$	90	0	YOCK	75 ELEC $Q > 7e$ or $< -7e$
> 6.	$\times 10^{-9}$		5	11 YOCK	74 CNTR $m > 6$ GeV
< 3.0	$\times 10^{-8}$		0	DARDO	72 CNTR
< 1.5	$\times 10^{-9}$		0	TONWAR	72 CNTR $m > 10$ GeV
< 3.0	$\times 10^{-10}$		0	BJORNOE	68 CNTR $m > 5$ GeV
< 5.0	$\times 10^{-11}$	90	0	BONES	67 ELEC $m=5-15$ GeV

- ALVIS 18 search for fractional charged flux of cosmic matter at Majorana demonstrator; no signal observed and limits are set on the flux of lightly ionizing particles for charge as low as $e/1000$.
- AGNESE 15 Fig. 6 for limits extending down to $Q = 1/200$.
- SAITO 90 candidates carry about 450 MeV/nucleon. Cannot be accounted for by conventional backgrounds. Consistent with strange quark matter hypothesis.
- MINCER 85 is high statistics study of calorimeter signals delayed by 20–200 ns. Calibration with AGS beam shows they can be accounted for by rare fluctuations in signals from low-energy hadrons in the shower. Claim that previous delayed signals including BJORNOE 68, DARDO 72, BHAT 82, SAKUYAMA 83b below may be due to this fake effect.
- SAKUYAMA 83b analyzed 6000 extended air shower events. Increase of delayed particles and change of lateral distribution above 10^{17} eV may indicate production of very heavy parent at top of atmosphere.
- BHAT 82 observed 12 events with delay $> 2. \times 10^{-8}$ s and with more than 40 particles. 1 eV has good hadron shower. However all events are delayed in only one of two detectors in cloud chamber, and could not be due to strongly interacting massive particle.
- MARINI 82 applied PEP-counter for TOF. Above limit is for velocity $= 0.54$ of light. Limit is inconsistent with YOCK 80 YOCK 81 events if isotropic dependence on zenith angle is assumed.
- YOCK 81 saw another 3 events with $Q = \pm 1$ and m about $4.5 m_p$ as well as 2 events with $m > 5.3 m_p$, $Q = \pm 0.75 \pm 0.05$ and $m > 2.8 m_p$, $Q = \pm 0.70 \pm 0.05$ and 1 event with $m = (9.3 \pm 3.) m_p$, $Q = \pm 0.89 \pm 0.06$ as possible heavy candidates.
- YOCK 80 events are with charge exactly or approximately equal to unity.
- BHAT 78 is at Kolar gold fields. Limit is for $\tau > 10^{-6}$ s.
- YOCK 74 events could be tritons.

Superheavy Particle (Quark Matter) Flux in Cosmic Rays

VALUE ($\text{cm}^{-2}\text{s}^{-1}\text{s}^{-1}$)	CL%	DOCUMENT ID	TECN	COMMENT
••• We do not use the following data for averages, fits, limits, etc. •••				
<5	$\times 10^{-16}$	90	1 ADRIANI	15 PMLA $4 < m < 1.2 \times 10^5 m_p$
<1.8	$\times 10^{-12}$	90	2 AMBROSIO	00B MCRO $m > 5 \times 10^{14}$ GeV
<1.1	$\times 10^{-14}$	90	3 ASTONE	93 CNTR $m \geq 1.5 \times 10^{-13}$ gram
<2.2	$\times 10^{-14}$	90	4 AHLEN	92 MCRO $10^{-10} < m < 0.1$ gram
<6.4	$\times 10^{-16}$	90	5 NAKAMURA	91 PLAS $m > 10^{11}$ GeV
<2.0	$\times 10^{-11}$	90	6 ORITO	91 PLAS $m > 10^{12}$ GeV
<4.7	$\times 10^{-12}$	90	7 LIU	88 BOLO $m > 1.5 \times 10^{-13}$ gram
<3.2	$\times 10^{-11}$	90	8 BARISH	87 CNTR $1.4 \times 10^8 < m < 10^{12}$ GeV
<3.5	$\times 10^{-11}$	90	9 NAKAMURA	85 CNTR $m > 1.5 \times 10^{-13}$ gram
<7.	$\times 10^{-11}$	90	10 ULLMAN	81 CNTR Planck-mass 10^{19} GeV
			10 ULLMAN	81 CNTR $m \leq 10^{16}$ GeV

- ADRIANI 15 search for relatively light quark matter with charge $Z = 1-8$. See their Figs. 2 and 3 for flux upper limits.
- AMBROSIO 00b searched for quark matter ("nuclearites") in the velocity range $(10^{-5}-1)$ c. The listed limit is for 2×10^{-3} c.
- ASTONE 93 searched for quark matter ("nuclearites") in the velocity range $(10^{-3}-1)$ c. Their Table 1 gives a compilation of searches for nuclearites.
- AHLEN 92 searched for quark matter ("nuclearites"). The bound applies to velocity $< 2.5 \times 10^{-3}$ c. See their Fig. 3 for other velocity/c and heavier mass range.
- NAKAMURA 91 searched for quark matter in the velocity range $(4 \times 10^{-5}-1)$ c.
- ORITO 91 searched for quark matter. The limit is for the velocity range $(10^{-4}-10^{-3})$ c.
- LIU 88 searched for quark matter ("nuclearites") in the velocity range $(2.5 \times 10^{-3}-1)$ c. A less stringent limit of 5.8×10^{-11} applies for $(1-2.5) \times 10^{-3}$ c.
- BARISH 87 searched for quark matter ("nuclearites") in the velocity range $(2.7 \times 10^{-4}-5 \times 10^{-3})$ c.
- NAKAMURA 85 at KEK searched for quark-matter. These might be lumps of strange quark matter with roughly equal numbers of u, d, s quarks. These lumps or nuclearites were assumed to have velocity of $(10^{-4}-10^{-3})$ c.
- ULLMAN 81 is sensitive for heavy slow singly charge particle reaching earth with vertical velocity 100–350 km/s.

Highly Ionizing Particle Flux

VALUE ($\text{m}^{-2}\text{yr}^{-1}$)	CL%	EVTs	DOCUMENT ID	TECN	COMMENT
••• We do not use the following data for averages, fits, limits, etc. •••					
<0.4	95	0	KINOSHITA	81B PLAS	Z/β 30-100

SEARCHES FOR BLACK HOLE PRODUCTION

VALUE	DOCUMENT ID	TECN	COMMENT
••• We do not use the following data for averages, fits, limits, etc. •••			
not seen	1 AABOUD	16P ATLS	13 TeV $pp \rightarrow e\mu, e\tau, \mu\tau$
	2 AAD	15AN ATLS	8 TeV $pp \rightarrow$ multijets
	3 AAD	14A ATLS	8 TeV $pp \rightarrow \gamma + \text{jet}$
	4 AAD	14AL ATLS	8 TeV $pp \rightarrow \ell + \text{jet}$
	5 AAD	14C ATLS	8 TeV $pp \rightarrow \ell + (\ell \text{ or jets})$
	6 AAD	13D ATLS	7 TeV $pp \rightarrow 2$ jets
	7 CHATRCHYAN	13A CMS	7 TeV $pp \rightarrow 2$ jets
	8 CHATRCHYAN	13AD CMS	8 TeV $pp \rightarrow$ multijets
	9 AAD	12AK ATLS	7 TeV $pp \rightarrow \ell + (\ell \text{ or jets})$
	10 CHATRCHYAN	12W CMS	7 TeV $pp \rightarrow$ multijets
	11 AAD	11AG ATLS	7 TeV $pp \rightarrow 2$ jets

- AABOUD 16P set limits on quantum BH production in $n = 6$ ADD or $n = 1$ RS models.
- AAD 15AN search for black hole or string ball formation followed by its decay to multijet final states, in pp collisions at $E_{\text{cm}} = 8$ TeV with $L = 20.3 \text{ fb}^{-1}$. See their Figs. 6–8 for limits.
- AAD 14A search for quantum black hole formation followed by its decay to a γ and a jet, in pp collisions at $E_{\text{cm}} = 8$ TeV with $L = 20 \text{ fb}^{-1}$. See their Fig. 3 for limits.
- AAD 14AL search for quantum black hole formation followed by its decay to a lepton and a jet, in pp collisions at $E_{\text{cm}} = 8$ TeV with $L = 20.3 \text{ fb}^{-1}$. See their Fig. 2 for limits.
- AAD 14C search for microscopic (semiclassical) black hole formation followed by its decay to final states with a lepton and ≥ 2 (leptons or jets), in pp collisions at $E_{\text{cm}} = 8$ TeV with $L = 20.3 \text{ fb}^{-1}$. See their Figures 8–11, Tables 7, 8 for limits.
- AAD 13D search for quantum black hole formation followed by its decay to two jets, in pp collisions at $E_{\text{cm}} = 7$ TeV with $L = 4.8 \text{ fb}^{-1}$. See their Fig. 8 and Table 3 for limits.
- CHATRCHYAN 13A search for quantum black hole formation followed by its decay to two jets, in pp collisions at $E_{\text{cm}} = 7$ TeV with $L = 5 \text{ fb}^{-1}$. See their Figs. 5 and 6 for limits.
- CHATRCHYAN 13AD search for microscopic (semiclassical) black hole formation followed by its evaporation to multiparticle final states, in multijet (including γ, ℓ) events in pp collisions at $E_{\text{cm}} = 8$ TeV with $L = 12 \text{ fb}^{-1}$. See their Figs. 5–7 for limits.
- AAD 12AK search for microscopic (semiclassical) black hole formation followed by its decay to final states with a lepton and ≥ 2 (leptons or jets), in pp collisions at $E_{\text{cm}} = 7$ TeV with $L = 1.04 \text{ fb}^{-1}$. See their Fig. 4 and 5 for limits.
- CHATRCHYAN 12W search for microscopic (semiclassical) black hole formation followed by its evaporation to multiparticle final states, in multijet (including γ, ℓ) events in pp collisions at $E_{\text{cm}} = 7$ TeV with $L = 4.7 \text{ fb}^{-1}$. See their Figs. 5–8 for limits.
- AAD 11AG search for quantum black hole formation followed by its decay to two jets, in pp collisions at $E_{\text{cm}} = 7$ TeV with $L = 36 \text{ pb}^{-1}$. See their Fig. 11 and Table 4 for limits.

REFERENCES FOR Other Particle Searches

AAD	21AL PRL 127 051802	G. Aad et al.	(ATLAS Collab.)
AAD	21BA JHEP 2111 2209	G. Aad et al.	(ATLAS Collab.)
AAD	21F PR D103 112006	G. Aad et al.	(ATLAS Collab.)
AAD	21X JHEP 2107 173	G. Aad et al.	(ATLAS Collab.)
AALJ	21V EPJ C81 261	R. Aaij et al.	(LHCb Collab.)
ACHARYA	21V PRL 126 071801	B. Acharya et al.	(MOEDAL Collab.)
AFEK	21 PR D104 012004	G. Afeke et al.	(YALE)
ALKHATIB	21A PRL 127 081802	I. Alkhatib et al.	(SuperCDMS)
ANDREEV	21 PRL 126 211802	Yu.M. Andreev et al.	(NA64 Collab.)
SIRUNYAN	21AF PR D104 052011	A.M. Sirunyan et al.	(CMS Collab.)
SIRUNYAN	21T EPJ C81 629	A.M. Sirunyan et al.	(CMS Collab.)
SIRUNYAN	21U PR D104 012015	A.M. Sirunyan et al.	(CMS Collab.)
TUMASYAN	21 PRL 127 261804	A. Tumasyan et al.	(ATLAS Collab.)
AAD	20AD PRL 125 131801	G. Aad et al.	(ATLAS Collab.)
AAD	20D PL B801 135114	G. Aad et al.	(ATLAS Collab.)
AAD	20J PR D101 052013	G. Aad et al.	(ATLAS Collab.)
AAD	20M PR D102 032006	G. Aad et al.	(ATLAS Collab.)
AAD	20P EPJ C80 450	G. Aad et al.	(ATLAS Collab.)
AAD	20T JHEP 2003 145	G. Aad et al.	(ATLAS Collab.)
AAD	20W JHEP 2006 151	G. Aad et al.	(ATLAS Collab.)
AALJ	20AL JHEP 2010 156	R. Aaij et al.	(LHCb Collab.)
AGUILAR-AR...	20B JHEP 2004 054	A. Aguilar-Arevalo et al.	(CONNIE Collab.)
BALL	20 PR D102 032002	A.H. Ball et al.	(MILLIQAN)
FEDDERKE	20 PR D101 115021	M.A. Fedderke, P.W. Graham, S. Rajendran	(STAN+)
SIRUNYAN	20A EPJ C80 3	A.M. Sirunyan et al.	(CMS Collab.)
SIRUNYAN	20AI JHEP 2005 033	A.M. Sirunyan et al.	(CMS Collab.)
SIRUNYAN	20AY PL B808 135578	A.M. Sirunyan et al.	(CMS Collab.)
SIRUNYAN	20C EPJ C80 75	A.M. Sirunyan et al.	(CMS Collab.)
SIRUNYAN	20N PL B806 135502	A.M. Sirunyan et al.	(CMS Collab.)
SIRUNYAN	20Z JHEP 2003 051	A.M. Sirunyan et al.	(CMS Collab.)
AABOUD	19AA EPJ C79 120	M. Aaboud et al.	(ATLAS Collab.)
AABOUD	19AE EPJ C79 481	M. Aaboud et al.	(ATLAS Collab.)
AABOUD	19AJ PL B795 56	M. Aaboud et al.	(ATLAS Collab.)
AABOUD	19AK PRL 122 151801	M. Aaboud et al.	(ATLAS Collab.)
AABOUD	19AM PR D99 052003	M. Aaboud et al.	(ATLAS Collab.)
AABOUD	19AO PR D99 052005	M. Aaboud et al.	(ATLAS Collab.)
AABOUD	19AT PR D99 092007	M. Aaboud et al.	(ATLAS Collab.)
AABOUD	19G PR D99 012001	M. Aaboud et al.	(ATLAS Collab.)
AABOUD	19H PR D99 012008	M. Aaboud et al.	(ATLAS Collab.)
AABOUD	19Q JHEP 1905 041	M. Aaboud et al.	(ATLAS Collab.)
AABOUD	19V JHEP 1905 142	M. Aaboud et al.	(ATLAS Collab.)
ALCANTARA	19 PR D99 103016	E. Alcantara, L.A. Anchordoqui, J.F. Soriano	
SIRUNYAN	19B PR D99 012005	A.M. Sirunyan et al.	(CMS Collab.)
SIRUNYAN	19BH PR D99 032011	A.M. Sirunyan et al.	(CMS Collab.)
SIRUNYAN	19BT PL B797 134876	A.M. Sirunyan et al.	(CMS Collab.)
SIRUNYAN	19CA PR D100 112003	A.M. Sirunyan et al.	(CMS Collab.)
SIRUNYAN	19CD PRL 123 231803	A.M. Sirunyan et al.	(CMS Collab.)
SIRUNYAN	19O JHEP 1902 074	A.M. Sirunyan et al.	(CMS Collab.)

Searches Particle Listings
Other Particle Searches

Table with 4 columns: Author(s), Experiment/Reference, Collaboration, and Notes. Lists various particle physics experiments and searches such as SIRUNYAN, AABOUD, AALTONEN, etc., along with their respective collaborations like ATLAS, CMS, and LHCb.

